 © 1989 The Chemical Society of Japan Bull. Chem. Soc. Jpn., 62, 1—4 (1989)

Natural-Abundance Oxygen-17 Magnetic Relaxation in Aqueous Solutions of Carbohydrates

Hisashi UEDAIRA,*,† Mitsuhiko IKURA,† and Hatsuho UEDAIRA††
†Department of Polymer Science, Faculty of Science, Hokkaido University, Sapporo 060
††Research Institute for Polymers and Textiles, Tsukuba, Ibaraki Pref. 305
(Received April 20, 1988)

The spin-lattice relaxation times, T_1, of $H_2{}^{17}O$ have been measured for aqueous solutions of several pentoses, hexoses, di-, and trisaccharides as a function of the concentration at 25 °C. The coordination numbers, n_h, and the rotational correlation times, τ_c^h, of water molecules around the sugars were estimated and compared with that of pure water, τ_c°. The value of $\tau_c^h/\tau_c^\circ=4.10$ for glucose is largest, while that of $\tau_c^h/\tau_c^\circ=2.82$ for ribose is the smallest, among these sugars. The value of n_h ($\tau_c^h/\tau_c^\circ-1$) was defined as the dynamic hydration number. The dynamic hydration numbers showed a good correlation with the mean number of the equatorial OH groups and the limiting diffusion coefficients.

Several attempts have been made to elucidate the relation between the hydration and the conformation of carbohydrates in aqueous solutions,[1] since Kabayama and Patterson[2] proposed a model that the conformation of β-D-glucose well matches the tridymite structure in water. Special attention has been paid to the fact that the sugar hydration is affected by the mean value of the number of equatorial OH groups, $n(e\text{-OH})$, existing in the various conformers of sugar ususally found in solutions.[3,4]

Recently, we reported that the values of partial molar heat capacities at infinite dilution,[5] the relative increments in the ultrasonic velocity,[6] and the limiting diffusion coefficients[7] of many pentose, hexose, and oligomers in aqueous solutions correlate well with $n(e\text{-OH})$. It was found that the denaturation temperatures of lysozyme and ovalbumin increase almost linearly with the $n(e\text{-OH})$ of the added sugars.[8,9] The permeable velocity of some hexose through the red cell membrane is inversely proportional to their values.[4] These results show that e-OH groups play an important role in the equilibrium, transport, and biochemical properties of aqueous solutions of sugars.

To prove the effect of $n(e\text{-OH})$ on the hydration of sugars, the magnetic relaxation method of oxygen-17 is extremely powerful, since the sugars possess exchangeable protons. As far as we know, Tait et al.[3] have measured only the linewidth of the NMR spectra of ^{17}O-enriched water in concentrated solutions of several monosaccharides. In this work, we report the spin-lattice relaxation times of the natural abundance ^{17}O of water for aqueous solutions of pentose, hexose, and oligosaccharides as a function of the concentration at 25 °C. The concentration dependence of the water-^{17}O relaxation rates is interpreted in terms of the effect of the e-OH groups on the sugar hydration. Then we discuss the relation between the diffusion coefficients and the dynamic hydration numbers of sugars.

Experimental

All of the sugars studied were of G. R. (Tokyo Kasei Co.) and has been purified by the method which has been reported previously.[8,10]

Distilled and deionized water was used.

All natural-abundance oxygen-17 NMR experiments were performed using a JEOL GX-500 spectrometer operating at 6.7 MHz. The oxygen-17 T_1 was measured by using the inversion recovery sequence (180°~τ~90°). For the oxygen-17 relaxation in neutral water, $T_2<T_1$ is observed in consequence of ^{17}O-^1H spin-spin coupling.[11] Therefore, the water and all the solutions were maintained at pH 3.5 by adding p-hydroxybenzoic acid,[3] since at this pH value the proton exchange becomes sufficiently fast, making $T_2=T_1$ in pure water.

The temperature was maintained at 25±0.3 °C by means of gas-thermostating.

Results and Discussion

The value of the oxygen-17 T_1 of water was 7.3 ms at 25 °C, in agreement with the data reported by Hindman et al. (6.8 ms).[12] In Figs. 1—3, the values of T_1°/T_1 for $H_2{}^{17}O$ in aqueous solutions of sugars are plotted against their concentrations, where T_1° and T_1 are the spin-lattice relaxation times of ^{17}O in pure water and

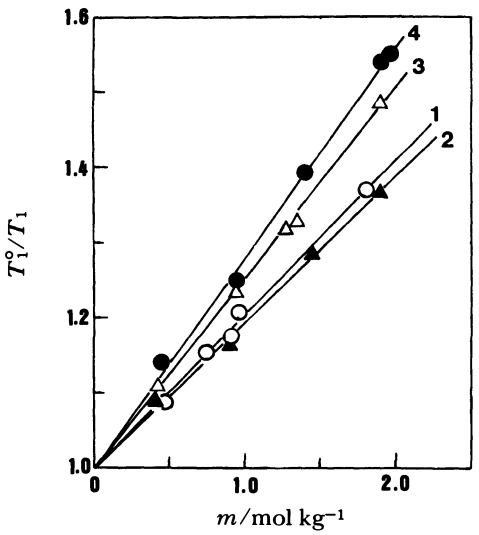

Fig. 1. T_1°/T_1 of $H_2{}^{17}O$ in solutions of monosaccharides as a function of the molality.
1 -○- deoxyribose; 2 -▲- ribose; 3 -△- arabinose; 4 -●- xylose.

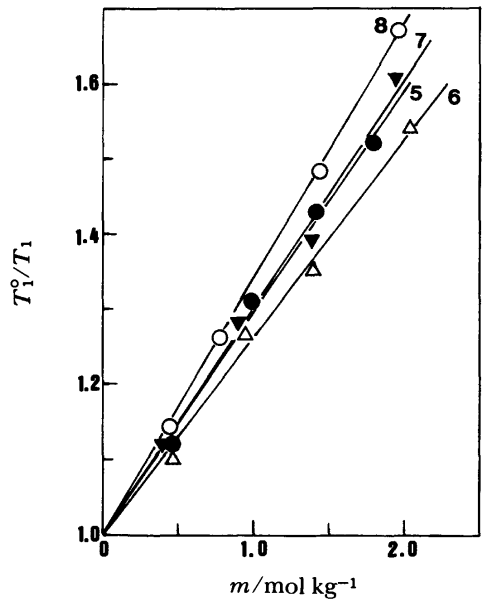

Fig. 2. T_1°/T_1 of $H_2{}^{17}O$ in solutions of monosaccharides as a function of the molality.
5 -●- fructose; 6 -△- mannose; 7 -▼- galactose; 8 -○- glucose.

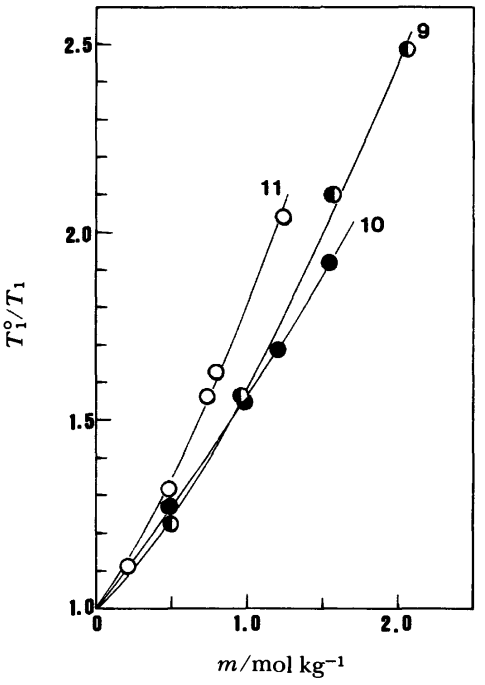

Fig. 3. T_1°/T_1 of $H_2{}^{17}O$ in solutions of oligosaccharides as a function of the molality.
9 -◐- sucrose; 10 -●- maltose; 11 -○- raffinose.

solutions respectively.

The values of T_1°/T_1 for sugar solutions are adequately represented by the empirical equation of this form:

$$T_1^\circ/T_1 = 1 + Bm + Cm^2 \qquad (1)$$

where m is the molality of the sugar. Especially, the values of T_1°/T_1 for monosaccharide solutions are well represented by the linear equation of molality, as is shown in Figs. 1 and 2. The solid line in these figures are those calculated by the least-squares method. The correlation coefficients were in the range of 0.997—0.990. The values of $55.5B$ (see Eq. 6) for sugars are given in the third colum in the table. The numbers on the lines and curves in all the figures denote the same sugars as in the table.

In the extreme motional narrowing condition, we obtain for the oxygen-17 relaxation rate:[13]

$$\frac{1}{T_1} = \frac{3}{125}\left(1 + \frac{\eta^2}{3}\right)\left(\frac{e^2qQ}{\hbar}\right)^2 \tau_c \qquad (2)$$

where η is an assymmetric parameter of the electrical field gradient, e^2qQ/h is the quadrupole coupling constant, and τ_c is the correlation time of molecular reorientation. The contribution of η will be omitted in the following discussion, since this value is usually small.[14] As the value of e^2qQ/h for pure water is 7.7 MHz,[3] we obtain τ_c°=2.4 ps from the value of T_1°; this is good agreement with the value (2.5 ps) which Hertz[14] obtained from the relaxation rate of the water protons.

In aqueous sugar solutions, the ^{17}O nuclei are distributed between two motional states with different intrinsic relaxation rates. If the exchange of water molecules between hydration water (mole fraction x_h) and bulk water is fast, the following relation is obtained;[15]

$$1/T_1 = (1 - x_h)/T_1^\circ + x_h/T_{1h} \qquad (3)$$

which, by the use of Eq. 2, can be rewritten as:[3,15]

$$\frac{T_1^\circ}{T_1} = 1 + n_h\left(K\frac{\tau_c^h}{\tau_c^\circ} - 1\right)\frac{m}{55.5} \qquad (4)$$

$$K \equiv (e^2qQ_h/\hbar)^2/(e^2qQ_0/\hbar)^2 \qquad (5)$$

where the subscripts h and zero refer to the water of the hydration sphere (cosphere) and bulk water respectively and n_h is the coordination number.[15] From a comparison of Eqs. 1 and 4, we obtain this relation;

$$55.5B = n_h\left(K\frac{\tau_c^h}{\tau_c^\circ} - 1\right) \qquad (6)$$

Then, if the value of n_h is known, we can estimate the value of τ_c^h/τ_c°. Since n_h is the number of the water molecule close to that of sugar, we supposed 6, 10, and 14 for mono-, di-, and trisaccharides respectively, according to Kabayama and Patterson's model.[2] Regarding the quadrupole coupling constant of hydration water, there are two viewpoints. It is usually assumed that e^2qQ/h is equal to that of pure water or ice. Generally, the former assumption is adopted in the case of electrolytes and nonelectro-

Table 1. Hydration Characteristics and Diffusion Coefficients of Sugars in Aqueous Solutions at 25 °C

No.	Sugar	$n(e\text{-OH})^{a)}$	$55.5B$	n_h	$\tau_c^h/\tau_c^{\circ b)}$	$\tau_c^h/\tau_c^{\circ c)}$	$D_0\times10^{10\,d)}$ / $m^2\ s^{-1}$
1	Deoxyribose	1.4	11.4	6	2.90		8.150
2	Ribose	2.1	10.9	6	2.82		7.795
3	Arabinose	2.6	14.0	6	3.32	4.38	
4	Xylose	3.5	15.5	6	3.58	4.72	7.495
5	Fructose	3	16.5	6	3.75	4.90	7.002
6	Mannose	3.3	14.7	6	3.45	4.55	
7	Galctose	3.6	16.6	6	3.76	4.96	
8	Glucose	4.6	18.6	6	4.10	5.41	6.75
9	Sucrose	6.3	25.2	10	3.52	4.64	5.223
10	Maltose	7.2	27.2	10	3.72	4.91	5.201
11	Raffinose	8.3	30.7	14	3.19	4.21	4.359

a) Refs. 5 and 7. b) $K=1$. c) $K=0.76$. d) Ref. 7.

lytes.[14,15] On the other hand, Tait et al.[3] took the e^2qQ/h value of ice as that of glucose and ribose solutions. According to these two assumptions for the value of e^2qQ/h, the values of K in Eq. 5 were calculated to be 1 and 0.76 respectively.

We show in the table the values of $n(e\text{-OH})$, n_h, and τ_c^h/τ_c° for each sugar. For monosaccharides, a sugar with more e-OH groups shows the larger value of τ_c^h/τ_c°. This means that the thermal motion of water molecules around sugar is more restricted than in bulk water and that the degree of restriction depends on $n(e\text{-OH})$. Glucose has the largest stabilization effect on the water structure. It is worthy of notice that the values of τ_c^h/τ_c° for deoxyribose and ribose with smaller $n(e\text{-OH})$ values than those of other sugars are smaller; that is to say, water molecules around both sugars are more mobile. This means that the assumption that the e^2qQ/h value of water in the hydration sphere equals that of ice is not appropriate in the case of these sugars. Accordingly, we did not use this assumption in calculating the values of τ_c^h/τ_c° for ribose and deoxyribose.

As is shown in the table, the values of τ_c^h/τ_c° for di- and trisaccharides are nearly equal to those of the constituted monosaccharides. Suggett and Clark[16] measured the dielectric relaxation of the concentrated sugar solutions and obtained the values of the dielectric relaxation, τ_r of water molecules in the hydration sphere. The values for glucose, mannose, maltose, and sucrose were 22.0, 21.0, 21.6, and 21.6 ps respectively,[17] which agree with the results of τ_c^h/τ_c° reported in this study. Recently, we also obtained the same τ_c^h/τ_c° value for the monomers and dimers of sulfonate ions.[18]

Previously, we calculated the translational frictional coefficients of oligomers in aqueous solutions and pointed out that the microviscosity around the oligomer is almost the same as that around the monomer.[19] Since the microviscosity around a solute molecule is closely related to the rotational correlation time of the solvent in the cosphere, the above results strongly support our idea. Thus, there is little correlation between $n(e\text{-OH})$ and τ_c^h/τ_c° for oligosaccharides.

The values of $n_h(\tau_c^h/\tau_c^\circ-1)$, which is equal to $55.5B$, is considered to signify the dynamic state of the water molecule in the cosphere relative to the bulk water formed by the same number of water molecules as the cosphere, as is clear from Eqs. 3 and 6. In this context, $n_h(\tau_c^h/\tau_c^\circ-1)$ is defined as the dynamic hydration number. The dynamic state of water molecules in the cosphere of sugar molecule depends on the interaction between water and sugar molecules, which is itself affected by $n(e\text{-OH})$. The number of water molecules in the cosphere is in proportion to the number of OH groups in the sugar molecule, as has been mentioned above. The e-OH groups are able to interact with water in a manner which forms a long-lived hydration structure, since e-OH groups on pyranose sugars match the unperturbed water lattice.[2] We proposed that the sugar molecule, which has a larger number of e-OH groups in a molecule, has a stronger stabilizing effect on the water structure.[4] It is reasonable, therefore, to express the stabilizing effect in the dynamic hydration number. The relation of the dynamic hydration number to $n(e\text{-OH})$ is shown in Fig. 4. This good correlation clearly indicates that the hydration of sugar is essentially determined by the $n(e\text{-OH})$ value.

Recently, we found that the limiting diffusion coefficients, D_0, of sugars in water serve as a linear function of $n(e\text{-OH})$. Therefore, it is of interest to examine the correlation between the dynamic hydration number and the value of D_0. The straight line shown in Fig. 5 is expressed in the following equation by the least-square method:

$$10^{10}D_0 = 10.15 - 0.1872(55.5B)\ (m^2\ s^{-1}) \qquad (7)$$

The first term on the right-hand side of Eq. 7 indicates the diffusion coefficient of a hypothetical molecule, which has the same interaction as a water–water one. If this hypothetical molecule is a ring formed by

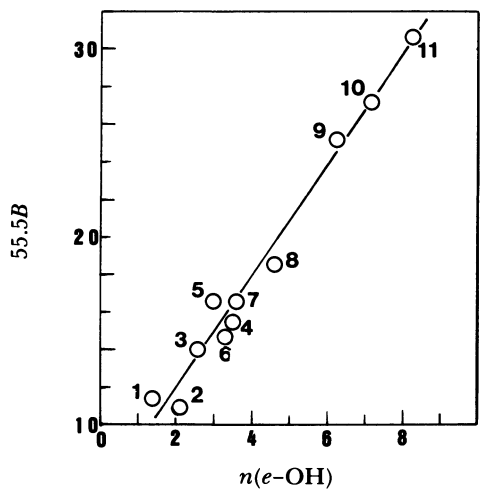

Fig. 4. The relation between $55.5B$ and $n(e\text{-OH})$. The numbers in figure denote the same sugar as in Table 1.

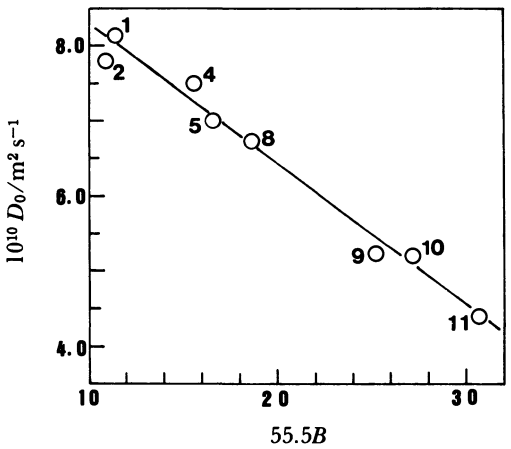

Fig. 5. The relation between D_0 and $55.5B$. The numbers in figure denote the same sugar as in Table 1.

several water molecules, we can calculate the D_0 value of the molecule by the use of the following equation:[19,20]

$$D_0 = D_w[11 \ln(L/r)/(6L/r)] \quad (8)$$

where D_w is the self-diffusion coefficient of pure water (2.3×10^{-9} m^{2}s^{-1} at 25 °C[21]). r is the radius of the water molecule, and L, the length of the ring. We obtain $D_0=10.4\times10^{-10}$ m^{2}s^{-1} for the ring consisting of four water molecules and $D_0=9.34\times10^{-10}$ m^{2}s^{-1} for the ring consisting of five such molecules. These results are reasonable in view of the model in which a molecule of monosaccharide is surrounded by six water molecules. Any other properties which depend on the sugar hydration may be consistently explained by the dynamic hydration number.

References

1) F. Franks, "Polysaccharides in Foods," ed by J. M. V. Blanshrd and L. R. Mitchel, Butterworths, London (1979), Chap. 3.
2) M. A. Kabayama and D. Patterson, *Can. J. Chem.*, **36**, 563 (1958).
3) M. J. Tait, A. Suggett, F. Franks, S. Ablett, and P. A. Quickenden, *J. Solution Chem.*, **1**, 131 (1972).
4) H. Uedaira, *Kagaku Sosetsu*, **11**, 191 (1976).
5) H. Uedaira and H. Uedaira, *J. Chem. Thermodynamics*, **17**, 901 (1985).
6) H. Uedaira and M. Ishimura, *Bull. Chem. Soc. Jpn.*, in press.
7) H. Uedaira and H. Uedaira, *J. Solution Chem.*, **14**, 27 (1985).
8) H. Uedaira and H. Uedaira, *Bull. Chem. Soc. Jpn.*, **53**, 2451 (1980).
9) H. Uedaira, *Sen-i Gakkaishi*, **37**, 436 (1982).
10) H. Uedaira and H. Uedaira, *Bull. Chem. Soc. Jpn.*, **42**, 2140 (1969).
11) S. Meiboom, *J. Chem. Phys.*, **34**, 375 (1961).
12) J. C. Hindman, A. Svirmickas, and M. Wood, *J. Phys. Chem.*, **74**, 1266 (1970).
13) A. Abragam, "The Principles of Nuclear Magnetism," Oxford University Press, London (1961).
14) H. G. Hertz, "Water," Vol. 3, ed by F. Franks, Plenum New York (1973), Chap.7.
15) H. G. Hertz, *Progress in NMR Spectroscopy*, **3**, 159 (1967).
16) A. Suggett and A. H. Clark, *J. Solution Chem.*, **5**, 1 (1976).
17) The relation between τ_c and τ_r is expressed as follows:[15]

$$1.5\tau_c < \tau_r < 3\tau_c$$

For example, the value of τ_c^h for glucose is 9.84 ps, satisfying this relation.
18) H. Uedaira and H. Uedaira, *Nippon Kagaku Kaishi*, **1986**, 1256.
19) H. Uedaira and H. Uedaira, *J. Phys. Chem.*, **74**, 2211 (1970).
20) R. Zwanzig, *J. Chem. Phys.*, **45**, 1858 (1966).
21) R. Mills, *J. Phys. Chem.*, **77**, 685 (1973).

 © 1989 The Chemical Society of Japan Bull. Chem. Soc. Jpn., 62, 5—10 (1989)

The Phase Transitions of 1,4-Dialkyl-1,4-diazoniabicyclo[2.2.2]octane Bis(tetrafluoroborate), C_n-DABCO-C_n-$(BF_4)_2$ ($10 \leqq n \leqq 22$)

Tohru TERADA, Takashi NOGAMI,* and Yasuhiko SHIROTA
Department of Applied Chemistry, Faculty of Engineering, Osaka University, Yamadaoka, Suita, Osaka 565
(Received May 27, 1988)

The phase transitions of a series of title compounds were investigated by means of DSC, IR absorption spectra, and measurements of ionic conductivities. All of the compounds exhibited phase transitions in the range of 77—110 °C. The IR absorption spectra clarified that conformational change in the alkyl chain occurred above the transition temperature. The temperature dependences of the ionic conductivities of BF_4^- showed conductivity jumps by a factor of 9—120 around the transition temperatures. A comparison of the DSC results and the ionic conductivities of BF_4-salts with those of the corresponding Br-salts showed that the former compounds have higher transition temperatures, smaller transition enthalpies (and, accordingly, smaller transition entropies), and smaller values of the conductivity jumps than the latter. These results show that BF_4-salts are more rigid than Br-salts in the low temperature phase and that the motion of the alkyl group of the former salts is less vigorous than the latter in the high-temperature phase. By observing the crystal with a polarization microscope under crossed Nicols condition, it was found that optical anisotropy was diminished gradually with the elevation of the temperature and disappeared completely above T_c without changing the crystal shape.

The phase transitions of various types of quaternary alkyl halide salts of 1,4-diazabicyclo[2.2.2]octane (DABCO) have been studied by means of measurements of the ionic conductivities of the halide anion, DSC, IR, and Raman spectroscopies.[1-7] Conductivity jumps of the halide anion by from two to three orders of magnitude were observed around the transition temperatures. The IR and Raman spectroscopies of the salts established that transitions are induced by the vigorous motion of the alkyl chain, accompanied with its conformational change.[8] Some of the unsymmetric bis(quaternary alkyl bromide) salts of DABCO gave a metastable state after having been heated above the transition temperature and then cooled.[4,5] The study of molecular motion in a solid is important as a model system for the melting of materials and the glass transition of polymers, etc. As an extension of the previous studies, we have investigated the phase transition of a series of symmetric bis(quaternary salts) of DABCO possessing the tetrafluoroborate anion. We adopted DABCO-BF_4 salts to see the effect of the different type of anion from the previous ones (spherical and monoatomic halide anion→tetrahedral and pentaatomic BF_4^-) on the phase transitions. The materials in this study will be abbreviated by the number of alkyl carbons. For example, 1,4-didodecyl-1,4-diazoniabicyclo[2.2.2]octane bis(tetrafluoroborate) is abbreviated to C_{12}-DABCO-C_{12}-$(BF_4)_2$. Thus, the materials in this study will generally be abbreviated as C_n-DABCO-C_n-$(BF_4)_2$.

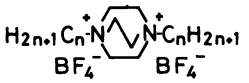

C_n-DABCO-C_n-$(BF_4)_2$

Experimental

Materials. All of the materials were synthesized by treating the corresponding C_n-DABCO-C_n-Br_2[1,2] with tetrafluoroboric acid. Table 1 summarizes the reaction media and precipitation media of C_n-DABCO-C_n-Br_2 and C_n-DABCO-C_n-$(BF_4)_2$ ($1 \leqq n \leqq 22$), the solvents of recrystallization, and the yields of C_n-DABCO-C_n-$(BF_4)_2$ after one recrystallization. C_n-DABCO-C_n-Br_2 ($1 \leqq n \leqq 9$) could not be purified by recrystallization because of their hygroscopic properties; therefore, they were directly used, without recrystallization, for the synthesis of tetrafluoroborate.[9] A protonated salt, H-DABCO-H-$(BF_4)_2$, was synthesized by the reaction of DABCO with tetrafluoroboric acid in ethyl alcohol; it is denoted as $n=0$ in Table 1. C_n-DABCO-C_n-$(BF_4)_2$ ($1 \leqq n \leqq 9$) and H-DABCO-H-$(BF_4)_2$ were recrystallized five times, and C_n-DABCO-C_n-$(BF_4)_2$ ($10 \leqq n \leqq 22$), three times, before the measurements. Most of the analytical data of C_n-DABCO-C_n-$(BF_4)_2$ ($10 \leqq n \leqq 22$) were satisfactory.[10] All of the materials decomposed above 300 °C without melting.

The synthetic method will be described for C_{16}-DABCO-C_{16}-$(BF_4)_2$ as typical. The reaction was conducted in a Teflon beaker. C_{16}-DABCO-C_{16}-Br_2 (0.723 g, 1 mmol) was dissolved into ethyl alcohol (20 ml), and then two molar amounts of tetrafluoroboric acid (42%) was stirred in. The homogeneous solution was then stirred into benzene (180 ml), and the mixture was cooled by ice in order to precipitate the product. The white precipitate was collected, dried in a vacuum, and recrystallized three times from ethyl alcohol.

Measurements. The ionic conductivities, DSC, and IR absorption spectra were measured by methods reported previously.[1,2]

Results and Discussion

DSC Measurements. The DSC measurements were made with a scan speed of 5 °C min^{-1}. C_n-DABCO-C_n-$(BF_4)_2$ ($10 \leqq n \leqq 22$) exhibited a single endothermic signal in the range of 77—110 °C. When they were

Table 1. Reaction and Precipitation Media,[a] Solvents of Recrystallization,[a] and Yields

n	C_n-DABCO-C_n-Br_2		C_n-DABCO-C_n-$(BF_4)_2$		Yield[d]
	Reaction/precipitation media	Solvent of recrystallization	Reaction/precipitation media	Solvent of recrystallization	%
0	—	—	EtOH/EtOH[c]	EtOH-H_2O	22.9
1	MeOH	b)	EtOH/EtOH[c]	EtOH-H_2O	43.2
2	MeOH	b)	EtOH/EtOH[c]	EtOH-H_2O	64.2
3	MeOH	b)	EtOH/EtOH[c]	EtOH-H_2O	21.1
4	MeOH	b)	EtOH/EtOH[c]	EtOH-H_2O	29.3
5	MeOH	b)	EtOH/EtOH[c]	EtOH-H_2O	40.0
6	MeOH	b)	EtOH/EtOH[c]	EtOH-H_2O	4.8
7	MeOH	b)	EtOH/EtOH[c]	EtOH-H_2O	21.1
8	MeOH	b)	EtOH/Bz	EtOH-H_2O	16.5
9	MeOH	b)	EtOH/Bz	EtOH-H_2O	6.3
10	MeOH/Bz	MeCN	EtOH/EtOH[c]	MeOH-Bz	40.0
11	MeOH/Ether	MeCN	EtOH/H_2O	MeOH-Bz	37.1
12	MeOH/Bz	MeCN	EtOH/H_2O	MeOH-Bz	43.2
13	MeOH/Ether	MeCN	MeOH/Bz	MeOH	65.8
14	MeOH/Bz	MeCN	MeOH/Bz	EtOH	86.4
15	MeOH/Ether	EtOH	MeOH/Bz	MeOH	82.4
16	MeOH/Bz	EtOH	EtOH/Bz	EtOH	82.3
17	MeOH/Bz	EtOH	MeOH/Bz	EtOH	86.2
18	MeOH/Bz	EtOH	EtOH/Bz	EtOH	74.5
22	MeOH/Bz	EtOH	EtOH/Bz	EtOH	78.2

a) MeOH=methyl alcohol, Bz=benzene, Ether=diethyl ether, MeCN=acetonitrile, EtOH=ethyl alcohol. b) Purification by recrystallization could not be done because of the hygroscopic property. c) The ethanol solution of the reaction was poured into a large amount of ethanol cooled by ice. d) Yields after one recrystallization.

Table 2. Transition Temperatures (T_c), Transition Enthalpies (ΔH), Transition Entropies (ΔS), and Ratios of the Ionic Conductivities below (σ_l) and above (σ_h) the Transition Temperature of C_n-DABCO-C_n-$(BF_4)_2$

n	T_c	ΔH	ΔS	σ_h/σ_l[a]
	°C	kJ mol^{-1}	J mol^{-1} deg^{-1}	
10	77	20.1	58	— (850)
11	84	23.7	66	14 (630)
12	89	40.5	112	42 (920)
13	95	34.8	94	13 (1500)
14	96	55.8	151	15 (1400)
15	99	42.7	115	47 (980)
16	102	67.8	181	20 (1200)
17	101	41.5	111	24 (3600)
18	106	74.1	196	120 (1400)
22	110	105.6	276	9 (2200)

a) The values in parentheses indicate σ_h/σ_l values observed for C_n-DABCO-C_n-Br_2 (after Ref. 2).

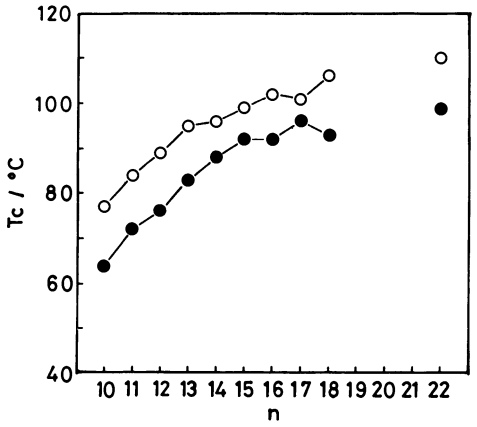

Fig. 1. The plot of the transition temperatures (T_c) against the carbon number of alkyl group (n) of C_n-DABCO-C_n-$(BF_4)_2$. The T_c-n plot of C_n-DABCO-C_n-Br_2 are also shown for the sake of comparison. ○ C_n-DABCO-C_n-$(BF_4)_2$, ● C_n-DABCO-C_n-Br_2.

cooled after having been heated above the transition temperature, they showed exothermic signals around the transition temperature. The values of the endothermic and exothermic heats of transition were almost equal, within the limits of experimental error. Thus, the phase transition is almost reversible. Part of Table 2 summarizes the transition temperatures, transition enthalpies, and transition entropies. The DSC signals expected for C_n-DABCO-C_n-$(BF_4)_2$ ($1 \leqq n \leqq 9$) were below the limit of sensitivity of the DSC apparatus. Figure 1 plots the transition temperatures (T_c) of C_n-DABCO-C_n-$(BF_4)_2$ ($10 \leqq n \leqq 22$) against the carbon number (n) of the alkyl group. T_c was obtained by the onset of the endothermic signal. This figure also shows the T_c-n plot of C_n-DABCO-C_n-Br_2 ($10 \leqq n \leqq 22$)[2] for the sake of comparison. T_c tends to increase with the increase in the carbon number of the alkyl group. As will be described below, the phase transition is induced by the vigorous motion of the alkyl chain above T_c. The increase in T_c with the increase in n is caused by the fact that the van der Waals force between alkyl groups of the neighboring molecules becomes larger as n increases, while the

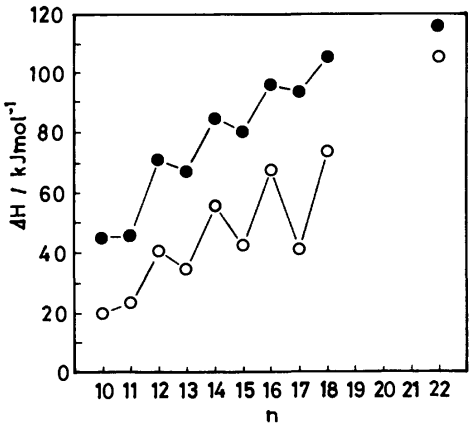

Fig. 2. The plot of the transition enthalpies (ΔH) against the carbon number of alkyl group (n) of C_n-DABCO-C_n-$(BF_4)_2$. The ΔH-n plot of C_n-DABCO-C_n-Br_2 are also shown for the sake of comparison. ○ C_n-DABCO-C_n-$(BF_4)_2$, ● C_n-DABCO-C_n-Br_2.

onset temperature of the motion of alkyl chain shifts to the higher temperature range with this increase. The transition temperatures of BF_4-salts were higher than those of the corresponding Br-salts. Thus, the former salts are harder than the latter in the low temperature phase. Figure 2 plots the transition enthalpies (ΔH) of C_n-DABCO-C_n-$(BF_4)_2$ ($10 \leqq n \leqq 22$) against the carbon number of the alkyl group (n). This figure also shows the ΔH-n plot of C_n-DABCO-C_n-Br_2 for the sake of comparison. The ΔH values of BF_4-salts were smaller than those of the corresponding Br-salts. The even-odd number effect of alkyl carbon on ΔH was clearly seen for BF_4-salts as well as Br-salts, and this effect became larger with the increase in n in BF_4-salts. It is well known that the melting points of normal alkanes show such an even-odd number effect. Accordingly, the distinct even-odd number effect shown in Fig. 2 suggests that the alkyl group of DABCO-salt plays an important role in the phase transitions. The plot of the transition entropies (ΔS) sgainst the carbon number of the alkyl group (not shown here) also showed an even-odd number effect similar to that in Fig. 2. The ΔS values of the BF_4-salts were likewise smaller than those of the Br-salts; this suggests that the motion of the alkyl group of the former salts is less vigorous than that of the latter in the high-temperature phase.

IR Absorption Spectroscopy. The temperature dependence of the IR-absorption spectra of C_{17}-DABCO-C_{17}-$(BF_4)_2$ was measured by means of the KBr method in order to gain more detailed information on the phase transitions. Figure 3 shows the IR spectra measured below and above the transition temperature (12 and 115 °C). The strong absorption around 1000—1150 cm^{-1} is ascribable to BF_4^-. The spectrum at 12 °C (Fig. 3(a)) exhibits fine structures (shown by the arrows). These structures are assigned to band

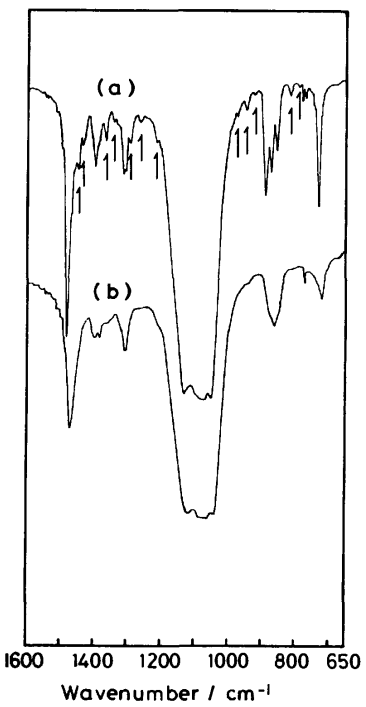

Fig. 3. IR absorption spectra of C_{17}-DABCO-C_{17}-$(BF_4)_2$.
(a) 12°C, (b) 115°C.

progressions of the alkyl chain[2] and are indicative of the trans-zigzag conformation of the alkyl chain in the low-temperature phase. Although a slight broadening was found, these band progressions were always observed with an elevation of the temperature up to the transition temperature. However, they disappeared suddenly around the transition temperature to give the structureless spectra shown in Fig. 3(b). The disappearance of the band progressions in the high-temperature phase indicates the conformational change in the alkyl chain induced by its vigorous motion in the solid.[2] Thus, the phase transitions of the present materials were attributable to be the same origin as C_n-DABCO-C_n-X_2 (X=Cl, Br, I).[1-7]

Ionic Conductivities. In the measurements of ionic conductivities, the charge carrier was usually determined by applying a DC voltage to the sample, while injecting the common carrier ion into the sample.[1,2] This was accomplished by mixing the authentic ionic conductor with the electrode material (graphite in many cases). Since the carrier concentration is maintained in such an experiment, the resistance of the sample does not change.[1] Unfortunately, since no BF_4^- conductor was reported, the above DC experiment could not be made for the present masterials. By analogy with previous studies,[1-7] C_n-DABCO-C_n-$(BF_4)_2$ is assumed to be the BF_4^- conductor. This assumption is plausible because, although the two candidates for the charge carrier[11] are quaternary DABCO cation and BF_4^-, the quaternary DABCO

cation is too big to transport in the solid. On the other hand, BF_4^- is much smaller than the quaternary DABCO cation, and can transport in the solid. In other words, if the quaternary DABCO cation, which occupies most of the volume of the material, could move in the solid, the materials would not remain solid, but would be converted into liquid, especially above T_c.

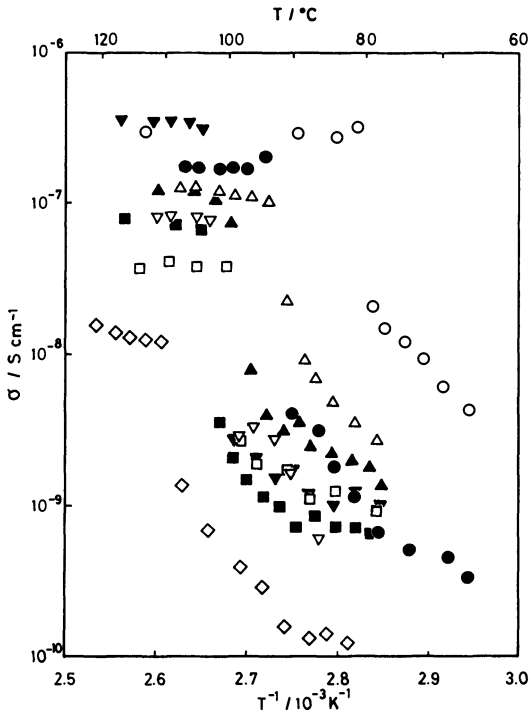

Fig. 4. Temperature dependence of the ionic conductivities of C_n-DABCO-C_n-$(BF_4)_2$.
○ n=11, ● n=12, △ n=13, ▲ n=14, □ n=15, ■ n=16, ▽ n=17, ▼ n=18, ◇ n=22.

The ionic conductivities were measured for compressed pellet samples by the AC method.[1,2] The temperature dependences of the ionic conductivities of C_n-DABCO-C_n-$(BF_4)_2$ are shown in Fig. 4. Conductivity jumps were observed within the temperature width of 1.7—5.7 °C[12] around the transition temperature[13] for all of the materials. Part of Table 2 summarizes the ratios of the ionic conductivities below (σ_l) and above (σ_h) the conductivity jumps. This table also shows the values of σ_h/σ_l in C_n-DABCO-C_n-Br_2 in parentheses for the sake of comparison. The σ_h/σ_l values of the BF_4-salts were found to be in the range of 9—120, whereas those of Br-salts were in the range of 850—3600.[2] Thus, the conductivity jumps of BF_4-salts were much smaller than those of Br-salts. This can be explained by the following reasons. The conductivity jumps proved to arise from the formation of voids (conduction channels) caused by the vigorous motion of the alkyl chain above T_c.[2-7] The DSC results showed that the motion of the alkyl chains of the BF_4-salts above T_c are less vigorous than those of the Br-salts. Therefore, the conduction channels of the BF_4^- are formed less effectively in the present materials than those of Br^- in C_n-DABCO-C_n-Br_2. Moreover, BF_4^- is a bigger anion than Br^-, and so the transport of BF_4^- is more retarded than that of Br^-. Accordingly, the ionic conductivities themselves of the BF_4-salts were lower than those of the Br-salts.[14] All of these effects lead to the smaller values of σ_h/σ_l for the BF_4-salts than those for the Br-salts. No correlation was found between the σ_h/σ_l values of C_n-DABCO-C_n-$(BF_4)_2$ ($11 \leqq n \leqq 22$) and those of the corresponding C_n-DABCO-C_n-Br_2 ($11 \leqq n \leqq 22$). Comparing the ionic conductivities themselves, C_n-DABCO-C_n-Br_2 showed almost identical values above T_c, irrespective of n,[2] although they were very different below T_c. On the other hand, the

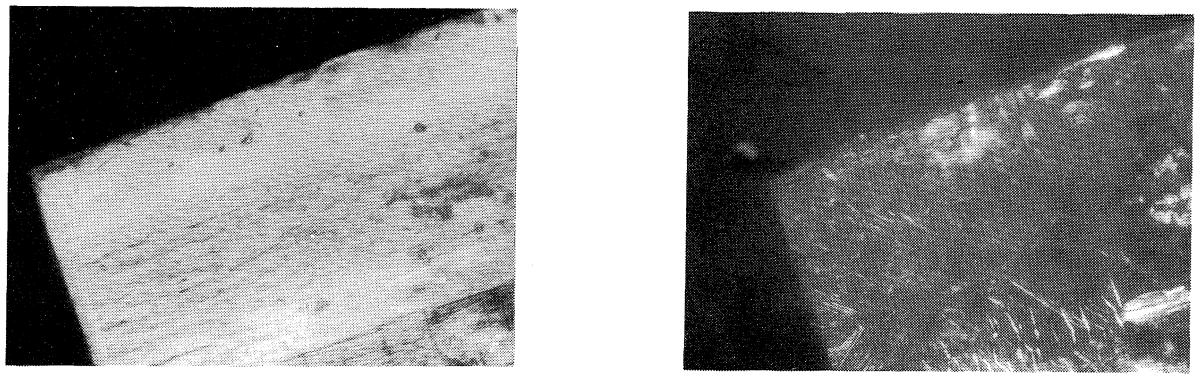

Fig. 5. Disapperance of optical anisotropy of C_{14}-DABCO-C_{14}-$(BF_4)_2$ observed by polarization microscope under a crossed Nicols condition.
(a) 60 °C, (b) 105 °C.

ionic conductivities of the present materials were very different below and above T_c. The reason for this remains to be clarified. The activation energies (ΔE) of the ionic conductivities were 0—13 and 16—94 kJ mol^{-1} above and below T_c respectively.[15] The small ΔE values of some of the materials above T_c suggest liquid-like anion transport in the solid.

Observation by Polarization Microscope. The IR absorption spectra of C_n-DABCO-C_n-$(BF_4)_2$ demonstrated a vigorous motion of the alkyl chain above T_c. The temperature dependence of the ionic conductivities of BF_4^- suggested a liquid-like anion transport above T_c. These phenomena can be visualized by observing the sample crystal under a polarization microscope. Figure 5 shows photographs of C_{14}-DABCO-C_{14}-$(BF_4)_2$ (T_c=96 °C) under a crossed Nicols condition at 60 and 105 °C as examples. The crystal looked bright far below T_c as a result of optical anisotropy (Fig. 5(a)). When the temperature of the sample was elevated, the optical anisotropy began to diminish around 80 °C, and it disappeared completely around 100 °C without changing the crystal shape (Fig. 5(b)). These phenomena were not so sharp as in the case of Br-salts.[16] In these cases, the disappearance of the optical anisotropy of the crystal occurred very sharply (within 1 °C). The wide temperature range of the disappearance of the optical anisotropy suggests that the movement of the alkyl group already begins below T_c and that it becomes more vigorous as the temperature is elevated. Although a single and sharp DSC signal was observed at T_c, it does not justify the simple picture that the movement of the alkyl group begins suddenly at T_c.[17]

Summary

The phase transitions of C_n-DABCO-C_n-$(BF_4)_2$ ($10 \leqq n \leqq 22$) were studied by means of DSC, the IR absorption spectra, and measurements of the ionic conductivities of BF_4^-. These materials exhibited conductivity jumps of BF_4^-, as in the cases of C_n-DABCO-C_n-X_2 (X=Cl, Br, I). The conductivity jumps were induced by the vigorous motion of the alkyl chain in the solid. A comparison of the conductivity jumps of BF_4-salts with those of Br-salts showed that the former gave smaller values of σ_h/σ_l by one to two orders of magnitude. When the T_c, ΔH, and ΔS values of BF_4-salts were compared with those of the corresponding Br-salts, the former were found to give higher T_c and smaller ΔH (and ΔS) than the latter. All of these experimental results led to the conclusions that BF_4-salts are harder than the corresponding Br-salts in the low-temperature phase and that the motion of the alkyl chain of the former salts is less vigorous than that of the latter in the high-temperature phase.

We are grateful to Professor Shigekazu Kusabayashi and Dr. Shunsuke Takenaka, Faculty of Engineering, Osaka University, for allowing us to use the DSC apparatus and the polarization microscope. The present work was supported by a Grant-in-Aid for Special Project Research on Chemical Sensors (No. 62217014) from the Ministry of Education, Science and Culture.

References

1) J. Shimizu, T. Nogami, and H. Mikawa, *Solid State Commun.*, **54**, 1009 (1985).

2) J. Shimizu, K. Imamura, T. Nogami, and H. Mikawa, *Bull. Chem Soc. Jpn.*, **59**, 1443 (1986).

3) K. Imamura, J. Shimizu, and T. Nogami, *Bull. Chem. Soc. Jpn.*, **59**, 2699 (1986).

4) J. Shimizu, K. Imamura, T. Nogami, and H. Mikawa, *Bull. Chem. Soc. Jpn.*, **59**, 3367 (1986).

5) K. Imamura, T. Nogami, and Y. Shirota, *Bull. Chem. Soc. Jpn.*, **60**, 111 (1987).

6) K. Imamura, T. Nogami, and Y. Shirota, *Bull. Chem. Soc. Jpn.*, **60**, 3499 (1987).

7) K. Imamura, T. Nogami, Y. Shirota, T. Ishioka, and M. Kobayashi, *Bull. Chem. Soc. Jpn.*, **60**, 3879 (1987).

8) The phase transition of DABCO has already been reported: T. Wada, E. Kishida, Y. Tomiie, H. Suga, S. Seki, and I. Nitta, *Bull. Chem. Soc. Jpn.*, **33**, 1317 (1960).

9) After the reaction, the methyl alcohol was evaporated to dryness and the residual solid was washed with hexane for $1 \leqq n \leqq 5$ or with benzene for $6 \leqq n \leqq 9$, and then dried in a vacuum.

10) Analytical data (%) of C_n-DABCO-C_n-$(BF_4)_2$ (Found/Calcd).

n=10:	C,	54.52/54.95;	H,	9.40/ 9.58;	N,	4.84/4.93.
n=11:	C,	56.39/56.24;	H,	9.82/ 9.80;	N,	4.61/4.70.
n=12:	C,	57.74/57.70;	H,	10.13/10.01;	N,	4.49/4.49.
n=13:	C,	58.89/58.90;	H,	10.26/10.19;	N,	4.22/4.29.
n=14:	C,	59.80/60.01;	H,	10.40/10.37;	N,	4.01/4.12.
n=15:	C,	60.85/61.02;	H,	10.57/10.53;	N,	3.95/3.95.
n=16:	C,	61.88/61.96;	H,	10.80/10.67;	N,	3.74/3.80.
n=17:	C,	62.74/62.83;	H,	10.81/10.81;	N,	3.65/3.66.
n=18:	C,	63.31/63.63;	H,	10.90/10.93;	N,	3.51/3.53.
n=22:	C,	65.76/66.36;	H,	11.25/11.36;	N,	3.02/3.10.

11) Since the samples were dried around 80 °C in a vacuum overnight before the measurements, the effect of the moisture on the ionic conductivity can be neglected.

12) The conductivity jumps were found to occur within the following temperature widths: 1.7 °C (n=11), 3.7 °C (n=12), 2.7 °C (n=13), 2.5 °C (n=14), 2.3 °C (n=15), 2.5 °C (n=16), 4.5 °C (n=17), 5.7 °C (n=18), 3.5 °C (n=22).

13) The transition temperatures of C_n-DABCO-C_n-$(BF_4)_2$, obtained by the use of the mid-points of the conductivity jumps, are as follows (they are close to those obtained by DSC (cf. Table 2)): 80 °C (n=11), 92 °C (n=12), 93 °C (n=13), 96 °C (n=14), 100 °C (n=15), 101 °C (n=16), 101 °C (n=17), 101 °C (n=18), 109 °C (n=22).

14) The ionic conductivities of BF_4-salts above T_c were by one to two orders of magnitude smaller than those of the Br-salts (cf. Ref. 2).

15) The activation energies (ΔE) of the ionic conductivities of C_n-DABCO-C_n-$(BF_4)_2$ are as follows (kJ mol^{-1}) (with the ranges of the temperature (°C) for the calculation of ΔE in the low-temperature phase shown in parentheses): Below

T_c: 55 (n=11, 67≦T≦79), 68 (n=12, 74≦T≦91), 56 (n=13, 79≦T≦89), 20 (n=14, 85≦T≦97), 32 (n=15, 79≦T≦98), 16 (n=16, 90≦T≦102), 94 (n=17, 87≦T≦98), 17 (n=18, 85≦T≦99), 65 (n=22, 88≦T≦107). Above T_c: 5 (n=11), 3 (n=12), 7 (n=13), 7 (n=14), 0 (n=15), 7 (n=16), 4 (n=17), 3 (n=18), 13 (n=22). The activation energies below the lower limit of the temperature shown in the parentheses are much smaller than those calculated especially for n=15, 16, 17, 18, and 22. The reasons for this remain to be clarified.

16) T. Nogami, *Kagaku*, **43**, 169 (1988).

17) Detailed measurements of the ^{1}H spin-lattice relaxation time of C_{10}-DABCO-C_{10}-X_2 (X=Br, I) demonstrated that the movement of the alkyl chain also begins below T_c. H. Nakayama, T. Eguchi, N. Nakamura, H. Chihara, T. Nogami, K. Imamura, and Y. Shirota, *Bull. Chem. Soc. Jpn.*, in press.

 © 1989 The Chemical Society of Japan Bull. Chem. Soc. Jpn., 62, 11—16 (1989)

Effect of Additives on Selective Formation of Isobutene from the CO-H_2 Reaction over ZrO_2

Ken-ichi MARUYA,* Takeshi FUJISAWA, Akihiro TAKASAWA, Kazunari DOMEN, and Takaharu ONISHI*

Research Laboratory of Resources Utilization, Tokyo Institute of Technology, 4259 Nagatsuta, Midori-ku, Yokohama 227

(Received June 22, 1988)

The CO-H_2 reaction over ZrO_2 was carried out in the presence of various organic additives. The addition of dimethyl ether, methylal, acetaldehyde, and dimethyl acetal showed the marked enhancement effects on the hydrocarbon formation keeping the high selectivity for isobutene. Ethylene was little effective. The addition of acetone, propanal, and propylene resulted in the decrease in the formation of isobutene and the increase in that of *n*-butenes. The presence of CO and H_2 was essential to the selective formation of isobutene. The formation pathways of isobutene and the other hydrocarbons are discussed.

The CO-H_2 reaction has been mostly performed using transition metal catalysts to produce a broad spectrum of compounds with linear carbon chains. Selective formation of saturated, branched-chain, aliphatic hydrocarbons has been carried out using the difficultly reducible oxide catalysts such as ThO_2[1] and Dy_2O_3[2] under very severe conditions and CdO catalysts combined with acid supports under mild conditions.[3] Recently, we found that the CO-H_2 reaction over ZrO_2 under mild conditions such as 673 K and atmospheric pressure produces isobutene selectively.[4,5]

The isosynthesis reaction[6] has been suggested to proceed via methanol which is formed as a primary product from CO and H_2.[1,2] He and Ekerdt[7,8] observed the appearance of methoxide species along with formate ion after the treatment of ZrO_2 with a mixture of CO and H_2 at reduced pressure and at reaction temperatures from 673 to 773 K followed by evacuation at 298 K, and proposed the following pathway for the formations of methanol and hydrocarbons from CO and H_2 over ZrO_2. This methanism is similar to that in the isosynthesis reaction, in that methanol is a precursor to hydrocarbons.

We have reported that the CO-H_2 reaction over ZrO_2 at 673 K forms the hydrocarbons consisting mainly of isobutene and that adsorbed species on the ZrO_2 surface during the reactions are both methoxide and formate species.[9] Therefore, the first question is how the methoxide species participates in the formation of hydrocarbons. We also reported that the formation path of isobutene is different from that of the other hydrocarbons such as C_2, C_3, and linear C_4 hydrocarbons on the basis of their different dependences on the reaction temperature and CO pressure,[5] i.e., the yields of C_2, C_3, and linear C_4 hydrocarbons are linearly plotted by the Arrhenius equation in the wide temperature range from 473 to 723 K, while that of isobutene increases rapidly above 573 K and the activation energy for the formation of isobutene is much higher than those of the other hydrocarbons. Furthermore, the formation rate of isobutene depends on the CO pressure nearly in the second order, while those of the other hydrocarbons do not. Therefore, the second question is how the formation of isobutene is correlated with that of the other hydrocarbons. Here we describe the relation of surface methoxide species to the formation of hydrocarbons and the effect of addition of various organic compounds having the carbon chain from C_1 to C_3 to the CO-H_2 reaction on the formations of isobutene and the other hydrocarbons.

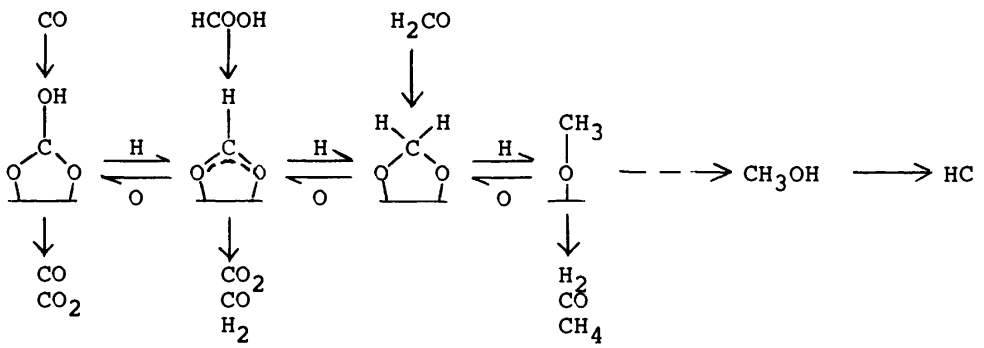

Experimental

Materials. ZrO_2 was prepared as described previously.[5] H_2 was purchased from Showa Denko Co. CO, ethylene, and propylene were purchased from Takachiho Kagaku Kogyo K. K. Iron carbonyl in CO gas was removed by active carbon cooled at Dry Ice or liquid nitrogen temperature. Oxygenates were purchased from Kanto Chemical Co. and used without further purification.

Procedures. Reactions were carried out in a conventional flow system with a quartz reactor of 12 mm in diameter and a glass vacuum system with a gas-circulating pump. The flow reactions with organic additives were carried out at 1 atm total pressure and at the total flow rate of 100 ml·min^{-1}. Feed of dimethyl ether was controlled finely by two needle valves and its concentration was determined by G.C. The other organic compounds were added using syringe. The glass vacuum system was used for the investigation of time course of the CO–H_2 reaction. Products were analyzed by GC as described previously.[5]

Results

1) Reaction of Methanol. The reaction of methanol over isosynthesis catalysts at 723 K and 300 atm has been reported to form the products of the same hydrocarbon distribution as the CO–H_2 reaction.[1,2] On the other hand, the reaction of methanol over ZrO_2 under mild conditions such as 643 K and 0.23 kPa of the methanol partial pressure produced only dimethyl ether in the steady state. Since the CO–H_2 reaction in the presence of 0.25 kPa of water produced only CO_2 of 0.15 kPa, no formation of hydrocarbons in the methanol reaction over the ZrO_2 catalyst will be due to the inhibition of the further reaction of dimethyl ether for the hydrocarbon formation by water.

2) Reaction of Dimethyl Ether. Since dimethyl ether is an anhydride of methanol, the reaction of dimethyl ether is expected to occur without the inhibition by water. Table 1 shows the conversion of dimethyl ether and the distribution of hydrocarbons formed. Increasing the feed of dimethyl ether from 0.012 to 2.5 ml·min^{-1} decreases the conversion from 99 to 28% and the total yield of C_1 to C_6 hydrocarbons based on the dimethyl ether consumed from 72 to 6%. At the highest feed, 50% of dimethyl ether consumed decomposes into CO and H_2. One of the reasons why the increase in the feed of dimethyl ether results in the low yield of hydrocarbons is likely that the decomposition of dimethyl ether increases with an increase in the feed. The product distribution in Table 1 shows that the reaction of dimethyl ether alone yields a broad spectrum of hydrocarbons. Although the highest yield in the hydrocarbons is achieved in C_2 hydrocarbons, the yield is low.

The addition of H_2 to the dimethyl ether reaction leads to the higher yield of hydrocarbons, which

Table 1. Effect of Additives to CO–H_2 Reaction on Hydrocarbon Yields[a]

Run	Feed rate/ml min^{-1}				DME conv.
	N_2	H_2	CO	DME	%
1	91	0	0	0.012	99
2	91	0	0	0.04	99
3	91	0	0	0.48	80
4	91	0	0	2.5	28
5	54	36	0	0.12	100
6	18	36	36	0	–
7	18	36	36	0.05	100
8	18	36	36	0.12	100
9	18	36	36	0.39	100
10	18	36	36	2.2	95
11	18	36	36	0.14[c]	100

Run	Hydrocarbon yield/carbon base μmol min^{-1}								$\sum C_i$[b]
	CO	CO_2	C_1	C_2	C_3	C_4	C_5	C_6	2(DME consumed) %
1	–	0	0.11	0.25	0.27	0.08	0.06	+	72
2	–	0	0.19	0.23	0.22	0.14	0.29	+	30
3	–	0	1.3	2.8	0.64	1.1	0.60	+	15
4	63	0	1.8	6.9	1.5	2.3	0.48	0.28	6
5	–	–	0.89	1.7	0.85	0.78	0.26	0.02	41
6	–	3.2	0.03	0.14	0.17	2.3	0.25	+	–
7	–	6.1	0.38	0.57	0.41	3.5	0.53	–	121
8	–	9.2	0.34	0.61	0.65	5.2	0.43	0.01	68
9	–	5.7	1.4	2.7	2.1	8.3	0.48	0.01	43
10	64	7.5	17	27	12	29	6.6	1.2	50
11	–	–	1.3	0.9	0.45	4.2	0.65	0.06	41[d]

a) ZrO_2: 4.0 g, reaction temperature: 643 K. b) Sum of carbon base yield of C_1 to C_6 hydrocarbons. c) Methylal was used instead of dimethyl ether. d) $\sum C_i/3$ (methylal consumed).

consist mainly of alkanes as shown in Table 1. The addition of CO instead of H_2 resulted in the rapid deactivation giving methane selectively.

3) Reaction of Dimethyl Ether in the Presence of CO and H_2. The conversion of dimethyl ether and the distribution of hydrocarbons formed in the presence of CO and H_2 are presented in Table 1. It is clear from the higher conversion of dimethyl ether and the higher yields of hydrocarbons that the presence of either CO or H_2 improves the reactivity of dimethyl ether. The main products are C_2 and C_4 hydrocarbons. The effect of CO and H_2 is particularly remarkable for the formation of C_4, because it is rather minor products in the absence of both CO and H_2. The yield of C_4 hydrocarbons in the absence of CO and H_2 is so low that it does not overcome the amount in the CO–H_2 reaction without dimethyl ether. The three reactant system of dimethyl ether, CO, and H_2 forms C_4 with much higher yield. The maximum yield is obtained at 2.2 ml·min^{-1} of the feed, above which the yield decreases with an increase in the feed.

Table 2 shows the isomer distribution in the C_4 hydrocarbons. In the absence of CO and H_2 the selectivity of isobutene increases, as the feed of dimethyl ether increases. In the presence of CO and H_2 the selectivity to isobutene is more than 90%.

At the dimethyl ether feed of 2.2 ml·min^{-1} in the three reactant system, the concentration of CO in the outlet of catalyst bed was higher by 4% than that in the inlet. This means that a large amount of dimethyl ether decomposes into CO and H_2 despite of the presence of CO and H_2. The carbon balance from CO formed and the hydrocarbons recovered shows that 16% of dimethyl ether consumed is still unrecovered, even though the decomposition into CO and H_2 is taken into account.

4) Relation between Formations of Methanol and Hydrocarbons. The enhancement effect of dimethyl ether on the isobutene formation mentioned above stimulated us to investigate the relation between the formation of methanol and hydrocarbons at low temperatures, where methanol is main in the products, the selectivity of isobutene in hydrocarbons is low,[5] and methoxide is one of the main adsorbed species on the catalyst surface.[9]

The time courses of the formation of methanol and dimethyl ether in the CO–H_2 reaction over ZrO_2 at 473 and 523 K are shown in Fig. 1. There are induction

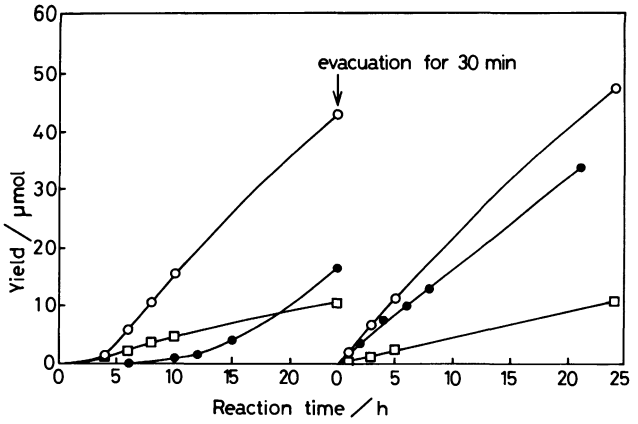

Fig. 1. Time course of methanol and dimethyl ether yields from CO and H_2 (CO/H_2=1/3) at 69 kPa over ZrO_2.
-●-; methanol at 473 K, -○-; methanol at 523 K, and -□-; dimethyl ether.

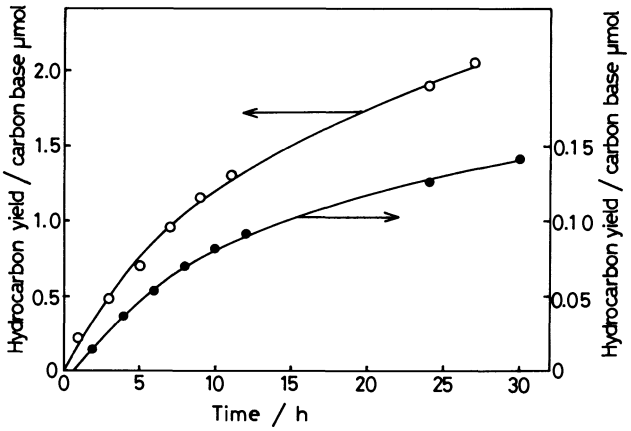

Fig. 2. Time course of hydrocarbon yields from CO and H_2 (CO/H_2=1/3) at 69 kPa over ZrO_2.
-●-; 473 K (hydrocarbon distribution after 24 h reaction is C_1: 18, C_2: 26, C_3: 12, C_4: 10 μmol, and C_5^+: trace), -○-; 523 K (hydrocarbon distribution after 24 h reaction is C_1: 56, C_2: 42, C_3: 12, C_4: 20 μmol, and C_5^+: trace).

Table 2. Isomer Distribution in C_4 Hydrocarbons

Run	Feed rate/ml·min^{-1}				Selectivity/%				
	N_2	CO	H_2	DME	C_4H_{10}	1-C_4H_8	t-2-C_4H_8	c-2-C_4H_8	i-C_4H_8
1	91	0	0	0.01	4	+	20	23	53
2	91	0	0	0.43	5	+	11	15	69
3	91	0	0	0.7	+	+	11	12	77
4	91	0	0	6.2	+	+	5	3	92
5	18	36	36	0	+	1	1	1	97
6	18	36	36	0.23	+	+	5	3	92
7	18	36	36	0.7	2	+	2	3	93
8	18	36	36	4.4	+	+	2	1	97
9	18	36	36	6.1[a]	+	+	2	1	97

a) Methylal was used instead of dimethyl ether.

Table 3. Effect of Olefin Addition to CO-H_2 Reaction on Hydrocarbon Distribution[a]

Run	Olefin[b]	Temp	Product/C-base μmol·min^{-1}				
		K	C_1	C_2	C_3	C_4	C_5
1	—	643	0.02	0.14	0.20	2.7	0.18
2	Ethylene	643	0.25	c)	1.2	6.0	0.20
3	—	633	0.08	0.26		2.1	0.10
4	Propylene	633	0.18	0.24	c)	2.4	0.10

Run	Selectivity in C_4 hydrocarbons/%				
	C_4H_{10}	1-C_4H_8	t-2-C_4H_8	c-2-C_4H_8	i-C_4H_8
1	+	+	1.5	1.5	97
2	1	+	2	2	84
3	+	+	1.5	1.5	97
4	1	14	26	24	35

a) Catalyst: 5.0 g, feed rate: 100 ml·min^{-1} ($CO/H_2/N_2$=40/40/20). b) Feed rate of olefin: 1.0 ml·min^{-1}. c) Conversions of olefins were less than few %.

Table 4. Effect of Oxygenate Addition to CO-H_2 Reaction on Hydrocarbon Distribution[a]

Run	Oxygenate	Product/carbon base μmol·min^{-1}					Selectivity in C_4 hydrocarbons/%				
	μmol·min^{-1}	C_1	C_2	C_3	C_4	C_5	C_4H_{10}	1-C_4H_8	t-2-C_4H_8	c-2-C_4H_8	i-C_4H_8
1	$C_2H_5OC_2H_5$ (96)	0.20	29	0.90	0.08	1.9	—	—	—	—	—
2	CH_3CHO[b] (1.2)	0.17	1.2	1.0	9.2	0.7	+	+	1	2	97
3	$CH_3CH(OCH_3)_2$ (2.2)	0.2	0.4	0.18	4.4	0.2	1	+	1	1	97
4	CH_3CH_2CHO (0.3)	0.2	0.4	2.7	0.40	5.0	18	17	29	29	24
5	CH_3COCH_3 (2.8)	0.34	0.30	2.2	0.44	0.15	—	—	—	—	—

a) Catalyst: 5.0 g, feed rate: 100 ml·min^{-1} ($CO/H_2/N_2$=40/40/20), temperature: 643 K. b) Acetaldehyde was used as a solution of methylal (12 μmol·min^{-1}).

times of 12 and 3 h for the formation of two oxygen-containing products at the temperatures, respectively. However, the induction times disappear in the repeated reaction after the reaction for 24 h followed by the evacuation for 30 min at the same temperatures.

At 523 K the CO-H_2 reaction was carried out for 1 h, during which no product was detected except for hydrocarbons by G.C. However, when the products trapped at liquid nitrogen temperature was dissolved into water and analyzed using GC-MS, a small amount of formaldehyde was detected. Almost the same amount of formaldehyde was found in the products collected from initial 1 to 2 h. Thus, within the induction time for methanol formation, hydrocarbons and formaldehyde were already formed.

On the other hand, the formation of hydrocarbons at 473 and 523 K is accompanied by no or a short induction time as shown in Fig. 2. The hydrocarbon distributions are rather similar to that in the reaction of dimethyl ether alone.

5) Effect of Organic Additives on the Formation of Isobutene. Table 3 shows the effect of the addition of ethylene and propylene to the CO-H_2 reaction. The addition of them seems to affect little the yield of hydrocarbons. However, in the addition of propylene, the main isomer in C_4 hydrocarbons changes into 1- and 2-butenes, although in the case of ethylene it is still isobutene.

Table 4 shows the effect of the addition of C_2 and C_3 oxygenates. The addition of diethyl ether only leads to produce mainly ethylene and C_4 hydrocarbons are minor. Acetaldehyde markedly enhanced the yield of hydrocarbons keeping the high selectivity for isobutene for initial few hours, after which the activity and selectivity were rapidly lowered to form yellow oily products. As it was very hard to control the amount of acetaldehyde added, dimethy acetal was used instead of C_2 aldehyde. The reaction was stable to form the higher yield of hydrocarbons with the high selectivity for C_4 hydrocarbons as shown in Table 4.

The addition of propanal leads to the decrease of C_4 hydrocarbons and the increase of the other hydrocarbons, especially C_5. The main isomer in C_4 hydrocarbons is changed from isobutene with the selectivity of 97% in the absence of propanal to 1- and 2-butenes with that of 75% in the presence of propanal. The addition of acetone also leads to the decrease of C_4 hydrocarbons. The most of acetone is converted to propylene.

Discussion

1) The Formation of C_2, C_3, and Linear C_4 Hydrocarbons. The treatment of ZrO_2 evacuated at 993 K with a mixture of CO and H_2 at room temperature results in the formation of some paraformaldehyde type adsorbed species.[5] The CO–H_2 reaction over ZrO_2 at 523 K produced formaldehyde in the initial stage of the reaction during the induction time for the formation of methanol and dimethyl ether. On the other hand, disappearance of induction time in repeated reaction shown in Fig. 1 may indicate that the induction time means the time taken to accumulate a surface intermediate which is not easily removed by evacuation at 523 K. Since formate and oxymethylene species on oxide surfaces are adsorbed forms of formyl and formaldehyde, respectively,[9–11] the formation of formaldehyde and methanol with and without induction time, respectively, may indicate the following relation of relative rates at the low temperatures,

$$CO + H_2 \longrightarrow CH_xO_y(a) \rightarrow \begin{cases} \xrightarrow{\text{fast}} CH_2O(g) \\ \xrightarrow{\text{slow}} CH_3O(a) \end{cases}$$

where $CH_xO_y(a)$ means adsorbed species such as formate, formyl, or formaldehyde.

On the other hand, the time course of hydrocarbon formations at 523 and 473 K shows no or a short induction time as shown in Fig. 2. Therefore, the hydrocarbons are not formed via methanol or methoxide species. Although dissociation of CO is possible for the common Fischer-Tropsch catalyst metals and polymerization of CH_2 formed from the carbon atoms and hydrogen is proposed as the mechanism of hydrocarbon formation,[12] there has been no report on the cleavage of C–O bond over oxide catalysts which requires a multiple catalyst site. We have no evidence for the cleavage also in the case of the reaction over ZrO_2. Since formaldehyde is formed without induction time, $CH_xO_y(a)$ is a possible candidate of the intermediate in the hydrocarbon formation. The formose reaction to form various carbohydrates having carbon-carbon bonds from formaldehyde in the presence of base catalysts[13] and the cleavage of carbon-oxygen bond of formaldehyde coordinated on zirconium complex[14] may suggest the possible pathway of direct hydrocarbon formation from the intermediate. Since the formation of C_2, C_3, and linear C_4 hydrocarbons are plotted by Arrhenius equation in the temperature range between 473 and 723 K, the formation path must be the same in the wide temperature range between 473 and 723 K.

2) The Formation of Isobutene. The formation of branched-chain hydrocarbons from CO and H_2 has been described by the pathway via the reaction of carbonyl of formaldehyde, acetaldehyde, and acetone coordinated on ZrO_2 with CO or methoxide species.[15,16] However, the present results that the addition of acetone or propanal to a mixture of CO and H_2 results in the decrease of C_4 hydrocarbons eliminate the formation of isobutene by either the carbonylation of acetone or propanal or the aldol condensation-type reaction of propanal.

The second order dependence of the isobutene formation on CO pressure[5] suggests that the formation of C_2 species from C_1 species is a slow process. The marked enhancement effect of C_2 oxygenate such as acetaldehyde or acetal on the isobutene formation may support the suggestion. On the other hand, the enhancement effect of dimethyl ether and the indispensability of CO and H_2 shown in Table 1 may suggest that methoxide or CH_xO_y species formed from dimethyl ether reacts with CO and H_2 to form the C_2 species. In the temperature range where isobutene is selectively formed, methanol and dimethyl ether are formed so fast as to be in equilibrium with a gas of CO and H_2. Thus, the following pathway is written. Further detailed mechanism is under investigation.

$$\left[\begin{matrix} CO + H_2 \\ \text{or} \\ CH_3OCH_3 \end{matrix}\right] \rightarrow \left[\begin{matrix} CH_xO_y(a) \\ \text{or} \\ CH_3O(a) \end{matrix}\right] \xrightarrow[CO + H_2]{\text{slow}} C_2 \text{ species}$$

$$\xrightarrow[CO + H_2]{\text{fast}} \xrightarrow[CO + H_2]{\text{fast}} CH_2{=}C(CH_3){-}CH_3$$

References

1) H. Pichler and K. H. Ziesecke, *Brennst. Chem.*, **30**, 13, 60, 81, 333 (1949).

2) R. Kieffer, J. Varela, and A. Deluzaruche, *J. Chem. Soc., Chem. Commun.*, **1983**, 763.

3) J. T. Miller and T. D. Nevitt, *J. Catal.*, **103**, 512 (1987).

4) T. Maehashi, K. Maruya, K. Domen, K. Aika, and T. Onishi, *Chem. Lett.*, **1984**, 747.

5) K. Maruya, T. Maehashi, T. Haraoka, S. Narui, Y. Asakawa, K. Domen, and T. Onishi, *Bull. Chem. Soc. Jpn.*, **61**, 667 (1988).

6) E. M. Cohn, "Catalysis," ed by P. H. Emmett, Vol. 4, Reinhold, New York (1956) p. 443.

7) M.-Y. He and J. G. Ekerdt, *J. Catal.*, **87**, 381 (1984).

8) M.-Y. He and J. G. Ekerdt, *J. Catal.*, **87**, 238 (1984); **90**, 17 (1984); **101**, 90 (1986).

9) H. Abe, K. Maruya, K. Domen, and T. Onishi, *Chem. Lett.*, **1984**, 1875.

10) T. Onishi, H. Abe, K. Maruya, and K. Domen, *J. Chem. Soc., Chem. Commun.*, **1986**, 103.

11) G.-W. Wang and H. Hattori, *J. Chem. Soc., Faraday Trans. 1*, **80**, 1039 (1984); G. Busca, J. Lamotte, J.-C. Lavalley, and V. Lorenzelli, *J. Am. Chem. Soc.*, **109**, 5197 (1987).
12) R. C. Brady III and R. Pettit, *J. Am. Chem. Soc.*, **103**, 1287 (1981).
13) e.g., T. Matsumoto, H. Yamamoto, and S. Inoue, *J. Am. Chem. Soc.*, **106**, 4829 (1984); Y. Shigemasa, Y. Sasaki, N. Ueda, and R. Nakashima, *Bull. Chem. Soc. Jpn.*, **57**, 2761 (1984).
14) G. Erker, *Acc. Chem. Res.*, **17**, 103 (1984).
15) T. J. Mazanec, *J. Catal.*, **98**, 115 (1986).
16) S. C. Tseng, N. B. Jackson, and J. G. Ekerdt, *J. Catal.*, **109**, 284 (1988).

 © 1989 The Chemical Society of Japan Bull. Chem. Soc. Jpn., 62, 17—22 (1989)

The Magnetic Predissociation of the $B^3\Pi_{0^+u}$ State of the Iodine Molecule

Masaaki BABA,* Misako KIMURA, Toshiyuki TSUBOI, Hajime KATÔ, and Saburo NAGAKURA†

Department of Chemistry, Faculty of Science, Kobe University, Nada-ku, Kobe 657

†Institute for Molecular Science, Myodaiji, Okazaki 444

(Received July 4, 1988)

It is shown that the predissociation of I_2 excited to the $B^3\Pi_{0^+u}$ state can occur through the coupling with the $2431^1\Pi_u$ state by gyroscopic and Zeeman interactions. The interaction matrix elements between the $B^3\Pi_{0^+u}$ and $2431^1\Pi_u$ states are shown to be nonzero, for the $2431^1\Pi_u$ state is mixed significantly with the $2431^3\Pi_{1u}$ state by the spin-orbit interaction. The v, J dependence of the magnetic-quenching ratios of the $B^3\Pi_{0^+u}$–$X^1\Sigma_g^+$ fluorescence intensity has been measured and analyzed. The rate constants of the magnetic predissociation in the $B^3\Pi_{0^+u}$ state have also been evaluated. The magnetic-field dependence of the hyperfine structure has been measured by means of the Doppler-free intermodulated fluorescence method.

In 1913, Steubing[1] found the quenching of the $B^3\Pi_{0^+u}$–$X^1\Sigma_g^+$ fluorescence by an external magnetic field. Turner[2] suggested that it was due to magnetic predissociation in the $B^3\Pi_{0^+u}$ state. Van Vleck[3] suggested that the mixing of the $B^3\Pi_{0^+u}$ state with the repulsive $^3\Pi_{0^-u}$ state causes the magnetic predissociation. The rate constants were determined by studies of the magnetic quenching of the fluorescence intensity.[4,5]

The natural predissociation (predissociation in a zero magnetic field) of the $B^3\Pi_{0^+u}$ state was found by analyzing the fluorescence lifetime and the absorption strength.[6–9] The vibrational quantum-number dependence of the natural predissociation was very similar to that of the magnetic predissociation. The predissociation was attributed to the gyroscopic interaction (heterogeneous electronic-rotational perturbation) and the hyperfine interaction between the $B^3\Pi_{0^+u}$ and $2431^1\Pi_u$ states.[10] Vigue et al.[11,12] found an interference effect between the natural and magnetic predissociations. Both the natural and magnetic predissociations in the $B^3\Pi_{0^+u}$ state were consequently assigned as originating from the coupling with the $2431^1\Pi_u$ state.[12] However, this study is not yet complete because the matrix elements of the coupling between the $^3\Pi_{0^+u}$ and $^1\Pi_u$ states have been calculated to be zero for the gyroscopic and Zeeman interactions.

In this paper, we shall show that the matrix elements of the Zeeman interaction between the $B^3\Pi_{0^+u}$ and $2431^1\Pi_u$ states are not zero, for the $2431^1\Pi_u$ state is mixed with the $2431^3\Pi_{1u}$ state by the spin-orbit coupling.[13,14] We have measured the magnetic quenching ratios of completely resolved rotational lines. By using these results and the fluorescence lifetime,[12] we shall reexamine the rate constants of the magnetic predissociation in the $B^3\Pi_{0^+u}$ state. The magnetic-field dependence of the hyperfine structure has been measured by the Doppler-free intermodulated fluorescence method; these results shall also be discussed.

Experimental

A single-mode tunable ring dye laser equipped with an autoscan system (Coherent 699-29) was used for excitation. A small amount of solid iodine was sealed in a Pyrex cell after trap-to-trap purifications. The residual gas pressure was lower than 1×10^{-5} Torr (1 Torr≈133.322 Pa). The vapour pressure of the iodine was controlled by cooling the sidearm of the cell. The cell was placed in the center of an electric magnet. The laser light was linearly polarized and propagated with its polarization parallel to the applied magnetic field. The fluorescence was detected by a photomultiplier (Hamamatsu R712) through a glass filter (Toshiba R66) to block the scattered laser light. The output of the photomultiplier was phase-sensitively detected through a lock-in amplifier (PAR Model 128) by chopping the laser light at 960 Hz.

The magnetic-quenching ratio for a rotational level was determined by measuring the change in the peak intensity with the applied magnetic field. The Doppler-limited line shape did not change with the magnetic field. Therefore, the height of the maximum intensity was proportional to the integrated line intensity. The assignment of the rotational line was carried out using the molecular constants obtained by Luc.[15]

The hyperfine structure was obseved by means of the intermodulated fluorescence method.[16] The laser light was split into two counter propagating beams which were chopped at 390 Hz and 570 Hz and which crossed in the center of the cell. We obtained the Doppler-free spectrum by detecting the fluorescence intensity at 960 Hz through a lock-in amplifier. The linewidth was about 10 MHz at the laser power of 30 mW mm^{-2} and the vapour pressure of 30 mTorr (with the sidearm cooled at 0 °C).

Theoretical

As Mulliken defined,[14] we shall denote the MO (molecular orbital) electronic configuration of the valence-shell state of the $\sigma_g^2\sigma_u^2\sigma_g^m\pi_u^p\pi_g^q\sigma_u^n$ type with $m+n+p+q=10$ as $mpqn$. The basic determinant wavefunctions of the iodine molecule are given by:

$$|2440^1\Sigma_g^+> = |\pi_{g+1}\bar{\pi}_{g+1}\pi_{g-1}\bar{\pi}_{g-1}|,$$
$$|2431^3\Pi_{0^+u}> = (2)^{-1/2}(|\pi_{g+1}\pi_{g-1}\bar{\pi}_{g-1}\sigma_u| -$$

$$
\begin{aligned}
&+|\pi_{g+1}\bar{\pi}_{g+1}\bar{\pi}_{g-1}\bar{\sigma}_u|),\\
|2431^3\Pi_{1u+}> &= (2)^{-1/2}(|\pi_{g+1}\bar{\pi}_{g+1}\pi_{g-1}\bar{\sigma}_u|\\
&+|\pi_{g+1}\bar{\pi}_{g+1}\bar{\pi}_{g-1}\sigma_u|),\\
|2431^3\Pi_{1u-}> &= (2)^{-1/2}(|\pi_{g+1}\pi_{g-1}\bar{\pi}_{g-1}\bar{\sigma}_u|\\
&+|\bar{\pi}_{g+1}\pi_{g-1}\bar{\pi}_{g-1}\sigma_u|),\\
|2431^1\Pi_{u+}> &= (2)^{-1/2}(|\pi_{g+1}\bar{\pi}_{g+1}\pi_{g-1}\bar{\sigma}_u|\\
&-|\pi_{g+1}\bar{\pi}_{g+1}\bar{\pi}_{g-1}\sigma_u|),\\
|2431^1\Pi_{u-}> &= (2)^{-1/2}(|\pi_{g+1}\pi_{g-1}\bar{\pi}_{g-1}\bar{\sigma}_u|\\
&-|\bar{\pi}_{g+1}\pi_{g-1}\bar{\pi}_{g-1}\sigma_u|),
\end{aligned}
\tag{1}
$$

where MO without a bar indicates with an α-spin, where MO with a bar indicates with a β-spin, and where a determinant such as $|\sigma_g(1)\bar{\sigma}_g(2)\pi_{u+1}(3)\bar{\pi}_{u+1}(4)\pi_{u-1}(5)\bar{\pi}_{u-1}(6)\pi_{g+1}(7)\bar{\pi}_{g+1}(8)\pi_{g-1}(9)\bar{\pi}_{g-1}(10)|/(10!)^{1/2}$ is briefly denoted as $|\pi_{g+1}\bar{\pi}_{g+1}\pi_{g-1}\bar{\pi}_{g-1}|$ in Eq. 1 by omitting the common MOs of a low energy. MOs $\pi_{g\pm1}$ and σ_u in Eq. 1 are, respectively, of the form $5p_{\pm1}-5p_{\pm1}$ and $5p_0+5p_0$, where $5p_0=5p_z$ and $5p_{\pm1}=\mp2^{-1/2}(5p_x \pm i5p_y)$.

As a set of basis functions, we use wavefunctions of simple products, $|\Lambda>|S\Sigma>|v>|J\Omega M>$. The function $|\Lambda>|S\Sigma>|v>$ is a wavefunction for a nonrotating molecule, where Λ and Σ represent the projections of the total electronic orbital and the total electronic spin angular momenta along the molecular axis respectively, while v represents the vibrational quantum number. All of these are expressed in molecule-fixed coordinates. The wavefunction $|J\Omega M>$ associated with the molecular rotation is expressed in laboratory-fixed coordinates, where the quantum numbers J and M specify the total angular momentum and its projection along the laboratory-fixed Z axis respectively and where $\Omega=\Lambda+\Sigma$. The eigenfunctions for the levels of the unperturbed states $2440^1\Sigma_g^+$, $2431^3\Pi_{0^+u}$ $2431^3\Pi_{1u}$, and $2431^1\Pi_u$, are expressed, respectively, as:[17]

$$
\begin{aligned}
|2440^1\Sigma_g^+vJM> &= |0^+>|00>|v>|J0M>,\\
|2431^3\Pi_{0^+u}vJM> &= |0^+>|10>|v>|J0M>,\\
|2431^3\Pi_{1u\pm}vJM> &= 2^{-1/2}(|1>|10>|v>|J1M1>\\
&\pm|-1>|10>|v>|J-1M>),\\
|2431^1\Pi_{u\pm}vJM> &= 2^{-1/2}(|1>|00>|v>|J1M>\\
&\pm|-1>|00>|v>|J-1M>),
\end{aligned}
\tag{2}
$$

where the electronic wavefunctions $|0^+>|00>$, $|0^+>|10>$, $|1>|10>$, $|-1>|10>$, $|1>|00>$, and $|-1>|00>$ are equal to $|2440^1\Sigma_g^+>$, $|2431^3\Pi_{0^+u}>$, $|2431^3\Pi_{1u+}>$, $|2431^3\Pi_{1u-}>$, $|2431^1\Pi_{u+}>$, and $|2431^1\Pi_{u-}>$ of Eq. 1, respectively.

The spin-orbit interaction induces a mixing of the singlet and triplet wavefunctions, and it occurs between the same J levels. The perturbed wavefunctions of I_2 at the equilibrium distance R_e of the ground state were calculated by Mulliken[14] as:

$$
\begin{aligned}
|X^1\Sigma_g^+vJM> &= |2440^1\Sigma_g^+vJM>\\
&- 0.153|2341^3\Pi_{0^+g}vJM>,\\
|B^3\Pi_{0^+u}vJM> &= 0.916|2431^3\Pi_{0^+u}vJM>\\
&- 0.378|1342^3\Pi_{0^+u}vJM>\\
&- 0.064|1441^1\Sigma_u^+vJM>,\\
|A^3\Pi_{1u\pm}vJM> &= 0.908|2431^3\Pi_{1u\pm}vJM>\\
&+ 0.419|2431^1\Pi_{u\pm}vJM>,\\
|2431^1\Pi_{u\pm}vJM> &= 0.419|2431^3\Pi_{1u\pm}vJM>\\
&- 0.908|2431^1\Pi_{u\pm}vJM>.
\end{aligned}
\tag{3}
$$

The magnetic field was applied along the Z-axis in laboratory-fixed coordinates. The basic electronic orbital and spin wavefunctions are expressed in molecule-fixed coordinates. The Zeeman interaction energy in the molecule-fixed coordinates is written as:[17]

$$
H_Z = -[2^{-1/2}(\mu_+ D_{01}^1 - \mu_- D_{0-1}^1) + \mu_Z D_{00}^1]H, \tag{4}
$$

where H is the magnetic field. $\mu_+ = -\mu_B\sum_i(l_+ + 2s_+)_i$, $\mu_- = -\mu_B\sum_i(l_- + 2s_-)_i$, and $\mu_Z = -\mu_B\sum_i(l_Z + 2s_Z)_i$ are the components of the magnetic moment of the molecule, and D_{MN}^J is the rotation matrix. We shall always use the representations of the rotation group, the angular momenta, the coupling coefficients, and the tensors as defined by Brink and Satchler.[18] The matrix element of the Zeeman interaction is zero between different spin states in Eq. 2,while the nonzero matrix elements for $|2431^3\Pi_{0^+u}v'JM>$ are calculated to be:

$$
\begin{aligned}
&<2431^3\Pi_{0^+u}v'JM|H_Z|\,2431^3\Pi_{1u-}vJ-1\,M>\\
&\quad = 4\mu_B H<v'|v>[(J-1)(J-M)(J+M)/2J(2J-1)(2J+1)]^{1/2},\\
&<2431^3\Pi_{0^+u}v'JM|H_Z|\,2431^3\Pi_{1u+}vJ\,M>\\
&\quad = 4\mu_B H<v'|v>M/[2J(J+1)]^{1/2},\\
&<2431^3\Pi_{0^+u}v'JM|H_Z|\,2431^3\Pi_{1u-}vJ+1\,M>\\
&= -4\mu_B H<v'|v>[(J+2)(J+1-M)(J+1+M)\\
&\quad /2(J+1)(2J+1)(2J+3)]^{1/2}.
\end{aligned}
\tag{5}
$$

Thus, the $2431^3\Pi_{0^+u}$ state can couple with the $2431^3\Pi_{1u}$ state by the Zeeman interaction. The Zeeman interaction between the $B^3\Pi_{0^+u}$ and $2431^1\Pi_u$ states has nonvanishing matrix elements, as can be seen from Eqs. 3 and 5.

The Hamiltonian of the gyroscopic interaction is written as:

$$
H_G = -(\hbar^2/2\mu R^2)(J_+L_- + J_-L_+), \tag{6}
$$

where μ is the reduced mass and where R is the internuclear distance. It causes perturbation between states that differ by $\Delta\Omega=\Delta\Lambda=\pm1$ and $\Delta S=0$. The gyroscopic interaction between the $B^3\Pi_{0^+u}$ and $2431^1\Pi_u$ states arises through the nonzero matrix element:

$$
\begin{aligned}
&<2431^3\Pi_{0^+u}v'JM|H_G|2431^3\Pi_{1u+}vJM> =\\
&\quad -G<v'|\hbar^2/2\mu R^2|v>[J(J+1)]^{1/2},
\end{aligned}
\tag{7}
$$

where G is defined as $<0^+|L_-|1>=<0^+|L_+|-1>=2^{-1/2}G$. The predissociation of I_2 excited to the $|B^3\Pi_{0^+u}v'JM>$ level can occur through the gyroscopic interaction

with the $|2431^1\Pi_{u+}vJM\rangle$ level; the rate is proportional to:

$$G^2|\langle v'|\hbar^2/2\mu R^2|v\rangle|^2 J(J+1). \quad (8)$$

In the presence of the magnetic field H along the Z axis, the predissociation of I_2 excited to the $|B^3\Pi_{0+u}v'JM\rangle$ level can occur through the Zeeman interaction with the $|2431^1\Pi_{u-}vJ-1M\rangle$, $|2431^1\Pi_{u+}vJM\rangle$, and $|2431^1\Pi_{u-}vJ+1M\rangle$ levels, as can be seen from Eqs. 3 and 5. The predissociation through the interaction between the $|B^3\Pi_{0+u}v'JM\rangle$ and $|2431^1\Pi_{u+}vJM\rangle$ levels can occur by both gyroscopic and Zeeman interactions. The rate of predissociation from the excited level $|B^3\Pi_{0+u}v'JM\rangle$ is proportional to:

$$\begin{aligned}&8\mu_B^2H^2|\langle v'|v\rangle|^2(J-1)(J-M)(J+M)/J(2J-1)(2J+1)\\&+|4\mu_BH\langle v'|v\rangle M[2J(J+1)]^{-1/2}\\&-G\langle v'|\hbar^2/2\mu R^2|v\rangle[J(J+1)]^{1/2}|^2\\&+8\mu_B^2H^2|\langle v'|v\rangle|^2(J+2)(J+1-M)(J+1+M)\\&/(J+1)(2J+1)(2J+3)=k_{p(M)}.\end{aligned} \quad (9)$$

The $B^3\Pi_{0+u}-X^1\Sigma_g^+$ transition is allowed through the nonvanishing transition moments of $\langle^3\Pi_{0+u}|\mu|^3\Pi_{0+g}\rangle$ and $\langle^1\Sigma_u^+|\mu|^1\Sigma_g^+\rangle$, where μ is an electric dipole moment. The dependence on J and M is the same for both these transition moments. For an excitation by a plane-polarized light with the electric vector along the Z axis, which is the case in our experiment, the nonvanishing moment of the $B^3\Pi_{0+u}$ $(v'JM)-X^1\Sigma_g^+(v''JM)$ transition is given by:

$$\begin{aligned}&\langle B^3\Pi_{0+u}v'JM|\mu_Z|X^1\Sigma_g^+v''J-1M\rangle\\&\quad=\mu(B-X)\langle v'|v''\rangle[(J-M)(J+M)/(2J-1)(2J+1)]^{1/2},\\\text{and}\quad&\langle B^3\Pi_{0+u}v'JM|\mu_Z|X^1\Sigma_g^+v''J+1M\rangle\\&\quad=\mu(B-X)\langle v'|v''\rangle[(J+1-M)(J+1+M)/\\&(2J+1)(2J+3)]^{1/2},\end{aligned} \quad (10)$$

where $\mu(B-X)$ is the electric dipole transition moment of the $B^3\Pi_{0+u}-X^1\Sigma_g^+$ transition.

The rate of the predissociation following the optical excitation is proportional to:

$$\begin{aligned}k_p=&(2J+1)^{-1}\sum_M k_{p(M)}\mu(B-X)^2|\langle v'|v''\rangle|^2\\&\times[(J-M)(J+M)/(2J-1)(2J+1)\\&+(J+1-M)(J+1+M)/(2J+1)(2J+3)],\end{aligned} \quad (11)$$

The summation over M is equal to averaging over the molecular orientation; one thus obtains:

$$\begin{aligned}k_p=&\mu(B-X)^2|\langle v'|v''\rangle|^2[16\mu_B^2H^2|\langle v'|v\rangle|^2(J+1)(11J-5)\\&/(2J-1)(2J+3)+G^2|\langle v'|\hbar^2/2\mu R^2|v\rangle|^2J(J+1)/3],\end{aligned} \quad (12)$$

where the first term is the contribution from the Zeeman interaction, while the second term is that from the gyroscopic interaction. It should be noted that the interference term disappears upon the averaging; hence, the interference can not be observed in our experiment. Accordingly, the rate of predissociation due to the Zeeman interaction can be written as:

$$k_{mpr}=bH^2, \quad (13)$$

while the rate of predissociation due to the gyroscopic interaction can be written as:

$$k_{gpr}=g\,J(J+1), \quad (14)$$

where b and g are constants.

Experimental Results and Discussion

A portion of the fluorescence excitation spectrum of the iodine molecule,which includes the band origin of the $B^3\Pi_{0+u}(v'=6)-X^1\Sigma_g^+(v''=4)$ transition, is shown in Fig. 1. Most of the lines are rotationally resolved and can be easily assigned. However, the hyperfine structure is not resolved because of the Doppler-width. We measured the magnetic quenching ratio of the line intensity of each rotational level. Since the lifetime of the $B^3\Pi_{0+u}$ state is relatively long (an order of ~μs), the fluorescence intensity is sensitive to optical saturation and molecular collisions. Therefore, the measurement should be made at as low a laser power and as low a vapour pressure as possible. All the measurements were carried out at 1 mW mm^{-2} and 30 mTorr; it was thus confirmed that the quenching ratio under these conditions was almost independent of the laser power.

We also measured the magnetic-quenching ratio I_H/I_0 of each rotational line, where I_H and I_0 are, respectively, the fluorescence intensity at the magnetic

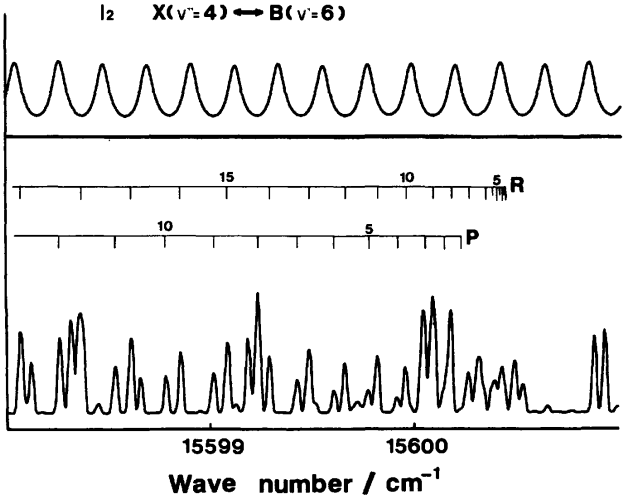

Fig. 1. Fluorescence excitation spectrum of I_2 around the band origin of the $B^3\Pi_{0+u}(v'=6)-X^1\Sigma_g^+(v''=4)$ transition. The assignment of each rotational line is shown above. The upper trace is the transmittance of the etalon (FSR=6.5 GHz) which is monitored to confirm the linearity of the scan and to detect a mode-hop of the laser line.

field H and at the zero magnetic field. The observed values of I_H/I_0 for J'=20—80 levels of v'=6 and 10 at H=0.78 and 1.67 T are shown in Fig. 2. The magnetic quenching ratio depends on the decay rate of the J' level. Hence, the values of the P and R lines of the identical J' are naturally the same. We measured the magnetic-field dependence of the quenching ratio for each rotational line. The ratios I_0/I_H of the P(35) lines of the $B^3\Pi_{0^+u}(v'=6)-X^1\Sigma_g^+(v''=4)$ and $B^3\Pi_{0^+u}(v'=10)-X^1\Sigma_g^+(v''=3)$ transitions are plotted against the square of the applied magnetic field in Fig. 3. The experimental error was ±1%.

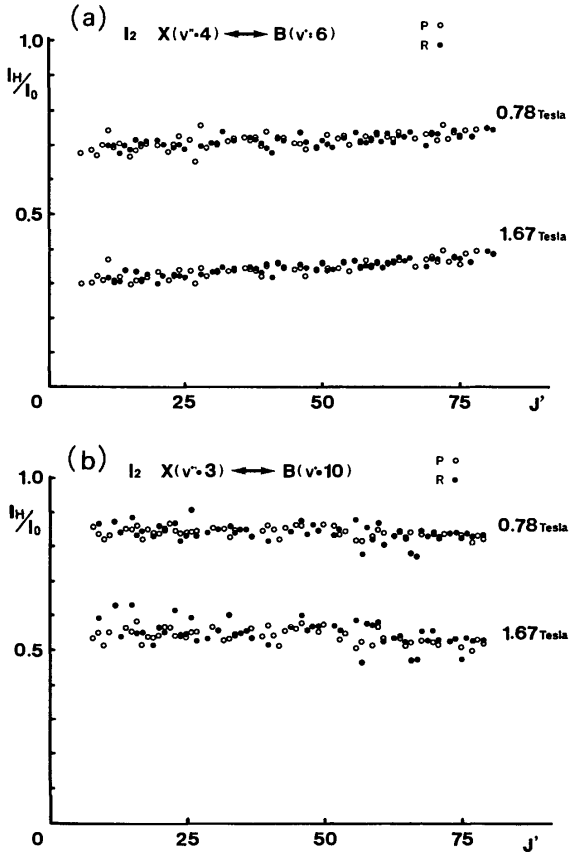

Fig. 2. The values of I_H/I_0 for J' levels of $B^3\Pi_{0^+u}$ (v'=6) at the magnetic field of 0.78 and 1.67 T are shown in (a). Those for J' levels of $B^3\Pi_{0^+u}(v'=10)$ are shown in (b).

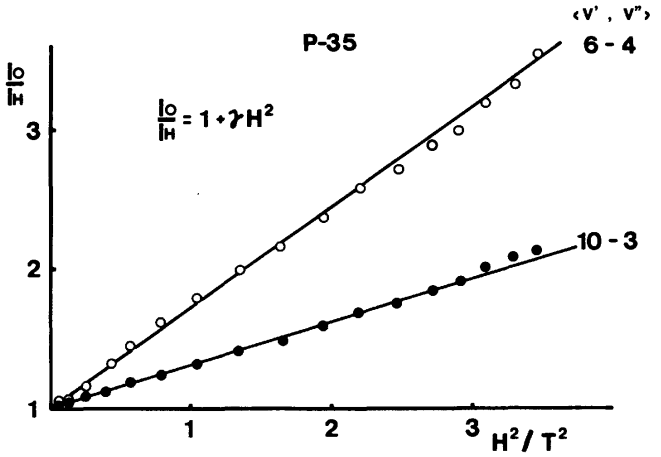

Fig. 3. Magnetic field dependence of the quenching ratio I_0/I_H of the P(35) lines of the $B^3\Pi_{0^+u}(v'=6)-X^1\Sigma_g^+(v''=4)$ and $B^3\Pi_{0^+u}(v'=10)-X^1\Sigma_g^+(v''=3)$ transitions.

The magnetic-quenching ratio of the fluorescence is expressed as:

$$I_H/I_0 = (k_{rad} + k_{col} + k_{npr}) / (k_{rad} + k_{col} + k_{npr} + k_{mpr}), \quad (15)$$

where k_{rad}, k_{col}, and k_{mpr} are, respectively, the rate of radiative decay, the rate of collisional quenching, and the rate of magnetic predissociation. k_{npr} is the rate of the natural predissociation, which is the sum of the rate of the gyroscopic predissociation k_{gpr} and the rate of the hyperfine predissociation k_{hpr}. The lifetime τ in the zero field is given by:

$$\tau = (k_{rad} + k_{col} + k_{npr})^{-1}. \quad (16)$$

From Eqs. 13, 15, and 16, one obtains:

$$I_0/I_H = 1 + \tau b H^2 = 1 + \gamma H^2. \quad (17)$$

One can determine the value of γ from the slope of I_0/I_H vs. H^2. We measured the J dependence of the magnetic-quenching ratios for various v' levels. The

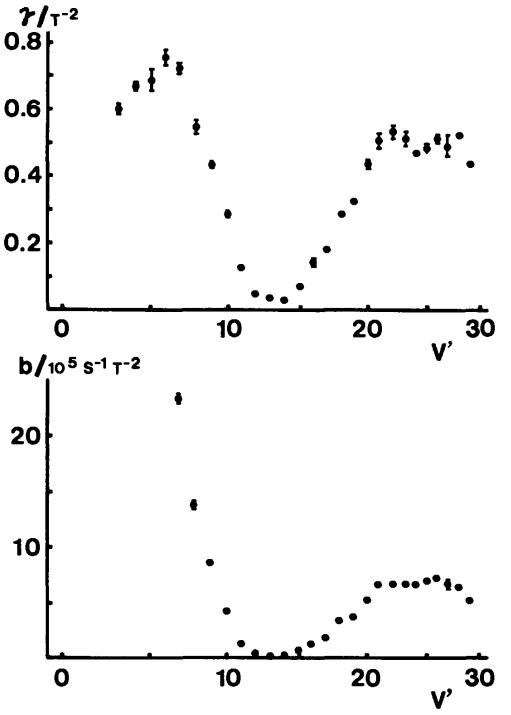

Fig. 4. Upper (a): Observed values of γ extrapolated to J=0 for various v levels. Lower (b): b values deduced from the observed γ values and the fluorescence lifetime at J=0 from Ref. 12.

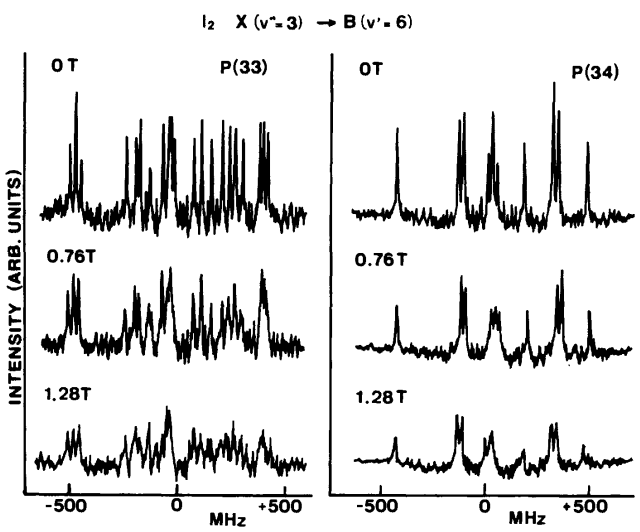

Fig. 5. Hyperfine structure of P(33) and P(34) lines of the $B^3\Pi_{0^+u}(v'=6)-X^1\Sigma_g^+(v''=3)$ transition, and the change with the magnetic field.

results of the extrapolation of the values of γ at $J=0$ are shown in Fig. 4(a). At $J=0$, the rate of the gyroscopic predissociation is zero. We evaluated the values of τ at $J=0$ by using the results obtained by Vigue et al.[12] Unfortunately, their results are limited for $v'>7$. Consequently we could obtain the b value at $J=0$ for $v'=7$—29; the b value obtained for each v' level is plotted in Fig. 4(b). The profile is very similar to that presented by Chapman et al.[5] and Vigue et al.,[12] but the absolute values are considerably different. We measured the magnetic-quenching ratio for many more rotationally resolved lines; hence, we could obtain more accurate values than the previous ones.

By using the intermodulated fluorescence technique,[16] we observed the hyperfine structure and the change with the magnetic field. The results for the P(33) and P(34) lines of the $B^3\Pi_{0^+u}(v'=6)-X^1\Sigma_g^+(v''=3)$ transition are shown in Fig. 5. The Pauli exclusion principle requires that odd J levels of the $B^3\Pi_{0^+u}$ state of $^{127}I_2$ can combine only with states of an even total nuclear spin ($I=0$, 2, and 4), while even J levels can combine only with states of an odd total nuclear spin ($I=1$, 3, and 5). Hence, 15 sublines are observed for an even J'' line and 21 sublines for an odd J'' line. In either the presence or absence of a magnetic field, no energy shift or line splitting of the hyperfine lines was observed. However, when a magnetic field was applied, a remarkable decrease of the intensity of each line was observed; the ratio of the change was almost the same for all lines.

The hyperfine structure could be explained by the nuclear electric quadrupole interaction and the nuclear spin-rotation interaction.[20,21] For a large value of $J(\gg I)$, the angular momentum $\boldsymbol{J}$ is almost parallel to $\boldsymbol{F}=\boldsymbol{J}+\boldsymbol{I}$. The Zeeman interaction energy with the nuclear spins may be expressed by:

$$E_{NZ} = g_I\mu_N(M_1 + M_2)H, \tag{19}$$

where M_i is the projection of the nuclear spin angular momentum of the nucleus i along the molecular-fixed z axis. g_I is a nuclear g-factor, and μ_N is the nuclear magneton. We used a linearly polarized light whose polarization was parallel to the magnetic field; hence,the transitions of $M'_F-M''_F=0$ are allowed by an electric dipole transition. The nuclear g-factors of the $B^3\Pi_{0^+u}$ and $X^1\Sigma_g^+$ states can be estimated to be almost the same, for no energy shift or line splitting of the hyperfine lines was observed when a magnetic field was applied.

Levenson and Schawlow[21] found that the nuclear spin-rotation interaction varied strongly with the vibrational quantum number v' of the $B^3\Pi_{0^+u}$ state. The coupling was found to increase rapidly near the dissociation limit of the $B^3\Pi_{0^+u}$ state. Broyer et al.[22] found that the lifetime extrapolated to $J=0$ shows a strong variation with v, very similar to that of b. They assigned the origin of this new predissociation to the hyperfine predissociation. In order to make this problem clear, more extensive studies of Doppler-free spectroscopy by using a molecular beam will be necessary.

A part of this work was supported by the Joint Studies Program (1987—1988) of the IMS. H. K. and M. B. wish to thank the Ministry of Education of Japan for a Grant-in-Aid for scientific research.

References

1) W. Steubing, *Verh d. D. Phys. Ges.*, **15**, 1181 (1913).
2) L. A. Turner, *Z. Phys.*, **65**, 464 (1930).
3) J. H. Van Vleck, *Phys. Rev.*, **40**, 344 (1932).
4) E. O. Degenkolb, J. I. Steinfeld, E. Wasserman, and W. Klemperer, *J. Chem. Phys.*, **51**, 615 (1969).
5) G. D. Chapman and P. R. Bunker, *J. Chem. Phys.*, **57**, 2951 (1972).
6) A. Chutjian, J. K. Link, and C. Brewer, *J. Chem. Phys.*, **46**, 2666 (1967).
7) A. Chutjian and T. C. James, *J. Chem. Phys.*, **51**, 1242 (1969).
8) J. Tellinghuisen, *J. Chem. Phys.*, **57**, 2397 (1972).
9) J. Tellinghuisen, *J. Chem. Phys.*, **58**, 2821 (1973).
10) M. Broyer, J. Vigue,and J. C. Lehmann, *J. Chem. Phys.*, **63**, 5428 (1975).
11) J. Vigue, M. Broyer, and J. C. Lehmann, *J. Chem. Phys.*, **62**, 4941 (1974).
12) J. Vigue, M. Broyer, and J. C. Lehmann, *J. Phys. (Paris)*, **42**, 937, 949, 961 (1981).
13) R. S. Mulliken, *Phys. Rev.*, **57**, 500 (1940).
14) R. S. Mulliken, *J. Chem. Phys.*, **55**, 288 (1971).
15) P. Luc, *J. Mol. Spectrosc.*, **80**, 41 (1980).
16) M. S. Sorem and A. L. Shawlow, *Opt. Comm.*, **5**, 148 (1972).
17) H. Katô, M. Baba, and I. Hanazaki, *J. Chem. Phys.*, **80**,

3936 (1984).
18) D. M. Brink and G. R. Satchler, *Angular Momentum*, Oxford University, Oxford, 1968.
19) G. A. Capella and H. P. Broida, *J. Chem. Phys.*, **58**, 4212 (1973).
20) M. Kroll, *Phys. Rev. Lett.*, **23**,631 (1969).
21) M. D. Levenson and A. L. Schawlow, *Phys. Rev.*, **A6**, 10 (1972).
22) M. Broyer, J. Vigue, and J. C. Lehmann, *J. Chem. Phys.*, **64**, 4793 (1976).

The Synthesis and Oxidation of Mixed Cobalt(III) Complexes with Dimethyldithiocarbamato and Diamine Ligands, and the Crystal Structure of $(+)^{CD}_{500}$-Dimethyldithiocarbamato-bis(ethylenediamine)cobalt(III) Bis[μ-(*R*,*R*)-tartrato]diantimonate(III) Pentahydrate

Masakazu KITA,*,† Kazuaki YAMANARI, and (the late) Yoichi SHIMURA
Department of Chemistry, Faculty of Science, Osaka University, Toyonaka, Osaka 560
(Received October 9, 1987)

Dithiocarbamato complexes, $[Co(dtc)_{3-n}(diamine)_n]^{n+}$ (n=1 and 2 and dtc=dimethyldithiocarbamate) were newly prepared and characterized by means of their absorption, CD, and MCD spectra. $(+)^{CD}_{500}$-$[Co(dtc)(en)_2][Sb_2(R,R\text{-}C_4H_2O_6)_2]\cdot 5H_2O$ crystallized in the monoclinic space group of $P2_1$ with a=14.630(3), b=9.300(1), c=12.023(5) Å, β=110.78(3)°, V=1529.4(8) Å^3, and Z=2. The refinement of 3346 reflections (Mo $K\alpha$ radiation) led to R=0.073. The dtc complex had a *Λ* configuration. The Co–N bond trans to the dtc sulfur atom was longer by 0.026 Å than the cis one. A novel oxidation derivative, $[Co\{(dimethylamino)thioxomethanesulfinato\text{-}O,S\}(en)_2]^{2+}$, was prepared and characterized by means of its XPS spectrum.

A large number of dithiocarbamato-metal complexes have been synthesized.[1] Several reports have been published on the crystal structures of dithiocarbamato cobalt(III) complexes: e.g., $[Co(S_2CNH_2)_3]$,[2] $[Co\{S_2CN(CH_3)_2\}_3]$,[3] and $[Co(S_2CN(C_2H_5)_2)_3]$.[4] No mixed chromophore systems of the $[Co(S)_2(N)_4]$ and $[Co(S)_4(N)_2]$ types have, however, been reported. The mixed chromophores are interesting in terms of their spectrochemistry because of the large difference in the ligand field strengths between dtc-sulfur and amine-nitrogen donors. Furthermore, sulfur donor groups with various chemical environments (thiolato, thioether, sulfenato, sulfinato, sulfito, thiosulfato, etc.) induce in cobalt(III) complexes the trans influence (structural trans effect) ranging in magnitude from 0.00 to 0.089 Å;[5] in contrast, however, no such trans influence of dithiocarbamato has yet been determined because the appropriate mixed complexes have not been synthesized.

This paper deals with the synthesis of a series of mixed cobalt(III) complexes with dimethyldithiocarbamate and diamine as the remaining ligands: $[Co(dtc)_{3-n}(diamine)_n]^{n+}$ (n=0, 1, and 2). The complexes were characterized by their electronic absorption, circular dichroism (CD), and magnetic circular dichroism (MCD) spectra. The X-ray crystal structure of $(+)^{CD}_{500}$-$[Co(dtc)(en)_2][Sb_2(R,R\text{-}C_4H_2O_6)_2]\cdot 5H_2O$ was determined. The H_2O_2 oxidation of dithiocarbamato complexes was also attempted.

The following abbreviations of the ligands are used in this paper: Hdtc=dimethyldithiocarbamic acid $(CH_3)_2NCS_2H$; Hdtsi=(dimethylamino)thioxomethanesulfinic acid $(CH_3)_2NC(S)SO_2H$; Hmtz=2-mercapto-2-thiazoline $\overline{S\text{–}CH_2\text{–}CH_2N=C}\text{–}SH$; en=ethylenediamine $NH_2CH_2CH_2NH_2$; *R*-pn=(*R*)-propylenediamine $NH_2CH_2CH(CH_3)NH_2$.

† Present address: Department of Chemistry, Faculty of Science, Nagoya University, Chikusa-ku, Nagoya 464.

Experimental

Preparation and Optical Resolution. (1) $[Co(dtc)(en)_2](ClO_4)_2$: To a solution of $Co(ClO_4)_2$ (0.018 mol) in 100 cm^3 of water we added a solution of ethylenediamine (2.2 g, 0.036 mol) in 100 cm^3 of methanol. To the mixture we then immediately added a solution of bis(dimethylthiocarbamyl) disulfide (2.2 g, 0.009 mol) in 200 cm^3 of ethanol, and the subsequent mixture was stirred at ca. 70 °C for 1 h. The resulting reddish purple precipitate was filtered off and washed with ethanol and diethyl ether. The precipitate was recrystallized by dissolving it in hot water (ca. 70 °C), filtering, and cooling to ca. 5 °C. The yield was 7.6 g (85%). Found: C, 16.75; H, 4.43; N, 13.81%. Calcd for $[Co(dtc)(en)_2](ClO_4)_2=C_7H_{22}N_5O_8S_2Cl_2Co$: C, 16.87; H, 4.45; N, 14.06%.

For optical resolution, to a solution of $[Co(dtc)(en)_2](ClO_4)_2$ (3.0 g, 0.006 mol) in 50 cm^3 of hot water we added a solution of $K_2[Sb_2(R,R\text{-}C_4H_2O_6)_2]\cdot 3H_2O$ (1.9 g, 0.003 mol) in 50 cm^3 of hot water. After a few minutes, the red-plate diastereomer $(+)^{CD}_{500}$-$[Co(dtc)(en)_2][Sb_2(R,R\text{-}C_4H_2O_6)_2]\cdot 5H_2O$ began to deposit; it was filtered off. The filtrate was cooled to induce the crystallization of $(-)^{CD}_{500}$-$[Co(dtc)(en)_2](ClO_4)_2$. The crystals were collected and recrystallized from hot water. Found for the less-soluble diastereomer: C, 19.64; H, 3.83; N, 7.58%. Calcd for $(+)^{CD}_{500}$-$[Co(dtc)(en)_2][Sb_2(R,R\text{-}C_4H_2O_6)_2]\cdot 5H_2O=C_{15}H_{36}N_5O_{17}S_2CoSb_2$: C, 19.64; H, 3.92; N, 7.57%. Found for the $(-)^{CD}_{500}$-complex: C, 16.97; H, 4.48; N, 14.01%. Calcd for $(-)^{CD}_{500}$-$[Co(dtc)(en)_2](ClO_4)_2=C_7H_{22}N_5O_8Cl_2S_2Co$: C, 16.87; H, 4.45; N, 14.06%. An adequate amount of anion-exchange resin (QAE-Sephadex A-25, chloride form) was added to a suspension of the less-soluble diastereomer, $(+)^{CD}_{500}$-$[Co(dtc)(en)_2][Sb_2(R,R\text{-}C_4H_2O_6)_2]\cdot 5H_2O$, in water, leading to a reddish brown supernatant. After the removal of the resin, sodium perchlorate was added to the filtrate; the crystals of $(+)^{CD}_{500}$-$[Co(dtc)(en)_2](ClO_4)_2$ were then deposited. Found: C, 16.80; H, 4.42; N, 13.98%. Calcd for $(+)^{CD}_{500}$-$[Co(dtc)(en)_2](ClO_4)_2=C_7H_{22}N_5O_8S_2Cl_2Co$: C, 16.87; H, 4.45; N, 14.06%.

(2) $[Co(dtc)_2(en)]ClO_4$: This green complex was obtained as a by-product (5%) from the mother liquor in the above preparation. The complex was also prepared in a

high yield by the following method. Bis(dimethylthiocarbamyl) disulfide (4.3 g, 0.0183 mol) was stirred into a solution of $Co(ClO_4)_2$ (0.036 mol) in 100 cm^3 of ethanol. To the mixture we then added a mixed solution of sodium dimethyldithiocarbamate dihydrate (6.4 g, 0.036 mol) and ethylenediamine (2.2 g, 0.036 mol) in 50 cm^3 of water. After a few minutes, the green precipitate began to deposit. The mixture was then stirred at ca. 70 °C for 1 h. The resulting green precipitate was filtered and washed with water (100 cm^3), ethanol (20 cm^3), chloroform (100 cm^3 each, three times), and then ether (100 cm^3). The water washings contained the complex $[Co(dtc)(en)_2](ClO_4)_2$, and the chloroform ones, $[Co(dtc)_3]$. The green precipitate was recrystallized by dissolving it in hot water–ethanol (2:1) and by then cooling it below 10 °C. The columnar green crystals were collected. The yield was 12 g (73%). Found: C, 20.80; H, 4.41; N, 12.17%. Calcd for $[Co(dtc)_2(en)]ClO_4=C_8H_{20}N_4O_4S_4ClCo$: C, 20.94; H,4.39; N, 12.21%.

(3) $(+)^{CD}_{580}$- and $(-)^{CD}_{580}$-$[Co(dtc)_2(R\text{-pn})]ClO_4$: The $[Co(dtc)_2(R\text{-pn})]ClO_4$ complexes were prepared by the same procedure as that used for $[Co(dtc)_2(en)]ClO_4$, except for the use of *R*-pn instead of en. The yield was 11 g (85%). The green crystals of $[Co(dtc)_2(R\text{-pn})]ClO_4$ were dissolved in a small amount of dimethyl sulfoxide (DMSO), adsorbed on a column of cation-exchange resin (SP-Sephadex C-25, Na^+ form), and eluted with a 0.5 M NaCl aqueous solution (1 M=1 mol dm^{-3}). The two green bands were eluted separately. The earlier eluate showed a negative CD at 17000 cm^{-1} and the latter one, a positive CD at 17000 cm^{-1}. Each perchlorate salt was obtained by adding a saturated aqueous solution of $NaClO_4$ to each eluate. Found for the $(-)^{CD}_{580}$-complex: C, 22.76; H, 4.70; N, 11.86%. Calcd for $(-)^{CD}_{580}$-$[Co(dtc)_2(R\text{-pn})]ClO_4=C_9H_{22}N_4O_4S_4ClCo$: C, 22.86; H, 4.69; N, 11.85%. Found for the $(+)^{CD}_{580}$-complex: C, 21.49; H, 4.86; N, 10.96%. Calcd for $(+)^{CD}_{580}$-$[Co(dtc)_2(R\text{-pn})]ClO_4\cdot 1.5H_2O=C_9H_{25}N_4O_{5.5}S_4ClCo$: C, 21.62; H, 5.04; N, 11.20%.

(4) $[Co(dtc)_3]$: This complex was obtained according to the method in the literature.[3] Found: C, 25.75; H, 4.37; N, 9.84%. Calcd for $[Co(dtc)_3]=C_9H_{18}N_3S_6Co$: C, 25.77; H, 4.32; N, 10.02%.

(5) $(-)^{CD}_{490}$-$[Co(dtsi)(en)_2](ClO_4)_2$: A mixed solution of 30% aqueous H_2O_2 (10 g) and 60% aqueous $HClO_4$ (10 g) was stirred into a solution of $(-)^{CD}_{500}$-$[Co(dtc)(en)_2](ClO_4)_2$ (5 g) in 50 cm^3 of DMSO below 5 °C to give an orange-red solution instantly. To the resulting solution we immediately added a mixture of diethyl ether (700 cm^3) and ethanol (300 cm^3). Orange-red crystals separated out on the inside of a beaker within a few minutes and were filtered off. The yield was ca. 1 g. Found: C, 16.19; H, 4.20; N, 13.18%. Calcd for $(-)^{CD}_{490}$-$[Co(dtsi)(en)_2](ClO_4)_2=C_7H_{22}N_5O_{10}S_2Cl_2Co$: C, 15.86; H, 4.18; N, 13.20%. The compound was stable in the solid state on exposure to light, but was unstable in an aqueous or DMSO solution, even in the dark, probably because of the solvolysis.

(6) $[Co(mtz)(en)_2](ClO_4)_2$: To a solution of $CoCl_2\cdot 6H_2O$ (4.8 g, 0.020 mol) in 40 cm^3 of ethanol–water (2:1) we added a solution of ethylenediamine (3.0 g, 0.050v mol) in 100 cm^3 of ethanol. To the mixture we then added a solution of 2-mercapto-2-thiazoline (2.4 g, 0.020 mol)[6] in 200 cm^3 of ethanol, after which the air oxidation was continued for 1 h. The resulting brown-purple precipitate was recrystallized by dissolving it in hot water, adding $NaClO_4$ (10 g), and cooling the mixture to ca. 5 °C. The yield was 2.5 g (25%). Found: C, 17.05; H, 4.11; N, 13.92%. Calcd for $[Co(mtz)(en)_2](ClO_4)_2=C_7H_{20}N_5O_8S_2Cl_2Co$: C, 16.94; H, 4.06; N, 14.11%.

For optical resolution, to a solution of $[Co(mtz)(en)_2](ClO_4)_2$ (0.5 g, 0.001 mol) in 20 cm^3 of hot water we added a solution of $K_2[Sb_2(R,R\text{-}C_4H_2O_6)_2]\cdot 3H_2O$ (0.3 g, 0.0005 mol) in 30 cm^3 of hot water. After a few minutes, purple thin plate crystals $(+)^{CD}_{506}$-$[Co(mtz)(en)_2][Sb_2(R,R\text{-}C_4H_2O_6)_2]\cdot 5H_2O$ began to deposit; they were filtered off. To the filtrate we added $NaClO_4$ (10 g), and then the crystals of $(-)^{CD}_{506}$-$[Co(mtz)(en)_2](ClO_4)_2$ deposited were collected and recrystallized from hot water. Found for the less-soluble diastereomer: C, 19.42; H, 3.94; N, 7.46%. Calcd for $(+)^{CD}_{506}$-$[Co(mtz)(en)_2][Sb_2(R,R\text{-}C_4H_2O_6)_2]\cdot 5H_2O=C_{15}H_{38}N_5O_{17}S_2Cl_2CoSb_2$: C, 19.43; H, 4.13; N, 7.55%. Found for $(-)^{CD}_{506}$-complex: C, 16.87; H, 4.07; N, 13.73%. Calcd for $(-)^{CD}_{506}$-$[Co(mtz)(en)_2](ClO_4)_2=C_7H_{20}N_5O_8S_2Cl_2Co$: C, 16.94; H, 4.06; N, 14.11%.

Spectroscopic Determination. The visible and ultraviolet absorption spectra were measured on a Hitachi 330 spectrophotometer. The CD spectra were recorded on a JASCO MOE-1 spectropolarimeter, and the MCD spectra on the same instrument in a 1.5 T magnetic field. The absorption, CD, and MCD measurements were made in aqueous, DMSO, and/or $CHCl_3$ solution at room temperature. The XPS measurements were carried out on a Shimadzu HIPS 70 apparatus. The binding energies relative to the Fermi level were determined by referring to the values of the Na-2s (64.0 eV) and S-$2p_{3/2}$ (169.5 eV) of Na_2SO_4, mixed with an appropriate amount of each sample.

X-Ray Analysis. The X-ray analysis of $(+)^{CD}_{500}$-$[Co(dtc)(en)_2][Sb_2(R,R\text{-}C_4H_2O_6)_2]\cdot 5H_2O$ was also performed. Crystal Data: monoclinic, $P2_1$, a=14.630(3) Å, b=9.300(1) Å, c=12.023(5) Å, β=110.78(3)°, V=1529.4(8) Å^3, Z=2, D_{calcd}=2.01, D_{obsd}=2.00 g cm^{-3}. An orange-red crystal, of appropriate dimensions (0.375×0.250×0.075 mm), was used for X-ray work. The diffraction intensities were measured using a Rigaku four-circle diffractometer, with graphite monochromatized Mo $K\alpha$ radiation (λ=0.71069 Å). Their intensities decreased progressively with the length of X-ray exposure. Furthermore, the linear absorption coefficient is μ(Mo $K\alpha$)=25.08 cm^{-1}. Therefore the damage[7] and absorption[8] corrections were applied. Out of a total of 3654 reflections ($5°<2\theta<55°$), 3346 corresponded to those with $I>3\sigma(I)$. The atomic scattering factors of the neutral atoms were taken from Ref. 9 for all the atoms, both the $\Delta f'$ and $\Delta f''$ components of anomalous dispersion were included for all nonhydrogen atoms.

All the computations were performed on an ACOS-S700 apparatus at the Crystallographic Research Center, Institute for Protein Research, Osaka University. The computer programs used were ABSC,[8] MFPA,[10] HBLS V and RHO,[11] DAPH,[12] and ORTEP.[13] The structure was solved by the usual heavy-atom method: conventional Patterson, Fourier, and least-squares refinement techniques. The absolute configurations of the asymmetric carbon atoms of bis[μ-(*R*,*R*)-tartrato(4−)]diantimonate(III) ion were fitted to those reported previously.[14] Therefore, the absolute configuration of the cobalt(III) complex, $(+)^{CD}_{500}$-$[Co(dtc)(en)_2]^{2+}$, was determined definitely. All nonhydrogen atoms except one water oxygen atom, which could not be found by the last

Table 1. Fractional Atomic Positional and Isotropic Thermal Parameters for Non-Hydrogen Atoms[a)]

Atom	x	y	z	$B^{b)}$ / Å^2
Co	0.29075(9)	0.33340(16)	0.05600(10)	1.70(3)
S(1)	0.2834(2)	0.5189(3)	−0.0704(2)	2.03(6)
S(2)	0.1389(1)	0.3151(3)	−0.0795(2)	2.43(6)
N(1)	0.2490(6)	0.4633(12)	0.1554(6)	2.6(2)
N(2)	0.2717(7)	0.1756(12)	0.1562(7)	2.8(3)
N(3)	0.4294(6)	0.3584(10)	0.1573(7)	2.6(2)
N(4)	0.3418(6)	0.1966(9)	−0.0327(6)	1.9(2)
C″	0.1643(7)	0.4643(11)	−0.1450(9)	2.1(2)
N″	0.1028(6)	0.5306(12)	−0.2363(7)	2.7(2)
C(Me1)	0.0017(8)	0.4699(21)	−0.2923(11)	4.3(4)
C(Me2)	0.1269(9)	0.6564(17)	−0.2903(15)	5.2(5)
C(11)	0.2440(9)	0.3873(17)	0.2625(8)	3.6(4)
C(12)	0.2063(9)	0.2354(18)	0.2171(12)	4.1(4)
C(21)	0.4908(8)	0.3079(15)	0.0874(9)	2.9(3)
C(22)	0.4450(7)	0.1682(13)	0.0280(9)	2.3(3)
Sb(1)	0.64581(5)	0.94213(9)	0.33258(5)	2.08(2)
Sb(2)	0.67639(5)	0.41774(9)	0.47306(6)	2.38(2)
O(11)	0.5218(5)	0.8399(9)	0.1997(5)	2.6(2)
O(12)	0.3963(6)	0.6965(12)	0.1779(7)	3.6(3)
O(13)	0.5883(5)	0.8392(9)	0.4349(5)	2.4(2)
O(14)	0.5600(5)	0.5226(9)	0.3690(6)	2.5(2)
O(15)	0.6355(5)	0.5406(10)	0.6031(6)	2.7(2)
O(16)	0.5185(6)	0.6796(13)	0.6205(7)	3.8(3)
C(31)	0.4698(7)	0.7646(12)	0.2418(9)	2.5(3)
C(32)	0.4995(7)	0.7616(13)	0.3782(8)	2.4(2)
C(33)	0.5079(7)	0.6067(12)	0.4219(9)	2.2(3)
C(34)	0.5559(8)	0.6124(14)	0.5603(8)	2.7(3)
O(21)	0.7056(5)	0.4048(10)	0.3107(6)	3.1(2)
O 22)	0.8057(6)	0.4938(10)	0.2230(7)	3.1(2)
O(23)	0.7754(5)	0.5689(9)	0.5003(5)	2.5(2)
O(24)	0.7137(5)	0.7739(9)	0.2940(6)	2.3(2)
O(25)	0.7801(5)	0.9388(10)	0.4811(6)	2.9(2)
O(26)	0.9274(6)	0.8379(12)	0.5482(7)	4.1(3)
C(41)	0.7740(7)	0.4886(12)	0.3063(9)	2.1(2)
C(42)	0.8186(7)	0.5874(12)	0.4137(8)	2.0(2)
C(43)	0.8100(7)	0.7445(13)	0.3699(8)	2.3(3)
C(44)	0.8433(7)	0.8437(13)	0.4755(10)	2.8(3)
O(W1)	0.2692(7)	0.8961(10)	0.0092(7)	3.7(3)
O(W2)	0.0921(10)	0.8512(23)	0.0477(16)	9.7(8)
O(W3)	0.0488(9)	0.5779(15)	0.0751(11)	5.8(4)
O(W4)	0.0089(7)	0.5542(17)	0.2802(10)	6.7(5)

a) The e.s.d. are shown in parentheses. The numberings are shown in Fig. 7. b) B is evaluated from the corresponding anisotropic thermal parameters according to Ref. 14. The isotropic thermal parameters are of the $\exp\{-B(\sin^2\theta/\lambda^2)\}$ form.

difference Fourier synthesis, were located and were assigned anisotropic parameters. The hydrogen atoms, except for those belonging to methyl-carbon atoms and water-oxygen atoms, were introduced into their geometrical positions,[15] but were not refined. The refinement of R and R_2 converged to 0.073 and 0.082 respectively.[16] The final positional parameters, the corresponding isotropic thermal parameters as calculated from the respective anisotropic parameters by Hamilton's method,[17] and their estimated standard deviations for nonhydrogen atoms are given in Table 1. The calculated positional parameters of the hydrogen atoms, the anisotropic thermal parameters for all the nonhydrogen atoms, and the complete list of $|F_o|$ and $|F_c|$ values are deposited as Document No. 8847 at the Office of the Editor of the Bull. Chem. Soc. Jpn.

Description of the Structure of $(+)^{CD}_{500}$-[Co(dtc)(en)$_2$]-[Sb$_2$(R,R-C$_4$H$_2$O$_6$)$_2$]·5H$_2$O and the Trans Influence Induced by the dtc Ligand. Figure 1 shows the numbering of the diastereomeric salt. Tables 2 and 3 show the nonhydrogen atom bond distances and angles respectively. Table 4 lists several selected plane equations, sets of deviations of atoms from the plane, and the dihedral angles between the pair of planes.

This dtc complex has the Λ-(δ,δ) configuration, judged from the asymmetric carbon atoms of the bis[μ-(R,R)-tartrato(4−)]diantimonate(III) ion.[14] The [Sb$_2$(R,R-C$_4$H$_2$O$_6$)$_2$]$^{2-}$ anion has reasonable bond distances and angles as compared with the results of an other structure analysis,[14] as is shown in Table 5. Table 6 shows the selected bond distances and angles of the present [Co(dtc)(en)$_2$]$^{2+}$ in comparison with those of [Co(dtc)$_3$].[4] There are no large differences between the two complexes concerning the dtc

ligand, the Co-S distances, and the bite angle, S-Co-S. The cobalt atom lies nearly on the plane of S_2CN (Table 4), but the S(1)-Co-S(2), S(1)-Co-N(2), and S(2)-Co-N(3) angles are 76.9, 169.9, and 172.4° respectively, accounting for the rather distorted octahedral structure shown in Table 2. More remarkable is the mean of the trans Co-N(2) and Co-N(3) distances, which is longer by 0.026 Å than the mean of cis Co-N(1) and Co-N(4). The magnitude of the trans influence induced by the dtc ligand is between those induced by the

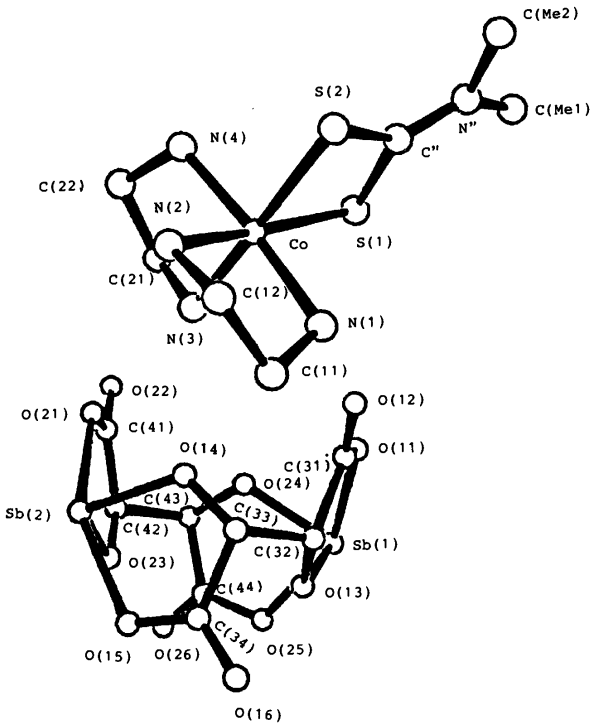

Fig. 1. A perspective view and numbering of $(+)^{CD}_{500}$-[Co(dtc)(en)$_2$][Sb$_2$(R,R-$C_4H_2O_6$)$_2$]·5H$_2$O (50% probability thermal ellipsoids).

Table 2. Intramolecular Bond Distances (l/Å)

For the Co(III) complex:			
Co-S(1)	2.277(3)	Co-S(2)	2.249(3)
Co-N(1)	1.950(8)	Co-N(2)	1.990(9)
Co-N(3)	1.978(8)	Co-N(4)	1.966(8)
S(1)-C"	1.724(10)	S(2)-C"	1.694(10)
C"-N"	1.317(13)	N"-C(Mel)	1.495(15)
N"-C(Me2)	1.447(16)	N(1)-C(11)	1.473(16)
C(11)-C(12)	1.562(18)	C(12)-N(2)	1.509(15)
N(3)-C(21)	1.532(14)	C(21)-C(22)	1.510(16)
C(22)-N(4)	1.459(13)		
For bis[μ-(R,R)-tartrato(4−)]diantimonate(III):			
Sb(1)-O(11)	2.167(6)	Sb(1)-O(13)	1.966(6)
Sb(1)-O(24)	1.987(7)	Sb(1)-O(25)	2.131(7)
Sb(2)-O(14)	1.968(7)	Sb(2)-O(15)	2.180(7)
Sb(2)-O(21)	2.142(8)	Sb(2)-O(23)	1.961(7)
O(11)-C(31)	1.260(12)	O(12)-C(31)	1.227(13)
O(13)-C(32)	1.423(12)	O(14)-C(33)	1.399(12)
O(15)-C(34)	1.280(12)	O(16)-C(34)	1.219(13)
C(31)-C(32)	1.555(14)	C(32)-C(33)	1.512(14)
C(33)-C(34)	1.575(14)	O(21)-C(41)	1.296(13)
O(22)-C(41)	1.242(13)	O(23)-C(42)	1.406(12)
O(24)-C(43)	1.409(12)	O(25)-C(44)	1.302(13)
O(26)-C(44)	1.239(14)	C(41)-C(42)	1.526(14)
C(42)-C(43)	1.550(14)	C(43)-C(44)	1.494(15)

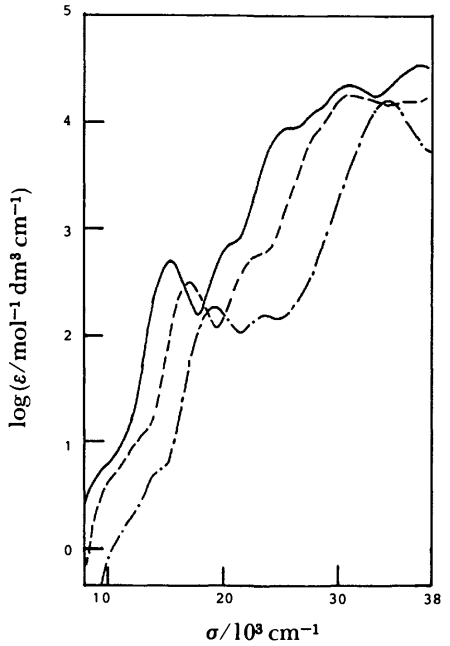

Fig. 2. Absorption spectra of [Co(dtc)$_{3-n}$(en)$_n$](ClO$_4$)$_n$ in DMSO solution: n=0 (——), n=1 (---), and n=2 (-·-).

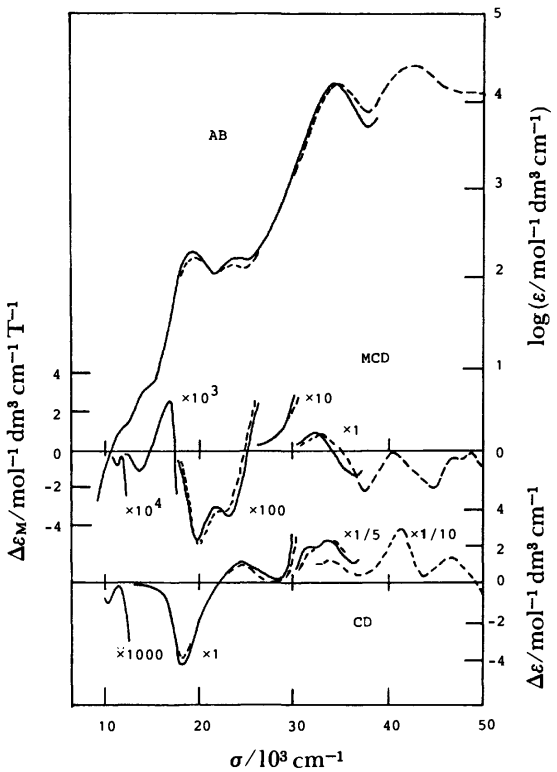

Fig. 3. Absorption, MCD, and CD spectra of [Co(dtc)(en)$_2$](ClO$_4$)$_2$ in DMSO (——) and H$_2$O (---) solution. For CD, $(-)^{CD}_{500}$-isomer (Δ-isomer) was used.

Table 3. Intramolecular Bond Angles (ϕ/°)

For the Co(III) complex:			
Metal coordination angles			
S(1)-Co-S(2)	76.90(9)	S(1)-Co-N(1)	89.5(3)
S(1)-Co-N(2)	169.9(3)	S(1)-Co-N(3)	96.7(3)
S(1)-Co-N(4)	93.6(2)	S(2)-Co-N(1)	92.7(3)
S(2)-Co-N(2)	94.0(3)	S(2)-Co-N(3)	172.4(3)
S(2)-Co-N(4)	91.2(2)	N(1)-Co-N(2)	86.5(3)
N(1)-Co-N(3)	91.3(3)	N(1)-Co-N(4)	175.5(3)
N(2)-Co-N(3)	92.7(4)	N(2)-Co-N(4)	90.9(3)
N(3)-Co-N(4)	85.1(3)		
Intraligand angles			
Co-S(1)-C″	85.3(3)	Co-S(2)-C″	86.9(4)
Co-N(1)-C(11)	111.7(7)	Co-N(2)-C(12)	105.8(7)
Co-N(3)-C(21)	106.8(6)	Co-N(4)-C(22)	111.8(6)
S(1)-C″-S(2)	110.8(6)	S(1)-C″-N″	124.4(8)
S(2)-C″-N″	124.8(8)	C″-N″-C(Me1)	119.0(9)
C″-N″-C(Me2)	123.4(9)	C(Me1)-N″-C(Me2)	117.5(9)
N(1)-C(11)-C(12)	104.9(9)	C(11)-C(12)-N(2)	107.1(9)
N(3)-C(21)-C(22)	106.2(9)	C(21)-C(22)-N(4)	106.6(8)
For bis[μ-(*R*,*R*)-tartrato(4−)]diantimonate(III):			
O(11)-Sb(1)-O(13)	79.2(3)	O(11)-Sb(1)-O(24)	80.7(3)
O(11)-Sb(1)-O(25)	153.1(3)	O(13)-Sb(1)-O(24)	97.9(3)
O(13)-Sb(1)-O(25)	86.7(3)	O(24)-Sb(1)-O(25)	78.5(3)
O(14)-Sb(2)-O(15)	78.8(3)	O(14)-Sb(2)-O(21)	81.4(3)
O(14)-Sb(2)-O(23)	100.1(3)	O(15)-Sb(2)-O(21)	150.9(3)
O(15)-Sb(2)-O(23)	82.8(3)	O(21)-Sb(2)-O(23)	79.9(3)
Sb(1)-O(11)-C(31)	115.1(6)	Sb(1)-O(13)-C(32)	118.1(6)
Sb(1)-O(24)-C(43)	117.8(6)	Sb(1)-O(25)-C(44)	114.8(7)
Sb(2)-O(14)-C(33)	118.8(6)	Sb(2)-O(15)-C(34)	115.4(6)
Sb(2)-O(21)-C(41)	114.2(6)	Sb(2)-O(23)-C(42)	117.1(5)
O(11)-C(31)-O(12)	123.9(10)	O(11)-C(31)-C(32)	116.2(9)
O(12)-C(31)-C(32)	119.9(9)	C(31)-C(32)-O(13)	111.4(8)
C(31)-C(32)-C(33)	110.0(8)	O(13)-C(32)-C(33)	112.0(8)
C(32)-C(33)-O(14)	111.8(8)	C(32)-C(33)-C(34)	106.6(8)
C(33)-C(34)-O(15)	114.2(8)	C(33)-C(34)-O(16)	120.7(9)
O(15)-C(34)-O(16)	125.1(9)	O(21)-C(41)-O(22)	124.9(9)
O(21)-C(41)-C(42)	115.3(9)	O(22)-C(41)-C(42)	119.8(9)
C(41)-C(42)-O(23)	113.2(8)	C(41)-C(42)-C(43)	108.8(8)
O(23)-C(42)-C(43)	111.2(8)	C(42)-C(43)-O(24)	110.3(8)
C(42)-C(43)-C(44)	109.2(8)	C(43)-C(44)-O(25)	116.4(9)
C(43)-C(44)-O(26)	120.9(10)	O(25)-C(44)-O(26)	122.6(10)
O(14)-C(33)-C(34)	112.5(8)	O(24)-C(43)-C(44)	112.2(8)

thiolato and thiosulfato ligands: SO_3^{2-}(0.089)>RSO^-(0.072)>RSO_2^-(0.049)>RS^-(0.040)>dtc$^-$(0.026)>$S_2O_3^{2-}$(0.019)>RSR′, RSSR′, or $RSNH_2$(0.000),[5] where the figures in parentheses indicate the difference (Å) between the trans Co-N distance and the average of the cis distances in the [Co(S)(N)$_5$] type. The dtc sulfur donor atoms do not induce so large a trans influence, presumably because of the little overlapping between the σ(dtc) MO and metal dσ AO attributable to the 4-membered acute chelation.

Results and Discussion

Synthesis and Characterization of [Co(dtc)$_{3-n}$(diamine)$_n$](ClO$_4$)$_n$(n=0, 1, and 2, and diamine means en or *R*-pn). The reduction of dialkyl disulfide by 2-equiv cobalt(II) ions with 10-equiv amines yields several [Co(thiolato)(amine)$_5$]$^{2+}$-type complexes.[18] In the present series, [Co(dtc)$_{3-n}$(diamine)$_n$]$^{n+}$ (n=0, 1, and 2, and diamine means en or *R*-pn), such a redox reaction between the disulfide and cobalt(II) ions produced the desired complexes in high yields, as has been described in the Experimental section.

The absorption spectra of three complexes [Co(dtc)$_{3-n}$(en)$_n$](ClO$_4$)$_n$(n=0, 1, and 2) in a DMSO solution are shown in Fig. 2. The energies of both the spin-allowed first (15000—20000 cm^{-1}) and second (20000—25000 cm^{-1}) d-d bands decrease with the increase in the number of dtc ligands. Such shifts correspond the weaker ligand field of the dtc sulfur donor than that of the en nitrogen one. The observed increase in the band intensity can be accounted for through the partial release of the Laporte forbidden d-d transitions by the mixing between the dπ(Co) and n(dtc) or π(dtc) and by the distortion from the octahedral-site structure around the central cobalt(III)

Table 4. Displacements of Atoms from the Least-Squares Plane and the Dihedral Angles between Planes

For the Co(III) complex:
Plane 1. [Co, S(1), S(2), N(2), and N(3)]
$0.5239X-0.6451Y-0.5562Z+0.2536=0$
Co 0.0070, S(1) −0.0891, S(2) 0.1035, N(2) −0.0465, N(3) 0.0509, C″ −0.0426, N″ −0.1439, C(Me1) −0.0691, C(Me2) −0.2346
Plane 2. [Co, S(1), N(1), N(2), and N(4)]
$-0.7902X-0.1947Y-0.5812Z+4.1017=0$
Co −0.0409, S(1) 0.1075, N(1) −0.1064, N(2) 0.1466, N(4) −0.0948
Plane 3. [Co, S(2), N(1), N(3), and N(4)]
$-0.3522X-0.7682Y+0.5346Z+3.4924=0$
Co 0.0321, S(2) −0.0724, N(1) 0.0710, N(3) −0.1009, N(4) 0.0773
Plane 4. [S(1), S(2), C″, and N″]
$-0.5517X+0.5697Y+0.6091Z+0.1889=0$
S(1) 0.0022, S(2) 0.0047, C″ −0.0101, N″ 0.0039, Co 0.1234, C(Me1) −0.0283, C(Me2) −0.0423
Dihedral angles (ϕ/°)

Between Planes 1 and 2	88.0
Between Planes 1 and 3	89.2
Between Planes 1 and 4	174.5
Between Planes 2 and 3	83.3

The X, Y, and Z coordinates in Å refer to the crystallographic axes.

Table 5. Selected Bond Distances (l/Å) and Angles (ϕ/°) for the $[Sb_2\{(R,R)\text{-}C_4H_2O_6\}_2]^{2-}$ Ion

	This work	$K_2[Sb_2(R,R\text{-}C_4H_2O_6)_2]\cdot 3H_2O$[11]
Bond	Average l/Å	Average l/Å
Sb-O[a]	2.155	2.16
Sb-O[b]	1.971	1.99
O[a]-C	1.285	1.27
O[b]-C′	1.409	1.40
Angle	Average ϕ/°	Average ϕ/°
O[a]-Sb-O[b]	79.1	78.3
Sb-O[a]-C	114.9	115.2
Sb-O[b]-C′	118.0	117.5

a) and b) oxygen atoms indicate the carboxyl and hydroxyl oxygen atoms of a tartrato(4−) anion.

Table 6. Selected Bond Distances (l/Å) and Angles (ϕ/°) for the Cobalt(III) Complexes Containing the dtc Ligand

	This work	$[Co(dtc)_3]$[19]
Bond	Average l/Å	Average l/Å
Co-S	2.263	2.264
S-C″	1.709	1.705
C″-N″	1.317	1.320
N″-C(Me)	1.460	1.450
Angle	Average ϕ/°	Average ϕ/°
S-Co-S	76.9	76.4
Co-S-C″	86.1	86.6
S-C″-S	110.8	110.4
S-C″-N″	124.6	124.9
C″-N″-C(Me)	121.2	121.4
C(Me)-N″-C(Me)	117.5	117.2

ion because of the 4-membered chelation of the dtc ligand. In the higher energy region (25000—35000 cm^{-1}), the energy of ligand-to-metal charge-transfer (LMCT) band, dσ*(Co)←σ(dtc), decreases and the band is split and widened with the increase of the number of the dtc ligands. These features may result from the increase in the sets of combination of the σ MOs of the dtc ligands.

The absorption, MCD, and CD spectra of the complex compound $(-)^{CD}_{500}$-$[Co(dtc)(en)_2](ClO_4)_2$, which has a *cis*-$[Co(S)_2(N)_4]$ chromophore, are shown in Fig. 3, while the numerical data are listed in Tables 7, 8, and 9. The weak shoulders in the absorption spectrum at ca. 12000 cm^{-1} and ca. 15000 cm^{-1} can be assigned to the spin-forbidden d-d transitions, $^3T_1$ and $^3T_2$←$^1A_1$ (O_h) respectively. In the MCD spectra, the negative peak at 11360 cm^{-1} and the pair of the negative peak at 13700 cm^{-1} and the positive one at 17000 cm^{-1} correspond to the transitions of $^3T_1$ (the first peak) and $^3T_2$ (the latter two peaks)←$^1A_1$(O_h). The absorption band at 19400 cm^{-1}, the negative CD peak at 18300 cm^{-1}, and the negative MCD at 19900 cm^{-1} are assigned to the spin-allowed first d-d transition of $^1T_1$←$^1A_1$ (O_h), and the absorption band at 23700 cm^{-1} the negative MCD peak at 23200 cm^{-1}, and the positive CD one at 24500 cm^{-1}, to the second d-d transition of $^1T_2$←$^1A_1$. The intense absorption bands at 34300 cm^{-1} and at 41000 cm^{-1} can be assigned to the LMCT band σ*(Co)←σ(dtc or sulfur) and the intra-

Table 7. Absorption Spectral Data

Complex/Solvent	$\sigma_{max}(\log \varepsilon)$[a]
$[Co(dtc)(en)_2](ClO_4)_2$	
DMSO	12.05(0.27)[sh], 14.93(0.76)[sh], 19.40(2.25), 23.71(2.18), 34.30(4.24)
H_2O	14.94(0.80)[sh], 19.60(2.21), 23.29(2.11), 34.75(4.21), 41.10(4.35)[sh], 42.90(4.43)
$[Co(dtc)_2(en)]ClO_4$	
DMSO	10.00(0.56)[sh], 12.99(1.06)[sh], 17.24(2.51), 23.00(2.76)[sh], 27.47(3.79)[sh], 31.25(4.27)
H_2O	17.39(2.49), 23.00(2.70)[sh], 28.17(3.78)[sh], 31.75(4.22), 35.71(4.11)[sh], 40.00(4.34)[sh], 41.90(4.45)
$[Co(dtc)_3]$	
DMSO	10.00(0.78)[sh], 15.38(2.70), 21.05(2.88)[sh], 25.74(3.95)[sh], 25.74(3.95)[sh], 27.89(4.08)[sh], 30.91(4.35), 35.90(4.49)[sh]
H_2O	10.00(0.74)[sh], 15.60(2.66), 21.05(2.85)[sh], 25.53(3.98)[sh], 25.53(3.98)[sh], 28.03(4.13)[sh], 31.08(4.34), 36.14(4.53)[sh], 37.40(4.55), 41.00(4.52)
Δ-$[Co(dtc)_2\{(R)$-pn$\}]ClO_4$	
DMSO	10.00(0.56)[sh], 12.99(1.03)[sh], 17.24(2.53), 23.00(2.77)[sh], 27.78(3.87)[sh], 31.25(4.29)
H_2O	17.39(2.52), 23.00(2.73)[sh], 28.17(3.84)[sh], 31.75(4.28), 35.71(4.17)[sh], 40.00(4.41)[sh], 41.67(4.52)
Λ-$[Co(dtc)_2\{(R)$-pn$\}]ClO_4$	
DMSO	10.00(0.57)[sh], 12.99(1.01)[sh], 17.24(2.54), 23.00(2.77)[sh], 27.78(3.89)[sh], 31.25(4.29)
H_2O	17.39(2.52), 23.00(2.75)[sh], 28.17(3.88)[sh], 31.25(4.29), 35.71(4.18)[sh], 40.00(4.42)[sh], 41.67(4.53)
Δ-$[Co(dtsi)(en)_2](ClO_4)_2$	
DMSO	20.94(2.49), 29.00(3.40)[sh], 37.74(4.40)
$[Co(mtz)(en)_2](ClO_4)_2$	
DMSO	11.95(0.43), 16.00(1.47)[sh], 19.20(2.18), 23.30(2.11), 33.33(3.66)[sh]
H_2O	19.50(2.10), 23.20(2.05), 33.33(3.68)[sh], 38.20(4.21), 44.00(4.25)[sh], 48.00(4.33)

a) Wavenumbers are given in $10^3\,cm^{-1}$ units, the $\log(\varepsilon/mol^{-1}\,dm^3\,cm^{-1})$ values are in parentheses, and sh indicates a shoulder.

Table 8. MCD Spectral Data

Complex/Solvent	$\sigma_{ext}(\Delta\varepsilon_M)$[a]
$[Co(dtc)(en)_2](ClO_4)_2$	
DMSO	11.36(−0.00008), 13.70(−0.0011), 16.95(+0.0026), 19.92(−0.048), 23.15(−0.035), 32.47(+0.983), 37.76(−1.37)
H_2O	20.00(−0.050), 22.73(−0.032), 33.11(0.898), 37.40(−2.10), 44.44(−2.04)
$[Co(dtc)_2(en)]ClO_4$	
DMSO	12.11(−0.0018), 14.29(+0.0031), 17.54(−0.066), 21.98(−0.041), 29.41(+1.91), 31.65(−1.96)
H_2O	29.85(+1.57), 32.26(−1.51), 42.55(−2.16)
$[Co(dtc)_3]$	
DMSO	11.24(−0.0025), 12.66(+0.0036), 15.95(−0.120), 20.53(−0.075), 24.10(+0.279), 27.17(+3.12), 28.99(−1.63), 35.71(−0.80)
$CHCl_3$	10.99(−0.0025), 12.82(−0.0033), 16.05(−0.106), 20.62(−0.064), 24.10(+0.317), 27.03(+3.35), 28.65(−1.96), 30.77(−0.66)[sh]

a) Wavenumbers are given in $10^3\,cm^{-1}$ units, the $\Delta\varepsilon_M$ (in parentheses) are given in $mol^{-1}\,dm^3\,cm^{-1}\,T^{-1}$ units, and sh indicates a shoulder.

ligand transition π^*(dtc or delocalized MO on S_2NC fragment)←n(dtc) respectively.

Figure 4 shows the absorption and MCD spectra of $[Co(dtc)_2(en)]ClO_4$, which has a *cis*-$[Co(S)_4(N)_2]$ chromophore. The first eluted $(-)^{CD}_{580}$-$[Co(dtc)_2(R$-pn$)]ClO_4$, which shows a negative CD at 17000 cm^{-1}, is assigned to the Δ absolute configuration by analogy with the assignment for $[Co(dtc)(en)_2](ClO_4)_2$. The CD curve due to the configurational contribution was calculated from these CD spectra on the basis of the assumed additivity of the CD contributions. It is noteworthy that the CD intensities of the bis-

Table 9. CD Spectral Data

Complex/Solvent	$\sigma_{ext}(\Delta\varepsilon)$[a]
Δ-[Co(dtc)(en)$_2$](ClO$_4$)$_2$	
DMSO	10.20(−0.0011), 18.25(−4.26), 24.51(+1.14), 31.45(+9.34), 33.56(+10.94)
H_2O	18.21(−3.87), 24.51(+0.99), 32.26(+9.24), 34.13(+11.13), 41.32(+28.47), 46.73(+12.87)
Δ-[Co(dtc)$_2${(*R*)-pn}]ClO$_4$	
DMSO	17.01(−9.79), 20.20(−1.04)^{sh}, 23.26(+3.98)^{sh}, 28.82(+57.16), 31.25(+41.25), 35.71(−44.71)^{sh}, 37.04(−64.73)
H_2O	17.24(−8.75), 20.41(−0.84)^{sh}, 23.26(+3.14)^{sh}, 29.07(+53.74), 31.75(+38.11), 37.59(−43.10), 40.49(+27.44), 43.29(+23.15), 46.51(−44.78)
Λ-[Co(dtc)$_2${(*R*)-pn}]ClO$_4$	
DMSO	16.86(+9.68), 20.41(+1.51)^{sh}, 22.99(−2.44)^{sh}, 28.49(−60.52), 31.25(−37.67), 36.90(+67.82)
H_2O	17.04(+9.11), 20.20(+1.36)^{sh}, 23.26(−2.21)^{sh}, 28.99(−58.97), 31.85(−37.51), 37.31(+49.28), 40.32(−30.16), 42.74(−16.15), 46.51(+53.27)
Δ-[Co(dtsi)(en)$_2$](ClO$_4$)$_2$	
DMSO	20.41(−0.443), 28.90(+0.645), 37.04(+3.827)
Δ-[C(mtz)(en)$_2$](ClO$_4$)$_2$	
DMSO	19.76(−2.26), 24.94(+1.02), 32.89(+5.17)

a) Wavenumbers are given in 10^{-1} cm^{-1} units, the $\Delta\varepsilon$ (in parentheses) are given in mol^{-1} dm^3 cm^{-1} units, and sh indicates a shoulder.

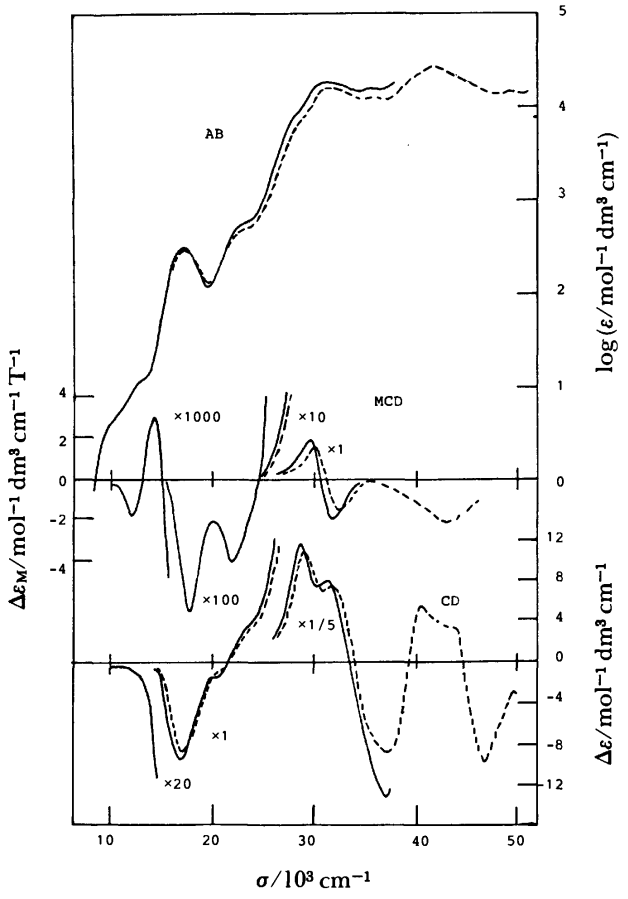

Fig. 4. Absorption and MCD spectra of [Co(dtc)$_2$(en)]-ClO$_4$, and CD curve of [(*Δ*-[Co(dtc)$_2$(*R*-pn)]ClO$_4$)−(*Λ*-[Co(dtc)$_2$(*R*-pn)]ClO$_4$)]/2 in DMSO (——) and H_2O (---) solutions.

(dithiocarbamate) complexes are about twice larger than that of the monodithiocarbamate one. This means the larger distortion from the octahedral-site structure is due to the increase in the numbers of the 4-membered dtc ligand. The shoulders of the absorption spectra at 10000 cm^{-1} and 13000 cm^{-1} are assigned to the spin-forbidden d–d transitions. A negative CD peak at 16900 cm^{-1} and a negative MCD peak at 17500 cm^{-1} are assigned to the splitting components of the first d–d transition. The two LMCT absorption bands at 27500 and 31300 cm^{-1} correspond to the two peaks of MCD at 29400 and 31700 cm^{-1} or to the two peaks of CD at 28700 and 31300 cm^{-1}. The absorption bands at 40000 and 41900 cm^{-1} are assigned to the dtc intraligand $\pi^*\leftarrow$n transitions. The vicinal contribution of asymmetric carbon or *R*-pn to the CD spectrum of [Co(dtc)$_2$(*R*-pn)]ClO$_4$ is shown in Table 9. It is interesting to note that the contribution depends significantly on the kind of solvent.

The absorption and MCD spectra of [Co(dtc)$_3$] with a [Co(S)$_6$] chromophore are shown in Tables 7 and 8. The absorption bands at 11200 and 12700 cm^{-1} are assigned to the spin-forbidden d–d transitions. The bands at 24100, 27200, and 29000 cm^{-1} are assigned to the LMCT transitions, and the band at 35900 cm^{-1}, to the dtc intraligand transitions. The positions of the absorption bands are the same as those of the MCD ones throughout the region observed.

The splitting components of the first d–d transition of the *cis*-S_2N_4- and *cis*-S_4N_2-type complexes were calculated semiempirically[21] on the basis of the observed d–d transition energies of [Co(en)$_3$]$^{3+}$ and

[Co(dtc)$_3$]. The calculated values are fairly consistent with the observed splittings: the energetically lower component corresponds to the CD peak, and the higher one, to the MCD extreme, as is shown in Table 10.

Synthesis and Characterization of the Oxidation Product [Co(dtsi)(en)$_2$](ClO$_4$)$_2$. The orange-red oxidation complex was prepared via the H_2O_2 oxidation of [Co(dtc)(en)$_2$](ClO$_4$)$_2$. The H_2O_2 oxidation of the coordinated dtc ligand in neutral aqueous solution was ineffective, but it was effective in acid media. Elemental analysis indicates that the calculated formula weight of the resulting species is consistent with two additional oxygen atoms compared with the starting material. Since it is reasonable to consider that the oxidation takes place at the sulfur moieties of the dtc ligand, there are two possibilities, $(CH_3)_2NC(SO)SO^-$ or $(CH_3)_2NC(S)SO_2^-$, as the oxidized dtc ligand. The XPS spectra of the [Co(dtc)(en)$_2$](ClO$_4$)$_2$ and [Co(dtsi)(en)$_2$](ClO$_4$)$_2$ are given in Fig. 5: they indicate the presence of two kinds of sulfur in the latter complex. The lower S-2p$_{3/2}$ binding energy (162.7 eV) in the dtsi complex is the same as that in the dtc complex. The higher peak (166.6 eV) is due to the oxidized sulfur atom with two oxygen atoms, for the S-2p$_{3/2}$ binding energy increases with the increase in

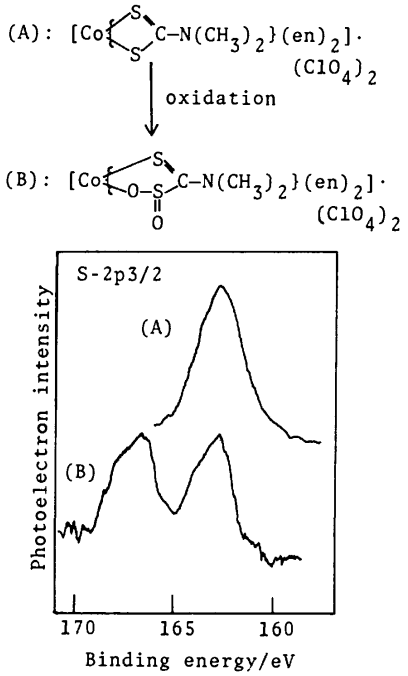

Fig. 5. XPS spectra of (A) [Co(dtc)(en)$_2$](ClO$_4$)$_2$ and (B) [Co(dtsi)(en)$_2$](ClO$_4$)$_2$ in the region of S-2p binding energy.

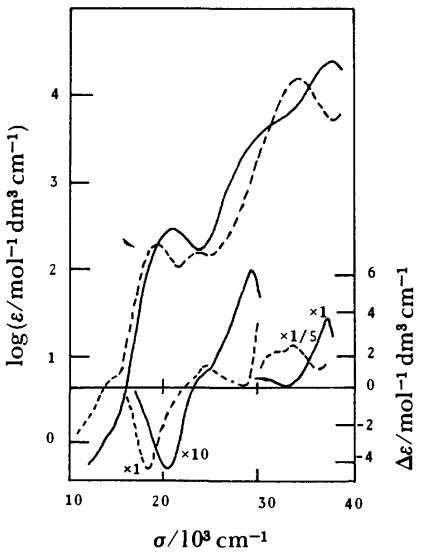

Fig. 6. Absorption and CD spectra of Δ-[Co(dtsi)(en)$_2$]-(ClO$_4$)$_2$ (——) and Δ-[Co(dtc)(en)$_2$](ClO$_4$)$_2$ (---) in DMSO solution.

Table 10. Splittings of the 1st Spin-Allowed d-d Transition.
(The wavenumber is given in 10^3 cm^{-1} units)

Type/Complex	Method	Splittings of the 1st d-d band
N_6		
[Co(en)$_3$]$^{3+}$	AB	21.3 (Standard)
Δ-isomer	CD	20.5(−)
S_6		
[Co(dtc)$_3$]	AB	15.4 (Standard)
	MCD	16.0(−)
cis-S_2N_4	Calcd	18.3, 19.8
[Co(dtc)(en)$_2$]$^{2+}$	AB	19.4
Δ-isomer	CD	18.3(−)
	MCD	19.9(−)
cis-S_4N_2	Calcd	16.8, 18.3
[Co(dtc)$_2$(en)]$^+$	AB	17.2
$(\Delta\varepsilon_{\Delta\text{-}R}-\Delta\varepsilon_{\Lambda\text{-}R})/2$	CD	16.9(−)
	MCD	17.5(−)
Δ-[Co(dtc)$_3$]	CD	15.50(−0.14) from Ref. 2

the sulfur oxidation numbers.[22] Since the intensities of the lower and higher energy bands are approximately equal, the dtsi complex should have oxidized and nonoxidized sulfur atoms compared with those of the original dtc complex. Thus, the dtsi ligand is represented by this formula: $(CH_3)_2NC(S)SO_2^-$. The present dtsi complex exhibits a new absorption band at ca. 29000 cm^{-1} as a broad shoulder in addition to the $\sigma^*(Co)\leftarrow\sigma(S)$ LMCT band at 37000 cm^{-1}, as is shown in Fig. 6. The *O*-bonded sulfinato cobalt(III) complex, $[Co(NH_2CH_2CH_2SO_2\text{-}O,N)(en)_2]^{2+}$, shows a similar absorption band at 31000 cm^{-1} without the $\sigma^*(Co)\leftarrow\sigma(S)$ LMCT band.[5] This fact indicates that the dtsi ligand coordinates through the sulfinato oxygen and thiocarbonyl sulfur atoms. This indicates the occurrence of the chelate ring expansion from a four-membered ring to a five-membered one during the oxidation process. The optically active complex $(-)_{490}^{CD}$-$[Co(dtsi)(en)_2]^{2+}$ can be assigned to the *Δ*-configuration on the basis of the CD sign at 20400 cm^{-1} in the first d-d band region (Fig. 6). Therefore, the oxidation reaction proceeds with a retention of the initial configuration of *Δ*-$[Co(dtc)(en)_2]^{2+}$, whose configuration was determined by X-ray structure analysis as has been described in the preceding section.

References

1) D. Coucouvanis, *Prog. Inorg. Chem.*, **11**, 233 (1970), **26**, 301 (1979), and the references cited therein.

2) C. L. Raston, A. H. White, and A. C. Willis, *J. Chem. Soc., Dalton Trans.*, **1975**, 2429.

3) S. Merlino, *Acta Crystallogr., Sect. B*, **24**, 1441 (1968).

4) H. Iwasaki and K. Kobayashi, *Acta Crystallogr., Sect. B*, **36**, 1657 (1980).

5) V. H. Houlding, H. Macke, and A. W. Adamson, *J. Am. Chem. Soc.*, **102**, 6888 (1980).

6) 2-Mercapto-2-thiazoline was neutralized by the excess ethylenediamine in the former solution.

7) N means the number '*n*' of the *n*th-measurement counting from the start of measurement of the reflection intensity.

8) T. Takano, N. Tanaka, and M. Kusunoki, "ABSC, The Universal Crystallographic Computing System-Osaka," The Computing Center, Osaka University (1979), p. 13.

9) "International Tables for X-Ray Crystallography," Kynoch Press, Birmingham(1974), Vol. IV.

10) N. Yasuoka and N. Tanaka, "MFPA, The Universal Crystallographic Computing System-Osaka," The Computation Center, Osaka University (1979), p. 16.

11) T. Ashida, "HBLS V, The Universal Crystallographic Computing System-Osaka," The Computation Center, Osaka University (1979), p. 53.

12) T. Ashida, "DAPH, The Universal Crystallographic Computing System-Osaka," The Computation Center, Osaka University (1979), p. 61.

13) C. K. Johnson, "ORTEP-II: A FORTRAN Thermal-Ellipsoid Plot Program for Crystal Structure Illustrations, ORNL--5138, March 1976. Oak Ridge National Laboratory."

14) M. E. Gress and R. A. Jacobson, *Inorg. Chim. Acta*, **8**, 209 (1974).

15) N-H=0.87 Å and C-H=0.97 Å were used.

16) $R=\sum||F_o|-|F_c||/\sum|F_o|$ and $R_2=\{\sum w(|F_o|-|F_c|)^2/\sum w|F_o|^2\}^{1/2}$.

17) W. G. Hamilton, *Acta Crystallogr.*, **12**, 609 (1959).

18) D. L. Nosco and E. Deutsch, *Inorg. Synth.*, Vol. XXI, 19 (1982).

19) C. J. Weschler and E. Deutsch, *Inorg. Chem.*, **12**, 2682 (1973).

20) M. Kita, K. Yamanari, and Y. Shimura, *Chem. Lett.*, **1983**, 141.

21) H. Yamatera, *Bull. Chem. Soc. Jpn.*, **31**, 95 (1958).

22) M. Kita, Y. Yamanari, K. Kishi, S. Ikeda, and Y. Shimura, *Chem. Lett.*, **1981**, 337.

 © 1989 The Chemical Society of Japan Bull. Chem. Soc. Jpn., 62, 33—38 (1989)

^{125}Te and ^{129}I Mössbauer Spectroscopic Studies of the Tetragonal and Orthorhombic Forms of Tellurium(IV) Oxide

Hiroshi SAKAI* and Yutaka MAEDA
Research Reactor Institute, Kyoto University,
Kumatori-cho, Sennan-gun, Osaka 590-04
(Received May 11, 1988)

^{125}Te and ^{129}I Mössbauer spectra have been measured for the tetragonal (α) and orthorhombic (β) forms of TeO_2. The Mössbauer data show that there are no significant differences between the two modifications in either the electronic structure or the chemical bonding of the tellurium atoms; this is consistent with the crystallographic data. From a comparison of the Mössbauer data for ^{125}Te with those for ^{129}I, we have concluded that the ^{129}I daughter nucleus, produced by the nuclear β^- decay of ^{129}Te, is present in the same lattice environment as the parent ^{129}Te nucleus in TeO_2. A $Cu^{125}I$ crystalline compound has been used as the Mössbauer source of ^{125}Te, which emits a single line of resonance γ-ray. The values of the isomer shift and line width for the source are found to be -0.13 mm s^{-1} relative to the ZnTe standard absorber and 6.53 mm s^{-1} respectively.

Tellurium(IV) oxide (TeO_2) is known to have two crystalline forms, a colorless tetragonal (α) form and a yellow orthorhombic (β) form.[1] In both modifications the coordination about the tellurium atom is a slightly distorted trigonal bipyramid, with one corner of the equatorial triangle unoccupied. The four Te–O bond distances are 1.903 Å (equatorial) and 2.082 Å (axial) for the tetragonal form and from 1.88 to 2.19 Å for the orthorhombic form. These bond distances suggest a considerable covalent character of the Te–O bonds, since the sum of the covalent bond radius for each atom is 2.03 Å.[2] The surroundings of the Te sites (the bond distances and the bond angles) in the trigonal bipyramid are similar in the two modifications, although a weak Te–Te bond with the distance of 3.17 Å exists in the β-form. This fact suggests that there are no significant differences in the electronic structure and the chemical bonding of the Te atoms for the α- and β-forms. However, the results of ^{129}I Mössbauer emission investigations have exploded the expectations based on the coordination figures.[3,4] The isomer shift observed in the ^{129}I Mössbauer emission spectrum of the α-form is considerably larger than that in the β-form. Warren et al.[4] have concluded that the difference in the isomer shifts arises from differences in the s-character of the parent Te–O bonds is the two forms. If this conclusion is correct, a difference in the isomer shifts should be observed in the ^{125}Te Mössbauer absorption spectra for the two modifications.

In the present paper we wish to report our results on the ^{125}Te Mössbauer absorption spectra for the tetragonal (α) and orthorhombic (β) forms of TeO_2. Further, the ^{129}I Mössbauer emission spectra were measured for these compounds in order to compare their values with the previous data. Thus, the specimens were investigated both as absorbers and as sources.

Experimental

Materials. The commercially available TeO_2 (Wako Pure Chemical) was found by X-ray powder diffraction analysis using graphite monochromated Cu $K\alpha$ radiation to be the orthorhombic (β) phase. The tetragonal (α) form prepared by melt-quenching was also confirmed by X-ray diffraction. The diffraction patterns of the α- and β-forms are given in Fig. 1; they are in good agreement with the values in the literature (ASTM cards 1-0870, 1-0117).

Measurements. ^{125}Te Mössbauer Absorption Spectra: $Cu^{125}I$ crystalline powder, prepared from the standard form of $Na^{125}I$ in a 0.1 mol dm^{-3} NaOH solution (New England Nuclear Co.), was used as the Mössbauer source of ^{125}Te. The radioactive compound had first been used as the

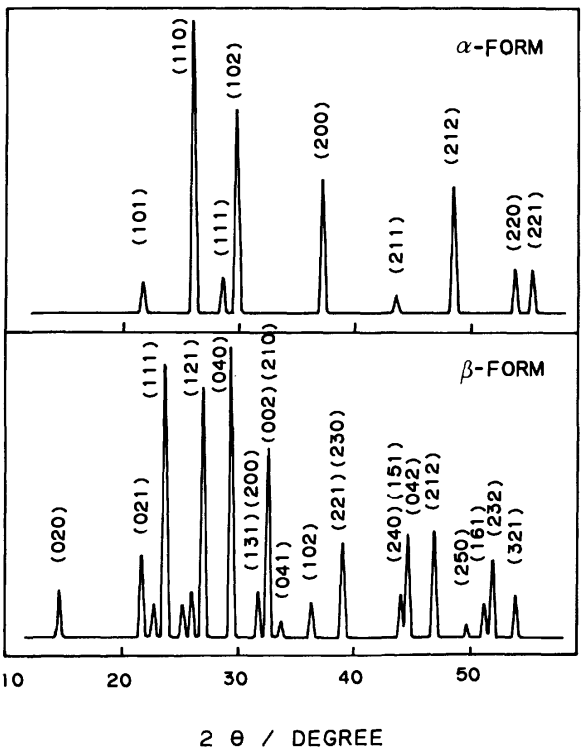

Fig. 1. X-Ray powder diffraction patterns of the tetragonal (α) and orthorhombic (β) forms of TeO_2 obtained by using graphiet monochromated Cu $K\alpha$ radiation.

γ-ray source for the ^{125}Te Mössbauer specitroscopy by Ambe and Ambe.[5] They found that the source emitted a single line of resonance γ-ray. In the present investigation, the source was also verified to be a single line from the spectra against a ZnTe absorber (2 mg cm^{-2} ^{125}Te) at 16 K and 77 K. The line width at half maximum was found to be 6.53 mm s^{-1} for the single absorption peak; this value was comparable to such other sources as ^{125}I or ^{125}Sb deposited on Cu foil and Zn^{125m}Te. The natural line width of ^{125}Te is calculated to be 5.20 mm s^{-1} from the lifetime of the 35.50 keV state. The Mössbauer spectra were measured in the transmission geometry by cooling the source and the absorber (each a modification of TeO_2; 3 mg cm^{-2} ^{125}Te) to 16 K by the use of a closed-cycle helium refrigerator. The 35.5 keV Mössbauer γ-ray was detected indirectly by counting the 5.8 keV escaped peak in a Xe-filled proportional counter. The velocity scale of the spectrometer was calibrated with a six-line spectrum of an Fe foil.

^{129}I Mössbauer Emission Spectra: About a 300-mg portion of each form of TeO_2 was used as a γ-ray source, irradiated at a thermal neutron-fluence rate of 2×10^{13} n cm^{-2} s^{-1} for 1 h in the Kyoto University Reactor (KUR). The Mössbauer experiments were performed with ^{129}I daughters produced by this nuclear reaction: ^{128}Te(n, γ) ^{129}Te$\xrightarrow{\beta^-}$ ^{129}I. The ^{128}Te abundance in natural tellurium is 31.8%, enough for it to serve as the source. A single line Cu^{129}I (10 mg cm^{-2} ^{129}I), used as a Mössbauer absorber, was prepared from Na^{129}I in a Na_2SO_3 solution in a manner similar to that used for Cu^{125}I. The absorber was checked, by means of a spectrum, against the standard ZnTe source at 16 K, in which the isomer shift and the line width were found to be -0.42 mm s^{-1} and 1.42 mms^{-1} respectively. Furthermore, the ^{129}I emission spectrum of the tellurium metal was measured at 16 K in order to calibrate the velocity scale of the spectrometer under the same experimental conditions; this was in addition to the measurement of the six-line spectrum of an Fe foil at room temperature. The Mössbauer measurements were carried out in the same way as those of ^{125}Te. The 27.8 keV γ-ray was detected by the use of a 1 mm-thick NaI(Tl) scintillation counter.

Results and Discussion

A. ^{125}Te Mössbauer Absorption Spectra. The ^{125}Te Mössbauer absorption spectra at 16 K of (a) ZnTe, (b) α-TeO_2, and (c) β-TeO_2 are shown in Fig. 2. The spectra were analyzed with Lorentzian curves by means of the least-squares method. The Mössbauer parameters, such as the isomer shift (δ) relative to the ZnTe standard absorber, the quadrupole splitting (2 ε), and the full width at half maximum (2Γ), are summarized in Table 1. Various δ values have been reported by different laboratories for the same Te compound, for example, TeO_2.[6] These discrepancies, as has been pointed out by Dobud and Jones,[7] seem to arise from the difficulties inherent in calibrating the spectrometer, for the ^{125}Te Mössbauer study requires a relatively high velocity region. Therefore, the standard Te compounds, such as Te metal and β-TeO_3, in addition to ZnTe, were measured under the same experimental conditions. The results are also given in Table 1, together with the δ values recommended by Stevens and Gettys.[8]

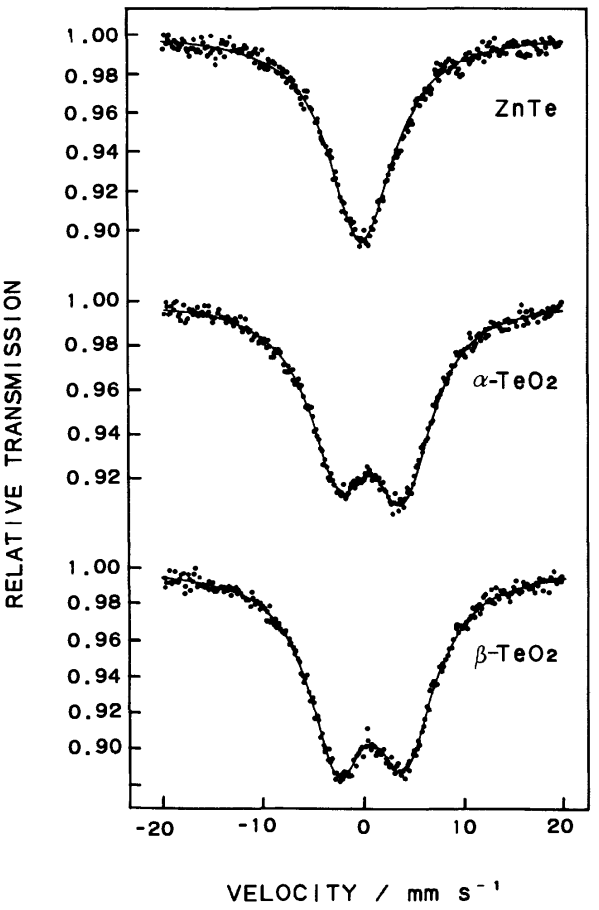

Fig. 2. ^{125}Te Mössbauer absorption spectra at 16 K of the ZnTe standard absorber, α-TeO_2, and β-TeO_2 against the Cu^{125}I source.

Table 1. ^{125}Te Mössbauer Parameters of α- and β-TeO_2, Te Metal, and β-TeO_3

	T	δ	2ε	2Γ
	K	mm s^{-1} ±0.08	mm s^{-1} ±0.08	mm s^{-1} ±0.10
α-TeO_2	16	0.73	6.48	7.25
β-TeO_2	16	0.70	6.80	7.10
Te metal	16	0.57 (0.66)	7.30	6.28
β-TeO_3	16	−1.11 (−1.11)	0	7.79
ZnTe	16	0	0	6.53

The δ values are relative to the ZnTe absorber. The δ values in parentheses are taken from Ref. 8.

The δ value of ZnTe against the Cu^{125}I source has been found to be +0.13 mm s^{-1}; this value is different from the recommended value (-0.02 mm s^{-1}) against the ^{125}I source deposited on a Cu foil.[8] The difference implies that the electronic structure of iodine in the CuI crystal is different from that in the Cu metal. As

will be shown below, the result we have obtained from the $Cu^{125}I$ source is reasonable, since the δ value of the $Cu^{129}I$ absorber against the $Zn^{129}Te$ source is about -0.4 mm s^{-1} in the ^{129}I Mössbauer study. It is of interest that the $Cu^{125}I$ source has given a single resonance line; that is, no anomalous charge state of ^{125}Te following the electron capture (EC) decay of ^{125}I has been observed for the spectrum. Violet and Booth[9] and Jung and Triftshäuser[10] observed four-line spectra for an $NaIO_3$ source. The latter authors concluded from the δ and 2ε values of two pairs of lines that the spectrum indicated the coexistence of Na_2TeO_3 and TeO_3, resulting from the K-capture decay of ^{125}I in $NaIO_3$ and the subsequent electron-rearrangements.

The ^{125}Te Mössbauer absorption spectra for the α- and β-forms of the TeO_2 crystal are similar to each other. The asymmetry in the spectrum of the α-form may be due to the preferred orientation of the specimen. The δ value of the α-form is in good agreement with that of the β-form, within the limits of experimental error. This result is apparently not in accord with that obtained from the ^{129}I Mössbauer emission spectra for both modifications. Warren et al.[4] have determined the isomer shift ratio, δ (^{125}Te)/ δ (^{129}I), for the ^{125}Te and ^{129}I nuclei in precisely the same lattices. They found this ratio to be $+0.29\pm0.03$ for several tellurium compounds. Therefore, if the ^{129}I resulting from the β^- decay of ^{129}Te finds itself in the same lattice environment as the parent TeO_2, the δ values relative to the ZnTe of the ^{129}I Mössbauer emission spectra should be observed to be about $+2.5$ mm s^{-1} for both modifications of the TeO_2 crystal, dividing the averaged δ value of ^{125}Te by 0.29. However, the δ values of ^{129}I for the α- and β-forms have been experimentally measured to be $+2.74\pm0.14$ mm s^{-1} and $+1.52\pm0.01$ mm s^{-1} respectively.[3,4] The deviation, in particular for the β-form, between the expected and measured δ values indicates that the resulting ^{129}I is no longer in the same lattice environment.

It is interesting to examine the δ value of the $Cu^{125}I$ source, for it is little used for ^{125}Te Mössbauer spectroscopy. The $Cu^{129}I$ absorber is often used for source experiments in the ^{129}I Mössbauer spetroscopy, and the δ value relative to the ZnTe source has been established as -0.41 mm s^{-1}.[11] Therefore, the δ value of the $Cu^{125}I$ source against the ZnTe absorber is estimated to be -0.12 mm s^{-1} from the isomer shift ratio for the ^{125}Te and ^{129}I nuclei; this value is in good agreement with the measured δ value (-0.13 mm s^{-1}). This implies that the ^{125}Te daughter nucleus, produced by the EC decay of ^{125}I, is present in the same lattice environment as the parent ^{125}I nucleus in the CuI crystal.

In the ^{125}Te Mössbauer absorption spectra, the quadrupole splitting $\{2\varepsilon=\frac{1}{2}e^2Qq(1+\frac{1}{3}\eta^2)^{1/2}\}$ of the α-form is slightly smaller than that of the β-form. This result also disagrees with that of the ^{129}I Mössbauer emission spectra, indicating that the quadrupole coupling constants (e^2Qq) for the α- and β-forms are $+812\pm21$ MHz and $+786\pm7$ MHz respectively.[3,4] Warren et al.[4] have determined the ratio of the quadrupole coupling constansts for ^{125}Te and ^{129}I nuclei, as well as the isomer shift ratio, in equivalent lattice sites as follows:

$$\frac{e^2Qq(^{125}\mathrm{Te})}{e^2Qq(^{129}\mathrm{I})}\left(1+\frac{1}{3}\eta^2\right)^{1/2}=0.45. \quad (1)$$

Langouche et al.[12] have also determined this ratio to be -0.48 ± 0.02 by means of a detailed examination of the ^{129}I and ^{125}Te Mössbauer spectra for several Te-thiourea compounds. Using this ratio and our result for 2ε of ^{125}Te, we can derive the e^2Qq values of ^{129}I for the α- and β-forms to be 773 MHz and 810 MHz respectively. The agreement between the measured and estimated e^2Qq values is insufficient.

It is important to note that in the ^{129}I Mössbauer emission measurements discrepancies in the values of δ and e^2Qq are often observed for an identical compound. For example, the δ and e^2Qq values for the tellurium metal have been reported to be $+0.71\pm0.03$ mm s^{-1} and -373 ± 6 MHz respectively by Pasternak and Bukshpan,[3] whereas they have been reported to be $+0.52\pm0.13$ mm s^{-1} and -349 ± 11 MHz respectively by Warren et al.[4] The values of δ and e^2Qq obtained in the present work are $+0.69\pm0.05$ mm s^{-1} and -403 ± 10 MHz respectively, values which are in good agreement with those of the more recent works of Langouche et al.[13] ($\delta=+0.77\pm0.04$ mm s^{-1}, $e^2Qq=-404\pm4$ MHz) and Kim and Boolchand[14] ($\delta=+0.80\pm0.03$ mm s^{-1}, $e^2Qq=-396\pm3$ MHz). Therefore, it is dangerous to conclude that the minor discrepancies in the reported and estimated δ and e^2Qq values for the two modifications of TeO_2 are to be attributed to the chemical effects accompanying the nuclear reaction and the β^- decay of the ^{129}Te nucleus.

B. ^{129}I Mössbauer Emission Spectra. ^{129}I Mössbauer emission spectra have been reinvestigated for both modifications of TeO_2 at 16 K, in order to examine in detail the chemical effects on the ^{128}Te (n, γ) ^{129}Te nuclear reaction and the β^- decay of the ^{129}Te and, furthermore, to clarify the origin of the large difference in the δ values of ^{129}I between the α- and β-forms previously reported. The spectra against the $Cu^{129}I$ standard absorber are shown in Fig. 3 (b) and (c); no anomalous peak is observed. These spectra were analyzed by the least-squares method using a single set of fitting parameters, δ, e^2Qq, the asymmetry parameter (η), the full width at half maximum (2Γ), each peak intensity, and the base line. The solid lines in the figures represent the best-fitting Lorentzian curves. The Mössbauer parameters obtained are given in Table

Table 2. ^{129}I Mössbauer Parameters of α- and β-TeO_2 and of Te Metal

	T	δ	e^2Qq	η	Ref.
	K	mm s^{-1}	MHz	%	
α-TeO_2	16	+2.44±0.12	+800±10	58±7	This work
	80	+2.74±0.14	+812±21	52±7	4
β-TeO_2	16	+2.36±0.12	+780±10	50±7	This work
	16	+2.40±0.12	+793±10	46±7	This work
	80	+1.52±0.01	+786± 7	55±5	3
Te metal	16	+0.69±0.05	+403±10	70±7	This work
ZnTe	16	−0.42±0.05	0	0	This work

a) The δ values are relative to the ZnTe source.

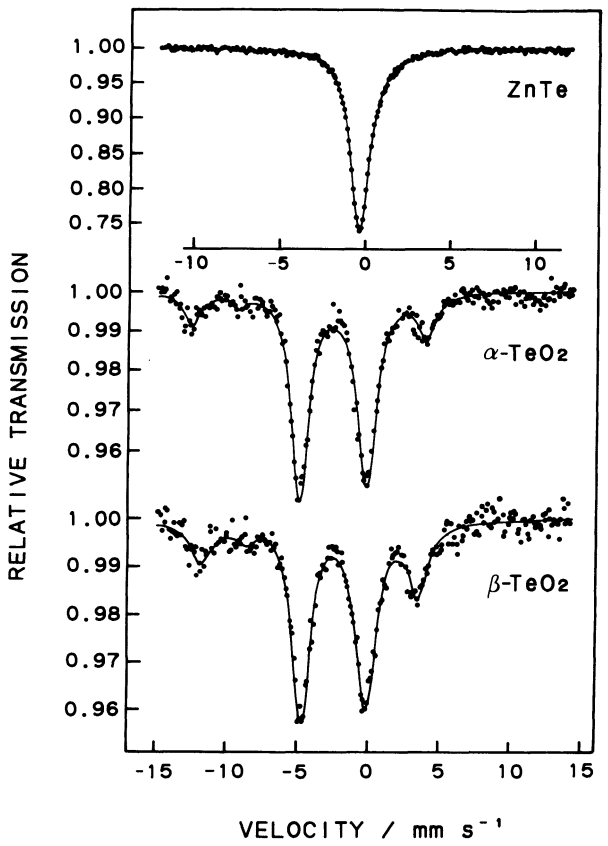

Fig. 3. ^{129}I Mössbauer emission spectra at 16 K of the ZnTe standard source, α-TeO_2, and β-TeO_2 against the $Cu^{129}I$ absorber.

2, together with the data of the previous works.[3,4] For the β-form of TeO_2, the measurements were independently carried out twice because of the large difference in the δ value between the previous data[3] and our data. The δ values are relative to a $Zn^{129}Te$ source, subtracting 0.42 mm s^{-1} (δ value for $Cu^{129}I$) from the actual δ values observed for the emission spectra.

The spectra observed in the present work are similar to the previously reported spectra independently measured by Pasternak and Bukshpan[3] and by Warren et al.[4] The values of e^2Qq and η for both modifications of TeO_2 are in good agreement with those reported by them, as may be seen in Table 2. However, the δ values, being close to each other for both modifications in this work, are different, especially for the β-form, from the previous data. The origin of the differences in the δ values is not clear. The differences might be attributable to the deviations between the ^{129}I spectra and ^{57}Fe calibrating spectra, since, in the ^{129}I Mössbauer measurements, the driving γ-ray source must be cooled in the cryostat, while the measurements of the ^{57}Fe calibrations are not accompanied by any such difficulty. One of the results obtained in the present investigation is that there are almost no differences in the δ values of ^{129}I for the α- and β-forms of TeO_2; this finding is consistent with that of the ^{125}Te absorption spectra. The isomer shift ratios of the ^{125}Te and ^{129}I nuclei are found to be 0.30 for both modifications of TeO_2. This value is very close to that to be expected when the ^{129}I daughter nucleus is present in the lattice site equivalent to the parent ^{129}Te site. On the other hand, the ratios of the quadrupole coupling constants of the ^{125}Te and ^{129}I nuclei are observed to be 0.46 for the α-form and 0.49 for the β-form. These values are in agreement with the value reported by Langouche et al.,[12] within the limits of experimental error of the ^{125}Te and ^{129}I Mössbauer measurements. Therefore, we have concluded, from a comparison of the values of δ and e^2Qq for ^{129}I with those for ^{125}Te, that the ^{129}I daughter nuclei, produced as a consequence of the nuclear β^- decay of ^{129}Te, are present in the same lattice environment as the parent ^{129}Te nuclei in both modifications of TeO_2.

C. Electronic Structures and Chemical Bondings. It is also of interest to consider the electronic structure and the chemical bonding of the tellurium atoms in the two forms of TeO_2. The tellurium atoms are present in a slightly distorted trigonal bipyramidal environment, and the Te–O bonds are predominantly covalent in character, judging from a consideration of the bond lengths. These crystallographic results

suggest that the bonding of the tellurium is characterized by sp^2 hybridization in the equatorial plane and by pd hybridization in the axial direction. Since, however, the $\angle$O-Te-O angles in the equatorial plane are 101°—102° for both modifications, the lone pair occupying one corner of the equatorial triangle may have significantly more s-character than that required in pure sp^2 hybridization. The contribution of the s-character to the bonding can be evaluated from the isomer shift (δ). The δ value reflects the s-electron density at the nucleus, $|\Psi_s(0)|^2$. Since the nuclear radius term $\Delta R/R$ is positive in sign for ^{125}Te, an increase in the s-electron density should lead to a more positive δ value. The 5s-electron density is shielded by outer 5p-electrons, therefore, δ is also dependent on the 5p-electron density. The removal of 5p-electrons of the tellurium atom in bonding will lead to an increase in the δ value, while the contribution of the 5s-electron to the bonding orbitals will directly decrease the δ value. These effects may be expressed quantitatively as follows:[15]

$$\delta = -2.6\,h_s + 0.44\,h_p - 0.16 \quad (2)$$
(mm s^{-1} for ZnTe reference material),

where h_s and h_p are the numbers of 5s- and 5p-electron holes respectively in the closed Te^{2-} configuration. The equation is obtained by multiplying the empirical formula of the ^{129}I Mössbauer isomer shift by 0.29, the isomer shift ratio, $\delta(^{125}Te)/\delta(^{129}I)$, described above.

The δ values observed for the two forms of TeO_2, smaller than those of the other Te(IV) compounds,[6] suggest that the s-electrons of the Te atoms take part in the bonding to some extent and that the Te-O bonds have a highly covalent character. Unfortunately, it is impossible to estimate independently the contribution of 5s-electrons to the bonding and the extent of the covalent character of the Te-O bonds. Dobud and Jones[7] have estimated the s-character in the bond to be about 9% for α-TeO_2, assuming that, in the absence of a 5s character, TeO_2 would have the same δ value as $TeCl_6^{2-}$ (+1.7 mm s^{-1}). The estimation has led to $5s^{1.6}$ $5p^{1.9}$ for the electronic configuration of the Te atom, i.e., an effective charge of +2.5 on the Te atom. It is thought that this estimated charge of +2.5 is the upper limit of the effective charge localized on the Te atom in the α-TeO_2, because the Te-O bonds would be expected, considering the Te-O and Te-Cl bond distances, to have a more covalent character than the Te-Cl bonds in $TeCl_6^{2-}$. The covalent character of the Te-Cl bond in $(NH_4)_2TeCl_6$ has been estimated to be 0.32 from the ^{35}Cl NQR measurements.[16] For the Te-O bonds in TeO_2 the covalent character would be larger.

It is important to assign the configuration of the iodine produced in α- and β-TeO_2 in order to examine the influence of the nuclear β^- decay of ^{129}Te. Since

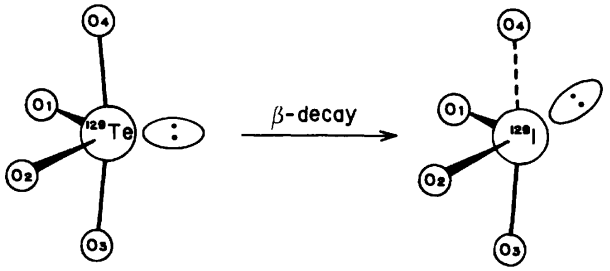

Fig. 4. Bonding configuration of the ^{129}I daughter atom produced by nuclear β^- decay of the ^{129}Te parent atom in TeO_2.

there are almost no differences in the values of δ, e^2Qq, and η between the two modifications, as has been described above, the resulting iodine species may be regarded to be identical. The values of δ, e^2Qq, and η observed for the iodine species in TeO_2 are very close to those for one iodine site (IO_3^-) in the I_2O_4 compound, consisting of two inequivalent iodine sites, IO^+ and IO_3^-.[17,18] The crystal structure of the I_2O_4 compound has not yet been established, but the IO_3^- part is believed to be similar to the configuration of HIO_3, judging from the similarity in the values of e^2Qq and η.[17] Therefore, we may infer that the iodine formed in TeO_2 is situated at a vertex of a distorted trigonal pyramid and that it has three nearest oxygen neighbors at an average distance of about 1.9 Å. The mean interbond angle O-I-O would be close to that of HIO_3 (98°). The formation of such an iodine species in the TeO_2 crystal can be understood as follows: one of the two axial Te-O bonds is severed by the β^- decay of ^{129}Te and subsequent electron rearrangements [see Fig. 4]. Such a process was also observed for the tellurium metal and tellurium atoms doped in the other elemental chalcogen hosts, in which the twofold coordination of tellurium involving π-bonding orbitals with two chalcogens-near-neighbors transforms into a nearly onefold coordination of iodine involving σ-bonding orbitals with a chalcogen-neighbor.[14]

In conclusion, the similarities between the Mössbauer spectra of the tetragonal (α) and orthorhombic (β) forms of TeO_2 indicate that there are no significant differences in the electronic structure and the chemical bonding of the tellurium atoms in the two modifications. In addition, the comparison of the Mössbauer data for ^{125}Te with those for ^{129}I indicates that the ^{129}I daughter nucleus, produced by the nuclear β^- decay of ^{129}Te, is present in the same lattice environment as the parent ^{129}Te nucleus in TeO_2.

We wish to thank Professor Sumio Ichiba and Dr. Kōji Yamada (Department of Chemistry, Hiroshima University) for the X-ray diffraction analysis. We are also grateful to Professor Takenobu Higashimura (Research Reactor Institute, Kyoto University) for his

useful discussions and encouragement. This work is partly supported by a Grant-in-Aid from the Ministry of Education (No. 62540330).

References

1) A. F. Wells, "Structural Inorganic Chemistry," 4th ed, Oxford University Press, London (1975), p. 581.
2) L. Pauling, "The Nature of the Chemical Bond," 3rd ed, Cornell University Press, Ithaca (1960), Chap. 7.
3) M. Pasternak and S. Bukshpan, *Phys. Rev.*, **163**, 297 (1967).
4) J. L. Warren, C. H. W. Jones, and P. Vasudev, *J. Phys. Chem.*, **75**, 2867 (1971).
5) F. Ambe and S. Ambe, private communication.
6) N. N. Greenwood and T. C. Gibb, "Mössbauer Spectroscopy," Chapman and Hall, London (1971).
7) P. Dobud and C. H. W. Jones, *J. Solid State Chem.*, **16**, 201 (1976).
8) J. G. Stevens and W. L. Gettys, "Mössbauer Isomer Shifts," ed by G. K. Shenoy and F. E. Wagner, North-Holland, Amsterdam (1978), Appendix 7.
9) C. E. Violet and R. Booth, *Phys. Rev.*, **144**, 225 (1966).
10) P. Jung and W. Triftshäuser, *Phys. Rev.*, **175**, 512 (1968).
11) H. DeWaard, "Mössbauer Effect Data Index 1973," ed by J. G. Stevens and V. E. Stevens, IFI/Plenum Press, New York (1974), p. 447.
12) G. Langouche, B. B. Triplett, N. S. Dixon, Y. Mahmud, and S. S. Hanna, *Phys. Rev. B*, **15**, 2504 (1977).
13) G. Langouche, M. Van Rossum, K. P. Schmidt, and R. Coussement, *Phys. Rev. B*, **9**, 848 (1974).
14) C. S. Kim and P. Boolchand, *Phys. Rev. B*, **19**, 3187 (1979).
15) B. M. Cheyne, J. J. Johnstone, and C. H. W. Jones, *Chem. Phys. Lett.*, **14**, 545 (1972).
16) D. Nakamura, K. Ito, and M. Kubo, *J. Am. Chem. Soc.*, **84**, 163 (1962).
17) Y. S. Grushko, B. G. Lur'e, and A. N. Murin, *Fiz. Tverd. Tela*, **11**, 2144 (1969) [*Sov. Phys. -Solid State*, **11**, 1733 (1970)].
18) C. H. W. Jones, *J. Chem. Phys.*, **62**, 4343 (1975).

 © 1989 The Chemical Society of Japan Bull. Chem. Soc. Jpn., 62, 39—44 (1989)

Solvent Effects on the Formation of Copper(II) Chloro Complexes in Acetonitrile-Dimethyl Sulfoxide Mixtures

Shin-ichi ISHIGURO,* Honoh SUZUKI, Bojana G. JELIAZKOVA,† and Hitoshi OHTAKI††
Department of Electronic Chemistry, Tokyo Institute of Technology at Nagatsuta, 4259, Nagatsuta-cho, Midori-ku, Yokohama 227
††Coordination Chemistry Laboratories, Institute for Molecular Science, Myodaiji, Okazaki 444
(Received May 26, 1988)

Complexation of copper(II) with chloride ions has been calorimetrically and spectrophotometrically studied in various acetonitrile (AN)-dimethyl sulfoxide (DMSO) mixtures at 25 °C. Complexation of copper(II) ion with DMSO as a ligand in AN has also been investigated calorimetrically. It is indicated that the solvent effect on the thermodynamic parameters of the complexation is dominated by two factors, (1) the preferential solvation of copper(II) ion with DMSO that mainly affects the enthalpies, and (2) the change in solvent-solvent interactions in the bulk that strongly affects the corresponding entropies.

Complexation of copper(II) with chloride ions is enhanced in *N,N*-dimethylformamide (DMF),[1] dimethyl sulfoxide (DMSO)[2] and acetonitrile (AN)[3] over water, although the donicity of DMF or DMSO is stronger than that of water,[4] i.e. an energy to break copper(II)-solvent bonds is larger in DMSO or DMF than in water. The enhanced complexation in these aprotic solvents is generally due to large and positive entropies, in contrast to small or even negative entropies in water. It is also found that the difference in the complexation of copper(II) with chloride ions is significant even in these aprotic donor solvents. Although the donicities of DMSO and DMF are not largely different, the complexation of copper(II) ions is weaker in the former solvent than in the latter. The difference is also mainly ascribed to the entropies. These facts suggest that the solvent-solvent interaction in the bulk solvent molecules plays an important role for the complexation, as the entropy difference may reflect that solvent molecules coordinating to metal and ligand ions are liberated and enter the bulk solvent of different structures.[5]

In order to throw more light on the role of solvent structure in the bulk for complexation reactions, we have examined the complexation in AN-DMF mixtures.[6] Both AN and DMF solvents have so weak solvent-solvent interactions that they distribute practically at random in the liquid phase.[7] In contrast to DMF, DMSO is a strongly self-associated donor solvent in the liquid at room temperature.[8-10] Then, in this work we further investigated the complex formation of the same copper(II)-chloride system in AN-DMSO mixtures. The complexation of copper(II) ion with DMSO as a ligand in AN was also explored to elucidate preferential solvation of copper(II) ion with DMSO molecules in the mixtures.

† Present address: Department of Analytical Chemistry, Sofia University, Anton Ivanov 1, Sofia, Bulgaria.

Experimental

Reagents. All chemicals used were of reagent grade and were prepared or purified as described previously.[1-3]

Measurements. Calorimetric measurements were carried out in a room thermostated at 25±0.5 °C by using a computer assisted titration calorimetry system. In the copper(II) chloride system, acetonitrile-dimethyl sulfoxide mixtures of 0.05 and 0.1 mole fraction DMSO were used as solvents. The ionic strength of test solutions was kept constant at 0.2 mol dm^{-3} by using $(C_2H_5)_4NClO_4$ throughout measurements. A copper(II) perchlorate solution (100 cm^3) was placed in a Dewar vessel kept at 25.0±0.0001 °C, filled with dry nitrogen gas and isolated from moisture with a P_2O_5 drying-tube, and was titrated with a 0.2 mol dm^{-3} $(C_2H_5)_4NCl$ solution. The concentration of copper(II) ions in the initial test solution was varied over the range 10—30 mmol dm^{-3} in the mixtures. In the copper(II) DMSO system, an AN solution of copper(II) perchlorate (50 cm^3) was titrated with DMSO (0.5 mol dm^{-3}) in AN in which the ionic strength was kept at 0.1 mol dm^{-3} with $(C_2H_5)_4NClO_4$. In both systems, heats observed at each titration point were corrected for heat of dilution of the titrant, which had been determined by separate experiments and found to be very small in all the solutions examined.

Heats of solution of anhydrous $CuCl_2$ crystals were measured in the AN-DMSO mixtures of the same composition as that used for titration calorimetry. Details of the measurements were described elsewhere.[3]

Electronic spectra were measured with an MPS-2000 spectrophotometer (Shimadzu) equipped with a PC-9801 VM computer (NEC) which recorded data at 1 nm intervals over the wavelength range 250—500 nm. A flow-cell with the pathlength of 0.5 cm was connected with a titration vessel through Teflon and glass tubes. A copper(II) perchlorate solution (20 cm^3) was placed in the vessel under a dry nitrogen atmosphere and was titrated with a 0.2 mol dm^{-3} $(C_2H_5)_4NCl$ solution. The measurements were carried out in AN-DMSO mixtures of 0.025, 0.05, 0.10, and 0.5 mole fraction DMSO. Absorbance data at selected 50 wavelengths over the range 250—500 nm were used for a least-squares calculation of formation constants.

Data Analysis. Calorimetric and spectrophotometric data obtained were analyzed by the same method described

previously.[11]

Results and Discussion

Copper(II) Chloride Complexes. Calorimetric titration curves obtained in AN-DMSO mixtures of 0.05 and 0.1 mole fraction DMSO are depicted in Fig. 1. As the heat of reaction q at each titration point depends on the volume of an aliquot of the titrant added δv and the concentration of ligand ions in the titrant $C_{X,tit}$, the $-q/(\delta v C_{X,tit})$ values are plotted against the ratio of the total concentrations of the ligand to the metal ion in solution C_X/C_M. The titration curves are well explained in terms of the formation of mononuclear $[CuCl_n]^{(2-n)+}$ (n=1—4) complexes in these mixtures, as well as in pure DMSO[2] and AN.[3] In Table 1 their formation constants and enthalpies simultaneously determined are summarized. The solid lines in Fig. 1 are calculated by using the constants in relevant mixtures in Table 1 and they well reproduce the experimental points over the whole range of C_X/C_M examined.

In Fig. 2 are shown typical electronic spectra measured in the AN-DMSO mixture of 0.025 mole fraction DMSO. The spectral changes with the concentration of chloride ions in the solution are similar in all the AN-DMSO mixtures examined.

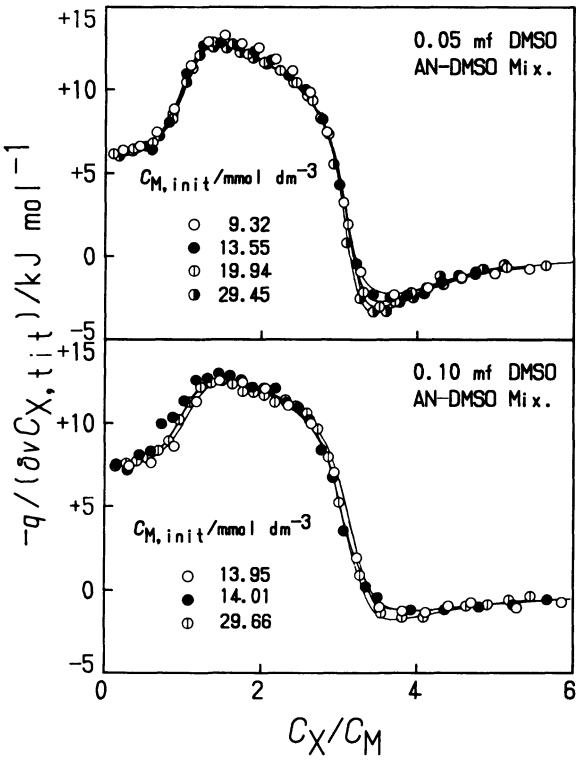

Fig. 1. Calorimetric titration curves for the copper(II) chloride system obtained in AN-DMSO mixtures at 25°C. Concentrations of copper(II) ions in the initial solutions $C_{M,init}$/mmol dm^{-3} are given. The solid lines show the curves calculated by using the constants in Table 1.

According to the analysis by the matrix rank method,[12] the number of species formed is five including the solvated copper(II) ion, each having appreciably different electronic spectra. The absorbance data are in fact satisfactorily explained in terms of the formation of $[CuCl_n]^{(2-n)+}$ (n=1—4) and their

Table 1. Overall Formation Constants, $\log(\beta_n/\text{mol}^{-n}\,\text{dm}^{3n})$, and Enthalpies, $\Delta H^\circ_{\beta n}$/kJ mol^{-1}, of $[CuCl_n]^{(2-n)+}$ (n=1—4) Obtained by Using Calorimetric Data in Acetonitrile-Dimethyl Sulfoxide Mixtures at 25°C

	DMSO content/mole fraction 0.05	0.1
$\log\beta_1$	6.0(0.3)	5.5(0.4)
$\log\beta_2$	10.5(0.6)	9.6(0.9)
$\log\beta_3$	15.0(0.7)	13.4(0.9)
$\log\beta_4$	17.2(0.8)	15.2(0.9)
$\Delta H^\circ_{\beta 1}$	5.9(0.3)	7.4(0.4)
$\Delta H^\circ_{\beta 2}$	24.2(1.4)	22.8(1.5)
$\Delta H^\circ_{\beta 3}$	29.4(0.3)	31.6(0.5)
$\Delta H^\circ_{\beta 4}$	23.5(0.3)	25.7(0.5)
U[a]	0.685	0.863
R[b]	0.0276	0.0362
N[c]	91	81

Values in parentheses refer to three standard deviations. a) Error-square sum. b) The Hamilton R factor. c) The number of data points.

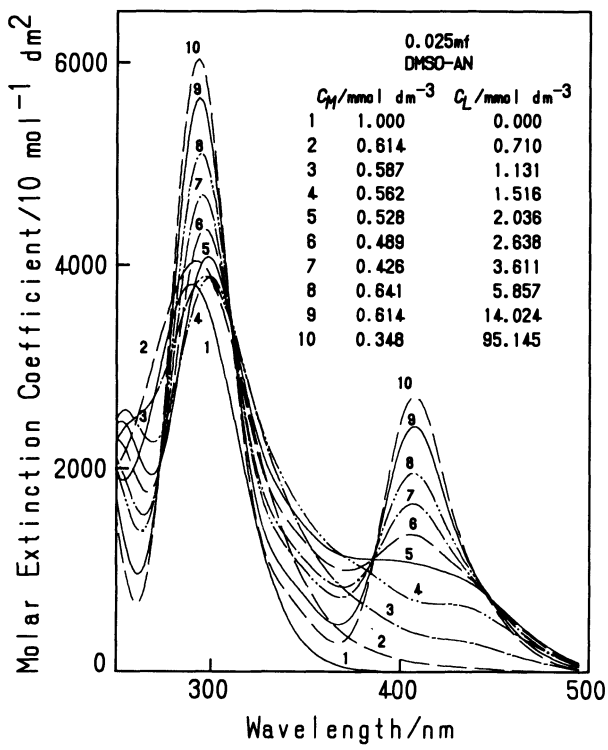

Fig. 2. Measured electronic spectra of copper(II) chloride solutions in the AN-DMSO mixture of 0.025 mole fraction DMSO. Intensities are normalized with the concentration of copper(II) ion in solution.

Table 2. Overall Formation Constants, $\log(\beta_n/\mathrm{mol}^{-n}\,\mathrm{dm}^{3n})$, of $[CuCl_n]^{(2-n)+}$ (n=1—4) Obtained by Using Spectrophotometric Data in Acetonitrile-Dimethyl Sulfoxide Mixtures at 25°C

	DMSO content/mole fraction			
	0.025	0.05	0.1	0.5
$\log\beta_1$	6.5(0.1)	6.06(0.07)	5.87(0.10)	4.67(0.09)
$\log\beta_2$	11.2(0.2)	10.4(0.1)	9.8(0.1)	7.4(0.1)
$\log\beta_3$	15.9(0.2)	14.6(0.1)	13.6(0.1)	10.1(0.1)
$\log\beta_4$	18.4(0.2)	16.9(0.1)	15.6(0.1)	11.3(0.1)
U[a]	0.0572	0.0270	0.0310	0.0503
R[b]	0.0056	0.0038	0.0042	0.0055
N[c]	3800	3850	3750	3800

Values in parentheses refer to three standard deviations. a) Error-square sum. b) The Hamilton R factor. c) The number of data points.

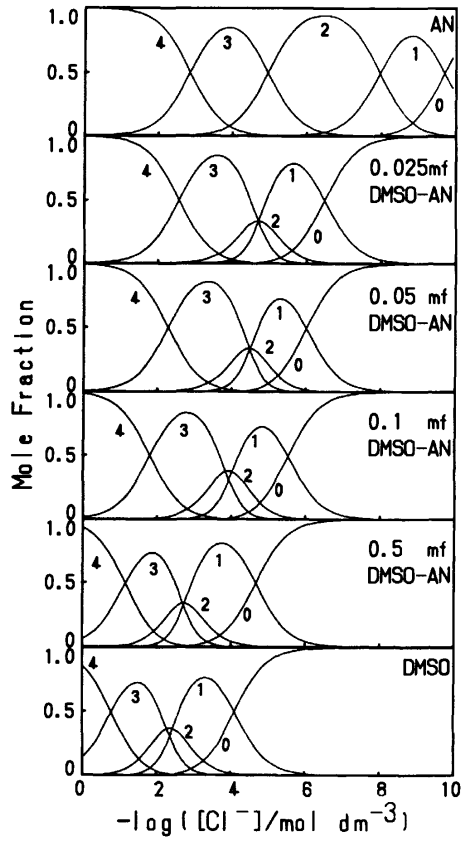

Fig. 3. Distribution of the copper(II) chloro complexes. The number represents n within $[CuCl_n]^{(2-n)+}$.

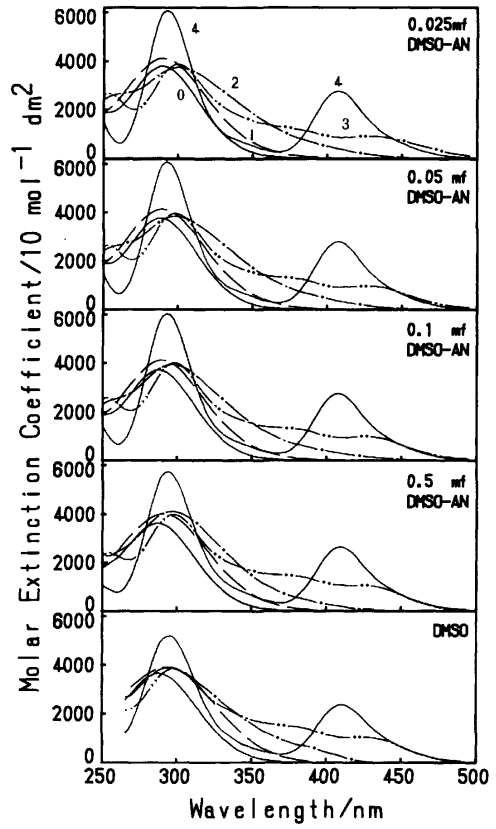

Fig. 4. Extracted electronic spectra of individual copper(II) chloro complexes. The number represents n within $[CuCl_n]^{(2-n)+}$.

formation constants were determined. The result is summarized in Table 2. The formation constants thus obtained by spectrophotometry in the 0.05 and 0.1 mole fraction DMSO mixtures are reasonably agreed with the respective values obtained by calorimetry in these solvents. The distribution of the species in these solutions, together with that in pure AN and DMSO, is shown in Fig. 3.

Extracted electronic spectra of the individual $[CuCl_n]^{(2-n)+}$ (n=1—4) complexes are depicted in Fig. 4. The electronic spectra of each species in all the AN-DMSO mixtures examined are practically the same as those in DMSO[2] and in DMF.[1] In DMF the structure of the distorted octahedral $[CuCl(dmf)_5]^+$ and the distorted tetrahedral $[CuCl_3(dmf)]^-$ and $[CuCl_4]^{2-}$ complexes has been determined by X-ray diffraction.[13] It is therefore expected that the corresponding chloro complexes of copper(II) ion in DMSO and in the AN-DMSO mixtures have essentially the same coordination structures as those in DMF.

Copper(II) DMSO Complexes. Calorimetric titration curves obtained by titrating copper(II) perchlorate with DMSO in AN are depicted in Fig. 5, in which the values $-q/(\delta v C_{L,tit})$ are plotted against C_L/C_M, where L denotes DMSO. The calorimetric data were

Table 3. Overall Formation Constants, $\log(\beta_n/\text{mol}^{-n}\,\text{dm}^{3n})$, and Enthalpies, $\Delta H^\circ_{\beta n}/\text{kJ mol}^{-1}$, of $[Cu(dmso)_n]^{2+}$ in Acetonitrile at 25 °C

	(1—4)	(1—5)	(1—4,6)	(1—6)
$\log\beta_1$	3.2(0.3)	3.1(0.2)	3.0(0.2)	3.1(0.2)
$\log\beta_2$	3.9(2)	5.3(0.2)	5.1(0.2)	5.2(0.2)
$\log\beta_3$	7.4(0.3)	7.4(0.2)	7.3(0.2)	7.4(0.2)
$\log\beta_4$	8.7(0.3)	9.2(0.2)	8.9(0.2)	9.1(0.2)
$\log\beta_5$	—	9.6(0.3)	—	9.5(0.8)
$\log\beta_6$	—	—	9.9(0.3)	10.0(1.7)
$\Delta H^\circ_{\beta 1}$	−14.5(0.5)	−14.5(0.4)	−14.4(0.4)	−14.4(0.4)
$\Delta H^\circ_{\beta 2}$	uncertain	−31(2)	−34(3)	−32(2)
$\Delta H^\circ_{\beta 3}$	−42(2)	−45(2)	−42(1)	−43(2)
$\Delta H^\circ_{\beta 4}$	−70.8(0.8)	−59(2)	−65(1)	−61(3)
$\Delta H^\circ_{\beta 5}$	—	−77(1)	—	−71(32)
$\Delta H^\circ_{\beta 6}$	—	—	−73.1(0.8)	−75(4)
U[a]	1.27	0.346	0.364	0.335
R[b]	0.0301	0.0157	0.0161	0.0155

Values in parentheses refer to three standard deviations. The number of data point is 244 including those obtained by back titrations. a) Error-square sum. b) The Hamilton R factor.

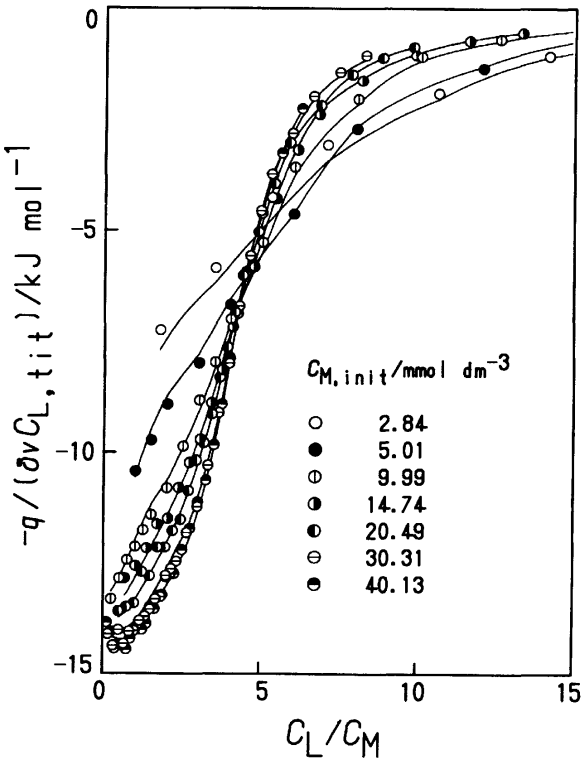

Fig. 5. Calorimetric titration curves for the copper(II) DMSO system in AN at 25 °C. Concentrations of copper(II) ions in the initial solutions $C_{M,init}$/mmol dm^{-3} are given. The solid lines show the curves calculated by using the constants for the set (1—6) in Table 3.

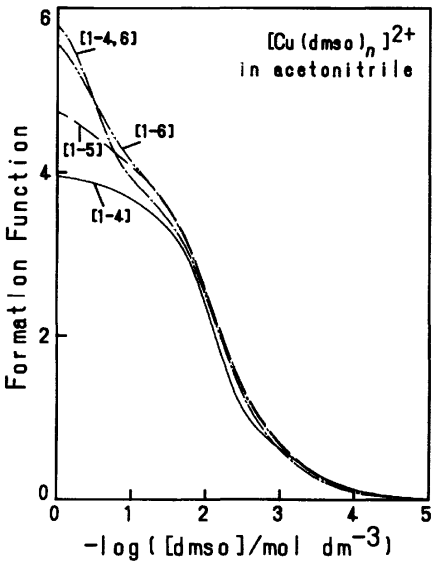

Fig. 6. Formation functions of $[Cu(dmso)_n]^{2+}$ for the various combinations of n's.

analyzed by assuming the formation of $[Cu(dmso)_n]^{2+}$ ($n \leqq 6$) complexes with various combinations of n's. The results of the least-squares analysis are summarized in Table 3. The Hamilton R factor for the set (1—4) assuming $[Cu(dmso)]^{2+}$, $[Cu(dmso)_2]^{2+}$, $[Cu(dmso)_3]^{2+}$ and $[Cu(dmso)_4]^{2+}$ only is appreciably larger than the values for the sets (1—5), (1—6) and (1—4,6). This evidently indicates that not only $[Cu(dmso)_n]^{2+}$ (n=1—4) but also higher species, $[Cu(dmso)_5]^{2+}$ and/or $[Cu(dmso)_6]^{2+}$, are formed in the solutions examined. The formation functions $\bar{n}$ calculated according to Eq. 1

$$\bar{n} = \Sigma n\beta_n[\text{dmso}]^n / (1 + \Sigma\beta_n[\text{dmso}]^n) \quad (1)$$

are shown in Fig. 6. The highest $\bar{n}$ reached in the present measurements is ca. 4.5, i.e., the formation of $[Cu(dmso)_5]^{2+}$ and/or $[Cu(dmso)_6]^{2+}$ is not extensive. In addition, the $\bar{n}$ curves for these sets are similar in the range $-\log([\text{dmso}]/\text{mol dm}^{-3}) > 1$, and thus it is hard to draw a unique conclusion for the formation of the pentakis- and/or hexakis(dimethyl sulfoxide) copper(II) complexes under the experimental conditions employed.

Enthalpies of Solution of Anhydrous $CuCl_2$ Crystal. By using the procedure described previously,[3] the enthalpies of solution for the following processes

$$CuCl_2(c) = Cu^{2+}(s) + 2Cl^-(s);\ \Delta H_s^\circ(Cu^{2+}, 2Cl^-) \quad (2)$$
$$CuCl_2(c) = [CuCl_2](s);\ \Delta H_s^\circ(CuCl_2) \quad (3)$$

where c and s stand for the crystalline and solution states, respectively, were determined in the AN–DMSO mixtures of 0.05 and 0.1 mole fraction DMSO. The result is given in Table 4. The $\Delta H_s^\circ(Cu^{2+}, 2Cl^-)$ values in the mixtures are significantly more negative than the value in AN, the fact also indicating that copper(II) ion is preferentially solvated with DMSO even in AN rich AN–DMSO mixtures. A similar trend, though much less marked, was found for the $\Delta H_s^\circ(CuCl_2)$ values.

Solvent Effects on the Formation of $[CuCl_4]^{2-}$. As seen in Table 5, the overall Gibbs energy value $\Delta G_{\beta 4}^\circ$ becomes less negative with an increase in the mole fraction of DMSO in the AN–DMSO mixtures. The $\Delta H_{\beta 4}^\circ$ value in any mixture is close to that in DMSO, but largely different from that in AN. The difference may be due to the preferential solvation of copper(II) ion with DMSO in the mixtures, i.e., an energy is needed to break Cu(II)–dmso bonds in the course of the reaction

$$[Cu(dmso)_6]^{2+} + 4Cl^- = [CuCl_4]^{2-} + 6dmso \quad (4)$$

in the mixtures. The values of $(\Delta H_{\beta 4}^\circ(AN) - \Delta H_{\beta 4}^\circ(mix))$ are −78.9 and −81.1 kJ mol^{-1} in the mixtures of 0.05 and 0.1 mole fraction DMSO, respectively, which are in fact close to the enthalpy of formation of $[Cu(dmso)_n]^{2+}$ (n=5 or 6) in AN. The result also implies that the solvation enthalpy of chloride ion may not be appreciably different in AN, DMSO, and their mixtures, as expected from the similar acceptor property of the solvents (the acceptor numbers are 19.3 for both DMSO and AN),[4] and the small enthalpy of transfer of chloride ion from AN to DMSO (−1.7 kJ mol^{-1}).[14]

It is known that DMSO molecules are associated in the liquid state at room temperature.[8–10] This is due to interactions between exposed dipoles at the molecular surface of DMSO[8] in contrast to embedded dipoles of AN, although these solvent molecules have similar dipole moments (μ_{AN}=12.9×10^{-30} C m, μ_{DMSO}=13×10^{-30} C m). A smaller molecular weight, or in other words, a smaller dispersion force, of AN than DMSO may also contribute to a weaker intermolecular interaction of the former. Donor–acceptor interactions between molecules may also be weaker in AN (the donor number D_N=14.1 and the acceptor number A_N=19.3) than in DMSO (D_N=29.8 and A_N=19.3). Consequently, AN is an unordered solvent with respect to pure DMSO. Dilute AN solutions of DMSO may be also unordered, i.e., DMSO–DMSO interactions are practically broken.

DMSO molecules solvate preferentially copper(II) ion to form $[Cu(dmso)_6]^{2+}$ in the AN–DMSO mixtures. The solvent molecules are liberated in the course of the complexation and enter the bulk solvent. As seen in Table 5 the $\Delta S_{\beta 4}^\circ$ values are all large and positive but significantly different. In AN, solvent molecules leave a relatively weak solvate structure for an unordered solvent, $\Delta S_{\beta 4}^\circ$ relatively low; in AN–DMSO mixtures, DMSO molecules leave a strong solvate structure for an unordered solvent, $\Delta S_{\beta 4}^\circ$ much larger; in DMSO, solvent molecules leave a strong solvate for an ordered solvent, again a low value of $\Delta S_{\beta 4}^\circ$, even lower than in AN. Thus, both solvate and solvent structures are responsible for the entropies of complexation.

Liberation of solvent molecules solvating chloride ion also occurs in the course of the complexation. However, the contribution of desolvation of chloride ion to the $\Delta S_{\beta 4}^\circ$ values may be small because of weak solvation of the ion in AN, DMSO, and their mixtures, as noted in a previous section.

The present work has been financially supported by Grant-in-Aid for Special Project Research No. 61134043 from the Ministry of Education, Science and Culture.

Table 4. Enthalpies of Solution, ΔH_s°/kJ mol^{-1}, of Anhydrous $CuCl_2$ in Acetonitrile–Dimethyl Sulfoxide Mixtures

y[a]	$\Delta H_s^\circ(CuCl_2)$	$\Delta H_s^\circ(Cu^{2+},2Cl^-)$
0	−15.9	0.6
0.05	−40.3	−64.5
0.1	−45.1	−67.9
1	−62.8	−83.3

a) DMSO content/mole fraction.

Table 5. Gibbs Energies, $\Delta G_{\beta 4}^\circ$/kJ mol^{-1}, Enthalpies, $\Delta H_{\beta 4}^\circ$/kJ mol^{-1}, and Entropies, $\Delta S_{\beta 4}^\circ$/J K^{-1} mol^{-1}, for the Reaction $Cu^{2+}+4Cl^-=[CuCl_4]^{2-}$, in Acetonitrile–Dimethyl Sulfoxide Mixtures at 25 °C

	DMSO content/mole fraction					
	0	0.025	0.05	0.1	0.5	1.0
$\Delta G_{\beta 4}^\circ$	−145.1	−105.2	−98.4	−86.9	−64.5	−54.6
$\Delta H_{\beta 4}^\circ$	−55.4	—	23.5	25.7	—	23.5
$\Delta S_{\beta 4}^\circ$	300	—	409	377	—	263

References

1) S. Ishiguro, B. G. Jeliazkova, and H. Ohtaki, *Bull. Chem. Soc. Jpn.*, **58**, 1143 (1985).
2) S. Ishiguro, H. Suzuki, B. G. Jeliazkova, and H. Ohtaki, *Bull. Chem. Soc. Jpn.*, **59**, 2407 (1986).
3) S. Ishiguro, B. G. Jeliazkova, and H. Ohtaki, *Bull. Chem. Soc. Jpn.*, **58**, 1749 (1985).
4) V. Gutmann, "The Donor-Acceptor Approach to Molecular Interactions," Plenum, New York (1978).
5) S. Ahrland, *Pure Appl. Chem.*, **51**, 2019 (1979).
6) S. Ishiguro, B. G. Jeliazkova, and H. Ohtaki, *Bull. Chem. Soc. Jpn.*, **59**, 1073 (1986).
7) H. Ohtaki, S. Itoh, T. Yamaguchi, S. Ishiguro, and B. M. Rode, *Bull. Chem. Soc. Jpn.*, **56**, 3406 (1983).
8) S. Itoh and H. Ohtaki, *Z. Naturforsch.*, **42a**, 858 (1987).
9) M. Sandsröm, *Acta Chem. Scand.*, **A32**, 627 (1978).
10) S. Ahrland, E. Hansson, Å. Iverfeldt, and I. Persson, *Acta Chem. Scand.*, **A35**, 275 (1981).
11) S. Ishiguro and H. Ohtaki, *J. Coord. Chem.*, **15**, 237 (1987).
12) Z Z. Hugus, Jr., and A. A. El-Awady, *J. Phys. Chem.*, **75**, 2954 (1971).
13) K. Ozutsumi, S. Ishiguro, and H. Ohtaki, *Bull. Chem. Soc. Jpn.*, **61**, 945 (1988).
14) S. Ahrland, S. Ishiguro, and R. Portanova, *Aust. J. Chem.*, **36**, 1805 (1983).

 © 1989 The Chemical Society of Japan Bull. Chem. Soc. Jpn., 62, 45—50 (1989)

Aggregation of Complexes Coordinated with *N,N'*-Bis(5-alkylsalicylidene)-ethylenediamine: ^{1}H NMR Peak Shifts and Paramagnetic Broadening Investigations

Kazuo MIYAMURA,* Keiki SATOH, and Yohichi GOHSHI
Department of Industrial Chemistry, Faculty of Engineering, The University of Tokyo, Hongo, Bunkyo-ku, Tokyo 113
(Received May 27, 1988)

Nickel(II) complexes coordinated with *N,N'*-disalicylideneethylenediamine (salen) substituted by a series of *n*-alkyl side chains have been synthesized. Drastic improvement in the solubility towards chloroform brought about by the increase in alkyl side chain lengths realised an extremely high concentration of 0.5 mol·dm^{-3}. Due to aggregation, their ^{1}H NMR spectra in $CDCl_3$ were strongly dependent on the concentration especially in the high concentration region. The alkyl chain length has very little influence on the dependency, indicating that the aggregation is caused by the complex–complex interaction rather than by the hydrophobic interaction between the alkyl side chains. Assuming a monomer–dimer equilibrium, the aggregation constant is determined from the concentration dependence. Further, the structure of the aggregate is estimated by combining the results of the concentration dependence, and the paramagnetic broadening caused by adding the corresponding copper(II) complex. The paramagnetic broadening investigation also indicated a close contact of copper(II) complex to nickel(II) complex.

The importance of aggregation in the field of coordination chemistry has been recognized recently from the studies on chlorophylls,[1–4] vesicles,[5,6] and others.[7–9] In particular, the intensive studies on the chlorophyll aggregate suggested it has different properties from the monomeric species. This is effectively used in photosynthesis.[2] It can be said that the aggregation of the chlorophyll molecules alters their photochemical properties. It is also well-known that some properties in highly dense solutions are not the mere extrapolation of those in thin solutions. It is the phenomenon of aggregation that is responsible for these changes. The changes accompanying the aggregation phenomenon, which in many cases have been treated as experimental errors, are now under investigation and have increasing importance.

Complexes of *N,N'*-disalicylideneethylenediamine, usually abbreviated as salen, are known to form dimers in the crystalline state.[10,11] They have been studied extensively because of some interesting properties which they exhibit. For example, cobalt(II) complex of salen coordinates a dioxygen molecule reversibly similar to that observed for hemoglobin.[12] The chemistry of salen is interesting not only because of its porphyrin-like nature, but also for the simplicity in its synthesis. Thus, it is relevant to examine the aggregating nature of salen complexes, and to investigate the property changes due to the aggregation.

However, a problem arises in studying the aggregation of salen complexes because of their low solubilities. Generally, the phenomenon of aggregation becomes conspicuous in the high concentration region, because high concentration creates extra occasions for solute molecules to meet and aggregate. However, at high concentrations, precipitation tends to occur as a result of molecular aggregation, and this interferes with the investigation of aggregation in solution. Thus it is important to increase the solubility of the solute to investigate the phenomenon of aggregation. The introduction of alkyl chains causes an increase in their solubility towards organic solvents, such as chloroform, consequently providing us an opportunity to investigate their behaviour in the high concentration region.[13]

In a previous letter,[14] we have reported briefly that the chloroform-*d* solution of salen type complexes, substituted by hexyl groups, exhibit concentration dependence in ^{1}H NMR due to aggregation. Such a phenomenon is not observed for the unsubstituted complex because of its low solubility. In this paper, the equilibrium of aggregation and the aggregating structure are discussed, together with the experimental procedures.

Experimental

5-Alkylsalicylaldehydes (alkyl=ethyl, butyl, hexyl, octyl) were synthesized by the Reimer-Tiemann reaction[15] from the corresponding commercially available (Kantoh Chemical Co.) *p*-alkylphenols. 5-Dodecyl-and 5-decylsalicyclaldehydes were synthesized by the same procedure from the corresponding *p*-alkylphenols obtained by ordinary Friedel-Crafts acylation and Clemmensen reduction from phenol and the corresponding alkanoyl chlorides, the procedure for which is given elsewhere.[16] All other reagents used were commercially available and were of reagent grade.

[*N,N'*-Bis(5-hexylsalicylidene)ethylenediaminato]nickel(II) [Ni(1-6)]. Nickel acetate tetrahydrate (0.50 g, 2 mmol) and ethylenediamine (0.12 g, 2 mmol) were added to 100 cm^3 of ethanol in a 200 cm^3 flask with stirring. After the mixture had become a clear blue solution, 5-hexylsalicylaldehyde (0.83 g, 4 mmol) was added drop by drop to the solution. The reaction mixture was then refluxed for 3 h. The precipitate formed was filtered and recrystallized from chloroform-ethanol mixed solvents. The yield was 0.7 g

(71%)

Found: C, 68.15; H, 7.75; N, 5.90%. Calcd for $C_{28}H_{38}N_2NiO_2$: C, 68.15; H, 7.75; N, 5.70%. ^{1}H NMR ($CDCl_3$) δ=0.87 (3H, t, J=6.9 Hz, CH_3CH_2-) 1.28 (10H, m), 1.52 (2H, t, J=6.9 Hz, benzyl-CH_2), 3.41 (2H, s, H_c), 6.74 (1H, d, J=2.1 Hz, H_c), 6.93 (1H, d, J=8.9 Hz, H_a), 7.02 (1H, dd, J=2.2 and 8.7 Hz, H_b), 7.33 (1H, s, H_d).

Other [*N,N'*-Bis(5-alkylsalicyclidene)ethylenediaminato]-nickel(II) [Ni(1-*n*)](*n*=2,4,8,10,12). A series of [*N,N'*-bis(5-alkylsalicylidene)ethylenediaminato]nickel(II) (alkyl=ethyl, butyl, octyl, decyl, dodecyl) were obtained from the corresponding 5-alkylsalicylaldehydes by a similar procedure to [*N,N'*-bis-(5-hexylsalicylidene)ethylenediaminato]nickel(II) as described above. The yields of the complexes tend to decrease with the complexes of longer alkyl chains, but they were never under 40%.

Found for [Ni(**1-2**)]: C, 63.15; H, 5.90; N, 7.35%. Calcd for $C_{20}H_{22}N_2NiO_2$: C, 63.05; H, 5.80; N, 7.35%. Found for [Ni(**1-4**)]: C, 65.20; H, 6.85; N, 6.25%. Calcd for $C_{24}H_{30}N_2NiO_2$: C, 65.20; H, 6.85; N, 6.35%. Found for [Ni(**1-8**)]: C, 69.80; H, 8.30; N, 4.95%. Calcd for $C_{32}H_{46}N_2NiO_2$: C, 69.95; H, 8.45; N, 5.10%. Found for [Ni(**1-10**)]: C, 71.55; H, 9.05; N, 4.60%. Calcd for $C_{36}H_{54}N_2NiO_2$: C, 71.40; H, 9.00; N, 4.65%. Found for [Ni(**1-12**)]: C, 72.55; H, 9.60; N, 4.10%. Calcd for $C_{40}H_{62}N_2NiO_2$: C, 72.60; H, 9.45; N, 4.25%.

[*N,N'*-Bis(5-hexylsalicylidene)ethylenediaminato]copper-(II) [Cu(1-6)]. Copper(II) acetate monohydrate (0.48 g, 2.4 mmol) and 5-hexylsalicylaldehyde (1.1 g, 5.3 mmol) were added to 100 cm^3 of ethanol in a 200 cm^3 flask with stirring. The mixture was then refluxed for 2 h. The green precipitate of bis(5-hexylsalicylaldehydato)copper(II) formed (0.8 g, 1.6 mmol) was filtered and dispersed again in ethanol. To this dispersion, ethylenediamine (0.11 g, 1.6 mmol) was added drop by drop. The reaction mixture was then refluxed for 3 h. The precipitate formed was filtered and recrystallized from hot ethanol. The yield was 0.4 g. (15%).

Found: C, 67.85; H, 7.20; N, 5.75%. Calcd for $C_{28}H_{38}CuN_2O_2$: C, 67.50; H, 7.70; N, 5.60%. Magnetic susceptibility μ_{eff}=1.89 B.M. (22 °C).

^{1}H NMR Measurements. The concentration dependence of ^{1}H NMR spectra was measured at 35 °C using a Hitachi R-40 90 MHz spectrometer. 400 MHz Superconducting ^{1}H NMR spectra were obtained with a JEOL spectrometer. The chloroform-d containing 1% of TMS supplied from Merck Japan Co., was used as solvent. A 5 cm^3 measuring flask was used to prepare the sample solution. The solutions of different concentration were prepared stepwise, adding the complex in small portions each time after the measurement had been completed.

Other Measurements. Visible absorption spectra were recorded with a Hitachi 340 spectrophotometer. Infrared spectra were obtained with a Jasoc IRA-2 spectrophotometer. Magnetic susceptibility measurements were performed with a Shimadzu torsion magnetometer MB-100 at Ochanomizu University.

Results and Discussion

The salen type ligands used in this paper have two alkyl (C_nH_{2n+1}) side chains of the same length, and are abbreviated as (**1-*n***). The results of elemental analyses accord well with the assumed structures. The IR spectra of nickel(II) and copper(II) complexes of (**1-*n***) exhibit a peak assignable to ν(C=N) at 1620 cm^{-1}, corresponding to the formation of a Schiff base in the complex.

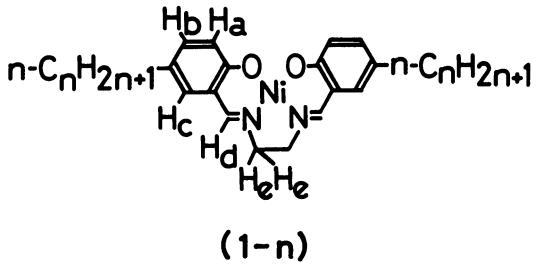

(1-n)

The nickel(II) and copper(II) complexes of (**1-*n***) in chloroform (2×10^{-4} mol·dm^{-3}) exhibit almost an identical electronic spectra regardless of their alkyl chain length, and also, they do not show notable change either in peak positions or in absorption coefficients in the concentration region of 2×10^{-5} to 4×10^{-4} mol·dm^{-3}. Thus, the spectra of the (**1-6**) complexes are given in Fig. 1 as the representatives of the series, together with those of the unsubstituted complexes. The spectral profiles of alkyl-substituted complexes are similar to that of the unsubstituted complexes, which adopt the square-planar 4 coordination geometry. Thus it can be concluded that the complexes of (**1-*n***) also adopt the square-planar geometry. This is confirmed by the magnetic susceptibility measurements of the crystal of [Ni(**1-12**)]. It shows that the [Ni(**1-12**)] is diamagnetic as are most of the square-planar nickel(II) complexes. The μ_{eff} values for [Cu(**1-*n***)] (n=6, 12) are 1.89 and 1.91

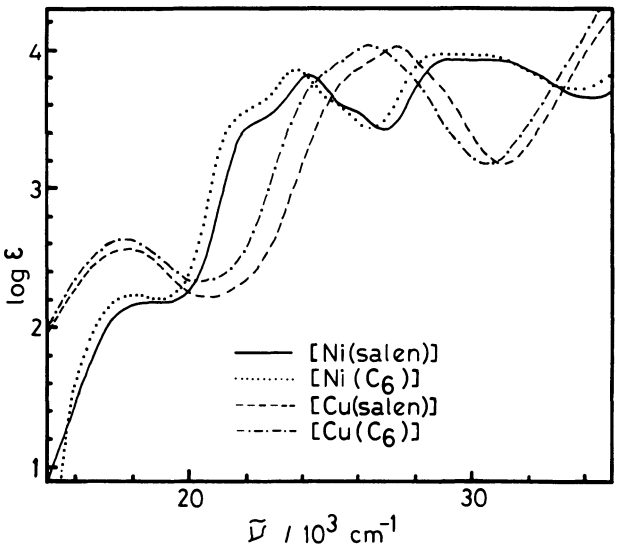

Fig. 1. Electronic spectra of [M(**1-6**)] and [M(salen)] (M=Ni, Cu).

B.M., which are in the range of normal monomeric copper(II) complexes.

However, a slight red shift on alkyl substitution can be noticed in the UV-region of the electronic spectra (Fig. 1). These red shifts are 500 and 1000 cm^{-1} for nickel(II) and copper(II) complexes, respectively. Similar red shifts are reported for the binuclear salen type complexes of (**2**).[17),18)] The shifts for nickel(II) and copper(II) complexes of (**2**) are 600 and 1200 cm^{-1} respectively. ESR study on the copper(II) complex of (**2**) revealed that the red shift is due to the interaction of two salen complex moieties in the complex. However, the concentration, at which the electronic spectra of (**1**-*n*) complexes are measured (2×10^{-4} mol·dm^{-3}), is far below the region of aggregation, as is shown later in this text. This means that the shift in electronic spectra of the (**1**-*n*) complexes cannot be attributed to the aggregation phenomenon dealt with in this paper. It can be considered that in (**1**-*n*), alkyl groups are directly attached to the benzene rings, possibly affecting the electronic state of salen moiety, while that is not the case in (**2**). It is, therefore, probable that the red shifts observed for the (**1**-*n*) complexes are due to the electronic effect of the substituted alkyl groups.

The Concentration Dependence in ^{1}H NMR. The ^{1}H NMR spectra of [Ni(**1**-*n*)] in chloroform-*d* are measured on a 400 MHz spectrometer, and almost all the peaks have been assigned. The assignment of the aromatic protons (H_a, H_b, and H_c) can be made by spin decoupling investigations. Geminal protons H_a and H_b split into doublets by the coupling, and a long-range coupling between H_b and H_c is also observed. Some other protons are also identified, on the basis of the assumed structure. ^{1}H NMR spectra of other nickel(II) complexes exhibit similar spectra and are assigned according to the same procedures. However, it is found that the positions of the peaks assigned to H_c and H_d differed slightly, each time one measures the ^{1}H NMR, although there are no differences in the sample solution except for their concentration.

On increasing the concentration, the signals assigned to the protons H_c and H_d, clearly showed up-field shifts. In Fig. 2 are given the concentration dependences of H_d for the nickel(II) complexes of (**1**-*n*). The shifts were observed only for H_c and H_d, and neither aliphatic protons nor the H_a and H_b protons of the benzene rings showed observable shifts. These up-field shifts become conspicuous above a concentration of ca. 10^{-3} mol·dm^{-3}, and, in the case of [Ni(**1**-**8**)], they move ca. 0.5 and 0.8 ppm upwards for H_c and H_d respectively, until the solution saturates at 0.51 mol·dm^{-3}.

The up-field shifts can be attributed to the aggregation of the complex, because there are no other interactions that are affected by the change in the concentration. It is well-known that the protons located above an aromatic ring exhibit a peak shift in

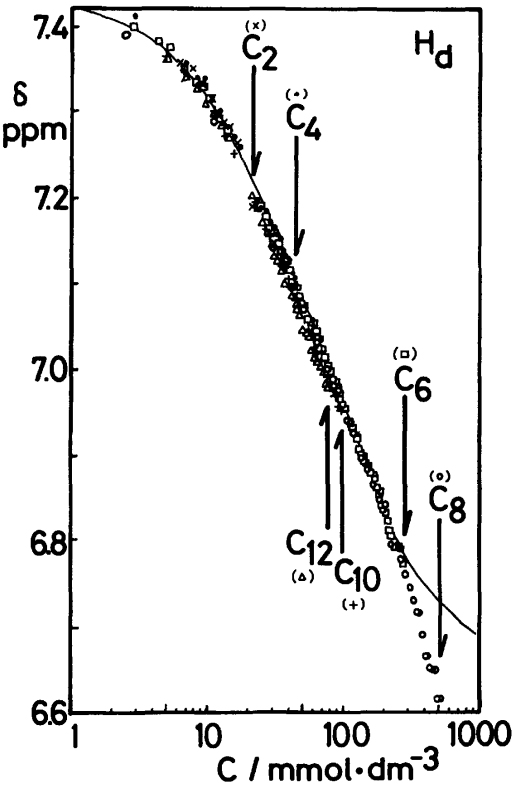

Fig. 2. Concentration dependence of ^{1}H NMR of [Ni(**1**-*n*)] in $CDCl_3$. Arrows indicate the concentration of saturation.

^{1}H NMR to an upper field due to the strong diamagnetic effect of the ring current formed in the aromatic ring.[19)] Thus, in the aggregate of [Ni(**1**-*n*)], the benzene ring of (**1**-*n*) is assumed to be placed above the protons H_c and H_d of another molecule of [Ni(**1**-*n*)], and vice versa. As the ^{1}H NMR spectrum of [Ni(**1**-*n*)] exhibits the shifts and not the splittings, a rapid equilibrium between the aggregate and the monomeric species is indicated.

The length of the alkyl chains have little effect on the concentration dependence. The major effect of the alkyl side chains is the modification of the solubility of the complex. The saturation concentration, which is indicated by arrows in Fig. 2, increases as the alkyl chain length increases, until it reaches its maxima for the (**1**-**8**) complex, and then decreases. The shift, on the other hand, has a slight tendency to increase with the alkyl length, but the amount is not large enough to be positively affirmed. However, it can be concluded that the complex-complex interaction rather than the hydrophobic interaction of the side chains is responsible for the aggregation.

Theoretical Treatment of the Concentration Dependences. The concentration dependence observed contains information on the distribution of the complex molecules present in the solution to the monomeric species and the aggregates. If the

aggregation occurs at low concentration, the shift of ^{1}H NMR should begin to appear at a low concentration. Therefore, the equilibrium constant of aggregate formation can be determined from the concentration dependence of the shift. At the primary stage of aggregation, i.e. in a relatively low concentration region, an equilibrium between the monomeric and dimeric species ought to be dominant in the solution. Assuming, therefore, an equilibrium between monomer and dimer for the first order approximation, the chemical shifts for a given proton (δ) at any concentration (C) are given as

$$\delta = \delta_d + (\delta_m - \delta_d)(\sqrt{1 + 8CK} - 1)/4CK$$

where K, δ_m, and δ_d stand for the equilibrium constant (=[dimer]/[monomer]^2), chemical shifts of monomer and dimer, respectively.[20] The shape of the curve for this equation is a sigmoidal curve, in which the δ value changes from δ_m (C=0) to δ_d (C=infinity).

Calculations to fit the theoretical curves to the observed data of H_c and H_d were performed, and the results are summarised in Table 1. The data for [Ni(**1-2**)] is insufficient to derive K and δ values, and the values calculated for [Ni(**1-4**)] are not accurate enough for the same reason. The curves given in Fig. 2 are those calculated for [Ni(**1-6**)]. The result shows that K, δ_m, and δ_d are almost identical regardless of the difference in the alkyl chain length. A slight increase of K in proportion to the chain length can be observed, but is not large enough to be confirmed. The calculated curves fit well to the data up to ca. 0.2 mol·dm^{-3}, but begin to drift apart from the data thereafter. In the case of [Ni(**1-8**)], the drift becomes extremely large because of the high concentration it reaches, and it shows completely different dependence from the theoretical curve. This is probably due to the formation of highly associated aggregates, such as trimers, etc.

Porphyrin complexes, including chlorophylls, also show this kind of up-field shifts.[20,21] The equilibrium constants for them are in the same order as the K values obtained here, indicating that the nickel complexes of (**1-*n***) are expected to have a similar aggregating ability to that of the porphyrin complexes. The differences between δ_m and δ_d for porphyrin complexes proved to be slightly larger than those observed for the (**1-*n***) complexes.

However, the ^{1}H NMR of the unsubstituted salen complex exhibited no observable shift. This is because the solubility of [Ni(salen)] (ca. 2×10^{-4} mol·dm^{-3}) is far lower than the concentration at which the salen type complex starts to aggregate. In other words, the crystallization takes place prior to the aggregation in [Ni(salen)]. It is apparent, therefore, that the effect of the aliphatic side chains is to increase the solubility of the complex, and to reveal the ability to aggregate in the solution, which is hidden in the complex of low solubility.

Paramagnetic Broadening Caused by Copper(II) Complex. Other information on aggregation phenomenon is obtained from the investigation of the paramagnetic broadening of ^{1}H NMR spectra caused by adding the corresponding copper(II) complex [Cu(**1-*n***)] to a $CDCl_3$ solution of [Ni(**1-*n***)]. In Fig. 3 is shown the spectral change of [Ni(**1-6**)] on adding [Cu(**1-6**)]. The change in the spectral profile becomes apparent on adding only 1% of the corresponding copper(II) complex. In Fig. 3, it is found that the peak at δ=3.4 (H_c) loses height drastically on the addition of the copper(II) complex. A similar phenomenon is also observed for the peaks at δ=6.6 (H_d) and 7.1 (H_c). Here again, the peaks of the protons H_c and H_d are broadened extensively, and in addition, the methylene protons of ethylenediamine moiety (H_e) are strongly affected. The intensity of the broadening observed is in the order of $H_c \approx H_d > H_e >$ other protons. It is found also that the peak width at half maxima and the amount of copper(II) complex added have a linear relation up to ca. 7%, although no special treatment such as deoxygenation was applied.

The paramagnetic broadening of ^{1}H NMR peaks is caused by the acceleration of the relaxation speed of activated protons placed near the unpaired electron of copper(II) complex (spin-spin relaxation).[22] Since the acceleration is due to the energy exchange between the spins of unpaired electrons of Cu^{2+} and ^{1}H nucleus, the observed paramagnetic broadening corresponds to the formation of [Ni(**1-6**)]-[Cu(**1-6**)] (abbr. Ni–Cu) aggregate. Protons subject to the intense

Table 1. Calculated Equilibrium Constants and δ Values for Monomer and Dimer of [Ni(**1-*n***)]

Complex	K/mol^{-1}·dm^3	H_c		H_d	
		δ_m	δ_d	δ_m	δ_d
[Ni(**1-2**)]		Not converged			
[Ni(**1-4**)]	9	6.81	6.07	7.44	6.40
[Ni(**1-6**)]	7.5	6.81	6.06	7.44	6.37
[Ni(**1-8**)]	8	6.81	6.00	7.47	6.25
[Ni(**1-10**)]	10	6.81	6.12	7.46	6.43
[Ni(**1-12**)]	9.5	6.80	6.09	7.45	6.40

In $CDCl_3$ at 35°C.

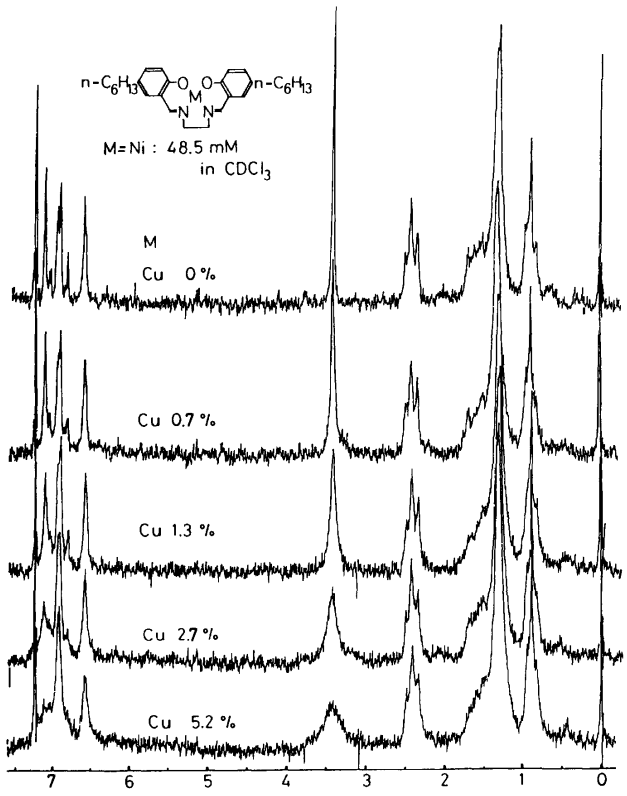

Fig. 3. Paramagnetic broadening of ^{1}H NMR spectra observed for [Ni(**1-6**)] by addition of [Cu(**1-6**)].

broadening, such as H_e and H_d, need to be placed near the Cu^{II} of [Cu(**1-6**)] in the Ni–Cu aggregate.

Paramagnetic broadening can also be caused by some other copper(II) complexes. Addition of bis(8-quinolinol)copper(II) or (*N,N'*-disalicylidene-1,3-propanediaminato)copper(II) also causes broadening in ^{1}H NMR spectrum of [Ni(**1-6**)]. This fact implies that [Ni(**1-6**)] aggregates with a variety of square-planar complexes. Thus, by observing the paramagnetic broadening, the structure of the heteronuclear aggregate of [Ni(**1-*n***)] and copper(II) complex can be investigated.

Structure of the Aggregate. The protons that are affected strongly in the peak shift (H_c and H_d) and paramagnetic broadening (H_c, H_d, and H_e), seem to be in the same part of the complex. These protons are all located around the imino groups. In other words, the spectral changes observed for Ni–Ni (abbr. for dimer of [Ni(**1-*n***)]) and Ni–Cu aggregates seem to be consistent with each other, implying similar structures for Ni–Ni and Ni–Cu aggregates. Assuming, therefore, that the structures of Ni–Ni and Ni–Cu aggregates are not very different, the structure of the aggregate in these systems can be evaluated from the amount and sign of the shift and broadening. The proposed structure for the aggregate in $CDCl_3$ solution is given in Fig. 4. In this aggregate, the protons H_c and H_d are placed above (and below) the aromatic rings, which lead to the

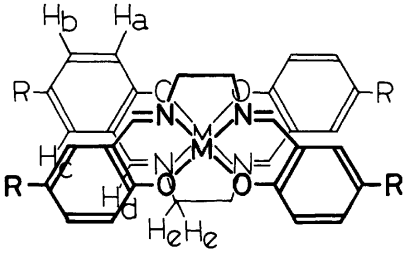

Fig. 4. Proposed aggregation structure (M=Ni, Cu).

shifts, and the protons H_c, H_d, and H_e are placed near to the Cu^{2+} of the neighbouring copper(II) complex, which cause broadening.

This structure of the dimer is different from that obtained for the crystal of [Cu(salen)]·$CHCl_3$ by the crystallographic study.[10] The dimer in the crystal has weak apical bonds between copper(II) of a [Cu(salen)] molecule and the coordinating oxygen atoms of another molecule in the dimer. This structure in the crystal does not explain the observation that the protons around the imino groups are strongly affected by aggregation. On the other hand, the proposed structure agrees well with that observed in [Co(salen)]·$CHCl_3$,[11] which is notable for its oxygen coordinating nature.[12] The result obtained here suggests that [Co(salen)]·$CHCl_3$ probably crystallizes in a dimeric form in $CHCl_3$.

Although an assumption that the homonuclear (Ni–Ni) and heteronuclear (Ni–Cu) aggregates take similar aggregating structures must be made, the combination of peak shift and broadening investigations proved effective in estimating the aggregating structure of the salen type complexes.

The authors thank Dr. Yutaka Fukuda of Ochanomizu University for his help in obtaining magnetic susceptibility data. The present work was partly supported by a Grant-in-Aid for Scientific Research No. 5950614 from the Ministry of Education, Science and Culture.

References

1) "Porphyrins and Metalloporphyrins," ed by K. M. Smith, Elsevier, Amsterdam (1975).

2) T. M. Cotton, A. D. Trifunac, K. Ballschmiter, and J. J. Katz, *Biochim. Biophys. Acta*, **368**, 181 (1974).

3) R. J. Abraham and K. M. Smith, *J. Am. Chem. Soc.*, **105**, 5734 (1983).

4) R. P. H. Kooyman and T. J. Shaafsma, *J. Am. Chem. Soc.*, **106**, 551 (1984).

5) K. Monserrat, M. Graetzel, and P. Tundo, *J. Am. Chem. Soc.*, **102**, 5527 (1980).

6) W. E. Ford, J. W. Otvos, and M. Calvin, *Nature (London)*, **274**, 507 (1978).

7) K. Miyamura and S. Yoshikawa, *Kagaku*, **36**, 1020 (1981).

8) J. Le Moigne and J. Simon, *J. Phys. Chem.*, **84**, 170 (1980).
9) A. Takeuchi, S. Yamada, and H. Yokoi, *Bull. Chem. Soc. Jpn.*, **58**, 2987 (1985).
10) E. N. Baker, D. Hall, and T. N. Waters, *J. Chem. Soc. A*, **1970**, 406.
11) W. P. Schaefer and R. E. Marsh, *Acta Crystallogr., Sect. B*, **25**, 1675 (1969).
12) M. Calvin, R. H. Bailes, and W. K. Wilmarth, *J. Am. Chem. Soc.*, **68**, 2254 (1946).
13) T. Yamamura, *Chem. Lett.*, **1977**, 773.
14) K. Miyamura and Y. Gohshi, *Chem. Lett.*, **1986**, 1145.
15) I. Fells and E. A. Moelwyn-Hughes, *J. Chem. Soc.*, **1959**, 398.
16) S. R. Sandler and W. Karo, "Organic Functional Group Preparations I," 2nd ed., Academic Press, New York (1983), p. 11.
17) T. Izumitani, H. Okawa, and S. Kida, *Chem. Lett.*, **1981**, 483.
18) T. Izumitani, M. Nakamura, H. Okawa, and S. Kida, *Bull. Chem. Soc. Jpn.*, **52**, 2122 (1982).
19) B. I. Ionin and B. A. Ershov, "NMR Spectroscopy in Organic Chemistry," Plenum Press, New York (1970), p. 101.
20) R. J. Abraham, B. Evans, and K. M. Smith, *Tetrahedron*, **34**, 1213 (1978).
21) R. J. Abraham, G. H. Barnett, E. S. Bretschneider, and K. M. Smith, *Tetrahedron*, **29**, 553 (1973).
22) "NMR of Paramagnetic Molecules," ed by G. N. La Mar, W. D. Horrocks, Jr., and R. H. Holm, Academic Press, New York (1973).

 © 1989 The Chemical Society of Japan Bull. Chem. Soc. Jpn., 62, 51—55 (1989)

Studies on Mixed Chelates. XVI. Mixed Copper(II) Chelates with 1,2-Dipiperidinoethane and β-Diketonates[1)]

Yutaka FUKUDA,* Masako CHO, and Kozo SONE*
Department of Chemistry, Faculty of Science, Ochanomizu University,
Otsuka, Bunkyo-ku, Tokyo 112
(Received June 14, 1988)

1,2-Dipiperidinoethane (dipe) forms mixed chelates of the type $[Cu(dike)(dipe)]ClO_4$ with $Cu(ClO_4)_2$ and various β-diketonate ions (dike); however, hexafluoroacetylacetonate (hfac) forms $[Cu(hfac)_2(dipe)]$ instead. The strong solvatochromism of the former, and the high solubility and volatility of the latter, were compared with those of similar chelates studied so far.

1,2-Dipiperidinoethane (dipe; Fig. 1a) is a potential chelating agent which has been only little studied. Its chelate ring structure is similar to that of *N,N,N',N'*-tetramethylethylenediamine (tmen), but the substituent groups on its N atoms ($-(CH_2)_5-$) are much larger, and form bulky piperidine rings with the N atoms. It is, therefore, expected to be a weaker ligand than tmen, since (i) the bulkiness and rigidity of the piperidine rings will hinder the formation of chelate ring, and (ii) even when the chelate ring is formed, the bulky ligand will disturb the proper arrangement of other ligands, and destabilize the whole complex.

In spite of these expectations, however, we could recently prepare a number of fairly stable metallic complexes containing dipe. One of them is a dimeric copper(II) complex, $[Cu_2(OH)_2(dipe)_2](ClO_4)_2$, which is very similar to the dimeric complexes formed by tmen and related diamines.[2)] In this paper, the preparations and various interesting properties of mixed copper(II) complexes with β-diketonate ions (dike) are reported.

Experimental

Preparation of the Complexes. (1) $[Cu(dike)(dipe)]ClO_4$ (dike=Dipivaloylmethanate (dipm), Acetylacetonate (acac), Benzoylacetonate (bzac), Dibenzoylmethanate (dibm), or Trifluoroacetylacetonate (tfac)): To an ethanolic solution of $Cu(ClO_4)_2 \cdot 6H_2O$ (10 mmol in 30 ml), a mixture of a β-diketone and KOH (10 mmol each) dissolved in 10 ml of ethanol (EtOH) is added, and dipe (Tokyo Kasei Co.; 10 mmol in 10 ml of EtOH) is dropped in it upon warming. The mixture is stirred for 10 minutes, filtered, and kept in a freezer overnight. The obtained precipitate is recrystallized from acetone. A similar complex with hexafluoroacetylacetonate (hfac) could not be obtained in this way, and a mixture of $[Cu(hfac)_2(dipe)]$ and unknown precipitate (maybe copper hydroxide) was obtained instead.

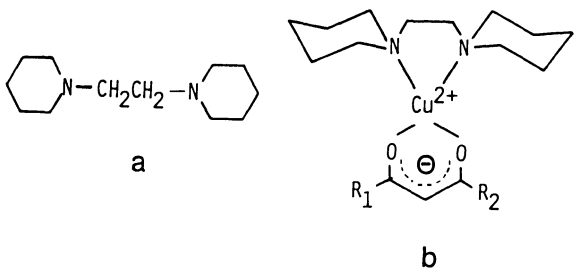

Fig. 1. Structures of dipe (a) and $[Cu(dike)(dipe)]^+$(b). The shape of the dipe moiety in (b) is assumed to be the same as that in $[Ni(NO_3)(acac)(dipe)]$, the structure of which was determined by an X-ray study (Y. Fukuda, C. Fujita, H. Miyamae, H. Nakagawa, and K. Sone, *Bull. Chem. Soc. Jpn.*, in press (1989)).

(2) $[Cu(hfac)_2(dipe)]$: To obtain this complex more easily, a mixture of hfacH and KOH (each 20 mmol, in 20 ml of EtOH) is added to an EtOH solution of $Cu(ClO_4)_2 \cdot 6H_2O$ (10 mmol in 20 ml), and then dipe (10 mmol in 10 ml of EtOH) is dropped in it upon warming. The mixture is stirred for 10 minutes, filtered, and evaporated until green crystals begin to appear. The crystals obtained are recrystallized from 1,2-dichloroethane (DCE).

Physical Measurements. Regarding measurements of UV-visible and IR spectra, magnetic susceptibilities, electric conductivities, and TG-DTA curves of the complexes obtained, one should review Ref. 3.

Results and Discussion

(A) The Complexes $[Cu(dike)(dipe)]ClO_4$ (dike=dipm, acac, bzac, dibm, and tfac). The colors, analytical data and magnetic moments of these complexes are given in Table 1. The strong resemblance of these data and the spectral data (vide infra) to those of the mixed chelates of the type $[Cu(dike)(diam)]ClO_4$ (diam=*N,N'*-polyalkylethylenediamine, e.g., tmen) studied before[4–7)] indicates that these complexes should be formulated as the perchlorates of the chelate cations shown in Fig. 1b.

Spectral Data. As in the case of $[Cu(dike)(diam)]ClO_4$, all these complexes are strongly solvatochromic. Table 2 and Fig. 2 show the shifts of their d–d absorption band observed in various solvents, which are remarkably similar to the corresponding data for $[Cu(dike)(tmen)]ClO_4$[4)] and $[Cu(dike)(teen)]ClO_4$[5)] (teen=*N,N,N',N'*-tetraethylethylenediamine). As with the latter two series of complexes, the $\tilde{\nu}_{max}$ for a certain complex decreases with an increase in the solvent donor number (DN),[8)] i.e., in the order 1,2-dichloroethane (DCE)→nitromethane (NM)→acetone (Me_2CO)→methanol (MeOH)→*N,N*-dimethylformamide (DMF)→

Table 1. Colors, Analytical Data, and Magnetic Moments of the Complexes

Complex	C/%[a]	H/%[a]	N/%[a]	μ_{eff}/B.M.
[Cu(dipm)(dipe)]ClO_4(**I**)(V)[b]	50.89(50.92)	7.97(7.99)	5.19(5.16)	1.85
[Cu(acac)(dipe)]ClO_4(**II**)(V)	43.31(44.54)	6.68(6.82)	5.83(6.11)	1.81
[Cu(bzac)(dipe)]ClO_4(**III**)(B)	50.52(50.77)	6.36(6.39)	5.35(5.38)	1.83
[Cu(dibm)(dipe)]ClO_4(**IV**)(D)	54.20(55.66)	5.98(6.06)	4.79(4.81)	1.80
[Cu(tfac)(dipe)]ClO_4(**V**)(B)	38.87(39.85)	5.48(5.31)	5.45(5.47)	1.80
[Cu(hfac)$_2$(dipe)](**VI**)(G)	38.33(39.21)	3.90(3.89)	4.11(4.16)	2.01

a) Calculated values are in parentheses. b) Colors: V=violet, B=blue, D=dark (nearly black), G=green.

Table 2. Electronic Spectra of the Complexes: $\tilde{\nu}_{max}$ and ε_{max} Values in Solid State and in Various Solvents

Complex[a]	$\tilde{\nu}_{max}/10^3\,cm^{-1}$ (ε_{max})							
	Solid	DMSO(a)	DMF(b)	MeOH(c)	Me_2CO(d)	MeCN(e)	NM(f)	DCE(g)[b]
I	17.3	16.1	16.4	16.8	17.2	17.2	18.8	19.2
		(129)	(137)	(133)	(130)	(152)	(157)	(159)
II	17.3	15.7	16.1	16.7	17.2	17.1	18.5	18.8
		(135)	(132)	(132)	(134)	(144)	(145)	(155)
III	17.2	15.8	16.1	16.7	17.2	17.1	18.3	18.5
		(152)	(143)	(154)	(154)	(163)	(176)	(173)
IV	17.5	15.7	16.1	16.7	17.1	16.9	18.3	18.3
		(147)	(144)	(171)	(166)	(166)	(212)	(180)
V	16.4	15.3	15.5	16.1	16.5	17.1	17.8	17.2
		(121)	(107)	(129)	(142)	(158)	(158)	(156)
VI	14.2	14.4	14.4	14.5	14.3	14.5	14.4	14.2
		(81)	(85)	(81)	(66)	(73)	(66)	(64)

a) Cf. Table 1. b) The DN values of the solvents a—g are, respectively, 29.8, 26.6, 19.1, 17.0, 14.1, 2.7, and 0.0.

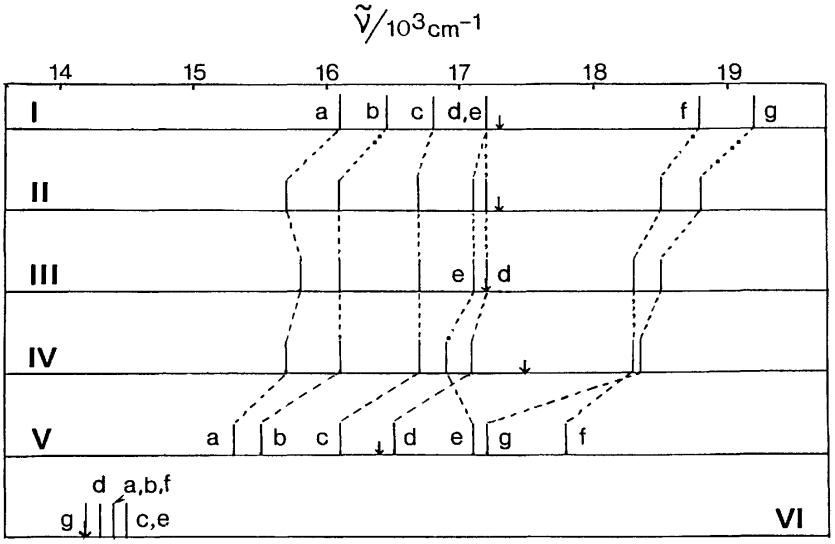

Fig. 2. Solvatochromism of the complexes: $\tilde{\nu}_{max}$ values of the complexes in various solvents. The $\tilde{\nu}_{max}$ in solid state are indicated by short arrows. As to the notations of the complexes (**I**—**VI**) and solvents (a—g), cf. Tables 1 and 2.

dimethyl sulfoxide (DMSO), while the $\tilde{\nu}_{max}$ in a certain solvent decreases with a decrease in the ligand field strength (l.f.s.) of dike, i.e., in the order dipm→acac→bzac→dibm→tfac. These resemblances prove, also in the present case, that the solvatochromism is caused by an axial coordination of solvent molecules onto the planar [Cu(dike)(dipe)]$^+$, which is strengthened by a decrease in the in-plane l.f.s. of the complex cation, as in the case of the tmen- and teen-containing complexes.[4,5]

An apparent exception from these general trends has now been found in the $\tilde{\nu}_{max}$ values in acetonitrile

(MeCN). The DN of this solvent (14.1) is sensibly lower than that of acetone (17.0), so that the $\tilde{\nu}_{max}$ in it should be higher than that in acetone. In fact, however, this is the case only with [Cu(tfac)(dipe)]-ClO_4, and with all other complexes (and also with the tmen- and teen-containing complexes, cf. Fig. 3), these two $\tilde{\nu}_{max}$ values are nearly equal, or slightly in the opposite order.

This spectral anomaly, which has been overlooked hitherto in this series of studies, may possibly be due to the slim, linear shape of MeCN molecule, and its "head-on" mode of coordination (i.e., the fact that $\angle$Cu–N–C=180°); these properties will facilitate the coordination of MeCN, especially when there is a steric hindrance, and so may make it an apparently stronger ligand than Me_2CO in certain cases. However, it may be due to another effect, i.e., the fact that the reacting particles in the present system (Cu^{2+} in the complex cation and MeCN) are rather "soft", and can form a "π-back bond" in the following way.

$$Cu^{2+} \longleftarrow N\equiv C-CH_3 \longleftrightarrow Cu^{2+} \overset{\pi}{\underset{\sigma}{\rightleftharpoons}} N=C-CH_3$$

Even a small contribution from this type of bonding will make the σ-bond synergetically stronger, and the apparent l.f.s. of MeCN notably higher. The sensitive dependence of the magnitude of the observed spectral anomaly on the electronic nature of dike, and similar spectral anomalies observed in MeCN solutions of [Ni(dike)(diam)]ClO_4,[9] seem to indicate the importance of the π-back bonding in the present case.

One more point of interest in Fig. 2 is a disappearance of the anomaly in DCE observed with [Cu(acac)(tmen)]ClO_4. It was formerly noted that the $\tilde{\nu}_{max}$ of this complex in DCE is apparently lower than that in NM, although the DN of DCE (=0) is lower than that of NM (=2.7). This anomaly was ascribed to the formation of ion pairs by means of an axial coordination of ClO_4^- in DCE; it was shown that the use of BPh_4^- instead of ClO_4^- eliminates this anomaly.[4,10]

Now this anomaly does not appear with [Cu(dipm)(dipe)]ClO_4 and [Cu(acac)(dipe)]ClO_4, and with [Cu(acac)(teen)]ClO_4, as shown in Fig. 3, i.e., $(\tilde{\nu}_{max})_{DCE} > (\tilde{\nu}_{max})_{NM}$ in every case. It is plausible that the bulky substituents on dipe and teen hinder the approach of ClO_4^- ions, and suppress ion-pair formation.

The values of $(\tilde{\nu}_{max})_{DCE}$ and $(\tilde{\nu}_{max})_{NM}$, however, get closer in going to [Cu(bzac)(dipe)]ClO_4 and [Cu(dibm)(dipe)]ClO_4, and in the case of [Cu(tfac)(dipe)]-ClO_4 the anomaly described above appears again more drastically. These facts, and the conductivity data shown below, lead to the following conclusion: the degree of ion-pair formation, which is low with the dipm and acac complexes, gradually increases in going to the bzac and dibm complexes, and then drastically in going to the tfac complex. In this last complex, in which the l.f.s. of tfac is the lowest among

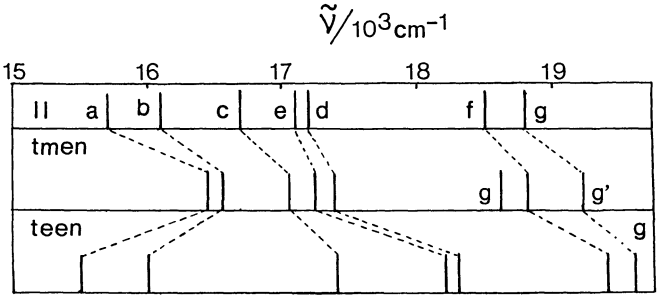

Fig. 3. Comparison of the solvatochromic changes of [Cu(acac)(dipe)]ClO_4, [Cu(acac)(tmen)]ClO_4, and [Cu(acac)(teen)]ClO_4. The notations of solvents are the same as those in Fig. 2. The $\tilde{\nu}_{max}$ of the tmen complex in DCE(g) is too low owing to the ion-pair formation (see text); the value for [Cu(acac)(tmen)]-BPh_4 (g') is therefore given for a better comparison.

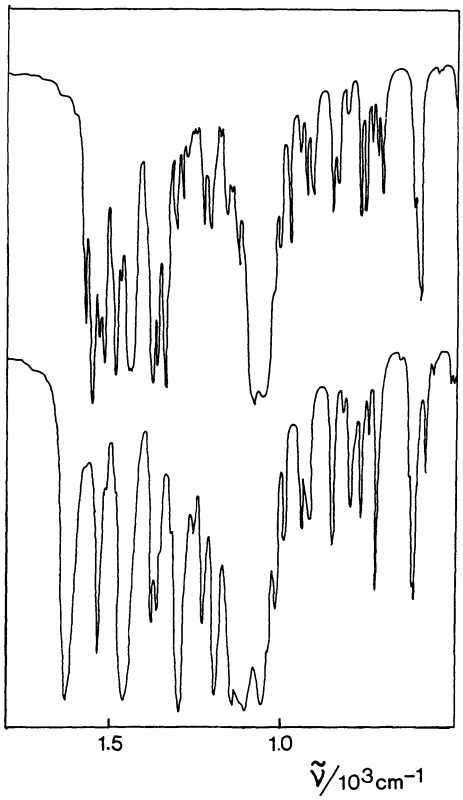

Fig. 4. Comparison of the IR spectra of [Cu(dipm)(dipe)]ClO_4 (above) and [Cu(tfac)(dipe)]ClO_4 (below).

the dike's used (or the positive charge on Cu(II) is highest), the bulkiness of dipe is seemingly insufficient to effectively hinder the coordination of ClO_4^-.

The coordination of ClO_4^- also occurs in crystals of the tfac complex. This can be seen from its IR spectrum, in which the peak of ClO_4^- near 1100 cm^{-1} is notably split, showing the deformation from T_d symmetry.[11] No such splitting takes place in the IR spectra of the other complex perchlorates. Figure 4 shows a part of the obtained spectra.[12]

Apart from such few anomalies, Fig. 2 may be taken

as a fairly regular array of solvents and dike ligands arranged in the order of their coordination abilities (DN of the solvents and l.f.s. of the dike's). In fact, these complexes of dipe (and those of teen, as reported before)[5,6] are even more strongly solvatochromic than [Cu(acac)(tmen)]ClO_4, which was often referred to as an excellent indicator of solvent DN.[7,13]

A comparison of the complexes of dipe, tmen, and teen given in Fig. 3 reveals some interesting trends. In going from tmen to teen, the d-d band moves to the blue in most solvents, except in solvents of very high DN (i.e., DMF and DMSO) where it moves to the red. This can be taken as an indication that (1) the thermal motion of the four ethyl groups of teen weakens the axial coordination of most solvents, making the complex more planar than in the case of tmen, while (2) strong solvent like DMF and DMSO can overcome this steric hindrance and get coordinated effectively, making the complex more regular octahedral, owing to the decreased in-plane l.f.s. produced by bulky teen, than in the case of tmen. On the other hand, in going from tmen to dipe, the d-d band of the complex [Cu(acac)(diam)]$^+$ moves to the red in all solvents, and the movement is larger in solvents of higher DN. In the dipe complex, the ends of the ethyl groups in teen are bound together in the form of piperidine rings, so that their free movements are strongly suppressed, and the movements toward axial directions become particularly difficult. The large steric hindrance to axial coordination in the teen complex is, thus, mostly lost in the dipe complex. Thus, it is probable that the spectral difference between the complex of dipe and that of tmen is mainly the result of the decreased l.f.s. of bulky and rigid dipe, which tends to make its complex more octahedral, in any solvent, than that of tmen.

Two factors which are expected to weaken the complexes of dipe were pointed out at the outset of this paper. The data in Fig. 3 indicate how the effects of both factors, i.e., the weakening of l.f.s. caused by large substituents, and steric hindrance to coordination of solvent molecules, can be recognized in solutions of the teen complex; however, only the first of them is apparent in those of the dipe complex, where the free motion of the substituent groups is restricted by ring formation.

Conductometric Data. Table 3a shows the molar conductivity values of the acac and tfac complexes in various solvents. They show, in general, that these complexes are 1:1 electrolytes.[14] One exception is the tfac complex in DCE; strong ion-pair formation is indicated here. Table 3b shows that the degree of ion-pair formation in DCE increases in the order dipm→acac→bzac→dibm→tfac, and also in the order teen→dipe→tmen. These results are in general agreement with the expectation from spectral data, if the ionic conductivities of the complex cations are reasonably assumed to be comparable to one another.

(B) The Complex [Cu(hfac)$_2$(dipe)]. When hfac is used as dike, no complex of the type (A) could be prepared, and a green, apparently 6-coordinated complex of this composition was obtained instead.[15] This complex is highly soluble in various nonpolar solvents, and it sublimes at ca. 175 °C (or at ca. 100 °C in vacuum) so that it can be purified by sublimation. The intermolecular attraction in this complex is therefore very weak; in this respect it is very similar to the complexes [Ni(dike)$_2$(diam)], and the corresponding Co(II) and Zn(II) complexes, studied before.[16,17]

The electronic spectra of this complex in organic solvents were also studied. Here, $\tilde{\nu}_{max}$ changes only slightly with solvent polarity, showing that there is no solvent molecule in the coordination sphere. A small shift to the blue, which occurs roughly in parallel with solvent acceptor number (AN),[8] is recognized. This may be due to an interaction of the solvent molecules, which now act as acceptors, with the twelve C-F groups covering the surface of the complex:

C—F·····Solvent (Acceptor).

A somewhat similar solvatochromism was recently observed in solutions of [Co(edta)]$^-$ and related

Table 3a. Molar Conductivities (Λ_M) of [Cu(acac)(dipe)]ClO_4 (**II**) and [Cu(tfac)(dipe)]ClO_4 (**V**) in Various Solvents at 25 °C. Concn: 5×10^{-3} mol dm^{-3}

Complex	Λ_M/ohm^{-1} cm^2 mol^{-1}						
	DCE	NM	MeCN	Me_2CO	MeOH	DMF	DMSO
II	20.8	95.9	159.2	147.2	96.6	68.2	33.8
V	8.9	93.1	157.8	139.0	97.2	77.8	34.5
Standard 1:1 electrolytes[14]	10—24	75—95	120—160	100—140	80—115	65—90	ca. 35

Table 3b. Molar Conductivities (Λ_M/ohm^{-1} cm^2 mol^{-1}) of Various Complexes in DCE at 25 °C. Concn: 5×10^{-3} mol dm^{-3}

Complex[a]	**I**	**II**	**III**	**IV**	**V**	**VI**	[Cu(acac)(tmen)]ClO_4	[Cu(acac)(teen)]ClO_4
Λ_M	22.0	20.8	18.1	17.2	8.95	0.22	16.9	28.1

a) Cf. Table 1.

macrocyclic complexes.[18]

The authors are grateful to the Ministry of Education, Science and Culture for supporting of this work through a Grant-in-Aid for Scientific Research (Grant No. 63540475).

References

1) Part XV: N. Hoshino, N. Kodama, Y. Fukuda, and K. Sone, *Bull. Chem. Soc. Jpn.*, **60**, 3947 (1987).

2) D. W. Meek, *Inorg. Chem.*, **4**, 250 (1965); B. J. Cole and W. H. Brumage, *J. Chem. Phys.*, **53**, 4718 (1970); E. D. Estes, W. E. Hatfield, and D. J. Hodgson, *Inorg. Chem.*, **13**, 1654 (1974).

3) Y. Fukuda, M. Yasuhira, and K. Sone, *Bull. Chem. Soc. Jpn.*, **58**, 3518 (1985).

4) Y. Fukuda, A. Shimura, M. Mukaida, E. Fujita, and K. Sone, *J. Inorg. Nucl. Chem.*, **36**, 1265 (1974).

5) Y. Fukuda, Y. Miura, and K. Sone, *Bull. Chem. Soc. Jpn.*, **50**, 142 (1977).

6) K. Sone and Y. Fukuda, "Ions and Molecules in Solution" ("Studies in Physical and Theoretical Chemistry," ed by N. Tanaka, H. Ohtaki, and R. Tamamushi, Elsevier, Amsterdam (1983), Vol. 27), p. 251.

7) K. Sone and Y. Fukuda, "Inorganic Thermochromism," Springer, Heidelberg (1987).

8) V. Gutmann, "The Donor-Acceptor Approach to Molecular Interactions," Plenum, New York (1978).

9) These complexes exist in an equilibrium of the type

$$[Ni(dike)(diam)]^+ + 2Solv \rightleftharpoons [Ni(dike)(diam)(Solv)_2]^+$$

(Solv=solvent molecule) in organic solvents; here the equilibrium in MeCN is shifted more strongly to the right hand side than that in Me_2CO, and the l.f.s. in $[Ni(dike)(diam)(MeCN)_2]^+$ is notably higher than that in $[Ni(dike)(diam)(Me_2CO)_2]^+$, probably owing to the same reason as in the case of the Cu(II) analogues. Cf. Ref. 7.

10) R. W. Soukup and K. Sone, *Bull. Chem. Soc. Jpn.*, **60**, 2286 (1987).

11) K. Nakamoto, "Infrared and Raman Spectra of Inorganic and Coordination Compounds," 3rd ed., Wiley, New York (1978).

12) Similar coordination of ClO_4^- in solid was observed formerly in the case of $[Cu(hfac)(tmen)]ClO_4$ and $[Cu(hfac)(teen)]ClO_4$. Cf. Refs. 4 and 5.

13) R. W. Soukup and R. Schmid, *J. Chem. Educ.*, **62**, 459 (1985).

14) W. J. Geary, *Coord. Chem. Rev.*, **7**, 81 (1971).

15) A similar complex was formerly prepared with teen: cf. Ref. 5.

16) Y. Saito, T. Takeuchi, Y. Fukuda, and K. Sone, *Bull. Chem. Soc. Jpn.*, **54**, 196 (1981).

17) Y. Shika, unpublished data; cf. Ref. 7.

18) N. Miura, M. Shimura, and H. Ogino, *Bull. Chem. Soc. Jpn.*, **60**, 1349 (1987); M. Fujiwara, M. Yoshitake, Y. Fukuda, and K. Sone, *Bull. Chem. Soc. Jpn.*, **61**, 2967 (1988).

X-Ray Crystal Structures of *trans*-(Chloromethyl)bis(2,4-pentanedionato)-(aqua and methanol)chromium(III) Complexes. Evidence for a Trans Influence Exerted in the Carbon-Bonded Chromium(III) Complexes

Yoichi ABE and Hiroshi OGINO*
Department of Chemistry, Faculty of Science, Tohoku University, Aoba, Sendai 980
(Received July 2, 1988)

The crystal and molecular structures of alkylchromium(III) complexes, *trans*-[Cr(CH_2Cl)$(acac)_2(H_2O)$]·EtOH and *trans*-[Cr(CH_2Cl)$(acac)_2$(MeOH)] ($acac^-$=2,4-pentanedionate anion, EtOH=ethanol, MeOH=methanol), have been determined by X-ray structure analyses. Both crystals are triclinic and the space group $P\bar{1}$; Z=2 with a=9.935(2), b=10.606(2), c=9.399(2) Å, α=90.39(2), β=92.44(2), γ=115.54(1)° for the aqua complex, and Z=4 with a=11.402(6), b=16.780(7), c=8.543(3) Å, α=98.83(3), β=102.00(4), γ=83.03(4)° for the methanol complex. Each complex has trans configuration. The carbon-bonded CH_2Cl group elongates specifically the Cr–O bond trans to the Cr–C bond in the aqua complex (Cr–O(H_2O)=2.134(6) Å) and methanol complex (Cr–O(MeOH)= 2.156(6), 2.136(6) Å).

Recently, we synthesized and isolated dichloromethyl- and chloromethyl-bonded chromium(III) complexes, *trans*-[CrR$(acac)_2$L] (R=$CHCl_2$, CH_2Cl; L=H_2O, MeOH, py).[1,2] Remarkably rapid substitution reactions

$$\textit{trans}\text{-[CrR(acac)}_2\text{(MeOH)]} + \text{L} \rightleftharpoons \textit{trans}\text{-[CrR(acac)}_2\text{L]} + \text{MeOH}$$

were observed for the complexes, where L denotes pyridine and its analogs. The X-ray crystal structure determinations of [Cr($CHCl_2$)$(acac)_2$(py)] and [Cr(CH_2Cl)-$(acac)_2$(py)][2] revealed that the geometries of both complexes are trans and the carbon-bonded ligands lengthen specifically the Cr–N bonds trans to the Cr–C bonds in [CrR$(acac)_2$(py)]. Therefore, the labilized ligand substitution reactions are ascribed to a strong electronic effect of the alkyl group on the bond trans to the Cr–C bond. However, there has been no direct evidence that the geometries of [CrR$(acac)_2(H_2O)$] and [CrR$(acac)_2$(MeOH)] are trans. In this work the structural determinations for the [Cr(CH_2Cl)$(acac)_2$L] (L=H_2O, MeOH) are described. The structural features are compared with those of [CrR$(acac)_2$(py)] (R=$CHCl_2$, CH_2Cl).

Experimental

The syntheses of *trans*-[Cr(CH_2Cl)$(acac)_2(H_2O)$]·EtOH and [Cr(CH_2Cl)$(acac)_2$(MeOH)] were carried out by the methods reported previously.[2] The single crystals of the aqua and methanol complexes were obtained by the recrystallizations from H_2O–ethanol (1:5) and H_2O–methanol (1:3), respectively.

Intensity data were collected on a Rigaku AFC-6A four-circle diffractometer with graphite-monochromated Mo $K\alpha$ radiation (λ=0.71073 Å). Crystallographic and experimental parameters for both complexes are listed in Table 1. During data collection, three standard reflections showed decrease in intensities of approximately 10% for both complexes. The reflection data were corrected for the decays as well as Lorentz and polarization factors. The structures were solved by the heavy-atom method and refined by the block-diagonal least-squares method. Refinement was carried out with anisotropic temperature factors for all non-hydrogen atoms. The positions of the hydrogen atoms of the chloromethyl groups and those of the methine groups of $acac^-$ ligands for both aqua and methanol complexes were calculated and fixed. All other hydrogen atoms were not included in the calculation. The atomic-scattering factors including the anomalous scattering factors were taken from Ref. 3 for non-hydrogen atoms and from Ref. 4 for hydrogen atom.

All the calculations were performed on Nippon Electric Co. ACOS-1000 and -2020 computers at the computer center of Tohoku University, using the Universal Crystallographic Computation Program System (UNICS III) and its local version.[5]

Results and Discussion

Positional and isotropic thermal parameters of the *trans*-[Cr(CH_2Cl)$(acac)_2(H_2O)$]·EtOH and [Cr(CH_2Cl)-$(acac)_2$(MeOH)] are listed in Tables 2 and 3,[6] respectively. The structures of the aqua and methanol complexes are shown in Figs. 1 and 2 with atom numbering schemes.

The geometries of *trans*-[Cr(CH_2Cl)$(acac)_2(H_2O)$]·EtOH and [Cr(CH_2Cl)$(acac)_2$(MeOH)] have been proved unequivocally to be trans by the crystal structure determinations. The ethanol molecule in *trans*-[Cr(CH_2Cl)$(acac)_2(H_2O)$]·EtOH is hydrogen-bonded to the coordinated water molecule (O(5)···O(6) 2.656(9) Å). The structures of two crystallographically independent molecules in *trans*-[Cr(CH_2Cl)$(acac)_2$(MeOH)] are almost the same, but different slightly in the orientation of the coordinated methanol molecules and the chloromethyl groups (Fig. 2).

Selected interatomic distances and angles are summarized in Tables 4 and 5. The most striking feature observed in the interatomic distances is that Cr–O-(H_2O) bond (2.134(6) Å) in the aqua complex is

Table 1. Crystal Data for *trans*-[Cr(CH_2Cl)(acac)$_2$(H_2O)]·EtOH and *trans*-[Cr(CH_2Cl)(acac)$_2$(MeOH)]

	trans-[Cr(CH_2Cl)(acac)$_2$(H_2O)]·EtOH	*trans*-[Cr(CH_2Cl)(acac)$_2$(MeOH)]
Formula	$C_{13}H_{24}ClCrO_6$	$C_{12}H_{20}ClCrO_5$
Formula weight	363.78	331.74
Crystal color	Reddish orange	Reddish orange
Crystal shape	Plate	Plate
Crystal dimensions (l/mm)	0.5×0.2×0.1 0.5×0.3×0.1	0.3×0.2×0.1
Crystal system	Triclinic	Triclinic
Space group	$P\bar{1}$	$P\bar{1}$
a(l/Å)	9.935(2)	11.402(6)
b(l/Å)	10.606(2)	16.780(7)
c(l/Å)	9.399(2)	8.543(3)
α(ϕ/°)	90.39(2)	98.83(3)
β(ϕ/°)	92.44(2)	102.00(4)
γ(ϕ/°)	115.54(1)	83.03(4)
U(v/Å^3)	892.4(3)	1573(1)
Z	2	4
D_c(d/g cm^{-3})	1.354	1.401
D_m(d/g cm^{-3})	1.34	—
μ(Mo $K\alpha$)(n/cm^{-1})	8.38	9.38
Temperature	Room temp	Room temp
Scan mode	ω-2θ	ω-2θ
Scan width (ω/°)	1.2+0.35 tanθ	1.2+0.5 tanθ
2θ range (ϕ/°)	3—55	3—55
Reflections measured	$\pm h$, $\pm k$, l	$\pm h$, $\pm k$, l
No. of reflections measured	4121	7273
No. of unique data used for calc. ($\|F_o\| > 3\sigma(\|F_o\|)$)	2493	3662
No. of parameters refined	191	360
R[a]	0.082	0.084
R_w[b]	0.107	0.114
Max. residual electron density (ρ/e Å^{-3})	0.86	0.83

a) $R=\sum||F_o|-|F_c||/\sum|F_o|$. b) $R_w=[\sum w(|F_o|-|F_c|)^2/\sum w|F_o|^2]^{1/2}$; $w=[\sigma^2(|F_o|)+aF_o^2]^{-1}$, where $a=0.030$ for the aqua complex and $a=0.005$ for the methanol complex.

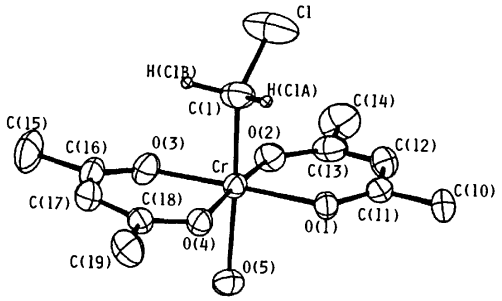

Fig. 1. ORTEP drawing of *trans*-[Cr(CH_2Cl)(acac)$_2$-(H_2O)] with the atom numbering schemes.

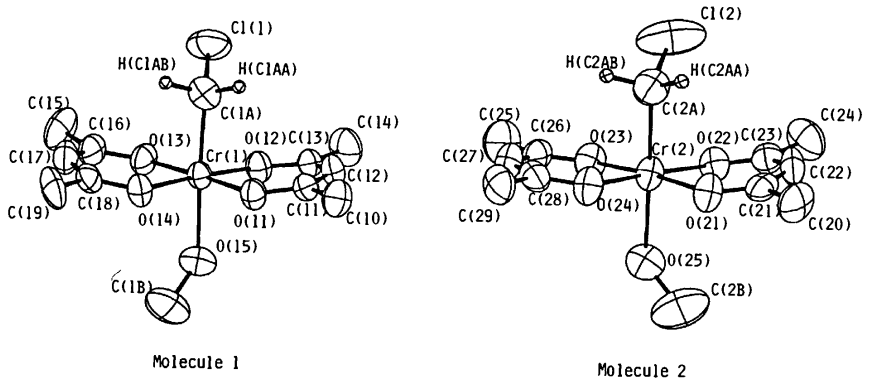

Fig. 2. ORTEP drawings of *trans*-[Cr(CH_2Cl)(acac)$_2$(MeOH)] with the atom numbering schemes.

considerably elongated, being compared to Cr–O(H_2O) bonds (1.975(4)—2.090(6) Å) in chromium(III) complexes which contain coordinated water molecules but have no Cr–C bonds.[7–12] This is also true for the methanol and pyridine complexes: The Cr–O(MeOH) bond (2.156(6) Å for molecule 1 and 2.138(6) Å for molecule 2) for the methanol complex and the Cr–N bond (2.201(4) Å) for the pyridine complex[2] are longer than those of *trans*-$[CrCl_2(MeOH)_4]^+$ (1.987 Å)[13] and *mer*-$[Cr(CF_3CO_2)_3(py)_3]$ (2.10 Å),[14] respectively. The trans influence exerted in the $[CrR(acac)_2L]$ complexes is responsible for the labilized ligand substitution rates.[2] It should be noted that similar ground-state distortion and kinetic effect are also observed for coenzyme B_{12} and related model complexes.[15–20]

Table 2. Final Positional ($\times10^4$) and Isotropic Thermal Parameters for *trans*-$[Cr(CH_2Cl)(acac)_2(H_2O)]\cdot EtOH$

Atom	x	y	z	B_{eq}/Å^2[a]
Cr	434(1)	3519(1)	1956(1)	3.8
Cl	2820(3)	2289(3)	3003(3)	11.7
O(1)	1920(4)	4779(4)	680(4)	4.3
O(2)	1631(5)	4582(5)	3614(5)	5.0
O(3)	−1059(5)	2324(5)	3241(5)	5.4
O(4)	−857(4)	2562(4)	291(4)	4.4
O(5)	−647(5)	4875(4)	1937(4)	5.1
O(6)[b]	15(8)	7010(7)	3757(6)	9.7
C(1)	1349(9)	2108(8)	1837(9)	6.2
C(10)	4199(8)	6429(8)	−186(9)	6.1
C(11)	3220(7)	5706(6)	1059(8)	4.8
C(12)	3754(7)	6094(7)	2447(8)	5.3
C(13)	2943(8)	5550(7)	3647(8)	5.7
C(14)	3586(11)	6102(10)	5132(10)	8.3
C(15)	−3160(11)	429(10)	4116(11)	8.5
C(16)	−2258(8)	1218(7)	2864(9)	5.7
C(17)	−2729(8)	763(7)	1480(9)	5.5
C(18)	−2059(7)	1453(7)	271(8)	4.6
C(19)	−2773(9)	872(9)	−1189(9)	6.5
C(2)[b]	−673(17)	7985(14)	3569(14)	13.7
C(3)[b]	−1685(15)	7599(17)	2414(15)	15.2

a) The equivalent isotropic thermal parameters for non-hydrogen atoms were computed using the following expression: $B_{eq}=4/3(\beta_{11}a^2+\beta_{22}b^2+\beta_{33}c^2+\beta_{12}ab\cos\gamma+\beta_{13}ac\cos\beta+\beta_{23}bc\cos\alpha)$. The β_{ij}'s are defined by $\exp[-(h^2\beta_{11}+k^2\beta_{22}+l^2\beta_{33}+2hk\beta_{12}+2hl\beta_{13}+2kl\beta_{23})]$. b) O(6), C(2), and C(3) denote the oxygen, methylene carbon, and methyl carbon atoms of EtOH solvate, respectively.

The Cr–C bond lengths of $[Cr(CH_2Cl)(acac)_2L]$ (L=H_2O, MeOH, py) lie in the range of the values (2.01—2.11 Å) reported for those of other carbon-bonded chromium(III) complexes.[21–23] The Cr–C bond lengths of the present complexes show a slight but interesting dependence on the ligand L trans to the Cr–C bond; i.e. py (2.077(6) Å)>H_2O (2.06(1) Å)≥MeOH (2.049(9) Å for molecule 1 and 2.052(9) Å for molecule 2). This order appears to indicate that the electron donating trans ligand L affects the length of the Cr–C bond.

The existence of the Cr–C bond has no substantial influence on the equatorial ligands. Table 6 shows that Cr–O(acac) bond lengths in the $[CrR(acac)_2L]$ complexes are essentially the same as those of $[Cr(acac)_3]$[24,25] and related complexes.[26–28]

It has been reported that the pentane moieties of two $acac^-$ chelates in $[Cr(CH_2Cl)(acac)_2(py)]$ are bent toward the CH_2Cl group.[2] This seems to be due to the intermolecular repulsion between a hydrogen atom of a chloromethyl group and a methyl group. Similar bending modes are observed for the aqua and methanol complexes. The degree of the bending can be expressed by the dihedral angles between the plane 1 (the least-squares plane which is defined by a chromium atom and the four oxygen atoms of two

Table 3. Final Positional ($\times10^4$) and Isotropic Thermal Parameters for *trans*-$[Cr(CH_2Cl)(acac)_2(MeOH)]$

Atom	x	y	z	B_{eq}/Å^2	Atom	x	y	z	B_{eq}/Å^2
Cr(1)	1635(1)	4092.7(7)	3813(1)	3.2	C(15)	−237(11)	3136(6)	6813(14)	6.6
Cr(2)	−3103(1)	699.2(8)	1312(2)	3.8	C(16)	266(7)	3195(5)	5329(11)	4.5
Cl(1)	3474(3)	3657(2)	7055(3)	7.3	C(17)	241(8)	2564(5)	4093(12)	4.8
Cl(2)	−3792(4)	1629(3)	4680(4)	11.0	C(18)	612(6)	2559(5)	2663(11)	4.2
O(11)	2503(5)	4325(3)	2231(6)	3.9	C(19)	453(9)	1836(6)	1366(14)	6.2
O(12)	2041(5)	5100(3)	5175(6)	3.9	C(1A)	3159(8)	3456(6)	4893(11)	4.8
O(13)	696(5)	3866(3)	5366(7)	4.2	C(1B)	−794(11)	4560(9)	1299(14)	8.1
O(14)	1112(5)	3132(3)	2356(7)	4.3	C(20)	−2826(11)	2729(6)	−1027(13)	6.5
O(15)	63(5)	4801(4)	2700(7)	4.8	C(21)	−3378(8)	2152(5)	−227(10)	4.5
O(21)	−2719(5)	1530(3)	166(7)	4.6	C(22)	−4567(8)	2364(5)	64(12)	4.9
O(22)	−4804(5)	1153(3)	994(7)	4.2	C(23)	−5194(7)	1853(5)	617(10)	4.3
O(23)	−3481(5)	−195(3)	2284(7)	4.6	C(24)	−6476(9)	2131(7)	787(15)	6.8
O(24)	−1427(5)	264(3)	1504(7)	4.6	C(25)	−3275(11)	−1322(6)	3725(14)	7.0
O(25)	−3556(5)	−75(4)	−916(8)	5.1	C(26)	−2735(9)	−709(5)	2978(10)	4.5
C(10)	3922(8)	4843(6)	1105(11)	5.3	C(27)	−1494(9)	−788(5)	3014(12)	5.3
C(11)	3247(7)	4865(5)	2452(10)	3.9	C(28)	−916(8)	−308(5)	2300(11)	4.7
C(12)	3458(7)	5422(5)	3780(10)	4.2	C(29)	437(8)	−471(6)	2371(13)	6.0
C(13)	2842(7)	5537(4)	5048(10)	4.0	C(2A)	−2660(9)	1397(6)	3504(12)	5.4
C(14)	3115(10)	6220(6)	6441(12)	6.0	C(2B)	−3597(13)	118(10)	−2491(16)	9.1

Table 4. Selected Interatomic Distances and Angles for *trans*-[Cr(CH_2Cl)(acac)$_2$(H_2O)]·EtOH

Bond length (l/Å)			
Cr-O(1)	1.968(5)	Cr-O(2)	1.943(5)
Cr-O(3)	1.954(5)	Cr-O(4)	1.951(5)
Cr-O(5)	2.134(6)	Cr-C(1)	2.06(1)
C(1)-Cl	1.73(1)		
O(6)-C(2)[a]	1.47(2)	C(2)-C(3)[a]	1.38(3)
Bond angle (ϕ/°)			
O(1)-Cr-O(2)	90.8(2)	O(1)-Cr-O(3)	177.9(2)
O(1)-Cr-O(4)	89.3(2)	O(1)-Cr-O(5)	89.8(2)
O(1)-Cr-C(1)	90.7(3)	O(2)-Cr-O(3)	88.5(2)
O(2)-Cr-O(4)	174.9(2)	O(2)-Cr-O(5)	87.8(2)
O(2)-Cr-C(1)	97.1(3)	O(3)-Cr-O(4)	91.4(2)
O(3)-Cr-O(5)	88.3(2)	O(3)-Cr-C(1)	91.3(3)
O(4)-Cr-O(5)	87.1(2)	O(4)-Cr-C(1)	88.1(3)
O(5)-Cr-C(1)	175.1(3)		
Cr-C(1)-Cl	119.6(5)		
O(6)-C(2)-C(3)[a]	112(1)		

a) O(6), C(2), and C(3) denote the oxygen, methylene carbon, and methyl carbon atoms of EtOH solvate, respectively.

Table 5. Selected Interatomic Distances and Angles for *trans*-[Cr(CH_2Cl)(acac)$_2$(MeOH)]

Bond length (l/Å)			
Molecule 1		Molecule 2	
Cr(1)-O(11)	1.941(6)	Cr(2)-O(21)	1.959(7)
Cr(1)-O(12)	1.946(5)	Cr(2)-O(22)	1.974(5)
Cr(1)-O(13)	1.973(7)	Cr(2)-O(23)	1.953(7)
Cr(1)-O(14)	1.953(5)	Cr(2)-O(24)	1.944(6)
Cr(1)-O(15)	2.156(6)	Cr(2)-O(25)	2.138(6)
Cr(1)-C(1A)	2.049(9)	Cr(2)-C(2A)	2.052(9)
C(1A)-Cl(1)	1.794(9)	C(2A)-Cl(2)	1.77(1)
O(15)-C(1B)	1.42(1)	O(25)-C(2B)	1.42(2)
Bond angle (ϕ/°)			
Molecule 1		Molecule 2	
O(11)-Cr(1)-O(12)	90.9(2)	O(21)-Cr(2)-O(22)	90.1(3)
O(11)-Cr(1)-O(13)	177.9(2)	O(21)-Cr(2)-O(23)	175.0(2)
O(11)-Cr(1)-O(14)	88.9(3)	O(21)-Cr(2)-O(24)	87.4(3)
O(11)-Cr(1)-O(15)	89.6(2)	O(21)-Cr(2)-O(25)	90.7(3)
O(11)-Cr(1)-C(1A)	89.6(3)	O(21)-Cr(2)-C(2A)	91.8(4)
O(12)-Cr(1)-O(13)	89.7(2)	O(22)-Cr(2)-O(23)	91.0(3)
O(12)-Cr(1)-O(14)	175.3(2)	O(22)-Cr(2)-O(24)	176.8(3)
O(12)-Cr(1)-O(15)	85.5(2)	O(22)-Cr(2)-O(25)	87.8(2)
O(12)-Cr(1)-C(1A)	92.8(3)	O(22)-Cr(2)-C(2A)	93.0(3)
O(13)-Cr(1)-O(14)	90.3(3)	O(23)-Cr(2)-O(24)	91.3(3)
O(13)-Cr(1)-O(15)	88.4(2)	O(23)-Cr(2)-O(25)	84.5(3)
O(13)-Cr(1)-C(1A)	92.5(3)	O(23)-Cr(2)-C(2A)	93.0(4)
O(14)-Cr(1)-O(15)	89.8(2)	O(24)-Cr(2)-O(25)	90.2(2)
O(14)-Cr(1)-C(1A)	91.9(3)	O(24)-Cr(2)-C(2A)	89.1(3)
O(15)-Cr(1)-C(1A)	178.0(3)	O(25)-Cr(2)-C(2A)	177.4(4)
Cr(1)-C(1A)-Cl(1)	114.3(5)	Cr(2)-C(2A)-Cl(2)	116.7(5)
Cr(1)-O(15)-C(1B)	127.9(7)	Cr(2)-O(25)-C(2B)	126.7(8)

$acac^-$ chelates) and the plane 2 (the least-squares plane which is defined by the two oxygen atoms of a $acac^-$ chelate and three skeletal carbon atoms of the $acac^-$ chelate). The values of the dihedral angles are 164.7(1)° for the pyridine complex,[2] 169.4(3)—173.5(4)° for the methanol complex, and 174.1(4) and 173.6(5)° for the aqua complex. The bending of the $acac^-$ chelates is again due to the interaction of molecules in the crystal. In the aqua and methanol complexes, it is seen that the nearest intermolecular non-bonding distances between two methyl groups of different molecules are close to or slightly shorter than the sum

Table 6. Average Interatomic Distances in the acac$^-$ Chelate Rings of *trans*-[CrR(acac)$_2$L] (R=$CHCl_2$, CH_2Cl; L=H_2O, MeOH, py) and Related Complexes

Complex	Bond length (l/Å)			
	Cr-O	O-C	C-C(methine)	C-C(methyl)
trans-[Cr(CH_2Cl)(acac)$_2$(H_2O)][a]	1.954(5)	1.274(7)	1.39(1)	1.52(2)
trans-[Cr(CH_2Cl)(acac)$_2$(MeOH)][a]	1.955(7)	1.27(1)	1.38(2)	1.52(2)
trans-[Cr(CH_2Cl)(acac)$_2$(py)][b]	1.960(3)	1.266(5)	1.400(7)	1.506(7)
trans-[Cr($CHCl_2$)(acac)$_2$(py)][b]	1.955(6)	1.29(1)	1.38(2)	1.54(2)
[Cr(acac)$_3$][c]	1.951(7)	1.26(2)	1.39(2)	1.52(2)
	1.962(5)	1.27(1)	1.38(1)	1.51(1)
[Cr(acac)$_2$(tn)]$^+$[d]	1.96(1)	1.28(2)	1.39(2)	1.53(2)
[Cr(acac)$_2$(μ-OMe)]$_2$[e]	1.965(5)	1.267(8)	1.38(1)	1.51(1)
[Cr^{II}(acac)$_2$][f]	1.982(3)	1.274(5)	1.399(6)	1.518(6)

a) This work. b) Ref. 2. c) Refs. 24 and 25. d) Ref. 26. e) Ref. 27. f) Ref. 28.

of the van der Waals radii for the methyl groups. In the aqua complex, there is an additional interaction between a chloromethyl group and the nearest methyl group of an ethanol. The inclination of the chloromethyl group may come from this repulsion.

This work was supported by a Grant-in-Aid for Scientific Research No. 60430011 from the Ministry of Education, Science and Culture.

References

1) Abbreviations used in this paper: Hacac, 2,4-pentanedione; MeOH, methanol; py, pyridine; EtOH, ethanol; tn, 1,3-diaminopropane.

2) H. Ogino, M. Shoji, Y. Abe, M. Shimura, and M. Shimoi, *Inorg. Chem.*, **26**, 2542 (1987).

3) "International Tables for X-ray Crystallography", Kynoch, Birmingham, England, Vol. IV, Tables 2.2A and 2.3.1 (1974).

4) R. F. Stewart, E. R. Davidson, and W. T. Simpson, *J. Chem. Phys.*, **42**, 3175 (1965).

5) T. Sakurai and K. Kobayashi, *Rikagaku Kenkyusho Houkoku*, **55**, 69 (1979).

6) Some additional bond lengths and angles, the positional and thermal parameters of hydrogen atoms, the final anisotropic thermal parameters, the projections of the unit cells for both complexes, and the F_o—F_c tables are deposited as Document No. 8849 at the Office of the Editor of the Bull. Chem. Soc. Jpn.

7) W. A. Wickramasinghe, P. H. Bird, M. A. Jamieson, N. Serpone, and M. Maestri, *Inorg. Chim. Acta*, **64**, L85 (1982).

8) X. Solans and M. Font-Altaba, *Acta Crystallogr., Sect. B*, **38**, 2899 (1982).

9) R. Temple, D. A. House, and W. T. Robinson, *Acta Crystallogr., Sect. C*, **40**, 1789 (1984).

10) R. Stomberg and I. Larking, *Acta Chem. Scand.*, **23**, 343 (1969).

11) P. Coggon, A. T. McPhail, F. E. Mabbs, A. Richards, and A. S. Thornley, *J. Chem. Soc. A*, **1970**, 3296.

12) J. V. McArdle, E. de Laubenfels, A. L. Shorter, and H. L. Ammon, *Polyhedron*, **1**, 471 (1982).

13) K. I. Hardcastle, D. O. Skovlin, and A. -H. Eidawad, *J. Chem. Soc., Chem. Commun.*, **1975**, 190.

14) L. M. Dikareva, A. S. Antsyshkina, M. A. Porai-Koshits, Y. V. Zefirov, and V. N. Ostrikova, *Koord. Khim.*, **9**, 1426 (1983).

15) P. J. Toscano and L. G. Marzilli, *Prog. Inorg. Chem.*, **31**, 105 (1984).

16) R. J. Guschl, R. S. Stewart, and T. L. Brown, *Inorg. Chem.*, **13**, 417 (1974).

17) K. L. Brown and A. W. Awtrey, *Inorg. Chem.*, **17**, 111 (1978).

18) R. C. Stewart and L. G. Marzilli, *J. Am. Chem. Soc.*, **100**, 817 (1978).

19) L. G. Marzilli, P. J. Toscano, L. Randaccio, N. Bresciani-Pahor, and M. Calligaris, *J. Am. Chem. Soc.*, **101**, 6754 (1979).

20) S. Bruckner, M. Calligaris, G. Nardin, and L. Randaccio, *Inorg. Chim. Acta*, **2**, 416 (1968).

21) J. J. Daly and R. P. A. Sneeden, *J. Chem. Soc. A*, **1967**, 736.

22) J. J. Daly, F. Sanz, R. P. A. Sneeden, and H. H. Zeiss, *J. Chem. Soc., Dalton Trans.*, **1973**, 73.

23) J. J. Daly, F. Sanz, R. P. A. Sneeden, and H. H. Zeiss, *J. Chem. Soc., Dalton Trans.*, **1973**, 1497.

24) B. Morosin, *Acta Crystallogr.*, **19**, 131 (1965).

25) R. Kuroda and S. F. Mason, *J. Chem. Soc., Dalton Trans.*, **1979**, 273.

26) K. Matsumoto and S. Ooi, *Bull. Chem. Soc. Jpn.*, **52**, 3307 (1979).

27) H. R. Fischer, J. Glerup, D. J. Hodgson, and E. Pedersen, *Inorg. Chem.*, **21**, 3063 (1982).

28) F. A. Cotton, C. E. Rice, and G. W. Rice, *Inorg. Chim. Acta*, **24**, 231 (1977).

 © 1989 The Chemical Society of Japan Bull. Chem. Soc. Jpn., 62, 61—67 (1989)

Mössbauer Spectroscopic Study of Superconducting Y-Ba-Cu(Fe)-O Ceramics and Gamma-Ray Irradiation Effect

Tetsuaki NISHIDA,* Hiroshi IDE, Yonezo MAEDA, Hiroyuki NASU,†
Toshirou YAGI,†† Akira SAKAI,†† and Yoshimasa TAKASHIMA
Department of Chemistry, Faculty of Science, Kyushu University 33,
Hakozaki, Higashiku, Fukuoka 812
†Department of Electrical Engineering, Faculty of Engineering, Hiroshima University,
Saijo, Higashi-Hiroshima 724
††Department of Physics, Faculty of Science, Kyushu University 33,
Hakozaki, Higashiku, Fukuoka 812
(Received July 22, 1988)

Mössbauer spectra of $YBa_2(Cu_{1-x}Fe_x)_3O_{7-\delta}$ ceramics (x=0.003, 0.008, and 0.017) measured at room temperature show a superposition of three quadrupole doublets. An outermost doublet (δ=0—0.04 mm s^{-1}, Δ=1.94—1.98 mm s^{-1}) is ascribed to high-spin Fe^{4+} ions present at substitutional sites of Cu^{2+} ions (Cu(2) site). An intermediate doublet (δ=−0.03—0.02 mm s^{-1}, Δ=1.12—1.17 mm s^{-1}) is ascribed to intermediate-spin Fe^{3+} ions present at substitutional sites of Cu^{3+} ions (Cu(1) site). An innermost doublet is ascribed to Fe^{3+} ions (high spin) with tetrahedral symmetry, present along the b-axis. A decrease in T_c from 72 to 60 K, observed when iron content (x) is increased from 0.008 to 0.017, is explained by a lowered layer structure composed of "dimpled" CuO_4 planes, owing to a displacement of O(4) oxygen atoms sharing CuO_5 tetragonal pyramids and CuO_4 square planars. One-dimensional chains composed of CuO_4 square planars proved to be primarily affected by γ-ray irradiation, whereas no change of T_c was observed. Low-temperature Mössbauer measurements revealed that "partial Debye temperatures" are 330 and 740 K for the chains and layer structure, respectively.

Since Bednorz and Müller exhibited a possibility of high-T_c superconductivity in oxide ceramics,[1] Ln-Ba-Cu-O ceramics, where Ln indicates lanthanide elements, have attracted much attention. Important findings of superconducting Y-Ba-Cu-O ceramics by Wu et al.[2] and Hikami et al.[3,4] suggested several practical applications at higher temperatures than so-called "liquid nitrogen temperature," e.g., fiber and thin film.[5-9] In addition to the applications and studies of physical properties (e.g. T_c and J_c), structure of Y-Ba-Cu-O superconductors has been studied by several groups. Using an electron probe microanalyzer (EPMA), Iwata et al.[10] elucidated that black-colored phase having a composition of Y:Ba:Cu=1:2:3 causes the superconductivity. Crystal structure of high-T_c $YBa_2Cu_3O_{7-\delta}$ was studied by Hazen et al.[11] and LePage et al.[12] by means of powder X-ray diffraction. As a result, it was revealed that orthorhombic (*Pmmm*) phase and tetragonal (*P4/mmm*) phase are present in $YBa_2Cu_3O_{7-\delta}$ ceramics. Powder neutron diffraction study combined with Rietveld analysis revealed that an orthorhombic (*Pmmm*) phase is concerned with the superconductivity in $YBa_2Cu_3O_{7-\delta}$ ceramics.[13-16] Beno et al.[13] elucidated that the orthorhombic phase is composed of distorted CuO_5 tetragonal pyramids, constituting "dimpled" CuO_4 layers in the a-b planes, and CuO_4 square planars constituting one-dimensional fence-like chains in the b-c planes. It was reported that the distorted CuO_5 tetragonal pyramids also constitute semiconducting $YBa_2Cu_3O_{7-\delta}$ ceramics (δ>0.5).[13] Most of the copper atoms in "dimpled" CuO_4 layers (denoted by Cu(2)) were reported to be divalent,[14] being in contrast to Cu^{3+} ions constituting one-dimensional CuO_4 square planars in the b-c planes.[15] Jorgensen et al.[14] revealed that Cu^{3+} ions in CuO_4 square planar chains (Cu(1)) play an important role in the conduction mechanism and that a depression of superconductivity is due to a loss of Cu^{3+} ions and/or a disordering of the one-dimensional chains. Similar conclusion has been drawn by Izumi et al.[16,17] in neutron diffraction studies.

^{57}Fe-Mössbauer spectroscopy has been utilized for a structural study of superconducting $GdBa_2Cu_3O_{7-\delta}$,[18,19] $YBa_2Cu_3O_{7-\delta}$,[20-27] and $EuBa_2Cu_3O_{7-\delta}$[28,29] ceramics. In a Mössbauer study of $GdBa_2(Cu_{0.94}Fe_{0.06})_3O_{7-\delta}$ ceramic at room temperature,[18,19] the spectrum was analyzed into two types of quadrupole doublets with isomer shifts (δ) of −0.12 and −0.17 mm s^{-1} and quadrupole splittings (Δ) of 1.97 and 1.05 mm s^{-1}, respectively. The former doublet peak with larger quadrupole splitting was ascribed to the Fe^{3+} ions present at substitutional sites of Cu^{2+} ions at Cu(1) site, whereas the latter peak was ascribed to the absorption due to Fe^{3+} ions present at substitutional sites of Cu^{3+} ions at Cu(2) site. In these studies,[18,19] a homogeneous single phase was recognized by X-ray diffraction method when the substitution of iron for copper was less than 15% in the $GdBa_2(Cu_{1-x}Fe_x)_3O_{7-\delta}$ ceramics. Furthermore, a Mössbauer spectrum proved to show a magnetic splitting at 4.2 K when the substitution of iron for copper was greater than 3%. A peak assignment similar to the case of $GdBa_2(Cu_{1-x}Fe_x)_3O_{7-\delta}$[18,19] ceramics was made for $YBa_2(Cu_{1-x}Fe_x)_3O_{7-\delta}$ ceramics by the same research group.[20] They indicated that T_c is decreased with increasing iron

content and that a superconductivity disappears when x is greater than 0.15. Isomer shift of $YBa_2(Cu_{1-x}Fe_x)_3O_{7-\delta}$ ceramic (x=0.06) also proved to be located around 0 mm s^{-1} with respect to a stainless steel.[20] On the other hand, quite a reverse assignment was made by several groups.[21,22,24,25,28] Nasu et al.[21] indicated that an asymmetric outermost doublet peak corresponds to high-spin Fe^{3+} ions (S=5/2) present at substitutional sites of Cu^{2+} ions (Cu(2) site), and that an intermediate doublet peak corresponds to intermediate-spin Fe^{3+} ions (S=3/2) present at substitutional sites of Cu^{3+} ions (Cu(1) site). An innermost weak doublet (δ=0.27 mm s^{-1} and Δ=0.52 mm s^{-1}) was ascribed to octahedral Fe^{3+} ions of high spin state.[21] Takano and Takeda[22] showed that both the outermost and intermediate doublet peaks correspond to intermediate-spin Fe^{3+} ions (S=3/2).

Structural information obtained by Mössbauer spectroscopy seems to be very useful because it is directly concerned with the mechanism of superconductivity in these ceramics. The present ^{57}Fe-Mössbauer study was carried out in order to elucidate a local (short-range) structure in $YBa_2(Cu_{1-x}Fe_x)_3O_{7-\delta}$ superconductors and also a long-range structure in connection with lattice dynamics of lower-dimensional chain and layer structures composed of copper (Cu^{2+} or Cu^{3+}) and oxygen atoms. Mössbauer measurements of ^{60}Co-γ ray (ca. 10^8 R) irradiated $YBa_2(Cu_{1-x}Fe_x)_3O_{7-\delta}$ superconductor were also performed in order to elucidate a sensitivity to gamma rays in connection with a short- or long-range structure.

Experimental

Superconducting $YBa_2(Cu_{1-x}Fe_x)_3O_{7-\delta}$ ceramics, in which x was chosen to be 0.003, 0.008, and 0.017, were prepared from Y_2O_3, $BaCO_3$, CuO, and $^{57}Fe_2O_3$ (^{57}Fe=96.03%), of a guaranteed reagent grade. Each of the mixtures containing weighed quantities of these reagents was ground in an agate mortar and dehydrated at 110 °C for 1 h on an electric heater. Each mixture in an alumina crucible was then heated at 900 °C for 5 h in an electric muffle furnace. After being cooled to room temperature, the mixture was pressed into a pellet with a diameter of 6 mm, under a hydrostatic pressure of 200 kg cm^{-2}. Superconducting $YBa_2(Cu_{1-x}Fe_x)_3O_{7-\delta}$ ceramics were prepared by sintering each pellet at 900 °C for 35 h. After the sintering, temperature in the electric muffle furnace was cooled down to 200 °C with a rate of 70 °C h^{-1}. All the procedures were performed in ambient atmosphere. The $YBa_2(Cu_{1-x}Fe_x)_3O_{7-\delta}$ ceramics prepared in this way are black in color. Mössbauer measurements were performed on pulverized samples by using a metallic iron foil enriched with ^{57}Fe as a reference of isomer shift. The iron foil was also used for calibrating the velocity of spectrometer. Cobalt-57 (10 mCi) diffused into a sheet of palladium foil was used as a Mössbauer source. Gamma-Ray irradiation was performed at the Cobalt-60 Irradiation Facilities of Kyushu University at an ambient temperature. During the Mössbauer measurements and ^{60}Co-γ ray irradiations ranging from 10^6 to 10^8 R, each sample was placed in a polyethylene bag filled with dry nitrogen gas in order to prevent it from absorbing atmospheric moisture. DC resistivity measurements were performed by a four-terminal method. Magnetic susceptibility was measured between room temperature and 78 K. DTA measurements were performed between room temperature and 800 °C with a heating rate of 5 °C min^{-1}. In DTA measurements, powder of α-Al_2O_3 was used as a standard material.

Results and Discussion

Mössbauer spectra of $YBa_2(Cu_{1-x}Fe_x)_3O_{7-\delta}$ ceramics (x=0.017, 0.008, and 0.003) are demonstrated in Fig. 1. Each Mössbauer spectrum shows a superposition of three quadrupole doublet peaks; an outermost peak with a quadrupole splitting of 1.94—1.98 mm s^{-1} (doublet (a)), an intermediate peak with a quadrupole splitting of 1.12—1.17 mm s^{-1} (doublet (b)), and an innermost peak with a quadrupole splitting of 0.46—0.56 mm s^{-1} (doublet (c)). The isomer shift of doublets (a) and (b) are located at 0—0.04 and −0.03—0.02 mm s^{-1}, respectively. The isomer shift of doublet (c) is 0.27—0.29 mm s^{-1}. It should be noted that the linewidth of doublet (b) is 0.46—0.49 mm s^{-1}, whereas the linewidth of doublets (a) and (c) is in a range of 0.28—0.30 mm s^{-1}. The latter values are characteristic of the absorption due to iron in crystalline compounds. On the other hand, the large linewidth (0.46—0.49 mm s^{-1}) of doublet (b) indicates distributed bond lengths and bond angles between iron and oxygen atoms, as observed in several Mössbauer studies of inorganic glasses.[30-38] This suggests a non-crystalline character of steric configuration around the iron concerned with doublet (b). The isomer shift of doublet (b) (−0.03—0.02 mm s^{-1}) indicates a much increased s-electron density at iron nucleus compared with that of high-spin Fe^{3+} ions.[30-38] Therefore, doublet (b) is ascribed to the absorption due to either

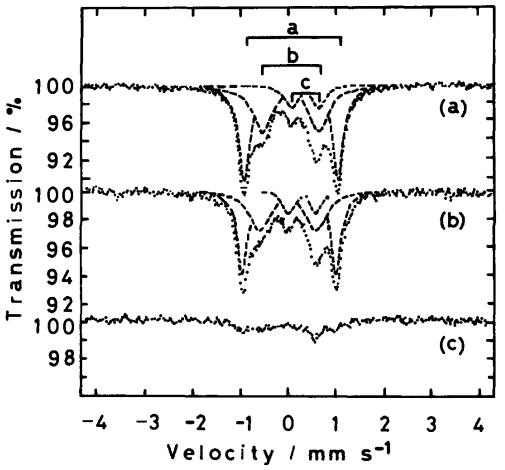

Fig. 1. Mössbauer spectra of superconducting $YBa_2(Cu_{1-x}Fe_x)_3O_{7-\delta}$ ceramics measured at room temperature. (a): x=0.017, (b): x=0.008, and (c): x=0.003.

high-spin Fe^{4+} ions or intermediate-spin Fe^{3+} ions ($S=3/2$).[39,40] If we take account of the small interatomic distance between Cu(1) and oxygen (O(1))[14,15] and therefore a strong ligand field at the copper (and also iron) site, we can speculate that iron is present at substitutional sites of Cu(1) in the form of intermediate-spin Fe^{3+} ($S=3/2$). In connection with this, Takano and Takeda[22] demonstrated a magnetically split peak at 1.5 K, which was assigned to Fe^{3+} ions of $S=3/2$, having an internal magnetic field (H_{int}) of about 33 T. A large linewidth of doublet (b) (0.46—0.49 mm s^{-1}), which is 30—75% greater than that of doublets (a) and (c), will reflect a decreased chain structure composed of CuO_4 chains in the b-c planes when Cu^{3+} (and small amounts of Cu^{2+}) ions are replaced by Fe^{3+} ions. In addition to the substitution of Fe^{3+} ions for Cu^{3+} (and also Cu^{2+}) ions, which preferentially conform CuO_4 square planars, incorporation of iron into $YBa_2Cu_3O_{7-\delta}$ ceramics will result in a formation of Fe^{3+}–oxygen polyhedra such as FeO_4 tetrahedra and FeO_6 octahedra. This will be discussed later.

Doublet (a) having a large quadrupole splitting is ascribed to Fe^{4+} ions present at substitutional sites of Cu^{2+} (and small amounts of Cu^{3+}) ions constituting CuO_5 tetragonal pyramids along the a-b planes. A bond length between copper (and also iron) present at Cu(2) site and an axial oxygen atom (O(4)), present at the apex of each pyramid, seems to be too longer[14,15] to form an intermediate spin state. Furthermore, isomer shift of high-spin Fe^{3+} ions present in tetragonal pyramids, having a coordination number 5, will be located around 0.4 mm s^{-1} with respect to metallic iron, i.e., between the isomer shift values of octahedra and tetrahedra.[30-40] A small isomer shift obtained for doublet (a) (0—0.04 mm s^{-1}) is explained by a decreased shielding effect of 4s-electron density by 3d-electrons when Fe^{3+} ($3d^5$) is oxidized to Fe^{4+} ($3d^4$). It seems that two-dimensional layers composed of "dimpled" CuO_4 planes constituting CuO_5 tetragonal pyramids along the a-b plane[13-17] will be less affected than one-dimensional chains composed of CuO_4 square planars (b-c plane), when Cu^{3+} and Cu^{2+} ions are replaced by Fe^{3+} and Fe^{4+} ions, respectively.

Doublet (c) having an isomer shift of 0.27—0.29 mm s^{-1} and a quadrupole splitting of 0.46—0.56 mm s^{-1} is ascribed to the absorption due to tetrahedral Fe^{3+} ions ($S=5/2$), because the isomer shift is characteristic of high-spin Fe^{3+} species with tetrahedral symmetry.[30-40] Magnetically-split Mössbauer spectra of $YBa_2(Cu_{1-x}Fe_x)_3O_{7-\delta}$ ceramics ($x=0.010$—0.067) observed at low temperatures, having an internal magnetic field (H_{int}) of about 49 T,[22,24,27] are consistent with the peak assignment described in this paper. In those papers, however, the magnetic peak was ascribed to octahedral Fe^{3+} ions.[22,24,27] It is generally known that H_{int} for octahedral Fe^{3+} species is greater than that of tetrahedral Fe^{3+} species, e.g. an H_{int} value of α-Fe_2O_3 at the corresponding temperature is about 54 T.[39] It seems that the FeO_4 tetrahedra are preferentially formed along the b-axis, because one-dimensional chain structure composed of CuO_4 square planars will be more favorable for the formation of FeO_4 tetrahedra than two-dimensional layer structure composed of CuO_5 tetragonal pyramids. The formation of FeO_4 tetrahedra along the b-axis will reduce a regular atomic arrangement, and some oxygen atoms will be located between one-dimensional chains composed of CuO_4 square planars. This will cause an increased unit cell length (lattice parameter a) along the a-axis, as reported by Maeno et al.[26] and Zhou et al.[27] If one-dimensional chains in the b-c planes carry supercurrent,[14-17,23] formation of FeO_4 tetrahedra along the b-axis will directly suppress the superconduction. As a result, a decrease in T_c will be observed. On the other hand, if two-dimensional layers in the a-b planes carry the supercurrent,[25,26] we have to consider a different mechanism concerning the decrease in T_c brought about by the formation of FeO_4 tetrahedra along the b-axis.

A decrease in T_c caused by increased iron content of superconducting $YBa_2(Cu_{1-x}Fe_x)_3O_{7-\delta}$ ceramics is shown in Fig. 2. By increasing iron content (x) from 0.008 (Fig. 2a) to 0.017 (Fig. 2b), it proved that T_c decreases from 72 to 60 K. These T_c's are lower than that of original $YBa_2Cu_3O_{7-\delta}$ ceramics (80 K) without iron.[2] Paramagnetic to diamagnetic transition around T_c is observed in $YBa_2(Cu_{1-x}Fe_x)_3O_{7-\delta}$ superconductor ($x=0.008$), as shown in Fig. 3. Temperature dependency of the magnetic susceptibility (χ) shows a good agreement with that of electrical resistivity shown in Fig. 2a. The formation of FeO_4 tetrahedra along the b-axis will lower the layer structure composed of "dimpled" CuO_4 planes (Cu(2) site), owing to a displacement of O(4) oxygen atoms sharing CuO_5 tetragonal pyramids and CuO_4 square planars. Therefore, if the superconduction is concerned with the a-b planes (Cu(2) site), displacement of O(4) oxygen will be the primary reason for the decrease in T_c. This is

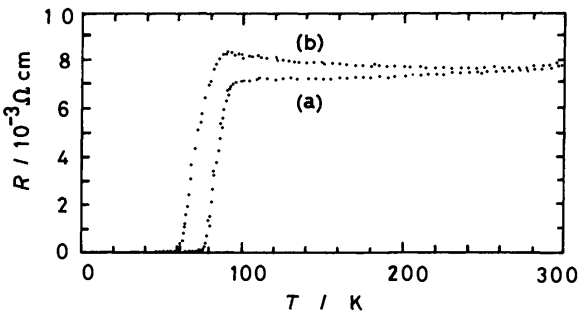

Fig. 2. Temperature dependency of electrical resistivity (R) of superconducting $YBa_2(Cu_{1-x}Fe_x)_3O_{7-\delta}$ ceramics. (a): $x=0.008$, (b): $x=0.017$.

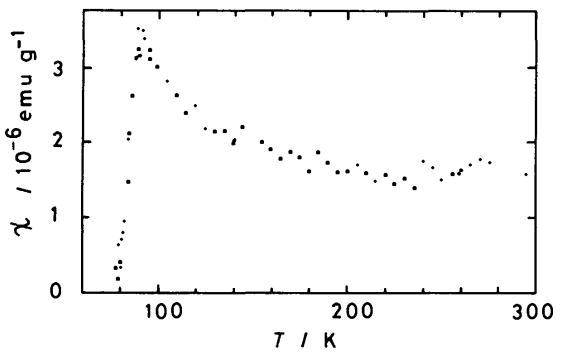

Fig. 3. Temperature dependency of magnetic susceptibility (χ) of superconducting $YBa_2(Cu_{0.992}Fe_{0.008})_3O_{7-\delta}$ ceramic.

also the case for the decrease in T_c observed in original $YBa_2Cu_3O_{7-\delta}$ ceramics when an oxygen content is decreased. Takano and Takeda,[22] reported that a relative absorption area corresponding to Cu(1) and Cu(2) sites depends on the oxygen content. This means that a decrease in T_c is not directly concerned with a relative occupation ratio of iron between Cu(1) and Cu(2) sites. Regarding the absorption and evolution of oxygen atoms, DTA measurements of superconducting $YBa_2(Cu_{1-x}Fe_x)_3O_{7-\delta}$ ceramics (x= 0.008 and 0.003) revealed a single and wide exothermic peak ranging from room temperature to about 680 °C (x=0.008) and 660 °C (x=0.003), followed by a continuous endothermic peak at the higher temperatures. The exothermic peak having a maximum at about 430 °C indicates a continuous oxygen absorption in this temperature range. At temperatures higher than 660—680 °C, evolution of oxygen will become frequent, indicating a phase transition from orthorhombic to tetragonal at the temperatures.

Mössbauer parameters of superconducting $YBa_2(Cu_{1-x}Fe_x)_3O_{7-\delta}$ ceramic (x=0.017) irradiated with ^{60}Co-γ rays are summarized in Table 1. Mössbauer spectra and most of the parameters except an absorption area proved to be independent of the irradiation. Experimental error of the isomer shift is estimated to be ±0.01 mm s^{-1} and that of quadrupole splitting and linewidth is ±0.02 mm s^{-1}. These results indicate that a local structure and a chemical bond around iron are scarcely affected by the ^{60}Co-γ ray irradiations. Actually, no change of T_c was observed after the γ-ray irradiation of 10^8 R. This is quite in contrast to the result of several oxide glasses,[31,33] in which a quantitative reduction of Fe^{3+} to Fe^{2+} or a change of isomer shift and/or quadrupole splitting was observed when irradiated with γ-rays$\geqq 10^6$ R. These experimental results demonstrate that $YBa_2(Cu_{1-x}Fe_x)_3O_{7-\delta}$ and also $YBa_2Cu_3O_{7-\delta}$ ceramics are highly resistant to γ-rays so far as a local structure is concerned. On the other hand, Table 1 indicates a dose-dependent change of relative absorption area. This is illustrated in Fig.

Table 1. Mössbauer Parameters of $YBa_2(Cu_{0.983}Fe_{0.017})_3O_{7-\delta}$ Ceramic Irradiated with ^{60}Co-γ Rays

Dose/R	δ[a]	Δ[b]	Γ[c]	A[d]
	mm s^{-1}	mm s^{-1}	mm s^{-1}	%
0	0.04	1.95	0.28	48.6
	0.02	1.17	0.46	39.1
	0.27	0.46	0.31	12.3
1×10^6	0.05	1.96	0.30	50.5
	0.03	1.17	0.47	36.3
	0.28	0.48	0.32	13.2
6×10^6	0.05	1.98	0.29	50.8
	0.03	1.16	0.39	36.7
	0.29	0.49	0.34	12.5
1×10^7	0.05	1.96	0.29	53.5
	0.03	1.16	0.39	30.6
	0.27	0.47	0.34	15.9
1×10^8	0.04	1.96	0.29	51.7
	0.03	1.15	0.50	30.8
	0.31	0.50	0.42	17.5

a) Isomer shift. b) Quadrupole splitting. c) Linewidth. d) Absorption area.

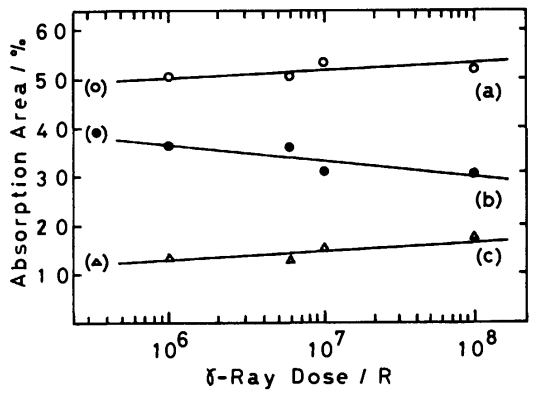

Fig. 4. Gamma-Ray dose dependency of relative absorption area (A) for superconducting $YBa_2(Cu_{0.983}Fe_{0.017})_3O_{7-\delta}$ ceramic. (a): doublet (a), (b): doublet (b), (c): doublet (c).

4, where plots in parentheses refer to the values before irradiation. We can understand from Fig. 4 that absorption area of doublet (b) decreases by the irradiation at the expense of absorption areas of doublets (a) and (c). This suggests a decrease in the recoil-free fraction f of Fe^{3+} ions present at substitutional sites of Cu(1) in one-dimensional chains. The reduced recoil-free fraction f will be closely concerned with the one-dimensional chain structure. This will be discussed later based on low-temperature Mössbauer measurements.

Mössbauer measurements of a superconducting $YBa_2(Cu_{0.992}Fe_{0.008})_3O_{7-\delta}$ ceramic were carried out at several temperatures ranging from room temperature to 78 K. As a result, no apparent spectral change was observed in any case. Temperature dependency of isomer shifts for the three doublets (a, b, and c) is shown in Fig. 5. It is obvious from Fig. 5 that all the isomer

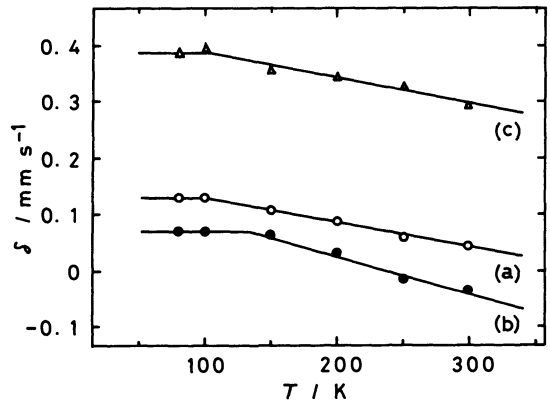

Fig. 5. Temperature dependency of isomer shift (δ). (a): doublet (a), (b): doublet (b), (c): doublet (c).

shift values are increased at lower temperatures owing to a decreased second-order Doppler effect. This suggests a decreased degree of atomic vibrations at iron and also copper sites, because a second-order Doppler shift is correlated with a mean square velocity of atomic vibration ($<v^2>$).[39] It can be known from Fig. 5 that a slope of doublet (b) is a little steeper than that of doublets (a) and (c). This means that a chemical bond between Fe^{3+} ion, present at substitutional sites of Cu(1) in one-dimensional chains, and four oxygen atoms is more affected by the lattice vibrations than two-dimensional Cu(2) sites or FeO_4 tetrahedra. In case of FeO_4 tetrahedra present along the b-axis, an atomic arrangement can be viewed to be three-dimensional because some oxygen atoms are located between two $Cu(1)O_4$ square planar chains, as described above. The experimental results shown in Fig. 5 are consistent with the result shown in Fig. 4. Another feature of Fig. 5 is that isomer shift is almost constant at 78 and 100 K. This result suggests that vibrational mode is changed at the onset of superconduction. The constant isomer shift values obtained at 78 and 100 K (and also at 150 K in case of doublet (b)) seem to suggest a retained amplitude (mean square velocity $<v^2>$) of lattice vibration, although we have only a few measuring points for each doublet peak. The present experimental results (Fig. 5) are consistent with the temperature dependencies of linewidth and absorption area shown in Figs. 7 and 8, respectively.

Figure 6 shows a temperature dependency of quadrupole splitting for each doublet peak. From Fig. 6, we can deduce on the average unchanged atomic configuration around Fe^{3+} or Fe^{4+} (and also Cu^{3+} or Cu^{2+}) ions and also unchanged 3d-electron configuration. In contrast to the quadrupole splitting values plotted in Fig. 6, linewidth (FWHM) of doublet (b) shows a significant decrease with increasing temperature (Fig. 7). The decrease in linewidth at higher temperatures is ascribed to a motional narrowing, which seems to be more frequent in case of one-

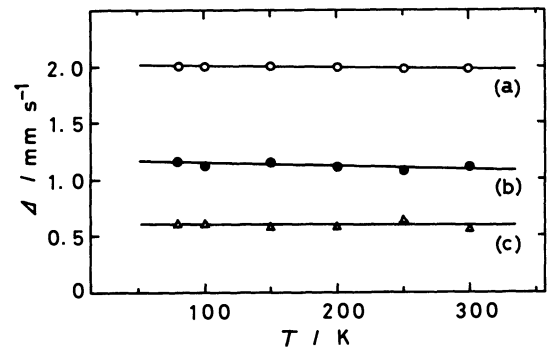

Fig. 6. Temperature dependency of quadrupole splitting (Δ). (a): doublet (a), (b): doublet (b), (c): doublet (c).

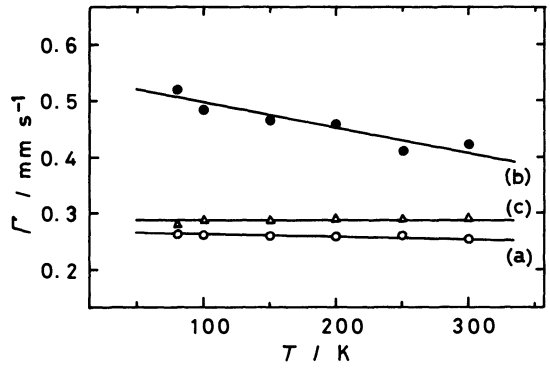

Fig. 7. Temperature dependency of linewidth (Γ). (a): doublet (a), (b): doublet (b), (c): doublet (c).

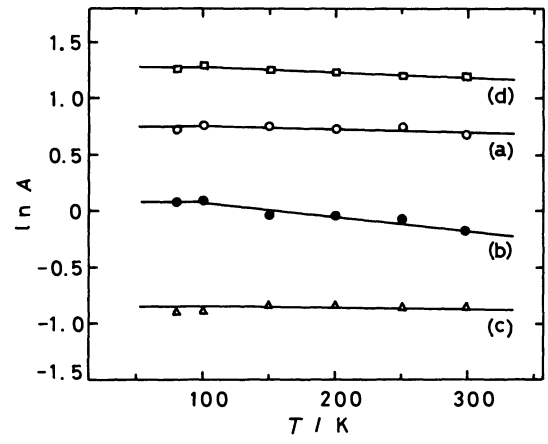

Fig. 8. Temperature dependency of absorption area (A). (a): doublet (a), (b): doublet (b), (c): doublet (c), (d): total absorption.

dimensional chains composed of CuO_4 square planars. A slight decrease in linewidth is observed in case of two-dimensional "dimpled" CuO_4 layers (doublet (a)). Figure 7 also indicates that a linewidth of doublet (c), corresponding to FeO_4 tetrahedra, is independent of the temperature.

Relative absorption area of three doublets is shown in Fig. 8. Characteristic feature of Fig. 8 is similar to

that of Figs. 5 and 7, i.e., absorption area of doublet (b) shows a pronounced decrease with increasing temperature. In contrast to this, absorption areas for doublets (a) and (c) are almost constant irrespective of the temperature, suggesting a high Debye temperature (Θ). A parameter of intermolecular force constant, Θ^2M, is calculated according to the formula,[41-43]

$$\Theta^2M = 3E^2/kc^2(-\mathrm{d}\ln f/\mathrm{d}T)^{-1}, \quad (1)$$

where M is the mass of Mössbauer nucleus and E is a Mössbauer transition energy. In Eq. 1, k and c are Boltzmann constant and velocity of light, respectively. When a very thin sample is measured, $\mathrm{d}\ln f/\mathrm{d}T$ can be approximated by $\mathrm{d}\ln A/\mathrm{d}T$,[41-43] where A and f are absorption area and recoil-free fraction, respectively. Several Θ^2M values have already been obtained for K_2O-GeO_2-SnO_2,[41] BaF_2-ZrF_4-FeF_2,[42] and K_2SO_4-$ZnSO_4$-$Fe_2(SO_4)_3$[43] glasses by Nishida et al. As a result, Θ^2M proved to be in a range of 1.9—8.7×10^6 in these glasses, depending on the composition and structure of the glass matrix. In case of BaF_2-ZrF_4-FeF_2 glasses,[42] a phase transition was observed around 225 K, where isomer shift and absorption area showed a different composition dependency. It is expected that Θ^2M of ionic compound will be much larger than those obtained for the glasses.[41-43] A Θ^2M value obtained from the total absorption area (Fig. 8d) amounts to 15.5×10^6, which corresponds to a Debye temperature (Θ) of 521 K if we substitute 57 for M. A little lower Debye temperatures have been obtained in Mössbauer studies of superconducting $YBa_2Cu_3O_{7-\delta}$[27] (455 K) and $EuBa_2Cu_3O_{7-\delta}$[28] (468 K) ceramics. Zhou et al.[27] reported that these Θ values are not exceptionally large. If we introduce a concept of "partial Debye temperature," which depends on each Mössbauer site, we can get some information corresponding to the amplitude of atomic vibrations at the individual sites. In this way, a Debye temperature of 330 K (Θ^2M= 6.2×10^6) is obtained from a slope of Fig. 8b. The relatively small Θ value is consistent with one-dimensional chains composed of $Cu(1)O_4$ square planars. On the other hand, "partial Debye temperature" amounts to 740 K (Θ^2M=31×10^6) in case of two-dimensional layers composed of "dimpled" $Cu(2)O_4$ planes (Fig. 8a). This higher Debye temperature will suggest a superconduction in the two-dimensional layers. "Partial Debye temperature" obtained from Fig. 8c (FeO_4 tetrahedra present along the b-axis) amounts to 1010 K (Θ^2M=58×10^6), for most of the absorption areas are almost constant irrespective of the temperature. Figure 8 indicates that an absorption area of each doublet measured at 78 K has the same magnitude as that measured at 100 K. Similar and more detailed results have recently been reported in case of ^{119}Sn-Mössbauer studies of $EuBa_2Cu_3O_{7-\delta}$[44] and $YBa_2Cu_3O_{7-\delta}$[45] superconductors doped with ^{119}Sn. In these studies,[44,45] it was suggested that phonons play an important role in electron pairing process. Temperature dependency of absorption area (Fig. 8) is similar to that of isomer shift shown in Fig. 5. It is understood from Figs. 5 and 8 that isomer shift is more sensitive to the change of temperature, because it is correlated with a square velocity ($\langle v^2 \rangle$) of atomic vibrations, as described above. Anyhow, when a superconduction occurs in $YBa_2Cu_3O_{7-\delta}$ ceramics, amplitude of atomic vibrations concerned with "dimpled" $Cu(2)O_4$ planes (and also $Cu(1)O_4$ square planars) will be retained in spite of the decrease in temperature. This will cause a strong phonon-electron coupling in the superconducting state.

The authors are grateful to Dr. Saburo Nasu of Osaka University and Prof. Yasukuni Matsumoto of Kinki University (Iizuka, Fukuoka) for useful comments and discussion. One of the authors (TN) is grateful to Kazuchika Ohkura Memorial Foundation for a financial support.

References

1) J. G. Bednorz and K. A. Müller, *Z. Phys. B*, **64**, 189 (1986).
2) M. K. Wu, J. R. Ashburn, C. J. Torng, P. H. Hor, R. L. Meng, L. Gao, Z. J. Huang, Y. Q. Wang, and C. W. Chu, *Phys. Rev. Lett.*, **58**, 908 (1987).
3) S. Hikami, T. Hirai, and S. Kagoshima, *Jpn. J. Appl. Phys.*, **26**, L314 (1987).
4) S. Kagoshima, S. Hikami, Y. Nogami, T. Hirai, and K. Kubo, *Jpn. J. Appl. Phys.*, **26**, L318 (1987).
5) M. Kawasaki, M. Funabashi, S. Nagata, K. Fueki, and H. Koinuma, *Jpn. J. Appl. Phys.*, **26**, L388 (1987).
6) H. Koinuma, T. Hashimoto, M. Kawasaki, and K. Fueki, *Jpn. J. Appl. Phys.*, **26**, L399 (1987).
7) T. Kumagai, H. Yokota, K. Kawaguchi, W. Kondo, and S. Mizuta, *Chem. Lett.*, **1987**, 1645.
8) T. Kumagai, H. Yokota, Y. Shindo, W. Kondo, and S. Mizuta, *Denki Kogaku*, **55**, 269 (1987).
9) H. Nasu, S. Makida, T. Kato, Y. Ibara, T. Imura, and Y. Osaka, *Chem. Lett.*, **1987**, 2403.
10) T. Iwata, M. Hikita, K. Semba, and S. Tsurumi, *Jpn. J. Appl. Phys.*, **26**, L647 (1987).
11) R. M. Hazen, L. W. Finger, R. J. Angle, C. T. Prewitt, W. L. Ross, H. K. Mao, C, S, Hadidiacos, P. H. Hor, R. L. Meng, and C. W. Chu, *Phys. Rev. B*, **35**, 7238 (1987).
12) Y. LePage, W. R. McKinnon, J. M. Tarascon, L. H. Greene, G. W. Hull, and D. M. Hwang, *Phys. Rev. B*, **35**, 7245 (1987).
13) M. A. Beno, L. Soderholm, D. W. Capone, II, D. G. Hinks, J. D. Jorgensen, J. D. Grace, I. K. Schuller, C. U. Segre, and K. Zhang, *Appl. Phys. Lett.*, **51**, 57 (1987).
14) J. D. Jorgensen, M. A. Beno, D. J. Hinks, L. Soderholm, K. J. Volin, R. L. Hitterman, J. D. Grace, I. K. Schuller, C. U. Segre, K. Zhang, and M. S. Kleefisch, *Phys. Rev. B*, **36**, 3608 (1987).
15) J. J. Capponi, C. Chaillout, A. W. Hewat, P. Lejay, M. Marezio, N. Nguyen, B. Raveau, J. L. Soubeyroux, J. L. Tholence, and R. Tournier, *Europhys. Lett.*, **3**, 1301 (1987).

16) F. Izumi, H. Asano, T. Ishigaki, E. Takayama-Muromachi, Y. Uchida, and N. Watanabe, *Jpn. J. Appl. Phys.*, **26**, L1193 (1987).
17) F. Izumi, H. Asano, T. Ishigaki, E. Takayama-Muromachi, Y. Uchida, and N. Watanabe, *Jpn. J. Appl. Phys.*, **26**, L1214 (1987).
18) H. Tang, Z. Q. Qiu, Y. W. Du, Gang Xiao, C. L. Chien, and J. C. Walker, *Phys. Rev. B*, **36**, 4018 (1987).
19) H. Tang, Z. Q. Qiu, Y. W. Du, and J. C. Walker, *Hyperfine Interact.*, **42**, 1243 (1988).
20) Z. Q. Qiu, Y. W. Du, H. Tang, and J. C. Walker, *Hyperfine Interact.*, **42**, 1239 (1988).
21) S. Nasu, H. Kitagawa, Y. Oda, T. Kohara, T. Shinjo, K. Asayama, and F. E. Fujita, *Physica B*, **148**, 484 (1987).
22) M. Takano and Y. Takeda, *Jpn. J. Appl. Phys.*, **26**, L1862 (1987).
23) Z. Q. Qiu, Y. W. Du, H. Tang, J. C. Walker, W. A. Bryden, and K. Moorjani, *J. Magn. Magn. Mater.*, **69**, L221 (1987).
24) T. Tamaki, T. Komai, A. Ito, Y. Maeno, and T. Fujita, *Solid State Commun.*, **65**, 43 (1988).
25) Y. Oda, H. Fujita, H. Toyoda, T. Kaneko, T. Kohara, I. Nakada, and Asayama, *Jpn. J. Appl. Phys.*, **26**, L1660 (1987).
26) Y. Maeno, M. Kato, Y. Aoki, and T. Fujita, *Jpn. J. Appl. Phys.*, **26**, L1982 (1987).
27) X. Z. Zhou, M. Raudsepp, Q. A. Pankhurst, A. H. Morrish, Y. L. Luo, and I. Maartense, *Phys. Rev. B*, **36**, 7230 (1987).
28) J. M. D. Coey and K. Donnelly, *Z. Phys. B*, **67**, 513 (1987).
29) A. Vértes, E. Kuzmann, Z. Homonnay, M. Gál, and K. Torkos, *Hyperfine Interact.*, **42**, 1247 (1987).
30) T. Nishida and Y. Takashima, *J. Non-Cryst. Solids*, **37**, 37 (1980).
31) T. Nishida, T. Shiotsuki, and Y. Takashima, *J. Non-Cryst. Solids*, **41**, 161 (1980).
32) T. Nishida, T. Hirai, and Y. Takashima, *J. Non-Cryst. Solids*, **43**, 221 (1981).
33) T. Nishida, T. Hirai, and Y. Takashima, *Phys. Chem. Glasses*, **22**, 94 (1981).
34) T. Nishida, T. Hirai, and Y. Takashima, *Bull. Chem. Soc. Jpn.*, **54**, 3735 (1981).
35) T. Nishida and Y. Takashima, "Application of Mössbauer Effect on the Crystallization of Several Glasses," in "Industrial Applications of the Mössbauer Effect," ed by G. J. Long and J. G. Stevens, Plenum Press, New York and London (1986), pp. 409—422.
36) T. Nishida, M. Ogata, and Y. Takashima, *Bull. Chem. Soc. Jpn.*, **60**, 2381 (1987).
37) T. Nishida, M. Ogata, and Y. Takashima, Proc. VI Int. Conf. Phys. Non-Cryst. Solids (Kyoto, 1987); J. Non-Cryst. Solids, **95/96**, 241 (1987).
38) T. Nishida, S. Saruwatari, and Y. Takashima, *Bull. Chem. Soc. Jpn.*, **61**, 2347 (1988).
39) N. N. Greenwood and T. C. Gibb, "Mössbauer Spectroscopy," Chapman and Hall Ltd., London (1971), Chaps. 3 and 5.
40) R. Ingalls, F. Van der Would, and G. A. Sawatzky, "Iron and Nickel" in "Mössbauer Isomer Shifts," ed by G. K. Shenoy and F. E. Wagner, North Holland Pub. Co., Amsterdam (1978), Chap. 7.
41) T. Nishida, M. Katada, and Y. Takashima, *Bull. Chem. Soc. Jpn.*, **57**, 3566 (1984).
42) T. Nishida, T. Nonaka, and Y. Takashima, *Bull, Chem. Soc. Jpn.*, **58**, 2255 (1985).
43) T. Nishida and Y. Takashima, *Bull. Chem. Soc. Jpn.*, **59**, 2789 (1986).
44) P. Boolchand, R. N. Enzweiler, I. Zitkovsky, J. Wells, W. Bresser, D. MacDaniel, R. L. Meng, P. H. Hor, C. W. Chu, and C. Y. Huang, *Phys. Rev. B*, **37**, 3766 (1988).
45) T. Yuen, C. L. Lin, J. E. Crow, G. N. Myer, R. E. Salomon, P. Schlottmann, N. Bykovetz, and W. N. Herman, *Phys. Rev. B*, **37**, 3770 (1988).

Syntheses of Acetyl-1-bromopyrenes

Masahiro MINABE,* Hidehiro MOCHIZUKI, Masaaki YOSHIDA, and Takashi TODA
Department of Applied Chemistry, Faculty of Engineering, Utsunomiya University, Ishiicho, Utsunomiya 321
(Received April 15, 1988)

The reaction of 1-bromopyrene with acetic anhydride in the presence of aluminium chloride afforded an *ipso*-substituted compound, 1-acetylpyrene, in addition to the expected compounds, 6-acetyl- and 8-acetyl-1-bromopyrene. 7-Acetyl-1-bromopyrene was prepared via the acetylation of 2-acetylamino-1-bromo-4,5,9,10-tetrahydropyrene. The structures of the acetylbromopyrenes were assigned according to the two-dimensional NMR spectra.

The chemistry of pyrene (**1**) is comparatively well-known in polycyclic aromatic hydrocarbons (PAHs).[1] An electrophilic substitution of **1** is known to take place preferentially at the 1-position,[2] and a second attack occurs at the 6- and 8-positions on bromination,[3] and at the 3-, 6-, and 8-positions on acetylation.[4] The isomeric 4- and 2-derivatives are easily obtained through the electrophilic substitutions of 1,2,3,6,7,8-hexahydropyrene[2,5,6] and of 4,5,9,10-tetrahydropyrene (**2**),[6-9] respectively. The reaction of 1-acetylpyrene (**3**)[2] with bromine afforded 1-bromoacetylpyrene as the main product.[10]

Recent development on synthetic programs of **1** has been classified into three categories: the first is the syntheses of derivatives of **1** as active metabolites.[11] Secondly, **1** is one of the useful starting materials to prepare PAHs for a carcinogenesis investigation and other purposes.[12,13] The third concerns the hydrogenated compounds of **1** as hydrogen donor solvents in the coal liquefaction process.[14]

During the course of the syntheses of indeno[1,2,3-*cd*]pyrenes, we have required some acetylbromopyrenes as precursors and for a consideration of the spectral characterization of indenopyrenes. The present paper deals with the Friedel–Crafts acetylation of 1-bromopyrene (**4**)[5] giving 6-acetyl- (**5**) and 8-acetyl-1-bromopyrene (**6**). The isomeric 7-acetyl-1-bromopyrene (**7**) was obtained from **2** through several steps. The structures of these isomers were assigned according to the NMR spectra.

Results and Discussion

The reaction of **4** with acetic anhydride in the presence of aluminium chloride yielded **3** (8%), **5** (23%), and **6** (34%), respectively, with the recovery of **4** (12%). The ratio of isomeric **5** and **6** was in fair agreement with the ratio on the diacetylation[4] of **1**. No detection of 1-acetyl-3-bromo isomer is similar to no isolation of 1,3-dibromopyrene in the bromination[3] of **4**, though different from the formation of 1,3-diacetylpyrene.[4] The formation of **3** is not due to the contaminating **1** in **4** because purity of **4** being over 98%: **3** was produced by the *ipso*-substitution of **4**.[15]

The first unknown compound in the sequence of the synthesis of **7** is 2-acetylamino-4,5,9,10-tetrahydropyrene (**8**): nitration of **2** with acetyl nitrate in acetic anhydride afforded 2-nitro derivative (**9**)[8] as the main product (74%), accompanied by 1-nitro isomer (**10**)[7] (8%). The resulting **9** was reduced to amine **11** by a procedure described elsewhere,[8] and the amino group was protected by the acetyl group to give **8**.

The synthesis of **7** from **8** is illustrated in Scheme 2. Bromination of **8** yielded, exclusively, 1-bromo derivative **12**. The Friedel–Crafts acetylation of **12** gave predominantly 7-acetyl derivative **13**: a steric repulsion

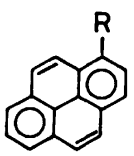

1 (R=H)
3 (R=Ac)
4 (R=Br)

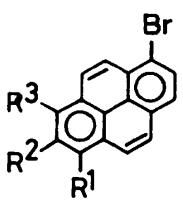

5 (R^1=Ac, R^2=R^3=H)
6 (R^3=Ac, R^1=R^2=H)
7 (R^2=Ac, R^1=R^3=H)

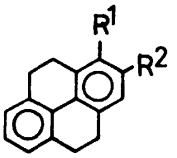

2 (R^1=R^2=H)
9 (R^1=H, R^2=NO_2)
10 (R^1=NO_2, R^2=H)
11 (R^1=H, R^2=NH_2)

Scheme 1.

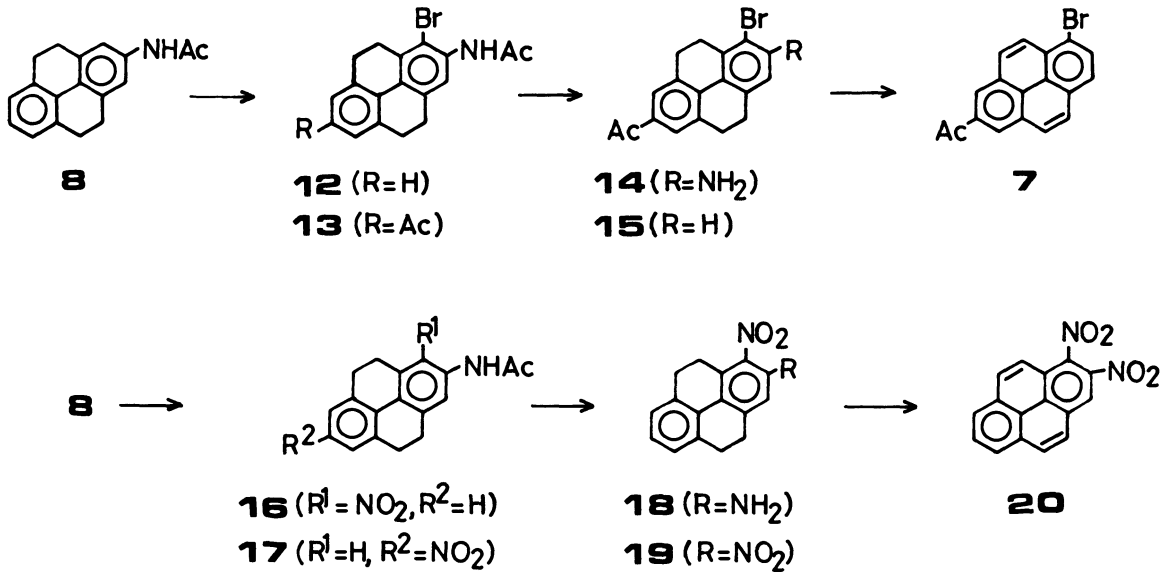

Scheme 2.

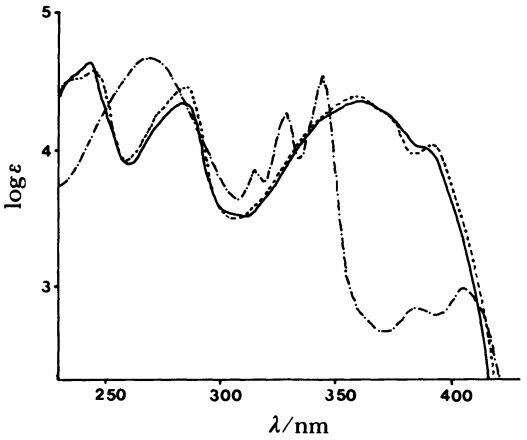

Fig. 1. Electronic absorption spectra of **5** (——), **6** (·····), and **7** (–·–·–·).

governs the regioselectivity of the acetylation giving no 3-acetyl isomer. Amine **14** was obtained by the hydrolysis of **13**, and a deamination of **14** gave 7-acetyl-1-bromo-4,5,9,10-tetrahydropyrene (**15**), followed by dehydrogenation to form **7**.

The IR and electronic spectra of **5** are very similar to those of **6**: carbonyl signals appear at 1668 cm^{-1} for **5** and 1664 cm^{-1} for **6**, and the absorption maxima were observed at 362 nm for **5** and 360 nm for **6**, respectively, having resemblance to those of **3** (389, 357, 285, 243, and 235 nm) (Fig. 1). On the contrary, those of **7** (1678 cm^{-1} and 345 nm) are significantly different from those of **5** and **6**. The absorptions at 345, 329, and 315 nm of **7** are very similar to those of **4** (347, 330, and 316 nm), showing a red shift from the parent **1** (337, 321, and 307 nm). This suggests that the 7-acetyl group of **7** can not conjugate effectively with an aromatic system, in comparison with those of **5** and **6**. This phenomenon should be similar to the "weak interaction" between the nitro group and the pyrenyl moiety of 2-nitropyrene.[6,11] These are ascribed to the different electron densities at the 1- and 2-position of parent **1**.[16]

The NMR signals of isomeric **5**, **6**, and **7** were assigned according to a 2D-NMR technique:[12,17] the chemical shifts and the ^3J coupling constants of ^1H NMR are summarized in Table 1. The characteristic peaks of **6**, compared with those of **5**, are a set of AB doublets at δ=8.09 and 8.10, corresponding to H_4 and H_5, respectively. The absorptions of peri and ortho protons to the acetyl group appear at 8.99 and 8.37 for **5** and 9.13 and 8.42 for **6**; these are in accord with those (ca. 9.0—9.1 and 8.4 ppm, respectively) for the diacetylpyrenes.[4] The signals of peri and ortho protons to the bromine absorb at 8.47 and 8.24 for **5**, at 8.57 and 8.29 for **6**, and at 8.48 and 8.29 ppm for **7**, respectively. The ^3J coupling constants of H_4/H_5 and H_9/H_{10} show large values upon substitutions of bromine and/or acetyl groups at the peri positions. It may demonstrate that the fairly good additivity by peri substituents is held on the coupling constants.

During a sequence of experiments, the nitration of **8** was examined in order to clarify the reactivity of **8**: the nitration of **8** gave two isomers, 2-acetylamino-1-nitro- (**16**) and 2-acetylamino-7-nitro-4,5,9,10-tetrahydropyrene (**17**), in a ratio of 60:40 (by HPLC). This finding is significantly different from the bromination of **8**: this is because of a higher regioselectivity of bromination than that of nitration.

Compound **16** was hydrolyzed to give free amine **18** followed by oxidation to yield 1,2-dinitro-4,5,9,10-tetrahydropyrene (**19**). The dehydrogenation of **19** afforded 1,2-dinitropyrene (**20**) (mp 246—248 °C, decomp). The NMR spectrum of **20** is the same as the reported values of the compound,[11,18] which was

Table 1. ^{1}H NMR of Acetyl-1-bromopyrenes, **5**, **6**, and **7**

Position in pyrene	Chemical shift δ/ppm (coupling const.[a]/Hz)		
	5	**6**	**7**
2	8.24(8.2)	8.29(8.2)	8.29(8.2)
3	8.02(8.2)	8.07(8.2)	8.05(8.2)
4	8.10(9.4)	8.09(8.7)	8.07(8.9)
5	8.99(9.4)	8.10(8.7)	8.16(8.9)
6	2.90[b]	8.21(8.1)	8.77(bs)[c]
7	8.37(8.1)	8.42(8.1)	2.88[b]
8	8.16(8.1)	2.92[b]	8.77(bs)[c]
9	8.09(9.3)	9.13(9.7)	8.26(9.3)
10	8.47(9.3)	8.57(9.7)	8.48(9.3)

a) Only ^3J are shown. b) Chemical shift of methyl protons. c) Broad singlet.

obtained by the nitration of 2-nitropyrene with nitric acid.

Experimental

All melting points are uncorrected. The NMR, IR, and electronic absorption spectra were recorded on a Varian VXR-300, a Jasco IR-G (KBr pellets), and a Hitachi U-3400 apparatus (EtOH). ^{1}H NMR were generally obtained using 3 mg of a sample dissolved in 0.62 ml of $CDCl_3$ in a 5 mm tube; ^{13}C NMR and 2D-NMR were measured using 11—14 mg of the specimen. Gas chromatograms were obtained by a Shimadzu GC-8AMP attached column (3 mm ID, 1 m) containing Dexsil 300 GC (5%) on Chromosorb WAW.

Materials. 1-Acetylpyrene (**3**) was obtained by the method described in the literature:[2] mp 87—90 °C (lit,[2] mp 88—90 °C); IR (C=O), 1660 cm^{-1}; ^{1}H NMR, δ=2.90 (3H, s), 8.04 (1H, t, J=7.7 Hz, H_7), 8.04 (1H, d, J=8.9 Hz, H_5), 8.14 (1H, d, J=8.1 Hz, H_3), 8.14 (1H, d, J=8.9 Hz, H_4), 8.21 (1H, d, J=9.5 Hz, H_9), 8.23 (1H, d, J=7.7 Hz, H_6), 8.24 (1H, d, J=7.7 Hz, H_8), 8.36 (1H, d, J=8.1 Hz, H_2), and 9.05 (1H, d, J=9.5 Hz, H_{10}); ^{13}C NMR, δ=30.5 (Me), 123.9 (C_3), 124.2 (C_{10c}), 124.9 (C_{10}), 125.0 (C_{10b}), 126.1 (C_5 or C_7), 126.3, 126.4, 127.0 (C_7 or C_5), 127.1 (C_2), 129.4 (C_{10a}), 129.6, 129.7, 130.4, 131.0, 131.8, 134.0 (C_1), and 202.1 (C=O).

1-Bromopyrene (**4**) was obtained by a method described in the literature:[5] mp 98.5—100.0 °C (lit,[5] mp 95—96.5 °C). Purity of **4** was determined to be over 98.0% (by GLPC, 245 °C) with contaminations of **1** (<0.2%) and dibromopyrenes (<1.8%). ^{1}H NMR of **4**, δ=7.99 (1H, d, J=8.1 Hz, H_3), 8.00 (1H, d, J=9.1 Hz, H_5), 8.02 (1H, t, J=7.5 Hz, H_7), 8.07 (1H, d, J=9.1 Hz, H_4), 8.15 (1H, d, J=9.3 Hz, H_9), 8.20 (1H, d, J=7.5 Hz, H_6 or H_8), 8.21 (1H, d, J=7.5 Hz, H_8 or H_6), 8.21 (1H, d, J=8.1 Hz, H_2), and 8.42 (1H, d, J=9.3 Hz, H_{10}); ^{13}C NMR, δ=119.9 (C_1), 124.0 (C_{10b}), 125.4 (C_5), 125.5 (C_8), 125.7 (C_6), 125.8 (C_{10c}), 125.9 (C_{10}), 126.5 (C_7), 127.1 (C_3), 127.7 (C_4), 128.9 (C_9), 129.6 (C_{10a}), 130.0 (C_2), 130.5 (C_{8a}), 130.9 (C_{5a}), and 131.1 (C_{3a}).

2-Nitro-4,5,9,10-tetrahydropyrene (**9**) was obtained by a method described elsewhere:[8] mp 108.5—110.5 °C (lit,[8] mp 110.8—111.6 °C); IR, 1528 and 1334 cm^{-1}; ^{1}H NMR, δ=2.9—3.0 (8H, m), 7.12 (2H, d, J=7.2 Hz, $H_{6,8}$), 7.22 (1H, t, J=7.2 Hz, H_7), and 7.95 (2H, s, $H_{1,3}$).

Isomeric **10** was isolated from the mother liquor of **9**: mp 142—144.5 °C; IR, 1518 and 1350 cm^{-1}; UV (CH_2Cl_2), λ_{max} 336, 279, and 271 nm; ^{1}H NMR, δ=2.8—3.0 (6H, m, $H_{4,5,9}$), 3.15 (2H, t, J=7.5 Hz, H_{10}), 7.13 (2H, d, J=7.5 Hz, $H_{6,8}$), 7.20 (1H, d, J=8.4 Hz, H_3), 7.22 (1H, t, J=7.5 Hz, H_7), and 7.73 (1H, d, J=8.4 Hz, H_2).

2-Amino-4,5,9,10-tetrahydropyrene (**11**) was obtained by a method described elsewhere:[8] mp 165.5—168 °C (decomp) (lit,[8] mp 168.8—169.6 °C); IR, 3390 and 3310 cm^{-1}; UV (CH_2Cl_2), λ_{max} 301 nm; ^{1}H NMR, δ=2.75—2.88 (8H, m, $H_{4,5,9,10}$), 3.65 (2H, bs, NH_2), 6.42 (2H, s, $H_{1,3}$), and 7.03 (3H, s, $H_{6,7,8}$).

Acetylation of 4. To a solution of **4** (323 mg, 1.2 mmol) in CH_2Cl_2 (5 ml) was added $AlCl_3$ (0.64 g, 4.8 mmol), and successively dropwise Ac_2O (0.49 ml, 5.2 mmol) over 3.5 h under ice-cooling. Upon stirring for an additional 0.5 h, the reaction mixture was quenched by an addition of ice. A small portion of the reaction mixture was analyzed by GLPC (at 245 °C with octacosane as an internal reference): **4** (retention time 5.6 min, 12.0%), **3** (7.9 min, 7.6%), **5** (19.7 min, 23.0%), and **6** (21.3 min, 34.0%) were confirmed to be contained.

The remaining part was percolated on silica gel (55 g) with PhH and separated into two fractions. The first eluate afforded a mixture (79 mg, mp 101—114 °C) of **1**, **4**, and dibromopyrenes. The second eluate gave a mixture (278 mg, mp 76—88 °C) of **3**, **5**, and **6**. The mixture was treated with LiChroprep Si-60 (E. Merck, 40—60 μm) using hexane-THF (95/5). The fraction between 1900—2200 ml gave 16 mg of **5**: mp 156.5—158.5 °C (from hexane); IR, 1668 cm^{-1}; UV, λ_{max} 390 (s, log ε 3.97), 362 (4.31), 285 (4.60), 244 (4.60), and 237 nm (s, 4.52); ^{13}C NMR, δ=30.5 (Me), 121.3 (C_1), 124.3 (C_{10c}), 124.5 (C_8), 125.2 (C_5), 125.4 (C_{10b}), 126.5 (C_3), 127.5 (C_7), 128.0 (C_{10}), 128.5 (C_9), 129.3 (C_4), 129.4 (C_{10a}), 129.5 (C_{5a}), 129.9 (C_{3a}), 130.6 (C_2), 132.6 (C_6), 133.6 (C_{8a}), and 202.1 (C=O); MS (70 eV), m/z 324, 322, 309, 307, 281, 279, and 200. Found: C, 66.76; H, 3.38%. Calcd for $C_{18}H_{11}OBr$: C, 66.89; H, 3.43%.

The fraction between 2400—2800 ml afforded 18 mg of **6**: mp 144—146 °C (hexane); IR, 1664 cm^{-1}; UV, λ_{max} 392 (log ε 4.01), 360 (4.39), 286 (4.47), 246 (4.60), and 238 nm (s, 4.53); ^{13}C NMR, δ=30.5 (Me), 121.2 (C_1), 124.3 (C_{10c}), 124.7 (C_6), 125.4 (C_{10b}), 126.5 (C_9), 126.7 (C_3), 127.3 (C_5), 127.5 (C_7), 128.1 (C_{10}), 129.0 (C_{10a}), 129.2 (C_4), 130.4 (C_{3a}), 130.5 (C_2), 130.6 (C_{8a}), 132.3 (C_8), 133.9 (C_{5a}), and 201.9 (C=O); MS (70 eV), m/z 324, 322, 309, 307, 281, 279, and 200. Found: C, 66.83; H, 3.40%. Calcd for $C_{18}H_{11}OBr$: C, 66.89; H, 3.43%.

2-Acetylamino-4,5,9,10-tetrahydropyrene (8). A mixture of **11** (4.972 g, 22 mmol) and Ac_2O (4.2 ml, 44 mmol) in PhH (100 ml) was refluxed for 1 h to give 5.797 g (99%) of **8**: mp 200.5—203.0 °C (decomp); IR, 3250, 1676, and 1648 cm^{-1}; UV, λ_{max} 314 (log ε 4.25), 300 (4.38), 290 (s, 4.28), and 237 nm

(3.70); ^{1}H NMR, δ=2.19 (3H, s, Me), 2.86 (8H, s, $H_{4,5,9,10}$), 7.04—7.14 (3H, m, $H_{6,7,8}$), 7.16 (1H, bs, NH), and 7.23 (2H, s, $H_{1,3}$); MS (20 eV), *m/z* 263, 221, and 200. Found: C, 81.84; H, 6.51; N, 5.22%. Calcd for $C_{18}H_{17}NO$: C, 82.10; H, 6.51; N, 5.32%.

Bromination of 2-Acetylamino-4,5,9,10-tetrahydropyrene (8). To a solution of **8** (1.315 g, 5 mmol) in $CHCl_3$ (180 ml) was added dropwise a solution of bromine (1.4 g, 7.8 mmol) in $CHCl_3$ (100 ml) under ice-cooling during a period of 2.5 h. Upon treatment with aq. $Na_2S_2O_3$ (3%), the organic layer afforded 1.55 g (91%) of **12**: mp 200.5—202.0 °C (decomp); IR, 3250 and 1660 cm^{-1}; UV, λ_{max} 296 (log ε 4.18) and 287 nm (4.19); ^{1}H NMR, δ=2.26 (3H, s, Me), 2.85—2.93 (6H, m, $H_{4,5,9}$), 2.98—3.06 (2H, m, H_{10}), 7.08 (1H, d, *J*=8.9 Hz, H_6 or H_8), 7.08 (1H, d, *J*=5.5 Hz, H_8 or H_6), 7.14 (1H, dd, *J*=5.5, 8.9 Hz, H_7), 7.73 (1H, s, NH), and 8.11 (1H, s, H_3); MS (20 eV), *m/z* 343, 341, 301, 299, and 262. Found: C, 62.98; H, 4.66; N, 4.08%. Calcd for $C_{18}H_{16}NOBr$: C, 63.17; H, 4.17; N, 4.09%.

Synthesis and Hydrolysis of 7-Acetyl-2-acetylamino-1-bromo-4,5,9,10-tetrahydropyrene (13). Aluminium chloride (7.04 g, 53 mmol) was added to a solution of **12** (3.762 g, 11 mmol) in CH_2Cl_2 (80 ml), and Ac_2O (1.7 ml, 18 mmol) was added dropwise at room temperature to the resulting mixture over 1 h. After the usual work-up, the crude materials were chromatographed on SiO_2 with CH_2Cl_2–AcOEt (8/2) to give 3.078 g (73%) of **13**: mp 248—250 °C (decomp); IR, 3260 and 1662 cm^{-1}; UV, λ_{max} 325 nm (log ε 4.37); ^{1}H NMR, δ=2.27 (3H, s, Me), 2.61 (3H, s, Me), 2.86—3.06 (8H, m, $H_{4,5,9,10}$), 7.68 (2H, s, $H_{6,8}$), 7.78 (1H, s, NH), and 8.18 (1H, s, H_3); MS (20 eV), *m/z* 385, 383, 343, 341, and 304. Found: C, 62.28; H, 4.55; N, 3.53%. Calcd for $C_{20}H_{18}NO_2Br$: C, 62.51; H, 4.72; N, 3.65%.

A mixture of **13** (1.215 g, 3.2 mmol), aq. HCl (20%, 25 ml), and EtOH (15 ml) was refluxed for 4.5 h to yield 825 mg (77%) of **14**: mp 176—177 °C (decomp); IR, 3460, 3340, and 1664 cm^{-1}; UV, λ_{max} 360 (log ε 4.35) and 246 nm (4.10); ^{1}H NMR, δ=2.60 (3H, s, Me), 2.75—3.05 (8H, m, $H_{4,5,9,10}$), 4.29 (2H, bs, NH_2), 6.57 (1H, s, H_3), and 7.66 (2H, d, *J*=1.8 Hz, $H_{6,8}$); MS (20 eV), *m/z* 343, 341, 328, and 326. Found: C, 62.80; H, 4.70; N, 3.91%. Calcd for $C_{18}H_{16}NOBr$: C, 63.17; H, 4.71; N, 4.09%.

7-Acetyl-1-bromopyrene (7). Amine **14** (724 mg, 2.1 mmol) was dissolved into a mixture of aq. HCl (18%, 20 ml) and THF (10 ml). The resulting mixture was diazotized with aq. $NaNO_2$ under ice-cooling, followed by stirring overnight with EtOH (16 ml) at room temperature. Upon a work-up by silica-gel column chromatography with CH_2Cl_2, **15** (448 mg, 65%) was obtained: mp 68—70 °C; IR, 1676 cm^{-1}; UV, λ_{max} 321 (s, log ε 4.35), 309 (4.39), 251 (s, 3.70), and 242 nm (3.89); ^{1}H NMR, δ=2.62 (3H, s, Me), 2.83—2.97 (6H, m, $H_{4,5,9}$), 3.02—3.07 (2H, m, H_{10}), 6.99 (1H, d, *J*=8.1 Hz, H_3), 7.43 (1H, d, *J*=8.1 Hz, H_2), and 7.69 (2H, s, $H_{6,8}$); MS (20 eV), *m/z* 328, 326, 313, 311, 203, and 202. Found: C, 65.97; H, 4.59%. Calcd for $C_{18}H_{15}OBr$: C, 66.07; H, 4.62%.

A mixture of **15** (115 mg, 0.35 mmol) and DDQ (397 mg, 1.75 mmol) in PhH (5 ml) was refluxed overnight, followed by column chromatography using alumina and PhH to give 62 mg (55%) of **7**: mp 157—159 °C; IR, 1678 cm^{-1}; UV, λ_{max} 406 (log ε 3.04), 385 (2.90), 345 (4.54), 329 (4.30), 315 (3.90), and 270 nm (4.71); ^{13}C NMR, δ=27.1 (Me), 120.4 (C_1), 124.8 (C_6), 124.9 (C_8), 125.2 (C_{10b}), 125.9 (C_3), 126.0 (C_{10c}), 126.6 (C_{10}), 127.8 (C_4), 128.0 (C_5), 129.2 (C_9), 130.1 (C_{10a}), 130.6 (C_{8a}), 130.9 (C_{5a}), 131.0 (C_{3a}), 131.1 (C_2), 134.4 (C_7), and 198.3 (C=O); MS (20 eV), *m/z* 324, 322, 309, 307, 281, 279, and 200. (Found: C, 66.28; H, 3.41%. Calcd for $C_{18}H_{11}OBr$: C, 66.90; H, 3.43%.)

Nitration of 8. A mixture of acetyl nitrate (4 mmol) in Ac_2O was added dropwise into a cold solution of **8** (526 mg, 2 mmol) in Ac_2O (50 ml); the reaction mixture was stirred for 40 min under ice-cooling. The resulting mixture was confirmed to contain **16** (48%), **17** (33%), and **8** (20%) by means of HPLC (LiChrosorb RP-18, CH_3CN). Upon work-up of the mixture with ice-water, the precipitate was chromatographed on SiO_2 with hexane–AcOEt (1/1) to give **16** (228 mg, 37%) and **17** (166 mg, 23%). **16**: mp 192—194 °C (decomp); IR, 3250, 1664, 1528, and 1368 cm^{-1}; UV, λ_{max} 288 (log ε 4.27) and 276 nm (s, 4.23); ^{1}H NMR, δ=2.22 (3H, s, Me), 2.8—3.0 (8H, m, $H_{4,5,9,10}$), 7.11 (2H, d, *J*=7.7 Hz, $H_{6,8}$), 7.19 (1H, d, *J*=7.7 Hz, H_7), 8.04 (1H, s, H_3), and 8.49 (1H, s, NH); MS (70 eV), *m/z* 308, 266, 250, and 249. Found: C, 70.19; H, 5.16; N, 9.07%. Calcd for $C_{18}H_{16}N_2O_3$: C, 70.11; H, 5.23; N, 9.09%.

17: mp 275—276 °C (decomp); IR, 3320, 1666, 1546, and 1334 cm^{-1}; UV, λ_{max} 370 (log ε 4.31), 261 (3.96), and 248 nm (3.96); ^{1}H NMR, δ=2.05 (3H, s, Me), 2.8—3.0 (8H, m, $H_{4,5,9,10}$), 7.40 (2H, s, $H_{1,3}$), 7.99 (2H, s, $H_{6,8}$), and 10.05 (1H, s, NH); MS (70 eV), *m/z* 308 and 266. Found: C, 70.26; H, 5.22; N, 9.04%. Calcd for $C_{18}H_{16}N_2O_3$: C, 70.11; H, 5.23; N, 9.09%.

In another experiment, **10** (263 mg, 1 mmol) was nitrated at a room temperature; in addition to 124 mg (40%) of **16**, 13 mg (4%) of 2-acetylamino-1,7-dinitro-4,5,9,10-tetrahydropyrene was isolated: mp 277 °C (decomp); IR, 3310, 1680, 1524, 1506, and 1348 cm^{-1}; ^{1}H NMR, δ=2.25 (3H, s, Me), 2.97—3.00 (8H, m, $H_{4,5,9,10}$), 7.99 (2H, s, $H_{6,8}$), 8.19 (1H, s, H_3), and 8.58 (1H, s, NH); MS (20 eV), *m/z* 353, 308, 294, and 249.

Synthesis of 1,2-Dinitro-4,5,9,10-tetrahydropyrene (19) and Dehydrogenation to 20. A mixture of **16** (681 mg, 2.2 mmol), aq. HCl (10%, 20 ml), and EtOH (35 ml) was refluxed for 2 h to give 515 mg (88%) of red needles of **18**: mp 159—161 °C; IR, 3470, 3370, 1514, and 1348 cm^{-1}; UV, λ_{max} 438 (log ε 3.04), 307 (s, 4.28), 296 (4.39), and 285 nm (4.37); ^{1}H NMR, δ=2.78—2.85 (6H, m, $H_{4,5,9}$), 3.00 (2H, t, *J*=6.6 Hz, H_{10}), 4.88 (2H, bs, NH_2), 6.62 (1H, s, H_3), and 7.04—7.15 (3H, m, $H_{6,7,8}$); MS (20 eV), *m/z* 266 and 249. Found: C, 72.06; H, 5.21; N, 10.48%. Calcd for $C_{16}H_{14}N_2O_2$: C, 72.16; H, 5.30; N, 10.52%.

To a solution of **18** (300 mg, 1.1 mmol) in $CHCl_3$ (10 ml) was added dropwise a solution of *m*-chloroperbenzoic acid (876 mg, 5.6 mmol) in $CHCl_3$ (15 ml) under ice-cooling; the resulting mixture was stirred at a room temperature for 2 h to give 242 mg (72%) of **19**: mp 192—194 °C (decomp); IR 1544, 1528, and 1330 cm^{-1}; UV, λ_{max} 351 nm (log ε 4.07); ^{1}H NMR, δ=2.84—3.07 (8H, m, $H_{4,5,9,10}$), 7.18 (2H, d, *J*=7.5 Hz, $H_{6,8}$), 7.32 (1H, t, *J*=7.5 Hz, H_7), and 7.96 (1H, s, H_3); MS (20 eV), *m/z* 296, 204, 203, and 202. Found: C, 64.94; H, 3.97; N, 9.37%. Calcd for $C_{16}H_{12}N_2O_4$: C, 64.86; H, 4.08; N, 9.46%.

A solution of **19** (141 mg, 0.48 mmol) in PhH (6 ml) was refluxed overnight with DDQ (1.081 g, 4.8 mmol). After filtration, the filtrate was chromatographed on alumina with PhH to give 122 mg (87%) of **20**: mp 246—248 °C (decomp); IR, 1557, 1536, and 1344 cm^{-1}; UV, λ_{max} 418 (log ε

3.10), 369 (3.15), 343 (3.64), 292 (4.02), and 249 nm (3.78); ^{1}H NMR,[11] δ=8.06 (1H, d, J=9.5 Hz), 8.22 (1H, d, J=9.2 Hz), 8.26 (1H, t, J=7.8 Hz), 8.38 (1H, d, J=9.2 Hz), 8.39 (1H, d, J=9.5 Hz), 8.41 (1H, d, J=7.8 Hz), 8.44 (1H, d, J=7.8 Hz), and 8.87 (1H, s, H_3); ^{13}C NMR (only tertiary carbons), δ=119.7, 120.5, 126.9, 128.0, 128.4, 129.0, 131.7, and 132.8; MS (20 eV), m/z 292, 262, 216, and 200.

Present work was partially supported by a Grant-in-Aid for Scientific Research (No. 61470022) from the Ministry of Education, Science and Culture. One of us (M. M.) is particularly indebted to Professor Ronald G. Harvey, the University of Chicago, for useful suggestions concerning the chemistry of pyrene.

References

1) E. Clar, "Polycyclic Hydrocarbons," Vol. 2, pp. 110—126, Academic Press, London (1964).

2) H. Vollmann, H. Becker, M. Corell, H. Streeck, and G. Langbein, *Justus Liebigs Ann. Chem.*, **531**, 1 (1937); *Chem. Abstr.*, **32**, 145 (1938).

3) J. Grimshaw and J. Trocha-Grimshaw, *J. Chem. Soc., Perkin Trans. 1*, **1972**, 1622.

4) R. G. Harvey, J. Pataki, and H. Lee, *Org. Prep. Proc. Internal.*, **6**, 144 (1984).

5) A. Streitwieser, Jr., R. G. Lawler, and D. Schwaab, *J. Org. Chem.*, **30**, 1470 (1965).

6) A. M. van den Braken-van Leersum, C. Tintel, M. van't Zelfde, J. Cornelisse, and J. Lugtenburg, *Recl. Trav. Chim. Pays-Bas*, **106**, 120 (1987).

7) Li Jang Ho and S. Hayano, The 52nd Spring Meeting of Chemical Society of Japan, Kyoto, Preprint, p. 895 (1986).

8) R. Bolton, *J. Chem. Soc.*, **1964**, 4637.

9) H. Lee and R. G. Harvey, *J. Org. Chem.*, **51**, 2847 (1986).

10) Sankyo Co., Ltd., Jpn. Kokai Tokkyo Koho, JP 81113728 (1981); *Chem. Abstr.*, **96**, 52044u (1982).

11) A. M. van den Braken-van Leersum, J. Cornelisse, and J. Lugtenburg, *J. Chem. Soc., Chem. Commun.*, **1987**, 1156.

12) B. P. Cho and R. G. Harvey, *Tetrahedron Lett.*, **28**, 861 (1987); *J. Org. Chem.*, **52**, 5668, 5679 (1987).

13) J. E. Rice, E. J. LaVoie, D. J. McCaustland, D. L. Fischer, and J. C. Wiley, Jr., *J. Org. Chem.*, **51**, 2428 (1986).

14) M. Minabe and K. Nakada, *Bull. Chem. Soc. Jpn.*, **58**, 1962 (1985).

15) H. Suzuki, *Yuki Gosei Kagaku Kyokai Shi*, **37**, 290 (1979), and references cited therein.

16) R. A. Hites and W. J. Simonsick, Jr., "Calculated molecular properties of polycyclic aromatic hydrocarbons," Elsevier, Amsterdam (1987), p. 45.

17) P. E. Hansen, *Org. Magn. Reson.*, **12**, 109 (1979); P. E. Hansen and A. Berg, *Acta Chem. Scand.*, **25**, 3377 (1971).

18) The melting point of **20** was not described in Ref. 11. In our experiment, the detailed assignment of NMR signals was failed because of low solubility of the specimen.

 © 1989 The Chemical Society of Japan Bull. Chem. Soc. Jpn., 62, 73—78 (1989)

Methylviologen-Accelerated Photoreduction of Tris(acetylacetonato)cobalt(III) with 1-Benzyl-1,4-dihydronicotinamide

Kohichi YAMASHITA, Shûta KAJIWARA, and Katsutoshi OHKUBO*
Department of Applied Chemistry, Faculty of Engineering, Kumamoto University, Kurokami, Kumamoto 860
(Received May 13, 1988)

The photoreduction of tris(acetylacetonato)cobalt(III) ($Co(acac)_3$) by 1-benzyl-1,4-dihydronicotinamide (BNAH) was examined with or without methylviologen in the wavelength range of 340—410 nm. The reaction rate of electron transfer from BNAH to $Co(acac)_3$ was considerably enhanced by methylviologen, especially, in lower polar environments; The weaker the hydrophobic interaction between BNAH and the substrate become, the more effectively methylviologen acts as an electron mediator for the above photoreaction. The reaction mechanism is also discussed with particular reference to the participation of the electron mediator in the elementary steps of the present photoinduced reaction.

The photochemistry of organic or inorganic compounds including biological ones is of general interest because of their importance in relation to solar energy conversion, new methods of organic synthesis, biomimetic photoinduced reactions, etc.[1] Recently, one of the biologically interesting compounds related to coenzyme NAD(P)H, 1,4-dihydropyridines (absorption maxima at 300—400 nm) have received considerable attention, since their reactivities as a reductant are enhanced remarkably by photoirradiation.[2–6]

In our previous work,[3] the photoactivated 1-benzyl-1,4-dihydronicotinamide (BNAH) was found to be very reactive for the reduction of cobalt(III) complexes such as tris(acetylacetonato)cobalt(III) ($Co(acac)_3$), especially in the presence of surfactant micelles which accelerate the reaction through the lengthening of the lifetime of the photoexcited BNAH and through the concentrating of BNAH and the substrates on the micellar surface.

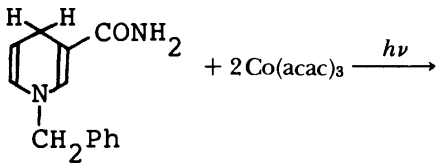

(BNAH)

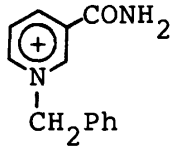

$$+ 2Co(acac)_3 + 2acac^- + H^+ \quad (1)$$

BNAH has an absorption maxima of $\pi \rightarrow \pi^*$ excitation on the dihydropyridine ring at 360 nm and an oxidation potential of about −2 V (vs. SCE)[4,7] in its photoexcitation state.

The electron transfer from photoactivated BNAH (BNAH*) to the substrate in the reaction expressed by Eq. 1 might be accelerated by using a good electron mediator such as methylviologen (MV^{2+}) (reduction potential of −0.69 V vs. SCE[6]). This can effectively trap the activated electron from the short-living BNAH* (0.93 ns in methanol).[5,6] The cationic radical of the methylviologen (MV^{+}) formed by the reaction of MV^{2+} and BNAH* might donate the electron to the substrate directly or indirectly.[8]

This report describes how methylviologen behaves as an electron mediator in the photoinduced reduction of $Co(acac)_3$ by BNAH, based on a kinetic analysis of the reaction.

Experimental

Materials. 1-Benzyl-1,4-dihydronicotinamide (BNAH) was prepared according to the previous method.[9] The commercially available $Co(acac)_3$ was purified by recrystallization from petroleum ether–benzene. Satisfactory elemental analyses were obtained for both BNAH and $Co(acac)_3$. Methylviologen (MV^{2+}) was also commercially available as its chloride and was used without further purification. The solvents methanol and water were distilled and deoxygenated before use by purging with gaseous nitrogen.

Reaction Procedure. The homogeneous 20—90% (v/v) methanol–0.02 mol dm^{-3} borate buffer (pH 9.0) solution, containing BNAH (1.25×10^{-3} mol dm^{-3}), $Co(acac)_3$ (1.25×10^{-3} mol dm^{-3}), and MV^{2+} (0—3.13×10^{-2} mol dm^{-3}), was irradiated in a Pyrex cell using a 400 W mercury lamp in the wavelength range $410>\lambda>340$ nm with Toshiba glass filter UV-35 and UV-D35. The reaction temperature was kept at 30±0.5 °C by stirring with a thermostated cell holder. The reaction rates of the photoreduction of $Co(acac)_3$ with BNAH were followed by the spectrophotometric determination of the decreased amount of $Co(acac)_3$ at λ_{max}=595 nm and that of BNAH at λ_{max}=360 nm using a JASCO UVIDEC-430A spectrophotometer. The light intensities were determined by Reinecke's salt actinometry.[10] The fluorescence spectrum of BNAH was measured by means of the JASCO FP-550A fluorescence spectrophotometer. The lifetime (τ) of photoexcited BNAH in the present reaction media was estimated from τ=0.93 ns of BNAH* in methanol[5] by measuring the fluorescence quantum yield relative to that obtained in methanol. Reduction potentials of MV^{2+} and $Co(acac)_3$ were determined by the cyclic voltammetry measurements which were performed on a Hokuto Denko Model HA-301 potentiostat/galvanostat at 298—313 K in 20—90% (v/v) methanol–borate buffer solution, using a standard calomel reference electrode (SCE).

Results and Discussion

When the reaction of BNAH and $Co(acac)_3$ was carried out in the 20—90% (v/v) methanol-0.02 mol dm^{-3} borate buffer solution (pH 9.0), in a nitrogen atmosphere at 30 °C, the photoirradiation of the reaction mixtures immediately caused the decrease in the absorbance of $Co(acac)_3$ at 595 nm, while such an absorption change of $Co(acac)_3$ was not observed during the thermal reaction in the dark for 6 h. Such an absorption decrease at 595 nm in the present photoreduction of $Co(acac)_3$ by BNAH was considerably accelerated by the presence of MV^{2+} (Fig. 2). All the reactions in Fig. 1 obeyed a pseudo-first-order rate law. The pseudo-first-order rate constants (k_{obs}) increased with increasing the concentration of MV^{2+}. In the case of the molar ratio of $[MV^{2+}]/[BNAH]=25$, the rate constant (k_{obs}) increased in value tenfold as compared with that in the absence of MV^{2+} (Fig. 3). The photoirradiation of the methanol-borate buffer solution containg BNAH and MV^{2+} caused electron transfer from the former to the latter with the formation of new absorption maxima of a reduced MV^{2+} (viz., MV^{+}) at 400 nm and 602 nm. These two peaks immediately disappeared by exposure to O_2 through the reaction of MV^{+} and O_2; Such a MV^{+} formation is also recognized in the photoreaction of NADH and MV^{2+}.[5] Therefore, the methylviologen cation radical, MV^{+}, formed by the photoirradiation of the reaction mixtures present (BNAH, MV^{2+}, and $Co(acac)_3$) participated in the reduction of $Co(acac)_3$.

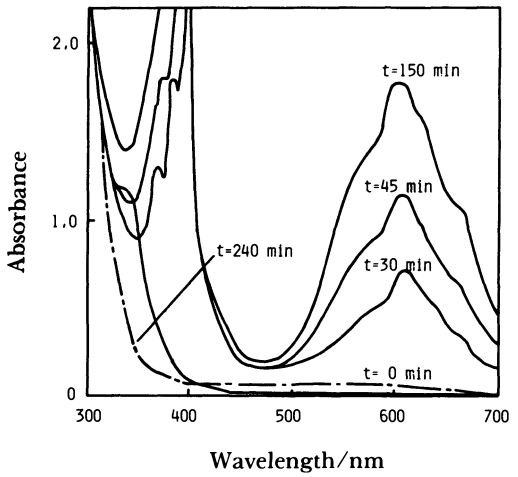

Fig. 1. Absorption spectral change during photoirradiation of BNAH and MV^{2+}. Broken line: O_2 bubling after t=240 min. $[BNAH]=1.25\times10^{-3}$ mol dm^{-3}, and $[MV^{2+}]=1.25\times10^{-3}$ mol dm^{-3} at 30 °C in 90% (v/v) methanol-borate buffer (pH 9.0) in a nitrogen atmosphere.

The quantum yield (Φ_{BNAH}) was evaluated on the basis of the amount of BNAH consumed by $Co(acac)_3$ or MV^{2+}. The Φ_{BNAH} value obtained in the present electron transfer reaction with MV^{2+} was characterized as the sum of the Φ_{BNAH} values evaluated in the reaction between BNAH* and MV^{2+} and in the reaction between BNAH* and $Co(acac)_3$. For instance, the presence of MV^{2+} in amounts equimolar with BNAH resulted in $\Phi_{BNAH}=7.31\times10^{-3}$, which was equal to the sum of the quantum yield for the reduction MV^{2+} by BNAH ($\Phi_{BNAH}=3.01\times10^{-3}$) and for the reduction of $Co(acac)_3$ by BNAH without MV^{2+} ($\Phi_{BNAH}=4.13\times10^{-3}$). Therefore, it is obvious that the photoinduced reduction of $Co(acac)_3$ by BNAH with MV^{2+} proceeds through the direct electron transfer from BNAH* to $Co(acac)_3$ and through the electron transfer from MV^{+}

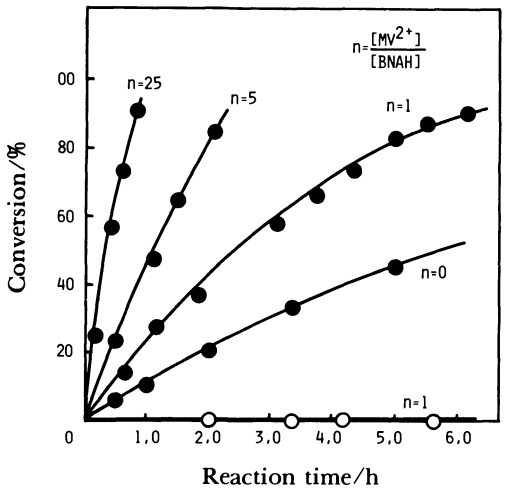

Fig. 2. Reduction of $Co(acac)_3$ with BNAH. Filled circle: Photoreduction, Empty circle: Thermal reduction. $n=[MV^{2+}]/[BNAH]$. $[BNAH]=1.25\times10^{-3}$ mol dm^{-3}, $[Co(acac)_3]=1.25\times10^{-3}$ mol dm^{-3}, at 30 °C in 90% (v/v) methanol-borate buffer (pH 9.0) in a nitrogen atmosphere.

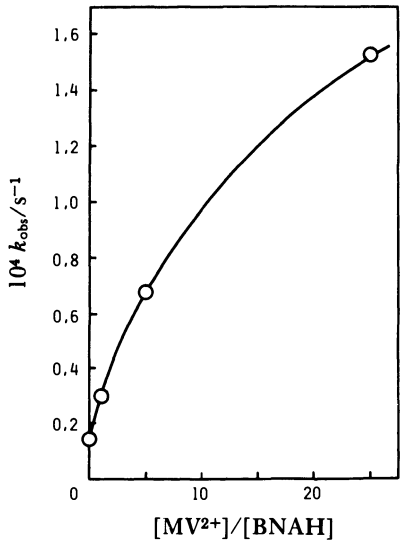

Fig. 3. The concentration effects of MV^{2+} on the pseudo-first-order rate constants in the photoreduction of $Co(acac)_3$ with BNAH. Reaction conditions are the same as Fig. 2.

(formed by the reaction of BNAH* and MV^{2+}) to $Co(acac)_3$. In this sense, the inactivation of BNAH* without the direct electron transfer to $Co(acac)_3$ is suppressed by the efficient electron mediator action of MV^{2+}.

In regard to the reaction mechanism of the present photoreduction of $Co(acac)_3$ by BNAH with MV^{2+}, the following multi-step electron transfer ($1e^-$, H^+, $1e^-$) mechanism (see Scheme) can be suggested as the most

$$\text{BNAH} \xrightarrow{h\nu} \text{BNAH}^* \quad (2a)$$

$$\text{BNAH}^* \xrightarrow{k_{ic}} \text{BNAH} \quad (2b)$$

$$\text{BNAH}^* \xrightarrow{k_f} \text{BNAH} + h\nu \quad (2c)$$

$$\text{BNAH}^* + MV^{2+} \xrightarrow{k_1} \text{BNAH}^{+\cdot} + MV^{+\cdot} \quad (2d)$$

$$\text{BNAH}^* + Co(acac)_3 \xrightarrow{k_1'} \text{BNAH}^{+\cdot} + Co(acac)_2 + acac^- \quad (2e)$$

$$\text{BNAH}^{+\cdot} \xrightarrow{k_2} \text{BNA}\cdot + H^+ \quad (2f)$$

$$\text{BNA}\cdot + MV^{2+} \xrightarrow{k_3} \text{BNA}^+ + MV^{+\cdot} \quad (2g)$$

$$\text{BNA}\cdot + Co(acac)_3 \xrightarrow{k_3'} \text{BNA}^+ + Co(acac)_2 + acac^- \quad (2h)$$

$$MV^{+\cdot} + Co(acac)_3 \xrightarrow{k_4} MV^{2+} + Co(acac)_2 + acac^- \quad (2i)$$

plausible mechanism.[6,11] In this mechanism, BNAH is activated to its singlet excited state, BNAH*, by photoirradiation (Reaction 2a), and the BNAH* once formed turns into a cationic radical ($BNAH^{+\cdot}$) by releasing one electron toward MV^{2+} or $Co(acac)_3$ via Reactions 2d, e, otherwise it is deactivated via Reactions 2b, c. A proton-releasing Reaction 2f is followed by the second electron-transfer step of the reaction between BNA· and the electron acceptor ($Co(acac)_3$ or MV^{2+}), as shown in Reaction 2g or 2h. The cationic radical ($MV^{+\cdot}$) formed by Reaction 2d and 2g donate the electron to $Co(acac)_3$ directly (Reaction 2i). These proton elimination and electron transfers might proceed very quickly because the pK_a value of $BNAH^{+\cdot}$ was 3.6 and the oxidation and reduction potentials (vs. SCE) of BNA·, MV^{2+}, and $Co(acac)_3$ were estimated to be -1.08, -0.47, and about -0.3 V respectively.[12,13] In practice, the accumulation of $MV^{+\cdot}$ ($\varepsilon_{max} \cong 12000$ mol^{-1} dm^3 cm^{-1} at 602 nm)[6] was not observed spectrophotometrically in the present photoreaction with MV^{2+}. It should be stressed that the amount of BNAH consumed by the thermal or photoinduced decomposition is negligibly small in comparison with that of BNAH reacted for the reduction of $Co(acac)_3$ and MV^{2+} in the present conditions (pH 9.0 at 30 °C), although 1,4-dihydropyridines such as BNAH undergo acid-catalyzed decomposition.[14]

From the reaction scheme (2a—i) the following Stern-Volmer equation (Eq. 3) was derived by a stationary state assumption of the concentration of BNAH*, $BNAH^{+\cdot}$, BNA·, and $MV^{+\cdot}$:

$$\frac{1}{\dfrac{1}{\Phi_{BNAH}} - 1} = \tau(k_1 MV^{2+} + k_1' Co(acac)_3) \quad (3)$$

where Φ_{BNAH}=quantum yield evaluated from the BNAH consumption and τ=lifetime of BNAH* in the absence of $Co(acac)_3$ and MV^{2+}. The Stern-Volmer equation (Eq. 3) can be rewritten as Eq. 4 or 5 for the present reaction without $Co(acac)_3$ and MV^{2+}, respectively.

$$\frac{1}{\Phi_{BNAH}} = \frac{1}{k_1\tau}\frac{1}{[MV^{2+}]} + 1 \quad (4)$$

$$\frac{1}{\Phi_{BNAH}} = \frac{1}{k_1' t}\frac{1}{[Co(acac)_3]} + 1 \quad (5)$$

As shown in Fig. 4, the linear relationship between $1/(1/\Phi_{BNAH}-1)$ and $[Co(acac)_3]$ was realized by the straight line of plots of $1/(1/\Phi_{BNAH}-1)$ vs. $[Co(acac)_3]$ for the photoreduction of $Co(acac)_3$ ($0.80-3.75\times10^{-3}$ mol dm^{-3}) with BNAH (1.25×10^{-3} mol dm^{-3}) in the presence of MV^{2+} (1.25×10^{-3} mol dm^{-3}); that is, the reaction sequences shown in scheme seems reliable for the present photoreactions. The k_1 and k_1' values in Eq. 3 were respectively estimated to be $(2.8\pm0.2)\times10^9$ and $(3.3\pm0.2)\times10^9$ mol^{-1} dm^3 s^{-1} from the above linear relationship by using the reported lifetime (τ=0.93 ns) value of BNAH*.[5] The relationship expressed by Eq. 4 or 5 was also satisfied in the photoreduction of $Co(acac)_3$ with BNAH or of MV^{2+} with BNAH (Fig. 5),

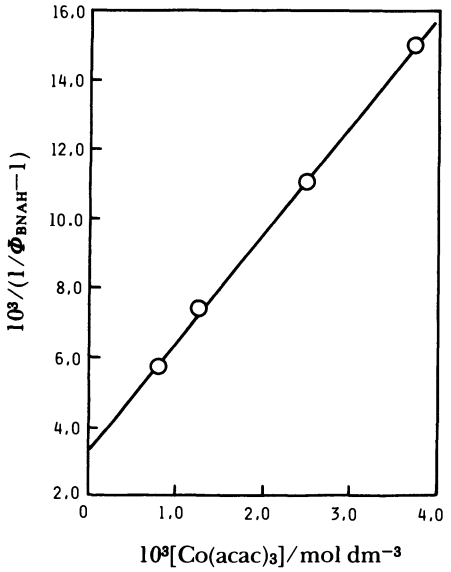

Fig. 4. Stern-Volmer plots for the photoreduction of $Co(acac)_3$ with BNAH in the presence of MV^{2+}. [BNAH]=1.25×10^{-3} mol dm^{-3}, and $[MV^{2+}]=1.25\times10^{-3}$ mol dm^{-3} at 30 °C in 90% (v/v) methanol-borate buffer (pH 9.0) in a nitrogen atmosphere.

and the straight lines in Fig. 5 resulted in $(3.0\pm0.2)\times10^9$ and $(3.4\pm0.2)\times10^9$ mol dm^{-3} s^{-1} for the k_1 and k_1' values, respectively. Notably, these two k_1 and k_1' values are approximately the same as those obtained from Eq. 3. This implies that both the electron-transfer reactions between BNAH and MV^{2+} and between BNAH and $Co(acac)_3$ are induced by the photoirradiation without interaction of $Co(acac)_3$ and MV^{2+} themselves.

The above-mentioned reaction mechanism suggests that the present photoreaction proceeds via the following photoactivation of such charge-transfer (CT) complexes as BNAH-MV^{2+}, if one takes account of the fact that 1,4-dihydropyridine compounds form CT-complexes with MV^{2+} in homogeneous or micellar solutions.[5]

$$\text{BNAH} + MV^{2+} \longrightarrow \text{BNAH-}MV^{2+} \quad (6)$$

$$\text{BNAH-}MV^{2+} \xrightarrow{h\nu} \text{BNAH-}MV^{2+*} \xrightarrow{Co(acac)_3} \text{BNAH}^{+} + Co(acac)_2 + MV^{2+} + acac^{-} \quad (7)$$

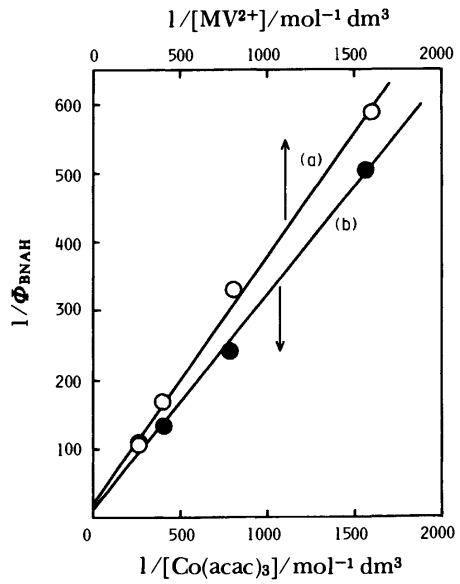

Fig. 5. Stern-Volmer plots for the photoreduction of (a) MV^{2+} and (b) $Co(acac)_3$ with BNAH. [BNAH]= 1.25×10^{-3} mol dm^{-3} at 30 °C in 90% (v/v) methanol-borate buffer (pH 9.0) in a nitrogen atmosphere.

However, such a CT-complex formation between BNAH and MV^{2+} can be negligible in the present reaction, because the present reaction did not generate the CT spectra of BNAH-MV^{2+} and the appreciable deviations of the observed data from the linear lines of the Stern-Volmer relationship by the CT-complex formation.

Since the lifetime (τ) of BNAH* and the reaction rate (k_1 or k_1') of BNAH* consumption by MV^{2+} or $Co(acac)_3$ might be affected by the reaction conditions, it is of interest to note how the present photoreduction of $Co(acac)_3$ by BNAH is dependent on the water content in the methanol-borate buffer solvent. As shown in Table 1, increasing the water content in the range of 10—80 vol.% accelerated Reaction 2e but retarded Reaction 2d. The reduction potentials of MV^{2+} and $Co(acac)_3$ seem not to be affected essentially by the increased water content. In a polar solvent the hydrophobic BNAH* can interact more easily with the hydrophobic $Co(acac)_3$ rather than with the hydrophilic MV^{2+}, so as to augment the k_1' value con-

Table 1. Solvent Effects on the Overall and Electron-Transfer Reaction Rates

Content of water	$10^{-9}k_1$[b]	$10^{-9}k_1'$[b]	τ[c]	$10^4 k_{obs}$[d]
vol.%	mol^{-1} dm^3 s^{-1}	mol^{-1} dm^3 s^{-1}	ns	s^{-1}
10	3.0±0.2	3.4±0.2	0.93±0.04	2.9±0.2
50	1.3±0.1	5.6±0.3	0.85±0.03	2.9±0.2
80	1.4±0.1	12.6±0.9	0.52±0.02	3.2±0.2

a) [BNAH]=1.25×10^{-3} mol dm^{-3}, [$Co(acac)_3$]=1.25×10^{-3} mol dm^{-3}, and [MV^{2+}]=1.25×10^{-3} mol dm^{-3} at 30°C in 90% (v/v) methanol-borate buffer (pH 9.0) in a nitrogen atmosphere. b) Respective rate constants (k_1 and k_1') for Reactions 2d and 2e. c) Lifetime of BNAH*. d) The pseudo-first-order rate constant for the overall reaction.

Table 2. Temperature Dependence of the k_1 and k_1' Values for the Elementary Electron-Transfer Processes of Reactions 2d and 2e

Temperature	τ[b]	$10^{-9}k_1$	$10^{-9}k_1'$	$10^3\Phi_{BNAH}$
K	ns	mol^{-1} dm^3 s^{-1}	mol^{-1} dm^3 s^{-1}	
293	1.16±0.05	2.9±0.2	2.9±0.2	8.9±0.4
298	1.04±0.05	3.1±0.3	3.1±0.3	8.1±0.4
303	0.93±0.04	3.0±0.2	3.4±0.2	7.3±0.4
313	0.71±0.02	3.3±0.2	4.4±0.2	7.0±0.4

a) [BNAH]=1.25×10^{-3} mol dm^{-3}, [$Co(acac)_3$]=1.25×10^{-3} mol dm^{-3}, and [MV^{2+}]=1.25×10^{-3} mol dm^{-3} in 90% (v/v) methanol-borate buffer (pH 9.0) in a nitrogen atmosphere. b) Lifetime of BNAH*.

Table 3. Estimated Values of the Activation Parameters ($\Delta G^{\neq}$, $\Delta H^{\neq}$, $\Delta S^{\neq}$) for the Reaction of BNAH* and MV^{2+} (Reaction 2d) and of BNAH* and $Co(acac)_3$ (Reaction 2e)

Elementary reaction	$\Delta G^{\neq}$/kJ mol^{-1} [a)]	$\Delta H^{\neq}$/kJ mol^{-1}	$T\Delta S^{\neq}$/kJ mol^{-1} [a)]
2d	19	2.3	−17
2e	19	15	−4.3

a) Calculated at 303 K.

siderably. However, the increased water content in the solvents shortened the lifetime of BNAH* (see Table 1), because BNAH* is inactivated by vibrational relaxation with water. Nevertheless, the increase of the water content in the solvents resulted in the slightly increased value of the pseudo-first-order rate constant (k_{obs}) of the overall reaction. This is probably because of the considerable acceleration of the elementary reaction between BNAH* and $Co(acac)_3$ at the higher water content in the solvents. In this sense, the extent of the contribution of MV^{2+} to the present photoreaction as an electron mediator via Reaction 2d is apparently large at low water contents of the solvents.

The present reaction also changes with the reaction temperature, as is shown in Table 2. The temperature elevation does not benefit the reaction in terms of the shortening of the lifetime of photoexcited BNAH* by increased vibrational relaxation of BNAH* in the solution.[15] However it does promote the electron transfer reactions expressed by Eqs. 2d and 2e , as reflected in the increased rate constants (k_1 and k_1') at higher temperatures. At any rate, the quantum yield (Φ_{BNAH}) given for the overall reaction in the presence of MV^{2+} decreased with increasing temperature, because the enhanced rate of BNAH* consumption by MV^{2+} or $Co(acac)_3$ did not affect the elevation of the Φ_{BNAH} value by overcoming the shortened lifetime of BNAH*. As reflected in the different extent of the rate change by the temperature difference between Reactions 2d and 2e, the magnitude of the contribution of MV^{2+} to the present reaction through the reaction with BNAH* suffers with the reaction temperature: the k_1 value (at 293 K) for the reaction between BNAH* and MV^{2+}, which was almost equal to the k_1' value (at 293 K) for the reaction between BNAH* and $Co(acac)_3$, was enhanced by the temperature elevation to a smaller extent as compared with the k_1' value in Reaction 2e; that is, the participation of MV^{2+} in the present reaction via Reaction 2d becomes less important at a temperature higher than 293 K.

Since linear Eyring relationships are obtainable from both the rate constants (k_1 and k_1') estimated at the temperature range of 293—313 K (Fig. 6), it is of interest to note the thermodynamic parameters (free energy of activation $\Delta G^{\neq}$, enthalpy of activation $\Delta H^{\neq}$, and entropy of activation $\Delta S^{\neq}$) for Reactions 2d and 2e.[16] Although the same $\Delta G^{\neq}$ values were obtained for Reactions 2d and 2e at 303 K, $T\Delta S^{\neq}$ value for Reaction 2e was less than that for Reaction 2e. This suggests that

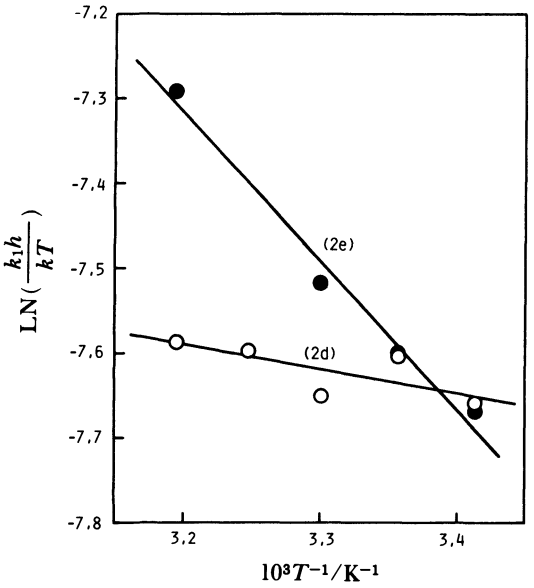

Fig. 6. Eyring relationships for the elementary reactions of 2d and 2e. Empty circle: Reaction 2d. Filled circle: Reaction 2e. [BNAH]=1.25×10^{-3} mol dm^{-3}, [MV^{2+}]=1.25×10^{-3} mol dm^{-3}, [$Co(acac)_3$]= 1.25×10^{-3} mol dm^{-3} in 90% (v/v) methanol-borate buffer (pH 9.0) in a nitrogen atmosphere.

BNAH and $Co(acac)_3$ react each other through a hydrophobic interaction as mentioned above.

Thus, it is concluded from the present study that the presence of hydrophilic MV^{2+} as an electron mediator in the photoreduction of hydrophobic $Co(acac)_3$ with hydrophobic BNAH accelerates the reaction considerably through the efficient acceptance of the electrons from the photoactivated BNAH*, especially in the lower polarity of the reaction conditions (viz., in the smaller content of water in the solvents in the present reaction) and, of course, through the smooth electron transfer from the electron mediator itself to $Co(acac)_3$.

References

1) J. H. Fendler, *J. Phys. Chem.*, **89**, 2730 (1985) and references cited theirin.

2) S. Fukuzumi, K. Hironaka, and T. Tanaka, *J. Am. Chem. Soc.*, **105**, 4722 (1983); N. Ono, R. Tamura, and A. Kaji, *ibid.*, **105**, 4017 (1983); K. Hironaka, S. Fukuzumi, and T. Tanaka, *J. Chem. Soc., Perkin Trans. 2*, **1984**, 1705; O. Ishitani, S. Yanagida, S. Takamuku, and C. Pac, *Bull. Chem. Soc. Jpn.*, **60**, 1801 (1987).

3) K. Ohkubo, K. Yamashita, and S. Sakaki, *J. Chem. Soc., Chem. Commun.*, **1984**, 787; K. Ohkubo, M. Chiba, and K. Yamashita, *J. Mol. Catal.*, **32**, 1 (1985).

4) F. M. Martens, J. W. Verhoeven, R. A. Gase, U. K. Pandit, and Th J. de Boer, *Tetrahedron*, **34**, 443 (1978).

5) F. M. Martens and J. W. Verhoeven, *Recl.: J. R. Neth. Chem. Soc.*, **100**, 228 (1981).

6) F. M. Marten and J. W. Verhoeven, *J. Photochem.*, **22**, 99 (1983).

7) S. Fukuzumi, K. Hironaka, N. Nishizawa, and T. Tanaka, *Bull. Chem. Soc. Jpn.*, **56**, 2220 (1983).

8) T. Endo and M. Okamura, *J. Org. Chem.*, **45**, 2663 (1980); T. Endo, K. Ageishi, K. Furusawa, and M. Okamura, *J. Mol. Catal.*, **18**, 351 (1983).

9) D. M. Mauterall and F. H. Westheimer, *J. Am. Chem. Soc.*, **77**, 2261 (1955).

10) E. E. Wegner and A. W. Adamson, *J. Am. Chem. Soc.*, **88**, 394 (1966).

11) A. Ohno, H. Yamamoto, and S. Oka, *J. Am. Chem. Soc.*, **103**, 2041 (1981); A. Ohno,T. Shio, H. Yamamoto, and S. Oka, *ibid.*, **103**, 2045 (1981).

12) S. Fukuzumi, S. Koumitsu, K. Hironaka, and T. Tanaka, *J. Am. Chem. Soc.*, **109**, 305 (1987).

13) As the reduction of $Co(acac)_3$ was irreversible, the determination of the reduction potential of $Co(acac)_3$ created some difficulty and the exact value of the reduction potential could not be obtained.

14) S. Shinkai, R. Ando, and T. Kunitake, *Bull. Chem. Soc. Jpn.*, **48**, 1914 (1975).

15) N. J. Turro,"Modern Molecular Photochemistry," The Benjamin/Cummings Publ. Co., Inc., Menlo Park (1978).

16) Y. Kaizu, M. Takano, and H. Kobayashi, *J. Phys. Chem.*, **89**, 332 (1985).

Selectivities of Aromatic Methyl Metalation.[1] Unexpectedly Strong Interactions of Carbanions with Aromatic Rings

Satoshi INAGAKI,* Takeo IMAI, and Yoshio MORI
Department of Chemistry, Faculty of Engineering, Gifu University,
Yanagido, Gifu 501-11
(Received May 25, 1988)

The site selectivities of the metalation reactions of dimethylnaphthalenes and dimethylanthracenes followed by MeOD quenching were investigated experimentally and theoretically. The 2(3)-methyl groups were found to be more effectively metalated than expected from the LUMO amplitudes of the aromatic rings. The MNDO calculations suggested that the naphthylmethyl and anthrylmethyl anions are not the aromatic rings perturbed by the carbanions, but the significantly different conjugated rings doubly bonded to the exocyclic carbon atoms. The unexpectedly strong interactions of the carbanion centers with the aromatic rings can account for the discrepancies between the selectivities and the LUMO amplitudes.

Aromatic compounds react with electrophiles (electron acceptors) and with nucleophiles (electron donors) at the positions where the HOMO and LUMO amplitudes are large, respectively. A similar expectation can be made for relative stabilities of aromatic compounds substituted by electron-releasing and -withdrawing groups. For example, aromatic compounds with an anionic center directly attached to the ring are expected to be stable when the LUMO amplitude is large on the substituted carbon atom. In fact, the acid dissociation constants[2] of isomeric naphthols and anthrols support the expectation: pK_a (H_2O, 20 °C)=9.85 for 1-naphthol and 9.93 for 2-naphthol; 9.88 for 1-anthrol and 9.92 for 2-anthrol. The LUMO of naphthalene and anthracene has greater extension at the 1- than 2-position (Fig. 1). However, the site-selectivity of the methyl metalation reactions of 1,2,3,4-tetramethylnaphthalenes observed by Dunkelblum and Hart[3] is opposite to the prediction based on the LUMO amplitudes. The metalation by butyllithium/*N*,*N*,*N*′,*N*′-tetramethylethylenediamine (*n*-BuLi/TMEDA) complex base preferentially occurs on the 2-methyl group (Eq. 1).

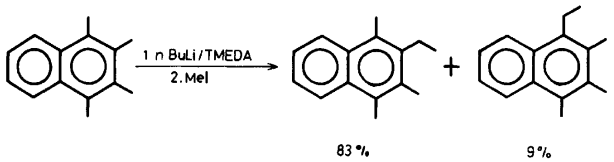

(1)

The anomaly was proposed[3] to come from steric origin: the C_2-methyls are closer to coplanarity with the naphthalene ring than the C_1-methyls, and *n*-BuLi/TMEDA, which is relatively large base, may attack the C_2-methyl to avoid the large steric interactions at the peri positions. A few years before, Kronzer and Sandel[4] estimated the kinetic parameters for the methylene rotation of the 1- and 2-naphthylmethyl (NM) organometallic compounds by the NMR spectroscopy. No appreciable difference was observed between the two isomers in the free energy of activation: ΔG^*(kcal mol^{-1}, 0 °C)=12.9±0.3 for 1-NM lithium and 12.8±0.5 for 2-NM lithium. In addition, Drakenberg et al.[5] reported the rotational barrier for the naphthoyl radicals. The barrier (ΔG^*) is lower for 1-naphthoyl radical (6.4 kcal mol^{-1}) than for 2-naphthoyl radical (8.2 kcal mol^{-1}). These rotational barriers throw a doubt on the steric explanation of the selectivity, rather than lend support to it.

We undertook experimental studies (Eq. 2) by employing 1,3-dimethylnaphthalene (DMN) and some dimethylanthracenes (DMA). The selectivity of the metalation reactions of the aromatic methyls was not always found to be in agreement with the LUMO amplitudes. The methyl metalations at the 2-positions of naphthalene and anthracene were shown to occur more preferentially than expected. The MNDO calculations suggested that methylnaphthalene and -anthracene, especially 2-methyl derivatives, might undergo more drastic structural change in the aromatic rings on metalation, which may account for the failure of the prediction based on the LUMO amplitudes.

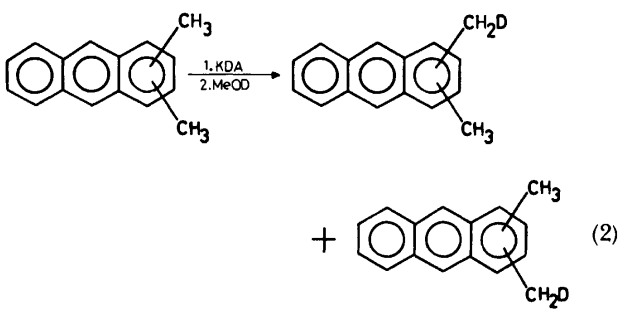

(2)

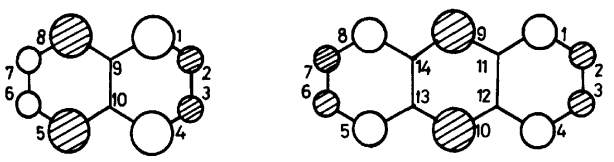

Fig. 1. The LUMO's of naphthalene and anthracene.

Results and Discussion

Selectivity. The metalation of 1,3-DMA preferentially occurred at the 3-methyl group, irrespective of the molar ratio of bases to the substrate (Fig. 2) and the reaction time (Fig. 3), although the LUMO amplitude is the smallest on C_3. For 1,10-DMA the 10-methyl metalation was preferred (Fig. 4). The LUMO amplitude is greater at the 9(10)-position(s). The selectivity is such as expected from the LUMO. The reactions of 2,9-DMA were not selective (Fig. 5), while the LUMO amplitude is much greater at the 9(10)-position(s). The absence of the selectivity is incompatible with the LUMO.

The reactions of 1,3-DMN were compared with 1,3-DMA. The 3-methyl metalation was preferred (Fig. 6). The selectivity is in good agreement with the observation by Dunkelblum and Hart.[3]

The selectivity consistent with the LUMO amplitude of the aromatic rings is only for 1,10-DMA. The other DMN and DMA examined here exhibited the opposite or inconsistent selectivities. The results present a striking contrast to the relative acidities of the isomeric naphthols and anthrols which can be explained in terms of the LUMO amplitudes.

MO Study. Molecular orbital study was undertaken to investigate the selectivity. Geometries of naphthylmethyl (NM) and anthrylmethyl (AM) carbanions were optimized by the MNDO molecular orbital calculations.[6] The relative stabilities of the isomeric anions are listed in Table 1.

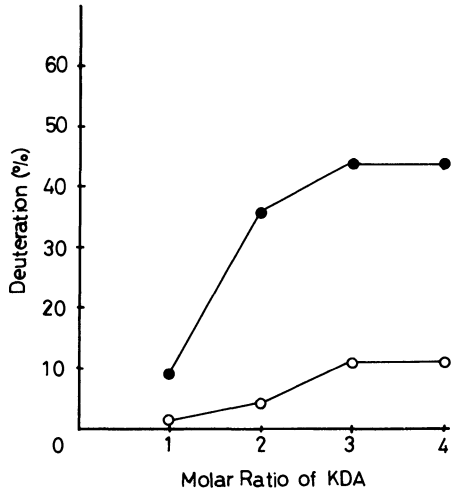

Fig. 2. The site selectivity of the metalation reactions of 1,3-dimethylanthracene (1,3-DMA). ○: 1-methyl, ●: 3-methyl.

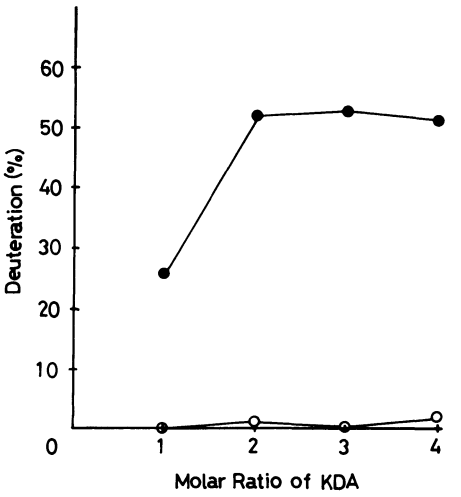

Fig. 4. The selectivity of the metalation reactions of 1,10-dimethylanthracene (1,10-DMA). ○: 1-methyl, ●: 10-methyl.

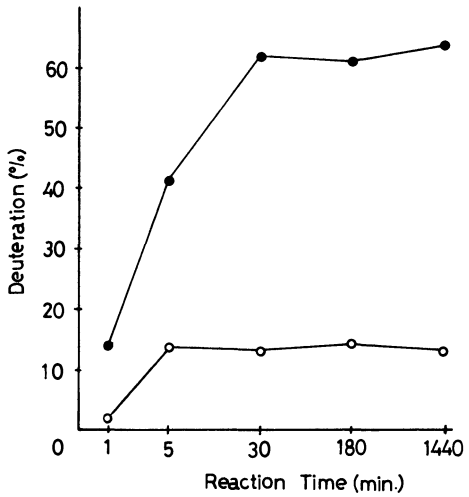

Fig. 3. The dependence of the selectivity on the reaction time for 1,3-dimethylanthracene (1,3-DMA). ○: 1-methyl, ●: 3-methyl.

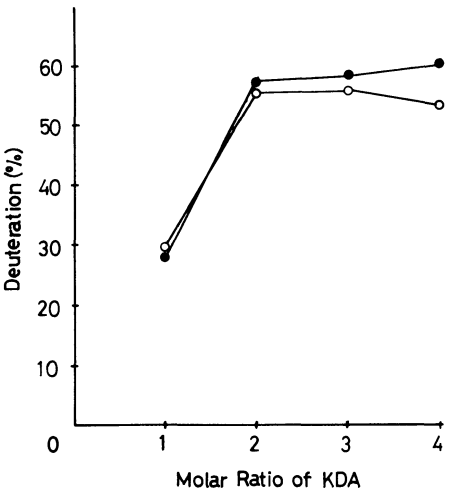

Fig. 5. The selectivity of the metalation reactions of 2,9-dimethylanthracene (2,9-DMA). ○: 2-methyl, ●: 9-methyl.

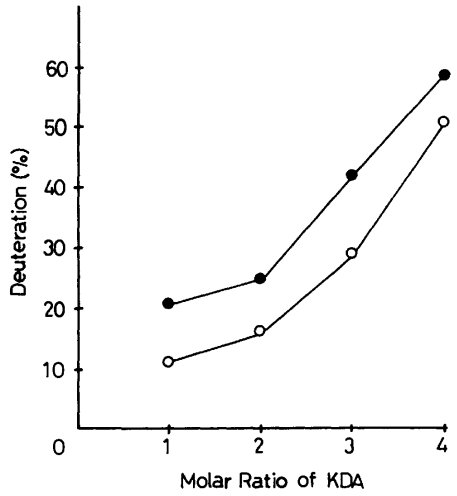

Fig. 6. The selectivity of the metalation reactions of 1,3-dimethylnaphthalene (1,3-DMN). ○: 1-methyl, ●: 3-methyl.

Table 1. Relative Energies[a] of Naphthylmethyl (NM) and Anthrylmethyl (AM) Anions

1-NM	2-NM	1-AM	2-AM	9-AM
0.0	−0.77	0.0	−0.29	−2.44

a) The results of the MNDO calculations in kcal mol^{-1}.

Although the calculated energy differences between 1- NM and 2-NM and between 1-AM and 2-AM anions are small, the relative stabilities are unexpectedly compatible with the observed selectivities of 1,3-DMN and 1,3-DMA. The 9-AM anion was shown to be the most stable. This result is in agreement with the prediction based on the LUMO amplitude and with the preferential C_{10} methyl metalation of 1,10-DMA. However, the result conflicts with the comparable extents of the C_2 and C_9 methyl metalations of 2,9-DMA. As a result, the 2-methyl metalation was concluded to occur more preferentially than expected from the calculated relative stabilities of the intermediate carbanions and the LUMO amplitudes of the aromatic rings.

Some interesting features were found in the optimized geometries (Fig. 7). The exocyclic bonds are surprisingly among the shortest in each species. These structures are not regarded as the aromatic rings perturbed by the methyl anions, but as entirely different conjugated rings doubly bonded to the methyl carbon atoms. The unexpected structural features can account for the failure in predicting the selectivity on the basis of the frontier orbital theory. The interactions of the carbanion centers with the naphthalene and anthracene rings are suggested to be too strong to be treated by the perturbation approach. The discrepancy between the LUMO amplitudes and the selectivities of the aromatic methyl metalations

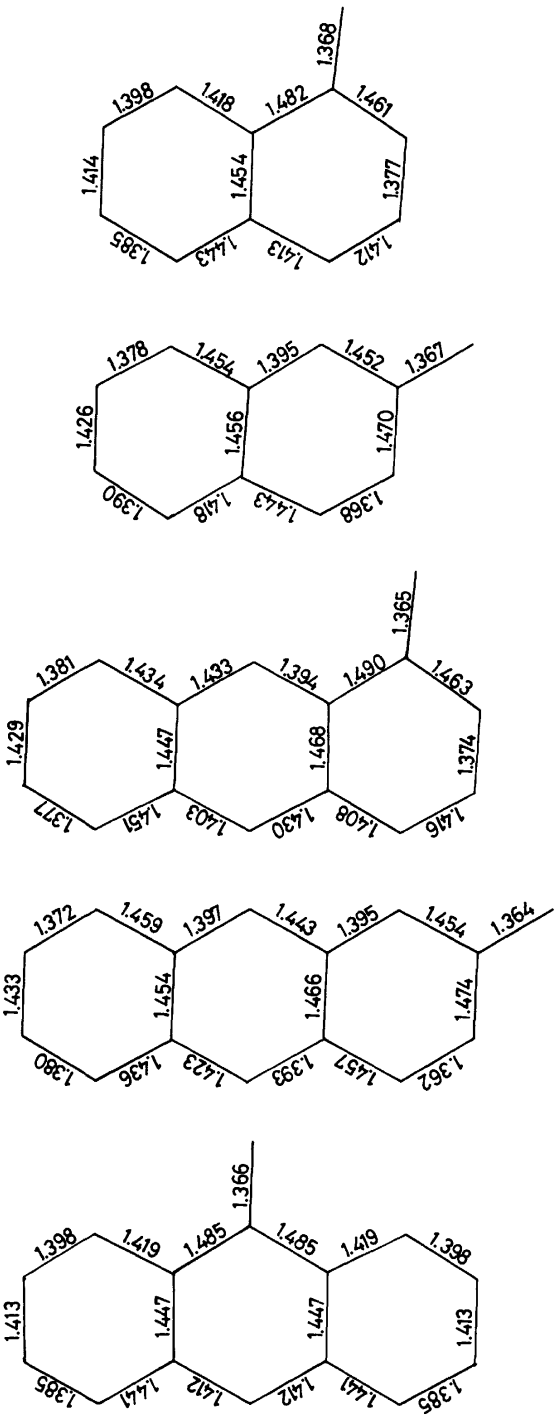

Fig. 7. The MNDO-optimized geometries of the naphthylmethyl (NM) and anthrylmethyl (AM) anions.

(the relative stabilities of the arylmethyl anions) is not necessarily incompatible with the success in explaining the relative acidities of the naphthols and anthrols. The oxy anions have n-orbitals at a lower energy level than the carbanions. The energy gaps between the n-orbitals and the LUMO of the aromatic rings are greater for the oxy anions. The frontier orbital interaction is weak enough to treat the

interactions of the oxy anions with the aromatic rings by the perturbational approach.

The bond alternations are remarkable all over the aromatic rings of the 2-NM and 2-AM anions. On the other hand, no appreciable bond alternation was found in the unsubstituted rings of the 1-NM, 1-AM, and 9-AM anions. The contrast was expected to give a clue to interpreting the preference of the 2-methyl metalation. Unfortunately, the explicit relation between the structural peculiarities and the selectivities still remains open to question.

Concluding Remarks

The selectivities of the methyl metalations of some dimethyl derivatives of naphthalene and anthracene were carried out under the same experimental conditions in order to examine the relation with the LUMO amplitudes of the aromatic rings. The preferential 3-methyl metalation of 1,3-DMN and 1,3-DMA is in conflict with the prediction from the LUMO amplitudes. The nonselective metalation of 2,9-DMA cannot be explained in terms of the LUMO which has much greater extension at the 9-position. The preference of the 10-methyl metalation of 1,10-DMA is in agreement with the LUMO amplitude. These results suggest that 2(3)-methyl group is more effectively metalated than expected from the LUMO amplitudes. The failure in predicting the selectivities from the LUMO presents a striking contrast to the success in predicting the acidities of the isomeric naphthols and anthrols.

The MNDO calculations suggested the strong interactions of the carbanions with the aromatic rings and the resulting double bond formation between them. The strong interaction rather than perturbation may be associated with the failure in the LUMO predictions of the relative stabilities of the isomeric arylmethyl anions or the selectivities of the aromatic methyl metalations. The successful explanation of the relative acidities of naphthols and anthrols can be understood in terms of weak interactions of the oxy anions with the aromatic rings due to lower n-orbital energies of the oxy anions.

Experimental

Materials. 1,3-, 1,4-, and 2,3-DMA's were prepared[7-9] from the anthraquinones.[10] 2,9- and 1,10-DMA's were obtained by Grignard synthesis from the anthrones.[11]

Metalation Reactions follwed by MeOD Quenching. DMA or DMN (0.1 g) was added to the KDA solution[12] which was prepared by mixing of t-BuOK into equimolar LDA in 10 ml of hexane under nitrogen atmosphere. The reaction mixtures immediately colored dark green for DMA and dark violet for DMN. The mixtures were stirred for a given period of time, and then quenched by a large excess of MeOD. After washing with dilute hydrochloric acid the organic layer was extracted by benzene and dried over sodium sulfate. The mixture was separated on the TLC. The ratios of methyl protons were determined by the 270 MHz FT-NMR spectroscopy on the basis of the 9- and 10-protons (2.0) for 1,3-DMA, the 9-proton (1.0) for 1,10-DMA, and the 10-proton (1.0) for 2,9-DMA.

The MNDO molecular orbital calculations were carried out on a HITAC M-680H computer, at the Institute for Molecular Science. NMR spectra were recorded on a JEOL JNM-GX 270 spectrometer, at the Center of Instrumentation, Gifu University. This work was partially supported by a Grant-in-Aid for Scientific Research from the Ministry of Education, Science and Culture.

References

1) Orbital Theory Provoked Experiments in Organic Chemistry: Part 4. Part 3: S. Inagaki, T. Okajima, and K. Tanaka, *Chem. Lett.*, **1988**, 1219.
2) K. Lauer, *Ber.*, **70B**, 1127 (1937).
3) E. Dunkelblum and H. Hart, *J. Org. Chem.*, **44**, 3482 (1979).
4) F. J. Kronzer and V. R. Sandel, *J. Am. Chem. Soc.*, **94**, 5750 (1972).
5) T. Drakenberg, J. Sandstörm, and J. Seita, *Org. Magn. Reson.*, **11**, 239, 246 (1978).
6) M. J. S. Dewar and W. Thiel, *J. Am. Chem. Soc.*, **99**, 4899 (1977).
7) L. F. Fieser, "Organic Experiments," Maruzen, Tokyo (1964), p. 195.
8) J. V. Braum and O. Bayer, *Ber.*, **59**, 914 (1926).
9) F. Griendt and H. Cerfontain, *Tetrahedron*, **36**, 317 (1980).
10) V. Stepan and J. Vodehnal, *Collect. Czech. Chem. Commun.*, **36**, 3964 (1971).
11) E. B. Barnett and N. F. Goodway, *J. Chem. Soc.*, **1929**, 1754.
12) B. Renger, H. Hügel, W. Wykypiel, and D. Seebach, *Chem. Ber.*, **111**, 2630 (1978); S. Raucher and G. A. Koolpe, *J. Org. Chem.*, **43**, 3794 (1978).

 © 1989 The Chemical Society of Japan Bull. Chem. Soc. Jpn., 62, 83—88 (1989)

Synthesis and Enantiomer Recognition of Dipodands and Crown Ethers Containing the 2,3:6,7-Dibenzobicyclo[3.3.1]nona-2,6-diene Residue as the Chiral Subunit

Koichiro NAEMURA,* Rinkō FUKUNAGA, Masanori KOMATSU, Masatoshi YAMANAKA, and Hiroaki CHIKAMATSU
Department of Chemistry, Faculty of Engineering Science, Osaka University, Toyonaka, Osaka 560
(Received May 31, 1988)

Five new optically active crown ethers and six optically active dipodands are reported. The crown ethers were synthesized by using (+)-(1*S*,4*R*,5*S*,8*R*)-2,3:6,7-dibenzobicyclo[3.3.1]nona-2,6-diene-4,8-diol and (+)-(1*S*,4*R*,5*S*,8*R*)-4,8-bis(hydroxymethyl)-2,3:6,7-dibenzobicyclo[3.3.1]nona-2,6-diene as a chiral subunit and the dipodands contained the 2,3:6,7-dibenzobicyclo[3.3.1]nona-2,6-diene residue as a chiral anchor group. The enantiomer recognition behaviour of these compounds was evaluated by the enantiomer differential transport of methyl (±)-phenylglycinate and (±)-1,2-diphenylethylamine hydrochloride through bulk liquid membrane.

A large number of chiral crown ethers have been synthesized and numerous reports have described their chiral recognition properties.[1] Chiral discrimination of an open-chained equivalent of crown ether, to which Vögtle and Weber have suggested the term "podand",[2] is also interesting in the host–guest chemistry. Although a variety of optically active podands have been prepared,[1] as far as we know, little has been reported on their chiral recognition behavior.

In a recent publication,[3] we have reported on the preparation of optically active crown ethers and dipodands, and their chiral recognition properties. The crown ethers contained the *trans*-tetrahydrofuran-2,5-diylbis(hydroxymethylene) residue as a chiral subunit and dipodands contained the same residue as a chiral anchor group. All of the dipodands showed the enantiomer selectivity toward chiral primary ammonium salts examined and the dipodand having two 2,3-benzo-1,4,7-trioxa-2-octen-1-yl groups as a donor arm as well as the chiral tetrahydrofuran anchor group exhibited higher enantiomer selectivity than the crown ether having the same chiral subunit. It was also showed that the enantiomer selectivity of dipodands in transport was considerably changed by selection of the end group.

These recent results prompted us to examine the chiral recognition property of dipodands and crown ethers, and to acquire further information about the change of the enantiomer selectivity of dipodands produced by the variation in the structure of donor arm. In this paper, we report the preparation of optically active crown ethers and dipodands having a chiral anchor group. These compounds contained the 2,3:6,7-dibenzobicyclo[3.3.1]nona-2,6-diene residue as a chiral subunit. Their enantiomer recognition behavior was evaluated by the enantiomer differential transport of racemic primary ammonium salts through bulk liquid membrane.

Results and Discussion

(+)-(2*S*,4*S*)-2,4-Diphenylglutaric acid (**1**), $[\alpha]_D$ +81.3° (EtOH), was obtained by treatment of the sparingly soluble quinine salt with concentrated hydrochloric acid followed by recrystallization from ethanol.[4] The absolute configuration of the compound has been unambigously determined by a chemical correlation with (−)-(*R*)-3-phenylbutanoic acid.[4] Treatment of (+)-**1** with concentrated sulfuric acid at 80—90 °C for 1 h gave (−)-**2** in 77% yield, recrystallization of which from methanol provided the optically pure specimen **2**, mp 195—197 °C; $[\alpha]_D$ −340° (EtOH).[4] Reduction of (−)-**2** with $LiAlH_4$ in dry tetrahydrofuran (THF) yielded (+)-**4**, mp 192—194 °C; $[\alpha]_D$ +87.2° (EtOH), in 97% yield. Reaction of (+)-**4** with methyl *p*-toluenesulfonate and NaH in dry *N*,*N*-dimethylformamide (DMF) at 45 °C gave (−)-**11**, mp 169—170 °C; $[\alpha]_D$ +15.0° ($CHCl_3$), in 57% yield. The another chiral subunit (+)-**5** having two hydroxymethyl groups was prepared from (−)-**2** as follows. Wittig reaction of

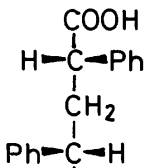

1

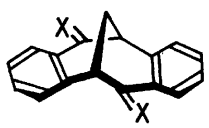

2 X = O

3 X = CH_2

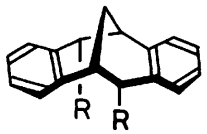

4 R = OH

5 R = CH_2OH

(−)-**2** with methyltriphenylphosphonium bromide using potassium *t*-butoxide and THF[5] gave (−)-**3**, mp 126—127 °C; $[\alpha]_D$ −391° (EtOH), in 92% yield. Treatment of (−)-**3** with diborane in THF led to the corresponding organoborane which was converted into (+)-**5**, mp 170—172 °C; $[\alpha]_D$ +143° (EtOH), in 85% overall yield by oxidation with 30% H_2O_2 in THF followed by treatment with 3 M (1 M=1 mol dm^{-3}) aqueous sodium hydroxide.

Using the diols (+)-**4** and (+)-**5** as a chiral subunit, we prepared optically active crown ethers. One of the ethylene glycol unit of 18-crown-6 and 15-crown-5 was replaced by the chiral diol (+)-**4** to give the chiral crown ethers **6** and **7** respectively. High-dilution condensation of (+)-**4** with pentaethylene glycol ditosylate in the presence of NaH in refluxing THF provided the crown ether (−)-**6**,[6] mp 115—117 °C; $[\alpha]_D$ −1.5° ($CHCl_3$), in 16% yield after alumina chromatography followed by recrystallization from hexane-benzene, and the formation of the dimeric crown ether formed by the condensation of two molecules of the diol **4** with two ditosylate molecules was not detected. By use of the same procedure, (+)-**4** was condensed with tetraethylene glycol ditosylate to give the mixture of crown ethers. Alumina chromatography of the mixture furnished (+)-**7**,[6] mp 72—74 °C; $[\alpha]_D$ +42.6° ($CHCl_3$) and the dimeric crown ether (+)-**8**,[6] mp 166—168 °C; $[\alpha]_D$ +5.4° ($CHCl_4$), in 11% and 12% yield, respectively. Their structures were confirmed on the basis of their mass and ^{1}H NMR spectra as well as elemental analyses. Analogously, condensation of (+)-**5** with pentaethylene glycol and tetraethylene glycol ditosylate in the presence of NaH in THF gave (+)-**9**,[6] $[\alpha]_D$ +51.2° ($CHCl_3$), (a glassy solid 12% yield) and (+)-**10**,[6] $[\alpha]_D$ +24.0° ($CHCl_3$), (a glassy solid 11% yield), respectively. In both cases, the formation of dimeric crown ethers was not detected and the dehydrated product (−)-**3** was isolated.

Cation-binding abilities for alkali metal ions (Li^+, Na^+, K^+, and Rb^+) of the crown ethers **6** and **7** were estimated by solvent extraction of aqueous solution of metal picrates with a chloroform solution containing crown ether, and the results are given in Table 1. As

Table 1. Extraction of Alkali Metal Picrates with Crown Ethers **6** and **7**

Crown ether	Extractability/%			
	Li^+	Na^+	K^+	Rb^+
6	<0.1	6	2	1
7	<0.1	5	1	<0.1

can be seen from Table 1, both crown ethers show almost negligible extractabilities for any of the alkali metal ions examined in this study. The introduction of the chiral subunit (+)-**4** into 18-crown-6 and 15-crown-5 enlarges a cavity of the crown ether ring and this may be the major reason for the extremely low extractability of the crown ethers **6** and **7**.

Our next task was the preparation of optically active dipodands having the 2,3:6,7-dibenzobicyclo[3.3.1]-nona-2,6-diene residue as a chiral anchor group. Condensation of (+)-**4** with 3-oxabutyl *p*-toluenesulfonate and NaH in dry DMF at 45—50 °C gave the dipodand (−)-**12** which possessed the methyl end group and two oxygen atoms in each donor arm. Both of the dipodands (−)-**13** and (−)-**14** contained two methyl end groups and they differed from each other in the number of donor atoms in a side chain. The dipodands (−)-**13** having three oxygen atoms in each side arm was prepared by condensation of (+)-**4** with 3,6-dioxaheptyl *p*-toluenesulfonate and the dipodand (−)-**14** having four oxygen atoms in each side arm was obtained from (+)-**4** and 3,6,9-trioxadecyl *p*-toluenesulfonate. The dipodands (−)-**15**, (−)-**16**, and (−)-**17**, all of which contained three oxygen atoms in a donor arm, differed from one another in the end group. Treatment of (+)-**4** with 3,6-dioxaoctyl, 3,6-dioxadecyl, and 7-phenyl-3,6-dioxaheptyl *p*-toluenesulfonate gave (−)-**15** having two ethyl end groups, (−)-**16** having two butyl end groups, and (−)-**17** having two benzyl end groups, respectively. All of the dipodands were obtained as a colorless oil and their structures were confirmed on the basis of their mass spectra as well as their ^{1}H NMR spectra.

Cation binding abilities of podands **13** and **14** were

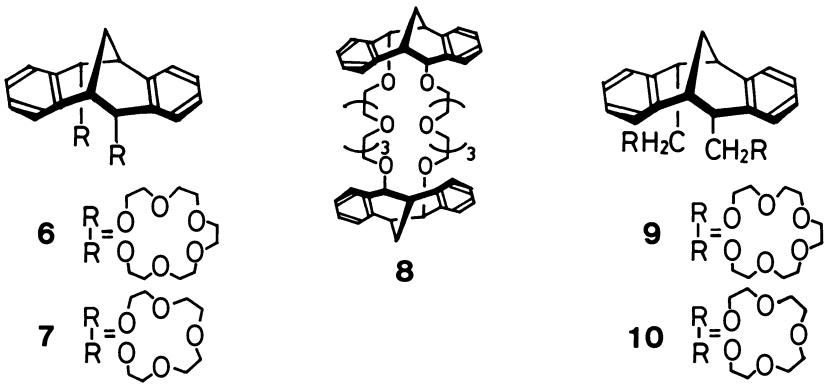

examined, but both compounds extracted hardly any of the metal ions.

Next we turned attention to examine the enantiomer recognition behavior of these crown ethers and dipodands in transport[7] of (±)-1,2-diphenylethylamine and methyl (±)-phenylglycinate hydrochloride through bulk liquid membrane containing the optically active host molecules. The results are summarized in Table 2.

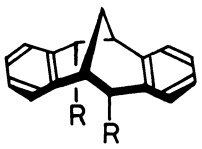

11 R = OCH_3

12 R = $O(CH_2)_2OCH_3$

13 R = $O(CH_2)_3OCH_3$

14 R = $O(CH_2)_4OCH_3$

15 R = $O(CH_2)_2OC_2H_5$

16 R = $O(CH_2)_2OC_4H_9$

17 R = $O(CH_2)_2OCH_2Ph$

As can be seen from Table 2, all crown ethers and dipodands transported dominantly 1,2-diphenylethylamine hydrochloride of the *S*-configuration and methyl phenylglycinate hydrochloride of the *R*-configuration. Entries 29 and 30 were carried out using the chloroform membrane which did not contain any host molecule. In these cases, methyl phenylglycinate hydrochloride scarcely transferred to the inner aqueous phase, but 4.0% of 1,2-diphenylethylamine hydrochloride moved to the receiving phase after 10 h. Entries 1, 2, 15, and 16 shows that the chiral compounds (+)-**4** and (−)-**11** containing no donor arm exhibited enantiomer selectivity, but their transportabilities were low. In Entries 3 and 4, the transport experiments were performed using the chloroform solution containing (+)-**4** and a small amount of achiral 18-crown-6. In these cases, the rate of transport of the guest molecules was obviously enhanced and the enantiomer selectivity was hardly changed by addition of 18-crown-6.

Table 2. Differential Transport of Enantiomeric Molecules through Bulk Liquid Membrane Containing Chiral Crown Ethers and Chiral Dipodands

Entry	Host	Guest[a]	Time	Transport	Configuration of dominant enantiomer	Optical purity
			h	%		%
1	(+)-**4**	a	10	7.0	*S*	37
2	(+)-**4**	b	180	5.0	*R*	4
3[b]	(+)-**4**	a	12	10	*S*	36
4[b]	(+)-**4**	b	44	11	*R*	6
5	(−)-**6**	a	2.5	10	*S*	69
6	(−)-**6**	b	36	10	—	0
7	(+)-**7**	a	2.4	10	*S*	67
8	(+)-**7**	b	8.5	10	*R*	25
9	(+)-**8**	a	1.5	12	*S*	53
10	(+)-**8**	b	42	11	*R*	5
11	(+)-**9**	a	2.2	10	*S*	32
12	(+)-**9**	b	36	12	—	0
13	(+)-**10**	a	1.7	10	*S*	80
14	(+)-**10**	b	24	11	*R*	11
15	(−)-**11**	a	5.0	11	*S*	29
16	(−)-**11**	b	180	2.0	—	—[d]
17	(−)-**12**	a	2.2	10	*S*	33
18	(−)-**12**	b	180	5.0	*R*	4
19	(−)-**13**	a	1.5	11	*S*	84
20	(−)-**13**	b	52	11	*R*	8
21	(−)-**14**	a	1.6	10	*S*	30
22	(−)-**14**	b	48	11	*R*	3
23	(−)-**15**	a	1.6	10	*S*	50
24	(−)-**15**	b	100	5.4	*R*	6
25	(−)-**16**	a	2.0	11	*S*	45
26	(−)-**16**	b	96	5.6	*R*	5
27	(−)-**17**	a	1.0	10	*S*	19
28	(−)-**17**	b	48	11	*R*	3
29[c]	No	a	10	4.0	—	—
30[c]	No	b	72	1	—	—

a) a: (±)-1,2-Diphenylethylamine hydrochloride, b: methyl (±)-phenylglycinate hydrochloride. b) The chloroform solution contained (+)-**4** (0.005 M) and 18-crown-6 (0.0005 M). c) The chloroform solution did not contain any host molecule. d) Circular dichroism was not measured.

The enantiomer selectivity of (+)-**7** and (+)-**10**, the cavity of which is smaller than that of (+)-**6** and (+)-**9**, is higher than the selectivity of (+)-**6** and (+)-**9**. The enantiomer selectivity of (+)-**10** toward 1,2-diphenylethylamine hydrochloride is the highest in crown ethers examined here and comparable to that of biphenanthryl crown ether,[8] which has been known to be a crown ether having a high chiral recognition property. The crown ether (+)-**7** is nearly equal to biphenanthryl crown ether with regard to its enantiomer recognition behavior toward methyl phenylglycinate hydrochloride.

Entries 17—22 shows that, among dipodands (−)-**12**, (−)-**13**, and (−)-**14**, all of which have two methyl end groups, the enantiomer selectivity of (−)-**13** having three oxygen atoms in each side chain is the highest of all and comparable to that of (+)-**10**. Transportability of (−)-**12** having only two donor atoms in each side chain is low, and a significant difference was not found in transportabilities of (−)-**13** and (−)-**14**. In Entries 19, 20, and 23—28, among dipodands (−)-**13**, (−)-**15**, (−)-**16**, and (−)-**17**, all of which contain three oxygen atoms in each side chain, (−)-**13** having two methyl end groups has the highest enantiomer selectivity. The bulky end groups reduce the enantiomer selectivity of dipodand, but there is no significant difference in transportabilities of these dipodands.

As noted above, the degree of enantiomer selectivity of dipodands in transport varied widely with variation in the structure of the donor arms, and in the case of dipodands reported here, the 1,4,7-trioxaoctyl group is the best subunit as the donor arm of the chiral dipodands.

Experimental

Melting points are uncorrected. Infrared spectra were recorded on a Hitachi 260-10 spectrometer. Ultraviolet spectra were taken on a Hitachi 220A spectrophotometer and circular dichroism data were corrected with a JASCO J-40 spectropolarimeter. Optical rotations were measured with a JASCO DIP-40 automatic polarimeter. ^{1}H NMR spectra were obtained from a JNM-MH-100 and a JNM-C-60 and chemical shift are reported in parts per million (δ) down field from tetramethylsilane. Mass spectra were taken with a Hitachi RMS-4 spectrometer.

(−)-2,3:6,7-Dibenzobicyclo[3.3.1]nona-2,6-diene-4,8-dione (2). (+)-2,4-Diphenylglutaric acid (**1**) (6.00 g, 0.0211 mol) $[\alpha]_D^{22}$ +79.1° (EtOH), which was obtained from the sparingly soluble quinine salt, was stirred in concentrated sulfuric acid (40 mL) for 1 h at 80—90 °C. The mixture was cooled to room temperature, poured into an ice-water, and extracted with benzene. The extract was washed with aqueous solution of sodium hydrogencarbonate and water, dried over $MgSO_4$, and concentrated in vacuo to give **2** (4.00 g, 77% yield), which was recrystallized from methanol to furnish (−)-**2**, mp 195—197 °C; $[\alpha]_D^{22}$ −340° (*c* 0.0220, EtOH). Found: C, 82.01; H, 4.81%. Calcd for $C_{17}H_{12}O_2$: C, 82.24; H, 4.67%.

(−)-4,8-Bis(methylene)-2,3:6,7-dibenzobicyclo[3.3.1]nona-2,6-diene (3). To a suspension of methyltriphenylphosphonium bromide[9] (36.0 g, 0.101 mol) in dry THF (450 mL) was added a suspension of potassium *t*-butoxide (11.3 g, 0.101 mol) in dry THF (190 mL), and then the mixture was stirred for 1 h at room temperature. A solution of (−)-**2** (5.00 g, 0.0202 mol); $[\alpha]_D$ −340°, in dry THF (30 mL) was added to the mixture and it was stirred for an additional 4 h at room temperature under nitrogen atmosphere. After water (15 mL) was added to the reaction mixture, it was stirred at room temperature for 1 h and an inorganic solid was filtered off. The filtrate was concentrated in vacuo and the residue was extracted with ether. The extract was washed with water, dried over $MgSO_4$, and concentrated in vacuo. After addition of hexane (200 mL) to the residue, the precipitated phosphine oxide was filtered off and the solvent was removed. The residue was chromatographed on alumina (eluted with hexane-benzene 1:1 v:v) to provide a solid, which was recrystallized from methanol to give (−)-**3** (4.52 g, 92% yield), mp 126—128 °C, $[\alpha]_D^{27}$ −391° (*c* 0.022, EtOH) (lit,[4] mp 124.2—124.6 °C; $[\alpha]_D$ +392° (EtOH)). Found: C, 93.25; H, 6.61%. Calcd for $C_{19}H_{16}$: C, 93.40; H, 6.60%.

(+)-2,3:6,7-Dibenzobicyclo[3.3.1]nona-2,6-diene-4,8-diol (4). To a suspension of $LiAlH_4$ (1.60 g, 0.0421 mol) in dry THF (50 mL) was added a solution of (−)-**2** (2.65 g, 0.0107 mol) in dry THF (50 mL) at 0 °C and then the mixture was stirred for 1 h at room temperature. After addition of 10% sulfuric acid to the reaction mixture with ice-cooling, an inorganic solid was filtered off and the filtrate was concentrated in vacuo. The residue was extracted with chloroform. The extract was washed with diluted HCl, aqueous solution of sodium hydrogencarbonate, and water, and dried over $MgSO_4$. The solvent was removed in vacuo to give a solid, which was recrystallized from hexane-benzene to provide (+)-**4** (2.48 g, 92% yield), mp 192—194 °C; $[\alpha]_D^{22}$ +87.0° (*c* 0.159, EtOH). Found: C, 80.75; H, 6.36%. Calcd for $C_{17}H_{16}O_2$: C, 80.92; H, 6.39%.

(+)-4,8-Bis(hydroxymethyl)-2,3:6,7-dibenzobicyclo[3.3.1]nona-2,6-diene (5). A freshly prepared solution of diborane (44.1 mL, 16.5 mmol) in THF was slowly added to a solution of (−)-**3** (4.04 g, 16.5 mmol) in dry THF (100 mL), and then the mixture was stirred for 1 h at room temperature under nitrogen atmosphere. After addition of a small amount of water, the reaction mixture was concentrated in vacuo to give a solid (7.78 g). The solid was dissolved in THF (100 mL), 3 M aqueous solution of sodium hydroxide (35 mL) was added, and the mixture was heated at 40 °C. 30% hydrogen peroxide (5.7 g) was added to the mixture and it was heated for an additional 2 h at this temperature. After water (50 mL) was added to the mixture, the organic phase was withdrawn and the aqueous solution was extracted with ether. The combined organic solutions were washed with water, dried over $MgSO_4$, and concentrated to give a solid, which was recrystallized from benzene to afford (+)-**5** (3.88 g, 85% yield), mp 170—172 °C; $[\alpha]_D^{27}$ +143° (*c* 0.524, EtOH); ^{1}H NMR (DMSO-d_6) δ=2.18 (2H, t J=3 Hz), 3.21 (2H, br s), 3.50 (2H, br s), 4.0—4.1 (4H, m), 4.70 (2H, br s), 6.9—7.5 (8H, m). Found: C, 81.20; H, 7.15%. Calcd for $C_{19}H_{20}O_2$: C, 81.39; H, 7.19%.

(−)-20,21:23,24-Dibenzo-2,5,8,11,14,17-hexaoxatricyclo-[16.3.3.1^{19,22}]pentacosa-20,23-diene (6). To a suspension of NaH (140 mg, 5.83 mmol) in dry THF (30 mL) was slowly

added a mixture of (+)-**4** (500 mg, 1.98 mmol) and pentaethylene glycol ditosylate[10] (1.20 g, 2.20 mmol) in dry THF (60 mL) over a period of 6 h under reflux in nitrogen atmosphere. After the mixture was refluxed for an additional 24 h, a small amount of water was added to the reaction mixture and the mixture was concentrated in vacuo. The residue was extracted with dichloromethane and the extract was washed with diluted HCl and aqueous solution of sodium hydrogencarbonate, and dried over $MgSO_4$. The solvent was evaporated in vacuo and the residue was chromatographed on alumina (eluted with chloroform) to give a solid, which was recrystallized from hexane-benzene to furnish (−)-**6** (140 mg, 16% yield), mp 115—117 °C; $[\alpha]_D^{26}$ −1.5°, $[\alpha]_{435}^{27}$ +30.7° (*c* 0.384, $CHCl_3$); ^1H NMR ($CDCl_3$) δ=2.20 (2H, d *J*=3 Hz), 3.3—4.1 (22H, m), 4.67 (2H, d *J*=4.5 Hz), 6.9—7.5 (8H, m); MS *m/z* 454 (M^+). Found: C, 71.03; H, 7.44%. Calcd for $C_{27}H_{34}O_6$: C, 71.34; H, 7.54%.

(+)-17,18:20,21-Dibenzo-2,5,8,11,14-pentaoxatricyclo[13.3.3.1^{16,19}]docosa-17,20-diene (7) and (+)-35,36:38,39:40,41:42,43-Tetrabenzo-2,5,8,11,14,20,23,26,29,32-decaoxapentacyclo[31.3.3.2^{15,18}.2^{16,19}.1^{34,37}]tetratetracosa-35,38,40,42-tetraene (8). Condensation of (+)-**4** (500 mg, 1.98 mmol) with tetraethylene glycol ditosylate[10] (1.10 g, 2.19 mmol) and NaH (140 mg, 5.83 mmol) was carried out according to a similar procedure described for the preparation of **6**. After the same work-up, chromatography on alumina provided **7** (90 mg, 11% yield, eluted with benzene) and **8** (100 mg, 12% yield, eluted with benzene-chloroform 4:1 v:v).

7: Mp 72—74 °C (recrystallized from hexane-benzene); $[\alpha]_D^{25}$ +42.6° (*c* 0.402, $CHCl_3$); ^1H NMR ($CDCl_3$) δ=2.18 (2H, t *J*=3 Hz), 2.7—3.7 (18H, m), 5.20 (2H,d *J*=7.5 Hz), 7.0—7.6 (8H, m); MS *m/z* 410 (M^+). Found: C, 72.80; H, 7.29%. Calcd for $C_{25}H_{30}O_5$: C, 73.14; H, 7.37%.

8: Mp 166—168 °C (recrystallized from benzene); $[\alpha]_D^{25}$ +5.4° (*c* 0.459, $CHCl_3$); ^1H NMR ($CDCl_3$) δ=2.12 (4H, t *J*=3 Hz), 3.1—3.4 (4H, m), 3.6—4.1 (32H, m), 4.63 (4H, d *J*=4.5 Hz), 6.8—7.4 (16H, m); MS *m/z* 820 (M^+). Found: C, 72.85; H, 7.33%. Calcd for $C_{50}H_{60}O_{10}$: C, 73.14; H, 7.37%.

(+)-21,23:25,26-Dibenzo-3,6,9,12,15,18-hexaoxatricyclo[18.3.3.1^{21,24}]heptacosa-22,25-diene (9). To a suspension of NaH (130 mg, 5.42 mmol) in dry THF (30 mL) was added a mixture of (+)-**5** (500 mg, 1.81 mmol) and pentaethylene glycol ditosylate (1.10 g, 2.01 mmol) in dry THF (60 mL) over a period of 15 h under reflux and then the mixture was refluxed for an additional 29 h in nitrogen atmosphere. After the same work-up described for the preparation of **6**, the crude product was chromatographed on alumina. Fractions eluted with benzene gave (−)-**3** (53 mg, 12% yield) and fractions eluted with benzene-chloroform (9:1 v:v) gave (+)-**9** (100 mg, 12% yield) as a glassy solid, $[\alpha]_D^{23}$ +51.2° (*c* 0.775, $CHCl_3$); ^1H NMR ($CDCl_3$) δ=2.20 (2H, br s), 3.2—4.0 (28H, m), 7.0—7.6 (8H, m); MS *m/z* 482 (M^+). Found: C, 71.80; H, 7.88%. Calcd for $C_{29}H_{38}O_6$: C, 72.17; H, 7.94%.

(+)-19,20:22,23-Dibenzo-3,6,9,12,15-pentaoxatricyclo[15.3.3.1^{18,21}]tetracosa-19,22-diene (10). The reaction of (+)-**5** (500 mg, 1.81 mmol) with tetraethylene glycol ditosylate (1.00 g, 1.99 mmol) and NaH (130 mg, 5.42 mmol) was performed by the same procedure described for the preparation of **6**. Alumina chromatography gave (−)-**3** (95 mg, 39% yield, eluted with benzene) and (+)-**10** (87 mg, 11% yield, eluted with benzene-chloroform 9:1 v:v) as a glassy solid, $[\alpha]_D^{24}$ +24.0° (*c* 0.566, $CHCl_3$); ^1H NMR ($CDCl_3$) δ=2.20 (2H, m), 3.3—4.0 (24H, m), 7.0—7.6 (8H, m); MS *m/z* 402 (M^+). Found: C, 71.45; H, 8.35%. Calcd for $C_{24}H_{34}O_5$: C, 71.61; H, 8.51%.

General Procedure for the Preparation of Monotosylates. To a solution of 2-(2-methoxyethoxy)ethanol (5.00 g, 0.0416 mol) in pyridine (30 mL) was slowly added *p*-toluenesulfonyl chloride (11.9 g, 0.0624 mol) with ice-cooling, and the mixture was kept overnight in a refrigerator. The reaction mixture was poured into ice-water, acidified with hydrochloric acid, and extracted with benzene. The extract was washed with aqueous solution of sodium hydrogencarbonate and water, and dried over $MgSO_4$. The solvent was throughly removed in vacuo to give 10.2 g (90% yield) of 3,6-dioxaheptyl *p*-toluenesulfonate which was used in the next reaction without further purification. The other monotosylates were prepared by the same procedure described here.

(−)-4,8-Dimethoxy-2,3:6,7-dibenzobicyclo[3.3.1]nona-2,6-diene (11). A mixture of (+)-**4** (302 mg, 1.20 mmol), NaH (115 mg, 4.79 mmol), and dry DMF (30 mL) was heated at 45 °C for 1 h. A solution of methyl *p*-toluenesulfonate (894 mg, 4.80 mmol) in dry DMF (20 mL) was added to the reaction mixture at 45 °C and then it was heated for an additional 48 h at 45—50 °C. After a small amount of water was added to the reaction mixture at room temperature, a solid was filtered off and the filtrate was concentrated in vacuo. To the residue was added diluted HCl and a precipitated solid was collected, washed with water, and recrystallized from ether-hexane to give (+)-**11** (190 mg, 57% yield), mp 169—170 °C; $[\alpha]_D^{25}$ +15.0° (*c* 0.360, $CHCl_3$); ^1H NMR ($CDCl_3$) δ=2.29 (2H, t *J*=3 Hz), 3.3—3.5 (2H, m), 3.70 (6H, s), 4.54 (2H, d *J*=5.2 Hz), 7.0—7.5 (8H, m). Found: C, 81.20; H, 7.16%. Calcd for $C_{19}H_{20}O_2$: C, 81.39; H, 7.19%.

(−)-4,8-(1,3-dioxapentyl)-2,3:6,7-dibenzobicyclo[3.3.1]-nona-2,6-diene (12). To a suspension of NaH (144 mg, 6.00 mmol) in dry DMF (30 mL) was added (+)-**4** (378 mg, 1.50 mmol) and the mixture was stirred for 1 h at room temperature. A solution of 3-oxabutyl *p*-toluenesulfonate (863 mg, 3.75 mmol) in dry DMF (20 mL) was added to the reaction mixture and then it was stirred for 24 h at 45—50 °C in nitrogen atmosphere. After a small amount of water was added to the reaction mixture, the solvent was removed in vacuo. The residue was extracted with chloroform and the extract was washed with water, dried over $MgSO_4$, and concentrated in vacuo. The residue was chromatographed on alumina and fractions eluted with hexane-benzene (1:1 v:v) gave a solid, which was recrystallized from hexane to provide (−)-**12** (435 mg, 79% yield), mp 66—67 °C; $[\alpha]_D^{20}$ −10.3° (*c* 0.283, $CHCl_3$); ^1H NMR ($CDCl_3$) δ=2.30 (2H, t *J*=3 Hz), 3.40 (6H, s), 3.3—4.3 (10H, m), 4.74 (2H, d *J*=5.2 Hz), 7.0—7.5 (8H, m). Found: C, 75.11; H, 7.70%. Calcd for $C_{23}H_{28}O_4$: C, 74.97; H, 7.66%.

(−)-4,8-Bis(1,4,7-trioxaoctyl)-2,3:6,7-dibenzobicyclo[3.3.1]-nona-2,6-diene (13). By using the same procedure described for the preparation of (−)-**12**, the compound **13** (650 mg, 86% yield) was obtained from (+)-**4** (470 mg, 1.66 mmol), 3,6-dioxaheptyl *p*-toluenesulfonate (1.14 mg, 4.15 mmol), and NaH (159 mg, 6.64 mmol) as a colorless oil after chromatography on alumina (eluted with hexane-benzene 1:1 v:v); $[\alpha]_D^{20}$ −34.0° (*c* 0.351, $CHCl_3$); ^1H NMR ($CDCl_3$) δ=2.32 (2H, t *J*=3 Hz), 3.36 (6H, s), 3.3—4.2 (18H, m), 4.74 (2H, d *J*=5.2 Hz), 7.0—7.5 (8H, m); MS *m/z* 456 (M^+). Found:

C, 69.98; H, 7.90%. Calcd for $C_{27}H_{36}O_6$: C, 71.02; H, 7.95%.

(−)-4,8-Bis(1,4,7,10-tetraoxaundecyl)-2,3:6,7-dibenzobicyclo-[3.3.1]nona-2,6-diene (14). The compound **14** (205 mg, 25% yield) was obtained from (+)-**4** (378 mg, 1.50 mmol), 3,6,9-trioxadecyl *p*-toluenesulfonate (1.19 g, 3.75 mmol), and NaH (144 mg, 6.00 mmol) as a colorless oil after chromatography on alumina (eluted with hexane–benzene 1:1 v:v); $[\alpha]_D^{20}$ −10.5° (*c* 0.721, $CHCl_3$); ^1H NMR ($CDCl_3$); δ=2.19 (2H, t *J*=3 Hz), 3.30 (6H, s), 3.3—4.2 (26H, m), 3.73 (2H, d *J*=4.5 Hz), 6.9—7.5 (8H, m); MS *m/z* 544 (M^+). Found: C, 68.28; H, 8.08%. Calcd for $C_{31}H_{44}O_8$: C, 68.36; H, 8.14%.

(+)-4,8-Bis(1,4,7-trioxanonyl)-2,3:6,7-dibenzobicyclo[3.3.1]-nona-2,6-diene (15). The compound **15** (250 mg, 34% yield) was obtained from (+)-**4** (378 mg, 1.50 mmol), 3,6-dioxaoctyl *p*-toluenesulfonate (1.08 g, 3.75 mmol), and NaH (144 mg, 6.00 mmol) as a colorless oil after chromatography on alumina (eluted with benzene); $[\alpha]_D^{22}$ +40.0° (*c* 0.520, $CHCl_3$); ^1H NMR ($CDCl_3$) δ=1.18 (6H, t *J*=6.8 Hz), 2.30 (2H, t *J*=3.2 Hz), 3.48 (4H, q *J*=6.8 Hz), 3.2—4.2 (18H, m), 4.74 (2H, d *J*=5.3 Hz), 7.0—7.6 (8H, m); MS *m/z* 484 (M^+). Found: C, 71.77; H, 8.28%. Calcd for $C_{29}H_{40}O_6$: C, 71.87; H, 8.32%.

(−)-4,8-Bis(1,4,7-trioxaundecyl)-2,3:6,7-dibenzobicyclo[3.3.1]-nona-2,6-diene (16). The compound **16** (380 mg, 54% yield) was obtained from (+)-**4** (327 mg, 1.30 mmol), 3,6-dioxadecyl *p*-toluenesulfonate (1.03 g, 3.25 mmol), and NaH (125 mg, 5.21 mmol) as a colorless oil after chromatography on alumina (eluted with benzene); $[\alpha]_D^{23}$ −9.80° (*c* 0.806, $CHCl_3$); ^1H NMR ($CDCl_3$) δ=0.88 (6H, t *J*=7 Hz), 1.0—1.7 (8H, m), 2.29 (2H, t *J*=3 Hz), 3.3—4.2 (22H, m), 4.74 (2H, d *J*=5.2 Hz), 7.0—7.5 (8H, m); MS *m/z* 540 (M^+). Found: C, 73.19; H, 8.89%. Calcd for $C_{33}H_{48}O_6$: C,73.30; H, 8.95%.

(−)-4,8-Bis(8-phenyl-1,4,7-trioxaoctyl)-2,3:6,7-dibenzo-bicyclo[3.3.1]nona-2,6-diene (17). The compound **17** (339 mg, 25% yield) was prepared from (+)-**4** (378 mg, 1.50 mmol), 7-phenyl-3,6-dioxaheptyl *p*-toluenesulfonate (1.31 g, 3.75 mmol), and NaH (144 mg, 6.00 mmol) as a colorless oil after chromatography on alumina (eluted with benzene); $[\alpha]_D^{22}$ −5.91° (*c* 0.551, $CHCl_3$); ^1H NMR ($CDCl_3$) δ=2.25 (2H, t *J*=3.2 Hz), 3.3—4.2 (20H, m), 4.72 (4H, d *J*=5.2 Hz), 7.0—7.5 (18H, m); MS *m/z* 608 (M^+). Found: C, 76.78; H, 7.15%. Calcd for $C_{39}H_{44}O_6$: C, 76.94; H, 7.29%.

Extraction Procedure. The aqueous solution (5 mL) of the metal picrate (2.4×10^{-4} M) and the chloroform solution (5 mL) containing the crown ether (2.4×10^{-4} M) were placed in a screw cap glass tube (30 mL) and the tube was shaken for 30 min at room temperature. Extraction of the picrate was followed by monitoring the absorbance at 357 nm of the aqueous phase.

Enantiomer Differential Transport. Enantiomer differential transport was carried out in a conventional apparatus which consisted of an outer cylindrical glass vessel (24.5 mm inner diameter) and a central glass tube (15.5 mm inner diameter). The 0.01 M chloroform solution of the optically active host molecule separated the inner aqueous phase (0.1 M hydrochloric acid) and the outer aqueous phase (0.08 M hydrochloric acid) which contained $LiPF_6$ (0.4 M) and the racemic guest molecule (0.08 M). The chloroform layer was gently stirred at a constant speed (60 rpm) at 20—25 °C, and transport was monitored by ultraviolet spectra and enantiomeric excess of the guest molecule transported was monitored by circular dichroism.

The present work was partially supported by a Grant-in-Aid for Scientific Research (No. 61540372) from the Ministry of Education, Science and Culture.

References

1) G. W. Gokel and S. H. Korzeniowski, "Macrocyclic Polyether Syntheses," Springer-Verlag, Berlin, Heiderberg, and New York (1982).

2) F. Vögtle and E. Weber, *Angew. Chem., Int. Ed. Engl.*, **18**, 753 (1979); E. Weber and F. Vögtle, *Inorg. Chim. Acta*, **45**, L65 (1980).

3) K. Naemura, I. Ebashi, A. Matsuda, and H. Chikamatsu, *J. Chem. Soc., Chem. Commun.*, **1986**, 666.

4) H. Tatemitsu, F. Ogura, Y. Nakagawa, M. Nakagawa, K. Naemura, and M. Nakazaki, *Bull. Chem. Soc. Jpn.*, **48**, 2473 (1975).

5) R. J. Anderson and C. A. Henrick, *J. Am. Chem. Soc.*, **97**, 4327 (1975).

6) K. Naemura, R. Fukunaga, and M. Yamanaka, *J. Chem. Soc., Chem. Commun.*, **1985**, 1560.

7) H. L. Rosano, J. H. Schulman, and J. B. Weisbuch, *Ann. N.Y. Acad. Sci.*, **92**, 457 (1961); B. Pressman, E. J. Harris, W. S. Jagger, and J. H. Johnson, *Proc. Natl. Acad. Sci. U.S.A.*, **58**, 1949 (1967).

8) K. Yamamoto, H. Fukushima, Y. Okamoto, K. Hatada, and M. Nakazaki, *J. Chem. Soc., Chem. Commun.*, **1984**, 1111.

9) G. Wittig and U. Schoellkopf, *Org. Synth.*, **40**, 66 (1960).

10) M. Newcomb, S. S. Moore, and D. J. Cram, *J. Am. Chem. Soc.*, **99**, 6405 (1977).

 © 1989 The Chemical Society of Japan Bull. Chem. Soc. Jpn., 62, 89—95 (1989)

The Decomposition of Arenediazonium Tetrafluoroborates with Halo- and Azidotrimethylsilanes in Nonaqueous Solvents

Takashi KEUMI,* Toshiaki UMEDA, Yoshinori INOUE,† and Hidehiko KITAJIMA
Department of Applied Chemistry, Faculty of Engineering, Fukui University, Bunkyo, Fukui 910
†Department of Industrial Chemistry, Shiga Prefectural Junior College, Hassaka-cho, 1900, Hikone 522
(Received June 4, 1988)

The reaction of arenediazonium tetrafluoroborates with chlorotrimethylsilane in a tetrahydrofuran/*N*,*N*-dimethylformamide (DMF) (5v/3v) solution afforded the protodediazotization products in high yields. The reactions of the diazonium salts with halotrimethylsilanes in DMF were found to give the corresponding haloarenes. Among the halodediazotization reactions, the iododediazotization with iodotrimethylsilane proceeded smoothly at room temperature to give the iodoarenes in excellent yields. In a similar manner, a variety of azidoarenes were obtained in consistently high yields by the treatment of arenediazonium tetrafluoroborates with azidotrimethylsilane in a DMF solution.

The reaction of arenediazonium salts is among the first to be studied in organic chemistry, and it has since been extensively studied not only because of its fundamental importance but also because of its industrial importance.[1] Arenediazonium halides, which are usually unstable, are prepared in situ by the diazotization of arylamines with sodium nitrite in an aqueous solution containing a mineral acid at a low temperature; subsequent reactions are immediately conducted in the same solution. The reactions carried out in the aqueous solution, however, frequently give rise to some by-products besides the desired products. For the purpose of lowering the amount of undesired products, there has been an attempt to use an isolated arenediazonium tetrafluoroborate salt in a nonaqueous medium. However, most of the tetrafluoroborate salts are too stable to be decomposed, and they are less soluble in organic solvents. Therefore, the decomposition of the diazonium salts has been performed by the addition of a strong base,[2] metals such as powdered zinc,[3] copper,[4] and copper(I) oxide,[5] or organometallic compounds, such as rhodium complexes[6] and tributyltin hydride.[7] Crown ether compounds,[4] poly(ethylene glycol),[8] or phase-transfer catalysts[9] have been used to improve the low solubility of the diazonium salts in organic solvents.

We have found that arenediazonium tetrafluoroborates readily decompose in the presence of halo- and azidotrimethylsilanes in a *N*,*N*-dimethylformamide (DMF) solution to afford the corresponding reduction products or substituted arenes in satisfactory yields. We wish to report herein the protodediazotization and halodediazotization induced by halotrimethylsilanes. The preparation of azidoarenes by the reaction of arenediazonium tetrafluoroborates with azidotrimethylsilane will also be reported.

$$ArN_2BF_4 \xrightarrow[\text{in DMF}]{Me_3SiX} ArY \qquad (1)$$

X = Cl, Br, I, N_3
Y = H, Cl, Br, I, N_3

Results and Discussion

The decomposition of 2-fluorenediazonium tetrafluoroborate was attempted in the presence of chlorotrimethylsilane (CTMS) in organic solvents. The results are summarized in Table 1. The diazonium salt was readily decomposed in a tetrahydrofuran (THF) suspension in the presence of an equivalent of CTMS at 60 °C for 10 min to give fluorene in a 69% yield and a trace amount of 2-chlorofluorene. The evolution of nitrogen gas was completed within ten minutes at 60 °C. In contrast, the salt was stable under these conditions in the absence of CTMS. The protodediazotization product was obtained in only a 13% yield, even after the salt has been heated under reflux for 90 min in a THF medium. Therefore, CTMS appears to induce the decomposition of the diazonium tetrafluoroborate. The homogeneous reaction conducted in DMF, which dissolved the salt, did not improve the yield of the protodediazotization product. On using a DMF/THF combined medium, however, the product yield was remarkably increased. In an attempt to apply this procedure as a general method for a reductive dediazotization, some arenediazonium tetrafluoroborates were subjected to a decomposition reaction with CTMS in a solution of THF/DMF (5v/3v) at 60 °C for 1 h. The results are shown in Table 2. Consistently high yields of the reductive dediazotization product were observed in a variety of arenediazonium tetrafluoroborates.

The decomposition of 2-fluorenediazonium tetrafluoroborate with halotrimethylsilanes in DMF or *N*,*N*-dimethylacetamide (DMA) was attempted in the presence of a halogenating reagent. The results are shown in Table 3. Although the reaction of 2-fluorenediazonium tetrafluoroborate with CTMS in DMF afforded only 2% of 2-chlorofluorene, the addition of *N*-chlorosuccinimide (NCS) to the reaction mixture increased the formation of the chloride to a 39% yield. In the reaction carried out in a solution of DMA/car-

Table 1. Protodediazotization of 2-Fluorenediazonium Tetrafluoroborate with Chlorotrimethylsilane (CTMS)[a]

Run	CTMS[c]	Solvent	Time	Yield of fluorene[b]
			min	%
1	None	Tetrahydrofuran (THF)	10	4
2	None	THF	20	6
3	None	THF	90	13
4	1.2	THF	10	69
5	1.2	THF	20	74
6	1.2	THF	60	76
7	1.2	*N,N*-Dimethylformamide (DMF)	60	63
8	1.2	THF/DMF (1v/1v)	60	78
9	1.2	THF/DMF (5v/3v)	60	98

a) Carried out at 60 °C. b) Determined by GLC using dibenzofuran as the internal standard. c) Molar equivalents to the diazonium tetrafluoroborate.

Table 2. Protodediazotization of Arenediazonium Tetrafluoroborates with Chlorotrimethylsilane[a]

Run	Ar (of ArN_2BF_4)	Yield of ArH/%[b]	Mp θ_m/°C	
			Found	Reported[10]
1	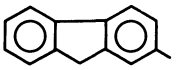	95	114—115	115—116
2	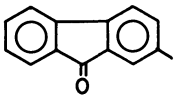	91	79—80	84—85
3	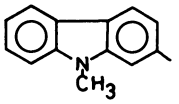	87	86—87	86—87
4	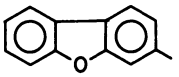	88	82—83	83—84
5	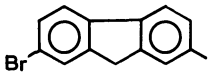	78	112	112—114
6	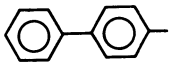	98	67—68	68—71
7	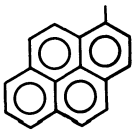	91	138—141	149—153

a) All the reactions were carried out in a solution of THF/DMF (5v/3v) in the presence of 1.2 equivalents of chlorotrimethylsilane at 60 °C for 1 h. b) Isolated yield.

bon tetrachloride in the presence of NCS, the yield of the chloride was increased to 59%. Similarly, the diazonium salt was decomposed with bromotrimethylsilane in the presence of *N*-bromosuccinimide (NBS) in a DMA solution to give 2-bromofluorene in a 71% yield, while the decomposition without NBS gave the bromide and the reduction products in 41% and 51% yields respectively.

On the other hand, the drop-by-drop addition of iodotrimethylsilane to a solution of 2-fluorenediazonium tetrafluoroborate in DMF violently evolved nitrogen gas at room temperature to give 2-iodofluorene and the reduction product in 55% and 30% yields respectively. The addition of iodomethane into the reaction mixture increased the fomation of 2-iodofluorene. The yield of the iodide increased with an increase in the amount of iodomethane added. Finally, 2-iodofluorene was obtained in a 98% yield in the reaction using a medium of iodomethane mixed with a minimum amount of DMF to dissolve the diazonium salt.

Table 3. Halodediazotization of 2-Fluorenediazonium Tetrafluoroborate with Halotrimethylsilane (X-TMS, X=Halide)[a]

Run	X	Additives (Molar equiv)	Solvent	Temp/°C	Product yield/%[b]	
					2-X-Fluorene	Fluorene
1	Cl	—	DMF	60	2	63
2	Cl	*N*-Chlorosuccinimide (NCS) (3)	DMF	60	39	41
3	Cl	NCS (3)	DMF/CCl_4 (1v/1v)	60	37	36
4	Cl	NCS (3)	DMA[c]/CCl_4 (1v/1v)	60	59	35
5	Br	—	DMF	60	41	51
6	Br	*N*-Bromosuccinimide (NBS) (1.5)	DMF	60	67	13
7	Br	NBS (3)	DMA	60	71	12
8	I	—	DMF	RT[d]	55	30
9	I	Methyl iodide (MI) (1.5)	DMF	RT	62	23
10	I	MI (3)	DMF	RT	77	13
11	I	MI (3)	DMA	RT	75	11
12	I	MI (33)	DMF	RT	98	Trace

a) Carried out with 1.2 equivalents of halotrimethylsilane. b) Determined by GLC using dibenzofuran as the internal standard. c) *N*,*N*-Dimethylacetamide. d) Room temperature.

Table 4. Iododediazotization of Arenediazonium Tetrafluoroborates with Iodotrimethylsilane[a]

Run	Ar (of ArN_2BF_4)	Yield/%[b]	Mp θ_m/°C	
			Found	Reported
1	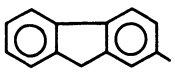	95	127—128	128[11]
2	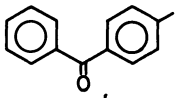	96	99—100	100—101[10]
3	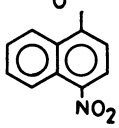	93	122—123	123[10]
4	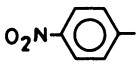	91	171—172	174[10]
5	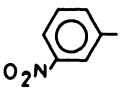	96	34—35	39[10]
6	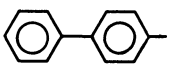	97	112—113	113—114[10]
7	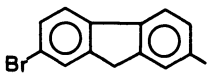	93	177—178	—
8	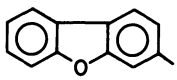	95	143—145	—

a) All the reactions were carried out in a solution of DMF/CH_3I in the presence of 1.2 equivalents of iodotrimethylsilane at room temperature for 1 h. b) Isolated yields.

This reaction procedure was also applied to the preparation of iodoarenes. Using the optimized conditions defined above, a variety of arenediazonium tetrafluoroborates were converted into the corresponding iodoarenes. The results are summarized in Table 4. 4-Iodobenzophenone, 1-iodo-4-nitronaphthalene, 4-iodo- and 3-iodo-1-nitrobenzenes, 4-iodobiphenyl, 7-bromo-2-iodofluorene, and 3-iododibenzofuran were obtained in excellent yields by this method.

When azidotrimethylsilane dissolved in DMF was

Table 5. Preparation of Azidoarenes by the Reaction of Arenediazonium Tetrafluoroborates with Azidotrimethylsilane[a]

Run	Ar (of ArN_2BF_4)	Yield/%[b]	Mp θ_m/°C	
			Found	Reported
1	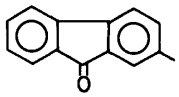	99	114—115	117[12]
2	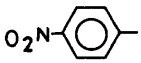	86	70—71	70—71[13]
3	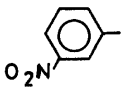	77	53—54	52[13]
4	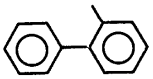	90	49—50	49—50[14]
5	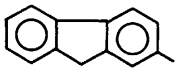	95	103—104	—
6	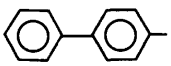	99	74—75	—
7	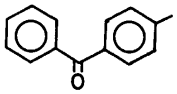	92	70—71	—
8	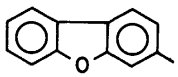	94	115—116	—
9	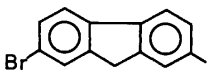	91	129—130	—
10	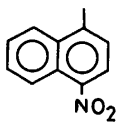	95	96—97	—

a) All the reactions were carried out in a solution of DMF in the presence of 1.2 equivalents of azidotrimethylsilane at room temperature for 1 h. b) Isolated yields.

added to a solution of 2-fluorenediazonium tetrafluoroborate in DMF at room temperature, nitrogen gas was immediately evolved to give 2-azidofluorene in an almost pure form in a 95% yield. No significant amount of the reduction product was observed. A variety of arenediazonium tetrafluoroborates were then reacted with azidotrimethylsilane in the DMF solution at room temperature. The yields and melting points of isolated azidoarenes are summarized in Table 5.

In all the cases examined here, the corresponding azidoarenes were obtained in satisfactory yields. The products, 2-azidofluorene, 4-azidobiphenyl, 4-azidobenzophenone, 3-azidodibenzofuran, 2-azido-7-bromofluorene, and 1-azido-4-nitronaphthalene, are new compounds. The IR spectra of these azides show the characteristic absorption peaks at 2180—2270 cm^{-1} due to the azide function. Their ^1H NMR spectral data are consistent with the desired structure.

Thus, halotrimethylsilanes (Cl, Br, I as the halide) and azidotrimethylsilane have been found to facilitate the decomposition of arenediazonium tetrafluoroborates to give the protodediazotization products or the corresponding haloarenes and azidoarenes. The acceleration effects of the trimethylsilyl compounds on the decomposition of 2-fluorenediazonium tetrafluoroborate in a DMF solution were in the sequence of: azido->iodo->bromo->chlorotrimethylsilanes. The ratio of halogenation to reduction products in the decomposition with halotrimethylsilanes was increased with the order of: iodo->bromo->chlorotrimethylsi-

lanes. According to the Hard and Soft Acids and Bases (HSAB) principle developed by Pearson,[15] the trimethylsilyl cation belongs to a hard acid group, while the halide ions, Br^- and I^-, and the azide ion, N_3^-, are classified as soft bases, the softness order being; $I^- > N_3^- > Br^- > Cl^-$. On the other hand, the tetrafluoroborate ion seems to be a hard base,[16] accounting for its good affinity to a hard acid, the trimethylsilyl cation. When CTMS is added to a solution of arenediazonium tetrafluoroborate in DMF, the hard acid species, the trimethylsilyl cation, would catch the hard-base anion, BF_4^-, to result in the formation of fluorotrimethylsilane, boron trifluoride, and arenediazonium chloride. This resultant diazonium chloride is usually less stable than the starting diazonium tetrafluoroborates, so it readily decomposes to give the corresponding chloroarenes or reduction products. The decomposition in the presence of the chlorinating reagent NCS increased the formation of chloroarenes. The addition of THF to the reaction medium DMF also remarkably increased the formation of the protodediazotization product. The decomposition appears to proceed by means of a radical mechanism. The decomposition with bromo-, iodo-, and azidotrimethylsilanes would also proceed by means of a process similar to that described above (Eqs. 2 and 3). The formation of fluorotrimethylsilane and boron trifluoride as well as the substituted arene was confirmed by ^1H NMR measurements of the reaction mixture of benzenediazonium tetrafluoroborate and azidotrimethylsilane in DMF/deuteriochloroform solutions. The full details of the confirmation will be given in the Experimental section.

$$ArN_2BF_4 + Me_3SiX \longrightarrow ArN_2X + Me_3SiF + BF_3 \quad (2)$$

$$ArN_2X \longrightarrow ArX + N_2 \quad (3)$$

The decompositions with iodo- and azidotrimethylsilanes proceed much more smoothly than that with CTMS. This may be due to the ease of both the exchange of the counter anion and the decomposition of the resultant diazonium salts.

In conclusion, halo- and azidotrimethylsilanes were found to be effective for the decomposition of arenediazonium tetrafluoroborates, which are usually difficult to decompose. Reduction products and haloarenes were obtained in satisfactory yields by the reaction of arenediazonium tetrafluoroborates with halotrimethylsilanes in a DMF solution. Azidoarenes were obtained in excellent yields by the reaction of arenediazonium tetrafluoroborates with azidotrimethylsilane. These reactions can be conducted in a DMF medium under mild conditions. There is no need to use any complex catalysts for the decompositions or any expensive additives to achieve dissolution in organic solvents. Thus, the reaction procedures described here will be useful for the preparation of arenes, haloarenes, and azidoarenes from arenediazonium tetrafluoroborates.

Experimental

Materials and Measurements. The melting points are uncorrected. The IR spectra were recorded on a Hitachi EPI-S2 model infrared spectrophotometer. The ^1H NMR spectra were recorded on a JEOL-FX 270 FT-NMR spectrometer in deuteriochloroform solutions, with teramethylsilane as the internal standard. GLC analysis was carried out on a Hitachi GC Model 163 gas chromatograph equipped with a hydrogen-flame ionization detector and a stainless steel column (length 3 m, i.d. 3 mm) packed with 3% Dexil 300 GC on Chromosorb W.

Preparation of Arenediazonium Tetrafluoroborates. All the diazonium salts were prepared by standard techniques (Ref. 17). The following salts have not been found in the above references. The yields, decomposition temperatures, and IR data for them are as follows.

1-Pyrenediazonium Tetrafluoroborate: 100% yield; mp 135—137 °C (decomp); IR (KBr) 2200, 1620, 1470, and 851 cm^{-1}.

9-Methyl-2-carbazolediazonium Tetrafluoroborate: 88% yield; mp 161—163 °C (decomp); IR (KBr) 2210, 1578, 1452, and 750 cm^{-1}.

3-Dibenzofurandiazonium Tetrafluoroborate: 69% yield; mp 160—163 °C (decomp); IR (KBr) 2260, 1626, 1432, 1200, and 750 cm^{-1}.

9-Oxo-2-fluorenediazonium Tetrafluoroborate: 89% yield; mp 159—162 °C (decomp); IR (KBr) 2275, 1723, 1608, 1590, and 765 cm^{-1}.

7-Bromo-2-fluorenediazonium Tetrafluoroborate: 90% yield; mp 139—140 °C (decomp); IR (KBr) 2230, 1591, 1170, and 818 cm^{-1}.

Protodediazotization Reactions. One procedure for the protodediazotization of 2-fluorenediazonium tetrafluoroborate is described as typical. Into a solution of 2-fluorenediazonium tetrafluoroborate (0.200 g; 0.714 mmol) in DMF (3 mL) cooled in an ice water bath, we added portion by portion a solution of CTMS (0.093 g; 0.857 mmol) in THF (5 mL) with stirring. After the mixture has then been heated at 60 °C with stirring for 1 h, it was poured into water. The resulting solid was filtered and washed with water to give fluorene (0.117 g; 98% yield; mp 104—107 °C). The recrystallization of the solid from ethanol gave a product with the mp of 114—115 °C (lit,[10] mp 115—116 °C).

Halodediazotization Reactions. The iododediazotization of 2-fluorenediazonium tetrafluoroborate will be described as a typical method. To a solution of iodotrimethylsilane (0.171 g; 0.857 mmol) and iodomethane (1.5 mL), we added drop by drop a solution of 2-fluorenediazonium tetrafluoroborate (0.200 g; 0.714 mmol) in DMF (1.5 mL) at room temperature under a nitrogen stream. After this addition, the mixture was stirred for 1 h at room temperature, poured into ice water, and then extracted with dichloromethane. The organic layer was washed with water and dried over anhydrous sodium sulfate. After the evaporation of the solvent, crude 2-iodofluorene was obtained (0.198 g; 95% yield; mp 126—127 °C). The recrystallization of the product from 80% ethanol gave a product with the mp of 127—128 °C (lit,[11] mp 128 °C). In a similar manner, the following iodoarenes were prepared.

3-Iododibenzofuran: 95% yield; mp 143—144 °C (from 90% EtOH); IR (KBr) 1453, 1440, 1183, 868, 810, and 748 cm^{-1}; ^1H NMR ($CDCl_3$) δ=7.32—7.70 (m, 5H) and 7.90—9.93 (m, 2H).

Found: C, 48.85; H, 2.38%. Calcd for $C_{12}H_7OI$: C, 49.01; H, 2.40%.

7-Bromo-2-iodofluorene: 93% yield; mp 177—178 °C (from EtOH); IR (KBr) 1452, 1393, 1003, and 802 cm^{-1}; ^1H NMR ($CDCl_3$) δ=3.85 (s, 2H, CH_2) and 7.47—7.87 (m, 6H).

Found: C, 41.83; H, 2.17%. Calcd for $C_{13}H_8BrI$: C, 42.09; H, 2.17%.

By means of a similar procedure, chlorodediazotization and bromodediazotization reactions of 2-fluorenediazonium tetrafluoroborates with CTMS and bromotrimethylsilane were carried out in the presence of NCS and NBS respectively.

Preparation of Azidoarenes. Into a solution of 2-fluorenediazonium tetrafluoroborate (0.200 g; 0.714 mmol) in DMF (1.5 mL), we dropped a solution of azidotrimethylsilane (0.099 g; 0.857 mmol) in DMF (1.5 mL) at room temperature. After the mixture has then been stirred for 1 h at that temperature, it was poured into ice water (about 100 mL). The resulting precipitate was filtered, washed with water, and dried to give 2-azidofluorene (0.14 g; 95% yield; mp 102—104 °C). The recrystallization of the solid from 80% ethanol gave a product with the mp of 103—104 °C; IR (KBr) 2200, 1580, 1450, 1289, and 761 cm^{-1}; ^1H NMR ($CDCl_3$) δ=3.88 (s, 2H, CH_2), 7.03 (d, J=3.0 Hz, 1H), 7.20 (s, 1H), 7.25—7.40 (m, 2H), 7.52 (d, J=8 Hz, 1H), and 7.72 (d, J=3 Hz, 2H).

Found: C, 75.54; H, 4.08; N, 20.19%. Calcd for $C_{13}H_9N_3$: C, 75.35; H, 4.38; N, 20.28%.

By a similar procedure, the following azidoarenes were prepared.

4-Azidobenzophenone: 92% yield; mp 70—71 °C (70% EtOH); IR (KBr) 2200, 1645, 1598, 1280, and 713 cm^{-1}; ^1H NMR ($CDCl_3$) δ=7.12 (d, J=3 Hz, 2H), 7.46—7.60 (m, 3H), 7.77 (d, J=3 Hz, 2H), and 7.85 (d, J=3 Hz, 2H).

Found: C, 69.95; H, 4.17; N, 18.51%. Calcd for $C_{13}H_9N_3O$: C, 69.95; H, 4.06; N, 18.82%.

1-Azido-4-nitronaphthalene: 95% yield; mp 96—97 °C (80% EtOH); IR (KBr) 2270, 1573, 1285, and 761 cm^{-1}; ^1H NMR ($CDCl_3$) δ=7.27 (d, J=3 Hz, 1H), 7.63 (t, J=3 Hz, 1H), 7.78 (t, J=3 Hz, 1H), 8.23 (d, J=3 Hz, 1H), 8.34 (d, J=3 Hz, 1H), and 8.68 (d, J=3 Hz, 1H).

Found: C, 56.42; H, 2.64; N, 25.85%. Calcd for $C_{10}H_6N_4O_2$: C, 56.08; H, 2.82; N, 26.16%.

4-Azidobiphenyl: 99% yield; mp 74—75 °C (80% MeOH); IR (KBr) 2200, 1485, 1290, 833, and 760 cm^{-1}; ^1H NMR ($CDCl_3$) δ=7.09 (d, J=3 Hz, 2H), 7.31—7.45 (m, 3H), and 7.54—7.59 (m, 4H).

Found: C, 73.60; H, 4.77; N, 21.37%. Calcd for $C_{12}H_9N_3$: C, 73.83; H, 4.65; N, 21.52%.

3-Azidodibenzofuran: 94% yield; mp 115—116 °C (70% EtOH); IR (KBr) 2200, 1602, 1453, 1288, and 779 cm^{-1}; ^1H NMR ($CDCl_3$) δ=7.03 (dd, J=3, 0.7 Hz, 1H), 7.23 (d, J=0.7 Hz, 1H), 7.34 (td, J=3, 0.4 Hz, 1H), 7.44 (td, J=3, 0.5 Hz, 1H), 7.55 (d, J=3 Hz, 1H), and 7.89 (d, J=3 Hz, 2H).

Found: C, 69.21; H, 3.52; N, 20.00%. Calcd for $C_{12}H_7N_3O$: C, 68.89; H, 3.37; N, 20.09%.

2-Azido-7-bromofluorene: 91% yield; mp 129—130 °C (80% EtOH); IR (KBr) 2200, 1613, 1457, 1293, and 798 cm^{-1}; ^1H NMR ($CDCl_3$) δ=3.85 (s, 2H, CH_2), 7.03 (dd, J=3, 0.7 Hz, 1H), 7.18 (s, 1H), and 7.47—7.70 (m, 4H).

Found: C, 54.45; H, 2.53; N, 14.54%. Calcd for $C_{13}H_8BrN_3$: C, 54.57; H, 2.83; N, 14.69%.

Confirmation of the Formation of Fluorotrimethylsilane and Boron Trifluoride. To a solution of benzenediazonium tetrafluoroborate (0.003 g) in DMF/deuteriochloroform (2v/8v) (1 mL) containing tetramethylsilane, we added a few drops of azidotrimethylsilane at 0—5 °C. After gas evolution had ceased, the mixture was subjected to ^1H NMR measurement at 27 °C. The NMR spectrum showed singlet peaks at 8.28, 3.36, 3.17, and 0.068 ppm in addition to the peaks due to DMF [7.99 (s, 1H), 2.96 (s, 3H), 2.85 (s, 3H)], azidobenzene [7.36 (t, 2H, J=7.3 Hz), 7.14 (t, 1H, J=7.3 Hz), 7.03 (d, 2H, J=8.3 Hz)], and azidotrimethylsilane [0.27 (s)]. The former three singlets (in a relative intensity of 1:3:3) were identified with those due to the DMF-boron trifluoride complex by comparing them with those observed in the ^1H NMR spectrum of a mixture of DMF and ethyl ehterboron trifluoride (1/1) in deuteriochloroform. The later singlet was identified as the peak due to fluorotrimethylsilane by being in accord with the chemical shift of that prepared from azidotrimethylsilane and KF in DMF/deuteriochloroform (2v/8v) solutions.

We wish to thank Fukui Chemical Industry Co. for its financial support of this work.

References

1) H. Zollinger, *Acc. Chem. Res.*, **6**, 335 (1973); H. Zollinger, *Angew. Chem., Int. Ed. Engl.*, **17**, 141 (1979); H. B. Ambroz and T. J. Kemp, *Chem. Soc. Rev.*, **8**, 353 (1979); Y. Hashida and S. Sekiguchi, *Yuki Gosei Kagaku Kyokai Shi*, **40**, 752 (1982).

2) P. R. Singh, B. Jayaraman, and H. K. Sing, *Chem. Ind.*, **1977**, 311.

3) A. Roe and J. R. Graham, *J. Am. Chem. Soc.*, **74**, 6297 (1952).

4) G. D. Hartman and S. E. Biffar, *J. Org. Chem.*, **42**, 1468 (1977).

5) A. H. Lewin and T. Cohen, *J. Org. Chem.*, **32**, 3844 (1967); S. H. Korzeniowski, L. Blum, and G. W. Gokel, *J. Org. Chem.*, **42**, 1469 (1977).

6) L. Toniolo and R. Eisenberg, *J. Chem. Soc., Chem. Commun.*, **1971**, 455; G. S. Max, *J. Org. Chem.*, **36**, 1725 (1971).

7) J. Nakayama, M. Yoshida, and O. Shimamura, *Tetrahedron*, **26**, 4609 (1970).

8) N. Suzuki, Y. Kaneko, T. Nomoto, and Y. Izawa, *J. Chem. Soc., Chem. Commun.*, **1984**, 1523.

9) S. H. Korzeniowski, L. Blum, and G. W. Gokel, *Tetrahedron Lett.*, **1977**, 1871.

10) H. Heibron, "Dictionary of Organic Compounds," Maruzen, Tokyo (1965).

11) A. Korczynski, G. Karlowska, and L. Kierzek, *Bull. Soc. Chim.*, **41**, 65 (1927).

12) A. Korczynski and St. Namylsloniski, *Bull. Soc. Chim.*, **35**, 1186 (1924).

13) H. O. Spauschus and J. M. Scott, *J. Am. Chem. Soc.*,

73, 210 (1956).

14) P. A. S. Smith and B. B. Brown, *J. Am. Chem. Soc.*, **73**, 2438 (1951).

15) R. G. Pearson, *J. Am. Chem. Soc.*, **85**, 3533 (1963); T. L. Ho, "Hard and Soft Acids and Bases Principle in Organic Chemistry," Academic Press, New York (1977), p. 5.

16) The negative charge of the tetrafluoroborate ion seems to be located on the fluorine atom according to the electroneutrality principle of the central atom of complex ions (L. Pauling, "The Nature of the Chemical Bond," Cornell University Press (1960), p. 172). Therefore, the ion is classified as a hard-base group, like the perchlorate ion.

17) N. Kornblum, *Org. React.*, **2**, 262 (1944); A. Roe, *ibid.*, **5**, 193 (1949); M. P. Doyle and W. J. Bryker, *J. Org. Chem.*, **44**, 1572 (1979).

Organic Photochemical Reactions. XXXI.[1] Photosensitized Ring-Cleavage Reactions of 2,2-Diaryloxetanes by Aromatic Nitriles

Kenichi NAKABAYASHI, Jun-ichi KOJIMA, Kimiko TANABE, Masahide YASUDA, and Kensuke SHIMA*
Department of Industrial Chemistry, Faculty of Engineering, Miyazaki University, Gakuen-Kibanadai, Miyazaki 889-21
(Received June 13, 1988)

Photosensitized reactions of 2,2-diaryloxetanes by 1,4-dicyanonaphthalene, 1-cyanonaphthalene, and 9,10-dicyanoanthracene, which give such ring-cleavage products as substituted benzophenones and alkenes, have been investigated. Quantum yields for the ring cleavage vary with the substituents on both the aryl group and oxetane ring. The quantum yield increases with increase in electron-donating ability of the oxetane. The limiting quantum yields in the case of 1,4-dicyanonaphthalene-photosensitized reaction of 2,2-di-*p*-tolyl- or 2,2-bis(*p*-methoxyphenyl)-3,3,4-trimethyloxetane exceed unity. The mechanism is discussed in terms of electron transfer from oxetanes to the excited singlet state of the sensitizer as well as the regeneration process of the oxetane cation radical involving the hole transfer from substituted benzophenone cation radicals to oxetanes in the chain process.

Cleavage of oxetane into carbonyl–olefin pairs is well-known to occur by the treatment with Brønsted acid or metal ion as well as by pyrolysis.[2] In these studies, the regio- and stereochemical control has been an interesting subject. On the other hand, photosensitized ring-cleavage reactions of such small ring compounds as cyclopropanes,[3] cyclobutanes,[4] oxiranes,[5] and aziridines[6] have received much attention from mechanistic and synthetic points of view. However, no photosensitized reactions of oxetanes have been reported. In order to develop the study of regioselective and efficient cleavage reactions of oxetanes, we attempted the ring cleavage of some 2,2-diaryloxetanes by photosensitization with such typical electron acceptor (S) as 1,4-dicyanonaphthalene (DCN), 1-cyanonaphthalene (CNN), and 9,10-dicyanoanthracene (DCA).

Results

Photoreaction. Photoreactions of 2,2-diaryloxetanes (**1a—h**) were carried out by irradiation of acetonitrile solutions at 313 nm for DCN and CNN runs and at 366 nm for DCA run, and the progress of the photoreactions was followed by gas chromatography. The photoproducts are shown in Scheme 1.

Pairs of substituted benzophenone (**2**) and alkenes (**3**) were formed by photosensitized reaction of **1a—h** with DCN. Such other products as 1,1-diaryl-2,2-dimethylethylene were not observed. The chemical yields of **2** and **3** in the photosensitized reaction with DCN are shown in Table 1. The formation of **2** occurred quantitatively whereas the yields of **3** were rela-

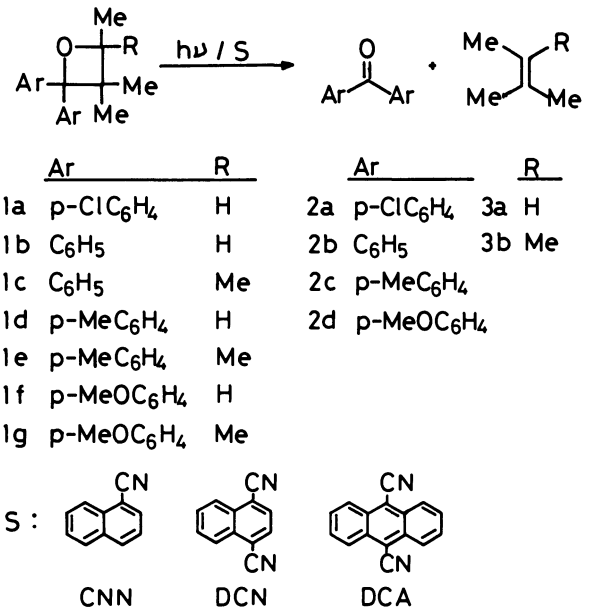

Scheme 1.

Table 1. Photosensitized Ring-Cleavage Reactions of Oxetanes (**1a—f**) with DCN[a]

Oxetane	Irradn time/h	Products (Yield/%)[b]	Conv. of **1**/%	Recov. of DCN/%
1a	24	**2a** (19) **3a** (11)	20	100
1b	20	**2b** (27) **3a** (20)	32	60
1c	24	**2b** (31) **3b** (24)	35	61
1d	10	**2c** (55) **3a** (55)	61	71
1e	25	**2c** (41) **3b** (17)	43	5
1f	4	**2d** (80) **3a** (71)	82	80

a) For acetonitrile solution (4 cm^3) containing **1** [0.05 mol dm^{-3}] and DCN [0.02 mol dm^{-3}]. b) GLC yields based on **1** used.

tively low in some cases except for the cases of **1d** and **1f**. DCN was recovered almost quantitatively except for the case of **1e** in which remarkable consumption of DCN was observed. Similarly, the photosensitized reaction of **1d** and **1f** with CNN or DCA proceeded to give **2** and **3** whereas no photosensitized reaction of **1a—c** with CNN or DCA occurred. The photosensitized reaction of **1f** with DCN and CNN did not proceed at all in less polar solvents such as benzene, dibutyl ether, dioxane, and tetrahydrofuran (THF) but proceeded slightly in ethyl acetate, 2-propanol, ethanol, and methanol. Acetonitrile was a better solvent for the occurrence of the efficient photoreactions. Moreover, it was confirmed that no reaction occurred at all in the dark or even upon direct irradiation of **1**.

Quantum Yields. The formation of **2** and **3** increased linearly with irradiation time up to 5% conversion. Limiting quantum yields were determined for the formation of **2** and **3** by the usual double-reciprocal plots of quantum yields (ϕ) vs. concentration of **1**. Figure 1 shows linear plots for the formation of **2** from DCN-photosensitized reaction of **1a—c,e,g**. Although such linear plots were also obtained from the formation of **3**, the slopes were steeper than those obtained from the formation of **2**, since the yields of **3** were lower than those of **2**. Such linear plots were not observed for the formation of **3b** from **1g**. Table 2 lists the intercept (I) and intercept-to-slope ratios (I/S) of the plots together with the limiting quantum yields for the formation of **2** and **3**. In the case of CNN and

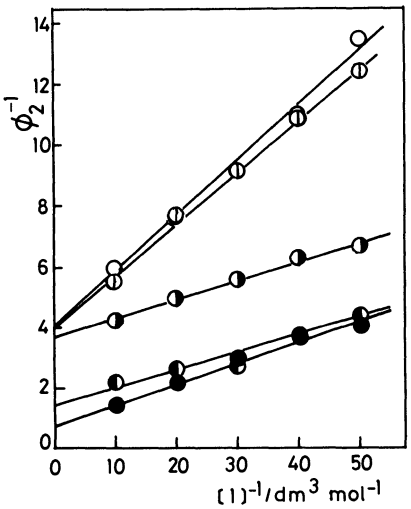

Fig. 1. Double-reciprocal plots of quantum yield for **2** formation vs. concentration of **1**: **1a** (-○-), **1b** (-◑-), **1c** (-◑-), **1e** (-◐-), and **1g** (-●-).

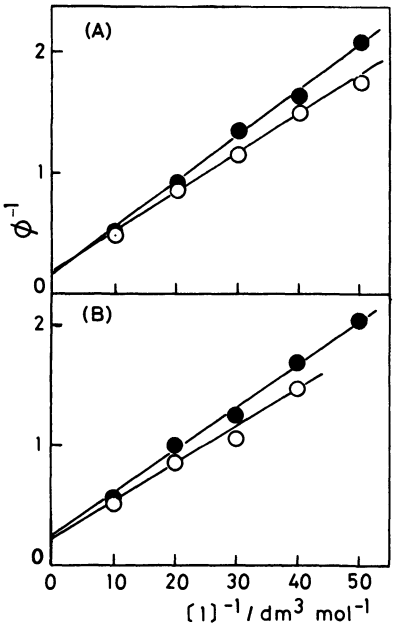

Fig. 2. Double-reciprocal plots of quantum yield for **2** (-○-) or **3a** (-●-) formation vs. concentration of **1**: (A) the case of DCN-**1d**, (B) the case of DCN-**1f**.

Table 2. Limiting Quantum Yields (ϕ) for the Formation of **2** and **3** and Fluorescence Quenching Rate Constants (k_q)

S (τ/ns)[a]	**1**	I[b]	I/S[b]	ϕ_2	ϕ_3	K_{SV} / dm^3 mol^{-1}	k_q / dm^3 mol^{-1} s^{-1}
DCN (9.5)	**1a**	3.9	21	0.26	0.21	33	3.5×10^9
	1b	4.1	24	0.25	0.23	44	4.6×10^9
	1c	3.7	58	0.27	0.25	56	5.9×10^9
	1d	0.20	6.3	5.0	5.2	79	8.3×10^9
	1e	1.5	27	0.68	0.47	90	9.5×10^9
	1f	0.22	7.1	4.7	4.3	161	1.7×10^{10}
	1g	0.88	13	1.1	—[c]	144	1.5×10^{10}
CNN (9.3, 12.3[d])	**1d**			0.02[e]		4	0.4×10^9
	1f			0.40[e]		146	1.6×10^{10}
	1f					161[d]	1.3×10^{10}[d]
DCA (15.3)	**1d**			0.03[f]		20	1.3×10^9
	1f			0.10[f]		182	1.2×10^{10}

a) Fluorescence lifetimes. b) The intercept (I) and the intercept-to-slope ratios (I/S) of the plots for the formation of **2** in Figs. 1 and 2. c) Not determined. d) In benzene. e) For the acetonitrile solution containing **1** [0.05 mol dm^{-3}] and CNN [0.01 mol dm^{-3}]. f) For the acetonitrile solutions containing **1** [0.05 mol dm^{-3}] and DCA [1×10^{-4} mol dm^{-3}].

DCA, the observed quantum yields at [1]=0.05 mol dm^{-3} are shown in Table 2. It should be noted that the limiting quantum yields for the formation of **2** and **3** from DCN-photosensitized reaction of **1d** or **1f** were more than unity as is shown in Fig. 2.

The quantum yields were measured for DCN-photosensitized reaction of **1d** in the presence of various concentrations of methanol and the plots of ϕ for the formation of **2** and **3** vs. [MeOH] are shown in Fig. 3. The ϕ_2 decreased to 0.38 when more than 0.4 mol dm^{-3} of methanol was added and ϕ_3 gradually decreased with increase of concentration of methanol.

Fluorescence Quenching. The fluorescence of aromatic nitriles was quenched by oxetanes following linear Stern-Volmer relationships (Eq. 1). Table 2 includes the Stern-Volmer constants (K_{SV}) and the fluorescence quenching rate constants (k_q) calculated from K_{SV} and the fluorescence life time (τ).[7-9]

$$I_F^0/I_F = 1 + K_{SV}[1] = 1 + k_q\tau[1] \quad (1)$$

Mass Spectrometry. The fragmentation of **1b—h** was studied by mass spectrometry at 70 eV. The relative intensities of the fragments are listed in Table 3 according to the fragmentation mode of Scheme 2 reported by Jones and McDonnell.[10]

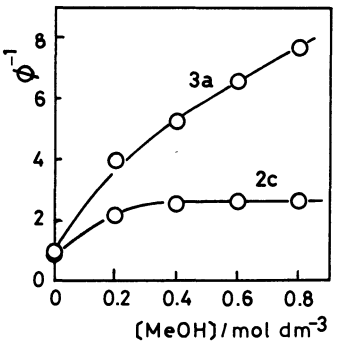

Fig. 3. Plots of the reciprocals of quantum yield for **2c** and **3a** vs. the concentration of methanol in DCN-photosensitized reaction of **1d**.

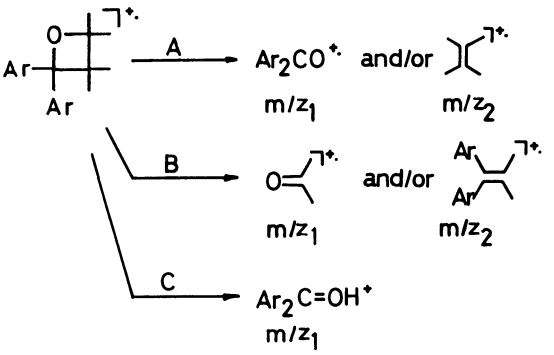

Scheme 2.

Table 3. Mass Spectral Data of Oxetanes (**1b—h**)[a]

Oxetane	Mode[b]	m/z_1	m/z_2	% Rel. Abundance[c]
1b	A	182 (12)[d]	70 (19)[e]	31
	B	44 (0)	208 (50)[f]	50
	C	183 (19)		19
1c	A	182 (6)[d]	84 (38)[g]	44
	B	58 (2)	208 (33)[f]	35
	C	183 (21)		21
1d	A	210 (11)[h]	70 (4)[e]	15
	B	44 (0)	236 (74)[i]	74
	C	211 (11)		11
1e	A	210 (8)[h]	84 (22)[g]	30
	B	58 (0)	236 (51)[i]	51
	C	211 (19)		19
1f	A	242 (11)[j]	70 (1)[e]	12
	B	44 (0)	268 (85)[k]	85
	C	243 (3)		3
1g	A	242 (11)[j]	84 (9)[g]	20
	B	58 (7)	268 (66)[k]	73
	C	243 (7)		7
1h	A	182 (47)[d]	56 (5)[l]	52
	B	44 (0)	194 (8)[m]	8
	C	183 (40)		40

a) % Relative abundance in parenthesis. b) Refers to Scheme 2. c) Sums of % relative abundance according to the mode. d) Includes relative intensity of m/z 105 (182—Ph). e) Includes relative intensity of m/z 55 (70—Me). f) Includes relative intensities of m/z 193 (208—Me) and 131 (208—Ph). g) Includes relative intensity of m/z 69 (84—Me). h) Includes relative intensity of m/z 119 (210—MeC_6H_4). i) Includes relative intensities of m/z 221 (236—Me) and 145 (236—MeC_6H_4). j) Includes relative intensity of m/z 135 (242—$MeOC_6H_4$). k) Includes relative intensities of m/z 253 (268—Me) and 161 (268—$MeOC_6H_4$). l) Includes relative intensity of m/z 41 (56—Me). m) Includes relative intensities of m/z 179 (194—Me) and 117 (194—Ph).

Discussion

Mechanism. There is no doubt that the photosensitization proceeds via the excited singlet state of aromatic nitriles since the rate constants for the fluorescence quenching of DCN by **1a—g** as well as the fluorescence quenching of DCA or CNN by **1f** are close to the diffusion-controlled rate in acetonitrile (2×10^{10} dm^3 mol^{-1} s^{-1}).[11] Moreover the intercept-to-slope ratio (I/S) obtained from quantum yield measurements shows reasonable agreement with the K_{SV} values for the fluorescence quenching in the case of DCN-**1a—c**. Table 4 lists the calculated free energy changes for the electron-transfer process from oxetanes to the excited singlet state of aromatic nitriles (^{1}S*) using the Rehm-Weller equation.[4,11] The calculated values for DCN-**1a—f** or DCA- and CNN-**1f** pairs are substantially negative. Therefore, it is strongly suggested that the electron transfer from oxetanes to ^{1}S* is responsible for the initiation process of photosensitized ring-cleavage reactions as reported for the photoreactions of some benzene derivatives with aromatic nitriles.[12] However, no photosensitized ring-cleavage reaction of **1f** with DCN or CNN in less polar solvents occur at all, though the fluorescence of S is efficiently quenched by **1f** in these solvents. From the above results, the cleavage of oxetane ring is suggested to proceed via the oxetane cation radical ($\mathbf{1}^{+\cdot}$) formed by the complete electron transfer from oxetanes to ^{1}S* rather than via exciplex formation. Consequently, mechanistic pathways for the photosensitized reaction with S are shown in Scheme 3. A usual kinetic treatment gives Eq. 2.

$$\phi^{-1} = \frac{1}{\alpha\beta}\left(1 + \frac{1}{k_A\tau[1]}\right) \qquad (2)$$

Since the oxidation potentials of 2,2-diaryloxetanes are similar to those of the corresponding benzene derivatives,[13] the positive charge in the photogenerated cation radicals of oxetanes is suggested to develop over the aryl groups. Therefore, the ring cleavage of $\mathbf{1}^{+\cdot}$ should be induced by the decrease of electron density in the C_2–C_3 σ bond through σ–π interaction between the aryl groups and the C_2–C_3 bond of the oxetane ring (Scheme 4). DCN-photosensitized reaction of *cis*-3,4-dimethyl-2,2-diphenyloxetane (**1h**) gave the mixture of *cis*- and *trans*-2-butene (**3c**) in 1:4—5 ratio and **2b** (Scheme 5). Such nonstereospecific cleavage of the oxetane ring arose from the stepwise bond-fission at C_2–C_3 of oxetane ring followed by free rotation around the C_3–C_4 bond. An alternative isomerization mechanism via the cation radical of **3c** is unlikely to operate in the photosensitized reaction of **1h**, since mass spectra of **1h** show that $\mathbf{3c}^{+\cdot}$ is scarcely produced from the fragmentation of $\mathbf{1h}^{+\cdot}$. Thus $\mathbf{2}^{+\cdot}$ and/or $\mathbf{3}^{+\cdot}$ are formed by the cleavage of the ring-opened cation radical and reduced with anion radical of S ($S^{-\cdot}$) to give **2** and **3**. The formation of $\mathbf{2}^{+\cdot}$ and/or $\mathbf{3}^{+\cdot}$ are also suggested by the fact that the quantum yields for the

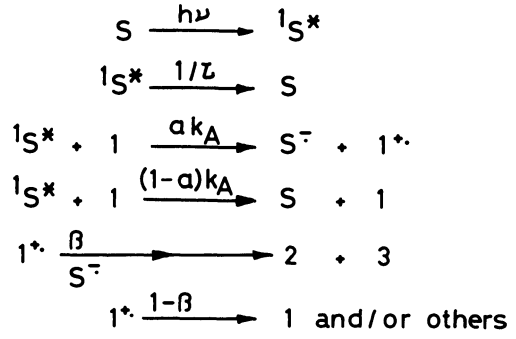

Scheme 3.

Table 4. Oxidation Potentials ($E^{ox}_{1/2}$) of **1a—f** and Calculated Free Energy Changes (ΔG) for Electron Transfer from **1a—f** to ^{1}S*

Oxetane	$E^{ox}_{1/2}$/V[a]	ΔG/kJ mol^{-1}[b]		
		DCN	CNN	DCA
1a	2.05	−39	55	23
1b	1.97	−47	48	15
1c	2.02	−42	52	19
1d	1.80	−63	31	−2
1f	1.44	−98	−3	−36

a) Half-wave oxidation potential vs. Ag/AgNO$_3$ in acetonitrile. b) Calculated values using the Rehm-Weller equation: see Refs. 4 and 11.

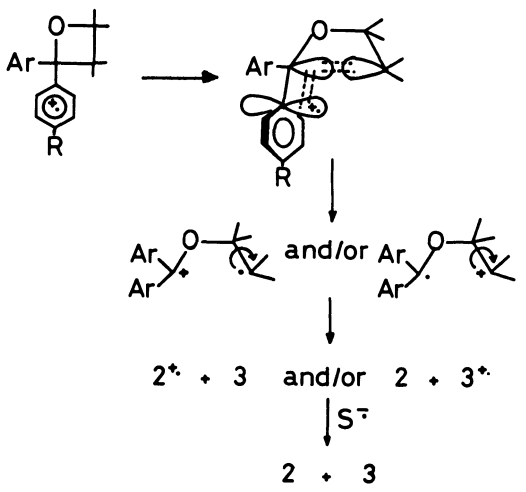

Scheme 4.

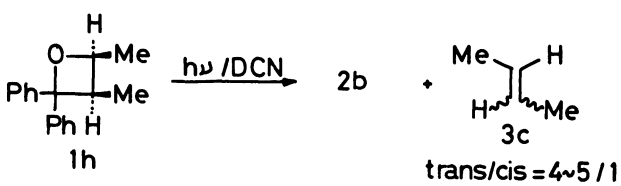

Scheme 5.

formation of **2** and **3** were diminished by the nucleophilic reaction of methanol in DCN-photosensitization of **1d** as shown in Fig. 3.

Consideration of Chain Mechanism. The chain mechanism should be taken into account in the case of **1d** and **1f** since the limiting quantum yields obtained from Fig. 2 exceed unity. The $2^{+\cdot}$ and $3^{+\cdot}$ generated from the cleavage of the oxetane cation radical are candidates for the chain carrier in the regeneration process of oxetane cation radicals. The hole transfer from $3^{+\cdot}$ to oxetanes is disadvantageous since the oxidation potentials of **3** are much lower than those of oxetanes showing that the hole-transfer process is substantially endothermic ($E^{ox}_{1/2}$=1.47 V for **3a** and 1.13 V for **3b**).[7] The hole transfer from $2^{+\cdot}$ to oxetane is conceivable for the regeneration pathways of $1^{+\cdot}$. Therefore, the reaction mechanism for DCN-photosensitization of **1d** and **1f** should include Eq. 3 in addition to Scheme 3. The I/S values for the chain process are much smaller than the K_{SV} values in Table 2. DCN-photosensitization of **1e** and **1g** in which I/S values are smaller than the K_{SV} values might proceed by a mechanism involving a chain mechanism.

$$2^{+\cdot} + 1 \longrightarrow 2 + 1^{+\cdot} \quad (3)$$

Jones and McDonnell reported that the fragmentation of the oxetane ring in mass spectra occurred according to the modes A, B, and C as is shown in Scheme 2.[10] Though the mass spectrometry features are different from those of photosensitized reactions, we can estimate the ratio of $2^{+\cdot}$ to $3^{+\cdot}$ generated from $1^{+\cdot}$ by the fragment intensity of mass spectra in mode A as shown in Table 3. It was found that the ratio of $2^{+\cdot}$ to $3^{+\cdot}$ in the case of **1d** and **1f** was greater than in the other cases. In other words, it is shown that the fragmentation of $1^{+\cdot}$ gives a pair of $2^{+\cdot}$ and **3** more than a pair of **2** and $3^{+\cdot}$ in the case of **1d** and **1f** in which the limiting quantum yield exceeds unity. Therefore, it is again indicated that $2^{+\cdot}$ plays an important role in the chain process.

In conclusion, the regioselective ring-cleavage reaction of oxetanes was accomplished by photosensitization with aromatic nitriles. The regioselectivity was caused by selective C_2–C_3 bond-fission of the oxetane cation radicals generated by photochemical electron transfer. Moreover, the reaction efficiencies were determined by the electron-donating abilities of oxetanes as well as by occurrence of chain processes.

Experimental

Instruments. Gas chromatography was performed on a Shimadzu GC-8A gas chromatograph using a 50 cm column of 2% OV-1 or 2% OV-17 on Chromosorb W for analyses of **1a**—h, **2a**—**d**, and DCN, a 3 m column of DC-550 on Uniport B for analyses of **3a**, a 1 m column of PEG-20M for analyses of **3b**, and a 2 m column of Unipak S (Gasukuro Kogyo) for analyses of **3c**. IR and ^{1}H NMR spectra were obtained on a Hitachi 260-50 spectrometer and a JEOL JNM60 spectrometer, respectively. The fluorescence quenching experiments were performed for degassed acetonitrile or benzene solutions (3 cm^3) containing DCN (1×10^{-3} mol dm^{-3}), CNN (1×10^{-3} mol dm^{-3}), or DCA (2×10^{-5} mol dm^{-3}) on a Hitachi MPF-4 spectrometer. Oxidation potentials of **1a**—**d**, f were determined by a Yanagimoto V10-PG cyclic voltammeter vs. Ag/$AgNO_3$ in acetonitrile using tetraethylammonium tetrafluoroborate as the supporting electrolyte.[14] Mass spectra were measured on a JEOL D-300S equipped with a JMA 2000 data analyzer.

Materials. Commercial 1-cyanonaphthalene was purified by the method described in a previous paper.[7] 9,10-Dicyanoanthracene was purified by repeated recrystallization from benzene. 1,4-Dicyanobenzene was prepared according to the literature method[15] and was purified by repeated recrystallization from benzene. The preparation of oxetanes was carried out by the irradiation of a benzene solution containing the substituted benzophenone and the alkene by high-pressure Hg lamp according to the procedure described in the literature.[16] The purification of the oxetanes was performed by column chromatography on silica gel and then by repeated recrystallization from methanol. Some data of oxetanes (**1a**—f) are as follows: **1a**, 80% of yield, mp 71—72 °C, ^{1}H NMR (CCl_4) δ=1.07 (s, 6H), 1.28 (d, 3H, J=6 Hz), 4.43 (q, 1H, J=6 Hz), 7.07—7.44 (m, 8H). **1b**, 88%, mp 104.5—105.5 °C, ^{1}H NMR (CCl_4) δ=0.98 (s, 6H), 1.18 (d, 3H, J=6 Hz), 2.17 (q, 1H, J=6 Hz), 6.92—7.43 (m, 10H). **1c**, 82%, mp 121.5—122 °C, ^{1}H NMR (CCl_4) δ=1.10 (s, 6H), 1.27 (s, 6H), 7.08—7.59 (m, 10H). **1d**, 77%, mp 99—100 °C, ^{1}H NMR (CCl_4) δ=0.95 (s, 6H), 1.15 (d, 3H, J=6 Hz), 4.34 (q, 1H, J=6 Hz), 6.79—7.30 (m, 8H). **1e**, 90%, mp 117—118 °C, ^{1}H NMR (CCl_4) δ=1.0 (s, 6H), 1.23 (s, 6H), 2.18 (s, 3H), 6.9 (d, J=8 Hz, 4H), 7.27 (d, J=8 Hz, 4H). **1f**, 87%, mp 91.5—92 °C, ^{1}H NMR (CCl_4) δ=0.97 (s, 6H), 1.20 (d, 3H, J=6 Hz), 4.40 (q, 1H, J=6 Hz), 6.55—7.42 (m, 8H). **1g**, 31%, mp 92—93 °C, ^{1}H NMR (CCl_4) δ=1.0 (s, 6H), 1.2 (s, 6H), 3.6 (s, 6H), 6.7 (d, J=8 Hz, 4H), 7.3 (d, J=8 Hz, 4H). **1h**, 75%, mp 87—88 °C, ^{1}H NMR (CCl_4) δ=0.83 (d, J=6 Hz, 3H), 1.3 (d, J=6 Hz, 3H), 3.03 (d-q, J=6 Hz, 6 Hz, 1H), 4.26 (d-q, J=6 Hz, 6 Hz, 1H), 6.9—7.26 (m, 10H).

Photoreactions and Determination of Quantum Yields. Photoirradiation was carried out with an Eikosha PIH-300 high-pressure Hg lamp under cooling with water using appropriate light filters and a "merry-go-round" turntable. A potassium chromate solution (0.2 g dm^{-3}, 10 mm path length) was used to isolate the 313-nm light, whereas the 366-nm light was obtained by the passage through a glass filter (Corning CS7-37) and 10% HCl aqueous solution of $BiCl_3$ (6.67 g dm^{-3}, 10 mm path length). A 2-hexanone actinometer and a trioxalatoferrate(III) actinometer were used for the determination of the quantum yields at 313 nm for the CNN and DCN-photosensitized reaction and at 366 nm for the DCA runs respectively.[17] The concentrations of DCN, CNN, and DCA were set in 0.02, 0.01, and 1×10^{-4} mol dm^{-3}, respectively. These were confirmed to be high enough for the complete absorption of the incident light during the photoreactions. Pyrex glass tubes (8 mm i.d.) were used as the common vessels for the photoreactions and actinometry.

The authors wish to thank Professor Chyongjin Pac, Osaka University, for his kind and helpful discus-

sions. We also thank Professor Toshinori Kokubu, Miyakonojo National College of Technology, for measurement of the oxidation potentials. This work was supported by a Grand-in-Aid for Scientific Research, No. 62550616, from the Ministry of Education, Science and Culture.

References

1) Part XXX: K. Shima, K. Tanabe, S. Furukawa, J. Saito, and K. Shirahashi, *Bull. Chem. Soc. Jpn.*, **57**, 1515 (1984).

2) D. R. Arnold, "Advances in Photochemistry," ed by W. A. Noyes, Jr., G. S. Hammond, and J. N. Pitts, Jr., John Wiley and Sons, New York (1968), Vol. 6, p. 301; G. Jones, II, "Organic Photochemistry," ed by A. Padwa, Marcel Dekker, New York (1981), Vol. 5, p. 1.

3) K. Mizuno, J. Ogawa, and Y. Otsuji, *Chem. Lett.*, **1981**, 741; V. R. Rao and S. S. Hixson, *J. Am. Chem. Soc.*, **101**, 6458 (1979).

4) C. Pac, T. Ohtsuki, Y. Shiota, S. Yanagida, and H. Sakurai, *Bull. Chem. Soc. Jpn.*, **59**, 1133 (1986); C. Pac, *Pure Appl. Chem.*, **58**, 1249 (1986).

5) A. P. Schaap, S. Siddiqui, S. D. Gagnon, and L. Lopez, *J. Am. Chem. Soc.*, **105**, 5149 (1983); A. P. Schaap, L. Lopez, and S. D. Gagnon, *J. Am. Chem. Soc.*, **105**, 663 (1983).

6) A. P. Schaap, G. Prasad, and S. Siddiqui, *Tetrahedron Lett.*, **25**, 3035 (1984).

7) C. Pac, M. Yasuda, K. Shima, and H. Sakurai, *Bull. Chem. Soc. Jpn.*, **55**, 1605 (1982).

8) P. K. Das, A. J. Muller, and G. W. Griffin, *J. Org. Chem.*, **49**, 1977 (1984).

9) J. Eriksen and C. S. Foote, *J. Phys. Chem.*, **82**, 2659 (1978).

10) G. Jones, II and L. P. McDonnell, *Org. Mass Spectrom.*, **10**, 1 (1975); *Tetrahedron Lett.*, **1975**, 4633.

11) D. Rehm and A. Weller, *Isr. J. Chem.*, **8**, 259 (1970).

12) S. Farid, "Organic Photochemistry," ed by A. Padwa, Marcel Dekker, New York, Vol. 6, p. 233.

13) J. Eriksen and C. S. Foote, *J. Am. Chem. Soc.*, **102**, 6083 (1980).

14) T. Majima, C. Pac, and H. Sakurai, *J. Am. Chem. Soc.*, **102**, 5265 (1980).

15) L. Heiss, E. F. Paulus, and H. Lehling, *Justus Liebigs Ann. Chem.*, **1980**, 1583.

16) D. R. Arnold, R. L. Hinman, and A. H. Glick, *Tetrahedron Lett.*, **1964**, 1425.

17) S. L. Murov, "Handbook of Photochemistry," Marcel Dekker, New York (1973), p. 119.

Diene-Containing Lipids as Probes for Phase-Transition Behavior of Lipids in Liposomes[1)]

Shinji TAKEOKA, Hidetaka IWAI, Hiroyuki OHNO, and Eishun TSUCHIDA*
Department of Applied Chemistry, Waseda University, Tokyo 160
(Received June 18, 1988)

The absorption maximum (λ_{max}) of 1,2-bis(2,4-octadecadienoyl)-*sn*-glycero-3-phosphorylcholine (DODPC), dispersed in an aqueous medium as liposomes, showed blue shift from 256.8 nm to 241.8 nm when these liposomes were cooled down from liquid crystalline state to gel state. The blue shift is explained to be due to stronger interaction between diene groups at gel state. This diene-containing lipid is examined to be an excellent membrane probe because it is typical phospholipid and miscible with several lipids. Furthermore, the dienoyl groups are known to be settled in the definite positions in bilayer membrane by suitable chemical modification. Phase transition behaviors of various 2,4-octadecadienoyl-containing phosphorylcholines as analogs for DODPC have also been investigated. Although they had similar spectral shifts at gel-to-liquid crystalline phase-transition temperature, their phase-transition temperatures and magnitude of λ_{max} shifts were revealed to be related directly and therefore be governed by the different packing of the diene groups in bilayer membrane. DODPC was mixed with 1,2-dipalmitoyl-*sn*-glycero-3-phosphorylcholine, or cholesterol, and phase behaviors of these mixed liposomes were also examined. Phase-transition of the mixed liposomes was detected easily by the shift of its λ_{max} with high sensitivity. Results were quite comparable to those obtained from other measurements, such as DSC, NMR, and so on.

We have already clarified various membrane properties through polymerization behaviors of polymerizable lipids as liposomes.[2-11)] 1,2-Bis(2,4-octadecadienoyl)-*sn*-glycero-3-phosphorylcholine (DODPC), which contains one diene group in every acyl chain, is effectively polymerized as liposomes with radical initiators. The polymerization profile was revealed to deeply depend on the characteristics of the applied radical initiators.[3,6)] However this monomeric lipid had polymerizable groups in the same 2,4-position in the 1- and 2-acyl chains, polymerization of diene groups in the 1-acyl chains was selectively initiated by azobis(isobutyronitrile) (AIBN) which was incorporated into a hydrophobic region of the bilayer membrane. On the contrary, the diene groups in the 2-acyl chains were polymerized by the addition of azobis(2-amidinopropane)dihydrochloride (AAPD), water-soluble radical initiators, suggesting that the diene groups in the 2-acyl chains were faced an aqueous phase.[3)] We also developed a new polymerization technique with which liposomes could be polymerized at any temperature.[10)] Polymerization was performed with AIBN and/or AAPD as photosensitizers and irradiating the UV-light of 360 nm at temperatures below or above the gel-to-liquid crystalline phase-transition temperature (T_c). Water-soluble AAPD penetrated lipid membrane at temperatures above T_c but not below.[10)] We prepared liposomes which possessed polymerized outer- or inner-half of bilayer with advantageous characteristics of impermeability of AAPD below the T_c.[10)] Change of microviscosity of lipid membrane at T_c was also analyzed with water-insoluble AIBN incorporated in hydrophobic region of the membrane. Initiation efficiency of the polymerization was affected by membrane microviscosity.[10)] We found that UV spectral shift for polymerizable lipids was attributed to the changes in lipid packing in the membrane. Here we describe this shift behavior in detail.

Experimental

Materials. 1,2-Bis(2,4-octadecadienoyl)-*sn*-glycero-3-phosphorylcholine (DODPC) was purchased from Nippon Oil & Fats Co., Ltd. 1-Palmitoyl-2-(2,4-octadecadienoyl)-*sn*-glycero-3-phosphorylchloline (POPC) was a gift from Toyo Soda Co., Ltd. 1,3-Bis(2,4-octadecadienoyl)-*rac*-glycero-2-phosphorylcholine (1,3-DPC) was synthesized according to the method as reported previously.[11)] 1,2-Dimyristoyl-*sn*-glycero-3-phosphorylcholine (DMPC), 1,2-dipalmitoyl-*sn*-glycero-3-phosphorylcholine (DPPC) and cholesterol were purchased from Sigma. The purity of lipids was confirmed with thin-layer chromatography (Merck, silica-gel plates) with chloroform/methanol/water (65:35:5 by vol) to show a single spot.[3)]

***rac*-1-*O*-(2,4-Octadecadienoyl)-2-*O*-octadecylglycerol:** 2-Phenyl-1,3-dioxan-5-ol was obtained according to the procedure of Hibbert et al.[12)] The product was then allowed to react with 1-bromooctadecane yielding 2-octadecyloxy-1,3-propanediol according to the procedures of Arnold.[13)] 2-Octadecyloxy-1,3-propanediol (5.00 g, 14.5 mM; 1 M=1 mol dm^{-3}) and 0.95 g pyridine (12 mM) were dissolved into 250 ml dry dichloromethane, and added dropwise to 40 ml dry dichloromethane containing 2,4-octadecadienoyl chloride (10 mM) at room temperature. After addition of 4-(dimethylamino)pyridine, the mixture was stirred overnight at room temperature under nitrogen atmosphere. The mixture was washed successively with 1M HCl aqueous solution, then with saturated NaCl aqueous solution. The organic layer was dried over anhydrous sodium sulfate and evaporated in vacuo. The purification of the residual product was carried out by passing through a silica gel column with benzene/ether (10/1 by vol.) as an eluent. The desired fraction was collected and solvents were removed under reduced pressure. *rac*-1-*O*-(2,4-Octadecadienoyl)-2-*O*-octadecylglycerol (3.74 g) was obtained with 62% yield. R_f=0.25 (benzene/

ether=9/1 v/v); MS: 606 (M^+); IR in cm^{-1} (KBr): 1720 (ester carbonyl), 1640, 1620 (diene), 3400 cm^{-1} (OH); Elementaly Anal. (calcd value for $C_{39}H_{74}O_4$ in parenthesis): C 77.17 (77.17), H 12.87 (12.29%); ^{13}C NMR ($CDCl_3$, TMS) (in ppm): 62.7, 62.0, 77.8 (glycerol backbone), 70.6 (-C-O-C-), 118.5, 128.3, 145.4, 145.9 (diene), 167.2 (ester carbonyl); mp: 44.5 °C.

1-*O*-(2,4-Octadecadienoyl)-2-*O*-octadecyl-*rac*-glycero-3-phosphorylcholine (OOPC): *rac*-1-*O*-(2,4-Octadecadienoyl)-2-*O*-octadecylglycerol (3.60 g, 5.93 mM) and trimethylamine (0.72 g, 7.1 mM) were dissolved in 50 ml of dry benzene. 2-Chloro-1,3,2-dioxophosphorane 2-oxide (1.01 g, 7.1 mM) in 5 ml of dry benzene was slowly added to the solution at 10 °C. After the mixture was stirred at room temperature in the dark for 12 h, formed precipitates were removed by filtration. The filtrate was evaporated and the residue was dried in vacuo. It was allowed to react with dry trimethylamine (20 ml) in the mixture of *N,N*-dimethylformamide and benzene (15 ml/30 ml) in a pressure bottle at 60 °C for 4 h. Distilled acetone (0.2 ml) was then added to the mixture, the precipitate formed was collected, washed with dehydrated acetone and dried in vacuo. The residue was purified by passing through the zwitterion-type ion-exchange chromatography (Bio-Rad, AG501-x8(D)) with chloroform/methanol (20 ml/20 ml) as an eluent. The fractions having the same R_f value as that of egg york lecithin were collected. Solvent was removed and the residual product was lyophilized from dry benzene/dry methanol (5/1 v/v) to give 2.70 g of 1-*O*-(2,4-octadecadienoyl)-2-*O*-octadecyl-*rac*-glycero-3-phosphorylcholine (OOPC): yield 59%; FAB-MS: 772 (M+1); elementary anal. (calcd value for $C_{44}H_{86}NO_7P$ in parenthesis): N: 1.70 (1.81%); IR in cm^{-1} (KBr): 1710 (ester carbonyl), 1640, 1620 (diene), 1250 (P=O), 1090 and 970 (phosphorylcholine); ^{13}C NMR ($CDCl_3$, TMS) (in ppm): 54.3 (choline methyl), 64.4, 76.6 (glycerol backbone), 59.5, 66.3 (choline ethyl), 70.6 (-C-O-C-) 118.8, 145.6, 128.2, 145.1 (diene), 167.1 (ester carbonyl).

Methods. A total of 0.20 g of lipids was dissolved in dehydrated chloroform and was slowly evaporated in a rotating sample tube to prepare thin films on the inner surface of the tube, then 20 ml of distilled water was added. Small unilamellar liposome suspension was prepared by sonication (Tip type, Tomy Seiko UR-200P) at 60 W for 20 min under nitrogen atmosphere.[4] As disordered lipid packing perturbs accurate measurement on the characteristics of the oriented lipids in liposomes, freshly prepared liposomes were incubated at 8 °C to increase liposome size and to minimize the disordered molecular packing through liposomal fusion.[8,14] Accurately diluted liposome suspension was put into quartz cell, and the absorption maximum corresponding to the diene groups was analyzed with UV spectrometry (Shimadzu MPS-2000) under heating or cooling (1.0 °C min^{-1}).

Results

1,2-Bis(2,4-octadecadienoyl)-*sn*-glycero-3-phosphorylcholine (DODPC), which possesses 2,4-diene groups in both 1- and 2-acyl chains, shows the absorption maximum (λ_{max}) at 262.3 nm in chloroform solution at 25 °C. The λ_{max} was almost independent of temperature as shown in Fig. 1. When DODPC lipids were dispersed into water by sonication, they assembled to form liposomes. Though the λ_{max} of DODPC liposomes was found at 256.8 nm at 25 °C, a blue shift from 256.8 nm to 241.8 nm was observed when the suspension was cooled from 19 °C to 12 °C as also shown in Fig. 1. The maximum λ_{max} shift was found at about 16 °C corresponding to the gel-to-liquid crystalline phase-transition temperature (T_c) of DODPC (18 °C: with DSC).[8] The T_c is known to be influenced by liposome size especially for small unilamellar liposomes,[15] and λ_{max} shift behavior was observed in related to the liposome size (data not shown here). Small unilamellar liposomes (SUVs) prepared with

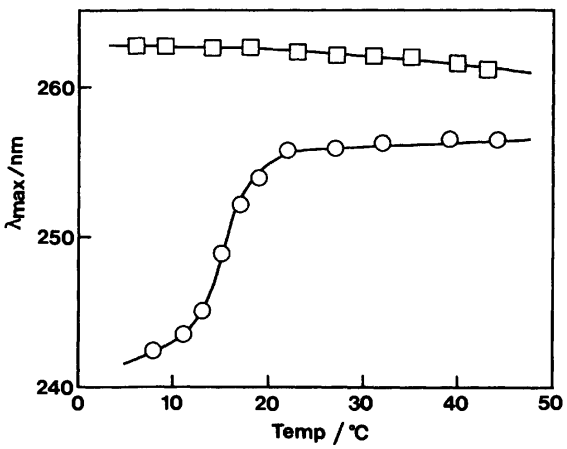

Fig. 1. Temperature dependence of wavelength at the absorption maximum for diene groups of DODPC. □: in chloroform. ○ in liposomes.

Table 1. λ_{max} and ε_{max} of Various Diene-Containing Lipid Liposomes at Temperatures below and above the Phase-Transition Temperature (T_c)

Lipid[a]	λ_{max}/nm		$\varepsilon_{max}\times10^{-4}$		T_{max}/°C	T_c/°C
	below T_c	above T_c	below T_c	above T_c		
DODPC	241.8	256.8	2.95	3.40	16.0	18.9
1,3-DPC	246.0	257.0	2.07	2.75	24.0	27.3
	(241.5	257.0	—	—	25.0)[b]	—
	(236.8	257.0	—	—	20.0)[c]	—
POPC	253.0	259.3	1.27	1.43	28.0	29.2
OOPC	245.0	255.0	1.48	1.70	39.0	40.1

a) Liposomes incubated at 8 °C for 12 h were used. b) Measured for the liposomes incubated for 7 days with elevating temperature. c) With lowering temperature.

sonication method were incubated at temperatures below T_c to prepare large unilamellar liposomes (LUVs) through liposomal fusion.[8,16] The LUVs with average radius of more than 35 nm are known to show almost the same phase-transition behavior.[8] The following measurements were therefore performed for LUVs with average radius of more than 35 nm. Those liposomes could be prepared by incubation at 8 °C for 12 h.

Spectral characteristics of other phospholipids having 2,4-octadecadienoyl group were also examined and summarized in Table 1. The temperature (T_{max}) which gave the maximum value of $d\lambda_{max}/dT$ was compared with a gel-to-liquid crystalline phase-transition temperature (T_c) obtained from DSC measurement. The blue shift of λ_{max} occurred at gel-to-liquid crystalline phase-transition temperature. The temperature dependence on the λ_{max} was normalized for all diene-containing lipids by drawing the relationship between $T-T_{max}$ and λ_{max} as summarized in Fig. 2. The absorption maxima of 1-palmitoyl-2-(2,4-octadecadienoyl)-*sn*-glycero-3-phosphorylcholine (POPC)[7] and 1-*O*-(2,4-octadecadienoyl)-2-*O*-octadecyl-*rac*-glycero-3-phosphorylcholine (OOPC) were measured in the temperature range from 5 °C to 60 °C. Though POPC or OOPC had one diene group in either 2- or 1-acyl chain, respectively, their λ_{max} shift behavior was quite different. In case of POPC, the λ_{max} shifted gradually from 253.0 nm to 259.3 nm on heating. The maximum shift was observed at 28 °C. While, OOPC showed a drastic shift from 245.0 nm to 255.5 nm at 39 °C. 1,3-Bis(2,4-octadecadienoyl)-*rac*-glycero-2-phosphorylcholine (1,3-DPC), an isomer of DODPC,[9] has 2,4-diene groups in 1- and 3-acyl chains. This 1,3-DPC also showed the λ_{max} shift from 246.0 nm to 257.0 nm at around 24 °C. However, 1,3-DPC liposomes were semistable and slowly changed their structure within a few days. When 1,3-DPC liposomes were incubated at 8 °C for 7 days, opalescent liposome dispersion was turbid indicating aggregation and fusion. In this system, λ_{max} changed from 241.5 nm to 257.0 nm (T_{max}=25 °C) with elevating temperature and from 257.0 nm to 236.8 nm (T_{max}=20 °C) with lowering temperature showing a hysteresis. This result was unique for 1,3-DPC liposomes.

The molar extinction coefficients (ε_{max}) of diene-containing lipid derivatives are also summarized in Table 1. ε_{max} for all lipids increased a little at temperatures above their phase-transition temperatures. As expected from the number of diene groups in one lipid molecule. ε_{max} of OOPC was almost identical as that of POPC and half of that of DODPC regardless of temperature.

The λ_{max} shift reflects the phase-transition temperature of diene-containing lipid liposomes. The ability of these lipids was also applied to analyze the phase-transition behavior of natural lipid assemblies. The λ_{max} shift for DODPC/DPPC (1:20 by mol) mixed liposomes was observed at 40 °C as shown in Fig. 3, corresponding to the gel-to-liquid crystalline phase-

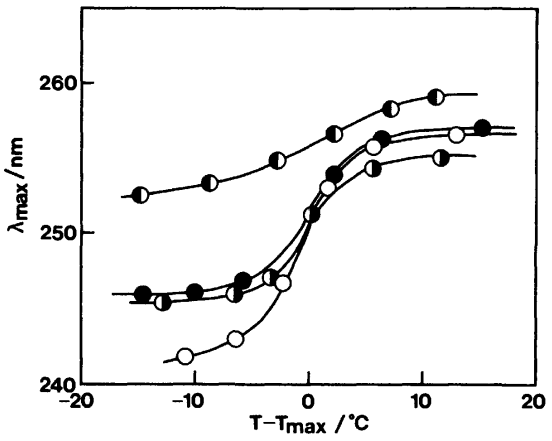

Fig. 2. Relationship betweeen $T-T_{max}$ and wavelength at the absorption maximum of DODPC (○), 1,3-DPC (●), OOPC (◑), and POPC (◐).

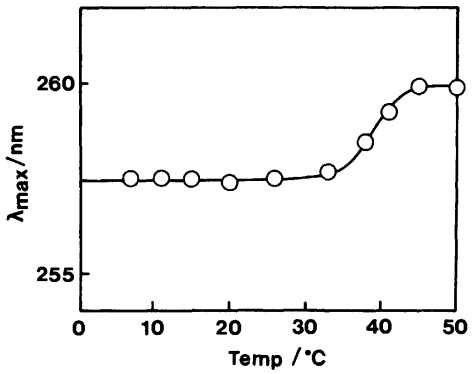

Fig. 3. Temperature dependence of wavelength at the absorption maximum of DODPC in DPPC/DODPC (20:1) mixed liposomes.

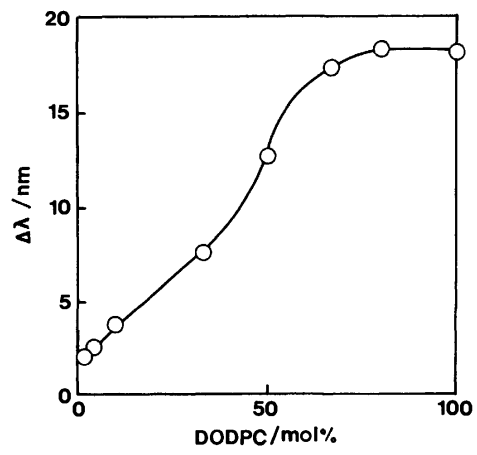

Fig. 4. Effect of DODPC mole fraction on the difference ($\Delta\lambda$) of wavelength between at the absorption maximum of DPPC/DODPC mixed liposomes at 5 °C and 260.0 nm. $\Delta\lambda$ at 0% of DODPC mole fraction corresponded to 258.5 nm.

transition temperature of DPPC, but not that of DODPC. The shift from 260.0 nm to 257.5 nm was different from that of DODPC (256.8 nm to 241.8 nm). This shift (2.5 nm) was very small compared with that of pure DODPC liposomes (15.0 nm). It is important to investigate λ_{max} shift behavior against composition of mixed liposomes. When DODPC fraction decreased, λ_{max} at temperatures below T_c significantly red-shifted while λ_{max} above T_c gradually saturated to 260.0 nm. The wavelength at 260.0 nm was considered to be limited value of longer wavelength. Differences ($\Delta\lambda$) between λ_{max} at gel state and that 260.0 nm against DODPC mole fraction were shown in Fig. 4. Since λ_{max} at 0% of DODPC mole fraction at gel state was 258.5 nm, the $\Delta\lambda$ was 1.5 nm. This increased with the DODPC composition and saturated to 18.2 nm when DODPC fraction exceeded 80%. In this case, T_{max} also reached the T_c of the pure DODPC liposomes. Furthermore, temperature range, at which the λ_{max} shift occurred, changed according to the composition of DODPC/DPPC mixed liposomes. There were two break points in the slope of temperature dependence of λ_{max}, namely, the onset and the offset blue shift. In mixed liposome system, temperatures of these two break points were significantly different. They were plotted against the molar ratio of DODPC to obtain an equilibrium phase diagram of DPPC and DODPC mixed liposome as shown in Fig. 5.[17] The temperature (T_f) of the onset blue shift drew the fluidus curve while the temperature (T_s) of the offset point did the solidus curve.

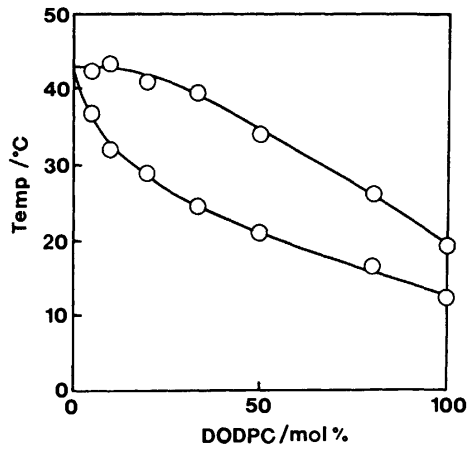

Fig. 5. Phase diagram of DODPC/DPPC mixed liposomes obtained from λ_{max} shift behavior. Upper curve was fluidus curve made of T_f and lower one was solidus curve made of T_s.

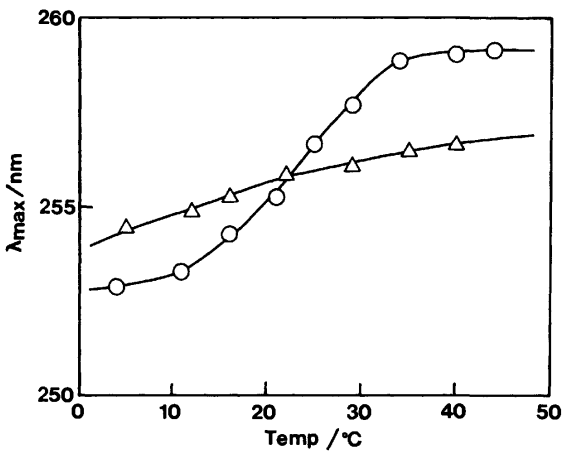

Fig. 6. Temperature dependence of the wavelength at the absorption maximum for diene groups of POPC (○) and POPC/cholesterol (1:1) mixed liposomes (△).

Effect of cholesterol on the phase-transition behavior was also analyzed with the λ_{max} shift. The λ_{max} for POPC/cholesterol (1:1 by mol) mixed liposome increased slightly from 254.2 nm to 256.7 nm when temperature was raised from 5 °C to 40 °C. The slope was smooth and continuous, and no distinct transition was found as shown in Fig. 6. This phenomenon can also be discussed in related to the well-known effect, so-called "Cholesterol Effect".[18,19]

Discussion

All diene-containing phospholipids analyzed here have at least one 2,4-dienoyl group in their acyl chains, and their absorption maximum was 262.3 nm in chloroform solution regardless of their structure. There was no temperature dependence on the λ_{max} in such a molecularly-dispersed homogeneous solution. Once these lipids formed molecular assemblies such as liposomes in an aqueous medium, the absorption maximum was observed at about 257 nm at temperatures above the gel-to-liquid crystalline phase-transition temperature (T_c) of corresponding lipid liposomes as shown in Table 1. All of diene-containing lipid liposomes showed blue shift of λ_{max} at temperatures below the T_c. The magnitude of λ_{max} shift at T_c was revealed to strongly depend on the chemical environment, acyl chain packing and conformation of dienoyl groups. Following three reasons can be presented to explain the blue shift of their λ_{max}.

(1) A structural change of conjugated dienoyl system may be induced at gel-to-liquid crystalline phase-transition temperature. If energy levels of electron orbitals for dienoyl group were changed by its structural change, the shift might occur.

(2) The λ_{max} for dienoyl groups is sensitive to solvent polarity. If polarity around dienoyl groups at temperatures below T_c was different from that above T_c because location of water molecules in bilayer membrane would change at T_c, the λ_{max} might therefore shift.

(3) The shifts in λ_{max} should be caused by the interaction of dienoyl groups in the lipid bilayer. In liquid-crystalline state, segmental motion of dienoyl groups is relatively high and they have more freedom

than those in the gel state. DODPC as liposomes in liquid-crystalline state showed a similar λ_{max} to that in homogeneous solution e.g. in methanol. Diene groups in gel state are oriented more regularly and interacted (stacked) with each other. It should therefore cause the blue shift of λ_{max}.[20]

To clarify the mean factor for this shift behavior, it is important to analyze the spectral characteristics for the diene group in the mixed bilayer membrane, where a little amount of diene-containing lipids is mixed with saturated normal lipids. In case of DPPC/DODPC (20:1 by mol) mixed liposomes (Fig. 3), the gel-to-liquid crystalline phase-transition temperature is almost the same as that of pure DPPC liposomes. However, the difference between λ_{max} below and above the T_c was much smaller than that of pure DODPC liposomes. If the λ_{max} shift was caused by the first and/or second reason, the mixed liposomes should have the same shift as that of the pure diene-containing lipid liposomes. In mixed liposome system, the wavelength of the absorption maxima at gel and liquid crystalline state approached to 258.5 nm and 260.0 nm, respectively in accordance with the increase of DPPC ratio as shown in Fig. 4. The wavelength of 258.5 nm was considered to be attributed to molecularly dispersed DODPC which had only intramolecular interaction of diene groups because the λ_{max} for not interacted diene group in bilayer membrane would be 260.0 nm. It was also supported from the result that the λ_{max} of molecularly-dispersed monodiene-type POPC was found at 260.0 nm at temperature below the T_c. The shift was therefore attributed to the direct interaction with diene groups of lipids. The third one is therefore concluded to be the most suitable explanation for this λ_{max} shift.

Generally, chromophores in stacked state show specific spectra reflecting their interaction. According to the molecular exciton model proposed by Kasha et al.,[13] direction and degree of λ_{max} shift were decided by inclination and distance among the transition dipoles. In bilayer membrane system, λ_{max} of chromophores, such as diene groups which constitute part of chains, is predicted to shift to a shorter wavelength because hydrocarbon chains extend perpendicularly to the membrane plane. The large blue shift however occurred only in gel state of the bilayer membrane as shown in Fig. 1. That was because the diene groups, packed closely with a good orientation manner in gel state, were disordered in liquid crystalline state. The λ_{max} shifted and approached to that of the molecularly dispersed diene-containing lipids (260.0 nm) at temperatures above T_c.

The λ_{max} shift for LUVs of some diene-containing lipids also reflected their structural characteristics as shown in Fig. 2. In case of DODPC, stacking of diene groups in the 1-acyl chains should be unequivalent with that in the 2-acyl chains because of their unsymmetrical chain packing in bilayer membrane.[4] The stacking between diene groups in the 1- and 2-acyl chains however also exists as described above. The comparison of the stacking of diene groups in the 1-acyl chains and that in the 2-acyl chains should be carried out with corresponding monodiene type lipids such as OOPC and POPC, respectively. λ_{max} of POPC was entirely longer than that of OOPC. This was attributed to the different orientation of diene groups of POPC to those of OOPC. Since diene groups in the 1-acyl chains of OOPC oriented perpendicularly to the membrane plane, stronger interaction was easily expected between these diene groups. While, those of POPC oriented with large inclination, and lots of dipoles aligned in the opposite direction with the same inclination. Interaction of 2,4-diene groups in the 2-acyl chains should therefore be very weak, leading to smaller blue shift of POPC than OOPC as shown in Fig. 2. The different packing of diene groups in the 1- and 2-acyl chains has already been shown from X-ray diffraction and D-NMR analyses on natural phospholipids.[21,22] It was also supported by our results on the selective polymerization of the 1- and 2-acyl chains by the addition of either water-soluble or -insoluble radical initiators.[4,6] Diene-groups in the 2-acyl chains of DODPC faced an aqueous phase while those in the 1-acyl chains located in a hydrophobic phase in consequence of perpendicular orientation of glycerol moieties to the liposome membrane plane. Diene-groups in the 2-acyl chains were therefore selectively polymerized with water-soluble radical initiators such as AAPD. POPC liposomes were accordingly polymerized with only water-soluble radical initiators.[7]

The spectral changes of azobenzene moieties of the assembled single chain amphiphiles have also been reported.[23] These amphiphiles are known to form bilayer structures in an aqueous medium, and the blue shift of λ_{max} was also found below the phase-transition temperature. This phenomenon was explained systematically with this exciton model in the one dimension because of card-like packing of azobenzene moieties in the membrane, and the λ_{max} shift was referred to the results from X-ray analyses.[24,25] In our system, the λ_{max} shift of diene groups was however smaller than those of azobenzene system. In the present paper, we discussed here the shift behavior with the two dimensional exciton model, i.e., molecular lamellar exciton model because diene group could be regarded as arrow.[26] We have to take the interaction of dipoles in two dimension into consideration. The treatment of interaction of dipoles with inclination to membrane plane is complicated because dipoles with the same inclination do not orient with the same direction in membrane plane.

Recently, O'Brien et al.[27] reported the shift of the absorption maxima for diene-containing lipids. They mentioned that the evidence for aggregation of diene

groups of DODPC and POPC in bilayer membrane could not be obtained from those lipids at 22 °C because those liposomes showed not so clear λ_{max} shift at that temperature. They should have taken the phase-transition temperature into account. The λ_{max} of around 260 nm for DODPC at 22 °C surely shifted to 243 nm at temperatures lower than the phase-transition temperature (16 °C) as shown in Fig. 1. In case of POPC, small shift of λ_{max} from 260.0 nm even below the phase-transition temperature (22 °C) occurred due to the different packing manner of diene groups in the 2-acyl chains as described above.

Temperature dependence of the absorption maxima was concluded to be essentially related to the lipid structure as shown in Table 1. Lipids having the same hydrophobic hydrocarbon number can be aligned in the following sequence by their T_c;

$$\text{DODPC}(18.9\,^\circ\text{C}) < \text{1,3-DPC}(27.3\,^\circ\text{C}) < \text{OOPC}(40.1\,^\circ\text{C}) < \text{DSPC}(55.0\,^\circ\text{C})$$

DSPC has two saturated acyl chains. OOPC has one diene group in 1-acyl chain. While DODPC or 1,3-DPC have two dienoyl groups in 1- and 2-acyl, or 1- and 3-acyl chains, respectively. This tendency has already been known for the natural lipids, i.e., the more the number of unsaturated bonds is, the lower the phase-transition temperature is. The difference of T_c between DODPC and 1,3-DPC was apparent to be due to the different lipid packing of these lipids in bilayer membrane. This lipid packing has already been analyzed with polymerization manner under the different point of view.[9] The diene-containing phospholipids are found to be applicable as probe molecules to analyze chemical environment of lipids in liposomes without disturbing the lipid packing. Furthermore, the position to be analyzed in bilayer membrane can be chosen by the location of diene groups in the acyl chains.

The molar extinction coefficient (ε_{max}) also shifted at gel-to-liquid crystalline phase-transition temperature. The ε_{max} decreased when temperature was set below the T_c. That was because the molar extinction coefficient of chromophore in a stacked stage was different (generally smaller) from that in the dispersed stage. The ε_{max} of POPC as liposomes was found to be smaller than that of OOPC as liposomes, though the ε_{max} values of POPC and OOPC were completely the same in organic solvents. It can be comprehended by the polarity around diene groups.[28] The absorption spectrum of diene group varies with solvent polarity. When the solvent polarity was higher, the ε_{max} tended to be smaller. The smaller ε_{max} of POPC indicated that the polarity of diene groups of POPC was higher than that of OOPC. The polarity of diene group in the 2-acyl chain is considered to be a little higher than that in the 1-acyl chain. These results strongly supported that 2,4-diene group of the 2-acyl chain faced an aqueous phase which had already been suggested from the analyses of polymerization behaviors of those lipids.[3,7] Furthermore, these spectroscopic analyses were quite suitable to measure the phase-transition of very dilute liposome suspension because the ε_{max} was large.

The λ_{max} for DPPC/DODPC (20:1 by mol) mixed liposomes shifted at 40 °C, corresponding to the T_c of this mixed liposome. The phase-transition temperature was almost the same as that of DPPC liposomes. Though diene-containing lipids can be used as membrane probe which detect the phase-transition temperature of lipid membrane, this probe itself is a lipid which has own phase-transition temperature. It is easy to reach the following conclusion that the present lipid system has effective to detect the T_c of the matrix membrane, it however has inevitable concentration dependence. It is favorable to use 5 mol% of the DODPC in order to detect the phase-transition of the matrix membrane because 5 mol% of DODPC is considered not to affect the phase-transition of the major component.[12] The shift for the mixed liposomes, however, was significantly smaller than that of pure diene-containing lipid liposomes. At this ratio, the shift was almost due to interaction of diene groups in 1- and 2-acyl chains of the lipid. Monodiene-type lipids therefore cannot be used as probes for phase-transition of matrix lipids. The lipid, having two diene groups which locate at the same position in bilayer membrane, is the best for this purpose because it is expected to be intramolecular interaction of diene groups.

When more than 5 mol% of DODPC was mixed to DPPC liposomes, λ_{max} shift also reflected the phase-transition of DODPC itself and it became broad.[29] It was a typical characteristic of mixed liposome systems. Two transition temperatures at which the onset and the offset of the blue shift occurred were related to T_f and T_s, respectively.[17] At temperatures above T_f, DODPC showed a constant value of λ_{max} because all of DODPC were in a liquid crystalline state. When the mixed liposome dispersion was cooled below T_f, gel phase of DODPC, which shows smaller λ_{max}, was formed in mixed liposomes. The portion of gel phase and the ratio of DODPC in the gel phase became larger by lowering temperature to T_s. It resulted that the value of λ_{max} gradually shifted to shorter wavelength. At temperatures below T_s, the mixed liposomes were totally in a gel state, showing a constant λ_{max} depending on the initial feed composition.

The phase-transition temperature is known to disappear by the addition of cholesterol, and slight temperature dependence of the λ_{max} was observed for cholesterol/POPC (1:1 by mol) mixed liposomes as shown in Fig. 6. The same phenomenon has already

been found with other measurements such as DSC,[18] NMR,[29] fluorescence spectroscopy[30] and so on. Cholesterol/POPC equimolar mixture system at 5 °C showed its λ_{max} at 254.2 nm which was longer wavelength than that for POPC (253.0 nm). Cholesterol shows an effect to fluidize the lipid membrane at temperatures below the T_c. It caused the decrease in the interaction between dienoyl groups of POPC below the T_c. The λ_{max} of cholesterol/POPC equimolar mixture liposomes (256.7 nm) at 40 °C, above the phase-transition temperature of POPC liposomes, was shorter than that of POPC liposomes (259.3 nm). That is considered to be the existence of some interaction of dienoyl groups due to less mobility of POPC in cholesterol containing lipid membrane. These spectral changes must be useful to detect the phase state of any lipid systems without disturbing their assembled structure.

Conclusion

The absorption maxima of diene-containing lipids as liposomes showed blue shift at gel state. The shift was resulted from the interaction of dienoyl groups, and it was explained by the exciton model. The different acyl chain packing of various diene-containing lipids was revealed to be the major factor to cause the temperature dependence of the absorption. The λ_{max} shift also reflected the phase-transition temperature of mixed liposomes. Besides the phase-transition temperature, the information about mobility and packing of diene groups were also obtained at any temperatures, which could not be observed by DSC measurement. The diene-containing lipids were concluded to be unique and quite potential compounds as membrane probes.

The authors thank Dr. Yoshihiko Nagata and Dr. Akira Akimoto of Toyo Soda Co. Ltd. for their kind supply of polymerizable lipid (POPC). This work was partially supported by a Grant-in-Aid for Scientific Research on Priority Area "Macromolecular Complexes" from the Ministry of Education, Science and Culture.

References

1) This is part 8 of the series. Part 7: Ref. 10.
2) H. Ringsdorf, B. Schlarb, and J. Venzmer, *Angew. Chem., Int. Ed. Engl.*, **27**, 113 (1988).
3) H. Ohno, Y. Ogata, and E. Tsuchida, *Macromolecules*, **20**, 929 (1987).
4) H. Ohno, Y. Ogata, and E. Tsuchida, *J. Polym. Sci., Polym. Chem. Ed.*, **24**, 2959 (1986).
5) H. Ohno, S. Takeoka, and E. Tsuchida, *Polym. Bull.*, **14**, 487 (1985).
6) H. Ohno, S. Takeoka, and E. Tsuchida, *Bull. Chem. Soc. Jpn.*, **60**, 2945 (1987).
7) H. Ohno, S. Takeoka, H. Iwai, and E. Tsuchida, *J. Polym. Sci., Polym. Chem. Ed.*, **25**, 2747 (1987).
8) H. Ohno, S. Takeoka, H. Iwai, and E. Tsuchida, *Macromolecules*, **21**, 319 (1988).
9) S. Takeoka, E. Hasegawa, H. Ohno, and E. Tsuchida, *Bull. Chem. Soc. Jpn.*, **61**, 2007 (1988).
10) H. Ohno, S. Takeoka, H. Iwai, and E. Tsuchida, *Macromolecules*, **22**, (1989) in press.
11) E. Hasegawa, K. Eshima, Y. Matsushita, H. Ohno, and E. Tsuchida, *Polym. Bull.*, **18**, 65 (1987).
12) H. Hibbert and N. M. Carter, *J. Am. Chem. Soc.*, **51**, 1601 (1929).
13) D. Arnold, H. U. Weltzien, and O. Westphal, *Justus Liebigs Ann. Chem.*, **709**, 234 (1967).
14) H. Ohno, Y. Maeda, and E. Tsuchida, *Biochem. Biophys. Acta*, **642**, 27 (1981).
15) H. Takemoto, S. Inoue, T. Yasunaga, M. Sukigara, and Y. Toyoshima, *J. Phys. Chem.*, **85**, 1032 (1981).
16) J. Suurkuusk, B. R. Lents, Y. Barenholz, R. L. Biltonen, and T. E. Thompson, *Biochemistry*, **15**, 1393 (1976).
17) E. J. Shimshick and H. M. McConnell, *Biochemistry*, **12**, 2351 (1973).
18) R. A. Demel and B. de Kruyff, *Biochim. Biophys. Acta*, **457**, 109 (1976).
19) E.-S. Wu, K. Jacobson, and D. Papahadjopoulos, *Biochemistry*, **16**, 3936 (1977).
20) M. Kasha, "Spectroscopy of the Excited State," ed by B. D. Bartolo, Plenum Press, New York (1976), p. 337.
21) A. Seelig and J. Seelig, *Biochim. Biophys. Acta*, **406**, 1 (1975).
22) P. B. Hitchcock, R. Mason, K. M. Thomas, and G. G. Shipley, *Proc. Natl. Acad. Sci. U.S.A.*, **71**, 3036 (1974).
23) M. Shimomura, R. Ando, and T. Kunitake, *Ber. Bunsenges. Phys. Chem.*, **87**, 1134 (1983).
24) H. Watanabe, K. Okuyama, Y. Ogata, K. Hirabayashi, M. Shimomura, T. Kunitake, and N. Yasuoka, *Nippon Kagaku Kaishi*, **1987**, 550.
25) T. Kunitake, M. Shimomura, T. Kajiyama, A. Harada, K. Okahata, and M. Takayanagi, *Thin Solid Films*, **121**, L89 (1984).
26) R. M. Hochstrasser and M. Kasha, *Photochem. Photobiol.*, **3**, 317 (1964).
27) P. N. Tyminski, I. S. Ponticello, and D. F. O'Brien, *J. Am. Chem. Soc.*, **109**, 6541 (1987).
28) R. M. Silverstein, G. C. Bassler, and T. C. Morrill, "Spectrometric Identification of Organic Compounds," 3d ed, John Wiley and Sons, Inc., New York (1974), p. 245.
29) J. R. Silvius, *Biochim. Biophys. Acta*, **857**, 217 (1986).
30) B. R. Lentz, *Biochemistry*, **19**, 1943 (1980).

 © 1989 The Chemical Society of Japan Bull. Chem. Soc. Jpn., 62, 109—113 (1989)

Asymmetric Transformation of (*RS*)-Cysteine via Formation of (*RS*)-4-Thiazolidinecarboxylic Acids

Tadashi SHIRAIWA,* Kazuo KATAOKA, Shinji SAKATA, and Hidemoto KUROKAWA
Faculty of Engineering, Kansai University, Yamate-cho, Suita, Osaka 564
(Received June 20, 1988)

Either (*R*)- or (*S*)-cysteine ((*R*)- or (*S*)-Cys) was efficiently obtained from (*RS*)-Cys by the asymmetric transformation via formation of (*RS*)-4-thiazolidinecarboxylic acid ((*RS*)-THC) or (*RS*)-2,2-dimethyl-4-thiazolidinecarboxylic acid ((*RS*)-DMT) and by using (2*R*,3*R*)- or (2*S*,3*S*)-tartaric acid ((*R*)- or (*S*)-TA), as a resolving agent, in acetic acid. The asymmetric transformation was carried out by combination of crystallization of less soluble salt of (*S*)-THC or -DMT with (*R*)-TA (or salt of (*R*)-THC or -DMT with (*S*)-TA) and epimerization of soluble diastereomeric salt. The (*R*)- and (*S*)-THCs from the less soluble salts gave approximately optically pure (*R*)- and (*S*)-Cys's, respectively, in 64% yield. The asymmetric transformation via formation of (*RS*)-DMT was more successfully achieved by adding 0.1 molar equivalent of salicylaldehyde; that is, hydrolysis of the obtained less soluble salt gave optically pure (*R*)- and (*S*)-Cys's, respectively, in 80% yield based on the (*RS*)-Cys used as the starting material.

(*RS*)-Cysteine (abbreviated as (*RS*)-Cys) has been optically resolved by preferential crystallization to obtain (*R*)-Cys, a useful material for medicines, food additives, and cosmetics, and (*S*)-Cys, a pharmaceutical material.[1-3] The optical resolution by preferential crystallization is useful for industrial purposes and gives both enantiomers. In many cases, only one enantiomer is demanded in large amounts, but the other is not in so large an amount. Asymmetric transformation has the possibility of converting a racemate solely into the desirable enantiomer. An asymmetric transformation has been carried out for (*RS*)-amino acid derivatives by combination of selective crystallization of a less soluble diastereomeric salt and epimerization of the other soluble one.[4-9] This paper describes an attempt to obtain either (*R*)- or (*S*)-Cys efficiently from (*RS*)-Cys.

(*R*)-4-Thiazolidinecarboxylic acid ((*R*)-THC), a material for antihypertensive agent, has been obtained by reacting (*R*)-Cys with formaldehyde.[10] We reported the asymmetric transformation of (*RS*)-THC via formation of its diastereomeric salts with equimolar (2*R*,3*R*)- or (2*S*,3*S*)-tartaric acid ((*R*)- or (*S*)-TA).[11] Although a treatment of (*R*)- or (*S*)-THC with hydroxylamine hydrochloride gives optically active Cys,[2,11] the overall yield based on initial (*RS*)-Cys is estimated to be 50%. It has been reported that optically active amino acids are racemized in the presence of aldehydes in an organic acid such as acetic acid.[12] If formation of (*RS*)-THC from (*RS*)-Cys, epimerization by excess formaldehyde of its soluble diastereomeric salt with TA, and crystallization of its less soluble salt take place simultaneously in one system, it is expectable to obtain optically active Cys in higher yield.

Optically active 2,2-dimethyl-4-thiazolidinecarboxylic acid (DMT) is rapidly formed by reacting optically active Cys with acetone in acetic acid and racemized simultaneously by excess acetone, as described in our previous paper.[13] DMT is more easily hydrolyzed in water to regenerate Cys than THC.[14,15] In addition, DMT seems to form easily the salt with equimolar TA similarly to THC.

On the basis of the above suggestions, the asymmetric transformation of (*RS*)-Cys was tried via formation of (*RS*)-THC and (*RS*)-DMT and by using optically active TA as a resolving agent.

Experimental

Materials. (*R*)- and (*RS*)-Cysteine hydrochloride monohydrates were purchased from Wako Pure Chemicals Ind. and Sigma Chemicals Co., respectively, and recrystallized from water. Aqueous solutions of the hydrochlorides were adjusted with concentrated aqueous ammonia to pH 6 to obtain (*R*)- and (*RS*)-Cys. (*R*)-Cys: $[\alpha]_D^{20}$ +6.5° (*c* 4.00, 5 mol dm^{-3} HCl). (*R*)- and (*S*)-TAs were purchased from Wako Pure Chemicals Ind.

Synthesis of 4-Thiazolidinecarboxylic Acid and 2,2-Dimethyl-4-thiazolidinecarboxylic Acid. (*RS*)- or (*R*)-Cys (0.0200 mol, 2.42 g) was dissolved in the presence of 1.62 g of 37% aqueous formaldehyde (0.0200 mol of formaldehyde) in 40 cm^3 of acetic acid at 50 °C, and the solution was cooled immediately to 30 °C. After stirring for 1 h at 30 °C, the solution was dried under reduced pressure at 40 °C. The THC obtained as the residue was washed thoroughly with methanol and dried. (*RS*)-THC: Yield 2.49 g (93.5%); mp 188—191 °C (decomp) (lit,[16] 183—184 °C, 195 °C (decomp)). (*R*)-THC: Yield 2.48 g (93.1%); mp 200—202 °C (decomp) (lit,[16] 196—197 °C, 205—209 °C (decomp); $[\alpha]_D^{20}$ −141° (*c* 0.500, water) (lit,[16] $[\alpha]_D$ −141° (water)).

(*R*)-DMT was obtained by reacting (*R*)-Cys with acetone in acetic acid and (*RS*)-DMT by racemization of (*R*)-DMT, as described in our previous paper.[13] (*R*)-DMT: Mp 144—145 °C (lit,[14] 138—140 °C); $[\alpha]_D^{20}$ −188° (*c* 0.100, acetone) (lit,[14] $[\alpha]_D$ −183° (acetone)). (*RS*)-DMT: Mp 150—152 °C.

Preparation of Standard Salts. A mixture of 0.0200 mol of (*R*)-Cys, 0.0200 mol of (*S*)-TA, and 0.0500 mol (2.90 g) of acetone in 10 cm^3 of acetic acid was refluxed for 30 min. After stirring the mixture for 30 min at room temperature, the formed salt of (*R*)-DMT with (*S*)-TA ((*R*)-DMT·(*S*)-TA salt) was collected by filtration, washed thoroughly with diethyl ether, and dried. The salt of (*R*)-DMT with (*R*)-TA

could not be obtained because the formed salt was strongly hygroscopic. The (*R*)-DMT·(*S*)-TA salt: Yield 5.95 g (95.6%); mp 172—174 °C (decomp); $[\alpha]_D^{20}$ −81.8° (*c* 0.500, methanol); Found C, 38.44; H, 5.47; N, 4.48% (Calcd for $C_{10}H_{17}NO_8S$: C, 38.58; H, 5.50; N, 4.50%).

The salt of (*R*)-THC with (*S*)-TA ((*R*)-THC·(*S*)-TA salt) and that of (*R*)-THC with (*R*)-TA ((*R*)-THC·(*R*)-TA salt) were prepared by the method described in our previous paper.[17] The (*R*)-THC·(*S*)-TA salt: Mp 171—173 °C (decomp); $[\alpha]_D^{20}$ −74.0° (*c* 0.500, water). The (*R*)-THC·(*R*)-TA salt: Mp 149—150 °C (decomp); $[\alpha]_D^{20}$ −55.8° (*c* 0.500, water).

Asymmetric Transformation. Procedure I: A mixture of 0.0200 mol of (*RS*)-Cys, 0.0200 mol of (*R*)- or (*S*)-TA, and 1.95 g of 37% aqueous formaldehyde (0.0240 mol of formaldehyde) in 40 cm³ of acetic acid was stirred for 0.5—2 h at 80 °C. After stirring the mixture for 15 min in an ice bath, the formed salt was collected by filtration, washed with diethyl ether, and dried. The salt was washed by stirring in 250 cm³ of ethanol for 1 h at 20 °C and then in 50 cm³ of methanol for 1 h to give (*R*)- or (*S*)-THC. The obtained (*R*)- and (*S*)-THCs (2.04 g) were treated with 1.5 molar equivalents of hydroxylamine hydrochloride in methanol to give 1.54 g of (*R*)- and (*S*)-Cys's, as described in our previous paper;[2] the yield based on 0.0200 mol of (*RS*)-Cys was 63.6%.

(*R*)-Cys (0.0200 mol) and 0.0200 mol of (*R*)-TA were dissolved in the presence of 1.62—2.44 g of 37% aqueous formaldehyde (0.0200—0.0300 mol of formaldehyde) in 40 cm³ of acetic acid at 70 °C. After stirring the mixture for 30 min at 30 °C and then for 1 h at 80 °C, the formed salt was filtered off and treated similarly to above.

Procedure II: A mixture of 0.0400 mol of (*RS*)-Cys, 0.0400 mol of (*R*)- or (*S*)-TA, and 0.200 mol of acetone in 15 cm³ of acetic acid was refluxed (approximately at 83 °C) for 2—10 h. The formed salt was filtered off, washed with diethyl ether, and dissolved in 80 cm³ of water. After refluxing for 2 h, the solution was dried under reduced pressure at 40 °C. The residue was stirred for 2 h in 100 cm³ of methanol to give (*R*)- or (*S*)-Cys.

Procedure III: After refluxing a mixture of 0.0400 mol of (*RS*)-Cys, 0.0400 mol of (*R*)- or (*S*)-TA, and 0.200 mol of acetone in 10 cm³ of acetic acid, 0.0040 mol of salicylaldehyde was added to the mixture. The mixture was refluxed (approximately at 77 °C) for 2—7 h and successively stirred for 30 min in an ice bath. The formed salt was filtered off, washed thoroughly with diethyl ether, and dried. The obtained salt was hydrolyzed to give (*R*)- or (*S*)-Cys and to recover TA. For example, 10.38 g of optically pure (*R*)-DMT·(*S*)-TA salt was added to a mixture of 10 cm³ of water and 100 cm³ of ethanol. After stirring the mixture for 1 h at 60 °C, crude (*R*)-Cys was filtered off: yield 5.61 g; $[\alpha]_D^{20}$ +4.7° (*c* 4.00, 5 mol dm⁻³ HCl). The (*R*)-Cys was washed by stirring for 30 min in 50 cm³ of methanol to give 3.88 g (80.1% yield) of optically pure (*R*)-Cys: $[\alpha]_D^{20}$ +6.5° (*c* 4.00, 5 mol dm⁻³ HCl) (lit,[18] $[\alpha]_D$ +6.5° (5 mol dm⁻³ HCl)). The ^{1}H NMR spectrum of the (*R*)-Cys in deuterium oxide showed no methyl protons. Drying of the above ethanol and methanol washings gave 4.96 g (82.6% recovery) of (*S*)-TA: $[\alpha]_D^{20}$ −12.1° (*c* 20.0, water) (lit,[19] (*R*)-TA $[\alpha]_D^{20}$ +11.98° (*c* 20%, water)).

Racemization Rate of (*R*)-2,2-Dimethyl-4-thiazolidinecarboxylic Acid. A mixture of 0.0200 mol of (*R*)-Cys and 30 cm³ of acetic acid was heated to 80 °C. After adding 0.100 mol of acetone and 0.0020 mol of acetaldehyde, benzaldehyde, 2-chlorobenzaldehyde, or salicylaldehyde, the resulting solution was stirred at 80 °C; (*R*)-Cys was dissolved completely by stirring for several minutes at 80 °C. One cm³ portions of the solution were pipetted out at 30 min intervals and diluted rapidly to 10 cm³ with acetic acid. The optical rotation at 589 nm was measured. The rate constant (k_R/h⁻¹) was calculated by the least-squares method from

$$\ln \alpha_0/\alpha_t = k_R t, \quad (1)$$

where α_t is the optical rotation at time *t* h and α_0 that extrapolated to zero time. The half-life period ($t_{1/2}$/h) was calculated on the basis of k_R values obtained by Eq. 1. The above solution was dried under reduced pressure after stirring for 3 h at 80 °C and the residue was washed thoroughly with diethyl ether. The ^{1}H NMR spectrum showed that the residue was DMT and not any 4-thiazolidinecarboxylic acid derivatives.

Measurements. Optical and specific rotations were measured by a Union Giken PM-101 digital polarimeter with a quartz cell of 0.50 dm path length. ^{1}H NMR spectra were recorded on a JEOL JNM—PMX 60 NMR spectrometer in deuterium oxide with no internal standard substance.

Results and Discussion

Asymmetric Transformation by Procedure I. (*RS*)-THC was easily formed by reacting (*RS*)-Cys with formaldehyde in acetic acid, as described in the experimental section. The diastereomeric salts of (*RS*)-THC with equimolar (*R*)-TA were separated into the less soluble (*S*)-THC·(*R*)-TA salt and the soluble (*R*)-THC·(*R*)-TA salt.[17] These results indicate a possibility that formation of (*RS*)-THC, selective crystallization of the (*S*)-THC·(*R*)-TA salt, and epimerization by excess formaldehyde of the (*R*)-THC·(*R*)-TA salt take place simultaneously in one system. The epimerization seems to be accelerated with an increase in amount of excess formaldehyde. However, the increase may result in dissolution of a part of the less soluble salt because 37% aqueous formaldehyde (37% FA) is employed. Optimization of the amount of 37% FA was conducted by stirring a mixture of 0.0200 mol of (*R*)-Cys, 0.0200 mol of (*R*)-TA, and 1.62—2.44 g of 37% FA (0.0200—0.0300 mol of formaldehyde) in acetic acid. These results are given in Table 1 and Fig. 1. The degree of transformation into the (*S*)-THC·(*R*)-TA salt in Fig. 1 was calculated by

$$\text{Degree of transformation}/\% = (\text{Yield}/\% \times \text{Optical purity}/\%)/100. \quad (2)$$

Although the use of 1.62 g of 37% FA (0.0200 mol of formaldehyde) gave the (*R*)-THC·(*R*)-TA salt, the salt was partially epimerized even by using equimole of formaldehyde to (*R*)-Cys, as indicated by its having 59.5% optical purity. The (*S*)-THC·(*R*)-TA salts with

Table 1. Asymmetric Transformation by Procedure I[a]

Conditions				Salt				THC		
Time h	Amount of formaldehyde[b] mol	Configuration Cys	Configuration TA	Configuration[c]	Yield g[%[d]]	Specific rotation[e] °	Optical purity[f] %	Configuration	Yield g[%[g]]	Optical purity[h] %
1	0.020	(*R*)	(*R*)	(*R*·*R*)	3.35[59.1]	−29.3	59.5	(*R*)	1.43[53.7]	65.2
1	0.022	(*R*)	(*R*)	(*S*·*R*)	3.66[64.6]	+59.3	77.3	(*S*)	1.59[59.7]	82.4
1	0.024	(*R*)	(*R*)	(*S*·*R*)	3.83[67.6]	+73.2	98.8	(*S*)	1.68[63.1]	99.3
1	0.026	(*R*)	(*R*)	(*S*·*R*)	3.57[63.0]	+72.4	97.5	(*S*)	1.56[58.6]	97.2
1	0.028	(*R*)	(*R*)	(*S*·*R*)	3.33[58.8]	+72.8	98.2	(*S*)	1.45[54.4]	98.6
1	0.030	(*R*)	(*R*)	(*S*·*R*)	3.08[54.4]	+72.1	97.1	(*S*)	1.33[49.9]	97.9
0.5	0.024	(*RS*)	(*R*)	(*S*·*R*)	3.46[61.1]	+67.0	89.2	(*S*)	1.47[55.2]	92.2
1	0.024	(*RS*)	(*S*)	(*R*·*S*)	4.56[80.5]	−73.8	99.7	(*R*)	1.98[74.4]	100
1.5	0.024	(*RS*)	(*R*)	(*S*·*R*)	4.68[82.6]	+73.2	98.8	(*S*)	2.04[76.6]	99.3
2	0.024	(*RS*)	(*S*)	(*R*·*S*)	4.68[82.6]	−73.7	99.5	(*R*)	2.04[76.6]	100

a) (*R*)- or (*RS*)-Cysteine (Cys) 0.0200 mol; (2*R*,3*R*)- or (2*S*,3*S*)-tartaric acid (TA) 0.0200 mol; acetic acid 40 cm³; temperature 80 °C; THC 4-thiazolidinecarboxylic acid. b) 37% aqueous formaldehyde (1.62 g) corresponds to 0.0200 mol of formaldehyde. (c) (*R*·*R*) represented the salt composed of equimolar amounts of (*R*)-THC and (*R*)-TA (*S*·*R*) the salt of (*S*)-THC and (*R*)-TA, and (*R*·*S*) the salt of (*R*)-THC and (*S*)-TA. d) The yield was calculated on the basis of 0.0200 ml (5.67 g) of the salt. e) $[\alpha]_D^{20}$ (*c* 0.500, water). f) The optical purity was determined on the basis of the specific rotation of the (*S*·*R*)-salt ($[\alpha]_D^{20}$ +74.0° (*c* 0.500, water)) and that of the (*R*·*R*)-salt ($[\alpha]_D^{20}$ −55.8° (*c* 0.500, water)). g) The yield was calculated on the basis of 0.0200 mol (2.66 g) of Cys. h) The optical purity was determined on the basis of the specific rotation of (*R*)-THC ($[\alpha]_D^{20}$ −141 ° (*c* 0.500, water)).

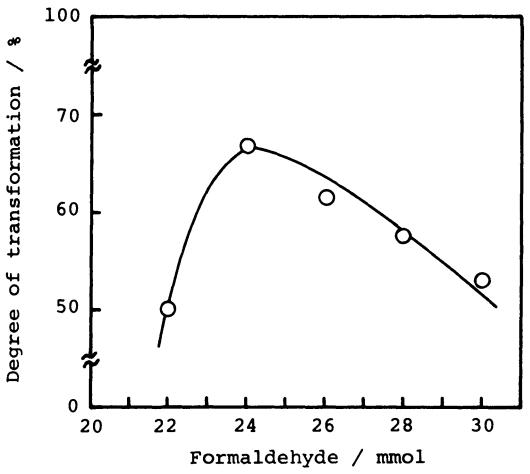

Fig. 1. Relationship between degree of transformation into salt of (*S*)-4-thiazolidinecarboxylic acid with (2*R*,3*R*)-tartaric acid and amount of formaldehyde. Conditions: (*R*)-Cysteine 0.0200 mol; (2*R*,3*R*)-tartaric acid 0.0200 mol; acetic acid 40 cm³; stirring time 1 h; temperature 80 °C; 1.62 g of 37% aqueous formaldehyde corresponds to 0.0200 mol of formaldehyde.

77—99% optical purity were obtained by using 1.79—2.44 g of 37% FA (0.0220—0.0300 mol of formaldehyde). As seen in Fig. 1, the (*S*)-THC·(*R*)-TA salt with 98.8% optical purity was obtained by using 1.95 g of 37% FA (0.0240 mol of formaldehyde) in the highest degree of transformation (66.7%). This salt gave (*S*)-THC with 99.3% optical purity in 63% yield based on the (*R*)-Cys used as the starting material.

Based on the above results, the asymmetric transformation was carried out by reaction of 0.0200 mol of (*RS*)-Cys, 0.0200 mol of (*R*)- or (*S*)-TA, and 1.95 g of 37% FA in 40 cm³ of acetic acid at 80 °C, as shown in Table 1. Although the asymmetric transformation was also attempted at 90 °C, the salt formed at lower temperature was dissolved on heating to 90 °C.

The (*R*)-THC·(*S*)-TA and (*S*)-THC·(*R*)-TA salts with approximately 100% optical purity were obtained in 83% yield by reaction for 1.5 and 2 h, respectively. These salts gave (*R*)- and (*S*)-THCs, respectively, in 77% yield. The obtained THCs were treated with hydroxylamine hydrochloride to give (*R*)- and (*S*)-Cys's, respectively, in 64% yield based on 0.0200 mol of (*RS*)-Cys.

Asymmetric Transformation by Procedure II. The asymmetric transformation by procedure I is more efficient than that described in our previous paper[11] in that it yields optically active Cys in higher yield. However, the treatment of THC with hydroxylamine hydrochloride is tedious and results in lowering of yield of the optically active Cys. Optically active DMT is racemized by acetone in acetic acid and hydrolyzed by adding water to reaction mixture to give (*RS*)-Cys in 97% yield.[13] The asymmetric transformation was tried for a mixture of 0.0400 mol of (*RS*)-Cys, 0.0400 mol of (*R*)-TA, and 0.200 mol of acetone in 15 cm³ of acetic acid under reflux (approximately at 83 °C), as shown in Table 2.

The salt of (*S*)-DMT with equimolar (*R*)-TA ((*S*)-DMT·(*R*)-TA salt) was crystallized as the less soluble diastereomeric salt and obtained in 61—75% yield with approximately 100% optical purity. Although the maximum yield was lower than that (83%) of the salt of THC obtained by procedure I, optically pure (*S*)-Cys was obtained in higher yield (71%) by hydrolysis in water. Therefore, DMT is a more favorable inter-

Table 2. Asymmetric Transformation by Procedure II[a]

Time	(*S*)-DMT·(*R*)-TA salt[b]			(*S*)-Cysteine	
	Yield	Specific rotation[d]	Optical purity[e]	Yield	Optical purity[g]
h	g [%[c]]	°	%	g [%[f]]	%
2	7.63[61.3]	+79.0	96.5	2.72[56.1]	92.3
4	8.69[69.8]	+81.2	99.2	3.15[65.0]	100
5	9.04[72.6]	+81.4	99.5	3.35[69.1]	98.5
6	8.99[72.2]	+81.4	99.5	3.43[70.8]	98.5
8	9.19[73.8]	+81.8	100	3.45[71.2]	100
10	9.28[74.5]	+81.6	99.7	3.46[71.4]	100

a) (*RS*)-Cysteine ((*RS*)-Cys) 0.0400 mol; (2*R*,3*R*)-tartaric acid ((*R*)-TA) 0.0400 mol; acetone 0.200 mol; acetic acid 15 cm^3; temperature 83 °C; DMT 2,2-dimethyl-4-thiazolidinecarboxylic acid. b) The (*S*)-DMT·(*R*)-TA salt is composed of (*S*)-DMT and (*R*)-TA. (c) The yield was calculated on the basis of 0.0400 ml (12.45 g) of the DMT salt. d) $[\alpha]_D^{20}$ (*c* 0.500, methanol). e) The optical purity was determined on the basis of the specific rotation of the (*R*)-DMT·(*S*)-TA salt ($[\alpha]_D^{20}$ −81.8° (*c* 0.500, methanol)) and that of equimolar mixture of (*RS*)-DMT and (*S*)-TA ($[\alpha]_D^{20}$ −2.9° (*c* 0.500, methanol)). f) The yield was calculated on the basis of 0.0400 mol (4.85 g) of Cys. g) The optical purity was determined on the basis of (*R*)-Cys ($[\alpha]_D^{20}$ +6.5° (*c* 4.00, 5 mol dm^{-3} HCl)).

mediate than THC to obtain optically active Cys by the asymmetric transformation.

Racemization by Using Aldehydes as Catalyst. The (*S*)-DMT·(*R*)-TA salt seems to be insoluble in acetone and to be more soluble in acetic acid than the (*S*)-THC·(*R*)-TA and (*R*)-THC·(*S*)-TA salts. Therefore, a relative decrease in amount of acetic acid (or an increase of acetone) may result in an increase in yield of the (*S*)-DMT·(*R*)-TA salt or its enantiomeric salt. However, such a system is refluxed at lower temperature and hence the epimerization rate for the soluble salt is reduced.[12,13] As seen in Tables 1 and 2, procedure I gives the (*S*)-THC·(*R*)-TA or (*R*)-THC·(*S*)-TA salt with high optical purity in 80% yield by reaction for 1 h, whereas procedure II requires long reaction time (over 5 h) to give the (*S*)-DMT·(*R*)-TA salt in over 70% yield. Therefore, aldehydes seem to be more favorable catalysts for epimerization than ketones.

The racemization rate of (*R*)-DMT was measured at 80 °C in the presence of 0.1 molar equivalent of acetaldehyde, benzaldehyde, 2-chlorobenzaldehyde, or salicylaldehyde as the catalyst. Since an addition of a small amount of water to this system resulted in hydrolysis of the formed DMT,[13] 37% FA was not employed as the catalyst. The racemizations using acetaldehyde, salicylaldehyde, or no aldehydes are illustrated in Fig. 2.

Figure 2 shows that linear relationships exist between ln α_0/α_t and time (t/h); the correlation coefficients are over 0.99. Therefore, these racemizations can be regarded as first-order reactions. The rate constant (k_R/h^{-1}) and half-life period ($t_{1/2}$/h) were calculated by Eq. 1 and given in Table 3.

Although the addition of aldehydes tended to accelerate the racemization of (*R*)-DMT, any aldehydes other than salicylaldehyde showed no extremely pronounced catalysis. The k_R value in the case using

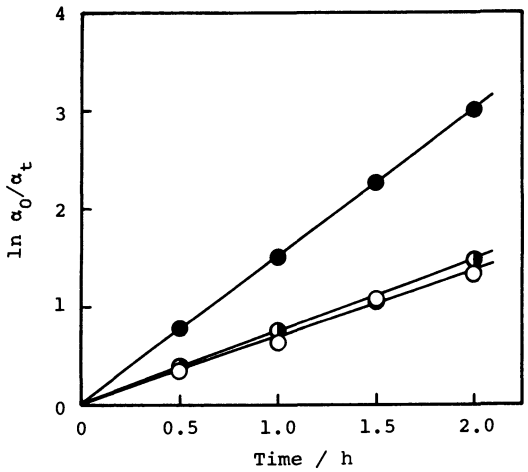

Fig. 2. Racemization of (*R*)-2,2-dimethyl-4-thiazolidinecarboxylic acid.
Conditions: (*R*)-Cysteine 0.0200 mol; aldehyde 0.0020 mol; acetone 0.100 mol; acetic acid 30 cm^3; temperature 80 °C. Aldehyde: ○ non; ◑ acetaldehyde; ● salicylaldehyde.

Table 3. Racemization of (*R*)-2,2-Dimethyl-4-thiazolidinecarboxylic Acid by Using Aldehydes as Catalyst[a]

Aldehyde	Rate constant	Half-life period
	h^{-1}	h
—	0.675	1.03
AA[b]	0.716	0.968
BA[c]	0.787	0.881
2-CBA[d]	0.683	1.01
SA[e]	1.51	0.459

a) (*R*)-Cysteine 0.0200 mol; acetone 0.100 mol; aldehyde 0.0020 mol; acetic acid 30 cm^3; temperature 80 °C. b) AA: Acetaldehyde. c) BA: Benzaldehyde. d) 2-CBA: 2-Chlorobenzaldehyde. e) SA: Salicylaldehyde.

Table 4. Asymmetric Transformation by Procedure III[a]

Time h	Configuration of TA	Salt				Cysteine		
		Configuration[b]	Yield g [%[c]]	Specific rotation[d] °	Optical purity[e] %	Configuration	Yield g [%[f]]	Optical purity[g] %
2	(*R*)	(*S*·*R*)	9.32[74.9]	+79.1	96.6	(*S*)	3.47[71.6]	93.8
3	(*R*)	(*S*·*R*)	9.79[78.6]	+79.8	97.5	(*S*)	3.68[75.9]	95.4
4	(*S*)	(*R*·*S*)	10.12[81.3]	−80.5	98.4	(*R*)	3.79[78.2]	98.5
5	(*R*)	(*S*·*R*)	10.36[83.2]	+81.8	100	(*S*)	3.88[80.1]	100
6	(*S*)	(*R*·*S*)	10.38[83.4]	−81.8	100	(*R*)	3.88[80.1]	100
7	(*R*)	(*S*·*R*)	10.38[83.4]	+81.8	100	(*S*)	3.88[80.1]	100

a) (*RS*)-Cysteine ((*RS*)-Cys) 0.0400 mol; (2*R*,3*R*)- or (2*S*,3*S*)-tartaric acid 0.0400 mol; salicylaldehyde 0.0040 mol; acetone 0.200 mol; acetic acid 10 cm^3; temperature 77 °C. b) (*S*·*R*) represented the salt composed of equimolar amounts of (*S*)-DMT and (*R*)-TA and (*R*·*S*) the salt of (*R*)-DMT and (*S*)-TA. c) The yield was calculated on the basis of 0.040 mol (12.45 g) of the DMT·TA salt. d) $[\alpha]_D^{20}$ (*c* 0.500, methanol). e) The optical purity was determined on the basis of the specific rotation of the (*R*)-DMT·(*S*)-TA salt ($[\alpha]_D^{20}$ −81.8° (*c* 0.500, methanol)) and that of equimolar mixture of (*RS*)-DMT and (*S*)-TA ($[\alpha]_D^{20}$ −2.9° (*c* 0.500, methanol)). f) The yield was calculated on the basis of 0.0400 mol (4.85 g) of Cys. g) The optical purity was determined on the basis of the specific rotation of (*R*)-Cys ($[\alpha]_D^{20}$ +6.5° (*c* 4.00, 5 mol dm^{-3} HCl)).

salicylaldehyde is 2.2 times that in the absence of aldehyde.

Asymmetric Transformation by Procedure III. Based on the above suggestion, the asymmetric transformation of (*RS*)-Cys was achieved in the presence of 0.1 molar equivalent of salicylaldehyde as the catalyst under reflux (approximately at 77 °C), as shown in Table 4. The ^{1}H NMR spectra of the obtained salts showed methyl protons and no aromatic protons.

The (*S*)-DMT·(*R*)-TA salt with 96.6% optical purity was obtained in 75% yield even by reaction for 2 h. This salt gave (*S*)-Cys with 93.8% optical purity in 72% yield. This yield corresponds to that to be obtained at 6 h by procedure II. Therefore, the epimerization was accelerated by adding salicylaldehyde.

The (*S*)-DMT·(*R*)-TA and (*R*)-DMT·(*S*)-TA salts with 98—100% optical purity were obtained in over 80% yield by reaction for 4—7 h. These salts were hydrolyzed in water to give (*R*)- or (*S*)-Cys, respectively, with 98—100% optical purity in 80% yield based on the initial (*RS*)-Cys. Further, (*R*)- and (*S*)-TAs, respectively, were recovered easily from these salts in over 80% recovery.

References

1) C. Inoue, Y. Kurima, and S. Moriguchi, Jpn. Patent, 70859 (1982); *Chem. Abstr.*, **97**, 163490 (1982).

2) T. Shiraiwa, Y. Sado, M. Komure, and H. Kurokawa, *Bull. Chem. Soc. Jpn.*, **60**, 3277 (1987).

3) T. Shiraiwa, H. Tazoh, M. Sunami, Y. Sado, and H. Kurokawa, *Bull. Chem. Soc. Jpn.*, **60**, 3985 (1987).

4) J. C. Clark, G. H. Phillipps, and M. R. Steer, *J. Chem. Soc., Perkin Trans. 1*, **1976**, 475.

5) S. Shibata, H. Matsushita, K. Kato, M. Noguchi, M. Saburi, and S. Yoshikawa, *Bull. Chem. Soc. Jpn.*, **52**, 2938 (1979).

6) K. Suzuki, S. Kiyooka, T. Miyagawa, and A. Kawai, *Nippon Kagaku Kaishi*, **1980**, 287.

7) C. Hongo, R. Yoshioka, M. Tohyama, S. Yamada, and I. Chibata, *Bull. Chem. Soc. Jpn.*, **56**, 3744 (1983).

8) R. Yoshioka, M. Tohyama, O. Ohtsuki, S. Yamada, and I. Chibata, *Bull. Chem. Soc. Jpn.*, **60**, 649 (1987).

9) R. Yoshioka, M. Tohyama, S. Yamada, O. Ohtsuki, and I. Chibata, *Bull. Chem. Soc. Jpn.*, **60**, 4321 (1987).

10) S. Ratner and H. T. Clarke, *J. Am. Chem. Soc.*, **59**, 200 (1937).

11) T. Shiraiwa, K. Kataoka, and H. Kurokawa, *Chem. Lett.*, **1987**, 2041.

12) S. Yamada, C. Hongo, and I. Chibata, *J. Org. Chem.*, **48**, 843 (1983).

13) T. Shiraiwa, K. Kataoka, S. Sakata, and H. Kurokawa, *Bull. Chem. Soc. Jpn.*, **61**, 4158 (1988).

14) G. E. Woodward and E. F. Schroeder, *J. Am. Chem. Soc.*, **59**, 1690 (1937).

15) J. C. Sheehan and D. H. Yang, *J. Am. Chem. Soc.*, **80**, 1158 (1958).

16) J. S. Davis, "Amino Acids and Peptides," Chapman and Hall, London, New York (1985), p. 302.

17) T. Shiraiwa, M. Nagata, K. Kataoka, Y. Sado, and H. Kurokawa, *Nippon Kagaku Kaishi*, in press.

18) Ref. 16, p. 130.

19) "Kagaku Daijiten," ed by Kagaku Daijiten Henshu Iinkai, Kyoritsu Shuppan, Tokyo (1971), Vol. 4, p. 693.

Studies on Ferrocene Derivatives. V.[1] Oxidation Reaction of (*o*-Substituted phenyl)ferrocenes

Yutaka Okada,* Noriyuki Yamamoto, and Takatoshi Hayashi
Department of Chemistry, Faculty of Science and Engineering,
Ritsumeikan University, Kita-ku, Kyoto 603
(Received June 30, 1988)

The oxidation reactivity of (*o*-substituted phenyl)ferrocenes with air was measured in acidic solution. The reactivity of *o*-acetyl, *o*-methoxycarbonyl, and *o*-methoxy derivatives was higher than that of the corresponding *p*-isomers. On the other hand, for *o*-hydroxy and *o*-methyl derivatives, the reactivity was lower than that of *p*-isomers. It was considered that the reactivity of *o*-isomers is influenced by the coordination ability of proton to iron atom. The coordination ability is governed by both the I-effect and steric effect of substituent.

Ferrocene (Fc) is very stable in air, and the oxidation from Fe(II) to Fe(III) is difficult. However, in an acidic solution, Fc is readily oxidized to ferrocenium ion[2] with air.

Investigations on oxidation reaction of substituted ferrocenes with air (or oxygen gas) in acidic solution have been done by several workers.[3,4] It has been reported that the rate of the reaction is influenced by electron-donating ability of a substituent.[3] The reaction mechanism was considered as follows:[4] ferrocenonium ion[2] is formed by coordination of a proton to iron atom of Fc, and is converted continuously to ferrocenium ion with loss of hydrogen atom by attack of oxygen (Eq. 1). That is to say,

$$Fc \xrightarrow{H^+} [Fc\text{-}H]^+ \xrightarrow{O_2} Fc^+, \quad (1)$$

where the active species on the oxidation reaction is ferrocenonium ion (protonated ferrocene). Therefore, it was considered that the rate of the reaction depends on the values of pK_a of catalytic acid.[5] Ferrocenonium ion was observed in $BF_3 \cdot H_2O$ by means of ^1H NMR.[6] However, in trifluoroacetic acid, the species was not found,[6] and the concentration of ferrocenonium ion was quite low.[4] On the other hand, the second step reaction was reported as follows:[4] In ferrocenonium ion, Cp groups are tilted by formation of Fe–H bond, and the metal orbitals are exposed to attack by O_2.[7] The oxidation reaction proceeded via insertion of O_2 into the Fe–H bond, followed by loss of $\dot{H}O_2$ radical.[4]

In our previous papers,[8,9] conformational studies on (*o*-substituted phenyl)ferrocenes were carried out by ^1H and ^{13}C NMR. It was clarified that the degree and orientation of the twist of the bond between phenyl (Ph) group and cyclopentadienyl (Cp) group vary with the kind of ortho substituent. In the present work, the oxidation reaction of (*o*-substituted phenyl)ferrocenes with air in acidic solution has been studied. The results were compared with those of the corresponding *p*-isomers. For acetyl, methoxycarbonyl, and methoxy derivatives, the oxidation reactivity of *o*-isomers was higher than that of corresponding *p*-isomers. On the other hand, for hydroxy and methyl derivatives, the reactivity of *o*-isomers was lower than that of *p*-isomers. Namely, no linear relationship was recognized between the oxidation reactivity and electron-donating ability of ortho substituent. Hence, the relation between the reactivity and the conformation is discussed.

Experimental

Preparation of Materials. The preparation and physical properties of (substituted phenyl)ferrocenes were reported in a preceding paper.[8]

Measurements of Oxidation Reactivity. Small three-necked flask fitted with reflux condenser, thermometer, and dropping funnel were employed for oxidation reaction. Air was introduced from the top of the condenser (Fig. 1). (Substituted phenyl)ferrocene (0.3 mmol) and 1,2-dichloroethane (50 ml) were added in the flask. Trichloroacetic acid (57 mmol) was dissolved in 10 ml of 1,2-dichloroethane. This solution was added through the dropping funnel. When all the materials were added, the reaction measurement was started. Reaction temperature was 40.0±0.1 °C, and air was introduced at a rate of 25±1 ml min^{-1}. The reaction mixture was stirred at 500 rpm by a magnetic stirrer with 25 mm length stirring bar. Sampling of reaction mixture was carried out at a regular interval. The sample was added

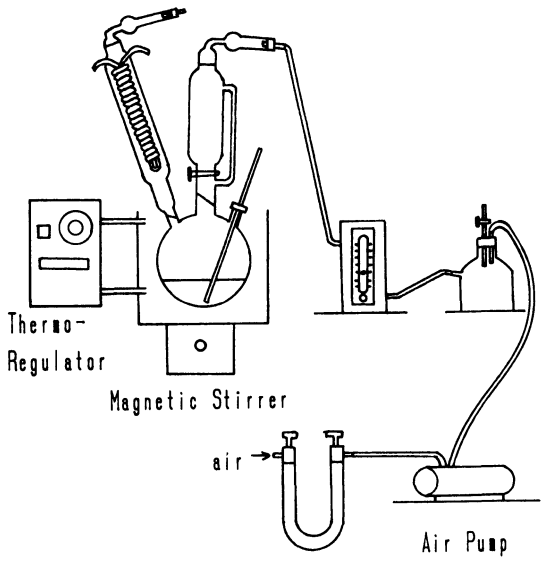

Fig. 1. Apparatus for oxidation reaction.

to water and vigorously stirred to stop the reaction. Then, the oxidation product (ferrocenium ion) was extracted in water; unreacted material and internal standard (nitrobenzene or 1,3,5-trichlorobenzene) remained in 1,2-dichloroethane layer. The amount of unreacted material in the presence of internal standard was determined by HPLC method. As mentioned above, the concentration of ferrocenonium ion in this solution was quite low.[4] Hence, it was considered that only ferrocenium ion was extracted in water. The conversion of the reaction is expressed by Eq. 2.

$$\text{Conversion} = ([Fc]_0 - [Fc])/[Fc]_0, \quad (2)$$

where [Fc] is the concentration of (substituted phenyl)ferrocene, and $[Fc]_0$ is the starting concentration. The rate constants were calculated as the pseudo-first order reaction about ferrocene derivatives; because the concentration of trichloroacetic acid was much higher than that of (substituted phenyl)ferrocene.

NMR Spectra. The method of NMR measurement was described in the preceding paper.[8]

IR Spectra. A JASCO IR-G type spectrometer was used. The measurements were done by the paste method (disperse medium: paraffin liquid).

Results and Discussion

Oxidation Reaction of (*p*-Substituted phenyl)ferrocenes. The conversions of the oxidation of (*p*-substituted phenyl)ferrocenes are shown in Fig. 2. The rate constants are presented in Table 1. The order of the reactivity was found as follows:

$$OH \fallingdotseq OCH_3 \fallingdotseq CH_3 > H > Cl > COCH_3 \fallingdotseq COOCH_3.$$

The order coincides approximately with that of electron-donating ability of para substituents. The relation between the Hammett constants[10] and the rate constants is shown in Fig. 3; a linear relationship was recognized. The reason was considered as follows. The electron density of the iron atom in the ferrocenes increased with an increase in electron-donating ability of para substituent. The coordination of catalytic proton to iron atom seems to be accelerated by higher electron density of iron atom. This order agrees with that of the polarographical oxidation potential value[11] of iron atom in ferrocene derivatives.

Oxidation Reaction of (*o*-Substituted phenyl)ferrocenes. The conversions of the oxidation of (*o*-substituted phenyl)ferrocenes are shown in Fig. 4. The rate constants are presented in Table 1. The order of the reactivity was found as follows:

$$OCH_3 > CH_3 \fallingdotseq COCH_3 > OH \fallingdotseq Cl \fallingdotseq COOCH_3.$$

The relation between the Hammett constants[10] and the rate constants is shown in Fig. 5. However, no linear relationship was recognized contrary to the case of the *p*-isomers.

The differences (Δk) of the rate constants between (*o*-substituted phenyl)ferrocenes and the correspond-

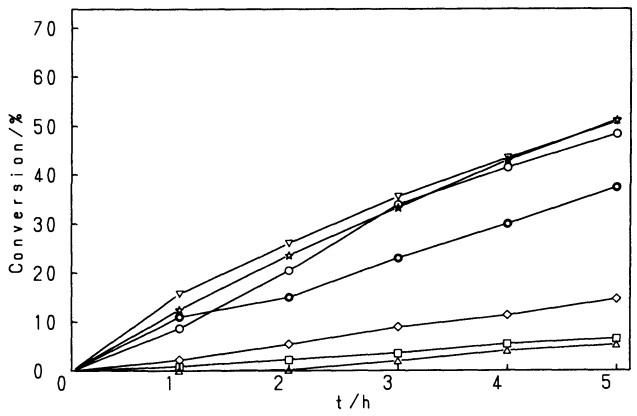

Fig. 2. Conversion of (*p*-substituted phenyl)ferrocenes. ●: H-, ○: *p*-CH_3-, ◇: *p*-Cl-, □: *p*-CH_3CO-, △: *p*-CH_3COO-, ▽: *p*-OH-, ☆: *p*-CH_3O-.

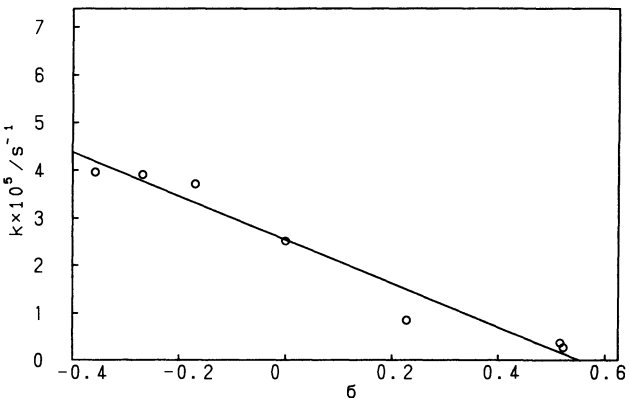

Fig. 3. Relation between Hammett constants and the rate constants of (*p*-substituted phenyl)ferrocenes.

Table 1. The Rate Constants of (Substituted phenyl)ferrocenes

	$k_{(p)}$[a]×10^5/s^{-1}	$k_{(o)}$[a]×10^5/s^{-1}	Δk[b]×10^5/s^{-1}
H	2.52	—	—
$COCH_3$	0.38	2.02	1.64
$COOCH_3$	0.28	1.04	0.76
CH_3O	3.92	7.10	3.18
OH	3.97	1.07	−2.90
CH_3	3.72	2.03	−1.69
Cl	0.86	1.04	0.18

a) $k_{(p)}$ and $k_{(o)}$ are the rate constants of *p*- and *o*-isomer, respectively. b) $\Delta k = k_{(o)} - k_{(p)}$.

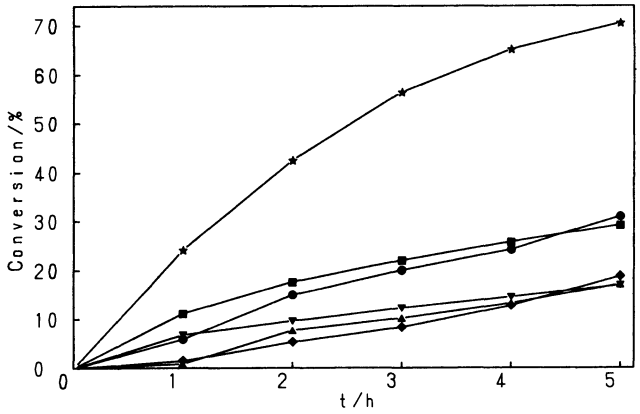

Fig. 4. Conversion of (*o*-substituted phenyl)ferrocenes. ●: *o*-CH_3-, ◆: *o*-Cl-, ■: *o*-CH_3CO-, ▲: *o*-CH_3COO-, ▼: *o*-OH-, ★: *o*-CH_3O-.

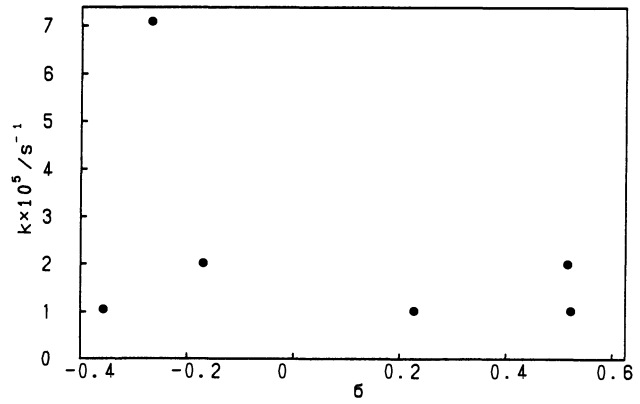

Fig. 5. Relation between Hammett constants and the rate constants of (*o*-substituted phenyl)ferrocenes.

ing *p*-isomers are presented in the right column of Table 1. (Substituted phenyl)ferrocenes can be classified into three groups by the values of Δk. The first group (acetyl, methoxycarbonyl, and methoxy derivatives) has positive values of Δk, and the second group (methyl and hydroxy derivatives) has negative values. In the third group (chloro derivative), the value is very small. The reason will be discussed later.

[Acetyl-, (Methoxycarbonyl)-, and Methoxyphenyl]-ferrocene: In [acetyl-, (methoxycarbonyl)-, and methoxyphenyl]ferrocene, the values of Δk were positive (Table 1). That is to say, the oxidation reactivity of the *o*-isomer was higher than that of the corresponding *p*-isomer (Fig. 6). In particular, the reactivity of (*o*-methoxyphenyl)ferrocene was highest in all the derivatives measured in this study. The reason will be discussed below.

As mentioned in the preceding paper,[8] the bond between Ph group and Cp group of (*o*-substituted phenyl)ferrocene is twisted. The twist is mainly produced by a steric repulsion between ortho substituent and α-proton of Cp group. It was considered that the degree of the twist in acetyl and methoxy-

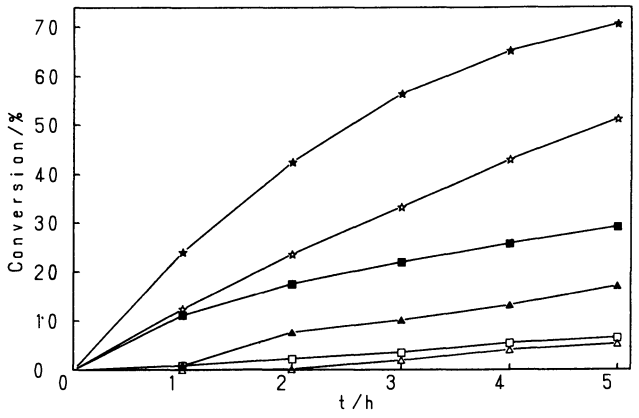

Fig. 6. Conversion of [methoxy-, acetyl-, and (methoxycarbonyl)phenyl]ferrocenes. ☆: *p*-CH_3O-, ★: *o*-CH_3O-, □: *p*-CH_3CO-, ■: *o*-CH_3CO-, △: *p*-CH_3COO-, ▲: *o*-CH_3COO-.

Table 2. The Values of $\Delta\delta$[a] of (Substituted phenyl)ferrocenes

	$H_{1'}$[b]	H_α[b]	H_β[b]	CH_3
p-CH_3CO	0.00	0.02	0.02	0.06
o-CH_3CO	0.01	0.01	0.02	0.06
p-CH_3COO	0.00	0.00	0.01	0.03
o-CH_3COO	0.02	0.01	0.02	0.04
p-CH_3O	0.02	0.02	0.03	0.02
o-CH_3O	0.03	0.05	0.06	0.02
p-CH_3	0.02	0.03	0.02	0.00
o-CH_3	0.01	0.02	0.01	0.00

a) $\Delta\delta=\delta'-\delta$, where δ' is proton chemical shift value measured in the presence of equimolar trichloroacetic acid and δ is the value at normal conditions.

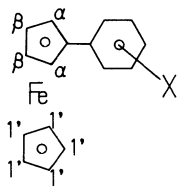

carbonyl derivative is almost equal.[8] On the other hand, the reactivity of acetyl derivative in *o*-isomer is higher than that of methoxycarbonyl derivative (Fig. 6). Therefore, it appears that the difference in this reactivity is not influenced by the I-effect which reflects on the twist of the bond between Ph group and Cp group, but depends on a different reason.

Proton chemical shift values of [acetyl- and (methoxycarbonyl)phenyl]ferrocene are shown in Table 2; the value of $\Delta\delta$ is defined as the difference between δ' and δ: δ' is the chemical shift value measured in the presence of equimolar trichloroacetic acid, and δ is the value at normal conditions. The value of $\Delta\delta$ was positive in all the protons of these derivatives. The values of $\Delta\delta$ of methyl groups in all the derivatives were larger than those of Cp groups. In Table 3, IR spectral data of (substituted phenyl)ferrocene are given. The values ν' measured in the presence of

Table 3. The Values of $\Delta\nu$ of [Acetyl- and (Methoxycarbonyl)phenyl]ferrocenes

	$\nu^{a)}/cm^{-1}$	$\nu'^{a)}/cm^{-1}$	$\Delta\nu^{b)}/cm^{-1}$
p-$COCH_3$	1666	1624	42
o-$COCH_3$	1680	1632	48
p-$COOCH_3$	1701	1686	15
o-$COOCH_3$	1710	1689	21

a) ν' is carbonyl streching frequency in the presence of trichloroacetic acid (ferrocene derivative: trichloroacetic acid=1 : 10) and ν is the value at normal conditions. b) $\Delta\nu=\nu-\nu'$.

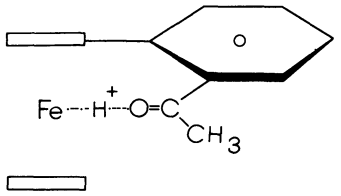

Fig. 7. Oxidation reaction of (*o*-acetylphenyl)ferrocene.

trichloroacetic acid were lower than the values ν measured at normal conditions. From these data, it was considered that coordination of proton occurs not only to iron atom but also to carbonyl oxygen. Hence, higher reactivity values of *o*-isomers are interpreted as follows: (i) Coordination of proton occurs to carbonyl oxygen at first. (ii) The proton was transferred to iron atom by formation of a chelate-like ring (Fig. 7). However, in *p*-isomer, the chelate-like ring is impossible to form.

If the oxidation reactions of [*o*-acetyl- and *o*-(methoxycarbonyl)phenyl]ferrocene are promoted by the chelating effect as shown in Fig. 7, the reactivity will be influenced by proton-coordinating ability or basicity of carbonyl oxygen. The basicity was examined by means of ^1H NMR.[12] The results indicate that basicity of acetyl group is higher than that of methoxycarbonyl group. Higher basicity of acetyl group was also shown by the IR spectral data in Table 3. (The values of $\Delta\nu$ of acetyl derivatives were larger than those of methoxycarbonyl derivatives.) Therefore, it was expected that the oxidation reactivity of (*o*-acetylphenyl)ferrocene is higher than that of methoxycarbonyl derivative. The experimental results agreed with this assumption. Namely, the difference in the reactivity between [*o*-acetyl- and *o*-(methoxycarbonyl)-phenyl]ferrocene can be explained by the chelating effect as shown in Fig. 7.

The unusually high reactivity of (*o*-methoxyphenyl)-ferrocene was considered by analogy. The values of $\Delta\delta$ of methyl groups in methoxy derivatives were positive (Table 2), whereas those in methyl derivatives were zero. Therefore, the oxidation reaction of this methoxy derivative seems to be promoted by the chelating effect as shown in Fig. 8. That is to say,

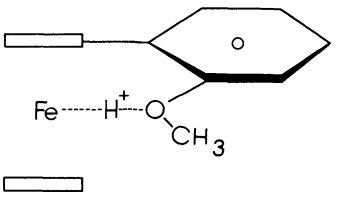

Fig. 8. Oxidation reaction of (*o*-methoxyphenyl)ferrocene.

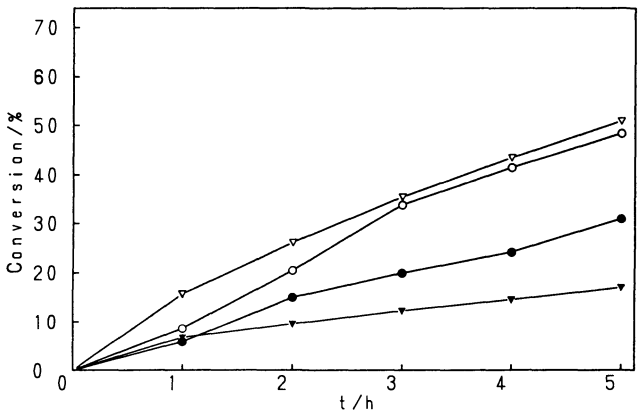

Fig. 9. Conversion of (hydroxy- and methylphenyl)-ferrocenes.
▽: *p*-OH-, ▼: *o*-OH-, ○: *p*-CH_3-, ●: *o*-CH_3-.

coordination of catalytic proton occurs at ethereal oxygen at first, and the proton transfer to iron atom follows by forming a chelate-like ring. Both the chelating effect of oxygen and the large I-effect of methoxyl group are presumed to raise the oxidation reactivity of (*o*-methoxyphenyl)ferrocene.

(Hydroxy- and Methylphenyl)ferrocene: In (hydroxy- and methylphenyl)ferrocene, the values of Δk were negative (Table 1), showing that the oxidation reactivity of the *o*-isomer is lower than that of the corresponding *p*-isomer (Fig. 9). The reason will be discussed below.

Displacing methyl group of (methoxyphenyl)ferrocene by hydrogen atom gives (hydroxyphenyl)ferrocene. The reactivity of two *o*-isomers, however, was strikingly different. Particular reactivity of methoxy derivative was mentioned above. The oxidation reactivity of (*o*-hydroxyphenyl)ferrocene was lowest in all the *o*-isomers examined in this study. The reason was considered in view of conformation of (*o*-hydroxyphenyl)ferrocene as follows. In this derivative, the degree of twist of the bond between Ph group and Cp group is distinctly large in spite of small size of hydroxyl group.[8] Furthermore, the endo conformation as in hydroxyl group is preferred than exo one. The driving force was suggested[8] to be an OH-d type hydrogen bond between hydroxyl group and d-electron of iron atom (Fig. 10). Therefore, it was considered that the electron density of iron atom in

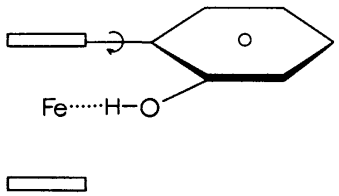

Fig. 10. Conformation of (*o*-hydroxyphenyl)ferrocene.

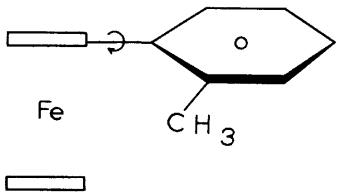

Fig. 11. Conformation of (*o*-methylphenyl)ferrocene.

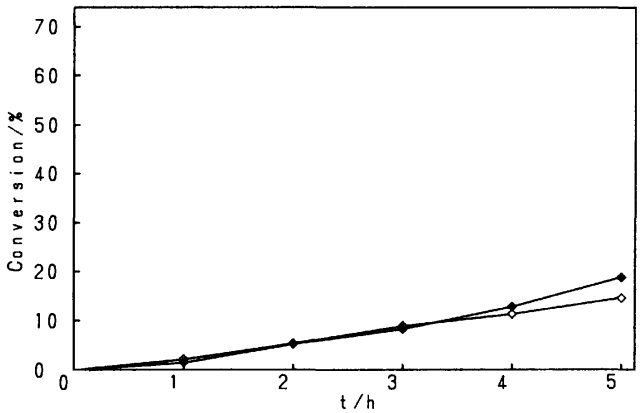

Fig. 12. Conversion of (chlorophenyl)ferrocene.
◇: *p*-Cl-, ◆: *o*-Cl-.

(*o*-hydroxyphenyl)ferrocene decreased strikingly by this hydrogen bond. Consequently, the oxidation reactivity of (*o*-hydroxyphenyl)ferrocene was remarkably low.

In (*o*-methylphenyl)ferrocene as well as hydroxy derivative, the endo conformation as in methyl group is preferred (Fig. 11).[8] The driving force to prefer the endo conformation is considered to be a CH-d type attractive interaction between methyl proton and d-electron of iron atom.[8] It is expected that the electron density of iron atom in (*o*-methylphenyl)ferrocene decreased slightly by this interaction. The CH-d type interaction will be weaker than the OH-d type hydrogen bond. Hence it seems that the electron density of iron atom in (*o*-methylphenyl)ferrocene is higher than that in (*o*-hydroxyphenyl)ferrocene. Consequently, the oxidation reactivity of methyl derivative was higher than that of hydroxy derivative.

(Chlorophenyl)ferrocene: In (chlorophenyl)ferrocene, the value of Δk was very small (Table 1),

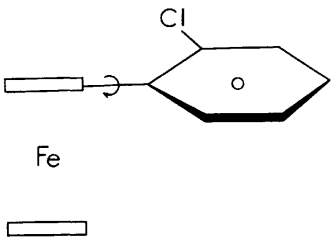

Fig. 13. Conformation of (*o*-chlorophenyl)ferrocene.

suggesting that no considerable difference exists in the reactivity between the *o*- and *p*-isomer (Fig. 12).

As mentioned in the previous paper,[8] the conformation of (*o*-chlorophenyl)ferrocene is considered as follows. The degree of twist of the bond between Ph group and Cp group is almost equal to that of (*o*-methylphenyl)ferrocene. However, in chloro derivative, the exo conformation (chlorine atom exists in exo position) is preferred (Fig. 13). The driving force to keep the exo conformation is considered to be an electronic repulsion between chlorine atom and d-electron of iron atom.[8] Therefore, it seems that the electron density of iron atom in chloro derivative does not decrease contrary to the case of methyl derivative. Consequently, the oxidation reactivity of (*o*-chlorophenyl)ferrocene was almost equal to that of *p*-isomer.

Conclusion

The reactivity of (substituted phenyl)ferrocene is influenced by the coordination ability of proton to iron atom. The coordination ability is governed by both the I-effect and the steric effect of the substituent.

References

1) Part IV: Y. Okada and T. Hayashi, *Nippon Kagaku Kaishi*, **1988**, 1998.
2) ferrocenium ion: Fc^+, ferrocenonium ion: $[Fe-H]^+$.
3) S. Muto, H. Kochi, and Y. Kamiya, *Sekiyu Gakkai Shi*, **17**, 50 (1974).
4) T. E. Bitterwolf and A. C. Ling, *J. Organomet. Chem.*, **40**, C29 (1972).
5) M. Aly, R. Bramly, J. Upadhyay, A. Wasserman, and P. R. Woolliams, *Chem. Commun.*, **1965**, 404.
6) T. J. Curphey, J. O. Santer, M. Rosenblum, and J. H. Rinchards, *J. Am. Chem. Soc.*, **82**, 5249 (1960).
7) T. E. Bitterwolf and A. C. Ling, *J. Organomet. Chem.*, **40**, 197 (1972).
8) T. Hayashi and Y. Okada, *Nippon Kagaku Kaishi*, **1987**, 208.
9) Y. Okada and T. Hayashi, *Nippon Kagaku Kaishi*, **1988**, 162.
10) H. H. Jaffé, *Chem. Rev.*, **53**, 191 (1953).
11) J. G. Mason and M. Rosenblum, *J. Am. Chem. Soc.*, **82**, 4206 (1960).
12) D. P. Eyman and R. S. Drago, *J. Am. Chem. Soc.*, **88**, 1617 (1966).

Preparation of New Nitrogen-Bridged Heterocycles. 19.[1] Smooth Syntheses of Thieno[3,2-*a*]- and Thieno[2,3-*b*]indolizine Derivatives

Akikazu KAKEHI,* Suketaka ITO, Tuneo FUJII, Yuichiro MORIMOTO, Shin-ichi MATSUMOTO, and Morio SHIOHARA

Department of Industrial Chemistry, Faculty of Engineering, Shinshu University, Wakasato, Nagano 380

(Received June 30, 1988)

The reactions of 2-(ethoxycarbonylmethylthio)indolizines having an acyl and/or a cyano group at the 1- and 3-positions under several alkaline conditions were examined, and title compounds, thieno[3,2-*a*]- and thieno[2,3-*b*]indolizine derivatives were obtained in fairly good yields. The cyclization modes observed in these transformation reactions were in accord with those expected by the molecular orbital calculations using some model compounds and by the stereochemical consideration of starting indolizines. The alkylations of 3-hydroxythieno[3,2-*a*]- and 3-hydroxythieno[2,3-*b*]indolizines were also investigated and the corresponding *O*- and *C*-alkylated heterocycles were formed in good yields.

In our previous communication[2] we have reported the smooth intramolecular cyclizations of the indolizines possessing an ethoxycarbonylmethylthio group at the 2-position and a cyano or an ethoxycarbonyl group at 1- or 3-position to ethyl 3-aminothieno[3,2-*a*]indolizine-2-carboxylates or ethyl 3-hydroxythieno-[2,3-*b*]indolizine-2-carboxylates under alkaline conditions. The regiospecificity of the reactions and the high synthetic value for the preparations of new heterocyclic skeletons prompted us to investigate further these intramolecular cyclizations using various 2-(ethoxycarbonylmethylthio)indolizines from the theoretical and practical standpoints of view. In this paper we wish to describe the formation of some thieno[3,2-*a*]- and thieno[2,3-*b*]indolizine derivatives from the alkaline treatment of polyfunctionalized indolizines and the comparison of the cyclization modes observed in these reactions with those expected by the molecular orbital calculations using model compounds.

Results and Discussion

Preparations of 2-(Ethoxycarbonylmethylthio)indolizines. These 2-(ethoxycarbonylmethylthio)indolizine derivatives **4a—t** were prepared in moderate to good yields by the treatment of the pyridinium salts **3a—t**, readily obtainable from the *S*-alkylations of the corresponding pyridinium-*N*-methylides **1a—j** with bromoacetonitrile **2a** or ethyl bromoacetate **2b**, with 1,8-diazabicyclo[5.4.0]undec-7-ene (DBU) at 0 °C followed by the addition of 2,3-dichloro-5,6-dicyano-*p*-benzoquinone (DDQ) as a dehydrogenating agent to the resulting reaction solutions. In the reactions of pyridinium salts **3e—j**, **o—t** possessing an acetyl or a benzoyl group, the formations of tricyclic thieno[2,3-*b*]-indolizines **5**[3] were also formed, but their yields were very low (<3%) (Scheme 1).

The structures of indolizines **4a—t** were determined

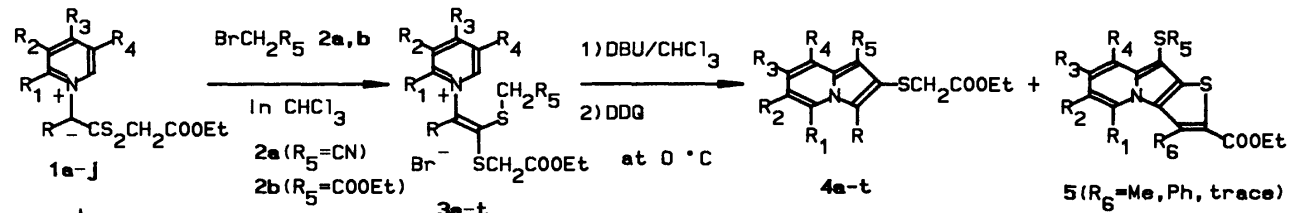

Ylide	R_1	R_2	R_3	R_4	R
1a	H	H	H	H	COOEt
1b	Me	H	H	H	COOEt
1c	H	H	Me	H	COOEt
1d	H	Me	H	Me	COOEt
1e	H	H	H	H	COMe
1f	Me	H	H	H	COMe
1g	H	H	Me	H	COMe
1h	H	Me	H	Me	COMe
1i	H	H	H	H	COPh
1j	H	H	Me	H	COPh

Prod.	Salt	R_1	R_2	R_3	R_4	R_5	R
4a	**3a**	H	H	H	H	CN	COOEt
4b	**3b**	Me	H	H	H	CN	COOEt
4c	**3c**	H	H	Me	H	CN	COOEt
4d	**3d**	H	Me	H	Me	CN	COOEt
4e	**3e**	H	H	H	H	CN	COMe
4f	**3f**	Me	H	H	H	CN	COMe
4g	**3g**	H	H	Me	H	CN	COMe
4h	**3h**	H	Me	H	Me	CN	COMe
4i	**3i**	H	H	H	H	CN	COPh
4j	**3j**	H	H	Me	H	CN	COPh

Prod.	Salt	R_1	R_2	R_3	R_4	R_5	R
4k	**3k**	H	H	H	H	COOEt	COOEt
4l	**3l**	Me	H	H	H	COOEt	COOEt
4m	**3m**	H	H	Me	H	COOEt	COOEt
4n	**3n**	H	Me	H	Me	COOEt	COOEt
4o	**3o**	H	H	H	H	COOEt	COMe
4p	**3p**	Me	H	H	H	COOEt	COMe
4q	**3q**	H	H	Me	H	COOEt	COMe
4r	**3r**	H	Me	H	Me	COOEt	COMe
4s	**3s**	H	H	H	H	COOEt	COPh
4t	**3t**	H	H	Me	H	COOEt	COPh

Scheme 1.

Table 1. ^{1}H NMR Spectral Data of 2-(Ethoxycarbonylmethylthio)indolizines

Compd[a] No.	C-5	C-6	C-7	C-8	CH_2CO_2Et		R			R_5	
4a	9.54	7.00	7.35	7.70	4.01	1.22	4.19	1.43	4.47	—	
	br d	dt	br t	br d	s	t	q	t	q		
4b	2.58	6.79	7.26	7.63	3.81	1.20	4.15	1.47	4.48	—	
	s	br d	q	br d	s	t	q	t	q		
4c	9.31	6.77	2.38	7.37	3.94	1.19	4.15	1.40	4.40	—	
	d	dd	s	br s	s	t	q	t	q		
4d	9.28	2.34	6.97	2.74	3.86	1.22	4.17	1.47	4.47	—	
	br s	s	br s	s	s	t	q	t	q		
4e	10.02	7.12	7.49	7.82	3.96	1.19	4.17	2.94		—	
	br d	dt	br t	br d	s	t	q	s			
4f	2.38	6.83	7.32	7.66	3.81	1.17	4.10	2.92		—	
	s	br d	q	br d	s	t	q	s			
4g	9.83	6.89	2.47	7.49	3.91	1.18	4.13	2.89		—	
	d	dd	s	br s	s	t	q	s			
4h	9.67	2.33	7.03	2.71	3.83	1.15	4.11	2.90		—	
	br s	s	br s	s	s	t	q	s			
4i	9.33	7.02	b)	b)	3.63	1.10	4.05	7.3—8.0		—	
	br d	dt			s	t	q	m			
4j	9.25	6.87	2.48	b)	3.61	1.07	4.03	7.3—7.9		—	
	d	dd	s		s	t	q	m			
4k	9.52	6.99	7.33	8.38	3.79	1.10	4.07	1.44	1.44	4.47	4.49[c]
	br d	dt	br t	br d	s	t	q	t	t	q	q
4l	2.53	6.67	7.15	8.28	3.73	1.10	4.07	1.43	1.43	4.43	4.46[c]
	s	br d	q	br d	s	t	q	t	t	q	q
4m	9.37	6.79	2.43	8.12	3.74	1.09	4.05	1.44	1.44	4.45	4.45[c]
	d	dd	s	br s	s	t	q	t	t	q	q
4n	9.27	2.30	6.84	2.44	3.68	1.13	4.10	1.41	1.44	4.43	4.46[c]
	br s	s	br s	s	s	t	q	t	t	q	q
4o	9.90	6.98	7.37	8.39	3.86	1.13	4.07	3.00		1.47	4.47
	br d	dt	br t	br d	s	t	q	s		t	q
4p	2.36	6.80	7.31	8.39	3.84	1.14	4.09	2.98		1.46	4.49
	s	br d	q	br d	s	t	q	s		t	q
4q	9.82	6.82	2.44	8.15	3.83	1.11	4.05	2.96		1.46	4.45
	d	dd	s	br s	s	t	q	s		t	q
4r	9.75	2.34	6.98	2.48	3.76	1.18	4.14	2.96		1.44	4.50
	br s	s	br s	s	s	t	q	s		t	q
4s	9.26	7.01	b)	8.48	3.58	1.05	4.01	7.2—8.0		1.46	4.50
	br d	dt		br d	s	t	q	m		t	q
4t	9.22	6.89	2.50	8.28	3.58	1.08	4.02	7.4—8.0		1.48	4.51
	d	dd	s	br s	s	t	q	m		t	q

a) These coupling constants are as follows: $J_{5,6}=J_{6,7}=7.0$, $J_{7,8}=9.0$, $J_{6,8}=2.0$, and $J_{Et}=7.0$ Hz. b) Overlapped with the phenyl proton signals. c) The signals due to these two ethoxycarbonyl groups could not be assigned.

by the analyses of their physical and spectral data and by the comparisons of their ^{1}H NMR (Table 1) and IR spectra (Table 4) with those of other indolizine derivatives prepared earlier by us[1,4] and other investigators.[5] For example, the elemental analyses of indolizines **4a—t** were in good accord with the proposed compositions and their ^{1}H NMR spectra showed distinct proton signals at near δ 1.15 (t, 3H, J=7.0 Hz, $OCH_2\underline{CH_3}$), 3.61—4.01 (s, 2H, SCH_2), and near 4.10 (q, 2H, J=7.0 Hz, $O\underline{CH_2}CH_3$) due to the 2-ethoxycarbonylmethylthio group, together with other proton signals on the indolizine ring. The presence of a saturated ester carbonyl group in the 2-substituent could be also confirmed by the absorption bands appeared at 1720—1740 cm^{-1} in their IR spectra. Interestingly, the up-field shift (10—30 cm^{-1}) of the absorption band of the carbonyl group at the 1-position in indolizines **4n**, **r** or at the 3-position in indolizines **4b**, **f**, **l**, **p** was observed. These shifts must be caused by the steric crowding of the carbonyl group with the 2-ethoxycarbonylmethylthio and the 5- or 8-methyl groups.

Preparations of Thieno[3,2-*a*]- and Thieno[2,3-*b*]-indolizines. Since these indolizines **4a—t** have an active methylene group in the 2-substituent and an acyl and/or a cyano group at the 1- or 3-position, the intramolecular reactions between these group should lead to the indolizine derivatives fused with a thiophene ring. Thus, the reactions of indolizines **4a—t** were examined under alkaline conditions in which the carbanion formation from the active methylene group could be expected.

Table 2. ^{1}H NMR Spectral Data of Thieno[3,2-*a*]indolizines

Compd[a,b] No.	C-7	C-6	C-5	C-4	C-3	R		COOEt		
6a	9.63	7.01	7.29	7.78	6.08	1.38	1.46	4.34	4.43[c]	
	br d	dt	br t	br d	br s	t	t	q	q	
6b	2.89	6.95	7.35	7.71	6.07	1.41	1.51	4.40	4.47[c]	
	s	br d	q	br d	br s	t	t	q	q	
6c	9.40	6.78	2.39	7.33	5.95	1.38	1.44	4.34	4.41[c]	
	d	dd	s	br s	br s	t	t	q	q	
6d	9.36	2.32	6.83	2.74	6.30	1.39	1.47	4.35	4.44[c]	
	br s	s	br s	s	br s	t	t	q	q	
6f	2.61	6.87	7.33	7.49	6.12	2.56		1.37	4.36	
	s	br d	q	br d	br s	s		t	q	
6h	9.97	2.33	7.00	2.88	6.37	2.51		1.40	4.34	
	br s	s	br s	s	br s	s		t	q	
6i	10.38	7.20	d)	d)	6.13	7.3—8.1		1.31	4.29	
	br d	dt			br s	m		t	q	
6j	10.10	6.93	2.48	d)	6.03	7.3—8.0		1.29	4.25	
	d	dd	s		br s	m		t	q	
9a	9.27	2.33	6.88	2.74	10.99	1.41	1.47	4.40	4.40[c]	
	br s	s	br s	s	br s	t	t	q	q	
9b	9.89	2.40	7.03	2.83	10.95	2.53		1.42	4.42	
	br s	s	br s	s	br s	s		t	q	
13a	9.38	2.35	6.93	2.74	4.16	1.42	1.48	4.41	4.44[c]	
	br s	s	br s	s	s	t	t	q	q	
13b	9.42	2.37	6.96	2.80	1.42	1.49	1.49	4.41	4.41	4.44[c]
	br s	s	br s	s	t	t	t	q	q	q
14a	9.23	2.34	7.07	2.87	—	1.41	4.42	1.21	4.21	1.87[e]
	br s	s	br s	s		t	q	t	q	s

a) The coupling constants are as follows: $J_{6,7}=J_{5,6}=7.0$, $J_{4,5}=9.0$, $J_{4,6}=2.0$, $J_{Et}=7.0$ Hz. b) The spectra of compound **6e** and **6g** could not be measured because of their low solubility. c) The signals due to these ethoxycarbonyl groups could not be assigned. d) Overlapped with the phenyl proton signals. e) The methyl signal on the C-2 position.

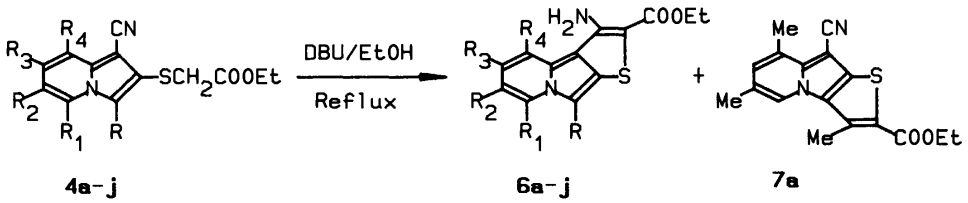

Prod.	React.	R_1	R_2	R_3	R_4	R
6a	**4a**	H	H	H	H	COOEt
6b	**4b**	Me	H	H	H	COOEt
6c	**4c**	H	H	Me	H	COOEt
6d	**4d**	H	Me	H	Me	COOEt
6e	**4e**	H	H	H	H	COMe

Prod.	React.	R_1	R_2	R_3	R_4	R
6f	**4f**	Me	H	H	H	COMe
6g	**4g**	H	H	Me	H	COMe
6h(+**7a**)	**4h**	H	Me	H	Me	COMe
6i	**4i**	H	H	H	H	COPh
6j	**4j**	H	H	Me	H	COPh

Scheme 2.

The treatment of indolizines **4a**—g, **i**, **j** having the 1-cyano group with DBU in refluxing ethanol gave smoothly ethyl 3-aminothieno[3,2-*a*]indolizine-2-carboxylates **6a**—g, **i**, **j**, in 50—94% yields, respectively, while the similar reaction of indolizine **4h** afforded also ethyl 9-cyano-3,6,8-trimethylthieno[2,3-*b*]indolizine-2-carboxylate **7a** in ca. 65% yield, together with the expected ethyl 9-acetyl-3-amino-4,6-dimethylthieno[3,2-*a*]indolizine-2-carboxylate **6h** (ca. 18%). Apparently, the formation of amino compounds **6a**—**j** results from the nucleophilic addition of the carbanion generated in situ to the 1-cyano group of indolizines **4a**—**j**, and that of product **7a** from the nucleophilic attack of the same species to the 3-acetyl group (Scheme 2).

On the other hand, the reactions of diethyl 1,3-indolizinedicarboxylates **4k**—n with DBU did not afford any significant products, but their reactions

Table 3. ^{1}H NMR Spectral Data of Thieno[2,3-*b*]indolizines

Compd[a] No.	C-5	C-6	C-7	C-8	C-3[b]		COOEt				
7a	8.19	2.36	6.88	2.67	2.94		1.42	4.38			
	br s	s	br s	s	s		t	q			
7b	8.57	6.82	7.29	8.33	2.99		1.42	1.47	4.40	4.44[c]	
	br d	dt	br t	br d	s		t	t	q	q	
7c	2.97	6.63	7.21	8.37	3.04		1.43	1.49	4.41	4.49[c]	
	s	br d	q	br d	s		t	t	q	q	
7d	8.23	6.53	2.39	7.94	2.84		1.42	1.46	4.38	4.40[c]	
	d	dd	s	br s	s		t	t	q	q	
7e	8.18	2.31.	6.87	2.87	2.96		1.44	1.49	4.41	4.41[c]	
	br s	s	br s	s	s		t	t	q	q	
7f	d)	6.57	d)	8.39	7.0—7.9		1.17	4.22	1.49	4.49	
		dt		br d	m		t	q	t	q	
7g	d)	6.42	2.39	8.15	7.0—7.9		1.18	4.22	1.49	4.48	
		dd	s	br s	m		t	q	t	q	
8a	8.59	6.83	7.31	8.27	10.53		1.42	1.45	4.41	4.41	
	br d	dt	br t	br d	br s		t	t	q	q	
8b	3.00	6.63	7.21	8.22	11.44		1.41	1.46	4.41	4.41	
	s	br d	q	br d	br s		t	t	q	q	
8c	8.39	6.63	2.42	7.97	8.70		1.41	1.44	4.39	4.39[c]	
	d	dd	s	br s	br		t	t	q	q	
11a	8.72	6.90	7.34	8.33	4.31		1.43	1.48	4.43	4.47[c]	
	br d	dt	br t	br d	s		t	t	q	q	
11b	2.97	6.65	7.23	8.28	4.11		1.43	1.48	4.41	4.45[c]	
	s	br d	q	br d	s		t	t	q	q	
11c	8.55	6.70	2.45	8.08	4.29		1.43	1.47	4.40	4.43[c]	
	d	dd	s	br s	s		t	t	q	q	
11d	8.70	6.85	7.31	8.30	1.40	1.46	1.50	4.37	4.43	4.56[c]	
	br d	dt	br t	br d	t	t	t	q	q	q	
11e	3.01	6.67	7.25	8.32	1.42	1.47	1.49	4.40	4.40	4.49[c]	
	s	br d	q	br d	t	t	t	q	q	q	
11f	8.57	6.71	2.46	8.08	1.41	1.46	1.50	4.38	4.43	4.56[c]	
	d	dd	s	br s	t	t	t	q	q	q	
12a	8.93	7.04	7.50	8.24	—		1.23	4.23	1.41	4.38	1.90[e]
	br d	dt	br t	br d			t	q	t	q	s
12b	3.14	6.77	7.42	8.50	—		1.26	4.25	1.44	4.41	1.91[e]
	s	br d	q	br d			t	q	t	q	s
12c	8.81	6.90	2.49	8.05	—		1.23	4.23	1.41	4.38	1.91[e]
	d	dd	s	br s			t	q	t	q	s

a) The coupling constants are as follows: $J_{5,6}=J_{6,7}=7.0$, $J_{7,8}=9.0$, $J_{6,8}=2.0$, $J_{Et}=7.0$ Hz. b) The proton signal due to the hydroxyl, methyl, methoxyl, or ethoxyl group. c) The signals due to these ethoxycarbonyl groups could not be assigned. d) Overlapped with the phenyl proton signals. e) The methyl signal on the C-2 position.

under the conditions for the Dieckmann reaction[6] gave the corresponding adducts: The treatment of indolizines **4k—m** with potassium *t*-butoxide in *N,N*-dimethylformamide (DMF) at room temperature followed by quenching the resulting mixture with diluted hydrochloric acid formed diethyl 3-hydroxythieno[2,3-*b*]indolizine-2,9-dicarboxylates **8a—c** in very good yields. Interestingly, similar reaction of compound **4n** did not give any compound of type **8**, but afforded only diethyl 3-hydroxy-4,6-dimethylthieno[3,2-*a*]indolizine-2,9-dicarboxylate **9a** in 89% yield. Analogously, the reactions of indolizines **4o—t** with potassium *t*-butoxide gave the corresponding cycloadducts **7b—d**, **7e+9b**, **7f**, and **7g**, respectively. Same products **7b**, **d**, **e**, were also obtained in 86, 74, and 59% yields by the reactions of indolizines **4o**, **q**, **r** with DBU. These results are shown in Scheme 3.

The structural assignments of thieno[3,2-*a*]indolizines **6a—j** and **9a**, **b** and thieno[2,3-*b*]indolizines **7a—g** and **8a—c** were accomplished mainly by their elemental and by ^{1}H NMR (Table 2 and 3) and IR (Table 5) spectral analyses. The structures of ethyl 3-aminothieno[3,2-*a*]indolizine-2-carboxylates **6a—j** could be easily decided by the appearances of two amino absorption bands (3300—3450 cm^{-1}) and the absence of the cyano band in their IR spectra and by the presence of amino proton signals (δ 5.95—6.37 (br s, 2H)) and the absence of the active methylene signals in their ^{1}H NMR spectra. Similarly, compounds **7a—g** were assigned to ethyl 3-methyl- or 3-phenylthieno[2,3-*b*]indolizine-2-carboxylates because the elimination of a water molecule from indolizines **4h**, **o—t** was confirmed by their elemental and by IR and ^{1}H NMR spectral analyses. On the other hand, the

Table 4. Some Data of 2-(Ethoxycarbonylmethylthio)indolizines

Compd No.	Salt(SM[a])	Method	Yield %	Mp θ_m/°C	$\nu^{KBr}_{CN\text{ and }CO}$/cm^{-1}			Formula[b]
4a	**3a** (**1a**,**2a**)	A	68	88—89	2208	1726	1676	$C_{16}H_{16}N_2O_4S$
4b	**3b** (**1b**,**2a**)	A	40	69—70	2208	1723	1716	$C_{17}H_{18}N_2O_4S$
4c	**3c** (**1c**,**2a**)	A	87	101—102	2200	1735	1670	$C_{17}H_{18}N_2O_4S$
4d	**3d** (**1d**,**2a**)	A	65	107—109	2211	1724	1680	$C_{18}H_{20}N_2O_4S$
4e	**3e** (**1e**,**2a**)	B	17	92—94	2218	1740	1630	$C_{15}H_{14}N_2O_3S$
4f	**3f** (**1f**, **2a**)	B	22	69—70	2210	1726	1661	$C_{16}H_{16}N_2O_3S$
4g	**3g** (**1g**,**2a**)	B	21	106—107	2201	1723	1634	$C_{16}H_{16}N_2O_3S$
4h	**3h** (**1h**,**2a**)	B	22	110—112	2217	1721	1626	$C_{17}H_{18}N_2O_3S$
4i	**3i** (**1i**, **2a**)	B	19	91—93	2200	1726	1610	$C_{20}H_{16}N_2O_3S$
4j	**3j** (**1j**, **2a**)	B	24	139—142	2201	1729	1612	$C_{21}H_{18}N_2O_3S$
4k	**3k** (**1a**,**2b**)	A	31	53	1729	1686	1670	$C_{18}H_{21}NO_6S$
4l	**3l** (**1b**,**2b**)	A	47	70—71	1720	1705	1675	$C_{19}H_{23}NO_6S$
4m	**3m**(**1c**, **2b**)	A	57	59—60	1726	1681	1670	$C_{19}H_{23}NO_6S$
4n	**3n** (**1d**,**2b**)	A	64	103—104	1725	1716	1671	$C_{20}H_{25}NO_6S$
4o	**3o** (**1e**, **2b**)	B	40	61—62	1720	1684	1617	$C_{17}H_{19}NO_5S$
4p	**3p** (**1f**, **2b**)	B	26	53—54	1723	1684	1652	$C_{18}H_{21}NO_5S$
4q	**3q** (**1g**,**2b**)	B	57	83—86	1720	1684	1620	$C_{18}H_{21}NO_5S$
4r	**3r** (**1h**,**2b**)	B	69	98—100	1734	1690	1639	$C_{19}H_{23}NO_5S$
4s	**3s** (**1i**, **2b**)	B	68	96—97	1723	1685	1620	$C_{22}H_{21}NO_5S$
4t	**3t** (**1j**, **2b**)	B	78	83—84	1721	1685	1608	$C_{23}H_{23}NO_5S$

a) Starting materials. b) Satisfactory analytical data (within 0.3% for C, H, and N) were obtained for all new compounds.

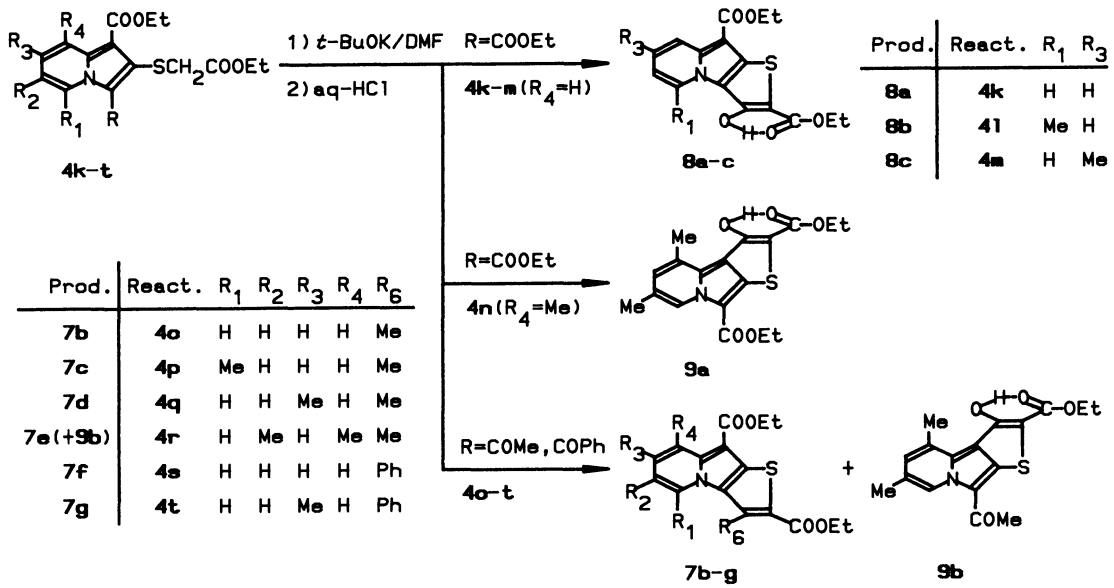

Scheme 3.

structures of products **8a**—**c** and **9a**, **b** could be determined by considering in detail the presence or absence of the anisotropic effect of the carbonyl group participating with the cyclizations: In the ^{1}H NMR spectra of compounds **8a**—**c**, for example, the chemical shifts (δ 7.97—8.27) due to the 8-proton were very similar to those (δ 8.12—8.38) of the starting indolizines **4k**—**m**, but the values (δ 8.59 and 8.39) for the 5-proton of cycloadducts **8a**, **c** were largely different from those (δ 9.52 and 9.37) of indolizine derivatives **4k** and **4m**. On the contrary, the chemical shifts (δ 9.27 and 9.89) owing to the 7-proton of compounds **9a**, **b** were almost same value (δ 9.27 and 9.75) with the 5-proton of indolizine **4n**, **r**. These facts mean that the 3-ester group was attacked in the formers (**4k**—**m**) and the 1-ester group in the latters (**4n**, **r**). That is to say, the cyclization modes can be decided clearly by the largely diminished anisotropic effect (δ ca. 1 ppm) for the protons at the position peri to the carbonyl group disappeared during the reactions. Furthermore, the presence of an enolic hydroxyl proton signal at δ 8.70—11.44 (1H, br s) shows definitely that these compounds **8a**—**c** and **9a**, **b** have an aromatic thiophene ring.

Table 5. Some Data of Thieno[3,2-*a*]- and Thieno[2,3-*b*]indolizines

Compd	React.	Method	Yield %	Mp θ_m/°C	$\nu^{KBr}_{NH_2 \text{ and } CO}$/cm^{-1}				Formula[a]
6a	**4a**	A	94	211—213	3442	3330	1650		$C_{16}H_{16}N_2O_4S$
6b	**4b**	A	50	170—172	3398	3320	1652		$C_{17}H_{18}N_2O_4S$
6c	**4c**	A	75	198—200	3438	3333	1677		$C_{17}H_{18}N_2O_4S$
6d	**4d**	A	89	183—184	3520	3360	1691	1648	$C_{18}H_{20}N_2O_4S$
6e	**4e**	A	73	270—271	3439	3341	1644		$C_{15}H_{14}N_2O_3S$
6f	**4f**	A	83	190—191	3385	3301	1666		$C_{16}H_{16}N_2O_3S$
6g	**4g**	A	82	175—176	3445	3333	1652		$C_{16}H_{16}N_2O_3S$
7a(+**6h**)[b]	**4h**	A	ca. 65	157—160	2200[c]		1693		$C_{17}H_{16}N_2O_2S$
6i	**4i**	A	73	270—271	3439	3341	1644		$C_{20}H_{16}N_2O_3S$
6j	**4j**	A	61	235—236	3422	3320	1654		$C_{21}H_{18}N_2O_3S$
8a	**4k**	B	86	159—161	1674	1635	d)		$C_{16}H_{15}NO_5S$
8b	**4l**	B	87	190—192	1660		d)		$C_{17}H_{17}NO_5S$
8c	**4m**	B	84	139—140	1685		d)		$C_{17}H_{17}NO_5S$
9a	**4n**	B	89	156—158	1674	1633	d)		$C_{18}H_{19}NO_5S$
7b	**4o**	B(A)	78(86)	194—195	1690	1670			$C_{17}H_{17}NO_4S$
7c	**4p**	B	67	149—150	1684	1659			$C_{18}H_{19}NO_4S$
7d	**4q**	B(A)	90(74)	173—174	1680	1665			$C_{18}H_{19}NO_4S$
7e	**4r**	A	59	127—128	1690	1669			$C_{19}H_{21}NO_4S$
9b(+**7e**)	**4r**	B	34(49)	192—194	1647	1600	d)		$C_{17}H_{17}NO_4S$
7f	**4s**	B	91	118—119	1684	1665			$C_{22}H_{19}NO_4S$
7g	**4t**	B	84	159—160	1672	1662			$C_{23}H_{21}NO_4S$
11a	**4k**, **10a**	C	78	126—128	1685	1670			$C_{17}H_{17}NO_5S$
11b	**4l**, **10a**	C	76	133—134	1689	1661			$C_{18}H_{19}NO_5S$
11c	**4m**,**10a**	C	74	136—138	1689	1666			$C_{18}H_{19}NO_5S$
11d	**4k**, **10b**	C	77	98—99	1680	1667			$C_{18}H_{19}NO_5S$
11e	**4l**, **10b**	C	74	137—139	1680				$C_{19}H_{21}NO_5S$
11f	**4m**,**10b**	C	83	128—130	1686	1675			$C_{19}H_{21}NO_5S$
12a(+**11a**)	**4k**, **10c**	C	63(15)	146—148	1724	1677	1650		$C_{17}H_{17}NO_5S$
12b	**4l**, **10c**	C	68	139—140	1720	1700	1650		$C_{18}H_{19}NO_5S$
12c(+**11c**)	**4m**,**10c**	C	67(7)	122—124	1725	1675	1650		$C_{18}H_{19}NO_5S$
13a	**4n**, **10a**	C	81	135—136	1695	1675			$C_{19}H_{21}NO_5S$
13b	**4n**, **10b**	C	86	126—128	1688	1667			$C_{20}H_{23}NO_5S$
14a	**4n**, **10c**	C	87	152—153	1725	1700	1669		$C_{19}H_{21}NO_5S$

a) Satisfactory analytical data (within 0.3% for C, H, and N) were obtained for all new compounds except **6h**. b) Other physical and analytical data of compound **6h** (ca. 18%) could not be measured because of the inaccessibility of its pure sample. c) Cyano absorption band. d) Distinct hydroxyl absorption band did not appear in the range of 4000—3000 cm^{-1}.

Preparations of *O*- and *C*-Alkylated Thienoindolizines. Since facile and effective syntheses of 3-hydroxythieno[2,3-*b*]indolizines **8a—c** and 3-hydroxythieno[3,2-*a*]indolizine **9a** could be established, the preparations of some derivatives using them were examined. The treatment of indolizines **4k—n** with potassium *t*-butoxide in DMF at room temperature followed by the addition of dimethyl **10a** and diethyl sulfate **10b** yielded the corresponding *O*-methylated **11a—c** and **13a** and *O*-ethylated thienoindolizines **11d—f** and **13b** in 74—88% yields. On the other hand, the reactions of indolizines **4k—n** using methyl iodide **10c** as an alkylating agent gave compounds **11a**+**12a**, **12b**, **11c**+**12c**, and **14a** in good yields, and the *C*-methylated thienoindolizines **12a—c** and **14a** were major or exclusive (Scheme 4).

The structures of methoxy- and ethoxythienoindolizines **11a—f** and **13a, b** were determined by the presence of the methoxyl (δ 4.11—4.31 (3H, s)) or ethoxyl proton signals (δ near 1.40 (3H, t, J=7.0 Hz) and near 4.45 (2H, q, J=7.0 Hz)) in addition to other proton signals which were very similar to those of hydroxythienoindolizines **8a—c** and **9a, b** in their ^{1}H NMR spectra. On the other hand, compounds **12a—c** and **14a** were assigned by the indications of a methyl group (δ near 1.90 (3H, s)) and of an ethoxycarbonyl group (δ near 1.25 (3H, t, J=7.0 Hz) and near 4.25 (2H, q, J=7.0 Hz)) attached to the tetrahedral carbon and by the considerably increased down-field shift of the 5-proton signal (δ 8.93 (**12a**) and 8.81 (**12c**)) in their ^{1}H NMR spectra.

Reaction Mechanisms and Molecular Orbital (MO) Calculations. Possible mechanisms for these intramolecular cyclizations are shown in Scheme 5. As was expected, these thieno[3,2-*a*]- **6a—j** and **9a, b** and thieno[2,3-*b*]indolizine derivatives **7a—g** and **8a—c** must be formed via the nucleophilic attack of carbanion **15** generated in situ by the alkaline treatment of indolizines **4a—t** to the cyano or carbonyl group at the 1- or 3-position followed by the aromatizations through hydrogen shifts or with the elimination. The formations of *O*-alkylated **11a—f**

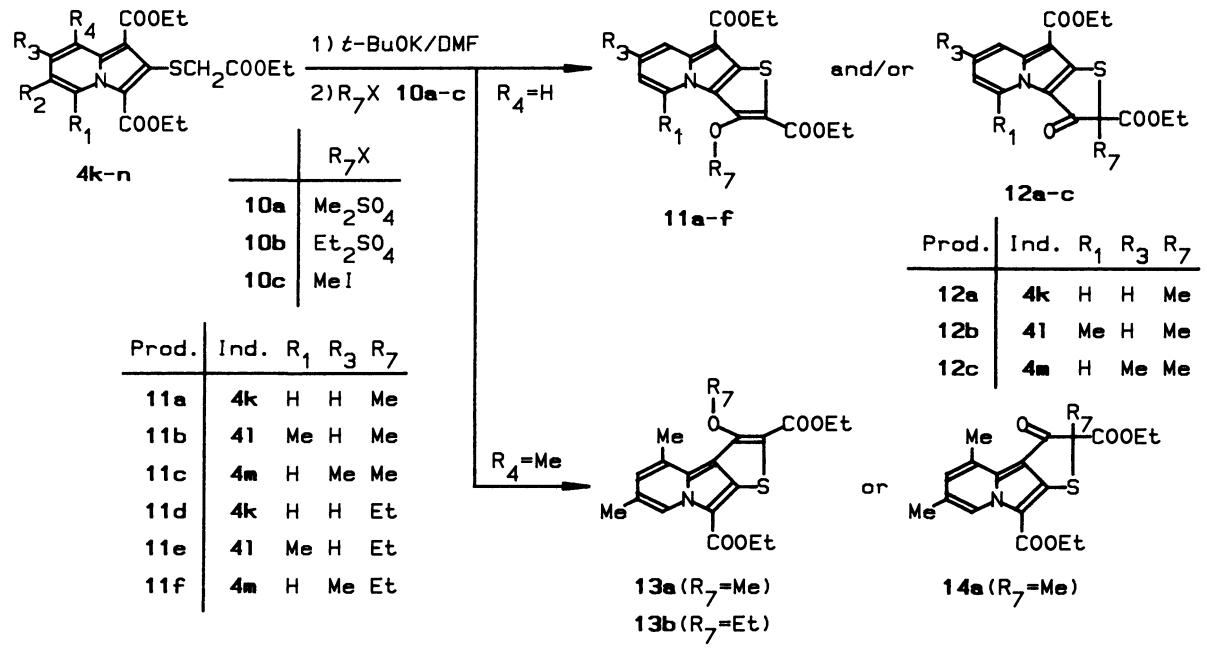

R_7X	
10a	Me_2SO_4
10b	Et_2SO_4
10c	MeI

Prod.	Ind.	R_1	R_3	R_7
11a	4k	H	H	Me
11b	4l	Me	H	Me
11c	4m	H	Me	Me
11d	4k	H	H	Et
11e	4l	Me	H	Et
11f	4m	H	Me	Et

Prod.	Ind.	R_1	R_3	R_7
12a	4k	H	H	Me
12b	4l	Me	H	Me
12c	4m	H	Me	Me

Scheme 4.

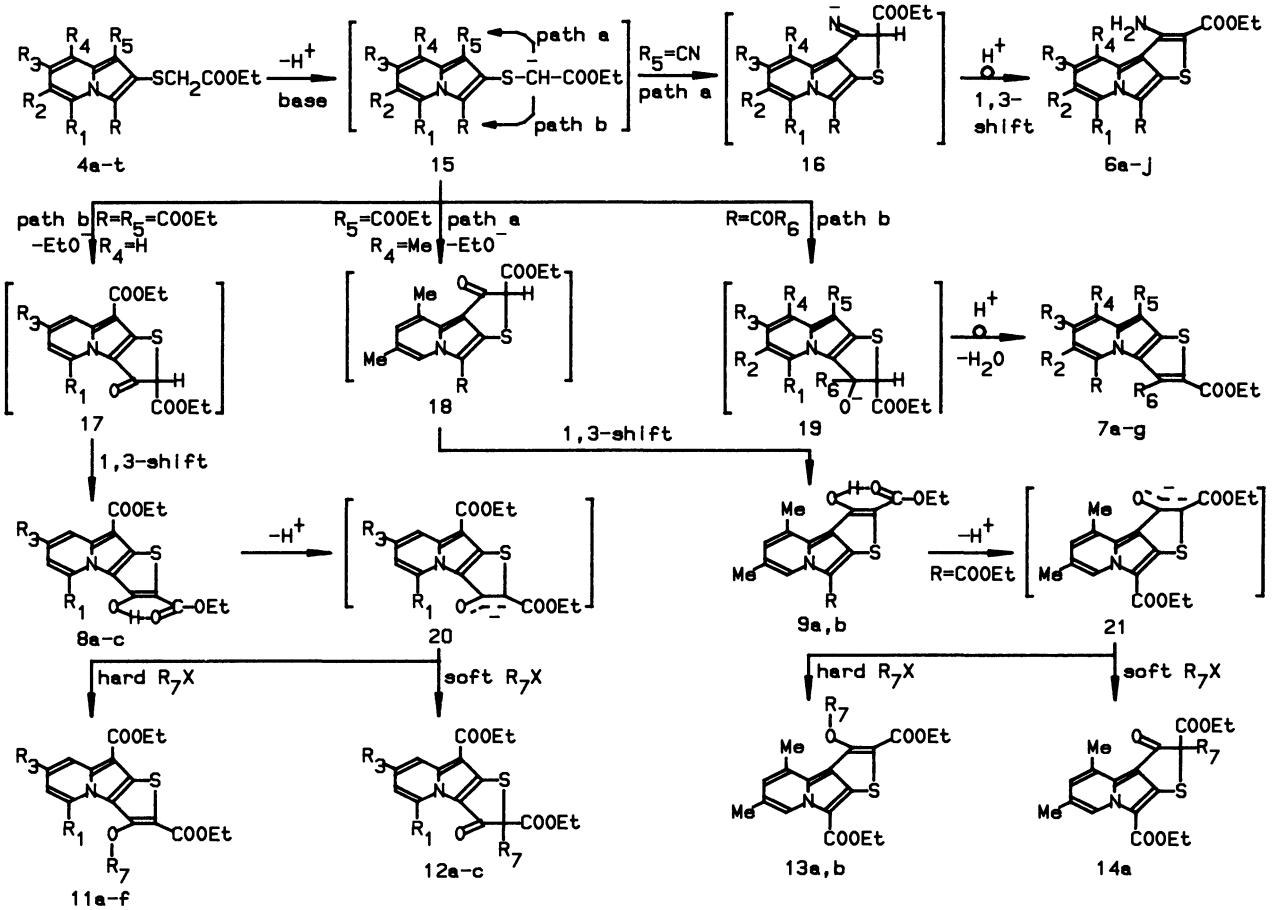

Scheme 5.

and **13a**, **b** and *C*-alkylated thienoindolizines **12a—c** and **14a** can be well-explained by the application of HSAB principle[7] to ambident anions **20** and **21**.

In order to obtain further information for the electrophilicity of the 1- and 3-substituents in the indolizine molecule, the MO calculations (PPP method)[8] of 1-cyano-3-indolizinecarboxylic acid **22a** and 1,3-indolizinedicarboxylic acid **22b** as models for

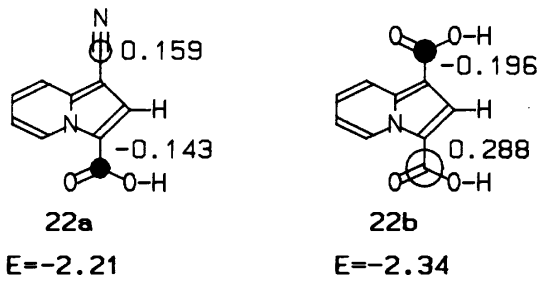

Fig. 1.

indolizines **4a**, **k** were carried out. The coefficients of the cyano and/or ester carbons at the 1- and 3-positions in the lowest unoccupied molecular orbitals (LUMO) of **22a**, **b** are shown in Fig. 1. Apparently, the order of the electrophilicity of the 1- and 3-substituent in these model compounds **22a**,**b** is 1-CN>3-COOH>1-COOH, and, except the cases of indolizines **4h**, n, **r**, parallel to that (1-CN>3-COMe or 3-COPh>3-COOEt>1-COOEt) observed. The formation of compound **7a** may be interpreted by considering the equilibrium (reversible) betweeen indolizine **4h** and 3-aminothieno[3,2-*a*]indolizine **6h** and an irreversible transformation of **4h** to **7a**. On the other hand, the nucleophilic attack leading to 3-hydroxythieno[3,2-*a*]indolizines **9a**, **b** can be explained in terms of the increased reactivity of the ester carbonyl carbon at the 1-position in indolizines **4n**, **r**, because the introduction of a 8-methyl group to the indolizine ring makes to shift the carbonyl absorption bands at the 1-position to considerably high (**4n**, 1716 cm^{-1}) and slightly high regions (**4r**, 1690 cm^{-1}).

Experimental

Melting points were measured with a Yanagimoto micromelting point apparatus and are uncorrected. The microanalyses were carried out on a Perkin-Elmer 240 elemental analyzer. The ^1H NMR spectra were determined with a Varian EM360A spectrometer in deuteriochloroform with tetramethylsilane as an internal standard and the chemical shifts are expressed in δ values. The IR spectra were taken with a Hitachi 260-10 infrared spectrophotometer.

Materials. Pyridinium ylides **1a—j** were prepared according to the procedure appeared in the literature.[3,9] Some physical and spectral data of new compounds are as follows: **1a**, 78%, yellow needles (from $CHCl_3$-ether), mp 131—132 °C, IR ν (KBr) 1740 and 1645 cm^{-1} (CO). Anal. ($C_{14}H_{17}NO_4S_2$) C, H, N. **1b**, 91%, yellow needles (from $CHCl_3$-ether), mp 136—137 °C, IR ν (KBr) 1720 and 1652 cm^{-1} (CO). Anal. ($C_{15}H_{19}NO_4S_2$) C, H, N. **1c**, 84%, yellow needles ($CHCl_3$-ether), mp 148—150 °C, IR ν (KBr) 1737 and 1650 cm^{-1} (CO). Anal. ($C_{15}H_{19}NO_4S_2$) C, H, N. **1d**, 85%, yellow needles ($CHCl_3$-ether), mp 178—179 °C, IR ν (KBr) 1724 and 1645 cm^{-1} (CO). Anal. ($C_{16}H_{21}NO_4S_2$) C, H, N. **1f**, 52%, yellow needles ($CHCl_3$-ether), mp 98—100 °C, IR ν (KBr) 1720 and 1590 cm^{-1} (CO). Anal. ($C_{14}H_{17}NO_3S_2$) C, H, N. **1h**, 81%, yellow needles ($CHCl_3$-ether), mp 171—172 °C, IR ν (KBr) 1721 and 1595 cm^{-1} (CO). Anal. ($C_{15}H_{19}NO_3S_2$) C, H, N.

Preparations of Indolizines. General Method A: A chloroform solution (20 ml) of pyridinium ylide **1a—d** (2 mmol) and bromoacetonitrile or ethyl bromoacetate (**2**, 2.2 mmol) was kept on standing until the ylide was completely alkylated (ca. 1—6 d). The resulting mixture was concentrated under reduced pressure at 50—55 °C and the residue was washed three times with ether to remove excess alkylating agents. Pyridinium salt thus obtained was again dissolved in chloroform (30 ml). To the solution DBU (0.38 g, 2.5 mmol) was added dropwise in an ice bath, and after stirring for additional 10 min, DDQ (0.45 g, 2 mmol) was added. The mixture was allowed to react for further 6—12 h in an ice bath and then concentrated under reduced pressure. The residue was separated by column chromatography (alumina) using chloroform as an eluent, and recrystallization from ethanol afforded the corresponding ethyl 2-(ethoxycarbonylmethylthio)indolizine-3-carboxylates **4a—d**, **k—n**.

Method B: A chloroform solution (30 ml) of ylide **1e—j** (2 mmol) and an alkylating agent (2.2 mmol) was kept on standing at room temperature until the ylide was completely disappeared. Without the removal of excess alkylating agent, the resulting solution was allowed to react with DBU (0.38 g, 2.5 mmol) and then with DDQ (0.45 g, 2 mmol) in an ice bath for 6—12 h. The similar work-ups of resulting mixtures gave other indolizine derivatives **4e—j**, **o—t**.

These results and some data are listed in Tables 1 and 4.

In the reactions of ylides **1e—j** ethyl 9-thiocyanato- and 9-(ethoxycarbonylthio)thieno[2,3-*b*]indolizine-2-carboxylates **5** were also obtained in below 3% yields but the preparations of pure samples could not be successful because of their low yields and of their thermal instability.

The application of Method A for the reactions of ylides **1e—j** having an acetyl or a benzoyl group gave complex mixtures and considerably diminished yields of the expected indolizines **4e—j**, **o—t** were observed. In these reactions indolizines and thieno[2,3-*b*]indolizines derived from pyridinium salts via the cis-trans-isomerization of the vinyl group were also detected.

Preparations of Thieno[3,2-*a*] and Thieno[2,3-*b*]indolizines. General Method A: An ethanolic solution (30 ml) of indolizine (1 mmol) was heated under the reflux temperature for 1—4 h. The solution was chilled overnight in a freezer and the precipitated substance was collected by filtration. Recrystallization from chloroform gave the corresponding thienoindolizines.

Method B: To a DMF solution (5 ml) of indolizine (1 mmol) potassium *t*-butoxide (0.14 g, 1.25 mmol) was added at room temperature and the mixture was kept on standing for an additional 1 h. After the acidification of the solution with diluted hydrochloric acid the precipitated substances were collected by filtration, washed with two portions (each 10 ml) of water, and dried in vacuum desiccator for 1 d. The separation of crude product by column chromatography (silica gel) using chloroform and recrystallization from ethanol provided the corresponding thienoindolizines.

These results and some physical and spectral data are summarized in Tables 2, 3, and 5.

Alkylations of Thienoindolizines. General Method: To a DMF solution (5 ml) of indolizine (1 mmol) potassium *t*-

butoxide (0.14 g, 1.25 mmol) was added at room temperature and the resulting mixture was kept on standing for an additional 1 h. An alkylating agent (2 mmol) was then added dropwise under stirring. After stirring for 1 h, the reaction solution was heated to 60—70 °C for further 10 min to complete the reaction. The work-ups gave the corresponding *O*-alkylated and/or *C*-alkylated thienoindolizine derivatives.

These results and some data are listed in Tables 2, 3, and 5.

References

1) For part 18 of this series, see A. Kakehi, S. Ito, N. Kinoshita, and Y. Abaka, *Bull. Chem. Soc. Jpn.*, **61**, 2055 (1988).

2) A. Kakehi, S. Ito, S. Matsumoto, and Y. Morimoto, *Chem. Lett.*, **1987**, 2043.

3) A. Kakehi, S. Ito, Y. Ohno, S. Shiba, and S. Kamata, *Bull. Chem. Soc. Jpn.*, **60** 3713 (1987).

4) A. Kakehi, S. Ito, S. Yonezu, K. Maruta, and K. Yuito, *Heterocycles*, **23**, 33 (1985); A. Kakehi, S. Ito, S. Yonezu, K. Maruta, K. Yuito, M. Shiohara, and K. Adachi, *Bull. Chem. Soc. Jpn.*, **60**, 1867 (1987).

5) C. Maseda, M. Sone, Y. Tominaga, R. Natsuki, Y. Matsuda, and G. Kobayashi, *Yakugaku Zasshi*, **94**, 839 (1974); Y. Tominaga, H. Fujito, K. Mizuyama, Y. Matsuda, and G. Kobayashi, *Chem. Pharm. Bull.*, **25**, 1519 (1977); Y. Tominaga, Y. Miyake, H. Fujito, K. Kurata, H. Awaya, Y. Matsuda, and G. Kobayashi, *ibid.*, **25**, 1528 (1977).

6) W. S. Johnson, B. Bannister, and R. Pappo, *J. Am. Chem. Soc.*, **78**, 6331 (1956); H. Sugihara, H. Mabuchi, and Y. Kawamatsu, *Chem. Pharm. Bull.*, **35**, 1919 (1987).

7) T.-L. Ho "Hard and Soft Acids and Bases Principle in Organic Chemistry," Academic Press, New York (1977).

8) R. Pariser and R. G. Parr, *J. Chem. Phys.*, **21**, 466 (1953); **21**, 767 (1953); J. A. Pople, *Trans. Faraday Soc.*, **49**, 1375 (1953); H. O. Pritchard and H. A. Skinner, *Chem. Rev.*, **55**, 745 (1955).

9) Y. Tominaga, H. Fujito, H. Norisue, A. Ushirogochi, Y. Matsuda, and G. Kobayashi, *Yakugaku Zasshi*, **99**, 1081 (1979).

Synthesis and Reactions of 2-Arylhydrazinotropones. II.[1] Synthesis of 5-Aryltropolones and B-Ring-Open Colchicine Analogues via Benzidine Type Rearrangement of 2-(2-Arylhydrazino)tropones[2]

Tetsuo NOZOE,* Kahei TAKASE,*,† Masafumi YASUNAMI,† Masayoshi ANDO,† Hiroaki SAITO,†,a) Kimiaki IMAFUKU,*,†† Bing-Zhu YIN,††,b) Masaaki HONDA,††,c) Yasutomo GOTO,††,d) Tadashi HANAYA,††† Yasushi HARA,†††,e) and Hiroshi YAMAMOTO*,†††

Tokyo Research Laboratories, Kao Corporation, Bunka, Sumida-ku, Tokyo 131
†Department of Chemistry, Faculty of Science, Tohoku University, Aoba, Sendai 980
††Department of Chemistry, Faculty of Science, Kumamoto University, Kurokami, Kumamoto 860
†††Department of Chemistry, Faculty of Science, Okayama University, Tsushima, Okayama 700

(Received July 7, 1988)

Treatment of a wide variety of 2-(2-arylhydrazino)tropones with ethanolic acid at 50—80°C readily gave the benzidine type rearrangement products, 2-amino-5-(4-aminoaryl)tropones, besides minor amounts of by-products of various type. The main products were conveniently led to the corresponding 5-aryltropolones. Similarly, 2-(2-arylhydrazino)tropones bearing an isopropyl and isopropenyl group at the 4-position afforded 4-substituted 2-amino-5-(4-aminoaryl)tropones as the main products, which were also led to 4-substituted 5-(4-acetamidoaryl)- and 5-(4-methoxyaryl)tropolones. Structural assignments of these products were made on the basis of ^{1}H NMR and other spectral data as well as of chemical transformations to known 5-phenyltropolone and also to 2-acetamido-8-hydroxy-10,10-dimethylcyclohept[*a*]inden-7(10*H*)-one. This synthetic scheme may possibly be utilized for a convenient synthesis of B-ring-open analogues of colchicine.

Colchicine (**1a**), a tricyclic natural troponoid, has attracted considerable attention owing to its marked antimitotic activity.[3] The total synthesis of **1a** has been accomplished so far by more than ten groups.[4] However, as all of these synthetic schemes involve lengthy multisteps and appear to lack general applicability particularly in large scale experiments, exploitation of a general, convenient synthetic method for colchicine analogues has been desired for the study of their structure-activity relationship.[5]

As for antimitotic agents, preparation of two types of the B-ring-open colchicine analogues **2** and **3**, (which can be derived from **1a** by the formal bond-disconnection at [a] and [b], respectively, see Scheme 1), was planned by one of us (T. N.) in order to obtain various information on tublinbinding sites. We have already reported the synthesis of various compounds of type **2**.[6] In the meantime, a synthetic approach for another, potentially useful compounds of type **3**, which are presumed to have a conformation close to that of **1a**, has been made as will be described below.

Although the tropolone nucleus is highly susceptible to various electrophilic substitutions (e.g., nitration, bromination, etc.), it does not undergo the Friedel–Crafts type alkylation and acylation by the usual method.[7,8] The reaction of organolithium or magnesium reagents with tropolones is known to afford C-3 and C-7 substitution products.[9] Thus, as for the preparation of 5-aryltropolones, only a few synthetic methods have been reported so far (see Scheme 2). Namely, 1) the permanganate oxidation of phenyltropilidene (**4**, derived from biphenyl) to give 5-phenyltropolone (**5**) in an extremely low overall yield (0.09%),[10] 2) the two-step conversion (amination and then hydrolysis) of a mixture of 4- and 5-phenyltropones (**7**, derived from phenyltropylium ion

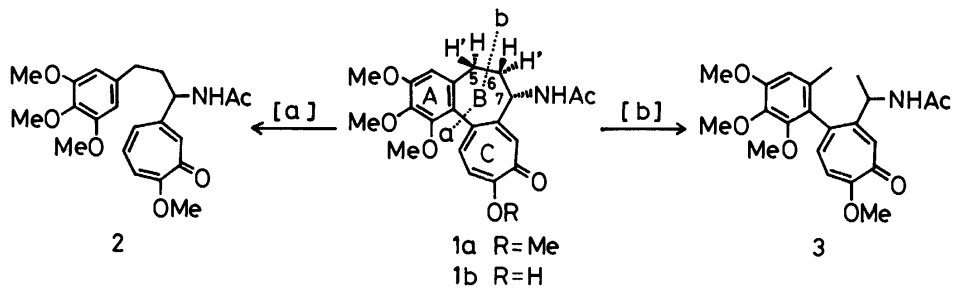

Scheme 1.

Present addresses: a) Sachigaoka, Asahi-ku, Yokohama-shi 241. b) Yanbian University, Yanji, Jilin, China. c) Koei Chemical Co., Ltd., Osaka 536. d) Fuji Photo Film Co., Ltd., Fujinomiya 418. e) Tosoh Co., Ltd., Shin-Nanyo-shi 746.

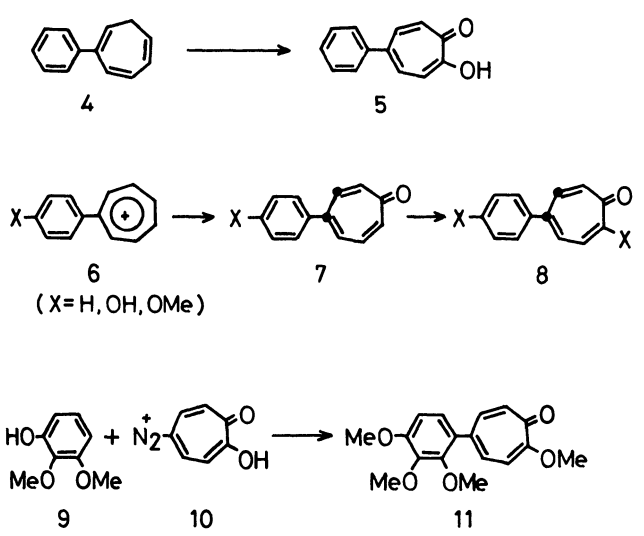

Scheme 2.

6)[11] to give, e.g., 2-methoxy-5-(4-methoxyphenyl)-tropone (**8**, X=OMe),[12] and 3) the thermolysis of 5-diazoniotropolone (**10**) either in benzene alone[7a] or in the presence of 2,3-dimethoxyphenol (**9**) to afford, after methylation, 2-methoxy-5-(2,3,4-trimethoxyphenyl)-tropone (**11**) (which exhibited an appreciable antimitotic activity).[3b,5a] However, all of these procedures have drawbacks either with respect to the low preparative yield or the regioselective control.[13] Thus, virtually no efficient, direct synthetic scheme has been established so far for preparation of 5-aryltropolones and much less tropolones having carbon substituents at both 4- and 5-positions.[13b]

Around 1973, Y. Sugimura[14] of Sankyo Co. (Tokyo) found that the treatment of some of 2-(2-phenylhydrazino)tropones **14** (see Scheme 3) with dilute hydrochloric acid readily afforded major products which he presumed to be derived through a benzidine-type

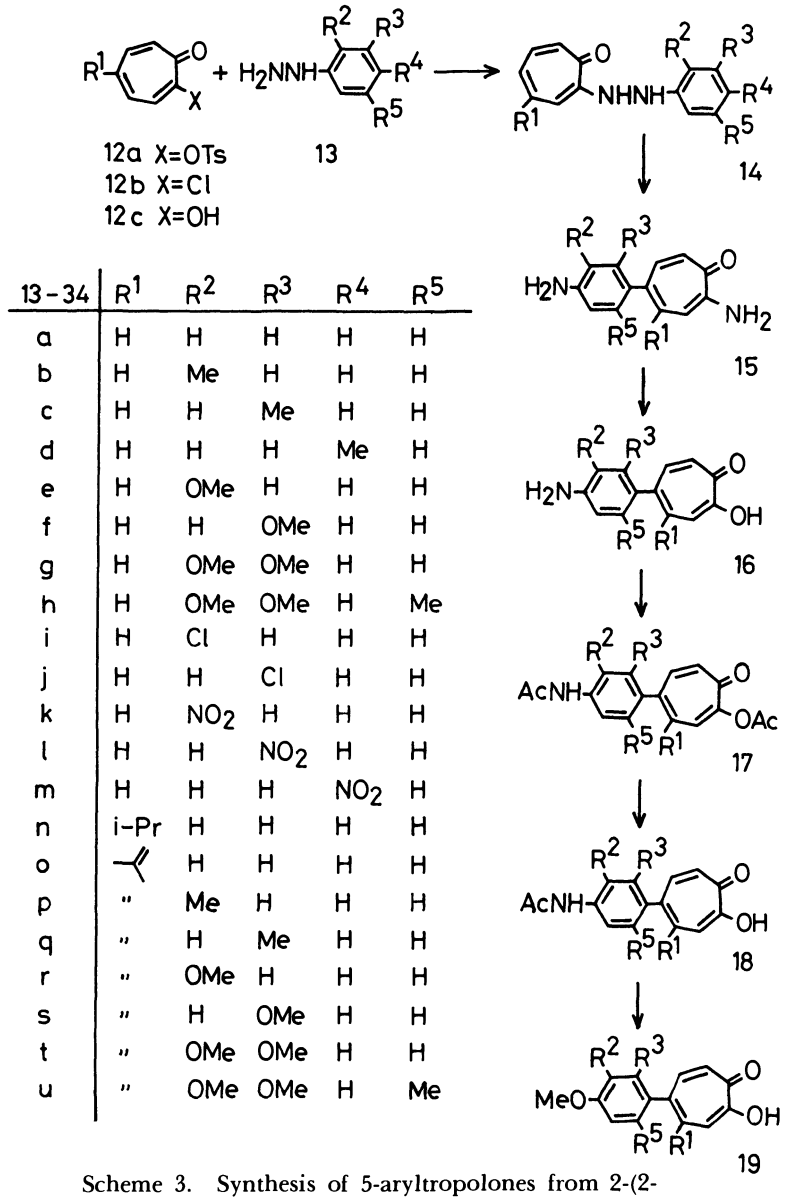

13-34	R^1	R^2	R^3	R^4	R^5
a	H	H	H	H	H
b	H	Me	H	H	H
c	H	H	Me	H	H
d	H	H	H	Me	H
e	H	OMe	H	H	H
f	H	H	OMe	H	H
g	H	OMe	OMe	H	H
h	H	OMe	OMe	H	Me
i	H	Cl	H	H	H
j	H	H	Cl	H	H
k	H	NO_2	H	H	H
l	H	H	NO_2	H	H
m	H	H	H	NO_2	H
n	i-Pr	H	H	H	H
o		H	H	H	H
p	"	Me	H	H	H
q	"	H	Me	H	H
r	"	OMe	H	H	H
s	"	H	OMe	H	H
t	"	OMe	OMe	H	H
u	"	OMe	OMe	H	Me

Scheme 3. Synthesis of 5-aryltropolones from 2-(2-arylhydrazino)tropones.

rearrangement. However, before establishing the precise structures of these products, the Sankyo research group had to interrupt this project for various reason and entrusted it to one of us (T. N.), who undertook further investigation in cooperation with the Tohoku Univ. research group. The structures of some of these acid-catalyzed products were then proved[2a] to be 2-amino-5-(4-aminophenyl)tropone (**15a**) and corresponding 5-(4-aminophenyl)tropones. Because of the Tohoku group's concentration on other research projects, the further study on this reaction was later carried out in cooperation with the Okayama and Kumamoto Univ. research groups.

We now wish to describe in this paper our detailed but frequently interrupted studies on this novel benzidine type rearrangement of a wide variety of 2-(2-arylhydrazino)tropones (aryl stands for substituted phenyls or 1-naphthyl hereafter) with or without a carbon-substituent at the 4-position to give 4-substituted (or unsubstituted) 2-amino-5-(4-aminoaryl)-tropones, which can be readily led to various 5-aryltropolones. This method is expected to be applicable to a convenient synthesis of analogues of colchicine (**1a**), such as those of type **3**.

Results and Discussion

Preparation of 2-(2-Arylhydrazino)tropones. We have recently reported[1] a series of 2-(2-phenylhydrazino)tropones **14** available by the condensation of 2-tosyloxytropone (**12a**) with substituted phenylhydrazines **13** (Scheme 3). The preparations of some of the 2-(2-phenylhydrazino)tropones, **14a—d**, **14l**, and **14m**, have also been investigated presently by using another reactive troponoid, 2-chlorotropone (**12b**), but the yields were found to be somewhat less satisfactory for most of these products compared with the case[1] from **12a**. Thus, in order to closely examine the benzidine-type rearrangement of **14** we have prepared a variety of 2-(2-phenylhydrazino)tropones **14a—u** by the reaction of **12a** with **13a—m** (among which **13g** and **13h** were newly prepared from 2,3-dimethoxyanilines **20** via diazonium compounds **21**, see Scheme 4 and the Experimental section).

In addition, for a further examination of the scope of the rearrangement of 2-(2-arylhydrazino)tropone system other than phenyl ring in the moiety, we have also prepared 2,2′-hydrazobis(tropone) (**23**) and 2-[2-(1-naphthyl)hydrazino]tropone (**24**) by the reaction of **12b** with 2-hydrazinotropone (**22**) and 1-naphthylhydrazine, respectively (Scheme 5). Physical data for these new 2-hydrazinotropones are described in the Experimental section and are consistent with their structures.

The Benzidine Type Rearrangement of 2-(2-Arylhydrazino)tropones and Reactions of the Rearranged Products. It was then found that the rearrangement was best effected, in most cases, by

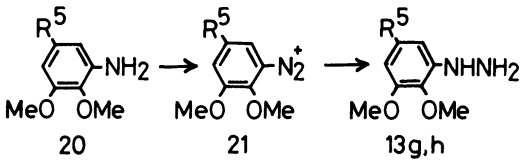

Scheme 4. Preparation of 2,3-dimethoxyphenylhydrazines. For R^5 of **13g**, **h**, see Scheme 3.

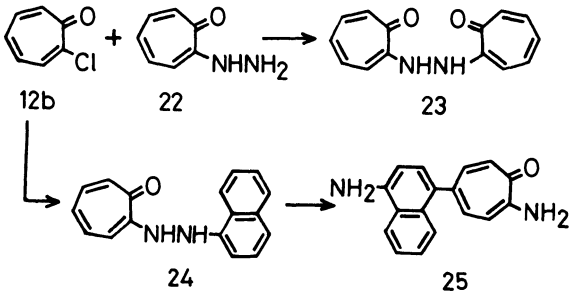

Scheme 5.

heating the arylhydrazinotropones **14a—u** at 50—80 °C in a ca. 1:10 mixture of 2 M hydrochloric acid (1 M=1 mol·dm^{-3}) and ethanol for 1—72 h under an inert atmosphere. The reactants were purified by recrystallization and/or silica-gel chromatography to yield 2-amino-5-(4-aminoaryl)tropones **15a—u** and other minor products **29—34** (see later), except for the case of the 2-(*p*-substituted phenylhydrazino)tropones **14d** and **14m**; the latter (**14m**) remained unchanged, while the former (**14d**) gave a mixture of several, air-sensitive products.[15] 2-[2-(1-Naphthyl)hydrazino]-tropone (**24**) similarly underwent the rearrangement to give 2-amino-5-(4-amino-1-naphthyl)tropone (**25**), whereas 2,2′-hydrazobis(tropone) (**23**) remained unchanged under the same acidic conditions (Scheme 5). The diamino compounds **15** stepwisely gave the monoacetyl and diacetyl derivatives as exemplified by treatment of **15a** with acetic anhydride in dichloromethane and in pyridine to give **15a′** and **15a″**, respectively (see Scheme 6).

Alkaline hydrolysis of **15** in ethanolic 2 M KOH under reflux for 10 h afforded 5-(4-aminophenyl)tropolones **16** (Scheme 3). As the 4-substituted 2-amino-5-(4-aminophenyl)tropones **15n—u** and tropolones **16n—u** were in general too air-sensitive to be isolated as pure compounds, they were immediately led to the *N,O*-diacetyl derivatives[16] **17n—u** and then 5-(4-acetamidophenyl)tropolones **18n—u** for characterization.

Structures of these newly isolated products **15—18** were established by spectroscopy [UV, IR, ^{1}H NMR, MS, and ^{13}C NMR (for some compounds, particularly **15a—c** and **25** in comparison with the spectra of the corresponding starting materials **14** and **24**)] and elemental analysis; their exact data and the rational assignments for the spectral parameters are described in the Experimental section. Yield of each product of

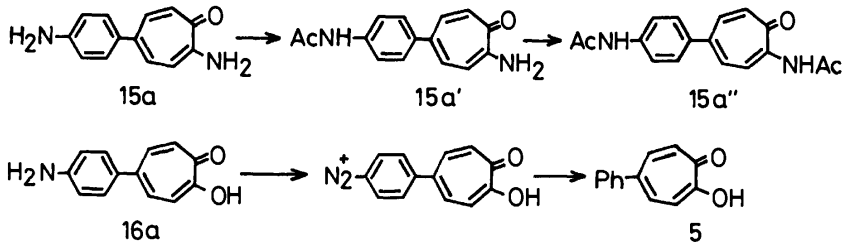

Scheme 6.

Table 1. Isolated Yields/% of 2-Amino-5-aryltropones **15**, **25**, 5-Aryltropolones **16**, **18**, Acetates **17**, and By-Products **29**—**34**

Starting material	**15(17)**[a]	**29**	Other product[b]	**16(18)**[c]
14a	78(55)	5		96
14a[d]	91			
14a[e]	—		**30** (1.5) **31** (5)	
14b	89			95
14c	87	10		98
14e	48		**32** (19)	87
14f	77	20		90
14g	34			67
14h	35			75
14i	77		**30** (2)	97
14j	79	17	**33** (1)	96
14k[f]	39		**34** (6)	50
14l[f]	49	5		71
14l[g]	33	5	**34** (17)	
14n	(91)			(86)
14o	(72)			(94)
14p	(85)			(100)
14q	(70)			(78)
14r	(48)			(96)
14s	(40)			(72)
14t	(30)			(92)
14u	(33)[h]			(93)
24			**25** (92)	

a) The value in parentheses is the overall yield of **17** from **14** (via **15** and **16**). b) Yield of each compound is shown in parentheses. c) The value in parentheses is the yield of **18** from **17**. d) Reaction time: 3.5 h. e) Reaction time: 10 min. f, g) The reaction was conducted in 3:2 dioxane–water and in 1-butanol, respectively (see the Experimental section). h) The value is for a mixture (3:2) of **17u** and **17u'**.

the above reactions is listed in Table 1.

The 4-aminophenyl substituent in **15** and **16** was confirmed to be on 5-position by converting a representative product **16a** into known 5-phenyltropolone[10,11] (**5**) upon treatment with nitrous acid, followed by reduction with phosphinic acid (Scheme 6). The unequivocal assignments of the isopropyl and isopropenyl groups of the rearranged products to the 4-position were based on the careful analysis of the 500 (or 200) MHz ^{1}H NMR data of **17** and **18n**—**u**, by taking into account the well-resolved parameters obtained presently for structurally related compounds, such as **1a**, colchiceine (**1b**), and tropolone itself (**12c**) (see Table 2). Characteristic features in the δ and J values for the representative examples of these 4,5-disubstituted tropolones **17** and **18** are summarized in Table 2, and these values have been effectively utilized in precisely determining the positions of substituents for the rest of the polysubstituted tropolones.

The conversion of the 4-acetamido group on the phenyl ring of **18** into 4-methoxyphenyl derivatives is exemplified by the transformations into **19n**, **p**, **q**, **u** upon treatment with ethanolic 1 M HCl under reflux and then with nitrous acid in aq methanol, followed by methylation with dimethyl sulfate in 1 M NaOH (Scheme 3).

Attempts to convert the 4-isopropyl and isopropenyl groups of **18** and **19** into the corresponding acetyl derivatives for the purpose of further manipulation[2b,6] of the functional group to suit more colchicine-like compounds have so far remained unsuccessful (Scheme 7). Namely, the selective ozonolysis of the isopropenyl group of **18o**, **p** was found to cause only profound decomposition in contrast to the successful conversion of 5-isopropenyltropolone to 5-acetyltropolone.[17] In order to obtain

Table 2. ^{1}H NMR (500 MHz) Parameters for Representative 4-Substituted 5- and 7-Aryltropolones and Their Acetates in $CDCl_3$[a]

Compd	HO-2 (AcO-2)	H-3	Me-C-4 (H_2C=C-4)	H-5	H-6
1a[b,c]	4.00[d]	7.49	e)	—	7.32 $J_{6,7}$=10.9
1b[b,c]	1.8	7.52	f)	—	7.57 $J_{6,7}$=12.0
12c	9.1	7.345 $J_{3,4}$=11.3	7.395 $J_{4,5}$=9.3	7.04 $J_{3,5}$=1.3	7.395 $J_{3,6}$=0.8
18r	1.6	7.43	1.60 (5.06, 5.08)	—	7.42 $J_{5,6}$=12.0
18s[h]	1.6	7.38	1.70[i] (4.85, 4.90[i])	—	7.34 $J_{6,7}$=11.5
17u	(2.38)	7.23	1.71[i] (4.85,[i] 4.87)	—	7.15 $J_{6,7}$=12.0
18u	1.6	7.36	1.74 (4.84, 4.85)	—	7.27 $J_{6,7}$=11.6
17u'	(2.27)	7.48 $J_{3,5}$=1.7	2.17[j] (5.33,[j] 5.46)	7.14 $J_{5,6}$=9.8	7.20
18u'	1.6	7.57 $J_{3,5}$=1.7	2.20[j] (5.34,[j] 5.45)	7.13 $J_{5,6}$=10.7	7.28

Compd	H-7	H-2' (MeO-2')	H-3' (MeO-3')	AcN-4' (MeO-4')	H-5'	H-6' (Me-6')
1a[b,c]	6.85	(3.65)	(3.94)	(3.90)	6.53	e)
1b[b,c]	7.33	(3.63)	(3.93)	(3.90)	6.55	f)
12c	7.345					
18r	7.27	6.84 $J_{2',6'}$=1.7	(3.86)	2.23 7.78[g]	8.36 $J_{5',6'}$=8.3	6.92
18s[h]	7.26	(3.73)	7.50 $J_{3',5'}$=2.0	2.20 7.24[g]	6.85 $J_{5',6'}$=8.0	7.03
17u	7.00	(3.66)	(3.83)	2.22 7.76[g]	8.02	(2.06)
18u	7.22	(3.61)	(3.89)	2.22 7.77[g]	8.01	(2.02)
17u'	—	(3.67)	(3.89)	2.22 7.74[g]	8.02	(2.05)
18u'	—	(3.65)	(3.91)	2.23 7.77[g]	8.08	(2.09)

a) Chemical shifts are δ values and coupling constants (J) in Hz (see the Experimental section). The δ value without J indicates either the absence of coupling with other protons or only a small magnitude of J (<ca. 0.5 Hz). b) Although approximate or inadequate data for **1a** (at 270 MHz) and **1b** (at 60 MHz) were reported (Ref. 6f), more accurately resolved, reliable parameters obtained at 500 MHz are shown here. c) The numbering of the A and C rings of **1a** and **1b** corresponds to that of **17** and **18** for the purpose of comparison. d) For MeO-1. e) The proton signals on the B ring (note the numbering of these protons are shown in the formula **1a**): δ=1.86 (1H, brtd, $J_{6,6'}$=11.9, $J_{6',7}$=11.8, $J_{5,6'}$=6.6, $J_{5',6'}\simeq$1.3 Hz, H-6'), 1.98 (3H, s, AcN-7), 2.28 (1H, brsept, $J_{5,6}$=12.7, $J_{6,7}$=6.6, $J_{5',6}$=6.5 Hz, H-6), 2.40 (1H, brtd, $J_{5,5'}$=13.7 Hz, H-5), 2.53 (1H, brdd, H-5'), 4.64 (1H, brdt, $J_{7,NH}$=6.7 Hz, H-7), and 7.02 (1H, brd, HN-7). f) The proton signals on the B ring (note the numbering of these protons are shown in the formula **1b**): δ=1.90 (1H, brsept, $J_{6,6'}$=12, $J_{6',7}$=12, $J_{5,6'}$=6.5, $J_{5',6'}\simeq$4 Hz, H-6'), 2.03 (3H, s, AcN-7), 2.29 (1H, brsept, $J_{5,6}$=12, $J_{6,7}$=6.5, $J_{5',6}$=6 Hz, H-6), 2.34 (1H, brtd, $J_{5,5'}$=13 Hz, H-5), 2.52 (1H, brdt, H-5'), 4.66 (1H, brdt, $J_{7,NH}$=6 Hz, H-7), and 6.21 (1H, brd, HN-7). g) For HN-4'. h) Measured at 200 MHz. i) $J\simeq$1.4 Hz. j) $J\simeq$0.8 Hz.

4-(1-azido-1-methylethyl) derivatives (e.g., **26b**) to effect the Schmidt-type reaction[17,18] (to give the corresponding 4-acetyl compounds), preparation of the bromo derivative **26a** was first sought by converting **19n** to the difluoroborane complex **19n'** and then by treatment with bromine under a tungsten light. However, **19n'** did not give **26a** but remained unchanged, most likely owing to the steric congestion around the 4-isopropyl side chain. On the other hand, the treatment of **18o, p** with sodium azide–concd sulfuric acid in chloroform resulted in, instead of the anticipated rearrangement to yield the acetyl derivatives,[17] a surprisingly facile ring closure to give indenotropolones (cyclohept[*a*]inden-7(10*H*)-one derivatives) **27o, p** (Scheme 7), which were led to acetates[16] **28o—p'** for characterization (see the Experimental section). The intramolecular cyclization was confirmed to readily proceed in the absence of sodium azide at room temperature, further supporting the neighboring positions of the aryl and isopropenyl

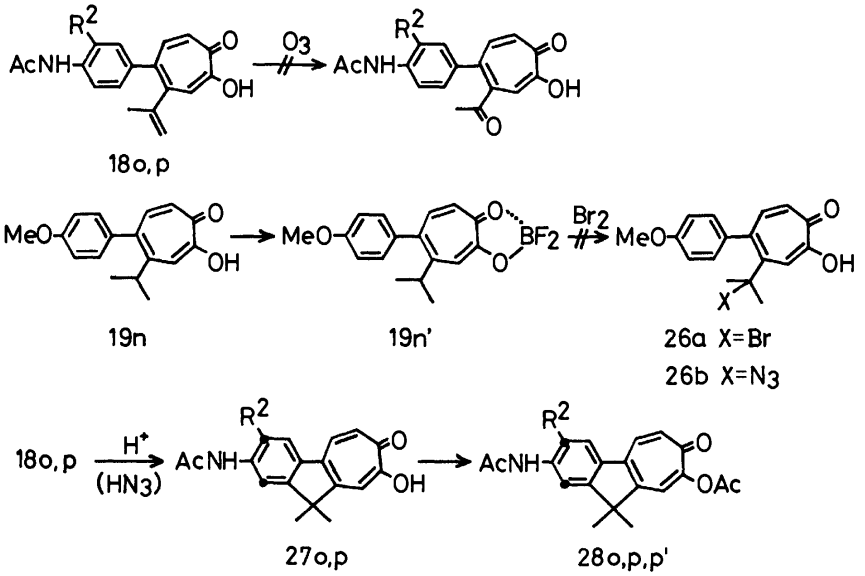

Scheme 7. Attempted preparations of 4-acetyl-5-aryltropolones. For R^2 of **18**, **27**, and **28o**, **p**, see Scheme 3.

groups on the tropolone ring in **18o—u**.

It is noteworthy that the rearrangement reactions of **14** resulted in the formation of minor amounts of by-products of various types. These were intensively studied in detail for the reactions of 2-(2-phenylhydrazino)tropones **14a—m**, and the following compounds were isolated (see Scheme 8):[15] a) The 3,*o*-type rearrangement products, indolotropones (6*H*-cyclohept[*b*]indol-6-one derivatives) **29**; b) the 5-semidine type rearrangement products, 5-anilino-2-arylazotropones **30**; c) the oxidative dimeric compound, 6,6'-bis(phenylhydrazono)-1,1'-[bi-2,4-cycloheptadien-1-yl]-7,7'-dione (**31**);[1] d) miscellaneous products, 2-aminotropone (**32**),[18] 2-arylazo-5-hydroxytropone (**33**), and *o*-[20] and *m*-nitroanilines[21] (**34**) (see Table 1 for yield of each compound).

Moreover, by a careful, chromatographic separation (after the alkaline hydrolysis and acetylation) of the reaction products of 2-[2-(2,3-dimethoxy-5-methylphenyl)hydrazino]-4-isopropenyltropone (**14u**), we isolated, besides the major 5,*p*-rearranged product **17u**, a minor amount of a by-product, whose structure was proved to be the 7,*p*-rearranged compound **17u'** by MS and ^{1}H NMR spectroscopy (see Scheme 9 and Table 2). It is noted that the signals due to 4-isopropenyl group in **17u'** were appreciably shifted to the downfield (ca. 0.5 ppm) from the corresponding signals of **17u** and appeared at δ 2.3 and 5.3—5.4 that coincide with the δ values of 4-isopropenyl group of β-dolabrin acetate,[22] thus supporting the assignment of the phenyl ring of **17u'** at the 7-position. This in turn shows the formation of a minor proportion of the corresponding 2-aminotropone **15u'** (Scheme 9) by the rearrangement of **14u**. Both **15u** and **15u'**, however, quickly turned into a dark tar during the attempted purification.

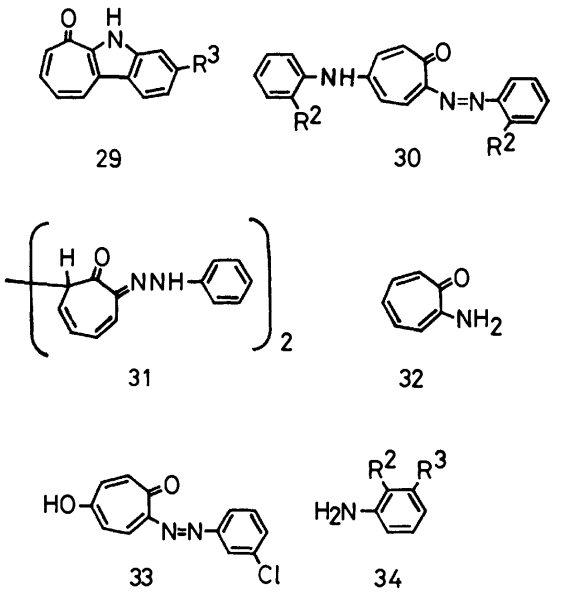

Scheme 8. Minor products of the rearrangement reaction. For R^2 and R^3 of **29**, **30**, and **34**, see Scheme 3.

Other remarks that would closely relate to the aspect of the reaction mechanism are as follows: 1) The presence of electron-donating substituents on the phenyl ring in **14** tends to accelerate the rearrangement, whereas that of an electron-withdrawing group markedly suppresses the reaction. 2) The rearrangement of **14o** proceeds much more smoothly than **14n**, suggesting that the presence of an electron-withdrawing group on the tropone ring of **14** appears to accelerate the reaction. 3) When substituent(s) is present at 3- (and 5-) position of the phenyl ring of **14**

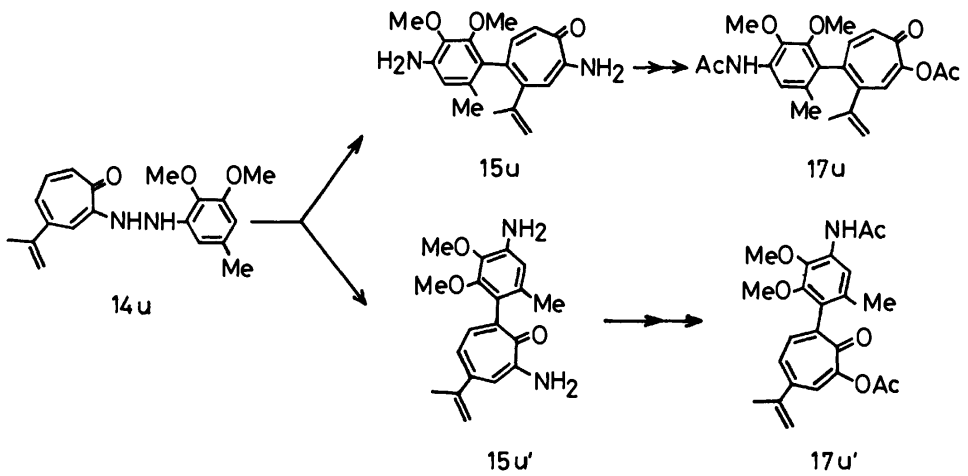

Scheme 9. The 5,*p*- and 7,*p*-rearrangement of **14u**.

and becomes bulkier, the yield of the product **15** tends to decrease and the amount of by-products increases.[15]

Closer studies on the rearrangement products using more variety of 2-arylhydrazinotropones of type **14**, particularly in connection with precursors bearing suitable substituents (e.g., R^1=CH(Me)NHAc and R^5=Me), are in progress.[15] Nevertheless, these findings in the present rearrangement are believed to be of value from the viewpoint of the development of the fundamental chemistry of troponoids,[7] and also to give important suggestions on further clarification of the reaction mechanism of benzidine rearrangement in general, which is still considered to contain certain ambiguity in many respects.[23] Moreover, present work demonstrates an effective way for preparation of a wide range of 5-aryltropolones having carbon-substituents at 4-position that are otherwise hardly available, and this methodology is expected to be useful in the development of a new, convenient route to colchicine analogues.

Experimental

Melting points were determined with a Thomas Hover MR or Yanagimoto MP-S3 instrument and are uncorrected. All reactions were monitored by TLC (Merck silica gel 60F, 0.25 mm) with an appropriate solvent system (mostly with MeOH-$CHCl_3$, $CHCl_3$-AcOEt, and/or AcOEt-hexane). Preparative TLC and column chromatography were performed with Merck Kiesel Gel 60G and Wako C-200 silica gel, respectively. Yields of products **15**—**18** and **29**—**34** are given in Table 1. The UV spectra were recorded in MeOH with a Hitachi EPS-3T spectrophotometer. The IR spectra were taken as KBr disk (unless otherwise stated) with a Shimadzu IR-27G, Hitachi 215, or JASCO A-102 spectrometer. The ^{1}H NMR spectra were measured in $CDCl_3$ (unless otherwise stated) with a Hitachi R24, R24B, or R-600 (60 MHz), Varian HA-100 (100 MHz), JEOL-FX200 (200 MHz) or Varian VXR-500 instrument (500 MHz, the SC-NMR Lab., Okayama Univ.) at 27 °C. Chemical shifts are recorded as δ values relative to tetramethylsilane as the internal standard measured at 60 MHz (unless otherwise stated). The assignments of all signals were made by employing a first-order analysis with the aid of decoupling technique and the parameters were confirmed by a computer-assisted simulation analysis. ^{13}C NMR spectra were recorded with a JEOL FX-100 (25 MHz) in DMSO-d_6. Mass spectra were taken on a Hitachi M-52 low-resolution or JEOL JMX-HX100 (with a JEOL JMA-DA5000 mass data system) high-resolution instrument and are given in terms of *m/z* (rel intensity) compared with the base peak.

Preparation of 2,3-Dimethoxy- (13g) and 2,3-Dimethoxy-5-methylphenylhydrazine (13h).[24] 2,3-Dimethoxyaniline[25] (15.9 g) was added dropwise to an ice-cooled 6 M HCl (40 cm^3), and then a solution of sodium nitrite (7.4 g) in water (20 cm^3) was added at 0—5 °C over a period of 30 min. Stirring was continued for 30 min at this temp. A solution of tin(II) chloride (110.6 g) in concd HCl (120 cm^3) was added at 0—5 °C over a period of 2 h. The mixture was stirred for 1 h at this temp and poured into an ice-cooled solution of NaOH (125.4 g) in water (314 cm^3). Black precipitates were filtered off and the filtrate was extracted with benzene. The combined organic layers were dried (Na_2SO_4) and concentrated in vacuo. The residue was distilled to give **13g** as pale yellow crystals (12.3 g, 75% yield): bp 122—124 °C/2 Torr (1 Torr=133.322 Pa), mp 78—82 °C; IR (neat) 3350 cm^{-1} (NH); ^{1}H NMR δ=3.72, 3.78 (3H each, 2s, MeO-2,3), 3.07—4.37 (3H, brm, $NHNH_2$), and 6.20—7.11 (3H, m, ArH*), *Aromatic H.

Anal. ($C_8H_{12}N_2O_2$) C, H, N.

Similar procedures starting with 2,3-dimethoxy-5-methylaniline[26] (20.9 g) afforded **13h** as a yellow viscous oil (16.1 g, 71%): bp 133—134 °C/3 Torr; IR (neat) 3400—3300 cm^{-1}; ^{1}H NMR δ=2.23 (3H, s, Me-5), 3.74, 3.80 (3H each, 2s, MeO-2,3), and 6.07—6.73 (2H, m, ArH).

Anal. ($C_9H_{14}N_2O_2$) C, H, N.

General Procedure for the Preparation of 2-(2-Arylhydrazino)tropones 14a—d, 14k, 14m, 23, and 24 from 2-Chlorotropone (12b). To a mixture of arylhydrazine **13** (1.2 mmol) and triethylamine (1.2 mmol, or 2.2 mmol when the arylhydrazine hydrochloride was used) in methanol (1 cm^3) was added **12b** (1.0 mmol) in methanol (2 cm^3) under nitrogen at room temp, and then the mixture was gently refluxed for 1.5—20 h; when the starting materials were not

soluble enough in MeOH alone, a certain amount of tetrahydrofuran (THF) was added as a co-solvent.

When the starting material **12b** almost disappeared (by TLC), the solvent was evaporated in vacuo. The residue was diluted with cold brine and extracted with $CHCl_3$ or CH_2Cl_2 (AcOEt or THF, if necessary). The combined organic layers were dried (Na_2SO_4) and evaporated in vacuo. The residue (when it was a solid) was recrystallized from an appropriate solvent (see below) to give the corresponding product; the filtrate was concentrated in vacuo and the residue was chromatographed in a column of silica gel, giving an additional amount of the product.

2-(2-Phenylhydrazino)tropone[27,28] (14a). Yellow prisms (48% yield from **12b** and **13a**, cf. Ref. 1, 66% yield using **12a**); mp 168 °C (from benzene, lit,[27] mp 168 °C); UV λ_{max} 246 (log ε 4.52), 335 (4.04), and 400 nm (4.05); IR 3270 (NH) and 1598 cm^{-1} (C=O); ^1H NMR (100 MHz, DMSO-d_6) δ=6.6—7.4 (10H, m, ArH), 8.1 (1H, brm, NH-1'), and 9.0 (1H, brm, NH-2); ^{13}C NMR δ=109.3 (C-3), 112.3 (C-2', 6'), 119.4 (C-4'), 123.3 (C-5), 129.3 (C-3', 5'), 130.3 (C-7), 136.4 (C-4), 137.1 (C-6), 147.1 (C-1'), 156.2 (C-2), and 176.2 (C-1); MS *m/z* 212 (M^+; 78.5), 105 (4), 93 (100), and 77 (17).

2-[2-(*o*-Tolyl)hydrazino]tropone (14b): Yellow prisms (40% yield from **12b** and **13b** hydrochloride, cf. Ref. 1, 82% yield using **12a**); mp 90—91 °C (from benzene); UV λ_{max} 246 (log ε 4.25), 335 (3.78), and 400 nm (3.76); IR 3270, 3250 (NH), and 1590 cm^{-1} (C=O); ^1H NMR (100 MHz, DMSO-d_6) δ=2.26 (3H, s, Me-2'), 6.4—7.5 (9H, m, ArH), 7.59 (1H, brs, NH-1'), and 8.98 (1H, brs, NH-2); ^{13}C NMR δ=17.4 (Me-2'), 109.2 (C-3), 110.7 (C-6'), 119.5 (C-4'), 122.3 (C-2'), 123.1 (C-5), 126.7 (C-3'), 129.9 (C-5'), 130.3 (C-7), 136.4 (C-4,6), 145.2 (C-1'), 156.7 (C-2), and 176.0 (C-1); MS *m/z* 226 (M^+; 100), 107 (95), and 106 (80).

Anal. ($C_{14}H_{14}N_2O$) C, H, N.

2-[2-(*m*-Tolyl)hydrazino]tropone (14c): Yellow prisms (57% yield from **12b** and **13c** hydrochloride, cf. Ref. 1, 72% yield using **12a**); mp 148 °C (from benzene); UV λ_{max} 246 (log ε 4.37), 358 (4.05), and 400 nm (3.91); IR 3300, 3240 (NH), 1600, and 1590 cm^{-1} (C=O); ^1H NMR (100 MHz, DMSO-d_6) δ=2.18 (3H, s, Me-3'), 6.48 (1H, brd, $J_{4',5'}$=8 Hz, H-4'), 6.52 (1H, brs, H-2'), 6.56 (1H, brd, $J_{3,4}$=10 Hz, H-3), 6.6—7.1 (1H, m, H-5), 6.67 (1H, brd, $J_{5',6'}$=8 Hz, H-6'), 6.87 (1H, brt, H-5'), 7.00 (1H, brd, $J_{6,7}$=11.5 Hz, H-7), 7.24 (1H, brt, $J_{4,5}$=10.0, $J_{4,6}$=1.5 Hz, H-4), 7.28 (1H, ddd, $J_{5,6}$=9.5 Hz, H-6), 8.0 (1H, brs, NH-1'), and 9.0 (1H, brs NH-2); ^{13}C NMR δ=21.1 (Me-3'), 109.2 (C-3), 109.8 (C-2'), 112.8 (C-6'), 120.0 (C-4'), 123.2 (C-5), 129.0 (C-5'), 130.0 (C-7), 136.3 (C-4,6), 138.1 (C-3'), 147.6 (C-1'), 156.1 (C-2), and 176.0 (C-1); MS *m/z* 226 (M^+; 73.4) and 106 (100).

Anal. ($C_{14}H_{14}N_2O$) C, H, N.

2-[2-(*p*-Tolyl)hydrazino]tropone (14d): Yellow needles (53% yield from **12b** and **13d** hydrochloride, cf. Ref. 1, 63% yield using **12a**); mp 162—164 °C (from benzene); UV λ_{max} 245 (log ε 4.60), 335 (4.12), and 402 nm (4.10); IR 3260 (NH) and 1600 cm^{-1} (C=O); ^1H NMR (100 MHz, DMSO-d_6) δ=2.30 (3H, s, Me-4'), 5.7 (1H, brm, NH-1'), 6.6—7.4 (9H, m, ArH), and 8.3 (1H, brm, NH-2); MS *m/z* 226 (M^+; 100), 107 (80), and 106 (91).

Anal. ($C_{14}H_{14}N_2O$) C, H, N.

2-[2-(*m*-Nitrophenyl)hydrazino]tropone (14k): Yellow prisms (53% yield from **12b** and **13k**, cf. Ref. 1, 62% yield using **12a**); mp 188—190 °C (from $CHCl_3$-benzene); UV λ_{max} 246 (log ε 4.75), 335 (4.25), and 398 nm (4.28); IR 3260 (NH) and 1600 cm^{-1} (C=O); ^1H NMR (100 MHz, DMSO-d_6) δ=6.6—7.7 (9H, m, ArH), 8.7 (1H, brs, NH-1'), and 9.3 (1H, brs, NH-2); MS *m/z* 257 (M^+; 100), 138 (13), and 121 (7).

Anal. ($C_{13}H_{11}N_3O_3$) C, H, N.

2-[2-(*p*-Nitrophenyl)hydrazino]tropone (14m): Yellow prisms (53% yield from **12b** and **13m**, cf. Ref. 1, 51% yield using **12a**); mp 185 °C decomp (from benzene); UV λ_{max} 243 (log ε 4.26), 340 (4.01), and 398 nm (4.09); IR 3300, 3200 (NH), and 1600 cm^{-1} (C=O); ^1H NMR (100 MHz, DMSO-d_6) δ=6.75 (2H, brd, J=9 Hz, H-2',6'), 6.755 (1H, brd, $J_{3,4}$=10 Hz, H-3), 6.76 (1H, brdd, $J_{4,5}$=10, $J_{5,6}$=9 Hz, H-5), 7.03 (1H, brd, $J_{6,7}$=11.5 Hz, H-7), 7.26 (1H, brt, H-4), 7.34 (1H, brdd, H-6), 8.08 (2H, brd, J=9 Hz, H-3',5'), 9.31 (1H, brs, NH-1'), and 9.4 (1H, brs, NH-2); MS *m/z* 257 (M^+; 100) and 138 (5).

Anal. ($C_{13}H_{11}N_3O_3$) C, H, N.

2,2'-Hydrazobis(tropone) (23): Pale yellow crystals (70% yield from **12b** and **22**); mp 190 °C (from $CHCl_3$-benzene); UV λ_{max} 245 (log ε 4.58), 336 (4.16), and 404 nm (4.27); IR 3300 (NH), 1610, and 1590 cm^{-1} (C=O); ^1H NMR (100 MHz, DMSO-d_6) δ=6.60 (2H, brd, $J_{3,4}$=9.5 Hz, H-3), 6.77 (2H, brdd, $J_{4,5}$=10.0, $J_{5,6}$=8.5 Hz, H-5), 7.06 (2H, brd, $J_{6,7}$=11.5 Hz, H-7), 7.24 (2H, brdd, H-4), 7.36 (2H, ddd, $J_{4,6}$=1.5 Hz, H-6), and 9.36 (2H, brs, NH-2); MS *m/z* 240 (M^+; 100), 121 (21), and 105 (4).

Anal. ($C_{14}H_{12}N_2O_2$) C, H, N.

2-[2-(1-Naphthyl)hydrazino]tropone (24): Yellow prisms (15% yield from **12b** and 1-naphthylhydrazine); mp 150 °C (from $CHCl_3$-benzene); IR 3300, 3200 (NH), and 1597 cm^{-1} (C=O); ^1H NMR (100 MHz, DMSO-d_6) δ=6.55 (1H, dd, J=7, 2.5 Hz, H-2'), 6.65—7.6 (9H, m, ArH), 7.86 (1H, brdd, J=6.5, 3 Hz, H-5'), 8.28 (1H, brdd, J=6.5, 3 Hz, H-8'), 8.70 (1H, m, NH-1'), and 9.25 (1H, brs, NH-2); ^{13}C NMR δ=104.9 (C-2'), 109.1 (C-3), 119.2, 121.5, 122.2 (C-8'a), 123.2 (C-5), 124.6, 126.0, 126.4, 128.1, 130.1 (C-7), 133.9 (C-4'a), 136.6 (C-4), 136.8 (C-6), 142.5 (C-1'), 156.0 (C-2), and 176.1 (C-1); MS *m/z* 262 (M^+; 100), 143 (46), 142 (21), and 105 (27).

Anal. ($C_{17}H_{14}N_2O$) C, H, N.

General Procedure for the Benzidine-Type Rearrangement of 2-(2-Arylhydrazino)tropones 14, 23, and 24. A. Procedure for 14a—f,i,j,m, 23, and 24: A mixture of **14** (or **23** or **24**) (1 mmol) and 2 M HCl (6.3 cm^3, 12.5 mmol) in ethanol (50 cm^3) was heated at 50—80 °C for 1 h (for **14a—f**, **24**), or refluxed for 5—6 h (for **14m**, **23**) or 12 h (for **14i,j**) under nitrogen. The mixture was neutralized with cold 2 M NaOH solution and extracted with ethyl acetate. The extract was washed with water and then with brine. The organic layer was dried (Na_2SO_4) and concentrated. When crystals were separated, they were collected and recrystallized. The filtrate was concentrated and chromatographed on preparative TLC plates (with chloroform, ethyl acetate, or diethyl ether). When no crystals appeared on evaporation of the AcOEt extract, the residue was directly chromatographed.

B. Procedure for 14g,h: A mixture of **14** (0.2 mmol) and 2 M HCl (1.3 cm^3) in ethanol (10 cm^3) was refluxed for 2 h under nitrogen. The reaction mixture was similarly worked up.

C. Procedure for 14k,l: A mixture of **14** (1 mmol) and 2 M HCl (6.3 cm^3) in 3:2 dioxane-water (50 cm^3) was refluxed for 72 h under nitrogen. The reaction mixture was similarly worked up.

D. Procedure for 14l: A mixture of **14l** (1 mmol) and

2 M HCl (6.3 cm^3) in 1-butanol (50 cm^3) was refluxed for 72 h under nitrogen. The reaction mixture was similarly worked up.

E. Procedure for 14n—u: A mixture of a 4-substituted 2-(2-arylhydrazino)tropone **14** (50 mg), ethanol (10 cm^3), and 2 M HCl (2.5 cm^3) was refluxed under nitrogen for 1—3.5 h. When the starting material **14** almost disappeared (by TLC), the mixture was concentrated at 40—50 °C under reduced pressure. When crystals separated, they were filtered off and washed with benzene to give crude **15** (as hydrochloride). This was stirred with cold, saturated aq $NaHCO_3$ under nitrogen and extracted with ethyl acetate, giving unstable **15** after recrystallization. If the hydrochloride of **15** did not precipitate, the reaction mixture was taken to pH 8 with cold 2 M KOH and the solvent was concentrated in vacuo. The residue was extracted with CH_2Cl_2 or AcOEt. The combined organic layers were dried (Na_2SO_4) and evaporated in vacuo to give crude **15n—u**. As these products were not stable enough to be purified, they were immediately subjected to the next step (see later).

2-Amino-5-(4-aminophenyl)tropone (15a): Yellow prisms; mp 203—204 °C (from $CHCl_3$-benzene); UV λ_{max} 240 (log ε 4.44), 375 (4.28), and 402sh nm (4.20); IR 3450, 3300 (NH), and 1610 cm^{-1} (C=O); ^1H NMR (100 MHz, DMSO-d_6) δ=5.2 (2H, brs, H_2N-4′), 6.7 (2H, brd, J=8.5 Hz, H-3′,5′), 7.3 (2H, brd, J=8.5 Hz, H-2′,6′), 7.5 (2H, m, H_2N-2), and 6.9—7.8 (4H, m, H-3,4,6,7); ^{13}C NMR δ=113.0 (C-3), 114.5 (C-3′,5′), 127.9 (C-2′,6′), 129.3 (C-7), 129.9 (C-1′), 133.9 (C-4), 136.0 (C-5,6), 148.2 (C-4′), 156.7 (C-2), and 174.6 (C-1); MS m/z 212 (M^+; 75.6) and 184 (100).

Anal. ($C_{13}H_{12}N_2O$) C, H, N.

Compound **15a** (50 mg, 0.24 mmol) was treated with acetic anhydride (0.22 cm^3) in 3:5 dichloromethane–benzene (8 cm^3) at 40 °C for 3 h under nitrogen to give 2-amino-5-(4-acetamidophenyl)tropone (**15a′**, 60 mg, 100% yield): Yellow crystals; mp>300 °C; IR 3425, 3250 (NH), 1680 (amide), and 1605 cm^{-1} (C=O); ^1H NMR (DMSO-d_6) δ=2.20 (3H, s, AcN), 7.02 (2H, brd, J=9 Hz, H-3′,5′), 7.0—7.8 (8H, m, ArH, H_2N-2), and 10.1 (1H, brm, NH-4′); MS m/z 254 (M^+; 100), 212 (5), and 182 (97).

Treatment of **15a′** (21 mg) with Ac_2O–pyridine at 20 °C for 2 h under nitrogen gave 2-acetamido-5-(4-acetamidophenyl)-tropone (**15a″**, 24 mg, 97%): Yellow crystals; mp>300 °C; IR 3350, 3250 (NH), 1701, 1678 (amide) and 1600 cm^{-1} (C=O); ^1H NMR (DMSO-d_6) δ=2.10 (3H, s, AcN-4′), 2.20 (3H, s, AcN-2), 6.9—8.0 (8H, m, ArH), 9.1, and 9.2 (1H each, brm, 2NH); MS m/z 296 (M^+; 80.0), 253 (100), 223 (27), and 184 (57).

2-Amino-5-(4-amino-3-methylphenyl)tropone (15b): Yellow prisms; mp 204 °C (from benzene); UV λ_{max} 244 (log ε 4.56) and 382 nm (4.40); IR 3450, 3325 (NH), 1610, and 1600 cm^{-1} (C=O); ^1H NMR (100 MHz, DMSO-d_6) δ=2.14 (3H, s, Me-3′), 4.0 (2H, m, H_2N-4′), 6.70 (1H, brd, J=8.5 Hz, H-5′), 6.9—7.3 (4H, m, H-3,7,2′,6′), 7.32 (2H, brm, H_2N-2), and 7.49 (2H, brdd, J=12, 2 Hz, H-4,6); ^{13}C NMR δ=17.3 (Me-3′), 112.1 (C-3), 114.0 (C-5′), 121.1 (C-3′), 124.3 (C-2′), 128.1 (C-6′), 128.7 (C-7), 130.0 (C-1′), 133.2 (C-4), 135.7 (C-5,6), 145.4 (C-4′), 155.6 (C-2), and 174.2 (C-1); MS m/z 226 (M^+; 100) and 198 (75).

Anal. ($C_{14}H_{14}N_2O$) C, H, N.

2-Amino-5-(4-amino-2-methylphenyl)tropone (15c): Yellow prisms; mp 153—155 °C (from benzene); UV λ_{max} 249 (log ε 4.51), 362 (4.15), and 410 nm (4.02); IR 3400—3100 (NH) and 1605 cm^{-1} (C=O); ^1H NMR (100 MHz, DMSO-d_6) δ=2.08 (3H, s, Me-2′), 4.99 (2H, brs, H_2N-4′), 6.42 (1H, brd, $J_{5',6'}$=8 Hz, H-5′), 6.46 (1H, brs, H-3′), 6.84 (1H, brd, H-6′), 7.3 (2H, brm, H_2N-2), and 6.9—7.4 (4H, m, H-3,4,6,7); ^{13}C NMR δ=19.8 (Me-2′), 111.3 (C-3,3′), 115.6 (C-5′), 128.0 (C-6′), 129.3 (C-7), 131.3 (C-1′), 134.8 (C-2′), 136.1 (C-5), 136.7 (C-4), 138.4 (C-6), 147.2 (C-4′), 156.7 (C-2), and 174.4 (C-1); MS m/z 226 (M^+; 76.6) and 198 (100).

Anal. ($C_{14}H_{14}N_2O$) C, H, N.

2-Amino-5-(4-amino-3-methoxyphenyl)tropone (15e): Yellow prisms; mp 185 °C (from benzene); UV λ_{max} 244 (log ε 3.92) and 387 nm (3.78); IR 3395, 3270 (NH), and 1615 cm^{-1} (C=O); ^1H NMR (DMSO-d_6) δ=3.87 (3H, s, MeO-3′), 4.85 (2H, brm, H_2N-4′), 6.5—7.8 (7H, m, ArH), and 7.35 (2H, brm, H_2N-2); MS m/z 242 (M^+; 100), 214 (43), 199 (24), 172 (13), and 171 (59).

Found: m/z 242.1063. Calcd for $C_{14}H_{14}N_2O_2$: M, 242.1056.

2-Amino-5-(4-amino-2-methoxyphenyl)tropone (15f): Yellow prisms; mp 185—187 °C (from benzene); UV λ_{max} 245 (log ε 4.64) and 380 nm (4.41); IR 3400, 3245 (NH), and 1605 cm^{-1} (C=O); ^1H NMR (DMSO-d_6) δ=3.70 (3H, s, MeO-2′), 5.2 (2H, brm, H_2N-4′), 7.25 (2H, brm, H_2N-2), 7.25—7.45 (7H, m, ArH); MS m/z 242 (M^+; 100), 214 (67), and 199 (13).

Anal. ($C_{14}H_{14}N_2O_2$) C, H, N.

2-Amino-5-(4-amino-2,3-dimethoxyphenyl)tropone (15g): Yellow prisms; mp 166—167 °C (from benzene); IR ($CHCl_3$) 3400, 3355 (NH), and 1610 cm^{-1} (C=O); ^1H NMR δ=3.66 (3H, s, MeO-2′), 3.92 (3H, s, MeO-3′), 6.09 (2H, brm, H_2N-4′), 6.55 (1H, d, $J_{5',6'}$=9Hz, H-5′), 6.89 (1H, d, H-6′), 6.96 (1H, d, $J_{6,7}$=11 Hz, H-7), 7.15—7.65 (3H, m, ArH), and 7.35 (2H, brm, H_2N-2); MS m/z 272 (M^+; 100), 244 (63), and 229 (6).

Found: m/z 272.1176. Calcd for $C_{15}H_{16}N_2O_3$: M, 272.1161.

2-Amino-5-(4-amino-2,3-dimethoxy-6-methylphenyl)tropone (15h): Yellow prisms; mp 120—122 °C (from benzene); IR ($CHCl_3$) 3380, 3350 (NH), and 1610 cm^{-1} (C=O); ^1H NMR δ=2.00 (3H, s, Me-6′), 3.59 (3H, s, MeO-2′), 3.85 (3H, s, MeO-3′), 6.30 (2H, brm, H_2N-4′), 6.42 (1H, s, H-5′), 6.95—7.2 (4H, m, ArH), and 7.35 (2H, brm, H_2N-2); MS m/z 286 (M^+; 100), 271 (8), 254 (45), and 243 (11).

Found: m/z 286.1321. Calcd for $C_{16}H_{18}N_2O_3$: M, 286.1317.

2-Amino-5-(4-amino-3-chlorophenyl)tropone (15i): Yellow prisms; mp 230 °C decomp (from ethanol), UV λ_{max} 245 (log ε 4.49) and 378 nm (4.37); IR 3330, 3205 (NH), and 1610 cm^{-1} (C=O); ^1H NMR (DMSO-d_6) δ=5.35 (2H, brm, H_2N-4′), 6.90 (1H, brd, $J_{5',6'}$=8.5 Hz, H-6′), 7.0—7.7 (6H, m, ArH), and 7.45 (2H, brm, H_2N-2); MS m/z 248 (M+2; 31), 246 (M^+; 92), 220 (34), 218 (100), 182 (13), 154 (11), 109 (19), and 91 (25).

Found: m/z 246.0560. Calcd for $C_{13}H_{11}N_2OCl$: M, 246.0560.

2-Amino-5-(4-amino-2-chlorophenyl)tropone (15j): Yellow prisms; mp 161—162 °C (from chloroform); UV λ_{max} 248 (log ε 4.11) and 363 nm (3.86); IR 3345 (NH) and 1605 cm^{-1} (C=O); ^1H NMR (DMSO-d_6) δ=5.45 (2H, brm, H_2N-4′), 6.4—7.7 (7H, m, ArH), and 7.45 (2H, brm, H_2N-2); MS m/z 248 (M+2; 33), 246 (M^+; 99), 220 (34), 218 (100), 182 (17), 154 (11), and 109 (18).

Found: m/z 246.0537. Calcd for $C_{13}H_{11}N_2OCl$: M, 246.0560.

2-Amino-5-(4-amino-3-nitrophenyl)tropone (15k): Yellow prisms; mp 253—254 °C (from ethyl acetate); UV λ_{max} 247 (log ε 4.54) and 372 nm (4.49); IR 3445, 3290 (NH), and 1635 cm^{-1} (C=O); ^{1}H NMR (DMSO-d_6) δ=5.60 (2H, brm, H_2N-4′), 6.8—7.5 (5H, m, H-3,4,6,7,5′), 7.52 (2H, brm, H_2N-2), 7.70 (1H, dd, $J_{5',6'}$=8, $J_{2',6'}$=2 Hz, H-6′), and 8.14 (1H, d, H-2′); MS *m/z* 257 (M^+; 100), 229 (36), and 183 (41).

Found: *m/z* 257.0799. Calcd for $C_{13}H_{11}N_3O_3$: M, 257.0800.

2-Amino-5-(4-amino-2-nitrophenyl)tropone (15l): Yellow prisms; mp 246—247 °C (from ethyl acetate); UV λ_{max} 250 (log ε 4.45), 358 (4.20), and 409 nm (4.07); IR 3420, 3280 (NH), and 1620 cm^{-1} (C=O), ^{1}H NMR (DMSO-d_6) δ=5.85 (2H, brm, H_2N-4′), 6.6—7.3 (7H, m, ArH), and 7.65 (2 H, brm, H_2N-2); MS *m/z* 257 (M^+; 100), 240 (11), 212 (18), 201 (22), 197 (33), 185 (20), 184 (36), 183 (28), 182 (45), 169 (43), and 154 (31).

Found: *m/z* 257.0805. Calcd for $C_{13}H_{11}N_3O_3$: M, 257.0800.

2-Amino-5-(4-amino-1-naphthyl)tropone (25): Yellow prisms; mp 173 °C (from benzene); IR 3350 (NH) and 1603 cm^{-1} (C=O); ^{1}H NMR (100 MHz, DMSO-d_6) δ=4.4 (2H, brs, H_2N-4′), 5.8 (2H, brs, H_2N-2), 6.74 (1H, d, $J_{2',3'}$=8 Hz, H-3′), 6.98 (1H, d, $J_{3,4}$=12 Hz, H-3), 7.19 (1H, d, H-2′), 6.9—7.5 (4H, m, H-4,6,6′,7′), 7.67 (1H, brdd, $J_{5',6'}$=7, $J_{5',7'}$=3Hz, H-5′), and 8.13 (1H, brdd, $J_{7',8'}$=6.5, $J_{6',8'}$=3 Hz, H-8′); ^{13}C NMR δ=112.1 (C-3), 122.9 (C-4′a), 124.0, 125.3, 126.0, 128.0 (C-2′), 129.0 (C-7), 132.0 (C-1′), 135.8 (C-5), 138.0 (C-4), 139.7 (C-6), 144.6 (C-8′a), 157.7 (C-4′), 159.5 (C-2), and 175.2 (C-1); MS *m/z* 262 (M^+; 72.2), 234 (100), and 217 (54).

Anal. ($C_{17}H_{14}N_2O$) C, H, N.

6*H*-Cyclohept[*b*]indol-6-one (29a):[29] Yellow prisms; mp 267 °C (from benzene, lit,[29] 245—246 °C).

3-Methyl-6*H*-cyclohept[*b*]indol-6-one (29c): Yellow prisms; mp 226 °C (from benzene); UV λ_{max} 229 (log ε 4.49), 282 (4.44), 312 (4.38), 326 (4.33), 394 (4.86), and 410 nm (3.99); IR 3200 (NH) and 1605 cm^{-1}; ^{1}H NMR (DMSO-d_6) δ=2.45 (3H, s, Me-3), 6.9—7.8 (5H, m, ArH), 8.00 (1H, d, $J_{1,2}$=8 Hz, H-1), 8.16 (1H, d, $J_{9,10}$=10 Hz, H-10), and 12.3 (1H, brm, HN-5); MS *m/z* 209 (M^+; 100), 181 (92), 180 (78), and 152 (16).

Found: *m/z* 209.0833. Calcd for $C_{14}H_{11}NO$: M, 209.0841.

3-Methoxy-6*H*-cyclohept[*b*]indol-6-one (29f): Yellow prisms; mp 251—252 °C (from benzene); UV λ_{max} 228 (log ε 4.42), 281 (4.23), 317 (4.46), 390 (3.75), 410 nm (3.85); IR 3180 (NH) and 1625 cm^{-1} (C=O); ^{1}H NMR (DMSO-d_6) δ=3.82 (3H, s, MeO-3), 6.7—7.7 (5H, m, ArH), 8.18 (1H, d, $J_{1,2}$=9 Hz, H-1), 8.30 (1H, d, $J_{9,10}$=11 Hz, H-10), and 12.4 (1H, brm, HN-5).

Anal. ($C_{14}H_{11}NO_2$) C, H, N.

3-Chloro-6*H*-cyclohept[*b*]indol-6-one (29j): Yellow prisms; mp 191—192 °C (from benzene); UV λ_{max} 233 (log ε 4.42), 272 (4.37), 280 (4.38), 314 (4.36), 386 (3.84), and 404 nm (3.96); IR 3175 (NH) and 1615 cm^{-1} (C=O); ^{1}H NMR (DMSO-d_6) δ=6.9—7.8 (5H, m, ArH), 8.32 (1H, brd, $J_{9,10}$= 11 Hz, H-10), 8.35 (1H, d, $J_{1,2}$=8 Hz, H-1), and 12.4 (1H, brm, HN-5); MS *m/z* 231 (M+2; 25), 229 (M^+; 79), 203 (34), 201 (100), and 166 (45).

Found: *m/z* 229.0246. Calcd for $C_{13}H_8NOCl$: M, 229.0295.

3-Nitro-6*H*-cyclohept[*b*]indol-6-one (29l): Yellow crystals; mp>300 °C (from benzene-methanol); UV λ_{max} 249 (log ε 4.29), 310 (4.39), 336 (4.17), 404 (3.81), and 420 nm (3.90); IR 3180 (NH) and 1620 cm^{-1} (C=O); ^{1}H NMR (DMSO-d_6) δ=7.0—8.65 (7H, m, ArH) and 12.9 (1H, brm, HN-5); MS *m/z* 240 (M^+; 100), 212 (43), 166 (73), and 139 (55).

Found: *m/z* 240.0537. Calcd for $C_{13}H_8N_2O_3$: M, 240.0535.

5-Anilino-2-phenylazotropone (30a): Dark red needles; mp 183—184 °C (from benzene); UV λ_{max} 235 (log ε 4.38), 320 (4.25), and 495 nm (4.31); IR ($CHCl_3$) 3000 (NH) and 1590 cm^{-1} (C=O); ^{1}H NMR δ=6.6—7.0 [1H, m, H-4″ (PhN-5)], 7.1—7.6 (10H, m, ArH), 7.66 (1H, d, $J_{3,4}$=10 Hz H-3), 7.8—8.05 [2H, m, H-2′,6′ (PhN=N-2)], and 9.3 (1H, brm, NH-5); ^{13}C NMR δ=111.3 (C-3), 122.4, 123.5, 124.6, 125.9, 126.6, 129.1, 129.9 (C-4), 131.3 (C-7), 137.6, 138.0, 151.3 (C-1″), 152.9 (C-1′), 155.7 (C-2), and 172.0 (C-1); MS *m/z* 301 (M^+; 16), 272 (9), 196 (41), 181 (26), 167 (87), 115 (8), and 77 (100).

Anal. ($C_{19}H_{15}N_3O$) C, H, N.

5-(2-Chloroanilino)-2-(2-chlorophenylazo)tropone (30i): Dark red prisms; mp 176 °C (from benzene-hexane); UV λ_{max} 266 (log ε 4.33), 272 (4.36), and 490 nm (4.54); IR ($CHCl_3$) 3010 (NH) and 1620 cm^{-1} (C=O); ^{1}H NMR δ=6.3—8.0 (12H, m, ArH) and 9.56 (1H, brm, NH).

Anal. ($C_{19}H_{13}N_3OCl_2$) C, H, N.

2-(3-Chlorophenylazo)-5-hydroxytropone (33): Dark red microcrystals; mp 117 °C decomp (from benzene); UV λ_{max} 299 (log ε 3.92) and 502 nm (3.87); IR ($CHCl_3$) 3260 (OH) and 1590 cm^{-1} (C=O); ^{1}H NMR δ=6.6—8.2 (8H, m, ArH) and 9.4 (1H, brm, OH); MS *m/z* 262 (M+2; 24), 260 (M^+; 74), 232 (8), 141 (10), 139 (33), 121 (100), and 111 (95).

Found: *m/z* 260.0356. Calcd for $C_{13}H_9N_2O_2Cl$: M, 260.0353.

General Procedure for Hydrolysis of 2-Amino-5-(4-aminoaryl)tropones 15. Compound **15** (0.5 mmol) was dissolved in ethanol (8 cm^3) and 6 M KOH (3.5 cm^3); if necessary, some THF was added as a co-solvent. The mixture was refluxed under nitrogen for 3—12 h, brought to pH 7 with 2 M HCl, and then concentrated in vacuo. When **16** separated as crystals, they were filtered off and washed with cold water (and then with a little benzene). The filtrate was extracted with AcOEt or CH_2Cl_2. The combined organic layers were dried (Na_2SO_4) and evaporated in vacuo to give additional **16**. The products **16n—u** were not stable enough for purification and therefore immediately acetylated (see later).

5-(4-Aminophenyl)tropolone (16a): Yellow prisms; mp 185—186 °C (from benzene-methanol); UV λ_{max} 238 (log ε 4.55), 256 (4.50), and 390 nm (4.38); IR 3440, 3360 (NH), 3150 (OH), and 1620 cm^{-1} (C=O); ^{1}H NMR δ=5.1 (3H, brm, H_2N-4′, HO-2), 6.70 (2H, brd, J=8.5 Hz, H-3′,5′), 7.1—7.2 (4H, m, ArH), and 7.25 (2H, brd, J=8.5 Hz, H-2′,6′); MS *m/z* 213 (M^+; 100) and 185 (98).

Anal. ($C_{13}H_{11}NO_2$) C, H, N.

Treatment of **16a** (54 mg) with cold nitrous acid, followed by reduction with phosphinic acid, gave 5-phenyltropolone (**5**)[10,11] as pale yellow plates (15 mg, 30% overall yield); mp 126 °C (lit,[10] 125—126 °C).

5-(4-Amino-3-methylphenyl)tropolone (16b): Yellow prisms; mp 157—158 °C (from benzene-methanol); UV λ_{max} 238 (log ε 4.50), 256 (4.44), and 393 nm (4.30); IR 3440, 3370 (NH), 3240 (OH), and 1615 cm^{-1} (C=O); ^{1}H NMR δ=2.20 (3H, s, Me-3′), 5.2 (3H, brm, H_2N-4′, HO-2), 6.69 (1H, brd, $J_{5',6'}$=9 Hz, H-5′), and 6.9—7.2 (6H, m, ArH).

Anal. ($C_{14}H_{13}NO_2$) C, H, N.

5-(4-Amino-2-methylphenyl)tropolone (16c): Yellow prisms; mp 115—117 °C (from benzene–methanol); UV λ_{max} 240sh (log ε 4.52), 251 (4.55), 358 (4.18), and 390sh nm (4.15); IR 3430 (NH), 3170 (OH), and 1615 cm^{-1} (C=O); ^1H NMR δ=2.15 (3H, s, Me-2′), 5.4 (3H, brm, H_2N-4′, HO-2), 6.50 (1H, brd, $J_{3',5'}$=2.5 Hz, H-3′), 6.51 (1H, brdd, $J_{5',6'}$=8.5 Hz, H-5′), 7.00 (1H, brd, H-6′), and 7.2—7.6 (4H, brs, ArH).

Anal. ($C_{14}H_{13}NO_2$) C, H, N.

5-(4-Amino-3-methoxyphenyl)tropolone (16e): Yellow prisms; mp 155—157 °C (from benzene–methanol); UV λ_{max} 238 (log ε 4.61), 257 (4.50), and 398 nm (4.37); IR 3460, 3320 (NH), 3200 (OH), and 1620 cm^{-1} (C=O); ^1H NMR δ=3.90 (3H, s, MeO-3′), 5.60 (3H, brm, H_2N-4′, HO-2), 6.67 (1H, brd, $J_{5',6'}$=8.5 Hz, H-5′), 6.84 (1H, brs, H-2′), and 7.1—7.8 (5H, brs, ArH).

Anal. ($C_{14}H_{13}NO_3$) C, H, N.

***5-(4-Amino-2-methoxyphenyl)tropolone* (16f):** Yellow prisms; mp 167—169 °C (from benzene–methanol); UV λ_{max} 237 (log ε 4.58), 256 (4.55), and 397 nm (4.30); IR 3470, 3380 (NH), 3200 (OH), and 1610 cm^{-1} (C=O); ^1H NMR δ=3.76 (3H, s, MeO-2′), 5.05 (3H, brm, H_2N-4′, HO-2), 6.15—6.45 (2H, m, H-3′,5′), 7.05 (1H, brd, $J_{5',6'}$=8 Hz, H-6′), and 7.2—7.65 (4H, m, ArH).

Anal. ($C_{14}H_{13}NO_3$) C, H, N.

5-(4-Amino-2,3-dimethoxyphenyl)tropolone (16g): Yellow prisms; mp 110—111 °C (from benzene); IR 3465, 3350 (NH), 3200 (OH), and 1605 cm^{-1} (C=O); ^1H NMR δ=3.69 (3H, s, MeO-2′), 3.84 (3H, s, MeO-3′), 5.45 (3H, brm, H_2N-4′, HO-2), 6.72 (1H, d, $J_{5',6'}$=8.5 Hz, H-5′), 7.0—7.65 (4H, m, ArH), and 7.03 (1H, d, H-6′).

Anal. ($C_{15}H_{15}NO_4$) C, H, N.

5-(4-Amino-2,3-dimethoxy-6-methylphenyl)tropolone (16h): Yellow prisms; mp 98—100 °C (from benzene); IR 3470, 3360 (NH), 3200 (OH), and 1610 cm^{-1} (C=O); ^1H NMR δ=2.06 (3H, s, Me-6′), 3.72 (3H, s, MeO-2′), 3.86 (3H, s, MeO-3′), 5.20 (3H, brm, H_2N-4′, HO-2), 6.72 (1H, s, H-5′), and 7.05—7.7 (4H, m, ArH).

Anal. ($C_{16}H_{17}NO_4$) C, H, N.

5-(4-Amino-3-chlorophenyl)tropolone (16i): Yellow prisms; mp 136—138 °C (from benzene–methanol); UV λ_{max} 238 (log ε 4.49), 256 (4.42), and 376 nm (4.32); IR 3450, 3350 (NH), 3200 (OH), and 1620 cm^{-1} (C=O); ^1H NMR δ=5.60 (3H, brm, H_2N-4′, HO-2), 6.76 (1H, brd, $J_{5',6'}$=8.5 Hz, H-5′), and 7.0—7.6 (6H, m, ArH).

Anal. ($C_{13}H_{10}NO_2Cl$) C, H, N.

5-(4-Amino-2-chlorophenyl)tropolone (16j): Yellow prisms; mp 161—163 °C (from benzene–methanol); UV λ_{max} 240sh (log ε 4.58), 256 (4.61), 355 (4.30), 358 (4.30), and 390sh nm (4.23); IR 3460, 3370 (NH), 3240 (OH), and 1605 cm^{-1} (C=O); ^1H NMR (DMSO-d_6) δ=5.10 (3H, brm, H_2N-4′, HO-2), 6.60 (2H, m, H-3′,5′), and 7.1—7.2 (5H, m, ArH).

Anal. ($C_{13}H_{10}NO_2Cl$) C, H, N.

5-(4-Amino-3-nitrophenyl)tropolone (16k): Yellow prisms; mp 272—275 °C (from chloroform–ethyl acetate); UV λ_{max} 241sh (log ε 4.49), 256 (4.52), 367 (4.41), and 390sh nm (4.36); IR 3480 (NH), 3180 (OH), and 1620 cm^{-1} (C=O); ^1H NMR (DMSO-d_6) δ=5.10 (3H, brm, H_2N-4′, HO-2) and 7.1—7.8 (7H, m, ArH).

Anal. ($C_{13}H_{10}N_2O_4$) C, H, N.

5-(4-Amino-2-nitrophenyl)tropolone (16l): Yellow prisms; mp 250—253 °C (from chloroform–ethyl acetate); UV λ_{max} 352 (log ε 4.58), 356 (4.31), 360 (4.32), and 394sh nm (4.25); IR 3480, 3380 (NH), 3180 (OH), and 1620 cm^{-1} (C=O); ^1H NMR (DMSO-d_6) δ=5.05 (3H, brm, H_2N-4′, HO-2) and 7.0—7.9 (7H, m, ArH).

Anal. ($C_{13}H_{10}N_2O_4$) C, H, N.

Acetylation of 5-(4-Aminoaryl)tropolones 16 to 5-(4-Acetamidoaryl)tropolone Acetates 17. A mixture of **16** (50 mg), pyridine (2.5 cm^3), and acetic anhydride (0.16 cm^3) was stirred overnight at 20 °C under argon. The volatile material was evaporated in vacuo and the residue was purified in a column of silica gel to give **17**. The complete characterization of **17n—t** was made as the corresponding tropolones **18n—t** after hydrolysis (see later).

5-(4-Acetamidophenyl)tropolone Acetate (17a): Yellow prisms; mp 215 °C (from benzene); UV λ_{max} 247 (log ε 4.07) and 354 nm (4.02); IR 3320—3200 (NH), 1755, 1695 (amide), and 1590 cm^{-1} (C=O); ^1H NMR (DMSO-d_6) δ=2.10 (3H, s, AcN-4′), 2.30 (3H, s, AcO-2), 7.1—8.0 (8H, m, ArH), and 10.0 (1H, brm, NH); MS *m/z* 297 (M^+; 24.0), 254 (100), 226 (13), 212 (11), and 184 (65).

Anal. ($C_{17}H_{15}NO_4$) C, H, N.

5-(4-Acetamidophenyl)-4-isopropyltropolone Acetate (17n): Yellow oil; ^1H NMR δ=1.01 (6H, d, J=7 Hz, Me_2C-4), 2.09 (3H, s, AcN-4′), 2.40 (3H, s, AcO-2), 2.75 (1H, sept, HC-4), 7.1—7.8 (7H, m, ArH), and 10.1 (1H, brs, NH).

5-(4-Acetamidophenyl)-4-isopropenyltropolone Acetate (17o): Yellow oil; ^1H NMR δ=1.56 (3H, brs, MeC-4), 2.18 (3H, s, AcN-4′), 2.36 (3H, s, AcO-2), 5.06 (2H, brs, H_2C=C-4), 7.1—7.8 (7H, m, ArH), and 8.43 (1H, brm, NH).

5-(4-Acetamido-3-methylphenyl)-4-isopropenyltropolone Acetate (17p): Yellow syrup; ^1H NMR δ=1.58 (3H, brs, MeC-4), 2.20 (3H, s, AcN-4′), 2.28 (3H, brs, Me-3′), 2.35 (3H, s, AcO-2), 5.05 (2H, brs, H_2C=C-4), and 7.1—8.0 (7H, m, ArH, NH).

5-(4-Acetamido-2-methylphenyl)-4-isopropenyltropolone Acetate (17q): Yellow syrup; ^1H NMR δ=1.59 (3H, brs, MeC-4), 2.16 (6H, brs, AcN-4′, Me-2′), 2.36 (3H, s, AcO-2), 4.92 (2H, brs, H_2C=C-4), and 7.05—7.85 (7H, m, ArH, NH).

5-(4-Acetamido-3-methoxyphenyl-4-isopropenyltropolone Acetate (17r): Yellow oil; ^1H NMR δ=1.59 (3H, brs, MeC-4), 2.23 (3H, s, AcN-4′), 2.37 (3H, s, AcO-2), 3.88 (3H, s, MeO-3′), 5.07 (2H, brs, H_2C=C-4), 6.2—7.57 (6H, m, ArH), and 7.82 (1H, m, NH).

5-(4-Acetamido-2-methoxyphenyl)-4-isopropenyltropolone Acetate (17s): Yellow oil; ^1H NMR δ=1.65 (3H, brs, MeC-4), 2.18 (3H, s, AcN-4′), 2.37 (3H, s, AcO-2), 3.78 (3H, s, MeO-2′), 4.90 (2H, brs, H_2C=C-4), and 6.95—8.1 (7H, m, ArH, NH).

5-(4-Acetamido-2,3-dimethoxyphenyl)-4-isopropenyltropolone Acetate (17t): Yellow oil; ^1H NMR δ=1.70 (3H, brs, MeC-4), 2.22 (3H, s, AcN-4′), 2.37 (3H, s, AcO-2), 3.73 (3H, s, MeO-2′), 3.89 (3H, s, MeO-3′), 4.92 (2H, brs, H_2C=C-4), 6.92 (1H, d, $J_{5',6'}$=8.5 Hz, H-6′), 7.12 (1H, d, $J_{6,7}$=11.0 Hz, H-7), 7.18 (1H, s, H-3), 7.39 (1H, d, H-6), 7.9 (1H, brm, NH), and 8.18 (1H, brd, H-5′).

5- and 7-(4-Acetamido-2,3-dimethoxy-6-methylphenyl)-4-isopropenyltropolone Acetates (17u,u′): A mixture (3:2 by ^1H NMR) of **17u** and **17u′** (respectively) was obtained as a yellow oil, which was rechromatographed in a prepacked silica-gel column (Merck Lobar, Size A) with 1:3 AcOEt–hexane to give only small proportions of pure **17u** and **17u′** (besides mostly overlapping fractions).

17u: Colorless prisms; mp 161.5—163 °C (from AcOEt–hexane); ^{1}H NMR (500 MHz), see Table 2; MS *m/z* 412 (M+1; 10.8) 411 (M^+; 40.7), 370 (26), 369 (100), 354 (22), 338 (15), 327 (13), 326 (16), 312 (44), 296 (44), 284 (15), 268 (21), 253 (16), and 252 (15).

Found: *m/z* 411.1666. Calcd for $C_{23}H_{25}NO_6$: M, 411.1682.

17u′: A pale yellow syrup; ^{1}H NMR (500 MHz), see Table 2; MS *m/z* 411 (M^+; 10.3), 381 (11), 380 (40), 369 (14), 354 (15), 340 (28), 339 (27), 338 (100), and 281 (10).

Found: *m/z* 411.1640. Calcd for $C_{23}H_{25}NO_6$: M, 411.1682.

Hydrolysis of 5-(4-Acetamidoaryl)tropolone Acetates 17 to 5-(4-Acetamidoaryl)tropolones 18. Compound **17** (50 mg) was treated with 1:1 1 M KOH–ethanol (4 cm^3) at 20 °C overnight. The solvent was evaporated in vacuo. The residue was diluted with cold water, taken to pH 4 with dil HCl, and extracted with CH_2Cl_2. The combined organic layers were dried (Na_2SO_4) and evaporated in vacuo. The residue was chromatographed in a column of silica gel to provide **18**.

5-(4-Acetamidophenyl)-4-isopropyltropolone (18n): Yellow needles; mp 250 °C decomp (from AcOEt); IR 3300 (OH, NH), 1675 (amide), and 1600 cm^{-1} (C=O); ^{1}H NMR δ=1.09 (6H, d, J=7 Hz, Me_2C-4), 2.09 (2H, s, AcN-4), 2.85 (1H, sept, HC-4), 7.1—7.8 (8H, m, ArH, OH), and 10.1 (1H, brs, NH); MS *m/z* 297 (M^+; 70.2), 282 (100), 254 (61), and 240 (15).

Found: *m/z* 297.1342. Calcd for $C_{18}H_{19}NO_3$: M, 297.1365.

5-(4-Acetamidophenyl)-4-isopropenyltropolone (18o): A pale yellow crystalline powder: mp 119—121 °C (from AcOEt–hexane); ^{1}H NMR δ=1.62 (3H, brd, J=1.5 Hz, MeC-4), 2.22 (3H, s, AcN-4′), 5.03, 5.06 (1H each, both brs, H_2C=C-4), 5.5 (1H, brm, HO-2), 7.25 (1H, d, $J_{6,7}$=11.5 Hz H-7), 7.26 (2H, brd, $J_{2',3'}=J_{5',6'}$=8 Hz, H-2′,6′), 7.39 (1H, d, H-6), 7.44 (1H, s, H-3), 7.49 (2H, brd, H-3′,5′), and 7.8 (1H, brm, NH); MS *m/z* 295 (M^+; 81.2), 280 (100), 252 (41), 238 (18), 210 (73), and 195 (31).

Found: *m/z* 295.1205. Calcd for $C_{18}H_{17}NO_3$: M, 295.1208.

5-(4-Acetamido-3-methylphenyl)-4-isopropenyltropolone (18p): Yellow prisms; mp 172—174 °C (from AcOEt–benzene, cf. Ref. 2b, mp 85 °C decomp[30]); ^{1}H NMR (500 MHz) δ=1.60 (3H, s, MeC-4), 2.23 (3H, brs, AcN-4′), 2.27 (3H, brs, Me-3′), 5.01, 5.05 (1H each, both brs, H_2C=C-4), 7.03 (1H, brm, NH), 7.13 (1H, brd, $J_{2',6'}$=1.7 Hz, H-2′), 7.15 (1H, brdd, $J_{5',6'}$=8.3 Hz, H-6′), 7.26 (1H, d, $J_{6,7}$=11.6 Hz, H-7), 7.38 (1H, d, H-6), 7.42 (1H, s, H-3), and 7.87 (1H, brd, H-5′); MS *m/z* 309 (M^+; 97.8), 294 (100), 266 (26), 252 (31), 238 (20), 224 (66), and 209 (46).

Found: *m/z* 309.1353. Calcd for $C_{19}H_{19}NO_3$: M, 309.1365.

5-(4-Acetamido-2-methylphenyl)-4-isopropenyltropolone (18q): Yellow prisms; mp 177—179 °C (from AcOEt–benzene); ^{1}H NMR (500 MHz) δ=1.63 (3H, brs, MeC-4), 2.12 (3H, brs, Me-2′), 2.19 (3H, brs, AcN-4′), 4.90 [1H, brs, (*E*)-HC=C-4], 4.94 [1H, brquint, J=1.3 Hz, (*Z*)-HC=C-4], 7.03 (1H, brd, $J_{5',6'}$=8.3 Hz, H-6′), 7.20 (1H, brm, NH), 7.23 (1H, d, $J_{6,7}$=11.7 Hz, H-7), 7.25 (1H, d, H-6), 7.31 (1H, brdd, $J_{3',5'}$=1.9 Hz, H-5′), 7.39 (1H, s, H-3), and 7.42 (1H, brd, H-3′); MS *m/z* 309 (M^+; 36.6), 294 (40), 266 (21), 250 (21), 224 (64), 222 (100), and 209 (40).

Found: *m/z* 309.1336. Calcd for $C_{19}H_{19}NO_3$: M, 309.1365.

5-(4-Acetamido-3-methoxyphenyl)-4-isopropenyltropolone (18r): Pale yellow needles; mp 169—171 °C (from AcOEt–hexane); ^{1}H NMR (500 MHz), see Table 2; MS *m/z* 325 (M^+; 100), 310 (20), 282 (82), 268 (94), 254 (52), 240 (66), 223 (28), 209 (24), 197 (15), and 195 (16).

Found: *m/z* 325.1296. Calcd for $C_{19}H_{19}NO_4$: M, 325.1314.

5-(4-Acetamido-2-methoxyphenyl)-4-isopropenyltropolone (18s): Pale yellow needles; mp 108—110 °C (from light petroleum); ^{1}H NMR (200 MHz), see Table 2; MS *m/z* 325 (M^+; 100), 310 (12), 282 (76), 268 (91), 254 (42), and 240 (53).

Found: *m/z* 325.1332. Calcd for $C_{19}H_{19}NO_4$: M, 325.1314.

5-(4-Acetamido-2,3-dimethoxyphenyl)-4-isopropenyltropolone (18t): Pale amber fine prisms: mp 159—159.5 °C (from AcOEt–cyclohexane); ^{1}H NMR (200 MHz) δ=1.73 (3H, brs, MeC-4), 2.22 (3H, s, AcN-4′), 3.63 (3H, s, MeO-2′), 3.88 (3H, s, MeO-3′), 4.83, 4.92 (1H each, both brs, H_2C=C-4), 6.85 (1H, d, $J_{5',6'}$=8.3 Hz, H-6′), 7.22 (1H, d, $J_{6,7}$=11.5 Hz, H-7), 7.33 (1H, s, H-3), 7.34 (1H, d, H-6), 7.79 (1H, brs, NH), and 8.06 (1H, brd, H-5′); MS *m/z* 355 (M^+; 16), 324 (19), 312 (11), 298 (12), and 43 (100).

Found: *m/z* 355.1435. Calcd for $C_{20}H_{21}NO_5$: M, 355.1420.

5- and 7-(4-Acetamido-2,3-dimethoxy-6-methylphenyl)-4-isopropenyltropolones (18u,u′): Pale yellow needles (a 3:2 mixture of **18u** and **18u′**, respectively, which were not separable even repeating chromatography); mp[§] 75 °C (from AcOEt–hexane).

18u: ^{1}H NMR[§] (500 MHz) see Table 1; MS[§] *m/z* 369 (M^+; 51), 338 (85), 326 (100), and 312 (31).

Found: *m/z* 369.1555. Calcd for $C_{21}H_{23}NO_5$: M, 369.1576.

18u′: ^{1}H NMR[§] (500 MHz) see Table 2.

General Procedure for the Preparation of 4-Substituted 5-(4-methoxyaryl)tropolones 19. A mixture of 5-(4-acetamidoaryl)-tropolone **18** (50 mg), ethanol (6 cm^3), and 2 M HCl (3 cm^3) was refluxed under argon for 12—36 h. The solvent was evaporated in vacuo. The residue was diluted with water (1 cm^3), EtOH (0.5 cm^3), and 2 M HCl (0.16 cm^3) at 0 °C, to which was slowly added, at 0 °C, sodium nitrite (1.2 equiv mol) dissolved in water (0.4 cm^3). The mixture was stirred at 5 °C for 2 h, diluted with water (50 cm^3), and then refluxed for 2 h under argon. The solvent was evaporated in vacuo. The residue was diluted with cold water and extracted with CH_2Cl_2. The combined organic layers were dried (Na_2SO_4) and evaporated in vacuo. The residue was suspended in cold water (1.5 cm^3) and 1 M NaOH (0.5 cm^3), and dimethyl sulfate (0.036 cm^3) was added. The mixture was stirred under argon at 5 °C for 30 min and then 70 °C for 1 h. After cooling, it was extracted with AcOEt and then with CH_2Cl_2. The combined organic layers were dried (Na_2SO_4) and evaporated in vacuo. The residue was chromatographed in a column of silica gel with benzene to provide **19**.

4-Isopropyl-5-(4-methoxyphenyl)tropolone (19n): Colorless needles (42% yield from **18n**); mp 114—115 °C (from

§ For specimen consisting of a ca. 3:2 mixture of **u** and **u′** form, because their separation could not be achieved.

benzene–cyclohexane); ^{1}H NMR δ=1.19 (6H, d, J=7.0 Hz, Me_2C-4), 3.01 (1H, brsept, J=7.0 Hz, HC-4), 3.89 (3H, s, MeO-4′), 6.93 (2H, brd, J=8.5 Hz, H-3′,5′), 7.11 (2H, brd, J=8.5 Hz, H-2′,6′), 7.19 (1H, d, $J_{6,7}$=12.0 Hz, H-7), 7.38 (1H, d, H-6), 7.43 (1H, s, H-3), and 7.45 (1H, brm, OH); MS m/z 270 (M^+; 100), 242 (36), 227 (43), 212 (11), and 196 (11).

Found: m/z 270.1224. Calcd for $C_{17}H_{18}O_3$: M, 270.1256.

4-Isopropyl-5-(4-methoxyphenyl)tropolone Difluoroborane Complex (19n′). Treatment of **19n** with an equivalent amount of boron trifluoride etherate in benzene–ether at 5 °C for 1 h, followed by purification using column chromatograhy on silica gel gave **19n′**: Colorless fine prisms (90% yield); mp 214—215 °C (from benzene–cyclohexane); ^{1}H NMR δ=1.20 (6H, d, J=7.0 Hz, Me_2C-4), 3.20 (1H, sept, J=7 Hz, HC-4), 3.88 (3H, s, MeO-4′), 7.01 (2H, brd, $J_{2',3'}=J_{5',6'}$=8.5 Hz, H-3′,5′), 7.18 (2H, brd, H-2′,6′), 7.62 (1H, d, $J_{6,7}$=11 Hz, H-6), 7.90 (1H, s, H-3), and 7.99 (1H, d, H-7); MS m/z 318 (M^+; 100), 290 (12), 275 (45), and 260 (11).

Found: m/z 318.1215. Calcd for $C_{17}H_{17}O_3BF_2$: M, 318.1239.

4-Isopropenyl-5-(4-methoxy-3-methylphenyl)tropolone (19p): Yellow needles (51% yield from **18p**); mp 146—147 °C (from ether–light petroleum); ^{1}H NMR δ=1.60 (3H, s, MeC-4), 2.22 (3H, s, Me-3′), 2.6 (1H, brm, OH), 3.86 (3H, s, MeO-4′), 5.04 (2H, brs, H_2C=C-4), 6.78 (1H, brd, $J_{5',6'}$=8.5 Hz, H-5′), 7.04 (1H, brs, H-2′), 7.06 (1H, brd, H-6′), 7.23 (1H, d, $J_{6,7}$=12.0 Hz, H-7), 7.40 (1H, d, H-6), and 7.42 (1H, s, H-3); MS m/z 282 (M^+; 100), 267 (80), 239 (71), 224 (51), 208 (22), and 181 (20).

Found: m/z 282.1198. Calcd for $C_{18}H_{18}O_3$: M, 282.1256.

4-Isopropenyl-5-(4-methoxy-2-methylphenyl)tropolone (19q): Pale yellow needles (40% yield from **18q**); mp 131—132 °C (from light petroleum); ^{1}H NMR δ=1.64 (3H, brs, MeC-4), 2.12 (3H, s, Me-2′), 3.85 (3H, s, MeO-4′), 4.93 (2H, m, H_2C=C-4), 6.71 (1H, brd, $J_{5',6'}$=8.5 Hz, H-5′), 6.77 (1H, brs, H-3′), 6.98 (1H, brd, H-6′), 7.20 (1H, d, $J_{6,7}$=12.0 Hz, H-7), 7.30 (1H, d, H-6), and 7.40 (1H, s, H-3); MS m/z 282 (M^+; 100), 267 (79), 239 (53), 224 (25), and 208 (9).

Found: m/z 282.1250. Calcd for $C_{18}H_{18}O_3$: M, 282.1256.

4-Isopropenyl-5- and 7-(2,3,4-trimethoxy-6-methylphenyl)-tropolone (19u,u′): A mixture (3:2) of **19u** and **19u′** (respectively) was obtained as a yellow syrup (49% yield from **18u,u′**), which was chromatographically inseparable.

19u: ^{1}H NMR[§] (500 M Hz) δ=1.25 (brs, HO-2), 1.74 (3H, brs, MeC-4), 2.00 (3H, brs, Me-6′), 3.69 (3H, s, MeO-2′), 3.87, 3.878 (3H each, 2s, MeO-3′,4′), 4.88 (2H, brs, H_2C=C-4), 6.50 (1H, brs, H-5′), 7.22 (1H, d, $J_{6,7}$=11.7 Hz, H-7), 7.27 (1H, d, H-6), and 7.38 (1H, s, H-3); MS[§] m/z 342 (M^+; 88), 327 (27), 312 (100), 311 (73), 292 (72), 281 (99), 268 (64), 253 (82), and 238 (81).

Found:[§] m/z 342.1428. Calcd for $C_{20}H_{22}O_5$: M, 342.1463.

19u′: ^{1}H NMR[§] (500 MHz) δ=1.25 (brs, HO-2), 2.04 (3H, brs, Me-6′), 2.20 (3H, brs, MeC-4), 3.69 (3H, s, MeO-2′), 3.88, 3.89 (3H each, 2s, MeO-3′,4′), 5.32, 5.45 (2H, 2brs, H_2C=C-4), 6.62 (1H, s, H-5′), 7.12 (1H, dd, $J_{5,6}$=10.7, $J_{3,5}$=1.7 Hz, H-5), 7.31 (1H, d, H-6), and 7.57 (1H, d, H-3).

2-Acetamido-8-hydroxy-10,10-dimethylcyclohept[*a*]inden-7(10*H*)-one (27o) and Its Acetate (28o). To a solution of **18o** (10 mg) in $CHCl_3$ (1 cm^3) was successively added concd sulfuric acid (0.5 cm^3) and sodium azide (3 mg) at 5 °C. The mixture was heated under argon at 70 °C for 2 h. The solvent was evaporated in vacuo. The residue was diluted with cold water, taken to pH 3 with $NaHCO_3$, and extracted with CH_2Cl_2. The combined organic layers were dried (Na_2SO_4) and evaporated in vacuo to give **27o** as a pale amber crystalline powder (6 mg, 60%): mp 295—300 °C decomp (from EtOH–AcOEt–benzene); ^{1}H NMR δ=1.50 (6H, s, Me_2C-10), 2.20 (3H, s, AcN-2), 7.36 (1H, brd, $J_{3,4}$=8.5 Hz, H-4), 7.42 (1H, d, $J_{5,6}$=11.5 Hz, H-6), 7.51 (1H, s, H-9), 7.62 (1H, brd, H-3), 7.63 (1H, d, H-5), and 7.72 (1H, brs, H-1); MS m/z 295 (M^+; 100), 280 (6), 267 (8), 253 (17), 225 (26), 210 (22), and 182 (8).

Found: m/z 295.1174. Calcd for $C_{18}H_{17}NO_3$: M, 295.1208.

The above reaction was effected in the absence of sodium azide at 20 °C within 5 h.

27o (6.0 mg) was dissolved in pyridine (1 cm^3) and acetic anhydride (0.5 cm^3), and the mixture was stirred overnight at 20 °C under argon. The volatile material was evaporated in vacuo and the residue was purified in a column of silica gel with AcOEt–hexane as an eluant, giving **28o** as amber prisms (5.1 mg, 74% yield): ^{1}H NMR (500 MHz) δ=1.47 (6H, brs, Me_2C-10), 2.22 (3H, s, AcN-2), 2.38 (3H, s, AcO-8), 7.32 (1H, d, $J_{5,6}$=10.6 Hz, H-6), 7.38 (1H, brs, H-9), 7.38 (1H, brd, $J_{3,4}$=8.4 Hz, H-4), 7.43 (1H, brm, NH), 7.46 (1H, brd, H-5), 7.62 (1H, brd, H-3), and 7.78 (1H, brs, H-1); MS m/z 337 (M^+; 11), 296 (90), 295 (100), 280 (21), 267 (29), 253 (53), 238 (14), 225 (63), 224 (27), 210 (48), 181 (30), 180 (21), and 43 (22).

Found: m/z 337.1285. Calcd for $C_{20}H_{19}NO_4$: M, 337.1314.

2-Acetamido-8-hydroxy-1,10,10- (and 3,10,10)-trimethylcyclohept[*a*]inden-7(10*H*)-one (27p) and Their Acetates (28p,p′). The similar treatment of **18p** (10 mg) as those for **27o** and **28o** gave the products as isomeric mixtures with regard to the 1- and 3-methyl group.

27p: A yellow powder (5 mg, 50% yield); ^{1}H NMR δ=1.49, 1.60* (6H, s, Me_2C-10), 2.21 (3H, brs, AcN-2), 2.35, 2.40* (3H, brs, Me-1,3), 6.9—8.2 (ca. 7H, m, ArH, NH, OH);* signals presumably due to the minor 1-methyl isomer (ca. 30%) in the chromatographically inseparable mixture; MS m/z 309 (M^+; 100), 294 (10), 268 (15), 267 (18), 239 (13), and 225 (10).

28p (3,10,10-trimethyl isomer): Yellow fine prisms (40% yield from **27p**) after separation from the minor product **28p′** (see below) by silica-gel column chromatography with 1:1 AcOET–hexane; mp 233—235 °C (from AcOEt); ^{1}H NMR δ=1.47 (6H, s, Me_2C-10), 2.22 (3H, brs, AcN-2), 2.35 (3H, brs, Me-3), 2.37 (3H, s, AcO-8), 7.30 (1H, d, $J_{5,6}$=11.0 Hz, H-6), 7.35 (1H, brs, H-9), 7.36 (1H, brs, H-4), 7.43 (1H, brd, H-5), 7.50 (1H, brs, H-1), and 8.05 (1H, brm, NH); MS m/z 351 (M^+; 5.2), 309 (100), 297 (10), 294 (9), 268 (13), 267 (15), 265 (11), 239 (17), 225 (16), 209 (10), and 43 (60).

Found: m/z 351.1452. Calcd for $C_{21}H_{21}NO_4$: M, 351.1471.

28p′ (1,10,10-trimethyl isomer): A yellow solid (25% yield from **27p** after the chromatographic purification); ^{1}H NMR δ=1.59 (6H, s, Me_2C-10), 2.21 (3H, brs, AcN-2), 2.38 (3H, s, AcO-8), 2.42 (3H, brs, Me-1), 7.32 (1H, d, $J_{5,6}$=11 Hz, H-6), 7.39 (1H, brs, H-9), 7.47 (1H, brd, $J_{3,4}$=8.5 Hz, H-4), 7.55 (1H, brd, H-5), 7.62 (1H, brd, H-3), and 7.95 (1H, brm, NH); MS m/z 351 (M^+; 3.3), 309 (100), 297 (18), 267 (18), 239 (15), 225 (11), 209 (10), and 43 (45).

Found: m/z 351.1445. Calcd for $C_{21}H_{21}NO_4$: M, 351.1471.

We are very indebted to Dr. Yukio Sugimura (Sankyo Co., Ltd., Tokyo) for his generously entrusting the early part of this study to us and also to Dr. Ko Hojo and Miss Masami Tsutsumi (Tokyo Kasei Kogyo Co., Ltd.) for kindly preparing the new phenylhydrazines **13g** and **13h** and supplying to us. Thanks are also due to Professor Hitoshi Takeshita (Kyushu Univ.) for the measurement of the ^{13}C NMR spectrum, Mr. Shin-ichi Takekuma (Kinki Univ.) for 200 MHz ^{1}H NMR and MS, and Dr. Hiromichi Matsuura (Wakunaga Pharmaceutical Co., Ltd.) for the high-resolution mass spectra. The present work was partially supported by Grant-in-Aids for Scientific Research Nos. 60540331 (to H. Y.), 60540336, and 61540381 (to K. I.) from the Ministry of Education, Science and Culture.

References

1) Part I: T. Nozoe, K. Imafuku, B.-Z. Yin, M. Honda, Y. Goto, Y. Hara, T. Ando, and H. Yamamoto, *Bull. Chem. Soc. Jpn.*, **61**, 2531 (1988).

2) A part of the results has been preliminarily presented: a) H. Saito, M. Yasunami, M. Ando, K. Takase, and T. Nozoe, 37th Nationl Meeting of the Chemical Society of Japan, Tokyo, April 1978, Abstr. No. 2D32; H. Saito, M.Sc. Thesis, Tohoku Univ. (1978); b) T. Nozoe, K. Takase, H. Saito, H. Yamamoto, and K. Imafuku, *Chem. Lett.*, **1986**, 1577.

3) See a) B. Bhattacharyya and J. Wolff, *J. Biol. Chem.*, **259**, 11836 (1984) and references cited therein. b) M. H. Zwig and C. F. Chignell, *Biochem. Pharmacol.*, **22**, 2141 (1973).

4) a) For an extensive review, see H.-G. Capraso and A. Brossi, "The Alkaloids," ed by A. Brossi, Academic Press, Orlando, Fla. (1984), Vol. 23, pp. 1—70. b) D. A. Evans, S. P. Tanis, and D. J. Hart, *J. Am. Chem. Soc.*, **103**, 5813 (1981) and references therein. c) C.-P. Mak and G. Büchi, *J. Org. Chem.*, **46**, 1 (1981).

5) See e.g., a) T. J. Fritzgerald, *Biochem. Pharmacol.*, **25**, 1383 (1976); b) M. Rossi, J. Link, and C. Lee, *Arch. Biochem. Biophys.*, **231**, 470 (1984).

6) a) T. Nozoe, K. Takase, Y. Kitahara, and K. Doi, 132nd National Meeting of the American Chemical Society, New York, Sept. 1957; b) T. Nozoe, *Experientia, Suppl. VII*, **1957**, 306; c) K. Suzuki, M.Sc. Thesis, Tohoku Univ. (1959); d) N. Kawabe, M.Sc. Thesis, Tohoku Univ. (1963); e) T. Nozoe, K. Takase, N. Kawabe, T. Asao, and H. Yamamoto, *Bull. Chem. Soc. Jpn.*, **56**, 3099 (1983); f) H. Yamamoto, A. Hara, S. Inokawa, and T. Nozoe, *ibid.*, **56**, 3106 (1983).

7) a) T. Nozoe, K. Takase, H. Matsumura, T. Asao, K. Kikuchi, and S. Itô, "Dai Yuki Kagaku (Comprehensive Organic Chemistry)," ed by M. Kotake, Asakura, Tokyo (1960), Vol. 13, pp. 1—692. b) F. Pietra, *Chem. Rev.*, **73**, 293 (1973). c) D. Lloyd, "Non-benzenoid Conjugated Carbocyclic Compounds," Elsevier, Amsterdam (1984), pp. 107—125.

8) The (2-acetyltropone)tricarbonyliron complexes were prepared by the Friedel-Crafts acylation of (tropone)-tricarbonyliron: M. Frank-Neumann, F. Brion, and D. Martina, *Tetrahedron Lett.*, **1978**, 5033.

9) T. Nozoe, T. Mukai, and J. Minegishi, *Proc. Jpn. Acad.*, **27**, 419 (1951); W. von E. Doering and C. F. Hisky, *J. Am. Chem. Soc.*, **74**, 5688 (1952); P. Akroyd, R. D. Haworth, and P. R. Jefferies, *J. Chem. Soc.*, **1954**, 266; R. D. Haworth and P. B. Tinker, *ibid.*, **1955**, 911; K. Kikuchi, *Nippon Kagaku Zasshi*, **77**, 1439 (1956); T. Nozoe, T. Mukai, and T. Asao, *Bull. Chem. Soc. Jpn.*, **33**, 1452 (1960); T. Nozoe, T. Mukai, and T. Tezuka, *ibid.*, **34**, 619 (1961).

10) W. von E. Doering and L. H. Knox, *J. Am. Chem. Soc.*, **75**, 297 (1953).

11) T. Ikemi, T. Nozoe, and H. Sugiyama, *Chem. Ind.*, **1960**, 932.

12) T. Nozoe and K. Takahashi, *Bull. Chem. Soc. Jpn.*, **38**, 665 (1965), *ibid.*, **40**, 1473 (1967); K. Takahashi, *ibid.*, **40**, 1462 (1967).

13) a) An indirect C–C bond formation has been reported for the synthesis of 3-, 4-, and 5-(substituted vinyl)tropolones from the corresponding halotropolones by means of palladium-catalyzed vinylic substitution; H. Horino, N. Inoue, and T. Asao, *Tetrahedron Lett.*, **22**, 741 (1981). b) A 4-aryl-2-methoxy-5-methyl-6-propyltropolone was prepared from a bicyclo[3.2.1]octane derivative by a five step sequence: see Ref. 4c.

14) Y. Sugimura, private communication to T. N.

15) These results including the approximate kinetics and the mechanistic problems of the rearrangement will be reported elsewhere: K. Imafuku, B.-Z. Yin, and T. Nozoe, to be published; H. Yamamoto, Y. Hidaka, T. Hanaya, and T. Nozoe, to be published.

16) The acetylation provided these tropolone acetates as single products. Although structures of **17** and **28** are conveniently represented by one of the two possible 2-acetoxytropone forms, the well-known temperature-dependent acetotropy is expected to proceed rapidly for these compounds in $CDCl_3$ at 27 °C; for the degenerate rearrangement of some tropolone acetates, see S. Masamune, A. V. Kemp-Jones, J. Green, D. L. Rabenstein, M. Yasunami, K. Takase, and T. Nozoe, *J. Chem. Soc., Chem. Commun.*, **1973**, 283.

17) H. Yamamoto, A. Hara, A. Noguchi, H. Kawamoto, S. Inokawa, and T. Nozoe, *Bull. Chem. Soc. Jpn.*, **55**, 1594 (1982) and references cited therein.

18) K. Doi, *Bull. Chem. Soc. Jpn.*, **34**, 501 (1961).

19) T. Nozoe, S. Seto, H. Takeda, S. Morosawa, and K. Matsumoto, *Proc. Jpn. Acad.*, **27**, 556 (1951).

20) J. H. Boyer, R. F. Reinisch, M. J. Danzig, G. A. Stoner, and F. Sahhar, *J. Am. Chem. Soc.*, **77**, 5688 (1955).

21) O. L. Brady, J. N. E. Day, and C. V. Reynolds, *J. Chem. Soc.*, **1929**, 2266.

22) K. Takase, M. Yasunami, and T. Nozoe, unpublished result.

23) For reviews of benzidine rearrangement, see M. J. S. Dewar, "Molecular Rearrangements," ed by P. de Mayo, Interscience, New York (1963), pp. 323—344; H. J. Shine, "Mechanism of Molecular Migration," ed by B. S. Thyagarajan, Interscience, New York (1969), Vol. 2, pp. 192—247.

24) These hitherto unreported compounds were kindly prepared by K. Hojo and M. Tsutsumi, Research Laboratory, Tokyo Kasei Kogyo Co., Ltd., Saitama and provided for us. The experimental procedures are described in this paper by the courtesy of Drs. K. Hojo and I. Takasu, Directors of the Research Laboratory.

25) F. Mauthner, *J. Prakt. Chem.*, **149**, 828 (1937).

26) W. K. Anslow, J. W. Ashley, and H. Raistrick, *J. Chem. Soc.*, **1938**, 439.
27) N. Soma, J. Nakazawa, T. Watanabe, Y. Sato, and G. Sunagawa, *Chem. Pharm. Bull.*, **13**, 457 (1965).
28) K. Imafuku, K. Kamachi, Y. Matsuda, and H. Matsumura, *Bull. Chem. Soc. Jpn.*, **52**, 2447 (1979).
29) T. Nozoe, J.-K. Sin, K. Yamane, and K. Fujimori, *Bull. Chem. Soc. Jpn.*, **48**, 314 (1975).
30) Although this value was reported, further purification of the specimen has raised the melting point to that described in this paper.

 © 1989 The Chemical Society of Japan Bull. Chem. Soc. Jpn., 62, 143—147 (1989)

Triethylborane-Induced Hydrodehalogenation of Organic Halides by Tin Hydrides

Katsukiyo MIURA, Yoshifumi ICHINOSE, Kyoko NOZAKI, Keigo FUGAMI, Koichiro OSHIMA,* and Kiitiro UTIMOTO
Department of Industrial Chemistry, Faculty of Engineering, Kyoto University, Yoshida, Kyoto 606
(Received July 7, 1988)

The reduction of organic halides with tributyltin hydride in the presence of a catalytic amount of triethylborane has been studied. (1) Alkyl iodides and alkyl bromides reacted easily with tin hydride at −78°C to give the corresponding hydrocarbons, while alkyl chlorides were sluggish to react and recovered unchanged. (2) The reduction of alkenyl halides such as 1-deuterio-1-iodo-1-dodecene and 1-iodo-1-triethylsilyl-1-dodecene proceeded nonstereospecifically. (3) The reduction of aryl halides with *n*-Bu_3SnH–Et_3B system was not so effective as the reduction of alkyl halides and alkenyl halides. Whereas aryl iodides were reduced at room temperature with *n*-Bu_3SnH, aryl bromides hardly reacted with *n*-Bu_3SnH even at 80 °C.

The free radical halogen abstraction from a C–Hal bond opens a broad variety of synthetic possibilities.[1,2] The simplest version is trapping of the outcoming radical by tin hydride, providing us with a facile route to replacement of halogen by hydrogen at the same carbon atom. The reactions are initiated by generation of tin radicals, which are produced mostly by radical initiators such as azobisisobutyronitrile (AIBN) or benzoyl peroxide. Recently we have found that Et_3B is an efficient radical initiator for generation of tin radicals from tin hydrides and applied this methodology to a couple of organic syntheses.[3] We would now like to report on a more detailed study on the reduction of organic halides with R_3SnH in the presence of Et_3B under mild reaction conditions.

Reduction of Alkyl Halides. A number of organic halides were reduced with *n*-Bu_3SnH–Et_3B system and the results are summarized in Table 1. Treatment of a solution of 1-bromododecane and tributyltin hydride in toluene with a catalytic amount of Et_3B (hexane solution, 10 mol%) gave dodecane quantitatively. It is worth noting that the reaction proceeded at low temperature such as −78 °C. Without Et_3B, 1-bromododecane was recovered quantitatively after treatment with *n*-Bu_3SnH in toluene at −78 °C for 3 h. Secondary bromoalkane and tertiary bromides were also easily reduced. The reactivity of the halides depends on the nature of the halogen. Iodides and bromides reacted easily with tin hydride in the presence of Et_3B, while chlorides were sluggish to react and were recovered practically unchanged. Heating a benzene solution of 1-chlorododecane with *n*-Bu_3SnH or Ph_3SnH in the presence of a catalytic amount of Et_3B at 70 °C for 5 h resulted in a recovery of the starting 1-chlorododecane quantitatively. Taking advantage of the difference in reactivity between bromide and chloride, it was possible to reduce one halogen in the presence of the other (Run 10).

Reduction of halides containing other functional groups such as ether, hydroxyl, or carbonyl proved that these functionalities could be present in the molecule without perturbing the course of reduction, although the nature of the functional group slightly influences the development of the reaction. For example, β-bromopropiophenone (Run 7) and ethylene acetal (Run 13) were reduced slowly at −78 °C. The reaction mixture was allowed to come to room temperature and then stirred for several hours to complete the reduction. 11-Bromo-1-undecanol could not be reduced at low temperature because of its low solubility in toluene and the reaction was perpformed at 0 °C.

Monodehalogenation of alkyl-substituted *gem*-dibromocyclopropanes with *n*-Bu_3SnH–Et_3B proceeded easily at −78 °C to provide stereoisomeric mixtures of monobromocyclopropanes. The isomeric ratios were almost the same as those obtained by reported ordinary procedure (without Et_3B).[4] The formation of *endo*- or *cis*-bromocyclopropanes as major products is explained as follows: (1) Tin radical attacks bromine to give a radical, (2) the intermediate radical equilibrates faster than hydrogen is transferred, (3) finally the less hindered approach of tin hydride provide endo or cis isomer selectively (Scheme 1). Reduction of monobromocyclopropanes to cyclopropanes did not proceed at −78 °C and it took prolonged reaction time (10 h) at

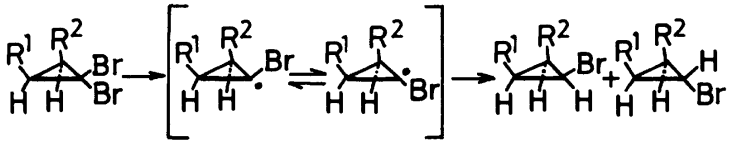

Scheme 1.

Table 1. Reduction of Alkyl Halides with n-Bu_3SnH–Et_3B

Run	Substrate	Reaction conditions Temp °C	Time h	Procedure	Yield of alkane %
1	1-Iodododecane	−78	0.5	A	95
2	2-Iodododecane	−78	0.5	A	90
3	1-Bromododecane	−78	0.5	A	100
4	2-Bromododecane	−78	0.5	A	98
5	1-Bromoadamantane	−78	0.5	A	75
6	$BrCH_2CH_2CH_2OTHP$	−78	0.5	B	77
7	$PhCOCH_2CH_2Br$	25	10	B	87
8	$HOCH_2(CH_2)_9CH_2Br$	0	0.5	B	94
9	$MeOOC(CH_2)_9CH_2Br$	−78	0.5	B	95
10	$Cl(CH_2)_3COO(CH_2)_3Br$	−78	0.5	B	87
11	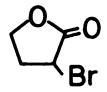	−78	0.5	B	90
12	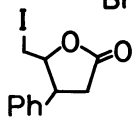	−78	0.5	B	87
13	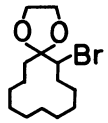	−78, 1; 20, 3		A	80
14	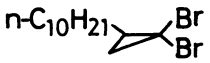	−78	1.0	A	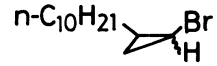 92(67/33)[a]
		20	15[b]	A	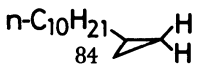 84
15		−78	1.0	A	Monobromide 80(82/18)[c]
16	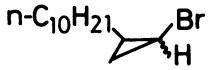	20	11	A	83
17	$CH_3(CH_2)_9CHBrCH_2Br$	−78	0.5	A	1-Dodecene 99
18	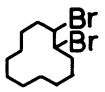	−78	0.5	A	Cyclododecene 96

a) Isomeric ratio (cis/trans). b) 2.2 mol of n-Bu_3SnH was employed. c) Isomeric ratio (endo/exo).

room temperature to complete the reaction. Treatment of dibromocyclopropanes with 2.2 mol of tin hydride at room temperature for 15 h afforded cyclopropanes directly in high yields.

β-Elimination has been achieved by treatment of *vic*-dibromoalkanes with n-Bu_3SnH–Et_3B system. *meso*-1,2-Dibromocyclododecane gave a mixture of *trans*- and *cis*-cyclododecene in an 1:1 ratio (Run 18).

Reduction of Alkenyl Halides. The reduction of alkenyl iodides and bromides was also examined in the presence of a catalytic amount of Et_3B. Whereas iodides reacted easily with tin hydrides at −78 °C, bromides reacted slowly compared with iodides and it took 10 h to complete the reduction at room temperature. The effectiveness of Et_3B catalyst was confirmed by the fact that treatment of a solution of (*E*)-1-bromo-1-dodecene with n-Bu_3SnH in the absence of Et_3B at room temperature for 15 h resulted in quantitative recovery of (*E*)-1-bromo-1-dodecene. The typical results are summarized in Table 2. Treatment of (*E*)-1-deuterio-1-iodo-1-dodecene or (*Z*)-isomer with n-Bu_3SnH–Et_3B at −78 ° resulted in a formation of similar isomeric mixtures of (*E*)- and (*Z*)-1-deuterio-1-dodecene (*E*:*Z*=61:39—63:37). Thus, the reduction proceeded nonstereospecifically. Same stereochemical results were obtained with n-Bu_3SnH–AIBN system. The reaction of (*E*)- or (*Z*)-1-deuterio-1-iodo-1-dodecene with n-Bu_3SnH in the presence of AIBN at 50 °C

provided similar isomeric mixtures of (*E*)- and (*Z*)-1-deuterio-1-dodecene (*E*:*Z*=60:40). The reduction of alkenyl halides having silyl group on the same carbon bearing iodine also followed non-stereospecific course (Runs 6 and 7). (*E*)-1-Iodo-1-triethylsilyl-1-dodecene (**1**) gave a mixture of (*Z*)-1-triethylsilyl-1-dodecene and (*E*)-isomer (*Z*:*E*=56:44) and (*Z*)-isomer **2** afforded a Z:*E*=57:43 mixture upon treatment with *n*-Bu_3SnH–Et_3B at −78 °C.[5] The results have been explained by fast equilibration of two configurations of the alkenyl radical before hydrogen transfer (Scheme 2).

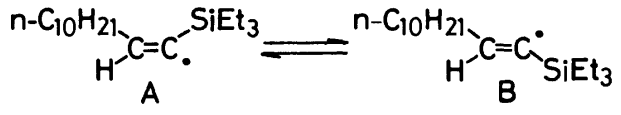

Scheme 2.

gem-Dibromoalkene provided monobromoalkene. For instance, reduction of 1,1-dibromo-1-dodecene gave an 1:1 mixture of 1-bromo-1-dodecene.

Reduction of Aryl Halides. The reduction of aryl iodides and bromides proceeded slowly with *n*-Bu_3SnH–Et_3B system.[6] 1-Iodonaphthalene reacted at room temperature, while 1-bromonaphthalene were inert. Aryl bromides were reduced at 80 °C, however, when more reactive Ph_3SnH was employed. The reaction was successively applied to the cyclization reaction. For instance, a mixture of five-membered ring and six-membered ring products was obtained upon treatment of aryl iodide **3** with *n*-Bu_3SnH–Et_3B (Scheme 3).

The Et_3B-induced reaction has following characteristics compared to ordinary reaction. (1) Tributyltin radical or triphenyltin radical can be generated at low

Table 2. Reduction of Alkenyl Halides with *n*-Bu_3SnH–Et_3B

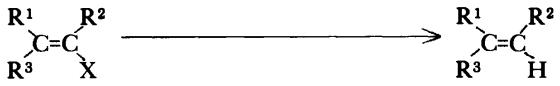

Run	Substrate	Reaction conditions Temp/°C	Time/h	Yield of alkene/%
1	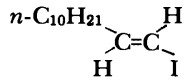	20	0.5	1-Dodecene 77
2	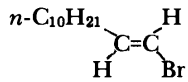	20	12	1-Dodecene 98
3	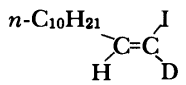	−78, 2;	20, 0.5	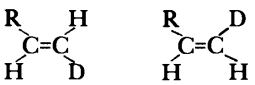 83 (63:37)
4	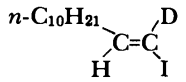	−78, 2;	20, 0.5	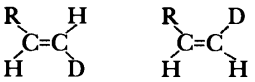 87 (61:39)
5	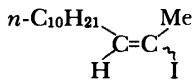	−78	0.5	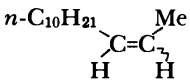 84
6	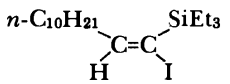 **1**	−78	0.5	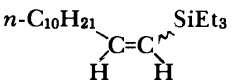 95 (*Z*/*E*=56/44)
7	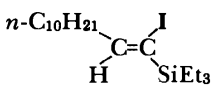 **2**	−78	0.5	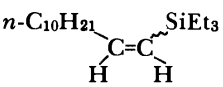 98 (*Z*/*E*=57/43)
8	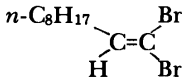	−78	0.5	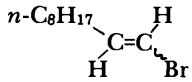 80 (*Z*/*E*=1:1)

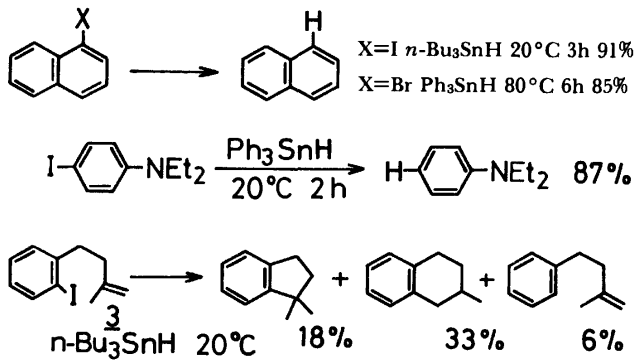

Scheme 3. Triethylborane-catalyzed reduction of aryl halides.

temperature such as −78 °C and thereby the reduction of organic halides (iodides and bromides) proceeds at lower temperature than that with *n*-Bu_3SnH–AIBN (or dialkyl peroxide) system. The mildness of the reaction will offer promising possibilities for selective reduction. (2) The reduction of organic halides with *n*-Bu_3SnH–Et_3B system takes place easily to give the corresponding hydrocarbons in comparable yields to previously reported procedure.

Triethylborane proved to be an effective radical initiator in the presence of trace amount of oxygen. Other role of Et_3B, however, is not clear. We are studying on this point from the intrinsic mechanistic interest.

Experimental

Distillation of the products was performed by use of Kugelrohr (Büchi), and boiling points are indicated by an air-bath temperature without correction. ^1H NMR and ^{13}C NMR spectra were taken on a Varian XL-200 spectrometer, $CDCl_3$ was used as solvent unless otherwise noted, chemical shifts being given in δ with tetramethylsilane as an internal standard. IR spectra were determined on a JASCO IR-810 spectrometer. The analyses were carried out by the staff at the Elemental Analyses Center of Kyoto University. Purification of products was performed by silica gel (Wakogel C-100) column chromatography.

Tributyltin Hydride and Triphenyltin Hydride. These compounds were prepared according to the reported procedure.[7]

Preparation of Alkyl Halides. Commercially available organic halides such as 1-bromododecane, 2-bromododecane, 1-iodododecane, 1-bromoadamantane, and α-bromo-γ-butyrolactone were used without further purification. Methyl 11-bromo undecanoate,[8] β-bromopropiophenone,[9] and 4,5-dihydro-5-iodomethyl-4-phenyl-2(3*H*)-furanone[10] were prepared according to the literature. *gem*-Dibromocyclopropanes were generated following the literature.[4] *vic*-Dibromides were prepared by treatment of 1-dodecene and *trans*-cyclododecene with bromine in ether.

3-Bromopropyl 4-Chlorobutyrate. A solution of 4-chlorobutyryl chloride (1.4 g, 10 mmol) in ether (10 ml) was added dropwise to a solution of 3-bromo-1-propanol (1.39 g, 10 mmol) and pyridine (1.6 g, 20 mmol) in ether (10 ml) at 0 °C under an argon atmosphere. The resulting mixture was stirred for 15 min at 0 °C, then for 2 h at room temperature. The mixture was diluted with ethyl acetate (20 ml) and poured into 1 M HCl (1 M=1 mol dm^{-3}) solution. Organic layer was separated and washed with 1 M HCl (2×20 ml) and brine (2×20 ml). Concentration of the dried (Na_2SO_4) organic layer gave a crude oil which was purified by silica-gel column chromatography followed by distillation to provide the title compound (1.8 g) in 74% yield. Bp 120 °C (bath temp, 2 Torr, 1 Torr=133.322 Pa); IR (neat) 2960, 1733, 1442, 1421, 1391, 1364, 1298, 1174, 1146, 1090, 1050, 1009, 785, 650 cm^{-1}; ^1H NMR ($CDCl_3$) δ=2.00—2.26 (m, 4H), 2.53 (t, J=7.3 Hz, 2H), 3.48 (t, J=6.5 Hz, 2H), 3.62 (t, J=6.3 Hz, 2H), 4.21 (t, J=6.1 Hz, 2H). Found: C, 34.68; H, 5.05%. Calcd for $C_7H_{12}O_2ClBr$: C, 34.52; H, 4.97%.

Preparation of Alkenyl Halides. (*E*)-1-Iodo-1-dodecene or (*E*)-1-bromo-1-dodecene were prepared by hydroalumination followed by treatment with iodine or bromine.[11]

(*E*)-1-Deuterio-1-iodo-1-dodecene. The compound was generated by hydroalumination of 1-deuterio-1-dodecyne followed by iodination. ^1H NMR ($CDCl_3$) δ=0.80—1.00 (m, 3H), 1.20—1.50 (m, 16H), 2.00—2.15 (m, 2H), 6.53 (tm, J=7.5 Hz, 1H).

(*Z*)-1-Deuterio-1-iodo-1-dodecene. Hydroalumination of 1-trimethylsilyl-1-dodecyne in hexane–ether (1:1) followed by the addition of D_2O gave (*Z*)-1-deuterio-1-trimethylsilyl-1-dodecene.[12] Iododesilylation[13] of alkenylsilane gave the title compound. ^1H NMR ($CDCl_3$) δ=0.75—0.95 (m, 3H), 1.10—1.50 (m, 16H), 2.00—2.20 (m, 2H), 6.18 (t, J=7.0 Hz, 1H).

2-Iodo-2-tridecene. The compound was prepared by iododesilylation according to the reported procedure.[13] A solution of iodine (0.25 g, 1.0 mmol) in dichloromethane (5.0 ml) was added to a solution of (*Z*)-2-trimethylsilyl-2-tridecene generated from 1-trimethylsilyl-1-dodecyne (0.25 g, 1.0 mmol)[14] in dichloromethane (5.0 ml) at 25 °C and the resulting mixture was stirred for 1 h. Work-up followed by purification by TLC (silica gel) gave 2-iodo-2-tridecene (0.20 g) in 65% yield as an isomeric mixture (*E*:*Z*=4:6). ^1H NMR ($CDCl_3$) δ=0.75—0.95 (m, 3H), 1.20—1.50 (m, 16H), 2.00 (m, 2H), 2.33 (s, 1.8H), 2.45 (s, 1.2H), 5.38 (tq, J=6.8, 1.5 Hz, 0.4H), 6.15 (tq, J=7.5, 1.7 Hz, 0.6H).

(*E*)-1-Iodo-1-triethylsilyl-1-dodecene and (*Z*)-1-Iodo-1-triethylsilyl-1-dodecene. These compounds were prepared from 1-triethylsilyl-1-dodecyne following the reported procedure.[12]

1,1-Dibromo-1-decene. The title compound was prepared from decanal, carbon tetrabromide, and triphenylphosphine.[15]

General Procedure for the Reduction of Alkyl Halides. (a) Procedure A: The hydrodehalogenation of 1-bromododecane is representative of procedure A. A dry 30-ml flask was equipped with septum inlet, a stirring bar, and three-way stop cock. One end of stop cock was connected to a balloon which was filled with argon. The inner atmosphere of the apparatus was replaced by argon. The flask was charged with a solution of 1-bromododecane (0.25 g, 1.0 mmol) in toluene (4.0 ml) and cooled to −78 °C with an Dry Ice–methanol bath. A solution of tributyltin hydride (0.33 g, 1.1 mmol) in toluene (4.0 ml) and a hexane solution of Et_3B (1.0 M, 0.1 ml, 0.1 mmol) was added successively. The solution was stirred

for 30 min at −78 °C. The disappearance of the starting material was confirmed by thin layer chromatographic assay. The resulting mixture was transferred into 100 ml round-bottomed flask using 25 ml of methanol. The solvent was evaporated as an azeotropic mixture to afford a crude oil which was submitted to silica-gel column chromatography (hexane as an eluant) to give dodecane (0.17 g) quantitatively. **(b) Procedure B:** The procedure was used for the reduction of the compounds which have polar functional groups such as hydroxyl or carbonyl in the molecule. The reduction of 11-bromo-1-undecanol to 1-undecanol is representative. A solution of tributyltin hydride (0.33 g, 1.0 mmol) in toluene (4.0 ml) was added to a solution of 11-bromo-1-undecanol (0.25 g, 1.0 mmol) in toluene (4.0 ml) at 0 °C. Et_3B (1.0 M hexane solution, 0.1 ml, 0.1 mmol) was added and the resulting mixture was stirred at 0 °C for 30 min. The reaction mixture was diluted with EtOAc (20 ml) and saturated aqueous potassium fluoride (2 ml) and anhydrous potassium fluoride (1.0 g) were added to remove tributyltin bromide.[16] The mixture was stirred for another 30 min and the precipitated tributyltin fluoride was removed by filtration and washed with ethyl acetate. Combined filtrates were washed with brine and dried over anhydrous sodium sulfate and concentrated in vacuo. The residual oil was purified by silica-gel column chromatography (hexane/ethyl acetate=5/1 as an eluant) to give 1-undecanol (0.16 g) in 94% yield.

General Procedure for the Reduction of Alkenyl Halides. The reactions were performed following the procedure A described for the reduction of alkyl halides. A solution of tributyltin hydride (0.33 g, 1.1 mmol) in toluene (4.0 ml) and Et_3B (1.0 M hexane solution, 0.1 ml, 0.1 mmol) were added successively to a solution of 1,1-dibromo-1-decene (0.30 g, 1.0 mmol) in toluene (4.0 ml) at −78 °C and the resulting mixture was stirred at −78 °C for 30 min. Concentration followed by purification by silica-gel column chromatography gave 1-bromo-1-decene (0.18 g) in 80% yield as an isomeric mixture (*E*/*Z*=1/1).

Reduction of Aryl Halide 3 with *n*-Bu_3SnH-Et_3B. A solution of *n*-Bu_3SnH (0.35 g, 1.2 mmol) in benzene (2.0 ml) was added dropwise over 2 h by syringe pump to a solution of aryl iodide **3** (0.24 g, 1.0 mmol) and Et_3B (1.0 M hexane solution, 0.1 ml, 0.1 mmol) in benzene (10 ml) at 20 °C. The resulting mixture was stirred more than 1 h after the completion of the addition. Work-up followed by purification by preparative TLC on silica gel gave a mixture of 1,1-dimethylindan (18%), 2-methyl-1,2,3,4-tetrahydronaphthalene (33%), and (3-methyl-3-butenyl)benzene (6%), whose spectra were identical with those of authentic samples.[17,18]

Financial support by the Ministry of Education, Science and Culture, Japanese Government (Grant-in-Aid for Scientific Research No. 63470074) is acknowledged.

References

1) M. Pereyre, J-P. Quintard, and A. Rahm, "Tin in Organic Synthesis," ed by B. M. Trost, Butterworths & Co. Ltd., (1987), Chap. 3, pp. 35—68; B. Giese, "Radicals in Organic Synthesis: Formation of Carbon Carbon Bonds," ed by J. E. Baldwin, Pergamon Press, Oxford (1986).

2) Reviews for the reduction with *n*-Bu_3SnH: W. P. Neumann, *Synthesis*, **1987**, 665; H. G. Kuivila, *ibid.*, **1970**, 499.

3) K. Nozaki, K. Oshima, and K. Utimoto, *J. Am. Chem. Soc.*, **109**, 2547 (1987); Y. Ichinose, K. Wakamatsu, K. Nozaki, J-L. Birbaum, K. Oshima, and K. Utimoto, *Chem. Lett.*, **1987**, 1647; Y. Ichinose, K. Nozaki, K. Wakamatsu, K. Oshima, and K. Utimoto, *Tetrahedron Lett.*, **28**, 3709 (1987); K. Nozaki, K. Oshima, and K. Utimoto, *Bull. Chem. Soc. Jpn.*, **60**, 3465 (1987); K. Nozaki, K. Oshima, and K. Utimoto, *Tetrahedron Lett.*, **29**, 1041 (1988); Y. Ichinose, K. Oshima, and K. Utimoto, *Chem. Lett.*, **1988**, 669.

4) Monodehalogenation by *n*-Bu_3SnH: D. Seyferth, H. Yamazaki, and D. L. Alleston, *J. Org. Chem.*, **28**, 703 (1963); T. Ando, H. Yamanaka, F. Namigata, and W. Funasaka, *J. Am. Chem. Soc.*, **89**, 5719 (1967); T. Ando, T. Ishihara, Y. Yanagi, *Mem. Fac. Eng., Kyoto Univ.*, **44**, 249 (1982). Cr(II): T. Shirafuji, K. Oshima, Y. Yamamoto, and H. Nozaki, *Bull. Chem. Soc. Jpn.*, **44**, 3161 (1971); H. Nozaki, T. Aratani, and R. Noyori, *Tetrahedron*, **23**, 3645 (1967).

5) Kuivila has reported that the reduction of 2-bromo-2-butene with *n*-Bu_3SnH at −78 °C followed a slightly stereospecific course. H. G. Kuivila, *Acc. Chem. Res.*, **1**, 229 (1968). On the other hand, Whitesides et al. have reported that the same mixture of 65% *trans*- and 35% *cis*-2-butene was obtained from the room temperature reduction of both *cis*- and *trans*-2-bromo-2-butene with *n*-Bu_3SnH. G. M. Whitesides, C. P. Casey, and J. K. Krieger, *J. Am. Chem. Soc.*, **93**, 1379 (1971).

6) Triphenylborane has been reported to accelerate the reduction of 4-bromobiphenyl. D. H. Lorenz, P. Shapiro, A. Stern, and E. I. Becker, *J. Org. Chem.*, **28**, 2332 (1963).

7) K. Hayashi, J. Iyoda, and I. Shiihara, *J. Organomet. Chem.*, **10**, 81 (1967); G. J. M. van der Kerk, J. G. Noltes, and J. G. A. Luijten, *J. Appl. Chem.*, **7**, 366 (1957).

8) H. C. Brown and C. F. Lane, *J. Am. Chem. Soc.*, **92**, 6660 (1970).

9) E. L. Foreman and S. M. McMlvain, *J. Am. Chem. Soc.*, **62**, 1436 (1940).

10) F. B. Gonzalez and P. A. Bartlett, *Org. Synth.*, **64**, 175 (1985).

11) G. Zweifel and C. C. Whitney, *J. Am. Chem. Soc.*, **89**, 2753 (1967).

12) J. J. Eisch and G. A. Damasevitz, *J. Org. Chem.*, **41**, 2214 (1976); K. Uchida, K. Utimoto, and H. Nozaki, *ibid.*, **41**, 2215 (1976).

13) T. H. Chan, P. W. K. Lau, and W. Mychajlowskij, *Tetrahedron Lett.*, **1977**, 3317; R. B. Miller and T. Reichenbach, *ibid.*, **1974**, 543.

14) K. Uchida, K. Utimoto, and H. Nozaki, *J. Org. Chem.*, **41**, 2941 (1976); *idem*, *Tetrahedron*, **33**, 2987 (1977).

15) E. J. Corey and P. L. Fuchs, *Tetrahedron Lett.*, **1972**, 3769.

16) J. E. Leibner and J. Jacobus, *J. Org. Chem.*, **44**, 449 (1979).

17) F. E. Juge, Jr. and A. Fry. *J. Org. Chem.*, **35**, 1876 (1970).

18) I. D. Rae and B. N. Umbrasas, *Aust. J. Chem.*, **28**, 2669 (1975).

Aromatic Hydroxylation with an Iron(III)-Catechol-H_2O_2 System. Mechanistic Implication of the Role of Catechol

Seizo TAMAGAKI, Kenji SUZUKI, and Waichiro TAGAKI*
Department of Applied Chemistry, Faculty of Engineering, Osaka City University, Sugimoto 3, Sumiyoshi-ku, Osaka 558
(Received July 8, 1988)

The role of catechol in benzene hydroxylation with Fe^{3+}/catechol/H_2O_2 system, the so-called Hamilton system, has been mechanistically investigated by using tiron as a substitute for pyrocatechol. The yield of phenol progresses linearly with reaction time. The phenol yield is dependent on the mole ratio of Fe^{3+} relative to tiron, and the ratio of more than unity is particularly important for the effective functioning of the catalyst system. The *o*-, *m*-, and *p*-product isomer distributions for a few aromatic hydrocarbons are nearly identical with those of the Fenton reaction. These and the separate experimental results are consistent with the mechanism involving the rate-limiting redox reaction between tiron and Fe^{3+} and then the follow-up radical chain sequence as in the Fenton reaction.

Since the first report of Udenfriend,[1] an enormous number of model peroxidase systems such as the Udenfriend[2] and Hamilton systems[3] have received considerable attention thus far. However, the reaction mechanisms for the majority of those systems are the least understood and quite speculative. This paper describes the results of detailed reexamination of mechanistic aspects of the aromatic hydroxylation by the Hamilton system consisting of Fe^{3+}, a catechol, and H_2O_2. The hydroxylation of aromatic hydrocarbons by this system has been studied in details by Hamilton.[3] The rate of the reaction was found to be first order in iron(III), H_2O_2, and catechol concentrations at a low concentration of catechol (2×10^{-4} M; 1 M=1 mol dm^{-3}). At higher concentrations of catechol, however, there was observed a decrease in rate, which may be due to the function of higher complexes of catechol with Fe^{3+} that is less reactive than the 1:1 complex. It has been postulated by Hamilton[4a] and has hitherto been cited in the literature and books[4b] that the reaction involves an *o*-quinone–iron oxide complex (**1**), which serves as an active oxidant to form a reactive intermediate **2**.

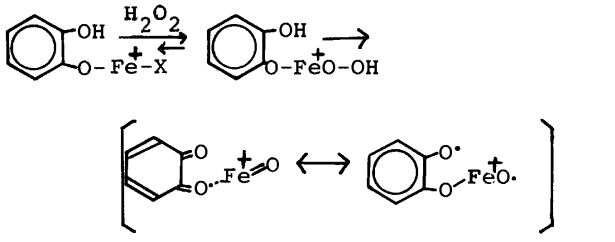

1

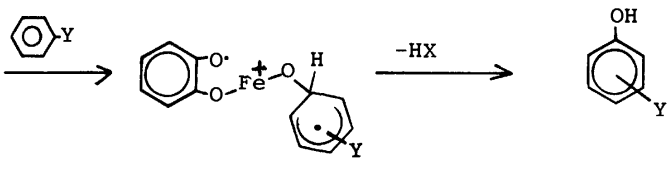

2

Recently, Richter and Waddell[5] have reported the evidence of a radical chain mechanism for the hydroxylation of a substrate, benzoic acid, with H_2O_2 in the presence of catalytic iron ion and 5-methyldihydrophenazine (H_2O_2/Fe^{3+}/MPH system) and have proposed the mechanism essentially resembling the classical Fenton reaction except that the new system requires the organic mediator (5-methyldihydrophenazine) to get the oxidized catalyst metal back to its original state. Thus, they classified this new system as the nonclassical Fenton system together with the Hamilton system. However, the mechanism for the Hamilton hydroxylation system is not yet perfectly understood, since no convincing evidence has been given; in particular, the functional roles of a catechol have not been exactly determined. In an attempt to find a mechanistic version of this reaction, we have replaced ordinarily used catechol by disodium catechol-3,5-disulfonate (tiron) which seems better suited for the mechanistic study of the Hamilton system with twofold reasons. (1) It is a bidentate ligand to form a deep blue Fe^{3+} complex, relatively far stable compared to the complex of catechol in a reaction pH range 2.0—3.5 and (2) it shows remarkable resistance to oxidative destruction during the reaction due to its bearing the aromatic ring highly substituted with two strongly electronegative sulfonato groups.

Experimental

Materials: Substituted catechols were commercially available as special grade and used without further purification.

Hydroxylation of Benzene: The hydroxylation were generally perfomed at ambident temperature in an aqueous solution of pH 3 adjusted with H_2SO_4 under nitrogen. A standard reaction was carried out in a two-phase system of H_2O (50 ml) and benzene (1 ml), containing $Fe_2(SO_4)_3$ (0.05 mmol) and tiron (0.1 mmol). Benzene was used in excess to minimize the further oxidation of product phenol. H_2O_2 (0.5 M, 2 ml, 1 mmol) was then added to the solution all at once. The mixing was performed with a mechanical shaker for 2.5 h. Analysis of products was done according to those described in the previous paper.[6] In any case, phenol

was obtained as the major product. No appreciable amount of by-products such as biphenyl, catechol, and quinone (if any, less than 1%) was detected. All the phenol yields were based on H_2O_2 added. Under the standard conditions the phenol yield was 38%.

Kinetics: The rate of decomposition of a Fe^{3+}-catechol complex in water was determined as follows: The equal volumes of the stock solutions of Fe^{3+} and a catechol (8×10^{-4} M each) was pipetted out and placed into a UV cell and the disappearance of the blue color due to the complex (λ_{max} shown in Table 1) was monitored with a Hitachi 220 spectrometer. The k_{obs} thus obtained was also listed in the third column of Table 1.

Table 1. Absorption Maximum and Redox Reaction Rate for Catecholate-Fe^{3+} Complexes (pH 3.0, 25 °C)

Catechol	λ_{max}/nm	k/min^{-1}
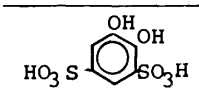	660(ε=1780)	0.018
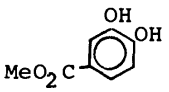	660	0.075
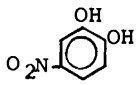	650	0.14
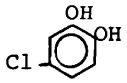	720	9.1
	720	too fast

Conditions: [Fe^{3+}], 4×10^{-4} M; [catechol], 4×10^{-4} M.

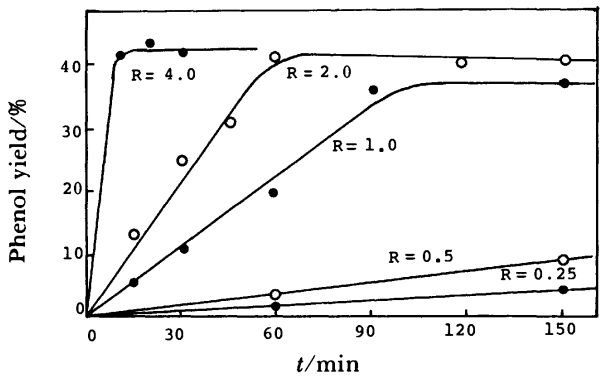

Fig. 1. Yield vs. time profile at varying [Fe^{3+}]/[tiron] ratio. R=[Fe^{3+}]/[tiron]. [Fe^{3+}]=2×10^{-3} M.

Results and Discussion

Time Course of Hydroxylation: First, the time courses for the hydroxylation were determined at varying mole ratios of Fe^{3+} to tiron, keeping the Fe^{3+} concentration fixed. Figure 1 shows the results. The yield of phenol increases linearly with time, indicating zero-order dependence of the rate on H_2O_2 concentration. Thus, H_2O_2 is not involved in the rate-limiting step.

Furthermore, a comparison of the rates at different mole ratios of Fe^{3+}/tiron, keeping the concentration of the Fe^{3+} constant, shows that the reaction at the ratio of 0.5 runs slower than that at 2.0, in spite of formation of a two-fold amount of the complex in the former; namely, the rate is independent of the quantities of the complex formed in solution, clearly demonstrating that, as opposed to the suggestion of Hamilton,[3] the Fe^{3+}-catechol complex itself can not be an active catalyst.

Effect of Fe^{3+}/Tiron Ratio on Phenol Yield. The effect of altering ratios of Fe^{3+}/tiron on the phenol yield was examined. The results are illustrated in Fig. 2. A plot of the phenol yield versus the mole ratio produces the characteristic sigmoidal profile; the phenol yield is quite low (<10%) in the ratio range below unity. This is not a result of formation of a lot of by-products but a result of no reaction, since the consumption of H_2O_2 was not observed.

The phenol yield begins to steeply rise as the ratio being close to unity, and then finally approaches a limiting value 40% when a slight excess of Fe^{3+} relative to tiron is added, suggesting that free Fe^{3+} is required for the activation of the catalyst system. As mentioned in the introductory section, tiron binds with Fe^{3+} to form only a 1:1 stable complex with an equilibrium constant $K\fallingdotseq10^4$ M^{-1} rather than highly coordinated Fe^{3+} complexes even at a large excess of tiron over

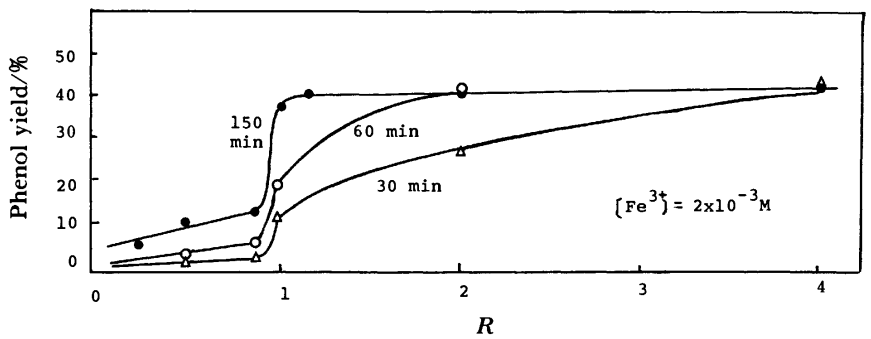

Fig. 2. Plots of phenol yield vs. [Fe^{3+}]/[tiron]. Reaction time: 30 (△); 60 (○); 150 min (●).

Fe^{3+} concentrations. Therefore, addition of an slight excess (less than 1.5 fold) of tiron brings about the complete lack of free Fe^{3+} in solution and would thus remarkably depress the phenol yield.

Kinetics of Tiron Oxidation with Fe^{3+}: In order to confirm further the above conclusion, the oxidation of tiron with iron(III) was kinetically examined at an Fe^{3+}/tiron mole ratio (R) of 1:1 by monitoring the disappearance of the absorption band of the tiron-Fe^{3+} complexes, holding the tiron concentration constant. The rate constants thus obtained are plotted as a function of R. Figure 3 shows those results. The rate is dependent on the ratio in the same characteristic fashion as observed in the benzene hydroxylation. That is, the reaction is extremely slow in the ratio range less than unity, while very fast in the range larger than unity. In the latter range, in particular, the rate increases linearly with increasing Fe^{3+} concentrations, explicitly demonstrating that an excess of Fe^{3+} over tiron is essential for the tiron oxidation as well as for the hydroxylation, and hence these two reactions commonly involve the oxidation of tiron by uncomplexed Fe^{3+} leading to a semiquinone and then to a quinone.

In Table 1 are listed the λ_{max} values of the complexes

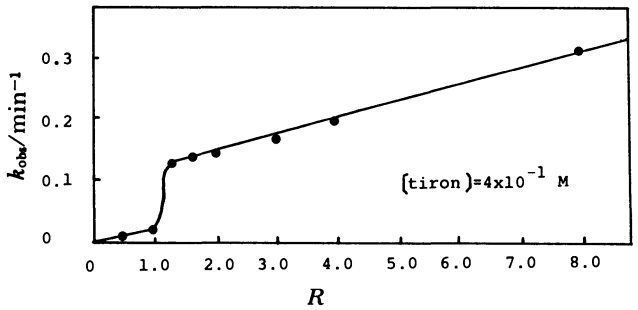

Fig. 3. Plot of the rate of the complex decomposition vs. $[Fe^{3+}]/[tiron]$. Varying concentrations of Fe^{3+} (0—3.2×10^{-3} M) in unbuffered solution (pH 3) changed the reaction pH from 3.0 to 2.6. In a separate experiment, however, such a pH change had no significant effect on the rate. Therefore, the solution was not buffered here. Rate/min^{-1} (pH): 0.14 (3.05); 0.151 (3.00); 0.148 (2.91); 0.150 (2.75); 0.145 (2.5); 0.104 (1.9); 0.060 (1.7).

Table 2. Effect of the Common Salt on the Redox Rate. Decomposition of the Tiron-Fe^{3+} Complex in the Presence of the Foreign Fe^{2+} Ion (25 °C)

Fe^{2+}/M	k_{obs}/min^{-1}
0	0.165
0.5	0.10
1.0	0.056
2.0	0.018
4.0	0.005

[tiron], 4×10^{-4} M; $[Fe^{3+}]$, 16×10^{-4} M.

due to the catecholate-to-Fe(III) charge-transfer band along with the rate constants for disappearance of their absorption bands (650—720 nm depending on catechols) at a 1:1 Fe^{3+}/catechol ratio.[7] The substitution of electron-donating groups on the catechol ring resulted in a red shift of the CT band and acceleration of the rate, as would be generally expected for oxidation reactions, while the electron-withdrawing ones decelerated the rates. Of these catechols studied here, tiron was the most stable with regard to its oxidation reaction.

Table 2 provides further evidence for the mechanism of tiron oxidation, i.e., the preequilibrium formation of the semiquinone, followed by the rate-determining semiquinone oxidation. According to this mechanism, an increase of Fe^{2+} in the reaction solution would move the equilibrium to the left, which should be attributable to the common ion effect of Fe^{2+} ion on the catechol-semiquinone preequilibrium. In fact, addition of foreign Fe^{2+} ion to the reaction system resulted in marked rate drop.

Baxendale et al.[8] undertook the kinetic study of the reaction between Fe^{3+} and catechol in detail and observed the deviation (Eq. 1) from the second-order kinetics attributable to the reverse reaction of Fe^{2+} with an intermediate. A mechanism (Scheme 1) involving a preequilibrium formation of the semiquinone intermediate was proposed there.

Scheme 1.

$$Fe^{3+} + H_2Q \underset{k_2}{\overset{k_1}{\rightleftharpoons}} Fe^{2+} + HQ + H^+$$

$$Fe^{3+} + HQ \xrightarrow{k_3} Fe^{2+} + Q + H^+$$

$$-d[H_2Q]/dt = k_1k_3[Fe^{3+}]^2[H_2Q]/(k_2[Fe^{2+}] + k_1[Fe^{3+}]) \quad (1)$$

***o*-, *m*-, and *p*-Products Distribution.** In order to understand the nature of hydroxylating species, the *o*-, *m*-, and *p*-isomer distributions in phenols derived from a few aromatics were examined under various conditions. The results are summarized in Table 3. The hydroxylating species generated from the present system reacts with phenylacetic acid and anisole to afford *o*-, *m*-, and *p*-hydroxyphenylacetic acids and anisoles with isomeric distributions of 49:29:22% and 82:8:10%, respectively.

Meanwhile, use of the modified Fenton reagent,[9] consisting of H_2O_2 and a stoichiometric amount of Fe^{2+} in the presence of Cu^{2+}, afforded 47:30:23 and 87:3:10%, respectively. The Fenton reagent has been established to produce hydroxyl radicals as the reactive hydroxylating species.[9] Therefore, a close parallelism between tiron and Fenton's systems in the patterns of isomeric distributions strongly supports that OH

radicals are reactive species common to these two hydroxylations.

Mechanism. The kinetic and yield data presently available are accounted for by the following reaction sequence in which elemental steps 1—5 combine to form an overall catalytic cycle. (Scheme 2)

The similarity in shape of the curvatures obtained on the hydroxylation (Fig. 2) and the redox reaction (Fig. 3) clearly indicates that both reactions take place through the same sequence up to the rate-determining step of the reaction. As Fig. 3 shows, the pseudo-first-order rate constant, k_{obs}, increases linearly with increasing [Fe^{3+}] in the range of the [Fe^{3+}]/[tiron] ratio>1, supporting that there is the reversible breakdown of the Fe^{3+}–tiron complex, yielding one semiquinone radical and one Fe^{2+} (1b), then followed by rate-determining attack of a second Fe^{3+} on the semiquinone radical, giving an *o*-quinone and Fe^{2+} (1c). The reversibility of step 1b is substantiated further by the observation of the common ion effect of foreign Fe^{2+} ions on the rate of the step 1b. The step 1c must be more rapid than the disproportionation of the semiquinone radical to the corresponding quinone and catechol (5), because the breakdown of the complex needs a second Fe^{3+}.

Fe^{2+} so formed triggers the Fenton reaction to yield an OH radical, immediately followed by steps 3 and 4, in which the OH radical attacks an aromatic ring giving rise to 1-hydroxycyclohexadienyl radical at a rate of almost diffusion control (10^{10} M^{-1} s^{-1}) and then the hexadienyl thus formed is oxidized by a quinone to phenol. The finding that quinones are good oxidants for such carbon radicals was reported by Steenken and Raghavan;[10] they estimated the rates of electron transfer between 1-methoxy-2-, 3-, and 4-hydroxycyclohexadienyl radical and *p*-benzoquinone to be 1.2×10^9, $<8\times10^5$, 4.4×10^9 M^{-1} s^{-1}, respectively. Thus, quinones are reduced back to the semiquinones or further to hydroquinones before the cyclohexadienyl radicals bimolecularly collapse to biphenyl, a coupling product. Actually, in sharp contrast to the original Fenton system, the present system gave no appreciable amount of biphenyl to be detected by HPLC analysis. The lifetime of an intermediate carbocation thus produced is $<1\times10^{-6}$ s[10] and hence phenol may be formed synchronously with the reduction of *p*-benzoquinone.

Meanwhile, the data of Table 4 shows that the isomer distribution is not appreciably affected by the presence

Table 3. Isomer Distributions in Phenolic Products from Phenylacetic Acid and Anisole

Catechol	Total yield %	*o*	*m* /%	*p*
Anisole				
(a) Tiron	9.4	82	8	10
(b) Catechol	18.4	67	3	30
(c) 4-Nitrocatechol	6.0	88	2	10
(d) Fenton	5.0	87	3	10
Phenylacetic acid				
(a) Tiron	44.6	49	29	22
(b) Catechol	24.6	49	29	24
(d) Fenton	4.5	47	30	23

Conditions: (a) Fe^{3+}(0.1 mmol)/tiron(0.1 mmol)/H_2O_2 (1.0 mmol)/phenylacetic acid(1.0 mmol)/50 ml H_2O (pH 3). (b,c) Fe^{3+}(0.1 mmol)/catechol(0.1 mmol)/H_2O_2 (1.0 mmol)/phenylacetic acid(1.0 mmol)/50 ml H_2O. (d) Fe^{2+}(1.0 mmol)/H_2O_2(1.0 mmol)/Cu^{2+}(1.0 mmol).

Table 4. Effect of Oxygen on the Phenol Yield and Isomer Distribution (pH 3, 2.5 h)

Conditions under	Benzene[a] Yield/%	Methyl phenylacetate[b] Total yield/%	*o*	*m* yield/%	*p*
N_2	36.2	36.2	46	29	25
Air	34.7	34.0	50	26	24
O_2	11.9	11.1	49	27	24

a) Tiron, 0.1 mmol; Fe^{3+}, 0.1 mmol; H_2O_2, 1.0 mmol; benzene, 2 ml; H_2O, 50 ml. b) Conditions were the same as a), except the substrate (1 mmol of methyl phenylacetate).

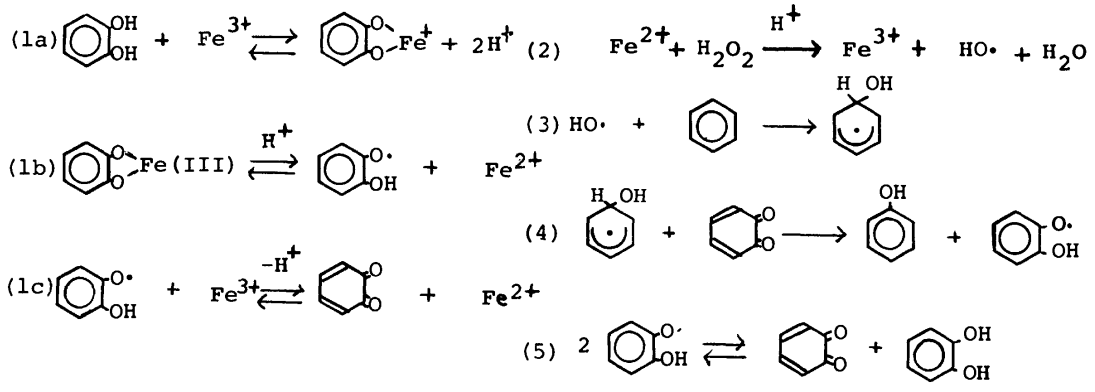

Scheme 2.

or absence of air. Under such a relatively low oxygen pressure the hexadienyl radical is more quickly oxidized to phenol than trapped by molecular oxygen. On the contrary, replacing air for the atmospheric pressure of oxygen considerably depressed the phenol yield more than 20%. This yield depression indicates the occurring of a concomitant irreversible trapping by molecular oxygen of the hexadienyl radical giving an intermediate 4-hydroxy-2,3-cyclohexadienylperoxyl radical, which would terminate the radical chain cycle; formation of such an intermediate in metal-catalyzed aromatic hydroxylation under an oxygen atmosphere was reported elsewhere.[11]

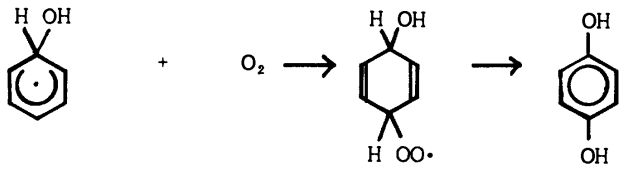

Thus, the overall mechanistic picture for the tiron system and related systems are basically similar to that for the MPH/Fe^{3+}/H_2O_2 system reported by Richter and Waddell. A catechol displays dual functions as a reductant toward Fe^{3+} and as an oxidant toward a 1-hydroxycyclohexadienyl radical through shuttling between catechol and quinone.

References

1) S. Udenfriend, C. T, Clark, J. Axelrod, and B. B. Brodie, *J. Biol. Chem.*, **208**, 731 (1954).

2) a) R. Breslow and L. N. Lukens, *J. Biol. Chem.*, **235**, 292 (1960). b) R. R. Grinstead, *J. Am. Chem. Soc.*, **82**, 3472 (1960).

3) a) G. A. Hamilton, R. J. Workman, and L. Woo, *J. Am. Chem. Soc.*, **86**, 3390 (1964). b) G. A. Hamilton, *ibid.*, **86**, 3391 (1964).

4) a) G. A. Hamilton, *J. Am. Chem Soc.*, **88**, 5266 (1966); b)Y. Ogata and Y. Sawaki, "Organic Syntheses by Oxidation with Metal Compounds," ed by W. J. Mijs and C. R. H. I. de Jonge, Plenum Press, New York (1986); M. M. T. Khan and A. E. Martell, "Homogeneous Catalysis by Metal Complexes," Vol. I, Academic Press, New York (1974).

5) H. W. Richter, M. A. Fetrow, R. E. Lewis, and W. H. Waddell, *J. Am. Chem. Soc.*, **104**, 1666 (1982); H. W. Richter and W. H. Waddell, *ibid.*, **104**, 4630 (1982).

6) S. Tamagaki, K. Suzuki, H. Okamoto, and W. Tagaki, *Tetrahedron Lett.*, **24**, 4847 (1983).

7) A. Avdeef, S. R. Sofen, T. L. Bregante, and K. N. Raymond, *J. Am. Chem. Soc.*, **100**, 5362 (1978); R. C. Hider, A. Mohd-Nor, and J. Silver, *J. Chem. Soc., Dalton Trans.*, **1981**, 609; D. D. Cox, S. J. Benkovic, L. M. Bloom, F. C. Bladley. M. J. Nelson, L. Que, Jr., and D. E. Wallick, *J. Am. Chem. Soc.*, **110**, 2026 (1988).

8) J. H. Barendle, H. R. Hardy, and L. H. Sutcliffe, *Trans. Faraday Soc.*, **47**, 963 (1951); E. Mentasi and E. Pelizzetti, *J. Chem. Soc., Dalton Trans.* **1973**, 2605; E. Mentasi, E. Pelizzetti, and G. Saini, *ibid.*, **1973**, 2609.

9) a) H. J. H. Fenton, *J. Chem. Soc.*, **65**, 899 (1894). b) C. Walling and R. A. Johnson, *J. Am. Chem. Soc.*, **97**, 363 (1975); C. Walling, *Acc. Chem. Res.*, **8**, 125 (1975).

10) S. Steenken and N. V. Raghavan, *J. Phys. Chem.*, **83**, 3101 (1979).

11) S. Ito, A. Kunai, H. Okada, and K. Sasaki, *J. Org. Chem.*, **53**, 296 (1988).

 © 1989 The Chemical Society of Japan Bull. Chem. Soc. Jpn., 62, 153—158 (1989)

Fe(III)-Catalyzed Aromatic Hydroxylation with H_2O_2 in the Presence of a Variety of Electron-Transfer Agents

Seizo TAMAGAKI, Masaaki SASAKI, and Waichiro TAGAKI*
Department of Applied Chemistry, Faculty of Engineering, Osaka City University, Sugimoto 3, Sumiyoshi-ku, Osaka 558
(Received August 4, 1988)

Electron-transfer agents such as *N,N,N',N'*-tetramethylphenylenediamine (TMPD), ferrocenes, and phenothiazines have been found to mediate the hydroxylation of benzene with H_2O_2 in the presence of Fe^{3+}. Of these, TMPD catalyst is the most effective to provide phenol in 80% or better yield based on added H_2O_2 under the optimized conditions. A general mechanism, involving the rate-determining reduction of Fe^{3+} to Fe^{2+} with such mediators, is suggested.

Since the initial report of Udenfriend,[1] many workers have studied the scope and mechanism of a number of non-enzymic hydroxylation systems, described by Udenfriend, Grinstead,[2] Hamilton,[3] and Ullich.[4] Richter and Waddell[5] studied the decomposition of H_2O_2 and hydroxylation of benzoic acid in the presence of catalytic Fe^{3+} and 5-methyldihydrophenazine (MPH) and have proposed that the oxidant inducing the aromatic hydroxylation is the hydroxyl radical produced in an iron-catalyzed one-electron reduction of H_2O_2. The rate was found to be expressed as $-d[H_2O_2]/dt=k[MPH]([Fe^{3+}]+\alpha)$. Recently, we have also shown that catechol-3,5-disulfonate, a substitute for catechol (CT), mediates electron transfer in the catalytic hydroxylation. Most of the phenomenon appears to be accounted for by the general features proposed by Richter and Waddell. The rate-determining step has been confirmed to be the redox reaction of Fe^{3+} with the catechol (Eq. 1), and the quinone or semiquinone thus formed is used to oxidize the 1-hydroxycyclohexadienyl radical intermediate (**8**) to phenol (Eq. 2). The catechol displays dual functions as a reductant toward Fe^{3+} and as an oxidant toward 1-hydroxycyclohexadienyl radical through shuttling between catechol and quinone.

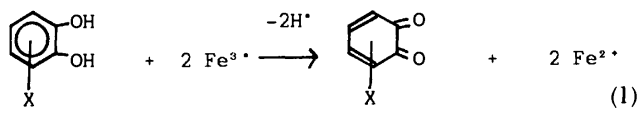

(1)

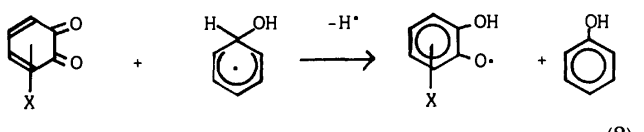

8 (2)

A set of these hydroxylating systems, referred to as a nonclassical Fenton reaction, have been suggested to commonly require catalytic electron-transfer agents (mediators) to return the oxidized Fe^{3+} to its reduced state.[5] However, only a limited number of mediators have been recognized so far; of these, the reduced 5-methylphenazinium cation has frequently been utilized in biological studies. The use of catechols has been reported by Hamilton[3] and by us.[6] We have recently reported 1,2-naphthoquinone-4-sulfonate to mediate the aromatic hydroxylation with H_2O_2 to produce phenols in 40% yields.[7]

In order to fully understand these hydroxylations, we consider it of interest to extend our studies to other new mediators. In this paper we present the results of a thorough kinetic study of the mediator-dependent hydroxylations.

Experimental

Materials. TMPD (**1**), (dimethylaminomethyl)ferrocene (DAMF, **2**), catechol (CT, **3**), hydroquinone (HQ), promethazine (PMZ, **4**), phenothiazine (PTZ, **5**), Methylene Blue (MB, **6**), thianthrene, *N*-methylacridinium iodide and ascorbic acid (AsH_2, **7**) were all commercially available as special grade and used as received. 10-Methyl-9,10-dihydroacridine (MDA) and the reduced Methylene Blue were prepared by the reduction of *N*-methylacridinium iodide and Methylene Blue, respectively. Moreover, 1,3,10-trimethyl-1,5-dihydroisoalloxazine (TMDIA) were synthesized according to the method described in the literature.[8]

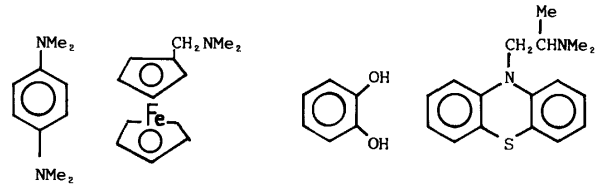

1 **2** **3** **4**

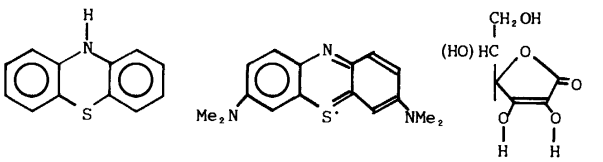

5 **6** **7**

Hydroxylation of Benzene. A standard hydroxylation procedure was effected as follows: Fe^{3+} (0.01 mmol, 0.2 mM; 1 M=1 mol dm^{-3}), an appropriate organic mediator (0.01 mmol, 0.2 mM), and benzene (1 ml) were added to 50 ml of H_2O adjusted with H_2SO_4 to pH 3. The air in the vessel was purged with nitrogen gas, and H_2O_2 (1 mmol, 2 mM) was

then added all at once. After mechanical shaking for 2.5 h, the solution was thoroughly extracted with ether and then the amount of phenol in the ether was determined with HPLC using anisole as an internal standard at 270 nm. The product yields are all based on an added amount of H_2O_2. When the yield was less than 5%, the reaction was examined again by increasing the amounts of Fe^{3+} and/or the mediator each ten-fold to obtain convenient rates. The results thus obtained are collected in Tables 1—5 along with Fig. 1.

Kinetics of the Reaction between Organic Mediator and Fe^{3+}. For the very fast redox reaction, the reaction rate was determined with a stopped flow apparatus with two mixing chambers (Union Giken Model RA 401) by monitoring the appearance of the absorption of the final products (radical cations), namely, at 610 nm for TMPD and at 615 nm for DAMF.[9] For PMZ having a relatively slow rate, a Hitachi 220 spectrophotometer equipped with temperature-controlled cell-holders was used to monitor the appearance of an increasing absorption at 513 nm. The initial concentrations of TMPD and DAMF were 5×10^{-5} and 1.25×10^{-4} M, respectively. The concentrations of Fe^{3+}(as $Fe_2(SO_4)_3$) were changed in the range 2.5—25×10^{-4} M, depending on mediators.

Isomer Distribution. The hydroxylation procedure was as usual except for employing methyl phenylacetate instead of benzene; conditions: TMPD, 0.01 mmol; Fe^{3+}, 0.01 mmol; H_2O_2, 1 mmol; methyl phenylacetate, 1 mmol in 50 ml of H_2O (pH 3) at 25 °C. The products were analyzed by using HPLC (Nihon Bunko Uniflow-221) with Packed Column SS-05 eluted with hexane/methyl acetate/methanol 9:1:1 at 290 nm. *o*-Methoxyphenol was an internal standard.

Results

It is clear from Table 1 that the optimum pH is about 3, just similar to that for the catechol-catalyzed hydroxylation reported previously by Hamilton.[3]

Table 2 shows that thianthrene, 10-methyl-9,10-dihydroacridine (MDA), ascorbic acid (AsH_2), and a pteridine are all ineffective even at a high level (2 mM) of catalyst concentrations. On the other hand, TMPD, DAMF, and CT work well even at a low level (0.2 mM) of these concentrations. The reaction solutions are

Table 1. . pH Effect on Phenol Yield (25 °C, 2.5 h, N_2)[a]

Mediator	pH	Yield/%
TMPD	1	9.7
	3	41.7(39.8)[b]
	5	2.3(1.9)[c]
DAMF	1	8.0
	3	38.8
	5	13.5

a) Conditions: mediator, 0.01 mmol; Fe^{3+}, 0.01 mmol; benzene, 1 ml; H_2O_2, 1 mmol; 50 ml H_2O. The solution was adjusted to a desired pH with H_2SO_4 or NaOH. b) 0.1 M acetate buffer, pH 3.19. c) 0.1 M acetate buffer, pH 5.0.

Table 2. Hydroxylation of Benzene with Fe^{3+}/Mediator/H_2O_2 Systems[a]

Run	Mediator/mmol		Fe^{3+}/mmol	Phenol yield/%[b]
1	None	—	0.1	1.9
2	TMPD	0.01	0.01	41.7
3	TMPD	0.01	0.001	12.0
4	DAMF	0.01	0.01	38.8
5	Ferrocene	0.01	0.01	40.9
6	CT	0.01	0.01	40.5
7	HQ	0.01	0.01	3.4
8	HQ	0.1	0.1	20.9
9	TMDIA	0.01	0.01	3.5
10	TMDIA	0.01	0.1	4.8
11	TMDIA	0.1	0.01	32.8
12	TMDIA	0.1	0.1	39.1
13	PMZ	0.01	0.01	1.8
14	PMZ	0.01	0.1	3.2
15	PMZ	0.1	0.01	1.5
16	PMZ	0.1	0.1	33.3
17	PTZ	0.01	0.01	5.3
18	PTZ	0.1	0.1	40.6
19	MB	0.01	0.01	3.2
20	MB	0.1	0.1	43.3
21	12N4S[d]	0.01	0.01	33.1[7]
22	Thianthrene	0.1	0.1	0.9
23	MDA	0.1	0.1	1.1
24	AsH_2	0.1	0.1	2.3
25	A18DS[e]	0.1	0.1	3.6[7]
26	Pteridine	0.1	0.1	6.0[c]
27	Cobaltcene	0.1	0.1	1.8

a) Unless otherwise noted, 2.5 h; 25 °C; benzene, 1 ml; H_2O_2, 1 mmol; 50 ml H_2O under N_2. b) The yield was based on H_2O_2 added. c) 2-Amino-4-hydroxy-6,7-dimethyl-5,6,7,8-tetrahydropteridine. d) 1,2-Naphthoquinone-4-sulfonate. e) Anthraquinone-1,8-disulfonate.

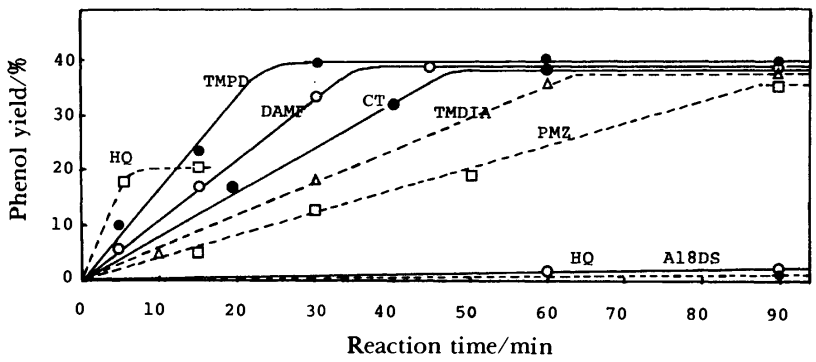

Fig. 1. Time course of hydroxylation with various mediators.
(——): Fe^{3+} 0.01 mmol; mediator 0.01 mmol. (---): Fe^{3+} 0.1 mmol; mediator 0.1 mmol. For reaction conditions, see text. Reaction conditions, see text.

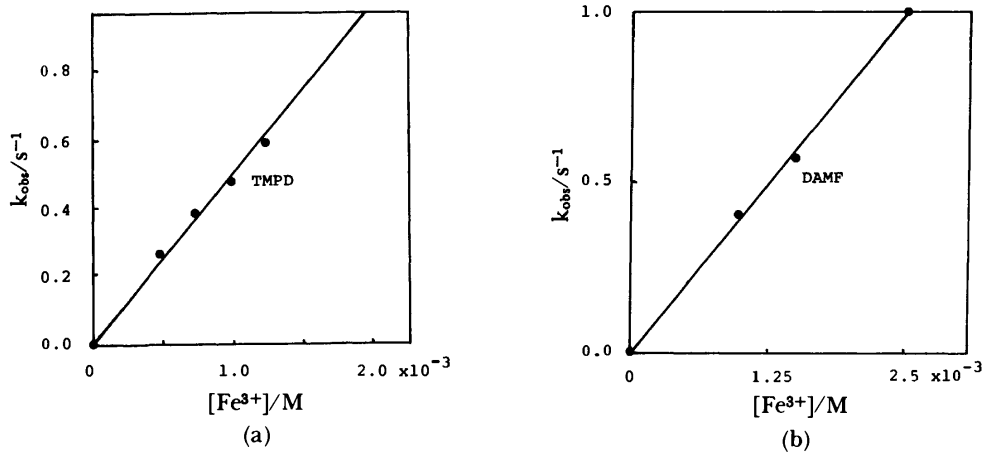

Fig. 2. Effect of concentration of Fe^{3+} on the redox rate. For reaction conditions, see text.

very clean and the formation of neither appreciable amount of by-products such as biphenyl and hydroquinone (<1%) nor dark deposit was observed. These mediators are at least an order of magnitude more active than TMDIA, PMZ, and PTZ. Figure 1 illustrates the profiles of the time courses of the reactions. Thus, the mediator dependency of the hydroxylation rate is obvious. The rate follows the order: TMPD>DAMF>CT>HQ>TMDIA>PMZ=PTZ. The phenol yields are found to increase linearly with reaction time and reach a limiting value irrespective of changing mediators. This linearity indicates that H_2O_2 is not involved in the rate-determining step of the reaction.

The highest reactivity of TMPD seems to be due to the fast redox reaction between Fe^{3+} and TMPD giving rise to Fe^{2+} and the TMPD radical cation. In order to ascertain this speculation, the kinetic experiments on the reaction of Fe^{3+} with TMPD and some other mediators was done under pseudo-first-order conditions in the presence of a 10-fold excess of Fe^{3+} in unbuffered aqueous solution of pH 2.5 at 25 °C by means of a stopped flow apparatus. In every case examined, the reaction is first-order with respect to each reactant and obeys strictly bimolecular kinetics; only representative data are shown in Fig. 2 and the second-order rate constants are given in Table 3. The rate is obviously mediator-dependent and follows the order: TMPD>DAMF>CT>HQ>PMZ. With regard to these effective mediators, this dependency clearly parallels the rate order for the hydroxylation, unambiguously indicating that the reduction of Fe^{3+} to Fe^{2+} takes place in the rate-determining step in these

Table 3. Second-Order Rate Constants for Oxidation of Some Mediators with Fe^{3+} (pH 2.5, 25 °C))

Mediator	$k_2/M^{-1}\,s^{-1}$
TMPD	492
DAMF	392
CT	60
HQ	27
PMZ	0.11

Table 4. Effect of Chelating Agents on Phenol Yield in the Hydroxylation with TMPD/H_2O_2 System (pH 3, 25 °C)[a] without Added Fe^{3+}[b]

Additive/mmol		Phenol yield/%
None	—	7.4
2,2′-Bipyridine	0.05	0.0
1,10-Phenanthroline	0.05	0.0
EDTA	0.05	0.0
Pyridine	0.05	5.8
Quinoline	0.05	3.2
8-Quinolinol	0.05	4.9

a) TMPD, 0.1 mmol; H_2O_2, 1 mmol; 50 ml H_2O. b) The reagents employed contain adventitious iron ions as trace contaminants.

Table 5. *o*-, *m*-, and *p*-Isomeric Distributions in Phenolic Products from Methyl Phenylacetate

Mediator	Total phenol yield/%	*o*	*m*	*p*
		Yield/mol%		
TMPD[a]	27.9	46	32	22
DAMF[a]	35.3	46	30	24
CT[a]	9.4	47	30	23
Fenton[b]	4.9	53	28	19
CT[c]	24.6	49	28	24
Fenton[c]	4.5	47	30	23

Unless otherwise noted, the reaction conditions were the same as the standard reaction. H_2O_2, 1 mmol; H_2O, 50 ml. a) Mediator, 0.01 mmol; Fe^{3+}, 0.01 mmol. b) Fe^{2+}, Cu^{2+}, 1 mmol each. c) Phenylacetic acid as the substrate.

hydroxylation reactions.

Meanwhile, addition of 1,10-phenanthroline, 2,2′-bipyridine, and EDTA, typical metal-chelating agents, in an excess over Fe^{3+} completely inhibited the progress of both the redox and the hydroxylation reactions, but pyridine and quinoline only slightly did it (Table 4). The implication is that the strong complexation of Fe^{3+} with, for example, EDTA leads to substantial lowering of the reduction potential of ferric ion from +0.7 to +0.17 (pH 4),[10] so that the redox reaction in question might not occur. Actually, in the presence of EDTA, no consumption of H_2O_2 was observed. The details will be discussed later.

In order to further elucidate reaction mechanisms whether OH radicals are formed, an examination of isomer distributions in the product phenols was carried out. In Table 5 are compared the *o*-, *m*-, and *p*-isomer distibutions for the present hydroxylating systems with that for the Fenton system. Methyl phenylacetate was the substrate. These *o*-, *m*-, and *p*-distributions are roughly the same for all mediators although far from a statistically random distribution of 2:2:1, supporting the occurrence of the hydroxyl radical as the reactive oxidant.

Discussion

The kinetic and yield data available could be accounted for by the essential steps 1)—4), as illustrated in Scheme 1, which combine to form a catalytic cycle; 1) the rate-determining reaction between Fe^{3+} and a reduced mediator giving Fe^{2+} and the corresponding oxidized mediator. 2) The production of an OH radical by the reaction of H_2O_2 with Fe^{2+}, followed by the subsequent phenol-forming steps 3) and 4) which include the 1-hydroxycyclohexadienyl radical as the key intermediate. Since TMPD and DAMF have no labile proton, Scheme 1, unlike the reaction mechanism proposed by Richter and Waddell, involves no protonation and deprotonation events accompanying the redox reaction; for example,

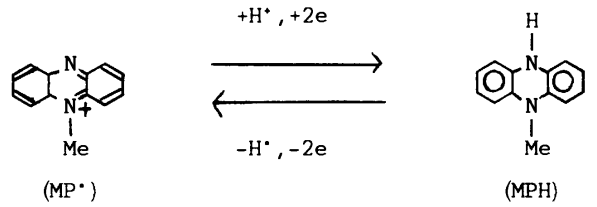

Scheme 1.

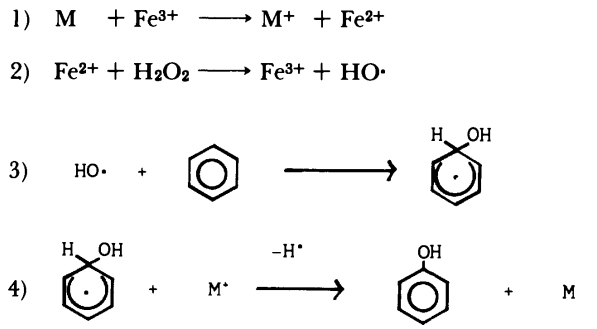

(M denotes an organic mediator in the reduced state.)

As can be seen from Table 2, MDA and AsH_2 are catalytically inactive. The two-electron redox potentials of MDA^{2+}/MDA (0 V) and dAs/AsH_2 (+0.17 V at pH 4; +0.06 V at pH 7)[10,11] are negative enough to reduce Fe^{3+}; nevertheless, those potentials seem to be too low to oxidize the 1-hydroxycyclohexadienyl radical to phenol. As for MDA, therefore, the one-electron oxidation by MDA^{2+} of the 1-hydroxylcyclohexadienyl redical (step 4) seems to be endothermic. The same argument can be given for catalytically inactive anthraquinonesulfonates[7] bearing a relatively low potential ($E°<-0.1$ V).[10,12] However, there is another explanation for the inactivity of ascorbic acid; dehydroascorbic acid (dAs) exists in hydrated form as the 2,3-bis-(gem-diol) in aqueous solution, which has no ability to oxidize the 1-hydroxycyclohexadienyl radical.

PMZ has a rather low activity, because it has a higher one electron-oxidation potential ($E°$=+0.86 V at pH 7)[13] than Fe^{3+}/Fe^{2+} couple ($E°$=+0.771 V; +0.74 at pH 3); hence, the reaction between Fe^{3+} and PMZ (step 1) is slightly endothermic. The lack of catalytic activity of thianthrene is due probably to the same reason.

Meanwhile, an organic mediator which possesses a redox potential somewhere between the $E°$ values of the Fe^{3+}/Fe^{2+} and 1-hydroxycyclohexadienyl radical/phenol couples, particularly, in the favorable range of about +0.2 and about +0.6 V, is quite effective. TMPD (+0.27 V), DAMF (+0.44 V), CT(+0.55 V), and HQ (+0.46 V)[13] meet well this requirement. These reactions follow the same mechanistic pattern. In addition, the oxidation potential of the 1-hydroxycyclohexadienyl radical is roughly estimated to lie somewhere between +0.1 and −0.1 V. Electrochemical potentials of various redox pairs are summarized in Fig. 3.

The effect of metal-chelating agents is quite interesting. The hydroxylations were inhibited by the addition of EDTA and 1,10-phenanthroline (Table 4) and no consumption of H_2O_2 was observed in both cases. However, the mechanistic features of the inhibition appear to be different with each chelating agent, because the redox potentials of iron–EDTA and iron–phenanthroline differ much: Since a redox potential of the iron–EDTA complex is far low compared to that of the standard Fe^{3+}/Fe^{2+} couple, the complexation with EDTA stabilizes the Fe(III) rather than Fe(II) state and thus would stop the progress of the Fe(II) formation (step 1). On the contrary, 1,10-phenanthroline complex (+1.03 V) stabilizes the Fe(II) rather than Fe(III) state to inhibit the generation of the OH radical (step 2). The hydroxylation in the presence of metal-chelating agents has been investigated by many workers.[14] Their roles have received much attention, but has not yet been fully understood and further studies will be needed.

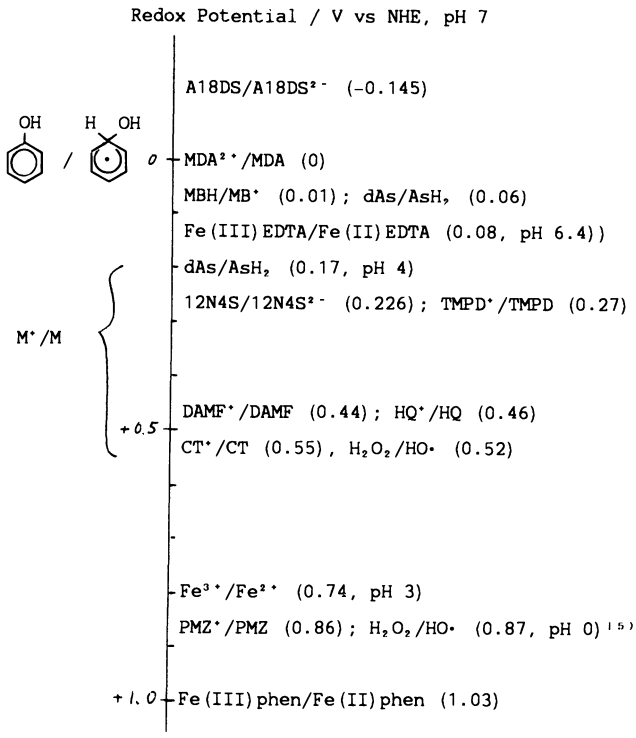

Fig. 3. Redox potentials (Volt vs. NHE, pH 7).

Table 6. Effect of Amounts of Benzene and H_2O_2 on Phenol Yield with $Fe^{3+}/TMPD/H_2O_2$

Benzene/ml	H_2O_2/mmol	Phenol yield/%
1	1	41.7
5	1	49.7
10	1	50.4
20	1	48.8
5	0.5	64.4
5	0.25	70.6
5	0.125	80.9

Reaction conditions: TMPD, 0.01 mmol; Fe^{3+}, 0.01 mmol; pH 3, 25 °C.

$$\underset{E°(V)\ 1.03}{\text{Fe(II)phen}} + H_2O_2 \xrightarrow{H^+,\ -H_2O} \underset{0.87}{\text{Fe(III)phen}} + HO\cdot$$

Finally, it is worth mentioning that, under the standard conditions, as Fig. 1 shows, the phenol production reaches about 40% regardless of used mediators. Although we can not offer a conclusive explanation for this observation, it should be noted, however, that the final phenol yield is substantially dependent on the initial concentration of added H_2O_2. Actually, as inspection of the data of Table 6 reveals, the TMPD-catalyzed reaction affords phenol in more than 80% yields, when, in order to maximize the conversion of H_2O_2 to phenol by minimizing further oxidation of product phenol and side reactions of H_2O_2, a five-fold excess of benzene and an eight-fold decreased amount of H_2O_2 were employed. Obviously, the presence of too much H_2O_2 is the major cause to decrease the phenol yield. Perhaps, a reaction shown below effectively competes with Reaction 3. It is well-known that the hydroperoxy radical will not participate in the hydroxylation of aromatic hydrocarbons.

$$H_2O_2 + HO\cdot \longrightarrow HOO\cdot + H_2O$$

Use of less Fe^{3+} improves the yield but only slightly. To our knowledge, more than 80% yield is the highest yet attained in the hydroxylations of unactivated aromatic hydrocarbons by hydroxyl radicals.

References

1) S. Udenfriend, C. T. Clark, J. Axelrod, and B. B.

Brodie, *J. Biol. Chem.*, **208**, 731 (1954).

2) R. R. Grinstead, *J. Am. Chem. Soc.*, **82**, 3472 (1960).

3) G. A. Hamilton, J. P. Friedman, and P. M. Campbell, *J. Am. Chem. Soc.*, **88**, 5266 (1966); G. A. Hamilton, J. W. Hanifin, and J. P. Friedman, *ibid.*, **88**, 5269 (1966).

4) V. Ullich, D. Hay, J. Staudinger, H. Buech, and W. Rummeln , *Biol. Phamacol.*, **16**, 2237 (1967).

5) H. W. Richter, M. A. Fetrow, R. E. Lewis, and W. H. Waddell, *J. Am. Chem. Soc.*, **104**, 1666 (1982); H. W. Richter and W. H. Waddell, *ibid.*, **104**, 4630 (1982).

6) S. Tamagaki, M. Sasaki, and W. Tagaki, *Bull. Chem. Soc. Jpn.*, in contribution.

7) S. Tamagaki, K. Suzuki, and W. Tagaki, *Tetrahedron Lett.*, **24**, 4847 (1983).

8) H. I. X. Mager and W. Berends, *Recuil Trav. Chim.*, **91**, 611 (1972); W. Berends et al., *ibid.*, **84**, 1329 (1965); **86**, 833 (1967).

9) L. Michaelis, M. P. Schubert, and S. Granick, *J. Am. Chem. Soc.*, **61**, 1981 (1939).

10) W. M. Clark, "Oxidation-Reduction Potentials of Organic Systems," R. E. Krieger Publ., N. Y. (1972); "Kagaku Binran, Kiso-hen," Maruzen, Tokyo (1975).

11) H. Borsook, H. W. Davenport, C. E. P. Jeffreys, and R. C. Warner, *J. Biol. Chem.*, **117**, 237 (1937).

12) K. B. Patel and R. L. Wilson, *J. Chem. Soc., Faraday Trans. 1*, **69**, 814 (1973).

13) B. W. Carlson, L. Miller, P. Neta, and J. Grodkowski, *J. Am. Chem. Soc.*, **106**, 7237 (1984); J. Grodkowski, P. Neta, B. W. Carlson, and L. Miller, *J, Phys. Chem.*, **87**, 3135 (1983); G. Borg, *Proc. Natl. Acad. Sci. U.S.A.*, **48**, 612, 623, 643, (1962); A. Obata, M. Yoshimori, K. Yamada, and H. Kawazuna, *Bull. Chem. Soc. Jpn.*, **58**, 437 (1985).

14) R. R. Grinstead, *J. Am. Chem. Soc.*, **82**, 3464 (1960); J. R. Hart, *Chem. Tech.*, **1987**, 313; S. Rahhal and H. W. Richter, *J. Am. Chem. Soc.*, **110**, 3126 (1988); J. D. Rush and W. H. Koppenol, *ibid.*, **110**, 4957 (1988).

15) W. H. Koppenol and J. Butler, *J. Adv. Free. Red. Biol. Med.*, **1**, 91 (1985).

 © 1989 The Chemical Society of Japan Bull. Chem. Soc. Jpn., 62, 159—163 (1989)

The Catalytic Role of a Flavin Analogue for Aromatic Hydroxylation with the Udenfriend System

Seizo TAMAGAKI, Masaaki SASAKI, and Waichiro TAGAKI*
Department of Applied Chemistry, Faculty of Engineering, Osaka City University, Sugimoto 3, Sumiyoshi-ku, Osaka 558
(Received August 11, 1988)

A new combination of the Udenfriend reagent and a flavin analogue was found to hydroxylate benzene to phenol. Effects of temperature and concentrations of reaction components, i.e., iron(II), flavin, and ascorbate, on the phenol yield were examined. In particular, decreasing ascorbate concentration increased the yield of phenol. Thus, 68% of the yield was obtained under better conditions. The mechanism of action of ascorbic acid and the flavin was discussed.

The Udenfriend system (Fe^{2+}/EDTA/ascorbate/O_2),[1] a model peroxidase, is a general method for the addition of a hydroxyl group into an aromatic substrate. Grinstead has examined the hydroxylation of benzoic and salicylic acids and has suggested a chain mechanism in which a hydroxyl radical is the reactive species that takes part in hydroxylation.[2] The reaction is relatively mild compared to other methods,[3] and the products obtained with the Udenfriend system in vitro are identical with that from the same compound in vivo. From a biomimetic or mechanistic viewpoint, the Udenfriend and related systems are still worthy of further investigations.[4]

Nevertheless, these systems usually afford only 3 to 25% yields depending on the substrate, the metal ion, and the complexing agent. Particularly, the hydroxylation of benzene gave rise to only less than 5% yield of phenol even under better conditions. This suggests that the Udenfriend system itself has yet a critical disadvantage of electron accepting/transferring relay in the catalytic cycle.

We report here that the 1,10-ethanoisoalloxazinium cation (a flavin analogue **1**)[5] markedly enhances the catalytic efficiency of the Udenfriend system. In this work, benzene was selected as a diagnostic substrate and for ease of the quantitative analysis of the product phenol.

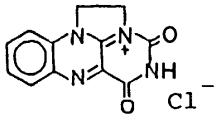

1

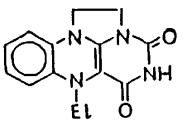

2

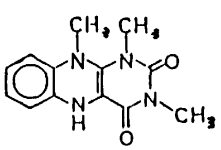

3

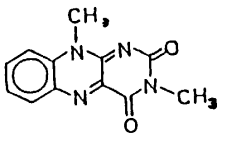

4

Experimental

Materials. EDTA, ascorbic acid, 1,10-phenanthroline, iron(II) sulfate were purchased from commercial suppliers and used without further purification. Flavins (**1**—**4**) were prepared by literature procedures.[6]

Hydroxylation. The standard hydroxylation was performed in a benzene (1 ml)-water (50 ml) two-phase system, containing 2 mM (1 M=1 mmol dm^{-3}) of Fe^{2+}, 2 mM of **1**, and 20 mM of ascorbic acid, at 50 °C under constant bubbling of oxygen through two needles with mechanical shaking. The pH of the reaction medium was initially adjusted to 3.0 with H_2SO_4. As the rate of the reaction is slow compared to dissolution of oxygen, the solution was assumed to be saturated with oxygen at all times. Benzene in excess of saturation was employed to keep the benzene concentration in the aqueous layer constant. The amount of phenol produced was determined with HPLC by using anisole as an internal standard as described previously.[7] All the percent yields are based on the added amount of ascorbate. Under the standard conditions (90 min), the yield was 31.0%. The results thus obtained are summarized in Figs. 1—4 and Tables 1—3. Unlike the original Fenton

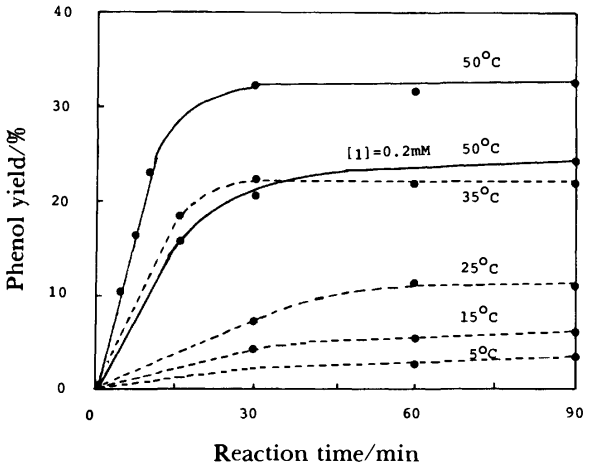

Fig. 1. Time courses of hydroxylation with Fe^{2+}/**1**/AsH_2/O_2.
Conditions: Fe^{2+}(2 mM)/**1**(2 mM)/AsH_2(20 mM) under O_2 at pH 3.

system, no biphenyl was detected by HPLC analysis in any cases. However, 10% of hydroquinone was produced.

Kinetics. The rate of reaction of **1** with ascorbic acid under N_2 at 25 °C was followed by the disappearance of the absorption peak due to **1** (λ_{max} 365 nm; ε 13500 in H_2O). Typical UV traces are shown in Fig. 5.

Results and Discussion

Figure 1 depicts the time plots for the benzene hydroxylation with the Fe^{2+}/**1**/ascorbic acid/O_2 system at various temperatures. The reaction is strongly temperature-dependent, and the phenol yield increases steadily with reaction time and reaches a limiting value at each reaction temperature. Table 1 compares the effect of changing structures of flavins on the yield under the standard conditions. The phenol yield for unblocked flavin **4** is only 1.1% and as poor as that for the control reaction in the absence of any flavins. On the other hand, flavin **1**, blocked with an ethano bridge at N-1 and N-10, afforded more than 30% yield. Further blocking at N-5 position (**2**) is far less effective than is the blocking at N-1 and N-10. Hemmerich and Massey[8] have studied the flavin-dependent molecular oxygen activation and have concluded that: (1) the more planar is the structure of a flavin molecule, the greater the reactivity toward O_2, (2) the substitution of 5-position with an alkyl group lowers the catalytic activity. On the basis of these criteria, the catalytic activity is expected to be in the order, **1**>**2**>**3**, just as was observed here.

A mechanism shown in Scheme 1 can be tentatively proposed for this reaction on the basis of this and other research. There are two catalytic cycles in the sequence; one is for the generation of hydrogen peroxide (Reactions 1, 2), the other for the production of phenol (Reactions 3—6). Although this mechanism is basically analogous to that previously reported for the nonclassical Fenton reaction (Fe^{3+}/MPH/O_2/NADH system),[9] the role of ascorbic acid (AsH_2) is somewhat different from that of NADH which has been proposed to reduce solely 5-methylphenazinium cation (MP^+). The details will be discussed later. In this mechanism, we presume the catalytic function of a flavin as follows; its fully reduced form (Fl_{red}) would be involved in formation of H_2O_2 from molecular oxygen via Reaction 2, while the oxidized form (Fl_{ox}) would be involved in phenol formation via Reaction 6 in which Fl_{ox} is converted to Fl_{sem} by abstracting one electron from the 1-hydroxycyclohexadienyl radical (**5**). The carbon cation thus formed is converted into phenol immediately after its formation (Reaction 6).[10] The Fl_{ox} could be reconverted to Fl_{red} either via disproportionation of Fl_{sem} (Reaction 7) or reduction with ascorbic acid (Reaction 1).

Thus, the lack of catalytic activity of unblocked flavin **4** is explained by its lower redox potential than that of ascorbic acid; hence, Reaction 1 is substantially endothermic. An altenative explanation may be possible. Reaction 6 would be also too endothermic to propagate the radical chain reaction, for the redox potential of **4** (Fl_{ox}) was estimated to be much lower than that of the hexadienyl radical.[7]

$$Fl_{ox} + AsH_2 \underset{(0.5)}{\overset{-H^+}{\rightleftharpoons}} Fl_{red}^- + dAs \quad (1)$$

$$Fl_{red} + O_2 \xrightarrow[(10^3)^{6)}]{+H^+} Fl_{ox} + H_2O_2 \quad (2)$$

$$2\,Fe(III) + AsH_2 \xrightarrow[(10^2)^{2)}]{-2\,H^+} 2\,Fe(II) + dAs \quad (3)$$

$$Fe(II) + H_2O_2 \xrightarrow[(50)^{13)}]{+H^+} Fe(III) + HO\cdot \quad (4)$$

$$HO\cdot + \bigcirc \xrightarrow[(10^{10})]{} \overset{H}{\underset{}{\bigcirc}}\!\!\overset{OH}{\cdot} \quad (5)$$

5

$$\overset{H}{\underset{}{\bigcirc}}\!\!\overset{OH}{\cdot} + Fl_{ox} \xrightarrow[(10^6-10^8)^{10)}]{-H^+} \bigcirc\!\!-\!\!OH + Fl_{sem} \quad (6)$$

$$2\,Fl_{sem} \underset{-H^+}{\overset{+H^+}{\rightleftharpoons}} Fl_{ox} + Fl_{red} \quad (7)$$

Scheme 1. Figures in parentheses are the 2nd-order rate constants, $M^{-1}\,s^{-1}$, where a flavin is **1**.

Table 1. Hydroxylation of Benzene by Fe^{2+}–AsH_2–O_2 in the Presence of Various Flavin Analogs[a]

Flavin	Phenol yield/%[b]
None (Udenfriend's conditions)	1.1
1	31.9
2	7.1
3	16.2
4	1.8

a) Conditions: Fe^{2+}(2.0 mM)/flavin(2.0 mM)/AsH_2(20 mM); reaction pH 3, 50 °C under O_2 for 90 min. b) Phenol yield based on added AsH_2.

In order to obtain better yields of phenol and to establish the reaction mechanism further, studies of variation of pH and concentrations of reaction components such as iron(II), flavin **1**, and ascorbic acid, and of effect of coordinating additives were performed. As **1** was found to be the most effective of all flavins at pH 3 (Table 2), only **1** was used for

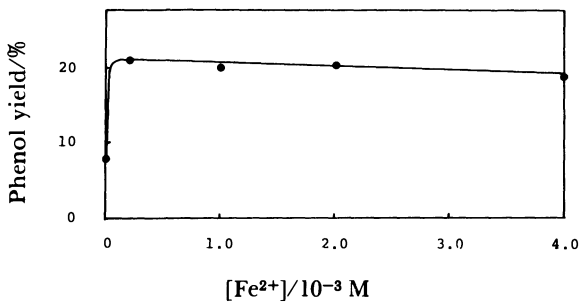

Fig. 2. Effect of Fe^{2+} concentration on phenol yield. Conditions: **1**(2 mM)/AsH_2(20 mM) under O_2 at pH 3 for 90 min.

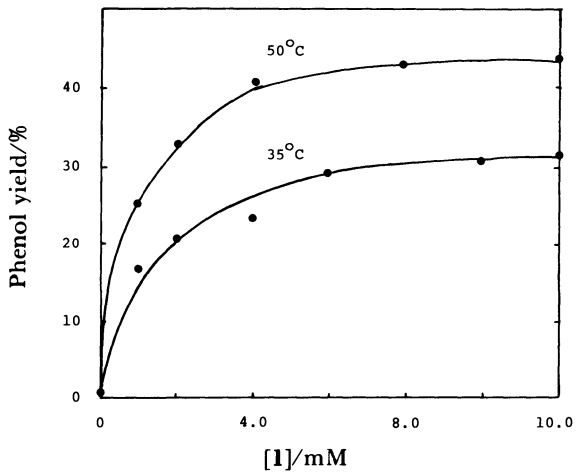

Fig. 3. Effect of concentration of **1** on phenol yield. Conditions: Fe^{2+}(2 mM)/AsH_2(20 mM) under O_2 for 90 min.

Table 2. Dependence of Phenol Yield on Reaction pH

pH\Flavin	Yield/%		
	1	**2**	**3**
1	23.3	6.0	24.0
3	31.9	7.1	16.2
5	11.8	2.6	9.2

Conditions: Fe^{2+}(2.0 mM)/flavin(2.0 mM)/AsH_2 (20.0 mM) under O_2 at 50°C for 90 min.

further investigations. The results are collected in Figs. 2 and 3. Figure 2 shows that the yield appears to be virtually independent of Fe^{2+} concentrations beyond 0.1 mM, indicating that neither the reduction (Eq. 3) nor the oxidation of metal ion (Eq. 4)[11] is rate-determining under the standard conditions. Moreover, the same Figure shows that even adventitious iron ion (no added Fe^{2+}), although less efficient, is capable of continuing the catalytic chain cycle. In these respects the present reaction follows a reaction pattern characteristic of the Fe^{3+}/MPH/O_2/NADH system.[9]

As can be seen from Table 3, the Fe^{2+}/**1**/H_2O_2 hydroxylating system, in which hydrogen peroxide is itself a reactant, is inhibited by addition of metal-complexing agents such as EDTA and 1,10-phenanthroline. Particularly, effect of EDTA is quite interesting. As was reported in the previous paper,[7] the mechanism for that hydroxylation is as indicated by the reaction sequence in Scheme 2. EDTA prevents the reaction of Fl_{red} (Fl_{sem}) with Fe^{3+} (Eq. 11) by markedly lowering the redox potential of Fe^{3+} below that of Fl_{red} (Fl_{sem}).

$$Fe(II) + H_2O_2 \xrightarrow[-H_2O]{+H^+} Fe(III) + \cdot OH \quad (8)$$

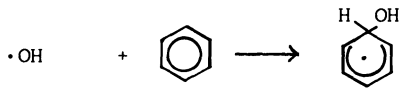

(9)

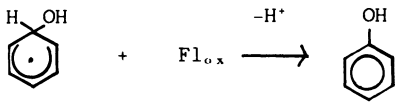

(10)

$$Fl_{red}(Fl_{sem}) + Fe(III) \longrightarrow Fl_{sem}(Fl_{ox}) + Fe(II) \quad (11)$$

$$2\,Fl_{sem} \underset{-H^+}{\overset{H^+}{\rightleftharpoons}} Fl_{red} + Fl_{ox} \quad (12)$$

On the other hand, EDTA in the present system had a little or no inhibitory effect on the phenol production, indicating that ascorbate must be used for

Table 3. Effect of Metal Ion-Chelating Agents (pH 3; 50°C)

Hydroxylating system	Fe^{2+}	**1**	% Phenol yield			
	mM	mM	None	EDTA[e]	DETAPAC[f]	Phen[g]
Present (a)	0.05	2.0	31.0	34.5	—	4.0
(b)	1.0	2.0	31.9	30.8	38.7	27.1
Udenfriend[c]	1.0	0.0	0.8	4.4	1.3	0.7
Fe^{2+}/**1**/H_2O_2[d]	1.0	2.0	41.0	7.3	6.5	4.8

a) Fe^{2+}/**1**/AsH_2(20 mM)/chelating agent(1 mM) under O_2 for 1.5 h. b) Fe^{2+}/**1**/AsH_2(20 mM)/chelating agent(2 mM) under O_2 for 1.5 h. c) No **1** was added. Fe^{2+}/AsH_2(20 mM)/chelating agent(2 mM) under O_2 for 1.5 h. d) Fe^{2+}/**1**/H_2O_2(1 mM)/chelating agent(2 mM) at 25°C under N_2 for 2.5 h. e) Ethylenediaminetetraacetic acid. f) Diethylenetriaminepentaacetic acid. g) 1,10-Phenanthroline.

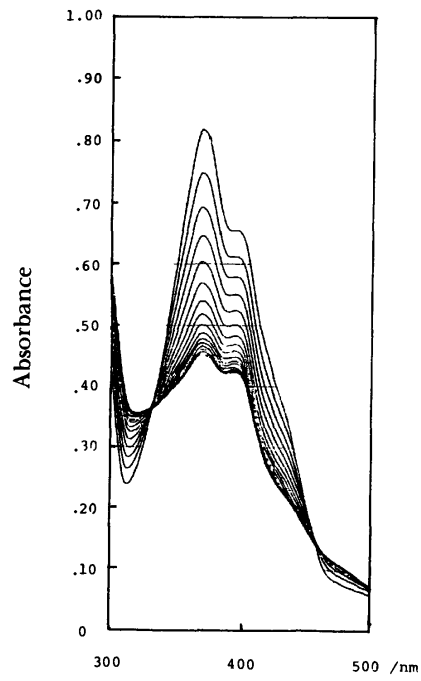

Fig. 4. UV traces for reaction of **1** with AsH_2 under N_2 at 25 °C at pH 3. The time interval is kept constant at 3 min. [**1**]=0.067 mM; $[AsH_2]_0$=2.68 mM.

reducing not only Fe^{3+} but also even the Fe(III)–EDTA chelate (Eq. 3). The Fe(II)–EDTA chelate have been well-known to react with H_2O_2 much more rapidly than the haxaaquairon(II) ion to produce reactive oxidants (Eq. 4).[11] As opposed to EDTA, 1,10-phenanthroline almost completely inhibited the production of phenol. This is probably because complexation of Fe^{3+} with 1,10-phenanthroline significantly stabilizes the Fe(II) rather than Fe(III) state and hence surpresses the generation of OH radical (Eq. 13).

$$\underset{E°(V)\ 1.03}{\text{Fe(II)-phen}} + H_2O_2 \not\longrightarrow \underset{0.72}{\text{Fe(III)-phen}} + HO\cdot \qquad (13)$$

Figure 3 illustrates the plots of the phenol yield as a function of varying concentrations of **1** over its concentration range 0—10 mM under the standard conditions, unless otherwise stated. With increase of the flavin concentrations, the yield increases steadily and approaches a limiting value of 32% at flavin concentrations greater than 4 mM. Similarly, comparison of time plots at 50 °C, shown as solid lines (a and b) in Fig. 1, reveals that the hydroxylation rate is proportional to the concentration of the catalyst flavin. These findings suggest again that either step associated with the formation of H_2O_2, i.e., Reaction 1 or 2, seems rate-determining. According to Bruice's calculation of the Gibbs free energy,[6] Reaction 2 is significantly exothermic as opposed to Reaction 1. Thus, the rate-determining step should be Reaction 1 rather than 2. Actually, this is evidenced further by

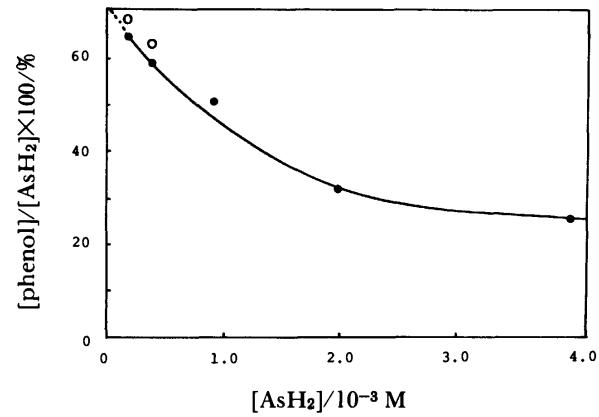

Fig. 5. Plots of phenyl yield vs. initial concentration of AsH_2. The yield is based on the initially added amount of AsH_2.
Conditions: (●) Fe^{2+}(2 mM)/**1**(2 mM); (○) Fe^{2+}(0.2 mM)/**1**(2 mM) under O_2 at pH 3 for 90 min.

Fig. 4, which illustrates the kinetic feature of reduction of Fl_{ox} with ascorbic acid in a 40-fold excess under nitrogen. The absorbance at λ_{max} 365 nm due to **1** decreases and finally the equilibrium is attained; as would be expected, the decreased peak returns to the original peak as soon as air has been introduced into the solution. The apparent 2nd-order rate constant for the reduction of Fl_{ox} thus obtained is 0.5 $M^{-1}\,s^{-1}$. This figure shows that the reduction in question is the slowest of all the reactions in Scheme 1. It is quite probable, therefore, that Reaction 1 is the rate-limiting step of the hydroxylation.

Meanwhile, the effect of altering ascorbic acid concentrations is particularly suggestive (Fig. 5). The yield of phenol increased steadily as the concentration of ascorbic acid is decreased; namely, the eight-fold decrease of ascorbic acid increases the yield up to 67.7%. This means that the presence of too much ascorbic acid in solution is a major important factor diminishing the phenol yield, where side reactions such as Reactions 14 and 15 might participate.

$$AsH_2 + \cdot OH \longrightarrow AsH\cdot + H_2O \qquad (14)$$

$$AsH_2 + H_2O_2 \longrightarrow dAs + 2\,H_2O \qquad (15)$$

Another inevitable side reaction would be ascribed to the reaction of the 1-hydroxycyclohexadienyl radical itself. As have often been reported by many workers,[12] the cyclohexadienyl radical will be trapped by molecular oxygen to give eventually hydroquinone. In fact, 10.0% of hydroquinone was produced under the standard conditions.

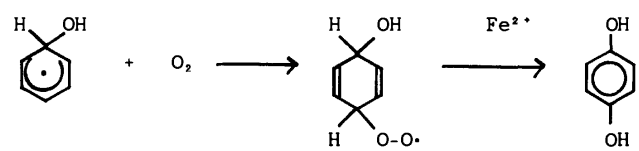

In conclusion, we have found that certain flavins markedly improve the Udenfriend hydroxylation system; a flavin plays versatile roles as catalyst for accepting and transferring electron(s). Ascorbic acid is merely the reductant toward Fl_{ox} and Fe^{3+}.

References

1) S. Udenfriend, C. T. Clarke, J. Axelrod, and B. B. Brodie, *J. Biol. Chem.*, **208**, 731 (1954); B. B. Brodie, J. Axelrod, P. A. Shore, and S. Udenfriend, *ibid.*, **208**, 741 (1954).

2) R. R. Grinstead, *J. Am. Chem. Soc.*, **82**, 3472 (1960).

3) G. A. Olah, A. P. Fung, and T. Kewn, *J. Org. Chem.*, **46**, 4305 (1981); I. Izumi, W. W. Dun, K. O. Wilborn, F. F. Fan, and A. J. Bard, *J. Phys. Chem.*, **84**, 3207 (1980); M. K. Eberhardt, G. A. Martinez, J. I. Rirerc, and A. Fuentes-Aponte, *J. Am. Chem. Soc.*, **104**, 7609 (1982); H. Sugimoto and D. T. Sawyer, *ibid.*, **106**, 4283 (1984).

4) S. Rehhal and H. W. Richter, *J. Am Chem. Soc.*, **110**, 3126 (1988); M. Masarwa, H. Cohen, D. Meyerstein, D. L. Hickman, A. Bakac, and J. H. Espenson, *ibid.*, **110**, 4293 (1988).

5) W. R. Knappe, *Chem. Ber.*, **108**, 2422 (1975).

6) G. Eberline and T. C. Bruice, *J. Am. Chem. Soc.*, **104**, 1449 (1982); **105**, 6679, 6685 (1983); H. I. X. Mager, R. Addink, and W. Berends, *Rec. Trav. Chim. Pays-Bas*, **91**, 611 (1967). M. Gladts and W. R. Knappe, *Chem. Ber.*, **107**, 3658 (1974).

7) S. Tamagaki, M. Sasaki, and W. Tagaki, *Bull. Chem. Soc. Jpn.*, in contribution.

8) T. Matuura, "Sanso Sanka Hanno," Maruzen, Tokyo (1977), p. 347.

9) H. W. Richter and W. H. Waddell, *J. Am. Chem. Soc.*, **104**, 4630 (1982); H. W. Richter, M. A. Fetrow, R. E. Lewis, and W. H. Waddell, *ibid.*, **104**, 1666 (1982).

10) S. Steenken and N. V. Raghavan, *J. Phys. Chem.*, **83**, 3101 (1979).

11) R. R. Grinstead, *J. Am. Chem. Soc.*, **82**, 3464 (1960).

12) I. Barakrishnan and M. P. Reddy, *J. Phys. Chem.*, **74**, 850 (1970); S. Ito, A. Kunai, H. Okada, and K. Sasaki, *J. Org. Chem.*, **53**, 296 (1988).

Synthesis, Structure, and Properties of Triple-Layered [2.2][2.2]Naphthalenophane[1)]

Tetsuo Otsubo,* Yoshio Aso, Fumio Ogura, Soichi Misumi,†
Atsushi Kawamoto,†† and Jiro Tanaka††
Department of Applied Chemistry, Faculty of Engineering, Hiroshima University, Saijo, Higashi-Hiroshima 724
†Institute of Scientific and Industrial Research, Osaka University, Ibaraki, Osaka 567
††Department of Chemistry, Faculty of Science, Nagoya University, Chikusa-ku, Nagoya 464
(Received July 11, 1988)

The title compound was synthesized in a similar manner to a simple access to triple-layered [2.2][2.2]paracyclophane. Its structure was elucidated by X-ray crystallographic analysis. The outer naphthalene rings are bent into a boat form and the inner naphthalene ring is bent into a twist form. These naphthalenes are stacked in layers within van der Waals contact. Therefore, there is a strong transannular π-electronic interaction between them, which brings about characteristic bathochromism, hyperchromism, and broadening in the electronic spectrum. These effects are more prominent than those of the double-layered homologue.

Multilayered cyclophanes are one of the most interesting compounds in the field of cyclophane chemistry.[2)] They show more unusual physical and chemical properties than double-layered phanes because their transannular π-electronic interactions between aromatic nuclei increase with an increase of the layers.[3)] However, the previous study has been limited only to benzene series.[2)] The extensive studies to fused aromatic ring series might be helpful in a comprehensive understanding of the transannular electronic interactions of cyclophanes which serve as an excimer model.[4)] In this report, we would like to present triple-layered [2.2][2.2]naphthalenophane (**1**) as the first example of multilayered phanes composed of fused aromatic nuclei. There have been some double-layered [2.2]naphthalenophanes of different stacking types mainly depending on the substitution mode of the bridging ethylenes. Haenel and Staab reported chiral [2.2](2,6)naphthalenophane (**2**), in which two aromatic rings were bridged at the 2- and 6-positions and obliquely overlapped each other.[5)] Blanck and Haenel later reported achiral isomer (**3**), which had the exact overlap of the two aromatic rings and accordingly was less stable than **2**.[6)] A study of a series of multilayered [2.2]paracyclophanes revealed that there was observed a dramatic enhancement in the electronic interaction with an increase in stacking layers from double to triple.[3)] Therefore, triple-layered naphthalenophane (**1**) is expected to show characteristic properties as compared to double-layered one **2** or **3**.

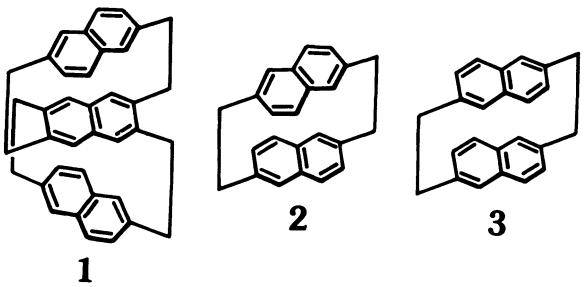

1 **2** **3**

Results and Discussion

Synthesis. Multilayered cyclophanes were previously synthesized in multisteps via double-layered ones.[3,7)] The same pathway is inapplicable to fused aromatic phanes because the functionalized double-layered intermediates are not readily accessible. Boekelheide et al., however, reported that a termolecular coupling of 1,2,4,5-tetrakis(bromomethyl)benzene

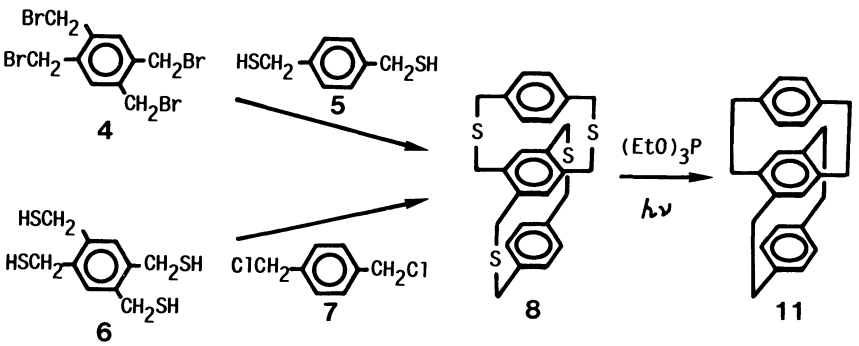

Scheme 1.

and 2 equiv of 2,6-bis(mercaptomethyl)pyridine followed by ring contraction using the Wittig rearrangement led to triple-layered pyridinoparacyclophane.[8] Such a termolecular reaction appears to provide a direct entry to triple-layered phanes, though it has a possibility of not only a low yield but also the formation of some regioisomers. Then, we have first examined its approach to triple-layered [2.2][2.2]paracyclophane (**11**) prior to the present target molecule **1**. As shown in Scheme 1, a termolecular coupling reaction of 1,2,4,5-tetrakis(bromomethyl)benzene (**4**) and 2 equiv of 1,4-bis(mercaptomethyl)benzene (**5**) in ethanol solution containing potassium hydroxide at room temperature gave triple-layered tetrathia[3.3][3.3]paracyclophane (**8**) in only 4.2% yield. On the other hand, a reaction of 1,2,4,5-tetrakis(mercaptomethyl)benzene (**6**) and two 1,4-bis(chloromethyl)benzenes (**7**) in refluxing ethanol gave the same compound **8** in 12% yield. There was no evidence for the formation of the other possible isomers **9** and **10**.

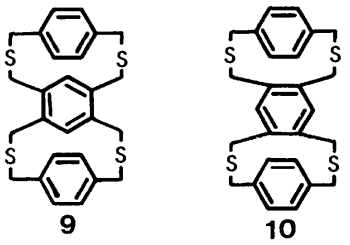

9 **10**

The photoinduced desulfurization of **8** with triethyl phosphite smoothly proceeded to give the desired compound **11** in 93% yield. The coupling yield is quite low, but the steps are few and the reactants **4**—**7** are readily available. As a result, this access constitutes the simplest one to **11**.

A similar method was applied to the synthesis of triple-layered [2.2][2.2]naphthalenophane (**1**) (Scheme 2). 2,3,6,7-Tetramethylnaphthalene (**12**) was prepared from 2,3-dimethylsuccinic anhydride and *o*-xylene according to the procedure of Dozen and Hatta[9] and brominated with *N*-bromosuccinimide to 2,3,6,7-tetrakis(bromomethyl)naphthalene (**13**) in 69% yield. A termolecular coupling reaction of **13** and two 2,6-bis(mercaptomethyl)naphthalenes (**14**) gave triple-layered tetrathia[3.3][3.3]naphthalenophane (**17**) in 9% yield. Alternatively, **13** on treatment with thiourea followed by alkaline hydrolysis was converted to 2,3,6,7-tetrakis(mercaptomethyl)naphthalene (**15**), which was coupled with two 2,6-bis(bromomethyl)naphthalenes (**16**) to give the same product **17** in 17% yield. The ^{1}H NMR spectrum demonstrates that the inner naphthalene protons resonate as a multiplet at δ 6.1—6.4. This indicates that **17** consists of an isomeric mixture of **17a—c**, which are quite difficult to separate. Another possible isomer **18** with a different substitution mode was not detected. The inner aromatic protons of **18** might be situated just above the outer naphthalene rings, so that the ^{1}H NMR spectrum should show a characteristic

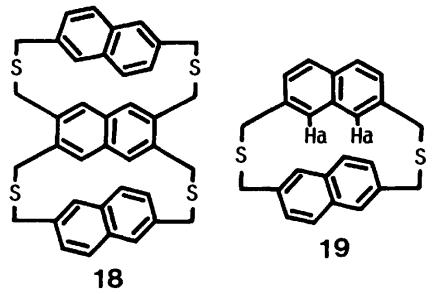

18 **19**

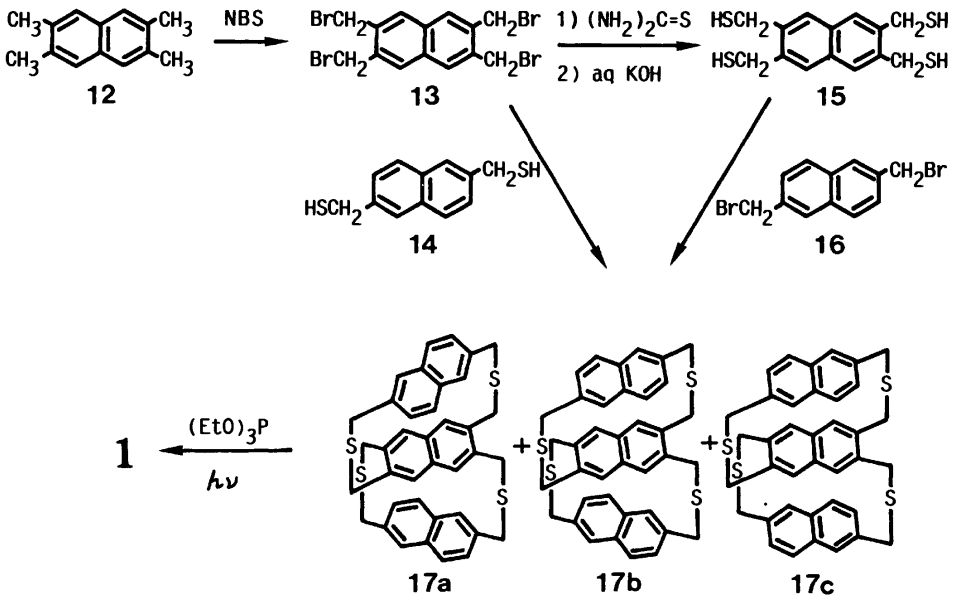

12 **13** **14** **15** **16** **1** **17a** **17b** **17c**

Scheme 2.

upfield shift like H_a protons (δ 5.82) of 2,15-dithia[3.3](2,6)(2,7)naphthalenophane (**19**) as a double-layered homologue.[10] The photolytic sulfur extrusion of **17** with triethyl phosphite gave the desired product **1** in 32% yield. Its structure was characterized by elemental analysis, spectroscopic measurements, and finally X-ray crystallographic analysis. No desulfurized isomers corresponding to the stacking types of **17b** and **17c** were observed. Probably a ring rotation occurred during the C–S bond fission on photolysis, leading to the sole formation of the more stable isomer **1**.

Molecular Structure. The crystal of **1** is triclinic with space group $P\bar{1}$ and the unit cell contains four molecules which form two distinct enantiomeric pairs. Table 1 lists final atomic parameters for the molecules (I) and (II). No essential difference in structure between the two distinct molecules is observed, so that only molecular structure I is discussed below. Figure 1 shows the side view of the ORTEP drawing. The three naphthalenes diagonally overlap each other and, on the whole, take a spiral structure. As seen from the top view of Fig. 2, the diagonal angle between the neighboring ones is 34°. The bridging ethylene bonds are torsional to avoid the eclipsing form. The torsional angle around C(1)–C(2) bond is 39°. Table 2 summarizes the C–C bond lengths and C–C–C bond angles. As a whole, they hold values close to normal except for a little elongation of the bridged ethylene bonds. On the other hand, Figs. 3 and 4 demonstrate that the outer naphthalene rings are bent into a boat form and the inner naphthalene ring is bent into a twist form. A mean plane (A) defined by C(4), C(5), C(11), and C(12) atoms inclines by 8.1° from a plane (molecular horizon) defined by C(5), C(6), C(10), and C(11), a plane (B) defined by C(3),

Table 1. Final Atomic Coordinates ($\times 10^4$) with Estimated Standard Deviations in Parentheses and Thermal Parameters ($Å^2$)[a] for Carbon Atoms of **1**

Atom	Molecule I				Molecule II			
	x	y	z	B_{eq}	x	y	z	B_{eq}
C(1)	6404(4)	7180(2)	1613(4)	4.02	6430(4)	−1529(2)	6698(4)	3.80
C(2)	6770(4)	7787(2)	2740(4)	3.98	6830(4)	−1907(2)	7842(4)	4.44
C(3)	6816(3)	7412(2)	3932(3)	3.40	6907(4)	−1470(2)	9028(4)	4.06
C(4)	7787(3)	7458(2)	4668(3)	3.35	7891(4)	−1011(2)	9729(4)	4.21
C(5)	7868(3)	6937(2)	5567(3)	3.30	7975(3)	−421(2)	10593(4)	3.79
C(6)	8859(3)	6909(2)	6223(4)	4.11	8981(4)	127(3)	11195(4)	4.77
C(7)	8908(3)	6270(3)	6788(4)	4.43	9025(4)	807(3)	11727(4)	4.74
C(8)	7963(4)	5619(3)	6730(3)	4.13	8076(4)	970(3)	11702(3)	4.25
C(9)	6983(3)	5685(2)	6286(3)	3.71	7103(4)	402(3)	11298(3)	4.29
C(10)	6906(3)	6338(2)	5691(3)	3.34	7010(3)	−313(2)	10738(3)	3.85
C(11)	5905(3)	6371(2)	5058(4)	3.80	6005(3)	−863(2)	10156(4)	4.39
C(12)	5856(3)	6887(2)	4214(4)	3.71	5955(4)	−1429(2)	9330(4)	4.25
C(13)	8039(4)	4845(3)	6964(4)	5.14	8145(4)	1788(3)	11881(4)	4.59
C(14)	8501(4)	4555(2)	5943(4)	4.49	8554(4)	2262(2)	10810(4)	4.09
C(15)	8015(3)	4749(2)	4699(3)	3.11	8051(3)	1784(2)	9599(3)	2.83
C(16)	8566(3)	5407(2)	4228(3)	2.84	8599(3)	1392(2)	9128(3)	2.45
C(17)	8049(3)	5758(2)	3314(3)	2.31	8060(3)	761(2)	8243(3)	2.21
C(18)	8589(3)	6386(2)	2696(3)	2.98	8594(3)	395(2)	7614(3)	2.65
C(19)	8052(3)	6760(2)	1937(3)	3.16	8052(3)	−273(2)	6890(3)	2.93
C(20)	6925(3)	6593(2)	1904(3)	3.00	6936(3)	−670(2)	6918(3)	2.66
C(21)	6370(3)	5920(2)	2346(3)	2.55	6386(3)	−271(2)	7368(3)	2.46
C(22)	6909(3)	5466(2)	2999(3)	2.13	6919(3)	469(2)	7973(3)	2.03
C(23)	6370(3)	4729(2)	3350(3)	2.49	6386(3)	937(2)	8319(3)	2.45
C(24)	6911(3)	4344(2)	4090(3)	2.85	6940(3)	1619(2)	9032(3)	2.83
C(25)	6422(3)	3482(2)	4057(4)	4.00	6430(4)	2222(2)	9001(4)	3.80
C(26)	6857(4)	3109(2)	3120(4)	4.48	6849(4)	2799(2)	8033(4)	4.28
C(27)	6935(4)	3535(2)	1984(4)	4.09	6906(3)	2388(2)	6893(4)	3.75
C(28)	7927(4)	3995(2)	1781(4)	4.31	7885(3)	2418(2)	6656(4)	3.59
C(29)	8029(4)	4572(2)	949(4)	4.06	7963(3)	1875(2)	5821(3)	3.34
C(30)	9036(4)	5115(3)	842(4)	5.39	8964(3)	1835(2)	5695(4)	3.87
C(31)	9099(4)	5787(3)	333(4)	5.36	9011(4)	1182(2)	5191(4)	4.18
C(32)	8152(4)	5953(3)	−127(4)	4.98	8064(3)	529(2)	4783(3)	3.58
C(33)	7169(4)	5386(3)	−221(3)	4.66	7078(4)	604(2)	4706(3)	3.72
C(34)	7079(4)	4681(2)	310(3)	4.00	7000(3)	1275(2)	5225(3)	3.29
C(35)	6059(4)	4134(3)	383(4)	4.35	5989(4)	1320(3)	5327(4)	4.05
C(36)	6000(4)	3583(2)	1193(4)	4.40	5947(4)	1861(2)	6127(4)	4.16
C(37)	8226(4)	6771(3)	−271(4)	5.81	8143(4)	−250(3)	4649(4)	4.57
C(38)	8595(4)	7245(3)	1007(4)	5.06	8557(4)	−499(3)	5932(4)	4.19

a) $B_{eq}=(4/3)\sum_{ij}\beta_{ij}(a_i \cdot a_j)$.

C(4), and C(12) atoms makes a dihedral angle of 7.9° with the plane A, and the C(2)–C(3) bond makes an angle of 9.7° with the plane B. These values are fairly smaller than the bending angles of [2.2]paracyclophane[11] or the multilayered homologues,[12] indicating that the outer naphthalene effectively disperses a strain throughout the fused system. On the other hand, the twist angle of the inner naphthalene, defined by the dihedral angle between mean planes of the two

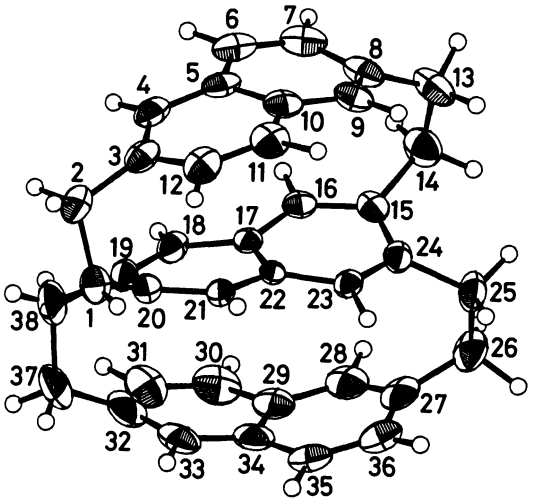

Fig. 1. A perspective view of molecule **1** with atom numbering scheme.

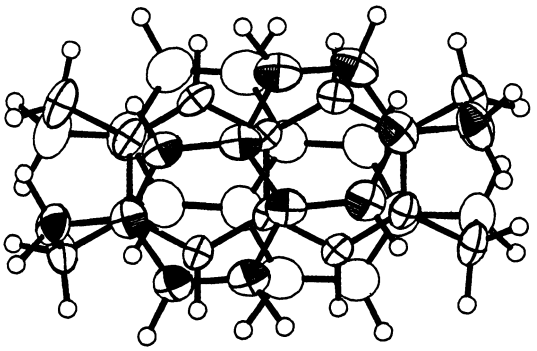

Fig. 2. A top view of molecule **1**.

Table 2. C–C Bond Lengths (Å) and C–C–C Bond Angles (°) in **1**

Bond length					
1–2	1.567(6),	2–3	1.508(6),	3–4	1.375(5)
4–5	1.419(5),	5–6	1.410(6),	6–7	1.372(7)
7–8	1.417(5),	8–9	1.365(7),	9–10	1.422(6)
10–5	1.425(5),	10–11	1.417(6),	11–12	1.361(6)
12–3	1.426(5),	8–13	1.511(8),	13–14	1.579(7)
14–15	1.514(5),	15–16	1.371(5),	16–17	1.413(5)
17–18	1.417(5),	18–19	1.361(6),	19–20	1.438(6)
20–1	1.505(7),	20–21	1.377(5),	21–22	1.416(5)
22–17	1.411(5),	22–23	1.420(4),	23–24	1.366(5)
24–15	1.437(5),	24–25	1.516(5),	25–26	1.565(7)
26–27	1.503(6),	27–28	1.385(6),	28–29	1.418(6)
29–30	1.417(6),	30–31	1.370(8),	31–32	1.418(8)
32–33	1.367(6),	33–34	1.427(7),	34–29	1.419(7)
34–35	1.423(6),	35–36	1.369(6),	36–27	1.418(7)
32–37	1.512(8),	37–38	1.568(7),	38–19	1.514(6)
Bond angle					
1–2–3	110.9(3),	2–3–4	121.1(4),	3–4–5	122.3(3)
4–5–6	123.5(3),	5–6–7	121.0(3),	6–7–8	121.0(4)
7–8–9	118.3(4),	8–9–10	121.1(4),	4–5–10	118.4(3)
6–5–10	117.4(4),	9–10–11	122.2(3),	9–10–5	119.4(4)
5–10–11	117.8(4),	10–11–12	121.5(4),	11–12–3	121.0(4)
2–3–12	120.4(3),	4–3–12	117.6(4),	7–8–13	120.7(5)
9–8–13	120.3(4),	8–13–14	111.4(4),	13–14–15	109.3(4)
14–15–16	119.6(3),	15–16–17	122.6(3),	16–17–18	125.0(3)
17–18–19	122.4(3),	18–19–20	118.7(3),	19–20–21	117.7(4)
1–20–19	121.7(3),	1–20–21	119.7(4),	2–1–20	109.6(3)
16–17–22	117.7(3),	18–17–22	117.4(3),	20–21–22	121.8(3)
21–22–23	123.9(3),	17–22–21	118.4(3),	17–22–23	117.7(3)
22–23–24	122.0(3),	23–24–25	119.6(3),	15–24–23	118.4(3)
15–24–25	120.9(4),	14–15–24	121.8(3),	16–15–24	117.5(3)
24–25–26	109.8(3),	25–26–27	111.4(4),	26–27–28	120.9(4)
27–28–29	121.1(5),	28–29–30	123.3(4),	29–30–31	121.1(5)
30–31–32	120.8(4),	31–32–33	118.5(5),	32–33–34	121.2(5)
28–29–34	118.6(4),	30–29–34	117.5(4),	33–34–35	121.7(5)
29–34–33	119.1(4),	29–34–35	118.4(4),	34–35–36	120.2(4)
27–36–35	122.0(4),	26–27–36	121.2(4),	28–27–36	117.1(4)
32–37–38	111.3(4),	31–32–37	120.1(4),	33–32–37	120.4(5)
19–38–37	109.6(3),	18–19–38	119.6(4),	20–19–38	121.0(4)

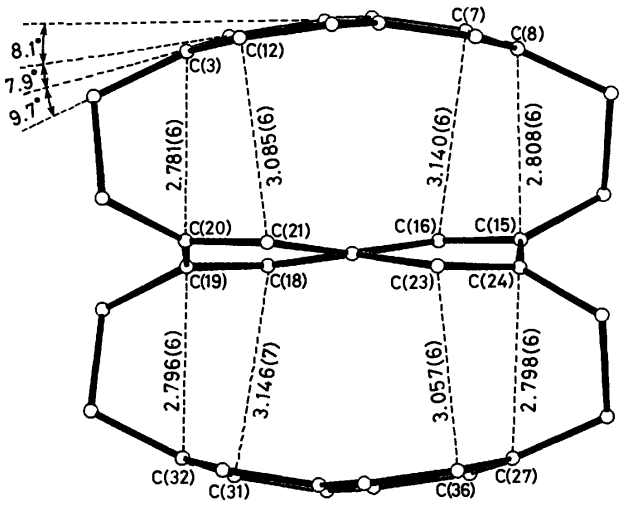

Fig. 3. A projection of the carbon skeleton of **1** along the transverse axis of the naphthalene with some short non-bonding atomic distances (Å).

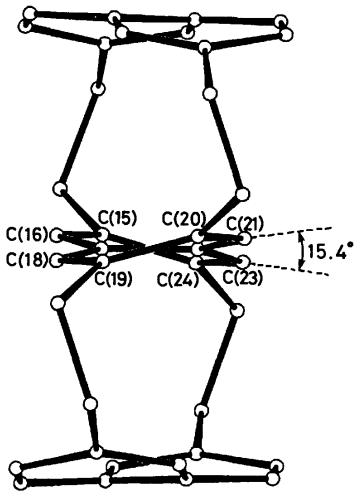

Fig. 4. A projection of the carbon skeleton of **1** along the longitudinal axis of the naphthalene.

benzene rings, is 15.4° so that a considerable strain exists in it. In addition, Fig. 3 shows the nearest nonbonded atomic distances between the neighboring aromatic rings to be situated in 2.8—3.1 Å. These values are quite smaller than van der Waals contact, causing a strong transannular interaction between the naphthalenes.

Spectroscopic Properties. The ^{1}H NMR spectra of cyclophanes are characterized by the magnetic anisotropic effect of the adjacent aromatic rings.[13] When the chemical shifts of three kinds of the aromatic protons in [2.2](2,6)naphthalenophane (**2**), δ 6.41 (noncoupled α-ArH), 6.83 (coupled β-ArH), and 7.09 (coupled α-ArH) are compared to the corresponding ones of 2,6-dimethylnaphthalene, δ 7.57, 7.24, and 7.64, the upfield shift on the noncoupled α-protons is marked, because they are more subject to a shielding

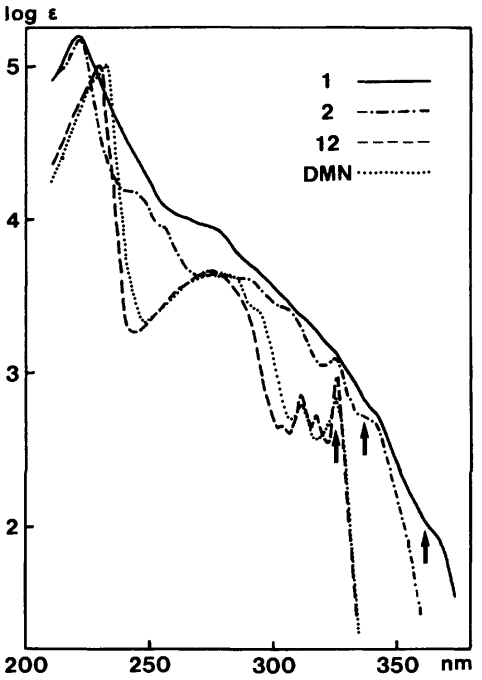

Fig. 5. The electronic spectra of triple-layered naphthalenophane (**1**), double-layered naphthalenophane (**2**), 2,3,6,7-tetramethylnaphthalene (**12**), and 2,6-dimethylnaphthalene (DMN) in tetrahydrofuran. The positions of the longest absorption bands are marked by arrows.

effect owing to the obliquely stacking structure.[5] The NMR spectrum of **1** suffers the additional anisotropy of the third naphthalene ring. The spiral stacking structure forces the noncoupled α-protons (δ 6.17) of the outer naphthalene to appear at a higher field than the coupled α-protons (δ 6.69) and β-protons (δ 6.91). The inner naphthalene protons are sandwiched between the two outer naphthalenes and accordingly the upfield shift of the signal (δ 5.55) relative to that (δ 7.44) of 2,3,6,7-tetramethylnaphthalene is especially large and corresponds to almost twice that for the α-protons of **2**.

The transannular π-electronic interactions of layered cyclophanes can be best understood by electronic spectroscopy. Figure 5 shows the electronic spectra of naphthalenophanes **1** and **2** in tetrahydrofuran. When 2,6-dimethylnaphthalene (DMN) or 2,3,6,7-tetramethylnaphthalene (**12**) is chosen as a standard, both compounds demonstrate common spectral characteristics of layered cyclophanes, i.e., bathochromism, hyperchromism, and broadening.[3] These effects are more eminent with an increase of the layers. For example, the longest absorption peaks of 2,6-dimethylnaphthalene and 2,3,6,7-tetramethylnaphthalene appear at 326 and 325 nm, respectively. In contrast, **2** has a shoulder at 336 nm as the longest band. Further, **1** has its band at 362 nm, indicating a stronger transannular π-electronic interaction as expected from the above crystal structure.

The strong transannular π-electronic interaction of **1** was also confirmed by its charge-transfer absorption with tetracyanoethylene (TCNE) as an electron acceptor. 2,6-Dimethylnaphthalene with TCNE exhibited two broad CT bands at λ_{max} 478 and 609 nm in dichloromethane. On the other hand, **2** showed the corresponding CT bands at 500(sh) and 644 nm, and **1** at 514 and 683 nm. Evidently, the bathochromic shifts for these naphthalenophanes indicate the enhancement of their donor abilities due to the transannular electronic interactions, which is more eminent in **1** than in **2**.

Experimental

General. Elemental analyses were determined by Mr. H. Iwatani, Microanalytical Laboratory of Department of Applied Chemistry, Hiroshima University. Melting points are uncorrected. NMR measurements were made on a JEOL PMX-60 instrumet (60 MHz) using deuteriochloroform as a solvent with tetramethylsilane as an internal standard. Mass spectra were taken on a JEOL JMS-DX 300 spectrometer at 70 eV using a direct insertion technique. Visible and ultraviolet spectra were measured with a Shimadzu UV-160 spectrophotometer.

1,2,4,5-Tetrakis(mercaptomethyl)benzene (6). A mixture of 1,2,4,5-tetrakis(bromomethyl)benzene (**4**)[14] 1.35 g (3 mmol) and thiourea 0.99 g (13 mmol) was refluxed in 20 cm³ of 95% ethanol for 5 h. The resulting tetrakis(thiouronium salt) was collected by filtration and washed with ethanol, 2.21 g. It was then refluxed with potassium hydroxide (4 g) in 15 cm³ of water for 4 h under nitrogen. The reaction mixture was acidified with 50% sulfuric acid on ice-cooling and extracted with dichloromethane. The extract was washed with brine, dried ($MgSO_4$), and evaporated. Recrystallization of the residue from benzene gave colorless needles 0.65 g (83%), mp 132—133 °C. ^{1}H NMR δ=1.83 (t, J=7 Hz, 4H, SH), 3.80 (d, J=7 Hz, 8H, CH_2), 7.21 (s, 2H, ArH). Calcd for $C_{10}H_{14}S_4$: C, 45.76; H, 5.38%. Found: C, 45.74; H, 5.38%.

Triple-Layered Tetrathia[3.3][3.3]paracyclophane (8). A solution of 1,2,4,5-tetrakis(mercaptomethyl)benzene (**6**) 1.048 g (4 mmol) and 1,4-bis(chloromethyl)benzene (**7**) 1.40 g (8 mmol) in 200 cm³ of benzene was slowly added into a refluxing solution of ethanol (1 dm³) containing potassium hydroxide (1.44 g) in a nitrogen atmosphere. The addition took one and a half day. After treated under reflux for additional half a day, the reaction mixture was concentrated in vacuo. The residue was taken up in dichloromethane and chromatographed on silica gel with dichloromethane. Recrystallization of the solid in the first eluate gave colorless plates of **8**, 228 mg (12%), decomp 210 °C. ^{1}H NMR δ=3.57 (d, J=14 Hz, 4H, CH_2), 3.66 (s, 8H, CH_2), 4.16 (d, J=14 Hz, 4H, CH_2), 6.26 (s, 2H, ArH), 6.71 (ABq, J=8 Hz, 8H, ArH). MS m/z 466 (M^+). Calcd for $C_{26}H_{26}S_4$: C, 66.91; H, 5.61%. Found: C, 67.17; H, 5.29%.

The same product (**8**) was obtained from a similar coupling reaction of 1,2,4,5-tetrakis(bromomethyl)benzene (**4**) 1.80 g (4 mmol) and 1,4-bis(mercaptomethyl)benzene (**5**) 1.36 g (8 mmol) at RT, yield 77 mg (4.2%).

Triple-Layered [2.2][2.2]Paracyclophane (11). A mixture of compound **8** 77 mg, triethyl phosphite 20 cm³, and benzene 20 cm³ was placed in a quartz tube and irradiated with a high-pressure mercury lamp (300 W) for 5 h in a nitrogen atmosphere. It was concentrated in vacuo, and the residue was chromatographed on silica gel with benzene to give the desired product **11** in the first eluate, 52 mg (93%). Recrystallization from carbon tetrachloride–acetone (1:3) gave colorless prisms, decomp 230 °C. It was consistent with the authentic sample in all respects.

2,3,6,7-Tetrakis(bromomethyl)naphthalene (13). 2,3,6,7-Tetramethylnaphthalene (**12**)[9] 3.68 g (20 mmol) was refluxed with *N*-bromosuccinimide 15.6 g (88 mmol) and a catalytic amount of benzoyl peroxide in 300 cm³ of carbon tetrachloride for 30 min under sunlight. The mixture was concentrated to about 50 cm³. The resulting solid was collected by filtration and thoroughly washed with hot water. The remainder was essentially pure product **13**, which was recrystallized from benzene to give colorless fine crystals, decomp 230 °C, 6.87 g (69%). ^{1}H NMR δ=4.85 (s, 8H, CH_2), 7.83 (s, 4H, ArH). Calcd for $C_{14}H_{12}Br_4$: C, 33.64; H, 2.42%. Found: C, 33.67; H, 2.36%.

2,3,6,7-Tetrakis(mercaptomethyl)naphthalene (15). 2,3,6,7-Tetrakis(bromomethyl)naphthalene (**13**) 6.87 g (13.7 mmol) was refluxed with thiourea 5.03 g (66 mmol) in 100 cm³ of 95% ethanol. The resulting tetrakis(thiouronium salt) was collected by filtration and washed with ethanol, 7.85 g. It was refluxed with potassium hydroxide (18 g) in 200 cm³ of water for 6 h under nitrogen. After the insoluble material was removed by filtration, the filtrate was acidified with 50% sulfuric acid on ice-cooling. The resulting solid was collected by filtration and recrystallized from chloroform to give colorless scales, 2.64 g (62%), mp 181—182 °C. ^{1}H NMR δ=1.83 (t, J=7 Hz, 4H, SH), 4.04 (d, J=7 Hz, 8H, CH_2), 7.69 (s, 4H, ArH). Calcd for $C_{14}H_{16}S_4$: C, 53.80; H, 5.16%. Found: C, 53.52; H, 5.02%.

Triple-Layered Tetrathia[3.3][3.3]naphthalenophane (17). A solution of 2,3,6,7-tetrakis(mercaptomethyl)naphthalene (**15**) 312 mg (1 mmol) and 2,6-bis(bromomethyl)naphthalene (**16**)[5] 646 mg (2.06 mmol) in 400 cm³ of benzene was slowly added into a refluxing solution of ethanol (800 cm³) containing potassium hydroxide (0.6 g) in a nitrogen atmosphere. The addition took 3 days. The solution was concentrated in vacuo, and the residue was chromatographed on silica gel with dichloromethane to give the desired product **17** in the first eluate, 52 mg (17%), colorless plates from chloroform, decomp 250 °C. ^{1}H NMR δ=3.5—4.5 (m, 16H, CH_2), 6.14, 6.21, 6.35 (each bs, 4H, inner ArH), 6.7—7.0 (m, 17H, outer ArH). MS m/z 616 (M^+). Calcd for $C_{38}H_{32}S_4$: C, 73.98; H, 5.23%. Found: C, 73.71; H, 5.27%.

A similar coupling reaction using 2,3,6,7-tetrakis(bromomethyl)naphthalene (**13**) 200 mg (0.4 mmol) and 2,6-bis(mercaptomethyl)naphthalene (**14**)[5] 167 mg (0.76 mmol) gave the same product **17**, 21 mg (9%).

Triple-Layered [2.2][2.2]Naphthalenophane (1). Triple-layered tetrathia[3.3][3.3]naphthalenophane (**17**) 72 mg, triethyl phosphite 20 cm³, and benzene 30 cm³ were placed in a quartz tube. The suspension was irradiated with a high-pressure mercury lamp for 12 h in a nitrogen atmosphere. It was evaporated, and the residue was purified by column chromatography on silica gel with benzene and then gel-permeation liquid chromatography with chloroform to give the desired product **1**, 18 mg (32%), colorless prisms from benzene, decomp 285 °C. ^{1}H NMR δ=2.3—3.3 (m, 16H,

CH_2), 5.55 (s, 4H, inner ArH), 6.17 (s, 4H, outer ArH), 6.69 (d, J=8 Hz, 4H, outer ArH), 6.91 (d, J=8 Hz, 4H, outer ArH). MS m/z 488 (M^+). Calcd for $C_{38}H_{32}$: C, 93.40; H, 6.60%. Found: C, 93.24; H, 6.71%.

Crystal Structure Analysis. The X-ray diffraction data were collected by using a Rigaku automated four-circle diffractometer with Cu $K\alpha$ radiation monochromatized by a graphite plate. Independent reflections 5750 with 2θ values up to 126° ($|F_o| \geqq 3.0\sigma(F_o)$) were used for analysis. Crystal data are as follows; colorless prism, $C_{38}H_{32}$, M=488.68, triclinic, space group $P\bar{1}$, a=13.515(3), b=18.748(3), c=11.143(2) Å, α=90.38(2), β=101.62(2), γ=110.30(1)°, V=2584.8(9) Å^3, D_m=1.237, D_c=1.256 g cm^{-3} for Z=4, u=4.574 cm^{-1}, crystal size 0.18×0.18×0.23 mm^3. The structure was solved by the Monte Carlo direct method[15] using the MULTAN-78 program system[16] and refined on F^2 by the full-matrix least-squares method with the analytical absorption correction.[17] Atomic scattering factors were taken from International Tables for X-ray Crystallography.[18] Anisotropic temperature factors were used for the refinement of carbon atoms. All H atoms were located from difference Fourier maps and their coordinates were refined with the isotropic temperature factors equivalent to that of the bonded carbon atoms. The R value converged to 0.066. Computations were carried out partly at the Information Processing Center of Hiroshima University and mainly at the Computation Center of Nagoya University using the library program of CRYSTAN system. Tables of structure factors, anisotropic thermal parameters, and coordinates of hydrogen atoms are deposited as Document No. 8850 at the Office of the Editor of Bull. Chem. Soc. Jpn.

One of the authors (T.O.) thanks Yamada Science Foundation for financial support.

References

1) This paper is dedicated to Professor Virgil Boekelheide on the occasion of his 70th birthday. A preliminary account of some of this work has appeared: T. Otsubo, F. Ogura, and S. Misumi, *Tetrahedron Lett.*, **24**, 4851 (1983).

2) For reviews, see S. Misumi and T. Otsubo, *Acc. Chem. Res.*, **11**, 251 (1987); S. Misumi, "Cyclophanes," ed by P. M. Keehn and S. M. Rosenfeld, Academic Press, New York (1983), Vol. II, p. 573.

3) T. Otsubo, S. Mizogami, I. Otsubo, Z. Tozuka, A Sakagami, Y. Sakata, and S. Misumi, *Bull. Chem. Soc. Jpn.*, **46**, 3519 (1973).

4) J. Ferguson, *Chem. Rev.*, **86**, 957 (1986).

5) M. Haenel and H. A. Staab, *Chem. Ber.*, **106**, 2203 (1973); *Tetrahedron Lett.*, **1970**, 3585.

6) N. E. Blank and M. W. Haenel, *Chem. Ber.*, **116**, 827 (1983).

7) T. Otsubo, H. Horita, and S. Misumi, *Synth. Commun.*, **6**, 591 (1976).

8) I. D. Reingold, W. Schmidt, and V. Boekelheide, *J. Am. Chem. Soc.*, **101**, 2121 (1979).

9) Y. Dozen and M. Hatta, *Bull. Chem. Soc. Jpn.*, **48**, 2842 (1975).

10) V. Boekelheide and C. H. Tsai, *Tetrahedron*, **32**, 423 (1976).

11) H. Hope, J. Bernstein, and K. N. Trueblood, *Acta Crystallogr., Sect. B*, **28**, 1733 (1972).

12) H. Mizuno, K. Nishiguchi, T. Toyoda, T. Otsubo, S. Misumi, and N. Morimoto, *Acta Crystallogr., Sect. B*, **33**, 329 (1977); Y. Koizumi, T. Toyoda, K. Miki, N. Kasai, and S. Misumi, *Bull. Chem. Soc. Jpn.*, **59**, 239 (1986).

13) T. Otsubo, S. Mizogami, Y. Sakata, and S Misumi, *Bull. Chem. Soc. Jpn.*, **46**, 3831 (1973).

14) W. Ried and H. Bodem, *Chem. Ber.*, **89**, 2328 (1956).

15) A. Furusaki, *Acta Crystallogr., Sect. A*, **35**, 220 (1979).

16) P. Main, S. E. Hull, L. Lessinger, G. Germain, J. P. Declercq, and M. M. Woolfson, MULTAN-78, (1978), Univ. of York, England, and Louvain, Belgium.

17) C. Katayama, N. Sakabe, and K. Sakabe, *Acta Crystallogr., Sect. A*, **28**, S207 (1972).

18) "International Tables for X-ray Crystallography," Kynoch Press, Birmingham, England (1974), Vol. IV.

 © 1989 The Chemical Society of Japan Bull. Chem. Soc. Jpn., 62, 171—179 (1989)

Synthesis of 4-[(*E*)-1-Alkenyl]-2-hydroxybutanolides and (*Z*)-4-Alkylidene-2-butenolides through Cycloadditions Using a Phosphorus-Functionalized Nitrile Oxide

Shuji KANEMASA,* Norihiko NAKAGAWA, Hiroyuki SUGA, and Otohiko TSUGE*
Institute of Advanced Material Study, and Department of Molecular Science and Technology,
Interdisciplinary Graduate School of Engineering Sciences,
Kyushu University, Kasugakoen, Kasuga 816
(Received July 15, 1988)

A sequence of cycloadditions of (diethoxyphosphinyl)acetonitrile oxide with α,β-unsaturated esters, the Raney Ni reduction of the resulting cycloadducts, the Horner–Emmons olefination, and the carbonyl reduction with sodium borohydride leads to 5-[(*E*)-1-alkenyl]-3-hydroxy-4,5-dihydro-2(3*H*)-furanones which can be converted into (*Z*)-5-alkylidene-2(5*H*)-furanones in two steps.

Unsaturated five-membered lactones, butenolides, are often the central skeletons of naturally occurring oxygen heterocycles.[1] Among the numerous reported syntheses of 2-butenolides,[2] the route by dehydration of 2-hydroxybutanolides is not familiar since availability of the starting 2-hydroxybutanolides[3] or their related derivatives[4] is quite narrow.

On the other hand, 2-isoxazoline-5-carboxylates which can be formed as cycloadducts in the cycloadditions of nitrile oxides with conjugated esters are synthetically equivalent to the α-hydroxy-γ-oxo ester functionality by a simple one-step procedure involving reductive N–O bond cleavage and hydrolysis. This cleavage can be conveniently and effectively carried out by the aid of Raney Ni.[5] Application of this sequence to the nitrile oxide bearing a functional group utilizable for olefination would lead to 2-hydroxy-4-oxo-5-alkenoates. These alkene esters must be the promising starting materials in the synthesis of 4-(1-alkenyl)-2-hydroxybutanolides (or 5-(1-alkenyl)-3-hydroxy-4,5-dihydro-2(3*H*)-furanones) and further 4-alkylidene-2-butenolides (or 5-alkylidene-2(5*H*)-furanones).

The present article describes a new synthetic method of butanolides and butenolides through the cycloaddition route using a phosphorus-functionalized nitrile oxide. Hereafter only the nomenclature as well as the compound numbering based on heterocyclic systems is employed in order to avoid confusion.

Results and Discussion

We have already reported that (diethoxyphosphinyl)-acetonitrile oxide (**1**) serves as a synthetically useful phosphorus-functionalized nitrile oxide[6,7] which undergoes regioselective cycloaddition with methyl acrylate to produce methyl 3-[(diethoxyphosphinyl)methyl]-2-isoxazoline-5-carboxylate (**2**).[8,9] Methyl 5-(diethoxyphosphinyl)-2-hydroxy-4-oxopentanoate (**3**)[9] can be obtained in a satisfactory yield via the Raney Ni reduction of the cycloadduct **2** in the presence of boric acid.

Though Horner–Emmons olefinations of 4-hydroxy-2-oxoalkylphosphonates are often accompanied by competitive dehydration and/or retro-aldol reaction, use of the combination of triethylamine (or 1,8-diazabicyclo[5.4.0]undec-7-ene (DBU)) and lithium bromide as a weak base system on the *O*-unprotected substrates was found effective enough to suppress these undesired side reactions.[10]

Under the equivalent conditions (lithium bromide–DBU in dry THF at 0 °C for 24 h), highly functionalized phosphonate **3** was smoothly converted into 2-hydroxy-4-oxo-5-alkenoates **4a—c** (Scheme 1). These olefinations were highly *E*-selective for all the aldehydes employed, no contamination by *Z*-isomers being observed. It should be emphasized that the reactions with aliphatic aldehydes provided the olefins in better yields than that with an aromatic aldehyde (**4a**: 80%; **4b**: 82%; **4c**: 52%).

Reduction of the conjugated carbonyl group at the 4-position of **4** with sodium borohydride was impracticably sluggish in ethanol at 0 °C and that at room

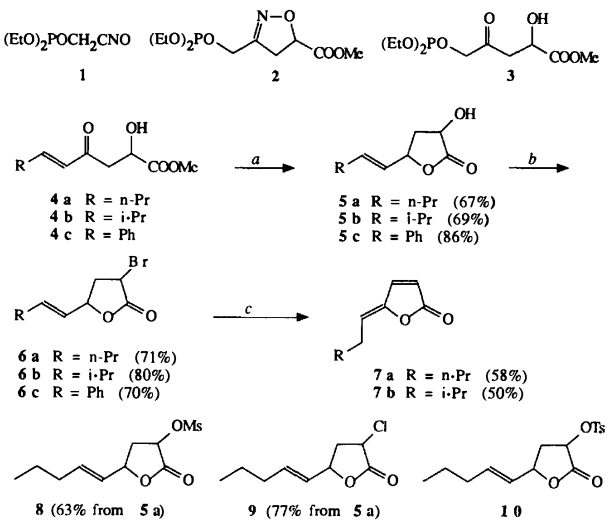

a $NaBH_4$ in MeOH at 0 °C then *p*-TsOH in CH_2Cl_2 at rt
b MsCl / NEt_3 in CH_2Cl_2 at 0 °C then LiBr in THF at rt
c DBU / hydroquinone (cat) in THF under reflux

Scheme 1.

temperature resulted in a complex mixture of many products. However in methanol a smooth reduction took place at 0 °C.[11] The reduction was carefully monitored on thin-layer chromatography (TLC) and as soon as the reduction was complete the crude reaction mixture containing the dihydroxy esters was subjected to lactonization without purification. Treatment of the crude reduction products with a catalytic amount of *p*-toluenesulfonic acid in dichloromethane at room temperature produced 5-(1-alkenyl)-3-hydroxy-4,5-dihydro-2(3*H*)-furanones **5a—c** as about 1 : 1 mixtures of 3,5-cis and 3,5-trans isomers. Although these two isomers can be separated from each other through careful column chromatography and in the present research their separation was actually carried out for characterization, this separation step may be omitted only for the purpose of synthesizing 2-butenolides.

As direct dehydration of **5a** by the aid of either of dicyclohexylcarbodiimide–copper(I) chloride (reflux in benzene for 5 h)[12] or methyltriphenoxyphosphonium iodide (at 80 °C for 1 h in hexamethylphosphoric triamide (HMPA))[13] ended in the formation of complex mixture, the hydroxyl group was replaced with a more effective leaving group such as mesyl, tosyl, or bromo substituent.

Though *O*-mesylation of **5a** with methanesulfonyl chloride–triethylamine (at 0 °C in dichloromethane) gave the mesylate **8** in a moderate yield, the product obtained on treating **5a** with *p*-toluenesulfonyl chloride–pyridine at room temperature was not the expected tosylate **10** but the chloride **9** (77%). On the other hand, only 18% yield of bromide **6a** was prepared by reacting **5a** with tribromophosphine–pyridine.

Base-induced dehydrohalogenation of chloride **9** and bromide **6a** was all unsuccessful (with triethylamine under reflux in diethyl ether, dichloromethane, or THF; with pyridine at 80 °C). Only when mesylate **8** was heated with DBU under reflux in THF, a low yield (5%) of the expected 2-butenolide **7a** was obtained. After some efforts, it was found that treating bromide **6a** with DBU under reflux in THF provided 2-butenolide **7a** in 58% yield. The structure of **7a** will be discussed below.

Therefore an effective synthetic route to bromides **6a—c** was searched. The aforementioned high-yield formation of chloride **9** in the attempted tosylation of **5a** indicates a possibility of the ready nucleophilic substitution of the tosylate **10** with a halide nucleophile under the quoted conditions. Accordingly hydroxy lactones **5a—c** were first mesylated and the crude mesylates were allowed to react with lithium bromide in THF at room temperature to give good yields of the expected bromides **6a—c** (Scheme 1). Since the starting hydroxy lactones **5a—c** were all mixtures of 3,5-cis and 3,5-trans isomers, **6a—c** were not stereochemically pure.

Dehydrobromination of bromides **6a—c** was carried out with DBU under reflux in THF where a catalytic amount of hydroquinone was used to inhibit the polymerization of products.[14] Though the 3-bromo-4,5-dihydro-2(3*H*)-furanones **6a—b** underwent smooth dehydrobromination, the phenyl-substituted analog **6c** led to complex mixture under all the employed conditions.

The structures of **7a—b** were assigned as *Z*-isomers of 5-alkylidene-2(5*H*)-furanones on the basis of spectral data where there newly appeared three olefin (3-, 4-, and 1′-Hs) and a pair of methylene (2′-H) protons and disappeared one set of trans-olefin. The *Z*-stereochemistry was confirmed by comparison of the chemical shifts of 1′-H (**7a**: δ=5.32; **7b**: 5.34) with those of *E*- and *Z*-isomers of 5-butylidene-2(5*H*)-furanone (*E*-isomer: 5.70; *Z*-isomer: 5.22),[3b] 5-ethylidene-3-methyl-2(5*H*)-furanone (*E*-isomer: 5.67; *Z*-isomer: 5.20),[15,16] or 3-methyl-5-(2-methylpropylidene)-2(5*H*)-furanone (*E*-isomer: 6.23; *Z*-isomer: 5.43).[17]

One application of the above furanone synthesis using nitrile oxide **1** enables the introduction of a methyl group at the 3-position of 5-alkylidene-2(5*H*)-furanones as shown in Scheme 2.

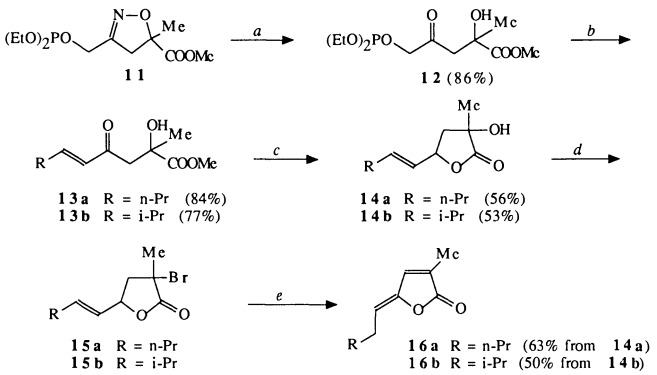

a Raney Ni / $B(OH)_3$ in aq EtOH at rt
b DBU / LiBr in THF at 0 °C then RCHO at 0 °C
c $NaBH_4$ in MeOH at 0 °C then *p*-TsOH in CH_2Cl_2 at rt
d MsCl / NEt_3 at 0 °C then LiBr in THF under reflux
e DBU / hydroquinone (cat) in THF under reflux

Scheme 2.

Regioselective cycloaddition of nitrile oxide **1** with methyl methacrylate and subsequent Raney Ni reduction of the cycloadduct **11** afforded ester phosphonate **12** (Scheme 2). Horner–Emmons olefination of **12** mediated by lithium bromide–DBU led to (*E*)-olefins **13a,b**. Sodium borohydride reduction of **13** proceeded in a stereoselective fashion to give 3-hydroxy-3-methyl-4,5-dihydro-2(3*H*)-furanones **14a,b** after acid-catalyzed lactonization. Three transformations consisting of mesylation of **14a,b**, bromination of the mesylates with lithium bromide, and the final dehydrobromination of the bromides **15a,b** were carried out in one procedure

without separation of the intermediate products to produce (*Z*)-3-methyl-5-pentylidene-2(5*H*)-furanone (**16a**) and (*Z*)-3-methyl-5-(3-methylbutylidene)-2(5*H*)-furanone (**16b**). No sign of the regioisomeric dehydrobromination leading to 2-methylenebutanolide was even observed.[18]

In conclusion, the cycloaddition route using the phosphorus-functionalized nitrile oxide **1** offers a useful preparation method of 3-hydroxy and 3-halo derivatives of (*E*)-5-(1-alkenylidene)-4,5-dihydro-2(3*H*)-furanones and (*Z*)-5-alkylidene-2(5*H*)-furanones. By a set of appropriate choices of conjugated esters in the cycloaddition step, carbonyl compounds in the olefination step, and nucleophiles in the functional group interconversion of the 3-hydroxyl moiety, this method can be further applied to their families bearing a variety of substitution patterns. Alkylation adjacent to the phosphinyl moiety of 2-isoxazolines **2** and **11** can be also combined.

Experimental

General. Melting points were determined on a Yanagimoto melting point apparatus and are uncorrected. IR spectra were taken with a JASCO IRA-1 spectrometer. ^{1}H NMR spectra were recorded on a JEOL GSX-270 instrument (270 MHz), and ^{13}C NMR on a JEOL FX-100 (25.05 MHz) or a JEOL GSX-270 spectrometer (67.94 MHz). Chemical shifts are expressed in parts per million downfield from tetramethylsilane as an internal standard. Mass spectra were measured with a JEOL-01SG-2 spectrometer at 70 eV of ionization energy. High-resolution mass spectra were obtained on the same instrument. Elemental analyses were performed on a Hitachi 026 CHN analyzer. Thin-layer chromatography (TLC) was accomplished on 0.2 mm precoated plates of silica gel 60 F-254 (Merck). For preparative column chromatography, Wakogel C-200, C-300 (Wako), and Silicagel 60 (Merck) were employed. Flash chromatography was carried out on an EYELA EF-10 apparatus using a column (20×180 mm) packed with Silicagel 60 (Merck, size: 0.04—0.063 mm). Solvents were evaporated with a Tokyo Rikakikai rotary evaporator type-V at about 50 °C unless otherwise stated.

Materials and Solvents. Generation of nitrile oxide **1**, its cycloaddition with methyl acrylate leading to 2-isoxazoline **2**, Raney Ni reduction of **2** furnishing **3**, its Horner-Emmons olefination with benzaldehyde giving **4c** were all previously reported.[8-10] Methyl methacrylate was distilled prior to use. Lithium bromide, 1,8-diazabicyclo[5.4.0]undec-7-ene (DBU), and hydroquinone are commercially available and were used without further purification. Tetrahydrofuran (THF) and dichloromethane were purified immediately before use by distillation from lithium aluminum hydride and calcium hydride, respectively, under nitrogen.

Methyl (*E*)-2-Hydroxy-4-oxo-5-nonenoate (4a). To a solution of lithium bromide (0.377 g, 3.88 mmol) in dry THF (5 ml) was added a solution of **3** (1.095 g, 3.88 mmol) in THF (5 ml). After stirring at room temperature for 10 min under nitrogen, a solution of DBU (0.561 g, 3.69 mmol) in THF (5 ml) was added dropwise at 0 °C. After 1 h at 0 °C, butanal (0.56 g, 7.76 mmol) was added, the mixture was stirred at 0 °C for 24 h, poured into ice water, and then extracted with dichloromethane (25 ml×2). The combined extracts were dried over magnesium sulfate and evaporated in vacuo. The residue was chromatographed on silica gel by using hexane–ethyl acetate (3:1 v/v) to give **4a** (0.624 g, 80%) as a single isomer (by ^{1}H NMR): Colorless liquid; IR (neat) 3480, 1740, 1660, 1620, 1430, 1200, 1100, 1030, and 975 cm^{-1}; ^{1}H NMR ($CDCl_3$) δ=0.95 (3H, t, J=7.3 Hz, *n*-Pr), 1.51 (2H, sx, J=7.3 Hz, *n*-Pr), 2.22 (2H, dt, J=7.3 and 7.0 Hz, *n*-Pr), 3.08 (1H, d, J_{3-2}=10.3 Hz, one of 3-H), 3.09 (1H, d, J_{3-2}=5.5 Hz, the other of 3-H), 3.50 (1H, br s, OH), 3.78 (3H, s, COOMe), 4.57 (1H, dd, J_{2-3}=10.3 and 5.5 Hz, 2-H), 6.11 (1H, d, J_{5-6}=16.1 Hz, 5-H), and 6.89 (1H, dt, J_{6-5}=16.1 and J_{6-7}=7.0 Hz, 6-H); ^{13}C NMR ($CDCl_3$) δ=13.69, 21.30, 34.57 (each *n*-Pr), 43.27 (3-C), 52.49 (COOMe), 67.19 (2-C), 130.42 (5-C), 149.11 (6-C), 174.28 (COOMe), and 197.70 (CO); MS *m/z* (rel intensity, %) 200 (M^+, 11), 141 (16), 97 (base peak), and 55 (57). HRMS Found: *m/z* 200.1050. Calcd for $C_{10}H_{16}O_4$: M, 200.1048.

Methyl (*E*)-2-Hydroxy-7-methyl-4-oxo-5-octenoate (4b). A similar procedure using lithium bromide (0.353 g, 4.06 mmol) in THF (5 ml), **3** (1.147 g, 4.06 mmol) in THF (5 ml), DBU (0.588 g, 3.86 mmol) in THF (5 ml), and 2-methylpropanal (0.586 g, 8.13 mmol) at 0 °C for 1 h after column chromatography on silica gel with hexane–ethyl acetate (3:1 v/v), gave **4b** (0.667 g, 82%) as a single isomer (by ^{1}H NMR): Colorless liquid; IR (neat) 3480, 1740, 1660, 1620, 1440, 1360, 1270, 1210, 1100, 1030, and 980 cm^{-1}; ^{1}H NMR ($CDCl_3$) δ=1.06 (6H, d, J=7.0 Hz, *i*-Pr), 2.3—2.7 (1H, m, *i*-Pr), 3.0—3.2 (2H, m, 3-H), 3.4—3.5 (1H, m, OH), 3.76 (3H, s, COOMe), 4.55 (1H, dd, J_{2-3}=10.0 and 5.5 Hz, 2-H), 6.04 (1H, dd, J_{5-6}=16.1 and J_{5-3}=1.5 Hz, 5-H), and 6.84 (1H, dd, J_{6-5}=16.0 and J_{6-7}=6.0 Hz, 6-H); ^{13}C NMR ($CDCl_3$) δ=21.18, 31.23 (each *i*-Pr), 43.27 (3-C), 52.50 (COOMe), 67.11 (2-C), 127.45 (5-C), 155.24 (6-C), 174.24 (COOMe), and 198.06 (CO); MS *m/z* (rel intensity, %) 200 (M^+, 5), 141 (14), 97 (base peak), 96 (13), 69 (11), and 41 (22). HRMS Found: *m/z* 200.1048. Calcd for $C_{10}H_{16}O$: M, 200.1048.

3-Hydroxy-5-[(*E*)-1-pentenyl]-4,5-dihydro-2(3*H*)-furanone (5a). To a solution of **4a** (0.787 g, 3.93 mmol) in methanol (10 ml) was added sodium borohydride (0.149 g, 3.93 mmol). After stirring at room temperature for 10 min, acetone (5 ml) was added at 0 °C. The mixture was stirred at 0 °C for 10 min, poured into ice water, and extracted with dichloromethane (20 ml×2). The combined extracts were dried over magnesium sulfate and evaporated in vacuo. The residue was dissolved in dichloromethane (10 ml) containing *p*-toluenesulfonic acid (0.075 g, 0.393 mmol), the mixture was stirred at room temperature for 3 h, poured into ice water, and then extracted with dichloromethane (20 ml×2). After dried over magnesium sulfate, the combined extracts were evaporated in vacuo and the residue was chromatographed on silica gel with hexane–ethyl acetate (2:1 v/v) to give **5a** (0.447 g, 67%) as a 1:1 mixture of two diastereomers (by ^{1}H NMR) which could be separated from each other by a careful column chromatography.

3,5-*trans*-5a: Colorless liquid; IR (neat) 3400, 1770, 1670, 1450, 1320, 1180, 1120, 970, and 940 cm^{-1}; ^{1}H NMR ($CDCl_3$) δ=0.90 (3H, t, J=7.3 Hz, *n*-Pr), 1.41 (2H, sx, J=7.3 Hz, *n*-Pr), 2.04 (2H, dt, J=7.3 and 7.0 Hz, *n*-Pr), 2.3—2.5 (2H, m, 4-H), 3.6—3.8 (1H, br s, OH), 4.53 (1H, dd, J_{3-4}=7.7 and 7.3 Hz, 3-H), 5.0—5.2 (1H, m, 5-H), 5.48 (1H, dd, $J_{1'-2'}$=15.0 and

$J_{1'-5}$=7.0 Hz, 1'-H), and 5.80 (1H, dt, $J_{2'-1'}$=15.0 and $J_{2'-3'}$=7.0 Hz, 2'-H); ^{13}C NMR ($CDCl_3$) δ=13.59, 21.91, 34.11 (each *n*-Pr), 36.47 (4-C), 67.32 (3-C), 78.74 (5-C), 127.14 (1'-C), 135.52 (2'-C), and 178.06 (2-C); MS (25 eV) *m/z* (rel intensity, %) 170 (M^+, 2), 98 (29), 83 (base peak), 82 (58), 81 (68), 70 (28), and 55 (21).

3,5-*cis*-5a: Colorless liquid; IR (neat) 3400, 1770, 1670, 1450, 1310, 1190, 1120, 960, and 900 cm^{-1}; ^{1}H NMR ($CDCl_3$) δ=0.91 (3H, t, J=7.3 Hz, *n*-Pr), 1.43 (2H, sx, J=7.3 Hz, *n*-Pr), 1.9—2.1 (3H, m, *n*-Pr and one of 4-H), 2.06 (1H, ddd, J_{gem}=12.5, J_{4-3}=8.0 Hz, and J_{4-5}=5.4 Hz, the other of 4-H), 3.6—3.8 (1H, br s, OH), 4.55 (1H, m, 3-H), 4.76 (1H, ddd, J_{5-4}=10.8, 5.4, and $J_{5-1'}$=7.7 Hz, 5-H), 5.50 (1H, dd, $J_{1'-2'}$=15.4 and $J_{1'-5}$=7.7 Hz, 1'-H), and 5.86 (1H, dt $J_{2'-1'}$=15.4 and $J_{2'-3'}$=7.0 Hz, 2'-H); ^{13}C NMR ($CDCl_3$) δ=13.95, 21.86, 34.11 (each *n*-Pr), 37.70 (4-C), 68.61 (3-C), 77.79 (5-C), 126.88 (1'-C), 137.27 (2'-C), and 177.88 (2-C); MS (25 eV) *m/z* (rel intensity, %) 170 (M^+, 1), 113 (47), 98 (24), 83 (base peak), 82 (47), 81 (59), and 70 (21).

No satisfactory analytical data were obtained due to hygroscopic nature of the both isomers of **5a**.

3-Hydroxy-5-[(*E*)-3-methyl-1-butenyl]-4,5-dihydro-2(3*H*)-furanone (5b). A similar procedure using **4b** (0.231 g, 1.15 mmol) in methanol (5 ml), sodium borohydride (0.044 g, 1.15 mmol), and *p*-toluenesulfonic acid (0.022 g, 0.115 mmol) in dichloromethane (5 ml) gave **5b** (0.135 g, 69%), after silica-gel column chromatography with hexane–ethyl acetate (5:1 v/v), as a 1:1 mixture of two diastereomers (by ^{1}H NMR). These two isomers could be separated from each other through a careful column chromatography.

3,5-*trans*-5b: Colorless prisms; mp 30—32 °C; IR (KBr) 3400, 1780, 1670, 1470, 1180, 1120, 1030, and 930 cm^{-1}; ^{1}H NMR ($CDCl_3$) δ=1.00 (6H, d, J=7.7 Hz, *i*-Pr), 2.2—2.5 (1H, m, *i*-Pr), 2.37 (1H, ddd, J_{gem}=13.2, J_{4-3}=7.7, and J_{4-5}=4.4 Hz, one of 4-H), 2.41 (1H, ddd, J_{gem}=13.2, J_{4-5}= 7.7, and J_{4-3}=7.3 Hz, the other of 4-H), 4.20 (1H, br s, OH), 4.55 (1H, ddd, J_{3-4}=7.7, 7.3, and J_{3-OH}=3.3 Hz, 3-H), 5.06 (1H, ddd, J_{5-4}=7.7, 4.4, and $J_{5-1'}$=7.0 Hz, 5-H), 5.43 (1H, ddd, $J_{1'-2'}$=15.4, $J_{1'-5}$=7.0, and $J_{1'-3'}$=1.5 Hz, 1'-H), and 5.78 (1H, ddd, $J_{2'-1'}$=15.4, $J_{2'-3'}$=6.6, and $J_{2'-5'}$=1.1 Hz, 2'-H); ^{13}C NMR ($CDCl_3$) δ=21.89, 30.65 (each *i*-Pr), 36.47 (4-C), 67.33 (3-C), 78.80 (5-C), 124.07 (1'-C), 142.41 (2'-C), and 177.98 (2-C); MS *m/z* (rel intensity, %) 142 (M^+—CO, 1), 99 (11), 95 (28), 93 (16), 84 (17), 83 (51), 82 (base peak), 81 (14), 73 (11), and 70 (41).

3,5-*cis*-5b: Colorless prisms; mp 36—38 °C; IR (KBr) 3400, 1780, 1660, 1460, 1320, 1180, 1120, 1030, 930, and 800 cm^{-1}; ^{1}H NMR ($CDCl_3$) δ=1.01 (6H, d, J=7.0 Hz, *i*-Pr), 2.03 (1H, ddd, J_{gem}=12.8, J_{4-3}=11.4, and J_{4-5}=10.6 Hz, one of 4-H), 2.2—2.5 (1H, m, *i*-Pr), 2.72 (1H, ddd, J_{gem}=12.8, J_{4-3}=8.1, and J_{4-5}=5.1 Hz, the other of 4-H), 4.12 (1H, s, OH), 4.60 (1H, ddd, J_{3-4}=11.4, 8.1, and J_{3-OH}=4.4 Hz, 3-H), 4.75 (1H, ddd, J_{5-4}=10.6, 5.1, and $J_{5-1'}$=7.7 Hz, 5-H), 5.45 (1H, ddd, $J_{1'-2'}$=15.4, $J_{1'-5}$=7.7, and $J_{1'-3'}$=1.5 Hz, 1'-H), and 5.83 (1H, dd, $J_{2'-1'}$=15.4 and $J_{2'-3'}$=6.6 Hz, 2'-H); ^{13}C NMR ($CDCl_3$) δ=21.84, 30.70 (each *i*-Pr), 37.74 (4-C), 68.64 (3-C), 77.91 (5-C), 123.94 (1'-C), 144.11 (2'-C), and 177.91 (2-C); MS *m/z* (rel intensity, %) 170 (M^+, 1), 95 (44), 93 (32), 84 (22), 83 (65), 82 (base peak), 81 (19), 79 (11), 77 (12), 73 (19), and 70 (35).

No satisfactory analytical results were obtained due to hygroscopic nature of the both isomers of **5b**.

3-Hydroxy-5-[(*E*)-2-phenylethenyl]-4,5-dihydro-2(3*H*)-furanone (5c). A similar procedure was applied to **4c** under the following conditions: **4c** (0.171 g, 0.73 mmol) in methanol (5 ml), sodium borohydride (0.028 g, 0.73 mmol), 10 min at 0 °C, acetone (2 ml), 10 min at room temperature, hydrolytic workup and extraction with dichloromethane, *p*-toluenesulfonic acid (0.014 g., 0.073 mmol) in dichloromethane (10 ml), 20 min at room temperature, hydrolytic workup and extraction with dichloromethane, silica-gel column chromatography with hexane–ethyl acetate. A 1:1 mixture (by ^{1}H NMR) of two diastereomers of **5c** (0.128 g, 86%) was obtained. These isomers could be separated through a careful column chromatography.

3,5-*trans*-5c: Colorless prisms (dichloromethane–hexane); mp 100—103 °C; IR (KBr) 3420, 1750, 1310, 1230, 1180, 1120, 930, 800, 750, and 690 cm^{-1}; ^{1}H NMR ($CDCl_3$) δ=2.49 (1H, ddd, J_{gem}=13.2, J_{4-3}=8.1, and J_{4-5}=2.2 Hz, one of 4-H), 2.51 (1H, ddd, J_{gem}=13.2, J_{4-3}=8.1, and J_{4-5}=4.8 Hz, the other of 4-H), 3.58 (1H, br s, OH), 4.59 (1H, t, J_{3-4}=8.1 Hz, 3-H), 5.28 (1H, ddd, $J_{5-1'}$=6.2, J_{5-4}=4.8, and 2.2 Hz, 5-H), 6.17 (1H, dd, $J_{1'-2'}$=15.8 and $J_{1'-5}$=6.2 Hz, 1'-H), 6.67 (1H, d, $J_{2'-1'}$=15.8 Hz, 2'-H), and 7.2—7.4 (5H, m, Ph); MS *m/z* (rel intensity, %) 204 (M^+, 9), 131 (12), 129 (12), 128 (16), 117 (15), 115 (30), 105 (17), 104 (base peak), 103 (14), 102 (13), 91 (32), 77 (18), 76 (40), 63 (14), and 51 (26). Found: C, 70.47; H, 5.92%. Calcd for $C_{12}H_{12}O_3$: C, 70.58; H, 5.92%.

3,5-*cis*-5c: Colorless prisms (dichloromethane–hexane); mp 135—138 °C; IR (KBr) 3450, 1750, 1320, 1200, 1120, 970, 910, 800, 760, and 690 cm^{-1}; ^{1}H NMR ($CDCl_3$) δ=2.12 (1H, ddd, J_{gem}=12.5, J_{4-5}=11.0, and J_{4-3}=10.8 Hz, one of 4-H), 2.84 (1H, ddd, J_{gem}=12.5, J_{4-3}=8.1, and J_{4-5}=5.5 Hz, the other of 4-H), 3.22 (1H, br s, OH), 4.61 (1H, dd, J_{3-4}=10.8 and 8.1 Hz, 3-H), 4.98 (1H, ddd, J_{5-4}=11.0, 5.5, and $J_{5-1'}$=7.3 Hz, 5-H), 6.19 (1H, dd, $J_{1'-2'}$=15.8 and $J_{1'-5}$=7.3 Hz, 1'-H), 6.72 (1H, d, $J_{2'-1'}$=15.8 Hz, 2'-H), and 7.2—7.4 (5H, m, Ph); MS *m/z* (rel intensity, %) 204 (M^+, 6), 129 (21), 128 (12), 117 (19), 115 (37), 104 (base peak), 103 (11), 91 (30), 78 (14), 77 (16), and 51 (22). Found: C, 70.47; H, 5.92%. Calcd for $C_{12}H_{12}O_3$: C, 70.57; H, 5.91%.

3-Bromo-5-[(*E*)-1-pentenyl]-4,5-dihydro-2(3*H*)-furanone (6a). To a solution of **5a** (0.06 g, 0.35 mmol) in dry dichloromethane (2 ml) were added, at 0 °C under nitrogen, triethylamine (0.043 g, 0.42 mmol) and methanesulfonyl chloride (0.055 g, 0.42 mmol). After stirring at 0 °C for 2 h, the mixture was poured into saturated aqueous ammonium chloride and extracted with dichlomethane (15 ml×2). The combined extracts were washed with saturated aqueous sodium hydrogencarbonate and dried over magnesium sulfate. The residue obtained by evaporation of the dichloromethane in vacuo was dissolved in dry THF (2 ml). After lithium bromide (0.061 g, 0.71 mmol) was added, the mixture was stirred at room temperature for 20 h under nitrogen, poured into water, and extracted with dichloromethane (15 ml×2). The combined extracts were dried over magnesium sulfate and evaporated in vacuo. The residue was chromatographed on silica gel with hexane–ethyl acetate (7:1 v/v) to give **6a** (0.058 g, 71%) as a 1:1 mixture (by ^{1}H NMR) of two diastereomers which could be separated from each other through a careful column chromatography.

3,5-*trans*-6a: Colorless liquid; IR (neat) 1780, 1670, 1460, 1430, 1380, 1320, 1180, 1030, 970, and 920 cm^{-1}; ^{1}H NMR ($CDCl_3$) δ=0.91 (3H, t, J=7.3 Hz, *n*-Pr), 1.43 (2H, sx, J=7.3 Hz, *n*-Pr), 2.07 (2H, dt, J=7.3 and 6.6 Hz, *n*-Pr),

2.47 (1H, ddd, J_{gem}=14.7, J_{4-5}=7.3, and J_{4-3}=6.6 Hz, one of 4-H), 2.59 (1H, ddd, J_{gem}=14.7, J_{4-5}=5.5, and J_{4-3}=2.2 Hz, the other of 4-H), 4.44 (1H, dd, J_{3-4}=6.6 and 2.2 Hz, 3-H), 5.14 ((1H, dt, J_{5-4}=$J_{5-1'}$=7.3, and J_{5-4}=5.5 Hz, 5-H), 5.50 (1H, dd, $J_{1'-2'}$=15.4 and $J_{1'-5}$=7.3 Hz, 1'-H), and 5.92 (1H, dt, $J_{2'-1'}$=15.4 and $J_{2'-3'}$=6.6 Hz, 2'-H); ^{13}C NMR ($CDCl_3$) δ=13.58, 21.81, 34.14 (each *n*-Pr), 38.96 (4-C), 40.16 (3-C), 80.31 (5-C), 125.65 (1'-C), 137.71 (2'-C), and 172.42 (2-C); MS *m/z* (rel intensity, %) 234 (M^++2, 18), 232 (M^+, 20), 191 (47), 189 (50), 153 (75), 109 (58), 81 (28), 78 (21), 69 (23), 67 (base peak), and 55. HRMS Found: *m/z* 232.0093. Calcd for $C_9H_{13}O_2Br$: M, 232.0099.

3,5-*cis*-6a: Colorless liquid; IR (Neat) 1780, 1660, 1450, 1320, 1265, 1160, 970, and 930 cm^{-1}; ^{1}H NMR ($CDCl_3$) δ=0.92 (3H, t, J=7.3 Hz, *n*-Pr), 1.43 (2H, sx, J=7.3 Hz, *n*-Pr), 2.07 (2H, dt, J=7.3 and 6.6 Hz, *n*-Pr), 2.38 (1H, ddd, J_{gem}=13.9, J_{4-5}=8.6, and J_{4-5}=8.4 Hz, one of 4-H), 3.02 (1H, ddd, J_{gem}=13.9, J_{4-3}=8.4, and J_{4-5}=6.2 Hz, the other of 4-H), 4.56 (1H, t, J_{3-4}=8.4 Hz, 3-H), 4.89 (1H, ddd, J_{5-4}=8.6, 6.2, and $J_{5-1'}$=7.7 Hz, 5-H), 5.60 (1H, dd, $J_{1'-2'}$=15.4 and $J_{1'-5}$=7.7 Hz, 1'-H), and 5.87 (1H, dt, $J_{2'-1'}$=15.4 and $J_{2'-3'}$=6.6 Hz, 2'-H); ^{13}C NMR ($CDCl_3$) δ=13.59, 21.80, 34.10 (each *n*-Pr), 37.91 (4-C), 39.77 (3-C), 79.98 (5-C), 126.49 (1'-C), 137.56 (2'-C), and 172.51 (2-C); MS *m/z* (rel intensity, %) 234 (M^++2, 43), 232 (M^+, 39), 191 (34), 189 (34), 153 (37), 109 (52), 78 (25), 67 (base peak), and 55 (84). HRMS Found: *m/z* 232.0086. Calcd for $C_9H_{13}O_2Br$: M, 232.0099.

3-Bromo-5-[(*E*)-3-methyl-1-butenyl]-4,5-dihydro-2(3*H*)-furanone (6b). A similar procedure was applied to **5b** under the following conditions: **5b** (0.287 g, 1.69 mmol) in dry dichloromethane (3 ml), triethylamine (0.205 g, 2.02 mmol), and methanesulfonyl chloride (0.263 g, 2.02 mmol) at 0 °C for 3 h, hydrolytic workup and extraction with dichloromethane (20 ml×2), lithium bromide (0.293 g, 3.37 mmol) in THF (3 ml), stirring at room temperature for 24 h, hydrolytic workup and extraction with dichloromethane, column chromatography on silica gel with hexane-ethyl acetate (7:1 v/v). A 1:1 mixture of two diastereomers of **6b** (by ^{1}H NMR, 0.315 g, 80%) was obtained by this procedure, which could be separated from each other through a careful column chromatography.

3,5-*trans*-6b: Colorless liquid; IR (neat) 1780, 1670, 1460, 1430, 1320, 1290, 1180, 1030, 970, and 920 cm^{-1}; ^{1}H NMR ($CDCl_3$) δ=1.02 (6H, d, J=7.0 Hz, *i*-Pr), 2.2—2.5 (1H, m, *i*-Pr), 2.49 (1H, ddd, J_{gem}=14.7, J_{4-5}=8.8, and J_{4-3}=6.2 Hz, one of 4-H), 2.59 (1H, ddd, J_{gem}=14.7, J_{4-5}=5.5, and J_{4-3}=1.8 Hz, the other of 4-H), 4.45 (1H, dd, J_{3-4}=6.2 and 1.8 Hz, 3-H), 5.12 (1H, ddd, J_{5-4}=8.8, 5.5, and $J_{5-1'}$=7.3 Hz, 5-H), 5.45 (1H, dd, $J_{1'-2'}$=15.4 and $J_{1'-5}$=7.3 Hz, 1'-H), and 5.90 (1H, dd, $J_{2'-1'}$=15.4 $J_{2'-3'}$=5.5 Hz, 2'-H); ^{13}C NMR ($CDCl_3$) δ=21.79, 30.71 (each *i*-Pr), 38.98 (4-C), 40.16 (3-C), 80.36 (5-C), 122.67 (1'-C), 144.47 (2'-C), and 172.39 (2-C); MS *m/z* (rel intensity, %) 234 (M^++2, 3), 232 (M^+, 3), 191 (38), 189 (41), 153 (53), 109 (96), 81 (27), 69 (92), 67 (51), and 55 (base peak). HRMS Found: *m/z* 232.0081. Calcd for $C_9H_{13}O_2Br$: M, 232.0099.

3,5-*cis*-6b: Colorless liquid; IR (neat) 1780, 1670, 1470, 1325, 1170, 975, and 930 cm^{-1}; ^{1}H NMR ($CDCl_3$) δ=1.02 (6H, d, J=7.0 Hz, *i*-Pr), 2.2—2.5 (1H, m, *i*-Pr), 2.37 (1H, ddd, J_{gem}=13.6, J_{4-3}=9.2, and J_{4-5}=8.8 Hz, one of 4-H), 3.02 (1H, ddd, J_{gem}=13.6, J_{4-3}=8.4, and J_{4-5}=6.2 Hz, the other of 4-H), 4.57 (1H, dd, J_{3-4}=9.2 and 8.4 Hz, 3-H), 4.88 (1H, dd, J_{5-4}=8.8, 6.2, and $J_{5-1'}$=7.3 Hz, 5-H), 5.54 (1H, dd, $J_{1'-2'}$= 15.4 and $J_{1'-5}$=7.3 Hz, 1'-H), and 5.85 (1H, dd, $J_{2'-1'}$=15.4 and $J_{2'-3'}$=6.6 Hz, 2'-H); ^{13}C NMR ($CDCl_3$) δ=21.77, 30.71 (each *i*-Pr), 37.82 (4-C), 39.80 (3-C), 80.04 (5-C), 123.54 (1'-C), 144.32 (2'-C), and 172.43 (2-C); MS *m/z* (rel intensity, %) 234 (M^++2, 2), 232 (M^+, 2), 191 (22), 189 (21), 153 (57), 109 (67), 81 (24), 79 (23), 69 (base peak), 67 (54), 56 (21), and 55 (94). HRMS Found: *m/z* 232.0074. Calcd for $C_9H_{13}O_2Br$: M, 232.0099.

3-Bromo-5-[(*E*)-2-phenylethenyl]-4,5-dihydro-2(3*H*)-furanone (6c). A similar procedure was applied to **5c** under the following conditions: **5c** (0.099 g, 0.048 mmol) in dichloromethane (3 ml), triethylamine (0.054 g, 0.53 mmol), and methanesulfonyl chloride (0.061 g, 0.53 mmol) in dichloromethane (1 ml) at −20 °C, stirring at 0 °C for 2 h, hydrolytic workup and extraction with dichloromethane (20 ml×2), lithium bromide (0.084 g, 0.97 mmol) in THF (2 ml), at room temperature for 24 h, hydrolytic workup and extraction, column chromatography on silica gel with hexane-ethyl acetate (7:1 v/v). A 1:1 mixture (by ^{1}H NMR) of two diastereomers of **6c** (0.09 g, 70%) was obtained, which could be separated from each other through a careful column chromatography.

3,5-*trans*-6c: Colorless liquid; IR (neat) 1770, 1490, 1440, 1370, 1305, 1170, 1030, 970, 920, and 760 cm^{-1}; ^{1}H NMR ($CDCl_3$) δ=2.5—2.8 (2H, m, 4-H), 4.48 (1H, dd, J_{3-4}=6.6 and 2.2 Hz, 3-H), 5.33 (1H, dt, J_{5-4}=8.8, 7.3, and $J_{5-1'}$=7.3 Hz, 5-H), 6.17 (1H, dd, $J_{1'-2'}$=15.8 and $J_{1'-5}$=7.3 Hz, 1'-H), 6.76 (1H, d, $J_{2'-1'}$=15.8 Hz, 2'-H), and 7.2—7.5 (5H, m, Ph).

3,5-*cis*-6c: Colorless liquid; IR (neat) 1770, 1480, 1440, 1380, 1330, 1165, 970, 920, and 750 cm^{-1}; ^{1}H NMR ($CDCl_3$) δ=2.49 (1H, ddd, J_{gem}=13.9, J_{4-3}=8.8, and J_{4-5}=7.7 Hz, one of 4-H), 3.12 (1H, ddd, J_{gem}=13.9, J_{4-3}=8.4, and J_{4-5}=6.6 Hz, the other of 4-H), 4.60 (1H, dd, J_{3-4}=8.8 and 8.4 Hz, 3-H), 5.11 (1H, ddd, J_{5-4}=7.7, 6.6, and $J_{5-1'}$=7.3 Hz, 5-H), 6.28 (1H, dd, $J_{1'-2'}$=15.8 and $J_{1'-5}$=7.3 Hz, 1'-H), 6.73 (1H, d, $J_{2'-1'}$= 15.8 Hz, 2'-H), and 7.2—7.5 (5H, m, Ph).

(*Z*)-5-Pentylidene-2(5*H*)-furanone (7a). To a solution of **6a** (0.276 g, 1.18 mmol) in dry THF (12 ml) were added hydroquinone (0.013 g, 0.118 mmol) and DBU (0.36 g, 2.37 mmol) in THF (8 ml). The mixture was heated under reflux for 2 h, poured into saturated aqueous ammonium chloride, and extracted with diethyl ether (20 ml×2). The combined ethers were washed with saturated aqueous sodium chloride, dried over magnesium sulfate, and evaporated in vacuo. The residue was chromatographed on silica gel with hexane-ethyl acetate (5:1 v/v) to give **7a**[3b] (0.105 g, 58%) as a single isomer (by ^{1}H NMR): Pale yellow liquid; IR (neat) 1780, 1670, 1550, 1460, 1180, 1120, 1100, 1060, 940, 870, and 830 cm^{-1}; ^{1}H NMR ($CDCl_3$) δ=0.92 (3H, t, J=7.0 Hz, *n*-Bu), 1.2—1.6 (4H, m, *n*-Bu), 2.41 (2H, dt, J=8.1 and 7.0 Hz, *n*-Bu), 5.32 (1H, t, $J_{1'-2'}$=8.1 Hz, 1'-H), 6.14 (1H, d, J_{3-4}=5.5 Hz, 3-H), and 7.35 (1H, d, J_{4-3}=5.5 Hz, 4-H); ^{13}C NMR ($CDCl_3$) δ=13.79, 22.36, 26.18, 31.04 (each *n*-Bu), 117.81 (1'-C), 118.90 (3-C), 143.72 (4-C), 149.74 (5-C), and 170.20 (2-C); MS *m/z* (rel intensity, %) 152 (M^+, 13), 109 (28), 81 (36), 80 (39), 68 (26), 67 (27), 55 (85), and 41 (base peak). HRMS Found: *m/z* 152.0839. Calcd for $C_9H_{12}O_2$: M, 152.0837.

(*Z*)-5-(3-Methylbutylidene)-2(5*H*)-furanone (7b). A similar prodedure was applied to **6a** under the following conditions: **6a** (0.34 g, 1.46 mmol), hydroquinone (0.016 g, 0.146 mmol), and DBU (0.444 g, 2.92 mmol) in dry THF (25 ml), heating under reflux for 2 h, hydrolytic workup and

extraction with diethyl ether (25 ml×2), column chromatography on silica gel with hexane–ethyl acetate (5:1 v/v). A single isomer (by ^{1}H NMR) of **7b** (0.111 g, 50%) was obtained: Pale yellow liquid; IR (neat) 1780, 1670, 1560, 1330, 1210, 1145, 1110, 1080, 950, 890, and 820 cm^{-1}; ^{1}H NMR ($CDCl_3$) δ=0.95 (6H, d, J=6.6 Hz, *i*-Bu), 1.7—1.9 (1H, m, *i*-Bu), 2.35 (2H, dd, J=8.1 and 6.6 Hz, *i*-Bu), 5.34 (1H, t, $J_{1'-2'}$=8.1 Hz, 1'-H), 6.15 (1H, d, J_{3-4}=5.5 Hz, 3-H), and 7.37 (1H, d, J_{4-3}=5.5 Hz, 4-H); ^{13}C NMR ($CDCl_3$) δ=22.33, 28.57, 35.32 (each *i*-Bu), 116.58 (1'-C), 118.96 (3-C), 143.65 (4-C), 150.22 (5-C), and 170.22 (2-C); MS *m/z* (rel intensity, %) 152 (M^+, 4), 81 (25), 80 (23), 56 (53), 55 (53), and 42 (base peak). HRMS Found: *m/z* 152.0835. Calcd for $C_9H_{12}O_2$: M, 152.0837.

3-(Methylsulfonyloxy)-5-[(*E*)-1-pentenyl]-4,5-dihydro-2(3*H*)-furanone (8). To a solution of **5a** (0.071 g, 0.42 mmol) in dry dichloromethane (2 ml) were added dropwise, at 0 °C under nitrogen, methanesulfonyl chloride (0.057 g, 0.5 mmol), and then triethylamine (0.046 g, 0.46 mmol). After stirring for 2 h at 0 °C, the mixture was poured into saturated aqueous ammonium chloride and extracted with dichloromethane (20 ml×2). The combined extracts were washed with water, dried over magnesium sulfate, and evaporated in vacuo. The residue was chromatographed on silica gel with hexane–ethyl acetate (3:1 v/v) to give **8** (0.066 g, 63%) as a 1:1 mixture of two diastereomers (by ^{1}H NMR) which could be separated from each other through a careful column chromatography.

***3,5-trans*-8:** Colorless liquid; IR (neat) 1780, 1670, 1460, 1370, 1170, 970, and 850 cm^{-1}; ^{1}H NMR ($CDCl_3$) δ=0.91 (3H, t, J=7.3 Hz, *n*-Pr), 1.43 (2H, sx, J=7.3 Hz, *n*-Pr), 2.07 (2H, ddt, J=7.3, 6.6, and 1.5 Hz, *n*-Pr), 2.50 (1H, ddd, J_{gem}=13.9, J_{4-3}=8.1, and J_{4-5}=4.8 Hz, one of 4-H), 2.67 (1H, dt, J_{gem}=13.9, J_{4-3}=J_{4-5}=7.0 Hz, the other of 4-H), 3.25 (3H, s, Me), 5.0—5.2 (1H, m, 5-H), 5.29 (1H, dd, J_{3-4}=8.1 and 7.0 Hz, 3-H), 5.48 (1H, ddt, $J_{1'-2'}$=15.4, $J_{1'-5}$=7.0, and $J_{1'-3'}$=1.5 Hz, 1'-H), and 5.86 (dt, $J_{2'-1'}$=15.4 and $J_{2'-3'}$=6.6 Hz, 2'-H); ^{13}C NMR ($CDCl_3$) δ=13.58, 21.79, 34.05 (each *n*-Pr), 35.09 (Me), 39.42 (4-C), 74.09 (3-C), 79.05 (5-C), 126.29 (1'-C), 136.77 (2'-C), and 171.25 (2-C); MS *m/z* (rel intensity, %) 153 (M^+—OMs, 1), 97 (13), 83 (11), 81 (35), 79 (57), 69 (13), 67 (35), and 55 (base peak).

***3,5-cis*-8:** Colorless liquid; IR (neat) 1780, 1670, 1460, 1370, 1180, 970, 840, and 760 cm^{-1}; ^{1}H NMR ($CDCl_3$) δ=0.92 (3H, t, J=7.3 Hz, *n*-Pr), 1.42 (2H, sx, J=7.3 Hz, *n*-Pr), 2.07 (2H, dt, J=7.3 and 6.6 Hz, *n*-Pr), 2.2—3.0 (2H, m, 4-H), 3.29 (3H, s, Me), 4.83 (1H, ddd, J_{5-4}=10.6, 8.4, and $J_{5-1'}$=7.7 Hz, 5-H), 5.37 (1H, dd, J_{3-4}=10.6 and 8.4 Hz, 3-H), 5.50 (1H, dd, $J_{1'-2'}$=15.4 and $J_{1'-5}$=7.7 Hz, 1'-H), and 5.91 (1H, dt, $J_{2'-1'}$=15.4 and $J_{2'-3'}$=6.6 Hz, 2'-H); ^{13}C NMR ($CDCl_3$) δ=13.56, 21.74, 34.07 (each *n*-Pr), 35.95 (Me), 39.65 (4-C), 74.28 (3-C), 77.82 (5-C), 126.10 (1'-C), 138.25 (2'-C), and 171.23 (2-C); MS *m/z* (rel intensity, %) 153 (M^+—OMs, 1), 152 (19), 109 (10), 108 (10), 107 (25), 97 (25), 95 (57), 83 (15), 81 (57), 80 (14), 79 (47), 69 (22), and 55 (base peak). Found: C, 48.53; H, 6.74%. Calcd for $C_{10}H_{16}O_5S$: C, 48.37; H, 6.50%.

3-Chloro-5-[(*E*)-1-pentenyl]-4,5-dihydro-2(3*H*)-furanone (9). To a solution of **5a** (0.1 g, 0.588 mmol) in pyridine (1 ml) was added *p*-toluenesulfonic acid (0.268 g, 1.41 mmol). The mixture was stirred at 0 °C for 3 h, at room temperature for 23 h, poured into water, and extracted with diethyl ether (15 ml×2). The combined extracts were washed with 1 M hydrochloric acid and then with water, dried over magnesium sulfate, and evaporated in vacuo. The residue was chromatographed on silica gel with hexane–ethyl acetate (7:1 v/v) to give a 1:1 mixture of two diastereomers (by ^{1}H NMR) which could be separated from each other through a careful column chromatography.

***3,5-trans*-9:** Colorless liquid; IR (neat) 1780, 1660, 1450, 1370, 1320, 1175, 960, and 930 cm^{-1}; ^{1}H NMR ($CDCl_3$) δ=0.91 (3H, t, J=7.3 Hz, *n*-Pr), 1.43 (2H, sx, J=7.3 Hz, *n*-Pr), 2.09 (2H, q, J=7.3 Hz, *n*-Pr), 2.4—2.6 (2H, m, 4-H), 4.44 (1H, dd, J_{3-4}=6.6 and 3.3 Hz, 3-H), 5.15 (1H, q, J_{5-4}=$J_{5-1'}$=7.3 Hz, 5-H), 5.48 (1H, dd, $J_{1'-2'}$=15.4 and $J_{1'-5}$=7.3 Hz, 1'-H), and 5.90 (1H, dt, $J_{2'-1'}$=15.4 and $J_{2'-3'}$=7.3 Hz, 2'-H); ^{13}C NMR ($CDCl_3$) δ=13.58, 21.84, 34.15 (each *n*-Pr), 39.58 (4-C), 51.27 (3-C), 79.84 (5-C), 125.84 (1'-C), 137.45 (2'-C), and 171.96 (2-C); MS *m/z* (rel intensity, %) 188 (M^+, 10), 153 (27), 145 (87), 109 (70), 88 (24), 82 (41), 79 (52), 77 (27), 69 (27), 67 (base peak), 65 (20), and 55 (79). HRMS Found: *m/z* 188.0492. Calcd for $C_9H_{13}O_2Cl$: M, 188.0603.

***3,5-cis*-9:** Colorless liquid; IR (neat) 1780, 1670, 1450, 1380, 1320, 1180, 970, and 930 cm^{-1}; ^{1}H NMR ($CDCl_3$) δ=0.91 (3H, t, J=7.3 Hz, *n*-Pr), 1.43 (2H, sx, J=7.3 Hz, *n*-Pr), 2.07 (2H, q, J=7.3 Hz, *n*-Pr), 2.26 (1H, m, one of 4-H), 2.96 (1H, m, the other of 4-H), 4.56 (1H, dd, J_{3-4}=10.3 and 8.4 Hz, 3-H), 4.8—4.9 (1H, m, 5-H), 5.54 (1H, dd, $J_{1'-2'}$=15.4 and $J_{1'-5}$=7.3 Hz, 1'-H), and 5.88 (1H, dt, $J_{2'-1'}$=15.4 and $J_{2'-3'}$=7.3 Hz, 2'-H); ^{13}C NMR ($CDCl_3$) δ=13.58, 21.80, 34.11 (each *n*-Pr), 39.55 (4-C), 51.30 (3-C), 78.89 (5-C), 126.40 (1'-C), 137.79 (2'-C), and 172.10; MS *m/z* (rel intensity, %) 188 (M^+, 17), 153 (34), 147 (29), 145 (73), 109 (68), 88 (32), 82 (39), 79 (54), 77 (25), 69 (29), 67 (base peak), 65 (21), and 55 (78). HRMS Found: *m/z* 188.0599. Calcd for $C_9H_{13}O_2Cl$: M, 188.0603.

Methyl 3-[(Diethoxyphosphinyl)methyl]-5-methyl-2-isoxazoline-5-carboxylate (11). To a solution of (diethoxyphosphinyl)acetaldehyde oxime (7.81 g, 40 mmol) in dry DMF (50 ml) was added dropwise at −20 °C a solution of NBS (14.2 g, 80 mmol) in dry DMF (50 ml). After stirring at −20 °C for 1 h and at 0 °C for 30 min, the mixture was diluted with dry diethyl ether (50 ml). A mixture of methyl methacrylate (8.01 g, 80 mmol) and triethylamine (4.05 g, 40 mmol) in diethyl ether (50 ml) was slowly added, the resulting mixture was stirred at room temperature for 18 h, poured into ice water, and extracted with dichloromethane (50 ml×2). The combined extracts were washed with water, dried over magnesium sulfate, and evaporated in vacuo. The residue was chromatographed on silica gel with hexane–ethyl acetate (5:1 v/v) to give **11** (7.62 g, 65%): Pale yellow liquid; IR (neat) 1740, 1670, 1440, 1390, 1340, 1250, 1020, 960, and 790 cm^{-1}; ^{1}H NMR ($CDCl_3$) δ=1.33 (6H, t, J=7.0 Hz, OEt), 1.60 (3H, s, Me), 2.95 (2H, d, J_{H-P}=22.0 Hz, PCH_2), 3.01, 3.59 (each 1H, dd, J_{gem}=18.0 and J_{H-P}=4.0 Hz, 4-H), 3.76 (3H, s, COOMe), and 4.11 (4H, dq, J=7.0 and J_{H-P}=8.0 Hz, OEt); ^{13}C NMR ($CDCl_3$) δ=16.39 (d, J_{C-P}= 5.9 Hz, OEt), 23.35 (Me), 26.26 (d, J_{C-P}=140.9 Hz, PCH_2), 47.04 (4-C), 52.89 (COOMe), 62.63 (d, J_{C-P}=5.9 Hz, OEt), 85.9 (5-C), 151.44 (d, J_{C-P}=9.8 Hz, 3-C), and 172.31 (COOMe); MS *m/z* (rel intensity, %) 293 (M^+, 1), 234 (base peak), 206 (28), 178 (59), and 160 (16). Satisfactory analytical result was not obtained because of its hygroscopic nature.

Methyl 5-(Diethoxyphosphinyl)-2-hydroxy-2-methyl-4-oxopentanoate (12). To a solution of **11** (7,62 g, 26 mmol) in

aqueous ethanol (17%, 78 ml) were added Raney Ni (W-2, suspension in ethanol, 6 ml) and boric acid (6.43 g, 104 mmol). The mixture was stirred at room temperature under hydrogen (1 atm) for 14 h. After removal of the catalyst by filtration through Celite 545, the filtrate was diluted with water and extracted with dichloromethane (30 ml×2). The combined extracts were dried over magnesium sulfate and evaporated in vacuo. The residue was chromatographed on silica gel with ethyl acetate to give **12** (6.6 g, 86%): Colorless liquid; IR (neat) 3340, 1740, 1710, 1450, 1390, 1250, 1020, 970, and 790 cm^{-1}; ^1H NMR ($CDCl_3$) δ=1.34 (6H, t, J=7.0 Hz, OEt), 1.41 (3H, s, Me), 3.04 (1H, d, J_{gem}=17.6 one of 3-H), 3.11 (2H, d, J_{H-P}=22.7 Hz, 5-H), 3.28 (1H, d, J_{gem}=17.6 Hz, the other of 3-H), 3.76 (3H, s, COOMe), 3.82 (1H, s, OH), and 4.14 (4H, dq, J=7.0 and J_{H-P}=7.5 Hz, OEt); ^{13}C NMR ($CDCl_3$) δ=16.31 (d, J_{C-P}=6.8 Hz, OEt), 26.26 (Me), 43.18 (d, J_{C-P}=127.2 Hz, PCH_2), 52.71 (COOMe), 52.86 (3-C), 62.72 (d, J_{C-P}=5.9 Hz, OEt), 72.45 (2-C), 176.01 (COOMe), and 200.79 (d, J_{C-P}=5.9 Hz, 4-C); MS m/z (rel intensity, %) 296 (M^+, 0.3), 237 (base peak), 167 (22), 139 (42), 123 (30), 42 (54), and 30 (20). HRMS Found: m/z 296.1023. Calcd for $C_{11}H_{21}O_7P$: M, 296.1023.

Methyl (*E*)-2-Hydroxy-2-methyl-4-oxo-5-nonenoate (13a). Under nitrogen, a solution of **12** (0.727 g, 2.45 mmol) in dry THF (5 ml) was added to a solution of lithium bromide (0.213 g, 2.45 mmol) in THF (2 ml). After stirring at room temperature for 10 min, a solution of DBU (0.355 g, 2.33 mmol) in THF (5 ml) was added at 0 °C, stirring was continued for 1 h, and then butanal (0.354 g, 4.19 mmol) was slowly added. After stirring at 0 °C for 24 h, the reaction mixture was poured into ice water and extracted with dichloromethane (20 ml×2). The combined extracts were dried over magnesium sulfate and evaporated in vacuo. The residue was chromatographed on silica gel by using hexane–ethyl acetate (3:1 v/v) as an eluent to give **13a** (0.443 g, 84%): Colorless liquid; IR (neat) 3510, 1750, 1670, 1630, 1460, 1380, 1300, 1210, 1120, and 990 cm^{-1}; ^1H NMR ($CDCl_3$) δ=0.94 (3H, t, J=7.3 Hz, n-Pr), 1.43 (3H, s, Me), 1.50 (2H, sx, J=7.3 Hz, n-Pr), 2.21 (2H, dq, J=7.3 and 1.5 Hz, n-Pr), 2.91, 3.26 (each 1H, J_{gem}=17.2 Hz, 3-H), 3.76 (3H, s, COOMe), 4.00 (1H, s, OH), 6.07 (1H, dt, J_{5-6}=15.8 and J_{5-7}=1.5 Hz, 5-H), and 6.88 (1H, dt, J_{6-5}=15.8 and J_{6-7}=7.3 Hz, 6-H); ^{13}C NMR ($CDCl_3$) δ=13.68, 21.24, 34.54 (each n-Pr), 26.28 (Me), 48.83 (3-C), 52.64 (COOMe), 72.74 (2-C), 130.29 (5-C), 149.24 (6-C), 176.32 (COOMe), and 199.00 (4-C); MS m/z (rel intensity, %) 214 (M^+, 5), 155 (27), 97 (base peak), 55 (62), 43 (51), and 41 (24). HRMS Found: m/z 214.1207. Calcd for $C_{11}H_{18}O_4$: M, 214.1208.

Methyl (*E*)-2-Hydroxy-2,7-dimethyl-4-oxo-5-octenoate (13b). A similar procedure was applied under the following conditions: **12** (1.439 g, 4.86 mmol) in dry THF (9 ml), lithium bromide (0.422 g, 4.86 mmol) in THF (2 ml), 10 min at room temperature, DBU (0.702 g, 4.61 mmol) in THF (9 ml) at 0 °C, stirring at 0 °C for 1 h, 2-methylpropanal (0.701 g, 9.71 mmol), stirring at 0 °C for 24 h, hydrolytic workup and extraction with dichloromethane (20 ml×2), column chromatography on silica gel with hexane–ethyl acetate (3:1 v/v). This procedure gave **13b** (0.805 g, 77%): Colorless liquid; IR (neat) 3500, 1740, 1670, 1630, 1460, 1370, 1200, 1120, and 990 cm^{-1}; ^1H NMR ($CDCl_3$) δ=1.07 (6H, d, J=7.0 Hz, i-Pr), 1.43 (3H, s, Me), 2.3—2.6 (1H, m, i-Pr), 2.92, 3.26 (each 1H, d, J_{gem}=17.2 Hz, 3-H), 3.76 (3H, s, COOMe), 3.99 (1H, s, OH), 6.02 (1H, dd, J_{5-6}=16.1 and J_{5-7}=1.5 Hz, 5-H), and 6.84 (1H, dd, J_{6-5}=16.1 and J_{6-7}=6.6 Hz, 6-H); ^{13}C NMR ($CDCl_3$) δ=21.17, 31.17 (each i-Pr), 26.25 (Me), 48.97 (3-C), 52.50 (COOMe), 72.61 (2-C), 127.45 (5-C), 155.06 (6-C), 176.25 (COOMe), and 199.07 (4-C); MS m/z (rel intensity, %) 214 (M^+, 4), 155 (29), 97 (base peak), 43 (34), and 41 (24). HRMS Found: m/z 214.1212. Calcd for $C_{11}H_{18}O_4$: M, 214.1204.

3-Hydroxy-3-methyl-5-[(*E*)-1-pentenyl]-4,5-dihydro-2(3*H*)-furanone (14a). A single isomer of **14a** (0.347 g, 56%) was obtained by a procedure similar to that employed for the preparation of **5a** from **4a** under the following conditions: **13a** (0.723 g, 3.37 mmol) in methanol (8 ml), sodium borohydride (0.128 g, 3.37 mmol), stirring at 0 °C for 10 min, acetone (4 ml), stirring at 0 °C for 10 min, hydrolytic workup and extraction with dichloromethane (20 ml×2), the crude product and p-toluenesulfonic acid (0.064 g, 0.337 mmol) in dichloromethane (8 ml), stirring at room temperature for 2 h, hydrolytic workup and extraction with dichloromethane (20 ml×2), column chromatography on silica gel with hexane–ethyl acetate (5:1 v/v): Colorless prisms; mp 49—51 °C; IR (KBr) 3400, 1750, 1440, 1380, 1320, 1180, 1120, 960, 920, and 600 cm^{-1}; ^1H NMR ($CDCl_3$) δ=0.91 (3H, t, J=7.3 Hz, n-Pr), 1.42 (2H, sx, J=7.3 Hz, n-Pr), 1.49 (3H, s, Me), 1.91 (1H, dd, J_{gem}=13.6 and J_{4-5}=8.4 Hz, one of 4-H), 2.05 (2H, q, J=7.3 Hz, n-Pr), 2.50 (1H, dd, J_{gem}=13.6 and J_{4-5}=6.2 Hz, the other of 4-H), 3.71 (1H, br s, OH), 5.05 (1H, ddd, J_{5-4}=8.4, 6.2, and $J_{5-1'}$=7.3 Hz, 5-H), 5.46 (1H, dd, $J_{1'-2'}$=15.1 and $J_{1'-5}$=7.3 Hz, 1'-H), and 5.84 (1H, dt, $J_{2'-1'}$=15.1 and $J_{2'-3'}$=7.3 Hz, 2'-H); ^{13}C NMR ($CDCl_3$) δ=13.59, 21.91 (each n-Pr), 23.92 (Me), 34.17 (n-Pr), 43.37 (4-C), 73.66 (3-C), 78.64 (5-C), 127.28 (1'-C), 136.22 (2'-C), and 178.54 (COOMe); MS m/z (rel intensity, %) 167 (M^+—OH, 0.4), 97 (20), 81 (34), 71 (26), 67 (19), 58 (17), 55 (18), and 43 (base peak). Found C, 64.92; H, 9.00%. Calcd for $C_{10}H_{16}O_3$: C, 65.19; H, 8.75%.

3-Hydroxy-3-methyl-5-[(*E*)-3-methyl-1-butenyl]-4,5-dihydro-2(3*H*)-furanone (14b). A similar procedure was applied to **13b** under the following conditions: **13b** (0.747 g, 3.49 mmol) in methanol (7 ml), sodium borohydride (0.132 g, 3.49 mmol) stirring at 0 °C for 10 min, acetone (3 ml), stirring at 0 °C for 10 min, hydrolytic workup and extraction with dichloromethane (15 ml×2), the crude product and p-toluenesulfonic acid (0.066 g, 0.349 mmol) in dichloromethane (7 ml), stirring at room temperature for 1 h, hydrolytic workup and extraction with dichloromethane (15 ml×2), silica-gel column chromatography with hexane–ethyl acetate (5:1 v/v). From this procedure was obtained a single isomer of **14b** (0342 g, 53%) which was contaminated by a trace amount of an unidentified product: Colorless prisms; mp 85—87 °C; IR (KBr) 3420, 1750, and 1670 cm^{-1}; ^1H NMR ($CDCl_3$) δ=0.90 (6H, d, J=7.0 Hz, i-Pr), 1.50 (3H, s, Me), 1.92 (1H, dd, J_{gem}=13.6 and J_{4-5}=8.4 Hz, one of 4-H), 2.50 (1H, dd, J_{gem}=13.6 and J_{4-5}=6.2 Hz, the other of 4-H), 3.76 (1H, m, OH), 5.05 (1H, ddd, J_{5-4}=8.4, 6.2, and $J_{5-1'}$=7.0 Hz, 5-H), 5.41 (1H, dd, $J_{1'-2'}$=15.4 and $J_{1'-5}$=7.0 Hz, 1'-H), and 5.82 (1H, dd, $J_{2'-1'}$=15.4 and $J_{2'-3'}$=6.2 Hz, 2'-H); ^{13}C NMR ($CDCl_3$) δ=21.89 (i-Pr), 23.99 (Me), 30.71 (i-Pr), 43.34 (4-C), 73.66 (3-C), 78.67 (5-C), 124.26 (1'-C), 143.06 (2'-C), and 178.50 (2-C); MS m/z (rel intensity, %) 167 (M^+—OH, 8), 95 (21), 81 (49), 71 (22), 55 (34), and 43 (base peak).

(*Z*)-3-Methyl-5-pentylidene-2(5*H*)-furanone (16a). To a solution of **14a** (0.23 g, 1.25 mmol) in dry dichloromethane

(5 ml) were added, at 0 °C under nitrogen, triethylamine (0.152 g, 1.5 mmol) and methanesulfonyl chloride (0.171 g, 1.5 mmol). After stirring at 0 °C for 3 h, the mixture was poured into saturated aqueous ammonium chloride and extracted with dichloromethane (15 ml×2). The combined extracts were washed with saturated aqueous sodium hydrogencarbonate, dried over magnesium sulfate, and evaporated in vacuo. The residue was dissolved in dry THF (5 ml) and lithium bromide (0.217 g, 2.5 mmol) was added. The mixture was refluxed under nitrogen for 1 h, poured into water, and extracted with dichloromethane (15 ml×2). The combined extracts were dried over magnesium sulfate and evaporated in vacuo. The residue was filtered through a short column packed by silica gel. The fraction eluted with hexane–ethyl acetate (5:1 v/v) was evaporated in vacuo to give crude **15a** (0.183 g). This product was disolved in dry THF (1 ml) and were added hydroquinone (0.014 g, 0.125 mmol) and DBU (0.38 g, 2.5 mmol). This mixture was refluxed under nitrogen for 1 h, poured into saturated aqueous ammonium chloride, and extracted with diethyl ether. The combined extracts were dried over magnesium sulfate and evaporated in vacuo. The residue was chromatographed on silica gel by using hexane–diethyl ether (5:1 v/v) to afford **16a** (0.131 g, 63%): Colorless luquid; IR (neat) 1780, 1670, 1620, 1460, 1050, 990, 890, and 760 cm^{-1}; ^1H NMR ($CDCl_3$) δ=0.91 (3H, t, J=7.0 Hz, *n*-Bu), 1.2—1.5 (4H, m, *n*-Bu), 1.99 (3H, d, J_{Me-4}=1.5 Hz, Me), 2.37 (2H, dt, J=7.7 and 7.0 Hz, *n*-Bu), 5.17 (1H, t, $J_{1'-2}$=7.7 Hz, 1'-H), and 7.02 (1H, q, J_{4-Me}=1.5 Hz, 4-H); ^{13}C NMR ($CDCl_3$) δ=10.47 (Me), 13.81, 22.36, 25.89, 31.26 (each *n*-Bu), 114.81 (1'-C), 128.85 (3-C), 137.91 (4-C), 148.43 (5-C), and 171.27 (2-C); MS *m/z* (rel intensity, %) 166 (M^+, 16), 123 (58), 110 (35), 96 (31), 95 (23), 81 (32), 69 (20), 68 (60), 67 (20), 60 (28), and 55 (base peak). HRMS Found: *m/z* 166.0990. Calcd for $C_{10}H_{14}O_2$: M, 166.0993.

(*Z*)-3-Methyl-5-(3-methylbutylidene)-2(5*H*)-furanone (16b). A similar procedure was performed under the following procedure: **14b** (0.339 g, 1.84 mmol) in dry dichloromethane (7 ml), addition of triethylamine (0.223 g, 2.21 mmol) and methanesulfonyl chloride (0.253 g, 2.21 mmol) at 0 °C, stirring at 0 °C for 3 h under nitrogen, hydrolytic workup and extraction with dichloromethane, the crude product and lithium bromide (0.32 g, 3.68 mmol) in THF (5 ml), heating under reflux for 1 h, hydrolytic workup and extraction with dichloromethane, filtration through a short column, the crude product (0.297 g) and hydroquinone (0.02 g, 0.184 mmol) and DBU (0.56 g, 3.68 mmol) in THF (4 ml), heating under reflux for 1 h, hydrolytic workup and extraction with diethyl ether, a silica-gel chromatography with hexane–diethyl ether (5:1). Thus a single isomer of **16b** (0.153 g, 50%) was obtained: Colorless liquid; IR (neat) 1770, 1680, 1620, 1460, 1060, 1040, 990, 890, and 760 cm^{-1}; ^1H NMR ($CDCl_3$) δ=0.94 (6H, d, J=6.6 Hz, *i*-Bu), 1.6—1.9 (1H, m, *i*-Bu), 1.99 (3H, d, J_{Me-4}=1.5 Hz, Me), 2.27 (2H, dd, J=8.1 and 7.3 Hz, *i*-Bu), 5.17 (1H, t, $J_{1'-2'}$=8.1 Hz, 1'-H), and 7.01 (1H, q, J_{4-Me}=1.5 Hz, 4-H); ^{13}C NMR ($CDCl_3$) δ=10.48 (Me), 22.32, 28.65, 35.06 (each *i*-Bu), 113.57 (1'-C), 128.95 (3-C), 137.76 (4-C), 148.89 (5-C), and 171.30 (2-C); MS *m/z* (rel intensity, %) 166 (M^+, 12), 123 (85), 111 (21), 95 (36), 68 (44), 67 (24), 56 (88), 54 (22), and 40 (base peak). HRMS Found: *m/z* 166.0992. Calcd for $C_{10}H_{14}O_2$: M, 166.0993.

The present work was partially supported by a Grant-in-Aid for Scientific Research (No. 61470095) from the Ministry of Education, Science and Culture.

References

1) As reviews: A. R. Katritzky, "Comprehensive Heterocyclic Chemistry," Pergamon Press, Oxford, New York, Toronto, Sydney, Paris, Frankfurt (1984), Vol. 4, p. 694; M. Matsumoto, *Yuki Gosei Kagaku Kyokai Shi*, **39**, 25 (1981); S. Kano, S. Shibuya, and T. Ebata, *Heterocycles*, **14**, 661 (1980); G. Pattenden, *Progr. Chem. Org. Natural Products*, **35**, 133 (1978); Y. S. Rao, *Chem. Rev.*, **76**, 625 (1976).

2) Some recent syntheses: S. Tsuboi, H. Wada, K. Muranaka, and A. Takeda, *Bull. Chem. Soc. Jpn.*, **60**, 2917 (1987); S. Tsuboi, H. Wada, S. Mimura, and A. Takeda, *Chem. Lett.*, **1987**, 937; C. M. Beechan and J. J. Sims, *Tetrahedron Lett.*, **1979**, 1649; H. Achenbach and J. Witzke, *ibid.*, **1979**, 1579; D. W. Knight and G. Pattenden, *J. Chem. Soc., Parkin Trans. 1*, **1979**, 70; G. A. Kraus and H. Sugimoto, *J. Chem. Soc., Chem. Commun.*, **1978**, 30; T. Wolfram, *Liebigs Ann. Chem.*, **1977**, 1707; Y. S. Rao, *Synth. Commun.*, **6**, 527 (1976).

3) a) G. A. Garcia, H. Munoz, and J. Tariz, *Synth. Commun.*, **13**, 569 (1983); b) T. Nakano and Y. Nagai, *J. Chem. Soc., Chem. Commun.*, **1981**, 815; c) A. G. Schultz and Y. K. Yee, *J. Org. Chem.*, **41**, 561 (1976).

4) S. Hanessian, P. J. Hodge, P. J. Murray, and S. P. Sahoo, *J. Chem. Soc., Chem. Commun.*, **1986**, 754; P. Brownbridge, E. Egert, P. G. Hunt, O. Kennard, and S. Warren, *J. Chem. Soc., Perkin Trans. 1*, **1981**, 2751; K. Iwai, H. Kosugi, and M. Kawai, *Bull. Chem. Soc. Jpn.*, **50**, 242 (1977); S. Inayama and T. Kawamata, *Chem. Pharm. Bull.*, **21**, 461 (1973); C. C. Price and J. M. Judge, *Org. Synth.*, Coll. Vol. 5, 255 (1973).

5) D. P. Curran, *J. Am. Chem. Soc.*, **105**, 5826 (1983); S. F. Martin and B. Dupre, *Tetrahedron Lett.*, **24**, 1337 (1983); A. P. Kozikowski and P. D. Stein, *J. Am. Chem. Soc.*, **104**, 4023 (1982); D. P. Curran, *ibid.*, **104**, 4024 (1982); R. H. Wollenberg and J. E. Goldstein, *Synthesis*, **1980**, 757;

6) O. Tsuge, S. Kanemasa, and H. Suga, *Chem. Lett.*, **1987**, 323.

7) O. Tsuge, S. Kanemasa, and H. Suga, *Bull. Chem. Soc. Jpn.*, **61**, 2133 (1988).

8) O. Tsuge, S. Kanemasa, and H. Suga, *Chem. Lett.*, **1986**, 183.

9) O. Tsuge, S. Kanemasa, H. Suga, and N. Nakagawa, *Bull. Chem. Soc. Jpn.*, **60**, 2463 (1987).

10) O. Tsuge, S. Kanemasa, N. Nakagawa, and H. Suga, *Bull. Chem. Soc. Jpn.*, **60**, 4091 (1987).

11) H. Seki, K. Koga, H. Matsuo, S. Ohki, I. Matsuo, and S. Yamada, *Chem. Pharm. Bull.*, **13**, 995 (1965); M. S. Brown and H. Rapoport, *J. Org. Chem.*, **28**, 3261 (1963).

12) P. J. Jerris and A. B. Smith, III, *J. Org. Chem.*, **46**, 577 (1981).

13) J. P. H. Verheyden and J. G. Moffatt, *J. Org. Chem.*, **35**, 2319 (1970); R. O. Hutchins, M. G. Hutchins, and C. A. Milewski, *ibid.*, **37**, 4190 (1972).

14) Polymer formation was observed either in the absence of hydroquinone or when the reaction was performed in rather high concentration.

15) P. J. Babidge and R. A. M. Westropp, *Aust. J. Chem.*,

34, 1745 (1981).
16) D. W. Knight and G. Pattenden, *J. Chem. Soc., Perkin Trans. 1*, **1979**, 62.
17) Y. Tanabe and N. Ohno, *J. Org. Chem.*, **53**, 1560 (1988).
18) Some preparations of 3-alkylidene-4,5-dihydro-2(3*H*)-furanones by the elimination of 3-alkyl-3-bromo derivatives are known: S. M. Ali and S. T. Roberts, *J. Chem. Soc., Chem. Commun.*, **1975**, 887; A. E. Greene, J.-C. Muller, and G. Ourisson, *J. Org. Chem.*, **39**, 186 (1974).

Acid-Catalyzed Transformation of α-Hydroxy-γ-oxo Acetals to γ-Oxo Esters. A Novel Deconjugation of 4-Oxo-2-alkenal Acetals

Shuji KANEMASA,* Norihiko NAKAGAWA, Hiroyuki SUGA, and Otohiko TSUGE*
Institute of Advanced Material Study, and Department of Molecular Science and Technology, Interdisciplinary Graduate School of Engineering Sciences, Kyushu University, Kasugakoen, Kasuga 816
(Received July 15, 1988)

Under acid catalysis, α-hydroxy-γ-oxo acetals which are readily available from the nitrile oxide cycloaddition route are smoothly converted into γ-oxo esters. This unusual and high-yield transformation involves rare acid-catalyzed deconjugation of the intermediary 4-oxo-2-alkenal acetals and is influenced by a substituent at the 5-position.

A sequence of cycloadditions of (diethoxyphosphinyl)acetonitrile oxide with olefins or acetylenes and reductive N–O bond cleavage of the cycloadducts provides 4-hydroxy-2-oxoalkylphosphonates.[1] The resulting functionalities are synthetically important when they are utilized in organic synthesis either separately, all together, or together with an additional function introduced from dipolarophiles.[2]

We were investigating a possibility of acid-catalyzed one-step transformation of 2-hydroxy-4-oxo-5-alkenal acetals into 5-alkylidene-2(3*H*)-furanones which are important heterocycles often seen in natural products.[3] During this investigation we came across an unusual and high-yield transformation of the acetals to γ-oxo esters. All the results with respect to this novel transformation and its reaction mechanism are discussed in the present article.

Results and Discussion

Acid-catalyzed ring closure of 2-hydroxy-4-oxo-5-alkenal acetals must be useful as a direct synthetic way to 5-alkylidene-2(3*H*)-furanones[4] when the starting acetals are easily available. Since we previously tested the synthetic value of Horner–Emmons olefination of 4-hydroxy-2-oxoalkylphosphonates,[5] its applications to the synthesis of 5-alkylidene-2(3*H*)-furanones were aimed.

(*E*)-6,6-Diethoxy-5-hydroxy-1-phenyl-1-hexen-3-one (**3**) as a starting compound, can be prepared by Horner–Emmons olefination of diethyl 5,5-diethoxy-4-hydroxy-2-oxopentylphosphonate (**2**) which is available by a sequence of 1,3-dipolar cycloaddition of (diethoxyphosphinyl)acetonitrile oxide with 3,3-diethoxypropene and Raney Ni reduction of the cycloadduct, 5-(diethoxymethyl)-3-[(diethoxyphosphinyl)-methyl]-2-isoxazoline (**1**).[1,5]

Treatment of **3** with hydrogen chloride in chloroform at room temperature unexpectedly led to quantitative formation of ethyl (*E*)-4-oxo-5-hexenoate (**4**) (Scheme 1). This reaction can be complete in 20 min at 0 °C and the same product **4** was obtained in 89% yield. Ester **4** showed quite high stability against acid. For example, **4** stayed unchanged even when heated under reflux in chloroform together with hydrogen chloride for a long time (18 h). This quantitative ester formation contrasts with the reported example[4] where an analogous acetal, 6-hydroxy-2,6-dimethyl-7,7-dimethoxy-2-hepten-4-one, gives 3-methyl-5-(2-methylpropylidene)-2(3*H*)-furanone in 72% yield under the comparable conditions. Although there are known several ring-closure reactions of γ-oxo esters or acids leading to 2-furanone derivatives,[1,6] the high stability of ester **4** indicates that the furanone synthesis cited in Ref. 4 has proceeded not via the corresponding γ-oxo ester intermediate.[7]

To see whether the double bond of **3** is requisite or not for this novel transformation, the saturated ketone **6** was prepared from **1**. The Horner–Emmons olefination of 2-isoxazoline **1** with benzaldehyde gave 5-(diethoxymethyl)-3-[(*E*)-2-phenylethenyl]-2-isoxazoline (**5**) in 82% yield, which was reductively cleaved on Raney Ni to provide 6,6-diethoxy-5-hydroxy-1-phenyl-3-hexanone (**6**) in 69% yield.

Similar treatment of **6** with hydrogen chloride in chloroform gave γ-oxo ester **7** albeit in a moderate yield (58%), indicating that the essential skeleton for the γ-oxo ester formation is an α-hydroxy-γ-oxo acetal framework. However, it should be emphasized that the double bond at the 5-position of **3** has certainly contributed to some stabilization of the corresponding intermediate. This will be discussed later.

As the reaction for α-hydroxy-γ-oxo acetal **6** most likely to undergo under acid catalysis would be dehydration, treatment of the dehydrated derivative, (*E*)-6,6-diethoxy-1-phenyl-4-hexen-3-one (**8**), with an acid was next examined. Compound **8** is readily obtained in 85% yield through a sequence of *O*-mesylation and triethylamine-mediated β-elimination. When **8** was allowed to react with hydrochloric acid, the expected γ-oxo ester **7** was obtained in 57% yield, confirming the intermediacy of 4-oxo-2-alkenal acetal **8**.

It was disappointing that phosphonate **2** as a pre-

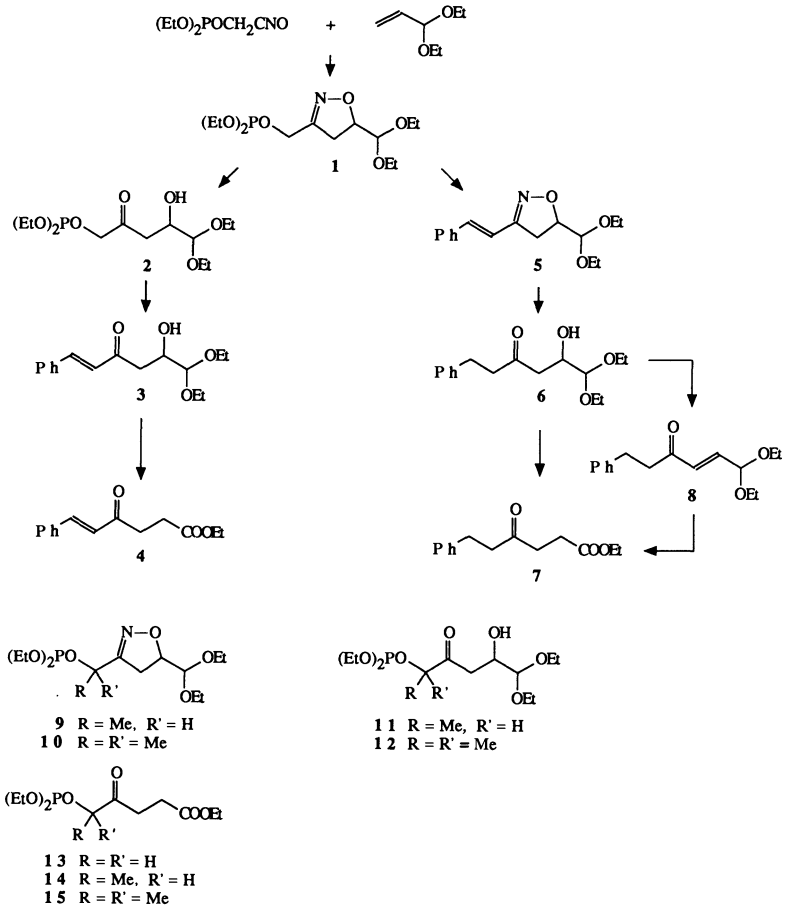

Scheme 1.

cursor of **3** underwent no such transformation into the corresponding γ-oxo ester **13** under similar conditions or even at −78 °C. The introduction of an alkyl moiety adjacent to the phosphinyl group (5-position) was of no use either. Thus phosphonate **2** as well as the methylated derivative **11** led to mixture of complex products.

Two methyl moieties were introduced adjacent to the phosphinyl moiety of **2** via 3-(1-phosphinyl-1-methylethyl)-2-isoxazoline **10** to give 2-(diethoxyphosphinyl)-6,6-diethoxy-5-hydroxy-2-methyl-3-hexanone (**12**). It was our delight to find that the dimethylated ketone **12** was smoothly converted into the corresponding γ-oxo ester **15** in 78% yield.

On the basis of the above results and observations, a possible reaction mechanism is illustrated in Scheme 2. Under acidic conditions the initial acid-catalyzed dehydration of **6** leads to enone **8** which then reversibly isomerizes into dienol intermediate **A**. Formation of **A** is facilitated by stabilization effect from the two ethoxyl groups attached at one end of the dienol conjugation. Since protonation occurs at the less congested α-position rather than the hindered γ-position, the isomerization equilibrates in favor for deconjugation leading to **B**. Under the reaction conditions, intermediate **B** is irreversibly hydrolyzed into γ-oxo ester **7**.

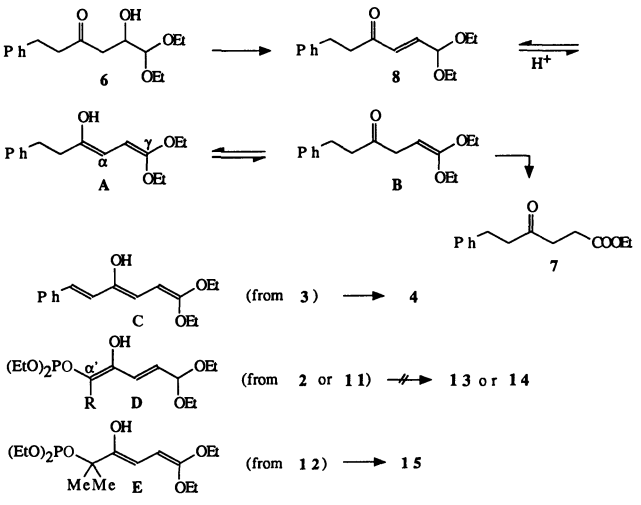

Scheme 2.

Although many synthetically useful examples are known for deconjugation processes under base catalyst[8] and under irradiation,[9] acid-catalyzed deconjugation was less important. As acid-catalyzed deconjugation is always a reversible reaction and often leads to a mixture of conjugated and deconjugated carbonyl compounds,[10] an irreversible step has to be involved for the process to be a useful synthetic reaction. In the

present case, the equilibrating intermediate **B** is irreversibly hydrolyzed by the water formed in the step of **6** to **8** under the applied conditions so that the equilibrium moves in favor for deconjugation.

The preexisting double bond of **3** provides some additional stabilization of the enolized intermediate **C** as a trienol. This is a reason why quantitative conversion of **3** into **4** has been achieved.

Since both the phosphonates **2** and **11** bear at least one highly acidic hydrogen at the α'- position, their enolization occurs exclusively at this position to form phosphorus-stabilized dienol intermediates **D** (R=H or Me) so that there is little chance for deconjugation. Only α',α'-dialkylated phosphonate **12** can undergo smooth conversion into γ-oxo ester **15** via dienol intermediate **E**.

In conclusion, 4-oxo-2-alkenal acetals are converted under acidic conditions into γ-oxo esters through a sequence of dehydration, enolization, deconjugation, and hydrolysis. Since both 3-(phosphinylmethyl)-2-isoxazoline **1** and 2-oxoalkylphosphonate **2** can be successfully employed for the introduction of a wide pattern of substituents by the aid of the phosphinyl moiety,[1] this transformation offers a general synthetic method of γ-oxo esters.

Experimental

General. Melting points were determined on a Yanagimoto melting point apparatus and are uncorrected. IR spectra were taken with a JASCO IRA-1 or a JASCO A-702 spectrometer. ^{1}H NMR spectra were recorded on a JEOL FX-100 (100 MHz) or a JEOL GSX-270 instrument (270 MHz), and ^{13}C NMR on a JEOL FX-100 (25.05 MHz) or a JEOL GSX-270 spectrometer (67.94 MHz). Chemical shifts are expressed in parts per million downfield from tetramethylsilane as an internal standard. Mass spectra were measured with a JEOL-01SG-2 spectrometer at 70 eV of ionization energy. High resolution mass spectra were obtained on the same instrument. Elemental analyses were performed on a Hitachi 026 CHN analyzer. Thin-layer chromatography (TLC) was accomplished on 0.2 mm precoated plates of silica gel 60 F-254 (Merck). For preparative column chromatography, Wakogel C-200, C-300 (Wako), and Silicagel 60 (Merck) were employed. Flash chromatography was carried out on an EYELA EF-10 apparatus using a column (20×180 mm) packed with Silicagel 60 (Merck, size: 0.04—0.063 mm). Micro vacuum distillation was carried out on a Sibata GTO-250R Kugelrohr distilling apparatus. Solvents were evaporated with a Tokyo Rikakikai rotary evaporator type-V at about 50 °C unless otherwise stated.

Materials and Solvents. 2-Oxoalkylphosphonate **2** and enone **3** were prepared according to the reported method starting from 2-isoxazoline **1**.[1,5] Tetrahydrofuran (THF) was distilled from lithium aluminum hydride under nitrogen immediately prior to its use.

Ethyl (*E*)-4-Oxo-6-phenyl-5-hexenoate (4): To a saturated solution of hydrogen chloride in chloroform (20 ml) was added dropwise a solution of **3** (0.067 g, 0.24 mmol) in chloroform (5 ml). The resulting solution was stirred at room temperature for 4 h, poured into ice water, and then extracted with chloroform (15 ml×2). The combined chloroform was washed with saturated aqueous sodium hydrogencarbonate, dried over anhydrous magnesium sulfate, and evaporated in vacuo. The residue was chromatographed over silica gel by using hexane–ethyl acetate (5:1 v/v) to give **4** (0.055 g, 98%). Similar reaction at 0 °C for 20 min afforded 89% of **4** and under reflux for 18 h 97%: Pale yellow liquid; IR (neat) 1730, 1680, 1660, 1610, 1575, 1490, 1445, 1360, 1200, 1160, 1100, 750, and 690 cm^{-1}; ^{1}H NMR ($CDCl_3$) δ=1.24 (3H, t, J=7.0 Hz, COOEt), 2.68, 3.01 (each 2H, t, J=6.5 Hz, 2- and 3-H), 4.14 (2H, q, J=7.0 Hz, COOEt), 6.73 (1H, d, J_{5-6}=16.0 Hz, 5-H), 7.1—7.8 (5H, m, Ph), and 7.57 (1H, d, J_{6-5}=16.0 Hz, 6-H); ^{13}C NMR ($CDCl_3$) δ=14.20 (COOEt), 28.24 (2-C), 35.26 (3-C), 60.62 (COOEt), 125.90, 128.32, 128.95 (each Ph), 130.52 (5-C), 134.44 (Ph), 142.86 (6-C), 172.87 (COOEt), and 198.04 (CO); MS m/z (rel intensity, %) 232 (M^+, 11), 131 (base peak), 103 (40), and 77 (30). HRMS Found: m/z 232.1107. Calcd for $C_{14}H_{16}O_3$: M, 232.1099.

5-(Diethoxymethyl)-3-(*E*)-2-phenylethenyl-2-isoxazoline (5): To a solution of **1** (0.522 g, 1.61 mmol) in dry THF (4 ml) was added, at −78 °C under nitrogen, butyllithium (15% in hexane, 1.14 ml, 1.78 mmol). After 1 h, benzaldehyde (0.343 g, 3.23 mmol) was added and the mixture was stirred at room temperature for 18 h. Saturated aqueous ammonium chloride was added to the mixture which was then extracted with dichloromethane (25 ml×2). The combined extracts were dried over magnesium sulfate and evaporated in vacuo. The residue was subjected to column chromatography over silica gel with hexane–ethyl acetate (5:1 v/v) to give **5** (0.363 g, 82%): Pale yellow liquid; IR (neat) 1630, 1495, 1450, 1370, 1060, 960, 900, 750, and 690 cm^{-1}; ^{1}H NMR ($CDCl_3$) δ=1.20, 1.25 (each 3H, t, J=7.0 Hz, OEt), 3.18 (1H, dd, J_{gem}=16.2 and J_{4-5}=10.6 Hz, one of 4-H), 3.28 (1H, dd, J_{gem}=16.2 and J_{4-5}=7.0 Hz, the other of 4-H), 3.5—3.9 (4H, m, OEt), 4.52 (1H, d, J_{CH-5}=4.8 Hz, $CH(OEt)_2$), 4.71 (1H, ddd, J_{5-4}=10.6, 7.0, and J_{5-CH}=4.8 Hz, 5-H), 6.76 (1H, d, J=16.5 Hz, -CH=), 7.06 (1H, d, J=16.5 Hz, PhCH=), and 7.2—7.5 (5H, m, Ph); ^{13}C NMR ($CDCl_3$) δ=15.28, 15.36 (each OEt), 34.46 (4-C), 63.45, 64.43 (each OEt), 81.45 (5-C), 102.23 ($CH(OEt)_2$), 117.69 (-CH=), 126.97, 128.84, 128.89 (each Ph), 135.82 (Ph), 136.60 (PhCH=), and 157.85 (3-C); MS m/z (rel intensity, %) 275 (M^+, 4), 230 (10), 103 (base peak), 75 (47), and 47 (22). Found: C, 69.79; H, 7.69; N, 5.09%. Calcd for $C_{16}H_{21}NO_3$: C, 69.97; H, 7.93; N, 4.98%.

6,6-Diethoxy-5-hydroxy-1-phenyl-3-hexanone (6): To a solution of **5** (0.363 g, 1.32 mmol) in aqueous ethanol (17%, 7.2 ml) were added Raney Ni (W-2, suspension in ethanol, 0.5 ml) and boric acid (0.326 g, 5.27 mmol). The mixture was stirred at room temperature under hydrogen (1 atm) for 12 h. All insoluble materials were filtered off by the aid of Celite 545. The filtrate was diluted with water and extracted with dichloromethane (25 ml×2). The combined extracts were dried over magnesium sulfate and evaporated in vacuo. The residue was chromatographed over silica gel by using hexane–ethyl acetate (5:1 v/v) to give **6** (0.256 g, 69%): Colorless liquid; IR (neat) 3430, 1705, 1600, 1490, 1445, 1370, 1060, 745, and 700 cm^{-1}; ^{1}H NMR ($CDCl_3$) δ=1.20, 1.22 (each 3H, t, J=7.3 Hz, OEt), 2.6—3.0 (7H, m, 1-, 2-, 4-H, and OH), 3.4—3.9 (4H, m, OEt), 4.09 (1H, dt, J_{5-4}=7.7, 4.8, and J_{5-6}=4.8 Hz, 5-H), 4.38 (1H, d, J_{6-5}=4.8 Hz, 6-H), and 7.1—7.3 (5H, m, Ph); ^{13}C NMR ($CDCl_3$) δ=15.32, 15.35 (each OEt), 29.47 (2-C), 44.15 (1-C), 45.18 (4-C), 63.51, 63.93 (each OEt), 68.74 (5-C), 104.03 (6-C), 126.07, 128.30, 128.46 (each

Ph), 140.97 (Ph), and 209.63 (3-C); Ms *m/z* (rel intensity, %) 235 (M^+—OEt, 4), 105 (37), 104 (27), 103 (base peak), 91 (63), 74 (56), 47 (58), and 43 (35). Found: C, 68.29; H, 8.94%. Calcd for $C_{16}H_{24}O_4$: C, 68.55; H, 8.63%.

Ethyl 4-Oxo-6-phenylhexanoate (7): A procedure similar to that employed for the formation of **4** from **3** was applied to **6** (0.093 g, 0.33 mmol). The reaction at room temperature for 2 h and the followed workup (silica-gel chromatography with hexane–ethyl acetate (7:1 v/v)) gave **7** (0.045 g, 58%). Compound **7** was also obtained by a similar procedure on **8** (room temperature for 1 h, in 57% yield): Pale yellow liquid; IR (neat) 1725, 1495, 1450, 1410, 1370, 1185, 1100, 1030, 750, and 700 cm^{-1}; ^1H NMR ($CDCl_3$) δ=1.24 (3H, t, *J*=7.3 Hz, COOEt), 2.57, 2.69, 2.78, 2.91 (each 2H, t, $J_{2-3}=J_{5-6}$=7.0 Hz, 2-, 3-, 5-, and 6-H), 4.12 (2H, q, *J*=7.3 Hz, COOEt), and 7.1—7.3 (5H, m, Ph); ^{13}C NMR ($CDCl_3$) δ=14.17 (COOEt), 27.99 (2-C), 29.69 (3-C), 37.23 (5-C), 44.26 (6-C), 66.65 (COOEt), 126.13, 128.29, 128.51 (each Ph), 140.96 (Ph), 172.79 (COOEt), and 208.00 (CO); MS *m/z* (rel intensity, %) 234 (M^+, 16), 105 (48), 101 (29), 91 (base peak), 76 (22), and 30 (30). HRMS Found: *m/z* 234.1254. Calcd for $C_{14}H_{18}O_3$: M, 234.1255.

***(E)*-6,6-Diethoxy-5-hydroxy-1-phenyl-4-hexen-3-one (8):** To a solution of **6** (0.1 g, 0.36 mmol) in dry dichloromethane (1 ml) were added, at −15 °C under nitrogen, triethylamine (0.108 g, 1.07 mmol) and methanesulfonyl chloride (0.049 g, 0.43 mmol). After stirring at −15 °C for 1 h and then at room temperature for 4 h, the reaction mixture was poured into ice water and then extracted with dichloromethane (20 ml×2). The combined extracts were dried over magnesium sulfate and evaporated in vacuo. The residue was chromatographed over silica gel with hexane–ethyl acetate (7:1 v/v) to provide **8** (0.08 g, 85%): Colorless liquid; IR (neat) 1680, 1640, 1605, 1500, 1450, 1370, 1330, 1130, 1060, 750, and 700 cm^{-1}; ^1H NMR ($CDCl_3$) δ=1.22 (6H, t, *J*=7.0 Hz, OEt), 2.9—3.0 (4H, m, 1- and 2-H), 3.4—3.8 (4H, m, OEt), 5.03 (1H, d, J_{6-5}=4.4 Hz, 6-H), 6.35 (1H, d, J_{4-5}=16.1 Hz, 4-H), 6.63 (1H, dd, J_{5-4}=16.1 and J_{5-6}=4.4 Hz, 5-H), and 7.1—7.4 (5H, m, Ph); ^{13}C NMR ($CDCl_3$) δ=15.19 (OEt), 29.83 (2-C), 41.96 (1-C), 61.50 (OEt), 99.54 (6-C), 126.12, 128.35, 128.48 (each Ph), 131.49 (Ph), 141.00, 141.35 (4- and 5-C), and 199.30 (CO); MS *m/z* (rel intensity, %) 262 (M^+, 1), 105 (24), 103 (base peak), 91 (93), 84 (30), 83 (21), 77 (22), 75 (33), 55 (34), and 47 (26). Found: C, 73.21; H, 8.83%. Calcd for $C_{16}H_{22}O_3$: C, 73.25; H, 8.45%.

5-(Diethoxymethyl)-3-[1-(diethoxyphosphinyl)ethyl]-2-isoxazoline (9): To a solution of **1** (0.53 g, 1.64 mmol) in dry THF (4 ml) was added, at −78 °C under nitrogen, butyllithium (15% in hexane, 1.15 ml, 1.8 mmol). After 30 min at −78 °C, methyl iodide (0.465 g, 3.28 mmol) was added and the mixture was stirred at room temperature for 18 h. It was then poured into saturated ammonium chloride and extracted with dichloromethane (20 ml×2). The combined extracts were dried over magnesium sulfate and evaporated in vacuo. The residue was subjected to column chromatography over silica gel by using hexane–ethyl acetate (5:1 v/v) to give **9** (0.388 g, 70%) as a 1:1 mixture (by ^{13}C NMR) of two diastereomers: Pale yellow liquid; IR (neat) 1610, 1440, 1390, 1375, 1250, 1160, 1120, 1060, 1020, 960, 885, and 790 cm^{-1}; ^1H NMR ($CDCl_3$) δ=1.20, 1.23 (each 3H, t, *J*=7.0 Hz, OEt), 1.34 (6H, t, *J*=7.0 Hz, OEt), 1.42, 1.49 (3H, each d, *J*=7.3 Hz, Me), 3.0—3.3 (3H, m, PCH and 4-H), 3.5—3.8 (4H, m, OEt), 4.15 (4H, dq, *J*=7.3 (HP) and 7.0 Hz, OEt), 4.44 (1H, d, *J*=5.1 Hz, $CH(OEt)_2$), and 4.5—4.7 (1H, m, 5-H); ^{13}C NMR ($CDCl_3$) δ=15.29 (Me), 15.33, 15.36 (each OEt), 16.46 (*J*=5.9 (CP) Hz, OEt), 32.09, 32.24 (each *J*=140.9 (CP) Hz, PCH), 36.47, 37.16 (each 4-C), 62.45, 62.50 (each *J*=6.9 (CP) Hz, OEt), 63.25, 63.37, 64.15, 64.33 (each OEt), 80.86, 80.89 (each 5-C), 102.17, 102.32 (each $CH(OEt)_2$), and 156.66 (*J*=6.9 (CP) Hz, 3-C); MS *m/z* (rel intensity, %) 292 (M^+—OEt, 26), 103 (base peak), 75 (50), and 47 (37). No satisfactory analytical result was obtained due to the hygroscopic nature of **9**.

5-(Diethoxymethyl)-3-[1-(diethoxyphosphinyl)-1-methylethyl]-2-isoxazoline (10): A similar procedure was employed under the following conditions: **1** (1.402 g, 4.34 mmol) in THF (9 ml), butyllithium (15% in hexane, 5.96 ml, 9.54 mmol) at −78 °C for 30 min, methyl iodide (2.462 g, 17.3 mmol), at room temperature for 17 h, silica-gel column chromatography with hexane–ethyl acetate (5:1 v/v). The dialkylated product **10** was obtained in 40% (0.61 g) yield: Pale yellow liquid; IR (neat) 1610, 1460, 1440, 1390, 1320, 1250, 1050, 1025, 960, 890, and 790 cm^{-1}; ^1H NMR ($CDCl_3$) δ=1.19, 1.23 (each 3H, t, *J*=7.0 Hz, OEt), 1.33 (6H, t, *J*=7.0 Hz, OEt), 1.44, 1.50 (each 3H, Me), 3.0—3.3 (2H, m, 4-H), 3.5—3.8 (4H, m, OEt), 4.14 (4H, dq, *J*=7.3 (HP) and 7.0 Hz, OEt), 4.43 (1H, d, *J*=5.5 Hz, $CH(OEt)_2$), and 4.5—4.7 (1H, m, 5-H); ^{13}C NMR ($CDCl_3$) δ=15.32 (OEt), 16.49 (*J*=4.9 (CP) Hz, OEt), 21.47, 21.69 (each Me), 36.72 (4-C), 37.64 (*J*=158.5 (CP) Hz, PC), 62.72 (*J*=7.8 (CP) Hz, OEt), 63.37, 64.16 (each OEt), 81.22 (5-C), 102.32 ($CH(OEt)_2$), and 160.32 (*J*=5.9 (CP) Hz, 3-C); MS *m/z* (rel intensity, %) 306 (M^+—OEt, 7), 103 (base peak), 75 (37), and 47 (24). No satisfactory analytical result was obtained due to the hygroscopic nature of **10**.

6,6-Diethoxy-2-(diethoxyphosphinyl)-5-hydroxy-3-hexanone (11): A procedure similar to that used to prepare **6** from **5** was employed to **9** under the following conditions: **9** (0.388 g, 1.15 mmol) in aqueous ethanol (17%, 9 ml), Raney Ni (W-2, suspension in ethanol, 0.5 ml), boric acid (0.284 g, 4.6 mmol), under hydrogen (1 atm) at room temperature for 12 h, silica-gel column chromatography with ethyl acetate. A 1:1 mixture (by ^{13}C NMR) of two diastereomers of **11** (0.271 g, 69%) was given: Colorless liquid; IR (neat) 3400, 1710, 1440, 1390, 1370, 1240, 1060, 1020, and 960 cm^{-1}; ^1H NMR ($CDCl_3$) δ=1.1—1.3 (6H, m, OEt), 1.33 (6H, t, *J*=7.0 Hz, OEt), 1.3—1.5 (3H, m, 1-H), 2.8—3.1 (3H, m, 2- and 4-H), 3.5—3.8 (4H, m, OEt), 4.13 (4H, dq, *J*=7.3 (CP) and 7.0 Hz, OEt), 4.0—4.2 (2H, m, 5-H), and 4.3—4.5 (1H, m, 6H); ^{13}C NMR ($CDCl_3$) δ=15.38 (1-C and OEt), 16.39 (*J*=5.9 (CP) Hz, OEt), 44.88 (4-C), 47.48, 47.57 (each *J*=126.2 (CP) Hz, 2-C), 62.55, 62.58 (each *J*=6.8 (CP) Hz, OEt), 63.44, 63.47, 63.97, 64.06 (each OEt), 68.78, 69.10 (each 5-C), 104.,04, 104.10 (each 6-C), 205.41, and 206.05 (each *J*=3.9 (CP) Hz, CO); MS *m/z* (rel intensity, %) 295 (M^+—OEt, 1), 236 (15), 103 (base peak), 74 (35), and 47 (23). No satisfactory analytical result was obtained due to the hygroscopic nature of **11**.

6,6-Diethoxy-2-(diethoxyphosphinyl)-5-hydroxy-2-methyl-3-hexanone (12): A procedure similar to that used to prepare **6** from **5** was employed to **10** under the following conditions: **10** (0.6 g, 1.71 mmol) in aqueous ethanol (17%, 10 ml), Raney Ni (W-2, suspension in ethanol, 2 ml), boric acid (0.422 g, 6.83 mmol), under hydrogen (1 atom) at room temperature for 22 h, silica-gel column chromatography with hexane–ethyl acetate (1:5 v/v). A 49% yield of **12** (0.298 g) was obtained and then the unreacted **10** was recov-

ered (0.132 g, 22%). **12**: Colorless liquid; IR (neat) 3400, 1710, 1460, 1450, 1395, 1370, 1240, 1025, 960, and 790 cm^{-1}; ^1H NMR ($CDCl_3$) δ=1.1—1.4 (6H, m, OEt), 1.32 (6H, t, J=7.0 Hz, OEt), 1.41, 1.47 (each 3H, 1-H and 2-Me), 2.8—3.1 (2H, m, 4-H), 3.5—3.9 (4H, m, OEt), 4.14 (4H, dq, J=7.3 (HP) and 7.0 Hz, OEt), 4.0—4.3 (2H, m, 5-H), and 4.42 (1H, d, J_{6-5}=4.8 Hz, 6-H); ^{13}C NMR ($CDCl_3$) δ=15.38 (OEt), 16.43 (J=5.9 (CP) Hz, OEt), 20.12, 20.19 (each 1-C and 2-Me), 40.92 (4-C), 50.79 (J=130.1 (CP) Hz, 2-C); 62.77 (J=6.8 (CP) Hz, OEt), 63.35, 63.84 (each OEt), 68.82 (5-C), 104.00 (6-C), and 208.73 (CO); MS m/z (rel intensity, %) 309 (M^+—OEt, 5), 251 (21), 180 (11), 123 (11), 103 (base peak), 76 (32), and 47 (22). No satisfactory analytical result was obtained due to the hygroscopic nature of **12**.

Ethyl 5-(Diethoxyphosphinyl)-2-methyl-4-oxohexanoate (15): A procedure similar to that used for the preparation of **4** from **3** was employed under the following conditions: **12** (0.092 g, 0.26 mmol) in chloroform (15 ml) saturated with hydrogen chloride, at room temperature for 5 h, silica-gel column chromatography with ethyl acetate. A 78% yield of **15** (0.062 g) was obtained: Colorless liquid; IR (neat) 1730, 1700, 1460, 1380, 1370, 1240, 1170, 1050, 1020, 960, and 790 cm^{-1}; ^1H NMR ($CDCl_3$) δ=1.25 (6H, t, J=7.0 Hz, OEt), 1.32 (6H, t, J=7.0 Hz, COOEt), 1.43, 1.49 (each 3H, s, 5-Me), 2.56, 3.05 (each 2H, t, J_{2-3}=6.6 Hz, 2- and 3-H), 4.12 (4H, q, J=7.0 Hz, COOEt), and 4.14 (4H, dq, J=7.3 (HP) and 7.0 Hz, OEt); ^{13}C NMR ($CDCl_3$) δ=14.20 (COOEt), 16.44 (J=5.9 (CP) Hz, OEt), 20.37, 20.45 (each 5-Me), 28.42 (2-C), 34.31 (3-C), 50.11 (J=131.1 (CP) Hz, 5-C), 60.55 (COOEt), 62.81 (OEt), 172.78 (COOEt), and 207.13 (CO); MS m/z (rel intensity, %) 308 (M^+, 5), 263 (20), 180 (base peak), 138 (41), 124 (21), 123 (43), 111 (20), 109 (45), 101 (36), 81 (46), 70 (25), 65 (23), and 55 (24). HRMS Found: m/z 308.1400. Calcd for $C_{13}H_{25}O_6P$: M, 308.1387.

The present work was partially supported by a Grand-in-Aid for Scientific Research (No. 61470095) from the Ministry of Education, Science and Culture. The authors thank Professor Akira Mori, Institute of Advanced Material Study, Kyushu University, for his useful suggestion to the reaction mechanism study.

References

1) O. Tsuge, S. Kanemasa, and H. Suga, *Chem. Lett.*, **1986**, 183; O. Tsuge, S. Kanemasa, and H. Suga, *Bull. Chem. Soc. Jpn.*, **60**, 2463 (1987).

2) O. Tsuge, S. Kanemasa, and H. Suga, *Chem. Lett.*, **1987**, 323; O. Tsuge, S. Kanemasa, and H. Suga, *Bull. Chem. Soc. Jpn.*, **61**, 2133 (1988).

3) As reviews: A. R. Katritzky, "Comprehensive Heteroxyclic Chemistry," Pergamon Press, Oxford, New York, Toronto, Sydney, Paris, Frankfurt (1984), Vol. 4, p. 694; M. Matsumoto, *Yuki Gosei Kagaku Kyokai Shi*, **39**, 25 (1981); S. Kano, S. Shibuya, and T. Ebata, *Heterocycles*, **14**, 661 (1980); G. Pattenden, *Progr. Chem. Org. Natural Products*, **35**, 133 (1978); Y. S. Rao, *Chem. Rev.*, **76**, 625 (1976).

4) An example of such transformation has been recently reported: Y. Tanabe and N. Ohno, *J. Org. Chem.*, **53**, 1560 (1988).

5) O. Tsuge, S. Kanemasa, N. Nakagawa, and H. Suga, *Bull. Chem. Soc. Jpn.*, **61**, 4091 (1988).

6) T. Wolfram, *Liebigs Ann. Chem.*, **1977**, 1707; A. G. Schultz and Y. K. Yee, *J. Org. Chem.*, **41**, 561 (1976); A. Samour, M. I. Selim, M. Elkassaby, and F. Elshahed, *Egypt. J. Chem.*, **17**, 645 (1974); E. Show, *J. Am. Chem. Soc.*, **68**, 2510 (1946).

7) A mechanism via a 2-methoxyfuran intermediate is proposed in Ref. 4.

8) E. Piers and Y. F. Lu, *J. Org. Chem.*, **53**, 926 (1988); E. Piers and A. V. Gavai, *J. Chem. Soc., Chem. Commun.*, **1985**, 1241; A. S. Kende and B. H. Toder, *J. Org. Chem.*, **47**, 167 (1982); E.-P. Krebs, *Helv. Chim. Acta*, **64**, 1023 (1981); H. J. Ringold and S. K. Malhotra, *Tetrahedron Lett.*, **1962**, 669.

9) R. Mortezaei, O. Piva, F. Henin, J. Muzart, and J. P. Pete, *Tetrahedron Lett.*, **27**, 2997 (1986); R. Ricard, P. Sauvage, C. S. K. Wan, A. C. Weedon, and D. F. Wong, *J. Org. Chem.*, **51**, 62 (1986); R. M. Duhaime, D. A. Lombardo, I. A. Skinner, and A. C. Weedon, *ibid.*, **50**, 873 (1985); I. A. Skinner and A. C. Weedon, *Tetrahedron Lett.*, **24**, 4299 (1983).

10) A. Kergomard and M. F. Renard, *Tetrahedron Lett.*, **1970**, 2319.

 © 1989 The Chemical Society of Japan Bull. Chem. Soc. Jpn., 62, 185—188 (1989)

Stopped-Flow Kinetics of the Formation and Decomposition of 2,4- and 4,4-Disubstituted Meisenheimer Complexes in the Reaction of 4-Piperidino-1,3-dinitrophenanthrene with Potassium Methoxide in Dimethyl Sulfoxide-Methanol[1)]

Hiroyuki TAKAHASHI, Takao HIRAIDE, Yohji HASHIDA, and Shizen SEKIGUCHI*
Department of Synthetic Chemistry, Tenjin-cho, Kiryu, Gunma 376
(Received July 21, 1988)

The formation of 2,4-disubstituted anionic σ complex, followed by the formation of 4,4-disubstituted one was confirmed by means of absorption and NMR spectra in the reaction of 4-piperidino-1,3-dinitrophenanthrene with potassium methoxide in DMSO–CH_3OH. The rates and activation parameters were determined by kinetic studies using stopped-flow and conventional spectrophotometers. It was found, compared with the previous results on the naphthalene system that the presence of H^5 of the title compound affects the rates differently.

Many Jackson–Meisenheimer complexes (anionic σ complex) have been prepared by nucleophilic attack on polynitroaromatic compounds (Eqs. 1a and 1b), in

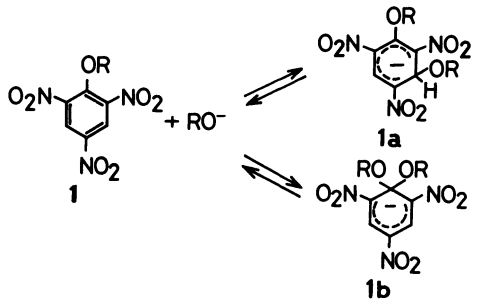

(1a)

(1b)

which at first **1a** (R: alkyl; hereafter called 1,3-disubstituted complex) is formed (kinetically controlled), subsequently rearranging into **1b** (hereafter called 1,1-disubstituted complex) (thermodynamically controlled.)[2)] Although many 1,3-disubstituted anionic σ complexes such as **1a** have been identified in the benzene or heteroaromatic systems, only a few ones such as **2a** (1,3-disubstituted complex) have been found in the naphthalene system (Eqs. 2a and 2b).[3–5)] The

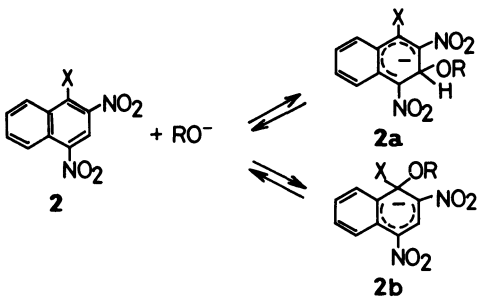

(2a)

(2b)

fact that **2a** (X; alkoxyl) is difficult to confirm in the reactions of **2** (X; alkoxyl) with alkoxide ions can be ascribed to its less stability than **1a**, mainly because the presence of nitro group para to the reaction site (C-3) stabilizes **1a** to much greater extent.[2)]

On the other hand, in the reactions with various nucleophiles, especially amines, the steric effects exerted by the structures of substrates or bulkiness of nucleophiles on the reaction mechanism have attracted much attention.[6–9)] In order to elucidate the effect of the structure of a substrate on the reaction rate, therefore, at first, we tried the reaction of 4-piperidino-1,3-dinitrophenanthrene (**3**) with potassium methoxide (CH_3OK) in DMSO–CH_3OH (90:10 v/v) (Eqs. 3a and 3b). We patterned the present experiments

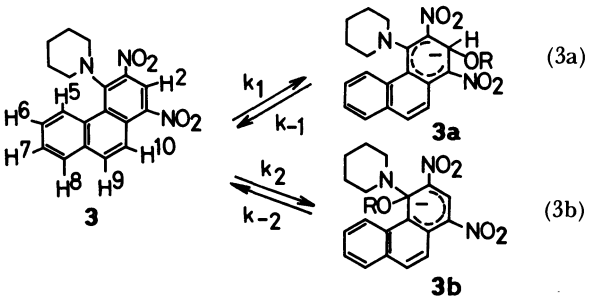

(3a)

(3b)

on those of the previous work.[5)]

This paper reports the stopped-flow kinetics of the formation of 2,4-disubstituted complex (**3a**) and of its decomposition or the formation of 4,4-disubstituted complex (**3b**), corresponding to **1b** and **2b**, and the comparison of the results with those for the naphthalene systems.[5)]

Results

General Features. Upon addition of excess CH_3OK to a DMSO–CH_3OH solution of **3**, Curve b appeared instantly, and then changed into Curve c at a relatively slow rate (Fig. 1), where the former could be attributed to **3a**, and the latter to **3b**.[4–7)] The results indicate that the reaction consists of the two seperate stages, i.e., the first rapid formation of **3a** and the second relatively slow decomposition of **3a** or the formation of **3b**.

NMR technique is expected to be useful for

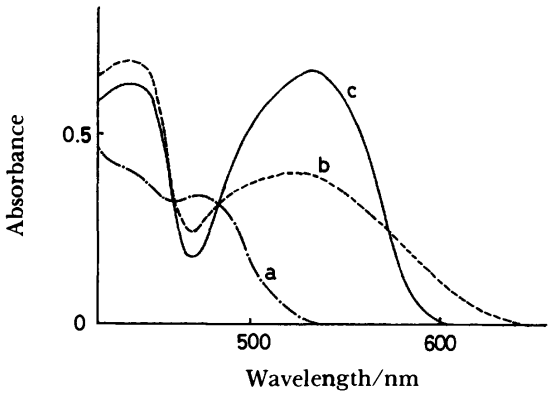

Fig. 1. Spectral change relevant to the reaction of 4-piperidino-1,3-dinitrophenanthrene (**3**) with CH_3OK in DMSO-CH_3OH (90:10, v/v); (a) **3** (3.87×10^{-5} M [M=mol dm^{-3}]) at room temperature; (b) just after addition of CH_3OK (2.95×10^{-2}); (c) 60 min.

elucidating the assignment mentioned above. Just after addition of methanolic CH_3OK (1.40×10^{-4} mol) to a DMSO-CH_3OH solution (0.5 ml) of **3** (1.40×10^{-4} mol), the solution turned red, suggesting the formation of a complex. Just upon addition of CH_3OK, H^2 sharp singlet (δ 8.25) of **3** shifted to δ 6.25, with a small singlet at δ 9.23, attributed to H^2 of **3b**, indicating the formation of **3a** (Eq. 3a) (sweep time 20 cps). This upfield shift is well-known to be characteristic of 2,4-disubstituted complex such as **3a**, corresponding to **2a** (1,3-disubstituted complex).[2] The H^2 singlet (δ 9.23) of **3b** increased in strength at the expense of the singlet at δ 6.25, which disappeared in 60 min. These results support the reaction path as shown in Eqs. 3a and 3b very well. It can be expected, therefore, that the separate kinetics of formation and decomposition of **3a** is possible.

Kinetics. Let us rewrite Eqs. 3a and 3b in a form convenient for quantitative discussion as Eq. 4. In the

$$3 + {}^-OCH_3 \underset{k_{-1}}{\overset{k_1}{\rightleftharpoons}} \mathbf{3a} \quad (4a)$$

$$\mathbf{3a} \underset{k_{-2}}{\overset{k_2}{\rightleftharpoons}} \mathbf{3b} \quad (4b)$$

$$K_1 = \frac{k_1}{k_{-1}}, \quad K_2 = \frac{k_2}{k_2}$$

kinetics on Stage I, Stage II can be neglected, since the former reaction is completed in several thousandths seconds, making contamination by the latter negligible from considering the time scale of reaction.

Stage I. The pseudo-first-order rate constant, k_ψ, for the attainment of an equilibrium is the sum of forward and reverse components.[8,9] Therefore, the following expression should hold:

$$k_\psi = k_1([{}^-OCH_3] + [\mathbf{3}]) + k_{-1} \quad (5)$$

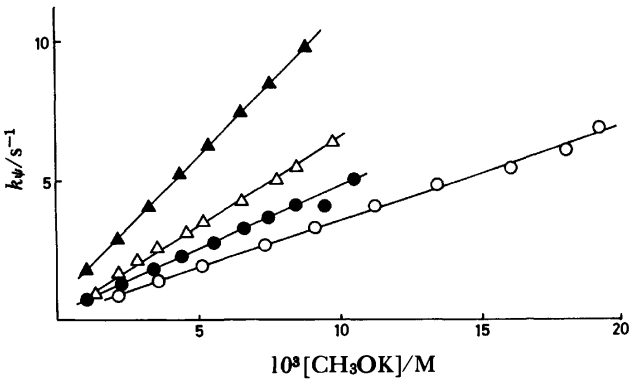

Fig. 2. Relationship between k_ψ and $[CH_3OK]$ in Stage I; $[\mathbf{3}]_0$ 1.53×10^{-4} M; μ 0.05 M ($KClO_4$); ○ 25 °C; ● 30 °C; △ 35 °C; ▲ 45 °C.

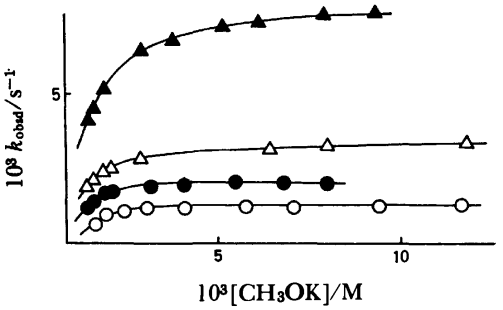

Fig. 3. Relationship between k_{obsd} and $[CH_3OK]$ in Stage II; $[\mathbf{3}]_0$ 1.99—6.00×10^{-5} M; μ 0.05 M ($KClO_4$); ○ 25 °C; ● 30 °C; △ 35 °C; ▲ 45 °C.

Under the usual conditions ($[{}^-OCH_3] \gg [\mathbf{3}]$), Eq. 5 is simplified to

$$k_\psi = k_1[{}^-OCH_3] + k_{-1} \quad (6)$$

As a result, dependence of k_ψ on $[{}^-OCH_3]$ would afford a linear relationship, and k_1 and k_{-1} are estimated from the slope and the intercept, respectively. The results in Fig. 2 are compatible with Eq. 6. Although the k_1 value can be exactly estimated from the slope, the k_{-1} one is very small relative to k_1, and has a large error. As a result, the k_{-1} value was calculated by the method described in the following paragraph.

Stage II. In considering the kinetics on Stage II, Stage I can be dealt with as a mobile equilibrium, lying almost entirely on the right under the conditions. Putting $[\mathbf{3}]_{st}=[\mathbf{3}]+[\mathbf{3a}]$ and K_1 the equilibrium constant for Stage I reaction, one obtains the following expression.

$$k_{obsd} = k_{-2} + \frac{k_2[{}^-OCH_3]}{1 + K_1[{}^-OCH_3]}, \quad (7)$$

where k_{obsd} is the pseudo-first-order rate coefficient for Stage II reaction, and k_2 and k_{-2} are the rate coefficients for forward and reverse reactions. Consequently, de-

Table 1. Rate and Equilibrium Constants for Stages I and II at Various Reaction Temperatures

Temp	k_1	k_{-1}	$10^{-3}K_1$[a]	k_2	$10^5 k_{-2}$	$10^{-5}K_2$[b]
°C	$M^{-1}s^{-1}$[c]	s^{-1}	M^{-1}[c]	$M^{-1}s^{-1}$[c]	s^{-1}	M^{-1}[c]
25	349± 8	0.16±0.05	2.18±0.73	2.90±0.06	1.24±0.03	2.33±0.01
30	437±12	0.24±0.03	1.82±0.27	4.06±0.07	1.50±0.04	2.70±0.01
35	576±16	0.36±0.02	1.60±0.13	5.63±0.11	2.66±0.11	2.49±0.02
45	973±27	0.77±0.04	1.26±0.01	10.5 ±0.22	7.90±0.33	1.32±0.02

a) $K_1=k_1/k_{-1}$. b) $K_2=k_2/k_{-2}$. c) $M^{-1}=dm^3\,mol^{-1}$.

pendence of k_{obsd} on [$^-OCH_3$] would afford a curvilinear relationship (convex upward), in which the curve would not pass through the origin (Fig. 3).

The exact k_2, k_{-2}, and k_1 values were estimated in the following way. First, k_1, k_{-1}, and K_1 ($=k_1/k_{-1}$) are obtained from the slope and intercept (Fig. 2), although k_{-1} has some extent of error. Second, in the plateau (Fig. 3) $K_1[^-OCH_3]\gg 1$, so the following relationship holds. In Eq. 8 it is clear from the previous work[5] that $k_2/k_1\gg k_{-2}$.

$$k_{obsd} = k_{-2} + \frac{k_2}{K_1} \qquad (8)$$

As a result, k_2 can be calculated by using the K_1 value obtained just above. Once k_2 and K_1 are estimated, k_{-2} can be calculated from Eq. 7 by using appropriate experimental values of k_{obsd} and methoxide concentration. Third, by substituting these values into Eq. 7 as initial values and using a nonlinear least squares method (Gauss-Newton Method), the optimum K_1, k_2, and k_{-2} values can be obtained, which are listed in Table 1.

From K_1 and k_1, k_{-1} can be estimated (Table 1). Calculated k_ψ and k_{obsd} obtained by substituting the values in Table 1 into Eqs. 6 and 7 are in agreement with the observed ones almost within <2% in almost all runs.

The rate and equilibrium constants and activation parameters, obtained by the Arrhenius plot are summarized in Table 2, together with those for the naphthalene system.[5]

Table 2. Rate and Equilibrium Constants and Activation Parameters[a] (1 cal_{th} = 4.184 J)

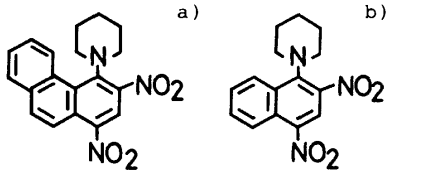

3 2

	3	2
$k_1/M^{-1}s^{-1}$[c,d]	349±8	480±35
k_{-1}/s^{-1}[c]	0.16±0.05	1.04±0.11
K_1[c]	2180±730	460±80
$\Delta H_1^{\neq}/kcal_{th}\,mol^{-1}$	9.6±0.7	11.5±2.3
$\Delta S_1^{\neq}/cal_{th}\,K^{-1}$	−14.8±2.5	−7.1±5.3
$\Delta H_{-1}^{\neq}/kcal_{th}\,mol^{-1}$	14.2±2.6	13.5±3.6
$\Delta S_{-1}^{\neq}/cal_{th}\,K^{-1}$	−11.5±5.3	−10.9±9.2
$\Delta H^0/kcal\,mol^{-1}$[c]	−4.6±1.2	−2.0±5.9
$\Delta S^0/cal_{th}\,K^{-1}$[c]	−3.3±2.0	3.8±14.5
$k_2/M^{-1}s^{-1}$[c]	2.90±0.06	2.53±0.29
k_{-2}/s^{-1}[c,d]	1.24±0.03×10^{-5}	1.80±1.31×10^{-4}
$\Delta H_2^{\neq}/kcal_{th}\,mol^{-1}$	11.5±2.2	12.2±2.5
$\Delta S_2^{\neq}/kcal_{th}\,K^{-1}$	−17.0±12.3	−15.4±10.2
$\Delta H_{-2}^{\neq}/kcal_{th}\,mol^{-1}$	20.6±5.1	27.2±7.2
$\Delta S_{-2}^{\neq}/cal_{th}\,K^{-1}$	−40±4.2	−15.8±1.5

a) Activation parameters at 25°C. b) Cited from Ref. 5. c) Cited from Table 1. d) $M^{-1}=dm^3\,mol^{-1}$. e) $\Delta H^0=\Delta H_1^{\neq}-\Delta H_{-1}^{\neq}$; $\Delta S^0=\Delta S_1^{\neq}-\Delta S_{-1}^{\neq}$.

Discussion

Stage I. The k_1 value is smaller for the phenanthrene system than for the naphthalene one, depending on $\Delta S_1^{\neq}$ rather than $\Delta H_1^{\neq}$. Such a result would stem from the following steric reason. When a methoxide ion attack C-2 of **3** or C-3 of **2**, the negative charge donated by the ion is delocalized over the ring to a larger extent for the phenanthrene system than the naphthalene one, which is reflected on $\Delta H_1^{\neq}$. This delocalization, however, would make $\Delta S_1^{\neq}$ decrease for the phenanthrene system as follows: both ortho-nitro groups to the reaction site could assume coplanarity to the ring upon delocalization, since the negative charge donated by the ion ($^-OCH_3$) delocalizes especially over these two nitro groups in the transition state of k_1 step.[6,7,10] The coplanarity of 3-nitro group of **3** would make the steric interference among 3-nitro, 4-piperidino, and H^5 groups severer than that of 2-nitro group of **2** would do among 2-nitro, 1-piperidino, and H^8 groups, and make the piperidyl ring almost perpendicular to the phenanthrene one, resulting in less freedom.

In k_{-1} step, both $\Delta H_{-1}^{\neq}$ and $\Delta S_{-1}^{\neq}$ are slightly unfavorable for the phenanthrene system, since **3a** is more stable by ca. 0.5 kcal mol^{-1} ($\Delta\Delta G^0=\Delta\Delta H^0-T\Delta\Delta S^0$) than **2a** owing to more extensive delocalization and, as a result, the reverse reaction is unfavorable. The fact the ΔG^0 is −3.6 and −3.1 kcal mol^{-1} for **3a** and **2a** respectively is very interesting indicating that **3a** and **2a** are more stable than **3** and **2** ($\Delta G^0=\Delta H^0-T\Delta S^0$), respectively.

Stage II. The k_2 value is larger for the phenanthrene system than for the naphthalene one, depending on

$\Delta H_2^{\neq}$ rather than $\Delta H_2^{\neq}$. The $\Delta\Delta H_2^{\neq}$ value ($=\Delta H_2^{\neq}$ for **2** $-\Delta H_2^{\neq}$ for **3**) is 0.7 kcal mol^{-1}, which makes k_2 for **3** ca. 3.3 times larger than k_2 for **2**, whereas the observed ratio is ca. 1.1 (Table 2). As a result, it can be seen that $\Delta S_2^{\neq}$ for **3** unfavorably affects k_2 to make the rate ratio of ca. 3.3 depending on $\Delta H_2^{\neq}$ reduce to ca. 1.1, although the $\Delta S_2^{\neq}$ values have large errors. In the transition state of k_2 step for the phenanthrene system, H^5 protrudes over between the piperidino and methoxyl (nucleophile) groups, and consequently the steric interference among H^5, piperidino, and 3-nitro groups would be relieved to some extent, compared with the transformation of **2** to **2b**, which is expected to lower the potential energy barrier between the reactants and transition state. This effect, however, would decrease $\Delta S_2^{\neq}$ to a larger extent for the phenanthrene system. In addition, delocalization of the negative charge donated by a methoxide ion is more extensive for the phenanthrene system than for the naphthalene one, and the larger resonance inhibition between the unshared electron pair on the piperidino nitrogen and the phenanthrene ring would make the nucleophilic attack on C-4 of a methoxide ion easier than for the naphthalene system. These effects would lower $\Delta H_2^{\neq}$ for the phenanthrene system.

Although the k_{-2} values can not be rigorously discussed because of large error in the case of **2**, they can be said to be much less smaller than the k_2 ones for the two systems. The large K_2 values indicate that **3b** and **2b** are very stable, compared with the reactants.

In conclusion it is found that H^5 of **3** exerts steric interference to the reaction site indirectly (Stage I) or directly (Stage II) in the reaction of 4-piperidino-1,3-dinitrophenanthrene (**3**) with $KOCH_3$ in DMSO–CH_3OH (9:1 v/v), which is very different from the fimilar reaction of the naphthalene analogue.

Experimental

NMR spectra were recorded on a Varian A-60D spectrometer and UV-VIS absorption spectra on a Hitachi Model 200-10 spectrophotometer.

Materials. 4-Piperidino-1,3-dinitrophenanthrene (**3**) was prepared from 4-chloro-1,3-dinitrophenanthrene (CDNP) and piperidine according to the method described previously.[11] The compound (CDNP) was prepared from 1,3-dinitro-4-phenanthrol, *p*-toluenesulfonyl chloride, and *N*,*N*-diethylaniline according to the method described previously.[10] Commercial dimethyl sulfoxide and methanol were purified according to the method described previously.[5] Commercial potassium perchlorate of special grade was used without further purification to keep the ionic strenght at 0.05 mol l^{-1} in rate measurements.

Rate Measurement. As regards the kinetics of formation of 2,4-disubstituted complex, an increase in the absorbance at 532 nm due to the complex was followed in order to estimate the apparent rate constants (k_ψ) with a thermostatted stopped-flow spectrophotometer (Otsuka Denshi Co.). In order to estimate k_{obsd}, a decrease in the absorbance at 600 nm due to 2,4-disubstituted complex was followed with a thermostatted Hitachi Model 200-10 spectrophotometer.

References

1) Aromatic Nucleophilic Substitution. 24; for part 23, see S. Sekiguchi, T. Horie, and T. Suzuki, *J. Chem. Soc., Chem. Commun.*, **1988**, 698.

2) M. J. Strauss, *Chem. Rev.*, **70**, 667 (1970); T. J. deBoer and I. P. Dirkx, "The Chemistry of the Nitro and Nitroso Groups," ed by H. Feuer, Interscience, New York (1968), Part I; C. F. Bernasconi, *Acc. Chem. Res.*, **11**, 147 (1978); F. Terrier, *Chem. Rev.*, **82**, 77 (1982).

3) S. Sekiguchi, K. Shinozaki, T. Hirose, K. Matsui, and T. Itagaki, *Tetrahedron Lett.*, **1974**, 1745.

4) S. Sekiguchi, S. Fujisawa, and Y. Ando, *Bull. Chem. Soc. Jpn.*, **49**, 1451 (1976).

5) S. Sekiguchi, T. Takei, K. Matsui, N. Tone, and N. Tomoto, *Bull. Chem. Soc. Jpn.*, **54**, 3009 (1981).

6) S. Sekiguchi, K. Tsutsumi, H. Shizuka, K. Matsui, and T. Itagaki, *Bull. Chem. Soc. Jpn.*, **49**, 1521 (1976).

7) S. Sekiguchi, T. Hirose, K. Tsutsumi, T. Aizawa, and H. Shizuka, *J. Org. Chem.*, **44**, 3921 (1979).

8) K. J. Laidler, "Chemical Kinetics," McGraw-Hill, (1965), p. 19.

9) C. F. Bernasconi, "Relaxation Kinetics," Academic Press, New York (1976), Chap. 2.

10) S. Sekiguchi, M. Hirai, E. Ota, H. Hiratsuka, Y. Mori, and S. Tanaka, *J. Org. Chem.*, **50**, 5105 (1985).

11) S. Sekiguchi, T. Itagaki, T. Hirose, K. Matsui, and K. Sekine, *Tetrahedron*, **29**, 3527 (1973).

 © 1989 The Chemical Society of Japan Bull. Chem. Soc. Jpn., 62, 189—192 (1989)

Polymer Reagents Derived from Sodium *p*-Styrenesulfonate: *N*-Methyl-*N*-nitroso-*p*-styrenesulfonamide and *p*-Styrenesulfinic Acid Polymers

Hiroyoshi KAMOGAWA* and Tomoo KITAMURA
Department of Applied Chemistry, Yamanashi University, Kofu 400
(Received July 25, 1988)

N-Methyl-*N*-nitroso-*p*-styrenesulfonamide (**1**) was synthesized starting with sodium *p*-styrenesulfonate (**3**). Monomer **1** and sodium *p*-styrenesulfinate (**2**), also synthesized starting with **3**, were polymerized and polymer of **2** was converted to corresponding free acid (**9**). The function of polymer of **1** as the reagent attaching the CH_2 group to the carbonyl carbon by insertion and that of polymer **9** as the catalyst for cis→trans isomerization were investigated for various compounds, including cyclohexanone and benzaldehyde and ethyl oleate. The effects of these polymer reagents as compared with those of the corresponding model compounds were discussed.

Sodium *p*-styrenesulfonate, now commercially available, is a versatile reagent for the syntheses of a variety of polymer reagents.[1-4] In the present article, we wish to report the synthesis of *N*-methyl-*N*-nitroso-*p*-styrenesulfonamide (**1**) polymer as a novel polymer reagent, together with *p*-styrenesulfinic acid polymer as a novel polymer catalyst, both being derived from sodium *p*-styrenesulfonate.

Thus, monomer **1** and sodium *p*-styrenesulfinate (**2**) were synthesized and homo- and copolymerized with *N*-vinyl-2-pyrrolidone (VP), respectively, to afford soluble polymers in appropriate solvents. VP was employed here to get copolymers soluble in reaction solvents.

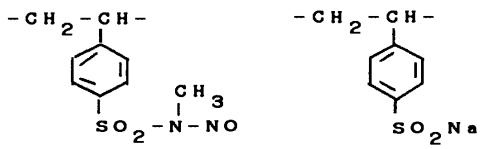

Polymer of 1 Polymer of 2

The CH_2 insertion and cis→trans isomerization reactions with polymer of **1** and the acid form of polymer of **2** were investigated, respectively.

Results and Discussion

Monomer **1** was synthesized starting with sodium *p*-styrenesulfonate (**3**) in the following manner (Eq. 1).

Compound **4** was synthesized from **3** in a high yield (91%) at 20 °C or below, without danger of polymerization.[1] Addition of an excess of methylamine to **4** provided **5** in a moderate yield (64%). Compound **5** in acetic acid was treated with aqueous sodium nitrite to afford crude monomer **1**. Reprecipitation from benzene–hexane by cooling followed by silica-gel column chromatography provided the purified monomer **1** in 62% yield. Analytical data (^{1}H NMR, IR, mass, and CHN) were all satisfactory.

Monomer **2** was synthesized also starting with **3**, as described in a previous paper.[2]

Monomer **1** was polymerized with α,α'-azobisisobutyronitrile (AIBN) in *N*,*N*-dimethylformamide (DMF) with 72% conversion to afford polymer of **1**, which was soluble in a ternary mixture of *N*,*N*-dimethylacetamide (DMA), ethanol, and water and suitable for the investigation of its function.

Polymer of **1** could also be prepared by means of the polymer reaction using the copolymerization product

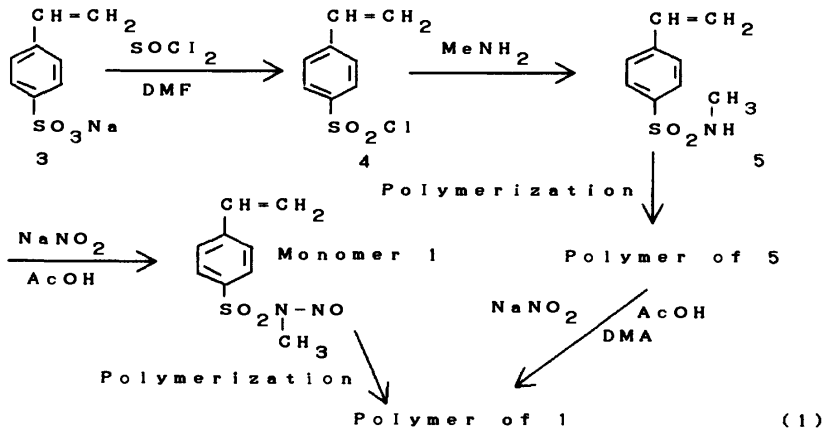

(1)

of **5** with VP in DMF (conversion, 70%) and consisting of nitrosation in a mixture of DMA, acetic acid, and water (conversion, 62%), as shown in Eq. 1.

Polymer of **2** was prepared by the copolymerization of **2** with VP in ethanol (conversion, 88%). Polymer of **2** in aqueous solution was converted to its acid form by acidification with concd HCl to produce polymer **9**, which was soluble in dioxane, the cis-trans reaction solvent, and immediately used as catalyst.

The functions adopted for homopolymer of **1** and polymer **9** were the same as those for the corresponding low-molecular-weight compounds, *N*-methyl-*N*-nitroso-*p*-toluenesulfonamide and *p*-toluenesulfinic acid (Eqs. 2 and 3).[5,6] However, separations of polymers **7** and **9** from products were easier.

Conversion from **6a—e** to **8a—e** and the extent of cis→trans isomerization were determined gas-chromatographically for the purified reaction mixtures, except for **6f—8f** and **6g—8g** mixtures, in which no standard samples of **8f,g** were available and the reaction products (**8f** and **8g**) were identified by IR, mass, and ^{1}H NMR and determined by ^{1}H NMR.

It can be seen in Table 1 that cyclic ketones such as **6a** and **6b** provided particularly low conversions under these conditions, presumably due to the poor accessbility of these bulky ketones to the functional portions of polymer molecules. *N*-Methyl-*N*-nitroso-*p*-toluenesulfonamide, the corresponding low-molecular-weight compound, afforded results similar to those observed for polymer of **1**. **8g**, a different kind of

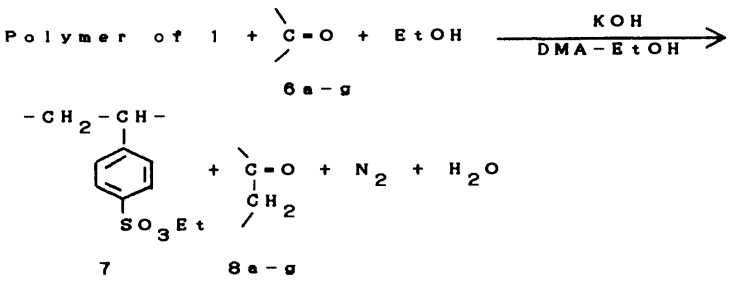

(2)

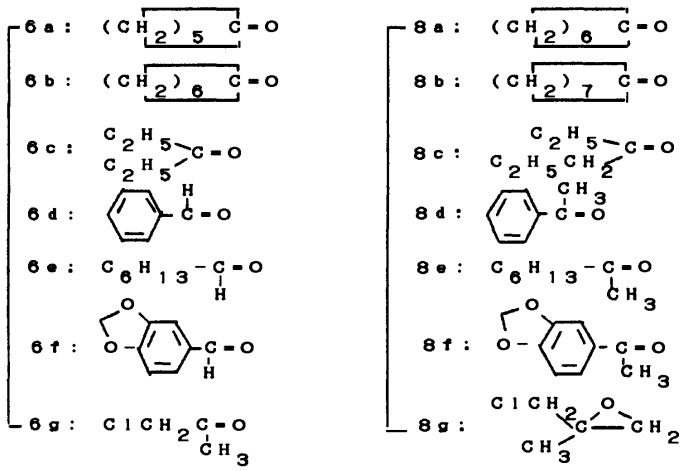

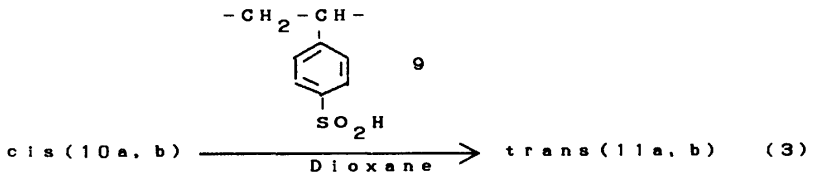

(3)

10a: Ethyl oleate
10b: cis-2-Octene

11a: Ethyl elaidate
11b: trans-2-Octene

Table 1. Function of Polymer of **1** According to Eq. 2[a]

Reactant	Product	Conversion/%
6a	**8a**	13(20[b])
6b	**8b**	17(23[b])
6c	**8c**	35(38[b])
6d	**8d**	35
6e	**8e**	65(65[b])
6f	**8f**[c]	67[d]
6g	**8g**[c]	57[d]

a) As for experimental conditions, see Experimental Section. b) For reference sample, *N*-methyl-*N*-nitroso-*p*-toluenesulfonamide. c) The identity of the product was determined only by ^{1}H NMR, IR, and mass spectra. d) Determined by ^{1}H NMR.

Table 2. Function of Polymer **9** According to Eq. 3[a]

Reactant	Product	Conversion/%
10a	**11a**	80(83[b])
10b	**11b**	83(88[b])

a) As for experimental conditions, see Experimental section. b) For reference sample, *p*-toluenesulfinic acid, as catalyst.

product from others, was the same as that obtained from **6g** with *N*-methyl-*N*-nitroso-*p*-toluenesulfonamide.[5]

Recycle of polymer of **1** could be carried out by the alkaline hydrolysis of polymer **7** to polymer containing **3** units, followed by conversion to polymer containing **1** units, which showed an enough function. This recycle could be repeated at least three times.

Table 2 also shows the results with polymer **9** according to Eq. 3. Conversions obtained with polymer **9** were also similar to those with the corresponding low-molecular-weight compound, *p*-toluenesulfinic acid. In this case, polymer **9** was not appreciably changed during the reaction and could be reused, if properly stored.

It is concluded from these results that, in the cases of the styrene polymers containing *N*-methyl-*N*-nitrososulfonamide and sulfinic acid functional groups, polymers bahave in reactions almost similarly to the corresponding low-molecular-weight reagents, but with more readiness of the separation of products from reagents as well as the possibility of recycling.

Experimental

The infrared (IR), ^{1}H NMR, and mass spectra were recorded on a Hitachi 215 spectrophotometer, a JNM-PMX60 spectrometer, and a Hitachi M808MS spectrometer, respectively, under standard conditions. Elemental analyses were made with a Perkin-Elmer 240 instrument. Gas chromatography was carried out with a Hitachi 164 gas chromatograph fitted with a SE-30 column under helium stream (30 ml min^{-1}).

***N*-Methyl-*p*-styrenesulfonamide (5).** A large excess of aqueous methylamine (25%; 10 ml, 80 mmol) was added dropwise to a stirred solution of *p*-styrenesulfonyl chloride (**4**; 4.4 g, 20 mmol), prepared from sodium *p*-styrenesulfonate (**3**) according to the method described in a previous report,[1] in ether (40 ml), cooled with an ice bath. Stirring was continued further for one hour, the resulting reaction mixture was extracted with ether (160 ml), and the organic layer was rinsed with water and dried over anhydrous sodium sulfate, followed by concentration on a rotary evaporator below 40 °C to leave a fluid in 64% yield. Found: C, 54.70; H, 5.65; N, 6.91%. Calcd for $C_9H_{11}NSO_2$: C, 54.75; H, 5.58; N, 7.09%. IR ($CHCl_3$) 3400 (NH), 1320, 1140 (SO_2), 990, 910 (vinyl) cm^{-1}. ^{1}H NMR (CCl_4) δ=2.5 (d, 3H, Me), 5.1—5.9 (m, 3H, CH_2=+NH), 6.7 (q, 1H, CH=), 7.5 (q, 4H, ArH). MS *m/z* 197 (M^+).

***N*-Methyl-*N*-nitroso-*p*-styrenesulfonamide (1).** A solution of sodium nitrite (0.84 g, 12 mmol) in water (2 ml) was added dropwise to a stirred solution of **5** (2.0 g, 10 mmol) in acetic acid (10 ml) containing a small quantity of water in an ice bath. Stirring was continued further for one hour. The reaction mixture was poured into aqueous sodium hydrogencarbonate (excess) containing ice, immediately followed by extraction with ether. The organic layer was washed thoroughly with water, dried over anhydrous sodium sulfate, and concentrated on the rotary evaporator to give crude **1**, which was reprecipitated from benzene (or ether)-hexane by cooling down to −20 °C, then subjected to silica-gel column chromatography to afford a purified fluid in 62% yield. Single spot by TLC. Found: C, 47.58; H, 4.46; N, 12.23%. Calcd for $C_9H_{10}N_2SO_3$: C, 47.79; H, 4.42; N, 12.40%. IR ($CHCl_3$) 1560, 1490 (N=O), 1360, 1110 (SO_2), 980 (vinyl) cm.$^{-1}$ ^{1}H NMR ($CDCl_3$) δ=3.2 (s, 3H, Me), 5.8 (q, 2H, CH_2=), 6.7 (q, 1H, CH=), 7.9 (q, 4H, ArH). MS *m/z* 196 (M^+—NO).

Preparation of Polymer of 1. (a) By Homopolymerization. A solution of monomer **1** (0.5 g) and purified α,α'-azobisisobutyronitrile (AIBN; 0.03 g) in DMF (1 ml) was put into a glass ampule, which was evacuated and sealed in the conventional manner. The ampule was then let stand at 50 °C for 72 h to effect polymerization. The content of the ampule was poured into a large amount of ether to afford precipitate in 72% conversion. $[\eta]$=0.06 dl g^{-1} (DMF, 25 °C). IR for polymer of **1** deposited on a KRS cell indicated the absorptions characteristic of the *N*-methyl-*N*-nitrososulfonamide portion of polymer, together with those at 2930—2860 cm^{-1} attributable to the vinyl polymer backbone.

(b) By Polymer Reaction Using Polymer of 5. Alternatively, polymer of **1** was prepared by a polymer reaction applied to polymer of **5**.

(i) Polymer of 5. A solution of **5** (1.0 g, 5 mmol), VP (10.0 g, 92 mmol), and AIBN (0.5 g) in DMF (20 ml) was gently stirred at 80 °C for 48 h under a nitrogen atmosphere. The resulting solution was diluted with DMF and poured into ether to afford precipitate in 70% conversion. $[\eta]$=0.21 dl g^{-1} (DMF, 25 °C). IR was satisfactory and the **5** to VP ratio in copolymer was 1:5.5 from the result of elemental analysis.

(ii) Polymer Reaction. To the stirred solution of polymer of **5** (5 g), prepared above, in a mixture of DMA (10 ml) and acetic acid (5 ml) cooled with an ice bath was added dropwise a solution of sodium nitrite (0.42 g, 6 mmol) in water (1 ml), followed by stirring for 2 h. The reaction mixture was

precipitated into ether to afford a sticky solid. IR was satisfactory and the conversion calculated from the results of elemental analysis was 62%.

Preparation of Polymer 9. (a) Polymer of 2. A solution of sodium *p*-styrenesulfinate (**2**; 0.2 g), prepared also starting with **3** as reported in a previous paper,[2] VP (1.0 g), and AIBN (0.06 g) in ethanol (2 ml) was put into an ampule, which was evacuated and sealed in the conventional manner and let stand at 70 °C for 72 h. The resulting viscous solution was precipitated into ether to afford polymer of **2** in 88% conversion. $[\eta]$ in water at 25 °C was 0.78 dl g^{-1} and the **2**/VP ratio in copolymer was 0.17 from elemental analysis.

(b) Polymer 9. A solution of polymer of **2** (0.5 g) prepared above in a small amount of water was acidified with concd HCl to afford precipitate, which was dried under reduced pressure (yield, 29%) and employed immediately for the reaction indicated in Eq. 3.

Function of Polymer of 1 According to Eq. 2. To a solution of polymer of **1** (0.5 g, 2 mmol), prepared by homopolymerization of monomer **1** as described above, in DMA (5 ml) were added with vigorous stirring ethanol (5 ml) and a carbonyl compound (**6a—g**; 2 mmol). To the resulting solution cooled in an ice bath, a solution of potassium hydroxide (0.2 g) in water (5 ml) was further added dropwise, followed by 3-h stirring of the resulting alkaline mixture below 20 °C. The reaction mixture was poured into an ice-water mixture, followed by ether extraction and conventional work up to afford a sample for gas chromatography. Polymer **7** remaining after the ether extraction as insoluble residue was hydrolyzed with 1 mol l^{-1} NaOH at 20 °C overnight to afford polymer of **3**, which was subjected to a reaction sequence analogous to that in Eq. 1 to recover polymer of **1**.

The position of peaks and their areas in the gas chromatograms of samples (column temperature: 80—100 °C) were compared with those of standard compounds to determine the **6a—e→8a—e** conversions. The results thus obtained are satisfactory and shown in Table 1. In the cases of **6f—g→8f—g** combinations, no standard compounds of **8f** and **8g** were available, so that quantitative comparison was not made by GC, but made by ^{1}H NMR. Conversions using a low-molecular-weight compound, *N*-methyl-*N*-nitroso-*p*-toluenesulfonamide, instead of polymer of **1**, were also determined and compared with the results obtained with polymer.

The result of recycle or polymer was 12 (1st), 10 (2nd), and 10% (3rd) in conversion for **6a→8a** in Table 1.

Function of Polymer 9 According to Eq. 3. A solution of polymer **9** (2.4 g, 2 mmol as $-SO_2H$), prepared above and a cis compound (**10a,b**; 2 mmol) in dry dioxane (10 ml) was heated under nitrogen stream. Reaction temperatures and times were 100 °C and 1 h and 70 °C and 6 h, respectively. Upon cooling, the reaction mixture was diluted with hexane to precipitate polymer **9**, which was removed by filtration and ready to another use. The filtrate was washed twice with sat. aq. NaCl, dried over anhyd. $MgSO_4$, and concentrated on a rotary evaporator to leave a sample for gas chromatography. The comparison of the positions and areas of peaks in the gas chromatogram with those for the corresponding standard compound was successfully done and provided the **10a,b→11a,b** conversion. The results thus obtained are shown in Table 2, in which the results with *p*-toluenesulfinic acid instead of polymer **9** are also given. Column temperatures were 210 and 80 °C for samples **10a** and **10b**, respectively.

The result of recycle of polymer was 75 (1st), 74 (2nd), and 70% (3rd) in conversion for **10a→11a** in Table 2.

References

1) H. Kamogawa, A. Kanzawa, M. Kadoya, T. Naito, and M. Nanasawa, *Bull. Chem. Soc. Jpn.*, **56**, 762 (1983).

2) H. Kamogawa and K. Maeda, *J. Polym. Sci., Polym. Chem. Ed.*, **22**, 1393 (1984).

3) H. Kamogawa, Y. Haramoto, Y. Misaka, Y. Asada, Y. Ohno, and M. Nanasawa, *J. Polym. Sci., Polym. Chem. Ed.*, **23**, 1517 (1985).

4) H. Kamogawa and T. Sueki, *J. Polym. Sci., Polym. Chem. Ed.*, **23**, 1963 (1985).

5) C. D. Cutsche, "Organic Reactions, VIII," Wiley, New York (1954), p. 365.

6) T. W. Gibson and P. Strassburger, *J. Org. Chem.*, **41**, 791 (1976).

 © 1989 The Chemical Society of Japan Bull. Chem. Soc. Jpn., 62, 193—197 (1989)

Replacement of an 11-Carbonyl Group of 11-Oxo Steroid by an Oxygen Atom. A New Partial Synthesis of 11-Oxaprogesterone[1)]

Hiroshi SUGINOME* and J. B. WANG
Organic Synthesis Division, Department of Chemical Process Engineering,
Faculty of Engineering, Hokkaido University, Sapporo 060
(Received July 28, 1988)

We describe the transformation of commercially available 3α-hydroxy-5β-pregnane-11,20-dione acetate (**1**) into 11-oxaprogesterone (**15**) in 11 steps including the regioselective β-scission of an alkoxyl radical as a key step.

Among oxamodification of steroids, the synthesis of 11-oxasteroids has been extensively investigated by Engel and his colleagues. In 1968 they achieved the transformation of hecogenin into the first oxasteroid, 11-oxaprogesterone (**15**) having a significant biological activity, in 22 steps.[2,3)] They have also reported the synthesis and biological evaluation of several related 11-oxasteroids.[4,5)] Recently, the partial synthesis of 11-oxaestradiol via dye-sensitized photooxygenation of a 3-hydroxy-1,3,5(10),9-estratetraen-17-one methyl ether has also been reported by Bonet and his colleagues.[6)]

We ourselves have reported new general methods for transforming steroidal five- and six-membered cyclic alcohols or cyclic ketones as starting materials into oxasteroids with the same ring size in 2 or 4 steps[7-9)] and synthesized 1-oxa-, 3-oxa-, 4-oxa-, 6-oxa-, 7-oxa-, 16-oxa-, and 17-oxasteroids effectively by these methods. We have also recently shown that the synthesis of 11-oxasteroids can be achieved by our general method by which cyclic ketones are transformed into the corresponding cyclic ethers and that the synthesis of 11-oxa-5β-pregnan-3α-ol can be achieved by the replacement of the 11-carbonyl group of a commercially available 3α-hydroxy-5β-pregnane-11,20-dione acetate (**1**).[10)]

We wish to describe here the partial synthesis of 11-oxaprogesterone (**15**) from pregnane dione **1** based on our method by which cyclic ketones are transformed into cyclic ethers.

Results

A selective reduction of the 20-carbonyl group of a commercially available pregnane derivative **1** with $NaBH_4$ at room temperature followed by acetylation by the standard method gave a mixture of 3α,20α- and 3α,20β-dihydroxy-5β-pregnan-11-one 3,20-diacetate (**3**) in 94% yield. The preparations of this mixture of epimers by the reduction of 5β-pregnane-3,11,20-trione or 3α-hydroxy-5β-pregnane-11,20-dione with $NaBH_4$ followed by acetylation,[11,12)] have been reported to give the 20β-epimer as the predominant product.[12)]

A Baeyer–Villiger oxidation of diacetates **3** with potassium peroxodisulfate in glacial acetic acid containing concd sulfuric acid for 10 days at room temperature led to a regio- and stereoselective oxidation of the carbonyl group and gave a crystalline mixture of 3α,20α- and 3α,20β-dihydroxy-11-oxa-*C*-homo-5β-pregnane-12-one 3,20-diacetate (**4**) in a 56% yield. The ratio of the 20β-isomer and 20α-isomer was estimated to be approximately 1.7:1 based on the area ratio of the signals due to the two 9α-protons of the

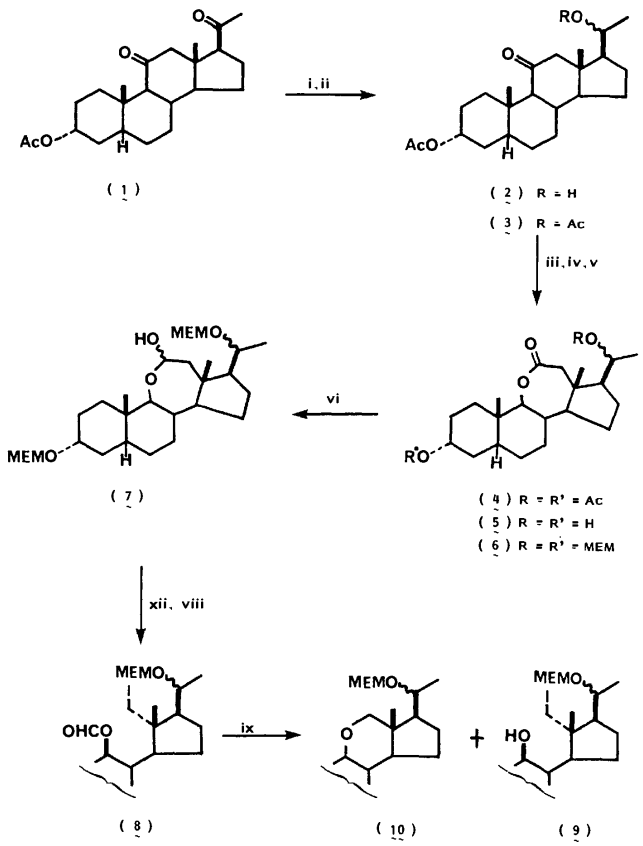

Scheme 1. Reagents: i) $NaBH_4$, EtOH, 20 °C, 5 h; ii) $(CH_3CO)_2O$, pyridine, 35 h; iii) AcOH, concd H_2SO_4, $K_2S_2O_8$, 20 °C, 10 d; iv) aq MeOH, Na_2CO_3, reflux, 18 h; v) CH_3CN, MEM·NH_4Cl, 16 h; vi) toluene, DIBAL, 20 °C, 1 d; vii) HgO, I_2, benzene, 20 °C; viii) *hν*, 20 °C, 4 h; ix) THF, $NaBH_4$, reflux, 1 d.

^{1}H NMR spectrum. To the best of our knowledge, no successful formation of lactones from 11-oxosteroids by means of the Baeyer–Villiger oxidation has previously been reported and the present example seems to be the first one. Examination of the oxidation product by means of TLC indicated that neither 9β-isomers nor 12-oxa-isomers of lactones **4** were present in the product. Its ^{1}H NMR spectrum exhibited two clear doublets at δ 4.27 and 4.38 with J=9.62 and 10.62 arising from the 9α-H of the 20-isomers.

Before transforming the lactone **4** into the corresponding lactols, the replacement of the 3α- and 20-acetyl groups by an MEM† group was necessary. The diacetate was therefore treated with sodium carbonate in aq methanol under reflux for 18 h to give the corresponding diol **5** in a 78% yield. The ratio of the two isomers with regard to the 20 position was 1:1.5. The treatment of diols **5** with [(2-methoxyethoxy)-methyl]triethylammonium chloride in acetonitrile under reflux for 16 h gave the corresponding MEM ether **6** in 76% yield. The dihydroxylactones protected by the MEM group was then transformed into the corresponding lactols **7** in a 73% yield by a treatment with DIBAL†† in toluene for one day at room temperature. The lactols **7** were then subjected to a regioselective homolytic cleavage of the 12,12a-carbon–carbon bond according to the procedure reported previously;[8] the lactols **7** in benzene were first transformed into the corresponding hypoiodite with 3 molar equivalents each of mercury(II) oxide and iodine and the solution was irradiated with a 100-W Hg arc for 4 h through a Pyrex to give iodo formates **8** in a 73% yield. Signals due to the formyloxy groups of the 20α-isomer and 20β-isomer in the ^{1}H NMR spectrum appeared at δ 8.23 and 8.33 as two singlets. The ratio of the two epimers estimated by the area ratio of these two singlets was 1:1.6.

The first attempt to cyclize the iodo formates **8** into the corresponding oxasteroids was made by heating the formates **8** in THF with $NaBH_4$ under reflux for 2 days. This procedure resulted, however, in only a low yield of oxasteroid **10** with an accompanying formation of 11β-ol **9** arose from hydrolysis. The crude oxasteroid **10**, isolated by means of preparative TLC, was immediately subjected to the removal of the protecting MEM group to give a mixture of 11-oxa-5β-pregnane-3α,20α- and 3α,20β-diol (**12**) by the standard method. The overall yield of oxasteroids **12** from iodo formates **8** was only 16%.

We obtained a much higher yield of oxasteroids **12**, however, by the initial removal of the MEM group of iodo formates **8** to iodo formates **11** followed by cyclization, although the intramolecular displacement of the iodo formates **8** in dichloromethane with $TiCl_4$ at room temperature gave a mixture of two epimers of iodo formates **11** in a 96% yield. The ratio of the two epimers estimated by the signal areas due to their 9α-H in the ^{1}H NMR was 1.1:1. The heating of iodo formates **11** in THF under reflux for 3 days gave a mixture of 11-oxa-5β-pregnane-3α,20α- and 3α,20β-diol (**12**) in a 51% yield with an accompanying formation of triols **13**.

Oxidation of 20-epimers of dihydroxyoxasteroids **12** in dichloromethane with PCC††† gave 11-oxa-5β-pregnane-3,20-dione (**14**) in a 84% yield. Further oxidation of dione **14** in dioxane with DDQ afforded 11-oxaprogesterone (**15**) and 11-oxapregna-1,4-diene-3,20-dione **16** in 11% and 31% yields. The transformation of the latter into the former by means of selective homogeneous hydrogenation with tris(triphenylphosphine)chlororhodium as a catalyst has already been achieved in 85% yield by Engel and his colleagues.[2]

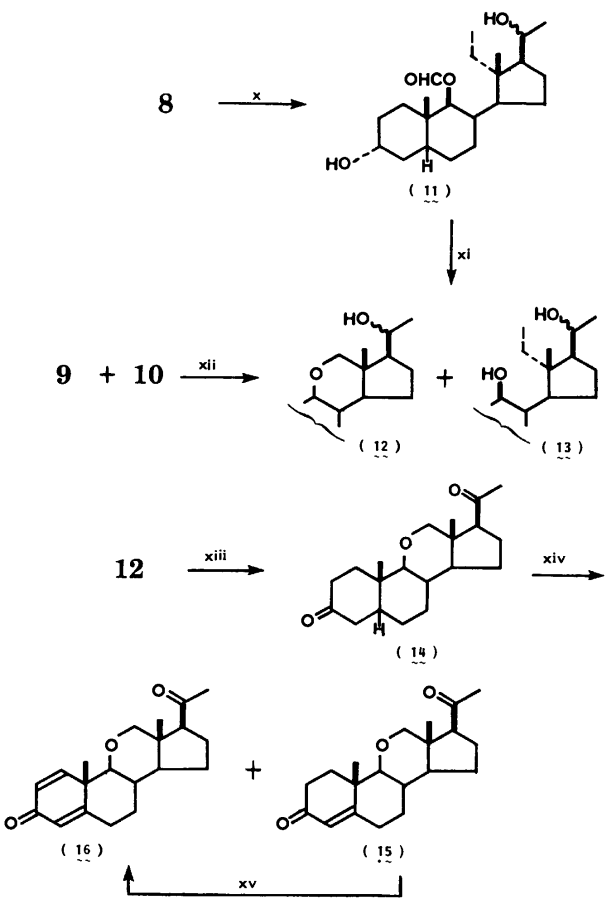

Scheme 2. Reagents: x) CH_2Cl_2, $TiCl_4$, 0°C, 20 min; xi) THF, $NaBH_4$, reflux, 3 d; xii) CH_2Cl_2, $TiCl_4$, 0°C, 40 min; xiii) CH_2Cl_2, PCC, 0°C, 12 h; xiv) dioxane, DDQ, reflux, 23 h; xv) benzene, H_2, $(Ph_3P)_3RuCl$, 20°C, 5 h.

† MEM; (2-methoxyethoxy)methoxy.

†† DIBAL; diisobutylaluminium hydride.

††† PCC; pyridinium chlorochromate.

Experimental

Mps were recorded with a Yanagimoto micro mp apparatus and are uncorrected. IR spectra were determined for Nujol mull with a JASCO IR 810 infrared spectrophotometer. ^{1}H NMR spectra were determined with JEOL JNM-FX 270 high-resolution FT-NMR spectrometer (270 MHz) (Solvent $CDCl_3$; $SiMe_4$ as internal standard) (Faculty of Pharmaceutical Sciences of this University). TLC was carried out on a Merck Kieselgel 60 PF_{254}. The high- and low-resolution mass spectra were determined with a JEOL JMA-D 300 spectrometer (70 eV) (Faculty of Agriculture or Faculty of Pharmaceutical Sciences of this University). Optical rotations were measured with a JASCO DIP-360 digital polarimeter.

3α,20α- and 3α,20β-Dihydroxy-5β-pregnan-11-one 3,20-Diacetates (3). Commercially available 3α-hydroxy-5β-pregnane-11,20-dione 3-acetate (**1**) (5 g) in ethanol (350 ml) was reduced with $NaBH_4$ (1 g) at room temperature for 5 h by the standard procedure to yield a mixture of 3α,20α- and 3α,20β-dihydroxy-5β-pregnan-11-one 3-acetates (**2**). The crude 20-ols **2** were immediately acetylated with acetic anhydride (25 ml) and pyridine (50 ml) for 35 h at room temperature. The solution was poured into water and the crystals were collected by filtration, washed with water and dissolved in dichloromethane. The solution was worked up in the usual way to yield 3,20-diacetates **3** (5.94 g). Recrystallization of the diacetates with hexane–ethyl acetate gave a stereoisomeric mixture of 3,20-diacetates **3** (5.24 g, 94%). Mp 161.5—163.0 °C (lit,[11] 160.5—161.0 °C)

Baeyer-Villiger Oxidation of 3α,20α-Dihydroxy-5β-pregnan-11-one 3,20-Diacetates. The diacetates (1.59 g), potassium peroxodisulfate (7 g) and concd sulfuric acid (7 ml) in glacial acetic acid (39 ml) in a vessel covered by aluminum foil was set aside for 10 days at room temperature. The reaction mixture was extracted with chloroform (ca. 40 ml× 5). The combined extracts were washed with 5% aqueous sodium thiosulfate, brine and water and dried over $MgSO_4$. The work-up of the solution gave a residue which was subjected to preparative TLC with 1:1 hexane–ethyl acetate to yield two fractions. The less polar fraction (1.06 g) was the starting material. The more polar fraction (300 mg) was a crude lactone **4** which was recrystallized from hexane–ethyl acetate. Mp 192—195 °C. (Found: M$^+$, 434.2676. $C_{25}H_{38}O_6$ requires M, 434.2668); IR 1727 (OAc and lactone C=O), 1244 and 1039 cm^{-1}; ^{1}H NMR δ=0.75 (3H, s, 18-H of 20α- and 20β-isomer), 1.08 (s, 19-H of 20α- and 20β-isomer), 1.17 (d, J=5.86 Hz, 21-H), 2.03 (s, OAc of 20α-isomer), 2.04 (s, OAc of 20β-isomer), 2.10 (s, OAc of 20β-isomer), 2.14 (s, OAc of 20α-isomer), 2.39 and 2.66 (each d, J=14.2 Hz, 12a-H of 20α-isomer), 2.51 and 3.22 (each d, J=13.9 Hz, 12a-H of 20β-isomer), 4.27 (d, J=9.52 Hz, 9aα-H of 20β-isomer), 4.38 (d, J=10.62 Hz, 9α-H of 20α-isomer), and 4.77 (m, 3β-H and 20-H of 20α- and 20β-isomers). EIMS m/z 434 (M$^+$, 4.8%). 374 [(M−CH_3CO_2H)$^+$, 11.4], 324 [(M−2CH_3COOH)$^+$, 18.6], and 43 (100).

3α,20α- and 3α,20β-Dihydroxy-5β-C-homo-11-oxapregnan-12-one (5). To the lactone **4** (270 mg) in methanol (20 ml), aq. saturated sodium carbonate (2 ml) was added. The solution was heated under reflux for 18 h. The removal of the solvent gave a residue which was dissolved in dichloromethane, then washed with a 5% hydrochloric acid, brine and water and dried over $MgSO_4$. The usual work-up gave a product (223 mg) which was purified by means of preparative TLC with ethyl acetate to give diol **5** as an amorphous solids (169 mg, 78%). (Found: M$^+$, 350.2471. $C_{21}H_{34}O_4$ requires M, 350.2457); IR 3380 (OH), 1708 (lactone C=O) and 1041 cm^{-1} (C-O-C); ^{1}H NMR δ=0.87 (s, 18-H of 20α-isomer), 0.93 (s, 18-H of 20β-isomer), 1.06 (s, 19-H of 20β-isomer), 1.07 (s, 19-H of 20α-isomer), 1.00 (d, J=6.23 Hz, 21-H of 20β-isomer), 1.16 (d, J=6.23 Hz, 21-H of 20α-isomer), 2.46 and 3.61 (each d, J=13.6 Hz, 12a-H of 20α-isomer), 2.52 and 3.26 (each d, J=13.6 Hz, 12a-H of 20β-isomer), 3.70 (2H, m, 3β-H and 20α- and 20β-H), 4.30 (d, J=9.89 Hz, 9α-H of 20α-isomer), and 4.40 (d, J=9.89 Hz, 9α-H of 20α-isomer); EIMS m/z 350 (M$^+$, 18.9), 322 [(M−H_2O)$^+$, 51.4], 341 [(M−2H_2O)$^+$, 50.0], and 81 (100%).

3α,20α- and 3α,20β-Dihydroxy-5β-C-homo-11-oxapregnan-12-one 3,20-MEM Ether (6). To diol **5** (163 mg) in dry acetonitrile (10 ml), MEM triethylammonium chloride (400 mg) was added. The solution was heated under reflux for 16 h and the solvent was removed under vacuum. The residue was dissolved in dichloromethane–acetone. The solution was washed with aq 5% sodium hydrogencarbonate, brine and then water and dried over $MgSO_4$. The usual work-up gave a crude MEM ether. Since the IR spectrum indicated the presence of the starting diol in this product, the crude MEM ether was again subjected to the above procedure to transform the starting diol into MEM ether. The product was purified by means of preparative TLC with ethyl acetate to give oily MEM ether **6** (187 mg, 76.3%). (Found: M$^+$, 526.3493. $C_{29}H_{50}O_8$ requires M, 526.3503); IR 1735 (lactone C=O), 1119 (C-O-C) and 1048 cm^{-1} (C-O-C); ^{1}H NMR δ=0.80 (s, 18-H of 20α-epimer), 0.83 (s, 18-H of 20β-epimer), 1.05 (s, 19-H of 20α-epimer), 1.06 (s, 19-H of 20β-epimer), 3.38 (s, OMe), 3.39 (s, OMe), 3.56—3.74 (m, -OCH_2CH_2O-), 4.28 (d, J=9.80 Hz, 9α-H of 20β-epimer), 4.38 (d, J=9.80 Hz, 9α-H of 20β-isomer), and 4.68—4.89 (4H, m, -OCH_2O-), EIMS: m/z 526 (M$^+$, 0.1), 89 (95.6), and 59 (100%).

Reduction of 3α,20α- and 3α,20β-Dihydroxy-5β-C-homo-11-oxapregnan-12-one 3,20-MEM Ether (6) with DIBAL. To lactone MEM ether **6** (195 mg) in dry toluene (10 ml), a DIBAL solution (0.53 ml) (1 M in toluene) was added dropwise at −78 °C in an atmosphere of nitrogen. The solution was stirred for 1 day at room temperature. After the solution had again been cooled to −78 °C, a more DIBAL solution (0.2 ml) was added and the solution stirred for 4 h at room temperature. The reaction was quenched by the addition of iced water and the solution was filtered. After the addition of chloroform and acetone, the solution was washed with brine and then with water and dried over $MgSO_4$. The usual work-up gave a product which was purified by means of preparative TLC with ethyl acetate to give only lactol **7** (143 mg, 73%). [Found: (M−H_2O)$^+$, 510.3573. $C_{29}H_{50}O_7$ requires M, 510.3557]: IR 3442 (OH), 1099 (C-O-C) and 1043 cm^{-1} (C-O-C); ^{1}H NMR δ=3.85 (d, J=9.52 Hz, 9α-H of 20α-epimer), 3.97 (d, J=9.65 Hz, 9α-H of 20α-epimer), 5.14 (m, 12-H of 20β-epimer), and 5.33 (m, 12-H of 20α-epimer); EIMS m/z 510 [(M−H_2O)$^+$, 0.19] and 59 (100%).

Preparation of 3α,20α- and 3α,20β-Bis[3-(2-methoxyethoxy)methoxy]-11-iodo-9,11-seco-C-nor-5β-yl Formates (8). Lactol **7** (155 ml) was dissolved in dry benzene (20 ml) containing pyridine (0.2 ml). To this solution mercury(II) oxide (200 mg) and iodine (230 mg) were added. The solution was then flashed with nitrogen and irradiated with a

100-W high-pressure Hg arc for 4 h. The solution was then filtered and the filtrate was washed with aq 5% sodium thiosulphate, brine and then water successively and dried over $MgSO_4$. The usual work-up of the solution gave a residue (193 mg) which was subjected to preparative TLC with a 1:2 hexane–ethyl acetate. The most mobile fraction (140 mg, 73%) was two 20-epimers of iodo formates **8**. IR 1721 (OCHO) and 1025—1175 (C-O-C); ^{1}H NMR δ= 0.93 (s, 18-H of 20α-epimer), 0.95 (s, 18-H of 20β-epimer), 1.04 (s, 19-H of 20α-epimer), 1.06 (s, 19-H of 20α-epimer), 3.39 (s, OMe), 3.51—3.78 (m, $-OCH_2CH_2O-$), 4.74—4.81 (m, $-OCH_2O-$), 5.21 (d, J=10.99 Hz, 9α-H of 20β-epimer); 5.32 (d, J=9.16 Hz, 9α-H of 20α-epimer), 8.23 (s, OCHO of 20α-epimer), and 8.33 (s, OCHO of 20β-epimer); EIMS: m/z 549 [(M−OMEM)$^+$, 0.14], 397 (2.1), 89 (100), and 59 (80.1%).

Preparation of 3α,20α- and 3α,20β-Dihydroxy-11-iodo-9,11-seco-*C*-nor-5β-pregnan-9β-yl Formate (11). To iodo formate **8** (50 mg) in dichloromethane (3 ml), titanium tetrachloride (0.2 ml) was slowly added at 0 °C. After the solution had been stirred for 20 min at 0 °C, concd aq ammonia was added. The combined organic layers were washed with brine and then with water and dried over $MgSO_4$. The usual work-up gave an oily product (50 mg) which was purified by means of preparative TLC with ethyl acetate to give amorphous formate **11** (35 mg, 96%). [Found: (M−HI−H_2O)$^+$, 332.2321, $C_{21}H_{32}O_3$ requires M 332.2351]; IR ($CHCl_3$) 3410 (OH), 1719 and 1189 (-OCHO); ^{1}H NMR δ=5.20 (d, J=10.99 Hz, 9α-H), 5.30 (d, J=10.99 Hz, 9α-H), 8.30 (s, OCHO), and 8.35 (s, OCHO); EIMS m/z 415 [(M−OCHO−H_2O)$^+$, 0.22], 332 [(M−HI−H_2O)$^+$, 2.8], 305 [(M−HCHO−I)$^+$, 2.3], 287 [(M−OCHO−H_2O)$^+$, 84.3], 269 [(M−HCHO−I−2H_2O)$^+$, 56.4], and 95 (100%).

11-Oxa-5β-pregnane-3α,20α and 3α,20β-diol (12). To iodo formates **11** (90 mg) in dry THF (10 ml), $NaBH_4$ (180 mg) was added and the solution was heated under reflux for 3 days. The removal of the solvent gave a residue which was dissolved in dichlorormethane. The solution was washed with brine and then with water and dried over anhydrous $MgSO_4$. The usual work-up of the solution gave a product (80 mg) which was subjected to preparative TLC with a 2:1 ethyl acetate–hexane to give three fractions. The most mobile fraction (10 mg) was the starting iodo formates **11**. The next mobile fraction (31 mg, 51%) was the amorphous epimers **12** of oxasteroid. (Found: M$^+$, 322.2523. $C_{20}H_{34}O_3$ requires M, 322.2508); IR 3280 (OH), 1114, 1085, and 1072 cm^{-1}; ^{1}H NMR δ=(the predominant epimer of the 20α- and 20β-isomers), 0.86 (3H, s, 18-H), 1.02 (3H, s, 19-H), 3.12 (1H, d, J=9.89 Hz, 9α-H), 3.18 (1H, d, J=10.63 Hz, 12-H), 3.61—3.75 (2H, m, 3β-H and 20ξ-H) and 4.15 (1H, d, J=10.63 Hz, 12-H).

The most polar fraction (30 mg, 35%) was an oily 11-iodo-*C*-nor-9,10-seco-5β-pregnane-3α,9β,20α- and 3α,9β,20β-triols. IR ($CHCl_3$) 3392 (OH) and 1094 cm^{-1} (C-O); ^{1}H NMR δ=3.04 (d, J=10.63 Hz, 11-H), 3.34 (d, J=9.90 Hz, 9α-H); 3.56—3.74 (m, 3α-H, 11-H, 20α-H, and 20β-H); the epimer, δ=3.26 (d, J=10.26 Hz, 11-H), 3.77 (d, J=10.26 Hz, 11-H), and 3.94 (d, J=9.90 Hz, 9α-H), ^{1}H NMR m/z 433 (0.27), 415 (1.08), 397 (0.68), 322 [(M−HI)$^+$, 36.1], 304 [(M−HI−H_2O)$^+$, 35.4], and 44 (100%).

Preparation of 11-Oxa-5β-pregnane-3,20-dione (14). To diol **13** (30 mg) in dichloromethane (5 ml), PCC (100 mg), and Celite (100 mg) were added at 0 °C and the solution was stirred for 12 h at room temperature. After the addition of diethyl ether, the solution was filtered. The removal of the solvent from the filtrate gave a residue which was purified by means of preparative TLC with a 2:3 hexane–ethyl acetate to give crystals of dione **14** (25 mg, 84%). The specimen for analysis was obtained by recrystallization from hexane–ethyl acetate. Mp 153.5—155.0 °C. (Found: C, 75.47; H, 9.60%. $C_{20}H_{30}O_3$ requires C, 75.43; H, 9.50%); $[\alpha]_D^{22}$ +48° (c 1, $CHCl_3$); IR 1715 and 1703 (C=O), 1078 and 1071 (C-O-C); ^{1}H NMR δ=0.77 (3H, s, 18-H), 1.10 (3H, s, 19-H), 2.07 (3H, s, 21-H), 3.26 (1H, d, J=9.53 Hz, 9α-H), 3.47 (1H, d, J=10.26 Hz, 12-H), and 4.16 (1H, d, J=10.26 Hz); EIMS: m/z 318 (M$^+$, 52.2), 300 (6.9), 288 (9.9), 233 (37.4), and 43 (100%).

Preparation of 11-Oxa-5β-pregnane-3,20-dione (14) from Iodo Formate 8 via 10 and 12. Iodo formate **8** (139 mg) in dry THF (6 ml) containing $NaBH_4$ (139 mg) was heated under reflux for 1 day in an atmosphere of dry nitrogen. To the solution a further amount (50 mg) of $NaBH_4$ was added and the solution was heated under reflux for 1 day. After the removal of the solvent the residue was dissolved in dichloromethane. The solution was washed with brine and then with water and dried over anhydrous $MgSO_4$. The removal of the solvent gave an oily product (120 mg) which was subjected to preparative TLC with a 1:1 hexane–ethyl acetate to give an oily product (80 mg). To the product in dichloromethane (5 ml), titanium tetrachloride (0.28 ml) was added and the solution was stirred for 40 min at 0 °C. To the solution concd aq ammonia was added and the organic layer was washed with brine and then with water and dried over anhydrous $MgSO_4$. The usual work-up of the solution gave a product (60 ml) which was subjected to preparative TLC with a 1:2 hexane–ethyl acetate to give oxasteroid **12** (15 mg) and triol **13** (35 mg). Oxasteroid **12** was oxidized with PCC to give a new dione **14** (11 mg) as described previously. The overall yield from **8** to **12** was 16%.

Synthesis of 11-Oxaprogesterone (15) and 11-Oxapregna-1,4-diene-3,20-dione (16). 11-Oxasteroid **14** (28 mg) in dry dioxane (3 ml) containing DDQ (30 mg) was heated under reflux for 23 h in an atmosphere of nitrogen. After the removal of the solvent, the residue was dissolved in acetone and the solution was filtered through aluminum oxide. The removal of acetone gave a yellow product which was subjected to preparative TLC (Merck, silica gel 60 F_{254}) with a 1:1 hexane–ethyl acetate to give three fractions. The most mobile fraction (10 mg) was the starting material. The second mobile fraction was crystals of 11-oxaprogesterone (**15**) (2 mg, 11% based on the converted oxasteroid **14**) which was recrystallized from dichloromethane–diethyl ether. Mp 179—180 °C (lit,[2] 181—182 °C). ^{1}H NMR δ=0.80 (3H, s, 18-H), 1.26 (3H, s, 19-H), 2.07 (3H, s, 21-H), 2.59 (1H, J=9.98 Hz, 9α-H), 3.44 (1H, J=10.26 Hz, 12-H), 4.16 (1H, J=10.26 Hz, 12-H), and 5.78 (1H, s, 4-H). EIMS m/z 316 (M$^+$, 28), 193 (84), and 43 (100%).

The most polar fraction (6 mg, 31% based on the converted starting steroid) was 11-oxapregna-1,4-diene-3,20-dione which was recrystallized from dichloromethane–diethyl ether to give a pure specimen. Mp 193—196 °C (lit,[2] 195—196 °C), $[\alpha]_D^{22}$ +104.8° (c 0.8 in $CHCl_3$) [lit,[2] $[\alpha]_D^{22}$ +104.3° (c 1.0 in $CHCl_3$)]. ^{1}H NMR δ=0.83 (3H, s, 18-H), 1.32 (3H, s, 19-H), 2.07 (3H, s, 21-H), 2.63 (1H, d, J=9.52 Hz, 9α-H), 3.48 (1H, d, J=10.26 Hz, 12-H), 4.18 (1H, d, J=10.26 Hz, 12-H), 6.12 (1H, s, 4-H), 6.25 (1H, d, J=10.3 Hz, 2-H), and 7.26 (1H, s, J=10.3 Hz, 1-H), EIMS: m/z 314 (M$^+$, 16.5), 286 (5.8), 193 (42.3), and 42 (100%).

References

1) Photoinduced Molecular Transformations. Part 99. Part 98. H. Suginome, Y. Kurokawa, and K. Orito, *Bull. Chem. Soc. Jpn.*, **61**, 4005 (1988).

2) C. R. Engel and M. N. R. Chowdhury, *Tetrahedron Lett.*, **1968**, 2107; C. R. Engel, R. C. Rastogi, and M. N. R. Chowdhury, *Steroids*, **19**, 1 (1972).

3) The Participation of the 20-oxo group in the acidic cyclization of 3,3:20,20-bis(ethylenedioxy)-9,10-secopregnane-9β,11-diol to 11-oxa-5α-pregnane-3,20-dione and its 17β-epimer has recently been reported by Nagano and his colleagues. H. Nagano, T. Iwadare, and M. Shiota, *J. Chem. Soc., Perkin Trans. 1*, **1986**, 2291.

4) C. R. Engel, S. Salvi, and M. N. R. Chowdhury, *Steroids*, **25**, 781 (1975); V. S. Salvi, D. Mukherjee, M. N. R. Chowdhury, and C. R. Engel, *Steroids*, **27**, 717 (1976).

5) C. R. Engel, D. Mukherjee, M. N. R. Chowdhury, G. Ramani, and V. S. Salvi, *J. Steroid Biochem.*, **6**, 585 (1975).

6) T. Planas and J. J. Bonet, 11 IUPAC Symposium on Photochemistry, Lisbon, July-August, 1986, Abstr. 3P-38.

7) H. Suginome and S. Yamada, *J. Org. Chem.*, **49**, 3753 (1984).

8) H. Suginome and S. Yamada, *J. Org. Chem.*, **50**, 2489 (1985).

9) H. Suginome and S. Yamada, *Bull. Chem. Soc. Jpn.*, **60**, 2453 (1987).

10) H. Suginome, J. B. Wang, and S. Yamada, *Chem. Lett.*, **1987**, 783.

11) O. Mancera, H. J. Ringold, C. Djerassi, G. Rosenkranz, and F. Sondheimer, *J. Am. Chem. Soc.*, **75**, 1286 (1953).

12) E. P. Oliveto and E. B. Hershberg, *J. Am. Chem. Soc.*, **75**, 488 (1953).

Design and Synthesis of Macromonocyclic Polyamines Composed of Natural Methylene Arrays

Masaaki IWATA* and Hiroyoshi KUZUHARA
RIKEN (The Institute of Physical and Chemical Research),
Wako, Saitama 351-01
(Received August 4, 1988)

A general synthetic method applicable to acyclic and cyclic polyamines was developed. The methodology was exemplified by systematical synthesis of twelve macromonocyclic polyamines, **1** ([17]N_4) through **12** ([35]N_8), composed of the combination of four natural polyamine segments, spermidine, spermine, thermine, and thermospermine. These twelve designed macrocycles are exhausted numbers of possible structures defined by three arbitrarily chosen criteria concerning with methylene chain arrays and nitrogen content (four to eight). The common elements of the structural characteristics were analyzed and were found to be reduced to readily available three classes of simple *N,N'*-ditosylalkanediamines derived from diamines and triamine. Nitrogen content was increased systematically through the reaction of *N,N'*-ditosylalkanediamine with one of three ω-phthalimidated electrophiles followed by regeneration of the same functionality at symmetrical both terminals as the starting materials via a series of transformation reaction, in excellent yields. Tractable formamide intermediate profits the facile synthesis of acyclic polyamines with long chains. Cyclization was achieved, under high dilution conditions, through the reaction of α,ω-bis(tosylamide) with α,ω-ditosylates in DMF in the presence of cesium carbonate. The cyclization occurred in practical synthetic yields even in the formation of multi-membered ring when the shorter electrophile and the longest α,ω-bis(tosylamide) reacted.

Knowledge of biological importance of natural polyamines as one of substances controlling cell functions[1] has stimulated much interest in intrinsic biological role of amino groups involved in, through the synthesis of selectively modified spermidines[2a] or through the studies on biological activities of polyamine analogues.[2b,c] Ubiquitous natural polyamines, spermidine and spermine, and rare species-specific polyamines, thermine[3a] and thermospermine,[3b] are correlated structurally in a sense of disposition of methylene chain blocks, in which both types of polyamines are composed, mysteriously, of the combination of the contiguous three and/or four methylene chain blocks. Difference lies only in the order of the methylene block disposed along the polyamine chain. Biosynthetically, this implys only the limited numbers of amino acid sources, methionine and ornithine. However, profound nature of their sequence might be concealed in their biological function because of their species-specific beings.

Cyclic polyamines, in which the studies had been initiated based on the interest in complexing reagents with high stability and/or selectivity for metal ions,[4a,b] have extended recently their subject fields in search of functions such as molecule or ion receptors, analogous to but much more different from crown ethers, which effect such functions as recognition, regulation, transport, and catalysis for guest molecules or ions.[4c] Since these functions are highly dependent on the molecular design of the macrocycles, synthetic feasibility of a given molecular architecture is crucial to access for investigation. The strategy in most cases has been to elaborate the substituted acyclic polyamine backbone from a simple amine and then close macrocycle late in the synthesis. Prior derivatization of a polyamine building block has resorted to rather limited methods.[2a,4d,e,f] Presently, the most effective molecular architecture for designed cyclic polyamines has been carried out through four main processes; (a) the synthesis of acyclic polyamines with α,ω-bis(tosylamide)s as nucleophiles, and (b) of electrophiles with electron-withdrawing groups at both terminals, followed by (c) cyclization between nucleophiles and electrophiles, and, finally, (d) deprotection of the protecting groups on the amino groups.[5] All the presently known methods, however, suffer from some synthetic drawback especially, in (a), (b), and (c) steps for efficient and generally adaptable architecture. In (a) step, it is desirable to accommodate every type of methylene chain blocks and to regenerate efficiently the same nucleophilic functionality in the shortest procedure.[2a] In (b) step, it is ideal to accommodate the tosyloxy group at both terminals.[6] In addition, when designed macrocycles might be constructed through several couples of α,ω-nucleophiles and α,ω-electrophiles in (c) step, it is ideal to select readily best couples according to a certain guiding principle.

Recently, we have developed two elemental reactions; the transformation reaction of phthalimides to formamides[7] (Eq. 1) and the rearrangement reaction of *N*-nitroso sulfonamides, which are quantitatively prepared by nitrosation of the corresponding sulfonamides, to tosylate[8] (Eq. 2). Through the

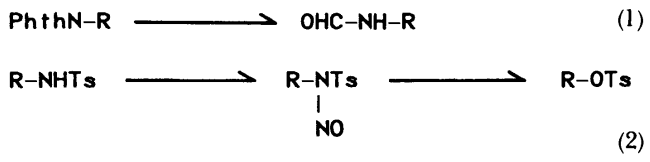

preliminary investigations concerning with applicability of the elemental reactions,[9] a new plan of molecular architecture for macromonocyclic polyamines was emerged. In the plan, firstly, our concern

was to provide cyclic polyamines, in which all the methylene blocks in the ring are composed of natural methylene arrays. This effort might provide functionally unique macrocycles which may reveal the biological significance of mysterious natural methylene arrays and of biological role of primary amino groups. Secondary, our concern was to elongate chain as long as possible, in order to know how much extent the elemental reactions could be tenable in polyamine synthesis. Therefore, most of the problems involved in the conventional methods are expected to be solved through the present study.

Results and Discussion

Concept of Design and Specification: In design of cyclic polyamines, three criteria, concerning with methylene chain arrays and amine content, were defined to limit arbitrariness of the structures and to reduce numbers of targets; i) every two or three contiguous methylene blocks bisected by nitrogen atoms are comparable to one of natural polyamine segments, spermidine, spermine, thermine, and thermospermine, ii) the cycle includes these four natural polyamine arrays at least once in the chain, and iii) four through eight nitrogen atoms exist in the chain. These three criteria generate logically twelve polyamines, **1** ([17]N_4) through **12** ([35]N_8), as exhausted numbers of possible structures to be synthesized. In order to minimize synthetic steps of the defined macrocycles, the common elements of the structural characteristics were analyzed; according to their

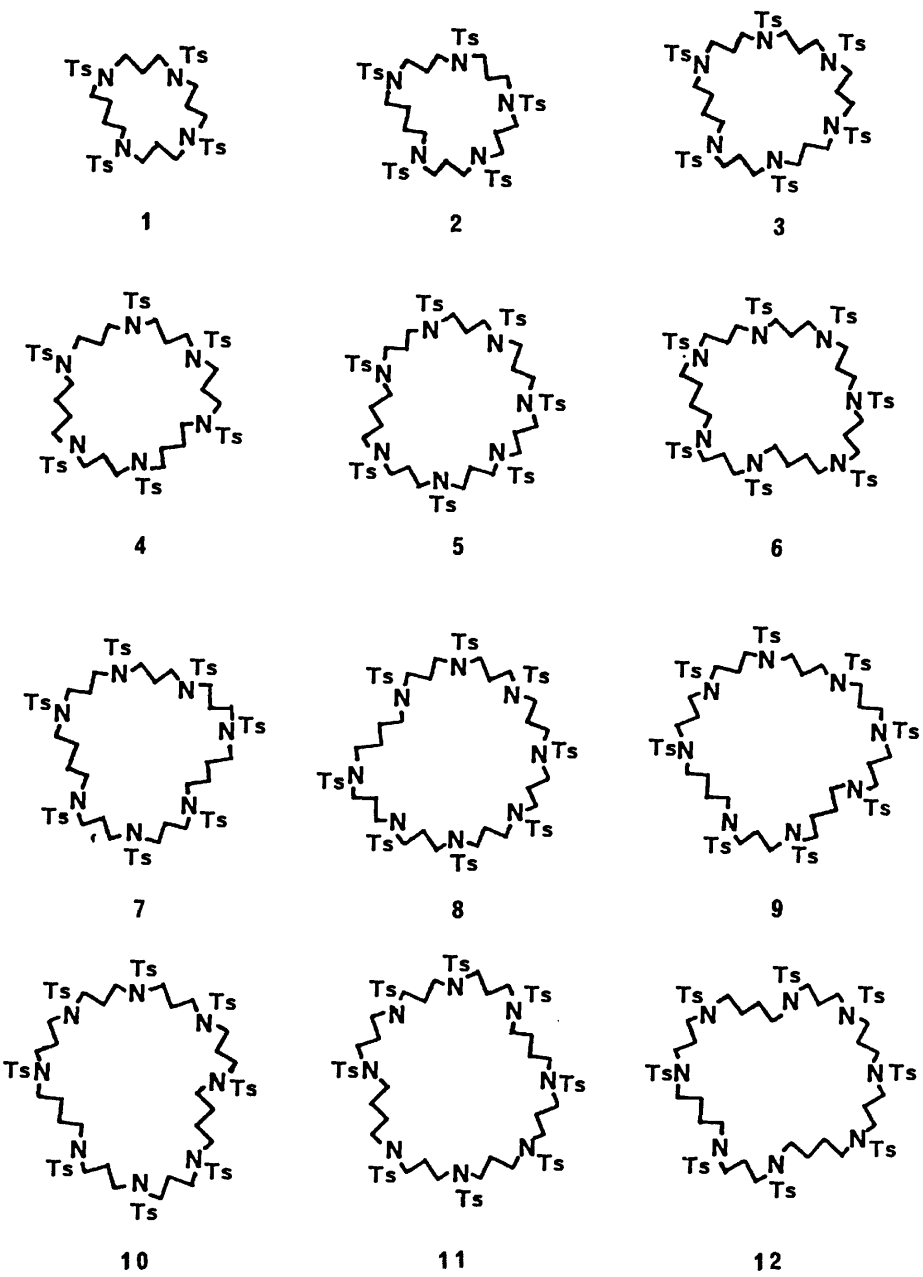

Table 1. The Flow Chart of Hierarchical Synthetic Design of Tosylated Acyclic and Cyclic Polyamines[a)]

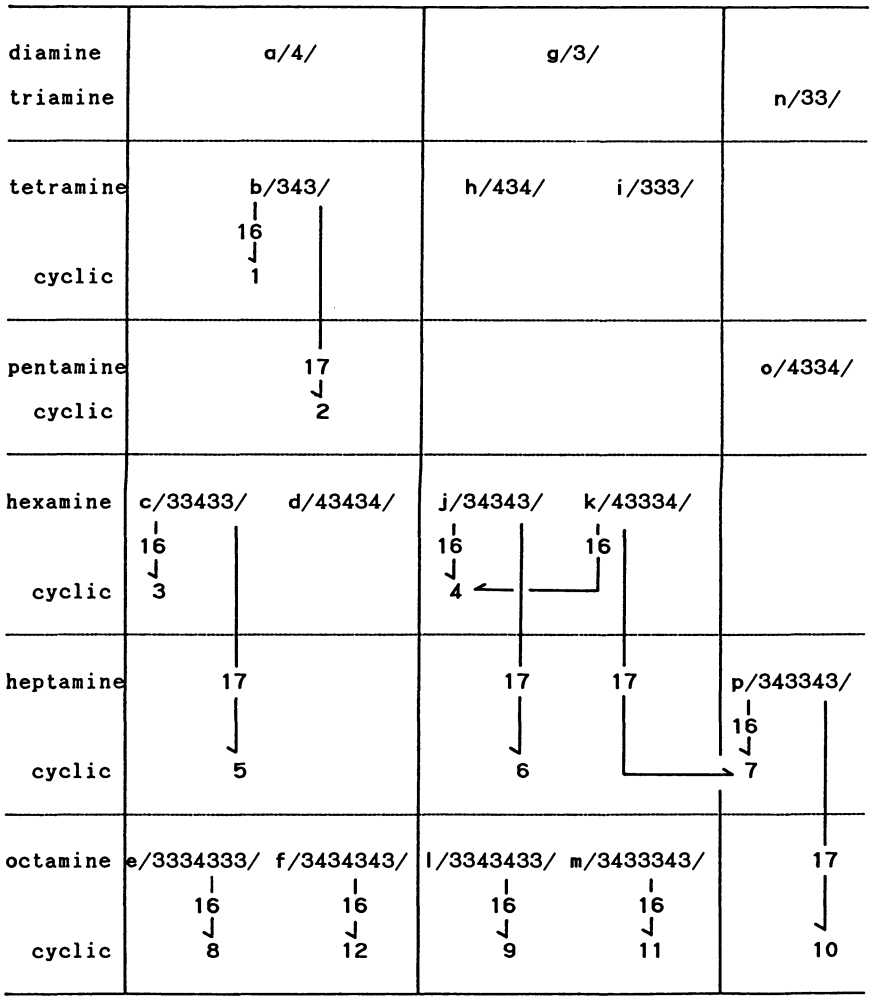

a) The chain type is shown by gothic alphabet and the chain composition is indicated by the contiguous methylene chain blocks in Arabic numerals with the default of nitrogen atoms between slant lines. Arrows in Table indicate a formal route from the acyclic to cyclic polyamines by use of α,ω-ditosylates (**16**, **17**) indicated in the arrow intermitted.

molecular symmetry, these twelve macrocycles designed were found to be divided into three classes. Starting from *N*,*N*′-ditosyl-1,4-butanediamine (**a**) as one core chain, six macrocycles, **1**, **2**, **3**, **5**, **8**, and **12** could be derived. Likewise, *N*,*N*′-ditosyl-1,3-propanediamine (**g**) as another core chain emerges four macrocycles, **4**, **6**, **9**, and **11**. N^1,N^7,4-Tritosyl-4-azaheptane-1,7-diamine (**n**) could be the other core for two macrocycles, **7** and **10**. Owing to their molecular symmetry, two macrocycles, **4** and **7**, might be synthesized through alternative combination.

Molecular Architecture: As shown in Table 1, nitrogen content could be increased hierarchically, for synthetic convenience, at both terminals with the same electrophiles. For example, diamine chains (**a**, **g**) will be source for tetramine chains, which, then, be source for hexamine and octamine chains. Thus, heptamine chain (**p**) will be derived from pentamine chain (**o**), which might have been derived from triamine chain (**n**). We expected that chain elongation from the lower to the higher nitrogen content and transformation to regenerate the same functionality at symmetrical both terminals as the starting α,ω-bis(tosylamide)s would be provided through the processes illustrated in Scheme 1; the reaction of α,ω-bis(tosylamide)s, **a**, **g**, or **n**, with ω-phthalimidated electrophiles, **13**, **14**, or **15**, will provide α,ω-diphthalimides (**A**) which then be transformed to α,ω-diformamides (**B**) and subsequently to α,ω-bis(tosylamide)s (**C**) to give **b**, **h**, or **o**, respectively, with the higher nitrogen content. The processes were expected to be recyclizable. Cyclization was expected to be achieved by the conventional process,[6)] using **C** and α,ω-ditosylated electrophiles, **16**, **17**, **18**, or **19**. As a result, in the strategy of our molecular architecture (in Table 1 and Scheme 1),

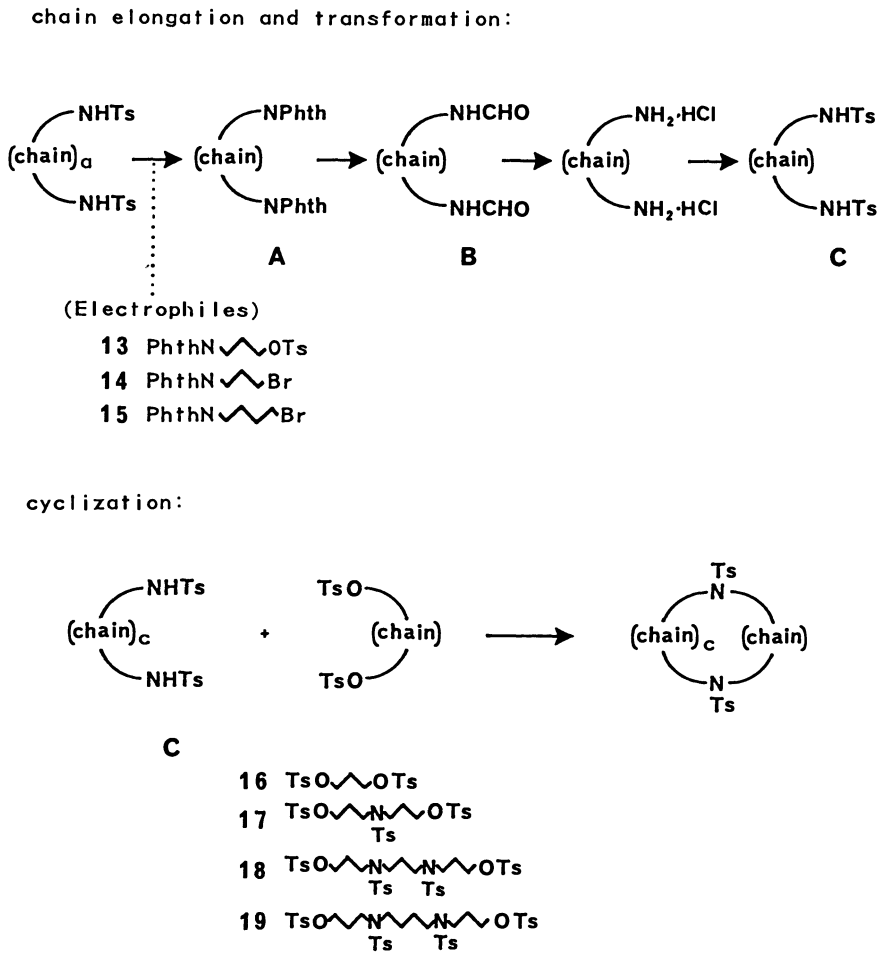

Scheme 1.

synthetic feasibility will be judged from the efficacy of repeated three reactions, chain elongation, **A** to **C** transformation, and cyclization. Therefore, efficient synthesis of electrophilic synthons, ω-phthalimidated electrophiles (**13**, **14**, **15**) and, α,ω-ditosylates (**16**, **17**, **18**, **19**), required for chain elongation and cyclization, should be the first issue.

Synthesis of Electrophiles: Elongative introduction of three methylene chain would be accommodated by *N*-(3-tosyloxypropyl)phthalimide (**13**) or *N*-(3-bromopropyl)phthalimide (**14**), and four methylene chain would be accommodated by *N*-(4-bromobutyl)phthalimide (**15**). It should be noted, as pointed previously,[9a] that the tosyloxy group is about five-fold more reactive than the bromo group. Thus, efficient synthesis of **13** was pursued. According to *N*-nitroso sulfonamide–sulfonate rearrangement reaction,[8a] *N*-(3-tosylaminopropyl)phthalimide (**20**) could be a precursor for **13**. Compound **20** was prepared via independent two routes; one route was via tosylation of commercially available 3-bromopropylamine hydrobromide (**21**) followed by condensation with potassium phthalimide (route A). The other route started with diphthalimidation of commercially available 1,3-dibromopropane (**23**) followed by treatment with hydrazine hydrate to afford a unique heterocycle, 3,4-dihydro-2*H*-pyrimido[2,1-*a*]isoindol-6-one (**25**).[10] After hydrolysis of **25**, tosylation in the presence of triethylamine gave **20** in quantitative yield (route B). Both routes proceeded in excellent yields. In economical point of view, compound **21** is expensive. Nitrosation of **20** proceeded quantitatively[8b] and the nitrosated product was rearranged in hot benzene to give **13** in 80% conversion yield. For the pur-

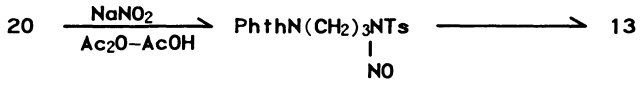

pose of reactivity comparison with **13**, compound **14** was prepared in 88% yield through the modification of the Gabriel method[11a] via the reaction of 1,3-dibromopropane with phthalimide. Since *N*-(4-tosyloxybutyl)phthalimide (**27**) has been unavailable in practical scale,[12] *N*-(4-bromobutyl)phthalimide (**15**), employed for accommodation of four methylene block throughout, was prepared in 68% yield through

(route A):

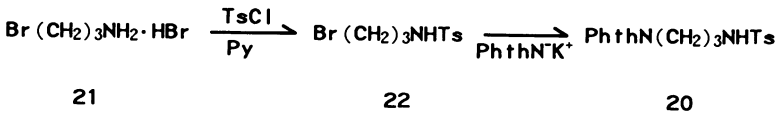

21 22 20

(route B):

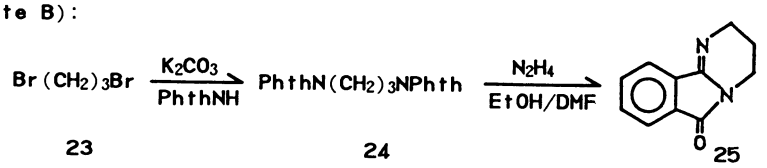

23 24 25

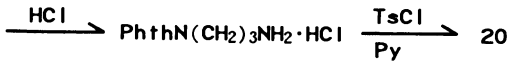

26

modification of the Gabriel method[11b] via the reaction of 1,4-dibromobutane (**28**) with phthalimide.

α,ω-Ditosylates, **16**, **17**, **18** and **19**, were prepared from the corresponding α,ω-bis(tosylamide)s, **Cg**, **Cn**, **Ci**, and **Cb**, respectively, through the nitrosation[8b] followed by the rearrangement reaction.[8a]

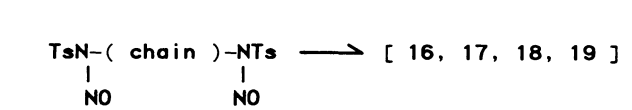

Chain Elongation and Transformation: Presently, three methods have been available for the condensation of electrophiles with α,ω-tosylamides (**C**) in synthetic polyamine chemistry; conventional use of potassium carbonate as base trigger in *N,N*-dimethylformamide (DMF), activation of α,ω-bis(tosylamino) groups via the formation of the corresponding Na salt,[6] and use of cesium carbonate[13] in DMF. When cesium carbonate was employed for the reaction of **Ca** with **13** in DMF at ambient temperature, the product **Ab** was obtained almost quantatively though the reaction proceeded very slowly (a day long). When the reaction temperature was elevated up to 80 °C for acceleration of the condensation, the reaction was not accelerated but decomposition of **13** turned out remarkable.

In preliminary experiments, tosylates were found to be decomposed considerably during the slow condensation reaction with potassium carbonate, probably due to the prolonged reaction time. When the reaction temperature was elevated, decomposition of the tosylate was accelerated as well as in the case of the use of cesium carbonate, resulting in marked decrease in product yield. When the Na salt of tosylamide of **Ca** reacted with **13** in DMF, the condensation occurred rapidly but yield of **Ab** never exceeded 40% in several runs. Therefore, in sacrifice of the reaction time, cesium carbonate was employed as a base for chain elongation throughout the present study. In addition, difference in reactivity between the tosyloxy group and the bromo group was not apparent due, probably, to mild reaction conditions. Thus, both **13** and **14** were employed for introduction of three methylene chains without intention and **15**, for accommodation of four methylene chains. Since the bromo group is more tough against base than the tosyloxy group, in a general sense, and more feasible in scaled-up synthesis, compound **14** was employed more often than **13**. Furthermore, it was an idea that ω-phthalimidated electrophile was added in slight excess amount so as to supply its amount lost by its decomposition during prolonged reaction time.

The transformation reaction of phthalimides to formamides[7] was applied satisfactorily to the conversion of α,ω-diphthalimides (**A**) to α,ω-diformamides (**B**) without exception and the yield of **B** became optimal when 20 mol equiv hydrazine hydrate to **A** was employed in hot DMF. Compound **B** was hydrolyzed with hot 2 M HCl (1 M=1 mol dm^{-3}) to give the corresponding hydrochloride salt. It was optional to isolate hydrochloride salt mostly as crystals. However, for the present purpose, the hydrochloride was treated, without neutralization, directly with tosyl chloride in pyridine in the presence of triethylamine to afford α,ω-bis(tosylamide) (**C**).

These series of reactions were found to be repeated successfully without decrease in product yields even if the chain was elongated to octamines. The results in repeated manipulation, **A** through **C**, are summarized in Table 2. Tractable formamide intermediate (**B**) profits greatly the facile synthesis of acyclic poly-

amines. In addition, operationally simplified tosylation by in situ neutralization of hydrochloride salt with triethylamine was found to be advantageous for increased yields of tosylamide (**C**) and decreased decomposition of unstable free amine.

Macrocyclization: The same three methods as those shown in the section of chain elongation and transformation have been available for cyclization reaction of the electrophiles with nucleophiles. Since the product yield in the chain elongation turned out optimal when cesium carbonate was used as a base, the same base seemed to be the best choice upon macrocyclization as well. Under high dilution conditions, α,ω-bis(tosylamide) and α,ω-ditosylate (1.2 mol equiv) reacted in the presence of cesium carbonate (2.5 mol equiv) in DMF (a day long). The results obtained are listed in Table 3. Compound **1** ([17]N_4) and **2** ([21]N_5) were obtained almost quantitatively. Since compound **1** had been prepared previously in 56% yield by the reaction of **Ci** with 1,4-dibromobutane in the presence of potassium carbonate in DMF at 120 °C,[13] the present method turned out to improve the product yield of cyclization to great extent. The difference in yields suggests how important the choice of base, reaction time, and types of electrophiles is for macrocyclization. The other cyclic polyamines, **3** through **12** containing six to eight nitrogens in the ring, were prepared in rather excellent yields for such large ring sizes. There was no by-product in any case. Unreacted nucleophile **C** was retrieved. However, α,ω-ditosylated electrophile was not retrieved but decomposed completely. This implys that conversion yield based on nucleophile **C** was quantitative in all cases. Thus, it is suggestive as for the conditions of optimal cyclization that yield will be elevated further if α,ω-ditosylated electrophile is added intermittently in a suitable time during the reaction.

Compounds **7** ([30]N_7), **9** ([33]N_8), and **11** ([34]N_8) were prepared, for comparison, by two sets of electrophile and nucleophile. The results reveal that a coupling of the electrophile with the shortest chain length and the nucleophile with the longest chain

Table 2. Product Yields (%) of α,ω-Diphthalimides (**A**), α,ω-Diformamides (**B**), and α,ω-Bis(tosylamide)s (**C**) in the Chain Elongation and Transformation Reactions (in Scheme 1)

Terminal groups → Chain type[a]	NPhth (**A**)	NHCHO (**B**)	NHTs (**C**)
a/4/	—	—	67
b/343/	99	83	98
c/33433/	88	74	84
d/43434/	96	78	83
e/3334333/	99	78	89
f/3434343/	92	85	90
g/3/	—	—	70
h/434/	98	92	82
i/333/	99	92	93
j/34343/	99	86	90
k/43334/	80	91	90
l/3343433/	95	80	90
m/3433343/	93	74	97
n/33/	95	98	94
o/4334/	98	79	78
p/343343/	89	80	69

a) The chain type is shown by gothic alphabet and the chain composition is indicated by the contiguous methylene chain blocks in Arabic numerals with the default of nitrogen atoms between slant lines.

Table 3. Macromonocyclization by the Reaction of α,ω-Ditosylates with α,ω-Bis(tosylamide)s (**C**)

Product		Reactants		Yield/%
Compd.	Type[a]	α,ω-Ditosyl ester[b]	**C**[b]	
1	(17)N4	**16**/3/	**b**/343/	99
2	(21)N5	**16**/3/	**q**/3433/	98
3	(25)N6	**16**/3/	**c**/33433/	61
4	(26)N6	**16**/3/	**j**/34343/	56
5	(29)N7	**17**/33/	**c**/33433/	55
6	(30)N7	**17**/33/	**j**/34343/	64
7	(30)N7	**17**/33/	**k**/43334/	66
		19/343/	**q**/3433/	47
8	(33)N8	**16**/3/	**e**/3334333/	75
9	(34)N8	**16**/3/	**l**/3343433/	86
		18/333/	**j**/34343/	37
10	(34)N8	**17**/33/	**p**/343343/	53
11	(34)N8	**16**/3/	**m**/3433343/	64
		19/343/	**c**/33433/	38
12	(35)N8	**16**/3/	**f**/3434343/	48

a) Ring size in the parentheses and nitrogen content in Arabic numerals are shown. b) The chain type is shown by gothic Arabic numerals or alphabet and the chain composition is indicated by the contiguous methylene chain blocks in Arabic numerals with the default of nitrogen atoms between slant lines.

length gives far better yield in each case.

Spectral Characteristics: Chemical shifts in ^{1}H NMR spectra are summarized in Tables 4 through 7. Table 4 includes all protons for macrocycles, **1** through **12**. Table 5 includes protons in the methylene region for α,ω-diphthalimide (**A**). Table 6 includes protons in the methylene region and the formamido group for typical α,ω-diformamide (**B**). Table 7 includes protons in the methylene region and tosylamino group for α,ω-bis(tosylamide) (**C**). All signals were perfectly assigned by ^{1}H–^{1}H spin decoupling technique.

^{1}H NMR spectra provide certain information about the ring flexibility in cyclic polyamines since FIN- and TIN-protons[15] indicate marked dependence on

Table 4. Chemical Shifts of All Protons in ^{1}H NMR Spectra for Cyclic Polyamines, **1** through **12**[a] (δ/ppm, in $CDCl_3$)

	Ring	FIN	TIN	FOU	TOU	ArMe	ArHme	ArHs
1	(17)N4	1.68	1.96	3.06	3.09, 3.13	2.43, 2.428	7.31, 7.32	7.64, 7.66
2	(21)N5	1.68	1.95, 1.96	3.09	3.13, 3.15, 3.16	2.40, 2.43	7.31	7.65, 7.66, 7.67
3	(25)N6	1.62	1.94, 1.97, 2.01	3.09	3.11, 3.13, 3.17	2.41, 2.42	7.28, 7.29, 7.30	7.63, 7.65
4	(26)N6	1.62	1.93	3.09	3.11, 3.13	2.407, 2.41	7.28, 7.29, 7.30	7.64
5	(29)N7	1.57	1.90	3.09	3.11	2.41	7.28, 7.29	7.64
6	(30)N7	1.58	1.89	3.10	3.11	2.41	7.28	7.64
7	(30)N7	1.57	1.89	3.09	3.10, 3.11	2.41	7.28, 7.29	7.64
8	(33)N8	1.53	1.89	3.08	3.11	2.40	7.28	7.63
9	(34)N8	1.54	1.88	3.08	3.10, 3.11	2.40	7.27	7.63
10	(34)N8	1.54	1.87	3.08	3.10	2.40	7.28, 7.29	7.63
11	(34)N8	1.54	1.88	3.07	3.09, 3.10	2.40, 2.40	7.27, 7.28	7.63, 7.64
12	(35)N8	1.54	1.86	3.08	3.08	2.40	7.28	7.64, 7.65

a) See Ref. 15 for the significance of abbreviated designation.

Table 5. Chemical Shifts of Methylene Protons in ^{1}H NMR Spectra for α,ω-Diphthalimides (**A**)[a] (δ/ppm, in $CDCl_3$)

	Compd	C1	C2	C3	C4	FIN	TIN	FOU	TOU
b	343	3.69	1.90	3.18		1.60		3.12	
c	33433	3.67	1.89	3.16		1.56	1.89	3.12	3.10
d	43434	3.65	1.64	1.55	3.11	1.54	1.84	3.11	3.11
e	3334333	3.67	1.89	3.16		1.53	1.86	3.10	3.10
f	3434343	3.66	1.83	3.15		1.55	1.86	3.10	3.10
h	333	3.70	1.90	3.20			1.98		3.15
i	434	3.67	1.67	1.56	3.11		1.85		3.10
j	34343	3.67	1.87	3.15		1.56	1.85	3.10	3.12
k	43334	3.65	1.64	1.55	3.11		1.87, 1.92		3.11, 3.13, 3.14
l	3343433	3.67	1.86	3.16		1.54	1.87	3.10	3.10
m	3433343	3.66	1.86	3.12		1.54	1.86	3.09	3.09, 3.12, 3.13
n	33	3.70	1.95	3.22					
o	4334	3.66	1.66	1.56	3.12		1.88		3.12
p	343343	3.66	1.86	3.15		1.55	1.86	3.10	3.11, 3.13

a) See Ref. 15 for the significance of abbreviated designation.

Table 6. Chemical Shifts of Main Protons in ^{1}H NMR Spectra for α,ω-Diformamides (**B**)[a] (δ/ppm, in $CDCl_3$)

	Compd	C1	C2	C3	C4	FIN	TIN	FOU	TOU	NH	CHO
b	343	3.40	1.77	3.13		1.58		3.09		6.38	8.20
c	33433	3.37	1.78	3.13		1.60	1.88	3.10	3.12	6.44	8.15
d	43434	3.30	1.57	1.63	3.07	1.63	1.90	3.14	3.11, 3.12	6.24	8.13
h	333	3.40	1.79	3.12			1.79		3.12	6.52	8.18
i	434	3.32	1.59	1.62	3.07		1.90		3.14	6.17	8.17
j	34343	3.36	1.77	3.12		1.58	1.88	3.10	3.11	6.43	8.16
k	43334	3.30	1.57	1.63	3.06		1.93, 1.94		3.11, 3.14, 3.17	6.30	8.12
n	33	3.40	1.80	3.15						6.29	8.19
o	4334	3.31	1.59	1.63	3.06		1.93		3.17	6.20	8.15

a) See Ref. 15 for the significance of abbreviated designation.

Table 7. Chemical Shifts of Main Protons in ^{1}H NMR Spectra for α,ω-Bis(tosylamide)s (**C**)[a] (δ/ppm, in $CDCl_3$)

	Compd	C1	C2	C3	C4	FIN	TIN	FOU	TOU	NH
b	343	2.98	1.77	3.12		1.53		3.07		5.31
c	33433	2.97	1.77	3.12		1.60	1.85	3.09	3.08, 3.09	5.40
d	43434	2.90	1.52	1.60	3.04	1.64	1.88	3.12	3.11, 3.13	5.16
e	3334333	2.95	1.77	3.09		1.56	1.86, 1.87	3.10	3.10	5.41
f	3434343	2.95	1.74	3.09		1.53	1.84	3.09	3.09	5.37
h	333	2.99	1.79	3.09			1.85		3.14	5.36
i	434	2.93	1.55	1.67	3.08		1.92		3.14	5.18
j	34343	2.96	1.75	3.11		1.55	1.86	3.08	3.09	5.34
k	43334	2.89	1.53	1.63	3.04		1.93, 1.98		3.11, 3.16	5.25
l	3343433	2.95	1.72	3.08		1.52	1.88, 1.89	3.04, 3.06	3.10, 3.11	5.39
m	3433343	2.95	1.75	3.10		1.54	1.89	3.06, 3.07	3.11	5.39
n	33	2.96	1.72	3.11						5.13
o	4334	2.91	1.54	1.64	3.06		1.94		3.12, 3.16	5.14
p	343343	2.95	1.74	3.10		1.54	1.89	3.06, 3.07	3.11	5.39

a) See Ref. 15 for the significance of abbreviated designation.

the ring size. In comparison of **1** and **12**, the difference in chemical shift values between them is 0.14 for FIN-protons and 0.1 for TIN-protons, respectively (Table 4). Since chemical shift values for all protons in **12** are almost the same as those for open-chain polyamines (**A**) to (**C**), compound **1** is fairly a rigid molecule. In viewpoint of the ring flexibility on the basis of chemical shift value, cyclic polyamines, **6** and **7** with thirty-membered ring, are the boundary ring size whether or not the ring is flexible. Thus, the macrocycles, **2** through **5**, are rather rigid molecules in comparison with the macrocycles, **8** through **12**. It is reasonable to predict that the trend observed is related closely to the nitrogen function in the molecule; that is, latent amine nitrogens involved in the polyamines, **8** through **12**, might behave equivalently, while each of those in polyamines, **1** through **5**, would function differently. Averaged chemical shift values for the terminal tosylamide proton (NHTs) in **C**, and the formamide proton (NHCHO) and the formyl proton in **B** are δ 5.30, 6.33, and 8.16, respectively.

Conclusion

Synthetic availability of the recently developed transformation reaction of phthalimides to formamides[7] and tosylamides to tosylates via *N*-nitrosotoluenesulfonamide intermediates[8] for polyamine synthesis was investigated through molecular architecture for designed polyamines with natural methylene arrays. Since chain elongation, transformation, and cyclization reactions proceeded very effectively, the present route provides a new adaptable method generally applicable to polyamine synthesis. Several problems involved in the traditional synthetic processes for cyclic polyamines has now been overcome perfectly. In addition, a guiding principle for the choice of better couple of nucleophiles and electrophiles upon cyclization has now been discovered. In the present synthesis, all the amino nitrogens are protected by the tosyl group, which makes it advantageous to monitor the proceeding reaction and isolation as well. Since effective detosylation methods are available for *N*-tosylated polyamines,[5,16] formal synthesis of acyclic and cyclic polyamines has now been established.

Experimental

The ^{1}H NMR spectra were recorded on JEOL GSX-500S (500 MHz) instrument with Me_4Si as the internal standard in $CDCl_3$ unless otherwise mentioned; chemical shifts (δ) and coupling constants (J) are in parts per million and hertz, respectively. Infrared spectra (IR) were obtained on a Shimadzu IR-27 apparatus. Merck silica gel 60 (Art. 7734, 0.063—0.02) was used for column chromatography, and fragmented Merck precoated silica gel 60 F_{254} plates (Art. 5715, 20×20 cm), for thin-layer chromatography (TLC). Product spots on TLC were detected either with UV-lamp or in an iodine vapor bath. The uncorrected melting points were measured in a bilayered coverglass (18 m/m, thickness 0.13—0.17 mm) with a micro melting point apparatus (Yanagimoto Seisakusho, Serial No. 2647).

Materials. *N*,*N*-Dimethylformamide (DMF) was dried over Molecular Sieves (Type A). Phthalimide, 3-bromopropylamine hydrobromide (**21**), 1,3-dibromopropane (**23**), and 1,4-dibromobutane (**28**) are commercially available. Potassium phthalimide was prepared according to the described method.[17] 1,3-Diphthalimidopropane (**24**)[11a] was prepared by the reaction of **23** with phthalimide in the presence of potassium carbonate in DMF. 3,4-Dihydro-2*H*-pyrimido[2,1-*a*]isoindol-6-one (**25**) was prepared from **24** through newly developed method.[10] *N*-(3-Bromopropyl)phthalimide (**14**) and *N*-(4-bromobutyl)phthalimide (**15**) were prepared by the reaction of **23** and **28**, respectively, with phthalimide in 88 and 68% yields respectively;[11] **14**, mp 73—75 °C (lit,[11a] mp 72—73 °C); **15**, mp 81—82 °C (lit,[11b] mp 80.5 °C). Synthesis of α,ω-

ditosylates, **16**, **17**, **18**, and **19**, from the corresponding α,ω-bis(tosylamide)s will be described elsewhere. *N,N'*-Ditosyl-1,4-butanediamine (**a**) and *N,N'*-ditosyl-1,3-propanediamine (**g**) were prepared from the correspoding diamines via the method previously reported.[18]

Synthesis of *N*-(3-Tosylaminopropyl)phthalimide (20). Route A; compound **21** (15 g, 69 mmol) and tosyl chloride (29.6 g, 1.5 mol equiv) pyridine (150 mL) was stirred at 0—5 °C for 2 h. The mixture was poured into water and extracted with chloroform. The chloroform layer was washed several times with 2 M HCl and, then, dried over $MgSO_4$. Chloroform was removed and the residue was chromatographed on a silica-gel column eluted with chloroform–acetone (95:5 v/v) to give 11.92 g (99% yield) of *N*-tosyl-3-bromopropylamine (**22**). A mixture of **22** (2.93 g, 10 mmol) and potassium phthalimide in DMF (50 mL) was heated at 80 °C for 3 h. The mixture was poured into brine and resulting precipitate was collected by filtration. The precipitate was recrystallized from ethanol to give 2.665 g (74% yield) of **20**.

Route B; compound **25** (1.23 g, 6.6 mol) was heated with 2 M HCl (28 mL) containing ethanol (5 mL) at 75 °C for 5 h. Solvents were removed under reduced pressure and the residue was recrystallized from ethanol to give 1.55 g (98% yield) of *N*-(3-aminopropyl)phthalimide hydrochloride (**26**); mp 192—194 °C. Calcd for $C_{11}H_{13}O_2N_2Cl$; C, 54.89; H, 5.44; N, 11.64; Cl, 14.73%. Found; C, 54.79; H, 5.45; N, 11.48; Cl, 15.02%. IR (KBr) ν 2400—2800 (NH_3^+), 1780 and 1710 (C=O) cm^{-1}.

Compound **26** (1.5 g, 6.2 mmol) and tosyl chloride (1.54 g, 1.3 mol eguiv to **26**) in pyridine (45 mL) and triethylamine (1 mL) were stirred at ambient temperature for 4 h. Solvents were removed and the residue was chromatographed on a silica-gel column eluted with chloroform–acetone (9:1 v/v) to afford 1.46 g (98% yield) of **20**; mp 170—171 °C. Calcd for $C_{18}H_{18}O_4N_2S$: C, 60.32; H, 5.06; N, 7.82; S, 8.95%. Found: C, 60.13; H, 5.08; N, 7.71; S, 8.91%. IR (KBr) ν 3290 (NH), 1770, 1705 (C=O), 1340, 1160 (SO_2) cm^{-1}. ^1H NMR; δ=1.83 (2H, quin, J=6.35, phthN-CH_2-CH_2-), 2.40 (3H, s, ArMe[15]), 3.74 (2H, t, J=6.35, phthN-CH_2-CH_2-), 3.93 (2H b-m, -CH_2-CH_2-NHTs), 5.25 (1H, b-t, NHTs), 7.27 (2H, d J=8.30, ArHme[15]), 7.75 (2H, d, J=8.30, ArHs[15]), 7.73 (2H, m, aromatic protons meta to phthaloyl carbonyl), 7.82 (2H, m, aromatic protons ortho to phthaloyl carbonyl).

Synthesis of *N*-(3-Tosyloxypropyl)phthalimide (13). Compound **20** (1.5 g, 4.2 mmol) was treated with sodium nitrite (0.713 g, 2 mol equiv to **20**) in a mixture of acetic anhydride (15 mL) and acetic acid (3 mL) at below 5 °C for 3 h. The mixture was poured into water and the resulting crystalline precipitate was collected by filtration. After dried in Drierite desiccator, the nitrosated compound was heated with benzene (80 mL) at 80 °C for 20 h. Solvent was removed and the residue was chromatographed on a silica-gel column eluted with chloroform–acetone (95:5 v/v) to give 0.87 g (59% yield) of **13**; mp 92—94 °C. Calcd for $C_{18}H_{17}O_5NS$: C, 60.15; H, 4.77; N, 3.90; S, 8.92%. Found: C, 60.15; H, 4.78; N, 4.25; S, 8.68%. IR (KBr) ν 1773, 1710 (C=O), 1357, 1188, 1175 (SO_2) cm^{-1}. ^1H NMR; δ=2.06 (2H, quin, J=6.83, phthN-CH_2-CH_2-), 2.44 (3H, s, ArMe[15]), 3.74 (2H, t, J=6.83, phthN-CH_2-CH_2-), 4.11 (2H, t, -CH_2-CH_2-OTs), 7.33 (2H, d, J=8.30, ArHme[15]), 7.78 (2H, d, J=8.30, ArHs[15]), 7.72 (2H, m, aromatic protons meta to phthaloyl carbonyl), and 7.83 (2H, m, aromatic protons ortho to phthaloyl carbonyl).

General Procedure for the Synthesis of α,ω-Diphthalimides (A) by the Reaction of α,ω-Tosylamides (C) with ω-Phthalimidated Electrophilies (13,14,15). A mixture of α,ω-bis(tosylamide) (**C**), one of ω-phthalimidated electrophiles (**13**,**14**,**15**) (2.2 mol equiv to **C**), and cesium carbonate (2.5 mol equiv to **C**) in DMF was stirred at ambient temperature for two days. The mixture was filtered through Celite and, then, the solvent was removed under reduced pressure. The residue was chromatographed on a silica-gel column eluted with chloroform–acetone (95:5 v/v) to give α,ω-diphthalimide (**A**).

General Procedure for the Synthesis of α,ω-Diformamides (B) from α,ω-Diphthalimides (A). To a solution of α,ω-diphthalimide (**A**) in DMF, hydrazine hydrate (20 mol equiv to **A**) was added and the mixture was heated at 75 °C for 23 h. After removal of DMF, the residue was chromatographed on a silica-gel column eluted with chloroform–methanol (9:1 v/v) to give α,ω-diformamide (**B**).

General Procedure for the Synthesis of α,ω-Bis(tosylamide)s (C) from α,ω-Diformamides (B). To a solution of α,ω-diformamide (**B**) in a small amount of ethanol, 2 M hydrochloric acid was added and heated at 80 °C for 4 h. Solvents were removed and the residue was stirred with tosyl chloride (2.6 mol equiv to **B**) in pyridine containing a small amount of triethylamine at ambient temperature for 4 h. Solvents were evaporated under reduced pressure and the residue was chromatographed on a silica-gel column eluted with chloroform–acetone (9:1 v/v) to give α,ω-bis(tosylamide)s (**C**).

***N,N'*-Bis(3-phthalimidopropyl)-*N,N'*-ditosyl-1,4-butanediamine (Ab).** By the reaction of a with either **13** or **14**, compound **Ab** was obtained as crystals; mp 201—202 °C (recryst. from ethanol–acetone). Calcd for $C_{40}H_{42}O_8N_4S_2$: C, 62.32; H, 5.49; N, 7.27; S, 8.32%. Found: C, 62.11; H, 5.47; N, 7.18; S, 8.36%. IR (KBr) ν 1770, 1720 (C=O), 1340, 1155 (SO_2) cm^{-1}. ^1H NMR, shown in Table 5.

***N,N'*-Bis(3-formamidopropyl)-*N,N'*-ditosyl-1,4-butanediamine (Bb).** By the reaction of **Ab** with N_2H_4 in DMF, compound **Bb** was obtained as viscous liquid; Calcd for $C_{26}H_{38}O_6N_4S_2$: C, 55.10; H, 6.76; N, 9.89; S, 11.32%. Found: C, 54.99; H, 6.72; N, 9.98; S, 11.11%. IR (KRS) ν 3350 (NH), 1670, 1520, 1450 (NHCHO), 1330, 1150 (SO_2) cm^{-1}. ^1H NMR, shown in Table 6.

***N,N'*-Bis[3-(tosylamino)propyl]-*N,N'*-ditosyl-1,4-butanediamine (Cb).** Through treatment of **Bb** with 2 M hydrochloric acid and, then, with tosyl chloride, compound **Cb** was obtained as viscous liquid; Calcd for $C_{38}H_{50}O_8N_4S_4$: C, 55.72; H, 6.15; N, 6.84; S, 15.66%. Found: C, 55.71; H, 6.29; N, 6.70; S, 15.55%. IR (KRS) ν 3280 (NH), 1330, 1160 (SO_2) cm^{-1}. ^1H NMR, shown in Table 7.

4,8,13,17-Tetratosyl-N^1,N^1:N^{20},N^{20}-diphthaloyl-4,8,13,17-tetraazaeicosane-1,20-diamine (Ac). By the reaction of **Cb** with either **13** or **14**, compound **Ac** was obtained as amorphous powder; Calcd for $C_{60}H_{68}O_{12}N_6S_4$: C, 60.34; H, 5.74; N, 7.04; S, 10.75%. Found: C, 60.14; H, 5.84; N, 6.87; S, 10.52%. IR (KBr) ν 1770, 1720 (C=O), 1340, 1155 (SO_2) cm^{-1}. ^1H NMR, shown in Table 5.

4,8,13,17-Tetratosyl-N^1,N^{20}-diformyl-4,8,13,17-tetraazaeicosane-1,20-diamine (Bc). By the reaction of **Ac** with N_2H_4 in DMF, compound **Bc** was obtained as amorphous

powder; Calcd for $C_{46}H_{64}O_{10}N_6S_4$: C, 55.84; H, 6.52; N, 8.50; S, 12.97%. Found: C, 56.10; H, 6.43; N, 8.73; S, 12.87%. IR (KRS) ν 3350 (NH), 1670, 1520, 1450 (NHCHO), 1330, 1150 (SO_2) cm^{-1}. ^1H NMR, shown in Table 6.

N^1,N^{20},4,8,13,17-Hexatosyl-4,8,13,17-tetraazaeicosane-1,20-diamine (Cc). Through treatment of **Bb** with 2 M hydrochloric acid and, then, with tosyl chloride, compound **Cc** was obtained as amorphous powder; Calcd for $C_{58}H_{76}O_{12}N_6S_6$: C, 56.10; H, 6.17; N, 6.77; S, 15.50%. Found: C, 55.92; H, 6.15; N, 6.53; S, 15.36%. IR (KRS) ν 3290 (NH), 1330, 1155 (SO_2) cm^{-1}. ^1H NMR, shown in Table 7.

5,9,14,18-Tetratosyl-N^1,N^1:N^{22},N^{22}-diphthaloyl-5,9,14,18-tetraazadocosane-1,22-diamine (Ad). By the reaction of **Cb** with **15**, compound **Ad** was obtained as viscous liquid; Calcd for $C_{62}H_{72}O_{12}N_6S_4$: C, 60.96; H, 5.94; N, 6.88; S, 10.50%. Found: C, 60.72; H, 5.86; N, 7.16; S, 10.36%. IR (KBr) ν 1770, 1710 (C=O), 1340, 1160 (SO_2) cm^{-1}. ^1H NMR, shown in Table 5.

5,9,14,18-Tetratosyl-N^1,N^{22}-diformyl-5,9,14,18-tetraazadocosane-1,22-diamine (Bd). By the reaction of **Ad** with N_2H_4 in DMF, compound **Bd** was obtained as viscous liquid; Calcd for $C_{48}H_{60}O_{10}N_6S_4$: C, 56.67; H, 6.74; N, 8.26; S, 12.61%. Found: C, 56.78; H, 6.74; N, 8.04; S, 12.75%. IR (KRS) ν 3350 (NH), 1670, 1520, 1450 (NHCHO), 1330, 1150 (SO_2) cm^{-1}. ^1H NMR, shown in Table 6.

N^1,N^{22},5,9,14,18-Hexatosyl-5,9,14,18-tetraazadocosane-1,22-diamine (Cd). Through treatment of **Bd** with 2 M hydrochloric acid and, then, with tosyl chloride, compound **Cd** was obtained as amorphous powder; Calcd for $C_{60}H_{80}O_{12}N_6S_6$: C, 56.75; H, 6.35; N, 6.62; S, 15.15%. Found: C, 56.61; H, 6.22; N, 6.56; S, 15.04%. IR (KBr) ν 3290 (NH), 1330, 1160 (SO_2) cm^{-1}. ^1H NMR, shown in Table 7.

4,8,12,17,21,25-Hexatosyl-N^1,N^1:N^{28},N^{28}-diphthaloyl-4,8,12,17,21,25-hexaazaoctacosane-1,28-diamine (Ae). By the reaction of **Cc** with **14** compound **Ae** was obtained as amorphous powder; Calcd for $C_{80}H_{94}O_{16}N_8S_6$: C, 59.46; H, 5.86; N, 6.94; S, 11.91%. Found: C, 59.34; H, 5.79; N, 6.68; S, 11.75%. IR (KBr) ν 1770, 1710 (C=O), 1340, 1160 (SO_2) cm^{-1}. ^1H NMR, shown in Table 5.

4,8,12,17,21,25-Hexatosyl-N^1,N^{28}-diformyl-4,8,12,17,21,25-hexaazaoctacosane-1,28-diamine (Be). By the reaction of **Ae** with N_2H_4 in DMF, compound **Be** was obtained as amorphous powder; IR (KBr) ν 3350 (NH), 1670, 1520, 1450 (NHCHO), 1330, 1150 (SO_2) cm^{-1}.

N^1,N^{28},4,8,12,17,21,25-Octatosyl-4,8,12,17,21,25-hexaazaoctacosane-1,28-diamine (Ce). Through treatment of **Be** with 2 M hydrochloric acid and, then, with tosyl chloride, compound **Ce** was obtained as amorphous powder; Calcd for $C_{78}H_{102}O_{16}N_8S_8$: C, 56.29; H, 6.18; N, 6.73; S, 15.42%. Found: C, 55.95; H, 6.15; N, 6.54; S, 15.30%. IR (KBr) ν 3290 (NH), 1330, 1155 (SO_2) cm^{-1}. ^1H NMR, shown in Table 7.

4,9,13,18,22,27-Hexatosyl-N^1,N^1:N^{30},N^{30}-diphthaloyl-4,9,13,18,22,27-hexaazatriacontane-1,30-diamine (Af). By the reaction of **Cd** with **14**, compound **Af** was obtained as amorphous powder; Calcd for $C_{82}H_{98}O_{16}N_8S_6$: C, 59.90; H, 6.01; N, 6.82; S, 11.70%. Found: C, 59.60; H, 5.96; N, 6.86; S, 11.49%. IR (KBr) ν 1770, 1710 (C=O), 1340, 1160 (SO_2) cm^{-1}. ^1H NMR, shown in Table 5.

4,9,13,18,22,27-Hexatosyl-N^1,N^{30}-diformyl-4,9,13,18,22,27-hexaazatriacontane-1,30-diamine (Bf). By the reaction of **Af** with N_2H_4 in DMF, compound **Bf** was obtained as amorphous powder; IR (KBr) ν 3350 (NH), 1670, 1520, 1450 (NHCHO), 1330, 1150 (SO_2) cm^{-1}.

N^1,N^{30},4,9,13,18,22,27-Octatosyl-4,9,13,18,22,27-hexaazatriacontane-1,30-diamine (Cf). Through treatment of **Bf** with 2 M hydrochloric acid and, then, with tosyl chloride, compound **Cf** was obtained as amorphous powder; IR (KBr) ν 3290 (NH), 1330, 1155 (SO_2) cm^{-1}. ^1H NMR, shown in Table 7.

***N*,*N*′-Bis(3-phthalimidopropyl)-*N*,*N*′-ditosyl-1,3-propanediamine (Ah).** By the reaction of **g** with either **13** or **14**, compound **Ah** was obtained as amorphous powder; Calcd for $C_{39}H_{40}O_8N_4S_2$: C, 61.89; H, 5.33; N, 7.40; S, 8.47%. Found: C, 61.76; H, 5.36; N, 7.20; S, 8.37%. IR (KBr) ν 1770, 1710 (C=O), 1335, 1150 (SO_2) cm^{-1}. ^1H NMR, shown in Table 5.

***N*,*N*′-Bis(3-formamidopropyl)-*N*,*N*′-ditosyl-1,3-propanediamine (Bh).** By the reaction of **Ah** with N_2H_2 in DMF, compound **Bh** was obtained as viscous liquid; Calcd for $C_{25}H_{36}O_6N_4S_2$: C, 54.32; H, 6.57; N, 10.14; S, 11.60%. Found: C, 54.10; H, 6.67; N, 9.97; S, 11.40%. IR (KRS) ν 3350 (NH), 1670, 1520, 1450 (NHCHO), 1330, 1160 (SO_2) cm^{-1}. ^1H NMR, shown in Table 6.

***N*,*N*′-Bis[3-(tosylamino)propyl]-*N*,*N*′-ditosyl-1,3-propanediamine (Ch).** Through treatment of **Bh** with 2 M hydrochloric acid and, then, with tosyl chloride, compound **Ch** was obtained as viscous liquid; Calcd for $C_{37}H_{48}O_8N_4S_4$: C, 55.20; H, 6.01; N, 6.96; S, 15.93%. Found: C, 55.56; H, 5.98; N, 6.93; S, 15.97%. IR (KRS) ν 3290 (NH), 1330, 1160 (SO_2) cm^{-1}. ^1H NMR, shown in Table 7.

***N*,*N*′-Bis(4-phthalimidobutyl)-*N*,*N*′-ditosyl-1,3-propanediamine (Ai).** By the reaction of **g** with **15**, compound **Ai** was obtained as amorphous powder; Calcd for $C_{41}H_{44}O_8N_4S_2$: C, 62.73; H, 5.65; N, 7.14; S, 8.17%. Found: C, 62.59; H, 5.68; N, 7.06; S, 8.14%. IR (KBr) 1770, 1710 (C=O), 1335, 1150 (SO_2) cm^{-1}. ^1H NMR, shown in Table 5.

***N*,*N*′-Bis(4-formamidobutyl)-*N*,*N*′-ditosyl-1,3-propanediamine (Bi).** By the reaction of **Ai** with N_2H_4 in DMF, compound **Bi** was obtained as viscous liquid; Calcd for $C_{27}H_{40}O_6N_4S_2$: C, 55.84; H, 6.94; N, 9.65; S, 11.04%. Found: C, 55.61; H, 6.83; N, 9.57; S, 10.78%. IR (KRS) ν 3350 (NH), 1670, 1520, 1450 (NHCHO), 1330, 1150 (SO_2) cm^{-1}. ^1H NMR, shown in Table 6.

***N*,*N*′-Bis[4-(tosylamino)buty]-*N*,*N*′-ditosyl-1,3-propanediamine (Ci).** Through treatment of **Bi** with 2 M hydrochloric acid and, then, with tosyl chloride, compound **Ci** was obtained as viscous liquid; Calcd for $C_{39}H_{52}O_8N_4S_4$: C, 56.22; H, 6.29; N, 6.73; S, 15.40%. Found: C, 55.94; H, 6.24; N, 6.76; S, 15.15%. IR (KRS) ν 3290 (NH), 1330, 1160 (SO_2) cm^{-1}. ^1H NMR, shown in Table 7.

4,9,13,18-Tetratosyl-N^1,N^1:N^{21},N^{21}-diphthaloyl-4,9,13,18-tetraazaheneicosane-1,21-diamine (Aj). By the reaction of **Ci** with either **13** or **14**, compound **Aj** was obtained as amorphous powder; Calcd for $C_{61}H_{70}O_{12}N_6S_4$: C, 60.67; H, 5.84; N, 6.96; S, 10.62%. Found: C, 60.59; H, 5.77; N, 6.56; S, 10.39%. IR (KBr) ν 1770, 1710 (C=O), 1335, 1150 (SO_2) cm^{-1}. ^1H NMR, shown in Table 5.

4,9,13,18-Tetratosyl-N^1,N^{21}-diformyl-4,9,13,18-tetraazaheneicosane-1,21-diamine (Bj). By the reaction of **Aj** with N_2H_4 in DMF, compound **Bj** was obtained as amorphous powder; Calcd for $C_{47}H_{66}O_{10}N_6S_4$: C, 56.26; H, 6.63; N, 8.38; S, 12.78%. Found: C, 55.92; H, 6.73; N, 8.57; S, 12.66%. IR (KRS) ν 3350 (NH), 1670, 1520, 1450 (NHCHO), 1330, 1150 (SO_2) cm^{-1}. ^1H NMR, shown in Table 6.

N^1,N^{21},4,9,13,18-Hexatosyl-4,9,13,18-tetraazaheneicosane-

1,21-diamine (Cj). Through treatment of **Bi** with 2 M hydrochloric acid and, then, with tosyl chloride, compound **Cj** was obtained as amorphous powder; Calcd for $C_{59}H_{78}O_{12}N_6S_6$: C, 56.43; H, 6.26; N, 6.69; S, 15.32%. Found: C, 56.71; H, 6.19; N, 6.54; S, 15.29%. IR (KBr) ν 3290 (NH), 1330, 1160 (SO_2) cm^{-1}. ^1H NMR, shown in Table 7.

5,9,13,17-Tetratosyl-N^1,N^1:N^{21},N^{21}-diphthaloyl-5,9,13,17-tetraazaheneicosane-1,21-diamine (Ak). By the reaction of **Ch** with **15**, compound **Ak** was obtained as viscous liquid; Calcd for $C_{61}H_{70}O_{12}N_6S_4$: C, 60.67; H, 5.84; N, 6.96; S, 10.62%. Found: C, 60.40; H, 5.83; N, 6.93; S, 10.56%. IR(KRS) ν 1770, 1710 (C=O), 1335, 1150 (SO_2) cm^{-1}. ^1H NMR, shown in Table 5.

5,9,13,17-Tetratosyl-N^1,N^{21}-diformyl-5,9,13,17-tetraazaheneicosane-1,21-diamine (Bk). By the reaction of **Ak** with N_2H_4 in DMF, compound **Bk** was obtained as viscous liquid; Calcd for $C_{47}H_{66}O_{10}N_6S_4$: C, 56.26; H, 6.63; N, 8.38; S, 12.78%. Found: C, 55.98; H, 6.63; N, 8.19; S, 12.76%. IR (KRS) ν 3350 (NH), 1670, 1520, 1450 (NHCHO), 1330, 1150 (SO_2) cm^{-1}. ^1H NMR, shown in Table 6.

N^1,N^{21},5,9,13,17-Hexatosyl-5,9,13,17-tetraazaheneicosane-1,21-diamine (Ck). Through treatment of **Bk** with 2 M hydrochloric acid and, then, with tosyl chloride, compound **Ck** was obtained as amorphous powder; Calcd for $C_{59}H_{78}O_{12}N_6S_6$: C, 56.43; H, 6.26; N, 6.69; S, 15.32%. Found: C, 56.38; H, 6.05; N, 6.40; S, 15.37%. IR (KBr) 3290 (NH), 1330, 1160 (SO_2) cm^{-1}. ^1H NMR, shown in Table 7.

4,8,13,17,22,26-Hexatosyl-N^1,N^1:N^{29},N^{29}-diphthaloyl-4,8,13,17,22,26-hexaazanonacosane-1,29-diamine (Al). By the reaction of **Cj** with **14**, compound **Al** was obtained as amorphous powder; Calcd for $C_{81}H_{96}O_{16}N_8S_6$: C, 59.68; H, 5.94; N, 6.88; S, 11.80%. Found: C, 59.60; H, 5.80; N, 6.79; S, 11.52%. IR (KBr) ν 1770, 1710 (C=O), 1335, 1150 (SO_2) cm^{-1}. ^1H NMR, shown in Table 5.

4,8,13,17,22,26-Hexatosyl-N^1,N^{29}-diformyl-4,8,13,17,22,26-hexaazanonacosane-1,29-diamine (Bl). By the reaction of **Al** with N_2H_4 in DMF, compound **Bl** was obtained as viscous liquid; IR (KRS) ν 3350 (NH), 1670, 1520, 1450 (NHCHO), 1330, 1150 (SO_2) cm^{-1}. It was very hard to obtain analytically pure sample by chromatography. Thus, the sample was directly subjected to the next reaction.

N^1,N^{29},4,8,13,17,22,26-Octatosyl-4,8,13,17,22,26-hexaazanonacosane-1,29-diamine (Cl). Through treatment of **Bl** with 2 M hydrochloric acid and, then, with tosyl chloride, compound **Cl** was obtained as amorphous powder; Calcd for $C_{79}H_{104}O_{16}N_8S_8$: C, 56.54; H, 6.25; N, 6.68; S, 15.29%. Found: C, 56.80; H, 6.09; N, 6.48; S, 15.17%. IR (KBr) ν 3290 (NH), 1330, 1160 (SO_2) cm^{-1}. ^1H NMR, shown in Table 7.

4,9,13,17,21,26-Hexatosyl-N^1,N^1:N^{29},N^{29}-diphthaloyl-4,9,13,17,21,26-hexaazanonacosane-1,29-diamine (Am). By the reaction of **Ck** with **14**, compound **Am** was obtained as amorphous powder; Calcd for $C_{81}H_{96}O_{16}N_8S_6$: C, 59.68; H, 5.94; N, 6.88; S, 11.80%. Found: C, 59.55; H, 5.82; N, 6.73; S, 11.88%. IR (KBr) ν 1770, 1710 (C=O), 1335, 1150 (SO_2) cm^{-1}. ^1H NMR, shown in Table 5.

4,9,13,17,21,26-Hexatosyl-N^1,N^{29}-diformyl-4,9,13,17,21,26-hexaazanonacosane-1,29-diamine (Bm). By the reaction of **Al** with N_2H_4 in DMF, compound **Bm** was obtained as viscous liquid; IR (KRS) ν 3350 (NH), 1670, 1520, 1450 (NHCHO), 1330, 1150 (SO_2) cm^{-1}. It was very hard to obtain analytically pure sample by chromatography. Thus, the sample was directly subjected to the next reaction.

N^1,N^{29},4,9,13,17,21,26-Octatosyl-4,9,13,17,21,26-hexaazanonacosane-1,29-diamine (Cm). Through treatment of **Bm** with 2 M hydrochloric acid and, then, with tosyl chloride, compound **Cm** was obtained as amorphous powder; Calcd for $C_{79}H_{104}O_{16}N_8S_8$: C, 56.54; H, 6.25; N, 6.68; S, 15.29%. Found: C, 56.47; H, 6.18; N, 6.50; S, 15.49%. IR (KBr) ν 3290 (NH), 1330, 1160 (SO_2) cm^{-1}. ^1H NMR, shown in Table 7.

N^1,N^1:N^7,N^7-Diphthaloyl-4-tosyl-4-azaheptane-1,7-diamine (An). By the reaction of **13** with **20** in the presence of cesium carbonate, compound **An** was obtained as crystals; mp 227—228 °C (recryst. from ethanol). Calcd for $C_{29}H_{27}O_6N_3S$: C, 63.84; H, 4.99; N, 7.70; S, 5.88%. Found: C, 63.85; H, 4.99; N, 7.66; S, 5.91%. IR (KBr) ν 1770, 1710 (C=O), 1335, 1150 (SO_2) cm^{-1}. ^1H NMR, shown in Table 5.

N^1,N^7-Diformyl-4-tosyl-4-azaheptane-1,7-diamine (Bn). By the reaction of **Al** with N_2H_4 in DMF, compound **Bm** was not obtained and, thus, was prepared via the separate path; the reaction of *N*-formyl-*N'*-tosyl-1,3-propanediamine[7] with **14** in the presence of cesium carbonate in DMF gave N^1-formyl-N^7-phthaloyl-N^4-tosyl-4-azaheptane-1,7-diamine in 93% yield, which was, then, treated with hydrazine hydrate in DMF to afford **Bn** in 98% yield; viscous liquid. Calcd for $C_{15}H_{23}O_4N_3S$: C, 52.76; H, 6.79; N, 12.31; S, 9.39%. Found: C, 52.81; H, 6.87; N, 12.20; S, 9.21%. IR (KRS) ν 3350 (NH), 1670, 1520, 1450 (NHCHO), 1330, 1150 (SO_2) cm^{-1}. ^1H NMR, shown in Table 6.

N^1,N^7,4-Tritosyl-4-azaheptane-1,7-diamine (Cn). Through treatment of **Bn** with 2 M hydrochloric acid and, then, with tosyl chloride, compound **Cn** was obtained as amorphous powder; Calcd for $C_{27}H_{35}O_6N_3S_3$: C, 54.61; H, 5.94: N, 7.08; S, 16.20%. Found: C, 54.29; H, 5.99; N, 7.03; S, 16.04%. IR (KBr) ν 3290 (NH), 1330, 1160 (SO_2) cm^{-1}. ^1H NMR, shown in Table 7.

5,9,13-Tritosyl-N^1,N^1:N^{17},N^{17}-diphthaloyl-5,9,13-triazaheptadecane-1,17-diamine (Ao). By the reaction of **Cn** with **15**, compound **Ao** was obtained as amorphous powder; Calcd for $C_{51}H_{57}O_{10}N_5S_3$: C, 61.48; H, 5.77; N, 7.03; S, 9.66%. Found: C, 61.66; H, 5.71; N, 7.06; S, 9.55%. IR (KBr) ν 1770, 1710 (C=O), 1335, 1150 (SO_3) cm^{-1}. ^1H NMR, shown in Table 5.

5,9,13-Tritosyl-N^1,N^{17}-diformyl-5,9,13-triazaheptadecane-1,17-diamine (Bo). By the reaction of **Ao** with N_2H_4, compound **Bo** was obtained as viscous liquid; Calcd for $C_{37}H_{53}O_8N_5S_3$: C, 56.11; H, 6.75; N, 8.84; S, 12.15%. Found: C, 55.90; H, 6.78; N, 8.79; S, 11.99%. IR (KRS) ν 3350 (NH), 1670, 1520, 1450 (NHCHO), 1330, 1150 (SO_2) cm^{-1}. ^1H NMR, shown in Table 6.

N^1,N^{17},5,9,13-Pentatosyl-5,9,13-triazaheptadecane-1,17-diamine (Co). Through treatment of **Bo** with 2 M hydrochloric acid and, then, with tosyl chloride, compound **Co** was obtained as amorphous powder; Calcd for $C_{49}H_{65}O_{10}N_5S_5$: C, 56.35; H, 6.27; N, 6.71; S, 15.35%. Found: C, 56.30; H, 6.15; N, 6.64; S, 15.36%. IR (KBr) ν 3290 (NH), 1330, 1160 (SO_2) cm^{-1}. ^1H NMR, shown in Table 7.

4,9,13,17,22-Pentatosyl-N^1,N^1:N^{25},N^{25}-diphthaloyl-4,9,13,17,22-pentaazapentacosane-1,25-diamine (Ap). By the reaction of **Co** with **14**, compound **Ap** was obtained as amorphous powder; Calcd for $C_{71}H_{83}O_{14}N_7S_5$: C, 60.10; H, 5.90; N, 6.91; S, 11.30%. Found: C, 60.33; H, 6.06; N, 6.76; S, 11.18%. IR (KBr) ν 1770, 1710 (C=O), 1335, 1150 (SO_2) cm^{-1}. ^1H NMR, shown in Table 5.

4,9,13,17,22-Pentatosyl-N^1,N^{25}-diformyl-4,9,13,17,22-penta-

azapentacosane-1,25-diamine (Bp). By the reaction of **Ap** with N_2H_4, compound **Bp** was obtained as viscous liquid; IR (KRS) ν 3350 (NH), 1670, 1520, 1450 (NHCHO), 1330, 1150 (SO_2) cm^{-1}. It was very hard to obtain analytically pure sample by chromatography. Thus, the sample was directly subjected to the next reaction.

***N*¹,*N*²⁵,4,9,13,17,22-Heptatosyl-4,9,13,17,22-pentaazapentacosane-1,25-diamine (Cp).** Through treatment of **Bp** with 2 M hydrochloric acid and, then, with tosyl chloride, compound **Cp** was obtained as amorphous powder; Calcd for $C_{79}H_{104}O_{16}N_8S_8$: C, 56.49; H, 6.25; N, 6.68; S, 15.30%. Found: C, 56.47; H, 6.10; N, 6.66; S, 15.28%. IR (KBr) 3290 (NH), 1330, 1160 (SO_2) cm^{-1}. ^1H NMR, shown in Table 7.

General Procedure for the Synthesis of Macromonocyclic Polyamines, (1) through (12). A mixture of α,ω-bis(tosylamide) (**C**), α,ω-ditosylate (**16**, **17**, **18**, or **19**) (1.2 mol equiv to **C**), and cesium carbonate (2.5 mol equiv to **C**) in DMF was stirred at ambient temperature for a day or two. The mixture was filtered through Celite and the solvent was, then, evaporated under reduced pressure. The residue as chromatographed on a silica-gel column eluted with chloroform–acetone (95:5 v/v) to afford cyclic polyamine.

1,5,9,13-Tetratosyl-1,5,9,13-tetraazacycloheptadecane (1): [17]N_4. By the reaction of **16** with **Cb**, compound **1** was obtained as amorphous powder. Compound **1** had been prepared via alternative route in less yield.[14] IR (KBr) ν 1335 and 1150 (SO_2) cm^{-1}. ^1H NMR data, listed in Table 4.

1,5,9,13,17-Pentatosyl-1,5,9,13,17-pentaazacycloheneicosane (2): [21]N_5. By the reaction of **16** with *N*¹,*N*¹⁶,4,8,13-pentatosyl-4,8,13-triazahexadecane-1,16-diamine (**Cq**), which was derived from tosylated spermidine in similar series of procedure to those for **Co** preparation from **An**, compound **2** was obtained as amorphous powder; Calcd for $C_{51}H_{67}O_{10}N_5S_5$: C, 57.22; H, 6.31; N, 6.54; S, 14.98%. Found: C, 56.89; H, 6.27; N, 6.32; S, 15.23%. Amorphous powder. IR (KBr) ν 1335 and 1150 (SO_2) cm^{-1}. ^1H NMR data, listed in Table 4.

1,5,9,13,17,21-Hexatosyl-1,5,9,13,17,21-hexaazacyclopentacosane (3): [25]N_6. By the reaction of **16** with **Cc**, compound **3** was obtained as amorphous powder; Calcd for $C_{61}H_{80}O_{12}N_6S_6$: C, 57.16; H, 6.29; N, 6.56; S, 15.01%. Found: C, 57.18; H, 6.29; N, 6.46; S, 15.08%. IR (KBr) ν 1335 and 1150 (SO_2) cm^{-1}. ^1H NMR data, listed in Table 4.

1,5,9,13,18,22-Hexatosyl-1,5,9,13,18,22-hexaazacyclohexacosane (4): [26]N_6. By the reaction of **16** with **Cj**, compound **4** was obtained as amorphous powder; Calcd for $C_{62}H_{82}O_{12}N_6S_6$: C, 57.47; H, 6.38; N, 6.49; S, 14.85%. Found: C, 57.63; H, 6.40; N, 6.12; S, 14.52%. IR (KBr) ν 1335 and 1155 (SO_2) cm^{-1}. ^1H NMR data, listed in Table 4.

1,5,9,13,17,21,25-Heptatosyl-1,5,9,13,17,21,25-heptaazacyclononacosane (5): [29]N_7. By the reaction of **17** with **Cc**, compound **5** was obtained as amorphous powder; Calcd for $C_{71}H_{93}O_{14}N_7S_7$: C, 57.11; H, 6.28; N, 6.57; S, 15.03%. Found: C, 57.21; H, 6.30; N, 6.42; S, 14.85%. IR (KBr) ν 1335 and 1155 (SO_2) cm^{-1}. ^1H NMR data, listed in Table 4.

1,5,9,13,17,22,26-Heptatosyl-1,5,9,13,17,22,26-heptaazacyclotriacontane (6): [30]N_7. By the reaction of **17** with **Cj**, compound **6** was obtained as amorphous powder; Calcd for $C_{72}H_{95}O_{14}N_7S_7$: C, 57.38; H, 6.35; N, 6.51; S, 14.90%. Found: C, 57.12; H, 6.42; N, 6.21; S, 14.64%. IR (KBr) ν 1335 and 1155 (SO_2) cm^{-1}. ^1H NMR data, listed in Table 4.

1,5,9,13,18,22,26-Heptatosyl-1,5,9,13,18,22,26-heptaazacyclotriacontane (7): [30]N_7. In order to examine the effect on cyclization yield by changing in a couple of electrophile and nucleophile, two couples were tested; by the reaction of **17** with **Co**, compound **7** was obtained as amorphous powder in 66% yield. Alternatively, by the reaction of **19** with **Cq**, compound **7** was obtained in 47% yield. Calcd for $C_{72}H_{95}O_{14}N_7S_7$: C, 57.38; H, 6.35; N, 6.51; S, 14.90%. Found: C, 57.52; H, 6.68; N, 6.14; S, 14.58%. IR (KBr) ν 1335 and 1155 (SO_2) cm^{-1}. ^1H NMR data, listed in Table 4.

1,5,9,13,17,21,25,29,-Octatosyl-1,5,9,13,17,21,25,29-octaazacyclotritriacontane (8): [33]N_8. By the reaction of **16** with **Ce**, compound **8** was obtained as amorphous powder; Calcd for $C_{81}H_{106}O_{16}N_8S_8$: C, 57.08; H, 6.27; N, 6.58; S, 15.05%. Found: C, 57.14; H, 6.35; N, 6.31; S, 14.78%. IR (KBr) ν 1335 and 1155 (SO_2) cm^{-1}. ^1H NMR data, listed in Table 4.

1,5,9,13,17,21,26,30-Octatosyl-1,5,9,13,17,21,26,30-octaazacyclotetratriacontane (9): [34]N_8. In order to examine the effect on cyclization yield by changing in a couple of electrophile and nucleophile, two couples were tested; by the reaction of **16** with **Cl**, compound **9** was obtained as amorphous powder in 86% yield. Alternatively, by the reaction of **18** with **Cj**, compound **9** was obtained in 37% yield. Calcd for $C_{82}H_{108}O_{16}N_8S_8$: C, 57.31; H, 6.34; N, 6.52; S, 14.93%. Found: C, 56.98; H, 6.36; N, 6.18; S, 14.54%. IR (KBr) ν 1335 and 1155 (SO_2) cm^{-1}. ^1H NMR data, listed in Table 4.

1,5,9,13,17,22,26,30-Octatosyl-1,5,9,13,17,22,26,30-octaazacyclotetratriacontane (10): [34]N_8. By the reaction of **17** with **Cp** compound **10** was obtained as amorphous powder; Calcd for $C_{82}H_{108}O_{16}N_8S_8$: C, 57.31; H, 6.34; N, 6.52; S, 14.93%. Found: C, 56.99; H, 6.34; N, 6.26; S, 14.92%. IR (KBr) ν 1335 and 1155 (SO_2) cm^{-1}. ^1H NMR data, listed in Table 4.

1,5,9,13,18,22,26,30-Octatosyl-1,5,9,13,18,22,26,30-octaazacyclotetratriacontane (11): [34]N_8. In order to examine the effect on cyclization yield by changing in a couple of electrophile and nucleophile, two couples were tested; by the reaction of **16** with **Cm**, compound **11** was obtained as amorphous powder in 64% yield. Alternatively, by the reaction of **19** with **Cc**, compound **11** was obtained in 38% yield. Calcd for $C_{82}H_{108}O_{16}N_8S_8$: C, 57.31; H, 6.34; N, 6.52; S, 14.93%. Found: C, 56.99; H, 6.38; N, 6.34; S, 14.62%. IR (KBr) ν 1335 and 1155 (SO_2) cm^{-1}. ^1H NMR data, listed in Table 4.

1,5,9,13,18,22,27,31-Octatosyl-1,5,9,13,18,22,27,31-octaazacyclopentatriacontane (12): [35]N_8. By the reaction of **16** with **Cf**, compound **12** was obtained as amorphous powder; Calcd for $C_{83}H_{110}O_{16}N_8S_8$: C, 57.54; H, 6.40; N, 6.47; S, 14.81%. Found: C, 57.45; H, 6.46; N, 6.29; S, 14.78%. IR (KBr) ν 1335 and 1155 (SO_2) cm^{-1}. ^1H NMR data, listed in Table 4.

We are indebted to Dr. Hiroshi Yamazaki and his staff in RIKEN for performing elemental analyses and to Dr. Jun Uzawa and Mrs. Tamiko Chijimatsu in RIKEN for measurement of ^1H NMR spectra. M. I. is grateful to Dr. Hideki Nagashima in RIKEN for helpful discussion in the molecular design and to the Ministry of Education, Science and Culture for a financial support by a Grant-in-Aid for Scientific Research (No. 62540397).

References

1) C. W. Tabor and H. Tabor, *Ann. Rev. Biochem.*, **53**, 749 (1984).

2) a) R. J. Bergeron, *Acc. Chem. Res.*, **19**, 105 (1986). b) H. Yanagawa, Y. Ogawa, and F. Egami, *Z. Allg. Mikrobiol.*, **16** 627 (1976). c) *Idem, J. Biochem.*, **80**, 891 (1976).

3) a) T. Ohshima, *Biochem. Biophys. Res. Commun.*, **63**, 1093 (1975). b) *Idem., J. Biol. Chem.*, **254**, 8720 (1979).

4) D. H. Busch and C. Cairns, "Progress in Macrocyclic Chemistry Vol. 3. Synthesis of Macrocycles,"ed by R. M. Izatt and J. J. Christensen, John Wiley and Sons, New York (1987), Chap. 1, p. 1. b)L. F. Lindoy, *ibid.*, Chap. 2, p. 53. c) P. G. Potvin and J.-M. Lehn, *ibid.*, Chap. 4, p. 167. d) B. Ganem, *Acc. Chem. Res.*, **15**, 290 (1982). e) H. H. Wasserman and J. S. Wu, *Heterocycles*, **17**, 581 (1982). f) J. E. Nordlander, M. J. Payne, M. A. Balk, J. L. Gress, F . D. Harris, J. S. Lane, R. F. Lewe, S. E. Marshall, D. Nagy, and D. J. Rachlin, *J. Org. Chem.*, **49**, 133 (1984) and references cited therein.

5) M. W. Hosseini and J.-M. Lehn, *Helv. Chim. Acta*, **69**, 587 (1986).

6) J. E. Richman and T. J. Attkins, *J. Am. Chem. Soc.*, **96**, 2268 (1974).

7) M. Iwata and H. Kuzuhara, *Chem. Lett.*, **1986**, 951.

8) a) M. Iwata and H. Kuzuhara, *J. Chem. Soc., Chem. Commun.*, **1985**, 918. b) *Idem, Bull. Chem. Soc. Jpn.*, **58**, 3395 (1985).

9) a) M. Iwata and H. Kuzuhara, *Chem. Lett.*, **1986**, 369. b) *Idem., ibid.*, **1985**, 1941.

10) The new transformation of *N,N'*-diphthaloyl-1,3-propanediamine (**24**) to **25** under specified conditions proceeded in 86% yield. Since the reaction was interested, particularly, in the formation mechanism, preparative procedure will be described in the separate report related to the work on mechanistic consideration of hydrazinolysis of phthalimides.

11) a) S. Gabriel and J. Weiner, *Ber.*, **21**, 2669 (1888). b) S. Gabriel and T. A. Maass, *ibid.*, **32**, 1266 (1899).

12) The reason why compound **27** is unavailable in the preparative scale is related closely to that why synthesis of *N*-(4-tosylaminobutyl)phthalimide is difficult.

13) B. K. Vriesema, J. Buter, and R. M. Kellogg, *J. Org. Chem.*, **49**, 110 (1984).

14) E. Kimura and T. Yatsunami, *Chem. Pharm. Bull.*, **28**, 994 (1980).

15) Cl- through C4-protons are the methylene protons at both terminals since all the molecules are symmetric. FIN-protons designate the internal two methylene protons of contiguous four methylene chains sectioned by nitrogen atom such as -N-CH_2-$C\underline{H}_2$-$C\underline{H}_2$-CH_2-N-. TIN-protons designate the central methylene protons of contiguous three methylene chains sectioned by nitrogen atom such as -N-CH_2-$C\underline{H}_2$-CH_2-N-. FOU-protons designate the external two methylene protons of contiguous four methylene chains sectioned by nitrogen atom such as -N-$C\underline{H}_2$-CH_2-CH_2-$C\underline{H}_2$-N-. TOU-protons designate the external two methylene protons of contiguous three methylene chains sectioned by nitrogen atom such as -N-$C\underline{H}_2$-CH_2-$C\underline{H}_2$-N-. ArMe-protons designate methyl protons attached to aromatic ring. ArHme-protons designate aromatic protons disposed at position ortho to the methyl group. ArHs-protons designate aromatic protons disposed at position ortho to the sulfonyl group.

16) T. Hamada, A. Nishida, and O. Yonemitsu, *J. Am. Chem. Soc.*, **108**, 140 (1986).

17) P. L. Salzberg and J. V. Supniwski, *Org. Synth.*, Coll. Vol. III., 119 (1956).

18) M. Iwata and H. Kuzuhara, *Bull. Chem. Soc. Jpn.*, **55**, 2153 (1982).

 © 1989 The Chemical Society of Japan Bull. Chem. Soc. Jpn., 62, 211—218 (1989)

A Mechanistic Study on the Reaction of Iminothiadiazolines with Activated Acetylenes: Competitive Pathway through Hypervalent Sulfurane and Zwitterion

Yohsuke YAMAMOTO,† Tohru TSUCHIYA, Masahide OCHIUMI, Shin-ichi ARAI, Naoki INAMOTO,* and Kin-ya AKIBA*,†

Department of Chemistry, Faculty of Science, The University of Tokyo, Hongo, Bunkyo-ku, Tokyo 113

(Received August 5, 1988)

The reaction of 3-aryl-5-benzoyl-2-imino-2,3-dihydro-1,3,4-thiadiazoles (**6**) with dimethyl acetylenedicarboxylate (**4b**) gave the corresponding thiazole (**8**) and benzoyl cyanide through sulfurane (**B**) by 1,3-dipolar cycloaddition and cis- (**9**) and trans-vinyl (**10**) compounds through zwitterion (**C**) by simple addition. Two types of addition reactions competed each other and the ratio of the two [R=**B**/**C**] depended solely on the solvent polarity (E_T). Dibenzoylacetylene behaved similarly. Several iminothiazolines and iminothiadiazolines reacted with activated acetylenes and the selectivity for the two types of addition reactions for each system was shown to be affected by quite subtle balance of electron-withdrawing ability of each heterocycle.

Many kinds of five-membered sulfur heterocycles have been used for cycloadditions as masked 1,3-dipoles. For example, aminothiatriazole,[1] dithiolanthiones,[2] dithiolethiones[3] and its aza-,[4] oxa-,[5] selena-[6] analogues have been reported to react with activated olefins, acetylenes, nitriles, and heterocumulenes. During our research on the role of hypervalent sulfur for ring-transformation,[7] we also reported the reaction of 5-imino-4,5-dihydro-1,2,4-thiadiazole (**1**) with activated acetylenes to give the corresponding 2-aminothiazole and nitrile and also that of the same compound with imidates to afford the corresponding adduct which has an aromatic 1,2,4-thiadiazole ring via hydrogen shift.[4g,7c] The characteristic feature of these reactions is that bond switching takes place at the central sulfur atom and the resulting products are adducts accompanied by ring-transformation or new heterocycles produced by elimination of small molecules from the adducts. Although almost all reactions are assumed to proceed through hypervalent sulfuranes, for example **A**, only a few mechanistic studies have been presented. Goerdeler reported the cycloaddition of 3-imino-3*H*-1,2,4-dithiazoles (**2**) with activated olefins,[4b] and found that fumarate and maleate reacted stereospecifically, which indicated that the reaction proceeded in a concerted manner. Another example is the reaction of cis- and trans-disubstituted dithiolanthiones (**3**) with activated acetylenes (**4**),[2a] and the former compound produced cis-olefin and vice versa (Scheme 2, Eqs. 2 and 3). The result also shows that any discrete polar or radical intermediate is not involved through the process.

During our study on the scope of these reactions, we found some complexity of the product depending on the change of electronic nature of the starting iminothiadiazolines. Closely related 2-imino-2,3-dihydro-1,3,4-thiadiazoles **5** and **6a** reacted with dibenzoylacetylene (**4a**: X=PhCO) to give different types of compounds as main product, that is, **7a** (81%) and **8d** (98%), respectively (vide infra, Scheme 3, Eqs. 4 and 5). Hence, there is still to be elucidated on mechanism of the reaction of activated acetylenes

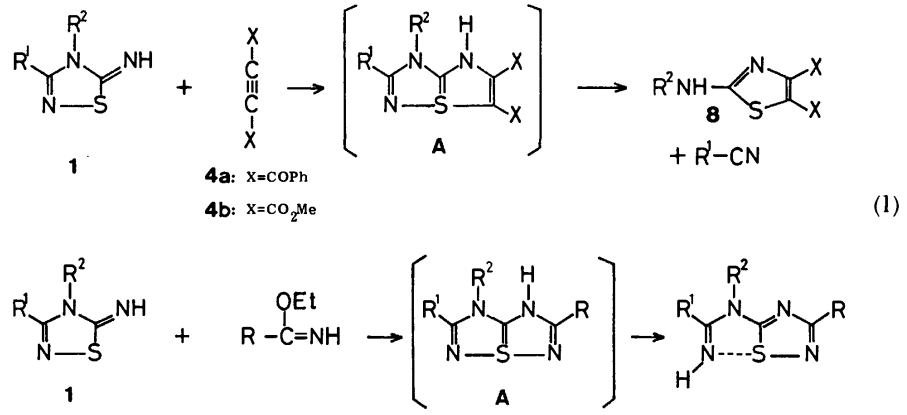

Scheme 1.

† Present address: Department of Chemistry, Faculty of Science, Hiroshima University, Higashisenda-machi, Naka-ku, Hiroshima 730.

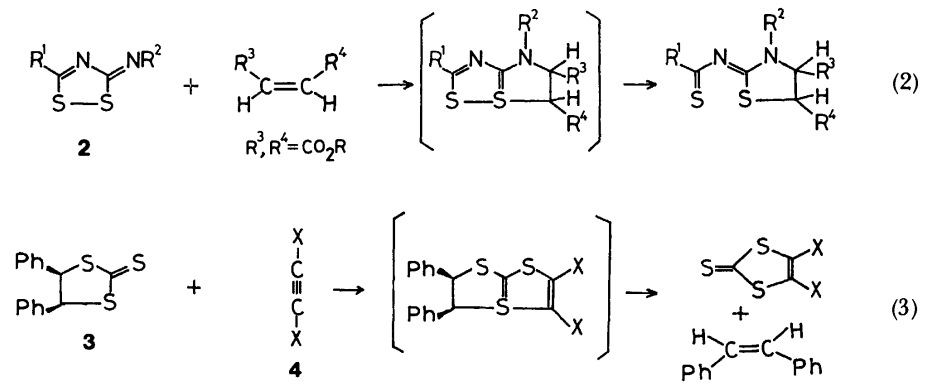

Scheme 2.

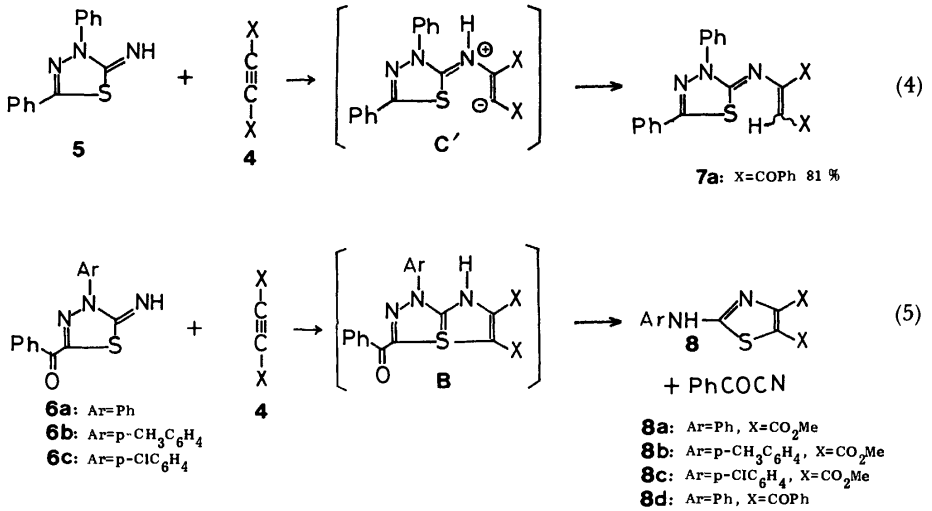

Scheme 3.

with those compounds. We examined the reaction of Eq. 5 in detail in comparison with Eq. 4 to obtain mechanistic insight of the reaction. It was concluded that the difference of the reaction course could be explained on the basis of competitive reactions which proceeded through two intermediates, sulfurane (**B**) and zwitterion (**C**).

Results and Discussion

Products of the Reaction of 6 with 4b. The reaction of 3-aryl-5-benzoyl-2-imino-2,3-dihydro-1,3,4-thiadiazoles (**6**) with dimethyl acetylenedicarboxylate (**4b**) was carried out in a variety of solvents at 50 °C for several hours (Eq. 5). In all cases examined, the main product was the thiazole (**8**), which could be recrystallized from the reaction mixture. When the reaction was carried out in nonpolar solvents the yield of **8** always amounted to ca. 90%. In order to scrutinize the reaction the products were separated by dry column chromatography (SiO_2) using dichloromethane as an eluent. Besides the thiazole (**8**), three products **9**, **10**, **11**, and benzoyl cyanide were obtained. The structure of **11** was confirmed by comparison with authentic samples prepared from **6** and benzoyl

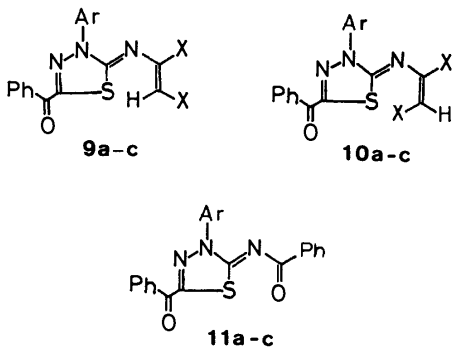

chloride. Structural assignment of **9** and **10** are based on the elemental analyses, ^1H NMR and mass spectra. ^1H NMR clearly shows that both products have an olefinic proton, and isomerization from **9** to **10** was observed by addition of a catalytic amount of chloroacetic acid. Therefore these are geometrical

isomers. By comparison of the ^{1}H NMR spectra of **9** and **10**, rather large difference was noticed between chemical shifts of olefinic protons (δ 5.5—5.7 and 6.2—6.4). As it is known that a greater deshielding of the vinyl proton occurs in fumarate ester than in maleate, the former compound with vinyl proton at higher field should be cis-vinyl **9** and the latter is trans-vinyl **10**.[8] By the same reason Dolfini[9] assigned structure of adduct (**12**) of aziridine with **4b** that **12** with a vinyl proton at higher field (δ 5.31) is **12a** and the another at lower field (δ 6.15) is **12b**. We were surprised to see that the thiazole (**8**), which is expected to result from sulfurane **B**, and vinyl compounds **9** and **10**, which should be produced through zwitterion **C**, were obtained together in aprotic solvents. Therefore we next examined the solvent and substituent effects on the reaction.

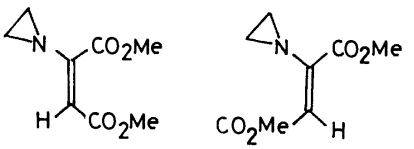

12a **12b**

Solvent and Substituent Effects on the Reaction of 6 with 4b. Reactions of **6b** with **4b** were carried out in eleven solvents to examine the solvent effect on the ratio of these products. A mixture of **4b** (1.2—1.4 mmol) and **6b** (0.99—1.01 mmol) in 50 ml of a dry solvent was heated at 50.0 °C for several hours. The reaction proceeded cleanly and four products were separated by chromatography. Total yield was almost quantitative (95—100%) and Table 1 shows the ratio of the four products. The formation of **11** is ascribed to the secondary reaction of **6b** with benzoyl cyanide which is produced together with **8** during the reaction. This was actually confirmed by a separate experiment.

Table 1. Solvent Effect on the Reaction of **6b** with **4b**[a]

Solvent	E_T	**8**	**9**	**10**	**11**	R[b]
PhH	34.5	86.4	2.1	0.9	10.6	28.8
CCl_4	32.5	90.6	3.3	0.1	6.0	26.6
THF	37.4	91.6	3.7	0.5	4.2	21.8
AcOEt	38.1	84.1	3.1	1.3	11.5	19.1
MeCOMe	42.2	72.8	6.3	1.6	19.2	9.2
Me_2SO	45.0	76.3	9.4	3.4	11.0	6.0
MeCN	46.0	73.9	14.7	1.5	9.9	4.6
t-BuOH	43.9	79.0	5.7	4.0	11.3	8.1
i-PrOH	48.6	71.9	5.3	12.4	10.4	4.1
EtOH	51.9	68.7	13.8	15.8	1.7	2.32
MeOH	55.5	41.8	38.5	18.9	0.8	0.73

a) Sum of the isolated yields of the four products were 95—100% and these values were normalized to correspond to the total yield of 100%. b) R=**8**/(**9**+**10**).

Important informations can be extracted from Table 1: (i) The yield of the main product **8** decreases and that of total vinyl compounds (**9**+**10**) increases according to the increase of polarity of solvents (E_T),[10] i.e., R ([**8**/(**9**+**10**)])[11] decreases according to the increase of E_T, (ii) vinyl compounds are produced even in nonpolar aprotic solvents and cis-vinyl (**9**) is the major one in all the aprotic solvents, (iii) ratio of cis-vinyl (**9**) to trans-vinyl (**10**) is dependent on the kind of alcohols used.

When log R was plotted against the parameter E_T, good linear relationship was observed (corr. coeff. 0.980) for all of the solvents (Fig. 1). This means that the ratio of **8** to total vinyl compounds (**9**+**10**) is determined solely by the polarity of the solvent irrespective of the participation of alcoholic protons in the formation of **9** and **10**. These can be explained by competitive reactios (Scheme 4), that is, the vinyl compounds and the thiazole are formed through different intermediates, i.e., nonpolar sulfurane (**B**) and polar one, zwitterion (**C**), the ratio of which is determined by the solvent polarity.

Table 2. Substituent Effect on the Reaction of **6** with **4b** in Methanol[a]

Ar	**8**	**9**	**10**	**11**	R[b]
p-MeC_6H_4	41.8	38.5	18.9	0.8	0.61
C_6H_5	45.3	35.6	18.9	0.2	0.83
p-ClC_6H_4	48.8	26.5	23.4	1.3	0.98

a) Sum of the isolated yields of the four products were 95—100% and these values were normalized to correspond to the total yield of 100%. b) R=**8**/(**9**+**10**).

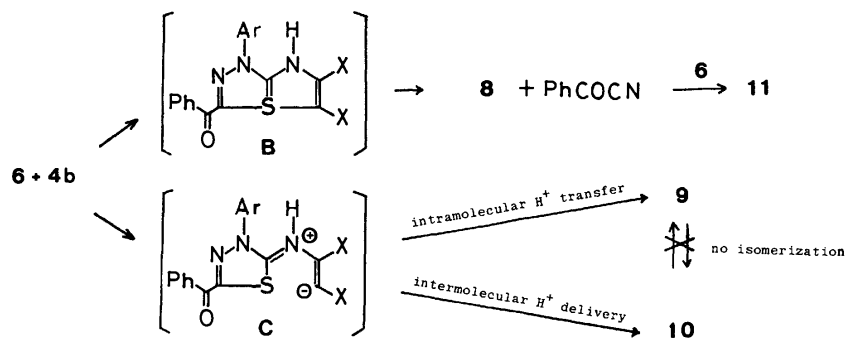

Scheme 4.

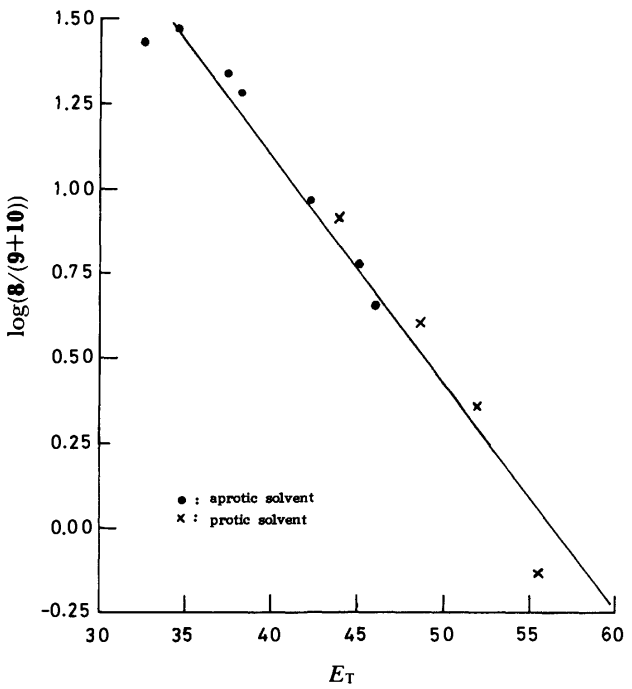

Fig. 1. Relationship between product distribution and solvent polarity E_T.

Substituent effect of the aryl group was examined in methanol as a solvent and results are shown in Table 2. These indicate that the ratio R increased according to the increase of the electron-withdrawing ability of substituent Ar. It is reasonable that formation of sulfurane (**B**) is favored and stability of zwitterion (**C**) is disfavored by increasing electron-withdrawing ability of Ar.

The cis–trans ratio of vinyl compounds (**9** and **10**) remained constant under the reaction conditions and workup procedure. The cis–trans ratio of vinyl compounds in methanol was examined at appropriate intervals by ^{1}H NMR and no change of the ratio was observed at 20, 25, 45, 70, and 138 h. In addition the isomerization during workup was carefully checked by subjecting the isolated vinyl compounds again to chromatography and no change of the ratio was confirmed. Therefore, it is concluded that the ratio of the vinyl compounds (**9** and **10**) was actually determined by the reaction. Such a ratio of vinyls is consistent with that of aziridine with **4b**.[9,12] It was reported that cis adduct **12a** formed via intramolecular path was exceedingly formed in aprotic solvent and trans adduct was predominant in methanol because intermolecular protonation by the solvent became favored. Also in our result, cis-vinyl **9** was invariably preferred to trans-vinyl **10** in aprotic solvents, which probably results from intramolecular prototropy. Ratios of **9** to **10** in protic solvents were quite different from those in aprotic ones, for example, the dramatic difference exists between acetonitrile (**9**/**10**=14.6/1.5) and 2-propanol (5.3/12.4) which have similar polarity (E_T). The ratios in alcohols seem to depend on bulkiness of alkyl groups and to acidity of alcohols. The result indicates that alcohols participate to form vinyl compounds (**9** and **10**) from **C**.

Reaction of Closely Related Thiazolines and Thiadiazolines with Activated Acetylenes. Now it is interesting to compare the results with closely related systems. We examined six types of compounds, **1**, **5**, **13**—**16** in addition to **6**. All these compounds reacted smoothly with activated acetylenes **4a** and **4b** at room temperature or at 50 °C within several hours. Results are summarized in Scheme 5. Reaction course was not affected by using either **4a** or **4b**.

In thiazolines (**13**—**15**), any ring-transformed thiazole was not obtained but only simple adduct was formed in high yield even in nonpolar aprotic solvents. On the other hand, 1,2,4-thiadiazolines, **1** and **16a** (Hector's base) reacted with dibenzoyl acetylene to give only ring-transformed thiazole in 96 and 74% yields and the same kind of results was obtained with dimethyl acetylenedicarboxylate. It is noteworthy here that the reaction of 1,3,4-thiadiazoline **6** with **4a** gave the ring-transformed thiazole as a main product (vide supra), but only simple adduct **7a** was obtained from **4a** and **5**, in which the benzoyl group at 2 position was substituted by a phenyl group (Scheme 3, Eqs. 4 and 5).

All these results can be interpreted by competitive reactions similarly to Scheme 4. That is, relative stability of the intermediate sulfurane **D** and zwitterion **E** determines the reaction course. It is well-known that the hypervalent bond, i.e., three-center four-electron bond, is stabilized by electronegative groups at apical positions.[13] In sulfurane **D** the hypervalent bond corresponds to 1, 6a, 6 bond, so that the groups at 1 and 6 positions are most important in order to form the sulfurane by 1,3-dipolar cycloaddition. In 1,2,4-thiadiazolines **1** and **16** (Hector's base) sulfurane **D** was formed due to the presence of an electronegative nitrogen atom at position-M. In three thiazolines, **13**—**15**, less electronegative carbon than nitrogen should come to position-M, thus not sulfurane (**D**) but zwitterion (**E**) was generated as an intermediate. In 1,3,4-thiadiazolines the nitrogen at position-L has electron-withdrawing effect but the effect is not so much as the nitrogen at position-M in 1,2,4-thiadiazolines. Thus the group at position-M became important in 1,3,4-thiadiazolines. The benzoyl group attached at position-M was electronegative enough to let **6** participate in cycloaddition to generate sulfurane **D** but the phenyl group was not enough so and **5** gave vinyl compounds via zwitterion **E**.

Conclusion

The reaction of iminothiadiazolines and 2-imino-4-

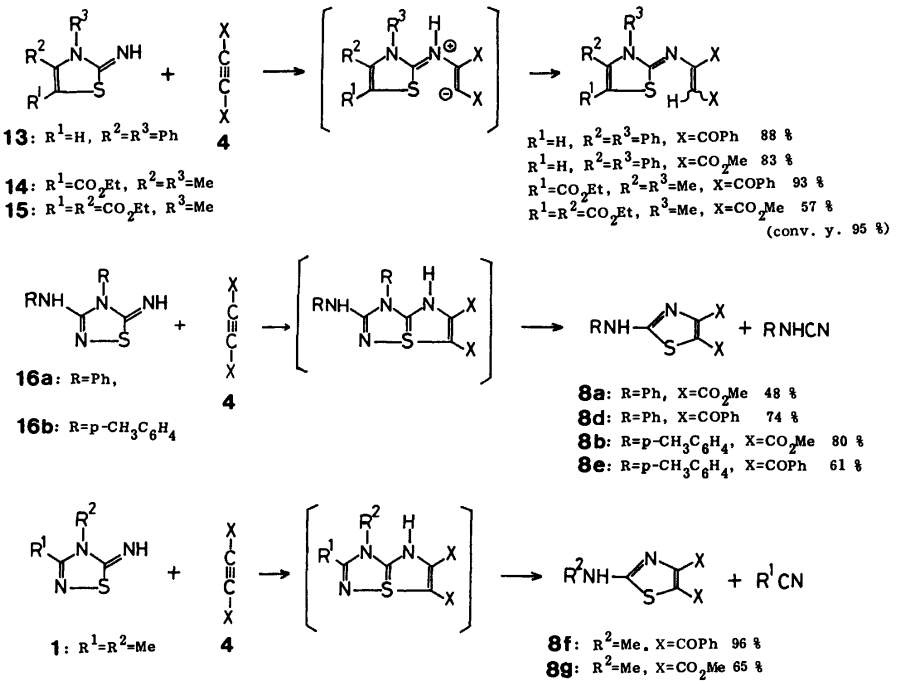

Scheme 5.

thiazolines with activated acetylenes can be understood by competitive reactions, invoking the formation of sulfurane **D** by concerted 1,3-dipolar cycloaddition and that of zwitterion **E** by simple addition. Selectivity between the two reactions stands on quite subtle balance of electron-withdrawing ability of the heterocycles. It is not yet clear whether sulfurane **D** can open to zwitterion **E** or **E** can close to **D** during the reaction, however, the presence of the two intermediates was verified for the present case, i.e., **6**+**4a**.

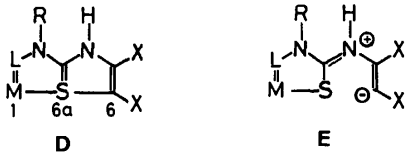

Experimental

IR spectra were recorded on a Hitachi EPI-G2 spectrometer. ^{1}H NMR spectra were determined with a Hitachi R-24B or a Hitachi R-20B spectrometer. UV spectra were measured with a EPS-G3 spectrometer. Mass spectra were obtained with a Hitachi RMU-6 and JEOL D-300 spectrometer. All melting points are uncorrected. All solvents employed in the reaction were purified as follows; methanol and ethanol were distilled from magnesium alkoxide. 2-Propanol, *t*-butyl alcohol, and benzene were distilled from sodium. Carbon tetrachloride and ethyl acetate were distilled from phosphorus pentaoxide and redistilled from anhydrous potassium carbonate. Acetone was treated with potassium permanganate and redistilled from potassium carbonate. Tetrahydrofuran was distilled from sodium/benzophenone. Dimethyl sulfoxide was distilled over calcium hydride. Acetonitrile was spectral grade stored over 4-A Molecular Sieves. Dibenzoyl acetylene (**4a**)[14] and dimethyl acetylenedicarboxylate (**4b**)[15] were prepared by the reported procedure.

5-Benzoyl-2-imino-3-phenyl-2,3-dihydro-1,3,4-thiadiazole (6a) was prepared from phenacyl thiocyanate and benzenediazonium chloride in ethanol-water-tetrahydrofuran solution at pH 4.[16]

6a: Yield 50%; mp 94—96 °C (lit, 89—90 °C);[16] UV (CH_2Cl_2) λ_{max} 265 (log ε=4.28), 375 nm (4.15); IR (KBr) 3310, 1640, 1600 cm^{-1}.

5-Benzoyl-2-imino-3-*p*-tolyl-2,3-dihydro-1,3,4-thiadiazole (6b). Yield 60%; mp 123—124 °C (lit, 112 °C);[16] UV (CH_2Cl_2) λ_{max} 265 (log ε=4.24), 377 nm (4.09); IR (KBr) 3250, 1640, 1600 cm^{-1}.

5-Benzoyl-2-imino-3-(*p*-chlorophenyl)-2,3-dihydro-1,3,4-thiadiazole (6c). Yield 60%; mp 139.5—141 °C (lit, 127 °C);[16] IR (KBr) 3300, 1640, 1600 cm^{-1}.

Reactions of 6 and 4b. General Procedure: A solution of **4b** (1.2—1.4 mmol) and **6** (0.99—1.01 mmol) in 50 ml of dry solvent was heated at 50 °C for several hours. After disappearance of **6** was checked by TLC, the solvent was evaporated. The reaction mixture was subjected to dry column chromatography (SiO_2) with chloroform as an eluent. This column was divided into four fractions, each of which was composed of **8**, **9**, **10** an **11**.

4,5-Bis(methoxycarbonyl)-2-(phenylamino)thiazole (8a). Mp 115—116 °C; IR (KBr) 3150, 3125, 1745, 1720, 1590 cm^{-1}; ^{1}H NMR ($CDCl_3$) δ=3.70 (s, 3H), 3.80 (s, 3H), 7.2—7.5 (m, 5H), 9.5 (brs, 1H); MS, *m/z* (relative intensity) 292 (M^+, 100), 232 (72). Calcd for $C_{13}H_{12}N_2O_4S$: C, 53.43; H, 4.14; N, 9.59%. Found: C, 53.37; H, 3.98; N, 9.33%.

4,5-Bis(methoxycarbonyl)-2-(*p*-tolylamino)thiazole (8b). Mp 173.5—175.5 °C; IR (KBr) 3200, 3150, 1730, 1690,

1600 cm^{-1}; ^1H NMR ($CDCl_3$) δ=2.40 (s, 3H), 3.80 (s, 3H), 3.85 (s, 3H), 7.1—7.4 (m, 4H), 8.85 (brs, 1H); MS, *m/z* (relative intensity) 306 (M^+, 100), 246 (87). Calcd for $C_{14}H_{14}N_2O_4S$: C, 54.90; H, 4.61; N, 9.15%. Found: C, 54.96; H, 4.61; N, 9.24%.

4,5-Bis(methoxycarbonyl)-2-(*p*-chlorophenylamino)thiazole (8c). Mp 191—192 °C; IR (KBr) 3220, 3170, 1730, 1690, 1600 cm^{-1}. Calcd for $C_{13}H_{11}N_2O_4SCl$: C, 47.79; H, 3.39; N, 8.51; S, 9.81; Cl, 10.85%. Found: C, 47.79; H, 3.53; N, 8.31; S, 9.97; Cl, 10.68%.

5-Benzoyl-3-phenyl-2-[[(*E*)-1,2-bis(methoxycarbonyl)vinyl]-imino]-2,3-dihydro-1,3,4-thiadiazole (9a). Mp 121.5—122.5 °C; UV (CH_2Cl_2) λ_{max} 272 (log ε=4.17), 318 (4.24), 381 nm (4.10); ^1H NMR ($CDCl_3$) δ=3.69 (s, 3H), 3.80 (s, 3H), 5.56 (s, 1H), 7.2—8.4 (m, 10H); MS, *m/z* (relative intensity) 423 (M^+, 4), 105 (100). Calcd for $C_{21}H_{17}N_3O_5S$: C, 59.57; H, 4.05; N, 9.93%. Found: C, 59.59; H, 3.91; N, 10.21%.

Compound 9b. Mp 123.5—124.5 °C; UV (CH_2Cl_2) λ_{max} 270 (log ε=4.21), 319 (4.16), 386 nm (4.09); ^1H NMR ($CDCl_3$) δ=2.35 (s, 3H), 3.70 (s, 3H), 3.85 (s, 3H), 5.65 (s, 1H), 7.1—8.4 (m, 9H); MS, *m/z* (relative intensity) 437 (M^+, 4), 105 (100). Calcd for $C_{22}H_{19}N_3O_5S$: C, 60.40; H, 4.38%. Found: C, 60.32; H, 4.37%.

Compound 9c. Mp 121.0—122.5 °C; ^1H NMR ($CDCl_3$) δ=3.75 (s, 3H), 3.90 (s, 3H), 5.70 (s, 1H), 7.2—8.4 (m, 9H). Calcd for $C_{21}H_{16}N_3O_5SCl$: C, 55.09; H, 3.52; N, 9.18%. Found: C, 54.51; H, 3.33; N, 8.90%.

5-Benzoyl-3-phenyl-2-[[(*Z*)-1,2-bis(methoxycarbonyl)vinyl]-imino]-2,3-dihydro-1,3,4-thiadiazole (10a). Mp 131.5—132.5 °C; UV (CH_2Cl_2) λ_{max} 272 (log ε=4.33), 380 nm (4.06); ^1H NMR ($CDCl_3$) δ=3.67 (s, 3H), 3.76 (s, 3H), 6.23 (s, 1H), 7.2—8.4 (m, 10H); MS, *m/z* (relative intensity) 423 (M^+, 18), 105 (100). Calcd for $C_{21}H_{17}N_3O_5S$: C, 59.57; H, 4.05; N, 9.93%. Found: C, 59.72; H, 4.07; N, 9.66%.

Compound 10b. Mp 148.5—149.5 °C; UV (CH_2Cl_2) λ_{max} 272 (log ε=4.34), 383 nm (4.03); ^1H NMR ($CDCl_3$) δ=2.40 (s, 3H), 3.71 (s, 3H), 3.80 (s, 3H), 6.35 (s, 1H),7.1—8.5 (m, 9H); MS, *m/z* (relative intensity) 437 (M^+, 5), 105 (100). Calcd for $C_{22}H_{19}N_3O_5S$: C, 60.40; H, 4.38; N, 9.61%. Found: C, 60.41; H, 4.11; N, 9.35%.

Compound 10c. Mp 161—162 °C; ^1H NMR ($CDCl_3$) δ=3.70 (s, 3H), 3.80 (s, 3H), 6.35 (s, 1H), 7.2—8.4 (m, 9H). Calcd for $C_{21}H_{16}N_3O_5SCl$: C, 55.09; H, 3.52; N, 9.18%. Found: C, 55.66; H, 3.70; N, 9.43%.

5-Benzoyl-2-benzoylimino-3-phenyl-2,3-dihydro-1,3,4-thiadiazole (11a) was prepared by the reaction of **6a** with benzoyl chloride in quantitative yield. Mp 202.5—204 °C. Calcd for $C_{22}H_{15}N_3O_5S$: C, 68.56; H, 3.92; N, 10.91%. Found: C, 68.56; H, 3.77; N, 10.79%.

Compound 11b. Mp 233.0—233.5 °C. Calcd for $C_{23}H_{17}N_3O_5S$: C, 69.15; H, 4.29; N, 10.52%. Found: C, 69.69; H, 4.18; N, 10.62%.

Compound 11c. Mp 216—217.5 °C. Calcd for $C_{22}H_{14}N_3O_2SCl$: C, 62.93; H, 3.36; N, 10.01%. Found: C, 62.91; H, 3.24; N, 9.92%.

Reaction of 6a with 4a. In 30 ml of THF **6a** (435 mg, 1.55 mmol) was mixed with **4a** (467 mg, 1.99 mmol). After stirring for 4 h at room temperature, the reaction mixture was recrystallized from benzene to give 4,5-dibenzoyl-2-(phenylamino)thiazole (**8d**) in 98% yield. Mp 173.5—175 °C; IR (KBr) 3200, 3150, 1680, 1620 cm^{-1}; ^1H NMR ($CDCl_3$) δ=7.0—7.9 (m, 15H), 8.75 (brs, 1H); MS, *m/z* (relative intensity) 384 (M^+, 100), 279 (29). Calcd for $C_{23}H_{16}N_2O_2S$: C, 71.87; H, 4.20; N, 7.29%. Found: C, 71.60; H, 3.95; N, 7.04%.

2-Imino-3,5-diphenyl-2,3-dihydro-1,3,4-thiadiazole (5) was prepared from a reported method.[17] Mp 99.5—101 °C (lit, 97 °C).[17]

Reaction of 5 with 4a. In 5 ml of THF **5** (33 mg, 0.13 mmol) was mixed with **4a** (113 mg, 0.48 mmol) at room temperature and heated at 50 °C for 2 h. The reaction mixture was submitted to TLC (SiO_2) with chloroform to give 52 mg (81%) of simple addition product. Mp 141—142.5 °C; IR (KBr) 1680, 1640 cm^{-1}; ^1H NMR ($CDCl_3$) δ=7.0 (s, 1H), 7.4—8.6 (m, 20H); MS, *m/z* (relative intensity) 487 (M^+, 10), 382 (71), 105 (100). Calcd for $C_{30}H_{31}N_3O_2S$: C, 73.90; H, 4.34; N, 8.62; S, 6.58%. Found: C, 73.92; H, 4.30; N, 8.32; S, 6.50%.

5-Imino-4-phenyl-3-phenylamino-4,5-dihydro-1,2,4-thiadiazole (16a). Hector's bases were prepared from the corresponding arylthioureas by oxidation with acidic hydrogen peroxide.[18] Yield 54%; mp 181—182 °C (lit, 181 °C).[18]

Compound 16b. Yield 47%; Mp 126—127 °C (lit, 127 °C).[18]

Reaction of 16a and 4b. To a stirred solution of **16a** (1.34 g, 5.01 mmol) in 100 ml of chloroform, **4b** (0.93 g, 6.6 mmol) in 20 ml of chloroform was added dropwise during 7 h at room temperature. After being stirred for 3 h, the reaction mixture was subjected to dry column chromatography (alumina) to give **8a** in 48% yield.

Reaction of 16a with 4a. To a solution of **16a** (1.34 g, 5.01 mmol) in 100 ml of chloroform, **4a** (1.53 g, 6.5 mmol) was added portionwise. After the mixture was stood for 1 h, the solvent was evaporated. The residual oil was crystallized from benzene-hexane to give 4,5-dibenzoyl-2-(phenylamino) thiazole (**8d**) in 74% yield.

4,5-Dibenzoyl-2-(*p*-methylphenylamino)thiadiazole (8e). Yield 61%; mp 203—204 °C; IR (KBr) 3200, 3150, 1680, 1620 cm^{-1}; ^1H NMR ($CDCl_3$) δ=2.3 (s, 3H), 7.0—7.8 (m, 14H), 8.7 (brs, 1H); MS, *m/z* (relative intensity) 398 (M^+, 97), 293 (23).

3,4-Dimethyl-5-imino-4,5-dihydro-1,2,4-thiadiazole (1) was prepared from a similar method described in the literature.[19] Mp 64—69 °C (lit, 66 °C);[19] IR (KBr) 3200, 1595, 1580 cm^{-1}; ^1H NMR ($CDCl_3$) δ=2.25 (s, 3H), 3.28 (s, 3H), 5.85 (brs, 1H).

Reaction of 1 with 4a. The solution of **4a** (1.07 g, 4.58 mmol) in 5 ml of THF was added dropwise to a solution of **1** (495 mg, 3.83 mmol) in 10 ml of THF. After stirring overnight at room temperature, the reaction mixture was crystallized from ethanol to give 4,5-dibenzoyl-2-(methylamino)thiazole (**8f**) in 96% yield. Mp 197—198.5 °C; IR (KBr) 3200, 1680, 1620 cm^{-1}. ^1H NMR ($CDCl_3$) δ=2.87 (bd, *J*=6 Hz, 3H), 7.2—7.8 (m, 10H), 8.4 (brm, 1H). Calcd for $C_{18}H_{14}N_2O_2S$: C, 67.06; H, 4.38; N, 8.69; S, 9.95%. Found: C, 67.10; H, 4.22; N, 8.68; S, 9.94%.

Reaction of 1 with 4b. To a solution of **1** (126 mg, 0.98 mmol) in 5 ml of hexane **4b** (142 mg, 1.00 mmol) was added dropwise at 0 °C. The reaction occurred exothermally to form precipitates. After 1 h, the solvent was evaporated and the residue was submitted to TLC (SiO_2, ether). 4,5-Bis(methoxycarbonyl)-2-(methylamino)-thiazole (**8g**) was obtained in 65% yield. Mp 156.5—158 °C

(recrystallized from benzene-hexane); IR (KBr) 3200, 3100, 1730, 1620 cm^{-1}; ^1H NMR ($CDCl_3$) δ=2.97 (d, J=6 Hz, 3H), 3.84 (s, 3H), 3.95 (s, 3H), 8.27 (bs, 1H); MS, m/z (relative intensity) 230 (M^+, 100), 199 (81), 172 (28). Calcd for $C_8H_{10}N_2O_4S$: C, 41.73; H, 4.38; N, 12.17; S, 13.93%. Found C, 41.62; H, 4.65; N, 12.05; S, 14.09%.

2-Imino-3,4-diphenyl-4-thiazoline (13) was prepared from a similar method described in the literature.[20] Mp 112—113 °C (lit, 111 °C).[20]

Reaction of 13 with 4a. To a solution of **13** (1.27 g, 5.05 mmol) in 50 ml of chloroform, **4a** (1.52 g, 6.51 mmol) was added portionwise at room temperature. After the mixture was stood overnight, the solvent was evaporated. The residual oil was crystallized from ethanol to give 3,4-diphenyl-2-[(1,2-dibenzoylvinyl)imino]-4-thiazoline in 88% yield. Mp 183.5—185.5 °C; IR (KBr) 1670, 1640 cm^{-1}; ^1H NMR ($CDCl_3$) δ=6.4 (s, 1H), 6.9 (s, 1H), 6.8—8.1 (m, 20H); MS, m/z (relative intensity) 486 (M^+, 14), 381 (65), 279 (100).

Reaction of 13 with 4b. To a stirred solution of **13** (1.26 g, 5.01 mmol) in 50 ml of chloroform, **4b** (933 mg, 6.57 mmol) in 50 ml of chloroform was added portionwise After the mixture was stood overnight, the solvent was evaporated. The residue was crystallized from ethanol to give 3,4-diphenyl-2-[[1,2-bis(methoxycarbonyl)vinyl]imino]-4-thiazoline in 83% yield. Mp 162—163 °C; IR (KBr) 1740, 1710, 1685 cm^{-1}; ^1H NMR ($CDCl_3$) δ=3.7 (s, 3H), 3.8 (s, 3H), 5.7 (s, 1H), 6.5 (s, 1H), 7.1—7.6 (m, 10H); MS, m/z (relative intensity) 394 (M^+, 78), 335 (94), 303 (100). Calcd for $C_{21}H_{18}N_2O_4S$: C, 63.95; H, 4.60; N, 7.10%. Found: C, 64.15; H, 4.67; N, 7.13%.

5-Ethoxycarbonyl-3,4-dimethyl-2-imino-4-thiazoline (14) was prepared by methylation of 2-amino-5-ethoxycarbonyl-4-methylthiazole[21] with trimethyloxonium tetrafluoroborate in 32% yield. Mp 76—77 °C; ^1H NMR ($CDCl_3$) δ= 1.30 (t, J=6 Hz, 3H), 2.50 (s, 3H), 3.30 (s, 3H), 4.20 (q, J=6 Hz, 2H), 6.85 (brs, 1H); High resolution MS, Calcd for $C_8H_{12}N_2O_2S$: 200.0617. Found: m/z 200.0496.

4,5-Bis(ethoxycarbonyl)-2-imino-3-methyl-4-thiazoline (15) was prepared by methylation of 2-amino-4,5-bis(ethoxycarbonyl)thiazole[22] with trimethyloxonium tetrafluoroborate in 35% yield. Oil; ^1H NMR ($CDCl_3$) δ=1.30 (t, J= 6 Hz, 3H), 1.40 (t, J=6 Hz, 3H), 3.30 (s, 3H), 4.20 (q, J= 6 Hz, 2H), 4.40 (q, J=6 Hz, 2H), 7.0—7.5 (brs, 1H); High resolution MS, Calcd for $C_{10}H_{14}N_2O_4S$: M, 258.0673. Found: m/z 258.0632.

Reaction of 14 with 4a. A mixture of **14** (418 mg, 2.09 mmol) and **4a** (554 mg, 2.37 mmol) in 25 ml of benzene was heated at 50 °C for one day. The reaction mixture was chromatographed (dry column chromatography, SiO_2) with dichlorometane as an eluent to give a vinyl compound in 93% yield. ^1H NMR ($CDCl_3$) δ=1.40 (t, J=6 Hz, 3H), 2.60 (s, 3H), 3.45 (s, 3H), 4.30 (q, J=6 Hz, 2H), 7.00 (s, 1H), 7.2—8.1 (m, 10H).

Reaction of 15 with 4b. A mixture of **15** (340 mg, 1.32 mmol) and **4b** (218 mg, 1.53 mmol) in 40 ml of methanol was heated at 50 °C for 5 h. About 1:1 mixture of vinyl compounds were obtained after chromatographic separation in 57% yield (And 40% of **15** was recovered). To the $CDCl_3$ solution was added chloroacetic acid, resulting in isomerization and the ratio of the compounds changed to 5:1. cis-vinyl: ^1H NMR ($CDCl_3$) δ=1.30 (t, J=7 Hz, 3H), 3.44 (s, 3H), 3.70 (s, 3H), 3.88 (s, 3H), 4.0—4.5 (m, 4H), 5.60 (s, 1H). trans-vinyl: ^1H NMR ($CDCl_3$) δ=1.41 (t, J=7 Hz, 3H), 3.44 (s, 3H), 3.70 (s, 3H), 3.81 (s, 3H), 4.1—4.6 (m, 4H), 6.29 (s, 1H).

References

1) a) G. L'abbé, *Tetrahedron*, **24**, 3537 (1982) and references therein; b) R. J. S. Beer and I. Hart, *J. Chem. Soc., Chem. Commun.*, **1977**, 143.

2) a) D. B. J. Easton, D. Leaver, and T. J. Rawlings, *J. Chem. Soc., Perkin Trans. 1*, **1972**, 41; b) B. R. O'Connor and F. N. Jones, *J. Org. Chem.*, **35**, 2002 (1970).

3) a) H. Behringer and R. Wiedenmann, *Tetrahedron Lett.*, **1965**, 3705; b) H. Behringer, D. Bender, J. Falkenberg, and R. Wiedenmann, *Chem. Ber.*, **101**, 1428 (1968).

4) a) G. Lang and J. Vialle, *Bull. Soc. Chim. Fr.*, **1967**, 2865; b) J. Goerdeler and H. W. Linden, *Tetrahedron Lett.*, **1975**, 3387; c) J. E. Oliver and R. T. Brown, *J. Org. Chem.*, **39**, 2228 (1978); d) K-y. Akiba, M. Ochiumi, T. Tsuchiya, and N. Inamoto, *Tetrahedron Lett.*, **1975**, 459; e) K-y. Akiba, T. Tsuchiya, and N. Inamoto, *ibid.*, **1976**, 1877; f) K-y. Akiba, T. Tsuchiya, N. Inamoto, K. Yamada, H. Tanaka, and H. Kawazura, *ibid.*, **1976**, 3819; g) K-y. Akiba, T. Tsuchiya, M. Ochiumi, and N. Inamoto, *ibid.*, **1975**, 455; h) M. S. Chauhan, M. E. Hassan, and D. M. McKinnon, *Can. J. Chem.*, **52**, 1738 (1974); i) A. Cuthbertson and C. Glidewell, *J. Mol. Struct.*, **90**, 227 (1982).

5) M. Baudy and A. Robert, *J. Chem. Soc., Chem. Commun.*, **1976**, 912.

6) M. V. Lakshmikantham and M. P. Cava, *J. Org. Chem.*, **41**, 879 (1976).

7) a) K-y. Akiba, K. Kashiwagi, Y. Ohyama, Y. Yamamoto, and K. Ohkata, *J. Am. Chem. Soc.*, **107**, 2721 (1985); b) Y. Yamamoto and K-y. Akiba, *ibid.*, **106**, 2713 (1984); c) K-y. Akiba, A. Noda, and K. Ohkata, *Phosphorus and Sulfur*, **16**, 111 (1983); d) K-y. Akiba, T. Kobayashi, and S. Arai, *J. Am. Chem. Soc.*, **101**, 5857 (1979); e) K-y. Akiba, S. Arai, T. Tsuchiya, Y. Yamamoto, and F. Iwasaki, *Angew. Chem., Int. Ed. Engl.*, **18**, 166 (1979).

8) The prefix cis and trans was based on the mode of addition, not on the configuration of the compound.

9) J. E. Dolfini, *J. Org. Chem.*, **30**, 1298 (1965).

10) K. Dimroth, C. Reichardt, T. Siepmann, and F. Bohlmann, *Justus Liebigs Ann. Chem.*, **661**, 1 (1963).

11) As previously noted **11b** was the secondary product and the ratio of thiazole to vinyls (**8b**/(**9b**+**10b**)) is meaningful.

12) R. Huisgen, B. Giese, and H. Huber, *Tetrahedron Lett.*, **1967**, 1883.

13) J. I. Musher, *Angew. Chem., Int. Ed. Engl.*, **8**, 54 (1969); J. C. Martin, *Science*, **221**, 509 (1983) and references cited therein.

14) R. E. Lutz and W. R. Smithey, *J. Org. Chem.*, **16**, 51 (1955).

15) E. H. Huntress, T. E. Lesslie, and J. Bornstein, *Org. Synth.*, Coll. Vol. 4, 329 (1963).

16) S. Shawali and O. Abdelhamid, *Tetrahedron Lett.*, **1975**, 163.

17) R. Fusco and C. Musante, *Gazz. Chim. Ital.*, **68**, 147 (1938).

18) D. S. Hector, *Ber.*, **22**, 1176 (1889); **23**, 357 (1890).

19) J. Goerdeler and W. Roth, *Chem. Ber.*, **96**, 534 (1963).
20) H. Bayer and G. Ruhlig, *Chem. Ber.*, **89**, 107 (1956).
21) R. M. Dodson and L. C. King, *J. Am. Chem. Soc.*, **67**, 2242 (1945).
22) L. H. Conover and D. S. Tarbell, *J. Am. Chem. Soc.*, **72**, 5221 (1950).

 © 1989 The Chemical Society of Japan Bull. Chem. Soc. Jpn., 62, 219—225 (1989)

Anodic Oxidation of (Trimethylsilyl)methanes with π-Electron Substituents in the Presence of Nucleophiles

Toshio KOIZUMI, Toshio FUCHIGAMI,* and Tsutomu NONAKA*
Department of Electronic Chemistry, Tokyo Institute of Technology,
4259 Nagatsuta, Midori-ku, Yokohama 227
(Received March 12, 1988)

It was found that oxidation potentials of methanes with π-electron substituents were decreased by introduction of a trimethylsilyl group. The anodic oxidation of benzyl-, allyl-, aryl(or alkyl)thiomethyl-, and aryloxymethyl-substituted trimethylsilanes smoothly proceeded in the presence of nucleophiles, e.g. alcohols and carboxylic acids, to eliminate the trimethylsilyl groups giving the corresponding alkoxylated and carboxylated products in moderate or high yields without full optimization of electrolytic conditions, while aminomethylsilanes did not undergo such a kind of anodic oxidation.

Anodic oxidation of organic compounds involves mostly a proton elimination step which sometimes governs overall efficiency and/or selectivity of the reaction. For instance, the anodic substitution of toluene involves the proton elimination from the methyl or phenyl group which is substituted by a nucleophile. The proton elimination step is generally influenced by reaction conditions, and in fact it has been found that the product selectivity of the toluene oxidation is sensitively affected by electrolytic conditions such as acidity/basicity of anolyte and anode material.[1-6]

In this work, it was attempted to control the proton elimination on the basis of a different principle in which the methyl group of toluenes was modified by a cationic leaving group. As leaving species more favorable than proton, NO^+, RCO^+, and I^+ have sometimes been used.[7] However, these are electron-withdrawing groups, which cause increases in the oxidation potential of the mother compounds. This should be a disadvantage for efficient anodic oxidation. In this work, a trimethylsilyl group was used as a cationic leaving group for the following reasons:[8] (a) A trimethylsilyl substituent increases HOMO energy level of π-electron system at β-position,[14-17] (b) a C–Si bond is more easily cleaved than a C–H one[18] (Bonding energy: CH_3–$SiMe_3$, 89.4 kcal mol^{-1}; CH_3–H, 104.8 kcal mol^{-1}[19]), (c) a silicon atom is more easily attacked by nucleophiles than a hydrogen one,[18] (d) silyl substituents contribute to stabilize β-carbocations, comparably to alkoxy ones,[18,20] (e) a C–Si bond is chemically stable,[18] and (f) trimethylsilyl compounds are easily prepared using trimethylsilyl chloride.[21]

The following anodic substitution reaction of (trimethylsilyl)methanes with π-electron substituents was examined in the presence of nucleophiles, e.g. alcohols and carboxylic acids.

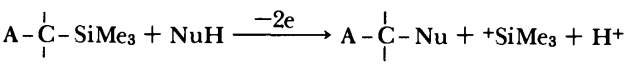

A: π-Electron substituent
NuH: Nucleophile

Results and Discussion

Trimethylsilylated compounds[(trimethylsilyl)methanes] such as benzyl-, allyl-, thiomethyl-, oxymethyl-, and aminomethyl-trimethylsilane (**1**—**5**), and related unsilylated compounds were used as the starting materials of the anodic oxidation.

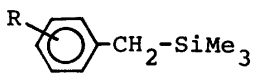

1a: R=H
1b: R=*p*-Me
1c: R=*o*-Me

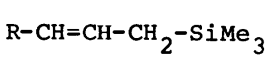

2a: R=H
2b: R=Ph

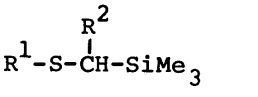

3a: R^1=Ph, R^2=H
3b: R^1=*p*-Me-C_6H_4, R^2=H
3c: R^1=Me, R^2=Ph

4

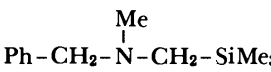

5

Oxidation Potentials of Trimethylsilanes. Benzyl- and thiomethyl-trimethylsilanes (**1a**, **b**, and **3a**, **c**) gave irreversible cyclic voltammetric waves at a platinum anode in 0.1 M (1 M=1 mol dm^{-3}) Bu_4NBF/MeCN (Scan rate, 100 mV s^{-1}). As shown in Table 1, their oxidation peak potentials (E_p^{ox}) are significantly less noble than those of the unsilylated parent compounds. Similar decreases in oxidation potentials of allyl- and aminomethyl-silanes have been found by Yoshida et al.[11] and Cooper and Owen,[22] respectively. These facts suggest that the decreases in oxidation potentials of the π-electron compounds can be induced by introduction of silyl groups to the α-positions.

Anodic Oxidation of Benzylsilanes (1a—c). Oxidation in Methanol: Benzylsilanes (**1a**, **b**) were oxidized at platinum and graphite anodes in methanol containing $NaClO_4$ to give mixtures of α-monomethoxy-

Table 1. Oxidation Potentials of Benzyl- and [Aryl(or alkyl)thiomethyl]trimethylsilanes, and Their Unsilylated Parent Compounds

Trimethylsilane	E_p^{ox}/V[a]	Unsilylated parent compound	E_p^{ox}/V[a]
1a	1.38	Ph-CH_3	1.98
1b	1.17	*p*-Me-C_6H_4-CH_3	1.70
3a	0.92	Ph-S-CH_3	1.05
3c	0.99	Me-S-CH_2-Ph	1.25

a) vs. $Ag/AgNO_3$ sat.

Table 2. Anodic Oxidation of Benzyltrimethylsilanes in Methanol[a]

Run	Benzyltrimethylsilane	Anode	Charge passed/×96500 C mol^{-1}	Yield[b]/%	
				6a/b	**7a/b**
1	**1a**	Pt	2.8	56	35
2	**1a**	Graphite	2.8	49	30
3	**1a**	Pt	4.7	38	52
4	**1a**	Graphite	4.7	44	49
5	**1b**	pt	3.0	47	32
6	**1b**	Graphite	3.0	25	39
7	**1b**	pt	5.0	8	65
8	**1b**	Graphite	5.0	0	61

a) Silanes (5 mmol) were electrolyzed at 1.0 A dm^{-2} of constant current in 0.57 M $NaClO_4$/MeOH (35 cm^3) in a divided cell. b) Determined by GLC.

toluenes (**6a, b**) and α,α-dimethoxytoluenes (**7a, b**) in good combined yields (Table 2). Any nucleus-methoxylated products were not formed. At smaller amounts of charge passed, the platinum anode seems somewhat favorable to the formation of **6**. Increases in charge passed resulted in evident decreases and increases in the yields of **6** and **7**, respectively. This fact suggests that **7** forms via **6**.

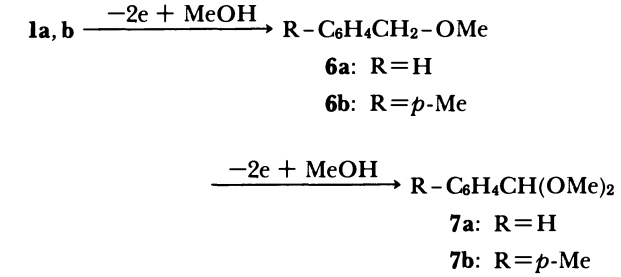

It is interesting to note that Yoshida et al.[11] have obtained **6** (R=H and *p*-Cl) as single products in high yields in the anodic oxidation of **1** at a graphite anode in Et_4NOTs/MeOH, though any reasoning for such a difference from the above result can not be made at present.

Oxidation in Dichloromethane: Allyl alcohol is easily oxidized because of its low oxidation potential.[23] Therefore, the anodic allyloxylation hardly takes place in general, since the oxidation of allyl alcohol itself occurs preferably to substrates to be allyloxylated. However, the benzylsilanes, of which the oxidation potentials are decreased by the introduction of trimethylsilyl groups, could be anodically allyloxylated in moderate yields under unoptimized conditions (Table 3: Runs 9 and 10).

The anodic substitution is reasonably affected by natures of nucleophiles used. In fact 2,2,2-trifluoroethanol, whose nucleophilicity should be extremely low due to the strongly electron-withdrawing CF_3 group, did not give the corresponding trifluoroethoxylated product (Run 11). On the other hand, somewhat nucleophilic trifluoroacetate ion gave benzyl trifluoroacetate along with benzyl alcohol as a by-product in the oxidation of **1a** (Run 12). The formation of benzyl alcohol may be due to water as a contaminant in the electrolyte or to hydrolysis of the main prodct during the work-up procedure. In Run 13 without any nucleophile added, **1a** itself played a role of nucleophile and benzyl(trimethylsilylmethyl)benzene was formed in 30% yield. In a quaternary ammonium tosylate solution (Run 14), tosylate ion did not act as a nucleoplile, but products such as bibenzyl and toluene were formed, probably, via benzyl radical intermediate species.

From the above results, a mechanistic scheme (Scheme 1) can be postulated as below. In the scheme, the elimination of trimethylsilyl cation from the cation radical intermediate species occurs superiorly to that of protons and the radical coupling process proceed under certain conditions.

In an acetonitrile solution (Run 15), **1a** was anodically acetamidated to give *N*-benzylacetamide in a low yield.

Anodic Oxidation of Allylsilanes (2a, b). Allyltrimethylsilane (**2b**) was anodically trifluoroethoxylated in a low yield in a divided cell (Table 4: Run 16), while benzyltrimethylsilane (**1b**) was not in an undivided cell (Run 11). Reasoning for this difference has not been clearly made, but it is likely that the trifluoroethoxylation is accelerated by acid electrogenerated

in the anode chamber of the divided cell. In fact, the yield was increased by addition of TsOH (Run 17).

Although benzylsilane (**1a**) did not give the corresponding tosylate but underwent the radical process as described above (Run 14), allyl tosylate was formed in the oxidation of allylsilane (**2a**) under similar conditions (Run 18). This may be rationalized due to a stronger electrophilicity of allyl cation than benzyl one

Table 3. Anodic Oxidation of Benzyltrimethylsilanes in Dichloromethane in the Presence and Absence of Nucleophiles[a]

Run	Benzyltrimethylsilane	Nucleophile	Electrolyte	Anode
9[b]	**1c**	CH_2=$CHCH_2OH$[c]	0.60 M Et_4NOTs	Graphite
10[b]	**1b**	CH_2=$CHCH_2OH$[c]	0.60 M Et_4NOTs	Graphite
11[b]	**1b**	CF_3CH_2OH[c]	0.60 M Et_4NOTs	Graphite
12[b]	**1a**	CF_3COO^-	0.57 M $CF_3COONBu_4$	Pt
13[f]	**1a**	—	0.57 M Bu_4NClO_4	Pt
14[f]	**1a**	—	0.46 M Et_4NOTs	Graphite
15[f]	**1a**	MeCN[g] + H_2O	0.57 M Bu_4NBF_4	Pt

Run	Charge passed/×96500 C mol^{-1}	Product (Yield/%)
9[b]	2.0	*o*-Me-C_6H_4-O-CH_2CH=CH_2 (36[d])
10[b]	2.0	*p*-Me-C_6H_4-O-CH_2CH=CH_2 (34[d])
11[b]	2.0	*p*-Me-C_6H_4-O-CH_2CF_3 (Not formed)
12[b]	3.0	$PhCH_2$-$OOCCF_3$ (24[e])
		$PhCH_2$-OH (8[e])
13[f]	1.5	$PhCH_2$-$C_6H_4SiMe_3$ (30[e])
14[f]	2.4	$PhCH_2CH_2Ph$ (9[d])
		$PhCH_3$ (trace)
15[f]	2.0	$PhCH_2$-NHCOMe[h] (17[d])

a) Silanes (5 mmol) were electrolyzed at 1.0 A dm^{-2} of constant current. b) An undivided cell was used. c) 20 mmol. d) Isolated yield. e) Determined by GLC. f) A divided cell was used. g) Used as solvent. h) Unknown products were also formed.

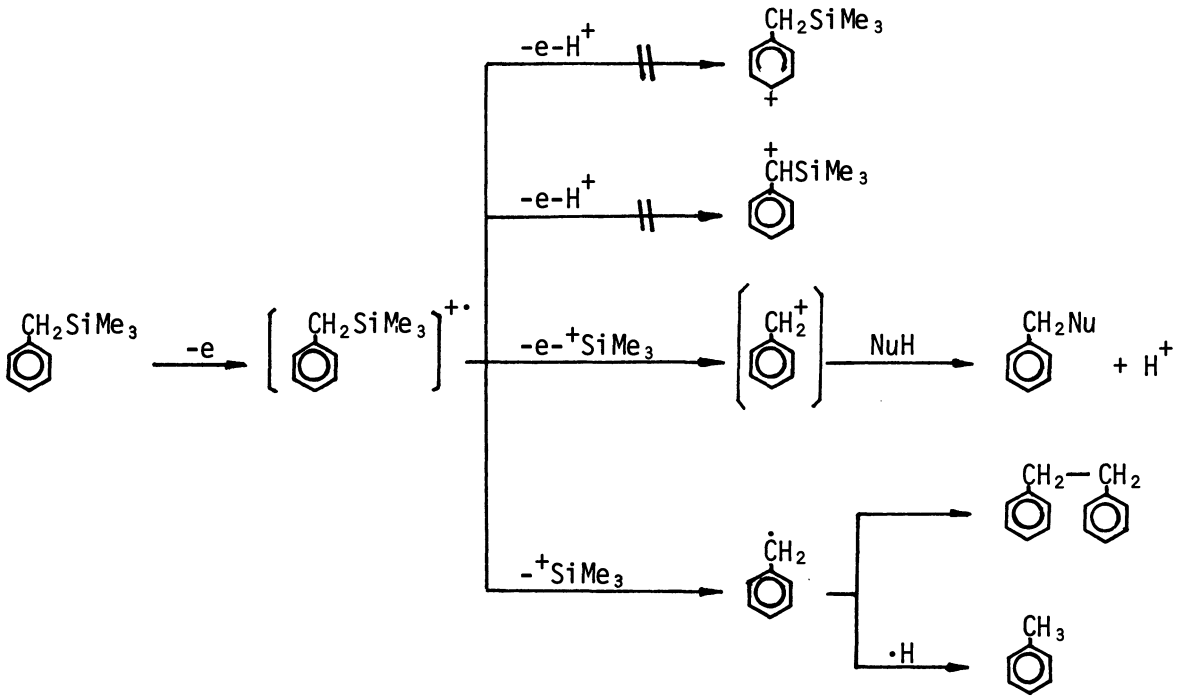

Scheme 1.

Table 4. Anodic Oxidation of Allylsilanes in the Presence of Nucleophiles[a]

Run	Allylsilane	Nucleophile	Electrolyte	Product (Yield[b]/%)
16	**2b**	CF_3CH_2OH (20 eq)	0.30 M Et_4NOTs	$PhCH{=}CHCH_2{-}OCH_2CF_3$ (10)
17[c]	**2b**	CF_3CH_2OH (20 eq)	0.30 M Et_4NOTs	$PhCH{=}CHCH_2{-}OCH_2CF_3$ (19)
18[d]	**2a**	TsO^-	0.30 M Et_4NOTs	$CH_2{=}CHCH_2{-}OTs$ (20)
19[d]	**2a**	CF_3COO^-	0.50 M $CF_3COONBu_4$	$CH_2{=}CHCH_2{-}OOCCF_3$ (Formed[e])

a) Electrolysis was carried out by passing 2×96500 C mol^{-1} of charge at 0.8 A dm^{-2} using a graphite anode in acetonitrile in a divided cell. b) Isolated yield. c) TsOH (1 equiv) was added to the anolyte. d) CH_2Cl_2 was used as solvent. e) Confirmed by GLC-MS.

Table 5. Anodic Oxidation of Thiomethylsilanes in the Presence of Alcohols[a]

$$R^1\text{-}S\text{-}\underset{\textbf{3}}{\underset{|}{\overset{R^2}{C}}}H\text{-}SiMe_3 \xrightarrow{-2e + ROH} R^1\text{-}S\text{-}\underset{\textbf{8}}{\underset{|}{\overset{R^2}{C}}}H\text{-}OR$$

Run	3	ROH	Yield[b] of 8/%
20[c]	**3a**	MeOH[d]	50[e]
21	**3a**	MeOH[d]	66[e]
22[f]	**3a**	MeOH[d]	56
23	**3a**	EtOH	65
24	**3a**	Me_2CHOH	49
25	**3a**	Me_3COH	25
26	**3a**	$CH_2{=}CHCH_2OH$	59[e]
27	**3a**	$CH_2{=}CHCH(Me)OH$	54[e]
28	**3a**	$Me_2C{=}CHCH_2OH$	58[e]
29	**3a**	PhOH	0
30	**3b**	$CH_2{=}CHCH_2OH$	42[e]
31	**3c**	CF_3CH_2OH	6[g]
32	**3c**	$CH_2{=}CHCH_2OH$	66[e]
33	**3c**	$Me_2C{=}CHCH_2OH$	77[e]

a) 2.5 mmol of **3** was electrolyzed by passing 2×96500 C mol^{-1} of charge at 1.0 A dm^{-2} of current density at a graphite anode in 0.60 M Et_4NOTs/MeCN containing 50 mmol of ROH in an undivided cell. b) Isolated yield. c) At 0.5 A dm^{-2} of current density. d) Used as solvent. e) Determined by GLC. f) At 1.5 A dm^{-2} of current density. g) By-products: $(CF_3CH_2O)_2$-CHPh (16%) and $(MeS)_2CHPh$ (32%).

whose positive charge is more highly delocalized. The anodic trifluoroacetoxylation of **2a** (Run 19) occurred as well as that of **1a**.

The reaction scheme of allylsilanes can be presented similarly to that of benzylsilanes (Scheme 1). Yoshida et al. reported interesting results from a mechanistic aspect and proposed a more detailed mechanism.[11]

Anodic Oxidation of [Aryl(or alkyl)thiomethyl]silanes (3a—c). Oxidation in the Presence of Alcohols: It is known that α-methoxylated sulfides can be obtained by the anodic methoxylation of sulfides.[24,25] However, the existence of electron-withdrawing groups at the α-positions of sulfide molecules seems to be necessary to accelerate deprotonation from cation radical intermediate species and to result in successful methoxylation. In fact, it was confirmed that methyl phenyl sulfide was anodically methoxylated in only 1% yield.

As shown in Table 5, [aryl(or alky)lthiomethyl]-trimethylsilanes (**3a—c**) could be alkoxylated in the anodic oxidation in the presence of a variety of alcohols such as primary (Runs 20—23, 26, 28, 30—33), secondary (Runs 24, 27) and tertiary (Run 25) alcohols. In most cases, the yields were considerably good, though reaction conditions were not fully optimized. Phenol (Run 29) and trifluoroethanol (Run 31) did not give satisfactory results due to their low nucleophilicities.

Although arylthiometyl ethers (**8**) are versatile synthetic reagents for C_1 homologation,[26] it is not so easy to prepare them except for methyl and aryl arylthiomethyl ethers.[27] The anodic alkoxylation should provide an efficient and useful method for the preparation of **8**.

It is noteworthy that the allyloxylation of (thiomethyl)silanes can be performed by the anodic method, though allyl alcohols have considerably less noble oxidation potentials. The anodic methoxylation of phenyl trifluoroethyl sulfide proceeds very efficiently (in 93% yield) by contribution of the electron-withdrawing trifluoromethyl group,[24] while the allyloxylation did not. This fact should clearly indicate a sufficient effect of the modification of sulfides by trimethylsilyl groups on the allyloxylation. It is expected that **8** with allyl groups are converted into the corresponding β,γ-unsaturated ketones by the [2,3]Wittig rearrangement using bases. In fact, **8** derived from **3c** and allyl alcohol in Run 32 gave the ketone in a good yield as follows:

$$MeS\text{-}\underset{|}{\overset{Ph}{C}}H\text{-}OCH_2CH{=}CH_2 \xrightarrow[-80\text{—}-20^\circ C]{LDA/THF} Ph\text{-}\overset{O}{\overset{\|}{C}}\text{-}CH_2CH{=}CH_2 \quad (74\%)$$

Oxidation in the Presence of Carboxylic Acids: As shown in Table 6, the anodic carboxylation of **3a** could smoothly proceed using a few kinds of aliphatic carboxylic acids. It is interesting to note that an unsilylated

Table 6. Anodic Oxidation of Phenylthiomethylsilane in the Presence of Carboxylic Acids[a]

$$\underset{\textbf{3a}}{\text{Ph-S-CH}_2\text{-SiMe}_3} \xrightarrow{-2e + \text{RCOOH}} \underset{\textbf{9}}{\text{Ph-S-CH}_2\text{OCOR}}$$

Run	RCOOH	Yield[b] of 9/%
34	MeCOOH	66
35[c]	MeCOOH	20
36	$Me_2CHCOOH$	61

a) 2.5 mmol of **3a** was electrolyzed by passing 2× 96500 C mol^{-1} of charge at 1.0 A dm^{-2} of current density at a graphite anode in 0.60 M Et_4NOTs/MeCN containing 50 mmol of RCOOH in an undivided cell. b) Isolated yield. c) At a Pt anode in 0.6 M MeCOONa/MeCOOH.

sulfide, $PhSCH_2CH_3$, was not acetoxylated at all under the same conditions.

A reaction scheme involving sulfenium ions as key intermediates would be written for the anodic alkoxylation and carboxylation of **3** analogously to Scheme 1.

Anodic Oxidation of Aryloxymethyl (4) and Aminomethyl (5) Silanes. (Phenoxymethyl)trimethylsilane (**4**), which is an oxygen analogue of **3a**, was anodically methoxylated (52% yield) under conditions presented in Table 5.

[(*N*-Methylbenzylamino)methyl]trimethylsilanes (**5**) did not undergo the alkoxylation,[28] but gave a diamine (**10**) in 40—68% yields in the presence of either methanol or ethanol. The diamine (**10**) was also formed chemically from *N*-methylbenzylamine and formaldehyde along with dimethyl or diethyl ether.

$$\text{PhCH}_2\text{N(Me)CH}_2\text{N(Me)CH}_2\text{Ph}$$

10

Experimental

Materials. Anodes: Platinum and graphite anodes were polished with fine alumina powder and emery paper, respectively, and then washed with acetone.

Solvents: Acetonitrile, dichloromethane, and methanol were dried using P_2O_5-CaH_2, CaH_2, and sodium metal, respectively, and then distilled in an atmosphere of nitrogen.

Benzyltrimethylsilanes (1a—c): A general method developed for preparing aryltrimethylsilanes[29] was applied. **1a**: Bp 84—85 °C (26 mmHg) (1 mmHg=133.322 Pa) [lit,[30] 93 °C) (35 mmHg)]. **1b**: Bp 84—85 °C (14 mmHg) (lit,[31] 211.5 °C). **1c**: Bp 82—83 °C (9 mmHg) (lit,[32] 210—211 °C.

Allyltrimethylsilanes (2a, b): The silane **2a** was prepared by the method of literature.[29] Bp 86—87 °C (lit,[29] 85 °C). The silane **2b** was also prepared similarly to **2a**. Bp 103—105 °C (10 mmHg); ^{1}H NMR [$CDCl_3$, relative to $Si(CH_3)_3$] δ=0.00 (s, 9H, $Si(CH_3)_3$), 1.5—1.7 (m, 2H, CH_2-Si), 6.1—6.4 (m, 2H, CH=CH), and 7.0—7.4 (m, 5H, C_6H_5).

[Aryl(or alkyl)thiomethyl]trimethylsilanes (3a—c): The silanes were prepared by methods of literatures. **3a**:[33,34] Bp 136—137 °C (32 mmHg) [lit,[35] 158.5 °C (52 mmHg)]. **3b**:[35] Bp 150—151 °C (30 mmHg) [lit,[35] 83—85 °C (1 mmHg)]. **3c**:[37] Bp 99—100 °C (8 mmHg); ^{1}H NMR ($CDCl^3$, relative to $Si(CH_3)_3$) δ=0.00 (s, 9H, $Si(CH_3)_3$), 1.87 (s, 3H, S-CH_3), 3.31 (s, 1H, CH), and 7.1—7.3 (m, 5H, C_6H_5).

Phenoxymethyltrimethylsilane (4): The silane was prepared by the method of literature.[38] Bp 86—87 °C (9 mmHg) (lit,[38] 83—84 °C (8 mmHg)).

[*N*-(Methylbenzylamino)methyl]trimethylsilane (5): The silane was prepared by the method of literature[39] and purified by column chromatography (Silica gel, hexane-ether (1:1)).

Electrolysis. The electrolysis was galvanostatically carried out at room temperature using a platinum (7.7 cm^2) or graphite (5.0 cm^2) anode in a divided (anolyte, 35—50 cm^3) or undivided (electrolyte, 15 cm^3) cell. Detailed electrolytic conditions are shown in the text.

Separation and Analysis of Products. After electrolysis, the electrolytic solution was poured into a saturated sodium chloride solution and extracted with ether or dichloromethane. The extract was dried over anhydrous sodium sulfate and concentrated under reduced pressure. The products were analyzed by GLC (2 m PEG 20 M and 2.25 m Silicone HV grease columns) and isolated by column chromatography (silica gel, hexane-dichloromethane (4:1) or benzene). Molecular structures of all the products were determined by ^{1}H NMR, MS and IR spectra, and/or elemental analysis. Data for the identification of some special products are given below.

[(Benzylphenyl)methyl]trimethylsilane: IR (neat) 3070, 3030, 2960, 2900, 1600, 1505, 1490, 1450, 1250, 1215, 1155, 850, 725, and 690 cm^{-1}; ^{1}H NMR ($CDCl_3$, relative to $SiCH_3$) δ=0.00, 0.02 (s, 9H, $Si(CH_3)_3$), 2.07, 2.13 (s, 2H, -CH_2-Si), 3.95 (s, 2H, C_6H_5-CH_2-C_6H_4), and 6.47—6.77 (m, 9H, C_6H_5-CH_2-C_6H_4); MS (70 eV) *m/z* (M^+); GLC 2 peaks with almost equal area, probably for *o*- and *p*-benzyl isomers.

3-Phenylallyl 2,2,2-Trifluoroethyl Ether: ^{1}H NMR ($CDCl_3$, TMS) δ=3.90 (q, 2H, CH_2CF_3), 4.35 (d, 2H, =CH-CH_2-O), 6.1—6.7 (m, 2H, CH=CH) and 7.2—7.6 (m, 5H, C_6H_5).

Methyl Phenylthiomethyl Ether:[40] IR (neat) 3070, 3000, 2940, 2900, 2830, 1590, 1480, 1440, 1185, 1080, and 900 cm^{-1}; ^{1}H NMR ($CDCl_3$, TMS) δ=3.47 (s, 3H, O-CH_3), 5.00 (s, 2H, S-CH_2-O), and 7.2—7.6 (m, 5H, C_6H_5); MS (70 eV) *m/z* 154 (M^+).

Ethyl Phenylthiomethyl Ether: IR (neat) 3070, 2990, 2940, 2900, 1590, 1480, 1440, 1080, 1015, 840, and 740 cm^{-1}; ^{1}H NMR ($CDCl_3$, TMS) δ=1.22 (t, 3H, CH_2CH_3), 3.67 (q, 2H, CH_2CH_3), 4.98 (s, 2H, S-CH_2-O), and 7.1—7.5 (m, 5H, C_6H_5); MS (70 eV) *m/z* 168 (M^+). Found: C, 64.29; H, 7.25%. Calcd for $C_9H_{12}SO$: C, 64.25; H, 7.19%.

Isopropyl Phenylthiomethyl Ether: ^{1}H NMR ($CDCl_3$, TMS) δ=1.17 (d, 6H, CH_3), 3.8—4.3 (m, 1H, CH), 5.00 (s, 2H, S-CH_2-O), 7.1—7.6 (m, 5H, C_6H_5); MS (70 eV) *m/z* 182 (M^+). Found: C, 65.58; H, 7.60%. Calcd for $C_{10}H_{14}SO$: C, 65.89; H, 7.74%.

***t*-Butyl Phenylthiomethyl Ether:** IR (neat) 3070, 2980, 2930, 1585, 1480, 1440, 1395, 1365, 1055, 1025, and 740 cm^{-1}; ^{1}H NMR ($CDCl_3$, TMS) δ=1.25 (s, 9H, CH_3), 4.87 (s, 2H, S-CH_2-O), and 7.1—7.5 (m, 5H, C_6H_5); MS (70 eV) *m/z* 196 (M^+). Found: C, 67.20; H, 8.18; S, 16.39%. Calcd for $C_{11}H_{16}SO$: C, 67.30; H, 8.22; S, 16.33%.

Allyl Phenylthiomethyl Ether: IR (neat) 3070, 3030, 2990,

2900, 2860, 1585, 1480, 1440, 1060, 1000, and 930 cm^{-1}; ^1H NMR ($CDCl_3$, TMS) δ=4.17 (d, 2H, O-C<u>H</u>$_2$-CH=), 5.00 (s, 2H, S-CH_2-O), 5.0—5.5 (m, 2H, CH=C<u>H</u>$_2$), 5.6—6.2 (m, 1H, C<u>H</u>=CH_2), and 7.2—7.6 (m, 5H, C_6H_5); MS (70 eV) *m/z* 180 (M^+). Found: C, 66.32; H, 6.86; S, 18.25%. Calcd for $C_{10}H_{12}SO$: C, 66.63; H, 6.71; S, 17.79%.

1-Methylallyl Phenylthiomethyl Ether: IR (neat) 3070, 2990, 2940, 2910, 1740, 1585, 1480, 1440, 1060, 1040, 1025, 995, and 930 cm^{-1}; ^1H NMR ($CDCl_3$, TMS) δ=1.26 (d, 3H, CH_3), 4.35 (quintet, 1H, O-C<u>H</u>(CH_3)CH=), 4.91 (s, 2H, S-CH_2-O), 5.1—5.3 (m, 2H, =CH_2), 5.5—5.9 (m, 1H, -CH=), and 7.2—7.5 (m, 5H, C_6H_5); MS (70 eV) *m/z* 194 (M^+). Found: C, 68.01; H, 7.30; S, 16.47%. Calcd for $C_{11}H_{14}SO$: C, 68.00; H, 7.26; H, 16.50%.

3-Methyl-2-butenyl Phenylthiomethyl Ether: IR (neat) 3060, 3030, 2980, 2910, 2880, 1670, 1585, 1480, 1440, 1200, 1060, 900, and 735 cm^{-1}; ^1H NMR ($CDCl_3$, TMS) δ=1.69 (s, 3H, CH_3), 1.75 (s, 3H, CH_3) 4.17 (d, 2H, O-C<u>H</u>$_2$-CH=), 5.00 (s, 2H, S-CH_2-O), 5.36 (t, 1H, CH_2-C<u>H</u>=), and 7.2—7.7 (m, 5H, C_6H_5). Found: C, 69.11; H, 7.79%. Calcd for $C_{12}H_{16}SO$: C, 69.19; H, 7.74%.

Allyl (*p*-Methylphenylthio)methyl Ether: IR (neat) 3075, 3030, 2980, 2920, 2900, 2860, 1640, 1595, 1490, 1060, 1000, and 920 cm^{-1}; ^1H NMR ($CDCl_3$, TMS) δ=2.33 (s, 3H, CH_3), 4.20 (d, 2H, O-C<u>H</u>$_2$-CH=), 5.00 (s, 2H, S-CH_2-O), 5.1—5.5 (m, 2H, CH=C<u>H</u>$_2$), 5.6—6.3 (m, 1H, C<u>H</u>CH_2), 7.08 (d, 2H, C_6H_4), and 7.38 (d, 2H, C_6H_4); MS (70 eV) *m/z* 194 (M^+). Found: C, 68.29; H, 7.68%. Calcd for $C_{11}H_{14}SO$: C, 68.00; H, 7.26%.

2,2,2-Trifluoroethyl Phenyl(methylthio)methyl Ether: ^1H NMR ($CDCl_3$, TMS) δ=1.98 (s, 3H, CH_3), 3.90 (q, 2H, -CH_2-), 5.73 (s, 1H, S-CH-O), and 7.4—7.8 (m, 5H, C_6H_5).

[Di(methylthio)]phenylmethane: ^1H NMR ($CDCl_3$, TMS) δ=2.10 (s, 6H, CH_3), 4.77 (s, 1H, S-CH-S), and 7.4—7.8 (m, 5H, C_6H_5).

Di(2,2,2-trifluoroethoxy)phenylmethane: ^1H NMR ($CDCl_3$, TMS) δ=3.90 (q, 2H, -CH_2-), 5.87 (s, 1H, O-CH-O), 7.12 (s, 5H, C_6H_5).

Allyl Phenyl(methylthio)methyl Ether: IR (neat) 3080, 3040, 3000, 2930, 2870, 1640, 1600, 1490, 1455, 1070, 1010, and 915 cm^{-1}; ^1H NMR ($CDCl_3$, TMS) δ=1.87 (s, 3H, CH_3), 4.1—4.3 (m, 2H, O-C<u>H</u>$_2$CH=), 5.1—5.6 (m, 2H, CH=C<u>H</u>$_2$), 5.60 (s, 1H, S-CH-O), 5.7—6.4 (m, 1H, C<u>H</u>=CH_2), and 7.1—7.6 (m, 5H, C_6H_5); MS (70 eV) *m/z* 194 (M^+). Found: C, 68.59; H, 7.53%. Calcd for $C_{11}H_{14}SO$: C, 68.00; H, 7.26%.

3-Methyl-2-butenyl Phenyl(methylthio)methyl Ether: IR (neat) 3075, 3040, 2995, 2930, 2870, 1670, 1605, 1495, 1455, 1080, 1060, 1030, and 725 cm^{-1}; ^1H NMR ($CDCl_3$, TMS) δ=1.70 (s, 3H, =C-CH_3), 1.78 (s, 3H, =C-CH_3), 1.90 (s, 3H, S-CH_3), 4.22 (d, 2H, O-C<u>H</u>$_2$-CH=), 5.47 (t, 1H, CH_2-C<u>H</u>=), 5.63 (s, 1H, S-CH-O), and 7.2—7.7 (m, 5H, C_6H_5). Found: C, 70.12; H, 8.27%. Calcd for $C_{13}H_{18}SO$: C, 70.23; H, 8.16%. The product **10** was also identified with an independently synthesized sample[41] by comparing their physical properties.

[2,3]Wittig Rearrangement Reaction of Allyl Phenyl(methylthio)methyl Ether. A THF solution (1 cm^3) of the titled ether (0.203 g, 1.0 mmol) was dropwise added to a mixed solution of diisopropylamine (2.2 mmol), 1.50 M butyllithium/hexane (1.5 cm^3, 2.2 mmol) and THF (5 cm^3) at −80 °C. The temperature was gradually elevated and reached to −20 °C after 4 h. The reaction mixture was poured into a saturated ammonium chloride solution and extracted with ether. The extract was dried over anhydrous sodium sulfate and evaporated under reduced pressure. Allyl phenyl ketone was isolated from the residue by preparative thin layer chromatography (Silica gel, hexane–chloroform (1 : 1)): Yield 0.108 g (74%). The ketone was converted into the 2,4-dinitrophenylhydrazone to be identified. IR (KBr) 3300, 3090, 1610, 1595, 1580, 1505, 1485, 1330, 1310, 1135, 1100, 980, and 920 cm^{-1}; MS (70 eV) *m/z* 326 (M^+). Found: C, 58.79; H, 4.18; N, 17.06%. Calcd for $C_{16}H_{14}N_4O_4$: C, 58.89; H, 4.32; N, 17.17%.

The authors are grateful to Dr. Junichi Yoshida (Osaka City University) for helpful discussion.

References

1) S. Torii, "Electroorganic Synthesis, Methods and Applications. Part. 1. Oxidations," Kodansha, Tokyo (1981), Chap. 3.

2) A. Nilsson, U. Palmquist, T. Petterson, and A. Ronlan, *J. Chem. Soc., Perkin Trans. 1*, **1978**, 708.

3) M. Rakoutz, D. Michelet, B. Brossard, and J. Varagnat, *Tetrahedron Lett.*, **1978**, 3723.

4) W. J. Koehl, Jr., U. S. Patent 3448021 (1969); *Chem. Abstr.*, **71**, 49605f(1969).

5) B. B. Dey and R. K. Maller, *J. Sci. Ind. Res.*, **12B**, 255 (1953); *Chem. Abstr.*, **47**, 12056g (1953).

6) J. S. Clarke, R. E. Ehigamusoe, and A. Kuhn, *J. Electroanal. Chem.*, **70**, 333 (1976).

7) J. March, "Advanced Organic Chemistry. Reactions, Mechanisms and Structures," 2nd ed, Mc-Graw Hill, New York (1977), Chaps. 11 and 12.

8) The authors[9,10] and Yoshida et al.[11–13] have independently reported briefly the anodic oxidation of allyl-, benzyl-, and phenylthiomethylsilanes.

9) T. Koizumi, T. Fuchigami, and T. Nonaka, *Chem. Express*, **1**, 355 (1986).

10) T. Koizumi, T. Fuchigami, and T. Nonaka, *Chem. Lett.*, **1987**, 1095.

11) J. Yoshida, T. Murata, and S. Isoe, *Tetrahedron Lett.*, **27**, 3373 (1986).

12) J. Yoshida, T. Murata, and S. Isoe, *Tetrahedron Lett.*, **28**, 211 (1987).

13) J. Yoshida and S. Isoe, *Chem. Lett.*, **1987**, 631.

14) J. C. Giovdan, *J. Am. Chem. Soc.*, **105**, 6544 (1983).

15) H. Bock and W. Kaim, *J. Am. Chem. Soc.*, **102**, 4429 (1980).

16) A. Hosomi and H. Sakurai, *Yuki Gosei Kagaku Kyokai Shi*, **43**, 406 (1985).

17) H. Sakurai, *Pure Appl. Chem.*, **57**, 1759 (1985).

18) I. Heming, *Chem. Soc. Rev.*, **1981**, 83.

19) R. Walsh, *Acc. Chem. Res.*, **14**, 246 (1981).

20) H. Sakurai, *Kagaku*, **39**, 609 (1984).

21) H. Matsumoto, *Yuki Gosei Kagaku Kyokai Shi*, **40**, 490 (1982).

22) R. E. Cooper and W. J. Owen, *J. Organomet. Chem.*, **29**, 33 (1971).

23) F. Sundholm and G. Sundholm, *Electrochim. Acta*, **19**, 565 (1974).

24) T. Fuchigami, Y. Nakagawa, and T. Nonaka, *Tetrahedron Lett.*, **27**, 3896 (1986).

25) M. Kimura, K. Koie, S. Matsubara, Y. Sawaki, and H. Iwamura, *J. Chem. Soc., Chem. Commun.*, **1987**, 122.

26) J. Otera, *Yuki Gosei Kagaku Kyokai Shi*, **44**, 459 (1986).
27) R. A. Holton and R. V. Nelson, *Synth. Commun.*, **10**, 911 (1980).
28) Yoshida el al. have briefly reported the anodic methoxylation of methoxymethyl and (methoxycarbonylamino)-methyl silanes, but the electrolytic conditions are not presented: J. Yoshida, T. Murata, and S. Isoe, 9th. Electroorganic Chemistry Symposium, Sendai, June 1987, Abstr. No. 23.
29) A. Hosomi, *Yuki Gosei Kagaku Kyokai Shi*, **37**, 1026 (1979).
30) H. Gilman and F. J. Marshall, *J. Am. Chem. Soc.*, **71**, 2066 (1949).
31) C. Eaborn and S. H. Parker, *J. Chem. Soc.*, **1955**, 126.
32) L. A. Leites, E. Sh. Finkelstein, V. M. Vdovin, and N. S. Nametkin, *Izv. Akad. Nauk USSR, Ser. Khim.*, **1965**, 1305.
33) H. Gilman and F. J. Webb, *J. Am. Chem. Soc.*, **62**, 987 (1940).
34) P. J. Kocienski, *Tetrahedron Lett.*, **21**, 1559 (1980).
35) G. D. Cooper, *J. Am. Chem. Soc.*, **76**, 3713 (1954).
36) H. Gilman, L. F. Cason, and H. G. Brooks, *J. Am. Chem. Soc.*, **75**, 3760 (1953).
37) S. Cabiddu, C. Floris, S. Melis, and F. Sotgiu, *Phosphorus and Sulfur*, **19**, 61 (1984).
38) J. J. Eisch, J. E. Galle, A. Piotrowski, and M.-R. Tsai, *J. Org. Chem.*, **47**, 5051 (1982).
39) J. E. Noll, J. L. Speier, and B. F. Daubert, *J. Am. Chem. Soc.*, **73**, 3867 (1951).
40) S. Hackett and T. Livinghouse, *J. Org. Chem.*, **51**, 879 (1986).
41) A. Padwa and W. Dent, *J. Org. Chem.*, **52**, 235 (1987).

The Ab Initio Modeling of Hammett-Type Correlations. The Separation of Inductive Effects from Mesomeric Effects in Aromatic Systems

Jun NIWA
College of General Education, Nagoya University, Chikusa, Nagoya 464-01
(Received April 13, 1988)

Substituent effects have been modeled using both substituted hydrogens and substituted benzenes perturbed with point charges in order to separate the inductive (field) effect from the mesomeric effect with the use of ab initio techniques. Several pure dipole 'substituents' have been introduced to derive the scale of inductive effects common to both aliphatic and aromatic systems. In the above systems the interaction energies have been estimated by dividing into electrostatic interaction and polarization. Calculations with the use of 4-31G basis set show satisfactory correlations with the experimentally determined substituent constants. The propriety of the present approach has also been examined for the gas-phase acidities of phenols.

Recently substituent effects in Hammett correlations have been investigated by Streitwieser et al. with the use of STO-3G basis set ab initio techniques,[1] where substituted benzenes are perturbed with pure point charges in order to model the nonbonded reaction center. They have concluded that most substituents have essentially the same polarizability and that they are, therefore, independent of the reaction-center-charge type.

They have, however, made no explicit estimate of the electrostatic interaction (ES) and polarization (PL) between substituent and probe. Comparison with experimentally determined substituent constants has also shown serious discrepancies in the substituents, such as Cl, CF_3, CHO, and $COCH_3$.

On the other hand, years of analyses of Hammett-type correlations have led to a separation of the inductive (field) effects from the mesomeric (resonance) effects in aromatic systems.[2] It has a priori been based on an implicit consensus that the inductive effect of a substituent is uniformly transmitted to the reaction center independently of any structure variation in the parent compounds throughout aliphatic and aromatic systems, while the mesomeric effect varies greatly depending on the extent to which the reaction center interacts with the substituent.

Several experimental and theoretical attempts have been made to derive the standard scale of the inductive effect inherent in each substituent itself.[2,3] Inconsistencies between the scales appear to be a consequence of how well the interactions other than the electrostatic interaction between substituent and reaction center or probe (namely, such effects as resonance, hyperconjugation, and polarization) are eliminated in the aliphatic systems adopted to derive the scale.

One of the major problems remaining in separating the inductive effects from mesomeric effects is to clarify theoretically whether or not such a standard scale of inductive effect inherent in each substituent can be derived. In order to settle this problem using ab initio techniques, we have chosen isodesmic reactions for the systems of substituted hydrogens, HX, and substituted benzenes, C_6H_5X, perturbed with point charges (+)/and(−)···HX (**1**) and (+)/and(−)····C_6H_5X (**2**), respectively, where point charges are located on the molecular axis in the former and in the para-direction in the latter.

The advantage of Systems **1** and **2** as the reference systems is that the HX molecules in System **1** contain no mesomeric interactions and that no mesomeric effects can be due to direct mesomerc interactions with the perturbing site in System **2**.

In the above systems, several pure dipole 'substituents' carrying different charges have been introduced in order to model pure 'inductive' (field) effect substituents and to make a standard scale of the inductive effect, one common to both aliphatic and aromatic systems. The electronic interactions between substituent and probe have been estimated by dividing into electrostatic interaction (ES) and polarization (PL) by utilizing the energy decomposition analysis.[4]

Furthermore, in order to ascertain the propriety of our approach we have attempted to separate the inductive effect from the mesomeric effect in the gas-phase acidities of phenols,[5] in which there exist strong direct mesomeric interactions between the substituent and the reaction center.

Calculation Methods

Calculations were performed using the IMSPAK series[6] of the computer program at the 4-31G basis level, in which the procedure of energy-decomposition analysis[4] was included. The procedure may be briefly described as follows. We express the Hartree–Fock (HF) wave function for the isolated molecule as ψ^0 and its energy as E_0. If we denote the HF wave function of the molecule perturbed with a point charge and its energy as ψ^1 and E_1 respectively, the HF total interaction energy, ΔE_{SCF}, is given by:

$$\Delta E_{SCF} = E_1 - E_0$$

The electrostatic interaction (ES) is the interaction

between the undistorted electron distribution of the molecule and the point charge. In our scheme, ES is calculated as the difference between E_2 and E_0, E_2 being the energy associated with the wave function ψ^0:

$$ES = E_2 - E_0$$

The polarization (PL) is the effect of the distortion of the electron distribution of the molecule by the point charge. Then the difference E_1-E_2 corresponds to the energy change due to the polarization by the point charge:

$$PL = E_1 - E_2$$

The geometries of the benzenoid rings were maintained constant for each substituent; r_{C-C}=1.39 Å r_{C-H}=1.083 Å, and all angles=120°. The geometries of the substituent groups were taken from the experimentally determined values.[7] In the geometry of a pure dipole 'substituent', we have taken the same geometry as Streitwieser et al.[1] used; that is, a positive pole carrying a charge (1.0e) was located at 1 Å from the hydrogen atom of the parent compound, and the distance between positive and negative poles was taken to be 0.72 Å so as to coincide with the dipole moment experimentally determined for nitromethane (3.5 D). The other dipole substituents were set up to carry 0.3e and 0.5e respectively.

The unit point charge of the probe was located at 1 Å from the hydrogen atom along the C-H bond in the para-position in C_6H_5X and at 5.21 Å in HX molecules so as to make their values equal to the distance from the positive pole of the dipole substituent in System **2** (see the Scheme 1 below).

As the means of evaluating the substituent effects on the above perturbed molecules, the following isodesmic reaction was used:

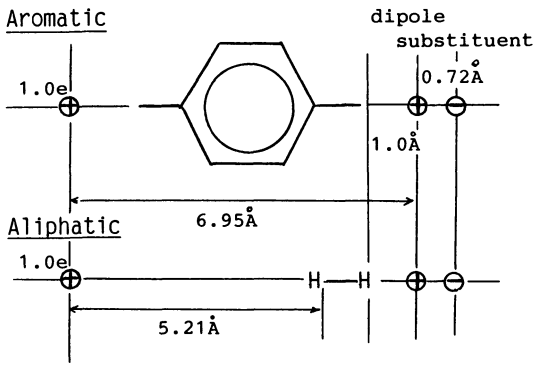

Scheme 1.

$$\underset{A}{RX} + (\pm)\cdots\underset{B}{RH} \rightarrow \underset{C}{RH} + (\pm)\cdots\underset{D}{RX} \quad (1)$$

where X represents a substituent, and RH, a parent compound. The total change in the energy($\delta\Delta E_{SCF}$) for the isodesmic reaction was obtained using Eq. 2. It corresponds to a substituent effect for the perturbed system:

$$\delta\Delta E_{SCF}=(E_C + E_D) - (E_A + E_B)=(E_D - E_A) - (E_B - E_C)=\Delta E_{subst} - \Delta E_H \quad (2)$$

A negative value in $\delta\Delta E_{SCF}$ corresponds to the energy which is stabilized compared with that of the parent compound.

Results and Discussion

The total energies, E_0, E_1, and E_2, are summarized in Tables 1 and 4. The respective energy changes, $\Delta E_{SCF}(\Delta E_{subst})$, are summarized in Tables 2 and 5, where they are also shown divided into electrostatic interactions (ES) and polarization (PL). As may clearly be seen from the tables, the contributions of PL

Table 1. Total Energies of Substituted Hydrogens (HX) and Those Perturbed with Point Charges (hartree)

Substituent	HX	Point charge (+)		Point charge (−)	
	E_0	E_1	E_2	E_1	E_2
1. CH_3	−40.13758	−40.13785	−40.13742	−40.13815	−40.13774
2. H	−1.12676	−1.12675	−1.12649	−1.12729	−1.12703
3. NH_2	−56.10365	−56.10128	−56.10098	−56.10659	−56.10631
4. OCH_3	−114.86845	−114.86403	−114.86365	−114.87362	−114.87325
5. CHO	−113.69106	−113.68696	−113.68651	−113.69606	−113.69562
6. $COCH_3$	−152.68400	−152.68115	−152.68058	−152.68796	−152.68742
7. CF_3	−336.33417	−336.32708	−336.32675	−336.34190	−336.34159
8. F	−99.88727	−99.87943	−99.87928	−99.89539	−99.89525
9. Cl	−459.56313	−459.55712	−459.55671	−459.56994	−459.56954
10. CN	−92.73133	−92.72297	−92.72252	−92.74058	−92.74015
11. NO_2	−204.27804	−204.26709	−204.26674	−204.28966	−204.28933
12. Dipole(1.0e)	−1.84658	−1.83566	−1.83543	−1.85798	−1.85775
13. Dipole(0.5e)	−1.29906	−1.29357	−1.29331	−1.30506	−1.30481
14. Dipole(0.3e)	−1.18511	−1.18181	−1.18155	−1.18893	−1.18868

Table 2. Energies of Electrostatic Interactions (ES) and Polarizations (PL) of Substituted Hydrogens (HX) Perturbed with Point Charges (kcal mol^{-1})

Substituent	Point charge (+)			Point charge (−)		
	ΔE_{SCF}[a)]	ES[a)]	PL[a)]	ΔE_{SCF}[a)]	ES[a)]	PL[a)]
1. CH_3	−0.17	0.10	−0.27	−0.36	0.10	−0.26
2. H	0.01	0.17	−0.16	−0.33	−0.17	−0.16
3. NH_2	1.49	1.68	−0.19	−1.85	−1.67	−0.18
4. OCH_3	2.77	3.01	−0.24	−3.24	−3.01	−0.23
5. CHO	2.57	2.85	−0.28	−3.14	−2.86	−0.28
6. $COCH_3$	1.79	2.15	−0.36	−2.49	−2.15	−0.34
7. CF_3	4.45	4.66	−0.21	−4.85	−4.66	−0.19
8. F	4.92	5.01	−0.09	−5.10	−5.01	−0.09
9. Cl	3.77	4.03	−0.26	−4.27	−4.02	−0.25
10. CN	5.25	5.53	−0.28	−5.81	−5.53	−0.28
11. NO_2	6.87	7.09	−0.22	−7.29	−7.09	−0.20
12. Dipole(1.0e)	6.85	7.00	−0.15	−7.15	−7.01	−0.14
13. Dipole(0.5e)	3.44	3.60	−0.16	−3.77	−3.60	−0.17
14. Dipole(0.3e)	2.07	2.23	−0.16	−2.40	−2.24	−0.16

a) Differences at two places below the decimal points show the limits of the accuracy of the present calculations.

Table 3. Isodemic Energies of Substituted Hydrogens (HX) Perturbed with Point Charges (kcal mol^{-1})

Substituent	Point charge (+)			Point charge (−)		
	$\delta\Delta E_{SCF}$	δES	δPL	$\delta\Delta E_{SCF}$	δES	δPL
1. CH_3	−0.2	−0.1	−0.1	0.0	0.1	−0.1
2. H	0.0	0.0	0.0	0.0	0.0	0.0
3. NH_2	1.5	1.5	0.0	−1.5	−1.5	0.0
4. OCH_3	2.8	2.8	0.0	−2.9	−2.8	−0.1
5. CHO	2.6	2.7	−0.1	−2.8	−2.7	−0.1
6. $COCH_3$	1.8	2.0	−0.2	−2.2	−2.0	−0.2
7. CF_3	4.4	4.5	−0.1	−4.5	−4.5	0.0
8. F	4.9	4.8	0.1	−4.8	−4.8	0.0
9. Cl	3.8	3.9	−0.1	−3.9	−3.9	0.0
10. CN	5.2	5.4	−0.2	−5.5	−5.4	−0.1
11. NO_2	6.9	6.9	0.0	−7.0	−6.9	−0.1
12. Dipole(1.0e)	6.8	6.8	0.0	−6.8	−6.8	0.0
13. Dipole(0.5e)	3.4	3.4	0.0	−3.4	−3.4	0.0
14. Dipole(0.3e)	2.1	2.1	0.0	−2.1	−2.1	0.0

Table 4. Total Energies of Monosubstituted Benzenes (C_6H_5X) and Those Perturbed with Point Charges (hartree)

Substituent	C_6H_5X	Point charge (+)		Point charge (−)	
	E_0	E_1	E_2	E_1	E_2
1. CH_3	−269.35678	−269.41059	−269.31329	−269.46820	−269.40033
2. H	−230.37710	−230.42667	−230.33085	−230.49016	−230.42333
3. NH_2	−285.32524	−285.38428	−285.28645	−285.43214	−285.36402
4. OCH_3	−344.07902	−344.13186	−344.03450	−344.19152	−344.12353
5. CHO	−342.92560	−342.96163	−342.86480	−343.05460	−342.98640
6. $COCH_3$	−381.90433	−381.94435	−381.84706	−382.03006	−381.96160
7. CF_3	−565.56236	−565.59608	−565.50083	−565.69051	−565.62389
8. F	−329.10717	−329.14647	−329.05174	−329.22877	−329.16260
9. Cl	−688.77574	−688.81668	−688.72013	−688.89871	−688.83135
10. CN	−321.96928	−321.99981	−321.90317	−322.10325	−322.03538
11. NO_2	−433.51752	−433.53859	−433.44307	−433.65925	−433.59197
12. Dipole(1.0e)	−231.09762	−231.12420	−231.03003	−231.23117	−231.16520
13. Dipole(0.5e)	−230.54858	−230.58686	−230.49185	−230.67171	−230.60531
14. Dipole(0.3e)	−230.43472	−230.47758	−230.38224	−230.55378	−230.48720

Table 5. Energies of Electrostatic Interactions (ES) and Polarizations (PL) of Substituted Benzenes (C_6H_5X) Perturbed with Point Charges (kcal mol^{-1})

Substituent	Point charge (+)			Point charge (−)		
	ΔE_{SCF}[a]	ES[a]	PL[a]	ΔE_{SCF}[a]	ES[a]	PL[a]
1. CH_3	−33.76	27.29	−61.05	−69.93	−27.33	−42.60
2. H	−31.10	29.02	−60.12	−70.94	−29.01	−41.93
3. NH_2	−37.05	24.34	−61.39	−67.08	−24.33	−42.75
4. OCH_3	−33.15	27.93	−61.08	−70.61	−27.93	−42.68
5. CHO	−22.61	38.15	−60.76	−80.96	−38.16	−42.80
6. $COCH_3$	−25.12	35.94	−61.06	−78.91	−35.94	−42.97
7. CF_3	−21.16	38.61	−59.77	−80.43	−38.62	−41.81
8. F	−24.66	34.78	−59.44	−76.30	−34.78	−41.52
9. Cl	−25.69	34.90	−60.59	−77.18	−34.90	−42.28
10. CN	−19.16	41.48	−60.64	−84.06	−41.48	−42.58
11. NO_2	−13.22	46.71	−59.93	−88.93	−46.71	−42.22
12. Dipole(1.0e)	−16.68	42.41	−59.09	−83.80	−42.40	−41.40
13. Dipole(0.5e)	−24.02	35.60	−59.62	−77.28	−35.60	−41.68
14. Dipole(0.3e)	−26.89	32.93	−59.82	−74.72	−32.94	−41.78

a) Differences at two places below the decimal points show the limits of the accuracy of the present calculations.

Table 6. Isodesmic Energies of Monosubstituted Benzenes (C_6H_5X) Perturbed with Point Charges (kcal mol^{-1})

Substituent	Point charge (+)			Point charge (−)		
	$\delta\Delta E_{SCF}$	δES	δPL	$\delta\Delta E_{SCF}$	δES	δPL
1. CH_3	−2.7	−1.7	−1.0	1.0	1.7	−0.7
2. H	0.0	0.0	0.0	0.0	0.0	0.0
3. NH_2	−6.0	−4.7	−1.3	3.9	4.7	−0.8
4. OCH_3	−2.1	−1.1	−1.0	0.3	1.1	−0.9
5. CHO	8.5	9.1	−0.6	−10.0	−9.1	−0.9
6. $COCH_3$	6.0	6.9	−0.9	−8.0	−6.9	−1.1
7. CF_3	9.9	9.6	0.3	−9.5	−9.6	0.1
8. F	6.4	5.8	0.6	−5.4	−5.8	0.4
9. Cl	5.4	5.9	−0.5	−6.2	−5.9	−0.3
10. CN	11.9	12.5	−0.6	−13.1	−12.5	−0.6
11. NO_2	17.9	17.7	0.2	−18.0	−17.7	−0.3
12. Dipole(1.0e)	14.4	13.4	1.0	−12.9	−13.4	0.5
13. Dipole(0.5e)	7.1	6.6	0.5	−6.3	−6.6	0.3
14. Dipole(0.3e)	4.2	3.9	0.3	−3.8	−3.9	0.1

to the total interaction energies, ΔE_{SCF}, are small compared with those of ES, except for X=H and CH_3 in Systerm **1**, while those of PL are much more than those of ES in System **2**. However, the contributions of PL to the isodesmic energies ($\delta\Delta E_{SCF}$) (Tables 3 and 6) are almost the same in magnitude in the two systems; as a whole, their contributions to the substituent effects are small compared with those of ES.

According to the comments of Streitwieser et al.[1] the original assumptions for the Hammett equation were that the susbstituent constants are independent of the nature of the reactions and that a different charge center changes only the sign of the reaction constant. Strictly speaking, these assumptons are valid only in an approximate sense. The latter assumption should be restricted only to the electrostatic interactions because the contributions of PL act as a disturbing factor for the assumption, even in the present model systems, which are perturbed only with point charges.

Figure 1-(a) shows plots of the $\delta\Delta E_{SCF}$ values in System **1** perturbed with positive and negative charges, where the dotted line of a unit slope is drawn through the points for the δ ES values. The deviations from the line show the contributions of PL to the substituent effects. Such contributions can almost be ignored in System **1**. The solid line shows the correlation between the $\delta\Delta E_{SCF}$ values of the systems (the value of slope: −0.99, correlation coefficient: r=0.998, goodness of 'fit':[8] f=0.03). These results practically satisfy the original assumptions for the Hammett equation including the dipole 'substituents'; this means that System **1** can be used as a reference system to derive a standard scale of the inductive effect independent of the charge type of the probe. On the other hand, the contributions of PL to the substituent effects in System **2** are rather too large to ignore (Fig.1-(b)), and those perturbed with positive point chrges are a little larger than those perturbed with negative point charges (r=0.985, f=0.13). These results imply that the standard σ^0 values experimentally derived in cationic

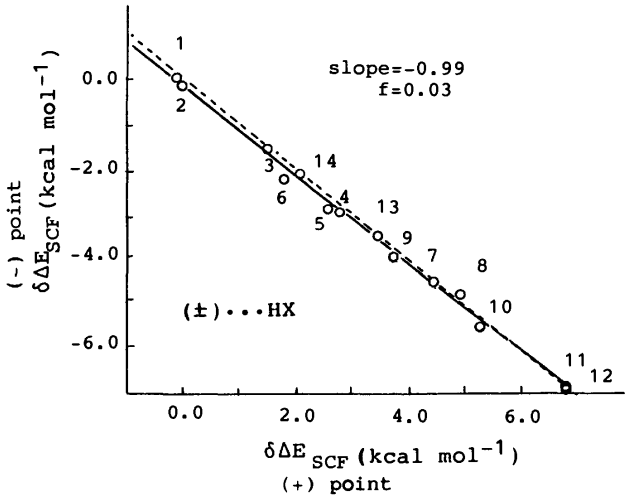

(a)

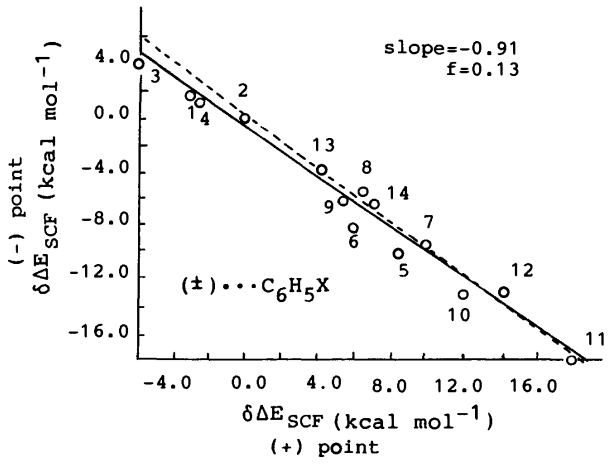

(b)

Fig. 1. (a) Plots of the isodesmic energy changes ($\delta\Delta E_{SCF}$) for point charge perturbed substituted hydrogens (HX).
(b) Plots of the isodesmic energy changes ($\delta\Delta E_{SCF}$) for point charge perturbed para-substituted benzenes (C_6H_5X). The dotted line connects the point for δES with a slope of −1.00. The regression line shown corresponds to the open circles. The numbering corresponds to that in Tables 3 and 6, respectively.

systems must be somewhat different from those derived in anionic systems. Therefore, in order to derive experimentally the 'inherent' substituent constants, it is necessary to choose the system in which there exists no polarization contribution arising from charged probe centers and in which complicating solvent effects have been eliminated as much as possible. Recently several attempts have been performed to derive 'inherent' substituent constants by utilizing gas-phase reactions.[9] However, all the reactions thus far examined have carried charged probe centers and also contained additive resonance interactions between the substituents and the reaction center.

Therefore, up to the present, the σ_R^0 values redefined

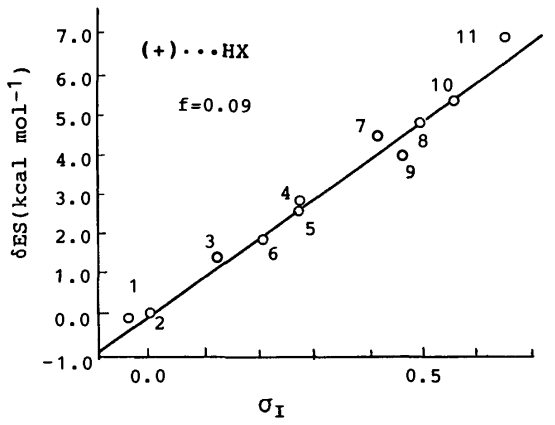

Fig. 2. Plots of δES against σ_I for the positive point charge perturbed substituted hydrogens (HX). The numbering corresponds to that in Table 3.

by Taft et al.[10] appear to be the nearest to the original assumptions for the Hammett equation; they have been determined on the basis of the substituent chemical shift, ^{13}C, at the para-position (C_p-SCS) of monosubstituted benzenes in diluted 'inert' solvents and, therefore, the ^{13}C 'probe' is a part of the 'neutral' aryl ring unperturbed by the charge. In the present analysis we will define the experimental 'inherent' substituent constants σ^0 (inh) using σ_I and σ_R^0 values determined by Taft et at.,[10] that is, $\sigma^0(\text{inh})=\sigma_I+\sigma_R^0$ (Table 2 in Ref. 10).

Figure 2 shows plots of the δ ES in System **1** against the σ_I values determined by Taft et al.,[10] where representative eleven substituents are chosen. The δES values obtained at 4-31G show a 'good' fit (r=0.989, f=0.09), while those at STO-3G show serious discrepancies in the substituents F, Cl, CF_3, CHO, and $COCH_3$.

Theoretical approaches to derive the field-effect parameter (σ_F) have also been performed by several workers, using the isodesmic reactions (NH_4^+/HX), measuring the polarization of a bond produced in an isolated moloecule by the HX molecule (HH/HX), and using the electrostatic potentials ($EP_{(HX)}$) obtained from the interaction of a positive charge at a determined geometry from a HX molecule, and so on.[3b] The third approach is essentially identical with that of Streitwieser et al.[1] The $\sigma_{F(theo)}$ values recommended by Topsom are summarized in Ref. 3b (Table 19 on p. 166). The correlation of δES and $\sigma_{F(theo)}$ values showed a 'good' fit (r=0.988, f=0.10, n=11), while that of δES and $EP_{(HX)}$ was properly excellent (r=0.997, f=0.05, n=9).

Figure 3 shows plots of the δES against values $\sigma^0(\text{inh})=(\sigma_I+\sigma_R^0)$[10] in System **2**. The δES values obtained at 4-31G also show a 'fair' fit for the eleven substituents (r=0.988, f=0.13). In this case, too, values obtained at STO-3G show serious discrepancies for the substituents, CF_3, CHO, $COCH_3$, and Cl. The correla-

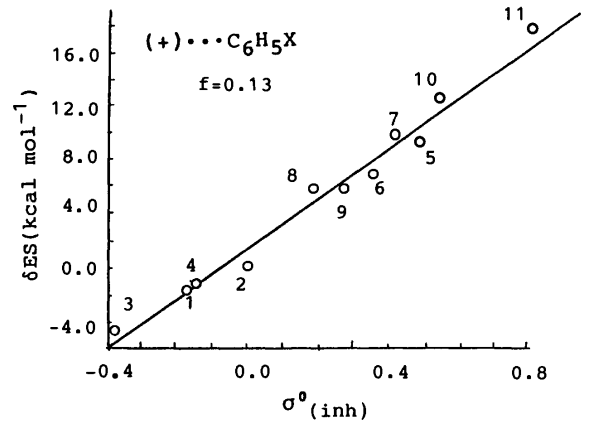

Fig. 3. Plots of δES against σ^0(inh)($=\sigma_I+\sigma_R^0$) for para-substituted benzenes (C_6H_5X). The numbering corresponds to that in Table 6.

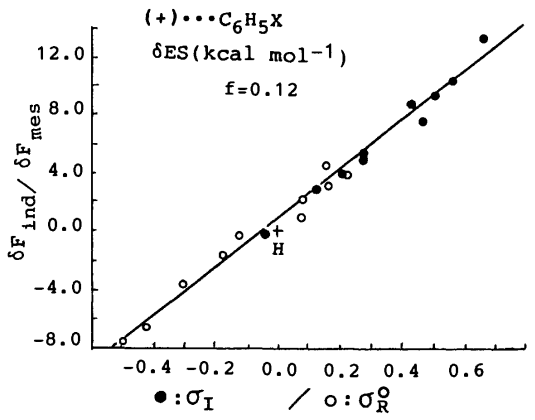

Fig. 5. Correlation between δF_{ind} and δF_{mes} against $\sigma_{I(inh)}$ and σ_R^0, respectively, on the same regression line.

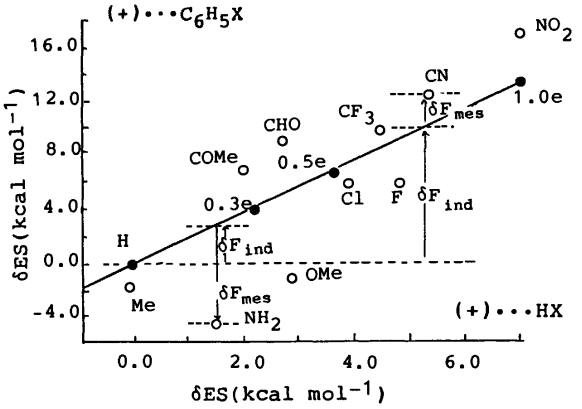

Fig. 4. Separation of inductive effects from mesomeric effects. Plots of δES for the positive point charge perturbed substituted hydrogens (HX) and benzenes (C_6H_5X). A regression line shows the correlation between hydrogen and dipole substituents. The deviations from the line (δF_{ind} and δF_{mes}) correspond to the inductive and mesomeric contributions of substituents in C_6H_5X.

tion between the $\delta\Delta E_{SCF}$ values which contain the contribution of PL and σ^0(inh) also shows a 'fair' fit (r=0.985, f=0.16 and r=0.988, f=0.13 for both systems, perturbed with positive and negative point charges respectively).

Figure 4 shows plots of the δES values in System **2** against those in System **1** perturbed with the positive point charge, where the correlation line is drawn for three 'dipole' substituents and hydrogen to derive the scale of inductive effects in aromatic systems (r=0.999, f=0.03). The intersecting point of a perpendicular line drawn from a substituent with the correlation line corresponds to its inductive effect, because it contains no mesomeric interactions and it is a quantity directly proportional to the inductive effect in System **1**. Points above the line correspond to π-destabilizing groups, while points below the line correspond to π-stabilizing groups. Thus, deviations from the correlation line correspond to the 'mesomeric effects' in the Hammett equations.

There can not be any direct mesomeric interactions between a substituent and a probe in System **2**. Therefore, the mesomeric contribution must be attributed to the field effect caused by the distribution of charges on the molecule, a distribution which stems from a strong interaction between the π-system of the benzene ring and suitable orbitals on the substituent group. Hereafter, we will abbreviate the former effect as δF_{ind}, and the latter, as δF_{mes}. The latter is expected to be proportional to the experimentally determined σ_R^0 values. The values of δF_{ind} and δF_{mes} are summarized in Table 9, while those of σ_I, σ_R^0, and σ_R^- (g)[5] are cited in Table 10.

Figure 5 shows plots of δF_{ind} against σ_I and those of δF_{mes} against σ_R^0. The correlation shows a 'fair' fit (r=0.991, f=0.12) on the same correlation line; no substituents examined show any serious deviations from the correlation line.

The theoretical σ_R^0 values have also been derived by the calculation of the overall π-electron transfer, $\sum q_\pi$, in monosubstituted benzenes and ethylenes.[3b] The correlation of δF_{mes} with the $\sigma_{R(theo)}^0$ values was 'fair' (r=0.986, f=0.18, n=11), while δF_{mes} was well correlated with the experimental σ_R values summarized by Topsom (Table 1 in p. 16 of Ref. 3b) (r=0.992, f=0.13, n=11).

Strictly speaking from the experimental point of view, a common scale of inductive effects exists, of course, only in an approximate sense. In the present approach, a common scale of inductive effects throughout the aliphatic and aromatic systems has been obtained by the introduction of the pure dipole 'substituents'. Our results imply that the hypothetical dipole of the substituent group in the aromatic system which corresponds to that of the aliphatic system can be estimated from the correlation line. Although the pure dipole 'substituents' are undoubtedly not actual,

the existence of the common scale is guaranteed since they are intrinsically of an abstract nature.

The propriety of the present approach has further been investigated for the gas-phase acidities of *p*-substituted phenols.[5] The corresponding isodesmic reaction is:

$$XC_6H_4OH + C_6H_5O^- \rightarrow XC_6H_4O^- + C_6H_5OH \quad (3)$$

where the geometries of the parent compounds, C_6H_5OH and $C_6H_5O^-$, were optimized by means of the energy-gradient method at the 3-21G level,[11] while those of the substituent groups were taken from the experimentally determined values.

The total energies calculated at 4-31G for *p*-substituted phenols and phenoxide ions are summarized in Table 7. The isodesmic energies ($\delta\Delta E_{SCF}$) are summarized in Table 8 and compared with the experimentally obtained values.[12] The calculations considerably overestimated the observed substituent effects ($\delta\Delta G^0$ (g) kcal mol^{-1}). As may clearly be seen from Fig. 6, however, the correlation between observed and calculated values shows almost a 'good' fit (r=0.993, f=0.11) for all the substituents measured.

Table 7. Total Energies of Phenols (XC_6H_4OH) and Phenoxide Ions ($XC_6H_4O^-$) (hartree)

Substituent	XC_6H_4OH	$XC_6H_4O^-$
1. CH_3	−344.06472	−343.46771
2. H	−305.12403	−304.53078
3. NH_2	−360.06859	−359.46623
4. OCH_3	−418.83220	−418.23581
5. OH	−379.86506	−379.27200
6. CHO	−417.67369	−417.10948
7. CF_3	−640.31004	−639.73952
8. F	−403.85238	−403.26757
9. CN	−396.71666	−396.15618
10. NO_2	−508.26620	−507.71714
11. Dipole(1.0e)	−305.84254	−305.27846
12. Dipole(0.5e)	−305.29428	−304.71565
13. Dipole(0.3e)	−305.18086	−304.59638

Table 8. Comparison of Experimental Values with Theoretical Calculations of the Relative Gas-Phase Acidities of Para-Substituted Phenols (kcal mol^{-1})

Substituent	$\delta\Delta G^0$(g)	$\delta\Delta E_{(SCF)}$
1. CH_3	1.1	2.4
2. H	0.0	0.0
3. NH_2	3.3	5.7
4. OCH_3	1.2	2.0
5. OH	1.2	−0.1
6. CHO	−15.8	−18.2
7. CF_3	−11.9	−14.1
8. F	−2.3	−5.3
9. CN	−16.6	−20.6
10. NO_2	−20.9	−27.7
11. Dipole(1.0e)	—	−18.3
12. Dipole(0.5e)	—	−9.2
13. Dipole(0.3e)	—	−5.5

In order to separate the inductive effects from the mesomeric effects in this case, too, the pure dipole 'substituents' have been introduced in the same way as in System **2**. Figure 7 shows the plots of the $\delta\Delta E_{SCF}$ values against the δES values in System **1** perturbed with negative point charge, where the correlation line

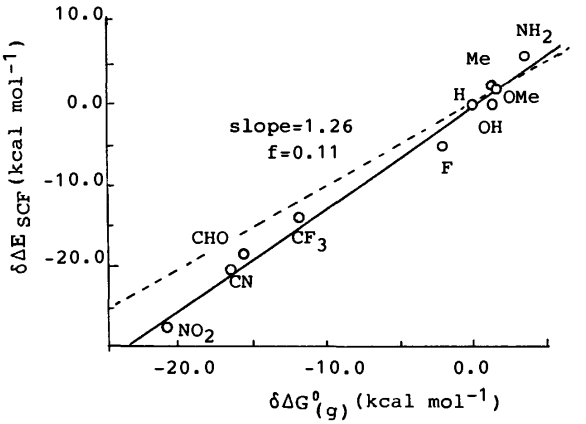

Fig. 6. Correlation of $\delta\Delta E_{SCF}$(calcd) against $\delta\Delta G^0$(g)-(obsd) for the isodesmic reactions for *p*-substituted phenols. The dotted line shows a unit slope.

Table 9. Values of δF_{ind} and δF_{mes} in Monosubstituted Benzenes (C_6H_5X), and Values of Inductive and Mesomeric Components ($\delta\Delta E_{ind}$ and $\delta\Delta E_{mes}$) in Isodesmic Reactions of *p*-Substituted Phenols (kcal mol^{-1})

Substituent	C_6H_5X		XC_6H_4OH	
	δF_{ind}	δF_{mes}	$\delta\Delta E_{ind}$	$\delta\Delta E_{mes}$
1. CH_3	−0.1	−0.3	0.2	2.2
2. H	0.0	0.0	0.0	0.0
3. NH_2	2.9	−7.6	−4.0	9.8
4. OCH_3	5.5	−6.5	−7.6	9.6
5. CHO	5.2	4.0	−7.2	−11.1
6. $COCH_3$	3.8	3.1	—	—
7. CF_3	8.6	1.0	−12.0	−2.1
8. F	9.3	−3.5	−13.0	7.7
9. Cl	7.4	−1.5	—	—
10. CN	10.3	2.2	−14.4	−6.2
11. NO_2	13.3	4.4	−18.6	−9.2

Table 10. Values of σ_I, σ_R^0, and σ_R^-(g)

Substituent	σ_I	σ_R^0	σ_R^-(g)
CH_3	−0.04(—)	−0.13	−0.09
H	0.00(0.00)[a]	0.00	0.00
NH_2	0.12(0.10)	−0.50	−0.24
OCH_3	0.27(0.25)	−0.42	−0.29
CHO	0.27(0.32)	0.22	0.46
$COCH_3$	0.20(0.22)	0.16	0.43
CF_3	0.42(0.43)	0.08	0.15
F	0.50(0.50)	−0.31	−0.38
Cl	0.46(0.46)	−0.18	−0.17
CN	0.56(0.58)	0.08	0.23
NO_2	0.65(0.65)	0.15	0.41

a) Values in parentheses are cited from Ref. 5.

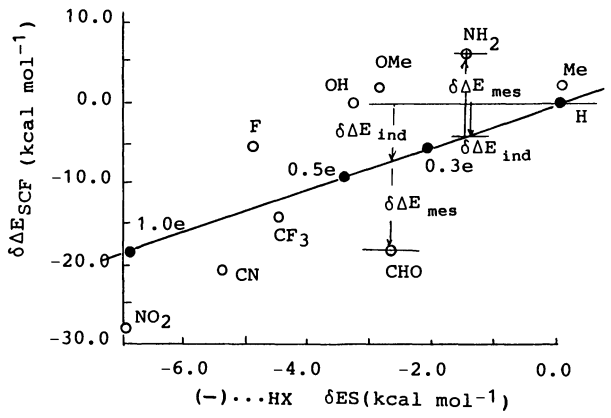

Fig. 7. Separation of inductive effects from mesomeric effects. Plots of the isodesmic energy changes ($\delta\Delta E_{SCF}$) for *p*-substituted phenols against δES for negaitive point charge perturbed hydrogens. A regression line shows the correlation between hydrogen and dipole substituents. The deviations from the line ($\delta\Delta E_{ind}$ and $\delta\Delta E_{mes}$) correspond to the inductive and mesomeric contributions of substituents.

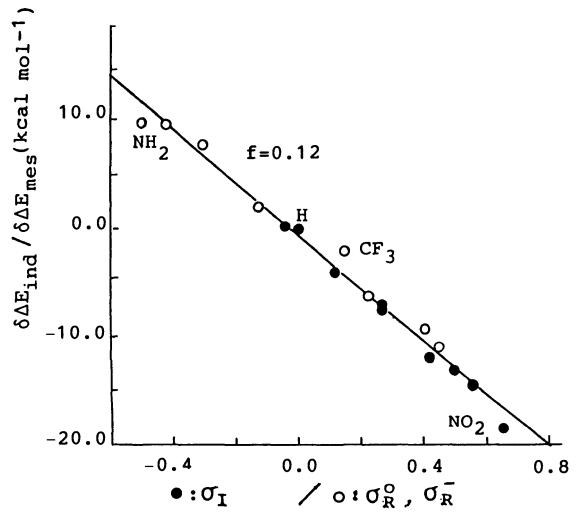

Fig. 8. Correlation between $\delta\Delta E_{ind}$ and $\delta\Delta E_{mes}$ against σ_I and σ_R^0(for EDG)/σ_R^-(g)(for EWG), respectively, on the same correlation line.

is drawn for three dipole 'substituents' and hydrogen. The correlation is very good (r=1.000, f=0.001). By the same procedure as that described in System **2**, the inductive effects ($\delta\Delta E_{ind}$) can be estimated. The points above the line correspond to π-destabilizing groups (electron donating groups; EDG), while the points below the line correspond to π-stabilizing groups (electron withdrawing groups; EWG). Thus, deviations from the correlation line correspond to mesomeric effects ($\delta\Delta E_{mes}$). Therefore, the deviations above the line may be expected to be proportional to the σ_R^0 values, while the downward deviations may be expected to be proportional to the σ_R^- (g) values.

Figure 8 shows plots of $\delta\Delta E_{ind}$ against σ_I and also plots of $\delta\Delta E_{mes}$ against σ_R^0 for EDG and against σ_R^- (g) for EWG. The correlation shows a 'fair' fit (r=0.992, f=0.12) on the same correlation line.[13]

The present approach provides us with theoretical grounds for the separation of the inductive effect from the mesomeric effect in aromatic systems. It can also be applied to gas-phase reactions in which the reaction center carries a positive charge. We will present the results of analyses of these in succeeding papers.

The numerical calculations were carried out on a FACOM M-382 computer at the Nagoya University Computation Center.

References

1) E. R. Vorpagel, A. Streitwieser, Jr., and S. D. Alexandratos, *J. Am. Chem. Soc.*, **103**, 3777 (1981).

2) "Steric Effects in Organic Chemistry," ed. by M. S. Newman, John Wiley, New York (1956), p. 556; "Advances in Liner Free Energy Relationships," ed. by N. B. Chapman and T. Shorter, Plenum Press, New York (1972), p. 11; "Correlation Analysis in Chemistry," ed. by N. B. Chapman and T. Shorter, Plenum Press, New York (1978), p. 119.

3) a) "Progress in Physical Organic Chemistry," ed. by R. W. Taft, John Wiley, New York (1983), Vol. 14, p. 247 and the references cited therein; b) "Progress in Physical Organic Chemistry," ed. by W. Taft, John Wiley, New York (1987), Vol. 16, pp. 16, 125 and the references cited therein.

4) S. Iwata and K. Morokuma, *J. Am. Chem. Soc.*, **95**, 7563 (1973); S. Yamabe and K. Morokuma, *ibid.*, **97**,4458 (1975); K. Morokuma, *Acc. Chem. Res.*, **10**, 295 (1977).

5) M. Fujio, R. T. McIver, Jr., and R. W. Taft, *J. Am. Chem. Soc.*, **103**, 4017 (1981).

6) The GAUSSIAN-70 and HONDO programs have been modified and revised in the form of the IMSPAK program at the Institute of Molecular Science (Japan).

7) "Tables of Interatomic Distance and Configuration in Molecules and Ions," Chem. Soc. London, Spec. Publ., No. 11 (1958).

8) "Correlation Analysis of Organic Reactivity," ed. by J. Shorter, Reseach Studies Press, New York (1982), p. 216.

9) "Progress in Physical Organic Chemistry," ed. by R. W. Taft, John Wiley, New York (1987), Vol. 16, p. 1.

10) J. Bromilow, R. T. Brownlee, V. O. Lopez, and R. W. Taft, *J. Org. Chem.*, **44**, 4766 (1979).

11) This level of theory has been demonstrated to be reliable in the calculation of molecular geometries for a wide variety of systems. See for example, D. J. DeFrees, B. A. Levi, S. K. Pollack, W. J. Hehre, J. S. Binkley, and J. A. Pople, *J. Am. Chem. Soc.*, **101**, 4085 (1979); W. J. Pietro, M. M. Francl, W. J. Hehre, D. J. DeFrees, J. A. Pople, and J. S. Binkley, *J. Am. Chem. Soc.*, **104**, 5039 (1982).

12) Calculations were also performed for some phenoxide ions with 4-31+G, where a diffuse sp function (exponent: 0.068) is taken into account. Althoguh the total energies were improved (for example, X=H; −304.54540, X=NO_2; −507.72919 (hartree)), the isodesmic energy was not so much affected ($\delta\Delta E_{SCF}$ for X=NO_2: −26.1 kcal mol^{-1}).

13) When σ_R^- (g) values were used for the EDG, the correlation partly collapsed for F and NH_2 (r=0.986, f=0.16).

Effective Doping of Polymer Anion during Chemical Polymerization of Pyrrole Using $Fe(OH)_3$ Oxidant

Akira OHTANI† and Takeo SHIMIDZU*
Division of Molecular Engineering, Graduate School of Engineering, Kyoto University, Sakyo-ku, Kyoto 606
†Central Research Laboratory, Nitto Electric Industrial Co., Ltd., Ibaraki, Osaka 567
(Received May 16, 1988)

Polypyrroles were prepared by the chemical polymerization of pyrrole using various combinations of Fe^{3+} oxidants and electrolytes. The morphology and yield of the resulting polymers were affected by the property of the electrolyte anion in the oxidative solution. The size of the particles of the resulting polymers was decreased by using a high-molecular-weight polymer anion as the electrolyte anion. Both the polymer anion and Cl^- were incorporated as a dopant into the polypyrrole matrix during the chemical polymerization of pyrrole, using an aqueous solution containing both $FeCl_3$ and the polymer anion. On the contrary, the polymer anion was effectively incorporated as a dopant into the polypyrrole matrix during the chemical polymerization of pyrrole, using an aqueous solution containing both $Fe(OH)_3$ and the polymer acid. A novel type of chemical preparation of the polypyrrole-polymer anion composite using the $Fe(OH)_3$ oxidant and the polymer acid was developed.

Conducting polypyrrole (PPy)[1-6] has applications in such equipment as electronic devices,[7,8] electrochromic displays,[9-11] polymer batteries,[12-15] polymer modified electrodes,[16] and functional membranes.[17-20] An electrochemical polymerization, a chemical polymerization, and a photo-electrochemical polymerization of pyrrole easily provided conducting PPy. Moreover, many hydridization procedures of PPy have been developed so as to improve the properties of PPy.[21-40] In electrochemical polymerization, dopant anions are freely chosen, since they act as supporting electrolytes. Many kinds of PPy-functional anion composites have been prepared.[21-23,32,33] The functional anions to be doped were such as electrochromic molecules, photosensitive molecules, nucleic acids, amino acids, tenside anion, and polymer anions. In the chemical polymerization of pyrrole in a solution containing both an oxidant and a functional anion, an anion of oxidant, e.g. Cl^- of $FeCl_3$, is easily incorporated as a dopant into the PPy matrix, though the doping of the functional anion is not efficient. However, chemical polymerization is a useful method for preparing of large amount of conducting polymers, since it is performed without electrodes.[41-45] In this study, $Fe(OH)_3$ was chosen as an oxidant; and discussions are presented concerning the effective doping of the polymer anion into the PPy matrix during the chemical polymerization of pyrrole in H_2O containing the $Fe(OH)_3$ oxidant and the polymer acid.

Experimental

Materials. Pyrrole (Aldrich Chemical) was distilled and stored under a N_2 atmosphere. $FeCl_3 \cdot 6H_2O$ (Wako Chemical), $Fe_2(SO_4)_3$ (Wako Chemical), sodium 1-propanesulfonate (PSNa) (Nakarai Chemical), and 1-propanesulfonic acid (PSH) (Kodak) were used without further purification. $Fe(OH)_3$ was prepared by adding a $FeCl_3$ aqueous solution to a NaOH aqueous solution; then, the precipitate of $Fe(OH)_3$ was filtered to remove Na^+ and Cl^-. Sodium polyethylenesulfonate (PESNNa) was prepared by the polymerization of sodium ethylenesulfonate (Tokyo Kasei), using a combination of potassium peroxodisulfate (Wako Chemical) and sodium hydrogensulfite (Wako Chemical) as a redox-initiator in H_2O. The degree of polymerization was controlled by varying the polymerization time. Polyethylenesulfonic acid (PESNH) and polystyrenesulfonic acid (PSSH) were obtained by an ion-exchange treatment of PESNNa and sodium polystyrenesulfonate (Toyo Soda) through ion-exchange column (DOWEX 50W-12; Dow Chemical), respectively.

Preparation of PPy. Reaction of Pyrrole with $FeCl_3$ and $Fe_2(SO_4)_3$ Aqueous Solutions: Pyrrole (0.187 ml) was added to a 10 ml $FeCl_3$ aqueous solution (0.54 mol dm^{-3}) or in 10 ml $Fe_2(SO_4)_3$ aqueous solution (0.27 mol dm^{-3}); the solution instantly acquired a black color as the PPy precipitate was formed. After 2 hours at room temperature, the mixture was filtered and the precipitate was washed with distilled water. After a final rinse with acetone, the black powder was dried in vacuo.

Reaction of Pyrrole with $FeCl_3$ Aqueous Solution Containing Polymer Anion: Pyrrole (0.187 ml) was added in 10 ml $FeCl_3$ aqueous solution (0.54 mol dm^{-3}) containing 1.62 mol dm^{-3} PESNNa; the solution instantly acquired a black color as the PPy precipitate was formed. After 2 hours at room temperature, the mixture was filtered and the precipitate was washed with distilled water. After a final rinse with acetone, the black powder was dried in vacuo.

Reaction of Pyrrole with $Fe(OH)_3$: An acid (PSH, PESNH, or PSSH) (0.0162 mol) was added to 10 ml of H_2O containing pyrrole (0.0027 mol) and suspended $Fe(OH)_3$ (0.0054 mol); the solution instantly acquired a black color. After 2 hours at room temperature, the mixture was filtered and the precipitate was washed with distilled water (in the case that the precipitate was obtained). On the contrary, when a precipitate was not obtained, the mixture was centrifuged at 3000 rpm; then, the supernatant was disposed of. The remaining mixture was filtered and the precipitate was washed with distilled water. After a final rinse with

acetone, the black powder was dried in vacuo.

Measurements. The conductivity was measured by using a standard van der Pauw method. The PPy powder was molded into a disk by pressing. Scanning and transmission electron microscopic (SEM and TEM) observations were carried out with a Hitachi S-450 and a Hitachi H-800, respectively. The preparation of ultrathin sections of the resulting polymers used for TEM observations was carried out by cutting the PPy powder dispersed PET film, which was embedded in epoxy resin (Polysciences), with an ultra microtome (Sorvall, MT-6000). An elementary analysis of Fe atoms in the PPy matrix was carried out with an X-ray Microanalyzer attachment (Hitachi H-8010).

Results and Discussion

Table 1 shows the conditions of the chemical polymerization of pyrrole using various Fe^{3+} oxidants and electrolytes, as well as the characteristics of the resulting polymers. Pyrrole was polymerized by $FeCl_3$ and $Fe_2(SO_4)_3$ aqueous solutions containing no other electrolyte. The resulting polymers (PPy/Cl^- and PPy/SO_4^{2-}) were precipitated, and black powders were obtained by filtration. On the contrary, pyrrole was not polymerized by $Fe(OH)_3$ suspended H_2O containing no electrolyte. Upon adding an electrolyte, PSNa or PESNNa, into the $Fe(OH)_3$ suspended H_2O, pyrrole was not polymerized either. It was considered that $Fe(OH)_3$ cannot oxidize pyrrole. Upon adding an acid, PSH, PESNH, or PSSH, into the $Fe(OH)_3$ suspended H_2O, $Fe(OH)_3$ was dissolved and pyrrole was polymerized. When PSH and low-molecular-weight PESNH (η_{inh}=0.05) were used as an electrolyte, the resulting polymers (PPy/PS^- and PPy/$PESN^-$(1)) were precipitated. In contrast, when high-molecular-weight PESNH (η_{inh}=0.19 and 0.24) and PSSH (η_{inh}=0.77) were used as an electrolyte, the resulting polymers (PPy/$PESN^-$(2), PPy/$PESN^-$(3), and PPy/PSS^-) were suspended. On the other hand, the resulting polymer (PPy/mix.) prepared by $FeCl_3$ aqueous solution containing PESNNa (η_{inh}=0.19) was precipitated. PPy/PS^-, PPy/mix., and PPy/$PESN^-$(1) were easily obtained by filtration. On the contrary, PPy/$PESN^-$(2) and PPy/$PESN^-$(3) were obtained by a combination of centrifugation (3000 rpm) and filtration. Particles of these polymers did not precipitate perfectly. The PPy/PSS^- did not precipitate upon centrifugation (3000 rpm). These results indicate that the size of the particles of the resulting polymer depended on the property of the electrolyte anion.

Table 2 shows elementary analysis and conductivity data of the resulting polymers. These PPy had as high conductivity (ca. 10^0 S cm^{-1}) as PPy prepared by electrochemical polymerization in H_2O.[37] The Cl/N and the S/N ratios allowed us to estimate the ratio of incorporated anions to the pyrrole moiety (f). As for the polymer anion, the present f-value does not necessarily indicate the doping ratio, since the existence of

Table 1. Conditions and Proceedings of Polymerization

Oxidant	Electrolyte[a]	Viscosity/η_{inh}[b]	Resulting polymer	Abbreviation
$FeCl_3$	None	—	Precipitated	PPy/Cl^-
$Fe_2(SO_4)_3$	None	—	Precipitated	PPy/SO_4^{2-}
$Fe(OH)_3$	None	—	Not polymerized	—
$Fe(OH)_3$	PSNa	—	Not polymerized	—
$Fe(OH)_3$	PSH	—	Precipitated	PPy/PS^-
$Fe(OH)_3$	PESNNa	0.19	Not polymerized	—
$FeCl_3$	PESNNa	0.19	Precipitated	PPy/mix.
$Fe(OH)_3$	PESNH	0.05	Precipitated	PPy/$PESN^-$ (1)
$Fe(OH)_3$	PESNH	0.19	Suspended	PPy/$PESN^-$ (2)
$Fe(OH)_3$	PESNH	0.24	Suspended	PPy/$PESN^-$ (3)
$Fe(OH)_3$	PSSH	0.77	Suspended	PPy/PSS^-

a) PSNa; sodium 1-propanesulfonate, PSH; 1-propanesulfonic acid PESNNa; sodium polyethylenesulfonate, PESNH; polyethylenesulfonic acid PSSH; polystyrenesulfonic acid. b) Logarithmic viscosity number of polyelectrolyte at 0.5 g dl^{-1}.

Table 2. Elemental Analysis and Conductivity of the Resulting Polymers

PPy	Elemental analysis/wt%					Mole ratio		f[a]	Conductivity
	H	C	N	S	Cl	Cl/N	S/N		S cm^{-1}
PPy/Cl^-	3.55	57.80	16.78	0	8.53	0.201	0	0.201	1.70
PPy/SO_4^{2-}	3.53	55.97	15.82	4.00	0	0	0.111	0.222[b]	2.80
PPy/mix.	3.83	54.26	14.66	4.95	1.34	0.036	0.147	0.183	0.73
PPy/$PESN^-$ (1)	4.12	44.19	10.92	9.53	0	0	0.381	0.381	2.70
PPy/$PESN^-$ (2)	4.16	46.12	11.28	9.25	0	0	0.359	0.359	1.20
PPy/$PESN^-$ (3)	3.93	43.22	10.79	9.33	0	0	0.378	0.378	0.18

a) f=Cl/N+S/N. b) f=S/N×2.

the undoped sulfonate moiety in the PPy matrix was observed (as mentioned below). PPy/PESN$^-$ had a higher f-value than PPy/Cl$^-$ and PPy/SO_4^{2-}. As for PPy/mix., because of the existence of Cl and S atoms in the PPy matrix, both Cl$^-$ and PESN$^-$ seemed to be incorporated as a dopant into the PPy matrix. Interestingly, the f-value of PESN$^-$ was 4-times larger than that of Cl$^-$, in spite of the same concentration of the two anions in the oxidative solution. A similar behavior was observed for the PPy prepared by electrochemical polymerization in H_2O containing both the polymer anion and ClO_4^- as an electrolyte anion.[46] This result indicates that the polymer anion was easily incorporated, compared with the small anion, owing to a multi-negative charge. However, doping by only the polymer anion was not expected when $FeCl_3$ was used as an oxidant. When $Fe(OH)_3$ was used as an oxidant, on the contrary, effective doping by the polymer anion seemed to be achieved, since only S atoms existed in the PPy matrix. Because the $Fe(OH)_3$ oxidant and PESN$^-$ gave the PESN-Fe and H_2O, the polymer anion was the only anionic species in the oxidative solution. Therefore, the polymer anion could be incorporated as a dopant into the PPy matrix.

Table 3 shows the molecular weight (MW) per residue of the resulting polymer and yield. The MW per residue was calculated by using the f-value, the MW of pyrrole moiety, and the MW of anion:

$$\text{MW per residue} = (\text{MW of pyrrole moiety}) + (\text{MW per one anion moiety}) \times f. \quad (1)$$

Assuming that the f-value corresponds to the real doping ratio, the theoretical yield was calculated in terms of the moles of the oxidant used, the f-value, and the MW per residue. $(2+f)$ electrons were consumed

Table 3. Molecular Weight per Residue of the Resulting Polymer and Yield

PPy	MW per residue	Theoretical yield/g	Experimental yield/g	Yield/%
PPy/Cl$^-$	72.2	0.177	0.180	102
PPy/SO_4^{2-}	75.8	0.184	0.180	98
PPy/mix.	82.3	0.203	0.208	102
PPy/PESN$^-$ (1)	106.9	0.241	0.233	97
PPy/PESN$^-$ (2)	103.9	0.238	0.176	74
PPy/PESN$^-$ (3)	106.0	0.241	0.158	66

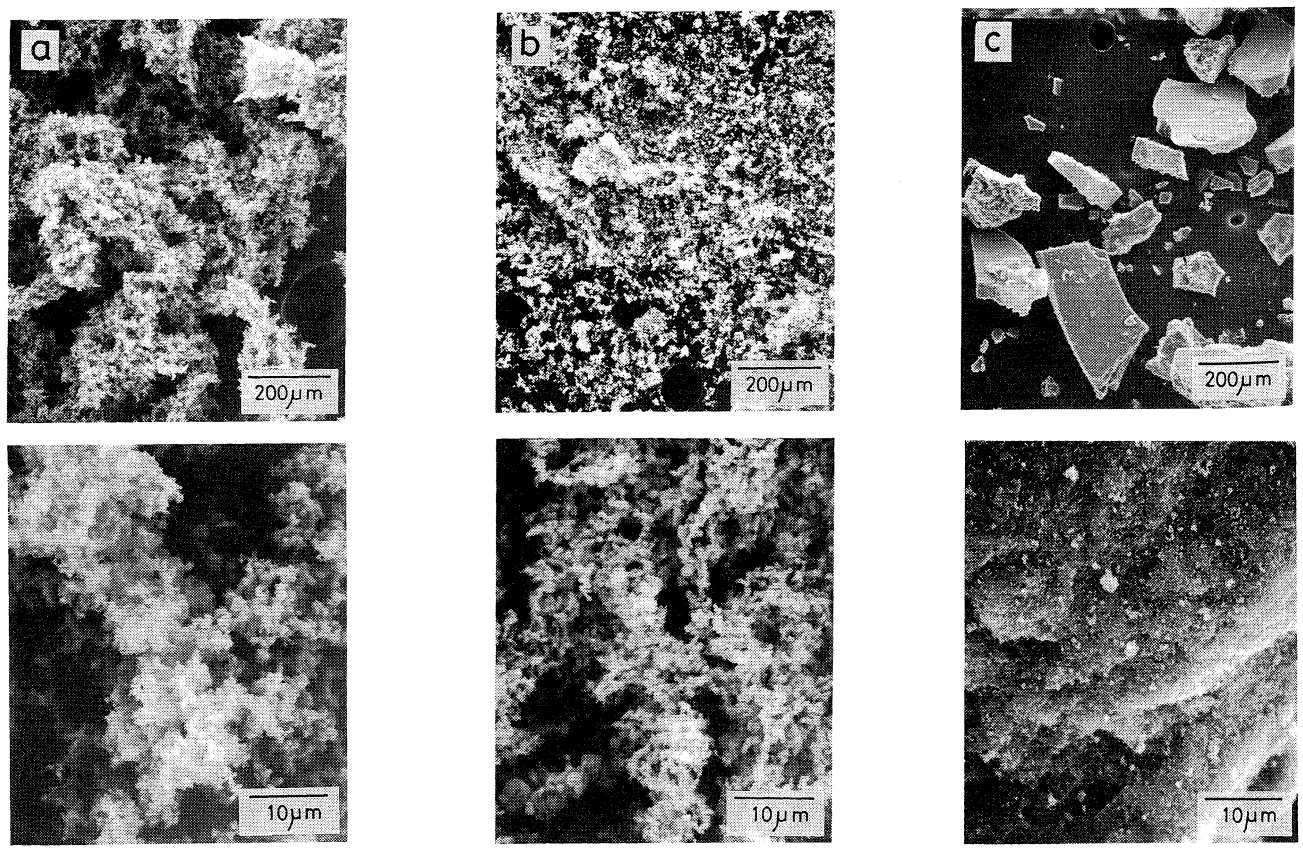

Fig. 1. Typical SEM photographs of the resulting polymers. Accelerating voltage was 15 kV. (a) PPy/SO_4^{2-}, (b) PPy/PESN$^-$(1), (c) PPy/PESN$^-$(3).

during the oxidative polymerization of one pyrrole. Thus,

$$\text{(mole of oxidant used)/(mole of pyrrole consumed)} = [2(x-1)+(fx)]/x;$$

$$\text{if } x \text{ is large,} \quad \simeq 2+f.$$

Here, x denotes the degree of polymerization. Accordingly,

$$\text{Theoretical yield} = [\text{(mole of oxidant used)}/(2+f)] \times \text{(MW per residue)}. \quad (2)$$

The yields for PPy/Cl^-, PPy/SO_4^{2-}, PPy/mix., and PPy/PESN$^-$(1), which were precipitated, were ca. 100%. The yields for PPy/PESN$^-$(2) and PPy/PESN$^-$(3), which were suspended, were low.

Figures 1(a)—(c) show typical SEM photographs for the resulting polymers. The morphology of the resulting polymers was affected by the size of the dopant. Powders of PPy with a small-size anion and PPy with a low-molecular-weight polymer anion have clusters of globules with void spaces between, as shown in Fig. 1(a) and (b). On the other hand, powders of PPy with a high-molecular-weight polymer anion were curds composed of very small particles, as shown in Fig. 1(c). Figures 2(a)—(d) show typical TEM photographs of the resulting polymers. The size of particles estimated by TEM photographs were 2800—4000 Å, 2000—2800 Å, 800—1200 Å, and 200—400 Å for PPy/Cl^-, PPy/mix., PPy/PESN$^-$(2), and PPy/PSS^-, respectively. The higher molecular-weight of the polymer anion seems to give a smaller size of PPy particle. PPy/mix. showed an intermediate property between PPy/Cl^- and PPy/PESN$^-$(2). These photograph observations indicates that the polymer anion, which has a multi-negative charge, acted as an inhibitor for the growth of PPy particles. The existence of a small amount of Fe atom was observed in the PPy matrix in the X-ray microanalysis measurement. The present Fe atom was considered to be a counter cation of sulfonic acid of the polymer anion, since it was removed from the PPy matrix by washing

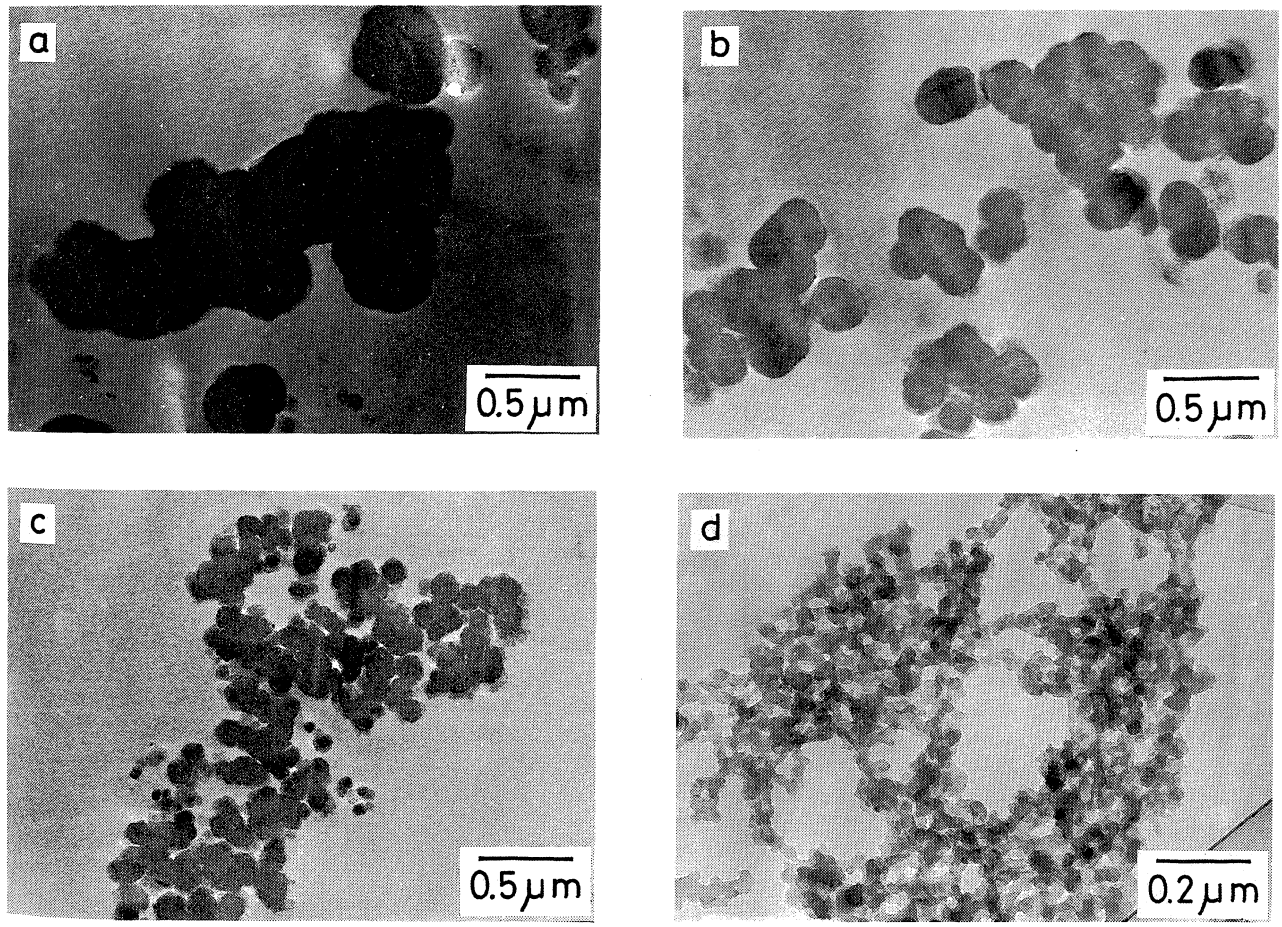

Fig. 2. Typical TEM photographs of the resulting polymers. Accelerating voltage was 100 kV. Ultra-thin section of (a) PPy/Cl^-, (b) PPy/mix., and (c) PPy/PESN$^-$(2), and dispersion of (d) PPy/PSS^-.

using an HCl aqueous solution. Moreover, PPy/PESN$^-$ had a higher doping ratio than PPy/Cl^- and PPy/SO_4^{2-}, as mentioned above. Thus, it was considered that there are a considerable amount of undoped polymer anions in the PPy matrix. It is speculated that during the chemical polymerization of pyrrole, the partly incorporated polymer anion into PPy has a considerable amount of free, undoped sulfonic acid, so that PPy was prevented from aggregation, owing to the high charge density of the remaining undoped sulfonic acid. Low yields of PPy/PESN$^-$(2) and PPy/PESN$^-$(3) could be explained by the unrecovered smaller particle of PPy. It was concluded that the $Fe(OH)_3$ oxidant has a capability to effectively dope the acid and that the morphology of the resulting polymers can be controlled by the property of the electrolyte anion.

The present method, using an $Fe(OH)_3$ oxidant and an acidic solution, is considered to be one of the effective hybridization procedures in conducting polymer syntheses.

We thank Mr. Hajime Tsuchiya, Nitto Technical Information Center, for his TEM observations.

References

1) A. F. Diaz, K. K. Kanazawa, and G. P. Gardini, *J. Chem. Soc., Chem. Commun.*, **1979**, 635.
2) K. K. Kanazawa, A. F. Diaz, R. H. Geiss, W. D. Gill, J. F. Kwak, J. A. Logan, J. F. Rabolt, and G. B. Street, *J. Chem. Soc., Chem. Commun.*, **1979**, 854.
3) A. F. Diaz and J. I. Castillo, *J. Chem. Soc., Chem. Commun.*, **1980**, 397.
4) A. F. Diaz, J. I. Castillo, J. A. Logan, and W.-Y. Lee, *J. Electroanal. Chem.*, **129**, 115 (1981).
5) A. F. Diaz, A. Martinez, K. K. Kanazawa, and M. Salmon, *J. Electroanal. Chem.*, **130**, 181 (1981).
6) A. F. Diaz, J. I. Castillo, K. K. Kanazawa, J. A. Logan, M. Salmon, and O. Fajardo, *J. Electroanal. Chem.*, **133**, 233 (1981).
7) H. S. White, G. P. Kittlesen, and M. S. Wrighton, *J. Am. Chem. Soc.*, **106**, 5375 (1984).
8) G. P. Kittlesen, H. S. White, and M. S. Wrighton, *J. Am. Chem. Soc.*, **106**, 7389 (1984).
9) F. Garnier, G. Tourillon, M. Gazard, and J. C. Dubois, *J. Electroanal. Chem.*, **148**, 299 (1983).
10) R. Bjorklund, S. Andersson, S. Allenmark, and I. Lundström., *Mol. Cryst. Liq. Cryst.*, **121**, 263 (1985).
11) S. Kuwabata, H. Yoneyama, and H. Tamura, *Bull. Chem. Soc. Jpn.*, **57**, 2247 (1984).
12) K. Kaneto and K. Yoshino, *Kino Zairyo*, **4**, 8 (1984).
13) A. Mohammadi, O. Inganas, and I. Lundström, *J. Electrochem. Soc.*, **133**, 947 (1986).
14) N. Mermilliod, J. Tanguy, and F. Petiot, *J. Electrochem. Soc.*, **133**, 1073 (1986).
15) T. Osaka, K. Naoi, H. Sasaki, and S. Ogano, *J. Electrochem. Soc.*, **134**, 285 (1987).
16) A. F. Diaz, *Chem. Scripta*, **17**, 145 (1981).
17) P. Burgmayer and R. W. Murray, *J. Am. Chem. Soc.*, **104**, 6139 (1982).
18) P. Burgmayer and R. W. Murray, *J. Phys. Chem.*, **88**, 2515 (1984).
19) B. Zinger and L. L. Miller, *J. Am. Chem. Soc.*, **106**, 6861 (1984).
20) H. Shinohara, M. Aizawa, and H. Shirakawa, *Chem. Lett.*, **1985**, 179.
21) R. A. Bull, F.-R. Fan, and A. J. Bard, *J. Electrochem. Soc.*, **130**, 1636 (1983).
22) R. Noufi, *J. Electrochem. Soc.*, **130**, 2126 (1983).
23) K. Okabayashi, O. Ikeda, and H. Tamura, *J. Chem. Soc., Chem. Commun.*, **1983**, 684.
24) R. B. Bjorklund and I. Lundström, *J. Electron. Mater.*, **13**, 211 (1984).
25) O. Niwa and T. Tamamura, *J. Chem. Soc., Chem. Commun.*, **1984**, 817.
26) S. E. Lindsey and G. B. Street, *Synth. Metals*, **10**, 67 (1984).
27) M-A. de Paoli, R. J. Waltman, A. F. Diaz, and J. Bargon, *J. Chem. Soc., Chem. Commun.*, **1984**, 1015.
28) N. Bates, M. Cross, R. Lines, and D. Walton, *J. Chem. Soc., Chem. Commun.*, **1985**, 871.
29) T. Ojio and S. Miyata, *Polym. J.*, **18**, 95 (1986).
30) F.-R. F. Fan and A. J. Bard, *J. Electrochem. Soc.*, **133**, 301 (1986).
31) H. Yoneyama, T. Hirai, S. Kuwabata, and O. Ikeda, *Chem. Lett.*, **1986**, 1243.
32) T. Iyoda, A. Ohtani, T. Shimidzu, and K. Honda, *Chem. Lett.*, **1986**, 687.
33) T. Iyoda, A. Ohtani, T. Shimidzu, and K. Honda, *Synth. Metals*, **18**, 725 (1987).
34) T. Shimidzu, A. Ohtani, T. Iyoda, and K. Honda, *J. Chem. Soc., Chem. Commun.*, **1986**, 1414.
35) T. Shimidzu, A. Ohtani, T. Iyoda, and K. Honda, *J. Chem. Soc., Chem. Commun.*, **1986**, 1415.
36) T. Shimidzu, A. Ohtani, T. Iyoda, and K. Honda, *J. Chem. Soc., Chem. Commun.*, **1987**, 327.
37) T. Shimidzu, A. Ohtani, T. Iyoda, and K. Honda, *J. Electroanal. Chem.*, **224**, 123 (1987).
38) T. Shimidzu, A. Ohtani, and K. Honda, *J. Electroanal. Chem.*, **251**, 323 (1988).
39) T. Shimidzu, A. Ohtani, and K. Honda, *Bull. Chem. Soc. Jpn.*, **61**, 2885 (1988).
40) T. Shimidzu, A. Ohtani, M. Aiba, and K. Honda, *J. Chem. Soc., Faraday Trans. 1*, in press.
41) M. Salmon, K. K. Kanazawa, A. F. Diaz, and M. Krounbi, *J. Polym. Sci., Polym. Lett. Ed.*, **20**, 187 (1982).
42) K. Yoshino, S. Hayashi, and R. Sugimoto, *Jpn. J. Appl. Phys. Part 2*, **23**, L899 (1984).
43) V. Bocchi and G. P. Cardini, *J. Chem. Soc., Chem. Commun.*, **1986**, 148.
44) R. E. Myers, *J. Electron. Mater.*, **15**, 61 (1986).
45) T. H. Chao and J. March, *J. Polym. Sci., Polym. Chem. Ed.*, **26**, 743 (1988).
46) K. Hyodo and M. Nozaki, *Electrochim. Acta*, **33**, 165 (1988).

 © 1989 The Chemical Society of Japan Bull. Chem. Soc. Jpn., 62, 239—243 (1989)

Highly Stereoselective Palladium(0)-Catalyzed Allylation of Active Methylene Compounds with Allyl Imidates under Neutral Conditions

Osamu SUZUKI, Seiichi INOUE, and Kikumasa SATO*
Department of Applied Chemistry, Faculty of Engineering, Yokohama National University, Tokiwadai, Hodogaya-ku, Yokohama 240
(Received July 22, 1988)

In the presence of a catalytic amount of Pd(0), active methylene compounds were allylated by allyl imidates under neutral conditions. In allylation with 3,3-disubstituted allyl imidates, e.g., geranyl and neryl imidate the effect of solvent and ligand to the *E/Z* ratio are investigated. The reaction in dimethyl sulfoxide by addition of diphosphine, e.g., 1,2-bis(diphenylphosphino)ethane, or large excess of triphenylphosphine as additive ligand gave best results. In these conditions, various active methylene compounds were allylated stereoselectively, especially complete retention of starting olefin geometry was achieved with neryl imidate.

Palladium-catalyzed allylation of carbanions is one of the useful methods for carbon–carbon bond formation; allyl acetates are commonly used as precursors of π-allylpalladium intermediates in the presence of a stoichiometric amount of bases such as NaH for the generation of a carbanion to be allylated.[1] It would be more valuable if the reaction could be carried out without addition of a base. Allylation using allyl carbonates under neutral conditions has also been reported.[1c]

Many bioactive compounds which have *trans*-isoprene units are known, and in recent years several kinds of polyprenols containing *cis*-isoprene units such as betulaprenols,[2,3] undecaprenol,[4] dolichols,[5] and others[6] have been isolated. An efficient method for stereoselective introduction of isoprene units is strongly desired, but stereoselective allylation via π-allylpalladium species had not been achieved until we recently reported that active methylene compounds were allylated by *O*-(allyloxycarbonyl)oximes with high stereoselectivity in the presence of catalytic amounts of bases.[7]

The present paper describes the highly stereoselective allylation of various active methylene compounds with allyl imidates under neutral conditions.

Results and Discussion

Although stoichiometric amounts of the bases were needed, palladium catalyzed allylic alkylation to active methylene compounds took place with allyl acetates smoothly. We anticipated that allylimidates **1**, imine analogues of esters, would be reactive toward palladium to generate π-allylpalladium species[8] and would also be capable of liberating imidate anions which are basic enough to generate carbon nucleophiles from active methylene compounds (Scheme 1).

A series of imidates was prepared by either the reaction of imidoyl chloride with alkoxide[9] or the reaction of ethyl imidate with allylic alcohols.[10]

The reaction of allyl *N*-phenylbenzimidate (**1a**)

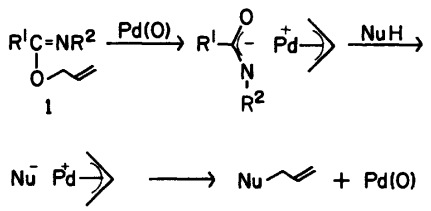

Scheme 1.

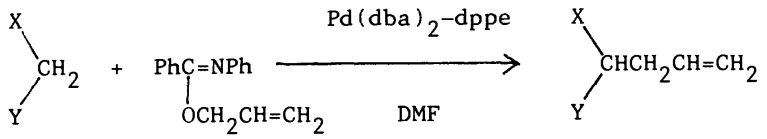

3 1a 4 + 5

Scheme 2.

Table 1. Palladium-Catalyzed Allylation of Active Methylene Compounds **3** with Allyl *N*-Phenylbenzimidate (**1a**)[a]

Compd	**3** (pK_a)			Time/h	Product (yield/%)[b]	
					4	**5**
3a:	X=Y=MeCO		(9)	1	**4a**: (25)	**5a**: (55)
3b:	X=MeCO	Y=CO_2Et	(11)	1.5	**4b**: (31)	**5b**: (35)
				3[c]	**4b**: (24)	**5b**: (29)
3c:	X=Y=CO_2Et		(13)	4	**4c**: (55)	**5c**: (28)
3d:	X=Ph	Y=PhCO	(16)	5	**4d**: (69)	
3e:	X=Ts	Y=MeCO		7[d]	**4e**: (58)	**5e**: (18)

a) The reaction was carried out by using 2 mol% of Pd(dba)$_2$-dppe in DMF at r.t. Ts=*p*-$CH_3C_6H_4SO_2$. b) Isolated yield. c) PPh_3 (4 equiv to Pd(0)) was used instead of dppe. d) The reaction was carried out at 85 °C.

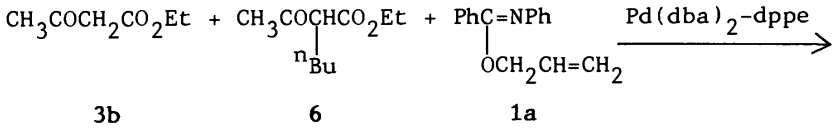

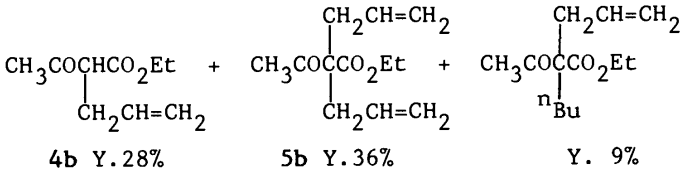

Scheme 3.

(R^1=Ph, R^2=Ph) with various active methylene compounds **3** was found to proceed smoothly in the presence of bis(dibenzylideneacetone)palladium (Pd(dba)$_2$) (2 mol%) and 1,2-bis(diphenylphosphino)ethane (dppe) (2 mol%) in *N*,*N*-dimethylformamide (DMF) to yield a mixture of monoallylated **4** and diallylated compounds **5** in good combined yields (Scheme 2). The results are summarized in Table 1. The ratio of diallylation to monoallylation products decreased in almost the reverse order of the acidity of active methylene compounds. Various kinds of imidates **1** (R^1=Ph, H, Me, R^2=Ph, H) were similarly effective for this allylation reaction. Tetrahydrofuran (THF), chloroform, benzene, acetonitrile, dimethyl sulfoxide (DMSO), and hexamethylphosphoric triamide (HMPA) were also effective as solvents; the addition of triphenylphosphine (PPh_3) or dppe is absolutely necessary, but the allylation did not take place with tributylphosphine, trimethyl phosphite, or tri-*o*-tolylphosphine.

To examine the concurrent formation of the diallylation products a competition experiment was conducted. When an equimolar mixture of ethyl acetoacetate (**3b**) and ethyl 2-butyl-3-oxobutanoate (**6**) was treated with imidate **1a**, the allylation of **6** took place only to a small extent (9% yield) in comparison with the formation of the diallylation product **5b** from **3b** in 36% yield (Scheme 3). These results imply that the allylation does not proceed by a simple mechanism. Hence, use of a large excess of active methylene compound was effective at suppressing the diallylation; when 10 equiv of **3b** was used, monoallylation product was obtained in 77% yield and the diallylated product was no longer formed.

The regiochemistry of allylation with unsymmetrically substituted allylic systems is an important problem from both synthetic and mechanistic viewpoints. The results of allylation of *p*-tolylsulfonylacetone (**3e**) with several substituted allyl imidates are summarized in Table 2. It is noteworthy that diallylated products were no longer detected. The less substituted site of the allylic system in the imidate reacted preferentially, and prenyl imidate **2d** gave only one regioisomer **7d**. Moreover, the 2-butenylated product **7b** was a pure trans isomer irrespective of the structure of the starting imidate **2b** or **2c**.

The stereochemistry of allylation with 3,3-disubstituted allyl imidates was next examined using geranyl imidate **2e** and neryl imidate **2f** (Scheme 4). In these types of allylation good yields were obtained only in polar solvents; in chloroform, benzene, or THF, the yields were poor or the reaction did not take place. In general, the reaction of the π-allylpalladium complex is strongly influenced by the solvent and the

Table 2. Allylation of *p*-Tolylsulfonylacetone (**3e**) with Substituted Allyl Imidate[a]

Imidate	Time/h	Yield[b]/%	Product (ratio[c]/%)	
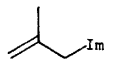 **2a**	7	98	**7a**: (100)	
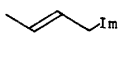 **2b**	22	85	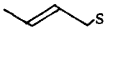 **7b**: (75)	**7c**: (25)
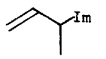 **2c**	19	57	**7b**: (71)	**7c**: (29)
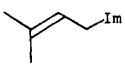 **2d**	19	61	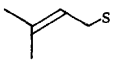 **7d**: (100)	

a) The reaction was carried out by using 2 mol% of Pd(dba)$_2$-dppe in DMF at 85 °C. Im=–OCH(=NPh); S=TsCHCOCH$_3$. b) Isolated yield. c) Determined by GLC.

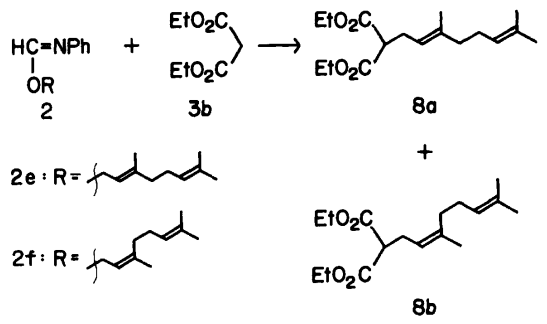

Scheme 4.

ligand.[1] However, few reports have been given with respect to the stereochemistry.[11] Therefore, initially, the effect of the solvent to the *E/Z* ratio of products was examined in detail (Table 3). When geranyl imidate **2e** was used in combination with dppe, the greater the donor number[12] of the solvent, the higher was the stereoselectivity. On the other hand complete retention of the stereochemistry of the starting neryl imidate **2f** was attained by the use of DMSO as solvent. It is well-known that the pathway for isomerization of the allyl moiety involves π-allyl to σ-allyl interconversion and bond rotation,[13] and this higher selectivity indicates that nucleophilic attack is faster than syn-anti isomerization. Indeed, the allylation proceeded most rapidly in DMSO among the solvent tested. When PPh$_3$ was used as ligand, the amount of PPh$_3$ was crucial for the stereoselectivity. No stereoselectivity (*Z*:*E*=50:50) was observed with 2 equiv. of PPh$_3$ to Pd(0) in allylation of diethyl malonate (**3c**) with **2f** in DMSO, satisfactory results were obtained with 8 equiv. of PPh$_3$ (*Z*:*E*=90:10). Notably complete retention of stereochemistry was attained by using a large excess (15 equiv to Pd(0)) of PPh$_3$. Similarly, no stereoisomer was formed with a large excess of methyldiphenylphosphine.

Table 3. Allylation of Diethyl Malonate (**3c**) with **2e** and **2f** in Several Polar Solvents[a]

Imidate	Solvent (donor No.)	Time h	Yield[b] %	*E/Z* ratio[c] **8a** : **8b**
2e	DMF (26.6)	7	79	76 : 24
2e	NMP[d] (27.3)	18	59	82 : 18
2e	DMSO (29.8)	4	79	97 : 3
2f	DMF	28	73	51 : 49
2f	DMAc[e]	19	48	52 : 48
2f	DMSO	5	76	0 : 100
2f	HMPA	19	65	52 : 48

a) The reaction was carried out by using 2 mol% of Pd(dba)$_2$-dppe at 85 °C. b) Isolated yield. c) Determined by GLC. d) *N*-Methyl-2-pyrrolidone. e) *N*,*N*-Dimethylacetamide.

Table 4. Stereoselective Allylation toward Various Active Methylene Compounds with **2e** and **2f**[a]

Compd	Imidate	Time/h	Yield[b]/%	*E/Z* ratio[c]
3b	**2e**	2	71[d]	100 : 0
4b	**2e**	1	91	99 : 1
3b	**2f**	3	73[d,e]	0 : 100
4b	**2f**	1	88	0 : 100
6	**2f**	1	82	0 : 100
3c	**2e**	4	79[f]	97 : 3
4c	**2e**	2	76	99 : 1
3c	**2f**	5	76[g]	0 : 100
4c	**2f**[h]	1	82	0 : 100
3e	**2e**[h]	15	81	98 : 2
3e	**2f**[h]	19	93	11 : 89
TsCH$_2$CO$_2$Et **3f**	**2e**[h]	18	73	96 : 4
3f	**2f**[h]	18	69[i]	1 : 99

a) The reaction was carried out by using 2 mol% of Pd(dba)$_2$-dppe in DMSO at 85 °C. b) Isolated yield. c) Determined by GLC. d) After hydrolysis and decarboxylation. e) Containing 15% of regioisomer. f) Containing 7% of regioisomer. g) Containing 14% of regioisomer. h) Excess of PPh$_3$ (15 equiv) to Pd(0)) was used instead of dppe. i) Containing 17% of regioisomer.

Table 4 shows the results of allylation of various active methylene compounds with geranyl imidate (**2e**) and neryl imidate (**2f**) in DMSO. Ethyl acetoacetate (**3b**) was allylated with **2e** and **2f** with complete retention of the olefin geometry to yield, after hydrolysis and decarboxylation, stereochemicaly pure geranylacetone

and nerylacetone in 71% and 73% yield, respectively. Substituted ethyl acetoacetates **4b**, **6** and diethyl malonate (**3c**), and diethyl allylmalonate (**4c**) were also allylated stereoselectively, especially with **2f**, no stereoisomer was observed. Sulfonylacetone **3e** and ethyl *p*-tolylsulfonylacetate (**3f**) were also allylated stereoselectively by using a large excess of PPh_3 as ligand.

In other neutral allylations, e.g., allylation with allyl carbonates, complete retention of stereochemistry was not achieved, especially the reaction of neryl carbonate with methyl acetoacetate which gave almost equal amounts of geranylacetone and nerylacetone.[1c] Therefore the present allylation with allyl imidates is thought to be valuable as a method for the stereoselective introduction of trisubstituted allylic moieties under neutral conditions.

Experimental

General. Boiling points are uncorrected. IR spectra were measured on a Hitachi 260-10 spectrometer. ^1H NMR spectra were obtained with a JEOL JNM-C-60M or a JEOL FT-90-Q using $CDCl_3$ as solvent and with tetramethylsilane as internal standard. Column chromatography was normally effected with Wakogel C-200 (Wako Pure Chemical Industries). GLC analyses were performed on a Shimadzu GC-9A chromatograph using a column packed with Silicone OV-17 (3 mm×2 m), and the peak areas were calculated on a Shimadzu chromatopack C-R3A.

Materials. $Pd(dba)_2$ was prepared according to a literature method.[14] The structure of the known compounds were established on the basis of their spectroscopic properties and from descriptions in the literature. Allylic imidates were prepared by methods described in the literature.[9] The following new compounds were prepared by the method of Roberts.[10]

3-Methyl-2-butenyl *N*-Phenylformimidate (2d): Bp 91—92 °C/0.45 mmHg (1 mmHg≈133.322 Pa); IR(neat) 1650, 1190, 770, and 700 cm^{-1}; ^1H NMR δ=1.71 (6H, s), 4.63 (2H, d, J=7 Hz), 5.35 (1H, t, J=7 Hz), 6.7—7.2 (5H, m), 7.47 (1H, s).

Found: C, 76.38; H, 7.68; N, 7.56%. Calcd for $C_{12}H_{15}NO$: C, 76.16; H, 7.99; N, 7.40%.

(*E*)-3,7-Dimethyl-2,6-octadienyl *N*-Phenylformimidate (2e): Bp 139—141 °C/0.38 mmHg; IR (neat) 1640, 1185, 760, and 700 cm^{-1}; ^1H NMR δ=1.59, 1.65, and 1.71 (9H, each s), 2.01 (4H, bs), 4.64 (2H, d, J=7 Hz), 4.98 (1H, bs), 5.33 (1H, t, J=7 Hz), 6.6—7.1 (5H, m), and 7.44 (1H, s).

Found: C, 79.15; H, 9.32; N, 5.29%. Calcd for $C_{17}H_{23}NO$: C, 79.33; H, 9.01; N, 5.44%.

(*Z*)-3,7-Dimethyl-2,6-octadienyl *N*-Phenylformimidate (2f): Bp 141—143 °C/0.35 mmHg; IR (neat) 1640, 1185, 760, and 700 cm^{-1}; ^1H NMR δ=1.59, 1.65, and 1.75 (9H, each s), 2.10 (4H, bs), 4.64 (2H, d, J=7 Hz), 5.01 (1H, bs), 5.37 (1H, t, J=7 Hz), 6.7—7.2 (5H, m), and 7.50 (1H, bs).

Found: C, 79.58; H, 9.20; N, 5.58%. Calcd for $C_{17}H_{23}NO$: C, 79.33; H, 9.01; N, 5.44%.

General Procedure for Allylation of Active Methylene Compounds. To a stirred mixture of active methylene compound (0.4 mmol), $Pd(dba)_2$ (5 mg, 2 mol%), and dppe (3 mg, 2 mol%) in DMF (10 ml), was added a solution of imidate (0.4 mmol) in DMF (2 ml). The resulting mixture was stirred at 85 °C under nitrogen, poured into water, and extracted with diethyl ether. The organic layer was washed with brine and dried over $MgSO_4$. After filtration, the solvent was removed and the residue was purified by column chromatography (silica gel; hexane/ethyl acetate).

Reaction of 2-Propenyl *N*-Phenylbenzimidate (1a) with Ethyl Acetoacetate (3b) and Ethyl 2-Butyl-3-oxobutanoate (6). To a stirred mixture of **3b** (406 mg, 3.1 mmol), **6** (581 mg, 3.1 mmol), $Pd(dba)_2$ (36 mg), and dppe (25 mg) in DMF (10 ml), was added a solution of **1a** (740 mg, 3.1 mmol) in DMF (2 ml). The resulting mixture was stirred at room temperature for 2 h and treated according to the general procedure, affording **4b** (149 mg, 28%), **5b** (118 mg, 36%) and ethyl 2-butyl-2-(2-propenyl)-3-oxobutanoate (64 mg, 9%).

Allylation of *p*-Tolylsulfonylacetone (3e) with Substituted Allyl Imidate (Table 2). Substituted allyl imidate (0.4 mmol) and **3e** (85 mg, 0.4 mmol) were stirred in DMF (10 ml) at 85 °C under nitrogen in the presence of $Pd(dba)_2$ (5 mg, 2 mol%) and dppe (3 mg, 2 mol%). Allylated sulfones were obtained according to the general procedure. The ratio of **7b** and **7c** was determined by GLC (column 230 °C, **7b**; retention time=7.6 min, **7c**; retention time=6.5 min).

Allylation of Diethyl Malonate (3c) with 2e and 2f in Several Polar Solvents (Table 3). To a stirred mixture of **3c** (311 mg, 1.9 mmol), $Pd(dba)_2$ (22 mg, 2 mol%), and dppe (15 mg, 2 mol%) in solvent (20 ml), was added a solution of imidate **2e** or **2f**. The resulting mixture was stirred at 85 °C under nitrogen, and treated according to the general procedure. The E/Z ratio was determined by GLC (column 180 °C, **8a**; retention time=9.9 min, **8b**; retention time=8.7 min).

Allylation toward Various Active Methylene Compounds with 2e and 2f (Table 4). To a stirred mixture of the active methylene compound (1.9 mmol), $Pd(dba)_2$ (22 mg, 2 mol%), and dppe (15 mg, 2 mol%) in DMSO (20 ml) was added a solution of imidate **2e** or **2f**. The resulting mixture was stirred at 85 °C under nitrogen, and treated according to the general procedure. The following new compound were obtained using the above procedure.

Ethyl (*E*)-2-(3,7-Dimethyl-2,6-octadienyl)-2-(2-propenyl)-3-oxobutanoate: IR (neat) 1735, 1710, 1215, and 920 cm^{-1}; ^1H NMR δ=1.26 (3H, t, J=7 Hz), 1.60 (6H, s), 1.68 (3H, S), 2.00 (4H, bs), 2.12 (3H, s), 2.58 (4H, d, J=7 Hz), 4.19 (2H, q, J=7 Hz), 4.8—5.1 (4H, m), 5.62 (1H, ddt, J=18, 9, 7 Hz).

Found: C, 74.57; H, 9.78%. Calcd for $C_{19}H_{30}O_3$: C, 74.47; H, 9.87%.

Ethyl (*Z*)-2-(3,7-Dimethyl-2,6-octadienyl)-2-(2-propenyl)-3-oxobutanoate: IR (neat) 1735, 1710, 1215, and 920 cm^{-1}; ^1H NMR δ=1.25 (3H, t, J=7 Hz), 1.60, 1.68 (6H, each s), 2.03 (4H, bs), 2.11 (3H, s), 2.57 (2H, d, J=7 Hz), 4.18 (2H, q, J=7 Hz), 4.88 (1H, t, J=7 Hz), 5.10 (1H, bs).

Found: C, 74.39; H, 10.64%. Calcd for $C_{20}H_{30}O_3$: C, 74.49; H, 10.63%.

Diethyl (*Z*)-2-(3,7-Dimethyl-2,6-octadienyl)-2-(2-propenyl)-malonate: IR (neat) 1730, 1220, and 920 cm^{-1}; ^1H NMR δ=1.24 (3H, t, J=7 Hz), 1.60 (3H, s), 1.68 (6H, s), 2.03 (4H, bs), 2.62 (H, d, J=7 Hz), 4.17 (4H, q, J=7 Hz), 4.9—5.2 (4H, m), 5.68 (1H, ddt, J=18, 9, 7 Hz).

Found: C, 71.68; H, 9.39%. Calcd for $C_{20}H_{32}O_4$: C, 71.39; H, 9.59%.

References

1) a) Reviews: B. M. Trost, *Acc. Chem. Res.*, **13**, 38 (1980); J. Tsuji, "Organic Synthesis with Palladium Compounds," Springer Verlag, (1980); b) B. M. Trost and R. S. Christopher, *J. Org. Chem.*, **49**, 468 (1984), and references cited therein; c) J. Tsuji, I. Schimizu, I. Minami, Y. Ohashi, T. Sugiura, and K. Takahashi, *ibid.*, **50**, 1523 (1985) and references cited therein; d) B. M. Trost, N. Schmuff, and M. Miller, *J. Am. Chem. Soc.*, **102**, 5979 (1980); e) Y. Tanigawa, K. Nishimura, A. Kawasaki, and S. Murahashi, *Tetrahedron Lett.*, **23**, 5549 (1982).

2) B. O. Lindgren, *Acta Chim. Scand.*, **19**, 1317 (1965).

3) A. R. Wellburn and F. W. Hemming, *Nature (London)*, **212**, 1364 (1966).

4) A. Wright, M. Dankert, P. Fennessey, and P. W. Robbins, *Proc. Natl. Acad. Sci. U.S.A.*, **57**, 1798 (1967).

5) J. Burgos, F. W. Hemming, J. F. Pennock, and R. A. Morton, *Biochem. J.*, **88**, 470 (1963).

6) A. R. Wellburn, J. Stevenson, F. W. Hemming, and R. A. Morton, *Biochem. J.*, **102**, 313 (1967); K. J. Stone, A. R. Wellburn, F. W. Hemming, and J. F. Pennock, *Biochem. J.*, **102**, 325 (1967); T. Suga and T. Shishibori, *J. Chem. Soc., Perkin Trans. 1*, **1980**, 2098; K. Ibata, M. Mizuno, T. Tanigawa, and Y. Tanaka, *Biochem. J.*, **213**, 305 (1983).

7) O. Suzuki, Y. Hashiguchi, S. Inoue, and K. Sato, *Chem. Lett.*, **1988**, 291.

8) T. Ikariya, Y. Ishikawa, K. Hirai, and S. Yoshikawa, *Chem. Lett.*, **1982**, 1815; T. G. Schenck and B. Bosnich, *J. Am. Chem. Soc.*, **107**, 2058 (1985).

9) G. D. Lander, *J. Chem. Soc.*, **1903**, 320.

10) R. M. Roberts and F. A. Hussein, *J. Am. Chem. Soc.*, **82**, 1950 (1960).

11) T. Cuvigny, M. Julia, and C. Roland, *J. Organomet. Chem.*, **285**, 395 (1985).

12) V. Gutmann, *Angew. Chem., Int. Ed. Engl.*, **9**, 843 (1970).

13) B. M. Trost and T. R. Verhoeven, *J. Am. Chem. Soc.*, **102**, 4370 (1982); E. Keinan and M. Sahai, *J. Chem. Soc., Chem. Commun.*, **1984**, 648.

14) Y. Takahashi, Ts. Ito, S. Sakai, and Y. Ishii, *J. Chem. Soc. D*, **1970**, 1065.

Synthesis and Reaction of a New Chiral Pyridoxamine Analogue; Some Doubt about the Stereochemical Process Tentatively Proposed for a Nonenzymatic Transamination Reaction

Makoto ANDO* and Hiroyoshi KUZUHARA*
Riken (The Institute of Physical and Chemical Research),
Wako-shi, Saitama 351-01
(Received August 8, 1988)

A pyridoxamine analogue-like chiral pyridinophane with two sulfonyl groups in the bridging chain, (*S*)-15-aminomethyl-14-hydroxy-2,8-dithia[9](2,5)pyridinophane *S,S,S',S'*-tetraoxide ((*S*)-**7**), was prepared by oxidation of the sulfide precursor, (*S*)-**2**. The amino group was successfully transferred from (*S*)-**7** to several 2-oxo carboxylic acids in methanol at room temperature in the presence of one-half equimolecular zinc(II) ion, giving (*R*)-amino acids in excess. The reaction rates of this nonenzymatic transamination using chiral (*S*)-**7** were much smaller than those of the corresponding reaction using chiral (*S*)-**2**. The enantiomeric excess of the amino acids obtained through the reactions of (*S*)-7 was compared with those of (*S*)-**2**, showing that (*S*)-**7** was more efficient than (*S*)-**2** for the preparation of (*R*)-alanine, but was less than that of (*S*)-**2** for the preparations of (*R*)-valine, (*R*)-leucine, and (*R*)-phenylalanine. These results aroused some doubt about the previous explanation of the stereochemical features of such nonenzymatic transamination reactions.

Transaminases, as well as other vitamin B_6-dependent enzymes, play a crucial role in amino acid metabolism, catalyzing the transfer of an amino group between amino acids and 2-oxo carboxylic acids. Two coenzymes, pyridoxal phosphate (PLP) and pyridoxamine phosphate (PMP), mediate the transfer of amino groups in such enzymatic reactions by forming Schiff bases with substrates, that undergo subsequent equilibration between their aldimine and ketimine forms (Scheme 1). The pioneering work of Snell[1] demonstrated that, in the simple model systems (in the absence of apoprotein), pyridoxal and pyridoxamine (with or without phosphate groups) duplicate the reaction of transaminases, and that the reaction rate is considerably increased when polyvalent metal cations are present. Martell[2] presented the first example of zinc(II) catalysis of a model transamination reaction in nonaqueous solvents, in which a simple isomerization from the ketimine to the aldimine reached near completion in the absence of large excesses of reagents (Scheme 2). Utilizing these fundamental discoveries, several groups[3] have pursued further development of new transaminase models capable of enantioface differentiation. We have succeeded in the preparation of pyridoxamine analogues with planar chirality, the (*R*) and (*S*) enantiomers of 15-aminomethyl-14-hydroxy-2,8-dithia[9](2,5)pyridinophane (**2**)[4] and 15-aminomethyl-14-hydroxy-5,5-dimethyl-2,8-dithia[9]-(2,5)pyridinophane (**3**).[5] Stereoselective transamination from chiral **3** (and **2** in a few cases) to various 2-oxo carboxylic acids (**1**) in methanol in the presence of

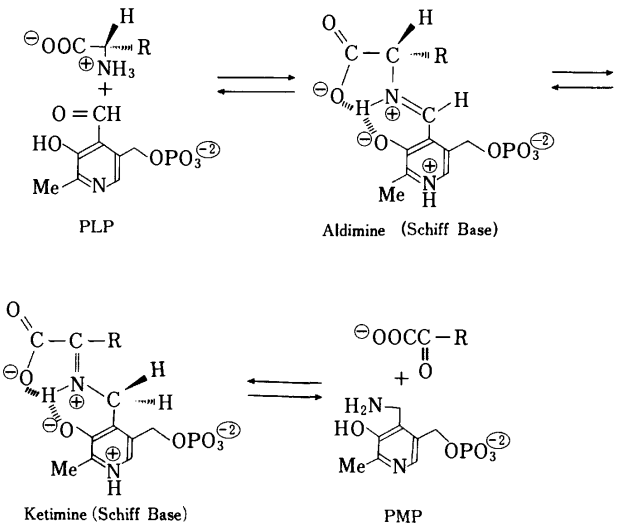

Scheme 1.

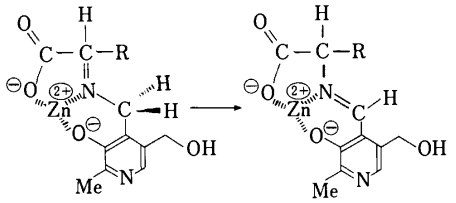

Scheme 2.

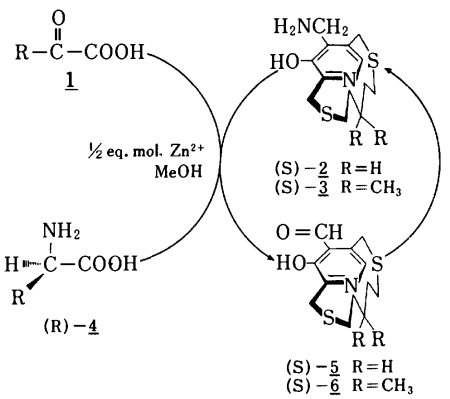

Scheme 3.

zinc(II), successfully produced α-amino acids (**4**) with enantiomeric excesses (e.e.) ranging from 60 to 96% depending on the substrates employed.[6] Interesting stereochemical features were observed in these transamination reactions. First, the reduction of the molar ratio of zinc(II) vs. chiral **3** from 1/1 to 0.5/1 resulted in a remarkable increase of the e.e. values of **4** produced, without affecting their chemical yields (about 70% in most cases). Second, the employment of the (*S*) enantiomer of **3** gave the (*R*) enantiomer of **4** in excess, and vice versa. In order to rationalize these phenomena, we tentatively proposed an octahedral zinc(II) chelate complex coordinated with two equimolecular Schiff base ligands as the key intermediate.[7] As is seen in Fig. 1,[8] a kinetically controlled stereoselective protonation would take place on one of the enantiofaces of the carbanion. The other enantioface is sterically hindered by one of the bulky sulfur atoms (circled in Fig. 1). If this hypothetical view is applicable to other cases, the replacement of the sulfur atoms of **3** (or **2**) with bulkier groups would result in the increase of the e.e. values of **4** produced by the model transamination reaction.

This paper describes syntheses of the racemate and the (*S*)-enantiomer of 15-aminomethyl-14-hydroxy-2,8-dithia[9](2,5)pyridinophane *S,S,S',S'*-tetraoxide (**7**) from **2**, and the zinc(II)-catalyzed transamination reactions of chiral **7** and chiral **2** with various kinds of **1**. The sulfonyl group in **7** is much bulkier than the thio group in **2** and would be expected to have little tendency to chelate metal ions, which is a necessary condition for the model transamination reactions to proceed smoothly. Although it has been shown that **3** shows higher efficiency in asymmetric induction than **2**,[6] the derivatives of **3** were generally much less soluble than those of **2**. Consequently, the asymmetric transaminations from **7** were compared with those from **2**, but not the sulfonyl analogue of **3** with **3**.

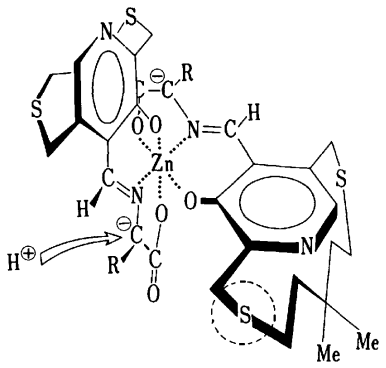

Fig. 1. *Λ*-Isomer of the octahedral zinc(II) chelate complex containing (*S*)-**3** Schiff base.

Synthesis of 7. Initially, racemic **7** was prepared for model studies. Acetylation of (*RS*)-**2** with acetic anhydride and pyridine at 100 °C gave crystalline 14-acetoxy-15'-diacetylamino derivative, (*RS*)-**9**, which revealed three carbonyl absorptions at 1690, 1710, and 1780 cm^{-1} but no NH absorption in the IR spectrum. Its ^1H NMR spectrum also revealed methyl protons of three acetyl groups around δ 2.30. In the spectrum, all gem-protons of the three pyridylmethylene groups appeared with the same characteristic pattern; i.e., one proton as a sharp doublet but the other as a broad doublet, suggesting that all acetyl groups undergo restricted rotation, and each rotamer influences one of the gem-protons in a different way. Oxidation of (*RS*)-**9** with *m*-chloroperbenzoic acid in chloroform gave almost equal amounts of two products in 82% total yield, which were separable by silica-gel chromatography. Both compounds revealed two absorption

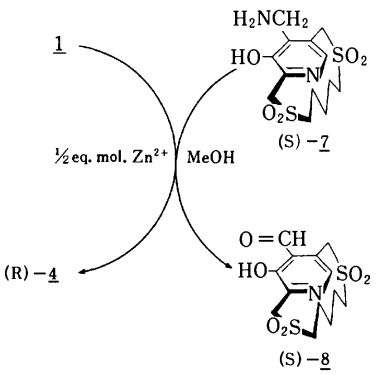

Scheme 4.

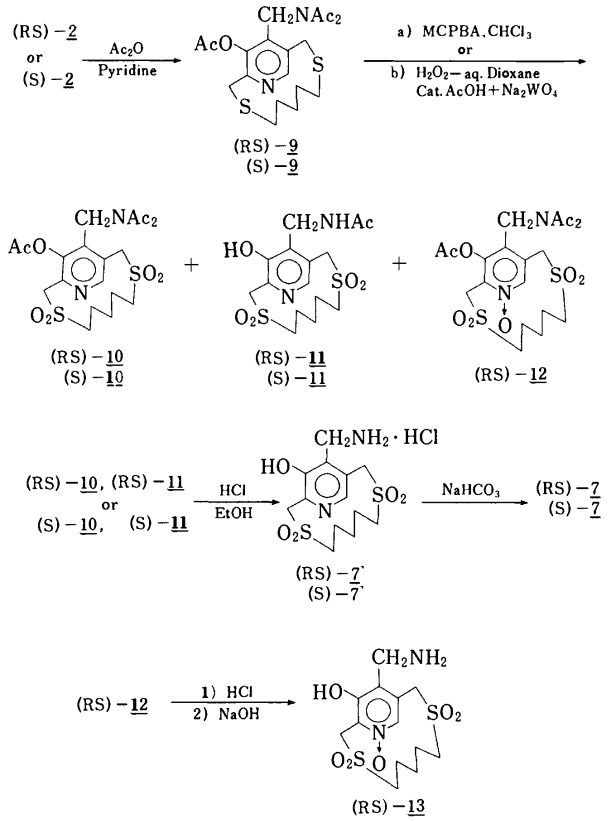

Scheme 5.

peaks of sulfonyl groups, at 1120—1130 and 1310—1320 cm^{-1} in their IR spectra. Elemental analyses of these products suggested that the less polar one was the expected (*RS*)-14-acetoxy-15-[(diacetylamino)methyl]-2,8-dithia[9](2,5)pyridinophane *S,S,S',S'*-tetraoxide ((*RS*)-**10**), and the other was *N,S,S,S',S'*-pentaoxide, (*RS*)-**12**. This identification was in good agreement with the results of our previous model oxidation experiment.[9] When the ^1H NMR spectrum of (*RS*)-**10** was compared with that of (*RS*)-**9**, four protons of 1- and 9-pyridylmethylene groups showed downfield shifts, appearing in the region of δ 4.36—5.24. One of the gem-protons of the (diacetylamino)methyl group, that appeared at 5.08 ppm as a broad doublet in the spectrum of **9**, was split into three sharp doublets at δ 5.07, 5.15, and 5.22 in the spectrum of **10**, with peak ratio 1:3:1. This presumably reflects the geometric proportion of the acetyl groups undergoing the restricted rotation. The ^1H NMR spectrum of (*RS*)-**12** revealed that one of the protons of the methylene group existing between the pyridine ring and the sulfonyl groups was missing, suggesting its easy replacement with the deuterium of the solvent (DMSO-d_6). Selective oxidation of the sulfur atoms in **9** to the corresponding sulfone was achieved by employing hydrogen peroxide as the oxidant. Although this oxidation also gave two compounds, the by-product was not **12** but **11**, a partially deacetylated derivative of **10**. Thus, when (*RS*)-**9** was treated in aqueous dioxane with hydrogen peroxide in the presence of catalytic amounts of acetic acid and sodium tungstate, (*RS*)-**10** and (*RS*)-15-[(acetylamino)-methyl]-14-hydroxy-2,8-dithia[9](2,5)pyridinophane *S,S,S',S'*-tetraoxide ((*RS*)-**11**) were obtained in a total yield of 62% with a ratio dependent on the reaction conditions employed. Both racemic **10** and **11** were deacetylated by treatment with hydrochloric acid, giving the same product, the racemic hydrochloride of **7** ((*RS*)-**7'**), which was quantitatively converted to the free base, (*RS*)-**7**, by neutralization with aqueous sodium hydrogencarbonate. In the ^1H NMR spectrum of (*RS*)-**7** using DMSO-d_6 as the solvent, all gem-protons of the pyridylmethylene groups appeared as three sets of sharp AB quartets, one of which was characteristic in showing a large difference of the chemical shifts between the A and B doublets (δ 3.97 and 4.98). (*RS*)-**12** could also be deprotected in a similar way, giving (*RS*)-**13**.

Chiral **7** was prepared from the corresponding **2** in the same way as the racemate model preparation. Thus, (*S*)-**2** was changed to (*S*)-**9**, which was oxidized by using the hydrogen peroxide–acetic acid–sodium tungstate system. Acidic hydrolysis of (*S*)-**10** and (*S*)-**11** gave (*S*)-**7'**, which was neutralized to give free (*S*)-**7** with the specific rotation of −352° at 589 nm.

Transamination Reactions. Transaminations from (*S*)-**7**, and from (*S*)-**2** were conducted employing four kinds of **1** as the reactants. The reaction conditions employed were the same, as those of the previous experiments mainly using chiral **3**,[6] except for the reaction time. A methanol solution containing the sodium salt of **1** (sodium pyruvate), (*S*)-**7** (or (*S*)-**2**), and one-half equivalent of zinc(II) was allowed to stand at room temperature, and the progress of the reaction was monitored by the change in its electronic absorption spectra with time (Fig. 2). The decrease in the initial absorption at 329 nm, due to the ketimine Schiff base zinc chelate complex, occurred simultaneously with an increase in the corresponding aldimine absorption at 390 nm. The time required for completion of the reaction reflected a large difference in the rate of the reactions of **2** and **7**. In the case of **2**, the isomerization from the ketimine to the aldimine was complete within 1 day, whereas it took more than 10 days in the reaction of **7**.

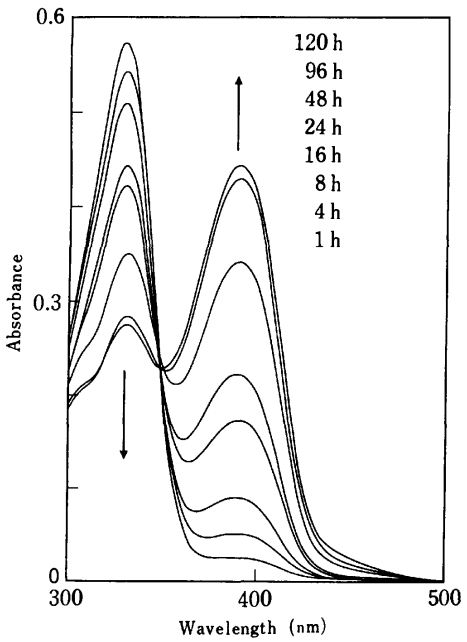

Fig. 2. Changes of the electronic absorption spectra with time for a methanol solution of (*S*)-**7** (0.1 mM), zinc perchlorate (0.05 mM), and sodium pyruvate (0.2 mM).

Various modifications of the procedures previously employed[6] were also required for isolation of amino acids from the zinc(II) chelate complexes of aldimine Schiff bases between **4** and **8** (Scheme 4). We have previously reported that the chelated aldimine intermediate derived from (*S*)-**2** was readily decomposed at room temperature by addition of dilute hydrochloric acid to the methanol solution of the reaction mixture. After extraction of (*S*)-**5** and excess of **1** with organic solvent, ion-exchange chromatography of the remaining aqueous solution gave (*R*)-**4**. Unexpectedly, this method failed in the present case, and the chelated aldimine intermediate derived from (*S*)-**7** resisted

Table 1. Transamination Reactions between (*S*)-**7** or (*S*)-**2** and RCOCOOH (**1**)

R	Reaction time/d		Recovered (*S*)-**7** or (*S*)-**2**/%		Products (amino acids) Major enantiomer		e.e./%		Chemical yield (isolation)/%		Name
	(*S*)-**7**	(*S*)-**2**	(*S*)-**7**	(*S*)-**2**	(*S*)-**7**	(*S*)-**2**	(*S*)-**7**	(*S*)-**2**	(*S*)-**7**	(*S*)-**2**	
Methyl	5	1	13	0	R	R	71	51	67 (77)[a]	80	Ala
Isopropyl	10	1	31	0	R	R	45	57	44 (64)	61	Val
Isobutyl	10	1	10	0	R	R	69	78	51 (58)	87	Leu
Benzyl	5	1	18	0	R	R	45	47	60 (73)	79	Phe

a) The values in the parentheses are the calculated ones on the basis of the amount of (*S*)-**7** consumed.

hydrolysis with dilute hydrochloric acid at room temperature, giving no amino acids. As the initial electronic absorption at 390 nm disappeared by addition of dilute hydrochloric acid it was replaced by a new stable absorption which appeared at 300 nm. It is possible that only zinc(II) ion was removed, leaving the acid-stable aldimine Schiff base in the solution. Therefore, the mixture in methanol–hydrochloric acid was evaporated and the residue redissolved in 1 M (1 M=1 mol dm^{-3}) hydrochloric acid. After heating at 100 °C for 5 h, extraction with ethyl acetate removed (*S*)-**8** and the excess of **1**. The aqueous solution was placed on a Dowex 50 W (H^+) column and successively eluted with water and aqueous ammonia to remove inorganic salts. In contrast to the case of transamination using (*S*)-**2**, concentration of the aqueous ammonia solution precipitated (*S*)-**7** unchanged. After filtration, the filtrate containing the amino acid **4** was passed through an Amberlite CG 50 (H^+) column, for complete removal of (*S*)-**7**. The combined yield of (*S*)-**7** recovered was in the range of 10—30%, depending upon the bulkiness of **1** employed. A small amount of brown-colored unidentified impurity was finally removed from the aqueous amino acid solution, using a LOBAR column.

Chemical yields and e.e. values of the amino acids isolated were determined on the basis of their weights and specific rotations measured. All results of the transamination reaction are tabulated in Table 1. The behavior of the *N,S,S,S',S'*-pentaoxide **13** in the transamination reaction is interesting, but no transamination was observed with (*RS*)-**13**.

Discussion

As mentioned above, the transamination reactions of (*S*)-**7** were different from those of (*S*)-**2** in several respects. For example, in the preparation of valine, the transamination using (*S*)-**2** was completed within 24 h and no (*S*)-**2** was left; whereas 31% of (*S*)-**7** was recovered even after standing for 10 days. Nevertheless, as the change of electronic absorption spectra showed, the reaction pattern producing chiral amino acids was essentially the same for both cases. The chemical yields of the amino acids produced by transamination using (*S*)-**2** or (*S*)-**7** did not differ much, when they

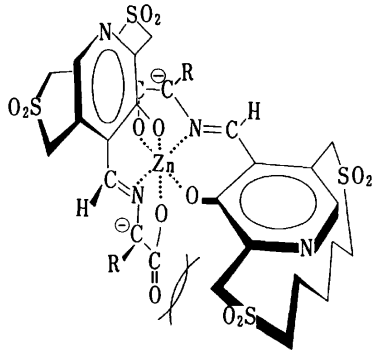

Fig. 3.

were calculated on the basis of the chiral pyridoxamine analogues consumed (the values in the parentheses for (*S*)-**7** in Table 1). The major enantiomer of amino acids obtained was *R* in all cases, suggesting that the transamination reaction using chiral **7** also obeys the rule established by the previous experiments using chiral **3** (and **2** in part); i.e., use of the (*S*)-enantiomer of the pyridoxamine analogues gives the (*R*)-amino acids in excess, and vice versa.[6] Contrary to the previous expectation of generally higher e.e. value by using (*S*)-**7** instead of (*S*)-**2**, it was actually so only in the single case of alanine. In the preparation of other amino acids such as valine, leucine, and phenylalanine, the efficiency of asymmetric induction by (*S*)-**7** was at most nearly equal to or lower than (*S*)-**2**. These unexpected results might be still rationalized with our view of the hypothetical reaction intermediate like Fig. 1, as described in the following. When the alkyl group in **1** is small like pyruvic acid (R=CH_3), the ketimine Schiff base resulted from its condensation with (*S*)-**7** might behave similarly to the Schiff base of (*S*)-**2**, forming a six-coordinated octahedral zinc(II) chelate complex. Isomerization from the ketimine to the aldimine involving the kinetically controlled stereoselective protonation would also take place within such chelate complex (see Fig. 1). These situations should have been considerably disturbed in the syntheses of other amino acids having bulkier alkyl groups (R in **1**). Namely, steric interaction should exist between the two bulky groups, R and sulfonyl group, as shown in

Fig. 3. This would labilize such zinc(II) chelate structure coordinated with two equimolecular Schiff base ligands. As a result, the geometry most favorably fixed for the ketimine-aldimine isomerization would be partially destroyed, lowering the steric effect of the sulfonyl group for enantioselectivity. This situation would lead not only to the increase of the amount of unchanged (*S*)-**7** but also to the decrease of the e.e. value of the amino acids.

The above speculative rationalization has been presented without any evidence. Therefore, an alternative process involving four- or five-coordinated zinc(II) chelate complex might better explain the whole stereochemical features of the nonenzymatic transamination reactions. Consideration of these possibilities and accumulation of the evidences for them will be made hereafter.

Experimental

General Procedures. Melting points were determined in a capillary tube using a Büchi melting point apparatus and are uncorrected. IR and UV-VIS absorption spectra were obtained with a Shimadzu IR 27G and a Varian-Cary 2290 spectrometer, respectively. Specific rotations were measured by using a Perkin-Elmer 241 polarimeter with a 1 dm 5 mL or a 1 dm 1 mL cell at room temperature. ^{1}H NMR spectra were obtained with a JEOL JNM GSX 500 s (500 MHz) using tetramethylsilane or sodium 3-(trimethylsilyl)propionate-d_4 as the internal references. Thin-layer chromatography (TLC) used precoated aluminium sheets from E. Merck (silica gel 60 F_{254}, 0.2 mm-thick for pyridinophanes, and cellulose F_{254}, 0.1 mm-thick for amino acids). The solvent systems used were as follows: chloroform–methanol for silica gel and 1-butanol–acetic acid–water for cellulose. The pyridinophanes on the silica gel layer were observed under a UV lamp or visualized by iodine vapor. The amino acids on the cellulose layer were visualized by ninhydrin–1-butanol and heating. Silica-gel column chromatography was performed using Merck silica gel 60 (0.063—0.200 mm in particle size) with solvent systems specified. Dowex 50 W×8 (100—200 mesh) and Amberlite CG 50 (Type 1) were purified in the usual way prior to use. Reversed-phase silica-gel column chromatography was carried out with a prepacked Merck LOBAR Column (Li Chroprep RP-8, 40—60 μm in particle size and 10×240 mm in column size) using water as the eluent. Ultrafiltration was performed using a Millex GS (0.22 μm in pore size and 4 cm^2 in effective area of filtration) purchased from Millipore, Japan Ltd.

(*RS*)-14-Acetoxy-15-[(diacetylamino)methyl]-2,8-dithia[9](2,5)pyridinophane ((*RS*)-9). A solution of (*RS*)-2[4] (10.00 g) in pyridine (100 mL) and acetic anhydride (100 mL) was stirred at 100 °C for 16 h, concentrated in vacuo at 70 °C, and poured into ice-water. The mixture was extracted with ethyl acetate and the extract was washed successively with aqueous sodium hydrogencarbonate and water, dried ($MgSO_4$), and concentrated in vacuo. The residual matter was chromatographed on silica gel with 100:1 (v/v) $CHCl_3$–MeOH as the eluent, giving (*RS*)-**9** (14.37 g, quantitative), mp 127—128 °C; UV ($CHCl_3$) 289 nm (ε 4.0×10^3); IR (KBr) 1780 (O-C=O) and 1710 and 1690 cm^{-1} (N-C=O); ^{1}H NMR (DMSO-d_6) δ=2.28 (s, 3H, $OCOCH_3$), 2.32 (s, 6H, N-$(COCH_3)_2$), 3.52 (d, 1H, J=13.0 Hz, =CCH_2S), 3.75 (broad, d, 1H, J=ca. 13 Hz, =CCH_2S), 3.87 (d, 1H, J=13.7 Hz, =CCH_2S), 4.01 (broad, d, 1H, J=ca. 14 Hz, =CCH_2S), 4.87 (d, 1H, J=16.2 Hz, =CCH_2N), 5.08 (broad, d, 1H, J=ca. 16 Hz, =CCH_2N), and 8.42 (s, 1H, N=CH). Found: C, 55.43; H, 6.38; N, 6.73; S, 15.62%. Calcd for $C_{19}H_{26}N_2O_4S_2$: C, 55.59; H, 6.38; N, 6.82; S, 15.62%.

(*S*)-14-Acetoxy-15-[(diacetylamino)methyl]-2,8-dithia[9](2,5)pyridinophane ((*S*)-9). The same treatments of (*S*)-**2** as those of the racemate described above resulted in (*S*)-**9** in 87% yield: mp 147—148 °C; $[\alpha]_D^{27}$ −42.6° (*c* 0.384, $CHCl_3$). Found: C, 55.57; H, 6.36; N, 6.85; S, 15.48%. Calcd for $C_{19}H_{26}N_2O_4S_2$: C, 55.59; H, 6.38; N, 6.82; S, 15.62%.

Oxidation of (*RS*)-9. (a) With *m*-Chloroperbenzoic Acid: A solution of *m*-chroroperbenzoic acid (85% purity, 7.50 g, 37 mmol) in chloroform (75 mL) was added dropwise at 5—10 °C for 1 h with stirring to a solution of (*RS*)-**9** (2.00 g, 4.9 mmol) in chloroform (100 mL), giving a precipitate. The mixture was stirred at 5—10 °C for another 1 h and at room temperature overnight. Meanwhile the precipitate completely dissolved. After addition of 20—30 mL of 5% aqueous sodium hydrogensulfite, the mixture was extracted with aqueous sodium hydrogencarbonate for removal of *m*-chlorobenzoic acid. The chloroform layer was washed with water, dried ($MgSO_4$), and concentrated in vacuo. The residue was chromatographed on silica gel, using 100:1 (v/v) $CHCl_3$–MeOH as the eluent, giving (*RS*)-**10** (0.95 g, 41%) and (*RS*)-**12** (0.97 g, 41%) in this elution order. (*RS*)-**10**: mp 202—204 °C; UV ($CHCl_3$) 282 nm (ε 4.2×10^3); IR (KBr) 1790 (O-C=O), 1710 and 1690 (N-C=O), and 1320 and 1120 cm^{-1} (SO_2); ^{1}H NMR (DMSO-d_6) δ=2.31 (s, 3H, $COOCH_3$), 2.32 (s, 6H, N$(COCH_3)_2$), 4.36—4.92 (m, 5H, =CCH_2S and =CCH_2N), 5.07 (d, 0.2H, J=17 Hz, =CCH_2N), 5.14 (d, 0.6H, J=16 Hz, =CCH_2N), 5.22 (d, 0.2H, J=17 Hz, =CCH_2N), and 8.81 (s, 1H, N=CH). Found: C, 47.74; H, 5.51; N, 5.68; S, 13.64%. Calcd for $C_{19}H_{26}N_2O_8S_2$: C, 48.09; H, 5.52; N, 5.90; S, 13.51%.

(*RS*)-**12:** Mp 201—202 °C (decomp); UV ($CHCl_3$) 287 nm (ε 11.9×10^3); IR (KBr) 1780 (O-C=O), 1710 and 1690 (N-C=O), 1310 (SO_2), 1290 (N→O), and 1130 cm^{-1} (SO_2); ^{1}H NMR (DMSO-d_6) δ=2.31 (s, 3H, $OCOCH_3$), 2.32 (s, 6H, N-$(COCH_3)_2$), 4.51 (d, 1H, J=13.5 Hz, =CCH_2S), 4.84 (d, 1H, J=14.2 Hz, =CCH_2S), 4.85 (d, 1H, J=15.9 Hz, =CCH_2N), 4.90 (d, 1H, J=14.2 Hz, =CCH_2S), 5.14 (d, 1H, J=15.9 Hz, =CCH_2N), and 8.81 (s, 1H, N=CH). Found: C, 46.33; H, 5.32; N, 5.67; S, 12.97%. Calcd for $C_{19}H_{26}N_2O_9S_2$: C, 46.52; H, 5.34; N, 5.71; S, 13.07%.

(b) With Hydrogen Peroxide: Aqueous hydrogen peroxide (30%, 2.43 mL, 24.5 mmol) was added dropwise with stirring at 60—65 °C for 30 min to a solution of (*RS*)-**9** (2.00 g, 4.9 mmol), acetic acid (ca. 15 mg), and sodium tungstate dihydrate (ca. 5 mg) in dioxane–water (2:1 v/v, 30 mL). The mixture was heated at 80—85 °C for 1 h, cooled, diluted with aqueous sodium hydrogensulfite (5%, 5—10 mL), and extracted with chloroform. The extract was dried ($MgSO_4$), concentrated, and chromatographed on silica gel with 100:1 (v/v) $CHCl_3$–MeOH as the eluent, giving (*RS*)-**10** (1.15 g, 50%). Further elution with 25:1 (v/v) $CHCl_3$–MeOH gave (*RS*)-**11** (0.22 g, 12%); mp>280 °C; UV ($CHCl_3$) 282 nm (ε 4.2×10^3); IR (KBr) 3350 (broad, NH, OH), 1650 (NHCO), and 1310 and 1140 cm^{-1} (SO_2); ^{1}H NMR

(DMSO-d_6) δ=1.87 (s, 3H, $NCOCH_3$), 4.34 (d, 1H, J=13.3 Hz, $=CCH_2S$), 4.35 (dd, 1H, J=14.8 and 6.1 Hz, $=CCH_2N$), 4.57 (dd, 1H, J=14.8 and 6.1 Hz, $=CCH_2N$), 4.67 (d, 1H, J=14.1 Hz, $=CCH_2S$), 4.95 (d, 1H, J=13.7 Hz, $=CCH_2S$), 5.00 (d, 1H, J=13.3 Hz, $=CCH_2S$), 8.37 (s, 1H, N=CH), 8.82 (t, 1H, J=5.8 Hz, NH), and 10.82 (s, 1H, OH). Found: C, 45.36; H,5.57; N, 6.89; S, 16.41%. Calcd for $C_{15}H_{22}N_2O_6S_2 \cdot 1/2H_2O$: C, 45.10; H, 5.80; N, 7.01; S, 16.05%.

Oxidation of (*S*)-9 with Hydrogen Peroxide. The same treatment of (*S*)-**9** with hydrogen peroxide-acetic acid-sodium tungstate gave a mixture of (*S*)-**10** and (*S*)-**11** in 33% and 30% yields, respectively. (*S*)-**10**: mp 204—205 °C; $[\alpha]_D^{31}$ −78° (c 0.363, $CHCl_3$). Found: C, 47.12; H, 5.40; N, 5.70; S, 13.45%. Calcd for $C_{19}H_{26}N_2O_8S_2 \cdot 1/2H_2O$: C, 47.19; H, 5.63; N, 5.79; S, 13.26%.

(*S*)-**11**: Mp 266—267 °C (decomp); $[\alpha]_D^{29}$ −168 ° (c 0.321, pyridine). Found: C, 43.97; H, 5.38; N, 6.68; S, 15.96%. Calcd for $C_{15}H_{22}N_2O_6S_2 \cdot H_2O$: C, 44.11; H, 5.92; N, 6.86; S, 15.70%.

(*RS*)-15-Aminomethyl-14-hydroxy-2,8-dithia[9](2,5)pyridinophane *S,S,S',S'*-Tetraoxide ((*RS*)-7) via Monohydrochloride of 7 ((*RS*)-7'). **(a) From (*RS*)-10:** A solution of (*RS*)-**10** (3.00 g, 7.3 mmol) in ethanol (15 mL) and 6 M hydrochloric acid (15 mL) was heated under reflux for 3 h and concentrated in vacuo. The residue was dissolved in a small amount of hot water, treated with charcoal, and diluted with ethanol, giving (*RS*)-**7'** (1.94 g, 80%): mp>280 °C; UV (H_2O) 333 (ε 3.7×10³), 301 (ε 4.1×10³), and 255 nm (ε 3.7×10³); IR (KBr) 3000, 1580, and 1500 (OH, $NH_2 \cdot HCl$) and 1320 and 1110 cm^{-1} (SO_2). Found: C, 40.56; H, 5.58; Cl, 8.85; N, 7.13; S, 16.54%. Calcd for $C_{13}H_{20}N_2O_5S_2 \cdot HCl$: C, 40.57; H, 5.50; Cl, 9.21; N, 7.28; S, 16.66%.

To a solution of (*RS*)-**7'** (1.414 g, 3.7 mmol) in water was added aqueous sodium hydrogencarbonate (310 mg, 3.7 mmol) and the mixture was stirred at room temperature for 30 min, giving (*RS*)-**7** (1.223 g, 91%) as a precipitate: mp 175—202 °C (decomp); UV (dioxane) 300 nm (ε 2.9×10³); IR (KBr) 3500 and 3350 (NH_2, OH) and 1300 and 1130 cm^{-1} (SO_2); ^{1}H NMR (DMSO-d_6)[10] δ=3.97 (d, 1H, J=12.4 Hz, $=CCH_2S$), 4.07 (d, 1H, J=15.6 Hz, $=CCH_2N$), 4.13 (d, 1H, J=15.3 Hz, $=CCH_2N$), 4.42 (d, 1H, J=14.0 Hz, $=CCH_2S$), 4.65 (d, 1H, J=13.7 Hz, $=CCH_2S$), 4.98 (d, 1H, J=12.4 Hz, $=CCH_2S$), and 7.78 (s, 1H, N=CH). Found: C, 42.58; H, 5.50; N, 7.57; S, 17.47%. Calcd for $C_{13}H_{20}N_2O_5S_2 \cdot H_2O$: C, 42.61; H, 6.05; N, 7.64; S, 17.50%.

(b) From (*RS*)-11: A solution of (*RS*)-**11** (0.85 g, 2.1 mmol) in ethanol (10 mL) and 6 M hydrochloric acid (10 mL) was heated under reflux for 3 h and worked up in the same way as described in (a), giving (*RS*)-**7'** (0.71 g, 86%), which was neutralized with sodium hydrogencarbonate to give (*RS*)-**7** (0.61 g, 90%).

(*S*)-15-Aminomethyl-14-hydroxy-2,8-dithia[9](2,5)pyridinophane *S,S,S',S'*-Tetraoxide ((*S*)-7) via Monohydrochloride of 7 ((*S*)-7'). Either (*S*)-**10** or (*S*)-**11** was treated with hydrochloric acid in the same way as the hydrolysis of the corresponding racemate, giving (*S*)-**7'** in 74% and 85% yields, respectively: mp>280 °C; $[\alpha]_D^{29}$ −317 ° (c 0.293, H_2O). Found: C, 40.40; H, 5.56; Cl, 9.10; N, 7.20; S, 16.59%. Calcd for $C_{13}H_{20}N_2O_5S_2 \cdot HCl$: C, 40.57; H, 5.50; Cl, 9.21; N, 7.28; S, 16.66%.

Neutralizing (*S*)-**7'** with equimolecular amount of sodium hydrogencarbonate similarly to the case of the racemate gave (*S*)-**7** in quantitative yield: mp 196—199 °C (decomp); $[\alpha]_D^{19}$ −352 ° (c 0.241, pyridine). Found: C, 42.69; H, 5.51; N, 7.52; S, 17.55%. Calcd for $C_{13}H_{20}N_2O_5S_2 \cdot H_2O$: C, 42.61; H, 6.05; N, 7.64; S, 17.50%.

(*RS*)-15-Aminomethyl-14-hydroxy-2,8-dithia[9](2,5)pyridinophane *N,S,S,S',S'*-Pentaoxide ((*RS*)-13). A solution of (*RS*)-**12** (1.92 g, 5.3 mmol) in ethanol (20 mL) and 6 M hydrochloric acid (20 mL) was heated under reflux for 3 h, treated with charcoal, and concentrated in vacuo. The residue was dissolved in a minimum amount of water and adjusted to pH 3 by addition of aqueous sodium hydroxide, giving (*RS*)-**13** (1.38 g, 97%) as a precipitate: mp>280 °C; UV (1 M HCl) 327 (ε 4.8×10³), 276 (ε 9.0×10³), and 240 nm (ε 23.7×10³); IR (KBr) 3400 (broad, NH_2, OH), 1360 (SO_2), 1280 (N→O), and 1130 cm^{-1} (SO_2); ^{1}H NMR (DCl-D_2O)[11] δ=3.86 (s, 2H, $=CCH_2N$), 4.20 (d, 1H, J=15.0 Hz, $=CCH_2S$), 4.46, (d, 1H, J=14.6 Hz, $=CCH_2S$), 4.50 (d, 1H, J=14.6 Hz, $=CCH_2S$), 5.02 (d, 1H, J=14.6 Hz, $=CCH_2S$), and 7.92 (s, 1H, N=CH). Found: C, 42.57; H, 5.58; N, 7.44; S, 17.43%. Calcd for $C_{13}H_{20}N_2O_6S_2$: C, 42.85; H, 5.53; N, 7.69; S, 17.65%.

Transamination Reactions. (a) Using (*S*)-2: A solution of (*S*)-**2** (85 mg, 0.3 mmol), sodium salts of **1** (0.6 mmol), and zinc perchlorate hexahydrate (56 mg, 0.15 mmol) in methanol (150 mL) was stirred at room temperature for 24 h. After addition of 1 M hydrochloric acid (6 mL), the resulting mixture was concentrated to dryness in vacuo. The residue was extracted with a mixture of water and ethyl acetate. The aqueous extract was concentrated to ca. 10 mL and put on a column packed with Dowex 50 W×8 (100—200 mesh,H^+ form, 50 mL). The column was successively eluted with water (1 L) and 0.1 M aqueous ammonia. The latter eluate was concentrated to give a residue, which was put on a column packed with Amberlite CG 50 (100—200 mesh, H^+ form, 20 mL). The column was eluted with water to collect the amino acid-containing fractions, and evaporated. Optical purities of **4** obtained were calculated on the basis of its measured optical rotations.

(b) Using (*S*)-7: The same reaction conditions were employed except for the longer reaction time. A solution of (*S*)-**7** (110 mg, 0.3 mmol), sodium salt of **1** (0.6 mmol), and zinc perchlorate hexahydrate (56 mg, 0.15 mmol) in methanol (150 mL) was stirred at room temperature, monitoring the reaction by the change of the electronic absorption spectrum. The reaction time employed was 5 days for preparations of alanine (from pyruvate) and phenylalanine (from phenylpyruvate), whereas 10 days were necessary for the preparation of valine (from 3-methyl-2-oxobutyrate) and leucine (from 4-methyl-2-oxovalerate). After the reaction was over, 1 M hydrochloric acid (6 mL) was added and the mixture was concentrated to dryness; the residue was dissolved again in 1 M hydrochloric acid (20 mL) and heated at 100 °C for 5 h. Concentration in vacuo followed by dilution with water was repeated several times to remove hydrochloric acid as much as possible. The final residue was extracted with a mixture of water and ethyl acetate. The aqueous extract was concentrated to a volume of 10 mL and put on a column packed with Dowex 50 W×8 (100—200 mesh, H^+ form, 50 mL). The column was successively eluted with water (1 L) and 0.1 M aqueous ammonia. The latter eluate was concentrated to a volume of 5 mL to give (*S*)-**7** unreacted as a precipitate, which was filtered off. The filtrate was put on a column packed with Amberlite CG 50

(100—200 mesh, H^+ form, 20 mL) and eluted with water. The amino acid-containing fractions were collected, concentrated, and put on a LOBAR column RP-8 (10×240 mm), which was eluted with water. Concentration of the eluate gave **4**. Before measurement of the optical rotations, the aqueous solutions of **4** obtained were passed through a membrane filter.

The authors wish to express their thanks to Miss Mutsuko Yoshida and her coworkers of this Institute for elemental analyses and to Dr. Jun Uzawa and Mrs. Tamiko Chijimatsu of this Institute for the measurements of ^1H NMR spectra.

This study was performed through Special Coordination Funds of the Science and Technology Agency of the Japanese Government.

References

1) D. E. Metzler, M. Ikawa, and E. E. Snell, *J. Am. Chem. Soc.*, **76**, 648 (1954), and earlier papers.

2) Y. Matsushima and A. E. Martell, *J. Am. Chem. Soc.*, **89**, 1331 (1967).

3) R. Breslow, A. W. Czarnik, M. Lauer, R. Leppkes, J. Winkler, and S. Zimmerman, *J. Am. Chem. Soc.*, **108**, 1969 (1986), and earlier papers; I. Tabushi, Y. Kuroda, M. Yamada, and H. Higashimura, *ibid.*, **107**, 5545 (1985), and earlier papers.

4) H. Kuzuhara, T. Komatsu, and S. Emoto, *Tetrahedron Lett.*, **1978**, 3563.

5) M. Ando, Y. Tachibana, and H. Kuzuhara, *Bull. Chem. Soc. Jpn.*, **55**, 829 (1982).

6) Y. Tachibana, M. Ando, and H. Kuzuhara, *Chem. Lett.*, **1982**, 1765.

7) Y. Tachibana, M. Ando, and H. Kuzuhara, *Chem. Lett.*, **1982**, 1769.

8) Alternative helical isomer, *Δ*, is unlikely to exist.

9) M. Ando and H. Kuzuhara, *Bull. Chem. Soc. Jpn.*, **60**, 818 (1987).

10) No signals assignable to OH and NH_2 protons were observed owing to their replacement wth deuterium of DMSO-d_6 taking place during the prolonged time for recording.

11) When ^1H NMR spectrum of **13** was obtained after **13** had been dissolved in DCl–D_2O as soon as possible, no replacement of the protons of the pyridylmethylene groups with deuterium of the solvents was observed.

The Electric Birefringence and Dichroism of a Nonlinear Optical Compound, 4-[2-[4-(Dimethylamino)phenyl]ethenyl]-1-ethylpyridinium Iodide, in the Presence of Poly(*p*-styrenesulfonate) and Poly(L-α-glutamate) in Solutions

Kiwamu YAMAOKA* and Yasumori HINO
Faculty of Science, Hiroshima University, Higashisenda-machi, Naka-ku, Hiroshima 730
(Received June 11, 1988)

The pulsed electric birefringence at 633 nm and dichroism at 462 nm of the title cationic compound (DAES) were measured at 20 °C over a wide electric field strength range (0.1—24 kV cm^{-1}) in the presence of poly(*p*-styrenesulfonate)(NaPSS) and poly(L-α-glutamate) (PGA) in aqueous solutions at various mixing ratios (*P/D*) of the polymer to the ligand. The steady-state electric birefringence δ of NaPSS–DAES complexes was positive, while that of NaPSS was negative. The optical anisotropy factor of bound DAES was responsible for the sign reversal. The reduced electric dichroism of NaPSS–DAES at a *P/D* of 1.9 was +0.38 at infinitely high fields. A value of ±50° was found for the average angle between the orientation axis of the complex and the direction of the optical transition moment at 462 nm of bound DEAS chromophores. No appreciable permanent dipole moment was present in any of the NaPSS–DAES systems. The field orientation was due mostly to counterion-induced moments. The rotational relaxation time was determined from the decay signals. For PAG–DAES and PGA at pH 6.4 and 4.1, the sign of δ was always positive, the magnitude differing from each other by only 10—20%.

4-[2-[4-(Dimethylamino)phenyl]ethenyl]-1-ethylpyridinium iodide (DAES) is one of the well-known nonlinear optical materials which exhibit a marked second harmonic generation (SHG) phenomenon, due mostly to their large hyperpolarizability in the crystalline state.[1] Attempts have been made to observe SHG in some stilbene derivatives in the dissolved state with a strong Nd:YAG laser beam.[2] The static electric field-induced SHG of the π-electronic conjugated system is generally weak; therefore, a high external field strength of about 100 kV cm^{-1} or more is required. If nonlinear optical compounds were oriented unidirectionally at much lower electric fields, as in the crystalline state, the SHG measurement could be facilitated with less powerful but easily available laser diodes as the light source; hence, a variety of practical applications would thus become feasible. This idea may be realized if the nonlinear materials are attached either covalently or electrostatically to the appropriate polymeric matrices, which are easily orientable by an external force. The electric field is particularly useful because the field orientation is fast and reversible, which would enable us to develop an on-off switching device.

In order to achieve the above objectives, a series of systematic studies will be necessary to determine the electrooptical properties of polymer-nonlinear optical material complexes. In this work, the field orientation behavior of DAES, a cationic stilbene derivative with a large permanent dipole moment, was studied in the presence of poly(sodium *p*-styrenesulfonate) (NaPPS)[3–8] and poly(sodium L-α-glutamate) (PGA),[9–11] both of which are known to be oriented easily in an aqueous solution by means of an external electric field. The interaction of polymer–ligand complexes is best studied by pulsed electric birefringence and electric dichroism, which measure the anisotropic electric, optical, and hydrodynamic properties.[3–14] Since a large change in permanent dipole moments between the ground and excited states of the nonlinear optical ligand effects an SHG phenomenon,[1] lower ratios of the polymer site to the ligand are chosen in this work.

Experimental

Materials. The DAES was purchased from Nippon Kankoh Shikiso Kenkyusho (Okayama) and was used without further purification. This compound was insensitive to the irradiation of the 320—450 nm light from a 150-W quartz-iodine lamp. The NaPSS was kindly supplied by the Tosoh Co. and was fractionated by the precipitation method. The weight-average molecular weight was estimated to be 1.63×10^6 from the intrinsic viscosity of 2.61 dl g^{-1} in 0.2 M (1 M=1 mol dm^{-3}) NaCl at 25 °C.[15] The PGA was a gift of Dr. Hiroshi Sato of the Mitsubishi Rayon Co. and was fractionated by successive precipitation. The weight-average molecular weight was estimated to be 1.04×10^5 from the intrinsic viscosity of 1.02 dl g^{-1} in 2 M NaCl at 25 °C. The polymer–DAES solution was prepared by adding the DAES solution to the polymer solution at a desired mixing ratio (denoted as *P/D*), which was expressed in terms of the polymer residue-to-DAES concentrations. The polymer concentration was kept constant at all *P/D* values, since the polymer conformation without added salt or at a low ionic strength is concentration-dependent.

Measurements. The absorption spectra in the absence of electric field were measured on a Shimadzu Model UV-250 recording spectrophotometer at 20 °C with quartz cells 0.3 and 1.0 cm in path length. The electric birefringence was measured at 20 °C on a high-speed, high-voltage He–Ne laser (632.8 nm) apparatus constructed in this laboratory. The electric dichroism was determined at 20 °C and at an absorption maximum of 462 nm of DAES on an instrument

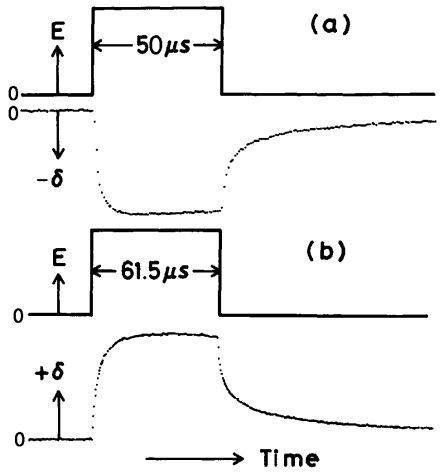

Fig. 1. Transient electric birefringence signals and applied electric square-pulse fields. (a) NaPSS: E=16.83 kV cm^{-1} and δ=−6.19° and (b) NaPSS-DAES at P/D=1.9: E=16.78 kV cm^{-1} and δ=+21.67°. Birefringence signal δ in (a) is an average of four accumulations, while the signal in (b) is the response to a single pulse. The sampling time of the signal detecting system was set at 200 ns. The instrumental time constant was adjusted to 100 ns for the buildup (or the rise) and 300 ns for the decay signal.

previously reported.[5,12] The output signals were digitized and processed with the transient wave memory-microcomputer system.[16] Figure 1 shows examples of the transient electric birefringence signals of NaPPS and its DAES complex.

Results and Discussion

Isotropic Absorption Spectra. Figure 2 shows the isotropic absorption spectra of DAES in the presence of NaPSS and PGA, together with those of DAES alone (P/D=0). The spectra of DAES in the presence of NaPSS differ from the reference spectrum of DAES, whose maximum at 450 nm is shifted toward red by 25 nm at higher P/D values, but shifted back to ca. 430 nm at a low P/D of about 1 probably because of the metachromatic effect of bound DEAS.[17] These changes are a strong indication of the formation of a complex by the electrostatic interaction between the anionic sulfonato group and the quarternized ring nitrogen of DAES.[17] The spectra of DAES in PGA differ only slightly from the DAES spectra at two pH's; thus, the binding of DAES to PGA appears to be very weak, regardless of the backbone conformations of PGA (helix at pH 4.1 and random coil at pH 6.4).

Steady-State Electric Birefringence. Figure 3 shows the steady-state birefringence of NaPSS-DAES complexes, expressed in terms of the optical phase retardation δ. Since DAES exhibits no electric birefringence in the absence of NaPSS over a field strength range of $E \leq 22.4$ kV cm^{-1}, the observed signals are all due to the NaPSS-DAES complex. It should be noted that the

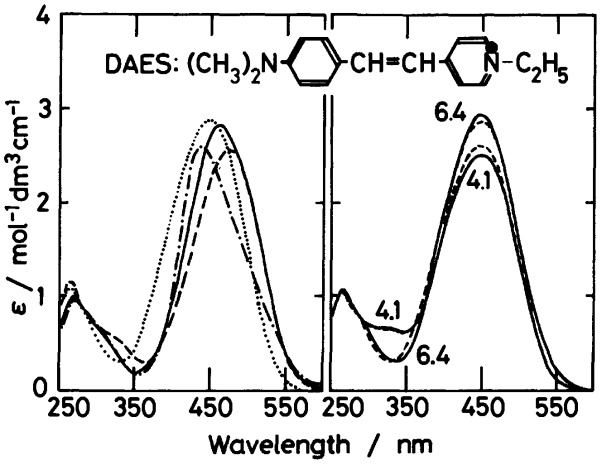

Fig. 2. Isotropic absorption spectra of DAES in the presence and the absence of NaPSS (left) and PGA (right). P/D for NaPSS at pH 6.4: 7.1 (——), 1.9 (——), 0.94 (—·—·—), and 0 (·····). P/D for PGA: 9.8 (——) and 0 (-----) at pH 4.1 and 5.4 (——) and 0 (-----) at pH 6.4; the numerals denote pH values. The molar absorption coefficient ε was expressed in terms of the concentration of DAES. The residue concentrations of polymers are constant: [NaPSS]= 0.202 mM containig 0.8 mM NaCl, [PGA]=0.389 mM.

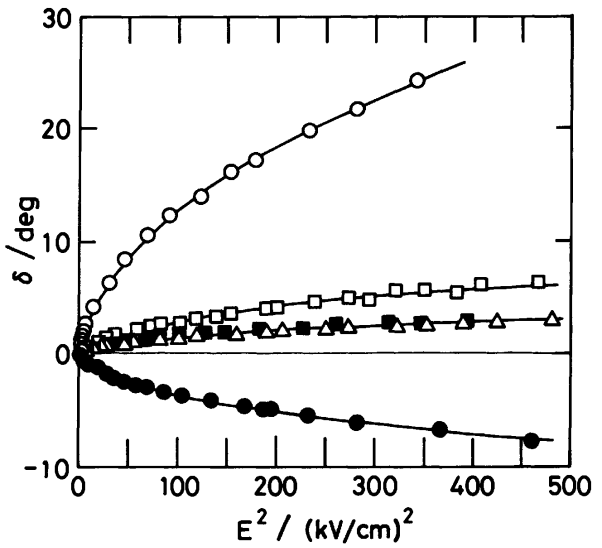

Fig. 3. The steady-state electric birefringence δ of NaPSS-DAES complexes and NaPSS versus the square of applied external electric field strength E^2. P/D: 7.1 (■), 4.7 (□), 1.9 (○), 0.94 (△), and ∞ (●). [NaPSS]=0.202 mM in 0.8 mM NaCl. Solid lines are theoretically calculated SUSID orientation functions (see text).

sign of δ for the complex is reversed to positive, while the sign is negative for NaPSS itself.[3,4,6-8] A large contribution of the bound DAES moiety to the observed δ values is evident. Since more than half of DAES present in solution are unbound at a low P/D ratio of 0.94, the δ values are much less than those of complexes at P/D=7.1—1.9, probably because of the

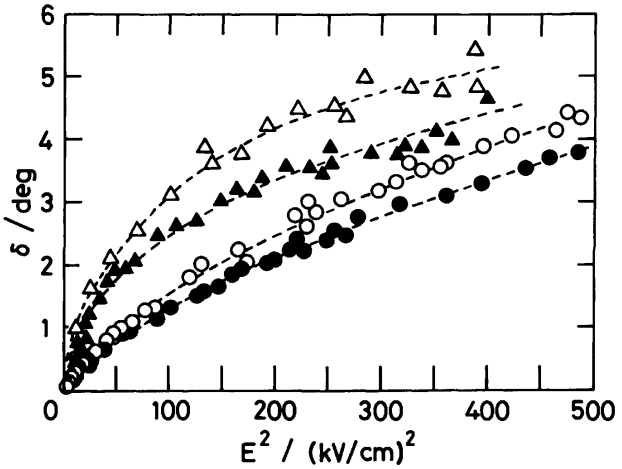

Fig. 4. The steady-state electric birefringence δ of PGA in the presence and the absence of DAES versus the square of field strength E^2. pH at 4.1: P/D=9.8 (○) and ∞ (●). pH at 6.4: P/D=5.4 (△) and ∞ (▲). [PGA]=0.389 mM.

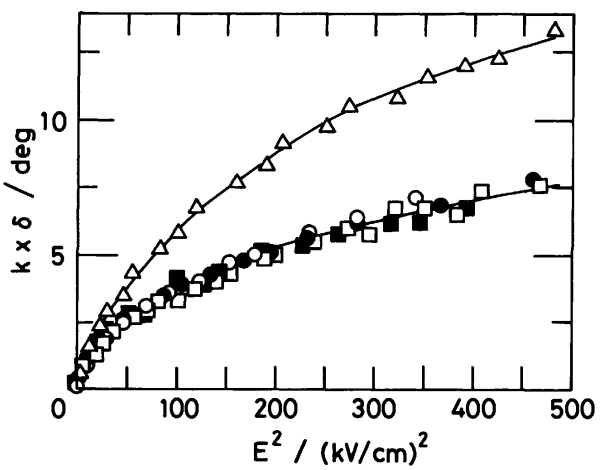

Fig. 5. The field strength dependence of δ multiplied by a normalization factor k for NaPSS-DAES complexes. k=−1.0 (∞), 2.3 (7.1), 1.3 (4.7), 0.29 (1.9), and 4.0 (0.94), P/D values being given in the parentheses. The symbols and other conditions are all the same as in Fig. 3.

presence of unbound DEAS in the solution.

Figure 4 shows the steady-state birefringence of DAES in the presence of PGA at pH 4.1 and 6.4. The magnitude of δ for DAES in the presence of PGA was found to differ from that of PGA by only 10—20% over the 0.1—22.4 kV cm^{-1} range, the sign of δ being positive in all cases. Hence, no appreciable DAES ions are oriented jointly with PGA by an applied field. It is now clear that, though positively charged at those pH's, DAES is not bound tightly to the side-chain carboxylate of PGA, as is also indicated by the spectral changes (cf. Fig. 2).

Electric birefringence is expressed by the product of the optical, $\Delta g/n$, and electric, $\Phi(E)$, terms; it is given as $\delta=(4\pi^2 C_v d/\lambda)(\Delta g/n)\Phi(E)$, where C_v is the volume fraction of orientable solutes (i.e., the NaPSS-DAES complex), d is the path length of a Kerr cell (1.0 cm), λ is the wavelength of the incident light (632.8 nm), Δg is the optical anisotropy factor, n is the refractive index of the solution, and $\Phi(E)$ is the orientation function, which describes the dependence of δ on the field strength.[7] If the field orientation of the NaPSS-DAES complexes and NaPSS is described by a common orientation function, the observed δ vs. E^2 plots in Fig. 3 should all be brought to coincide with one another. In such a case, $\delta \times k=\Phi(E)$, where k is a constant, since the optical term is independent of the field strength. Figure 5 shows that all the δ vs. E^2 plots except for P/D=0.94 are now brought into a good coincidence with the appropriate constants, k, evaluated in the low field region. This indicates that a single orientation function is sufficient to describe the field orientation of NaPSS (P/D=∞) and the complexes (P/D=7.1, 4.7, 1.9).

It has been shown that NaPSS is oriented because of its large induced dipole moment.[3,4,8] The results shown in Fig. 5 indicate that NaPPS-DAES complexes also possess practically no net permanent dipole moment μ along the molecular axis of field orientation. If all the DEAS molecules in a solution are bound, the average number of DEAS molecules bound on each NaPSS polyanion would be about 1110(at P/D=7.1)—4150(at P/D=1.9). Because of the permanent dipole moment of ca. 7 Debye units for each DAES molecule, the vectorial sum of μ would be roughly as large as 7000—29000 Debyes if all bound DAES moieties were aligned in parallel fashions like an arrow along a rodlike NaPSS backbone. This case is inconsistent with the present results. Possible explanations are: (1) the bound DAES molecules are so arranged that the individual dipole moments, μ_{DAES}, cancel each other out and/or (2) the overall conformation of the complexes is not rigidly rodlike, but coiled, so that the net moment μ is negligibly small.

In order to analyze the experimentally obtained δ vs. E^2 plots for ionized polymers, which are lacking in the permanent dipole moment and are, therefore, oriented by induced dipole moment(s), a new orientation function is needed. For this purpose, a theoretical function was recently derived on the assumption that an ionized polymer possesses both saturable ($\Delta\sigma E$) and unsaturable ($\Delta\alpha E$) induced dipole (SUSID) moments.[18] These two types of induced dipole moments are responsible for the interaction with the electric field. The former ($\Delta\sigma E$) is induced by the counterion and is saturated at the critical electric field E_0, while the latter ($\Delta\alpha E$) is partly electronic and partly ionic. Here, $\Delta\alpha$ is the electronic polarizability anisotropy, and $\Delta\sigma$ is the ionic polarizability anisotropy (the details are given in Ref. 18). The theoretical curves based on the SUSID mechanism (solid lines) in Fig. 3 reproduce all

Table 1. Optical, Electric, and Hydrodynamic Properties of NaPSS and NaPSS-DAES Complexes at 20°C

P/D	δ_∞[a]	$\Delta g/n$[b]	$(\Delta g/n)_{DAES}$[c]	$\Delta\alpha$	$\Delta\sigma$	E_0	τ_w	l
	deg		$mol^{-1}\,dm^3$	$10^{-33}F\,m^2$	$10^{-31}F\,m^2$	$kV\,cm^{-1}$	μs	Å
0.94	5.9	7.01	112	1.8	0.3	2.0	4.1	620
1.9	49.3	58.7	704	1.2	7.1	0.1	15.4	1020
4.7	11.0	13.1	700	1.2	7.1	0.1	18.1	1080
7.1	6.2	7.37	849	1.2	7.1	0.1	18.4	1090
∞	−14.3	−17.0	—	1.2	7.1	0.1	26.7	1250

a) The optical phase retardation at infinitely high fields. b) Values are estimated by curve-fitting. c) The reduced optical anisotropy factor contributed by DAES, defined as [((Δg/n) of NaPSS-DAES complex)−(Δg/n) of NaPSS)]/(DAES concentration).

the observed δ vs. E^2 plots quite well. The degree of orientation at a high field of 22.4 kV cm^{-1} is calculated from those theoretical curves to be 0.53 for NaPSS and for NaPSS-DAES at P/D=7.1—1.9 and 0.56 for NaPSS-DAES at P/D=0.94; these values constitute strong evidence for the ease of the orientation of these polymer systems by external pulse fields. Table 1 shows the optical and electric properties, which were evaluated by means of the curve-fitting.[18] It is interesting to note in Table 1 that the reduced optical anisotropy factor ($\Delta g/n$) of the NaPSS-DAES complexes varies greatly with the P/D ratio, while the ($\Delta g/n$) value per DAES molecule, $(\Delta g/n)_{DAES}$, remains nearly constant in the P/D range of 7.1—1.9, where the DAES molecules in the solution are probably almost all bound to NaPSS.[17]

Relaxation Time from Decay Signal. Figure 6 shows the birefringence-average relaxation time of the NaPSS and NaPSS-DAES complexes, $\langle\tau\rangle_{EB}$, which was obtained by means of the area method from the decay signal upon the removal of the applied pulse field (cf. Fig. 1).[19] The values of $\langle\tau\rangle_{EB}$ rapidly decrease in the low field region; however, they reach constant levels at higher pulse fields ($E \geq 10$ kV cm^{-1}). This feature is mostly due to the polydispersity of the NaPSS sample.[20] The value of $\langle\tau\rangle_{EB}$ at infinitely high fields is reduced to the weight-average relaxation time τ_w which is given in Table 1. The τ_w value of 27 μs for NaPSS is the largest, while it is only 4 μs for NaPSS-DAES at P/D=0.94. Considering that the weight-average degree of polymerization is 7890, the contour length of NaPSS would be as long as 19700 Å (=2.5 Å×7890). For a rigidly rodlike model with this length and a radius of 9 Å, the rotational relaxation time should be ca. 52.6×10^3 μs, as calculated with the aid of the Broersma equation.[7,21] A comparison of this value of 52.6×10^3 μs with the observed value of 27 μs reveals that the backbone chain is probably folded and that the overall shape of NaPSS and its DAES complex may be approximated by an ellipsoid.[7] The apparent length l (=2a) is given in Table 1 for this model, with a probable semi-minor axis b of 32 Å,[7] as calculated with the Perrin equation: $\tau^{-1}=(9kT/4\pi\eta_0 a^3)\cdot[\ln(2p)-0.5]$, where η_0 is the viscosity of the solvent, $p=a/b$ (the axial ratio), and a is the semi-major axis.

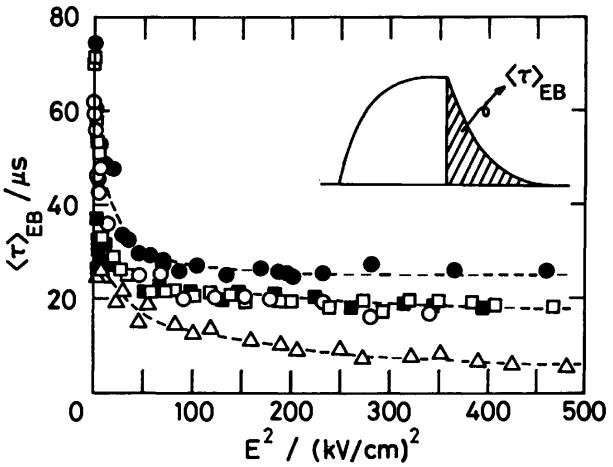

Fig. 6. The birefringence-average relaxation time $\langle\tau\rangle_{EB}$ of NaPSS and NaPSS-DAES complexes. Symbols are all the same as in Fig. 3.

(In this calculation, the NaPSS sample was assumed to be monodisperse.) The most likely reason for the absence of the net permanent dipole moment μ in the DAES-bound NaPSS is the extensive folding of the polymer chain.[7] The whole shape, approximated by an ellipsoid, apparently becomes more compact with the decrease in the P/D values.

Electric Dichroism of the NaPSS-DAES Complex. Since the value of $\Delta g/n$ was positive for the NaPSS-DAES complexes, in contrast with the case of NaPSS (cf. Table 1), the DAES chromophore is probably bound to the ionized sulfonate group in such a way that the angle θ between the orientation axis of the complex and the optical transition moment direction of the 462-nm absorption band of bound DAES is less than ±54.7°.[5,12] In order to confirm this inference, the steady-state electric dichroism of the NaPSS-DAES complex at P/D=1.9 was measured over a wide field-strength range. Figure 7 shows the field-strength dependence of the reduced dichroism $\Delta A/A$ at 462 nm, which is given as $\Delta A/A=(A_{/\!/}-A_\perp)/A=(3/2)(3\cos^2\theta-1)\times\Phi(E)$, where A is the absorbance at 463 nm of the solution in the absence of an applied field.[12] As in the case of the electric birefringence shown in Fig. 3, the experimental plot was fitted to a SUSID theoretical

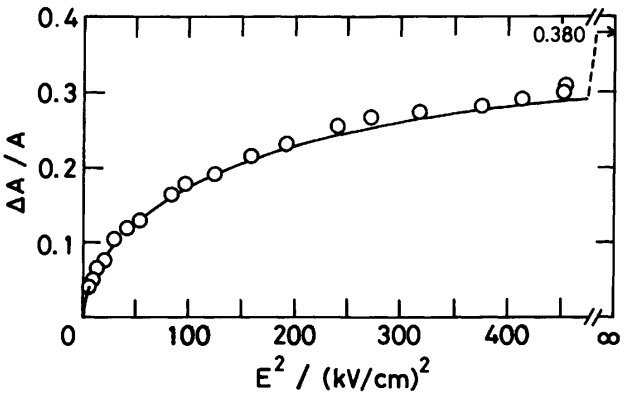

Fig. 7. The field strength dependence of the steady-state reduced electric dichroism $\Delta A/A$ at 462 nm of NaPSS-DAES complex at P/D=1.9. [NaPSS]= 0.10l in 0.4 mM NaCl. Circles are experimentally obtained. Solid line is calculated with the SUSID orientation function with the following values: $\Delta\alpha=4.4\times10^{-33}$ F m², $\Delta\sigma=4.4\times10^{-31}$ F m², $\Delta\sigma E_0$=4000 Debyes, and E_0=0.3 kV cm^{-1}.

curve in order to estimate the intrinsic or saturated reduced dichroism, $(\Delta A/A)_s=(3/2)(3\cos^2\theta-1)$, at infinitely high fields. This value was found to be +0.38, from which the angle θ was calculated to be ±50°. The 462-nm transition moment is directed along the long axis of the DAES molecule, which, therefore, makes an angle of ±50° with respect to the orientation axis of the complex. (This angle represents an *average* of all the bound DAES chromophores and should not be construed as meaning that each and every DAES molecule is bound at this fixed angle.)

The positive $\Delta g/n$ value (cf. Fig. 3 and Table 1) is now verified to result from the angle θ, which is less than ±54.7° (where $(\Delta A/A)_s=0$)[12] for all NaPSS-DAES complexes. It is also clear that the angle is nearly constant over P/D values from 7.1 to 1.9, as is indicated by the $(\Delta g/n)_{DAES}$ values in Table 1. The average angle of ±50° of bound DAES chromophores indicates that the component of the ground-state permanent dipole moment μ_3 along the orientation axis of the NaPSS-DAES complex (the 3-axis)[7] should amount to approximately 4.5 (=7cos50°) Debyes per bound DAES. Considering the number of DAES on each NaPSS chain, the total moment of μ_3 might be expected to make a large contribution to the field orientation, but the experimental finding is contrary, as has been discussed above. If the conformational deformation of the whole NaPSS-DAES complex backbone or the local motion of the bound DAES moiety should occur as the result of an applied electric field, the $\Delta A_{/\!/}/A=-2\Delta A_\perp/A$ relationship generally breaks down between the parallel $\Delta A_{/\!/}$ and prependicular $\Delta A_\perp$ dichroism (Eq. 3 of Ref. 12). This relationship was confirmed to hold up to $E\leq22.4$ kV cm^{-1} in the present work; therefore, in this field range no electrochromic effect[22] is expected in NaPSS-DAES complexes.

The steady-state dichroism signal of DAES at 450 nm was very small in the presence of PGA either at pH 4.1 or at 6.4, again indicating that the interaction between DAES and PGA is weak.

Conclusion

In brief summary, NaPSS-DAES complexes can be oriented by external electric fields to exhibit considerable electric birefringence and dichroism signals, but a complete orientation is still difficult to attain at a practical field strength of about 25 kV cm^{-1}. The overall permanent dipole moment of the complex is nearly zero; the cooperative addition of individual moments of DAES did not occur upon binding to NaPSS. A host polymeric matrix with a larger electric moment must be explored to improve the degree of field orientation. The contribution of the first-order hyperpolarizability anisotropy of the NaPSS-DAES complex to the field orientation seems to be of no special significance. The orientation behavior can be described satisfactorily by the interaction between the electric (linear) polarizability anisotropies $\Delta\alpha$ and $\Delta\sigma$ of the NaPSS chain and the applied field E.

PGA is a rigid and rodlike helix in the low pH region, each residue having a permanent dipole moment of 5—4 Debye units;[9-11] thus, it was thought to be very suitable as the host to cationic DAES and other 2-styrylpyridinium derivatives which show optical nonlinearity.[1] Unfortunately, no appreciable binding occurs in these host-ligand systems, probably because of the weak basicity of the quarternary ring nitrogen atom of DAES and also the weak acidity of the carboxylate of the glutamyl residue. In order for bound optically nonlinear materials to show a larges SHG effect, a smaller molecular weight and rigidly rodlike NaPSS, and other host polyelectrolytes may have to be explored. At the same time, the bound ligands may have to be arranged in such a manner that their permanent dipole moments are additive. In this fashion, a large difference in the excited and ground state moments can be expected; this is one of the conditions for the optical SHG phenomenon.[1]

References

1) R. J. Twieg and K. Jain, "Nonlinear Optical Properties of Organic and Polymeric Materials," ed by D. J. Williams, ACS Symposium Series No. 233, American Chemical Society, Washington, D. C. (1983), pp. 58—80.

2) J. L. Oudar, *J. Chem. Phys.*, **67**, 446 (1977).

3) K. Kikuchi and K. Yoshioka, *J. Phys. Chem.*, **77**, 2101 (1973).

4) K. Yamaoka and K. Ueda, *J. Phys. Chem.*, **84**, 1422 (1980).

5) K. Matsuda and K. Yamaoka, *Bull. Chem. Soc. Jpn.*, **55**, 69 (1982).

6) M. Tricot and C. Houssier, *Macromolecules*, **15**, 854

(1982).
7) K. Yamaoka and K. Ueda, *Bull. Chem. Soc. Jpn.*, **56**, 2390 (1983).
8) K. Yamaoka and K. Matsuda, *J. Phys. Chem.*, **89**, 2779 (1985).
9) M. Matsumoto, H. Watanabe, and K. Yoshioka, *Biopolymers*, **9**, 1307 (1970).
10) S. Kobayasi and A. Ikegami, *Biopolymers*, **14**, 543 (1975).
11) K. Yamaoka, T. Ichibakase, K. Ueda, and K. Matsuda, *J. Am. Chem. Soc.*, **102**, 5109 (1980).
12) K. Yamaoka and K. Matsuda, *Macromolecules*, **14**, 595 (1981).
13) A. Yamagishi and F. Watanabe, *J. Phys. Chem.*, **85**, 2129 (1981).
14) A. Yamagishi, *J. Phys. Chem.*, **88**, 305 (1984).
15) A. Takahashi, T. Kato, and M. Nagasawa, *J. Phys. Chem.*, **71**, 2001 (1967).
16) K. Yamaoka, S. Yamamoto, and I. Kosako, *Polym. J.*, **19**, 951 (1987).
17) K. Yamaoka, T. Matsuda, D. Shiba, and M. Takatsuki, *Bull. Chem. Soc. Jpn.*, **55**, 1300 (1982), and the references cited therein.
18) K. Yamaoka and K. Fukudome, *J. Phys. Chem.*, **92**, 4994 (1988).
19) K. Yoshioka and H. Watanabe, *Nippon Kagaku Zasshi*, **84**, 626 (1963).
20) K. Yamaoka and K. Fukudome, *Bull. Chem. Soc. Jpn.*, **56**, 60 (1983).
21) S. Broersma, *J. Chem. Phys.*, **32**, 1626 (1960).
22) K. Yamaoka and E. Charney, *J. Am. Chem. Soc.*, **94**, 8963 (1972).

 © 1989 The Chemical Society of Japan Bull. Chem. Soc. Jpn., 62, 257—261 (1989)

Polymerization of Amino Acids in Liposomal Membrane under Reduced Pressure and Normal Pressure

Akira SHIBATA,* Sinsuke YAMASHITA,† Satoru UENO, and Takuya YAMASHITA
Faculty of Pharmaceutical Sciences, Tokushima University, Shomachi, Tokushima 770
†Department of Chemistry, Naruto University of Education, Takashima, Naruto 772
(Received July 4, 1988)

Incorporation of polypeptides with hydrophobic side groups into lipid bilayers was achieved by the polymerization of *N*-carboxy anhydrides of γ-dodecyl L-glutamate and of γ-benzyl D-glutamate in DMPC liposomal membrane under reduced pressure and normal pressure. The effects of polypeptide conformations on the barrier properties of liposomal membrane incorporating polypeptide were examined. There was little difference in the trapping volume when liposomes prepared under reduced pressure and normal pressure were compared. The incorporation of polypeptides into the membrane bilayer had a tendency to decrease the volume trapping efficiencies. It was found that in the membrane-free aqueous phase, polymerization of *N*-carboxy amino acid anhydrides promoted formation of β-structure and in the membrane bilayer formation of α-helix structure was enhanced. The content of α-helical polypeptide was maximum for liposomes prepared under reduced pressure. The activation energies for water permeation across the liposomal membrane were lowered by the incorporation of polypeptdes into the membrane bilayer. The incorporation of α-helical polypeptide was more ceffective than that of β-structured one for the lowering of activation energies. The permeability barrier properties of liposomal membrane were larger for liposome incorporating poly(γ-dodecyl L-glutamate) (PDOLG) than for liposome incorporating poly(γ-benzyl D-glutamate)(PBDG). This seems to be due to a difference in miscibilities with lipid in the membrane bilayer.

The interactions of liposomes with a variety of polypeptides have been studied as attractive models for the molecular interactions occuring in biological membranes. The interactions cause major changes in the permeability of the membrane bilayer,[1-3] the polypeptide conformation,[4,5] and the morphology of the liposomes.[6] Poly(L-glutamic acid) interacts on the surface of the phosphatidylcholine liposomes and remains in random coil configuration upon complexation with the liposome.[7] Poly(L-lysine) goes from a random coil to an α-helix when it interacts with phosphatidylserine.[5] The copolypeptide lysine–tyrosine has only a small effect on the membrane conductance and it gives a β-structure upon interaction with phosphatidylserine or phosphatidylcholine liposome.[4] Most results so far reported have been obtained by the use of a variety of water-soluble polypeptides that were adsorbed by electrostatic interaction to the outer surface of liposomal membrane. It is now well-recognized that nonpolar interactions play a major role in the determination of protein tertiary structure, catalytic activity, and ligand binding activities and it is to be anticipated that such interactions would also play an important role in lipid-proton interactions of the cell membrane. Our attention has been focused on the incorporation of hydrophobic polypeptide into the membrane bilayer and the effects of their conformations.[8]

In the present study, polypeptides with nonpolar side groups were used as a lipophilic protein model which was embedded into the hydrophobic domain of the membrane. Incorporation of polypeptides with hydrophobic side groups into the membrane bilayer was achieved by polymerization of *N*-carboxy anhydrides of γ-dodecyl L-glutamate and of γ-benzyl D-glutamate in DMPC liposomal environment under reduced pressure and normal pressure. The effects of conformation and hydrophobic side group of polypeptides on the water permeability of liposomal membrane incorporating polypeptide were studied by the osmotic method.

Experimental

Materials. Dimyristoylphosphatidylcholine (DMPC) and dihexadecyl hydrogenphosphate (DHP) were obtained from Sigma. *N*-Carboxy anhydrides of γ-dodecyl L-glutamate (DOLG-NCA) and γ-benzyl D-glutamate (BDG-NCA) were prepared by the method of Blout and Karlson.[9] Diethyl ether and dichloromethane were distilled under nitrogen atmosphere. Water was distilled, the second time from alkaline potassium permanganate solution.

Preparation of Liposome. Large unilamellar liposomes were prepared according to the ether injection method of Deamer and Bangham[10] with some modifications. Injecting lipid solution was prepared by solubilizing DMPC, DHP, and *N*-carboxy amino acid anhydride in mixture of diethyl ether and dichloromethane (3:2 (v/v)) at an appropriate molar ratio (1:0.1:1). This solution was gradually injected with the aid of a mechanical drive through a needle into an aqueous phase, located within the internal chamber of the modified Liebig condenser. 45 ml of the lipid solution (2.5 μmol ml^{-1}) was injected into 6 ml distilled water at 60 °C under normal pressure. For the preparation of liposomes under reduced pressure the apparatus was placed under water vacuum. The temperature of the aqueous phase inside the water vacuum line was maintained at 35 °C for 460 mmHg (1 mmHg≈133.322 Pa) and 45 °C for 510 mmHg. *N*-Carboxy amino acid anhydride represents a class of high-energy amino acid derivatives which polymerize to form

polypeptides. Since the negative-charged portion on the liposomal surface was expected to be favorable for the spontaneous polymerization of *N*-carboxy amino acid anhydrides,[11] the preparation of liposome was evolved for DMPC liposome containing 10 mol% of DHP.

Isolation of Polypeptides from Liposomes. The liposome suspension prepared was filtered through gel column (Cellulofine-GC-700) to remove residual organic solvent, non-incorporated monomer and polymer. To isolate polypeptide from liposomes incorporating polypeptide (150 μmol DMPC), the liposome suspension was first lyophilized and the residue was added to 10 ml diethyl ether or methanol. After shaking, a dispersed precipitant appeared. The precipitated polypeptide was filtered off, washed with methanol, and dried in vacuo.

Osmotic Shrinkage Measurements. For the osmotic shrinkage measurements the liposome suspension was mixed quickly by using a rapid mixing device (Otsuka Electronics MX-7) with hypertonic glucose solution (100 mM) and a 1:1 mixing ratio. The osmotic shrinking of liposomes was followed by the time-course of turbidity change at 450 nm. For osmometers with membrane completely impermeable to the solute a proportionality exists betweem the volume change and the difference in osmotic pressure of the outer and inner volume. Since the initial volume change is directly proportional to the relative initial shrinkage rate (initial absorbance change), r_0, the following relation holds:[12,13]

$$r_0 = 1/A_0(\mathrm{d}A/\mathrm{d}t) = k(\mathrm{d}V/\mathrm{d}t) = kP_wSRT\Delta C \qquad (1)$$

where $1/A_0(\mathrm{d}A/\mathrm{d}t)$ is the initial shrinkage rate, $\mathrm{d}V/\mathrm{d}t$ is the volume change with time, P_w is the permeability coefficient for water, S is the area occupied by the membrane, R is the gas constant, T is the absolute temperature, and ΔC is the concentration difference in the permeable solutes between the inside and outside the liposome, respectively. On the assumption that permeability coefficients could be expressed in the form of Arrhenius's equation

$$P_w = P_w^0 \exp(-\Delta E_a/RT) \qquad (2)$$

one can obtain from Eqs. 1 and 2:

$$r_0/T = 1/A_0\,(\mathrm{d}A/\mathrm{d}t)/T = KP_w^0 \exp(-\Delta E_a/RT) \qquad (3)$$

where K ($=kSR\Delta C$) is a constant at fixed ΔC. An activation energy, ΔE_a, for water permeation across the liposomal membrane could be determined by plotting the logarithms of r_0/T as a function of the reciprocal of absolute temperature.

Results and Discussion

Effects of Conditions for Preparing Liposome on Trapping Volume. Polypeptides isolated from the liposomes prepared under reduced pressure and normal pressure were in yields of 20% and 14% for PDOLG and of 12% and 9% for PBDG. The incorporation of these polypeptides into the liposomal membrane tends to be somewhat larger for reduced pressure (460 mmHg) than for normal pressure.

A parameter we have used to characterize ether injection liposomes is the trapping volume, calçulated by the solute diffusion method.[14] Table 1 summarizes the typical values of volume trapping efficiencies of the liposomes with the without polypeptide prepared under reduced pressure and normal pressure. We observed little difference between the trapping volume of the liposomes prepared under reduced pressure polypeptides into the bilayer tended to decrease volume trapping efficiencies. The values of the trapping volume ranged from 8 to 11 l mol^{-1} and were larger than the values for the typical sonicated liposome by a factor of about 10.

Conformation of Polypeptides Prepared in Membrane Bilayer. Figures 1 and 2 show the infrared spectra for PDOLG and PBDG isolated from liposomes prepared under reduced pressure (460 mmHg) and normal pressure, together with that for the same polypeptides obtained by polymerizing *N*-carboxy amino acid anhydrides in membrane-free aqueous phase. The spectra which are characteristic of poly-

Table 1. Effects of Conditions for Preparing Liposome on Volume Trapping Efficiencies

Composition	*P*	*T*	Trapping volume
	mmHg	°C	l mol^{-1}
DMPC:DHP	760	60	11.2
	460	35	10.8
DMPC:DHP: DOLG-NCA	760	60	8.7
	460	35	8.3
DMPC:DHP: BDG-NCA	760	60	8.8
	460	35	9.3

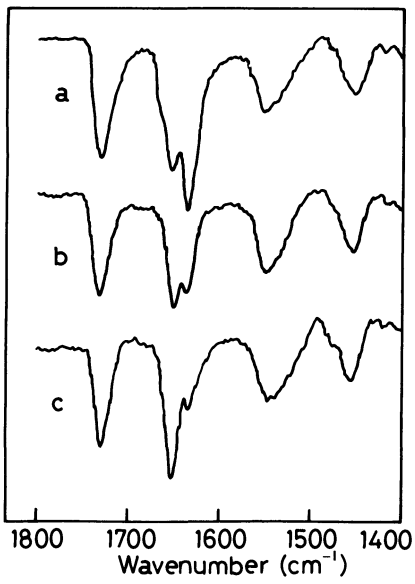

Fig. 1. Infrared spectra of poly(γ-dodecyl L-glutamate) polymerized in membrane free aqueous phase(a), isolated from liposomes prepared under normal pressure(b) and reduce pressure(c).

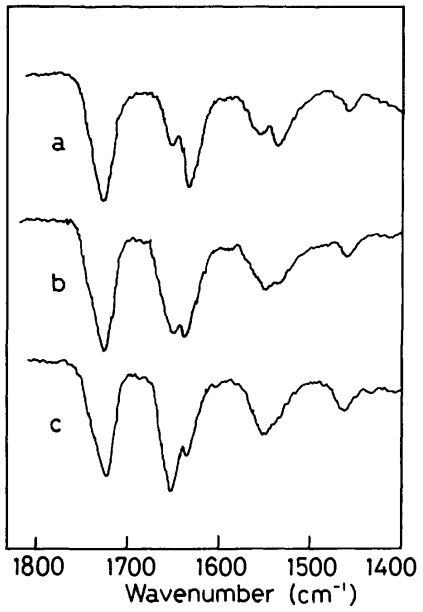

Fig. 2. Infrared spectra of poly(γ-benzyl D-glutamate). Symbols, a, b, and c, are the same as in Fig. 1.

peptide having α-helix structure show major diagonostic at about 1650 cm^{-1} for the amide I band and 1550 cm^{-1} for the amide II band. The β-structure gives rise to a strong band at lower frequecy (about 1635 cm^{-1} for the amide I band and 1520 cm^{-1} for the amide II band) than the α-helix structure. The contents of α-helix structure and β-structure are qualitatively estimated by the comparison of the peak height between 1650 and 1635 cm^{-1} for the amide I band. The conformations of PDOLG and PBDG polymerized in the membrane-free aqueous phase were enhanced in the β-structure (Figs. 1-a and 2-a). Taking into account the fact that both PDOLG and PBDG polymerized in organic solvent (dioxane or anisole) take the α-helix structure,[8] the hydrophilic environments for the polymerization of *N*-carboxy amino acid anhydrides may promote the formation of the β-structure. Yaron et al.[15] have reported that the helical structure of poly[N^5-(3-hydroxypropyl)-L-glutamine] was stabilized under hydrophobic environments such as methanol or *N*,*N*-dimethylformamide and that the addition of water into this solution resulted in a lowering of the helix content. Apparently the presence of water as a protein solvent is not necessarily the most favorable environment for helical structures of polypeptide. On the other hand, polymerization of DOLG-NCA and of BDG-NCA in the membrane bilayer under normal pressure increased the α-helical content (Figs. 1-b and 2-b) and under reduced pressure led to further increase of the α-helix structure (Figs. 1-c and 2-c). Although the α-helicities of PDOLG and PBDG have a tendency to change with the reaction environments, PDOLG differs from PBDG in the α-helix content of polypeptides prepared under different conditions. The polymerization of DOLG-NCA in the membrane-free aqueous phase gave spectra of the β-configuration. PDOLG prepared in the bilayer under normal pressure was enhanced in α-helix, and under reduced pressure the α-helix structure was present in much larger quantities. For the polymerization of BDG-NCA in the membrane-free aqueous phase, on the other hand, the spectra showed mostly β-structure, similar to that of DOLG-NCA. The content of α-helix for PBDG prepared in the bilayer under normal pressure was nearly equal to that of the β-structure, and under reduced pressure the helical content again became much larger than that of the β-structure.

From the results mentioned above, it is found that in the membrane-free aqueous phase the polymerization of *N*-carboxy anhydrides of γ-dodecyl L-glutamate and of γ-benzyl D-glutamate promotes the formation of the β-structure, while in the lipid bilayer membrane the α-helix structure predominates. The content of α-helical polypeptide was maximum for liposomes prepared under reduced pressure. Considering these results, we suggest that the hydrophobic anchor side groups of these *N*-carboxy anhydrides are embedded locally with some degree of translational or rotational freedom into the lipid bilayer matrix of liposomes, and functional groups of *N*-carboxy anhydrides may be brought into positions favorable to the formation of spiral arrangements of the molecules. Consequently, this will induce the formation of the α-helical structure. It is important to delineate the factors affecting the conformation of biological macromolecules. The force dictating the conformation of polypeptide can arise from intramolecular forces, from intermolecular forces, from the solvent, or from surrounding dissimilar medium (environments), which represents a special type of intermolecular interaction. The liposomal environments found to be favorable for the preparation of α-helical polypeptide.

Water Permeation through Liposomal Membrane. The water permeability of liposomal membrane incorporating polypeptide is a sensitive function of the extent of interaction between polypeptides and membrane lipids, and was studied by the measurements of initial osmotic shrinkage rates.

Figures 3, 4, and 5 show the experimental data for the polypeptide-free liposome, and the polypeptide incorporating liposomes prepared under reduced pressure (460 and 500 mmHg) and normal pressure. A linear relationship between the logarithms of r_0/T and the reciprocal of absolute temperature as in Eq. 3 was obtained in all cases investigated. The activation energies estimated from the gradient in Figs. 3—5 are given in Table 2. The values listed in columns 2 and 3 are the pressure and the temperature of the aqueous phase, respectively.

The activation energies for water permeation which

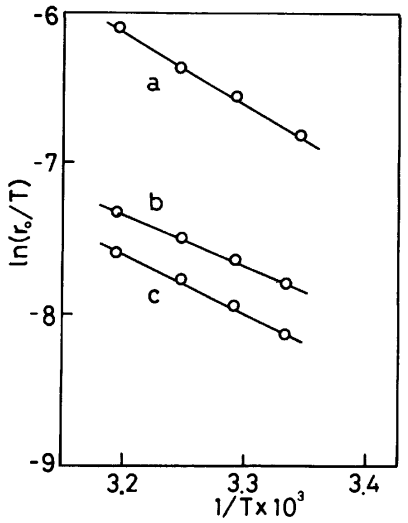

Fig. 3. Arrhenius plots for water permeability across lipid bilayers of liposomes prepared under normal pressure and at 60°C.
a) Polypeptide free liposome, b) liposome incorporating poly(γ-dodecyl L-glutamate), c) liposome incorporating poly(γ-benzyl D-glutamate).

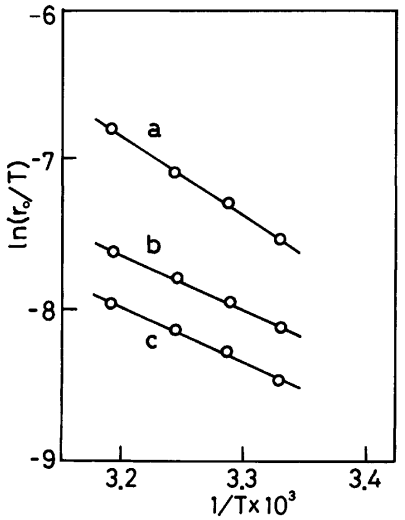

Fig. 4. Arrhenius plots for water permeability across lipid bilayers of liposomes prepared under reduced pressure of 510 mmHg and at 45°C. Symbols, a, b, and c, are the same in Fig. 3.

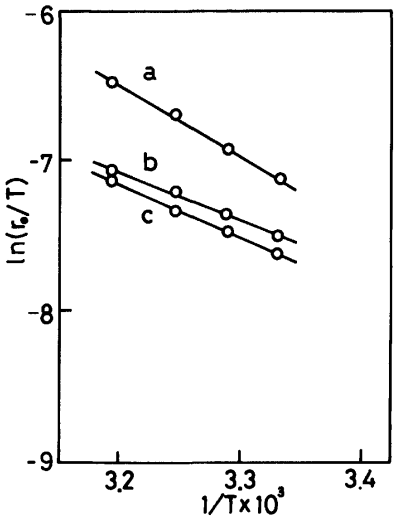

Fig. 5. Arrhenius plots for water permeability across lipid bilayers of liposomes prepared under reduced pressure of 460 mmHg and at 35°C. Symbols, a, b, and c, are the same in Fig. 3.

Table 2. Activation Energies for Permeation of Water across Liposomal Membranes under Different Conditions

Composition	P	T	ΔE_a
	mmHg	°C	kcal mol^{-1}
DMPC:DHP	760	60	9.6
	510	45	10.3
	460	35	9.5
DMPC:DHP:	760	60	8.6
DOLG-NCA	510	45	8.3
	460	35	7.2
DMPC:DHP:	760	60	7.6
BDG-NCA	510	45	7.1
	460	35	6.3

DMPC:DHP=1:0.1(mol/mol). DMPC:DHP:NCA=1:0.1:1(mol/mol).

laid in the range 6.3—10.3 kcal mol^{-1} were dependent of the conditions for preparing liposomes. The preparation of polypeptide incorporating liposomes under reduced pressure tended to increase α-helical polypeptide in membrane bilayer as shown in Figs. 1 and 2. This lowers the activation energies for water permeation through polypeptide incorporating liposomal membrane. That is to say, the incorporation of α-helical polypeptide was more effective than that of β-structured one for the lowering of activation energies. Another reason why the activation energies are lowered in the presence of polypeptide is in miscibility between polypeptide and DMPC. Much information has been gained by the recognition of analogies between monomolecular films and biological membranes.[16] PDOLG and PBDG form a monomolecular film at the air-water interface, and the surface-pressure-area (π-A) curves are shown in Fig. 6. The curves of PDOLG with alkyl side groups and PBDG with benzyl side groups have differences related to hydrophobic side chain interactions and side chain flexibility.[17,18] Therefore, the difference in properties of monomolecular films must be reflected in the orientation and the packing of DMPC in polypeptide incorporating membrane bilayer which is associated in permeability barrier properties. Actually, we obtained the results that the permeability barrier properties were larger for liposome incorporating PDOLG than for that incorporating PBDG (Table 2).

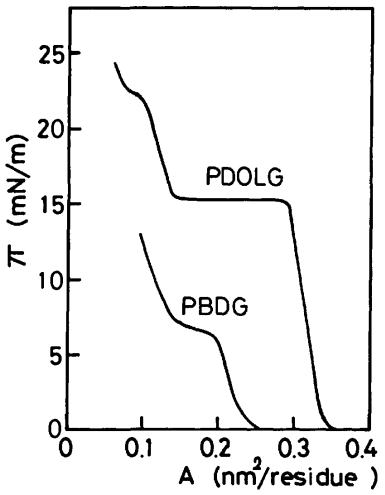

Fig. 6. Surface pressure-area (π-A) curves of poly-(γ-dodecyl L-glutamate) and poly(γ-benzyl D-glutamate).

Conclusion

Incorporation of polypeptides with hydrophobic side groups into lipid bilayers was achieved by the polymerization of DOLG-NCA and BDG-NCA in DMPC liposomal membrane under reduced pressure and normal pressure. Polymerization of *N*-carboxy amino acid anhydrides in the liposomal membrane promoted formation of the α-helix structure. The presence of polypeptides in membrane bilayer resulted in a lowering of activation enegries for permeation of water across the liposomal membrane, and the lowering was maximum for incorporation of α-helical polypeptide.

References

1) D. Bach, *J. Membr. Biol.*, **14**, 57 (1973).
2) H. K. Kimelberg and D. Papahadjopoulos, *J. Biol. Chem.*, **246**, 1142 (1971).
3) I. M. Cambell and H. B. Pawag, *Can. J. Biochem.*, **57**, 1099 (1978).
4) D. Bach, K. Rosenheck, and I. R. Miller, *Eur. J. Biochem.*, **53**, 265 (1975).
5) G. G. Hammes and S. E. Schullery, *Biochemistry*, **9**, 2555 (1970).
6) "Recent Progress in Surface Science," ed by J. F. Danielli, A. C. Riddiford, and M. D. Rosenberg, Academic Press, New York (1970), Vol. 3.
7) K.-Y. Yu, J. J. Baldassare, and C. Ho, *Biochemistry*, **13**, 4375 (1974).
8) A. Shibata, S. Yamashita, Y. Ito, and T. Yamashita, *Biochim. Biophys. Acta*, **854**, 147 (1986).
9) E. R. Blout and R. H. Karlson, *J. Am. Chem. Soc.*, **78**, 941 (1956).
10) D. W. Deamer and A. D. Bangham, *Biochim. Biophys. Acta*, **443**, 629 (1976).
11) H. Tsuyuki, H. Van Kley, and M. A. Stahmann, *J. Am. Chem. Soc.*, **78**, 764 (1956).
12) M. C. Block, L. L. M. Van Deenen, and J. De Gier, *Biochim. Biophys. Acta*, **443**, 1 (1976).
13) T. Inoue, H. Kamaya, and I. Ueda, *Biochim. Biophys. Acta*, **812**, 393 (1985).
14) D. W. Deamer, *Ann. N. Y. Acad. Sci.*, **308**, 250 (1978).
15) A. Yaron, N. Lupu, M. Sela, and A. Berger, *Biochim. Biophys. Acta*, **69**, 430 (1963).
16) N. J. Malcolm, "Biological Interface," Elsevier Sci. Pub. Co., Amsterdam (1975).
17) B. R. Malcolm, *Adv. Chem. Ser.*, **145**, 338 (1975).
18) T. Yamashita, A. Shibata, and S. Yamashita, *Bull. Chem. Soc. Jpn.*, **51**, 2751 (1978).

Studies of the Hydrous Niobium(V) Oxide Ion Exchanger. V. Effect of Heat Treatment on the Sodium Isotopic Exchange Rates between Hydrous Niobium(V) Oxide in Na^+ Form and Aqueous Solutions

Yasushi INOUE,* Hiromichi YAMAZAKI, and Mitsuji IKEDA
Department of Nuclear Engineering, Faculty of Engineering, Tohoku University, Aramaki, Sendai 980
(Received April 15, 1988)

The effect of a heat treatment was studied on the sodium isotopic exchange rate between the hydrous niobium(V) oxide in the Na^+ form and aqueous solutions. The rate was controlled by the particle diffusion of sodium ions and increased with the heat-treatment temperature. The increase in the rate for the exchanger heat-treated at 200 °C was due to a decrease in the effective particle radius brought about by cracks which developed in the particles. A further increase in the rate at temperatures higher than 200 °C could be explained in terms of an increase in the Na^+-diffusion coefficient, which was produced by an increase in the pore size responsinble for the movement of sodium ions.

A radiochemical experiment was previously undertaken in order to measure the isotopic exchange rate of sodium ions between hydrous niobium(V) oxide in the Na^+ form and aqueous solutions of sodium salts, indicating that the rate in Na^+ solutions higher than 0.1 mol dm^{-3} was controlled by the particle diffusion.[1] On the other hand, this material may be useful for applications at high temperatures, since it is appreciably stable under heat treatment.[2] This aroused the interest of the present authors regarding a study of the effect of a heat treatment on the ion-exchange rate of this material. In addition, this study will greatly contribute to an understanding of the ion-exchange mechanism of hydrous niobium(V) oxide by clarifying the relation between the properties of the exchanger matrix and the ion-exchange rates.

The present paper describes the effect of a heat treatment in air on the isotopic exchange rates of sodium ions between the hydrous niobium(V) oxide and aqueous solutions, and discusses the important properties of the material which strongly governs the isotopic exchange rate.

Experimental

Sample Preparation. The hydrous niobium(V) oxide prepared by the previously recommended method was classified into four particle sizes by using Japan Industrial Standard sieves (mesh size; −48+60, −70+80, −100+120, −145+200) and then converted to the H^+ form.[1,3]

Two- to four-gram portions of the exchanger were heated in air to a constant weight at constant temperature (200, 350, and 450 °C). After being cooled, the exchanger was immersed in water overnight, followed by drying to a constant weight in a desiccator containing a saturated NH_4Cl solution (relative humidity, 79%).

The exchanger was then converted to the Na^+ form by treating it with a 0.05 mol dm^{-3} $Na_2B_4O_7$ buffer solution at pH 9.3. The buffer solution was used for preventing any part of the exchanger from dissolving, since the exchanger is chemically unstable in strong basic solutions. The particale size was again made uniform by using sieves, since the exchanger would be broken down during a heat treatment. The exchanger was then labeled with ^{22}Na by equilibrating it with a ^{22}Na-solution having the same chemical composition as the above-mentioned solution for 2d at room temperature. After having been washed with a 0.05 mol dm^{-3} $Na_2B_4O_7$ solution (free from ^{22}Na), the exchanger was used for a rate meassurement.

Properties of the Exchangers. The properties of each sample were all referred to the exchanger in the H^+ form dried in the desiccator. The average particle radius was estimated by approximating the particle shape by a sphere, from the particle-size distribution measured in an 83 wt% glycerol solution by using a Seishin Enterprise Micron-Photo-Sizer, Model SKC-2000S. The specific surface area of the sample, after heated at 110 °C to a constant weight, was determined by the BET method (N_2 adsorption at −196 °C) using a Yanagimoto Surface Area Measuring Apparatus (Model GSA-10). The pore-size distribution and the pore volume of each sample were calculated by Inkley's method from the adsorption isotherm of N_2 at −196 °C.[4] The density of the exchanger was measured in the usual manner by using a 25-cm^3 pycnometer. The exchange capacity of the sample for Na^+ ions was measured in a 0.05 mol dm^{-3} $Na_2B_4O_7$ solution (pH 9.3) by a column method. The water content was determined from the weight loss of the exchanger heated at 850 °C. X-Ray diffraction patterns were obtained by means of a Shimadzu X-ray diffraction unit, Model XD-3A, using Ni-filtered Cu $K\alpha$-radiation.

Measurement of the Isotopic Exchange Rate. All the rate measurements were performed in a nitrogen atmosphere by using the same apparatus as described earlier.[5] The rate was measured in solution with the same compositions as those used for converting the exchanger to the Na^+ form. A portion less than 0.2 gram of the sample was placed in a cage and immersed in 200 cm^3 of a solution of a desired composition while the cage was being rotated. The solution had been adjusted in advance to a constant temperature (within ±0.1 °C). Aliquots of the solution (0.2 cm^3) were taken out at appropriate time intervals in order to measure the radioactivity with a well-type NaI(Tl)-scintillation counter (Aloka Model ARC-361). The time of contact of the exchanger with the solution was taken as the elapsed time between immersing

the cage and withdrawing an aliquot of the solution. The fractional attainment of equilibrium, $F(t)=C_t/C_\infty$, was calculated from these results; here, C_t is the total radioactivity of the solution at time t and C_∞ at $t=\infty$. C_∞ was calculated using $C_\infty=C_iM/(M+m)$, where C_i is the initial total radioactivity of the exchanger, and m and M the total amounts of Na^+ in the exchanger and in solution, respectively. Although the rate was measured by a batch method, the infinite solution-volume approximation was closely obeyed under the present experimental conditions: less than 0.2 g of the exchanger per 200 cm^3 of the solution.

Results and Discussion

Analysis of the Results. The exchange rate for the exchanger without heat treatment was confirmed to be controlled by the diffusion of ions in the spherical particles.[1] When the infinite solution volum approximation is obeyed, as is the case in the present experimental condition, Bt vs. t plots must give a straight line passing through the point of origin,and the slope of the line, i.e., B, is inversely proportional to the square of particle radius. Here,

$$B = \pi^2 D/r^2, \quad (1)$$

where D is the self-diffusion coefficient of the ions in the exchanger and r refers to the radius of the particles. Bt can be calculated from the measured values of the fractional attainment of equilibrium ($F(t)$) by using the equation derived by Reichenberg:

$$Bt = 2\pi - \frac{\pi^2}{3}F(t) - 2\pi\left(1 - \frac{\pi}{3}F(t)\right)^{1/2}. \quad (2)$$

This equation gives a fairly good approximation in the region where $F(t)$ is less than 0.85.[6] In putting the rate data in order, therefore, Bt values were plotted against t.

Effect of Heat Treatment on the Properties of the Exchanger. Table 1 shows some properties of the exchanger in the H^+ form heat-treated in air, together with those without heat treatment (designated sample as R.T.). These results were obtained for the sample of −145+200 mesh, but were essentially the same for those of differrent particle sizes.

When the samples were heated at 200 °C, the exchange capacity and the water content, respectively, decreased to about 60 and 70% of the original values, and then gradually decreased with temperature. The density increased with temperature, reaching a constant value at 350 °C. The specific surface area decreased with temprature, but the fractional pore volume was independent of the temperature of the heat treatment. Figure 1 shows distribution curves of the pore size as form of the frequency polygon, in which the percentage of the volume of pores of each size to the total pore volume is shown at intervals of 1 nm of the diameter. The distribution curves gradually shifted to the lager-pore side with increasing temperature during a heat treatment and became considerably broadened at 450 °C. The reason for the broad distribution curve for a sample heat-treated at 200 °C is not clear, but may be attributable to an incomplete relaxation of the distortion of the structure of the exchanger matrix, by considering an increase in the density of the exchanger at a heat treatment temperature between 200 and 350 °C.

Effect of Heat Treatment on the Exchange Rate. The Na^+-isotopic exchange rates for samples heat-treated at various temperatures, together with those for sample

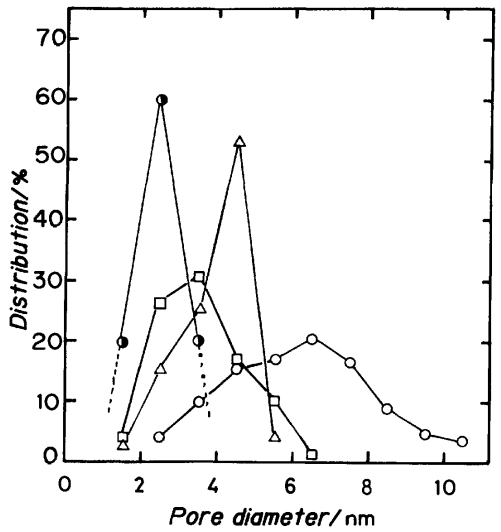

Fig. 1. Pore size distribution curves.
Temperature for heat treatment, ◑: R.T., □: 200 °C, △: 350 °C, ○: 450 °C. Particle size:−145+200 mesh.

Table 1. Properties of Exchangers[a]

Temp of treatment	Composition[c]	Density	Ion-exchange capacity[d]	Specific surface area	Pore volume
°C	mol H_2O(mol Nb_2O_5)$^{-1}$	g cm^{-3}	mol(mol Nb_2O_5)$^{-1}$	m^2 cm^{-3}	ml cm^{-3}
R.T.[b]	6.45±0.06	2.39±0.05	0.665±0.008	758±20	0.50
200	4.61±0.05	2.70±0.05	0.401±0.004	610±18	0.63
350	4.03±0.05	2.95±0.05	0.297±0.003	519±17	0.54
450	3.59±0.04	2.91±0.05	0.205±0.003	329±15	0.63

a) Particle size: −145+200 mesh. b) Sample without heat treatment. c) The water content was determined from the weight loss at 850 °C. d) Exchange capacity for Na^+ at pH 9.3 (0.05 mol dm^{-3} $Na_2B_4O_7$).

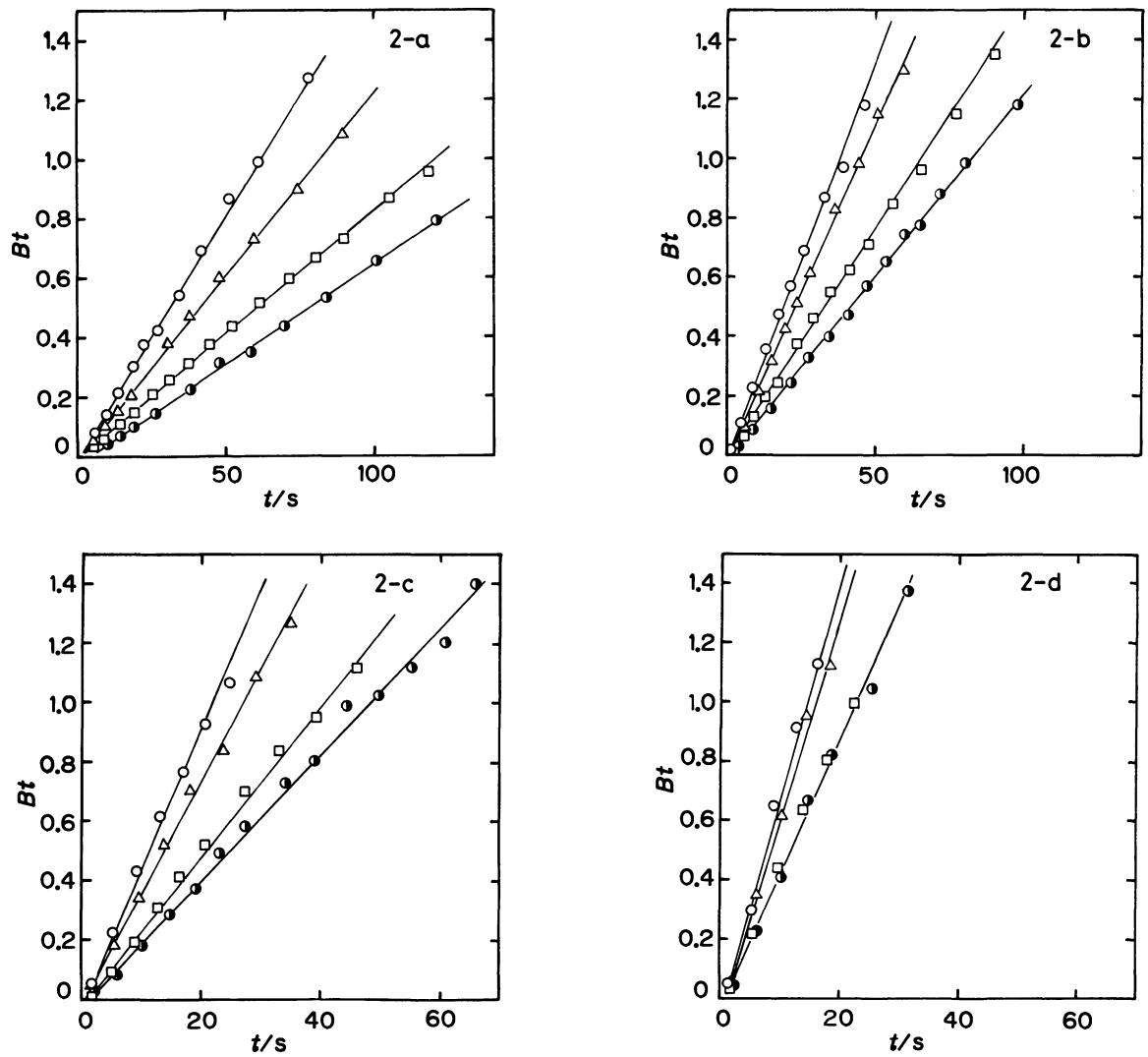

Fig. 2. Effect of heat treatment on the isotopic exchange rate.
Temperature, 5.1 °C; 0.10 mol dm^{-3} Na^+; temperature for heat treatment, ◑: R.T., □: 200 °C, △: 350 °C, ○: 450 °C. Particle size/mesh, 2-a:−48+60, 2-b:−70+80, 2-c:−100+120, 2-d:−145+200.

R.T., are shown in Figs. 2-a through 2-d. These figures indicate that the heat treatment enhanced the exchange rate in such different ways as to depend on the particle size; the rate increased monotonously with temperature in −48+60 mesh, but abruptly between 200 and 350 °C in −145+200 mesh. These figures also show that plots of Bt vs. t gave straight lines passing through the point of origin, irrespective of the heat-treatment temperature. Hence, the exchange rate is controlled by the rate of diffusion of sodium ions in the exchanger particles.

When this is true, the slopes of the straight lines (B) must be inversely proportional to the square of the particle radii (r). As is shown in Fig. 3, however, the exchangers which were heat-treated did not follow this relation, unlike sample R. T. This inconsistency may be ascribed to a dependence of the effective particle radius responsible for the diffusion of sodium ions or of the diffusion coefficient of Na^+ ions, on the apparent particle size. The latter is improbable for the following reason. As shown in Fig. 2, when the samples were heat-treated at 200 °C, an exchanger of small particle size (−145+200 mesh) showed the same rate as sample R. T. whereas the heat treatment appreciably increased the rate in the case of exchangers of large particle size. We can, therefore, conclude that the effective radius of the exchanger particles was decreased from the apparent radius estimated from the particle size distribution.

The decrease in the effective particle size is considered to be brought about by cracks developed during heating in the particles which are stressed due to a condensation of the hydroxyl groups. Naturally, the cracks build up more in large than in small particles; that is, the ratio of the effective to apparent radius becomes smaller when

Table 2. Particle Size of Samples Heat-Treated at 200 °C

Particle size	Apparent particle radius (r)	B_0[a]	B'[b]	Effective[c] particle radius (r')	Volume[d] ratio
mesh	μm	$\times 10^{-2}$ s^{-1}	$\times 10^{-2}$ s^{-1}	μm	%
−48+60	145±4	0.67±0.02	0.84±0.04	130±5	72±4
−70+80	107±3	1.24±0.02	1.56±0.05	95±3	71±3
−100+120	74±2	2.13±0.09	2.54±0.11	68±3	77±5
−145+200	52±2	4.45±0.13	4.67±0.22	51±2	94±5

a) Slope of Bt vs. t plot for the sample R.T. b) Slope of Bt vs. t plot for the sample heated at 200 °C. c) Effective radius of the exchanger heated at 200 °C, determined by the equation: $r'=(B_0/B')^{1/2}r$. d) Ratio of the effective volume to the apparent volume determined from particle size distribution.

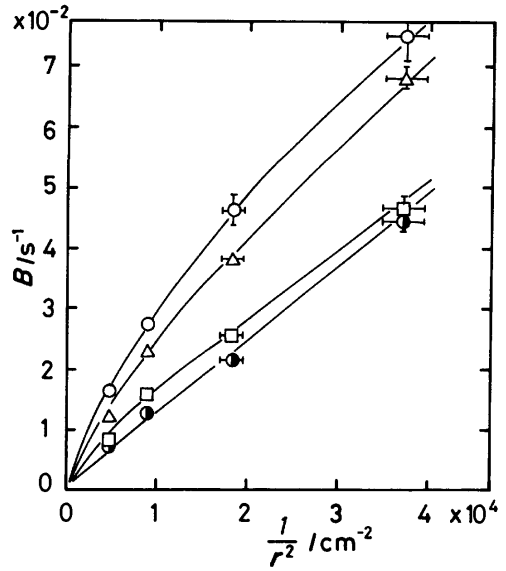

Fig. 3. Relationship between B and $1/r^2$.
Temperature, 5.1 °C; 0.10 mol dm^{-3} Na^+; temperature for heat treatment, ◑: R.T., □: 200 °C, △: 350 °C, ○: 450 °C.

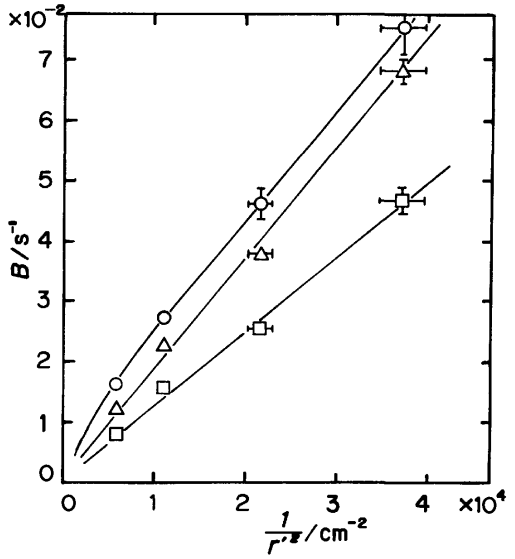

Fig. 4. Relationship between B and $1/r'^2$.
Temperature, 5.1 °C; 0.10 mol dm^{-3} Na^+; temperature for heat treatment, □: 200 °C, △: 350 °C, ○: 450 °C.

the apparent radius is larger. Based on this view, by assuming a constant Na^+-diffusion coefficient, the effective particle radius (r') was calculated by using the equation $r'/r=(B_0/B')^{1/2}$, where B_0 and B', respectively, are the B values for samples without a heat treatment and those heat-treated at 200 °C; where r refers to the apparent particle radius of the exchanger. Table 2 shows the effective particle radii of exchangers heated at 200 °C of various apparent particle sizes. This table reveals that, although the effective radius of the exchanger particle of −145+200 mesh heated at 200 °C was nearly the same as its apparent radius, those of larger particles decreased considerably with heating at 200 °C.

By using the r' estimated for samples heat-treated at 200 °C (Table 2), B vs. $1/r'^2$ plots were made for samples heat-treated at higher temperatures, together with those for the samples heated at 200 °C for a comparison (Fig. 4). In the case where a sample was heated at 350 °C, the plot followed a straight line passing through the point of origin. Therefore, it is considered that cracking does not proceed further and that the effective particle radii are unchanged when the temperature for a heat treatment is raised from 200 to 350 °C. The larger slopes of the straight lines for the samples heated at 350 °C than at 200 °C indicate an increasing D with temperature on account of Eq. 1. At 450 °C, the factors contributing to an increase of the rate cannot be unequivocally determined, because a precise proportionality does not hold between B and $1/r'^2$, but may be a combination of the two factors mentioned above.

If we consider the situation microscopically, the hydrous niobium(V) oxide consists of two phases: the solid framework and the interstitial pore phase. Ions diffuse mainly through the pore phase, since a very large specific surface area of the samples (Table 1) indicates that the solid framework occupies only a small fraction of the exchanger particle. The diffusion is necessarily slower in the medium of the pore phase than in a homogeneous phase having the same medium as the pore phase. This is the situation for two reasons. First, the diffusion path is obstructed by the framework and is, thus, tortuous rather than straight. Secondly, the movement of the diffusing species in the pore phase

may be reduced by friction or other interactions with the pore walls, together with a retarding effect of the electrostatic interaction between the ions and the exchange sites. The change of the Na^+-diffusion coefficient by heat treatment can be explained by one or combinations of these factors.

As was shown in Table 1, the fractional pore volume of the exchanger was unchanged upon heat treatment. Therefore, an increase in the diffusion coefficient in the exchanger with heating at 350 °C cannot be explained by a diminution in the tortuosity of the diffusing path or in the obstruction by the matrix. The retarding effect due to the electrostatic interaction between the ions and the exchange sites is also not effective, since changes of the exchange capacity for sodium ions and the electronic density on the fixed ionic groups of the exchanger have no influence on the exchange rate, as was described in a preceding report.[1] Collisions of ions and their friction with pore walls slow down the movement of the ions in the pore phase when the pores are not large enough compared to the size of the ions. From the large water content and fractional pore volume of the exchanger, sodium ions are considered to exist as hydrated ions in the exchangers. The diameter of hydrated sodium ions has been reported to be 1.2 to 1.4 nm.[7] Pores of dimeter smaller than 2.4 to 2.8 nm, therefore, strongly interrupt the movement of ions. On the other hand, such a retarding effect must be relaxed in pores lager than such a boundary value. As shown in Fig. 1, the peak, appearing in the vicinity of this boundary, of the distribution curve of the pore size in the exchanger heated at 200 °C shifted to the larger side of the boundary when the sample was heated at 350 °C. The large value of the Na^+-diffusion coefficient in the exchanger heated at 350 °C, therefore, is attributable to the large pore size, twice as large as the diameter of hydrated sodium ion, though some ambiguity remains concerning the effect of the broadness of the distribution curves. The further increase of the exchange rate for a sample heated at 450 °C may be partly due to a further increase in the diffusion coefficient produced by an increase in the pore diameter to 6.5 nm. Figure 5 shows the X-ray diffraction patterns of the samples, indicating an enhanced crystallization of the exchanger heated at 450 °C. If the retarding effect of pore walls on the diffusion of ions is small in a well-ordered exchanger matrix, the effective diffusion coefficient of ions may be increased by crystallization. As an example, Nancollas reported that the effective diffusion coefficient of sodium ions in hydrons thorium(IV) oxide was increased by the crystallization of the matrix.[8]

The effect of heating on the isotopic exchange rates of sodium ions for the hydrous niobium(V) oxide can be summarized as follows.

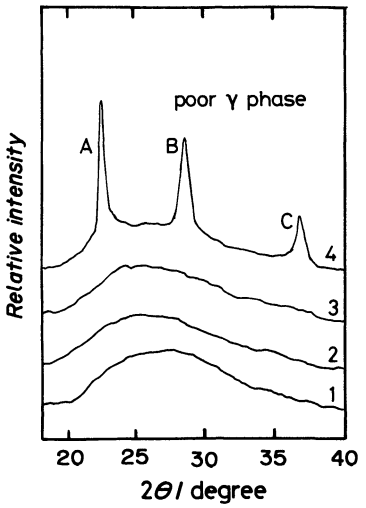

Fig. 5. X-Ray diffraction patterns.
Temperature of treatment, 1: R.T., 2: 200 °C, 3: 350 °C, 4: 450 °C. Interplaner distance/nm, A: 0.393, B: 0.315, C: 0.246.
γ-Niobium(V) oxide: low temperature phase of the compound reported by Brauer[9] and by Holtzberg et al.[10]

When an exchanger of large particle size is heated at 200 °C, the effective radius of the exchanger particle is decreased due to cracks which develop in the exchanger particles, resulting in an increased rate in the exchange reaction. A further increase in the exchange rate, when samples are heated at temperatures higher than 200 °C, can be explained in terms of an increase in the diffusion coefficient of sodium ions due to a reduction of the interactions between the ions and the pore walls, and the collisions of ions in the pores.

References

1) Y. Inoue, H. Yamazaki, and M. Ikeda, *Bull. Chem. Soc. Jpn.*, **61**, 1147 (1988).
2) Y. Inoue, H. Yamazaki, and Y. Matsuda, *Bull. Chem. Soc. Jpn.*, **58**, 2955 (1985).
3) Y. Inoue, H. Yamazaki, and Y. Kimura, *Bull. Chem. Soc. Jpn.*, **58**, 2481 (1985).
4) F. A. Inkley and R. W. Crauston, *Adv. Catal.*, **9**, 143 (1957).
5) Y. Inoue and Y. Yamada, *Bull. Chem. Soc. Jpn.*, **56**, 705 (1983).
6) D. Reichenberg, *J. Am. Chem. Soc.*, **75**, 589 (1953).
7) R. Kunin, "Ion Exchange Resins," John Wiley and Sons, New York (1958), p. 27.
8) G. H. Nancollas and R. Paterson, *J. Inorg. Nucl. Chem.*, **22**, 259 (1961).
9) G. Brauer, *Z. Anorg. Allg. Chem.*, **248**, 1 (1941).
10) F. Holtzberg, A. Reisman, M. Berry, and M. Berkenblit, *J. Chem. Soc.*, **79**, 2039 (1957).

 © 1989 The Chemical Society of Japan Bull. Chem. Soc. Jpn., 62, 267—274 (1989)

The Synthesis and Chemical Reaction of Magnesium and Calcium Bis(phosphorodiamidates) with Acids

Shoji SATO, Takao TAKAYANAGI, and Makoto WATANABE*
Department of Industrial Chemistry, Chubu University,
Matsumoto-cho, Kasugai, Aichi 487
(Received June 30, 1988)

Magnesium bis(phosphorodiamidate) hexahydrate and calcium bis(phosphorodiamidate) dihydrate were made by adding an aqueous solution of magnesium chloride or calcium chloride to a sodium phosphorodiamidate solution. These phosphorodiamidates reacted with the water of crystallization and/or adsorbed water to produce phosphoramidate and orthophosphate. They also reacted with HCl gas, acetic acid, and oxalic acid to make polyphosphates and phosphates with amino and/or imino groups. Several typical reactions are as follows:

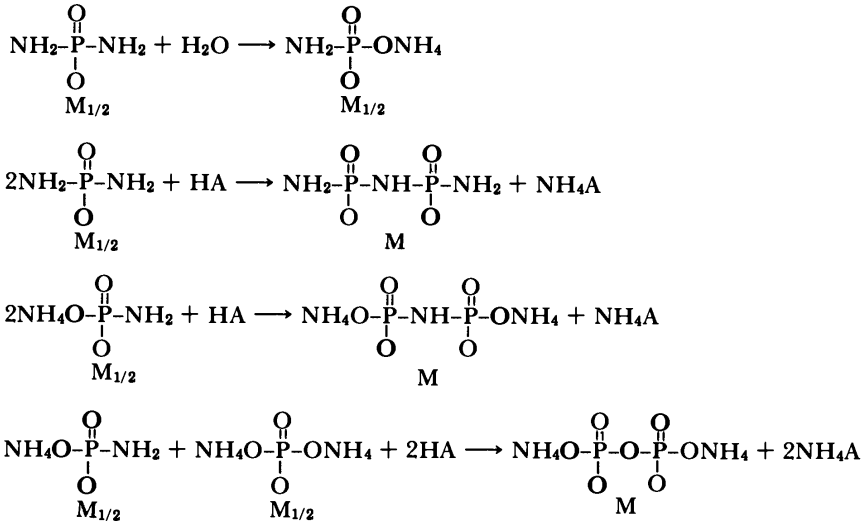

where M and HA stand for alkaline earth metal and acid respectively.

There are many kinds of phosphorus-nitrogen compounds. Among these compounds, the phosphazenes may be the best known and the most intesively studied ones. These compounds have attracted much attention from the theoretical, synthetic, mechanistic, and technological points of view.[1] There are a series of phosphorus-nitrogen compounds which have amino groups on a phosphorus atom. These compounds can be used as fertilizers, flame retarders, and starting materials for the preparation of organic and inorganic phosphorus compounds.[2] The present authors have previously reported the syntheses and thermal behavior of several phosphoramidates.[3-8] When the phosphoramidates were heated in air at a moderately high temperature (100—1000 °C), they mainly produced ortho- and polyphosphates, although a small amount of polyphosphates containing imino groups was also formed. The present authors also studied the synthesis and thermal behavior of sodium phosphorodiamidate.[9] The phosphorodiamidate was finally converted to sodium metaphosphate when it was heated in air above 300 °C. An amino group on these phosphoramidates was, accordingly, thermally unstable in air, and it was difficult to prepare phosphates containing imino groups from phosphoramidates by means of thermal condensation. The chemical reactions of alkaline earth bis(phosphorodiamidates) with hydrogen chloride, acetic acid, and oxalic acid have now been carried out in order to study the condensation and decomposition of the amino groups in the phosphorodiamidates.

Experimental

Preparation of Phosphorodiamidates. Sodium phosphorodiamidate pentahydrate was made by the method described in our previous paper.[9] The phosphorodiamidate (20.8 g) was dissolved in 100 cm^3 of water, and then 100 cm^3 of a 0.5-mol dm^{-3} solution of magnesium chloride or calcium chloride was added. Acetone (500 cm^3) was put into the resulting mixed solution, and a white precipitate was filtered off. The product was dissolved in 150 cm^3 of water, and the residue was removed by filtration. The product was recrystallized by adding 300 cm^3 of acetone to the solution. The recrystallized product was filtered off, washed with 75 Vol%-aqueous acetone, and then dried in a silica-gel desiccator at room temperature for several days.

Reaction of Phosphorodiamidates with Hydrogen Chloride. About 3—4 g of a phosphorodiamidate sample was placed in a reaction glass tube. The air in the tube was replaced with

dried nitrogen gas. Dried hydrogen chloride, which had been prepared by adding concentrated hydrochloric acid to concentrated sulfuric acid and by then passing the resulting gas through concentrated sulfuric acid, was introduced into the reaction tube. The reaction product was washed quickly with ethanol to remove the HCl gas adsorbed on the product.

Reaction of Phosphorodiamidates with Acetic Acid. Magnesium phosphorodiamidate (5 g) or calcium phosphorodiamidate (4 g) was placed in a mixed solution of 2 cm^3 of acetic acid and 20 cm^3 of chloroform. The mixture was then heated at 25 or 60 °C in a water bath while being stirred. The solid product was filtered off and washed with ethanol.

Reaction of Phosphorodiamidates with Oxalic Acid. Phosphorodiamidate (2 g) and oxalic acid (3 g) were added to 100 cm^3 of ethanol. The mixture was then heated at 25 or 60 °C in a water bath, after which the solid product was filtered off and then washed with ethanol.

Chemical Analysis. Alkaline earth cations, phosphorus, and nitrogen in a sample solution were determined by, respectively, the EDTA (disodium dihydrogen ethylenediaminetetraacetate dihydrate) titration method with a BT indicator, Molybdenum Blue colorimetric analysis, and the Kjeldahl technique.

The Paper Chromatography and Colorimetry of Phosphates. A sample (0.1 g) was dissolved in 10 cm^3 of a 6% EDTA solution by adjusting the pH of the solution to 9—10. The paper-chromatographic separation and colorimetric determination of the phosphate species in the solution were carried by the methods described in our previous paper.[3] A modified stock solution of a molybdenum(V)-molybdenum(VI) reagent was used.[10]

HPLC Technique. The HPLC analysis which was developed by Yoza was employed to separate and determine the phosphate species in a sample.[11] A separation column (2.6 mm×500 mm) with TSK-GEL (SAX-F0011), a Shimadzu spectrophotometer (UV-110-02), and KCI eluents (0.20 and 0.40 mol dm^{-3}) were used for the analysis. About 10 mg of a sample was dissolved in 10 cm^3 of water or a 6% EDTA solution, and 200 mm^3 of the solution was injected into the column.

X-Ray Diffractometry. An X-ray diffraction diagram of a powder sample was taken with nickel-filtered Cu $K\alpha$ radiation using a Rigaku X-ray diffractometer, RAD-1B.

IR Spectrophotometry. An IR spectrum of a sample was recorded on a JASCO IR spectrophotometer, A-3, using the KBr disc method.

^{31}P NMR Measurement. A sample was dissolved in water or a 6% EDTA solution. The ^{31}P NMR spectrum of the sample solution was taken by means of a JNM-GX 270 spectrograph. The chemical shifts are reported relative to external 85%-orthophosphoric acid, with the positive shifts being downfield.

Results and Discussion

Composition of Phosphorodiamidates. The phosphorodiamidates gave a single ^{31}P NMR peak at +14.4 ppm at pH 9. (The peak shifted to +8.5 ppm at pH 5—4.) Found for magnesium salt: Mg, 7.5; P, 19.7; N, 17.5%. Found for calcium salt: Ca, 15.1; P, 23.5; N, 21.1%. Calcd for $Mg[PO_2(NH_2)_2]_2 \cdot 6H_2O$: Mg, 7.5; P, 19.2; N, 17.4%. Calcd for $Ca[PO_2(NH_2)_2]_2 \cdot 2H_2O$: Ca, 15.1; P, 23.3; N, 21.1%. Accordingly, the products are magnesium bis(phosphorodiamidate) hexahydrate and calcium bis(phosphorodiamidate) dihydrate. The yields of the products were about 80%. The magnesium phosphorodiamidate was stable below 5 °C, but it gradually decomposed above room temperature (15—25 °C). On the other hand, the calcium phosphorodiamidate was stable at room temperature.

Reaction with Hydrogen Chloride. When hydrogen chloride gas was introduced into the reaction tube, an elevation of the temperature in the tube was observed. The highest temperature was about 50—60 °C. The analytical data of the nitrogen content and the X-ray diffraction analysis of the reaction products are given in Table 1. (Since the paper-chromatographic separation between phosphate species in the products could not be achieved with the developing solvents employed in this experiment, the analytical data of the composition of the products as obtained by paper chromatography are not given in the table.) According to the results shown in the table, the magnesium phosphorodiamidate reacted with HCl gas to produce an ammonium ion. In the case of the reaction of the calcium phosphorodiamidate, the reaction rate seemed much slower than that of the magnesium salt. The IR spectral data in Fig. 1 show the absorption of NH_4^+ at 1400 cm^{-1} in good agreement with the results in Table 1. The IR spectra of the products also give peaks due to P–O–P and/or P–NH–P linkages at 920 and 730 cm^{-1}. This means that the phosphorodiamidates produce polymers associated with P–O–P and/or P–NH–P linkages by the reaction with HCl gas. The

Table 1. Nitrogen Content and X-Ray Diffraction Data of the Reaction Products of Phosphorodiamidates with HCl Gas

Phosphorodiamidate	Reaction time/min	Total N/%	N as NH_4^+/%	X-Ray dif.
$Mg[PO_2(NH_2)_2]_2 \cdot 6H_2O$	60	17.4	8.4	NH_4Cl, UK
	180	15.8	9.5	NH_4Cl, UK
	300	15.5	9.3	NH_4Cl, UK
$Ca[PO_2(NH_2)_2]_2 \cdot 2H_2O$	60	20.7	—	SM
	180	20.7	—	SM
	300	19.7	—	SM

UK and SM stand for the unknown crystalline substance and the starting material respectively.

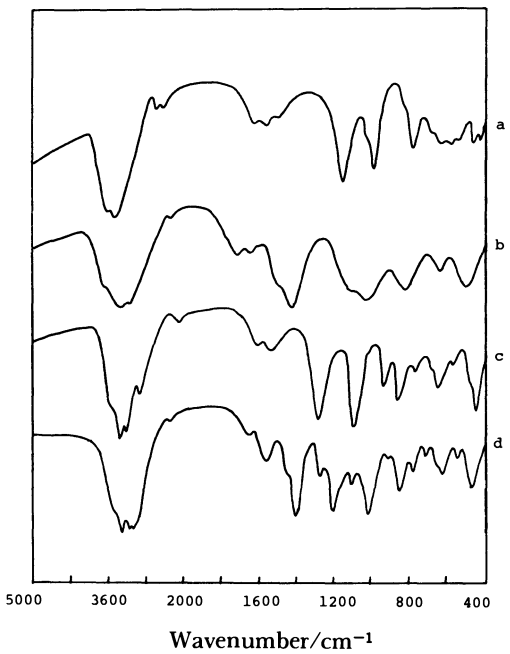

Fig. 1. IR spectra of the phosphorodiamidates and the reaction products of the phosphorodiamidates with HCl gas for 300 min.
a: $Mg[PO_2(NH_2)_2]_2 \cdot 6H_2O$, b: reaction product of $Mg[PO_2(NH_2)_2]_2 \cdot 6H_2O$, c: $Ca[PO_2(NH_2)_2]_2 \cdot 2H_2O$, d: reaction product of $Ca[PO_2(NH_2)_2]_2 \cdot 2H_2O$.

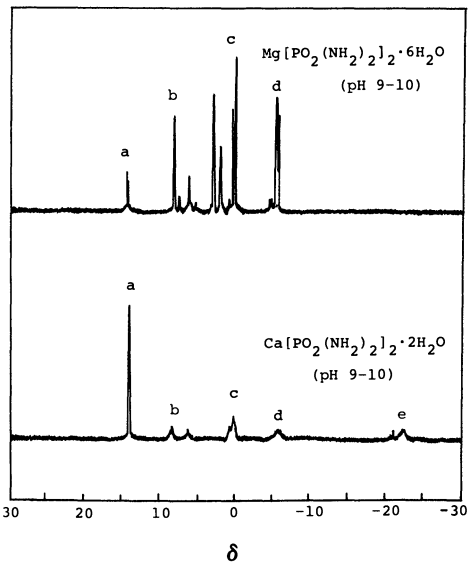

Fig. 2. ^{31}P NMR spectra of the reaction products of the phosphorodiamidates with HCl gas for 300 min.
a: Phosphorodiamidate, b: phosphoramidate, c: orthophosphate, d: end-PO_4 group, e: middle-PO_4 group.

^{31}P NMR spectral data in Fig. 2 give the peaks of phosphoramidate, orthophosphate, an end-PO_4 group, a middle-PO_4 group, and unknown materials other than phosphorodiamidate. The unknown peaks which appeared in lower fields than that of orthophosphate might be caused by compounds with amino

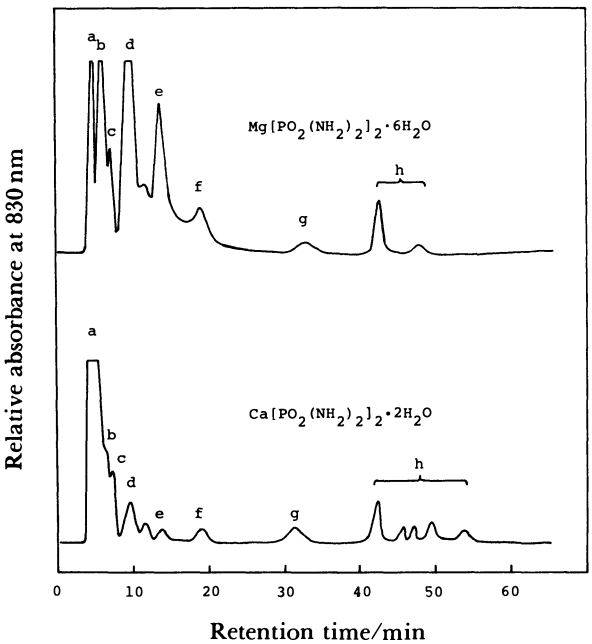

Fig. 3. HPLC profiles of the reaction products of the phosphorodiamidates with HCl gas for 300 min.
a: Phosphorodiamidate, b: phosphoramidate, c: orthophosphate, d: imidodiphosphate, e: diphosphate, f: triphosphate, g: chain polyphosphates, h: ring and higher chain polyphosphates.

and/or imino groups.[12] The HPLC profile of the products in Fig. 3 indicates that the products contain phosphorodiamidate, phosphoramidate, orthophosphate, diphosphate, imidodiphosphate, triphosphate, and higher-chain and ring polyphosphates with P–O–P and P–NH–P linkages. According to the results, the following reaction processes can be written for the reaction systems:

(1) Decomposition

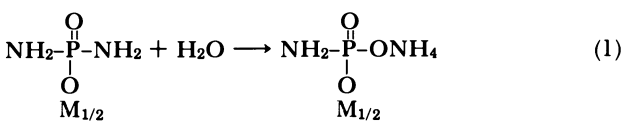

(1)

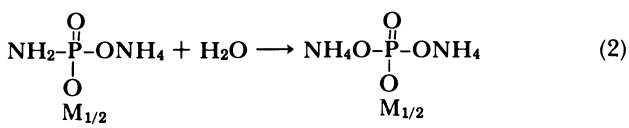

(2)

The water in the above reaction can come from the water of crystallization and/or the adsorbed water of the phosphorodiamidates and from the slight amount of water in the gas in the reaction systems.

(2) Condensation

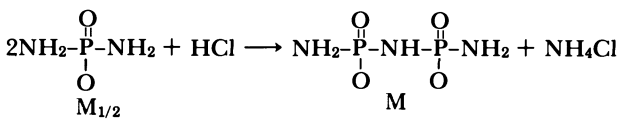

(3)

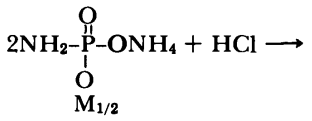

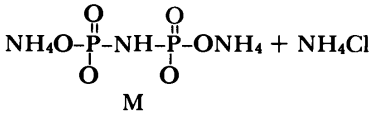

(4)

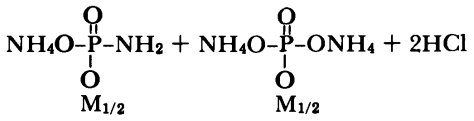

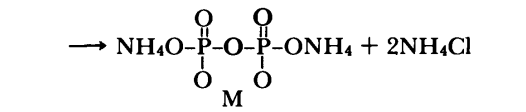

(5)

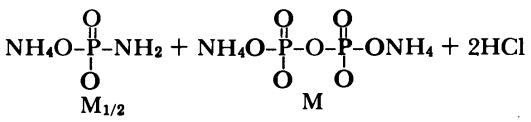

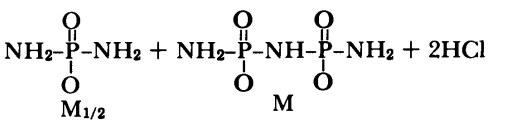

(6)

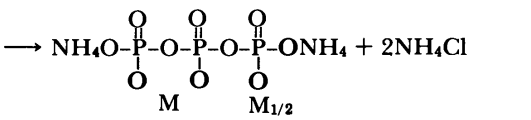

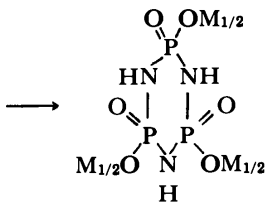

+2NH4Cl (7)

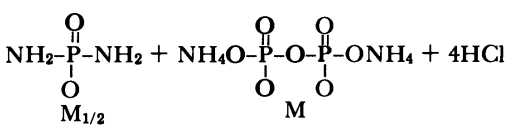

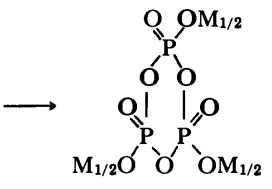

+4NH4Cl (8)

where M stands for alkaline earth metal. (Only typical reactions are shown above.)

The phosphoramidate with an OH group was considered to from a zwitterion:[2]

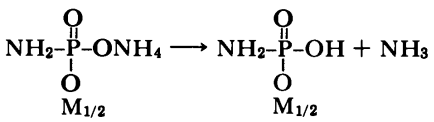

(9)

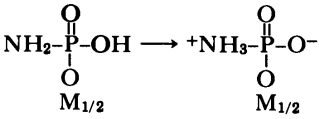

(10)

The zwitterion is very active and can react with water, phosphoramidates, and phosphates to produce orthophosphate, polyphosphates, and phosphates with amino and/or imino groups:

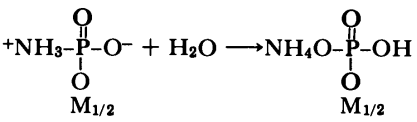

(11)

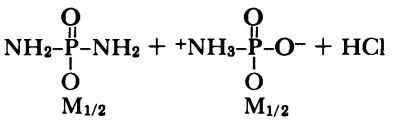

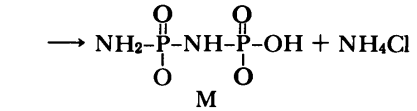

(12)

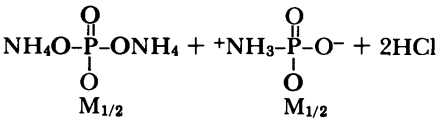

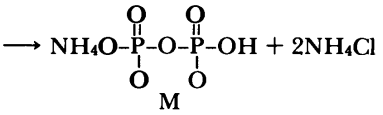

(13)

It was difficult, however, to obtain exact information about the zwitterion, so it is impossible to decide which process is most reasonable for the reaction systems.

Reaction with Acetic Acid. The nitrogen content and the results of the X-ray diffraction analysis of the reaction products of the phosphorodiamidates with acetic acid are listed in Table 2. The results show that the amino group in the phosphorodiamidates was converted to an ammonium ion by the reaction with acetic acid. The IR spectra of the products in Fig. 4 exhibit an absorption of an NH_4^+ ion at 1400 cm^{-1}. The results agree well with those in Table 2. The IR spectra also show that the products have P-O-P and/or P-NH-P linkages by means of the absorption at 920 cm^{-1}. The ^{31}P NMR spectra of the reaction products in Fig. 5 give peaks due to orthophosphate, phosphoramidate, and an end-PO_4 group, a middle-PO_4 group, and unknown materials. As has been men-

Table 2. Nitrogen Content and X-Ray Diffraction Data of the Reaction Products of Phosphorodiamidates with Acetic Acid

Phosphorodiamidate	Reaction temp/°C	Reaction time/h	Total N/%	N as NH_4^+/%	X-Ray dif.
$Mg[PO_2(NH_2)_2]_2 \cdot 6H_2O$	25	15	14.3	4.1	SM
		25	14.0	4.1	UK
	60	15	11.1	7.6	AM
		25	8.1	6.5	AM
$Ca[PO_2(NH_2)_2]_2 \cdot 2H_2O$	25	15	15.1	2.8	SM
		25	12.8	3.8	UK
	60	15	11.6	5.9	AM
		25	9.5	5.4	AM

SM, UK, and AM stand for the starting material, the unknown crystalline substance, and the amorphous product respectively.

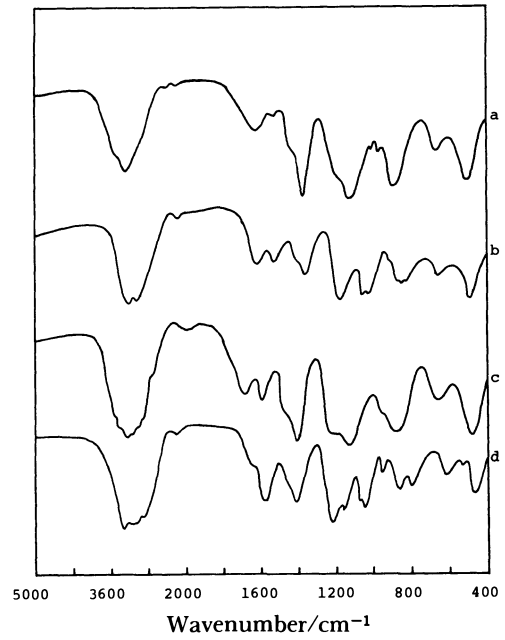

Fig. 4. IR spectra of the reaction products of the phosphorodiamidates with acetic acid for 25 h. a: $Mg[PO_2(NH_2)_2]_2 \cdot 6H_2O$ at 60 °C, b: $Mg[PO_2(NH_2)_2]_2 \cdot 6H_2O$ at 25 °C, c: $Ca[PO_2(NH_2)_2]_2 \cdot 2H_2O$ at 60 °C, d: $Ca[PO_2(NH_2)_2]_2 \cdot 2H_2O$ at 25 °C.

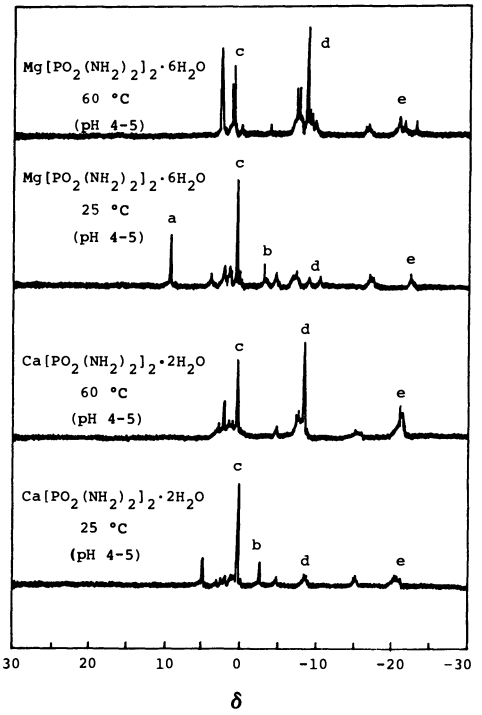

Fig. 5. ^{31}P NMR spectra of the reaction products of the phosphorodiamidates with acetic acid for 25 h. a: Phosphorodiamidate, b: phosphoramidate, c: orthophosphate, d: end-PO_4 group, e: middle-PO_4 group.

tioned above, the peaks in the magnetic fields lower than that of orthophosphate seemed to be attributable to the peaks of phosphates associated with amino and/or imino groups. The HPLC profiles of the products in Fig. 6 give peaks of orthophosphate, phosphoramidate, diphosphate, imidodiphosphate, triphosphate, and higher-chain and ring polyphosphates containing P–O–P and/or P–NH–P linkages. Accordingly, the same decomposition reactions as in Eqs. 1 and 2 can be given for the reaction systems. The following condensations of phosphate species with acetic acid can be described for the systems:

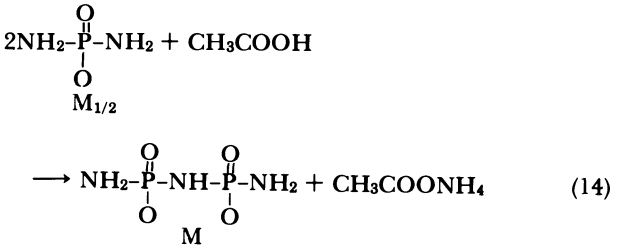

(14)

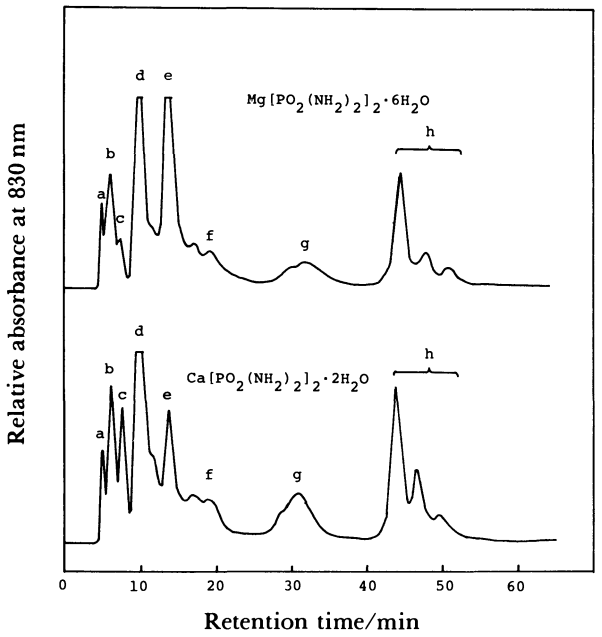

Fig. 6. HPLC profiles of the reaction products of the phosphorodiamidates with acetic acid at 60°C for 15 h.
a: Phosphorodiamidate, b: phosphoramidate, c: orthophosphate, d: imidodiphosphate, e: diphosphate, f: triphosphate, g: chain polyphosphates, h: ring and higher chain polyphosphates.

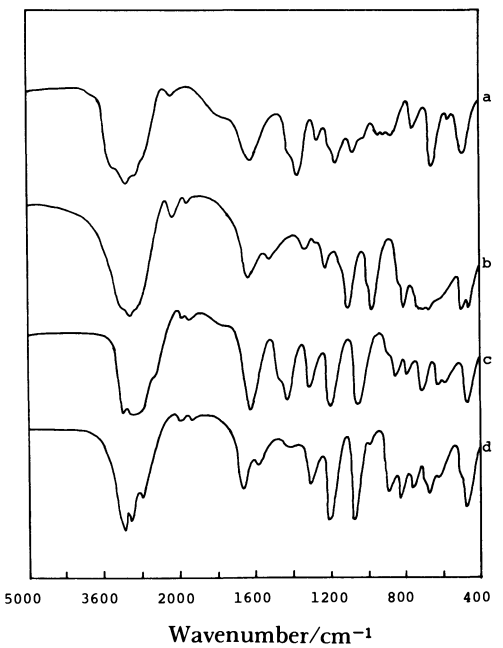

Fig. 7. IR spectra of the reaction products of the phosphorodiamidates with oxalic acid for 25 h.
a: $Mg[PO_2(NH_2)_2]_2 \cdot 6H_2O$ at 60°C, b: $Mg[PO_2(NH_2)_2]_2 \cdot 6H_2O$ at 25°C, c: $Ca[PO_2(NH_2)_2]_2 \cdot 2H_2$ at 60°C, d: $Ca[PO_2(NH_2)_2]_2 \cdot 2H_2O$ at 25°C.

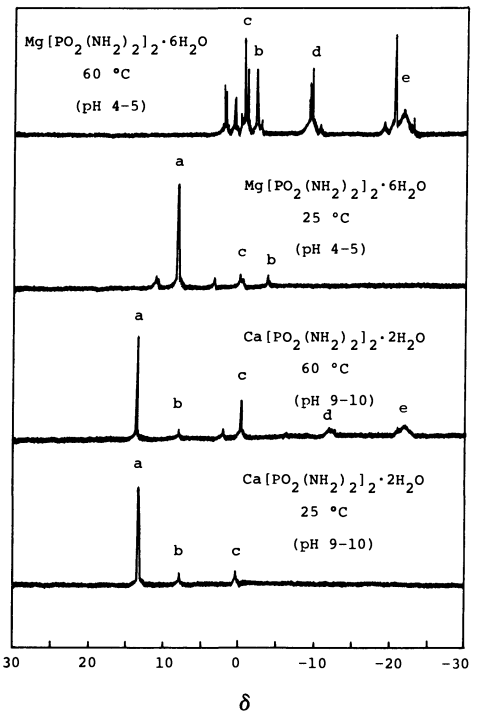

Fig. 8. ^{31}P NMR spectra of the reaction products of the phosphorodiamidates with oxalic acid for 25 h.
a: Phosphorodiamidate, b: phosphoramidate, c: orthophosphate, d: end-PO_4 group, e: middle-PO_4 group.

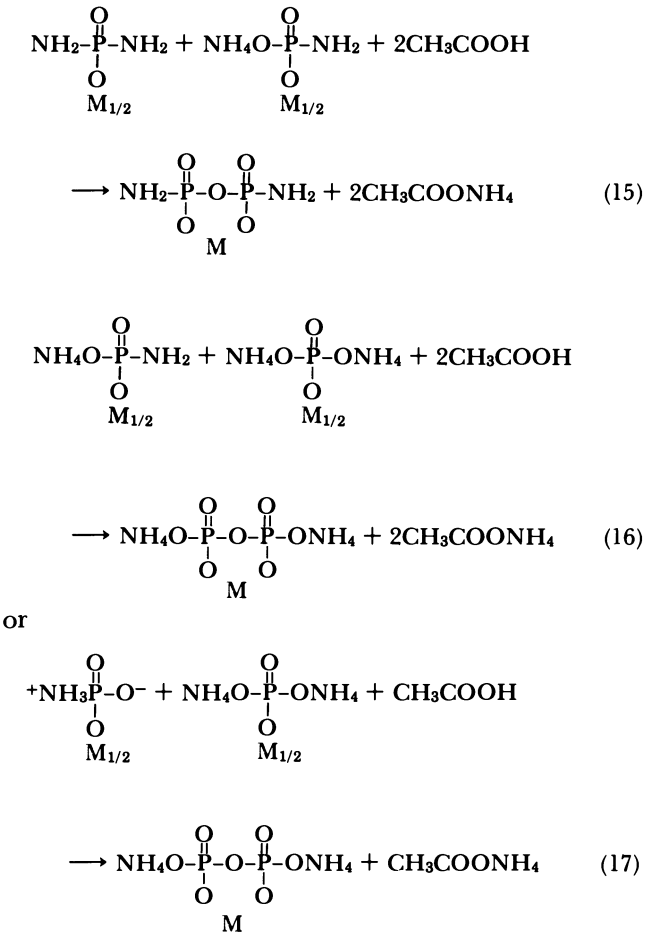

Table 3. Nitrogen Content and X-Ray Diffraction Data of the Reaction Products of Phosphorodiamidates with Oxalic Acid

Phosphorodiamidate	Reaction temp/°C	Reaction time/h	Total N/%	N as NH_4^+/%	X-Ray dif.
$Mg[PO_2(NH_2)_2]_2 \cdot 6H_2O$	25	15	17.0	0.3	SM
		25	16.5	0.5	SM
	60	15	13.0	6.0	UK
		25	10.9	7.2	UK
$Ca[PO_2(NH_2)_2]_2 \cdot 2H_2O$	25	15	20.2	0.4	SM
		25	19.4	0.9	SM
	60	15	18.2	2.1	SM
		25	14.0	4.8	SM

SM and UK stand for the starting material and the unknown crystalline substance respectively.

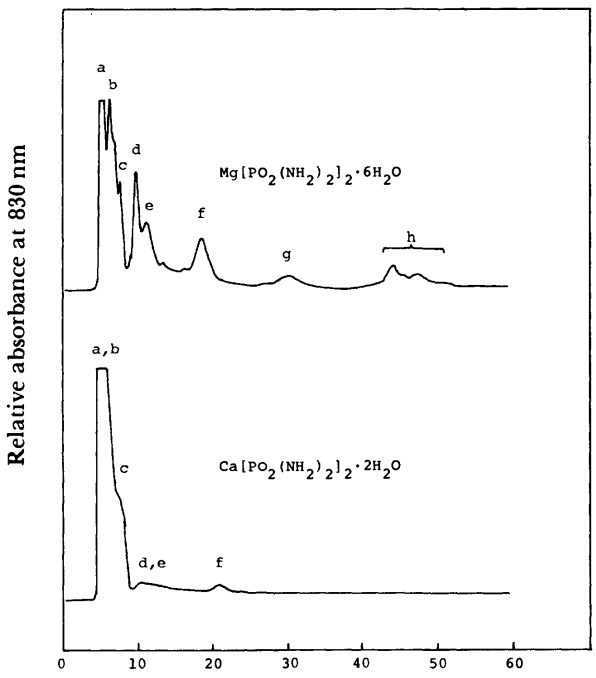

Fig. 9. HPLC profiles of the reaction products of the phosphorodiamidates with oxalic acid at 60 °C for 15 h.
a: Phosphorodiamidate, b: phosphoramidate, c: orthophosphate, d: imidodiphosphate, e: diphosphate, f: triphosphate, g: chain polyphosphates, h: ring and higher chain polyphosphates.

(Only a few typical reaction models are described here.)

Reaction with Oxalic Acid. The chemical analysis of the nitrogen content and X-ray diffraction data of the products in Table 3 show that the phosphorodiamidates react little with oxalic acid at 25 °C. The amino group in the phosphorodiamidates is converted to an ammonium ion at 60 °C. The IR spectra of the reaction products in Fig. 7 show an absorption of NH_4^+ at 1400 cm^{-1} and support the results in Table 3. The ^{31}P NMR spectra of the products of the magnesium phosphorodiamidate in Fig. 8 indicate large peaks of orthophosphate, phosphoramidate, an end-PO_4 group, a middle-PO_4, group, and unknown species. The ^{31}P NMR spectra of the other reaction products gave a large peak of phosphorodiamidate and very small peaks of the other species. This means that the rates of the reactions other than that of the magnesium salt at 60 °C are very small. These results are well supported by the HPLC data in Fig. 9. According to the above results, one can write the same decomposition reactions as Eqs. 1 and 2, and the condensation reaction processes similar to those of acetic acid for the reactions with oxalic acid, thus:

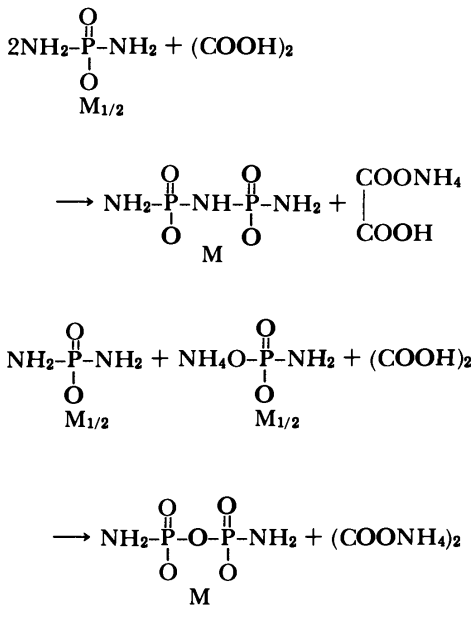

(18)

(19)

(Only typical reactions are shown.)

References

1) H. A. Allcock, "Phosphorus-Nitrogen Compounds," Academic Press, New York and London (1972).
2) D. E. C. Corbridge, "Phosphorus," Elsevier, Amsterdam (1980), p. 219.
3) M. Watanabe, T. Inagaki, and S. Sato, *Bull. Chem. Soc. Jpn.*, **56**, 458 (1983).
4) M. Watanabe, T. Inagaki, Y. Morii, and T. Yamada, *Setsuko To Setsukai*, **184**, 111 (1983).
5) M. Watanabe, Y. Morii, and S. Sato, *Bull. Chem. Soc. Jpn.*, **57**, 2087 (1984).
6) M. Watanabe, Y. Morii, and S. Sato, *Bull. Chem. Soc. Jpn.*, **57**, 2914 (1984).
7) S. Sato, M. Watanabe, and T. Yamada, *Setsuko To Setsukai*, **199** 357 (1985).
8) S. Sato and M. Watanabe, *Bull. Chem. Soc. Jpn.*, **58**, 3513 (1985).
9) M. Watanabe and S. Sato, *J. Mater. Sci.*, **21**, 2623 (1986).
10) Y. Hirai, N. Yoza, and S. Ohashi, *Anal. Chim. Acta*, **115**, 269 (1980).
11) N. Yoza, N. Okazawa, T. Hashi, and S. Ohashi, presented at the 4th Symposium of Inorganic Phosphorus Chemistry, Nagoya, November, 1983.
12) M. M. Crutchfield, C. H. Dungan, J. H. Letcher, V. Mark, and J. R. Van Wazer, "^{31}P Nuclear Magnetic Resonance, Topics in Phosphorus Chemistry," Interscience Publishers, New York (1967), Vol. 5, p. 227, and the references cited therein.

 © 1989 The Chemical Society of Japan Bull. Chem. Soc. Jpn., 62, 275—278 (1989)

Hydrothermal Synthesis of Gallium Orthophosphate Crystals

Shin-ichi HIRANO* and Pan-chae KIM
Department of Applied Chemistry, Faculty of Engineering, Nagoya University,
Furo-cho, Chikusa-ku, Nagoya 464
(Received July 27, 1988)

Synthesis and crystal growth of $GaPO_4$ have been carried out in order to elucidate the properties of gallium orthophosphate. Single crystals were hydrothermally grown in the low temperature range from 150 to 180 °C. Solubility of $GaPO_4$ was measured under hydrothermal conditions, and the temperature coefficient of solubility was found to be negative in H_3PO_4 solution. Single crystals have morphologies bounded by the major rhombohedral $(10\bar{1}1)$ faces under lower temperature and pressure conditions. Polymorphs of $GaPO_4$ exist corresponding to low quartz type, low and high cristobalite types.

On the study of orthophosphate crystals M(III)PO_4, with M=Al, Ga, Fe, or Mn, compared with the extensive studies on berlinite ($AlPO_4$), little has been done on other crystals. It is well known that the single crystal of $AlPO_4$ has a larger piezoelectric coupling constant than quartz.[1] Single crystals of $GaPO_4$ which have a similar structure to $AlPO_4$ have potential as a promising material with interesting piezoelectric properties. However, the synthesis and properties of $GaPO_4$ single crystals have not been well investigated. This work describes the following studies; (1) synthesis of $GaPO_4$ particles as a single phase, (2) measurement of solubility of $GaPO_4$ in 4 mol dm^{-3} H_3PO_4 hydrothermal solution, (3) growth of $GaPO_4$ single crystals in H_3PO_4 solution at low temperatures below 180 °C, (4) phase transition of $GaPO_4$ single crystals.

Experimental

The starting particles of $GaPO_4$ were prepared by the solid state reaction of a stoichiometric mixture of Ga_2O_3 (99.99% purity) and $NH_4H_2PO_4$ (>99.0% purity) at 1000 °C for 24 h, and subsequently by the hydrothermal treatment at 180 °C and 14.7 MPa for 24 h in 4 mol dm^{-3} H_3PO_4 solution.[2,3] The hydrothermal runs were carried out in a test-tube type pressure vessel. The temperature was controlled with a calibrated chromel-alumel thermocouple set in the pressure vessel. The pressure was measured with a calibrated Heise gauge with an accuracy of ±0.5%. The solubility was determined by the weight loss method with a gold capsule of about 0.4 cm^3 in inner volume with recrystallized powders. The powders and H_3PO_4 solution were sealed hermetically in the gold capsule, and placed in a pressure vessel. Solubility runs were carried out at desired temperatures and pressures. Equilibrium was achieved after 3 d. Therefore, the solubility was measured by experimental runs for longer than 3 d, which were found to be enough to reach the equilibrium by preliminary experiments. The pressure vessel was quenched into cold water, the capsule was cut-open, and the powders were rinsed on a filter, dried and weighed. Synthesis runs of $GaPO_4$ single crystals were carried out by the following two methods because of its negative temperature coefficient of solubility; runs were performed by an inverse method with the nutrient in a lower temperature region and the others by the temperature increase method. The hydrothermal growth conditions are a temperature of 150—180 °C, a pressure of 14.7 MPa, a solvent of 4 mol dm^{-3} H_3PO_4 and a run duration of 3—7 d. The morphology of the grown single crystals was observed by optical microscopy. Phase transitions of $GaPO_4$ single crystals were investigated by DTA and XRD.

Results and Discussion

Synthesis of the Starting Particles. In order to investigate the solid state reaction process between Ga_2O_3 and $NH_4H_2PO_4$, DTA-TG analysis was carried out at a heating and cooling rate of 10 °C min^{-1} (Fig. 1). Endothermic peaks at about 200 and 300 °C are ascribed to the two step decomposition reactions of $NH_4H_2PO_4$.[2] The partial reaction of Ga_2O_3 with P_2O_5 produced from $NH_4H_2PO_4$ took place at about 450 °C to form $GaPO_4$, associated with amorphous $Ga(H_2PO_4)_3$ compound. The XRD indicated the formation of crystalline $GaPO_4$. Amorphous $Ga(H_2PO_4)_3$ decomposed to $Ga(PO_3)_3$ at about 550 °C. $GaPO_4$ was formed in a highly crystallized state associated with evaporation of P_2O_5 above about 850 °C. The formation of $GaPO_4$ crystalline powders took place by the decomposition of $Ga(PO_3)_3$ to loose P_2O_5, at which a little weight loss occurred. The products reacting up to 800 °C were consist with Ga_2O_3, P_2O_5, $GaPO_4$, and $Ga(PO_3)_3$. The formation reaction of $GaPO_4$ completed above 800 °C. The prepared powders treated at 1000 °C for 24 h and then cooled to room temperature were composed of the low temperature type $GaPO_4$, P_2O_5 glass and the high

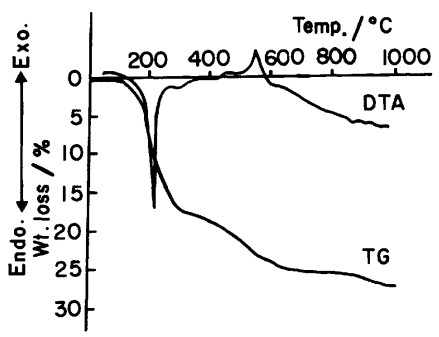

Fig. 1. Thermogravimetric and differential thermal analysis of the reaction product between Ga_2O_3 and $NH_4H_2PO_4$.

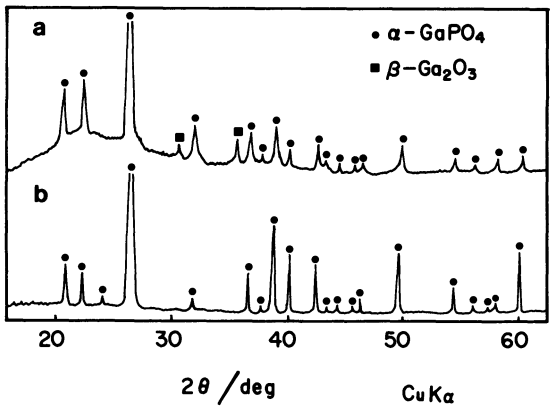

Fig. 2. X-Ray diffraction profiles of Ga_2O_3-$NH_4H_2PO_4$ mixture, (a) reacted twice at 1000 °C for 24 h, and (b) hydrothermally treated at 180 °C and 14.7 MPa for 24 h in 4 mol dm^{-3} H_3PO_4 solution.

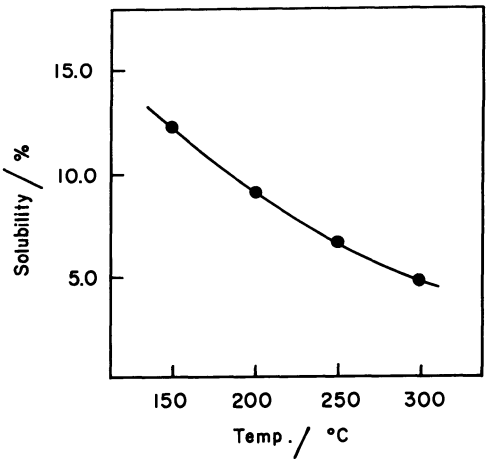

Fig. 3. Weight percent solubility of $GaPO_4$ as a function of temperature at 14.7 MPa in 4 mol dm^{-3} H_3PO_4 solution.

temperature type Ga_2O_3 as shown in Fig. 2 (a). The above results indicate a solid state reaction process to form $GaPO_4$ as follows:

$$2NH_4H_2PO_4 \rightarrow P_2O_5 + 2NH_3\uparrow + 3H_2O\uparrow \text{ (200 and 300 °C)}$$

$$Ga_2O_3 + 3P_2O_5 + 6H_2O \rightarrow 2Ga(H_2PO_4)_3 \text{ (ca. 450 °C)}$$
$$(Ga_2O_3 + P_2O_5 \rightarrow 2GaPO_4)$$

$$Ga(H_2PO_4)_3 \rightarrow Ga(PO_3)_3 + 3H_2O\uparrow \text{ (ca. 550 °C)}$$

$$Ga(PO_3)_3 \rightarrow GaPO_4 + P_2O_5\uparrow \text{ (>800 °C)}$$

In order to prepare the $GaPO_4$ particles as a single phase, these mixture powders were hydrothermally treated at 180 °C and 14.7 MPa for 24 h in 4 mol dm^{-3} H_3PO_4 solution. As shown in Fig. 2 (b), it was confirmed that only the low temperature type of $GaPO_4$ formed as a single phase. Single phase $GaPO_4$ particles were used for the solubility measurement and crystal growth.

Solubility. Solubilities in 4 mol dm^{-3} H_3PO_4 hydrothermal solution were measured as a function of temperature and pressure over the range 150—300 °C and 14.7—44.1 MPa. Figure 3 shows the solubility of $GaPO_4$ as a function of temperature at 14.7 MPa in 4 mol dm^{-3} H_3PO_4 solution. In turns out that the temperature coefficient of solubility at constant pressure, $(\partial S/\partial T)_p$, is negative over the range 150—300 °C. This fact indicated several features of importance to crystal synthesis, i.e. it is eventually required to proceed the crystal growth with supersaturation provided by a temperature difference under hydrothermal conditions where the nutrient was sustained in the low temperature region of the pressure vessel. The solubility was re-plotted as a relation of log (solubility) with $1/T$, in order to investigate the dissolution behavior of $GaPO_4$ in 4 mol dm^{-3} H_3PO_4

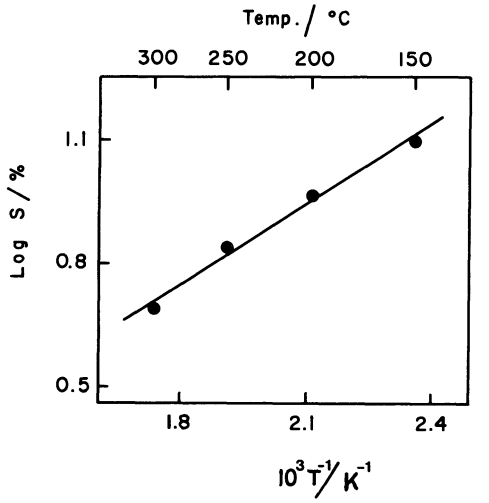

Fig. 4. Log solubility (Log S) of $GaPO_4$ as a function of $1/T$ at 14.7 MPa in 4 mol dm^{-3} H_3PO_4 solution.

$$S = \frac{\text{Wt. of dissolved } GaPO_4}{\text{Wt. of } H_3PO_4 \text{ solution}} \times 100\ (\%)$$

hydrothermal solution at 14.7 MPa (Fig. 4). The figure reveals that the van't Hoff equation was well obeyed. From the slope of Fig. 4, the heat of dissolution with the solvent, ΔH, was calculated to be about −5.4 kJ mol^{-1}. Figure 5 shows the solubility of $GaPO_4$ as a function of pressure in 4 mol dm^{-3} H_3PO_4 solution at constant temperature. The result indicates that the solubility increases with pressure under these conditions. Therefore, the general solubility behavior of $GaPO_4$ at low concentrations of H_3PO_4 solution is similar to that at relatively high concentrations.[3] However, as far as the growth experiment is concerned, the concentration of hydrothermal solvent must be especially considered because the viscosity of H_3PO_4 solution increases with increase of concentra-

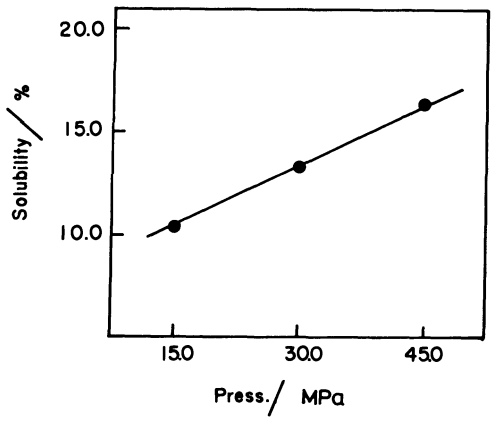

Fig. 5. Weight percent solubility of $GaPO_4$ as a function of pressure at 180 °C in 4 mol dm^{-3} H_3PO_4 solution.

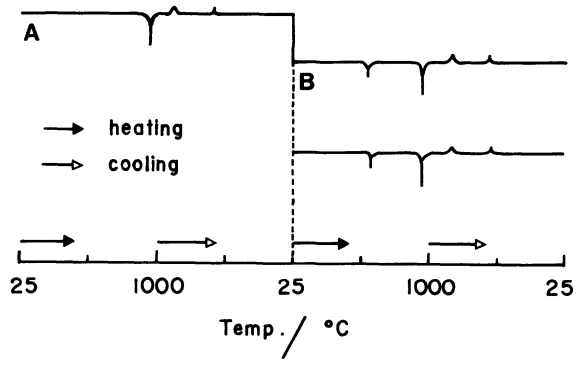

Fig. 7. Typical differential thermal analysis curves of $GaPO_4$ heated and cooled at 10 °C min^{-1}, (A) the first $GaPO_4$ run, and (B) the second $GaPO_4$ run of reverse changes.

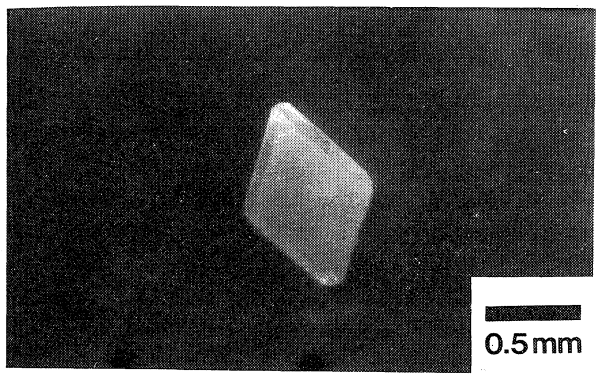

Fig. 6. Microscopic photograph of an α-quartz type $GaPO_4$ single crystal grown hydrothermally in 4 mol dm^{-3} H_3PO_4 solution at 150—180 °C and 14.7 MPa for 3 d.

tion such as 4 mol dm^{-3} H_3PO_4 solution; 4.5×10^{-3} Pa s, 6 mol dm^{-3} H_3PO_4 solution; 5.0×10^{-3} Pa s and 7.25 mol dm^{-3} H_3PO_4 solution; 5.6×10^{-3} Pa s. It becomes more difficult to avoid taking up the highly viscous solution within grown single crystals in highly concentrated solution.

Synthesis of $GaPO_4$ Single Crystals. Based on the results of solubilities, preliminary synthesis runs were carried out under the following conditions: temperature, 150—180 °C; heating rate, 10 °C d^{-1}; pressure, 14.7 MPa; run duration, 3 d; solvent, 4 mol dm^{-3} H_3PO_4 solution. Under these conditions, synthesis of single crystals was achieved by heating the saturated solution at the constant heating rate, i.e. the temperature increase method. As a result, spontaneously nucleated crystals were obtained at the lower part of the gold capsules (higher temperature region) and a typical grown crystal is shown in Fig. 6. At lower growth temperature in 4 mol dm^{-3} H_3PO_4 solution, typical grown crystals tended to be bounded by well developed major rhombohedral ($10\bar{1}1$) faces. The alternative technique was applied to grow $GaPO_4$ crystals, i.e. the inversely placed method, at 180 °C and 14.7 MPa in 4 mol dm^{-3} H_3PO_4 solution for 7 d. In a gold capsule, nutrient was set in a basket at the upper (cooler) part and the seeds were placed at the lower (hotter) part. Consequently, seeds were suspended in the hotter region and the excess nutrient in the cooler region. Also, a modified technique was used, that is the combination of the temperature increase method with inversely placed arrangement under several conditions. The growth features of the crystals did not depend on the growth method, but varied with the growth condition, e.g. at 240 °C and 25 MPa in 7.25 mol dm^{-3} H_3PO_4 solution, the crystals tended to be bounded by prism ($10\bar{1}0$) faces and terminated by small major rhombohedral ($10\bar{1}1$) faces and minor rhombohedral ($01\bar{1}1$) faces.[3]

Phase Transition of $GaPO_4$ Single Crystals. A few studies of phase transition on $GaPO_4$ have been reported.[4-6] However, the transition behavior has not been clarified yet with use of single crystals. In this work, the phase transitions of $GaPO_4$ single crystals were studied by the X-ray diffraction method and by the differential thermal analysis technique. The starting single crystals of $GaPO_4$ were identified by X-ray diffraction at room temperature. It was confirmed to consist of only the low temperature quartz type of $GaPO_4$. Typical differential thermal analysis curves for $GaPO_4$ single crystals are shown in Fig. 7. In the curve (A) of the first cycle run, the transition temperature with endothermic peak was observed at about 976 °C on the heating cycle, and those with exothermic peaks at about 915 and 576 °C on cooling. In the second heating cycle (B), the transition temperature with endothermic peaks were observed at about 608 and 957 °C on heating, and those with exothermic peaks at about 928 and 576 °C on cooling, respectively. The behavior of phases at the transition temperature was investigated by X-ray diffraction on the quenched

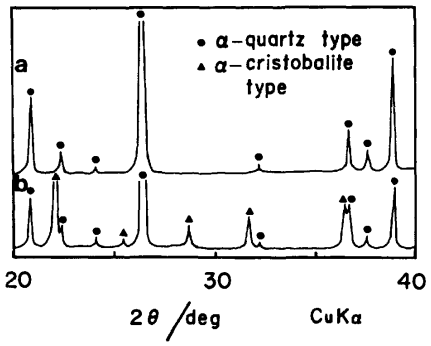

Fig. 8. X-Ray diffraction profiles of the starting $GaPO_4$, (a) the first $GaPO_4$ form, and (b) the second $GaPO_4$ form (in the data of Fig. 7).

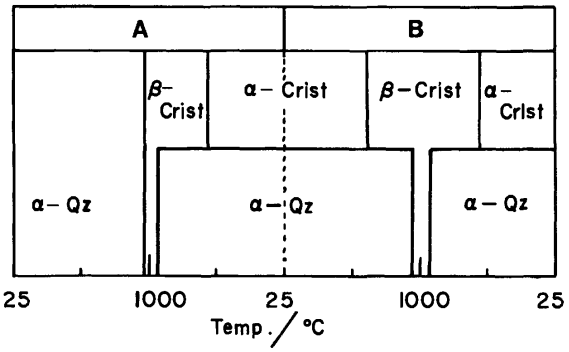

Fig. 9. The phase transition scheme of $GaPO_4$, (A) curve A, and (B) curve B of differential thermal analysis (in the data of Fig. 7).
α-Qz; low temperature quartz type, α-Crist; low temperature cristobalite type, β-Crist; high temperature cristobalite type.

specimens. In the curve (A) of the first run, it is shown that the phase transition from α-quartz type to β-cristobalite type $GaPO_4$ at around 970 °C on heating occurs, while on cooling, β-cristobalite type $GaPO_4$ was partially transformed to α-quartz type $GaPO_4$ and β-cristobalite type remained untransformed was subsequently transformed to α-cristobalite type $GaPO_4$. In the curve (B) of the second run, the phase transition from α-cristobalite type to β-cristobalite type $GaPO_4$ was observed at 608 °C. The α-quartz type transformed to β-cristobalite type $GaPO_4$ at 957 °C on heating, and the phase transition behavior on cooling was similar to the curve (A). From the above results, the starting phase of the first run was composed only of α-quartz type $GaPO_4$ of a single phase as shown in Fig. 8 (a). After cooled to room temperature from 1000 °C, α-quartz type and α-cristobalite type $GaPO_4$ coexisted, as shown in Fig. 8 (b). The results of these phase transitions were summarized in Fig. 9 on cycles.

Conclusion

α-Quartz type $GaPO_4$ particles were synthesized as a single phase by the solid state reaction of Ga_2O_3 with $NH_4H_2PO_4$ and subsequent hydrothermal treatment. Solubilities of α-quartz type $GaPO_4$ were measured under hydrothermal conditions over the range 150—300 °C and 14.7—44.1 MPa, and the temperature coefficient was found to be negative in 4 mol dm^{-3} H_3PO_4 solution. The solubility increased with increase of pressure in 4 mol dm^{-3} H_3PO_4 solution. The solubility of $GaPO_4$ obeyed the van't Hoff equation. The heat of dissolution with the solvent, ΔH, was about −5.4 kJ mol^{-1}. α-Quartz type $GaPO_4$ single crystals could be grown at lower temperature, pressure and concentration of solution, i.e. at 150—180 °C and 14.7 MPa in 4 mol dm^{-3} H_3PO_4 solution. Typical grown single crystals were bounded by well developed major rhombohedral ($10\bar{1}1$) faces. On heating, the phase transition from α-quartz type to β-cristobalite type $GaPO_4$ occurred at about 976 °C. On cooling, β-cristobalite type transformed to α-quartz type $GaPO_4$ at about 915 °C, and subsequently transformed to α-cristobalite type $GaPO_4$ at about 576 °C. On heating in successive runs, the phase transition from the α-cristobalite type to the β-cristobalite type $GaPO_4$ occurred at about 608 °C, and the α-quartz type which remained untransformed was transformed to the β-cristobalite type $GaPO_4$ at about 957 °C. On cooling, the β-cristobalite type transformed to the α-quartz type $GaPO_4$ at about 928 °C, and subsequently transformed to the α-cristobalite type $GaPO_4$ at about 576 °C.

References

1) Z. P. Chang and G. R. Barsch, IEEE Trans. Sonics Ultrasonics, SU-23, 127 (1976).
2) S. Hirano, K. Shibata, K. Miwa, and S. Naka, *Jpn. J. Assoc. Cryst. Growth*, **12**, 100 (1985).
3) S. Hirano, K. Miwa, and S. Naka, *J. Cryst. Growth*, **79**, 215 (1986).
4) A. Perloff, *J. Am. Ceram. Soc.*, **39**, 83 (1956).
5) E. C. Shafer and R. Roy, *J. Am. Ceram. Soc.*, **39**, 330 (1956).
6) L. H. Cohen and W. JR. Klement, *Philos. Mag.*, **39**, 399 (1979)

 © 1989 The Chemical Society of Japan Bull. Chem. Soc. Jpn., 62, 279—284 (1989)

A Calorimetric Study on the β' Phase in the System Tin-Antimony. Enthalpies of Mixing and Formation

Walid Ahmad BADAWI
Department of Chemistry, Faculty of Science, Al-Fateh University, Tripoli, Libya
(Received July 15, 1987)

Calorimetric studies on the behavior of the enthalpy of formation at 573 K in the system tin-antimony have been carried out at the compositions 44, 50, 57 at-% Sb using a presently constructed calorimeter. The enthalpy of mixing at 943 K has been determined in the whole range of composition. The relation of the behavior of mixing to that of formation is found as predicted earlier. The enthalpy of formation displays a pronounced temperature dependence above 623 K. The thermodynamic properties of the alloy SnSb at the three compositions exclude a transformation from β to β' phase around 600 K. Also estimated entropy terms indicate the absence of such a transformation. Earlier reported additional β phase in the system Sn-Sb seemed therefore not to be present.

In our previous studies[1,2] on the enthalpy of formation in the systems Bi-Sb and Sn-Sb, it was observed that the enthalpy of formation depends insignificantly on the temperature. On the other hand, Wittig and Schöffl[3] reported a pronounced temperature dependence of the heat of formation in the systems Al-Ag and Al-Zn. Such a temperature dependence was claimed to be a typical property of all metallic alloys. In order to determine the range of temperature for which this statement could be valid we have again been studying the system Sn-Sb, however, using a different procedure and a presently constructed isoperibolic calorimeter. This should also confirm the results obtained from our study[2] on the enthalpy of formation in this system and consequently test the accuracy of our calorimeter.

The phase boundaries in the system Sn-Sb have not yet been precisely predicted and diverging opinions and results exist with regard to the structures of the phases present and their transformations. Hansen and Anderko[4] rerported the existence of β and β' phases in the system Sn-Sb. According to their studies the transformation from β to β' phase should be accompanied by a change in the structure so that the β phase with a NaCl-structure exists above 598 K, while the β' phase with a distorted rhombohedral structure appears below 598 K in the region 42—58% Sb.

The present study on the system tin-antimony has been carried out in order to determine the existence of the β phase and its transformation. This would be possible by studying the thermodynamic properties of this system.

Experimental

Sample. The metals used were of extra purity grade (Riedel de Haen Co.). The preparation, treatment, and testing of the samples were all the same as reported earlier.[2]

High Temperature Diffraction Study. X-Ray (powder) photographs for samples at the compositions 58 and 50 at-% Sb were taken at 598 and 698 K (Table 1). They revealed nearly the same values for the lattice constant as those at room temperature.[2]

High Temperature Calorimetry. The calorimeter operates quasi-isothermally and represents an isoperibolic type of calorimeter. The cylindrical calorimeter of Thermax steel (Thermax 10, production No. 4742, Ger.) with a mass of 202 g is used as a sample container. The hollow space of the calorimeter is coated with a layer of aluminium oxide and its purpose was to prevent reaction of the sample with the calorimeter. The cover of the calorimeter, also coated with a layer of Al_2O_3, has three wells for the tube of the drop device, stirrer (made of ceramic) and Pt-to-(Pt+10 mass per cent Rh) thermopile. The calorimeter is suspended inside a metallic shield system of V2A steel which contains two cylindrical compensating systems of Thermax steel placed below and above the calorimeter. The lower compensating body has wells of each 3.5 mm diameter for the twelve differential thermopiles. The whole assembly is placed in a vertical tube furnace (R=41 Ω). Another tube furnace (R=35 Ω) is placed above the cooling system which in turn was placed at the mouth of a tube of silica glass containing the whole assembly. The purpose of the second tube furnace was to warm the sample before its final drop in the calorimeter.

The temperature difference between the calorimeter and lower compensating system are measured by means of a set of twelve differential thermopiles. These were calibrated on a standard Pt-PtRh thermopile. The accuracy obtained was found to be ±0.1 K. The thermal potential of the thermopiles is measured by means of a digital millivoltmeter (Hewlett-Packard 2401 C). The temperature drifts of the calorimeter from the lower compensating system are of negligible importance. The observed short-term fluctuation of the null-point is measured to 2×10^{-4} K min^{-1}. Excellent regulation of the temperature was obtained by means of a p-regulator.[5] The derived temperatures are judged to correspond with the IPTS-68 within 0.01 K at 500 K and 0.1 K at 1000 K. In fact the precision is considerably better, and the temperature increments are measured to 0.0003 K.

The calibration of the calorimeter occured on exactly measured enthalpy of tin sample.[3] The calibration factor is determined with an accuracy of 0.3% to an average value: ϕ=85.0±0.31 mV^{-1} min^{-1}.

The operation with this calorimeter can be explained with the aid of Table 2 and Fig. 1 which describe the process and evaluation of a measurement on alloy sample as follows:
Using the quasi-isothermal procedure, the calorimeter equation of 1st order becomes

$$Q = k \cdot \int_0^n (\vartheta - \bar{\vartheta}_v)\mathrm{d}t = K \cdot A \qquad (1)$$

where Q is the heat produced in the calorimeter in J, K the constant of heat interchange in $W K^{-1}$, ϑ the difference between the temperature of the calorimeter and that of the thermostat (compensating system) in the main period which represents the sum of all reads in the main period, and $\bar{\vartheta}_v$ the average value of all reads in the null-point periods: $\bar{\vartheta}_v=(\vartheta_v+\vartheta_n)/n$. A refers to the area under the curve as shown in Fig. 1 and t to the time in second. The determination of A and calculation of the heat content of an alloy sample are illustrated in Table 2: Subtraction of the average value of $\bar{\vartheta}_v$ and ϑ_n from all reads in the main period yields a reduced quantity which represents the deviations in the temperature of the calorimeter from the null-point in the pre- and post-period. The reduced quantity will be integrated according to the trapezoidal rule: The sum of the first and last reads in the main period will be devided by 2. Addition of this result to the sum of all reads between the first and last one gives the area A.

Table 1. Lattice Constants of the Alloy SnSb

T/K	x_{Sb}	a/Å
598	0.500	6.120
	0.580	6.116
698	0.500	6.117
	0.580	6.118

Procedure of Enthalpy Measurement. The enthalpy of mixing of liquid tin and liquid antimony can be determined

Table 2. The Process and Evaluation of a Measurement on a Sample of the Tin-Antimony Alloy

Pre-period	Main-period	Post-period
3.188 mV min	3.307 264	3.186
3.187	3.612 254	3.187
3.187	3.564 254	3.187
3.187	3.522 236	3.187
3.187	3.488 229	3.187
3.187	3.456 222	3.187
3.187	3.426 215	3.186
3.187	3.400 209	3.187
3.186	3.376 204	3.187
3.187	3.355 200	3.187
	3.336 197	
	3.318 194	
	3.303 191	
	3.289 190	
	3.276 189	

ϑ_v=187 mV min ϑ_n=188.6 mV min $A=(A_1+A_2)/2$=3.66 mV min

$A_1=\sum(\vartheta_i-3)-t\cdot\sum(\vartheta_v-3)$=3.657 mV min $H=A\cdot\varphi$=311.7 J

$A_2=\sum(\vartheta_i-3)-t\cdot\sum(\vartheta_n-3)$=3.657 mV min h=28076 J mol^{-1}

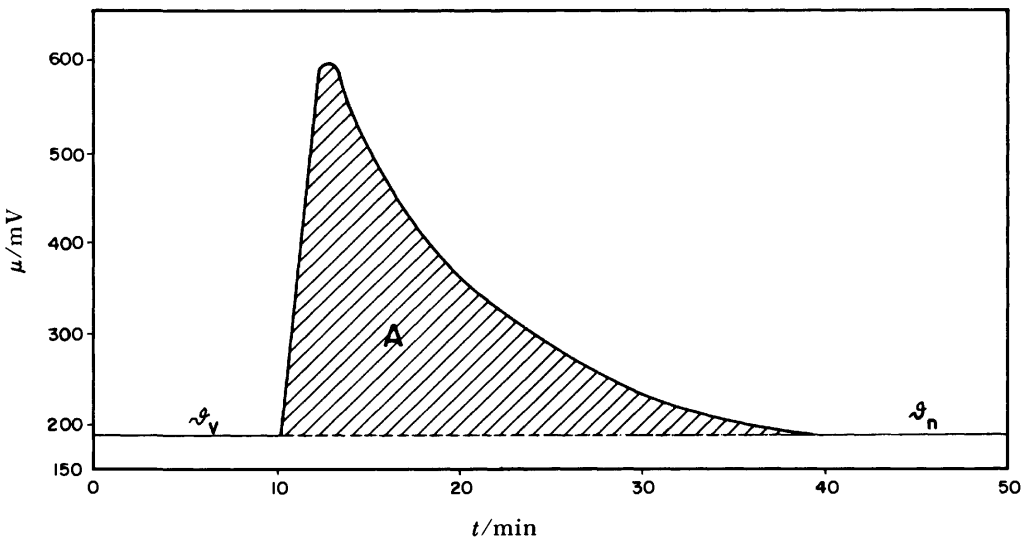

Fig. 1. Plot of the thermal potential μ versus the time t for a measurement on alloy sample using the present calorimeter.

at the temperature T through the equations

$$-(1-x_2)\cdot \mathrm{Sn}(l,T) - x_2\mathrm{Sb}(l,T) + \mathrm{Sn}_{1-x_2}\mathrm{Sb}_{x_2}(l,T) = 0 \quad (2)$$

$$h^{\mathrm{M}} = -(1-x_2)\cdot h_1(T) - x_2 h_2(T) + h_3(T) \quad (3)$$

where h^{M} is the enthalpy of mixing of liquid tin and liquid antimony, h_3 the enthalpy of the alloy at the mole fraction of antimony x_2.

The enthalpy of mixing has been determined at 943 K in the whole range of composition (Table 3).

The enthalpy of formation is the special form of the enthalpy of reaction evolved by the formation of the substance from the elements. In the case of the tin-antimony alloy, the formation reaction is

$$-(1-x_2)\cdot \mathrm{Sn}(\mathrm{s},T_0) - x_2\cdot \mathrm{Sb}(\mathrm{s},T_0) + \mathrm{Sn}_{1-x_2}\mathrm{Sb}_{x_2}(\mathrm{s},T_0) = 0. \quad (4)$$

The enthalpy of formation is then

$$h^{\mathrm{F}} = -(1-x_2)\cdot h_1(T_0) - x_2\cdot h_2(T_0) + h_3(T_0) \quad (5)$$

Indices 1, 2, and 3 refer to tin, antimony, and the alloy, respectively.

Subtraction of Eq. 5 from Eq. 3, yields

$$h^{\mathrm{M}} - h^{\mathrm{F}} = -(1-x_2)[h_1(T) - h_1(T_0)] - x_2[h_2(T) - h_2(T_0)] + [h_3(T) - h_3(T_0)] = {}^{\mathrm{e}}h(T) - {}^{\mathrm{e}}h(T_0) \quad (6)$$

where ${}^{\mathrm{e}}h(T)-{}^{\mathrm{e}}h(T_0)$ is the difference in the excess enthalpy of the alloy. The term $h_3(T)-h_3(T_0)$ is the enthalpy difference of the alloy; this was measured at even temperature interval of 10 K in the range 298.15 K to 923 K and tabulated together with the difference of the excess enthalpy at even temperature interval of 50 K in the same range of temperature. The enthalpy difference of tin and antimony are measured accurately (Table 4). All these heat contents have been measured using the present technique: The solid sample can be tempered at any temperature using a pre-furnace (see the description of the calorimeter) before the drop in a liquid phase of the same substance and composition existing inside the calorimeter. In this case the pre-dissolving of the sample is not required since the melting occurs in a liquid phase having the same composition as that of the sample so that the complications of the solution-calorimetry can be avoided. This also enables us to obtain the enthalpy difference between the solid and liquid phases.

The procedure for measurement of the enthalpy of formation (refer to Eq. 6) can be illustrated with reference to the following schema:

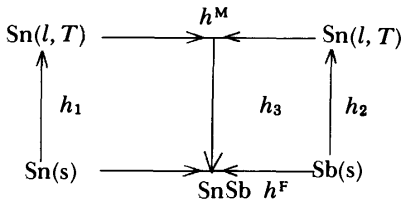

The non-measurable process of the enthalpy of formation will be substituted by (1) heating of tin and antimony at T, (2) measurement of the enthalpy of mixing at T, and (3) measurement of the enthalpy difference of the single miscible phase between T_0 and T. The value of h^{F} has been determined at three compositions (Table 7) employing the present procedure.

Results and Discussion

(i) Lattice Constant. Results of the lattice constant determinations at 598 and 698 K for the compositions 50 and 58 at-% Sb in the system Sn-Sb are presented in Table 1. They compare surprisingly well with those at room temperature.[2] These results are compatible to those expected for a β' phase with distorted rhombohedral structure.[4] This gives the first signal for the non-existence of further β phase claimed to be present in the phase diagram of the system SnSb.[4]

(ii) Enthalpy of Mixing. In Table 3 are listed the values of the enthalpy of mixing as determined in the present study. The results have been least squares fitted by a polynomial expression with a standard deviation of 0.3% for a single measurement. The present value of h^{M} is in good agreement with that by Hultgren et al.[6] and Wittig.[7] Also the result by Kleppa[8] who gives an accuracy of 1% for his measurements is in reasonable agreement with the present one.

(iii) Enthalpies. Table 4 illustrates values for $h_1(T)-h_1(298.15\ \mathrm{K})$ and $h_2(T)-h_2(298.15\ \mathrm{K})$ as measured in the present study. The average error of the individual measurements was found to be 0.32%, while the deviation for a single measurement of earlier reported data[6] was estimated to be 1—2%.

Table 3. Enthalpy of Mixing in the Tin-Antimony System at 943 K in J mol^{-1}. Estimated Standard Deviations in Parenthesis

x_{Sb}	$-h^{\mathrm{M}}$	x_{Sb}	$-h^{\mathrm{M}}$
0.0	0	0.6	1310(4)
0.1	497(2)	0.7	1101(3)
0.2	788(3)	0.8	794(2)
0.3	1180(4)	0.9	419(1)
0.4	1352(4)	1.0	0
0.5	1395(4)		

Table 4. Experimentally Determined Enthalpy Differences of Tin and Antimony in J mol^{-1}. M(Sn)=118.7 g mol^{-1}; M(Sb)=121.76 g mol^{-1}

T/K	$h_1(T)-h_1(298.15\ \mathrm{K})$	$h_2(T)-h_2(298.15\ \mathrm{K})$
298.15	0	0
400	2850	2612
500	5820	5329
600	15755	7912
700	18617	10670
800	21462	13541
900	24309	16552
923	24995	37160

Table 5. Experimentally Determined Enthalpy and Excess Enthalpy Differences in the System Tin-Antimony in J mol^{-1}

	$h_3(T)-h_3(298.15\,K)$			${}^{e}h(T)-{}^{e}h(298.15\,K)$		
x_2	0.44	0.50	0.57	0.44	0.50	0.57
T/K						
298.15	0	0	0	0	0	0
323	750	650	650	−12	−21	−22
373	1990	1990	1890	−12	−83	−88
423	3370	3170	3370	−59	−136	−143
473	4820	4580	4530	−141	−136	−165
523	6350	6040	5950	−4356	−3742	−3467
573	8010	7530	7240	−3569	−3586	−3335
623	12310	9100	8980	−528	−3336	−3105
673	22480	16370	12450	9850	2950	−669
723	26920	26140	24910	13513	11665	11431
773	28330	27630	27980	13619	11780	13318
823	29700	28060	29620	13701	11780	13647
873	30475	30210	30980	13771	11738	13669
923	32430	31460	32340	4684	1282	461

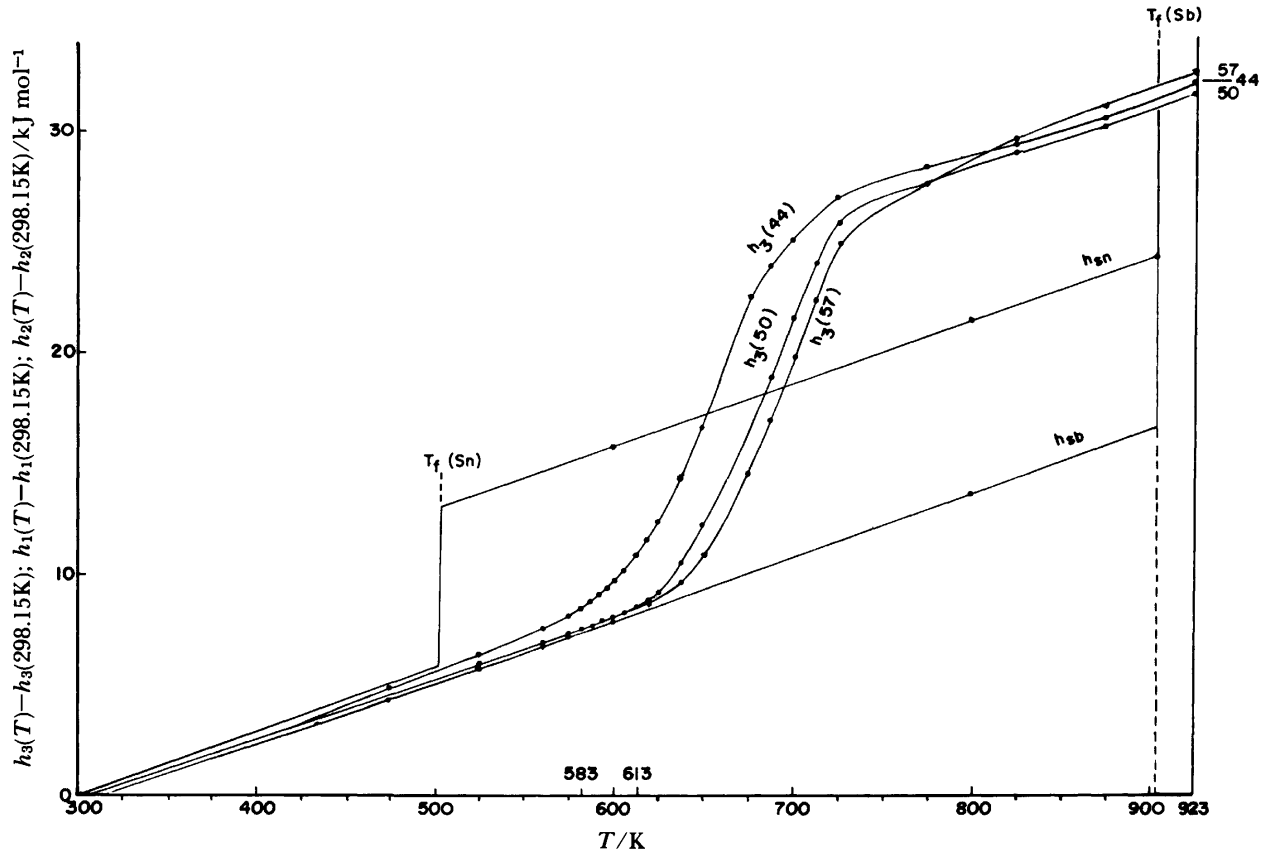

Fig. 2. Dependence of the enthalpy difference of Sn, Sb, and the alloy at the compositions 44, 50, and 57 at-% Sb on the temperature T.

In Table 5 are listed the present values of the enthalpy and excess enthalpy differences of the alloy SnSb in the region 298.15 to 923 K. The estimated standard deviation is 0.35% for a single measurement. Figure 2 shows the curves of the enthalpy differences of Sn and Sb against temperature in the range 300 to 923 K together with those for the enthalpy differences of the alloy at 44, 50, and 57 at-% Sb in the same range of temperature. The values of $h_3(T)-h_3(298.15\,K)$ for the three compositions in the region 583 to 618 K (as a part of the whole range 298.15 to 923 K) are obtained from a separate series of experiments using the present calorimeter and Wittig's one[7] for C_p measurements. The purpose of these additional measurements was to find

Table 6. Thermodynamic Properties of the Alloy SnSb for Selected Temperature in the Range 298.15 to 923 K

	C_P			$h_3^\circ(T)-h_3^\circ(298.15\,K)$			$S^\circ(T)-S^\circ(298.15\,K)$		
	$J\,K^{-1}\,mol^{-1}$			$J\,mol^{-1}$			$J\,K^{-1}\,mol^{-1}$		
x_2	0.44	0.50	0.57	0.44	0.50	0.57	0.44	0.50	0.57
T/K									
583	31.14	26.67	26.72	8900	7625	7610	20.88	17.88	17.91
589	31.13	26.86	26.81	9125	7850	7841	21.19	18.28	18.25
593	31.38	26.91	26.88	9225	7905	7889	21.58	18.50	18.48
595	31.49	26.98	26.91	9305	7955	7949	21.76	18.59	18.59
597	31.51	26.98	26.96	9399	8007	8001	21.88	18.73	18.73
600	31.79	26.99	26.99	9602	8075	8063	22.23	18.87	18.87
603	32.11	26.99	27.01	9805	8189	8175	22.62	19.01	19.02
606	33.08	26.99	27.03	10195	8211	8202	23.46	19.14	19.17
613	34.24	27.00	27.03	10800	8390	8377	24.77	19.46	19.48
618	35.85	27.00	27.07	11500	8750	8721	26.13	19.68	19.73

thorough trace for the trends of $h_3(T)-h_3(298.15\,K)$ around 600 K in order to detect any phase transformation which should occur around this temperature.[4]

In the case of a phase transformation, the curve of h_3 should indicate an abrupt rise in a form of a sharp bent around 600 K. Since this is not observed experimentally, such a transformation can be excluded (refer to Fig. 2).

(iv) Thermodynamic Properties of the Alloy. Table 6 represents values of C_p, $h_3^\circ(T)-h_3^\circ(298.15\,K)$, and $S^\circ(T)-S^\circ(298.15\,K)$ of the alloy SnSb at the compositions 44, 50, and 57 at-% Sb for selected temperatures in the range 298.15 to 923 K. The C_p for the composition 44 at-% Sb indicates a somewhat significant increasing trend due to the partially melting of the alloy in accordance with the phase diagram of the system Sn-Sb, while C_p for 50 and 57 at-% Sb increases insignificantly with the temperature. This is due to the fact that the alloy at the last two compositions can persist until 618 K. Since C_p at 698 K dose not display an abruptly increasing trend which could point out phase transformation, the β phase seems not to be producible.

Further important evidence for the absence of a transformation from β' to β phase is obtained from the quantitative information of the entropy terms: With reference to Table 6, the increase in the entropy change between 597 and 600 K is 0.45 J K^{-1} mol^{-1} for 44 at-% Sb, and 0.04 J K^{-1} mol^{-1} for 50 and 57 at-% Sb; and that between 593 and 600 K is 0.47, 0.39, and 0.39 J K^{-1} mol^{-1} for 44, 50, and 57 at-% Sb, respectively. Also the increase in the entropy change between 593 and 603 is not much larger 1.04, 0.54, and 0.54 J K^{-1} mol^{-1} for 44, 50, and 57 at-% Sb, respectively). Such a very small increase in the entropy change corresponds to usual increase in the enthalpy due to the rise in the temperature but not due to phase transformation.

(v) Enthalpy of Formation. The data in Table 7 represent values for the integral and partial molar enthalpy of formation at 573 K as obtained from the present study for the compositions 44, 50, and 57% Sb. A number in parenthesis is the estimated standard deviation (esd). The present data of h^F could confirm those obtained earlier[2] by using the Wittig's calorimeter.[7] This means that the present calorimeter could be useful for measurements of heat contents with an accuracy of 0.8% and reproducibility of 0.3%.

Table 7. Integral and Partial Molar Enthalpies of Formation in the System Tin-Antimony at 573 K in $J\,mol^{-1}$. Estimated Standard Deviations in Parenthesis

x_2	$-h^F$	$-h_1^F$	$+h_2^F$
0.44	3986(13)	9242	2606
0.50	3216(12)	10158	3752
0.57	2152(11)	11506	4924

From curve-fitting calculations, the following polynomial function for h^F is derived:

$$h^F = -5.655 - 4.101\,x_2 + 18.01\,x_2^2 \quad (7)$$

This equation would produce a curve for h^F similar to that one illustrated in Figs. 2 and 3 in the previous study.[2]

For the partial molar enthalpies of formation of tin and antimony, the following equations are derived:

$$h_1^F = -5.655 - 18.01\,x_2^2 \quad (8)$$

$$h_2^F = 8.254 - 18.01\,(x_2 - 1)^2 \quad (9)$$

These equations would also produce nearly the same curves as shown earlier.[2] The behavior of the enthalpy of formation and its partial quantities in relation to the composition has been discussed previously.[2] Also the behavior of the enthalpy of mixing and its partial quantities in relation to that of the enthalpy of formation is found as predicted earlier.[2] The discussion on the data of h^F will be here restricted to the dependence of h^F on the temperature and the transformation from β' to β phase.

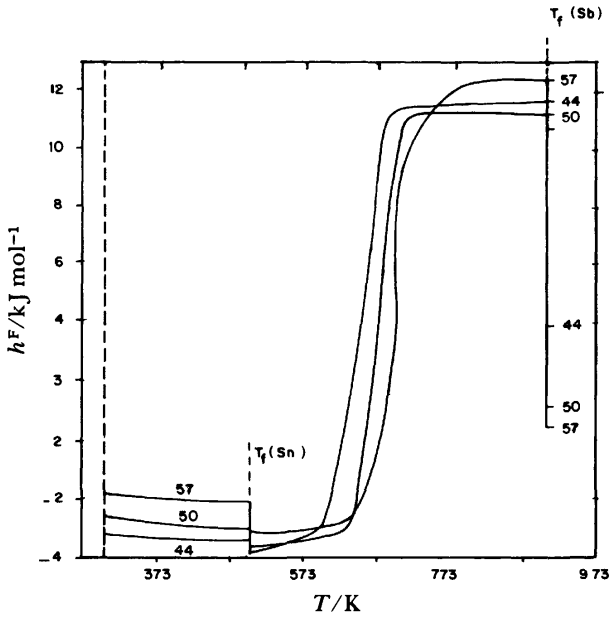

Fig. 3. Dependence of the enthalpy of formation, h^F, at the compositions 44, 50, and 57 at-% Sb on the temperature T.

With reference to the previous data,[2] the enthalpy of formation depends insignificantly on the temperature. This is only valid for the range 298.15 to 504 K. As shown in Fig. 3, h^F changes abruptly at the same temperatures around 505 and 904 K at the three compositions 44, 50, and 57 at-% Sb. This is due to the melting of Sn and Sb. Figure 3 also illustrates that h^F displays a pronounced temperature dependence above 623, 648, and 668 K at 44, 50, and 57 at-% Sb, respectively. This is due to the fact that the alloy can not persist until 623 K but partially melts in accordance with the phase diagram. The continuous formation of the liquid phase should be accompanied with continuous increasing enthalpy of formation. After completion of the liquid formation and disappearing of the β' phase, h^F increases insignificantly and drops finally due to the melting of antimony at 904.02 K (see Fig. 3).

Assuming that a β phase could exist at 598 K in equilibrium with the original one (β' phase), the entropy change for the sample with x_2=0.44 at 598 K would be

$$\Delta S = S(\beta) + S(\text{liquid}) - S(\beta') = n_s \cdot S^F_{x_s} + n_l[(1 - x_l)S^{fus}_{Sn} + x_l \cdot S^{fus}_{Sb} + S^M_{x_l}] - S^F_{x_2} \quad (10)$$

where $S^F_{x_s}$ and $S^F_{x_2}$ are the entropies of formation at the mole fractions of the solid x_s and antimony x_2, respectively. S^{fus}_{Sn} and S^{fus}_{Sb} refer to the entropies of Sn and Sb, respectively. $S^M_{x_l}$ is the entropy of mixing at the mole fraction of the liquid x_l.

With reference to the phase diagram of the system Sn-Sb[4] and applying the level rule, the number of moles of the liquid will be $n_l = \frac{x_2 - x_s}{x_l - x_s} = 0.132$ mol, and that of the solid is $n_s = 1 - n_l = 0.868$ mol (x_l=0.216; x_s=0.474; x_2=0.44).

Substitution of these values in Eq. 10 together with the entropy terms, yields

$$\Delta S = [(-0.868 \times 5.644) + 0.132\{(0.784 \times 13.916^{6}) + (0.216 \times 21.589^{6}) - 2.408^{7}\} + 6.366]\ \text{J K}^{-1}\ \text{mol}^{-1}$$

$$\Delta S = [3.205]\ \text{J K}^{-1}\ \text{mol}^{-1}.$$

The value of ΔS (3.205 J K^{-1} mol^{-1}) seems to be too large compared with that obtained for the increase in the change of the entropy between 593 and 603 K as 1.04 J K^{-1} mol^{-1} (see, Table 6 and p. 283). This means that our assumption of the existence of further β phase in equilibrium with the β' phase was incorrect and hence the first one seems not to be present. These views together with the above cited ones (C_p and [$h_3(T) - h_3$(298.15 K)] behavior around 598 K (the transformation temperature), estimated entropy terms and the results of the high temperature diffraction study) exclude a transformation from β to β' phase. It is also noteworthy that some strong views support the existence of only one phase.[9]

References

1) W. A. Badawi, *Bull. Chem. Soc. Jpn.*, **60**, 2599 (1987).
2) W. A. Badawi, *Bull. Chem. Soc. Jpn.*, **60**, 3771 (1987).
3) F. E. Wittig and L. Schöffl, *Z. Metalk.*, **52**, 700 (1960).
4) M. Hansen and K. Anderko, "Constitution of Binary Alloys," McGraw, New York (1958), pp. 1175—1177.
5) F. E. Wittig, *Chemie-Ingenieur-Technik*, **32**, 1037 (1960).
6) Hultgren et al., "Selected Values of Thermodynamic Properties of Binary Alloys," Amer. Soc. for Metals, and Alloys, Metals Park, Ohio (1973).
7) F. E. Wittig and E. Gehring, *Ber. Bunsenges. Phys. Chem.*, **71**, 372 (1967).
8) O. J. Kleppa, *Phys. Chem.*, **59**, 175 (1955).
9) L. Gmelin, "Handbuch der Anorganischen Chemie," Verlag Chemie, Darmstadt (1974), p. 4.

 © 1989 The Chemical Society of Japan Bull. Chem. Soc. Jpn., 62, 285—289 (1989)

Behaviors of the Enthalpies of Mixing and Formation in the System Lead-Indium

Walid Ahmad BADAWI
Department of Chemistry, Faculty of Science, Al-Fateh University, Tripoli, Libya
(Received January 5, 1988)

The paper presents results of calorimetric studies on the enthalpies of mixing and formation in the system lead-indium. The enthalpy of formation is negative and becomes more negative at higher composition. The partial enthalpy of formation of lead is negative but increases at higher composition. The partial enthalpy of formation of indium is also negative and decreases with increasing the composition. The enthalpy of formation displays a considerable temperature dependence which seems to be smaller than that observed for the enthalpy of formation in other systems.

The studies of the behavior of the enthalpy of formation, $\Delta_f H°$, in binary systems begun in the previous papers[1,2] are now continued with another system, namely lead-indium. The phase diagram of this system has been previously studied by Hansen[3] and Elliott.[4] Also the enthalpy of solution has been measured by Hultgren et al.[5] However, no determination of the enthalpy of formation in the system Pb-In seems to be reported so far. Hence we report here values for the enthalpy of formation at 298.15 K and 423 K.

The studies by Wittig and Schöffl[6] on the enthalpy of formation in the systems Al-Ag and Al-Zn revealed a pronounced temperature dependence of $\Delta_f H°$. Such a temperature dependence was claimed to be a general property of all metallic alloys. On the other hand, the increase of the heat of formation due to an increase in the temperature was attributed to lattice defects of greater expansion of aluminum lattice in the alloys compared with the expansion in pure aluminum metal. However, such a lattice defect caused by the increase in the temperature is not common to all metallic solid solutions. Thus, further studies on other systems are required in order to decide if a pronounced temperature dependence of $\Delta_f H°$ is general property of all metallic alloys. For this reason, we have been studying the system Pb-In which was selected due to its large range of miscibility in the solid state.

Experimental

Sample. The metals used were of extra purity grade (Riedel de Haen Co.). The preparation, treatment, and testing of the samples were all the same as described before.[1] The samples were tempered for 6 h at 420 K, 6 h at 350 K, and 190 h at 320 K. The procedure adopted was similar to that used earlier.[2] In the measurement process, the samples of different masses (1.352—1.525 g) were dropped in a liquid phase (having the same composition and material as that of the solid sample) existing inside the calorimeter.

Apparatus. The calorimeter operates quasi-isothermally and represents an isoperibolic calorimeter. Figure 1 shows the apparatus which consists of a cooling system (10) in which a tube of silica glass (20), of 85 mm diameter and 800 mm height, with lower closed end was fixed by means of sealing-wax. The tube of silica glass contains a cylindrical shield system of V2A steel (13) being connected to a ring of brass by means of three rods of V2A steel. The ring of brass is placed in the lower part of the cooling system.

A set of plates of Nickel (12) are connected to the cover of the shield by means of three rods of V2A steel and their purpose was to distribute the heat radiation.

The cylindrical shield (ϕ_c=80 mm, ϕ=68 mm, h=200 mm) contains two cylindrical compensating systems of Thermax steel (14, 18) placed below and above a calorimeter also of Thermax steel (Thermax 10, production no. 4742, Germany). The hollow space of the calorimeter (16) is coated with a layer of aluminum oxide in order to provide better

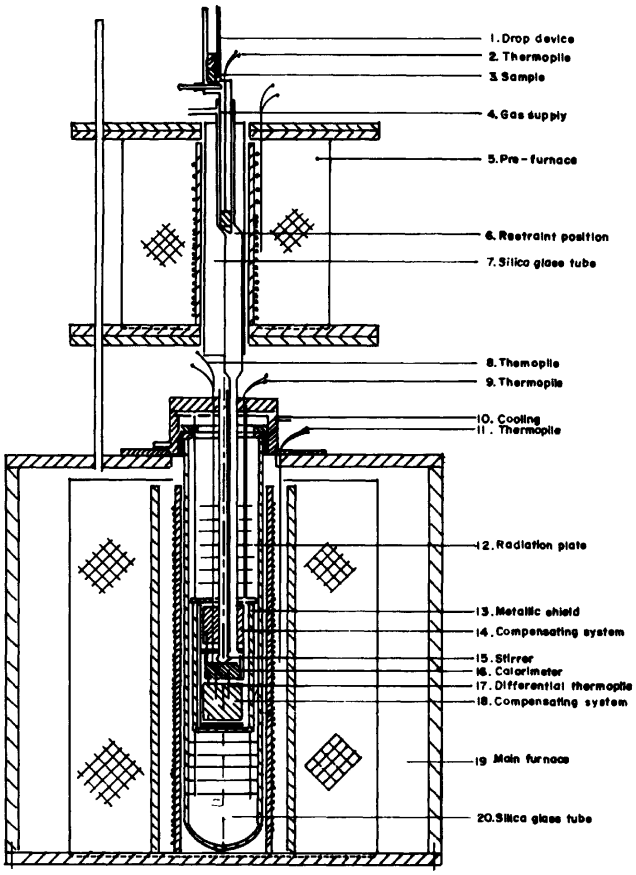

Fig. 1. Apparatus.

interchange of heat and to prevent reaction with the sample since the calorimeter was used as a sample container. The lower compensating system (18) was connected to a plate of V2A steel by means of two rods of the same material. This plate was used as a cover of the shield.

The change of the calorimeter after completion of a series of experiments occurs by moving the upper compensating system upwards.

The lower compensating system is connected to the calorimeter by means of a set of twelve differential Pt-to-(Pt+10 mass per cent Rh) thermopiles. These were calibrated on a standard Pt-PtRh thermopile. The cover of the calorimeter (sprayed with Al_2O_3) has three wells for the thermopile of the calorimeter (8), stirrer made of ceramic (15) and the silica glass tube of the drop device.

The upper compensating system (14) having the same dimensions as those of the lower one is placed on three studs made of ceramic. The differential thermopiles (17) and other ones have leeds which go through wells in the cover of the cooling system. These are sealed by means of lip sealing in form of rubber rings.

The whole assembly is placed in a vertical tube furnace (19) of 41 Ω resistance. Another vertical tube furnace (5) of 35 Ω resistance is placed above the cooling system. The role of the second furnace was to warm the sample before its final drop in the calorimeter. The drop of the sample to a position lying close to the center of the upper tube furnace occurs by means of a drop device (1). The restrain development (6) allows the sample to be tempered at any temperature. The final drop of the samle occurs by moving the upper part of the drop device upwards. The drop device is connected with argon gas supply (4) being connected with a purification and distribution device. The role of Ar gas is to prevent oxidation.

The temperature differences between the calorimeter and the lower compensating system were measured by means of a set of twelve differentical Pt-PtRh thermopiles. The sensibility of the thermopiles was increased due to isolation of their soldered joints with a layer of aluminum oxide instead of tubes of ceramic. This also reduced the dead time of the calorimeter. Excellent regulation of the temperature of the furnace was obtained by means of p-regulator.[7] The temperature of the guard body is kept 0.2 K below that of the shield, while the temperature of the furnace is kept 5 K lower to secure satisfactory operation of the control units. The calibration of the calorimeter was conducted measuring the enthalpy of a standard sample of tin.[8] The calibration factor was determined with an accuracy of 0.3%. The time needed to reach equilibrium was registered to 300 s. The calorimeter sensibility is 625 $\mu V\,K^{-1}$. The short-term fluctuation of the null point was measured to 2.1×10^{-2} K min^{-1}. The temperature drifts of the calorimeter from the lower compensating system were of negligible importance. The derived temperatures are judged to correspond with the IPTS-68 to within 0.01 K at 500 K and 0.1 K at 1000 K. In fact, the precision is considerably better and, the temperature increments were measured to 0.0003 K. The measurement of the thermal potential of the thermopiles occured by means of a digital millivoltmeter (Hewlett-Packard 2401 C).

Results and Discussion

(i) Enthalpies. Table 1 presents values of $H_1^\circ(T)-H_1^\circ(298.15\,K)$; $H_1^\circ(T)-H_1^\circ(423\,K)$ and $H_2^\circ(T)-H_2^\circ(298.15\,K)$; $H_2^\circ(T)-H_2^\circ(423\,K)$ as determined in the present study. The average error of the individual measurements was found to be 0.34% while the deviation for a single measurement of earlier reported data[5] was estimated to 1%.

Table 2 summarizes values of $[H_3^\circ(670\,K)-H_3^\circ(298.15\,K)]$ and $[H_3^\circ(720\,K)-H_3^\circ(423\,K)]$. The deviation is 0.32% for a single measurement.

(ii) Enthalpy of Mixing. The enthalpy of mixing of lead-indium at the temperature T_1 has been determined according to the following equations:

$$-(1-x_2)\cdot \mathrm{Pb}(l,T_1) - x_2\cdot \mathrm{In}(l,T_1) + \mathrm{Pb}_{1-x_2}\mathrm{In}_{x_2}(l,T_1) = 0 \quad (1)$$

$$\Delta_m H^\circ = -(1-x_2)H_1^\circ(T_1) - x_2H_2^\circ(T_1) + H_3^\circ(T_1) \quad (2)$$

where $\Delta_m H^\circ$ is the enthalpy of mixing of liquid Pb-In and H_3° is the enthalpy of the alloy at the mole fraction of indium x_2.

Table 1. Experimentally Determined Enthalpy Differences of Lead and Indium. M(Pb)=207.2 g mol^{-1}; M(In)=114.82 g mol^{-1}

T/K[a]	$H_1^\circ(T)-H_1^\circ(298.15\,K)$	$H_1^\circ(T)-H_1^\circ(423\,K)$	$H_2^\circ(T)-H_2^\circ(298.15\,K)$	$H_2^\circ(T)-H_2^\circ(423\,K)$
	kJ mol^{-1}	kJ mol^{-1}	kJ mol^{-1}	kJ mol^{-1}
298.15	0	—	0	—
400.01	2.796	—	2.509	—
429.45(s)	—	—	3.509	—
429.45(l)	—	—	7.168	3.460
499.98	5.726	2.189	9.243	5.547
600.45(s)	8.891	6.275	12.162	8.496
600.45(l)	14.361	10.545	—	—
670.03	16.407	12.617	14.188	10.521
700.11	17.280	13.503	15.053	11.391
719.97	17.860	14.089	15.627	11.970
800.13	20.151	16.412	17.916	14.272
900.02	22.960	19.259	20.075	17.125

a) The approximate temperature increments can be infered from the adjacent mean temperature.

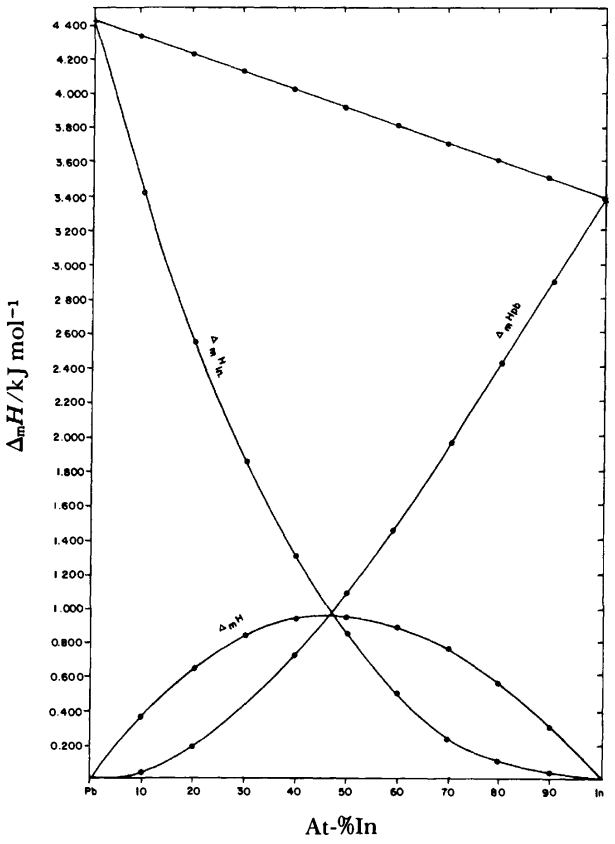

Fig. 2. The integral and partial molar enthalpies of mixing; the ξ-function at 670 K in the system Pb-In.

Table 3 collects the values of the integral and partial molar enthalpy of mixing and the ξ-values at 670 and 720 K in the whole range of composition. A number within parenthesis is the estimated standard deviation (esd). The accuracy obtained is 1% for $\Delta_m H°$ at 670 K and 0.6% for $\Delta_m H°$ at 720 K. The present value is in acceptable agreement with that by Hultgren et al.[5] From curve-fitting calculations, the following polynomial functions for $\Delta_m H$ are derived:

$T = 670$ K;

$$\Delta_m H° = 4.438x_2 - 5.467x_2^2 + 1.029x_2^3, \quad (3)$$

$T = 720$ K;

$$\Delta_m H° = 5.129x_2 - 6.363x_2^2 + 1.224x_2^3. \quad (4)$$

The curve of $\Delta_m H°$ against the composition is shown in Figs. 1 and 2. Figure 2 illustrates the trend of $\Delta_m H°$ at 670 and 720 K. From the data in Table 3 one may conclude that the enthalpy of mixing is small compared with that for other systems e.g. Sn-Sb.[2] This is due to excellent mixing of Pb with In. The enthalpy of mixing is positive and increases with the increase of indium mole fraction to reach a maximum at x_{In}=0.5 (Figs. 1, 2); after that the enthalpy of mixing decreases with the increase of the composition. The partial molar quantities of an integral thermodynamic property, Y, is given by

$$y_1 = Y - x_2 \cdot (\partial Y/\partial x_2)_{T,p} \quad (5)$$

and

$$y_2 = Y - (x_2 - 1) \cdot (\partial Y/\partial x_2)_{T,p} \quad (6)$$

Using Eqs. 3, 4, 5, and 6, we obtain

$T = 670$ K;

$$\Delta_m H_1^\circ = 5.467x_2^2 - 2.058x_2^3, \quad (7)$$

Table 2. Enthalpy Differences of the PbIn Alloys in kJ mol^{-1}. M(Pb)=207.2 g mol^{-1}; M(In)=114.82 g mol^{-1}

x_{In}	H_3°(670 K)−H_3°(298.15 K)	H_3°(720 K)−H_3°(423 K)
0.600	25.861	21.950
0.650	25.866	21.940
0.700	25.862	21.917
0.750	25.872	21.914

Table 3. Integral and Partial Molar Enthalpies of Mixing; ξ-Values in the System Lead-Indium in kJ mol^{-1}. Estimated Standard Deviations in Parenthesis. M(Pb)=207.2 g mol^{-1}; M(In)=114.82 g mol^{-1}

x_{In}	T=670 K				T=720 K			
	$\Delta_m H°$	$\Delta_m H_1^\circ$	$\Delta_m H_2^\circ$	ξ	$\Delta_m H°$	$\Delta_m H_1^\circ$	$\Delta_m H_2^\circ$	ξ
0.000	0	0	4.438	4.438	0	0	5.129	5.129
0.100	0.390(6)	0.034	3.428	4.335	0.447(4)	0.061	3.956	5.007
0.200	0.669(8)	0.202	2.577	4.232	0.776(5)	0.235	2.969	4.884
0.300	0.859(8)	0.436	1.871	4.129	1.005(5)	0.506	2.153	4.762
0.400	0.957(9)	0.743	1.301	4.026	1.109(5)	0.860	1.494	4.639
0.500	0.972(9)	1.110	0.852	3.924	1.135(6)	1.282	0.976	4.517
0.600	0.899(8)	1.524	0.513	3.821	1.051(4)	1.758	0.586	4.395
0.700	0.781(7)	1.973	0.272	3.718	0.892(4)	2.273	0.307	4.272
0.800	0.578(9)	2.445	0.112	3.615	0.670(6)	2.813	0.127	4.150
0.900	0.308(8)	2.928	0.026	3.512	0.365(3)	3.361	0.029	4.027
1.000	0	3.409	0	3.409	0	3.905	0	3.905

$$\Delta_m H_2^\circ = 4.438 - 10.934x_2 + 8.554x_2^2 - 2.058x_2^3. \quad (8)$$

$T = 720$ K;

$$\Delta_m H_1^\circ = 6.353x_2^2 - 2.448x_2^3, \quad (9)$$

$$\Delta_m H_2^\circ = 5.129 - 12.706x_2 + 10.025x_2^2 - 2.448x_2^3. \quad (10)$$

Table 3 also illustrates the ξ-values. For $\xi\,(T)$, the following equation was used:

$$\xi(T) = \Delta_m H^\circ(T)/x_2 \cdot (1 - x_2). \quad (11)$$

The polynomial functions for $\Delta_m H^\circ(T)$ were employed together with Eq. 11 to derive the following relations for ξ:

$$\xi(670\,\text{K}) = 4.438 - 1.029x_2, \quad (12)$$

$$\xi(720\,\text{K}) = 5.129 - 1.224x_2. \quad (13)$$

With reference to these equations, $\xi(T)$ exhibits a linear function. Figure 3 represents the experimentally determined values for ξ.

(iii) Enthalpy of Formation. The enthalpy of formation is the special form of the enthalpy of reaction evolved by the formation of the substance from the elements. In the case of lead-indium alloy, the formation reaction is

$$-(1 - x_2)\cdot \text{Pb(s, } T_0) - x_2 \cdot \text{In(s, } T_0) + \text{Pb}_{1-x_2}\text{In}_{x_2}\text{(s, } T_0) = 0 \quad (14)$$

where T_0 is the intial temperature.

The enthalpy of formation is then

$$\Delta_f H^\circ = -(1 - x_2)\cdot H_1^\circ(T_0) - x_2 \cdot H_2^\circ(T_0) + H_3^\circ(T_0) \quad (15)$$

The indices 1, 2, and 3 indicate lead, indium, and the alloy, respectively.

Subtraction of Eq. 15 from Eq. 2, yields

$$\Delta_m H^\circ - \Delta_f H^\circ = -(1 - x_2)\cdot[H_1^\circ(T_1) - H_1^\circ(T_0)] - x_2 \cdot [H_2^\circ(T_1) - H_2^\circ(T_0)] + [H_3^\circ(T_1) - H_3^\circ(T_0)]. \quad (16)$$

The term $[H_3^\circ(T_1) - H_3^\circ(T_0)]$ which appears in Eq. 16 is the enthalpy difference of the alloy; this was measured between 298.15 and 670 K; between 423 and 720 K. The enthalpy differences $[H_1^\circ(T) - H_1^\circ(T_0)]$ and $[H_2^\circ(T) - H_2^\circ(T_0)]$ are measured accurately (see Table 1).

The following schema illustrates the above given procedure for determining of $\Delta_f H^\circ$:

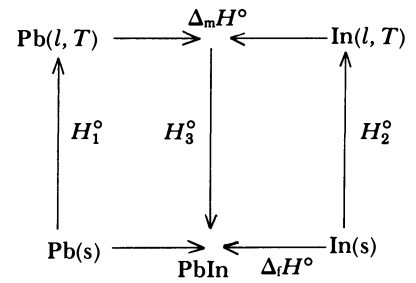

The non-measurable process of the enthalpy of formation will be substituted by (1) heating of lead and indium at T_1, (2) measurement of the enthalpy of mixing at T_1, and (3) measurement of the enthalpy difference of the single miscible phase between T_0 and T_1. Employing this procedure, the enthalpy of formation at 298.15 and 423 K has been determined at four compositions.

The integral and partial molar enthalpies of formation at 298.15 and 423 K are presented in Table 4 for four compositions. A number within parenthesis is the estimated standard deviation (esd). The average error of the individual measurement was found to be 0.2% for T=298.15 K and 0.3% for T=423 K. Using the

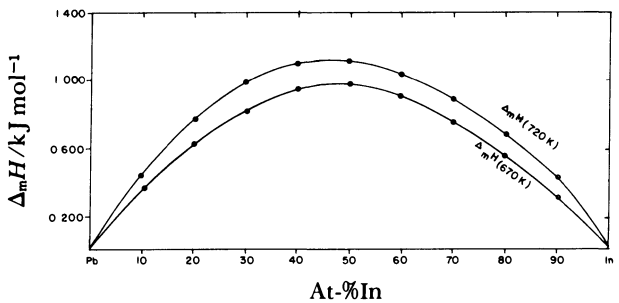

Fig. 3. The enthalpies of mixing at 670 and 720 K in the system Pb–In.

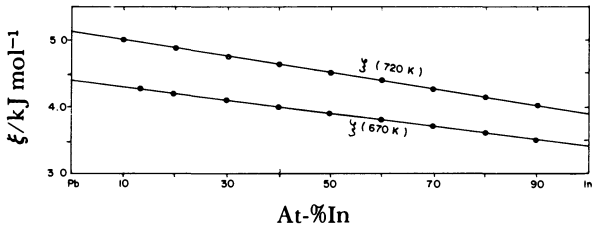

Fig. 4. The ξ-function at 670 and 720 K in the system Pb–In.

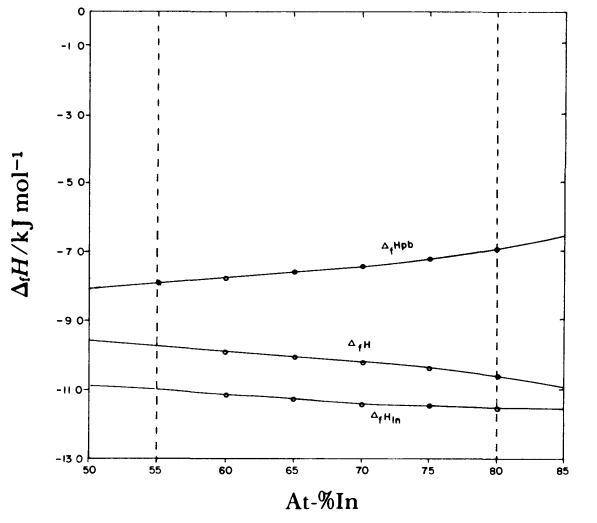

Fig. 5. The integral and partial molar enthapies of formation at 298.15 K in the system Pb–In.

Table 4. Integral and Partial Molar Enthalpy of Formation of the β-Phase in the System Lead-Indium in kJ mol^{-1}. Estimated Standard Deviations in Parenthesis. M(Pb)=207.2 g mol^{-1}; M(In)=114.82 g mol^{-1}

x_{In}	T=298.15 K			T=423 K		
	$-\Delta_f H°$	$-\Delta_f H_1°$	$-\Delta_f H_2°$	$-\Delta_f H°$	$-\Delta_f H_1°$	$-\Delta_f H_2°$
0.600	9.868(18)	7.827	11.228	8.081(21)	6.426	9.219
0.650	10.044(1)	7.642	11.339	8.247(1)	6.247	9.310
0.700	10.227(10)	7.442	11.517	8.628(14)	6.110	9.389
0.750	10.444(28)	7.227	11.517	8.628(53)	5.933	9.456

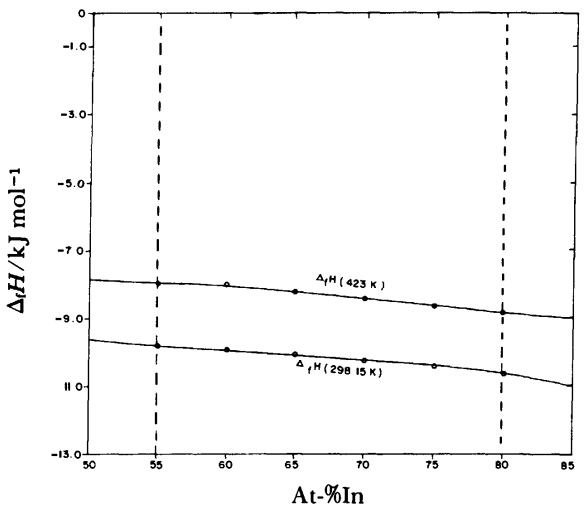

Fig. 6. The enthalpies of formation at 298.15 and 423 K in the system Pb-In.

data in Table 4, it was possible to derive equations which produce the curves shown in Fig. 5 as follows:

$$\Delta_f H°(298.15\,K) = -8.886 + 0.119x_2 - 2.908x_2^2 - 0.028x_2^3, \quad (17)$$

$$\Delta_f H°(423\,K) = -7.296 + 0.098x_2 - 2.388x_2^2 - 0.023x_2^3. \quad (18)$$

It is apparent that the enthalpy of formation displays a somewhat pronounced temperature dependence. However, it appears that $\Delta_f H°$ in other systems e.g. Al-Zn[6] exhibits larger temperature dependence.

The enthalpy of formation in the system Pb-In is negative and becomes more negative at higher composition. This is due to the insertion of the smaller indium atom in the structure of PbIn which becomes more stable at higher mole fraction of indium.

With reference to the definitions of the partial quantities (Eqs. 5 and 6), and using Eqs. 17 and 18, the following equations for $\Delta_f H_1°$ and $\Delta_f H_2°$ are derived:

T = 298.15 K;

$$\Delta_f H_1° = -8.886 + 2.908x_2^2 + 0.056x_2^3, \quad (19)$$

$$\Delta_f H_2° = -8.767 - 5.816x_2 + 2.824x_2^2 + 0.056x_2^3. \quad (20)$$

T = 423 K;

$$\Delta_f H_1° = -7.296 + 2.388x_2^2 + 0.046x_2^3, \quad (21)$$

$$\Delta_f H_2° = -7.198 - 4.776x_2 + 2.319x_2^2 + 0.046x_2^3. \quad (22)$$

The curve in Fig. 4 shows that the partial enthalpy of formation of lead is negative but increases at higher composition. However, $\Delta_f H_1°$ is always negative. This means that the structure remains stable even when the composition increases. The partial molar enthalpy of formation of indium is also negative and becomes more negative at higher composition. For a heteropolar behavior, the delivery of electrons from indium to lead would increase with the increase of indium mole fraction so that the partial molar enthalpy of formation of indium should increase with the increase of the composition.

References

1) W. A. Badawi, *Bull. Chem. Soc. Jpn.*, **60**, 2599 (1987).
2) W. A. Badawi and A. E. Eid, *Bull. Chem. Soc. Jpn.*, **60**, 3771 (1987).
3) M. Hansen, "Constitution of Binary Alloys," McGraw-Hill, (1958).
4) R. P. Elliott, "Constitution of Binary Alloys, First Supplement," McGraw-Hill, (1956).
5) Hultgren et al., "Selected Values of Thermodynamic Properties of Binary Alloys," Amer. Soc. Met., Metal Park, Ohio (1973).
6) F. E. Wittig and L. Schöffl, *Z. Metalk.*, **51**, 700 (1960).
7) F. E. Wittig, *Chemie-Ingenieur-Technik*, **32**, 1037 (1960).
8) F. E. Wittig and E. Gehring. *Z. Naturforsch. A*, **18**, 351 (1963).

Optical and Magnetic Resonance Studies of the Interaction of Metallotetraphenylchlorin and Octaethylporphyrin with Trinitrofluorenone

Biswajit CHOUDHURY and T. K. CHANDRASHEKAR*
Department of Chemistry, Indian Institute of Technology, Kanpur 208016, India
(Received November 2, 1987)

The interaction of metallo derivatives of tetraphenylchlorin (TPC) and octaethylporphyrin (OEP) with 2,4,7-trinitrofluorenone (TNF) is described in terms of 1 : 1 molecular complexes. The binding constants vary as CuOEP>ZnOEP>CuTPC>ZnTPC and this variation is accounted in terms of the structure of the macrocycle and the substituents present on it. ESR studies of the complexes reveal that the π-complexation results in changes in the electronic structure of the central metal ion. The magnitude of different proton shifts of the acceptor in ^{1}H NMR spectra of the complexes are used to arrive at the possible solution structure of the complexes.

Molecular complexation of macrocyclic tetrapyrrole pigments with organic molecules has been the subject of numerous studies because of their presence and participation in many reactions of chemical and biochemical interest.[1-3] It has been shown that the major source of stabilization in such complexes is π-π interaction between the donor and acceptor and charge transfer forces contribute to a small extent to the binding strength.[4,5] The recent X-ray crystallographic work on the photosynthetic bacterial reaction center has revealed that the orientation of the donor and the acceptor relative to each other is crucial in such complexes to prevent back electron transfer.[6] Thus a systematic study of the molecular complexes of porphyrins and related macrocycles with electron acceptors is important to get information about the factors and forces responsible for stability of such complexes in a particular orientation. We have been interested in the molecular complexation behavior of tetrapyrrole pigments and our earlier studies have indicated that the stability of the complexes depends both on the metal ion present in the cavity of the macrocycle as well as on the compatibility in sizes of the donor and acceptor.[7-9] In the present study the metal derivatives (Cu and Zn) of tetraphenylchlorin (TPC) and octaethylporphyrin (OEP) were employed as donors and 2,4,7-trinitro-9-fluorenone (TNF) as an acceptor (Fig. 1). Electronic absorption spectral method was used to evaluate the bindig constants while the ^{1}H NMR and ESR measurements were recorded to ascertain the site of interaction in these complexes. The results of this study were used to derive information regarding the relative orientation of the donor and acceptor in the complexes in solution.

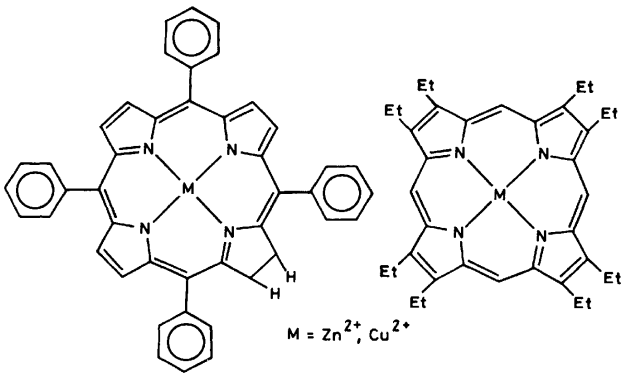

Tetraphenylchlorin Octaethylporphyrin

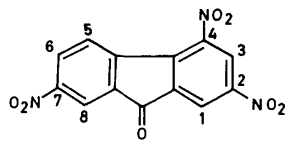

2,4,7-Trinitro-9-fluorenone

Fig. 1. Structure of metallomacrocycles and 2,4,7-trinitro-9-fluorenone.

Experimental

TPC was prepared from tetraphenylporphyrin (TPP) following the literature procedure.[10] OEP and TPP were obtained from Strem Chemicals, USA. TNF was procured from Aldrich Chemicals, USA. The metal derivatives of OEP and TPC were synthesized by refluxing the corresponding metal acetate with the macrocycle in DMF.[11] The purity was checked by NMR and optical spectra. All the solvents employed in the study were distilled before use. The preparation of the solutions and all the manipulations were carried out in dim light. The spectra of the solutions were recorded immediately after mixing.

The electronic absorption method employed for the evaluation of association constants involved the measurement of absorbance of the Q-bands of the porphyrins in the solvent $CHCl_3$ on increasing addition of TNF. The concentration of the donor was held constant (approx. 10^{-5} M; 1 M=1 mol dm^{-3}) and the range of concentration of TNF employed was 1.0×10^{-4} to 2.0×10^{-2} M.

The optical absorption spectra were recorded on Shimadzu double beam spectrophotometer. The ^{1}H NMR spectra of the complexes were recorded on a Bruker WH 400 FT NMR spectrometer usig $CDCl_3$ as solvent and TMS as internal standard. The ESR spectra were recorded on a Varian E-109 ESR spectrometer using toluene as solvent. The spectra were recorded at about 100 K using liquid nitrogen. The IR spectra of the complexes were recorded on

a Perkin Elmer 580/7358 IR spectrometer. The 1:1 complexes for ^{1}H NMR, ESR, and IR studies were prepared as follows. To a solution of porphyrin [10^{-3} M] in $CHCl_3$, TNF [10^{-3} M] was added and the mixture was stirred for an hour. Slow evaporation of solvent over a water bath gave the required complex. The air-dried complex was dissolved in appropriate solvents and used for spectral studies.

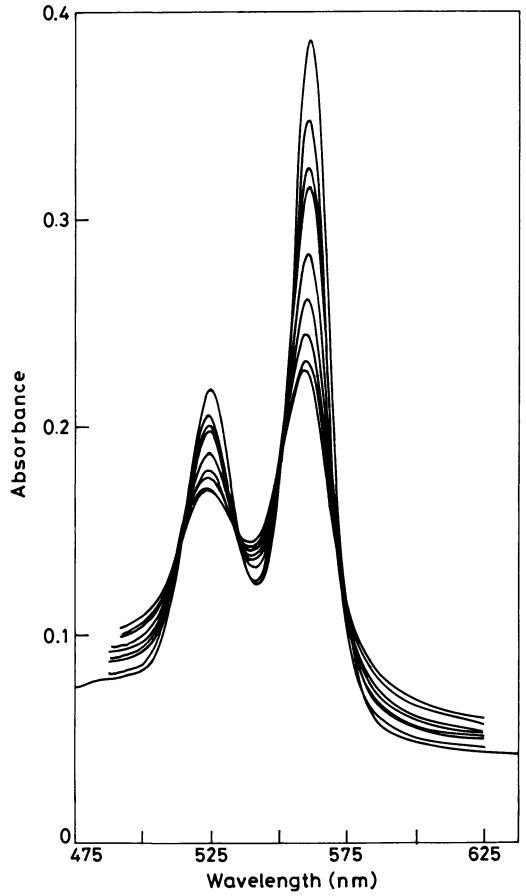

Fig. 2. Visible absorption spectra of CuOEP [1.06×10^{-5} M] containing increasing amounts of TNF [1.356×10^{-4}—2.712×10^{-3} M].

Results and Discussion

The metal derivatives of TPC and OEP exhibited intense absorption bands (Q-bands) in the visible region (500—600 nm) in $CHCl_3$. The acceptor, TNF, did not absorb in this region and showed intense absorption only in UV region. Addition of increasing amounts of TNF to $CHCl_3$ solutions of MTPC and MOEP derivatives progressively decreased the intensity of the Q-bands of the donors with the appearance of isosbestic points (Fig. 2). These observations are consistent with the formation of molecular complexes between TNF and the macrocycle.[12] The decrease in absorbance of donor upon increasing concentrations of the acceptor was analyzed for the calculation of association constant (K) using Nash equation.[13] The linearity of the plots of $d^0/(d^0-d)$ versus $1/C_A$, where d^0 and d denote the absorbance values of donor in the absence and presence of TNF and C_A is the concentration of the acceptor, indicated that the predominant species that existed in solution is the 1:1 complex (Fig. 3). The possible existence of 1:2 (donor-acceptor) complexes in solution was then analyzed using the method of Bent and French.[14] The slopes of the logarithmic plots yielded values in the range from 0.9—1.7 indicating the existence of higher order complexes.[15] It was difficult to quantify the stability constants of these higher order complexes as they were present in only very low concentrations. However, the presence of these complexes did not alter the magnitudes of K-values calculated for 1:1 complexes appreciably. The association constants determined for 1:1 complexes are listed in Table 1.

An inspection of Table 1 reveals that the values of K vary as CuOEP>ZnOEP>CuTPC>ZnTPC. A comparison of these K values with other structurally similar macrocycles is also made in the table. The increase in K-values upon going from OEP to TPC derivatives can be attributed to the presence of eight strong electron-donating ethyl groups as the pyrrole

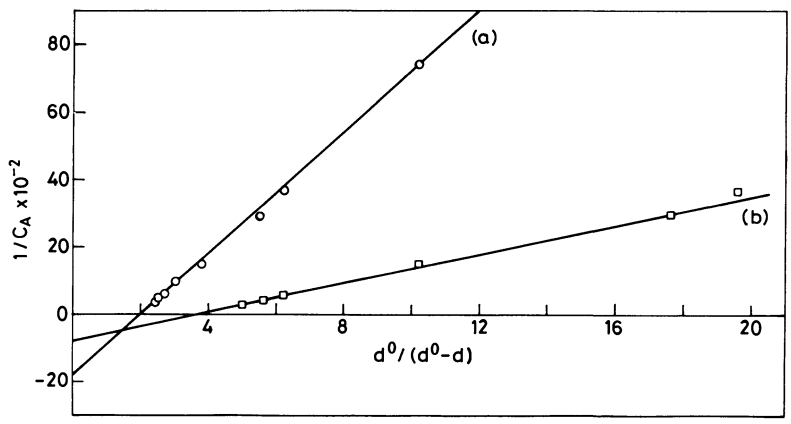

Fig. 3. Plot of $1/C_A$ versus $d^0/(d^0-d)$ for (a) CuOEP-TNF and (b) ZnOEP-TNF at 30°C.

substituents in OEP relative to TPC. Also, the presence of one reduced pyrrole ring in TPC decreases the conjugation thereby decreasing its donating ability. It should be mentioned here that the recent ESR study on the charge transfer complexation between OEP and TPP metal derivatives indicates that the effects of the interaction are generally much larger for OEP complexes than for TPP complexes, supporting our observation.[16] The higher values of K for pheophytin may arise due to the presence of an additional electron-rich cyclopentanone ring in pheophytin relative to chlorin. The limited study made here did not allow us to quantify the role of metal ions on the magnitude of K-values.

The ESR spectra of CuTPC and CuOEP and their 1:1 complexes in toluene at 100 K displayed characteristic features in parallel and perpendicular regions permitting evaluation of ESR parameter (Table 2).[17] The observed effects on ESR parameters upon complexation with TNF are (i) a small decrease in $g_{\parallel}$ and $g_{\perp}$, and $A_{\parallel}^{Cu}$ values and (ii) a small increase in $A_{\perp}^{Cu}$, $A_{\parallel}^{N}$, and $A_{\perp}^{N}$ values. These effects were consistent with the formation of molecular complex.[18] It was anticipated that the π-complexation would lead to a small change in the distribution of π-electrons over the macrocycle perturbing the electronic levels of central metal orbitals. Indeed, Iwaizumi et al.[16] in their recent EPR and ENDOR studies on OEP and TPP complexes of Co and Cu have shown that the charge transfer complex formation with π-acceptors perturbs the metal d-orbital states. If this is true, then one would expect the covalency of the (Cu-N) σ-bond to get perturbed upon complexation. Therefore, bonding parameter α^2 of the (Cu-N) σ-bond was calculated using the $A_{\parallel}^{Cu}$ hyperfine tensor using the equation:[19]

$$\alpha^2 = -\left(\frac{A_{\parallel}^{Cu}}{P}\right) + (g_{\parallel} - 2) + \frac{3}{7}(g_{\perp} - 2) + C$$

A value of P=0.0354 cm^{-1} was used for copper complexes. From Table 2 it can be seen that the α^2 value decreases slightly upon complexation with TNF for both CuTPC and CuOEP. This decrease in α^2

Table 1. K Values for Complexation of TNF with Different Macrocycles at 30°C

Complex	K/dm^{-3} mol^{-1}	Reference
ZnTPC-TNF	47.0	This work
CuTPC-TNF	133.0	This work
ZnOEP-TNF	1083.0	This work
CuOEP-TNF	1863.0	This work
CuTPP-TNF	435.0±95	a)
ZnTPP-TNF	40.0±5.0	a)
ZnPheo-TNF	1030.0±8	b)

a) T. K. Chandrashekar and V. Krishnan, *Bull. Soc. Chim. Fr.*, Part I, 1-42, 1984. b) P.R. Droupadi and V. Krishnan, *J. Phys. Chem.*, **89**, 909 (1985).

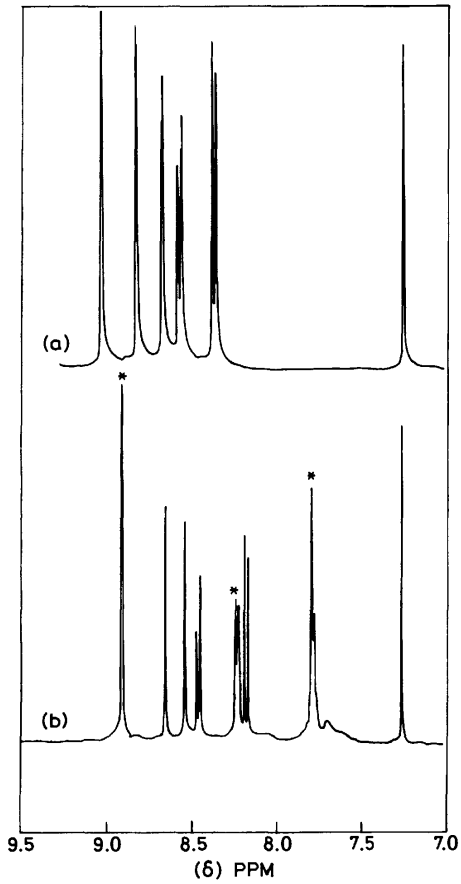

Fig. 4. ^{1}H NMR spectra of (a) TNF and (b) 1:1 complex of ZnTPC-TNF. The peaks marked * correspond to ZnTPC protons.

Table 2. ESR Parameters for the Interaction of CuTPC and CuOEP with TNF in Toluene at 100 K

Complex	$g_{\parallel}$	$g_{\perp}$	$10^4 A_{\parallel}^{Cu}$ / cm^{-1}	$10^4 A_{\perp}^{Cu}$ / cm^{-1}	$10^4 A_{\parallel}^{N}$ / cm^{-1}	$10^4 A_{\perp}^{N}$ / cm^{-1}	α^2
CuTPC	2.185	2.047	208.10	31.55	14.70	15.70	0.7949
CuTPC-TNF (1:1)	2.180	2.031	206.64	32.24	15.27	16.15	0.7771
CuOEP	2.187	2.047	204.90	25.10	17.01	14.58	0.7878
CuOEP-TNF (1:1)	2.180	2.043	202.10	26.20	17.30	15.12	0.7693
CuOEP-TNF[a] (diluted in NiOEP)	2.175	2.044	202.00	25.00	17.50	14.90	0.7645

a) Taken from Ref. 18.

Table 3. ^{1}H NMR Data of TNF Protons and Their Shifts (ppm) in Molecular Complexes with ZnTPC and ZnOEP in $CDCl_3$

Complex	H_3	H_1	H_8	H_6	H_5
TNF	9.04	8.84	8.69	8.58	8.38
ZnTPC-TNF	−0.12	−0.18	−0.19	−0.37	−0.59
ZnOEP-TNF	−0.75	−1.16	−1.27	−1.33	−1.63

(−) Upfield shift.

value indicates an increase in the covalency of the (Cu–N) σ-bond. This was also supported by the experimental observation of a slight increase in both $A_{\parallel}^{N}$ and $A_{\perp}^{N}$ values upon interaction with TNF. These two observations qualitatively indicated that there is a slight rearrangement in the electronic environment of the central metal ion upon π-complexation.

In view of the observation that the interactions are essentially localized in the π-system of macrocycles, the ^{1}H NMR spectral studies were undertaken to arrive at the relative orientations of the molecules in solution. We examined the effect of complexation from proton resonance shifts experienced by acceptor and donors (ZnOEP and ZnTPC). Figure 4 shows the ^{1}H NMR of TNF and ZnTPC–TNF (1:1) complex. The assignment of TNF proton resonance was made according to the literature.[20] It is seen from the spectra that all the protons of TNF are upfield shifted in the complexes relative to pure TNF indicating that the TNF is positioned in the diamagnetic shielding zone of the macrocycle. A similar shielding of the acceptor proton resonances have been observed in the charge-transfer complexes with aromatic donors.[21] The proton resonance of donor [β-pyrrole, *o*-, *m*-, and *p*-hydrogens of aryl groups in TPC and ethyl substituents in OEP] also showed both upfield and downfield shifts. The magnitude of shifts were very small (0.15—0.2 ppm). The shifts observed for different proton resonances of TNF upon complexation are listed in Table 3. Examination of Table 3 clearly reveals that the magnitude of shifts observed for TNF protons is much higher for ZnOEP complex than those observed for ZnTPC complex. This may be due to the stronger donating capacity of OEP relative to TPC. This was also reflected in the magnitude of *K*-values. Moreover, the table also illustrates that among the different protons of TNF, the upfield shift experienced by H_5 and H_6 are relatively large compared to other protons [H_3, H_1, and H_8] consistent with the observation made by Hill et al. for the interaction of Co(II) and Ni(II) mesoporphyrin dimethyl ester with TNF.[20] These results indicate that the protons H_5 and H_6 are closer to the π-system of the macrocycle relative to other protons of TNF.

The spectral data obtained in the present study provides some insight into the proposition of possible overlap structures of donor and the acceptor in solution. The observation that the strong IR vibrations of

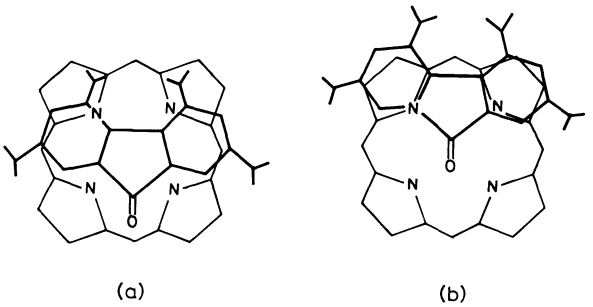

Fig. 5. Possible overlap pictures of the donor and the acceptor in solution. (a) The C_4 axis of the porphyrin is coincident with the C_5 axis of the fluorenone skeleton and (b) the carbonyl group of the fluorenone is tilted away from the metal ion (see text). For clarity the double bonds and the substituents on porphyrin are omitted.

the acceptor [ν(CO) and ν(NO_2)] were not perturbed upon complexation clearly rules out any possibility of coordinative type of interaction of the acceptor with the metal. Thus the major stabilization for the complexes arises from the π–π interaction of the donor and acceptor. Several structures could be perceived by juxtapositioning the acceptor over the macrocycle keeping the intermolecular distance at van der Waals interaction level. CPK models indicate that one can visualize two structures in terms of plane to plane overlap.

In structure (a), the acceptor can be placed over the porphyrin plane such that the axis passing through the five membered ring of the fluorenone is coincident with the C_4 axis of the porphyrin. This would dispose TNF protons over the porphyrin core. In this case all the protons of TNF would experience a uniform shielding since both the planes are exactly parallel. In the alternate structure, (b), the acceptor can be displaced over the porphyrin plane such that the carbonyl group of TNF is tilted away from the metal center (Fig. 5). This will bring H_5 and H_6 protons of TNF near to the porphyrin core. In this case the protons H_5 and H_6 of TNF are expected to shield more relative to other protons. ^{1}H NMR shift data seems to support the structure (b).[5,18,20] These proposed overlap structures are in general agreement with the only reported X-ray crystallographic structure for the 1:2 [porphyrin–acceptor] charge transfer complex[23] of a nickel porphyrin with tetranitrofluorenone. In this structure the porphyrin and the fluorenone rings are both approximately planar and the angle between the porphyrin and the fluorenone ring is 11.4°. The only difference between the proposed structure in the present study and the X-ray study lies in the fact that the carbonyl oxygen is tilted towards the metal ion while in the present case it is tilted away from the metal ion. This difference might arise from the fact that the X-ray structure reported is for a 1:2 complex while our data is for a 1:1 complex. Secondly, the choice of the

porphyrin is different from the reported structural study. In conclusion, the solution structure described here is strongly supported by experimental data presented. Further confirmation of the structure must come from X-ray crystallographic studies.

Financial support by the Department of Science and Technology, Govt. of India is gratefully acknowledged.

References

1) K. Alston and C. B. Storm, *Biochemistry*, **18**, 4292 (1979).
2) M. A. Slifkin, "Charge Transfer Interactions of Biomolecules," Academic Press, New York (1971), pp. 116—131.
3) H. A. O. Hill, P. J. Sadler, R. J. P. Williams, and C. D. Barry, *Ann. N. Y. Acad. Sci.*, **206**, 247 (1973).
4) B. Pullman, C. Spantaars, and G. Berthier, *Proc. Natl. Acad. Sci.*, **46**, 1011 (1960).
5) G. P. Fulton and G. N. Lamar, *J. Am. Chem. Soc.* **98**, 2124 (1976).
6) J. Deisenhofer, O. Epp, K. Miki, R. Huber, and H. Michel, *J. Mol. Biol.*, **180**, 385 (1984).
7) T. K. Chanrashekar and V. Krishnan, *Inorg. Chem.*, **20**, 2782 (1981).
8) T. K. Chandrashekar and V. Krishnan, *Inorg. Chim. Acta*, **62**, 259 (1982).
9) T. K. Chandrashekar and V. Krishnan, *Can. J. Chem.*, **62**, 475 (1984).
10) H. W. Whitlock, Jr., R. Hanauer, M. Y. Oester, and B. K. Bower, *J. Am. Chem. Soc.*, **91**, 7485 (1969).
11) G. D. Darough, J. R. Miller, and F. M. Huennekens, *J. Am. Chem. Soc.*, **73**, 4315 (1951).
12) H. A. O. Hill, P. J. Sadler, and R. J. P. Williams, *J. Chem. Soc.*, **1973**, 1663.
13) C. J. Nash, *Phys. Chem.*, **64**, 950 (1960).
14) H. E. Bent and C. L. French, *J. Am. Chem. Soc.*, **63**, 568 (1941).
15) Plots of $\log[(A_i-A_o)/(A_c-A_i)]$vs. [A], where A_o, A_i, and A_c represent absorbance values of porphyrin only, porphyrin containing increasing amounts of acceptor, and porphyrin with large excess of acceptor, respectively and [A] concentration of the acceptor used for MOEP-TNF interactions were constructed. These plots are linear with the slopes varying from 0.9—1.7.
16) M. Iwaizumi, Y. Ohba, H. Iida, and M. Hirayama, *Inorg. Chim. Acta*, **82**, 47 (1984).
17) The exact evaluation of perpendicular components of g and A were done by simulated spectra. Estimated errors are ± 0.001 for g and $\pm 1\times10^{-4}$ cm^{-1} for A^{Cu} and $\pm 0.1\times10^{-4}$ cm^{-1} for A^{N} values. The A^{N} values are determined from partially enlarged spectrum.
18) H. Yokoi and M. Iwaizumi, *Bull. Chem. Soc. Jpn.*, **53**, 1489 (1980).
19) D. Kivelson and R. Nieman, *J. Chem. Phys.*, **35**, 149 (1961).
20) C. D. Barry, H. A. O. Hill, B. E. Mann, P. J. Sadler, and R. J. P. Williams, *J. Am. Chem. Soc.*, **95**, 4545 (1973).
21) R. Foster and C. A. Fyfe, in progress in "Nuclear Magnetic Resonance Spectroscopy," ed by J. W. Emsley and L. H. Sutcliff, Pergamon, Oxford (1969), Vol. 4.
22) C. D. Barry, H. A. O. Hill, P. J. Sadler, and R. J. P. Williams; *Proc. R. Soc. London, Ser. A*, **334**, 493 (1973).
23) R. Grigg, J. T. Grimshaw, and T. J. King, *J. Chem. Soc., Chem. Commun.*, **1978**, 571.

 © 1989 The Chemical Society of Japan Bull. Chem. Soc. Jpn., 62, 295—303 (1989)

Spectral Studies on the Cooperative Binding Mechanism of Evans Blue to Poly(*N*-vinyl-2-pyrrolidone)

Meenakshi MARUTHAMUTHU* and E. SUBRAMANIAN
Department of Physical Chemistry, University of Madras,
Guindy Campus, Madras 600025, India
(Received March 7, 1988)

The binding of Evans Blue (EB) to poly(*N*-vinyl-2-pyrrolidone) (PVP) was studied at two pH's 7.2 and 11.2 spectrophotometrically by absorbance change method. At pH 7.2, the absorption spectrum of EB changed unusually on adding PVP and this indicated the formation of two types of spectroscopically distinguishable PVP–EB complexes. At very low [PVP], a weak complex was formed which got converted into a strong complex at high [PVP]. Positive cooperativity was found to be operative in this conversion and in the strong complex at higher [PVP]. Scatchard, Hill, and Schwarz methods were employed to analyze this cooperativity and to determine the binding parameters. The analysis revealed: (i) the binding constants for the weak and strong complexes were of the order of 10^4 and 10^5 dm^3 mol^{-1} respectively; (ii) positive cooperativity at higher [PVP] was due to the interaction of neighboring binding sites on different polymer chains. At pH 11.2, only one type of complex was formed with higher affinity. But the binding behavior remained the same as at pH 7.2.

Evans Blue, a bisazo dye (C. I. No. 23860) is employed in blood volume determination. The basis behind this is its high binding affinity to plasma albumin. Resembling with serum albumin in many respects, for example, in binding behavior and in having amide linkage, the water-soluble synthetic polymer, poly(*N*-vinyl-2-pyrrolidone) (abbreviated as PVP) is physiologically and pharmaceutically an important macromolecule. In our earlier study,[1] the binding of the dye, Evans Blue (EB) to PVP was analyzed using a simple method, namely the Klotz's spectrophotometric method.[2] The significant finding of the study was that the dye binds mainly through electrostatic interaction. In the present work, employing absorbance change method[3] instead of the Klotz's method, we have attempted to investigate the cooperative binding mechanism, the binding forces and the nature of binding. Further, the unusual spectral change of EB with PVP, an interesting observation, has been found to be due to the formation of two types of spectroscopically distinguishable complexes. Thus all these features inspired us to make a thorough investigation of the system.

Experimental

Materials. PVP (average molecular weight=40000) and EB were purchased from Loba Chemie Indo Austranal Co., India. Urea, sodium chloride, and buffer reagents used were of analytical grade.

Method. The binding experiments were carried out at pH 7.2 in KH_2PO_4–Na_2HPO_4 buffer and at pH 11.2 in Na_2HPO_4–Na_3PO_4 buffer, both of 0.05 mol dm^{-3} concentration. All spectroscopic measurements were made at room temperature (ca. 25 °C) using Carl Zeiss Specord UV VIS spectrophotometer with matched 1 cm path length quartz cuvettes. The measuring pipettes and the cuvettes were prerinsed with the dye solution to reduce its concentration loss by adsorption onto the walls. Viscosities of PVP and PVP–EB solutions were measured at 30 °C with an Ubbelohde suspended level viscometer which has a flow time of 141 s for water.

For the binding studies, a dye concentration range of 7.5 to 25.0 μmol dm^{-3} was selected as admitted by the Beer-Lambert's law and PVP was employed in a wide concentration range from 1.11×10^{-7} mol dm^{-3} to 2.78×10^{-4} mol dm^{-3}, expressed in terms of polymer molecular weight. Urea and NaCl were used as additives in a range with maximum concentrations of 4.0 mol dm^{-3} and 1.6 mol dm^{-3} respectively.

Results and Discussion

Since the studies were conducted at two different pH's 7.2 and 11.2 and the binding behavior is almost the same at both the pH's, at first, the results obtained at pH 7.2 have been discussed in detail.

Quantification of Binding. The spectral shift of EB, at pH 7.2, from the λ_{max} of 609 nm to 639 nm on adding PVP forms the basis for the absorbance change method adopted in the present work. The absorbances of the dye were measured at 639 nm (at 609 nm when the pH is 11.2) (i) in the unbound or free condition (D_1), (ii) in the fully-bound condition (D_2) i.e., at the highest [PVP] and (iii) in the partially bound condition (D). Substituting all these values in Eq. 1, the bound dye concentration, C_B was calculated.

$$C_B = \frac{(D_1 - D)}{(D_1 - D_2)} \times C_T \qquad (1)$$

C_T is the total initial dye concentration, a known quantity. The conditions proposed for the application of the absorbance method are: (i) obeying of Beer-Lambert's law by both the free and the bound dye and (ii) the constancy of the molar extinction coefficient value of the complex with the variation of [dye]/[polymer] ratios. These have been found to be fulfilled in the present system and hence the dye-aggregation in the free as well as in the complexed states has been ruled out. Nonoccurrence of any blueshifts in the spectrum of EB with PVP also excludes, as pointed out by Takagishi et al.,[4] the association of dye molecules.

Scatchard method,[5] for which the equation is given

below, was followed to determine the binding parameters for the PVP–EB system.

$$\frac{r}{C_F} = nK - rK \qquad (2)$$

where r = the ratio, in moles, of bound dye to total polymer,
C_F = the unbound or free dye concentration,
n = the total number of binding sites per mole of polymer,
and K = the intrinsic binding constant, a measure of the strength of binding.

From the slope and intercept of the Scatchard plot, the binding parameters were calculated both in the absence and in the presence of the additives, 2.0 mol dm^{-3} urea and 0.4 mol dm^{-3} NaCl. Table 1 displays these values and Fig. 1 illustrates the representative Scatchard plots. Freedman and Johnson[6] have reported the K value of 4×10^5 dm^3 mol^{-1} for the human serum albumin–Evans Blue system at pH 7.3 in buffer–NaCl (0.12 mol dm^{-3}) mixture. This literature value is comparable with that of the PVP–EB system ($K=1.03\times10^5$ dm^3 mol^{-1}) in 0.4 mol dm^{-3} NaCl, admitting the fact that we have used a higher [NaCl] which has certainly a binding-reducing effect.

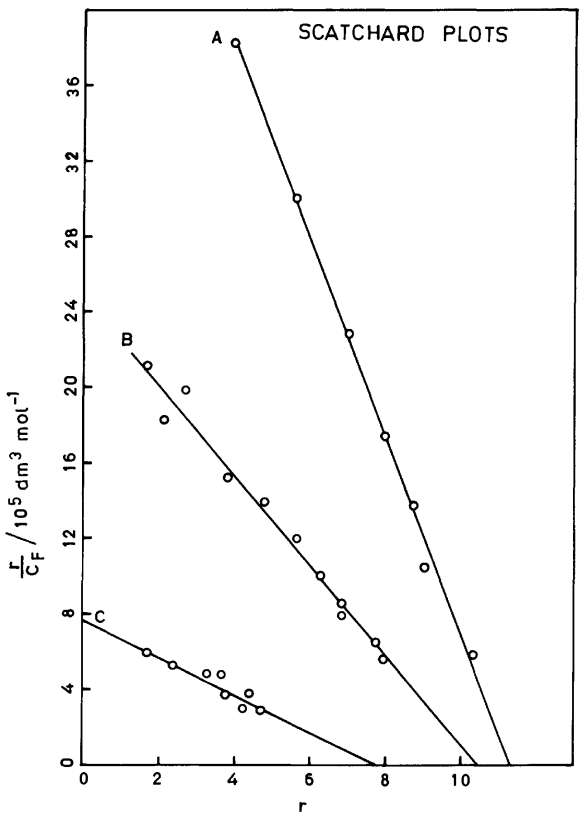

Fig. 1. Scatchard plots for the PVP–EB system at pH 7.2.
(A) PVP+2.0 mol dm^{-3} urea; (B) PVP only; (C) PVP+0.4 mol dm^{-3} NaCl, [PVP]=1.39 μmol dm^{-3} for B and C and 1.0 μmol dm^{-3} for A with varying [EB].

Spectroscopically Distinguishable Complexes. The spectrum of the dye, EB undergoes a peculiar shift (Fig. 2) when PVP is added from the lowest to the highest concentration of the range specified earlier. First, at very low [PVP], absorption at the λ_{max} of the free dye (609 nm or 16.42×10^3 cm^{-1}) decreases without any shift and it continues upto a [PVP] of 0.53 μmol dm^{-3}. In this condition, as evident from the isosbestic point at 635 nm, only two kinds of spectral species—the unbound dye and a weak PVP–EB complex—are existing in solution, maintaining equilibrium between themselves. When the added [PVP] is higher than 0.53 μmol dm^{-3}, two things happen: (i) spectral shifting to 639 nm (or 15.64×10^3 cm^{-1}) starts and (ii) the decreased absorption at 609 nm begins to increase with the disappearance of the isosbestic point. This drastic change indicates the

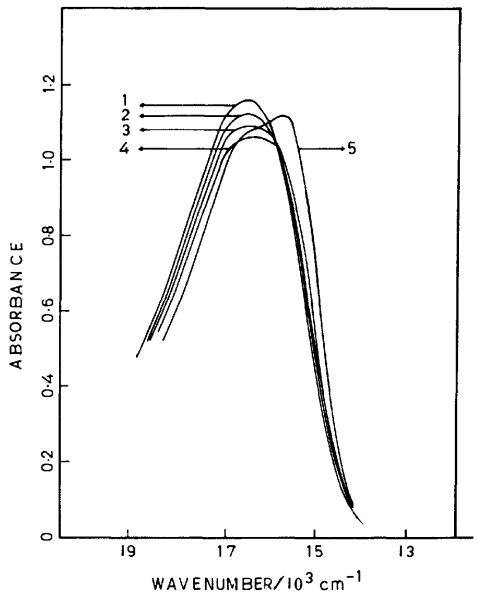

Fig. 2. Absorption spectra of EB and PVP–EB complex at pH 7.2. [EB]=2.0 μmol dm^{-3}.
1: EB only (λ_{max}=609 nm); (2—5): EB+PVP (λ_{max} for 5=639 nm) with [PVP] (in μmol dm^{-3})=0.2, 0.33, 0.53, and 2 respectively. Isosbestic point for the PVP–EB complex=635 nm.

Table 1. Binding Parameters[a] for the PVP–EB System at pH 7.2
[PVP]=1.39 μmol dm^{-3}; Temperature=25 °C

Parameter	PVP only	PVP[b]+2.0 mol dm^{-3} urea	PVP+0.4 mol dm^{-3} NaCl
n	10.36	11.24	7.57
$K/10^5$ dm^3 mol^{-1}	2.40	5.26	1.03

a) Calculated by the least-square method. b) [PVP]=1.0 μmol dm^{-3}.

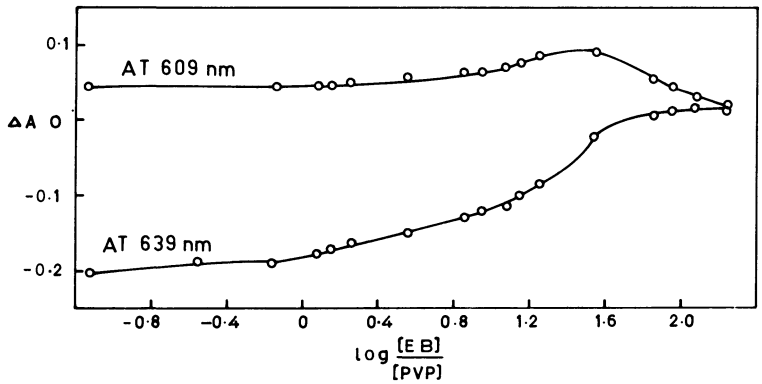

Fig. 3. Variation of absorbance difference ($\Delta A = D_1 - D$) with [EB]/[PVP] ratios at pH 7.2.
D_1=absorbance of the free dye; D=absorbance of PVP+EB mixture. [EB]=20.0 μmol dm^{-3}; [PVP]= 0.11 to 278.0 μmol dm^{-3}.

formation of the strong PVP-EB complex by the conversion of the weak one.

Figure 3 illustrates clearly the change in absorbance of the dye (20 μmol dm^{-3}) with [PVP] at the two wavelengths 609 nm and 639 nm. Upto [EB]/[PVP]$\geqslant$25, i.e, until log([EB]/[PVP]) reaches a value of 1.4, ΔA i.e., ($D_1 - D$) at 609 nm (ΔA_{609}) increases while ΔA_{639} first remains constant and then decreases. Since the changes of ΔA occur in two opposite directions upto the ratio of 25, it indicates the presence of two types of PVP-EB complexes in solution under equilibrium condition. Below the ratio of 25, change in ΔA_{609} as well as ΔA_{639} occurs in one direction only, i.e., a decrease and then constancy. This points out the existence of one complex i.e., the strong complex. Since all the experiments for determining the binding parameters in Table 1 were carried out at sufficiently high [PVP], the ratio [EB]/[PVP] is always less than 25 and hence the data correspond to the strong complex only. The designations 'strong' and 'weak' given to the complex, are purely relative and have been assigned only on the basis of the binding constant values.

Cooperativity and [PVP] Effect. Generally in ligand-polymer binding studies, cooperativity will be manifested at high [ligand]/[polymer] ratios only. Because, at this condition the number of available free sites will be much less than the free ligand concentration. Reeves et al.[7] have noticed cooperative binding at high dye concentrations only in 4-phenylazo-1-naphthol-2-sulfonate and the corresponding disulfonate-PVP systems. But on the contrary, in the present system cooperativity is explicit at the low [EB]/[PVP] ratio only i.e., a high [PVP] induces cooperativity. This is clearly seen from the convex Scatchard plots of Fig. 4 drawn for the set of a fixed [EB] with varying [PVP]. These plots obviously show that the operation of positive cooperativity is a function of [PVP]. This inference is again confirmed

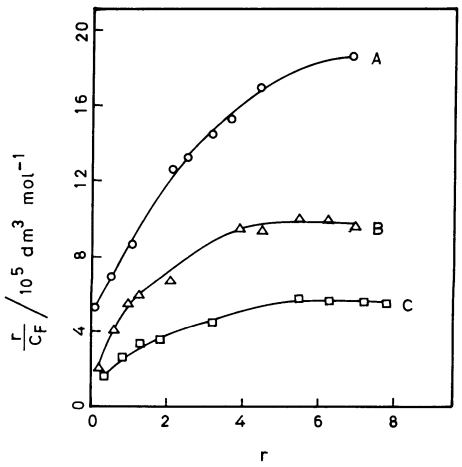

Fig. 4. Convex Scatchard plots for the PVP-EB system at pH 7.2. [PVP]=0.11 to 278.0 μmol dm^{-3}; [EB] (in μmol dm^{-3})=(A) 7.5; (B) 15.0 and (C) 25.0.

by the sigmoidal shape binding isotherm also i.e., r versus C_F plot (figure not shown). Figure 4 apparently shows that as the [EB]/[PVP] ratio is increased (e.g., at [EB]=25 μmol dm^{-3}), the extent of convexity is reduced. Therefore if we had used a still higher dye concentration, we would have obtained a concave Scatchard plot also indicative of negative cooperativity. But the experimental constraints did not allow us to do so. However in the reverse approach i.e. fixing the [PVP] constant and varying the dye concentration, an inverted 'U' shaped Scatchard plot (figure not shown) was obtained, suggesting the operation of both the positive and negative cooperativities.

The alternate inference from the afore-mentioned Scatchard plots is the ligand-mediated and ligand-facilitated association of polymer molecules. This possibility is ruled out on the grounds that the shapes and intersection of the theoretical Scatchard plots proposed by Cann[8] for the association of polymer

molecules do not coincide with that for the PVP-EB system. Moreover the values of the binding constants should be raised, if the polymer molecules were to associate through ligands. This was also not observed in the present system. Hence the above scatchard plots indicate only the operation of a 'mixed' cooperativity i.e., positive cooperativity at lower [EB]/[PVP] ratios and negative cooperativity at higher ratios. If the [PVP] is much less, the upward rising portion of the Scatchard curve disappears and only a linear down-ward plot (Fig. 1) is obtained, implying a simple model of binding.

Analysis of Cooperativity. Two methods—the well-known Hill method[9] and the Schwarz method[10]—have been employed for the analysis of cooperativity. Molyneux and Lentzos[11] have already applied these methods. For the use of both the methods an essentially accurate n value should have been known. The n value of 10.36 in Table 1 was verified by the difference spectrum method.[12] The difference spectrum of EB (20 μmol dm^{-3}) in varying [PVP] was recorded with the dye solution of same concentration as reference. The λ_{max} of the spectrum (661.4 nm) does not change upto a [PVP] of 2 μmol dm^{-3} and above this, it blueshifts to 651.5 nm. This observation demonstrates that one mole of PVP, on an average, can bind 10 moles of EB without any change in the nature of the complex. A higher [PVP] promotes a less polar environment around the already existing complex resulting in the blue-shift.

In Fig. 5 are shown the Hill plots constructed according to the Eq. 3.

$$\log\left(\frac{r}{n-r}\right) = \log K_a + n_H \log C_F \qquad (3)$$

Where K_a is the apparent binding constant and n_H the Hill coefficient. Figure 5 (Plot A) which exhibits clearly the operation of positive cooperativity in binding is the plot of the data obtained from a set of experiments with [EB]=7.5 μmol dm^{-3} and varying [PVP]. This plot is linear for 5 to 66% saturation of the binding. The curved portions at very low and very high degrees of saturation which reflect the single-site binding are extrapolated back to the abscissa to evaluate the first (K_1) and the last (K_n) ligand binding constants. These were used in calculating the

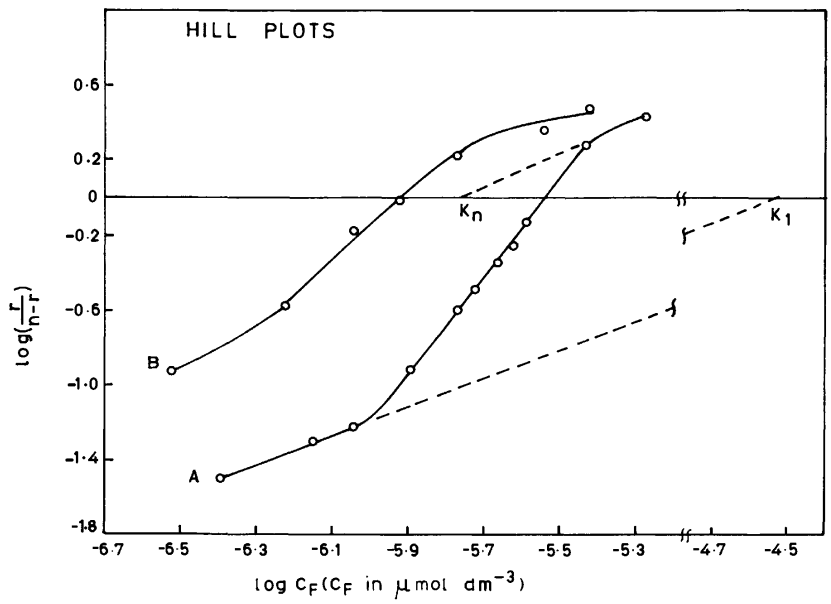

Fig. 5. Hill plots for the PVP-EB system.
(A): pH 7.2; [EB]=7.5 μmol dm^{-3}; [PVP]=0.28 to 22.2 μmol dm^{-3}. (B): pH 11.2; [EB]=12.5 μmol dm^{-3}; [PVP]=1.0 to 10.0 μmol dm^{-3}.

Table 2. Binding Parameters from the Hill Method at pH 7.2.
[PVP]=0.28 to 22.20 μmol dm^{-3}; Temperature=25 °C

[EB]	n_H	K_a	n_H[a]	K_1	n_H[b]	K_n	ΔG_{int}
μmol dm^{-3}		10^5 dm^3 mol^{-1}		10^5 dm^3 mol^{-1}		10^5 dm^3 mol^{-1}	kcal mol^{-1}
7.5	2.45	3.36	0.80	0.33	0.87	5.79	1.69
25.0[c]	2.32	1.08	—	—	—	—	—

a) and b) Values from the extrapolations at the very low and very high degrees of saturation respectively. c) Extrapolations not possible due to the experimental constraints.

interaction energy,[13] ΔG_{int} as given by Eq. 4.

$$\Delta G_{int} = RT \ln \frac{K_n}{K_1} \quad (4)$$

The values of the Hill parameters are presented in Table 2. When [EB] is increased from 7.5 μmol dm^{-3} to 25 μmol dm^{-3}, the Hill plot becomes linear for the entire data (3—76% saturation) and here K_a has a lower value. It is obvious from Table 2 that as [EB] is increased, the extent of positive cooperativity is diminished and thereby it supplements the Scatchard plots in Fig. 4. The values of the Hill coefficient imply that there is a constructive interaction between the two neighboring binding sites and that it is this interaction which promotes positive cooperativity. In the other experimental approach i.e., keeping the [PVP] constant and varying [EB], the Hill equation is not obeyed indicating the operation of a mixed cooperativity. PVP-EB system has an interaction energy of 1.69 kcal mol^{-1} (1 cal=4.184 J) or 163 cal/site which is less relative to the hemoglobin-O_2 system (3.0 kcal mol^{-1} or 750 cal/site).[13] This marked difference reflects the poor elevation of the binding strength in the PVP-EB system on each successive step of ligand binding.

Figure 6 shows the Schwarz isotherm at the [EB]=7.5 μmol dm^{-3}. The linearity of the plot suggests the obeying of the Schwarz equation given below:

$$\frac{(1-2\theta)\sqrt{C_F}}{\sqrt{\theta(1-\theta)}} = \frac{1}{\sqrt{K_0}} - \alpha C_F \sqrt{K_0} \quad (5)$$

Here θ = the fractional occupancy i.e., r/n,
K_0 = the intrinsic binding constant for a site when the sites on either side of it are unoccupied,
and α = the cooperativity parameter i.e., the increment in K_0 when one neighboring site is filled.

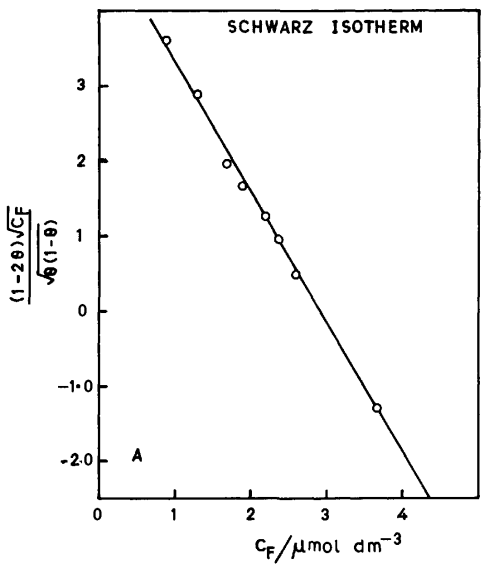

Fig. 6. Schwarz isotherm for the PVP-EB system at pH 7.2.
[EB]=7.5 μmol dm^{-3}; [PVP]=0.28 to 22.2 μmol dm^{-3}.

From the slope and intercept, α and K_0 were calculated and are given in Table 3 along with the Hill parameters. Table 3 shows that K_0 and K_1 are comparable as well as αK_0 and K_a, within the limits of experimental error. Thus the two methods, by virtue of their nature, provide the binding constant value (K_0 and K_1) of the PVP-EB weak complex also. Obeying of Schwarz model in the present system implies that at the lowest [PVP] (i.e. [EB]/[PVP]>25), when every polymer chain has only one EB molecule bound to the site, the complex exists as a weak one. But when further PVP is added, site-site interaction of two neighboring binding sites occurs leading to the conversion of the weak complex into the strong one.

Thus it is brought out from the above discussion that positive cooperativity is exhibited at two instances: (i) in the conversion of the weak to the strong complex and (ii) in the strong complex at higher [PVP]. But at the low [PVP] in the strong complex, no cooperativity is observed. Incorporating all these features, the following mechanism is proposed:

$$\underset{\text{(at the lowest concentration)}}{\text{PVP}} + \text{EB} \rightleftharpoons \text{Weak complex} \quad (6)$$

$$\text{Weak complex} + \text{PVP} \overset{\text{Cooperativity}}{\rightleftharpoons} \text{Strong complex} \quad (7)$$

$$\text{Strong complex} + \text{PVP} \overset{\text{Cooperativity}}{\rightleftharpoons} \text{Cooperative PVP-EB Strong complex} \quad (8)$$

Nature of the Complexes. The nature of the complexes formed depends on the structures of the polymer and the dye. PVP consists of nonpolar methylene and methine (CH) groups and the polar amide linkage. Due to the operation of keto-enol tautomerism, the heterocyclic N and the carbonyl O atoms acquire fractional positive and negative charges respectively to the extent of 0.37 units.[14] EB is a bisazo dye with two phenyl-substituted hydroxyl groups at

Table 3. Binding Parameters from the Schwarz and Hill Methods. pH=7.2; [EB]=7.5 μmol dm^{-3}; Varying [PVP]; Temperature=25 °C

Schwarz	Hill
$\frac{K_0}{\text{dm}^3\,\text{mol}^{-1}} = 3.89 \times 10^4$	$\frac{K_1}{\text{dm}^3\,\text{mol}^{-1}} = 3.33 \times 10^4$
$\alpha = 8.83$	
$\frac{\alpha K_0}{\text{dm}^3\,\text{mol}^{-1}} = 3.44 \times 10^5$	$\frac{K_a}{\text{dm}^3\,\text{mol}^{-1}} = 3.36 \times 10^5$

the ortho positions with respect to the azo groups. It also has hydrophilic ($-SO_3H$, $-NH_2$) and hydrophobic (biphenyl) groups in its structure (refer to Scheme 1). Two other structurally similar dyes, Trypan Blue (TB) and Benzopurpurin 4B (BP) have been chosen to determine the nature of the PVP–EB complexes. TB is a positional isomer of EB, the difference being in the position of the four sulfonato groups. In TB, two of the four sulfonato groups are very near to the azo groups i.e., at the ortho positions; the other two sulfonato groups are meta to the amino groups. This difference in position of the sulfonato groups between EB and TB reflects in the binding constant value also (as shown in the ensuing discussion). BP has the same basic skeleton as of EB and TB but without two hydroxyl and two sulfonato groups.

A comparison of the spectral behavior of these dyes at pH 7.2 shows that except BP, EB and TB exhibit, at first a decreased absorption at their respective λ_{max}'s with very low [PVP] and then a red shift at higher [PVP]. BP, on the other hand, shows only a redshift. At pH 11.2, the spectral behavior of EB (Fig. 9) gets changed from that at pH 7.2 and resembles that of BP. The reason for this is the ionization of the two phenolic hydroxyl groups at this alkaline pH. Correlation of these observations with the structures of the dyes leads to the interpretation that the initial decrease in absorption of EB and TB is mainly due to the -OH group of the dye and hence the formation of the weak complex. A similar decrease in absorption is also observed when NaCl is added to EB. From this, it is concluded that the formation of weak complex produces a polar environment around the dye, relative to that present with the dye alone. When urea is added to the weak complex the decreased absorption begins to increase at 0.5 mol dm^{-3} urea and at 4.0 mol dm^{-3}, the spectrum of the complex coincides with that of the free dye, suggesting the total collapse of the weak complex. Thus the urea effect, coupled with the above spectral studies indicates that the hydrogen bonding is the main force in the weak complex formation.

A brief description about the weak complex, emerging from the foregoing discussion is as follows: Since the [PVP] is very low, the polymer molecules would exist as single entities only. Hydrogen bonding interaction from the two -OH groups and the electrostatic interaction from the two sulfonato groups (far from the azo groups) favor its formation. Both the azo groups and the other two sulfonato groups (para to the amino groups) do not seem to involve in binding but get exposed to the solvent medium. Thereby they make the environment of the complex more polar.

In the strong complex, the electrostatic interactions originating from the two remaining sulfonato groups, the dipolar and the hydrophobic interactions from the biphenyl part are the additional interacting forces. Now the azo group is present in a less polar environment as indicated by the redshift of the spectrum. Since the [PVP] is high, the PVP chains would be in somewhat coiled form and thereby make a less polar environment. All these features strengthen the PVP–EB attachment and hence the binding constant is enhanced by 7 times the value of the weak complex. Scheme 1 illustrates the model for the PVP–EB strong complex. In this model, the rectangle represents the PVP binding site with coiled chain.

The two sulfonato groups para to the amino groups are near to the azo groups, when compared to the other two sulfonato groups. The former sulfonato groups start interacting with PVP, only in the strong complex but not in the weak complex. This conclusion was made because of the following inference. The interaction from the anionic groups nearer to the azo group appears to contribute significantly to the binding affinity. The supporting evidences for this are: (i) $-O^-$ rather than -OH is the stronger interacting group, as revealed by the studies at pH 11.2; (ii) the PVP–TB strong complex has been observed to have a higher binding constant value than the PVP–EB strong complex. Since the azo group interaction is more pronounced in the strong complex only, the above logical conclusion was arrived at.

Further addition of PVP to the strong complex e.g., at a [PVP] of 10 or 20 μmol dm^{-3}, the polymer coils of the unoccupied sites interact hydrophobically, create a still less polar environment and thereby induces the site–site cooperative interaction. This is possible because at higher [PVP], intermolecular interactions such as polymer entanglement or interpenetration of polymer chains are unavoidable and therefore the site–site interaction is feasible. Creation of nonpolar environment and hence the positive cooperativity is proved by (i) change in λ_{max} of the difference spectrum, (ii) effect of urea on binding at higher [PVP] (discussed

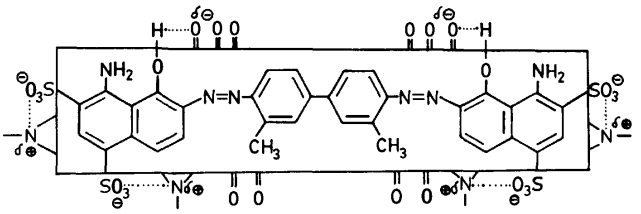

Scheme 1. PVP–EB strong complex.

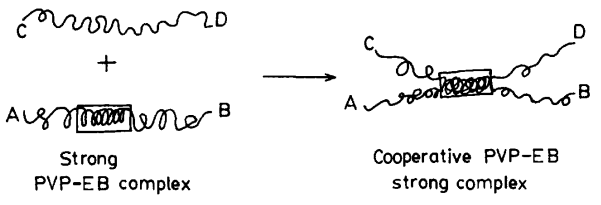

Scheme 2. Cooperative interaction in the strong PVP–EB complex.

Table 4. Viscosity of PVP and PVP-EB Complex at pH 7.2. 0.05 mol dm^{-3} Buffer; Temperature=30 °C [EB]=25.0 μmol dm^{-3}

Sample	Intrinsic viscosity
	ml g^{-1}
PVP	20.62
PVP+EB	21.56

later) and (iii) cooperativity as a function of [PVP] previously illustrated by Scatchard and Hill plots. Scheme 2 pictorially represents the cooperative interaction. In this model AB and CD are two different polymer chains and the rectangle denotes the bound dye molecule.

The question of positive cooperativity due to the interaction between adjacent sites on the same polymer chain rather than on different polymer chains is ruled out because, if it were the case, we should have observed cooperativity at the very low [PVP] also. But it is not the case. Further cooperativity of sites on the same polymer chain would facilitate the dye binding on a single macromolecule resulting in the overall conformational change. This was also not encountered as indicated by the viscosity data in Table 4. Thus from the foregoing arguments, it is clear that the observed positive cooperativity in the strong complex is exclusively due to the interaction between the sites on different polymer chains. The viscosity data also reveal the absence of coulombic repulsion between the bound dye molecules and hence the chain elongation.

Influence of Additives on Binding. In our previous article[1] we have reported that both urea and NaCl reduce the binding constant values at higher [PVP]. But at lower [PVP], urea enhances the binding constant while NaCl decreases it. In other words, urea plays a dual role while NaCl has only one effect i.e., the binding reducing effect. The trend at lower [PVP] is observed in the present work also (Table 1). The explanation for this is based on the effect of these additives on the formation of weak and strong complexes. Decrease in absorbance at 609 nm (D^{609}) and the increase in absorbance at 639 nm (D^{639}) of the PVP-EB mixture, relative to the absorbance of the free dye (D_1) have been considered as to signify the formation of the weak and strong complexes respectively. Therefore if the addition of urea or NaCl decreases the value of D^{609}, it is considered as to favor the formation of the weak complex. If D^{609} is increased, it indicates the inhibition of the weak complex formation. Oppositely, the increase in D^{639} represents the facile formation of the strong complex and the decrease in D^{639}, the inhibition.

Figure 7 exhibits clearly the urea effects (4.0 mol dm^{-3}) in terms of the plot ΔA or $(D-D_1)$ versus [EB] at both the wavelengths. At the [PVP] of 0.4 μmol dm^{-3},

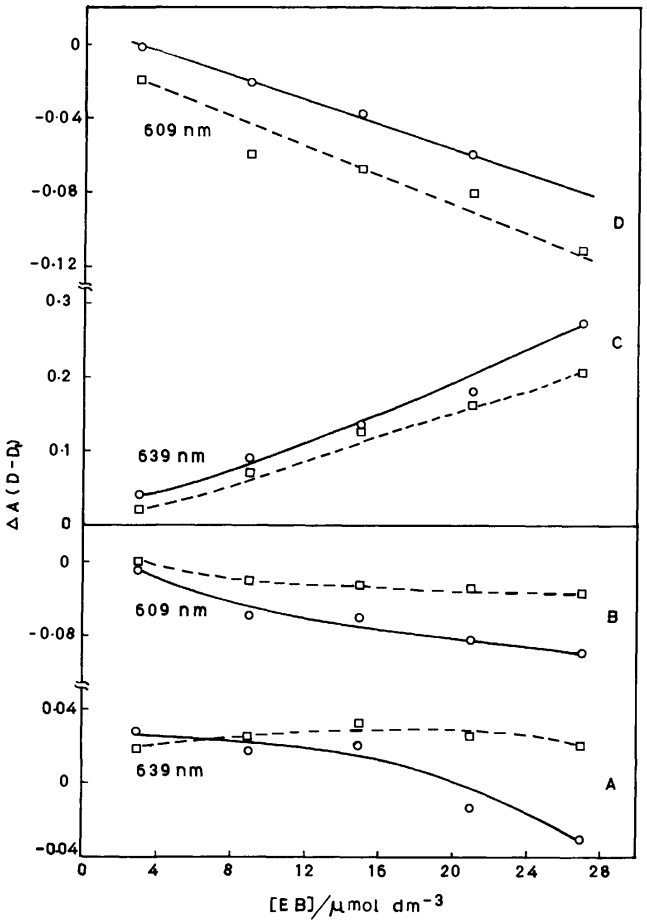

Fig. 7. Difference in absorbance, ΔA and urea effects at pH 7.2, [urea]=4.0 mol dm^{-3}.
For A and B [PVP]=0.4 μmol dm^{-3} and for C and D [PVP]=50.0 μmol dm^{-3}. Solid line: PVP+EB; dotted line: PVP+EB+urea. D=absorbance of the complex; D_1=absorbance of the free dye; $\Delta A = D-D_1$.

addition of urea to PVP-EB mixture increases the absorbance at both the wavelengths. This means that the strong complex formation is favored at the decay of the weak complex. But at higher [PVP] (50 μmol dm^{-3}), urea produces the opposite effect i.e., absorbances are decreased at both the wavelengths. This decrease in absorbance at 609 nm of the PVP+EB mixture by urea (the set of two lines D in Fig. 7) should not be taken as an indication of the formation of weak complex. Because, at this higher [PVP], as already stated, only one type of complex i.e., the strong complex alone can exist. Therefore, this decreased absorbance at 609 nm, as already discussed in the nature of the PVP-EB weak complex, could be considered only as reflecting a more polar environment around the PVP-EB strong complex. Thus at higher [PVP], the strong complex formation is hindered by urea, as a result of the change in polarity of the binding environment.

The underlying principle for both the urea effects is

the water-structure breaking action. It has been already established that for the effective interaction of different polar groups in aqueous solution in close proximities, the water structure around these groups is an inhibiting factor. As already mentioned, in the conversion of weak to strong complex, additional electrostatic and dipolar interactions from the sulfonato, azo, and biphenyl groups begin to operate. Therefore the breaking of water structure around the hydrophilic groups by urea in the weak complex favors an effective interaction between PVP and EB and facilitates the conversion of weak to strong complex. Conversely at higher [PVP], the nonpolar interactions operating between different polymer chains in the cooperative PVP–EB strong complex is disfavored to some extent by urea through the destruction of iceberg structure of water. This type of inhibition of hydrophobic interactions by urea has already been noticed in many studies.[15] This effect leads to the exposure of the PVP–EB strong complex to a relatively less nonpolar environment and hence reduces the binding affinity. Now the urea effect is summarized as follows:

$$\text{At lower [PVP] : Weak complex} \xrightarrow{\text{Urea}} \text{Strong complex} \quad (9)$$

$$\text{At higher [PVP] : Strong complex (in nonpolar environment)} \xrightarrow{\text{Urea}} \text{Strong complex (in less nonpolar environment)} \quad (10)$$

Thus these two types of effects are responsible for the dual role played by urea.

On the contrary to urea, NaCl decreases the absorbances of the complex at both the wavelengths at all PVP concentrations. This means that the strong complex formation is hindered by NaCl, irrespective of the [PVP] employed. Since the present work is mainly concerned with the strong complex, the observed effect of NaCl is only a reduced binding at all PVP concentrations. This effect may be caused in two ways: (i) the water-structure breaking action and (ii) the interaction of Na^+ ions with the hydrophilic groups e.g. the sulfonato and the azo groups. The latter way appears to be the predominant one because, the strong complex formation to which the contribution from the electrostatic interaction is very much, is hindered.

Binding Forces. The forces involved in binding need not be discussed in detail because the operation of electrostatic forces, hydrogen bonding and hydrophobic interaction in the system has already been mentioned. Besides these, the dipolar forces may also operate between the easily polarizable aromatic moieties and the >C=O group in PVP. Figures 8A and 8B illustrate respectively the UV spectra of PVP and EB in the presence of the other component. The $n\rightarrow\pi^*$ transition of both the components get redshifted with decreased intensity. This clearly demonstrates the creation of a less polar environment and in turn the mutual delocalization of electrons and the ground state stabilization. All these aspects facilitate the polar interactions.

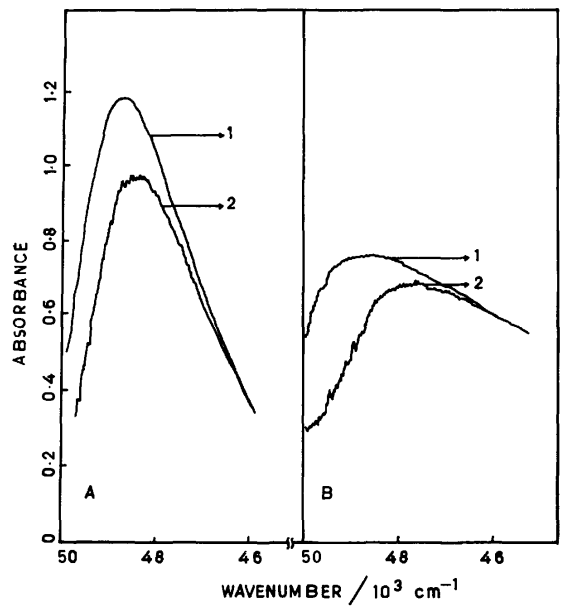

Fig. 8. UV spectra of PVP and EB at pH 7.2. [PVP]=1.0 μmol dm^{-3} and [EB]=20.0 μmol dm^{-3}. A: (1) Spectrum of PVP alone (λ_{max}=205.2 nm); (2) Spectrum of PVP in the presence of EB (λ_{max}=206.4 nm). B: (1) Spectrum of EB alone (λ_{max}=205.3 nm); (2) Spectrum of EB in the presence of PVP (λ_{max}=210 nm).

Studies at pH 11.2. At this alkaline pH, the two phenolic hydroxyl groups are ionized ($pK_a \simeq 10$) and the dye acquires 6 negative charges. Unlike at pH 7.2, only one type of complex is formed at pH 11.2. This is shown in Fig. 9 with the spectral change in only one direction. The free dye has λ_{max} at 570 nm and the bound dye at 609 nm. Because of this spectral shift, a very attractive instantaneous color change can be seen, when one drop of PVP solution is added to the dye solution. The isosbestic point at 573.4 nm is an additional proof for the existence of only one type of complex. Since the λ_{max} of the bound dye coincides with that of the free dye at pH 7.2 (609 nm), it is concluded that the EB molecule in the PVP–EB complex, at the alkaline pH, should be present with the two phenoxide anions involved in ion-pair formation with the fractionally positively charged N atom of the pyrrolidone ring. This ion-pair formation is very much facilitated because of the nonpolar environment provided by the PVP molecular chains. Such ion-pair formation as this, has already been

Table 5. Binding Parameters for the PVP-EB System at pH 11.2. Temperature=25 °C

Scatchard method[a]	Hill method[b]	Schwarz method[b]
K=8.14×10^5	K_n=8.17×10^5	K_0=2.78×10^5
n=11.49	n_H=1.75	α=2.91
		αK_0=8.11×10^5

All the binding constants are in dm^3 mol^{-1} unit. a) [PVP]=1.0 μmol mol^{-3} with varying [EB]. b) [EB]=12.5 μmol dm^{-3} with varying [PVP].

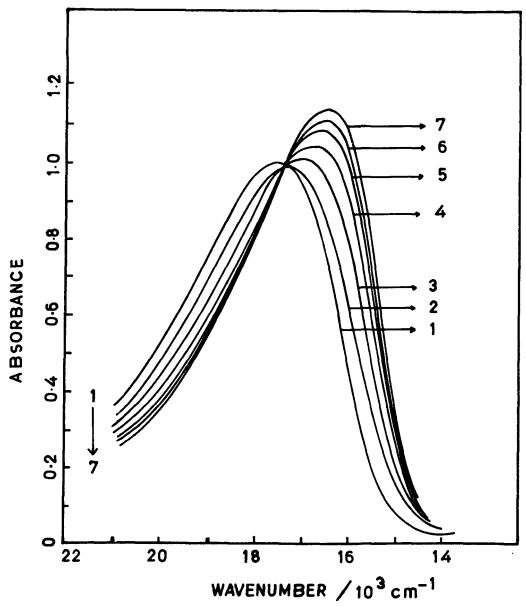

Fig. 9. Spectra of EB and PVP-EB complex at pH 11.2.
[EB]=27.5 μmol dm^{-3}. (1) EB only (λ_{max}=570 nm); (2—7): EB+PVP (λ_{max} for 7=609 nm) with [PVP] (in μmol dm^{-3})=0.5, 1, 2, 5, 10 and 25 respectively. Isosbestic point for the PVP-EB complex=573.4 nm.

reported in the bovine serum albumin-Methyl Orange system.[16]

Eventhough only one type of complex is formed, the entire binding behavior is the same as in pH 7.2. The binding parameters determined from various methods are given in Table 5. Extrapolations in the Hill plot (plot B; Fig. 5) to evaluate K_1 and K_n were not possible under the experimental conditions at pH 11.2. The dye has higher affinity at this pH and this is due to the involvement of two more electrostatic interacting sites ($-O^-$ ions) in binding. The cooperativity parameter α is one-third of the value at pH 7.2 and this may be due to the absence of weak complex in initial stage. Incorporating all these, the following mechanism is put forward.

$$\text{PVP} + \text{EB} \rightleftharpoons \text{Complex} \quad (11)$$

$$\text{Complex} + \text{PVP} \overset{\text{Cooperativity}}{\rightleftharpoons} \text{Cooperative PVP-EB complex} \quad (12)$$

Comparison of the binding studies at the two pH's points out that the two phenolic hydroxyl groups play the key role in establishing the binding behavior in the PVP-EB system. From the whole study the conclusion arrived at is that although a synthetic polymer, PVP can be placed in equal rank with the protein molecules as the former is also able to exhibit a cooperative mechanism like the biomacromolecules in the binding of ligands.

The financial assistances offered by CSIR and UGC, New Delhi are gratefully acknowledged. Sincere thanks are due to Dr. P. Molyneux, Macrophile Associates, London, for his help.

References

1) M. Maruthamuthu and E. Subramanian, *Polym. Bull.*, **14**, 207 (1985).
2) I. M. Klotz, *J. Am. Chem. Soc.*, **68**, 2299 (1946).
3) A. R. Peacocke and J. N. H. Skerrett, *Trans. Faraday Soc.*, **52**, 261 (1956).
4) T. Takagishi, S. Fujii, and N. Kuroki, *J. Colloid Interface Sci.*, **94**, 114 (1983).
5) G. Scatchard, *Ann. N.Y. Acad. Sci.*, **51**, 660 (1949).
6) F. B. Freedman and J. A. Johnson, *Am. J. Physiol.*, **216**, 675 (1969).
7) R. L. Reeves, S. A. Harkaway, and A. R. Sochor, *J. Polym. Sci., Polym. Chem. Ed.*, **19**, 2427 (1981).
8) J. R. Cann, *Methods in Enzymology*, **XLVIII** (Part F), 299 (1978).
9) A. V. Hill, *J. Physiol. (London)*, **40**, iv (1910).
10) G. Schwarz, *Eur. J. Biochem.*, **12**, 442 (1970).
11) P. Molyneux and M. C. Lentzos, *Colloid Polym. Sci.*, **257**, 855 (1979).
12) P. C. Huang and S. Gabay, *Biochem. Pharmacol.*, **23**, 957 (1974).
13) J. Wyman, *Adv. Protein Chem.*, **19**, 223 (1964).
14) P. Molyneux, "The Physical Chemistry and Pharmaceutical Applications of Polyvinylpyrrolidone," Proceedings of the International Symposium on Povidone, Kentucky, U.S.A. (1983), p. 1.
15) G. Nemethy, *Angew. Chem., Int. Ed. Engl.*, **6**, 195 (1967).
16) I. M. Klotz, R. K. Burkhard, and J. M. Urquhart, *J. Phys. Chem.*, **56**, 77 (1952).

Behavior of the Enthalpies of Dissolution and Formation in the System Silver-Indium

Walid Ahmad BADAWI*,† and Ahmed M. OUN
Department of Chemistry, Faculty of Science, Al-Fateh University, Tripoli, Libya
(Received March 28, 1988)

The enthalpy of dissolution in the system Ag-In has been measured at 1100 K in the whole range of composition. The behavior of the enthalpy of dissolution points out the existence of the compound Ag_3In in the liquid state. The enthalpy of formation in the range of the γ phase has also been determined at 623 and 773 K. The enthalpy of formation is negative. The partial molar enthalpy of formation of silver is negative but increase with the increase of the composition, and that of indium is negative and decreases with increasing composition. The enthalpy of formation depends insignificantly on the temperature. A pronounced temperature dependence of the enthalpy of formation seemed not to be a general property of all metallic alloys as reported earlier.

The behavior of the thermodynamic functions of alloys depends on (1) the ratio of the atomic radii of the components, (2) the electronegativity and (3) the valence electron concentration (C_{ve}) which is given by

$$C_{ve} = v_1 + x_2 \cdot (v_2 - v_1), \quad (1)$$

where v_1 is the valence of the first component in the binary alloy. x_2 and v_2 refer to the mole fraction and the valence of the second component, respectively. Based upon these factors, it was possible to derive systematic statements for the behavior of the enthalpy of mixing in liquid alloys.[1,2] The quantity C_{ve} (Eq. 1), and in some cases the above given factors (2) and (3) contribute in determining the trend of the enthalpy of formation. However, solid solutions differ from liquid ones in that they include miscibility gaps and phases of different structures. This led to a need of more detailed information on common factors which are responsible for predicting the behavior of the enthalpy of formation in solid solutions. Hence, we now extend our previous studies[3–5] to include more observations on the properties of the enthalpy of formation by studying the system silver-indium which has been selected due to its somewhat large range of miscibility in the solid state, and due to the existence of a γ phase[6] which has not been studied before.

Another point of interest is to see if the enthalpy of formation displays a pronounced temperature dependence and to decide if this temperature dependence is a general property of all metallic alloys as claimed by Wittig and Schöffl.[7]

Experimental

Sample. The metals used were: indium of extra purity grade (E. Merck Co.) and 99.88 mass percent silver (Riedel de Haen Co., Germany). The preparation, treatment and testing of the samples were all the same as described before.[1] The samples were tempered for 10 h at 773 K, and 170 h at 623 K. In the measurement process of the enthalpy of dissolution, the solid samples of silver with different masses (12.970—0.160 g) were dropped in liquid samples of indium (1.534 g) being heated at 1100 K. For measurement of the enthalpy difference of the single miscible phase, the solid alloy samples with masses lying between 1.435 and 1.545 g were dropped at 623 and 773 K in a liquid phase (having the same composition as that of the solid alloy sample) which exists at 1100 K inside the calorimeter.

Calorimetric Technique. The calorimeter used in the present study has been described in detail elsewhere.[5] The cylindrical calorimeter of Themax steel which represents a sample container has a hollow space coated with a layer of aluminum oxide. The role of this Al_2O_3 layer is to prevent reaction of the sample with the calorimeter. The cover of the calorimeter, also coated with a layer of aluminum oxide, has three wells for the tube of the drop device, stirrer (made of ceramic) and the thermocouple. The calorimeter is suspended inside a metallic shield system of V2A steel. This contains two cylindrical compensating systems of Thermax steel placed below and above the calorimeter. The lower compensating system has wells of each 3.5 mm diameter for the twelve differential Pt-to-(Pt+10 mass percent Rh) thermocouples. The whole assembly is placed in a vertical tube furnace. Another vertical tube furnace is placed above the cooling system which in turn was placed at the mouth of a silica glass tube which contains the whole assembly. The role of the second tube furnace was to temper the sample at any high temperature before its final drop in the calorimeter. The calibration of the thermocouples used was based on a standard Pt-PtRh thermocouple. A digital millivoltmeter (Hewlett-Packard 2401 C) was used for a registration of the thermal potential of the thermocouples. The temperature drifts of the calorimeter caused by the lower compensating body were negligible. The derived temperatures are judged to correspond with the IPTS-68 to within 0.01 K at 500 K and 0.1 K at 1000 K. The temperature was regulated by means of a p-regulator.[8]

The calibration of the calorimeter was conducted by measuring the enthalpy of a standard tin sample.[9] The calibration factor is determined with an accuracy of 0.3%.

Results and Discussion

(i) Enthalpies. Values of $[H_1^\circ(T)-H_1^\circ(623\text{ K})]$; $[H_1^\circ(T)-H_1^\circ(773\text{ K})]$ and $[H_2^\circ(T)-H_2^\circ(623\text{ K})]$; $[H_2^\circ(T)-H_2^\circ(773\text{ K})]$ are presented in Table 1. The deviation for a single measurement is 0.35%.

† P. O. Box 13539, Tripoli, Libya.

Table 1. Experimentally Determined Enthalpy Differences of Silver and Indium
M(Ag)=107.868 g mol^{-1}; M(In)=114.82 g mol^{-1}

T/K	$H_1^\circ(T)-H_1^\circ$(623 K)	$H_1^\circ(T)-H_1^\circ$(773 K)	$H_2^\circ(T)-H_2^\circ$(623 K)	$H_2^\circ(T)-H_2^\circ$(773 K)
	kJ mol^{-1}	kJ mol^{-1}	kJ mol^{-1}	kJ mol^{-1}
700	2.100	—	2.332	—
800	4.978	0.759	5.362	0.817
900	8.027	3.680	8.391	3.847
1000	11.815	6.772	11.420	6.876
1100	14.673	10.034	14.449	9.905
1200	18.198	13.467	17.479	12.935

Table 2. Enthalpy Differences of the AgIn Alloys in kJ mol^{-1}
M(Ag)=107.868 g mol^{-1}; M(In)=114.82 g mol^{-1}

x_{In}	H_3°(1100 K)$-H_3^\circ$(623 K)	H_3°(1100 K)$-H_3^\circ$(773 K)
0.300	24.446	19.611
0.350	24.513	19.690
0.400	24.726	19.732
0.450	24.719	—

Table 3. Integral and Partial Molar Enthalpies of Dissolution at 1100 K in the System Ag-In in kJ mol^{-1}. Estimated Standard Deviations in Parenthesis
M(Ag)=107.868 g mol^{-1}; M(In)=114.82 g mol^{-1}

x_2	$-\Delta_s H^\circ$	$-\Delta_s H_1^\circ$	$+\Delta_s H_2^\circ$
0.000	0	0	—
0.100	2.862(20)	1.087	—
0.200	4.551(20)	3.502	−12.614
0.300	5.630(18)	6.190	− 4.381
0.400	5.138(24)	8.386	− 0.207
0.500	4.142(10)	9.611	+ 1.347
0.600	3.025(15)	9.675	+ 1.432
0.700	1.977(11)	8.679	+ 0.945
0.800	1.132(15)	7.003	+ 0.355
0.900	0.525(10)	5.329	+ 0.052
1.000	0	4.616	0

Table 2 collects values for the enthalpy differences of the alloys: [H_3°(1100 K)$-H_3^\circ$(623 K)] and [H_3°(1100 K)$-H_3^\circ$(773 K)] as measured in the present study. The deviation is 0.4% for a single measurement.

(ii) Enthalpy of Dissolution. The enthalpy of dissolution of solid silver in liquid indium at the temperature T_1 can be determined according to the following equations:

$$-(1-x_2)\cdot \mathrm{Ag(s}, T_1) - x_2\cdot \mathrm{In}(l, T_1) + \mathrm{Ag}_{1-x_2}\mathrm{In}_{x_2}(l, T_1) = 0, \quad (2)$$

$$\Delta_s H^\circ = -(1-x_2)\cdot H_1^\circ(T_1) - x_2\cdot H_2^\circ(T_1) + H_3^\circ(T_1), \quad (3)$$

where $\Delta_s H^\circ$ is the enthalpy of dissolution of Ag in In, and H_3° is the enthalpy of the alloy at the mole fraction of indium x_2. Table 3 summarizes the values of the integral and partial molar enthalpies of dissolution at 1100 K in the whole range of composition. A number within parenthesis is the estimated standard deviation (esd). The accuracy

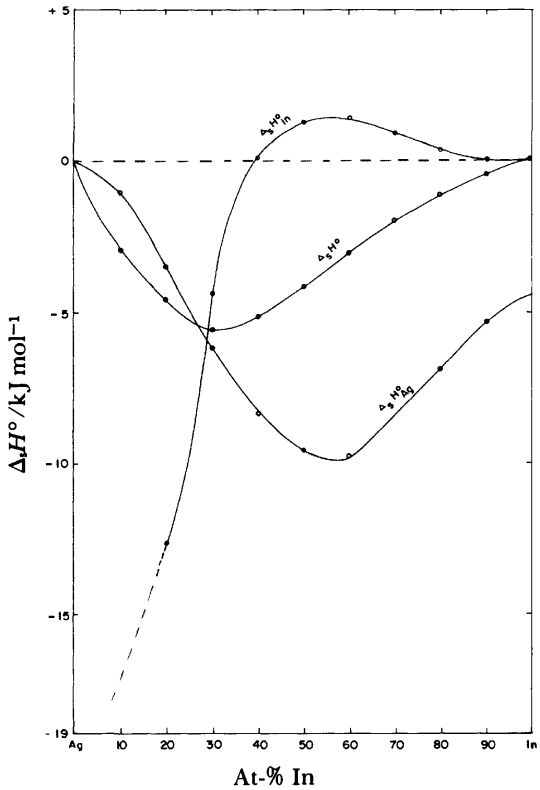

Fig. 1. The integral and partial molar enthalpies of dissolution at 1100 K in system Ag-In.

obtained is 0.8%. The present value is in excellent agreement with that obtained by Hultgren et al.[6]

From curve-fitting calculations, the following polynomial function for $\Delta_s H^\circ$ is derived:

$$\Delta_s H^\circ = -48.448x_2+132.302x_2^2-123.876x_2^3+40.022x_2^4. \quad (4)$$

Figure 1 shows the plot of the integral and partial molar enthalpies of dissolution $\Delta_s H^\circ$, $\Delta_s H_{Ag}^\circ$, $\Delta_s H_{In}^\circ$,

against the composition. The integral enthalpy of dissolution is negative and decreases with the increase of the composition to reach a minimum at x_2=0.3; after that the enthalpy of dissolution increases with the increase of indium mole fraction. This behavior of $\Delta_s H°$ with a minimum lying at x_2=0.3 points out the existence of a compound with the form Ag_3In. This may be quantitatively explained by using the Wagner effect:[10] assuming that we have to deal with a heteropolar system with the compound Ag_3In, the minimum of $\Delta_s H°$ should lie at the composition of the compound: $x_{In}=1-3/(1+3)=0.25$, where Ag is considered to be the donor and In the acceptor (see Ref. 11). With reference to Eq. 4, $\Delta_s H°$ at x_2=0.3 is equal to -5.648 kJ mol^{-1}, while $\Delta_s H°$ at x_2=0.25 is equal to -5.622 kJ mol^{-1}. The deviation between the two values (26 J mol^{-1}) is not much larger than the value expected from the experimental uncertaintities (14—18 J). It is also possible that the Wagner effect is overlapped by another dissolution effect so that the minimum of the enthalpy of dissolution is shifted to the composition x_2=0.3. This means that we have to deal with a non-ideal Wagner effect (see Ref. 11). It is also noteworthy that such behavior of the enthalpy of dissolution which suggests the existence of a compound at x_2=0.3 indicates that the maximum of the volume of dissolution may also lie at x_2=0.3.

With reference to the definition of the partial molar quantities:

$$y_1 = Y - x_2 \cdot (\partial Y/\partial x_2)_{T,p}, \quad (5)$$

$$y_2 = Y - (x_2 - 1) \cdot (\partial Y/\partial x_2)_{T,p}, \quad (6)$$

and using Eq. 4, we obtain:

$$\Delta_s H_1^\circ = -132.302x_2^2 + 247.752x_2^3 - 120.066x_2^4, \quad (7)$$

$$\Delta_s H_2^\circ = -48.448 + 264.604x_2 - 503.930x_2^2 + 407.840x_2^3 - 120.066x_2^4. \quad (8)$$

Figure 1 shows the partial molar enthalpies of dissolution of silver and indium against the composition. The partial molar enthalpy of dissolution of silver $\Delta_s H^\circ_{Ag}$ is negative and takes a minimum at the composition 58 at-% In. This is due to the delivery of electrons from silver to indium. Such a delivery of electrons increases with the increase of indium mole fraction so that $\Delta_s H^\circ_{Ag}$ becomes more negative to reach a minimum at equilibrium being established at the maximum of the C_{ve} which lies at x_2=0.58. The partial molar enthalpy of dissolution of indium, $\Delta_s H^\circ_{In}$ is negative in the range 0 to 40 at-% In but increases with the increase of the composition to take positive values above 40 at-% In with a maximum at x_2=0.58. This behavior is also understandable: The insertion of the somewhat larger indium atom in the structure causes a positive deformation work which increases with increasing composition since the lattice suffers higher tension. The maximum of $\Delta_s H^\circ_{In}$ at x_2=0.58 (the same composition of $\Delta_s H^\circ_{Ag}$ minimum) also represents the maximum of C_{ve} at equilibrium.

(iii) Enthalpy of Formation. The enthalpy of formation can be calculated from the enthalpy of dissolution using the method as described before.[2] The procedure can be explained through the following equations:

$$-(1 - x_2) \cdot \mathrm{Ag(s, } T_0) - x_2 \cdot \mathrm{In(s, } T_0) + \mathrm{Ag_{1-x_2}In_{x_2}(s, } T_0) = 0. \quad (9)$$

This reaction represents the formation reaction of the alloy from Ag and In at the initial temperature T_0. The enthalpy of formation of the alloy AgIn is:

$$\Delta_f H° = -(1 - x_2) \cdot H(T_0) - x_2 \cdot H_2^\circ(T_0) + H_3^\circ(T_0). \quad (10)$$

The indices 1, 2, and 3 indicate silver, indium, and the alloy, respectively.

Subtraction of Eq. 10 from Eq. 3, yields:

$$\Delta_s H° - \Delta_f H° = -(1 - x_2) \cdot [H_1^\circ(T_1) - H_1^\circ(T_0)] - x_2 \cdot [H_2^\circ(T_1) - H_2^\circ(T_0)] + [H_3^\circ(T_1) - H_3^\circ(T_0)]. \quad (11)$$

The term $[H_3^\circ(T_1)-H_3^\circ(T_0)]$ which appears in Eq. 11 is the enthalpy difference of the alloy; this was measured between 623 and 1100 K and between 773 and 1100 K. The differences $[H_1^\circ(T)-H_1^\circ(T_0)]$ and $[H_2^\circ(T)-H_2^\circ(T_0)]$ are measured accurately (Table 1).

Table 4 presents values for the integral and partial molar enthalpies of formation at 623 and 773 K. A number within parenthesis is the estimated standard deviation (esd). The average error of the individual measurement was found to be 0.6% for the enthalpy of formation at 623 K and 0.36% for that at 773 K. There exists no report on the enthalpy of formation in the

Table 4. Integral and Partial Molar Enthalpies of Formation of the γ Phase in the System Silver-Indium in kJ mol^{-1}. Estimated Standard Deviations in Parenthesis M(Ag)=107.868 g mol^{-1}; M(In)=114.82 g mol^{-1}

x_{In}	T=773 K			T=623 K		
	$-\Delta_f H°$	$-\Delta_f H_1^\circ$	$-\Delta_f H_2^\circ$	$-\Delta_f H°$	$-\Delta_f H_1^\circ$	$-\Delta_f H_2^\circ$
0.300	15.488(129)	15.984	14.260	15.264(0)	15.782	14.068
0.350	15.373(0)	15.937	14.368	15.158(23)	15.736	14.169
0.400	15.257(141)	15.882	14.470	14.964(142)	15.682	14.264
0.450	15.204(125)	15.821	14.566	—	—	—

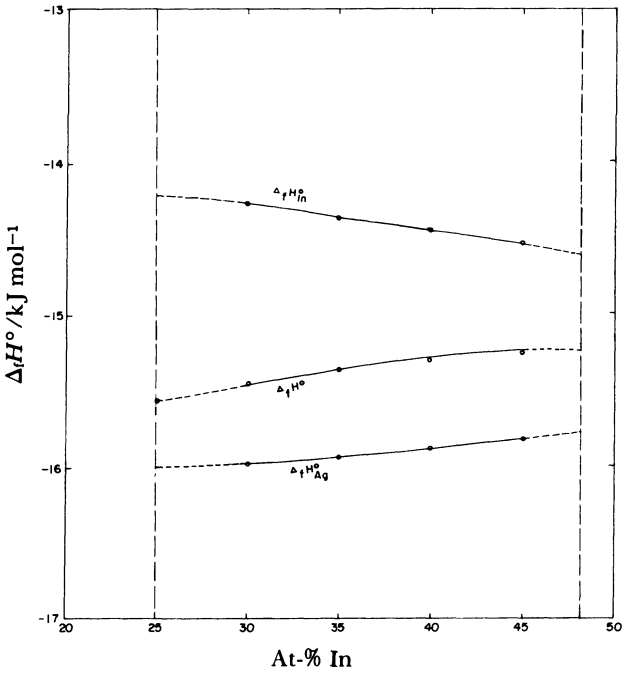

Fig. 2. The integral and partial molar enthalpies of formation at 623 K in the range of the γ phase in the system Ag–In.

literature, hence a comparison with the present data can not be made.

From curve-fitting calculations it was possible to derive equations for the relation of the enthalpy of formation to the mole fraction of indium:

$$\Delta_f H^\circ(623\ \mathrm{K}) = -16.117 + 2.641x_2 - 1.506x_2^2 + 0.050x_2^3, \quad (12)$$

$$\Delta_f H^\circ(773\ \mathrm{K}) = -15.914 + 2.607x_2 - 1.486x_2^2 + 0.049x_2^3. \quad (13)$$

These equations produce the curves of the enthalpies of formation against the temperature as shown in Fig. 3. It is clearly observable that the enthalpy of formation depends insignificantly on the temperature. This is a somewhat surprising observation since Wittig and Schöffl[7] claimed in their study on the system Al–Zn that a pronounced temperature dependence of the enthalpy of formation is a typical property of all metallic alloys. However, it appears that Wittig's conclusion was incorrect: The pronounced temperature dependence of the enthalpy of formation in the system Al–Zn was attributed to lattice defects of greater expansion of aluminum lattice in the alloy compared with the expansion in pure aluminum metal. Since such a lattice defect in the structure due to an increase in the temperature is not common to all metallic alloys, a pronounced temperature dependence of the enthalpy of formation (which is not observed on the system Ag–In) seemed

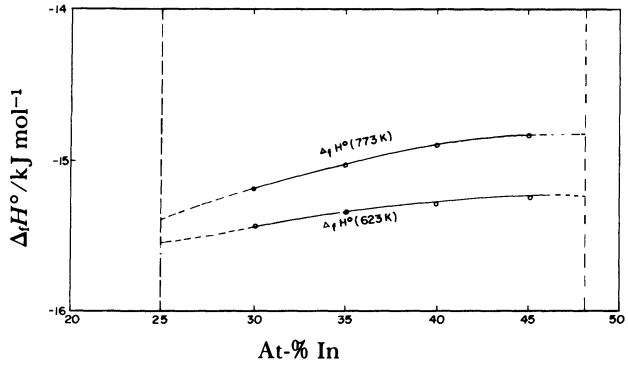

Fig. 3. The enthalpies of formation at 623 and 773 K in the range of the γ phase in the system Ag–In.

not to be a general property of all metallic alloys. The relation of the enthalpy of formation to temperature depends on the type of the system and on the range of temperature and composition in which the phase can exist. This was deduced from our study on the system Sn–Sb[5] where the pronounced temperature dependence was attributed to the continuous formation of liquid from the solid solution (the β' phase) in accordance with the phase diagram.

As illustrated in Table 4 and Figs. 2 and 3, the enthalpy of formation is negative and increases slightly with the increase of the composition due to the insertion of indium atom in the structure. The insertion of indium atom which is not much larger than silver atom in the structure leads to a small positive deformation work so that the enthalpy of formation depends slightly on the composition. The charging of the Brillouin zones is always the reason for the increase of the enthalpy of formation with the increase of the composition (see Ref. 3).

With reference to the definition of the partial molar quantities (Eqs. 5 and 6), we obtain through Eqs. 12 and 13 the following equations for $\Delta_f H_1^\circ$ and $\Delta_f H_2^\circ$:

$T = 623$ K

$$\Delta_f H_1^\circ = -16.117 + 1.506x_2^2 - 0.100x_2^3, \quad (14)$$

$$\Delta_f H_2^\circ = -13.476 + 3.012x_2 + 1.356x_2^2 - 0.100x_2^3 \quad (15)$$

and

$T = 773$ K

$$\Delta_f H_1^\circ = -15.914 + 1.486x_2^2 - 0.098x_2^3, \quad (16)$$

$$\Delta_f H_2^\circ = -13.307 - 2.972x_2 + 1.486x_2^2 - 0.098x_2^3. \quad (17)$$

Figure 2 shows that the partial molar enthalpy of silver is negative and becomes more negative at higher composition. A hypothetical illustration of this behavior is probably that a poor fraction of silver s-electrons forms a weak bond with indium ions. At higher composition, the equilibrium shifts for the benefit of the delivery of further electrons on indium.

The partial molar enthalpy of formation of indium is also negative, but increases at higher composition. The negative trend in the whole range of the γ phase indicates the stability of the structure. However, this stability decreases at higher composition due to the insertion of the somewhat larger indium atom in the structure: the structure exhibits a higher tension resulting from a small deformation work which is associated with the insertion of the indium atom in the structure.

References

1) F. E. Wittig, *Z. Electrochem.*, **63**, 327 (1959).
2) W. A. Badawi, *Bull. Chem. Soc. Jpn.*, **61**, 1351 (1988).
3) W. A. Badawi, *Bull. Chem. Soc. Jpn.*, **60**, 2599 (1987).
4) W. A. Badawi, *Bull. Chem. Soc. Jpn.*, **60**, 3771 (1987).
5) W. A. Badawi, *Bull. Chem. Soc. Jpn.*, **62**, 285 (1989).
6) Hultren et al., "Selected Values of the Thermodynamic Properties of Binary Alloys," Am. Soc. Metals, Ohio (1973).
7) F. E. Wittig and L. Schöffl, *Z. Metalk.*, **51**, 700 (1960).
8) F. E. Wittig, *Chemie-Ingenieur-Technik*, **32**, 1037 (1960).
9) F. E. Wittig and E. Gehring, *Z. f. Naturforschung*, **18a**, 351 (1963).
10) C. Wagner, "Thermodynamics of Alloys, Reading, Mass.," Addison-Wesley, (1952).
11) W. A. Badawi, *Bull. Chem. Soc. Jpn.*, **61**, 2261 (1988).

 © 1989 The Chemical Society of Japan Bull. Chem. Soc. Jpn., 62, 309—316 (1989)

Conductimetric Studies of Ionic Association of Tetraalkylammonium Halides and Tetraphenylborate in *N,N*-Dimethylformamide-Methyl Ethyl Ketone Mixtures at 25 °C

Nurul Islam,* S. B. A. Zaidi, and Aijaz Ahmad Ansari
Department of Chemistry, Aligarh Muslim University, Aligarh-202002, India
(Received April 18, 1988)

The molar conductivities of Et_4NBr, n-Pr_4NBr, n-Bu_4NBr, and n-Bu_4NBPh_4 have been measured in *N,N*-dimethylformamide–methyl ethyl ketone (DMF–MEK) mixtures ($34.5 \geqslant D \geqslant 20.10$) over the maximum concentration range ($2 \times D^3 \times 10^{-7}$ mol dm^{-3}) along with the densities and viscosities of the solvent mixtures at 25 °C. The conductance data have been analyzed by using the Fuoss-1978 (F78) conductance equation and the results compared with those obtained from the Justice (J) and the Fuoss-Onsager-Skinner (FOS) equations. The molar conductivities at infinite dilution (Λ_0), the thermodynamic association constant (K_A) and the distance or the ion-size parameter (R or $a°$) are evaluated from these data. A better fit of the parameters was provided by the F78 equation which yielded K_A and R values. The Λ_0 and the K_A values are found to increase with decrease in the dielectric constant of the medium and in a given solvent mixture they follow the order $Et_4NBr > n$-$Pr_4NBr > n$-$Bu_4NBr > n$-Bu_4NBPh_4.

Extensive studies on the electrolytic conductivities in various pure and mixed aprotic solvents have been made[1–8] to examine the magnitude and the nature of ion–ion and ion–solvent interactions in terms of the limiting molar conductance, the ion-size parameter and the ionic association constant. The solvent properties like the viscosity and the dielectric constant have also been taken into account in determining the extent of ionic association and the solute–solvent interactions which enabled many to interpret the unique structure of the solvent.

The present study deals with the mixtures of *N,N*-dimethylformamide and methyl ethyl ketone (DMF–MEK) both of which are dipolar aprotic and in the pure state have no tendencies[9–11] to self-association through the dipole–dipole interactions. Recently,[12] it has been reported that the physical properties of DMF–MEK mixtures over the entire composition range show an ideal behavior for the physicochemical investigations in the cases of 1:1 electrolytes. Consequently, the investigation of conductance behavior of tetraalkylammonium halides and tetraphenylborate has been undertaken with a view to examining the suitability of the F78[13,14] conductance equation over those of the Justice[15] and the FOS[16] conductance equations.

Experimental

Methyl ethyl ketone was treated several times with saturated potassium carbonate solution to remove the acid impurities and the two layers thus obtained were separated. After removing most of the water by distillation, the ketone was dried over sodium sulfate and anhydrous potassium carbonate for several days. The decanted liquid was fractionally distilled several times until the measured density (0.7999 kg m^{-3}), viscosity (0.379 kg m^{-1} s^{-1}) and specific conductance: (2—3.5)$\times 10^{-8}$ S cm^{-1} at 25 °C were found to be comparable with those of the corresponding literature values.[12,17]

N,N-Dimethylformamide was purified by keeping it over anhydrous sodium carbonate for 24 hours and was then distilled under reduced pressure in a dry nitrogen atmosphere and the fraction distilling at 73 °C/57 mmHg (1 mmHg≈133.322 Pa) was collected. The purified solvent had a density: 0.9443 kg m^{-3}; viscosity: 0.795 kg m^{-1} s^{-1} and specific conductance: (1—2)$\times 10^{-7}$ S cm^{-1}, which agree well with those of the reported[18,19] values.

Tetrabutylammonium tetraphenylborate (n-Bu_4NBPh_4) was prepared[20] by dissolving sodium tetraphenylborate in conductivity water (2% solution) and filtered to remove a small amount of insoluble impurities. To this, an equivalent amount of tetrabutylammonium bromide in 2% aqueous solution was slowly added. The bulky white precipitate thus obtained was washed five times by decantation. After preliminary drying, the product was recrystallized four times from 1:3 water–acetone mixture and finally dried for several days at 40 °C and 10^{-4} mmHg pressure (mp 223—225 °C).

The pure samples of Et_4NBr, n-Pr_4NBr (both, Fluka, AG), and n-Bu_4NBr (Eastman, AG) procured from the supplier were used as such.

Conductance measurements were carried out by the IMPEDENCE BRIDGE, 1608-A (General Radio & Co., U.S.A.) at a constant frequency of 1 kHz with an accuracy of ±0.05—0.005%. The Pyrex conductivity cell (cell constant, 0.7891 cm^{-1}) having bright platinum disc electrodes was used. The cell was calibrated by the method of Lind and co-workers[21] using the decinormal potassium chloride solutions. The overall reproducibility of the conductance measurement was found to be within ca. ±0.025%.

The solvent mixtures were prepared by weight and in each case initially a concentrated electrolytic solution ($C_{max} = 2 \times D^3 \times 10^{-7}$)[22] of the salt was prepared and several solutions of different concentrations were prepared by the method of dilution. Dielectric constants of the solvent mixtures were taken from the literature.[12]

All the measurements were carried out in an atmosphere of pure and dry nitrogen at 25±0.01 °C in a thermostated oil bath.

Table 1. Properties of Solvent Mixtures at 25 °C

Solvent No.	$X_{DMF\%}$	ρ / g cm^{-3}	η / cP[a]	D	q/Å[b]
1	00.00	0.7999 (0.79987)[c]	0.3790 (0.3795)[c]	18.01[c]	15.10
2	11.46	0.8157	0.419	20.10	13.94
3	22.55	0.8311	0.452	21.84	12.83
4	33.29	0.8456	0.487	23.53	11.90
5	43.70	0.8613	0.527	25.40	11.03
6	53.80	0.8768	0.569	27.40	10.23
7	73.10	0.9043	0.655	31.01	9.04
8	82.32	0.9179	0.699	32.95	8.50
9	91.29	0.9312	0.745	34.50	8.12
10	100.00	0.9443 (0.9440)[c]	0.795 (0.796)[c]	36.71[c]	—

a) 1 P=0.1 Pa s. b) Bjerrum distance. c) Ref. 35.

Results and Discussion

The physical properties of the solvents employed in computation are listed in Table 1. The molar conductivities, Λ(S cm^2 mol^{-1}) of dilute electrolytic solutions of varying concentrations, C(mol dm^{-3}) of Et_4NBr, n-Pr_4NBr, n-Bu_4NBr, and n-Bu_4NBPh_4 in mixtures of DMF–MEK are recorded at 25 °C (Table 2).

The concentration dependence of the above conductance data has been analyzed in terms of the F78 equation[13,14] and the parameters thus obtained are compared with those obtained by employing the J and the FOS equations.[15,16]

The F78 equation[13,14] based on the concept of diffusion controlled steady state approach is of the form,

$$\Lambda = [1 - \alpha(1 - \gamma)][\Lambda_0(1 + \Delta x/x) + \Delta\Lambda_e] \quad (1)$$

where Λ_0 is the limiting equivalent conductance, the term $\Delta x/x$ represents the relaxation effect, $\Delta\Lambda_e$ the electrophoretic effect, while γ denotes the fraction of solute present as free ions and α is the contact pair parameter. Both Δx and $\Delta\Lambda_e$ depend on the values of the diameter of the Gurney cosphere, R, the dielectric constant and the viscosity of the medium. The parameters and the auxilliary variables are related by a set of the following equations:

$$K_R = (1 - \alpha)(1 - \gamma)/C\gamma^2 f^2 = (4\pi NR^3/3000)\exp(\beta/R) \quad (2)$$

$$K_S = \alpha/(1 - \alpha) \quad (3)$$

The conductometric association constant, K_A is given by

$$K_A = (1 - \gamma)/C\gamma^2 f^2 = K_R/(1 - \alpha) \quad (4)$$

while the activity coefficient, f, is

$$-\ln f = \beta\kappa/2(1 + \kappa R) \quad (5)$$

in which $\beta = e^2/DkT$ and $\kappa^2 = 8\pi\beta\gamma n = \pi\beta NC/125$. The relevant terms have their usual significance. For this purpose, the PARACOND[23] computer program designed for the symmetrical electrolytes has been used.

Similarly, each set of conductance data has been analyzed using Justice's modification[15] of the Fuoss-Hsia equation[24] and the relevant constants derived by employing the Fernandez-Prini equation.[1] The Fuoss-Hsia equation is given by,

$$\Lambda = \Lambda_0 - S(C\gamma)^{1/2} + E\gamma C\ln(C\gamma) + J_1 C\gamma - J_2(C\gamma)^{3/2} - \Lambda C f_\pm^2 \gamma K_A \quad (6)$$

where γ is the degree of dissociation, $f_\pm$ the mean molar activity coefficient, and all other terms have their usual significance. The thermodynamic association constant is given by

$$K_A = (1 - \gamma)/C\gamma^2 f_\pm^2 \quad (7)$$

in which the activity coefficient for the neutral ion pair is taken as unity. The activity coefficients are obtained using the Debye–Hückel equation,

$$\ln f_\pm = -A(\gamma C)^{1/2}/\{1 + BR_j(C\gamma)^{1/2}\}. \quad (8)$$

As proposed by Justice,[15] the distance parameter, R_j of Eq. 8 has been taken as the Bjerrum critical distance, q ($=e^2/2DkT$). The analysis of the data in terms of Eq. 6 has been carried out by a pit-mapping method[25] in which Λ_0, R_j, and K_A are varied until a minimum is located for the standard error of estimate. This latter quantity, σ_Λ is defined by

$$\sigma_\Lambda = \{\sum(\Lambda_{obs} - \Lambda_{calc})^2/(N - 3)\}^{1/2}. \quad (9)$$

Finally, the above set of conductance data (Table 2) has been analyzed in terms of the FOS equation,[16]

$$\Lambda = \Lambda_0 - S(C\gamma)^{1/2} + EC\gamma\log(6E'_1 C\gamma) + LC\gamma - C\gamma f_\pm^2 \Lambda K_A \quad (10)$$

for associated electrolytes. The symbols used have their usual meaning. Kay's computer program[26] based on the least square method of calculation is employed here.

The values of the best fit parameters of Λ_0, K_A, and the distance or the ion-size parameter (R or a°)

Table 2. Molar Conductivities, Λ(S cm^2 mol^{-1}) and Molar Concentrations, C(mol dm^{-3}) of Et_4NBr, n-Pr_4NBr, n-Bu_4NBr, and n-Bu_4NBPh_4 in DMF-MEK Mixtures at 25 °C

Et_4NBr		n-Pr_4NBr		n-Bu_4NBr		n-Bu_4NBPh_4	
$C\times10^4$	Λ	$C\times10^4$	Λ	$C\times10^4$	Λ	$C\times10^4$	Λ
			Solvent 2				
14.127	102.51	15.842	99.95	16.697	97.72	16.277	80.29
11.772	106.52	13.941	102.44	12.987	102.13	12.660	82.66
8.829	112.77	11.617	106.01	9.740	106.97	9.495	85.23
7.063	117.43	8.713	111.42	7.546	111.09	6.330	88.42
5.886	121.11	6.280	117.21	5.844	114.87	4.682	90.53
2.943	133.56	3.645	125.76	2.922	123.68	2.843	93.49
1.762	140.92	1.741	134.79				
			Solvent 3				
17.453	97.38	17.246	96.16	14.889	94.08	20.432	74.75
15.177	100.29	14.996	98.81	12.947	96.06	17.945	76.02
12.467	104.35	12.318	102.45	10.635	98.71	13.051	78.93
9.696	109.41	9.077	107.91	8.272	101.93	10.246	80.95
6.981	115.67	6.898	112.51	5.956	105.78	8.512	82.39
3.491	127.17	5.174	116.95	2.978	112.42	5.932	85.01
2.327	132.67	3.449	122.52	1.489	117.16	3.589	88.04
			Solvent 4				
24.743	94.68	23.315	89.48	25.470	86.16	25.351	71.52
21.516	97.44	19.429	92.41	16.621	92.36	21.126	73.23
18.328	100.56	15.753	95.66	12.994	95.71	17.484	74.92
14.996	104.39	12.953	98.57	10.526	98.41	13.000	77.44
12.372	108.05	8.831	103.91	8.475	101.01	9.219	80.08
8.837	113.91	5.251	110.14	5.129	106.31	5.548	83.42
5.438	121.52	2.913	115.79	3.570	109.51	2.533	87.33
2.472	131.16						
			Solvent 5				
22.840	95.42	21.182	86.26	30.771	82.58	13.388	73.55
19.861	97.99	18.419	88.37	26.758	84.61	11.642	74.58
16.918	100.96	15.130	91.16	22.793	87.02	9.917	75.76
13.051	105.56	11.768	94.71	18.101	90.16	7.650	77.43
10.151	109.81	8.826	98.32	13.987	93.54	5.950	79.06
7.613	114.26	7.061	101.01	9.458	98.19	4.463	80.48
4.567	121.16	4.236	106.12	6.680	101.91	2.231	83.37
2.284	128.29	2.118	111.34	4.734	105.06	1.336	84.91
			Solvent 6				
30.107	90.08	29.914	80.82	29.779	79.75	23.945	67.33
26.494	92.36	25.482	83.27	24.815	82.24	19.156	69.16
22.078	95.56	21.501	85.80	20.121	85.04	15.963	70.56
17.901	99.08	17.201	89.04	16.544	87.46	13.683	71.71
14.719	102.28	13.761	92.10	12.408	90.85	10.642	73.43
10.036	107.96	9.382	96.93	7.445	96.07	7.982	75.21
7.360	112.18	6.880	100.41	3.223	101.62	4.368	78.24
3.310	120.65	3.440	106.64			2.395	80.48
			Solvent 7				
31.754	85.77	32.989	77.53	31.714	75.47	31.903	62.44
28.225	87.91	28.686	79.63	27.578	77.21	27.741	63.57
23.815	90.77	24.436	81.91	22.653	79.87	23.632	64.79
19.052	94.41	19.993	84.63	17.619	82.78	19.335	66.29
15.242	98.01	15.344	88.04	12.686	86.38	15.951	67.58
9.145	105.16	11.376	91.58	7.611	91.18	11.601	69.55
5.716	110.67	7.368	95.99	5.074	94.26	7.569	71.76
3.629	114.95	3.924	101.06	3.171	97.11	4.579	73.92
						3.187	75.17
			Solvent 8				
28.677	80.63	29.444	75.89	22.086	71.51	17.945	62.57
24.580	82.91	26.767	77.07	17.436	73.71	15.834	63.34
19.118	86.44	23.555	78.63	13.251	75.89	13.459	64.28

Table 2. (Continued)

Et_4NBr		n-Pr_4NBr		n-Bu_4NBr		n-Bu_4NBPh_4	
$C\times10^4$	Λ	$C\times10^4$	Λ	$C\times10^4$	Λ	$C\times10^4$	Λ
			Solvent 8				
14.388	90.18	19.629	80.75	9.465	78.48	10.767	65.50
8.603	95.99	14.722	83.83	6.023	81.26	7.690	67.06
6.145	99.26	9.815	87.68	3.614	83.68	5.984	68.12
3.441	103.64	4.907	92.89	2.581	85.01	3.230	70.11
		2.181	96.73			1.795	71.49
			Solvent 9				
31.214	78.28	28.693	73.66	28.587	69.05	22.468	60.52
26.755	80.19	24.594	75.12	23.823	70.65	18.617	61.66
20.809	83.13	19.129	77.63	17.867	72.97	14.480	63.04
14.406	87.01	14.346	80.12	12.994	75.24	10.860	64.45
8.644	91.58	7.173	84.96	10.210	76.77	7.082	66.24
5.402	94.86	4.304	87.56	5.105	80.25	4.287	67.87
3.745	96.91	3.311	88.63	3.576	81.59	2.603	69.11

corresponding to the minimum standard deviations from the relevant (F78, J and FOS) equations are listed in Tables 3-I, 3-II, and 3-III, respectively.

The above calculations have been carried out on a VAX-11/780 computer.

A comparison of the applicability of the above three equations to the conductance is made here. The computed values of Λ_0 for the salts under study in various DMF–MEK mixtures obtained using the F78, the J and the FOS equations are found to be close to each other. On the one hand, these Λ_0 show the usual decrease in their values with increase in the size of the ions in the order: $Et_4\overset{+}{N}>n\text{-}Pr_4\overset{+}{N}>n\text{-}Bu_4\overset{+}{N}>Ph_4B^-$ in accord with the trend in the behavior of their parent Λ values. On the other hand, the Λ_0 values are found to increase with decrease in the dielectric constant of the solvent mixtures. Such a situation has also been reported earlier for several pure[11,27] and mixed aprotic solvents[28,29] and has been attributed to a number of effects such as the solvent structure and the ion–solvent interactions. The solvent structure effects are apparently reflected by the viscosity behavior which is marked by its increase with increase in the mol% of DMF. The excess thermodynamic parameters[12] of the present system show an ideal mixing which suggest the absence of intermolecular interactions in DMF–MEX mixtures similar to those observed for the DMF–acetone system.[6]

The K_A values (Table 3) obtained using the F78 equation are found to be ca. 23.26% and ca. 30.38% higher than those obtained from the J and the FOS equations, respectively. An increase in the K_A values with decrease in the dielectric constant of the medium is in accordance with those reported earlier[27–33] for similar system. The applicability of the various theories of ion association can be examined in terms of the dependence of $\log K_A$ upon $1/D$ (Fig. 1). The nonlinearity of the plot suggests the applicability of the F78, FOS and Justice theories of ionic association.

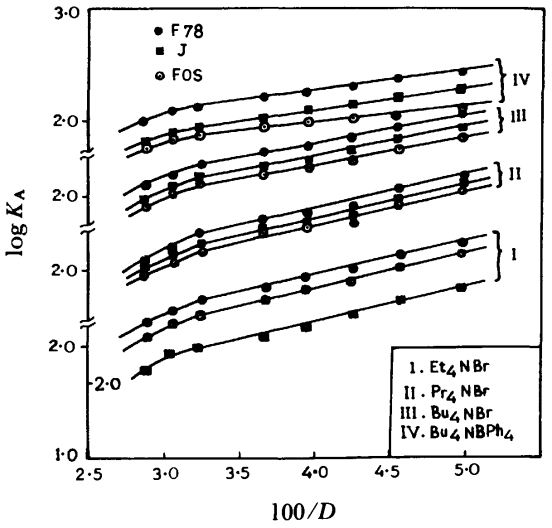

Fig. 1. $\log K_A$ vs. $100/D$.

Further, it is evident from Table 3 that the K_A values for all the salts in a given dielectric constant decrease with the increasing size of the cations in the order, $Et_4\overset{+}{N}>n\text{-}Pr_4\overset{+}{N}>n\text{-}Bu_4\overset{+}{N}\approx BPh_4^-$, similar to those observed earlier[11,30,34,35] due to apparent decrease in the ion–dipole interaction.

The distance or the ion-size parameter (R or $a°$) values obtained using different equations are compared with the crystallographic radii of the salts under study. The values of R_j or $a°$ obtained using the J and the FOS equations in some of the solvent mixtures (Tables 3-II and 3-III) are less than the corresponding crystallographic radii of the ion pairs and are, therefore, not understandable. The F78 equation, on the other hand, predicts meaningful values of R as 11.40 to 17.55 Å in the media of $34.50\geqslant D\geqslant 20.10$ which are also more than the Bjerrum critical distance, q ($=e^2/2DkT$) unlike the R_j or $a°$ values (of J or the FOS equations) which are found to be less than the q values. It may, however, be noted that the J equation

Table 3-I. Best Fit Parameters for Et_4NBr, n-Pr_4NBr, n-Bu_4NBr, and n-Bu_4NBPh_4 in DMF-MEK Mixtures at 25°C, Using the F78 Conductance Equation

Salt	Λ_0 / S cm^{2}mol^{-1}	K_A / dm^3 mol^{-1}	K_R	K_S	α	R / Å	σ_Λ/%
			Solvent 9				
Et_4NBr	104.43±0.01	164.81	18.82	7.76	0.885	12.80	0.01
n-Pr_4NBr	94.51±0.04	143.48	21.09	5.80	0.853	13.65	0.04
n-Bu_4NBr	86.99±0.01	128.16	22.53	4.69	0.824	14.15	0.01
n-Bu_4NBPh_4	72.72±0.01	111.34	26.32	3.23	0.763	15.36	0.01
			Solvent 8				
Et_4NBr	113.09±0.03	223.98	16.62	12.48	0.926	11.40	0.03
n-Pr_4NBr	102.42±0.03	179.08	17.63	9.16	0.902	11.85	0.03
n-Bu_4NBr	90.23±0.05	159.54	21.46	6.34	0.864	13.35	0.06
n-Bu_4NBPh_4	74.74±0.01	127.15	27.46	3.63	0.784	15.30	0.02
			Solvent 7				
Et_4NBr	127.39±0.05	276.92	20.66	12.40	0.925	12.40	0.03
n-Pr_4NBr	111.51±0.05	233.44	23.09	9.11	0.901	13.30	0.03
n-Bu_4NBr	105.21±0.06	209.88	24.11	7.70	0.885	13.65	0.05
n-Bu_4NBPh_4	80.30±0.02	137.41	30.15	3.56	0.780	15.50	0.02
			Solvent 6				
Et_4NBr	134.02±0.04	308.08	27.32	10.27	0.911	13.20	0.02
n-Pr_4NBr	118.49±0.01	291.98	30.33	8.62	0.896	14.15	0.00
n-Bu_4NBr	112.29±0.03	244.59	31.17	6.85	0.872	14.40	0.02
n-Bu_4NBPh_4	85.92±0.01	165.90	34.17	3.85	0.794	15.24	0.01
			Solvent 5				
Et_4NBr	141.23±0.02	392.53	31.82	11.34	0.918	13.50	0.01
n-Pr_4NBr	121.00±0.05	327.13	35.22	8.28	0.892	14.50	0.03
n-Bu_4NBr	119.29±0.05	281.78	37.82	6.45	0.866	15.20	0.03
n-Bu_4NBPh_4	89.36±0.04	194.13	39.80	3.88	0.795	15.70	0.05
			Solvent 4				
Et_4NBr	146.95±0.05	462.65	38.29	11.08	0.917	14.10	0.02
n-Pr_4NBr	129.16±0.02	361.53	42.25	7.56	0.883	15.15	0.01
n-Bu_4NBr	123.04±0.02	322.51	43.88	6.35	0.864	15.55	0.01
n-Bu_4NBPh_4	94.56±0.01	213.59	46.66	3.58	0.782	16.20	0.01
			Solvent 3				
Et_4NBr	152.25±0.01	650.28	42.92	14.15	0.934	13.90	0.01
n-Pr_4NBr	143.83±0.02	552.89	45.91	11.04	0.917	14.70	0.006
n-Bu_4NBr	126.15±0.01	380.57	53.43	6.12	0.859	16.45	0.006
n-Bu_4NBPh_4	98.00±0.02	254.28	57.31	3.44	0.775	17.25	0.02
			Solvent 2				
Et_4NBr	161.05±0.01	823.58	52.02	14.83	0.936	14.35	0.005
n-Pr_4NBr	150.97±0.02	650.72	58.10	10.19	0.911	15.80	0.01
n-Bu_4NBr	142.45±0.04	540.16	61.16	7.83	0.886	16.45	0.02
n-Bu_4NBPh_4	103.41±0.02	284.32	66.78	3.26	0.765	17.55	0.014

yields higher values of R_j ($25.40 \geqslant D \geqslant 20.10$) than the crystallographic radii of the ion pairs. Although not too much can be deduced from the best-fit R values as they are particularly susceptible to the choice of conductance equation. However, some generalization can be made about the R values obtained from the F78 equation since this presupposes that ion pairs may be of solvent-separated or contact ion pair variety. For a contact ion pair (CIP), R is simply taken as the sum of the ionic radii whereas for the solvent separated ion pair (SSIP), $R=\bar{a}+ds$, where $\bar{a}$ is taken as the sum of the ionic radii and ds is the diameter of solvent molecules. The ds value estimated to be 4.98 Å for MEK and 5.03 Å for DMF. Consequently, the resultant association constant is greater for smaller ions than those for the larger ones because the smaller ion prefers to form an additional CIP with the formation of SSIP in DMF-MEK mixtures and it is apparent from Table 3-I that the SSIP formation constant, K_R increases and CIP formation constant, K_S

Table 3-II. Best Fit Parameters for Et_4NBr, n-Pr_4NBr, n-Bu_4NBr, and n-Bu_4NBPh_4 in DMF-MEK Mixtures at 25°C, Using the J Conductance Equation

Salt	Λ_0 / S cm² mol⁻¹	K_A / dm³ mol⁻¹	R_j / Å	σ_Λ/%
		Solvent 9		
Et_4NBr	104.40±0.01	134.53	2.43	0.01
n-Pr_4NBr	94.42±0.05	107.06	5.98	0.05
n-Br_4NBr	86.96±0.01	91.01	5.07	0.01
n-Bu_4NBPh_4	72.72±0.01	69.029	4.46	0.01
		Solvent 8		
Et_4NBr	113.06±0.04	197.48	1.79	0.03
n-Pr_4NBr	102.37±0.03	149.45	5.24	0.03
n-Bu_4NBr	90.30±0.06	127.15	3.48	0.05
n-Bu_4NBPh_4	74.76±0.02	83.44	3.79	0.02
		Solvent 7		
Et_4NBr	127.21±0.06	239.68	5.42	0.04
n-Pr_4NBr	111.27±0.04	189.88	6.54	0.03
n-Bu_4NBr	105.05±0.12	166.64	6.98	0.09
n-Bu_4NBPh_4	80.28±0.03	87.73	6.80	0.03
		Solvent 6		
Et_4NBr	133.86±0.04	261.70	7.28	0.02
n-Pr_4NBr	118.39±0.01	241.44	6.83	0.01
n-Bu_4NBr	110.58±0.16	157.49	7.73	0.12
n-Bu_4NBPh_4	85.90±0.01	110.20	8.47	0.01
		Solvent 5		
Et_4NBr	141.10±0.02	340.04	7.69	0.01
n-Pr_4NBr	120.86±0.04	267.17	8.71	0.03
n-Bu_4NBr	119.07±0.05	216.46	9.28	0.04
n-Bu_4NBPh_4	89.34±0.05	128.41	9.96	0.05
		Solvent 4		
Et_4NBr	146.70±0.04	396.24	9.44	0.02
n-Pr_4NBr	129.05±0.02	293.08	9.52	0.02
n-Bu_4NBr	122.88±0.01	249.46	10.19	0.01
n-Bu_4NBPh_4	94.56±0.01	140.15	10.57	0.01
		Solvent 3		
Et_4NBr	152.11±0.03	581.75	8.94	0.02
n-Pr_4NBr	143.62±0.01	476.67	9.87	0.01
n-Bu_4NBr	126.14±0.01	298.95	10.28	0.01
n-Bu_4NBPh_4	97.94±0.02	162.05	11.87	0.02
		Solvent 2		
Et_4NBr	160.83±0.01	739.32	10.27	0.005
n-Pr_4NBr	150.83±0.02	558.91	10.93	0.01
n-Bu_4NBr	142.23±0.02	440.31	11.94	0.014
n-Bu_4NBPh_4	103.34±0.01	179.30	13.27	0.010

decrease with increasing the size of the cations in a given dielectric constant of the medium.

Thus, in view of the above findings the F78 equation seems to be better suited for explaining the conductance behavior of the present system. The successful applicability of this equation seems to stem from the consideration of the solvated radii of ions present in solution in the diffuse steady state and consequently gives significantly better fit parameters compared to the other available conductance equations.

We are grateful to Prof. R. M. Fuoss, Prof. R. L. Kay, and Prof. J. C. Justice for sending the details of their equations and computer programs. One of us (S.B.A.Z.) thanks the U.G.C., Government of India for financial assistance.

Table 3-III. Best Fit Parameters for Et_4NBr, n-Pr_4NBr, n-Bu_4NBr, and n-Bu_4NBPh_4 in DMF–MEK Mixtures at 25°C, Using the FOS Conductance Equation

Salt	Λ_0 / S cm² mol⁻¹	K_A / dm³ mol⁻¹	$a°$ / Å	σ_Λ/%
		Solvent 9		
Et_4NBr	104.40±0.05	129.69	6.41	0.02
n-Pr_4NBr	94.41±0.10	99.46	5.40	0.06
n-Bu_4NBr	86.95±0.02	84.51	5.86	0.01
n-Bu_4NBPh_4	72.72±0.01	66.17	7.22	0.01
		Solvent 8		
Et_4NBr	113.00±0.15	189.48	6.60	0.02
n-Pr_4NBr	102.40±0.06	142.92	6.35	0.04
n-Bu_4NBr	90.31±0.11	126.64	8.60	0.06
n-Bu_4NBPh_4	74.76±0.03	79.92	7.50	0.03
		Solvent 7		
Et_4NBr	127.20±0.16	230.27	6.38	0.06
n-Pr_4NBr	111.20±0.10	177.95	6.77	0.04
n-Bu_4NBr	105.10±0.15	159.49	6.68	0.09
n-Bu_4NBPh_4	80.26±0.05	79.10	6.80	0.04
		Solvent 6		
Et_4NBr	133.80±0.11	245.57	6.80	0.04
n-Pr_4NBr	118.30±0.05	226.36	7.07	0.02
n-Bu_4NBr	112.10±0.11	174.59	6.56	0.04
n-Bu_4NBPh_4	85.87±0.01	92.33	6.54	0.01
		Solvent 5		
Et_4NBr	141.10±0.07	320.13	7.25	0.03
n-Pr_4NBr	120.80±0.15	244.51	6.82	0.02
n-Bu_4NBr	118.90±0.18	186.17	6.63	0.06
n-Bu_4NBPh_4	89.32±0.08	105.38	6.07	0.06
		Solvent 4		
Et_4NBr	146.60±0.12	360.50	6.44	0.04
n-Pr_4NBr	128.90±0.09	256.36	6.44	0.03
n-Bu_4NBr	122.70±0.06	210.16	6.27	0.02
n-Bu_4NBPh_4	94.43±0.05	97.85	5.97	0.03
		Solvent 3		
Et_4NBr	152.00±0.09	545.70	7.85	0.04
n-Pr_4NBr	143.50±0.11	434.37	7.35	0.02
n-Bu_4NBr	126.10±0.04	259.24	7.40	0.02
n-Bu_4NBPh_4	97.74±0.08	101.88	5.78	0.03
		Solvent 2		
Et_4NBr	160.70±0.01	686.47	7.94	0.04
n-Pr_4NBr	150.70±0.10	502.16	7.61	0.03
n-Bu_4NBr	142.00±0.10	372.66	6.89	0.02
n-Bu_4NBPh_4	103.10±0.07	97.67	5.81	0.02

References

1) R. Fernandez-Prini, "Physical Chemistry of Organic Solvent Systems," ed by A. C. Covington and T. Dickinson, Plenum Press, London (1973).

2) J. Barthel, R. Watcher, and H. J. Gores, "Modern Aspects of Electrochemistry," Vol. 13, ed by B. E. Conway and J. O'M. Bockris, Plenum Press, London (1979).

3) R. Jasinski, "Advances in Electrochemistry and Electrochemical Engineering," Vol. 8, ed by C. W. Tobias, Wiley-Interscience, New York (1971).

4) Y. Matsuda and H. Satake, *J. Electrochem. Soc.*, **127**, 877 (1980).

5) Y. Matsuda, H. Nakashima, M. Morita, and Y. Takasu, *J. Electrochem. Soc.*, **128**, 2552 (1981).

6) D. S. Gill and H. Schneider, *Ind. J. Chem.*, **19A**, 313 (1980).

7) O. Fischer, J. Vrba, and E. Vischerova, *Colln. Czeck. Commun.*, **41**, 695 (1976).

8) D. S. Gill and A. N. Sharma, *J. Chem. Soc., Faraday Trans. 1*, **78**, 465 (1982).

9) J. B. Kissinger, M. M. Tannahill, M. S. Greenberg,

and A. I. Popov, *J. Phys. Chem.*, **77**, 2444 (1973).
10) N. E. Hill and W. E. Vaugham, "Dielectric Properties and Molecular Behaviour," Van Nostrand, Reinhold, New York (1969), p. 31.
11) P. G. Sears, D. Wilhoit, and L. R. Dawson, *J. Phys. Chem.*, **59**, 373 (1955).
12) O. Fischer and M. S. K. Niazi, *Electrochim. Acta*, **27**, 791 (1982).
13) R. M. Fuoss, *J. Phys. Chem.*, **82**, 2427 (1978).
14) R. M. Fuoss, *Proc. Natl. Acad. Sci. U.S.A.*, **75**, 16 (1978).
15) J. C. Justice, *J. Chim. Phys.*, **65**, 353 (1968).
16) R. M. Fuoss, L. Onsager, and J. F. Skinner, *J. Phys. Chem.*, **69**, 2581 (1965).
17) G. J. Janz and M. J. Tait, *Can. J. Chem.*, **45**, 1101 (1967).
18) R. C. Paul, D. S. Gill, and S. P. Narula, *Ind. J. Chem.*, **8**, 936 (1970).
19) J. E. Prue and P. J. Sherrington, *Trans. Faraday Soc.*, **57**, 1795 (1961).
20) F. Accascina, S. Petrucci, and R. M. Fuoss, *J. Am. Chem. Soc.*, **81**, 1301 (1959).
21) J. E. Lind, Jr., J. J. Zwolenik, and R. M. Fuoss, *J. Am. Chem. Soc.*, **81**, 1557 (1959).
22) R. M. Fuoss, *J. Phys. Chem.*, **81**, 1829 (1977).
23) R. M. Fuoss, "PARACOND", Dept. of Chemistry, Yale University, New Heaven, Connecticut, 1978.
24) R. M. Fuoss and K. L. Hsia, *Proc. Natl. Acad. Sci. U.S.A.*, **57**, 1550 (1967).
25) M. Salomon and E. Plichta, *Electrochim. Acta*, **28**, 1681 (1983).
26) R. L. Kay, *J. Am. Chem. Soc.*, **82**, 2099 (1960).
27) D. F. Evans, C. Zawoyski, and R. L. Kay, *J. Phys. Chem.*, **69**, 3878, 4208 (1965).
28) D. S. Gill, *J. Chem. Soc., Faraday Trans. 1*, **77**, 751 (1981).
29) L. Bahadur and M. V. Ramannamurti, *J. Chem. Soc., Faraday Trans. 1*, **76**, 1409 (1980).
30) M. A. Matesich, J. A. Nadas, and D. F. Evans, *J. Phys. Chem.*, **74**, 4568 (1970).
31) R. L. Kay and T. L. Broadwater, *J. Solution Chem.*, **5**, 57 (1976).
32) W. H. Lee and R. J. Wheaton, *J. Chem. Soc., Faraday Trans. 2*, **75**, 1128 (1979).
33) J. C. Justice, *J. Phys. Chem.*, **79**, 454 (1975).
34) R. L. Kay, C. Zawoyski, and D. F. Evans, *J. Phys. Chem.*, **69**, 4208 (1965).
35) S. R. C. Hughes and D. H. Price, *J. Chem. Soc. A*, **7**, 1093 (1967).

 © 1989 The Chemical Society of Japan Bull. Chem. Soc. Jpn., 62, 317—320 (1989)

Infrared and Raman Studies of the $[VO(O_2)_2F]^{2-}$ Ion

E. M. Nour*,††, A. B. El-Sayed,† and S. A. Sadeek
Department of Chemistry, Faculty of Science, Zagazig University, Zagazig, Egypt
†Department of Chemistry, Faculty of Science, Ain Shams University, Cairo, Egypt
(Received January 5, 1988)

The IR and Raman spectra of $Cs_2[VO(O_2)_2F]$ are recorded. The spectra are interpreted on the basis of C_s symmetry of the $[VO(O_2)_2F]^{2-}$ ion. The ν(V=O), ν_s(O-O), and ν_{as}(O-O) are assigned at 950, 890, and 875 cm^{-1}, respectively. The calculated values of the force constants $f_{V=O}$, f_{O-O}, f_{V-O}, $f_{V-O'}$, and f_{V-F} are 670, 298, 262, 273, and 248 N m^{-1}, respectively. The band assignments and the force constant values are discussed in view of the bonding and structure of the $[VO(O_2)_2F]^{2-}$ ion.

In recent years the study of the peroxovanadium chemistry has attracted considerable interest and growing importance,[1-7] since the compounds have much relation to the various types of metal-centered biological systems such as the oxygen carriers as well as the peroxidase and catalase enzymes.[8-10] Most of these studies on peroxovanadium compounds are concerned mainly with their syntheses and structures and in some cases along with vibrational qualitative assignments of the bands, relatively few detailed vibrational works have been elucidated.

Although the reaction between vanadium(V) and H_2O_2 is complicated and pH dependent, many peroxovanadium(V) species have recently been prepared in pure forms. In 1980 Jere and Kaushik[4] reported the isolation of the first fluoro-peroxo species of vanadium(V), $K_2[VO(O_2)_2F]$. A general method for the preparation of different alkali fluorooxodiperoxovanadates(V), $A_2[VO(O_2)_2F]$, was later reported by Chaudhuri and Ghosh.[11].

In previous communications[12-14] detailed vibrational studies have been successfully carried out for many peroxometal species. In this work we report the quantitative vibrational assignments for an oxodiperoxovanadium species based on the IR and Raman spectra of $Cs_2[VO(O_2)_2F]$ and with the aid of normal coordinate analysis. The force constant values for the different bonds and angle bends are calculated. This enable an assessment of the type of bonding and structure inherent in this type of oxodiperoxo compounds.

Experimental

The soild oxodiperoxo compound $Cs_2[VO(O_2)_2F]$ was prepared according to the published method.[11] The chemical composition and IR spectrum agreed with the literature data.[11]

Spectroscopic Measurements. The Raman spectrum of $Cs_2[VO(O_2)_2F]$ was measured using a Carry Model 82 spectrometer and a Coherent Radiation Innova 12 argon ion laser with excitation lines 488.0 and 514.5 nm. To prevent photochemical and thermal decomposition by the laser beam, the sample, as a pressed disc, (20% by weight in KBr), was spun at approximately 2000 rpm in a conventional rotating disc holder. The IR spectrum of the compound was recorded for the sample as a KBr disc using a Pye Unicam SP 2000 spectrometer.

Results and Discussion

The IR spectrum of $Cs_2[VO(O_2)_2F]$ is shown in Fig. 1, and its Raman spectrum recorded using the

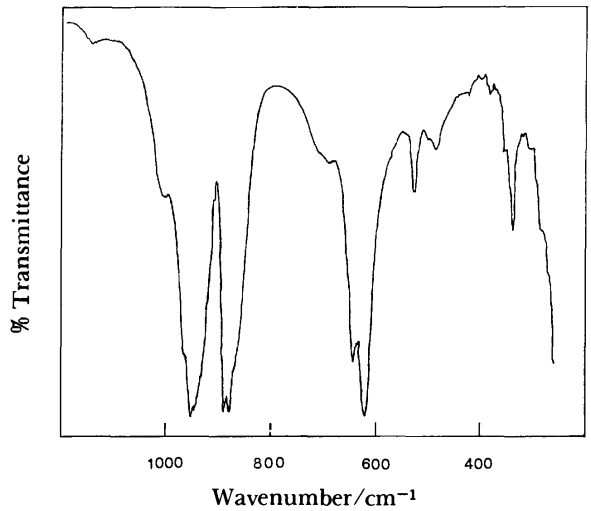

Fig. 1. Infrared spectrum of $Cs_2[VO(O_2)_2F]$.

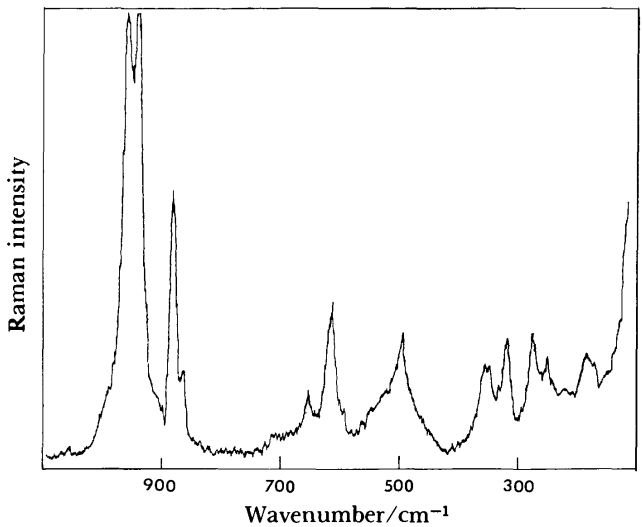

Fig. 2. Raman spectrum of $Cs_2[VO(O_2)_2F]$.

†† Present address: Department of Chemistry, Qatar University, Doha 2713, Qatar (Arabian Gulf).

488.0 nm excitation line is shown in Fig. 2. Before discussing the assignments of these spectra, the geometry of the ion $[VO(O_2)_2F]^{2-}$ must be considered. Here, the vanadium is six coordinate and from the IR and Raman band activities of the O_2^{2-} groups (Table 2), it is clear that each of the peroxy groups acts as a bidentate ligand forming a triangular shape with a vanadium. In this case two structures for the $[VO(O_2)_2F]^{2-}$ are possible. In the first structure both the vanadyl oxygen and the fluoride occupy the two axial positions while the two peroxo groups occupy the four equatorial positions. In this case the ion belongs to the C_{2v} symmetry. The other possible structure contains the two peroxo groups and the fluoride coordinated to vanadium in one plane with the vanadyl oxygen perpendicular to such a plane (Fig. 3). In this case the $[VO(O_2)_2F]^{2-}$ ion belongs to the C_s symmetry. This C_s structure may be the most probable one based on the fact that the reported crystal structure[7] of the related species $NH_4[VO(O_2)_2(NH_3)]$ indicates that the vanadium(V) is bonded to five oxygens and one nitrogen atoms: the coordination structure can best be described as a pentagonal pyramid. The four oxygens of the two peroxo groups, which are related by the mirror plane, and the ammonia nitrogen form the base of a distorted pyramid, and the vanadyl oxygen occupies the apical position. The V-O, V=O, V-N, and O-O bond lengths are 1.883, 1.606, 2.110, and 1.472 Å, respectively. Moreover, the predicted C_s structure for $[VO(O_2)_2F]^{2-}$ ion is also related to those of $[CrO(O_2)_2py]$ and $[CrO(O_2)_2(H_2O)]$.[15,16] Accordingly, the modes of vibrations of $[VO(O_2)_2F]^{2-}$ ion with the pentagonal pyramidal structure in the C_s symmetry, are distributed amongst the vibrational representation: $9A'+6A''$. This gives 15 non-degenerate modes, all are being both infrared and Raman active. From the fifteen fundamentals two modes of the type A′ belong to V=O and V-F bond stretches. The diperoxovanadium unit, $V(O_2)_2$ which possesses a local symmetry of C_{2v}, has six modes of bond vibrations, $3A'+3A''$. These are designated as ν(O-O); A′, ν(O-O); A″, ν(V-O); 2A′, and ν(V-O); 2A″. The remaining seven modes, 4A′ and 3A″ are associated with the different angle bends.

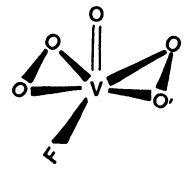

Fig. 3. Geometry of the $[VO(O_2)_2F]$ ion.

Table 1. Force Constants for $[VO(O_2)_2F]^{2-}$ Ion

Symbol	Description	Value[a]
f_Q	V=O	670
f_R	O-O	298
f_r	V-O	262
$f_{r'}$	V-O′	273
f_W	V-F	248
f_β	O=V-O	87
$f_{\beta'}$	O=V-O′	96
f_α	F-V-O′	93
f_ϕ	O=V-F	105
f_τ	O-V-O	116
f_{rr}		13
f_{Rr}		11
$f_{r'r'}$		14
$f_{r'w}$		8
$f_{\beta\beta}$		9
$f_{\alpha\alpha}$		12
$f_{\beta\beta'}$		9
$f_{\beta'\beta'}$		10

a) Stetching constants in N m^{-1}, bending constants in N m^{-1} Rad.^{2}.

Band Assignments. The observed IR and Raman bands are quantitatively assigned as indicated in Table 2 based on the C_s symmetry and the band intensities and with the aid of a complete normal coordinate analysis. This analysis was carried out on the basis of Wilson's GF matrix method;[17] a general quadratic potential energy function was applied utilizing no nonbonded interactions. A version of the Schachschneider programs[18] was used in the computation process. The details of the calculations are similar to those described previously.[19,20] However, in the calculation we faced with the problem that the number of the force constants exceeds the number of the observed frequencies which made it difficult to determine a complete set of force constants for $[VO(O_2)_2F]^{2-}$ ion. Therefore, the force field was simplified to include only the most effective interaction constants beside the diagonal constants. The initial set of force constants involved only the diagonal constants was first introduced and these were chosen in comparison with the known values of related peroxo compounds.[12] These values were systematically refined to obtain the best fit between the observed and calculated frequencies. The next step was to determine the effective off-diagonal constants by studying the effect of change in the value of each of the interaction force constants on values of the calculated frequencies as well as the physically acceptable potential energy distributions as shown in Table 2. This type of simplifying the force field has been successfully used by many workers.[21,22] The final set of the force constant values and their description are given in Table 1. The ν(V=O); A′ is assigned to the IR band at 952 cm^{-1} and to the Raman doublet at 955 and 942 cm^{-1}. This doublet structure may infer the existence of solid-solid interaction between the vanadyl oxygen of one ion and the vanadium of another.[7] This assignments for ν(V=O) agree well with the known values reported for other vanadyl species.[4,11,23]

Table 2. Observed and Calculated Frequencies (cm^{-1}), Potential Energy Distributions and Quantitative Vibrational Assignments for $[VO(O_2)_2F]^{2-}$ Ion

Frequency			Potential energy distribution									Assignment
Obsd		Calcd										
IR	Raman		f_Q	f_R	f_r	$f_{r'}$	f_w	f_β	$f_{\beta'}$	f_α	f_ϕ	f_π	
952s	955vs 942vs	953	100	0	0	0	0	0	0	0	0	0	A′ : ν(V=O)
890s	882s	883	0	81	6	8	0	0	0	1	0	4	81% ν(O–O), 6% ν(V–O), 8% ν(V–O′).
653m	650m	641	0	0	21	32	34	1	1	2	3	5	21% ν(V–O), 32% ν(V–O′), 34% ν(V–F).
—	495m	497	0	3	54	2	37	0	0	0	0	4	54% ν(V–O), 37% ν(V–F).
485m	—	489	0	5	13	52	24	0	0	2	0	4	13% ν(V–O), 52% ν(V–O′), 24% ν(V–F).
340ms	323m	342	1	0	0	1	6	4	21	3	59	5	21% δ(O=V–O′), 59% δ(O=V–F).
—	280m	274	0	3	0	2	4	2	4	26	5	55	26% δ(F–V–O′), 55% δ(O–V–O).
—	248w	241	1	0	0	0	0	76	15	2	3	2	76% δ(O=V–O), 15% δ(O=V–O′).
—	180	175	0	0	0	0	0	20	51	0	29	0	20% δ(O=V–O), 51% δ(O=V–O′), 29% δ(O=V–F).
875s	872w	879	0	62	16	19	0	0	0	3	0	0	A″: 62% ν(O–O), 16% ν(V–O , 19% ν(V–O′).
618s	622s	629	0	34	27	32	0	3	4	0	0	0	34% ν(O–O), 27% ν(V–O), 32% ν(V–O′).
526m	522w	520	0	0	54	46	0	0	0	0	0	0	54% ν(V–O), 46% ν(V–O′).
365w	363m	366	0	0	3	2	0	43	50	2	0	0	43% δ(O=V–O), 50% δ(O=V–O′).
250w	—	257	0	2	0	0	0	1	1	96	0	0	96% δ(F–V–O′).
—	—	169	0	0	0	0	0	55	45	0	0	0	55% δ(O=V–O), 45% δ(O=V–O′).

Normalized to total 100 for the diagonal force constant distributions. Vibrations with more than 5% contribution are only listed.

The O–O bond vibrations are assigned to the bands around 890 and 875 cm^{-1} due to the ν_s(O–O); A′ and ν_{as}(O–O); A″, respectively. The observation of these two modes in both the IR and Raman spectra supports the triangular structure of $V(O_2)$ units (Fig. 3). Under such a structure, ν_s(O–O) and ν_{as}(O–O) belong to A′ and A″ symmetries, respectively, and both should be IR and Raman active. These values of ν(O–O) occur at much higher frequencies compared with that of the simple peroxide salts. The ν(O–O) in Li_2O_2 occurs at 802 cm^{-1}.[24] The higher value of ν(O–O) in our ion $[VO(O_2)_2F]^{2-}$ may be due to the π-donation from the filled π^* orbitals of the O_2^{2-} to the empty d-orbitals of vanadium(V); the peroxide bond order, and hence its frequency should be increased. However, we believe that such π-donation from the peroxide should be much stronger than that reflected as an increase in the ν(O–O) value. This conclusion is based on the P.E.D. values (Table 2) which demonstrate a relatively strong coupling between the ν(O–O) and the ν(V–O) vibrations; the coupling is expected to lower the ν(O–O) value. The assignments of the other ν(V–O) and ν(V–F) frequencies are rather difficult. This arises from the very strong coupling between these motions as indicated from the P.E.D. values for each band as shown in Table 2. This type of strong mixing is expected from the closed system of $V(O_2)_2$ beside the existence of all of these atoms in one plane. However, the ν_s(V–O) and ν_{as}(V–O) could be assigned to the infrared and Raman bands observed around 650 and 620 cm^{-1}, respectively. The corresponding frequencies for the V–O′ bond vibrations are 485 and 526 cm^{-1}. The ν(V–F) is assigned to the Raman band at 495 cm^{-1}.

The calculated force constant values for the O–O and V=O bonds are 298 and 670 N m^{-1} respectively, while the average value of the V–O bonds is 268 N m^{-1}.

The higher value of the $f_{V=O}$ agrees with the double bond character of the vanadyl bond. Using the bond stretching force constant as an approximate measure of the relative equilibrium bond strength, it appears that the vanadyl link is ≈2.5 times stronger than the vanadium-peroxo link.

We are grateful to Professor J. Laane of Texas A & M University for the Raman facilities.

References

1) M. K. Chaudhuri and S. K. Ghosh, *Inorg. Chem.*, **23**, 534 (1984).
2) M. K. Chaudhuri and S. K. Ghosh, *J. Chem. Soc., Dalton Trans.*, **1984**, 507.
3) P. Schwendt, *Collect. Czechos. Chem. Commun.*, **48**, 248 (1983).
4) C. V. Jere and S. M. Kaushik, *Synth. React. Inorg. Met.-Org. Chem.*, **10**, 255 (1980).
5) D. Begin, F. W. B. Einstein, and J. Field, *Inorg. Chem.*, **14**, 1785 (1975).
6) V. P. Schwendt, P. Petrovic, and D. Dskert, *Z. Anorg. Allg. Chem.*, **466**, 232 (1980).
7) R. E. Drew and F. W. B. Einstein, *Inorg. Chem.*, **11**, 1079 (1972).
8) R. Guilard, J. Latoar, C. Lecompte, and J. Marchon, *Inorg. Chem.*, **17**, 1228 (1978).
9) C. Djordgevic, *Chem. Ber.*, **18**, 554 (1982).
10) M. M. T. Khan and A. E. Martell, "Homogeneous Catalysis by Metal Complexes," Academic Press, New York & London (1974), Chap. 2.
11) M. K. Chaudhuri and S. K. Ghosh, *Polyhedron*, **1**, 553 (1982).
12) E. M. Nour and S. Morsy, *Inorg. Chim. Acta*, **117**, 45 (1986).
13) R. E. Hester and E. M. Nour, *J. Raman Spect.*, **11**, 49 (1981).
14) E. M. Nour, *Pak. J. Sci. Ind. Res.*, **30**, 356 (1987).
15) R. Stomberg, *Ark. Kemi*, **22**, 29 (1964).
16) R. E. Hester and E. M. Nour, *J. Raman Spect.*, **11**, 39 (1981).
17) E. B. Wilson, J. C. Decius, and P. C. Cross, "Molecular Vibrations," McGraw-Hill, New York (1955).
18) J. H. Schachtschneider, "Vibrational Analysis of Polyatomic Molecules," Shell Co., Emeryville, CA (1964), Vols. V and VI.
19) E. M. Nour, *Spectrochim. Acta*, **42A**, 1411 (1986).
20) E. M. Nour, M. Zaky, and SH. Sallam, *Polyhedron*, **5**, 929 (1986).
21) K. O. Christe, E. C. Curtis, C. J. Schack, and D. Pilipovich, *Inorg. Chem.*, **11**, 1679 (1972).
22) R. R. Holmes, R. M. Deiters, and J. A. Golen, *Inorg. Chem.*, **8**, 2612 (1969).
23) J. K. Basumatary, M. K. Chaudhuri, R. N. D. Purkayastha, and Z. Hiese, *J. Chem. Soc., Dalton Trans.*, **1986**, 710.
24) L. Vasks, *Acc. Chem. Res.*, **9**, 175 (1976).

 © 1989 The Chemical Society of Japan Bull. Chem. Soc. Jpn., 62, 321—324 (1989)

Synthesis and Spectral Analysis of Some Schiff Bases Containing Long Alkyl Chains

Sushree SENAPATI, Bijaya Kumar MISHRA, Gopa Bandhu BEHERA,* and Prem Prakash MAHENDROO†
Centre of Studies in Surface Science and Technology, Department of Chemistry,
Sambalpur University, Burla 768 019, India
†Alcon Laboratories, Inc., 6201 South Freeway, Fort Worth, Texas 76134, U.S.A.
(Received July 30, 1987)

Schiff bases containing hydrophobic alkyl chains have been synthesized and the IR, ^{1}H NMR, ^{13}C NMR, and mass spectral data of some of the compounds have been reported.

In view of the biological importance[1-5] of the Schiff bases, we have reported in this paper the synthesis of Schiff bases (**1** and **2**) from hexadecyloxybenzaldehydes and diamines and have discussed the IR, ^{1}H NMR, ^{13}C NMR, and mass spectra of some of these compounds. Recently Becker et al.[6] have also reported the synthesis of a similar Schiff base derived from 11-*cis*-retinal and have studied their photophysical and photochemical behavior in nonionic micellar solutions.

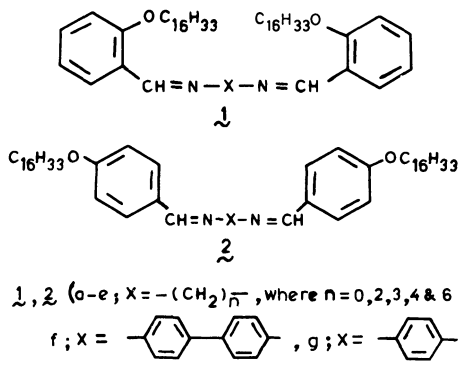

Experimental

General. Melting points were determined on a sulfuric acid bath and are uncorrected. IR (KBr) spectra were recorded on a Perkin-Elmer 398 spectrophotometer (Table 1). ^{1}H NMR (Table 2) and ^{13}C NMR (Table 3) spectra of the compounds (**1a,b,d** and **2b—e**) were recorded in $CDCl_3$ using TMS as an internal standard. Mass spectra of the compounds (**1a,b** and **2b,d**) were obtained from CDRI Lucknow.

***p*-(Hexadecyloxy)benzaldehyde:** About 0.5 g (0.02 mol) of sodium was dissolved in 50 ml ethanol and to it a solution of *p*-hydroxybenzaldehyde (2.44 g, 0.02 mol) in 20 ml ethanol were added with stirring. To this, hexadecyl bromide (10 ml, 0.02 mol) was added gradually and the total mixture was refluxed at 120 °C for 15 h. A solid separated after cooling the reaction mixture to 0 °C. It was then washed with water, extracted from ether, and crystallized from acetonitrile. Yield 45%; mp 50 °C, IR 2910, 2840 (CH_2), 1690 cm^{-1} (CH=O).

o-(Hexadecyloxy)benzaldehyde was prepared similarly by treating salicylaldehyde with hexadecyl bromide. Yield 45%; mp 46 °C; IR 2910, 2840 (CH_2), 1680 cm^{-1} (CH=O).

***N,N'*-Bis[*p*-(hexadecyloxy)benzylidene]diamines (2b):** A solution of *p*-(hexadecyloxy)benzaldehyde (0.692 g, 0.002 mol) and ethylenediamine (0.06 ml, 0.001 mol) in ethanol (20 ml) was refluxed for 30 min in presence of one to two drops of piperidine. A white compound obtained at room temperature was then crystallized from absolute ethanol. Yield 80%; mp 91 °C.

Other Schiff bases (**1** and **2**) were prepared similarly by treating appropriate diamines with *o*- or *p*-(hexadecyloxy)-benzaldehyde, respectively, with varying reflux time. Compounds **2a, f, g** were crystallized from benzene and the rest were from ethanol. Compound **1c** was found to be gummy and could not be crystallized. The diamines used for the synthesis of Schiff bases together with mp, analytical, and IR data of the compounds are given in Table 1.

Results and Discussion

IR Spectra: The IR spectra of all the compounds exhibit characteristic absorption in the range of 2920—2840 cm^{-1} for the $-CH_2-$, 1635—1570 cm^{-1} for the -C=N-, 1255—1240 cm^{-1} for the C-O-C, and 770—720 cm^{-1} for the aromatic -C-H. The IR absorption of the C=N group occurs at a lower energy region for compounds **a, f, g**, of both series, which may be due to extended conjugation in the molecule. The absorption due to aromatic C-H groups for Schiff bases **2**

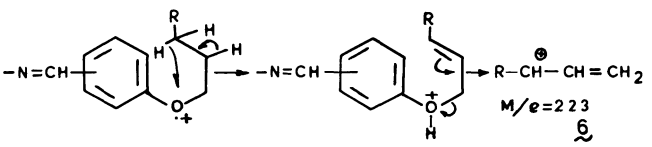

Scheme 1.

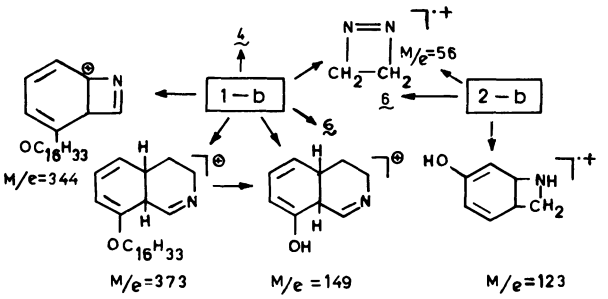

Scheme 2.

Table 1. Melting Point, Analytical Data, and IR Spectral Data of the Schiff Bases **1** and **2**

Compound	Schiff base nature of X	Diamines used for condensation	Reflux time / h	Mp θ_m/°C
1a	Nil	NH_2NH_2	8	81
1b	$-(CH_2)_2-$	$NH_2(CH_2)_2NH_2$	8	54
1c	$-(CH_2)_3-$	$NH_2(CH_2)_3NH_2$	24	gummy
1d	$-(CH_2)_4-$	$NH_2(CH_2)_4NH_2$	8	66
1e	$-(CH_2)_6-$	$NH_2(CH_2)_6NH_2$	10	44
1f	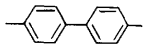	Benzidine	0.5	75
1g		*p*-Phenylenediamine	0.5	77
2a	Nil	NH_2NH_2	0.5	116
2b	$-(CH_2)_2-$	$NH_2(CH_2)_2NH_2$	0.5	91
2c	$-(CH_2)_3-$	$NH_2(CH_2)_3NH_2$	0.5	75
2d	$-(CH_2)_4-$	$NH_2(CH_2)_4NH_2$	0.5	83
2e	$-(Ch_2)_6-$	$NH_2(CH_2)_6NH_2$	0.5	87
2f	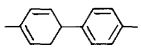	Benzidine	0.5	130(d)
2g		*p*-Phenylenediamine	0.5	127

Compound	Found (Calcd)		IR/cm^{-1}			
	C%	H%	$-CH_2-$	-C=N-	Ar-O-C	Ar-H
1a	80.87	11.12	2920	1625	1255	770
	(80.23)	(11.04)	2850	1605		
1b	80.51	11.20	2910	1630	1245	750
	(80.45)	(11.17)	2840	1595		
1c	—	—	2920	1630	1245	750
			2845	1595		
1d	80.71	11.31	2910	1630	1245	760
	(80.65)	(11.29)	2850	1600		
1e	80.85	11.43	2910	1630	1245	750
	(80.83)	(11.40)	2840	1595		
1f	82.91	10.05	2920	1610	1250	760
	(82.86)	(10.00)	2850	1595		
1g	81.70	10.51	2920	1615	1250	755
	(81.68)	(10.47)	2850	1600		
2a	80.43	11.16	2910	1620	1250	720
	(80.23)	(11.04)	2840	1600		
2b	80.34	11.23	2910	1635	1250	720
	(80.45)	(11.17)	2840	1600		
2c	80.45	11.30	2910	1635	1250	720
	(80.55)	(11.23)	2850	1600		
2d	80.53	11.35	2920	1635	1240	720
	(80.65)	(11.29)	2850	1600		
2e	80.68	11.49	2910	1630	1250	720
	(80.83)	(11.40)	2840	1600		
2f	82.91	10.05	2900	1600	1250	720
	(82.86)	(10.00)	2840	1570		
2g	81.70	10.55	2910	1605	1250	720
	(81.68)	(10.47)	2840	1570		

appears at a lower energy region than that for **1**.

^{1}H NMR Spectra: The ^{1}H NMR spectral data of the compounds are given in Table 2. The chemical shift values indicate that the influence of the 'O' and 'N' atoms is not observed beyond three bonds (i.e. about 4 Å distance). The 'q' and the 'y' protons in the compounds **1d**, **2d**, and **e** appear at the same δ value. Hence, the extent of inductive effect due to the 'O' and 'N' atoms is same at the second carbon (i.e., by a bond distance of about 3 Å). The 'y' protons for the compound **2c**, however, appear at a down field because these protons experience the inductive effect from both the nitrogen atoms to an equal extent whereas in **2d** and **2c** the influence is due to one nitrogen only. The signal due to the methine protons ($-CH_w$=N) is generally shifted downfield for the ortho series

Table 2a. ^{1}H NMR Chemical Shifts (δ) of Schiff Bases **1**

Compound	Nature of X	Positions of proton[a)]			
		o	p	q	r
1a	Nil	0.88, t, 6H, J=6.6	1.25, 52H	1.82, qn, 4H	4.0, t, 4H, J=5.86, 6.6
1b	$-(CH_2)_2-$	0.88, t, 6H, J=5.86, 7.33	1.26, 52H	1.74, qn, 4H	3.92, t, 4H, J=6.6
1d	$-(CH_2)_4-$	0.88, t, 6H, J=6.6	1.26, 52H	1.80, qn, 4H	3.97, t, 4H, J=6.6

Compound	Positions of proton[a)]		
	s	t	u
1a	6.90, d, 2H, J_{st}=8.06	7.36, dt, 2H, J_{st}=8.06, J_{tu}=7.33, J_{tv}=1.47	6.99, t, 2H, J_{tu}=7.33, J_{uv}=8.06
1b	6.83, d, 2H, J_{st}=8.06	7.29, dt, 2H, J_{st}=8.06, J_{tu}=7.33, J_{tv}=1.47	6.91, t, 2H, J_{tu}=7.33, J_{uv}=7.33
1d	6.85, d, 2H, J_{st}=8.06	7.3, dt, 2H, J_{st}=8.06, J_{tu}=7.33, J_{tv}=1.47	6.92, t, 2H, J_{tu}=7.33, J_{uv}=8.06

Compound	Positions of proton[a)]			
	v	w	x	y
1a	8.13, dd, 2H, J_{uv}=8.06, J_{tv}=1.47	9.1, s, 2H	—	—
1b	7.94, dd, 2H, J_{uv}=8.06, J_{tv}=1.47	8.74, s, 2H	3.97, s, 4H	—
1d	7.26, dd, 2H, J_{uv}=7.33, J_{tv}=1.47	8.72, s, 2H	3.67, 2, 4H	1.80, qn, 4H

s=singlet, d=doublet, t=triplet, qn=quintet, dd=doublet of a doublet, dt=doublet of a triplet, J=values in Hz. a) o—r, hexadecyl; s—v, benzene; w, methine; x, y, *N*-methylene.

Table 2b. ^{1}H NMR Chemical Shifts (δ) of Schiff Bases **2**

Compound	Nature of X	Positions of proton[a)]		
		o	p	q
2b	$-(CH_2)_2-$	0.88, t, 6H	1.26, 52H	1.77, qn, 4H
2c	$-(CH_2)_3-$	0.88, t, 6H, J=5.86, 6.6	1.26, 52H	1.78, qn, 4H
2d	$-(CH_2)_4-$	0.88, t, 6H, J=5.86, 7.33	1.26, 52H	1.78, qn, 4H
2e	$-(CH_2)_6-$	0.88, t, 6H, J=5.87, 7.33	1.26, 52H	1.75, qn, 4H

Compound	Positions of proton[a)]		
	r	s+t	u+v
2b	3.94, t, 4H, J=6.6	6.86, d, 4H, J=8.8	7.61, d, 4H, J=8.8
2c	3.96, t, 4H, J=6.6	6.89, d, 4H, J=8.8	7.64, d, 4H, J=8.06
2d	3.97, t, 4H, J=6.6	6.89, d, 4H, J=8.8	7.63, d, 4H, J=8.8
2e	3.96, t, 4H, J=6.6	6.89, d, 4H, J=8.8	7.63, d, 4H, J=8.8

Compound	Positions of proton[a)]			
	w	x	y	z
2b	8.20, s, 2H	3.90, s, 4H	—	—
2c	8.23, s, 2H	3.66, t, 4H	2.08, qn, 4H	—
2d	8.19, s, 2H	3.61, 4H	1.78, qn, 4H	—
2e	8.17, s, 2H	3.56, t, 4H, J=6.6, 7.33	1.75, qn, 4H	1.26, s, 4H

a) o—r, hexadecyl; s—v, benzene; w, methine; x—z, *N*-methylene.

Table 3a. ^{13}C Chemical Shifts (ppm) of Schiff Base **1**

Carbon No.	Chemical shift values		
	1a	**1b**	**1d**
(1) Hexadecyl carbons			
C_1	14.091	14.037	13.983
C_2	22.699	22.615	22.615
C_3	31.950	31.895	31.895
C_4	29.359	29.306	29.306
C_5—C_{11}	29.683	29.629	29.629
C_{12}—C_{14}	26.122	26.068	26.068
C_{15}	29.683	29.629	29.629
C_{16}	68.580	68.420	68.420
(2) *o*-Phenylene carbons			
C_{17}	158.7 (157.7)	158.469	158.199
C_{18}	112.1 (114.3)	111.962	111.962
C_{19}	132.14 (129.0)	131.439	131.331
C_{20}	120.5 (121.0)	120.432	120.540
C_{21}	127.3 (127.5)	127.284	127.284
C_{22}	123.13 (123.60)	125.072	125.126
(3) -CH=N-$(CH_2)_n$ carbons			
C_{23}	157.3	158.307	156.689
C_{24}	—	62.055	61.78
C_{25}	—	—	29.198

Table 3b. ^{13}C Chemical Shifts (ppm) of Schiff Base 2

Carbon No.	Chemical shift values			
	2b	**2c**	**2d**	**2e**
(1) Hexadecyl carbons				
C_1	14.037	14.091	14.091	14.037
C_2	22.669	22.699	22.723	22.669
C_3	31.895	31.949	31.949	31.895
C_4	29.359	29.350	29.413	29.359
C_5—C_{11}	29.683	29.683	29.683	29.629
C_{12}—C_{14}	26.014	26.014	26.068	26.014
C_{15}	29.683	29.683	29.413	29.359
C_{16}	68.10	68.10	68.30	68.15
(2) *o*-Phenylene carbons				
C_{17}	161.960 (160.4)	161.170	161.170	161.113
C_{18}, C_{19}	114.60 (114.3)	114.60	114.50	114.50
C_{20}—C_{22}	129.30 (127.5)	129.30	129.40	129.40
(3) -CH=N-$(CH_2)_n$ carbons				
C_{23}	161.221	160.40	160.196	159.90
C_{24}	61.80	59.00	61.46	61.515
C_{25}	—	32.216	31.949	30.978
C_{26}	—	—	—	27.149

compared to that for para series because of the possibility of hydrogen bond formation (**3**) in the former. The signal is further shifted downfield in **1a** because its most probable conformation is the H-bonded structure.

^{13}C NMR Spectra: The assignment of the chemical shift values to the carbon atoms has been worked out by applying additive rules proposed by Lindman and Adam.[7] The substituents used are the $-OCH_3$ in place of the $-OC_{16}H_{33}$ and the $-CH=CH_2$ in place of the -C=N- due to unavailability of data and similarity in behavior. The calculated values (given in parentheses) fit well with the observed values within an error of ±0.7 ppm.

Mass Spectra: None of the compounds show a molecular ion peak but the fragmentation pattern conforms to the expected structures of the compounds. The fragmentation pattern due to a straight alkyl chain, peaks at m/z=43 due to $C_3H_7^+$, at 105 due to **4** (for ortho series) and **5** (for para series), a prominent peak at 223 (Scheme 1) for all compounds are discernible. The fragmentation pattern of the compounds **1b** and **2b** are given in Scheme 2.

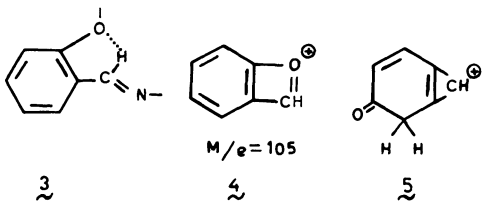

3 **4** **5**

The authors thank the University Grants Commission, New Delhi for funding the project, CDRI Lucknow for mass spectra and Sambalpur University for laboratory facilities.

References

1) E. Grazi, T. Cheng, and B. L. Horecker, *Biochem. Biophys. Res. Commun.*, **7**, 250 (1962).

2) G. A. Hamilton and F. H. Westheimer, *J. Am. Chem. Soc.*, **81**, 6332 (1959).

3) R. A. Morton and G. A. J. Pitt, *Prog. Chem. Org. Natl. Prood*, **14**, 244 (1957).

4) R. K. Chaturvedi and E. H. Cordes, *J. Am. Chem. Soc.*, **89**, 4631 (1967).

5) H. C. Dunathan, *Adv. Enzymol.*, **35**, 79 (1971).

6) R. S. Becker, K. Freedman, and C. Lenoble, *J. Phys. Chem.*, **90**, 4334 (1986).

7) L. P. Lindman and J. Q. Adams, *Anal. Chem.*, **43**, 1245 (1973).

 © 1989 The Chemical Society of Japan Bull. Chem. Soc. Jpn., 62, 325—329 (1989)

Studies on Tetramethyldithizone Isomers and Their Reactions with Metal Ions

A. M. KIWAN,* F. M. HASSAN, and W. HAMDAN
Department of Chemistry, University of Kuwait, P. O. Box 5969 Safat, 13060 Safat, Kuwait
(Received February 17, 1988)

Six bis(dimethylphenyl) analogues of dithizone are prepared, characterized and their reactions with metal ions in a two phase system are reported. The extraction equilibria of their complexes with Cd(II), Co(II), Hg(II), Pb(II), Tl(I), Zn(II), and Bi(III) as well as their spectral characteristics are described. Complete extraction of these metal chelates requires higher pH's than those needed for the unsubstituted dithizone. The molar absorptivities of Bi(III) complexes with bis(3,4-dimethylphenyl)-, and bis(3,5-dimethylphenyl) analogues are higher than the corresponding value of Bi(III) dithizonate. The molar absorptivities of Cu(II) and Hg(II) (in CCl_4) complexes with bis(3,5-dimethylphenyl) analogue are also higher than the corresponding values of the unsubstituted dithizone complexes.

Dithizone (3-mercapto-1,5-diphenylformazan) is a well-known sensitive analytical reagent used for the determination of many metals in various substances.[1] It is also effective for the separation and preconcentration of traces of metals from different materials prior to their determination by highly sensitive methods.[2] The sensitivity and/or selectivity of dithizone are affected by introducing substituents in the phenyl rings. In a preceding paper, the effects of introducing four chlorine atoms (as electron-withdrawing groups) into the phenyl rings of dithizone on the extraction parameters and spectral characteristics of six new tetrachlorodithizone isomers and their metal complexes were reported.[3]

This paper describes the effects of introducing four methyl groups (as electron-releasing groups) into the phenyl rings of dithizone and their spectral characteristics as well as those of their metal complexes.

Results and Discussion

Visible Spectra of Tetramethyldithizone Analogues. These compounds are black crystalline solids which are insoluble in water. They are fairly soluble in

Table 1. Spectral Characteristics of Isomeric Tetramethyldithizones in Chloroform and Carbon Tetrachloride

Compound[a]	Solvent	$\lambda_{max,1}$ nm	$\lambda_{max,2}$ nm	λ_{min} nm	$\varepsilon_{max,1}$[b] $\times10^{-3}$	$\varepsilon_{max,2}$[b] $\times10^{-3}$	ε_{min}[b] $\times10^{-3}$	R	ΔR[c]
Unsubstituted	$CHCl_3$	605	442	504	41.5	16.0	6.8	2.59[e]	0.0
			440[f]		41.4[f]	15.9[f]	—	2.59[f]	
	CCl_4	620	450	515	34.6	20.0	—	1.73[f]	0.0
2,3-	$CHCl_3$	614	452	510	44.4	12.2	7.2	3.64	1.05
	CCl_4	625	458	528	39.5	15.5	7.6	2.55	0.82
2,4-	$CHCl_3$	625	456	514	50.7	11.8	7.4	4.30	1.71
	CCl_4	632	460	524	48.5	16.2	7.4	2.99	1.26
2,5-	$CHCl_3$	622	455	512	43.6	10.9	6.1	4.0	1.41
	CCl_4	630	460	536	39.0	14.6	4.4	2.67	0.94
2,6-	$CHCl_3$	588	420	484	34.2	12.2	6.5	2.80	0.21
	CCl_4	606	434	500	34.5	14.5	5.9	2.38	0.65
3,4-	$CHCl_3$	618	450	514	50.3	14.2	12.2	3.54	0.95
	CCl_4	627	446	516	43.8	19.0	7.2	2.31	0.58
3,5-	$CHCl_3$	611	446	507	43.4	13.5	7.11	3.21	0.62
	CCl_4	622	452	515	37.5	20.3	7.05	1.85	0.12
2-	$CHCl_3$	610[d]			49.5[d]				
		612[e]	450		43.5[e]			3.38[e]	0.79
								3.32[f]	0.73
	CCl_4	628[g]	460[g]		38.1[g]			2.31[f]	0.58
3-	$CHCl_3$	610[e]	451[e]	506[e]	43.2[e]	14.7[e]	6.5[e]	3.03[e]	0.44
								3.04[f]	0.45
	CCl_4							1.92[f]	0.19
4-	$CHCl_3$	616[e]	452[e]		49.5[e]	13.4[e]		3.76[e]	1.17
								3.74[f]	1.15
	CCl_4	630[g]	456[g]		46.4[g]				
		632[h]			44.2[h]			2.30[f]	0.57

a) Position of methyl substituents on both phenyl rings. b) Molar absorptivity (l mol^{-1} cm^{-1}). c) $\Delta R=R_s-R_u$ where R_s and R_u are the peak ratios for the substituted and unsubstituted dithizone, respectively. d) Ref. 4. e) Ref. 7. f) Ref. 1. g) Ref. 5. h) Ref. 6.

organic solvents such as chloroform and carbon tetrachloride to give green solutions with two distinct absorption bands in the visible region. The positions and intensities of these bands were found to depend on the position of methyl groups in the phenyl rings as well as on the nature of solvents (Table 1). The solutions of these compounds were found to be stable for about one week if they are kept refrigerated.

Inspection of the spectral data in Table 1 shows the following:

1) Both $\lambda_{max,1}$ and $\lambda_{max,2}$ of all tetramethyldithizone isomers (except bis(2,6-dimethylphenyl) analogue of dithizone) are shifted towards longer wavelengths. This trend is qualitatively similar to what was found with dimethyldithizone isomers[4-7] and also with the tetrachlorodithizone isomers.[8]

2) The $\varepsilon_{max,1}$ values of all tetramethyldithizone derivatives (except that of bis(2,6-dimethylphenyl) analogue) have increased, whereas the $\varepsilon_{max,2}$ values have decreased. This effect is the opposite to what was found with the tetrachlorodithizone analogues whose $\varepsilon_{max,1}$ values have generally decreased.[8]

3) As a result of the effects on $\varepsilon_{max,1}$ and $\varepsilon_{max,2}$ mentioned above, all peak ratio (R) values ($= \varepsilon_{max,1}/\varepsilon_{max,2}$) of all tetramethyldithizone derivatives are higher than the corresponding value of the unsubstituted dithizone. Substituent effects on the R values of dimethyldithizone analogues were observed[4-7] where opposite effects on the R values of tetrachlorodithizone analogues has been found.[8]

The existence of two absorption bands in the visible spectra of dithizone solutions in organic solvents are generally attributed to thione–enethiol tautomerism.[1,3,9] The longer wavelength band is attributed to the thione (**1**) whereas the shorter wavelength band corresponds to the thiol tautomer (**2**). It has been also suggested that the peak ratio, R, represents the relative concentration of the two tautomers. The findings that the R values of all tetramethyldithizone isomers are higher than the corresponding values of the unsubstituted dithizone, may then be accounted for by the shifting of equilibria towards the thione tautomer.

However, some authors have attempted to reconsider the thione–enethiol hypothesis of dithizone; firstly by the preparation of *S*-methyl derivative of dithizone and comparing its spectrum with that of the parent compound. This failed, for while authentic *S*-methyldithizone have been synthesized by Irving and Bell,[10] its initially permanganate pink solution in chloroform (λ_{max} 270 and 550 nm, ε_{550} 1225 $m^2\,mol^{-1}$) isomerizes rapidly by first-order kinetics to a yellow isomer (λ_{max} 280, 420, and 540 nm, ε_{420} 1775 $m^2\,mol^{-1}$) the band at 550 nm becoming less intense as that at 420 nm increases.

Some of the doubts concerning the existence and structure of thiol and thione tautomers of dithizone would be also resolved if *N*-methyl derivatives such as PhNH–N(CH_3)–C(=S)–N=N–Ph or PhN(CH_3)–NH–C(=S)–N=N–Ph could be prepared. Many authors have attempted such syntheses but without success.[11-13]

The ^1H and ^{13}C NMR spectroscopy has also been applied by some authors[14-17] to examine the thione–enethiol hypothesis. Owing to its low solubility in organic solvents, Coleman et al.[14] examined the more soluble analogue 1,5-bis(2-ethylphenyl) thiocarbazone in $CDCl_3$. They observed δ 1.4 (6H, triplet, CH_3), 3.0 (4H quartet, CH_2), 7.3, 8.1 (8H, multiplet, ArH), and 12.0 (1.6H, singlet, NH). The latter resonance which disappeared on addition of CH_3OD, showed no signs of splitting over the range of +50 to −45 °C, and the authors ruled out the hypothesis of tautomeric equilibrium in favor of a single symmetrical species **3** essentially that subsequently established for the solid-state structure by X-ray crystallography.[18]

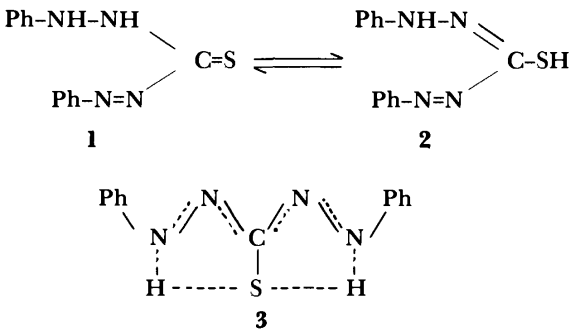

1 **2**

3

Hutton[17] has recently investigated the ^1H and ^{13}C NMR spectroscopy of dithizone and seven of its alkyl-substituted analogues and his results showed that their NH singlets at ca. δ 12.50—12.80, always integrated for 2 protons, i.e. confirming Coleman's results.[14]

On the other hand, Wagler and Koch[19] have recently reported a mathematical analysis of the spectra of dithizone in four organic solvents which supports the thione–enethiol tautomerism. Their analysis allowed the calculation of the individual thione and thiol forms and also estimation of the position of tautomeric equilibria in different organic solvents. However, despite that thione–enethiol tautomerism is still unresolved, dithizone (as well as some of its analogues) remains among the best known sensitive analytical reagents.

Visible Spectra of Metal Complexes: The metal complexes of tetramethyldithizone analogues are highly colored and their electronic spectra are characterized by strong absorption bands in the visible region. Table 2 summarizes their spectral characteristics which indicate the following main features:

1) The metal complexes of bis(2,3-, 2,4-, 2,5-, and 2,6-(dimethylphenyl) analogues of dithizone exhibit λ_{max}'s at shorter wavelengths and have lower values of ε_{max} than the corresponding values of unsubstituted

dithizone metal complexes.

2) On the other hand, almost all complexes of bis(3,4- and 3,5-dimethylphenyl) analogues of dithizone exhibit λ_{max}'s at longer wavelengths and have relatively higher ε_{max} values than the corresponding complexes of the unsubstituted dithizone.

3) The molar absorptivities of Bi(III) complexes with bis(3,4-dimethylphenyl)-, and bis(3,5-dimethylphenyl) analogues are higher than the corresponding value with the unsubstituted dithizone. The molar absorptivities of Cu(II) and Hg(II) (in CCl_4) complexes with bis(3,5-dimethylphenyl) analogue are also higher than the corresponding values of the unsubstituted dithizone complexes.

Table 2. Spectral Characteristics of Metal Complexes with Tetramethyldithizone Analogues in Chloroform

Compd.[a] Metal	Unsubs.[c] dithizone		2,3-Dimethyl		2,4-Dimethyl	
	λ_{max}	$10^{-3}\varepsilon_{max}$[b]	λ_{max}	$10^{-3}\varepsilon_{max}$[b]	λ_{max}	$10^{-3}\varepsilon_{max}$[b]
Cd(II)	517 (520)[d]	88.4 (88.0)	506	69.9	518	67.6
Co(II)	540	68.3		I[f]		I[f]
Cu(II)	546	48.2	530	41.4	540	43.2
Hg(II)	485	72.2	478	54.1	494	56.6
	484[e]	71.2[e]	478[e]	55.0[e]	486[e]	62.6[e]
Pb(II)	515	68.8	496	52.6	510	55.6
Tl(I)	506	34.8	500	25.8	514	30.3
Zn(II)	526	91.1	516	68.2	530	74.9
Bi(III)[e]	490	80.0	476	68.4	500	48.5

Compd.[a] Metal	2,5-Dimethyl		2,6-Dimethyl		3,4-Dimethyl		3,5-Dimethyl	
	λ_{max}	$10^{-3}\varepsilon_{max}$[b]	λ_{max}	$10^{-3}\varepsilon_{max}$[b]	λ_{max}	$10^{-3}\varepsilon_{max}$[b]	λ_{max}	$10^{-3}\varepsilon_{max}$[b]
Cd(II)	515	63.5	478	52.2	518	84.1	518	82.8
Co(II)	526	60.4	520	18.2	550	63.2	545	48.7
Cu(II)	536	43.8	518	58.4	556	45.9	545	58.1
Hg(II)	484	52.7	440	42.3	498	75.3	491	68.4
			448[e]	41.5[e]	498[e]	73.8[e]	486[e]	77.8[e]
Pb(II)	506	50.2	466	45.2	525	70.4	520	63.4
Tl(I)	506	25.7	465	23.4	518	34.3	532	44.0
Zn(II)	526	65.7	488	56.0	538	91.8	534	85.7
Bi(III)[e]	480	65.6	No reaction		500	95.1	496	92.6

a) Position of dimethyl substituents on both phenyl rings are indicated. b) Molar absorptivities (l mol^{-1} cm^{-1}). c) Ref. 7. d) Ref. 1. e) In CCl_4. f) Incomplete reaction.

Table 3. Extraction Data for Metal Complexes with Tetramethyldithizone Analogues from 0.5 mol dm^{-3} Sodium Perchlorate Solutions into $CHCl_3$

Compd.[a] Metal	Unsubs.[b] dithizone		2,3-Dimethyl		2,4-Dimethyl	
	$\log K_{ext}$	$pH_{1/2}$	$\log K_{ext}$	$pH_{1/2}$	$\log K_{ext}$	$pH_{1/2}$
Cd(II)	0.34	3.81	−4.21	6.11	−4.13	6.07
Co(II)	−2.4	5.2	−8.62	8.31	−6.60	7.30
Cu(II)	7.3	0.35	0.50	3.75	1.20	3.40
Hg(II)	26.86	−9.43	19.9	−5.95	19.65	−5.83
Pb(II)	−0.56	4.28	−3.30	5.65	−4.68	6.34
Tl(I)	−4.17	8.17	−5.73	9.73	−5.93	9.93
Zn(II)	0.40	3.80	−4.35	6.18	−3.36	5.68
Bi(III)[c]	9.89[c]	0.70[c]	5.30[c]	2.33[c]	2.1[c]	3.3[c]

Compd.[a] Metal	2,5-Dimethyl		2,6-Dimethyl		3,4-Dimethyl		3,5-Dimethyl	
	$\log K_{ext}$	$pH_{1/2}$	$\log K_{ext}$	$pH_{1/2}$	$\log K_{ext}$	$pH_{1/2}$	$\log K_{ext}$	$pH_{1/2}$
Cd(II)	−3.69	5.85	−3.21	5.61	−0.89	4.45	−1.10	4.55
Co(II)		—	−5.26	6.63	−3.29	5.65	−5.16	6.58
Cu(II)	0.80	3.59	5.30	1.35	7.63	0.18	3.38	2.31
Hg(II)	20.39	−6.20	19.45	−5.73	21.76	−6.88	22.85	−7.43
Pb(II)	−4.25	6.13	−4.0	6.0	0.50	3.75	−1.55	4.78
Tl(I)	−5.66	9.66	−5.24	9.24	−4.78	8.78	−2.97	6.97
Zn(II)	−3.75	5.88	−3.05	5.53	−1.25	4.63	−3.15	5.58
Bi(III)[c]	3.5[c]	2.83[c]		—	9.05[c]	0.98[c]	8.97[c]	1.01[c]

a) Position of dimethyl substituents on both phenyl rings are indicated. b) Ref. 7. c) In CCl_4.

Table 4. Elemental Analysis and Some Characteristic IR Data for Tetramethyldithizone Analogues

Bis(dimethylphenyl) analogue	Mp θ_m/°C	Elemental analysis[a] C/%	H/%	Main IR bands (KBr)/cm^{-1}
2,3-	152	65.20	6.51	3460, 2910, 1595, 1585, 1490, 1465, 1415, 1280, 1260, 1235, 1190, 1140, 1090, 1050, 780, 700, 580, 465
2,4-	143	65.45	6.38	3440, 2915, 1605, 1505, 1435, 1385, 1215, 1165, 1145 1095, 805
2,5-	136	65.27	6.45	3440, 2910, 1630, 1465, 1450, 1250, 1230, 1190, 1145, 1095, 805, 585, 450
2,6-	138	65.18	6.40	3410, 3280, 3175, 2960, 1290, 1260, 1200, 1150, 1095, 1020, 930, 860, 790, 765, 630, 575, 510, 465
3,4-	125	65.52	6.27	3420, 2910, 1485, 1450, 1315, 1255, 1215, 1175, 1140, 815, 460
3,5-	128	65.15	6.42	3440, 2910, 1600, 1490, 1315, 1245, 1190, 1160, 1120, 840, 770, 660, 475

a) The theoretical results are 65.35% C, and 6.45% H.

Extraction Equilibria. The metal extraction equilibria may be represented by the following general equation:

$$n(CH_3)_4H_2Dz + M^{n+} \rightleftharpoons M[(CH_3)_4HDz]_n + nH^+$$

Table 3 lists the extraction data from which the following conclusions may be drawn:

i) The extraction constants, K_{ext} of tetramethyldithizone metal complexes are considerably smaller than those of the unsubstituted dithizone or the tetrachlorodithizone complexes.[8]

ii) Complete extraction of the metal chelates require higher pH's than those needed for the unsubstituted dithizone complexes as suggested by their higher $pH_{1/2}$.

iii) Unlike bis(2,6-dichlorophenyl) analogue of dithizone,[8] the bis(2,6-dimethylphenyl) analogue of dithizone can extract Cu(II) rather more efficiently than the other tetramethyldithizone isomers (except bis(3,4-dimethylphenyl) analogue.

iv) Bis(3,5-dimethylphenyl) analogue seems more efficient than the unsubstituted dithizone in the separation of Cd(II) from Zn(II).

Experimental

Reagents and Chemicals: The bis(2,3-, 2,4-, 2,5-, 2,6-, 3,4-, and 3,5-dimethylphenyl) analogues of dithizone were prepared from the corresponding arylamines by the nitroformazyl method.[20] The nitroformazan derivatives were converted to the tetramethyldithizone analogues and were finally purified by crystallization from chloroform–cyclohexane mixtures. The elemental analysis data, melting points and some characteristic IR frequencies are given in Table 4.

Deionized water was used throughout, and the usual precautions were taken as with dithizone.[3,21,22]

Procedures. The spectral characteristics (λ_{max} and ε_{max}) of the tetramethyldithizone isomers and their metal complexes were determined in the usual way.[3,21,22] The composition of metal complexes and their extraction constants were also determined as described elsewhere.[8]

The visible spectra of ligands and their complexes were recorded on a Unicam SP8000 spectrophotometer and the infrared spectra on a Unicam SP1000, a Radiometer 64 pH-meter was used for pH measurements. The elemental analyses were done at the Alfred Bernhardt Mikroanalytisches Laboratorium, Elbach, F. R. G.

The authors are grateful to the Research Council of the University of Kuwait for the financial support (SC026) of this work.

References

1) H. M. N. H. Irving, "Dithizone, Analytical Sciences Monographs No. 5," The Chemical Society, London (1977) and references therein.

2) H. Irving, *Fresenius Z. Anal. Chem.*, **263**, 264 (1973).

3) E. B. Sandell and H. Onishi, "Photometric Determination of Traces of Metals," John Wiley and Sons, New York (1978), Part I, Chap. 6G, and references therein.

4) B. E. McClellan and H. Freiser, *Anal. Chem.*, **36**, 2262 (1964).

5) S. Takei and T. Kato, *Tech. Report of Tohoku Univ. Report VII, XXVI*, 20 (1962).

6) A. I. Busev and L. A. Bazhanova, *Russ. J. Inorg. Chem.*, **6**, 1417 (1961).

7) A. M. Kiwan et al., unpublished results.

8) A. M. Kiwan and G. A. Wanas, *Anal. Chim. Acta*, **144**, 165 (1982).

9) P. S. Pelkis and R. G. Dubenko, *Ukr. Khim. Zh.*, **33**, 748 (1957); *Chem. Abstr.*, **52**, 14551 (1958); **49**, 1314 (1954); **48**, 9943 (1954); *Zh. Obs. Khim.*, **24**, 1640 (1954).

10) H. Irving and C. F. Bell, *Nature (London)*, **169**, 756 (1952); *J. Chem. Soc.*, **1954**, 4253.

11) A. H. Corwin and G. R. Jackson, *J. Am. Chem. Soc.*, **71**, 3698 (1949).

12) H. M. N. H. Irving, personal communication.

13) D. S. Tarbell, C. W. Todd, M. C. Paulson, E. G. Lindstrom, and V. P. Wystrach, *J. Am. Chem. Soc.*, **70**, 1381 (1948).

14) R. A. Coleman, W. H. Foster, J. Kazan, and M. Mason, *J. Org. Chem.*, **35**, 2039 (1970).

15) A. H. Nabilsi, Ph. D. Thesis, University of Leeds (1972).

16) P. Rashidi Ranjbar and I. Yavari, *Org. Mag. Res.*, **16**, 168 (1981).
17) A. T. Hutton, *Polyhedron*, **6**, 13 (1987).
18) M. Laing, *J. Chem. Soc., Perkin Trans. 2*, **1977**, 1248.
19) H. Wagler and H. Koch, *Talanta*, **31**, 1101 (1984).
20) D. M. Hubbard and E. W. Scott, *J. Am. Chem. Soc.*, **65**, 2390 (1943).
21) L. S. Landry and S. F. Rodendo, *Anal. Chem.*, **26**, 732 (1954).
22) H. Irving and J. J. Cox, *Analyst*, **83**, 526 (1958).

On the Relationship between the Chemical Structure and the Carcinogenicity of Polycyclic Aromatic Compounds and Heterocyclic Nitrogen Compounds, as Studied by ^{13}C NMR

Yohko SAKAMOTO* and Yuko SAKAMOTO
School of Pharmaceutical Sciences, Toho University, Funabashi, Chiba 274
(Received May 25, 1988)

Synopsis. The relationship between the chemical structure and the carcinogenicity of eighty polycyclic aromatic compounds and heterocyclic nitrogen compounds was investigated by ^{13}C NMR. The averaged chemical shifts of the carcinogenic polycyclic aromatic compounds were within the range from δ 126.80 to 127.87, while those of the carcinogenic heterocyclic nitrogen compounds were within the range from δ 129.48 to 132.12. The carcinogenicity of several compounds were predicted according to the index.

The information on the electronic structure and electronic state of polycyclic aromatic compounds was obtained by the calculation of the averaged chemical shifts for all the carbons in the ring structure of the molecules, as has been described previously.[1]

The purpose of this paper is to confirm the previous "carcinogenic index" in eighty polycyclic aromatic compounds, either carcinogenic, noncarcinogenic or undetermined.

Polycyclic Aromatic Hydrocarbons 1—51: It has been reported that compounds **1** and **2** are carcinogenic.

The averaged chemical shifts of these carcinogenic compounds are within the index range from δ 127.11 to 127.87, as has reported in a previous paper.[1]

The averaged chemical shift of two other carcinogenic compounds, **3** and **4**, were δ 126.99 and 126.80 respectively. Thus, we can expand the upper limit of the "carcinogenic index" at a high field from δ 127.11 to 126.80.

Compounds **5—8** and **10—13**, previously reported to be noncarcinogenic,[2,3] were confirmed to be out of the "carcinogenic index".

All the fluorene compounds **10—13** can similarly be expected to be noncarcinogenic.

Compounds **14—22**, **24**, **31**, and **37—46** have been reported to be either carcinogenic or noncarcinogenic, depending on the reports.[2-4] According to the "index range", the possibility that compounds **15**, **16**, **18**, **19**, **24**, **31**, **37**, **39**, **42**, and **46** are carcinogenic is high. On the other hand, the possibility that compounds **14**, **17**, **20—22**, **38**, **40**, **41**, and **43—45** are carcinogenic is low.

Compound **9**, previously reported to be noncarcinogenic,[3] fell in the borderline region of the "carcinogenic index", where the judgement of carcinogenicity was difficult.

Heterocyclic Nitrogen Componds 52—80: The averaged chemical shifts in the carcinogenic compounds **52—60** were within the range from δ 129.48 to 132.12.

Table 1. The Averaged ^{13}C NMR Chemical Shifts over All the Ring Carbons of Polycyclic Aromatic Hydrocarbons, and Their Carcinogenicities

Compound	Averaged chemical shift δ/ppm	Predicted carcinogenicity[a]	Carcinogenicity[b] literature
Dibenzo[*a,l*]pyrene (**1**)	127.47	+	+ (2, 3)
Phenanthro[4,5-*bcd*]thiophene (**2**)	127.64	+	+ (3)
Dibenzo[*a,i*]pyrene (**3**)	126.99	+	+ (2, 3, 4)
Dibenzo[*a,h*]pyrene (**4**)	126.80	+	+ (2, 3, 4)
Benzo[*e*]pyrene (**5**)	126.66	−	− (2)
Picene (**6**)	126.08	−	− (2)
Coronene (**7**)	125.78	−	− (2)
1-Methylbenz[*a*]anthracene (**8**)	129.47	−	− (2)
Benzo[*b*]chrysene (**9**)	127.12	+	− (3)
Fluorene (**10**)	130.52	−	− (3)
Fluoranthene (**11**)	129.08	−	− (3)
Benzo[*b*]fluorene (**12**)	124.58	−	− (3)
Benzo[*ghi*]fluoroanthene (**13**)	128.75	−	− (3)
Benzo[*c*]phenanthrene (**14**)	128.40	−	± (3, 4)
Anthanthrene (**15**)	126.97	+	± (2, 4)
Benzo[*ghi*]perylene (**16**)	126.79	+	± (2, 3)
Cyclopenta[*cd*]pyrene (**17**)	128.29	−	± (2, 3)
Benzo[*b*]triphenylene (**18**)	127.26	+	± (3)
Chrysene (**19**)	127.10	+	± (3)

Table 1. (Continued)

Benzo[*c*]chrysene (**20**)	127.92	−	± (3)
Indeno[1,2,3-*cd*]pyrene (**21**)	128.17	−	± (3, 4)
Perylene (**22**)	128.32	−	± (3, 4)
Rubrene (**23**)	130.57	−	
Dibenzo[*a,j*]anthracene (**24**)	127.06	+	± (2, 3, 4)
9-Phenylanthracene (**25**)	129.83	−	
9,10-Diphenylanthracene (**26**)	130.64	−	
9,10-Dihydroanthracene (**27**)	129.94	−	
Acenaphthylene (**28**)	129.15	−	
Acenaphthene (**29**)	130.96	−	
1,2,2a,3,4,5-Hexahydroacenaphthylene (**30**)	132.36	−	
1-Methylphenanthrene (**31**)	127.66	+	± (4)
2-Methylphenanthrene (**32**)	128.23	−	
3-Methylphenanthrene (**33**)	128.20	−	
3,6-Dimethylphenanthrene (**34**)	128.68	−	
1,2,3,4-Tetrahydrophenanthrene (**35**)	128.56	−	
1,2,3,4,5,6,7,8-Octahydrophenanthrene (**36**)	131.94	−	
1-Methylchrysene (**37**)	127.44	+	± (3)
2-Methylchrysene (**38**)	128.49	−	± (3)
3-Methylchrysene (**39**)	127.76	+	± (3)
4-Methylchrysene (**40**)	128.61	−	± (3)
5-Methylchrysene (**41**)	128.34	−	± (3)
6-Methylchrysene (**42**)	127.38	+	± (3)
Benzo[*b*]naphtho[1,2-*d*]thiophene (**43**)	129.62	−	± (3)
Benzo[*b*]naphtho[2,1-*d*]thiophene (**44**)	131.53	−	± (3)
Benzo[*b*]naphtho[2,3-*d*]thiophene (**45**)	128.04	−	± (3)
Benzo[2,3]phenanthro[4,5-*bcd*]thiophene (**46**)	127.83	+	± (3)
Dibenzo[*a,e*]fluoroanthrene (**47**)	128.78	−	
Benzo[*a*]fluoroanthene (**48**)	129.44	−	
Benzo[*b*]fluoroanthene (**49**)	128.68	−	
Benzo[*j*]fluoroanthene (**50**)	129.25	−	
Benzo[*k*]fluoroanthene (**51**)	129.31	−	
Acridine (**52**)	132.12	+	+ (4)
Benz[*a*]acridine (**53**)	130.67	+	+ (4)
Benz[*c*]acridine (**54**)	130.85	+	+ (4)
10-Azabenzo[*a*]pyrene (**55**)	129.48	+	+ (3)
Dibenz[*a,c*]acridine (**56**)	129.58	+	+ (3)
Dibenz[*a,h*]acridine (**57**)	130.19	+	+ (3)
Dibenz[*a,j*]acridine (**58**)	129.95	+	+ (3)
Dibenz[*c,h*]acridine (**59**)	130.33	+	+ (3)
Dibenz[*a,i*]acridine (**60**)	130.24	+	+ (4)
2-Methylpyridine (**61**)	137.49	(−)[c]	
3-Methylpyridine (**62**)	137.95	(−)	
4-Methylpyridine (**63**)	140.39	(−)	
2,3-Dimethylpyridine (**64**)	138.57	(−)	
2,4-Dimethylpyridine (**65**)	139.98	(−)	
2,5-Dimethylpyridine (**66**)	138.77	(−)	
3,4-Dimethylpyridine (**67**)	139.90	(−)	
3,5-Dimethylpyridine (**68**)	138.96	(−)	
3-Ethyl-4-methylpyridine (**69**)	140.80	(−)	
Quinoline (**70**)	133.38	(−)	
Quinazoline (**71**)	138.50	(−)	
Phenanthridine (**72**)	130.56	+	
Benzo[*f*]quinoline (**73**)	130.70	+	
Benzo[*h*]quinoline (**74**)	131.03	+	
2-Methylquinoline (**75**)	133.51	(−)	
4-Methylquinoline (**76**)	133.40	(−)	
2,4-Dimethylquinoline (**77**)	134.03	(−)	
2,6-Dimethylquinoline (**78**)	134.36	(−)	
5,6,7,8-Tetrahydroquinoline (**79**)	138.71	(−)	
Quinoxaline (**80**)	136.90	(−)	

a) − for noncarcinogenic and + for carcinogenic. b) Carcinogenicity reported previously. It may be based on biochemical evidence or molecular orbital calculation. −: for noncarcinogenic, +: for carcinogenic, ±: for either noncarcinogenic or carcinogenic. c) (−): the carcinogenicities of these compounds were assigned by adopting the noncarcinogenic range for the chlorinated monocyclic aromatic compounds.

The carcinogenicity of the other compounds **61—80** have not been determined. Compounds **72**, **73**, and **74** may be expected to be carcinogenic, according to the above "index range". The "carcinogenic index" of the heterocyclic nitrogen compounds (δ 129.48—132.12) was similar to that of chlorinated monocyclic aromatic compounds (δ 127.76—132.64);[1] both were shifted to a lower field than that from the polycyclic aromatic compounds (δ 126.80—127.87).

There have been no reports on attempts to determine the noncarcinogenic range of noncarcinogenic heterocyclic nitrogen compounds.

However, compounds **61—71** and **75—80** may be expected to be noncarcinogenic by analogy with the chlorinated monocyclic aromatic compounds.

The polar atoms attract the electrons in the ring by the δ-I effect. Thus, the averaged chemical shifts of heterocyclic and chlorinated compounds move downfield as a whole compared with those of polycyclic aromatic compounds, resulting in the difference in the "carcinogenic index" between the two types of compounds.

The present study, like the previous report,[1] shows a close relationship among the carcinogenicity, the averaged chemical shifts, and the electronic structure in aromatic hydrocarbons. Thus, the "index" will be useful in predicting whether or not compounds are carcinogenic.

The authors are heartily grateful to Professor Taichi Ohmoto of Toho University for his encouragement.

References

1) Y. Sakamoto and S. Watanabe, *Bull. Chem. Soc. Jpn.*, **59**, 3033 (1986).

2) E. L. Cavalieri, E. G. Rogan, R. W. Roth, R. K. Saugier, and A. Hakam, *Chem.-Biol. Interactions*, **47**, 87 (1983).

3) "Spectral Atlas of Polycyclic Aromatic Compounds," ed by W. Karcher, R. J. Fordham, J. J. Dubois, P. G. J. M. Glaude, and J. A. M. Ligthart, D. Reidel Publishing Company (1983).

4) IARC Monographs on the evaluation of the carcinogenic risk of chemicals to humans., Vol. 32, *IARC*, Lyon, 1983.

5) A. C. Allison and T. Nash, *Nature (London)*, **197**, 758, (1963).

Ion Association of Tetrabutylammonium Halides in 1,1- and 1,2-Dichloroethane and 4-Methyl-2-pentanone

Satoshi KUSAKABE,* Masahiro SHINODA, and Kaoru KUSAFUKA
Department of Chemistry, Science University of Tokyo,
Kagurazaka, Shinjuku-ku, Tokyo 162
(Received April 1, 1988)

Synopsis. The ion-association equilibrium of tetrabutylammonium chloride, bromide, and iodide in the titled solvents has been investigated by solvent extraction at 298 K. In each solvent the association constants have been found to be of similar magnitude among these three salts. This is explained in terms of the larger degree of hydration in the smaller anions. The influence of coextracted water on the equilibrium is discussed.

Solvent extraction has been applied to studies on equilibrium in water-immiscible solvents.[1,2] The solvent is, however, intrinsically saturated with water and even though its amount is usually small, it may cause some effects on the equilibrium. In some solvent extraction systems a certain amount of water is extracted together with the substance in question and the coextraction of water is attributed to the hydration of the chemical species in the organic phase.[3–6] In the present study, the distribution of tetrabutylammonium halides (TBAX; X=Cl, Br, and I) is measured between an aqueous solution and three aprotic solvents; 1,1-dichloroethane (1,1-DCE, relative permittivity[7] ε_r=9.90), 1,2-dichloroethane (1,2-DCE, ε_r=10.37), and 4-methyl-2-pentanone (MIBK, ε_r=13.11); and the association constant of these salts in the organic phase is calculated. The water content of the equilibrated 1,1- and 1,2-DCE is also measured in order to compare the degree of hydration of the salts in these solvents.

Experimental

The reagents employed were of reagent grade. Both 1,1- and 1,2-DCE were washed with aqueous sodium hydrogencarbonate and then water. The former solvent was distilled and the middle distillate was used. MIBK was washed with diluted perchloric acid, an aqueous sodium hydroxide solution, and then water. Tetrabutylammonium halides were recrystallized from ethanol and ether. Their stock solutions were titrated with a standardized silver nitrate solution using uranine as the indicator.

A portion of an aqueous TBAX solution and an equal volume of an organic solvent were mechanically agitated for half an hour in a thermostated room at 298 K. The TBA^+ in the organic phase was stripped with water. When the stripping was not quantitative with water only, a certain amount of carbon tetrachloride (to DCE) or hexane (to MIBK) was added. TBA^+ both in the stripping solution and in the equilibrated aqueous phase was extracted into chloroform as its picrate, and the concentration was determined by spectrophotometry. The water content in the equilibrated 1,1- and 1,2-DCE solutions was measured with a Karl Fischer titrator. Since the extraction of TBACl was poor, the aqueous chloride-ion concentration was enhanced to 2 mol dm^{-3} by adding lithium chloride in order to attain a measurable amount of coextracted water.

Since the salt concentrations in both the aqueous and organic solutions were low, formation of ion pairs in the aqueous phase and any association of ions other than one-to-one adducts in the organic phase are assumed to be negligible. The equilibria and distribution ratio can then be written as follows using the extraction constant, K_{ex}, and the association constant, K_{as}.

$$TBA^+_{(aq)} + X^-_{(aq)} \rightleftarrows TBA^+X^-_{(org)}$$

$$K_{ex} = [TBA^+X^-]_{org}[TBA^+]_{aq}^{-1}[X^-]_{aq}^{-1}f_{\pm}^{-2} \quad (1)$$

$$TBA^+_{(org)} + X^-_{(org)} \rightleftarrows TBA^+X^-_{(org)}$$

$$K_{as} = [TBA^+X^-]_{org}[TBA^+]_{org}^{-1}[X^-]_{org}^{-1} \quad (2)$$

$$D = ([TBA^+X^-]_{org} + [TBA^+]_{org})/[TBA^+]_{aq} \quad (3)$$

Using the charge balance in both phases, $[TBA^+]_{aq} = [X^-]_{aq}$ and $[TBA^+]_{org} = [X^-]_{org}$, Eq. 4 can be obtained.

$$D/f_{\pm} = K_{ex}[TBA^+]_{aq}f_{\pm} + (K_{ex}/K_{as})^{1/2} \quad (4)$$

The mean activity coefficient in the aqueous solution, $f_{\pm}$, was calculated using Debye-Hückel's expression with the closest ion-ion distance 0.6 nm. The activity coefficient of the ionic species in the organic phase is considered to be unity because the dissociated amount of the salts in it should be very small. The distribution data were treated by a least squares program.

Since TBA^+ can be regarded as anhydrous in 1,1-DCE as well as in 1,2-DCE,[3,5] the coextracted water interacts with the anions and the apparent mean hydration number of the anion in the solvents, n_h, is calculated by Eq. 5;

$$n_h = (w_t - w_0)/[TBAX]_{org,total} \quad (5)$$

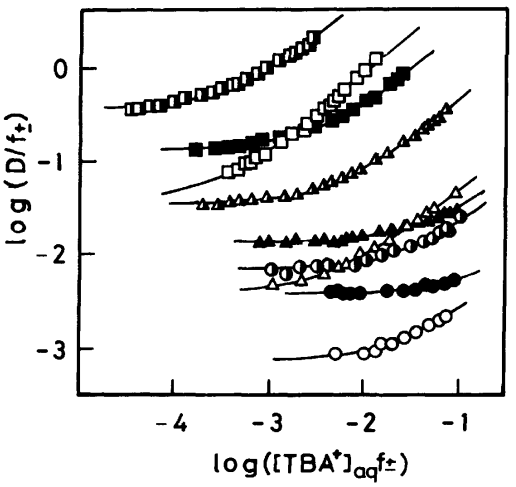

Fig. 1. Distribution ratio of TBAX against the equilibrated salts concentration in the aqueous phase compensated with the activity of the ions in the aqueous phase. X: Cl^- (circles), Br^- (triangles), and I^- (squares). Solvent: 1,1-DCE (open), 1,2-DCE (half filled), and MIBK (filled). Solid lines give the calculated values by using the constants in Table 1.

Table 1. Extraction and Association Constants of Tetrabutylammonium Halides and Apparent Hydration Number of the Halide Ion in the Organic Solvents

X^-	K_{ex}			K_{as}			n_h	
	1,1-DCE	1,2-DCE	MIBK	1,1-DCE	1,2-DCE	MIBK	1,1-DCE	1,2-DCE
Cl^-	3.2×10^{-2}	0.29	3.8×10^{-2}	5.7×10^{4}	6.0×10^{3}	2.3×10^{3}	2.1	2.7
Br^-	0.80	7.0	0.38	4.8×10^{4}	5.7×10^{3}	1.9×10^{3}	1.38	2.0
I^-	1.1×10^{2}	7.0×10^{2}	3.9	7.6×10^{4}	5.3×10^{3}	2.3×10^{3}	0.61	0.88

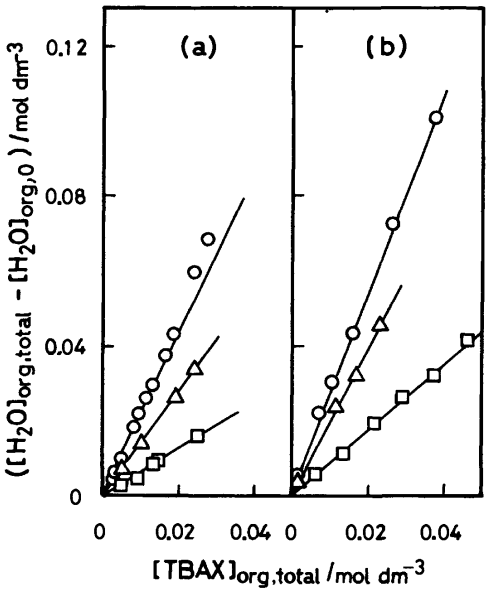

Fig. 2. Coextracted water with TBAX into 1,1-DCE (a) and 1,2-DCE (b). X: Cl^- (○), Br^- (△), and I^- (□). The solid lines are with the slope of n_h in Table 1.

where w_t and w_0 represents the water concentrations in the organic phase equilibrated with an aqueous solution containing and without containing TBAX, respectively.

Results and Discussion

The distribution data are given in Fig. 1 and the calculated constants are shown in Table 1. The ion-association equilibrium of tetraalkylammonium salts has often been studied by several methods. The association constant for the present salts and solvents is available in the literature only for the iodide in DCE. By electrolytic conductivity the values for dry and water-saturated 1,1-DCE have been compared as; 7.30×10^4 (dry) and 6.54×10^4 (wet), and for 1,2-DCE, 6.70×10^3 (dry) and 5.83×10^3 (wet).[8] Another value for dry 1,2-DCE is reported to be 8.0×10^3 [9] From the solvent extraction data in Ref. 10, it can be calculated to be 5.37×10^4 for 1,1-DCE and 5.89×10^3 for 1,2-DCE, respectively.

The amount of the water uptake of the salts is shown in Fig. 2. After agitation with pure water, 1,1-DCE and 1,2-DCE contained 0.066 mol dm^{-3} and 0.126 mol dm^{-3} of water, respectively. These values were used as w_0 in the calculation of the hydration number for the iodide and the bromide. When equilibrated with 2 mol dm^{-3} of aqueous lithium chloride solution, 1,1-DCE contained 0.060 mol dm^{-3} of water and 1,2-DCE did 0.120 mol dm^{-3}. These were used in the calculation of n_h for the chloride. The extraction of lithium chloride was negligible. The difference of the water concentration between these two experiments is caused by the decrease of water activity in the lithium chloride solution.[11] However, since the initial concentration of TBAX was at most 0.1 mol dm^{-3}, the water activity change should be slight in each aqueous TBAX solution so that each w_0 is valid for the different concentrations of TBAX. In Fig. 2 the plots for the chloride in 1,1-DCE show upper deviation with increasing salt concentration. In this case the extrapolated value onto the lower concentration was taken as its n_h. The obtained values of n_h are given in Table 1.

A wet solvent can be regarded as a mixed solvent with water. Since water has large relative permittivity (78.3), the wet solvents discussed here have larger permittivity than the dry ones. Assuming the linear contribution of water to the permittivity of the solution and using w_0 and the relative permittivity values of pure solvent and water, the permittivity of the water-saturated 1,1-DCE is calculated to be 10.2 instead of 9.9 for the pure solvent. Similar calculations give 10.8 for the water-saturated 1,2-DCE instead of 10.4.[12] The experimentally observed enhancement for 1,2-DCE is, however, reported to be only 0.105 (10.387 instead of 10.282) when it contains 0.118 mol dm^{-3} of water which is close to saturation.[13] On the basis of Fuoss's expression,[14] the decrease in the association constant caused by the change of the permittivity of the water-saturated solvents is estimated to be around 10% both for 1,1-DCE (for the increase from 9.9 to 10.2) and for 1,2-DCE (from 10.3 to 10.4).[15] Ito et al.[8] have compared the association constants of TBAI between several dry and wet solvents and concluded that the saturated amount of water reduces the association constants around 15% irrespective of the solvents examined. Therefore, even when the permittivity change by the coexisting water seems to be small, it should be considered in a precise discussion.

The values of n_h in Table 1 are in the order chloride>bromide>iodide in both solvents. This order is that of the hydration tendency of the anions. It means that the organic solvent molecules solvate weakly and the hydrated water molecules are only partially replaced. For three anions the n_h values are always smaller in 1,1-DCE than in 1,2-DCE. This has been explained by Diamond[5] in terms of the acidity of the solvent, namely, the capability of hydrogen-bond formation with the anions which is stronger in 1,1-DCE. Water dissolves into MIBK up to 0.8 mol dm^{-3}, which interferes with the determination of a

reliable hydration number of the anions in this solvent. Since MIBK is a basic solvent, water will react as an acid with the MIBK molecules. This may also change the properties of the solvent.

As seen in Table 1, the association constants of TBAX in MIBK are almost equal for the three salts. This is totally different from the order observed in dry basic aprotic solvents;[16] for example in acetone, the association constant of TBA^+ salts is 435 for the chloride, 264 for the bromide, and 143 for the iodide. It is also known that the order of K_{as} for halide salts in solvating type solvents such as alcohols is chloride<bromide<iodide.[16] Not only for MIBK, none of the K_{as} in Table 1 follow the two typical orders. Considering the n_h values together, this may be explained by the opposite tendency being overlapped; the hydrated water gives a solvating effect and the bulk solvent remains almost inert. In other words, the effective radius of the anions in each solvent should be similar in the three halide ions by hydration. If the ion-ion distance of the ion pairs is similar, whatever ions are solvated or hydrated, the association constants should be of similar magnitude.

The influence of the coextracted water will be larger for the extraction of the more hydrating species and, in the opposite extreme, comparison of the behavior of anhydrating substances in wet and dry solvents will give information about the net change of the physical properties of the solvent induced by the coexisting water.

References

1) K. Gustavii and G. Schill, *Acta Pharm. Suecica*, **3**, 259 (1966).

2) T. Sekine and Y. Hasegawa, "Solvent Extraction Chemistry," Dekker, New York (1977), pp. 141—154.

3) T. Kenjo and R. M. Diamond, *J. Phys. Chem.*, **76**, 2454 (1972).

4) V. L. Kheifets, N. A. Yakovleva, and B. Ya. Krasil'shchik, *Zh. Prikl. Khim.*, **46**, 521 (1973).

5) T. Kenjo and R. M. Diamond, *J. Inorg. Nucl. Chem.*, **36**, 183 (1973).

6) I. M. Ivanov and V. P. Zaitsev, I. S. E. C., **1980** paper 80—54.

7) The values for the relative permittivity are taken from J. A. Riddick, W. B. Bunger, and T. K. Sakano, "Techniques of Chemistry Volume II, Organic Solvents," 4th ed, John Wiley & Sons, New York (1986).

8) K. Ito, E. Iwamoto, and Y. Yamamoto, *Bull. Chem. Soc. Jpn.*, **55**, 2143 (1982).

9) R. L. Louis, *Inorg. Nucl. Chem. Lett.*, **2**, 817 (1970).

10) E. Iwamoto, K. Ito, and Y. Yamamoto, *J. Phys. Chem.*, **85**, 894 (1981).

11) W. L. Masterton and M. C. Gendrano, *J. Phys. Chem.*, **70**, 2895 (1966).

12) The 1,2-DCE consists of gauche and trans isomers. Since the more polar gauche form is preferable in the vicinity of the polar solute, the "effective" permittivity of this solvent is estimated to be around 11.8 by electrolytic conductivity measurements. See a) J. T. Denison and J. B. Ramsey, *J. Am. Chem. Soc.*, **77**, 2615 (1955) and b) Y. H. Inami and J. B. Ramsey, *J. Chem. Phys.*, **31**, 1297 (1959).

13) T. F. Lin, S. D. Christian, and H. E. Affsprung, *J. Phys. Chem.*, **71**, 1133 (1967).

14) R. M. Fuoss, *J. Am. Chem. Soc.*, **80**, 5059 (1958).

15) The association constant is expressed in Ref. 14 as;

$$K_{as} = (4\pi N\mathring{a}^3/3000)\cdot\exp(e^2/\mathring{a}\varepsilon_r kT)$$

where $\mathring{a}$ is the distance of the ions in a pair in the unit of cm. At 298 K we obtain the following equation.

$$\log K_{as} = 21.40 + 3\log\mathring{a} + 2.43\times10^{-6}/\mathring{a}\varepsilon_r$$

If the value of $\mathring{a}$ is supposed to be constant, e.g. 5×10^{-8} cm, the final term of the above equation is about $50/\varepsilon_r$. Assuming the $\mathring{a}$ value to be constant, we can estimate the $\log K_{as}$ values for different ε_r with this equation.

16) U. Mayer, *Coord. Chem. Rev.*, **21**, 159 (1976).

Photochemical Reaction of Benzophenones with Allylic Silanes

Akio TAKUWA,* Naomi FUJII, Hiroyuki TAGAWA, and Hidetoshi IWAMOTO
Department of Chemistry, Faculty of Science, Shimane University,
Nishikawatsu-cho, Matsue 690
(Received June 20, 1988)

Synopsis. Photocycloaddition and hydrogen abstraction reactions between benzophenones and allylic silanes have been investigated. The high regioselective oxetane formations were explained in terms of an additional stability due to the σ_{Si-C}–p_π hyperconjugation of β-silyl radicals in diradical intermediates. Allyl radical substituted by a trimethylsilyl group, which was generated from a hydrogen abstraction reaction, recombined with benzophenone ketyl radical at the γ position. No electron transfer products were observed in the reactions.

Although a photochemical reaction of allylic silanes has been recently developed, most of them are focused on a photoinduced electron-transfer reaction between allylic silanes and electron acceptors such as iminium salts,[1] cyano aromatics,[2] and imides,[3] in which a cation radical generated by an electron transfer from allylic silanes readily undergoes desilylation; the resulting allyl radical attacks the substrates to afford allylated products. However, little is known about the reactivity of allylic silanes as an olefin[4] to the photoexcited carbonyl group. In this paper we wish to describe the Paterno-Büchi reaction and the hydrogen abstraction reaction between benzophenones and allylic silanes.

Results and Discussion

Irradiation of a N_2-purged acetonitrile solution of benzophenone (**1a**, 1 equiv) and allyltrimethylsilane (**2a**, 6 equiv) with a high-pressure Hg lamp through a Pyrex filter afforded a regioisomeric mixture of oxetanes (**3a** and **4a**, 41%) and (*E*)-1,1-diphenyl-4-trimethylsilyl-3-buten-1-ol (**5a**, 26%), and benzopinacol (**6a**, 15%). These products were separated by preparative thin-layer chromatography on silica gel. Each regioisomer of oxetanes could be separated into **3a** and **4a** by medium-pressure liquid chromatography. The structural identification of these isolated products was elucidated by spectral analyses and chemical transformation.

The configuration of the oxetanes, **3a** and **4a**, was determined by ^{1}H NMR (270 MHz): the signals at δ 3.85 (m), 4.38 (dd, J=5.1 and 5.4 Hz), and 4.82 (dd, J=5.4 and 8.3 Hz) were assignable, respectively, to Ha and Hb or Hc of 2,2-diphenyl-3-(trimethylsilylmethyl) oxetane (**3a**), whereas 2,2-diphenyl-4-(trimethylsilylmethyl)oxetane (**4a**) showed the signals at δ 2.94 (dd, J=7.6 and 9.9 Hz, Hb′ or Hc′), 3.32 (dd, J=6.7 and 9.9 Hz, Hb′ or Hc′), and 4.98 (m, Ha′). The isomeric distribution of the oxetanes was estimated by integrations of these signals before separation. The catalytic hydrogenation of the hydrogen abstraction product (**5a**) gave 1,1-diphenyl-4-trimethylsilyl-1-butanol. The *E* configuration of **5a** was confirmed by the coupling constant (J=18 Hz) between the olefinic protons. The irradiation of other benzophenones with **2a** under similar conditions afforded **3**—**6**; the results are summarized in Table 1.

Unsymmetrical allylic silane, (3-methyl-2-butenyl)-trimethylsilane (**2b**) also reacted with the benzophenones to afford oxetanes, hydrogen abstraction product, and benzopinacol (see Table 1).

It is well-known[5] that electronically excited benzophenones in the triplet state react with olefins to yield [2+2]cycloadducts (oxetanes) and, in fewer cases, allyl alcohols (reduction products), formed by the abstraction of an allylic hydrogen from the olefin by photoexcited benzophenone and a recombination of the two resulting radicals. This reaction pattern also holds for the present reactions, as shown in Scheme 1.

An extremely high regioselectivity of oxetane formation was observed in a reaction of **1** with **2a** (**3**:**4**=24—32:1, see Table 1); this is noteworthy. The regioselectivity of oxetane formation is usually predicted in terms of stability of diradical intermediates.[5] However these high regioselectivities in the present reactions could not be simply explained on the

Table 1. Photochemical Reaction of Benzophenones with Allyl- and (3-Methyl-2-butenyl)trimethysilanes

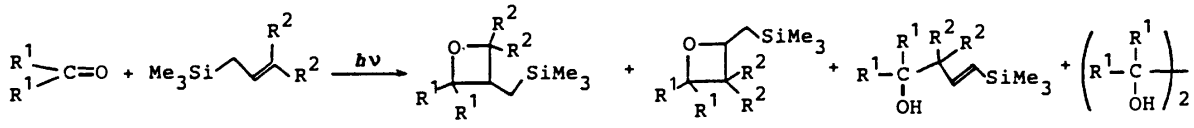

1 2 3 4 5 6

Benzophenone	Ailylic silane	Yield of products/%			
		3+4	[3 :4]	5	6
1a (R^1=Ph)	**2a** (R^2=H)	**3a**+**4a** (41)	[24:1]	**5a** (26)	**6a** (15)
1b (R^1=*p*-ClC$_6$H$_4$)	**2a**	**3b**+**4b** (38)	[32:1]	**5b** (14)	**6b** (16)
1c (R^1=*p*-CH$_3$C$_6$H$_4$)	**2a**	**3c**+**4c** (36)	[24:1]	**5c** (27)	**6c** (13)
1a	**2b** (R^2=CH$_3$)	**3d**+**4d** (54)	[1 :2.8]	**5d** (14)	**6a** (13)
1c	**2b**	**3e**+**4e** (45)	[1 :2.8]	**5e** (16)	**6c** (11)

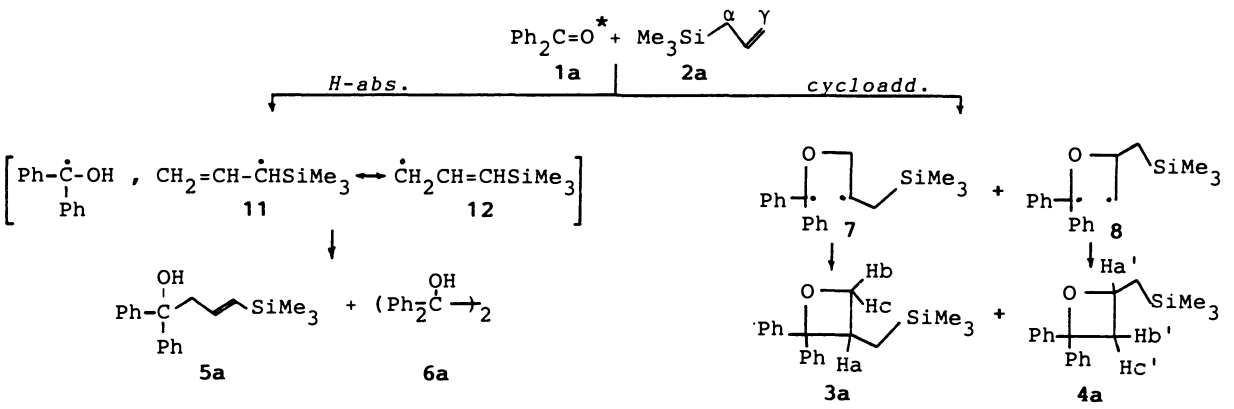

Scheme 1.

basis of the stability differences of primary and secondary radicals, because Yang et al.[6] reported that 1:9 mixtures of oxetanes (**9**:**10**) were produced in the photocycloaddition of benzophenone with isobutene or 3-methyl-2-butene. The diradical **7** could be more stabilized than expected, probably due to a σ_{Si-C}–p_π hyperconjugation.[7]

This additional stabilizing effect by the σ_{Si-C}–p_π conjugation was further supported by the isomeric distribution of oxetanes formed in the reaction with **2b**. Although isomer **4** predominates, the selectivity (**3**:**4**=1:2.8, see Table 1) is less than that which we had expected (1:9)[6] from the results of oxetane formation between **1** and isobutene. This also clearly indicates that the diradical **3'** is more stable than the diradical **9'** (R=H) owing to the σ_{Si-C}–p_π conjugation of β-silyl radical.

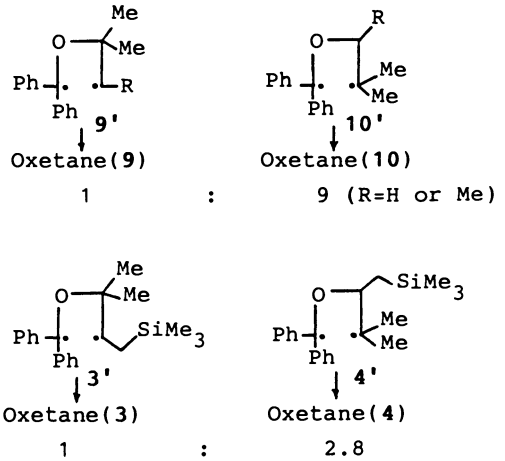

A 1-(trimethylsilyl)-2-propenyl radical formed by an H-abstraction of **1a** from **2a** recombined exclusively at the γ position with ketyl radical to give **5a**; nevertheless, radical **11** can be expected to be more stable than radical **12**. This suggests that the coupling at the α position is strongly hindered by a steric interaction between the trimethylsilyl and phenyl groups. 1-(Trimethylsilyl)-3-methyl-2-butenyl radical generated from **2b** also coupled at the γ position with a ketyl radical.

We recently reportred a photoinduced electron-transfer reaction between benzophenones and allylic stannanes,[8] however, no electron-transfer reaction products (homoallyl alcohols) could be detected in the present reactions. This is understandable on the bases of the endothermicity of the present reactions, since the free energy changes calculated by Rehm–Weller equation[9] for an electron transfer from allylsilane to photoexcited triplet benzophenones were estimated to be positive (+0.88—+1.21 eV).

Experimental

^{1}H NMR spectra were recorded on a JEOL MH-100 or GX-270 spectrometer using TMS or chloroform as the internal standard in deuteriochloroform. Infrared spectra were taken with a Hitachi 260-50 spectrometer. Medium-pressure liquid chromatography was performed on a Yamazen FFLC-254 chromatograph equipped with a Lobar column (Merck Si-60). Mass spectra were recorded with a ESCO EMD-05A spectrometer. Elemental analyses were carried out using a Yanaco MT-2 CHN corder. Benzophenones and allyltrimethylsilane were commercially available and used after recrystallization or distillation. (3-Methyl-2-butenyl)trimethylsilane was prepared by a method described in the literature.[10]

General Procedure. After a N_2-purged acetonitrile or benzene solution (15 ml) of a benzophenone (0.5 mmol) and allylic silane (3 mmol) was irradiated with a high-pressure Hg lamp through a Pyrex filter for 15 h, the solvent was evaporated, and products were separated by preparative TLC (ether–hexane). The isomeric mixture of oxetanes could be separated into each isomer by liquid chromatography. The yields of the products are shown in Table 1. Benzopinacols (**6a**—**6c**) gave satisfactory spectroscopic data.

Identification of the Products. 2,2-Diphenyl-3-(trimethylsilylmethyl)oxetane (3a): Oil; ^{1}H NMR δ=−0.03 (s, 9H), 0.41 (t, 1H, J=14 Hz), 0.65 (dd, 1H, J=3 and 14 Hz), 3.85 (m, 1H), 4.38 (dd, 1H, J=5.1 and 5.4 Hz), 4.82 (dd, 1H, J=5.4 and 8.3 Hz), and 7.25—7.43 (m, 10H); IR (CCl_4) 2945, 2853, 1487, 1442, 1245, 980, 860, 840, and 700 cm^{-1}; MS m/z 296 (M^+). Found: C, 76.59; H, 8.22%. Calcd for $C_{19}H_{24}OSi$: C, 76.97; H, 8.16%.

2,2-Diphenyl-4-(trimethylsilylmethyl)oxetane (4a): Oil; ^{1}H NMR δ=0.01 (s,9H), 1.18 (dd, 1H, J=10.5 and 13.5 Hz), 1.32 (dd, 1H, J=5.4 and 13.5 Hz), 2.94 (dd, 1H, J=7.6 and 9.9 Hz), 3.32 (dd, 1H, J=6.7 and 9.9 Hz), 4.98 (m, 1H), and 7.16—7.49 (m, 10H); IR(CCl_4) 2945, 2905, 1490, 1445, 1245, 940, 860, 838, and 700 cm^{-1}; MS m/z 296 (M^+). Found: C, 76.81; H, 7.79%. Calcd for $C_{19}H_{24}OSi$: C, 76.97; H, 8.16%.

(*E*)-1,1-Diphenyl-4-trimethylsilyl-3-buten-1-ol (5a): Oil; ^{1}H NMR δ=0.01 (s, $SiMe_3$), 2.54 (s, OH), 3.14 (t, CH_2, J=2.7 Hz), 5.87 (m, CH=CH), and 7.22—7.46 (m, aromatic protons); IR ($CHCl_3$) 3550, 2997, 2945, 1605, 1440, and 1245 cm^{-1}. Found: C, 77.12; H, 8.03%. Calcd for $C_{19}H_{24}OSi$: C, 76.97; H, 8.16%. The alcohol (24 mg, 0.08 mmol) was hydrogenated in methanol (5 ml) in the presence of 5% Pd-C (3 mg) to give 1,1-diphenyl-4-trimethylsilyl-1-butanol: oil(63%); ^{1}H NMR δ=0.00 (s, $SiMe_3$), 0.60 (t, CH_2, J=8.3 Hz), 1.38 (m, CH_2), 2.19 (s, OH), 2.36 (t, CH_2, J=8.8 Hz), and 7.25—7.49 (m, aromatic protons); IR ($CHCl_3$) 3600, 3010, 2950, 1450, and 1250 cm^{-1}; MS m/z 298 (M^+).

2,2-Bis-(*p*-chlorophenyl)-3-(trimethylsilylmethyl)oxetane (3b): Oil; ^{1}H NMR δ=−0.05 (s, 9H), 0.38 (t, 1H, J=14 Hz), 0.55 (dd, 1H, J=4.6 and 14 Hz), 3.66 (m, 1H), 4.24 (t, 1H, J=5.9 Hz), 4.70 (dd, 1H, J=5.9 and 8.2 Hz), and 7.30 (8H); MS m/z 365 (M^+). Found: C, 62.66; H, 5.70%. Calcd for $C_{19}H_{22}OCl_2Si$: C, 62.46; H, 6.07%.

2,2-Bis(*p*-chlorophenyl)-4-(trimethylsilylmethyl)oxetane (4b): Oil; ^{1}H NMR δ=0.01 (s, 9H), 1.20 (dd, 1H, J=9.3 and 14 Hz), 1.37 (dd, 1H, J=4.7 and 14 Hz), 2.83 (dd, 1H, J=8.4 and 10.2 Hz), 3.23 (dd, 1H, J=8.4 and 11.2 Hz), 5.20 (m, 1H), and 7.33 (8H); MS m/z 365 (M^+).

(*E*)-1,1-Bis(*p*-chlorophenyl)-4-trimethylsilyl-3-buten-1-ol (5b): Oil; ^{1}H NMR δ=−0.01 (s, $SiMe_3$), 2.51 (s, OH), 3.04 (d, CH_2, J=6 Hz), 5.77 (dt, C-CH=C, J=6 and 18 Hz), 5.89 (d, C=CH-Si, J=18 Hz), and 7.21—7.46 (m, aromatic protons); MS m/z 365 (M^+). Found: C, 62.22; H, 5.91%. Calcd for $C_{19}H_{22}OCl_2Si$: C, 62.46; H, 6.07%.

2,2-Di-*p*-tolyl-3-(trimethylsilyl)methyloxetane (3c): Oil; ^{1}H NMR δ=−0.02 (s, 9H), 0.44 (t, 1H, J=14 Hz), 0.64 (dd, 1H, J=2.9 and 14 Hz), 2.36 (s, 6H), 3.74 (m, 1H), 4.30 (dd, 1H, J=5.5 and 7.8 Hz), 4.73 (dd, 1H, J=5.5 and 8.3 Hz), and 7.18—7.26 (m, 8H); MS m/z 324 (M^+). Found: C, 78.00; H, 8.77%. Calcd for $C_{21}H_{28}OSi$: C, 77.72; H, 8.70%.

2,2-Di-*p*-tolyl-4-(trimethylsilylmethyl)oxetane (4c): Oil; ^{1}H NMR δ=0.03 (s, 9H), 1.22 (dd, 1H, J=10.3 and 13.5 Hz), 1.38 (dd, 1H, J=5.3 and 13.5 Hz), 2.36 (s, 6H), 2.85 (dd, 1H, J=7.4 and 11.2 Hz), 3.23 (dd, 1H, J=7.4 and 11.2 Hz), 4.96 (m, 1H), and 7.15—7.26 (m, 8H); MS m/z 324 (M^+).

1,1-Di-*p*-tolyl-4-trimethylsilyl-3-buten-1-ol (5c): Oil; ^{1}H NMR δ=0.07 (s, $SiMe_3$), 2.38 (s, Me), 2.55 (s, OH), 3.16 (br.s, CH_2), 5.95 (br.s, CH=CH), and 7.17 (d, 4H, J=8.3 Hz), and 7.37 (d, 4H, J=8.3 Hz); IR ($CHCl_3$) 3550, 3000, 2955, 2925, 1613, 1508, 1250, 860, and 837 cm^{-1}; MS m/z 324 (M^+). Found: C, 77.96; H, 9.00%. CalCd for $C_{21}H_{28}OSi$: C, 77.72; H, 8.70%.

2,2-Dimethyl-4,4-diphenyl-3-(trimethylsilylmethyl)oxetane (3d): Oil; ^{1}H NMR δ=0.04 (s, 9H), 0.45 (dd, 1H, J=12 and 15 Hz), 0.52 (dd, 1H, J=4 and 15 Hz), 1.26 (s, 3H), 1.35 (s, 3H), 3.38 (dd, 1H, J=4 and 12 Hz), and 7.09—7.36 (m, 10H); IR ($CHCl_3$) 2995, 2950, 1445, 1370, 1250, 1000, 875, and 860 cm^{-1}; MS m/z 324 (M^+). Found: C, 77.54; H, 8.87%. Calcd for $C_{21}H_{28}OSi$: C, 77.72; H, 8.70%.

3,3-Dimethyl-2,2-diphenyl-4-(trimethylsilylmethyl)oxetane (4d): Needles from methanol; mp 88 °C ^{1}H NMR δ=0.13 (s, 9H) 0.69 (dd, 1H, J=5.4 and 14.2 Hz), 0.99 (s, 3H), 1.00 (s, 3H), 1.02 (dd, 1H, J=10.3 and 14.2 Hz), 4.51 (dd, 1H, J=5.4 and 10.3 Hz), and 7.11—7.63 (m, 10H); IR (KBr) 2950, 1490, 1460, 1445, 1245, 1000, 940, 860, and 710 cm^{-1}; MS m/z 324 (M^+). Found: C, 77.59; H, 8.86%. Calcd for $C_{21}H_{28}OSi$: C, 77.72; H, 8.70%.

2,2-Dimethyl-2,2-diphenyl-4-trimethylsilyl-3-buten-1-ol (5d): Oil; ^{1}H NMR δ=0.07 (s, $SiMe_3$), 1.17 (s, Me), 2.46 (s, OH), 5.84 (d, C-CH=C, J=19.3 Hz), 6.34 (d, C=CHSi, J=19.3 Hz), and 7.21—7.55 (m, aromatic protons); IR ($CHCl_3$) 3600, 2955, 1605, 1495, 1450 1255 870, and 842 cm^{-1}. Found: C, 77.46; H, 8.99%. Calcd for $C_{21}H_{28}OSi$: C, 77.72; H, 8.70%.

2,2-Dimethyl-4,4-di-*p*-tolyl-3-(trimethylsilylmethyl)oxetane (3e): Oil; ^{1}H NMR δ=−0.03 (s, 9H), 0.47 (dd, 1H, J=12 and 15 Hz), 0.54 (dd, 1H, J=4 and 15 Hz), 1.30 (s, 3H), 1.40 (s, 3H), 2.37 (s, 6H), 3.40 (dd, 1H, J=4 and 12 Hz), and 7.05—7.33 (m, 8H); IR ($CHCl_3$) 2980, 2950, 1370, 1245, 1155, 1005, and 860 cm^{-1}; MS m/z 352 (M^+). Found: C, 78.39; H, 8.88%. Calcd for $C_{23}H_{32}OSi$: C, 78.35; H, 9.15%.

3,3-Dimethyl-2,2-di-*p*-tolyl-4-(trimethylsilylmethyl)oxetane (4e): Prisms; mp 79—80 °C; ^{1}H NMR δ=0.13 (s, 9H), 0.71 (dd, 1H, J=4.9 and 14 Hz), 1.00 (s, 6H), 1.01 (dd, 1H, J=10 and 14 Hz), 2.28 (s, 3H), 2.29 (s, 3H), 4.50 (dd, 1H, J=5.1 and 10 Hz), and 7.06—7.49 (m, 8H); IR (KBr) 2945, 2910, 1605, 1460, 1245, 993, 945, 860, and 815 cm^{-1}; MS m/z 352 (M^+). Found: C, 78.60; H, 9.00%. Calcd for $C_{23}H_{32}OSi$: C, 78.35; H, 9.15%.

2,2-Dimethyl-2,2-di-*p*-tolyl-4-trimethylsilyl-3-buten-1-ol (5e): Oil; ^{1}H NMR δ=0.10 (s, $SiMe_3$), 1.20 (s, Me), 2.23 (s, Me), 2.38 (s, OH), 5.80 (d, C=CH-Si, J=19 Hz), 6.45 (d, C-CH=C, J=19 Hz), and 7.05—7.40 (m, aromatic protons); IR ($CHCl_3$) 3590, 2990, 2945, 1605, 1500, 1245, 863, and 840 cm^{-1}; MS m/z 352 (M^+). Found: C, 78.21; H, 9.46%. Calcd for $C_{23}H_{32}OSi$: C, 78.35; H, 9.15%.

References

1) P. S. Mariano, *Acc. Chem. Res.*, **16**, 130 (1983); K. Ohga, U. S. Yoon, and P. S. Mariano, *J. Org. Chem.*, **49**, 213 (1984).

2) K. Mizuno, M. Ikeda, and Y. Otsuji, *Tetrahedron Lett.*, **26**, 461 (1985); K. Mizuno, K. Terasaka, M. Ikeda, and Y. Otsuji, *ibid.*, **26**, 5819 (1985).

3) Y. Kubo, T. Imaoka, T. Shiragami, and T. Araki, *Chem. Lett.*, **1986**, 1749.

4) Cyclobutane ring formation was reported in the reaction of 1,4-naphthoquinone or 1-cyanonaphthalene with allylsilane. M. Ochiai, M. Arimoto, and E. Fujita, *J. Chem. Soc., Chem. Commun.*, **1981**, 460. K. Mizuno, M. Yasueda, and J. Otsuji, the Symposium on Photochemistry, Sendai, Japan, August 1987, Abstr., p. 35.

5) N. J. Turro, "Modern Molecular Photochemistry," Benjamin, Menlo Park, Cal. (1978).

6) N. C. Yang, M. Nussim, M. J. Jorgenson, and S. Murov, *Tetrahedron Lett.*, **1964**, 3657. See also D. R. Arnold, R. L. Hinman, and A. H. Glick, *ibid.*, **1964**, 1425.

7) The hyperconjugation of β-silyl radical has been also reported. H. Sakurai, A. Hosomi, and M. Kumada, *J. Org. Chem.*, **34**, 1764 (1969); T. Kawamura, P. Meaakin, and J. K. Kochi, *J. Am. Chem. Soc.*, **94**, 8065 (1972); M. C. R. Symons, *ibid.*, **94**, 8589 (1972); D. Giller and K. U. Ingold, *ibid.*, **95**, 6459 (1973); M. Kira, M. Watanabe, and H. Sakurai, *ibid.*, **102**, 5202 (1980).

8) The photochemical reaction of benzophenones with allylic stannanes proceeded via electron transfer reaction to give homoallyl alcohols (1,1-diphenyl-3-buten-1-ol) as major products. A. Takuwa, H. Tagawa, H. Iwamoto, O. Soga, and K. Maruyama, *Chem. Lett.*, **1987**, 1091.

9) The free energy changes (ΔG_2) calculated by Rehm-Weller equation for electron transfer from allylsilane to the excited triplet benzophenones were estimated to be positive (+0.88—+1.21 eV). D. Rehm and A. Weller, *Isr. J. Chem.*, **8**, 259 (1970).

10) A. Hosomi, H. Hashimoto, and H. Sakurai, *J. Org. Chem.*, **43**, 2551 (1978).

Convenient Synthesis of Cyclic Trithiocarbonates from 1,2- or 1,3-Dihaloalkanes and Sodium Trithiocarbonate in the Presence of Phase-Transfer Catalyst

Akira SUGAWARA,* Tsukasa SATO, and Ryu SATO*,†
Department of Industrial Chemistry, Tsuruoka Technical College, Tsuruoka, Yamagata 997
†Department of Resource Chemistry, Faculty of Engineering Iwate University, Morioka 020
(Received June 22, 1988)

Synopsis. Cyclic trithiocarbonates, such as 1,3-dithiolane-2-thiones and 1,3-dithiane-2-thiones, were conveniently synthesized by treating 1,2- or 1,3-dihaloalkanes with sodium trithiocarbonate in the presence of a phase-transfer catalyst.

Much attention has been paid to the synthesis of cyclic trithiocarbonates, which are very important intermediates for the preparation of insecticides,[1] biologically active compounds[2] and the donor of a superconductor.[3] Many procedures for the synthesis of cyclic trithiocarbonates have hintherto been developed: for example, a reaction of potassium *O*-methyl dithiocarbonate or carbon disulfide with epoxide[4,5] a reaction of potassium *O*-methyl dithiocarbonate with 2-chloroethanols,[6] a reaction of sodium trithiocarbonate with 1,3-trimethylene dimesylates,[2] and a reaction of ammonium trithiocarbonates with α,ω-dithioalkanes.[7] These procedures have, however, some problems reparding the availability of the starting materials. In the course of our investigations on the synthesis of alkanediyl and alkyl aryl trithiocarbonates,[8] we found a convenient synthesis of cyclic trithiocarbonates, 1,3-dithiolane-2-thione (**2a—d**) and 1,3-dithiane-2-thione (**4a—c**), from 1,2- or 1,3-dihaloalkanes with sodium trithiocarbonate in phase-transfer catalyst (PTC) systems (Eqs. 1 and 2).

Trioctylmethylammonium chloride (TOMAC) was employed as a phase-transfer catalyst. As shown in Table 1, 1,3-dithiolane-2-thione (**2a**) was obtained in high yield from 1,2-dibromoethane (Run 4). The reaction in the absence of PTC resulted in a poor yeild of 4-methyl-1,3-dithiolane-2-thione (**2b**) (Runs 8—10). Surprisingly, 1,2-ethanedithiol also afforded 1,3-

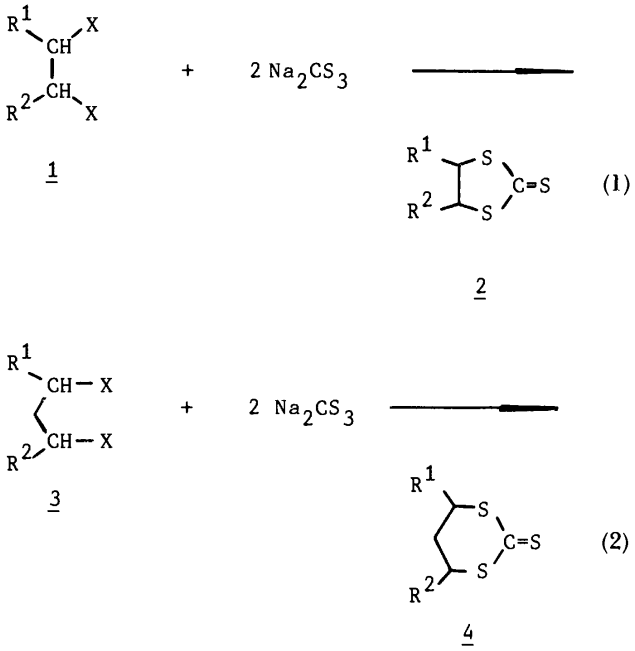

Table 1. Reaction of Substituted 1,2-Dihaloethane and Sodium Trithiocarbonate in the Presence of PTC

Run[a]	Substrate **1**			React		Catalyst	Yield of **2**	
	R^1	R^2	X	Temp/°C	Time/h	mmol	%[b]	
1	H	H	Br	60	8	0	84	**2a**
2	H	H	Br	60	8	0.02	92	**2a**
3	H	H	Br	60	3	0.02	76	**2a**
4	H	H	Br	60	8	0.08	97	**2a**
5[c]	H	H	SH	Reflux	2	0	90	**2a**
6	H	H	Cl	60	8	0.08	58	**2a**
7	H	H	I	60	8	0.08	—[d]	
8	CH_3	H	Br	60	8	0	25	**2b**
9	CH_3	H	Br	60	8	0.08	67	**2b**
10	CH_3	H	Br	60	20	0.08	81	**2b**
11	C_2H_5	H	Br	60	20	0.08	72	**2c**
12	CH_3	CH_3	Br	60	25	0.08	10	**2d**
13	C_6H_5	C_6H_5	Br	60	8	0.08	—[d]	

a) 1,2-Dihaloethane, 2 mmol; Na_2CS_3, 6 mmol. b) Isolated yield based on substrate. c) 1,2-Ethanedithiol, 2 mmol; CS_2, 6 mmol; NaOH, 2.5 mmol. d) Products were ethene derivatives.

dithiolane-2-thione (**2a**) in high yield upon treating with carbon disulfide and sodium hydroxide, as shown in Table 1 (Run 5). It should be noted that the treatment of 1,2-diiodoethane and 1,2-dibromo-1,2-diphenylethane with sodium trithiocarbonate gave *trans*-1,2-diphenylethene, since the ethene was a dehalogenates product from the diiodide or dibromide (Runs 7 and 12).[9] Interestingly, 4-mercaptomethyl-1,3-dithiane-2-thione (**5**) was obtained in good yield upon treating 2,3-dibromo-1-propanol (59%) and 1,3-dibromo-2-propanol (37%) with sodium trithiocarbonate. The formation of **5** may be interpreted in terms of a substitution of the hydroxyl group with trithiocarbonate followed by cyclization as depicted in Scheme 1. The novel thiolane **5** is conceived to be a useful intermediate for the synthesis of biologically active compounds, based on previous results.[2]

Next, we studied the synthesis of 4-methyl-1,3-dithiane-2-thione (**4b**) by a reaction of 1,3-dibromobutane (**3**) with sodium trithiocarbonate in the presence of PTC. As shown in Table 2, three 1,3-dithiane-2-thiones (**4a—c**) were obtained in moderate yields. The treatment of 1,4-dibromobutane with sodium trithiocarbonate by the above-mentioned method was not prepared seven-membered cyclic trithiocarbonate.

As mentioned above, 1-3-dithiolane-2-thione **2** and 1,3-dithiane-2-thione **4** were synthesized in satisfactory yields by a reaction of the corresponding 1,2- or 1,3-dihaloalkanes with sodium trithiocarbonate in the presence of PTC. A plausible pathway for this reaction may be considered to be an internal nucleophillic attack of the thiolate anion of intermediate (**6**) as shown in Scheme 2. This novel method for the preparation of cyclic trithiocarbonates has a great advantage from the point of synthetic convenient and utility.

Experimental

All melting points were uncorrected. IR spectra were obtained on a Jasco IR-G spectrophotometer and NMR spectra

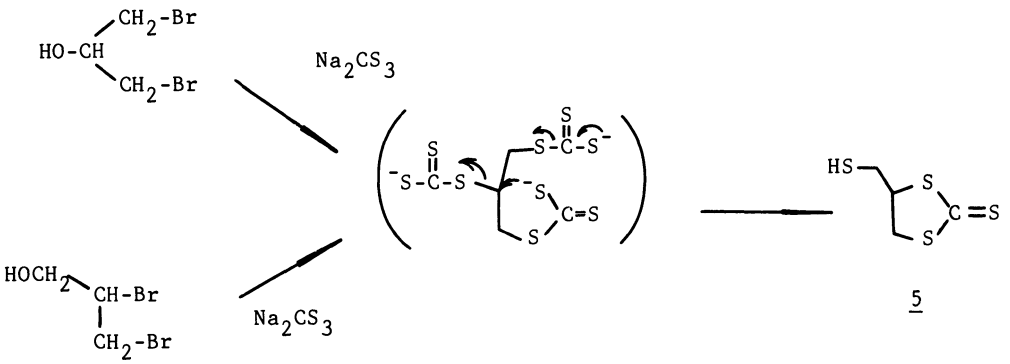

Scheme 1.

Table 2. Synthesis of 1,3-Dithiane-2-thiones **4** from Substituted 1,3-Dibromopropane with Na_2CS_3 in the Presence of PTC

Run[a]	Substrate **3**			React		Yield of **4**/%[b]	
	R^1	R^2	X	Temp/°C	Time/h		
1[c]	H	H	Br	60	1	7	**4a**
2	H	H	Br	60	1	38	**4a**
3[d]	H	H	SH	100	3	45	**4a**
4	CH_3	H	Br	rt	1	23	**4b**
5[c]	CH_3	H	Br	60	1	17	**4b**
6	CH_3	H	Br	60	1	60	**4b**
7	CH_3	H	Br	60	5	66	**4b**
8	CH_3	CH_3	Br	60	20	31	**4c**

a) 1,3-Dibromopropane, 2 mmol; Na_2CS_3, 6 mmol; TOMAC, 0.08 mmol. b) Isolated yield based on substrate **3**. c) Absence of TOMAC. b) 1,3-Propanedithiol, 2 mmol; CS_2, 6 mmol; NaOH, 2.5 mmol.

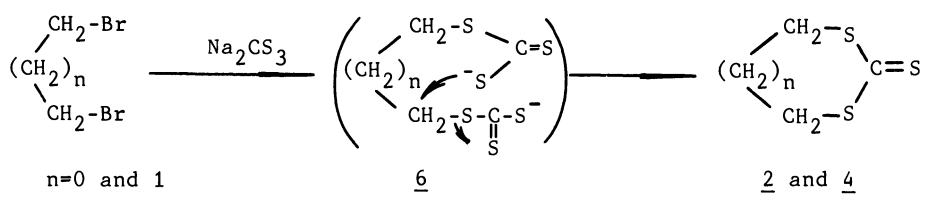

Scheme 2.

were measured with a Varian Gemine-200 spectrophotometer (200 MHz) in $CDCl_3$ using TMS as in internal standerd. Elemental analyses were determined with a Yanagimoto MT-3.

General Procedure. To a solution of 1,2-dibromoethane (2 mmol) in benzene (5 ml) were added Na_2CS_3 30% aqueous solution (6 mmol) and trioctylmethylammonium chloride (0.08 mmol); then, the mixture was heated with stirring at 60 °C for 8 h. After completion of the reaction, the benzene layer was washed with water and then dried on sodium sulfate. A yellow oil obtained by the evaporation of benzene was chromatographed on silica gel using dichloromethane–hexane (3:1) as an eluent to give the desired 1,3-dithiolane-2-thione (**2a**) in a yield of 97%. The structures of the products were characterized by ^1H NMR, IR, MS, and elemental analyses. The physical and spectral data of thione **2a**, **4a**, and **4b** were identified with those of authentic samples.[2,9,10]

4-Methyl-1,3-dithiolane-2-thione (2b): Oil; IR (neat) 1032, 1048, and 1077 cm^{-1}; ^1H NMR ($CDCl_3$) δ=1.65 (d, 3H, J=6,6 Hz, CH_3), 3.70 (q, 1H, J=11.8, 7.4 Hz, CH), 4.04 (q, 1H, 7.4, 5.7 Hz, CH), and 4.55 (m, 1H, J=11.8, 6.6, and 5.7 Hz, CH). Found ; C, 32.19; H, 4.09%. Calcd for $C_4H_6S_3$: C, 31.96; H, 4.02%.

4-Ethyl-1,3-dithiolane-2-thione (2c): Oil; IR (neat) 1048 and 1088 cm^{-1}; ^1H NMR ($CDCl_3$) δ=1.09 (t, 3H, J=7.4 Hz, CH_3), 1.99 (m, 2H, CH_2), 3.72 (q, 1H, J=12.0, 7.6 Hz, CH), 4.00 (q, 1H, J=12.0, 5.6 Hz, CH), and 4.34 (m, 1H, CH). Found: C, 36.70; H, 4.97%. Calcd for $C_5H_8S_3$: C, 36.54; H, 4.91%.

4,5-Dimethyl-1,3-dithiolane-2-thione (2d): Oil; IR (neat) 1050, 1065, and 1090 cm^{-1}; ^1H NMR ($CDCl_3$) (mixture of cis and trans) δ=1.52, 1.60 (d, 6H, CH_3) and 4.10, 4.50 (m, 2H, CH). Found: C, 36.69; H, 4.66%. Calcd for $C_5H_8S_3$: C, 36.54; H, 4.91%.

4,6-Dimethyl-1,3-dithiane-2-thione (4c): Oil; IR (neat) 930, 990, and 998 cm^{-1}; ^1H NMR ($CDCl_3$) δ=1.46 (d, 6H, J=7.0 Hz, CH_3), 2.19 (t, 2H, J=6.0 Hz, CH_2), and 3.64 (m, 2H, J=7.0, 6.0 Hz, CH_2). Found: C, 40.65; H, 5.76%. Calcd for $C_6H_{10}S_3$; C, 40.40; H, 5.63%.

4-Mercaptomethyl-1,3-dithiolane-2-thione (5): Oil; IR (neat) 2500 and 1060 cm^{-1}; ^1H NMR ($CDCl_3$) δ=1.77 (t, 1H, J=9.0 Hz, SH), 3.05 (m, 2H, CH_2), 3.99 (q, 1H, J=12.2, 4.4 Hz, CH), 4.19 (q, 1H, J=12.2, 5.4 Hz, CH), and 4.36 (m, 1H, CH). Found: C, 26.45; H, 3.32%. Calcd for $C_4H_6S_4$: C, 26.34; H, 3.32%.

References

1) O. Serpold, H. J. Renner, J. Weissflog, and H. Schneider, Ger. (East) Patent 11045 (1956); *Chem. Abstr.*, **53**, 6519c (1959)

2) S. Kubota, E. Taniguchi, M. Eto, and K. Maekawa, *Agric. Biol. Chem.*, **41**, 1621 (1977).

3) D. B. J. Easton and D. Leaver, *J. Chem. Soc., Chem. Commun.*, **1965**, 585.

4) S. M. Iqbal and L. N. Owen, *J. Chem. Soc.*, **1960**, 1030; C. G. Overberger and A. Drucker, *J. Org. Chem.*, **29**, 360 (1964); J. A. Durden, Jr., H. A. Stansbury, Jr., and W. H. Catlette, *J. Am. Chem. Soc.*, **82**, 3082 (1960).

5) P. Alain and T. Clande, Fr. Patent 1510016 (1966); *Chem. Abstr.*, **70**, 46876p (1969).

6) N. Sawa, M. Hoda, and Y. Hosokawa, Jpn. Patent 7343741 (1973); *Chem. Abstr.*, **81** 13781e (1974).

7) Y. Hori, Y. Nagano, T. Fukuhara, S. Teramoto, and H. Taniguchi, *Nippon Kagaku Kaishi*, **1987**, 1408.

8) A. Sugawara, M. Shirahata, S. Sato, and R. Sato, *Bull. Chem. Soc. Jpn.*, **57**, 3353 (1984); A. Sugawara, K, Hasegawa, K. Suzuki, Y. Takahashi, and R. Sato, *ibid.*, **60**, 435 (1987).

9) J. Nakayama, H. Machida, and M. Hoshino, *Tetrahedron Lett.*, **24**, 3001 (1983).

10) S. Tanimoto, T. Oida, K. Hatanaka, and T. Sugimoto, *Tetrahedron Lett.*, **22**, 655 (1981).

The β-Sheet Structure-Disrupting Potential of Electron-Donor and -Acceptor Solvents and Role of Mixed Solvents in Solvation of Peptides[1)]

Mitsuaki NARITA,* Shinya HONDA, and Satoshi OBANA
Department of Industrial Chemistry, Faculty of Technology, Tokyo University of Agriculture and Technology, Koganei 184
(Received July 27, 1988)

Synopsis. The β-sheet structure-disrupting potential of hydrogen-donor and -acceptor solvents was in the good relationship with their electron-acceptor and -donor numbers (AN and DN), respectively. As AN and DN of solvents are larger, their β-sheet structure-disrupting potential becomes higher. Based on the results of the β-sheet structure disruption in the three component solvent system, it can also be clarified that combinations of homogeneous solvents are suitable for peptide and protein synthesis, but those of heterogeneous ones are not effective. The results of this study are of quite significance for the search for effective solvents in peptide and protein synthesis.

The elucidation of dissolution mechanism of peptides in organic solvents is of practical significance because the insolubility of peptide intermediates, protected peptides, is a serious obstacle in peptide and protein synthesis.[2,3)] In previous papers,[4–10)] we showed that the insolubility of peptides in high-polar organic solvents such as DMF, NMP, DMSO, and HMPA was caused by a β-sheet aggregation formed by peptide chains of equal to or larger than an octa- or nonapeptide sequence. Furthermore, in a recent paper,[11)] we demonstrated that the hydrogen donating and accepting ability of solvent played an important role in disrupting a β-sheet aggregation, and that strongly hydrogen-donating HFIP had a high peptide-solubilizing potential.

In this paper, using a solvent-titration technique,[12)] we first demonstrate that the β-sheet structure-disrupting potential of hydrogen-donor and -acceptor solvents is in the good relationship with their electron-acceptor and -donor numbers (AN and DN),[13)] respectively. Next, we examine the β-sheet structure disruption in the three component solvent system and discuss the criteria to search for effective solvents in peptide and protein synthesis.

Experimental

Materials. The sample of Boc-Val-Gly-Phe-Gly-Leu-Ile-Leu_2-OBzl is that prepared before.[4)] The purity of the peptide was confirmed by elemental and amino acid analyses. It gave a single peak on high-performance liquid chromatography.

IR Measurements. The IR absorption spectra of the sample in CH_2Cl_2 were recorded at room temperature with a JEOL Model JIR-100 FT-IR spectrometer by employing 0.5 mm-path length cells with sodium chloride windows. The concentration of the peptide was kept 1.0×10^{-3} M (1 M=1 mol dm^{-3}).

Results and Discussion

The β-Sheet Structure-Disrupting Potential of Electron-Donor and -Acceptor Solvents. As a β-sheet structure of peptides is disrupted by hydrogen bonding between solvents and peptide main chains such as N-H···O=C, N-H···O=S, N-H···O=P, and C=O···H-O, the β-sheet structure-disrupting potential of hydrogen-acceptor solvents such as DMF, NMP, DMSO, and HMPA is expected to correlate with their DN. Actually, as shown in Fig. 1, plots of log $[S_{0.5}]_0$ vs. DN for HMPA, DMSO, TMP, and PC gave a straight line. The apparent molarity of titrating solvents, $[S_{0.5}]_0$, corresponds to that at the half value of the initial intensity of 1630-cm^{-1} band in the solvent-titration curves of Boc-Val-Gly-Phe-Gly-Leu-Ile-Leu_2-OBzl[11)] when molarity of titrating solvents is used as abscissa instead of vol-%.

In this paper, we further investigated the relationship between the β-sheet structure-disrupting potential and AN of electron-acceptor solvents. As expected from the result of electron-donor solvents, the fine straight line relationship between log $[S_{0.5}]_0$ and AN for AcOH, MeOH, EtOH and *i*-PrOH was also obtained by the solvent titration curves of the peptide in CH_2Cl_2 using electron-acceptor solvents as titrating solvents (Fig. 1). As AN and DN of titrating solvents are larger, their β-sheet structure-disrupting potential clearly becomes higher. The straight lines observed between log $[S_{0.5}]_0$ and AN or DN indicate that AN and DN of solvents are a measure of their solvating power for peptide C=O and N-H bonds, respectively, and that the hardness of a peptide C=O bond as a base and a

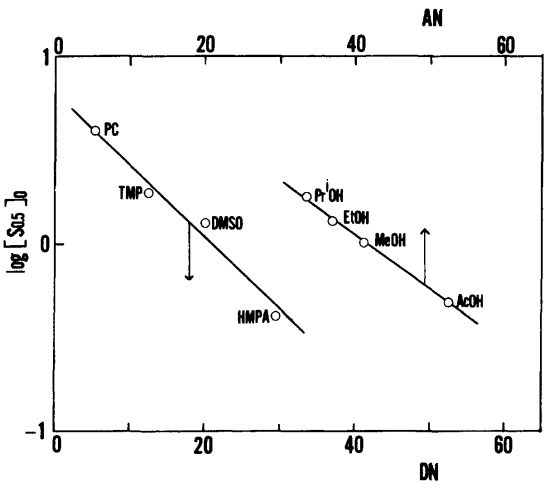

Fig. 1. Plots of log $[S_{0.5}]_0$ vs. AN for AcOH, MeOH, EtOH, and *i*-PrOH and DN for HMPA, DMSO, TMP, and PC.

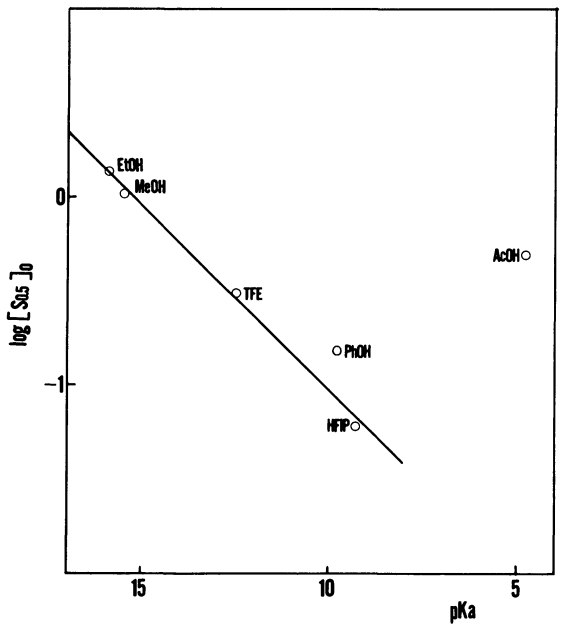

Fig. 2. The linear relationship between $\log[S_{0.5}]_0$ and pK_a values of hydrogen-donor solvents.

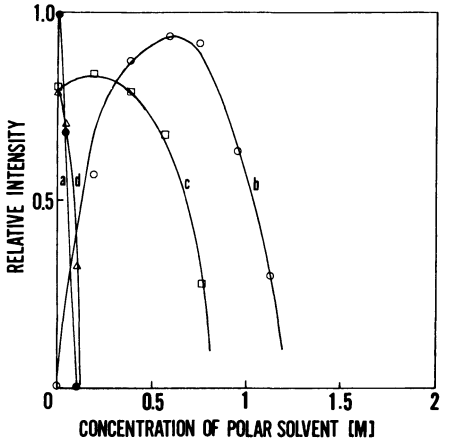

Fig. 3. The solvent-titration curves of the peptide in CH_2Cl_2 (a), HMPA-CH_2Cl_2 (b), DMSO-CH_2Cl_2 (c), and EtOH-CH_2Cl_2 (d) using HFIP as a titrating solvent. Each molar concentration of DMSO, HMPA, and EtOH in CH_2Cl_2 was 0.7 M.

peptide N–H bond as an acid is similar to that of triethylphosphine oxide and antimonyl(V) chloride, respectively.[13] Furthermore, although the AN values using triethyphosphine oxide as an electron donor are not reported for HFIP, PhOH, TFE, and *n*-BuOH, the linear relationship observed by AcOH, MeOH, EtOH, and *i*-PrOH suggests that the values of $[S_{0.5}]_0$ for HFIP (0.05), PhOH (0.14), TFE (0.33), and *n*-BuOH (1.5) give their AN values in the case that peptide C=O bonds act as an electron donor. Thus, from Fig. 1, the AN values are estimated to be 88 for HFIP, 70 for PhOH, 59 for TFE, and 36 for *n*-BuOH, respectively.

Figure 2 shows the fine correlation of the β-sheet structure-disrupting potential of hydrogen donor solvents with their pK_a values. The β-sheet structure-disrupting potential of hydrogen-donor solvents except AcOH has the linear relationship with their pK_a values, being in the following order: HFIP>PhOH>TFE>AcOH>MeOH>EtOH>*n*-BuOH>*i*-PrOH, and the lower the pK_a value of hydrogen-donor solvents is, the higher their β-sheet structure-disrupting potential becomes. The straight line observed between $\log[S_{0.5}]_0$ and pK_a values also indicates that pK_a values of hydrogen-donor solvents are a measure of their solvating power for a peptide C=O bond. Since AcOH is predominantly present in the dimeric form in CH_2Cl_2, AcOH has the potential lower than that expected from its pK_a value. In fact, the IR spectrum of AcOH in CH_2Cl_2 shows bands stronger at 1720—1708 cm^{-1} (dimer) than at 1760 cm^{-1} (monomer).

The β-Sheet Structure Disruption in the Three Component Solvent System. In peptide and protein synthesis, a mixture of aprotic high-polar solvents such as NMP, DMSO, and HMPA is generally used for coupling reactions between large peptide fragments because the solubilizing potential of their mixture is higher than that of them alone. Therefore, it is of practical significance to clarify why mixed solvents were more effective in peptide and protein synthesis.

On the other hand, the fine correlation of the β-sheet structure-disrupting potential of hydrogen-donor and -acceptor solvents with their AN and DN strongly suggests that combinations of homogeneous solvents are suitable for peptide and protein synthesis but those of heterogeneous ones are not effective. For example, in CH_2Cl_2, HMPA functions as a strong electron donor and HFIP, as a strong electron acceptor. Thus, in a mixture of HMPA and CH_2Cl_2, addition of HFIP is estimated to interrupt hydrogen bonding of HMPA to a peptide N–H bond and to reduce the peptide-solubilizing potential of a mixture of HMPA and CH_2Cl_2. Therefore, the investigation of the β-sheet structure-disrupting behavior in the three component solvent system is expected to offer significant information for the search for effective solvents in peptide and protein synthesis. Thus, we examined the β-sheet structure-disrupting behavior of the peptide in the three component solvent systems. Figure 3 shows the solvent-titration curves of the peptide in DMSO-CH_2Cl_2, HMPA-CH_2Cl_2, and EtOH-CH_2Cl_2 using HFIP as a titrating solvent. Figure 4 presents the solvent-titration curves of the peptide in DMSO-CH_2Cl_2 and EtOH-CH_2Cl_2 using HMPA as a titrating solvent. In Figs. 3 and 4, the molar concentration of each high-polar solvent was 0.7 M.

In Fig. 3, the curve b gives a clear-cut role of HMPA and HFIP in the β-sheet structure disruption. In the absence of HFIP, the peptide is completely solvated by HMPA in the HMPA-CH_2Cl_2 solution, being free from the β-sheet aggregation, and successive addition of HFIP induces the onset and increase in the β-sheet aggregation. These phenomena signify that HFIP counteracts hydrogen bonding between peptide N–H bonds and HMPA P=O bonds, and that HFIP functions as a strong hydrogen donor not for peptide C=O bonds but for HMPA P=O bonds since the DN of

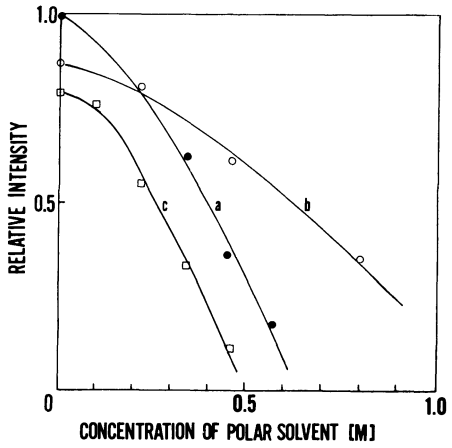

Fig. 4. The solvent-titration curves of the peptide in CH_2Cl_2 (a), EtOH-CH_2Cl_2 (b), and DMSO-CH_2Cl_2 (c) using HMPA as a titrating solvent. Each molar concentration of EtOH and DMSO in CH_2Cl_2 was 0.7 M.

a HMPA P=O bond is higher than that of amide C=O bonds.[13] Further addition of HFIP clearly causes the β-sheet structure disruption. In the DMSO-CH_2Cl_2 solution, HFIP also functions as a strong hydrogen donor for DMSO S=O bonds (Fig. 3, c). These results show that a mixture of electron-donor and -acceptor solvents is not suitable for disruption of the β-sheet structure in peptide and protein synthesis. On the other hand, successive addition of HFIP to the EtOH-CH_2Cl_2 solution induces a remarkable decrease in the 1630-cm^{-1} band due to disruption of the β-sheet structure (Fig. 3, d). In this case, HFIP and EtOH act independently as hydrogen donors for peptide C=O bonds since the DN of EtOH and HFIP is estimated to be lower than that of peptide C=O bonds. Similarly, a combination of HMPA and DMSO, which are strong hydrogen acceptors for peptide N-H bonds, showed effective disruption (Fig. 4, c) since no competition between HMPA and DMSO takes place by mixing. In addition, in the HFIP-EtOH-CH_2Cl_2 and HMPA-DMSO-CH_2Cl_2 solvent systems, each solvent can independently play an important role in effective solvation of peptide side chains in peptide and protein synthesis. We have the view that the results in this study clarify the criteria of the search for effective solvents in peptide and protein synthesis.

The authors wish to thank Central Glass Co., Ltd., for generous gift of HFIP and TFE.

References

1) This paper forms Part XI of "Designs of Three-dimensional Structures of Peptides and Proteins and the Synthetic Route for Peptides and Proteins" series. For part X of this series, see Ref. 11. The abbreviations for amino acid residues are the following: Val, L-valine; Gly, glycine; Phe, L-phenylalanine; Leu, L-leucine; Ile, L-isoleucine. Additional abbrevitions used are the following: Boc, *t*-butoxycarbonyl; OBzl, benzyl ester; HFIP, 1,1,1,3,3,3-hexafluoro-2-propanol; IR; infrared; DMF, *N*,*N*-dimethylformamide; NMP, *N*-methylpyrrolidone; DMSO, dimethyl sulfoxide; HMPA, hexamethylphosphoric triamide; TMP, trimethyl phosphate; PC, propylene carbonate; AcOH, acetic acid; MeOH, methanol; EtOH, ethanol; *i*-PrOH, 2-propanol; PhOH, phenol; TFE, 2,2,2-trifluoroethanol; *n*-BuOH, 1-butanol.

2) M. Narita, K. Ishikawa, J.-Y. Chen, and Y. Kim, *Int. J. Peptide Protein Res.*, **24**, 580 (1984).

3) M. Narita, T. Fukunaga, A. Wakabayashi, K. Ishikawa, and H. Nakano, *Int. J. Peptide Protein Res.*, **23**, 306 (1984).

4) M. Narita, J.-Y. Chen, H. Sato, and Y. Kim, *Bull. Chem. Soc. Jpn.*, **58**, 2494 (1985).

5) M. Narita, T. Ogura, K. Sato, and S. Honda, *Bull. Chem. Soc. Jpn.*, **59**, 2433, 2439, 2445 (1986).

6) M. Narita, M. Doi, and T. Nakai, *Bull. Chem. Soc. Jpn.*, **60**, 3255 (1987); M. Narita, M. Doi, and H. Takegahara, *ibid.* **60**, 2445 (1987).

7) M. Narita, S. Nagasawa, J.-Y. Chen, H. Sato, and Y. Tanaka, *Makromol. Chem.*, **185**, 1069 (1984); M. Narita, N. Ohkawa, S. Nagasawa, and S. Isokawa, *Int. J. Peptide Protein Res.*, **24**, 129 (1984); S. Isokawa, T. Asakura, and M. Narita, *Macromolecules*, **18**, 871 (1985); S. Isokawa, I. Tominaga, T. Asakura, and M. Narita, *ibid.*, **18**, 878 (1985).

8) M. Narita, M. Doi, H. Sugasawa, and K. Ishikawa, *Bull. Chem. Soc. Jpn.*, **58**, 1473 (1985); M. Narita, K. Ishikawa, H. Sugasawa, and M. Doi, *ibid.*, **58**, 1731 (1985).

9) M. Narita, M. Doi, K. Kudo, and Y. Terauchi, *Bull. Chem. Soc. Jpn.*, **59**, 3553 (1986).

10) M. Narita, S. Honda, and H. Umeyama, *Bull. Chem. Soc. Jpn.*, **60**, 4127 (1987).

11) M. Narita, S. Honda, H. Umeyama, and S. Obana, *Bull. Chem. Soc. Jpn.*, **61**, 281 (1988).

12) C. Toniolo, G. M. Bonora, M., Mutter, and F. Maser, *J. Chem. Soc., Chem. Commun.*, **1983**, 1298.

13) V. Gutmann, *Electrochim. Acta*, **21**, 661 (1976); U. Mayer, V. Gutmann, and W. Gerger, *Mh. Chem.*, **106**, 1235 (1975).

Temperature Dependence of Conductivities and Ion-Association Constants of Potassium Sulfate in Water

Haruhiko YOKOYAMA* and Tomoko OHTA
Department of Chemistry, Yokohama City University, 22-2 Seto, Kanazawa-ku, Yokohama 236
(Received May 13, 1988)

Synopsis. From the temperature dependence of the ion-association constants between K^+ and SO_4^{2-} at 0 to 50 °C, the contact ion-pair formation and short-range interactions are discussed while considering the hydration of the anion. The limiting molar conductivities of SO_4^{2-} are expressed as a cubic equation of the temperature.

In a previous conductivity study[1] of $KClO_4$ and KNO_3 in water, we found that their ion-association constants have minimum values at certain temperatures between 0 and 50 °C. This phenomenon was explained as indicating the presence of specific interactions within contact ion pairs, the formations of which were considered to be helped by a weak hydration of the ions. The sulfate ion, one of the oxoacid anions, also has been known to associate with the potassium ion.[2] It is of interest to examine the temperature dependence of the ion-association constant between these ions, especially whether the specific interactions are characteristic of oxoacid anions.

Although a sulfate ion is one of the most usual types of inorganic anions, details concerning the temperature dependence of its limiting molar conductivity have not yet clarified.[3,4] In the present study, the precise conductivities of potassium sulfate in aqueous solutions were measured at eleven temperatures between 0 and 50 °C in order to clarify these problems.

Experimental

Materials. Potassium sulfate (Wako Pure Chemical Industries, reagent grade) was recrystallized twice from conductivity water and then air-dried at room temperature. It was further dried at about 150 °C and kept over diphosphorus pentaoxide in a desiccator under reduced pressure. This salt was confirmed to be anhydrous by the Karl-Fischer method with an AQ-5 Aquacounter of Hiranuma Sangyo Co. The quantity of adsorption water was less than 0.003 wt%.

Solutions. All solutions were made by weight and the molar concentration at each temperature was calculated by using the solution densities estimated from those at 25 °C (as previously described).[1,5] The conductivity of the water used[1] was always lower than 1×10^{-7} S cm^{-1} at 25 °C after dissolved carbon dioxide was removed. Eight solutions of 0.00025 to 0.0023 mol dm^{-3} were examined.

Measurements. Conductivity measurements were made with a Fuso 360 linear-bridge conductometer in a manner described previously.[1,5] The change of the cell constant (0.13720 cm^{-1} at 25 °C) with temperature was corrected to be regarded as −0.0014% for an elevation of 1 °C.[1] The reproducibility of conductivity measurements was within 0.05%. The precision of temperature measurements was ±0.003 °C and the accuracy of the temperature was ±0.01 °C.

Results and Discussion

Analysis of Conductivity Data. The observed molar conductivities, $\Lambda(K_2SO_4/2)$,[6] were analyzed by assuming the following ion-association (ion-pair formation) equilibrium between the ions, as made by Jenkins and Monk:[2]

$$K^+ + SO_4^{2-} \rightleftharpoons K^+SO_4^{2-}.$$

Representing the fraction of the free sulfate ion as α and the ionic molar conductivity as λ, we can express $\Lambda(K_2SO_4/2)$, based on the mixed rule, by

$$\Lambda(K_2SO_4/2) = \alpha[\lambda(K^+) + \lambda(SO_4^{2-}/2)] + (1-\alpha)[\lambda(K^+) + \lambda(K^+SO_4^{2-})]/2 = \alpha\Lambda_{12} + (1-\alpha)\Lambda_{11}/2,$$

where Λ_{12} and Λ_{11} correspond to the molar conductivities of hypothetical 1:2 and 1:1 electrolytes completely dissociated. In the present study Λ_{12} and Λ_{11} were expressed by means of the Robinson-Stokes equation[3] as follows:

$$\Lambda_{12} = [\lambda^\infty(K^+) + \lambda^\infty(SO_4^{2-}/2)] - S\sqrt{I}/(1 + Ba\sqrt{I}) \quad (1)$$

and

$$\Lambda_{11} = [\lambda^\infty(K^+) + \lambda^\infty(K^+SO_4^{2-})] - S\sqrt{I}/(1 + Ba\sqrt{I}), \quad (2)$$

where λ^∞ is the limiting molar ionic conductivity, a is the closest distance of approach of ions, S and B have their usual meanings[3] and I is the ionic strength, $I=c(1+2\alpha)$, where c is the molar concentration of the salt. According to the treatment of Jenkins and Monk,[2] the $\lambda^\infty(K^+SO_4^{2-})$ was approximated as $0.6\lambda^\infty(SO_4^{2-}/2)$ and S in Eqs. 1 and 2 were taken as those in hypothetical solutions for $\alpha=1$ and 0, respectively. The activity coefficients of the ions, y_i, were expressed by the Debye-Hückel equation involving a.[3] The values of a were assumed to be 3.66 Å, considering the crystallographic radius of K^+ (1.33 Å)[3] and the effective ionic radius of SO_4^{2-} (2.33 Å), which was estimated from its ionic partial molar volume by means of Glueckauf's equation.[1,5] The values of $\lambda^\infty(K^+)$ were obtained from the following cubic equation in which parameters had been given by Harned and Owen:[1,4]

$$\lambda^\infty(t\,°C) = \lambda^\infty(25\,°C) + a(t-25) + b(t-25)^2 + c(t-25)^3. \quad (3)$$

On these assumptions, the $\lambda^\infty(SO_4^{2-}/2)$ and the ion-association constant,

$$K = (1-\alpha)/[c\alpha(1+\alpha)y_{2-}],$$

were determined by a least-squares procedure, minimizing σ, where $\sigma^2=\sum[\Lambda(\text{obsd})-\Lambda(\text{calcd})]^2/(n-2)$. Further details of the calculation have been described

Table 1. Ion-Association Constants (K) and Limiting Molar Ionic Conductivities (λ^∞)

t	K	$\lambda^\infty(SO_4^{2-}/2)$	$\lambda^\infty(K^+)$	σ
°C	dm³ mol⁻¹	S cm² mol⁻¹	S cm² mol⁻¹	S cm² mol⁻¹
0	8.1±0.6	41.55±0.04	40.72	0.0342
5	7.8±0.6	48.49±0.04	46.72	0.0343
10	7.9±0.5	55.80±0.03	53.03	0.0277
15	8.0±0.4	63.47±0.03	59.61	0.0246
20	8.1±0.4	71.50±0.03	66.44	0.0291
25	8.2±0.4	79.84±0.04	73.50	0.0331
30	8.4±0.4	88.54±0.04	80.76	0.0381
35	8.6±0.5	97.54±0.06	88.20	0.0535
40	8.6±0.5	106.81±0.08	95.79	0.0703
45	9.0±0.6	116.52±0.09	103.52	0.0870
50	9.4±0.8	126.52±0.13	111.35	0.1231

Table 2. Experimental and Theoretical Values of Standard Enthalpy and Entropy of Ion Association at Several Temperatures (a=3.66 Å)

	Experimental		Theoretical[a]	
t	$\Delta H°$	$\Delta S°$	$\Delta H°$	$\Delta S°$
°C	kJ mol⁻¹	J K⁻¹ mol⁻¹	kJ mol⁻¹	J K⁻¹ mol⁻¹
5	−0.2±1.7	16.6±6.2	2.71	26.9
15	1.1±0.9	20.9±3.3	3.27	28.9
25	2.4±0.7	25.7±2.3	3.86	30.9
35	4.0±1.0	30.9±3.5	4.49	33.0
45	5.8±2.2	36.5±7.0	5.16	35.2

a) Ref. 9.

previously.[1,5]

Ion-Association Constants and Their Temperature Dependence. The obtained values of K, $\lambda^\infty(SO_4^{2-}/2)$ and σ are shown in Table 1 together with the used values of $\lambda^\infty(K^+)$.[7] The results at 25 °C are in practical agreement with those of Jenkins and Monk:[2] K=9 dm³ mol⁻¹ and $\lambda^\infty(SO_4^{2-}/2)$=79.98 S cm² mol⁻¹.[8] The values of K are apparently comparable to the theoretical ones:[9] K/dm³ mol⁻¹=7.75 (0 °C), 8.08 (10 °C), 8.48 (20 °C), 8.93 (30 °C), 9.45 (40 °C), and 10.05 (50 °C) for a=3.66 Å. However, as shown in Fig. 1, the difference in the temperature dependence between the theoretical and experimental values is found, especially at lower temperatures, even if the scattering of the experimental values is taken into consideration. The full line fitted to the log K values in Fig. 1 was drawn by using the following equation:[1]

$$\log K = p(t - t_{min})^2 + \log K_{min}, \quad (4)$$

with $p=(3.9\pm0.8)\times10^{-5}K^{-2}$, $t_{min}=6.4\pm3.7$ °C, and $\log K_{min}=0.899\pm0.001$ (obtained by a least-squares calculation). The standard enthalpy and entropy of ion association, $\Delta H°$ and $\Delta S°$, were estimated by the use of Eq. 4 and are shown for several temperatures in Table 2, compared with the theoretical values.[9] The experimental and theoretical values ($\Delta H°$ and $\Delta S°$) are close to each other at higher temperatures. However, the experimental values deviate more with decreasing temperature.

The temperature dependence of K between K^+ and SO_4^{2-} is similar to that for KNO_3 and $KClO_4$, for which the K values were considerably larger than the theoretical ones and became minimum at higher

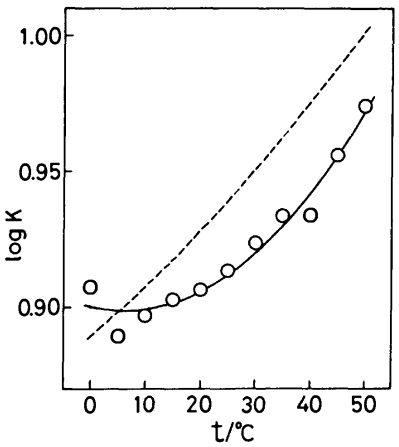

Fig. 1. Temperature dependence of the ion-association constants: experimental (O) and theoretical (----) values.

temperatures: 30 °C for KNO_3 and 36 °C for $KClO_4$.[1] These results have been explained as indicating the presence of specific short-range interactions within the contact ion pairs of which formations were helped by the weak hydration of the ions.[1] The present results can be explained by considering the relatively strong hydration of SO_4^{2-} compared to that of NO_3^- and ClO_4^-.[10] The appearance of t_{min} may suggest the presence of short-range interactions within contact ion pairs,[11] as observed for KNO_3 and $KClO_4$.[1] The lower t_{min} is due to the relatively large energy requirement for the partial release of hydration water molecules around SO_4^{2-} by the contact ion-pair formation. The

not so large values of K (in spite of the possibility of the presence of specific interactions) is due to a strong hydration of SO_4^{2-}, which hinders contact ion-pair formation. A similar hydration effect has been found concerning the ion association between Na^+ and SO_4^{2-}, of which the K value, 6.7 $dm^3 mol^{-1}$,[2] is relatively small compared to that for K^+. This has been attributed to a stronger hydration of Na^+ than of K^+.[10]

The Temperature Dependence of Limiting Molar Conductivities of SO_4^{2-}. Equation 3 was used to represent the temperature dependence of $\lambda^\infty(SO_4^{2-}/2)$. The parameters were determined to be as follows: $\lambda^\infty(25\,°C)$=79.83 S $cm^2 mol^{-1}$, a=1.7027 S $cm^2 mol^{-1} K^{-1}$, b=6.70×10^{-3} S $cm^2 mol^{-1} K^{-2}$, and c=−5.4×10^{-6} S $cm^2 mol^{-1} K^{-3}$. By using Eq. 3 with these parameter values, the experimental $\lambda^\infty(SO_4^{2-}/2)$ could be reproduced with an average deviation of ±0.03 S $cm^2 mol^{-1}$.

References

1) H. Yokoyama and T. Ohta, *Bull. Chem. Soc. Jpn.*, **61**, 3073 (1988).

2) I. L. Jenkins and C. B. Monk, *J. Am. Chem. Soc.*, **72**, 2695 (1950).

3) R. A. Robinson and R. H. Stokes, "Electrolyte Solutions," 2nd ed, Butterworths, London (1959), Chaps. 4, 6, and 7 and Appendixes.

4) H. S. Harned and B. B. Owen, "The Physical Chemistry of Electrolytic Solutions," 3rd ed, Reinhold, New York (1958), p. 233.

5) H. Yokoyama, *Bull. Chem. Soc. Jpn.*, **57**, 1304 (1984); H. Yokoyama and M. Nishimura, *ibid.*, **58**, 1094 (1985).

6) The table of the observed molar conductivities are deposited as Document No. 8836 at the Office of the Editor of Bull. Chem. Soc. Jpn.

7) The values of K are somewhat dependent on the assumptions for $\lambda^\infty(K^+SO_4^{2-})$ and a: for example, we obtain $K(25\,°C)/dm^3 mol^{-1}$=7.8±0.4 by assuming $\lambda^\infty(K^+SO_4^{2-})$=0.5$\lambda^\infty(SO_4^{2-}/2)$ and 8.8±0.4 by assuming a=4.16 Å. However, the following discussion in this study is qualitatively unaltered.

8) Obtained from the analysis with the Onsager limiting equation;[3] we can obtain K=8.5±0.9 $dm^3 mol^{-1}$ and $\lambda^\infty(SO_4^{2-}/2)$=79.85±0.06 S $cm^2 mol^{-1}$ with the Robinson-Stokes equation by reanalyzing their data in the concentration range examined in the present study.

9) H. Yokoyama and H. Yamatera, *Bull. Chem. Soc. Jpn.*, **48**, 1770, 3002 (1975); although the theoretical equation of the ion-association constant has been derived for symmetrical electrolytes, it was assumed to be also applicable to unsymmetrical electrolytes.

10) Y. Marcus, "Ion Solvation," John Wiley & Sons, New York (1985), Chap. 5.

11) About half of ion pairs are presumed to be contact ion pairs, since the formation constants of separated ion pairs are theoretically estimated as follows: 3.9, 4.4, and 5.0 $dm^3 mol^{-1}$ at 0, 25, and 50 °C, respectively,[9] where the closest distance of approach was taken as 6.4$_2$ Å equal to the sum of 3.66 and 2.7$_6$ Å (diameter of water molecule).

 © 1989 The Chemical Society of Japan Bull. Chem. Soc. Jpn., 62, 349—353 (1989)

Selective Formation of Ethene from CO Hydrogenation Reaction over In_2O_3-CeO_2, -La_2O_3, and -Y_2O_3 Mixed Oxide Catalysts

Toru ARAI, Ken-ich MARUYA,* Kazunari DOMEN, and Takaharu ONISHI*
Research Laboratory of Resources Utilization, Tokyo Institute of Technology,
4259 Nagatsuta, Midori-ku, Yokohama 227
(Received June 9, 1988)

CO hydrogenation over mixed oxides of 3A and 4A Groups (Y_2O_3, La_2O_3, CeO_2, and ZrO_2) with 3B Group (Al_2O_3, Ga_2O_3, and In_2O_3) was carried out. The addition of Ga_2O_3 or In_2O_3 to Y_2O_3, La_2O_3, and CeO_2 enhances the formation of light alkenes. An In_2O_3-CeO_2 catalyst shows the highest selectivity (43%) for ethene with the lowest selectivity (0.5%) for ethane in total hydrocarbons produced. The addition of In_2O_3 to CeO_2 results in an increase in activity for the CO hydrogenation reaction. From the results of an ethene hydrogenation reaction over mixed oxide catalysts, the high selectivity for alkene formation over In_2O_3-containing catalysts is due to a suppression of alkene hydrogenation by the addition of In_2O_3. Indium in CeO_2 is highly dispersed while keeping an oxidation state of +1 or +3 under the reaction conditions.

The selective, direct formation of light alkenes from CO hydrogenation has been studied over specifically supported metal catalysts under limited conditions. Propene is selectively formed over an Al_2O_3-supported $Fe_3(CO)_{12}$ catalyst at the initial stage of the reaction,[1,2] and also over a Co-zeolite catalyst reduced by Cd vapor.[3] Ott et al.[4] reported that the formation of ethene and propene proceeds with selectivity of 25% over freshly reduced Fe-Ru alloys. Vannice et al.[5-7] found that ethene is formed with a selectivity of 25—30% over K-promoted Fe-Mn cluster catalysts; however, the activity decreases rapidly upon carbon deposition due to a CO disproponation reaction. These metal catalysts are generally not so stable as to keep the high activity for a long-time reaction and are not selective for ethene formation.

On the other hand, CO hydrogenation over oxide catalysts, such as ThO_2, known as an iso-synthesis catalyst, proceeds to form branched hydrocarbons selectively under severe conditions such as at 723—743 K and 30—60 MPa.[8] Maehashi et al.,[9] reported that isobutene is selectively formed over ZrO_2 under moderate conditions, such as at 623—673 K and 67—2000 kPa. The formation of branched hydrocarbons with specific selectivity[10] is a characteristic of oxide catalysts on the CO hydrogenation reaction.

In this paper, we report on the CO hydrogenation reaction over mixed oxide catalysts: 3A and 4A group metal oxides with 3B Group metal oxides and the role of In_2O_3, which is the most effective for the selective formation of ethene among the added 3B Group oxides.

Experimental

Catalyst Preparation. Oxide catalysts (CeO_2, La_2O_3, Y_2O_3, and ZrO_2) were prepared as follows: Metal hydroxide was precipitated by the hydrolysis of each metal(III) nitrate with a 5% aqueous ammonia solution, washed with distilled water, dried overnight at 393 K, and then calcined to form oxide at 773 K for 3 h. Mixed oxide catalysts were prepared by co-precipitation from a mixed aqueous solution of each metal nitrate via the same procedure as that of the oxide. The atomic ratios of M_I (Al, Ga, and In) to M_{II} (Y, La, Ce, and Zr) were 1 : 10. All catalysts used were evacuated at 973 K for 3 h before the reaction, except for La_2O_3 and its mixed oxides which were evacuated at 973 K for 1 h.

Chracterization. The surface areas of the used catalysts were measured by the BET method. The crystal structures were determined by X-ray diffraction (Rigaku geigerflex rad-B system). Surface analyses of the catalysts were conducted by using an X-ray photoelectron spectrometer equipped with a glovebox (Shimadzu ESCA-750). The binding energies were corrected by Au $4f_{7/2}$ (83.8 eV).

Procedure. CO hydrogenation reactions were carried out over catalysts in a closed circulation system. A typical reaction was performed at 673 K and the initial pressure was 67 kPa (H_2 : CO=3 : 1).

Ethene hydrogenation reactions were carried out over catalysts at 195 and 273 K, and 60 kPa (H_2 : C_2H_4=20 : 1). The activities were obtained from the initial rate of ethane formation.

Analyses. Products, except for methane, were collected by a liquid-nitrogen trap. Quantitative analyses were conducted by a GC equipped with a Porapak-Q column for hydrocarbons, CO_2, and H_2O, VZ-7 and VZ-10 columns for C_2 and C_3 hydrocarbons and isomers of C_4 hydrocarbons, and a Molecular Sieve-5A column for CH_4 and CO.

Results and Discussion

CO Hydrogenation over Oxide and Mixed Oxide Catalysts. Table 1 shows the activity and selectivity for hydrocarbon formation over catalysts which were stable for 17.5 h, except for In_2O_3 and Ga_2O_3. The products were hydrocarbons, CO_2, H_2O, and a small amounts of oxygenates, such as methanol and dimethyl ether.

Y_2O_3, La_2O_3, CeO_2, and ZrO_2 showed a relatively high selectivity for C_4, C_5, and C_6 hydrocarbons which consist mainly of branched alkenes, while Ga_2O_3 produced only CH_4. In_2O_3 was rapidly reduced to metallic indium under the reaction conditions and produced large amounts of CO_2 and H_2O with no hydrocarbons from CO hydrogenation. The addition of In_2O_3 or Ga_2O_3 to CeO_2, La_2O_3, and Y_2O_3 resulted in an

Table 1. The CO Hydrogenation over Oxide and Mmixed Oxide Catalysts at 673 K and 67 kPa ($H_2/CO=3$)

Catalysts[a] (surface area)[c]	Activity[b]		Selectivity (carbon-base %)					
	Hydrocarbons	CO_2	C_1	C_2	C_3	C_4	C_5	C_{6+}
Y_2O_3 (51)	18 (0.35)[d]	30	10	4(67)[e]	7(86)[e]	30	23	26
Al_2O_3-Y_2O_3 (60)	10 (0.17)	12	6	6(75)	9	42	26	11
Ga_2O_3-Y_2O_3 (50)	16 (0.32)	13	5	21(90)	16	41	16	2
In_2O_3-Y_2O_3 (47)	18 (0.38)	15	5	19(94)	22(90)	34	13	7
La_2O_3 (17)	9 (0.53)	18	15	7(40)	8(60)	19	21	30
Al_2O_3-La_2O_3 (53)	10 (0.19)	16	9	7(47)	9	27	31	17
Ga_2O_3-La_2O_3 (59)	9 (0.15)	6	7	24(90)	16	28	22	3
In_2O_3-La_2O_3 (17)	12 (0.71)	14	7	34(92)	16(93)	20	16	7
CeO_2 (21)	43 (2.0)	34	25	29(96)	9(84)	21	8	8
Al_2O_3-CeO_2 (64)	180 (2.8)	130	18	30(97)	13(91)	24	13	2
Ga_2O_3-CeO_2 (59)	160 (2.7)	130	25	43(97)	14(96)	15	3	+
In_2O_3-CeO_2 (28)	160 (5.7)	130	24	43(99)	10(94)	13	7	3
ZrO_2 (50)	10 (0.20)	14	5	6(64)	7(90)	77	5	+
Al_2O_3-ZrO_2 (81)	6 (0.07)	8	19	14(85)	14	49	4	+
Ga_2O_3-ZrO_2 (59)	13 (0.22)	13	36	16(90)	14	21	5	8
In_2O_3-ZrO_2 (39)	23 (0.59)	47	99	1(96)	+	+	+	+
In_2O_3-Al_2O_3 (164)	9 (0.05)	76	100	+	+	+	+	+
Ga_2O_3 (18)	3 (0.17)	3	100	+	+	+	+	+
In_2O_3[f] (60)	+ (0)	200	−	−	−	−	−	−

a) The amounts of catalysts used were 1.5 g except CeO_2 and CeO_2 mixed oxide catalysts (0.5 g) and the atomic ratios of Al_2O_3, Ga_2O_3, and In_2O_3 to Y_2O_3, La_2O_3, CeO_2, and ZrO_2 were 1/10. b) The values are the average rates from initial 2.5 to 17.5 h in carbon-base $\mu mol \cdot g\text{-cat.}^{-1} \cdot h^{-1}$. c) $m^2 \cdot g^{-1}$. d) Parentheses show the specific activity based on surface area in carbon-base $\mu mol \cdot m^{-2} \cdot h^{-1}$. e) Parentheses show the selectivity for alkenes. f) In_2O_3 was reduced to metallic indium under the reaction conditions.

increase in the selectivity for C_2 and C_3 hydrocarbons, while CH_4, C_4, C_5, and C_{6+} hydrocarbons decreased. The alkene selectivities in C_2 and C_3 hydrocarbons also increased. Especially, the In_2O_3-CeO_2 catalyst exhibited the highest selectivity (43%) for C_2 hydrocarbons which consist of 99% ethene. The addition of Al_2O_3, Ga_2O_3, or In_2O_3 to ZrO_2 resulted in an increase in the selectivity for methane. In_2O_3-Al_2O_3 produced methane only. These results indicate that In_2O_3- or Ga_2O_3-combined 3A group oxides are effective for the selective formation of ethene and that In_2O_3 is the most effective among the additives.

The catalytic activity, based on the surface area of the oxide and mixed oxide catalysts (Table 1), show that CeO_2 and its mixed oxides exhibit a high specific activity. Especially, In_2O_3-CeO_2 indicates the highest value among them and the addition of In_2O_3 to CeO_2 leads to an enhancement of the activity for hydrocarbon formation. The activity of In_2O_3-Y_2O_3 and In_2O_3-La_2O_3 are nearly equal to that of Y_2O_3 and La_2O_3, respectively.

The Effect of In_2O_3 Addition to CeO_2, La_2O_3, and Y_2O_3 on the Hydrocarbon Formation. The product distribution change upon the addition of In_2O_3 suggests that the role of In_2O_3 is to retard the rate of carbon-carbon bond formation and to accelate the rate of the hydrogenation of surface species. However, the facts that the addition of In_2O_3 does not increase the selectivity for methane and that it retards alkane formation seem to be inconistent with the above-mentioned suggestion. Although there is a little difference among the three oxides, it may be a common feature that the addition of In_2O_3 to 3A Group oxides results in the retardation of the carbon-carbon bond formation and alkane formation, including methane, without lowering the activity for hydrocarbon formation.

CO Hydrogenation Reaction over In_2O_3-CeO_2 and Effect of In_2O_3 Addition. Figures 1 and 2 show the time course of the activity and selectivity for hydrocarbon formation over In_2O_3-CeO_2, respectively. The constant catalytic activity and the selectivity for hydrocarbon formation were observed during 2—48 h reactions. Large amounts of CO_2 and H_2O (totally 600 $\mu mol\ g^{-1}$) were formed at the initial stage (0—1 h), but decreased remarkably after 1 h, the reaction proceeded with a good material balance during 2—48 h reactions.

Figure 3 shows the dependence of the reaction temperatures on the selectivity over In_2O_3-CeO_2 and CeO_2 catalysts. In_2O_3-CeO_2 shows the high selectivity (40—45%) for C_2 hydrocarbons, which consist of 98—99% ethene in the temperature range 573—723 K.

In the case of a single CeO_2 catalyst, the selectivity for C_2 hydrocarbons is only 4% at 573 K, and the ethene content in C_2 hydrocarbons is 71%; however, these values increase to 36 and 96%, respectively, at 723 K.

The activity of the In_2O_3-CeO_2 catalyst based on the surface area is remarkably high in comparision with that of CeO_2 at temperatures below 673 K, as shown in Fig. 4. Thus, the addition of In_2O_3 to CeO_2 leads to an

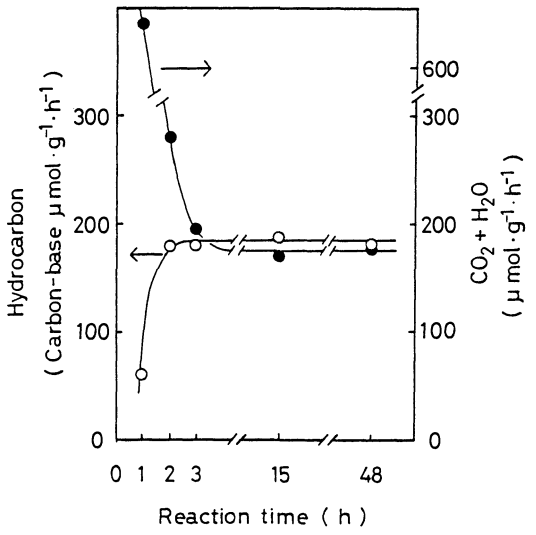

Fig. 1. Time course of the activity over In_2O_3-CeO_2 at 673 K, 67 kPa, and H_2:CO=3. This long run reaction of 48 h was carried out in the closed circulation system by exchanging the reaction gas to maintain the pressure about 60—67 kPa.
(○): Hydrocarbon, (●): CO_2+H_2O.

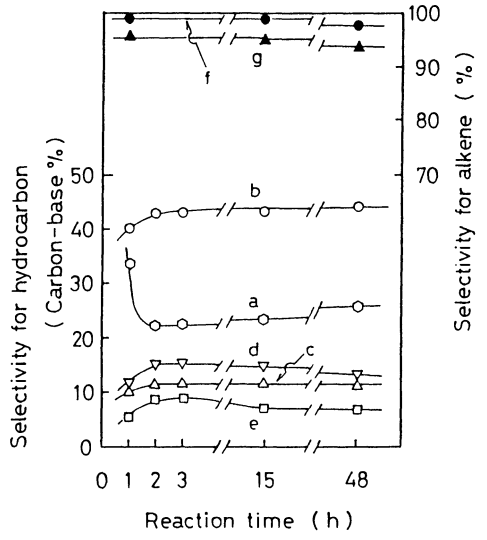

Fig. 2. Time course of the selectivity over In_2O_3-CeO_2 at 673 K, 67 kPa, and H_2:CO=3.
a(○): C_1 hydrocarbon, b(○): C_2, c(△): C_3, d(▽): C_4, e(□): C_{5+}.
f(●): C_2H_4 in C_2 hydrocarbons, g(▲): C_3H_6 in C_3 hydrocarbons.

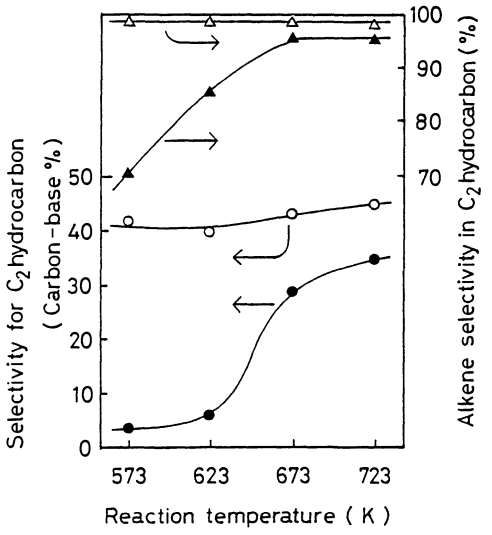

Fig. 3. The effect of reaction temperature on the selectivity.
a(○): In_2O_3-CeO_2; selectivity for C_2 hydrocarbons. b(●): CeO_2; selectivity for C_2 hydrocarbons. c(△): In_2O_3-CeO_2; selectivity for ethene in C_2 hydrocarbons. d(▲): CeO_2; selectivity for ethene in C_2 hydrocarbons.

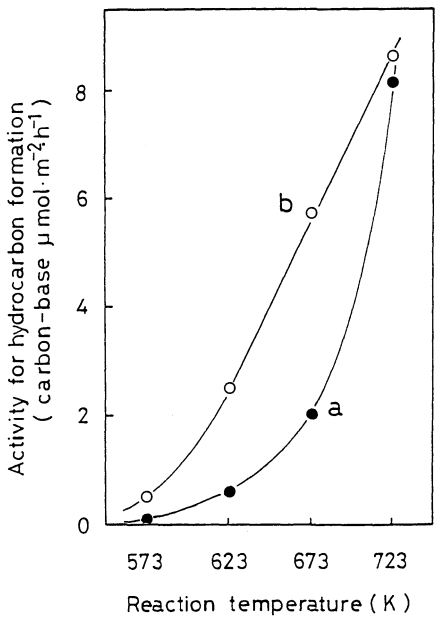

Fig. 4. The effect of reaction temperature on the activity for hydrocarbon formation.
a(●): CeO_2 and b(○): In_2O_3-CeO_2.

increase in the activity for hydrocarbon formation, the selectivity for C_2 hydrocarbons, and the selectivity for alkene. These effects become clearer at lower reaction temperatures.

C_2H_4 Hydrogenation Reaction over Single and In_2O_3-Containing Mixed Oxides. The rates of C_2H_4 hydrogenation at 195 and 273 K over CeO_2, La_2O_3, and Y_2O_3 and their mixed oxides with In_2O_3 are shown in Table 2. The rates of C_2H_4 hydrogenation over CeO_2 and In_2O_3-CeO_2 are much slower than those over the other oxide catalysts. The addition of In_2O_3 results in a decrease in the rate of C_2H_4 hydrogenation. The catalysts which have the lower rate for the C_2H_4 hydrogenation show a higher selectivity for alkene, as shown in Fig. 5. This indicates that the high selectivity for alkene formation over CeO_2 and In_2O_3-containing mixed oxides is due to the low rate of alkene hydrogenation as a side reaction of CO hydrogenation.

Among single oxides, CeO_2 shows the lowest and

La_2O_3 shows the highest activity for ethene hydrogenation, respectively, as reported by Minachev et al.[11] To the contrary, the activity for a CO hydrogenation reaction is highest over CeO_2 and lowest over La_2O_3. These facts show that there is a great difference between the hydrogenation reactions of C_2H_4 and CO. These results suggest the following possibilities: (1) a key step of hydrocarbon formation from CO and H_2 is neither the step of hydrogenation nor the activation of H_2, (2) the activation site or process of CO is different from that of C_2H_4, and (3) the hydrogen species which reacts with CO or intermediates to form hydrocarbons is different from that which reacts with ethene.

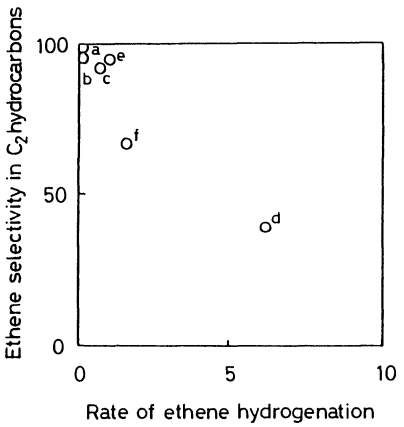

Fig. 5. Correlation between the ethene selectivity (%) in C_2 hydrocarbon on CO hydrogenation reaction at 673 K and the rate (10^3 μmol g-cat.$^{-1}$ h^{-1}) of ethene hydrogenation at 195 K.
a; In_2O_3-CeO_2,b; CeO_2, c; In_2O_3-La_2O_3, d; La_2O_3, e; In_2O_3-Y_2O_3, and f; Y_2O_3.

Table 2. Rate of Hydrogenation of C_2H_4

Catal.[a]	Rate (μmol g-cat^{-1} h^{-1})	
	273 K	195 K
CeO_2	20	0(0)[b]
In_2O_3-CeO_2	3	0(0)
La_2O_3	fast	6100(360)
In_2O_3-La_2O_3	fast	680(40)
Y_2O_3	fast	1500(30)
In_2O_3-Y_2O_3	fast	940(20)

a) Catalysts of 0.1 g (La_2O_3, Y_2O_3, and their In_2O_3-containing mixed oxides) or 0.5 g (CeO_2 and In_2O_3-CeO_2) were used on C_2H_4 hydrogenation reaction as maintaining the conversion below ca. 30%. b) Parentheses show the activity based on specific surface area, μmol m^{-1} h^{-1}.

The addition of In_2O_3 to CeO_2 enhances CO hydrogenation while supressing C_2H_4 hydrogenation. Therefore, the role of added In_2O_3 is different in the hydrogenation of CO and alkene.

Characterization of In_2O_3-Containing Mixed Oxides. XRD and XPS results of the oxides and In_2O_3-containing mixed oxides are shown in Table 3. For In_2O_3-CeO_2, only the diffraction patterns of CeO_2 (fluorite type) were observed, although the catalyst contained 10% In_2O_3. On the other hand, a slight amount of $LaInO_3$ and $YInO_3$ in addition to La_2O_3 and Y_2O_3 were observed for In_2O_3-La_2O_3 and In_2O_3-Y_2O_3, respectively. However, no peaks due to In_2O_3 appeared for all In_2O_3-containing mixed oxides. The binding energies of In $3d_{5/2}$ for the mixed oxides after the reaction were observed between 444.4 and 444.7 eV. The values are higher than that at 443.3 eV for metallic indium. Indium in the mixed oxides still kept the higher oxidation state under the reaction conditions.

The surface composition on the In_2O_3-CeO_2 catalyst was estimated from the peak area of Ce3d and In3d and corrected by the ionization cross section[13] and escape depth[14] using formula,[15]

$$\frac{C_{In}}{C_{Ce}} = \frac{A_{In}}{A_{Ce}} \times \frac{I_{Ce}}{I_{In}} \times \frac{D_{Ce}}{D_{In}}$$

where C, A, I, and D denote the surface concentration, peak area, total ionization cross section, and escape depth, respectively.

It was found that the surface ratio of In/Ce is close to the bulk ratio, as shown in Table 3.

From these results, it can be seen that indium in CeO_2 is highly dispersed as small crystalline forms of

Table 3. Characterization of the Oxides and In_2O_3-Containing Mixed Oxides

Catal.	XRD	XPS	
		Binding energy of In $3d_{5/2}$ (eV)	Surface ratio (%) of In to M (Ce, La, or Y)
CeO_2	CeO_2	—	—
In_2O_3-CeO_2	CeO_2	444.4	11
La_2O_3	La_2O_3	—	—
In_2O_3-La_2O_3	La_2O_3+($LaInO_3$)	444.5	9
Y_2O_3	Y_2O_3	—	—
In_2O_3-Y_2O_3	Y_2O_3+($YInO_3$)	444.7	5
In_2O_3	In_2O_3	444.4	—
In[a]	—	443.3	—

a) Commercial metallic indium (99.99%) was spattered by Ar ion bomberdment before the measurement, and the binding energy obtained for $In3d_{5/2}$ agreed with the literature.[12]

In_2O_3 or as a substitutional solution state, and that indium in La_2O_3 and Y_2O_3 exists partialy as mixed oxide compounds of $LaInO_3$ and $YInO_3$, while keeping the oxidation state under the reaction conditions. To the contrary, single In_2O_3 is rapidly reduced to metallic indium and forms no hydrocarbons from a mixture of CO and H_2 under the above-stated reaction conditions. The valency of indium could not be determined by XPS, since the binding energies of In^+ and In^{3+} are close to each other. On the other hand, In_2O_3-CeO_2 produces large amounts of CO_2 and H_2O (total ca. 600 $\mu mol\,g^{-1}$) during the initial stage (0—1 h). It is known that In_2O_3 is easily reduced[16] and that CeO_2 is partially reduced to CeO_{2-x} (x=0—0.5)[17] to form Ce^{3+},[18] under the reductive conditions, such as the CO hydrogenation reaction. Single CeO_2 forms relative small amounts of CO_2 and H_2O (totally ca. 50 $\mu mol\,g^{-1}$) during the initial stage of the reaction at 673 K. These facts indicate that the In_2O_3 addition to CeO_2 enhances the reduction of the catalyst to form In^+ and/or Ce^{3+}. CeO_2 exhibits a high activity and selectivity for ethene formation, similar to In_2O_3-CeO_2, at a high reaction temperature of 723 K (Figs. 3 and 4). This means that the active centers for hydrocarbon formation exist on cerium ions in In_2O_3-CeO_2. Details concerning the active center for CO hydrogenation reaction over In_2O_3-CeO_2 will be published elsewhere.

References

1) F. Hugues, B. Besson, and J. M. Basset, *J. Chem. Soc. Chem. Commun.*, **1980**, 719.

2) F. Hugues, P. Bursiere, J. M. Basset, D. Commereuc, and Y. Chauvin, Proceedings Intnl Congr. Catal. 1980 A28 Tokyo.

3) D. Fraenkel and B. G. Gates, *J. Am. Chem. Soc.*, **102**, 2478 (1980).

4) G. L. Ott, T. Fleisch, and W. N. Delgass, *J. Catal.*, **60**, 394 (1979).

5) A. A. Chen, M. Kaminsky, G. L. Geoffroy, and M. A. Vannice, *J. Phys. Chem.*, **90**, 4810 (1986).

6) J. Venter, M. Kaminsky, G. L. Geoffroy, and M. A. Vannice, *J. Catal.*, **103**, 450 (1987).

7) G. B. McVicker and M. A. Vannice, *J. Catal.*, **63**, 25 (1980).

8) H. Pichler and K. H. Ziesecke, *Brennst. Chem.*, **30**, 13, 60, 81, 333 (1949).

9) T. Maehashi, K. Maruya, K. Domen, K. Aika, and T. Onishi, *Chem. Lett.*, **1984**, 747.

10) K. Maruya, A. Inaba, T. Maehashi, K. Domen, and T. Onishi, *J. Chem. Soc., Chem. Commun.*, **1985**, 487.

11) Kh. M. Minachev, Yu. S. Khodakov, and V. S. Nakhshunov, *J. Catal.*, **49**, 207 (1977).

12) K. Yoshihara, T. Shiokawa, K. Maeda, Y. Nakai, and K. Seto, *Chem. Lett.*, **1973**, 879.

13) J. H. Scofield, *J. Electron Spectrosc. Relat. Phenom.*, **8**, 129 (1976).

14) D. R. Penn, *J. Electron Spectrosc. Relat. Phenom.*, **9**, 29, (1976).

15) C. J. Powell, *American Lab.*, **10**, 17 (1978).

16) K. Otuka, S. Shibuya, and A. Morikawa, *Chem. Lett.*, **1982**, 987.

17) M. Brysse, M. Geenin, and J. Veron, *J. Catal.*, **28**, 54 (1973).

18) T. Jin, Y. Zhou, G. J. Mains, and J. M. White, *J. Phys. Chem.*, **91**, 5931 (1987).

Intermolecular Interactions of Fluorine Atoms in the Crystal of 1,3-Dimethyl-5-fluorouracil and Its Mixed Crystal with 1,3-Dimethyluracil

Tooru TAGA,* Noriko YAMAMOTO, and Katsunosuke MACHIDA
Faculty of Pharmaceutical Sciences, Kyoto University, Sakyo-ku, Yoshidashimoadachi-cho, Kyoto 606
(Received June 20, 1988)

A crystal of 1,3-dimethyl-5-fluorouracil can be used to solve large amounts of 1,3-dimethyluracil as a solid-solution crystal. The crystal structure has been determined by an X-ray method. The planar molecules are arranged in a parallel sheet, and the molecules within the same sheet interact with each other through short CH···O and CH···F contacts. The short intermolecular C···F distance is 2.999(6) Å. The stability of a mixed crystal could be explained in terms of intermolecular interactions around the fluorine atom.

A mixed crystal of organic compounds is generally formed in the case that two component molecules have similar sizes and shapes.[1] On the other hand, the similarity of the atomic sizes between a fluorine atom and a hydrogen atom is one of the important characteristics for fluorine-substitution effects.[2] Thus, a rigid organic compound and its fluorine substituent have a high possibility to form a mixed crystal. We therefore tried to form a mixed crystal between 1,3-dimethyluracil (DMU) and 1,3-dimethyl-5-fluorouracil (DNFU), and obtained fairly stable mixed crystals over a wide range of their mixing ratios. The DMU and DMFU compounds were obtained by methylations of uracil and 5-fluorouracil. The 5-fluorouracil is a well-known antitumor-active agent, and its fluorine-substitution effects have received special attention.[2] The crystal structure of DMU had already been reported by Banerjee et al.[3] However, the crystal structure of DMFU was unknown, and the mixed crystal was isomorphic to the DMFU crystal. Thus, the present X-ray analyses of the DMFU and mixed crystals were performed in order to study the fluorine-substitution effects in the mixed crystals.

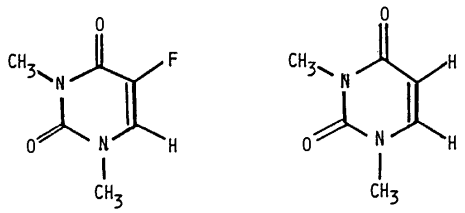

Scheme 1.

Experimental

Structure Determination of DMFU. The colorless single crystals of DMFU were obtained from an ethanol solution and a crystal (0.1×0.3×0.3 mm) was mounted on a Rigaku AFC-5RU diffractometer with graphite-monochromated Cu$K\alpha$ radiation (λ=1.54178 Å). The crystal data were $C_6H_7N_2O_2F$, M_r=158.13, orthorhombic, $P2_12_12_1$, a=6.605(2), b=8.455(2), c=12.621(2) Å, V=704.8 Å^3, Z=4, D_x=1.490 Mg m^{-3}. Intensity data of 638 reflections were collected within $2\theta<120°$ (h 0—6, k 0—8, l 0—14) in a 2θ-ω scan mode with a scan width of $0.8°+0.5°\tan\theta$ and scan speed 2° ω/min. The intensity fluctuation during data collection was less than 2% for three standard reflections measured at every 56 reflections. Intensities were corrected for Lorentz and polarization factors, but no absorption correction was applied (μ=11.54 cm^{-1}). The structure was solved by MULTAN78[4] and refined by a full-matrix least-squares method using a modified version of the program ORFLS.[5] The minimized quantity was $\sum w(|F_o|-k|F_c|)^2$, where k is a scale factor and w is a weight equal to $[\sigma(F_o)+(0.023\ F_o)^2]^{-1}$. All hydrogen atoms were located on a difference Fourier map. The refinement of C, N, O and F atoms with anisotropic temperature factors and of H atoms with isotropic temperature factors converged an R value to 0.047 (wR=0.057) for 541 unique reflections with $F_o>2\sigma(F_o)$, in which (200) reflection was omitted due to a large extinction effect.

Mixed Crystal Formed between DMFU and DMU. Condensed ethanol solutions of DMFU-DMU mixtures with 1 : 1, 2 : 3, 1 : 2, and 1 : 5 molar ratios for DMFU : DMU were prepared at room temperature (27 °C). Transparent columner crystals were obtained by cooling the solution in a refringerator (5 °C) for a few days. The HPLC analyses using a Shimadzu LC-3A apparatus equipped with an SPD-2A UV detector showed that the molar content of DMU in the obtained crystals were 0.36, 0.50, 0.61, and 0.77, corresponding to the above-mentioned solutions. Preliminary microscopic and X-ray photographic studies indicated that the mixed crystals were isomorphic to the DMFU crystal. The mixed crystal obtained from a 1 : 1 DMFU : DMU solution was subjected to a single-crystal X-ray analysis. The crystal size was 0.3×0.3×0.3 mm, and the unit cell dimensions were a=6.634(1), b=8.439(1), and c=12.530(1) Å, V=703.6 Å^3. The calculated crystal density was 1.425 Mg m^{-3} for Z=4. Data collections and structure refinements were performed in the same way as in the case of the DMFU crystal. Intensity data of 652 reflections (h 0—6, k 0—8, l 0—14) were collected. Disorders of the F(5) and H(5) atoms were assumed in the structure, and an occupancy of 0.6 was assigned for the F(5) atom. The disordered structre was refined to R=0.075 (wR=0.125) for 540 reflections with $F_o>3\sigma(F_o)$.

The atomic scattering factors used for all atoms were obtained from the International Table for X-ray Crystallography.[6] All computations were undertaken on a FACOM M382 in the Data Processing Center of Kyoto University,

using the program KPPXRAY.[7]

Results and Discussion

Molecular Structure of DMFU. The atomic coordinates and thermal parameters for nonhydrogen atoms are listed in Tables 1 and 2.[8] A perspective view of the DMFU molecule with the atomic numbering is given in Fig. 1. The molecule is planar within 0.04 Å, except for the hydrogen atoms of the methyl groups. Bond distances and bond angles, except for the C(4)-C(5)-C(6) angle (Table 3), agree well with those

Table 1. Atomic Coordinates and Temperature Factors of DMFU (Estimated Standard Deviations in Parentheses)

Atom	x	y	z	B_{eq}/Å^{2} a)
F(5)	0.2536(11)	0.2097(3)	0.3405(1)	6.62
C(1)	0.2545(21)	0.6354(5)	0.5865(5)	6.36
C(2)	0.2488(15)	0.3629(4)	0.6489(2)	4.08
C(3)	0.2545(21)	0.0876(6)	0.7109(4)	6.29
C(4)	0.2476(13)	0.1412(4)	0.5214(3)	4.22
C(5)	0.2494(15)	0.2600(4)	0.4418(2)	4.40
C(6)	0.2504(16)	0.4126(4)	0.4628(2)	4.13
N(1)	0.2518(15)	0.4652(3)	0.5655(2)	4.19
N(3)	0.2464(11)	0.2036(3)	0.6238(2)	4.08
O(2)	0.2467(14)	0.4090(3)	0.7401(2)	6.07
O(4)	0.2490(16)	−0.0007(3)	0.5049(2)	6.30

a) $B_{eq}=(4/3)(\beta_{11}a^2+\beta_{22}b^2+\beta_{33}c^2)$.

Table 2. Atomic Coordinates and Temperature Factors of DMFU-DMU Meixed Crystal (Estimated Standard Deviations in Parentheses)

Atom	x	y	z	B_{eq}/Å^{2} a)
F(5)	0.2547(18)	0.2069(7)	0.3383(4)	7.21
C(1)	0.2525(18)	0.6319(8)	0.5830(7)	7.66
C(2)	0.2459(14)	0.3609(6)	0.6450(3)	4.42
C(3)	0.2504(20)	0.0854(8)	0.7080(6)	6.89
C(4)	0.2483(14)	0.1390(7)	0.5166(5)	5.08
C(5)	0.2523(12)	0.2556(7)	0.4364(4)	5.08
C(6)	0.2477(12)	0.4079(8)	0.4582(4)	4.90
N(1)	0.2453(11)	0.4614(5)	0.5607(3)	4.71
N(3)	0.2498(11)	0.2005(6)	0.6195(4)	4.66
O(2)	0.2510(13)	0.4056(6)	0.7367(3)	7.29
O(4)	0.2558(15)	−0.0043(5)	0.5010(4)	7.20

a) $B_{eq}=(4/3)(\beta_{11}a^2+\beta_{22}b^2+\beta_{33}c^2)$.

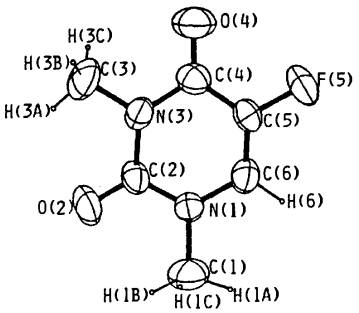

Fig. 1. The molecular structure of DMFU with the numbering scheme.

Table 3. Bond Distances and Bond Angles of DMFU and DMFU-DMU Mixed Crystals (Estimated Standard Deviations in Parentheses)

Bond distance (l/Å)	DMFU	Mixed
F(5)-C(5)	1.348(3)	1.296(7)
C(1)-N(1)	1.463(5)	1.467(8)
C(2)-N(1)	1.363(4)	1.355(6)
C(2)-N(3)	1.384(4)	1.391(7)
C(2)-O(2)	1.215(4)	1.210(6)
C(3)-N(3)	1.474(6)	1.474(9)
C(4)-C(5)	1.421(5)	1.407(8)
C(4)-N(3)	1.396(5)	1.390(8)
C(4)-O(4)	1.218(4)	1.226(7)
C(5)-C(6)	1.317(5)	1.314(9)
C(6)-N(1)	1.370(4)	1.361(6)
Bond angle (ϕ/°)	**DMFU**	**Mixed**
N(1)-C(2)-N(3)	116.2(2)	115.5(4)
N(1)-C(2)-O(2)	121.9(3)	123.1(5)
N(3)-C(2)-O(2)	121.9(3)	121.4(5)
C(5)-C(4)-N(3)	112.8(3)	113.7(5)
C(5)-C(4)-O(4)	125.1(3)	125.1(6)
N(3)-C(4)-O(4)	122.1(3)	121.1(6)
F(5)-C(5)-C(4)	116.6(3)	117.1(6)
F(5)-C(5)-C(6)	120.0(3)	120.5(5)
C(4)-C(5)-C(6)	123.4(3)	122.4(5)
C(5)-C(6)-N(1)	120.5(3)	121.4(5)
C(1)-N(1)-C(2)	119.0(3)	117.7(5)
C(1)-N(1)-C(6)	119.4(3)	120.3(5)
C(2)-N(1)-C(6)	121.6(3)	121.9(5)
C(2)-N(3)-C(3)	118.5(3)	117.9(5)
C(2)-N(3)-C(4)	125.4(3)	125.2(5)
C(3)-N(3)-C(4)	116.0(3)	116.9(5)

of the usual uracil derivatives.[9] The C(5)-F(5) bond distance of 1.348(3) Å is close to the usual values, but the C(4)-C(5)-C(6) bond angle of 123.4(3)° is significantly larger than the average value of 120.7° for those of other uracil derivatives. A similar trend regarding such a large bond angle has been observed in several compounds which have a conjugated ring substituted with a fluorine atom, e.g. fluorobenzens[10] and *m*-, *o*-, *p*-fluorobenzoates.[11-13]

Molecular Packing of DMFU. The planar DMFU molecules form a sheet parallel to the *bc* plane. Such sheets cross the *a*-axis at $a=1/4$ and 3/4 with the interplaner distance of 3.3 Å. The projection of the molecular stacking along the *a*-axis is shown in Fig. 2. The molecules related by the 2_1-axis along the *a*-axis are close to each other, the short van der Waals distances being 3.32(1) Å between C(4) and C(6), 3.33(1) Å between C(2) and F(5), 3.37(1) Å between N(3) and F(5), and 3.40(1) Å between N(3) and C(5). The molecular stacking pattern is different from those of other uracil crystals. However, the molecular overlapping, such as the fluorine atom which lies near the adjacent uracil ring, resembles those observed in purine and halogenated pyrimidine complexes.[14] This type of molecular stacking may be favorable for dipole-induced dipole interactions between the fluorine atom and the conjugated ring.

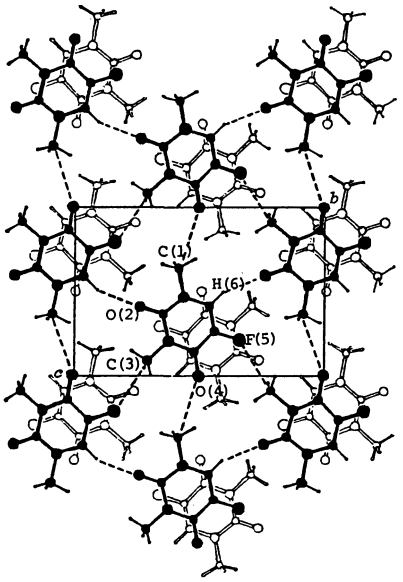

Fig. 2. Projection of the crystal structure viewed along the *a*-axis.

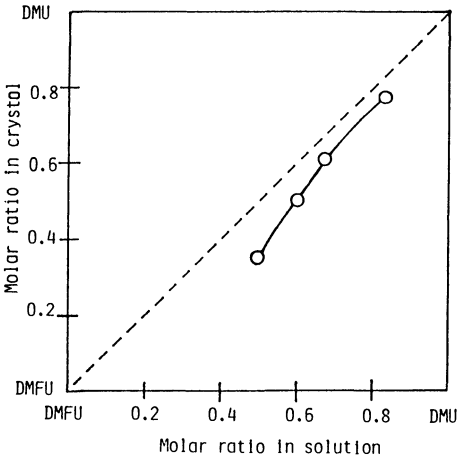

Fig. 3. Plots of the molar ratios in the prepared solutions and in the crystals.

CH ··· O Hydrogen Bonds. As shown in Fig. 2, one DMFU molecule is surrounded by six neighbor molecules within the same sheet; very short intermolecular contacts, C(6)H ··· O(2) (C ··· O 3.190(4) Å and H ··· O 2.28(3) Å) and C(1)H_3 ··· O(4) (C ··· O 3.245(5) Å and H ··· O 2.63(4) Å) were observed within the sheet. The C ··· O and H ··· O distances are significantly shorter than the sum of the van der Waals radii, 1.75, 2.0, 1.50, and 1.20 Å for C, CH_3, O, and H, respectively.[15] Similar short NCH_3 ··· O contacts have been observed in the DMU crystal,[3] and similar short C(aromatic)-H ··· O contacts have been also observed in the benzoquinone crystal.[16] The short CH ··· O interactions may be classified into the CH ··· O hydrogen-bonds[17–19] which strongly bind to the planar molecules in the sheet.

Mixed Crystal Formation between DMFU and DMU. The crystal structure of DMFU is quite different from that of DMU, and the mixed crystal has an isomorphic form to the DMFU crystal. A comparison of the molar ratios in the prepared solutions and in the obtained mixed crystals are given in Fig 3. The observed line is located below the dotted diagonal line, and the DMU amounts in the mixed crystal are smaller than those in the solution. However, very large amounts of DMU can be mixed into a DMFU crystal. Even if the DMU molar ratio is 77%, the mixed crystal has the same DMFU form. In this mixed crystal, the larger the amounts of DMU molecules are solved, the more the unit cell volume of the mixed crystal decreases, though the decrement of the unit cell volume is smaller than the expected value for the DMU amounts; for instance, a volume decrement of 1.2 $Å^3$ for a mixed crystal with a 0.4 DMU/DMFU molar ratio corresponds to about half of the volume change estimated from the van der Waals volumes. Thus, the small volume change is one of the unique properties of this mixed crystal. Usually a mixed crystal formed without any volume change is classified into a block solution in which impurity molecules occupy defect sites of the crystal or are located at the boundaries of mosaic blocks. However, in the present case it must be a true substitutional solid solution in which the host molecules are replaced with guest molecules at random. The structure of such a solid solution model was successfully refined by a least-squares method for the 0.4 molar ratio DMU mixed crystal. The refined structure was essentially the same as that of the DMFU crystal, although the C-F bond in the mixed crystal seems to be slightly shortened.

Intermolecular NCH_3 ··· F Interaction. The fluorine atom in the DMFU crystal has a short intermolecular contact to the methyl group of the neighbouring molecule with an F(5) ··· C(3) distance of 2.999(6) Å. According to Nyburg and Faerman,[20] the van der Waals radius for a fluorine atom varies from 1.30 to 1.38 Å, depending on the directions of the intermolecular contacts. The present F ··· C distance is shorter than the van der Waals sum of the smallest F radius (1.30 Å) and the C radius (1.75 Å), and it is the shortest in the resemble F ··· CH_3 contacts observed so far.[21,22] The Coulomb interaction between the approached F and CH_3 is attractive; the interaction energy is about -11 kJ mol^{-1} for a simple point charge model with net charges of -0.195 a.u. on F and 0.124 a.u. on CH_3. Thus, the replacement of F by H in a mixed crystal will cause a loss of Coulomb energy. On the other hand, the van der Waals interaction between the F and CH_3 is repulsive in the DMFU crystal because of the very short F ··· CH_3 distance. Thus, the replacement of F by H will decrease the van der Waals energy; the estimated energy gain is about 2.7 kJ mol^{-1} for the coefficients by Williams and Houpt.[23] The entropy effect, owing to a mixing of two components, also decreases the free energy of the mixed crystal, though

this contribution (maximum -3 kJ mol^{-1} for an ideal case) is small if the mixing ratio is different from 1 : 1.

In conclution, the DMFU crystal consists of very stable sheets of planar DMFU molecules which are bonded by CH $\cdots$ O hydrogen bonds. Repulsive van der Waals interactions at short F $\cdots$ CH_3 contacts cause the DMFU crystal to become a stable solid solution for DMU over a wide range of mixing ratios. Such easy replacement of fluorine substituents must be one of the important properties of a fluorine atom in considering the fluorine-substitution effects.

The authors wish to thank Professor Kenji Osaki for his motivation of this work. They also thank Dr. Takashi Harayama and Dr. Reiko Yanada for their kind supply of 1,3-dimethyl-5-fluorouracil.

References

1) A. I. Kitaigorodsky, "Mixed Crystal," Springer-Verlag, Berlin (1984).
2) P. Goldman, *Science*, **164**, 1123 (1969).
3) A. Banerjee, J. K. Dattagupta, W. Saenger, and A. Rabczenko, *Acta Crystallogr., Sect. B*, **33**, 90 (1977).
4) P. Main, S. E. Hull, L. Lessinger, G. Germain, J.-P. Declercq, and M. M. Woolfson, MULTAN78; "A System of Computer Programs for the Automatic Solution of Crystal Structure from X-ray Diffraction Data," Univs. of York, England, and Louvain, Bergium (1978).
5) W. R. Busing, K. O. Martin, and H. A. Levy, ORFLS, Report ORNL-TM-305, Oak Ridge National Laboratory, Tenesee (1963).
6) "International Tables for X-ray Crystallography," Vol. IV, Birmingham, Kynoch Press (1974).
7) T. Taga, T. Higashi, and H. Iizuka, KPPXRAY; "Kyoto Program Package for X-ray crystal structure analysis," Kyoto Univ., Kyoto (1985).
8) The anisotropic temperature factors for the non-hydrogen atoms, the atomic coordinates for the hydrogen atoms, and the lists of structure factors are deposited as Document No. 8852 at the Office of the Editor of the Bull. Chem. Soc., Jpn.
9) D. Voet and A. Rich, *Prog. Nuclaic Acid Res. Mol. Biol.*, **10**, 183 (1970).
10) M. Colapietro, A. Domenicano, and G. P. Ceccarini, *Acta Crystallogr., Sect. B*, **35**, 890 (1979).
11) T. Taga, N. Yamamoto, and K. Osaki, *Acta Crystallogr., Sect. C*, **41**, 153 (1985).
12) G. Ferguson and K. M. S. Islam, *Cryst. Struct. Commun.*, **4**, 389 (1975).
13) M. Colapietro, A. Domenicano, and G. P. Ceccarini, *Acta Crystallogr., Sect. B*, **35P**, 890 (1979).
14) C. E. Bugg, J. M. Thomas, M. Sundaralingam, and S. T. Rao, *Biopolymers*, **10**, 175 (1971).
15) L. Pauling, "The Nature of the Chemical Bonds," 3rd ed., Cornell University Press, Itaca, N. Y. (1960).
16) Z. Berkovitch-Yellin and L. Leiserowitz, *Acta Crystallogr., Sect. B*, **40**, 159 (1984).
17) D. J. Sutor, *J. Chem. Soc.*, **1963**, 1105.
18) J. Donohue, "Structural Chemistry and Molecular Biology," edited by A. Rich and N. Davidson, p. 443, San Francisco, Freeman (1968).
19) R. Taylor and O. Kennerd, *J. Am. Chem. Soc.*, **104**, 5063 (1982).
20) S. C. Nyburg and C. H. Faerman, *Acta Crystallogr., Sect. B*, **41**, 274 (1985).
21) T. Dahl, *Acta Crystallogr., Sect. B*, **33**, 3021 (1977).
22) N. Yamamoto, K. Machida, T. Taga, and H. Ogoshi, *Acta Crystallogr., Sect. C*, **42**, 1573 (1986).
23) D. E. Williams and D. J. Houpt, *Acta Crystallogr., Sect. B*, **42**, 286 (1986).

Photochromic Properties of a New Spirobenzothiopyran Compound

Shin-ichiro TAMURA,* Nobutoshi ASAI, and Jun'etsu SETO
Sony Corporation Research Center, 174 Fujitsuka-cho, Hodogaya-ku, Yokohama 240
(Received July 26, 1988)

Photochromic processes of 1'-hexyl-5',8-dimethoxy-3',3'-dimethyl-6-nitrospiro[2*H*-1-benzothiopyran-2,2'-indoline] were investigated with laser flash techniques. Photocoloration was found to proceed via the excited singlet state, and the quantum yield of coloration was an order of magnitude smaller than those of ordinary spirobenzopyrans. The main route of the decoloration was found to be the thermal reaction. Remarkably different solvent effects for the thermal fading rate of the colored form were observed, which indicates that the zwitterionic structure is more significant for the new spirobenzothiopyran than ordinary spirobenzopyrans. Repetitive cycles of photocoloration and thermal fading were achieved.

Photochromism of spirobenzothiopyran was first reported by Becker and Kolc.[1] They synthesized 1',3',3'-trimethylspiro[2*H*-1-benzothiopyran-2,2'-indoline], and observed its colored form at 77 K. The colored form was thermally unstable, and bleached at elevated temperatures. The photochemical processes of coloration and decoloration have not as yet been investigated.

Recently, a new series of spirobenzothiopyrans was synthesized.[2] The thermal stability of the colored forms observed at room temperature upon irradiation with UV light of these new compounds was improved by introducing a nitro group in the benzothiopyran ring. The absorption spectra of the colored forms in a polymer matrix are reported to extend to wavelengths as long as 900 nm, and application as optical recording media for laser is expected.

In the present work, the photochromic reactions of a typical compound of the new spirobenzothiopyrans, 1'-hexyl-5',8-dimethoxy-3,3'-dimethyl-6-nitrospiro-[2*H*-1-benzothiopyran-2,2'-indoline] (Scheme 1), were investigated with laser flash techniques. The solvent effect on the fading rate and the absorption spectrum was also studied in order to assign the structure of the colored form.

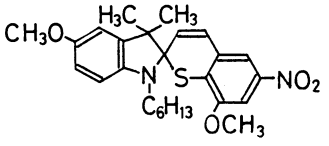

Scheme 1.

Results and Discussion

Coloration and Decolortation Processes. The absorption spectrum of the colorless form is independent of the kind of solvent, and has maxima at 310 nm and 400 nm. Fluorescence was not detected at room temperature, which is in agreement with the result of Becker and Kolc.[1] Although they attempted to observe emission at 77 K, no emission characteristics of 1',3',3'-trimethylspiro[2*H*-1-benzothiopyran-2,2'-indoline] was detected.

The photocoloration process was investigated in aerated and degassed solutions of ethanol (EtOH) and *N*,*N*-dimethylformamide (DMF). The colorless form was excited at 360 nm. Figure 1 shows the transient absorption spectra in aerated and degassed EtOH solutions, measured immediately after the laser pulse. There is no significant difference between the two spectra. The shape of the spectrum was that of the colored form, and no reaction intermediates were detected. Similar results were obtained in aerated and degassed DMF solutions.

Kinetic measurements of the coloration process were made at the wavelength of the absorption maximum of the colored form (620 nm in EtOH, 660 nm in DMF). The absorbance of the colored form was proportional to the laser energy, indicating a single photon process. Figure 2 shows the result of the kinetic measurements of the coloration process in EtOH solution. The time that the absorption change lags behind the time-integrated laser intensity is very small. We assumed a linear response of the reaction to the laser pulse, and obtained a good fit of the experimental results with the calculated absorption changes using various rate constants. The coloration proceeds by first-order kinetics, and the colorlation rates were determined to be 7×10^7 s^{-1} in EtOH and 8×10^7 s^{-1} in DMF. No significant

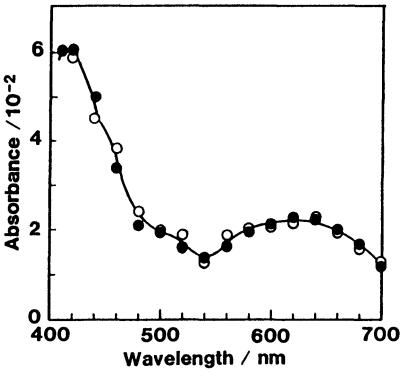

Fig. 1. Transient absorption spectrum observed 30 ns after a laser pulse in aerated(○) and degassed(●) EtOH solutions.

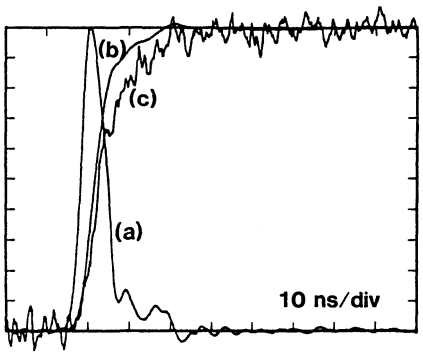

Fig. 2. The photocoloration process in ethanol solution. The laser profile(a), its time-integrated intensity(b), and the absorption change of the colored form(c) are shown. Each curve is normalized to unity.

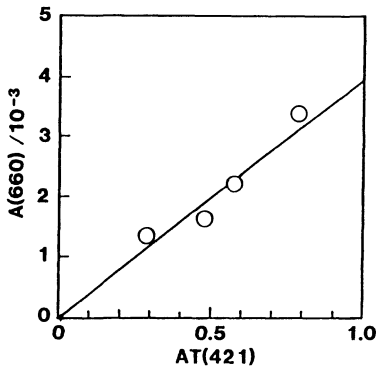

Fig. 3. The plot of the absorption of the colored form in degassed DMF, $A(660)$ vs. the triplet-triplet absorption of anthracene, $AT(421)$.

difference was found in the observed rate constants for degassed and aerated solutions, or for aprotic and protic solvents.

In order to determine the reaction state of the coloration process, we performed triplet quenching experiments on the photoexcited colorless form in degassed EtOH solution using ferrocene (triplet energy 159 kJ mol^{-1} [3]) as a quencher. It is reasonable to assume that the triplet energy level of the colorless form is much higher than that of ferrocene, so the triplet-triplet energy transfer from the colorless spirobenzothiopyran to ferrocene may proceed with the diffusion-controlled rate constant, k_d ($=9.2\times10^9$ s^{-1} [4]). The observed rate of the coloration, k, is given by $k=k_0+k_d$ [Ferr], where k_0 is the coloration rate constant in the absence of ferrocene. However, even when ferrocene was added up to a concentration of 1×10^{-1} mol dm^{-3}, the observed rate of the coloration was not changed. These results indicate that the coloration does not proceed via the triplet state of the uncolored form. Therefore, the reaction state must be the excited singlet state.

Quantum yields of the coloration reaction were determined in degassed solutions of EtOH and DMF by using the triplet-triplet absorption of anthracene in degassed EtOH solution as a relative standard as described in Ref. 5. Figure 3 shows the relationship between the absorption of the colored form at 660 nm, $A(660)$, in degassed DMF and the triplet-triplet absorption of anthracene at 421 nm, $AT(421)$. The quantum yield is estimated from the slope of the plot, and is 4.8×10^{-2} in EtOH and 1.8×10^{-2} in DMF. These values are an order of magnitude smaller than those of the ordinary spirobenzopyrans,[6] which indicates that the deactivation process due to the sulfur atom is efficient for the new spiro compound.

We also carried out laser flash experiments on the decoloration reaction, in which the colored form was excited in the wavelength region on the longer wavelength side of the absorption spectrum. In aerated solutions, decoloration was observed, while, in degassed solutions, no decoloration of the colored form was observed under these experimental conditions. Therefore, the photodecoloration observed in aerated solution was due to photooxidation, and the conversion of the colored form to the colorless form mainly occurs by way of a thermal reaction in the ground state.

Solvent Effect. The thermal stability of the colored form is affected by the solvent polarity. A number of studies have been made for the ordinary spirobenzopyrans, and the colored forms are best regarded as zwitterionic species.[7] The logarithm of the fading rate constant decreases linearly with increasing Kosower's Z or Brownstein's S values. However, the plot against the $(D-1)/(D+2)$ gives a nonlinear graph, and is different for protic and aprotic solvents, where D is the dielectric constant of the solvent. These results can be interpreted in terms of the hydrogen bonding between the colored form and protic solvents.[7]

For the new spirobenzothiopyran, the thermal fading rate, k_T, at 25 °C and the wavenumber of the absorption maximum of the colored form, $\tilde{\nu}_{max}$ was measured in methanol (MeOH), ethanol (EtOH), isobutyl alcohol (i-BuOH), tetrahydrofuran (THF), N,N-dimethylformamide (DMF), and dimethyl sulfoxide (DMSO), and summarized in Table 1. Remarkably different solvent effects for the thermal fading rate were observed for this compound. Figure 4 shows the plot of the logarithm of k_T against Dimroth's E_T

Table 1. Effects on the Solvent Polarity on the Rate Constant of Thermal Fading, k_T, (25 °C) and the Wavenumber of the Absorption Maximum of the Colored Form, $\tilde{\nu}_{max}$

Solvent	Dielectric constant(D)	E_T	k_T	$\tilde{\nu}_{max}$
		kJ mol^{-1}	s^{-1}	cm^{-1}
MeOH	32.6	232	2.8×10^{-4}	1.66×10^4
EtOH	24.3	217	6.9×10^{-3}	1.61×10^4
i-BuOH	15.2	196	9.4×10^{-3}	1.59×10^4
DMSO	48.9	188	4.3×10^{-4}	1.56×10^4
DMF	36.7	183	2.8×10^{-3}	1.51×10^4
THF	7.93	156	3.1×10^{-1}	1.39×10^4

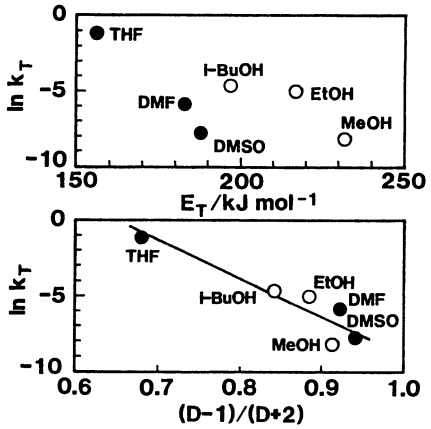

Fig. 4. The plots of ln k_T vs. E_T (upper half) and $(D-1)/(D+2)$ (lower half). The solid circle represents the aprotic solvent, and the open circle protic solvent.

values[8] (E_T is linearly related to the S and Z values) and $(D-1)/(D+2)$. With increasing value of E_T and $(D-1)/(D+2)$, k_T decreases. A linear relationship was obtained against $(D-1)/(D+2)$, rather than against E_T, which is contrary to the ordinary spirobenzopyrans. For the new spirobenzothiopyran, the hydrogen bonding effect on the thermal stability of the colored form in protic solvents as observed in the ordinary spiropyran was not marked.

For the structure of the colored form of the new spirobenzothiopyran, two resonance forms, the thione structure **I** and the zwitterionic structure **II** (Scheme 2) are considered. Becker and Kolc assigned the structure of the colored form of a spirobenzothiopyran to be similar structure to **I**, by comparing the spectral characteristics at 77 K with the colored forms of the chromenes, 2*H*-1-benzothiopyrans, and spiro[benzopyran-2,2′-indolines].[1]

However, the dependence of k_T on the $(D-1)/(D+2)$ value can not be explained in terms of the thione structure **I**. The k_T value for the new spirobenzothiopyran is on the same order (ca. 10^{-4} s^{-1}) as that for the ordinary spirobenzopyran[7] in a highly polar solvent such as MeOH. On the other hand, k_T for the new spirobenzothiopyran in THF is about 10 times larger than that for the ordinary spirobenzopyran, and the colored form of the new spirobenzothiopyran becomes very

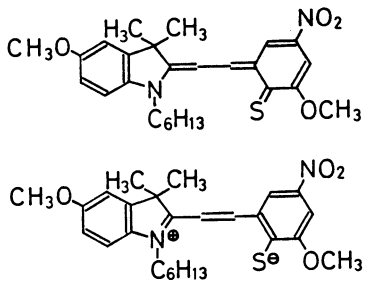

Scheme 2.

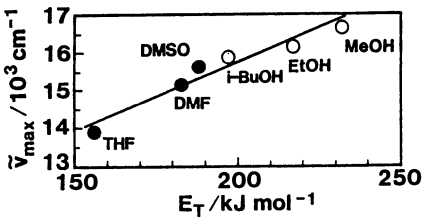

Fig. 5. The plots of $\tilde{\nu}_{max}$ vs. E_T. The solid circle represents the aprotic solvent, and the open circle the protic solvent.

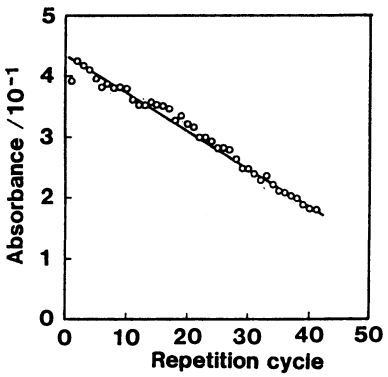

Fig. 6. The absorption decay of the colored form on the repetitive UV coloration and thermal fading cycles.

unstable in a solvent with a small $(D-1)/(D+2)$ value. These results imply that the contribution of the zwitterionic structure is even larger for the new spirobenzothiopyran than for the ordinary spirobenzopyran.

Figure 5 shows the plots of the wavenumber of the absorption maximum of the colored form, $\tilde{\nu}_{max}$, against the Dimroth's E_T value. $\tilde{\nu}_{max}$ increases with increasing value of E_T, and a hypsochromic effect was observed. A linear plot was obtained against the E_T value. This result indicates that the polarity of the colored form in the excited state is lower than that in the ground state, which can be interpreted in terms of the zwitterionic structure **II**.

Cycle Lifetime and Recording Characteristics. The new spirobenzothiopyran could be repetitively colored and bleached by irradiating with UV and by thermal treatment respectively. We performed repetitive coloration and decoloration in degassed DMF solution containing 10^{-4} mol dm^{-3} of the spirobenzothiopyran. With 2 minutes of UV irradiation, more than 30 cycles were achieved before the absorption of the colored form at the maximum decreased to 50% of the initial value (Fig. 6). The value of the cycle lifetime is on the order of 10 even in a dilute solution, which is promising with regard to practical application.

We examined the recording characteristics of a disk medium with a multilayer structure, in which the new spirobenzothiopyran was used as the sensitive material. The recording was carried out with a laser diode lasing at 780 nm. A carrier-to-noise ratio of more than

54 dB was achieved with a carrier frequency of 1 MHz.[9]

In conclusion, we first investigated the photochromic processes of a spirobenzothiopyran compound, and found that photocoloration proceeds via the excited singlet state, and the quantum yield of coloration is an order of magnitude smaller than those of ordinary spirobenzopyrans. The main route of the decoloration was found to be the thermal reaction. Remarkably different solvent effects for the thermal fading rate were observed, and the zwitterionic structure was significant for the new spirobenzothiopyran than for ordinary spirobenzopyrans.

Experimental

The spirobenzothiopyran was synthesized as described elsewhere.[1] All the solvents used methanol (MeOH), ethanol (EtOH), isobutyl alcohol (*i*-BuOH), tetrahydrofuran (THF), *N,N*-dimethylformamide (DMF), dimethyl sulfoxide (DMSO)) were spectral-grade. Typical concentration of the spiropyran was 1×10^{-4} mol dm^{-3}.

Photochemistry of the coloration and decoloration process was investigated in aerated and degassed solution of EtOH and DMF. Excitation was from a pulsed dye laser (FWHM>8 ns, output>10 mJ) optically pumped by a XeCl excimer laser. The absorption change was detected by a K-367 laser kinetic spectrometer (Applied Photophysics). The photomultiplier signal was recorded on a Tektronix 7912AD programmable digitizer, and analyzed by using a personal computer. Quantum yields of coloration were determined by using the triplet-triplet absorption of anthracene in degassed EtOH solution as a relative standard. The values used were 5.2×10^{4} dm^{3}mol^{-1} cm^{-1} for the molar extinction coefficient[10] and 0.7 for the triplet yield.[11] The molar absorption coefficient of the spiropyran was estimated by the extrapolation of the coloration curves in degassed solutions to be 8.5×10^{3} dm^3 mol^{-1} cm^{-1} (620 nm) in EtOH and 8.0×10^{3} dm^3 mol^{-1} cm^{-1} (660 nm) in DMF.

The solvent effect on the thermal fading and the absorption spectra in various solvents were monitored with a Hitachi 320 spectrophotometer. A 500 W high pressure mercury lamp with a Toshiba UV-D36 and a IRA-25S glass filters was used for the coloration source for the repetitive coloration and thermal fading experiments.

References

1) R. S. Becker and J. Kolc, *J. Phys. Chem.*, **72**, 997 (1968).

2) S. Arakawa, H. Kondo, and J. Seto, *Chem. Lett.*, **1985**, 1805.

3) A. Farmilo and F. Wilkinson, *Chem. Phys. Lett.*, **34**, 575 (1975).

4) L. Murov, "Handbook of Photochemistry," Marcel Dekker Inc., New York (1973), p. 55.

5) S. Tamura, K. kikuchi, K. Kokubun, and A. Weller, *Z. Phys. Chem. Neue Folge*, **121**, 165 (1980).

6) S. Kholmanskii, A. V. Zubkov, and K. M. Dyumaev, *Russ. Chem. Rev.*, **50**, 305 (1981).

7) C. Bertelson, "Photochromism," ed. by G. H. Brown, Wiley-Interscience, New York (1971), p. 171, and references therein.

8) S. Arakawa, H. Kondo, S. Tamura, N. Asai, and J. Seto, Conference of Lasers and Electro-Optics, Technical Digest, (1986), p. 358.

9) C. Reichardt, *Agnew. Chem., Int. Ed. Engl.*, **4**, 29 (1965).

10) K. Kikuchi, H. Kokubun, and M. Koizumi, *Bull. Chem. Soc. Jpn.*, **44**, 1524 (1971).

11) T. Medinger and F. Wilkinson, *Trans. Faraday Soc.*, **61**, 620 (1965).

The X-Ray Photoelectron Spectra of 1:1 and 1:2 Salts Formed from Triethylammonium and 7,7,8,8-Tetracyanoquinodimethane

Jun Okubo, Toshihiko Hoshi,* Isao Ono, Kaori Karube, and Michio Kobayashi†
Department of Chemistry, College of Science and Engineering, Aoyama Gakuin University, Setagaya-ku, Tokyo 157
†Department of Chemistry, Technological University of Nagaoka, Nagaoka 940-21
(Received July 27, 1988)

The X-ray photoelectron spectra of the 1:1 and 1:2 salts formed from the triethylammonium cation ($TEAH^+$) and 7,7,8,8-tetracyanoquinodimethane (TCNQ) have been measured and analyzed in order to investigate the electronic structures and conformations of the salts. The N 1s band (398.2 eV) degenerated in the free TCNQ molecule splits into two bands (398.4 eV and 400.3 eV) in the 1:1 salt. This is due to the unequal interactions of the nitrogen atoms of the TCNQ anion radical ($TCNQ^{\cdot-}$) with $TEAH^+$. In the 1:2 salt, the degenerated N 1s bands of two free TCNQ molecules split into three bands (398.5, 400.0, and 401.8 eV). This implies that the negative charge is inhomogeneously distributed over two TCNQ molecules, supporting the idea that the electronic structure of the 1:2 salt can be represented approximately as $TEAH^+$-$TCNQ^{\cdot-}$-$TCNQ^0$. It is found that, in the 1:2 salt, the neutral TCNQ molecule ($TCNQ^0$) is weakly bound to the TCNQ anion radical ($TCNQ^{\cdot-}$) of the strongly bound 1:1 salt, with their molecular planes parallel.

7,7,8,8-Tetracyanoquinodimethane (TCNQ) is a strong electron-acceptor and easily forms CT (charge transfer) complexes with such electron donors as tetrathiafulvalene and *p*-phenylenediamine.[1-13] Melby et al. have synthesized salts of TCNQ with many electron donors and investigated their physicochemical properties.[1] The ion-radical salt of TCNQ with triethylammonium ($TEAH^+$) was also synthesized by them, and its EPR, IR and UV spectra were measured. The analyses of these spectra have revealed that the electronic structure of the 1:1 salt between $TEAH^+$ and TCNQ can be described as $TEAH^+$-$TCNQ^{\cdot-}$; i.e., the TCNQ molecule exists as an anion radical in the crystal. Kobayashi et al. have determined the crystal structure of the 1:2 salt between $TEAH^+$ and TCNQ by means of X-ray diffraction and have shown that the TCNQ in the crystal has two kinds of electronic structures, $TCNQ^{\cdot-}$ and $TCNQ^0$; i.e., the negative charge is inhomogeneously distributed over two TCNQ molecules.[2] In contrast, Filhol et al. showed, by means of the neutron diffraction, that the electronic structure of the 1:2 salt is $TEAH^+$-$TCNQ^{-1/2}$-$TCNQ^{-1/2}$.[3a] However, they have since corrected the results to $TEAH^+$-$TCNQ^{-3/5}$-$TCNQ^{-2/5}$;[3b] i.e., the two TCNQ molecules in the 1:2 salt are not equivalent, but the negative charge is delocalized significantly over the two TCNQ molecules.

In this investigation we have measured and analyzed the X-ray photoelectron spectra (XPS) of the 1:1 and 1:2 salts formed from $TEAH^+$ and TCNQ in order to investigate the electronic structures and conformations of these salts.

Experimental

Commercial triethylamine hydrochloride (TEA-HCl) (Wako Pure Chemical Industries, Ltd.) was purified by sublimation after several recrystallizations from ethyl alcohol. Commercial TCNQ (Tokyo Kasei Co., Ltd.) was purified by sublimation in vacuo (0.28 mmHg/220 °C; 1 mmHg=133.322 Pa). The 1:1 and 1:2 salts of $TEAH^+$ and TCNQ were synthesized according to the procedure reported by Melby et al. and purified by recrystallization from acetonitrile.[1] The salts thus obtained were identified by means of their IR and UV spectra and elemental analysis. The XPS spectra were measured with a Shimadzu ESCA-750 apparatus, employing Mg $K\alpha$ (1253.6 eV) radiation as the X-ray source. Powdered samples are fixed on an adhesive tape put on the holder. The binding energies for the XPS bands were calibrated by the use of that for the $4f_{7/2}$ band of Au powder.

MO Calculation

MO calculation for the π-electron system of TCNQ was performed by using a modified PPP method[14] which can deal, at the same time, with mutually perpendicular π and π' systems as presented in the triple bonds of the cyano groups of TCNQ.

Results and Discussion

The XPS spectra for TEA-HCl, TCNQ, and the 1:1 salt between $TEAH^+$ and TCNQ are compared in Fig. 1, while the spectrum for the 1:2 salt is shown in Fig. 2. According to Ikemoto et al., the N 1s band of the TCNQ salt changes in shape upon X-ray irradiation.[4] In order to confirm this fact, we have measured the XPS spectra of the TCNQ salts at various accumulation times. As a result, the shape of the spectra was found not to change within three accumulation times, but the band shape did vary slightly at five accumulation times. Thus, in this investigation, the spectra accumulated three times are used. The dotted lines shown for each XPS band are the reduced spectra, which are obtained assuming Gaussian curves. The peak positions and integrated intensities (in percent) of these reduced spectra are summarized in Table 1 for all of the compounds investigated here.

XPS Spectra of TEA-HCl and TCNQ. TEA-HCl shows a fairly wide C 1s band at 285.4 eV, the half-width being 2.5 eV. This band consists, therefore, of

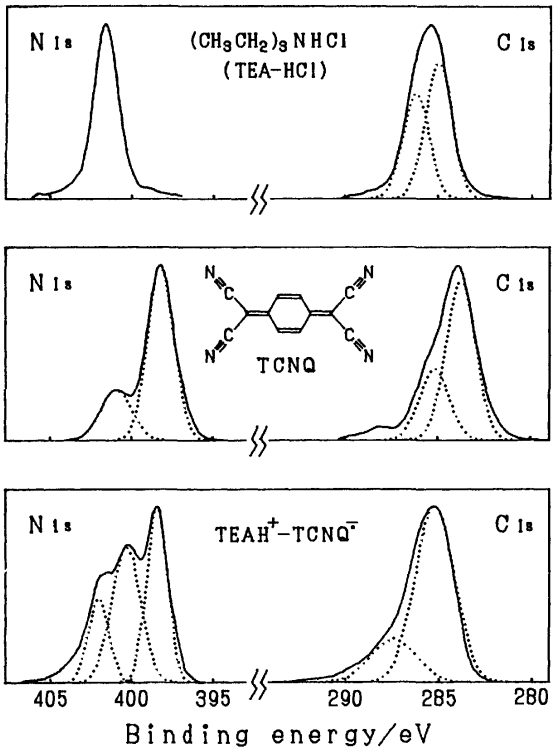

Fig. 1. Comparison of XPS spectra of TEA-HCl, TCNQ, and the 1:1 salt between $TEAH^+$ and TCNQ.

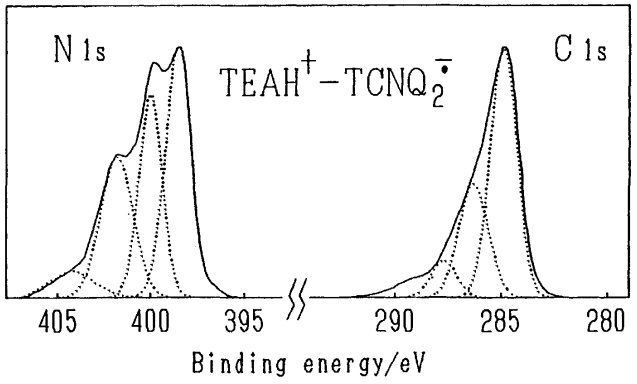

Fig. 2. XPS spectrum for the 1:2 salt between $TEAH^+$ and TCNQ.

two bands with nearly equal intensities whose peak positions are, as determined from the reduced spectra, at 285.0 and 286.2 eV. The higher-energy band at 286.2 eV is assigned to the 1s orbital of the electron-deficient carbon atom adjacent to the electron-withdrawing nitrogen atom with the higher electronegativity, and the lower energy band at 285.0 eV, to that of the outer methyl carbon atom. The N 1s band of TEA-HCl is positioned at 401.6 eV, with a narrow half width.

TCNQ has a C 1s band consisting of a main peak at 283.8 eV and a weak band (a shoulder in the original spectrum) at 285.2 eV. To assign these bands in the reduced spectrum, we have performed a modified PPP

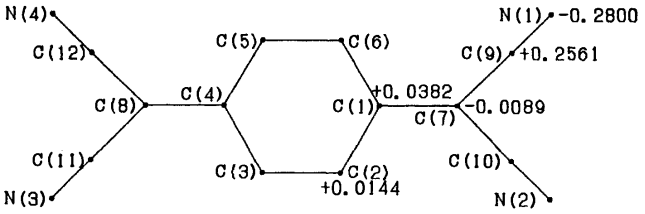

Fig. 3. The formal charge on each atom of TCNQ estimated by a modified PPP calculation.

Table 1. The C 1s and N 1s Binding Energies and Intensities for TEA-HCl, TCNQ, $TEAH^+$-$TCNQ^{\cdot}$, and $TEAH^+$-$TCNQ_2^{\cdot}$, as Estimated from the Reduced Spectra

Compound	Core level	Binding energy/eV	Intensity (in percent)
TEA-HCl	C 1s	288.0	57
		286.2	43
	N 1s	401.6	100
TCNQ	C 1s	283.8	69
		285.2	31
	N 1s	398.2	74
		400.9	26
$TEAH^+$-$TCNQ^{\cdot}$ (1:1)	C 1s	285.2	78
		287.4	22
	N 1s	398.4	37
		400.3	40
		402.0	17
$TEAH^+$-$TCNQ_2^{\cdot}$ (1:2)	C 1s	284.8	60
		286.2	31
		278.6	9
	N 1s	398.5	39
		400.0	27
		401.8	27
		404.2	7

calculation (as explained in the previous section) and have estimated the formal charge on each atom of TCNQ, the results being illustrated in Fig. 3. The formal charges on the central carbon atoms C(1)-C(8) constituting the quinodimethane skeleton are small in magnitude, but those on carbon atoms C(9)-C(12) constituting the cyano groups are large (positive values). From the viewpoint of potential depth, the lower-energy band at 283.8 eV and the higher-energy band at 285.2 eV are assigned to carbon atoms C(1)-C(8) and C(9)-C(12), respectively. This assignment predicts the intensity ratio of the 283.8 eV band to the 285.2 eV band (which is equal to the ratio of the numbers of carbon atoms assigned to each band) to be 2:1, in considerable agreement with the observed value (69:31) given in Table 1.

The N 1s band of TCNQ consists of a main band at 398.2 eV and a sub-band at 400.9 eV. The band contour and band positions agree well with those reported by Ikemoto et al.[5] They have suggested that the sub-band is attributable to a shake-up process involving intramolecular transitions between the π-electron

molecular orbitals.

XPS Spectrum of the 1 : 1 Salt between $TEAH^+$ and TCNQ. As may be seen from Fig. 1, the N 1s band of the 1 : 1 salt shows a complex band contour not explained by the simple addition of the N 1s band of $TEAH^+$ to that of TCNQ; i.e., an extra or new N 1s band has emerged on the formation of the salt. This extra band is too intense to be assigned to only a shake-up band,[4,5] i.e., the shake-up band is considered to be buried in the intense extra band. It is, therefore, demonstrated that the N 1s band is sensitive to the salt formation; in other words, the interaction between $TEAH^+$ and $TCNQ^{\cdot-}$ in the 1 : 1 salt is manifest in the behavior of the N 1s band. This may be due to the fact that the salt is in such a conformation that $TEAH^+$ interacts entirely with the nitrogen atoms located on the outer part of the TCNQ molecule, as will be discussed below in detail. The N 1s band of the 1 : 1 salt consists of three bands —at 398.4, 400.3, and 402.0 eV (Table 1) which are now assigned on the basis of the previously proposed ionic structure ($TEAH^+$-$TCNQ^{\cdot-}$) of the salt.[1]

From the viewpoint of the potential depth on atoms for the free molecule, it is natural to expect that the N 1s band of the triethylammonium cation ($TEAH^+$) is positioned on a higher-energy side than that of the TCNQ anion radical ($TCNQ^{\cdot-}$). Therefore, the highest-energy band at 402.0 eV can be assigned to the N 1s band originating from the $TEAH^+$ of $TEAH^+$-$TCNQ^{\cdot-}$. The N 1s band originating from the $TEAH^+$ of $TEAH^+$-$TCNQ^{\cdot-}$ is on a somewhat higher-energy side than that of $TEAH^+$-Cl^-. This may be due to the fact that the effective positive charge of the proton in $TEAH^+$-$TCNQ^{\cdot-}$ is larger than that in $TEAH^+$-Cl^-; this is because the ionic radius of $TCNQ^-$ is larger than that of Cl^-. Thus, the other two N 1s bands —at 398.4 and 400.3 eV— of the salt can be attributed to the ionization from the N 1s orbital of $TCNQ^{\cdot-}$. This implies that the N 1s bands of free $TCNQ^{\cdot-}$, which are degenerated, are split into two bands because $TEAH^+$ interacts with the nitrogen atoms of $TCNQ^{\cdot-}$ unequally. The unequal interaction of $TEAH^+$ with the nitrogen atoms of $TCNQ^{\cdot-}$ just mentioned may be possible when the configuration of $TEAH^+$ and $TCNQ^{\cdot-}$ is linear in the 1 : 1 salt, as is illustrated in Fig. 4a. The N 1s bands (398.4 and 400.3 eV) of the $TCNQ^{\cdot-}$ of the 1 : 1 salt are positioned on a higher-energy side than that (398.2 eV) of the free TCNQ. This fact is rather surprising, since, in general, an XPS band of a neutral molecule is on a higher-energy side than that of negatively charged species.

As is well-known, the position of the XPS band is dependent on the potential depth on the atom. In the present case, the potential depth may be influenced by two factors: the effects of the π-electron density, and the positive charge of the proton. The increase in the binding energy of the N 1s bands of the $TCNQ^{\cdot-}$ of the 1 : 1 salt in comparison with that of the free TCNQ molecule may indicate that the effect of the proton is superior to that of an extra odd electron. Thus, the 400.3 eV band is assigned to the N 1s band of the nitrogen atoms 1 and 2, which interact with the proton of $TEAH^+$ directly, and the 398.4 eV band to those of the nitrogen atoms 3 and 4 (Fig. 4a). In conformity with these assignments, the observed intensity ratio (37 : 40 : 17) of the N 1s bands is in good agreement with the theoretical one (2 : 2 : 1) estimated from the number of nitrogen atoms assigned to each N 1s band. It is interesting to notice here that the 400.3 eV N 1s band of the salt has a wide half width. We have considered that this band broadening is derived from the singlet-triplet splitting due to the biradical nature of the ionized state of $TCNQ^{\cdot-}$ and/or from superimposition of the shake-up band.[5] The unpaired electron in $TCNQ^{\cdot-}$ may be localized mainly at nitrogen atoms 1

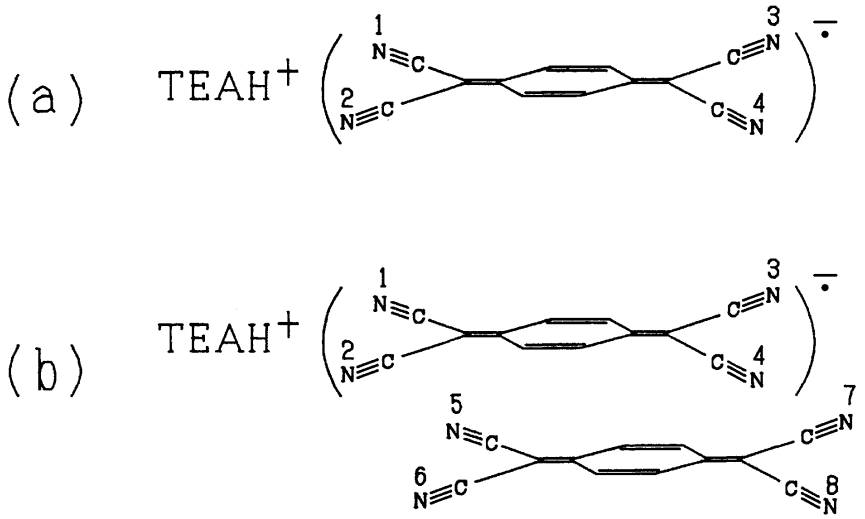

Fig. 4. Conformations of (a) the 1 : 1 salt ($TEAH^+$-$TCNQ^{\cdot-}$) and (b) the 1 : 2 salt ($TEAH^+$-$TCNQ^{\cdot-}$-$TCNQ^0$).

and 2 through the electrostatic attraction by $TEAH^+$, resulting in the concentration of the biradical nature of the ionized state of $TCNQ^-$ on nitrogen atoms 1 and 2 (Fig. 4a). This may be the reason why only the 400.3 eV N 1s band of the salt, which stems from the ionization of the nitrogen atoms 1 and 2, is broadened. The band broadening mentioned above may, therefore, be evidence for the presence of an unpaired electron in the CT-structure ($TEAH^+$-$TCNQ^-$) of the 1 : 1 salt.

In contrast to the N 1s band, the C 1s band of the 1 : 1 salt has a broad and rather structureless band shape; i.e., the C 1s bands of donor and acceptor are not separated, but are overlapped to give a broad band, demonstrating that the C 1s band is insensitive to the salt formation. The broad C 1s band of the 1 : 1 salt can, however, be decomposed into two bands of the Gaussian type positioned at 285.2 and 287.4 eV, whose intensity ratio is 78 : 22 (Table 1), as is shown in Fig. 1. The intense band at 285.2 eV results, as has been explained above, from a complete overlap of the band originating from the 283.8 eV C 1s band of the free TCNQ molecule, which is assigned to the central carbon atoms C(1)-C(8) of TCNQ (Fig. 3), and that originating from the C 1s band of TEA-HCl. The weak band at 287.4 eV may originate from the 285.2 eV C 1s band of the free TCNQ molecule, which is assigned to the carbon atoms C(9)-C(12) of TCNQ; this assignment is based on the fact that the theoretical intensity ratio (7 : 2) is in good agreement with the observed one (78 : 22). According to these assignments of the C 1s bands of the salt, the two C 1s bands at 283.8 and 285.2 eV of the free TCNQ molecule are shifted to energies higher by 1.4 and 2.2 eV respectively by the formation of the salt. This rather surprising result may be also explained by the same reason as that presented for the higher-energy shift of the N 1s band of $TCNQ^-$.

XPS Spectrum of the 1 : 2 Salt between $TEAH^+$ and TCNQ. The N 1s band of the 1 : 2 salt shows, like that of the 1 : 1 salt, a complex band contour not explained by the simple addition of N 1s bands of the cation and the anion; i.e., at least, an additional N 1s band has emerged on the formation of the salt. Indeed, it has shown, as will be discussed below, that the splitting pattern of the N 1s bands is a good indicator of the donor-acceptor interaction in the salt or of the conformation and electronic structure of the salt.

The N 1s band of the 1 : 2 salt consists of four bands —at 398.5, 400.0, 401.8, and 404.2 eV, with the intensity ratio of 39 : 27 : 27 : 7 (Table 1). The assignment of these bands is the basis for the study of the donor-acceptor interaction in the 1 : 2 salt and for the verification of the previously proposed models for the electronic structure of the 1 : 2 salt. By analogy with the case of the 1 : 1 salt, the N 1s band of $TEAH^+$ may be expected to shift to a higher-energy side on forming the 1 : 2 salt, the 401.8 or 404.2 eV band being a candidate for the N 1s band of $TEAH^+$ in the salt. We have considered that the 401.8 eV N 1s band can not be assigned to the N 1s band of $TEAH^+$ for the following two reasons: (1) the band has, as will be discussed later, a wide half width and, hence, resembles the 400.3 eV N 1s band of the $TCNQ^-$ of the 1 : 1 salt, and (2) the intensity of the band is too large to be assigned to $TEAH^+$. Thus, the 404.2 eV N 1s band is assigned to $TEAH^+$, while three N 1s bands at 398.5, 400.0, and 401.8 eV must be assigned to the two TCNQ molecules in the 1 : 2 salt. In other words, it has been demonstrated that the degenerated N 1s bands of two free TCNQ molecules are split into three bands in the 1 : 2 salt. This splitting pattern of the N 1s bands is possible only when the following two conditions are fulfilled: (a) the negative charge is inhomogeneously distributed over two TCNQ molecules, and (b) the unequal, in the same sense as in the 1 : 1 salt, interaction of $TEAH^+$ with the nitrogen atoms of the one TCNQ molecule is stronger (or weaker) than that with the nitrogen atoms of the other TCNQ molecule. The first condition is necessary for the second one to be fulfilled, rather supporting the electronic structure of $TEAH^+$-$TCNQ^-$-$TCNQ^0$ previously determined by means of X-ray diffraction.[2] The second condition may be fulfilled when the 1 : 2 salt is in the conformation illustrated in Fig. 4b. As may be seen from Fig. 4b, $TEAH^+$ interacts strongly with $TCNQ^-$ with just the same conformation as that of the 1 : 1 salt, and $TCNQ^0$ interacts weakly with $TCNQ^-$, with their molecular planes parallel.

The conformational model shown in Fig. 4b makes possible a further assignment of the three N 1s bands at 398.5, 400.0, and 401.8 eV. There seem to be formally two alternative assignments for the lowest-energy band at 398.5 eV: one is the assignment to the four nitrogen atoms of the $TCNQ^0$ positioned at 5—8, and the other, to the nitrogen atoms at 3, 4, 7, and 8 (Fig. 4b). Following the latter assignment, the highest-energy band at 401.8 eV is assigned to the nitrogen atoms 1 and 2, which are bound with the proton of $TEAH^+$ most strongly, and the band at 400.0 eV to the nitrogen atoms 5 and 6. As a result, the energy difference between the two split bands of $TCNQ^-$ in the 1 : 2 salt amounts to 3.3 (=401.8—398.5) eV, which is very different from that (1.9 eV) in the 1 : 1 salt; thus, the latter assignment can be ruled out. Since, however, the 401.8 eV band is assigned to the nitrogen atoms 1 and 2, and the 400.0 eV band, to the nitrogen atoms 3 and 4, the former assignment reasonably predicts the above-mentioned energy difference to be 1.8 (=401.8—400.0) eV, which corresponds well to the value (1.9 eV) observed in the 1 : 1 salt. The theoretical intensity ratio (2 : 1 : 1) for the three N 1s bands assigned as above is also in agreement, though only qualitatively, with the observed one (39 : 27 : 27). It is interesting to note that the two split N 1s bands of $TCNQ^-$ in the 1 : 2 salt are both shifted to a higher-energy side by ca. 1.5 eV compared with those in the 1 : 1 salt. This may be because a small amount of the unpaired electron of $TCNQ^-$

migrates to $TCNQ^0$, for that $TCNQ^0$ is bound to $TCNQ^{\cdot-}$ via the weak CT-type interaction ($TCNQ^{\cdot-}$ behaves as an electron donor with respect to $TCNQ^0$). The unique similarity between the N 1s bands of the 1 : 2 salt and those of the 1 : 1 salt is the existence of the broad band assigned to the nitrogen atoms (1 and 2) of $TCNQ^{\cdot-}$ directly interacting with $TEAH^+$. That is, the 401.8 eV N 1s band of the 1 : 2 salt, which is assigned to the nitrogen atoms (1 and 2) directly interacting with $TEAH^+$, exhibits a band broadening based on the same mechanism as that in the 1 : 1 salt. This is a further confirmation of the band assignment based on the conformation and electronic structure of the 1 : 2 salt presented in Fig. 4b.

The C 1s band of the 1 : 2 salt shows an ill-resolved band shape which is very similar, in spite of the presence of $TCNQ^{\cdot-}$ in the salt, to that of the C 1s band of the free TCNQ molecule. Indeed, the two lower-energy reduced bands at 284.8 and 286.2 eV, which are assigned, respectively, to the central carbon atoms of $TCNQ^{\cdot-}$ and $TCNQ^0$ and to the carbon atoms constituting the cyano groups of $TCNQ^{\cdot-}$ and $TCNQ^0$, have an energy separation of 1.4 eV and an intensity ratio of 60 : 31, comparable to those values (1.3 eV and 69 : 31) for the C 1s band of the free TCNQ molecule (see Table 1). It can, therefore, be understood that the C 1s-band positions of $TCNQ^{\cdot-}$ coincide, following the electronic structure of $TEAH^+$-$TCNQ^{\cdot-}$-$TCNQ^0$ for the 1 : 2 salt, with those of $TCNQ^0$. We have considered this coincidence to be a further confirmation of the already mentioned general tendency for the core level of the carbon atom to be scarcely affected by valence electrons.[5] The C 1s band of $TEAH^+$ in the 1 : 2 salt might be buried under the C 1s bands of $TCNQ^{\cdot-}$ and $TCNQ^0$.

References

1) L. R. Melby, R. J. Harder, W. R. Hertler, W. Mahler, R. E. Benson, and W. E. Mochel, *J. Am. Chem. Soc.*, **84**, 3374 (1962).

2) H. Kobayashi, Y. Ohashi, F. Marumo, and Y. Saito, *Acta Crystallogr., Sect. B*, **26**, 459 (1970).

3) a) A. Filhol, C. M. E. Zeyen, P. C. Chenavas, J. Gaultier, and P. Delhaes, *Acta Crystallogr., Sect. B*, **36**, 2719 (1980); b) A. Filhol and M. Thomas, *Acta Crystallogr., Sect. B*, **40**, 44 (1984).

4) I. Ikemoto, M. Yamada, T. Sugano, and H. Kuroda, *Bull. Chem. Soc. Jpn.*, **53**, 1871 (1980).

5) I. Ikemoto, J. M. Thomas, and H. Kuroda, *J. Chem. Soc., Faraday Discuss.*, **54**, 208 (1972).

6) L. J. Aarons, M. Barber, J. A. Connor, M. F. Guest, I. H. Hillier, I. Ikemoto, J. M. Thomas, and H. Kuroda, *J. Chem. Soc., Fraday Trans. 2*, **69(2)**, 270 (1973).

7) H. T. Jonkman and J. Kommandeur, *Chem. Phys. Lett.*, **15**, 946 (1972).

8) P. Nielsen, A. J. Epstein, and D. J. Sandman, *Solid State Commun.*, **15**, 53 (1974).

9) Y. Ohashi and T. Sakata, *Bull. Chem. Soc. Jpn.*, **46**, 3330 (1973).

10) K. Komaras, G. Gruner, and G. A. Swatzky, *Solid State Commun.*, **27**, 1171 (1987).

11) M. A. Butler. J. P. Ferraris, A. N. Bloch, and D. O. Cowan, *Chem. Phys. Lett.*, **24**, 600 (1974).

12) W. D. Grobman, R. A. Pollak, D. E. Eastman, E. T. Maas, Jr., and B. A. Scott, *Phys. Rev. Lett.*, **32**, 534 (1974).

13) M. G. Kaplunov, Yu. M. Shulga, K. I. Pokhodnya, and Yu. G. Borodko, *Phys. Status Solidi B*, **73**, 335 (1976).

14) M. Kobayashi, T. Hoshi, J. Okubo, H. Hiratsuka, T. Harazono, M. Nakagawa, and Y. Tanizaki, *Bull. Chem. Soc. Jpn.*, **57**, 2905 (1984).

Spectroscopic Evidence of α,α-Dihydroxy Ketone in Biacetyl Aqueous Solutions

Kaori MIYATA, Kenichi NAKASHIMA,† and Motohiko KOYANAGI*
Department of Chemistry, Faculty of Science, Kyushu University, Hakozaki, Higashi-ku, Fukuoka 812
(Received July 27, 1988)

From the analysis of emission, excitation, absorption, and ^{1}H NMR spectra of 2,3-butanedione (i.e., biacetyl), it has been established that about two thirds of the molecule in aqueous solutions exists as 3,3-dihydroxy-2-butanone (i.e., a hydrated form of biacetyl). For the first time, two different types of emission are discriminated: Emission is mostly due to the fluorescence spectrum of the monoketone upon irradiation of light with a shorter wavelength than 320 nm while it is due to the strong phosphorescence spectrum of biacetyl itself upon irradiation of light with a longer wavelength than 350 nm. The almost stoichiometric molecular rearrangement from the hydrated (monoketone) form in a water phase to the ordinary (diketone) form in a hydrocarbon phase has been found to take place.

The molecule, 2,3-butanedione (i.e., biacetyl; hereafter abbreviated as BA), has extensively been studied both on the energy decay dynamics[1-9] and on the electronic and molecular structures in the excited states.[10-14] Its substantially high phosphorescence quantum yield in fluid solutions still gives intriguing problems to molecular spectroscopists. The fundamental interpretations of the photochemical and photophysical processes were reviewed earlier.[15,16] Many optical studies thereof have so far been carried out in nonaqueous solvents or in the free molecule, on one hand. From the spectroscopic interest of cage effects, on the other hand, room temperature phosphorescence materials (including BA) in cyclodextrins and in micelles have recently come to attract attention;[17,18] the surrounding environments being water for these cases.

At an early stage of the ^{1}H NMR instrumental development, Greenzaid et al. observed the spectra of several aliphatic aldehydes and ketones in aqueous solutions and found that there, more or less, exists equilibrium between the hydration-dehydration reaction for each molecule.[19] Further, unusual absorption behavior was found for BA in water.[20-25] Substantial hydration was pointed out to occur in such solutions although several other photochemical processes were suggested.[22] Spectroscopically, no further developed optical study has been pursued from this point of view despite its importance: In fact, several authors seem to encounter similar problems recently.[17,18,23-25] Most all these works are thus likely to contain some erroneous conclusions because they did not necessarily take into account this molecular rearrangement reaction in the water phase.

The purpose of this paper is to give an additional piece of evidence for the equilibrium by means of the usual emission technique.

Experimental

The materials (i.e., BA, acetone, 3-hydroxy-2-propanone, 3-hydroxy-2-butanone, and 1,3-dihydroxy-2-propanone: all Tokyo Kasei GR grade reagents) were several times distilled in vacuo. The absorption and emission spectra were recorded on a Hitachi Absorption Spectrometer EPS-2 and on a Hitachi Fluorometer F-3000, respectively. The NMR spectra were measured on a 400 MHz Japan Electric NMR Spectrometer type JNM-GX400 using D_2O and C_6D_6 (both E. Merck reagents). The other solvents were all Dotite spectroscopic grade reagents. Dioxane (DX) and tetrahydrofuran (THF) were used immediately after the neat solvents were purged with nitrogen gas for several minutes.

Results and Discussion

Absorption Spectra. To our knowledge, there is not a suitable solvent which is miscible with water and is of an "inert" nature. As the next best choice, DX and THF were employed although these never fulfilled the latter requirement. In order to obtain reproducible (and thus reliable) spectral data, we measured the absorption spectra immediately after the sample solutions were prepared. Further, we paid a special caution to prevent the solutions from coming into contact with air under room light. The absorption spectra of BA at a constant concentration in THF-H_2O mixed solvents were measured with changing the molar fraction of H_2O. The results are partially shown in Fig. 1. An increase in absorption intensity around 260 nm with a decrease in H_2O concentration may largely be attributed to peroxides which still coexist in THF.

First we consider a chemical equilibrium between the hydration-dehydration reaction as follows:

$$BA + n\,H_2O \leftrightarrow BA[H_2O]_n. \quad (1)$$

Then we obtain a stoichiometric equation by using an analytical method[26,27] as follows:

$$\frac{1}{\varepsilon - \varepsilon_A} = \frac{1}{(\varepsilon'_A - \varepsilon_A)KC^n} + \frac{1}{\varepsilon'_A - \varepsilon_A} \quad (2)$$

where ε'_A and ε_A are the molar extinction coefficients of the hydrated (monoketone) form and the diketone form of BA, respectively; ε an apparent absorption

† Present address: Laboratory of Chemistry, College of Liberal Arts, University of Saga, Honjo, Saga 840.

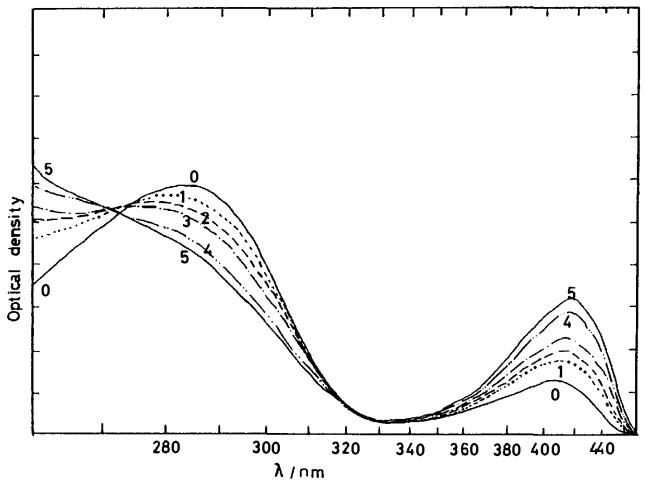

Fig. 1. Absorption spectra of BA in H_2O–THF mixed solvents at 25 °C. BA concentration is fixed at 2.6×10^{-2} mol dm^{-3}. H_2O concentrations (in mol dm^{-3} units) are: (0)55, (1)38.5, (2)33, (3)27.5, (4)16.5, and (5)11.

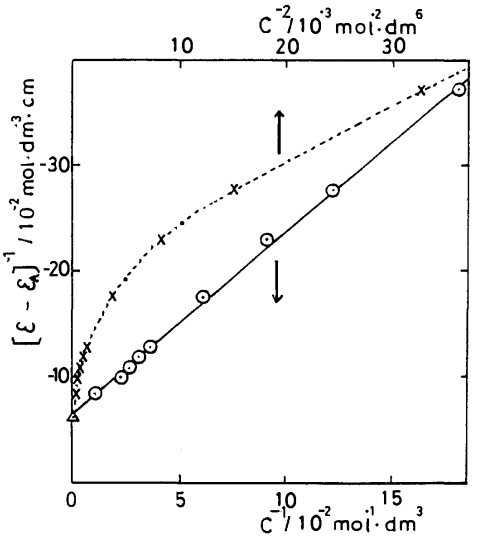

Fig. 2. Plots of $(\varepsilon-\varepsilon_A)^{-1}$ against C^{-n} (C: H_2O concentrations; and n=1,2) at 410 nm. For ○, n=1; for ×, n=2; and for △, see text.

coefficient of the system as a function of wavelengths; and C the total concentration of water. Plots of $(\varepsilon-\varepsilon_A)^{-1}$ against C^{-n} may give a straight line as far as Eq. 1 holds. In Fig. 2, $(\varepsilon-\varepsilon_A)^{-1}$ at 410 nm was plotted against C^{-1} and C^{-2}. It should be noted that a linear relation was obtained for case n=1, but not for n=2 (and also not for n=0.5). The hydration number n is thus 1. From the slope and the intercept of the straight line in Fig. 2, the values of K and ε'_A were estimated to be 3.61×10^{-2} dm^3 mol^{-1} and ca. 0 dm^3 mol^{-1} cm^{-1}, respectively. As shown in Table 1, the obtained K value is close to that evaluated by Bell et al. for another solvent system at 25 °C under the assumption that the 420 nm absorption system is completely due to the $S_1(n\pi^*)\leftarrow S_0$ transition of the ordinary diketone form of

Table 1. Equibrium Constant K at 25 °C

Solvent system[a]	Means[b]	$K/10^{-2}$ dm^3 mol^{-1}	α[c]
H_2O-DX	Abs.	3.8±0.5	0.48±0.07
H_2O-THF	Abs.	3.7±0.5	0.49±0.08
H_2O-EtOH	Abs.	1.9±1.0	0.95±0.4
D_2O	NMR	3.4±0.3	0.53±0.05
H_2O[d]	NMR	(3.6)[e]	0.500
H_2O-DX[f]	Abs.	(6.0)[e]	0.299

a) DX: dioxane; THF: tetrahydrofuran; EtOH: ethanol. b) Abs.: absorption. c) Molecular ratio: [unhydrate]/[hydrate]. d) Taken from Ref. 19. e) Calculated from the reported α-value by using 55.4 mol dm^{-3} for pure water at 25 °C. f) Taken from Ref. 21.

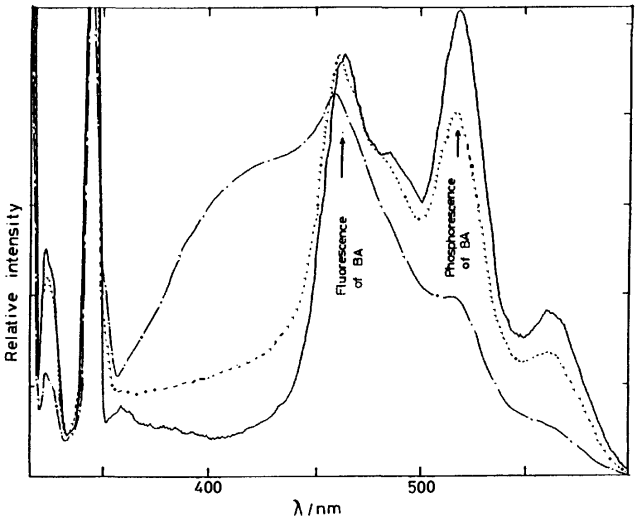

Fig. 3. Emission spectra of ca. 10^{-3} mol dm^{-3} BA in H_2O–THF mixed solvents at 20 °C. Water concentrations are: (——), 0 vol%; (----), 5 vol%; and (-·-·-), 10 vol%. Several sharp bands in the 330—350 nm range are due to Raman lines of the solvents. λ_{exc}=313 nm; slit widths (in light wavelength units): 1.5 nm.

BA.[21] The present (more general) treatment confirms that Bell and McDougall's assumption is almost acceptable because of the obtained $\varepsilon'_A\approx 0$ in the 380—430 nm range. The same method was applied to the 270—320 nm absorption system. However, no reliable correlation was obtained for n=1 (and n=2).

Emission Spectra. When BA in aqueous solutions is irradiated with light monochromated at 313 nm, a broad emission spectrum appears around 420 nm, near the absorption maximum of the $S_1(n\pi^*)\leftarrow S_0$ absorption of BA (see also Fig. 1). This band shows an increase in intensity with an increase in water concentration (see Fig. 3) while no such an anomalous emission was observed for ca. 10^{-3} mol dm^{-3} BA in nonaqueous solvents such as toluene, methylcyclohexane, and hexane. With a further increase in water concentration, the intensity of the 420 nm band comes to surpass those of the three bands at 457 nm (fluorescence of BA), at 512 nm (phosphorescence of BA), and at 560 nm (phosphorescence of BA). Such an example (in ca. 100% H_2O) is shown in Fig. 4 (see the solid line

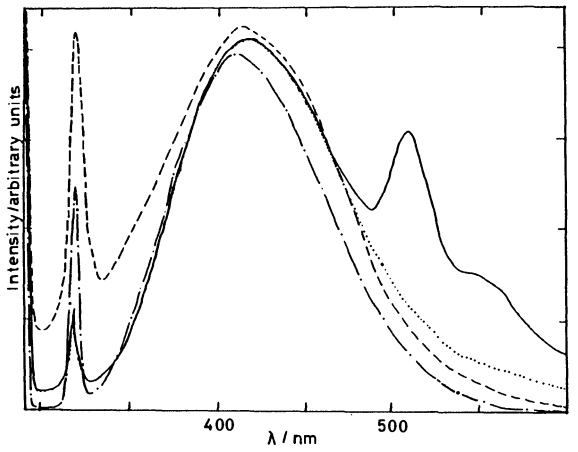

Fig. 4. Emission spectra of ca. 10^{-3} mol dm^{-3} ketones in aqueous solutions at 20°C. λ_{exc}=313 nm. Slit widths: 1.5 nm. (——) and (– – – –): BA in the absence and existence of oxygen, respectively; (– – –): 3-hydroxy-2-propanone; and (–·–·–): 3-hydroxy-2-butanone (acetoin). Bands around 320 nm are attributed to Raman lines of H_2O.

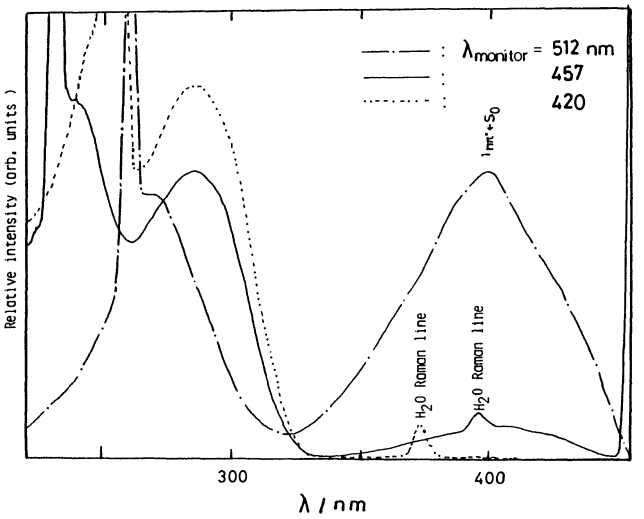

Fig. 5. Excitation spectra of ca. 10^{-3} mol dm^{-3} BA in aqueous solutions at 20°C. Slit widths: 1.5 nm. Note that 2nd order excitation light appears with large intensity below 260 nm since no light filter was employed.

curves). For comparison, fluorescence spectra of the four monoketones (i.e., 3-hydroxy-2-propanone (hydroxyacetone), 3-hydroxy-2-butanone (acetoin), 1,3-dihydroxy-2-propanone (dihydroxyacetone), and acetone) were measured at 20°C in aqueous solutions. Excitation light was all the same. For space saving, the spectra of the former two are shown in Fig. 4. A similarity between the 420 nm emission spectrum of BA in aqueous solutions and the fluorescence spectrum of each monoketone strongly suggests that the former is due to the monoketone species (namely, the hydrated form of BA, $CH_3C(OH)_2CO\text{-}CH_3$). Several other optical properties (such as band width, emission quantum yield, Stokes shift, etc.) resemble the general optical features of monoketones.[28,29]

Excitation Spectra. In order to identify this additional species more clearly, we observed several excitation spectra of BA in aqueous solutions at various wavelengths of the emission spectra monitored. Only three spectra are shown in Fig. 5. Obviously, there are big differences in the spectral locations and in the intensity distribution patterns when emission is monitored at 512 nm (the peak wavelength of the normal phosphorescence) and at 420 nm (that of the anomalous fluorescence): In between is the remainder which was measured at $\lambda_{monitored}$=457 nm (the peak wavelength of the normal fluorescence spectrum of BA). The different spectral dependence is a manifestation that there are chemically different emitting species: one with an absorption maximum at 400 nm and another with that at 285 nm.

Further, we studied the emission, absorption, and excitation spectra of the four monoketones, loc. cit., in aqueous solutions at 20°C. Although small spectral shifts of the absorption maxima were found from molecule to molecule, these emission spectra were very

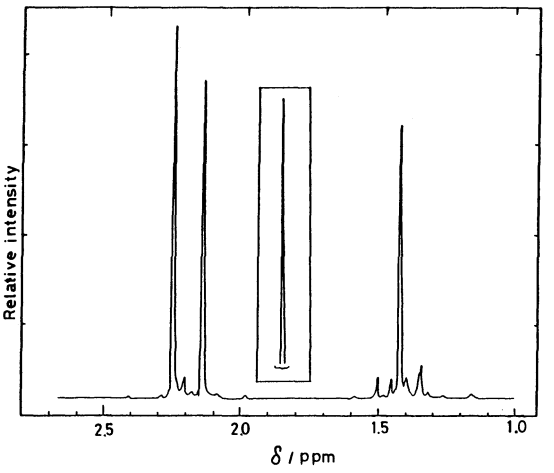

Fig. 6. 400 MHz ^{1}H NMR spectra of 1.5×10^{-2} mol dm^{-3} BA in D_2O at 20°C. The inserted shows only one peak obtained from BA in C_6D_6.

similar to each other (vide supra). It was confirmed that each excitation spectrum showed a close correlation to the corresponding absorption spectrum. All these results lead us to the conclusion that the 420 nm emission in BA aqueous solutions is due to the hydrated form of BA.

^{1}H NMR Spectra. The ^{1}H chemical shifts and integrated intensities of BA were measured for two solvent systems: D_2O and C_6D_6. The concentration of BA was of ca. 10^{-2} mol dm^{-3} for each case. The results are shown in Fig. 6. Three prominent peaks were observed in D_2O solutions while only one prominent peak in C_6D_6 solutions. Without doubt, the strong single peak at δ 1.86 in C_6D_6 solutions is due to the six equivalent protons of $C^1H_3COCOC^1H_3$. The relative integrated intensity ratio among the three prominent

peaks in D_2O solutions was approximately 1.8 (for the peak at δ 2.25): 1.0 (for the peak at δ 2.14): 1.0 (for the peak at δ 1.42). That the integrated intensities of the latter two peaks are almost equal to each other allows the assignment to be the same as proposed by Greenzaid et al.:[19] the peak at δ 2.25 as the six equivalent protons in the ordinary diketone form of BA; and the peak at 2.14 ppm as the three equivalent protones of C^1H_3CO- and the peak at δ 1.42 as the three remainder (i.e., $C^1H_3C(OD)_2-$) in the hydrated form. Many small peaks are due to several impurities produced photochemically during the experimental procedure.

Greenzaid et al. found that the molecular ratio of the dehydrated to the hydrated form of BA in H_2O was 0.50,[19] a little bit smaller value with reference to 0.54 for our BA-D_2O system. This small difference is, however, within the experimental errors ($\pm$0.05).

Reversibility of the Molecular Rearrangement and Equilibrium Constants. Another important aspect is that the hydration-dehydration reaction takes place in equilibrium on going from one phase to another. We confirmed this by measuring the ^1H NMR spectra of BA first in aqueous solution (phase 1), secondly in C_6D_6 solution (phase 2) after extraction of the BA from the phase 1 solution by fresh perdeuterated benzene, and lastly in D_2O solution (phase 3) after extraction of the BA from the C_6D_6 (phase 2) solution by fresh heavy water. Apart from the contaminated ^1HDO signal at δ 4.74 in D_2O and at δ 1.60 in C_6D_6 solution, the triplet to singlet and the singlet to triplet signal pattern changes were well reproduced. This means that the BA molecule exists extensively as the hydrated form in the water phase while they are almost completely as the ordinary diketone form in the benzene phase.

This equilibrated molecular rearrangement was also confirmed by measuring emission and excitation spectra of two-phases-forming (i.e., unmiscible) H_2O-methylcyclohexane (MCH) solution systems. The chemical treatments are the same as mentioned above, but for a system of H_2O and MCH instead that of D_2O and C_6D_6. Both the emission and excitation spectra are almost completely ascribed to the ordinary diketone form of BA in the MCH phases while those are due to the both forms in the water phases.

The equilibrium constants obtained for the hydration-dehydration reaction of BA in several aqueous solvent systems are briefly summarized in Table 1 together with the data reported previously by other investigators.[19,21] Apart from some differences in the K-values, all the data establish that there occurs an extensive hydration reaction of BA in such aqueous solutions. An interesting issue may arise on this molecuar rearrangement and on the decay dynamics of BA around an interface of oil-water as well as around those of micelle-water and cyclodextrin-water. This reversibility in the molecular rearrangement strongly suggests that there is a possibility of BA (as well as benzil[30]) to become a new probing reagent for studies of such hydrophobic/hydrophilic macromolecular phenomena. At least, this polymorphous nature of BA should fully be taken into account on the discussion of the dynamics and structures in micelles,[17,18] in cyclodextrins,[18] and in water-contained organic solvents.[23,24]

The authors are thankful to Professor Ryoichi Shimada for his encouragement and to Miss Kayoko Ogi for her kind assistence in obtaining the ^1H NMR spectra. This work was in part supported by Grant-in-Aid for Scientific Research from the Ministry of Education, Science and Culture (No. 62540358).

References

1) H. L. J. Böckström and K. Sandros, *Acta Chem. Scan.*, **12**, 823 (1958); **14**, 48 (1960).
2) L. S. Forster, S. A. Greenberg, R. J. Lyon, and M. E. Smith, *Spectrochim. Acta*, **16**, 128 (1960).
3) J. T. Dubois and F. J. Wilkinson, *J. Chem. Phys.*, **39**, 899 (1963).
4) G. M. McClelland and J. T. Yardley, *J. Chem. Phys.*, **38**, 4368 (1973).
5) C. S. Parmenter and H. M. Poland, *J. Chem. Phys.*, **51**, 1551 (1969).
6) H. W. Sidebottom, C. C. Badcock, J. G. Calvert, B. R. Rabe, and K. Damon, *J. Am. Chem. Soc.*, **94**, 13 (1972).
7) M. B. Robin, *J. Lumin.*, **12/13**, 131 (1976).
8) J. C. André, M. Bouchy, and W. R. Ware, *Chem. Phys.*, **37**, 119 (1979).
9) R. Rima, M. Bouchy, J. C. André, and M. L. Viriot, *Chem. Phys.*, **106**, 333 (1984).
10) S. Kamei, K. Okuyama, H. Abe, N. Mikami, and M. Ito, *J. Phys. Chem.*, **90**, 93 (1986).
11) J. W. Sidman and D. S. McClure, *J. Am. Chem. Soc.*, **77**, 6461 (1955).
12) J. C. D. Brand and A. W. H. Mau, *J. Am. Chem. Soc.*, **96**, 4380 (1974).
13) E. Drent and K. Kommandeur, *Chem. Phys. Lett.*, **14**, 321 (1972).
14) D. Ben-Amotz and I. T. Chan, *J. Phys. Chem.*, **86**, 2428 (1982).
15) W. A. Noyes, Jr., G. B. Porter, and J. E. Jolly, *Chem. Rev.*, **56**, 49 (1956).
16) M. B. Rubin, *Fortsch. Chem. Forsch.*, **13**, 251 (1969).
17) J. J. Donkerbrock, C. Gooijer, N. H. Velthorst, and R. W. Frei, *Anal. Chem.*, **54**, 891 (1982).
18) F. J. DeLuccia and L. J. C. Love, *Anal. Chem.*, **56**, 2811 (1984).
19) P. Greenzaid, Z. Luz, and D. Samuel, *J. Am. Chem. Soc.*, **89**, 749 (1967).
20) L. S. Forster, *J. Am. Chem. Soc.*, **77**, 1417 (1955).
21) R. P. Bell and A. O. McDougall, *Trans. Faraday Soc.*, **56**, 1281 (1960).
22) J. Lemaire, *J. Phys. Chem.*, **71**, 2653 (1967).
23) G. Favaro, *J. Photochem.*, **6**, 139 (1976/1977).
24) G. Favaro, *J. Chem. Soc., Perkin Trans. 2*, **1976**, 869.
25) A. Gupta, R. Mukhtar, and S. Seitzen, *J. Phys. Chem.*, **84**, 2356 (1980).
26) V. P. Senthilnathan and S. Singh, *Spectrochim. Acta,*

29A, 881 (1973).
27) K. Nakashima and M. Koyanagi, *Photochem. Photobiol.*, **44**, 169 (1986).
28) P. A. Hackett and D. Phillips, *J. Chem. Phys.*, **78**, 665 (1974).
29) M. Koyanagi and L. Goodman, *Chem. Phys.*, **5**, 107 (1974); and references cited therein.
30) Benzil is well-known to emiss both phosphorescence and fluorescencence with remarkable emission yields in fluid solutions (e.g., see Ref. 31). Very recently, we have studied absorption spectra of benzil in various solvents. In contrast to the results obtained thereof (Ref. 32), no anomalous absorption intensification of BA was observed in hydrogen donating solvents. The environmental intensification scheme of BA thus seems to be close to the cases of acetone and cyclopentanone (Ref. 33). Reversely, no evidence of the reactions of hydration and methylation has not been obtained for benzil.
31) F. J. Arnett and P. S. McGlynn, *J. Phys. Chem.*, **79**, 626 (1975).
32) K. Miyata and M. Koyanagi, *Bull. Chem. Soc. Jpn.*, **61**, 3813 (1988).
33) K. Nakashima, K. Uchida-Kai, M. Koyanagi, and Y. Kanda, *Bull. Chem. Soc. Jpn.*, **55**, 415 (1982).

Electronic Properties of New Organic Conductors Based on 2,7-Bis(methylthio)-1,6-dithiapyrene (MTDTPY) with TCNQ and *p*-Benzoquinone Derivatives

Kenichi IMAEDA,* Toshiaki ENOKI,† Takehiko MORI, Hiroo INOKUCHI, Mitsuru SASAKI,††
Kazuhiro NAKASUJI,†† and Ichiro MURATA††
Institute for Molecular Science, Okazaki 444
††Department of Chemistry, Faculty of Science, Osaka University, Toyonaka, Osaka 560
(Received August 8, 1988)

The electronic properties of charge-transfer (CT) complexes based on a new organic donor MTDTPY with TCNQ and *p*-benzoquinone derivatives (fluoranil (FLL), chloranil (CHL), bromanil (BRL), and DDQ) have been investigated by means of electrical conductivity, thermoelectric power, ESR, and band calculation. β-MTDTPY-TCNQ, MTDTPY-CHL, and MTDTPY-BRL show a metallic electrical conduction. MTDTPY-CHL and MTDTPY-BRL are the first organic metals among the CT complexes with *p*-benzoquinone derivatives. The metal-insulator (M-I) transition takes place around 110, 240, and 125 K for β-MTDTPY-TCNQ, MTDTPY-CHL, and MTDTPY-BRL, respectively. The sharp ESR linewidth and large anisotropy of the transfer integral for β-MTDTPY-TCNQ and MTDTPY-CHL suggest a one-dimensional electronic property. Thus, the M-I transition for these complexes is considered to be caused by a Peierls instability. MTDTPY-CHL undergoes a first-order phase transition in the semiconducting phase. This phase transition disappears by applying pressure.

The findings of metallic conductivity in TTF-TCNQ and superconductivity in $(TMTSF)_2PF_6$ have attracted the interest of many chemists and physicists dealing with organic conductors. These new phenomena have mainly been discovered in charge-transfer (CT) complexes based on TTF and its derivative donors. It is required to explore a new class of donors for the purpose of extending the range of research for organic conductors. It is well known that polycyclic aromatic hydrocarbons form CT complexes with various acceptors. Among them, a perylene-bromine complex is famous for the first organic semiconductor with a high conductivity of $\rho_{RT}\approx 1\ \Omega$ cm.[1] Thereafter, metallic conductivities down to 200 K have been observed in perylene-X (X=PF_6 and AsF_6) crystals obtained using an electrochemical technique.[2]

For the development of a new class of donors based on polycyclic aromatic hydrocarbons, we intended to introduce sulfur atoms in perylene and pyrene skeletons in order to increase the polarizability and decrease the ionization potential. 3,10-Dithiaperylene (DTPR) and 1,6-dithiapyrene (DTPY) were synthesized on the basis of such a molecular design. Most of their CT complexes were semiconductors, despite relatively high conductivities.[3] Bechgaard et al. prepared a single crystal of DTPY-TCNQ and found metallic conductivity down to 4 K.[4,5] In order to enhance the dimensionality through interchain interactions, we synthesized 2,7-bis(methylthio)-1,6-dithiapyrene (MTDTPY) substituted with two methylthio groups to DTPY. The molecular structure of MTDTPY is illustrated in Fig. 1. We reported on the synthesis and gave a brief of the physical properties of MTDTPY and their CT complexes in a previous paper,[6] which

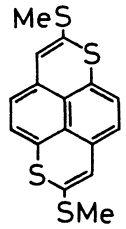

Fig. 1. Molecular structure of MTDTPY.

presents the metallic conductivities of MTDTPY complexes with TCNQ, chloranil (CHL), and bromanil (BRL). In this paper, we present the experimental results of electrical conductivity, thermoelectric power, ESR, and band calculation for MTDTPY complexes with TCNQ, fluoranil (FLL), CHL, BRL, and 2,3-dichloro-5,6-dicyano-*p*-benzoquinone (DDQ) and discuss the electronic structures in relation to their dimensionalities. The difference in electronic properties between DTPY-TCNQ and MTDTPY-TCNQ is also discussed.

Experimental

Single crystals of MTDTPY with TCNQ were prepared by a diffusion method in a CH_3CN solution. Two kinds of black needle crystals were obtained as lustrous crystal and lusterless crystal. X-Ray studies have shown that each crystal phase has a different crystal structure, where the former (α-form) is monoclinic and the latter (β-form) is triclinic.[6] The black needle crystals of MTDTPY complexes with FLL, CHL, and BRL were prepared by a slow concentration of the mixed solutions of the donor and the acceptor in CH_2Cl_2. MTDTPY-DDQ was obtained as black needle crystal by a diffusion method in a C_6H_5CN solution. All the complexes were shown to have a composition of 1 : 1 from elemental analyses. The electrical conductivity for all complexes along the long crystal axis, which corresponds to the stacking axis for β-MTDTPY-TCNQ and MTDTPY-CHL, was meas-

† Present address: Department of Chemistry, Faculty of Science, Tokyo Institute of Technology, Ookayama, Meguro-ku, Tokyo 152.

ured by a two-probe method for α-MTDTPY-TCNQ and a four-probe method for the other complexes using gold paste as electrical contacts. The conductivity under pressure up to 10 kbar for MTDTPY-CHL was carried out by means of a BeCu clamp cell with a manganin pressure sensor using Idemitsu Daphne oil #7373 as a pressure fluid medium. The thermoelectric power for β-MTDTPY-TCNQ and MTDTPY-CHL along the long crystal axis was measured by the Chaikin and Kwak method.[7] An ESR measurement was performed using a conventional X-band spectrometer Varian E112 equipped with a continuous-flow helium cryostat Oxford ESR9. A static magnetic field was applied perpendicular to the long axis of the crystals with dimensions of about 1×0.1×0.03 mm^3 for β-MTDTPY-TCNQ and about 2×0.2×0.03 mm^3 for MTDTPY-CHL. The absolute value of the spin susceptibility was determined with DPPH as a reference. Molecular orbital calculations for β-MTDTPY-TCNQ and MTDTPY-CHL were performed by the extended Hückel method.[8,9] The intermolecular overlap integral was calculated between the conduction molecular orbitals which correspond to the highest occupied molecular orbital (HOMO) for a donor and the lowest unoccupied molecular orbital (LUMO) for an acceptor. The energy band structure was obtained using the tight-binding approximation.

Results

MTDTPY-TCNQ. α-MTDTPY-TCNQ shows a simple semiconductive behavior with a resistivity at room temperature ρ_{RT} of 2.7×10^5 Ω cm and an activation energy E_a of 0.26 eV. This result can be easily understood in terms of a mixed stack structure by an X-ray diffraction study and a small degree of charge transfer of 0.3—0.4 estimated by IR and X-ray procedures.[6] On the contrary, β-MTDTPY-TCNQ with a segregated stack structure and a partial CT of 0.6—0.7[6] shows a metallic conduction with $\rho_{RT}=9.5\times10^{-3}$ Ω cm (Fig. 2). The resistivity gradually decreases down to 275 K, where it shows a broad minimum. Below 150 K, the resistivity increases steeply with an inflection in the slope around 110 K. The activation energy below 90 K is estimated to be 0.056 eV. The temperature dependence of the thermoelectric power S for β-MTDTPY-TCNQ is also shown in Fig. 2. S is almost constant down to 200 K with a negative value of −8.5 μV K^{-1} at room temperature, and it then gradually increases. Its sign changes to a positive side around 150 K. Then, S shows a maximum at 110 K and decreases rapidly.

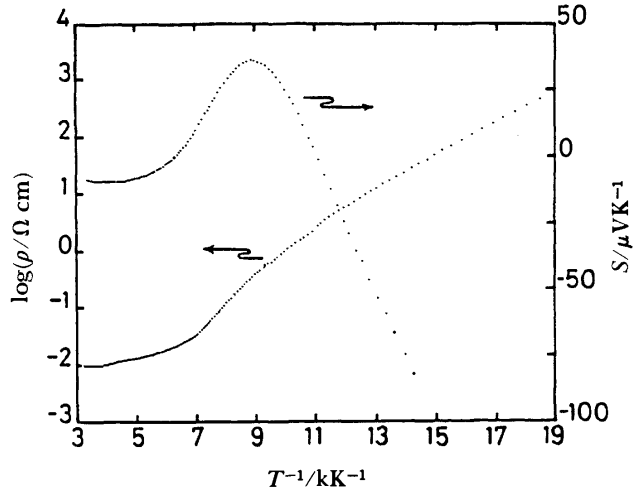

Fig. 2 .Temperature dependence of the resistivity and the thermoelectric power for β-MTDTPY-TCNQ.

β-MTDTPY-TCNQ shows a sharp ESR spectrum with a Lorentzian line shape with a g-value of 2.0024 and a linewidth of 0.87 G (1G=10^{-4} T) at room temperature. The g-value is independent of the temperature down to 110 K (Fig. 3). The ESR spectra split into two components below 110 K. The g-value of one component remains unchanged down to 50 K, around the g-value of the spectra above 110 K, while that of the other component gradually increases to 2.0034 at 50 K. Below 50 K, the two signal components approach each other. The signal with a smaller g-value is assigned to electron spins on TCNQ molecules, since its value is very close to 2.0025 of the reported value for $TCNQ^-$ anion in the LiTCNQ salt.[10] The signal with a larger g-value is assigned to electron spins on MTDTPY molecules, since the large g-shift ($\delta g=g-g_0$, g_0: g-value for free electron spin) is caused by a large spin-orbit coupling due to sulfur atoms in an MTDTPY molecule. The temperature dependence of the linewidth is also shown in Fig. 3. The linewidth decreases linearly with decreasing temperature in the metallic region. Below 110 K at the biginning of the splitting in the

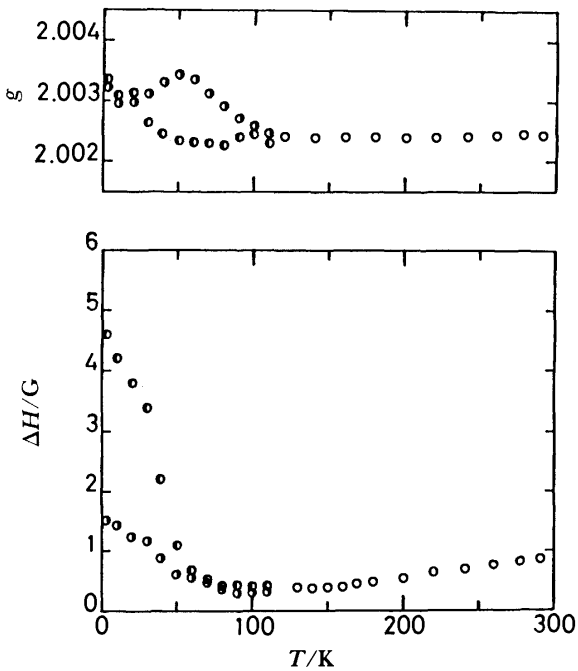

Fig. 3. Temperature dependence of the g-value and the linewidth (ΔH) in ESR spectra for β-MTDTPY-TCNQ. The half-open circles indicate the g-value and the linewidth of two components of the ESR spectra deconvoluted by a computer simulation (◑: MTDTPY, ●: TCNQ).

spectra, the linewidths for two signal components increase with lowering temperature. The signal for TCNQ chains becomes broader than that for MTDTPY chains, where 4.5 G for the former signal and 1.5 G for the latter signal at 3 K. Figure 4 shows the temperature dependence of the spin susceptibility χ_s for β-MTDTPY-TCNQ. χ_s gradually decreases in the metallic region and then decreases steeply below 150 K. Below 110 K, it decreases exponentially and has a Curie tail due to lattice irregularities below 50 K. The estimated concentrations of localized spins are about 0.04 and 0.07% for MTDTPY and TCNQ molecules, respectively.

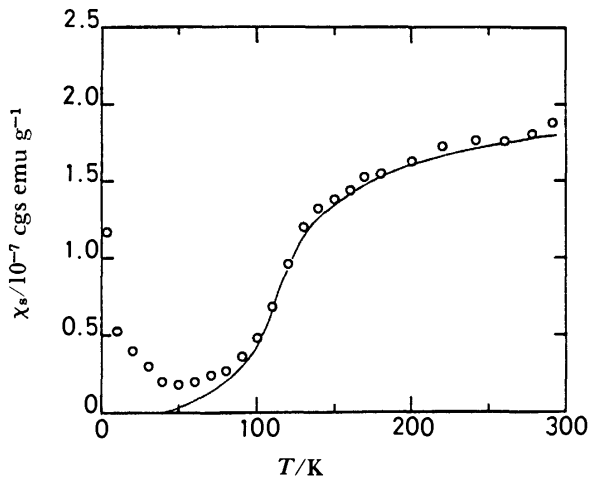

Fig. 4. Temperature dependence of the spin susceptibility (χ_s) for β-MTDTPY-TCNQ. The solid line is obtained after a subtraction of the Curie tail at low-temperatures.

Figure 5 shows the charge distribution of the HOMO in an MTDTPY molecule. The charge density on the inner sulfur atom is ten times as large as that on the outer sulfur atom. Table 1 summarizes the calculated intermolecular overlap integrals for the HOMO of MTDTPY, the LUMO of TCNQ, and the HOMO-LUMO between MTDTPY and TCNQ in β-MTDTPY-TCNQ. Both MTDTPY and TCNQ molecules have the largest overlap integrals along the stacking direction parallel to the c-axis. The ratio ($t_{\parallel}/t_{\perp}$) between intrachain and interchain transfer integrals is 24 and 44 for MTDTPY and TCNQ columns, respectively. According to IR and X-ray studies, β-MTDTPY-TCNQ has a degree of charge-transfer of 0.6—0.7.[6] The energy band structure under the degree of CT of 0.6 is shown in Fig. 6. The upper energy band corresponds to TCNQ, while the lower one corresponds to MTDTPY. Both MTDTPY and TCNQ sheets display completely one-dimensional band structures having an energy dispersion only along the stacking axis and almost flat Fermi surface.

MTDTPY-*p*-Bbenzoquinone Derivatives. MTDTPY-

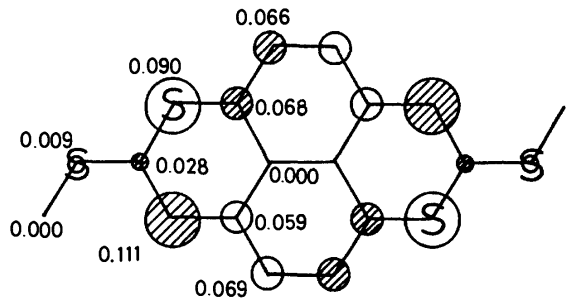

Fig. 5. Charge distribution of the HOMO for MTDTPY.

Table 1. Overlap Integrals of the HOMO, the LUMO, and the HOMO-LUMO in β-MTDTPY-TCNQ

Molecules	Crystal direction[a]	Overlap integral $\times 10^{-3}$
MTDTPY-MTDTPY	c	11.11
MTDTPY-MTDTPY	a−c	0.46
MTDTPY-MTDTPY	a	−0.10
TCNQ-TCNQ	c	6.96
TCNQ-TCNQ	a+c	0.16
TCNQ-TCNQ	a	−0.07
MTDTPY-TCNQ	a/2+b/2+c/2	0.22

a) The definition of the crystal axes is described in Ref. 6.

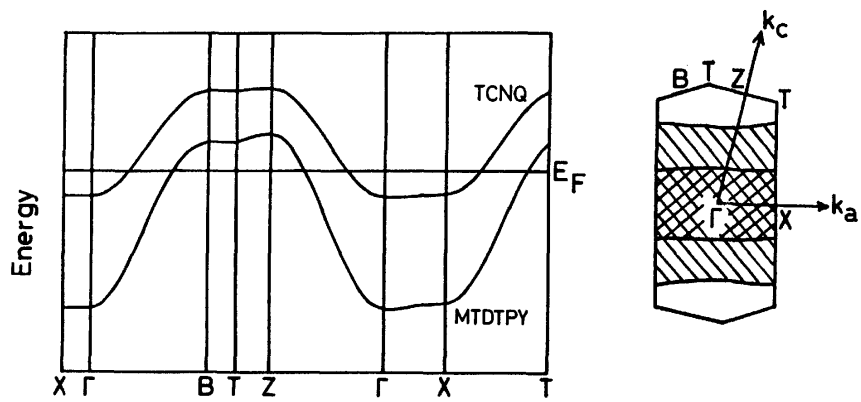

Fig. 6. Energy band structure and Fermi surface of β-MTDTPY-TCNQ. The regions shaded with // slashes and \\ slashes indicate the electron-like parts for MTDTPY and TCNQ, respectively.

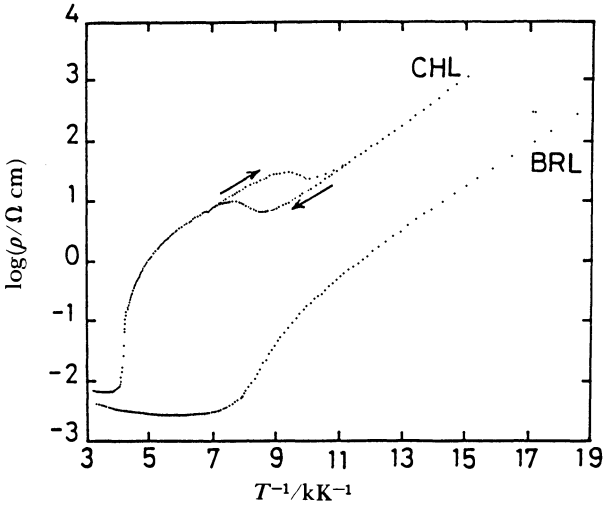

Fig. 7. Temperature dependence of the resistivities for MTDTPY-chloranil (CHL) and MTDTPY-bromanil (BRL). The arrows indicate the cooling and heating runs.

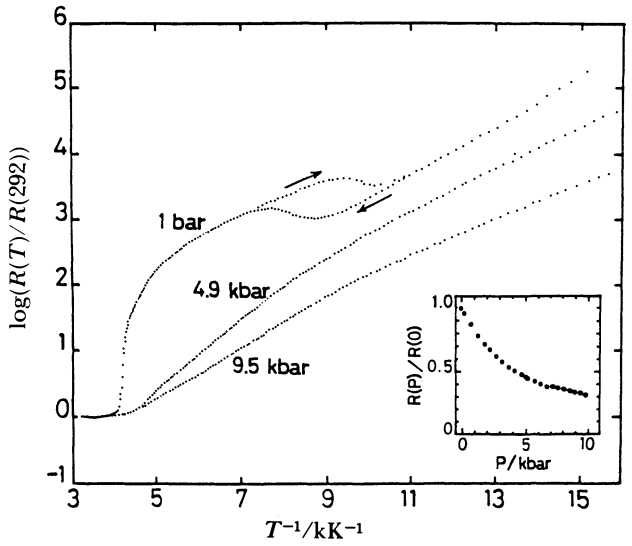

Fig. 8. Temperature dependence of the resistivities under 1 bar, 4.9 kbar, and 9.5 kbar for MTDTPY-chloranil. The inset shows the pressure dependence of the resistance at room temperature.

FLL shows a simple semiconductive behavior with E_a=0.13 eV in spite of fairly low resistivity with ρ_{RT}=5.5×10^{-2} Ω cm. MTDTPY-DDQ is also a semiconductor with ρ_{RT}=5.4 Ω cm and E_a=0.14 eV. On the other hand, MTDTPY-CHL shows a metallic conduction with ρ_{RT}=7.0×10^{-3} Ω cm (Fig. 7). The resistivity slowly decreases down to 280 K, where it shows a broad minimum. Then, the resistivity suddenly increases at 240 K. A hysteresis of the resistivity is observed around 110 K. The results of the resistivity under pressure for MTDTPY-CHL are shown in Fig. 8. The pressure dependence of the resistance at room temperature is shown in the inset. The resistance decreases monotonously with increasing pressure and the resistance at about 10 kbar becomes about one-third of that at 1 bar. Under 4.9 kbar, the metal-insulator transition temperature (T_{MI}) is lowered to 220 K compared with 240 K under 1 bar. What is noticeable is that the hysteresis of the resistivity disappears above this pressure. The activation energy E_a is 0.10 eV just below the M-I transition under 4.9 kbar. When the pressure increases to 9.5 kbar, T_{MI} is unchanged and E_a just below the M-I transition decreases to 0.078 eV due to a reduction of the band gap by pressure.

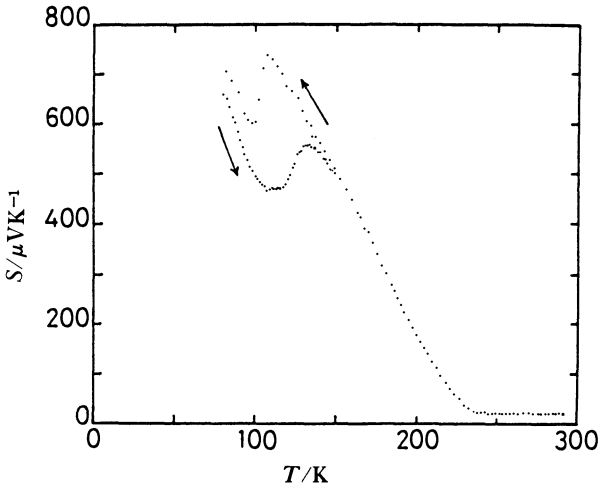

Fig. 9. Temperature dependence of the thermoelectric power for MTDTPY-chloranil. The arrows indicate the cooling and heating runs.

Figure 9 shows the temperature dependence of the thermoelectric power S for MTDTPY-CHL. S is steadily constant down to 240 K and then increases steeply. The hysteresis in the thermoelectric power is observed around the same temperature as that in the resistivity.

MTDTPY-CHL shows an ESR spectrum with a Lorentzian line shape with a g-value of 2.0059 and a linewidth of 2.2 G at room temperature. The splitting of the ESR spectra was not observed over the entire temperature region, unlike β-MTDTPY-TCNQ. The g-value is entirely independent of the temperature. Figure 10 shows the temperature dependence of the linewidth ΔH and the spin susceptibility χ_s for MTDTPY-CHL. ΔH gradually decreases down to about 120 K and then increases to 2.9 G at 3 K. χ_s gradually decreases down to 240 K, and below this temperature it decreases exponentially. Below 80 K, χ_s shows a Curie tail due to lattice irregularities in the crystal. The concentration of localized spins is about 0.03%.

Table 2 summarizes the intermolecular overlap integrals for MTDTPY-CHL. The overlap integrals along the stacking axis are largest for both donor and acceptor columns. $t_{\parallel}/t_{\perp}$ is 7 and 45 for MTDTPY and CHL columns, respectively. The degree of CT of MTDTPY-CHL has not been determined precisely.

From X-ray analysis, the bond lengths of C=C and C=O of a CHL molecule in MTDTPY-CHL are larger than those of a neutral CHL. These values are close to those in TMPD (*N,N,N',N'*-tetramethyl-1,4-phenylenediamine)-CHL with a degree of CT of ca. 0.6.[6] Figure 11 shows the energy band structure of MTDTPY-CHL, assuming that the degree of CT is 0.6. The energy bands for MTDTPY and CHL show a one-dimensional character with a strong dispersion along the stacking direction. They cross each other and the band gaps come out at the crossing points. This manner is in contrast with the parallel bands in

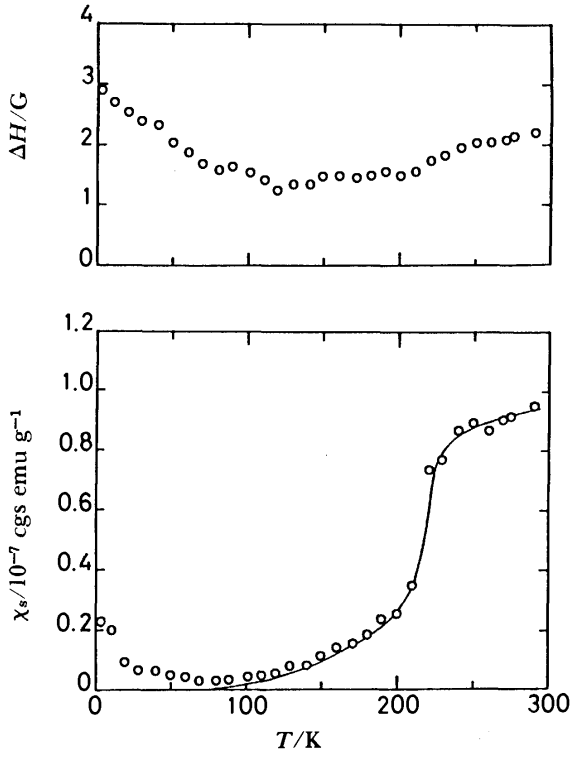

Fig. 10. Temperature dependence of the linewidth (ΔH) and the spin susceptibility (χ_s) for MTDTPY-chloranil. The solid line is obtained after a subtraction of the Curie tail at low-temperatures.

β-MTDTPY-TCNQ. The band structure is semimetallic with electron and hole carriers at the Fermi energy. Accordingly, electron and hole pockets coexist at the Fermi surface in the Brillouin zone.

Next, we present the results concerning the electrical property of MTDTPY-BRL. As shown in Fig. 7, MTDTPY-BRL has a metallic character down to 125 K. The resistivity at room temperature is 4.3×10^{-3} Ωcm, which is lower than 7.0×10^{-3} Ωcm of MTDTPY-CHL. The resistivity decreases gradually down to 175 K and shows a broad minimum, and then increases gradually. Thereafter, the resistivity increases sharply below 125 K, which suggests the occurrence of a metal-insulator transition. This transition temperature is lower compared with 240 K of MTDTPY-CHL. MTDTPY-BRL does not show any hysteresis in the resistivity, dissimilar to MTDTPY-CHL.

Discussion

β-MTDTPY-TCNQ. In a β-MTDTPY-TCNQ crystal, MTDTPY and TCNQ molecules are segregately stacked to form uniform columns along the c-axis with interplanar spacings of 3.48 Å for MTDTPY stacks and 3.27 Å for TCNQ stacks.[6] The degree of CT was evaluated to be 0.6—0.7 from the CN stretching frequency and the bond length in a TCNQ molecule. Such a segregated stack structure and partial CT, which are favorable for realizing organic metals, give a

Table 2. Overlap Integrals of the HOMO, the LUMO, and the HOMO-LUMO in MTDTPY-Chloranil

Molecules	Crystal direction[a]	Overlap integral $\times10^{-3}$
MTDTPY-MTDTPY	c	−6.81
MTDTPY-MTDTPY	a+b+c	−1.01
MTDTPY-MTDTPY	a+b	−0.32
CHL-CHL	c	10.35
CHL-CHL	a+b	−0.23
MTDTPY-CHL	a/2+b+c	0.15

a) The definition of the crystal axes is described in Ref. 6.

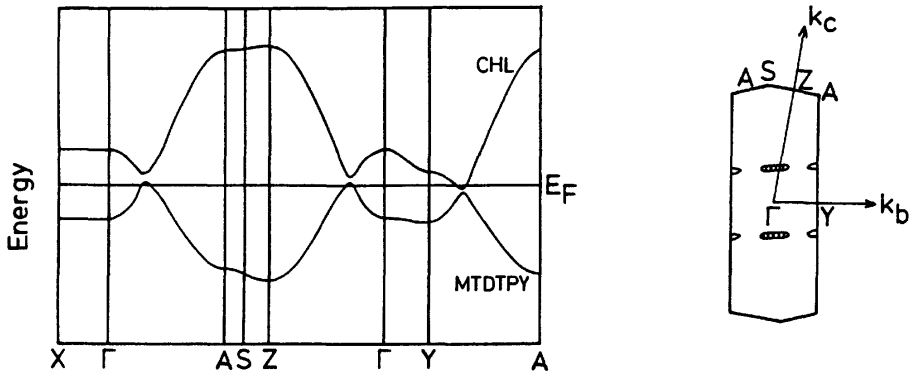

Fig. 11. Energy band structure and Fermi surface of MTDTPY-chloranil. The shaded and non-shaded regions indicate the hole and electron parts, respectively.

metallic conductivity. β-MTDTPY-TCNQ has a two-chain conducting system due to a partial CT from MTDTPY to TCNQ. A thermoelectric power measurement is useful for determining which carrier is dominant in electrical conduction. The negative thermoelectric power at high-temperature means that the electron carriers on TCNQ columns predominate in electrical conduction. The shift of its sign below 150 K implies that the sort of carriers which play the main role of electrical conduction changes from electron carriers on TCNQ columns to hole carriers on MTDTPY columns. The change of the main conduction path affects the electronic properties, since the resistivity starts to increase steeply below 150 K.

A band calculation presents a one-dimensional electronic structure with large anisotropy of the transfer integral between MTDTPY molecules and between TCNQ molecules, and weak intermolecular interaction between MTDTPY and TCNQ molecules. The sharp ESR linewidth of 0.87 G at room temperature is also suggestive of the one-dimensionality of this complex. The linewidth with the Lorentzian line shape can be expressed by the inverse of the spin-lattice relaxation time. The linewidth observed in a one-dimensional metal is extremely narrow, since spin-lattice relaxation through spin-orbit coupling based on the Elliott mechanism is prohibited due to the lack of interchain hopping for pure one-dimensional conductors.[11,12] The spin susceptibility gradually decreases in the metallic region, which deviates from temperature-independent Pauli paramagnetic behavior seen in simple metals. The temperature-dependent Pauli susceptibility has been observed in typical one-dimensional organic metal TTF-TCNQ.[13] The Pauli susceptibility χ_P is related to the density of states at the Fermi energy $N(E_F)$ in the equation $\chi_P=\mu_B{}^2N(E_F)$. For a one-dimensional system, a Peierls gap as a fluctuation already exists in the metallic state and reduces $N(E_F)$. Since the fluctuation is enhanced with lowering temperature, the spin susceptibility shows a decreasing behavior with temperature, even in the metallic region.

β-MTDTPY-TCNQ undergoes an M-I transition around 110 K, judging from an activated behavior in the spin susceptibility χ_s and a decrease proportional to T^{-1} in the thermoelectric power below this temperature. The exponential decrease in χ_s suggests a stabilization of a singlet ground state below T_c. The magnetic activation energy Δ is evaluated to be 0.042 eV with the equation $\chi_s=(C/T)\exp(-\Delta/T)$. This value is in good agreement with E_a of 0.056 eV in the resistivity. The thermoelectric power for intrinsic semiconductors can be approximately expressed in the Boltzmann-transport theory by

$$S = -\frac{k}{|e|}\left(\frac{b-1}{b+1}\cdot\frac{E_a}{kT}+A\right),$$

where b is the mobility ratio μ_e/μ_h between electron and hole carriers, and A is a constant term.[14] The mobility ratio b is calculated to be 2.8 from the slope below 110 K using E_a value of 0.056 eV in the resistivity. This fact means that electron carriers move faster than hole carriers in the semiconductive phase. In the metallic phase, the ESR spectra show a single absorption line due to motional narrowing through interchain coupling between donor and acceptor. Below T_c, the ESR spectra split into two signal components. The splittings of the spectra in the semiconducting phase are attributed to a reduction of the interchain electron hopping rate. The hopping rate is evaluated to be ca. 2×10^{-7} s at 110 K with an absorption line shape simulation for electron hopping model between two sites.[15,16] This rate is quite slow, which means that the interactions between MTDTPY and TCNQ columns are very weak. (The hopping rate for TTF-TCNQ metal is estimated to be 3.7×10^{-12} s from an NMR experiment by Soda et al.[17])

We now discuss the differences in the electronic properties between DTPY-TCNQ and β-MTDTPY-TCNQ. Both complexes possess segregated stacks of donor and acceptor molecules in their crystals. The significant difference is the manner of interatomic contact between an S atom in a donor molecule and an N atom in a TCNQ molecule. DTPY-TCNQ has a contact of 3.40 Å (van der Waals distance: 3.35 Å) between S atom with the high charge density and N atom,[4,5] while β-MTDTPY-TCNQ has a contact of 3.50 Å between the outer S atom with the low charge density and N atom.[6] According to our band calculation of DTPY-TCNQ, the intermolecular overlap integrals are -3.7×10^{-3} for DTPY stacks, 32.1×10^{-3} for TCNQ stacks, and -6.0×10^{-3} between DTPY and TCNQ stacks. Noticeably, the intermolecular overlapping between DTPY and TCNQ molecules is perceptibly large, which is comparable to that for DTPY stacks and is one-fifth of that for TCNQ stacks. The enhancement of the dimensionality through interchain interactions between DTPY and TCNQ stacks is considered to suppress the Peierls transition in the DTPY-TCNQ system. In the case of β-MTDTPY-TCNQ, the intermolecular interaction between MTDTPY and TCNQ stacks is very weak with a minute overlap integral. The marked one-dimensionality may give rise to the Peierls transition at a higher temperature.

MTDTPY-CHL. The electronic property in the metallic state of MTDTPY-CHL closely resembles that of β-MTDTPY-TCNQ. According to an X-ray diffraction study, the MTDTPY-CHL crystal possesses a uniform segregated stack structure with interplanar distances of 3.47 Å for MTDTPY stacks and 3.22 Å for CHL stacks.[6] The bond lengths of CHL in MTDTPY-CHL complex suggest a partial CT state. These facts realize a metallic conduction in this complex. A theoretical calculation exhibits the semimetal-

lic band structure with electron and hole carriers. The positive thermoelectric power of 20 $\mu V K^{-1}$ at room temperature tells that the electrical conduction is dominated by hole carriers. The one-dimensional nature of this complex is shown in the narrow ESR linewidth of 2.2 G at room temperature, the large $t_{\parallel}/t_{\perp}$ for both MTDTPY and CHL stacks and the weak interchain interaction between MTDTPY and CHL stacks. Hence, the Pauli susceptibility depends on the temperature, even in the metallic state, due to a one-dimensional fluctuation.

MTDTPY-CHL is considered to have a Peierls transition at 240 K, since below this temperature the resistivity increases abruptly and the thermoelectric power increases proportionally to T^{-1} and the spin susceptibility decreases in an activated manner with Δ=0.091 eV. Characteristically, MTDTPY-CHL shows a first-order phase transition with the hysteresis in the resistivity and the thermoelectric power around 110 K, which suggests the presence of some transformation in the crystal structure. This first-order phase transition is smeared out upon applying pressure above ca. 5 kbar.

Finally, we briefly mention of the relation between the conductivity and the ionicity of the complex. The ionicity of the complex is mainly goverened by the difference (I_p−E_A) between an ionization energy I_p of a donor and an electron affinity E_A of an acceptor. A small (I_p−E_A) gives an ionic complex, while a large one gives a neutral complex. A complex with a partial CT is realized under the condition (I_p−E_A)≈E_M (E_M: crystal Madelung energy).[18] As to *p*-benzoquinone derivatives used in this work, the ability of an acceptor increases in BRL≈CHL≪DDQ. MTDTPY-BRL and MTDTPY-CHL show high conductivities owing to a partial CT of ca. 0.6. MTDTPY-DDQ shows the highest resistivity, 5.4 Ωcm, since the ionicty of the complex approaches the ionic state with a decrease of (I_p−E_A).

Summary

α-MTDTPY-TCNQ, MTDTPY-FLL, and MTDTPY-DDQ are semiconductors, whereas β-MTDTPY-TCNQ, MTDTPY-CHL, and MTDTPY-BRL show metallic conductivity. X-Ray diffraction studies confirm that metallic conductions in β-MTDTPY-TCNQ and MTDTPY-CHL are owing to uniform segregated stacks and a partial charge-transfer state. MTDTPY-CHL and MTDTPY-BRL are the first organic metals among the *p*-benzoquinone derivatives complexes ever known. Theoretical calculations give one-dimensional electronic structures for β-MTDTPY-TCNQ and MTDTPY-CHL. ESR measurements also suggest one-dimensionality with a narrow linewidth and temperature-dependent Pauli susceptibility. Thus, the origin of the metal-insulator (M-I) transitions at 110 and 240 K for β-MTDTPY-TCNQ and MTDTPY-CHL, respectively, can be attributed to a Peierls instability. These complexes show novel behaviors in the semiconducting region. In the case of β-MTDTPY-TCNQ, the ESR spectra are separated into two components below T_{MI}. The splittings of the spectra can be explained by a slow interchain hopping rate of electrons between MTDTPY and TCNQ molecules. MTDTPY-CHL has a first-order phase transition around 110 K. This phase transition is easily suppressed by pressure above ca. 5 kbar. MTDTPY-BRL, without a first-order phase transition, shows a lower M-I transition temperature of 125 K.

β-MTDTPY-TCNQ and MTDTPY-CHL have two-dimensional networks in the crystals through interchain S-S contacts less than the van der Waals distance.[6] However, their electronic properties are one-dimensional, as presented in the results of ESR and band calculation. The selection of the other acceptors or another chemical modifications will be needed to achieve an intention for enhancing the dimensionality to stabilize a metallic state.

The authors are grateful to Dr. Shunji Bandow of Institute for Molecular Science for his helpful support in the ESR simulation.

References

1) H. Akamatu, H. Inokuchi, and Y. Matsunaga, *Nature (London)*, **173**, 168 (1954).

2) H. J. Keller, D. Nöthe, H. Pritzkow, D. Wehe, M. Werner, P. Koch, and D. Schweitzer, *Mol. Cryst. Liq. Cryst.*, **62**, 181 (1980).

3) K. Nakasuji, H. Kubota, T. Kotani, I. Murata, G. Saito, T. Enoki, K. Imaeda, H. Inokuchi, M. Honda, C. Katayama, and J. Tanaka, *J. Am. Chem. Soc.*, **108**, 3460 (1986).

4) N. Thorup, G. Rindorf, C. S. Jacobsen, K. Bechgaard, I. Johannsen, and K. Mortensen, *Mol. Cryst. Liq. Cryst.*, **120**, 349 (1985).

5) K. Bechgaard, *Mol. Cryst. Liq. Cryst.*, **125**, 81 (1985).

6) K. Nakasuji, M. Sasaki, T. Kotani, I. Murata, T. Enoki, K. Imaeda, H. Inokuchi, A. Kawamoto, and J. Tanaka, *J. Am. Chem. Soc.*, **109**, 6970 (1987).

7) P. M. Chaikin and J. F. Kwak, *Rev. Sci. Instrum.*, **46**, 218 (1975).

8) T. Mori, A. Kobayashi, Y. Sasaki, H. Kobayashi, G. Saito, and H. Inokuchi, *Bull. Chem. Soc. Jpn.*, **57**, 627 (1984).

9) T. Mori, Ph. D Thesis, The University of Tokyo, Tokyo, Japan (1985).

10) M. Kinoshita and H. Akamatu, *Nature (London)*, **207**, 291 (1965).

11) R. J. Elliott, *Phys. Rev.*, **96**, 266 (1954).

12) Y. Tomkiewicz, E. M. Engler, and T. D. Schultz, *Phys. Rev. Lett.*, **35**, 456 (1975).

13) Y. Tomkiewicz, A. R. Taranko, and J. B. Torrance, *Phys. Rev. B*, **15**, 1017 (1977).

14) P. M. Chaikin, R. L. Greene, S. Etemad, and E. Engler, *Phys. Rev. B*, **13**, 1627 (1976).

15) K. Kuwata and G. Soda, "Kanwagenshō No Kagaku,"

ed by K. Higashi and S. Nagakura, Iwanami, Tokyo (1973), Chap. 2.
16) A. Carrington and A. D. McLachlan, "Introduction to Magnetic Resonance," Chapman and Hall, London (1979), Chap. 12.
17) G. Soda, D. Jerome, M. Weger, J. M. Fabre, and L. Giral, *Solid State Commun.*, **18**, 1417 (1976).
18) J. B. Torrance, J. E. Vazquez, J. J. Mayerle, and V. Y. Lee, *Phys. Rev. Lett.*, **46**, 253 (1981).

Computer Simulations of Gel Filtration Chromatograms of Rapidly Self-Associating Systems

Noriaki FUNASAKI,* Sakae HADA, and Saburo NEYA
Kyoto Pharmaceutical University, Yamashina-ku, Kyoto 607
(Received August 8, 1988)

A computer simulation method for gel filtration chromatography (GFC), based on plate theory and mass action law, is developed for rapidly self-associating systems and compared with asymptotic theory. For ovalbumin, a non-associable protein, whose elution volume increases linearly with increasing concentration, the leading boundary is predicted to be broader than the trailing. Computer simulations are used to estimate the aggregation numbers and the equilibrium constants for dimerization of carbonylhemoglobin and hexamerization of α-chymotrypsin. The concentration, C_{min}, at the plateau region of the trailing boundary is shown to be close to cmc by asymptotic theory. The present computer simulation and derivative GFC patterns serve to estimate monomer concentration and micellar size of surfactants from analysis of GFC data.

Gel filtration chromatography (GFC) is routinely used for separation of materials different in size and for estimation of the molecular weights of proteins and synthetic polymers. GFC patterns for self-associating or complex forming systems are often complicated and troublesome for the above purposes. An appropriate analysis of these systems, however, may provide useful information on molecular association. The dissociation of the hemoglobin subunits is an instance for such applications.[1] Since the assumption of a sharp (no broadening) boundary simplifies the analysis of complicated patterns for chemically reacting systems, this assumption (hereafter called asymptotic theory) has been used for analyses of GFC, sedimentation velocity,[2] and electrophoretic data. These analyses have established the stoichiometry of the reactions by using mass action law.[1-4] Furthermore, these transport properties are often represented as derivative patterns. These patterns have been analyzed by the asymptotic theory.[2-4]

The GFC method has also been used to investigate the aggregation properties of surfactants,[5] such as the aggregation number,[6] monomer concentration,[7,8] micellar size,[8-10] and mixed micelle formation.[11,12] However, since the aggregation number of surfactants is usually much larger than that of proteins, GFC elution curves of the surfactants have been analyzed on the basis of phase separation model intuitively,[8] by the asymptotic theory,[7] or by plate theory.[12,13] As a result, different analyses have been done for surfactants and proteins. For micellization of surfactants, mass action model is superior to the phase separation model; e.g., it is suggested by GFC that monomer concentration of a surfactant increases with increasing surfactant concentration above the critical micelle concentration (cmc).[7,8] Therefore the above-mentioned results for surfactants[5-13] should be analyzed in terms of the mass action model by reference with those of proteins. Furthermore, derivative GFC profiles often provide more detailed information than original profiles. No derivative GFC pattern except ours has been reported for surfactants.[10]

The major advantage of the asymptotic theory is that analytical solutions of the characteristic constants of self-associating systems are obtained from the elution curve and its derivative. Therefore this theory has been applied to surfactants and proteins.[1-7] Computer simulation procedures of transport properties (including GFC) of self-associating systems have been published.[14] These procedures require a number of parameters involved in column beds and materials used. Plate theory[15] based on the phase separation model has been applied to surfactants.[12,13] This theory is superior to the asymptotic theory, since the former predicts a more realistic profile than the latter. Another advantage of the plate theory over other theories[14] is that the adjustable parameter for the column characteristics is only the number of plates.

In the present work, we developed plate theory based on mass action model, demonstrated its usefulness for simulations of GFC profiles of proteins and surfactants, and revealed the scope and limitations of the asymptotic theory.

Computational Methods

Plate Theory. A gel column is assumed to be composed of n plates as shown schematically in Fig. 1. Each plate consists of the mobile and stationary phases. The total volume of the mobile phase equals to the void volume V_0 of the column. When a solution of volume of V_f is applied from the "zero-th" plate (the top) of the column, the mobile phase of volume V_f is flown down to the nearest neighboring plate throughout the column till another solution of the same volume flows from the n-th plate (the bottom). Then we assumed a rapid establishment of the partition equilibrium of the solute between the mobile and stationary phases at each plate.[12,13,15]

When the partition equilibrium has been established after addition of a solution of volume iV_f, the total amount of the solute at the j-th plate may be written as

$$(M_{i,j}+S_{i,j})V_f=(M_{i-1,j-1}+S_{i-1,j})V_f. \quad (1)$$

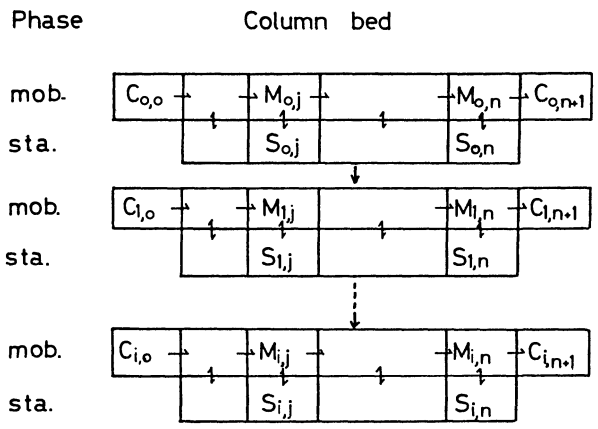

Fig. 1. Schematic elution process based on plate theory. The integers i and j indicate the numbers of transfer and plate, respectively.

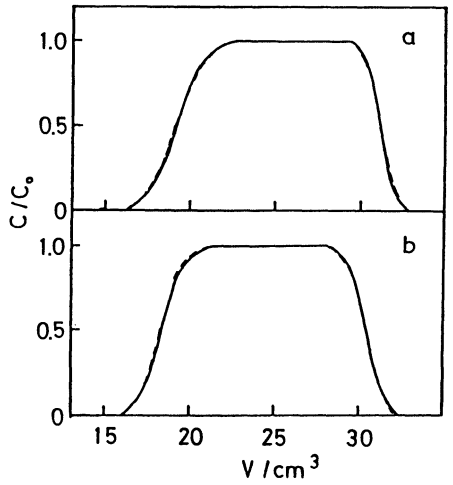

Fig. 2. Effects of concentration dependence of elution volumes upon the protein distribution for ovalbumin at (a) 12.0 g dm^{-3} and (b) 1.6 g dm^{-3}. The observed results (solid lines) are taken from Ref. 19 and the dashed lines are calculated from plate theory by using the following parameters; V_0=12.53 cm^3, n=250, and P=0.00638C_0+0.45092.

Here $M_{i,j}$ and $S_{i,j}$ are "concentrations" at the j-th plate in terms of the volume of the mobile phase (V_f). The same equilibration is made for all plates (j=1 to n). In Eq. 1, for the first plate (j=1) $M_{i-1,0}=C_{i-1,0}$ and for the n-th plate $M_{i-1,n}=C_{i,n+1}$. This procedure is repeated for different numbers of transfer (i=1 to i) starting from zero. The relation between $C_{i,n+1}$ and iV_f presents the theoretical elution curve. The partition ratio, P, of a solute between the stationary and mobile phases may be written as

$$P=S_{i,j}/M_{i,j}=(V_e-V_0)/V_0, \tag{2}$$

where V_e is the elution volume of the solute.

For analysis of GFC data two methods for charging a sample are used, viz., the small size (zonal) method and the large sample size (frontal) method.[16] The latter examples are shown in Fig. 2. When an enough volume of solution at concentration C_0 is charged, the solution of the same concentration C_0 appears on the elution curve. If a small volume of the sample is charged, the sample is diluted during elution in the column. Therefore, since the zonal method cannot be used for quantitative analysis of elution curves for self-associating systems,[9] we will consider only the frontal method. For the frontal method we may assume $C_{i,0}=C_0$ for $1\leqq i\leqq k$ and $C_{i,0}=0$ for $i>k$, where k is sufficiently large to produce the plateau region on the elution curve, as shown in Fig. 2.

For the self-associating system, monomer$\rightleftarrows m$-mer, we may write the equilibrium constant K in the mobile phase as

$$K=C_m/C_1^m, \tag{3}$$

where C_1 and C_m denote concentrations of the monomer and m-mer on a monomer basis. The total concentrations in the mobile and stationary phases may be written as

$$M_{i,j}=C_1+C_m=C_1+KC_1^m \tag{4}$$

and

$$S_{i,j}=P_1C_1+P_mC_m=P_1C_1+P_mKC_1^m, \tag{5}$$

where P_1 and P_m are the partition ratios for the monomer and m-mer.

Assuming appropriate values for V_0, n, P_1, P_m, K, m, and C_0, we can simulate the theoretical elution curve (C vs. V) and its first-derivative curve (dC/dV vs. V). The derivative curve provides useful information on self-associating systems.[4,10,17,18]

Asymptotic Theory. As Fig. 2 shows for the frontal method, the boundaries at the initiation (leading) and termination (trailing) of solute elution are diffuse. Approximately we may assume that the equivalent sharp boundary for the solute zone leading or trailing boundary is the first moment (centroid) of the elution profile and satisfies the relationships:

$$V_C=\int_0^{C_0} V\mathrm{d}C/C_0 \qquad \text{(leading boundary)} \tag{6}$$

and

$$V_C'=\int_0^{C_0} V\mathrm{d}C/C_0+S \qquad \text{(trailing boundary)}. \tag{7}$$

Here S is the charged volume of the sample. For these determinations the volume coordinate V is assigned a zero value when the leading boundary of the charged sample enters the column bed. This theory predicts the elution profile of a rectangle (C_0 in height and S in width) for the non-associating system.[4,16]

When this theory is applied to the self-associating system, monomer$\rightleftarrows m$-mer, we may determine the aggregation number m from the trailing boundary and the equilibrium constant K from either the leading or trailing boundary. At $m\geqq 3$, the derivative profile for the trailing boundary is expected to exhibit a min-

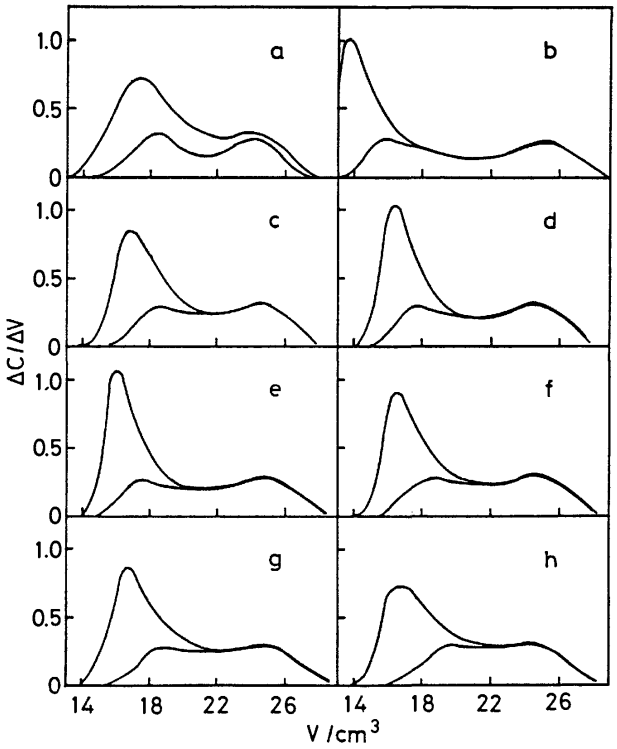

Fig. 3. Derivative chromatograms of α-chymotrypsin at concentrations of 5.0 g dm^{-3} (upper curve) and 2.4 g dm^{-3} (lower curve); Fig. a is observed[17] and Figs. b–h are calculated by using the parameters shown in Table 2.

imum (V_{min}) and two maxima ($V_{1p}>V_{mp}$), as shown in Fig. 3, and m and K may be evaluated from

$$m=(3V_{min}-V_1-2V_m)/(3V_{min}-2V_1-V_m) \quad (8)$$

and

$$K=(m-2)\{2(m^2-1)\}^{m-1}/[\{(m(2m-1)\}^m(C_{min})^{m-1}]. \quad (9)$$

Here C_{min} may be taken as the concentration corresponding to the minimum on the derivative curve and V_1 and V_m are the centroid elution volumes of the monomer and m-mer, respectively. At $m=2$, only one maximum (V_{max}') is expected for the derivative curve in the trailing boundary and K may be evaluated from

$$K=\lambda(m+\lambda)^{m-1}/(m^m C_e^{m-1}). \quad (10)$$

Here C_e may be taken as the concentration at the maximum and $\lambda=(V_1-V_{max}')/(V_{max}'-V_m)$.

For the leading boundary the centroid volume V_e may be written as

$$V_e=\alpha V_1+(1-\alpha)V_m, \quad (11)$$

where α is the weight fraction of monomeric species in the plateau region. Substitution of $C_1=C_0\alpha$ and $C_m=C_0(1-\alpha)$ into Eq. 3 yields

$$K=(1-\alpha)/(C_0^{m-1}\alpha^m), \quad (12)$$

where α may be taken as $(V_e-V_m)/(V_1-V_m)$ from Eq. 11.[3-5,16] Thus, the main advantage of the asymptotic theory over the plate theory is to provide the analytical solutions for m and K. However, the values of m and K estimated from the asymptotic theory may be used as a first approximation.

Results and Discussion

Concentration Dependence of Elution Volumes. Generally speaking, the elution volume increases with increasing solute concentration slightly.[16] In the case where the elution volume of a nonassociable solute increases with increasing concentration, the leading boundary becomes broader than the trailing one.[19] This elution pattern is the reverse found for self-associating solutes.[17]

Figure 2 shows the elution curves for ovalbumin at 1.6 g dm^{-3} and 12 g dm^{-3}. From such results V_e (and V_e') has been determined as a function of C_0:

$$V_e=18.18+0.080C_0. \quad (13)$$

In the experiments $S=12.0$ cm^3 and $V_0=12.53$ cm^3 (estimated in this work). Substitution of these values and Eq. 13 into Eq. 2 yields

$$P=0.00638C_0+0.45092. \quad (14)$$

Based on the plate theory by using P (Eq. 14), V_0 (12.53 cm^3), C_0 (1.6 or 12 g dm^{-3}) and $n=250$, we can simulate the elution curve. These theoretical curves are drawn by the dashed lines. At the low concentration of the protein, the leading and trailing boundaries are almost symmetric, whereas at the high concentration the leading boundary is broader than the trailing. These results are well reproduced, showing the utility of the plate theory to predict the shape of the elution pattern. Asymptotic theory always predicts a rectangular elution pattern for a non-associable solute. The results of Fig. 2 have also been explained by the Houghton theory.[19,20] This theory is applicable for the system where the concentration dependence of V_e is small.

Table 1. Comparison between the Observed and Theoretical Values of V_e for Dimerization of Human Carbonylhemoglobin as a Function of Concentration

C_0	V_{obsrd}[a]	V_{calc}[b]			
		Asymptotic theory		Plate theory	
mmol dm^{-3}	cm^3	K=0.25	K=0.31	K=0.25	K=0.31
0.3×10^{-6}	37.8	37.79	37.75	37.79	37.75
1	37.4	37.45	37.37	37.46	37.38
2	36.95[c]	37.15	37.05	37.16	37.05
5	36.5	36.68	36.57	36.69	36.58
8	36.45[c]	36.43	36.32	36.44	36.33
10	36.2	36.32	36.22	36.33	36.23
12	36.17[c]	36.23	36.13	36.24	36.14
14	36.2	36.15	36.06	36.17	36.07

a) Taken from Ref. 3. b) $V_1=38.0$ cm^3, $V_m=34.9$ cm^3, and $V_0=15.6$ cm^3 were used. c) Average of two or three data.

Dimerization of Carbonylhemoglobin. The equilibrium constant of dimerization of human carbonylhemoglobin has been determined from Sephadex G-200 column experiments.[3] In Table 1 the observed and theoretical V_c values from the leading boundary are shown as a function of protein concentration. From the experiments at 10^{-8} mol dm^{-3} and 10^{-3} mol dm^{-3}, the V_c values for the monomer and dimer have been estimated to be 38.0 and 34.9 cm^3, respectively. These values may be regarded as independent of concentration. The void volume has been determined to be 15.6 cm^3 from V_c of tobaco mosaic virus.[3]

By substituting m=2, the observed values of V_m, V_1, and C_0, and an assumed K value in Eq. 12, we can calculate the theoretical V_c value for dimerization. In Table 1 the calculated V_c values for two K values are shown; a K value of 0.25 dm^3 mmol^{-1} has been reported by the original workers[3] and 0.31 dm^3 mmol^{-1} is our best fitted value. A K value of 0.28 dm^3 mmol^{-1} has been estimated from porous disk diffusion measurements for the same protein.[3] Agreement between the K values estimated from the two methods is very good, showing that these values are reliable.

From the plate theory we can calculated V_c by using the observed values of V_0, V_1, and V_m and assumed values of K and n. The V_c values for the cases n=200 and K=0.25 and 0.31 are included in Table 1. Agreement between the asymptotic and plate theories is excellent.

Hexamerization of Chymotrypsin at Neutral pH. Winzor and Scheraga have reported frontal elution patterns and their derivatives for α-chymotrypsin at pH 7.9.[17] In the elution curve the leading boundary was sharper than the trailing. This feature is common for self-associating systems and is in contrast with nonassociating concentration-dependent systems, as shown in Fig. 2. This characteristic has been explained by the asymptotic theory[16] and is also explicable on the basis of the plate theory (computed results are omitted).

The derivative trailing patterns for several protein concentrations have been reported.[17] The data at two concentrations of them, 5.0 and 2.8 g dm^{-3}, are shown in Fig. 3, since most of the main features appear herein. Extrapolation of the monomer elution volume to C_0=0 permits us to estimate a value of V_1=25.0 cm^3.[3] One of the main problems encountered in the use of GFC patterns to characterize self-associating systems is the absence of the definite value of V_m.[16] As expected from Table 2, one of the estimation methods is to choose the gel phase from which the polymer is excluded.[4] Then V_m may be identified with V_0, the void volume of the column bed. By this reasoning Ackers and Thompson have taken V_m as 11.9 cm^3.[3] Substituting these values in Eq. 8, together with an estimate of V_{min}=21.5 cm^3 (inferred from Fig. 3a), they estimated a value of m=6.[3] Furthermore a C_{min} value of 1.4 g dm^{-3} has been inferred[4] from the size of the more slowly migrating part of the bimodal trailing boundary reported by Winzor and Scheraga. By using these m and C_{min} values, a K value of 0.015 dm^{15} g^{-5} has been estimated from Eq. 9.[4] However, we should be alert to the above analysis since an estimated V_0 value has been used. In this connection it is noted that the sedimentation velocity patterns of Massey et al.[21] yielded a slightly higher estimate of C_{min} (1.8 g dm^{-3}), from which a value of K=0.004 dm^{15} g^{-5} has been obtained on the basis of asymptotic theory.[4]

Table 2. Seven Sets of the Parameters to Simulate Polymerization of α-Chymotrypsin at Neutral pH on the Basis of Plate Theory[a]

Set	m	K / g^{m-1} dm^{3m-3}	V_1 / cm^3	V_m / cm^3
b	6	0.015	25.0	11.9
c	6	0.010	23.9	15.5
d	6	0.010	23.9	14.0+0.298C_m
e	6	0.009	24.5	13.2+0.357C_m
f	5	0.014	24.5	13.2+0.357C_m
g	5	0.015	24.5	14.5
h	4	0.020	24.5	12.0+0.357C_m

a) n=100 is used for simulation.

Taking these uncertainties of K and V_m values into consideration, we made simulations for many sets of the values of m, V_1, V_m, K, and n. Seven sets of them are shown in Table 2. In the following calculations, we used n=100. In set b, the values used in the above analysis based on the asymptotic theory are employed. As Fig. 3b shows, the polymer peaks have much smaller V_m values than the observed ones (Fig. 3a). This discrepancy may be ascribed to inadequate values for V_m or V_0 (or both) suggested by Ackers and Thompson. The most uncertain parameter in this simulation is V_m. Therefore we considered larger V_m values and their concentration dependences (sets c—e). Determann and Nichel reported a calibration relation between molecular weights and elution volumes for many proteins from the literature.[22] From this relation we can estimate a value of V_0=13.1 cm^3. The V_m values in Table 2 are chosen by taking this V_0 value into consideration. As Figs. 3c—e show, the simulated polymer peak at 5 g m^{-3} is slightly sharper than the observed one. Therefore we considered smaller aggregation numbers. As Fig. 3f shows, the simulated curve at C_0=2.4 g dm^{-3} gives a slightly broader peak than the observed. A value of m=5 (Figs. 3f and 3g) gives as good fittings as m=6. None of the simulations (b—h) very well reproduce the experimental result (a). This discrepancy may be ascribed to the inaccuracy in both the experimental result and the plate theory. Asymptotic theory predicts unrealistic derivative patterns.[4]

Comparison between Asymptotic and Plate Theories. In application of Eq. 8 the practical upper limit

lies in the region $m<10$, since the denominator of Eq. 8 approaches experimental errors in the determination of the elution volume.[3] Therefore we made model calculations in the case of hexamerization to compare the two theories.

For these theories we used the same parameters, viz., V_1=230.0, V_m=130.0, V_0=100.0, and K=1. Concentration dependence of these parameters was neglected. Substitution of these values and m=6 in Eqs. 8 and 9 yielded V_{min}=203.3 and C_{min}=0.649. According to the asymptotic theory, these values should be independent of C_0. Furthermore V_c for the leading boundary can be calculated from Eq. 12 and is shown in Table 3.

From the plate theory, we also calculated the frontal elution curve and its derivative, by assuming n=100. From these curves we determined several characteristic values. These are shown in Table 3. The equilibrium monomer concentration C_1 was calculated from Eq. 3 and included herein. In this table V_{mp} and V_{lp} are the elution volumes at maxima ($V_{mp}<V_{lp}$) in the trailing boundary of the derivative curve.

The V_{min} value calculated from the plate theory increases with increasing concentration, in contrast with concentration independence expected from the asymptotic theory. The experimental V_{min} data on chymotrypsin support the prediction of the plate theory (e.g., see Fig. 3). Therefore the estimation of m from Eq. 8 may be generally regarded as a first approximation. The value of C_{min} from the plate theory is also concentration-dependent and is smaller than that of the asymptotic theory. It is notable that C_{min} is smaller than C_1. Combination of Eqs. 9 and 12 yields

$$C_e/C_0=\{(m-2)(2m-2)^{m-1}\alpha^m\}^{1/(m-1)}/\{(2m^2-m)(1-\alpha)\}^{1/(m-1)}. \quad (15)$$

At the limit $m\to\infty$

$$C_{min}\to C_0\alpha=C_1. \quad (16)$$

Here the equation $C_e=C_{min}$ is used since $m\geqq 3$. The same conclusion (Eq. 16) was obtained from the plate theory based on phase separation model for micelle formation.

Table 3 shows that the plate theory predicts the increase of V_1 and the decrease of V_m with increasing concentration. Concentration dependence of the elution volume of the monomer and m-mer does not always indicate size changes of these species. These results are consistent with the experimental data on chymotrypsin.[17]

The difference between the V_c values calculated from the two theories is 0.5, regardless of C_0. Since this difference (close to $V_0/2/n$) decreases with increases in n, we can conclude that the two theories predict the same V_c value for the leading boundary. This conclusion may justify applications of the asymptotic theory to leading boundary data for self-associating systems, such as hemoglobin[1] and carbonylhemoglobin (Table 1).

Implications to Micellization of Surfactants. The above results may be useful for quantitative analyses of GFC data on surfactants. The aggregation number of surfactants is usually larger than that of proteins, e.g., typically $m>50$. Hence phase separation model ($m=\infty$) has been used to analyze GFC data for pure and mixed surfactants.[11-13] This model is useful, but is less accurate than mass action model since m is a definite value. Furthermore, most of the GFC data on surfactants have been analyzed on the basis of the asymptotic theory.[6-8]

The monomer concentration C_1 for hexaethylene glycol dodecyl ether ($C_{12}E_6$) has been estimated by two interpretations of GFC data. First approach[7] used Eq. 11 and second approach assumed the equality of $C_{min}=C_1$.[8] As expected, the former approach yielded greater C_1 values than the latter.[7,8] However, both approaches must be reconsidered, as shown below.

According to Phillips' definition of the cmc, the cmc is a C_0 value which satisfies the equation $d^3(C_1+C_m/m)/dC_0^3=0$.[23] By using this definition and Eq. 3, we can obtain

$$\text{cmc}=[Km(2m-1)/(m-2)]^{1/(1-m)}. \quad (17)$$

This equation can be also obtained from the equation $d^3C_1/dC_0^3=0$.[24] On the other hand, we can write C_{min} at $m\geqq 3$ from Eq. 9 as

$$C_{min}=\left\{\frac{K[m(2m-1)]^m}{(m-2)[2(m^2-1)]^{m-1}}\right\}^{1/(1-m)} \quad (18)$$

When m is large enough, we can thus obtain

$$C_{min}\cong\text{cmc}\cong(2Km)^{1/(1-m)}. \quad (19)$$

This equation provides the physical meaning of C_{min} and a GFC method for cmc determination without interpolation of any property. The C_{min} value for $C_{12}E_6$ increased with increasing C_0, whereas the plate theory

Table 3. Comparison between Two Theories in Hexamerization[a]

C_0	C_1	Plate theory[b]					Asymptotic theory[c]
		C_{min}	V_{min}	V_{mp}[d]	V_{lp}[d]	V_c	V_c
0.125	0.125	—[e]	—[e]	—[e]	229.8	230.5	230.0
0.25	0.250	—[e]	—[e]	—[e]	229.8	230.4	229.9
0.5	0.487	—[e]	—[e]	—[e]	230.0	227.8	227.3
1	0.778	0.624	196.5	175.2	232.1	208.3	207.8
2	1.000	0.589	203.4	146.7	233.5	180.5	180.0
4	1.188	0.587	205.0	138.0	234.3	160.2	159.7
8	1.371	0.582	206.5	134.0	235.0	147.6	147.1
16	1.560	0.581	207.5	132.5	236.0	140.3	139.8
32	1.765	0.579	208.5	131.5	236.5	136.0	135.5
64	1.990	0.576	209.3	131.2	237.0	133.6	133.1

a) V_1=230.0, V_m=130.0, V_0=100.0, and K=1 are used for calculations. b) n=100 is used. c) C_{min}=0.649 and V_{min}=203.3 were obtained from Eqs. 8 and 9, regardless of C_0. d) These values are the volumes at maxima in the derivative elution curves. e) Not observed.

predicts a slight decrease of C_{min} (e.g., see Table 3) and the asymptotic theory predicts the constancy. This discrepancy between theory and experiment may be ascribed to the increase of m with increasing C_0 for $C_{12}E_6$.[8,10]

In GFC, generally, large particles have smaller elution volumes than small ones. For self-associating systems, however, the elution volume depends on C_0 as well as size of species. As Fig. 3 shows, the polymer peak shifts toward smaller volume side with increasing C_0. This is not due to the increase of m. For $C_{12}E_6$, the elution volume of the micelle decreased with increasing C_0. This decrease has all been ascribed to the increase of m. The V_m value in Eq. 11 should correspond to true size of the micelle, and is not equal to the elution volume of the micelle at the concentration of the solution used.[10]

Conclusion

To demonstrate the scope and limitations of asymptotic theory and plate theory based on mass action law for self-associating systems, we investigated the elution patterns for ovalbumin (nonassociable protein), dimerization of carbonylhemoglobin, hexamerization of chymotrypsin, and micellization of surfactants. The asymptotic theory has an advantage of giving analytical expressions (V_c, C_{min}, V_{min}, and others) for elution patterns of self-associating systems. Equation 11, which was supported by the plate theory, gives the basis for the estimation of monomer concentrations of such systems. For surfactants C_{min} is very close to the cmc (Eq. 19). The plate theory has an advantage of requiring only a limited number of parameters over other theories.[14] It correctly predicts that the trailing boundary becomes sharper with increasing C_0 when the elution volume of a nonassociable solute increases linearly with C_0. Derivative elution profiles of self-associating systems were well simulated to make possible estimation of m and K and prediction of concentration dependence of V_{min} and C_{min}. These predictions will be useful to analyze experimental GFC data on surfactants.[18]

This work was supported by a Grant-in-Aid from the Scientific Research Foundation of Kyoto Pharmaceutical University.

References

1) R. Valdes and G. K. Ackers, *J. Biol. Chem.*, **252**, 74 (1977).
2) G. A. Gilbert, *Disc. Faraday Soc.*, **20**, 68 (1955); *Proc. R. Soc. London, Ser. A*, **250**, 377 (1959).
3) G. K. Ackers and T. E. Thompson, *Proc. Natl. Acad. Sci. U.S.A.*, **53**, 342 (1965).
4) L. W. Nichol and D. J. Winzor, "Migration of Interacting Systems," Clarendon Press, Oxford (1972), Chap. 3.
5) T. Sasaki, *Yukagaku*, **16**, 49 (1967).
6) H. Suzuki, *Bull. Chem. Soc. Jpn.*, **49**, 375 (1976).
7) T. Sasaki, M. Yasuoka, and H. Suzuki, *Bull. Chem. Soc. Jpn.*, **50**, 2538 (1977).
8) A. Goto, R. Sakura, and F. Endo, *J. Colloid Interface Sci.*, **67**, 491 (1978).
9) C. Tanford, Y. Nozaki, and M. F. Rohde, *J. Phys. Chem.*, **81**, 1555 (1977).
10) N. Funasaki, S. Hada, and S. Neya, *J. Phys. Chem.*, **92**, 3488 (1988).
11) F. Tokiwa, K. Ohki, and I. Kokubo, *Bull. Chem. Soc. Jpn.*, **41**, 2845 (1968).
12) T. Nakagawa and H. Jizomoto, *Kolloid-Z. Z. Polym.*, **234**, 1124 (1970).
13) T. Nakagawa and H. Jizomoto, "Proceedings of the IVth International Congress on Surface Active Substances," Barcelona (1968), p. 299.
14) J. L. Bethune and G. Kegeles, *J. Phys. Chem.*, **65**, 1761 (1961); J. K. Zimmerman, D. J. Cox, and G. K. Ackers, *J. Biol. Chem.*, **246**, 4242 (1971); L. M. Gilbert and G. A. Gilbert, *Methods Enzymol.*, **48**, 195 (1978); D. J. Cox, *ibid.*, **48**, 212 (1978); G. Kegeles and J. R. Cann, *ibid.*, **48**, 248 (1978).
15) A. J. P. Martin and R. L. M. Syringe, *Biochem. J.*, **35**, 1358 (1941).
16) G. K. Ackers, *Adv. Protein Chem.*, **24**, 343 (1970).
17) D. J. Winzor and H. A. Scheraga, *Biochemistry*, **2**, 1263 (1963).
18) N. Funasaki, S. Hada, and S. Neya, *J. Phys. Chem.*, in press.
19) D. J. Winzor and L. W. Nichol, *Biochim. Biophys. Acta*, **104**, 1 (1965).
20) G. Houghton, *J. Phys. Chem.*, **67**, 84 (1963).
21) V. Massey, W. F. Harrington, and B. S. Hartley, *Disc. Faraday Soc.*, **20**, 24 (1955).
22) H. Determann and W. Michel, *J. Chromatogr.*, **25**, 303 (1966).
23) J. N. Phillips, *Trans. Faraday Soc.*, **51**, 561 (1951).
24) S. Ikeda, "Colloid Chemistry," Shokabo, Tokyo (1986), Chap. 6.

Photoelectrochemical Properties of Thin Films of Zinc Porphyrin Derivatives with Pyridyl Group

Kohshin TAKAHASHI,* Teruhisa KOMURA, and Hiroto IMANAGA
Department of Chemistry and Chemical Engineering, Faculty of Technology, Kanazawa University, Kodatsuno, Kanazawa 920
(Received August 8, 1988)

The cathodic photocurrents of the film electrodes of $ZnPyP_3P(3)$ and $ZnPyP_3P(4)$, ($PyP_3P(n)$, 5-(2-, 3-, and 4-pyridyl)-10,15,20-triphenylporphyrin, where (n) denotes the position of free bond of pyridyl group), were almost four times larger than that of ZnTPP (TPP, 5,10,15,20-tetraphenylporphyrin) in 0.01 mol dm^{-3} quinhydrone aqueous solution at pH 5. On the other hand, the very small anodic photocurrent was observed with the film electrodes of ZnTPyP(3) and ZnTPyP(4) (TPyP(n),5,10,15,20-tetra(2-, 3-, and 4-pyridyl)porphyrin). The photoelectrochemical properties of $ZnPyP_3P(2)$ and ZnTPyP(2) were distinct from those of other structural isomers, but approximately similar to those of ZnTPP. The conductivities of $ZnPyP_3P(n)$ films were about three oders of magnitude larger than those of ZnTPP and ZnTPyP(n) films. It was found from the absorption and resonance Raman spectra that the pyridyl group in porphyrin coordinated to zinc in another porphyrin in the solid films as well as in toluene and dichloromethane solutions. The molecular arrangement of zinc porphyrin in the solid film probably influenced the photoelectrochemical properties and the conductivity.

Much attention has been drawn to the photoelectrochemical properties of metalloporphyrin films from the standpoint of the conversion of solar to chemical and/or electrical energy.[1-8] The cathodic photocurrent is observed with the metalloporphyrin film electrode because of the formation of the blocking contact between a p-type semiconductor such as the metalloporphyrin film and an electrolytic solution.[1] The photocurrent quantum yield increases with a decrease in the first ring oxidation potential of metalloporphyrins,[2-5] and also with an increase in π-π interactions between neighbouring molecules.[5] On the other hand, the film of 5,10,15,20-tetra(3-pyridyl)porphyrin acts as an n-type semiconductor.[6]

In the present paper, the photoelectrochemical properties of zinc porphyrins as illustrated in Fig. 1 are investigated in a quinhydrone solution and compared with those of ZnTPP. We report that the pyridyl group in zinc porphyrins plays an important role in the photoelectrochemical behavior because of its coordination to zinc in another porphyrin.

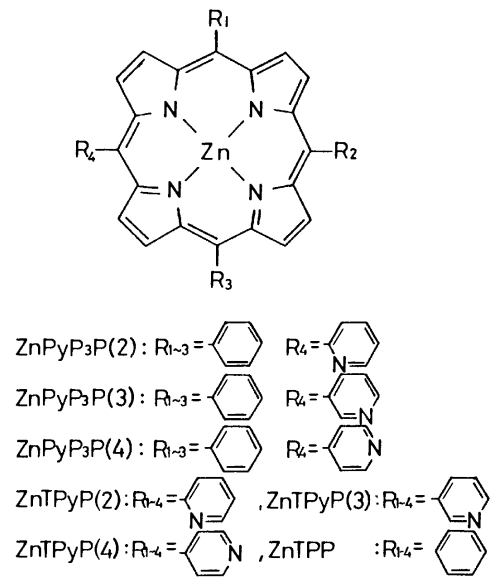

Fig. 1. Structures and abreviations of zinc porphyrins.

Experimental

H_2TPP, and $H_2PyP_3P(n)$ as well as $H_2TPyP(n)$ were synthesized and purified by the literature method.[9-11] Contamination with chlorine was oxidized by 2,3-dichloro-5,6-dicyano-*p*-benzoquinone.[12] ZnTPP and $ZnPyP_3P(n)$ as well as ZnTPyP(n) were synthesized by the literature method.[13] The products were purified by column chromatography on alumina. *p*-Benzoquinone was used after sublimation. Potassium chlorid and tetraethylammonium perchlorate (Et_4NClO_4) were used after double recrystallization from water. Toluene and dichloromethane were purified twice by distillation. *N*,*N*-Dimethylformamide (DMF) was twice distilled under reduced pressure in a N_2 atmosphere after dehydration by Molecular Sieves (4A 1/16) and barium oxide. Pyridine was twice distilled after dehydration by KOH. Other chemicals (reagent grade) were used without purification. All aqueous solutions were prepared with twice distilled water.

Absorption and second-derivative absorption spectra were taken on a Hitachi U-3210 spectrophotometer. The exciting radiation for resonance Raman spectra was provided by a Ar^+ laser (488 nm, Nippon Denki GSL3200). The scattering radiation was dispersed by a double monochromator (Jobin Yovon Ramanor HG2S), and detected by a cooled photomultiplier tube (Hamamatsu Photonics R464) and a photon-counter (Hamamatsu Photonics C1230). Porphyrin films were prepared on a Pt or glass plate by sublimation at pressure 4×10^{-3} Pa. Film electrodes were insulated from the electrolyte with epoxy resin except for the portion to be exposed to light (1 cm^2). A 500W xenon arc lamp (Ushio UXL-500D-O) was used as a white light source. The light was passed through a color filter (Toshiba L-39) and water (1 cm), and irradiated onto a film electrode in a N_2-purged solution thermostated at 25 °C. The light source for photo-

current action spectra measurements consisted of a 750 W halogen-tungsten lamp and a monochromator (Jasco CT-10). Monochromatic light intensity was measured with a chemical actinometer of $K[Cr(NH_3)_2(NCS)_4]$.[14] Photocurrent-voltage curves of the film electrodes were measured by using a potentiostat (Nikko Keisoku NPG-301), a potential sweeper (Nikko Keisoku NPG-2), and a three-electrode configuration. An X-Y plotter (Riken Denshi F-3B) was used to record current-voltage curves. A platinum wire (30 cm^2) was used as a counter electrode and a commercially available Ag/AgCl (in 3.33 M KCl aqueous solution, 1 M=1 mol dm^3) as the reference electrode. The conductivity of a surface-type cell of the solid film in vacuum was determined from a linear relationship between voltage and current. The measurements of current and voltage were performed by a picoammeter and a DC voltage source (Yokogawa Hewlet Packard 4140B). Cyclic voltammetry was performed in a N_2-purged solution by a Pt disk (diameter, 1 mm) as the working electrode, a Pt wire as the counter electrode, and Ag/0.01 M $AgNO_3$ in acetonitrile as the reference electrode. Half-wave potentials were measured with the scan rate of 100 mV s^{-1}, and as the average of cathodic and anodic peak potentials.

Results and Discussion

Dimerization of (ZnPyP$_3$P(n)) in Toluene and CH_2Cl_2. In nonbonding solvents such as toluene and CH_2Cl_2, $ZnPyP_3P(n)$ was slightly soluble and ZnTPyP(n) was insoluble, but in coordinating solvents such as DMF and pyridine, $ZnPyP_3P(n)$ and ZnTPyP(n) were soluble. The addition of pyridine to ZnTPP in toluene gave rise to a red shift of the absorption peak in the B and Q regions because of the formation of a monopyridine complex.[15] On the other hand, the absorption peak in the Q region of $ZnPyP_3P(2)$ in toluene was observed at a longer wavelength than that of ZnTPP in toluene, and the addition of pyridine gave rise to a blue shift of the Q band of $ZnPyP_3P(2)$. The Soret band of $ZnPyP_3P(2)$ in toluene and CH_2Cl_2 exhibited very broad spectra with very small molar extinction coefficients at the absorption peak (about 3×10^5 M^{-1} cm^{-1}) in comparison with those of other zinc porphyrins such as ZnTPP, $ZnPyP_3P(3)$ and $ZnPyP_3P(4)$, but in the solution containing pyridine, the sharp Soret band was observed with $ZnPyP_3P(2)$ as well as other zinc porphyrins. It was found from the second-derivative absorption spectra that the Soret band of $ZnPyP_3P(2)$ in CH_2Cl_2 consisted of two components and the peak wavelengths were 418 and 436 nm. The $Q_{1.0}$ bands of $ZnPyP_3P(n)$ in toluene and CH_2Cl_2 were broad. It was found from the second-derivative absorption spectra that the broad $Q_{1.0}$ bands consisted of two components and the peak wavelengths were near 550 and 565 nm. However, the absorption spectra in solution containing pyridine exhibited only one component near 560 nm. The absorption spectra of ZnTPP and $ZnPyP_3P(2)$ are shown in Fig. 2, and the absorption spectra features of zinc porphyrin derivatives are summarized in Table 1.

The absorption spectra of $ZnPyP_3P(n)$ in toluene distinctly changed in the range of 25 to 65 °C although that of ZnTPP hardly changed. Figure 3 shows the temperature-dependence of the absorption and second-

Table 1. Absorption Spectral Features of Zinc Porphyrins in Solutions at 25 °C and Solid Films at Room Temperature

Porphyrin	Media	$B_{0.0}$	$Q_{1.0}$	$Q_{0.0}$
		nm		
ZnTPP	CH_2Cl_2	419(59.5)[b]	548(2.16)	586(0.36)
	Toluene	424(48.8)	550(2.15)	589(0.34)
	1.2 M pyridine-toluene[a]	428(62.3)	562(2.01)	602(0.91)
	Film	435	553	590
$ZnPyP_3P(2)$	CH_2Cl_2	418(28.0)	566(1.63)	613(0.49)
	Toluene	424(29.4)	565(1.63)	612(0.43)
	1.2 M pyridine-toluene	428(57.9)	562(1.97)	602(0.74)
	Film	436	570	617
$ZnPyP_3P(3)$	CH_2Cl_2	420(44.6)	563(1.78)	605(0.73)
	Toluene	424(46.8)	561(1.49)	605(0.52)
	1.2 M pyridine-toluene	428(62.3)	563(2.02)	602(0.88)
	Film	445	570	610
$ZnPyP_3P(4)$	CH_2Cl_2	419(55.6)	558(1.50)	604(0.55)
	Toluene	423(49.5)	552(1.81)	600(0.34)
	1.2 M pyridine-toluene	428(63.1)	562(2.12)	602(0.84)
	Film	444	568	610
ZnTPyP(2)	1.2 M pyridine-CH_2Cl_2[c]	428	560	599
	Film	437	571	616
ZnTPyP(3)	1.2 M pyridine-CH_2Cl_2	429	563	601
	Film	446	570	610
ZnTPyP(4)	1.2 M pyridine-CH_2Cl_2	428	561	600
	Film	445	568	608

a) Toluene containing 1.2 M pyridine. b) The values in parentheses are molar extinction coefficients ($\varepsilon/10^4$ M^{-1} cm^{-1}). c) Dichloromethane containing 1.2 M pyridine.

derivative spectra in the Q region of $ZnPyP_3P(2)$ in toluene. The absorption spectra indicated two isobestic points at 530 and 557 nm. The minima of second-derivative absorption spectra corresponded to the absorption peaks, and thus two absorption peaks were present in the $Q_{1,0}$ region of the toluene solution at relatively high temperature. The absorbances of the absorption peaks at 568 and 613 nm decreased with an increase in temperature, while that at 551 nm increased.

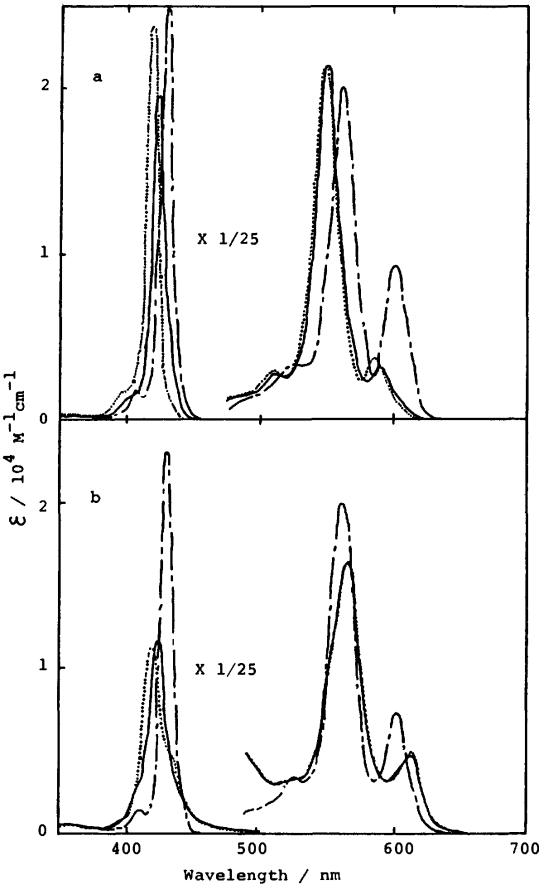

Fig. 2. Absorption spectra of ZnTPP(a) and $ZnPyP_3P(2)$(b) in toluene (——), CH_2Cl_2 (----), and toluene containing 1.2 M pyridine (-·-·-) at 25 °C.

The above results suggested that the pyridyl group in porphyrin coordinated to zinc in another porphyrin in nonbonding solvents such as toluene and CH_2Cl_2. However, the absorption spectra of $ZnPyP_3P(n)$ in toluene exhibited the temperature-dependence because the coordination bond between porphyrin molecules was relatively weak. Kirksey et al. demonstrated by means of ^1H NMR that the exchange between coordinated and uncoordinated pyridine was rapid in the solution of ZnTPP.[16] It was therefore presumed that the exchange between coordinated and uncoordinated $ZnPyP_3P(n)$ occurred in the toluene and CH_2Cl_2 solutions. Further, the dimer and monomer probably coexisted in the solution of $ZnPyP_3P(n)$ because the

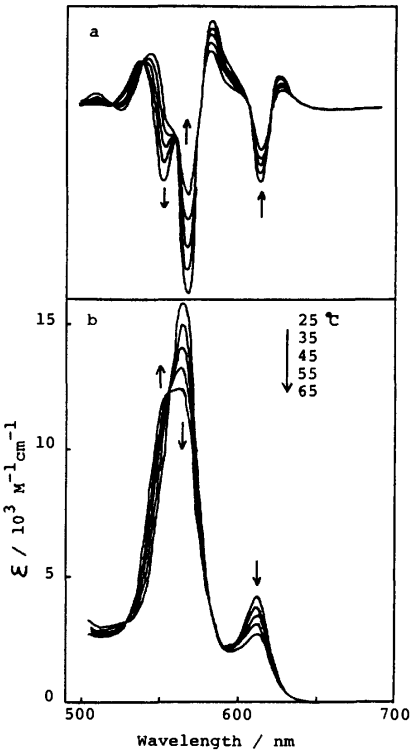

Fig. 3. Temperature-dependence of second-derivative(a) and absorption spectra(b) of $ZnPyP_3P(2)$ in toluene.

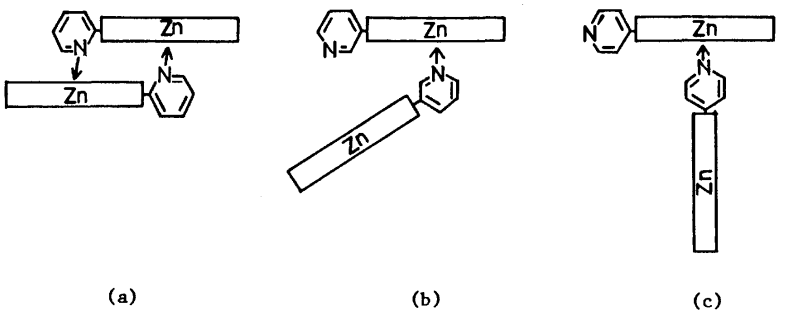

Fig. 4. Typical schematic dimer models of $ZnPyP_3P(2)$(a), $ZnPyP_3P(3)$(b) and $ZnPyP_3P(4)$(c).
□ Denotes porphyrin ring, and N→Z coordination between Zn and N (pyridyl group).

absorption spectra at different temperatures passed through isobestic points. On the other hand, the Soret band of $ZnPyP_3P(2)$ in toluene and CH_2Cl_2 was especially broad in comparison with those of $ZnPyP_3P(3)$ and $ZnPyP_3P(4)$. Figure 4 shows typical schematic dimer models of $ZnPyP_3P(n)$. The π-π interaction between porphyrin rings in a dimer of $ZnPyP_3P(2)$ was probably large because only $ZnPyP_3P(2)$ can form a dimer of the face-to-face type. Therefore, the Soret band of $ZnPyP_3P(2)$ was broadened considerably.

The Photoelectrochemical Properties of Zinc Porphyrin Films. The photovoltaic effect was observed with the film electrodes of zinc porphyrin derivatives in a quinhydrone aqueous solution. Figure 5 shows the dependence of the short circuit photocurrent on the film thickness. The film electrodes of $ZnPyP_3P(3)$ and $ZnPyP_3P(4)$ exhibited the maximum cathodic photocurrent at the film thickness of 70 nm (about -12 $\mu A\ cm^{-2}$), and above 70 nm the photocurrent slightly decreased with an increase in film thickness. The film electrodes of $ZnPyP_3P(2)$, ZnTPyP(2), and ZnTPP exhibited the maximum cathodic photocurrent at the film thickness of 40—80 nm (-3—-8 $\mu A cm^{-2}$), and then the photocurrent suddenly decreased with an increase in film thickness. On the other hand, the film electrodes of ZnTPyP(3) and ZnTPyP(4) generated the very small anodic photocurrent (about 1 $\mu A cm^{-2}$). The dependence of the photocurrent of $ZnPyP_3P(2)$ and ZnTPyP(2) on the film thickness was distinct from that of other structural isomers, but approximately similar to that of ZnTPP. The film electrodes were consequently classified into three groups, (a) $ZnPyP_3P(3)$ and $ZnPyP_3P(4)$, (b) $ZnPyP_3P(2)$, ZnTPP, and ZnTPyP(2), (c) ZnTPyP(3) and ZnTPyP(4). The film electrode of each group indicated the different dependence of photocurrent on the film thickness because porphyrin of each group in the solid film may be oriented in different pattern. The molecular arrangement for porphyrin in the solid film will be discussed later. Figure 6 shows the photocurrent-voltage curves of the film electrodes of $ZnPyP_3P(4)$ and ZnTPyP(3) in 0.01 M quinone and hydroquinone solutions containing 0.2 M KCl at pH 5. The cathodic photocurrent was observed with $ZnPyP_3P(4)$ below the electrode potential of 0.5—0.6 V vs. AgCl/Ag in the quinone solution, and also the small anodic and cathodic photocurrents were observed in the hydroquinone solution because of the increase of conductivity of a zinc porphyrin film under irradiation. The onset potential of cathodic photocurrent in the quinone solution was larger than the reduction potential of quinone. The film electrodes of groups (a) and (b) indicated similar photocurrent-voltage curves to $ZnPyP_3P(4)$. These film electrodes consequently behaved as p-type semiconductors. The very thin film electrode of ZnTPyP(3) exhibited the anodic photocurrent above the electrode potential of -0.05 V vs. AgCl/Ag in the hydroquinone solution, and also the film electrode of ZnTPyP(4) (group (c)) indicated a similar photocurrent-voltage curve to ZnTPyP(3). Thus the film electrodes of group (c) exhibited different photocurrent-voltage curves from those of groups

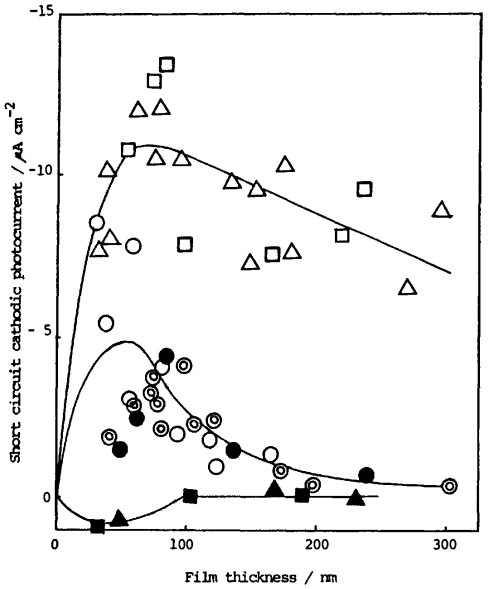

Fig. 5. Dependence of short circuit photocurrents of zinc porphyrins on film thickness in 0.01 M quinhydrone aqueous solution containing 0.2 M KCl at pH 5. A white light source was a 500 W xenon lamp.
◎: ZnTPP, ○: $ZnPyP_3P(2)$, □: $ZnPyP_3P(3)$, △: $ZnPyP_3P(4)$, ●: ZnTPyP(2), ■: ZnTPyP(3), ▲:, ZnTPyP(4).

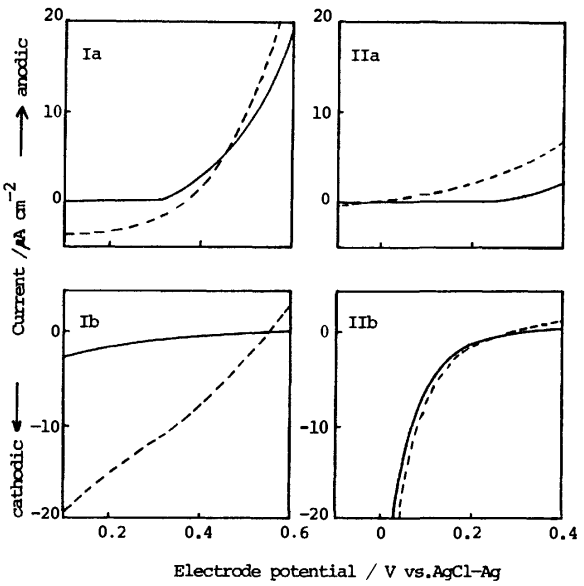

Fig. 6. Current-voltage curves of film electrodes of $ZnPyP_3P(4)$ (I, thickness 140 nm) and ZnTPyP(3) (II. thickness 30 nm) in 0.01 M hydroquinone(a) and quinone(b) aqueous solutions containing 0.2 M KCl at pH 5. A white light source was a 500 W xenon lamp.
——, in dark; ----, under irradiation.

(a) and (b). Figure 7 shows the short circuit photocurrent action spectrum of $ZnPyP_3P(4)$ film electrode in 0.01 M quinhydrone solution containing 0.2 M KCl at pH 5. The photocurrent was normalized in such a way that the incident light on the film electrode was constant (300 $\mu W\,cm^{-2}$). The photocurrent quantum yield of $ZnPyP_3P(4)$ was 0.16% at the irradiation wavelength of 440 nm. The action spectra were approximately the same as the absorption spectrum of the film. Therefore, the result suggested that the excited state of a zinc porphyrin molecule took part in the generation of the photocurrent.

The conductivities of $ZnPyP_3P(2)$, $ZnPyP_3P(3)$, and $ZnPyP_3P(4)$, which have only one pyridyl group in a molecule, were 8.3×10^{-11}, 6.6×10^{-10}, and 3.4×10^{-10} $S\,cm^{-1}$, respectively, and larger than that of ZnTPP (3×10^{-13} $S\,cm^{-1}$). On the other hand, the conductivities of ZnTPyP(n), which has four pyridyl groups in a molecule, were nearly equal to that of ZnTPP. The photoconductivity was observed with these films. The conductivities of zinc porphyrin films are summarized in Table 2. The pyridyl group in a porphyrin molecule was probably concerned with the molecular arrangement of porphyrin in the solid film because the conductivity was dependent on the number of the pyridyl group.

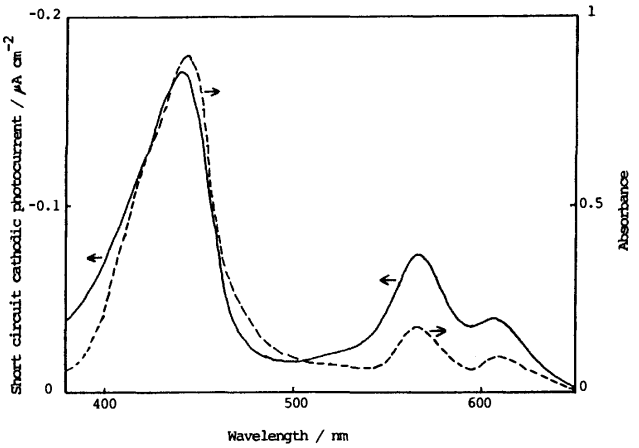

Fig. 7. Absorption(----) and photocurrent(——) action spectra of $ZnPyP_3P(4)$ film electrode (thickness 80 nm). An electrolytic solution was 0.01 M quinhydrone aqueous solution containing 0.2 MKCl at pH 5.

The photocurrent quantum yield of porphyrin film electrodes may be influenced by the following factors,[4] (i) the ease of charge carrier formation, (ii) packing of porphyrin molecules in the solid film, and (iii) the extent of π-π overlap between the porphyrin rings. The charge carrier may be easily formed with a decrease in the first ring oxidation potential of metalloporphyrins.[2-4] Table 3 summarizes the redox potentials of zinc porphyrin derivatives. ZnTPyP(n) was easily reduced but not oxidized in comparison with ZnTPP because of electron withdrawing of the pyridyl group in porphyrin. However, the redox potential of $ZnPyP_3P(n)$ was nearly equal to that of ZnTPP. Therefore, the difference of the photoelectrochemical properties of zinc porphyrin derivatives was not attributable to that of redox potentials. On the other hand, factors (ii) and (iii) presumably facilitated energy and electron transfers.[4]

The absorption peaks in the Q region of $ZnPyP_3P(n)$ and ZnTPyP(n) films were observed at longer wavelengths than that of a ZnTPP film (Table 1). The resonance Raman spectra were observed with zinc porphyrin films. We presumed that the signals in the range of 382 to 395 cm^{-1} were greatly ascribed to the stretching vibration of Zn-N (pyrole). The signals of $ZnPyP_3P(n)$ and ZnTPyP(n) were observed at lower wavenumbers than that of a ZnTPP film at 395 cm^{-1}

Table 2. Conductivities in the Dark (σ_d) and under Irradiation (σ_i)[a] of Zinc Porphyrin Films at Room Temperature

Porphyrin	σ_d/S cm^{-1}	σ_i/S cm^{-1}
ZnTPP	3×10^{-13}	9×10^{-12}
$ZnPyP_3P(2)$	8.3×10^{-11}	1.1×10^{-9}
$ZnPyP_3P(3)$	6.6×10^{-10}	5.3×10^{-9}
$ZnPyP_3P(4)$	3.4×10^{-10}	2.8×10^{-9}
ZnTPyP(2)	5×10^{-13}	1.5×10^{-11}
ZnTPyP(3)	8×10^{-13}	1.4×10^{-11}
ZnTPyP(4)	6×10^{-13}	4×10^{-12}

a) A white light source was a 500 W xenon lamp.

Table 3. Half-Wave Potentials of Zinc Porphyrins in DMF and Pyridine Solution Containing 0.1 M Et_4NClO_4 at Room Temperature

Porphyrin	Solvent	Reduction potential[a]/V		Oxidation potential[a]/V	
		2nd	1st	1st	2nd
ZnTPP	DMF	−2.15	−1.73	0.46	0.72[c]
$ZnPyP_3P(2)$	DMF	−2.14[b]	−1.71	0.50	0.75[c]
$ZnPyP_3P(3)$	DMF	−2.12	−1.68	0.54	0.77[c]
$ZnPyP_3(4)$	DMF	−2.08[b]	−1.67	0.53	0.79[c]
ZnTPyP(2)	Pyridine		−1.62	0.58[c]	
ZnTPyP(3)	Pyridine	−2.01[b]	−1.56	0.67[c]	
ZnTPyP(4)	Pyridine		−1.52	0.72[c]	

a) Measured against Ag/0.01 M $AgNO_3$ in acetonitrile. b) Cathodic-peak potential (irreversible reduction). c) Anodic-peak potential (irreversible oxidation).

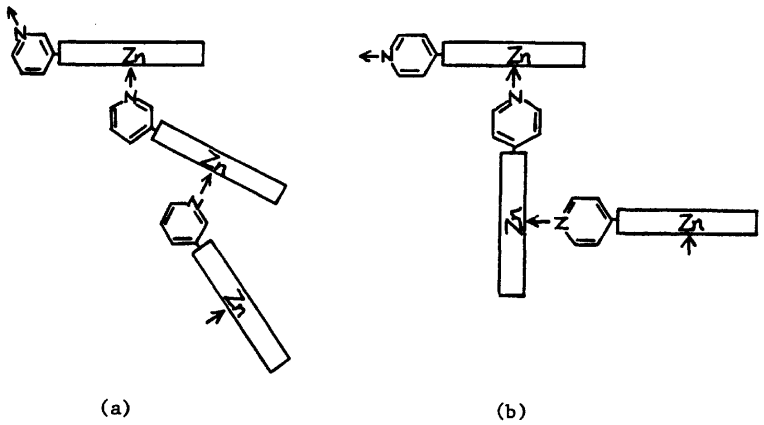

Fig. 8. Typical schematic models of molecular arrangement of $ZnPyP_3P(3)$ (a) and $ZnPyP_3P(4)$ (b) in a solid film.
▭ Denotes porphyrin ring, and N→Z coordination between Zn and N (pyridyl group).

(difference, 8—13 cm^{-1}). The results suggested that the pyridyl group in porphyrin coordinated to zinc in another porphyrin in the solid film as well as in the toluene and CH_2Cl_2 solutions. $ZnPyP_3P(3)$ and $ZnPyP_3P(4)$ can form linear polymers as shown in Fig. 8 because the porphyrins have only one pyridyl group in a molecule, but ZnTPyP(3) and ZnTPyP(4) can form cross-linked polymers because of four pyridyl groups in a molecule. A linear polymer in porphyrin film facilitated the energy and electron transfers, but a cross-linked polymer interfered these transfers. On the other hand, $ZnPyP_3P(2)$ and ZnTPyP(2) can not form a polymer because of dimer formation of the face-to-face type (Fig. 4) and/or the steric hindrance by the porphyrin ring although a oligomer can be formed. Therefore, the absorption peaks in the Soret region of $ZnPyP_3P(2)$ and ZnTPyP(2) films were observed at shorter wavelengths than those of other structural isomer films, and at the same wavelength as that of ZnTPP film (Table 1). The film electrodes of $ZnPyP_3P(2)$ and ZnTPyP(2) consequently exhibited the same photoelectrochemical properties as a ZnTPP film electrode.

References

1) K. Yamashita, Y. Harima, and Y. Matsumura, *Bull. Chem. Soc. Jpn.*, **58**, 1761 (1985).
2) F. J. Kampas, K. Yamashita, and J. Fajer, *Nature*, **40**, 284 (1980).
3) T. Katsu, K. Tamagake, and Y. Fujita, *Chem. Lett.*, **1980**, 289.
4) K. Yamashita, *Chem. Lett.*, **1982**, 1085.
5) K. Yamashita, Y. Harima, H. Kubota, and H. Suzuki, *Bull. Chem. Soc. Jpn.*, **60**, 803 (1987).
6) K. Yamashita, Y. Matsumura, Y. Harima, S. Miura, and H. Suzuki, *Chem. Lett.*, **1984**, 489.
7) T. Kawai, K. Tanimura, and T. Sakata, *Chem. Phys. Lett.*, **56**, 541 (1978).
8) H. Jimbo, H. Yoneyama, and H. Tamura, *Photochem. Photobiol.*, **32**, 319 (1980).
9) A. D. Adler, F. R. Longo, J. D. Finarelli, J. Goldmacher, J. Assour, and L. Korsakoff, *J. Org. Chem.*, **32**, 476 (1967).
10) R. G. Little, J. A. Anton, P. A. Loach, and J. A. Ibers, *J. Heterocycl. Chem.*, **12**, 343 (1975).
11) K. Kalyanasundaram, *Inorg. Chem.*, **23**, 2453 (1984).
12) G. H. Barnett, M. F. Hadson, and K. M. Smith, *J. Chem. Soc., Perkin Trans. 1*, **1975**, 1401.
13) A. D. Adler, F. R. Longo, F. Kampas, and J. Kim, *J. Inorg. Nucl. Chem.*, **32**, 2443 (1970).
14) E. E. Wegner and A. W. Adamson, *J. Am. Chem. Soc.*, **88**, 394 (1966).
15) J. R. Miller and G. D. Dorough, *J. Am. Chem. Soc.*, **74**, 3977 (1952).
16) C. H. Kirksey, P. Hambright, and C. B. Storm, *Inorg. Chem.*, **8**, 2141 (1969).

High-Resolution ^{13}C NMR Study of (1→3)-β-D-Glucans in the Solid State: DMSO-Induced Conformational Change and Conformational Characterization by Spin-Relaxation Measurements

Hazime SAITÔ* and Motoko YOKOI
Biophysics Division, National Cancer Center Research Institute, Tsukiji 5-chome, Chuo-ku, Tokyo 104
(Received August 17, 1988)

High-resolution ^{13}C NMR spectra of a variety of (1→3)-β-D-glucans were recorded in the solid state after lyophilization from DMSO solution in order to study resulting conformations free from the triple-helix conformation. Lyophilization from DMSO solution caused conformational change of laminaran from *Laminaria species* ($\overline{Dp}$=38) from the triple helix to the oligomer-type form (form I). On the contrary, single-chain conformation (form II) of high molecular-weight curdlan was unchanged before and after lyophilization from DMSO solution. Further, DMSO induced conformational change of both single-chain (form II) and triple-helical (form III) conformations of acid-degraded curdlan ($\overline{Dp}$=14) to the form I. These findings support our view that the single-chain conformation is a major form in curdlan powder. We found that these three forms are distinguished by either the ^{13}C spin-lattice relaxation times (T_1^C's) of the laboratory frame or proton spin-lattice relaxation times in the rotating frame ($T_{1\rho}^H$). In particular, the form I was distinguishable from others by its prolonged T_1^C values (3.5—12 s) of C-6 carbon. In addition, the $T_{1\rho}^H$ of the triple helix of annealed curdlan was one order of magnitude longer than that of the single chain, reflecting their difference in the manner of molecular packing.

Linear or branched (1→3)-β-D-glucans function as structural components in cell walls of plant cell or microorganism and also act as reserve polysaccharides.[1] Such function depends on secondary structure of polysaccharides, single or triple helix or others, which is strongly affected by a number of structural and physical parameters such as the degree of polymerization and/or of branching, the extent of annealing, etc. In this connection, it appears that conformational elucidation of these polysaccharides in the solid state is essential for better understanding in their function as well as solution properties. However, conformational characterization by X-ray diffraction is not feasible for noncrystalline samples which are in many instances important in relation to their solution/gel properties.

For this purpose, we have demonstrated that high-resolution solid-state ^{13}C NMR spectroscopy can be conveniently used as an alternative means for characterization of secondary structures of a number of molecular systems,[2-4] because this method is equally applied to noncrystalline as well as crystalline substances. In fact, we demonstrated that three types of conformations, form I (laminaripentaose or laminariheptaose), form II (curdlan-type) and form III (laminarn-type), are readily distinguishable for (1→3)-β-D-glucans in the solid, on the basis of the conformation-dependent displacements of ^{13}C chemical shifts (up to 8 ppm).[5-7] Most of samples adopting these conformations were obtained by lyophilization or spray-drying, except for the annealed curdlan. Nevertheless, we found that conformations of the forms I and II are not always completely disordered as anticipated, because the C-3 ^{13}C NMR peaks of these forms (δ 91.2±0.4 and 89.6±0.5 for the forms I and II, respectively) are significantly displaced downfield by 5—6 ppm as compared from those of disordered state achieved in aqueous solution (δ 84.5).[5] This finding is in contrast to the case of amorphous (1→4)-α-D-glucans whose C-1 peak is so broad and shows a remarkably large chemical shift range (δ 94—106). Further, the weighted average of amorphous C-1 shift is similar to the chemical shift in aqueous solution.[8] Accordingly, these forms should be considered as locally ordered conformations as judged by ^{13}C NMR spectroscopy, which is sensitive to change of the local conformations, although they are disordered as determined by X-ray diffraction.

In this connection, we previously proposed the existence of *single*-helix[9] conformation in (1→3)-β-D-glucans of higher molecular-weight (curdlan and pachyman) obtained by spray-drying or lyophilization,[5,6] although this form might not be always straightforwardly acceptable, as an energetically stable form on the basis of calculation of molecular mechanics.[10] It is easily recognized, however, that this sort of form could be isolated as anhydrous form as a result of lyophilization. The evaluation of relative proportion of such single chains is very important to clarify molecular architecture of their resulting gel networks and gelation mechanism.[11-16] Then, it is expected that single-stranded chains can be obtained if (1→3)-β-D-glucans dissolved in DMSO solution are lyophilized, because DMSO molecules tend to disperse the triple-helical chains into single chains and to yield conformations free from the triple-helix form. As a result, direct evidence as to the existence of the single chain is available by means of the conformation-dependent ^{13}C chemical shifts.

In the present article, we aimed to study conformational change of various types of (1→3)-β-D-glucans lyophilized from DMSO solution. In addition, we measured ^{13}C spin-lattice relaxation times in the laboratory frame (T_1^C's)[17] and proton spin-lattice relaxation time in the rotating frame ($T_{1\rho}^H$'s)[18] to gain

information as to dynamic features of these three kinds of conformations.

Experimental

Curdlan powder ($\overline{Dp}$=540) was provided by Takeda Chemical Industries, Osaka, Japan. Laminaran from *Laminaria species* ($\overline{Dp}$=38) was purchased from Nutritional Biochemistry Corporation, Ohio, USA. Laminaran from *Eisenia araborea* was purchased from Nakarai Chemical Industry, Kyoto, Japan (Lot. No. M6G2275). Preparation of acid-degraded curdlan, $\overline{Dp}$=14, was described in our previous paper.[5] Laminaripentaose and laminariheptaose were purchased from Seikagaku Kogyo, Tokyo (Lot No. 407191). Lentinan and HA-β-glucan, branched (1→3)-β-D-glucans,[5] were generous gift from Dr. G. Chihara and Dr. Y. Yoshioka of this Institute, respectively. Lyophilized solid samples from DMSO solution were prepared by dissolving the glucans in DMSO or DMSO-d_6, followed by lyophilization in vacuo.

High-resolution ^{13}C NMR spectra in the solid state were recorded on a Bruker CXP-300 spectrometer by means of cross polarization-magic angle spinning (CP-MAS) method. Samples were contained in a ceramic rotor used for the double air-bearing type MAS system and spun as fast as 3—3.5 kHz. The duration of 90° pulse was 4 μs. The contact, sampling and repetition times were 1 ms, 20—30 ms, and 4 s, respectively. The ^{13}C chemical shifts were referred to TMS through the peak position of the glycine carboxyl group (δ 176.0).

The ^{13}C spin-lattice relaxation times were measured by the method of cross polarization enhancement, with an inversion of proton-spin temperature.[17] The peak intensity $M_{net}(t)$ at the delay time t after turning off the ^{13}C H_1 field decays exponentially from its initial value, $2M_{cp}(0)$ as shown by Eq. 1,

$$M_{net}(t)=2M_{cp}(0)\exp(-t/T_1^C) \quad (1)$$

Thus, the T_1^C values were obtained by a semilog plot of the peak-intensity against the delay time t. Carbon-resolved proton spin-lattice relaxation times in the rotating frame ($T_{1\rho}^H$'s) were obtained from the exponential decrease in ^{13}C NMR peak-intensity of longer contact time.[18] Namely, the ^{13}C peak-intensity $M(t)$ is given by

$$M(t)\approx M_0\exp(-t/T_{1\rho}^H)/(1-T_{CH}/T_{1\rho}^H) \quad (2)$$

where M_0 and T_{CH} stand for the maximum peak-intensity and cross polarization relaxation time, respectively. Thus, we obtained the $T_{1\rho}^H$ values from a semilog plot of $M(t)$ vs. t.

The proton spin-lattice relaxation times of the laboratory frame (T_1^H's) were measured by the pulse sequence via ^{13}C CP-MAS, in which 180° pulse and variable delay time were inserted prior to standard cross polarization.[19] So, the T_1^H values were obtained by a semilog plot of ^{13}C NMR intensity vs. t, as in a similar manner to the inversion-recovery measurement in liquid state.

Results

Figure 1 shows that the C-3 ^{13}C NMR peak of laminaran from *Laminaria species* lyophilized from DMSO solution (δ 90.8) (Fig. 1B) is displaced downfield by 3.9 ppm from that of untreated sample[6] (δ 86.9; form III, triple helix) (Fig. 1A). These ^{13}C chemical shifts of (1→3)-β-D-glucans in the solid state were assigned on the basis of the data recorded in DMSO-d_6 solution, as summarized in Table 1. The relative peak-positions

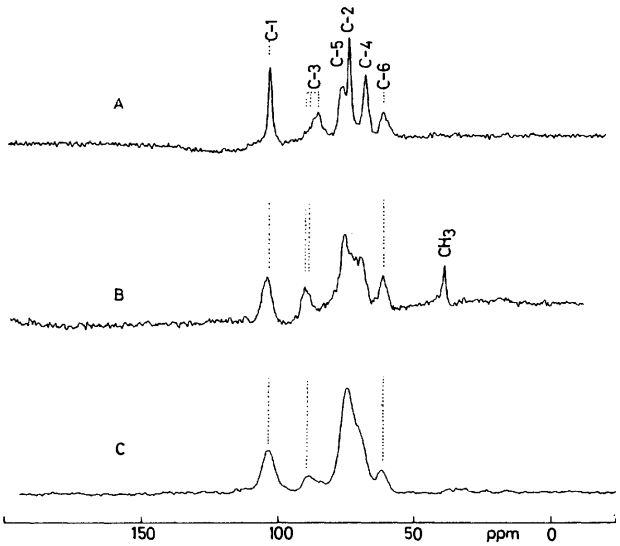

Fig. 1. ^{13}C NMR spectra of laminarans taking different conformations in the solid state.
(A) laminaran ($\overline{Dp}$=38) from *Laminaria species* (from Ref. 6), (B) laminaran ($\overline{Dp}$=38); lyophilized from DMSO solution, and (C) laminaran from *Eisenia araborea*.

Table 1. ^{13}C Chemical Shifts of (1→3)-β-D-Glucans in Various Conformations (ppm from TMS)[a]

	Form I (oligomer-type)			Form II (single chain)		Form III (triple helix)		DMSO
	Laminari-heptaose	Curdlan ($\overline{Dp}$ 14) from DMSO	Laminaran from DMSO	Curdlan from DMSO	Curdlan powder[b]	Annealed curdlan[b]	Laminaran[b]	soln.
C-1	104.0	103.8	104.7	103.8	104.1	103.7	103.4	103.7
C-2	72.9	72.4	c	71.1[d,e]	74.0[d,e]	74.3	74.3	73.8
C-3	91.3	90.7	90.8	89.1	89.7	87.1	86.9	87.0
C-4	69.7	69.1	71.0	67.1	69.3	68.6	68.4	69.3
C-5	76.4	76.1	75.7	75.0[d]	76.1[d]	78.0	76.7	77.0
C-6	61.5	61.8	62.1	61.0	62.3	62.2	62.1	61.8
CH_3	—	38.9	39.9	39.5	—	—	—	39.6

a) Estimated error ±0.3 ppm. b) Data taken from Ref. 6. c) Not well resolved from the C-5 peak.
d) Assignment reversible. e) Estimated error ±1.5 ppm.

of the C-5 and C-2 carbons in the form III were previously confirmed by measurements of the ^{13}C spin-lattice relaxation times of the laboratory frame,[6] although these are obscured in the form II due to overlap of peaks. The C-3 NMR peak-position of laminaran lyophilized from DMSO solution is very close to that of the form II (single-chain conformation; δ 89.6±0.5[5]) but is resonated slightly at a low-field position (90.8 ppm), corresponding to that of the form I[5,6] (δ 91.2±0.4) (Table 1). In contrast to the above-mentioned water-soluble species, the ^{13}C NMR peak-positions of water-insoluble laminaran from *Eisenia araborea* (Fig. 1C) are similar to those of curdlan powder (form II; Fig. 2B), although the individual peaks of the former were considerably broadened as compared with those of the latter, reflecting the enhancd extent of disorder. Figure 2 illustrates the ^{13}C NMR spectra of curdlan and its acid-degraded fraction ($\overline{Dp}$=14) lyophilized from DMSO solution, together with those of annealed curdlan (at 180°) and curdlan powder as reported previously.[5,6] Again, the ^{13}C NMR spectrum of acid-degraded fraction ($\overline{Dp}$=14) lyophilized from DMSO solution is found to be very similar to that of laminaripentaose or laminariheptaose (form I), as judged from the C-3 peak-positions and the splitting pattern of the C-5, C-2, and C-4 peaks (Fig. 2D and 2E). However, the ^{13}C NMR pattern of curdlan powder (high molecular-weight) is unchanged

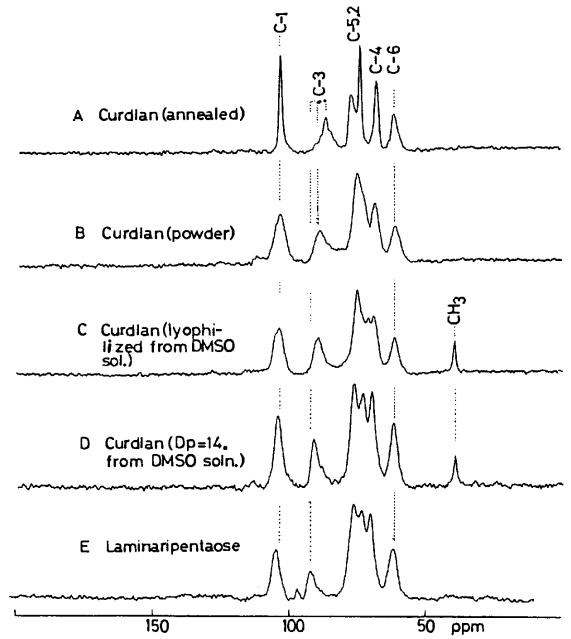

Fig. 2. ^{13}C NMR spectra of a variety of (1→3)-β-D-glucans in the solid state. (A) Annealed curdlan at 180° (Ref. 6), (B) curdlan powder (Ref. 6), (C) curdlan lyophilized from DMSO solution, (D) acid-degraded curdlan ($\overline{Dp}$=14) lyophilized from DMSO solution, and (E) laminaripentaose.

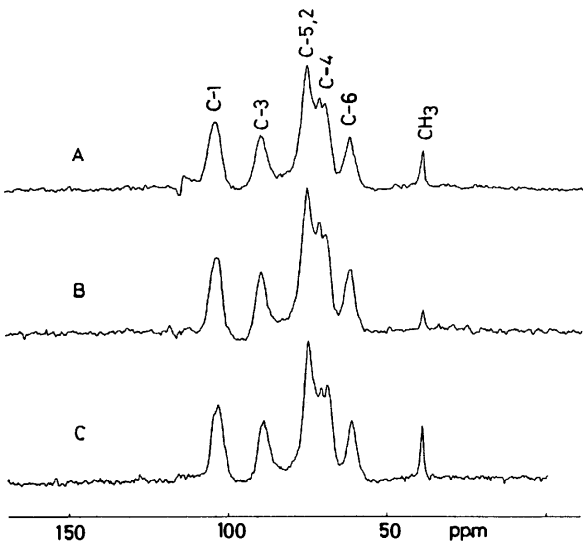

Fig. 3. ^{13}C NMR of curdlan lyophilized from DMSO-d_6 solution (A and B) and from DMSO solution (C). Contact time; 2 ms for A, 1 ms for B and C.

Table 2. DMSO-Induced Conformational Change of (1→3)-β-D-Glucans[a]

	$\overline{Dp}$	Conformation before and after DMSO treatment	
		Before[b]	After
Curdlan	540	Single chain (90%) + Triple helix (10%)	Single chain
Laminaran	38	Triple helix	Single chain
Curdlan	14	Single chain (60%) + Triple helix (40%)	Form I

a) Conformations based on the displacement of the C-3 ^{13}C chemical shifts. b) Data taken from Refs. 5 and 6.

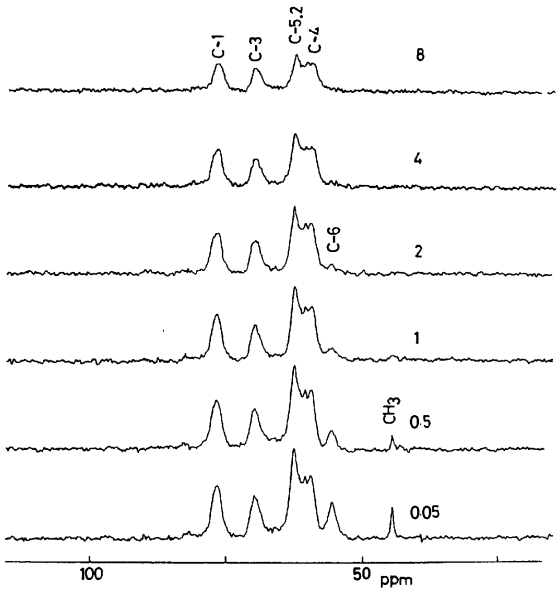

Fig. 4. Stacked plot of ^{13}C NMR peak-intensities of curdlan lyophilized from DMSO, obtained by cross polarization for the T_1^C measurements. Delay times (s) are given in the right-hand side.

before and after lyophilization from DMSO solution (form II, Figs. 2B and 2C). Obviously, the ^{13}C NMR pattern of the triple-helix (form III) is readily distinguishable from those of the forms I and II. The DMSO-induced conformational change of (1→3)-β-D-glucans as described above was summarized in Table 2.

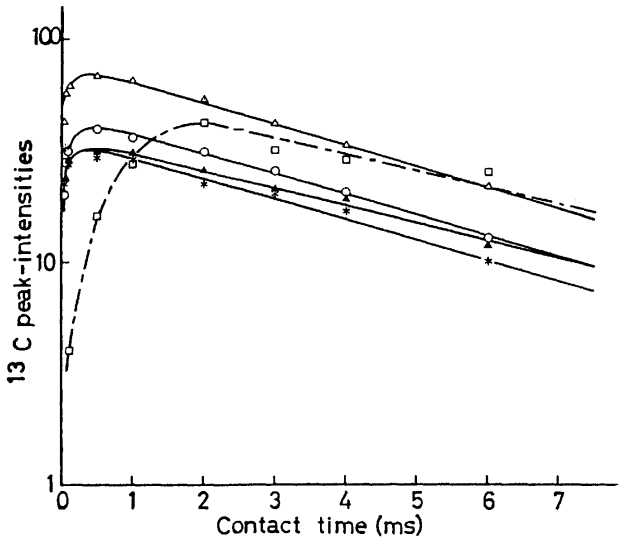

Fig. 5. Plot of the ^{13}C peak-intensities of curdlan lyophilized from DMSO against the contact time: (○) C-1; (*) C-3; (△) C-5,2; (●) C-6; (□) CH_3

As demonstrated in Fig. 3, the methyl ^{13}C NMR signal of perdeuterated DMSO is clearly visible (with approximate 30% peak-intensity as compared with that of protonated DMSO: see Figs. 3B and C) in spite of the absence of nearby protons. The peak-intensity of the methyl signal is enhanced by increasing the contact time from 1 ms to 2 ms (Fig. 3A). Figure 4 illustrates a typical stacked plot of the ^{13}C NMR spectra of curdlan lyophilized from DMSO solution for measurements of the ^{13}C spin-lattice relaxation times. It is evident from Fig. 4 that the methyl, C-6 and other ^{13}C signals decay with different time constant. The T_1^C values based on these stacked plots were summarized in Table 3.

Figure 5 illustrates a typical plot of the ^{13}C peak-intensity vs. the contact time for curdlan lyophilized from DMSO solution. The maximum peak-intensity of curdlan polymer was achieved at the contact time of 500 μs, whereas the maximum peak of DMSO was at 2 ms. Carbon-resolved $T_{1\rho}^H$ and T_1^H values were summarized in Table 4.

Discussion

Conformation of (1→3)-β-D-Glucans Lyophilized from DMSO Solution. Linear (1→3)-β-D-glucans are not soluble in aqueous media when the degree of polymerization ($\overline{Dp}$) is larger than 14.[20] This is a

Table 3. ^{13}C Spin-Lattice Relaxation Times (T_1^C's) in the Laboratory Frame of (1→3)-β-D-Glucans in the Solid State (s)

	Form I (oligomer-type)			Form II(single chain)		Form III (triple helix)
	Oligomers			Curdlan		Annealed curdlan[c]
	n=5	n=6	$\bar{n}$=14[b]	Powder[c]	from DMSO soln.	
C-1	32	17	22	14	15	16
C-2	25[a]	11[a]	15[a]	10	11	18
C-3	38	15	29	11	16	16
C-4	34	17	22	7.8	10	8.2
C-5	30[a]	14[a]	15[a]	10	9.7	9.3
C-6	12	3.5	4.2	1.0	1.6	1.2
CH_3 (DMSO)	—	—	0.6	—	0.4	—

a) Interchangeable. b) Lyophilized from DMSO solution. c) Data taken from Ref. 6.

Table 4. Proton Spin-Lattice Relaxation Times in the Laboratory (T_1^H's) and Rotating Frame ($T_{1\rho}^H$'s)

	Single chain (form II)				Triple helix (form III)		
	Curdlan from DMSO		Curdlan powder	Lentinan powder	Annealed curdlan		HA-β-gluca
	$T_{1\rho}^H$/ms	T_1^H/s	$T_{1\rho}^H$/ms	$T_{1\rho}^H$/ms	$T_{1\rho}^H$/ms	T_1^H/s	$T_{1\rho}^H$/ms
H-1	4.9	0.34	3.9	4.7	31	0.51	7.2
H-2	4.8[a]	0.34	3.3	4.4	34	0.51	8.4
H-3	4.8	0.31	4.3	4.5	29	0.48	7.8
H-4	4.8	0.33	4.5	4.4	31	0.52	7.7
H-5	5.7[a]	0.34	3.3	4.4	36	0.62	8.4
H-6	5.6	0.30	4.8	5.7	37	0.48	8.2
$(CH_3)_2SO$	6.6	0.28	—	—	—	—	—

a) Assignment interchangeable.

consequence of adopting regular secondary structure which causes aggregation of polymer chains in aqueous media. In particular, we previously showed that (1→3)-β-D-glucans with $\overline{Dp}$=14—131 take considerable fraction of the triple helix conformation (ca. 40%).[5] On the contrary, relative fraction of the triple helix is reduced to less than 10%[5] for the glucans with $\overline{Dp}$ larger than ca. 200, which possess gel-formig ability.[20] Branched glucans such as lentinan and schizophyllan, on the other hand, form soft gel when the glucans of higher concentration are dissolved in aqueous media.[21] In any cases, ^{13}C NMR peak-intensity of these gel samples is suppressed partially or completely,[21] depending on the extent of polymer chains participated in formation of the triple helix.

On the other hand, full peak-area is observed in DMSO solution due to complete disruption of the triple-helix conformation.[22] As a result, the high-field shoulder or peak at δ 87.0 arising from the triple-helix coformation (form III) (approximately 10, 40, and 100% contribution for curdlan, acid-degraded fraction ($\overline{Dp}$=14), and laminaran, respectively) disappeared almost completely for preparations lyophilized from DMSO solution. In fact, (1→3)-β-D-glucans take effectively disordered conformation in DMSO solution, as substantiated from the displacement of peaks as well as relaxation parameters.[22] This view was also supported by the data of light scattering, viscosity and refractometry as applied to DMSO solution of schizophyllan, a branched glucan.[23,24]

Nevertheless, it is interesting to note that the lyophilized samples from DMSO solution do not necessarily take completly disordered conformation but adopt local regular secondary forms, either the forms I or II, depending on their chain-lengths, as judged from the peak-position of the C-3 signal which exhibits conformation-dependent displacement (see Figs. 1 and 2).[3-7] In general, lyophilization results in retaining ordered solution conformation in the solid state, if solvent molecules do not play dominant role to adopt ordered conformation in solution, as demonstrated previously for a number of sequential polypeptides and silk fibroin.[25,26] On the contrary, the present finding indicates that rather regular secondary structure (at least as viewed as a local conformation) is formed during the course of freezing followed by lyophilization, even if solution conformation is completely disordered as in DMSO solution. This situation is not unexpected, because conformational freezing around the minimum conformational energy could occur during the freezing step of lyophilization. Similar result was obtained for formation of silk I-like form by lyophilization from disordered aqueous fibroin solution (unpublished). As summarized in Table 2, achieved conformations differ as in the single chain or form I, depending on $\overline{Dp}$ of the glucans. It is emphasized that the latter form is also single-stranded by taking the condition for formation into account. In any cases, the present result demonstrates that DMSO causes conformational change of (1→3)-β-D-glucans from the triple helix to the form I or form II (single chain) These findings clearly support our view about the existence of the single chains in gel-forming linear glucans such as curdlan. On the contrary, the reverse conformational change from the single chain to triple helix is associated with hydration or hydration/annealing of samples, as illustrated schematically in Fig. 6. In other word, it is seen that the present conformational transitions are mainly caused by either hydration or dehydration process.

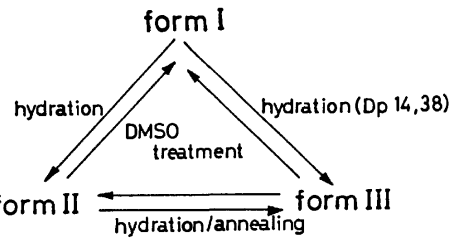

Fig. 6. Schematic representation of conformational changes.

It is interesting that DMSO molecules are always present in lyophilized samples from DMSO solution (less than 1/2 DMSO molecules per single residue), as seen by the methyl ^{13}C NMR signal from DMSO (Figs. 1—3). This is again true for the ^{13}C NMR peak of DMSO-d_6, in spite of the absence of nearby proton. This means that build-up of the DMSO signal is caused by intermolecular cross-polarization with protons from the glucan due to short proton-carbon distance (the order of 10 Å or less).[27]

Conformational Characterization by Spin-Lattice Relaxation Times. As pointed out previously, noncrystalline samples characterized by X-ray diffraction are not necessarily motionally disordered, because there appears no distinction of the ^{13}C T_1 values between curdlan powder and annealed curdlan[6] (see Table 3). In many instances, it appears that the presence of methyl or hydroxymethyl groups, undergoing rapid reorientational motions with correlation time at the order of 10^{-8} s, strongly affects the spin-lattice relaxation times of nearby carbons due to dipolar coupling, instead of slow overall motions ineffective to the T_1 process of the laboratory frame.[6,28-30] In fact, very long T_1^C values (50—800 s) were reported for highly crystalline cellulose samples where there exists no rapid reorientation in the C-6 hydroxymethyl groups.[31,32] Thus, the T_1^C values of the C-4 and C-5 carbons in the single-chain (form II) and triple-helical (form III) conformations are appreciably shortened by the dipolar couplings to the C-6 hydroxymethyl protons undergoing rapid internal rotation (Table 3),[6] since the extent of the dipolar couplings is proportional to r^{-6} where r is the interatomic distance. On the contrary, the corresponding C-6 T_1^C values in the oligomer-type form (form I) (3.5—12 s) are much

longer than those (1.0—1.6 s) of the above-mentioned polymers adopting the forms II and III. Therefore, the T_1^C values of the oligomers are generally longer than those of the polymer samples. For this, it is tempted to explain that this is simply caused by difference in molecular packing. However, these two types of samples were not obtained by crystallization but by lyophilization. Thus, it is reasonable to assume that conformation of the olilgomer-type (form I) is altered, especially at the site of C-6 hydroxymethyl group, from the single-chain conformation. In this connection, it is worthwhile to take into account the plausible conformational diversity at C-6 as viewed from the C-6 ^{13}C chemical shifts which are sensitive to C-6 conformation (i.e. tg, gt, or gg).[33,34] No such differences, however, are found for the spectra and therefore there is no evidence for conformational diversity at C-6. Thus, the longer T_1^C values for the oligomers may reflect a closer-packed, more immobile local structure.

Interestingly, very short ^{13}C spin-lattice relaxation times (0.4—0.6 s) arose from the methyl carbons of DMSO molecules which undergo rapid rotational reorientation in the solid state (Table 3). It is rather surprising to note, however, that the presence of such rapid motion of the methyl groups in DMSO is not effective for shortening of the T_1^C's of nearby carbons from the glucans as a fast relaxation center for dipolar couplings. In fact, there appear no significant differences in the T_1^C values between samples with and without DMSO. The most probable explanation is that DMSO molecules are not closely located at a short (2—3 Å) distance to any of carbons in the glucans, as an effective center for further shortening of the T_1^C values, even if they are bound to either the hydroxyl groups at the C-2, C-4, or C-5 carbons.

In contrast, only averaged values are observed for both proton spin-lattice relaxation times in the laboratory and rotational frame due to efficient spin diffusion[35] (Table 4). The $T_{1\rho}^H$ values of the single-chain (1→3)-β-D-glucans are almost the same among three kinds of glucans (4—5 ms), irrespective of differences in the primary structures. However, the $T_{1\rho}^H$'s of triple-helical annealed curdlan are almost one order of magnitude longer than those of the single-chain conformation. In the case of a branched glucan adopting the triple helix (HA-β-glucan), the $T_{1\rho}^H$ values are not substantially prolonged as in the annealed curdlan but are still prolonged as compared with those of the single-chain glucans (Table 4). Such distinction seems to be accounted for by differences in molecular packing: the latter molecules are not crystalline but lyophilized. In general, the T_1^H's are sensitive to spatially dependent proton-proton spin diffusion as well as spectral density of ^1H dipolar modulation. In this connection, it appears that the above-mentioned difference between the triple and single helix is a consequence of differential motional state rather than spin-diffusion process.

Conclusion

We have shown that (1→3)-β-D-glucans lyophilized from DMSO solution undergo substantial conformational change from the triple helix to single-chain or oligomer-type form, depending on their chain lengths. The present finding supports our view about the existence of the single chains in gel-forming high molecular-weight (1→3)-β-D-glucans. Further, we found that three types of conformations are distinguishable by either ^{13}C spin-lattice relaxation times in the laboratory frame or proton spin-lattice relaxation times in the rotating frame.

The authors are grateful to Drs. Goro Chihara and Yûko Yoshioka for their generous gift of lentinan and HA-β-glucan, respectively.

References

1) J. J. Marshall, *Adv. Carbohydr. Chem. Biochem.*, **30**, 257 (1974).

2) H. Saitô, R. Tabeta, A. Shoji, T. Ozaki, I. Ando, and T. Asakura, "Magnetic Resonance in Biology and Medicine," ed by G. Govil and C.L. Kheterapal, and A. Saran, Tata McGraw-Hill, New Delhi (1985), pp. 195—215.

3) H. Saitô, *Magn. Reson. Chem.*, **24**, 835 (1986).

4) H. Saitô and I. Ando, *Ann. Rep. NMR Spectrosc.*, **21**, 209 (1989).

5) H.Saitô, R. Tabeta, T. Sasaki, and Y. Yoshioka, *Bull. Chem. Soc. Jpn.*, **59**, 2093 (1986).

6) H. Saitô, R. Tabeta, M. Yokoi, and T. Erata, *Bull. Chem. Soc. Jpn.*, **60**, 4259 (1987).

7) H. Saitô, R. Tabeta, Y. Yoshioka, C. Hara, T. Kiho, and S. Ukai, *Bull. Chem. Soc. Jpn.*, **60**, 4267 (1987).

8) M. J. Gidley and S. M. Bociek, *J. Am. Chem. Soc.*, **110**, 3820 (1988).

9) In our previous series of papers,[5-7] form II conformation was ascribed to the "single helix" form based on the similarity of peak positions between the powder and gel sample. However, we found on the basis of ^{13}C NMR data that the single-helix conformation as seen in the gel state is the same as that of the "swollen form" (A. J. Stipanovic and P. J. Giammatteo, "Industrial Polysaccharides: Genetic Engineering, Structure/Property Relations and Applications," ed by M. Yalpani, Elsevier, Amsterdam, (1987), p. 281), rather than the form II (to be published). For this reason, it is more appropriate to ascribe the form II to "single chain" form.

10) R. H. Marchessault and Y. Deslandes, *Carbohydr. Res.*, **75**, 231 (1979).

11) H. Saitô, "Solution Properties of Polysaccharides," ed. by D. A. Brant, ACS Symp. Ser. No. 150, pp. 125—147 (1981).

12) H. Saitô, T. Ohki, and T. Sasaki, *Biochemistry*, **16**, 908 (1977).

13) H. Saitô, E. Miyata, and T. Sasaki, *Macromolecules*, **11**, 1244 (1978).

14) N. Kasai and T. Harada, "Fiber Diffraction Methods," ed. by A. D. French and K. H. Gardner, ACS Symp. Ser. No. 141, pp. 363—383 (1980).

15) W. S. Fulton and E. T. Atkins, "Fiber Diffraction Methods," ed. by A. D. French and K. H. Gardner, ACS Symp. Ser. No. 141, pp. 385—410 (1980).
16) It was shown that intense ^{13}CNMR signals are visible (70—80%) in curdlan gel at the temperature of swelling (54 °C; translucent low set gel) by conventional high-resolution spectrometer (Ref. 11). The conformation of such a portion is not a random coil but an ordered form (single helix) with increased flexibilty of chains as viewed from the significant displacements of the C-3 signals from those of aqueous solution and condition of acquisition of spectra, in contrast to the cases of a variety of gels formed by chemically cross-linked synthetic polymers. This means that major conformation of starting curdlan powder is not the triple-helical but single-chain form (form II), in contrast to the expectation based on the previous X-ray diffraction studies (Refs. 10 and 15). In fact, conversion from the single to triple helix is at most 50%, even if annealing of the gel sample is made at 150—180° and resulting samples were cooled rapidly (Ref. 6).
17) D. A. Torchia, *J. Magn. Reson.*, **30**, 613 (1978).
18) E. O. Stejskal, J. Schaefer, M. D. Sefcik, and R. A. McKay, *Macromolecules*, **14**, 275 (1981).
19) M. J. Sullivan and G. E. Maciel, *Anal. Chem.*, **52**, 1615 (1982).
20) H. Saitô, E. Miyata, and T. Sasaki, *Macromolecules*, **11**, 1244 (1978).
21) H. Saitô, T. Ohki, and T. Sasaki, *Carbohydr. Res.*, **74**, 227 (1979).
22) H. Saitô, T. Ohki, and T. Sasaki, *Biochemistry*, **16**, 908 (1977).
23) Y. Kashiwagi, T. Norisuye, and H. Fujita, *Macromolecules*, **14**, 1220 (1981).
24) T. Sato, T. Norisuye, and H. Fujita, *Macromolecules*, **16**, 185 (1983)
25) H. Saitô, R. Tabeta, T. Asakura, Y. Iwanaga, A. Shoji, T. Ozaki, and I. Ando, *Macromolecules*, **17**, 1405 (1984).
26) H. Saitô, R. Tabeta, A. Shoji, T. Ozaki, T. Ando, and T. Miyata, *Biopolymers*, **23**, 2279 (1984).
27) J. Schaefer, M. D. Sefcik, E. O. Stejskal, and R. A. McKay, *Macromolecules*, **14**, 188 (1981).
28) H. Saitô and R. Tabeta, "Peptide Chemistry 1987," ed by T. Shiba and S. Sakakibara, Protein Research Foundation, Osaka, pp. 53—58 (1988).
29) A. Naito, S. Ganapathy, K. Akasaka, and C. A. McDowell, *J. Magn. Reson.*, **54**, 235 (1983).
30) R. Teeaar and E. Lippmaa, *Polym. Bull.*, **12**, 315 (1984).
31) F. Horii, A. Hirai, and R. Kitamaru, *J. Carbohydr. Chem.*, **3**, 641 (1984).
32) D. L. VanderHart, *J. Magn. Reson.*, **72**, 13 (1987).
33) H. Saitô, G. Izumi, T. Mamizuka, S. Suzuki, and R. Tabeta, *J. Chem. Soc., Chem. Commun.*, **1982**, 1386.
34) F. Horii, A. Hirai, and R. Kitamaru, *Polym. Bull.*, **10**, 357 (1983).
35) A. Abragam, "The Principle of Nuclear Magnetism," Claredon Press, Oxford(1963), Chap. V.

 © 1989 The Chemical Society of Japan Bull. Chem. Soc. Jpn., 62, 399—402 (1989)

^{1}H and ^{79}Br NMR in 1,4-Didecyl-1,4-diazoniabicyclo[2.2.2]octane Dibromide and Diiodide

Hirokazu NAKAYAMA,† Taro EGUCHI,† Nobuo NAKAMURA, Hideaki CHIHARA,* Takashi NOGAMI,††
Kengo IMAMURA,†† and Yasuhiko SHIROTA††
Department of Chemistry, Faculty of Science, Osaka University, Toyonaka, Osaka 560
†Institute of Chemistry, College of General Education, Osaka University, Toyonaka, Osaka 560
††Department of Applied Chemistry, Faculty of Engineering, Osaka University, Yamada-oka, Suita, Osaka 565
(Received August 25,1988)

Temperature dependence of ^{1}H NMR spin-lattice relaxation time was measured in solid 1,4-didecyl-1,4-diazoniabicyclo[2.2.2]octane dibromide and diiodide (C_{10}-DABCO-C_{10}-Br_2 and C_{10}-DABCO-C_{10}-I_2). ^{79}Br NMR spin-lattice relaxation time and chemical shift measurements in the high-temperature phase were also performed in C_{10}-DABCO-C_{10}-Br_2. It was found that the cation rotates isotropically, while the anion diffuses at a correlation time of ca. 10^{-8} s in the high-temperature phase of C_{10}-DABCO-C_{10}-Br_2. The activation energies for these modes are 30 and 34 kJ mol^{-1}, respectively. Methyl reorientation is activated in the low-temperature phase (E_a=11.8 kJ mol^{-1} in C_{10}-DABCO-C_{10}-Br_2 and E_a=12.0 kJ mol^{-1} in C_{10}-DABCO-C_{10}-I_2). Near the phase-transition temperature some motion of decyl chain is observed (E_a=57 kJ mol^{-1} in C_{10}-DABCO-C_{10}-Br_2 and E_a=35.5 kJ mol^{-1} in C_{10}-DABCO-C_{10}-I_2).

A series of symmetric bis(quaternary alkyl halide) salts of 1,4-diazabicyclo[2.2.2]octanes (DABCO) exhibit first order solid-solid phase transitions above room temperature.[1,2] For these compounds the halide anion conductivities in the high-temperature phases are higher than those in the room-temperature phases by two or three orders of magnitude.[1,2] This characteristic phase transition has been studied extensively by DSC, IR, and powder X-ray diffraction.[1,2] It was revealed that the longer the alkyl chain, the higher the transition temperature becomes in both bromide and iodide salts. If the carbon number of alkyl groups is the same, the transition temperature rises in the order of chloride, bromide, and iodide. Temperature dependence of the IR spectra shows abrupt disappearance of the band progressions[1] above the transition temperatures. These results indicate that the phase transition is accompanied by a conformational change of the alkyl chains. In the case of the unsymmetric bis(quaternary alkyl halide) salts of 1,4-diazabicyclo[2.2.2]octanes, similar phase transitions have been observed.[3,4]

The conductivities of these compounds are of the order of 10^{-5} $(\Omega\,cm)^{-1}$ in the high-temperature phases, being considerably low compared with typical superionic conductors in which conductivities of the order of 10^{-1} to 10^{-3} $(\Omega\,cm)^{-1}$ have been observed. However, they possess the characteristic feature which is not seen in the other ionic conductors, i.e., the conductivity as well as the transition temperature to the conductive phase can be controlled by changing the length and the assortment of side alkyl chains. Therefore, the compounds of DABCO series are potential candidates of new type of electrical conductors which possess highly controllable characteristics. The extensive works on this series will thus open a new area of the molecular design.

Althougth we have been engaged in a number of experimental work as mentioned above, the microscopic mechanisms of the phase transitions and of the high electrical conduction in the high-temperature phases of DABCO series compounds have not yet been clarified. In order to shed light upon these points, we conducted measurements of ^{1}H NMR spin-lattice relaxation times in 1,4-didecyl-1,4-diazoniabicyclo-[2.2.2]octane dibromide (C_{10}-DABCO-C_{10}-Br_2) and 1,4-didecyl-1,4-diazoniabicyclo[2.2.2]octane diiodide (C_{10}-DABCO-C_{10}-I_2), and ^{79}Br NMR spin-lattice relaxation times and chemical shift in C_{10}-DABCO-C_{10}-Br_2.

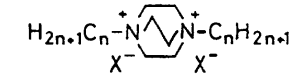

C_n-DABCO-C_n-X_2(X=Br, I)

Experimental

C_{10}-DABCO-C_{10}-Br_2 and C_{10}-DABCO-C_{10}-I_2 were synthesized by the method described in a previous paper.[1] ^{1}H NMR spin-lattice relaxation times (T_1) were measured with the saturation-τ-$\pi/2$ pulse sequence by a MATEC pulsed spectrometer between 77 and 400 K. The resonance frequencies were 20.5 MHz for C_{10}-DABCO-C_{10}-Br_2 and 19.5 MHz for C_{10}-DABCO-C_{10}-I_2.

The specimen were sealed in a glass ampoule with a small amount of helium gas for heat exchange. The sample temperatures were measured with Chromel-*P*-Constantan thermocouples and controlled to within 0.1 K during each run.

^{79}Br NMR spin-lattice relaxation time (T_1) and line shape measurements were carried out by a MATEC pulsed spectrometer with a wide-bore (130 mmϕ) Oxford superconducting magnet (4.72 T). The sample temperature was regulated by using a home-made cryostat of liquid flow type. T_1 was measured after 256 signal accumulation by using the saturation-τ-$\pi/2$ pulse sequence. The line shape was determined by the Fourier transformation after the 1024 accumulation of FID signals (sampling interval=2 μs and sampling points= 2048). The aqueous solution of NaBr and powder NaBr

were used as standard reagents of ^{79}Br NMR.

Results and Discussion

Temperature dependence of ^1H NMR spin-lattice relaxation times (T_1) for both compounds is shown in Fig. 1. T_1's change abruptly at 337 K in C_{10}-DABCO-C_{10}-Br_2 and at 361 K in C_{10}-DABCO-C_{10}-I_2. These temperatures agree well with the transition temperatures determined by DSC within the experimental error.[1,2]

The T_1 minima around 150 K are attributed to reorientation of terminal methyl groups for the following reasons. The spin-lattice relaxation rate due to methyl reorientation is expressed[5] by

$$T_1^{-1} = A \cdot B(\omega_0 \cdot \tau_c)\,\omega_0^{-1},$$

where

$$A = \frac{3}{5}\gamma^4 \hbar^2 r^{-6} I(I+1),$$

$$B(\omega_0 \cdot \tau_c) = \frac{\omega_0 \cdot \tau_c}{1+(\omega_0 \cdot \tau_c)^2} + \frac{4\omega_0 \cdot \tau_c}{1+4(\omega_0 \cdot \tau_c)^2},$$

and

$$\tau_c = \tau_0 \exp(E_a/kT)$$

where ω_0 is the nuclear Larmor frequency, τ_c is the correlation time, r is the interproton distance within the methyl group, I is the spin quantum number, and E_a is the activation energy. Using A as an adjustable parameter, we can reproduce T_1 as shown in Fig. 1. The activation energies obtained are given in Table 1. According to the BPP theory,[5] the methyl reorientation contributes to A by an amount of $8.9\times10^8\,s^{-2}$ assuming that all methylene protons are rigid and do not undergo any relaxation, and that the spin-temperature approximation holds in the present system. This value agrees very well with the experimental ones (8.5×10^8 s^{-2} in C_{10}-DABCO-C_{10}-Br_2 and 8.0×10^8 s^{-2} in C_{10}-DABCO-C_{10}-I_2). We found also that the above experimental results satisfy well an empirical relation between E_a and the temperature at which T_1 minimum occurs[6] for both compounds. The T_1 minima around 150 K are, therefore, attributed to the terminal methyl group reorientation.

Temperature dependence of T_1 near the phase-transition temperature is shown in Fig. 2. In the low-

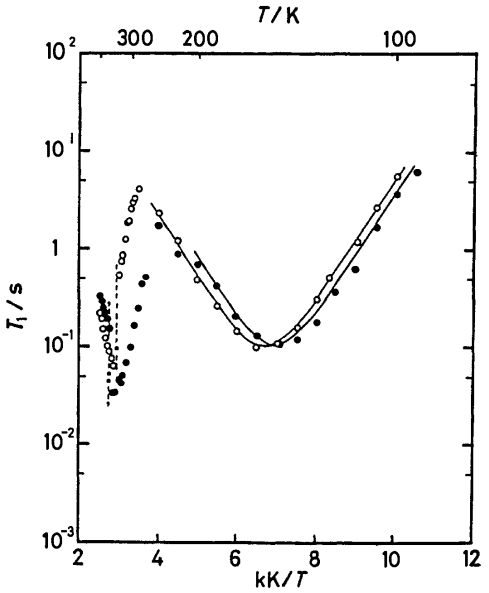

Fig. 1. Temperature dependence of ^1H NMR spin-lattice relaxation times (T_1) in C_{10}-DABCO-C_{10}-Br_2 (○) and C_{10}-DABCO-C_{10}-I_2 (●). The measuring frequencies are 20.5 and 19.5 MHz for C_{10}-DABCO-C_{10}-Br_2 and C_{10}-DABCO-C_{10}-I_2, respectively. Solid lines are the theoretical curves by assuming the methyl reorientations. The phase-transition temperatures are indicated by vertical broken lines.

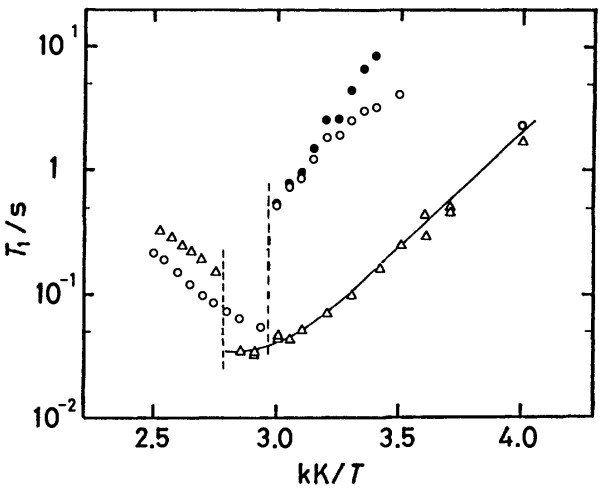

Fig. 2. Temperature dependence of ^1H NMR spin-lattice relaxation times (T_1) near the phase-transition temperatures in C_{10}-DABCO-C_{10}-Br_2 (○) and C_{10}-DABCO-C_{10}-I_2 (△). For C_{10}-DABCO-C_{10}-Br_2 T_1 is contributed by the methyl reorientation and another undefined mode (●). The measuring frequencies are 20.5 and 19.5 MHz for C_{10}-DABCO-C_{10}-Br_2 and C_{10}-DABCO-C_{10}-I_2, respectively.

Table 1. Activation Energies in C_{10}-DABCO-C_{10}-Br_2 and C_{10}-DABCO-C_{10}-I_2

	Low-temperature phase		High-temperature phase
	CH_3 rotation	Large angle oscillation?	Overall rotation
	E_a/kJ mol^{-1}	E_a/kJ mol^{-1}	E_a/kJ mol^{-1}
C_{10}-DABCO-C_{10}-I_2	12.0	35.5	28.0
C_{10}-DABCO-C_{10}-Br_2	11.8	57	30

temperature phase near the phase-transition point, the T_1 decreases with increasing temperature. For C_{10}-DABCO-C_{10}-Br_2 T_1 is contributed by two components in this temperature region. One is the contribution of methyl reorientation mentioned above. The other component discussed here is also shown in Fig. 2 as solid circles. The mechanism of this relaxation can not be pinned down at present stage: A large angle oscillation of the decyl chain is the most probable candidate. The activation energies for this mode are 57 kJ mol^{-1} for C_{10}-DABCO-C_{10}-Br_2 and 35.5 kJ mol^{-1} for C_{10}-DABCO-C_{10}-I_2. In the high-temperature phases, the T_1's become longer with increasing temperature with apparent activation energies of 30 kJ mol^{-1} for C_{10}-DABCO-C_{10}-Br_2 and 28 kJ mol^{-1} for C_{10}-DABCO-C_{10}-I_2. The free induction decays (FID) are shown in Fig. 3 where T_2*=33 μs in the high-temperature phase in comparison with T_2*=8 μs in the room-temperature phase. In the high-temperature phase the line widths, which are equal to the inverse of T_2*, are relatively wide and comparable with those often encountered in liquid crystalline phase or plastic phase. In addition, the polarizing microscope study[1] gave an evidence that the high-temperature phase is isotropic. The IR spectra showed that the ordered trans-zigzag conformation of the alkyl chain is lost in the high-temperature phase.[2] All these facts suggest that overall rotation of the cation is excited in the high-temperature phase.

In the high-temperature phase, the activation energies for these two compounds are almost the same. This fact suggests strongly that the cations in both materials are in similar environment. On the other hand, the activation energy for large-amplitude motion in the low-temperature phase is significantly lower in C_{10}-DABCO-C_{10}-I_2 than in C_{10}-DABCO-C_{10}-Br_2, due probably to larger void space available to the cations, which is brought about by larger size of

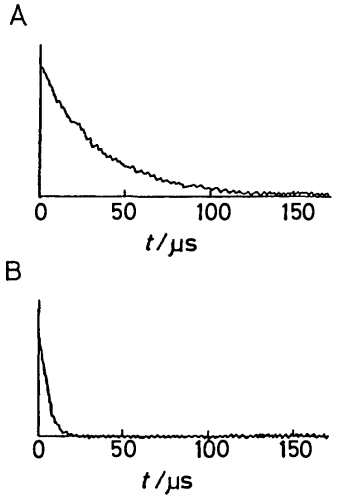

Fig. 3. Free induction decays of ^{1}H NMR in C_{10}-DABCO-C_{10}-Br_2 (A) in the high-temperature phase and (B) in the room-temperature phase.

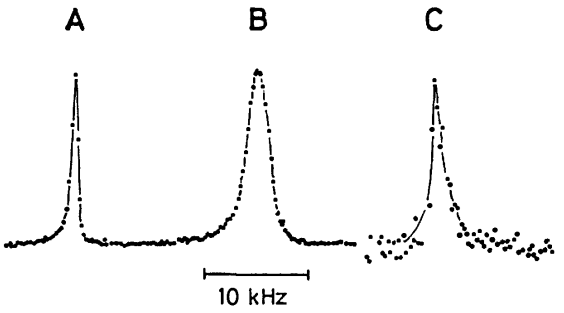

Fig. 4. ^{79}Br FT-NMR spectra A) in NaBr water solution, B) in NaBr powder, and C) in C_{12}-DABCO-C_{12}-Br_2.

the anion in the former material. Since the cationic motion is highly excited in C_{10}-DABCO-C_{10}-I_2, the difference in the Gibbs energy in low- and high-temperature phases is certainly small compared with C_{10}-DABCO-C_{10}-Br_2 and the transition temperature of C_{10}-DABCO-C_{10}-I_2 is significantly higher than that of C_{10}-DABCO-C_{10}-Br_2.

^{79}Br NMR of C_n-DABCO-C_n-Br_2 (n=10, 12, 14) were observed only in the high-temperature phases. The line shape in C_{12}-DABCO-C_{12}-Br_2 at 363 K is shown in Fig. 4 together with those in aqueous solution of NaBr and powdered NaBr. The line shapes and the line widths in C_{10}-DABCO-C_{10}-Br_2 and C_{14}-DABCO-C_{14}-Br_2 are nearly the same as those in C_{12}-DABCO-C_{12}-Br_2. In NaBr crystals Br nuclei are located at the sites of cubic symmetry so that the electric field gradient (EFG) at the Br site vanishes. Hence one expects neither first order splitting nor second order shift of the ^{79}Br resonance in NaBr. The finite line width in this compound shown in Fig. 4 is due probably to imperfection of the crystal lattice and to the magnetic dipole interaction which can be hardly estimated because of the lack of the crystal-structure data. The resonance frequency in NaBr crystals coincides with that in aqueous solution of NaBr listed in Table 2. The line width in C_n-DABCO-C_n-Br_2 (Fig. 4) is narrower than that in powdered NaBr, indicating that the EFG at the Br site vanishes and moreover, any extrinsic EFG due to lattice imperfection and magnetic dipole interaction are averaged out due to rapid translational diffusion of Br^- as will be discussed later. In the low-temperature phases the ^{79}Br NMR could not be observed due to large quadrupolar line broadening. The most remarkable point in Table 2 is that C_n-DABCO-C_n-Br_2 (n=10, 12, or 14)

Table 2. ^{79}Br NMR Frequencies, Line Widths, and Chemical Shifts

System	ν/MHz	$\Delta\nu$/kHz	δ/ppm
C_n-DABCO-C_n-Br_2 (n=10, 12, 14)	50.5360	1.5	3660
NaBr powder	50.3517	3.0	0
NaBr solution	50.3517	1.0	0

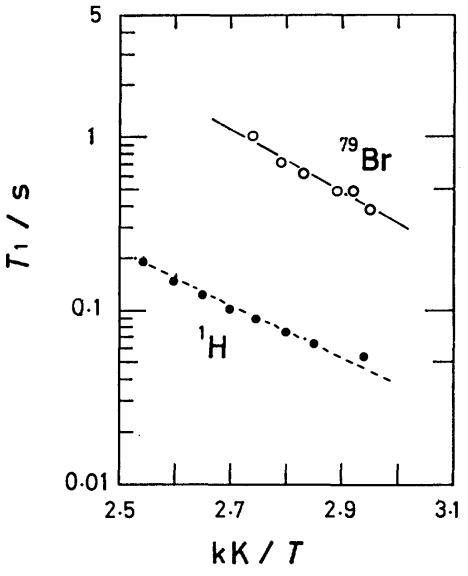

Fig. 5. Temperature dependence of ^{79}Br (50.5 MHz) and ^{1}H NMR (20.5 MHz) T_1's in the high-temperature phase of C_{10}-DABCO-C_{10}-Br_2.

show a very large down-field chemical shift. The interpretation by a second-order quadrupole effect is ruled out because of very narrow, symmetric line shape as shown in Fig. 4. Thus one must consider that there exists some special mechanism to generate a large paramagnetic term in the DABCO series compounds. At present we cannot identify the origin of such a large paramagnetic shift.

The temperature dependence of ^{79}Br and ^{1}H T_1's in C_{10}-DABCO-C_{10}-Br_2 are shown in Fig. 5. ^{79}Br T_1 is longer than ^{1}H T_1 by an order of magnitude, and its temperature slope is slightly larger. ^{79}Br T_1 (solid line in Fig. 5) shows that $\omega_0\tau_c<1$ and leads to E_a=34±3 kJ mol^{-1} which can be attributed to the translational diffusion of Br^- anions. Since the overall rotation of cations as well as anionic diffusion is highly excited in the isotropic high-temperature phase, this phase can be classified as an ionic plastic crystal. NH_4NO_3,[7] $TlNO_3$,[8] CH_3NH_3I[9] have been considered to belong to this category.

In conclusion, the methyl reorientation is first activated in the low-temperature phase (E_a=11.8 kJ mol^{-1} in C_{10}-DABCO-C_{10}-Br_2 and E_a=12.0 kJ mol^{-1} in C_{10}-DABCO-C_{10}-I_2). On further increase in temperature the large angle oscillation of the decyl chains may govern the relaxation mechanism (E_a=35.5 kJ mol^{-1} and 57 kJ mol^{-1} in C_{10}-DABCO-C_{10}-I_2 and C_{10}-DABCO-C_{10}-Br_2). In the high-temperature phase the overall rotation of cations are excited (E_a=28.0 kJ mol^{-1} and 30 kJ mol^{-1} in C_{10}-DABCO-C_{10}-I_2 and C_{10}-DABCO-C_{10}-Br_2). Furthermore, the anions diffuse at a rate higher than 10^8 s^{-1} with an activation energy of E_a=34 kJ mol^{-1}.

References

1) J. Shimizu, T. Nogami, and H. Mikawa, *Solid State Commun.*, **54**, 1009 (1985).

2) J. Shimizu, I. Imamura, T. Nogami, and H. Mikawa, *Bull. Chem. Soc. Jpn.*, **59**, 1443 (1986).

3) J. Shimizu, K. Imamura, T.Nogami, and H. Mikawa, *Bull. Chem. Soc. Jpn.*, **59**, 3367 (1986).

4) K. Imamura, J. Shimizu, and T. Nogami, *Bull. Chem. Soc. Jpn.*, **59**, 2699 (1986).

5) A. Abragam, "The Principles of Nuclear Magnetism," Clarendon Press, Oxford (1961).

6) T. Eguchi and H. Chihara, *J. Magn. Reson.*, **76**, 143 (1988).

7) M. T. Riggin, R. R. Knispel, and M. M. Pintar, *J. Chem. Phys.*, **56**, 2911 (1972).

8) K. Moriya, T. Matsuo, and H. Suga, *J. Phys. Chem. Solids*, **44**, 1103 (1983).

9) H. Ishida, R. Ikeda, and D. Nakamura, *Bull. Chem. Soc. Jpn.*, **59**, 915 (1986).

 © 1989 The Chemical Society of Japan Bull. Chem. Soc. Jpn., 62, 403—409 (1989)

The Electrocapillary Curves of the Phosphatidylcholine Monolayer at the Polarized Oil-Water Interface. II. Double Layer Structure of Dilauroylphosphatidylcholine Monolayer at the Nitrobenzene-Water Interface

Takashi KAKIUCHI, Masatoshi NAKANISHI, and Mitsugi SENDA*
Department of Agricultural Chemistry, Faculty of Agriculture, Kyoto University, Sakyo-ku, Kyoto 606
(Received August 25, 1988)

Electrocapillary curves have been measured at the polarized nitrobenzene-water interface in the presence of dilauroylphosphatidylcholine (DLPC) in the nitrobenzene phase. DLPC formed a saturated monolayer when the concentration of DLPC was above 10 μmol dm^{-3}. The area occupied by a DLPC molecule in the saturated monolayer was 0.93 nm^2, indicating that the monolayer was in the liquid-expanded state. The stability of the monolayer was strongly affected by the electrical potential difference across the interface. The monolayer was stable when the interface was negatively polarized, i.e., the potential in the aqueous phase was negative with respect to that in the oil phase. The potential of zero charge shifted to a negative potential as the adsorption of DLPC increased, which indicated the specific adsorption of lithium ions in the aqueous phase to the head group of the DLPC molecules exposed to the aqueous phase. When the interface was positively polarized, the adsorption of DLPC abruptly decreased and the monolayer appeared to be disrupted.

Phospholipid monolayers formed at the air-water interface and at the oil-water interface have been extensively used to study the surface properties of the monolayers, which are expected to represent, to some extent, the surface properties of phospholipid bilayers as well as those of biological membranes.[1,2] Among those monolayers, the monolayer formed at the polarizable oil-water interface is particularly suitable for studying the electrochemical properties of phospholipid monolayers, since the potential drop across the interface can be accurately controlled externally at this interface.[3] Thus, the monolayer at the polarized oil-water interface enables us to study its electrochemical properties in detail, e.g., the double layer structure in the vicinity of the monolayer and the ion-transfer reaction across the monolayer. The electrochemical study of the retardation of the ion transfer across the oil-water interface in the presence of a phospholipid monolayer has been reported by Koryta et al.,[4] Girault and Schiffrin,[5] and Cunnane et al.[6] However, the properties of the monolayer, itself, formed at these interfaces are not yet fully understood. To make full use of the advantage of the monolayer at the polarized interface, it is important to elucidate the properties of the phospholipid monolayers formed at the polarized interface. For example, knowledge regarding the double layer structure seems indispensable to correctly interpret the measured change of the rate constant of the ion-transfer reaction, e.g., taking account of the Frumkin correction.[7] Several attempts have been made to characterize the phospholipid monolayer at the polarized oil-water interface. We reported the conditions of the monolayer formation of L-α-dilauroylphosphatidylcholine (DLPC) at the nitrobenzene-water interface after measuring the double layer capacitance of the interface.[8] Although double layer capacitance is a sensitive measure which can be used to detect any structural change of the interface, the basic properties of the interface, such as the absolute amount of adsorbed substances and the excess surface charge density, can be estimated thermodynamically only through electrocapillary curve measurements. Girault and Schiffrin have studied the electrocapillary curves at the 1,2-dichloroethane-water interface in the presence of egg york phosphatidylcholine and phosphatidylethanolamine.[9] They have also studied the effect of pH in the aqueous side of the interface on the electrocapillary curves at different concentrations of phosphatidylcholine.[10] However, a detailed analysis of the electrocapillary curves has not yet been reported. In Part I of this study, we found that an equilibrium electrocapillary curve can be obtained for the DLPC monolayer at the polarized nitrobenzene-water interface in the potential range where the potential of the aqueous phase was negative with respect to that in the nitrobenzene phase.[11] In the present communication, we will focus our attention mainly on the electrocapillary curves in this potential region of the interface recorded at various concentrations of DLPC.

Experimental

The interfacial tension was measured at 25±0.05 °C using a computer-aided pendant drop method.[12,13] Details of this method were described in Part I.[11] In the measurement, the drop of an aqueous solution was formed in the nitrobenzene phase to make sure that the amount of the DLPC was sufficient to make up a saturated monolayer. A laboratory-made four-electrode potentiostat of the type proposed by Samec et al.[14] was used to control the potential drop across the polarized interface. The nitrobenzene used as a solvent of the oil phase was distilled and then treated with active alumina. DLPC was purchased from Sigma and was used without further purification. DLPC was dissolved in a 3:2 toluene-chloroform mixture as a stock solution. The nitrobenzene solution of DLPC for the measurement was prepared so that the final concentration of a 3:2 toluene-chloroform mixture in nitrobenzene was 10% (v/v). The

methods for the preparation of tetrapentylammonium tetraphenylborate (TPnATPB) and of the tetrapentylammonium chloride (TPnACl) solution have been described elsewhere.[15] All other chemicals were of reagent grade. The nitrobenzene solution was equilibrated with an aqueous solution of lithium chloride prior to a measurement.

Results

The electrochemical cell employed in the present study was

I	II	III	IV	V	VI	VII
Ag	AgCl	0.02 M† TPnACl (W)	0.1 M TPnATPB + $x\mu$M DLPC (NB)	0.05 M LiCl (W)	AgCl	Ag

The interface between Phases IV and V was a polarized nitrobenzene-water interface. The other nitrobenzene-water interface between Phases III and IV was a nonpolarized interface.[15] The potential of the right hand side of cell with respect to the left is denoted as E^{W-}_{O+}, where the super- and subscripts, W− and O+, indicate that the right-hand side and left-hand side reference electrodes are reversible to an anion (Cl^-) in Phase V and a cation ($TPnA^+$) in Phase IV, respectively. The electrocapillary curves were recorded between x=0 and 50 in the cell two hours after the formation of an interface in order to ensure the establishment of adsorption equilibrium.[11]

The potential of zero charge, E_{pzc}, of this system was found to be 0.32 V (Fig. 2) when x=0. Since at E_{pzc} the Galvani potential difference between the nitrobenzene and the aqueous phases is very small in the absence of specific adsorption,[16] the potential referring to E_{pzc} at x=0 can be taken as a convenient measure of the Galvani potential difference, $\Delta^W_O\phi$. As we have shown in Part I, the DLPC monolayer gives an equilibrium electrocapillary curve when $\Delta^W_O\phi<0$, i.e., in Region I (see Fig. 1). In the more positive potential range, Region II, the interfacial tension, γ, abruptly increased and the data in this region were much less reproducible (Fig. 1). Below, we mainly deal with the electrocapillary curves measured in Region I.

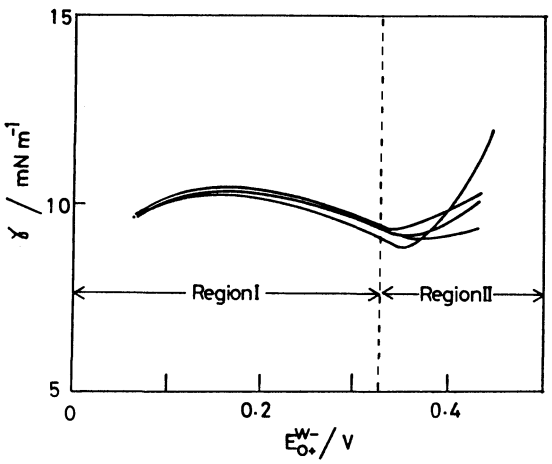

Fig. 1. The reproducibility of the electrocapillary curve when c_{DLPC}=10 μmol dm^{-3}.

The electrocapillary curves at x=0, 0.5, 1, 2, 5, 10, 20, and 50 are shown in Fig. 2. Each point represents the average value of triplicate measurements. For the electrocapillary curves at the four higher concentrations, only data from Region I are plotted. In Region I, the interfacial tension decreased as the concentration of DLPC was increased. Here, γ is plotted against the logarithm of the concentration of DLPC in the nitrobenzene phase, $\ln c_{DLPC}$, at different values of E^{W-}_{O+} (Fig. 3). At a higher concentration of DLPC, the γ vs. $\ln c_{DLPC}$ curve at any value of E^{W-}_{O+} gave a straight line. This

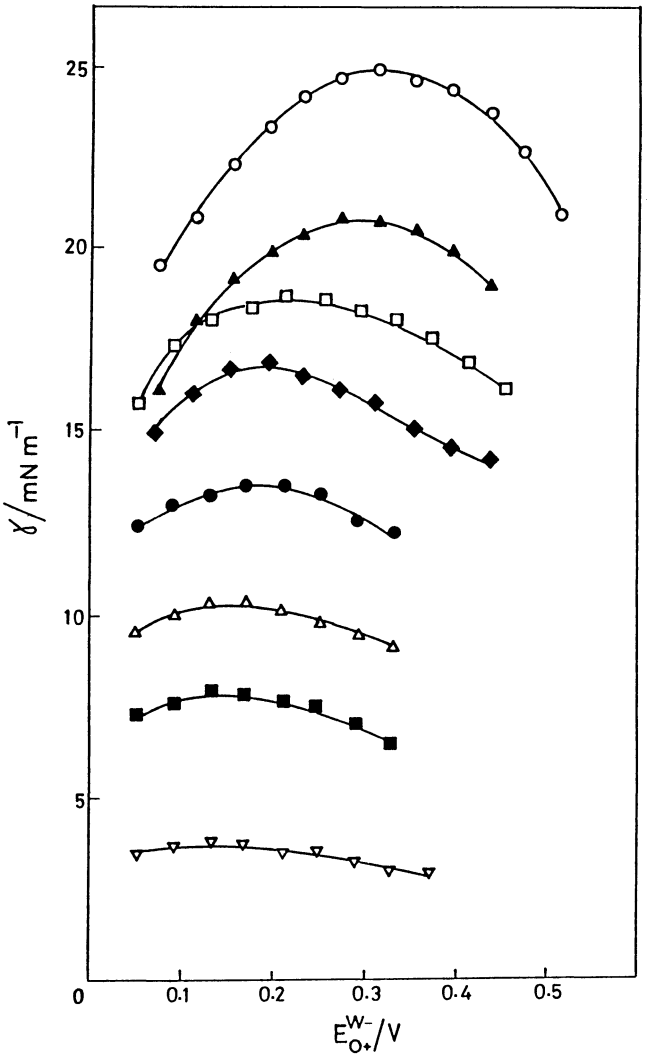

Fig. 2. The electrocapillary curves at 25°C for the interface between the nitrobenzene solution of 0.1 mol dm^{-3} TPnATPB and the aqueous solution of 0.05 mol dm^{-3} LiCl in the presence of x μmol dm^{-3} DLPC in the nitrobenzene phase: x=0(○), 0.5(▲), 1(□), 2(◆), 5(●), 10(△), 20(■), and 50(▽).

† 1 M=1 mol dm^{-3}.

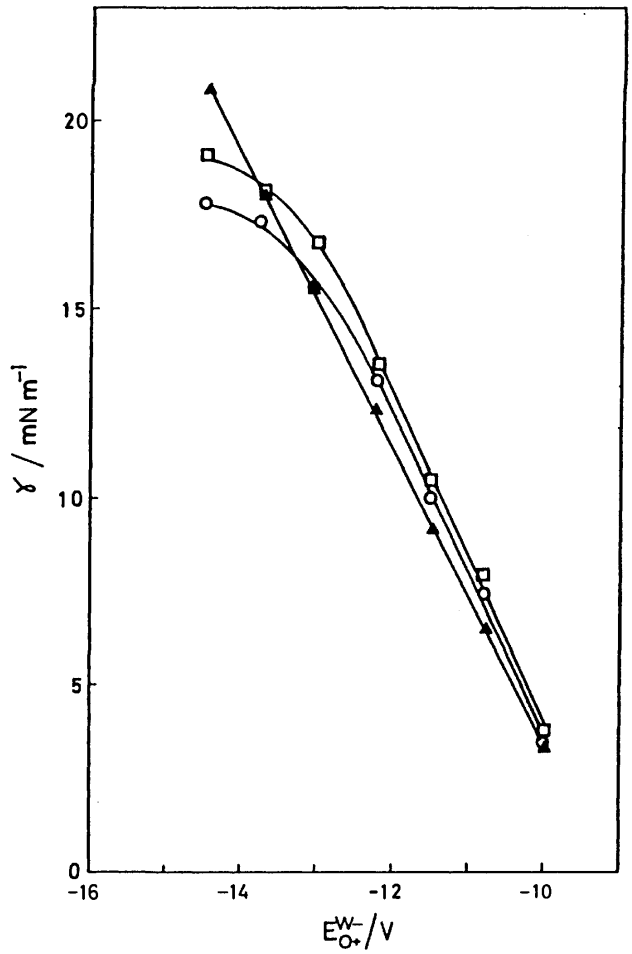

Fig. 3. γ vs. ln c_{DLPC} curves at E^{W-}_{O+}=0.09(▲), 0.15(□), and 0.33(○) V.

linear dependence indicates the formation of a saturated monolayer of DLPC at the interface. The possibility of micelle formation of the DLPC in the nitrobenzene phase is excluded within the concentration range studied, because of the lack of a break point in the curves. The adsorbed amount of DLPC was calculated from the slope of the curves in Fig. 3 using the thermodynamic relation based on the electrocapillary equation at the polarized oil-water interface:[17]

$$\Gamma_{DLPC} = -\frac{1}{RT}(\partial\gamma/\partial \ln a^{NB}_{DLPC})_{E^{W-}_{O+},\mu_i}, \quad (1)$$

where Γ_{DLPC} is the relative surface excess of DLPC, a^{NB}_{DLPC} the activity of the DLPC in the nitrobenzene phase, R the gas constant, and T the absolute temperature. The subscripts of the parenthesis in the right-hand side of Eq. 1 indicate that the derivative must be taken while keeping E^{W-}_{O+} and the chemical potentials of components except for DLPC constant. In the calculation, a^{NB}_{DLPC} was taken to be equal to the concentration of DLPC in the nitrobenzene phase, c_{DLPC}. Since the concentration of the DLPC in the nitrobenzene phase is small, Γ_{DLPC} can be equated to the adsorbed amount of DLPC at the interface. The adsorption isotherm of DLPC at E^{W-}_{O+}=0.210 V is shown in Fig. 4. The maximum adsorption of DLPC, Γ^{m}_{DLPC}, calculated from the limiting slope of the γ vs. lnc_{DLPC} curves was plotted as a function of E^{W-}_{O+} in Fig. 5. Γ^{m}_{DLPC} was independent of E^{W-}_{O+} between E^{W-}_{O+}=0.08 and 0.280 V; the monolayer was stable in this potential range. This is in accordance with our previous results, obtained from differential capacitance measurements of the DLPC monolayer at the same interface.[8] The Γ^{m}_{DLPC} in this potential range was found to be 1.76×10^{-10} mol cm^{-2}, which corresponds to the value of the occupied area of a DLPC molecule (0.93 nm^2). The isotherm fitted well to the Frumkin isotherm (Fig. 4). The solid curve in Fig. 4 is a regression curve using the Frumkin isotherm:[18]

$$Bc_{DLPC} = \frac{\theta}{1-\theta}\exp(-2a\theta), \quad (2)$$

where B is the adsorption coefficient, $\theta=\Gamma_{DLPC}/\Gamma^{m}_{DLPC}$, and a is the interaction parameter. In the regression

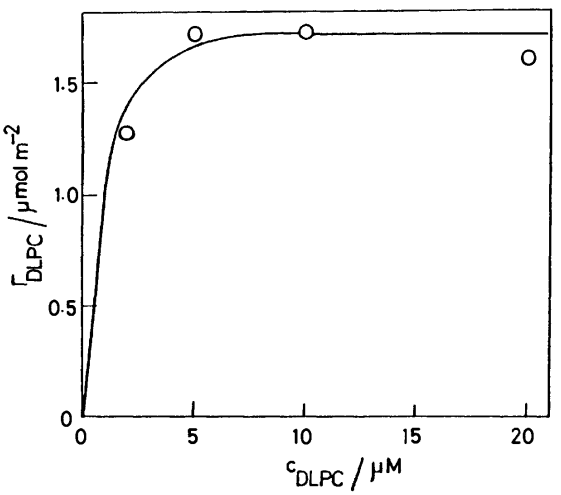

Fig. 4. Adsorption isotherm of DLPC at E^{W-}_{O+}=0.210 V. The solid line is the regression curve using the Frumkin isotherm.

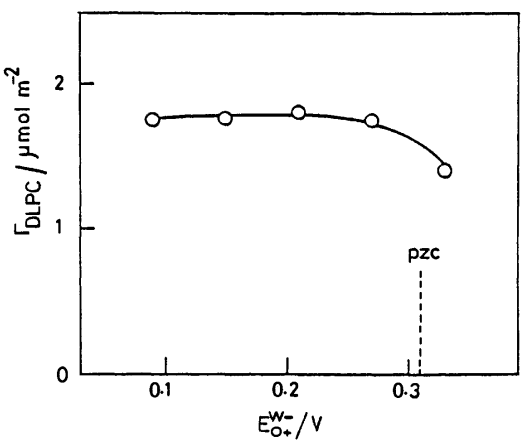

Fig. 5. Dependence of Γ_{DLPC} at c_{DLPC}=10 μmol dm^{-3} on the applied potential.

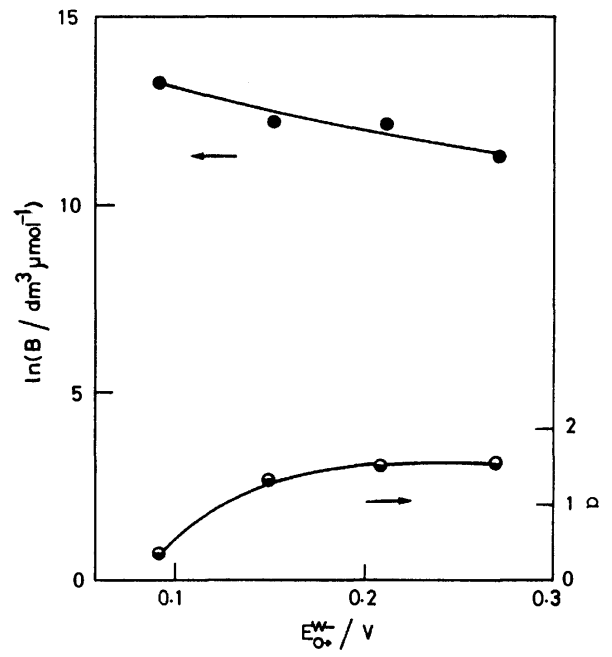

Fig. 6. Dependence of the logarithm of the adsorption coefficient, ln$B$, and the interaction parameter, a on the applied potential.

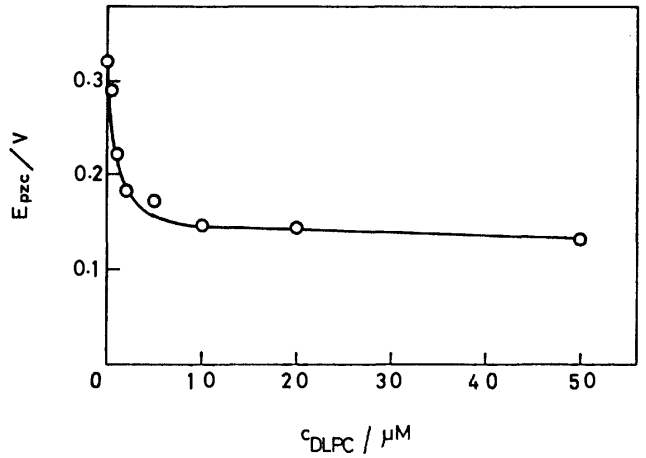

Fig. 7. Shift of the potential of zero charge, E_{pzc}, with the increase of the DLPC concentration.

analysis, the value of Γ^{m}_{DLPC}, estimated from the limiting slope of the γ vs. lnc_{DLPC} plot, was employed. The adsorption isotherm in Fig. 4 ensures the absence of multi-layer formation at the interface. The logarithm of B and a are plotted in Fig. 6 as a function of E^{w-}_{o+}. As can be seen in Fig. 2, the potential of zero charge, E_{pzc}, shifted to a negative potential with the increase of c_{DLPC} (Fig. 7). The shift reached 170 mV when the saturated monolayer was formed.

Discussion

Figures 3, 4, and 5 clearly manifest the formation of a saturated DLPC monolayer at the polarized nitrobenzene-water interface. The monolayer was stable when the $\Delta^{w}_{o}\phi$ was negative. This confirms our previous conclusion concerning the monolayer formation of DLPC obtained from capacitance measurement.[8] The value of the area occupied by a DLPC molecule in the saturated monolayer, 0.93 nm^2, is 20% greater than the value estimated from the capacitance measurements using the spread monolayer technique.[8] If we take account of the uncertainty intrinsic to the spread method, i.e., the necessary extrapolation of the capacitance value to the value at t=0,[8] the values from the two independent methods agree with each other and suggest that the saturated monolayer is in the liquid-expanded state.[19] The ln$B$ was weekly dependent on the applied potential (Fig. 6) and decreased with a positive increase in the potential. The value of ln$B$ at E^{w-}_{o+}=0.22 V was 12.5, corresponding to an adsorption free energy of 31 kJ mol^{-1}. This is in agreement with the value estimated from the capacitance measurement at the same polarization.[8] Wandlowski et al. reported a similar value from the capacitance measurements.[20] The a parameter was also varied with the applied potential, yet the value of a was always positive.

The negative shift of the E_{pzc} with an increase in the DLPC adsorption (Fig. 7) means that there exists a Galvani potential difference at the E_{pzc}, such that the inner potential in the aqueous phase becomes more negative with respect to the inner potential in the nitrobenzene phase. There are four possible sources for this shift of the E_{pzc}: the nitrobenzene and the water molecules at the interface, the head group and the carbonyl group of the adsorbed DLPC molecules, and the specific adsorption of ions in the presence of the monolayer. The contribution from the first factor would be very small, because the $\Delta^{w}_{o}\phi$ at the E_{pzc} in the absence of the specific adsorption of ions at the interface is very small.[16] The second and third factors are the permanent dipole moments of the DLPC molecules oriented at the interface. The phosphatidylcholine molecule has a zwitterion group, whose isoelectric point is at pH=5.5.[19] The pH of the aqueous solution studied was typically 5.8, and, hence, all the head groups exposed to the aqueous side of the interface were in zwitterionic form. The dipole moment of the zwitterion group is so large that even its minute orientation normal to the interface should give rise to large dipole potential. However, neutron diffraction studies of the phosphatidylcholine bilayer have demonstrated a coplaner arrangement of the choline segment, i.e., with the P-N dipole approximately parallel to the plane of the bilayer.[21] A similar conclusion has been reached in a study of the phosphatidylcholine monolayer at the air-water interface.[22] Moreover, since the phosphate group is directly attached to the glyceride part of the phosphatidylcholine and the trimethylammonio group is away from it, the deviation of the orientaion of the zwitterionic group from the parallel position, if any, should result in a shift of the pzc to the positive direction, which is at variance with the

present results. On the other hand, the C=O bond of the carbonyl group in the phosphatidylcholine monolayer at the air-water interface is oriented with its oxygen atom pointing toward the aqueous phase and with the angle of C=O axis being within 20° with respect to the interface.[23] If the carbonyl group is oriented similarly in the polarized nitrobenzene-water interface, the contribution of this oriented dipole is estimated to be 70 mV at the saturation coverage. This contribution to the surface potential, however, can explain only part of the shift of the E_{pzc} observed experimentally. Consequently, the above-mentioned three possible contributions arising from the oriented dipoles cannot fully account for the observed shift of 170 mV. The remaining factor that can account for the observed change of the E_{pzc} is the specific adsorption of an Li^+ ion in the aqueous phase to the hydrophilic head group of the adsorbed monolayer. This specific adsorption should result in a potential difference in the aqueous phase, such that the potential at the inner Helmholtz plane (IHP) where the Li^+ ion is specifically adsorbed, ϕ_1, is positive with respect to the bulk of the aqueous phase. This direction of the shift is in harmony with the observed trend of E_{pzc}. The specific adsorption of Li^+ ions to the phospholipid surface has been found in the liposomes made of phosphatidylcholine.[24] Pospisil et al. reported the specific effect of Li^+ ion on the phase transition of dipalmitoylphosphatidylcholine adsorbed at the mercury-solution interface.[25] The specific binding of Li^+ ion to a lipid bilayer made of a phosphatidylserine membrane was found to significantly affect its physicochemical properties and physiological functions.[26]

If the specific adsorption of Li+ does occur at the interface, the shift of E_{pzc} is expected to depend on the concentration of Li^+ ion in the aqueous phase. Figure 8 shows that the shift of E_{pzc} with the LiCl concentration exceeds the shift attributable to a change in the potential of the reference electrode in the aqueous phase (dotted line). The latter change was calculated using the Davies equation[27] for an evaluation of the mean ionic activity of LiCl. The observed large shift of E_{pzc} with the Li^+ ion concentration (solid line) confirms the presence of the specific adsorption of Li^+. If we make a simplified assumption, that the distribution of the nonspecifically adsorbed ions in the aqueous phase follows the Gouy-Chapman theory, we can estimate the degree of the Li^+ ion binding to the interface. The shift of E_{pzc}, after subtracting the potential drop due to the oriented carbonyl group, which was assumed to be 70 mV irrespective of the $\Delta_o^w\phi$ and of the LiCl concentration, should correspond to ϕ_1. Although ϕ_1 is in general larger than the potential at the outer Helmholtz plane (OHP), ϕ_2, which passes through the center of the nonspecifically adsorbed Li^+ ion at its closest approach to the interface, the error would be small if we equate ϕ_1 with ϕ_2, because some of the nonspecifically adsorbed ions can enter beyond the OHP due to the sparse distribution of the adsorbed DLPC molecules(cf. Figs. 9a and 9b). Then, by using the Gouy-Chapman theory, the surface charge density corresponding to the ϕ_2 potential at a given concentration of LiCl can be calculated. This surface charge density may be taken as the specifically adsorbed amount of Li+ ions, since the potential is at the E_{pzc} and there is no excess surface charge density in the nitrobenzene phase. The specifically adsorbed amount of Li^+ ion, ${}^i\Gamma_{Li}$, and the degree of the counterion binding, $\alpha={}^i\Gamma_{Li}/\Gamma_{DLPC}$, thus obtained, are listed in Table 1. The Γ_{DLPC} was assumed to be constant over the concentration range of LiCl studied.

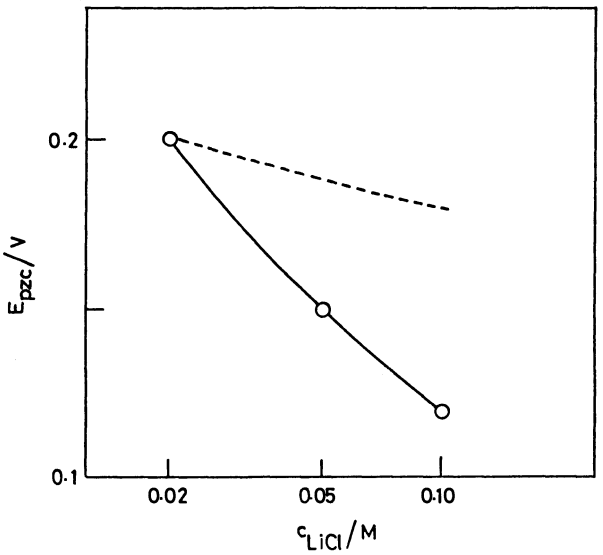

Fig. 8. Shift of the potential of zero charge with the concentration of DLPC in the nitrobenzene phase. The dotted line is the expected curve in the case of no specific adsorption.

In the case of the phosphatidylcholine bilayer, lipophilic anions are much more strongly adsorbed at the membrane surface than lipophilic cations.[28] Flewelling and Hubbell attributed this asymmetric adsorbability to the potential drop across the membrane surface and then estimated for the egg yolk phosphatidylcholine membrane that the potential at the membrane surface is 240±70 mV positive with respect to the bulk solution.[29] It is interesting that this magnitude of the membrane potential is comparable with the amount of the shift of the E_{pzc} found in the present study. The double-layer structure of the nitrobenzene-water interface in the presence of the satu-

Table 1. Specific Adsorption of Li^+ Ion to the Dilauroylphosphatidylcholine Monolayer

c(LiCl)	ΔE_{pzc}	$F{}^i\Gamma_{Li}$	α
mol dm^{-3}	mV	μC cm^{-2}	%
0.02	55	2	12
0.05	100	9	50
0.10	100	13	74

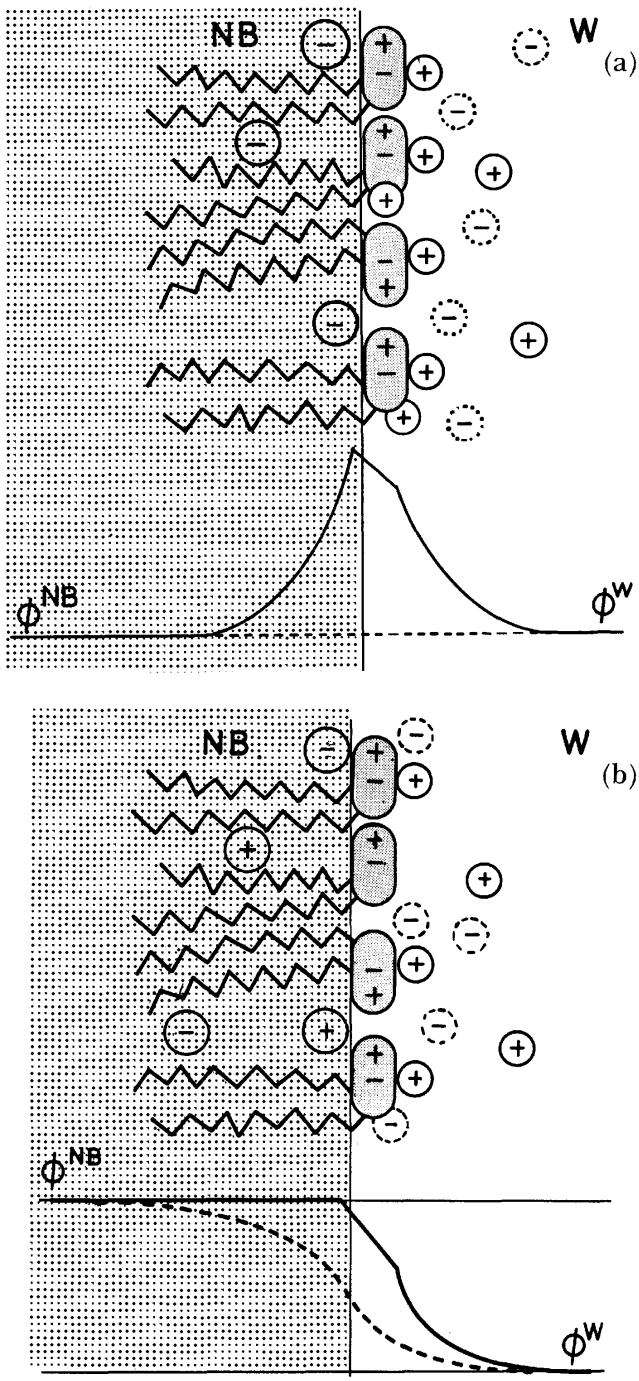

Fig. 9. Schematic representation of the double layer structure and the potential profile of the interface between the nitrobenzene solution of TPnATPB and the aqueous solution of LiCl in the presence (——) and in the abscence (----) of DLPC adsorption: a) at the E_{pzc} for the base electrolyte, b) at the E_{pzc} for the saturated DLPC monolayer.

rated DLPC monolayer, deduced from the present analysis, is illustrated in Fig. 9a at E_{O+}^{W-}=0.32 V ($\Delta_O^W\phi\simeq 0$) and in Fig. 9b at the E_{pzc} for the saturated DLPC monolayer, respectively. The inner Helmholtz plane in the aqueous phase was postulated to lie on the line passing through the centers of the specifically adsorbed Li^+ ions. Also, schematically illustrated are the penetration of $TPnA^+$ and TPB^- ions in the nitrobenzene phase into the hydrocarbon part of the DLPC monolayer and the random orientation of the zwitterion group in the plane parallel to the interface.

The abrupt increase in the interfacial tension (Fig. 1) when the potential was increased from Region I to II would predict the appearance of a peak on the corresponding equilibrium capacitance vs. potential curve. However, experimentally no such peak at this potential was observed on the differential capacitance vs. potential curves.[8,20,30] In the presence of the adsorption of a surface active substance, the capacitance, $C=(\partial q/\partial E)_c$, is generally composed of two terms:[31]

$$\left(\frac{\partial q}{\partial E}\right)_c = \left(\frac{\partial q}{\partial E}\right)_\Gamma + \left(\frac{\partial q}{\partial \Gamma}\right)_E \left(\frac{\partial \Gamma}{\partial E}\right)_c , \qquad (3)$$

where q is the excess surface charge density, E the electrical potential difference, c the bulk concentration of the adsorbate, and Γ the surface excess of the adsorbate. The first term on the right-hand side of Eq. 3 is a quantity called "true capacitance" and the second term is the "adsorption pseudocapacitance." In Region I, the Γ_{DLPC} is practically independent of E_{O+}^{W-} (Fig. 5) and, hence, the second term makes no significant contribution to the total capacitance. On the other hand, in Region II, the desorption of DLPC from the interface certainly takes place, judging from the recovery of the interfacial tension (Fig. 1). Then, the $(\partial\Gamma/\partial E)_c$ term in Eq. 3 is not generally negligible. When the adsorption is a diffusion limited process, which is likely to be the case for the DLPC adsorption, because of the low value of c_{DLPC}, the second term in Eq. 3 may be rewritten as[31]

$$\left(\frac{\partial q}{\partial \Gamma}\right)_E \left(\frac{\partial \Gamma}{\partial E}\right)_c = \left(\frac{\partial q}{\partial \Gamma}\right)_E \left(\frac{\partial \Gamma}{\partial E}\right)_{c,\omega=0} \frac{b+2}{(b+1)^2+1} , \qquad (4)$$

where $(\partial\Gamma/\partial E)_{c,\omega=0}$ is $(\partial\Gamma/\partial E)_c$ at $\omega\to 0$, $\omega=2\pi f$ is the angular frequency, and f is the ac frequency employed in a capacitance measurement. The b is given by

$$b=(2\omega/D)^{1/2}(\partial\Gamma/\partial c)_E, \qquad (5)$$

where D is the diffusion coefficient of the adsorbate. Only when b is small, can the measured capacitance be seen as being the thermodynamic capacitance.[32] In the case of the Frumkin isotherm,

$$(\partial\Gamma/\partial c)_E = \frac{\Gamma_m}{c}\,\frac{\theta(1-\theta)}{1-2a\theta(1-\theta)} . \qquad (6)$$

If we assume that the diffusion coefficient of the DLPC in the nitrobenzene is the same as that of dilauroylphosphatidylethanolamine, 3.8×10^{-6} cm^2 s^{-1},[33] we obtain $b=6.38\sqrt{\omega}$ when c=10 μmol dm^{-3}, a=1, and θ=0.5. Accordingly, even at f=1 Hz the last factor of the right hand side of Eq. 4 is significantly smaller than 1, resulting in the disappearance of the expected peak on a measured capacitance vs. potential curve. If the adsorption-desorption process is sluggish giving a

"frozen" monolayer, the second term in Eq. 3 is again smaller than the equilibrium value. Thus, the measured capacitance in Region II is in any case smaller than the equilibrium capacitance and the integration of the measured capacitance vs. potential curve would not give the excess surface charge density.

The abrupt increase of the interfacial tension in the adsorption of egg yolk phosphatidylcholine at the 1,2-dichloroethane-water interface has been suggested to be due to the protonation of the phosphatidylcholine molecules at the interface.[9] In the experimental conditions employed in the present study, this protonation model is not applicable. The pK_a of the phosphate group of phosphatidylcholines at the air-water interfaces is of the order of 3.0.[34] On the other hand, in the present study the ϕ_2 potential in the aqueous phase does not exceed 30 mV,[16] even in the positive extreme of Region II, because of the relatively high concentration of LiCl. Accordingly, the surface pH is not lower than 4.5 and, hence, practically all the DLPC molecules at the interface should be in a zwitterionic form,[34] even when the change of pH in the vicinity of the interface is taken into account. A probable explanation of the abrupt rise of γ would be a desorption of the DLPC molecules from the interface accompanied by the process of the facilitated Li^+ ion transfer in Region II.

This work was supported by a Grant-in-Aid for Scientific Research No. 60211017 and a Grant-in-Aid for Scientific Research on Priority Areas "Macromolecule-Complexes (No. 62612003)" from the Ministry of Education, Science and Culture.

References

1) S. Ohki, C. B. Ohki, and N. Duzgunes, *Adv. Colloid Interface Sci.*, **5**, 271 (1976).
2) L. I. Boguslavsky, "Progress in Surface Science," ed by S. G. Davison, Vol. 19, p. 1, Pergamon Press, New York (1985).
3) T. Kakiuchi and M. Senda, *Bull. Chem. Soc. Jpn.*, **56**, 1322 (1983).
4) J. Koryta, Le Q. Hung, and A. Hofmanová, *Studia Biophys.*, **90**, 25 (1982).
5) H. H. Girault and D. J. Schiffrin. "Charge and Field Effect in Biosystems," ed by M. J. Allen and P. N. R. Usherwood, Abacus Press, England (1984).
6) V. J. Cunnane, D. J. Schiffrin, M. Fleischmann, G. Geblewicz, and D. Williams, *J. Electroanal. Chem. Interfacial Electrochem.*, **243**, 455 (1988).
7) A. N. Frumkin, *Z. Phys. Chem.*, **164A**, 121 (1933).
8) T. Kakiuchi, M. Yamane, T. Osakai. and M. Senda, *Bull. Chem. Soc. Jpn.*, **60**, 4223 (1987).
9) H. H. J. Girault and D. J. Schiffrin, *J. Electroanal. Chem. Interfacial Electrochem.*, **179**, 277 (1984).
10) H. H. J. Girault, private communication.
11) T. Kakiuchi, M. Nakanishi, and M. Senda, *Bull. Chem. Soc. Jpn.*, **61**, 1845 (1988).
12) H. H. Girault, D. J. Schiffrin, and B. D. V. Smith, *J. Electroanal. Chem. Interfacial Electrochem.*, **137**, 207 (1982).
13) H. H. J. Girault, D. J. Schiffrin, and B. D. V. Smith, *J. Colloid Interface Sci.*, **101**, 257 (1984).
14) Z. Samec, V. Mareček, J. Koryta, and M. W. Khalil, *J. Electroanal. Chem. Interfacial Electrochem.*, **83**, 393 (1977).
15) T. Kakiuchi and M. Senda, *Bull. Chem. Soc. Jpn.*, **60**, 3099 (1987).
16) T. Kakiuchi and M. Senda, *Bull. Chem. Soc. Jpn.*, **56**, 1753 (1983).
17) T. Kakiuchi and M. Senda, *Bull. Chem. Soc. Jpn.*, **56**, 2912 (1983).
18) A. N. Frumkin, *Z. Phys. Chem.*, **116**, 466 (1925).
19) M. C. Phillips and D. Chapman, *Biochim. Biophys. Acta*, **163**, 301 (1968).
20) T. Wandlowski V. Mareček, and Z. Sămec, *J. Electroanal. Chem. Interfacial Electrochem.*, **242**, 277 (1988).
21) D. L. Worcester, "Biological Membranes," ed by D. Chapman and D. F. H. Wallach, Vol. 3, p. 1, Academic Press, New York(1976).
22) M. M. Standish and B. A. Pethica, *Trans. Faraday Soc.*, **64**, 1113 (1968).
23) F. Paltauf, H. Hauser, and M. C. Phillips, *Biochim. Biophys. Acta*, **249**, 539 (1971).
24) H. Trauble, *Naturwiss.*, **58**, 277 (1971).
25) L. Pospĭsil, J. Kůta, E. Müller, and H. Dörfler, *J. Electroanal. Chem. Interfacial Electrochem.*, **106**, 359 (1980).
26) H. Hauser and G. G. Shipley, *Biochemistry*, **22**, 2171 (1983); G. Cevec, J. M. Seddon, and D. Marek, *Biochim. Biophys. Acta*, **814**, 141 (1985).
27) C. W. Davies, *J. Chem. Soc.*, **1938**, 2093.
28) R. F. Flewelling and W. L. Hubbell, *Biophys. J.*, **49**, 531 (1986).
29) R. F. Flewelling and W. L. Hubbell, *Biophys. J.*, **49**, 541 (1986).
30) T. Wandlowski, S. Račinský, V. Mareček, and Z. Samec, *J. Electroanal Chem. Interfacial Electrochem.*, **227**, 281 (1987).
31) A. N. Frumkin and V. I. Melik-Gaikazyan, *Dokl. Akad. Nauk USSR*, **77**, 855 (1951).
32) M. Senda and I. Tachi, *Rev. Polarogr. (Kyoto)*, **10**, 89 (1962).
33) T. Kakiuchi, M. Kotani, and M. Senda, in preparation.
34) H. Hauser and M. C. Phillips, "Progress in Surface and Membrane Science," ed by D. A. Cadenhead and J. F. Danielli, Vol. 13, p. 360, Academic Press, New York (1979).

Surface Adsorption and Micelle Formation of Dodecyltrimethylammonium Chloride and Decylammonium Chloride Mixture

Norihiro IKEDA,* Eiji SHIOTA, Makoto ARATONO, and Kinsi MOTOMURA
Department of Chemistry, Faculty of Science, Kyushu University 33, Fukuoka 812
(Received September 13, 1988)

The surface tension of the aqueous solution of dodecyltrimethylammonium chloride (DTAC) and decylammonium chloride (DeAC) mixture was measured as a function of the total molality and composition of the surfactants at 298.15 K under atmospheric pressure. To make clear the miscibility of surfactants, the compositions in the mixed adsorbed film and micelle were calculated by use of the thermodynamic equations developed previously. The results indicated that both adsorbed film and micelle are richer in DTAC molecules than the bulk solution. Furthermore, the composition in the adsorbed film at the critical micelle concentration (cmc) was evaluated and compared with that in the micelle. It was found that the composition of DeAC in the micelle is smaller than that in the adsorbed film. This forms a striking contrast to the previous observation of dodecylammonium chloride (DAC)-DeAC mixture. It was concluded that the structure and size of polar head group of surfactants have a significant influence on the miscibility of surfactants.

In our previous paper on the subject of the adsorption of dodecylammonium chloride (DAC) and decylammonium chloride (DeAC) mixture from its micellar solution, we have evaluated thermodynamically the compositions of the surfactants in the mixed adsorbed film and micelle.[1] It has been proved that they, though fairly similar with each other, are remarkably different from that in the solution.

Now another combination of surfactants will give us an information about the miscibility of surfactants in the adsorbed film and micelle and make sure of the usefulness of our thermodynamic treatment. In the present study we choose the dodecyltrimethylammonium chloride (DTAC)-DeAC mixture because (i) we have already investigated the adsorption of DTAC from the micellar solution, the effect of *N*-methylation of DAC on the adsorption and micelle formation, and the phase transition of the adsorbed film of DTAC and DeAC mixture at a low concentration,[2-4] (ii) the critical micelle concentration (cmc) of DTAC is smaller than that of DeAC while the surface tension at the cmc is larger, and (iii) an information is expected to be provided about the influence of the chemical structure of polar head group of surfactant on the miscibility.

The surface tension of the aqueous solution of DTAC-DeAC mixture is measured as a function of the total concentration and composition of the mixture at concentrations around the cmc at constant temperature under atmospheric pressure and analyzed by use of the thermodynamic equations advanced by the authors.[1,4,5] Further, the results are compared with those of the DAC-DeAC system.

Experimental

Dodecyltrimethylammonium chloride and decylammonium chloride were synthesized and purified by the method described previously.[6,7] Water was distilled triply, the second and third stages being from dilute alkaline permanganate solution. Surface tension was measured under atmospheric pressure at 298.15 K by the drop volume method described in the previous paper.[8] The surface tension values were reproducible to ± 0.05 mN m^{-1}.

Results and Discussion

To obtain the compositions in the adsorbed film and micelle in equilibrium with the aqueous solution of surfactant mixture, the total molality m of surfactants in the solution defined by

$$m = m_1 + m_2 \quad (1)$$

and the composition of the surfactant 2 in the total surfactant defined by

$$X_2 = m_2/m \quad (2)$$

were adopted as the experimental variables at constant temperature and pressure.[1,4,5] Here m_i is the molality of surfactant i.

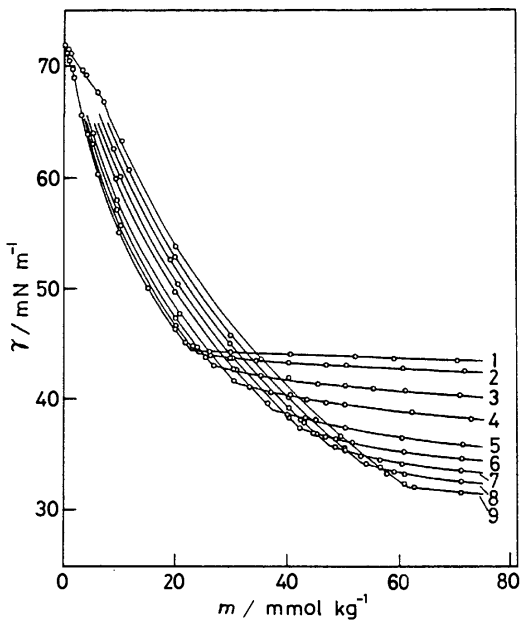

Fig. 1. Surface tension vs. total molality curves at constant composition: (1) X_2=0; (2) 0.1000; (3) 0.3017; (4) 0.5002; (5) 0.7021; (6) 0.8026; (7) 0.8932; (8) 0.9506; (9) 1.

The surface tension of the aqueous solution of dodecyltrimethylammonium chloride and decylammonium chloride mixture was measured as a function of m at fixed composition X_2 of DeAC and at 298.15 K under atmospheric pressure. The results are shown in Fig. 1. It is seen that the γ vs. m curve changes its shape gradually with X_2 from the curve of DTAC to that of DeAC. The curve has a distinct break point arising from the formation of micelles; the concentration at the break point is referred to as the critical micelle concentration (cmc). The cmc value increases with increasing X_2 and the surface tension at the cmc γ^{cmc} decreases. Here, it should be noted that the slope of γ vs. m curve of the micellar solution of mixture has a larger absolute value than those of pure DTAC and DeAC.

Taking up the γ values at a given m value from Fig. 1, the γ vs. X_2 curves are obtained and shown in Fig. 2 together with the γ^{cmc} vs. X_2 curve. It is seen that the value of γ increases with increasing X_2 while that of γ^{cmc} decreases. On the other hand, the m vs. X_2 curves at a given surface tension obtained from Fig. 1 are shown in Fig. 3 with the cmc vs. X_2 curve. It is found that both values of m and cmc increase with X_2.

Now let us evaluate the total surface density of surfactant mixture Γ^H defined by

$$\Gamma^H=\Gamma_1^H+\Gamma_2^H, \tag{3}$$

where Γ_i^H is the surface excess number of moles per unit area of surfactant i with respect to the two dividing planes chosen so as to make the surface excess numbers of moles of water and air zero. Assuming that the solution is ideal, the total surface density is calculated by use of the equation

$$\Gamma^H=-(m/2RT)(\partial\gamma/\partial m)_{T,p,X_2}, \tag{4}$$

where T is the temperature, p the pressure, and R the gas constant. The evaluated values of Γ^H are plotted against m at various compositions in Fig. 4. It should be noted that the value of Γ^H increases with decreasing the composition at low concentrations, while it decreases at high concentrations. Taking into account that the DTAC molecule has a larger head group than the DeAC molecule, the large size of the polar head group of DTAC molecule is said to reduce considerably the adsorption of surfactants at a high surface density even though the DTAC molecule has a longer

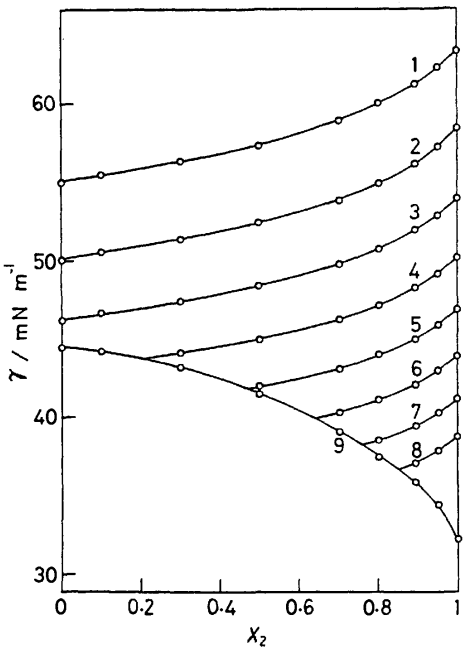

Fig. 2. Surface tension vs. composition curves at constant total molality: (1) m=10 mmol kg^{-1}; (2) 15; (3) 20; (4) 25; (5) 30; (6) 35; (7) 40; (8) 45; (9) γ^{cmc} vs. X_2.

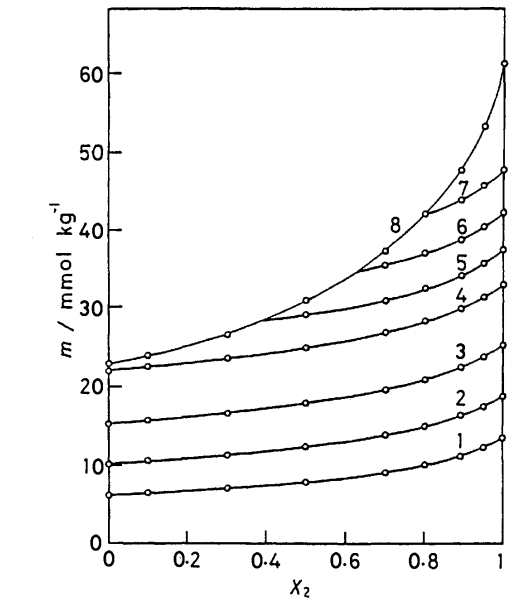

Fig. 3. Total molality vs. composition curves at constant surface tension: (1) γ=60 mN m^{-1}; (2) 55; (3) 50; (4) 45; (5) 42.5; (6) 40; (7) 37.5; (8) cmc vs. X_2.

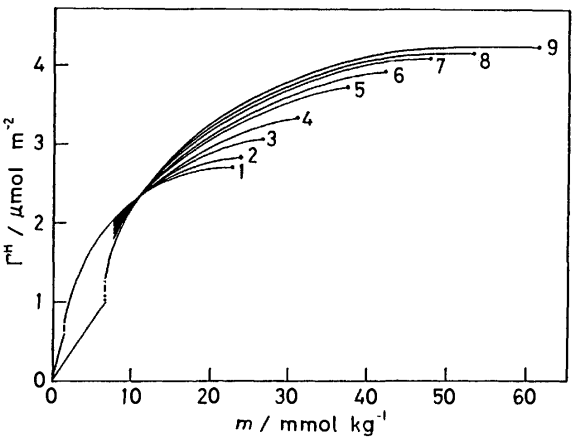

Fig. 4. Total surface density vs. total molality curves at constant composition: (1) X_2=0; (2) 0.1000; (3) 0.3017; (4) 0.5002; (5) 0.7021; (6) 0.8026; (7) 0.8932; (8) 0.9506; (9) 1; (●) total surface density at the cmc $\Gamma^{H,cmc}$.

hydrocarbon chain.

It has been shown that the plots of γ at constant m and of m at constant γ against the composition of DeAC in the adsorbed film X_2^H provide us the useful information to examine the miscibility of surfactants in the mixed adsorbed film. Here the composition X_2^H is defined by

$$X_2^H = \Gamma_2^H / \Gamma^H. \tag{5}$$

The values of X_2^H at constant m are calculated by applying the relation

$$X_2^H = X_2 - [(1-X_2)X_2/RT\Gamma^H](\partial\gamma/\partial X_2)_{T,p,m} \tag{6}$$

to the γ vs. X_2 curves given in Fig. 2 with the Γ^H values of Fig. 4 and those at constant γ by applying the relation

$$X_2^H = X_2 - [2(1-X_2)X_2/m](\partial m/\partial X_2)_{T,p,\gamma} \tag{7}$$

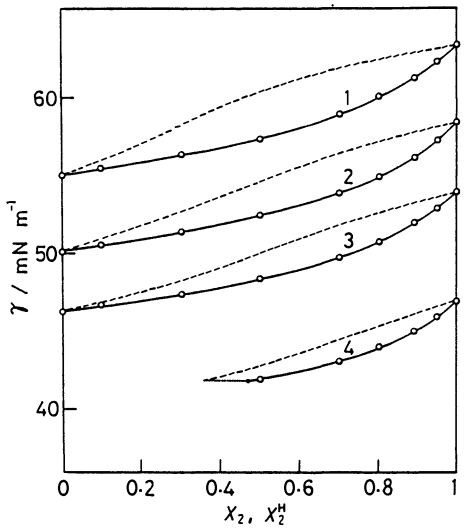

Fig. 5. Surface tension vs. composition curves at constant total molality; (1) m=10 mmol kg^{-1}; (2) 15; (3) 20; (4) 30; (●) γ^{cmc}; (——) X_2; (----) X_2^H.

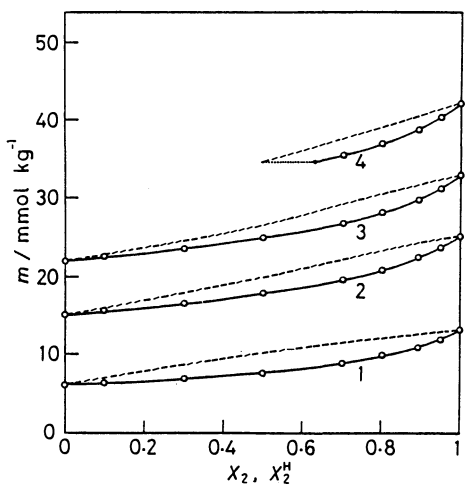

Fig. 6. Total molality vs. composition curves at constant surface tension: (1) γ=60 mN m^{-1}; (2) 50; (3) 45; (4) 40; (●) cmc; (——) X_2; (----) X_2^H.

to the m vs. X_2 curves given in Fig. 3.[1,4] Both results are respectively shown in Figs. 5 and 6. These diagrams take the shape of cigar and are similar to the three-dimensional phase diagram of an ideal system. Therefore we can say that the DTAC and DeAC molecules are perfectly miscible in the adsorbed film. It is also seen that the adsorbed film is richer in DTAC molecules. This implies that the mixed adsorbed film abounds in the surfactant having a lower surface tension at a given concentration. Further the qualitative feature of the diagram is almost the same as that of the DAC-DeAC mixture.[1] However, the diagrams in Fig. 5 seem to be thinner than the corresponding ones of the DAC-DeAC mixture. This is visualized by plotting the difference in composition between the solution and the adsorbed film $X_2 - X_2^H$ against X_2 (Fig. 7); the differences of the DTAC-DeAC mixture are much smaller than those of the DAC-DeAC mixture both at a given γ and at a given m. Taking into account that the DTAC and DAC molecules are different only in the structure and size of the polar head group, it is concluded that the large head group of DTAC increases the composition of DeAC and decreases the total surface density remarkably at high concentrations.

Next, let us discuss the miscibility of the surfactants in the mixed micelle. We define the thermodynamic quantity of micelle as the excess one in reference to the spherical dividing surface which makes the excess number of moles of water zero[5] and the composition of DeAC in the mixed micelle X_2^M as

$$X_2^M = N_2^M/(N_1^M+N_2^M), \tag{8}$$

where N_i^M is the number of surfactant i in the micelle particle. The value of X_2^M is calculated by application of the relation[1,5]

$$X_2^M = X_2 - [2(1-X_2)X_2/\mathrm{cmc}]\,(\partial \mathrm{cmc}/\partial X_2)_{T,p} \tag{9}$$

to the cmc vs. X_2 curve given in Fig. 3. The cmc vs. X_2^M

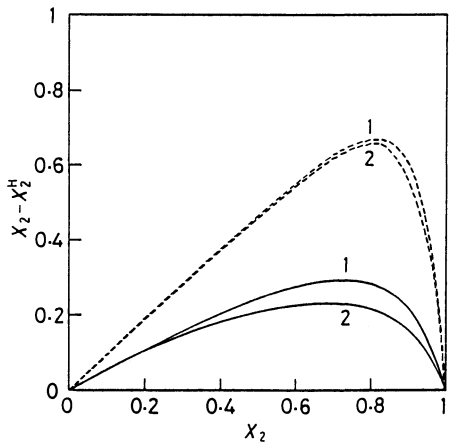

Fig. 7. Difference in composition between the solution and the adsorbed film vs. composition curves at constant molality and constant surface tension: (1) m=14 mmol kg^{-1}; (2) γ=50 mN m^{-1}; (——) DTAC-DeAC system; (----) DAC-DeAC system.

curve is depicted together with the cmc vs. X_2 curve in Fig. 8. It is seen that the diagram has the shape of a swollen cigar and the micelle is richer in DTAC molecules than the solution. Since the mixed adsorbed film is in equilibrium with the bulk solution containing the micelles at a concentration above the cmc, it is useful to compare the compositions in the micelle and adsorbed film. The composition in the adsorbed film at the cmc $X_2^{H,cmc}$ is obtained by virtue of the equation

$$X_2^{H,cmc} = X_2^M - [(1-X_2)X_2/RT\Gamma^{H,cmc}]\,(\partial\gamma^{cmc}/\partial X_2)_{T,p}, \quad (10)$$

where $\Gamma^{H,cmc}$ is the total surface density at the cmc.[1] By applying this equation to the γ^{cmc} vs. X_2 curve given in Fig. 2 and using the X_2^M value in Fig. 8, the values of $X_2^{H,cmc}$ were evaluated; the results are also depicted in

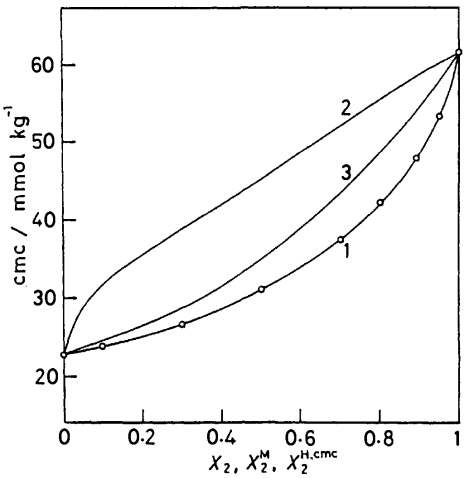

Fig. 8. Critical micelle concentration vs. composition curves: (1) cmc vs. X_2; (2) cmc vs. X_2^M; (3) cmc vs. $X_2^{H,cmc}$.

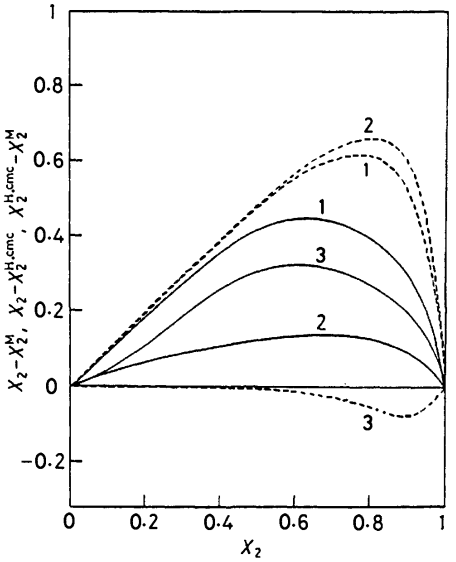

Fig. 9. Difference in composition vs. composition curves at the cmc: (1) $X_2-X_2^M$ vs. X_2; (2) $X_2-X_2^{H,cmc}$ vs. X_2; (3) $X_2^{H,cmc}-X_2^M$ vs. X_2; (——) DTAC-DeAC system; (----) DAC-DeAC system.

the form of the cmc vs. $X_2^{H,cmc}$ curve in Fig. 8. We can see that the adsorbed film at the cmc is also richer in DTAC molecules than the bulk solution. However, it is noteworthy that the composition of DeAC in the adsorbed film is larger than that in the micelle. This behavior forms a striking contrast to that of the DAC-DeAC system.[1]

Now let us consider the values of $X_2-X_2^M$, $X_2-X_2^{H,cmc}$, and $X_2^{H,cmc}-X_2^M$ to elucidate the relation among the compositions in the bulk, surface, and micelle. They are plotted against X_2 in Fig. 9. It is clearly seen that the $X_2-X_2^M$ value is considerably large compared with the $X_2-X_2^{H,cmc}$ value. However, on looking at the corresponding ones of the DAC-DeAC system depicted also in Fig. 9, we notice that the $X_2-X_2^M$ and the $X_2-X_2^{H,cmc}$ values are not so different than each other. This fact indicates that the difference in composition between the adsorbed film and micelle stems from that in geometrical shape when the polar head groups of surfactants are different in shape and size. Furthermore, taking into account that the $X_2-X_2^{H,cmc}$ values of the two systems are fairly different though the $X_2-X_2^M$ values are relatively close to each other, it is concluded that the miscibility in the adsorbed film is influenced more significantly by the structure of polar head group than that in the micelle. A similar conclusion has been drawn from the effect of the *N*-methylation of dodecylammonium chloride on the entropies of interface and micelle formation.[3] There is one more important difference between the two systems; that is, the value of $X_2^{H,cmc}-X_2^M$ is positive for the present system, while negative for the DAC-DeAC system. We can say therefore that the bigger head group is favorable to the micelle formation.

Finally, it is possible to show that the γ^{cmc} vs. composition diagram is helpful to understand the variation of the surface tension of surfactant mixture in the range of concentration above the cmc. It is seen from Fig. 10 that as the total molality m of surfactant mixture increases at a given overall composition X_2, the composition X_2^M in the mixed micelle increases and

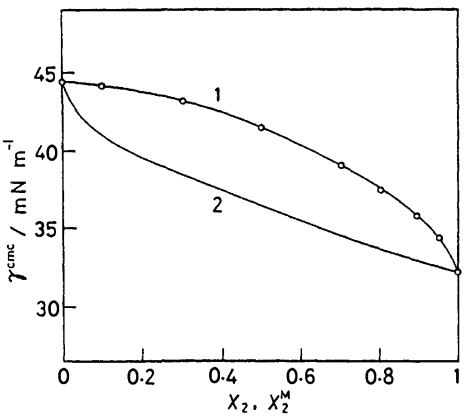

Fig. 10. Surface tension at the cmc vs. composition curves: (1) γ^{cmc} vs. X_2; (2) γ^{cmc} vs. X_2^M.

approaches X_2 at an infinite m. Consequently the surface tension of the micellar solution of mixture is expected to decrease gradually with increasing m. Inspecting Fig. 1, the γ vs. m curve of mixture is found to have a larger negative slope than those of pure DTAC and DeAC at concentrations above the cmc. This is consistent with the above expectation.

References

1) K. Motomura, H. Matsukiyo, and M. Aratono, *ACS Symp. Ser.*, **311**, 163 (1986).

2) M. Aratono, T. Okamoto, and K. Motomura, *Bull. Chem. Soc. Jpn.*, **60**, 2361 (1987).

3) M. Aratono, T. Okamoto, N. Ikeda, and K. Motomura, *Bull. Chem. Soc. Jpn.*, **61**, 2773 (1988).

4) S. Uryu, M. Aratono, M. Yamanaka, K. Motomura, and R. Matuura, *Bull. Chem. Soc. Jpn.*, **56**, 3219 (1983).

5) K. Motomura, M. Yamanaka, and M. Aratono, *Colloid Polym. Sci.*, **262**, 948 (1984).

6) M. Aratono, S. Uryu, Y. Hayami, K. Motomura, and R. Matuura, *J. Colloid Interface Sci.*, **98**, 33 (1984).

7) M. Aratono, S. Uryu, Y. Hayami, K. Motomura, and R. Matuura, *J. Colloid Interface Sci.*, **93**, 162 (1983).

8) K. Motomura, S. Iwanaga, Y. Hayami, S. Uryu, and R. Matuura, *J. Colloid Interface Sci.*, **80**, 32 (1981).

 © 1989 The Chemical Society of Japan Bull. Chem. Soc. Jpn., 62, 415—418 (1989)

In-Situ X-Ray Diffraction Study of Metal Hydride Formation in Palladium and Palladium-Based Alloy Electrodes under Cathodic Hydrogen Charging

Ken-ichi MACHIDA† and Michio ENYO*
Research Institute for Catalysis, Hokkaido University, Sapporo 060
(Received September 28, 1988)

An in situ X-ray diffraction (XRD) technique reported earlier was improved and employed to study the hydride formation in Pd and Pd-Au alloy foils and amorphous Pd-Zr alloy ribbons during cathodic hydrogen charging or its reverse process. The phase transformation from α- to β-PdH_x in the Pd electrode, accompanied by an increase in the cell volume, was demonstrated to take place by the formation of a β phase domain in the bulk during the cathodization. The lattice constant was discontinuously changed from $a \simeq 3.92$ to 4.04 Å and such a discontinuous change was observed on the $Pd_{90}Au_{10}$ alloy as well. However, no phase transformation was observed on the Pd-Au alloys with the Pd content of 70 at.% or below, where the lattice constant increased continuously with an increase in the negative potential for the cathodic polarization. No crystallization in the amorphous Pd-Zr alloy ribbon electrodes was detected after hydrogen charging.

Electrochemical oxidation/reduction reactions are often accompanied by the occlusion of electrolysis products into the electrode, which may cause a phase transformation or formation of other phases. A typical example is the hydride formation due to hydrogen absorption into electrodes of some metals or alloys.[1] An X-ray diffraction (XRD) technique may be used to detect such changes. A set of ex situ XRD measurements on a relationship between the α and β phases of Pd and its alloys has demonstrated that the phase transformation proceeds even electrochemically and also is modified by the alloying element and its content.[2-4] However, the measurements should preferably be made in situ, as the new phases formed may be unstable when the electrodes are taken out of the system in which the electrochemical environment has been controlled.

Uno Falk et al.[5] have reported, by using an in situ XRD technique, clear phase changes during charging and discharging of Cd, Fe, or Ni electrode in Jungner and Edison secondary cells. Recently, Nazri and Müller[6] have applied this technique to a Li electrode in nonaqueous solutions. The present authors also have reported the phase transformation accompanied by the hydride formation in Pd electrodes.[7] In this work, the in situ XRD technique is improved for accepting samples with low crystallinity and applied to the study of hydride formation in Pd, Pd-Au, and amorphous Pd-Zr alloy electrodes as a function of the cathodization conditions.

Basic Relations in Hydrogen Electrode Reaction. The hydrogen electrode reaction on Pd, Pd-Au, or amorphous Pd-Zr alloy electrodes has been shown to proceed via the Volmer-Tafel reaction scheme.[8-10] In this mechanism, the equivalent hydrogen pressure $\overline{P}_{H_2}$ during the polarization as referred to its value $\overline{P}_{H_2,o}$ at equilibrium potential is related to the overpotential component η_2' for the Tafel step, $2H(ads) \rightarrow H_2$, by the relation,[8]

$$-\eta_2' = (RT/2F) \ln (\overline{P}_{H_2}/\overline{P}_{H_2,o}) \quad (1)$$

This overpotential component can readily be evaluated from electrode potential-time transient curves.[8] Although this relation has been substantiated by various analyses, a direct demonstration under an in situ condition is desirable. The in situ XRD analysis by monitoring the η_2' may be expected to give conclusive information about the metal hydride phase relation in hydrogen absorbing metal or alloy electrodes under cathodic polarization.

Experimental

Electrodes. The test electrodes used were Pd foil and $Pd_{100-x}Au_x$ (x=10, 30, 45, and 60) alloy foils of 10×10 mm in size and 12.5 or 50 μm in thickness which were spot-welded to Ta wires sealed beforehand into glass tubings. Similarly, an amorphous $Pd_{35}Zr_{65}$ ribbon (0.8 mm wide and ca. 20 μm in thickness) was cut to pieces of 10 mm long, which were spot-welded on a Ta net of 10×10 mm, followed by etching in dilute HF solution for several ten seconds in order to remove a catalytically inactive ZrO_2 surface layer.

Apparatus and Method. A syringe-type electrochemical cell[11] consisting of the working electrode, a Pt net counter electrode, a Ag/AgCl reference electrode, and a window of Kapton foil (polyimid sheet) for X-ray observations[7] was used (Fig. 1). In order to make the cell applicable to samples of low crystallinity (e.g. oxides or, particularly, amorphous-like samples), a modification was introduced to minimize the background signal from the Kapton foil window, especially in a low 2θ angle region, in such a way that X-ray beams passed vertically through the window over the whole scan angle. The glass cell was mounted on a Rigaku θ-θ scan goniometer which had a fixed and horizontal sample stage, rotatable X-ray source and a detector. The X-ray radiation used was Mo $K\alpha$ (λ=0.71069 Å) monochromatized with a graphite plate. All the electrochemical measurements were carried out at room temperature (about 293 K) in 0.5 M H_2SO_4 (M=mol dm^{-3}) under H_2 atmosphere. The XRD data obtained were calibrated by using silicon powder comounted with epoxy resin on the electrode. All potentials were

† Present address: Department of Applied Chemistry, Faculty of Engineering, Hokkaido University, Sapporo 060.

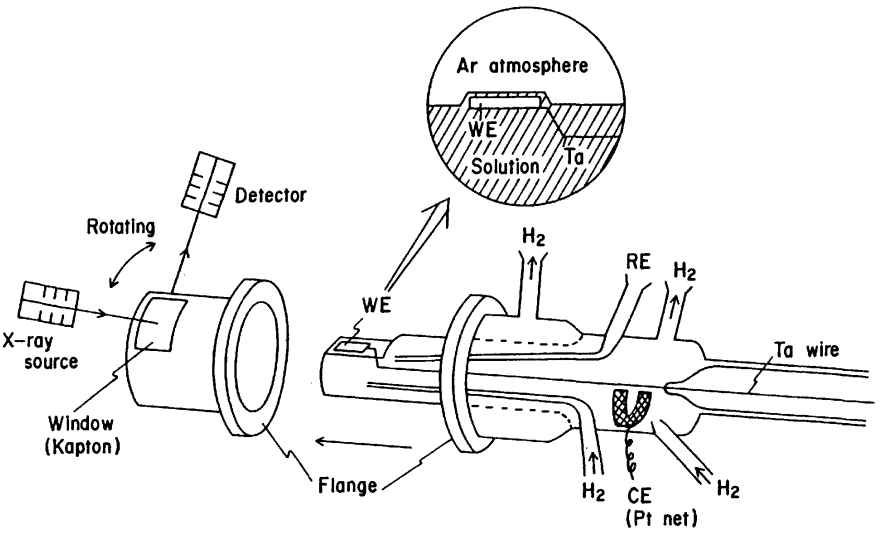

Fig. 1. A syringe type electrochemical cell for the in situ XRD study. WE; working electrode, CE; counter electrode, RE; reference electrode.

represented based on a reversible hydrogen electrode potential.

Results and Discussion

Pd Foil Electrodes. The in situ XRD patterns obtained on a Pd foil electrode under polarization are shown in Fig. 2. The conditions for polarization were chosen in such a way that η_2' was shifted in sequence towards more negative potentials. This process leads to adsorption of hydrogen into the Pd electrode bulk (the absorption hemicycle). The patterns on Pd foil electrode before the polarization or polarized at $\eta_2'>50$ mV were assigned to α phase of the Pd-H system, viz. a cubic system with space group of $Fm3m$. The lattice constant is gradually increased from $a\simeq3.89$ to 3.91 Å along with the negative shift of the polarization potential.

At the η_2' value of 49 mV, the β phase (which belongs to the same cubic system as the α phase) of the Pd-H system started to appear, leading to the α-β coexistence phase. The presence of signals of both α and β phases indicates that the transformation takes place by the partial formation of β-PdH_x domain in the Pd foil electrode. The lattice constants of the specimen at $\eta_2'=49$ mV were 3.92 and 4.40 Å for the α and β phase, respectively. The η_2' value of 49 mV is equivalent to $\overline{P}_{H_2}\simeq2.5$ kPa according to Eq. 1, which is in agreement with that usually observed in the process of gaseous hydrogen charging into Pd.[12] Nevertheless, the complete transformation to β phase at $\eta_2'=46$ or 49 mV needed a long time of polarization and the condition of $\eta_2'=0$ or -38 mV was suitable to achieve a uniform β phase. In addition, the specimen polarized at $\eta_2'=-38$ mV gave rise to enlargement of the lattice constant ($a=4.08$ Å). This clearly indicates that the hydrogen content x in the β-PdH_x further increased with cathodic polarizations at more negative potentials.

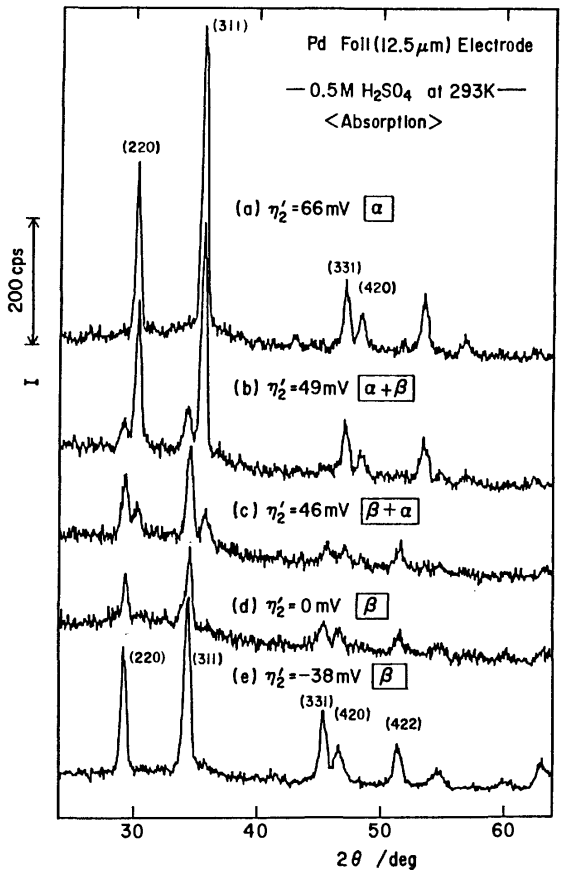

Fig. 2. In situ XRD patterns observed on a Pd foil electrode at various η_2' values during the hydrogen absorption hemicycle. The polarization time was 0.5 h for $\eta_2'=-38$ and 0 mV or 3 h for $\eta_2'=46$, 49, and 66 mV. 0.5 M H_2SO_4.

Figure 3 shows the in situ XRD patterns obtained on a Pd foil electrode under polarization, together with that under a blank condition. The data were collected

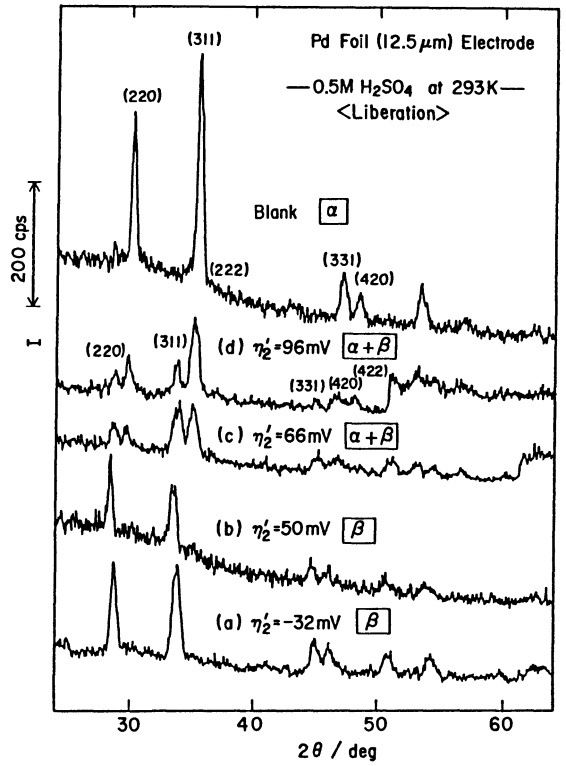

Fig. 3. In situ XRD patterns observed on a Pd foil electrode at various η_2' values during the hydrogen liberation hemicycle. Polarization time was 0.5 h for η_2'=−32 mV or 3 h for η_2'=50, 66, and 96 mV. 0.5M H_2SO_4.

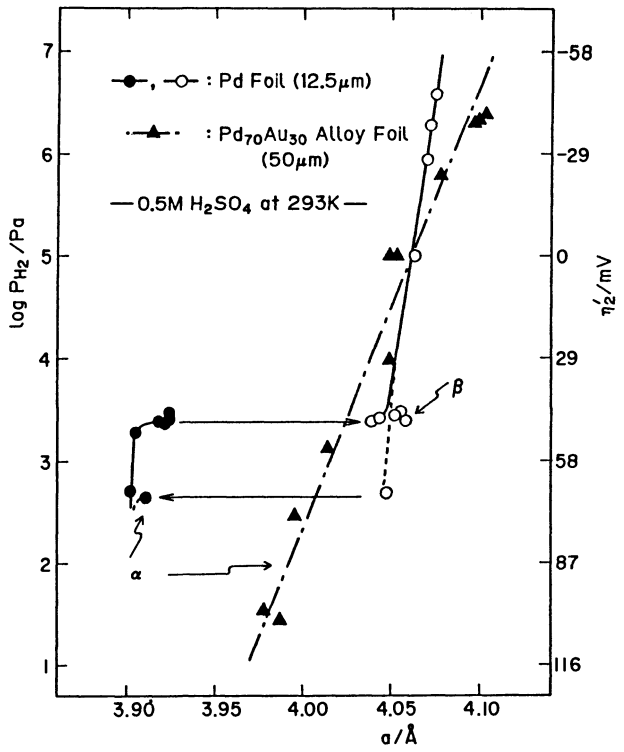

Fig. 4. Relationships between the η_2' (or $\overline{P}_{H_2}$) and lattice constant observed for α and β phases on the Pd-H and $Pd_{70}Au_{30}$-H systems.

under the condition in which electrode potential was shifted stepwise to more positive potentials up to η_2'=96 mV (a hydrogen liberation hemicycle). The β phase in the Pd foil electrode was kept even under the polarization of η_2'=50 mV, but it was partly retransformed to α phase at η_2'= 66 mV, giving the XRD signal originated from α phase which has a comparable intensity with β phase. The amount of α phase increased with increase of the potential for polarization, viz. η_2'=96 mV. On the other hand, no retransformation to α phase was observed at the potential in the α-β transformation region during the hydrogen absorption hemicycle (η_2'=50 mV), even after a longer

Table 1. Lattice Constants for a Series of $Pd_{100-x}Au_x$ Alloy Foils before and after Cathodic Polarization (in 0.5 M H_2SO_4)

Alloy	Lattice constant/Å	
	before	after[a)]
$Pd_{90}Au_{10}$	3.90	4.07
$Pd_{70}Au_{30}$	3.93	4.05
$Pd_{55}Au_{45}$	3.95	4.04
$Pd_{40}Au_{60}$	3.97	4.03

a) Cathodization potential η_2'=ca. −5 mV.

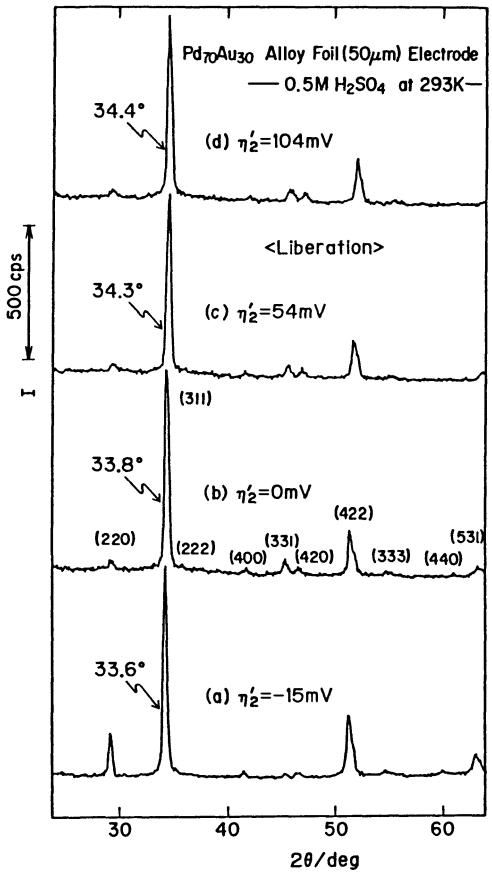

Fig. 5. In situ XRD patterns observed on a $Pd_{70}Au_{30}$ alloy foil electrode at various η_2' values during the hydrogen liberation hemicycle. Polarization time was 0.5 h. 0.5 M H_2SO_4.

polrization period, e.g. 20 h.

The relationship between the η_2' (or $\overline{P}_{H_2}$) and lattice constant observed on the Pd foil are shown in Fig. 4. A clear hysteresis is seen on the hydrogen pressure versus hydrogen content curves between the hydrogen liberation and absorption hemicycles. Such a hysteresis well corresponds to that observed in the hydrogen charging-discharging cycle in gaseous H_2,[12] with the extent dependent on the duration of the polarization.

Pd-Au Alloy Foil Electrodes. The lattice constants of a series of Pd-Au alloy electrodes before and after the polarization at $\eta_2' \simeq -5$ mV are summarized in Table 1. The increase of the Au content in the Pd-Au alloys resulted in an enlargement of the lattice constants (see data in Table 1), while the inverse tendency was observed after the cathodic polarization. This indicates that the Pd-Au alloys become difficult to absorb hydrogen with an increase in the Au content. This observation agrees with results obtained on Pd alloyed with Au[3] or the other group IB metals.[4]

In Fig. 5, the in situ XRD patterns obtained on the $Pd_{70}Au_{30}$ electrode in the hydrogen liberation hemicycle are shown. There was no discontinuous change in the lattice constant obtained at various η_2' values and, instead, the 2θ value of (311) reflection from the α phase changed continuously from 33.6 to 34.4° as indicated in the figure, which gave the lattice constant of 3.986—4.078 Å. In this way, the α-β phase transformation such as that observed on Pd foils did not take place in the $Pd_{70}Au_{30}$ alloy foil electrode. This result is in good agreement with similar characters observed in the case of absorption of hydrogen into Pd-Au alloys.[3]

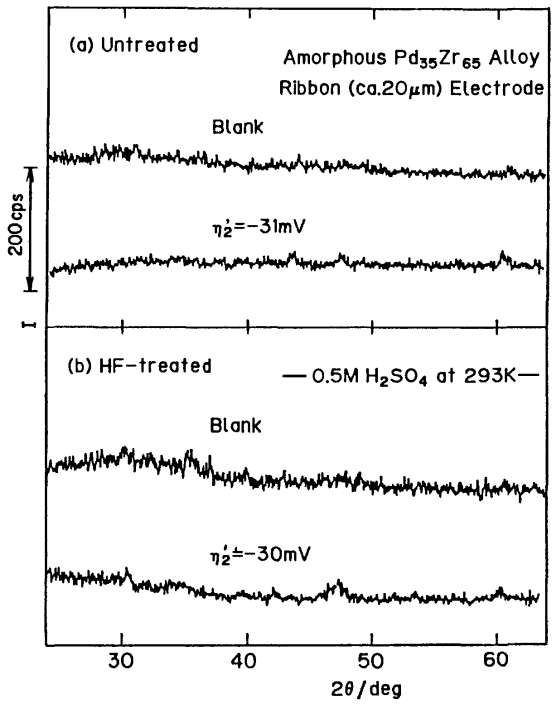

Fig. 6. In situ XRD patterns observed on an amorphous $Pd_{35}Zr_{65}$ ribbon electrode at various η_2' during the hydrogen absorption hemicycle. Polarization time was 1 h. 0.5 M H_2SO_4.

Amorphous $Pd_{35}Zr_{65}$ Alloy Ribbon Electrodes. Figure 6 shows in situ XRD patterns observed on amorphous $Pd_{35}Zr_{65}$ alloy ribbon electrodes before and after the etching treatment in dilute HF solution. Both the untreated and HF-treated specimens before the polarization gave no peak in the XRD patterns originating from crystalline phases (see blank one). Further, no XRD peak corresponding to hydrides was detected even under the cathodic polarization conditions (η_2'=ca. −30 mV). This result may be important in suggesting that the amorphous alloy materials are not likely to encounter hydrogen embrittlement due to recrystallization even under strong hydrogen charging conditions such as the one in the electrochemical cathodic polarization, and thus they may be used in hydrogen storage-type batteries.

Conclusion

An in situ XRD technique was developed and applied to the studies of phase changes during metal hydride formation in Pd and Pd-Au alloy foil and amorphous Pd-Zr ribbon electrodes. The technique may be applicable to studies of composition or structure changes in other electrochemical processes. The α-β phase transformation in PdH_x or no such phase changes in Au-rich Pd-Au alloy foils and amorphous Pd-Zr alloy ribbons were indicated.

The present work has been partly supported by Grants-in-Aid for Scientific Reseasrch from the Ministry of Education, Science and Culture.

References

1) "Hydrogen for Energy Storage," ed by A. F. Andressen and A. J. Maeland, Pergamon Press, New York (1978), p. 19.
2) F. A. Lewis, "The Palladium Hydroge System," Academic Press, New York (1967), pp. 70—93.
3) A. Maeland and T. B. Flanagan, *J. Phys. Chem.*, **69**, 3575 (1965).
4) A. W. Carson and F. A. Lewis, *Trans. Faraday Soc.*, **63**, 1453 (1967); R. Burch and R. G. Buss, *J. Chem. Soc., Faraday Trans. 1*, **71**, 913 (1975).
5) S. Uno Falk, *J. Electrochem. Soc.*, **107**, 661 (1960); A. J. Salkind, C. J. Venuto, and S. Uno Falk, *ibid.*, **111**, 493 (1964).
6) G. Nazri and R. H. Müller, *J. Electrochem. Soc.*, **132**, 1385, 2051, 2054 (1985).
7) K. Machida and M. Enyo, *Chem. Lett.*, **1986**, 1437.
8) T. Maoka and M. Enyo, *Electrochim. Acta*, **26**, 607, 615 (1981).
9) M. Enyo, *J. Res. Inst. Catal., Hokkaido Univ.*, **30**, 11 (1982).
10) M. Enyo, T. Yamazaki, K. Kai, and K. Suzuki, *Electrochim. Acta*, **28**, 1573 (1983).
11) K. Kunimatsu, *Hyomen (Surface)*, **20**, 197 (1982).
12) Ref. 2, p. 33.

 © 1989 The Chemical Society of Japan Bull. Chem. Soc. Jpn., 62, 419—423 (1989)

Ionization and Dissociation of Picric Acid in 4-Methyl-2-pentanone Solutions at Various Water Concentration

Tatsuya SEKINE* and Hirochika NAGANAWA
Department of Chemistry, Science University of Tokyo, Kagurazaka, Shinjuku-ku, Tokyo 162
(Received May 26, 1988)

The spectrum of picric acid in 4-methyl-2-pentanone solutions which contained the acid and water at several concentrations was determined in the wavelength range from 330 to 500 nm and the data were statistically analyzed. It was concluded that picric acid molecules formed ion pairs together with four water molecules in these solutions and the ion pairs thus formed dissociated partially. Both of the ion pairs and dissociated picrate ions in these solutions had strong absorption in the visible range where no absorption was found with the acid molecules but the spectra of these two species were different. The formation and dissociation constants of the ion pairs were also calculated from the data and the role of water in these chemical reactions was considered.

In a previous paper,[1] the dissociation of picric acid in water-saturated 4-methyl-2-pentanone was studied by a liquid-liquid distribution method and the results were compared with those of perchloric and nitric acid. It was concluded that picric acid in this medium was a weak acid (pK_a=4.7) which was weaker than perchloric acid (pK_a=3.5) but stronger than nitric acid (pK_a=6.0). An acid in the undissociated form in such organic solvents may be present in two different chemical forms; the acid molecule and the ion pair. However, it was not possible to know only from these liquid-liquid distribution data whether the undissociated picric acid was in one of these chemical forms or it was a mixture of both. In the present study, the spectrum of picric acid in 4-methyl-2-pentanone solutions was determined at various concentrations of the acid and water. The data were statistically analyzed and the spectrum of the ion pairs was estimated. Furthermore, the molar ratio of the two chemical forms of undissociated acid species was calculated. The formation constant of the ion pairs from the acid molecules as well as the dissociation constant of the ion pairs thus formed were determined at several water concentrations and the role of water for these reactions was considered.

Experimental

All the materials were of a reagent grade. A small amount of picric acid was stored in a reduced pressure desiccator. The 4-methyl-2-pentanone was distilled twice. All the procedures were carried out in a thermostated room at 298 K. A picric acid solution of water-saturated 4-methyl-2-pentanone was prepared by shaking the solvent with an aqueous solution which contained a certain amount of the acid. In order to prepare a picric acid solution of 4-methyl-2-pentanone at a certain acid concentration and a desired water concentration, a water-saturated solution containing the acid was mixed with a calculated amount of dry solvent in a stoppered polypropylene tube. Use of glass vessels was found to be unfavorable for the experiments. When glass vessels were used, the reproducibility of the data was poor but by use of polypropylene vessels, it was much improved. This is probably due to that a part of water and/or the acid are adsorbed on the surface of glass. The absorbance of the picric acid solutions which contained water was measured from 330 to 500 nm. The acid concentration was determined as follows. A portion of the solution was transferred into another tube and ten times volume of hexane was added in order to make the back extraction of the acid more easily. Then the solution was shaken with a 1×10^{-3} mol dm^{-3} aqueous sodium hydroxide solution and the optical absorption of the aqueous phase at 380 nm where the molar absorptivity was 1.34×10^4 was measured. The spectrum of tetrabutylammonium picrate of 4-methyl-2-pentanone solutions at different water concentrations was determined in a similar manner as previously reported.[2] Quartz cells of 1 to 10 mm optical path were used for this spectrophotometry. The water concentration in the solution was determined by the Karl-Fischer titration. A spectrophotometer (Hitachi 556 type) which was connected with a personal computer (NEC 9801 VM type) through a 12 bit interface (Microscience Co. DAS-1898BPC type) was used throughout the experiments.

Data Analysis

In a 4-methyl-2-pentanone solution, picric acid may be present in three forms; an acid molecule ($Hpic(H_2O)_p$), an ion pair ($H^+pic^-(H_2O)_q$), and a picrate ion ($pic^-(H_2O)_r$) which has released a proton ($H^+(H_2O)_s$). Each of the value of p, q, r, and s in the above chemical formulas could be different when the water concentration is different but these values can not be determined in the present study. Thus the total concentration of picric acid in the solution may be written as;

$$[\mathrm{Acid}]_{\mathrm{total}} = \sum[Hpic(H_2O)_p] + \sum[H^+pic^-(H_2O)_q] + \sum[pic^-(H_2O)_r] \quad (1)$$

The water concentration experimentally determined is the sum of the associated and unassociated water with the acid. However, since the water concentration in the present study (0.5 to 0.8 mol dm^{-3}) is in a large excess to the acid, the concentration of total water could be regarded as that of the unassociated water. The ionization of acid is caused by the water in the medium. If the number of water molecules which are necessary for the formation of an ion pair from an acid molecule is always the same even when the water concentration in the medium is different, the following

statistical treatments are possible. Under such conditions, each of p, q, r, and s could be treated as a fixed value in the equations in order to make a simpler expression. The equilibrium for the formation of ion pairs from the acid molecules may generally be written as;

$$Hpic(H_2O)_p + n\ H_2O \rightleftarrows H^+pic^-(H_2O)_q$$

$$K_{ip} = \frac{[H^+pic^-(H_2O)_q]}{[Hpic(H_2O)_p]\,[H_2O]^n} \quad (2)$$

Part of the ion pairs may undergo dissociation. The equilibrium can be written as;

$$H^+pic^-(H_2O)_q \rightleftarrows H^+(H_2O)_s + pic^-(H_2O)_r$$

$$K_{dis} = \frac{[H^+(H_2O)_s]\,[pic^-(H_2O)_r]}{[H^+pic^-(H_2O)_q]} \quad (3)$$

Since several properties of the medium such as the dielectric constant etc. could be different when the water concentration is different, the value of dissociation constant of the ion pairs may be affected by the change in the concentration of water.

The overall acid dissociation constant in the medium may be written as;

$$K_a = \frac{[H^+(H_2O)_s]\,[pic^-(H_2O)_r]}{[Hpic(H_2O)_p] + [H^+pic^-(H_2O)_q]} \quad (4)$$

This can also be rewritten as;

$$K_a = \frac{K_{dis}\,K_{ip}[H_2O]^n}{1 + K_{ip}[H_2O]^n} \quad (5)$$

The absorbance of the solution, A, may be written as;

$$A = \varepsilon_{mol}[Hpic(H_2O)_p] + \varepsilon_{ip}[H^+pic^-(H_2O)_q] + \varepsilon_{ion}[pic^-(H_2O)_r] \quad (6)$$

where ε_{mol}, ε_{ip}, and ε_{ion} is the molar absorptivity of acid molecules, ion pairs, and dissociated picrate ions, respectively, at a certain wavelength.

From Eqs. 1 to 6, the following equation is obtained;

$$A = \frac{1}{2}K_a(\sqrt{1 + 4K_a^{-1}[Acid]_{total}} - 1) \times \left\{\frac{1}{2}\varepsilon_u(\sqrt{1 + 4K_a^{-1}[Acid]_{total}} - 1) + \varepsilon_{ion}\right\} \quad (7)$$

where ε_u is the molar absorptivity of the acid in the undissociated form which can be written as;

$$\varepsilon_u = \frac{\varepsilon_{ip}K_{ip}[H_2O]^n + \varepsilon_{mol}}{1 + K_{ip}[H_2O]^n} \quad (8)$$

When the water concentration is different, the value of ε_u should not be the same as seen from this equation.

In the present study, the spectra of solutions were determined at various acid and water concentrations and the data were analyzed by a successive approximation method using a least squares computer program.

Results

In the present study, the spectra of the following 98 sample solutions were measured. The water concentration was 0.801 (water saturated), 0.751, 0.701, 0.651, 0.601, 0.551, and 0.501 mol dm^{-3} and the total picric acid concentration was 14 different values from 5×10^{-6}

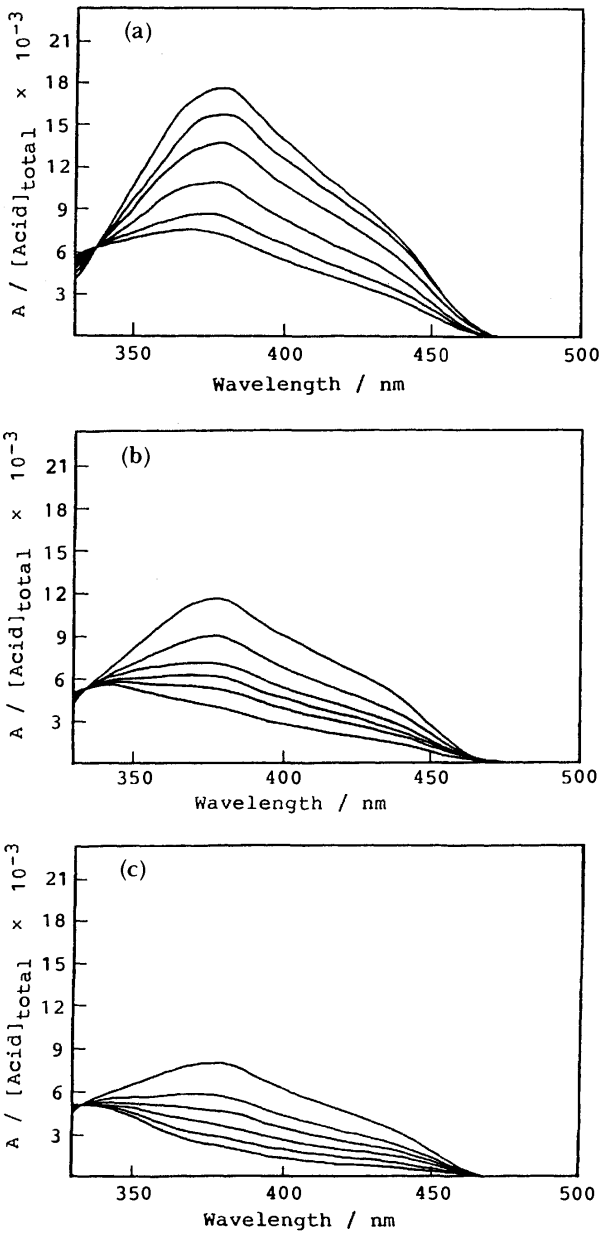

Fig. 1. Examples of spectra of picric acid in 4-methyl-2-pentanone which contained water. The total acid concentration, $[Acid]_{total}$, for each curve in the figures is from the top to the bottom in the right side. (a) $[H_2O]_{total}$ is 0.801 mol dm^{-3} (water saturated) and $[Acid]_{total}$ is 4.77×10^{-6}, 1.45×10^{-5}, 2.90×10^{-5}, 8.25×10^{-5}, 2.03×10^{-4}, and 3.45×10^{-4} mol dm^{-3}. (b) $[H_2O]_{total}$ is 0.651 mol dm^{-3} and $[Acid]_{total}$ is 1.96×10^{-5}, 4.94×10^{-5}, 1.10×10^{-4}, 1.60×10^{-4}, 2.50×10^{-4}, and 6.02×10^{-4} mol dm^{-3}. (c) $[H_2O]_{total}$ is 0.501 mol dm^{-3} and $[Acid]_{total}$ is 2.10×10^{-5}, 5.25×10^{-5}, 9.39×10^{-5}, 1.84×10^{-4}, 3.29×10^{-4}, and 8.05×10^{-4} mol dm^{-3}.

to 1×10^{-3} mol dm^{-3} for each water concentration. Figures 1(a) to 1(c) give the spectra obtained when the water concentration was 0.801, 0.651, and 0.501 mol dm^{-3} as examples of the experimental data.

The absorbance of the 14 solutions of the same water concentration but different $[Acid]_{total}$ was measured from 330 to 500 nm at an interval of 1 nm. Since the absorbance due to the solvent could not be canceled out when the wavelength was lower than 330 nm, no optical data were obtained in this lower wavelength range. From these data, the value of ε_u was determined on the basis of Eq. 7 for each wavelength to give the best-fit with the optical data at a certain given value of K_a. By repeating these procedures, a value of K_a which was common for the data of all the wavelengths and a value of ε_u for each wavelength (total 171 values of ε_u in the above wavelength range) were calculated for each given water concentration. Table 1 lists the values of K_a for the seven water concentrations thus obtained. The spectra of the undissociated species were calculated as shown in Fig. 2. When the water concentration in the medium was very low, for example, such as 5×10^{-3} mol dm^{-3}, no absorption due to the ion pairs and/or due to the dissociated picrate ions was found in the visible range and the spectrum from 330 to 500 nm was essentially similar to that of picric acid in cyclohexane obtained by separate experiments. For this reason, it was concluded that only the spectrum of the acid molecules was observed under such conditions. This spectrum is also given in Fig. 2. It was found that the spectrum of 1×10^{-5} mol dm^{-3} of tetrabutylammonium picrate in 4-methyl-2-pentanone was not affected by water in the concentration range of the present study. The salt could be regarded to dissociate nearly completely at this concentration at least in the water-saturated medium.[2] From these, it could be assumed that the molar absorptivity of the dissociated picrate ions, ε_{ion}, is not affected by water under the conditions of the present study.

The above results indicate that water is indispensable for the formation of ion pairs in the medium. From the values of ε_u, the value of n and of K_{ip} were calculated on the basis of Eq. 8 by the successive approximation method. After trials, the number of water molecules which were necessary to form the ion pairs from acid molecules in 4-methyl-2-pentanone, n in Eq. 2, was found to be 4.0. The value of K_{ip} is found to be $10^{-0.35}$ as given in Table 1. Furthermore, the value of K_{dis} at each water concentration was determined by introducing a set of values of K_a, K_{ip}, and n into Eq. 5 as listed in Table 1. Figure 3 gives the spectra of the three chemical species of picric acid. The spectrum of ion pairs was obtained by the above calculation but that of acid molecules and of dissociated picrate ions were obtained by separate experiments under conditions where only one of these species was found in the solution.

Table 1. Summary of the Values Obtained by Analysis of Data

$[H_2O]_{total}$	log K_a	log K_{ip}[a]	log K_{dis}	n[b]	R[c]
0.801	−4.51	−0.35	−3.70	4.0	0.156
0.751	−4.61	−0.35	−3.71	4.0	0.125
0.701	−4.73	−0.35	−3.72	4.0	0.098
0.651	−4.87	−0.35	−3.74	4.0	0.075
0.601	−5.01	−0.35	−3.75	4.0	0.056
0.551	−5.15	−0.35	−3.75	4.0	0.040
0.501	−5.33	−0.35	−3.77	4.0	0.028

a) In the successive approximation procedures of data analysis, K_{ip} in Eq. 2 was assumed to be constant even when the water concentration was different. The range of error for this value obtained is ±0.07. b) The number of water molecules which are necessary to form an ion pair from one acid molecule. The range of error for this value obtained is ±0.14. c) The molar ratio of ion pairs to the acid in the undissociated form; $R=[H^+pic^-]/([Hpic]+[H^+pic^-])$.

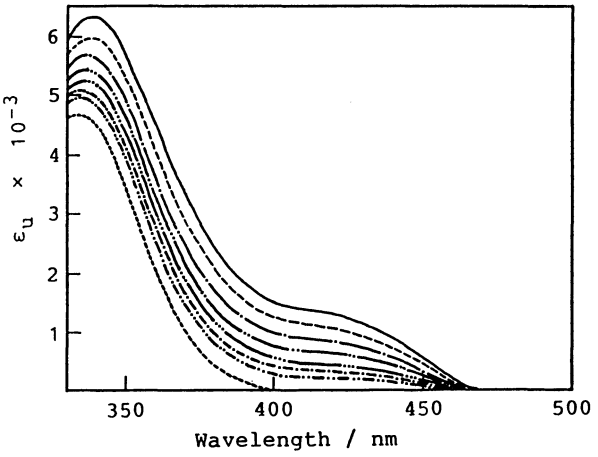

Fig. 2. Calculated spectrum of picric acid in the undissociated form when the $[H_2O]_{total}$ is different. The $[H_2O]_{total}$ is 0.801, 0.751, 0.701, 0.651, 0.601, 0.551, 0.501, and 5.0×10^{-3} mol dm^{-3} from the top to the bottom.

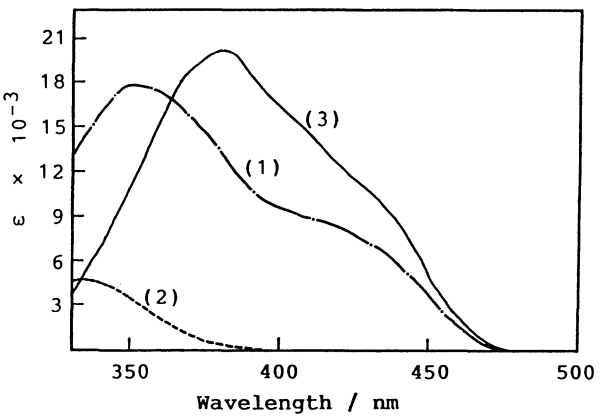

Fig. 3. Absorption spectrum of (1) ion pairs obtained by calculation and that of (2) acid molecules and (3) dissociated picrate ions obtained by separate experiments. The solvent is 4-methyl-2-pentanone containing water.

Discussion

In the previous paper,[1] the dissociation constant of picric acid in water-saturated 4-methyl-2-pentanone was determined by a liquid-liquid distribution method to be $10^{-4.7}$. This value is approximately similar to that in the water-saturated medium obtained by the spectrophotometry in the present study, $10^{-4.51}$. The water concentration in the solvent was the same throughout the experiments and no spectrophotometric measurements were made in this previous liquid-liquid distribution study. For this reason, the chemical form of the undissociated acid and the role of water for the acid dissociation could not be concluded. However, the following conclusions can be drawn from the results in the present study. (i) Since the spectrum of picric acid in this solvent at lower water concentrations is quite similar to that in cyclohexane, all the acid should be in the form of acid molecule under these conditions. Thus the change in the spectrum by the change in the water concentration in 4-methyl-2-pentanone can well be explained in terms of ion-pair formation from one acid molecule with four water molecules and that of the dissociation of ion pairs thus formed. In other words, water is an essential base which has an electron donating oxygen atom and causes the ion-pair formation. However, 4-methyl-2-pentanone should be a too weak base for this. (ii) Since the value of K_{dis} was not affected very much by the change in the water concentration as is seen from Table 1, the change in the physical properties of the medium should be only slight in the concentration range of water of the present study. (iii) The overall acid dissociation constant, K_a in Eq. 4, is dependent on the water concentration but the dissociation constant of the ion pairs, K_{dis} in Eq. 3, is only slightly dependent on it. Thus the dependence of the overall acid dissociation constant on the water concentration is an apparent effect. This is because although the ionization of the acid is caused by water, K_a in Eq. 4 does not contain the term of water concentration. The effect of water can be normalized by Eq. 5. (iv) The value of K_{dis} in water-saturated solvent ($10^{-3.70}$) is similar to that of the dissociation constant of sodium and potassium salt of this acid ($10^{-3.60}$ for sodium salt and $10^{-3.61}$ for potassium salt) in the same medium as reported in the previous paper.[2] This indicates that the degree of dissociation of the ion pairs is rather similar to that of sodium or potassium salt of this acid in the same medium. Furthermore, the spectrum of the ion pairs in Fig. 3 is quite similar to that of the ion pairs of sodium or potassium picrate in water-saturated 4-methyl-2-pentanone.[2] Both of the spectrum of lithium picrate in the ion-pair form and in the dissociated ion form in 2-butanone previously reported by Gilkerson and Roberts[3] are quite similar to that of picric acid in the corresponding chemical form obtained in the present study. (v) Since four water molecules should hydrate a proton when the acid is ionized, the cation, $H_9O_4^+$, may be formed in such a medium like in aqueous solutions[4,5]. This cation could be present in the dissociated form or in the ion-pair form with a picrate ion in 4-methyl-2-pentanone.

Iwachido, Oosawa, and Tôei studied the dissociation of picric acid in 4-methyl-2-pentanone, 2-butanone, and acetone by spectrophotometry and by vapor-pressure osmometric method.[6] In this previous paper, the dissociation equilibrium in the following equation was considered.

$$HA_{x(H_2O)} + nH_2O \rightleftarrows H^+_{y(H_2O)} + A^-_{z(H_2O)}$$

From Fig. 1 in this previous paper, the pK_a in water-saturated 4-methyl-2-pentanone can be read as $10^{-4.3}$. Furthermore, the hydration number of proton was concluded to be 4.0 in this previous study. However, as seen from Fig. 2 in the present study, the spectrum of the undissociated acid, which is the cumulative spectrum of both the acid molecules and ion pairs, is dependent on the water concentration. This is due to the difference in the proportion of the ion pair species in the undissociated acid when the water concentration is different. Thus when the acid dissociation is determined by spectrophotometry and when the formation of ion pairs is not taken into account, the fraction of ion pairs is not involved in the fraction of the undissociated acid but it is involved in the fraction of the dissociated picrate ions. This should cause an overestimation of the acid dissociation. Furthermore, as seen from Fig. 3, the spectra of ion pairs and dissociated picrate ions are different and this causes an error in the estimation of the dissociation constant when the wavelength to be used for the data analysis is different. Table 1 also gives the calculated molar ratio of the ion pairs to the undissociated acid at each water concentration. This ratio should be independent from the acid concentration when the water concentration is the same as seen from Eq. 2. When ion pairs are formed, a careful correction for this species should be made for the determination of the acid dissociation constant by spectrophotometry. Such a correction should not be necessary when the medium is high dielectric as water or it is low dielectric as cyclohexane. This is because in the former, the formation of ion pairs is negligible and in the latter, the dissociation of the ion pairs is negligible. However, in a moderately dielectric medium as in 4-methyl-2-pentanone (dielectric constant=13.1, dry solvent at 293 K), consideration on the effect for the optical absorption due to the ion pairs is important under certain conditions. This should be necessary in order to make a reasonable estimation of the dissociation equilibrium of the acid.

The authors are grateful to Dr. Satoshi Kusakabe for his valuable discussion.

References

1) T. Sekine, T. Yoshikata, and T. Saitou, *Bull. Chem. Soc. Jpn.*, **57**, 2748 (1984).
2) H. Naganawa and T. Sekine, *Anal. Sci.*, **3**, 427 (1987).
3) W. R. Gilkerson and A. M. Roberts, *J. Am. Chem. Soc.*, **102**, 5181 (1980).
4) R. Grahn, *Arkiv Fysik.*, **1**, 13 (1962).
5) H.-G. Lee, Y. Matsumoto, T. Yamaguchi, and H. Ohtaki, *Bull. Chem. Soc. Jpn.*, **56**, 443 (1983).
6) T. Iwachido, S. Oosawa, and K. Tôei, *Bull. Chem. Soc. Jpn.*, **58**, 2415 (1985).

Syntheses, and Crystal and Molecular Structures of Tetraethylammonium, and Tetrapropylammonium Tris(thiocyanato)cadmates(II), $[R_4N][Cd(SCN)_3]$, ($R=C_2H_5$, C_3H_7)

Masahiro TANIGUCHI* and Akira OUCHI
Department of Chemistry, College of Arts and Sciences, The University of Tokyo, Komaba, Meguro-ku, Tokyo 153
(Received July 23, 1988)

The title complexes have been synthesized and their crystal and molecular structures determined by a single crystal X-ray diffraction technique. $[(C_2H_5)_4N][Cd(SCN)_3]$ (**1**) is orthorhombic with a space group of $A2_1am$; $a=10.773(2)$, $b=16.574(4)$, $c=9.871(2)$ Å, and $Z=4$, while $[(C_3H_7)_4N][Cd(SCN)_3]$ (**2**) is triclinic with a space group of $P\bar{1}$; $a=10.297(5)$, $b=11.542(5)$, $c=9.374(3)$ Å, $\alpha=90.10(3)$, $\beta=91.61(4)$, $\gamma=80.94(4)°$, and $Z=2$. In **1**, the metal atom has a 3*N*,3*S*-hexa-coordinated octahedral geometry, and three ligated N atoms take *fac*-configuration. Each pair of a metal atoms are bridged by three thiocyanate (SCN) ions, where two SCN ions are *S*-coordinated, while the other is *N*-coordinated to the same side metal atom, forming a linear polymeric form. In **2**, the metal atom is in a 3*N*,2*S*-penta-coordinated trigonal-bipyramidal geometry, where one non-bridging SCN ion is *N*-coordinated equatorially, while four bridging SCN ions are ligated with two N (axially), and two S atoms (equatorially), respectively. Each pair of metal atoms is bridged by two SCN ions, forming a linear polymeric form. The respective tetraalkylammonium ions in **1** and **2** are not bridged to the complex anions, but are bonded only electrostatically. The final *R* values obtained are: **1**, 0.042 and **2**, 0.052.

Several reports about the thiocyanato complexes of cadmium, in which the metal atoms are bridged by thiocyanate (SCN) ions, have already been published.[1-9] Many of the complexes are the neutral Lewis base adducts of cadmium(II) thiocyanates,[1-7] but there are some, not many, anionic thiocyanato complexes where the central cadmium atoms are coordinated only to SCN ions.[8,9] These anionic complexes have their own polymeric form, respective types of bridging structures. The $M[Cd(SCN)_3]$ type tris(thiocyanato)-cadmates of rubidium,[9] cesium,[9] and tetramethylammonium[8] are in two-, three-, and one-dimensional polymeric form, respectively. Moreover, in the case of the tetramethylammonium salt, we could obtain another type of thiocyanatocadmate, $[(CH_3)_4N]_2[Cd(SCN)_4]$, which has a different type of polymeric chain.[8] Therefore, it was thought to be very interesting to synthesize and to clarify the structures of the other kinds of tetraalkylammonium thiocyanatocadmates.

From this aspect, we have synthesized the title two new complexes, and their crystal and molecular structures were determined by the single-crystal X-ray diffraction method.

Experimental

Synthesis of Tetraethylammonium and Tetrapropylammonium Tris(thiocyanato)cadmates(II). Cadmium(II) thiocyanate, as well as tetraethyl- and tetrapropylammonium thiocyanates were obtained by metathetical reactions between their chlorides and potassium thiocyanate in methanol, respectively, by the method of Singh.[10]

The tetraethylammonium salt, $[(C_2H_5)_4N][Cd(SCN)_3]$ (**1**), was obtained as follows. Cadmium thiocyanate (0.57 g, 2.5 mmol) was dissolved into 10 cm^3 of methanol, and the acetone solution (5 cm^3) of tetraethylammonium thiocyanate (0.47 g, 2.5 mmol) was added. The mixture was stirred and was left standing for about 1 h at ambient temperature; the crystalline product precipitated. Yield: 0.56 g (1.34 mmol, 54%). Found: Cd, 26.88; C, 31.63; H, 4.76: N, 13.29%. Calcd for $CdC_{11}H_{20}N_4S_3$: Cd, 26.96; C, 31.69; H, 4.84; N, 13.44%.

The tetrapropylammonium salt, $[(C_3H_7)_4N][Cd(SCN)_3]$ (**2**), was obtained almost by the same method as that for **1**, using an aqueous solution of cadmium thiocyanate (0.57 g, 2.5 mmol, in 5 cm^3 of water) and the acetone solution of tetrapropylammonium thiocyanate (0.61 g, 2.5 mmol, in 7 cm^3 of the solvent). Yield: 0.60 g (1.27 mmol, 51%). Found: Cd, 23.83; C, 37.85; H, 5.88; N, 11.85%. Calcd for $CdC_{15}H_{28}N_4S_3$: Cd, 23.76; C, 38.09; H, 5.97; N, 11.84%.

Intensity Data Collection. The crystallographic data as well as various experimental conditions used to obtain the intensity data of both complexes are listed in Table 1. The used crystals of both complexes were colorless. The reflections were collected on a Rigaku AFC-6A automated 4-circle X-ray diffractometer with graphite monochromated Mo $K\alpha$ radiation ($\lambda=0.71073$ Å). The observed intensities were corrected for Lorentz and polarization factors, but not for absorption and extinction.

Structure Determination. The structures were solved by the heavy-atom method. The positions of the metal, sulfur, and some other atoms were deduced from their three-dimensional Patterson maps; the other non-hydrogen atoms were located by means of successively Fourier syntheses. Their positional, isotropic and then anisotropic thermal parameters were refined by means of a block-diagonal least-squares method.

In a crystal of **1**, the ab-plane is a mirror plane, and the cadmium atom as well as one bridging SCN ion, S(2)–C(2)–N(2), are on it, while the other two bridging SCN ions are arranged on both sides of the plane, since one is the mirror image of the other (Fig. 3).

The N(3) atom of the tetraethylammonium ion is also in the mirror plane. Although only one set of its carbon atoms are shown in Fig. 3, another set of carbon atoms also exists at the respective mirror image positions, and the occupancy factors of each pair should be equal, 0.5, except for those of C(4) and C(6), 1.0, which are in the mirror plane.

As the respective electron clouds of the pairs of C(3) and $C(3^i)$, as well as of C(5) and $C(5^i)$, which are on both sides of

Table 1. Crystallographic Data and Some Experimental Conditions Regarding the Collection of the Intensity Data of Tetraethylammonium and Tetrapropylammonium Tris(thiocyanato)cadmates

Complex	$[(C_2H_5)_4N]$-$[Cd(SCN)_3]$	$[(C_3H_7)_4N]$-$[Cd(SCN)_3]$
F. W.	416.91	473.02
Crystal system	Orthorhombic	Triclinic
Space group	$A2_1am$	$P\bar{1}$
$a(l/Å)$	10.773(2)	10.297(5)
$b(l/Å)$	16.574(4)	11.542(5)
$c(l/Å)$	9.871(2)	9.374(3)
$\alpha(\phi/°)$	90.0	90.10(3)
$\beta(\phi/°)$	90.0	91.61(4)
$\gamma(\phi/°)$	90.0	80.94(4)
$U(v/Å^3)$	1762.5(7)	1099.7(8)
$D_m(d/g\ cm^{-3})$	1.56(3)	1.41(3)
$D_x(d/g\ cm^{-3})$	1.57	1.43
Z	4	2
$\mu(MoK\alpha)(n/cm^{-1})$	15.7	12.7
Number of reflection measured	3640	4111
Reflections used for calculation	1107	2795
Measured range$(2\theta/°)$	3—65	3—50
Scan width$(\theta/°)$	1.00+0.5tanθ	1.06+0.5tanθ
Size of crystal (v/mm^3)	0.03×0.25×0.30	0.13×0.16×0.27
R (R_w)	0.042(0.050)	0.052(0.067)
R_r (R_{rw})	0.043(0.051)	
F_w	0.024	0.024

$R=\sum||F_o|-|F_c||/\sum|F_o|$
$R_w=[\sum w(|F_o|-|F_c|)^2/\sum wF_o^2]^{1/2}$, where $w=1/[\{\sigma(|F_o|)\}^2+(F_w\times F_o)^2]$
R_r (R_{rw}): The R_r and R_{rw} values for the structure of inversed chirality. As these values are higher than the normal ones, they are not adopted. Moreover, as the differences between the corresponding values of the normal and inversed chirality are only a little, any more stereochemical investigations were not attempted.

the mirror plane symmetrically, are hardly separated, they are too large to be regarded as being at one position in the mirror plane. Therefore, in the final step of refinement, as a device to converge their positional parameters, two of their thermal parameters, B_{23} and B_{13}, were fixed to be 0, and were refined as usual. No such problem was found concerning the C(7) and C(9) atoms. An attempt to separate the C(8) atomic position into two was not successful: probably their positions are too close to be distinguished from each other.

All of the calculations were carried out on a HITAC M-682H or M-680H computer at the Computer Center of the University of Tokyo, using the UNICSIII program.[11] The atomic scattering factors were taken from Ref. 12.

Infrared Spectrum Measurement. The infrared spectra of these complexes were obtained by means of a JASCO 202-A infrared spectrophotometer, using liquid paraffin and hexachloro-1,3-butadiene mull.

Results and Discussion

The final atomic parameters of **1** and **2**, together with their isotropic equivalent temperature factors, are listed in Tables 2 and 3; their bond lengths and bond angles are tabulated in Tables 4 and 5, respectively.[13] A perspective drawing of the skeletons of complexes **1** and **2**, together with the numbering scheme of the atoms, are shown in Figs. 1 and 2. Projections of the unit cell of **1** and **2** along c-axis are given in Figs. 3 and 4. The numbering scheme of the tetraalkylammonium cations of **1** and **2** are shown in Figs. 3 and 4,

Table 2. Final Atomic Coordinates (×10⁴) of the Non-Hydrogen Atoms and Their Equivalent Isotropic Temperature Factors of Tetraethylammonium Tris(thiocyanato)cadmate(II) (Estimated Standard Deviations in Parentheses)

Atom	x	y	z	$B_{eq}/Å^{2\,a)}$
Cd	0	233.4(4)	0	4.0
S(1)	1277(2)	932(1)	2088(3)	5.3
S(2)	3612(3)	−1616(2)	0	6.0
N(1)	3644(6)	368(4)	1546(8)	5.1
N(2)	1327(8)	−817(5)	0	4.8
N(3)	2461(9)	3477(5)	0	3.9
C(1)	2669(6)	598(4)	1754(7)	3.3
C(2)	2280(9)	−1144(6)	0	3.8
C(3)	3425(20)	2977(10)	858(17)	5.3
C(4)	4390(19)	2584(12)	0	8.7
C(5)	3054(17)	4149(9)	−862(17)	4.9
C(6)	3914(18)	4689(8)	0	7.8
C(7)	1657(14)	3899(10)	1094(18)	4.9
C(8)	728(12)	3273(6)	1718(13)	8.3
C(9)	1709(19)	2907(8)	−910(18)	5.3

a) The equivalent isotropic temperature factors were computed by the following expression: $B_{eq}=4/3(B_{11}a^2+B_{22}b^2+B_{33}c^2)$. The B_{ij}'s are defined by: $T=\exp[-(h^2B_{11}+k^2B_{22}+l^2B_{33}+2hlB_{13}+2klB_{23}+2hkB_{12})]$.

Table 3. Final Atomic Coordinates (×10⁴) and Their Equivalent Isotropic Temperature Factors of Tetrapropylammonium Tris(thiocyanato)-cadmate(II) (Estimated Standard Deviations in Parentheses)

Atom	x	y	z	$B_{eq}/Å^{2\,a)}$
Cd	2685.8(5)	4048.3(5)	4201.5(7)	4.0
S(1)	6694(3)	4181(2)	7133(3)	6.4
S(2)	2456(3)	158(3)	2201(4)	8.4
S(3)	2108(2)	4359(2)	6842(2)	4.8
N(1)	4845(6)	3550(8)	5170(8)	5.2
N(2)	2752(7)	2350(6)	3203(9)	6.0
N(3)	−526(6)	5355(6)	6644(8)	5.0
N(4)	2481(6)	8269(5)	7922(6)	3.6
C(1)	5593(7)	3846(6)	5995(9)	4.0
C(2)	2613(8)	1451(8)	2783(9)	4.9
C(3)	542(7)	4927(6)	6689(8)	3.6
C(4)	2019(7)	7820(7)	6481(8)	3.9
C(5)	753(8)	8543(8)	5883(10)	5.7
C(6)	373(10)	7999(8)	4489(10)	6.1
C(7)	1434(8)	8277(8)	9047(8)	4.7
C(8)	1035(11)	7084(9)	9320(10)	6.8
C(9)	−96(12)	7295(13)	10423(12)	9.4
C(10)	3742(7)	7421(7)	8317(8)	4.3
C(11)	4429(9)	7745(8)	9687(9)	5.6
C(12)	5622(9)	6790(9)	9987(10)	6.1
C(13)	2732(8)	9548(6)	7801(9)	4.3
C(14)	3702(9)	9734(7)	6676(11)	5.7
C(15)	3901(11)	11028(8)	6746(13)	7.3

a) See footnote of Table 2.

Table 4. Selected Bond Lengths and Bond Angles of Tetraethylammonium Tris(thiocyanato)cadmate(II), with Their Standard Deviations in Parentheses

Bond length	(l/Å)	Bond length	(l/Å)
Cd-S(1)	2.753(2)	Cd^{iv}-S(2)	2.736(3)
Cd^{iv}-N(1)	2.336(7)	Cd-N(2)	2.253(8)
S(1)-C(1)	1.633(7)	S(2)-C(2)	1.635(10)
N(1)-C(1)	1.135(9)	N(2)-C(2)	1.160(13)
Cd···Cd^{iv}	5.442(1)		
Bond angle	**(ϕ/°)**	**Bond angle**	**(ϕ/°)**
S(1)-Cd-$S(1^{i})$	97.78(7)	S(1)-Cd-N(2)	90.48(15)
S(1)-Cd-$N(1^{ii})$	170.92(18)	$S(1^{i})$-Cd-$N(1^{iii})$	90.90(16)
$S(1^{i})$-Cd-$S(2^{ii})$	85.43(6)	$S(2^{ii})$-Cd-N(2)	173.8(2)
$N(1^{ii})$-Cd-$N(1^{iii})$	81.6(3)	Cd-S(1)-C(1)	99.6(3)
Cd^{iv}-S(2)-C(2)	94.6(4)	Cd^{iv}-N(1)-C(1)	147.1(7)
Cd-N(2)-C(2)	157.2(8)	S(1)-C(1)-N(1)	178.7(7)
S(2)-C(2)-N(2)	179.2(9)		

Key to the symmetry operations: i, x, y, $-z$; ii, $-0.5+x$, $-y$, z; iii, $-0.5+x$, $-y$, $-z$; iv, $0.5+x$, $-y$, z.

Table 5. Selected Bond Lengths and Bond Angles of Tetrapropylammonium Tris(thiocyanato)cadmate(II), with Their Standard Deviations in Parentheses

Bond length	(l/Å)	Bond length	(l/Å)
Cd-$S(1^{i})$	2.572(2)	Cd-S(3)	2.573(3)
Cd-N(1)	2.363(7)	Cd-N(2)	2.163(7)
Cd-$N(3^{ii})$	2.338(7)	S(1)-C(1)	1.625(8)
S(2)-C(2)	1.619(9)	S(3)-C(3)	1.644(7)
N(1)-C(1)	1.165(11)	N(2)-C(2)	1.137(12)
N(3)-C(3)	1.132(9)	Cd···Cd^{i}	5.373(3)
Cd···Cd^{ii}	5.855(3)		
Bond angle	**(ϕ/°)**	**Bond angle**	**(ϕ/°)**
N(1)-Cd-$N(3^{ii})$	176.1(3)	$S(1^{i})$-Cd-S(3)	116.68(9)
N(2)-Cd-$S(1^{i})$	122.0(2)	N(2)-Cd-S(3)	121.2(2)
N(1)-Cd-$S(1^{i})$	91.7(2)	N(1)-Cd-S(3)	82.8(2)
N(1)-Cd-N(2)	92.3(3)	$N(3^{ii})$-Cd-$S(1^{i})$	87.4(2)
$N(3^{ii})$-Cd-S(3)	94.2(2)	$N(3^{ii})$-Cd-N(2)	91.4(3)
Cd-$S(1^{i})$-$C(1^{i})$	98.3(3)	Cd-S(3)-C(3)	100.8(3)
Cd-N(1)-C(1)	143.1(6)	Cd-N(2)-C(2)	169.5(7)
Cd-$N(3^{ii})$-$C(3^{ii})$	160.9(6)	S(1)-C(1)-N(1)	171.5(11)
S(2)-C(2)-N(2)	170.6(11)	S(3)-C(3)-N(3)	169.5(11)

Key to the symmetry operations: i, 1.0−x, 1.0−y, 1.0−z; ii, $-x$, 1.0−y, 1.0−z.

respectively.

In **1**, each cadmium atom, which is in the mirror plane, has a 3*N*3*S*-hexa-coordinated octahedral geometry: the nitrogen atoms as well as sulfur atoms are in the *fac*-configuration, respectively. Each pair of cadmium atoms is bridged triply by three SCN ions, where the ions are coordinated to one side of the metal atom with 2N and 1S atoms, while to the other side of the metal atom with 1N and 2S atoms, respectively. This type of triple SCN bridging structure is only found in this complex, **1**, and in $[(CH_3)_4N][Cd(SCN)_3]$ (**3**);[8] it is never found in any other metal thiocyanato complexes.

The complex is linked approximately linearly along the a-axis. The cadmium atoms lie along the planes

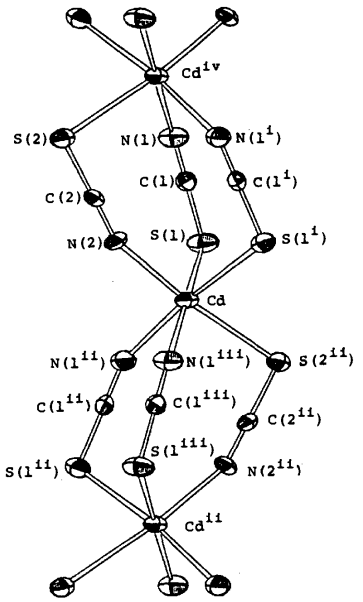

Fig. 1. A perspective drawing of the structure of $[(C_2H_5)_4N][Cd(SCN)_3]$ with the numbering scheme. (i, x, y, $-z$; ii, $-0.5+x$, $-y$, z; iii, $-0.5+x$, $-y$, $-z$; iv, $0.5+x$, $-y$, z.)

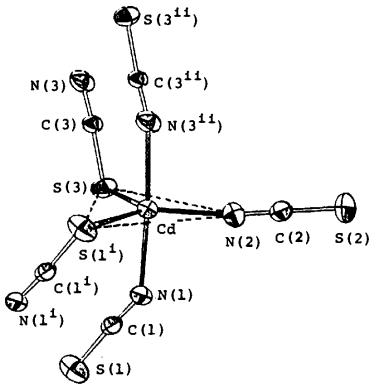

Fig. 2. A perspective drawing of the structure of $[(C_3H_7)_4N][Cd(SCN)_3]$ with the numbering scheme. (i, 1.0−x, 1.0−y, 1.0−z; ii, $-x$, 1.0−y, 1.0−z.)

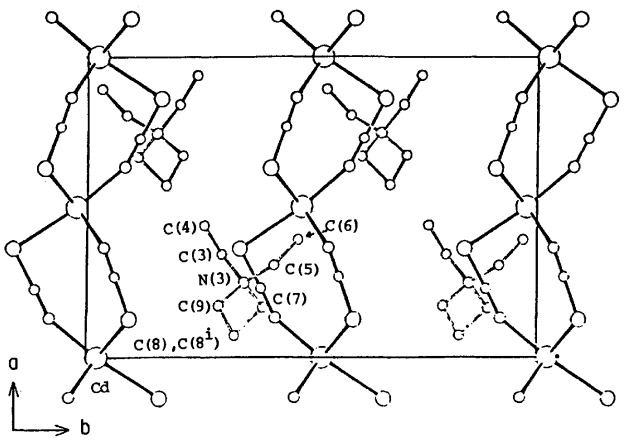

Fig. 3. A projection of the unit cell of $[(C_2H_5)_4N][Cd(SCN)_3]$ along c-axis. (i, x, y, $-z$.)

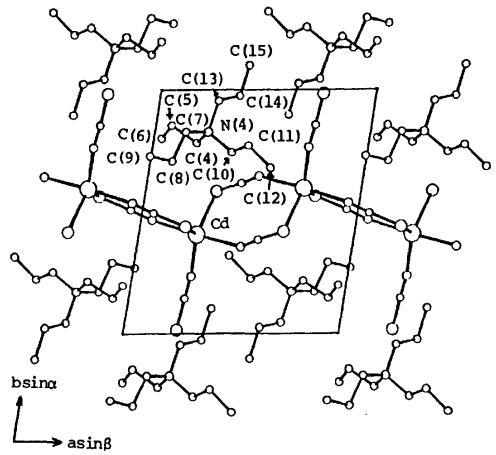

Fig. 4. A projection of the unit cell of $[(C_3H_7)_4N][Cd(SCN)_3]$ along c-axis.

parallel to the bc-plane, which cross the a-axis at 0 and 0.5.

As shown in Table 4, the average Cd-S and Cd-N bond lengths are shorter than the sum of the Shannon's ionic radii of Cd-S and Cd-N.[14] The average Cd-S and Cd-N bond lengths of **3**, 2.720 and 2.334 Å,[8] are not much different from the corresponding ones of **1**.

Similar to the Cd-N-C angles of **3** (155.5(7), 145.6(10), and 144.5(11)°),[8] the corresponding bond angles of **1**, Cd^{iv}-N(1)-C(1) (iv, 0.5+x, $-y$, z) and Cd-N(2)-C(2) (147.1(7) and 157.2(8)°), are much smaller than the angles of common thiocyanato complexes, 160—180°.

On the other hand, the Cd-S-C bond angles of **1** are in the range of the common angle of the other cadmium thiocyanato complexes (90—100°).[1-9]

The Cd··· Cd^{iv} distance is 5.442(1) Å, which is not much different from that of **3**, 5.373(3) Å, but a little shorter than the values found in the other double-SCN-chain neutral cadmium thiocyanate adducts.[1-7]

However, the chains of complexes **1** and **3** are a little different from each other. As shown in Fig. 3, all complex chains of **1** are exactly parallel, while those of **3** are not, because their neighboring chains are different in their zigzag bending structure from each other. Consequently, their corresponding SCN ions are not exactly parallel.

Complex **1** is less closely packed than **3**. Their unit-cell volumes are; **1**, 1762.5(7), and **3**, 1370(7) Å^3, respectively, where both of them are Z=4, and their respective D_x are: **1**, 1.57 and **3**, 1.75.

In **2**, the cadmium atom is 3*N*2*S*-penta-coordinated trigonal bipyramidal geometry: two nitrogen atoms, N(1) and $N(3^{ii})$, are at the axial positions, while two sulfur, $S(1^{i})$ and S(3), and one nitrogen, N(2), atoms are ligated equatorially. The angle N(1)-Cd-$N(3^{ii})$ is 176.1(3)°, which is approximately a straight line, while the positional deviation of the Cd atom from the plane of N(2), S(3), and $S(1^{i})$ atoms is only 0.04 Å.

Since, the complex **2** has a smaller coordination number, 5, than the octahedral ones, the Cd-S as well as the Cd-N bond lengths are expected to be shorter than the latter type complexes. In fact, Shannon's ionic radii of divalent cadmium in coordination number 6 and 5 are 0.95 and 0.87 Å, respectively.[14] Really the Cd-S lengths of **2** (2.573 Å on the average are shorter than those of **1** (2.745 Å on the averge). However, against expectation, the Cd-N length of **2** (2.288 Å on the average) is not much different from those of **1** (2.295 Å on the average). In **2**, the axially bridging Cd-N(1), and Cd-$N(3^{ii})$ bond lengths (2.351 Å on the average) are longer than that of the equatorially coordinated non-bridging SCN ion, Cd-N(2) (2.163(7) Å). This fact is probably due to a steric hindrance caused by packing SCN-bridging complexes in the crystal, which may originate for the same reason, since their Cd-N-C bond angles are abnormally small (143.1(6) and 160.9(6)°), compared with the corresponding angles of any common thiocyanato complexes, 180—160°. The angle of Cd-N(2)-C(2) is 169.5(7)°, which is less deviated from 180°, and which is expected to be less hindered (sterically) in the crystal.

Each pair of cadmium atoms is bridged by two SCN ions, forming a linear polymeric chain laid approximately parallel to the a-axis: Cd··· Cd^{i} and Cd··· Cd^{ii} are 5.373(3) and 5.855(3) Å, respectively. Two cadmium atoms, the central one and the next one in the line, and the atoms of two SCN ions, which bridge the two metal atoms, form an eight-membered ring. The rings on both sides of a metal atom, are in the respective planes: the deviations of the atomic positions of the rings from the respective mean-square planes are less than 0.1 Å. The dihedral angle between the two planes is 78.1°.

Some temperature factors of propyl carbon atoms of **2** are a little large; however, no clear disorder was found.

This type of penta-coordinated complex is the first example in the anionic thiocyanato complexes of cadmium. Even among the neutral adducts of cadmium(II) thiocyanates, only one example, bis(thiocyanato)-{tri(*m*-tolyl)phosphine}cadmium(II) (**4**), has been reported.[1] In **4**, one S and one N atom of SCN ions are ligated to the axial directions, while one each of P(phosphine), S(SCN), and N(SCN) atoms occupy the equatorial positions. The axial Cd-S and Cd-N bond lengths are 2.792(2) and 2.297(6) Å, while the equatorial ones are, 2.595(2) and 2.256(6) Å. Compared with the corresponding bond lengths of **2**, in **4**, the Cd-S (equatorial) is about the same, while Cd-N (equatorial) is not so short as that of **2**. This fact is probably because of the steric hindrance of the large size phosphine ligand, as well as because of the fact that the equatorial SCN ion is a bridging one in **4**.

The infrared spectra of **1** and **2** were examined. The ν(CN) band at 2100 cm^{-1} of **1** is approximately a sin-

glet, although some fine structure of the peak was recognized. On the other hand, the band of **2** appeared in two peaks (2100 and 2140 cm^{-1}), other than the additional fine structures of both peaks. The splitting of the band of **2** is probably due to the existence of two types of SCN ions as above mentioned. The ν(CS) (760 cm^{-1}), and δ (SCN) (458 cm^{-1}) bands were found in both spectra of **1** and **2**: both of them are singlets and no clear wavenumber differences were recognized between the corresponding peaks of **1** and 2.

References

1) R. G. Goel, W. P. Henry, M. J. Oliver, and A. L. Beauchamp, *Inorg. Chem.*, **20**, 3924 (1981).

2) M. Cannas, G. Carta, A. Cristini, and G. Marongiu, *Inorg. Chem.*, **16**, 288 (1977).

3) L. Cavalca, M. Nardelli, and G. Fava, *Acta Crystallogr.*, **13**, 125 (1960).

4) M. Taniguchi, M. Shimoi, and A. Ouchi, *Bull. Chem. Soc. Jpn.*, **59**, 2299 (1986).

5) M. Taniguchi and A. Ouchi, *Bull. Chem. Soc. Jpn.*, **60**, 1192 (1987).

6) M. Taniguchi, Y. Sugita, and A. Ouchi, *Bull. Chem. Soc. Jpn.*, **60**, 1321 (1987).

7) M. Taniguchi and A. Ouchi, *Bull. Chem. Soc. Jpn.*, **60**, 4172 (1987).

8) Y. Kuniyasu, Y.Suzuki, M. Taniguchi, and A. Ouchi, *Bull. Chem. Soc. Jpn.*, **60**, 179 (1987).

9) G. Thiele and D. Messer, *Z. Anorg. Allg. Chem.*, **464**, 255 (1980).

10) P. P. Singh and A. K. Gupta, *Inorg. Chem.*, **17**, 1 (1978).

11) T. Sakurai and K. Kobayashi, *Rikagaku Kenkyusho Hokoku*, **55**, 69 (1979).

12) "International Tables for X-Ray Crystallography," Kynoch Press, Birmingham (1974), Vol. IV, pp. 72, 150.

13) The final F_o—F_c tables, and some additional data of bond lengths and bond angles of **1** and **2**, are deposited as Document No. 8851 at the Office of the Editor of Bull. Chem. Soc. Jpn.

14) R. D. Shannon, *Acta Crystallogr., Sect. A*, **32**, 751 (1976). According to this report, the ionic radii are as follows: Cd(valence, 2+; coordination number, 6), 0.95, (valence, 2+, coordination number, 5), 0.87; S(valence, 2—; coordination number, 6), 1.84 Å; N(valence, 3—; coordination number, 4), 1.46 Å. Therfore, Cd-S and Cd-N in **1** are calculated to be 2.79 and 2.41 Å, while the values of **2**, 2.71 and 2.33 Å, respectively.

 © 1989 The Chemical Society of Japan Bull. Chem. Soc. Jpn., 62, 429—434 (1989)

Preparation of Crystalline $LiNb_xTa_{1-x}O_3(0 \leqq x \leqq 1)$ Films from Metal Alkoxide Solutions

Shin-ichi HIRANO* and Kazumi KATO
Department of Applied Chemistry, Faculty of Engineering, Nagoya University,
Furo-cho, Chikusa-ku, Nagoya 464
(Received August 3, 1988)

Crystalline $LiNb_xTa_{1-x}O_3(0 \leqq x \leqq 1)$ films were prepared from complex alkoxide solutions, controlling the ratio of Nb to Ta by means of a dip-coating method. The present work revealed the dependence of the film thickness on the concentration of the solution and the speed of the withdrawal of the substrate from the solution, the effects of water on the crystallization of the films, and the effects of the structures of the substrates on the crystallinity of the prepared films.

$LiNbO_3$ and $LiTaO_3$ are very attractive materials for use in piezoelectric and electrooptic devices. They have the same crystal structure and form a solid solution. The growth of single crystals had been studied mainly by means of the Czochlarski method for a long time. In both the Li_2O-Nb_2O_5 system and the Li_2O-Ta_2O_5 system, there are solid solution ranges around the stoichiometric compositions. Single crystals could be grown not from the stoichiometric melts, but from the congruent melts. The congruent compositions of $LiNbO_3$ and $LiTaO_3$ are 48.45 mol% Li_2O[1] and 48.75 mol% Li_2O[2] respectively. For SAW devices and integrated optics, $LiNbO_3$ and $LiTaO_3$ thin films were prepared by several techniques, including RF sputtering,[3-7] vapor transport,[8] epitaxial growth by melting (EGM),[9] and the liquid-phase epitaxial (LPE) growth,[10-13] in which the chemical composition has hitherto been quite difficult to control. The precise control of the composition is important in these systems, though, since their properties depend greatly on the Li_2O composition.

We ourselves previously reported the synthesis of stoichiometric $LiNbO_3$ powders and $LiNbO_3$ films by the controlled hydrolysis of carefully prepared alkoxide.[14-16] By this method, we could synthesize stroichiometric crystalline fine powders of $LiNbO_3$ at temperature as low as 250 °C,[14] and also crystalline $LiNbO_3$ films on Si and sapphire substrates.[15,16] It was found that the crystallinity of the initial thin film coating of $LiNbO_3$ affected the crystallization of films deposited subsequently. By crystallizing the initial thin film at 400 °C on a sapphire substrate, the subsequently coated film on it could be made to crystallize, even at 250 °C, without any cracks. Films on sapphire substrates crystallized with the preferred orientation, but not these on Si substrates. Several workers[17,18] have followed us in the preparation of $LiNbO_3$ films and $LiTaO_3$ films by this method because this method is a promising chemical technique by which highly pure products with desiable composition can be synthesized at low temperatures.

In this paper, we will discuss the conditions desirable for preparing $LiNbO_3$ and $LiTaO_3$ films with and without the preferred orientation from alkoxide solutions by means of the dip-coating method, we will also examine the crystallization process of these prepared films. This paper will also focus on the preparation of $LiNb_xTa_{1-x}O_3(0 \leqq x \leqq 1)$ films.

Experimental

Lithium ethoxide (99.99% pure), niobium pentaethoxide (99.999% pure), and tantalum pentaethoxide (99.9999% pure) were used as sources. Both $LiOC_2H_5$ and $M(OC_2H_5)_5$ (M=Nb,Ta) in the molar ratio of 1 : 1 were dissolved in absolute ethanol; then the mixture was stirred and refluxed carefully at 78.5 °C for 24 h in order to prepare a complex alkoxide solution.[14] For the partial hydrolysis of this solution, an adequate amount of CO_2-free, distilled water with ethanol was dropped in slowly. After the mixture had then been stirred and refluxed for 24 h, it was concentrated in order to adjust the viscosity and the density of the solutions by measuring with a rotational viscometer and a picnometer.

Optically polished Si and sapphire (α-Al_2O_3) with various crystallographic orientations (such as (100) and (111) for Si and (012), (110), and (001) for α-Al_2O_3) were used as substrates. These substrates were cleaned by ethanol before the dipping procedure.

Substrates were dipped into the solutions and withdrawn at fixed rates. Thin films formed on the substrates after they had dried for several minutes at room temperature. The coated substrates were then heated up to various temperatures at the rate of 2 °C min^{-1} and kept for 1 h at that temperature in a flow of a water-vapor and oxygen mixture, after while they were heated further for 0.5 h in dry oxygen. To examine the effect of the atmosphere on the crystallization during heat treatment, the entire heating procedure was also carried out in a flow of dry oxygen.

The crystallization of films was examined by means of XRD and FT-IR. The film thicknesses were determined by means of ellipsometry, while the morphologies of the films were observed by means of SEM.

Results and Discussion

The parameters which influenced the homogeneity, the thickness, the crystallization, and the crystallinity of the films prepared by the dip-coating method were as follows; the partial hydrolysis of alkoxide solutions, the concentration of alkoxide solutions, the speed of the withdrawal of substrates from the solutions, the crystal system and the crystallographic orientation of

the substrates, and the heating conditions.

Effects of Concentration of Alkoxide Solution and Withdrawal Speed on Film Thickness. For the composition of Li_2O-Nb_2O_5, homogeneous, transparent, and stable solutions were prepared after a partial hydrolysis of the double alkoxide solution. An amount of water equal to the amount of the double alkoxide, $R_w(H_2O/LiNb(OEt)_6)=1.0$, was essential for the partial hydrolysis if we were to prepare a stable homogeneous alkoxide solution. The viscosities and the densities of the solutions for various concentrations are shown in Table 1. Homogeneous gel films could be prepared not from a 1.3 mol dm^{-3} solution, which was almost saturated, but from solutions of up to 1.0 mol dm^{-3}. Figure 1 shows the thickness of $LiNbO_3$ films crystallized at 400 °C as a function of the concentration of the solution. It was found that the film thickness changed linearly with the concentration of the solution. Another parameter which determined the film thickness was the withdrawal speed. Figure 2 shows the effect of the withdrawal speed (U) on the thickness (t) of $LiNbO_3$ films crystallized at 400 °C. Linear relationships are observed for the log t-log U plots. This linear relation has also been observed for a solution of styrene and hexyl methacrylate in toluene,[19] for alkoxy-derived films,[20] and for $BaTiO_3$ films from alkoxide solutions.[21] In the present work on $LiNbO_3$ films, a slope of 0.45—0.54 has been observed.

Table 1. Viscosities and Densities of Solutions for Preparation of $LiNbO_3$ Films (20 °C)

Concn of soln / mol dm^{-3}	Viscosity / 10^{-3} N s m^{-2}	Density / g m^{-3}
0.2	6	0.82
0.6	7	0.86
0.8	8	0.89
1.0	8	0.92
1.3	8	0.95

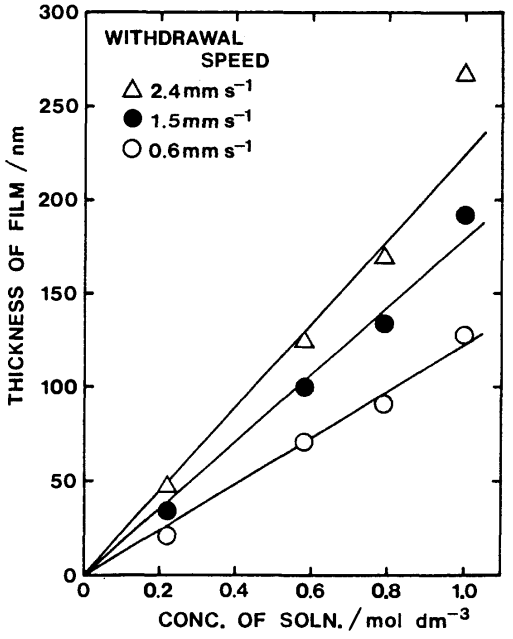

Fig. 1. Change of film thickness with concentration of solution for $LiNbO_3$ films crystallized at 400 °C.

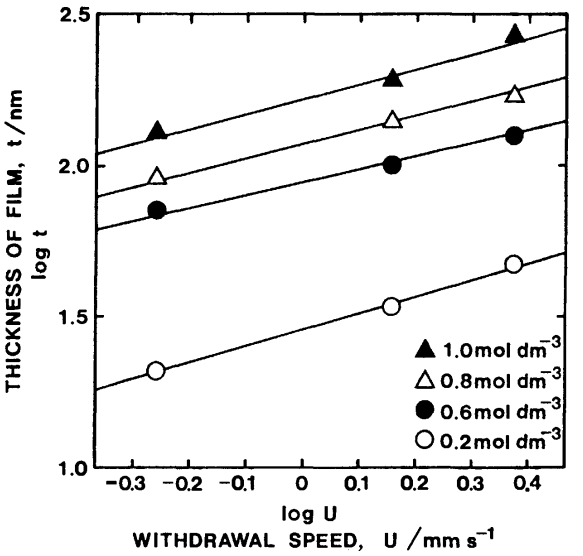

Fig. 2. Change of film thickness (t) with withdrawal speed (U) for $LiNbO_3$ films crystallized at 400 °C expressed in logarithmic scale.

Table 2. Viscosities and Densities of Solutions for Preparation of $LiTaO_3$ Films (20 °C)

Concn of Soln / mol dm^{-3}	Viscosity / 10^{-3} N s m^{-2}	Density / g m^{-3}
0.2	6	0.83
0.6	7	0.91

Table 3. Concentrations of Solutions and Thicknesses of $LiTaO_3$ Films Crystallized at 500 °C

Concn of soln / mol dm^{-3}	Film thickness / nm		
	Withdrawal speed / mm s^{-1}		
	0.6	1.5	2.4
0.2	27	40	50
0.6	86	126	180

The alkoxide solution with the Li_2O-Ta_2O_5 composition was more sensitive to water than the solution with the Li_2O-Nb_2O_5 composition. Even though a very small amount of water (R_w=1/4) was added, the solution came to be opaque colloidal, which was not appropriate for the dip-coating. Therefore, $LiTaO_3$ films were prepared from the double alkoxide solution without partial hydrolysis. The viscosities and the densities of the solutions are shown in Table 2. The saturated concentration of the solution with the Li_2O-Ta_2O_5 composition was about 0.7 mol dm^{-3}. Therefore, the relationships between the concentration of the solution and the thickness of films crystallized at

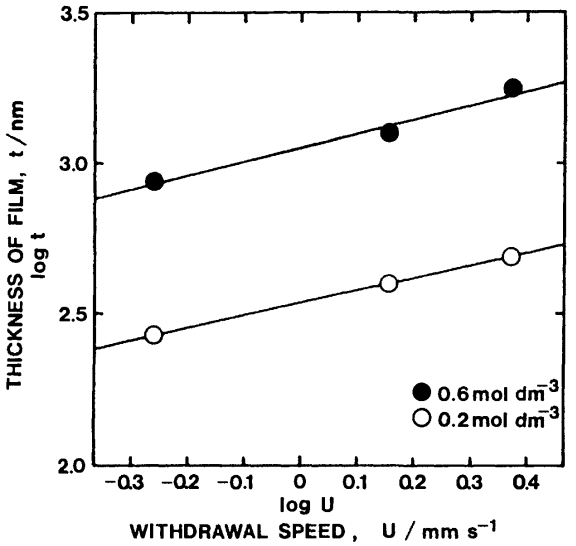

Fig. 3. Change of film thickness (t) with withdrawal speed (U) for $LiTaO_3$ films crystallized at 500 °C expressed in logarithmic scale.

500 °C, and the withdrawal speed and the film thickness, were measured for the solutions up to 0.7 mol dm^{-3} (Table 3 and Fig. 3). The film thickness was found to increase linearly with the concentration of the solution, also, it depended on the withdrawal speed to a power in the range from 0.41 to 0.47.

Effect of Water on Crystallization of Films. The as-prepared $LiNbO_3$ films on Si substrates, which had been prepared from the solution with R_w=1.0, were amorphous. Figure 4(a) shows the FT-IR spectra of films heated in the flowing of a water vapor and oxygen mixture. The as-prepared film showed an absorption band at 540 cm^{-1} attributable to a Nb-O bond. The band shifted to the higher frequency side because of the strengthening of the Nb-O bond with the crystallization of the film, and the film heated at 400 °C showed a strong absorption band at 590 cm^{-1}. It has been confirmed by the electron-diffraction method that the film heated at 250 °C was polycrystalline, and the film crystallized at 400 °C on Si showed the same XRD pattern as did crystalline $LiNbO_3$ powders.[15] On the contrary, a $LiNbO_3$ film which had been prepared from a solution without partial hydrolysis (R_w=0) and then heated to 400 °C showed a broader absorption band on the lower-frequency side, as is shown in Fig. 4(b). From the XRD pattern of this film, the crystallinity was found to be lower than that of films prepared from the solution with the partial hydrolysis. This result clearly indicates the importance of controlled partial hydrolysis for the crystallization of films.

Figures 5(a) and (b) show the FT-IR spectra of $LiTaO_3$ films heated in the flow of a water vapor and oxygen mixture, and in one of dry oxygen, respectively. The films which were crystallized at 500 °C in the flow of a water vapor and oxygen mixture showed

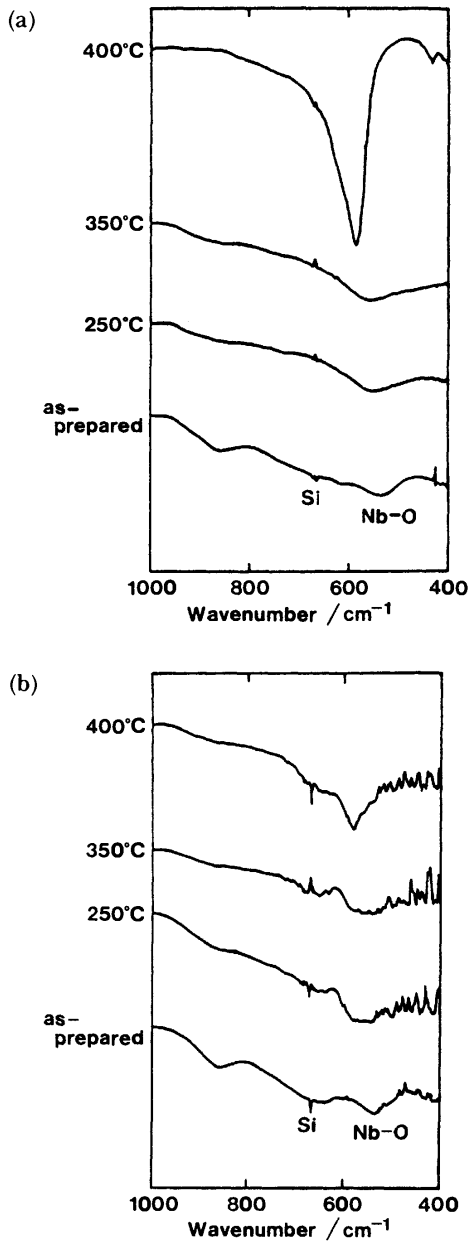

Fig. 4. FT-IR spectra of $LiNbO_3$ films, which were prepared from (a) solution with the partial hydrolysis (R_w=1.0) and (b) solution without partial hydrolysis (R_w=0), heated in a flowing mixture of water vapor and oxygen on Si.

a strong absorption band at 590 cm^{-1} attributable to a Ta-O bond. In contrast with this film, the film heat-treated at 500 °C in a flow of dry oxygen showed only a broad absorption band on the lower-frequency side, plus another absorption band on 860 cm^{-1} attributable to the residual CO_3^{2-} groups. Figure 6 shows the XRD profiles of $LiTaO_3$ films on Si(111) substrates heated in the flow of a water vapor and oxygen mixture, which revealed the occurrence of the crystallization. However, the film heated in the flow of a dry oxygen without water vapor stream did not crystallize at the same temperature of 500 °C.

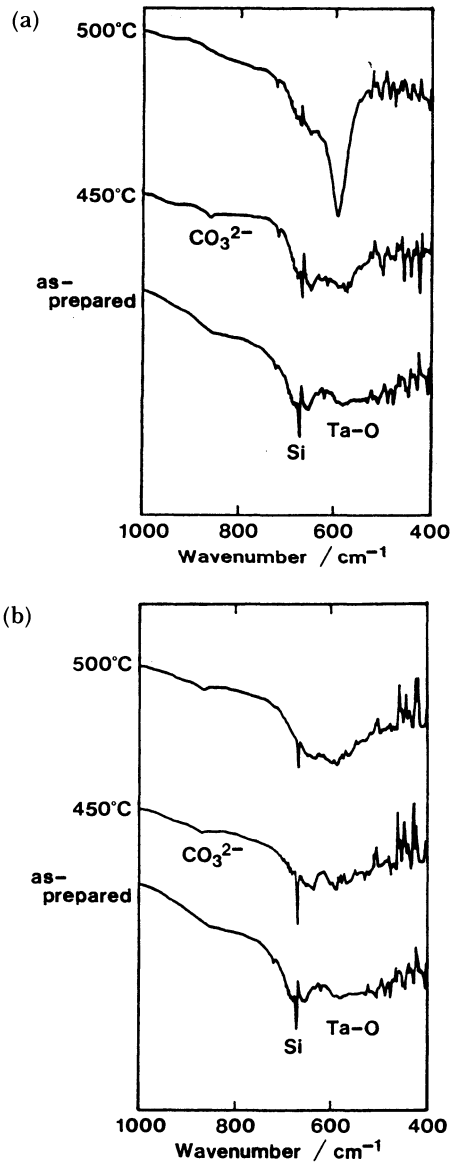

Fig. 5. FT-IR spectra of $LiTaO_3$ films on Si heated in flow (a) of water vapor and oxygen mixture and (b) of dry oxygen.

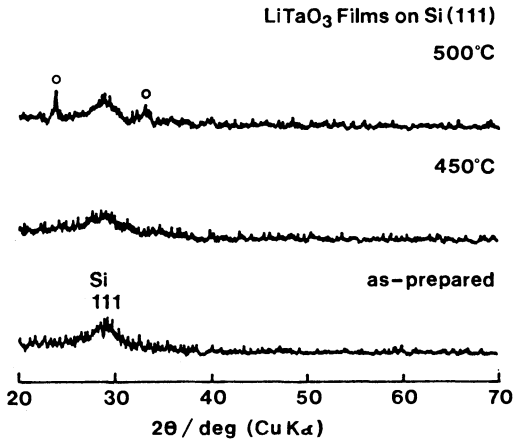

Fig. 6. XRD profiles of $LiTaO_3$ films heated in flow of water vapor and oxygen mixture on Si(111) substrates.

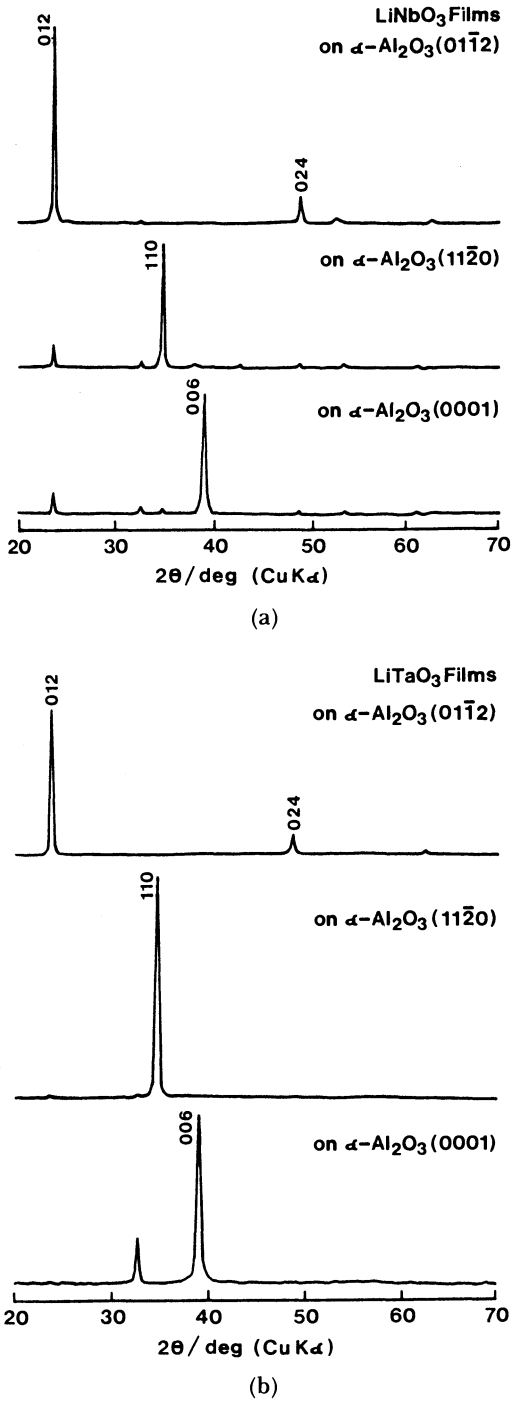

Fig. 7. XRD profiles of (a) $LiNbO_3$ films crystallized at 400 °C on sapphire substrates and (b) $LiTaO_3$ films crystallized at 500 °C on sapphire substrates.

Effects of Substrates on Crystallinity. Both $LiNbO_3$ films and $LiTaO_3$ films on Si substrates were polycrystalline and showed the same XRD profiles as those of $LiNbO_3$ powders and $LiTaO_3$ powders respectively. On the contrary, these films on sapphire substrates, which have the same type of oxygen packing as $LiNbO_3$ and $LiTaO_3$, crystallized with the preferred orientation along each orientation, such as (012), (110), and (001) sapphire. Figures 7(a) and (b) show

the XRD profiles of $LiNbO_3$ films crystallized at 400 °C on sapphire substrates, and of $LiTaO_3$ films crystallized at 500 °C on sapphire substrates, respectively. The crystallographic orientation of the sapphire substrates controls the preferred orientation of the crystallized $LiNbO_3$ and $LiTaO_3$ films.

Formation of $LiNb_xTa_{1-x}O_3(0 \leqq x \leqq 1)$ Films. Complex alkoxide solutions with a stoichiometric composition were prepared by controlling the molar ratio of niobium pentaethoxide to tantalum pentaethoxide. The alkoxide solutions without partial hydrolysis were used for the preparation of films in order to prevent any deviation from the nominal ratio of the composition. Typical XRD profiles of $LiNb_{0.5}Ta_{0.5}O_3$ films crystallized at 500 °C on sapphire substrates are shown in Fig. 8. These films also showed the preferred orientation as the films of the edge compounds, just like $LiNbO_3$ and $LiTaO_3$. Figure 9 shows the relationships between the composition and the lattice constants of films crystallized at 500 °C on sapphire (110) and (001) substrates. The *a* lattice constant increased slightly while the *c* lattice constant decreased, with the composition. These data obey Vegard's law. That such behavior of the lattice parameter changes with the composition could also be observed by Peterson et al.[22,23] and Fukuda et al.[24]

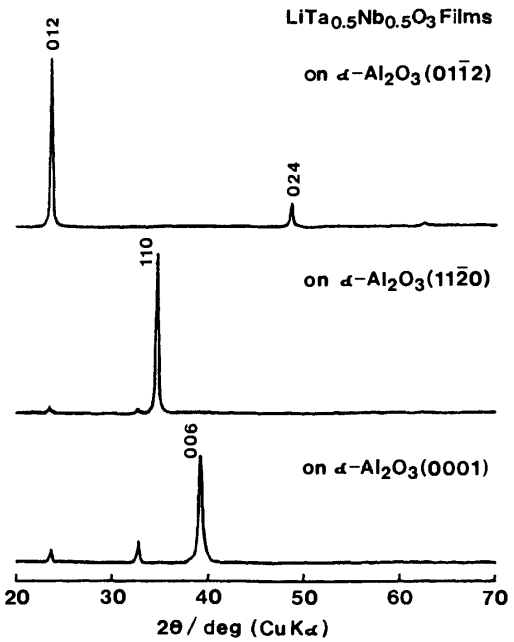

Fig. 8. XRD profiles of $LiNb_{0.5}Ta_{0.5}O_3$ films crystallized at 500 °C on sapphire substrates.

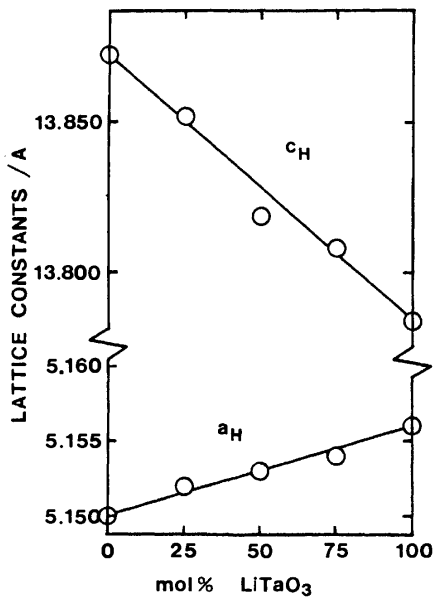

Fig. 9. Change of lattice constants of $LiNb_xTa_{1-x}O_3(0 \leqq x \leqq 1)$ with composition.

Conclusion

Crystalline $LiNbO_3$ films and $LiTaO_3$ films were prepared from double alkoxide solutions by the dip-coating method at lower temperatures. The film thickness could be controlled by adjusting the concentration of the solution and the withdrawal speed from the solution. The water for the partial hydrolysis and the water vapor stream during the heat treatment were found to be very effective for the decomposition and the elimination of organic groups and is promoting the crystallization. The crystallinity of the films was affected by the kind of substrate and the crystallographic orientation. $LiNbO_3$ films and $LiTaO_3$ films on sapphire substrates showed the preferred orientation along each orientation, such as (012), (110), and (001), whereas these films on Si(100) and (111) had the same crystallinity as $LiNbO_3$ and $LiTaO_3$ powders, without any preferred orientation. Solid solution $LiNb_xTa_{1-x}O_3(0 \leqq x \leqq 1)$ films could also be prepared from the complex alkoxide solutions. The composition of the films were found to be controlled by the formation of the complex alkoxide solution and could be strictly monitored from the linear relationships between the compositions and the lattice constants of the films.

References

1) H. M. O'Bryan, P. K. Gallagher, and C. D. Brandle, *J. Am. Ceram. Soc.*, **68**, 493 (1985).
2) S. Miyazawa and H. Iwasaki, *J. Cryst. Growth*, **10**, 276 (1971).
3) S. Takada, M. Ohnishi, H. Hayakawa, and N. Mikoshiba, *Appl. Phys. Lett.*, **24**, 490 (1974).
4) G. H. Hewig, K. Jain, F. O. Sequeda, R. Tom, and Po-Wen Wang, *Thin Solid Films*, **88**, 67 (1982).
5) G. Griffel, S. Ruschin, A. Hardy, M. Itzkovitz, and N. Croiyoru, *Thin Solid Films*, **126**, 185 (1985).
6) P. R. Meek, L. Holland, and P. D. Townsend, *Thin Solid Films*, **141**, 251 (1986).
7) T. Kanata, Y Kobayashi, and K. Kubota, *J. Appl. Phys.*, **62**, 2989 (1987).
8) S. Fushimi and K. Sugii, *Jpn. J. Appl. Phys.*, **13**, 1895 (1974).

9) S. Miyazawa, *Appl. Phys. Lett.*, **23**, 198 (1973).
10) A. A. Ballman, H. Brawn, P. K. Tien, and S. Riva-Sanseverino, *J. Cryst. Growth*, **29**, 289 (1975).
11) S. Kondo, S. Miyazawa, S. Fushimi, and K. Sugii, *Appl. Phys. Lett.*, **26**, 489 (1975).
12) T. Fukuda and H. Hirano, *Appl. Phys. Lett.*, **28**, 575 (1976).
13) R. R. Neurgaonkar, J. R. Oliver, and E.T. Wu, *J. Cryst. Growth*, **84**, 409 (1987).
14) S. Hirano and K. Kato, *Adv. Ceram. Mater.*, **2**, 142 (1987).
15) S. Hirano and K. Kato, *J. Non-Cryst. Solids*, **100**, 538 (1988).
16) S. Hirano and K. Kato, *Adv. Ceram. Mater.*, **3**, 503 (1988).
17) D. J. Eichorst and D. A. Payne, (to be published).
18) T. Furusaki, G. Tei, K. Kodaira, S. Shimada, and T. Matsushita, *Yogyo Kyokai Shi*, **95**, 209 (1987).
19) C-C. Yang, J. Y. Josefowicz, and L. Alexandru, *Thin Solid Films*, **74**, 117 (1980).
20) H. Dislich and E. Hussmann, *Thin Solid Films*, **77**, 129 (1981).
21) S. Sakka, K. Kamiya, K. Makita, and Y. Yamamoto, *J. Non-Cryst. Solids*, **63**, 223 (1984).
22) G. E. Peterson, J. R. Carruthers, and A. Carnevale, *J. Chem. Phys.*, **46**, 4009 (1967).
23) G. E. Peterson, J. R. Carruthers, and A Carnevale, *J. Chem. Phys.*, **53**, 2436 (1970).
24) T. Fukuda and H. Hirano, *J. Cryst. Growth*, **35**, 127 (1976).

 © 1989 The Chemical Society of Japan Bull. Chem. Soc. Jpn., 62, 435—438 (1989)

Synthesis and Properties of Copper(II) Halide Complexes with Imino Oximes

Songping WAN,* Wasuke MORI,† Shoichiro YAMADA,† and Shun-Ichi MURAHASHI
Faculty of Engineering Science, Osaka University, Toyonaka 560
†College of General Education, Osaka University, Toyonaka 560
(Received August 22, 1988)

Two types of imino oxime copper(II) complexes were obtained by the reactions of copper(I) halides CuX (X=Br, I) with imino oximes (3-[2-[(alkylamino)ethyl]imino]-2-butanone oximes or 3-[2-[(dialkylamino)ethyl]-imino]-2-butanone oximes, abbreviated as Hdox-enRR′). One type contains the binuclear complexes $[Cu_2(dox\text{-}enRR')_2]^{2+}$ and uncoordinated halide anions. The magnetic susceptibilities measured over the temperature range 77—320 K show a strong antiferromagnetic spin coupling interaction through the N-O bridge in these complexes. The magnetic behavior can be explained by using the Bleaney-Bowers equation. It is assumed that the complexes of the other type consist of copper(I) and copper(II) in 2:1 ratio without spin-coupling interaction between the copper ions. The plot of the reciprocal magnetic susceptibilities versus temperatures is linear.

Previous reports on the metal complexes with imino oximes **1** have shown a variety of structural and magnetic properties, which depend upon the substituents R and R′, metal ions and counter anions.[1-5] For

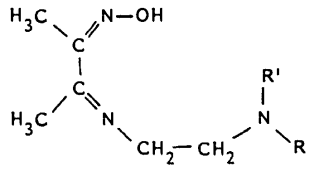

1a Hdox-enR(R′=H,R=alkyl)
1b Hdox-enR$_2$(R′=R=alkyl)
1

example, the reactions of nickel(II) with imino oximes **1** gave two types of complexes, namely hexa-coordinated and tetra-coordinated nickel(II) complexes. These results show a significant effect of the counter anions.[1] We have extended similar studies to several other metals and found that in the copper(II) thiocyanato complexes, imino oximes **1** are coordinated to copper(II) ion as a bridging quadridentate ligand, and the thiocyanate anion is coordinated through nitrogen atom to form a group of penta-coordinated binuclear copper(II) complexes.[4] It is worthwhile to investigate the effect of the anions on the structure and the bonding of copper(II) complexes formed. Reported here are the results of some of our work with the copper(II) halide complexes, together with their comparison with the corresponding nickel(II) complexes and thiocyanato copper(II) complexes.

Experimental

Materials. Biacetyl monoxime, *N*-alkylethylenediamine, *N,N*-dialkylethylenediamine, and copper halides CuX (X= Br, I) were commercially available and used as received.

Synthesis. Cu(dox-enMe)I (R′=H,R=Me; 2a). A mixture of biacetyl monoxime (1.01 g, 0.01 mol) and *N*-methylethylenediamine (0.74 g, 0.01 mol) in ethanol (40 cm^3) was heated at 60 °C for 2.5 h. Copper(I) iodide (0.95 g, 0.005 mol) was added to the solution at 50 °C, stirred for several hours and filtered off. The solution was evaporated spontaneously at room temperature and a dark-green precipitate was collected by filtration and washed with ethanol to give the complex (0.5 g) in 27% yield. Mp: 147 °C. Found: C, 25.99; H, 4.91; N, 11.37%. Calcd for $C_7H_{14}N_3OCuI \cdot 1/2EtOH$: C, 25.74; H, 4.55; N, 11.29%.

Cu(dox-enR$_2$)I (R′=R=Me, Et; 2b, 2c). These complexes were prepared by the method similar to that for Cu(dox-enMe)I except that *N,N*-dimethylethylenediamine and *N,N*-diethylethylenediamine, respectively, were used instead of *N*-methylethylenediamine. On adding a small amount of ether and ethanol when the reaction solution was almost evaporated nearly to dryness, complex **2b** (0.6 g) and complex **2c** (0.6 g) were obtained as dark-green crystals in 33% yield and 31% yield, respectively. Mp: **2b**, 141 °C; **2c**, 142 °C. Found: C, 26.40; H, 4.48; N, 11.42%. Calcd for $C_8H_{16}N_3OCuI$ (**2b**): C, 26.64; H, 4.47; N, 11.65%. Found: C, 31.20; H, 5.24; N, 10.70%. Calcd for $C_{10}H_{20}N_3OCuI$ (**2c**): C, 30.90; H, 5.19; N, 10.81%.

Cu(dox-enBu$_2$)I (R′=R=Bu; 2d). A mixture of biacetyl monoxime (1.11 g, 0.011 mol) and copper(I) iodide (0.95 g, 0.005 mol) in methanol (40 cm^3) was heated at 70 °C for 1 h. *N,N*-dibutylethylenediamine (1.72 g, 0.01 mol) was added and the mixture was stirred for 1 h. Addition of a small amount of ether and ethanol, followed by evaporation of the solvent almost to dryness, gave dark-green crystals (0.5 g) of the complex **2d** in 23% yield. Mp: 124 °C. Found: C, 37.90; H, 6.39; N, 9.44%. Calcd for $C_{14}H_{28}N_3OCuI$: C, 37.80; H, 6.34; N, 9.45%.

Cu(dox-enRR′)Br (R′=R=Me, Et; 2e, 2f). To a solution of copper(I) bromide (0.36 g, 0.0025 mol) in ethanol (20 cm^3) was added the ligand Hdox-enRR′ (0.005 mol) which was prepared beforehand.[1] The mixture was stirred at 70 °C for 1.5 h. The solution was filtered and evaporated spontaneously at room temperature. On adding a small amount of ether when the solution was almost evaporated nearly to dryness, the complex **2e** (0.2 g) and complex **2f** (0.63 g) were obtained as dark-green crystals in 24% yield and 66% yield respectively. Mp: **2e**, 150 °C; **2f**, 137 °C. Found: C, 29.12; H, 5.45; N, 12.65%. Calcd for $C_8H_{16}N_3OCuBr \cdot H_2O$ (**2e**): C, 28.91; H, 5.47; N, 12.67%. Found: C, 34.50; H, 6.03; N, 12.04%. Calcd for $C_{10}H_{20}N_3OCuBr \cdot 1/2H_2O$ (**2f**): C, 34.24; H, 6.03; N, 11.98%.

Cu$_3$(dox-enPr$^i_2$)$_3$I (R′=R=Pr^i; 3a). A mixture of bi-

acetyl monoxime (1.11 g. 0.011 mol) and copper(I) iodide (0.95 g, 0.005 mol) in ethanol (40 cm^3) was heated at 60 °C for 2 h. *N,N*-Diisopropylethylenediamine (1.44 g, 0.01 mol) was added to the solution and the mixture was stirred for 1 h. On concentrating the solution to 20 cm^3, a green precipitate (0.1 g) was obtained in a very low yield. Mp>300 °C. Found: C, 41.19; H, 7.09; N, 11.64%. Calcd for $C_{36}H_{72}N_9O_3Cu_3I \cdot 3H_2O$ C, 41.15; H, 7.48; N, 12,00%.

Cu_3(dox-enPr$^i_2$)$_3$Br (R′=R=Pr^i; 3b). A mixture of biacetyl monoxime (1.11 g, 0.011 mol) and CuBr (0.72 g, 0.005 mol) in methanol (50 cm^3) was heated at 60 °C for 3 h. At room temperature a solution of *N,N*-diisopropylethylenediamine (1.44 g, 0.01 mol) in ethanol (10 cm^3) was added to the reaction mixture above, and the mixture was heated at 60 °C for several hours. Evaporation of the filtered solution at room temperature gave a green precipitate (0.7 g) in 14% yield. Mp>300 °C. Found: C, 44.49; H, 7.55; N, 12.73%. Calcd for $C_{36}H_{72}N_9O_3Cu_3Br \cdot H_2O$: C, 44.69; H, 7.60; N, 13.03%.

Measurements. Electronic absorption spectra were measured at room temperature with a Shimadzu MPS 5000 spectrophotometer. Infrared absorption spectra were recorded as Nujol mulls on a Perkin-Elmer 938G infrared spectrophotometer. Room temperature magnetic moments were determined with the Gouy-method using H_2O as a susceptibility standard, and magnetic susceptibilities at temperatures 77 K to 320 K were measured by the Faraday method in a manner as described previously.[6] Pascal's constants were used to estimate the diamagnetic corrections for imino oximes, Br, I, and Cu.[7]

Results and Discussion

Synthesis of the Copper(II) Halide Complexes with Imino Oximes. In the present work, the reactions of copper(I) salts CuX (X=I, Br) with the imino oximes (Hdox-enRR′; **1**) gave two types of copper(II) complexes depending on the nature of R and R′:

i) Cu(dox-enRR′)X (**2**; R′=H, R=Me, X=I; R′=R=Me, Et, X=I, Br; R′=R=Bu, X=I).

ii) Cu_3(dox-enPr$^i_2$)$_3$X (**3**; X=I, Br)

The following features are to be noted about the synthesis of these complexes:

i) By the reactions of copper(I) halides CuX (X=I, Br) with 3-[[2-(alkylamino)ethyl]imino]-2-butanone oximes (**1a**), the complex Cu(dox-enMe)I (**2a**) was obtained exclusively. Attempts to isolate copper(II) complexes by the reactions of copper(I) chloride with imino oximes (Hdox-enRR′) have so far been unsuccessful. It seems to be difficult to crystallize out the desirable copper(II) complexes because of their high solubilities in an organic solvent.

ii) Using copper(I) halide salts CuX (X=I, Br) as a starting material, we succeeded in preparing the imino oxime copper(II) complexes (**2**). In this method, the copper(I) ion was oxidized by atmospheric oxygen under the reaction conditions employed. This method has been applied with success to the preparation of other copper(II) complexes.[4] By similar procedures, using copper(II) bromide in place of copper(I) bromide, the desirable copper(II) complex could not be isolated as solid. The following equations can be considered:

$$CuX + \text{Hdox-enRR}' \xrightarrow{O_2} \text{Cu(dox-enRR}')X + H_2O \quad (1)$$

$$CuX_2 + \text{Hdox-enRR}' \longrightarrow \text{Cu(dox-enRR}')X + HX \quad (2)$$

According to the Eq. 2, the reaction of copper(II) salt with imino oximes produces HX, which induced the decomposition of ligand Hdox-enRR′ and hence the formation of the complexes Cu(dox-enRR′)X becomes unfavorable; however using copper(I) salt as starting substance, beside the desirable complexes only H_2O is formed as shown in Eq. 1.

iii) As shown in the experimental section, the crystals of complexes were obtained by adding a small amount of ether when the reaction solution was evaporated nearly to dryness. It also reflects the high solubility of these complexes in alcohol.

Characterization of the Copper(II) Halide Complexes (2) of Imino Oximes. As discussed later in more detail, d-d bands and magnetic properties indicate that the complexes **2** isolated are copper(II) complexes. The composition determined by the elemental analysis indicates that the imino oximes lose a proton on coordination to the copper(II) ion.

Infrared spectra of the complexes **2** exhibit no vibrations in 3140—3253 cm^{-1}, showing that the deprotonated imino oxime monoanions are coordinated to the copper(II) ion, in agreement with the assumption that the complexes **2** are copper(II) complexes. Moreover, the bands due to imino oxime C=N (Table 1) are shifted from the vibration of the free ligand at 1623—1630 cm^{-1}, indicating that the nitrogen atom of imino oxime C=N is bound to the copper(II) ion.

Electronic absorption spectra of the copper(II) complexes **2** show one broad band in the visible region (Table 1), where d-d bands of square planar copper(II) complexes are expected to be occur.[8,9] Since the magnetic moments of these coeper(II) complexes at room temperature are subnormal, the spin-coupling interaction between copper(II) ions is presumed to be present. In the light of previous studies on the corresponding thiocyanato copper(II) complexes,[4,5] a similar binuclear structure $[Cu_2(\text{dox-enRR}')_2]^{2+}$ (shown in **2**) may

Table 1. The Main Data for Copper(II) Halide Complexes of Imino Oximes

	R	R′	X	μ/BM	d-d/$10^3 cm^{-1}$	$\nu_{C=N}$/cm^{-1}
2a	Me	H	I	0.79	18.4	1654
2b	Me	Me	I	0.73	18.0	1642
2c	Et	Et	I	0.60	16.1	1637
2d	Bu	Bu	I	0.59	16.8	1636
2e	Me	Me	Br	0.70	16.7	1642
2f	Et	Et	Br	0.60	15.8	1641
3a	Pr^i	Pr^i	I	1.08	17.0	1624
3b	Pr^i	Pr^i	Br	1.06	16.9	1624

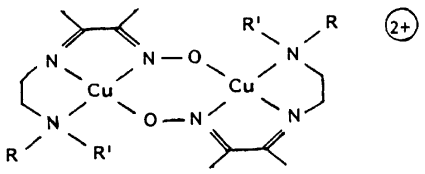

$[Cu_2(dox\text{-}enRR')_2]^{2+}$
2

also be proposed for the copper(II) halide complexes in the present work. Since the coordination ability of halide anions, particularly iodide anion, is much lower than that of thiocyanate, it is reasonable to assume that the halide anions are not coordinated to copper(II) ion in the complexes **2**. In agreement with this seems to be the finding in the present work that the d-d bands of the copper(II) halide complexes shift to higher energy region, as compared with those of thiocyanato copper(II) complexes.[4] It is well-known that the d-d bands of the square-planar copper(II) complex undergo a bathochromic shift when the fifth ligand is bound to the planar copper(II) ion.[8,9]

Investigation on the temperature dependence of the magnetic susceptibility of copper(II) complex is very important and useful for understanding the nature of spin-coupling interaction and the structure of complexes. There have been many studies on the magnetic properties of copper(II) complexes, which have binuclear structures and show spin-coupling interaction between two copper(II) ions through the bridging oxygen atom[10-12] or bridging group N-O.[13,14] As discussed above, the magnetic moments of the complexes **2** are much smaller than that of the normal $3d^9$ system, showing that there exists a spin-coupling interaction between two copper(II) ions. Magnetic susceptibilities of complexes **2** were measured over the temperature range 77—320 K. One of the examples is shown in Fig. 1. The temperature dependence of the magnetic susceptibility shows the presence of a strong spin-coupling interaction between copper(II) ions in these binuclear complexes. The magnetic behaviors can be explained using the Bleaney-Bowers equation (Eq. 3)

$$\chi_A = \frac{Ng^2\beta^2}{kT}\frac{1}{3+\exp(-2J/kT)} + N\alpha \qquad (3)$$

or its modification (Eq. 4)

$$\chi_A = \frac{Ng^2\beta^2}{kT}\frac{1}{3+\exp(-2J/kT)}\cdot(1-p) + \frac{Ng^2\beta^2}{4kT}\cdot p + N\alpha \qquad (4)$$

The symbols in Eqs. 3 and 4 have their usual meanings. Figure 1 exhibits the good agreement between the experimental and calculated values. The exchange parameters for the halide copper(II) complexes **2** are given in Table 2. It is interesting that the values of $-2J$ of the halide copper(II) complexes are greater than those of the thiocyanato copper(II) complexes. This result implies that the spin-coupling interaction between two copper(II) ions is stronger in the halide complexes than that in the thiocyanato complexes, and may be considered to arise from the apical bonding of the thiocyanate anion to the copper(II) ion in the latter. Thus all the findings combined are consistent with the assumption that the complexes **2** adopts a binuclear structure $[Cu_2(dox\text{-}enRR')_2]^{2+}$ and that there exists a strong antiferromagnetic interaction between two copper(II) ions through two bridging N-O groups. This result is in contrast to that of similar nickel(II) complexes, in which there is little interaction between two nickel(II) ions having d^8 system.[1]

Depending upon the nature of ligand and the steric conditions, copper(II) ion would form various complexes with different coordination numbers and different structures. The results of the present work show that although the main skeleton of copper(II) complexes was determined by imino oximes used, the different anions form the complexes with different coordination numbers and structures.[4,5,15]

Characterization of Complexes 3. The characterization of complexes **3** was investigated in the same way as that for complexes **2**. The composition of the elemental analysis leads to the empirical formula

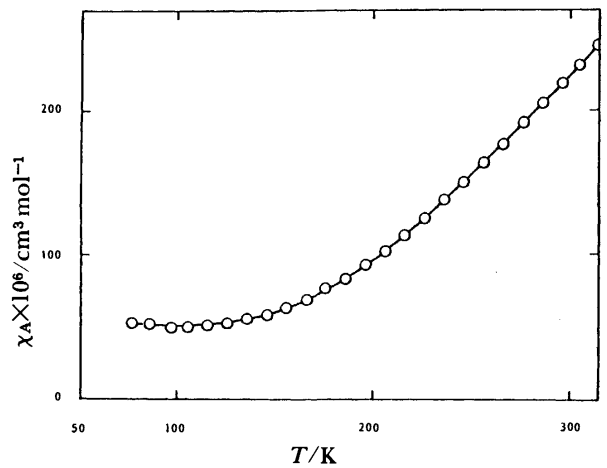

Fig. 1. Temperature dependence of the magnetic susceptibilities for $Cu(dox\text{-}enMe_2)Br$. The solid line was calculated from Eq. 3 with $2J/k=-1060$ K, $N\alpha=46\times10^{-6}$ cm^3mol^{-1}.

Table 2. Magnetic Susceptibilities at Room Temperature and Magnetic Parameters of Copper(II) Halide Complexes of Imino Oximes

	χ_g / cm^3g^{-1}	g	$-2Jk^{-1}$ / K	$N\alpha\times10^6$ / cm^3mol^{-1}	p
2a	0.26	2.02	861	57	
2b	0.14	2.21	972	31	
2c	−0.11	2.29	1160	44	0.01
2d	−0.22	2.21	1130	18	0.06
2e	0.12	2.29	1060	46	0.01
2f	−0.09	2.26	1240	68	

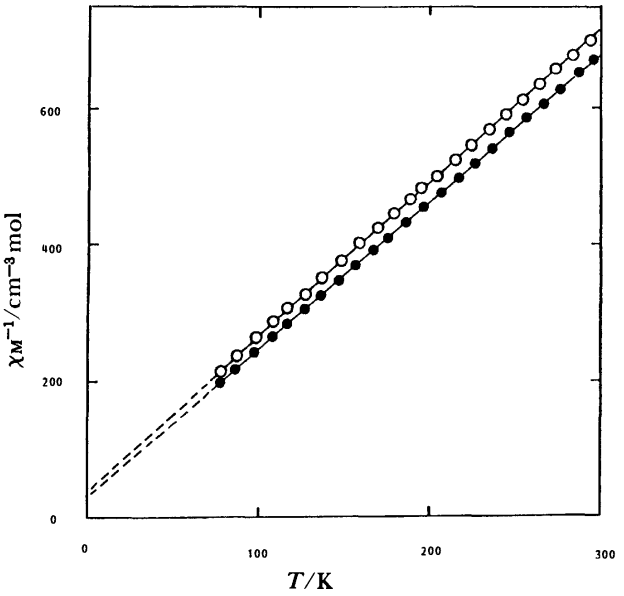

Fig. 2. Reciprocal susceptibility vs. temperature for $Cu_3(dox\text{-}enPr^i_2)_3$ Br (○) and $Cu_3(dox\text{-}enPr^i_2)_3$ I (●). The susceptibility is calculated per formula unit, e.g., for three copper ions. The curves show the theoretical susceptibilities calculated by the Curie-Weiss equation with the parameters described in the text.

$Cu_3(dox\text{-}enPr^i_2)_3X \cdot nH_2O$ (X=I, Br), which is significantly different from that of the complexes **2**. This formulation, which involves the imino oxime monoanion as ligand, requires that copper be present as a mixture in 1+ and 2+ oxidation states. It is also noted that the imino oxime C=N infrared vibrations of complexes **3** occur at wavenumbers around 1624 cm^{-1} distant from the corresponding ones of **2** showing that the structure of **3** differs from that of **2**. The d-d bands (Table 1) indicate that the coordination geometry around copper(II) ion is square-planar. No specific feature of the electronic spectrum could be assigned as an intervalence transfer transition. This difference between complexes **2** and **3** probably arises from the presence of the bulky diisopropylamino groups $-N(Pr^i)_2$ in **3**, which may interfere with the coordination of the $-N(Pr^i)_2$ part. More direct evidence for the existence of a mixed-valence copper complex comes from measurements of the magnetic susceptibility. The magnetic moment calculated per copper ion is μ_{eff}=1.06—1.08 BM (BM=9.274×10^{-24} JT^{-1}). This value is consistent with the presence of Cu(I) and Cu(II) in 2 : 1 ratio without spin-coupling interaction between the copper ions. Variable temperature magnetic susceptibility measurements are also consistent with the existence of copper(I) and almost magnetically independent copper(II) centers. Over the temperature range 77—300 K the plot of reciprocal susceptibility versus temperature is linear (Fig. 2). The data fit well to the Curie-Weiss law (Eq. 5), with C=0.443 emu K mol^{-1} and θ=−18 K for X=Br, and C=0.462 emu K mol^{-1} and θ=−14 K for X=I, where C and θ are Curie and Weiss constant, respectively.

$$\chi^{-1} = C^{-1}(T-\theta) \quad (5)$$

Thus the present compounds are considered to be class I mixed-valence compounds, which contain noninteracting copper(I) and copper(II) sites.[16] Precise structure for these complexes must await further studies using X-ray methods. In any case, however, it is evident that the structure of copper complexes with imino oxime $Hdox\text{-}enPr^i_2$ is different from that of the corresponding dialkylamino analogues. The present study thus demonstrates one of those cases, in which the *N*-isopropyl-substituted ligands tend to form metal complexes with structure different from that of the corresponding normal alkyl analogues, owing to the bulky isopropyl groups.[17]

References

1) S. P. Wan, H. Kuma, and S. Yamada, *Synth. React. Met.-Org. Chem.*, **16**, 1049 (1986).
2) S. P. Wan, W. Mori, and S. Yamada, *Synth. React. Met.-Org. Chem.*, **16**, 1273 (1986).
3) H. Tanaka, H. Kuma, and S. Yamada, *Synth. React. Met.-Org. Chem.*, **15**, 699 (1985).
4) S. P. Wan, W. Mori, S. Yamada, and S.-I. Murahashi, *Bull. Chem. Soc. Jpn.*, **61**, 2833 (1988).
5) S. P. Wan, H. Kuma, S. Yamada, S.-I. Murahashi, and Y. Namba, Abstracts of XXVI. ICCC, Portugal, 1988.
6) W. Mori, M. Kishita, and M. Inoue, *Inorg. Chim. Acta*, **42**, 11 (1980).
7) A. Earnshaw, "Introduction to Magnetochemistry," Academic Press Inc., New York (1968).
8) a) A. B. P. Lever, "Inorganic Electronic Spectroscopy," Elsevier, Amsterdam, 1984. b) S. Yamada, "Structural Coordination Chemistry," Kagakudojin, Kyoto (1980), p. 155.
9) B. J. Hathaway and A. A. G. Tomlinson, *Coord. Chem. Rev.*, **5**, 1 (1970).
10) a) L. Walz, H. Paulus, and W. Haase, *J. Chem. Soc., Dalton Trans.*, **1985**, 913. b) L. Schwabe and W. Haase, *J. Chem. Soc., Dalton Trans.*, **1985**, 1909.
11) M. Mikuriya, M. Nakamura, H. Okasawa, and S. Kida, *Inorg. Chim. Acta*, **68**, 111 (1983).
12) L. Strinna Erre, G. Micera, P. Piu, F. Cariati, and G. Ciani, *Inorg. Chem.*, **24**, 2297 (1985).
13) G. A. Nicholson, C. R. Lazarus, and B. J. McCormick, *Inorg. Chem.*, **19**, 192 (1980).
14) S. Baral and A. Chakravorty, *Proc. Indian Acad. Sci.*, **86A**, 45 (1977).
15) M. Nasakkala, H. Saarinen, and J. Korvenranta, *Finn. Chem. Lett.*, **1980**, 6.
16) M. B. Robin and P. Day, *Adv. Inorg. Chem. Radiochem.*, **10**, 247 (1967).
17) S. Yamada and A. Takeuchi, *Coord. Chem. Rev.*, **43**, 187 (1982).

 © 1989 The Chemical Society of Japan Bull. Chem. Soc. Jpn., 62, 439—443 (1989)

Halogenation Using Quaternary Ammonium Polyhalides. XIV.[1] Aromatic Bromination and Iodination of Arenes by Use of Benzyltrimethylammonium Polyhalides-Zinc Chloride System

Shoji KAJIGAESHI,* Takaaki KAKINAMI,† Masayuki MORIWAKI, Toshio TANAKA, Shizuo FUJISAKI, and Tsuyoshi OKAMOTO†

Department of Industrial Chemistry, Faculty of Engineering, Yamaguchi University, Tokiwadai, Ube 755
†Department of Industrial Chemistry, Ube Technical College, Tokiwadai, Ube 755

(Received May 18, 1988)

The reaction of arenes with benzyltrimethylammonium tribromide or benzyltrimethylammonium dichloroiodate in acetic acid in the presence of $ZnCl_2$ at room temperature or at 70 °C gave bromo- or iodo-substituted arenes in good yield, respectively.

The aromatic bromination of arenes (**1**) with molecular bromine has usually been brought about in the presence of a catalytic amount of iodine or iron filings.[2] The reaction of **1** with NBS and aqueous sulfuric acid gives bromo-substituted arenes (**2**).[3] Reactive **1** can be (mono)brominated by the use of NBS in DMF.[4] Trifluoroacetyl hypobromite (CF_3COOBr),[5] which is prepared by a reaction of bromine with silver trifluoroacetate, and copper(II) bromide[6] have also been used as brominating agents for arenes.

A direct iodination of **1** using I_2 can be accomplished with the use of HNO_3[7] or HIO_3/H_2SO_4[8] to oxidize HI to I_2 and so displace the equilibrium. A mixture of I_2 and $HIO_4 \cdot 2H_2O$ is conveniently used for the direct iodination of polyalkylbenzenes.[9] Iodoarene (**3**) have also been synthesized by a reaction of **1** with I_2 and an equimolecular mixture of $AlCl_3$ and $CuCl_2$.[10] Activated **1** can be iodinated by the use of I_2 and $Cu(OAc)_2$ in acetic acid.[11]

We have recently shown that quaternary ammonium polyhalides, such as benzyltrimethylammonium tribromide (BTMA Br_3)[12] or benzyltrimethylammonium dichloroiodate (BTMA ICl_2),[13] are useful brominating or iodinating agents for reactive aromatic compounds. In this paper, we wish to report on the bromination and iodination of **1** by the use of BTMA Br_3-$ZnCl_2$ and BTMA ICl_2-$ZnCl_2$, respectively.

Results and Discussion

The reaction of **1** with a calculated amount of BTMA Br_3 and $ZnCl_2$ or BTMA ICl_2 and $ZnCl_2$ in acetic acid (at room temperature or at 70 °C) gave **2** or **3** in good yields, respectively. The results are summarized in Table 1.

While such reactive aromatic compounds as phenols, aromatic amines, aromatic ethers, and acetanilides have been easily brominated by BTMA Br_3 in dichloromethane in the presence of methanol, the reaction of **1** (less reactive compounds) with BTMA Br_3 in dichloromethane-methanol did not proceed at all, even under reflux for many hours. However, **1** could be smoothly brominated by use of this reagent in acetic acid with the aid of the Lewis acid $ZnCl_2$. Thus, the combined effect of BTMA Br_3 and $ZnCl_2$ in acetic acid provides a new excellent bromination procedure for **1**.

BTMA ICl_2 is slightly soluble in acetic acid at room temperature. However, an addition of $ZnCl_2$ makes this reagent soluble in acetic acid, and the iodination reaction of **1** readily proceeds under mild conditions.

In these cases, it turned out that an equimolar amount of $ZnCl_2$ was required for BTMA Br_3 or BTMA ICl_2. We, thus, assumed the existence of complexes formed from the polyhalides and $ZnCl_2$ as active species, and proposed that a reaction scheme which affords **2** (mono-bromoarenes) or **3** (mono-iodoarenes) may be described according to the following equations:

$$PhCH_2(CH_3)_3N^+XY_2^- + ZnCl_2 \longrightarrow [PhCH_2(CH_3)_3N]^+[ZnCl_2Y_2]^{2-}X^+ \quad (1)$$

$$\underset{\mathbf{1}}{Ar\text{-}H} + [PhCH_2(CH_3)_3N]^+[ZnCl_2Y_2]^{2-}X^+ \longrightarrow \underset{\mathbf{2}\text{ or }\mathbf{3}}{Ar\text{-}X} + PhCH_2(CH_3)_3N^+Y^- + ZnCl_2 + HY. \quad (2)$$

That is, the reaction appeared to occur in accord with the following stoichiometry:

$$\underset{\mathbf{1}}{H\text{-}Ar} + PhCH_2(CH_3)_3N^+XY_2^- \xrightarrow{ZnCl_2} \underset{\mathbf{2}\text{ or }\mathbf{3}}{Ar\text{-}X} + PhCH_2(CH_3)_3N^+Y^- + HY. \quad (3)$$

(X=Y=Br for BTMA Br_3; X=I, Y=Cl for BTMA ICl_2)

Incidentally, we found that $ZnCl_2$ was a more effective Lewis acid catalyst than other $AlCl_3$, $AlBr_3$, $FeCl_3$, and $ZnBr_2$.

As shown in Table 1, the bromination of **1** using BTMA $Br_3/ZnCl_2$ proceeded more easily than the iodination of **1** using BTMA $ICl_2/ZnCl_2$. Avramoff et al. have already reported the bromination of **1** with tetramethylammonium tribromide (TMA Br_3) in acetic acid under reflux.[44] However, TMA Br_3 is not easy to handle, compared with stable BTMA Br_3 due to its hygroscopic character. Unfortunately, by our method the bromination of benzene did not proceed

Table 1. Bromination and Iodination of **1** by Use of BTMA $Br_3/ZnCl_2$ and BTMA $ICl_2/ZnCl_2$ in AcOH

Substrate **1**	Molar ratio (BTMA Br_3/**1** / BTMA ICl_2/**1**)	Reaction conditions: time/h	Reaction conditions: temp/°C	Product (**2**: X=Br / **3**: X=I)		Yield[a] %	Mp(°C) or Bp(°C/mmHg): Found	Mp(°C) or Bp(°C/mmHg): Reported
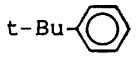 (**1a**)	1.1	2	70	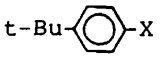	**2a-1**	95	228/760	228—229/740[14]
	1.1	24	70		**3a-1**	92	258/760	116—118/9[15]
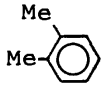 (**1b**)	1.1	2	rt	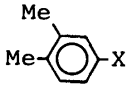	**2b-1**	69	215—216/760	214—215/760[16]
	1.1	24	rt		**3b-1**	40	229/760	228—235/760[17]
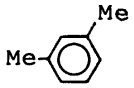 (**1c**)	1.1	1	rt	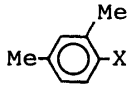	**2c-1**	73	205.5—207/760	200—205/760[18]
	1.1	24	rt		**3c-1**	66	233/760	232/760[19]
1c	2.1	120	70	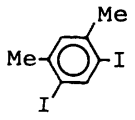	**3c-2**	60	66—68	72[17]
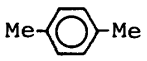 (**1d**)	1.0	2	rt	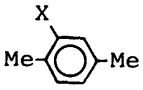	**2d-1**	84	203—204/760	205/760[20]
	1.0	16	rt		**3d-1**	75	232—233/760	110—113/19[21]
1d	2.1	72	70	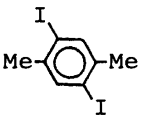	**3d-2**	67	103—104	104—105[19]
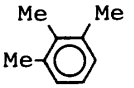 (**1e**)	1.0	1	rt	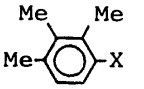	**2e-1**	99	231/760	229.5/750[22]
	1.0	43	rt		**3e-1**	90	270/760	144—145/22[23]
1e	3.1	24	70[b]	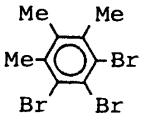	**2e-3**	99	241—242	246[24]
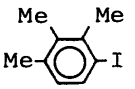 (**3e-1**)	2.1	78	70[b]	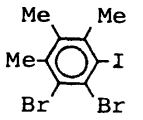		93	223—224	—
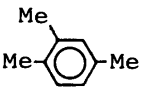 (**1f**)	3.1	24	70[b]	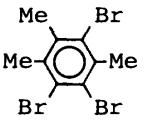	**2f-3**	99	230—231	232[25]
1f	1.0	48	rt	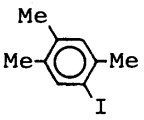	**3f-1**	97	36—37	36—37[23]
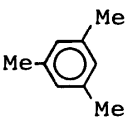 (**1g**)	1.1	6	reflux[c]	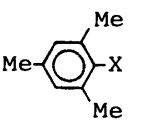	**2g-1**	93	223/760	78—80[26]
	1.0	3	rt		**3g-1**	90	30.5—31	30.5—31[27]
1g	2.0	0.5	rt	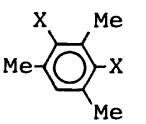	**2g-2**	96	62—63	64[28]
	2.0	28	70		**3g-2**	99	82	82[29]
1g	3.1	24	70[b]	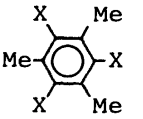	**2g-3**	96	224	224—225[30]
	3.1	120	70		**3g-3**	54	206—207	208[31]

Table 1. (Continued)

Substrate 1	Molar ratio (BTMA Br_3/1 / BTMA ICl_2/1)	Reaction conditions time/h	temp/°C	Product (2: X=Br / 3: X=I)		Yield[a] %	Mp(°C) or Bp(°C/mmHg) Found	Reported
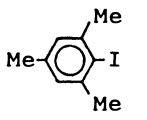 (3g-1)	1.0	18	rt	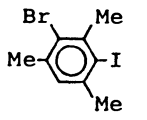		77	42—43	—
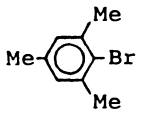 (2g-1)	1.0	24	70	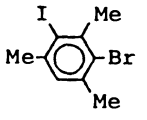		87	42—43	—
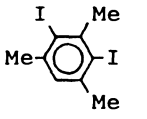 (3g-2)	1.1	78	70[b]	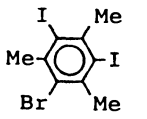		87	184—185	—
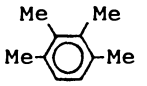 (1h)	1.0	2	rt	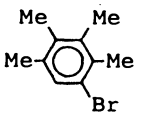	2h-1	96	30	29—30[32]
1h	2.1	2	rt	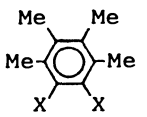	2h-2	85	209—210	208[32]
	2.1	24	70		3h-2	88	189—190	191—192[33]
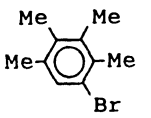 (2h-1)	1.1	24	70	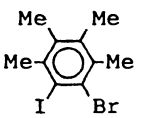		93	188	190—191[33]
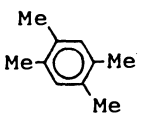 (1i)	1.0	24	rt	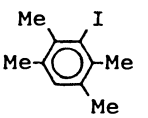	3i-1	90	78	78—80[34]
1i	2.1	3	rt	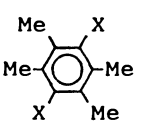	2i-2	90	202—203	200[32]
	2.1	48	70		3i-2	76	138—139	140—141[33]
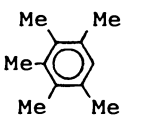 (1j)	1.1	2	rt	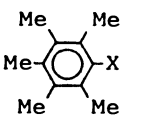	2j-1	95	163.5—164.5	159—160[35]
	1.1	6	rt		3j-1	99	140	141—142[34]
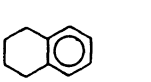 (1k)	1.0	1	rt	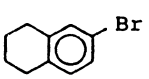	2k-1	93	241/760	238—239/760[36]
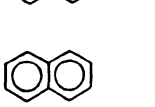 (1l)	1.0	3	rt	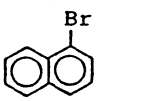	2l-1	96	272/760	272—273/740[37]
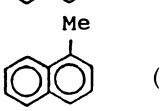 (1m)	1.0	3	rt	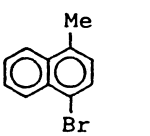	2m-1	99	298—300/760	140—142/8[38]
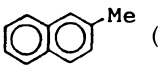 (1n)	1.0	0.5	rt	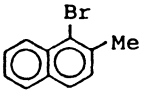	2n-1	99	290—292/760	154—154.5/13[39]
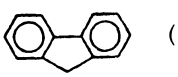 (1o)	1.0	0.5	rt	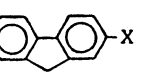	2o-1	99	102—103	101—102[40]
	1.0	3	rt		3o-1	94	124—125	126—127[41]
1o	2.1	6	rt	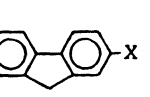	2o-2	97	165—166	166.5—167[42]
	2.1	3	70		3o-2	95	214—215	155.5[43]

a) Yield of isolated product. b) Reaction was carried out by shading the light in order to prevent a side chain bromination. c) 1,2-Dichloroethane-methanol was used as solvent instead of acetic acid contained $ZnCl_2$.

and the bromination of toluene gave a mixture of *o*-, *p*-bromo and dibromo derivatives.

The reaction of **1** with equimolar amount of BTMA ICl_2 and $ZnCl_2$ at room temperature usually gave monoiodoarenes, and with 2-equiv of BTMA ICl_2 and $ZnCl_2$ at 70 °C usually gave diiodoarenes. Thus, the objective mono-, or diiodoarenes could be obtained selectively from **1** by the use of a calculated amount of BTMA ICl_2 and $ZnCl_2$ in acetic acid. However, by our method the iodination of less reactive benzene hardly proceeded; otherwise, the iodination of monoalkylbenzenes, such as toluene and ethylbenzene, gave a mixture of *o*-, *p*-iodo and diiodo derivatives, respectively, with nonselective manners. In the case of *t*-butylbenzene (**1a**), only a *p*-iodo compound **3a-1** was obtained, owing to a steric hindrance of the large *t*-butyl moiety.

Keefer et al. have reported the iodination of **1** such as 1,3,5-trimethylbenzene (**1g**) and 1,2,3,4,5-pentamethylbenzene (**1j**) by the use of ICl and $ZnCl_2$ in acetic acid.[27] However, it takes a long time to obtain the iodo compound, compared with our iodination method. Furthermore, ICl is not easy to handle quantitatively because of its viscous character.

Experimental

All melting points are uncorrected. The ^1H NMR spectra were recorded on a JMN-MH-100 spectrometer with tetramethylsilane as an internal standard.

Benzyltrimethylammonium Tribromide (BTMA Br_3). A partially improved preparative method is as follows: Benzyltrimethylammonium chloride (9.3 g, 50 mmol) and sodium bromate (3.8 g, 25 mmol) was dissolved in water (80 ml); dichloromethane (50 ml) was then added to the aqueous solution. To an ice-cold mixture of the above-mentioned solution was added dropwise 47% hydrobromic acid (30.2 g, 175 mmol) under stirring over a period of 15 min. The dichloromethane layer (dark red) was separated and the water layer was extracted with dichloromethane (20 ml×3). The combined organic solution was dried over magnesium sulfate and evaporated in vacuo to give a residue which was recrystallized from dichloromethane-ether (5:1) affording BTMA Br_3 as orange crystals; yield 16.6 g (85%); mp 100—101 °C (lit,[45] mp 100—101 °C).

2,5-Dimethyl-1-bromobenzene (2d-1). Typical Procedure of Bromination at Room Temperature: To a solution of 1,4-dimethylbenzene (**1d**) (0.50 g, 4.71 mmol) in acetic acid (30 ml) was added BTMA Br_3 (1.84 g, 4.71 mmol) and $ZnCl_2$ (0.7 g, 5.13 mmol). The mixture was stirred for 2 h at room temperature until the initial orange color faded. To the mixture was added water (20 ml) and 5% aq. solution of $NaHSO_3$ (10 ml). The mixture was extracted with hexane (40 ml×4). The organic layer was dried over magnesium sulfate and passed through a short alumina-column. The elute (hexane solution) was concentrated in vacuo to give **2d-1** as colorless oil; yield 0.74 g (84%); bp 203—204 °C/760 mmHg (lit,[20] bp 205 °C/760 mmHg; 1 mmHg≈133.322 Pa).

1-Bromo-4-*t*-butylbenzene (2a-1). Typical Procedure of Bromination at 70 °C. To a solution of *t*-butylbenzene (**1a**) (0.50 g, 3.73 mmol) in acetic acid (20 ml) was added BTMA Br_3 (1.60 g, 4.10 mmol) and $ZnCl_2$ (0.7 g, 5.13 mmol). The mixture was stirred for 2 h at 70 °C until the initial orange color faded. A subsequent work-up as mentioned above gave **2a-1** as colorless oil; yield 0.75 g (95%); bp 228 °C/760 mmHg (lit,[14] bp 228—229 °C/740 mmHg).

1-Iodo-2,4,6-trimethylbenzene (3g-1). Typical Procedure of Iodination: To a solution of 1,3,5-trimethylbenzene (**1g**) (0.50 g, 4.16 mmol) in acetic acid (20 ml) was added BTMA ICl_2 (1.45 g, 4.17 mmol) and $ZnCl_2$ (0.6 g, 4.40 mmol). The mixture was stirred for 3 h at room temperature. The yellow color of the solution gradually changed to light brown. To the mixture was added water (20 ml) and 5% aq. solution of $NaHSO_3$ (10 ml). Then, the mixture was extracted with hexane (50 ml×3). The organic layer was dried over $MgSO_4$ and passed through a short alumina-column in order to remove any trace amount of acetic acid. The hexane solution was concentrated in vacuo to give **3g-1** as colorless crystals; yield 0.92 g (90%); mp 30.5—31 °C (lit,[27] mp 30.5—31 °C).

1,2-Dibromo-3-iodo-4,5,6-trimethylbenzene: This compound was obtained as colorless crystals; mp 223—224 °C (from ethanol). ^1H NMR ($CDCl_3$) δ=2.30, 2.45, and 2.58 (9H, three s, three CH_3). Found: C, 27.00; H, 2.05%. Calcd for $C_9H_9IBr_2$: C, 26.77; H, 2.25%.

1-Bromo-3-iodo-2,4,6-trimethylbenzene: Mp 42—43 °C (from ethanol-water (1:3)). ^1H NMR ($CDCl_3$) δ=2.30, 2.35, and 2.70 (9H, three s, three CH_3), and 6.88 (1H, s, 5-H). Found: C, 33.27; H, 3.01%. Calcd for $C_9H_{10}IBr$: C, 33.26; H, 3.10%.

1-Bromo-3,5-diiodo-2,4,6-trimethylbenzene: This compound was obtained as colorless crystals; mp 184—185 °C (from ethanol). ^1H NMR ($CDCl_3$) δ=2.77 (6H, s, 2- and 6-CH_3), and 2.93 (3H, s, 4-CH_3). Found: C, 24.25; H, 2.01%. Calcd for $C_9H_9I_2Br$: C, 23.98; H, 2.01%.

2,7-Diiodofluorene (3o-2): Mp 214—215 °C (from ethanol-water (1:1)). (lit,[43] mp 155.5 °C). ^1H NMR ($CDCl_3$) δ=3.80 (2H, s, CH_2) and 7.4—8.0 (6H, m, Harom). Found: C, 37.29; H, 1.87%. Calcd for $C_{13}H_8I_2$: C, 37.35; H, 1.93%.

We wish to thank Dr. Mamoru Nakai and Mr. Katsumasa Harada, Ube Laboratory, Ube Industries, Ltd., for elemental analysis.

References

1) Part XIII of this series: S. Kajigaeshi, T. Kakinami, M. Moriwaki, S. Fujisaki, and M. Tashiro, *Rep. Inst. Adv. Mater. Stud. Kyushu Univ.*, **2**, 87 (1988).

2) W. A. Wisansky and S. Ansbacher, *Org. Synth.*, Coll. Vol. III, 138 (1955).

3) F. L. Lambert, W. D. Ellis, and R. J. Parry, *J. Org. Chem.*, **30**, 304 (1965).

4) R. H. Mitchell, Y-H. Lai, and R. V. Williams, *J. Org. Chem.*, **44**, 4733 (1979).

5) R. N. Haszeldine and A. G. Sharpe, *J. Chem. Soc.*, **1952**, 993.

6) D. C. Nonhebel, *Proc. Chem. Soc.*, 307 (1961).

7) F. B. Dains and R. Q. Brewster, *Org. Synth.*, Coll. Vol. I, 323 (1941).

8) H. O. Wirth, O. Königstein, and W. Kern, *Justus Liebigs Ann. Chem.*, **634**, 84 (1960).

9) H. Suzuki, K. Nakamura, and R. Goto, *Bull. Chem.*

Soc. Jpn., **39**, 128 (1966); H, Suzuki, *Org. Synth.*, **51**, 94 (1971).
10) T. Sugita, M. Idei, Y. Ishibashi, and Y. Takegami, *Chem. Lett.*, **1982**, 1482.
11) C. A. Horiuchi and J. Y. Satoh, *Bull. Chem. Soc. Jpn.*, **57**, 2691 (1984).
12) S. Kajigaeshi and T. Kakinami, *Yuki Gosei Kagaku Kyokai Shi*, **46**, 986 (1988) and references cited therein.
13) S. Kajigaeshi, T. Kakinami, H. Yamasaki, S. Fujisaki, M. Kondo, and T. Okamoto, *Chem. Lett.*, **1987**, 2109; S. Kajigaeshi, T. Kakinami, H. Yamasaki, S. Fujisaki, and T. Okamoto, *Bull. Chem. Soc. Jpn.*, **61**, 600 (1988); S. Kajigaeshi, T. Kakinami, M. Moriwaki, M. Watanabe, S. Fujisaki, and T. Okamoto, *Chem. Lett.*, **1988**, 795.
14) L. M. Stock and H. C. Brown, *J. Am. Chem. Soc.*, **81**, 5615 (1959).
15) J. B. Shoesmith and A. Mackie, *J. Chem. Soc.*, **1927**, 2334.
16) R. L. Datta and N. R. Chatterjee, *J. Am. Chem. Soc.*, **38**, 2545 (1916).
17) P. S. Varma and K. S. V. Raman, *J. Indian Chem. Soc.*, **12**, 343 (1935).
18) R. W. Maxwell and R. Adams, *J. Am. Chem. Soc.*, **52**, 2959 (1930).
19) H. Hammerich, *Ber.*, **23**, 1634 (1890).
20) G. E. Philbrook, H. F. Gober, and C. L. Henry, *J. Am. Chem. Soc.*, **73**, 2382 (1951).
21) E. C. Taylor, F. Kienzle, and A. McKillop, *Org. Synth.*, **55**, 70 (1976).
22) L. I. Smith and C. L. Moyle, *J. Am. Chem. Soc.*, **58**, 1 (1936).
23) H. Suzuki and T. Sugiyama, *Bull. Chem. Soc. Jpn.*, 46, 586 (1973).
24) V. N. Ipatieff, H. Pines, and M. Savoy, *J. Am. Chem. Soc.*, **69**, 1948 (1947).
25) G. Lowe, F. G. Torto, and B. C. L. Weedon, *J. Chem. Soc.*, **1958**, 1855.
26) L. J. Andrews and R. M. Keefer, *J. Am. Chem. Soc.*, **78**, 4549 (1956).
27) R. M. Keefer and L. J. Andrews, *J. Am. Chem. Soc.*, **78**, 5623 (1956).
28) R. E. Lutz and C. L. Kibler, *J. Am. Chem. Soc.*, **62**, 1520 (1940).
29) H. Suzuki and R. Goto, *Bull. Chem. Soc. Jpn.*, **36**, 389 (1963).
30) G. F. Hennion and J. G. Anderson, *J. Am. Chem. Soc.*, **68**, 424 (1946).
31) P. S. Varma and T. S. Subrahmanian, *J. Indian Chem. Soc.*, **13**, 192 (1936).
32) L. I. Smith and C. L. Moyle, *J. Am. Chem. Soc.*, **55**, 1676 (1933).
33) H. Suzuki and Y. Haruta, *Bull. Chem. Soc. Jpn.*, **46**, 589 (1973).
34) H. Suzuki, T. Sugiyama, and R. Goto, *Bull. Chem. Soc. Jpn.*, **37**, 1858 (1964).
35) L. I. Smith and J. W. Horner, Jr., *J. Am. Chem. Soc.*, **62**, 1349 (1940).
36) N. V. Sidgwick and H. D. Springall, *J. Chem. Soc.*, **1936**, 1532.
37) J. S. Whitehurst, *J. Chem. Soc.*, **1951**, 221.
38) L. H. Klemm and S. S. Rawlins, *J. Org. Chem.*, **17**, 613 (1952).
39) J. F. Bunnett and T. K. Brotherton, *J. Am. Chem. Soc.*, **78**, 6265 (1956).
40) W. R. Hodgkinson and F. E. Matthews, *J. Chem. Soc.*, **43**, 163 (1883).
41) P. Chanussot, *An. Quim.*, **25**, 5 (1927); *Chem. Abstr.*, **21**, 3360 (1927).
42) W. E. Truce and D. D. Emrick, *J. Am. Chem. Soc.*, **78**, 6130 (1956).
43) P. S. Varma and V. S. Rao, *J. Indian Chem. Soc.*, **15**, 72 (1938).
44) M. Avramoff, J. Weiss, and O. Schächter, *J. Org. Chem.*, **28**, 3256 (1963).
45) S. Kajigaeshi, T. Kakinami, H. Tokiyama, T. Hirakawa, and T. Okamoto, *Bull. Chem. Soc. Jpn.*, **60**, 2667 (1987).

Reaction of 9-Diazofluorene with 2,3-Dichloro-5,6-dicyano-*p*-benzoquinone: The Structure and the Behaviors of the Resulting Product

Tadao SHINGAKI,* Hiro KUMA, Yoshihiko KUSHI, and Toshikazu NAGAI
Institute of Chemistry, College of General Education, Osaka University, Toyonaka, Osaka 560
(Received June 6, 1988)

The title reaction gave 3′,4′-dichloro-1′,6′-dicyanospiro[fluorene-9,7′-[3′]norcarene]-2′,5′-dione (**2**) in a good yield. Recrystallizations of **2** from solvents such as benzene, dioxane, acetonitrile, and acetone gave each molecular complex consisting of a **2**/solvent molar ratio of 1 : 1. The structure of **2** was determined by the use of one complex, **2**·CH_3COCH_3, by an X-ray crystallographic analysis, which revealed that an interaction between **2** and acetone was not very strong. Such a host-guest interaction was shown also from ^1H NMR spectroscopy and a differential thermal analysis of the complex. Compound **2** afforded the corresponding spiroacetals of 9-fluorenone through reactions with ethylene glycol and 1,3-propanediol.

Diazoalkanes are best represented as resonance hybrids comprising linear structures with opposing dipoles.[1a,b] They react with electrophiles (largely at carbon) and with nucleophiles (at nitrogen).[1c] Furthermore, these diazo compounds behave as 1,3-dipoles[2] or carbene precursors.[3] On the other hand, quinones have conjugated two carbonyl groups and two carbon-carbon double bonds and can be considered as being dipolarophiles.[4] In particular, the quinones substituted by electronegative groups, such as halogen and/or cyano group(s),[5] become strong electron acceptors.[6] Thus, the reactions of diazoalkanes with quinones have aroused wide interest from mechanistic or synthetic points of view and have been described by various authors.[7]

Generally speaking, diazoalkanes achieve 1,3-dipolar cycloaddition to the carbon-carbon double bonds of *p*-benzoquinone and of incompletely blocked *p*-quinones to give pyrazoline derivatives,[8] while the diazo compounds attack the carbonyl group(s) of completely blocked *p*-quinones to afford oxiranes[8c,d,9], with the evolution of nitrogen. Needless to say, the oxirane formation from the former quinones[8e,9a] and the pyrazoline formation from the latter[8f,10] have also been reported.

In a previous paper,[11] we stated that we had obtained 2,3-dichloro-5,6-dicyanodispiro[2,5-cyclohexadiene-1,2′-oxirane-3′,9″-fluoren]-4-one (**1**) through a reaction of 9-diazofluorene (9-DF) with 2,3-dichloro-5,6-dicyano-*p*-benzoquinone (DDQ). The instability of the 9-fluorenylidene-DDQ adduct in an acetone-d_6 solution precluded its characterization by ^{13}C NMR spectroscopy. However, chemical support of the structure (**1**) was deduced from the seemingly straightforward formation of acetals by reactions of the adduct with alcohols (as described hereinafter). We recently undertook an X-ray analysis of a crystal which included acetone used for recrystallization of the adduct, and determined its structure to be that of 3′,4′-dichloro-1′,6′-dicyanospiro[fluorene-9,7′-[3′]-norcarene]-2′,5′-dione (**2**) rather than that of **1**.

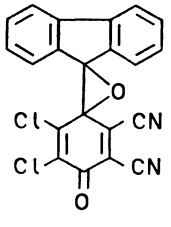

1

Results and Discussion

Reaction of 9-DF with DDQ. A solution of 9-DF in acetonitrile was added drop by drop with stirring into a solution of DDQ of acetonitrile at room temperature. The evolution of nitrogen was immediately observed and an orange substance was obtained, accompanied by 9,9′-bifluorenylidene (**3**). The substance, upon standing under vacuum for several hours, turned from orange to a yellow powder, **2**.

Regarding the formation of **2** from 9-DF and DDQ, the following routes can be suggested: (A) 1,3-Dipolar cycloaddition of the diazo compound to a quinone carbon-carbon double bond takes place to give substituted 3a,4,7,7a-tetrahydro-3*H*-indazole-4,7-dione (**4**), and then the loss of nitrogen gives **2**. In fact, such dipolar cycloadducts have been isolated in the many

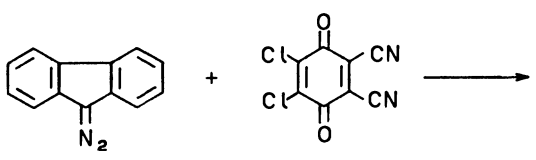

9-DF DDQ

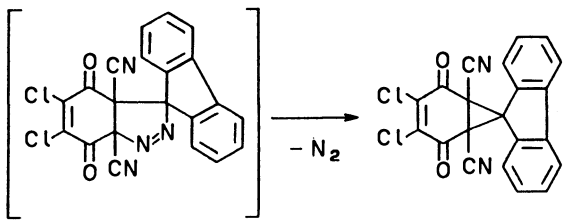

4 2

reactions of diazo compounds and quinones.[8] It has been reported that the reactions of 9-DF with *p*-benzoquinone and with 1,4-naphthoquinone give the dihydroxy-3*H*-indazole derivatives.[12] On the other hand, it has been noted that, upon sufficiently raising the temperature in these reactions (in refluxing benzene), a dipolar reaction and a loss of nitrogen occur to give cyclopropanes while the dienolization to form dihydroxy-3*H*-indazole derivatives can be effectively avoided.[13] In our reaction system of 9-DF with DDQ bearing electron-withdrawing groups, the 3*H*-indazole was not isolated because of its instability, even under the present reaction condition. Cycloaddition, however, was observed to occur in the double bond of the cyano group site in DDQ in preference to that of the chloro site. This finding can be explained according to a difference in electron-withdrawing ability between the chloro and the cyano groups. (B) A direct nucleophilic attack of the diazo carbon on the carbon atom adjacent to the cyano group in DDQ leads to the for-

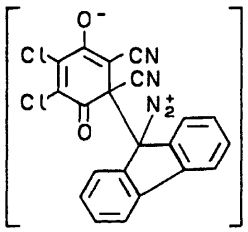

5

mation of a diazonium betain intermediate (**5**), which gives **2** through a loss of nitrogen and a ring closure. This route may be ruled out for the formations of indazole derivatives from diazo compounds and quinones. (C) A charge-transfer complex of DDQ and 9-DF may be formed as the first step, followed by the formation of a radical ion pair prior to the free radical ions,[14] which may combine to give the pyrazoline (**4**) as a precursor of **2**. The 1 : 1 charge-transfer complexes of DDQ with durene[15] and with *p*-phenylenediamine[16] have been isolated. The formations of a DDQ radical anion in a DDQ–diphenyldiazomethane system[17] and of a radical ion pair for DDQ and 9-DF[14] have been observed by means of their electron spin resonance and electronic absorption spectra. From the point of view of the one-electron redox potentials, $E_{1/2}$(+0.51[18] and +1.21[19] V vs. SCE in acetonitrile for DDQ and 9-DF, respectively), it seems unlikely to us that the above-mentioned pyrazoline formation proceeds through the radical ions.

Inclusion of Some Solvents. Upon recrystallization from acetone, **2** slowly precipitated as big yellowish-orange columnar crystals, which exhibited the values of elementary analysis for a molecular compound consisting of one molecule of **2** and one molecule of acetone. The mass spectra of the molecular complex (**2**·CH_3COCH_3) revealed *m/z* 390 (M^+ −58 (C_3H_6O)) as the highest peak. The ^1H NMR spectra (in $CDCl_3$) of **2**·CH_3COCH_3 were all similar to superimposed spectra of the components; none of the peak shifts were observed. This finding shows that **2**·CH_3COCH_3 completely dissociates into the components in the solvent because of a week interaction between **2** and the ketone. When the big crystals of **2**·CH_3COCH_3 were stored in a dry-seal desiccator, their surfaces gradually changed to yellow powder. When crushed crystals of **2**·CH_3COCH_3 were kept in vacuo by use of a rotary oil pump for one hour or so, they completely changed to yellow powder, **2**. The recrystallization of **2** or **2**·CH_3COCH_3 from ethyl methyl ketone gave a new molecular complex (**2**·$C_2H_5COCH_3$) having a molar ratio of **2** to the ethyl methyl ketone of 1 : 1 in either case; the complex showed the same behavior as those of **2**·CH_3COCH_3 in its characterization by mass and ^1H NMR spectroscopy. In addition, **2** forms crystalline molecular complexes of 1 : 1 stoichiometry with a variety of guest molecules such as benzene, tetrahydrofuran, dioxane, and acetonitrile. Furthermore, these host-guest compounds make a change in the guests upon recrystallization from the other solvents,[11] as mentioned above regarding the conversion of **2**·CH_3COCH_3 into **2**·$C_2H_5COCH_3$. Differential thermal analyses (DTA) of each host-guest compound gave endothermic peaks at respective temperatures between 74 and 107 °C (for six kinds of samples), all of the compounds recorded the start of exothermic peaks at temperature 185—187 °C.[11] Although the host-guest compounds with polar additives (acetonitrile and ketones) have a tendency to indicate higher DTA endothermic peak points than the boiling points of these additives, the

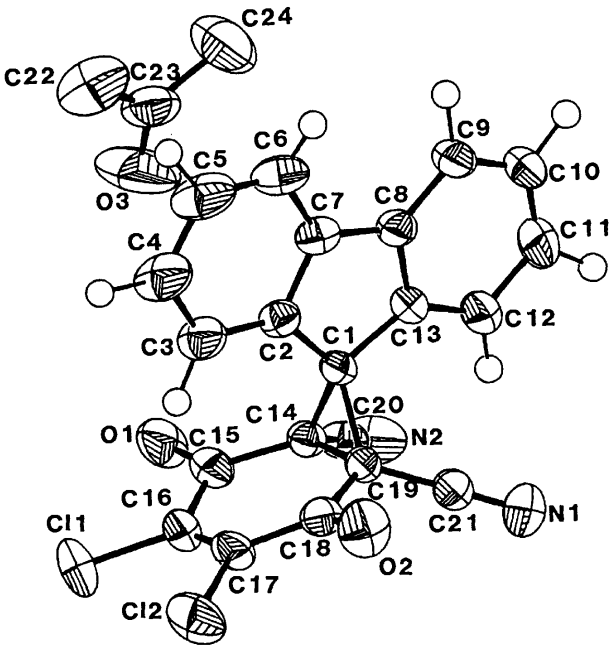

Fig. 1. ORTEP drawing of **2**·CH_3COCH_3.

relationship of the peak points to the natures of the additives is not clear.

X-Ray Crystal Structure. A perspective view of a complex, **2**·CH_3COCH_3, is shown in Fig. 1 by an ORTEP drawing[20] together with the atomic numberings. The bond distances and the bond angles are listed in Tables 1 and 2, respectively.

The cyclopropane ring of **2** is formed with a short bond, C14-C19 (1.505 Å), and two longer bonds, C1-C14 (1.542 Å) and C1-C19 (1.556 Å). The bond angles in the cyclopropane ring are 58.1° (C14-C1-C19), 61.4° (C1-C14-C19) and 60.5° (C1-C19-C14), respectively. These facts show a cyclopropane ring having a tendency to be an isosceles triangle.

Table 1. Bond Distances (in Å) of **2**·CH_3COCH_3 with Estimated Standard Deviations in Parentheses

Bond	Distance	Bond	Distance	Bond	Distance
C1-C2	1.518(4)	C2-C3	1.379(4)	C3-C4	1.390(5)
C4-C5	1.365(5)	C5-C6	1.377(5)	C6-C7	1.390(5)
C2-C7	1.404(4)	C7-C8	1.441(4)	C8-C9	1.393(4)
C8-C13	1.400(4)	C9-C10	1.375(5)	C10-C11	1.381(5)
C11-C12	1.380(5)	C12-C13	1.392(4)	C13-C1	1.507(4)
C1-C14	1.542(3)	C14-C15	1.515(4)	C15-O1	1.201(4)
C15-C16	1.485(4)	C16-CL1	1.698(3)	C16-C17	1.337(4)
C17-CL2	1.703(3)	C17-C18	1.477(4)	C18-O2	1.200(4)
C18-C19	1.516(4)	C19-C21	1.444(4)	C21-N1	1.138(4)
C19-C14	1.505(3)	C19-C1	1.556(3)	C14-C20	1.445(4)
C20-N2	1.138(5)	O3-C23	1.202(6)	C22-C23	1.483(6)
C23-C24	1.485(7)				

The projected view of the crystal structure of the complex, **2**·CH_3COCH_3, is represented in Fig. 2. The shortest distance between the acetone molecule and **2** is that of O2-C22 (X, $1+Y$, Z) (3.286 Å). This distance reveals the existence of a hydrogen bond,[21] though it is very weak, judging from the sum (3.40 Å[21]) of the van der Waals radii of a methyl group and an oxygen atom.

Reaction of 2 with Diols. It was found that, in acetonitrile at room temperature, **2** reacted with diols to give spiroacetals (**6**). Besides **6**, an almost quantitative amount of 2,3-dichloro-5,6-dicyanohydroquinone ($DDQH_2$) was isolated along with 9-fluorenone (**7**). The formation of the by-product, **7**, can be ascribed to the action of residual water present in the used solvent and/or of the water used in the treatment of the reaction mixture.

Table 2. Bond Angles (in Degree) of **2**·CH_3COCH_3 with Estimated Standard Deviations in Parentheses

Bond	Angle	Bond	Angle	Bond	Angle
C2-C1-C13	104.8(2)	C14-C1-C19	58.1(2)	C1-C2-C7	107.2(3)
C3-C2-C7	119.5(3)	C2-C3-C4	119.2(3)	C3-C4-C5	121.1(3)
C4-C5-C6	120.7(3)	C5-C6-C7	119.0(3)	C2-C7-C6	120.4(3)
C2-C7-C8	110.3(3)	C7-C8-C13	109.5(3)	C9-C8-C13	120.2(3)
C8-C9-C10	119.2(3)	C9-C10-C11	120.6(3)	C10-C11-C12	121.1(3)
C11-C12-C13	119.0(2)	C8-C13-C12	119.8(3)	C1-C13-C8	108.1(3)
C1-C14-C15	120.3(2)	C1-C14-C20	117.8(2)	C1-C14-C19	61.4(2)
C14-C15-C16	118.5(2)	O1-C15-C14	119.7(3)	O1-C15-C16	121.8(3)
C15-C16-C17	122.9(3)	CL1-C16-C15	115.2(2)	CL1-C16-C17	121.8(2)
C16-C17-C18	122.8(3)	CL2-C17-C16	122.5(2)	CL2-C17-C18	114.6(2)
C17-C18-C19	118.0(2)	O2-C18-C17	122.7(2)	O2-C18-C19	119.3(2)
C14-C19-C18	118.9(3)	C18-C19-C21	110.7(3)	C14-C19-C21	120.3(3)
C1-C19-C14	60.5(2)	N2-C20-C14	179.6(3)	N1-C21-C19	178.5(3)
O3-C23-C22	120.8(4)	O3-C23-C24	118.9(4)	C22-C23-C24	120.3(4)

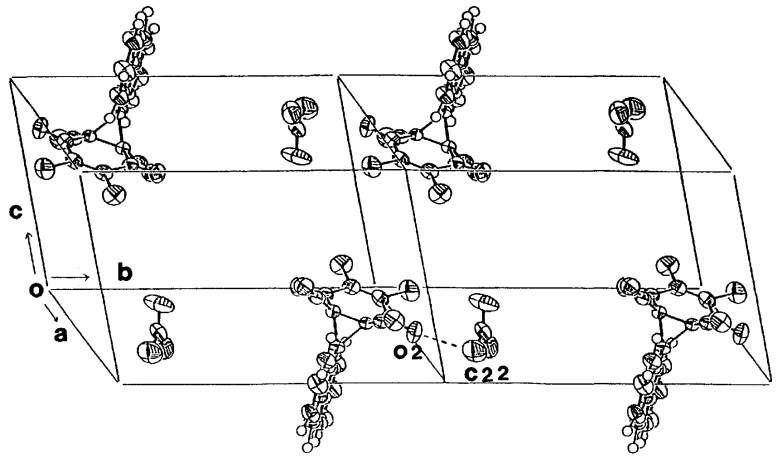

Fig. 2. The projected view of the crystal structure of **2**·CH_3COCH_3.

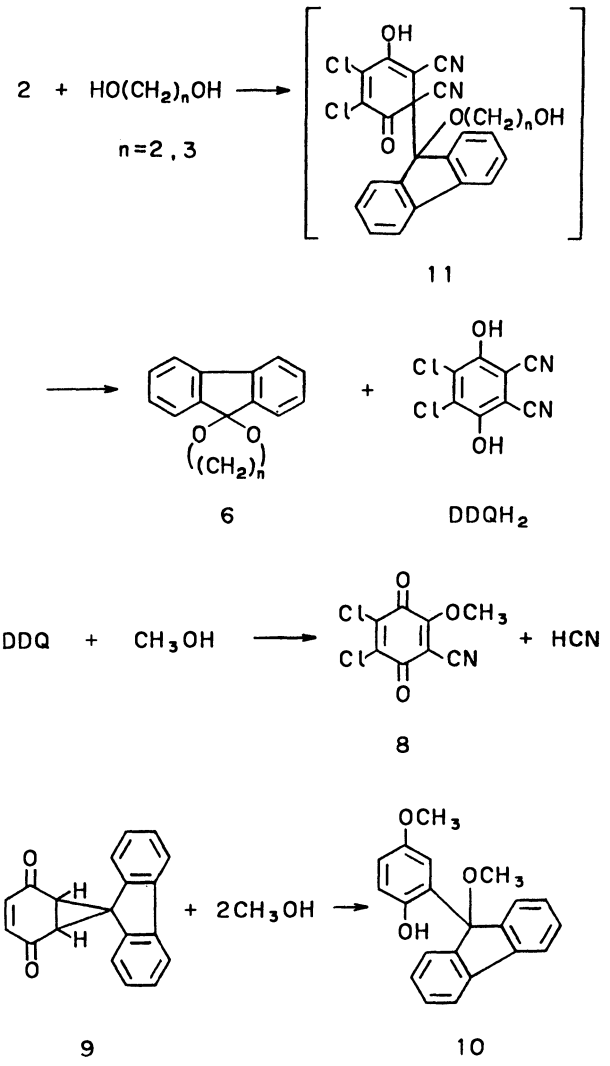

The nucleophilic displacement of the cyano group in DDQ by methanol proceeds to give 2,3-dichloro-5-cyano-6-methoxy-*p*-benzoquinone (**8**) at room temperature,[22] and the nucleophilic ring opening of the cyclopropane in spiro[fluorene-9,7′-[3′]norcarene]-2′,5′-dione (**9**) by methanol proceeds to afford 4-methoxy-2-(9-methoxy-9-fluorenyl)phenol (**10**).[13] In respect that the reaction of **2** with the diols has led to the production of the corresponding acetals and $DDQH_2$; the intermediate (**11**) represented above may be formed prior to the acetals. The cyclopropane ring of **2** provides electron-withdrawing cyano, carbonyl, and 9-fluorenylidene groups as well as strains inherent in a three-membered cyclic alkane. A nucleophilic attack of the diol takes place on the spiro carbon atom, leading to the ring opening; the follow-up proton migration occurs from the resulting oxonio hydrogen to the carbonyl oxygen to give **11**. In this intermediate, because of the strong electron-withdrawal of the DDQ moiety, the 9-fluorenylidene site is most likely subject to an internal nucleophilic attack by the other alcohol oxygen atom. Thus, an internal acetalization and an aromatization of the DDQ moiety provide **6** and $DDQH_2$. Here, it is left as a possibility that **11** undergoes an intermolecular nucleophilic attack with another molecule of the diol to give the corresponding noncyclic acetal. However, the noncyclic acetals could not be isolated also in the presence of more excess diols than those in the above-mentioned runs.

As mentioned above, a small amount of 9,9′-bifluorenylidene (**3**) was obtained in the reaction of 9-DF and DDQ. Whereas, from a stirred acetonitrile solution of **2** and 9-DF, **3** was not detected by means of high-performance liquid chromatography, both of the starting materials were recovered unchanged. Such a result was also shown by employing diphenyldiazomethane instead of 9-DF. Mechanistically, **3** could be derived from the diazonium betain intermediate, which had been provided by a nucleophilic attack of the diazo carbon on one carbonyl oxygen in DDQ, as described for the stilbene derivative formation in the reactions of aryldiazomethanes with chloranil.[9c,d]

Experimental

The melting points were determined on a Laboratory Devices Melt-Temp instrument and uncorrected. The infrared spectra were recorded on a Hitachi 260-10 spectrometer. The ^1H NMR spectra were taken on a Varian EM-390 spectrometer (90 MHz) and the ^{13}C NMR spectra were taken on a JEOL FX-200 spectrometer at 50.10 MHz (measured at NMR Application Laboratory, Nippon Denshi LTD., Tokyo, Japan) by the use of tetramethylsilane as an internal standard in acetone-d_6 or chloroform-d_3. Mass spectral data were obtained with a Hitachi RUM-6E mass spectrometer at an ionization potential of 70 eV. The DTA was accomplished with a Shimadzu DTA-system (thermal analysis instrument 30-series), all the samples being heated at a rate of 10 K min^{-1} from room temperature to 190 °C.

Materials. 9-Diazofluorene[23] and diphenyldiazomethane[24] were prepared by oxidation of the corresponding hydrazones with yellow mercury(II) oxide, the former; mp 99 °C[25] (from ether), the latter; mp 29—30 °C[26] (from light petroleum). Although 9-DF can be preserved for a long time in a refrigerator, the diazomethane must be prepared just before use. Benzene, acetone, ethyl methyl and diethyl ketones, acetonitrile, and dioxane were used after the commercial reagents had been purified according to the published directions.[27] DDQ was obtained from a commercial source and recrystallized from dichloromethane; mp 213—214 °C.[28] The diols were distilled under reduced pressure before use after the commercial materials were dried over Molecular Sieves 3A.

Reaction of 9-DF with DDQ. To a stirred solution of DDQ (3.63 g, 16 mmol) in acetonitrile (100 ml) was added dropwise over 40 min at 22—27 °C a solution of 9-DF (2.88 g, 15 mmol) in acetonitrile (50 ml); the evolution of nitrogen began immediately. Stirring was allowed to continue until the gas evolution was no longer observed after completing the addition. The evolved nitrogen was almost the theoretical amount, based on the diazo compound used. The orange-yellow flocculent precipitate formed under stirring was collected and washed with a small quantity of cold acetonitrile. A further crop was obtained by concentrating the

mother liquor under reduced pressure. The combined products were crystallized from dichloromethane to give **2** (5.45 g, 93%) as a yellow powder. Evaporating the acetonitrile mother liquor, treating the residue with ether, and cooling yielded red crystals of **3** (0.10 g, 2%). Upon employing acetone, dichloromethane, and benzene as the reaction solvent, the yield of **2** (70—90%) decreased with an increase in the yield of **3**. 3′,4′-Dichloro-1′,6′-dicyanospiro[fluorene-9,7′-[3′]norcarene]-2′,5′-dione (**2**): Mp 183 °C (decomp). Found: C, 64.39; H, 2.12; N, 7.16%. Calcd for $C_{21}H_8N_2O_2Cl_2$: C, 64.47; H, 2.06; N, 7.16%. MS *m/z* 390 (M^+). IR (KBr) 2250 (C≡N), 1710 (C=C), 1450, 1280, and 730 cm^{-1}. ^{13}C NMR ($(CD_3)_2CO$) δ=40.97 (s, fluorenylidene 9-C), 53.93 (s, C-CN), 112.60 (s, CN), 134.41 (s, CCl), 175.73 (s, CO), 136.43, 142,09, 144.27, 147.39 (each s), 122.37, 123.50, 123.83, 126.66, 129.37, 130.24 (each d), and 132.70 (d, 2C). 9,9′-Bifluorenylidene (**3**): Red needles (from ether); mp 189—190 °C. Found: C, 95.00; H, 4.88%. Calcd for $C_{26}H_{16}$: C, 95.09; H, 4.91%. MS *m/z* 328 (M^+). IR (KBr) 3050, 1600 (C=C), 1440, 1340, 760, and 720 cm^{-1}.

Host-Guest Compounds. A general method is exemplified in the adduct formation of **2** with ethyl methyl ketone as follows. The powder of **2** was dissolved in 10 ml of the ketone placed in a 30-ml Erlenmeyer flask at about 40 °C. The top of the flask was covered by a piece of powder paper which had been perforated with a pin; the saturated solution was left to stand at room temperature for crystallization, which gave big yellowish-orange columnar crystals. The adduct, **2**·$C_2H_5COCH_3$, was filtered off before use: Found: C, 64.81; H, 3.48; N, 6.05; Cl, 15.31%. Calcd for $C_{25}H_{16}N_2O_3Cl_2$: 64.79, H, 3.31; N, 5.90; Cl, 15.21%. MS *m/z* 390 (M^+−72). ^1H NMR ($CDCl_3$) δ=1.20 (t, $CH_2C\underline{H}_3$), 2.12 (s, CH_3), 2.44 (q, CH_2), and 7.0—8.2 (8H, aromatic H).

All of the following adducts made in this way revealed the mass spectra having the highest peak at *m/z* 390 and the ^1H NMR spectra (in $CDCl_3$) having peaks attributable to the fluorenylidene protons and the original peaks of their respective guests.

2·CH_3COCH_3: Found: C, 64.02; H, 3.13; N, 6.16%. Calcd for $C_{24}H_{14}N_2O_3Cl_2$: C, 64.16; H, 3.14; N, 6.24%.

2·CH_3CN: Found: C, 64.10; H, 2.42; N, 9.70%. Calcd for $C_{23}H_{11}N_3O_2Cl_2$: C, 63.90; H, 2.57; N, 9.72%.

2·Tetrahydrofuran: Found: C, 64.70; H, 3.46; N, 6.12%. Calcd for $C_{25}H_{16}N_2O_3Cl_2$: C, 64.81; H, 3.48; N, 6.05%.

2·1,4-Dioxane: C, 62.58; H, 3.38; N, 5.90%. Calcd for $C_{25}H_{16}N_2O_4Cl_2$: C, 62.64; H, 3.37; N, 5.85%.

2·Benzene: Found: C, 68.88; H, 3.00; N, 6.01%. Calcd for $C_{27}H_{14}N_2O_2Cl_2$: C, 69.09; H, 3.01; N, 5.97%.

2·Tetrahydropyran: Found: C, 65.22; H, 3.78; N, 5.80%. Calcd for $C_{26}H_{18}N_2O_3Cl_2$: C, 65.42; H, 3.80; N, 5.87%.

2·$C_2H_5COC_2H_5$: Found: C, 65.51; H, 3.90; N, 5.68%. Calcd for $C_{26}H_{18}N_2O_3Cl_2$: C, 65.42; H, 3.80; N, 5.87%.

As for a change of the guests, for example, **2**·$C_2H_5COCH_3$ was recrystallized from acetonitrile, by a manner similar to that described above, to give the **2**·CH_3CN adduct as orange columnar crystals.

Spiro Acetals. To a solution of 1.00 g (2.6 mmol) of **2** in acetonitrile (30 ml) was added 1.00 g (16 mmol) of ethylene glycol; the solution was then stirred for 4 h at room temperature. The removal of the solvent under reduced pressure gave a pale-yellow oil. To the residue was added benzene (30 ml or so), and insoluble $DDQH_2$ was filtered off and washed with benzene. The washing and filtrate parts were combined, washed with a 5% solution of sodium carbonate (15 ml×3), followed by rinsing with a saturated solution of sodium chloride (15 ml×3) and drying over anhydrous magnesium sulfate. The concentration of the benzene solution gave an oily substance, which was chromatographed on alumina (about 300 mesh). Careful successive elution gave **7** (0.12 g, 26%) with benzene-ether (5 : 1) and a spiro acetal, **6a**, (0.32 g, 56%) with benzene-ether (1 : 1). The reaction of **2** with 1,3-propanediol, by the same method as described above, gave **7** (0.17 g, 37%) and **6b** (0.31 g, 51%) besides $DDQH_2$. The structures of $DDQH_2$ and **7** were assigned

Table 3. Fractional Atomic Coordinates with e.s.d.'s in Parentheses and Equivalent Isotropic Thermal Parameters (in Å^2)

(H atoms refined isotropically)

Atom	X	Y	Z	B_{eq}[a]	Atom	X	Y	Z	B_{eq}[a]
CL1	0.50857(9)	0.82840(7)	0.33643(11)	7.7	C14	0.9334(3)	0.7085(2)	0.3108(3)	4.0
CL2	0.55325(9)	1.01443(6)	0.23356(11)	7.3	C15	0.7800(3)	0.7193(2)	0.3208(3)	4.9
O1	0.7539(3)	0.6473(2)	0.3461(3)	7.9	C16	0.6677(3)	0.8206(2)	0.3037(3)	5.0
O2	0.8275(3)	0.9612(1)	0.1671(3)	7.2	C17	0.6864(3)	0.8997(2)	0.2598(3)	4.7
O3	1.0173(4)	0.1625(3)	0.3877(3)	11.4	C18	0.8199(3)	0.8935(2)	0.2233(3)	4.5
N1	1.2240(3)	0.8428(2)	0.3995(3)	7.0	C19	0.9535(2)	0.7981(2)	0.2621(3)	3.8
N2	1.1717(3)	0.5963(2)	0.5337(3)	7.1	C20	1.0669(3)	0.6460(2)	0.4357(3)	4.9
C1	0.9345(3)	0.7025(2)	0.1426(3)	3.8	C21	1.1056(3)	0.8220(2)	0.3400(3)	4.7
C2	0.7920(3)	0.7007(2)	−0.0226(3)	4.1	C22	0.8476(5)	0.1800(3)	0.1082(5)	9.1
C3	0.6309(3)	0.7390(2)	−0.0740(3)	5.3	C23	1.0034(4)	0.1459(2)	0.2492(4)	7.1
C4	0.5288(3)	0.7250(2)	−0.2385(4)	6.4	C24	1.1446(6)	0.0891(4)	0.2210(6)	11.5
C5	0.5855(4)	0.6741(3)	−0.3492(4)	6.7	HC3	0.593(3)	0.774(2)	0.002(3)	2.7
C6	0.7457(4)	0.6334(2)	−0.3001(3)	6.0	HC4	0.420(3)	0.752(2)	−0.274(3)	3.9
C7	0.8497(3)	0.6459(2)	−0.1360(3)	4.4	HC5	0.512(4)	0.666(2)	−0.453(4)	4.6
C8	1.0199(3)	0.6103(2)	−0.0555(3)	4.5	HC6	0.782(3)	0.597(2)	−0.373(4)	3.9
C9	1.1264(4)	0.5532(2)	−0.1186(3)	6.1	HC9	1.084(4)	0.532(2)	−0.233(4)	4.2
C10	1.2856(4)	0.5273(2)	−0.0148(4)	6.9	HC10	1.368(4)	0.481(2)	−0.053(4)	5.2
C11	1.3398(3)	0.5568(2)	0.1503(4)	6.5	HC11	1.448(4)	0.535(3)	0.227(4)	5.1
C12	1.2364(3)	0.6130(2)	0.2155(3)	5.4	HC12	1.274(3)	0.632(2)	0.326(3)	3.7
C13	1.0748(3)	0.6399(2)	0.1120(3)	4.2					

a) $B_{eq}=4/3\sum_i\sum_j B_{ij}a_ia_j$.

upon comparisons with the authentic samples.

Spiro[1,3-dioxolane-2,9′-fluorene] (6a): Mp 133—134 °C (from ether). Found: C, 80.26; H, 5.41%. Calcd for $C_{15}H_{12}O_2$: C, 80.33; H, 5.39%. MS *m/z* 224 (M^+). IR (KBr) 2860, 1440, 1110, 1060, 980, 935, 760, and 725 cm^{-1}. ^1H NMR ($CDCl_3$) δ=4.35 (s, 4H) and 7.1—7.7 (m, 8H).

Spiro[1,3-dioxane-2,9′-fluorene] (6b): Mp 172—173 °C (form ether). Found: C, 80.44; H, 5.92%. Calcd for $C_{16}H_{14}O_2$: C, 80.64; H, 5.92%. MS *m/z* 238 (M^+). IR (KBr) 2880, 1450, 1082, 1010, 960, 930, 770, and 740 cm^{-1}. ^1H NMR ($CDCl_3$) δ=1.9—2.2 (m, 2H), 4.35 (t, 4H, J=5.4 Hz, OCH_2), and 7.1—7.8 (m, 8H).

Crystallographic Measurements. The crystal of $2 \cdot CH_3COCH_3$ was sealed in a Lindemann glass capillary with the mother liquor, because it gradually lost acetone molecules. Three dimensional X-ray data were collected using a crystal (0.4×0.3×0.2 mm) by Ni-filtered Cu $K\alpha$ radiation on a Rigaku automated four-circle diffractometer. The ω-2θ scan mode was employed at a rate of 10 ° min^{-1} (in ω). The backgrounds were counted for 2 s before and after each scan. A total of 3751 reflections was collected up to 2θ=125° and 2989 ($|F_o|>3\sigma|F_o|$) reflections were used in the analyses. The structure was solved by the direct method (MULTAN 74)[29] and refined by a block-diagonal least squares method (HBLS-V).[30] Anisotropic temperature factors were used for nonhydrogen atoms. The positions of the hydrogen atoms were calculated based on the molecular geometry. The methyl hydrogen atoms of the acetone molecule were neglected. These hydrogen atoms with isotropic temperature factors were included in further refinement. The final R and R_w values were 0.057 and 0.076, respectively. The weighting scheme used was $w=1/(\sigma(F_o)^2+0.0015(F_o)+0.0001(F_o)^2)$. The atomic scattering factors for all atoms were taken from Ref. 31. The final atomic coordinates are listed in Table 3†.

Crystal Data: $C_{24}H_{14}N_2O_3Cl_2$, F.W.=449.3, triclinic, space group $P\bar{1}$, a=9.848(1), b=13.972(1), c=9.222(1) Å, α=101.27(1), β=117.78(1), γ=71.96(1), V=1065.5(2) $Å^3$, D_c=1.401 $g \cdot cm^{-3}$, Z=2.

All the computations were carried out on an ACOS computer at the Computation Center, Osaka University, and on an ACOS S-850 computer at the Crystallographic Research Center, Institute for Protein Research, Osaka University.

† Tables of anisotropic temperature factors, and of observed and calculated structure factors are deposited as Document No. 8848 at the office of Bull. Chem. Soc. Jpn.

References

1) a) G. W. Cowell and A. Ledwith, *Q. Rev. Chem. Soc.*, **24**, 119 (1970); b) S. Sorriso, "Structural Chemistry," in "The chemistry of diazonium and diazo groups," ed by S. Patai, John Wiley & Sons Inc., New York (1978), Part 1, Chap. 3; c) A. F. Hegarty, "Kinetics and mechanisms of reactions involving diazonium and diazo groups," in *ibid.*, Part 2, Chap. 12.

2) a) R. Huisgen, *Angew. Chem., Int. Ed. Engl.*, **2**, 633 (1963); b) R. Huisgen, *J. Org. Chem.*, **33**, 2291 (1968); c) R. Huisgen, *ibid.*, **41**, 403 (1976); M. Regitz and H. Heydt, "Diazoalkanes," in "1,3-Dipolar Cycloaddition Chemistry," ed by A. Padwa, John Wiley & Sons Inc., New York (1984), Vol. 1, Chap. 4.

3) W. Kirmse, "Carbene Chemistry," Academic Press, New York (1964).

4) K. T. Finley, "The addition and substitution chemistry of quinones," in "The chemistry of the quinonoid compounds," ed by S. Patai, John Wiley & Sons Inc., New York (1974), Part 2, Chap. 17; G. Bianchi, C. De. Micheli, and R. Gandolfi, "The Chemistry of Double-Bonded Functional Groups," eb by S. Patai, John Wiley & Sons Inc., New York (1977), Chap. 6.

5) D. Walker and J. D. Hiebert, *Chem. Rev.*, **67**, 153 (1967); A. B. Turner, "2,3-Dichloro-5,6-dicyano-*p*-benzoquinone (DDQ)," in "Synthetic Reagents," ed by J. S. Pizey, John Wiley & Sons Inc., New York (1977), Vol. 3, Chap. 2.

6) G. Briegleb, *Angew. Chem.*, **76**, 326 (1964).

7) C. D. Gutsche, "The Reaction of Diazomethane and its Derivatives with Aldehydes and Ketones," in "Organic Reaction," ed by R. Adams, John Wiley & Sons Inc., New York (1945), Vol. 8, Chap. 8.

8) a) H. von Pechmann, *Ber.*, **28**, 855 (1895); L. F. Fieser and J. L. Hartwell, *J. Am. Chem. Soc.*, **57**, 1479 (1935); E. Bergmann and F. Bergmann, *J. Org. Chem.*, **4**, 125 (1939); F. M. Dean, P. G. Jones, and P. Sidisunthorn, *J. Chem. Soc.*, **1962**, 5186; F. M. Dean, P. G. Jones, P. B. Morton, and P. Sidisunthorn, *ibid.*, **1963**, 5336; F. M. Dean and P. G. Jones, *ibid.*, **1963**, 5342; B. Eistert, J. Riedinger, G. Küffner, and W. Lazik, *Chem. Ber.*, **106**, 727 (1973); b) H. von Pechmann and E. Seel, *Ber.*, **32**, 2292 (1899); B. Eistert. K. Pfleger, and P. Donath, *Chem. Ber.*, **105**, 3915 (1972); c) M. F. Aldersley, F. M. Dean, and B. E. Mann, *J. Chem. Soc., Chem. Commun.*, **1983**, 107; d) B. Eistert, H. Fink, and A. Müller, *Chem. Ber.*, **95**, 2403 (1962); e) Rundel and P. Kastner, *Justus Liebigs Ann. Chem.*, **737**, 87 (1970); B. Eistert, L. S. B. Goubran, C. Vamvakaris, and T. J. Arachal, *Chem. Ber.*, **108**, 2941 (1975); f) B. Eistert, H. Fink, J. Riedinger, H-G. Hahn, and H. Durr, *ibid.*, **102**, 3111 (1969); g) L. F. Fieser and M. A. Peters, *J. Am. Chem. Soc.*, **53**, 4080 (1931).

9) a) B. Eistert and G. Bock, *Chem. Ber.*, **92**, 1247 (1959); B. Eistert, H. Fink, K. Pfleger, and G. Küffner, *Justus Liebigs Ann. Chem.*, **735**, 145 (1970); b) L. I. Smith and W. B. Pings, *J. Org. Chem.*, **2**, 95 (1937); c) For oxetane formation, T. Oshima and T. Nagai, *Bull. Chem. Soc. Jpn.*, **53**, 726 (1980); d) For ether formation, T. Oshima and T. Nagai, *ibid.*, **53**, 3284 (1980); e) For ether formation, T. Oshima and T. Nagai, *ibid.*, **54**, 2039 (1981); T. Oshima, R. Nishioka, S. Ueno, and T. Nagai, *J. Org. Chem.*, **47**, 2114 (1982); T. Oshima and T. Nagai, *Tetrahedron Lett.*, **26**, 5317 (1985).

10) a) W. C. Howell, M. Ktenas, and J. M. MacDonald, *Tetrahedron Lett.*, **1964**, 1719; b) H-D. Becker, B. W. Skelton, and A. H. White, *Aust. J. Chem.*, **34**, 2189 (1981).

11) T. Shingaki, M. Tsujita, and T. Nagai, *Chem. Lett.*, **1986**, 1639.

12) L. Horner and E. Lingnau, *Justus Liebigs Ann. Chem.*, **591**, 21 (1955); cf. Ref. 8f; N. Latif, I. Zeid, and N. Mishriky, *J. Prakt. Chem.*, **312**, 209 (1970).

13) G. W. Jones, D. R. Kerur, Y. Yamazaki, and H. Shechter, *J. Org. Chem.*, **39**, 492 (1974).

14) T. Oshima and T. Nagai, *Tetrahedron Lett.*, **1977**, 3715.

15) P. R. Hammond, *J. Chem. Soc.*, **1963**, 3113.

16) A. Ottenberg, R. L. Brandon, and M. E. Browne, *Nature (London)*, **201**, 1119 (1964).

17) T. Oshima, A. Yoshioka, and T. Nagai, *Tetrahedron Lett.*, **1977**, 1789.

18) M. E. Peover, *J. Chem. Soc.*, **1962**, 4540.

19) F. Pragst and W. Jugelt, *Electrochim. Acta*, **15**, 1543

(1970).
20) C. K. Johnson, ORTEP-II, Report ORNL—5138, Oak Ridge National Laboratory, Oak Ridge, Tennessee (1976).
21) D. J. Sutor, *J. Chem. Soc.*, **1963**, 1105.
22) H-D. Becker, *J. Org. Chem.*, **34**, 1203 (1969).
23) H. Staudinger and O. Kupfer, *Ber.*, **44**, 2197 (1911); R. Baltzly, N. B. Behta, P. B. Russell, R. E. Brooks, E. M. Gribsky, and A. M. Steinberg, *J. Org. Chem.*, **26**, 3669 (1961).
24) L. I. Smith and K. L. Howard, *Org. Synth.*, Coll. Vol. III, 351 (1955).
25) A. Schönberg, W. I. Awad, and N. Latif, *J. Chem. Soc.*, **1951**, 1368.
26) D. Bethell and J. D. Callister, *J. Chem. Soc.*, **1963**, 3801; T. Oshima, A. Yoshioka, and T. Nagai, *J. Chem. Soc., Perkin Trans. 2*, **1978**, 1283.
27) J. A. Riddic, W. B. Gunger, and T. K. Sakano, "Organic Solvents," in "Techniques of Chemistry," 4th ed, ed by A. Weissberger, John Wiley & Sons Inc., New York (1986), Vol. II.
28) D. Walker and T. D. Waugh, *J. Org. Chem.*, **30**, 3240 (1965).
29) P. Main, S. E. Hull, L. Lessinger, G. Germain, J. P. Declercq, and M. M. Woolfson, MULTAN 78; "A System of Computer Programs for the Automatic Solution of Crystal Structures from X-Ray Diffraction Data," University of York, England, and Louvain, Belgium (1978).
30) T. Ashida, HBLS-V, "The Universal Crystallographic Computing System-Osaka," The Computation Center, Osaka University (1979), pp. 53—59.
31) "International Tables for X-Ray Crystallography," Kynoch Press, Birmingham (1974), Vol. IV, p. 71.

Selective Synthesis of Halogeno Derivatives from 5-Acetoxytropolone

Tomohiro NAGAO, Akira MORI,† and Hitoshi TAKESHITA*,†
Graduate School of Engineering Sciences, 39, Kyushu University, Kasuga-koen, Kasuga, Fukuoka 816
†Institute of Advanced Material Study, 86, Kyushu University, Kasuga-koen, Kasuga, Fukuoka 816
(Received June 25,1988)

5-Acetoxytropolone was successfully halogenated by means of benzyltrimethylammonium tribromide and sulfuryl chloride to give 3-halotropolones and 3,7-dihalotropolones which were converted to the corresponding halogenated *p*-tropoquinone derivatives. From 3,7-dihalo-*p*-tropoquinones, 3,4,7-trichloro-5-hydroxytropolone was prepared in good yields via a Thiele-type addition reaction with hydrochloric acid. By a similar treatment, 5-hydroxytropolone gave a complex mixture.

Recently, we have shown that tropolones polysubstituted with acetoxyl group and/or halogens undergo reductive dehydrohalogenation during acetyl trifluoroacetate (ATA)-mediated acetolysis.[1] This was particularly interesting in connection to the reduction of *p*-tropoquinones to 5-hydroxytropolones by heating in acetic acid which suffered an oxidative decarboxylation.[2,3] Previous attempts of electrophilic bromination of 5-hydroxytropolone (**1**)[4] have so far been unsuccessful: a treatment of **1** with bromine has been known to give an intractable material.[5] Refluxing acetic acid of **1** with bromine,[2] however, gave 2,10-dihydroxydicyclohepta[*b,d*]furan-3,9-dione and its dibromo derivatives and dibromo-5-hydroxytropolones, which were a mixture of 3,6-, 3,7-, and 4,6-dibromo derivatives, indicating the operation of an oxidation-addition mechanism via tropoquinones.[6]

Herein, we discuss the electrophilic substitution reactions of the derivatives of **1** with benzyltrimethylammonium tribromide (**2**)[7] and sulfuryl chloride (**3**) halogenations to selectively form 3-halo or 3,7-dihalotropolones.

First of all, **1** was acetylated to 5-acetoxytropolone (**4**)[4] and treated with two molar equivalents of **2** to form product (**5**) in quantitative yield. The structure of **5** was deduced to be 5-acetoxy-3,7-dibromotropolone by conversion to known 3,7-dibromo-5-hydroxytropolone (**6**).[6]

The reaction was mild and selective. The present procedure gave 3,7-dibromo derivatives selectively. However, an excess amount of **2** resulted in the formation of cyclohexadienones; probably, the product, **5**, was oxidized with **2** to 3,7-dibromo-*p*-tropoquinone (**7**) or its equivalent which further ring-contracted via a benzil-benzilic acid rearrangement, in a protic solvent to 3,5-dibromo-4-hydroxy-4-methoxycarbonyl-2,5-cyclohexadienone (**8**).[6] On the other hand, a monobromo derivative, 5-acetoxy-3-bromotropolone (**9**), was obtained in good yield by the use of a controlled amount of **2**. A mild acid hydrolysis of **9** in aqueous acetic acid gave 3-bromo-5-hydroxytropolone (**10**).

In parallel, chlorination of **4** was also successful by use of **3**: A treatment of **4** with **3** in benzene gave 5-acetoxy-3,7-dichlorotropolone (**11**), which could be quantitatively hydrolyzed to 3,7-dichloro-5-hydroxytropolone (**12**). The controlled chlorination of **4** yielded 5-acetoxy-3-chlorotropolone (**13**) together with an accompanied formation of 16% of **11**. An acid hydrolysis of **13** gave 3-chloro-5-hydroxytropolone (**14**).

The DDQ (2,3-dichloro-5,6-dicyano-*p*-benzoquinone)-oxidation of these halogenated compounds, **6**,[6] **10**, **12**, and **14**, afforded the corresponding *p*-tropoquinone derivatives (**7**,[6] **15**, **16**, and **17**) in high yields. A comparable result could be obtained by silver acetate-oxidation[6] of the 5-hydroxytropolones, as verified, in the case of **6** to **7**. As predicted, concd hydrochloric acid treatment of **17** and **16** in tetrahydrofuran (THF) gave 3,6-dichloro-5-hydroxytropolone (**18**) and 3,4,7-trichloro-5-hydroxytropolone (**19**). The **7** also gave **19** via a halogen exchange. Interestingly, **6** or **10** did not react with concd hydrochloric acid to **12** or **14**; the exchange should be operative only with quinones, prior to the Thiele-type addition step. Further, DDQ-oxidation of **19** was unsuccessful.

In conclusion, we have now obtained products of electrophilic substitution reactions of the derivative of **1** with halogens. Related studies concerning the development of the functional materials starting these troponoids are progressing.

Experimental

Bromination of 4 to 5-Acetoxy-3,7-dibromotropolone (5). A 1 : 1-mixture of MeOH and CH_2Cl_2 (10 cm^3) containing **4** (100 mg) was treated with **2** (476 mg) and $CaCO_3$ (120 mg) at room temperature for 1 h. The mixture was then treated with 1 M HCl (1 M=1 mol dm^{-3}), extracted with EtOAc, and dried over $MgSO_4$. Silica-gel column chromatography of the organic material obtained by removal of the solvent afforded **5** [greenish-yellow needles, mp 188—190 °C, 187 mg; 98%. Found: C, 31.85; H, 2.00%. Calcd for $C_9H_6O_4Br_2$: C, 31.99; H, 1.79%. ^{1}H NMR[8] δ=2.27 (3H, s) and 7.95 (2H, s). ^{13}C NMR δ=21.1, 123.9 (2C), 135.5 (2C), 139.4, 172.4 (2C), and 175.1. IR ν: 3155, 1760, 1615, 1595, 1565, 1330, 1195, 1155, 915, 810, and 760 cm^{-1}. UV λ_{max}^{MeOH}: 267 nm (ε=29300), 335 (9000, sh), 346 (12200), 418 (9400, sh), and 438 (14400)].

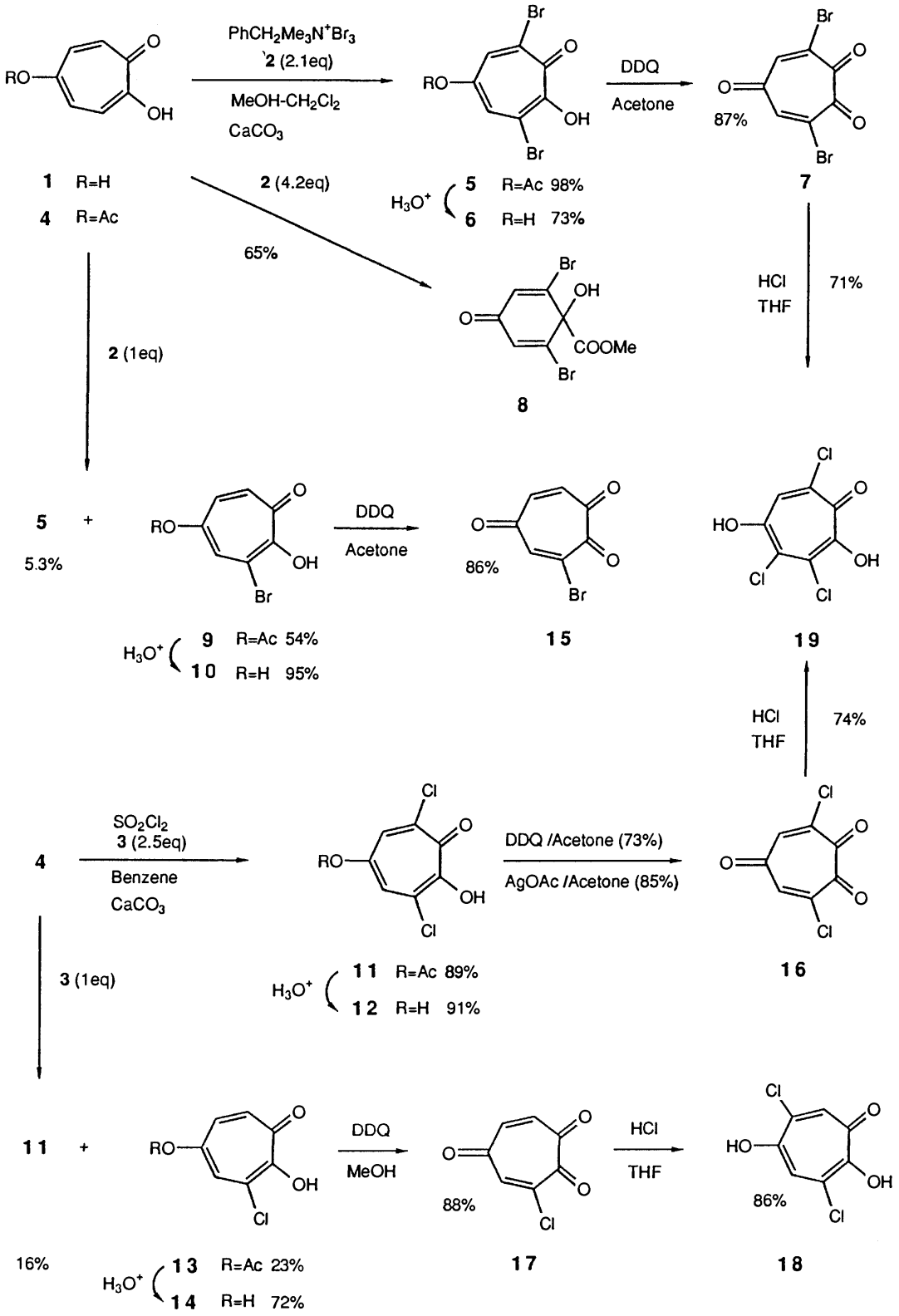

Hydrolysis of 5 to 3,7-Dibromo-5-hydroxytropolone (6). An aqueous AcOH solution (50%, 9 cm^3) of **5** (75 mg) was heated at 100 °C for 6 h. The mixture was then heated in vacuo to remove the solvent and the separated crystals were collected by filtration to give **6** [yellow needles, mp 232—234 °C (decomp) (lit,[6] 166—167 °C), 49 mg; 73%] together with the recovered **5** (17 mg; 23%).

Formation of 3,5-Dibromo-4-hydroxy-4-methoxycarbonyl-2,5-cyclohexadienone (8) by Treatment of 4 with Excess of 2. A 1 : 1-mixed solution consisted of MeOH and CH_2Cl_2 (5 cm^3) of **4** (50 mg) was treated with **2** (458 mg, 4.2 mol equiv) in the presence of $CaCO_3$ (60 mg) at room temperature for 1 h. The same work-up of the mixture gave **8** [colorless prisms, mp 161—162 °C, 59 mg; 65%. Found: C, 29.72; H,

2.05%. Calcd for $C_8H_6O_4Br_2$: C, 29.48; H, 1.86%. ^{1}H NMR δ=3.90 (3H, s) and 6.78 (2H, s). ^{13}C NMR δ=55.6, 77.4, 131.1 (2C), 142.8 (2C), 168.8, and 181.1. IR ν: 3350, 1750, 1650, 1600, 1300, 1225, 1115, 900, and 705 cm^{-1}. UV λ_{max}^{MeOH}: 249 nm (ε=14400) and 280 (4100)].

Controlled Bromination of 4 to 5-Acetoxy-3-bromotropolone (9). To an MeOH solution (20 cm^3) of **4** (200 mg) and $CaCO_3$ (60 mg), a CH_2Cl_2 solution (20 cm^3) of **2** (433 mg) was added drop by drop at room temperature for 2 h. After being stirred for another 2 h, the mixture was acidified with dil HCl, extracted with EtOAc, and dried over $MgSO_4$. Silica-gel column chromatography of the organic material afforded **9** [pale-yellow needles, mp 152—154 °C, 155 mg; 54%. Found: C, 41.86; H, 2.66%. Calcd for $C_9H_7O_4Br$: C, 41.73; H, 2.72%. ^{1}H NMR δ=2.33 (3H, s), 7.15 (1H, dd, J=11.4, 2.6 Hz), 7.30 (1H, d, J=11.4 Hz), and 7.96 (1H, d, J=2.6 Hz), ^{13}C NMR δ=20.9, 118.5, 128.3, 130.2, 137.5, 146.7, 164.3, 169.3, and 169.9. IR ν: 3245, 1765, 1610, 1565, 1210, 1150, 915, and 810 cm^{-1}. UV λ_{max}^{MeOH}: 258 nm (ε=29300), 318 (6200, sh), 335 (9700), 342 (9500, sh), 373 (4600, sh), 391 (5500), and 420 (4800)] together with **5** (20 mg; 5.3%) and the recovered **4** (35 mg; 18%).

Hydrolysis of 9 to 3-Bromo-5-hydroxytropolone (10). Similarly, **9** (93 mg) was treated with aqueous AcOH (33%, 10 cm^3) at 100 °C for 6 h to afford **10** [yellow needles, mp 226—228 °C (decomp), 74 mg; 95%. Found: C, 38.52; H, 2.30%. Calcd for $C_7H_5O_3Br$: C, 38.74; H, 2.32%. ^{1}H NMR δ=7.37 (1H, dd, J=11.7, 2.9 Hz), 7.67 (1H, d, J=11.7 Hz), and 8.15 (1H, d, J=2.9 Hz). ^{13}C NMR δ=127.6, 128.2, 134.2, 134.4, 161.7, 162.1, and 164.9. IR ν: 3300—2300, 1605, 1510, 1465, 1315, 1215, 1080, 870, and 760 cm^{-1}. UV λ_{max}^{MeOH}: 253 nm (ε=14700), 346 (6800), 389 (4900, sh), 401 (5100), and 431 (2800, sh)].

Chlorination of 4. Formation of 5-Acetoxy-3,7-dichlorotropolone (11). An anhydrous benzene suspension (10 cm^3) of **4** (2.0 g) and $CaCO_3$ (560 mg) was treated with SO_2Cl_2 (3.75 g) and refluxed for 2 h. After removing the solvent, the residue was acidified with dil HCl and extracted with $CHCl_3$. Silica-gel column chromatography of the organic material afforded **11** [greenish-yellow crystals, mp 168—170 °C, 2.46 g; 89%. Found: C, 43.12; H, 2.40%. Calcd for $C_9H_6O_4Cl_2$: C, 43.40; H, 2.43%. ^{1}H NMR δ=2.29 (3H, s) and 7.77 (2H, s). ^{13}C NMR δ=20.7, 133.9 (2C), 134.2 (2C), 144.9, 165.7 (2C), and 171.0. IR ν: 3200, 1765, 1600, 1575, 1340, 1200, 1155, and 855 cm^{-1}. UV λ_{max}^{MeOH}: 251 nm (ε=22400, sh), 262 (32600), 333 (9500, sh), 344 (12300), 396 (4100, sh), 412 (6800, sh), and 436 (10000)].

Hydrolysis of 11 to 3,7-Dichloro-5-hydroxytropolone (12). An aqueous acetone solution (33%, 15 cm^3) of **11** (1.84 g) was refluxed for 4 h. Silica-gel column chromatography of the residue, obtained from the mixture, afforded **12** [yellow crystals, mp 253—255 °C (decomp), 1.39 g; 91%. Found: C, 40.91; H, 2.06%. Calcd for $C_7H_4O_3Cl_2$: C, 40.61; H, 1.95%. ^{1}H NMR δ=7.50 (2H, s). ^{13}C NMR δ=127.4 (2C), 136.9 (2C), 154.8, and 162.8 (2C). IR ν: 3400—2400, 1605, 1575, 1530, 1420, 1360, 1220, 1110, 860, and 760 cm^{-1}. UV λ_{max}^{MeOH}: 255 nm (ε=25500), 349 (8800), 395 (6400, sh), 412 (7300), and 438 (4800, sh)].

Controlled Chlorination of 4. Formation of 5-Acetoxy-3-chlorotropolone (13). To an anhydrous benzene suspension (100 cm^3) of **4** (3.0 g), an anhydrous benzene solution (20 cm^3) of SO_2Cl_2 (2.24 g) was added drop by drop for 1 h. After being refluxed for another 2 h, the mixture was heated in vacuo to remove the solvent. The residue was chromatographed on a silica-gel column to give recovered **4** (1.05 g; 35%), **11** (645 mg; 16%), and **13** [pale-yellow needles, mp 148—150 °C, 834 mg; 23%. Found: C, 50.49; H, 3.25%. Calcd for $C_9H_7O_4Cl$: C, 50.37; H, 3.29%. ^{1}H NMR δ=2.33 (3H, s), 7.13 (1H, dd, J=11.4, 2.6 Hz), 7.32 (1H, d, J=11.4 Hz), and 7.73 (1H, d, J=2.6 Hz). ^{13}C NMR δ=20.9, 118.3, 129.9, 134.5, 136.8, 146.6, 164.7, 169.2, and 169.5. IR ν: 3270, 1750, 1610, 1575, 1220, 1155, 920, 845, and 775 cm^{-1}. UV λ_{max}^{MeOH}: 215 nm (ε=29900), 314 (6200, sh), 332 (10000), 342 (9200, sh), 373 (4700, sh), 390 (5500), and 415 (3700)].

Hydrolysis of 13 to 14. An aqueous acetone solution (33%, 15 cm^3) of **13** (300 mg) was refluxed for 4 h. The mixture was then heated in vacuo to remove the solvent; the residue was crystallized from EtOH to give **14** [pale-yellow crystals, mp 218—220 °C (decomp) (lit,[6] 221—223 °C (decomp)). ^{1}H NMR δ=7.03 (1H, d, J=11.4, 2.6 Hz), 7.35 (1H, d, J=11.4 Hz), and 7.70 (1H, d, J=2.6 Hz)].

DDQ-Oxidation of 6. Formation of 3,7-Dibromo-*p*-tropoquinone (7). An acetone suspension (2 cm^3) of **6** (100 mg) was treated with DDQ (93 mg) at room temperature for 30 min. The mixture was then heated in vacuo to remove the solvent; the residue was chromatographed on a silica-gel column to give **7** [yellow crystals, mp 93—95 °C (lit,[6] 96—97 °C (decomp)), 86 mg; 87%].

DDQ-Oxidation of 10 to 3-Bromo-*p*-tropoquinone (15). Similarly, an acetone solution (5 cm^3) of **10** (40 mg) was treated with DDQ (42 mg) at room temperature for 30 min. The mixture was then heated in vacuo to remove the solvent; the residue was chromatographed to give **15** [yellow crystals, mp 59—61 °C, 34 mg; 86%. Found: C, 39.25; H, 1.53%. Calcd for $C_7H_3O_3Br$: C, 39.10; H, 1.41%. ^{1}H NMR δ=6.78 (2H, d, J=0.7 Hz) and 7.53 (1H, t, J=0.7 Hz). ^{13}C NMR δ=133.8, 136.5, 138.5, 141.1, 181.9, 184.6, and 185.2. IR ν: 3045, 1670, 1640, 1610, 1595, 1320, and 1160 cm^{-1}].

DDQ-Oxidation of 12. Formation of 3,7-Dichloro-*p*-tropoquinone (16). An acetone suspension of **12** (200 mg) was treated with DDQ (200 mg) at room temperature for 1 h. After removing the solvent, the residue was chromatographed on a silica-gel column to give **16** [yellow crystals, mp 53—55 °C, 145 mg; 73%. Found: C, 41.50; H, 1.15%; M$^+$, 203.9414. Calcd for $C_7H_4O_3Cl_2$: C, 41.01; H, 0.98%; M, 203.9381. ^{1}H NMR δ=7.30 (2H, s). ^{13}C NMR δ=136.9 (2C), 142.5 (2C), 180.3, and 181.5 (2C). IR ν: 1695, 1630, 1610, 1330, 1190, and 895 cm^{-1}].

AgOAc-Oxidation of 12. An acetone suspension (5 cm^3) of **12** (100 mg) was treated with AgOAc (160 mg) at room temperature for 1 h with stirring. After removing the solvent in vacuo, the residue was passed through a short Celite column and chromatographed on a silica-gel column to give **16** (84 mg; 85%).

Concentrated HCl-Treatment of 16 to 3,4,7-Trichloro-5-hydroxytropolone (19). A THF solution (5 cm^3) of **16** (145 mg) and concd HCl (0.03 cm^3) was stirred at room temperature for 30 min. After removing the solvent in vacuo, the residue was washed with $CHCl_3$ and recrystallized from MeOH to give **19** [greenish-yellow crystals, mp 190 °C (decomp), 126 mg; 74%. Found: C, 34.98; H, 1.25; Cl, 43.90%. Calcd for $C_7H_3O_3Cl_3$: C, 34.82; H, 1.25; Cl, 44.06%. ^{1}H NMR δ=7.59 (1H, s). ^{13}C NMR δ=123.7, 133.3, 135.9, 137.8, 151.4, 161.2, and 163.3. IR ν: 3200—2400, 1510, 1430, 1310, 1190, 1140, 870, and 835 cm^{-1}. UV λ_{max}^{MeOH}: 263 nm (ε=23600), 329 (2900, sh), 355 (6200), 370 (6300), 397 (6400, sh), 416 (7500), and 440 (5800, sh)].

Concentrated HCl-Treatment of 7. Formation of 19. Similarly, a THF solution (5 cm^3) of **7** (195 mg) was treated with concd HCl (0.03 cm^3) at room temperature for 30 min. After removing the solvent, the residue was washed with $CHCl_3$ and recrystallized from MeOH to give **19** (114 mg; 71%). Its identity with the sample obtained from **12** was confirmed by a direct comparison.

DDQ-Treatment of 14. Formation of 3-Chloro-*p*-tropoquinone (17). An MeOH solution (4 cm^3) of **14** (150 mg) was treated with DDQ (200 mg) at room temperature for 30 min. The mixture was then chromatographed on a silica-gel column to give **17** [yellow crystals, mp 68—69 °C (lit,[6] 73—74 °C), 130 mg; 88%].

Concentrated HCl-Treatment of 17 to 3,6-Dichloro-5-hydroxytropolone (18). A THF solution (5 cm^3) containing concd HCl (0.03 cm^3) of **17** (130 mg) was stirred at room temperature for 1 h. After removing the solvent, the residue was recrystallized from EtOH to give **18** [pale-yellow crystals, mp 181—183 °C (decomp), 136 mg; 86%. Found: C, 40.52; H, 2.02%. Calcd for $C_7H_4O_3Cl_2$: C, 40.61; H, 1.95%. ^1H NMR δ=7.70 (1H, s) and 7.96 (1H, s). ^{13}C NMR δ=124.6, 129.6, 130.9, 139.7, 153.5, 159.2, and 168.1. IR ν: 3400—2800, 1525, 1450, 1335, 1220, 1130, and 830 cm^{-1}. UV λ_{max}^{MeOH}: 255 nm (ε=27000), 351 (8100), 365 (8200), 391 (8900, sh), 408 (9800), and 434 (6400, sh)].

Attempted DDQ-Oxidation of 19. An anhydrous acetone solution (5 cm^3) of **19** (100 mg) was treated with DDQ(85 mg) at room temperature for 1 h. After removing the solvent in vacuo, the residue was chromatographed on a silica-gel column to give 14 mg of solid material, whose ^1H NMR spectrum indicated a mixture. Despite the intensive effort, no compound was isolable, and the absence of starting **19** in the mixture was assured by mass spectrometry.

References

1) H. Takeshita, A. Mori, T. Kusaba, and H. Watanabe, *Bull. Chem. Soc. Jpn.*, **60**, 4325 (1987).

2) H. Takeshita, T. Kusaba, and A. Mori, *Chem. Lett.*, **1982**, 701.

3) H. Takeshita, T. Kusaba, and A. Mori, *Chem. Lett.*, **1983**, 1371.

4) T. Nozoe, S. Seto, S. Ito, M. Sato, and T. Katono, *Proc. Jpn. Acad.*, **28**, 488 (1952).

5) T. Nozoe, K. Takase, and H. Matsumura, "Dai Yuki Kagaku(Comprehensive Organic Chemistry)," ed by M. Kotake, Asakura Shoten, Tokyo (1960), Vol. 13, p. 294,

6) H. Takeshita, T. Kusaba, and A. Mori, *Bull. Chem. Soc. Jpn.*, **55**, 1659 (1982).

7) S. Kajigaeshi, T. Kakinami, H. Tokiyama, T. Hirakawa, and T. Okamoto, *Chem. Lett.*, **1987**, 627.

8) The NMR spectra were measured in $CDCl_3$ solutions, and the chemical shifts were expressed in δ unit (internal Me_4Si).

 © 1989 The Chemical Society of Japan Bull. Chem. Soc. Jpn., 62, 455—458 (1989)

Novel Synthesis of Carbamic Ester from Carbon Dioxide, Amine, and Ortho Ester

Shigeru Ishii, Hidenobu Nakayama, Yasuhiko Yoshida,* and Tadataka Yamashita
Department of Applied Chemistry, Faculty of Engineering, Toyo University, Kujirai, Kawagoe, Saitama 350
(Received June 30, 1988)

Carbon dioxide reacted with aliphatic amines and ortho esters to form carbamic esters in good yields. The influence of different ortho esters on the carbamate synthetic reaction is described. In the case of orthocarbonates, carbamic esters were obtained in high yields. The reaction of carbon dioxide, amines, and ortho esters may involve a competitive reaction between the esterification of carbamic acid produced by a reaction of carbon dioxide with amine, and the alkylation of amine.

In recent years, great efforts have been made to find alternative raw materials for organic syntheses, instead of using diminishing fossil fuel. Carbon dioxide is hoped to be made available as a potential carbon source for future use since it is an almost inexhaustible resource. However, it has a great disadvantage due to its inertness in chemical reactions.

A large number of the fixation reactions of carbon dioxide has so far been studied. Especially, recent interest in the fixation of carbon dioxide has been leading to a starting material for the direct synthetic reactions of carbamic esters.[1-9] The usual synthetic methods for carbamic esters[10] are the reaction of alcohol with isocyanate or carbamoyl chloride, and the reaction of amine with chloroformate. However, a new process for preparing carbamic esters without these compounds should be developed, since these reagents are very toxic. Carbamic esters have not been obtained by a direct esterification of carbamic acid, since carbamic acid has been known only as a transient intermediate in the reaction of isocyanate with water, or the hydrolysis of carbamic ester,[11] and is not isolable.

Carbamic acid can also be obtained by a reaction of carbon dioxide with aliphatic amine (Eq. 1). However, carbon dioxide is not fixed by only the reaction with amine, because of an easy dissociation to carbon dioxide and amine.[12]

$$R_2NH + CO_2 \rightleftarrows R_2NCOOH \qquad (1)$$

We reported previously the following reactions using carbamic acid as the reaction intermediate: the reaction of carbon dioxide and amines with epoxides to obtain 2-hydroxyalkyl carbamates in high yields,[3] the reaction with vinyl ethers to form 1-alkoxyalkyl carbamates selectively,[2] and the reaction with alkyl halides to yield the corresponding alkyl carbamates.[5] In the course of our studies concerning the fixation of carbon dioxide, a direct esterification of carbamic acid using ortho esters was found.

In this paper we describe this reaction of carbon dioxide, aliphatic amines, and ortho esters to afford directly carbamic esters.

Results and Discussion

Carbon dioxide reacted with amines and ortho esters to give carbamic esters in good yields, depending on the reactivities of amines and ortho esters, and the reaction conditions.

$$CO_2 + R_2NH + R'C(OR'')_3 \longrightarrow R_2NCOOR'' \qquad (2)$$

Figure 1 suggests a dependence of the carbamate

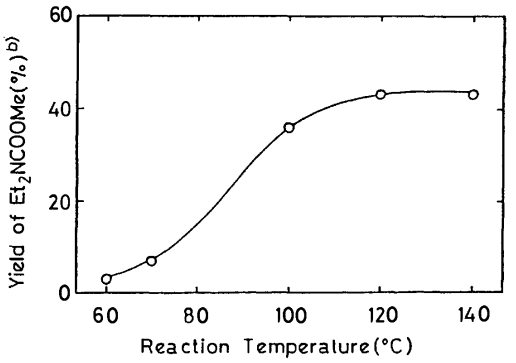

Fig. 1. The dependence of methyl diethylcarbamate yield on the reaction temperature.[a]
a) Et_2NH; 0.2 mol, $HC(OMe)_3$; 0.1 mol, CO_2; 40 atm, for 45 h.
b) Yield based on $HC(OMe)_3$.

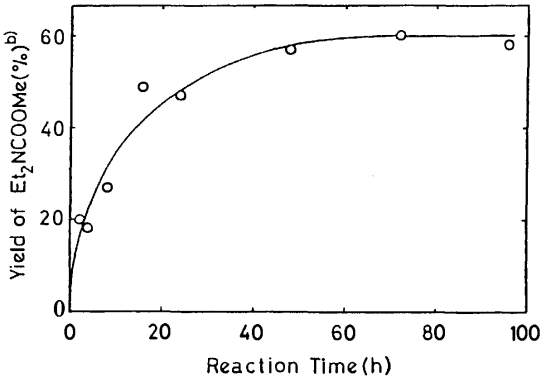

Fig. 2. The dependence of methyl diethylcarbamate yield on the reaction time.[a]
a) Et_2NH; 0.2 mol, $HC(OMe)_3$; 0.1 mol, CO_2; 40 atm, at 120°C.
b) Yield based on $HC(OMe)_3$.

Table 1. Reaction of CO_2, Amines, and Ortho Esters[a]

No.	Amine	Ortho ester	Yield of products (%)[b]			
			Carbamate	Yield	Amide	Yield
1	Et_2NH	$CH_3C(OMe)_3$	$Et_2NCOOMe$	60	Et_2NCOCH_3	100
2	Et_2NH	$HC(OMe)_3$	$Et_2NCOOMe$	43	Et_2NCHO	88
3	Et_2NH	$HC(OEt)_3$	$Et_2NCOOEt$	83	Et_2NCHO	93
4	Et_2NH	$C(OMe)_4$	$Et_2NCOOMe$	127	—	—
5	Et_2NH	$C(OEt)_4$	$Et_2NCOOEt$	156	—	—
6		$HC(OMe)_3$	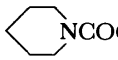	27	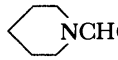	100
7		$HC(OEt)_3$	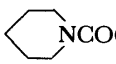	76	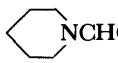	100
8		$HC(OMe)_3$	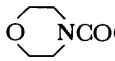	23	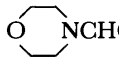	100
9		$HC(OEt)_3$	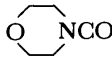	70	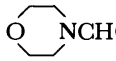	99
10	n-$PrNH_2$	$HC(OMe)_3$	n-PrNHCOOMe	67	n-PrNHCHO	13
11	PhMeNH	$HC(OEt)_3$	—	0	—	0

a) Amine; 0.2 mol, ortho ester; 0.1 mol, CO_2; 40 atm, 120 °C, 45 h. b) Yield based on ortho ester by GLC.

yield upon the reaction temperature in a reaction of diethylamine, carbon dioxide, and trimethyl orthoformate for 45 h. The yield of methyl diethylcarbamate was 3% at 60 °C, though the yield increased with the reaction temperature. The yield of methyl diethylcarbamate was 43% at 120 °C.

The relation between the reaction time and the yield of methyl diethylcarbamate is shown in Fig. 2. In this case, a longer reaction time enhanced the carbamate yield to 60% after 72 h.

The results for the reaction of carbon dioxide, various amines, and ortho esters at 120 °C for 45 h are summarized in Table 1. While aliphatic amines gave the carbamic esters in good yields (Table 1, Nos. 1—10), aromatic amine, such as *N*-methylaniline, did not give the carbamic ester (Table 1, No. 11). It appeared that aromatic amine does not react with carbon dioxide, since the basicities of aromatic amines are lower than those of aliphatic amines.

A reaction using orthoacetate gave a carbamic ester in higher yield than that of orthoformate (Nos. 1 and 2.). With orthocarbonates, the yields of methyl and ethyl carbamates were 127 and 156%, respectively (Nos. 4 and 5)

The reaction with ethyl ortho esters gave the corresponding carbamic esters in higher yields than those of methyl ortho esters (Nos. 2—9), even in the case of using any of the aliphatic secondary amines. The primary aliphatic amine reacted with methyl ortho ester to give the corresponding carbamic ester in a good yield (No. 10).

In order to obtain more details concerning the reaction mechanism, the by-products of the reaction with amines, carbon dioxide, and ortho esters at 120 °C for 45 h were studied in greater detail. The results are summarized in Table 2. The reaction of diethylamine, carbon dioxide, and triethyl orthoformate gave ethyl diethylcarbamate in 83% yield with *N*,*N*-diethylformamide, ethyl alcohol, and triethylamine as by-products in 93, 186, and 6%, respectively (Table 2, No. 1). From these results, the reaction mechanism is considered to be as follows. At first, carbamic acid, formed from a reaction of carbon dioxide with amine (Eq. 1), reacted with ortho ester to form carbamic ester, alcohol, and

Table 2. Reaction Mixture Obtained by the Reaction of CO_2, Amines, and Ortho Esters[a]

No.	Amine	Ortho ester	Reaction mixture	Yield (%)[b]
1	Et_2NH	$HC(OEt)_3$	Et_2NH	20
			Et_3N	6
			EtOH	186
			$HC(OEt)_3$	5
			$Et_2NCOOEt$	83
			Et_2NCHO	93
2		$HC(OMe)_3$		64
				23
				100
3		$HC(OEt)_3$		30
				70
				99
4	Et_2NH	$C(OEt)_4$	Et_2NH	21
			Et_3N	0
			EtOH	151
			$C(OEt)_4$	13
			$Et_2NCOOEt$	156
			$(EtO)_2CO$	31

a) Amine; 0.2 mol, ortho ester; 0.1 mol, CO_2; 40 atm, 120 °C, 45 h. b) Yield based on ortho ester by GLC.

carboxylic ester corresponding to ortho ester (Eq. 3). Then, the formed carboxylic ester reacted with amine (being present in large excess into the reaction system) to give the corresponding amide and alcohol (Eq. 4). The alkylation of amine by ortho ester also occurred to form tertiary amine (Eq. 5).

$$R_2NCOOH + R'C(OR'')_3 \longrightarrow R_2NCOOR'' + R''OH + R'COOR'' \quad (3)$$

$$R'COOR'' + R_2NH \longrightarrow R_2NCOR' + R''OH \quad (4)$$

$$R_2NH + R'C(OR'')_3 \longrightarrow R_2NR'' + R''OH + R'COOR'' \quad (5)$$

Using methyl orthoformate, the alkylation of morpholine was preferred to the esterification of carbamic acid to give *N*-methylmorpholine in good yield (No. 2). The reaction with ethyl orthoformate gave the carbamic ester in higher yield (No. 3).

When tetraethyl orthocarbonate was used in the synthetic reaction of the carbamic ester, ethyl diethylcarbamate was formed in a yield over 100%, based on the amount of ortho ester. The reaction of carbamic ester with tetraethyl orthocarbonate is considered to give ethyl diethylcarbamate, diethyl carbonate and ethyl alcohol in equimolar amounts (Eq. 6). Diethyl carbonate easily reacted with the amine to form carbamic ester (Eq. 7),[13-15] which corresponded to the amide obtained by reactions with orthoformate or orthoacetate.

$$R_2NCOOH + C(OR')_4 \longrightarrow R_2NCOOR' + (R'O)_2CO + R'OH \quad (6)$$

$$(R'O)_2CO + R_2NH \longrightarrow R_2NCOOR' + R'OH \quad (7)$$

The reaction of amines, carbon dioxide, and ortho esters is considered to involve competitive reactions between the esterification of carbamic acid and the alkylation of amine,[16,17] depending on the reactivities of the amines and ortho esters.

In conclusion, aliphatic amines react with carbon dioxide and ortho esters to give carbamic esters in good yields, though aromatic amines give no products at all. The reactions of carbon dioxide and amines with ethyl ortho esters give the carbamic esters selectively in high yields.

Experimental

Material. Commercially available amines and ortho esters were purified by employing the usual procedures and stored under a nitrogen atmosphere. Commercially high-purity carbon dioxide gas was introduced into an autoclave directly from a gas cylinder without further purification.

Measurements. IR spectra were recorded on Hitachi EPG-G3 and 260-50 equipment. NMR spectra on a Hitachi 24B spectrometer operating at 60 MHz and JEOL FX90Q at 90 MHz, using hexamethyldisiloxane (HMDS) as an internal standard. The GC-MS spectra were recorded on a Shimadzu QP1000 GC-MS spectrometer. Gas liquid chromatography (GLC) analyses were performed on a Shimadzu GC-4C apparatus with a thermal conductor, using a 3 mm×5 m column packed with Silicon OV-17 with helium as the carrier gas.

Syntheses of Carbamic Esters. Ethyl Diethylcarbamate: The typical reaction of amines and carbon dioxide with ortho esters is noted as follows. The mixture of diethylamine (0.2 mol; 20.7 cm^3) and triethyl orthoformate (0.1 mol; 16.6 cm^3) was added into a 100 cm^3 stainless autoclave, and carbon dioxide gas was introduced directly from a gas cylinder until the pressure reached 40 atm (4.05×10^6 Pa). After the autoclave was allowed to stand in an oil bath controlled at 120 °C for 45 h, an excess of carbon dioxide gas was released. The reaction mixture was subjected to fractional distillation under reduced pressure in order to isolate the product, ethyl diethylcarbamate (bp 60.8—61.2 °C/13 mmHg, (1 mmHg≈133.322 Pa) 11.0 g, 76%).

Preparations of other carbamic esters were carried out by a similar manner.

Identification of the Carbamic Ester. Methyl Diethylcarbamate: Bp 155—156 °C (lit,[18] bp 154—155 °C); IR (neat) 1695 cm^{-1} (C=O); ^1H NMR ($CDCl_3$) δ=0.99 (6H, t, $(C\underline{H}_3CH_2)_2N$), 2.88 (4H, q, $(CH_3C\underline{H}_2)_2N$), 3.21 (3H, s, CH_3O).

Ethyl Diethylcarbamate: Bp 60.8—61.2 °C/13 mmHg (lit,[19]; Bp 62—63 °C/14 mmHg); IR (neat) 1700 cm^{-1} ((C=O), ^1H NMR ($CDCl_3$) δ=1.1 (9H, t, CH_3), 3.24 (4H, q, $(CH_3C\underline{H}_2)_2N$), 4.12 (2H, q, $OC\underline{H}_2CH_3$).

***N*-Methoxycarbonylpiperidine:** Bp 101.0—101.5 °C/30 mmHg (lit,[20] bp 100 °C/30 mmHg); IR (neat) 1700 cm^{-1} (C=O); ^1H NMR ($CDCl_3$) δ=1.4 (6H, m, methylenes of piperidine ring), 3.2 (4H, m, CH_2N), 3.46 (3H, s, CH_3O).

***N*-Ethoxycarbonylpiperidine:** Bp 57.7—58.0 °C/1.5 mmHg (lit,[20] bp 55—56 °C/0.9 mmHg); IR (neat) 1705 cm^{-1} (C=O); ^1H NMR ($CDCl_3$) δ=0.97 (3H, t, $C\underline{H}_3CH_2O$), 1.3 (6H, m, methylene of piperidine ring), 3.2 (4H, m, CH_2N), 3.75 (2H, q, $CH_3C\underline{H}_2O$).

Methyl Propylcarbamate: Bp 79.0—80.0 °C/21 mmHg (lit,[22] bp 76 °C/20 mmHg); IR (neat) 1710 cm^{-1} (C=O); ^1H NMR ($CDCl_3$) δ=0.82 (3H, t, $C\underline{H}_3CH_2CH_2N$), 1.45 (2H, m, $CH_3C\underline{H}_2CH_2N$), 3.08 (2H, q, $CH_2C\underline{H}_2N$), 3.48 (3H, s, CH_3O), 5.1 (1H, s, NH).

***N*-Methoxycarbonylmorpholine:** Bp 59.7 °C/1.5 mmHg; IR (neat) 1700 cm^{-1} (C=O); ^1H NMR ($CDCl_3$) δ=3.3 (8H, m, methylene of morpholine ring), 3.57 (3H, s, CH_3O); Found: C, 49.42, H, 7.87; N, 9.46%. Calcd for $C_6H_{11}NO_3$: C, 49.46; H, 7.64; N, 9.64%.

***N*-Ethoxycarbonylmorpholine:** Bp 72.6—72.8 °C/2.3 mmHg. IR (neat) 1705 cm^{-1} (C=O); ^1H NMR ($CDCl_3$) δ= 1.13 (3H, t, $C\underline{H}_3CH_2O$), 3.4 (8H, m, methylene of morpholine ring), 4.01 (2H, q, $CH_3C\underline{H}_2O$); Found: C, 52.68; H, 8.36; N, 8.76%. Calcd for $C_7H_{13}NO_3$; C, 52.82; H, 8.23; N, 8.80%.

References

1) T. Toda, *Chem. Lett.*, **1977**, 957; T. Asano, N. Saito, S. Ito, K. Hatakeda, and T. Toda, *ibid.*, **1978**, 311.

2) Y. Yoshida and S. Inoue, *Chem. Lett.*, **1977**, 1375.

3) Y. Yoshida and S. Inoue, *Chem. Lett.*, **1978**, 139; Y. Yoshida and S. Inoue, *J. Chem. Soc., Perkin Trans. 1*, **1979**, 3140.

4) Y. Yoshida and S. Inoue, *Bull. Chem. Soc. Jpn.*, **51**, 559 (1978).

5) Y. Yoshida, S. Ishii, and T. Yamashita, *Chem. Lett.*, **1984**, 1571.
6) N. Saito, K. Hatakeda, S. Ito, T. Àsano, and T. Toda, *Bull. Chem. Soc. Jpn.*, **59**, 1629 (1986).
7) Y. Sakaki and P. H. Dixneuf, *J. Chem. Soc., Chem. Commun.*, **1986**, 79.
8) Y. Sakaki and P. H. Dixneuf, *J. Org. Chem.*, **52**, 314 (1987).
9) Y. Yoshida, S. Ishii, A, Kawato, T. Yamashita, M. Yano, and S. Inoue, *Bull. Chem. Soc. Jpn.*, **61**, 2913 (1988).
10) P. Adams and F. A. Baron, *Chem. Rev.*, **65**, 567 (1965).
11) H. Al. Rawi and A. Williams, *J. Am. Chem. Soc.*, **99**, 2671 (1977).
12) J. T. Edsall, "Biophysical Chemistry," Academic Press, New York (1958), Vol. I, p. 571.
13) M. M. Baizer and J. R. Clark, *J. Org. Chem.*, **22**, 1595 (1955).
14) B. R. Delaly, A. Sekera, P. Chabrier, and P. Piganiol, *Bull. Soc. Chim. Fr.*, **1951**, 392.
15) C. R. M. Acheson, *Acc. Chem. Res.*, **4**, 177 (1971).
16) R. H. Dewolfe, "Carboxylic Ortho Acid Derivatives," Academic Press, New York (1970), p. 192.
17) R. A. Swaringen, Jr., J. F. Eaddy, and T. R. Henderson, *J. Org. Chem.*, **45**, 3986 (1980).
18) M. Barker, L. Hunyer, and G. Reynolds, *J. Chem. Soc.*, **1948**, 874.
19) O. Schmit, *Chem. Ber.*, **36**, 2477 (1954).
20) W. Ried, H. Hillenbrand, and G. Oertel, *Ann. Chem.*, **590**, 123 (1954).
21) K. Osugi, *J. Pharm. Soc. Jpn.*, **78**, 1313 (1958).
22) M. Montagne, *Bull. Soc. Chim. Fr.*, **14**, 125 (1947).

 © 1989 The Chemical Society of Japan Bull. Chem. Soc. Jpn., 62, 459—468 (1989)

Electronic Control of Stereoselectivity in the Metal Hydride Reductions of 1,2,3,4-Tetrahydro-1,4-methanonaphthalen-9-ones[1]

Keiji Okada,* Seiji Tomita, and Masaji Oda*
Department of Chemistry, Faculty of Science, Osaka University, Toyonaka, Osaka 560
(Received July 11, 1988)

Stereoselectivity in the metal hydride reduction of a series of substituted 1,2,3,4-tetrahydro-1,4-methanonaphthalen-9-ones was investigated in relation to their homoconjugation character. The observed stereoselectivity sequence was found to be parallel with the homoconjugation sequence: the portion of anti-attack increases as the benzene ring becomes electron-rich. The results are rationalized in terms of the transition state model proposed by Cieplak or of the contribution of the nonclassical carbocation in the transition state.

Since Dauben, Fonken, and Noyce presented a rationalization of "product development control" for the predominant axial attack of nucleophiles on cyclohexanones in 1956,[2] a number of ingenious rationalizations as well as many experimental investigations on the nucleophilic addition to cyclic ketones have appeared.[3] 7-Norbornenone has also attracted attention in its relationship to the homoconjugation character between the carbonyl group and the endocyclic double bond. Brown and Muzzio originally expected that the anti/syn-stereoselectivity towards 7-norbornenone might reflect the homoconjugation property. Such interaction would lead to the preferential anti-attack. However, the opposite selectivity was observed.[4] Experimental data so far available show that the nucleophiles stereoselectively attack the carbonyl group from the syn-side of the double bond. For example, the reactions with sodium borohydride,[4] Grignard reagents,[5,6] alkyllithium reagents,[7] diazomethane,[8] and with sulfonium[9] or sulfoxonium[6] ylides gave the products of syn-attack in a stereoselective or stereospecific manner. Exceptions can be seen in the reaction with vinyllithium[10] and phenyllithium.[11] Mechanistic problems as to whether the observed stereoselectivity is due to steric or electronic effects are controversial. Attack from the anti-side of the double bond seems to be slightly more hindered owing to the steric repulsion between the exo-protons of ethano-bridge and the incoming nucleophiles. An empirical calculation evaluating congestion or torsion-corrected congestion, however, suggests that attack from the side of the double bond is slightly more hindered, leading to a consideration that the stereoselectivity may be due to a chelating effect of the double bond rather than a steric or torsional effect.[12] A similar electronic interpretation was also proposed by Bly and Bly.[6] An insight into this selectivity can be drawn by the experiments reported by Tanida who investigated the metal hydride reductions of monosubstituted benzonorbornenones **1** as a reference for the solvolysis experiments of the corresponding anti-brosylates. A maximum variation for the selectivity of anti/syn-alcohol was obtained in the disiamylborane reduction (52/48 for Z=Cl, 45/55 for Z=H, 36/64 for Z=OMe). However, the author argued the selectivity in terms of the subtle change of steric environment because the change of stereoselectivity was too small in comparison with the large variation of solvolysis rates.[13] For demonstration of the electronic effect, much widely variable selectivity is desirable. We wish to report the metal hydride reductions of a series of substituted 1,2,3,4-tetrahydro-1,4-methanonaphthalen-9-ones (9-benzonorbornenones),[14] **2a—f**. Because of simplicity, the name "9-benzonorbornenone" is used in the text hereafter.

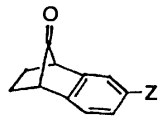

1

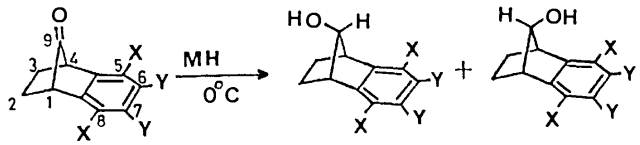

2a-f **3a-f** **4a-f**

a: X=Y=F, b: X=Y=Cl, c: X=Y=H, d: X=OMe; Y=H, e: X=H; Y=OMe, f: X=Y=OMe

Results and Discussion

Synthesis. Compounds **2a**, **2b**, **2c**, and **2d** were synthesized according to the literature procedures.[15,16] Dimethoxy derivatives **2e**, **8e** and tetramethoxy derivatives **2f** and **8f** are new compounds. At first, we attempted the syntheses of **2e** and **2f** from the corresponding isopropylidene derivatives **8e** and **8f**, which were prepared by cycloaddition of 6,6-dimethylfulvene (**6**) with the appropriate benzynes, followed by reduction of the endocyclic double bond, in total yields of 38 and 44%, respectively (Scheme 1). Ozonolysis or oxidative cleavage ($KMnO_4$-$NaIO_4$, OsO_4-$NaIO_4$) of the isopropylidene derivatives gave **2e** and **2f** in very poor yields because of facile oxidation of the benzene rings. More rewarding routes to **2e** and **2f** are also outlined in Scheme 1. Cycloaddition of 6-phenylfulvene (**9**) with 4,5-dimethoxybenzyne gave the adduct **10** in 24% yield. Reduction of the endocyclic double bond and

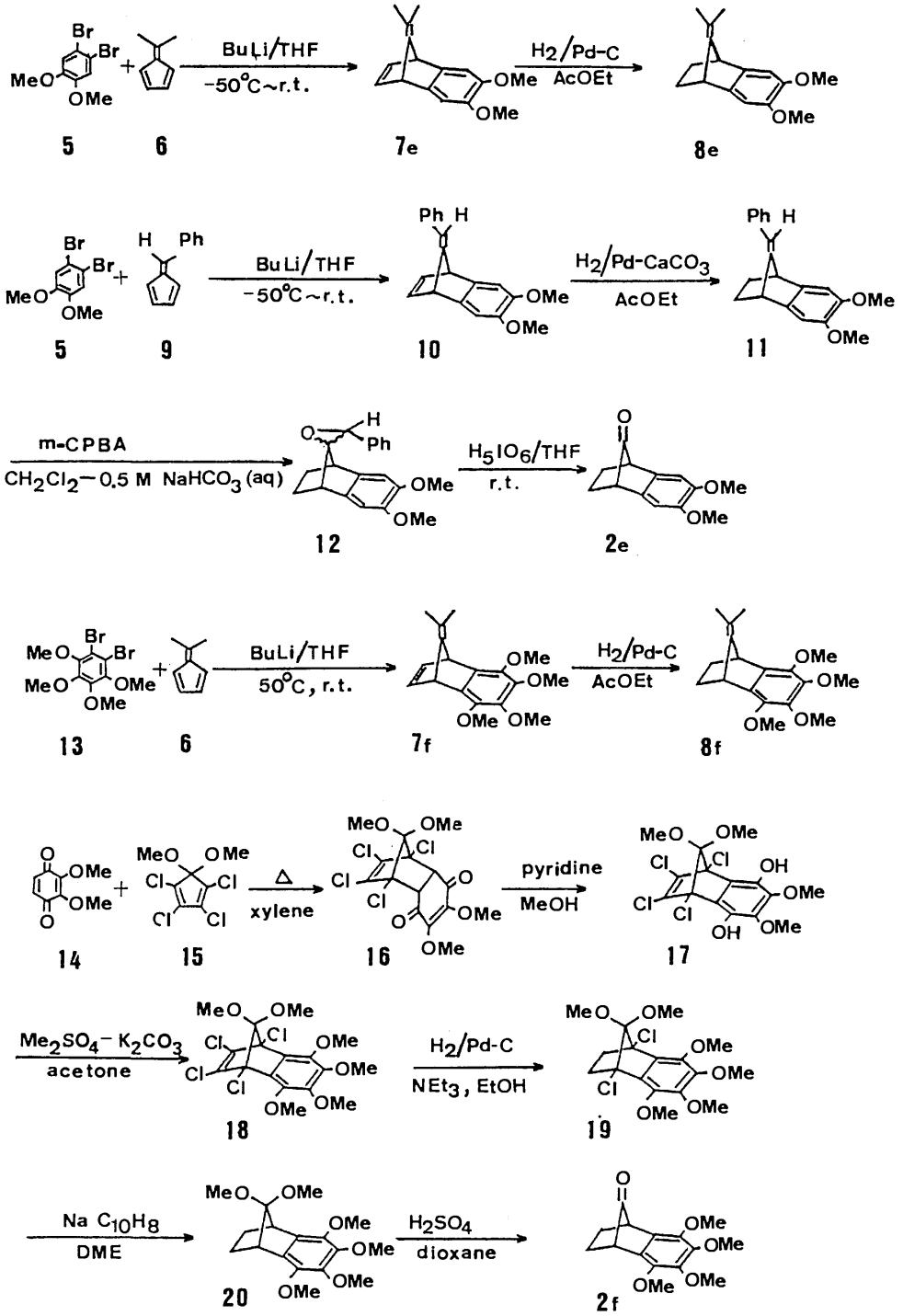

Scheme 1.

successive epoxidation followed by oxidative cleavage with H_5IO_6 in THF produced the desired **2e** in 28% yield from **10**. Compound **2f** was synthesized by a modification of the reported method.[16] Cycloaddition of 2,3-dimethoxy-*p*-benzoquinone (**14**) with 5,5-dimethoxy-1,2,3,4-tetrachlorocyclopentadiene (**15**) gave **16** in 97% yield. Enolization followed by *O*-methylation afforded dimethyl acetal **18** in 78% yield. Direct transformation of **18** to **20** with metal reduction (Li/*t*-BuOH-THF) failed and a mixture of the dimethoxy and trimethoxy derivatives was obtained instead. This conversion was achieved by two step reduction with use of H_2/Pd-C-Et_3N-EtOH and sodium naphthalenide/DME. Acidic hydrolysis of **20** gave **2f** in 85% yield.

Stereochemistry of Anti- (3a—f) and Syn-Alcohols (4b—f). ^{1}H NMR data of the produced anti- (**3a—f**) and syn-alcohols (**4b—f**) are listed in Table 1. Stereochemistry of the anti- and syn-alcohols were determined by use of a NMR shift reagent, Eu(fod)$_3$. The

Table 1. Chemical Shifts (δ)[a] and Relative Shift Values[b] Induced by $Eu(fod)_3$ for Protons of **3a**—f and **4b**—f

	OH	$H_{1,4}$	$H_{2,3}$-endo	$H_{2,3}$-exo	H_9	Methoxy protons	Aromatic protons
X=Y=F	2.02	3.42	1.22	2.19	3.82		
3a		(1.00)	(0.76)	(1.23)	(2.02)		
X=Y=Cl	2.02	3.46	1.23	2.24	3.92		
3b		(1.00)	(0.66)	(1.20)	(2.16)		
X=Y=H	1.87	3.11	1.18	2.10	3.80		7.06
3c		(1.00)	(0.65)	(1.20)	(2.09)		(0.21)[c]
X=OMe, Y=H	2.02	3.11	1.17	2.10	ca. 3.7	3.72	6.54
3d		(1.00)	(0.62)	(1.18)	(2.0)	(0.11)	(0.96)
X=H, Y=OMe	2.12	3.07	1.14	2.08	3.81	3.82	6.77
3e		(1.00)	(0.65)	(0.76)	(1.44)	(1.44)	(1.71)
X=Y=OMe	1.98	3.34	1.03	2.16	3.82	3.83, 3.86	
3f		(1.00)	(0.66)	(0.83)	(1.38)	(0.55, 1.24)	
X=Y=Cl	1.76	3.52	1.18	2.08	4.20		
4b		(1.00)	(0.35)	(0.36)	(1.71)		
X=Y=H	1.58	3.16	1.11	1.96	4.10		6.99—7.30
4c		(1.00)	(0.35)	(0.39)	(1.82)		(0.34)[c]
X=OMe, Y=H	1.63	3.40	1.12	1.92	4.06	3.73	6.61
4d		(1.00)	(0.37)	(0.42)	(1.81)	(0.20)	(0.26)
X=H, Y=OMe	1.72	3.11	1.08	1.94	4.11	3.86	6.89
4e		(1.00)	(0.36)	(0.39)	(1.87)	(0.25)	(0.55)
X=Y=OMe	1.58	3.42	1.18	2.00	4.11	3.85, 3.90	
4f		(1.00)	(0.33)	(0.35)	(1.57)	(0.36, 0.54)	

a) Measured in $CDCl_3$ (ca. 25—30 mg/0.3 ml). b) In parenthesis; averaged values determined by successive addition of 5 mg of $Eu(fod)_3$ up to ca. 25 mg. c) An averaged value of the two kind of protons.

relative shift values (1.00 for $H_{1,4}$-protons in both alcohols) induced by $Eu(fod)_3$ for $H_{2,3}$- and other protons are also summarized in Table 1. It is clear that $H_{2,3}$-exo protons in anti-alcohols (**3b—f**) have larger relative shifts (0.76—1.20) than those (0.35—0.42) of syn-alcohols (**4b—f**). The same trend is observed for $H_{2,3}$-endo protons. These results clearly elucidate the stereochemistry of the alcohols as assigned in the text. Although the partial coordination of $Eu(fod)_3$ onto methoxyl groups is also recognizable from the table, this coordination would not much affect the shift of $H_{2,3}$-protons for the relatively long distance between these protons and the coordinated metal center. The assignment is also supported by the fact that H_9-methine protons of anti-alcohols appear in higher field (δ ca. 3.7—3.92) than those of syn-alcohols (δ 4.06—4.20) because of the anisotropy effect of the benzene rings. Similarly, hydroxyl protons of anti-alcohols have lower chemical shifts (δ 1.87—2.12) than those (δ 1.58—1.76) of syn-alcohols in usual concentration (ca. 25—30 mg/0.3 ml $CDCl_3$). It is interesting to note that the shift of aromatic protons of **3e** and **4e** is larger than those of **3d** and **4d** upon the contact with $Eu(fod)_3$. This may suggest that the two adjacent methoxyl groups might form a better ligand for $Eu(fod)_3$ than the two methoxyl groups at *p*-position. It may be also interesting to refer to GC retention time (column; OV-17) of these alcohols: syn-alcohols have shorter retention time than anti-alcohols in all cases. This may be a reflection of the expected hydrogen bond between the hydroxyl group and the benzene π-bond. This relation might be used as a convenient method of stereochemical assignment for the related compounds.

Homoconjugation Interaction of the Carbonyl Group and the Benzene Ring. Although the expectation that anti/syn-stereoselectivity may reflect the homoconjugation interaction in 7-norbornenone was rather disappointing,[4] it is worthy to reconsider the possibility that the same expectation may be realized in a series of substituted 9-benzonorbornenones. Before entering the section of stereoselective metal hydride reduction, the donating ability of the substituted benzene rings is discussed here in relation to the homoconjugation property. As to 7-norbornenone, extensive studies by means of ^{13}CNMR,[17] PES,[18] and CD (for unsymmetrically deutrated or substituted derivatives)[19] spectra have shown the homoconjugation interaction between the endocyclic double bond and the carbonyl group. The similar homoconjugation interaction is expectable if the endocyclic double bond is replaced by the benzene ring. Electron-donating substituents on the benzene ring of 9-benzonorbornenones (**2a—f**) would decrease the double bond character of the carbonyl group. Therefore, the homoconjugation in **2a—f** may be revealed in IR stretching frequency of the carbonyl groups. Initially, we thought that electron-donating property would increase in the sequence of **2a**→**2b**→**2c**→**2d**→**2e**→**2f**. However, the observed frequency for **2f** falls in the range between **2b** and **2c**: [IR(CCl_4, $\nu_{C=O}$); 1793 for **2a**: 1786 ($CHCl_3$) for **2b**: 1782 for **2c**: 1781 for **2d**: 1778 for

2e: 1785 cm^{-1} for **2f**]. This may suggest that tetramethoxybenzo moiety may not be an effective electron donor, contrary to our initial expectation. To elucidate this point, other reliable methods to evaluate the electron-donating ability of the substituted benzene rings favorably using the related molecules were sought. 9-Isopropylidenebenzonorbornenes are known to be homoconjugated compounds.[16,20,22] In these compounds, it has been established that the degree of homoconjugation can be evaluated by ^{13}C NMR parameter, $\Delta\delta$ (C_9–C_{10})[20,22] and also by the anti/syn-stereoselectivity in the reaction with singlet oxygen and other electrophiles.[22] For these reasons, 9-isopropylidene analogues **8e** and **8f** were prepared and their ^{13}C NMR and the reactions with singlet oxygen were examined. Table 2 shows the results together with the reported data.[16,22] Both $\Delta\delta$ (C_9–C_{10}) and the anti/syn-attack selectivity indicate the poor electron-donating ability of tetramethoxybenzene ring: the ^{13}C NMR parameters and the stereoselectivities for **8a—f** are roughly lined in the order of **8a**≃**8b**→**8f**→**8c**→**8d**→**8e**. This is the same sequence with that the IR experiments showed for **2a—f**. From these results, we conclude that the donating ability of the substituted benzene rings increases in the order of **2(8)a**≃**2(8)b**→**2(8)f**→**2(8)c**→**2(8)d**→**2(8)e**. The poor electron-donating property in **2(8)f** is probably due to nonplanar conformation of tetramethoxybenzo moiety arising from the steric congestion of four adjacent methoxyl groups.

Stereoselective Metal Hydride Reductions of 9-Benzonorbornenones. The reductions of substituted 9-benzonorbornenones (**2a—f**) with various metal hydrides gave the corresponding anti- (**3a—f**) and syn-alcohols (**4b—f**) in high yields (71—99%). The produced alcohols can be separated by the preparative TLC or gas chromatography. Table 3 summarizes the results of the reductions with various typical reagents along with the reaction conditions. In spite of considerably different sizes and reactivities of the reagents, the portion of anti-attack (syn-alcohol) increases in the order of **2a**→**2b**→**2f**→**2c**→**2d**→**2e** with slight deviation. Especially, the reduction with diisobutylaluminum hydride (DIBALH), and bis(1,2-dimethylpropyl)-borane (common name "disiamylborane" is used hereafter) follows this sequence. A small change in the sequence is observed for other reagents. In addition, the following features are notable from Table 3. (1) **2a**

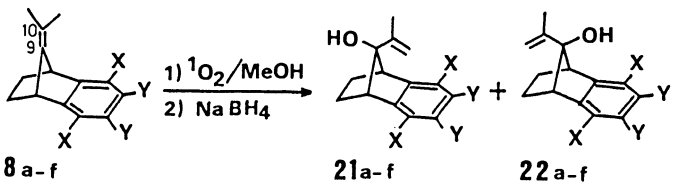

a: X=Y=F, b: X=Y=Cl, c: X=Y=H, d: X=OMe; Y=H, e: X=H; Y=OMe, f: X=Y=OMe

Table 2. ^{13}C NMR Parameters[a] and Anti/Syn-Stereoselectivity in the Singlet Oxygen Reaction of **8a—f**

	8a[b,c]	**8b**[b,c]	**8c**[b,c]	**8d**[b,c]	**8e**	**8f**
$\delta(C_9)$	145.26	145.74	148.61	148.03	148.34	146.80
$\delta(C_{10})$	113.94	114.62	110.88	109.42	109.74	111.09
$\Delta\delta(C_9-C_{10})$	31.3	31.1	37.7	38.6	38.6	35.7
$^1O_2$; anti(**21**) : syn(**22**)	44 : 56	41 : 59	76 : 24	83 : 17	91 : 9	72 : 28

a) Measured in $CDCl_3$. b) L. A. Paquette, L. W. Hertel, R. Gleiter, M. C. Böhm, M. A. Beno, and G. G. Christoph, *J. Am. Chem. Soc.*, **103**, 7106 (1981). c) K. Okada and T. Mukai, *J. Am. Chem. Soc.*, **100**, 6509 (1978); L. A. Paquette, L. W. Hertel, R. Gleiter, and M. Böhm, *ibid.*, **100**, 6512 (1978).

Table 3. Product Ratios (**3a—f** : **4a—f**) in the Metal Hydride Reductions of **2a—f**[a]

Reagent	Solvent	**2a**	**2b**	**2c**	**2d**	**2e**	**2f**
LAH	THF	100 : 0	92 : 8	62 : 38	45 : 55	51 : 49	59 : 41
LAH	Ether	100 : 0	95 : 5	81 : 19	79 : 21	64 : 36	78 : 22
DIBALH	Ether	100 : 0	86 : 14	43 : 57	37 : 63	26 : 74	60 : 40
LTBA[b]	Ether	100 : 0	100 : 0	93 : 7	93 : 7	95 : 5	96 : 4
$NaBH_4$	EtOH	100 : 0	95 : 5	81 : 19	79 : 21	81 : 19	89 : 11
$(BH_3)_2$	THF	100 : 0	93 : 7	75 : 25	70 : 30	54 : 46	70 : 30
Sia_2BH[c]	Diglyme	100 : 0	—[d]	57 : 43	46 : 54	22 : 78	61 : 39

a) All reactions were performed at 0 °C. b) Lithium tri-*t*-butoxyaluminum hydride. c) Bis(1,2-dimethylpropyl)borane (Disiamylborane). d) 70—95% recovery.

and **2b** show high syn-selectivity toward all the reagents giving anti-alcohols. (2) High selectivity of syn-attack is observed in the reduction with tri-*t*-butoxyaluminum hydride for all the substrates. (3) The anti/syn-selectivity is widely varied in the reduction with lithium aluminum hydride in THF, diisobutylaluminum hydride, and disiamylborane: in these cases, the main product is switched from anti- to syn-alcohol when the benzene ring becomes electron-donating. Obviously, steric effect of the substituents on the benzene ring or the $H_{2,3}$-exo protons do not provide a rationalization for the observed stereoselectivity sequence. On the other hand, this sequence is the one that was discussed in homoconjugation interaction, strongly indicating the importance of electronic effects.

Several electronic factors have been previously reported on the stereoselectivity in the nucleophilic addition to cyclic ketones. Especially with regard to cyclohexanones, the origin of the selectivity is highly controversial: product development control, torsional strain,[23] orbital interaction,[24] antiperiplanar interaction with axial hydrogen,[25] steric effect of axial hydrogen at C_4,[26] and electrostatic potential field[27] have been proposed. Recently, Hudec and Giddings reported a new view of "twist-angle," which is determined by the relative signs of coefficients of $p_{x,y,z}$-orbitals of carbonyl carbon in LUMO of ketones, to rationalize the stereoselectivity in the nucleophilic addition to cyclic ketones including 7-norbornenone.[28] For 7-norbornenone, they predicted that the endocyclic double bond facilitates the syn-attack and rationalized the result of syn-attack in sodium borohydride reduction. However, our experiments clearly show that anti-attack increases when the electron-donating substituents are situated on the benzene ring. Therefore, the model proposed by Hudec and Giddings cannot explain our results. A related but more successful transition state model has been recently reported by Cieplak.[29] He assumed that the incipient C-Nu bond is weak and essentially electron-deficient and therefore can be characterized as a σ^*-orbital. In his model, nucleophiles preferably attack the carbonyl group from the direction such that the σ^*-orbital can interact with the electron-donating orbitals neighboring the carbonyl group. Le Noble and co-workers recently reported that the model developed by Cieplak reasonably explained the stereoselectivity of a series of substituted adamantanones.[30] Participation of donor orbitals on the stabilization of polarized carbonyl group of the adamantanones may be supported by the recent X-ray study of the complex, 5-phenyl-2-adamantanone-pentachloroantimony reported by Laube and Stilz.[31]

Application of Cieplak's model to our system gives a satisfactory rationalization. Qualitative transition models are illustrated in **A** for anti-attack and in **B** for syn-attack. In **A**, the transition state is much stabilized

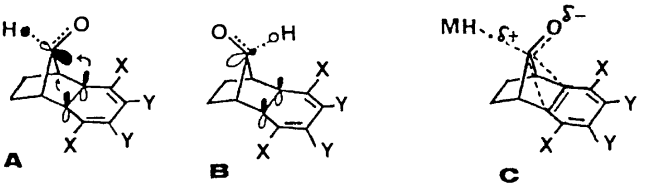

by the large bonding overlap of back side lobe of σ^*-orbital with benzene π-orbital, compared with the transition state in **B**. Thus, increase of electron-donating character of the benzene ring would increase the anti-attack. Furthermore, Cieplak predicts that coordination of metal ions to the carbonyl oxygen would decrease the energy of σ^*-orbital, so that higher stereoselectivity would be observed. This can explain higher anti-attack for **2d** and **2e** in the reduction with diisobutylaluminum hydride and disiamylborane, both of which have a Lewis acid character and would coordinate onto the carbonyl oxygen in the transition state. Lithium ion in THF is also known to coordinate onto carbonyl groups.[32] Thus, Cieplak's model satisfactorily explains our results.

However, similar rationalization is also provided by the contribution of nonclassical carbocation. As Cieplak pointed out that the incipient C-H bond is electron-deficient and polarized in nature, some positive charge remains on the carbonyl carbon to a greater extent than in the ground state. Coordination onto the carbonyl oxygen must assist this polarization. When the benzene ring becomes electron-rich, the transition state for anti-attack would be stabilized as shown in **C**. Thus, the explanations with Cieplak's and nonclassical carbocation models lead to the similar conclusion in this system. We do not have choice of one from the two explanations because of their totally different languages.

It is interesting to compare the results of anti/syn-stereoselectivity in metal hydride reduction of **2a—f** with that in singlet oxygen addition to isopropylidene derivatives **8a—f**. As can be recognized from Tables 2 and 3, higher selectivity of anti-attack for the substrates which have the same substituents on the benzene ring is observed in the reaction with singlet oxygen (e.g. anti/syn-attack for singlet oxygen; 76/24 for **8c**, for LAH reduction with THF; 38/62 for **2c**). High anti-selectivity of addition of other electrophiles to **8** have been reported.[16,22] The different selectivity in the two systems is probably related to the difference of the approach of the reagents to the C=C and C=O bond. Electrophiles would attack from the center of C=C in the transition state because of the bonding nature of HOMO of C=C. Whereas nucleophiles would attack the carbonyl group from the side of carbonyl carbon with obtuse angle of Nu-C-O[33] because of the anti-bonding nature of LUMO of C=O. From this consideration, nucleophilic attack toward 9-benzonorbornenones or 7-norbornenone would involve much severe steric repulsion with $H_{2,3}$-exo protons in com-

parison with electrophilic addition to the corresponding 9-isopropylidene analogues. High selectivity of syn-attack in the reduction with very bulky tri-*t*-butoxyaluminum hydride for all the substrates may be ascribed to this factor. In this case, the contribution of the electronic factor would be minimized.

Higher syn-selectivity toward **2a** and **2b** for all the metal hydrides may be due to several factors. The expected small electronic contribution via Cieplak's model or nonclassical carbocation as well as steric repulsion with $H_{2,3}$-exo protons, which would be similar in all the substrates, would suggest more or less syn-attack. However exclusive syn-attack for **2a** may indicate that certain level of special electronic factor such as electrostatic potential field is exerted. Such field calculation in the related isopropylidene system has been reported by Paquette and Gleiter et al.[16,22]

In summary, we have demonstrated electronic control of stereoselectivity in the metal hydride reductions of a series of 9-benzonorbornenones: anti-attack prevails when benzene ring becomes electron-rich. Brown's original expectation that anti/syn-stereoselectivity in the nucleophilic addition may reflect the homoconjugation character is realized in this paper. Rationalizations are provided by Cieplak's model or by the contribution of nonclassical carbocation. Since both explanations are related to HOMO-LUMO interaction between *p*-orbital of the polarized carbonyl carbon with benzene π-orbital in the transition state, the observed stereoselectivity must be lined parallel with the homoconjugation interaction which is related to the interaction of weakly polarized C=O and benzene π-orbitals in the ground state. A steric effect of $H_{2,3}$-exo protons must be also important for the metal hydride reductions. However, such effect is very similar in the series of 9-benzonorbornenones for the given metal hydrides. High syn-selectivity of **2a** is probably due to the special electrostatic potential field effect.

Experimental

General. Melting points were measured on a Mettler FP2 apparatus and are uncorrected. IR spectra were recorded with a Hitachi EPI-G3 grating spectrophotometer and wavenumbers were corrected with use of polystyrene film. The wavenumbers of the carbonyl stretching for **2a**—f were directly read from the spectrophotometer at their maximum absorptions. ^{1}H NMR spectra were obtained at 90 MHz on a JEOL FX-90Q, or 100 MHz on a Varian XL-100. ^{13}C NMR spectra were taken with a JEOL FX-90Q (22.5 MHz). Mass spectra were measured on a JEOL JMS-01SG-2 mass spectrometer. GLC analyses were performed on a Hitachi 063 gas chromatography with a glass column packed with Silicone OV-17 (3%) on Chromosorb W AW DMCS (1 m). Column chromatography was carried out with Merck Kieselgel 60 or Merck Aluminiumoxide 90 and preparative TLC with Merck Kieselgel GF_{254} (Type 60). Lithium aluminum hydride, sodium borohydride, lithium tri-*t*-butoxyaluminum hydride, and diisobutylaluminum hydride were commercial products and used without purification. Diborane and disiamylborane were generated in situ prior to use.[34] Compounds **2a**,[15] **2b**,[15] **2c**,[15] and **2d**[16] were prepared according to the reported methods. All the solvent were distilled before use.

1,4-Dihydro-9-isopropylidene-6,7-dimethoxy-1,4-methanonaphthalene (7e). In a 300 ml three-necked round bottom flask equipped with a dropping funnel was placed 100 ml of dry THF, 10.0 g (33.9 mmol) of 1,2-dibromo-4,5-dimethoxybenzene (**5**) and 4.70 g (44.3 mmol) of 6,6-dimethylfulvene (**6**). The mixture was flashed with nitrogen, cooled to −50 °C, and magnetically stirred while 55 mmol of butyllithium in 34 ml hexane solution (1.63 M; 1 M=1 mol dm^{-3}) was slowly added over 40 min from the dropping funnel. The solution was stirred at −50—−34 °C for 1 h, and allowed to come up slowly to ambient temperature. After being stirred for 1 h, the mixture was treated dropwise with 80 ml of water and then 60 ml of ether. The separated organic layer was dried, filtered, and concentrated. Chromatography over 50 g silica gel (eluent; hexane : ethyl acetate=10 : 1) gave 3.08 g (37%) of **7e**. Recrystallization from hexane gave colorless prisms; mp 79—80 °C; IR (KBr) 2930, 2900, 1603, 1488, 1462, 1295, 1208, 1086, 1050, 754 cm^{-1}; ^{1}H NMR (100 MHz, $CDCl_3$) δ=1.53 (s, 6H), 3.80 (s, 6H), 4.30 (dd, 2H, J=1.8, 1.8 Hz), 6.83—6.95 (m, 4H); MS (75 eV) m/z (%) 242 (M^+; 40), 227 (7), 188 (14), 115 (100). Found: C, 79.27; H, 7.49%. Calcd for $C_{16}H_{18}O_2$: C, 79.31; H, 7.49%.

1,2,3,4-Tetrahydro-9-isopropylidene-6,7-dimethoxy-1,4-methanonaphthalene (8e). To a 50 ml two-necked flask containing 50 mg of 5% Pd on charcoal was added 4.00 g (16.5 mmol) of **7e** dissolved in 20 ml of ethyl acetate. The suspension was flashed with hydrogen (1 atm) and stirred for 3 h at 0 °C. Filtration through Celite and evaporation of the solvent produced almost pure **8e**. Recrystallization from hexane gave colorless prisms; mp 82—84 °C; IR (KBr) 2945, 2860, 1601, 1499, 1468, 1458, 1323, 1312, 1287, 1252, 1215, 1196, 1110, 1103, 1088, 1020, 794 cm^{-1}; ^{1}H NMR (100 MHz, $CDCl_3$) δ= 1.18 (m, 2H), 1.59 (s, 6H), 1.86 (m, 2H), 3.69 (dd, 2H, J= 1.8, 1.8 Hz), 3.80 (s, 6H), 6.75 (s, 2H); ^{13}C NMR ($CDCl_3$) δ=27.34, 43.78, 56.30, 109.74, 139.73, 147.89. Found: C, 78.29; H, 8.21%. Calcd for $C_{16}H_{20}O_2$: C, 78.65; H, 8.25%.

1,4-Dihydro-6,7-dimethoxy-9-benzylidene-1,4-methanonaphthalene (10). To a solution of 6.00 g (20.3 mmol) of 1,2-dibromo-4,5-dimethoxybenzene (**5**) and 4.70 g (30.5 mmol) of 6-phenylfulvene (**9**) in 60 ml of dry THF cooled to −50 °C under nitrogen was added 16.2 ml (26.2 mmol) of a hexane solution of butyllithium (1.62 M) dropwise via syringe over 25 min. After being stirred at −50—−60 °C for 1 h, the solution was gradually warmed up to room temperature and further stirred for an additional 1 h. Ether (40 ml) and water (50 ml) were added to the mixture. The separated organic layer was dried, filtered, and concentrated under reduced pressure. Column chromatography over 80 g silica gel (eluent; hexane : ethyl acetate=5 : 1) afforded 1.42 g (24%) of **10**. Recrystallization from ethanol gave colorless prisms; mp 123—125 °C; IR (KBr) 3000, 2935, 2900, 2830, 1680, 1603, 1490, 1297, 1219, 1095, 1074, 1054, 853, 771, 712 cm^{-1}; ^{1}H NMR (100 MHz, $CDCl_3$) δ=3.81 (s, 3H), 3.82 (s, 3H), 4.20 (m, 1H), 4.70 (m, 1H), 5.49 (s, 1H), 6.89—7.04 (m, 4H), 7.08—7.41 (m, 5H); MS (75 ev) m/z (%) 290 (M^+; 100), 275 (11), 259 (14). Found: C, 82.40; H, 6.31%. Calcd for $C_{20}H_{18}O_2$: C, 82.73; H, 6.25%.

1,2,3,4-Tetrahydro-6,7-dimethoxy-9-benzylidene-1,4-methanonaphthalene (11). A solution of 1.06 g (3.66 mmol)

of **10** in 10 ml of ethyl acetate in the presence of 100 mg of 1.2% Pd on calcium carbonate[35] was stirred under hydrogen (1 atm) at 0 °C. During hydrogenation, the absorption of volume of hydrogen was measured. After 16 h, the solution was filtered and evaporated under reduced pressure. Recrystallization of the crude product from ethanol gave 0.977 g (92%) of **11** as colorless needles; mp 56—58 °C; IR (KBr) 2930, 2860, 1690, 1610, 1498, 1470, 1327, 1316, 1285, 1220, 1104, 1088, 1020, 793, 706 cm^{-1}; ^1H NMR (100 MHz, $CDCl_3$) δ=1.32 (m, 2H), 2.05 (m, 2H), 3.58 (m, 1H), 3.82 (s, 3H), 3.84 (s, 3H), 4.14 (m, 1H), 5.92 (s, 1H), 6.82 (s, 1H), 6.84 (s, 1H), 7.09—7.42 (m, 5H); Found: C, 81.89; H, 6.96%. Calcd for $C_{20}H_{20}O_2$: C, 82.16; H, 6.90%.

1,2,3,4-Tetrahydro-6,7-dimethoxy-1,4-methanonaphthalen-9-one (2e). To a solution of 450 mg (1.54 mmol) of **11** in 15 ml of dichloromethane was added 5 ml of aqueous sodium hydrogen carbonate (0.5 M) and *m*-chloroperbenzoic acid (310 mg, 1.79 mmol). The mixture was stirred for 2 h at room temperature. The progress of the reaction was followed by TLC. To this mixture was further added 100 mg (0.578 mmol) of *m*-chloroperbenzoic acid. After 1 h of stirring, dichloromethane (15 ml) was added to the mixture and the organic layer was washed with 20 ml of 10% sodium hydrogensulfite solution, 20 ml of saturated sodium hydrogencarbonate solution, and brine prior to drying over magnesium sulfate. After filtration and evaporation of the solvent, the mixture was passed through a short alumina column to give a mixture of epoxides **12** (284 mg; 60%, anti : syn=7 : 1 from NMR analysis). The mixture of epoxides was used for the next step without separation. To a stirred solution of 230 mg (1.01 mmol) of periodic acid in dry THF (3 ml) at 0 °C was added a solution of 284 mg (0.922 mmol) of **12** in 6 ml of dry THF. After 1 h, ether (15 ml) was added to the mixture. The organic layer was washed with saturated sodium hydrogencarbonate, dried and evaporated. Chromatography over 18 g of silica gel (eluent; hexane : ethyl acetate=5 : 1) of the crude products gave 100 mg (50%) of **2e**. Recrystallization from hexane-benzene gave colorless prisms; mp 142—143 °C; IR (CCl_4) 2975, 1778, 1493, 1466, 1321, 1278, 1225, 1078, 1013, 856 cm^{-1}; ^1H NMR (100 MHz, $CDCl_3$) δ= 1.34 (m, 2H), 2.18 (m, 2H), 3.30 (dd, 2H, J=1.8, 1.8 Hz), 3.86 (s, 6H), 6.89 (s, 2H); ^{13}C NMR ($CDCl_3$) δ=23.01, 47.49, 56.35, 106.22, 132.93, 148.69; MS (75 eV) *m/z* (%) 218 (M^+; 14), 190 (100), 175 (32). Found: C, 71.32; H, 6.44%. Calcd for $C_{13}H_{14}O_3$: C, 71.54; H, 6.47%.

1,4-Dihydro-9-isopropylidene-5,6,7,8-tetramethoxy-1,4-methanonaphthalene (7f). To a stirred solution of 3.36 g (9.44 mmol) of 1,2-dibromo-3,4,5,6-tetramethoxybenzene (**13**) and 2.00 g (18.8 mmol) of 6,6-dimethylfulvene (**6**) in 25 ml of dry THF cooled at −50 °C under nitrogen was added dropwise butyllithium (12 mmol) in 7.6 ml of hexane solution (1.62 M) over 10 min via syringe. The mixture was stirred for 1 h at −50—−44 °C and slowly allowed to come up to room temperature. After 1 h of stirring, water (20 ml) and ether (20 ml) was added. The separated organic layer was dried and evaporated under reduced pressure. Chromatography over 70 g silica gel (eluent; hexane : ethyl acetate=15 : 1) afforded 1.38 g (48%) of **7f**. Recrystallization from hexane gave colorless prisms; mp 51—53 °C; IR (KBr) 2990, 2965, 2925, 1471, 1451, 1409, 1402, 1350, 1262, 1190, 1116, 1071, 1027, 1020, 973, 959, 751 cm^{-1}. ^1H NMR (90 MHz, $CDCl_3$) δ=1.55 (s, 6H), 3.86 (s, 12H), 4.60 (dd, 2H, J=1.8, 1.8 Hz), 6.90 (dd, 2H, J=1.8, 1.8 Hz); MS (75 eV) *m/z* (%) 302 (M^+; 100), 287 (50). Found: C, 71.39; H, 7.33%. Calcd for $C_{18}H_{22}O_4$: C, 71.50; H, 7.33%.

1,2,3,4-Tetrahydro-9-isopropylidene-5,6,7,8-tetramethoxy-1,4-methanonaphthalene (8f). According to the similar procedure with the preparation of **11**, 1.00 g (3.31 mmol) of **7f** was converted to the hydrogenated **8f** (936 mg, 3.08 mmol, 93%). Recrystallization from ethanol-water gave as colorless plates; mp 55—59 °C; IR (KBr) 2980, 2950, 2920, 1471, 1449, 1410, 1360, 1291, 1268, 1120, 1108, 1081, 1060, 1025, 1007, 966 cm^{-1}; ^1H NMR (90 MHz, $CDCl_3$) δ=1.32 (m, 2H), 1.63 (s, 6H), 1.86 (m, 2H), 3.87 (s, 12H), 3.97 (dd, 2H, J=1.8, 1.8 Hz); ^{13}C NMR ($CDCl_3$) δ=19.89, 27.10, 40.43, 61.23, 61.28, 110.09, 135.15, 142.73, 144.30. Found: C, 70.87; H, 8.00%. Calcd for $C_{18}H_{24}O_4$: C, 71.03; H, 7.95%.

1,2,3,4-Tetrahydro-5,6,7,8-tetramethoxy-1,4-methanonaphthalen-9-one (2f). A solution of 702 mg (4.18 mmol) of 2,3-dimethoxy-1,4-benzoquinone (**14**) and 1.60 g (6.06 mmol) of 5,5-dimethoxy-1,2,3,4-tetrachlorocyclopentadiene (**15**) in 5 ml of xylene was refluxed for 20 h with stirring under nitrogen. After evaporation of the solvent under reduced pressure, the mixture was separated with chromatography over 40 g silica gel (eluent; hexane : ethyl acetate=2 : 1) to give 1.76 g (97%) of the endo adduct **16**. Recrystallization from hexane-benzene gave colorless prisms; mp 121—122 °C; IR (KBr) 2950, 2845, 1698, 1680, 1594, 1458, 1330, 1294, 1259, 1247, 1189, 1148, 1121, 1044, 1015, 1009, 979, 957, 910, 815, 623 cm^{-1}. ^1H NMR (100 MHz, $CDCl_3$) δ=3.57 (s, 5H), 3.66 (s, 3H), 3.97 (s, 6H); MS (75 eV) *m/z* (%) 434 (M^++4, 4), 432 (M^+ +2, 8), 430 (M^+, 5), 401 (5), 399 (34), 397 (95), 395 (100). Found: C, 41.80; H, 3.29; Cl, 32.61%. Calcd for $C_{15}H_{14}O_6Cl_4$: C, 41.70; H, 3.27; Cl, 32.82%. A solution of 800 mg (1.85 mmol) of **16** and 0.3 ml (3.7 mmol) of pyridine in 10 ml dry methanol was refluxed for 20 h. To the cooled solution were added 30 ml of dichloromethane and 20 ml of hydrochloric acid (1 M). The separated organic layer was washed with brine, dried, and concentrated. Separation with chromatography over 30 g silica gel (eluent; hexane : ethyl acetate=2 : 1) gave 625 mg (78%) of **17**. Recrystallization from hexane-benzene gave colorless plates; mp 144—145 °C; IR (KBr) 3490, 3390, 2950, 2845, 1603, 1477, 1438, 1305, 1260, 1190, 1131, 1078, 1007, 950, 781, 763, 699, 682, 664 cm^{-1}. ^1H NMR (100 MHz, $CDCl_3$) δ=3.52 (s, 3H), 3.64 (s, 3H), 3.91 (s, 6H), 5.67 (s, 2H). Found: C, 42.01; H, 3.32; Cl, 32.73%. Calcd for $C_{15}H_{14}O_6Cl_4$: C, 41.70; H, 3.27; Cl, 32.82%. A solution of 460 mg (1.06 mmol) of **17** in 10 ml of dry acetone containing 0.20 ml (2.1 mmol) of dimethyl sulfate and 3.1 g (22 mmol) of anhydrous potassium carbonate was refluxed for 15 h with vigorous stirring. The cooled solution was treated with 20 ml of water and stirred for 30 min at room temperature. The mixture was extracted with 20 ml of ether twice, and the ethereal layer was washed with brine and dried. Evaporation of ether afforded almost pure **18**. Recrystallization from hexane gave colorless prisms; mp 99—100 °C; IR (KBr) 2930, 2820, 1607, 1471, 1410, 1348, 1273, 1184, 1100, 1026, 1004, 987, 964, 940, 822, 771, 693, 682, 653 cm^{-1}; ^1H NMR (100 MHz, $CDCl_3$) δ=3.50 (s, 3H), 3.66 (s, 3H), 3.82 (s, 6H), 3.92 (s, 6H). Found: C, 44.41; H, 3.91; Cl, 30.96%. Calcd for $C_{17}H_{18}O_6Cl_4$: C, 44.37; H, 3.94; Cl, 30.82%. A solution of 2.43 g (5.28 m mol) of **18** in a mixture of triethylamine (25 ml) and ethanol (50 ml) containing 300 mg of 5% palladium on charcoal was stirred for 3 h under hydrogen (1 atm) at room temperature. Filtration through Celite and evaporation of the solvent gave almost pure **19** (1.88 g,

91%). Recrystallization from hexane afforded colorless prisms; mp 113—115 °C; IR (KBr) 2925, 2820, 1470, 1410, 1359, 1291, 1253, 1189, 1105, 1067, 1040, 997, 977, 933, 842, 810, 710, 620 cm^{-1}; ^1H NMR (100 MHz, $CDCl_3$) δ=1.77 (m, 2H), 2.50 (m, 2H), 3.53 (s, 3H), 3.73 (s, 3H), 3.83 (s, 6H), 3.92 (s, 6H). Found: C, 51.87; H, 5.64; Cl, 18.16%. Calcd for $C_{17}H_{22}O_6Cl_2$: C, 51.92; H, 5.64; Cl, 18.03%. To a solution of 2.00 g (15.6 mmol) of naphthalene in 30 ml dry DME under nitrogen at 0 °C was added sodium (290 mg, 12.6 mmol). To this sodium naphthalenide solution was added dropwise at 0 °C a solution of 1.00 g (2.54 mmol) of **19** in 10 ml of dry DME. After 30 min, the mixture was slowly treated with 10 ml of ethanol, 60 ml of water, and extracted with 70 ml of ether twice. The ether layer was washed with brine and dried. Purification with chromatography over 30 g silica gel (eluent; hexane : ethyl acetate=6 : 1) afforded 750 mg (91%) of acetal **19**. Recrystallization from hexane gave colorless prisms; mp 69—70 °C; IR (KBr) 2945, 2825, 1472, 1413, 1369, 1302, 1277, 1179, 1138, 1089, 1064, 1031, 958, 801 cm^{-1}; ^1H NMR (100 MHz, $CDCl_3$) δ=1.16 (m, 2H), 2.12 (m, 2H), 3.12 (s, 3H), 3.29 (s, 3H), 3.50 (dd, 2H, J=1.8, 1.8 Hz), 3.83 (s, 6H), 3.88 (s, 6H). Found: C, 62.92; H, 7.45%. Calcd for $C_{17}H_{24}O_6$: C, 62.95; H, 7.46%. To a solution of 666 mg (2.06 mmol) of **19** in 10 ml of dioxane was added a solution of 20% aqueous sulfuric acid (20 ml) at 0 °C. After 11 h of stirring at 50 °C, the solution was cooled, poured into 30 ml of water, and extracted with 50 ml of ether twice. The combined ether layer was washed with brine, dried, and concentrated. Purification with chromatography over 10 g silica gel (eluent; hexane : ethyl acetate=5 : 1) afforded 485 mg (85%) of **2f**. Recrystallization from hexane gave colorless prisms; mp 92—94 °C; IR (CCl_4) 2925, 1785, 1481, 1420, 1410, 1360, 1302, 1272, 1121, 1084, 1063, 1032, 1012 cm^{-1}; ^1H NMR (100 MHz, $CDCl_3$) δ=1.43 (m, 2H), 2.24 (m, 2H), 3.54 (dd, 2H, J=1.8, 1.8 Hz), 3.86 (s, 6H), 3.90 (s, 6H); ^{13}C NMR ($CDCl_3$) δ=22.59, 44.02, 61.38, 61.49, 127.50, 144.16, 145.65; MS (75 eV) m/z (%) 278 (M+; 23), 250 (100), 235 (80), 207 (16). Found: C, 64.70; H, 6.52%. Calcd for $C_{15}H_{18}O_5$: C, 64.73; H, 6.52%.

Prototypical Procedure for Reductions with Lithium Aluminum Hydride. To a suspension of 28 mg (0.74 mmol) of lithium aluminum hydride in 5 ml of dry ether under nitrogen at 0 °C was added dropwise a solution of 100 mg (0.63 mmol) of **2c** in 5 ml of dry ether. After 30 min, the reaction was quenched by addition of 0.1 ml of water. The ether layer was dried over magnesium sulfate and directly subjected to GLC analysis (**3c** : **4c**=81 : 19). Separation with preparative TLC gave 80 mg (0.50 mmol) of **3c** and 20 mg (0.13 mmol) of **4c** in total yield of 99%. The yields for other derivatives were as follows; in ether: 96% for **2a**, 79% for **2b**, 99% for **2d**, 89% for **2e**, and 80% for **2f**, in THF: 98% for **2a**, 71% for **2b**, 97% for **2c**, 99% for **2d**, 91% for **2e**, and 90% for **2f**. The anti/syn ratio of the alcohols are listed in Table 3. A large volume (80—100 ml) of solvents were used to dissolve 100 mg of **2b**. Physical data for the alcohols **3a**—f and **4b**—f are as follows; **3a**: colorless prisms from hexane; mp 122—124 °C; IR (KBr) 3300, 2905, 1500, 1482, 1301, 1139, 1032, 951, 888, 777 cm^{-1}; ^1H NMR (100 MHz, $CDCl_3$) δ=1.22 (m, 2H), 1.90—2.38 (m, 3H), 3.42 (m, 2H), 3.82 (m, 1H). Found: C, 56.79; H, 3.43%. Calcd for $C_{11}H_8OF_4$: C, 56.90; H, 3.47%. **3b**: colorless needles from hexane; mp 133—135° C; IR (KBr) 3255, 2920, 1371, 1294, 1101, 1065, 678 cm^{-1}; ^1H NMR (100 MHz, $CDCl_3$) δ=1.23 (m, 2H), 2.02 (br s, 1H), 2.24 (m, 2H), 3.46 (m, 2H), 3.92 (m, 2H). **4b**: colorless needles from hexane; mp 162—165 °C; IR (KBr) 3260, 2945, 1374, 1309, 1132, 1122, 1070 cm^{-1}; ^1H NMR (100 MHz, $CDCl_3$): δ=1.18 (m, 2H), 1.76 (br s, 1H), 2.08 (m, 2H), 3.52 (m, 2H), 4.20 (br s, 1H). Found: C, 44.14; H, 2.72; Cl, 47.41%. Calcd for $C_{11}H_{18}OCl_4$: C, 44.34; H, 2.71; Cl, 47.59%. **3c**:[13,24] colorless needles from hexane; mp 103—105 °C; IR (KBr) 3250, 2970, 1350, 1337, 1105, 1080, 747 cm^{-1}; ^1H NMR (100 MHz, $CDCl_3$) δ=1.18 (m, 2H), 1.87 (br s, 1H), 2.10 (m, 2H), 3.11 (ddd, 2H, J=1.8, 1.8, 1.8 Hz), 3.80 (br s, 1H), 7.06 (s, 4H). **4c**:[13,23,24] colorless needles from hexane; mp 114—115 °C; IR (KBr) 3250, 2970, 1458, 1370, 1271, 1151, 1124, 1068, 750 cm^{-1}; ^1H NMR (100 MHz, $CDCl_3$) δ= 1.11 (m, 2H), 1.58 (br s, 1H), 1.96 (m, 2H), 3.16 (ddd, 2H, J=1.8, 1.8, 1.8 Hz), 4.10 (br s, 1H), 6.99—7.30 (m, 4H). **3d**: colorless needles from hexane; mp 107—108 °C; IR (KBr) 3560, 3530, 2950, 2835, 1508, 1468, 1459, 1446, 1298, 1260, 1165, 1093, 1065, 969, 811, 800, 717 cm^{-1}; ^1H NMR (100 MHz, $CDCl_3$) δ=1.17 (m, 2H), 1.95—2.21 (m, 3H), 3.11 (ddd, 2H, J=1.8, 1.8, 1.8 Hz), 3.72 (s, 6H), ca 3.7 (m, 1H), 6.54 (s, 2H). Found: C, 70.69; H, 7.28%. Calcd for $C_{13}H_{16}O_3$: C, 70.88; H, 7.32%. **4d**: colorless needles from hexane; mp 68—70 °C; IR (KBr) 3945, 3920, 2945, 2880, 1502, 1463, 1302, 1259, 1168, 1075, 1032, 961, 794, 715 cm^{-1}; ^1H NMR (100 MHz, $CDCl_3$) δ=1.12 (m, 2H), 1.63 (br s, 1H), 1.92 (m, 2H), 3.40 (ddd, 2H, J=1.8, 1.8, 1.8 Hz), 3.73 (s, 6H), 4.06 (t, 1H, J=1.8), 6.61 (s, 2H). Found: C, 70.83; H, 7.28%. Calcd for $C_{13}H_{16}O_3$: C, 70.88; H, 7.32%. **3e**: colorless needles from hexane; mp 118—119 °C; IR (KBr) 3520, 2930, 1499, 1463, 1331, 1248, 1216, 1097, 1069, 771 cm^{-1}; ^1H NMR (100 MHz, $CDCl_3$) δ=1.14 (m, 2H), 1.97—2.23 (m, 3H), 3.07 (ddd, 2H, J=1.8, 1.8, 1.8 Hz), 3.81 (m, 1H), 3.82 (s, 6H), 6.77 (s, 2H). Found: C, 71.00; H, 7.41%. Calcd for $C_{13}H_{16}O_3$: C, 70.88; H, 7.32%. **4e**: colorless prisms from hexane-benzene; mp 107—108 °C; IR (KBr) 3325, 2965, 1500, 1491, 1461, 1328, 1282, 1121, 1092, 1074, 1039, 783 cm^{-1}; ^1H NMR (100 MHz, $CDCl_3$) δ=1.08 (m, 2H), 1.72 (br d, 1H, J=ca. 9.0 Hz), 1.94 (m, 2H), 3.11 (ddd, 2H, J=1.8, 1.8, 1.8 Hz), 3.86 (s, 6H), 4.11 (m, 1H), 6.89 (s, 2H). Found: C, 70.82; H, 7.38%. Calcd for $C_{13}H_{16}O_3$: C, 70.88; H, 7.32%. **3f**: colorless needles from hexane; mp 105—106 °C; IR (KBr) 3315, 2970, 2940, 1478, 1417, 1319, 1295, 1126, 1065, 1027, 1005 cm^{-1}; ^1H NMR (100 MHz, $CDCl_3$) δ=1.03 (m, 2H), 1.93—2.27 (m, 2H), 3.34 (ddd, 2H, J=1.8, 1.8, 1.8 Hz), 3.82 (m, 1H), 3.83 (s, 6H), 3.86 (s, 6H). Found: C, 63.96; H, 7.14%. Calcd for $C_{15}H_{20}O_5$: C, 64.27; H, 7.19%. **4f**: colorless needles from hexane; mp 121—124 °C; IR (KBr) 3320, 2935, 1472, 1413, 1364, 1309, 1089, 1068, 1032, 1020, 973 cm^{-1}; ^1H NMR (100 MHz, $CDCl_3$) δ=1.18 (m, 2H), 1.58 (d, 1H, J=9.0 Hz), 2.00 (m, 2H), 3.42 (ddd, 2H, J=1.8, 1.8, 1.8 Hz), 3.85 (s, 6H), 3.90 (s, 6H), 4.11 (dt, 1H, J=9.0, 1.8 Hz); Found: C, 64.00; H, 7.17%. Calcd for $C_{15}H_{20}O_5$: C, 64.27; H, 7.19%.

Prototypical Procedure for Reductions with Diisobutylaluminum Hydride. To a solution of 100 mg (0.633 mmol) of **2c** in 10 ml of dry ether under nitrogen at 0 °C was added dropwise a 1.43 ml hexane solution of diisobutylaluminum hydride (2.50 mmol). After being stirred for 30 min at 0 °C, the mixture was treated with 2 ml of ethanol and 8 ml of aqueous hydrochloric acid (2 M). The separated ether layer was washed with brine and dried over magnesium sulfate. GLC analysis of the mixture gave the ratio of **3c** : **4c**=43 : 57. The products were separated with preparative TLC to give 35 mg (0.22 mmol) of **3c** and 47 mg (0.29 mmol) of **4c** in total yield of 81%. Yields for other derivatives were 86% for **2a**, 83% for **2b**, 76% for **2d**, 92% for **2e**, and 80% for **2f**.

Prototypical Procedure for Reductions with Lithium Tri-

***t*-butoxyaluminum Hydride.** To a suspension of 640 mg (2.52 mmol) of lithium tri-*t*-butoxyaluminum hydride in 5 ml of dry ether under nitrogen at 0 °C was added a solution of 100 mg (0.633 mmol) of **2c** in 5 ml of dry ether. After 30 min of stirring at 0 °C, the mixture was treated with 3 ml of ethanol and 8 ml of aqueous hydrochloric acid (2 M). The separated ether layer was washed with brine, dried over magnesium sulfate, and subjected to GLC analysis (**3c**:**4c**=93:7). The products were purified with preparative TLC to give 92 mg (0.58 mmol) of **3c** and 7 mg (0.04 mmol) of **4c** in total yield of 98%. The yields for other derivatives were 99% for **2a**, 79% for **2b**, 97% for **2d**, 99% for **2e**, and 97% for **2f**.

Prototypical Procedure for Reductions with Sodium Borohydride. To a solution of 26 mg (0.69 mmol) of sodium borohydride in 5 ml of dry ethanol at 0 °C was added a solution of 100 mg (0.633 mmol) of **2c** in 8 ml of dry ethanol. After being stirred for 30 min at 0 °C, the mixture was treated with 30 ml of water and extracted with 20 ml of ether twice. The ether layer was washed with brine and dried over magnesium sulfate. GLC analysis afforded the anti/syn ratio (**3c**:**4c**=81:19). Separation with preparative TLC gave 76 mg (0.48 mmol) of **3c** and 19 mg (0.12 mmol) of **4c** in 94% total yield. The yields for other derivatives were 99% for **2a**, 77% for **2b**, 94% for **2d**, 89% for **2e**, and 88% for **2f**.

Prototypical Procedure for Reductions with Diborane. To a suspension of 48 mg (1.3 mmol) of sodium borohydride in 10 ml of anhydrous THF under nitrogen at 15—18 °C was added dropwise 0.21 ml (1.7 mmol) of boron trifluoride etherate. After being stirred for 30 min, a solution of 100 mg (0.633 mmol) of **2c** in 5 ml of THF was added to the mixture at 0 °C. After 30 min, the mixture was treated with 3 ml of ethanol and 8 ml of aqueous hydrochloric acid (2 M) and extracted with 15 ml of ether twice. The organic layer was washed with brine and dried over magnesium sulfate. GLC analysis provided the anti/syn ratio (**3c**:**4c**=75:25). The products were separated with preparative TLC to give 68 mg (0.43 mmol) of **3c** and 23 mg (0.14 mmol) of **4c** in total yield of 90%. The yields for other derivatives were 91% for **2a**, 81% for **2b**, 92% for **2d**, 96% for **2e**, and 82% for **2f**. For the reduction of **2b**, **2b** was added as solids.

Prototypical Procedure for Reductions with Disiamylborane. To a suspension of 48 mg (1.3 mmol) of sodium borohydride and 0.35 ml (3.3 mmol) of 2-methyl-2-butene in 10 ml of dry diglyme under nitrogen at 0 °C was added 0.21 ml (1.7 mmol) of boron trifluoride etherate. The mixture was stirred for 30 min at 0 °C. To this suspension was added a solution of 100 mg (0.633 mmol) of **2c** in diglyme (5 ml) at 0 °C. After 3 h, 13 ml of aqueous sodium hydroxide (3 M) and 10 ml of 30% aqueous hydrogen peroxide were added to the mixture. After being stirred for overnight at room temperature, the mixture was poured into ice-water and extracted with 25 ml of ether twice. The ether layer was washed with brine, dried over magnesium sulfate, and subjected to GLC analysis (**3c**:**4c**=57:43). Separation with preparative TLC gave 56 mg (0.35 mmol) of **3c** and 38 mg (0.24 mmol) of **4c** in total yield of 93%. The yields for other derivatives were 86% for **2a**, 92% for **2d**, 89% for **2e**, and 72% for **2f**. Under similar conditions, **2b** was inert, resulting in 70—95% of recovery.

Prototypical Procedure for Singlet Oxygen Reactions. A water cooled solution of 200 mg (0.820 mmol) of **8e** and rose bengal (10 mg) in 50 ml of methanol was irradiated with sodium lamp (55 W×4) while oxygen was bubbled through the solution. After 8 h, the solvent was concentrated under reduced pressure to ca. 10 ml. The mixture was treated with 310 mg (8.20 mmol) of sodium borohydride and stirred at room temperature for 12 h. After addition of 30 ml of water, the products was extracted with 30 ml of ether twice. The ether layer was washed with brine and dried over magnesium sulfate. The mixture was carefully separated with preparative TLC to give 7 mg (0.03 mmol) of the recovered **8e**, 176 mg (0.677 mmol) of **21e**, and 18 mg (0.069 mmol) of **22e**. The anti/syn ratio was 91/9. **21e**: Colorless prisms; mp 110—112 °C; IR (KBr) 3590, 2940, 1492, 1467, 1422, 1330, 1286, 1250, 1222, 1116, 1098, 1078, 1007, 901 cm^{-1}; ^1H NMR (100 MHz, $CDCl_3$) δ=1.19 (m, 2H), 1.71 (m, 4H), 2.30 (m, 2H), 3.19 (dd, 2H, J=1.8, 1.8 Hz), 3.82 (s, 6H), 4.75 (m, 1H), 4.88 (m, 1H), 6.71 (s, 2H). Found: C, 73.63; H, 7.76%. Calcd for $C_{16}H_{20}O_3$: C, 73.82; H, 7.74%. **22e**: colorless prisms from hexane; mp 112—115 °C; IR (KBr) 3540, 2950, 1490, 1465, 1328, 1285, 1248, 1222, 1167, 1120, 1099, 1062 cm^{-1}; ^1H NMR (100 MHz, $CDCl_3$) δ=1.09 (m, 2H), 1.65—2.11 (m, 6H), 3.27 (dd, 2H, J=1.8,1.8 Hz), 3.87 (s, 6H), 5.08 (m, 1H), 5.16 (m, 1H), 6.91 (s, 2H). Found: C, 73.54; H, 7.73%. Calcd for $C_{16}H_{20}O_3$: C, 73.82; H, 7.74%. Under similar conditions **21c** and **22c** were obtained from **8c** in total yield of 95% with the ratio of **21c**:**22c**=80:20. Similarly, **21f** and **22f** were produced in total yield of 85% with the ratio of **21f**:**22f**=72:28. **21f**: colorless prisms from hexane. mp 81—82 °C; IR (KBr) 3585, 2925, 1476, 1460, 1416, 1368, 1301, 1271, 1123, 1077, 1068, 1017, 1006, 900 cm^{-1}; ^1H NMR (100 MHz, $CDCl_3$) δ=1.27 (m, 2H), 1.67—1.81 (m, 4H), 2.34 (m, 2H), 3.46 (dd, 2H, J=1.8,1.8 Hz), 3.83 (s,6H), 3.86 (s, 6H), 4.76 (m, 1H), 4.93 (m, 1H). Found: C, 67.37; H, 7.57%. Calcd for $C_{18}H_{24}O_5$: C, 67.48; H, 7.55%. **22f**: oil; IR (CCl_4) 3550, 2935, 1475, 1418, 1369, 1299, 1276, 1132, 1093, 1071, 1035, 1021, 908 cm^{-1}; ^1H NMR (100 MHz, $CDCl_3$) δ=1.16 (m, 2H), 1.79 (br s, 1H), 1.90—2.16 (m, 5H), 3.54 (dd, 2H, J=1.8,1.8 Hz), 3.88 (s, 6H), 3.91 (s, 6H), 5.10 (m, 1H), 5.18 (m, 1H). Found: C, 67.21; H, 7.58%. Calcd for $C_{18}H_{24}O_5$: C, 67.48; H, 7.55%.

NMR Shift Reagent Study. The $Eu(fod)_3$ used was taken directly from a fresh bottle of commercial product. The purified alcohols (**3a**—f, **4b**—f) were each dissolved in $CDCl_3$ (25—30 mg/0.3 ml) in a NMR tube. The shift reagent, $Eu(fod)_3$, was weighed out and added into the solution five times in about 5 mg portions, and ^1H NMR spectrum was measured each time. The plots of the observed relative shift of each proton of the alcohol vs. the amount of added $Eu(fod)_3$ gave fairly good straight lines. From the slope of each proton, the relative shift value was calculated.

References

1) A part of this study has been reported as a preliminary communication; K. Okada, S. Tomita, and M. Oda, *Tetrahedron Lett.*, **27**, 2645 (1986).

2) W. G. Dauben, G. J. Fonken, and D. S. Noyce, *J. Am. Chem. Soc.*, **78**, 2579 (1956).

3) D. C. Wigfield, *Tetrahedron*, **35**, 449 (1979) and references therein.

4) H. C. Brown and J. Muzzio, *J. Am. Chem. Soc.*, **88**, 2811 (1966).

5) J. Warkentin, *Can. J. Chem.*, **48**, 1391 (1970).

6) R. K. Bly and R. S. Bly, *J. Org. Chem.*, **28**, 3165 (1963).

7) F. R. S. Clark and J. Warkentin, *Can. J. Chem.*, **49**,

2223 (1971).
8) R. S. Bly, F. B. Culp, Jr., and R. K. Bly, *J. Org. Chem.*, **35**, 2235 (1970).
9) N. F. Feiner, G. D. Abrams, and P. Yates, *Can. J. Chem.*, **54**, 3955 (1976).
10) J. A. Berson, T. Miyashi, and G. Jones, II, *J. Am. Chem. Soc.*, **96**, 3468 (1974).
11) E. C. Ashby and J. T. Laemmle, *Chem. Rev.*, **75**, 521 (1975).
12) W. T. Wipke and P. Gund, *J. Am. Chem. Soc.*, **98**, 8107 (1976).
13) H. Tanida, *Farumashia*, **2**, 400 (1966).
14) IUPAC name: 1,2,3,4-tetrahydro-1,4-methanonaphthalen-9-one or 2,3-benzo-2-norbornen-7-one.
15) B. Hankinson, H. Heaney, A. P. Price, and R. P. Sharma, *J. Chem. Soc., Perkin Trans. 1*, **1973**, 2569.
16) L. A. Paquette, L. W. Hertel, R. Gleiter, M. C. Böhm, M. A. Beno, and G. G. Christoph, *J. Am. Chem. Soc.*, **103**, 7106 (1981).
17) Gurudata and J. B. Stothers, *Can. J. Chem.*, **47**, 3601 (1969); J. B. Stothers, J. R. Swenson, and C. T. Tan, *ibid.*, **53**, 581 (1975); R. Bicker, H. Kessler, A. Steigel, and G. Zimmermann, *Chem. Ber.*, **111**, 3215 (1978).
18) D. Chadwick, D. C. Frost, and L. Weiler, *J. Am. Chem. Soc.*, **93**, 4962 (1971); G. Hentrich, E. Gunkel, and M. Klessinger, *J. Mol. Struct.*, **21**, 231 (1974).
19) D. A. Lightner, J. K. Gawroński, A. E. Hansen, and T. D. Bouman, *J. Am. Chem. Soc.*, **103**, 4291 (1981).
20) E. Heilbronner and H.-D. Martin, *Helv. Chim. Acta*, **55**, 1490 (1972).
21) R. W. Hoffmann and H. Kurz, *Chem. Ber.*, **108**, 119 (1975) and references therein.
22) K. Okada and T. Mukai, *J. Am. Chem. Soc.*, **100**, 6509 (1978); L. A. Paquette, L. W. Hertel, R. Gleiter, and M. Böhm, *ibid.*, **100**, 6512 (1978); K. Okada and T. Mukai, *Tetrahedron Lett.*, **1979**, 3429; R. W. Hoffmann and N. Hauel, *ibid.*, **1979**, 4959; L. W. Hertel, L. A. Paquette, *J. Am. Chem. Soc.*, **101**, 7620 (1979).
23) M. Chérest and H. Felkin, *Tetrahedron Lett.*, **1968**, 2205.
24) J. Klein, *Tetrahedron Lett.*, **1973**, 4307; J. Klein, *Tetrahedron*, **30**, 3349 (1974).
25) J. Huet, Y. Maroni-Barnaud, N. T. Anh, and J. Seyden-Penne, *Tetrahedron Lett.*, **1976**, 159; N. T. Anh and O. Eisenstein, *Noveau J. de Chemie*, **1**, 61 (1977).
26) D. C. Wigfield and F. W. Gowland, *J. Org. Chem.*, **42**, 1108 (1977).
27) J. Royer, *Tetrahedron Lett.*, **1978**, 1343.
28) M. R. Giddings and J. Hudec, *Can. J. Chem.*, **59**, 459 (1980).
29) A. S. Cieplak, *J. Am. Chem. Soc.*, **103**, 4540 (1981).
30) C. K. Cheung, L. T. Tseng, M.-H. Lin, S. Srivastava, and W. T. le Noble, *J. Am. Chem. Soc.*, **108**, 1598 (1986).
31) T. Laube and H. U. Stilz, *J. Am. Chem. Soc.*, **109**, 5876 (1987).
32) E. C. Ashby, F. R. Dobbs, and H. P. Hopkins, Jr., *J. Am. Chem. Soc.*, **97**, 3158 (1975).
33) H. B. Bürgi, J. M. Lehn, and G. Wipff, *J. Am. Chem. Soc.*, **96**, 1956 (1974).
34) H. C. Brown and A. W. Moerikofer, *J. Am. Chem. Soc.*, **84**, 1478 (1962).
35) M. Busch and H. Stöve, *Ber.*, **49**, 1063 (1916).

 © 1989 The Chemical Society of Japan Bull. Chem. Soc. Jpn., 62, 469—473 (1989)

The Structure of Rotungenoside, a New Bitter Triterpene Glucoside from *Ilex Rotunda*

Munehiro NAKATANI,* Shuichi HATANAKA, Hajime KOMURA,† Takashi KUBOTA,†† and Tsunao HASE
Department of Chemistry, Faculty of Science, Kagoshima University, 1-21-35 Korimoto, Kagoshima 890
†Suntory Institute for Bioorganic Research, Shimamoto-cho, Mishima-gun, Osaka 618
††Department of Chemistry, Faculty of Science, Osaka City University, Sugimoto-cho, Sumiyoshi-ku, Osaka 558
(Received July 27, 1988)

A new bitter triterpene ester glucoside have been isolated along with known bitter triterpene glucoside pedunclosside and some minor triterpenes ulsolic acid, rotundic acid, and rotungenic acid from the unripe fruits of *Ilex rotunda*. The structure was characterized as β-D-glucopyranosyl 3β,19α,24-trihydroxyurs-12-en-28-oate by spectral data and chemical means.

Ilex rotunda Thunb. (Aquifoliaceae) yields red fruits in winter. Birds pick up the ripe fruits in early spring but don't the unripe ones. Some triterpenoids have been isolated from this plant, i.e. a triterpene rotundic acid (**1**) from the seeds[1] and a triterpene glucoside pedunclosside (**2**) from the leaves.[2] But there is no detailed study on the constituents of the fruits. Then we were interested in the difference of their constituents and first investigated on the ripe fruits to get new triterpenes rotungenic acid (**3**) and rotundioic acid (**4**).[3] We now studied the constituents of the unripe fruits and isolated a new bitter triterpene ester glucoside rotungenoside (**5**) as minor glucoside along with major pedunclosside (**2**) and minor triterpenes ulsolic acid, rotundic acid (**1**), and rotungenic acid (**3**). These bitter glucosides **1** and **2** exhibited a weak insect antifeedant activity against the larvae of *Spodoptera litura* Fab. with the leaf disk choice test.

Results and Discussion

The fresh unripe fruits of *Ilex rotunda* were extracted with methanol. After concentration to one-tenth of its original volume, the extract was suspended in water and then extracted with ethyl acetate. The extract was roughly divided into two groups by passing through LH-20 column, one of which was a mixture of triterpenes and the other contained some triterpene glycosides. Triterpenoids were detected by the red-violet colour given by the Liebermann-Burchard test. Crystallization of the glycoside fraction afforded a mixture of two compounds which were separated to a major known pedunclosside (**2**) (28-β-D-glucopyranosyl 3β,19α,23-trihydroxyurs-12-en-28-oate) and minor new rotungenoside (**5**) on a DCCC(droplet countercurrent chromatography) using chloroform–methanol–water solvent system in ascending mode. From the triterpene fraction, three known compounds ulsolic acid, rotundic acid (**1**) (3β,19α,23-trihydroxyurs-12-en-28-oic acid) and rotungenic acid (**3**) (3β,19α,24-trihydroxyurs-12-en-28-oic acid) were isolated.

Rotungenoside (**5**), an amorphous white powder, $[\alpha]_D^{25}$ +5° (MeOH), was assigned the molecular formula $C_{36}H_{58}O_{10}$ from SIMS (*m/z* 673[M+Na]$^+$). Its IR and UV spectra showed the presence of hydroxyl and ester groups (3450 and 1720 cm^{-1}) and double bond (209 nm: ε 3000). Its ^{13}C NMR spectrum revealed thirty-six carbon signals (CH_3-X6, -CH_2-X9, >CH-X4, -<u>C</u>-X5, -CH_2-OX2, >CH-OX5, -<u>C</u>-OX1, -CH<O,O> X1, >C=CH-X1, -CO-OX1). The SI mass spectrum showed a characteristic peak at *m/z* 489 denoting the loss of 1 mol of glucose and two peaks of 471 and 453 indicated further successive loses of 1 and 2 mol of water. The ^{13}C NMR experiment (Table 1) suggested that this glycoside **5** had the same sugar (β-D-glucopyranose) with pedunclosside (**2**) which was linked to the aglycone with ester linkage. The anomeric carbon of **5** was also found at a higher field (δ 95.7) owing to the esterification effect;[4] pedunclosside (**2**): δ 96.0. Careful examination of ^{13}C NMR spectra of these aglycone part, clarified that these compounds had very similar aglycone; the only difference is the substitution around C-3 and C-4 in 3,18-dihydroxyurs-12-en-18-oic skeleton. In particular, the exchange of

Table 1. ^{13}C NMR Data of Pedunclosside (**2**) and Rotungenoside (**5**) in Py-d_5 Solution

Carbon No.	2	5	Carbon No.	2	5
1	39.1t	38.9t	20	42.3d	42.1d
2	27.8t	28.5t	21	26.9t	26.8t
3	74.2d	80.4d	22	37.9t	37.8t
4	43.0s	43.2s	23	68.2t	23.7q
5	48.8d	48.0d	24	13.2q	64.7t
6	19.0t	19.4t	25	17.7q	17.4q
7	33.5t	33.9t	26	16.9q	16.8q
8	40.8s	40.6s	27	24.8q	24.6q
9	48.0d	48.0d	28	177.2s	177.0s
10	37.4s	37.2s	29	27.2q	27.1q
11	24.3t	24.4t	30	16.3q	16.2q
12	128.7d	128.4d			
13	139.5s	139.3s	1′	96.0d	95.5d
14	42.3s	42.1s	2′	73.9d	74.1d
15	29.5t	29.3t	3′	79.3d	79.3d
16	26.3t	26.2t	4′	71.4d	71.3d
17	48.8s	48.7s	5′	79.0d	79.0d
18	54.6d	54.5d	6′	62.6t	62.4t
19	72.9s	72.7s			

the signal at δ 13.2 to δ 23.7 led to the conclusion that the C-23 methyl was replaced with a hydroxymethyl group since the signal of the C-24 methyl in most ursene triterpenoids having 3β-OH group has been observed to about 10 ppm higher field than the C-23 methyl signal.[5,6]

The glucoside **5** was acetylated to give the hexaacetate **6**. Its ^{1}H NMR spectrum (Table 2) supported very well the ester linked β-anomeric configuration (δ 5.52, 1H, d, J= 8Hz; H-1′) including glucose moiety and showed the presence of an 3β-acetoxyl group (δ 4.58, 1H, dd, J=11 and 5.5 Hz; H-3α). A signal at δ 2.53 (1H, br s; H-18) suggested the presence of the 19-*O*-substituted urs-12-ene skeleton,[7] while the 4-acetoxylmethylene signals at δ 4.14 and 4.36 (each d, J=12 Hz) showed the large down-field shift of 0.25 and 0.67 ppm compared to those of **7** (hexaacetate of **2**), which also suggested the 4β-CH_2OH configuration in **5**.

The aglycone of **3** was obtained by alkaline hydrolysis and identified as **3** by means of ^{13}C NMR and mass spectroscopies. It follows that **5** can be formulated as 28-β-D-glucopyranosyl 3β,19α,24-trihydroxyurs-12-en-28-oate. In the ^{1}H NMR spectrum of the diacetate (**8**), a W-type long-range coupling was observed between the H-3α signal at δ 4.58 (dd, J=10.5 and 5 Hz) and higher one of the axial 4β-acetoxymethyl signals at δ 4.38 and 4.12 (each d, J=11.5 Hz) but not observed in the hexaacetate **6**, which suggested a conformation change in the glucoside **6**.

Acid hydrolysis of **5** with hydrochloric acid in methanol afforded glucose (identified by TLC and paper chromatography) and a mixture of conjugated and nonconjugated dienes **9** and **10**. The dehydration product **9** showed a hindered conjugated diene system at 229 nm (ε 3400) in its UV spectrum and the ^{1}H NMR spectrum showed the presence of one olefinic methyl group at δ 1.75. On the other hand, compound **10** had a nonconjugated UV absorption at 207.5 nm (ε 6500) and showed two olefinic methyl signals at δ 1.53 and 1.63 in its ^{1}H NMR spectrum. These compounds were also obtained from rotungenic acid (**3**) by the acid treatment. A similar dehydration has been observed in the reaction of 19-hydroxyurs-12-ene or 19-hydroxyolean-12-enes[8,9] and so the compounds from **3** and **5**

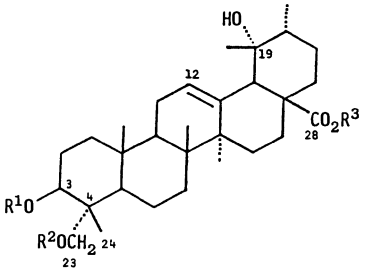

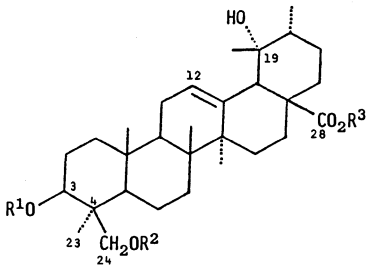

	R^1	R^2	R^3
1:	H	H	H
2:	H	H	glu
4:	H	4α-CO_2H	H
7:	Ac	Ac	glu(Ac)

	R^1	R^2	R^3
3:	H	H	H
5:	H	H	glu
6:	Ac	Ac	glu(Ac)
8:	Ac	Ac	H

Table 2. ^{1}H NMR Data of Acetylglucosides **6** and **7**, and Acetylrotungenic Acid (**8**)

H	Aglycone								H	Glucosyl			
	6			**7**		**8**				**6**		**7**	
	δ	Mult	J/Hz	δ	Mult J/Hz	δ	Mult	J/Hz		δ	Mult J/Hz	δ	Mult J/Hz
3	4.58	dd	11, 5.5	4.80	dd 11, 5	4.58	dd	10.5, 5	1′	5.52	d 8	5.52	d 8
12	5.38	brt	3.5	5.38	brt 3	5.35	brt	3.5	2′	5.17	dd 9, 8	5.17	dd 9, 8
18	2.53	brs		2.53	brs	2.54	brs		3′	5.25	t 9	5.25	t 9
23	0.95	s		3.69	d 11.5	0.95	s		4′	5.12	dd 10, 9	5.12	dd 10, 9
				3.89	brd 11.5				5′	3.78	ddd 10, 4.5, 2.3	3.78	ddd 10, 4.5, 2.2
24	4.14	d	12	0.84	s	4.12	brd	11.5	6′	4.05	dd 12, 2.3	4.05	dd 12, 2.2
	4.36	d	12			4.38	d	11.5		4.27	dd 12, 4.5	4.27	dd 12, 4.5
25	1.02	s		0.98	s	1.02	s		Ac	2.01	s	2.01	s
26	0.71	s		0.72	s	0.73	s			2.02	s	2.02	s
27	1.22	s		1.21	s	1.22	s			2.02	s	2.03	s
29	1.25	s		1.25	s	1.26	s			2.07	s	2.07	s
30	0.94	s		0.94	s	0.96	s						
Ac	2.03	s		2.03	s	2.03	s						
	2.06	s		2.06	s	2.05	s						

Measured in $CDCl_3$.

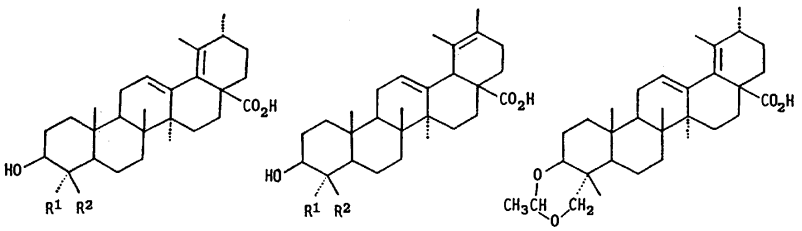

9: R^1= CH_3, R^2= CH_2OH 10: R^1= CH_3, R^2= CH_2OH 13

11: R^1= CH_2OH, R^2= CH_3 12: R^1= CH_2OH, R^2= CH_3

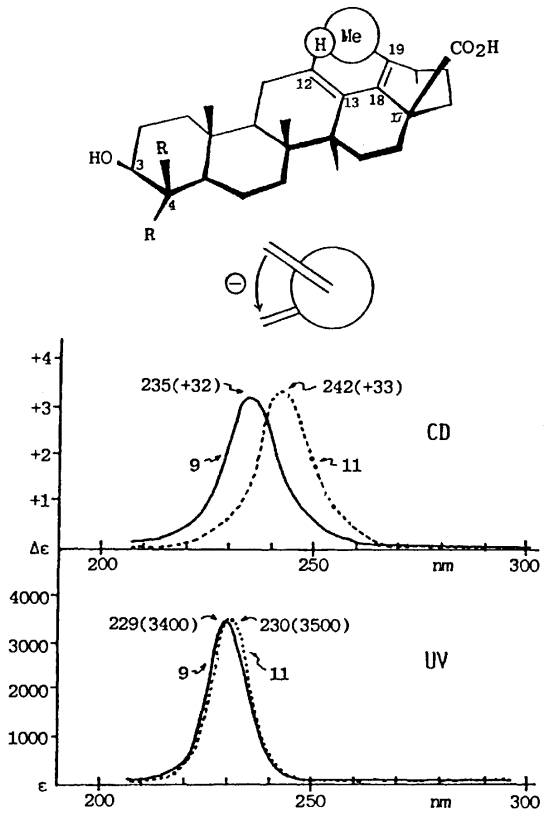

Fig. 1. UV and CD spectra of conjugated diene **9** and **11**.

were formulated as structures **9** and **10**. In the case of the reaction of **2** with dil sulfuric acid in ethanol, an acetal **13** was given in addition to dehydration products **11** and **12**.

The conjugated diene **9** exhibited a strong positive Cotton effect in the CD spectrum at 235 nm ($\Delta\varepsilon$ +32) like **11** (242 nm; $\Delta\varepsilon$ +33) due to π-π^* transition of conjugated diene (Fig. 1). The positive Cotton effect was well correlated with the chirarlity of chromophore, which is positive when the planes of the two double bonds are skewed in a right-handed helix. In the heteroannular cisoid diene, the sign of π-π^* cd is opposite to the chirality of the diene system.[10] Thus the positive effect expected for the negative chirality of the diene system in **9**, as predicted from its Dreiding model, was observed.

Among the compounds isolated in this work, pedunclosido and rotungenoside were active as an insect antifeedant against the larvae of *Spodoptera litura* Fab.

Experimental

Mps are uncorrected. Concentrations were performed under reduced pressure at bath temperatures not exceeding 50 °C. ^{1}H NMR spectra were obtained at 360 MHz and ^{13}C NMR spectra at 25.2 MHz. All the compounds were finally purified by HPLC on a C_{18} semiprep column using H_2O/MeOH solvent system. UV spectra were measured in methanol (MeOH).

Plant Material. Unripe fruits of the plant were collected at Kagoshima University in December 1983.

Extraction and Isolation. The unripe fruits (2 kg) were extracted with MeOH (3×10 l). After concn to 500 ml, H_2O (300 ml) was added and extracted with ethyl acetate (AcOEt) to give 18 g of an extract, which was passed through LH-20 column with MeOH to give two fractions. The first eluted fraction (7.2 g) was crystallized twice from AcOEt to give 2.1 g of a mixture of glucosides. The mixture (165 mg) was separated to a major component **2** (134 mg; 81.3%) and minor one **5** (14 mg; 8.4%) on a DCCC using $CHCl_3$-MeOH-H_2O (7 : 13 : 8 v/v) in ascending mode. The major component was eluted out at fractions 70—100 and the minor one at fractions 104—136. The elution of the compounds was monitored by TLC. Chromatography of the second fraction (3.4 g) on silica gel afforded ulsolic acid (25 mg) and a mixture of two triterpenes (1.2 g), which was separated to **1** (840 mg) and **3** (43 mg) by recrystallization from MeOH followed by HPLC (solvent; 20% H_2O/MeOH).

Rotungenoside (5). A white amorphous powder; $[\alpha]_D^{25}$ +5° (*c* 0.04, MeOH); UV 209 nm (ε 3000); IR (Nujol) 3500—3200, 1720 cm^{-1}; SIMS *m/z* 673 $(M+Na)^+$, 651 $(M+1)^+$, 581, 535, 489 $(651-C_6H_{11}O_5)^+$, 471 $(489-H_2O)^+$, 461, 453 $(471-H_2O)^+$, 435, 425, 407. Calcd for $C_{36}H_{59}O_{10}$: M+1, 651.

Pedunclosido (2). Prisms from AcOEt mp 213—214°C; $[\alpha]_D^{25}$ +22° (*c* 0.05, MeOH); SIMS *m/z* 673 $(M+Na)^+$, 489 $(M+1-C_6H_{11}O_5)^+$, 471 $(489-H_2O)^+$, 425, 407; IR (Nujol) 3500—3200, 1720 cm^{-1}; UV 210 nm (ε 4500). Found: C, 66.32; H, 8.83%. Calcd for $C_{36}H_{58}O_{10}$: C, 66.47; H, 8.92%.

Ursolic Acid. Mp 290 °C; EIMS *m/z* 456 $(M)^+$, 438, 410, 248, 207, 203, 189, which was identified by direct comparison (IR and MS) with an authentic sample.

Rotundic Acid (1). Prisms from MeOH, mp 272—274 °C (decomp); $[\alpha]_D^{25}$ +24° (*c* 0.1, MeOH); SIMS *m/z* 511 $(M+Na)^+$; EIMS *m/z* 488 $(M)^+$, 470, 452, 442, 264, 246, 223,

201, 175, 146; IR (Nujol) 3500—2600, 1690, 1640 cm^{-1}; UV 209 nm (ε4000); ^{13}C NMR (py-d_5) δ=13.1 (C-24), 16.0 (C-30), 16.8 (C-26), 17.3 (C-25), 18.8 (C-6), 24.1 (C-11), 24.7 (C-27), 26.5 (C-16), 27.0 (C-21), 27.2 (C-29), 27.7 (C-2), 29.4 (C-15), 33.4 (C-7), 37.3 (C-10), 38.5 (C-22), 38.9 (C-1), 40.4 (C-8), 42.2 (C-14), 42.4 (C-20), 42.9 (C-4), 47.9 (C-9), 48.3 (C-17), 48.8 (C-5), 54.7 (C-18), 68.2 (C-23), 72.7 (C-19), 73.7 (C-3), 128.1 (C-12), 140.0 (C-13), 180.7 (C-28). HRMS Found: m/z 488.3503. Calcd for $C_{30}H_{48}O_5$: M, 488.3502.

Rotungenic Acid (3). Column from H_2O-MeOH, mp 295—298 °C (decomp); $[\alpha]_D^{24}$ +50° (c 0.07, MeOH); SIMS m/z 489 $(M+1)^+$; EIMS m/z 488 $(M)^+$, 470, 452, 442, 264, 246, 223, 219, 205, 201, 175, 146; IR (Nujol) 3500—2600, 1690, 1640 cm^{-1}; UV 209 nm (ε 4000): ^{13}C NMR (py-d_5) δ=16.1 (C-30), 16.8 (C-26), 17.2 (C-25), 19.3 (C-6), 23.7 (C-23), 24.3 (C-11), 24.7 (C-27), 26.5 (C-16), 27.0 (C-21), 27.2 (C-29), 28.5 (C-2), 29.4 (C-15), 34.0 (C-7), 37.2 (C-10), 38.6 (C-22), 38.8 (C-1), 40.4 (C-8), 42.1 (C-14), 42.4 (C-20), 43.2 (C-4), 47.9 (C-9), 48.4 (C-17), 54.7 (C-18), 56.6 (C-5), 64.6 (C-24), 72.8 (C-19), 80.3 (C-3), 127.9 (C-12), 140.0 (C-13), 180.8 (C-28). HRMS Found: m/z 488.3504. Calcd for $C_{30}H_{48}O_5$: M, 488.3502.

Hexaacetylrotungenoside (6). Rotungenoside (**5**) (4 mg) was treated with acetic anhydride (Ac_2O) in py at 60 °C for 24 h to give the hexaacetate **6** (4 mg), mp 141—142.5 °C; $[\alpha]_D^{25}$ +15° (c 0.1, MeOH); IR (Nujol) 3450, 1740, 1720 cm^{-1}; UV 208 nm (ε 3700). Found: C, 63.77; H, 7.95%. Calcd for $C_{48}H_{70}O_{16}$: C, 63.84; H, 7.81%.

Hexaacetylpeduncloside (7). Peduncloside (**2**) (17 mg) was treated with Ac_2O in py at 60 °C for 24 h to give the hexaacetate **7** (15 mg), mp 160—161 °C; $[\alpha]_D^{25}$ +47° (c 0.1, MeOH); IR (Nujol) 3500, 1745, 1720 cm^{-1}; UV 209 nm (ε 3800). Found: C, 63.89; H, 7.92%. Calcd for $C_{48}H_{70}O_{16}$: C, 63.84; H, 7.81%.

3,24-Diacetylrotungenic Acid (8). Compound **3** (4.5 mg) was acetylated with Ac_2O in py to give the diacetate **8** (3 mg), mp 164—167 °C; EIMS m/z 554 $(M-H_2O)^+$, 526, 512, 264, 246.

Alkaline Hydrolysis of Rotungenoside (5). Rotungenoside (**5**) (11 mg) was treated with 10% aq potassium carbonate (K_2CO_3) (400 mg) in MeOH (10 ml) under reflux for 3 h. The crude product gave **3** (7 mg) as plates from MeOH, mp 295—298 °C (decomp).

Alkaline Hydrolysis of Peduncloside (2). Compound **2** (11 mg) was treated with 10% aq K_2CO_3 in MeOH under reflux for 10 h. Work-up as usual gave **1** (6.5 mg) as plates from H_2O-MeOH, mp 272—275 °C (decomp).

Acid Hydrolysis of Rotungenoside (5). Compound **5** (10 mg) was treated with 2M hydrochloric acid (HCl; 1M=1 mol dm^{-3}) (2 ml) in MeOH (10 ml) under reflux for 4 h. The product was extracted with ether and the extract was purified by HPLC (17.5% H_2O/MeOH) to give **9** (3 mg) and **10** (1 mg). Compound **9**, mp 198—199 °C as plates from MeOH; IR (Nujol) 3500—2500, 1690, 1650 cm^{-1}; UV 229 nm (ε 3400); CD (MeOH) 235 nm ($\Delta\varepsilon$ +32); EIMS m/z 470 $(M)^+$, 424 $(M-HCO_2H)^+$, 246, 223, 205, 201, 69 (base peak); ^1H NMR ($CDCl_3$) δ=0.88, 0.92, 0.97 (each 3H, s), 1.09 (3H, d, J=7.1 Hz), 1.25 (3H, s), 1.75 (3H, s) 3.34 (1H, br d, J=11.4 and 3.7 Hz), 3.45 (1H, br dd, J=11.5 and 5.0 Hz), 4.21 (1H, d, J=11.2 Hz), 5.44 (1H, dd, J=4.2 and 3.7 Hz). HRMS Found: m/z 470.3387. Calcd for $C_{30}H_{46}O_4$: M, 470.3395. Compound **10**; UV 207.5 nm (ε 6500); CD (MeOH) 210 nm ($\Delta\varepsilon$ −5.2); EIMS m/z 470 $(M)^+$, 472 $(M-H_2O)^+$, 426 $(M-CO_2)^+$, 424, 313, 246, 223, 205, 201, 149, 75 (base peak); ^1H NMR ($CDCl_3$) δ= 0.81, 0.90, 0.96, 1.24, 1.53, 1.63 (each 3H, s), 3.16 (1H, br s), 3.34 (1H, br d, J=11.4 Hz), 3.44 (1H, br dd, J=12 and 4 Hz), 4.21 (1H, d, J=11.2 Hz), 5.48 (1H, t, J=3.7 Hz). HRMS Found: m/z 470.3335. Calcd for $C_{30}H_{46}O_4$: M, 470.3395.

Methyl Ester of 9. Compound **9** was methylated with diazomethane (CH_2N_2) in MeOH to give the methyl ester **14**, a white amorphous powder; EIMS m/z 484 $(M)^+$, 260, 247, 201; ^1H NMR ($CDCl_3$) δ=0.84 (3H, s; 9-Me), 0.92 (3H, s; 4α-Me), 0.96 (3H, s; 11-Me), 1.07 (3H, d, J=7Hz; 20-Me), 1.25 (3H, s; 14-Me), 1.72 (3H, s; 19-Me), 3.34 (1H, m; 3-H), 3.45 (1H, br dd, J=11.5 and 4 Hz; 24-H), 4.21 (1H, d, J=11.5 Hz; 24-H), 5.35 (1H, dd, J=4 and 3.5 Hz; 12-H).

Methyl Ester of 10. Compound **10** was methylated with CH_2N_2 in MeOH to give the methyl ester **15**, mp 264—267 °C; EIMS m/z 484 $(M)^+$, 260, 248, 247, 215, 201 187; ^1H NMR ($CDCl_3$) δ=0.79 (3H, s; 9-Me), 0.90 (3H, s; 4α-Me), 0.95 (3H, s; 11-Me), 1.25 (3H, s; 14-Me), 1.53 (3H, s; 20-Me), 1.63 (3H, s; 19-Me), 3.20 (1H, br, s; 18-H), 3.33 (1H, br d, J=11 Hz; 3-H), 3.44 (1H, br dd, J=11.5 and 4 Hz; 24-H), 4.20 (1H, d, J=11.5 Hz; 24-H), 5.47 (1H, t, J=3.5 Hz; 12-H).

Acid Hydrolysis of Peduncloside (2). (i) Compound **2** (95 mg) was refluxed with 2 M HCl in MeOH for 3 h. HPLC separation of the crude product gave **11** (42 mg) and **12** (8 mg). Compound **11**, mp 145—146 °C; IR (Nujol) 3500—2500, 1690, 1650 cm^{-1}; UV 230 nm (ε 3500); CD (MeOH) 242 nm ($\Delta\varepsilon$ +33); SIMS m/z 493 $(M+Na)^+$, 471 $(M+1)^+$; ^1H NMR ($CDCl_3$) δ=0.87, 0.98, 1.03, 1.08 (each 3H, s), 1.09 (3H, d, J=7 Hz), 1.74 (1H, s), 3.45 (1H, d, J=10.5 Hz), 3.67 (1H, dd, J=9 and 7 Hz), 3.74 (1H, d, J=10.5 Hz), 5.46 (1H, t, J=4 Hz). HRMS Found: m/z 470.3391. Calcd for $C_{30}H_{46}O_4$: M, 470.3395. Compound **12**, mp 165—167 °C; IR (Nujol) 3500—2500, 1680, 1650 cm^{-1}; UV 207 nm (ε 4000); ^1H NMR ($CDCl_3$) δ=0.86, 0.89, 0.97, 1.01, 1.54, 1.61 (each 3H, s), 3.17 (1H, br s), 3.43 (1H, d, J=10.5 Hz), 3.64 (1H, dd, J=9 and 7 Hz), 3.73 (1H, d, J=10.5 Hz), 5.49 (1H, t, J=3.8 Hz). HRMS Found: m/z 470.3319. Calcd for $C_{30}H_{46}O_4$: M, 470.3395. (ii) Compound **2** (97 mg) was refluxed with 1 M sulfuric acid (15 ml) in ethanol (20 ml) for 5 h. Chromatography of the crude product on silica gel afforded an acetal **13** (8 mg) in addition to a mixture of **11** and **12**. Compound **13**, mp 215—216 °C; IR ($CHCl_3$) 3200—2500, 1690,1600 cm^{-1}; UV 247 nm (ε 4500); SIMS m/z 497 $(M+1)^+$, 451 $(497-HCO_2H)^+$, 404 $(451-CH_3CHO)^+$; ^1H NMR ($CDCl_3$) δ=0.87, 0.98, 1.03, 1.08 (each 3H, s), 1.09 (3H, d, J=7 Hz), 1.35 (3H, d, J=5.3 Hz; $C\underline{H}_3CH\begin{matrix}O\\O\end{matrix}$), 3.24 (1H, d, J=10.4 Hz; 23-H), 3.55 (1H, dd, J=10 and 4.5 Hz; 3-H), 3.77 (1H, d, J=10.4 Hz; 23-H), 4.74 (1H, q, J=5.3 Hz; $CH_3C\underline{H}\begin{matrix}O\\O\end{matrix}$), 5.42 (1H, t, J=3.5 Hz). SIMS Found: m/z 497. Calcd for $C_{32}H_{49}O_4$: M+1, 497.

Reaction of Rotungenic Acid (3) with Acid. Compound **3** (7 mg) was refluxed with 2 M HCl in MeOH for 3 h. Work-up as usual gave **9** (3 mg) and **10** (1 mg).

Reaction of Rotundic Acid (1) with Acid. Compound **1** was treated with 2 M HCl in a manner similar to **3**. The crude product gave **11** and **12**.

Insect Antifeedant Activity. The triterpenoids **1**, **2**, **3**, and **5** were tested against the larvae of the pest insect *Spodoptera litura* Fab. with the leaf disk method.[11] Peduncloside (**2**) and rotungenoside (**5**) showed the antifeedant activity at 2000 ppm concn.

We are grateful to Dr. Hideo Naoki and Takashi Iwashita (Suntory Institute for Bioorganic Research) for MS and NMR spectra and to Mr. Mitsuo Tahara (Sankei Chemical Co., Ltd.) for the supply of the insect.

This work was partially supported by Grant-in-Aid for the Scientific Research (No. 60540355) from the Ministry of Education, Science and Culture.

References

1) T. Oyama, H. Aoyama, K. Yamada, T. Mitsuhashi, and N. Sugiyama, *Tetrahedron Lett.*, **1968**, 4639.

2) T. Hase, H. Hagii, M. Ishizu, M. Ochi, N. Ichikawa, and T. Kubota , *Nippon Kagaku Kaishi*, **1973**, 778.

3) M. Nakatani, Y. Miyazaki, T. Iwashita, H. Naoki, and T. Hase, *Phytochemistry*, in press.

4) K. Yamasaki, H. Kohda, T. Kobayashi, R. Kasai, and O. Tanabe, *Tetrahedron Lett.*, **1976**, 1005.

5) P. J. Houghton and L. M. Lian, *Phytochemistry*, **25**, 1939 (1986).

6) R. Chemli, A. Badadjamian, R. Faure, K. Boukef, G. Balansard, and E. Vidal, *Phytochemistry*, **26**, 1785 (1987).

7) I. Yoshioka, T. Sugawara, and I. Kitagawa, *Chem. Pharm. Bull.*, **19**, 1700 (1971).

8) C. H. Brieskorm and H. Wandere, *Chem. Ber.*, **100**, 1252 (1967).

9) J. Bermejo, J. L. Breton, G. de la Fuente, and A. G. Gonzalez, *Tetrahedron Lett.*, **1967**, 4649.

10) A. W. Burgstahler and R. C. Barkhurst, *J. Am. Chem. Soc.*, **92**, 7601 (1970).

11) I. Kubo, M. Taniguchi, A. Chapya, and K. Tsujimoto, *Planta Med.*, **1980**, 185.

The Synthesis of 1,3-Dithiolan-2-ones on the Reaction of Oxiranes with Carbon Disulfide under High Pressure

Yoichi TAGUCHI,* Masahiko YASUMOTO, Isao SHIBUYA, and Yasuo SUHARA
National Chemical Laboratory for Industry, Higashi, Tsukuba, Ibaraki 305
(Received July 27, 1988)

An equimolar reaction of 2-hexyloxirane with carbon disulfide in hexane was run in the presence of triethylamine under 800 MPa at 100 °C for 20 h, and gave 63% of 4-hexyl-1,3-dithiolan-2-one (**3a**), 21% of 4-hexyl-1,3-dithiolane-2-thione (**1a**) and 5% of 5-hexyl-1,3-oxathiolan-2-one (**4a**). Hexane, benzene, and diisopropyl ether were good solvents for the reaction. The reaction of a variety of oxiranes with carbon disulfide produced 1,3-dithiolan-2-ones as the main products under 500 MPa at 100 °C for 20 h. Upon a reaction of 2-hexyloxirane with carbon disulfide, 5-hexyl-1,3-oxathiolane-2-thione (**2a**), and 2-hexylthiirane (**5a**) were produced during the first stage of reaction. The formation of **1a** and **4a** began immediately, whereas, the formation of **3a** required a long induced period. A feasible mechanism for the formation of **3a** is proposed to be a rearrangement of **2a** in the presence of triethylamine, free from carbon disulfide.

Many organic reactions are accelerated by compression.[1,2] It has recently been reported that the reactions of many thiiranes with carbon disulfide in the presence of triethylamine under high pressure give 1,3-dithiolane-2-thiones nearly quantitatively.[3] The reactions of many oxiranes with carbon disulfide are also accelerated by compression to give 1,3-dithiolane-2-thiones (**1**) as a main product.[4] **1** is considered to be formed via 1,3-oxathiolane-2-thiones (**2**),[4] and the relative ratio of **2** to the total yield is high during the early period of the reaction. Therefore, it is expected that **2** is formed with high yield and selectivity by the choice of suitable reaction conditions. The equimolar reaction of oxiranes and carbon disulfide in a solvent was investigated under high pressure for this purpose. As a result, an interesting rearrangement was found to occur without yielding **2**.

In this paper, we report on reactions in which no **2** was obtained and 1,3-dithiolan-2-ones (**3**) were newly formed as the main products upon the reaction of oxiranes with carbon disulfide. When excess carbon disulfide was used, **3** was not found.[4] The formation of **3** is considered to include some rearrangement, since **3** can not be formed by a simple addition reaction. There have been no reports on a similar rearrangement under high pressure. The effects of the pressure, temperature, reaction time, molar ratio of reactants, the amount and kind of catalysts, and the kind of solvents have been investigated in detail with regard to the reaction of 2-hexyloxirane with carbon disulfide. The mechanism for the formation of the products is also discussed.

Results and Discussion

A reaction of 2-hexyloxirane with excess carbon disulfide at 100 °C for 20 h under 800 MPa gave 71% of 4-hexyl-1,3-dithiolane-2-thione (**1a**), 5% of 5-hexyl-1,3-oxathiolane-2-thione (**2a**) and 12% of 5-hexyl-1,3-oxathiolan-2-one (**4a**).[4] However, an equimolar reaction in hexane under the same reaction conditions gave 63% of 4-hexyl-1,3-dithiolan-2-one (**3a**), 21% of **1a** and 5% of **4a**; no **2a** was produced.

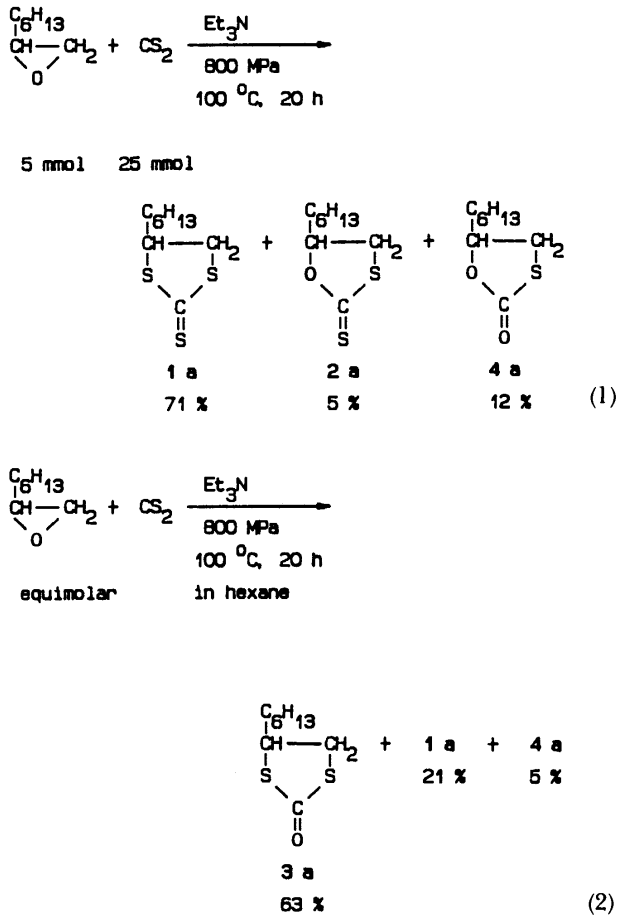

Table 1 shows the effects of pressure, temperature, and reaction time on the reaction. The reaction under ordinary pressure gave no products (Run 1); this fact shows that this reaction can be remarkably accelerated by compression. At a pressure higher than 500 MPa, **3a** was the main product and none of **2a** was produced unexpectedly (Runs 3—7). Under 200 MPa, both products **2a** and **3a** were obtained and 29% of 2-

Table 1. Reaction of 2-Hexyloxirane with CS_2[a]

Run	Press.	Temp	Time	Conv.	Yield/%					
	MPa	°C	h	%	**1a**	**2a**	**3a**	**4a**	**5a**	Total
1	0.1[b]	100	20	19	—	—	—	—	—	—
2	200	100	20	95	18	19	12	2	29	80
3	500	70	20	100	12	—	55	4	15	86
4	500	100	20	100	16	—	68	5	—	89
5	800	70	20	100	12	—	33	1	25	71
6	800	100	7	100	13	—	44	—	8	65
7	800	100	20	100	21	—	63	5	—	89

a) 2-Hexyloxirane 5 mmol; CS_2 5 mmol; Et_3N 0.5 mmol; hexane 3 ml. b) In a sealed glass tube.

Table 2. Effect of Solvents on the Reaction of 2-Hexyloxilane with CS_2[a]

Run	Press.	Solvent	Conv.	Yield/%					
	MPa		%	**1a**	**2a**	**3a**	**4a**	**5a**	Total
1	500	Hexane	100	16	—	68	5	—	89
2	500	Benzene	100	17	4	72	5	—	98
3	500	IPE	100	16	—	70	5	—	91
4	500	CH_3CN	100	25	—	43	—	—	68
5	800	$CHCl_3$	100	16	—	31	4	11	62
6	500	Acetone	100	14	—	3	—	1	18
7	500	DMF	91	10	1	1	—	6	18

a) 2-Hexyloxilane 5 mmol; CS_2 5 mmol; Et_3N 0.5 mmol; reaction time 20 h; reaction temperature 100 °C.

Table 3. Effect of Various Catalysts on the Reaction of 2-Hexyloxirane with CS_2[a]

Run	Catalyst	Press.	Temp	Time	Conv.	Yield/%					
		MPa	°C	h	%	**1a**	**2a**	**3a**	**4a**	**5a**	Total
1	*N*-Methylmorpholine	200	100	20	17	—	2	—	—	8	10
2	*N*-Methylmorpholine	500	70	20	81	4	31	—	1	4	40
3	*N*-Methylmorpholine	800	70	20	100	18	48	—	5	10	81
4	*N*-Methylmorpholine	800	100	7	100	16	—	60	1	14	91
5	Pyridine	200	100	20	33	2	14	—	—	7	23
6	Tributylamine	800	100	20	100	29	—	54	5	—	88
7	2,6-Dimethylpyridine	800	100	20	74	6	26	—	4	—	36

a) 2-Hexyloxirane 5 mmol; CS_2 5 mmol; catalyst 0.5 mmol; hexane 3 ml.

Table 4. Effects of the Amount of Triethylamine and Molar Ratio of Reactants[a]

Run	Press.	Et_3N	CS_2	Conv.	Yield/%					
	MPa	mmol	oxirane	%	**1a**	**2a**	**3a**	**4a**	**5a**	Total
1	500	0.05	1	58	1	19	—	—	6	26
2	500	0.10	1	95	20	28	13	5	11	77
3	500	0.15	1	97	16	16	39	5	17	93
4	500	0.25	1	98	16	1	63	7	7	94
5	500	0.50	1	100	16	—	68	5	—	89
6	500	1.00	1	100	20	—	66	7	—	93
7	500	6.00	1	100	24	—	60	1	—	85
8	800	0.50	1.5	100	66	3	16	9	—	94
9	800	0.50	0.5	100	1	—	3	3	—	7

a) 2-Hexyloxirane 5 mmol; hexane 3 ml; reaction time 20 h; reaction temperature 100 °C.

hexylthiirane (**5a**) was also formed (Run 2).

Table 2 shows the effect of solvents. **3a** was formed in high yields in hexane, benzene, and diisopropyl ether (IPE); however, in polar solvents, such as acetone and *N*,*N*-dimethylformamide (DMF), the yield of **3a** decreased.

Table 3 shows the effect of catalysts. When *N*-methylmorpholine was used as a catalyst under 800 MPa at 100 °C, **3a** was obtained as the main product (Run 4), but under lower pressure or at a lower

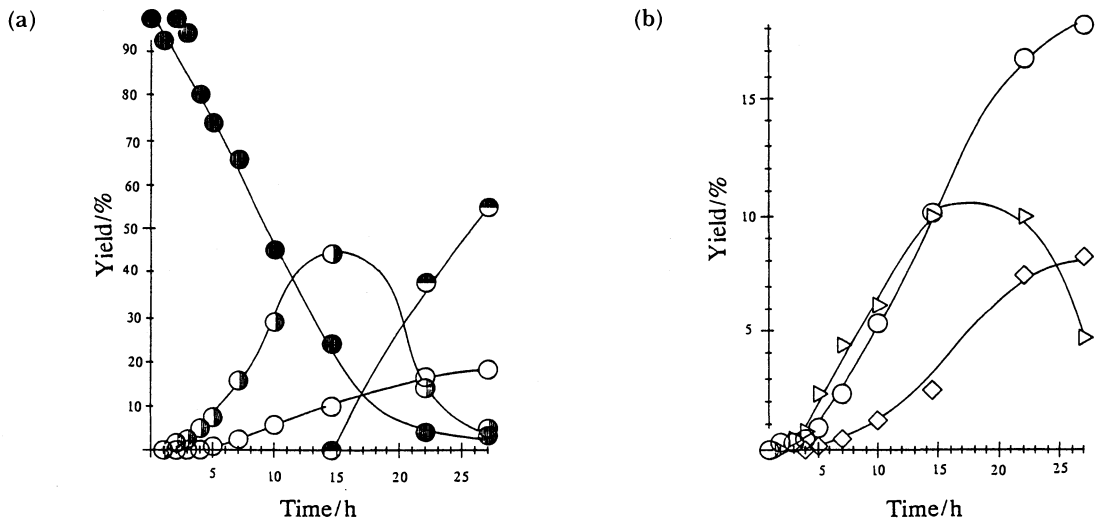

Fig. 1. Relation of the yields of products and reaction time on the reaction of 2-hexyloxirane with CS_2. Reaction temperature: 70 °C, pressure: 300 MPa, 2-hexyloxirane: 50 mmol, CS_2: 50 mmol, Et_3N: 5 mmol, heptane: 30 ml, tetradecane: 0.50 g.
—●—: 2-hexyloxirane, —○—: **1a**, —◑—: **2a**, —◒—: **3a**, —◇—: **4a**, —▷—: **5a**.

temperature **3a** was not formed (Runs 1—3).

Table 4 shows the relation between the yields of the products and the amount of triethylamine used as a catalyst on the reaction. Since the rate of the reaction of thiiranes with carbon disulfide is proportional to the amount of triethylamine catalyst,[3] it is considered that the rate of the reaction of 2-hexyloxirane is proportional to the amount of triethylamine in the range of 0.05—0.50 mmol. When 0.05 mmol of triethylamine was used, **2a** was formed as the main product and **3a** was not formed (Run 1); also, none of **2a** was detected and **3a** was given as the main product when 0.50 mmol of triethylamine was used (Run 5). As a result, it is suggested that **3a** is formed by the conversion of **2a**. When a slight excess of carbon disulfide was used, **1a** was obtained as the main product and the yield of **3a** decreased (Run 8). This shows that the ratio of products depends upon the molar ratios of oxiranes and carbon disulfide; but when the ratio of carbon disulfide was reduced, the polymerization of 2-hexyloxirane proceeded preferentially (Run 9).

Figure 1 shows the relation between the yields of the products and the reaction time on the reaction in heptane under 300 MPa at 70 °C. During the initial stage, **2a** was formed as the main product, and no **3a** was formed. **3a** was first detected at 22 h after starting ; **2a**

Table 5. Reaction of Various Oxiranes with CS_2[a]

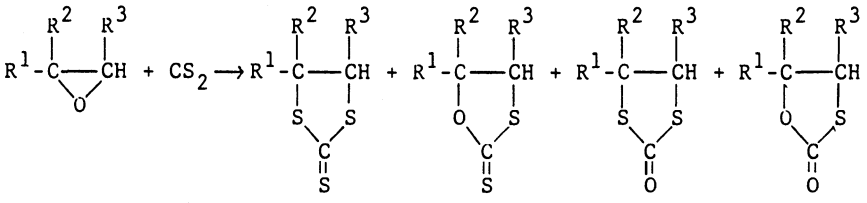

1 **2** **3** **4**

Run	Product			Solvent	Et_3N	Yield/%				
	R^1	R^2	R^3		mmol	**1**	**2**	**3**	**4**	Total
1	CH_3	H	H	Hexane	0.50	44	—	22	—	66
2	CH_3	H	H	Benzene	0.10	17	31	34	5	87
3	C_2H_5	H	H	Hexane	0.50	24	—	47	5	76
4	CH_3	CH_3	H	Hexane	0.50	4	54	30	—	88
5	Ph	H	H	Hexane	0.50	Trace	—	Trace	—	Trace
6	Ph	H	H	Hexane	0.05	48	—	9	—	57
7	Ph	H	H	Benzene	0.05	29	—	36	—	65
8	H	$(CH_2)_4$		Hexane	0.50	31	15	—	11	46
9	H	$(CH_2)_4$		Benzene	0.10	27	—	10	4	41

a) Oxirane 5 mmol; CS_2 5 mmol; Et_3N 0.5 mmol; pressure 500 MPa; reaction temperature 100 °C; reaction time 20 h.

was reduced greatly. These phenomena verify that **2a** changes to **3a**, and that the formation of **3a** has a long induced period. In contrast to the production of **3a**, **1a** and **4a** were already detected at an early time, and increased as the reaction proceeded. The formation mechanisms of **1a** and **4a** are considered to be the same mechanisms as mentioned previously.[4]

Table 5 shows the products and yields for the reactions of various oxiranes with carbon disulfide. 2-Phenyloxirane and 2-methyloxirane which produce **1** easily upon reacting with excess carbon disulfide,[4] produced **3** as the main product under suitable reaction conditions (Runs 2 and 7). 2,2-Dimethyloxirane, which gave **2** as the main product on the reaction with excess carbon disulfide, also gave **2** as the main product, though **3** was obtained with 30% yield (Run 4).

An equimolar reaction of 2-hexyloxirane with carbon disulfide in the presence of triethylamine seems to proceed as follows:

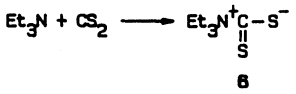

(3)

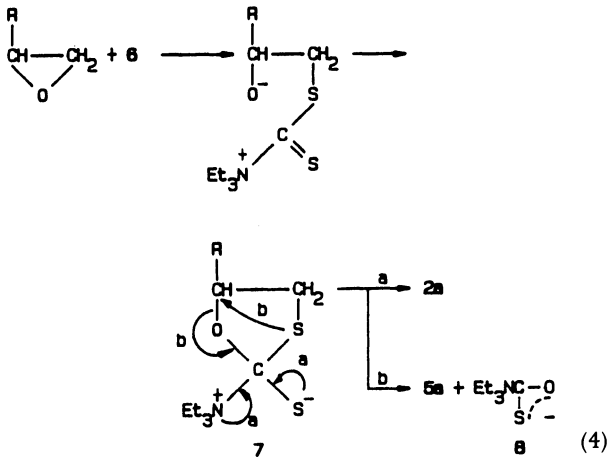

(4)

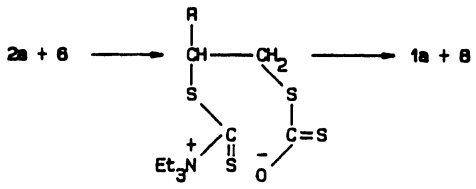

(5)

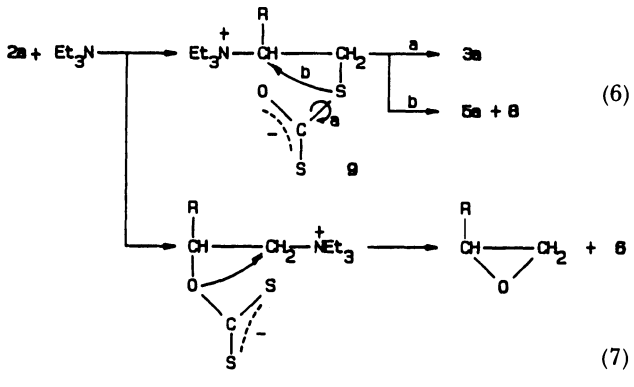

(6)

(7)

Adduct **6** attacks 2-hexyloxirane to give **2a** and **5a** (Eq. 4). **1a** is obtained through a reaction of **2a** with **6**, as mentioned previously (Eq. 5). When carbon disulfide is almost consumed and free triethylamine is present without producing **6** with carbon disulfide, **2a** reacts with triethylamine to give adduct **9**. **3a** is formed by a rotation of the C-S bond of **9**. A similar rotation has been reported regarding the isomerization of *N*-phenyl-1,3-dioxolan-2-imine.[5] To confirm this mechanism, **2a** in hexane was heated at 100 °C in the presence of triethylamine under 800 MPa for 20 h to form **3a** as the main product (Eq. 8). In contrast, a similar reaction in carbon disulfide gave **1a** as the main product; **3a** was not obtained (Eq. 9). It is considered that the reaction of Eq. 7 is also achieved, because the formations of **1a** and **4a** in Eq. 8 need 2-hexyloxirane and **6**.

$$\mathbf{2a} \xrightarrow[800\ \text{MPa, 100 °C}]{\text{Et}_3\text{N, Hexane}} \underset{9\%}{\mathbf{1a}} + \underset{18\%}{\mathbf{2a}} + \underset{52\%}{\mathbf{3a}} + \underset{6\%}{\mathbf{4a}} + \underset{15\%}{\mathbf{5a}} \quad (8)$$

$$\mathbf{2a} + CS_2 \xrightarrow[800\ \text{MPa, 100 °C}]{\text{Et}_3\text{N}} \underset{73\%}{\mathbf{1a}} + \underset{7\%}{\mathbf{2a}} + \underset{9\%}{\mathbf{4a}} + \underset{2\%}{\mathbf{5a}} \quad (9)$$

Of Eqs. 3—7, it has been reported[3,4] that the compression have an accelerating effect on reactions in Eqs. 3—5. The reactions of Eqs. 6 and 7 seem to also be accelerated by compression since a rearrangement of **2a** did not occur under ordinary pressure under similar reaction conditions to Eq. 8.

Some products[6-9] which are derived from **3** are known to be accricides, fungicides, or insecticides. Though various synthetic methods of 1,3-dithiolan-2-one have been reported,[10-14] the materials used for its derivatives are rather inaccessible. Synthesis of its derivatives by reactions of oxirane with carbon disulfide under high pressure have the advantage since many kinds of oxiranes may be obtained commercially.

Experimental

Apparatus. The apparatus used for the reaction under high pressure was the same as that described previously.[15]

Measurement. GLC was carried out using a JEOL 20KF chromatograph with 20% SE-30 columns. ^{1}H NMR spectra were measured with a Hitachi R-40 spectrometer. Mass spectra were measured with a JEOL D-300 GC-MS spectrometer by the CI (chemical ion) method with isobutane. IR spectra were obtained with a JASCO A-302 spectrophotometer.

Reaction of Oxiranes with Carbon Disulfide. A typical procedure is as follows: A homogeneous mixture of 2-hexyloxirane (5 mmol), carbon disulfide (5 mmol), and triethylamine (0.5 mmol) in a sealed Teflon tube was compressed to 800 MPa, heated at 100 °C, and maintained for 20 h in a high-pressure apparatus. The resulting mixture was subjected to evaporation and the residue was distilled with a Kugelrohr. The distillate was separated by column chromatography on silica gel using a mixture of hexane and chloroform (7 : 3 v/v) as an eluent. The spectral data of **1a** and **4a** agreed with the known data.[3,4] The structure of **3a** was identified by a comparison of ^{1}H NMR and IR spectra of **3a** with

those of **1a**, **2a**, **4a**, and 1,3-dithiolan-2-one.[10] **3a**: IR 1642 cm^{-1} ; ^1H NMR δ=0.89 (t, 3H, CH_3), 1.31 (s, 8H, $\{CH_2\}_4$), 1.65—2.10 (m, 2H, CH_2), 3.24—3.86 (m, 2H, CH_2), and 3.91—4.37 (m, 1H, CH); QM^+ 205.

2-Methyloxirane, 2-ethyloxirane, 2,2-dimethyloxirane, 2,3-tetramethyleneoxirane, and 2-phenyloxirane were treated with carbon disulfide similarly to 2-hexyloxirane. The spectral data of **1**, **2**, and **4** from these reactions agreed with the known data.[3,4] The spectral data of the other products of these reactions are as follows:

4-Methyl-1,3-dithiolan-2-one: IR 1642 cm^{-1}; ^1H NMR δ=1.60 (d, J=6.3 Hz, 3H, CH_3), 3.22—3.53 (dd, J=7.2 and 11.7 Hz, 1H, one proton of CH_2), 3.58—3.85 (dd, J=4.5 and 11.7 Hz, 1H, one proton of CH_2), and 4.00—4.42 (m, 1H, CH); QM^+ 135.

4-Ethyl-1,3-dithiolan-2-one: IR 1642 cm^{-1}; ^1H NMR δ= 1.06 (t, 3H, CH_3), 1.93 (quin, 2H, CH_2), 3.30—3.56 (dd, J=7.2 and 11.7 Hz, 1H, one proton of CH_2), 3.60—3.87 (dd, J=5.4 and 11.7 Hz, 1H, one proton of CH_2), and 3.89—4.22 (m, 1H, CH); QM^+ 149.

4,4-Dimethyl-1,3-dithiolan-2-one: IR 1643 cm^{-1}; ^1H NMR δ=1.70 (s, 6H, $2CH_3$), and 3.47 (s, 2H, CH_2); QM^+ 149.

4,5-Tetramethylene-1,3-dithiolan-2-one: IR 1624 cm^{-1}; ^1H NMR δ=1.2—2.3 (m, 8H, $4CH_2$), and 3.70—3.95 (m, 2H, 2CH); QM^+ 175.

4-Phenyl-1,3-dithiolan-2-one: IR 1651 cm^{-1}; ^1H NMR δ=3.71 (d, J=9 Hz, 2H, CH_2), 5.23 (t, 1H, CH), and 7.10—7.70 (m, 5H, C_6H_5); QM^+ 197.

Rearrangement of 2a in Hexane. A homogeneous mixture of **2a** (43.1 mg), triethylamine (4.0 mg), tetradecane (7.3 mg), and hexane (0.3 ml) in a sealed Teflon tube was compressed to 800 MPa, heated at 100 °C, and maintained for 20 h in a high-pressure equipment. The GLC analysis using tetradecane as a standard showed that 52% of **3a** was obtained.

Reaction of 2a with Carbon Disulfide. A homogeneous mixture of **2a** (43.3 mg), carbon disulfide (200 mg), triethylamine (3.8 mg), and tetradecane (5.9 mg) in a sealed tube was compressed to 800 MPa, heated at 100 °C, and maintained for 20 h in a high-pressure apparatus. A GLC analysis using tetradecane as a standard showed that 71% of **1a** was obtained.

References

1) K. Matsumoto, A. Sera, and T. Uchida, *Synthesis*, **1985**, 1.
2) K. Matsumoto and A. Sera, *Synthesis*, **1985**, 999.
3) Y. Taguchi, K. Yanagiya, I. Shibuya, and Y. Suhara, *Bull. Chem. Soc. Jpn.*, **60**, 727 (1987).
4) Y. Taguchi, K. Yanagiya, I. Shibuya, and Y. Suhara, *Bull. Chem. Soc. Jpn.*, **61**, 921 (1988).
5) G. A. Sperange and W. J. Peppel, *J. Org. Chem.*, **23**, 1922 (1958).
6) N. Yasuda, T. Yamatani, T. Ohnuki, and M. Okutsu, *J. Heterocycl. Chem.*, **21**, 1845 (1984); *Chem. Abstr.*, **103**, 1655z (1985).
7) P. Siegle, E. Kuehle, I. Hammann, and W. Behrenz, Ger. Offen., 2357930 (1975); *Chem. Abstr.*, **83**, 96702t (1975).
8) G. Zumach, P. Siegle, I. Hammann, and P. E. Frohberger, Ger. Offen., 2203050 (1973); *Chem. Abstr.*, **79**, 105232m (1973).
9) R. W. Addor, U. S. Patent, 3281430 (1966); *Chem. Abstr.*, **66**, 65483s (1967).
10) S. Satumabayashi, H. Takahashi, T. Tanaka, and S. Motoki, *J. Org. Chem.*, **38**, 3953 (1973).
11) P. Koch and E. Perrotti, Ger. Offen., 2437132 (1975); *Chem. Abstr.*, **82**, 156282x (1975).
12) S. Sakai, H. Niimi, and Y. Ichii, *J. Organomet. Chem.*, **72**, 103 (1974).
13) C. G. Overberger and P. V. Bonsigner, *J. Am. Chem. Soc.*, **80**, 5427 (1958).
14) V. S. Etlis, L. N. Grobov, and G. A. Razuvaev, *Zh. Obshch. Khim.*, **32**, 2940 (1962); *Chem. Abstr.*, **58**, 7817a (1963).
15) M. Kurabayashi, K. Yanagiya, and M. Yasumoto, *Bull. Chem. Soc. Jpn.*, **44**, 3413 (1971).

Reversible Bond Switch with Participation of Hypervalent Sulfurane in a Thiadiazole Ring System and Its Kinetic Study in a Protonated System

Yohsuke YAMAMOTO† and Kin-ya AKIBA*,††

Department of Chemistry, Faculty of Science, The University of Tokyo, Hongo, Bunkyo-ku, Tokyo 113

††Department of Chemistry, Faculty of Science, Hiroshima University, Higashisenda-machi, Naka-ku, Hiroshima 730

(Received August 15, 1988)

The existence of ring transformation equilibrium (bond switch) in 5-(1-aminoethylideneamino)-3-methyl-1,2,4-thiadiazole (**5a**) was confirmed by nitrogen-15 labeling experiment. Kinetic studies were carried out under neutral or acidic conditions. Kinetic parameters of the intramolecular equilibration of the monoprotonated **5a** (**5a**-H^+) were obtained by line shape analyses of the ^1H NMR, i.e., $\Delta G^{\ddagger}_{273}=14.8\pm0.2$, $\Delta H^{\ddagger}=11.6\pm1.0$ kcal·mol^{-1} $\Delta S^{\ddagger}=-12\pm3$ eu, $k_{273}=9$ s^{-1}. Position of protonation was determined at the nitrogen of the ethylideneamino part of the amidino group. It was concluded that the central sulfur atom moves back and forth in the range of 0.38 Å nine times a second at 0 °C, that is, bond switching.

Labile and polarizable nature of three-center four-electron bond in hypervalent molecules has been amply demonstrated by X-ray analyses of organic molecules of main group elements and sulfuranes are typical examples among them. Sulfurane **1** was synthesized by Martin,[1a] and two S-O bond lengths are longer than usual covalent bond and differ by 0.25 Å. The S-S bond length in 1,6,6a-trithiapentalene system (**2**) lies close to 2.36 Å but fluctuates within the range of 0.4 Å according to substituents.[2] The lability of bond length is one of the characteristics of hypervalent bond. The apparent bond switch in the 1,3-dipolar cycloaddition of five-membered sulfur containing heterocycles with activated acetylenes and so on have been considered to proceed through unsymmetrical trithiapentalene type intermediates.[3] Large difference of reactivity with activated acetylenes was noticed between isoelectronic 3(2*H*)- and 5(2*H*)-isothiazolethiones (**3** and **4**), that is, the latter was much more reactive than the former, because the central sulfur atom could participate in the 1,3-dipolar cycloaddition.[3f] Reid and co-workers reported the bond switch in the trithiapentalene-tungsten complexes.[4]

We have communicated a facile bond switch in some 1,2,4-thiadiazol-5(4*H*)-imine system by methylation or protonation,[5] and simplified the system in order to observe reversible bond switch via symmetrical sulfurane as an intermediate. In this system the sulfur-nitrogen bond was switched by prototropy, and the facility of the equilibration would suggest that the stability of the intermediate **A** reduced the activation energy (Eq. 1).[6] This type of equilibration does not take place at all when an oxygen is substituted for the sulfur.

In this paper the observed phenomenon was confirmed to be bond switching by introducing ^{15}N to the amidino group and kinetic studies on equilibration were carried out under neutral and acidic conditions.[7]

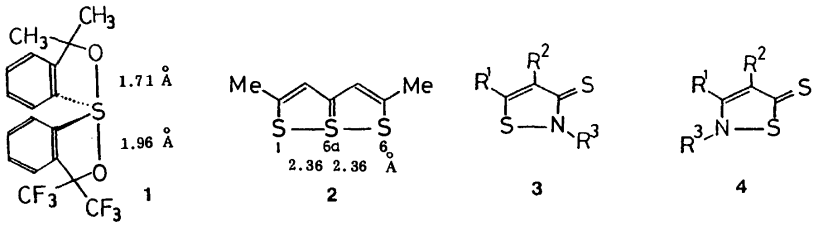

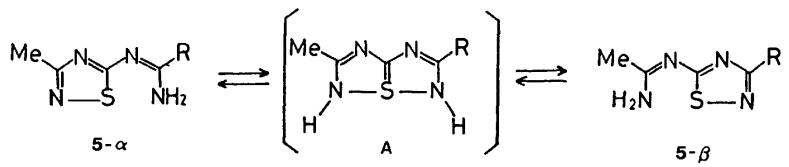

(1)

5a: R=Me
5b: R=CH_2Cl
5c: R=Ph
5d: R=p-$CH_3C_6H_4$
5e: R=p-ClC_6H_4

† Present address: Department of Chemistry, Faculty of Science, Hiroshima University, Higashisenda-machi, Naka-ku, Hiroshima 730.

Results and Discussion

Confirmation of Bond Switch by ^{15}N Labeling Experiment and Estimation of the Rate under Neutral Conditions. As described before 5-(1-substituted 1-aminomethyleneamino)-3-methyl-1,2,4-thiadiazole (**5α**) was considered to be in equilibrium with the bond-switched **5β**. The conclusion was drawn by the following facts: (i) in the ^1H NMR spectra of unsymmetrical **5b** and so on signals due to the methyl and the substituent (R) appeared as a pair, respectively, but those of symmetrical **5a** (R=Me) showed only two peaks due to two different methyl groups; (ii) relative intensity of the methyl corresponded exactly to that of the other substituent (R). In order to present an unambiguous evidence for bond switch, **5c** was synthesized also from 5-amino-3-phenyl-1,2,4-thiadiazole (**6b**)[8] and acetonitrile in the presence of aluminum trichloride to give an identical compound with previously prepared one from 5-amino-3-methyl-1,2,4-thiadiazole (**6a**) and benzonitrile[6] (Eq. 2). Further

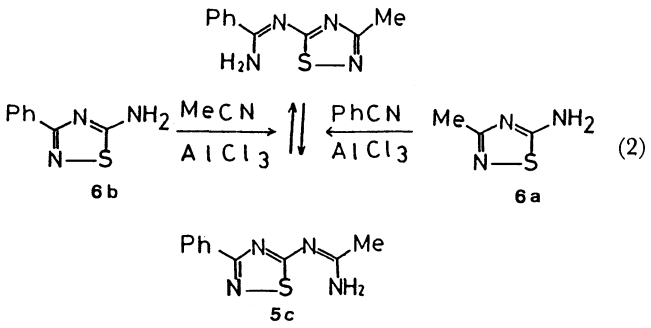

(2)

conclusive evidence came from the ^{15}N labeling experiment. Thus an imidate **7** was prepared from **6a** and triethyl orthoacetate in 95% yield. The imidate **7** was converted with ammonia at room temperature to give **5a**, which was identical with the compound synthesized previously. This method was mild and efficient thus it was applied to the synthesis of ^{15}N labeled **5a** in 60% yield using $^{15}NH_3$ (in situ prepared from [^{15}N]ammonium chloride (^{15}N 99% enriched) and 1 equiv of potassium hydroxide). In the proton

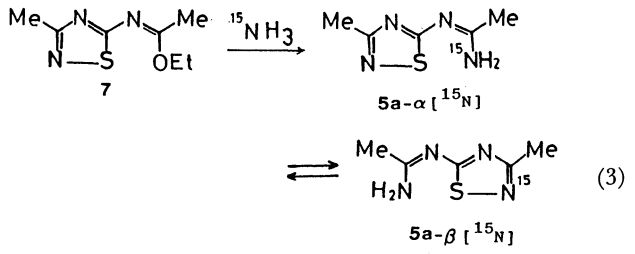

(3)

decoupled ^{15}N NMR spectrum of **5a**[^{15}N] two peaks with almost equal height were observed. The chemical shifts of these nitrogens were obtained from that of nitromethane as an external reference and were calculated into the values from liquid ammonia.[9a] The peak at δ 104.1 was observed as a triplet (J_{NH}=91 Hz) in nondecoupled conditions, thus it is assigned to the nitrogen of the amino group in the amidino group. It is reasonable that the other peak at δ 240.7 (singlet in nondecoupled conditions) is assigned to the N(2) of the thiadiazole ring by comparison with reported chemical shift data.[9b] Off-resonance ^{15}N NMR spectrum of **5a**[^{15}N] is shown in Fig. 1. Therefore bond switch was evidently confirmed to take place.

It is interesting that ^{15}N NMR chemical shift of the amino nitrogen is in somewhat lower field than usual and that of the N(2) of the thiadiazole is in higher field.[9b] This tendency can be understood by contribution of intramolecular electron shift from the electron-rich amidino group into the electron-deficient five-membered thiadiazole ring.[9c] The explanation can also be applied to the electronic effects of the subsituents on the equilibrium ratio (β/α), that is, 2.14 in **5b** (R=CH_2Cl), 5.99 in **5d** (R=*p*-MeC_6H_4), 14.5 in **5c** (R=C_6H_5), and ca. 50 in **5e** (R=*p*-ClC_6H_4) (all values in $CDCl_3$ at 34 °C). Thus β-forms are further stabilized in polar solvents (**5b**: 2.14 in $CDCl_3$, 6.46 in CD_3CN). Measurements of the equilibrium ratios of **5b** in several solvents at various temperatures were carried out to give thermodynamic parameters of the bond switch. The results are shown in Table 1. It was found that ΔS was about zero and ΔH was almost responsible for the equilibrium ratio.

The rather large difference between the equilibrium ratio in $CDCl_3$ and CD_3OD (2.9 and 10.7 at −26 °C) was tried to use for the determination of the rate of the equilibration. Thus, to a $CDCl_3$ solution of **5b** (β/α=3) at −50 °C precooled CD_3OD (−50 °C) was added and ^1H NMR spectrum of the mixture was measured quickly at that temperature. In the first measurement which was done during 2—3 min after mixing, the ratio (β/α) was determined to be ca. 7 and in

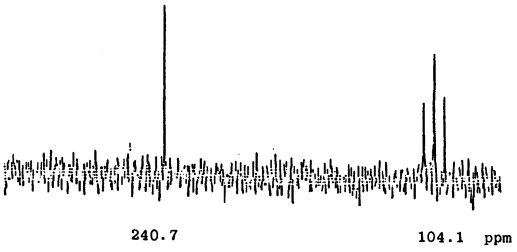

Fig. 1. Off-resonance ^{15}N NMR of **5a**[^{15}N] in neutral solution ($CDCl_3$).

Table 1. Solvent Effect on the Thermodynamic Parameters between **5bα** and **5bβ**

Solvent	Polarity E_T	β/α (34 °C)	ΔG_{307} kcal mol^{-1}	ΔH kcal mol^{-1}	ΔS eu
$CDCl_3$	39.1	2.14	−0.48	−0.75	−0.9
CD_2Cl_2	41.1	3.28	−0.72	−0.77	−0.2
CD_3CN	46.0	6.46	−1.14	−1.02	+0.4
CD_3OD	55.5	6.53	−1.15	−1.28	−0.4

the next measurement (4—5 min after mixing) a new equilibrium ratio (β/α=8) was observed. Therefore it was concluded that the exchange process between α- and β-forms was fairly fast even at −50 °C. Although the ratios thus obtained contain large experimental error, the rate of equilibration ($\alpha \rightarrow \beta$) was roughly estimated to be ca. 10^{-2} s^{-1} at −50 °C by reversible first order approximations and $\Delta G^{\ddagger}_{223}$ was estimated to be about 14—15 kcal mol^{-1}(1 cal=4.184 J). Therefore the coalescence method was employed to determine the rate. A solution of **5b** in *o*-dichlorobenzene and DMSO-d_6 was heated until 170 °C in an NMR probe, but coalescence between two signals of the methyl (or chloromethyl) group was not observed. Free energy of activation ($\Delta G^{\ddagger}_{443}$) of the bond switch is calculated to be over 23 kcal mol^{-1} at 170 °C.

Accurate and detailed kinetic studies were carried out for a similar system **8** under neutral conditions

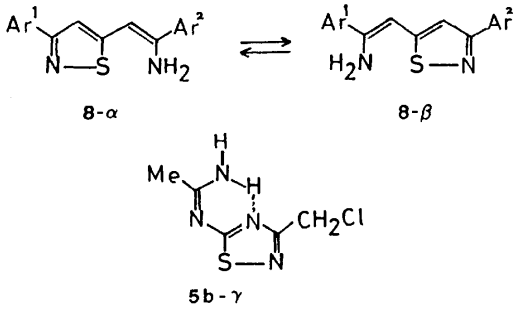

and kinetic parameters were obtained as $\Delta H^{\ddagger}$=12.2 kcal mol^{-1}, $\Delta S^{\ddagger}$=−41 eu, and $\Delta G^{\ddagger}$=24.4 kcal mol^{-1} (R^1=R^2=*p*-ClC_6H_4) (Eq. 4).[10a] The large negative value of activation entropy is characteristic and a much larger value is expected for **5**, because **5b**-γ is hydrogen-bonded intramolecularly in the ground state.[10b] Detailed discussion on the mechanism of the bond switch under neutral conditions was carried out for **8**.

Bond Switch under Acidic Conditions. When an acid was added to a solution of **5**, rate of bond switching was greatly accelerated and only one methyl signal could be observed at room temperature. Figure 2 shows that downfield shift of the methyl protons in **5a** takes place according to the amount of trifluoroacetic acid (TFA). Good linear relationship was observed until the added acid reached to one equiv to **5a**. When it exceeded one equiv, chemical shift of the methyl signal became constant even with large excess of TFA (6 equiv) or trifluoromethanesulfonic acid (13 equiv), indicating that only monoprotonation occurred and di- or polyprotonation did not. pK_a of **5a** was measured to be 4.87±0.02 by potentiometry, therefore the acidity of TFA (pK_a 0.23)[11] is high enough to protonate **5** stoichiometrically. The position of protonation will be discussed in a later section.

In order to determine the rate of equilibration under acidic conditions ^{1}H NMR of **5b** was measured in $CDCl_3$-DMSO-d_6 at low temperatures. By lowering the temperature two pairs of two singlets appeared again when a limited amount of TFA was added (Table 2). The fact that the signal split into two pairs indicates the bond switch between monoprotonated species [(**5b**-α-H^++**5b**-α)⇄(**5b**-β-H^++**5b**-β)] was to be observed. But in excess of TFA it was impossible to observe split because β/α ratio became large (> 15) according to the amount of TFA. Therefore in order to observe this exchange equilibration between protonated α- and β-forms, ^{1}H NMR of **5a** was measured. In the case of **5a**, protonated forms (**5a**-α-H^+⇄**5a**-β-H^+) are identical before and after the bond switch, therefore only two singlets were observed. After comparison of the experimental spectra with computer simulated ones,[12] the obtained rate constants were applied to the Eyring equation. In every case the spectra used to obtain one rate constant were measured at six to eight temperatures and the statistical errors of $\Delta H^{\ddagger}$ and $\Delta S^{\ddagger}$ were rendered very small by deliberate experiments. The activation free energy ($\Delta G^{\ddagger}$) and the rate were calculated from $\Delta H^{\ddagger}$ and $\Delta S^{\ddagger}$, and the $\Delta G^{\ddagger}$ was consistent with the value calculated from coalescence temperature (T_c) within 0.2 kcal mol^{-1}. In Table 3-A the effect of concentration of TFA is shown while that of **5a** is kept almost constant. Solubility of **5a** was much larger in CD_3OD and CD_3CN in comparison

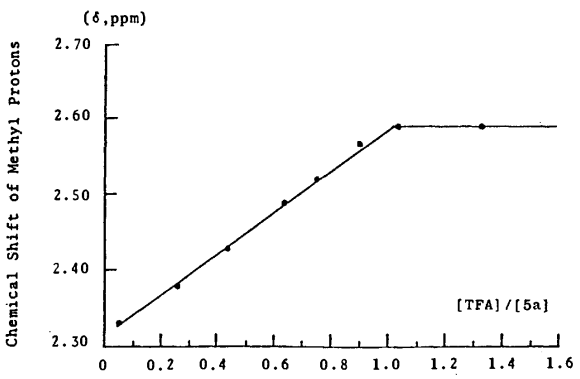

Fig. 2. Relation of chemical shift of methyl protons in **5a** and the amount of added TFA (CD_2Cl_2). [**5a**]=0.3—0.4 M.

Table 2. Low Temperature ^{1}H NMR Data of **5b** in the Presence of TFA[a,b]

TFA (equiv)	Temp °C	δ/ppm β	δ/ppm α	β/α
0	9	2.17, 4.61	2.49, 4.23	6
0.06	9	2.18, 4.63	2.48, 4.25	8
0.13	−17	2.21, 4.66	2.51, 4.27	9
0.31	−47	2.31, 4.73	2.51, 4.28	15
0.68	−47	2.48, 4.78		
1.02	−47	2.59, 4.78		
3.26	−47	2.59, 4.83		

a) $CDCl_3$-DMSO-d_6 as a solvent. b) The upfield signals are due to the methyl group and the downfield ones are assigned to methylene protons of the chloromethyl group.

with CD_2Cl_2 and so on, and in addition split widths ($\Delta\nu$) in polar solvents were larger than those in non-polar ones, therefore only CD_3OD and CD_3CN were used in the presence of more than one equiv of TFA. A remarkable point in Table 3-A was that the kinetic parameters in 1.23 equiv of TFA were considerably different from those in other cases. For example, free energy of activation ($\Delta G^{\ddagger}_{273}$) became larger from 13.5 (0.66 equiv) to 14.7 (1.23 equiv) kcal mol^{-1}, hence the rate (k_{273}) decreased considerably. So the effect of concentration of **5a** was studied with less than one equiv of TFA (Table 3-B) and it was clear that $\Delta G^{\ddagger}$ and the rate were dependent on the concentration. These facts imply that intermolecular process (ex. **5a**-α+**5a**-β-$H^+ \rightleftarrows$**5a**-α-H^++**5a**-β) played an important role for the bond switching in the presence of less than one equiv of TFA (Eq. 5). This intermolecular process cannot take part in the bond switching in the presence of more than one equiv of TFA. In fact both effects of concentration of **5a** and the ratio of the acid were not observed (Table 3-C). That is, $\Delta G^{\ddagger}_{273}$ was almost constant although split width ($\Delta\nu$) and coalescence temperature (T_c) changed with polarity of the solvent system. Evidently intramolecular reversible bond switching was observed under these conditions. Even when trifluoromethanesulfonic acid was used instead of TFA almost no change of kinetic parameters was observed. Therefore, the possibility that the equilibration proceeded through small amount of diprotonated intermediates can be ruled out. In CD_3CN different values of $\Delta H^{\ddagger}$ and $\Delta S^{\ddagger}$ were obtained probably due to the effect of solvation but $\Delta G^{\ddagger}$ was nealy equal to that in CD_3OD.

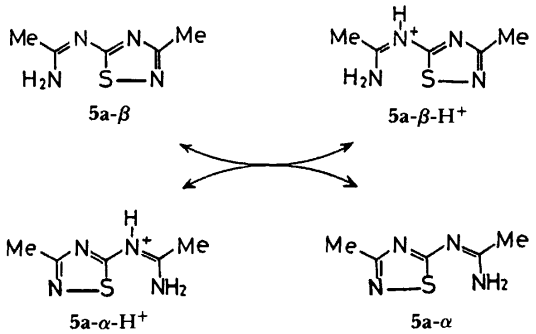

(5)

Position of Protonation and Mechanism of Bond Switching. There can be several types of monopro-

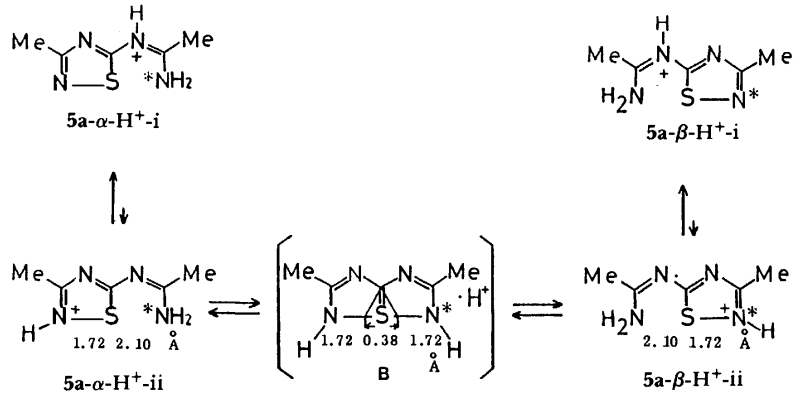

(6)

Table 3. Kinetic Parameters of the Ring Transformation of **5a**

	Run	Solv.	[5a]	[Acid][a)]/[5a]	$\Delta\nu$ / Hz	T_c / °C	$\Delta G^{\ddagger}_{273}$ / kcal mol^{-1}	$\Delta H^{\ddagger}$ / kcal mol^{-1}	$\Delta S^{\ddagger}$ / eu	k_{273} / s^{-1}
A	1	CD_2Cl_2	0.35	0.05	15.7	−29	13.5	4.3±0.4	−34±2	90
	2		0.29	0.28	10.1	−40	13.9	2.2±0.4	−43±2	43
	3	CD_3OD	0.43	0.06	16.9	−10	13.8	8.4±0.6	−20±2	55
	4		0.39	0.13	15.9	−13	13.6	8.7±1.2	−18±5	79
	5		0.39	0.48	11.3	−21	13.7	6.8±0.4	−25±2	63
	6		0.41	0.66	9.1	−25	13.5	7.8±1.1	−21±5	91
	7		0.39	1.23	4.4	−4	14.7	11.2±1.0	−13±4	11
B	8	CD_2Cl_2	0.08	0.21	11.8	−13	14.2	4.7±0.8	−35±3	27
	9	CD_3OD	0.71	0.13	15.9	−16	13.5	8.9±1.3	−17±5	91
	10		0.15	0.13	16.7	+13	14.4	8.7±1.0	−21±4	18
C	11	CD_3OD	0.37	1.9	4.7	−4	14.6	11.3±1.5	−12±6	11
	12		0.10	3.5	6.1	+6	14.9	11.7±0.9	−12±3	7
	13		0.43	6.5	3.7	−7	14.7	11.1±0.4	−13±2	10
	14		0.11	6.5	5.6	−1	14.7	11.8±1.0	−11±4	9
	15[a)]		0.11	12.8	9.5	+21	15.1	11.9±1.1	−12±4	5
	16	CD_3CN	0.09	6.0	11.9	+3	14.4	15.1±0.3	+3±1	19

a) TFA was used throughout Run 1 to 14 (60 MHz), 16 (90 MHz) and trifluoromethanesulfonic acid was used for Run 15 (90 MHz).

tonated species, we conclude the structure of monoprotonated species observed in solution is **5a**-α-H^+-i (≡**5a**-β-H^+-i) among them. ^{15}N NMR peaks in the presence of 1.42 equiv of TFA at −20 °C ($CDCl_3$-CD_3CN=3 : 1) appeared at δ 129.3 and 242.5 under complete proton decoupled conditions and the latter was observed as a singlet and the former as a triplet (J_{NH}=92 Hz) under nondecoupled conditions, respectively. This indicates that the protonation took place at the nitrogen of the amino group in the amidino group which is *not* labeled by ^{15}N. Basicity of both N(2) and N(4) of the thiadiazole ring is very much smaller than that of **5**,[13] thus monoprotonation at those cannot be the case. Thus the possibility of Eq. 7

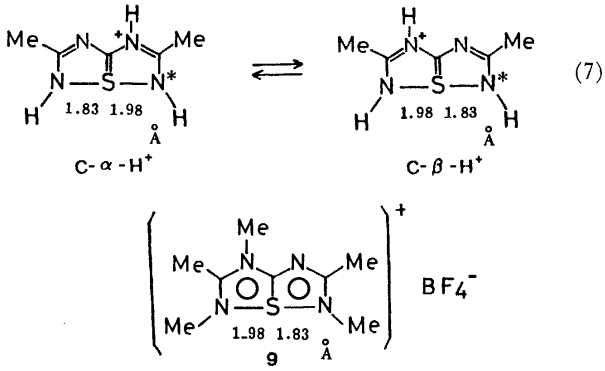

(7)

can be ruled out. But it is unlikely that **5a**-α-H^+-i is an appropriate precursor of the bond switch because of the much lowered nucleophilicity of the amidino group than **5a**. In contrast, **5a**-α-H^+-ii should be the precursor in the point that S-N bond in the thiadiazole ring is weakened by protonation at N(2) and the sulfur atom becomes highly susceptible to nucleophilic attack by the amino group. Kinetic data for the bond switching in Eq. 6 (Table 3-C) are summarized as $\Delta G^{\ddagger}_{273}$=14.8±0.2, $\Delta H^{\ddagger}$=11.6±1.0 kcal mol^{-1}, $\Delta S^{\ddagger}$=−12±3 eu, k_{273}=9 s^{-1}. The equilibrium ratio of (**5a**-α-H^+-i/**5a**-α-H^+-ii) is very difficult to estimate. It is not so unreasonable to assume that the ratio can be estimated by the difference between pK_a values in **5a** (4.87) and isothiazole (−0.51)[14] or 5-amino-3-phenyl-1,2,4-thiadiazole (1.4).[15] Thus the equilibrium ratio is estimated to be in the range of $10^{4.9-1.4}$ to $10^{4.9-(-0.5)}$. Then the real rate of the ring transformation should be in the range of $9\times10^{3.5}$ to $9\times10^{5.4}$ s^{-1} at 0 °C and the activation free energy ($\Delta G^{\ddagger}_{273}$) from **5a**-$\alpha$-$H^+$-ii to **5a**-$\beta$-$H^+$-ii is calculated to be from 8.0 to 10.3 kcal mol^{-1}. Such a low barrier of the bond switch can be attributed to the stability of the intermediate thiapentalenium salt **B** and also to the essential weakness of the hypervalent N-S^{IV}-N bond.

Total N-S^{IV}-N bond length of the intermediate (or transition state) **B** can be estimated based on the structure of thiapentalenium salt **9**, which was synthesized by us and the structure was determined by X-ray diffraction.[5,16] The N-S bond length in **5a**-α-H^+-ii can be estimated by the data for an isothiazolium salt to be 1.72 Å[17] then S-N bond length becomes 2.10 Å. It can be visualized that the central sulfur atom moves back and forth as a pendulum in the range of 0.38 Å nine times a second at 0 °C, that is, bond switching. This can be regarded as a model of reversible S_N2 reaction at the central sulfur (Eq. 6) and really is the first experimental evidence to show the presence of double minimum in energy in trithiapentalene analogous system, i.e., so called no-bond resonance compound.

Experimental

IR spectra were recorded on Hitachi EPI-G2 spectrometer. ^1H NMR spectra were obtained with Hitachi R-20B or R-24B spectrometer, and kinetic measurements were done mainly with JEOL FX-60 spectrometer. Partial measurement of kinetics in ^1H NMR and all work for ^{15}N NMR were carried out with JEOL FX-90Q and Hitachi R-90H spectrometer. All melting points were uncorrected.

Alternative Synthesis of 5-(1-Aminoethylideneamino)-3-phenyl-1,2,4-thiadiazole (5c). A mixture of 5-amino-3-phenyl-1,2,4-thiadiazole (**6b**) (480 mg, 2.7 mmol), anhydrous aluminum trichloride (414 mg, 3.1 mmol), and acetonitrile (0.18 ml, 3.5 mmol) was heated at 100 °C for 1 h, and it was poured into ca. 20 ml of aq HCl (0.5 M; 1 M=1 mol dm^{-3}) and the product was extracted with chloroform (50 ml×3). After drying ($MgSO_4$) and evaporation of the solvent, the residue was subjected to dry column chromatography to give 18% yield of **5c**, which was identical with the previously prepared compound from 5-amino-3-methyl-1,2,4-thiadiazole (**6a**) and benzonitrile by mp (148.0—148.7 °C), NMR and IR spectroscopy.[6]

5-(1-[^{15}N]Aminoethylideneamino)-3-methyl-1,2,4-thiadiazole (5a[^{15}N]). A mixture of 5-amino-3-methyl-1,2,4-thiadiazole (1.96 g, 17.0 mmol) and triethyl orthoacetate (8.01 g, 49.4 mmol) was heated at 110 °C for 16 h. After removal of the excess orthoacetate, the residue was distilled under reduced pressure to give 5-(1-ethoxyethylideneamino)-3-methyl-1,2,4-thiadiazole (**7**) as colorless liquid. Yield 3.00 g (95%); bp 70—71 °C/1 mmHg (1 mmHg≈133.322 Pa); ^1H NMR (CCl_4) δ=1.31 (t, 3 H, J=7 Hz), 2.11 (s, 3 H), 2.40 (s, 3 H), 4.20 (q, 2 H, J=7 Hz).

Aqueous ammonia (28%) (1.5 ml, 22.5 mmol) was added to a solution of **7** (1.02 g, 5.51 mmol) in 10 ml of ethanol at 0 °C, and the mixture was stirred for 3 h. After the solvent was evaporated the residue was recrystallized from benzene-hexane to give 701 mg (82%) of **5a**, which was identical with the previously synthesized compound by mp (109.5—111.5 °C), NMR and IR spectroscopy.[6]

To a solution of ammonium chloride (^{15}N 99% enriched, 105 mg, 1.93 mmol) in 5 ml of methanol a solution of potassium hydroxide (85%, 130 mg, 1.97 mmol) in 2 ml of methanol was added at 0 °C, and then **7** (346 mg, 1.87 mmol) was added to the mixture. After it was stirred for 5 h at room temperature, the solvent was evaporated and the residue was recrystallized from benzene-hexane to give 176 mg (60%) of **5a**[^{15}N]. Mp 108—110.5 °C. ^1H NMR ($CDCl_3$) δ=2.19 (s, 3H), 2.50 (s, 3H), 6.5 (bm, 2H). ^{15}N NMR ($CDCl_3$) δ=104.1 (t, J=91 Hz), 240.7 (s).

The Measurement of Bond Switching Equilibrium between 5b-α and 5b-β. About 10 to 15 mg of **5b** was dissolved in several solvents in an NMR sample tube (concen-

trations were kept almost the same (ca. 0.2 M)). The sample tube was cooled and the equilibrium ratio of the α- and β-isomers was measured from the peak area of both signals of the methyl protons and that of the methylene protons of the chloromethyl group. Integral ratios were measured four to six times for each condition and the average ratio was obtained. Thermodynamic parameters were calculated using the average ratios at five to six temperatures between 34 and −26 °C.

Low-Temperature ^{1}H NMR Measurement of 5b in the Presence of TFA. 34—38 mg of **5b** in $CDCl_3$ (510—600 mg) and DMSO-d_6 (199—234 mg) in the presence of the various amounts of TFA (0.06—3.26 equiv) were cooled to 9, −17, and −47 °C in an NMR tube and ^{1}H NMR were measured. Separation of peaks of methyl and chloromethyl groups could not be observed in the presence of more than 0.68 equiv of TFA.

Low-Temperature ^{1}H NMR Measurement of 5a in the Presence of TFA and Trifluoromethanesulfonic Acid. The chemical shift difference of the separated signals of the two methyl groups became constant at low temperatures (ca. −50—−60 °C) for each run in CD_3OD and CD_3CN and this constant value was employed as the line separation width without exchange ($\Delta\nu$). Computer calculation of all data were carried out using DNMR-3 program with Hitac 8700/8800 or Hitac M-200H computer in the University of Tokyo. The rate of exchange was determined by superimposing the simulated spectra on the observed ones.

This work was supported in part by a Grant-in-Aid for Scientific Research (No. 57430006) from the Ministry of Education, Science and Culture. We thank Prof. Naoki Inamoto for his helpful discussion and also wish to thank prof. Michinori Ōki for his kind permission to use the DNMR 3 program.

References

1) a) L. J. Adzima and J. C. Martin, *J. Org. Chem.*, **42**, 4001 (1977). b) For a review of hypervalent compounds: J. C. Martin, *Science*, **221**, 509 (1983).

2) a) C. T. Pederson, *Sulfur Reports*, **1**, 1 (1980); b) R. Gleiter and R. Gygax, *Top. Curr. Chem.*, **63**, 49 (1976); c) N. Lozac'h, *Adv. Heterocycl. Chem.*, **13**, 161 (1971).

3) a) H. Behringer and R. Wiedenmann, *Tetrahedron Lett.*, **1965**, 3705; b) G. Lang and J. Vialle, *Bull. Soc. Chim. Fr.*, **1967**, 2865; c) B. R. O'Connor and F. N. Jones, *J. Org. Chem.*, **35**, 2002 (1970); d) D. B. Easton, D. Leaver, and T. J. Rawlings, *J. Chem. Soc., Perkin Trans. 1*, **1972**, 41; e) J. E. Oliver and R. T. Brown, *J. Org. Chem.*, **39**, 2228 (1974); f) M. S. Chauhan, M. E. Hassan, and D. M. McKinnon, *Can. J. Chem.*, **52**, 1738 (1974); g) J. Goerdeler and H. W. Linden, *Tetrahedron Lett.*, **1975**, 3387; h) K-y. Akiba, M. Ochiumi, T. Tsuchiya, and N. Inamoto, *Tetrahedron Lett*, **1975**, 459; i) K-y. Akiba, T. Tsuchiya, and N. Inamoto, *Tetrahedron Lett.*, **1976**, 1877; j) K-y. Akiba, T. Tsuchiya, N. Inamoto, K. Yamada, H. Tanaka, and H. Kawazura, *Tetrahedron Lett.*, **1976**, 3819; k) G. L'abbe, *Tetrahedron*, **24**, 3537 (1982); l) A. F. Cuthbertson and C. Glidewell, *J. Mol. Struct.*, **90**, 227 (1982); m) Y. Yamamoto, T. Tsuchiya, M. Ochiumi, S. Arai, N. Inamoto, and K-y. Akiba, *Bull. Chem. Soc. Jpn.*, **62**, 211 (1989).

4) P. J. Pogorzelec and D. H. Reid, *J. Chem. Soc., Chem. Commun.*, **1983**, 289.

5) a) K-y. Akiba, S. Arai, T. Tsuchiya, Y. Yamamoto, and F. Iwasaki, *Angew. Chem., Int. Ed. Engl.*, **18**, 166 (1979); b) K-y. Akiba, S. Arai, and F. Iwasaki, *Tetrahedron Lett.*, **1978**, 4117.

6) K-y. Akiba, T. Kobayashi, and S. Arai, *J. Am. Chem. Soc.*, **101**, 5857 (1979).

7) Portions of this work have been communicated in preliminary form: Y. Yamamoto and K-y. Akiba, *J. Am. Chem. Soc.*, **106**, 2713 (1984).

8) J. Goerdeler, *Chem. Ber.*, **87**, 57 (1954).

9) a) G. C. Levy and R. L. Lichter, "Nitrogen-15 Nuclear Magnetic Resonance Spectroscopy," John Wiley & Sons, New York (1979); b) Chemical shift data (δ/ppm) in ^{15}N NMR: isothiazole 298.4; aniline 56.5; N (1) in tetramethyl-2-phenylguanidine 55.0. c) K-y. Akiba, S. Arai, N. Inamoto, K. Yamada, H. Tanaka, and H. Kawazura, *Chem. Lett.*, **1978**, 1415.

10) a) K-y. Akiba, K. Kashiwagi, Y. Ohyama, Y. Yamamoto, and K. Ohkata, *J. Am. Chem. Soc.*, **107**, 2721 (1985); b) F. Iwasaki and K-y. Akiba, *Acta Crystallogr., Sect. B*, **37**, 185 (1981).

11) A. L. Henno and C. J. Fox, *J. Am. Chem. Soc.*, **73**, 2323 (1951).

12) Computer simulations were carried out by using a DNMR-3 program with a Hitac M-200H computer.

13) R. Zahradnik and J. Koutecky, *Collect. Czechoslov. Chem. Commun.*, **26**, 156 (1961).

14) K. R. H. Wooldridge, *Adv. Heterocycl. Chem.*, **14**, 16 (1973).

15) J. Goerdeler and A. Fincke, *Chem. Ber.*, **89**, 1033 (1956).

16) Y. Yamamoto and K-y. Akiba, *Heterocycles*, **13**, 297 (1979).

17) A. Hordvik and K. Julsham, *Acta Chem. Scand.*, **26**, 343 (1972).

 © 1989 The Chemical Society of Japan Bull. Chem. Soc. Jpn., 62, 485—489 (1989)

Reactivities of Stable Rotamers. XXV. Deprotonation at the 9-Position of 9-(2-Substituted 1-naphthyl)fluorene Rotamers with Butyllithium[1,2]

Kazuhiro MORIYAMA, Mikio NAKAMURA, Nobuo NAKAMURA, and Michinori ŌKI*,†
Department of Chemistry, Faculty of Science, The University of Tokyo, Bunkyo-ku, Tokyo 113
(Received August 15, 1988)

Deprotonation of 9-(2-substituted 1-naphthyl)fluorene rotamers, where the substituent is a dimethylamino, a methoxy, or a methylthio, has been carried out with butyllithium in hexane-benzene. While the reactions of the *ap*-isomers were generally slower than those of the *sp*-isomers, the difference in the methoxy compounds was the greatest among the compounds examined. The results are discussed on the basis of the ease of ligation of the substituent and the steric effects that prevail in the *ap*-isomers, together with the distance between 9-position and the ligation site in the subsituent.

Since the successful isolation of stable rotamers at room temperature,[3] we have been interested in reactivities of rotamers and have been able to show some interesting differences in their reactivities.[4] Among those examined so far, the difference in the rates of deprotonation of 9-(2-methoxy-1-naphthyl)fluorene rotamers (**1**: X=O) was one of the greatest.[2] We have thus been interested to explore further to understand the reactivity differences of these rotamers and have carried out the similar reactions of 9-(2-substituted 1-naphthyl)fluorene (**1**) rotamers where X is NCH_3, O, or S. This paper is to report the results and to discuss the interesting differences observed in the investigation.

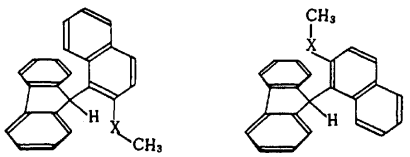

sp-1 *ap*-1

The syntheses of the dimethylamino compound (**1**: X=CH_3N) and the methoxy compound (**1**: X=O) were already reported.[5,6] The methylthio compound (**1**: X=S) was synthesized in the following way. 1-Bromo-2-methylthionaphthalene (**2**) was lithiated with butyllithium and was treated with 9-fluorenone to afford a mixture of *ap*- and *sp*-9-(2-methylthio-1-naphthyl)-9-fluorenol (**3**) which was reduced with hydriodic acid to give the desired compound (**1**: X=S). The rotamers were separated by chromatography on silica gel.

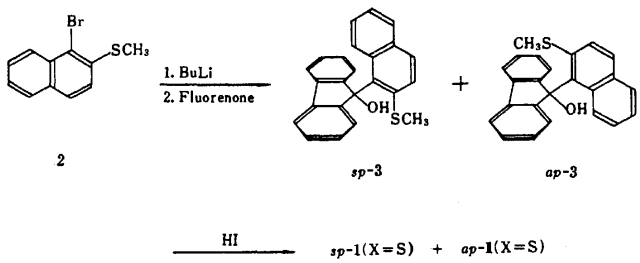

2 *sp*-3 *ap*-3

† Present address: Department of Chemistry, Faculty of Science, Okayama University of Science, Ridaicho, Okayama 700.

The barriers to isomerization of the dimethylamino and the methoxy compounds have been reported.[5,6] The barrier to rotation of the methylthio compound was determined. It was 29.6 kcal mol^{-1} (1 cal=4.184 J) for the *ap*→*sp* process and 31.0 kcal mol^{-1} for the reverse process at 101 °C. The equilibrium constant, *sp*/*ap*, was 7.31 at the same temperature. Calculation of the rate constants of isomerization was carried out by assuming that the entropy of activation was zero[6,7] to find that the rates of deprotonation described below were larger than the rates of isomerization by a factor of more than 100 if the deprotonation was carried out at 34 °C in the cases of the dimethylamino and the methylthio compounds. However, the rates of deprotonation of the methoxy compound were only 5 times faster than those of isomerization from the *ap*-form to the *sp* at the same temperature.

We had to compromise, between the isomerization and the deprotonation, and decided to run the reaction with butyllithium in hexane-benzene at low temperatures where the contamination by the other rotamer, that might be formed by rotation under the reaction conditions, was minimal and the reaction rates were large enough for the conventional measurements. Because of the technical reasons, the reactions of the *ap*-forms were generally carried out only at 34 °C and the rates of the reactions were followed by the NMR integration, whereas those of the *sp*-forms below 40 °C and followed by mass spectra after decomposition of the lithiated product with trifluoroacetic acid-*d*. Therefore the rates of the reaction were compared by calculation of those of the *sp*-isomers with the use of kinetic parameters obtained from the results at low temperatures. The kinetics apparently followed the pseudo-first-order rate law in the substrate for both rotamers of **1**. The results are shown in Table 1, in which the second-order rate constants were compared with those of 9-(2-methyl-1-naphthyl)fluorene rotamers[8] that do not carry heteroatoms in the substituent.

The results indicate that the reaction rates are enhanced when a heteroatom is introduced to the 1-substituent of the naphthalene nucleus. It is well known that butyllithium forms a hexamer in hydro-

Table 1. Second-Order Rate Consants ($\times 10^5/s^{-1}$ mol^{-1} L) of Lithiation of **1** at 34.0 °C

2-Substituent	$N(CH_3)_2$	OCH_3	SCH_3	CH_3[a]
sp	34.2	1090	13.1	0.14
ap	27.8	2.73	4.68	1.0

a) At 42 °C.[8] Due to the change in precedence of the substituent in the sequence rule, that shown in the line of *sp* is actually the *ap* form and vice versa. This arrangement is taken for the convenience of the comparison.

carbon solvents.[9] Therefore, butyllithium is a very bulky reagent under the reaction conditions unless some assistance for deaggregation by the substrate is not available. We conclude therefore that the heteroatom in the substituent acts to deaggregate butyllithium in this instance as in the cases of solvents with heteroatoms.[10]

The enhancement is larger in the *sp* forms than in the *ap* forms. This might be attributed to the fact that in the ligated form of the *ap* (oversimplified as *ap*-**4**) the distance between the butyllithium and the 9-H is too far for the deprotonation to occur directly, whereas the direct deprotonation from the ligated form of *sp*, which is also shown by an oversimplified form (*sp*-**4**), is possible.

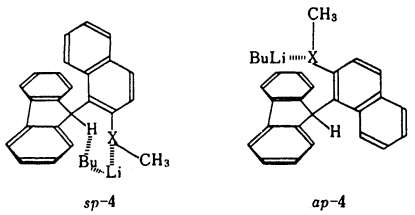

sp-4 *ap*-4

However, the enhancement is not very remarkable for both *ap* and *sp* forms of the compounds examined here, an only exception being *sp*-**1** (X=O). When one compares the rates of the reactions of *ap*-forms, the largest enhancement is seen in the nitrogen compound (*ap*-**1**: X=NCH_3) but the enhancement in the oxygen and the sulfur compounds is only a factor of ca. 5 relative to the compound which carries no heteroatoms, *sp*-9-(2-methyl-1-naphthyl)fluorene. This will mean that the deaggregation due to ligation of the heteroatom in the substituent in the *ap*-form is not efficient in the enhancement of the reaction rates.

To make a sharp contrast, the enhancement of the rates was distinct in the *sp*-isomers, the smallest case, sulfur, giving the enhancement of a factor of ca. 100, when one compares the rates with that of the methyl compound. Especially large is the enhancement by the oxygen-substituent, the factor being ca. 10^4.

We should like to attribute the results both to the steric effects that become operative on ligation of the heteroatom to the lithium cation and the ability of the heteroatom to ligate to the lithium. Although the amino-nitrogen is known to be the best ligating heteroatom to the lithium cation,[11] if the ligation takes place to the amino-nitrogen in compound **1** (X=NCH_3) the steric effects will be great even in the *sp*-form (*sp*-**4**): since alkyllithium is known to be largely covalent,[12] the butyl group will accompany the lithium atom in every case and the situation will not change to a large extent even when the ligation of the heteroatom takes place.[13] We believe that the stable conformation of the dimethylamino group in *sp*-**1** (X=NCH_3) is such that the lone-pair electrons of the nitrogen atom directs to the 9-H to minimize the steric effects and probably due to the presence of a weak hydrogen bond between the 9-CH of the fluorene and the heteroatom in the 2-substituent of the naphthalene.[15] However this conformation is no longer stable if the amino-nitrogen ligates to the lithium cation because of the accompanying steric effects.

By contrast, the oxygen and the sulfur atom have two pairs of unshared electrons, one of which can be used to ligate to the lithium cation without causing too much steric hindrance in these cases. The largest enhancement by the oxygen-substituent in the *sp* must be attributed to this effect. The sulfur atom is known to be a weakly ligating atom to the lithium cation.[16] The results observed here are derived by this nature together with the factor that the sulfur atom has two pairs of the unshared electrons.

Coming back to the data of *ap*-isomers, we still see the effect of the ligating atom: the amino compound gives the largest rate constant for the lithiation. It is also interesting to note that, while the *ap*-rotamers of 9-(2-dimethylaminomethyl-, methoxymethyl-, or methylthiomethyl-1-naphthyl)fluorene, which has one extra methylene group inserted between the 1-naphthyl-carbon and the heteroatom of **1**, exhibit reaction rates that obey second-order rate law,[14] the *ap*-forms of **1** all exhibit practically pseudo-first-order rates. The difference in the reaction conditions between the present case and that reported is the concentrations of the substrates: in the earlier paper, concentrations were higher than those used in this work by ca. 10. These suggest that the rates of the reactions we observe might involve both the second-order and the first-order ones. Thus we carried out the study on the effects of concentration of the substrate on the methoxy compound (*ap*-**1**: X=O).

The results shown in Table 2 indicate that there is indeed the effects of concentration observed: the higher concentration enhances the lithiation rates. However,

Table 2. The Effect of Concentration on the Apparent Pseudo-First-Order Rate Constants of Lithiation of *ap*-**1** (X=O) at 34 °C

Concentration/10^{-3} mol L^{-1}	Rate const/10^{-5} s^{-1}
6.34	2.48
12.7	2.62
31.3	3.11

there is one thing we have to take into account before discussing the data in Table 2. That is, the rates of rotation of the methoxy compound (**1** : X=O) are large enough, so that we cannot neglect the contribution of isomerization by rotation, especially at 40 °C.

We assumed that the rates of rotation under the reaction conditions were equal to those without the added butyllithium. Then the rates of isomerization can be calculated by the activation parameters reported previously.[6] Fortunately the rates of reaction of the *sp*-form, which was formed by isomerization, was large enough to assume that it reacted instantaneously to form the lithiated compound under the conditions. Then we can write the following equation for the decrease in the amount of the *ap*-form.

$$k_{obs} = k_{ap} + k_{iso} \quad (1)$$

where k_{ap} is the rate constant of lithiation of *ap*-**1** (X=O) and k_{iso} the rate of isomerization. Using these assumptions, we obtain the rates of lithiation of *ap*-**1** (X=O) as shown in Table 3. This kind of consideration will not be necessary for the compounds, in which X=$N(CH_3)_2$ or S, because their barrier to rotation is higher than the oxygen compound.

$$k_{obs} = k_1 + k_{iso} + k_2[ap\text{-}\mathbf{1}] \quad (2)$$

Then using the data in Tables 2 and 3 together with Eq. 2, we obtain k_2 as 2.55×10^{-4} s^{-1} $L\,mol^{-1}$. Thus, whereas the contribution of the second-order reaction at the concentration of 6.34×10^{-3} mol L^{-1} is only 6.5%, that at the concentration of 31.3×10^{-3} mol L^{-1} is 26%. It is clear that at the concentration reported previously (0.31 mol L^{-1}) the contribution of the first-order reaction is very minor.

Although detailed discussion of the reaction rates of the *ap* forms is precluded because of various unknown factors, we believe the first-order rate constant of the methoxy compound is significantly larger than that of the hydrocarbon. Probably this is caused by the fact that the methoxyl group is smaller than the methyl group to make the access of the deprotonation reagent to the 9-H easier by rotation of the naphthyl group.

The largest rates of the reaction of the dimethylamino compound in the *ap* series may involve factors of the most favorable ligation of the amino-nitrogen, the steric effects on ligation, and unassisted deprotonation. The detailed discussion of the factors is not possible at present.

Table 3. Observed Rate Constants, Calculated Isomerization Rate Constants, and True Rates of Lithiation of Compound **1** (X=O) at 34 °C

Temp/°C	$k_{obs}/s^{-1}(\times10^5)$	k_{iso}/s^{-1} $(\times10^5)$	$k_1/s^{-1}(\times10^5)$
20	0.607	0.192	0.415
26	1.14	0.429	0.710
34	2.48	1.19	1.29
40	4.40	2.48	1.92

a) For the definition of k_1 and k_{iso}, see text.

Table 4. Apparent Pseudo-First-Order Rate Constants $(\times10^5/s^{-1})$ of Lithiation of **1**

Form	Substituent	Rate constants(Temp/°C)
sp	$N(CH_3)_2$	3.07 (0.0), 6.88 (10.0), 9.22 (15.0), 12.7 (20.0)
sp	OCH_3	5.67 (−18.0), 9.04 (−14.0), 13.7 (−10.0), 25.1 (−5.0)
ap	OCH_3	0.607 (20.0), 1.14 (26.0), 2.48 (34.0), 4.40 (40.0)
sp	SCH_3	1.85 (10.0), 4.36 (20.0), 9.18 (30.0), 17.7 (40.0)

Table 5. Activation Parameters for the Lithiation of **1**

Form	Substituent	ΔH^*/kcal mol^{-1}	ΔS^*/cal mol^{-1} K^{-1}
sp	$N(CH_3)_2$	10.8±0.5	−39.3±1.8
sp	OCH_3	14.9±1.7	−18.9±6.4
ap	OCH_3	13.3±1.9	−37.7±6.2
sp	SCH_3	12.7±1.2	−35.2±3.9

The products obtained after protonation of the lithiated compounds were *sp*-**1** in all the cases examined. We believe this is caused by the fact that the lithium compound obtained from the *sp* form is stabilized by ligation of the heteroatom in the substituent. The protonation of organolithium compounds is known to proceed with retention of stereochemistry,[17] there must be reasons for the isomerization of *ap*-**1** to *sp*-**1**. We believe that, in the *ap*-form, the initially formed lithium compound may be *ap* as well but, due to the fact that a larger substituent in the 9-position of the 9-arylfluorenes reduces the barrier height,[18] the rotation about the C_9(fluorene)-to-C_1(naphthalene) bond becomes easier and thermodynamically stable form is taken.

Experimental

Materials. 9-(2-Methoxy-1-naphthyl)fluorene rotamers were prepared according to the method described previously[6] with a minor modification. Since the method described earlier gives *ap*-isomer as a minor product which isomerizes easily at room temperature, the purification of this form is rather tedious. We thus prepared *ap*-**1** (X=O) by treating the corresponding phenol as described below. 9-(2-Dimethylamino-1-naphthyl)fluorene rotamers (**1**: X=NCH_3) were prepared by the method described in the literature.[5]

***ap*-9-(2-Methoxy-1-naphthyl)fluorene [*ap*-1 (X=O)].** To a solution of 2.0 g (6.5 mmol) of *ap*-1-(9-fluorenyl)-2-naphthol[6] in 100 mL of ether was added 4.3 mL (6.5 mmol) of a ca. 15% solution of butyllithium in hexane at −78 °C under a nitrogen atmosphere. After addition of 1.0 mL (8.8 mmol) of methyl trifluoromethanesulfonate, the mixture was warmed up to room temperature, and was stirred for 30 min. The mixture was poured into water. The ether layer was separated and the aqueous layer was extracted with ether. The combined ether solution was dried over magnesium sulfate. Evaporation of the solvent gave a crude product of which recrystallization from hexane-dichloromethane afforded 1.5

g (72%) of the desired product.[6] ^{1}H NMR ($CDCl_3$) δ=3.00 (3H, s), 5.81 (1H, s), 6.9—7.9 (13H, m), 8.3—8.5 (1H, m).

9-(2-Methylthio-1-naphthyl)fluoren-9-ol (3). To a solution of 10 g (40 mmol) of 1-bromo-2-methylthionaphthalene[19] in 300 mL of dry benzene was added 27 mL (41 mmol) of a ca. 15% hexane solution of butyllithium at ca. 0 °C under a nitrogen atmosphere. After stirring for 4 h at room temperature, 7.2 g (40 mmol) of 9-fluorenone was added rapidly. The mixture was refluxed for 4 h, cooled to room temperature, and treated with ca. 5% hydrochloric acid. The ether layer was separated and the aqueous layer was extracted with ether. The combined ether solution was dried over magnesium sulfate and filtered. After evaporation of the solvent from the filtrate, the residue was chromatographed on silica gel with 4 : 1 hexane-dichloromethane eluent to give 13 g (93%) of the desired product which consisted of the *sp* and the *ap* rotamers in 10 : 1 ratio. This product was used directly for the next reaction. The following ^{1}H NMR data ($CDCl_3$, δ) were collected: *sp* 2.72 (3H, s), 6.7—8.8 (14H, m); *ap* 1.89 (3H, s), 9.5—9.7 (1H, m).

9-(2-Methylthio-1-naphthyl)fluorene (1: X=S). A mixture of 10 g (28 mmol) of the product obtained above in 1 L of acetic acid and 100 mL of ca. 57% hydriodic acid was stirred for 30 min at room temperature and then poured into water. The mixture was extracted with ether and the combined ether solution was washed with aqueous sodium hydrogensulfite and then with aqueous sodium hydrogencarbonate. After drying over magnesium sulfate, the solvent was evaporated and the residue was submitted to chromatography on silica gel. Elution with hexane afforded 2.7 g (28%) of the *sp* rotamer which was purified by recrystallization from acetonitrile and then that with 10 : 1 hexane-dichloromethane did 4.0 g (42%) of the *ap* rotamer which was also purified by recrystallization from acetonitrile.

ap-**1** (X=S), mp 158.5—159.5 °C. Found: C, 85.47; H, 5.43; S, 9.60%. Calcd for $C_{24}H_{18}S$: C, 85.17; H, 5.36; S, 9.47%. ^{1}H NMR ($CDCl_3$) δ=1.91 (3H, s), 6.06 (1H, s), 7.0—7.9 (13H, m), 8.3—8.5 (1H, m).

sp-**1** (X=S), mp 145.5—146.0 °C. Found: 84.99; H, 5.36; S, 9.54%. Calcd for $C_{24}H_{18}S$: C, 85.17; H, 5.36; S, 9.47%. ^{1}H NMR ($CDCl_3$) δ=2.70 (3H, s), 6.52 (1H, s), 6.3—8.0 (14H, m).

Determination of Barriers to Rotation. *ap*-**1** (X=S) which was the unfavorable rotamer at equilibrium was dissolved in toluene-d_8 (30 mg of the sample in 0.4 mL of the solvent) and the solution was placed in an NMR sample tube. The tube was heated in a boiling water bath and the decrease in the starting material and the increase in *sp*-**1** (X=S) were determined by integration of the respective NMR signals with a Varian EM 390 spectrometer. The equilibrium constant was obtained after 96 h heating. The rate constant was obtained by assuming reversible unimolecular reactions.

Kinetic Study of Lithiation. A solution of ca. 0.03 mmol of an *sp*-rotamer in 2.0 mL of benzene was prepared as a stock solution. Eight portions of 0.2 mL each of the stock solution were placed in small tubes and frozen at −78 °C under a nitrogen atmosphere. To the sample solutions, 0.3 mL each of ca. 15% hexane solution of butyllithium was added. The mixture was immersed in a thermostatted bath and the rates of the reaction were determined by quenching the sample solution at an appropriate time interval with 0.1 mL of trifluoroacetic acid-*d* in 1 mL of toluene at −78 °C. The ratios of the 9-deuterio compound to the 9-protio compound were determined by the intensities of the molecular ion peaks in the mass spectra. Correction for the natural abundance of isotopes that give [M^+ +1] peaks was made according to the literature.[20] The results are shown in Table 4. *ap*-**1** (X=O) was treated similarly.

Table 4 shows the calculated activation parameters from the second-order rate constants. Entropies of activation are very large negative in every case to indicate that the reaction has the nature that the freedom of the substrates is restricted in the transition state.

For the determination of the rates of lithiation of the *ap* isomers, intensities of the proton signals in NMR spectra were used. A solution of 44 mmol (0.13 mmol) of the sample in 0.2 mL of benzene-d_6 was placed in an NMR sample tube and frozen at −78 °C under a nitrogen atmosphere. After addition of 0.3 mL of ca. 15% solution of butyllithium in hexane, the mixture was warmed with stirring to make a homogeneous solution and kept at 34 °C. It is known that, when lithiation takes place, the proton signals due to 4-H and 5-H of the fluorene ring appears at δ 8.0—8.3 and that at δ 8.2—8.5 due to 8-H of the naphthalene ring in the *ap* series disappears.[14] The intensities of these signals as well as those due to the 9-H of the fluorene ring could be directly used for the determination of the rates in the cases of the *sp*-isomers. For the *ap*-isomers, initial concentration of the substrate was calculated by dividing the sum of intensities of signals at δ 8.0—8.5 and at δ ca. 6 by 2. The amount of the lithiated compound was calculated by subtracting the intensity of the signal at δ ca. 6 from that at δ 8.0—8.5 and dividing the difference by 2. The results are shown in Table 1.

The quantity of the butyllithium in the solution was calculated from the signal intensity due to the α-protons of butyllithium. It was ca. 0.9 mol L^{-1}. This confirms that the pseudo-first-order conditions are satisfied.

The ^{1}H NMR spectra were obtained with a Varian EM 390 spectrophotometer and the mass spectra on a JEOL D300.

This work was supported by a Grant-in-Aid for Fundamental Scientific Research (62124035) of the Ministry of Education, Science and Culture.

References

1) For Part 24, see M. Ōki, T. Tanuma, Y. Tanaka, and G. Yamamoto, *Bull. Chem. Soc. Jpn.*, **61**, 4309 (1988).

2) A preliminary report has been published: M. Nakamura and M. Ōki, *Chem. Lett.*, **1975**, 671.

3) M. Ōki, *Angew. Chem., Int. Ed. Engl.*, **15**, 87 (1976); *Top. Stereochem.*, **14**, 1 (1983).

4) M. Ōki, *Acc. Chem. Res.*, **17**, 154 (1984).

5) K. Moriyama, M. Nakamura, N. Nakamura, and M. Ōki, *Gazz. Chim. Ital.*, **117**, 655 (1987).

6) M. Nakamura and M. Ōki, *Bull. Chem. Soc. Jpn.*, **53**, 3248 (1980).

7) R. Saito and M. Ōki, *Bull. Chem. Soc. Jpn.*, **55**, 2508 (1982).

8) M. Nakamura, N. Nakamura, and M. Ōki, *Bull. Chem. Soc. Jpn.*, **50**, 1097 (1977).

9) D. Margerison and J. P. Newport, *Trans. Faraday Soc.*, **59**, 2058 (1963).

10) T. L. Brown, *Adv. Organomet. Chem.*, **3**, 365 (1966).

11) W. X. Xu and J. Smid, *J. Am. Chem. Soc.*, **106**, 3790

(1984).

12) R. B. Bates and C. A. Ogle, "Carbanion Chemistry," Springer-Verlag, Berlin (1983), pp. 3, 4.

13) We have discussed that on ligation of a Lewis base to organolithiums the C-Li bond may be lengthened and the ionic character of the bond may increase.[14] At the extreme case of the ligation, the bond will be ionic. However, the discussion presented here holds in those cases as well, because the carbanion will form an intimate ion pair which is as bulky as the covalent species.

14) M. Nakamura, Y. Suzuki, and M. Ōki, *Bull. Chem. Soc. Jpn.*, **58**, 2370 (1985).

15) We have noticed that in various rotational isomers of the 9-arylfluorene series those (*sp*) which carry a heteroatom in proximity of the 9-H of the fluorene ring very easily discolor on standing, whereas such phenomenon is not observed in the *ap*. This phenomenon is most easily explained if one assumes the presence of the hydrogen bond between the 9-CH, which is acidic, and the heteroatom in the substituent of the aryl group, because the interaction will facilitate the oxidation at the 9-position of the fluorene ring.

16) T. L. Ho, "Hard Soft Acids and Bases Principle in Organic Chemistry," Academic Press, New York (1977).

17) D. Y. Curtin and W. J. Koehl, Jr., *J. Am. Chem. Soc.*, **84**, 1967 (1962).

18) E. A. Chandross and C. F. Sheley, *J. Am. Chem. Soc.*, **90**, 4345 (1968); K. Albert and A. Rieker, *Chem. Ber.*, **110**, 1804 (1977).

19) D. L. Tuleen and D. N. Buchanan, *J. Org. Chem.*, **32**, 495 (1967).

20) K. Biemann, "Mass Spectrometry," McGraw-Hill, New York (1962), p. 204.

Stereoselective Syntheses of 2-Deoxy-β-*C*-arabino- and ribopyranosides: 2-Deoxy-β-arabino- and ribopyranosyl Cyanides

Kuniaki TATSUTA,* Jun HAYAKAWA, and Yukio TATSUZAWA
Department of Applied Chemistry, Faculty of Science and Technology, Keio University, Hiyoshi, Kohoku, Yokohama 223
(Received August 17, 1988)

2-Deoxy-β-arabino- and ribopyranosyl cyanides, which should be suitable for the syntheses of biologically active products, were stereoselectively prepared from the reaction of the enones, 1,5-anhydro-2-deoxy-*erythro*-hex-1-en-3-ulose derivatives, with acetone cyanohydrin, followed by the stereoselective reduction of the producing ketones with $NaBH_4$-$CeCl_3 \cdot 7H_2O$ and L-Selectride, respectively.

The C-C bond formation at the anomeric center of carbohydrates has become an increasingly important area in synthetic oraganic chemistry. In particular, a wide variety of medicinally imporatant *C*-nucleosides[1] have been discovered as well as several *C*-glycosyl flavonoids[2] and other structurally diverse *C*-glycosides.[3] Although a lot of stereoselective routes exist for *C*-glycopyranosides,[4] little synthetic strategies have been reported for 2-deoxy-*C*-glycosides.[5] Efficient and stereocontrolled methods for the 2-deoxy-*C*-glycosidation remain an imporatant synthetic objective, not only for the preparation of biologically active 2-deoxy-*C*-glycosides including antiviral[6] *C*-nucleosides but also for the homologation of carbohydrates to serve as chiral sources for other synthetic targets.

As part of an ongoing program in these and related areas, we wish to report the stereoselective syntheses of 2-deoxy-β-*C*-glycopyranosides: 2-deoxy-β-*C*-arabino- and ribopyranosyl cyanides by using acetone cyanohydrin, which is a tractable and inexpensive reagent.

Our strategy is based on the following considerations: i) the 1,4-addition of the cyanide ion[7] to the anomeric position of such enones as **1** and **8** in basic conditions to give thermodynamically the β-glycosyl cyanides; ii) the stereoselective reduction of the producing ketones such as **2** and **9** by $NaBH_4$-$CeCl_3 \cdot 7H_2O$[8] and bulky L-Selectride to give predominantly the arabino- and ribopyranosides, respectively, because of the significant influence of the C-4 substituent and the ring oxygen atom.[9]

Thus, reaction of acetone cyanohydrin[7] with the conjugated enone, 4-*O*-acetyl-1,5-anhydro-2,6-dideoxy-L-*erythro*-hex-1-en-3-ulose[10] (**1**) was best realized by using *N*,*N*-diisopropylethylamine as a catalytic base in acetonitrile to afford the intermediary 1,4-adduct **2**, which in turn was exclusively converted into the 2-deoxy-β-*C*-glycosides **3** and **4**. The 1,4-addition was also done by use of Na_2CO_3 as a catalyst in aqueous acetonitrile, but in a lower yield.

The keto cyanide **2** was submitted to the hydride reduction with $NaBH_4$ in the presence of $CeCl_3 \cdot 7H_2O$ in methanol, followed by acetylation to give predominantly 3,4-di-*O*-acetyl-2,6-dideoxy-β-L-arabinopyranosyl cyanide (**3**) in a 64% yield with the corresponding β-L-ribopyranosyl cyanide (**4**) in a 15% yield. The borohydride reduction without $CeCl_3$ gave a mixture of **3** and **4** in 23% and 22% yields without stereoselectivity. These selectivities suggested that $CeCl_3$ decreased the participation of the ring oxygen atom[9] and, relatively, $NaBH_4$ could approach to the C-3 carbonyl group from the same site of the C-4 acetoxyl group by the interaction.

In the transformation, other hydride reagents [$LiBH_4$, $Zn(BH_4)_2$, $LiBHEt_3$, $NaBH_3CN$, Bu_4NBH_4, Me_4NBH_4, $Me_4NBH(OAc)_3$, Red-Al, DIBAL, and $LiAlH_4$] were assayed in several solvents (MeOH, ether, THF, and dichloromethane), but they gave **3** and **4** in lower yields.

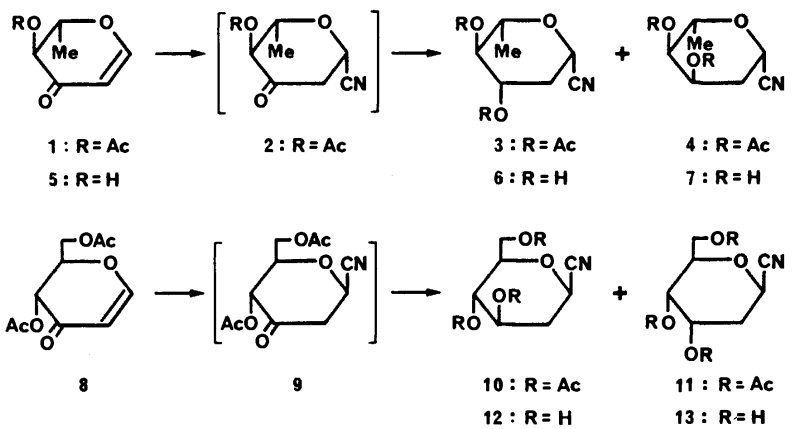

However, remarkably, the L-Selectride reduction in THF resulted the predominant formation of the ribopyranoside **4** in a 59% yield with only a 6% yield of the arabinopyranoside **3**. This result was reasonably supported by the consideration that the approach of the bulky hydride reagent to the C-3 carbonyl group would be restricted to the opposite site of the C-4 acetoxyl group by the steric hindrance as well as the aid of the ring oxygen atom[9] to give exclusively the cis-3,4-diol **4**.

The corresponding α-glycosyl cyanides were not recognized as detectable amounts in the aforesaid reactions.

The de-*O*-acetylated enone **5** was treated with the similar manner through borohydride reductions, but it gave **3** and **4** only in very low yields after acetylation.

The compounds **3** and **4** were de-*O*-acetylated by 7% methanolic ammonia solution to 2,6-dideoxy-β-L-arabino- and ribopyranosyl cyanides (**6** and **7**) in 95% and 87% yields, respectively, while the deacetylation with MeONa occurred in moderate yields.

When 4,6-di-*O*-acetyl-1,5-anhydro-2-deoxy-D-*erythro*-hex-1-en-3-ulose[10] (**8**) was used for the aforesaid addition, the corresponding products, 3,4,6-tri-*O*-acetyl-2-deoxy-β-D-arabino-and β-D-ribopyranosyl cyanides (**10** and **11**) were provided in almost same yields as described above, after borohydride reduction and acetylation. Namely, through the $NaBH_4$-$CeCl_3$ reduction, **10** and **11** were produced in 60% and 20% yields, while, through the L-Selectride reduction, **10** and **11** were in 4% and 60% yields.

Both compounds **10** and **11** were similarly de-*O*-acetylated to **12** and **13** in high yields, respectively. The latter compound **13** was slightly labile even on keeping in a refrigerator.

In conclusion, an efficient and stereoselective preparation of 2-deoxy-β-*C*-glycosides: 2-deoxy-β-arabino- and ribopyranosyl cyanides has been developed, starting from 1,5-anhydro-2-deoxy-*erythro*-hex-1-en-3-ulose derivatives (**1** and **8**) by using the addition of acetone cyanohydrin followed by borohydride reduction.

Experimental

Melting points were determined on a micro hot-stage Yanaco MP-S3 and were uncorrected. Optical rotations were measured with a JASCO DIP-360 photoelectric polarimeter in chloroform and methanol. IR spectra were recorded on a Hitachi Perkin-Elmer 225 spectrometer, and ^{1}H NMR spectra on a JEOL GX-400 spectrometer in $CDCl_3$ and CD_3OD using TMS as internal standard. Mass spectra were measured with a Hitachi M-80 mass spectrometer. TLC was carried out on Merck TLC plates (60F-254, 0.25 mm). Column chromatography was performed on silica gel, Merck Kieselgel 60. In general, organic solvents were purified and dried by the appropriate procedures, and evaporation was carried out under reduced pressure below 35 °C.

The starting materials, 4-*O*-acetyl-1,5-anhydro-2,6-dideoxy-L-*erythro*-hex-1-en-3-ulose (**1**), 1,5-anhydro-2,6-dideoxy-L-*erythro*-hex-1-en-3-ulose (**5**), and 4,6-di-*O*-acetyl-1,5-anhydro-2-deoxy-D-*erythro*-hex-1-en-3-ulose (**8**), were prepared according to the Czernecki's procedures.[10]

3,4-Di-*O*-acetyl-2,6-dideoxy-β-L-arabinopyranosyl Cyanide (3) and 3,4-Di-*O*-acetyl-2,6-dideoxy-β-L-ribopyranosyl Cyanide (4). A) By $NaBH_4$-$CeCl_3$: A mixture of **1** (1.74 g), acetone cyanohydrin (2.8 ml) and *N*,*N*-diisopropylethylamine (0.36 ml) in acetonitrile (17 ml) was stirred at 70 °C for 3 days, and then evaporated to a residue (approximately 3.5 g) containing **2**. A solution of the residue in methanol (100 ml) was stirred with $CeCl_3 \cdot 7H_2O$ (4.18 g) at 5 °C for 20 min, and $NaBH_4$ (1.0 g) was added. The mixture was stirred at the same temperature for 1.5 h and then at room temperature for 18 h. The reaction mixture was neutralized with Amberlite CG-50 (H type), filtered and evaporated to a residue, which was stirred with acetic anhydride (10 ml) in pyridine (30 ml) at room temperature for 24 h. After addition of ethanol, the mixture was evaporated and co-evaporated with toluene to a residue, which was chromatographed on silica gel (100 g) with 15:1 chloroform-ethyl acetate to give **3** (1.58 g, 64%) and **4** (0.37 g, 15%) having the R_f-values 0.45 and 0.37 (10:1 chloroform-ethyl acetate).

3: Needles from ethyl acetate-hexane; mp 102 °C; $[\alpha]_D^{31}$ −100° (*c* 1.1, $CHCl_3$); IR (KBr): 1720, 1240, and 1220 cm^{-1} (OAc); ^{1}H NMR (400 MHz, $CDCl_3$); δ=1.25 (3H, d, Me-5, *J*=6.2 Hz), 2.03 (1H, m, H-2ax), 2.04 and 2.08 (each 3H, s, OAc), 2.40 (1H, ddd, H-2eq, *J*=13.2, 5.1, and 1.5 Hz), 3.94 (1H, dq, H-5, *J*=9.6 and 6.2 Hz), 4.76 (1H, t, H-4, *J*=9.6 and 9.5 Hz), 4.86 (1H, dd, H-1, *J*=5.8 and 1.5 Hz), and 5.22 (1H, ddd, H-3, *J*=11.7, 9.5 and 5.1 Hz); MS *m/z* 242 (M^++1).

Found: C, 54.89; H, 6.11%. Calcd for $C_{11}H_{15}NO_5$: C, 54.77; H, 6.27%.

4: Syrup; $[\alpha]_D^{31}$ −157° (*c* 1.1, $CHCl_3$); IR (neat): 1740, 1245, and 1220 cm^{-1} (OAc); ^{1}H NMR (400 MHz, $CDCl_3$): δ=1.24 (3H, d, Me-5, *J*=6.1 Hz), 2.07 and 2.19 (each 3H, s, OAc), 2.26 (2H, m, H-2ax and 2eq), 4.31 (1H, dq, H-5, *J*=9.6 and 6.1 Hz), 4.61 (1H, dd, H-4, *J*=9.6 and 3.0 Hz), 4.77 (1H, dd, H-1, *J*=5.6 and 2.7 Hz), and 5.37 (1H, dd, H-3, *J*=6.3, 3.0 and 0 Hz); MS *m/z* 242 (M^++1).

Found: C, 54.64; H, 6.34%. Calcd for $C_{11}H_{15}NO_5$: C, 54.77; H, 6.27%.

B) By L-Selectride: A sample of **1** (1.70 g) was treated by the same procedure as described in the Section A. To a stirred solution of the residue (approximately 3.5 g) containing the adduct **2** in THF (100 ml) was added dropwise a 1 M L-Selectride solution in THF (25 ml) at −78 °C, and then stirring was continued for 1 h at the same temperature. After addition of 50% acetic acid, the mixture was partitioned between ethyl acetate and water. The combined organic layers were dried and evaporated to a residue, which was acetylated as described in the Section A. After silica-gel column chromatography, **3** (0.14 g, 6%) and **4** (1.42 g, 59%) were obtained.

2,6-Dideoxy-β-L-arabinopyranosyl Cyanide (6). A sample of **3** (335 mg) was stirred in 7% methanolic ammonia solution (3.4 ml) at 5 °C for 3 h. The reaction mixture was evaporated to a residue, which was chromatographed on silica gel (10 g) with 1:2 benzene-ethyl acetate to give a syrup of **6** (207 mg, 95%): R_f 0.33 (2:1 chloroform-acetone); $[\alpha]_D^{29}$ −66° (*c* 1.0, MeOH); IR (neat): 2230 cm^{-1} (CN); ^{1}H NMR (400 MHz, CD_3OD): δ=1.29 (3H, d, Me-5, *J*=6.0 Hz), 1.85 (1H, ddd, H-2ax, *J*=14, 11.5, and 6.0 Hz), 2.15 (1H, ddd, H-2eq, *J*=14, 4.8, and 1.6 Hz), 2.93 (1H, t, H-4, *J*=9.2 and 9.0

Hz), 3.59 (1H, dq, H-5, J=9.2 and 6.0 Hz), 3.71 (1H, ddd, H-3, J=11.5, 9.0 and 4.8 Hz), and 4.96 (1H, dd, H-1, J=6.0 and 1.6 Hz); MS m/z 157 (M^+).

Found: C, 53.01; H, 6.91%. Calcd for $C_7H_{11}NO_3$: C, 53.49; H, 7.05%.

2,6-Dideoxy-β-L-ribopyranosyl Cyanide (7). A sample of **4** (359 mg) was deacetylated by the procedure described in the preparation of **6**, and then worked up to give needles of **7** (203 mg, 87%) after recrystallization from ethyl acetate-hexane: R_f 0.32 (2:1 chloroform-acetone); mp 162 °C; $[\alpha]_D^{29}$: −107° (c 0.87, MeOH); IR (KBr): 2230 cm^{-1} (CN); ^1H NMR (400 MHz, CD_3OD): δ=1.25 (3H, d, Me-5, J=6.1 Hz), 2.1 (2H, m, H-2ax and 2eq), 3.17 (1H, dd, H-4, J=9.4 and 4.0 Hz), 4.03 (1H, dd, H-1, J=6.3 and 2.9 Hz), 4.04 (1H, dq, H-5, J=9.4 and 6.1 Hz), and 4.79 (1H, t, H-3, J=4.0 and 0 Hz); MS m/z 157 (M^+).

Found: C, 53.42; H, 7.11%. Calcd for $C_7H_{11}NO_3$: C, 53.49; H, 7.05%.

3,4,6-Tri-*O*-acetyl-2-deoxy-β-D-arabinopyranosyl Cyanide (10) and 3,4,6-Tri-*O*-acetyl-2-deoxy-β-D-ribopyranosyl Cyanide (11). A) By $NaBH_4$-$CeCl_3$: A mixture of **8** (1.02 g), acetone cyanohydrin (1.85 ml) and *N,N*-diisopropylethylamine (0.16 ml) in acetonitrile (10 ml) was stirred at room temperature for 3 days, and then evaporated to a residue containing **9**. The residue was treated with $NaBH_4$ and $CeCl_3 \cdot 7H_2O$ followed by acetylation as described in the preparation (Section A) of **3** and **4**, and then worked up to give **10** (0.80 g, 60%) and **11** (0.26 g, 20%) having the R_f-values 0.37 and 0.32 (8:1 chloroform-ethyl acetate).

10: Needles from ethyl acetate-hexane; mp 156 °C; $[\alpha]_D^{26}$ +63° (c 0.93, $CHCl_3$); IR (KBr): 1730 and 1220 cm^{-1} (OAc); ^1H NMR (400 MHz, $CDCl_3$): δ=2.05, 2.07 and 2.10 (each 3H, s, OAc), 2.11 (1H, ddd, H-2ax, J=13.8, 11.7 and 5.9 Hz), 2.42 (1H, ddd, H-2eq, J=13.8, 5.0 and 1.5 Hz), 4.05 (1H, ddd, H-5, J=9.6, 4.8 and 1.8 Hz), 4.12 (1H, dd, H-6, J=12.8 and 1.8 Hz), 4.35 (1H, dd, H-6′, J=12.8 and 4.8 Hz), 4.94 (1H, dd, H-1′, J=5.9 and 1.5 Hz), 5.02 (1H, dd, H-4, J=9.6 and 9.2 Hz), and 5.27 (1H, ddd, H-3, J=11.7, 9.2, and 5.0 Hz); MS m/z 300 (M^++1).

Found: C, 52.13; H, 5.54%. Calcd for $C_{13}H_{17}NO_7$: C, 52.17; H, 5.73%.

11: Needles from ethyl acetate-hexane; mp 92 °C; $[\alpha]_D^{26}$ +102° (c 1.0, $CHCl_3$); IR (KBr): 1730 and 1220 cm^{-1} (OAc); ^1H NMR (400 MHz, $CDCl_3$): δ=2.05, 2.09, and 2.21 (each 3H, s, OAc), 2.28 (2H, m, H-2ax and 2eq), 4.20 (1H, dd, H-6, J=12.7 and 1.9 Hz), 4.35 (1H, dd, H-6′, J=12.7 and 4.6 Hz), 4.42 (1H, ddd, H-5, J=9.8, 4.6, and 1.9 Hz), 4.85 (1H, dd, H-1, J=4.3 and 3.2 Hz), 4.89 (1H, dd, H-4, J=9.8 and 2.8 Hz), and 5.43 (1H, dd, H-3, J=6.0, 2.8 and 0 Hz); MS m/z 300 (M^++1).

Found: C, 51.90; H, 5.51%. Calcd for $C_{13}H_{17}NO_7$: C, 52.17; H, 5.73%.

B) By L-Selectride: A mixture of **8** (1.14 g), acetone cyanohydrin (2.05 ml), and *N,N*-diisopropylethylamine (0.17 ml) in acetonitrile (11 ml) was stirred at room temperature for 3 days, and then evaporated to a residue. The residue was treated with L-Selectride followed by acetylation as described in the preparation (Section B) of **3** and **4** to give **10** (0.060 g, 4%) and **11** (0.89 g, 60%).

2-Deoxy-β-D-arabinopyranosyl Cyanide (12). A sample of **10** (550 mg) was de-*O*-acetylated by the procedure described in the preparation of **6**, and then worked up to give needles of **12** (282 mg, 89%) after recrystallization from ethyl acetate-hexane: R_f 0.37 (6:1 chloroform-methanol); mp 129 °C; $[\alpha]_D^{29}$ +90° (c 1.0, MeOH); IR (KBr): 2340 cm^{-1} (CN); ^1H NMR (400 MHz, CD_3OD): δ=1.86 (1H, ddd, H-2ax, J=13.6, 11.6, and 5.3 Hz), 2.16 (1H, ddd, H-2eq, J=13.6, 4.8, and 1.4 Hz), 3.27 (1H, t, H-4, J=9.2 Hz), 3.55 (1H, ddd, H-5, J=9.20, 5.0 and 2.0 Hz), 3.71 (1H, dd, H-6, J=12 and 5.0 Hz), 3.77 (1H, ddd, H-3, J=11.6, 9.20, and 4.8 Hz), 3.85 (1H, dd, H-6′, J=12 and 2.0 Hz), and 5.04 (1H, dd, H-1, J=5.3 and 1.4 Hz); MS m/z 173 (M^+).

Found: C, 48.32; H, 6.39%. Calcd for $C_7H_{11}NO_4$: C, 48.55; H, 6.40%.

2-Deoxy-β-D-ribopyranosyl Cyanide (13). A sample of **11** (510 mg) was de-*O*-acetylated by the procedure described in the preparation of **6**, and then worked up to give a syrup of **13** (236 mg, 80%): R_f 0.34 (6:1 chloroform-methanol); $[\alpha]_D^{29}$ +83° (c 0.56, MeOH); IR (neat): 2330 cm^{-1} (CN); ^1H NMR (400 MHz, CD_3OD): δ=2.10 (2H, m, H-2ax and 2eq), 3.50 (1H, dd, H-4, J=9.6 and 3.2 Hz), 3.70 (1H, dd, H-6, J=12.2 and 5.3 Hz), 3.84 (1H, dd, H-6′, J=12.2 and 2.3 Hz), 3.98 (1H, ddd, H-5, J=9.6, 5.3, and 2.3 Hz), 4.07 (1H, dd, H-3, J=6.1, 3.2, and 0 Hz), and 4.85 (1H, d, H-1, J=4.3 and 0 Hz); MS m/z 174 (M^++1).

Found: C, 48.74; H, 6.42%. Calcd for $C_7H_{11}NO_4$: C, 48.55; H, 6.40%.

We are grateful to the Institute of Microbial Chemistry for the generous support of our program. Financial support by the Ministry of Education, Science and Culture (Grant-in-Aid for Scientific Research) is gratefully acknowledged.

References

1) G. D. Daves and C. C. Cheng, *Prog. Med. Chem.*, **13**, 303 (1976); S. Hanessian and A. G. Pernet, *Adv. Carbohydr. Chem. Biochem.*, **33**, 111 (1976).

2) R. A. Eade and H.-P. Pham, *Aust. J. Chem.*, **32**, 2483 (1979); R. A. Eade, F. J. McDonald, and J. J. H. Simes, *ibid.*, **28**, 2011 (1975).

3) J. E. Hochlowski, J. D. Faulkner, G. K. Matsumoto, and J. Clardy, *J. Am. Chem. Soc.*, **105**, 7413 (1983); W. Keller-Schlierlein, M. Brufani, and S. Barcza, *Helv. Chim. Acta*, **51**, 1257 (1968).

4) A. O. Stewart and R. M. Williams, *J. Am. Chem. Soc.*, **107**, 4289 (1985); T. Kametani, K. Kawamura, and T. Honda, *ibid.*, **109**, 3010 (1987); P. DeShong, G. A. Slough, and V. Elango, *ibid.*, **107**, 7788 (1985); M. D. Lewis, J. K. Cha, and Y. Kishi, *ibid.*, **104**, 4976 (1982).

5) K. Narasaka, Y. Ichikawa, and H. Kubota, *Chem. Lett.*, **1987**, 2139; P. Lesimple, J.-M. Beau, and P. Sinay, *J. Chem. Soc., Chem. Commun.*, **1985**, 894.

6) H. Mitsuya and S. Broder, *Proc. Natl. Acad. Sci. U.S.A.*, **83**, 1911 (1986).

7) B. E. Betts and W. Davey, *J. Chem. Soc.*, **1958**, 4193; K. Utimoto, M. Obayashi, Y. Shishiyama, M. Inoue, and H. Nozaki, *Tetrahedron Lett.*, **21**, 3389 (1980).

8) A. L. Gemal and J.-L. Luche, *J. Am. Chem. Soc.*, **103**, 5454 (1981); L. A. Paquette and W. H. Ham, *ibid.*, **109**, 3025 (1987).

9) K. Tatsuta, K. Akimoto, M. Annaka, Y. Ohno, and M. Kinoshita, *Bull. Chem. Soc. Jpn.*, **58**, 1699 (1985).

10) S. Czernecki, K. Vijayakumaran, and G. Ville, *J. Org. Chem.*, **51**, 5472 (1986).

Hydrogenation of Carbon Monoxide, Aldehydes, and Unsaturated Hydrocarbons on Titania-Supported Palladium Catalysts

Jihong Wu,* Masaki Funakoshi, Hidetoshi Nagamoto, Hiroshi Komiyama, and Hakuai Inoue
Department of Chemical Engineering, Faculty of Engineering, The University of Tokyo,
Hongo, Bunkyo-ku, Tokyo, 113
(Received August 19, 1988)

Pd/TiO_2 catalysts prepared by different methods showed quite different catalytic activities in the hydrogenation of CO and other unsaturated compounds. The catalyst prepared by coprecipitation of Pd acetate and titanium tetraisopropoxide contained smaller Pd particles than those in catalysts prepared by impregnation methods. In the hydrogenation of CO, activities of the catalysts increased with increase in the Pd dispersion. The coprecipitated catalyst was much more active for this reaction than the other catalysts and showed high activity for methanol formation under normal pressure. In the hydrogenation of propionaldehyde to 1-propanol, the catalysts showed similar behavior to that in the CO/H_2 reaction. However, in hydrogenation of C=C double bonds, the activity order of the catalysts was reverse. Higher activity was obtained on the impregnated catalysts with larger Pd particle size and this trend was stronger in hydrogenation of the conjugated butadiene and C=C bond in acrylaldehyde than in the hydrogenation of ethylene.

Pd is widely used as a catalyst for the hydrogenation of various compounds. In some cases, supported Pd exhibits catalytic behavior much different from that of the bulk metal, and its activity and selectivity are quite sensitive to the nature of the supporting materials or other factors in preparation. Much research has been done concerning this problem. However, there is currently no agreement about a reliable way of describing the changes observed in the catalytic properties of a supported metal. In the case of Pd, hydrogenation of carbon monoxide is often studied for this purpose. Catalysts of Pd supported on various oxides were found to have very different activity and selectivity to this reaction.[1,2] Based on information obtained from the CO/H_2 reaction, there are mainly two ways of interpreting such variations in catalytic activity. One concerns the changes in the supported state of Pd caused by the interaction between Pd and the support, as suggested in the researches by Driessen[3] or by Fleisch.[4] On the other hand, some authors[5] have explained the support effect by the concept of ensemble effect wherein the support provides specific sites directly involved in the reaction rather than by considering changes in Pd. In the present work, we approach this problem from an alternate point of view. Titania-supported Pd catalysts with different Pd dispersions were prepared by coprecipitation and impregnation methods. The catalytic properties of these catalysts were investigated in hydrogenation of carbon monoxide, acrylaldehyde, propionaldehyde, 1,4-butadiene, and ethylene. The effect of Pd dispersion over titania was discussed on the basis of the activity order of the catalysts observed in the various reactions.

Experimental

Catalyst. The Pd/TiO_2 catalysts were prepared by three methods. (The resulting catalysts are denoted as A, B, and C respectively.) Catalyst A was prepared by coprecipitation by hydrolysis of $Ti(O\text{-}Pr^i)_4$ in its ether solution with $Pd(OAc)_2$. Diethyl ether was found to be a suitable solvent for the preparation, since alcoholic solvents such as methanol, ethanol, and propanols reduced the Pd salts and made it difficult to obtain a stable solution prior to the hydrolysis step. As soon as water was added to the solution hydrolysis took place. The yellow-brown color of $Pd(OAc)_2$ rapidly faded away from the solution along with the solid formation, indicating that the Pd salt had been adsorbed rapidly by the solid produced. Catalyst B was prepared by impregnating a commercial TiO_2 support (FA-50, 10 $m^2\ g^{-1}$, anatase, from Kogakogyo Corp.) with an ether solution of $Pd(OAc)_2$. Excess liquid was removed by evaporation. Catalyst C was prepared by impregnating the same FA-50 TiO_2 with a solution of $PdCl_2$ (0.25 ml/g-TiO_2), using the aqueous incipient wetness technique suggested by Tauster et al.[6] After coprecipitation or impregnation, the catalysts were dried in air at about 150 °C and then treated at assigned temperatures for use in the reactions.

Reaction Procedure. Reactions were carried out in conventional flow reactors and the products were analyzed by gas chromatography. For the hydrogenation of CO, a VZ-10 column was used to analyze hydrocarbons and a PEG-6000 column to analyze methanol and other oxygenates. For reactions of alkenes the products were also determined by a VZ-10 column, and for reactions of aldehydes a PEG-1000 column was used.

Other Measurements. Surface areas of catalysts were measured by N_2 adsorption. The irreversible adsorption of CO and H_2 was measured at room temperature using a pulse flow technique. Dispersion calculated from the adsorption amount of hydrogen (the atomic ratio H_{ad}/Pd) was used as the criterion to evaluate the specific activity of the catalysts. Measurements by X-ray diffraction and electron microscopy were also performed for characterization of the catalysts.

Results

Characterization of Catalysts. The different preparation methods resulted in catalysts with remarkably different Pd dispersions. Average Pd particle size calculated from the line broadening of the X-ray diffraction peak of Pd(111) are shown in Table 1. The measured surface area and the adsorption properties of the catalysts are also given in that table. Catalyst A, pre-

Table 1. Properties of Catalysts

Catalysts	Surf. area/ $m^2 g^{-1}$	Pd particle size from XRD/Å	Dispersion (H/Pd)
5.6% A H_2 300 °C 3 h	207	45	0.67
5.2% A[a] H_2 300 °C 3 h		51	0.54
1.7% A H_2 300 °C 3 h		83	0.50
5.6% A air 300 °C 2 h/H_2 300 °C 0.3 h		65	0.32
5.6% A air 300 °C 2 h/H_2 300 °C 1 h		65	0.34
5.2% B H_2 300 °C 2 h	8.9	186	0.17
5.2% B air 300 °C 1 h/H_2 300 °C 1 h			0.15
4.4% C H_2 300 °C 2 h	8.9	285	0.067
4.4% C air 300 °C 2 h/H_2 300 °C 1h			0.050

a) $Pd(OAc)_2$ was impregnated on the untreated solid obtained from hydrolysis of $Ti(O\text{-}Pr^i)_4$.

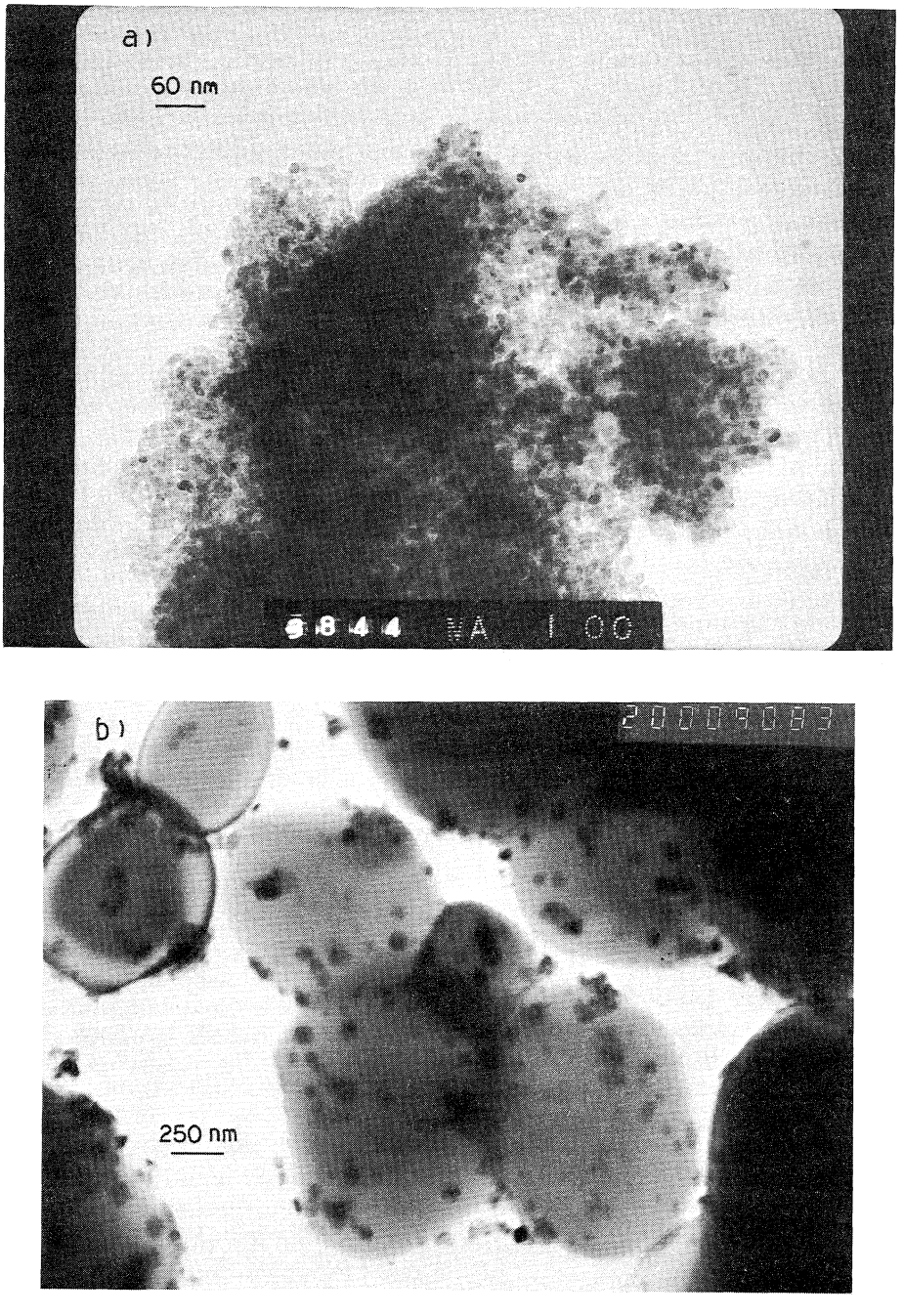

Fig. 1. TEM for a) coprecipitated catalyst A and b) impregnated catalyst B.

pared by coprecipitation of $Pd(OAc)_2$ and $Ti(O\text{-}Pr^i)_4$, achieved the highest surface area and the finest Pd particles among the three catalysts. Figure 1 shows TEM photographs for catalysts A and B. The distinction between the coprecipitated catalyst and the impregnated one is clearly seen. In the former, as a result of the preparation procedure, both Pd and the support were very fine particles and the two components were in such a well-mixed state that it is difficult to distinguish one from the other.

As shown in Table 1, a number of samples were prepared for each of the three catalysts with some variations in the conditions of heat treatment or in the preparation procedure to ensure reappearance by the preparation methods and the effects of the preparation conditions. Similar properties were generally achieved in the same group. For catalyst A, the amount of hydrogen adsorption apparently decreased after air treatment but no significant increase was seen in Pd particle size, as indicated by XRD.

The amount of hydrogen adsorption is presented as the ratio H_{ad}/Pd. Figure 2 gives a plot of H_{ad}/Pd vs. the reciprocal of average Pd particle size from XRD. The correlation between these two variables is approximately linear. The two air-treated samples of catalyst A deviated somewhat from the line. This is probably because during the air treatment the support crystal developed from its initial amorphous state and in that process some of the Pd might be wrapped inside the support. As a result, the adsorption capacity of the catalyst decreased without actual increase in Pd particle size. Though the proportional constant between the two amounts was not the same as that in the calculated equation[7] shown in the figure, the linear relationship shows that either of them can be used as a criterion to measure the relative difference of the catalysts. Here the value of H_{ad}/Pd is used to evaluate the specific activity of the catalysts.

Hydrogenation of CO. The main products of this reaction were methane and methanol. Under the pre-

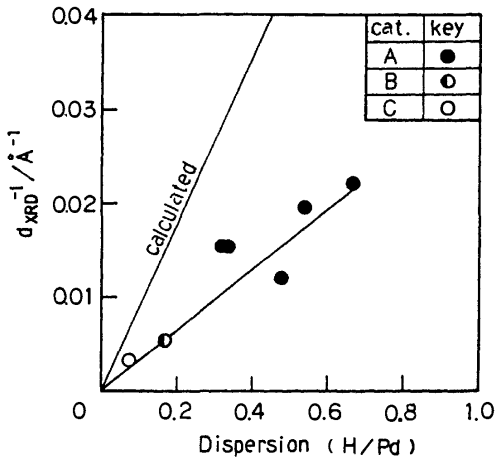

Fig. 2. Reciprocal of Pd particle diameter from XRD vs. Pd dispersion from hydrogen adsorption.

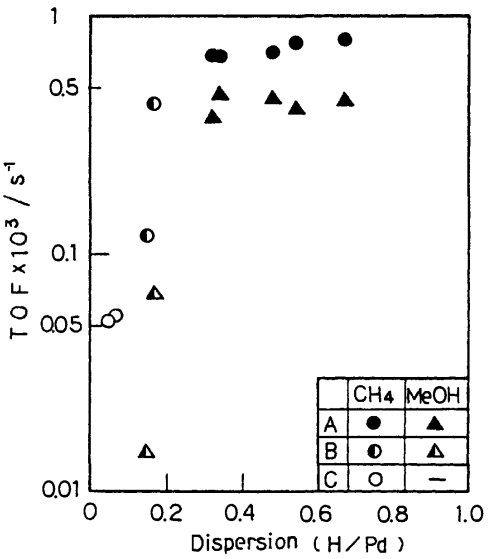

Fig. 3. Specific activity for formation of methane and methanol in the hydrogenation of CO: 1 atm, 230 °C, $CO:H_2=1:4$.

sent experimental conditions, the rate of methanol formation was affected significantly by equilibrium limitation as temperature increased beyond about 260 °C. Reactions were carried out mainly at 230 °C. Methanol production increased in the initial period of about two or three hours and then maintained a constant rate. Methane production deviated only slightly with time. Specific activities after reaching steady state are shown in Fig. 3 in terms of TOF (Turnover Frequency) based on hydrogen adsorption. Specific activity of the catalysts increased in the order C<B<A and this trend was especially remarkable for methanol formation. All the samples of catalyst A exhibited very similar activity and selectivity to each other and the production rate for methanol reached about 9 mmol/(g-Pd·h), which is quite high in comparison with the reported values for methanol synthesis on Pd catalysts at normal pressure.[1,8] However, catalyst C produced almost no methanol under the same conditions.

Hydrogenation of Acrylaldehyde (CH_2=CH-CHO) and Propionaldehyde (CH_3CH_2CHO). Acrylaldehyde is the simplest unsaturated aldehyde containing two kinds of double bonds—a C=C bond and a C=O bond. When hydrogenation of this compound was carried out at increasing temperature, at first the C=C bond was hydrogenated at comparatively low temperature and formed propionaldehyde. Then the second step of hydrogenating the formyl group took place at elevated temperature to produce 1-propanol. Catalyst A was found to be the only one on which the second step for 1-propanol formation occurred without completion of the first step. However, in the same temperature regime, though the hydrogenation of acrylaldehyde to propionaldehyde proceeded quite rapidly on catalysts B and C the resulting saturated aldehyde was not hydrogenated in spite of the completion of the first step.

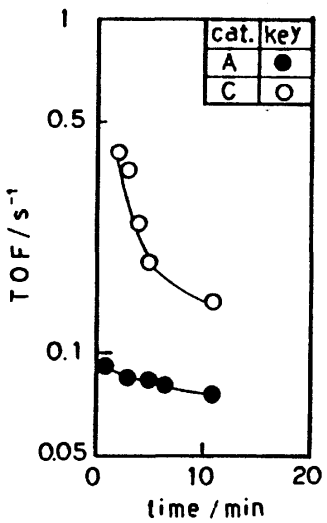

Fig. 4. Time dependence of activity for propionaldehyde formation in the hydrogenation of acrylaldehyde: acrylaldehyde 0.42%, H_2 33%, He 66.5%, 80°C.

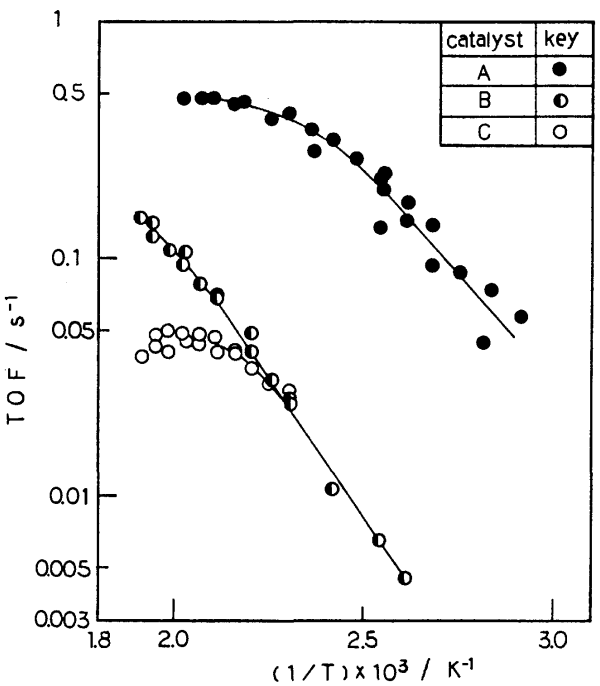

Fig. 5. Specific activity for 1-propanol formation in the hydrogenation of propionaldehyde: propionaldehyde 0.015%, H_2 33%, He 67%, 80°C.

Figure 4 shows the time dependence of the turnover frequency obtained at 80°C for catalysts A and C. In these experiments the total conversion was kept less than 10%. Under these conditions only propionaldehyde was produced and no 1-propanol was detected. The initial activity of catalyst C was about four times higher than that of catalyst A, when compared in terms of TOF.

However, in contrast to the C=C bond in acrylaldehyde, hydrogenation of the C=O bond in the formyl group was found to be quite different. In this case the relative activity of the catalysts showed a similar trend to that in the CO hydrogenation, with catalyst A being the most active one. Figure 5 shows the results from the reaction using propionaldehyde as the reactant. The figure is plotted as the temperature dependence of the production rate of 1-propanol. The activity of catalyst A was about one magnitude higher than that of the other two impregnated catalysts. The apparent slowness in increase of production rate observed in the high temperature region was due to the decomposition of the alcohol formed.

Hydrogenation of 1,4-Butadiene and Ethylene. Products of the hydrogenation of 1,4-butadiene included 1-butene, *trans*- and *cis*-2-butene and butane. Selectivities for the products are shown in Fig. 6, corresponding to the total conversion. All the catalysts had nearly the same selectivity and the general features of the product distribution were also consistent with those previously reported for Pd catalyst.[9] Among the products, *cis*-2-butene was produced only in a small amount. The fraction of butane was very low at small conversion but increased with the conversion, indicating that this product was a secondary product from successive hydrogenation of the butenes formed.

Remarkable differences in catalytic activity among the three catalysts were also observed in this reaction.

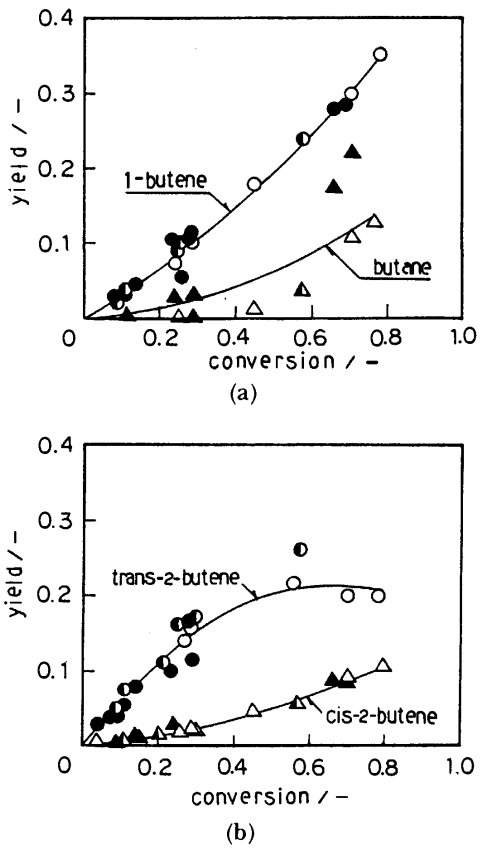

Fig. 6. Product distribution in the hydrogenation of 1,4-butadiene. ●▲ catalyst A, ◐◭ catalyst B, ○△ catalyst C.

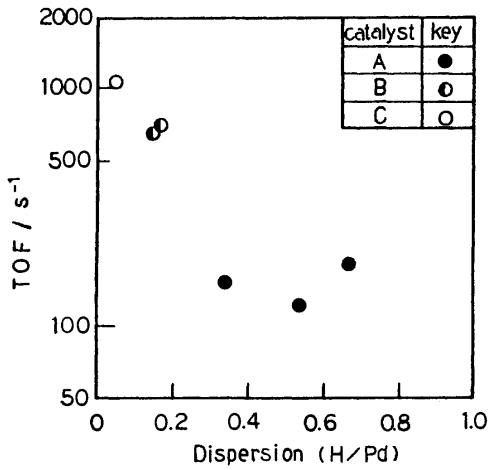

Fig. 7. Specific activity of catalysts in the hydrogenation of 1,4-butadiene: 1,4-C_4H_6 5%, H_2 95%, 80°C.

Figure 7 gives a comparison of the initial activity of the catalysts, which was in the order C>B>A, with the most poorly dispersed catalyst being the most active one. This trend is similar to the results for hydrogenation of acrylaldehyde to propionaldehyde but contrary to those for hydrogenation of CO and propionaldehyde.

Hydrogenation of ethylene was carried out in a similar way. In this reaction, catalyst C seemed to be the most active one but the difference among the catalysts was not so strong as was observed in the other reactions. Average values of TOF for each catalyst are given in Table 2, together with the results obtained in the other reactions.

Discussion

The preparation methods used in this study gave Pd/TiO_2 catalysts showing quite different catalytic behavior from one another. Table 2 gives a summary of the reaction results. Activities were compared in terms of TOF based on hydrogen adsorption capacity. In the hydrogenation of CO, both the total activity and the individual activities for formation of CH_4 and CH_3OH were in the order of A>B>C. The well-dispersed catalyst A in particular was much more active than the other two. The same trend was observed in the hydrogenation of the C=O double bond in an formyl group. However, with the C=C double bonds the activity order of the catalysts was reversed. For the hydrogenation of ethylene, the simplest olefin, the difference in TOF among the three catalysts was not very remarkable. But in the hydrogenation of a C=C bond which was conjugated with another C=C or C=O bond, as in butadiene or in acrylaldehyde, a catalyst with higher dispersion showed lower activity.

In interpreting the difference in the activity of the catalysts, the concept of ensemble effect as having been mentioned above does not seem to be applicable to our case. This concept places stress on the differences in support properties, but in the present study, the two catalysts B and C, for which the same particles of TiO_2 were used as support, also showed quite different activities in the reactions. Here, it might be more useful to study the reaction results in relation to the nature of the different reactants.

In the five reactions examined, as listed in Table 2, the activity order of the catalysts observed in the hydrogenation of CO and propionaldehyde showed a contrary trend to that observed in the other reactions. By looking at the reactants, one can find some significantly different features between the first two and the other three. In carbon monoxide and a formyl group, the oxygen atom inclines to draw the electron because of its large electronegativity and thereby makes the molecule of CO or the CO bond of the aldehyde less electron-donative. In the case of an olefin, however, the C=C bond is usually electronically rich with its π-electron and has a tendency toward electron donation. This electron-rich state becomes stronger in a conjugated compound, where overlapping of the π-electron orbitals causes higher electron density on the molecule. Such different properties of the reactants are expected to bring about different patterns in their ways of interactions with the catalyst. Changes in the work-function of a metal when a compound is adsorbed on it provides one way of indicating the electronic interaction between the adsorbent and the metal. According to previous reports, adsorption of CO on Pd surface causes a positive shift in the work-function of Pd of 0.82 eV[10] while with adsorption of ethylene the work-function of Pd shifts about 0.8 eV negatively.[11] Thus with adsorption of CO, the electron transfers from Pd to CO, but with ethylene the electron transfer occurs in the opposite direction. It has been found for

Table 2. Average Activities of Catalysts A, B, and C

Reactions		T/°C	TOF/s^{-1}		
			A	B	C
Hydrogenation of CO	methane	230	7.3×10^{-4}	2.8×10^{-4}	5.5×10^{-5}
	methanol		4.3×10^{-4}	4.0×10^{-5}	0
Hydrogenation of propionaldehyde		80	1.6×10^{-1}	4.5×10^{-3}	4.5×10^{-3}
Hydrogenation of ethylene		80	380	500	580
Hydrogenation of C=C bond in acrylaldehyde		80	0.09		0.4
Hydrogenation of 1,4-butadiene		80	150	680	1050

Pt, one of the metals which show very similar properties to those of Pd, that the work-function of a Pt surface shifted 0.2 eV positively with adsorption of CO in contrast to the negative shifts of 0.8 eV and 1.6 eV with adsorption of ethylene and butadiene, respectively.[12] This further indicates that donation of π-electron to the metal occurs to a larger extent on the conjugated diene than on ethylene. In corresponding to the relative extent of charge transfer on CO, ethylene and butadiene, our results showed that dependence of catalytic activity on Pd dispersion varied in reactions of these compounds. Activity for the hydrogenation of CO increased with increase in Pd dispersion. For the hydrogenation of ethylene, activity decreased slightly with the increase in Pd dispersion and in the reaction of 1,4-butadiene this decrease was much more obvious. As for the other two reactions of propionaldehyde and acrylaldehyde, the former behaved similarly to carbon monoxide while the latter was rather near to 1,4-butadiene as expected from the conjugating system composed of the C=C double bond and the aldehyde group in this molecule.

Pd with higher dispersion showed higher activity in the hydrogenation of electron-attractive compounds while in the hydrogenation of the electronically donative olefin bonds, Pd with lower dispersion was more active. These facts inversely suggest some changes in the electronic state of Pd, depending on its dispersed state on the support. According to the many studies of the hydrogenation of CO on Pd catalysts, it is known that bulk Pd metal is rather inactive in spite of its CO adsorption capacity.[7,13] Previous study[14] of a Pd alloy catalyst has shown that its catalytic activity was effectively increased after the alloy catalyst was treated in air to produce an oxidative state of Pd. These results indicated that the reaction of CO is favored by the oxidative state of Pd. In relation to these reported facts, the coprecipitated catalysts prepared in the present work are thought to be in a more oxidative state than Pd on the other catalysts.

The catalytic properties of supported metal catalysts may be affected by various factors and the situations are usually very complicated, making it difficult to determine the true state of the metal-support interaction. In this paper the experimental results obtained in the present work were discussed in relation to knowledge from past research and an interpretation of the different behavior observed for catalysts prepared by different methods was suggested by considering the electronic properties of the reactants and their interaction with Pd. The most plausible reason for the differences among the catalysts is thought to be the strength of the interaction between Pd and the TiO_2 support. Stronger interaction is expected on a catalyst prepared by coprecipitation which possesses a very large interface between Pd and the support.

The authors wish to express their thanks to Mr. Koji Adachi, the Engineering Research Institute of University of Tokyo, and Mr. Mineya Kuno, Sumitomo Electric Industries, Ltd., for orbtaining the measurement results of TEM.

References

1) M. Ichikawa and K. Shikakura, *Shokubai*, **21**, 253 (1979).
2) Y. A. Ryndin, R. F. Hicks, and A. T. Bell, *J. Catal.*, **70**, 287 (1981).
3) J. M. Driessen, E. K. Poels, J. P. Hindermam, and V. Ponec, *J. Catal.*, **82**, 26 (1983).
4) T. H. Fleisch, R. F. Hicks, and A. T. Bell, *J. Catal.*, **87**, 398 (1984).
5) M. A. Vannice, C. Sudhakar, and M. Freeman, *J. Catal.*, **108**, 97 (1987).
6) S. J. Tauster, S. C. Fung, and R. L. Garten, *J. Am. Chem. Soc.*, **100**, 170 (1978).
7) C. Sudhakar and M. A. Vannice, *J. Catal.*, **95**, 227 (1985).
8) Y. Kikuzono, S. Kagami, S. Naito, and T. Onishi, *Chem. Lett.*, **1981**, 1249.
9) H. Hattori, *Shokubai*, **26**, 47 (1984).
10) B. E. Nieuwenhuys, *Surf. Sci.*, **105**, 505 (1981).
11) P. E. C. Franken and V. Ponec, *Surf. Sci.*, **53**, 431 (1975).
12) M. Ichikawa and M. Hidai, "Kinitsu-Shokubai To Fukinitsu-Shokubai Nyumon," Maruzen, Tokyo (1983), Chap. 5.
13) S.-Y. Wang, S. H. Moon, and M. A. Vannice, *J. Catal.*, **71**, 167 (1981).
14) H. Komiyama, T. Jomura, M. Funakoshi, and H. Inoue, 17th Autumn Meeting of the Soc. of Chem. Engrs. Japan, Sendai, Sept. 1983, Preprints, No. SB309c.

Footprint Catalysis. III.[1,2] Inducible Alteration of Substrate Specificities of Silica(Alumina) Gel Catalysts for 2,4-Dinitrophenolysis of Toluic Anhydrides by Footprint Imprinting

Kensaku MORIHARA,* Eiko TANAKA, Yuko TAKEUCHI, Kazue MIYAZAKI, Nami YAMAMOTO, Yoshimi SAGAWA, Eriko KAWAMOTO, and Toyoshi SHIMADA
Department of Chemistry, Faculty of Science, Nara Women's University, Kitauoyanishi-machi, Nara 630
(Received April 26, 1988)

A tailor-made catalyst design was attempted for a required substrate specificity by the authors' footprint imprinting method. Two silica(alumina) footprint catalysts were prepared by imprinting with *N*-benzoylbenzenesulfonamide (**1**) and *N*-(*p*-toluoyl)-*p*-toluenesulfonamide (**2**) from the same aluminum ion-doped silica gel. Their catalytic effects upon 2,4-dinitrophenolysis of benzoic anhydride, *p*-, *m*-, and *o*-toluic anhydrides were compared in order to find any difference in substrate specificities. The catalyst prepared by imprinting with **1** showed the largest specificity(k_{cat}/K_m) toward benzoic anhydride, whereas the catalyst prepared with **2** showed the largest specificity toward *p*-toluic anhydride. This finding evidently demonstrated that the substrate specificities of footprint catalytic sites are alterable, as required through selecting appropriate transition state analogs as template molecules for footprint marking.

Previous papers[1,2] of this series reported that unusual catalytic sites of Lewis acid could be marked by imprinting on a silica gel surface like the footprints of the template molecules with a complementary structure to them, and that these "footprint" catalytic sites possessed an exact molecular recognition capability toward the template molecules used in the imprinting process, a capability which was revealed as being an abnormally strong competitive inhibition in a catalysis. This molecular recognition of footprint catalytic sites should also be revealed in their substrate specificity, which would lead to a catalyst design for a required substrate specificity in demand.

During the course of previous studies,[1,2] butanolysis[3] of benzoic anhydride using a potentiometric titration[4] was employed as a catalytic activity assay system. However, several kinds of technical problems were encountered in which the butanolyses of benzoic anhydride proceeded very slowly, accompanying the uncatalyzed reaction in significant quantities. Also, potentiometric titration[4] was rather troublesome, lacking sensitivity, and less reliable for an accurate assay. Accordingly, an improved assay system has been necessarily required for the further investigation of substrate specificities upon the footprint catalytic sites.

The present report deals with two matters. The first is with regard to a new photometric assay system for catalytic activity using 2,4-dinitrophenolysis of benzoic anhydride, and its application to a method for catalytic sites titration with the aid of pyridine poisoning of the catalysts. The second regards an attempt to alter the substrate specificities of silica(alumina) catalysts by selecting appropriate transition state analogs for the reaction of the substrate as template molecules. The kinetic parameters in 2,4-dinitrophenolysis of two footprint catalysts and of a control silica(alumina) catalyst were measured upon four anhydride substrates, i.e., benzoic anhydride and *p*-, *m*-, *o*-toluic anhydrides; induced alterations of substrate specificities were clearly demonstrated.

Experimental

Materials. All chemicals were of the guaranteed grade of Nacalai Tesque Co., Ltd., if not specified.

Templates and Inhibitors: *N*-Benzoylbenzenesulfonamide (Ph-SO_2-NH-Bz, **1**) and *N*-(*p*-toluoyl)-*p*-toluenesulfonamide (CH_3-C_6H_4-SO_2-NH-CO-C_6H_4-CH_3, **2**), and dibenzamide (Ph-CO-NH-CO-Ph, **3**) were of the same preparations as those previously reported.[1,2] Pyridine and 2,6-dimethylpyridine were of guaranteed grade reagents and were used without further purification.

Silica Gel: Merck Kieselgel 60, art. no. 7754, particle size 0.06—0.20 mm, mesh 70—230, was used.

Substrate: Benzoic anhydride was recrystallized from benzene-petroleum benzine, mp 42 °C (lit,[5] 42 °C). Three toluic anhydrides were prepared according to a procedure described in the literature.[6] *p*-Toluic anhydride was recrystallized from ethanol, mp 95—95.5 °C (lit,[7] 95 °C). IR (Perkin-Elmer 1740) (KBr) 3050 (arom.), 1775, 1715 (C=O, anhydride), 1609 (arom.), 1449, 1376 (methyl), 840, 824 cm^{-1} (*p*-, arom.). *m*-Toluic anhydride was recrystallized from ether-petroleum ether, mp 67.0—68.5 °C (lit,[8] 71 °C). IR (KBr) 3070, 3036 (arom.), 1784, 1718 (C=O), 1591 (arom.), 1487, 1378 (methyl), 803, 743, 724 cm^{-1} (*m*-, arom.). *o*-Toluic anhydride was recrystallized from ether-petroleum benzine, mp 36.5—38.0 °C (lit,[9] 36—38 °C, 39 °C). IR (KBr) 3074 (arom.), 1784, 1719 (C=O), 1456, 1381 (methyl), 733 cm^{-1} (*o*-, arom.).

Nucleophile: Potassium 2,4-dinitrophenolate was prepared through the neutralization of 2,4-dinitrophenol in a minimum amount of methanol with concd aqueous potassium hydroxide; the salt was recrystallized from hot water, and dried at 130 °C in vacuo.

Solvent: Acetonitrile, previously dehydrated with calcium chloride, was dried over phosphorus pentoxide overnight, and distilled using a Hempel fractionating column, bp 81—82 °C. To the distillate was added calcium hydride and distillation was repeated to remove perfectly any trace of water or acidic impurities.

Catalysts: Three footprint catalysts were prepared according to an imprinting method which was previously described in detail,[1] using **1**, **2**, **3**, as templates, respectively, (they are referred hereafter as catalyst {**1**}, {**2**}, and {**3**} in text.) as follows.

Kieselgel (100 g) was refluxed for 6 h with concd hydrochloric acid (300 cm^3), and washed thoroughly (by decantation) with water (5 dm^3) and dil aqueous ammonia (pH 7.0—8.0). The gel sludge was immediately treated with an aluminium chloride aqueous solution (0.2 M†, 50 cm^3 per the gel sludge equivalent to 10 g of dry weitht) for two days for aluminium ion doping. The pH of the supernatant of the mixture was kept at 7.0—8.0 by occasional adjustments with aqueous ammonia. The aluminium ion-doped gel sludge, isolated by decantation from the supernatant and precipitated aluminium hydroxide and washed with dil hydrochloric acid (pH 4.0), was divided into parts for imprinted (gel) catalysts and a control (gel) catalyst. A part of the doped gel was added to an acetone solution of a template (2×10^{-3} M of **1**, **2**, or **3**, 30 cm^3 per the gel sludge equivalent to 10 g of dry weight) and the pH of the supernatant of the mixture was adjusted to 4.0 with dil hydrochloric acid (pH 1.0). The mixture was allowed to stand for 2—5 days. For the control (gel) catalyst preparation, a template was omitted, other procedure being the same those as above mentioned. The gel, washed with dil hydrochloric acid (pH 4.0) and collected by filtration, was dried in a desiccator over calcium chloride for one day at room temperature and atmospheric pressure, and for further two days at reduced pressure of 25 mmHg.†† Finally, it was dried at 120—140 °C and the pressure of 3 mmHg, to give an "imprinted" (gel) catalyst. In the study on substrate specificity alteration, the two imprinted catalysts {**1**} and {**2**}, and one control catalyst without the imprinting were prepared in particular from the same origin of aluminium ion-doped silica gel preparation for exact comparison of the imprinting effects on the substrate specificity.

Acidic properties characterizations were carried out by methods of Benesi[10] with Hammett indicators for acid strength determination, and of Pines and Haag[11] with phenolphthalein for Lewis acid sites detection.[1]

Apparatus. The spectrophotometers used were the Hitachi 124 and Shimadzu UV-160. Triple-wavelength measurements were carried out with the latter using its internal data-processing program.

Kinetic Measurement. An appropriate amount of stock benzoic anhydride solution freshly prepared (1.5×10^{-2} M in acetonitrile) was diluted to 29 cm^3 with acetonitrile (final substrate concentration, 1—5 $\times10^{-3}$ M) in a glass-stoppered flask. To this solution was added 30 mg of a catalyst; the mixture was equilibrated at 30 °C for 10 min under gentle stirring. One cm^3 of stock 2,4-dinitrophenolate solution (5.0×10^{-3} M, prepared by dissolving 27.8 mg of potassium 2,4-dinitrophenolate and equivalent molar of 18-crown-6 in 25 cm^3 acetonitrile) was added in order to initiate the reaction under vigorous stirring. An aliquot, 3 cm^3, was taken out at proper intervals (2—3 min) and was filtered to remove off catalyst gel particles as quickly as possible, and the O.D. at 430 nm was recorded. When a triple-wavelength photometer was available, this filtration procedure was omissible by selecting wavelengths at 400, 430, and 500 nm; thereby, a more reliable determination was achieved than by the filtration procedure. First-order rate constants, k_{obs}, were calculated from the decrease in O.D. at 430 nm. In inhibition studies, the catalyst was equilibrated with an inhibitor in acetonitrile for 1 h at 30 °C; after the addition of the substrate solution, equilibration was continued for a further 5—10 min. The following procedures were the same as those mentioned before. Kinetic parameters, K_m and $k_{obs.max}$ (V_{max} in Michaelis-Menten kinetics) were obtained from Lineweaver-Burk plots using a least-squares method, and k_{cat} s were calculated from the $k_{obs.max}$ divided by the catalytic sites molarities obtained from a catalytic sites titration (see text).

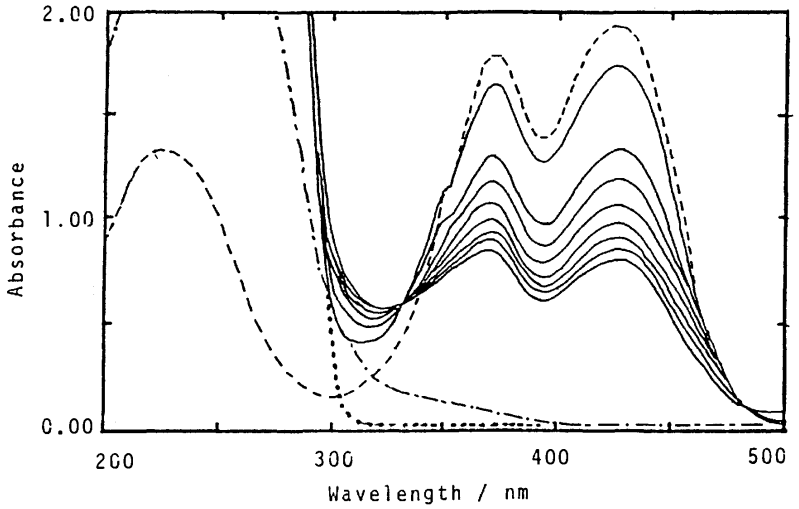

Fig. 1. Spectra changes in 2,4-dinitrophenolysis of benzoic anhydride by the footprint catalyst {**3**}.
——: reaction mixture, 4 min intervals. ----: nucleophile, 2,4-dinitrophenolate anion (1.67×10^{-4} M). ····: substrate, benzoic anhydride (1×10^{-3} M). —·—: product, 2.4-dinitrophenyl benzoate (ca. 1.67×10^{-4} M).

† 1 M=1 mol dm^{-3}.
†† 1 mmHg=133.322 Pa.

Results and Discussion

Photometric Assay of 2,4-Dinitrophenolysis. As can be seen in Fig. 1, the absorption spectra of 2,4-dinitrophenolate changed rapidly in the visible region (376, 430 nm) with the progress of the reaction; changes were evidently caused only by the catalytic 2,4-dinitrophenolysis, since no change was detected without a catalyst or substrate under the same reaction conditions.

Since no absorption of benzoic anhydride (substrate) or authentic 2,4-dinitrophenyl benzoate (product) was found in the region over 400 nm, the reaction rates could be simply determined through the O.D. decrease at 430 nm. After an initial slight curvature (within 8 min), linear semi-log plots of O.D. vs. time were usually observed over at least 1 half life, demonstrating that the reactions obey first-order kinetics with respect to the 2,4-dinitrophenolate concentration; the rate constants, $k_{obs.}$ s, were determined in the usual manner.

As a nucleophile, 2,4-dinitrophenolate was preferred to *p*-nitrophenolate, since the latter caused a too rapid *p*-nitrophenolysis of benzoic anhydride to determine the reaction rate, accompanying an uncatalyzed reaction in considerable quantities. The reverse reactions of the above-mentioned phenolyses, in which *p*-nitrophenyl benzoate or 2,4-dinitrophenyl benzoate were substrates and benzoate anion serves as a nucleophile[12] also caused a problem in that the release of phenolate anions was hindered by their adsorption on the gel surface.

As shown in Figs. 2 and 3 ([I])=0), the k_{obs} s obey Michaelis-Menten kinetics with respect to the anhydride substrates concentration. This fact suggests that

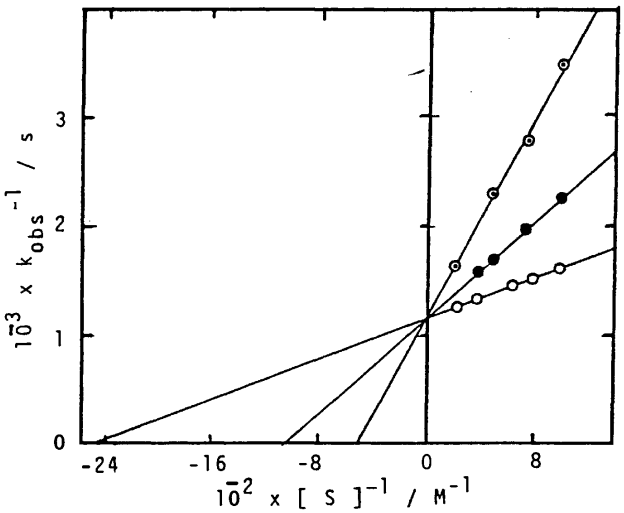

Fig. 2. Lineweaver-Burk plots for 2,4-dinitrophenolysis of benzoic anhydride catalyzed by the footprint catalyst {3}.
[S]: benzoic anhydride concentration. [I]: inhibitor **3** (Bz-NH-Bz) concentration. O: [I]=0. ●: [I]=2.89×10^{-7} M. ⊙: [I]=5.78×10^{-7} M. K_i=1.88×10^{-7} M.

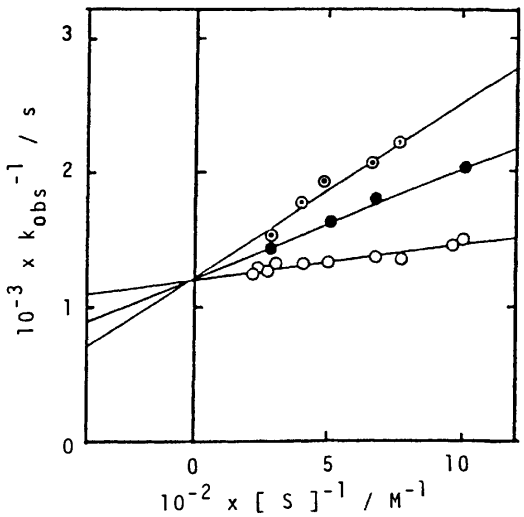

Fig. 3. Linewerver-Burk plots of footprint catalyst {1}.
[S]: substrate (benzoic anhydride) concentration. [I]: inhibitor **1**$^-$(Ph-SO_2-N^--Bz) concentration. O: [I]=0, ●: [I]=3.14×10^{-8} M, ⊙: [I]=7.48×10^{-8} M. K_m=2.22×10^{-4} M, K_i=2.30×10^{-8} M, K_m/K_i=9.65×10^3.

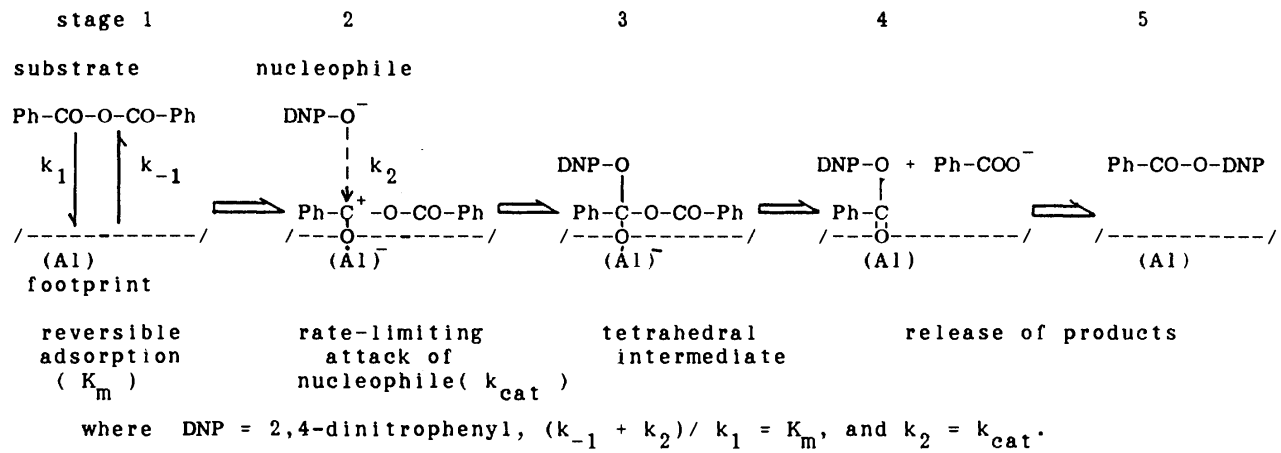

Scheme 1. Catalytic process of dinitrophenolysis of benzoic anhydride.

the reactions proceed through a Rideal-Eley mechanism with a rate-limiting nucleophilic attack (Scheme 1) similar to the butanolysis of benzoic anhydride previously reported.[1] The rate law is also expressed as follows.

$$\text{rate} = \frac{k_{cat}[\text{catalyst}][\text{benzoic anhydride}][\text{2,4-dinitrophenolate}]}{K_m + [\text{benzoic anhydride}]}$$

All of the imprinted catalysts under investigation were confirmed to possess footprint catalytic sites by the criterion that they showed typical competitive inhibition by the original template molecules with huge K_m/K_i values (K_i is the dissociation constant of the inhibitor bound on a catalytic site), as shown in Figs. 2, 3, and 4. Additionally to note, conjugate bases of the template molecules were used as inhibitors in the latter two cases (Figs. 2 and 3) and were found to be more (10-fold) effective than the free bases. This fact demonstrates that conjugate bases are probably the intrinsic footprint marking species in the imprinting process.

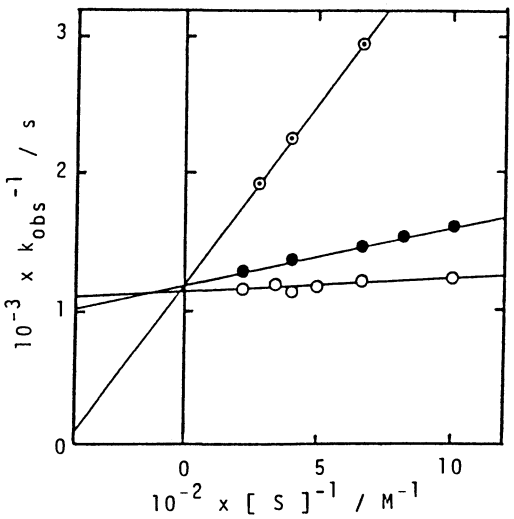

Fig. 4. Lineweaver-Burk plots of footprint cataltst {2}.
Substrate: *p*-toluic anhydride.
Inhibitor: 2-(CH_3-C_6H_4-SO_2-N^--CO-C_6H_4-CH_3).
○: [I]=0, ●: [I]=1.35×10^{-7} M, ◉: [I]=4.41×10^{-7} M.
K_m=7.85×10^{-5} M, K_i=2.45×10^{-8} M, K_m/K_i=3.2×10^3.

Regarding the acidic properties of the catalysts, all of the catalysts were positive to some Hammett indicators (Neutral Red, pK_a +6.8; Methyl Red, pK_a +4.8; 4-(phenylazo)diphenylamine, pK_a +1.5) and to phenolphthalein for Lewis acid (purple), which were the same as those reported previously.[1]

The kinetic parameters are summarized in Table 1, in which data of the butanolysis[1] analyzed by the potentiometric titration are also cited for a comparison. As can be seen, remarkable differences, 3 orders of magnitude, can be observed in the binding steps (K_m s, K_i s) between the 2,4-dinitrophenolysis and the butanolysis, These differences are presumably caused by the poor solvating ability of aprotic acetonitrile,[13] as compared with that of protic 1-butanol, i.e., all the substrate, inhibitors and footprint catalytic sites[14] might be less solvated or more "naked" in acetonitrile than in 1-butanol. The binding steps, thereby, would be strikingly enhanced. The huge rate enhancements observed in catalytic steps (k_{cat} s) (5 order of magnitude), are also explainable by the strengthened nucleophilicity of "naked" 2,4-dinitrophenolate anions solublized into dipolar acetonitrile with the aid of a crown ether.[15-17] The two effects mentioned above result in an enormous rate enhancement for the overall reaction (k_{cat}/K_m), 7 orders of magnitude.

By the application of this enhanced reaction in acetonitrile to an assay of a catalysis, a photometric method is successfully established as required, i.e., the butanolysis method needs 2.26 g of the substrate, 700 mg of a catalyst, and 120 min of reaction time at 55 °C per a measurement, whereas the new dinitrophenolysis method requires only 6.8 mg of the substrate, 30—50 mg of a catalyst, and 25 min at 30 °C per measurement.

Table 1. Kinetic Parameters of the Reactions

Catalyst imprinted with { }	k_{cat}[cat]	k_{cat}[a]	K_m	k_{cat}[cat]/K_m	k_{cat}/K_m	K_1	K_m/K_1
	s^{-1}	$M^{-1}s^{-1}$	M	$M^{-1}s^{-1}$	$M^{-2}s^{-1}$	M	
2,4-Dinitrophenolysis of benzoic anhydride in acetonitrile at 30 °C.[b]							
{Ph-SO_2-NH-Bz}[c]	2.9×10^{-2}	1.5×10^3	4.5×10^{-4}	6.5X10	3.2×10^6	1.8×10^{-7}	2580
{Bz-NH-Bz}[d]	2.9×10^{-2}	2.8×10^3	4.1×10^{-4}	7.1X10	6.9×10^6	1.9×10^{-7}	2220
Control	2.8×10^{-2}		1.8×10^{-3}	1.6X10		No inhibition	
Butanolysis in 1-butanol-benzene (30:70, v/v) at 55 °C.[e]							
{Ph-SO_2-NH-Bz}	5.4×10^{-7}		2.0×10^{-1}	2.7×10^{-6}		2.0×10^{-4}	970
{Bz-NH-Bz}	4.9×10^{-7}		1.6×10^{-1}	3.0×10^{-6}		Not determined	
{Bz-NH-Bz}	4.8×10^{-7}		1.3×10^{-1}	3.7×10^{-6}		4.7×10^{-5}	2770
Control 1	1.6×10^{-6}		1.7	9.8×10^{-7}		No inhibition	
Control 2	5.7×10^{-7}		1.3	4.6×10^{-7}		No inhibition	

a) Calculated with the molarities of catalytic sites per g determined by titration (see text).
b) This study. c) Molarity of catalytic sites, 2.01×10^{-5} mol per g. d) 1.03×10^{-5} mol per g.
e) Data from previous paper,[1] of which V_{max} values were devided by initial 1-butanol concentration and normalized per second and per g catalyst.

Catalytic Sites Titration by Pyridine Poisoning. Figure 5 demonstrates typical Lineweaver-Burk plots for an irreversible poisoning of the catalytic sites of {3} with pyridine. Similar plots for the poisoning have also been observed with the catalysts, {1}, {2} and control (plots are not shown). This poisoning by pyridine was applied to a titration method for a molarity of catalytic sites which is a requisite for k_{cat} calculation. As shown for the example in Fig.6, the amounts of catalytic sites of {3} could be determined from extrapolations of the linear k_{obs} vs. pyridine concentration plots to intercept on abscissa, since pyridine showed no other effect on 2,4-dinitrophenolysis. The titration was so accurate that the amounts of catalytic sites per g of a catalyst {3} (0.99—1.03×10^{-5} mol) obtained from 30 and 40 mg of the samples were practically identical within the experimental error. Similar titration by pyridine poisoning for the butanolysis of benzoic anhydride was rather difficult because the excess pyridine induced a general base catalysis which promoted butanolysis. As can be seen in Fig. 7,[18] where k_{obs} vs. pyridine plots had a break, the number of catalytic sites (6.92×10^{-5} mol per g) calculated from the ambiguous break point was not so reliable in accuracy as that from the dinitrophenolysis method. However, the finding that estimates of the same orders of the catalytic sites per g have been found from both butanolysis and dinitrophenolysis supports the hypothesis that these two reactions are catalyzed by the same catalytic sites, though remarkable differences have been observed in the kinetic parameters.

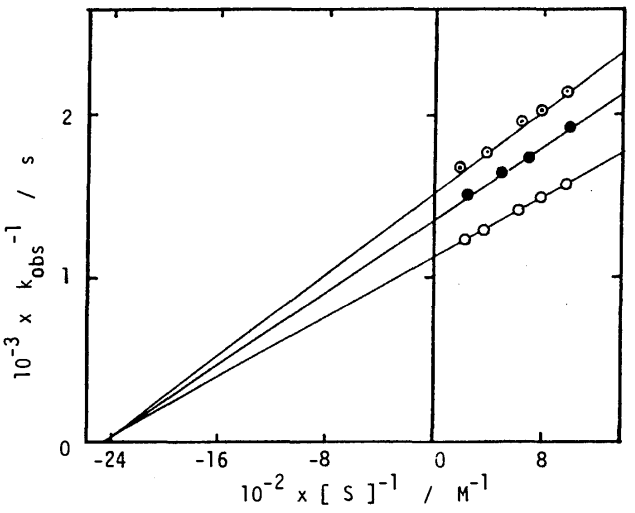

Fig. 5. Poisoning of the footprint catalyst {3} by pyridine; irreversible inhibition.
[S]=benzoic anhydride concentration. [I]=pyridine concentration. ○: [I]=0. ●: [I] 1.28×10^{-6} M. ◉: [I]=2.56×10^{-6} M.

It is worth mentioning here that the magnitude of the molarity of footprint catalytic sites, e.g., 2.0×10^{-5} mol per g for a catalyst {1}, is so large that the footprints cover about 2—3 percent of the surface of Kieselgel, assuming that the surface area of the gel is 500 m^2 per g and that of the template **1** is about 100 Å^2 per molecule. This larfge coverage by footprints would be effectively applicable to the design of specific adsorbents for a kind of affinity chromatography.

Effect of 2,6-Dimethylpyridine (Noninhibition). Figure 6 also shows that the addition of 2,6-dimethylpyridine gives rise to a noninhibitory effect on catalytic sites. This finding evidently confirms the idea that the footprint catalytic sites possess Lewis acid

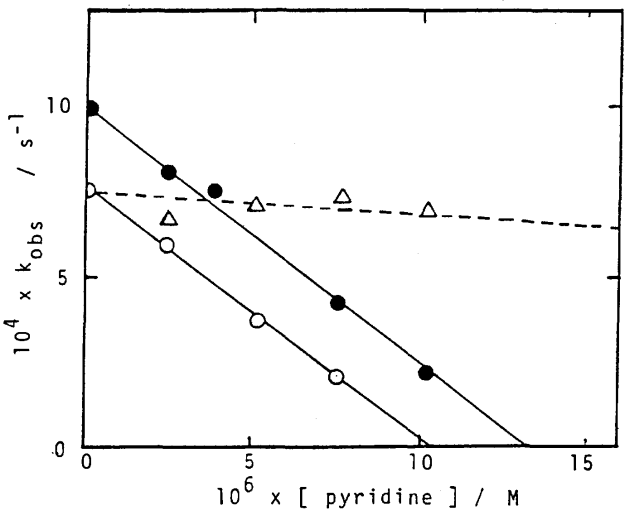

Fig. 6. Catalytic sites titration of the footprint catalyst {3} by pyridine poisoning in 2,4-dinitrophenolysis of benzoic anhydride.
[benzoic anhydride]: 2.5×10^{-3} M. ○: 30 mg catalyst. titre; 1.03×10^{-5} mol per g. ●: 40 mg catalyst. Titre; 9.96×10^{-6} mol per g. △: 2,6-dimethylpyridine to 30 mg catalyst (no inhibitory effect).

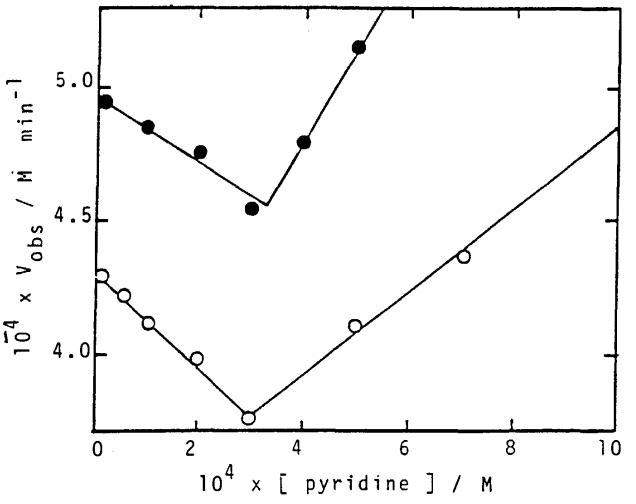

Fig. 7. Catalytic sites titration of a footprint catalyst {3} and a control catalyst by pyridine poisoning in butanolysis of benzoic anhydride. (Data from Ref. 18 referred for comparison.) Assay procedure was the same as descrelbed in Ref. 1.
○: control catalyst. titre; 6.00×10^{-5} mol per g. ●: catalyst{3}. titre; 6.92×10^{-5} mol per g.

sites, as previously discussed, since if the catalytic sites are Brønsted acid sites, they should lose their catalytic activities by neutralization with 2,6-dimethylpyridine. However, Lewis acid sites were still active because they cannot form acid-base complexes with 2,6-dimethylpyridine through steric hindrance to two methyl groups. It should be noted that a footprint catalyst and 2,6-dimethylpyridine forms an unusual reaction medium in which an acid and a base cannot act on each other like the case of "wolf and lamb" reaction,[19] and its potential utility as a concerted acid-base catalysis might be promising.

Alteration of Substrate Specificities. In order to distinguish the footprint effects of different catalytic sites on the substrate specificities, phthalic anhydride is not adequate, though it has been used once as a substrate in a previous study.[1] This is because its much higher reactivity than benzoic anhydride has covered (by leveling off) the difference in the catalytic effects, which had been observed in the catalysis for benzoic anhydride, between the imprinted catalytic sites (of {1} and {2}) and the native Lewis acid sites of the control catalyst. Consequently, benzoic anhydride and its *p*-, *o*-, *m*-methyl derivatives are selected here as a set of substrates to be used to compare the catalytic activities, since they have similar original reactivities, and also have similar binding capabilities due to their weak hydrophobic interactions with a silicate surface of the catalyst.

The four anhydride substrates were subjected to catalyzed reactions by the three catalysts, {1}, {2} and the control catalyst, to give twelve Lineweaver-Burk plots. They showed fairly good plots (see correlation coefficients r in Table 2) except one (r=0.6362) for *m*-toluic anhydride by catalyst {1} for uncertain reasons. Some typical plots are shown in Figs. 8 and 9.

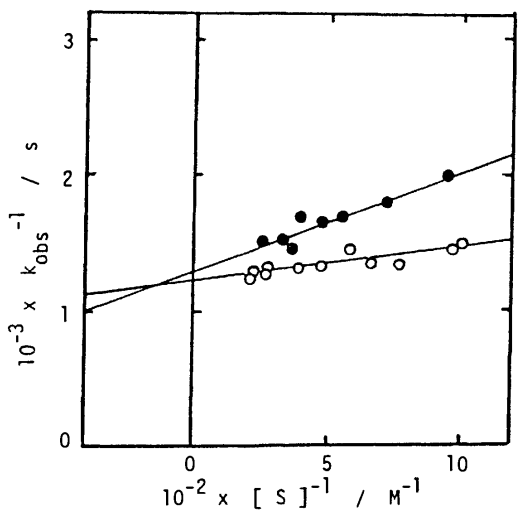

Fig. 8. Catalytic effects of footprint catalyst {1} upon benzoic anhydride and *o*-toluic anhydride.
[S]: anhydride concentration. ○: benzoic anhydride. ●: *o*-toluic anhydride.

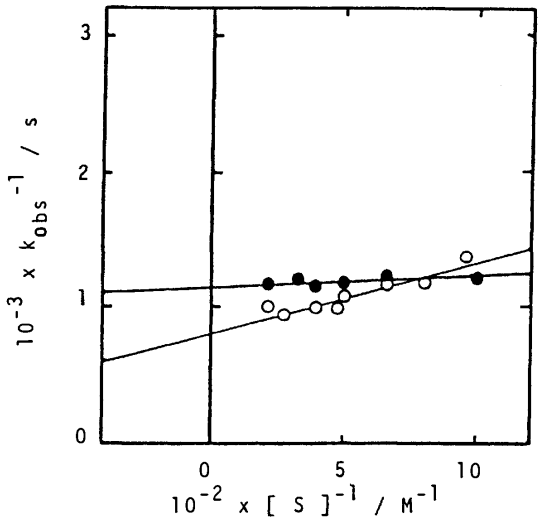

Fig. 9. Catalytic effects of footprint catalyst {2} upon benzoic anhydride and *p*-toluic anhydride.
○: benzoic anhydride. ●: *p*-toluic anhydride.

In Table 2 are summarized the kinetic parameters for the catalyzed reactions. Since the four anhydride substrates have still different reactivities in Lewis acid catalyzed reactions, the kinetic parameters have been normalized by dividing by the corresponding values of the control catalyst. With the aid of these normalized values, the characteristic catalytic effects of the footprint catalytic sites can be revealed separately from the original specificities of the control catalyst. The values of k_{cat}/K_m are reasonable to express and compare the substrate specificities of catalysts, as often used in enzyme kinetics.[20] The normalized k_{cat}/K_m values, otherwise, may represent "substrate specificity enhancement," a factor of alteration of the original specificity of "native" catalytic sites of the control catalyst by imprinting.

As can be seen in Table 2, remarkable differences in specificities exist between catalysts {1} and {2}. Though they have originated from the same aluminum ion-doped silica gel preparation, the former prefers benzoic anhydride (normalized k_{cat}/K_m=2.49) to other anhydrides (0.55—0.82), whereas the latter prefers *p*-toluic anhydride (3.97) to other anhydrides (1.04—1.26). These significant alterations in specificities are not brought about by changes in k_{cat} values (normalized values of 0.89—1.25 for catalyst {1}, 1.05—1.15 for {2}), but mainly come from changes in K_m values, owing to the exact molecular recognition of footprint catalytic sites.[2] Consequently, catalyst {1} shows the largest affinity (normalized K_m=0.36) to benzoic anhydride, possibly due to an inclusion effect of footprint sites through a best fitting with maximal interactions, and less affinities (1.46—1.79) to others due to exclusion effects of footprints through a steric hindrance to the methyl group of the substrates. However, catalyst {2} displays the largest affinity (0.31) to

Table 2. Kinetic Parameters and Substrate Specificities

Catalysts	Kinetic parameters	Substrate anhydrides			
		Benzoic	*p*-,	*m*-,	*o*-Toluic
Cat.{**1**}[c]	n[a]	11	14	15	8
	r[b]	0.9180	0.8447	0.6362	0.9286
	$K_m/10^{-4}$M	2.22	4.54	5.13	5.90
	(K_m)[d]	(0.36)[d]	(1.79)	(1.46)	(1.74)
	$k_{cat}/10^3\,M^{-1}s^{-1}$	1.07	0.97	1.07	1.04
	(k_{cat})	(0.89)	(1.25)	(1.20)	(0.95)
	$k_{cat}/K_m/10^6M^{-2}s^{-1}$	4.81	2.15	2.08	1.77
	(k_{cat}/K_m)	(2.49)	(0.70)	(0.82)	(0.55)
Cat. {**2**}[e]	n	8	6	8	5
	r	0.9406	0.7971	0.8805	0.9816
	$K_m/10^{-4}$M	6.85	0.79	3.97	2.97
	(K_m)	(1.09)	(0.31)	(1.12)	(0.87)
	$k_{cat}/10^3\,M^{-1}s^{-1}$	1.39	0.96	1.26	1.15
	(k_{cat})	(1.15)	(1.23)	(1.41)	(1.05)
	$k_{cat}/K_m/10^6\,M^{-2}s^{-1}$	2.02	12.19	3.17	3.85
	(k_{cat}/K_m)	(1.04)	(3.97)	(1.26)	(1.20)
Control[f]	n	4	4	4	4
	r	0.9925	0.9961	0.9581	0.8992
	$K_m/10^{-4}$M	6.28	2.53	3.52	3.40
	$k_{cat}/10^3\,M^{-1}s^{-1}$	1.21	0.77	0.89	1.09
	$k_{cat}/K_m/10^6M^{-2}s^{-1}$	1.93	3.07	2.52	3.21
		(1.00)	(1.00)	(1.00)	(1.00)

a) Numbers of data points on Lineweaver-Burk plots. b) Correlation coefficients. c) Molarity of catalytic sites, 2.58×10^{-5} mol per g. d) Figures in parentheses mean normalized values obtained by dividing with the corresponding values of the control catalyst. e) 3.08×10^{-5} mol per g. f) 2.93×10^{-5} mol per g.

p-toluic anhydride and also less affinity (1.0) to benzoic anhydride, though the latter can be bound onto the footprints of catalyst {**2**} without any steric hindrance. This fact suggests that the catalyst {**2**} can differentiate not only an inert methyl group in the *p*-, *m*-, or *o*-psition through the inclusion or exclusion effects, but also can recognize even a lack of the methyl group through a slight difference in their weak hydrophobic interactions.

Thus, the exact "complementarity" of the footprints to a template is clearly demonstrated to act effectively on substrate specificities in a catalytic reaction.

Conclusion

Substrate specificities of silica(alumina) catalysts can be inductively altered by the authors' imprinting method with a choice of appropriate template molecules, which would be the fundamental base of a practical tailor-made catalyst design.

References

1) Part I: K. Morihara, S. Kurihara, and J. Suzuki, *Bull. Chem. Soc. Jpn.*, **61**, 3991 (1988).

2) Part II: K. Morihara, E. Nishihata, M. Kojima, and S. Miyake, *Bull. Chem. Soc. Jpn.*, **61**, 3999 (1988).

3) K. Tarama, S. Teranishi, K. Hattori, and T. Ishibashi, *Shokubai (Tokyo)*, **4**, 69 (1962).

4) E. J. Greenhow, *Analyst*, **97**, 346 (1972).

5) "Beilstein Handbuch der Organischen Chemie," **IX**, 164.

6) H. Adkins and Q. E. Thompson, *J. Am. Chem. Soc.*, **71**, 2242 (1949).

7) "Beilstein Handbuch der Organischen Chemie," **IX**, 485.

8) "Beilstein Handbuch der Organischen Chemie," **IX**, 476.

9) "Beilstein Handbuch der Organischen Chemie," **IX**, 464.

10) H. A. Benesi, *J. Phys. Chem.*, **61**, 970 (1957).

11) H. Pines and W. O. Haag, *J. Am. Chem. Soc.*, **82**, 2471 (1960).

12) J. Hajdu and G. M. Smith, *J. Am. Chem. Soc.*, **103**, 6192 (1981).

13) V. Gutmann, "The Donor-Acceptor Approach to Molecular Interaction," Plenum Press, New York (1978).

14) E. A. Williams, J. Cargioli, and R. W. Larochelle, *J. Organomet. Chem.*, **108**, 153 (1976).

15) "Synthetic Multidentate Macrocyclic Compounds," ed by R. T. Izatt and J. J. Christensen, Academic Press, New York (1978).

16) C. L. Liotta, H. P. Harris, M. McDermott, T. Gonzalez, and K. Smith, *Tetrahedron Lett.*, **1974**, 2417.

17) C. L. Liotta, E. E. Grisdale, and H. P. Hopkins, *Tetrahedron Lett.*, **1975**, 4205.

18) K. Morihara and Y. Sagawa, unpublished data.

19) B. J. Cohen, M. A. Kraus, and A. Patchornik, *J. Am. Chem. Soc.*, **103**, 7620 (1981).

20) A. Fersht, "Enzyme Structure and Mechanism," Chap. 3, W. H. Freeman & Co., Ltd., Reading, San Francisco (1977).

Synthetic Photochemistry. XLVI.[1] Cycloaddition of *exo, endo*-2,7-Bis(methoxycarbonyl)-11,12-dioxatetracyclo[6.2.1.1^{3,6}.0^{2,7}]dodeca-4,9-diene and Conjugated Enones and *p*-Quinones

Guan Rong TIAN,† Akira MORI, Nobuo KATO, and Hitoshi TAKESHITA*
Institute of Advanced Material Study, 86, Kyushu University, Kasuga-koen, Kasuga, Fukuoka 816
(Received June 23, 1988)

Photocycloaddition of *exo,endo*-2,7-bis(methoxycarbonyl)-11,12-dioxatetracyclo[6.2.1.1^{3,6}.0^{2,7}]dodeca-4,9-diene with conjugated enones and *p*-quinones occurred exclusively at the exo-addition moiety to give [2+2]-cycloadducts. From cyclohexenone, all four possible photoadducts were obtained. A single photoadduct from cyclopentenone was a cis-transoid-cis isomer. Upon thermolysis, cyclobutene derivatives were formed from these photoadducts. An acid treatment of oxetane derivatives derived from photoadducts of *p*-quinones afforded Michael adducts instead of dienone-phenol rearrangement products.

Recently, we have shown that the thermal cycloaddition of 2,3-bis(methoxycarbonyl)-7-oxabicyclo[2.2.1]-heptadiene (**1**) and tropones,[2] cyclohepta[*b*]furan-2-ones,[3] and anthracenes[4] gave Diels-Alder adducts. Subsequent thermolysis of the adducts yielded homobarrelenones and dibenzobarrelenes. Therefore, **1** should be a useful "transfer reagent"[5,6] for acetylene. If **1** were applicable as an acetylene substitute in a photochemical version to form cyclobutenes, the utility of **1** should be extended to a great extent, since photoreactions of acetylenes with olefins were known to be contaminated by the formation of bicyclopropyl derivatives.[7] An irradiation of **1** with methyl 2,4-dioxopentanoate (**2**), however, solely gave a photoisomer of **1**, 7-oxaquadricyclane derivative (**3**),[8] but no intermolecular adduct. Instead of **1**, the reaction with *exo,endo*-2,7-bis(methoxycarbonyl)-11,12-dioxatetracyclo[6.2.1.1^{3,6}.0^{2,7}]dodeca-4,9-diene (**4**),[9] a 1 : 2-adduct of dimethyl butynedioate to furan, was investigated because the intramolecular process was prohibited. Herein, we describe our findings.

Photoadditions with *p*-Quinones. The UV-irradiation of **4** and *p*-benzoquinone (**5**) by means of a high-pressure mercury lamp gave a single photoadduct (**6**) in 78% yield. The ^{1}H NMR spectrum of **6** showed it to be a 1 : 1-adduct having an oxetane structure. The reactive double bond of **4** was identified as depicted in the structure, since the exo,exo-isomer (**7**) was photochemically inactive toward **5** under the conditions used. In addition, an iodolactonization[10] of **6** gave two isomeric iodo lactones (**8** and **9**), in 32 and 31% yields, respectively. Although the structures of **8** and **9** could not be differentiated at this stage, it is certain that the reaction occurred at the anti C=C bond in **4**.[11] The oxetane ring was deduced to have an exo-stereochemistry from the coupling constants (J_{ab}=J_{cd}= 0 Hz).

The UV-irradiation of **4** and 1,4-naphthoquinone (**10**) similarly gave a single product (**11**) in 44% yield. Again, the reaction occurred at the exo-C=C bond from the chemical shift of the remaining C=C carbons at δ=137.0 and 138.5 and the formation of two isomeric iodo lactones (**12** and **13**). The oxetane ring of **11** had an exo-stereochemistry according to the coupling constants (J_{ab}=J_{cd}=0 Hz). Its 1,4-dihydronaphthalene ring was exo from the observation of a high-field-shifted H$_c$ signal (δ=4.47), than the H$_c$ signal (δ=4.94 or 5.01) of **6**. An exclusive oxetane formation in *p*-quinones is a well-known reaction mode.[12,13]

It is interesting that in the ^{13}C NMR spectra the olefinic carbon signals of both photoadducts (**6** and **11**) appeared at nearly the same positions; in **6**, they were at 136.9 and 138.5, while those in **11** were at 137.0 and 138.5. These were also the case for photoadducts from the cycloalkanones and **2** (vide infra) and could be employed to deduce the structures of the products.

Photoadditions with Cyclic Enones. Similar UV-irradiation of **4** with 2-cyclohexenone (**14**) afforded four 1 : 1-adducts (**15—18**). The olefinic carbon signals of **15—18** appeared around 138 ppm, showing the occurrence of a reaction at the same C=C bond of **4**. The ^{1}H NMR spectra of **15—18** indicated that **14** attacked the exo site of **4**, but no further stereochemical information could be obtained at this stage. However, with potassium fluoride on Florisil,[14] **15** and **18** were converted to **17** and **16**, respectively; the newly-generated ring junctures of **16** and **17** were, thus, established to be cis.

Further chemical transformations clarified the remaining stereochemistry: When **16** was refluxed in xylene for 60 h, thermolysates (**19—21**) were obtained together with 3,4-bis(methoxycarbonyl)furan (**22**). Another cis-isomer **17** gave the thermolysate (**23**). Products **20** and **21** were identical with bicyclo[4.2.0]oct-7-en-2-one[15,16] and cyclooctadienone.[17] Since the ^{1}H NMR spectra of **19** and **23** were not informative to elucidate stereochemistries, an oxidation with *m*-chloroperbenzoic acid (MCPBA) was carried out; **19** gave a lactone (**24**), whereas **23** gave no oxidation product. The ^{1}H NMR spectrum of **24** showed a proton on the carbon bearing a lactonic oxygen atom at 4.39 (H$_a$, dd, J=6.6, 2.6 Hz). The nuclear Overhauser effect (NOE) experiments of **24** showed that the satura-

† On leave from Yanbian University, Yanji, Jilin, People's Republic of China.

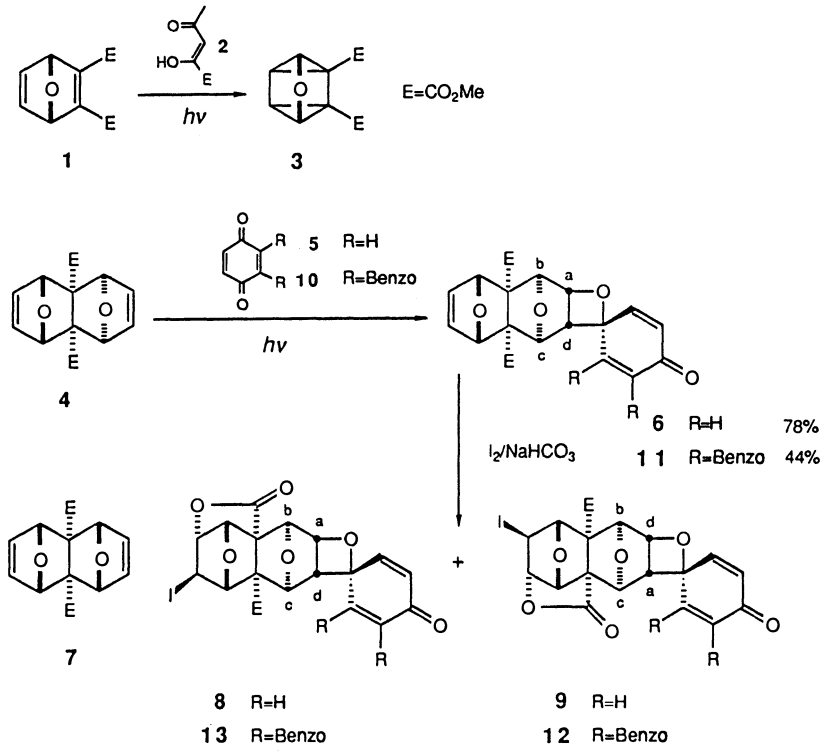

Scheme 1.

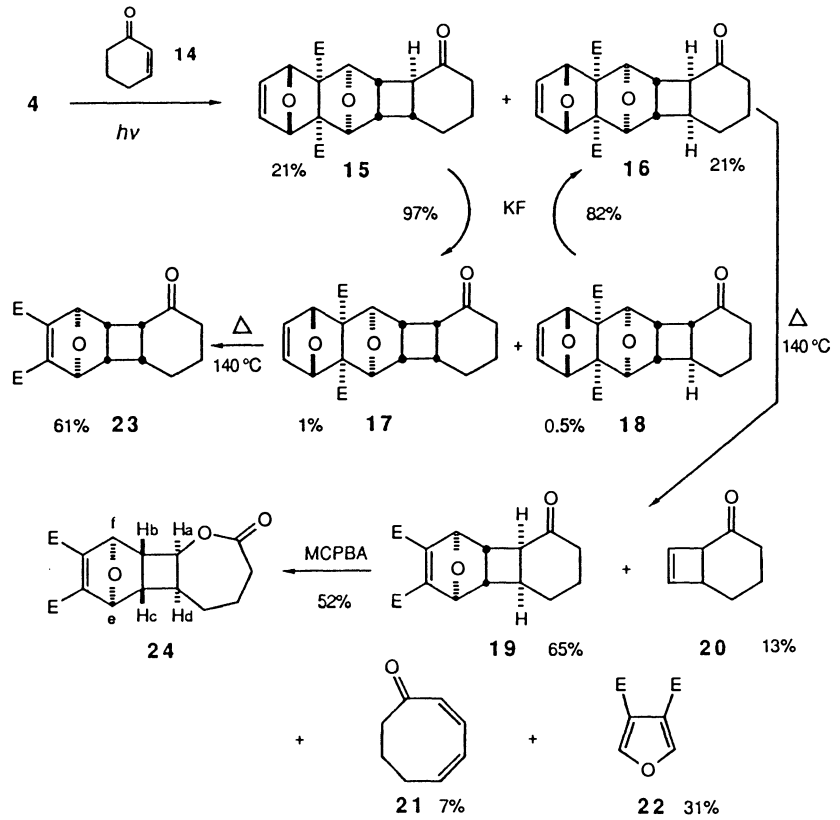

Scheme 2.

tion of the lower methine signal (H_f) resulted in an enhancement of both signals of H_a and H_b at 2.73 (1H, ddd, J=6.9, 2.6, 1.0 Hz), and the stereochemistry of **24** must be cis-transoid-cis. From these observations and the epimerization experiments, **16** and **17** were determined to be cis-transoid-cis and cis-cisoid-cis, respectively, and **15** and **18** were the corresponding trans epimers, as shown in Scheme 2.

On the other hand, the irradiation of **4** with 2-cyclopentenone (**25**) gave a single product (**26**) in 50% yield. The stereochemistry of **26** was shown to be parallel to that of **16**: its thermolysis gave **27** and **28** in 60 and 12% yields, by refluxing in a xylene solution. The ^{1}H NMR spectrum of **28** was identical with that of the reported bicyclo[3.2.0]hept-6-en-2-one.[18,19] An MCPBA-oxidation of **27** did indeed occur to form a single lactone (**29**), whose ^{1}H NMR spectrum showed a proton signal on the lactonic carbon at δ=4.53 (H_a, dd, J=7.7, 2.9 Hz), which coupled to two signals (H_b and H_d) around 2.4 and 2.6, but not to a signal (H_c) at 2.32, being confirmed from the COSY spectrum. An irradiation of the lower methine signal (H_f) enhanced the signal of H_a.

The difference in the product distributions in reactions with **14** and **25** should be due to, at least in part, a large strain energy for *trans*-bicyclo[3.2.0]heptanone framework, which should have arisen from the latter (**25**).

Photoaddition with Methyl 2,4-Dioxopentanoate (2). An irradiation of **4** with **2** gave a single product (**30**) via a [2+2] addition and a retro-aldol process.[20] The stereochemistry of **30** was determined to be as shown in Scheme 4 from the appearance of H_b as a doublet (J=8.4 Hz). A reductive cyclization of **30** with titanium(II) chloride[21] gave two 1,2-diols (**31** and **32**) in 60 and 20% yields. The NOE experiments of **31** and **32** established the cis relationship between the methyl group and protons H_a and H_b. Acetal formations of **31** to dioxolanes (**33**) and **32** to an uncyclized orthoformate (**34** or **35**) determined the *cis*- and *trans*-glycols, respectively.

All of the photoadducts from **4** with enones and *p*-quinones were derived by reactions at the anti C=C bond to the methoxycarbonyl groups. The inertness of the syn C=C bond toward photocycloaddition has been established without exception. The marked difference in the photochemical reactivity of these double bonds is interesting.

Thermal Cycloreversions of Photoadducts. As mentioned in the preparations of **19** and **27**, further cycloreversed products, **20** and **28**, were formed in 13 and 12% yields, respectively. Heating photoadduct **15** at 140 °C gave two products (**23** and **36**) in 44 and 38% yields, respectively. The latter **36** was quantitatively

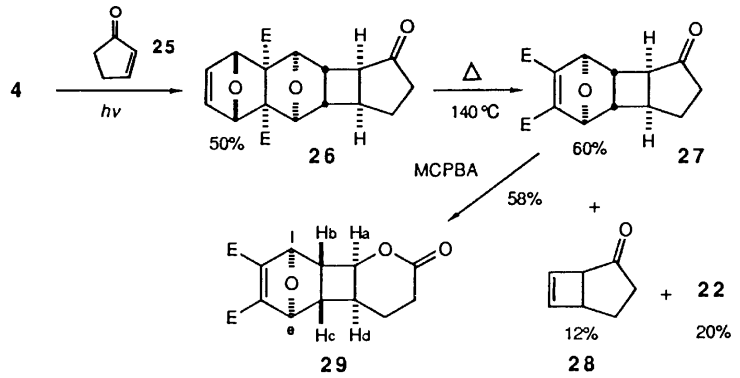

Scheme 3.

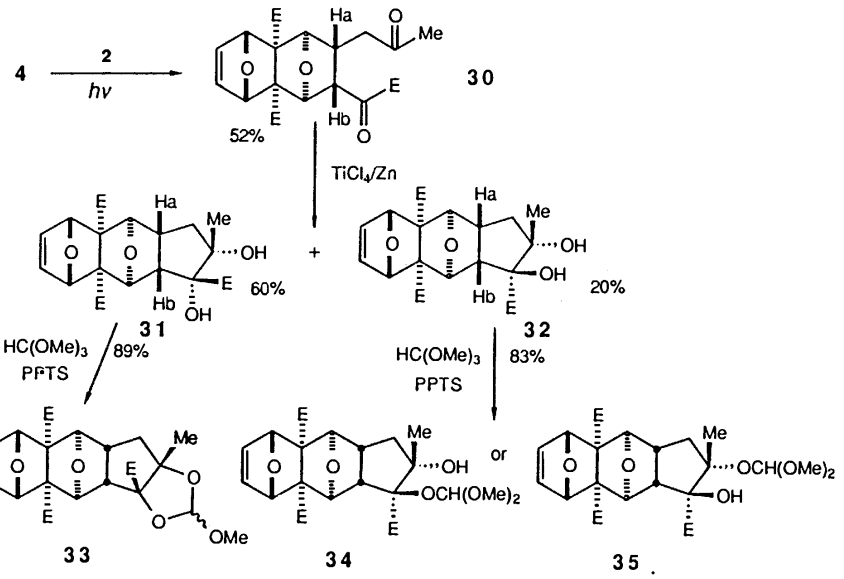

Scheme 4.

epimerized to **23** at 220 °C and the former **23** was obtained in 61% from the cis-cisoid-cis photoadduct **17**. Thermolysis of **19** and **23** at 330 °C gave **20** in 44 and 45% yields. While **27** was heated at 140 °C for 48 h, **28** was obtained in 52% yield together with **22**.

Subsequently, when **31** was thermolysed at 140 °C, thermolysates (**37** and **38**) were obtained in 67 and 7% yields. The former was converted to the latter in 63% yield at 220 °C.

Acid Treatments of Photoadducts from *p*-Quinones. Since photoadducts from *p*-quinones have a 2,5-cyclohexadienone chromophore, a dienone-phenol rearrangement would be expected.[12,13] When **6** was heated with hydrochloric acid in ethanol, two products (**39** and **40**) were formed in 61 and 13% yields. The major **39** had an aromatic ring with two ethoxyl groups, which were located at C-2 and C-4. The stereochemistry of the hydroxyl group was exo, from the coupling constant of H_a signal. The minor **40** had an enone chromophore and an oxetane ring. From the mass spectrum and an elemental analysis, **40** was shown to be a Michael adduct of hydrochloric acid. Two singlet signals of H_b and H_c appeared at 4.94 and 5.01 in **6**, whereas corresponding signals at 4.97 and 5.35 in **40**. One of them moved to the lower field upon the introduction of a chlorine atom. Therefore, the

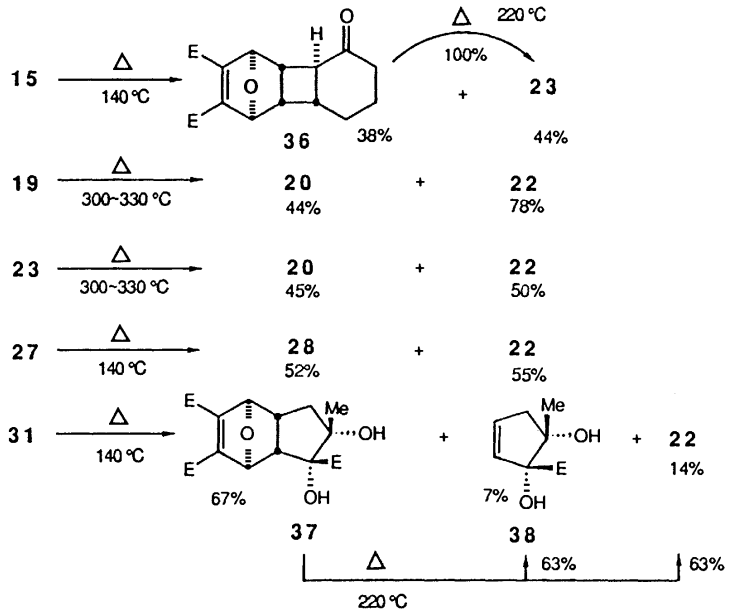

Scheme 5.

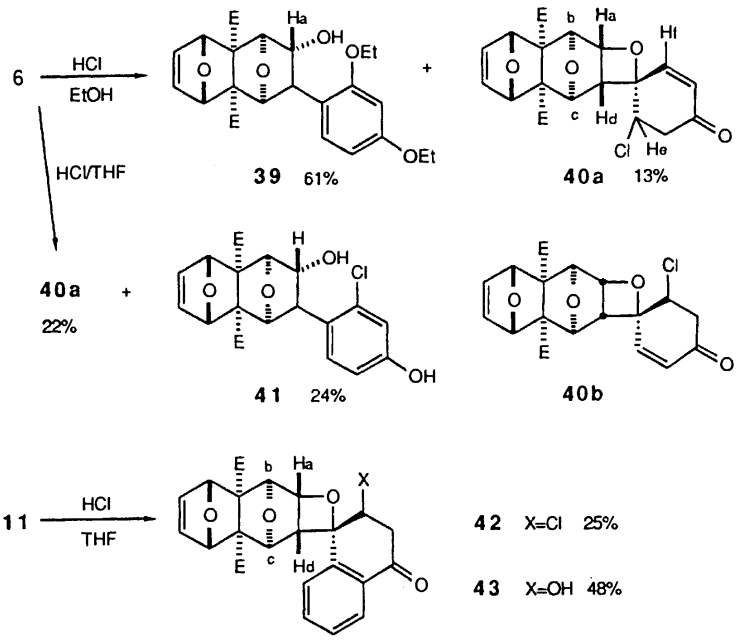

Scheme 6.

structure **40a** should be as depicted. The stereochemistry of the chlorine atom was quasi-axial due to an observation of a long-range coupling between H_e and H_f. To minimize the Michael adduct formation, the reaction was carried out in tetrahydrofuran; a new chlorophenol derivative (**41**) was obtained along with **40a**. Similarly, **11** gave two Michael adducts (**42** and **43**) as shown in Scheme 6. A chlorine atom of **42** was quasi-equatorial because a methylene signal appeared as two doublets of doublets at 3.02 (J=18.7, 12.8 Hz) and 3.28 (J=18.7, 5.5 Hz), while the hydroxyl group of **43** was quasi-axial from the splittings of the methylene signals at 2.89 (dm, J=18.9 Hz) and 2.98 (dd, J=18.9, 2.7 Hz). The chemical shifts of H_b and H_c (5.10 and 4.24) of **42** were similar to those (5.19 and 4.47) of **11**.

Thus, a dienone-phenol rearrangement did not occur in these particular photoadducts from *p*-quinones.

Conclusion

As has been described, **4** was photochemically reactive with cyclic enones and a further thermal cycloreversion of the photoadducts afforded 1,2-unsubstituted cyclobutene derivatives. Photochemical additions of **4** were regioselective. The cis-transoid-cis isomer formed exclusively from **25** and predominantly from **14**. Ready thermolyses to cyclobutene and cyclopentene derivatives indicate that **4** is useful as cycloaddend in alicyclic synthesis.

Experimental

Elemental analyses were performed by Miss S. Hirashima, of Institute of Advanced Material Study, Kyushu University. NMR spectra were measured by a JEOL 270H spectrometer in $CDCl_3$ solution (unless otherwise specified): chemical shifts are expressed in the unit δ. Mass spectra were measured with a JEOL OISG-2 spectrometer. IR spectra were taken as KBr disks or as a $CHCl_3$ solution using a Jasco IR-A 102 spectrometer. UV spectra were measured by a Hitachi U-3200 spectrophotometer.

Photoreaction of 1 and Methyl 2,4-Dioxopentanoate (2). Formation of 7-Oxaquadricyclane Derivative (3). A $CDCl_3$ solution (0.5 cm^3) of **1** (40 mg) and **2** (16.2 mg) was irradiated with a 400-W high-pressure mercury lamp and the reaction was monitored by ^1H NMR spectroscopy. After 1 h, new signals [2.83(2H, d, J=3 Hz), 3.70 (6H, s), and 4.93 (2H, d, J=3 Hz)] of **3** appeared, which was identical with the spectrum of the authentic **3**.[8]

Photoreaction of 4 and *p*-Benzoquinone (5). a) A $CDCl_3$ solution (0.5 cm^3) of **4** (35 mg) and **5** (14.5 mg) was irradiated. After 20 min, the solvent was evaporated and the residue was chromatographed on a silica-gel column to isolate **6** [colorless crystals, mp 191—192 °C, 12.6 mg; 78%. Found: C, 62.19; H, 4.64%. Calcd for $C_{20}H_{18}O_8$: C, 62.18; H, 4.70%. ^1H NMR δ=3.26 (1H, d, J=5.1 Hz, H_d), 3.70 (3H, s), 3.74 (3H, s), 4.71 (1H, d, J=1.8 Hz), 4.84 (1H, d, J=1.8 Hz), 4.94 (1H, s, H_b or H_c), 5.01 (1H, s, H_c or H_b), 5.21 (1H, d, J=5.1 Hz, H_a), 6.14 (1H, dd, J=10.3, 2.2 Hz), 6.21 (1H, dd, J=10.3, 2.2 Hz), 6.54 (1H, dd, J=5.9, 1.8 Hz), 6.67 (1H, dd, J=5.9, 1.8 Hz), 7.28 (1H, dd, J=10.3, 2.9 Hz), and 7.69 (1H, dd, J=10.3, 2.9 Hz). ^{13}C NMR δ=49.1, 52.8, 72.0, 72.8, 79.3, 80.0, 80.2, 80.3, 81.2, 84.0, 127.1, 128.3, 130.5, 136.9, 138.5, 144.7, 148.7, 170.4, 170.5, and 185.2. IR ν: 1715, 1665, 1625, 1260, and 1220 cm^{-1}. UV (MeOH): 237.6 nm (ε=12450)] together with **5** [10 mg] and **4** [12 mg]. **b)** A $CDCl_3$ solution (0.8 cm^3) of **5** (138 mg) and a 3 : 1-mixture (476 mg) of **4** and **7** was reacted by similar manner. Product **6** [193 mg, 54%] was obtained together with recovered **5** [10 mg] and a mixture [204 mg] of **4** and **7**.

Photoreaction of 4 and 1,4-Naphthoquinone (10). A $CHCl_3$ solution (1 cm^3) of **4** (341 mg) and **10** (156 mg) was irradiated to give **11** [colorless crystals, mp 179—181 °C, 150 mg; 44%. Found: C, 65.81; H, 4.58%. Calcd for $C_{24}H_{20}O_8$: C, 66.05; H, 4.62%. ^1H NMR δ=3.24 (1H, d, J=4.8 Hz, H_d), 3.60 (3H, s), 3.75 (3H, s), 4.47 (1H, s, H_c), 4.66 (1H, br s), 4.87 (1H, br s), 5.19 (1H, s, H_b), 5.36 (1H, d, J=4.8 Hz, H_a), 6.29 (1H, d, J=10.3 Hz), 6.53 (1H, dd, J=5.9, 1.8 Hz), 6.64 (1H, dd, J=5.9, 1.8 Hz), 7.47 (1H, ddd, J=7.7, 7.0, 1.5 Hz), 7.64 (1H, ddd, J=7.7, 7.0, 1.5 Hz), 7.68 (1H, d, J=10.3 Hz), 8.06 (1H, dd, J=7.0, 1.5 Hz), and 8.52 (1H, dd, J=7.0, 1.5 Hz). ^{13}C NMR δ=51.7, 52.7, 52.9, 72.5, 73.6, 79.2, 80.0, 80.2, 81.4, 83.3, 83.7, 126.3, 126.5, 128.6, 129.9, 130.7, 132.3, 137.0, 138.5, 138.7, 153.0, 170.4 (2C), and 184.6. IR ν: 1720, 1670, 1597, and 1260 cm^{-1}. UV (MeOH): 244.2 (ε=11600), 278.8 (5000), and 312.0 nm (2200)] and recovered **4** [211 mg] and **10** [33 mg].

Photoreaction of 4 and Cyclohexenone (14). A $CHCl_3$ solution (2 cm^3) of **4** (824 mg) and **14** (2.03 g) was irradiated for 60 h to give **15** [colorless crystals, mp 126—127 °C, 221 mg: 21%. Found: C, 64.12; H, 5.95%. Calcd for $C_{20}H_{22}O_7$: C, 64.16; H, 5.92%. ^1H NMR δ=1.6—2.5 (6H, m), 2.45—2.6 (1H, m), 2.83 (1H, dd, J=9.1, 5.5 Hz), 3.05 (1H, dd, J=13.6, 6.6 Hz), 3.33 (1H, dd, J=6.6, 5.5 Hz), 3.68 (3H, s), 3.69 (3H, s), 4.64 (1H, s), 4.71 (1H, br s), 4.76 (1H, br s), 4.97 (1H, s), 6.58 (1H, dd, J=5.5, 1.1 Hz), and 6.64 (1H, dd, J=5.5, 1.1 Hz). ^{13}C NMR δ=24.9, 26.7, 39.3, 41.6, 42.9, 45.9, 51.7, 52.5 (2C), 71.7, 73.8, 79.2, 80.3, 82.2, 83.9, 137.7, 138.9, 171.4, 171.5, and 206.6. IR ν: 1720, 1260, 1207, and 904 cm^{-1}], **16** [colorless crystals, mp 181—183 °C, 220 mg; 21%. Found: C, 64.05; H, 5.87%. Calcd for $C_{20}H_{22}O_7$: C, 64.16; H, 5.92%. ^1H NMR δ=1.5—1.6 (1H, m), 1.65—1.8 (1H, m), 1.8—1.9 (1H, m), 1.95—2.1 (1H, m), 2.24 (1H, ddd, J=18.0, 8.4, 6.6 Hz), 2.46 (1H, dt, J=18.0, 5.9 Hz), 2.5—2.6 (2H, m), 2.66 (1H, dd, J=8.1, 4.4 Hz), 2.81 (1H, dd, J=5.9, 4.4 Hz). 3.68 (3H, s), 3.69 (3H, s), 4.72 (2H, s), 4.76 (1H, br s), 4.81 (1H, s), 6.58 (1H, dd, J=5.5, 1.8 Hz), and 6.62 (1H, dd, J=5.5, 1.8 Hz). ^{13}C NMR δ=20.3, 27.5, 36.2, 39.6, 43.0, 44.0, 45.9, 52.5 (2C), 72.0, 72.2, 79.9 (2C), 84.5, 84.6, 138.1, 138.3, 171.2, 171.5, and 214.6. IR ν: 1725, 1697, 1262, 1210, and 905 cm^{-1}], **17** [colorless crystals, mp 185 °C, 7.5 mg, 1%. Found: C, 64.32; H, 5.97%. Calcd for $C_{20}H_{22}O_7$: C, 64.16; H, 5.92%. ^1H NMR δ=1.5—2.0 (4H, m), 2.2—2.35 (2H, m), 2.8—3.0 (3H, m), 3.18 (1H, dd, J=9.2, 6.6 Hz), 3.67 (3H, s), 3.68 (3H, s), 4.69 (1H, br s), 4.73 (1H, br s), 4.89 (1H, s), 4.91 (1H, s), 6.56 (1H, dd, J=5.5, 1.8 Hz), and 6.64 (1H, dd, J=5.5, 1.8 Hz). ^{13}C NMR δ=20.3, 21.5, 34.0, 39.6, 41.0, 42.6, 43.5, 52.8 (2C), 72.6, 72.8, 80.1, 80.2, 81.3, 82.6, 138.0, 138.9, 171.6 (2C), and 214.4. IR ν: 1720, 1695, 1260, and 1207 cm^{-1}], **18** [colorless crystals, mp 162—164 °C, 5 mg, 0.5%. Found: C, 64.30; H, 5.88%. Calcd for $C_{20}H_{22}O_7$: C, 64.16; H, 5.92%. ^1H NMR δ=1.5—1.9 (3H, m), 2.0—2.2 (4H, m), 2.4—2.5 (1H, m), 2.9—3.1 (2H, m), 3.68 (6H, s), 4.66 (1H, s), 4.72 (2H, br s), 5.28 (1H, s), 6.59 (1H, dd, J=5.5, 1.8 Hz), and 6.64 (1H, dd, J=5.5. 1.8 Hz). ^{13}C NMR δ=26.0, 29.0, 39.1,

42.6, 43.4, 45.1, 52.7, 52.8 (2C), 71.9, 73.8, 79.4, 80.6, 81.0, 83.9, 138.1, 139.1, 171.7, 171.8, and 206.7. IR ν: 1740, 1710, 1280, 1255, 1225, and 1080 cm^{-1}], and recovered **4** [47 mg].

Photoreaction of 4 and Cyclopentenone (25). A $CHCl_3$ solution (2 cm^3) of **4** (584 mg) and **25** (1.76 g) was irradiated for 80 h to give **26** [a colorless oil, 245 mg; 50%. Found: m/z 360.1208 (M^+). Calcd for $C_{19}H_{20}O_7$: 360.1208. ^1H NMR δ=1.9—2.4 (4H, m), 2.55—2.8 (4H, m), 3.69 (3H, s), 3.70 (3H, s), 4.71 (1H, br s), 4.74 (1H, br s), 4.79 (1H, s), 4.81 (1H, s), 6.59 (1H, dd, J=5.5, 1.8 Hz), and 6.62 (1H, dd, J=5.5, 1.8 Hz). ^{13}C NMR δ=27.6, 36.7, 36.9, 42.1, 45.1, 47.2, 52.5 (2C), 72.0, 72.4, 79.8, 79.9, 84.2, 84.9, 138.1, 138.2, 171.1, 171.4, and 221.3. IR ν: 1730, 1265, and 1220 cm^{-1}] and recovered **4** [211 mg] and **25** [454 mg].

Photoreaction of 4 and Methyl 2,4-Dioxopentanoate (2). A $CHCl_3$ solution (2 cm^3) of **4** (485 mg) and **2** (620 mg) was irradiated for 60 h to give **30** [colorless crystals, mp 175—176 °C, 269 mg; 52%. Found: C, 56.78; H, 5.26%. Calcd for $C_{20}H_{22}O_{10}$: C, 56.87; H, 5.25%. ^1H NMR δ=2.10 (3H, s), 2.55 (1H, dd, J=19.0, 8.4 Hz), 2.62 (1H, dd, J=19.0, 7.0 Hz), 3.23 (1H, td, J=8.4, 7.0 Hz, H_a), 3.67 (3H, s), 3.68 (3H, s), 3.89 (3H, s), 4.15 (1H, d, J=8.4 Hz, H_b), 4.48 (1H, d, J=1.5 Hz), 4.83 (1H, d, J=0.7 Hz), 4.95 (1H, d, J=1.1 Hz), 5.01 (1H, d, J=1.5 Hz), 6.62 (1H, dd, J=5.9, 1.5 Hz), and 6.71 (1H, dd, J=5.9, 1.1 Hz). ^{13}C NMR δ=30.2, 40.0, 43.3, 49.4, 52.5, 52.6, 53.3, 72.4, 72.5, 79.7 (2C), 83.2. 86.4, 137.6, 138.8, 161.0, 170.9, 171.1, 193.1, and 207.4. IR ν: 1730, 1270, and 1207 cm^{-1}] and recovered **4** [145 mg] and **2** [192 mg].

Iodolactonization of 6. A CH_3CN solution (6 cm^3) of **6** (100 mg), I_2 (120 mg), and $NaHCO_3$ (210 mg) was stirred for 2 d. A mixture was washed with an $NaHSO_3$ solution and extracted with $CHCl_3$. The solvent was evaporated and the residue was chromatographed on a silica-gel column to give **8** [colorless crystals, mp 240 °C, 36 mg; 32%. Found: C, 46.08; H, 3.19%. Calcd for $C_{19}H_{15}O_8I$: C, 45.80; H, 3.03%. ^1H NMR (DMSO-d_6) δ=3.40 (1H, d, J=5.1 Hz), 3.72 (3H, s), 4.10 (1H, s), 4.82 (1H, s), 4.88 (1H, s), 5.00 (1H, s), 5.11 (1H, d, J=5.5 Hz), 5.21 (1H, d, J=5.1 Hz), 5.51 (1H, J=5.5 Hz), 6.1—6.2 (2H, m), and 7.45—7.5 (2H, m). ^{13}CNMR (DMSO-d_6) δ=46.8, 53.2, 58.0, 74.0, 78.9, 79.1, 79.5, 80.2, 81.3, 81.9, 83.7, 84.5, 126.1, 129.8, 144.6, 149.5, 167.8, 170.5, and 184.7. IR ν: 1800, 1740, 1660, 1620, 1250, and 1000 cm^{-1}. UV (MeOH): 237.6 nm (ε=13500)], **9** [colorless crystals, mp 189—191 °C, 35 mg; 31%. Found: C, 45.99; H, 3.11%. Calcd for $C_{19}H_{15}O_8I$: C, 45.80; H, 3.03%. ^1H NMR (DMSO-d_6) δ=3.25 (1H, d, J=5.1 Hz), 3.74 (3H, s), 4.14 (1H, s), 4.82 (1H, s), 4.92 (1H, s), 5.09 (1H, d, J=5.1 Hz), 5.12 (1H, s), 5.30 (1H, d, J=5.1 Hz), 5.38 (1H, d, J=5.1 Hz), 6.12 (1H, dd, J=9.9, 2.2 Hz), 6.20 (1H, dd, J=10.3, 2.2 Hz), 7.46 (1H, dd, J=9.9, 2.9 Hz), and 7.54 (1H, dd, J=10.3, 2.2 Hz). ^{13}CNMR (DMSO-d_6) δ=46.7, 53.3, 59.0, 73.7, 77.8, 78.9 (2C), 79.1, 82.3, 83.3, 84.4 (2C), 126.3, 129.8, 144.6, 149.5, 167.7, 170.6, and 184.7. IR ν: 1797, 1740, 1660, 1620, and 1250 cm^{-1}. UV (MeOH): 237.4 nm (ε= 14500)], and recovered **6** [12 mg].

Iodolactonization of 11. A CH_3CN solution (6 cm^3) of **11** (117 mg), I_2 (164 mg), and $NaHCO_3$ (210 mg) was stirred for 4 d. A similar work-up as mentioned above gave **12** [colorless crystals, mp 240 °C, 13 mg; 9%. Found: C, 50.00; H, 2.99%. Calcd for $C_{23}H_{17}O_8I$: C, 50.29; H, 3.12%. ^1H NMR (DMSO-d_6) δ=3.16 (1H, d, J=4.8 Hz), 3.75 (3H, s), 4.12 (1H, s), 4.28 (1H, s), 5.05 (1H, d, J=5.1 Hz), 5.08 (1H, s), 5.15 (1H, s), 5.32 (1H, d, J=5.1 Hz), 5.48 (1H, d, J=4.8 Hz), 6.31 (1H, d, J=10.3 Hz), 7.57 (1H, ddd, J=7.7, 7.0, 1.1 Hz), 7.70 (1H, td, J=7.0, 1.5 Hz), 7.85 (1H, d, J=10.3 Hz), 7.94 (1H, dd, J=7.7, 1.5 Hz), and 8.38 (1H, dd, J=7.0, 1.1 Hz). ^{13}CNMR (DMSO-d_6) δ=49.7, 53.3, 59.4, 74.2, 77.8, 78.4, 79.2, 82.3, 82.6, 83.2, 83.9, 84.2, 125.7 (2C), 128.7, 129.4, 130.2, 131.6, 138.6, 153.4, 167.7, 170.5, and 183.5. IR ν: 1800, 1740, 1660, and 1595 cm^{-1}. UV (MeOH): 242.0 (ε=11850) and 277.8 nm (5100)] and **13** [colorless crystals, mp 249 °C, 27 mg: 18%. Found: C, 50.63; H, 3.04%. Calcd for $C_{23}H_{17}O_8I$: C, 50.29; H, 3.12%. ^1H NMR (DMSO-d_6) δ=3.39 (1H, d, J=4.8 Hz), 3.61 (3H, s), 4.04 (1H, s), 4.27 (1H, s), 4.92 (1H, s), 4.99 (1H, s), 5.11 (1H, d, J=5.1 Hz), 5.41 (1H, d, J=4.8 Hz), 5.55 (1H, d, J=5.1 Hz), 6.30 (1H, d, J=10.3 Hz), 7.55 (1H, dd, J=7.7, 7.3 Hz), 7.68 (1H, dd, J=7.7, 7.3 Hz), 7.86 (1H, d, J=10.3 Hz), 7.93 (1H, d, J=7.7 Hz), and 8.36 (1H, d, J=7.7 Hz). ^{13}CNMR (DMSO-d_6) δ=49.6, 53.2, 58.5, 74.5, 78.3, 79.1, 79.8, 81.3, 82.3, 83.1, 83.9, 84.5, 125.6 (2C), 128.7, 129.3, 130.3, 131.7, 138.3, 153.3, 167.8, 170.6, and 183.5. IR ν: 1800, 1750, 1675, 1597, and 1240 cm^{-1}. UV (MeOH): 243.2 (ε=11900) and 278.2 nm (5100)].

Epimerization of 15. An MeOH solution (16 cm^3) of **15** (90 mg) and KF (520 mg) was stirred in the presence of Florisil (540 mg) at room temperature for 2 d. After the solvent was removed, the residue was extracted with $CHCl_3$. The solvent was evaporated and the residue was chomatographed to give **17** [87 mg, 97%].

Epimerization of 18. An MeOH solution (5 cm^3) of **18** (43.6 mg) and KF (250 mg) was stirred with Florisil (300 mg) overnight to give **16** [35.7 mg, 82%].

Thermolysis of 16. A xylene solution (1.5 cm^3) of **16** (110 mg) was refluxed for 60 h in a sealed tube. The solvent was evaporated and the residue was chromatographed on a silica-gel column to give **19** [a colorless oil, 51.6 mg, 65%. Found: C, 62.54; H, 5.90%. Calcd for $C_{16}H_{18}O_6$: C, 62.74; H, 5.92%. ^1H NMR δ=1.6—2.0 (4H, m), 2.2—2.6 (6H, m), 3.79 (3H, s), 3.81 (3H, s), 5.09 (1H, s), and 5.17 (1H, s). ^{13}C NMR δ=20.2, 27.4, 33.9, 39.5, 39.9, 41.6, 43.4, 52.4 (2C), 82.6, 83.0, 141.8, 142.5, 162.5, 162.9, and 213.3. IR ν: 1720, 1260, and 1206 cm^{-1}], **20**[15,16] [a colorless oil, 4.1 mg, 13%], **21**[17] [a colorless oil, 2.1 mg; 7%], **22** [14.7 mg, 31%], and recovered **16** [12.5 mg].

Thermolysis of 17. A xylene solution (1 cm^3) of **17** (87 mg) was refluxed for 30 h to give **23** [a colorless oil, 26 mg; 61%. Found: C, 62.75; H, 6.02%. Calcd for $C_{16}H_{18}O_6$: C, 62.74; H, 5.92%. ^1H NMR δ=1.6—2.3 (6H, m), 2.50 (1H, dd, J=8.1, 7.0 Hz), 2.83 (1H, dd, J=9.5, 6.2 Hz), 2.9—3.1 (2H, m), 3.79 (6H, s), 5.20 (1H, s), and 5.32 (1H, s). ^{13}C NMR δ=20.2, 21.3, 30.7, 39.2, 39.4 (2C), 40.5, 52.3 (2C), 79.8, 80.4, 142.4, 142.7, 162.6, 162.7, and 213.0. IR ν: 1730, 1630, and 1215 cm^{-1}] and recovered **17** [34.7 mg].

Thermolysis of 15. A xylene solution (2 cm^3) of **15** (220 mg) was refluxed for 20 h to give **23** [61.8 mg, 44%], **36** [a colorless oil, 52.9 mg, 38%. Found: C, 62.50: H, 5.90%. Calcd for $C_{16}H_{18}O_6$: C, 62.74; H, 5.92%. ^1H NMR δ=1.8—2.3 (6H, m), 2.35—2.5 (2H, m), 2.89 (1H, dd, J=12.9, 6.6 Hz), 3.15 (1H, dd, J=6.6, 5.5 Hz), 3.79 (3H, s), 3.81 (3H, s), 4.99 (1H, s), and 5.31 (1H, s). ^{13}C NMR δ=25.4, 27.4, 39.7, 40.6, 41.5, 42.6, 50.6, 52.3, 52.4, 81.1, 81.9, 141.9, 144.9, 162.4, 162.8, and 206.7. IR ν: 1735, 1720. 1700, and 1210 cm^{-1}], and recovered **15** [49 mg].

Epimerization of 36 to 23. Compound **36** (19 mg) was placed in a sealed tube and pyrolyzed at 220 °C to give **23** [19 mg; 100%].

Thermolysis of 19. The compound **19** (70 mg) was passed through a glass tube heated at 300—330 °C under an

N_2 stream to give **20** [8 mg; 44%], **22** [21.5 mg; 78%], and recovered **19** [24 mg].

Thermolysis of 23. Similarly, compound **23** (70 mg) was pyrolyzed at 300—330 °C under an N_2 stream to give **20** [6 mg; 45%], **22** [10 mg, 50%], and recovered **23** [36.6 mg].

Thermolysis of 26. A xylene solution (1 cm^3) of **26** (150 mg) was refluxed for 2 d to give **27** [a colorless oil, 48 mg, 60%. Found: *m/z* 292.0948 (M^+). Calcd for $C_{15}H_{16}O_6$: 292.0946. ^1H NMR δ=2.0—2.4 (6H, m), 2.55—2.7 (2H, m), 3.79 (3H, s), 3.81 (3H, s), 5.17 (1H, s), and 5.19 (1H, s). ^{13}C NMR δ=27.3, 36.4, 36.6, 39.3, 42.7, 45.4, 52.4 (2C), 82.7, 83.0, 142.0, 142.3, 162.4, 162.8, and 219.8. IR ν: 1730, 1630, 1260, and 1210 cm^{-1}. UV (MeOH): 227.8 nm (ε=5400)], **28**[18,19] [a colorless oil, 3.5 mg, 12%], **22** [10 mg, 20%], and recovered **26** [51 mg].

Thermolysis of 27. A xylene solution (1 cm^3) of **27** (58 mg) was refluxed for 2 d to give **28** [5 mg, 52%], **22** [9 mg, 55%], and recovered **27** [32.2 mg].

MCPBA-Oxidation of 19. A $CHCl_3$ solution (1.5 cm^3) of **19** (33 mg) and MCPBA (50 mg) was kept in a refrigerator for 10 h. The mixture was washed with aqueous $NaHSO_3$ and $NaHCO_3$ solutions and a $CHCl_3$ layer was dried on Na_2SO_4 and evaporated. The residue was chromatographed on a silica-gel column to give **24** [colorless crystals, mp 107—109 °C, 18 mg, 52%. Found: C, 59.80; H, 5.74%. Calcd for $C_{16}H_{18}O_7$: C, 59.62; H, 5.63%. ^1H NMR δ=1.6—1.8 (1H, m), 1.8—1.95 (3H, m), 2.1—2.2 (1H, m), 2.22 (1H, dd, *J*=7.0, 4.0 Hz), 2.4—2.5 (2H, m, H_c and H_d), 2.73 (1H, ddd, *J*=6.9, 2.6, 1.0 Hz, H_b), 3.80 (3H, s), 3.82 (3H, s), 4.39 (1H, dd, *J*=6.6, 2.6 Hz, H_a), 5.08 (1H, s, H_e), and 5.12 (1H, s, H_f). ^{13}C NMR δ=20.5, 24.8, 31.9, 36.8, 40.5, 43.1, 52.4, 52.5, 73.6, 81.4, 82.1, 141.8, 143.3, 162.2. 162.6, and 172.8. IR ν: 1737, 1690, 1615, and 1290 cm^{-1}. UV (MeOH): 232.2 nm (ε=6000)].

MCPBA-Oxidation of 23. A $CHCl_3$ solution (3 cm^3) of **23** (63 mg) and MCPBA (60 mg) was refluxed for 10 h. Same work-up gave no product.

MCPBA-Oxidation of 27. A $CHCl_3$ solution (3 cm^3) of **27** (97 mg) and MCPBA (80 mg) was kept for 1 d in a refrigerator. Same work-up gave **29** [colorless crystals. mp 144—145 °C, 59 mg, 58%. Found: C, 58.52; H, 5.34%. Calcd for $C_{15}H_{16}O_7$: C, 58.44; H, 5.23%. ^1H NMR δ=1.9—2.0 (1H, m), 2.15—2.2 (1H, m), 2.32 (1H, dd, *J*=7.0, 3.3 Hz, H_c), 2.35—2.5 (2H, m), 2.5—2.6 (2H, m, H_b and H_d), 3.81 (3H, s), 3.82 (3H, s), 4.53 (1H, dd, *J*=7.7, 2.9 Hz, H_a), 5.14 (1H, s, H_e), and 5.22 (1H, s, H_f). ^{13}C NMR δ=22.8, 28.6, 31.3, 40.6, 46.1, 52.5 (2C), 74.0, 81.5, 82.0, 141.7, 143.6, 162.2, 162.7, and 171.2. IR ν: 1720, 1630, and 1230 cm^{-1}. UV (MeOH): 231.8 nm (ε=5900)].

$TiCl_2$-Mediated Cyclization of 30. To an anhydrous THF solution (20 cm^3) of $TiCl_4$ (0.1 cm^3), Zn (0.1 g) was added at −60 °C under stirring. After warming to room temperature, pyridine (0.1 cm^3) was added. To the resultant suspension, a THF solution (10 cm^3) of **30** (102 mg) was added drop by drop. After stirring overnight, the mixture was quenched with aqueous K_2CO_3 and extracted with $CHCl_3$. The organic layer was dried on Na_2SO_4 and evaporated. The residue was chromatographed on silica-gel to give **31** [colorless crystals, mp 200—202 °C, 63 mg; 60%. Found: C, 56.55; H, 5.74%. Calcd for $C_{20}H_{24}O_{10}$: C, 56.60; H, 5.70%. ^1H NMR δ=1.13 (3H, s), 1.75 (1H, dd, *J*=14.3, 4.0 Hz), 2.31 (1H, dd, *J*=14.3, 9.6 Hz), 2.88 (1H, ddd, *J*=9.6, 7.3, 4.0 Hz), 3.15 (1H, d, *J*=7.3 Hz), 3.69 (6H, s), 3.79 (3H, s), 3.80 (1H, s, OH), 4.44 (1H, s, OH), 4.69 (1H, s), 4.77 (1H, s), 4.80 (1H, s), 5.12 (1H, s), and 6.64 (2H, s). ^{13}C NMR δ=22.2, 43.0, 43.7, 52.0, 52.3, 52.6 (2C), 71.6, 72.1, 79.5 (2C), 81.0, 82.6, 85.0, 87.0, 138.2, 138.3, 171.1, 171.2, and 173.9. IR ν: 3370, 1720, 1260, 1235, and 1215 cm^{-1}] and **32** [colorless crystals, mp 199—201 °C, 21 mg; 20%. Found: C, 56.62; H, 5.65%. Calcd for $C_{20}H_{24}O_{10}$: C, 56.60; H, 5.70%. ^1H NMR δ=1.26 (3H, s), 1.46 (1H, dd, *J*=13.2, 9.5 Hz), 2.00 (1H, dd, *J*=13.2, 8.1 Hz), 3.11 (1H, dt, *J*=9.5, 8.1 Hz), 3.21 (1H, d, *J*=8.1 Hz), 3.34 (1H, s, OH), 3.69 (3H, s), 3.71 (3H, s), 3.77 (1H, s, OH), 3.86 (3H, s), 4.64 (1H, s), 4.77 (1H, d, *J*=1.1 Hz), 4.82 (1H, d, *J*=1.1 Hz), 5.08 (1H, s), 6.60 (1H, d, *J*=4.0 Hz), and 6.67 (1H, d, *J*=4.0 Hz). ^{13}C NMR δ=20.4, 41.7, 44.4, 52.3, 52.5, 52.6, 52.9, 71.5, 72.3, 79.5, 80.0, 82.5, 84.3, 84.9, 85.3, 137.8, 138.6, 171.3, 171.4, and 173.7. IR ν: 3500, 1725, 1260, and 1215 cm^{-1}].

Dioxolane Formation of 31. A trimethyl orthoformate solution (2 cm^3) of **31** (37 mg) and PPTS (10 mg) was stirred overnight. The mixture was washed with aqueous Na_2CO_3 and extracted with $CHCl_3$. The solvent was evaporated to give **33** [colorless crystals, a 1 : 2.5-mixture of isomers, mp 161—168 °C, 36 mg, 89%. Found: C, 56.73; H, 5.68%. Calcd for $C_{22}H_{26}O_{11}$: C, 56.65; H, 5.62%. ^1H NMR of a major isomer δ=1.35 (3H, s), 1.95 (1H, dd, *J*=14.3, 7.3 Hz), 2.17 (1H, dd, *J*=14.3, 9.9 Hz), 2.93 (1H, ddd, *J*=9.9, 8.1, 7.3 Hz), 3.41 (1H, d, *J*=8.1 Hz), 3.46 (3H, s), 3.68 (6H, s), 3.80 (3H, s), 4.60 (1H, s), 4.75 (2H, s), 4.76 (1H, s), 5.95 (1H, s), and 6.6—6.7 (2H, m) and a minor isomer δ=1.26 (3H, s), 2.00 (1H, dd, *J*=14.3, 7.3 Hz), 2.37 (1H, dd, *J*=14.3, 9.2 Hz), 2.85 (1H, ddd, *J*=9.2, 8.1, 7.3 Hz), 3.43 (3H, s), 3.62 (1H, d, *J*=8.1 Hz), 3.66 (6H, s), 3.78 (3H, s), 4.57 (1H, s), 4.74 (1H, s), 4.78 (1H, s), 5.00 (1H, s), 6.04 (1H, s), and 6.6—6.7 (2H, m)].

Orthoformate Formation of 32. A trimethyl orthoformate solution (2 cm^3) of **32** (22.5 mg) and PPTS (10 mg) gave **34** or **35** [a colorless oil, 22 mg, 83%. ^1H NMR δ=1.42 (1H, dd, *J*=14.4, 9.6 Hz), 1.46 (3H, s), 2.50 (1H, dd, *J*=14.4, 8.0 Hz), 2.96 (1H, ddd, *J*=9.6, 8.0, 5.6 Hz), 3.21 (3H, s), 3.27 (3H, s), 3.66 (1H, d, *J*=5.6 Hz), 3.69 (6H, s), 3.80 (3H, s), 4.59 (1H, s), 4.82 (1H, s), 4.87 (1H, s), 5.03 (1H, s), 5.19 (1H, s), and 6.65 (2H, s)].

Thermolysis of 31. A xylene solution (1.5 cm^3) of **31** (93 mg) was refluxed for 1.5 d to give **37** [a colorless oil, 40 mg; 67%. Found: C, 54.06; H, 5.94%. Calcd for $C_{16}H_{20}O_9$:C, 53.93; H, 5.66%. ^1H NMR δ=1.14 (3H, s), 1.86 (1H, dd, *J*=14.3, 2.9 Hz), 2.38 (1H, dd, *J*=14.3, 9.5 Hz), 2.62 (1H, ddd, *J*=9.5, 7.7, 2.9 Hz), 2.84 (1H, d, *J*=7.7 Hz), 3.8 (1H, s, OH), 3.80 (3H, s), 3.82 (3H, s), 3.88 (3H, s), 4.39 (1H, s, OH), 5.02 (1H, s), and 5.42 (1H, s). ^{13}C NMR δ=22.4, 41.5, 42.4, 51.7, 52.2, 52.5, 52.8, 81.4, 81.9, 83.0, 85.1, 143.5, 144.1, 162.2, 162.4, and 174.1. IR ν: 3475, 3400, 1725, 1640, 1260, and 1220 cm^{-1}. UV (MeOH): 226.6 nm (ε=6200)], **38** [a colorless oil, 2 mg, 7%. Found: *m/z* 172.0736 (M^+). Calcd for $C_8H_{12}O_4$: 172.0736. ^1H NMR δ=1.24 (3H, s), 2.5—2.65 (2H, m), 3.80 (3H, s), 5.63 (1H, dt, *J*=6.2, 1.8 Hz), and 6.13 (1H, dt, *J*=6.2, 2.2 Hz). ^{13}C NMR δ=23.2, 46.4, 53.3, 80.4, 87.7, 130.8, 136.4, and 174.8. IR ν: 3500, 1725, 1250, and 1207 cm^{-1}], and **22** [4.4 mg, 14%], and recovered **32** [23 mg].

Thermolysis of 37. Compound **37** (36 mg) was placed in a tube equipped with a Dry-Ice cold finger and pyrolyzed at 220 °C under reduced pressure (1300 Pa) to give **38** [9.3 mg, 63%], **22** [10 mg: 63%], and recovered **37** [5.4 mg].

HCl-Catalyzed Reaction of 6. a) An EtOH solution (6 cm^3) of **6** (70 mg) and concd HCl (1 drop) was stirred for 30 min at room temperature. The solvent was evaporated and the residue was chromatoraphed on a silica-gel column to give **39** [colorless crystals, mp 139—141 °C, 51 mg; 61%.

Found: C, 62.62; H, 6.40%. Calcd for $C_{24}H_{28}O_9$: C, 62.60; H, 6.13%. ^{1}H NMR δ=1.37 (1H, d, J=9.2 Hz, OH), 1.40 (3H, t, J=7.0 Hz), 1.41 (3H, t, J=7.0 Hz), 3.68 (3H, s), 3.73 (3H, s), 4.02 (4H, q, J=7.0 Hz), 4.23 (1H, d, J=7.0 Hz), 4.50 (1H, dd, J=9.2, 7.0 Hz, H_a), 4.77 (1H, d, J=1.5 Hz), 4.87 (1H, d, J=1.8 Hz), 4.93 (1H, d, J=1.1 Hz), 5.02 (1H, d, J=1.8 Hz), 6.45 (1H, d, J=2.6 Hz), 6.47 (1H, dd, J=8.1, 2.6 Hz), 6.60 (1H, dd, J=5.9, 1.8 Hz), 6.75 (1H, dd, J=5.9, 1.8 Hz), and 7.40 (1H, d, J=8.1 Hz). ^{13}C NMR δ=14.8 (2C), 43.9, 52.5, 52.9, 63.5, 63.9, 71.4, 72.7, 73.3, 79.2, 80.1, 86.3, 88.5, 100.2, 105.0, 117.7, 128.6, 137.0, 139.2, 158.5, 159.4, 171.4, and 171.5. IR ν: 3530, 1740, 1717, 1607, 1575, 1500, 1280, 1255, 1217, 1175, 1115, and 1035 cm^{-1}. UV (MeOH): 208.8 (ε=17200), 228.6 (10100), and 279.2 nm (3000)] and **40a** [colorless crystals, mp 202—203 °C, 10 mg; 13%. Found: C, 57.07; H, 4.56%. Calcd for $C_{20}H_{19}O_8Cl$: C, 56.81; H, 4.53%. ^{1}H NMR δ=2.70 (1H, dd, J=20.4, 2.9 Hz), 2.78 (1H, dd, J=20.4, 2.9 Hz), 2.95 (1H, d, J=5.5 Hz, H_d), 3.70 (3H, s), 3.72 (3H, s), 4.62 (1H, d, J=5.5 Hz, H_a), 4.77 (1H, q, J=2.9 Hz, H_e), 4.80 (1H, d, J=1.8 Hz), 4.84 (1H, s), 4.97 (1H, d, J=1.5 Hz, H_b), 5.35 (1H, d, J=1.5 Hz, H_c), 5.93 (1H, d, J=9.9 Hz), 6.52 (1H, dd, J=9.9, 2.9 Hz, H_f), 6.60 (1H, dd, J=5.9, 1.8 Hz), and 6.67 (1H, dd, J=5.9, 1.8 Hz). ^{13}C NMR δ=37.3, 52.7, 52.8, 55.4, 65.4, 71.4, 72.6, 79.1, 79.8, 82.3, 83.1, 83.8, 88.1, 126.9, 136.9, 138.5, 145.9, 170.6, 170.8, and 194.9. IR ν: 1720, 1685, 1260, and 1225 cm^{-1}. UV (MeOH): 204.6 (ε=11500) and 219.6 nm (12200)].

b) A THF solution (6 cm^3) of **6** (51 mg) and concd HCl (1 drop) was stirred for 3 h at room temperature to give **40a** [12 mg; 22%] and **41** [colorless crystals, mp 158—159 °C, 13.3 mg; 24%. Found: C, 56.97; H, 4.71%. Calcd for $C_{20}H_{19}O_8Cl$: C, 56.81; H, 4.53%. ^{1}H NMR δ=1.38 (1H, d, J=9.2 Hz, OH), 3.68 (3H, s), 3.72 (1H, d, J=7.0 Hz), 3.73 (3H, s), 4.52 (1H, dd, J=9.2, 7.0 Hz), 4.80 (1H, d, J=1.8 Hz), 4.86 (1H, s), 4.92 (1H, s), 4.95 (1H, d, J=1.8 Hz), 5.64 (1H, s), 6.60 (1H, dd, J=5.9, 1.8 Hz), 6.74 (1H, dd, J=5.9, 1.8 Hz), 6.97 (1H, d, J=8.4 Hz), 7.20 (1H, dd, J=8.4, 2.2 Hz), and 7.44 (1H, d, J=2.2 Hz). ^{13}C NMR δ=51.0, 52.7 (2C), 71.4, 72.5, 74.0, 79.3, 80.0, 87.3, 88.2, 116.5, 120.4, 129.6, 129.7, 130.7, 137.0, 139.0, 150.7, 171.0, and 171.1. IR ν: 3600—2800, 1720, 1495, 1430, 1270, and 1220 cm^{-1}. UV (MeOH): 220.6 (ε=9500), 230.6 (7800), and 281.2 nm (2200)].

HCl-Catalyzed Reaction of 11. A THF solution (10 cm^3) of **11** (85 mg) and concd HCl (1 drop) was stirred for 2 h at room temperature to give **42** [colorless crystals, mp 190 °C (decomp), 8 mg, 25%. Found: C, 61.04; H, 4.68%. Calcd for $C_{24}H_{21}O_8Cl$: C, 60.96; H, 4.48%. ^{1}H NMR δ=3.02 (1H, dd, J=18.7, 12.8 Hz), 3.28 (1H, dd, J=18.7, 5.5 Hz), 3.57 (3H, s), 3.60 (1H, d, J=5.1 Hz, H_d), 3.72 (3H, s), 4.24 (1H, s, H_c), 4.48 (1H, dd, J=12.8, 5.5 Hz), 4.77 (1H, d, J=1.8 Hz), 4.89 (1H, d, J=1.8 Hz), 5.10 (1H, s, H_b), 5.34 (1H, d, J=5.1 Hz, H_a), 6.54 (1H, dd, J=5.5, 1.8 Hz), 6.66 (1H, dd, J=5.5, 1.8 Hz), 7.46 (1H, td, J=7.7, 1.1 Hz), 7.68 (1H, ddd, J=7.7, 7.3, 1.5 Hz), 7.91 (1H, dd, J=7.7, 1.5 Hz), and 8.16 (1H, dd, J=7.3, 1.1 Hz). ^{13}C NMR δ=44.0, 45.4, 52.6, 52.8, 61.5, 72.2, 73.0, 79.4, 80.2, 80.7, 82.1, 82.9, 87.9, 126.6, 128.9, 129.9, 130.7, 134.2, 136.9, 138.7, 140.3, 170.5, 170.6, and 193.6. IR ν: 1720, 1690, 1590, 1280, and 1265 cm^{-1}. UV (MeOH): 204.6 (ε=27300), 250.6 (6400), and 293.0 nm (1300)], **43** [colorless crystals, mp 201—202 °C, 15 mg; 48%. Found: C, 63.44; H, 5.13%. Calcd for $C_{24}H_{22}O_9$: C, 63.43; H, 4.88%. ^{1}H NMR δ=2.49 (1H, s, OH), 2.89 (1H, dm, J=18.9 Hz), 2.98 (1H, dd, J=18.9, 2.7 Hz), 3.17 (1H, d, J=4.8 Hz), 3.58 (3H, s), 3.73 (3H, s), 4.41 (1H, s), 4.71 (1H, br s), 4.77 (1H, m), 4.85 (1H, br s), 5.13 (1H, s), 5.17 (1H, d, J=4.8 Hz), 6.54 (1H, dd, J=5.9, 1.8 Hz), 6.65 (1H, dd, J=5.9, 1.8 Hz), 7.43 (1H, t, J=7.7 Hz), 7.65 (1H, dd, J=7.7, 7.3 Hz), 7.97 (1H, d, J=7.7 Hz), and 8.18 (1H, d, J=7.3 Hz). ^{13}C NMR δ=40.0, 47.7, 52.7, 52.9, 72.2, 73.1, 73.9, 79.3, 80.0, 80.2, 80.8, 83.2, 87.0, 126.3, 128.5, 130.9 (2C), 133.8, 137.0, 137.6, 138.7, 170.5, 170.6, and 194.5. IR ν: 3500, 1720, 1680, 1590, 1270, and 1220 cm^{-1}. UV (MeOH): 250.4 (ε=14100) and 292.6 nm (4600)], and recovered **11** [55 mg].

References

1) Part XLV: G. R. Tian, S. Sugiyama, A. Mori, and H. Takeshita, *Bull. Chem. Soc. Jpn.*, **61**, 4397 (1988).

2) G. R. Tian, S. Sugiyama, A. Mori, and H. Takeshita, *Chem. Lett.*, **1987**, 1557.

3) G. R. Tian, S. Sugiyama, A. Mori, H. Takeshita, M. Higashi, and H. Yamaguchi, *Chem. Lett.*, **1988**, 941.

4) G. R. Tian, S. Sugiyama, A. Mori, and H. Takeshita, *Kyushu Daigaku Kino Busshitsu Kagaku Kenkyuka Hokoku*, **2**, 95 (1988): *idem, Kyushu Daigaku Sogo Rikogaku Kenkyuka Hokoku*, **10**, 171 (1988).

5) R. N. Warrener, R. A. Russell, R. Solomon, I. G. Pitt, and D. N. Butler, *Tetrahedron Lett.*, **28**, 6503 (1987).

6) D. N. Butler, D. L. Officer, I. G. Pitt, R. A. Russell, and R. N. Warrener, *Tetrahedron Lett.*, **28**, 6507 (1987).

7) R. Askani, *Chem. Ber.*, **98**, 3618 (1965); W. Hartmann, *ibid.*, **104**, 2864 (1971).

8) H. Prinzbach, M. Arguelles, and E. Druckrey, *Angew. Chem., Int. Ed. Engl.*, **5**, 1039 (1966).

9) A. W. McCulloch, D. G. Smith, and A. G. McInnes, *Can. J. Chem.*, **51**, 4125 (1973).

10) P. A. Bartlett and J. Myerson, *J. Am. Chem. Soc.*, **100**, 3950 (1978).

11) It is true that exo-Diels-Alder adducts of furans or pyrrols give γ-lactone derivatives via a skeletal rearrangement. However, the ^{13}C NMR of **8** and **9** confirmed the retention of the original skeleton in this reaction. See J. A. Berson and R. Swinder, *J. Am. Chem. Soc.*, **75**, 1721 (1953).

12) D. Bryce-Smith, A. Gilbert, and M. G. Johnson, *J. Chem. Soc. C*, **1967**, 383.

13) A. Mori and H. Takeshita, *Bull. Chem. Soc. Jpn.*, **58**, 1581 (1985); *idem, Chem. Lett.*, **1975**, 599.

14) N. Kato, S. Tanaka, H. Kataoka, and H. Takeshita, *Chem. Lett.*, **1987**, 2295.

15) R. L. Cargill and J. W. Crawford, *J. Org. Chem.*, **35**, 356 (1970).

16) M. I. Struchkova, A. Kh. Margaryan, and E. P. Serebryakova, *Izv. Akad. Nauk SSSR, Ser. Khim.*, **1980**, 56.

17) T. S. Cantrell and J. S. Solomon, *J. Am. Chem. Soc.*, **92**, 4656 (1970).

18) T. Svensson, *Chemica Scripta*, **3**, 171 (1973).

19) L. A. Paquette and O. Cox, *J. Am. Chem. Soc.*, **89**, 5633 (1967).

20) H. Takeshita and N. Kato, *Yuki Gosei Kagaku Kyokai Shi*, **44**, 1081 (1986).

21) T. Mukaiyama, T. Sato, and J. Hanna, *Chem. Lett.*, **1973**, 1041; J. E. McMurry and M. P. Fleming, *J. Am. Chem. Soc.*, **96**, 4708 (1974).

Protease-Catalyzed Peptide Formation under High Pressure

Shigeru KUNUGI,* Kazuo TANABE, Kouji YAMASHITA, Yoshio MORIKAWA, Takanobu ITO, Toshihiro KONDOH, Kouichirou HIRATA, and Akihiko NOMURA
Department of Applied Chemistry, Fukui University, Bunkyou 3-9-1, Fukui 910
(Received July 11, 1988)

The effect of high pressure on peptide formation by the catalysis of carboxypeptidase Y (substitution of ester or peptide by amino acid derivative) or by thermolysin (condensation of *N*-acylamino acid and amino acid amide) was studied. The carboxypeptidase Y-catalyzed substitution reaction of *N*-[3-(2-furyl)acryloyl]-phenylalanine ethyl ester with glycinamide or phenylalaninamide showed a six-fold higher total peptide yield at 200 MPa than at atmospheric pressure. In the case of the reaction of *N*-acyldipeptide and amino acid amide, both the peptide yield and substitution efficiency were improved at elevated pressure and the wasteful hydrolysis of the substrate was highly depressed by increasing pressure. The pressure was also effective to get rid of the substrate inhibition by the amino acid ester in the reaction between the *N*-acylamino acid ester and the amino acid ester and to yield much dipeptide ester at high pressure. An improvement of the peptide yield by pressure for the reaction of thermolysin was observed in a combination of less specific substrates, *N*-benzyloxycarbonyl-L-aspartic acid and phenylalanine methyl ester, since the high catalytic activity of this enzyme under elevated pressure was significant only in the case that the peptide yield was kinetic-controlled.

During the course of our studies on the reaction mechanisms of several proteases by examining the influence of hydrostatic pressure on the reactions,[1-3] we found that the pressure affected one type of activity of some enzymes in a considerably different manner from the other, depending on the nature of the scissile bond of the substrate. Also, a certain enzyme show a considerable apparent pressure-activation. One example of the former is carboxypeptidase from yeast (CPase Y),[2] which is grouped into serine carboxypeptidase.[4] The intrinsic carboxypeptidase activity of this enzyme (Eq. 1, where AA_i and R denote amino acid residue and alkyl group, respectively) was highly depressed by increasing the pressure, while an esterase (Eq. 2) or amidase (Eq. 3) reaction was less influenced by pressure; e.g., at 100 MPa the rate of hydrolysis of *N*-[3-(2-furyl)acryloyl]phenylalanine ethyl ester and amide was 85 and 75%, respectively, of that at atmospheric circumstance, while that of *N*-[3-(2-furyl)-acryloyl]glycylphenylalanine was decreased to less than 15% by the same pressure increase (pH 6, 25 °C). This resulted mainly from the difference in the ionic nature of the substrate and the discouraged electrostatic interaction at the elevated pressure to avoid any increase in the molar volume due to liberated hydration water around ionic groups.

$$---AA_1\text{-}AA_2 \longrightarrow ---AA_1 + AA_2 \quad (1)$$
$$---AA_1\text{-}OR \longrightarrow ---AA_1 + ROH \quad (2)$$
$$---AA_1\text{-}NH_2 \longrightarrow ---AA_1 + NH_3 \quad (3)$$

An example of the apparent pressure-activation was seen in the case of thermolysin, a zinc-containing

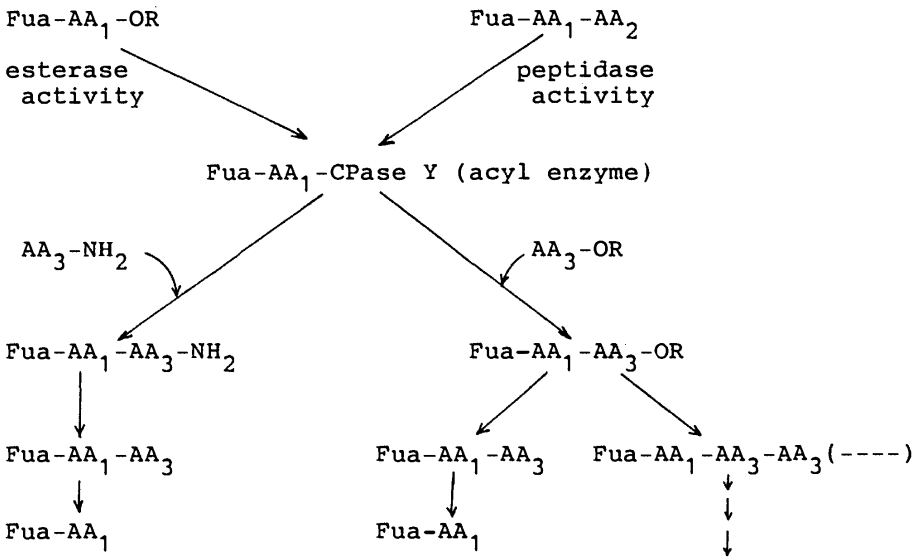

Scheme 1. Possible pathways of peptide formation and degradation of the primary product in CPase Y system.
AA_i, amino acid residue; R, alkyl group.

endoprotease from *B. thermoproteolyticus*. A pressure increase of up to 100 MPa gave about a 15-fold higher second-order rate for the hydrolysis of *N*-acyldipeptide amide catalyzed by this enzyme.[3] This could be explained in terms of a change of the structure and a subsequent change in the hydration state of the protein coupled with the progress of the reaction. These findings led us to inspect the pressure effect on the protease-catalyzed peptide formation reactions, since both of these enzymes are known to catalyze such kinds of reactions.[5] Actually, in a preliminary study we found a strong influence of pressure on a peptide formation reaction by CPase Y.[6]

In this report we describe the pressure effect on various types of peptide formation reactions catalyzed by CPase Y and thermolysin. With CPase Y, peptides can be formed by a nucleophilic attack by an amino acid derivative on the acylated intermediate[7] (Scheme 1), which is derived from either an ester substrate[8] or a peptide substrate.[9] Nucleophile can be either an amino acid amide (X=NH_2) or an amino acid ester (X=OR). The reverse reaction of the hydrolysis, starting from e.g. *N*-acylamino acid and amino acid (Eq. 4), might also give peptides.[10] With thermolysin, peptide can be formed only by a reaction of this type and the carboxyl part of AA_2 should be capped (-X).

$$---AA_1 + AA_2(-X) \longrightarrow ---AA_1\text{-}AA_2(-X) \quad (4)$$

Experimental

Materials. CPase Y was kindly donated by Oriental Yeast Co. (Osaka, Japan) (Lot 21003001) and thermolysin was obtained from Daiwa Kasei Co. (Osaka, Japan) (Lot T4KB31,32). *N*-[3-(2-Furyl)acryloyl]amino acids (Fua-amino acids) and *N*-[3-(2-furyl)acryloyl]dipeptides including the standard samples for the chromatographic analysis were prepared by the *N*-hydroxysuccinimide method,[11] as previously reported.[1-3] This chromophoric acyl group was chosen since it facilitates product detection and since we had made some kinetic studies on the proteases by using this type of substrate. The principle obtained from the present results may be applicable to substrates with other acyl groups. Buffer reagents were purchased from Dojindo Laboratories (Kumamoto, Japan) and other amino acid derivatives were of commercial reagent grade. The authentic sample of *N*-benzyloxycarbonyl-Asp-Phe methyl ester (Cbz-Asp-Phe-OMe) was a kind gift from Prof. Y. Okahata, Tokyo Institute of Technology, Japan.

Methods. The reaction solution contained an appropriate amount of organic solvent (depending on the reaction species; dimethyl sulfoxide [DMSO], *N*,*N*-dimethylformamide [DMFA], or acetonitrile [MeCN]), enzyme and substrates, buffered at described pH with 2-morpholinoethanesulfonic acid, 2-[4-(2-hydroxyethyl)-1-piperazinyl]ethanesulfonic acid, 2-amino-2-hydroxy-methyl-1,3-propanediol, 3-[[2-hydroxy-1,1-bis(hydroxymethyl)ethyl]amino]-1-propanesulfonic acid, or 3-cyclohexylamino-1-propanesulfonic acid.

It was divided into two parts; one part was sealed in a small polypropylene-made bottle, placed in a stainless-steel pressure vessel located in a thermostated bath, while the other part was incubated under atmospheric pressure at a controlled temperature. Kerosene was used as the pressure medium.

After a prescribed period the reaction mixture was taken out from each part of the solution and quenched by adding 5 volumes of a mixture of acetonitrile and 5 mM-aqueous phosphoric acid (1M=1 mol dm^{-3}). Portions were then analyzed by liquid chromatography (Shimadzu LC6A-Cosmosil 5C18-P). The eluent was a 40—60% mixture of acetonitrile with 5 mM of aqueous phosphate (pH 2.5—3) containing 50 mM Na_2SO_4 or triethylamine. The amount of each species was calculated from the integration of the eluent curve (Shimadzu Chromatopak C-R6A) after corrections with the extinction coefficient measured on a spectrophotometer (Uvidec 610-B) independently.

Results and Discussion

Carboxypeptidase Y. Table 1 shows the product distribution of the CPase Y-catalyzed reaction of Fua-Phe-OEt with Gly-NH_2 or Phe-NH_2 at atmospheric pressure and at 200 MPa. With Gly-NH_2, Fua-Phe, and Fua-Phe-Gly-NH_2 were detected as the products and the yield of the dipeptide amide was larger at high pressure. As reported before,[12] this enzyme shows carboxamidopeptidase activity towards Fua-Phe-Gly-NH_2 and, therefore, the primarily produced dipeptide amide can be directly hydrolyzed to Fua-Phe and Gly-NH_2. With Phe-NH_2, a dipeptide having free carboxylate (Fua-Phe-Phe), was also detected in the reaction mixture. This *N*-acyldipeptide was produced by the amidase activity on the primary product, Fua-Phe-Phe-NH_2. Thus, Fua-Phe was produced by the hydrolysis of either Fua-Phe-OEt or Fua-Phe-Phe (Eq. 5). (For Fua-Phe-Phe-NH_2 CPase Y shows no carboxamidopeptidase activity.[1])

Table 1. Effect of Pressure on CPase Y-Catalyzed Formation of Dipeptide Amide from Fua-Phe-OEt and Amino Acid Amide[a]

Nucleophile	Pressure	Yield (%)		
	MPa	Fua-Phe	Fua-Phe-Xxx-NH_2	Fua-Phe-Xxx
Gly-NH_2	0.1	84.6	15.4	0
	200	60.6	39.4	0
Phe-NH_2	0.1	91.2	2.3	6.5
	200	45.4	16.1	38.5

a) pH 8.0, [CPaseY]=0.6 μM, [Fua-Phe-OEt]= 2 mM, [Xxx-NH_2·HCl]= 0.1 M, 15 (v/v)% DMFA, 3 h reaction at 30 °C.

Table 2. Effect of Pressure on CPase Y-Catalyzed Hydrolysis of Fua-Dipeptide Amide[a]

Substrate	pH	Pressure	Product yield/%[b]		
		MPa	Fua-Xxx	Fua-Xxx-Yyy	Fua-Xxx-Yyy-NH_2
Fua-Gly-Phe-NH_2	5.0	0.1	54.6	0.2	45.3
		100	24.5	38.1	37.5
	7.5	0.1	84.7	0.5	14.8
		100	54.2	22.4	23.4
Fua-Phe-Gly-NH_2	5.0	0.1	46.7	0.0	53.3
		100	41.5	0.0	58.5
	7.5	0.1	53.5	0.0	46.0
		100	52.8	0.0	46.9
Fua-Phe-Phe-NH_2	5.0	0.1	75.4	14.8	9.8
		100	65.9	26.1	8.0
	7.5	0.1	60.9	39.2	0.0
		100	57.0	43.0	0.0

a) [Substrate]=0.25 mM, [CPase Y]=0.5 μM, 30 °C, 2.0 (v/v)% DMSO. b) Amount of each product found in the reaction mixture after 3 h incubation. Xxx and Yyy indicate Gly or Phe.

Table 3. Effect of Pressure on CPase Y-Catalyzed Dipeptide Formation from Fua-Gly-Phe and Leu-NH_2[a]

[Enzyme]	pH	Pressure	Product yield/%				Ratio[b]
μM		MPa	Fua-Gly-Phe	Fua-Gly	Fua-Gly-Leu-NH_2	Fua-Gly-Leu	
1.0	6.5	0.1	0	88.5	11.5	0	11.5
		100	4.3	68.5	22.6	4.5	23.4
	7.0	0.1	0	91.6	8.4	0	8.4
		100	42.3	40.5	14.0	3.2	24.3
2.0	6.5	0.1	0	95.7	4.3	0	4.3
		100	0	78.4	18.3	3.2	18.3
	7.0	0.1	0	96.1	3.9	0	3.9
		100	17.1	63.2	16.6	3.1	20.0

a) [Fua-Gly-Phe]=0.25 mM, [Leu-NH_2·HCl]=0.1 M, 3 h reaction at 35 °C, 2.5 (v/v)% DMFA.
b) (amount of Fua-Gly-Leu-NH_2)/(total hydrolyzed substrate).

$$\text{Fua-Phe-Phe-NH}_2 \rightarrow \text{Fua-Phe-Phe} \rightarrow \text{Fua-Phe} \quad (5)$$
$$\text{NH}_3 \qquad\qquad \text{Phe}$$

At 200 MPa, the total peptide yield was increased approximately six-fold. This result could be explained by considering the effect of pressure on the hydrolysis of Fua-dipeptide amides by this enzyme (Table 2). By increasing the pressure, the carboxypeptidase activity was retarded more rigorously than the amidase or the carboxamidopeptidase activity and, as a result, a dipeptide with a carboxylate end was obtained in higher yield.

An acyl-enzyme can be also produced from an *N*-acyldipeptide substrate which is attacked by amino acid amide to form an *N*-acyldipeptide amide. A time course of such a reaction under atmospheric pressure is shown in Fig. 1. After 3 h the reaction was completed. Table 3 shows the effect of pressure on such a peptide formation reaction: namely, the product distribution of a combination of Fua-Gly-Phe+Leu-NH_2 after 3 h reaction at 0.1 and 100 MPa. At elevated pressure the yield of Fua-Gly-Leu-NH_2 increased. At the same time the amount of remaining unreacted substrate, Fua-Gly-Phe, also increased, which was brought about by a strong retardation of the peptidase activity by pressure. This means that the pressure depressed the wasteful hydrolysis of the substrate.

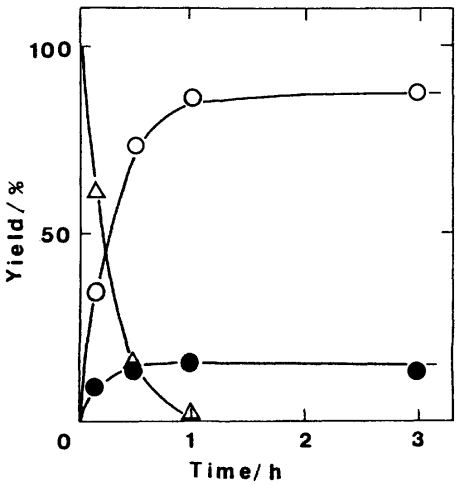

Fig. 1. Time course of CPase Y-catalyzed peptide formation from Fua-Gly-Phe and Leu-NH_2. Relative amounts of Fua-Gly (○), Fua-Gly-Phe (△), and Fua-Gly-Leu-NH_2 (●) are shown. [Fua-Gly-Phe]= 0.25 mM, [Leu-NH_2·HCl]=0.1 M, [enzyme]=1.0 μM, pH 6.5 (0.1 M Hepes), 2.5%(v/v) DMFA, 35 °C.

When the enzyme concentration was increased, *N*-

Table 4. Effect of Pressure on CPase Y-Catalyzed Dipeptide Formation from Fua-Phe-OEt and Phe-OEt[a)]

[Phe-OEt·HCl]	Pressure	Product yield/%					
M	MPa	Fua-Phe-OEt	Fua-Phe	Fua-(Phe)$_2$-OEt	Fua-(Phe)$_2$	Fua-(Phe)$_3$-OEt	Fua-(Phe)$_3$
0.05	0.1	0.2	53.2	1.4	40.9	0	4.3
	100	0.1	54.4	2.2	38.9	0	4.4
0.08	0.1	8.4	40.7	4.2	39.9	0.7	6.1
	100	0.1	47.5	10.5	36.0	0.6	5.1
0.1	0.1	37.0	24.4	13.8	20.0	2.1	2.3
	100	0.7	45.2	19.9	28.8	1.8	3.4
0.15	0.1	83.7	5.4	8.5	2.1	0.2	0
	100	17.8	37.4	28.9	12.9	1.3	0.9

a) [Fua-Phe-OEt]=1.0 mM, 30 °C, pH 9.5, [CPase Y]=9.5 nM, 7.0 (v/v)% MeCN, reaction time 3 h.

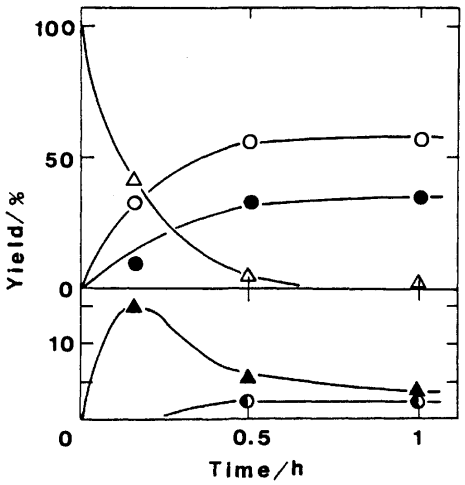

Fig. 2. Time course of CPase Y-catalyzed peptide formation from Fua-Phe-OEt and Phe-OEt. Relative amounts of Fua-Phe (○), Fua-Phe-OEt (△), Fua-Phe-Phe (●), Fua-Phe-Phe-OEt (▲), and Fua-Phe-Phe-Phe (◐) are shown. [Fua-Phe-OEt]=1.0 mM, [Phe-OEt·HCl]=0.05 M, [enzyme]=10 nM, pH 9.5, 7.0%(v/v) MeCN, 30 °C, 0.1 M NaCl.

acyldipeptide (Fua-Gly-Leu) appeared in the product, due to the amidase activity of this enzyme on the once produced dipeptide amide coupled with the highly depressed carboxypeptidase activity at elevated pressure. With this carboxypeptide used as an acyl donor, however, the peptide yield was relatively low, at most around 30%, even at elevated pressure.

Next, the reaction between *N*-acylamino acid ester and amino acid ester was examined. In this case the peptide ester once produced can further act as a substrate[8)] and the peptide chain can be extended, as shown in Fig. 2. Table 4 shows an example of the effect of pressure on such a reaction; Fua-Phe-OEt+Phe-OEt. At low Phe-OEt concentration the effect was practically negligible, since the esterase activity was affected by pressure to a smaller extent. Most of the product was *N*-acyldipeptide and small portions were dipeptide ester and tripeptide ester.

When the nucleophile (Phe-OEt) concentration was increased in order to increase the substitution efficiency, the amount of unreacted substrate increased, since this component also acted as a kind of inhibitor, of which the inhibition constant was estimated to be about 10 mM from the reported data.[4)] The pressure was highly effective to get rid of such a substrate inhibition and the yield of the dipeptide ester product was increased under high pressure.

Table 5. Effect of Pressure on Thermolysin-Catalyzed Peptide Formation Reaction

Reaction	pH	Pressure	Product yield
		MPa	%
Fua-Gly+Leu-NH_2[a)]	7.0	0.1	83.0
		200	52.1
	8.0	0.1	78.0
		200	62.6
Cbz-Asp+Phe-OMe[b)]	6.0	0.1	6.1
		150	35.8
	6.0	0.1	12.8[c)]
		150	55.8[c)]
	7.0	0.1	15.3
		150	33.6

a) [Fua-Gly]=1 mM, [Leu-NH_2·HCl]=50 mM, [TLN]=1.1 μM, 30 °C, 5 (v/v)% DMSO. Incubation time 6 h. b) [Cbz-Asp]=5 mM, [Phe-OMe·HCl]=100 mM, [TLN]=5 μM, 30 °C, 5 (v/v)% DMSO 50 (v/v)% MeCN. Incubation time 4 h. c) [TLN]=7.5 μM, 35 °C. Other conditions are as above.

Thermolysin. This enzyme effectively catalyzes the condensation reaction of *N*-acylamino acid and amino acid amide. Table 5 shows the result on the effect of pressure on thermolysin-catalyzed peptide condensation.

For a reaction to form a specific dipeptide substrate, such as Fua-Gly+Leu-NH_2→Fua-Gly-Leu-NH_2 (the second-order rate constant of the hydrolysis of this substrate by thermolysin is about 2×10^4 $M^{-1}s^{-1}$ at pH 6.5, 25 °C), the condensation efficiency is very high, much higher than other proteases when we compare their hydrolytic activities.[13)] Though the condensed product did not precipitate under the present experimental conditions (the concentration of the acyl substrate was set well below the solubility of the product; monophasic system), the reaction proceeded fast (as shown in Fig. 3-a) and the product yield was deter-

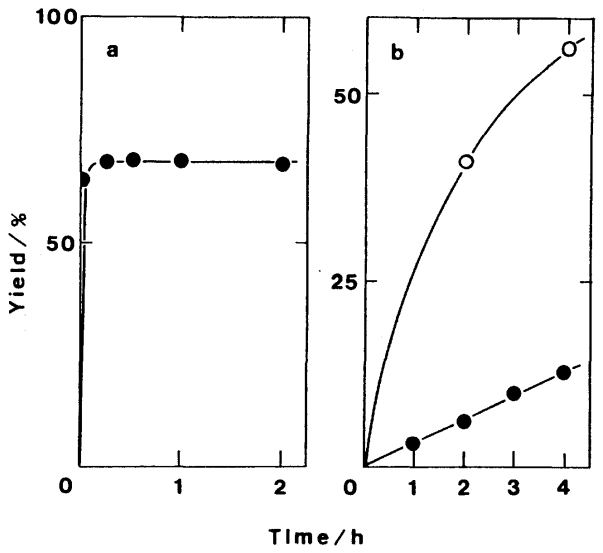

Fig. 3. Time course of thermolysin-catalyzed peptide formation from Fua-Gly+Leu-NH_2 (a) and Cbz-Asp+Phe-OMe (b). Yield of *N*-acyldipeptide amide (a) or ester (b) is shown.
(a) [Fua-Gly]=1mM, [Leu-NH_2·HCl]=0.1M, [TLN]=1.0 μM, pH 7.0 (Hepes 0.1M), 5% DMSO, 37°C.
(b) [Cbz-Asp]=5mM, [Phe-OMe·HCl]=0.1 M. [TLN]=7.5 μM, pH 6.0, 5% DMSO, 50% MeCN, 35°C.
●, at 0.1MPa; ○, at 150 MPa.

mined mostly by the equilibrium of the reaction (thermodynamic-controlled). At increased pressure the electrostriction of the water around the carboxylate and ammonium ions of the *N*-acylamino acid and amino acid amide, respectively, is favored in order to decrease the partial volumes in the system which in turn forces the reaction to proceed towards the dissociated (hydrolyzed) side and results in a lower yield of the peptide formation. At such a pressure as discussed in the present study the volume change contribution of enzyme protein structure is far less significant and that of the hydration change of the substrate (or protein) plays dominant roles.[14]

On the contrary the combination of Cbz-Asp and Phe-OMe (which is known as a reaction to produce a precursor of a sweetener[15]) is 'non-specific' to this enzyme and the reaction proceeded slowly (Fig. 3-b). Thus, the yield is determined rather "kinetically." In such a case the higher catalytic activity performed by the increased pressure is sufficient to exceed the negative factor given by the substrate hydration and, hence, a nearly six-fold increase in the peptide formation was observed under the present conditions.

These results indicate that pressure can be an important parameter in improving the peptide yield in a reaction catalyzed by proteolytic enzymes; this principle will be applied to other systems with different types of the substrate and enzyme. Though the pressure had been used to influence and improve various organic (or inorganic) syntheses,[16] the present example shows that the effect of pressure is exerted through molecular recognition and a reaction by a macromolecular catalyst which can amplify the effect to enable the control of reactions at relatively low pressure.

References

1) S. Kunugi, M. Fukuda, and N. Ise, *Biochim. Biophys. Acta*, **704**, 107 (1980); M. Fukuda, S. Kunugi, and N. Ise, *Bull. Chem. Soc. Jpn.*, **56**, 3308 (1983); M. Fukuda, H. Shima, and S. Kunugi, *ibid.*, **58**, 1349 (1985); M. Fukuda, H. Shima, and S. Kunugi, *J. Biochem. (Tokyo)*, **98**, 517 (1985); M. Fukuda and S. Kunugi, *ibid.*, **101**, 233 (1987).

2) M. Fukuda and S. Kunugi, *Eur. J. Biochem.*, **149**, 657 (1985).

3) M. Fukuda and S. Kunugi, *Eur. J. Biochem.*, **142**, 565 (1984).

4) R. Hayashi, S. Moore, and W. H. Stein, *J. Biol. Chem.*, **248**, 2296, 8366 (1973); R. Hayashi, Y. Bai, and T. Hata, *ibid.*, **250**, 5221 (1975); R. Hayashi, Y. Bai, and T. Hata, *J. Biochem. (Tokyo)*, **77**, 69 (1975); Y. Bai, R. Hayashi, and T Hata, *ibid.*, **77**, 83 (1975).

5) J. S. Fruton, *Adv. Enzymol.*, **53**, 239 (1982).

6) S. Kunugi, K. Tanabe, M. Fukuda, S. Makimoto, and Y. Taniguchi, *J. Chem. Soc., Chem. Commun.*, **1987**, 1335.

7) K.T. Douglas, Y. Nakagawa, and E. T. Kaiser, *J. Am. Chem. Soc.*, **98**, 8231 (1976); S. Kunugi and M. Fukuda, 30th IUPAC Congress (Manchester), 5p-55 (1985).

8) K. Breddam and F. Widmer, *Carlsberg Res. Commun.*, **48**, 231 (1983); F. Widmer, K. Breddam, and J. T. Johansen, *ibid.*, **45**, 453 (1980).

9) K. Breddam, F. Widmer, and J. T. Johansen, *Carlsberg Res. Commun.*, **45**, 237 (1980); K. Breddam, J. T. Johansen, and M. Ottesen, *ibid.*, **49**, 457 (1984).

10) R. Hayashi, 55th Ann. Meeting of Chem. Soc. Jpn., 1987.

11) S. Blumberg and B. L. Vallee, *Biochemistry*, **14**, 2410 (1975).

12) S. Kunugi, K. Tanabe, K.Yamashita, and M. Fukuda, *Bull. Chem. Soc. Jpn.*, **60**, 1399 (1987).

13) K. Morihara, *Tanpakushitsu Kakusan Koso*, **26**, 1979 (1981).

14) R. Jaenicke, *Ann. Rev. Biophys. Bioeng.*, **12**, 1 (1981); G. S. Greany and G. N. Somero, *Biochemistry*, **22**, 1888 (1983).

15) Y. Isowa, M. Ohmori, T. Ichikawa, K. Mori, Y. Nonaka, K. Kihara, K. Oyama, H. Satoh, and S. Nishimura, *Tetrahedron Lett.*, **1979**, 2611 ; K. Oyama, K. Kihara, and Y. Nonaka, *J. Chem. Soc., Perkin Trans. 2*, **1981**, 356.

16) W. J. le Noble and H. Kelm, *Angew. Chem., Int. Ed. Engl.*, **19**, 841 (1980).

 © 1989 The Chemical Society of Japan Bull. Chem. Soc. Jpn., 62, 519—523 (1989)

Cr(III) or Ce(IV) Impregnated Perfluorinated Resin-Sulfonic Acid Catalyst for the Oxidation of Alcohols

Shigekazu KANEMOTO,† Hiroyuki SAIMOTO,†† Koichiro OSHIMA,* Kiitiro UTIMOTO, and Hitosi NOZAKI†††
Department of Industrial Chemistry, Faculty of Engineering, Kyoto University, Yoshida, Kyoto 606
(Received July 26, 1988)

Several polymer supported catalysts are prepared by treatment of Nafion®551 (abbreviated NAFK below) with metal salts. Cr/NAFK and Ce/NAFK are found to be effective catalysts for the dehydrogenative oxidation of alcohols to the corresponding ketones by means of *t*-butyl hydroperoxide. Selective oxidation of secondary alcohols in the presence of primary ones was performed using a Ce/NAFK-$NaBrO_3$ system.

Polymer supported reagents are receiving considerable attention. The advantages of the use of polymeric reagents in organic synthesis have been described in a number of papers which are summarized in a monograph.[1] Major advantages of this approach are (1) the ease of purification of the final product and (2) the effective recycling use.

Two kinds of polymer reagents for the oxidation of alcohols to the corresponding aldehydes and ketones are described in literature. One is a reagent generated from poly(*p*-methylthiostyrene) and chlorine,[2] and the other is a polymeric analogue of pyridinium chlorochromate[3] or pyridinium dichromate.[4-6] The oxidation reactions using such stoichiometric reagents is easy to perform, but suffers from a couple of disadvantages including the requirement of a large amount of the reagent and a large volume of the solvent, because the exchange capacity of the polymer oxidant is usually low. Furthermore recycling of the reagents requires troublesome step of workup which prohibits the practical use. It is anticipated that the use of a catalytic amount of a polymer reagent in the presence of suitable co-oxidant such as *t*-BuOOH and $NaBrO_3$ could solve these disadvantages.[7] Here we wish to report convenient oxidation of alcohols with *t*-butyl hydroperoxide using a new type of polymer supported catalysts, i.e. Cr(III) and Ce(IV) impregnated perfluorinated resin-sulfonic acids.[8]

The structure of NAFK[9] is shown in Fig. 1. The perfluorinated resin has high stabilities thermally, chemically, and physically. NAFH (Nafion-H) has been widely used as a solid-state superacid reagent in several reactions.[10] Exchange of the counter metal on the polymer sulfonate was easily performed by treatment of the polymer potassium salt (NAFK) with the desired metal salts in deionized water. For instance, stirring of a mixture of NAFK and chromium(III) acetate for 36 h at 25 °C provided chromium impregnated catalyst (Cr/NAFK). Titrations of the generated catalyst indicated a capacity of 0.68 mmol of Cr(III) per gram which corresponds to 75% of the theoretical capacity of a fully loaded resin. Several kinds of metal impregnated perfluorinated resin-sulfonic acid catalysts were prepared and examined in the oxidation of 1-phenylethanol to acetophenone with anhydrous *t*-butyl hydroperoxide.[11] Among them, chromium(III) and cerium(IV) salts proved to efficiently catalyze the oxidation of alcohols. In contrast, polymer-supported catalysts carrying metals such as Cu(II), Ni(II), and Mn(II) were found less effective. The alcohols were only partly (at most 30%) converted into ketones with latter catalysts under the same reaction conditions.

Oxidation of secondary alcohols into ketones was studied using Cr/NAFK-*t*-BuOOH system in a

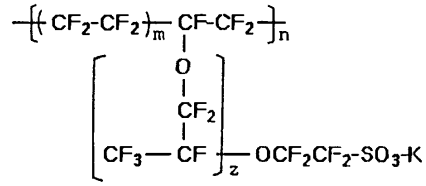

Nafion®511 (NAFK)

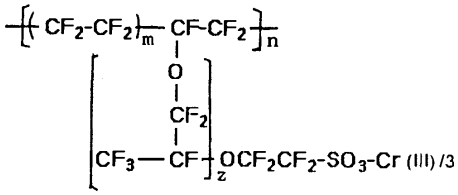

Cr / NAFK

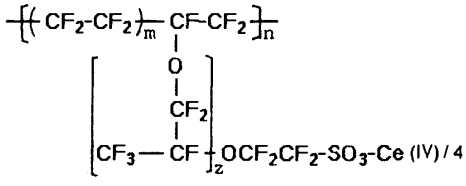

Ce / NAFK

Fig. 1.

† Present address: The Institute of Physical and Chemical Research (RIKEN), 2-1 Hirosawa, Wako-shi, Saitama 351-01.

†† Present address: Dept. Industrial Chemistry, Faculty of Engineering, Tottori University, Koyama-cho, Minami 4-101, Tottori 680.

††† Present address: Dept. Applied Chemistry, Okayama University of Science, Ridai-cho, Okayama 700.

Table 1. Oxidation of Alcohols with Cr/NAFK-*t*-BuOOH System[a,b]

Run	Substrate	Product	Yield /%
1	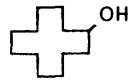	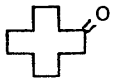	86
2	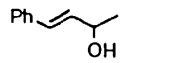	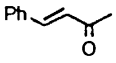	81
3	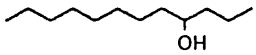	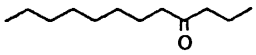	81
4	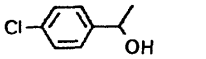	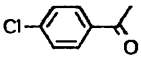	93
5	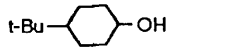	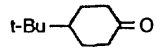	81
6	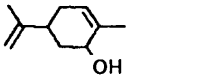	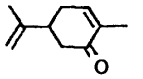	82
7	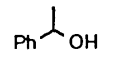	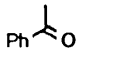	95
8	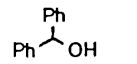	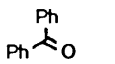	98

a) *t*-BuOOH (4.0 mmol) and Cr/NAFK (50 mg, 0.034 mmol) were employed per one mmol of alcohol. b) Yields represent isolated, purified products.

Table 2. Oxidation of Alcohols with Ce/NAFK-*t*-BuOOH System[a,b]

Run	Substrate	Product	Yield /%
1	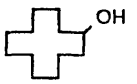	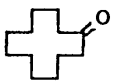	82
2	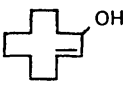	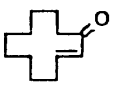	82
3	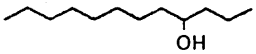	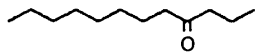	71
4	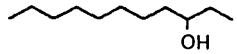	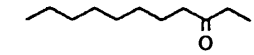	79
5	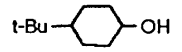	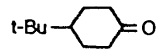	98
6	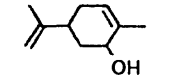	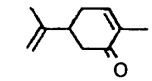	98
7	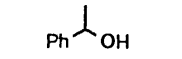	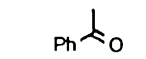	93
8	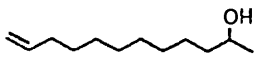	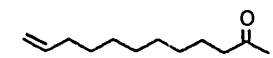	80

a) The hydroxy compounds (1.0 mmol), *t*-BuOOH (1.5 ml, 4.0 mmol), and Ce/NAFK (50 mg, 0.027 mmol) were combined in benzene and the mixture was stirred for 6 h at 80°C. b) Isolated and purified yields.

number of solvents under heating. Among them, chlorobenzene gave the best result. Reaction in benzene required a longer reaction time which caused contamination by undesired products. Toluene, which has similar boiling point to chlorobenzene, was not suitable for the oxidation of alcohols, because it was oxidized into benzaldehyde under the reaction conditions. The reaction proceeded upon heating a mixture of a substrate, an oxidant, and the resin catalyst suspended in chlorobenzene at 85 °C for several hours. The resin catalyst was filtered off and washed with ethyl acetate. Workup and purification of crude product gave the desired ketone effectively. Typical examples with Cr/NAFK-*t*-BuOOH chlorobenzene are summarized in Table 1. Secondary alcohols were converted into the corresponding ketones in good yields. Meanwhile, oxidation of primary alcohols generally gave complex mixtures of the unchanged substrates, the desired aldehydes, and the overoxidized carboxylic acids under the same reaction conditions. Ratios of these products were dependent on the reaction conditions (time, temperature). Prolonged reaction time or higher temperature naturally increased the formation of the carboxylic acids.

Recycling of the catalyst could be accomplished by simple filtration, washing with ethyl acetate, and drying. Titration of the recovered catalyst showed that more than 95% of chromium remained on the resin. Thus, 1-phenylethanol was oxidized to acetophenone in 92% (the second run) and 90% (the third run) yields by utilizing the recovered catalyst.

The resin cerium salt (Ce/NAFK) also has proved to be an efficient catalyst for the oxidation of alcohol by means of *t*-butyl hydroperoxide or sodium bromate. The catalyst, Ce/NAFK was prepared by stirring of a mixture of NAFK and $(NH_4)_2Ce(NO_3)_6$ for 36 h at 25 °C. In this catalytic system, the reaction proceeded at lower temperatures than Cr/NAFK-*t*-BuOOH system, so that benzene was found to be the preferred solvent. Table 2 shows the results of the oxidation of secondary alcohols. In contrast to the previously reported $(NH_4)_2Ce(NO_3)_6$-$NaBrO_3$ system,[12] the present system was not interfered with olefinic moiety in the substrates. Thus, 2-cyclododecen-1-ol and 11-dodecen-2-ol as well as carveol gave the corresponding olefinic ketones in good yields upon treatment with Ce/NAFK-*t*-BuOOH. Noteworthy is the fact that the cerium catalytic system does not oxidize primary alcohols into aldehydes. For example, 1-dodecanol was recovered practically unchanged under the general reaction conditions.

Reagents which are sufficiently selective to distinguish between functional groups of the same class are exceedingly valuable in syntheses. Recently several methods have been reported that permit the oxidation of secondary alcohols in the presence of primary ones.[13] It was anticipated that the treatment of primary, secondary diols with our new system would provide another method for selective formation of hydroxy ketones. This was indeed the case and selective oxidation of secondary hydroxyls in the presence of primary ones has been achieved as shown in Scheme

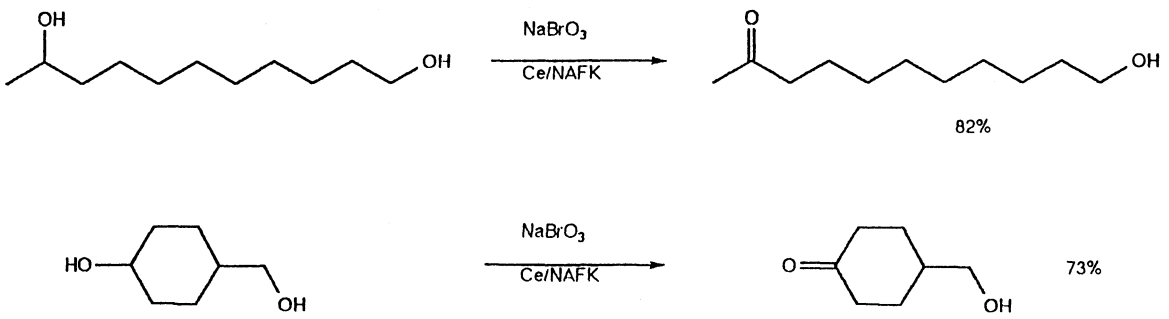

Scheme 1.

1, where choice of solvent and oxidant was critical. Oxidation in benzene with Ce/NAFK-*t*-BuOOH proceeded sluggishly and the desired products were contaminated by some unidentified by-products. For instance, oxidation of 1,10-undecanediol gave only 30% yield of 11-hydroxy-2-undecanone. The optimum yield of 82% was obtained with $NaBrO_3$ as a co-oxidant in AcOH at 55 °C. In similar fashion, 4-hydroxymethyl-1-cyclohexanol was converted into 4-hydroxymethyl-1-cyclohexanone in 73% yield with Ce/NAFK-$NaBrO_3$.

The Cr(III) and Ce(IV) catalysts prepared from Nafion-H (NAFH) also were effective for the transformation of alcohol into carbonyl compounds, but the products were contaminated by the di-*t*-butyl acetals which were generated by the NAFH catalyzed acetalization of the ketones.[14]

Experimental

Infrared spectra of neat liquid film samples were determined on a Hitachi grating infrared spectrometer 215, or JASCO IR 810, mass spectra and exact mass on a Hitachi M-80. NMR spectra were recorded on a Varian EM-390, or Varian XL-200 spectrometer using TMS as an internal standard unless otherwise noted. Multiplicity is designated as s, singlet; d, doublet; t, triplet, q, quartet; m, multiplet. Preparative TLC plates were prepared with Merck Kieselgel PF_{254}. Column chromatography was carried out with silica gel (Wakogel C-200) at atmospheric pressure.

Preparation of Metal/NAFK Catalyst. Preparation of Cr/NAFK is representative. Anhydrous chromium(III) acetate (0.69 g, 3.0 mmol) was dissolved in deionized water (30 ml). NAFK (1.1 g, 1.0 mmol of sulfonate) was added and the suspension was stirred for 36 h at 25 °C. The polymer catalyst was filtered off and washed with deionized water (10 ml×5) until the washings became practically colorless. The recovered polymer catalyst was dried in vacuo to constant weight, and used.

Capacity of thus prepared resin catalyst was confirmed as follows. Dried resin catalyst (500 mg) was suspended in aqueous hydrochloric acid (6 M; 1 M=1 mol dm^{-3} prepared with deionized water, 3 ml), and stirred for 5 h. The polymer was filtered off and washed with hydrochloric acid (5 ml×2). The recovered polymer catalyst was suspended again in hydrochloric acid (6 M, 3 ml) and the washing processes were repeated twice. Whole washings were collected and chromium(III) dissolved was titrated with ethylenediaminetetraacetic acid according to a described method.[15] Titration showed that 0.68 mmol of Cr(III) per gram was supported on the resin catalyst.

Preparation of Ce/NAFK. To a solution of $(NH_4)_2Ce(NO_3)_6$ (1.75 g, 3.0 mmol) in deionized water (30 ml) was added NAFK (1.1 g, 1.0 mmol of sulfonate), and the whole was stirred for 36 h at 25 °C. Titration of the dried resin indicated that 0.54 mmol of Ce(IV) per gram was loaded on the resin catalyst.

Other metal/NAFK catalysts prepared were Cu(II) (from $CuSO_4$ or $Cu(OAc)_2$), Ni(II) ($Ni(OAc)_2$), and Mn(II) ($Mn(OAc)_2$). Titration indicated that each metal/NAFK had capacity of more than 70% of theoretical one of fully loaded resin.

General Procedure for the Oxidation of Secondary Alcohols with *t*-Butyl Hydroperoxide Using Cr/NAFK as Catalyst. A solution of 1-phenylethanol (0.12 g, 1.0 mmol) in chlorobenzene (2.0 ml) was added to a suspension of Cr/NAFK (50 mg. 0.034 mmol as chromium(III) salt) in chlorobenzene (1.0 ml). A solution of *t*-butyl hydroperoxide in benzene (2.64 M, 1.5 ml, 4.0 mmol) was added and the whole was heated at 85 °C for 6 h. The solid catalyst was filtered off and washed with ethyl acetate. The filtrate and washings were combined and washed with aqueous sodium hydrogensulfite and brine successively. Purification of the concentrated crude product by silica gel column chromatography gave acetophenone (0.11 g) in 95% yield.

Oxidation of 1-Dodecanol with *t*-Butyl Hydroperoxide Using Cr/NAFK as Catalyst. To a suspension of Cr/NAFK (50 mg, 0.034 mmol of chromiun(III) salt) in chlorobenzene (2.0 ml) was added 1-dodecanol (0.18 g, 1.0 mmol) and *t*-butyl hydroperoxide in benzene (2.64 M, 1.5 ml. 4.0 mmol). The whole mixture was heated at 80 °C and stirred for 12 h. The resin catalyst was filtered off and the filtrate was treated with aqueous sodium hydrogensulfite. The water layer was acidified with aqueous hydrochloric acid (6 M, 2.0 ml) and extracted with ethyl acetate. Concentration of combined organic layer followed by separation by silica gel column chromatography gave dodecanal (0.07 g. 39%) and dodecanoic acid (0.03 g, 15%). Unchanged 1-dodecanol was also recovered (0.04 g, 24%).

General Procedure for the Oxidation of Secondary Alcohols with *t*-Butyl Hydroperoxide Using Ce/NAFK as Catalyst. Oxidation of carveol to carvone was representative. Carveol (0.15 g, 1.0 mmol) and *t*-butyl hydroperoxide (2.64 M benzene solution, 1.5 ml, 4.0 mmol) were added to a suspension of Ce/NAFK (50 mg, 0.027 mmol of cerium(IV) salt) in benzene (2.0 ml). The mixture was stirred for 2 h at 80 °C.

The resulting mixture was diluted with ethyl acetate, then Ce/NAFK catalyst was filtered off and washed with ethyl acetate on a glass filter. The organic layer was washed with aqueous sodium hydrogensulfite and brine, and dried over anhydrous sodium sulfate. Concentration gave a residual oil which was submitted to silica-gel column chromatography to give carvone (0.15 g) in 98% yield.

11-Hydroxy-2-undecanone: To a suspension of sodium bromate (0.15 g, 1.0 mmol) and Ce/NAFK (0.1 g, 0.054 mmol) in acetic acid (2.0 ml) was added a solution of 1,10-undecanediol (0.19 g, 1.0 mmol) in the same solvent (1.0 ml). The resulting mixture was stirred at 55 °C for 3 h. The resin catalyst was filtered off and washed with ethyl acetate. The filtrate and washings were combined and treated with aqueous sodium hydrogencarbonate, sodium hydrogensulfite, and brine. Concentration and purification by silica-gel column chromatography (hexane:ethyl acetate=2:1) gave the title compound (0.16 g) in 82% yield. Mp 42—43 °C; IR (neat) 3424, 1709, 1358, 1042 cm^{-1}; ^1H NMR (CCl_4) δ=1.1—1.8 (m, 14H), 2.09 (s, 3H), 2.36 (t, J= 6.6 Hz, 2H), 3.58 (t. J=6.8 Hz, 2H), 3.78 (b, 1H). Found: C, 70.65; H, 11.90%. Calcd for $C_{11}H_{22}O_2$: C, 70.92; H, 11.90%.

4-Hydroxymethyl-1-cyclohexanone: The product was identical with the authentic sample.[16]

Oxidation of 4-*t*-Butylcyclohexanol with *t*-Butyl Hydroperoxide Using Ce/NAFH as Catalyst. Ce/NAFH catalyst was generated in the same manner as the preparation of Ce/NAFK. Titration indicated the capacity of 0.60 mmol of Ce(IV) per one gram of resin. To a suspension of Ce/NAFH (50 mg, 0.03 mmol of Ce(IV) salt) in benzene (4.0 ml) was added 4-*t*-butylcyclohexanol (0.16 g, 1.0 mmol) and *t*-butyl hydroperoxide (2.64 M in benzene, 1.5 ml, 4.0 mmol) and the resulting mixture was stirred at 80 °C. The starting alcohol was consumed within 1.5 h and the resulting mixture was diluted with ethyl acetate. The resin catalyst was separated and washed with ethyl acetate. The filtrate and washings were treated with aqueous sodium hydrogensulfite and brine, dried over anhydrous sodium sulfate and concentrated. Purification of crude oil by silica-gel column chromatography (hexane:ethyl acetate=10:1) gave 4-*t*-butylcyclohexanone (0.05 g, 30%) and 4-*t*-butylcyclohexanone di-*t*-butyl acetal (0.15 g, 50%).

Buffering the reaction mixture by adding sodium hydrogencarbonate improved the yield of 4-*t*-butylcyclohexanone and suppressed the formation of acetal. Treatment of a mixture of Ce/NAFH (50 mg, 0.03 mmol of cerium(IV) salt), 4-*t*-butylcyclohexanol (0.16 g, 1.0 mmol) and sodium hydrogencarbonate (0.04 g, 0.5 mmol) in benzene (4.0 ml) with *t*-butyl hydroperoxide (2.64 M in benzene, 1.5 ml, 4.0 mmol) gave 4-*t*-butylcyclohexanone (0.11 g, 68%) which was contaminated by small amount of acetal (7%). Oxidation proceeded somewhat slower than the reaction without sodium hydrogencarbonate (80 °C, 3 h).

References

1) ACS Symp. Ser. 308 "Polymeric Reagents and Catalysts," ed by W. T. Ford, American Chemical Society, Washington, DC (1986).

2) G. A. Crosby, N. M. Weinshenker, and H. S. Uh, *J. Am. Chem. Soc.*, **97**, 2232 (1975).

3) J. M. J. Fréchet, J. Warnock, and M. J. Farrall, *J. Org. Chem.*, **43**, 2618 (1978).

4) J. M. J. Fréchet, P. Darling, and M. J. Farrall, *J. Org. Chem.*, **46**, 1728 (1981).

5) Several polymer reagents have been reported for the oxidation of olefins and carbonyl compounds. Epoxidation of olefin: F. Helfferich and D. B. Luten, Jr., *J. Appl. Polym. Sci.*, **8**, 2899 (1964); W. J. Hamilton, K. J. Krause, and H. B. Wagner, *ibid.*, **18**, 1039 (1974); T. Takagi, *Polym. Lett.*, **5**, 1031 (1967); T. Takagi and M. Aoyama, *ibid.*, **12**, 681 (1974); J. M. J. Fréchet and K. E. Haque, *Macromolecules*, **8**, 130 (1975); C. R. Harrison and P. Hodge, *J. Chem. Soc., Chem. Commun.*, **1974**, 1009; *idem, J. Chem. Soc., Perkin Trans. 1*, **1976**, 605. Baeyer-Villiger reaction: S. E. Jacobson, F. Mares, and P. M. Zambri, *J. Am. Chem. Soc.*, **101**, 6938, 6946 (1979).

6) Oxidation of alcohols with chromic acid on Amberlyst A 26, a macroreticular anion-exchange resin has been also reported. G. Cainelli, G. Cardillo, M. Orena, and S. Sandri, *J. Am. Chem. Soc.*, **98**, 6737 (1976).

7) For instance, vanadium and molybdenum salts supported on polymeric amine or dithiocarbamate have been used as the catalyst for the epoxidation: M. Nishizawa, T. Yokoyama, T. Kimura, and T. M. Suzuki, *Chem. Lett.*, **1983**, 1413; T. Yokoyama, M. Nishizawa, T. Kimura, and T. M. Suzuki, *ibid.*, **1983**, 1703; G. L. Linden and M. F. Farona, *J. Catal.*, **48**, 284 (1977); S. Bhaduri, A. Ghosh, and H. Khwaja, *J. Chem. Soc., Dalton Trans.*, **1981**, 447; S. Bhaduri and H. Khwaja, *ibid.*, **1983**, 415. Polystyrene-bound benzeneleninic acid-*t*-butyl hydroperoxide, for oxidation of benzyl alcohol: R. T. Taylor and L. A. Flood, *J. Org. Chem.*, **48**, 5160 (1983). Electrolytic oxidation of alkylbenzene using polymeric electron carrier. J. Yoshida, K. Ogura, and N. Kawabata, *J. Org. Chem.*, **49**, 3419 (1984).

8) A part of this work was published in a communication form: S. Kanemoto, H. Saimoto, K. Oshima, and H. Nozaki, *Tetrahedron Lett.*, **25**, 3317 (1984).

9) Nafion is a registered trademark of E. I. du Pont de Nemours & Co. See J. D. McMlure and S. G. Brandenberger, U. S. Patent, 4038213 (1977). Recent reports on Nafion reagents in organic synthesis: S. Murata and R. Noyori, *Tetrahedron Lett.*, **21**, 767 (1980); H. Saimoto, T. Hiyama, and H. Nozaki, *Bull. Chem. Soc. Jpn.*, **56**, 3078 (1983); G. A. Olah, S. C. Narang, R. Malhotra, and J. A. Olah, *J. Am. Chem. Soc.*, **101**, 1805 (1979). We thank Mitsui Fluorochemical Co. for a generous gift of NAFK.

10) NAFK was converted into the H^+ form according to the reported procedure. J. Kaspi and G. A. Olah, *J. Org. Chem.*, **43**, 3142 (1978).

11) J. G. Hill, B. E. Rossiter, and K. B. Sharpless, *J. Org. Chem.*, **48**, 3607 (1983). Reactions in aqueous media resulted in a considerable loss of capacity. Approximately 80% of chromium dissolved out from resin after the reaction with 70% aqueous *t*-butyl hydroperoxide.

12) H. Tomioka, K. Oshima, and H. Nozaki, *Tetrahedron Lett.*, **23**, 537 (1982).

13) M. E. Jung and L. M. Spelts, *J. Am. Chem. Soc.*, **98**, 7882 (1976); M. E. Jung and R. W. Brown, *Tetrahedron Lett.*, **1978**, 2771; G. H. Posner, R. B. Perfetti, and A. W. Runquist, *ibid.*, **1976**, 3499; M. A. Neirabeyeh, J. C. Ziegler, and B. Gross, *Synthesis*, **1976**, 811; Y. Ueno and M. Okawara, *Tetrahedron Lett.*, **1976**, 4597.

14) The present work has its origin in the finding that 4-methyl-1-phenyl-2-pentyne-1,4-diol is converted into the corresponding ynone quantitatively on treatment with NAFH in 70% aqueous *t*-BuOOH. H. Saimoto, M. Shinoda,

S. Matsubara, K. Oshima, T. Hiyama, and H. Nozaki, *Bull. Chem. Soc. Jpn.*, **56**, 3088 (1983). We are grateful to Dr. Tamejiro Hiyama for helpful discussions.

15) J. Kimunen and B. Wennerstrand, *Chemist. Annalyst*, **46**, 92 (1957).

16) C. G. Overberger, J. H. Kozlowski, and E. Radlmann, *J. Polym. Sci. A-1*, **10**, 2265 (1972).

Development of a Facile Method for Polypeptide Synthesis. Synthesis of Bovine Pancreatic Trypsin Inhibitor (BPTI)

Saburo AIMOTO,* Noriko MIZOGUCHI, Hironobu HOJO, and Shoko YOSHIMURA
Institute for Protein Research, Osaka University, Yamakaoda, Suita, Osaka 565
(Received July 27, 1988)

A new method for the preparation of pure polypeptides based on the minimun-protection strategy is described. Its effectiveness was demonstrated by a synthesis of bovine pancreatic trypsin inhibitor (BPTI). Protected peptide segments of Z-[Arg(Tos)^{1}, Asp(O*c*Hex)^{3}, Cys(Acm)^{5}, Glu(O*c*Hex)^{7}]-BPTI(1—13), Boc-[Cys(Acm)^{14,30}, Lys(Z)^{15,26}]-BPTI(14—36), and [Cys(Acm)^{38,51,55}, Lys(Z)^{41,46}]-BPTI(37—58) were prepared by modifying the products obtained by solid-phase peptide syntheses. The protected peptides corresponding to BPTI(14—36) and BPTI(37—58) were coupled by an active ester method to give protected BPTI(14—58). Next, protected BPTI(1—13) was coupled to the BPTI(14—58) by an active ester method after removing the Boc group from the protected BPTI(14—58). All of the protecting groups on BPTI(1—58) were removed, and the resulting peptide was oxidized to give the native form of BPTI in a very pure form. The synthetic BPTI was shown to be identical with the native BPTI in an elution experiment on ion-exchange chromatography and in its inhibitory activity. The new method proved to be very effective for a rapid preparation of pure polypeptide.

Solid-phase peptide synthesis permits effective peptide-chain elongation on a solid support within a short time.[1] However, purification of the final product becomes more difficult with increasing peptide size. On the other hand, a liquid-phase synthesis of a polypeptide is extremely tedious, even for an experienced peptide chemist. To overcome these problems, several approaches have been proposed.[2-5]

We have reported a facile method[6] for the preparation of a cyclic peptide using a protected peptide derived from the product obtained by a solid-phase method. The results suggested that the method could be applied to the preparation of polypeptides.

In this paper, we describe a novel method for the preparation of polypeptide. Its effectiveness was demonstrated by the synthesis of a well-studied small protein, BPTI. This method should be applicable to the syntheses of other peptides of this size.

Results and Discussion

Preparation of Protected Peptide Segments. As shown in Fig. 1, BPTI was divided into three peptide segments: BPTI (1—13), BPTI (14—36), and BPTI (37—58). To avoid racemization during segment coupling, their carboxyl-terminal amino-acid residues were designed to be a glycine or proline residue.

Since BPTI (1—13) contains aspartyl and glutamyl residues, selective protection of α- and ω-carboxyl groups of this peptide segment was realized by the solid-phase method involving N^{α}-(3-nitro-2-pyridinesulfenyl) amino acids (Npys-amino acid) and N^{α}-(9-fluorenylmethyloxycarbonyl) amino acids (Fmoc-amino acid) as shown in Fig. 2. Preparation of the Npys-prolyl resin **6** and chain elongation by using Npys-amino acid were carried out by Matsueda's method.[7] Fmoc-Cys(Acm) was introduced according

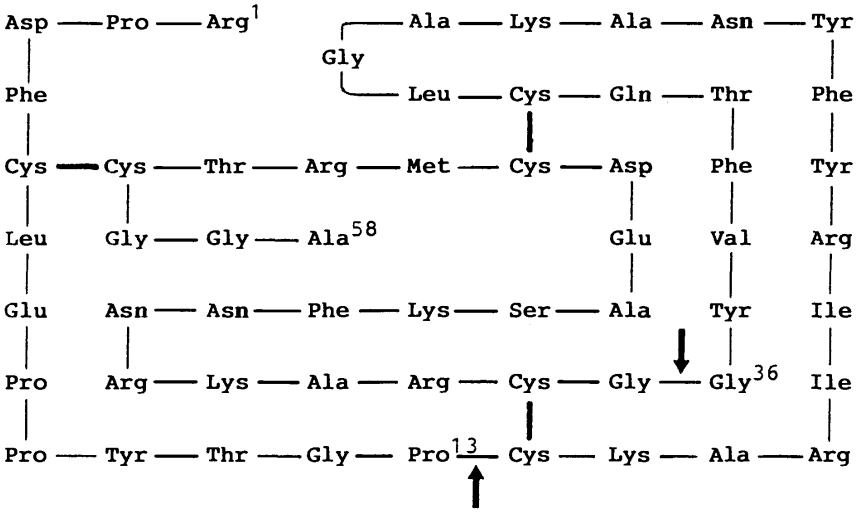

Fig. 1. Primary sequence of bovine pancreatic trypsin inhibitor (BPTI). Arrows indicate the sites where segment coupling was carried out.

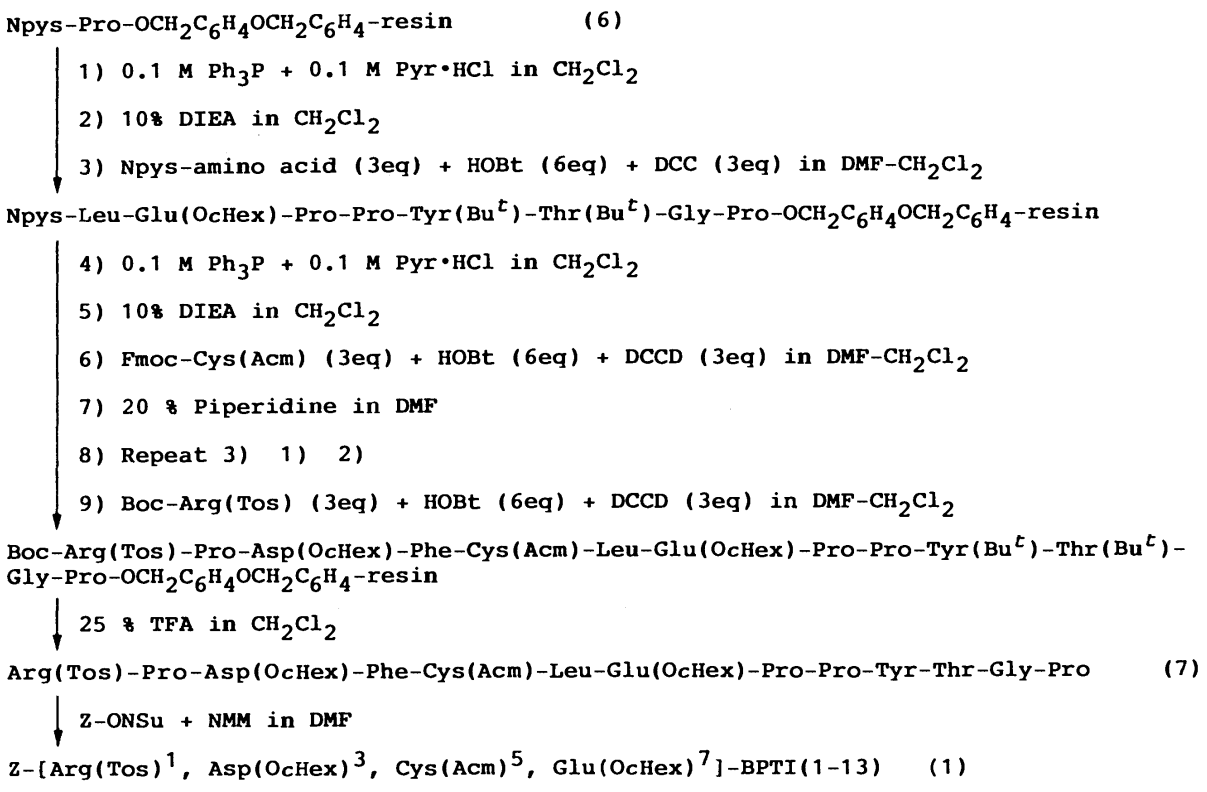

Fig. 2. Synthetic scheme of partially protected BPTI(1—13) **1**

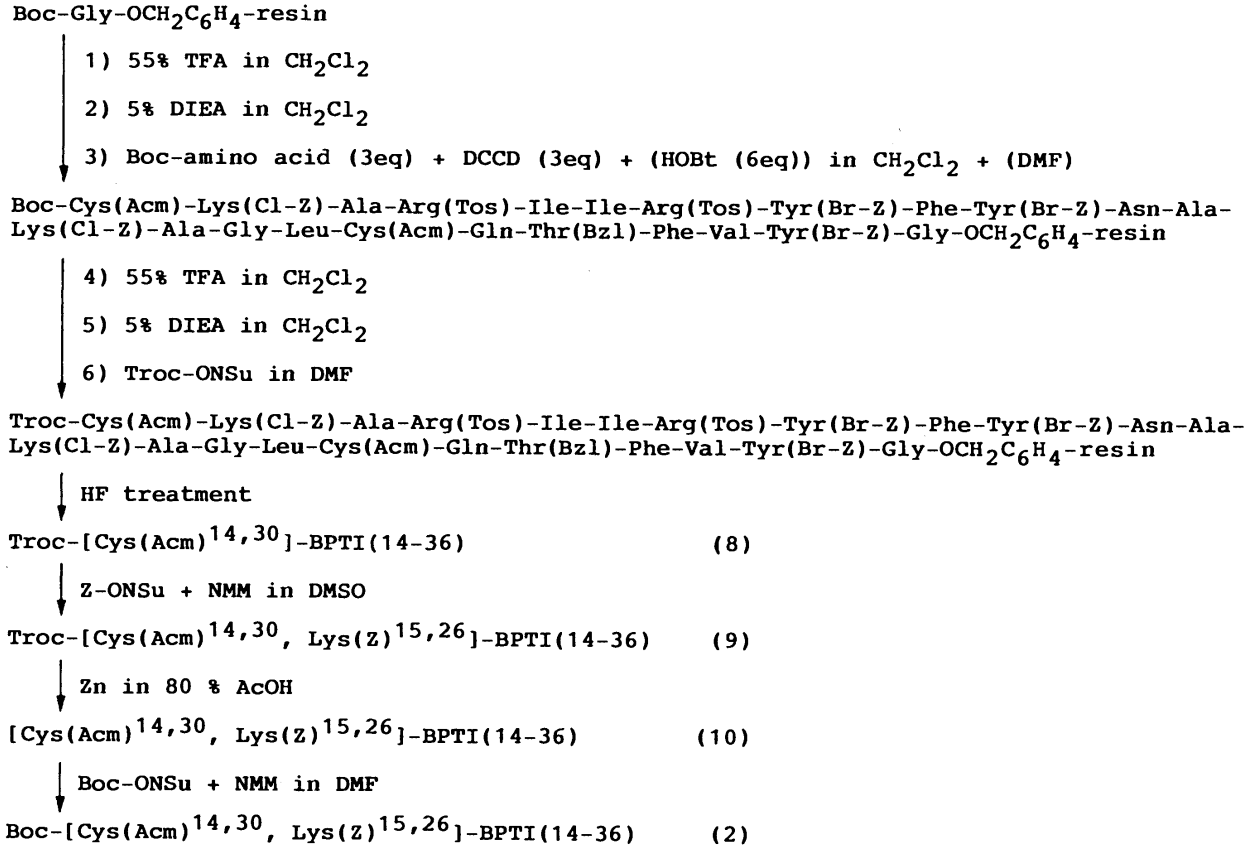

Fig. 3. Synthetic scheme of partially protected BPTI(14—36) **2**

to Chan et al. with slight modifications.[8] After completion of the peptide chain assembly, the protected peptide resin was treated with 25% trifluoroacetic acid (TFA) in CH_2Cl_2 to obtain protected peptide **7**. This peptide was hydrophobic, but very soluble in aqueous acetonitrile and easily purified by reversed-phase high-pressure liquid chromatography (HPLC). To the amino terminal of the purified peptide, the benzyloxycarbonyl (Z) group was introduced using *N*-(benzyloxycarbonyloxy)succinimide (Z-ONSu) in the presence of 4-methylmorpholine (NMM) as a base to give partially protected BPTI(1—13) **1** in a yield of about 30% based on crude peptide **7**. Confirmations of the protected peptides were carried out by a combination of amino acid analysis and fast atom bombardment (FAB) mass spectrometry.

Since BPTI(14—36) contains no side-chain carboxyl group, the protected BPTI (14—36) **2** was prepared by a solid-phase method involving N^{α}-(*t*-butoxycarbonyl) amino acids (Boc-amino acid). To the Boc-glycyl resin, which was prepared by Gisin's method,[9] Boc-amino acids were successively introduced by the standard Merrifield method,[1] in which the completion of each coupling reaction was checked by a Kaiser test.[10] After completion of the chain elongation, the terminal amino group was blocked by an acid-stable 2,2,2-trichloroethoxycarbonyl (Troc) group[6,11-13] to realize the selective protection of α- and ω-amino groups (Fig. 3). Treatment of the protected peptide resin with anhydrous hydrogen fluoride gave Troc-peptide **8**, which was converted to peptide **9** by a treatment with Z-ONSu in the presence of NMM. Treatment of peptide **9** with zinc dust in aqueous acetic acid gave peptide **10**, which was purified on HPLC. To the generated α-amino group of peptide **10**, a Boc group was introduced by a treatment with *N*-(*t*-butoxycarbonyloxy)succinimide (Boc-ONSu) in the presence of NMM to obtain partially protected BPTI (14—36) **2**. The yield of peptide **2** was as low as 3%, based on crude peptide **8**. Peptides **9**, **10**, and **2** tended to form gels in aqueous acetonitrile. This seemed to be responsible for the low recovery yield of the peptide after purification on HPLC.

Partially protected BPTI (37—58) **3** was prepared using the same strategy adopted for the synthesis of protected peptide **2** (Fig. 4). The yield of peptide **3** was about 30%, based on crude peptide **11**.

Segment Coupling of Partially Protected Peptides. Protected BPTI (1—58) **5** was prepared according to the scheme shown in Fig. 5. Peptide **2** was converted to the corresponding active ester in the presence of sevenfold molar excess of *N*-hydroxysuccinimide (HONSu) with a fivefold molar excess of 1-ethyl-3-(3-dimethylaminopropyl)carbodiimide hydrochloride (WSCI·HCl). The ester-formation reaction was monitored by HPLC and FAB mass measurements. The ester was precipitated with the aid of ether, then washed successively with ethyl acetate, dioxane, and water and dried. The obtained powder was dissolved in dimethyl sulfoxide (DMSO) and peptide **3** and NMM were added. The resulting solution was stirred overnight at room temperature. The product, isolated by HPLC, was

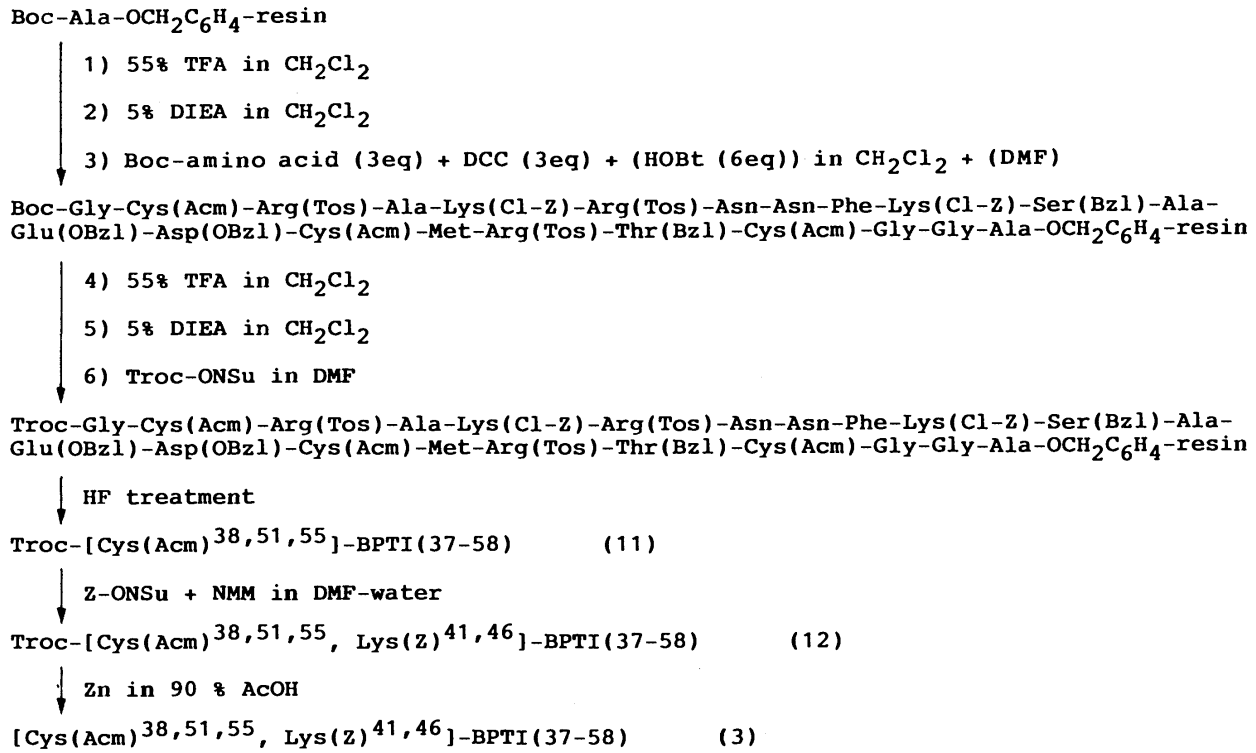

Fig. 4. Synthetic scheme of partially protected BPTI(37—58) **3**.

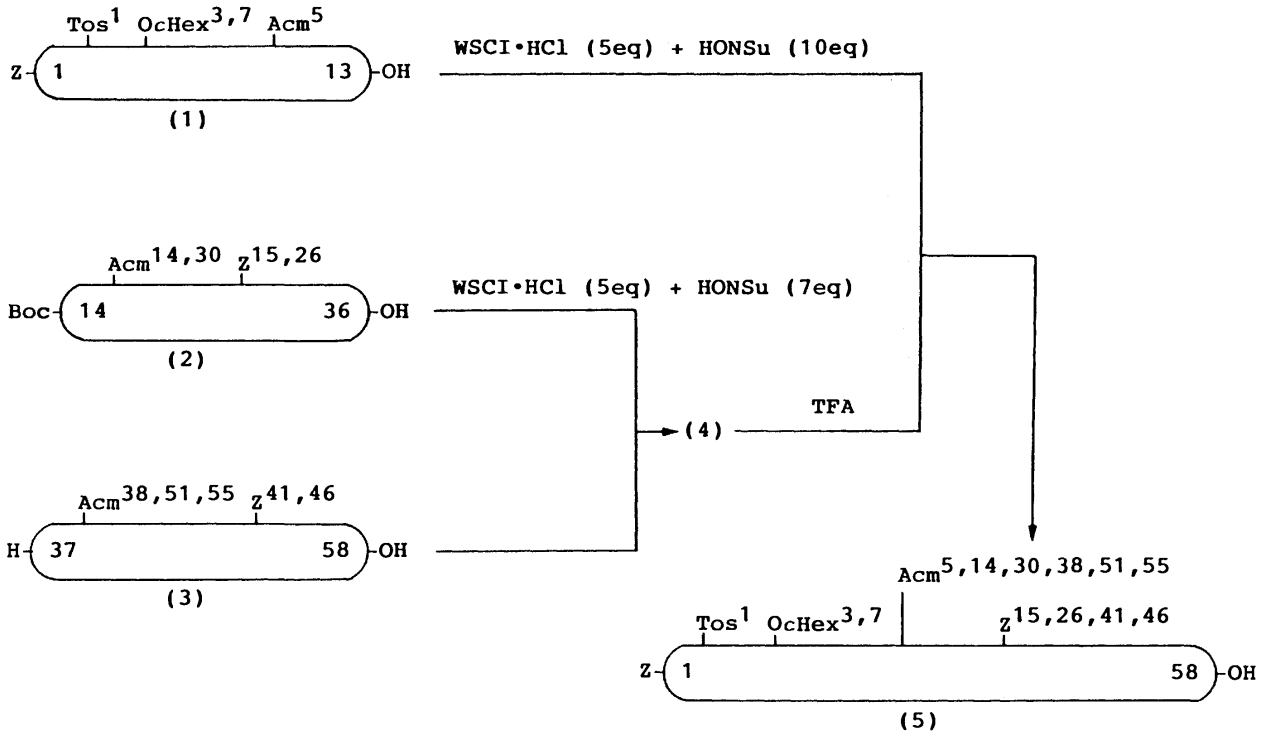

Fig. 5. Synthetic route leading to protected BPTI(1—58) **5** by segment coupling.

confirmed by amino acid analysis to be the desired product **4**, in a yield of about 50%. The active ester of peptide **1**, which was prepared as described above, and the amino-component peptide, which was obtained by TFA treatment of peptide **4**, were mixed in a 2 to 1 molar ratio in DMSO containing 5% NMM, and stirred overnight. Judging from the HPLC profile of the reaction mixture, the amino component reacted almost completely with the active ester to give a product. The amino acid analysis data of the product agreed with the theoretical values expected of protected BPTI (1—58) **5**. Though the segment coupling proceeded almost completely, the yield of the purified peptide **5** was about 30%. The low recovery yield seems to be due to the adsorption of the product on a reversed-phase column during the isolation process.

Generation of the Native Form of BPTI from Peptide 5 and Its Characterization. Protected BPTI (1—58) **5** was treated successively with anhydrous hydrogen fluoride, $Hg(AcO)_2$, and dithiothreitol (DTT) according to the procedure shown in Fig. 6. The reduced form of synthetic BPTI was oxidized in the presence of 1,2-dithiane-4,5-diol (the oxidized form of DTT) according to the method described by Creighton.[14] The native form of synthetic BPTI, thus generated, was adsorbed on TSK gel CM-5PW and eluted with a $AcONH_4$ (pH 8.6) linear gradient (0.01—1 M† $AcONH_4$), as shown in Fig. 7. The main product was eluted at the same position as that of native BPTI. The amino acid analysis data of the product agreed

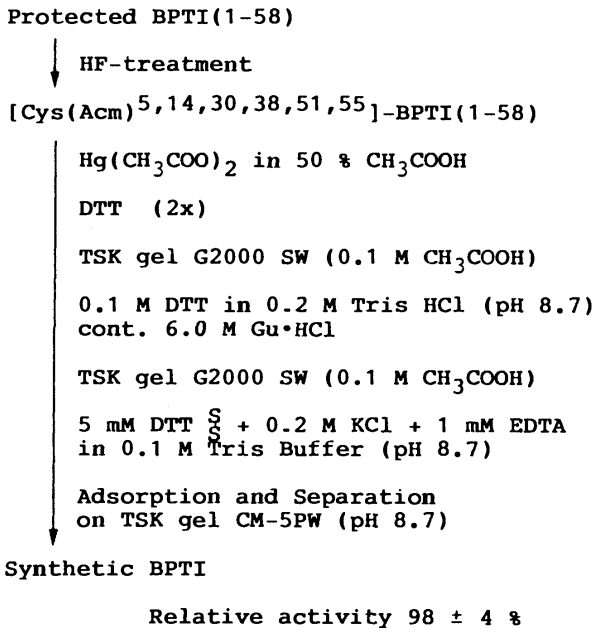

Fig. 6. Operation procedure leading to the native form of synthetic BPTI from protected BPTI(1—58) **5**. DTT^{S}_{S} indicates the oxidized form of DTT.

well with that of native BPTI (Table 1). Furthermore, the product had practically the same inhibitory activity (98±4%) against trypsin as native BPTI. These data show that highly pure BPTI was successfully synthesized.

Evaluation of the Newly Developed Method. Each of the protected peptide segments **1**, **2**, and **3** could be

†1 M=1 mol dm^{-3}.

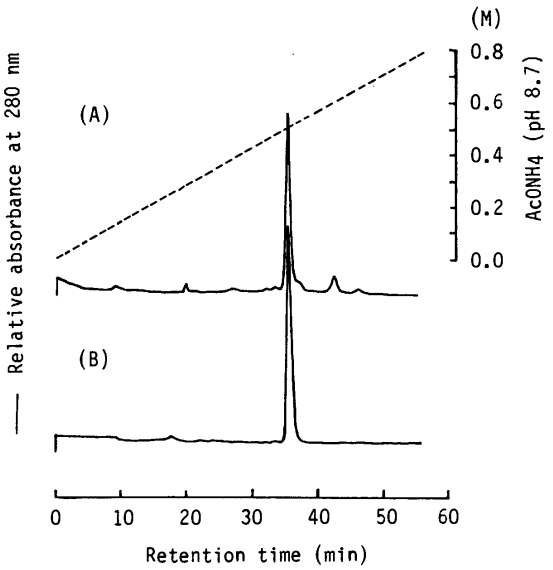

Fig. 7. Ion-exchange chromatogram of synthetic BPTI on TSK gel CM-5PW. (A) The elution profile of crude synthetic BPTI obtained by oxidation with DTT^{S}_{S}. (B) The elution profile of native BPTI. Broken line indicates the concentration of $AcONH_4$ in the buffer.

Table 1. Amino Acid Composition of Synthetic BPTI

	Synthetic BPTI	Native BPTI	Expected
Asp	5.33	5.18	5
Thr	2.98	2.94	3
Ser	1.19	1.03	1
Glu	3.29	3.22	3
Pro	4.02	4.08	4
Gly	6.16	6.14	6
Ala	6	6	6
1/2·Cys	5.11	5.26	6
Val	1.10	1.07	1
Met	0.94	0.96	1
Ile	1.24	1.28	2
Leu	2.07	2.07	2
Tyr	3.96	4.06	4
Phe	4.00	4.06	4
Lys	3.82	3.99	4
Arg	5.84	5.88	6

easily prepared within 2 to 3 weeks starting from the corresponding amino-acyl resins, and the total synthesis of BPTI was accomplished within 2 months. Therefore, the newly developed method enabled a very rapid polypeptide synthesis, which has a very important practical advantage. The minimum-protection strategy worked well on segment coupling. When NMM was used as a base, undesirable side reactions, such as acylation of alcoholic or phenolic hydroxyl groups, were not observed during segment coupling. Furthermore, the elution profile of the native form of BPTI (Fig. 7) revealed that a main product was eluted at the same retention time as native BPTI, and that the peak width of the main product was the same as that of the native one. These facts suggest that all the procedures involved in the synthesis of BPTI proceeded almost perfectly to give highly pure protected BPTI (1—58). Consequently, the pure final product, the native form of synthetic BPTI, could be obtained without employing affinity chromatography. One problem which did arise was the low recovery yield of peptide after HPLC purification. Other than this, we found our method to be useful for the preparation of pure polypeptides of this size.

Materials and Methods

All the amino acids used were of the L-configuration, except for glycine. Boc-amino acids and Bz-Arg-*p*NA·HCl were purchased from Peptide Institute Inc. (Minoh, Japan). Npys-amino acids except for Npys-Glu(O*c*Hex) and Npys-Asp(O*c*Hex), Npys-Cl, Fmoc-Cys(Acm), and *p*-alkoxybenzyl alcohol resin were purchased from Kokusan chemical Works, Ltd. (Tokyo, Japan). Trypsin (bovine pancreas) and bovine pancreatic trypsin inhibitor were purchased from Sigma Chemical Co. Troc-Cl and *trans*-1,2-dithiane-4,5-diol were purchased from Aldrich Chem. Co. *p*-Guanidinobenzoic acid *p*-nitrophenyl ester was purchased from Nacalai Tesque, Ltd. (Kyoto, Japan). All solvents used were of guaranteed grade. High-performance liquid chromatography (HPLC) was carried out on a handmade column of the YMC-Gel ODS S5 100 Å A-type (8×300 mm) (Yamamura Chemical Laboratory Co., Ltd., Kyoto, Japan). Amino acid analysis was carried out using a Jasco amino acid analysis system after acid hydrolysis of a peptide with 4 M methanesulfonic acid (Pierce Chemical Co.) at 110 °C for 24 h. Mass measurement was carried out using a Jeol double-focusing mass spectrometer JMS-HX100, equipped with a fast atom bombardment ion source. Sonication was carried out using a Branson Model B-220. The melting points were determined by the capillary method and are given as uncorrected values. Optical rotations were determined with a Perkin-Elmer Model 241 polarimeter. Abbreviations used are those recommended by IUPAC-IUB: *J. Biol. Chem.*, **247**, 977 (1972). Additional abbreviations: Acm, acetamidomethyl; Cl-Z, 2-chlorobenzyloxycarbonyl; Bzl, benzyl; Br-Z, 2-bromobenzyloxycarbonyl; O*c*Hex, cyclohexyl ester; DCHA, dicyclohexylamine.

Synthesis

Troc-ONSu. Troc-Cl (2.12 g, 10 mmol) and HONSu (1.27 g, 11 mmol) were mixed in dioxane (20 ml) in the presence of triethylamine (TEA) (1.82 ml, 13 mmol) at room temperature for 2 h. The solution was dried, and the product was dissolved in ethyl acetate, washed successively with diluted hydrochloric acid and water, and crystallized from a mixture of ethyl acetate and hexane to obtain Troc-ONSu (2.21 g, 76.0%), mp 105.5—106.0 °C. Found: C, 29.00; H, 2.00; N, 4.79; Cl, 36.48%. Calcd for $C_7H_6O_5NCl_3$: C, 28.94; H, 2.08; N, 4.82; Cl, 36.62%.

Npys-Glu(O*c*Hex)·DCHA. This compound was prepared from Npys-Cl and Glu(O*c*Hex) in the presence of TEA according to a method of Matsueda and Walter.[15] Npys-Glu(O*c*Hex)·DCHA; mp 150—151 °C, $[\alpha]_D^{23}$ +42.7° (*c* 1, ethanol). Found: C, 59.32; H, 7.92; N, 9.94%. Calcd for $C_{28}H_{44}O_6N_4S$: C, 59.55; H, 7.85; N, 9.92%.

Npys-Asp(OcHex)·DCHA. This compound was prepared from Npys-Cl and Asp(OcHex) in the presence of TEA according to a method of Matsueda and Walter.[14] Npys-Asp(OcHex)·DCHA; mp 157—158 °C, $[\alpha]_D^{23}$ +18.9° (*c* 1, ethanol). Found: C, 58.62; H, 7.77; N, 10.13%. Calcd for $C_{27}H_{42}O_6N_4S$: C, 58.87; H, 7.69; N, 10.18%.

Npys-Pro-OCH$_2$C$_6$H$_4$-O-CH$_2$C$_6$H$_4$-Resin (6). Npys-Pro (3.61 g, 13.4 mmol) was coupled to *p*-alkoxybenzyl alcohol resin (5 g, 0.67 meq OH/g) in the presence of 4-dimethylaminopyridine (DMAP) (1.64 g, 13.4 mmol) and dicyclohexylcarbodiimide (DCC) (2.76 g, 13.4 mmol) in *N*,*N*-dimethylformamide (DMF) (30 ml) at room temperature for 14 h. The resin, thus obtained, was treated twice with acetic anhydride (4 ml) in pyridine (20 ml) at room temperature for 30 min and gave 6.3 g of resin **6**. The proline content in the resin was determined to be 0.58 mmol g^{-1} by measuring the absorbance of the solution at 338 nm (ε=6330) after treatment of the resin with a dichloromethane solution containing 0.1 M triphenylphosphine in the presence of 0.1 M pyridine hydrochloride.[7]

Arg(Tos)-Pro-Asp(OcHex)-Phe-Cys(Acm)-Leu-Glu(OcHex)-Pro-Pro-Tyr-Thr-Gly-Pro (7). Npys-Pro resin (**6**) (0.86 g, 0.5 mmol) was placed in a reaction vessel, and the synthesis was carried out manually according to the following protocol by using Npys derivatives of Gly, Thr(Bu^t), Tyr(Bu^t), Pro, Glu(OcHex), Leu, Phe, and Asp(OcHex): (1) washing, CH_2Cl_2 (3×1 min); (2) deprotection, 0.1 M triphenylphosphine and 0.1 M pyridine hydrochloride/CH_2Cl_2 (1×1 min, 2×30 min); (3) washing, CH_2Cl_2 (3×1 min); (4) washing, 2-propanol (2×1 min); (5) washing, CH_2Cl_2 (3×1 min); (6) neutralization, 10% DIEA/CH_2Cl_2 (v/v) (3×1.5 min); (7) washing, CH_2Cl_2 (3×1.5 min) (8) coupling, Npys-amino acid (1.5 mmol) and 1-hydroxybenzotriazole (HOBt) (3 mmol)/DMF(5 ml) and DCC (1.5 mmol)/CH_2Cl_2 (5 ml) (1×1 h); (9) washing, DMF (3×1 min); (10) washing, CH_2Cl_2 (3×1 min); (11) washing, 2-propanol (3×1 min). Cys(Acm) was introduced to the peptide by using an Fmoc derivative under the coupling conditions used for Npys-amino acid; then, a peptide resin was washed successively with DMF, 2-propanol, and CH_2Cl_2. After that, the resin was treated as follows: (1) washing, CH_2Cl_2 (2×1 min); (2) washing, DMF (2×1 min); (3) deprotection, 20% piperidine/DMF (v/v) (1×1 min, 1×20 min); (4) washing, DMF (3×1 min); (5) washing, CH_2Cl_2 (3×1.5 min). The resin was coupled with Npys-Phe. Arg(Tos) was introduced by using its Boc derivative, and washed with DMF, CH_2Cl_2, and 2-propanol. The weight of the peptide resin, thus obtained, was 1.59 g. The whole resin was treated with 25 ml of 25% TFA/CH_2Cl_2 (v/v) for 30 min at room temperature. The resin was removed by filtration, and the filtrate was concentrated to dryness under reduced pressure, leaving a powder (720 mg). This crude product was purified on HPLC with the acetonitrile concentration increasing from 30% to 80% in 0.05% aq TFA at a flow rate of 2 ml min^{-1} and, gave 217.7 mg of compound **7**. Amino acid analysis: $Asp_{0.97}Thr_{1.01}Glu_{0.89}$ $Gly_{1.00}$ 1/2$Cys_{0.14}$ $Leu_{0.92}$ $Tyr_{0.93}Phe_{0.97}Arg_{0.27}Pro_{3.98}$. Found: *m*/*z* 1881.0 $(M+H)^+$ Calcd for $C_{90}H_{130}N_{17}O_{23}S_2$: 1881.0.

Z-[Arg(Tos)^1, Asp(OcHex)^3, Cys(Acm)^5, Glu(OcHex)^7]-BPTI(1—13) (1). Peptide **7** (23.4 mg, 12.4 μmol) and Z-ONSu (8 mg, 32.2 μmol) were dissolved in DMF (1 ml) containing NMM (10 μl), and the solution was stirred for 2 h. A product was precipitated by the addition of ether to the solution, and washed successively with ethyl acetate and dioxane. The product was further purified on HPLC under the same conditions as compound **7** and gave 14.0 mg of compound **1**. Amino acid analysis: $Asp_{0.98}Thr_{0.95}Glu_{0.97}Pro_{3.77}$ $Gly_{1.00}$ 1/2$Cys_{0.29}Leu_{0.99}Tyr_{1.00}Phe_{0.98}Arg_{0.36}$. Found: *m*/*z* 2014.9 $(M+H)^+$. Calcd for $C_{98}H_{136}N_{17}O_{25}S_2$: 2015.1.

Troc-Cys(Acm)-Lys-Ala-Arg-Ile-Ile-Arg-Tyr-Phe-Tyr-Asn-Ala-Lys-Ala-Gly-Leu-Cys(Acm)-Gln-Thr-Phe-Val-Tyr-Gly (Troc-[Cys(Acm)^{14,30}]-BPTI(14—36)) (8). Boc-Gly-OCH$_2$C$_6$H$_4$-resin (Gly 0.66 mmol g^{-1}, 2 g) was placed in a reaction vessel, and the synthesis was carried out manually using the Boc derivatives of Tyr(Br-Z), Val, Phe, Thr(Bzl), Gln, Cys(Acm), Leu, Gly, Ala, Lys(Cl-Z), Asn, Arg(Tos), and Ile. The schedule was as follows: (1) washing, CH_2Cl_2 (2×1 min); (2) deprotection, 55% TFA/CH_2Cl_2 (1×5 min, 1×15 min); (3) washing, CH_2Cl_2 (2×1 min); (4) washing, 33% dioxane/CH_2Cl_2 (1×2 min); (5) washing, CH_2Cl_2 (1×1 min); (6) washing, 33% dioxane (2×1 min); (7) washing, CH_2Cl_2 (3×1 min); (8) neutralization, 5% DIEA/CH_2Cl_2 (2×5 min); (9) washing, CH_2Cl_2 (3×1 min); (10) coupling, 3 equiv of Boc-amino acid/CH_2Cl_2 and 3 equiv of DCC/CH_2Cl_2 (1×120 min) except for Boc derivatives of Gln, Asn and Arg(Tos). For the coupling of Boc-Gln, Boc-Asn, or Boc-Arg(Tos), 3 equiv of Boc-amino acid and 6 equiv of HOBt/DMF, and 3 equiv of DCC/CH_2Cl_2 (1×120 min); (11) washing, CH_2Cl_2 (1×1 min); (12) washing, 2-propanol (1×2 min); (13) washing, CH_2Cl_2 (1×1 min); (14) washing, 2-propanol (1×2 min); (15) washing, CH_2Cl_2 (1×1 min); (16) Kaiser test.[10] When an unreacted amino group was detected at step 16, steps 9 to 16 were repeated. The terminal Troc group was introduced by adding 3 equiv of Troc-ONSu/DMF (2×150 min) after step 9. The weight of the protected-peptide resin, thus obtained, was 5.46 g. An aliquot of the resin (754 mg) was treated with anhydrous HF containing 10% anisole (v/v) at 0 °C for 70 min to give 374 mg of crude product **8** after lyophilization. This crude peptide was used for the preparation of compound **9** without further purification. An aliquot of the product was purified on HPLC, giving peptide **8**, which was confirmed as follows. Found: *m*/*z* 3002.0 $(M+H)^+$. Calcd for $C_{133}H_{201}N_{35}O_{34}S_2Cl_3$: 3001.6. Amino acid analysis: $Asp_{0.93}Thr_{0.90}Glu_{0.97}Gly_{1.89}Ala_{3.00}$1/2$Cys_{0.00}Val_{0.85}Ile_{0.89}$ $Leu_{0.91}Tyr_{2.74}Phe_{1.84}Lys_{1.86}$ $Arg_{1.78}$.

Troc-[Cys(Acm)^{14,30}, Lys(Z)^{15,26}]-BPTI(14—36) (9). Crude compound **8** (255 mg, ca. 85 μmol) was dissolved in DMSO (4 ml) containing NMM (0.4 ml). Z-ONSu (106 mg, 425 μmol) was added to the solution which was allowed to react for 3 h with stirring. Ether was added to the solution to precipitate a peptide, and the precipitate was washed with ethyl acetate and then dioxane. The product was purified on HPLC with the acetonitrile concentration increasing from 20% to 80% in 0.05% aq TFA at a flow rate of 2 ml min^{-1} and gave 43 mg of compound **9**. Found: *m*/*z* 3270.2 $(M+H)^+$. Calcd for $C_{149}H_{213}N_{35}O_{38}S_2Cl_3$: 3269.7. Amino acid analysis: $Asp_{0.98}$ $Thr_{0.96}Glu_{1.01}Gly_{1.92}Ala_{3.00}$1/2$Cys_{0.00}Val_{0.89}Ile_{0.87}Leu_{0.97}$ $Tyr_{2.73}Phe_{1.93}Lys_{1.89}Arg_{1.82}$.

[Cys(Acm)^{14,30}, Lys(Z)^{15,26}]-BPTI(14—36) (10). Compound **9** (40 mg) was dissolved in 80% aq acetic acid (6 ml) and zinc dust (100 mg) was added under mild sonication over 4 h at room temperature. The remaining zinc dust was removed by centrifugation. Water was added to the supernatant and the precipitate which formed was washed with water and dried, leaving a powder (35 mg). This powder was purified by HPLC under the conditions used for compound **9** to obtain compound **10** (24 mg); Found: *m*/*z* 3096.1 $(M+H)^+$. Calcd

for $C_{146}H_{212}N_{35}O_{36}S_2$: 3095.7. Amino acid analysis: $Asp_{0.98}Thr_{0.97}Glu_{0.98}Gly_{1.98}Ala_{3.00}l/2Cys_{0.81}Val_{0.84}Ile_{0.77}Leu_{0.97}Tyr_{2.76}Phe_{1.90}Lys_{1.86}Arg_{1.80}$.

Boc-[Cys(Acm)^{14,30}, Lys(Z)^{15,26}]-BPTI(14—36) (2). Compound **10** (21.7 mg) was dissolved in DMSO (0.5 ml) containing NMM (10 μl), and Boc-ONSu (20 mg) was added to the solution which was then stirred for 3 h at room temperature. Ethyl acetate was added to the solution to form a precipitate, which when washed with dioxane and freeze-dried gave a powder (19.0 mg). This was purified by HPLC under the conditions used for compound **7** and 8.2 mg of compound **2** was obtained. Found: m/z 3196.0 $(M+H)^+$. Calcd for $C_{151}H_{220}N_{35}O_{38}S_2$: 3195.8. Amino acid analysis: $Asp_{0.98}Thr_{0.95}Glu_{0.96}Gly_{1.97}Ala_{3.00}l/2Cys_{0.60}Val_{0.86}Ile_{0.80}Leu_{0.96}Tyr_{2.73}Phe_{1.90}Lys_{1.87}Arg_{1.83}$.

Troc-Gly-Cys(Acm)-Arg-Ala-Lys-Arg-Asn-Asn-Phe-Lys-Ser-Ala-Glu-Asp-Cys(Acm)-Met-Arg-Thr-Cys(Acm)-Gly-Gly-Ala (Troc-[Cys(Acm)^{38,51,55}]-BPTI(37—58)) (11). Boc-Ala-$OCH_2C_6H_4$-resin (Ala 0.53 mmol g^{-1}, 4.2 g) was placed in a reaction vessel, and peptide-chain elongation and introduction of a Troc group were carried out according to the schedule used for compound **8**, using Boc derivatives of Gly, Cys(Acm), Thr(Bzl), Arg(Tos), Met, Asp(OBzl), Glu(OBzl), Ser(Bzl), Lys(Cl-Z), Phe, and Asn. The weight of the protected peptide resin was 10.4 g. This resin (4.0 g) was treated with anhydrous HF (40 ml) containing anisole (4 ml) at 0 °C for 70 min and gave 1.16 g of crude peptide **11**, which was purified by HPLC with the acetonitrile concentration increasing from 10 to 45% in 0.05% aq TFA at a flow rate of 2 ml min^{-1}. Freeze-drying of the main fraction gave 414 mg of compound **11**. Found: m/z 2761.6 $(M+H)^+$. Calcd for $C_{104}H_{172}N_{38}O_{36}S_4Cl_3$: 2762.3. Amino acid analysis: $Asp_{2.95}Thr_{0.70}Ser_{0.92}Glu_{0.96}Gly_{2.82}Ala_{3.00}l/2Cys_{0.47}Met_{0.93}Phe_{0.94}Lys_{1.95}Arg_{2.95}$.

Troc-[Cys(Acm)^{38,51,55}, Lys(Z)^{41,46}]-BPTI(37—58) (12). Compound **11** (400 mg, 145 μmol) was dissolved in a mixture of DMF (5 ml) and water (2.5 ml). Z-ONSu (361 mg, 1.45 mmol) and NMM (500 μl) were then added, and the solution was stirred for 2 h at room temperature. Methanol (10 ml) was added to the solution to form a precipitate, which was washed with methanol (4×) and then with water (1×); it was then dried to give compound **12** (318 mg). Found: m/z 3031.0 $(M+H)^+$. Calcd for $C_{120}H_{184}N_{38}O_{40}S_4Cl_3$: 3030.4. Amino acid analysis: $Asp_{3.02}Thr_{0.74}Ser_{0.95}Glu_{1.00}Gly_{2.82}Ala_{3.00}l/2Cys_{0.24}Met_{0.94}Phe_{0.98}Lys_{1.92}Arg_{2.92}$.

[Cys(Acm)^{38,51,55}, Lys(Z)^{41,46}]-BPTI(37—58) (3). Compound **12** (318 mg, 105 μmol) was dissolved in 90% aq acetic acid (12 ml). Zinc dust (300 mg) was added with mild sonication under a nitrogen atmosphere over 3 h at room temperature. A product was isolated by HPLC with the acetonitrile concentration increasing from 25 to 50% in 0.05% aq TFA at a flow rate of 2 ml min^{-1}; 212 mg of compound **3** was obtained. Found: m/z 2856.6 $(M+H)^+$. Calcd for $C_{117}H_{138}N_{38}O_{38}S_4$: 2856.5. Amino acid analysis: $Asp_{3.04}Thr_{0.74}Ser_{0.95}Glu_{0.96}Gly_{3.07}Ala_{3.00}l/2Cys_{0.15}Met_{0.96}Phe_{0.97}Lys_{1.95}Arg_{2.99}$.

Z-[Cys(Acm)^{14,30,38,51,55}, Lys(Z)^{15,26,41,46}]-BPTI(14—58) (4). Compound **2** (7.4 mg, ca 2.2 μmol) was dissolved in DMSO (200 μl). HONSu (1.7 mg, 15 μmol) and WSCI·HCl (1.9 mg, 10 μmol) were added and the solution was stirred for 2 h at room temperature. Ether was added to the solution to form a precipitate, which was washed successively with ethyl acetate (1×), dioxane (1×), and water (2×) and dried. The obtained powder and compound **3** (12 mg, ca. 4.2 μmol) were dissolved in DMSO (100 μl) containing NMM (10 μl), and stirred overnight at room temperature. A product was isolated by HPLC with the acetonitrile concentration rising from 20 to 80% in 0.05% aq TFA to give 6.0 mg of compound **4**. Amino acid analysis of compound **4**: $Asp_{3.92}Thr_{1.61}Ser_{0.92}Glu_{1.98}Gly_{4.99}Ala_{6.00}l/2Cys_{0.57}Val_{0.83}Met_{0.83}Ile_{0.73}Leu_{0.98}Tyr_{2.42}Phe_{2.69}Lys_{3.70}Arg_{4.53}$.

Z-[Arg(Tos)^1, Asp(O*c*Hex)^3, Glu(O*c*Hex)^7, Cys(Acm)^{5,14,30,38,51,55}, Lys(Z)^{15,26,41,46}]-BPTI(1—58) (5). Compound **1** (4.35 mg, ca. 2.2 μmol), WSCI·HCl (0.42 mg, 2.2 μmol) and HONSu (1.1 mg, 10 μmol) were dissolved in DMSO (50 μl), and allowed to react for 3 h at room temperature. Ether was added to the solution and a precipitate of an active ester of compound **1** was formed. Compound **4** (6.0 mg, ca. 1 μmol) was treated with TFA (200 μl) at room temperature for 30 min. Freeze-drying of the solution in a test tube gave a solid mass. To the test tube, the active ester dissolved in DMSO (100 μl) and NMM (5 μl) were added. The resulting solution was stirred overnight at room temperature. A product was isolated from the reaction mixture by HPLC under the conditions used for compound **4** and 2.35 mg of compound **5** was obtained. Amino acid analysis: $Asp_{5.56}Thr_{3.35}Ser_{0.90}Glu_{3.67}Pro_{4.40}Gly_{6.51}Ala_{6.00}l/2Cys_{0.00}Val_{0.83}Met_{0.88}Ile_{0.77}Leu_{2.69}Tyr_{4.28}Phe_{4.50}Lys_{3.63}Arg_{5.36}$.

Generation of the Native Form of a Synthetic BPTI. Compound **5** (1.70 mg, 0.21 μmol) was treated with anhydrous HF (1 ml) containing anisole (0.1 ml) for 70 min at 0 °C. After evaporation of HF and anisole, the peptide was dissolved in 50% aq acetic acid (200 μl), and treated with $Hg(CH_3COO)_2$ (3 mg, 10 μmol) for 3 h at room temperature. DTT (5 mg, 32 μmol) in water (200 μl) was added and the precipitate that formed was removed by centrifugation after 30 min. To the supernatant, DTT (5 mg) was added. The solution was left for 2 h at room temperature, and then peptide was isolated by gel filtration on TSK-gel G2000 SW (7.5×600 mm), using 0.1 M aq acetic acid as a buffer. Fractions containing peptide were freeze-dried to obtain a powder, which was treated with DTT (2 mg, 13 μmol) in 0.2 M Tris·HCl (pH 8.7, 200 μl) containing 6.0 M guanidine hydrochloride under a nitrogen atmosphere for 5 h at room temperature. The solution was acidified by acetic acid, and the peptide was isolated by passing through TSK-gel G2000 SW (0.1 M acetic acid). Peptide-containing fractions were collected, and the peptide was oxidized in a buffer (13.44 ml) containing 0.2 M KCl, 1 mM EDTA, and 5 mM of the oxidized form of DTT after adjusting the pH of the buffer to 8.7 with solid tris(hydroxylmethyl)aminomethane at room temperature for 2 h. The solution was diluted to 150 ml with water. At each time, 50 ml of the solution was adsorbed on TSK-gel CM-5PW (7.5×75 mm) and eluted with a buffer (pH 8.7), increasing the ammonium acetate concentration from 0.01 M to 1 M over 70 min at a flow rate of 1 ml min^{-1}. This procedure was repeated three times. The total amount of the peptide in the main fractions was determined to be 27.6 nmol (13.1%) by amino acid analysis.

As a control experiment, native BPTI (76.9 nmol) was reduced and oxidized under the same conditions. The regenerated BPTI was isolated under the same procedure to obtain the native form of BPTI (11 nmol, 14%).

Inhibitory Activity of Synthetic BPTI. Active trypsin concentration was determined according to Chase and Shaw.[16] The trypsin inhibitor concentration was deter-

mined by amino acid analysis after acid hydrolysis of BPTI by 4 M methanesulfonic acid at 110 °C for 24 h. The remaining tryptic activity was measured according to Kassell by employing N^{α}-benzoyl-L-arginine *p*-nitroanilide (BAPNA).[17] Trypsin (1.69×10^{-5} M, 100 μl) and an appropriate amount of synthetic or native BPTI were added into 3 ml of 0.1 M tris buffer (pH 7.8) containing 0.02 M $CaCl_2$. The resultant solution was incubated for 3 min at 25 °C and then 100 μl of BAPNA solution (10 mg ml^{-1} of DMF) was added. The Δ OD_{405} per min was measured with a Hitachi 124 spectrophotometer. The activity of synthetic BPTI was measured at four different concentrations of synthetic BPTI. The specific activity of synthetic BPTI toward the native one was calculated to be 98±4%.

The authors wish to express their thanks to Professor Yasutsugu Shimonishi and Dr. Toshifumi Takao of the Institute for Protein Research, Osaka University for allowing use of the facilities for mass spectra measurement.

References

1) R. B. Merrifield, *J. Am. Chem. Soc.*, **85**, 2149 (1963).
2) J. Blake, *Int. J. Peptide Protein Res.*, **27**, 191 (1986).
3) J. Blake, D. Yamashiro, K. Ramasharma, and C. H. Li, *Int. J. Peptide Protein Res.*, **28**, 468 (1986).
4) J. M. Sabatier, M. Tessier-Rochat, C. Granier, J. Van Rietschoten, E. Pedoroso, A. Grandas, F. Albericio, and E. Giralt, *Tetrahedron*, **43**, 5973 (1987).
5) S. H. Nakagawa and E. T. Kaiser, *J. Org. Chem.*, **48**, 678 (1983).
6) S. Aimoto, *Bull. Chem. Soc. Jpn.*, **61**, 2220 (1988).
7) S. Ikeda, T. Yokota, K. Watanabe, M. Kan, Y. Takahashi, T. Ichikawa, K. Takahashi, and R. Matsueda, *Peptide Chem. 1985* ed. by Y. Kiso, Protein Research Foundation, Osaka, 115 (1986).
8) C. D. Chan, A. M. Felix, M. H. Jimenez, and J. Meienhofer., *Int. J. Protein Res.*, **15**, 485 (1980).
9) B. F. Gisin, *Helv. Chim. Acta*, **56**, 1476 (1973).
10) E. Kaiser, R. L. Colescott, C. D. Bossinger, and P. I. Cook, *Anal. Biochem.*, **34**, 595 (1970).
11) R. B. Woodward, K. Heusler, J. Gosteli, P. Naegeli, W. Oppolzer, R. Ramage, S. Ranganathan, and H. Vorbruggen, *J. Am. Chem. Soc.*, **88**, 852 (1966).
12) T. B. Windholz and D. B. R. Johnston, *Tetrahedron Lett.*, **1967**, 2555.
13) H. Yajima, H. Watanabe, and M. Okamoto, *Chem. Pharm. Bull.*, **19**, 2185 (1971).
14) T. E. Creighton, *J. Mol. Biol.*, **87**, 563 (1974).
15) R. Matsueda and R. Walter, *Int. J. Peptide Protein Res.*, **16**, 392 (1980).
16) T. Chase, Jr. and E. Shaw, *Biochem. Biophys. Res. Commun.*, **29**, 508 (1967).
17) B. Kassell, *Methods Enzymol.*, **19**, 844 (1970).

Novel Structures of 1 : 1 Complexes of 1,4,7,10,13-Pentaoxa-, 1,13-Dioxa-4,7,10-trithia[13]- and 1,4,7,10,13,16-Hexaoxa[16](1,1′)-ruthenocenophanes with $HgCl_2$: Metal–Metal (Ru–Hg) Bond Formation

Sadao SATO,† Masaru SATO,†† and Sadatoshi AKABORI*
Department of Chemistry, Faculty of Science, Toho University, Funabashi, Chiba 274
†Analytical and Metabolic Research Laboratories, Sankyo Co., Hiromachi, Shinagawa-ku, Tokyo 140
††Chemical Analysis Center, Saitama University, Urawa, Saitama 338
(Received August 9, 1988)

The structures of 1 : 1 complexes (**3b**, **4b**, and **5b**) of 1.4,7,10,13-pentaoxa-, 1,13-dioxa-4,7,10-trithia[13]- and 1,4,7,10,13,16-hexaoxa[16](1,1′)ruthenocenophanes (**3a**, **4a**, and **5a**) with $HgCl_2$, and **3a** have been determined by the single-crystal X-ray diffraction method. The complexing forms of the three complexes are quite similar to each other. Crystal data: **3b**, triclinic, space group $P\bar{1}$, a=12.043(3), b=10.759(2), c=8.529(2) Å, α=98.76(2), β=101.22(2), γ=77.03(2)°, U=1049.5 Å^3, Z=2, D_c=2.19 g cm^{-3}, μ(Mo $K\alpha$)=84 cm^{-1}. **4b**, triclinic, space group $P\bar{1}$ a=17.100(3), b=8.986(1), c=8.618(2) Å, α=105.17(1), β=62.24(1), γ=100.54(1)°, U=1128.1 Å^3, Z=2, D_c=2.18 g cm^{-3}, μ(Mo $K\alpha$)=81 cm^{-1}. **5b**, monoclinic, a space group $P2_1/a$, a=26.881(7), b=10.344(3), c=8.414(2), β=96.97(2)°, U=2322.2 Å^3, Z=4, D_c=2.11 g cm^{-3}, μ(Mo $K\alpha$)=76 cm^{-1}. **3a**, triclinic, space group $P\bar{1}$, a=11.107(1), b=8.816(1), c=9.788(1) Å, α=70.48(1), β=99.76(1), γ=101.31(1)°, U=877.6(2) Å^3, Z=2, D_c=1.59 g cm^{-3}, μ(Mo $K\alpha$)=9 cm^{-1}. Only the Ru atom of the ruthenocene nucleus of these complexes was coordinated to $HgCl_2$ with a slightly distorted trigonal-planar configuration. The distances between the Ru and the Hg atoms are 2.683(3), 2.704(1), and 2.696(2) Å, respectively.

Many research groups have recently attempted to investigate modified crown ethers in order to develop a new functionality for them.[1] For example, the syntheses of many kinds of macrocyclic compounds containing aza, thia, phosphorus, arsenic, and/or other coordinatable atoms have been reported. In this connection, several research groups have reported new-type crown ethers, thiacrown ethers, and oxathiacrown ethers which contain a ferrocene unit as an integral part of a ring member.[2] However, the complexes of crown ethers,[3] thiacrown ethers[4] and azacrown ethers[5] with $HgCl_2$ are rare, although a number of the complexes of crown ethers including ferrocenocrown ethers have already been reported.[2] In connection with this viewpoint, we have studied the preparation and structures of the complexes of metallocenocrown ethers with an interest in the electron-transfer interaction between the complexed cation and the metal atom of the metallocene nucleus.[6] In a previous paper,[7] we reported on the molecular structure of a 1 : 1 complex (**1b**) of 4,7,10,13-tetraoxa-1,16-dithia[16](1,1′)ruthenocenophane (**1a**) with $HgCl_2$, in which the linear Cl–Hg–Cl moiety was found to be held perpendicularly in the central cavity of the macrocyclic moiety. The distance between the Ru atom and the Hg atom is longer than 3.6 Å, which is too long for a direct Ru–Hg interaction. We have also previously reported[8] on the complexes (**2b**—**4b**) of polyoxa- and 1,n-dioxathia[n]ruthenocenophanes (**2a**—**4a**) with $HgCl_2$ (or $AgNO_3$) (**2**—**4**) and the presence of a strong electron-transfer interaction between the Ru atom and the Hg atom in **3a** and **4a** from the ^{1}H NMR and UV spectral data. The Ru–Hg interaction may be explained by two possible complexing manners: i) the Hg atom incorporated into the crown ether moiety interacts with the Ru atom; ii) the Hg atom is directly coordinated to the Ru atom from the opposite side of the macrocyclic ring. The result is very different from that of the 1:1 silver complex **2b** in which the Ag atom incorporated in the crown ether cavity of the host molecule does not interact with the Ru atom of the ruthenocene. In this paper,[9] we report on the molecular structures of **3b**, **4b** and the 1 : 1 complex **5b** of 1,4,7,10,13,16-hexaoxa[16](1,1′)ruthenocenophane (**5a**) in order to clarify the nature of the Ru–Hg interaction. An X-ray analysis of ruthenocenophane (**3a**) was also carried out in order to compare the structural change of the organic moiety by complexing.

Complexes **3b**, **4b**, and **5b** were prepared by the same method as mentioned in a previous paper.[8]

The molecular structures of **3a** and its $HgCl_2$ complex **3b** are illustrated in Fig. 1. Also, the molecular structures of **4b** and **5b** are also illustrated in Fig. 2. The final atomic parameters for **3b**, **4b**, **5b**, and **3a** are listed in Tables 1—4, and the bond lengths as well as the bond and torsion angles are given in Tables 5—8 for **3b**, **4b**, **5b**, and **3a**, respectively. In the complexes (**3b**—**5b**) the Hg atom is coordinated directly to the Ru atom of the ruthenocene nucleus from the opposite side of the crown ether moiety, with a slightly distorted trigonal-planar configuration. The Ru–Hg interatomic distances in **3b**, **4b**, and **5b** are 2.683(3), 2.704(1), and 2.696(2) Å, respectively, which essentially equal the sum (2.68 Å) of the covalent radii of Ru and Hg atoms.[10] The results differ completely from that of **1b** in which the Hg atom incorporated in the central cavity of the macrocyclic moiety forms a distorted hexagonal-bipyramidal geometry with the two chlo-

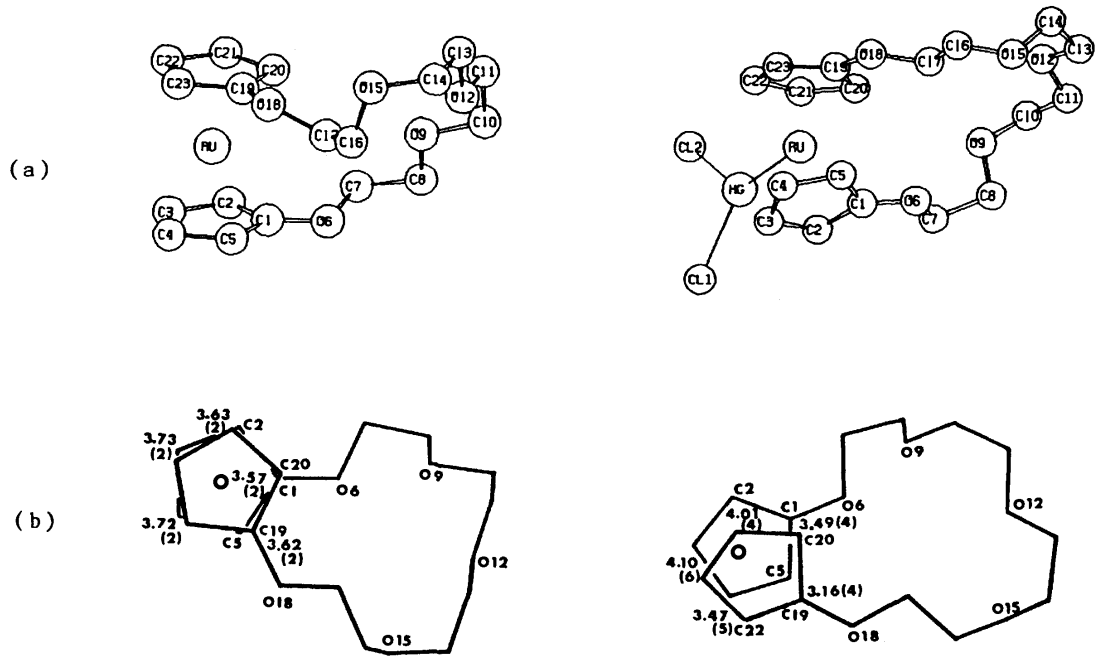

Fig. 1. (a) A perspective view of the molecules with atom numbering. (b) Projection of the organic ligand moiety on the Cp ring containing the C(1) atom are also given with the C·····C distances (Å) between the rings. An open circle denotes the Ru atom.

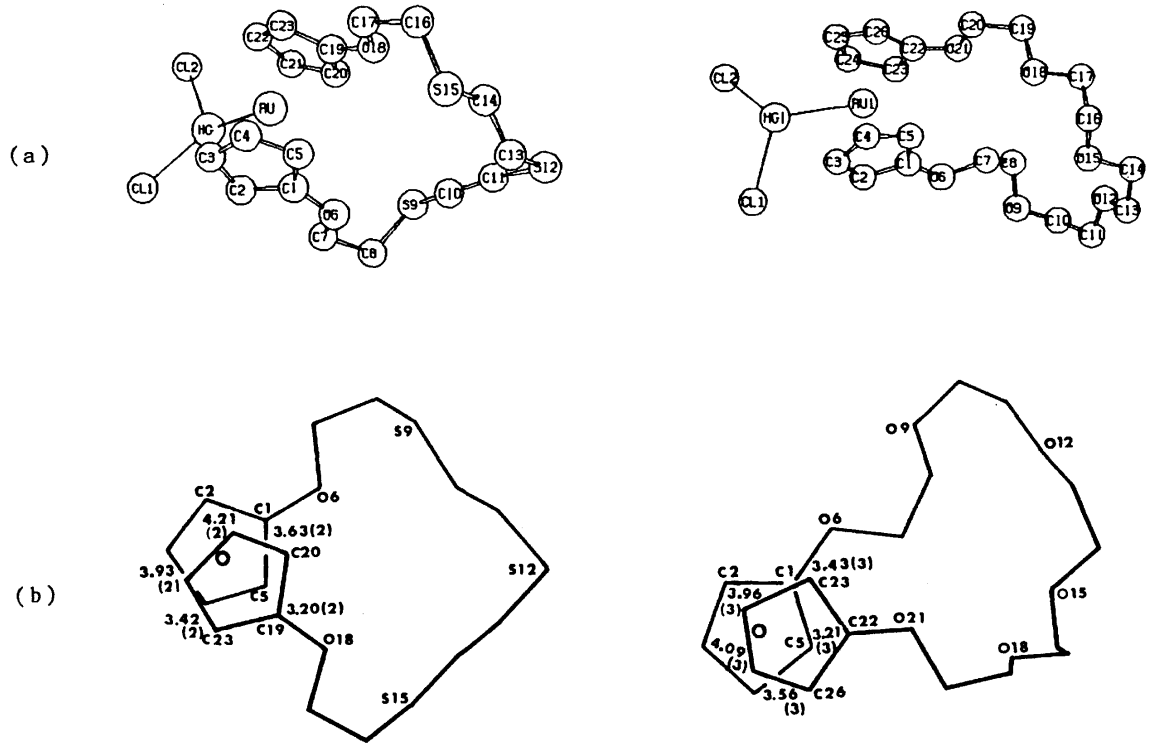

Fig. 2. (a) A perspective view of the molecules with atom numbering. (b) Projection of the organic ligand moiety on the Cp ring containing the C(1) atom are also given with the C·····C distances (Å) between the rings. An open circle denotes the Ru atom.

Table 1. Fractional Atomic Coordinates ($\times 10^4$; $\times 10^3$ for C, O) and Thermal Parameters (Å^2), with Estimated Standard Deviations in Parentheses of **3b**

Atom	x	y	z	B_{eq}[19]
Hg	−190.6(11)	9352.4(12)	2731.8(15)	4.8
Ru	1476(2)	7572(2)	1546(3)	3.9
Cl(1)	5(7)	11559(6)	4126(8)	5.0
Cl(2)	−2284(7)	9481(8)	2101(10)	5.8
C(1)	310(2)	752(3)	333(3)	3.9(0.5)
C(2)	235(2)	871(3)	359(3)	4.3(0.5)
C(3)	225(4)	934(4)	218(5)	7.7(0.9)
C(4)	280(3)	847(3)	101(4)	6.2(0.7)
C(5)	331(3)	733(3)	176(4)	5.0(0.6)
O(6)	358(2)	659(2)	421(3)	5.4(0.4)
C(7)	306(3)	665(3)	567(4)	5.8(0.7)
C(8)	333(3)	532(4)	626(5)	7.1(0.9)
O(9)	258(3)	458(3)	515(3)	8.5(0.7)
C(10)	251(5)	339(5)	565(6)	10.4(1.3)
C(11)	342(4)	241(5)	538(6)	9.6(1.2)
O(12)	341(2)	211(3)	361(3)	8.2(0.7)
C(13)	442(3)	131(4)	335(5)	7.1(0.9)
C(14)	460(3)	127(4)	166(5)	7.0(0.8)
O(15)	487(2)	242(2)	134(3)	6.9(0.6)
C(16)	409(3)	318(4)	35(4)	6.7(0.8)
C(17)	306(3)	395(3)	104(4)	5.4(0.6)
O(18)	243(2)	478(2)	−12(3)	5.6(0.5)
C(19)	149(2)	561(3)	17(3)	4.0(0.5)
C(20)	98(2)	571(3)	177(3)	4.0(0.5)
C(21)	−2(3)	667(3)	136(4)	4.7(0.6)
C(22)	−14(3)	720(3)	−4(4)	5.5(0.7)
C(23)	82(3)	654(3)	−71(4)	4.8(0.6)

Table 2. Fractional Atomic Coordinates ($\times 10^4$) and Thermal Parameters (Å^2), with Estimated Standard Deviations in Parentheses of **4b**

Atom	x	y	z	B_{eq}[19]
Hg	650.9(4)	−296.7(7)	1322.7(9)	3.7
Ru	1529.0(7)	2072.4(7)	2677.1(12)	2.4
Cl(1)	911(3)	−3026(4)	455(6)	5.4
Cl(2)	−992(2)	−242(4)	2101(5)	3.7
C(1)	2930(8)	1564(15)	847(17)	2.9
C(2)	2425(8)	117(15)	1028(20)	3.4
C(3)	2023(9)	85(17)	2921(19)	3.7
C(4)	2313(9)	1464(18)	3776(19)	4.2
C(5)	2850(9)	2416(17)	2541(18)	3.5
O(6)	3469(6)	2079(11)	−702(12)	3.3
C(7)	3332(11)	1204(17)	−2247(18)	4.1
C(8)	3837(11)	2127(20)	−3702(20)	5.0
S(9)	3366(4)	3908(6)	−3303(8)	8.5
C(10)	3905(27)	5219(25)	−2067(36)	18.4
C(11)	4059(19)	6613(31)	−2094(33)	13.8
S(12)	4644(3)	8135(5)	−1267(6)	5.3
C(13)	4582(10)	7545(19)	659(21)	4.9
C(14)	3690(10)	7717(18)	2186(21)	4.7
S(15)	3695(3)	7038(6)	4015(6)	5.1
C(16)	2585(10)	7339(18)	5698(20)	4.3
C(17)	1925(9)	6009(17)	5664(18)	3.4
O(18)	1892(6)	5744(10)	3945(12)	3.4
C(19)	1298(8)	4580(15)	3699(18)	2.9
C(20)	1236(9)	4129(14)	2052(17)	3.0
C(21)	514(9)	3021(14)	2309(19)	3.5
C(22)	146(9)	2707(16)	4054(20)	3.6
C(23)	629(9)	3707(16)	4963(18)	3.2

Table 3. Fractional Atomic Coordinates ($\times 10^4$) and Thermal Parameters (Å^2), with Estimated Standard Deviations in Parentheses of **5b**

Atom	x	y	z	B_{eq}[19]
Hg	5062.3(3)	3336.8(9)	3958.7(9)	3.5
Ru	5636(1)	2818(2)	1621(2)	2.6
Cl(1)	5528(2)	4556(5)	6515(6)	3.1
Cl(2)	4495(2)	1931(6)	5278(6)	3.8
C(1)	6419(7)	3637(22)	1876(24)	3.0
C(2)	6159(7)	4113(19)	3101(20)	4.7
C(3)	5752(8)	4863(19)	2389(22)	5.6
C(4)	5752(8)	4740(20)	736(23)	7.3
C(5)	6151(7)	3969(21)	399(21)	9.0
O(6)	6848(5)	2975(18)	2195(15)	6.6
C(7)	7078(8)	2521(29)	841(26)	5.7
C(8)	7404(9)	1457(35)	1378(34)	6.1
O(9)	7794(7)	1902(26)	2564(21)	6.0
C(10)	8263(9)	1336(32)	2555(28)	5.6
C(11)	8570(9)	2030(28)	1479(29)	5.5
O(12)	8357(6)	1846(19)	−84(17)	4.8
C(13)	8529(9)	2731(28)	−1182(31)	5.0
C(14)	8214(9)	2583(28)	−2763(25)	4.4
O(15)	7736(6)	3122(19)	−2596(17)	4.6
C(16)	7400(9)	3006(26)	−4017(25)	4.1
C(17)	7101(9)	1786(27)	−4133(24)	3.6
O(18)	6706(5)	1895(16)	−3184(16)	2.9
C(19)	6328(9)	906(23)	−3514(23)	3.2
C(20)	5900(8)	1180(21)	−2608(22)	4.3
O(21)	6042(5)	865(14)	−973(14)	4.0
C(22)	5693(7)	1100(19)	0(20)	2.9
C(23)	5793(8)	739(18)	1670(21)	3.2
C(24)	5331(9)	958(19)	2305(22)	2.3
C(25)	4978(8)	1541(22)	1110(26)	4.3
C(26)	5211(8)	1672(18)	−301(20)	3.5

Table 4. Fractional Atomic Coordinates ($\times 10^4$) and Thermal Parameters (Å^2), with Estimated Standard Deviations in Parentheses of **3a**

Atom	x	y	z	B_{eq}[19]
Ru	607.5(10)	2464.0(14)	2467.7(12)	2.0
C(1)	985(13)	1321(16)	961(15)	2.7
C(2)	−10(13)	297(17)	1718(15)	2.8
C(3)	−984(13)	1171(19)	1386(17)	3.5
C(4)	−623(13)	2767(20)	409(16)	3.5
C(5)	637(14)	2876(19)	129(15)	3.2
O(6)	2109(8)	1002(12)	869(9)	2.7
C(7)	2493(14)	−397(17)	2038(16)	3.3
C(8)	3847(14)	−286(19)	2049(18)	3.8
O(9)	4446(9)	891(13)	2748(12)	4.1
C(10)	5813(14)	966(21)	2928(21)	4.9
C(11)	6397(16)	2159(22)	3670(19)	4.8
O(12)	6336(10)	3733(13)	2722(11)	4.0
C(13)	6873(17)	5015(23)	3344(20)	5.2
C(14)	6736(14)	6632(21)	2360(19)	4.4
O(15)	5480(9)	6990(13)	2163(12)	4.4
C(16)	4636(14)	6417(18)	1125(17)	3.6
C(17)	3702(15)	4968(20)	1729(21)	5.1
O(18)	2851(8)	5492(11)	2425(11)	2.8
C(19)	2044(12)	4243(17)	3214(16)	2.8
C(20)	2269(14)	2612(18)	4068(16)	3.1
C(21)	1153(14)	1821(20)	4788(15)	3.5
C(22)	308(14)	2958(20)	4381(16)	3.8
C(23)	836(13)	4434(18)	3428(16)	3.3

Table 5. Bond Lengths (Å) and Bond and Torsion Angles (°) in the Organic Ligand of **3b**

1	2	3	4	1-2	1-2-3	1-2-3-4
Pentaoxa-crown moiety						
O(6)	C(1)	C(2)	C(3)	1.30(4)	134(3)	174(3)
O(6)	C(1)	C(5)	C(4)		116(3)	−176(3)
C(2)	C(1)	O(6)	C(7)			15(5)
C(5)	C(1)	O(6)	C(7)			−163(3)
C(1)	O(6)	C(7)	C(8)		114(2)	159(3)
O(6)	C(7)	C(8)	O(9)	1.48(4)	110(3)	−75(4)
C(7)	C(8)	O(9)	C(10)	1.53(5)	106(3)	−168(3)
C(8)	O(9)	C(10)	C(11)	1.45(5)	116(3)	−80(5)
O(9)	C(10)	C(11)	O(12)	1.43(6)	114(5)	−65(6)
C(10)	C(11)	O(12)	C(13)	1.37(8)	109(4)	169(4)
C(11)	O(12)	C(13)	C(14)	1.50(6)	109(3)	−164(3)
O(12)	C(13)	C(14)	O(15)	1.36(5)	111(3)	72(4)
C(13)	C(14)	O(15)	C(16)	1.49(6)	113(3)	−112(4)
C(14)	O(15)	C(16)	C(17)	1.42(5)	119(3)	75(4)
O(15)	C(16)	C(17)	O(18)	1.35(5)	116(3)	174(3)
C(16)	C(17)	O(18)	C(19)	1.50(5)	107(3)	−178(3)
C(17)	O(18)	C(19)	C(20)	1.43(4)	121(2)	2(4)
C(17)	O(18)	C(19)	C(23)			175(3)
O(18)	C(19)	C(20)	C(21)	1.32(4)	123(2)	−177(3)
O(18)	C(19)	C(23)	C(22)		130(3)	177(3)
Cyclopentadienyl ring						
C(1)	C(2)	C(3)	C(4)	1.41(4)	105(3)	8(4)
C(2)	C(3)	C(4)	C(5)	1.45(5)	109(3)	−5(5)
C(3)	C(4)	C(5)	C(1)	1.41(6)	106(3)	−1(4)
C(4)	C(5)	C(1)	C(2)	1.43(5)	109(3)	6(4)
C(5)	C(1)	C(2)	C(3)	1.39(4)	110(3)	−9(4)
C(19)	C(20)	C(21)	C(22)	1.59(4)	97(2)	−5(4)
C(20)	C(21)	C(22)	C(23)	1.44(4)	118(3)	2(4)
C(21)	C(22)	C(23)	C(19)	1.37(5)	104(3)	3(4)
C(22)	C(23)	C(19)	C(20)	1.39(5)	113(3)	−6(4)
C(23)	C(19)	C(20)	C(21)	1.37(4)	108(2)	6(3)
Hg coordination						
Ru	Hg	Cl(1)			2.683(3)	126.3(2)
Ru	Hg	Cl(2)				1281(2)
Ru	Hg	Cl(1′)				99.4(2)
Cl(1)	Hg	Cl(2)			2.528(9)	103.7(3)
Cl(1′)	Hg	Cl(1)			2.943(9)	89.9(3)
Cl(2)	Hg	Cl(1′)			2.451(9)	93.0(3)
Cl(1′)	$-x$, 2−y, 1−z.					

Table 6. Bond Lengths (Å) and Bond and Torsion Angles (°) in the Organic Ligand of **4b**

1	2	3	4	1-2	1-2-3	1-2-3-4
Trithia-crown moiety						
O(6)	C(1)	C(2)	C(3)	1.367(18)	127.4(14)	175.8(13)
O(6)	C(1)	C(5)	C(4)		122.4(13)	−174.4(12)
C(2)	C(1)	O(6)	C(7)			16(2)
C(5)	C(1)	O(6)	C(7)			−168.5(14)
C(1)	O(6)	C(7)	C(8)		114.1(12)	168.6(12)
O(6)	C(7)	C(8)	S(9)	1.46(2)	106.0(14)	−70.0(16)
C(7)	C(8)	S(9)	C(10)	1.51(3)	114.5(13)	89(2)
C(8)	S(9)	C(10)	C(11)	1.80(2)	100.8(16)	151(3)
S(9)	C(10)	C(11)	S(12)	1.80(5)	123(4)	−172.6(14)
C(10)	C(11)	S(12)	C(13)	1.24(6)	135(3)	−28(5)
C(11)	S(12)	C(13)	C(14)	1.74(3)	103.1(13)	−74.3(17)
S(12)	C(13)	C(14)	S(15)	1.823(19)	111.6(13)	178.3(2)
C(13)	C(14)	S(15)	C(16)	1.48(3)	107.8(13)	179.9(12)
C(14)	S(15)	C(16)	C(17)	1.837(19)	101.0(8)	89.7(13)
S(15)	C(16)	C(17)	O(18)	1.789(18)	115.2(12)	−62.4(16)
C(16)	C(17)	O(18)	C(19)	1.49(2)	107.2(12)	−178.3(12)
C(17)	O(18)	C(19)	C(20)	1.464(18)	115.3(11)	−175.8(11)
C(17)	O(18)	C(19)	C(23)			8(2)
O(18)	C(19)	C(20)	C(21)	1.366(19)	121.4(14)	−174.6(13)
O(18)	C(19)	C(23)	C(22)		129.1(14)	175.9(15)
Cyclopetadienyl ring						
C(1)	C(2)	C(3)	C(4)	1.43(2)	105.9(14)	−1.3(19)
C(2)	C(3)	C(4)	C(5)	1.45(2)	107.2(14)	3(2)
C(3)	C(4)	C(5)	C(1)	1.40(2)	110.6(15)	−2.9(19)
C(4)	C(5)	C(1)	C(2)	1.41(2)	106.1(14)	2.0(19)
C(5)	C(1)	C(2)	C(3)	1.42(2)	110.1(14)	−0.4(19)
C(19)	C(20)	C(21)	C(22)	1.42(2)	106.6(14)	−2.9(19)
C(20)	C(21)	C(22)	C(23)	1.41(2)	1103(14)	3(2)
C(21)	C(22)	C(23)	C(19)	1.42(2)	107.2(14)	−1.4(19)
C(22)	C(23)	C(19)	C(20)	1.44(2)	106.4(14)	−0.3(19)
C(23)	C(19)	C(20)	C(21)	1.44(2)	109.5(13)	1.9(19)
Hg coordination						
Ru	Hg	Cl(1)		2.704(1)	128.0(1)	
Ru	Hg	Cl(2)			122.1(1)	
Ru	Hg	Cl(2′)			106.0(1)	
Cl(1)	Hg	Cl(2)		2.430(5)	104.6(2)	
Cl(2)	Hg	Cl(2′)		2.574(4)	85.0(1)	
Cl(2′)	Hg	Cl(1)		2.885(4)	99.2(2)	
Cl(2′)	$-x$, $-y$, $-z$.					

rine atoms coordinated axially and the Cl-Hg-Cl skelton is almost linear with an angle of 172.7(2)°.[7] The complexing manner is very similar to that of the 1 : 1 complex[3] of dibenzo-18-crown-6 with $HgCl_2$.

In the ^1H NMR spectra of the ruthenocenophanes (**3a** and **4a**), the chemical shift differences between α- and β-protons of the Cp rings are only 0.41 and 0.38 ppm, respectively.[8] The results suggest that the two Cp rings are nearly parallel[11] to each other. Furthermore, CPK model inspections suggest that cavity sizes of **3a** and **4a** are sufficient to encapsule the Hg atom. Also, if the Hg atom is incorporated into the crown ether part of **3b** and **4b**, the Hg atom has to take a distorted pentagonal-bipyramidal geometry with two Cl atoms coordinated axially. However, interestingly, the Hg atom in **3b** and **4b** is directly bonded to the Ru atom of the ruthenocene nucleus from the opposite side of the crown ether moiety. The result suggests that, in the complexes **3b** and **4b**, the pentagonal-bipyramidal geometry of the Hg atom is unstable compared with its hexagonal-bipyramidal geometry in **1b**, although some other factors can not be ruled out. It is noteworthy that the Hg atom in **5b**, which has the same ring number of the crown ether moiety as **1b**, is directly bonded to the Ru atom from the opposite site of the crown ether moiety with a slightly distorted trigonal-planar configuration, although the Hg atom in **1b** is incorporated into the macrocyclic moiety with a distorted hexagonal-bipyramidal geometry (as described above). The difference in the complexing mode of **5b** and **1b** is attributed to the presence of the two sulfur atoms in the crown ether moiety in **1b**, since the sulfur atom coordinates more strongly with the Hg atom than does the oxygen atom. In the complexes (**3b**, **4b**, and **5b**), the sums of the three bond angles about each Hg atom are 358.1, 354.7, and 345.7°, and

Table 7. Bond Lengths (Å) and Bond and Torsion Angles (°) in the Organic Ligand of **5b**

1	2	3	4	1-2	1-2-3	1-2-3-4
Hexaoxa-crown moiety						
O(6)	C(1)	C(2)	C(3)	1.40(3)	122(2)	173.7(19)
O(6)	C(1)	C(5)	C(4)		130(2)	−176(2)
C(2)	C(1)	O(6)	C(7)			179(2)
C(5)	C(1)	O(6)	C(7)			0(4)
C(1)	O(6)	C(7)	C(8)		117(2)	−158(2)
O(6)	C(7)	C(8)	O(9)	1.44(4)	108(3)	−63(3)
C(7)	C(8)	O(9)	C(10)	1.44(5)	110(3)	−144(3)
C(8)	O(9)	C(10)	C(11)	1.43(4)	117(3)	88(3)
O(9)	C(10)	C(11)	O(12)	1.39(4)	112(3)	−68(3)
C(10)	C(11)	O(12)	C(13)	1.48(4)	109(2)	164(2)
C(11)	O(12)	C(13)	C(14)	1.38(3)	114(2)	−171(2)
O(12)	C(13)	C(14)	O(15)	1.42(3)	109(2)	72(3)
C(13)	C(14)	O(15)	C(16)	1.50(4)	107(2)	−178(2)
C(14)	O(15)	C(16)	C(17)	1.42(3)	112(2)	90(3)
O(15)	C(16)	C(17)	O(18)	1.41(3)	114(2)	78(3)
C(16)	C(17)	O(18)	C(19)	1.49(4)	109(2)	165.9(19)
C(17)	O(18)	C(19)	C(20)	1.41(3)	113.3(18)	−173.3(18)
O(18)	C(19)	C(20)	O(21)	1.44(3)	109.7(19)	−75(2)
C(19)	C(20)	O(21)	C(22)	1.48(3)	108.6(18)	178.3(16)
C(20)	O(21)	C(22)	C(23)	1.42(4)	115.1(16)	176.4(16)
C(20)	O(21)	O(22)	C(26)			−4(3)
O(21)	C(22)	C(23)	C(24)	1.34(2)	119.0(17)	−172.7(17)
O(21)	C(22)	C(26)	C(25)		131.2(19)	173.2(2)
Cyclopentadienyl ring						
C(1)	C(2)	C(3)	C(4)	1.40(3)	108.0(18)	5(2)
C(2)	C(3)	C(4)	C(5)	1.41(3)	106.2(18)	−1(3)
C(3)	C(4)	C(5)	C(1)	1.40(3)	110.3(19)	−2(3)
C(4)	C(5)	C(1)	C(2)	1.39(3)	106.6(19)	5(3)
C(5)	C(1)	C(2)	C(3)	1.40(3)	108.5(19)	−6(3)
C(22)	C(23)	C(24)	C(25)	1.45(3)	104.7(18)	−5(3)
C(23)	C(24)	C(25)	C(26)	1.43(3)	110(2)	1(3)
C(24)	C(25)	C(26)	C(22)	1.43(3)	108(2)	3(3)
C(25)	C(26)	C(22)	C(23)	1.41(3)	107.3(18)	−7(2)
C(26)	C(22)	C(23)	C(24)	1.42(3)	109.9(19)	7(2)
Hg coordination						
Ru	Hg	Cl(1)		2.696(2)	115.3(1)	
Ru	Hg	Cl(2)			130.6(1)	
Ru	Hg	Cl(1′)			115.5(1)	
Cl(1)	Hg	Cl(2)		2.670(6)	99.8(2)	
Cl(1′)	Hg	Cl(1)		2.697(6)	87.0(1)	
Cl(2)	Hg	Cl(1′)		2.466(6)	99.1(2)	
Cl(1′)	1−x, 1−y, 1−z.					

Table 8. Bond Lengths (Å) and Bond and Torsion Angles (°) in the Organic Ligand of **3a**

1	2	3	4	1-2	1-2-3	1-2-3-4
Pentaoxa-crown moiety						
O(6)	C(1)	C(2)	C(3)	1.355(14)	130.4(13)	−176.0(15)
O(6)	C(1)	C(5)	C(4)		119.3(13)	176.6(12)
C(2)	C(1)	O(6)	C(7)			−21(2)
C(5)	C(1)	O(6)	C(7)			−163.8(13)
C(1)	O(6)	C(7)	C(8)		113.9(11)	−163.1(11)
O(6)	C(7)	C(8)	O(9)	1.454(19)	107.0(13)	78.2(15)
C(7)	C(8)	O(9)	C(10)	1.486(19)	107.6(10)	174.8(13)
C(8)	O(9)	C(10)	C(11)	1.428(17)	111.0(8)	−178.9(13)
O(9)	C(10)	C(11)	O(12)	1.489(16)	109.7(11)	−73.4(19)
C(10)	C(11)	O(12)	C(13)	1.46(2)	110.1(16)	179.3(15)
C(11)	O(12)	C(13)	C(14)	1.39(2)	115.0(11)	−176.8(14)
O(12)	C(13)	C(14)	O(15)	1.440(18)	113.7(17)	74(2)
C(13)	C(14)	O(15)	C(16)	1.45(3)	112.9(16)	−82.9(19)
C(14)	O(15)	C(16)	C(17)	1.457(16)	116.5(9)	105.4(17)
O(15)	C(16)	C(17)	O(18)	1.414(16)	116.1(17)	68.6(19)
C(16)	C(17)	O(18)	C(19)	1.50(2)	107.5(14)	−171.1(13)
C(17)	O(18)	C(19)	C(20)	1.473(16)	114.4(13)	35(2)
C(17)	O(18)	C(19)	C(23)			−151.3(14)
O(18)	C(19)	C(20)	C(21)	1.375(12)	127.9(14)	175.0(14)
O(18)	C(19)	C(23)	C(22)		123.4(14)	175.2(14)
Cyclopentadienyl ring						
C(1)	C(2)	C(3)	C(4)	1.42(2)	107.8(14)	0.1(19)
C(2)	C(3)	C(4)	C(5)	1.38(2)	104.0(15)	0(2)
C(3)	C(4)	C(5)	C(1)	1.44(2)	108.2(15)	−0.1(19)
C(4)	C(5)	C(1)	C(2)	1.45(2)	104.8(14)	0.2(19)
C(5)	C(1)	C(2)	C(3)	1.43(2)	110.2(13)	−0.2(19)
C(19)	C(20)	C(21)	C(22)	1.45(2)	105.9(14)	−0.6(19)
C(20)	C(21)	C(22)	C(23)	1.46(2)	108.4(15)	0(2)
C(21)	C(22)	C(23)	C(19)	1.42(2)	109.1(15)	0(2)
C(22)	C(23)	C(19)	C(20)	1.41(2)	108.2(14)	−0.5(19)
C(23)	C(19)	C(20)	C(21)	1.44(2)	108.4(13)	0.7(19)

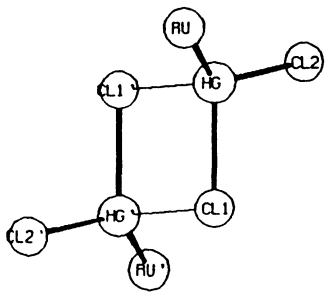

Fig. 3.

the deviations of the Hg atom from the Cl(1)-Ru-Cl(2) plane are 0.201, 0.340, and 0.562 Å, respectively. The deviation of the Hg atom from the Cl(1)-Ru-Cl(2) plane in **5b** is larger than those found in **3b** and **4b**. These values mean that the coordination of the Hg atom found in the present complexes is very close to trigonal, and that most probably those bonds are formed by sp^2 hybridization. This configuration of the Hg atom is very similar to those of $N(CH_3)_4HBr_3$[12] and $[(C_5H_5)_2Ru]_2 3HgCl_2$.[13] A slight distortion from sp^2 hybridization which would require an exactly planar configuration is due to the interaction with the adjacent molecule as described below. Furthermore, one Cl atom of the complex, which is the atom with the longer distance in the two Hg-Cl bonds, is linked by a weak bond to the Hg atom of the adjacent complex, as shown in Fig. 3. The bond length between Hg-Cl(2) (1−x, 1−y, 1−z) in **5b** which is responsible for the dimer formation is 2.697(6) Å, and the value is shorter than those (2.943 and 2.885 Å) for **3b** and **4b**, respectively. These distances for **3b**, **4b**, and **5b** are about 0.35—0.6 Å shorter than the sum of the van der Waals radii[10] of Hg and Cl atoms. These results indicate that the complexes (**3b**, **4b**, and **5b**) consist of a dimer of the Hg-Cl′ bond in crystals. Therefore, the total coordination sphere of the Hg atom can be described as a trigonal pyramid with the chlorine of the adjacent molecule in the apex.

The deviations of the dihedral angle between the plane of Cl(1)-Ru-Cl(2) and the average plane of the Cp rings in **5b**, 69.4(6) and 75.2(7)°, respectively, were also smaller than those (90.2 and 89.0°, 84.5 and 91.4°) for **3b** and **4b**, respectively. These results are thought to be due to differences in the ring numbers of the crown ether moieties in **3b**, **4b**, and **5b**.

^{13}C NMR Spectra. The ^{13}C NMR spectra of complex **5b** and the ruthenocenophane (**5a**) in DMSO-d_6 were obtained. The bridge-head carbon signal of **5b** is shifted up-field (10.40 ppm) and the α- and β-ring carbon signals down-field (1.0 and 1.1 ppm) compared with those of the ruthenocenophane (**5a**), although the methylene carbon signals are slightly shifted up-field (0.2 ppm). In the ^{13}C NMR spectra of **3b** and **4b**, however, the signals of the bridge-head carbon are shifted only 2.0 and 1.9 ppm up-field compared with those in the corresponding metal free ligands. Seyferth et al.[14] reported that the signal of the bridge-head carbon in (1,1′-ferrocenediyl)phenylphosphine, in which the Cp rings are highly tilted, is shifted up-field about 58 ppm compared with that of the corresponding acyclic compound (diphenylphosphinoferrocene). Also Osborne et al.[15] observed similar results in [1]ferrocenophanes. As shown in Fig. 2, the Cp rings of **5b** are tilted back to allow an interaction of the Hg atom to the ruthenium atom. The angles between the Cp ring planes in **5b** (22.1(9)°), **3b** (23.1(4)°), and **4b** (22.5(7)°) are larger than those found in **3a** (3.8(7)°) and **5a** (2.5°).[16] The angles of **5b** are comparable to those obtained for **3b** (23.1(4)°) and **4b** (22.5(7)°), and the differences in the tilt angles between **3a** and **3b**, **5a** and **5b** are nearly the same. However, the main conformational change in **5b** is reflected in the overlapping pattern between the two Cp rings compared with **3b** and **4b**. The torsion angle C(1)-Cp(1)-Cp(2)-C(22) (Cp1 and Cp2 are centroids of the Cp rings) in **5b** is 53.4°, although those of **3b** and **4b** are 69.3 and 75.9°, respectively. Therefore, the large shift of the bridge-head carbon in **5b** is not attributed only to the tilting of the Cp rings. The distances between the bridge-head carbon atom and C(22) and/or C(23) carbon atoms in the opposite Cp ring in **5b** are also nearly equal to those in **3b** and **4b**. Therefore, the large shift of the bridge-head carbon in **5b** is also not attributed to a steric compression.[17]

At present the reason is not clear.

Experimental

^{13}C NMR spectra were obtained on a JEOL FX-90Q spectrometer with TMS as internal standard.

Materials. 1,4,7,10,13-Pentaoxa[13](1,1′)ruthenocenophane (**3a**), 1,13-dioxa-4,7,10-trithia[13](1,1′)ruthenocenophane (**4a**), dichloro(1,4,7,10,13-pentaoxa[13](1,1′)ruthenocenophane)mercury(II) (**3b**), dichloro(1,13-dioxa-4,7,10-trithia[13](1,1′)ruthenocenophane)mercury(II) (**4b**), and dichloro(1,4,7,10,13,16-hexaoxa[16](1,1′)ruthenocenophane)-mercury(II) (**5b**) were prepared by the same manner as in described in the previous paper. Mercury(II) chloride used was reagent grade. Solvents were dried in appropriate methods and then purified by distillation under nitrogen.

^{13}C NMR Spectra (in DMSO-d_6). **3a**, 128.3(Cb), 60.2(C_β), 64.8(C_α), 71.2, 70.4, 69.8, 69.1(CH_2). **3b**, 130.3(Cb), 64.4(C_α), 61.5(C_β), 72.0, 66.5(CH_2). **4a**, 128.1(Cb), 60.2(C_β), 65.2(C_α), 72.5, 33.7, 32.5, 31.6(CH_2). **4b**, 130.0(Cb), 66.0(C_α), 61.4(C_β), 71.2, 70.3, 69.8, 69.0(CH_2). **5a**, 128.2(Cb), 60.1(C_β), 64.9(C_α), 71.0, 70.3, 70.0, 69.9, 69.1(CH_2). **5b**, 117.8(Cb), 65.9(C_α), 61.2(C_β), 71.0, 70.3, 69.9, 69.1(CH_2).

X-Ray Crystallography. Crystals of dimensions 0.5×0.5×0.2 mm, 0.5×0.2×0.1 mm, 0.4×0.2×0.2 mm, and 0.5×0.2×0.05 mm for the metal free ligand **3a**, complexes **3b**, **4b**, and **5b** were used for X-ray crystallography. Crystal data are as follows: **3a**, $C_{18}H_{24}O_5Ru$, Mw=421.5, triclinic, space group $P\bar{1}$, a=11.107(1), b=8.816(1), c=9.788(1) Å, α=70.48(1), β=99.76(1), γ=101.31(1)°, U=877.6(2) Å^3, Z=2, D_x=1.59 g cm^{-3}, μ(Mo $K\alpha$)=9 cm^{-1}. **3b**, $C_{18}H_{24}O_5RuHgCl_2$, Mw=693.0, triclinic, space group $P\bar{1}$, a=12.043(3), b=10.759(2), c=8.529(2) Å, α=98.76(2), β=101.22(2), γ=77.03(2)°, U=1049.5 Å^3, Z=2, D_x=2.19 g cm^{-3}, μ(Mo $K\alpha$)=84 cm^{-1}. **4b**, $C_{18}H_{24}O_2S_3RuHgCl_2$, Mw=741.2, triclinic, space group $P\bar{1}$, a=17.100(3), b=8.986(1), c=8.618(2) Å, α=105.17(1), β=62.24(1), γ=100.54(1)°, U=1128.1 Å^3, Z=2, D_x=2.18 g cm^{-3}, μ(Mo $K\alpha$)=81 cm^{-1}. **5b**, $C_{20}H_{28}O_6RuHgCl_2$, Mw=737.04, monoclinic, space group $P2_1/a$, a=26.881(7), b=10.334(3), c=8.414(2) Å, β=96.97(2)°, U=2322.2 Å^3, Z=4, D_x=2.11 g cm^{-3}, μ(Mo $K\alpha$)=76 cm^{-1}.

Intensity data for $2\theta \leq 50°$ were recorded on a Rigaku AF C-5R with graphite-monochromatized Mo $K\alpha$ radiation. Among totals of 3084 (**3a**), 3689 (**3b**), 3946 (**4b**), and 4070 (**5b**) independent reflections collected, 2996, 3244, 3394, and 3142 were considered to be observed at the 2.0σ (F_o) level and were corrected for Lorentz and polarization factors, but not for absorption. The structures of **3a**, **3b**, **4b**, and **5b** were solved by the heavy-atom method, and refined by a block-diagonal least-squares method. The positions of the hydrogen atoms could be estimated by using standard geometry. The final refinements with anisotropic temperature factors for the nonhydrogen atoms and isotropic temperature factors for the hydrogen atoms lowered the R values to 0.097 (R_w=0.123, $w=1/\sigma^2(F_o)$), 0.107 (R_w=0.128, w=1.0), 0.055 (R_w=0.057, $w=1/\sigma(F_o)$), and 0.067 (R_w=0.056, $w=1/\sigma^2(F_o)$) for **3a**, **3b**, **4b**, and **5b**, respectively. But, for **3b** the isotropic temperature factors were used for the O and C atoms because of the negative values of several atoms on the anisotropic refinements for the nonhydrogen atoms. Anomalous dispersion corrections were applied to the scattering factors of Hg, Ru, Cl, and S.[18]

Lists of structural factors, anisotropic thermal parameters, and H-atom coordination are being kept at the Chemical Society of Japan (Document No. 8853).

References

1) R. E. Izatt and J. J. Christensen, "Synthetic Multidentate Macrocyclic Compounds," Academic Press, New York (1977).

2) G. Oepen and F. Vögtle, *Libigs Ann. Chem.*, **1976**, 1094; J. F. Biernat and T. Wilezewski, *Tetrahedron*, **36**, 2521 (1980); A. P. Bell and D. Hall, *J. Chem. Soc., Chem. Commun.*, **1980**, 163; P. J. Hammond, P. D. Beer, and C. D. Hall, *J. Chem. Soc., Chem. Commun.*, **1983**, 1161; P. D. Beer, *J. Organomet. Chem.*, **297**, 313 (1985); P. D. Beer, *J.*

Chem. Soc., Chem. Commun., **1985**, 1115; G. Zhang, H. Zhu, and Q. Ding, *Yingyong Hauxue*, **2**, 70 (1985); M. P. Andrews, C. Blackurn, J. F. McAleer, and V. D. Patel, *J. Chem. Soc., Chem. Commun.*, **1987**, 1122; T. Saji and I. Kinoshita, *J. Chem. Soc., Chem. Commun.*, **1986**, 716; T. Saji, *Chem. Lett.*, **1986**, 275; T. Izumi, T. Tezuka, S. Yusa, and A. Kasahara, *Bull. Chem. Soc. Jpn.*, **57**, 2435 (1984); B. Czech, A. Czech, S. I. Kang, and R. A. Bartsch, *Chem. Lett.*, **1984**, 37.

3) Y. Kawasaki and Y. Matuura, *Chem. Lett.*, **1984**, 155.

4) N. W. Alcock, N. Herron, and P. Moore, *J. Chem. Soc., Dalton Trans.*, **1987**, 394.

5) N. W. Alcock, E. H. Curson, N. Herron, and P. Moore, *J. Chem. Soc., Dalton Trans.*, **1987**, 1979.

6) S. Akabori, S. Sato, K. Kawazoe, M. Sato, and Y. Habata, *Bull. Chem. Soc. Jpn.*, **61**, 1695 (1988); M. Sato, K. Suzuki, and S. Akabori, *Chem. Lett.*, **1987**, 2239; M. Sato, S. Akabori, M. Katada, I. Motoyama, and H. Sano, *Chem. Lett.*, **1987**, 1847; S. Akabori, S. Sato, Y. Habata, K. Kawazoe, C. Tamura, and M. Sato, *Chem. Lett.*, **1987**, 787.

7) S. Akabori, H. Munegumi, Y. Habata, S. Sato, K. Kawazoe, C. Tamura, and M. Sato, *Bull. Chem. Soc. Jpn.*, **58**, 2185 (1985).

8) S. Akabori, Y. Habata, and M. Sato, *Chem. Lett.*, **1985**, 1063; Y. Habata, S. Akabori, and M. Sato, *Bull. Chem. Soc. Jpn.*, **58**, 3540 (1985).

9) Preliminary report: S. Akabori, S. Sato, K. Kawazoe, C. Tamura, M. Sato, and Y. Habata, *Chem. Lett.*, **1987**, 1783.

10) L. Pauling, "The Nature of Chemical Bond," 3rd ed, ed by Cornel University Press, Ithaca, New York (1960).

11) G. B. Sul'pin and M. I. Rybinskaya, *Russ. Chem., Rev.*, **1974**, 716.

12) J. G. White, *Acta Crystallogr.*, **16**, 397 (1963).

13) A. I. Gusev and Y. T. Struckkov, *Zh. Struct. Kim.*, **12**, 1121 (1971).

14) D. Seyferth and H. P. Whithers, Jr., *J. Organomet. Chem.*, **185**, Cl (1980).

15) A. G. Osborne and R. H. Whitely, *J. Organomet. Chem.*, **193**, 345 (1980).

16) S. Akabori et al., unpublished results. to be published to Bull. Chem. Soc. Jpn.

17) "Topics in Carbon-13 NMR Spectroscopy," ed by G. C. Levy, John Wiley and Sons, New York (1979), Vol. 3, p. 199.

18) "International Tables for X-Ray Crystallography," Kynoch Press, Birmingham (1974),Vol. IV, pp. 72—98, 149, and 150.

 © 1989 The Chemical Society of Japan Bull. Chem. Soc. Jpn., 62, 539—544 (1989)

3,3′-Carbonylbis[5-phenyl-1,3,4-oxadiazole-2(3*H*)-thione]: A Novel, Reactive, and Versatile Condensing Agent for Amide, Ester, Thiol Ester, Urea, Carbonate, Polyamide, and Polyurea Syntheses

Yasuo SAEGUSA,* Tatsushi WATANABE, and Shigeo NAKAMURA
Department of Applied Chemistry, Faculty of Engineering, Kanagawa University, Kanagawa-ku, Yokohama 221
(Received August 30, 1988)

A novel condensing agent, 3,3′-carbonylbis[5-phenyl-1,3,4-oxadiazole-2(3*H*)-thione] (**3**), was readily prepared by the reaction of 5-phenyl-1,3,4-oxadiazole-2(3*H*)-thione with trichloromethyl chloroformate in benzene. The reagent **3** was found to be very useful for the one-pot or direct preparation of amide, ester, thiol ester, urea, and carbonate under mild conditions. The one-pot or direct polycondensation of several dicarboxylic acids with aromatic diamines and of aromatic diamines using **3** proceeded smoothly at ambient temperature to produce high-molecular-weight polyamides and polyureas, respectively.

Heterocyclic amides, such as imidazolides,[1-5] pyrazolide,[6] triazolide,[7] and oxadiazolides,[8] are very useful and popular condensing agents for the preparation of amides, esters, ureas, carbonates, and particularly peptides by a one-pot or direct procedure. The acylation or coupling reaction by the use of these reagents, however, takes a relatively long period. They also are generally very sensitive even to atmospheric moisture and must be handled with special cautions. The studies on the more reactive and even hydrolytically stable condensing agents have been successfully progressed.[9-18]

In the preceding article, we demonstrated that *N*- and *S*-acyl derivatives of 5-aryl-1,3,4-oxadiazole-2(3*H*)-thiones are novel highly reactive acylating agents for the synthesis of amide and polyamides under mild conditions.[19,20] This finding prompted us to develop further a novel condensing agent, 3,3′-carbonylbis[5-phenyl-1,3,4-oxadiazole-2(3*H*)-thione] (**3**), for the synthesis of amide and polyamides from carboxylic acids via *N*-acyl derivatives of 5-phenyl-1,3,4-oxadiazole-2(3*H*)-thione (**1**) as an active intermediate. This reagent might be also expected to be highly reactive for nucleophiles such as amines and alcohols.

We now report that amide, ester, thiol ester, urea, carbonate, and polyamides and polyureas with moderate to high molecular weights can be easily obtained from carboxylic acids and/or the corresponding nucleophiles by a one-pot or direct procedure using **3** under mild conditions.

Results and Discussion

Preparation of 3,3′-Carbonylbis[5-phenyl-1,3,4-oxadiazole-2(3*H*)-thione] (3). A novel and versatile condensing agent, 3,3′-carbonylbis[5-phenyl-1,3,4-oxadiazole-2(3*H*)-thione] (**3**), was conveniently prepared by the reaction of 5-phenyl-1,3,4-oxadiazole-2(3*H*)-thione (**1**) with trichloromethyl chloroformate (**2**) in a 1 : 1 molar ratio in benzene under reflux conditions (Scheme 1).

The reagent **3** is a pale yellow crystalline solid melting at 202 °C and has excellent hydrolytic stability compared with conventional condensing agents. Hence, this can be easily handled. The condensing agent **3** may be kept for a long period of time under atmospheric pressure.

The structure of **3** was assigned on the basis of infrared (IR) spectroscopy and elemental analysis. The IR spectrum exhibited a strong carbonyl absorption at 1760 cm^{-1} and a thiocarbonyl stretching absorption at 1355 cm^{-1}.

Reaction of 3 with Benzoic Acid (4), Isophthalic Acid (7a), and Adipic Acid (7b). In order to clarify the reactivity of **3** for carboxylic acids and the reaction pathway for the synthesis of amide, ester, thiol ester, and polyamides, the reaction of **3** with benzoic acid (**4**) was carried out in a variety of solvents including chloroform, tetrahydrofuran (THF), *N*,*N*-dimethylacetamide (DMA), *N*,*N*-dimethylformamide (DMF), and *N*-methyl-2-pyrrolidone (NMP) at room temperature (ca. 15°C) for 2 h in the presence or absence of pyridine as a tertiary base to form benzoate ion.

The condensing agent **3** reacted rapidly with **4** with the liberation of carbon dioxide and gave active amide intermediate, 5-phenyl-3-benzoyl-1,3,4-oxadiazole-2(3*H*)-thione[19] (**5**), in good yields (Table 1, Scheme 2). The use of pyridine was somewhat effective for the

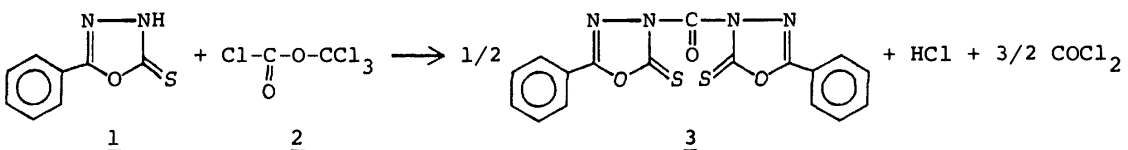

1 2 3

Scheme 1.

Table 1. Preparation of Active Amides **5**, **8a**, and **8b** Using Condensing Agent **3**

Carboxylic acid	Reaction conditions[a]			Product	
	Solvent	Base	Time	Type	Yield
	mL	mmol	h		%
4	CF[b](4)	Py[c](1)	2	**5**	90
4	THF(4)	Py(1)	2	**5**	89
4	DMA(4)	None	2	**5**	88
4	DMA(4)	Py(1)	2	**5**	91
4	DMF(4)	None	2	**5**	92
4	DMF(4)	Py(1)	2	**5**	96
4	NMP(2)	None	2	**5**	94
4	NMP(2)	Py(1)	2	**5**	99
4	NMP(2)	TEA[d](1)	2	**5**	68
7a	DMA(8)	Py(2)	4	**8a**	89
7a	DMF(8)	Py(2)	4	**8a**	91
7a	NMP(4)	None	4	**8a**	93
7a	NMP(4)	Py(2)	2	**8a**	74
7a	NMP(4)	Py(2)	4	**8a**	98
7b	NMP(4)	None	4	**8b**	94
7b	NMP(4)	Py(2)	4	**8b**	97

a) Reaction was carried out with 1 mmol of **4**, **7a**, or **7b** using 1 and 2 mmol of **3** for **4** and for **7a** and **7b**, respectively, at room temperature. b) CF: chloroform. c) Py: pyridine. d) TEA: triethylamine.

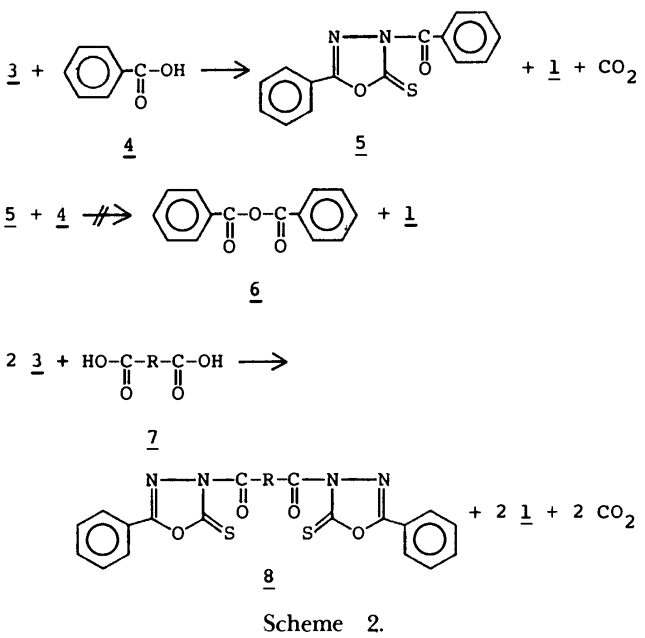

Scheme 2.

formation of **5**. No definite effect of medium on the reaction was, however, observed. Probable active intermediate benzoic anhydride (**6**) was not detected nor isolated entirely from the reaction mixtures. The use of triethylamine was attempted in place of pyridine, but was found less suitable as a base.

Similarly, active bisamide intermediates, 3,3′-isophthaloylbis[5-phenyl-1,3,4-oxadiazole-2(3*H*)-thione][19] (**8a**) and 3,3′-adipoylbis[5-phenyl-1,3,4-oxadiazole-2(3*H*)-thione][19] (**8b**), were both isolated in quantitatively from the condensation of **3** with isophthalic acid (**7a**) and adipic acid (**7b**), respectively (Table 1, Scheme 2).

Active amide intermediates **5**, **8a**, and **8b** obtained here were identified by melting point and IR spectroscopy. They, the actual acylating agents, have been characterized by high reactivity toward aminolysis.

Preparation of Benzanilide (10), Phenyl Benzoate (12a), and *S*-Phenyl Benzothioate (12b). Based on these results, we first studied the preparation of benzanilide (**10**), phenyl benzoate (**12a**), and *S*-phenyl benzothioate (**12b**) from benzoic acid (**4**) and aniline (**9**), phenol (**11a**), and thiophenol (**11b**), respectively, by a one-pot procedure using **3**. This efficient procedure consists of reacting **3** with **4** in chloroform, THF, DMA, DMF, or NMP at ambient temperature for 2 h in the presence or absence of pyridine affording **5** as an active intermediate (step 1) and subsequently with the respective nucleophiles at that temperature for a prescribed period (step 2).

The reaction with **9** as a nucleophile proceeded smoothly even without pyridine to furnish amide **10** in high yields (Table 2, Scheme 3). NMP as a solvent was somewhat more favorable than the others in the preparation of **10**. Both the reactions with **11a** and **11b** progressed much more slowly, but almost quantitative conversions to ester **12a** and thiol ester **12b** could be achieved in 2 and 8 d, respectively (Table 2, Scheme 3). An increase in the reaction temperature above 50 °C in step 2, however, accelerated dramatically the alcoholysis of **5**. Esterification at room temperature required an equimolar quantity of pyridine and above to nucleophiles **11a** and **11b**.

Table 2. One-Pot Preparation of Amide **10**, Ester **12a**, and Thiol Ester **12b** Using Condensing Agent **3**

Amine or alcohol	Reaction conditions			Product	
	Step 1[a]		Step 2[b]		
	Solvent	Pyridine	Time	Type	Yield
	mL	mmol			%
9	CF(4)	1	2h	**10**	85
9	THF(4)	1	2h	**10**	89
9	DMA(4)	1	2h	**10**	86
9	DMF(4)	1	2h	**10**	96
9	NMP(2)	0	2h	**10**	91
9	NMP(2)	1	2h	**10**	99
11a	CF(4)	2	4d	**12a**	99[c]
11a	THF(4)	2	4d	**12a**	91
11a	DMA(4)	2	4d	**12a**	85
11a	DMF(4)	2	4d	**12a**	91
11a	NMP(2)	0	4d	**12a**	Trace
11a	NMP(2)	0	12h[d]	**12a**	89
11a	NMP(2)	1	4d	**12a**	99[c]
11a	NMP(2)	2	1d	**12a**	67
11a	NMP(2)	2	2d	**12a**	95
11b	NMP(2)	0	8d	**12b**	Trace
11b	NMP(2)	2	8d	**12b**	86

a) Reaction was carried out with 1 mmol of **3** and **4** for 2 h at room temperature. b) Reaction was carried out with 1 mmol of **9**, **11a**, or **11b** at room temperature unless otherwise noted. c) A trace amount of **5** was contained. d) Reaction was carried out at 50°C.

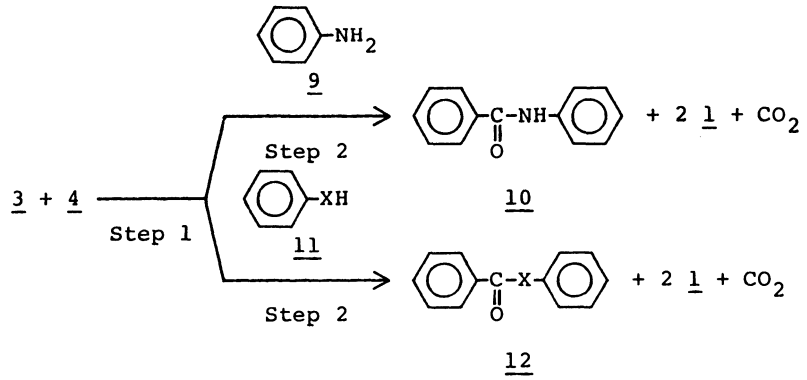

Scheme 3.

Preparation of *N,N'*-Diphenylurea (14) and Diphenyl Carbonate (16). The direct aminolysis and alcoholysis of **3** were next investigated to demonstrate the feasibility of the reactions for urea and carbonate formations, respectively. The reactions of **3** with twice-molar amounts of **9** and **11a** were conducted using chloroform, THF, DMA, DMF, and NMP as media at ambient temperature for a predetermined duration in the presence or absence of pyridine.

As shown in Table 3, **3** underwent aminolysis within a short time in the solvents to provide excellent yields of *N,N'*-diphenylurea (**14**) (Scheme 4). The use of NMP significantly affected the reaction rate of the aminolysis. Thus, the direct aminolysis of **3** is a facile, high-yield reaction which can be used for the synthesis of polyureas. The direct alcoholysis of **3** leading to diphenyl carbonate (**16**) took place relatively slow and required prolonged reaction time (much more than 8 d) for its completion (Table 3, Scheme 4). Raising the reaction temperature favored markedly the alcoholysis. Alcoholysis at room temperature required an equimolar quantity of pyridine to **11a**.

It is interesting to note that the treatments of **3** with an equimolar amounts of **9** and **11a** also afford high yields of **14** and **16**, respectively. This points to the following pathway (Scheme 4). A half-molar amount of **3** reacts first with **9** and **11a** to form 5-phenyl-3-anilinocarbonyl-1,3,4-oxadiazole-2(3*H*)-thione (**13**) and 5-phenyl-3-phenoxycarbonyl-1,3,4-oxadiazole-2(3*H*)-thione (**15**), respectively. The products **13** and **15** are more reactive than **5** as activated acylating agents and are less stable, and their enhanced reactivities cause them to react more rapidly with unreacted **9** and **11a**, respectively. Therefore, the formation of **13** and **15** is the rate-determining step in the proposed sequence of reactions.

Synthesis of Polyamides (18a—d). Facile one-pot amide preparation using the novel condensing agent **3** provides a promising route to polyamides. The polycondensation of dicarboxylic acids **7a** and **7b** with aromatic diamines including 4,4'-oxydianiline (**17a**) and 4,4'-methylenedianiline (**17b**) using **3** was therefore investigated by a one-pot procedure. Thus, the

Table 3. Direct Preparation of Urea **14** and Carbonate **16** Using Condensing Agent **3**

Amine or alcohol	Reaction conditions[a]			Product	
	Solvent	Pyridine	Time	Type	Yield
mmol	mL	mmol			%
9 (2)	CF(4)	0	2h	**14**	91
9 (2)	THF(4)	0	2h	**14**	91
9 (2)	DMA(4)	0	2h	**14**	89
9 (2)	DMF(4)	0	2h	**14**	93
9 (1)	NMP(2)	0	1h	**14**	95[b]
9 (2)	NMP(2)	0	1h	**14**	96
11a(2)	DMA(4)	2	8d	**16**	91
11a(2)	DMF(4)	2	8d	**16**	96
11a(1)	NMP(2)	1	4d	**16**	80[b]
11a(2)	NMP(2)	0	1d[c]	**16**	86
11a(2)	NMP(2)	2	4d	**16**	85
11a(2)	NMP(2)	2	8d	**16**	97

a) Reaction was carried out with 1 mmol of **3** at room temperature unless otherwise noted. b) The yield was calculated on the basis of half-molar quantities of **3**. c) Reaction was carried out at 60°C.

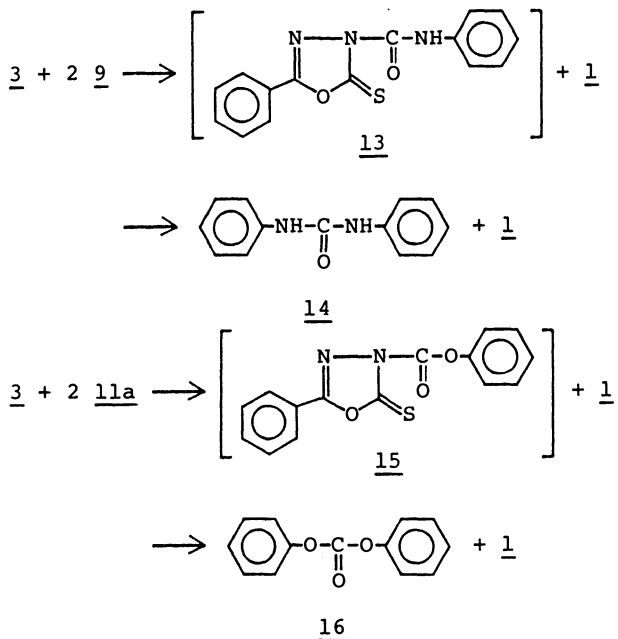

Scheme 4.

Table 4. One-Pot Synthesis of Polyamides **18a—d** Using Condensing Agent **3**

Carboxylic acid	Amine	Reaction conditions		Polymer			
		Step 1[a]	Step 2[b]				
		Pyridine	Time	Type	Yield	η_{sp}/c[c]	Remark[d]
		mmol	d		%	dL g^{-1}	
7a	**17a**	0	1	**18a**	92	0.13	P
7a	**17a**	2	1	**18a**	99	0.35	S
7a	**17a**	2	3	**18a**	99	0.37	G
7a	**17b**	2	1	**18b**	99	0.29	G
7b	**17a**	2	1	**18c**	99	0.33	G
7b	**17b**	2	1	**18d**	98	0.34	G

a) Reaction was carried out with 2 mmol of **3** and 1 mmol of **7a** or **7b** in 4 mL of NMP for 5 h at room temperature. b) Polymerization was carried out with 1 mmol of **17a** or **17b** at room temperature. c) Measured at a concentration of 0.5 g dL^{-1} in concentrated sulfuric acid at 30°C. d) P: polymer precipitation; S: homogeneous solution; G: apparent gelation.

Table 5. Direct Synthesis of Polyureas **19a** and **19b** Using Condensing Agent **3**

Amine	Reaction conditions[a]		Polymer			
	Salt[b]	Time	Type	Yield	η_{sp}/c[c]	Remark
				%	dL g^{-1}	
17a	None	1d	**19a**	98	0.26	G
17a	LiOH	1d	**19a**	99	0.78	S
17a	LiCl	1h	**19a**	99	0.67	S
17a	LiCl	1d	**19a**	99	0.87	S
17b	None	1d	**19b**	97	0.24	G
17b	LiCl	1d	**19b**	99	0.68	S

a) Polymerization was carried out with 1 mmol of **3** and **17a** or **17b** in 2 mL of NMP at room temperature. b) 5 wt% of the salt to NMP was added. c) Measured at a concentration of 0.5 g dL^{-1} in NMP at 30°C.

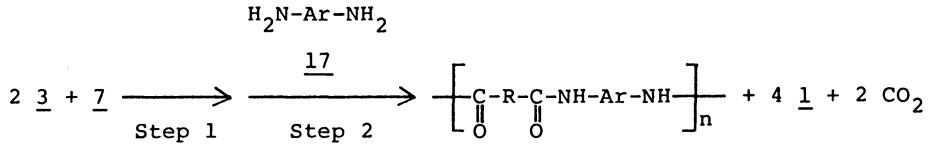

18

Scheme 5.

activation of the dicarboxylic acids was carried out by the addition of **3** to the respective NMP solutions of **7a** and **7b** at room temperature in the presence or absence of pyridine. After 5 h of stirring the diamine **17a** or **17b** was added, and the mixture was further stirred at that temperature for 1 or 3 d. The polyamides were isolated in the ordinary manner.

As can be seen from the reduced viscosities in Table 4, the corresponding polyamides (**18a—d**) with moderate molecular weights were easily synthesized in quantitative yields with pyridine (Scheme 5). Remarkable effect of pyridine on the polycondensations was observed.

Synthesis of Polyureas 19a and 19b. In order to further demonstrate the synthetic utility and versatility of the novel condensing agent **3**, it was applied to the synthesis of aromatic polyureas. The direct polycondensation leading to polyureas **19a** and **19b** was conducted in solution at ambient temperature for 1 h or 1 d in the presence of **3** using **17a** and **17b** as aromatic diamines. Equimolar amounts of the condensing agent and diamines were used. Polar aprotic solvent NMP was employed as a selected polymerization medium.

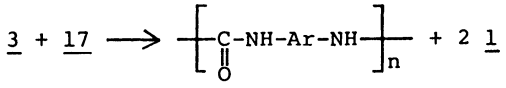

19

Scheme 6.

Although the polyureas were isolated in excellent yields, the molecular weights remained low, presumably due to the formation of a quasi-gel of polymers (Table 5, Scheme 6). High molecular weights were successfully attained by the addition of inorganic salts

such as lithium hydroxide and lithium chloride to the system in which the polymers remained dissolved.

In conclusion, these experimental results indicate that the novel condensing agent **3** is very useful for the preparation of amide, ester, thiol ester, urea, and carbonate and moderate- to high-molecular-weight polyamides and polyureas under mild conditions. Furthermore, **3** is a crystalline solid and is handled more easily than the conventional condensing agents.

Experimental

Melting points (mp) were uncorrected. Infrared (IR) spectra were recorded in potassium bromide on a JASCO IR-810 spectrophotometer. 5-Phenyl-1,3,4-oxadiazole-2(3*H*)-thione (**1**) was prepared as reported previously.[21] Trichloromethyl chloroformate (**2**), supplied by Hodogaya Chemical Industries Ltd., was used without further purification. The other reagents and solvents were obtained commercially and were used after purification by the usual manner. The products obtained were identified by spectral comparison and/or mp and mixed mp with the corresponding authentic samples unless otherwise noted.

3,3′-Carbonylbis[5-phenyl-1,3,4-oxadiazole-2(3*H*)-thione] (3). A mixture of **1** (17.8 g, 0.1 mol) and **2** (12 mL, 0.1 mol) in benzene (300 mL) was refluxed with stirring for 1 d. The solvent was removed in vacuo and the residue was recrystallized twice from benzene to give pale yellow granular crystals. Yield: 14.9 g (78%). Mp 202 °C (by differential thermal analysis); IR (KBr), 1760 (C=O), 1610 (C=N), and 1355 cm^{-1} (C=S).

Found: C, 53.52; H, 2.62; N, 14.76%. Calcd for $C_{17}H_{10}N_4O_3S_2$: C, 53.39; H, 2.64; N, 14.65%.

Reaction of 3 with Benzoic Acid (4). To a solution of **4** (0.122 g, 1 mmol) and/or pyridine (0.079 g, 1 mmol) in a solvent (2 or 4 mL) was added **3** (0.382 g, 1 mmol) followed by stirring at room temperature for 2 h. The reaction mixture was poured into 1% aqueous sodium hydrogencarbonate (50 mL). The resulting precipitate was collected, washed several times with water, and dried.

Reaction of 3 with Isophthalic Acid (7a) or Adipic Acid (7b). The condensing agent **3** (0.764 g, 2 mmol) was added to a solution of **7a** or **7b** (1 mmol) and/or pyridine (0.158 g, 2 mmol) in a solvent (4 or 8 mL). The solution was stirred at ambient temperature for 2 or 4 h, and then poured into 1% aqueous sodium hydrogencarbonate (100 mL). The solid, so formed, was filtered off, rinsed repeatedly with water, and dried.

Benzanilide (10). To a stirred solution of **4** (0.122 g, 1 mmol) and/or pyridine (0.079 g, 1 mmol), **3** (0.382 g, 1 mmol) at room temperature was added. After 2 h of the reaction aniline (**9**) (0.093 g, 1 mmol) was added, and the solution was stirred at that temperature for an additional 2 h. The product was isolated by pouring the solution into 1% aqueous sodium hydrogencarbonate (100 mL). It was gathered, washed thoroughly with water, and dried.

Phenyl Benzoate (12a) and *S*-Phenyl Benzothioate (12b). A mixture of **3** (0.382 g, 1 mmol), **4** (0.122 g, 1 mmol), and/or pyridine (1 or 2 mmol) in a solvent (2 or 4 mL) was stirred at ambient temperature for 2 h and phenol (**11a**) or thiophenol (**11b**) (1 mmol) was added. Stirring was further continued at that temperature or 50 °C for 12 h, 1, 2, 4, or 8 d. The reaction mixture was worked up as reported for **10**.

***N,N′*-Diphenylurea (14).** The condensing agent **3** (0.382 g, 1 mmol) was added to a solution of **9** (1 or 2 mmol) in a solvent (2 or 4 mL). This solution was stirred at room temperature for 1 or 2 h followed by treating as described.

Diphenyl Carbonate (16). A solution of **3** (0.382 g, 1 mmol), **11a** (1 or 2 mmol), and/or pyridine (1 or 2 mmol) in a solvent (2 or 4 mL) was reacted with stirring at ambient temperature or 60 °C for 1, 4, or 8 d. The work-up of the product was as usual.

Judging from IR and ^1H NMR spectra and the mp, all the products were virtually pure without any purifications.

Polyamides 18a—d. The condensing agent **3** (0.764 g, 2 mmol) was allowed to react with **7a** or **7b** (1 mmol) in *N*-methyl-2-pyrrolidone (NMP) (4 mL) in the presence or absence of pyridine (0.158 g, 2 mmol) and stirred at ambient temperature for 5 h. Diamine 4,4′-oxydianiline (**17a**) or 4,4′-methylenedianiline (**17b**) (1 mmol) was then added to this mixture. After 1 or 3 d of stirring at this temperature the polymer was separated by reprecipitation with 1% aqueous sodium hydrogencarbonate (300 mL). It was isolated, rinsed well with hot methanol, and dried. The reduced viscosity was measured at a concentration of 0.5 $g dL^{-1}$ in concentrated sulfuric acid at 30 °C.

Polyureas 19a and 19b. A mixture of **3** (0.382 g, 1 mmol) and **17a** or **17b** (1 mmol) in NMP or NMP (2 mL) containing 5 wt% of lithium hydroxide or lithium chloride reacted with stirring at room temperature for 1 h or 1 d. The polymerization solution was treated as described for **18**. The reduced viscosity was measured in NMP.

References

1) H. A. Staab, *Justus Liebigs Ann. Chem.*, **609**, 75 (1957).
2) G. W. Anderson and R. Paul, *J. Am. Chem. Soc.*, **80**, 4423 (1958).
3) R. Paul and G. W. Anderson, *J. Org. Chem.*, **27**, 2094 (1962).
4) Y. Nomura, *Yuki Gosei Kagaku Kyokai Shi*, **21**, 585 (1963), and references cited therein.
5) H. A. Staab and W. Rohr, "Newer Methods of Preparative Organic Chemistıy," ed by W. Foerst, Verlag Chemie, Weinheim (1976), Vol. V, p. 61.
6) W. Ried and B. M. Beck, *Justus Liebigs Ann. Chem.*, **646**, 96 (1961).
7) H. C. Beyerman and W. Maasen Van Den Brink, *Recl. Trav. Chim. Pays-Bas*, **80**, 1372 (1961); *Chem. Abstr.*, **58**, 5781e (1963).
8) T. Fujii and M. Miyoshi, *Chem. Lett.*, **1972**, 949.
9) T. Shioiri, *Yuki Gosei Kagaku Kyokai Shi*, **37**, 856 (1979), and references cited therein.
10) H. Ogura and K. Takeda, *Nippon Kagaku Kaishi*, **1981**, 836, and references cited therein.
11) Y. Nagao, *Kagaku Zokan*, **96**, 173 (1982).
12) T. Kunieda and M. Hirobe, *Yuki Gosei Kagaku Kyokai Shi*, **41**, 77 (1983), and references cited therein.
13) M. Ueda, H. Oikawa, N. Kawaharasaki, and Y. Imai, *Bull. Chem. Soc. Jpn.*, **56**, 2485 (1983).
14) M. Ueda, N. Kawaharasaki, and Y. Imai, *Bull. Chem. Soc. Jpn.*, **57**, 85 (1984).
15) M. Ueda, A. Mochizuki, I. Hiratsuka, and H. Oikawa, *Bull. Chem. Soc. Jpn.*, **58**, 3291 (1985).

16) M. Ueda and H. Oikawa, *J. Org. Chem.*, **50**, 760 (1985).
17) M. Ueda and H. Oikawa, *J. Polym. Sci., Polym. Chem. Ed.*, **23**, 1607 (1985).
18) M. Ueda and A. Mochizuki, *Macromolecules*, **18**, 2353 (1985).
19) Y. Saegusa, S. Nakamura, N. Chau, and Y. Iwakura, *J. Polym. Sci., Polym. Chem. Ed.*, **21**, 637 (1983).
20) Y. Saegusa, N. Akano, S. Nakamura, N. Chau, and Y. Iwakura, *J. Polym. Sci., Polym. Chem. Ed.*, **23**, 2727 (1985).
21) N. Chau, Y. Saegusa, and Y. Iwakura, *J. Heterocycl. Chem.*, **19**, 541 (1982).

Manganese(III)-Mediated Formylation of Aromatic Compounds in the Presence of Malonic Acid

Hiroshi NISHINO,* Katsunori TSUNODA, and Kazu KUROSAWA
Department of Chemistry, Faculty of Science, Kumamoto University, Kurokami 2-39-1, Kumamoto 860
(Received August 31, 1988)

The reaction of naphthalenes with malonic acid in the presence of manganese(III) acetate gives naphthalenecarbaldehydes and naphthalenecarboxylic acids. Similar reactions of anthracene, pyrene, and methoxybenzenes also yield formylated and carboxylated products. It was found that the formyl group introduced to the aromatic ring was not derived from carboxymethyl radical generated directly by the thermolysis of manganese(III) acetate, but from a dicarboxymethyl radical formed by the interaction of malonic acid and manganese(III) acetate. In addition, it was also found that the dicarboxymethyl radicals attacked the position of the highest electron density on the aromatic ring and that this formylation was effective when the ionization potential of the aromatic compound was lower than 7.8 eV.

It is known that the reaction of aromatic compounds with manganese(III) acetate, $[Mn_3O(OAc)_6(OAc)(HOAc)]\cdot 5H_2O$ (which is usually abbreviated to $[Mn_3O]$),[1] gives mainly acetoxymethylated products together with small amounts of carboxymethyl, diacetoxymethyl or formyl, and carboxyl derivatives.[2] This reaction is caused by carboxymethyl radicals, $\cdot CH_2CO_2H$, which are formed by the pyrolysis of manganese(III) acetate.[3] Kurosawa and McOmie have obtained a propellane, 7-oxa-10,11-benzotricyclo[4.3.2.0]undeca-2,4,10-trien-8-one, by the use of a similar oxidation of biphenylene.[4] On the other hand, Kurz and Chen have reported on the nitromethylation of aromatic hydrocarbons promoted by manganese(III) acetate.[5] A key of this nitromethylation is the formation of nitromethyl radicals, $\cdot CH_2NO_2$, formed by the

Table 1. Oxidation of Aromatic Compounds with Manganese(III) Acetate in the Presence of Malonic Acid in Boiling Acetic Acid

Entry	Compound	Molar ratio[a]	Time	Product (yield/%)[b]		
			min	Aldehyde	Acid	Others
1	**1a**	1:4:4	1	**2a** (55)		
2	**1a**	1:4:8	1	**2a** (50)		
3	**1a**	1:4:12	2	**2a** (39)		
4[c]	**1a**	1:8:8	10	**2a** (30)		
5[d]	**1a**	1:8:8	3	**2a** (34)		
6	**1a**	1:8:8	1	**2a** (59)		
7	**1a**	1:12:8	1	**2a** (46)		
8	**1b**	1:4:4	1	**2b** (44)		
9	**1b**	1:8:8	1	**2b** (46)	**3b** (12)	
10	**1c**	1:4:4	1	**2c** (33)		
11	**1c**	1:8:8	1	**2c** (25)	**3c** (8)	
12	**1d**	1:8:8	1	**2d** (58)		
13	**1e**	1:8:8	1	**2e** (53)		
14	**1f**	1:8:8	1	**2f** (34)		
15	**1g**	1:8:8	1	**2g** (26)		
				2g′ (22)		
				4 (13)		
16	**1h**	1:8:8	1	**2h** (13)	**3h** (39)	
17	**1i**	1:8:8	1	**2i** (6)	**3i** (22)	
18	**1j**	1:8:8	1	**2j** (5)	**3j** (26)	
19	**1k**	1:8:8	1		**3k** (43)	**5** (9)
20	**1l**	1:8:8	1		**3l** (29)	
21	**6**	1:4:4	1	**8** (12)	**10** (15)	**7** (28) **9** (13)
22	**6**	1:8:8	1	**8** (12)		**7** (16) **9** (10)
23	**11**	1:8:8	1	**12** (25)	**14** (10)	**13** (22)
24	**15a**	1:8:8	1		**17a** (5)	
					17a′ (9)	
25	**15b**	1:8:8	1	**16b** (9)	**17b** (9)	
26	**15c**	1:8:8	1	**16c** (t)	**17c** (9)	

a) Naphthalene: malonic acid: manganese(III) acetate. b) Yields based on the amount of naphthalene consumed. c) The reaction was carried out at 70°C. d) The reaction was carried out at 100°C.

interaction of manganese(III) acetate and nitromethane. Recently, we have found the spiroannulation of alkenes by the use of a malonic acid-manganese(III) acetate system.[6] Fristad and Hershberger suggested that dicarboxymethyl radicals, $\cdot CH(CO_2H)_2$, produced in the oxidation system participated in this spiroannulation.[7] In connection with these manganese(III) acetate oxidations, we tried to apply a malonic acid-manganese(III) acetate system to aromatic hydrocarbons in order to obtain aromatic lactone annulation, such as the formation of propellane[4] or di-γ-lactone.[8] When aromatic compounds were oxidized with manganese(III) acetate in the presence of malonic acid, a reaction involving dicarboxymethyl radicals actually occurred. However, no aromatic lactone annulation was observed and the dicarboxymethyl group was introduced in the aromatic ring, followed by decarboxylation to give the corresponding aldehydes or further by oxidation to yield carboxylic acids. This paper now describes the results of our investigation into this reaction as regards synthetic utility, scope, limitations, and mechanistic pathway.

Results and Discussion

2,7-Dimethoxynaphthalene (**1a**) was selected as an aromatic substrate for the reason that the reaction products were readily separated from **1a** by TLC and could be easily characterized by spectrometry. When **1a** was oxidized with manganese(III) acetate in the presence of malonic acid under various reaction conditions (Table 1), 2,7-dimethoxy-1-naphthalenecarbaldehyde (**2a**) was obtained in moderate yield (Entries 1—7). Especially, the oxidation at a molar ratio of **1a**: malonic acid: $[Mn_3O]$=1 : 8 : 8 at reflux temperature gave **2a** in the best yield (Entry 6). Then, methoxynaphthalenes (**1b—f**) were oxidized at a molar ratio of 1 : 8 : 8 at reflux temperature, giving the corresponding naphthalenecarbaldehydes (**2b—f**) in moderate yields together with a small amount of naphthalenecarboxylic acids (**3b** and **3c**) as a by-product (Entries 8—14). The reaction of **1g** gave dicarbaldehyde (**4**) in addition to two kinds of carbaldehydes (**2g** and **2g'**) (Entry 15). In a similar oxidation of **1h**, 6,7-dimethoxy-1-naphthalenecarboxylic acid (**3h**) was mainly produced in 39% yield (Entry 16). When methylnaphthalenes (**1i—k**) and naphthalene (**1l**) were oxidized under similar reaction conditions, naphthalenecarboxylic acids (**3i—l**) were formed in 22—43% yields along with a small amount of carbaldehydes (**2i** and **2j**) and 1-(diacetoxymethyl)naphthalene (**5**) (Entries 17—20).

Anthracene (**6**) was oxidized with the manganese(III) acetate-malonic acid system to give four products: 9-acetoxyanthracene (**7**), 9-anthracenecarbaldehyde (**8**), 9-(diacetoxymethyl)anthracene (**9**), and 9-anthracenecarboxylic acid (**10**) (Entries 21, 22). Pyrene (**11**) also yielded an aldehyde (**12**), a diacetoxymethyl derivative (**13**), and a carboxylic acid (**14**)

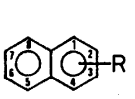

1a: R=2,7-$(CH_3O)_2$
b: R=1-CH_3O
c: R=2-CH_3O
d: R=1,5-$(CH_3O)_2$
e: R=1,3-$(CH_3O)_2$
f: R=2,6-$(CH_3O)_2$
g: R=1,7-$(CH_3O)_2$
h: R=2,3-$(CH_3O)_2$
i: R=1-CH_3
j: R=2-CH_3
k: R=1,8-$(CH_3)_2$
l: R=H
m: R=1-NO_2

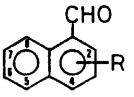

2a: R=2,7-$(CH_3O)_2$
b: R=4-CH_3O
c: R=2-CH_3O
d: R=4,8-$(CH_3O)_2$
e: R=2,4-$(CH_3O)_2$
f: R=2,6-$(CH_3O)_2$
g: R=4,6-$(CH_3O)_2$
g': R=2,8-$(CH_3O)_2$
h: R=6,7-$(CH_3O)_2$
i: R=4-CH_3
j: R=2-CH_3
4: R=5-CHO-4,6-$(CH_3O)_2$

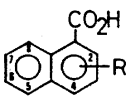

3b: R=4-CH_3O
c: R=2-CH_3O
h: R=6,7-$(CH_3O)_2$
i: R=4-CH_3
j: R=2-CH_3
k: R=4,5-$(CH_3)_2$
l: R=H

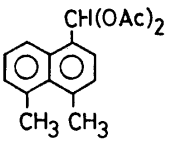

5

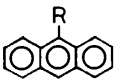

6: R=H
7: R=OAc
8: R=CHO
9: R=$CH(OAc)_2$
10: R=CO_2H

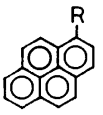

11: R=H
12: R=CHO
13: R=$CH(OAc)_2$
14: R=CO_2H

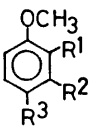

15a: $R^1=R^2=R^3=H$
b: $R^1=R^3=H$, $R^2=CH_3O$
c: $R^1=R^2=CH_3O$, $R^3=H$
16b: $R^1=H$, $R^2=CH_3O$, $R^3=CHO$
c: $R^1=R^2=CH_3O$, $R^3=CHO$
17a: $R^1=CO_2H$, $R^2=R^3=H$
a': $R^1=R^2=H$, $R^3=CO_2H$
b: $R^1=H$, $R^2=CH_3O$, $R^3=CO_2H$
c: $R^1=R^2=CH_3O$, $R^3=CO_2H$

Fig. 1.

under the similar reaction conditions (Entry 23).

On the contrary, anisole (**15a**), 1,3-dimethoxybenzene (**15b**), and 1,2,3-trimethoxybenzene (**15c**) were rather inactive under these oxidation conditions to afford only a small amount of benzaldehydes (**16b** and **16c**) and benzoic acids (**17a—c**) (Entries 24—26).

It is well-known that carboxymethyl radicals react with aromatic compounds and eventually give acetoxymethyl derivatives.[3] The acetoxymethylated products can be further oxidized with manganese(III) acetate to form diacetoxymethyl and/or formyl derivatives.[9] Aratani and Dewar have briefly reported that the oxidations of 1- and 2-methoxynaphthalene with manganese(III) acetate at 100 °C gave acetoxynaphthalenes and naphthoquinones.[10] When we repeated the oxidation of 2,7-dimethoxynaphthalene (**1a**) at a reflux temperature in which the carboxymethyl radicals could be formed more readily,[3] naphthalenecarbaldehyde, however, was not detected and the results were similar to those described in the literature (Scheme 1). Heiba and co-workers reported that a radical reaction preferentially occurred by the addition of acetic anhydride in a manganese(III) oxidation system.[3] The oxidation of **1a** was then carried out at reflux temperature under anhydrous conditions, but only acetoxymethylated product (**20**) was obtained, which was not further oxidized to give aldehyde under these reaction conditions (Scheme 2). It follows, therefore, that the formylation of aromatic compounds in the reaction of manganese(III) acetate–malonic acid system could not be caused by an attack of carboxymethyl radicals on the aromatic ring, but that malonic acid played an important role in this system. In order to clarify the source of formyl carbon, the reaction of **1a** was run by the use of malonic acid-d_4 in anhydrous benzene. As a result, a mixture of **2a** and 1-(formyl-*d*)naphthalene (**21**) was obtained in 24% yield (Scheme 3). Xanthene (**22**) was oxidized in a manganese(III) acetate–malonic acid system to give 9-(carboxymethyl)-xanthene (**23**) (Scheme 4). These facts indicate that dicarboxymethyl radicals directly attack the aromatic ring. The formation of **2a** in the reaction of **1a** with malonic acid-d_4 is probably due to a deuterium–hydrogen exchange between malonic acid-d_4 and acetic acid ligands of manganese(III) acetate. Accordingly, the mechanism for the manganese(III)-mediated formylation was depicted by the evidence mentioned above, as shown in Scheme 5, which involves double

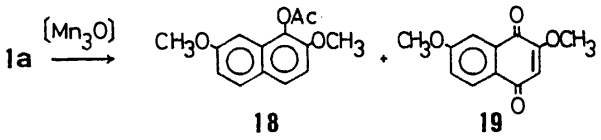

Scheme 1.

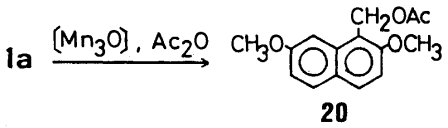

Scheme 2.

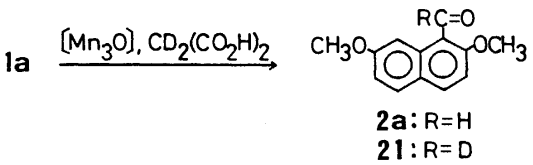

Scheme 3.

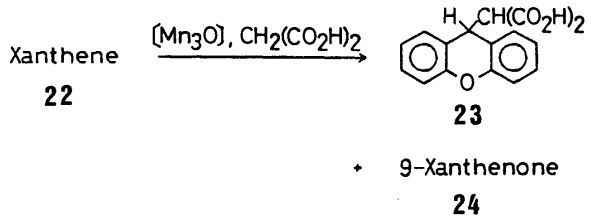

Scheme 4.

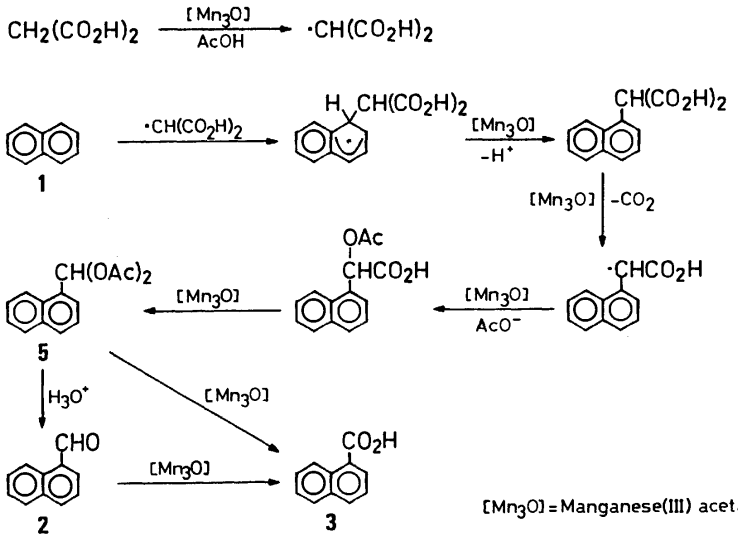

Scheme 5.

Table 2. Ionization Potentials of Aromatic Compounds and the Yields of Aldehydes and Carboxylic Acids in the Manganese(III) Oxidation

Entry	Compound	Ionization potential[a]/eV	Product(yield/%)	
			Aldehyde	Carboxylic acid
1	Anthracene (**6**)	7.36	**8**+**9** (25)	**10** (7)
2	Pyrene (**11**)	7.37	**12**+**13** (47)	**14** (10)
3	2,7-Dimethoxynaphthalene (**1a**)	7.58[b]	**2a** (59)	**3a** (0)
4	1-Methoxynaphthalene (**1b**)	7.70	**2b** (46)	**3b** (12)
5	2-Methoxynaphthalene (**1c**)	7.82	**2c** (25)	**3c** (8)
6	1,8-Dimethoxynaphthalene (**1k**)	7.92[c]	**5** (7)	**3k** (43)
7	1-Methylnaphthalene (**1i**)	7.96	**2i** (6)	**3i** (22)
8	2-Methylnaphthalene (**1j**)	8.04	**2j** (5)	**3j** (26)
9	Naphthalene (**1l**)	8.12	**2l** (0)	**3l** (29)
10	Anisole (**15a**)	8.39	**16a** (0)	**17a**+**17a'**(14)
11	1-Nitronaphthalene (**1m**)	8.59	**2m** (0)	**3m** (0)

a) Ref. 11. b) The ionization potential shows the value of **1f**. c) The ionization potential shows the value of 2,6-dimethylnaphthalene.

decarboxylation. The isolation of diacetoxymethyl derivatives (**5**, **9**, and **13**) (Table 1) would also support this mechanism. As can be seen in Fig. 1, a substituent group, such as formyl, diacetoxymethyl, or carboxyl group, is introduced at the position of the highest electron density on the aromatic ring, except for the case of 2,3-dimethoxynaphthalene (**1h**). This fact corroborates that the dicarboxymethyl radical has an electrophilic nature. Perhaps, in the case of **1h**, the attack of a bulky dicarboxymethyl radical was inhibited by a steric hindrance of the vicinal methoxyl groups. The manganese(III)-mediated formylation in the presence of malonic acid occurs preferentially to aromatic compounds which have an ionization potential in the range 7.36 to 7.82 eV (Table 2). Aromatic hydrocarbons having an ionization potential higher than these levels tend to be oxidized up to carboxylic acids, though they come to be less reactive to manganese(III) oxidation. This has been shown in cases of **1h**—**l** in which the corresponding aldehydes or diacetoxymethyl derivatives may be more readily oxidized with manganese(III) than the parent compounds. Aromatic substrates having an ionization potential over 8.4 eV could not react in this oxidation system. This aptness is similar to the direct diacetylmethylation of aromatic compounds with tris(2,4-pentanedionato)manganese(III), which is pyrolyzed in acetic acid to generate diacetylmethyl radicals.[11] The formylation of anthracene (**6**) was restrained, since a direct reaction between **6** and manganese(III) acetate via an electron-transfer mechanism took place and 9-acetoxyanthracene (**7**) was formed.[12] At this point, the behavior of **6** is seen to be different from that of **6** in direct diacetylmethylation with tris(2,4-pentanedionato)manganese(III) (only radical reaction including diacetylmethyl radicals occurs in the reaction of **6** with tris(2,4-pentanedionato)-manganese(III)).[11]

In conclusion, this manganese(III)-mediated formylation could be applied to the aromatic compounds having a relatively lower ionization potential (≦7.82 eV), although the formylation of aromatic compounds is known as Vilsmeier, Gattermann, Gattermann-Koch, Reimer-Tiemann reaction, and etc. It should be emphasized that the reaction time is extremely short (within 1 min).

Experimental

Measurements. The ^{1}H NMR spectra were measured in deuteriochloroform on a JEOL JNM-PMX60SI spectrometer at room temperature. Chemical shifts are recorded in the δ scale, relative to TMS as an internal standard. The IR spectra were taken in chloroform on a JASCO A-102 infrared spectrophotometer, and the IR spectral data are expressed in cm^{-1}. The mass spectra were obtained with a JEOL JMS-DX300 mass spectrometer at 70 eV of ionization energy. All melting points were determined with a Yanagimoto micro-melting point apparatus and were uncorrected. Thin-layer chromatography was carried out on silica gel (Wakogel B-10) with chloroform as a developing solvent.

Materials. Methoxynaphthalenes and polymethoxybenzenes were synthesized by the methylation of the corresponding naphthols and phenols with dimethyl sulfate. Naphthalene, anthracene, pyrene, and anisole were commercially available. Manganese(III) acetate was prepared by the method described in the literature.[3]

Oxidation of Aromatic Compounds with Manganese(III) Acetate in the Presence of Malonic Acid. The typical procedure for the oxidation of aromatic compounds with manganese(III) acetate in the presence of malonic acid was as follows. To a heated solution of aromatic compound (1 mmol) and malonic acid (8 mmol) in acetic acid (25 cm^3), manganese(III) acetate (1.98 g, 8 mmol for Mn(III)) was added. The mixture was heated under reflux until its dark-brown color turned opaque white. The solvent was removed in vacuo, and the residue was triturated with 2 M (1 M=1 mol dm^{-3}) HCl (25 cm^3), followed by extraction with chloroform. The chloroform extract was washed with an aqueous sodium hydrogencarbonate solution and concentrated. The aqueous solution was acidified with concentrated hydrochloric acid and subsequently extracted with ethyl acetate.

The solvent was removed in vacuo and the residue was treated with diazomethane in methanol. The neutral and esterified products, respectively, were separated on TLC. The yields are summarized in Table 1.

Oxidation Products. 2,7-Dimethoxy-1-naphthalenecarbaldehyde (2a): Mp 97.7—98.7 °C (from ethanol) (lit,[13] mp 98 °C); IR 1665 (CHO); ^{1}H NMR δ=3.86 (3H, s, OCH_3), 3.90 (3H, s, OCH_3), 6.86 (1H, d, J=9.0 Hz, H-3), 6.95 (1H, dd, J=9.0, 2.4 Hz, H-6), 7.51 (1H, d, J=9.0 Hz, H-4 or H-5), 7.78 (1H, d, J=9.0 Hz, H-5 or H-4), 8.73 (1H, d, J=2.4 Hz, H-8), and 10.75 (1H, s, CHO); MS m/z (rel intensity), 216 (100, M^+), 187 (25), 159 (53), 144 (20), 115 (31), and 102 (20). Found: C, 71.99; H, 5.59%. Calcd for $C_{13}H_{12}O_3$: C, 72.21; H, 5.59%.

6,7-Dimethoxy-1-naphthalenecarbaldehyde (2h): Mp 108—109 °C (from ethanol); IR 1682 (CHO); ^{1}H NMR δ=3.98 (3H, s, OCH_3), 4.05 (3H, s, OCH_3), 7.07 (1H, s, H-5), 7.35—8.18 (3H, m, arom. H), 8.70 (1H, s, H-8), and 10.21 (1H, s, CHO); MS m/z (rel intensity), 216 (100, M^+), 188 (37), 173 (26), and 145 (54). Found: m/z 216.0770. Calcd for $C_{13}H_{12}O_3$: M, 216.0786.

Methyl Ester of 6,7-Dimethoxy-1-naphthalenecarboxylic Acid (3h): Mp 189—190 °C (from ethanol); IR 1709 (C=O) and 1254 (C-O-C); ^{1}H NMR δ=3.96 (6H, s, 2×OCH_3), 4.00 (3H, s, OCH_3), 6.99 (1H, s, H-5), 7.20 (1H, t, J=8.0 Hz, H-3), 7.74 (1H, dd, J=8.0 and 2.4 Hz, H-4), 8.06 (1H, dd, J=8.0 and 2.4 Hz, H-2), and 8.47 (1H, s, H-8); MS m/z (rel intensity), 246 (100, M^+), 215 (41), 187 (15), 173 (20), and 145 (14). Found: m/z 246.0895. Calcd for $C_{12}H_{14}O_4$: M, 246.0891.

4,6-Dimethoxy-1,5-naphthalenedicarbaldehyde (4): Mp 185—186 °C (from ethanol); IR 1680 and 1703 (CHO); ^{1}H NMR δ=3.93 (1H, s, OCH_3), 4.00 (1H, s, OCH_3), 6.88 (1H, d, J=8.0 Hz, H-3), 7.40 (1H, d, J=9.0 Hz, H-7), 7.76 (1H, d, J=8.0 Hz, H-2), 9.41 (1H, d, J=9.0 Hz, H-8), 10.09 (1H, s, CHO), and 10.61 (1H, s, CHO); MS m/z (rel intensity), 244 (100, M^+), 229 (20), 213 (30), 199 (15), 115 (55), and 102 (40). Found: C,68.57; H, 5.02%. Calcd for $C_{14}H_{12}O_4$: C, 68.84; H, 4.95%.

1-Diacetoxymethyl-4,5-dimethylnaphthalene (5): Mp 130.4—131.4 °C (from light petroleum); IR 1240 (O-CO), 1760 (OAc); ^{1}H NMR δ=2.10 (6H, s, 2×OAc), 2.90 (6H, s, 2×CH_3), 7.1—7.5 (3H, m), 7.52 (1H, d, J=8.0 Hz), 8.09 (1H, dd, H-8), and 8.16 (1H, s, -CH<). Found: C, 71.43; H, 6.42%. Calcd for $C_{17}H_{18}O_4$: C, 71.31; H, 6.34%.

4-Methoxy-1-naphthalenecarbaldehyde (2b) (lit,[14] mp 34 °C); **2-methoxy-1-naphthalenecarbaldehyde (2c)**, mp 82.2—83.1 °C (lit,[15] mp 82.0—83.5 °C); **4,8-dimethoxy-1-naphthalenecarbaldehyde (2d)**, mp 126.8—127.6 °C (lit,[16] mp 126 °C); **2,4-dimethoxy-1-naphthalenecarbaldehyde (2e)**, mp 161.8—162.3 °C (lit,[17] mp 161—162 °C); **2,6-dimethoxy-1-naphthalenecarbaldehyde (2f)**, mp 90.3—90.8 °C (lit,[13] mp 90 °C); **4,6-dimethoxy-1-naphthalenecarbaldehyde (2g)**, mp 103.5—104.4 °C (lit,[18] mp 104 °C); **2,8-dimethoxy-1-naphthalenecarbaldehyde (2g')** (lit,[18] mp 90 °C); **4-methyl-1-naphthalenecarbaldehyde (2i)**, liquid (lit,[19] bp 160—165 °C/1.3×10^3 Pa); **2-methyl-1-naphthalenecarbaldehyde (2j)**, mp 50—51 °C (lit,[20] mp 51.5—52 °C); **methyl esters of 4-methoxy-1-naphthalenecarboxylic acid (3b);**[21] **2-methoxy-1-naphthalenecarboxylic acid (3c)** (lit,[22] mp 52—53 °C); **4-methyl-1-naphthalenecarboxylic acid (3i)** (lit,[23] bp 192—194 °C/1.6×10^3 Pa); **2-methyl-1-naphthalenecarboxylic acid (3j)** (lit,[23] bp 168—170 °C/2×10^3 Pa); **4,5-dimethyl-1-naphthalenecarboxylic acid (3k)**[24] and **1-naphthalenecarboxylic acid (3l)** (lit,[25] bp 100—102 °C/5.3 Pa) were characterized by its ^{1}H NMR, IR spectrum, and by comparison of the melting point or the boiling point with those of literatures.

1-Acetoxyanthracene (7): Pale yellow needles (from ethanol), mp 132—133 °C (lit,[26] mp 134—135 °C); IR 1765 (OAc); ^{1}H NMR δ=2.59 (3H, s, OAc), 7.2—8.1 (8H, m, arom. H), and 8.31 (1H, s, H-10).

9-Anthracenecarbaldehyde (8): Mp 103.5—104.5 °C (from ethanol) (lit,[27] mp 104—105 °C).

9-Diacetoxymethylanthracene (9): Mp 138—139 °C (from ethanol); IR 1760 (OAc); ^{1}H NMR δ=2.08 (6H, s, 2×OAc), 7.18—8.80 (8H, m, arom. H), 8.48 (1H, s, H-10), and 9.25 (1H, s, -CH<); MS m/z (rel intensity), 308 (14, M^+), 206 (100), 178 (95), and 151 (29). Found: m/z 308.0955. Calcd for $C_{19}H_{16}O_4$: M, 308.1048.

1-Pyrenecarbaldehyde (12): Mp 125.5—126.5 °C (from ethanol) (lit,[28] mp 127 °C).

1-Diacetoxymethylpyrene (13): Mp 151—152 °C (from ethanol); IR 1761 (OAc); ^{1}H NMR δ=2.10 (6H, s, 2×OAc), 7.27—8.76 (9H, m, arom. H), and 9.21 (1H, s, -CH<); MS m/z (rel intensity), 332 (17, M^+), 230 (35), 201 (36), and 181 (100). Found: m/z 332.1048. Calcd for $C_{21}H_{16}O_4$: M, 332.1048.

Methyl Ester of 1-Pyrenecarboxylic Acid (14): Mp 100—101 °C (from ethanol) (lit,[29] mp 101—102 °C).

The structures for the benzaldehydes (**16b, c**) and the methyl esters of 9-anthracenecarboxylic acid (**10**) (lit,[30] mp 297—298 °C), benzoic acids (**17a, a', b, c**) were determined by the analyses of their IR and ^{1}H NMR spectral data.

Oxidation of 2,7-Dimethoxynaphthalene (1a) with Manganese(III) Acetate. A modified procedure of Aratani and Dewar[10] was used for the oxidation of **1a** with manganese(III) acetate. A mixture of **1a** (1 mmol) and manganese(III) acetate (4 mmol for Mn(III)) was heated under reflux for 13 min in acetic acid (25 cm^3). The solvent was removed in vacuo and the residue was triturated with 2 M HCl (30 cm^3). The aqueous solution was extracted with chloroform and the obtained products were purified on TLC to give 1-acetoxy-2,7-dimethoxynaphthalene (**18**, 25%) and 2,7-dimethoxy-1,4-naphthoquinone (**19**, 39%). These compounds have the same spectral properties as those in the literature.[10]

Oxidation of 2,7-Dimethoxynaphthalene (1a) with Manganese (III) Acetate in the Presence of Acetic Anhydride. A mixture of **1a** (1 mmol), manganese(III) acetate (4 mmol for Mn(III)), and acetic anhydride (40 mmol) was heated under reflux for 4 min in acetic acid (25 cm^3). The reaction mixture was treated with the method described above to yield 1-(acetoxymethyl)-2,7-dimethoxynaphthalene (**20**, 54%).[3]

Reaction of 2,7-Dimethoxynaphthalene (1a) with Manganese(III) Acetate in the Presence of Malonic Acide-d_4. A mixture of **1a** (1 mmol), malonic acid (4 mmol), and manganese(III) acetate (4 mmol for Mn(III)) was heated under reflux for 12 h in dry benzene (25 cm^3) instead of acetic acid. After the work-up, **2a** was obtained in a 23% yield. Then, a similar reaction was carried out in the presence of malonic acid-d_4 instead of malonic acid to afford a mixture of **2a** (12%) and 1-(formyl-d)-2,7-dimethoxynaphthalene (**21**, 12%).

Oxidation of Xanthene (22) with Manganese(III) Acetate in the Presence of Malonic Acid. To a heated solution of xanthene (**22**, 1 mmol) and malonic acid (4 mmol) in acetic acid (25 cm^3), manganese(III) acetate (4 mmol for Mn(III)) was added. The mixture was heated under reflux for 1 min. The solvent was removed off and the residue was treated with

2 M HCl (25 cm^3). The aqueous solution was extracted with chloroform, which was subsequently washed with aqueous sodium hydrogencarbonate solution. The aqueous solution was acidified with concentated hydrochloric acid and then extracted with ethyl acetate. The acidic products obtained was methylated with diazomethane in methanol. The neutral and esterified products were separated on TLC to give a dimethyl ester of 9-dicarboxymethylxanthene (**23**, 20%) and 9-xanthenone (**24**, 6%).

Dimethyl Ester of 23: IR 1735, 1755 (OAc); ^{1}H NMR δ=3.53 (6H, s, 2×OCH_3), 3.54 (1H, d, J=8.4 Hz, -CH<), 4.83 (1H, d, J=8.4 Hz, -CH<), 6.89—7.43 (8H, m, arom.H); MS m/z (rel intensity), 312 (8, M^+), 196 (33), 181 (98), 168 (29), 139 (20), and 82 (100). Found: m/z 312.0988. Calcd for $C_{18}H_{16}O_5$: M, 312.0997.

The authors wish to thank Associate Professor Akira Mori of the Research Institute of Industrial Science, Kyushu University, and Dr. Teruyoshi Marunaka of the Taiho Pharmaceutical Co., Ltd., Tokushima, for their arrangement for the measurements of the mass spectra. The present work was supported by a Grant-in-Aid for Encouragement of Young Scientists No. 62740301 from the Ministry of Education, Science and Culture (1987).

References

1) L. W. Hessel and C. Romers, *Recl. Trav. Chim. Pays-Bas*, **88**, 545 (1969).

2) R. A. Sheldon and J. K. Kochi, "Metal-Catalyzed Oxidations of Organic Compounds," Academic Press (1981), pp. 120—151; W. J. de Klein, "Reactions with Manganese(III) Acetate," in "Organic Syntheses by Oxidation with Metal Compounds," ed by W. J. Mijs and C. R. H. J. de Jonge, Plenum Press (1986), pp. 261—314.

3) E. I. Heiba, R. M. Dessau, and W. J. Koehl, Jr., *J. Am. Chem. Soc.*, **91**, 138 (1969).

4) K. Kurosawa and J. F. W. McOmie, *Bull. Chem. Soc. Jpn.*, **54**, 3877 (1981); K. Kurosawa, T. Takamura, Y. Ueno, J. F. W. McOmie, and N. D. Pearson, *ibid.*, **57**, 1914 (1984).

5) M. E. Kurz and T. R. Chen, *J. Org. Chem.*, **43**, 239 (1978).

6) N. Ito, H. Nishino, and K. Kurosawa, *Bull. Chem. Soc. Jpn.*, **56**, 3527 (1983).

7) W. E. Fristad and S. S. Hershberger, *J. Org. Chem.*, **50**, 1026 (1985).

8) H. Nishino and K. Kurosawa, *Bull. Chem. Soc. Jpn.*, **56**, 2847 (1983).

9) H. Nishino and K. Kurosawa, *Bull. Chem. Soc. Jpn.*, **56**, 474 (1983).

10) T. Aratani and M. J. S. Dewar, *J. Am. Chem. Soc.*, **88**, 5479 (1966).

11) H. Nishino, *Bull. Chem. Soc. Jpn.*, **59**, 1733 (1986).

12) S. A. Zonis, *Sbornik Statei Obshchei Khim.*, **2**, 1091 (1953); *Chem. Abstr.*, **49**, 5414 g (1955); P. J. Andrulis, Jr. and M. J. S. Dewar, *J. Am. Chem. Soc.*, **88**, 5483 (1966).

13) N. P. Buu-Hoi and D. Lavit, *J. Chem. Soc.*, **1955**, 2776.

14) S. Israelashvili, Y. Gottlieb, M. Imber, and A. Habas, *J. Org. Chem.*, **16**, 1519 (1951).

15) A. Rieche, H. Gross, and E. Höft, *Chem. Ber.*, **93**, 88 (1960).

16) N. P. Buu-Hoi and D. Lavit, *J. Org. Chem.*, **20**, 1191 (1955).

17) N. P. Buu-Hoi and D. Lavit, *J. Org. Chem.*, **21**, 1022 (1956).

18) N. P. Buu-Hoi and D. Lavit, *J. Org. Chem.*, **21**, 1257 (1956).

19) G. Lock and R. Schneider, *Chem. Ber.*, **91**, 1770 (1958).

20) F. M. Aslam, P. H. Gore, and M. Jehangir, *J. Chem. Soc., Perkin Trans. 1*, **1972**, 892.

21) M. J. S. Dewar and P. J. Grisdale, *J. Am. Chem. Soc.*, **84**, 3539 (1962).

22) R. C. Fuson and F. W. Wassmundt, *J. Am. Chem. Soc.*, **78**, 5409 (1956).

23) F. Mayer and A. Siegliz, *Ber.*, **55B**, 1835 (1922).

24) W. J. Mitchell, R. D. Topsom, and J. Vaughan, *J. Chem. Soc.*, **1962**, 2526.

25) C. C. Price and C. F. Huber, *J. Am. Chem. Soc.*, **64**, 2136 (1942).

26) R. Van Helden and E. C. Kooyman, *Recl. Trav. Chim. Pays-Bas*, **80**, 57 (1961).

27) L. E. Hinkel, E. E. Ayling, and J. H. Beynon, *J. Chem. Soc.*, **1936**, 339.

28) G. Saint-Ruf, N. P. Buu-Hoi, and P. Jacquignon, *J. Chem. Soc.*, **1958**, 48.

29) O. Neunhoeffer and H. Woggon, *Justus Liebigs Ann. Chem.*, **600**, 34 (1956).

30) H. Meerwein and A. Migge, *Ber.*, **62B**, 1046 (1929).

Study on Conjugated Redox Membranes Containing an Intercellular Component of Wool as an Electron Carrier

Yoshiharu NAKAMURA,* Noriaki KAMON, and Teruo HORI
Department of Applied Chemistry, Faculty of Engineering, Fukui University, Bunkyo 3-9-1, Fukui 910
(Received June 2, 1988)

To realize artificially such a conjugated redox reaction as that which is drived across the biological cell membrane, two enzymic redox reactions were conjugated across a hydrogel membrane prepared with urethane prepolymer holding stabilized isocyanate groups. As redox couples, glucose 6-phosphate (G6P)/glucose 6-phosphate dehydrogenase (G6PD)/gluconolactone 6-phosphate (GL6P) and glutathione oxidized form (GSSG)/glutathione reductase (GRD)/glutathione reduced form (GSH) were chosen together with their common coenzyme, $NADP^+$/NADPH. The driving of a system consisting of two redox couples separated with the hydrogel membrane containing the coenzyme $NADP^+$ was intiated by the reduction of $NADP^+$ on the membrane surface in contact with the G6PD/G6P solution. The conjugated redox reaction proceeded by electron exchange between coenzymes in the membrane and the reproducing of $NADP^+$, which was accompanied with the GRD/GSSG solution. The rate of electron transfer across the urethane membrane was markedly accelerated by incorporating a nonkeratinous intercellular cement compound extracted from wool into the membrane. From cyclic voltammograms of a methyl viologen mediator, using a bare electrode and an intercellular compound modified carbon electrode, it was confirmed that the intercellular component could surely act as a good electron carrier.

In a previous paper[1] it was shown that methylene blue (MB) can be reduced to its leuco-form in an aqueous bath containing untreated wool fibers. However, no reduction occurred in the presence of wool fibers lacking an intercuticular cement material (δ_L component) by extraction with formic acid. In order to clarify this phenomenon a model experiment was contrived using thioglycolic acid (TGA) as a simple model compound having an -SH group like wool. According to expectations, the decolorization rate of MB was accelerated markedly by the addition of the δ_L component, indicating that the reduction of MB by -SH groups of wool could be mediated by the δ_L component.

Such a consideration was also made by Koga et al.;[2] they had observed a reverse oxidation reaction of leuconaphthazarin to naphthazarin on wool fibers in an aqueous bath and explained it by considering the reduction of disulfide (-SS-) groups of wool mediated by the δ_L component.

These two experimental facts described above suggest such a possibility that the δ_L component can work as an electron carrier for a redox system.

On the other hand, in connection with cell membranes there were a number of redox systems across membrane models such as micelles,[3] bilayer membranes,[4] and liquid membranes.[5] Such redox systems are, however, not suitable for practical uses because of such disadvantages as leakage of carrier or solvents from these membranes. To overcome such disadvantages, Endo et al., have devised some new systems for electron transfer across a synthetic solid membrane with a covalently bound electron mediator[6-8] and demonstrated redox reactions across the membrane. However, in the above-mentioned investigations enzymes were not used at all, which surely participate for driving the redox in real biological cell membranes.

In this study, we purposed to construct a new conjugated redox membrane system in which dehydrogenase and reductase separately adhere to both sides of a positively-charged polyurethane membrane containing $NADP^+$/NADPH as an electron mediator, and to demonstrate the driving of a redox reaction across the membrane. The intended purpose of this investigation involved improving a hitherto known conjugated redox system,[9] in which both enzymes are mixed together with their substrates and, hence, both products are also obtained in the mixture. In addition, the effect of incorporating the δ_L component into the membrane on the driving rate was investigated. It is worth noting that the δ_L component extracted from wool can truly work as an electron carrier. Except for cytochrome C, this is a unique example regarding the use of a natural electron carrier, although a large number of synthetic ones have been used.[10]

Experimental

Materials. Glucose 6-phosphate dehydrogenase (from yeast) G6PD and glutathione reductase (from yeast) GRD, nicotinamide-adenine dinucleotide phosphate $NADP^+$ and its reduced form NADPH were purchased from Oriental Yeast Co., Ltd. Glutathione, oxidized form GSSG, its reduced form GSH and glucose 6-phosphate **G6P** were all obtained commercially (Sigma) and were not further purified. The other reagents were analytical grade and used without further purifications.

Membrane. The requisites of a membrane for a conjugated redox system are as follows: the membrane should be hydrophilic because of use in aqueous system, it is charged positively to hold the negative charged coenzyme $NADP^+$/NADPH in it, and the pore size in the swollen membrane should be so adequate as to permit the thermal motion of the δ_L component in the membrane so as to diminish the leakage of enzymes, substrates, and products through the membrane.

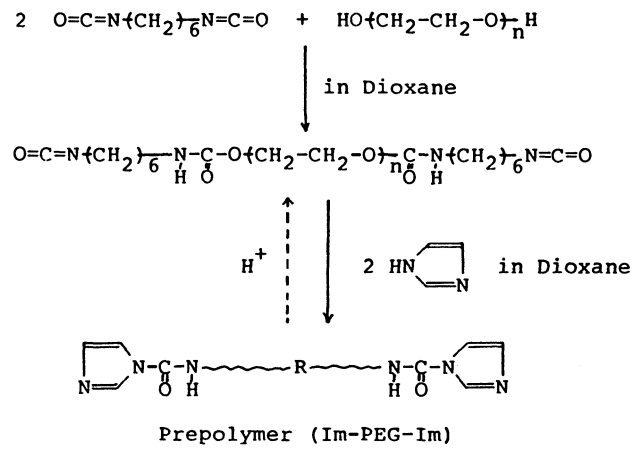

Scheme 1. Synthesis of urethane prepolymer.

For this purpose the recently developed method to prepare an enzyme-fixed hydrophilic urethane gel membrane[11] was modified to make the membrane at lower temperature. The preparation process of the prepolymer is shown in Scheme 1.

Polyethylene glycol (PEG) (#600, Nakarai Chemicals Co., Ltd.,) (46.7 g) and hexamethylene diisocyanate (HMDI) (Tokyo Chem. Ind. Co., Ltd.,) (26.2 g) were dissolved in dioxane and heated with stirring up to 80—90 °C. The reaction was continued until the amount of an isocyanate (-NCO) group in the reaction mixture was reduced to one-half its initial value to prevent any further reaction, allophanation. The -NCO content was determined by the Sigga-Hanna method.[12] To protect the end -NCO group of produced poly(oxyethylene) bis(6-isocyanatehexylcarbamate), it was reacted with 2 molar imidazole in dioxane at 40 °C for 24 h. The prepared prepolymer (Im-PEG-Im) was stable for at least 6 months under dry conditions. Considerably strong and thin hydrogel membranes could be prepared by casting the mixture of the prepolymer Im-PEG-Im and 20% excess of aqueous solution of diethylenetriamine (DETA 0.5 mol dm^{-3}) as a cross-linking agent on a glass plate framed by a circled silicone rubber at room temperature for 2 days. The membrane was immersed in water for 1 to 2 weeks to remove dioxane and released imidazole.

Electron Carrier. The extraction of the nonkeratinous δ_L component was carried out by the usual method, described by Bradbury et al.[13] The Cu^{2+} content in the δ_L component was determined to be 1.65 mmol g^{-1} by using the Bathocuproin method.[14] From the amino acid analysis it became clear that the δ_L contained a relatively large amount of histidine, compared with the other fractions of wool.[1]

The incorporation of the δ_L component into the membrane was carried out as follows: the δ_L component (10 mg) dissolved in an aqueous solution of DETA (0.5 mol dm^{-3}, 1 ml) was mixed with Im-PEG-Im (1 g); the mixture was then cast on a glass plate to form a membrane.

Measurements. Cyclic Voltammetry: In order to confirm that the δ_L component can act as an electron carrier, cyclic voltammetry was employed. A Yanaco Voltammetric Analyzer P-1000/Function Generator FG-121B was used with an X-Y recorder for cyclic voltammetry. The electrode assembly consisted of a carbon electrode GC-P2, Yanaco P_{010} (not-modified or δ_L-modified) as a working electrode, a sodium chloride saturated calomel electrode (SSCE) as a reference electrode and a platinum spiral as a counter electrode. 1.0-M $NaClO_4$ solutions (1 M=1 mol dm^{-3}) adjusted to pH 7.0 with 0.02-M phosphate buffer, was used as the supporting electrolytic solution. The δ_L modified carbon electrode was prepared by casting a formic acid solution of the δ_L component (10 mg/g) on the electrode surface and drying it in air. The concentration of MV was 0.25-mM. As a model of δ_L, a 1-mM aqueous solution of Cu^{2+}-histidine (mixture of $CuSO_4$ and aqueous histidine solution in a molar ratio of 1 : 10) was also measured using a bare carbon electrode as the working electrode.

Differential Pulse Polarograhy: The reaction kinetics was followed by measuring the concentration of GSH and GSSG in the reaction system by means of a differential pulse polarographic method (DPP method), which is based on the fact that the reduction peak for GSSG in the DPP chart is shifted to a larger negative potential upon adding $NADP^+$; however, that for GSH it is not shifted.[15] The instrument used was a Yanaco Voltammetric Analyzer P-1000 with a Watanabe X-Y recorder WX4401. A stock solution of 4-M $NaNO_3$ containing a 0.08-M phosphate buffer was mixed with a sample solution of GSSG, GSH or both mixture and NADPH in appropriate ratio; the solution was then transferred to an electrochemical cell. The differential pulse polarograms of the sample solutions were measured at the scan rate 5 mV s^{-1}. From the corresponding peaks the amounts of GSSG, GSH, and NADPH were determined.

Membrane Potential: The membrane potential was determined in a cell that consists of two compartments as shown previously.[16] The potential was measured by means of a Digital Multimeter TR6843 (Takeda Riken Co., Ltd.) with pin-hole type of Ag/AgCl/sat. KCl electrodes (Horiba Co., Ltd. #2010). The mean value of two measurements obtained by exchanging the electrodes in both compartments was taken as a reliable membrane potential. The concentration of the KCl solution was kept constant in one compartment at $1{,}0 \times 10^{-3}$ M and in the other compartment at 1.0×10^{-4} M. The temperature was controlled at 25±0.2 °C.

Driving of Conjugated Redox Reaction: A conjugated redox reaction was performed by using a two-compartment cell, as shown in Scheme 2. Both compartments **I** and **II** were filled with a 35.0 ml phosphate buffer solution of pH 7.8, an optimum pH for activating both enzymes. To support the driving of the conjugated reaction a coenzyme, NADPH or $NADP^+$ was added to compartment **I** and adsorbed in the membrane. At the same time, the diffusion flux $J_{NADP(H)}$ of NADP(H) through the membrane was measured. The NADP(H) concentration was determined spectrophotometrically (molar extinction: 6.20×10^3 l mol^{-1} cm^{-1} at 340 nm). After this measurement, the solutions were taken away and a 0.25-mM $NADP^+$ aqueous buffer solution was again freshly filled in both compartments and the 1 mmol

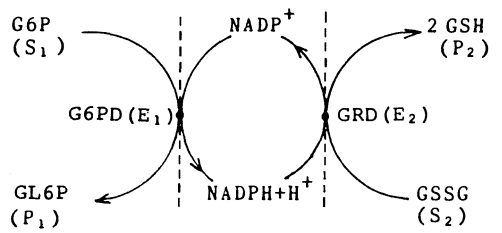

Scheme 2. A conjugated redox-enzyme system.

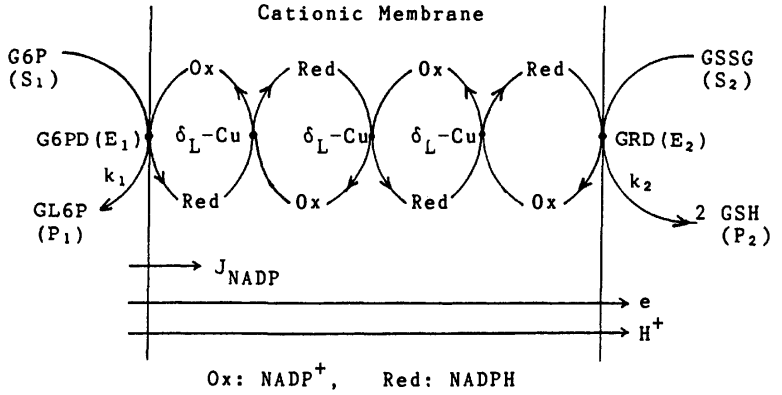

Scheme 3. Effect of δ_L-Cu as electron carrier on the conjugated redox system.

G6P and 0.6 mmol GSSG in compartments **I** and **II**, respectively. The reaction was started by adding 0.3 mg of G6PD to compartment **I** and 0.35 mg GRD to the compartment **II** at same time, respectively. The concentration change of GSSG and GSH in both compartments with time was followed by the method described above. Before the measurements it was confirmed that both the enzymes G6PD and GRD could not permeate through the membrane, perhaps because of their large molecular sizes and their high affinity against positively charged membranes.

The cyclic voltammetry, the differential pulse polarography and the conjugated redox reaction were performed in the O_2-free solutions.

Results and Discussion

Some characteristics of the membranes prepared are summarized in Table 1. Membrane Code 0 was prepared without the incorporation of the δ_L component, while Membrane Code δ was obtained by mixing the δ_L component. The thickness of these membranes was almost the same (ca. 120 μm). However, the pore sizes of the membranes were considerably different from each other: 0.22 and 0.12 μm for Membrane Code 01 and δ2, respectively. It is clear from the large negative membrane potential that both membranes were charged positively. This means that negative charges in the δ_L component, appearing at the adjusted pH of the test solution, could not overcome positive charge in the urethane membrane.

Figure 1 shows cyclic voltammograms of MV using (a) a bare carbon electrode and (b) a δ_L-modified carbon electrode. The electrode reaction proceeds as

Table 1. Properties of Prepared Urethane Membranes

Membrane code	Thickness	Pore size	Membrane potential
	μm	μm	mV
01	120	0.22	−54.8
02	148	0.18	−51.0
δ1	106	0.14	−52.6
δ2	123	0.12	−49.6

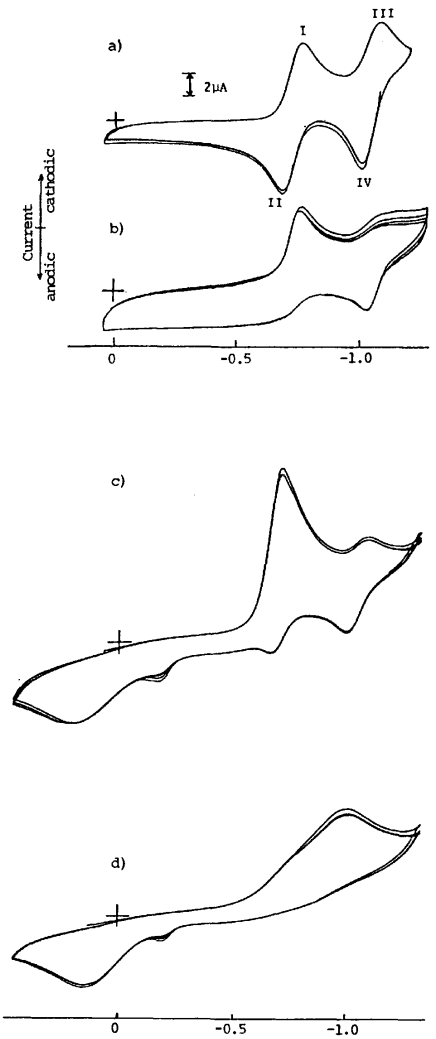

Fig. 1. Cyclic voltammograms of methyl viologen, supporting electrolyte: 1 M $NaClO_4$, pH 7.0 (0.02 M phosphate buffer), sweep rate: 150 mV s^{-1}.
a) Bare carbon electrode, 0.25 mM MV. b) carbon electrode modified with δ_L, 0.25 mM MV. c) Bare carbon electrode, 0.2 mM MV+0.8 mM Cu^{2+}-histidine*. d) Bare carbon electrode, 1 mM Cu^{2+}-histidine*. * molar ratio, Cu^{2+}: histidine=1:10.

follows:[17,18]

$$MV^{2+} + e \underset{II}{\overset{I}{\rightleftharpoons}} MV^{+\cdot} \quad (1)$$

$$MV^{+\cdot} + e \underset{IV}{\overset{III}{\rightleftharpoons}} MV^{\circ} \quad (2)$$

The numbers in **I—IV** correspond to those on the peaks of the curves in Fig. 1. The second reduction peak and the second oxidation peak were found to be smaller for the electrode (a), probably because the $MV^{+\cdot}$ produced in the first reduction step could be consumed by Cu^{2+} ions contained in the δ_L component. This could be confirmed from the fact that the same decrease in the peaks of CV was observed for a measurement of an aqueous MV solution containing a Cu^{2+}-histidine complex (Fig. 1c).

A typical feature of the conjugated redox reaction is shown in Fig. 2 for the case of a membrane containing δ_L. In this figure the concentrations of GSSG and GSH in components II are plotted against time. From the fact that the concentration of GSSG decreased and that of GSH increased after elapsed time, and the latter approached nearly double the initial concentration of GSSG, it is suggested that the recycle reaction between $NADP^+$ and NADPH occurs in the membrane, even if only small amounts of $NADP^+$ or NADPH (much fewer than one equibalent of the substrate) were added to the system. It should be noted that two GSH molecules are produced from one GSSG molecule. In this figure, the total concentration of glutathione in GSSG-form in both compartments was also plotted. This concentration decreases after a certain time, increases again and approaches a constant value equal to the initial concentration. This could be considered to be caused by the interaction of GSSG with the coenzyme adhering in the membrane (the interaction of GSSG with $NADP^+$ observed in DPP measurement).

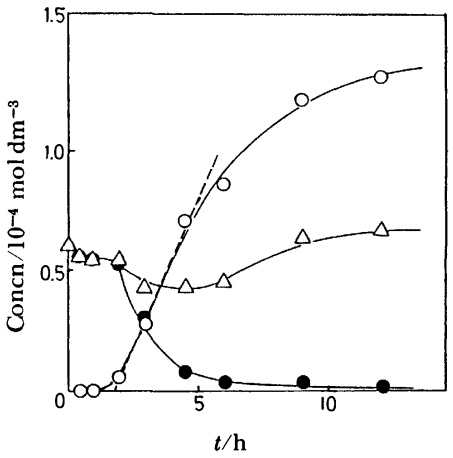

Fig. 2. Reduction of GSSG(●) and production of GSH(○) in compartment II in a conjugated redox reaction across the membrane containing δ_L component.
Membrane thickness; 90 mm(sustained Cu-treatment). △ shows the sum of GSSG and GSH (reduced to GSSG form).

For cases of membranes without δ_L, similar results were obtained, except that the concentration change of GSSG and GSH were much slower. The maximum production rate of GSH and the permeation time-lag were obtained from the slope and the intercept on the time-axis of the asymptote of the GSH-production curve (see Fig. 2), respectively. The effect of the electron carrier was estimated using the electron-transfer efficiency (ETE value),

$$ETE = J_{NADP(H)\leftarrow GSH} / J_{NADP(H)}, \quad (3)$$

where $J_{NADP(H)\leftarrow GSH}$ is an imaginary diffusion flux of NADP(H) reduced under the assumption that the production of GSH proceeds stoichiometrically according to the amount of NADPH diffused out through the membrane ($GSSG+NADPH+H^+ \rightarrow 2\ GSH+NADP^+$).

Kinetic data on the driving of the conjugated redox reaction through the membrane under various conditions are summarized in Table 2. Experiments No. 1 to 3 were made using membranes without the electron carrier δ_L component. No. 1 was driven without a prepermeation of the coenzyme, while Nos. 2 and 3 were driven after prepermeations of $NADP^+$ and NADPH, respectively. All of the values, d[GSH]/dt,

Table 2. Kinetic Data on the Driving of Conjugated Redox Reaction through the Urethane Membrane

Exp. No.	Membrane code	$J_{NADP(H)}\times10^{11}$ mol cm^{-2}s^{-1}	d(GSH)/d$t\times10^5$ mol l^{-1}s^{-1}	Time-lag h	$J_{NADP\leftarrow GSH}\times10^{11}$ mol cm^{-2}s^{-1}	Substrate conversion ratio (%)	ETE-value (ETE)[a]
1	01		3.10	2.5	2.76	90	1.6 (2.0)
2	01_{NADP^+}	1.75	6.20	2.0	5.68	94	3.2 (4.2)
3	01_{NADPH}	(1.36)	6.85	2.0	6.26	95	3.6 (4.6)
4	$\delta2_{NADP^+}$	0.613	2.55	4.5	2.33	37	3.8
5	$\delta2_{CudNADP^+}$	0.592	0.00	0.0	—	0	0.0
6	$\delta2_{Cu\ NADP^+}$	0.166	64.1	4.5	58.7	78	353

a) Calculated by using J_{NADPH}.

time-lag, $J_{NADP(H)\leftarrow GSH}$ and ETE-values were found to be almost same for both experiments. Of interest is the fact that the ETE-value is larger than 1. This means that the production of GSH in component II does not proceed based only on a simple diffusion of NADPH. Considering the fact that the time-lag of No. 3, in which NADPH was prepermeated, was not shorter than that of No. 2, an ETE-value larger than 1 can be explained considering either: that the electron exchange in the membrane took place between $NADP^+$ and NADPH, if they are ordered side by side in the membrane; or that not only the substrate, but the enzyme also could be condensed in the membrane because of the positive charge of the membrane. The latter should be meaningless, considering the following additional experiment: i.e. GSH was produced only in the compartment in contact with the membrane surface, on which GRD was previously adsorbed, when GSSG and NADPH were added to both compartments.

Of special interest are the results of experiments Nos. 4, 5, and 6 in the driving through the membrane entrapping the δ_L component. In these cases, the diffusion flux of $NADP^+$ is rather smaller and the time-lag are larger, compared with those in the cases of membranes without the δ_L component, perhaps because of a slightly smaller pore size, owing to the incorporation of the δ_L component in the membrane.

Experiment No. 5 was carried out by using the δ_L incorporated membrane after it was dipped in an aqueous $CuSO_4$ solution (1.6×10^{-6} mol dm^{-3}) for 24 h and slightly rinsed. In this case, GSH was not produced. An additional experiment showed that free copper ions inhibit the enzymic reaction in this system. Thus, the membrane was rinsed in water for 1 week and then used for driving experiment No. 5. A very interesting result was obtained wherein the rate of GSH-production was much larger, compared with those through the other membrane, although the diffusion flux J_{NADP} was considerably lower (1.6×10^{-12} mol cm^{-2} s^{-1}). Consequently, the ETE-value went up to over 300. In the case of the δ_L-incorporated membrane, the association of the substrates and coenzyme in the membrane could also be one of the causes of the extremely high ETE-value, though it does not seem likely considering the relatively small intake of coenzyme, and the considerably large time-lag. Therefore, it can be concluded that the large ETE-value for experiment No. 6 is achieved by the aid of the membrane-incorporated δ_L component catalyzing the electron-transfer reaction between the coenzymes. This consideration is shown schematically in Scheme 3. It is presumed that the electron can be transferred advantageously through the coenzymes probably adsorbed on the δ_L-component, a complex of Cu^{2+} with basic amino residues of polypeptides. However, further details of this electron-transfer mechanism have not yet been clarified.

Conclusion

Modeled on a biological cell membrane, an artificial conjugated redox membrane was constructed which incorporated dehydrogenase and reductase separately on both membrane surfaces. The conjugated redox reaction across the membrane was successfully demonstrated. The driving of redox reactions owes much to electron exchanges between $NADP^+$ and NADPH in the membrane. The electron-transfer efficiency (ETE value) could be improved by two orders of magnitude by incorporating the δ_L component extracted from wool fibers, compared with the fact that the ETE value was changed with the Cu^{2+} content in the δ_L component. The Cu^{2+} complex ions were regarded as being a cooperator for the electron transfer: they accelerate the electron-exchange reaction between coenzymes in the membrane.

The authors wish to express their hearty thanks to Professor Mitsugi Senda of the Kyoto University for valuable advice regarding CV measurements and to Associate Professor Shigeru Kunugi of Fukui University for useful discussions. Thanks are also due to Mrs. Yoshitaka Saito, Toshie Kobayashi, and Tomohiko Sugawara for their assistance in the experimental work.

The present work was supported by a Grant-in-Aid for Scientific Research No. 61550655 from the Ministry of Education, Science and Culture.

A part of this study was presented in the 3rd Membrane Symposium held by the Society of Fiber Science and Technology, Japan in 1987.

References

1) N. Nakamura, K. Kosaka, T. Tada, K. Hirota, and S. Kunugi, Proc. 7th Int.Wool Text. Res. Conf., Tokyo, **1**, 171 (1985).

2) J. Koga and T. Shibano, *Proc. Ann. Meeting Soc. Fiber Sci. Tech., Jpn.*, p. 193 (1987).

3) I. Tabushi and M. Funakura, *J. Am. Chem. Soc.*, **98**, 4684 (1976).

4) J. J. Gremalde, S. Boileau, and J. M. Lehn, *Nature (London)*, **256**, 229 (1977); K. Takuma, T. Sakamoto, and T. Matsuo, *Chem. Lett.*, **1981**, 815.

5) T. Sugimoto, J. Miyazaki, T. Kokubo, S. Tanimoto, M. Okano, and M. Matsumoto, *Tetrahedron Lett.*, **22**, 373 (1981).

6) Y. Nambu, T. Endo, and K. Tashiro, *J. Polym. Sci., Polym. Chem. Ed.*, **23**, 223 (1985).

7) Y. Nambu, T. Endo, and K. Tashiro, *J. Polym. Sci., Polym. Chem. Ed.*, **23**, 409 (1985).

8) Y. Ishikawa, Y. Nambu, and T. Endo, *J. Polym. Sci., Polym Chem. Ed.*, in press.

9) T. M. S. Chang, and C. Malouf, *Trans. Am. Soc. Artif. Int. Organs*, **24**, 18 (1978).

10) T. Osaka and N. Oyama, *Membrane*, **11**, 261 (1986).

11) S. Kunugi, Y. Morikawa, I. Ishida, and Y. Nadamura, *Polym. J.*, **19**, 269 (1987).

12) S. Sigga and J. G. Hanna, *Anal. Chem.*, **20**, 108 (1948).
13) J. H. Bradbury, J. D. Leeder, and I. C. Watt, *Appl. Polym. Symp.*, **18**, 227 (1971); D. E. Peters and J. H. Bradbury, *J. Biol. Sci.*, **29**, 43 (1976).
14) B. Zak and N. Resser, *Anal. Chem.*, **28**, 1158 (1956).
15) Y. Nakamura and Y. Saito, *Review of Polarography*, **32**, 68 (1986).
16) Y. Kimura and T. Iijima, *J. Membrane Sci.*, **18**, 285 (1984), Y. Nakamura, I. Tabata, and T. Hori, *Memor. of the Faculty of Eng., Fukui Univ.*, **36**, 183 (1988).
17) P. M. Allen and W. R. Bowen, *Trends in Biotech.*, **3**, 145 (1985).
18) N. S. Lewis and M. S. Wrighton, *Science*, **211**, 944 (1981).

 © 1989 The Chemical Society of Japan Bull. Chem. Soc. Jpn., 62, 557—562 (1989)

The Desulfurization of Polynuclear Aromatic Sulfur Compounds with a Raney Nickel

Masatoshi NAGAI,* Hideo URIMOTO,†,†† Kazuya UETAKE,†
Noriyuki SAKIKAWA,† and Richard D. GONZALEZ†††
Department of Chemical Engineering, Tokyo University of Agriculture and Technology, Koganei, Tokyo 184
†Department of Industrial Chemistry, Nihon University, Chiyoda-ku, Tokyo 101
†††Department of Chemical Engineering, University of Illinois at Chicago, Chicago, Illinois 60680, U.S.A.
(Received July 16, 1988)

The mechanism of the desulfurization of the polynuclear thiophene compounds with a Raney nickel was studied in ethanol at atmospheric pressure and from 0 to 78.3 °C. The desulfurization rate was initially fast but reached zero in about 30 minutes. The major products were biphenyl in the desulfurization of dibenzothiophene (**1**), 1-phenylnaphthalene in the desulfurization of benzo[*b*]naphtho[1,2-*d*]thiophene (**2**), and 2-phenylnaphthalene in the reaction of benzo[*b*]naphtho[2,3-*d*]thiophene (**3**) and benzo[*b*]naphtho[2,1-*d*]thiophene (**4**). The desulfurization extent for the four compounds decreased in this sequence: **3**>**1**>**2**>**4**. The extent of the desulfurization of the polynuclear thiophene compound was not related to the reaction indices, Fr(E), Fr(N), and Fr(R), of the sulfur atom of the compounds, which were calculated by using a simple Hückel theory; rather, it was related to both the free valence and the π-electron density. Therefore, the polynuclear thiophene compounds were considered to adsorb on a Raney nickel through the free-electron pair of the sulfur atom; consequently, the adsorption led to the C-S bond scission.

The hydrodesulfurization of heavy petroleum feedstocks and coal-derived liquids requires the conversion of high-molecular-weight compounds like dibenzothiophene and benzonaphthothiophenes.[1,2] There are several studies in the literature which deal with the mechanism of the hydrodesulfurization of polynuclear thiophene compounds on cobalt or nickel molybdenum catalysts at high pressures and high temperatures.[3-5] However, there are only a few studies which relate the chemical reactivity of polynuclear thiophene compounds to their electronic structure,[6] although the adsorption and hydrodesulfurization of simple sulfur compounds, e.g., thiophene, have been studied recently using Hückel theory.[7,8]

There is competition between the different processes (hydrogenation and desulfurization) during the reaction. The hydrodesulfurization occurs through the extrusion of a sulfur atom to give the corresponding hydrocarbon, with some hydrogenation of the aromatic ring occurring either prior to or following the removal of the sulfur. It is difficult to understand the relationship between desulfurization and the electronic properties of the compounds under reaction conditions. However, a Raney nickel extrudes a sulfur atom from the molecule to form hydrocarbons without hydrogenation at a low temperature in a solvent. In the present investigation, the desulfurization studies are performed in a batch reactor over a Raney nickel. The sulfur compounds used here are dibenzothiophene, benzo[*b*]naphtho[1,2-*d*]thiophene, benzo[*b*]naphtho[2,3-*d*]thiophene, and benzo[*b*]naphtho[2,1-*d*]thiophene (Fig. 1). The dependence of the desulfurization extent on the electronic structure of the compounds was considered using simple Hückel molecular orbital calculations. The mechanism of the adsorption and desulfurization of benzonaphthothiophenes and dibenzothiophene is also discussed.

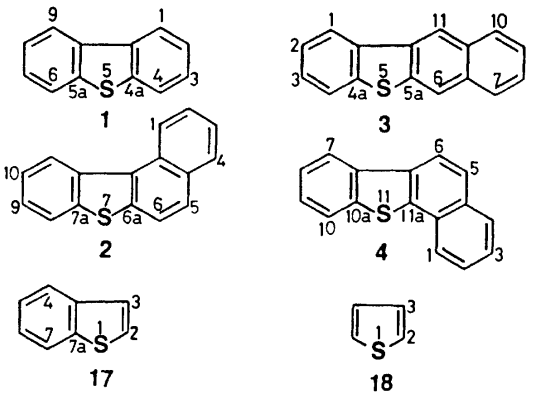

Fig. 1. Various thiophene compounds.

Experimental

Raney Nickel. The procedure was similar to that used in the preparation of W-7 Raney nickel described by Adkins et al.[9] A solution of 100 g of sodium hydroxide in 500 ml of H_2O at 50 °C was carefully added to 100 g of the Raney nickel alloy (41% Ni; Koso Chemical Co.). The addition was completed in approximately four and a half hours. The residue was washed by decantation with water and then by stirring with three successive portions of ethanol. The procedure was repeated three times using equal amounts of diethyl ether. The Raney nickel was used after it had then been stored in diethyl ether at 0 °C for more than one month.

Reactants. Dibenzothiophene (1): Compound **1** was synthesized according to the method of Gilman and Jacoby.[10] Mp 100.5—101 °C (lit, 99 °C[10])); Found: C, 78.29; H, 4.40; S, 17.31%. (Calcd: C, 78.22; H, 4.38; S, 17.40%).

Benzo[*b*]naphtho[1,2-*d*]thiophene (2): **2** was synthesized by dehydrogenating 5,6-dihydrobenzo[*b*]naphtho[1,2-*d*]-

†† Present address: Fukube Pharmaceutical Co., Ohatano, Kanagawa 257.

thiophene (**8**) in the presence of a Pd-C catalyst by the method of Campaigne and Osborn.[11] Compound **8** was obtained by the cyclization of 2-phenylthio-1-tetralone (**9**) in the presence of phosphorus pentaoxide. Compound **9** was prepared by reacting thiophenol with 2-bromo-1-tetralone. Mp 100.5—102 °C (lit, 102—102.5 °C,[10] 101.5—102 °C[11]); Found: C, 82.17; H 4.39% (Calcd: C, 82.01; H, 4.30%).

Benzo[*b*]naphtho[2,3-*d*]thiophene (3): **3** was synthesized in five stages from **1** and succinic anhydride as the starting compounds. Using 4-(dibenzothiophen-2-yl)-4-oxobutanoic acid, prepared by the Friedel Craft's reaction from the two starting compounds,[10] 4-(dibenzothiophen-2-yl)butanoic acid (**10**) was synthesized by the Huang-Minlon modification of the Wolff-Kishner reduction.[11] 9,10-dihydrobenzo[*b*]-naphtho[2,3-*d*]thiophen-7(8*H*)one (**11**) was synthesized by the cyclization of **10**.[12] Compound **3** was prepared by the dehydrogenation of the tetrahydrobenzo[*b*]naphtho[2,3-*d*]thiophene (**12**) with amorphous selenium. Compound **12** was synthesized by the reduction of **11** using the Wolff-Kishner procedure by the method of Campaigne and Osborn.[11] Mp 158.5—160 °C (lit, 160.5—161 °C,[11] 159—160 °C[13]).

Benzo[*b*]naphtho[2,1-*d*]thiophene (4): **4** was synthesized by a three stage reaction using 2-bromocyclohexanone (**13**) and 1-naphthalenethiol (**14**) as the starting compounds, while 2-(1-naphtylthio)cyclohexanone (**15**) was prepared by condensing **13** and **14**, which had been synthesized according to the method of Rabindran and Tilak.[12] Compound **4** was synthesized by the dehydrogenation of 7,8,9,10-tetrahydrobenzo[*b*]naphtho[2,1-*d*]thiophene (**16**) using amorphous selenium powder.[12] **16** was prepared by heating a mixture of **15** and phosphorus pentaoxide.[9] Mp 184—185 °C (lit, 182—184 °C,[11] 184—185 °C,[12] 186—187 °C[13]).

Apparatus and Procedure. Ten ml of abs. ethanol was placed in a pear-shaped flask equipped with a thermometer, a Dimroth condenser, and an electric stirrer. The Raney nickel (ca. 0.2 g) was weighted into the flask. An amount of the sample (0.2—1.47 mmol) was added to a certain solvent with the Raney nickel. The flask was then immediately placed in a glycerol bath at room temperature. After the solution had quickly been raised to the desired temperature, the stirrer was started and the initiation time was recorded. After the reaction, the flask was removed from the glycerol bath and cooled to room temperature. The catalyst was removed by filtration and washed with ethanol. The reaction mixture was then concentrated by evaporation to remove the solvent.

Analysis. The reaction products were analyzed by the use of conventional gas chromatography (Column packing: Apiezon Greese 20% Chromosorb W or Silicone OV-17 5% Uniport HP), using acenaphthene as the internal standard. The reaction products were identified by comparing the retention times with those obtained for known samples. No H_2S was observed during the reaction. Hydrogen sulfide was not trapped as zinc sulfide when an aqueous solution of zinc acetate was used for trapping. The extent of desulfurization, R, (mmol/g-Raney nickel), was calculated by the use of the following equation: $R=(A_0-A)/W$. A_0 is the initial number of moles of the reactant, while A is the number of moles of the reactant which have not reacted. W is the weight of the Raney nickel.

The simple Hückel theory (NEC microcomputer, Model PC-9801VM2) was used to calculate the π-electron density of a sulfur atom in addition to such other reaction indices as the π-bond order, free valence, and Fr(E), Fr(N), and Fr(R) introduced from the highest occupied, lowest unfilled, and singly occupied orbital (HOMO, LUMO, and SOMO) coefficients. In addition, benzothiophene (**17**) and thiophene (**18**) were studied in order to compare their behavior with that of the above compounds.

Results

Desulfurization of Dibenzothiophene. The extent of the desulfurization of dibenzothiophene with the Raney nickel in the ethanol solvent is shown in Fig. 2. Biphenyl was the principal product, with other compounds being formed only in trace amounts. The rate of desulfurization was fast initially, but reached zero in each case following a reaction time of about 30 minutes. This observation suggested that the activity of the Raney nickel was extremely high initially and that it then gradually diminished with the reaction. Therefore, for the time being, we shall assume that the desulfurization activity of the Raney nickel can be estimated by means of the initial rate of the desulfurization, v_0, at the starting time. The initial rates are 2.1, 1.5, 1.2, and 0.23 mmol/g-cat·h at 78.3, 48.8, 20.0, and 0 °C respectively.

A plot of log v_0 vs. $1/T$ gives an activation energy of 18.4 kJ mol^{-1} for the desulfurization of dibenzothiophene. This result is in good agreement with those obtained by Bartsch and Tanilian,[14] who studied the hydrodesulfurization of benzothiophene and dibenzothiophene, in dodecane as a solvent, over a sulfided $CoMo/Al_2O_3$ catalyst under atmospheric pressure and at 300—400 °C. These authors reported activation energies of 20.5 (for benzothiophene) and 22.5 kJ mol^{-1} (for dibenzothiophene). Moreover, a value of 15.5 kJ mol^{-1} was observed by Satterfield and Robert[15] for the

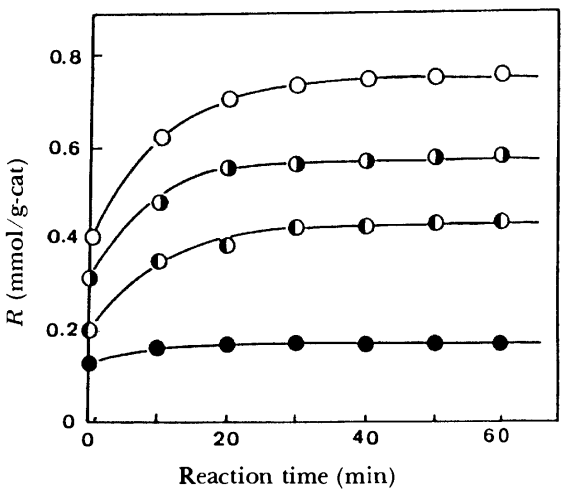

Fig. 2. The extent of desulfurization of dibenzothiophene with the Raney nickel in the ethanol solvent. The initial amount of the sample was 0.294 mmol and the catalyst weight was 0.2 g, ○: 78.3; ◑: 48.8; ◐: 20.0; ●: 0 °C.

hydrodesulfurization of thiophene over a sulfided $CoMo/Al_2O_3$ catalyst at 234—265 °C and at atmospheric pressure using a continuous-flow, stirred-tank reactor. On the other hand, in a previous gas phase study carried out in a fixed-bed microreactor,[16] an activation energy of 102 kJ mol^{-1} for the hydrodesulfurization of dibenzothiophene over a sulfided $NiMo/Al_2O_3$ catalyst was obtained. This is significantly higher than the 18.4 kJ mol^{-1} reported in the present study, which was performed in ethanol at low temperatures. These different results appear to be attributable to differences in the diffusion limitation for reactions carried out in the gas phase as opposed to the liquid phase.

The Initial Rate vs. the Extent of Desulfurization at 60 min. The Raney nickel initially exhibited a very high activity with dibenzothiophene, even though the reaction occurred before the reaction temperature reached the desired temperature. It is difficult to measure accurately the high initial rate of dibenzothiophene in the solvent of hydrocarbons, and there is a poor reproducibility in estimating the values of the desulfurization of benzonaphthothiophenes in small amounts. The Raney nickel gradually became less active during the reaction, though the extent of desulfurization was constant 60 min after the reaction had started. The extent of desulfurization at 60 min showed the total activity of the Raney nickel over the reaction time. Figure 3 shows that the extent of desulfurization at 60 min was proportional to the initial rate of desulfurization. Therefore, the extent of desulfurization at 60 min will be applied to further measurements of the desulfurization of dibenzothiophene and benzonaphthothiophenes with the Raney nickel.

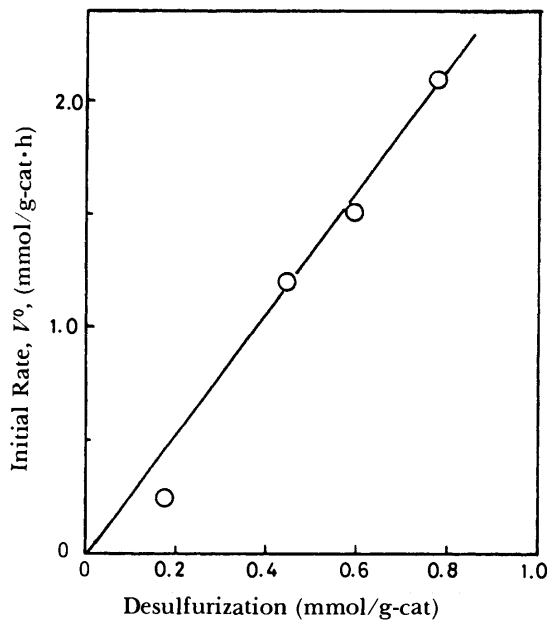

Fig. 3. The extent of desulfurization of dibenzothiophene at 60 min was proportional to the initial rate of desulfurization at 78.3 °C.

Effects of Solvents on the Desulfurization of Dibenzothiophene. The effects of the solvents on the desulfurization of dibenzothiophene by the Raney nickel at 78.3 °C for 60 min are shown in Table 1. The solvents exhibited a strong effect on the desulfurization activity of the Raney nickel. A high extent of desulfurization was observed when nonpolar solvents such as benzene or xylenes were used as solvents. This observation suggests that the nonpolar solvent blocks the Raney-nickel surface to a smaller extent than do other solvents. On the other hand, protic solvents, such as acetic acid and formic acid, depress the desulfurization. The extent of the desulfurization of dibenzothiophene in the presence of formic acid, acetic acid, and ethanol decreases with a decrease in the Y values of formic acid (Y value, +2.05), acetic acid (−1.64), and ethanol (−2.03). Since the Y value represents the ability of ionization of a solvent to the Raney nickel,[17] the protic solvents appear to decrease the activity of the Raney nickel because of the ionization of the nickel atom of the Raney nickel. Furthermore, formic acid poisons the surface of the Raney nickel by its carbonyl group.

Raney nickel contains hydrogen.[18,19,20] The carbon-sulfur bond of dibenzothiophene is split, and biphenyl formation occurs after the hydrogen has been used up. The solvent also reacted with this hydrogen of the Raney nickel. Methyl ethyl ketone was hydrogenated by the hydrogen. Therefore, the desulfurization of dibenzothiophene on the Raney nickel was depressed by the solvents because of the decrease in the amount of hydrogen in the Raney nickel, as well as because of the poisoning effect of the solvents and because of the ionization of the nickel atom of the Raney nickel.

Reactivity of Dibenzothiophene and Benzonaphthothiophenes. The desulfurization of dibenzothiophene and benzonaphthothiophenes over a Raney nickel in the ethanol solvent was performed at 78.3 °C for a period of 60 min. The major products (biphenyl **5** in the desulfurization of **1**, 1-phenylnaphthalene (**6**) in the desulfurization of **2**, and 2-phenylnaphthalene (**7**)

Table 1. Influence of Solvents on the Desulfurization of Dibenzothiophene

Solvent	R mmol/g-Raney nickel
Methyl ethyl ketone	0.44
Acetic acid	0.23
Formic acid	0.07
Ethanol	0.78
Benzene	1.27
Toluene	0.76
o-Xylene	1.01
m-Xylene	0.97
p-Xylene	0.80

Reaction time, 60 min; reaction temperature, 78.3°C; solvent volume: 10 ml.

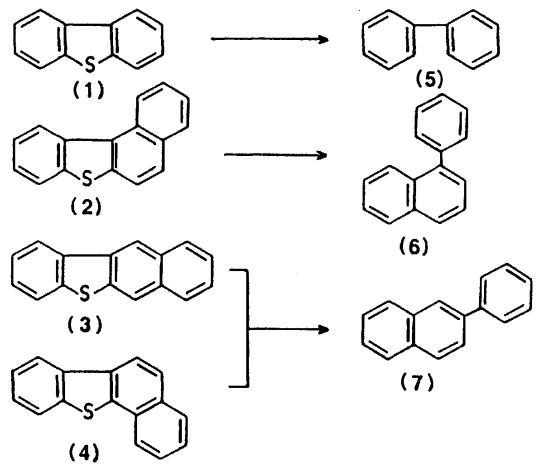

Fig. 4. The desulfurized compounds from the desulfurization of dibenzothiophene and benzonaphthothiophenes.

Table 2. The Desulfurization of the Four Compounds with a Raney Nickel at 78.3°C for 60 min

Compound	1	2	3	4
R (mmol/g-Raney nickel)	0.78	0.63	0.86	0.58

Initial mole of the sample, 0.2 mmol; weight of the Raney nickel, 0.2 g.

in the desulfurization of **3** and **4**) are shown in Fig. 4. Observation of these products shows that the reaction occurs through the extrusion of a sulfur atom to give the corresponding hydrocarbon, without any hydrogenation of the aromatic ring occurring either prior to or following the removal of sulfur. This indicates that the perpendicular adsorption of these compounds to the nickel atom is preferred during the reaction.

The results of the desulfurization of the four compounds with the Raney nickel in the ethanol solvent at 78.3 °C for 60 min are shown in Table 2. The extent of desulfurization for the four compounds decreased in this sequence: **3>1>2>4**. These results show that the tricyclic thiophene compound is not always more reactive than the tetracyclic compounds, since the reactivity of dibenzothiophene is lower than that of compound **3**. This last result is consistent with that obtained by Sapre et al.,[3] who found **3** more reactive than **1** on a sulfided $CoMo/Al_2O_3$ catalyst. This suggests that the reactivity of polynuclear thiophene compounds is not governed solely by the size of the molecule, but also by other elements which are related to the molecular structure.

Electronic-Structure Calculations. Parameters appropriate for the thiophene molecule are given in review articles by Zahradník[21,22] and Zdražil et al.[23] In this parameterization, $\alpha(S)=\alpha(C)+\beta(CC)$, $\alpha(C_\alpha)=\alpha(C)+0.1\beta(CC)$, and $\alpha(C_\alpha S)=0.8\beta(CC)$. Duben[24] studied thiophene using the simple Hückel molecular theory. He reported that, after a few trials had been made with other parameters, the only differences noted

Table 3. π-Electron Density and π-Bond Order of the Thiophene Compounds as Determined by a Simple Hückel Molecular Orbital Theory

Compound	q_s[a]	q_s-q_c[b]	πBond order of C-C bond	π-Bond order of C-S bond
			(2-3)	(4a-5) (5-5a)
3	1.732	0.685	0.597	0.384 0.384
			(4-4a)	(4a-5)
1	1.722	0.677	0.614	0.393
			(9-10)	(7a-7) (7-6a)
2	1.706	0.645	0.632	0.402 0.405
			(5-6)	(10a-11) (11-11a)
4	1.697	0.637	0.747	0.400 0.420
			(2-3)	(7a-1) (1-2)
17	1.663	0.543	0.755	0.421 0.472
			(2-3)	(1-2)
18	1.599	0.501	0.794	0.508

a) The π-electron density of the sulfur atom in the compounds. b) The difference between the π-electron density of the sulfur atom and the highest π-electron density of the carbon atom in the compounds.

Table 4. The Reaction Indices

Compound	1	2	3	4
Fr(E)[a]	0.372	0.660	0.110	0.315
Fr(N)[b]	0.000	0.047	0.068	0.083
Fr(R)[c]	0.186	0.354	0.089	0.199

a) $2(C_{HOMO,S})^2$. b) $2(C_{LUMO,S})^2$. c) $(C_{HOMO,S})^2+(C_{LUMO,S})^2$.

were some small changes in the orbital coefficients. For this reason, it was decided that the parameters specified in Zahradinik's article[21] could be used. Using these parameters, the Hückel molecular orbitals of polynuclear thiophenic compounds which are not adsorbed on the catalyst surface were calculated. The π-electron density of the sulfur atom and the π-bond order of the C-S bond are shown in Table 3, while the reaction indices, Fr(E), Fr(N), and Fr(R), of the sulfur atoms are presented in Table 4. Fr(E), Fr(N), and Fr(R) represent the ease of electrophilic, nucleophilic, and radical reactions at the sulfur atom of the compounds respectively. The π-electron density of the four compounds decreased in the following order: **3>1>2>4**. This order is in agreement with that of the desulfurization, but not with those of the reaction indices, Fr(E), Fr(N), and Fr(R).

Discussion

Relation between Desulfurization and Electron Structure. It was shown that the extents of desulfurization of the four compounds in ethanol at 78.3 °C for 60 min were 0.86, 0.78, 0.63, and 0.58 mmol/g-Raney nickel respectively. The correlation between the π-electron density of the sulfur atom of the polynuclear thiophene compounds and the extent of desulfurization is shown in Fig. 5. These data demonstrate that the desulfurization extent is proportional to the π-electron density of the sulfur atom. It appears, there-

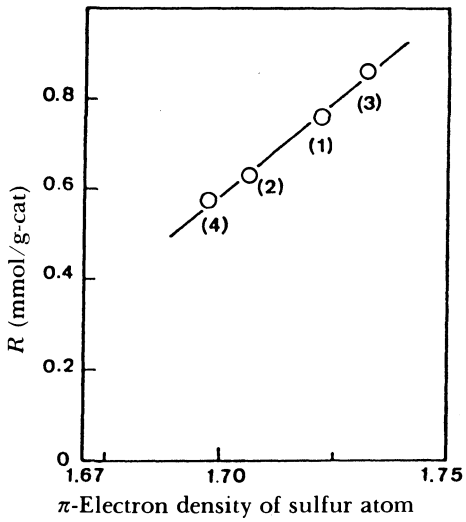

Fig. 5. Relationship between the extent of desulfurization of the polynuclear sulfur compounds and the π-electron density of their sulfur atom. The initial amount of sample was 0.2 mmol and the weight of the Raney nickel was 0.2 g.

fore, that the desulfurization which occurs on a Raney nickel depends on the π-electron density of the sulfur atom. This, in turn, is related to the strength of the adsorption of sulfur to a surface nickel atom of the Raney nickel. Hauptmann and Wladislaw[25] have also reported that the desulfurization was responsible for the first step of the reaction, that is, the adsorption of the organic compound on the metallic surface. This interaction with the Raney nickel is accomplished through the free-electron pair of sulfur. The sulfur can then readily split off from the ring without saturation occurring.

4 might be expected to exist a steric hindrance on the desulfurization, since it has the benzene ring in the compound on the side of the sulfur atom. Table 3 shows, however, that the π-bond order of C_{11a}-S_{11} of **4** is greater than that of C_{10a}-S_{11} of **4** which is similar to that of C_{7a}-S_7 of **2** and that, therefore, **4** is more easily desulfurized than expected, even though it has a steric hindrance. Thus, the preferential fission of the C-S bond can offset the effect of steric hindrance. Therefore, the interaction of the π electrons of the sulfur atom with the Raney nickel surface is more important than the molecular size for the desulfurization of polynuclear thiophene compounds over a Raney nickel.

Desulfrization Mechanism. Eisch and his coworkers[26] have undertaken a mechanistic study of the desulfurization of dibenzothiophene by the (2,2′-bipyridyl)nickel (0) complex and reported that a radical anion of the thiophene nucleus was formed and that this subsequently underwent C-S bond cleavage into S^- and aromatic radicals. However, it is obvious that there is no correlation between the desulfurization rate and the reaction indices, Fr(E), Fr(N), and Fr(R), as is shown in Table 4. These results suggest that there is no evidence in this study for either electron transfer or nucleophilic attack. Moreover, the radical reaction is not the rate-determining step in the desulfurization of the thiophene compounds on the Raney nickel, although the mechanism of desulfurization over a Raney nickel is most generally a free-radical mechanism.[25,27,28] Therefore, the rate-determining step in this reaction is not a C-S bond breaking, but the adsorption of the sulfur compound to a nickel atom of the Raney-nickel surface, with a competitive adsorption of the solvent. This adsorption leads to the removal of the sulfur from the thiophene compound. The sulfur reacts with the nickel atom of the Raney nickel to form nickel sulfide, but not hydrogen sulfide.

In the first step, the unshared electron pair of the sulfur is attracted to a low-valent nickel atom of the Raney-nickel surface. The compound is adsorbed on the surface through the unshared electron pair of sulfur, which acts as an electron donor. The carbon-sulfur bond is, therefore, weakened, and a free radical is formed. The hydrogen present on the Raney-nickel surface[18,19,20] then reduces the radical to the corresponding hydrocarbon.

On the other hand, for the monocyclic and bicyclic thiophene compounds, the hydrogenation of the C_2-C_3 bonds of **17** and **18** appears to take place competitively with the fission of the C-S bond. The difference (q_s—q_c) between the π-electron density of the sulfur atom and that of the carbon atom (C_3) (the carbon atom with the highest π-electron density) is small, although the charge density index refers to the nature of the molecule before allowance is made for perturbing effects due to the approaching reactant. Furthermore, the bond order of the C_2-C_3 bonds of **17** and **18** is larger than that of the others. For this reason, these two molecules must chemisorb by a multi-point mechanism.[29] According to the multi-point mechanism, thiophene molecules are chemisorbed in such a way that the C_2-C_3 bond is coordinated to an anion vacancy at the surface, with the adjacent sulfur center interacting with a contiguous sulfur atom on the surface. The mechanism by which the tricyclic and tetracyclic thiophene compounds are desulfurized is, therefore, quite different from that of the monocyclic and bicyclic compounds, **17** and **18**.

References

1) R. B. Lucke, D. W. Later, C. W. Wright, E. K. Chess, and W. C. Weimer, *Anal. Chem.*, **57**, 633 (1985).

2) R. C. Kong, M. L. Lee, M. Iwao, Y. Tominaga, R. Pratap, R. D. Thompson, and R. N. Castle, *Fuel*, **63**, 702 (1984).

3) A. V. Sapre, D. H. Broderick, D. Fraenkel, B. C. Gates, and N. K. Nag, *AIChE J.*, **26**, 690 (1980).

4) P. Geneste, A. Guida, and D. Levache, *Bull. Soc. Chim. Fr.*, **II**-170 (1983).

5) W. S. O'Brien, J. W. Chen, R. V. Nayak, and G. S. Carr, *Ind. Eng. Chem., Process Des. Dev.*, **25**, 221 (1986).

6) P. Geneste, A. Guida, and D. Levache, *Bull. Soc. Chim. Fr.*, II-136 (1983).
7) S. Harris and R. R. Chianelli, *J. Catal.*, **86**, 400 (1984).
8) J. Joffre, P. Geneste, and D. A. Lerner, *J. Catal.*, **97**, 543 (1986).
9) H. Adkins and H. R. Billia, *J. Am. Chem. Soc.*, **70**, 695 (1948).
10) H. Gilman and A. L. Jacoby, *J. Org. Chem.*, **3**, 108 (1938).
11) E. Campaigne and S. W. Osborn, *J. Heterocycl. Chem.*, **5**, 655 (1968).
12) K. Rabindran and B. D. Tilak, *Proc. Indian Acad. Sci.* **37A**, 564 (1953).
13) L. K. Klemm, J. J. Karckesy, and R. F. Lawrence, *J. Heterocycl. Chem.*, **15**, 773 (1978).
14) R. Bartsch and C. Tanielian, *J. Catal.*, **35**, 353 (1974).
15) C. N. Satterfield and G. W. Roberts, *AIChE J.*, **14**, 159 (1968).
16) M. Nagai, T. Satoh, and A. Aiba, *J. Catal.*, **97**, 52 (1986).
17) K. Shinoda, "Youkai to Youkaido (Soluble and Solubility)," Maruzen, Tokyo (1970); F. A. Carey and R. J. Sundberg, "Advanced Organic Chemistry, Part A," Plenum, New York (1984), p. 202.
18) G. R. Pettit and E. E. Van Tamelen, "Organic Reactions," John Wiley, New York (1962), Vol. 12, p. 356.
19) "Shokubai Binran (Handbook of Catalysts)," ed by A. Ozaki, K. Tamaru, and S. Nishimura, Chijinkan, Tokyo (1967), p. 492.
20) I. Nicolau and R. B. Anderson, *J. Catal.*, **68**, 339 (1981).
21) R. Zahradník, C. Párkányi, V. Horák, and J. Koutecký, *Coll. Czeck. Chem. Commum.*, **28**, 776 (1963).
22) R. Zahradník and C. Párkányi, *Coll. Czeck. Chem. Commum.*, **30**, 195 (1965).
23) M. Zdražil and J. Sedláček, *Coll. Czeck. Chem. Commum.*, **42**, 3133 (1977).
24) A. J. Duben, *J. Phys. Chem.*, **82**, 348 (1978).
25) H. Hauptmann and B. Wladislaw, *J. Am. Chem. Soc.*, **72**, 707, 710 (1950).
26) J. J. Eisch, L. E. Hawrence, and K. I. Han, *J. Org. Chem.*, **48**, 2963 (1983).
27) K. Mitsui, "Sesshoku Kangen (Catalytic Reduction)," Tokyo Kagaku Dojin, Tokyo (1970), p. 62; S. Nishimura and Y. Takagi, "Sesshoku Suisoka Hannou (Catalytic Hydrogenation)," Tokyo Kagaku Dojin, Tokyo (1987).
28) G. M. Badger and W. H. F. Sasse, *J. Chem. Soc.*, **1957**, 3862.
29) H. Kwart, G. C. A. Schuit, and B. C. Gates, *J. Catal.*, **61**, 128 (1980).

 © 1989 The Chemical Society of Japan Bull. Chem. Soc. Jpn., 62, 563—570 (1989)

The Adsorption and Desorption of Nitrogen Oxide by the Aqueous Dispersion of the Chelate Resin-Immobilized Iron(II) Complex

Naoki TOSHIMA,* Hiroyuki ASANUMA, Kazuaki YAMAGUCHI,† and Hidefumi HIRAI††
Department of Industrial Chemistry, Faculty of Engineering, The University of Tokyo, Hongo, Bunkyo-ku, Tokyo 113
(Received August 19, 1988)

Aqueous dispersions of the chelate resin-iron(II) complex were prepared by ion-exchange in water from iron(II) sulfate and a chelate resin containing iminodiacetic acid moieties. The resulting dispersions in water (50 cm^3) can adsorb 78% of the nitrogen oxide (NO) from 6 dm^3 of nitrogen gas containing 1000 ppm of nitrogen oxide at 25 °C. The adsorption rate of NO by the dispersions depends greatly on both the particle size of the chelate resin used and the concentration of iron(II) in the supernatant. A fast adsorption of nitrogen oxide can be achieved by using small particles of the chelate resin and by dissolving a large amount of iron(II) ions in the aqueous part of the dispersions. The adsorption and desorption of nitrogen oxide can be understood in terms of a 1 : 1 reversible coordination of NO to the iron(II) ion immobilized on the chelate resin. The equilibrium constant, enthalpy change, and entropy change for the above adsorbing reaction were 3.11×10^4 $dm^3\,mol^{-1}$, −45.6 $kJ\,mol^{-1}$, and −68.2 $J\,K^{-1}\,mol^{-1}$ respectively. Since the adsorbing reaction of NO in this system is reversible, the adsorbed NO can be released by heating the dispersions which have already adsorbed NO. The amount of the released NO can be predicted from the equilibrium constant at the releasing temperature. Moreover, a concentrated recovery of the NO can be achieved by the present aqueous dispersions system.

The concentration of NO in the atmosphere has never decreased in the past decade in spite of many efforts. Since NO is toxic for the human body and causes photochemical smog through nitrogen dioxide, advanced technology for the removal of NO is strongly desired. At the present time, the catalytic reduction of NO into innoxious nitrogen by using a gaseous reducing agent like ammonia or hydrogen is a well-known practical method for the removal of NO.[1-4] This method has, however, some disadvantages, such as a rapid deactivation of the catalyst by the contaminated gases (sulfur dioxide) or dust. On the other hand, aqueous absorbents for NO have been studied because of the relatively high durability against these contaminants. The typical solution systems involve: 1) an aqueous solution of sodium hydroxide, where NO is absorbed by the aqueous solution after the oxidation of NO to NO_2 by contact with O_3,[5] and 2) an aqeous solution of iron(II)-ethylenediaminetetraacetic acid (Fe(II)-EDTA), where NO can form a complex with Fe(II)-EDTA.[6-9] Among these methods, the aqueous solution of Fe(II)-EDTA is noteworthy for its high capability for the absorption of NO and its possible application for the simultaneous removal of NO and sulfur dioxide.[9] This solution, however, has disadvantages in the recovery of the Fe(II)-EDTA complex for the recyclic usage, since the complex is easily dissolved in water and the Fe(II) ions are easily oxidized into inactive Fe(III) ions.

In the present investigation, the immobilization of Fe(II) ions on the chelate resin involving iminodiacetic acid moieties (Fig. 1) instead of EDTA and the dispersion of the resulting Fe(II)-chelate resin complex (CR-Fe(II)) into water were examined for the purpose of establishing a method of ensuring easy handling, a concentrated recovery of NO, and an improvement in the durability against oxygen. In general, the immobilization of metal ions on the polymer resin gives rise to the following advantages:[10] 1) Easy recovery and repeated use of the metal complex; 2) the stabilization of the complex or protection of the active species by the polymer matrix against oxygen or water, and 3) an improvement in the activity by the polymer field. Many successful results supporting these advantages have been reported in the macromolecular metal complex catalyst system.[11] In the present paper, the preparation and characterization of aqueous dispersions of the chelate resin-immobilized Fe(II) complex, and its properties for the adsorption and desorption of NO will be described in detail.[12,13]

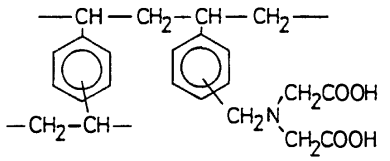

Fig. 1. Structure of the chelate resin.

Experimental

Materials. The chelate resin (Diaion CR-10; mean diameter of the particles, 0.5 mm), purchased from Mitsubishi Chemical Industries, Ltd., was used without further purification. The commercial resin was swollen with water. One gram of the swollen substance was determined by the pH-titration method to contain 0.98 mmol of iminodiacetic acid moieties. One gram of the resin dried in vacuo, on the other hand, had 2.78 mmol of the moieties. A mass of the chelate resin in a dry or a swollen state containing 21.0 mmol of iminodiacetic acid moieties was used at one time for the preparation of each aqueous dispersion.

† Present address: Applied Research Laboratory 1, Lion Co., Hirai, Edogawa-ku, Tokyo 132.
†† Present address: Department of Industrial Chemistry, Faculty of Engineering, Science University of Tokyo, Kagurazaka, Shinjuku-ku, Tokyo 162.

The iron(II) sulfate 7 hydrate, iron(II) perchlorate 6 hydrate, and iron(II) chloride *n* hydrate (*n* was determined to be 4.59 by the 1,10-phenanthroline method[14]) were used without further purification.

Mixed gases of NO and nitrogen of the designed NO concentration were purchased from Takachiho Shoji, Ltd., and were used without further purification.

The chelate resin in a small size was prepared by grinding the commercial chelate resin with an agate mortar and a pestle. Its mean particle size was proved to be 10 μm by measurement with an optical microscope. In order to avoid any differences in the particle size in the experimental lots, the chelate resin was previously ground on a large scale, and all the dispersion systems were prepared by using samples of the same lot.

Preparation of Absorbents or Adsorbents. (1) Aqueous Dispersions of the Chelate Resin-Immobilized Iron(II) Complex: Chelate resin containing 21.0 mmol of iminodiacetic acid moieties (21.4 g in the swollen state, or 7.53 g in the dry state) was added to 15 cm^3 of water in which a desired amount of Fe(II) sulfate had been dissolved under nitrogen. The resulting mixtures were shaken for 48 h with a mechanical shaker or magnetic stirrer to immobilize the Fe(II) ions on the chelate resin.

(2) An Aqueous Solution of the Iron(II)-EDTA Complex: An aqueous solution of the Fe(II)-EDTA complex, used as a conventional absorbent of NO, was prepared by dissolving 0.139 g (0.50 mmol) of $FeSO_4$ $7H_2O$ and 0.187 g (0.50 mmol) of EDTA 2Na $2H_2O$ in 50 cm^3 of water under oxygen-free conditions.

(3) An Aqueous Solution of Iron(II) Salt: Various kinds of Fe(II) solutions were prepared by dissolving 31.4 mmol of various Fe(II) salts in water under oxygen-free conditions, adjusting the total volume of the solution to 50 cm^3.

(4) Dispersions of the Chelate Resin-Immobilized Iron(II) Complex in an Aqueous Iron(II) Solution at a Designed Concentration: After the preparation of aqueous dispersions of the immobilized complex from 7.53 g of the ground chelate resin and 8.72 g (31.4 mmol) of $Fe(II)SO_4$ $7H_2O$, the supernatant of the dispersions was removed by use of a centrifuge. Adding 15 cm^3 of a fresh aqueous solution of $FeSO_4$ $7H_2O$ at a desired concentration provided dispersions of the immobilized Fe(II) complex in a Fe(II) solution. The exact concentration of the Fe(II) ions in the supernatant was determined by the 1,10-phenanthroline method.[14]

Characterization of Aqueous Dispersions of the Chelate Resin-Iron(II) Complex. (1) Electronic Spectra of the Complexes: The electronic spectra of the aqueous solutions of the complexes were measured with a Hitachi model 340 spectrophotometer. The electronic spectrum of the dry or wet chelate resin-immobilized Fe(II) complex was measured at room temperature with the same spectrophotometer equipped with an integrated reflection apparatus.

(2) Measurement of the Amount of the Iron(II) Ions Immobilized on the Chelate Resin: The amount of immobilized Fe(II) ions was measured by the following method. Fifty cm^3 of an aqueous solution of $FeSO_4$ with an exact, desired amount was added to 7.53 g of the dry chelate resin (containing 21.0 mmol of iminodiacetic acid moieties), after which the mixture was stirred for 48 h. After the immobilization of the Fe(II) ions on the chelate resin, the concentration of the Fe(II) ions in the supernatant was measured by the 1,10-phenanthroline method,[14] while the amount of immobilized Fe(II) ions was calculated from the decrease in the concentration of Fe(II) ions in the aqueous phase.

Adsorption and Desorption Experiment on NO. (1) Adsorption of NO: Adsorption experiments on NO were carried out by using the closed-circulation system illustrated in Fig. 2. After removing the remaining gas in the system with a vacuum pump, 6 dm^3 of nitrogen containing 1000 ppm (or 980 ppm) of NO (the total amount of NO was 0.246 mmol) was introduced into this apparatus at room temperature and then circulated inside the apparatus, bubbling the aqueous dispersions through by means of a gas pump at the rate of 1.6 $dm^3\,min^{-1}$. The adsorbent was kept at the desired temperature in a water bath with a thermostat.

Changes in the NO concentration in nitrogen were traced by sampling 23.8 cm^3 of the mixed gas in a 100 mm-cell and by measuring the absorbance at 226.5 nm.

(2) Dependence of the Amount of Adsorbed NO at Equilibrium on the Partial Pressure of NO: After placing the dispersions in contact with 6 dm^3 of nitrogen containing 980 ppm of NO until the equilibrium had been reached, the gas remaining in the system was removed and another 6 dm^3 of nitrogen with NO was introduced; the gas was then circulated again for the further adsorption of NO with the same dispersions. The amount of adsorbed NO was obtained from the sum of those NO values from the first and second runs. The concentration of NO in the second run corresponded to the partial pressure of NO at equilibrium. By repeating the above operation, the relationship between the amount of NO adsorbed and the partial pressure of NO was measured.

(3) Desorption of NO: The desorption of NO was carried out by the following two methods of heating and purging with pure nitrogen.

Heating: After the dispersions had been equilibrated with the mixed NO gas at 25 °C, the gas circulation was stopped and the system was left as it was. Then the temperature of the dispersions was raised to 80 °C, below which temperature the resin was known to be stable enough; the gas was then circulated again at the rate of 1.6 $dm^3\,min^{-1}$. Repeated adsorption-desorption cycles were carried out by raising and dropping the temperature of the dispersions without exchanging the initially introduced mixed gas.

Purging with Pure Nitrogen: After the dispersions had been equilibrated with the mixed NO gas at 25 °C, the gas remaining in the circulation system was removed by the use

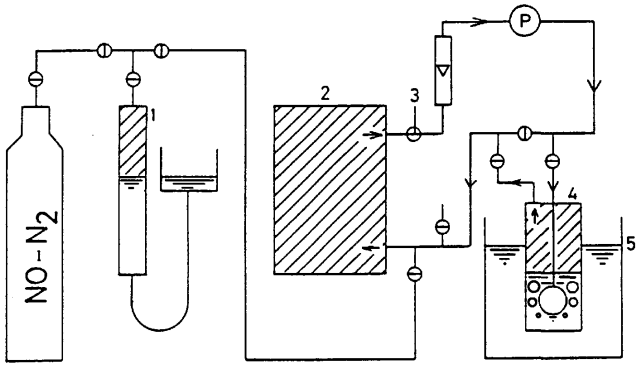

Fig. 2. Schematic diagram of gas adsorption apparatus.
1. Gas burette. 2. Gas holder. 3. Sampling outlet. 4. Adsorbing vessel. 5. Constant temperature water bath.

of a vacuum pump and 6 dm^3 of a pure nitrogen gas was freshly introduced into the system (except for the adsorbing vessel containing the dispersions). The nitrogen was then circulated through the dispersions at 25 °C. The error caused by the gas remaining in the adsorbing vessel was corrected in each run.

Results

Preparation and Characterization of an Aqueous Dispersion of the Chelate Resin-Immobilized Iron(II) Complex. The immobilization of Fe(II) ions on the chelate resin proceeds rapidly when the solution of Fe(II) ions is mixed with the chelate resin. The light green color of the solution gradually fades because of the decrease in the concentration of the Fe(II) ions in the supernatant. The immobilization was also observed in the electronic spectra. The chelate resin before the immobilization of the Fe(II) ions is white and has a peak at 280 nm in its electronic spectrum due to benzene chromophores in the matrices, as is shown by broken line in Fig. 3. The color of the resin changes from white to light green upon the immobilization of the Fe(II) ions, and a new peak appears at around 320 nm which does not exist in the electronic spectrum of an aqueous solution of $FeSO_4$ and the chelate resin. The exposure to NO gives new shoulder peaks around 450 and 600 nm, as is shown by the solid line in Fig. 3. A similar change has also been observed in the case of the adsorption by an aqueous solution of the Fe(II)-EDTA complex.[7,8] The release of NO by the heating of the adsorbed resin led to the disappearance of the two shoulder peaks and gave the same electronic spectrum as that of the original chelate resin-Fe(II) complex before the adsorption of NO.

Adsorption of NO by the Aqueous Dispersions of the Iron(II)-Chelate Resin Complex. Figure 4 shows the adsorption curves of various absorbents and adsorbents. An aqueous solution of Fe(II)-EDTA, a typical absorbent of NO, rapidly absorbs NO, even at a low concentration of NO. The absorption capacity, however, gradually decreases, probably because of the deterioration of the adsorbent by the trace amount of oxygen being contaminated by the leakage in air at the circulating pump. An aqueous solution of $FeSO_4$, the starting material of the dispersion system, absorbs only 3% of the initially charged amount of NO, as is shown by the open circles in Fig. 4. The mixture (the dispersions) prepared by adding the above aqueous solution of $FeSO_4$ to the chelate resin can adsorb enough NO, though its adsorption rate is not very fast. When these dispersions were separated into an aqueous part (the supernatant) and a solid part, however the aqueous part did not absorb NO, but the solid part did. This fact clearly indicates that Fe(II) ions immobilized on the chelate resin are the active species for the adsorption of NO.

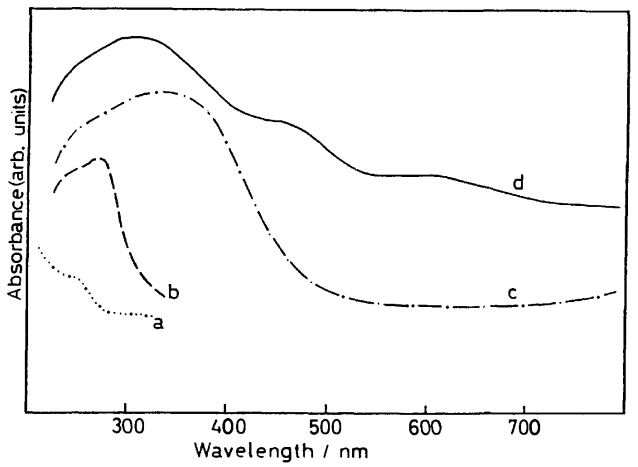

Fig. 3. Electronic spectra of the NO adsorbent and the related materials. a(·····): $FeSO_4$ solution in water, b(— —): chelate resin, c(·–·–): NO adsorbent before adsorption of NO, d(——): NO adsorbent after adsorption of NO.

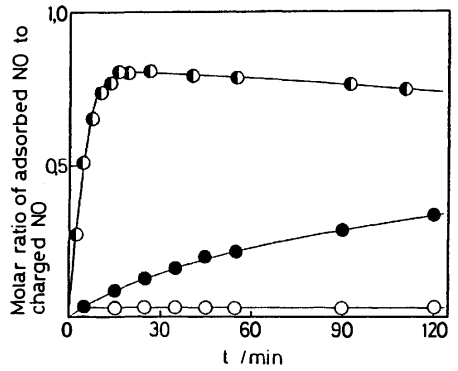

Fig. 4. Adsorption of NO at 25°C by Fe(II)-EDTA solution (◐, 0.01 mol dm^{-3}), Fe(II)-SO_4 solution (○, 0.36 mol dm^{-3}), and resin-immobilized adsorbent dispersion prepared by mixing 18 mmol of Fe(II)SO_4 and 21.4 g of the chelate resin in water by using a shaker (●). The adsorbents were contacted with 6 dm^3 of nitrogen containing 1000 ppm of NO.

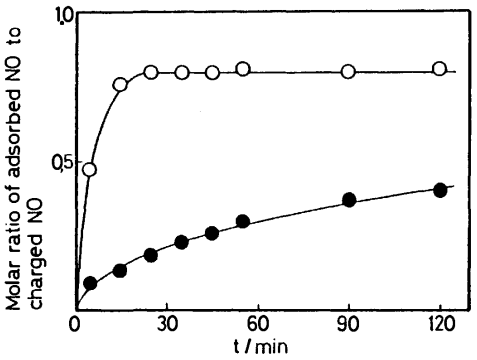

Fig. 5. Adsorption of NO at 25°C by the resin-immobilized Fe(II) adsorbents prepared from commercial beads (●) and from fine beads ground with agate mortar and pestle (○). Adsorption of NO was carried out by the contact with 6 dm^3 of nitrogen containing 980 ppm of NO at the rate of 1.6 dm^3 min^{-1}.

Figure 5 shows the NO adsorption curves of the dispersions of the adsorbents prepared by using the resin in a small size (10 μm) as well as in a commercial size (0.5 mm). The equilibrium is achieved within 25 min in the case of the small size resin by adsorbing 78% of NO at 25 °C, as Fig. 5 shows. Moreover, no deterioration by the contaminated oxygen as is seen in the case of an aqueous solution of Fe(II)-EDTA is observed in this system.

Figure 6 shows the dependence of the amount of adsorbed NO at equilibrium on the charged amount of Fe(II). The capital letter R in the figure shows the molar ratio of the initially charged amount of Fe(II) ions to the IDA moieties in the resin. The amount of NO adsorbed at equilibrium increases with the increase in the amount of charged Fe(II) ions and reaches saturation at the point where the amount of Fe(II) is half as much as the molar amount of IDA moieties in the resin by adsorbing 68% of the NO at 30 °C. The amount of immobilized Fe(II) ions, which are the active species for the adsorption of NO, reaches saturation over R=0.7, no further immobilization of the Fe(II) ions on the chelate resin was observed beyond this point.

The aqueous dispersions prepared from various Fe(II) salts with the different counter anions listed in Table 1 have almost the same activity for the adsorption of NO, while the aqueous solution of each Fe(II) salt absorbs only 6% of the NO. Thus, no significant difference in the adsorbing capability caused by the Fe(II) salts used was observed.

The adsorption rate of NO increased with the increase in the amount of charged Fe(II), as is shown in Fig. 7. The increase in the rate was observed after the saturation of Fe(II) immobilization, while the amount of adsorbed NO was at the saturation point.

The amount of NO adsorbed at equilibrium depends strongly on both the partial pressure of NO and the temperature. Figure 8 shows the relationship between the partial pressure of NO at equilibrium and the amount of NO adsorbed. As this figure shows, the

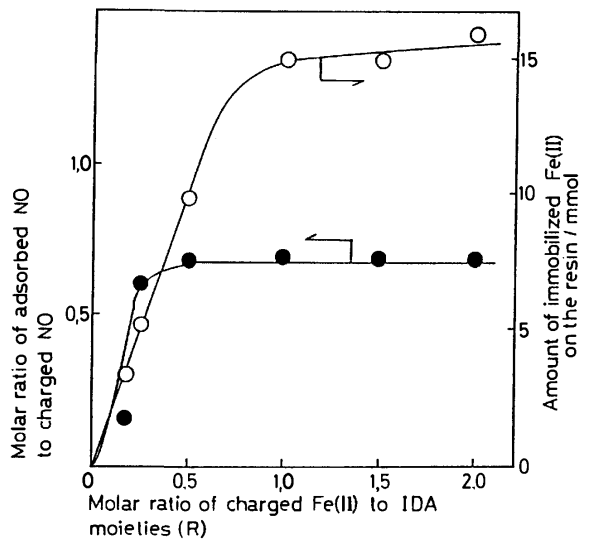

Fig. 6. Relationship between the amount of adsorbed NO at equilibrium (●) and the amount of immobilized Fe(II) on the resin (○) at various amount of Fe(II) charged. Initially charged amount of chelate resin was 7.53 g containing 21.0 mmol of IDA moieties.

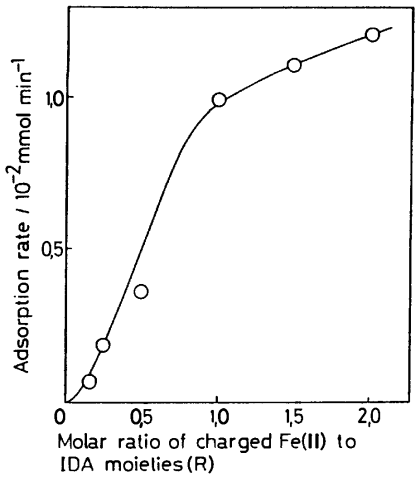

Fig. 7. Dependence of initial adsorption rate of NO on molar ratio (R) of the charged amount of Fe(II) to the amount of iminodiacetic acid moieties in the chelate resin by the contact with 6 dm^3 of nitrogen containing 980 ppm of NO at the rate of 1.6 dm^3 min^{-1} with the adsorbent dispersions prepared from 7.53 g of chelate resin containing 21.0 mmol of IDA moieties and designed amount of $FeSO_4$.

Table 1. Adsorption of NO with Fe(II) Complexes from Various Salts[a)]

Fe(II) complex		IDA[b)] of chelate resin/mmol	Molar ratio of adsorbed NO to charged NO
Fe(II) salt			
Formula	Amount/mmol		
$FeSO_4$	18	0	0.033
$FeSO_4$	31	21	0.776
$Fe(ClO_4)_2$	31	0	0.061
$Fe(ClO_4)_2$	31	21	0.700
$FeCl_2$	30	0	0.067
$FeCl_2$	30	21	0.767

a) Initial amount of NO=0.246 mmol. b) 21.0 mmol of the iminodiacetic acid (IDA) moieties were included by 21.4 g of the chelate resin.

amount of adsorbed NO increases linearly with the increase in the partial pressure of NO. As for the temperature-dependence, the increase in the temperature decreases the amount of NO adsorbed. Thus, the dispersions adsorbed 78% of NO at 25 °C; this figure decreased to 11% at 80 °C.

Desorption and Recyclic Use. Figure 9 shows the adsorption and desorption cycles of NO upon treatment with heat. The concentration of NO rapidly decreases to 220 ppm in 90 min when it is in contact with the dispersions at 25 °C. By elevating the temperature of the dispersions to 80 °C, the NO is smoothly released from the dispersions and the concentration of NO recovers to 876 ppm. In other words, 85% of the NO adsorbed is released, while only 12% of the NO charged remains in the dispersions at 80 °C. The adsorption-desorption cycles were repeated for 5 times without any deterioration.

The desorption of NO is also possible by letting pure nitrogen flow through the dispersions. Twenty-three percent (0.041 mmol) of the adsorbed NO was recovered at the concentration of 167 ppm by circulating 6 dm^3 of bubbling pure nitrogen through the dispersions, which had previously adsorbed NO (0.18 mmol) from 6 dm^3 of the mixed gas at 25 °C.

From the viewpoint of the recovery of NO as chemical resources, the recovery of NO at a higher concentra-

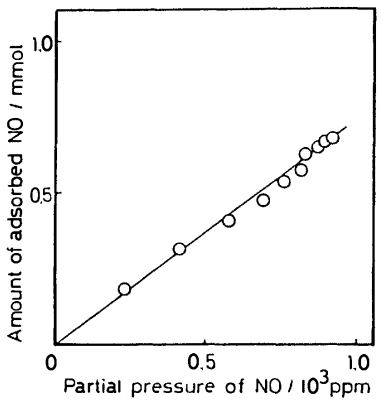

Fig. 8. Dependence of the amount of adsorbed NO at equilibrium on the concentration of NO. Adsorption experiment was carried out by the contact with 6 dm^3 of nitrogen containing 980 ppm of NO at 30 °C by the adsorbent dispersions prepared from 7.53 g of chelate resin containing 21.0 mmol of IDA moieties and 8.72 g of $FeSO_4$.

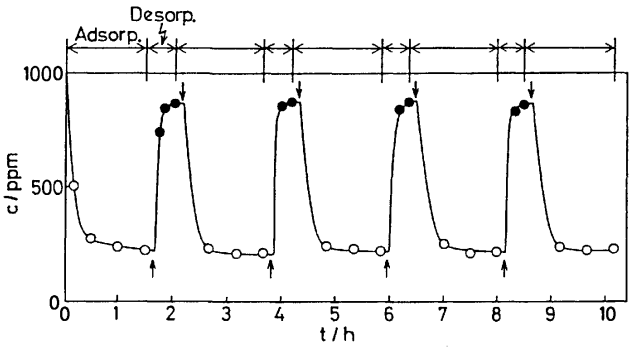

Fig. 9. Changes of the concentration (c) of NO in the gas phase with time (t) during the adsorption (○) of NO at 25 °C by Fe(II)-chelate resin adsorbent and desorption (●) of NO at 80 °C from the adsorbent. To adjust the temperature to a desired value, adsorbent was kept in the thermostat for 10 min without circulating the gas after adsorption (↑) or desorption (↓) of NO.

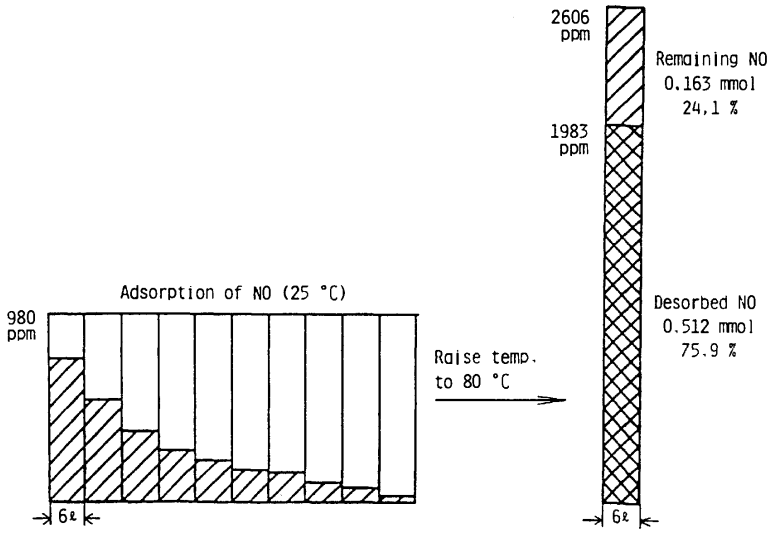

Fig. 10. The schematic presentation of the release of the cumulatively adsorbed NO from the adsorbent. Desorption of NO was carried out by circulating 6 dm^3 of pure nitrogen through the dispersions at the rate of 1.6 dm^3 min^{-1} till the equilibrium was attained after the dispersion was saturated with 980 ppm of NO by the contact with 6 dm^3 of nitrogen containing 980 ppm of NO for 10 times at 25 °C.

tion than that of the original gas is important. In order to test this possibility, the accumulated adsorption of NO was examined. After the first 6-dm^3 bag of the mixed gas had been circulated at 25 °C through the adsorbent until the equilibrium was reached, the remaining gas in the gas phase of the system was replaced by another 6 dm^3 of the fresh mixed gas, followed by a second circulation through the adsorbent. Ten repetitions of this procedure caused the adsorbent to be equilibrated with 980 ppm of NO. The total amount of NO adsorbed on the dispersions was 0.675 mmol. Then, 6 dm^3 of pure nitrogen was newly introduced into the system and circulated at 80 °C through the aqueous dispersions already saturated with 980 ppm of NO. This treatment released 0.512 mmol of NO, which corresponded to 76% of the total amount of that adsorbed , at the concentration of 1983 ppm. The above results are schematically illustrated in Fig. 10. These facts indicate that the concentrated NO can be obtained from the dilute one; that is, the concentrated recovery of NO is possible by using the present dispersion system.

Discussion

Complex Formation and Determination of the Equilibrium Constant. The appearance of a new peak at 320 nm upon the immobilization of the Fe(II) ions on the resin suggests the complex formation of Fe(II) with IDA moieties in the resin, as this peak does not exist in the separate spectra of Fe(II) and chelate resin. The new shoulder peaks at 450 nm and 600 nm appearing in the immobilized resin upon the contact with NO correspond to the charge-transfer band caused by the complex formation between NO and Fe(II). The appearance of such a charge-transfer band is observed in the case of an aqueous solution of an $Fe(II)SO_4$ or a monomeric Fe(II)-polyamine-*N*-carboxylic acid complex such as Fe(II)-EDTA.[15] These facts indicate that the adsorption of NO by the present aqueous dispersions proceeds through the complex formation between Fe(II) and NO, as in the case of the homogeneous aqueous solution of Fe(II)-EDTA or Fe(II).[16]

The above adsorbing reaction is considered to start from the dissolution of gaseous NO into water and to proceed according to Eqs. 1 and 2. Assuming the first-order reaction for the NO adsorption, i.e.:

$$NO_{gas} \rightleftharpoons NO_{aq} \quad (1)$$

$$n(NO_{aq}) + \text{CR-Fe(II)} \overset{K}{\rightleftharpoons} \text{CR-Fe(II)-(NO)}_n \quad (2)$$

$$K = [\text{CR-Fe(II)-NO}]/([\text{CR-Fe(II)}] \times [NO_{aq}])$$
$$= [\text{CR-Fe(II)-NO}] \times H/([\text{CR-Fe(II)}] \times p_{NO}) \quad (3)$$

$$K = n_{NO} \times H/([\text{CR-Fe(II)}]_0 \times p_{NO})$$
$$K \times p_{NO}/H = n_{NO}/[\text{CR-Fe(II)}]_0 \quad (4)$$

the 1 : 1 complex formation of NO with the Fe(II) ion (n=1 in Eq. 2), Eq. 3 can be obtained from Eq. 2, where p_{NO} and H are the partial pressure of NO (atm) and Henry's constant respectively. The amount of Fe(II) ions immobilized on the chelate resin, [CR-Fe(II)] in mmol, can have a linear relation with the amount of adsorbed NO n_{NO}; the uncoordinated amount is obtained by substracting the n_{NO} from the amount of the initially immobilized Fe(II) ions, $[\text{CR-Fe(II)}]_0$. As the CR-Fe(II) exists in a large excess to the adsorbed NO ($[\text{CR-Fe(II)}]/n_{NO}$=22 in the present case), however, the amount of unreacted CR-Fe(II), [CR-Fe(II)], can be regarded as the amount of the initially immobilized Fe(II) ions, $[\text{CR-Fe(II)}]_0$. Thus, Eq. 3 is transformed into Eq. 4. Equation 4 indicates that the partial pressure of NO at equilibrium should be in proportion to the amount of NO adsorbed when the 1 : 1 complex formation proceeds. In fact, the amount of NO adsorbed is in good proportion to the partial pressure of NO, as is shown in Fig. 8, which also indicates that the equilibrium constant, K, of the adsorbing reaction can be calculated according to Eq. 3.

Table 2 shows the equilibrium constant at each temperature obtained according to Eq. 3. The equilibrium constant decreases with the increase in the temperature because of the fall in the amount of NO adsorbed. The van't Hoff plots form a straight line, as is shown in Fig. 11, and the equilibrium constants K_c can be expressed as follows by using the temperature T as a parameter:

$$K_c = 3.32 \times 10^{-4} \times \exp(45.6 \times 10^3/RT) \quad (5)$$

where R=8.314 J K^{-1} mol^{-1}.

The enthalpy (ΔH) and entropy (ΔS) changes were obtained as −45.6 kJ mol^{-1} and −68.2 J K^{-1} mol^{-1} respectively. The enthalpy change in the absorbing reaction of NO with an aqueous solution of Fe(II)-EDTA was reported to be −66.1 kJ mol^{-1} [18] (−15.8 kcal mol^{-1}), which is lower by 20.5 kJ mol^{-1}

Table 2. Adsorption of NO by the Chelate Resin-Immobilized Fe(II) Complex at Various Temperatures

Temp/°C	Adsorbed NO[a]/mmol	Apparent equilibrium constant	
		$K_c H^{-1}$/atm^{-1}	K_c/dm^3 mol^{-1}
25.0	0.191(0.78)[b]	60.1	31.1 ×10^3
39.5	0.134(0.58)	23.2	14.8 ×10^3
59.8	0.069(0.29)	7.00	5.35×10^3
80.0	0.025(0.11)	2.02	1.67×10^3

a) Initial amount of NO=0.246 mmol. b) Molar ratio of adsorbed NO to charged NO.

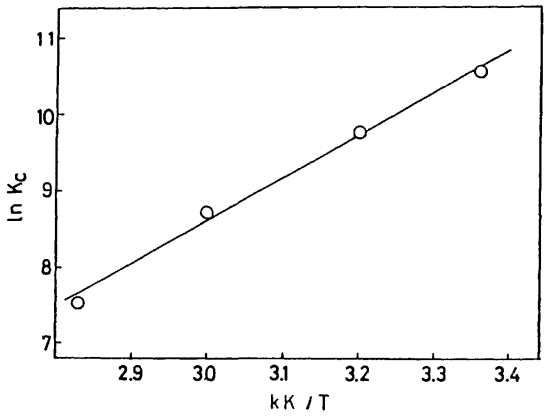

Fig. 11. The van't Hoff's plots for the adsorption of NO. The equilibrium constant at different temperature was calculated from the amount of adsorbed NO and partial pressure of NO at equilibrium according to the eq. 4. Adsorption experiment was carried out by circulating 6 dm^3 of nitrogen containing 980 ppm of NO at the rate of 1.6 dm^3 min^{-1}.

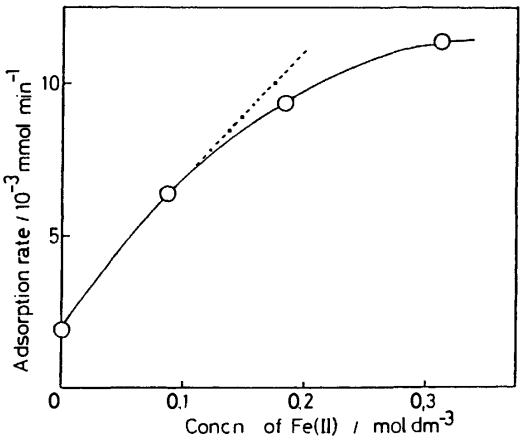

Fig. 12. Dependence of adsorption rate of NO on the concentration of $FeSO_4$ in the supernatant. In this system, amount of Fe(II) ion immobilized was kept constant (saturated) with 14.7 mmol. Adsorption experiment was carried out by circulating 6 dm^3 of nitrogen containing 1000 ppm of NO.

than that of CR-Fe(II). The strong NO-adsorbing capability of Fe(II)-EDTA is considered to be derived from the strong back-donation from Fe(II) to the NO molecule due to the increase in the electron density of the iron atom. In the case of the CR-Fe(II) complex, however, the coordination of NO to the Fe(II) ion is relatively weak due to the electron-releasing effect of the benzyl group compared with the case of the EDTA ligand.

Adsorption Rate. The increase in the rate of NO adsorption with small particles of the chelate resin suggests that the rate-determining step is the diffusion of the NO dissolved in the water into the resin inside. The adsorbing reaction is considered to occur by means of the following two steps: 1) the dissolution of NO into the supernatant of the dispersions, and 2) the adsorption of the NO dissolved by the CR-Fe(II) complex in the resin. The dissolution of the NO into the supernatant, the first step of the adsorption, is rapid and can always be brought to saturation by vigorous bubbling. The adsorption of the NO dissolved by the CR-Fe(II) complexes, the second step, occurs first on the surface of the resin, and then the NO adsorbed diffuses from the surface to the inside of the resin. This NO diffusion from the surface to the inside of the resin proceeds along with the diffusion of the aqueous solution in the resin. Therefore, the diffusion will be rather slow because of the low mobility of the solution in the resin. Thus, the adsorption of NO will proceed smoothly when large parts of the CR-Fe(II) complex exist near the surface of the resin. The fact that the CR-Fe(II) complex prepared from the ground resin adsorbs NO more rapidly than that prepared from the original resin can be explained by the 50-fold increase in the surface area of the resin by grinding the particles to from 0.5 mm to 10 μm in diameter.

The adsorption rate also increases with the increase in the charged amount of Fe(II) ions as is shown in Fig. 7. The increase in the rate is thought to be attributable to the increase in the amount of the CR-Fe(II) complex in the resin when the ratio (R) of the charged Fe(II) ions to the IDA moieties lies below 0.7. When R is over 0.7, the adsorption rate still increases, even though the immobilization of the Fe(II) ions is saturated in this region. This fact strongly suggests that the Fe(II) ions in the supernatant are closely connected with the adsorption rate of NO. Figure 12 shows the effect of the concentration of Fe(II) ions in the supernatant on the NO-adsorption rate. In this experiment, the amount of the CR-Fe(II) complexes was kept at saturation. In this case, no diffusion of the Fe(II) ions into the supernatant from the resin was observed because of the strong chelating interaction of the Fe(II) with the IDA moieties. Therefore, these experiments were performed under the same conditions except for the concentration of Fe(II) ions in the supernatant. Moreover, the amount of NO adsorbed at equilibrium was kept constant in each run. Even under these conditions, the adsorption rate depended greatly on the concentration of Fe(II) in the supernatant. The increase in the concentration of Fe(II) in the supernatant brought about the increase in the adsorption rate. On the contrary, the rate was extremely diminished by the exchange of the supernatant with distilled water. It is proposed from these facts that the Fe(II) ions in the supernatant work as accelerators, not as active species, of NO adsorption.

The concentration of NO in the supernatant is calculated to be 1.93×10^{-6} mol dm^{-3} by means of Henry's law when the supernatant is displaced by distilled water and is equilibrated with 1000 ppm of NO in the gas phase at 25 °C. In contrast, if the concentration of Fe(II) ions in the supernatant is 0.2 mol dm^{-3}, the concentration of Fe(II)-NO in the supernatant is calcu-

lated to be 1.27×10^{-4} mol dm^{-3} under the same conditions from the equilibrium constant of Eq. 6 (K_1=0.634 atm^{-1}).[16] Thus, when the supernatant contains Fe(II) ions, the concentration of NO in the supernatant 66 times higher than that in the case of the supernatant of pure water. Therefore, the Fe(II) ions work as carriers of NO molecules:

$$NO_{aq} + Fe(II) \overset{K_1}{\rightleftharpoons} Fe(II)\text{-}NO \quad (6)$$

$$K_1 = [Fe(II)\text{-}NO]/([NO]_{aq} \times [Fe(II)]) \quad (7)$$

$$Fe(II)\text{-}NO + CR\text{-}Fe(II) \overset{K_2}{\rightleftharpoons} CR\text{-}Fe(II)\text{-}NO + Fe(II) \quad (8)$$

$$NO_{aq} + CR\text{-}Fe(II) \rightleftharpoons CR\text{-}Fe(II)\text{-}NO \quad (9)$$

$$d[CR\text{-}Fe(II)\text{-}NO]/dt = k_1[Fe(II)\text{-}NO] \times [CR\text{-}Fe(II)] + k_2[NO]_{aq} \times [CR\text{-}Fe(II)] \quad (10)$$

$$d[CR\text{-}Fe(II)\text{-}NO]/dt = k_1K_1[NO]_{aq} \times [Fe(II)] \times [CR\text{-}Fe(II)] + k_2[NO]_{aq} \times [CR\text{-}Fe(II)] \quad (11)$$

These considerations suggest the following adsorption mechanism and equations. First, the dissolved NO reacts not only directly with CR-Fe(II) complexes, but also with Fe(II) ions in the solution, thus forming Fe(II)-NO complexes. The Fe(II)-NO complexes can transfer the NO molecules to the CR-Fe(II) complexes according to Eq. 8. The above reaction of Eq. 6 is rapidly equilibrated by the vigorous bubbling of NO, and the equilibrium constant K_1 is expressed as Eq. 7. The aqueous solution of NO resulting from Eq. 1 reacts directly with the CR-Fe(II) complexes to form CR-Fe(II)-NO complexes according to Eq. 9 as well as through the Fe(II)-NO complexes according to Eqs. 6 and 8. Under these conditions, the initial adsorption rate is expressed as Eq. 10 from Eqs. 8 and 9 by neglecting the diffusion of NO into the resin. Consequently, Eq. 11 is obtained by substituting [Fe(II)-NO] by using Eq. 7. This equation theoretically predicts that the adsorption rate will increase with the concentration of Fe(II) ions in the supernatant. In fact, the adsorption rate first increases linearly with the increase in the concentration of Fe(II). When the concentration of Fe(II) is zero, the adsorption proceeds according to Eqs. 1 and 9. At a high concentration of Fe(II) ions, the plots deviated from the line, probably due to the limitation of transferring the NO molecule of the Fe(II)-NO complex to CR-Fe(II).

The equilibrium constant K_2 of Eq. 8 is expressed as Eq. 12. The product of K_1 and K_2 corresponds to an equilibrium constant of the total reaction K, which should coincide with the K of Eq. 3. This means that the quantity of adsorbed NO is determined from the quantity of CR-Fe(II) and the concentration of NO, and that the concentration of Fe(II) ions does not affect the quantity of NO adsorbed at equilibrium:

$$K_2 = [CR\text{-}Fe(II)\text{-}NO] \times [Fe(II)]/([Fe(II)\text{-}NO] \times [CR\text{-}Fe(II)]) \quad (12)$$

$$K_1 \times K_2 = K$$

Desorption of NO. The adsorbed NO is easily desorbed by heating the dispersions or by bubbling in pure nitrogen. The latter is an operation equivalent to the lowering of the partial pressure of NO. The NO adsorbed at 25 °C can be released by elevating the temperature to 80 °C, leaving 12% of NO in the dispersions; this amount corresponds to the amount of NO adsorbed at 80 °C. This means that the quantity of NO released can be estimated from the difference between the quantities of NO equilibrated at the temperatures of adsorption and desorption. Moreover, no deterioration was observed after five repetitions; this clearly indicates that the adsorbing reaction of NO by the present dispersions proceeds reversibly according to Eq. 2 and that no side reaction, such as the reduction of NO by the Fe(II) ions into N_2O, occurs under these conditions. The reversible adsorption can clearly be understood by the desorption experiment using bubbling pure nitrogen. The amount of desorbed NO coincides again with the amount of NO (0.040 mmol) predicted from the equilibrium constant.

The present work was partially supported by a Grant-in-Aid for Scientific Research from the Ministry Education, Science and Culture.

References

1) S. Kasaoka, E. Sasaoka, and S. Nakashima, *Nenryo Kyokai Shi*, **63**, 54 (1984).
2) T. Inui, T. Otowa, M. Kawata, and Y. Takegami, *Nenryo Kyokai Shi*, **62**, 762 (1983).
3) I. Mochida, K. Suetsugu, H. Fujitsu, and K. Takeshita, *J. Catal.*, **77**, 519 (1982).
4) T. Shikada, T. Oba, K. Fujimoto, and H. Tominaga, *Ind. Eng. Chem., Prod. Res. Rev.*, **23**, 417 (1984).
5) S. Takasaki, *Netsu Kanri To Kogai*, **29** (2), 37 (1976).
6) M. Teramoto, S. Hiramine, Y. Shimada, Y. Sugimoto, and H. Teranishi, *J. Chem. Eng. Jpn.*, **11**, 450 (1978).
7) K. Ogura and T. Ozeki, *Denki Kagaku*, **51**, 762 (1983).
8) Y. Hishinuma, R. Kaji, H. Akimoto, F. Nakajima, T. Mori, T. Kamo, Y. Arikawa, and S. Nozawa, *Bull. Chem. Soc. Jpn.*, **52**, 2863 (1979).
9) E. Sada, H. Kumazawa, and H. Machida, *Ind. Eng. Chem. Res.*, **26**, 2016 (1987).
10) H. Hirai and N. Toshima, "Tailored Metal Catalysts," ed by Iwasawa, D. Reidel Publishing Company (1986), p. 87; "Kobunshi Sakutai Shokubai (Macromolecular Complex Catalysts)," ed by H. Hirai and N. Toshima, Japan Scientific Societies Press, Tokyo (1982).
11) H. Hirai and H. Asanuma, *Hyomen*, **25**, 40 (1987).
12) H. Hirai, H. Asanuma, and N. Toshima, *Chem. Lett.*, **1985**, 655.
13) H. Hirai, H. Asanuma, and N. Toshima, *Chem. Lett.*, **1985**, 1921.
14) Japanese Industrial Standard (JIS) K1010.
15) K. Ogura and T. Ozeki, *Electrochim. Acta*, **26**, 877 (1981).
16) K. Pearsall and F. Bonner, *Inorg. Chem.*, **21**, 1978 (1982).

Crystal Structure of an 8,5′-Iminocarbonyloxy-Bridged Guanine Nucleoside Methanol Solvate

Katsumaro MINAMOTO,* Niro SHIOMI, Kazumoto KONDO, Shoji EGUCHI, Masako HONDA,†
Chuji KATAYAMA,† Atsushi KATAYAMA,† and Jiro TANAKA†
Institute of Applied Organic Chemistry, Faculty of Engineering, Nagoya University, Furo-cho, Chikusa-ku, Nagoya 464
†Department of Chemistry, Faculty of Science, Nagoya University, Furo-cho, Chikusa-ku, Nagoya 464
(Received May 18, 1988)

Synopsis. The crystal structure of 8,5′-[(allylimino)-carbonyloxy]-2-*N*-dimethylaminomethylene-9-(2′,3′-*O*-isopropylidene-β-D-ribofuranosyl)guanine (**2a**) methanol solvate was determined by X-ray analysis. Its base-sugar torsion angle conforms to the CD spectral behavior of the partially deprotected compound **2b** in the sense of anti-conformation.

A recent report from this laboratory has described the direct cyclization of 8-allylamino-2-*N*-dimethylaminomethylene-2′,3′-*O*-isopropylideneguanosine (**1**) to 8,5′-[(allylimino)carbonyloxy]-2-*N*-dimethylaminomethylene-9-(2′,3′-*O*-isopropylidene-β-D-ribofuranosyl)guanine (**2a**) with the use of diphenyl carbonate or *N*,*N*′-carbonyldiimidazole (CDI) in an attempt to realize a general synthesis of purine 8,5′-imino- and substituted imino cyclonucleosides (**3**) (Scheme 1).[1] Compound **2a** was deblocked to 8,5′-[(allylimino)-carbonyloxy]-9-(2′,3′-*O*-isopropylidene-β-D-ribofuranosyl)guanine (**2b**) (the allyl group was used as a *N*-protective group[2]). The facile formation of **2a** was interesting in view of our recent efforts to synthesize long-bridged cyclonucleosides for expanding the range of model base-sugar conformations[3] and hence we decided to determine the base-sugar torsion angle (Φ_{CN}) of the cyclized system **2** by X-ray analysis. Although the crystals of both **2a** and **2b** more or less had a propensity to effloresce in open atmosphere, the former proved to be more amenable to manipulation, and accordingly the results of its X-ray analysis are described herein.

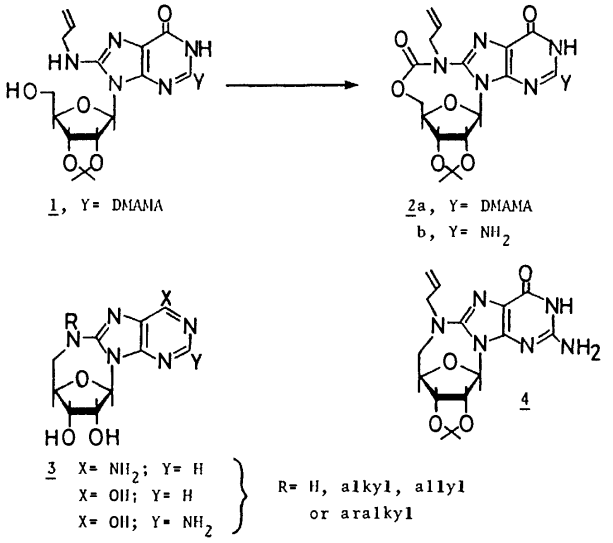

Scheme 1.

Experimental

Compound **2a** (100 mg) was dissolved in methanol (1.5 ml) at 40 °C and left at room temperature. Small hexahedral crystals appeared after 24 h and were allowed to grow for 2 weeks. Since these crystals (mono-methanolate) proved to have a tendency to effloresce with releasing methanol of crystallization,[4] a crystal was quickly sealed inside a glass capillary containing a tiny volume of the saturated mother liquor at the tip. D_m was measured by flotation in a mixture of acetone and chloroform. All subsequent X-ray measurements were conducted using a Rigaku automated four-circles diffractometer, AFC-5, employing graphite monochromatized Cu $K\alpha$ radiation (λ=1.5418 Å). $C_{20}H_{25}N_7O_6 \cdot CH_3OH$, M_r=491.51, triclinic, $P\bar{1}$, a=9.556 (1), b=11.171 (1), c=5.987(1) Å; α=106.28(1), β=83.70(1), γ=106.16(1)°; V=588.9(1) Å^3, D_x=1.386 g cm^{-3}, D_m=1.381 g cm^{-3}; Z=1; crystal size, 0.32×0.20×0.80 mm; 2156 measured reflections, $2\theta_{max}$=126.0°, $-11 \leqq h \leqq 10$, $-11 \leqq k \leqq 12$, $-4 \leqq l \leqq 0$, R_{int}=0.007. Three standard reflections after every 100 reflections (decay less than 18%). The structure was solved by the Monte-Carlo direct method[5] with the aid of MULTAN 78 program[6] using 1880 non-zero unique reflections, and refined by the full-matrix least-squares procedure with the analytical absorption correction.[7] Non-H atoms assigned anisotropic temperature factors. All the H atoms (except for some H atoms of **2a**) could be located on a difference Fourier map and refined with the equivalent isotropic temperature factors to that for the bonded carbon or nitrogen atoms.

$R=0.063$, $S=[\sum W(|F_o|^2-|F_c|^2)^2/(m-n)]^{1/2}=2.9$, $W=1/\sigma^2(F^2)$, $\Delta\rho_{max}$=1.0 e Å^{-3}.

Atomic scattering factors from International Tables for X-Ray Crystallography.[8] ORTEP employed for drawing the molecular structure. All the calculations were done on a FACOM M-382 computer at the Computation Center of Nagoya University.[9]

Discussion

Figures 1 and 2 show the selected bond lengths and bond angles of **2a**, respectively. When compared with the normal ribo-, deoxyribonucleosides or guanosine itself, it is seen from these figures that (a) the N9-C10-O18 (=N^9-$C_{1'}$-$O_{1'}$)[10] bond angle in **2a**, 113.9°, is significantly larger than 108—109° commonly shown by natural ribonucleosides[11] and the angle C13-C14-O15 ($C_{4'}$-$C_{5'}$-$O_{5'}$), 107.7°, is significantly smaller than normal 111—112°,[11] (b) the C13-C14 (=$C_{4'}$-$C_{5'}$) as well as C14-O15 (=$C_{5'}$-$O_{5'}$) bond length, 1.527 and 1.447 Å, respectively, is longer than corresponding values 1.507—1.514 and 1.42—1.43 Å for the normal nucleosides,[11] and (c) the N7-C8 (=N^7-C_8) bond length of the base, 1.298 Å, is shorter but the C8-N9 (=C_8-N^9) bond length, 1.414 Å, is significantly longer than the corresponding values, 1.306

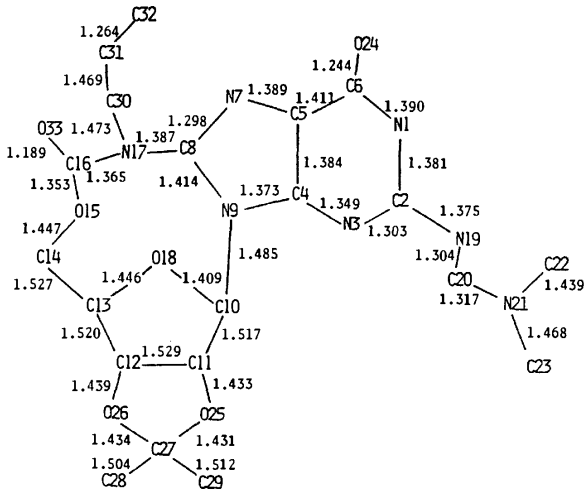

Fig. 1. Bond lengths of **2a** (l/Å).

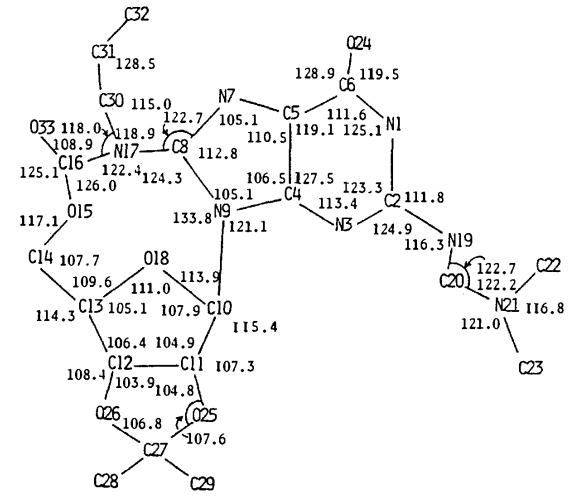

Fig. 2. Bond angles of **2a** (ϕ/°).

and 1.369 Å, shown by guanosine. These differences of the bond parameters seem to suggest the presence of some steric tension in the tricyclo[6.2.1] system including the bridge, which is probably reflected in our unsuccessful attempts to safely deisopropylidenate this type of compounds.

Figure 3 shows ORTEP drawing of the molecule as seen from over the base plane. It is recognized from this figure that the $O_{5'}$-CO-N^8(allyl)-bridge is located over the front side (2′,3′-side) of the nearly flat sugar ring. The base-sugar torsion angle (Φ_{CN}) defined as an angle from the $C_{1'}$-$O_{1'}$ bond was calculated as −90.20°, using the bond lengths and angles in Figs. 1 and 2. Here, the torsion angle was approximated by the dihedral angle between the plane C8-N9-C10 (=C_8-N^9-$C_{1'}$) and the plane O18-C10-N9 (=$O_{1'}$-$C_{1'}$-N^9). Similarly, the dihedral angle between the plane O18-C10-N9 (=$O_{1'}$-$C_{1'}$-N^9) and the plane C12-C10-N9 (=$C_{3'}$-$C_{1'}$-N^9) was calculated as −83.10° using appropriate bond parameters. Thus, the base-sugar torsion angle of **2a** has proved to reside between the two directions, $C_{1'}$-$C_{2'}$ and $C_{1'}$-$C_{3'}$, and quite near the $C_{1'}$-$C_{3'}$ line.

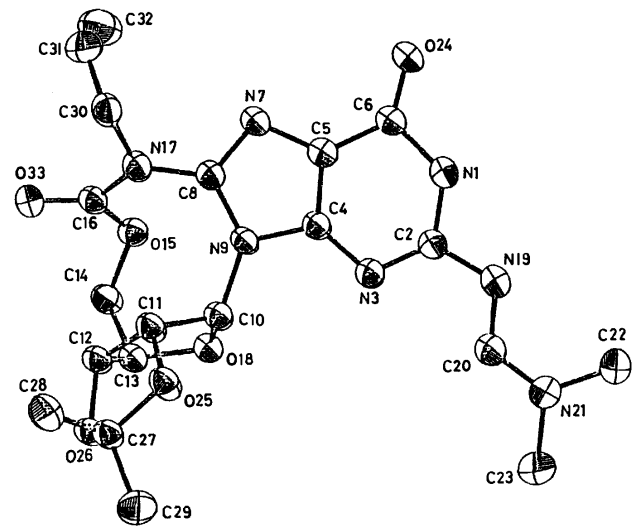

Fig. 3. An ORTEP drawing of **2a** as seen from the upside of the base plane. The H atoms and methanol of crystallization have been omitted for clarity (Thermal ellipsoids 30% probability level).

Table 1. UV and CD Spectra of **2b** and **4** in Methanol

Compd	UV[a] λ_{max}/nm (ε)	CD λ_{max}/nm (θ)
2b	269 (25900)	259 (+66500) 222 (−20000)
4	263 (15600) 283 (7500)[b]	259 (+28600) 223 (−4400)

a) Cited from Ref 1. b) Inflection.

CD spectra[13] of **2b** and 8,5′-allylimino-9-(5′-deoxy-2′,3′-*O*-isopropylidene-β-D-ribofuranosyl)guanine (**4**)[1] as an extreme anti conformer model are given in Table 1 together with their UV absorptions cited from Ref. 1. Although direct comparison between **2a** having an 8-iminocarbonyloxy group and **4** having an 8-amino group is rather inadequate, the strong positive Cotton effects of both compounds are in accord with the notion of the anti conformations of purine nucleosides.[14] It is anticipated that this type of long-bridged purine nucleosides in completely deprotected form would afford a different torsion angle or/and a different stereochemistry of the sugar part with releasing steric strain and further studies along this line are under way.

References

1) K. Minamoto, Y. Fujiki, N. Shiomi, Y. Uda, and T. Sasaki, *J. Chem. Soc., Perkin Trans. 1*, **1985**, 2337.
2) J. A. Montgomery and H. J. Thomas, *J. Org. Chem.*, **30**, 3253 (1965).
3) T. Sasaki, K. Minamoto, S. Yamashita, K. Yamaguchi, and K. Miyake, *J. Org. Chem.*, **46**, 5176 (1981). T. Sasaki, K. Minamoto, S. Yamashita, and Y. Fujiki, *ibid.*, **47**, 4465 (1982). T. Sasaki, K. Minamoto, and H. Nakade, Nucleic Acid Res., Symposium Series No. 11, **1982**, 57.
4) Solvent-free **2a** is a crystalline powder.[1]
5) A. Furusaki, *Acta Crystallogr., Sect. A*, **35**, 220 (1979).
6) P. Main, S. E. Hull, L. Lessinger, G. Germain, J. P.

DeClercq, and M. M. Woolfson, "MULTAN 78," Universities of York and Louvain (1978).

7) C. Katayama, N. Sakabe, and K. Sakabe, *Acta Crystallogr., Sect. A*, **1972**, 207.

8) "International Tables for X-Ray Crystallography," Kynoch Press, Birmingham, England (1974), Vol. 4.

9) Listing of atomic parameters, thermal parameters and F_o-F_c table are deposited as Document No. 8854 at the Office of the Editor of Bull. Chem. Soc. Jpn.

10) The atom numberings in the parentheses are those commonly used to designate the atoms in the purine bases and furanoses.

11) W. Saenger, "Principles of Nucleic Acid Structure," Springer-Verlag, New York (1984), p. 70.

12) "Synthetic Procedures in Nucleic Acid Chemistry," Vol. 2, ed by W. W. Zorbach and R. S. Tipson, Wiley-Interscience, New York, N. Y. (1973), p. 520.

13) The CD spectra were recorded on a JASCO J-500 Spectropolarimeter equipped with a JASCO DP-500 data processor for CD.

14) Ref. 10, p. 199.

The Relationship between the Acoustic Property and the Hydration of Saccharides

Hisashi UEDAIRA* and Miyuki ISHIMURA
Department of Polymer Science, Faculty of Science, Hokkaido University, Sapporo 060
(Received May 18, 1988)

Synopsis. Values of the relative increment of the sound velocity, A, in aqueous solutions of sugars were calculated from the experimental sound velocities. The values of A correlated well with the mean number of equatorial OH groups in a sugar molecule.

Recently, it was found that the limiting diffusion coefficients[1] and the partial molar heat capacities[2] for saccharides in water correlate well with the mean number of equatorial OH groups, $n(e\text{-OH})$, in a sugar molecule. These properties, which are affected by hydration, depend sensitively on the conformation of saccharides in aqueous solution. The accoustic properties of aqueous solutions of saccharides are also thought to depend on the degree of their hydration. Høiland and Holvik,[3] however, showed that the isoentropic partial molar compressibilities of saccharides do not correlate with the number of e-OH groups. Sarvazyan and his co-workers[4,5] theoretically indicated that the relative increment of the sound velocity, $A=(U-U_0)/(U_0m)$, sensitively reflects the solute-water interactions, where U and U_0 are the sound velocity in solutions and pure water respectively, and m is the concentration. In this paper, we report on the values of A calculated from the densities and compressibilities of aqueous saccharides solutions and discuss the relation between the values of A and the conformations of saccharides.

Results and Discussion

Høiland and Holvik obtained the following equations for the densitites, d, and compressibilities, β_s, of the saccharides solutions at 25 °C:

$$d=d_0+\sum_{i=1}^{3} a_i m^i \tag{1}$$

and

$$\beta_s=\beta_s^0+\sum_{i=1}^{3} b_i m^i, \tag{2}$$

where d_0 and β_s^0 are the density and compressibility of pure water, respectively. We obtained the following relation for A in the low concentration range; this relation was calculated from Eqs. 1 and 2 by means of the Laplace relation for the sound velocity:

$$A=-(a_1/d_0+b_1/\beta_s^0), \tag{3}$$

where a_1 and b_1 are the coefficients of the terms proportional to m in Eqs. 1 and 2, respectively.

We calcualted the values of A from Eq. 3 by the use of Høiland and Holvik's data.[3] The values obtained are plotted against $n(e\text{-OH})$ for saccharides in Fig. 1. We used the values of $n(e\text{-OH})$ which were previously calculated.[1,2] The straight line in Fig. 1 was determined by the method of least squares and is represented by

$$A\times10^2=1.297+0.780\,n(e\text{-OH}), \tag{4}$$

with a very high correlation coefficient of 0.965.

The change of sound velocity in solution is ascribed to two effects: (1) an increase in the sound velocity by the introduction of incompressible solute molecule, and (2) a change in the water structure around the molecule.[6,7] If the solute molecule stabilizes the water structure, the sound velocity in the solution is hastened. We found that the sound velocity in aqueous solutions of alkali chlorides increases with increasing the degree of structure making of an ion, but in a cessium chloride solution, which is the strong structure-breaking ion, it is smaller than that in pure water.[7]

In Eq. 3, the value of a_1 depends on the total number of OH groups in a sugar molecule and the intrinsic volume.[3,8] The value of b_1 depends only on the sugar OH group-water interactions, which differ in different orientation of the OH group. The values of a_1 are positive, but those of b_1 are negative for all the saccharides in Fig. 1.[3] Since $A>0$ for all the saccharides in Fig. 1, the absolute values of a_1/d_0 are smaller than those of b_1/β_s^0. Thus, the value of A mainly reflects the second effect between the above two, and increases with an increase in the degree of hydration.

The e-OH groups in a sugar molecule may be effectively substituted for a water molecule within the water structure; therefore, the hydration of sugar hydroxyl groups has a stereospecific nature. Thus, a

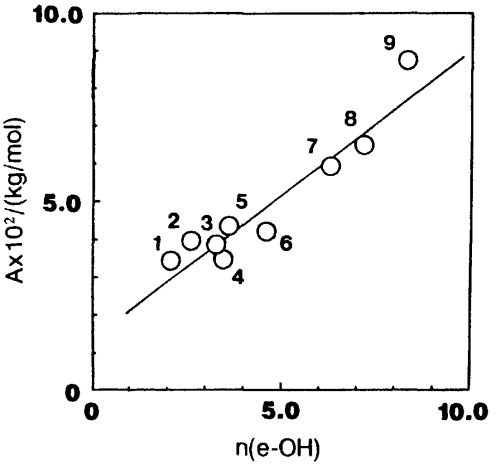

Fig. 1. The relationship between the values of A and the mean number of e-OH groups in each sugar molecule.
1. Ribose, 2. arabinose, 3. mannose, 4. xylose, 5. galactose, 6. glucose, 7. sucrose, 8. maltose, 9. raffinose.

sugar molecule which has a larger number of *e*-OH groups in the molecule has a stronger stabilizing effect on the water structure.[1,9] We showed that ribose, which has only 2.1 *e*-OH groups, hardly affects the water structure.[1] The result of Fig. 1, therefore, is explained by the effect of *e*-OH groups on the water structure. The relative increments of the sound velocities in aqueous solutions of saccharides clearly show the conformation dependence of their molecules.

We wish to thank Dr. Hatsuho Uedaira for her helpful discussions.

References

1) H. Uedaira and H. Uedaira, *J. Solution Chem.*, **14**, 27 (1985).
2) H. Uedaira and H. Uedaira, *J. Chem. Thermodyn.*, **17**, 901 (1985).
3) H. Høiland and H. Holvik, *J. Solution Chem.*, **7**, 587 (1978).
4) A. P. Sarvazyan and D. P. Kharakoz, *J. Phys. Chem.*, **83**, 1796 (1979).
5) A. P. Sarvazyan and V. A. Buchin, *J. Phys. Chem.*, **84**, 692 (1980).
6) F. Hirata and K. Arakawa, *Bull. Chem. Soc. Jpn.*, **45**, 2715 (1972).
7) H. Uedaira and Y. Suzuki, *Bull. Chem. Soc. Jpn.*, **52**, 2787 (1979).
8) F. Shahidi, P. G. Farrell, and J. T. Edward, *J. Solution Chem.*, **5**, 807 (1976).
9) M. J. Tait, A. Suggett, F. Franks, S. Ablett, and A. J. Quickenden, *J. Solution Chem.*, **1**, 131 (1972).

Gamma-X Ray Coincidence Mössbauer Study with $FeSO_4 \cdot 7H_2O(^{57}Co)$

Takayuki KOBAYASHI
Department of Physics, Shiga University of Medical Science, Otsu, Shiga 520-21
(Received May 24, 1988)

Synopsis. The anomalous charge states formed after the EC decay of ^{57}Co in $FeSO_4 \cdot 7H_2O$ doped with ^{57}Co are investigated in detail using the gamma-X ray coincidence Mössbauer spectroscopy. The mechanism to form these states is explained in terms of the H_2O and SO_4^{2-} coordination shells around the decaying atom.

Anomalous states formed after a nuclear decay in insulating materials (aftereffects) have been usually investigated using the emission Mössbauer spectroscopy.[1-4] In hydrated divalent metallic compounds doped with ^{57}Co, anomalous Fe^{3+} states are usually formed and are considered to be due to the oxidation of Fe^{2+} by free OH radicals produced through radiolysis of the H_2O ligands.[5] This mechanism was examined in detail with cobalt chloride hydrates using the gamma-X ray coincidence Mössbauer spectroscopy,[6] and a determinant role of the nearest and the next nearest H_2O coordination shells according to the densities of H_2O molecules was noticed. In the recent study with metallic sulfate hydrates,[7] the influence of both H_2O and SO_4^{2-} ligands to the aftereffects has been suggested, but its detailed mechanism remains unknown. In the present work, a further investigation of the aftereffects in $FeSO_4 \cdot 7H_2O$ is therefore given using the gamma-X ray coincidence Mössbauer spectroscopy.

The principle of the experiment is based on the fact that the influence of low-energy electrons emitted during the Auger cascade after the EC decay of ^{57}Co on the surroundings of the decaying atom in the K-Auger process is approximately two times larger than that in the case of the K-X ray emission. A Mössbauer spectrum observed by using the coincidence technique only when K-X rays are emitted is, therefore, expected to give new information for the mechanism of the aftereffects on careful comparison with a conventional emission Mössbauer spectrum. More detailed explanations of the principle are described elsewhere.[6,8,9]

A sample of $FeSO_4 \cdot 7H_2O$ doped with ^{57}Co was prepared at room temperature from a very small amount of 0.25 $mol \cdot dm^{-3}$ H_2SO_4 solution of iron(II) sulfate including few μCi of ^{57}Co. The detectors used for 6.5 keV X-rays and 14.4 keV γ-rays were NaI(Tl) crystals with 1-inch diameter and 1-mm thickness. The coincidence spectrum was recorded by the conventional slow coincidence technique. The other experimental details including the block diagram of the measuring system has been given in our previous paper.[6]

The Mössbauer spectra observed and parameters obtained are shown in Fig. 1 and Table 1, respectively. The normal state in $FeSO_4 \cdot 7H_2O$ is represented by $Fe^{2+}(1)$ in Table 1, and the others are anomalous states. Figure 2 shows graphically the relative intensities of the components. The reason why the intensity of $Fe^{2+}(1)$ in the coincidence spectrum is large compared with that in the conventional spectrum can be explained obviously from the experimental principle.

The densities of the H_2O and SO_4^{2-} molecules in $FeSO_4 \cdot 7H_2O$ as a function of distance from the iron atom to the oxygen atom is shown in Fig. 3, which were calculated by considering the structure of the compound.[10] Two distinct coordination shells of H_2O and SO_4^{2-} are noticed at approximately 2 Å and 4 Å, respectively, from the iron atom. The component Fe^{3+} is considered to arise from a free OH radical pro-

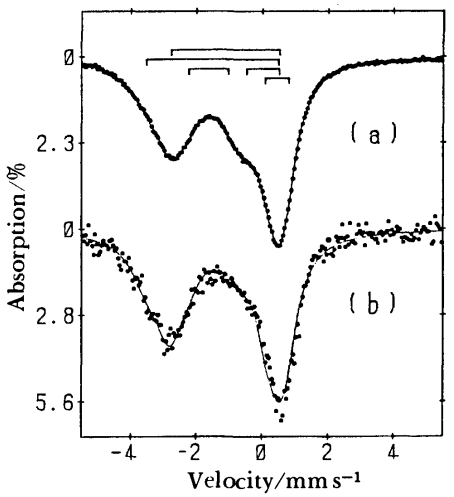

Fig. 1. Observed Mössbauer spectra; (a) conventional, (b) coincidence. The bar diagram represents the individual component peaks.

Table 1. Obtained Mössbauer Parameters of the Conventional and Coincidence Spectra

State	I.S.[a]	Q.S.	[Conventional] Width	[Conventional] Intensity	[Coincidence] Width	[Coincidence] Intensity
	mm s^{-1}	mm s^{-1}	mm s^{-1}	%	mm s^{-1}	%
$Fe^{2+}(1)$	−1.15±0.01	3.31±0.03	1.01±0.03	32.9	1.10±0.08	51.7
$Fe^{2+}(2)$	−1.52±0.04	3.97±0.06	1.24±0.06	18.4	1.22±0.15	23.7
$Fe^{2+}(3)$	−1.64±0.01	1.22±0.03	1.09±0.02	19.7	0.87±0.16	9.5
Fe^{3+}	−0.02±0.03	0.99±0.06	0.72±0.02	14.9	0.62±0.10	4.0
Fe*	0.43±0.02	0.69±0.02	0.72±0.02	14.1	0.62±0.10	11.1

a) Relative to α-iron at room temperature.

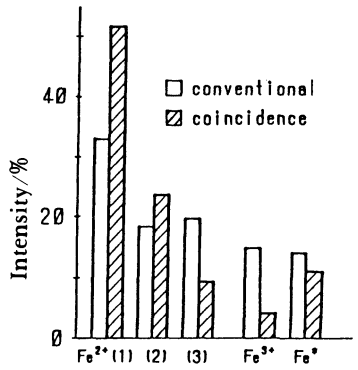

Fig. 2. Relative intensities of the component peaks in the spectra.

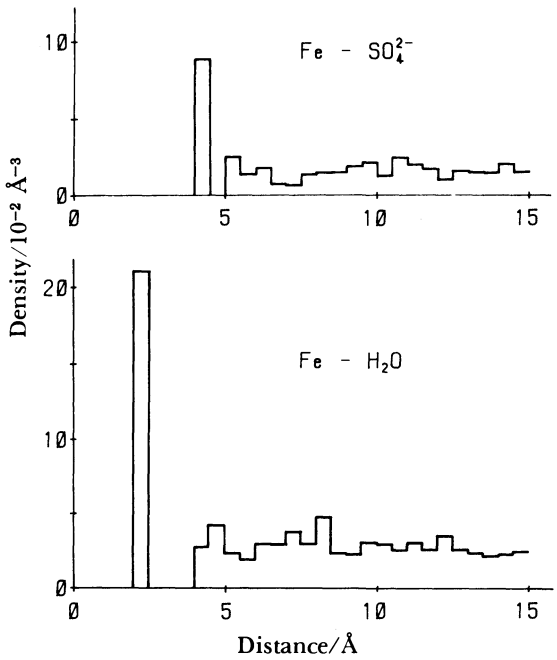

Fig. 3. Densities of H_2O or SO_4^{2-} molecules as a function of distance from a Fe atom in $FeSO_4 \cdot 7H_2O$.

duced through radiolysis of a H_2O ligand in the shell being nearest to the decaying atom, because its intensity in the coincidence spectrum is much smaller than that in the conventional spectrum. The species of Fe* having the unusual value of its isomer shift (I.S.) is unknown, but is probably a high-charged state.

The formation of the $Fe^{2+}(2)$ state can be attributed to the effect of radiolysis of SO_4^{2-} lingands. Owing to a relatively long distance between the decaying atom and a SO_3^- radical produced through radiolysis of a SO_4^{2-} ligand, this radical can hardly oxidize the iron ion which is produced after the decay of ^{57}Co. When this radical recombines with O^-, which is also produced through radiolysis, or remains in its state for a while, the local symmetry around the iron ion becomes lower and this results in a large Q.S. value. It is not easy to show the mechanism of the formation of the $Fe^{2+}(3)$ state, which has a smaller Q.S. value than the other divalent states and a similar I.S. value to the $Fe^{2+}(2)$ component. As in the case of $CoCl_2 \cdot 2H_2O$, where an equivalent component appears,[6] the ligands being further than those in the two H_2O and SO_4^{2-} shells may be involved in the formation of the $Fe^{2+}(3)$ state. The decreased $Fe^{2+}(3)$ intensity in the coincidence spectrum in comparison with that in the conventional spectrum supports this explanation. Owing to the reduction of the flux of low-energy electrons under the coincidence conditions, the number of electrons passing through the H_2O and SO_4^{2-} shells then decreases, which results in a low intensity of the component. The cause of the small Q.S. value of $Fe^{2+}(3)$ compared with that of the other divalent components is unknown.

The results obtained in the present work matches collectively with those of $CoCl_2 \cdot nH_2O$ (n=2,6).[6]

Miss Kazuko Fukumura should be acknowledged for her cooperation in preparing the sample material and in measuring the spectra.

References

1) R. Ingalls, G. J. Coston, G. de Pasquali, H. G. Drickamer, and J. J. Pinajian, *J. Chem. Phys.*, **45**, 1057 (1966).
2) J. M. Friedt, G. K. Shenoy, G. Absteiter, and R. Poinsot, *J. Chem. Phys.*, **59**, 3831 (1973).
3) Y. Sakai, K. Endo, and H. Sano, *Bull. Chem. Soc. Jpn.*, **54**, 3587 (1981).
4) D. L. Nagy, R. Doerfler, G. Ritter, J. Waigel, N. Zeman, and B. Molnár, *Phys. Lett.*, **95A**, 400 (1983).
5) J. M. Friedt and J. Danon, *At. Energy Rev.*, **18**, 893 (1981).
6) T. Kobayashi and J. M. Friedt, *Bull. Chem. Soc. Jpn.*, **59**, 631 (1986).
7) T. Kobayashi, *Radiochim. Acta*, **42**, 139 (1987).
8) T. Kobayashi, K. Fukumura and T. Kitahara, *Nucl. Instrum. Methods*, **166**, 257 (1979).
9) T. Kobayashi, *Radiochim. Acta*, **35**, 43 (1984).
10) W. H. Baur, *Acta Crystallogr.*, **17**, 1167 (1964).

The Thermodynamics of the Micelle Formation of Sodium α,ω-Alkanediyl Disulfate

Kenji IKEDA,* Tomoko NAKASIMA, Kunio ESUMI, and Kenjiro MEGURO
Department of Applied Chemistry, Institute of Colloid and Interface Science, Science University of Tokyo, Kagurazaka, Shinjuku-ku, Tokyo 162
(Received July 14, 1988)

Synopsis. The critical micelle concentrations of a α,ω-type surfactant: (sodium α,ω-alkanediyl disulfate: n=12, 14, 16) in an aqueous solution have been determined by studying the electrical conductivity, and the free energies of the micelle formation have then been estimated from these data. The free energy of micelle formation of a α,ω-type surfactant was smaller than that of a normal-type surfactant with the same alkyl chain length as the α,ω-type one. The free-energy changes per -(CH_2)- segment was also calculated from these data. It is found that the free-energy change per -(CH_2)- segment of the α,ω-type surfactant is −11.1 [kJ mol^{-1}].

A α,ω-type (bola form) surfactant has two head groups, are at each end of the hydrocarbon chain.[1-14] Interest in this surfactant has increased steadily in recent years from the standpoint of fundamental studies and applications. Studies of α,ω-type surfactant in aqueous solutions can be made from three points of view. First is how the α,ω-type surfactants are built up at the air-water interface. Second is how the micelle of the α,ω-type surfactants is formed in aqueous solutions and what kind of conformation the α,ω-type surfactants form in the micelle. Third is how the liquid crystalline phase of the α,ω-type surfactants is made up in a surfactant-water system. The critical micelle concentration and molecular areas have been determined by measuring the surface tension as a step in studying the carbon chain conformation in the air-water interface.[6,8] It has been suggested that the α,ω-type surfactant forms vertical "wicket-like" loops at the air-water interface. With regard to the micelle formation of α,ω-type surfactants, Zana et al.[10] have investigated the micelle properties of C_nMe_6 (N,N'-polymethylenebis(triethylammonium) dibromide: n= 12, 16, 22) by means of the P-jump and the ultrasonic absorption; they have concluded that the $C_{22}Me_6$ alkyl chain is probably folded in micelles, as the properties of $C_{22}Me_6$ are the same as those of normal alkyl-chain surfactant whose chain length is half that of $C_{22}Me_6$. We ourselves have investigated the micelle properties of $C_{20}Et_6$ in aqueous solutions by means of the ^{1}H NMR (FT PGSE technique)[12] and ^{13}C, ^{14}N NMR relaxation methods.[13] From the water, surfactant, and micelle self-diffusion coefficients, the length of alkyl carbon chain is obtained to be close to the micelle diameter. ^{13}C and ^{14}N NMR relaxation and NOE measurements indicate that the alkyl-carbon chain of $C_{20}Et_6$ is stretched out rather than folded.

The determination of the thermodynamic parameter of micelle formation has been studied by measuring the cmc at various temperatures. This kind of study is important in discussing the micelle property. In this study, several α,ω-type surfactants such as sodium α,ω-alkanediyl disulfate (n=12, 14, 16) were synthesized, and the cmc values at different temperatures were compared with that of a normal type surfactant, sodium alkyl sulfate.[16,17]

Experimental

Materials. The $C_{12}Na_2$ (sodium α,ω-dodecane disulfate) was prepared as has been described previously.[8] The $C_{14}Na_2$ and $C_{16}Na_2$ were synthesized via α,ω-alkanediol by using α,ω-alkanedioic acid (n=14, 16) (Tokyo Kasei Co.) as the starting material via α,ω-alkanediol. Normal alkanedioic acids were reduced to α,ω-alkanediol by using the borane-THF complex (Aldrich Chem. Co.). After the product has been recrystallized twice with benzene, the complete reduction to α,ω-alkanediol was confirmed by measuring the IR spectrum. The diol thus prepared was reacted with chlorosulfuric acid to give α,ω-alkane disulfate. Then, this disulfate was neutralized with sodium hydroxide. After the product has been recrystallized three times with an acetone-ethanol mixture and three times with an ethyl acetate-ethanol mixture, it was washed twice with diethyl ether and then dried more than 72 h under a vacuum. The purity of the white crystalline product was confirmed to be above 99% by means of elemental analysis, isotachophoresis (IP-3A: Shimadzu Co., Ltd.), NMR, and the surface tension.

Measurement. The electroconductivity of the solution was measured by means of a conductivity meter (Model CM-30ET Toa Denpa Co.) at 20, 25, 30, 40, 50, and 60 ±0.1 °C.

Results and Discussion

The cmc values were determined from plots of the specific conductance, κ, against the molar concentration, C, at several temperatures. These values are tabulated in Table 1. The cmc values decreased with the increase in the carbon chain lengths of the surfactant, while the cmc values of each surfactant increased with the increasing the temperature. Some cmc data taken from the literature[16] for hydrocarbon surfactants, sodium alkyl sulfates, are also shown in Fig. 1 for comparison with those for the α,ω-type surfactants. As the change in the cmc is small between 25 °C and 40 °C, the data for monoalkyl sulfate are used at 40 °C.[20] The C_nNa_2's cmc change against the carbon-chain length was smaller than that of the normal-type surfactant. From these results, it can be said that the

Table 1. cmc's Against the Temperature (×10^{-3} mol kg^{-1})

Temp/°C	$C_{12}Na_2$	$C_{14}Na_2$	$C_{16}Na_2$	$C_{18}Na_2$
20	60	—	—	—
25	61	—	—	—
30	63	—	—	—
40	64	38	—	—
50	65	41	—	—
60	68	46	11.8	—
70				7.6[a]

a) This value is taken from Ref. 7.

chain length of a α,ω-type surfactant is smaller than half the length of a normal-type surfactant.[19] Zana et al. reported that the C_nMe_6's cmc's change against the carbon-chain length was smaller than those of the C_nMe_3. This also suggests that the α,ω-type surfactant may be regarded as shorter than half the length of the normal-type surfactant. The micelle formation free energies of sodium α,ω-alkanediyl disulfate were calculated[15] from cmc measurements at different temperatures. These free energy values are shown in Table 2. A phase separation model was used for these calculations.[16] The following equation was used for the calculation of the micelle formation free energy:

$$\Delta G^\circ = (3-2\alpha)\, RT \ln \text{cmc} \qquad (1)$$

where α is the counterion binding of the micelle, R, the gas constant, and T, the absolute temperature. Each α value was also obtained by conductivity measurement. The micelle-formation free energies of C_nNa_2 were slightly decreased with increase in the temperature. The micelle-formation entropy changes in C_nNa_2 were also calculated from the cmc's at different temperatures, but the entropy changes of C_nNa_2 (n=12, 14) were negligibly small. These results show that the entropy change is not very important in forming the micelle in the case of n=12 or 14. In other words, the "iceberg" structure of water is not much destroyed when the C_nNa_2 (n=12, 14) micelle forms.[18] However, any further discussion of entropy change would be meaningless because these calculations of entropy changes contain many errors. Figure 2 shows the micelle formation free energy changes against the alkyl chain length at 60 °C. The free energy decreases with the increase in the alkyl carbon chain length. Increasing the alkyl carbon chain serves to increase in the hydrophobic effect and further to make micelle formation easier. The free energy change against the $-(CH_2)-$ segment of C_nNa_2 was -11.1 [kJ mol^{-1}].

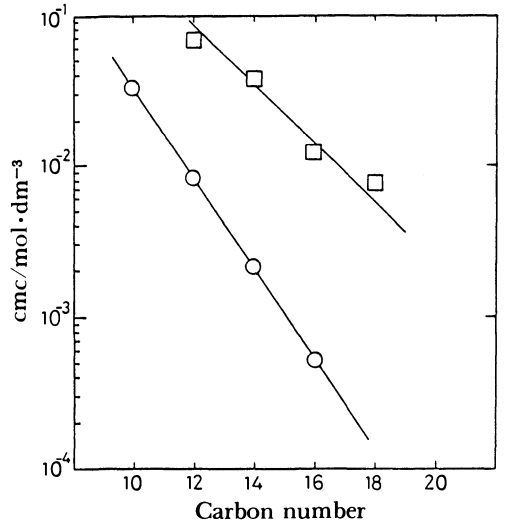

Fig. 1. cmc's of sodium n-alkyl sulfate and sodium α,ω-alkanediyl disulfate as a function of hydrocarbon chain length.
(□): C_nNa_2, (○): C_nNa.

Table 2. The Free-Energy Change of Micelle Formation

	Temp/°C	G_m/kJ mol^{-1}
$C_{12}Na_2$	20	−10.7
	30	−11.2
	40	−11.2
	50	−11.4
	60	−11.6
$C_{14}Na_2$	40	−11.4
	50	−11.5
	60	−12.1
$C_{16}Na_2$	60	−15.7
$C_{18}Na_2$	70	−17.8

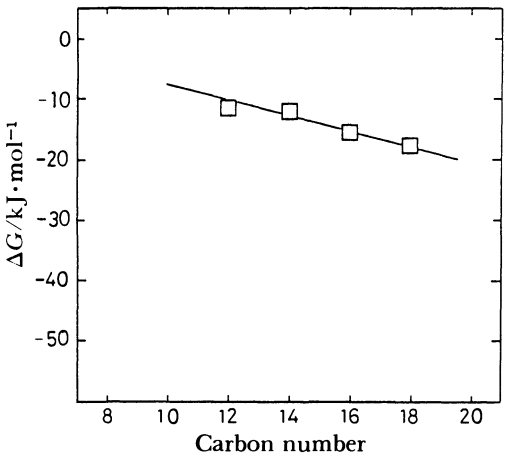

Fig. 2. Standard free energy of sodium α,ω-alkanediyl disulfate as a function of hydrocarbon chain length.
(□): C_nNa_2.

References

1) P. H. Elworthy, *J. Pharm. Pharmacol.*, **11**, 557 (1959).
2) P. H. Elworthy, *J. Pharm. Pharmacol.*, **11**, 624 (1959).
3) T. L. Broadwater and D. F. Evans, *J. Phys. Chem.*, **73**, 164 (1969).
4) O. D. Bonner and S. Kim, *J. Phys. Chem.*, **73**, 1367 (1969).
5) M. Ueno, T. Hikota, T. Mitama, and K. Meguro, *J.A.O.C.S.*, **49**, 250 (1972).
6) F. M. Menger and S. Wrenn, *J. Phys. Chem.*, **78**, 1387 (1974).
7) M. Ueno, S. Yamamoto, and K.Meguro, *J.A.O.C.S.*, **51**, 373 (1974).
8) K. Meguro, K. Ikeda, A. Otsuji, M. Taya, M. Yasuda, and K. Esumi, *J. Colloid Interface Sci.*, **118**, 372 (1987).
9) A. Cipiciami, M. Fracassini, R. Germani, G. Savelli, and C. A. Bunton, *J. Chem. Soc., Perkin Trans. 2*, **1987**, 547.
10) S. Yiv, K. M. Kale, J. Lang and R. Zana, *J. Colloid Interface Sci.*, **80**, 2651 (1976); S. Yiv and R. Zana, *ibid.*, **77**, 449 (1980); R. Zana and S. Yiv, *ibid.*, **77**, 456 (1980).
11) D. C. Mckenzie, C. A. Bunton, D. F. Nicoli, and G. Savelli, *J. Phys. Chem.*, **91**, 5709 (1987).
12) K. Ikeda, K. Meguro, A. Kahn, and B. Lindman, *J. Colloid Interface Sci.*, submitted for publication.
13) T. Wong, K. Ikeda, K. Meguro, U. Ollson, O. Sederman, and B. Lindman, *J. Phys. Chem.*, in press.
14) R. Zana, Y. Muto, K. Esumi, and K. Meguro, *J. Colloid Interface Sci.*, **123**, 502 (1988).
15) P. Mukerjee, K. Korematsu, M. Okawauchi, and G. Sugihara, *J. Phys. Chem.*, **89**, 5308 (1985).

16) S. S. Berr, *J. Phys. Chem.*, **91**, 4760 (1987).
17) N. J. Chang and E. W. Kaler, *J. Phys. Chem.*, **89**, 2996 (1985).
18) C. Tanford, "The Hydrophobic Effect," 2nd ed, Wiley-Interscience, New York (1980).
19) J. L. Israel and Y. Zimmels, in "Micellization, Solubilization, and Microemmulsions," ed by K. L. Mittal, Plenum Press, New York (1977), Vol. 1, p. 455.
20) J. Powney and C. C. Addison, *Trans. Faraday Soc.*, **33**, 1243 (1937).

Single Crystals Coimaged with the Gigantic Rod-Like Micelles in Viscoelastic Cationic Surfactant-Aromatic Additive Systems

Hirotaka HIRATA* and Yuko SAKAIGUCHI
Department of Physical Chemistry, Niigata College of Pharmacy, 2-13-5 Kamishin'eicho, Niigata 950-21
(Received July 22, 1988)

Synopsis. In a system of hexadecyltrimethylammonium bromide (HTAB)-salicylic acid (SA) in which a remarkable viscoelasticity is induced, we noticed the existence of single crystals coimaged with the infinitely elongated rod-like micelles. The single crystal implied the formation of a new species, a complex which resulted from the interaction of HTAB and aromatic additives.

Previously, we reported the clear detection, under an electron microscope, of gigantic rod-like micelle images in a solution of several cationic surfactants, such as HTAB and hexadecylpyridinium bromide, with some aromatic substances added.[1] These solutions were always accompanied by a remarkable viscoelasticity.[2] The gigantic rod-like micelles showed an infinite length, and they were heavily entangled with each other, like cobwebs, in the electron micrographs.[3,4] It seemed that those aspects provided a sufficient explanation of the solution behavior in all senses.

In the course of carrying out the image observation of the elongated gigantic micelles under an electron microscope, we recently became aware of the existence of a few single crystals always together with the rod-like micelles in almost all of the surfactant and aromatic additive systems. The images of these single crystals are exhibited in Fig. 1.

The crystals in a system of HTAB-SA typically have a well grown shape in electron micrography. The image contrast to the background suggests that the crystal thickness is nearly the same as the rod-like micelle diameter or at least of the same order.

It is obvious that the crystals found in these photos are different from those of each component, CTAB or SA, for there is a clear difference in the apparent shapes of the component crystals, excluding such cases of a plausible coming out of the crystalline materials of each component from the solutions, especially of the precipitation of the surfactants below their Krafft points.

The analysis of the sharp spots caused by the electron diffraction from these single crystals are being successfully carried out in many gigantic rod-like micelle-producing systems. The spot patterns were also clearly different from those of each component crystal. The results will be reported in another place.[5]

In this context, it is worthwhile mentioning that in one of the most remarkable viscoelastic solutions, the HTAB-*o*-iodophenol system, we obtained crystalline materials which were unambiguously indicated through the elementary analysis to be composed of HTAB and *o*-iodophenol in a one-to-one molar ratio.[6] This fact distinctly reveals that a certain kind of interaction between HTAB, a quaternary ammonium, and aromatic additives acts to provide a complex.[7]

Commercially available HTAB was used after one recrystallization from an acetone-methanol mixture

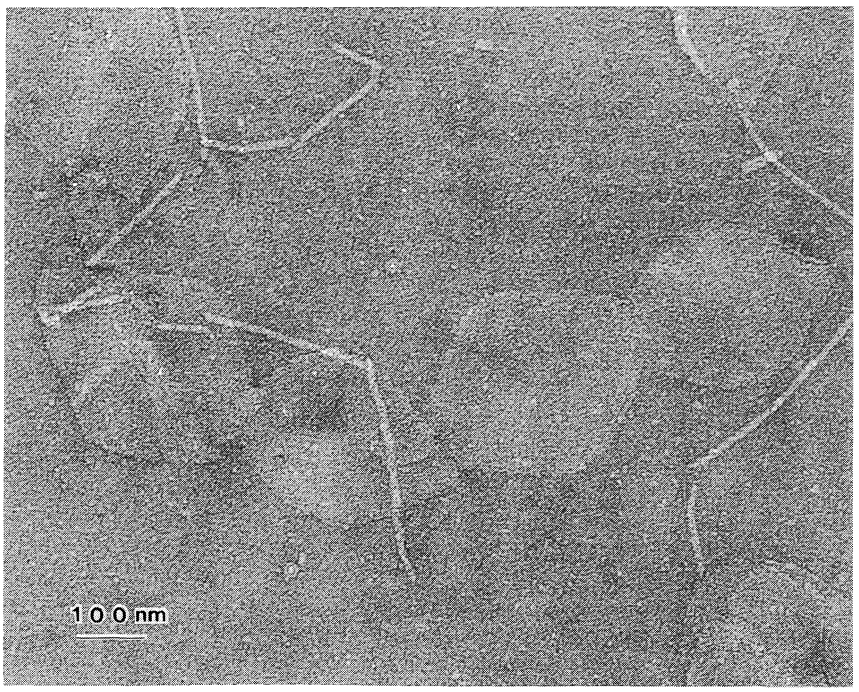

(a)

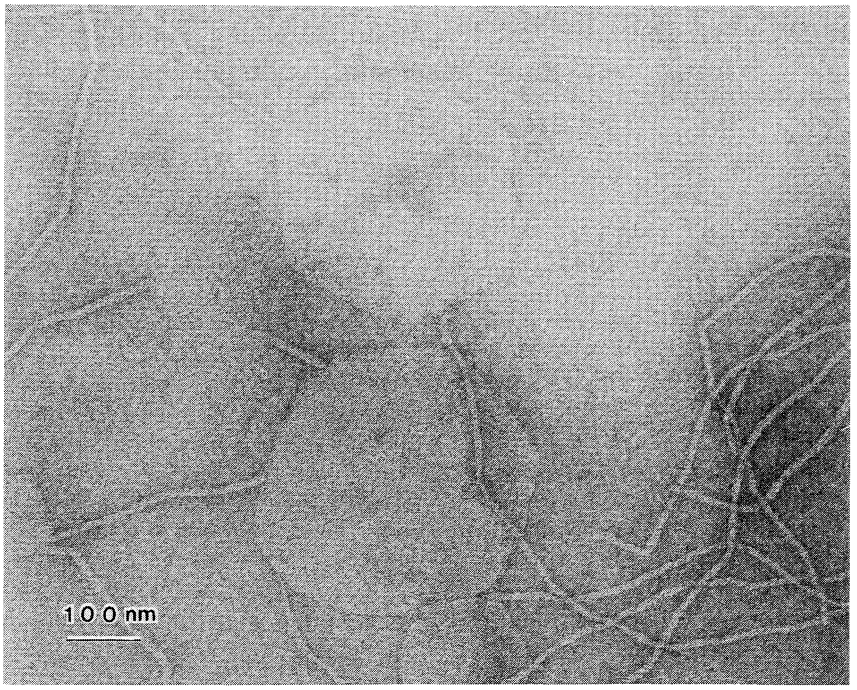

(b)

Fig. 1. Single crystals coimaged in the transmission electron micrograph of CTAB-SA system in the magnification of 97,500. Specimens were prepared from 1×10^{-3} mol l^{-1} CTAB solution at mixing molar ratio of SA/CTAB=0.8. As for the details see Ref. 3.
a) Rhombus shaped single crystals are seen with a definite angle between edges.
b) Apparent hexagonal shaped single crystals are seen. The angles between edges are equal to each other as well.

while SA in a special pure grade was used as purchased. Transmission electron microscopy was carried out upon a JEOL 100CX apparatus operated at 80 kV. All the images were obtained by negative staining techniques with uranyl acetate.

We are very grateful for having received many suggestive comments on this subject from Mr. Atsuo Koreeda in the Institute of Scientific and Industrial Research of Osaka University and also for the ardent encouragement of Dr. Yoshie Kitayama of the Engineering Chemistry Department of Niigata University.

References

1) T. Shikata, Y. Sakaiguchi, H. Urakami, A. Tamura, and H. Hirata, *J. Colloid Interface Sci.*, **119**, 291 (1987).
2) J. Ulmius, H. Wennerstrom, L. B. Johansson, G. Lindblom, and S. Gravsholt, *J. Phys. Chem.*, **83**, 2232 (1979).
3) Y. Sakaiguchi, T. Shikata, H. Urakami, A. Tamura, and H. Hirata, *J. Electron Microsc.*, **36**, 168 (1987).
4) Y. Sakaiguchi, T. Shikata, H. Urakami, A. Tamura, and H. Hirata, *Colloid Polym. Sci.*, **265**, 750 (1987).
5) H. Hirata, Y. Sakaiguchi, and J. Akai, *J. Colloid Interface Sci.*, in press.
6) Y. Sakaiguchi, T. Shikata, and H. Hirata, presented at the 62nd Colloid & Surface Science Symposium, Penn. State Univ. (1988).
7) C. A. Bunton and M. J. Minch, *J. Phys. Chem.*, **78**, 1490 (1974).

Enhancement of Catalytic Activity of Copper Ion-Exchanged Y Type Zeolites for the Decomposition of Nitrogen Monoxide

Masakazu IWAMOTO,* Hidenori YAHIRO, Takashi KUTSUNO,† Sukehiro BUNYU,† and Shuichi KAGAWA†
Department of Industrial Chemistry, Faculty of Engineering, Miyazaki University, Miyazaki 889-21
†Department of Industrial Chemistry, Faculty of Engineering, Nagasaki University, Nagasaki 852
(Received August 31, 1988)

Synopsis. Catalytic activity of Y zeolites containing copper ions (CuY) for decomposition of nitrogen monoxide was enhanced through additional exchange of other metal ions or evacuation treatment around 923—973 K. In the first case, Co^{3+} or Ni^{2+} ions increase the catalytic activity while Ca^{2+}, Mn^{2+}, Fe^{2+}, and Zn^{2+} diminish the catalytic activity of CuY. In the second case, the catalytic activity of CuY evacuated at 973 K was twice that of CuY without the evacuation treatment, which is discussed in connection with the increment of Cu ions active for the decomposition.

Decomposition of nitrogen monoxide (NO) has been reported to be catalyzed over partially copper(II) ion-exchanged Y zeolites (CuY).[1] This process is the simplest method for the removal of harmful NO because any reducing agents or absorbents are not necessary.[2] Very recently we have also reported that copper ion-exchanged ZSM-5 zeolites are more active than the CuY.[3] However, much more metal ions can be exchanged into Y-type zeolite lattice than into ZSM-5, and Y zeolite can be synthesized more easily and more cheaply. From the viewpoint of practical use of the zeolite catalyst, therefore, it would be very desirable to enhance the catalytic activity of the CuY. In the present work, we have found two possible ways; an additional exchange of other metal ions or evacuation treatments at higher temperatures caused an increase in the catalytic activity of the decomposition.

Experimental

Experimental apparatus and procedures were similar to those reported previously.[1,3] The reactant gas containing 5 vol% of NO and 95% helium was passed through the catalyst bed at 773 or 823 K and the extents of conversion of NO and to N_2 and O_2 were measured by gas chromatography. The total flow rate of feed gases was 30 cm^3 min^{-1}, catalyst weight being 2.0 g. Zeolite samples prepared by the conventional ion exchange of a NaY zeolite (Linde SK-40). In the two-component zeolites (containing copper ion and additional metal ion), zeolites were ion-exchanged first with copper ion and then with the other metal ion, or in the reverse order. Exchange levels of copper and other metal ions in the two component systems were each ca. 30%.

Results and Discussion

The decomposition activities of the two-component zeolites at 773 K are summarized in Table 1. The reaction products at this temperature were N_2, O_2, and NO_2. The formation of N_2O was not observed. In the table it should be noted that the extent of converted NO was approximately twice as much as that of produced N_2. This is due to the oxidative reaction of NO with generated O_2 to yield NO_2, $2NO+O_2 \rightarrow 2NO_2$ as discussed in the previous paper.[1]

Two interesting observations should be pointed out concerning Table 1. First the activity was increased by the coexistence of Co^{3+} or Ni^{2+}, while Ca^{2+}, Mn^{2+}, Fe^{2+}, and Zn^{2+} ions diminished the decomposition ability of CuY. Secondly, the catalytic activities of the two-component zeolites were little dependent on the order of ion exchange, as shown in the table. This fact suggests that the locations of metal ions over various exchangeable sites are decided by the difference between preferences of two kinds of metal ions toward the sites and not by the order of ion exchange.

It was confirmed in separate experiments that Co^{3+} or Ni^{2+} exchanged zeolites (without Cu^{2+} ions) showed no catalytic activity for the NO decomposition, while these ions had an effect for enhancement of the catalytic activity of the CuY. This suggests that the Co^{3+} or Ni^{2+} ions presumably occupy preferentially inner sites S_I and/or $S_{I'}$ which are generally inert for the catalytic reactions, and more Cu^{2+} ions would locate on the super cage-sites. However, one can not deny the possibility that some interaction of Cu^{2+} with Co^{3+} (or Ni^{2+}) resulted in the enhancement of the activity.

Next, pretreatments for the activation of a CuY zeolite (exchange level=70%) were examined. In a pretreatment, the zeolite sample was heated to 773 K in a dynamic vacuum, exposed to oxygen for 30 min, and then reevacuated for 30 min at the same temperature to remove such impurities on the zeolite surface as water, carbon dioxide, and possibly hydrocarbons. Subsequently, the sample was again heated to a desired temperature in a dynamic vacuum and evacuated at this temperature for 1 h. The catalytic run was carried out at 823 K and the results are shown in Fig. 1. It is

Table 1. Catalytic Activities of Various Two Components Zeolites Containing Copper(II) Ions for the Decomposition of Nitrogen Monoxide at 773 K

Exchanged metal ion	CuMY[a]		MCuY[a]	
	Conversion(%)[b] of NO	to N_2	Conversion(%)[b] of NO	to N_2
Cu	10.5	6.4	—	—
Ca-Cu	4.4	2.9	7.4	3.6
Mn-Cu	6.1	3.7	10.6	4.1
Fe-Cu	6.7	3.0	5.9	5.3
Co-Cu	13.5	7.1	12.2	6.1
Ni-Cu	15.5	8.4	16.6	11.4
Zn-Cu	9.2	5.0	6.7	3.0
Ag-Cu	7.5	7.1	8.9	6.4

a) CuMY indicates the order of ion-exchange first with copper ion and then with another metal ion, while MCuY was ion-exchanged in the reverse order. b) These values were calculated on the basis of the amount of NO fed.

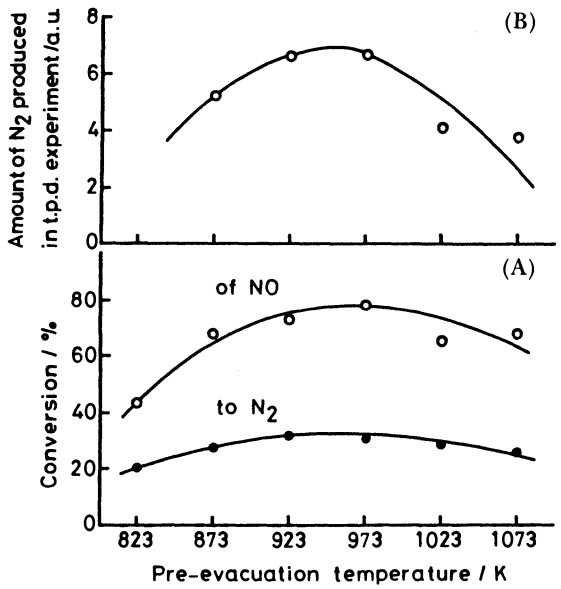

Fig. 1. Effect of the pre-evacuation temperature of the CuY zeolite (70%) on the catalytic activity for the NO decomposition at 823 K (A) and on the amounts of N_2 generated in TPD experiments (B).

evident that the evacuation at higher temperatures caused an increase in decomposition activity of the CuY, though too high evacuation temperatures resulted in a decrease in catalytic activity. The activity of the CuY evacuated at 973 K attained a level of two times as great as that of CuY without the evacuation treatment. The best temperature for evacuation were in the range 923—973 K. No deterioration of the effectiveness of the catalyst was found even after 10 h of continuous service.

To gather more evidence for the activity change of CuY catalysts, temperature programmed desorption (TPD) profiles of NO absorbed on the respective catalysts were investigated by means of the experimental method similar to that of Ref. 4. The amounts and temperatures of NO and N_2O desorbed remained roughly unchanged irrespective of the evacuation treatment. By contrast, the amounts of N_2 desorbed during the TPD procedures were dependent on the evacuation temperatures, though the desorption temperature did not change with the treatment. The amounts of N_2 are plotted in Fig. 1(B) as a function of the evacuation temperatures, indicating a bell-shaped dependence. It is noteworthy that the dependences of catalytic activities in flow system on the evacuation temperature is almost the same as that of N_2 formation in the TPD experiments. It was further confirmed in a separate TPD experiment that N_2 molecules did not chemically adsorb on the CuY surface at room temperature, indicating that the desorption of N_2 in the TPD experiments of adsorbed NO is due to the decomposition or reaction of some surface intermediates. Therefore, it follows that the increase in catalytic activity due to the evacuation around 923—973 K results from the increment of the number of active sites for the decomposition and not from the increment of turnover frequency per active site.

We have recently suggested that the active sites for the decomposition reaction would be copper(I) ions on zeolites.[3] In addition, it has also been reported that an evacuation treatment at higher temperatures above 873 K resulted in the desorption of oxygen molecules.[5,6] The desorption of oxygen would cause formation of copper(I) ions from copper(II) ions owing to charge transfer from anionic oxygen species to metal ions, which would result in the increase in the activity. The decrease in activity of CuY evacuated above 1023 K might be due to partial destruction of the zeolite lattice,[7] though we could not observe it by X-ray analysis.

In conclusion, the additional ion exchange of Co^{3+} or Ni^{2+} or the evacuation treatment around 923—973 K have been shown to enhance the catalytic activity of the CuY for the NO-decomposition.

This work was partially supported by a Grant-in-Aid for Scientific Research from the Ministry of Education, Science and Culture.

References

1) M. Iwamoto, S. Yokoo, K. Sakai, and S. Kagawa, *J. Chem. Soc., Faraday Trans. 1*, **77**, 1629 (1981).

2) J. W. Hightower and D. A. Van Leirsburg, "The Catalytic Chemistry of Nitrogen Oxides," ed R. L. Klimisch and J. G. Larson, Plenum, London (1975), p. 63.

3) M. Iwamoto, H. Furukawa, and S. Kagawa, "New Development in Zeolite Science Technology," ed by Y. Murakami et al., Elsevier, New York (1986), pp. 943—949.

4) S. Kagawa, H. Furukawa, and M. Iwamoto, Proc. 7th. Inter. Congr. Catal., Part B (1981), p. 1406.

5) M. Iwamoto, M. Nakamura, H. Nagano, S. Kagawa, and T. Seiyama, *J. Phys. Chem.*, **86**, 153 (1982).

6) M.Iwamoto, K. Maruyama, N. Yamazoe, and T. Seiyama, *J. Phys. Chem.*, **81**, 622 (1977); P. A. Jacobs and H. K. Beyer, *J. Phys. Chem.*, **83**, 1174 (1979).

7) I. E. Maxwell, R. S. Downing, and S. A. J. Van Langen, *J. Catal.*, **61**, 485 (1980); I. E. Maxwell, J. J. de Boer, and R. S. Drowning, *J. Catal.*, **61**, 493 (1980).

The Formation and Stereochemistry of $[Co^{III}_3(L\text{-cys-}N,S)_n(aet)_{6-n}]^{3-n}$ Type *S*-Bridged Complexes (n=0—6, L-cys=L-cysteinate, and aet=2-aminoethanethiolate)

Takumi KONNO,* Sen-ichi AIZAWA, and Jinsai HIDAKA
Department of Chemistry, University of Tsukuba, Tsukuba, Ibaraki 305
(Received June 27, 1988)

Synopsis. Three kinds of *S*-bridged trinuclear complexes, $\Delta_{LLL}\Delta_{LLL}$-$[Co_3(L\text{-cys-}N,S)_6]^{3-}$, $\Delta_{LLL}\Delta$- and $\Delta_{LLL}\Lambda$-$[Co_3(L\text{-cys-}N,S)_3(aet)_3]^0$, and $[Co_3(aet)_6]^{3+}$,[1] were formed by the reaction of a mixture of Δ_{LLL}-*fac*-$[Co(L\text{-cys-}N,S)_3]^{3-}$ (L-cys=L-cysteinate) and *fac*-$[Co(aet)_3]$ (aet=2-aminoethanethiolate) with $[CoCl(NH_3)_5]^{2+}$. The reaction with an excess amount of Co^{2+} led to the formation of seven kinds of *S*-bridged complexes, $[Co_3(L\text{-cys-}N,S)_n(aet)_{6-n}]^{3-n}$($n$=0—6).

Several *S*-bridged trinuclear metal complexes with L-cysteinate (L-cys) or 2-aminoethanethiolate (aet) have been investigated because of their stereochemical and spectrochemical interest.[2-12] Recently, it was found that the formation of $[M^{III}\{Co^{III}(L\text{-cys-}N,S)_3\}_2]^{3-}$ (M=Co, Fe) by the reaction of Δ_{LLL}-*fac*-$[Co^{III}(L\text{-cys-}N,S)_3]^{3-}$ with an excess amount of Co(II) or Fe(II) was accompanied by the inversion of the starting Δ_{LLL} complex and that only the $\Delta_{LLL}\Delta_{LLL}$ isomer was formed.[9-11] On the other hand, the reaction with Co(III) or Fe(III) proceeded with a retention of the Δ_{LLL} configuration, and the $\Delta_{LLL}\Delta_{LLL}$ isomer was selectively formed.[9-11] However the mechanism of this inversion is still unknown. In order to elucidate the stereoselectivity and the mechanism of the inversion for the *S*-bridged trinuclear complexes with L-cysteinate, an attempt was made to investigate the mixed-type trinuclear complexes containing L-cysteinate and 2-aminoethanethiolate. In this paper, we report the reactions of a mixture of Δ_{LLL}-*fac*-$[Co^{III}(L\text{-cys-}N,S)_3]^{3-}$ and *fac*-$[Co^{III}(aet)_3]$ with Co(III) and with Co(II). The reaction products were characterized on the basis of the absorption and CD spectra and their column chromatographic behavior in comparison with that of $[Co_3(L\text{-cys-}N,S)_6]^{3-}$ and $[Co_3(aet)_6]^{3+}$.

Experimental

1a) Reaction with Co(III). To a solution of $[CoCl(NH_3)_5]Cl_2$ (0.18 g, 0.72 mmol) in 15 cm^3 of water was added *fac*-$[Co(aet)_3]$[3] (0.20 g, 0.70 mmol), followed by the dropwise addition of a solution containing Δ_{LLL}-*fac*-$K_3[Co(L\text{-cys-}N,S)_3]9H_2O \cdot 0.5KCl$[11] (0.51 g, 0.70 mmol) in 5 cm^3 of water. The mixture was stirred at room temperature for 30 min and then filtered to remove any insoluble materials. The dark brown filtrate was poured onto a cation-exchange column (SP-Sephadex C-25 Na^+ form, 3.5 cm×90 cm). The negative-charged band (green) containing $\Delta_{LLL}\Delta_{LLL}$-$[Co_3(L\text{-cys-}N,S)_6]^{3-}$ [10,11,13] was eluted quickly with water, and then the neutral band was eluted slowly with water and finally separated into two bands, F-1 (brown) and F-2 (green), in this order. The formation ratio of the two isomers was about 1:1. Each eluate was concentrated to dryness with a rotary evaporator. The crude F-2 isomer was recrystallized from water and the F-1 isomer from water by adding a large amount of ethanol. Found for F-1: C, 22.83; H, 5.24; N, 9.86%. Calcd for $[Co_3(L\text{-cys-}N,S)_3(aet)_3] \cdot 4H_2O \cdot 0.5C_2H_5OH = C_{16}H_{44}N_6O_{10.5}S_6Co_3$: C, 22.41; H, 5.17; N, 9.80%. Found for F-2: C, 20.01; H, 5.52; N, 9.31%. Calcd for $[Co_3(L\text{-cys-}N,S)_3(aet)_3] \cdot 8H_2O = C_{15}H_{49}N_6O_{14}S_6Co_3$: C, 19.87; H, 5.45; N, 9.27%. ^{13}C NMR for F-1: δ 19.50 (CH_3 of ethanol), 34.89 (CH_2S of aet), 38.36 (CH_2S of L-cys), 49.79 (CH_2NH_2 of aet), 60.13 (CH_2 of ethanol), 66.36 (CH of L-cys), 177.96 (COO of L-cys). The ^{13}C NMR spectrum of the F-2 isomer could not be measured because of its low solubility in water. The remaining band, adsorbed on the top of the column, contained only $[Co_3(aet)_6]^{3+}$, which was eluted with a 0.2 mol dm^{-3} aqueous NaCl solution and separated into two bands, meso ($\Delta\Lambda$, brown) and racemic ($\Delta\Delta$ and $\Lambda\Lambda$, green) isomers[4,13,14] in this order.

1b) Reaction with Co(II). To a solution of $CoCl_2 \cdot 6H_2O$ (1.0 g, 4.2 mmol) in 15 cm^3 of water was added *fac*-$[Co(aet)_3]$[3] (0.2 g, 0.70 mmol), followed by the dropwise addition of a solution containing Δ_{LLL}-*fac*-$K_3[Co(L\text{-cys-}N,S)_3] \cdot 9H_2O \cdot 0.5KCl$[11] (0.51 g, 0.70 mmol) in 5 cm^3 of water. The mixture was stirred at room temperature for 30 min and then filtered to remove any insoluble materials. The dark brown filtrate was poured onto a cation-exchange column (SP-Sephadex C-25, Na^+ form, 3.5 cm×90 cm). The negative-charged NC band was quickly eluted with water, and then the neutral A band was slowly eluted with water and finally separated into four bands, A-1 (brown), A-2 (green), A-3 (brown), and A-4 (green), in this order. After the neutral A band had been eluted with water, the positive-charged band adsorbed on the top of the column was eluted with a 0.2 mol dm^{-3} aqueous NaCl solution. The first-eluted B band was separated into four bands; B-1 (brown), B-2 (green), B-3 (brown), and B-4 (green), the secondly eluted C band into three bands; C-a (pink), C-1 (brown), and C-2 (green), and the last-eluted D band containing $[Co_3(aet)_6]^{3+}$ into two bands; meso (D-1, brown) and racemic (D-2, green) isomers.[4,13,14] The NC eluate was poured onto an anion-exchange column (QAE-Sephadex A-25, Cl^- form, 3.5 cm×90 cm). No band was eluted with water. After the column had been swept with water, the negative-charged band adsorbed on the top of the column was eluted with a 0.2 mol dm^{-3} aqueous NaCl solution. The first-eluted B′ band was separated into three bands; B′-1 (green), B′-2 (brown), and B′-3 (green), and the secondly eluted C′ band into two bands; C′-1 (brown) and C′-2 (green). Finally, the green D′ band containing $\Delta_{LLL}\Delta_{LLL}$-$[Co_3(L\text{-cys-}N,S)_6]^{3-}$ [10,11,13] was eluted. The pink C-a band was found to be an unreacted Co^{2+} species from its absorption spectrum. In this reaction, the complex could not be isolated from each eluate because of its quite small amount. Accordingly, the concentration of each eluate was estimated on the basis of the extinction coefficients of $[Co_3(aet)_6]^{3+}$ [14] and $[Co_3(L\text{-cys-}N,S)_6]^{3-}$.[11]

2) Measurements. The electronic absorption specta were recorded with JASCO UVIDEC-1 and UVIDEC-610 spectrometers, and the CD spectra with a JASCO J-20 spectropolarimeter. The ^{13}C NMR spectrum was recorded with a JEOL JNM-FX-90Q NMR spectrometer in a D_2O solvent at the probe temperature. Sodium 2,2-dimethyl-2-silapentane-5-sulfonate (DSS) was used as the internal reference.

Results and Discusston

Three configurations, $\Delta\Delta$, $\Lambda\Lambda$, and $\Delta\Lambda$, with respect to the absolute configuration of the two terminal *fac*-[Co(bidentate-*N*,*S*)$_3$] moieties are possible for each of the *S*-bridged trinuclear complexes, [Co$_3$(L-cys-*N*,*S*)$_n$(aet)$_{6-n}$]$^{3-n}$ (n=0—6) (Fig. 1). In addition, another type of isomers arising from the arrangement of the L-cys-*N*,*S* and aet ligands are possible for each of the [Co$_3$(L-cys-*N*,*S*)$_n$(aet)$_{6-n}$]$^{3-n}$ (n=0—6) complexes (Table 1). The reaction of a mixture containing Δ_{LLL}-*fac*-[Co(L-cys-*N*,*S*)$_3$]$^{3-}$ and *fac*-[Co(aet)$_3$] with [CoCl(NH$_3$)$_5$]$^{2+}$ produced the F-1 (brown) and F-2 (green) neutral isomers besides $\Delta_{LLL}\Delta_{LLL}$-[Co$_3$(L-cys-*N*,*S*)$_6$]$^{3-}$ and [Co$_3$(aet)$_6$]$^{3+}$. Figure 2 illustrates the absorption and CD spectra of the F-1 and F-2 isomers. The absorption spectra of the F-1 and F-2 isomers coincide well with those of [Co$_3$(L-cys-*N*,*S*)$_6$]$^{3-}$ [10-12] and [Co$_3$(aet)$_6$]$^{3+}$. [4,14]

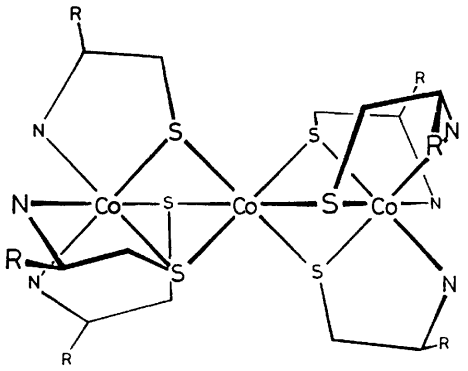

Fig. 1. Structure of [Co$_3$(L-cys-*N*,*S*)$_n$(aet)$_{6-n}$]$^{3-n}$ having the $\Delta\Lambda$ configuration. (R=H for aet, R=COO$^-$ for L-cys)

The CD spectra of the F-1 and F-2 isomers are in good agreement with those of $\Delta_{LLL}\Lambda_{LLL}$-[Co$_3$(L-cys-*N*,*S*)$_6$]$^{3-}$ [12] and $\Delta_{LLL}\Delta_{LLL}$-[Co$_3$(L-cys-*N*,*S*)$_6$]$^{3-}$ [10,11] respectively. These facts suggest that the green isomer is $\Delta_{LLL}\Lambda$-[Co$_3$(L-cys-*N*,*S*)$_3$(aet)$_3$], while the brown isomer is the $\Delta_{LLL}\Lambda$ one. Thus, for the reaction with [CoCl(NH$_3$)$_5$]$^{2+}$ the starting Δ_{LLL}-*fac*-[Co(L-cys-*N*,*S*)$_3$]$^{3-}$ and/or *fac*-[Co(aet)$_3$] complexes bridge to the Co(III) ion through the facial thiolato donor atoms, forming three types of trinuclear complexes; $\Delta_{LLL}\Delta_{LLL}$-[Co$_3$(L-cys-*N*,*S*)$_6$]$^{3-}$, $\Delta_{LLL}\Delta$- and $\Delta_{LLL}\Lambda$-[Co$_3$(L-cys-*N*,*S*)$_3$(aet)$_3$]^0, and [Co$_3$(aet)$_6$]$^{3+}$. This formation mechanism is consistent with the fact that the reaction of Δ_{LLL}-*fac*-[Co(L-cys-*N*,*S*)$_3$]$^{3-}$ with [CoCl(NH$_3$)$_5$]$^{2+}$ produced only $\Delta_{LLL}\Delta_{LLL}$-[Co$_3$(L-cys-*N*,*S*)$_6$]$^{3-}$, retaining the absolute configuration of the starting Δ_{LLL} complex. [10,11] The overall absorption spectra of the $\Delta_{LLL}\Lambda$ (green) and $\Delta_{LLL}\Lambda$ (brown) isomers are similar to each other, but a notable difference is observed in the lowest energy region; the $\Delta_{LLL}\Lambda$ (green) isomer has an absorption peak at 18.18×10^3 cm^{-1}, while the corresponding absorption component for the $\Delta_{LLL}\Lambda$ (brown) isomer appears as a shoulder at 18.9×10^3 cm^{-1} (Fig. 2). A similar difference in the absorption spectra between the $\Delta\Delta$ or $\Lambda\Lambda$ isomer (green) and the $\Delta\Lambda$ isomer (brown) was also observed for [Co$_3$(L-cys-*N*,*S*)$_6$]$^{3-}$ [10-12] and [Co$_3$(aet)$_6$]$^{3+}$. [4,14]

In contrast with the reaction with [CoCl(NH$_3$)$_5$]$^{2+}$, the reaction with an excess amount of Co^{2+} gave a number of trinuclear complexes, of which absorption and CD spectral behavior agrees well with that of [Co$_3$(L-cys-*N*,*S*)$_6$]$^{3-}$ and [Co$_3$(aet)$_6$]$^{3+}$. The last-eluted D band of a cation-exchange column and the last-eluted D′ band of an anion-exchange column contained [Co$_3$(aet)$_6$]$^{3+}$ and $\Lambda_{LLL}\Lambda_{LLL}$-[Co$_3$(L-cys-*N*,*S*)$_6$]$^{3-}$

Table 1. Possible Isomers and Formation Ratio of Isomers for [Co$_3$(L-cys-*N*,*S*)$_n$(aet)$_{6-n}$]$^{3-n}$(n=0—6)

Complexes	Possible Isomers	Eluates	Assignments	Formation Ratio (%)	Δ:Λ
[Co$_3$(aet)$_6$]$^{3+}$	$\Delta\Delta$, $\Lambda\Lambda$	D-1(brown)	$\Lambda\Lambda$	2.6	50:50
	$\Delta\Lambda$	D-2(green)	$\Delta\Lambda+\Lambda\Lambda$ (1:1)	2.7	
[Co$_3$(L-cys-*N*,*S*)(aet)$_5$]$^{2+}$	$\Delta_L\Delta$, $\Lambda_L\Lambda$	C-1(brown)	$\Lambda\Lambda$	7.6	38:62
	$\Delta_L\Lambda$, $\Delta\Lambda_L$	C-2(green)	$\Delta\Lambda+\Lambda\Lambda$ (1:3)	7.3	
[Co$_3$(L-cys-*N*,*S*)$_2$(aet)$_4$]$^+$	$\Delta_{LL}\Delta$, $\Delta_L\Delta_L$	B-1(brown)	$\Lambda\Lambda$	2.4	29:71
	$\Lambda_{LL}\Lambda$, $\Lambda_L\Lambda_L$	B-2(green)	$\Delta\Delta$	1.7	
	$\Delta_{LL}\Lambda$, $\Delta_L\Lambda_L$	B-3(brown)	$\Lambda\Lambda$	7.6	
	$\Delta\Lambda_{LL}$	B-4(green)	$\Lambda\Lambda$	11.2	
[Co$_3$(L-cys-*N*,*S*)$_3$(aet)$_3$]	$\Lambda_{LLL}\Delta$, $\Delta_{LL}\Delta_L$	A-1(brown)	$\Delta\Lambda$	2.1	20:80
	$\Lambda_{LLL}\Lambda$, $\Lambda_{LL}\Lambda_L$	A-2(green)	$\Lambda\Lambda$	7.3	
	$\Delta_{LLL}\Lambda$, $\Delta_{LL}\Lambda_L$	A-3(brown)	$\Delta\Lambda$	7.1	
	$\Delta_L\Lambda_{LL}$, $\Delta\Lambda_{LLL}$	A-4(green)	$\Lambda\Lambda$	6.0	
[Co$_3$(L-cys-*N*,*S*)$_4$(aet)$_2$]$^-$	$\Delta_{LLL}\Delta_L$, $\Delta_{LL}\Delta_{LL}$	B′-1(green)	$\Lambda\Lambda$	2.1	14:86
	$\Lambda_{LLL}\Lambda_L$, $\Lambda_{LL}\Lambda_{LL}$	B′-2(brown)	$\Delta\Lambda$	4.5	
	$\Delta_{LLL}\Lambda_L$, $\Delta_{LL}\Lambda_{LL}$ $\Delta_L\Lambda_{LLL}$	B′-3(green)	$\Lambda\Lambda$	9.1	
[Co$_3$(L-cys-*N*,*S*)$_5$(aet)]$^{2-}$	$\Delta_{LLL}\Delta_{LL}$, $\Lambda_{LLL}\Lambda_{LL}$	C′-1(brown)	$\Delta\Lambda$	0.8	5:95
	$\Delta_{LLL}\Lambda_{LL}$, $\Delta_{LL}\Lambda_{LLL}$	C′-2(green)	$\Lambda\Lambda$	6.6	
[Co$_3$(L-cys-*N*,*S*)$_6$]$^{3-}$	$\Delta_{LLL}\Delta_{LLL}$, $\Lambda_{LLL}\Lambda_{LLL}$ $\Delta_{LLL}\Lambda_{LLL}$	D′(green)	$\Lambda\Lambda$	11.4	0:100

The number of the subscript L for Δ or Λ denotes the number of the L-cys-*N*,*S* ligand in the terminal moiety.

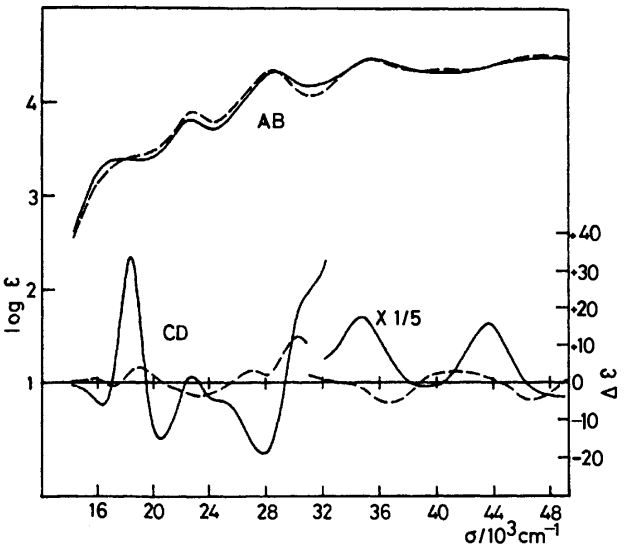

Fig. 2. Absorption and CD spectra of the $\Delta_{LLL}\Delta$ (——) and $\Delta_{LLL}\Lambda$ (----) isomers of $[Co_3(L\text{-cys-}N,S)_3(aet)_3]$.

respectively. Taking these absorption and CD spectral and column chromatographic behavior into consideration, it is probable that the C, B, A, B′, and C′ adsorbed bands contained the *S*-bridged trinuclear complexes, $[Co_3(L\text{-cys-}N,S)(aet)_5]^{2+}$, $[Co_3(L\text{-cys-}N,S)_2(aet)_4]^{+}$, $[Co_3(L\text{-cys-}N,S)_3(aet)_3]^{0}$, $[Co_3(L\text{-cys-}N,S)_4(aet)_2]^{-}$, and $[Co_3(L\text{-cys-}N,S)_5(aet)]^{2-}$ respectively. The formation of all seven kinds of complexes, $[Co_3(L\text{-cys-}N,S)_n(aet)_{6-n})]^{3-n}$ (n=0—6), indicates that the L-cys-*N*,*S* and aet ligands dissociate from the starting Δ_{LLL}-*fac*-$[Co(L\text{-cys-}N,S)_3]^{3-}$ and *fac*-$[Co(aet)_3]$ complexes through the reaction with Co^{2+}, followed by the rearrangement of these ligands to form a trinuclear structure. The green isomers showing an absorption peak at ca. 18×10^3 cm^{-1} are assignable to take the $\Delta\Delta$ or $\Lambda\Lambda$ configuration, while the brown isomers showing a shoulder at ca. 19×10^3 cm^{-1} take the $\Delta\Lambda$ configuration (vide supra). Moreover, the CD spectra of the isomers are classified into the three CD patterns of $\Delta_{LLL}\Delta_{LLL}$-, $\Delta_{LLL}\Lambda_{LLL}$-, and $\Lambda_{LLL}\Lambda_{LLL}$-$[Co_3(L\text{-cys-}N,S)_6]^{3-}$.[10-12] Accordingly, the absolute configuration ($\Delta\Delta$, $\Delta\Lambda$, or $\Lambda\Lambda$) for each trinuclear isomer can be assigned on the basis of the absorption and CD spectra as given in Table 1, although it is difficult to determine the arrangement of the L-cys-*N*,*S* and aet ligands. The formation ratios of the isomers obtained by the reaction with an excess amount of Co^{2+} are summarized in Table 1. The ratio of the Δ and Λ terminals in each trinuclear complex ($\Delta:\Lambda$) was evaluated from the values of the formation ratio of the $\Delta\Delta$, $\Delta\Lambda$, and $\Lambda\Lambda$ configurations (Table 1). No $\Delta\Delta$ isomer was formed for $[Co_3(L\text{-cys-}N,S)_6]^{3-}$, $[Co_3(L\text{-cys-}N,S)_5(aet)]^{2-}$, $[Co_3(L\text{-cys-}N,S)_4(aet)_2]^{-}$, and $[Co_3(L\text{-cys-}N,S)_3(aet)_3]$, which contain the $[Co(L\text{-cys-}N,S)_3]^{3-}$ and/or $[Co(L\text{-cys-}N,S)_2(aet)]^{-}$ terminals. Of these complexes, $[Co_3(L\text{-cys-}N,S)_6]^{3-}$ gave only the $\Lambda_{LLL}\Lambda_{LLL}$ isomer (D′), as in the case of the reaction of Δ_{LLL}-*fac*-$[Co(L\text{-cys-}N,S)_3]^{3-}$ with an excess amount of Co^{2+}[10,11] and the two isomers of $[Co_3(L\text{-cys-}N,S)_5(aet)]^{2-}$, $\Lambda_{LLL}\Delta_{LL}$ (C′-1) and $\Lambda_{LLL}\Lambda_{LL}$ (C′-2), were formed in a ratio of about 1:8. This behavior indicates that the $[Co(L\text{-cys-}N,S)_3]^{3-}$ and $[Co(L\text{-cys-}N,S)_2(aet)]^{-}$ terminals prefer strongly the Λ configuration to the Δ one. The Λ configurational preference is observed even for the $[Co(L\text{-cys-}N,S)(aet)_2]^{+}$ terminal; the C-2 eluate containing $\Delta_L\Delta$- and $\Delta_L\Lambda$-$[Co_3(L\text{-cys-}N,S)(aet)_5]^{2+}$ showed the same CD spectral pattern as did $\Lambda_{LLL}\Lambda_{LLL}$-$[Co_3(L\text{-cys-}N,S)_6]^{3-}$,[10,11] suggesting that the $\Delta_L\Lambda$ isomer is dominant in the C-2 eluate.[15] Thus, the L-cys-*N*,*S* ligand exerts a significant influence on the Λ configurational selectivity for the trinuclear structure, and the influence for each trinuclear complex can be estimated from the ratios of $\Delta:\Lambda$. That is, the values of the Λ terminal increase almost in proportion to the number of the L-cys-*N*,*S* ligand in the trinuclear complex (Table 1). This result is in contrast with the fact that mononuclear complexes with the L-cys-*N*,*S* ligand prefer the Δ configuration.[16-18]

References

1) In this paper, the chemical formulas of $[Co_3(L\text{-cys-}N,S)_6]^{3-}$ and $[Co_3(aet)_6]^{3+}$ are used instead of $[Co\{Co(L\text{-cys-}N,S)_3\}_2]^{3-}$ and $[Co\{Co(aet)_3\}_2]^{3+}$ (Refs. 10—12,14).

2) D. C. Jicha and D. H. Busch, *Inorg. Chem.*, **1**, 872, 878 (1962).

3) D. H. Busch and D. C. Jicha, *Inorg. Chem.*, **1**, 884 (1962).

4) G. R. Brubaker and B. E. Douglas, *Inorg. Chem.*, **6**, 1562 (1967).

5) C. H. Wei and L. F. Dahl, *Inorg. Chem.*, **9**, 1878 (1970).

6) R. E. DeSimone, T. Ontko, L. Wardman, and E. L. Blinn, *Inorg. Chem.*, **14**, 1313 (1975).

7) E. L. Blinn, P. Bulter, K. M. Chapman, and S. Harris, *Inorg. Chim. Acta*, **24**, 139 (1977).

8) P. R. Bulter and E. L. Blinn, *Inorg. Chem.*, **17**, 2037 (1978).

9) M. J. Heeg, E. L. Blinn, and E. Deutsch, *Inorg. Chem.*, **24**, 1118 (1985).

10) T. Konno, S. Aizawa, K. Okamoto, and J. Hidaka, *Chem. Lett.*, **1985**, 1017.

11) K. Okamoto, S. Aizawa, T. Konno, H. Einaga, and J. Hidaka, *Bull. Chem. Soc. Jpn.*, **59**, 3859 (1986).

12) S. Aizawa, K. Okamoto, H. Einaga, and J. Hidaka, *Bull. Chem. Soc. Jpn.*, **61**, 1601 (1988).

13) The eluate showed absorption and CD spectra identical with those of the complex characterized in previous papers (Refs. 4, 10, 11, 14).

14) S. Miyanowaki, T. Konno, K. Okamoto, and J. Hidaka, *Bull. Chem. Soc. Jpn.*, **61**, 2987 (1988).

15) The formation ratio, $\Delta_L\Delta:\Delta_L\Lambda$, roughly calculated from the CD intensity was about 1:3.

16) R. D. Gillard and R. Maskill, *Chem. Commun.*, **1968**, 160.

17) M. Kita, K. Yamanari, and Y. Shimura, *Bull. Chem. Soc. Jpn.*, **55**, 2873 (1982).

18) H. C. Freeman, C. J. Moore, W. G. Jackson, and A. M. Sargeson, *Inorg. Chem.*, **17**, 3513 (1978).

Cis to Trans Photoisomerization of $[CoCl_2\{(CH_3)_2PCH_2CH_2CH_2P(CH_3)_2\}_2]^+$, $[CoCl(H_2O)\{(CH_3)_2PCH_2CH_2P(CH_3)_2\}_2]^{2+}$ and Related Complexes

Kazuma OGUNI, Tomoji OHISHI,† Masakazu KITA, Kazuo KASHIWABARA, and Junnosuke FUJITA*
Department of Chemistry, Faculty of Science, Nagoya University, Chikusa-ku, Nagoya 464
(Received August 22, 1988)

Synopsis. Ligand field irradiation of *cis*-$[CoCl_2\{(CH_3)_2PCH_2CH_2CH_2P(CH_3)_2\}_2]^+$ in methanol and *cis*-$[CoCl(H_2O)\{(CH_3)_2PCH_2CH_2P(CH_3)_2\}_2]^{2+}$ in acetonitrile at 5 °C led to isomerization to the trans isomer with quantum yields of 0.010 and 0.070, respectively. The same cis to trans photoisomerization of $[CoCl_2(R_2PCH_2CH_2PR_2)_2]^+$ (R=CH_3, C_4H_9) occurred with much smaller quantum yields (ca. 1×10^{-4}) and *cis*-$[CoCl_2\{(C_6H_5)_2PCHCHP(C_6H_5)_2\}_2]^+$ was reduced to cobalt(II) species on irradiation.

Although photochemistry of cobalt(III) complexes has been studied extensively, reactions with a high quantum yield are limited to a few complexes.[1] Recently, Houlding and Miskowski[2] have reported the photoaquation of $[Co\{(CH_3O)_2PCH_2CH_2P(OCH_3)_2\}_3]^{3+}$ with a high quantum yield of 0.26. In this paper we report photoisomerizations of several *cis*-bis(diphosphine)cobalt(III) complexes to trans isomers in methanol or aceotnitrile solutions. The phosphine ligands are $(CH_3)_2PCH_2CH_2P(CH_3)_2$=dmpe, $(CH_3)_2PCH_2CH_2CH_2P(CH_3)_2$=dmpp, $(C_4H_9)_2PCH_2CH_2P(C_4H_9)_2$=dbpe, and *cis*-$(C_6H_5)_2PCHCHP(C_6H_5)_2$=dpee.

Experimental

Materials. The complexes were prepared as described peviously.[3] Methanol and acetonitrile used for solvents were purified and dried by standard methods, and purged with dry nitrogen for 10 min prior to use.

Quantum Yield Determinations. Photolyses were carried out with solutions (3.0 cm^3, ca. 3.0×10^{-4} to 3.0×10^{-3} mol dm^{-3}) in a 1.0 cm length spectrophotometer cell which was thermostated at 5±0.5 °C. Solutions in the cell were stirred during irradiation. The light source was a 150 W Xenon short arc lamp of Ushio Co., Ltd. with a mirror to enhance the light intensity on the cell window. Irradiation light was made monochromatic by use of a JASCO CT-10 monochrometer. The incident photon flux on the cell window as measured by trioxalatoferrate(III)[4] and reineckate actinometry[5] ranged from 6.4×10^{-9} to 3.2×10^{-8} einstein cm^{-2} s^{-1}. Absorption spectral changes of a solution were recorded on a JASCO UVIDEC 650 or a HITACHI U-3400 spectrophotometer at appropriate intervals during irradiation. Quantum yields were determined from the spectral data for less than 20% reactions according to the method of Adamson et al.[6] The values were corrected for thermal reactions (isomerization) in the dark, which were, however, negligibly slow under the experimental conditions (5 °C).[3]

Results and Discussion

Figures 1 and 2 show absorption spectra of *cis*- and *trans*-$[CoCl_2(dmpp)_2]^+$ and *cis*- and *trans*-$[CoCl(H_2O)(dmpe)_2]^{2+}$, respectively. In a previous paper,[3] we assigned the band at 16700 cm^{-1} of *trans*-$[CoCl_2(dmpp)_2]^+$ to the split component (Ia) of the first d-d band ($^1T_{1g}\leftarrow{}^1A_{1g}(O_h)$), and the broad band (17000—22000 cm^{-1}) and the shoulder around 25000 cm^{-1} of *cis*-$[CoCl_2(dmpp)_2]^+$ to the first and the second

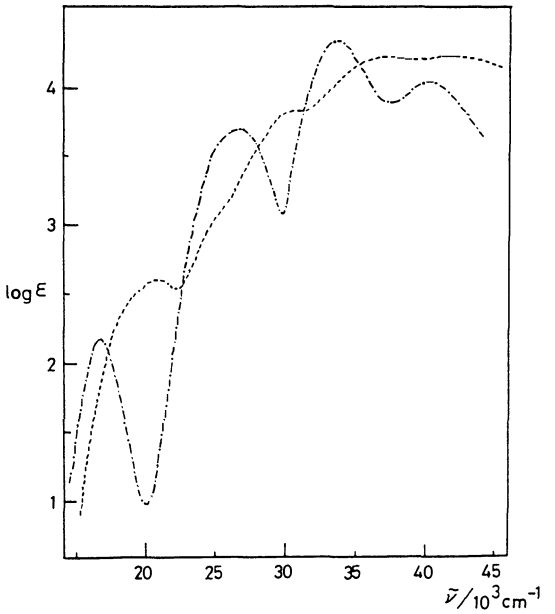

Fig. 1. Absorption spectra of *cis*- and *trans*-$[CoCl_2(dmpp)_2]^+$, (——) and (–·–·–).

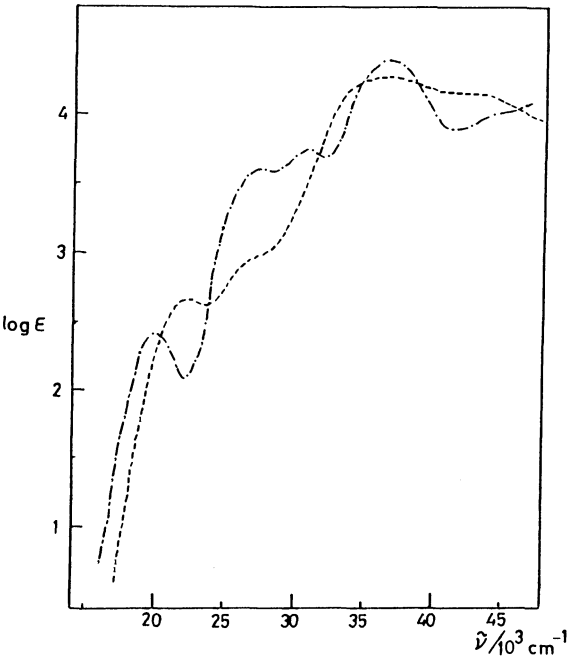

Fig. 2. Absorption spectra of *cis*- and *trans*-$[CoCl(H_2O)(dmpe)_2]^{2+}$, (——) and (–·–·–).

† Present address: Hitachi Research Laboratory, Hitachi Ltd., Hitachi, Ibaraki 319-12.

($^1T_{2g} \leftarrow {}^1A_{1g}(O_h)$) d-d bands, respectively. The ligand field spectra of other $[CoCl_2L_2]^+$ (L=dmpe, dbpe, dpee) are very similar to those of the corresponding isomers of the dmpp complex except that the absorption maxima are slightly shifted to higher energy in the order L=dpee<dbpe<dmpp<dmpe. For $[CoCl(H_2O)(dmpe)_2]^{2+}$, the trans isomer shows the first band at 20100 cm^{-1}, and the cis isomer gives the first band at 22400 cm^{-1} and the second one around 27000 cm^{-1} as a shoulder. Other strong bands in the higher energy region are all attributable to charge-transfer transitions from ligands to cobalt(III).

Figure 3 shows the changes in absorption spectrum at 5 min intervals that occur upon 480 nm irradiation of *cis*-$[CoCl_2(dmpp)_2]^+$ in methanol at 5 °C. Two clear isosbestic points were found at 442 nm and 571 nm. After 3 h irradiation the spectrum almost coincided with that of *trans*-$[CoCl_2(dmpp)_2]^+$. The *trans*-$[CoCl_2(dmpp)_2]^+$ isomer showed no spectral change by the same irradiation even for more than 10 h. Thus the photolysis of *cis*-$[CoCl_2(dmpp)_2]^+$ is concluded to afford only the trans isomer. Photolyses with 545 and 452 nm lights gave similar results. The quantum yields were determined according to the method of Adamson et al.,[6] and are listed in Table 1.

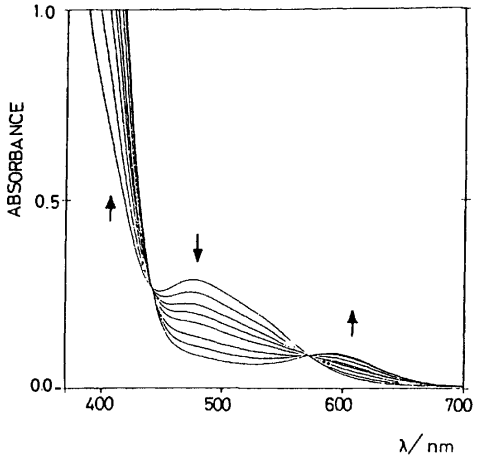

Fig. 3. Sequence of absorption spectra on 480 nm irradiation of *cis*-$[CoCl_2(dmpp)_2]^+$ in methanol at 5°C (5 min intervals).

Table 1. Quantum Yields of the Complexes at 5°C

Complex	Irradiation wavelength / nm	Quantum yield (ϕ)
cis-$[CoCl_2(L)_2]X$[a]		
L=dmpp, X=BF_4	545	0.011±0.003
	480	0.010±0.001
	452	0.010±0.001
	334	0.012±0.001
	254	0.014±0.001
L=dmpe, X=ClO_4	452	ca. 1×10^{-4}
	254	0.0051±0.0004
L=dbpe, X=PF_6	480	ca. 1×10^{-4}
	254	b)
L=dpee, X=BF_4	504	b)
	254	b)
cis-$[CoCl(H_2O)(dmpe)_2](PF_6)_2$[c]	452	0.070±0.007
	254	0.046±0.013

a) Solvent; methanol. b) Reductions to Co(II) species. c) Solvent; acetonitrile.

Ligand field irradiation of *cis*-$[CoCl_2(L)_2]^+$ (L=dmpe and dbpe) caused very small changes in the absorption spectra. The changes have isosbestic points and also indicate the isomerization to the trans isomers. However, the quantum yields were about 1×10^{-4}. In the case of the dpee complex, the spectrum changed with no isosbestic points and the intensity decreased. The changes indicate that the reduction of cobalt(III) to cobalt(II) took place by irradiation, although the photolysis products were not characterized. Thus the *cis*-dichloro complexes of 1,2-diphosphines exhibited different photochemical behavior from that of the 1,3-diphosphine, dmpp complex.

In contrast to rather photoinert *cis*-$[CoCl_2(dmpe)_2]^+$, *cis*-$[CoCl(H_2O)(dmpe)_2]^{2+}$ in acetonitrile yielded the trans isomer on irradiation at 452 nm with a quantum yield of 0.070. This value is about 700 times as large as that of *cis*-$[CoCl_2(dmpe)_2]^+$. The trans isomer was photoinert under the same conditions. Sheridan and Adamson[6] reported similar photoisomerization for an ethylenediamine (en) analog, *cis*-$[CoCl(H_2O)(en)_2]^{2+}$ in 0.2 mol dm^{-3} HCl; the complex undergoes cis to trans isomerization on 488 nm irradiation with a quantum yield of 0.0042, while the trans isomer is photoinert. Thus both chloroaqua complexes of en and dmpe exhibit similar photoreactivity, but the quantum yield of the former is smaller than that of the latter by a factor of about 10.

On irradiation with ultraviolet light (254 and 334 nm) *cis*-$[CoCl_2(L)_2]^+$ (L=dmpe and dmpp) and *cis*-$[CoCl(H_2O)(dmpe)_2]^{2+}$ isomerized to the trans isomers. In the spectral changes, isosbestic points were almost kept until about 45, 50, and 80% reactions of the dichloro complexes of dmpe and dmpp, and the chloroaqua complex of dmpe, respectively. Further photolyses led to apparent deviation from the isosbestic points. The deviations will be attributable to photoreaction of the reaction products, trans isomers, since all of these trans isomers undergo photolyses on 254 nm irradiation at moderate rates. These reactions are supposed to be reduction of cobalt(III) to cobalt(II), since ligand field bands characteristic of cobalt(III) complexes disappear. The quantum yields were obtained from the spectral data for less than 20% reactions. The value of *cis*-$[CoCl_2(dmpp)_2]^+$ was nearly the same as those obtained by ligand field irradiation. The independence on the wavelength of irradiation light suggests a reaction from a low energy excited state, although the mechanism is not clear at present. For most photoreactions of cobalt(III) complexes with strong ligands such as CN^- a ligand field triplet pathway has been postulated.[1] However, the value of *cis*-$[CoCl_2(dmpe)_2]^+$ obtained by 254 nm irradiation is about fifty times as large as that by 452 nm irradiation. No explanation can be given to the difference between the dmpp and dmpe complexes at present. The dbpe and dpee complexes were more susceptible to photoreduction on irradiation at 254 nm and the quantum

yields were not determined.

The authors wish to thank the Ministy of Education for Scientific Research Grant-in-Aid No. 61430013.

References

1) P. C. Ford, D. Wink, and J. Dibenedetto, *Prog. Inorg. Chem.*, **30**, 213 (1983). P. C. Ford, *Chem. Rev.*, **44**, 61 (1982). E. Zinato, "Concept of Inorganic Photochemistry," ed by A. W. Adamson, P. D. Fleischauer, Wiley-Interscience, New York, (1975), Chap. 4 and references therein.

2) V. H. Houlding and V. M. Miskowski, *Inog. Chem.*, **23**, 4671 (1984).

3) T. Ohishi, K. Kashiwabara, and J. Fujita, *Bull. Chem. Soc. Jpn.*, **60**, 575 (1987).

4) C. G. Hatchard and C. A. Parker, *Proc. R. Soc. London, Ser. A*, **235**, 518 (1956).

5) E. E. Wegner and A. W. Adamson, *J. Am. Chem. Soc.*, **88**, 394 (1966).

6) P. S. Sheridan and A. W. Adamson, *J. Am. Chem. Soc.*, **96**, 3032 (1974).

A Mild Selective Monobromination Reagent System for Alkoxybenzenes; *N*-Bromosuccinimide-Silica Gel

Hisatoshi KONISHI,* Katsutomo ARITOMI, Tamon OKANO, and Jitsuo KIJI
Department of Environmental Chemistry & Technology, Tottori University, Koyama-minami, Tottori 680
(Received May 2, 1988)

Synopsis. The monobromination of alkoxybenzenes with *N*-bromosuccinimide catalyzed by silica gel in carbon tetrachloride occurred preferentially at the para-position. *m*-*t*-Butylmethoxybenzene yielded 4-bromo-3-*t*-butyl-1-methoxybenzene with a selectivity of 74% even in the presence of a bulky substituent at the meta-position.

A variety of methods for the selective nuclear bromination of activated aromatic compounds has been developed in view of the importance of the brominated compound in organic syntheses. The monobromination of 1,3-dimethoxybenzenes was conducted using a dioxane-bromine complex.[1] The reagent is somewhat troublesome to use due to its hygroscopic property and thermal instability at room temperature.

Silica-gel-catalyzed chlorination of aromatic compounds has attracted much interest owing to its simplicity and selectivity.[2-5] Various types of chlorinating agents may be used. These studies prompted us to examine the silica-gel-catalyzed nuclear bromination of activated aromatic compounds with *N*-bromosuccinimide (NBS). Recently, the bromination of indoles and benzimidazoles with NBS-silica gel has been reported.[6] Here, we would like to describe a facile method for the selective monobromination of reactive alkoxybenzenes and to briefly discuss the role of silica gel in the reaction.

Results and Discussion

The results of bromination are summarized in Table 1. The reaction of *m*-dimethoxybenzene with a slight excess of NBS in carbon tetrachloride containing silica gel at 30 °C for 2 h gave 1-bromo-2,4-dimethoxybenzene in quantitative yield. No trace of the dibromo compound was detected. In the absence of silica gel, no bromination was observed. The rate of the reaction was largely dependent upon the amount of silica gel and the stirring speed. This was due to the heterogeneity of the reaction. A variety of silica gels showed the catalytic activity of bromination; an acidic silica gel (Microbead 3A, chromatographic material, Fuji-Davison) is very effective.

A similar treatment of *o*-dimethoxybenzene and 1-methoxynaphthalene gave monobrominated products in excellent yields. Methoxybenzene and ethoxybenzene required a longer time. The bromination is highly para-selective. Methoxybenzene gave a para-isomer of >98.5% purity. In the cases of substrates with a para-substituent, such as *p*-dimethoxybenzene and 2-methoxynaphthalene, ortho bromination occurred in moderate yields.

The reaction of *m*-dimethoxybenzene with 2.2 equivalent of NBS for 45 h gave 1,5-dibromo-2,4-dimethoxybenzene in 80% yield. In other cases, dibromination is of no practical value, due to the slow reaction.

In order to obtain some insight into the mechanism of bromination, the reaction of a series of *m*-alkylmethoxybenzenes was carried out. Electrophilic bromination with NBS in polar solvents has been reported,[7,8] and it was considered that NBS was activated on the polar silica-gel surface. It was expected that the regioselectivity of the bromination by a bulky electrophile is affected by a substituent at the meta position. However, the bromination of *m*-methyl-, *m*-ethyl-, and *m*-isopropylmethoxybenzenes occurred exclusively at the para-position to the methoxyl group. It was particularly noteworthy that *m*-*t*-butylmethoxybenzene yielded 4- and 6-bromo-3-*t*-butyl-1-methoxybenzene in a ratio of 74:26. These

Table 1. Bromination of Alkoxybenzenes with *N*-Bromosuccinimide/Silica Gel in Carbon Tetrachloride[a]

Alkoxybenzene	Time / h	Product	Yield / %
m-Dimethoxybenzene	2	1-Bromo-2,4-dimethoxybenzene	99
o-Dimethoxybenzene	4	4-Bromo-1,2-dimethoxybenzene	98
p-Dimethoxybenzene	24	2-Bromo-1,4-dimethoxybenzene	58
1-Methoxynaphthalene	4	4-Bromo-1-methoxynaphthalene	99
2-Methoxynaphthalene	18	1-Bromo-2-methoxynaphthalene	66
Methoxybenzene	20	*p*-Bromomethoxybenzene	90
Ethoxybenzene	40	*p*-Bromoethoxybenzene	96
m-Methylmethoxybenzene	40	4-Bromo-3-methyl-1-methoxybenzene	87
m-Ethylmethoxybenzene	20	4-Bromo-3-ethyl-1-methoxybenzene	90
m-Isopropylmethoxybenzene	20	4-Bromo-3-isopropyl-1-methoxybenzene	78
m-*t*-Butylmethoxybenzene	20	4- and 6-Bromo-3-*t*-butyl-1-methoxybenzene	85[b]

a) Substrate (2 mmol), NBS (2.1 mmol), Silica gel (Microbead 3A, 1g), CCl_4 (20 ml), 30°C.
b) Product distribution (4-/6-=74/26).

results were entirely unexpected, since electrophilic aromatic substitution at the ortho-position to a *t*-butyl group is highly suppressed due to its bulkiness.[9] Indeed, the iron-catalyzed bromination of *m*-*t*-butylmethoxybenzene yielded only 6-bromo-3-*t*-butyl-1-methoxybenzene. These findings imply that the steric repulsion between a *m*-alkyl substituent and a brominating species is not a dominant factor for controlling the isomer distribution.

Thallium(III)-induced bromination of meta-alkylmethoxybenzenes has been reported to be para selective.[10] The formation of 4-bromo-3-*t*-butyl-1-methoxybenzene with ca. 40% selectivity was attributed to the electronic control. In the present system, NBS is slightly polarized on the silica-gel surface; it can, therefore, be presumed that the brominating species has a considerable soft character. The regioselectivity in the electrophilic aromatic substitution by soft electrophiles is determined by the frontier electron density,[11] the reaction is expected to occur preferentially at the para-position for the methoxybenzene.

The regioselectivity is affected by the nature of the silica gels. Neutral and basic silica gels gave somewhat better selectivity, though the conversion was lower than that catalyzed by Microbead 3A. The silica gel, conversion/% at 10 h, and the selectivity for the 4-bromo-3-*t*-butyl-1-methoxybenzene were follows: Microbead 3A, 97, 74; Microbead 4B (neutral, Fuji-Davison), 62, 79; Microbead 5D (basic, Fuji-Davison), 51, 86; Wakogel C-300 (Wako Chemicals), 38, 84; Kieselgel 60 (Merck), 51, 82.

The commercial availability of the reagent, simple reaction conditions, no evolution of hydrogen bromide and excellent yields of the monobrominated products make our method valuable from a preparative point of view.

Experimental

N-Bromosuccinimide was recrystallized from water and dried over phosphorus pentaoxide. Silica gels were used as received. The bromination was conducted in the dark. ^{1}H NMR and ^{13}C NMR spectra were recorded on a JEOL GX-270 spectrometer in $CDCl_3$ operating at 270 and 67.9 MHz with tetramethylsilane as an internal standard. IR spectra were obtained with a JASCO IRA-1 spectrophotometer. GC-MS measurements were carried out on a Hitachi M-52 mass spectrometer. The IR and mass spectral properties of the products were in accord with the assigned structure. Analytical gas chromatography was performed on a Yanagimoto G-180 with a flame ionization detector using 3 m×3 mm Silicone OV-17(2%)/Chromosorb W, Silicone DC-560 (10%)/Chromosorb W, and PEG 20M(25%)/Shimalite columns. The GLPC analyses of the isolated products indicated the purity of >98%.

Silica-Gel-Catalyzed Bromination of *m*-Dimethoxybenzene with NBS: A Typical Procedure: To a solution of *m*-dimethoxybenzene (276 mg, 2 mmol) in carbon tetrachloride (20 ml) were added *N*-bromosuccinimide (374 mg, 2.1 mmol) and Microbead 3A (1.00 g). The mixture was vigorously stirred at 30 °C for 2 h. The insoluble material was removed by filtration, washed with aqueous sodium thiosulfate, and dried over anhydrous sodium sulfate. Filtration, removal of the solvent, and Kugelrohr distillation (bath temperature 133 °C, 2.7 kPa) yielded 433 mg (99%) of 1-bromo-2,4-dimethoxybenzene. ^{1}H NMR ($CDCl_3$); δ=3.862 (MeO), 3.897 (MeO), 6.393 (H-5, dd, J_{35}, 2.4 Hz, J_{56}, 8.7 Hz), 6.482 (H-3, d), 7.398 (H-6, d).

4-Bromo-1,2-dimethoxybenzene (135 °C, 2.7 kPa). ^{1}H NMR ($CDCl_3$); δ=3.834 (MeO), 3.867 (MeO), 6.732 (H-6, d, J_{56}, 8.6 Hz), 6.976 (H-3, d, J_{35}, 2.3 Hz), 7.029 (H-5, dd).

2-Bromo-1,4-dimethoxybenzene (133 °C, 2.7 kPa). ^{1}H NMR ($CDCl_3$); δ=3.758 (MeO), 3.842 (MeO), 6.81 (H-5 and H-6, m), 7.116 (d, J_{45}, 2.6 Hz).

4-Bromo-1-methoxynaphthalene (105 °C, 25 Pa). ^{1}H NMR ($CDCl_3$); δ=3.920 (MeO), 6.617 (H-2, d, J_{23}, 8.0 Hz), 7.50 (H-7, m), 7.59 (H-6, m), 7.628 (H-3, d), 8.148 (H-5, d, J_{56}, 8.0 Hz), 8.250 (H-8, d, J_{78}, 8.0 Hz).

1-Bromo-2-methoxynaphthalene (110 °C, 30 Pa). ^{1}H NMR ($CDCl_3$); δ=4.008 (MeO), 7.250 (H-3, d, J_{34}, 9.0 Hz), 7.38 (H-6, m), 7.55 (H-7, m), 7.757 (H-5, d, J_{56}, 8.0 Hz), 7.788 (H-4, d), 8.216 (H-8, d, J_{78} 8.7 Hz).

***p*-Bromomethoxybenzene** (120 °C, 3.3 kPa). ^{1}H NMR ($CDCl_3$); δ=3.756 (MeO), 6.76 and 7.36 (AA'BB').

***p*-Bromoethoxybenzene** (123 °C, 3.0 kPa). ^{1}H NMR ($CDCl_3$); δ=1.399 (CH_3, t, *J* 6.9 Hz), 3.990 (CH_2, q) 6.75 and 7.34 (AA'BB').

4-Bromo-3-methyl-1-methoxybenzene (123 °C, 3.3 kPa). ^{1}H NMR ($CDCl_3$); δ=2.360 (CH_3), 3.765 (MeO), 6.607 (H-6, dd, J_{56}, 8.6 Hz, J_{26}, 3.0 Hz), 6.781 (H-2, d), 7.391 (H-5, d).

4-Bromo-3-ethyl-1-methoxybenzene (112 °C, 1.9 kPa). ^{1}H NMR ($CDCl_3$); δ=1.212 (CH_3, t, *J*, 7.5 Hz), 2.713 (CH_2, q), 3.781 (MeO), 6.615 (H-6, dd, J_{56}, 8.6 Hz, J_{26}, 3.0 Hz), 6.786 (H-2, d), 7.269 (H-5, d).

4-Bromo-3-isopropyl-1-methoxybenzene (116 °C, 2.1 kPa). ^{1}H NMR ($CDCl_3$); δ=1.228 (CH_3, d, *J*, 6.9 Hz), 3.310 (CH, sep), 3.788 (MeO), 6.606 (H-6, dd, J_{26} 2.9 Hz, J_{56} 8.7 Hz), 6.826 (H-2, d), 7.411 (H-5, d).

6-Bromo-3-*t*-butyl-1-methoxybenzene: To a mixture of *m*-*t*-butylmethoxybenzene (20 mmol) and a trace amount of iron powder was added a solution of bromine (20 mmol) in carbon tetrachloride (20 ml). The mixture was stirred for 2 h, and poured into water (50 ml). After the conventional work-up, 6-bromo-3-*t*-butyl-1-methoxybenzene was obtained by Kugelrohr distillation (125 °C, 2.0 kPa) in 85% yield. ^{1}H NMR ($CDCl_3$); δ=1.314 (*t*Bu), 3.900 (MeO), 6.857 (H-4, dd, J_{24}, 2.2 Hz, J_{45}, 8.3 Hz), 6.918 (H-2, d), 7.425 (H-5, d). ^{13}C NMR ($CDCl_3$); δ=31.1 (q), 34.7 (s), 55.9 (q), 108.3 (C-6, s), 109.5 (C-2, d), 118.8 (C-4, d), 132.4 (C-5, d), 152.0 (C-3, s), 155.2 (C-1. s).

Bromination of *m*-*t*-Butylmethoxybenzene with NBS–Silica Gel: Silica-gel-catalyzed bromination was carried out in a similar manner as described above for 20 h. ^{1}H and ^{13}C NMR analysis of the distillate indicated that it consisted of two components in a ratio of 74:26. The NMR spectral data of the minor component was identical with those of 6-bromo-3-*t*-butyl-1-methoxybenzene. On the basis of the ^{1}H and ^{13}C NMR data, the major component was assigned to 4-bromo-3-*t*-butyl-1-methoxybenzene: ^{1}H NMR ($CDCl_3$) δ= 1.492 (*t*Bu), 3.781 (MeO), 6.577 (H-6, dd, J_{26}, 3.2 Hz, J_{56}, 8.7 Hz), 6.997 (H-2, d), 7.465 (H-5, d). ^{13}C NMR ($CDCl_3$); δ=29.6 (q), 36.6 (s), 55.3 (q), 111.5 (C-6, d), 113.0 (C-4, s), 115.3 (C-2, d), 136.1 (C-5, d), 148.9 (C-3, s), 158.6 (C-1, s).

References

1) D. C. Schlegel, C. D. Tipton, and K. L. Rinehart, Jr., *J. Org. Chem.*, **35**, 849 (1970).

2) C. Yaroslavsky, *Tetrahedron Lett.*, **1974**, 3395.

3) M. Hojo and R. Masuda, *Synth. Commun.*, **5**, 169 (1975).

4) K. Smith, M. Butters, W. E. Paget, and B. Nay, *Synthesis*, **1985**, 1155.

5) H. Konishi, K. Yokota, Y. Ichihashi, T. Okano, and J. Kiji, *Chem. Lett.*, **1980**, 1423.

6) A. G. Mistry, K. Smith, and M. R. Bye, *Tetrahedron*

Lett., **27**, 1051 (1986).
7) S. D. Ross, M. Finkelstein, and R. C. Petersen, *J. Am. Chem. Soc.*, **80**, 4327 (1958).
8) R. H. Mitchell, Y-H. Lai, and R. V. Williams, *J. Org. Chem.*, **44**, 4733 (1979).
9) L. M. Stock and H. C. Brown, *J. Am. Chem. Soc.*, **81**, 5615 (1959).
10) K. L. Erickson and H. W. Barowsky, *J. Chem. Soc., Chem. Commun.*, **1971**, 1596.
11) G. Klopman, *J. Am. Chem. Soc.*, **90**, 223 (1968).

Cyclization of Penta- and Hexapeptide Active Esters Related to Gramicidin S and Gratisin

Makoto TAMAKI,* Michiaki TAKIMOTO, Mitsuo HAYASHI,† and Ichiro MURAMATSU††
Department of Chemistry, Faculty of Science, Toho University, Miyama, Funabashi-shi, Chiba 274
†Medicinal Research Laboratories, Toyo Jozo Co., Ltd., Ohito, Shizuoka 410-23
††Department of Chemistry, College of Science, Rikkyo University, Nishi-Ikebukuro, Tokyo 171
(Received July 13, 1988)

Synopsis. Four pentapeptide *N*-hydroxysuccinimide esters [X-Orn(Z)-Leu-Y-Pro-ONSu (X=Val or D-Val, and Y=Phe or D-Phe)] related to gramicidin S were allowed to cyclize in pyridine. The peptides with a L-Phe residue preceding Pro tend to form various cyclic polymers, while ones with a D-Phe residue exclusively yielded a cyclic monomer or cyclic dimer. Peptides with a D-Val residue at the N-terminal produced monomerization products. The observed tendencies were similar for cyclization of four hexapeptide *N*-hydroxysuccinimide esters [X-Val-Orn(Z)-Leu-Y-Pro-ONSu (X=Tyr(Bzl) or D-Tyr($BzlCl_2$), and Y= Phe or D-Phe)] related to gratisin.

An antibiotic peptide, gramicidin S (GS),[1] is a cyclic decapeptide consisting of two identical pentapeptide sequences of -Val-Orn-Leu-D-Phe-Pro- (Fig. 1).[2] In 1957, Schwyzer and Sieber reported that the cyclization of the H-Val-Orn(Tos)-Leu-D-Phe-Pro *p*-nitrophenyl ester produced cyclic decapeptide (the ditosyl derivative of GS) instead of cyclic pentapeptide.[3] Since then, various analogs of GS have been synthesized by this cyclic dimerization method.[4] In an investigation of the influence of substitution of each amino acid residue in the H-$\overset{1}{\text{Val}}$-$\overset{2}{\text{Orn}}$(Z)-$\overset{3}{\text{Leu}}$-D-$\overset{4}{\text{Phe}}$-$\overset{5}{\text{Pro}}$ *p*-nitrophenyl ester to the cyclization, Izumiya et al. reported that the steric hindrance of the side chains of amino acid residues at the N-terminal and at position 4 in the active esters greatly affects the reaction.[4] However, the effects of an alteration of the configurations of the constituent amino acid have been little studied.

In present studies, four pentapeptide *N*-hydroxysuccinimide esters related to GS, X-Orn(Z)-Leu-Y-Pro-ONSu (X= Val or D-Val, and Y=Phe or D-Phe) (Fig. 2), were cyclized in order to examine the influence of the configurations of amino acid residues at the N-terminal and position 4. In addition, a similar investigation was carried out concerning four hexapeptide *N*-hydroxysuccinimide esters related to gratisin (GR) (Fig. 1),[5,6] X-Val-Orn(Z)-Leu-Y-Pro-ONSu [X=Tyr(Bzl) or D-Tyr($BzlCl_2$), and Y=Phe or D-Phe] (Fig. 2).

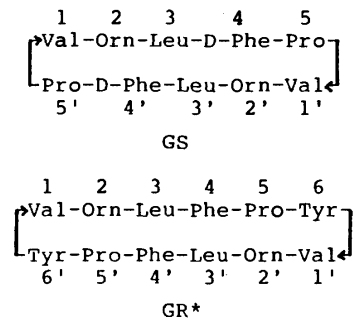

Fig. 1. Primary structures of GS and GR.
*The configuration of each amino acid residue has not been established yet.

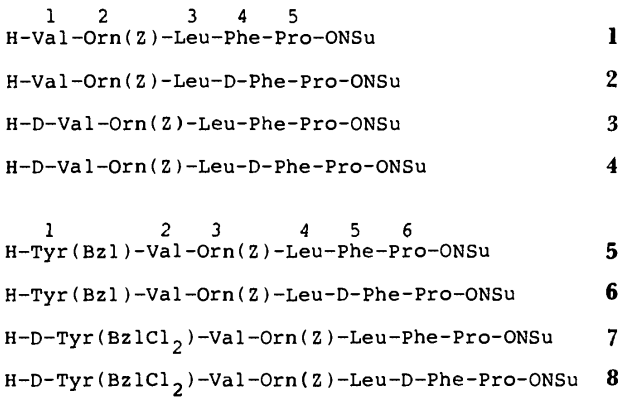

Fig. 2. Primary structures of penta- and hexapeptide active esters.

Boc-penta- and -hexapeptides were prepared by a conventional method.[6,7] Boc-penta- and -hexapeptides were converted into the penta- and hexapeptide-ONSu trifluoroacetates, which were cyclized in pyridine for 1 d at 25 °C (concentration of peptides in pyridine: 3×10^{-3} M). The ratio of the cyclic products was determined by high-performance liquid chromatography (HPLC) analysis. The molecular weight of each cyclic product isolated by semipreparative HPLC was determined by fast atom bombardment (FAB) or secondary ion mass spectrometry.

HPLC profiles of crude cyclic products are shown in Figs. 3 and 4. Cyclic peptides were eluted in order of the ring sizes.

Data of the cyclization are summarized in Table 1. Compounds **1** and **3**, both of which contain a L-Phe residue preceding Pro, gave cyclic products with widely distributed molecular weights. The former yielded the cyclic dimer, trimer, tetramer, and pentamer (roughly evenly), but not the cyclic monomer. The latter produced the cyclic monomer, dimer, trimer, and tetramer. Compound **2** yielded exclusively the cyclic dimer, diZ-GS, while Izumiya et al. reported that compound **2** gave a considerable amount of the cyclic monomer under similar conditions.[4,8] Compound **4** gave the cyclic monomer as a sole product. In the cases of the hexapeptide esters (**5**—**8**), each gave its cyclic monomer and dimer regardless of the configurations of the constituent amino acids. The ester con-

† 1 M=1 mol dm^{-3}.

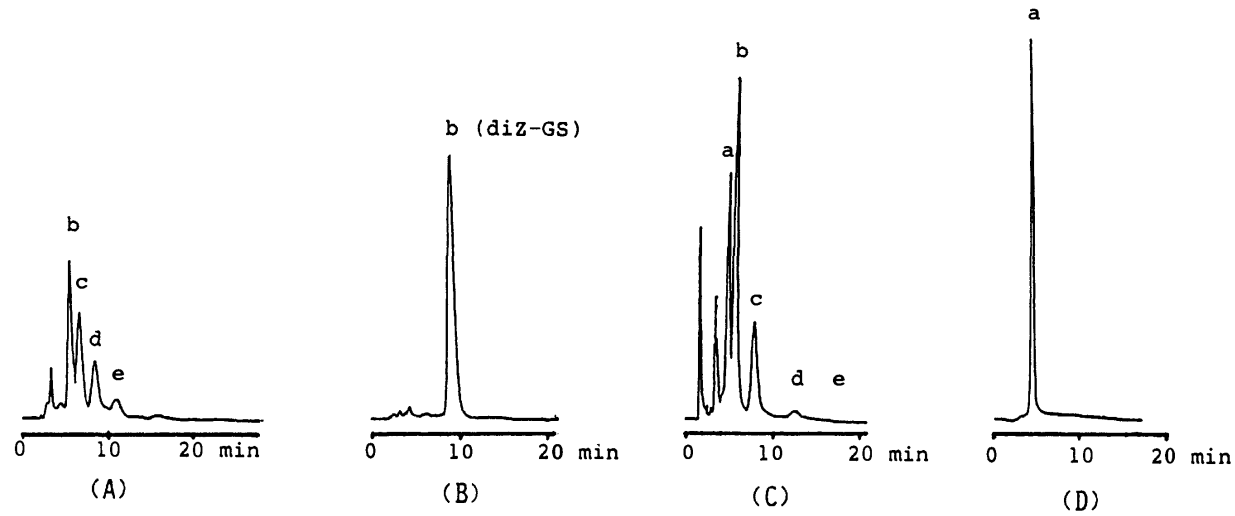

Fig. 3. HPLC profiles of crude products in cyclization of active esters related to GS.
The starting compounds are: (A), **1**; (B), **2**; (C), **3**; (D), **4**.
(a: cyclic monomer, b: cyclic dimer, c: cyclic trimer, d: cyclic tetramer, e: cyclic pentamer)

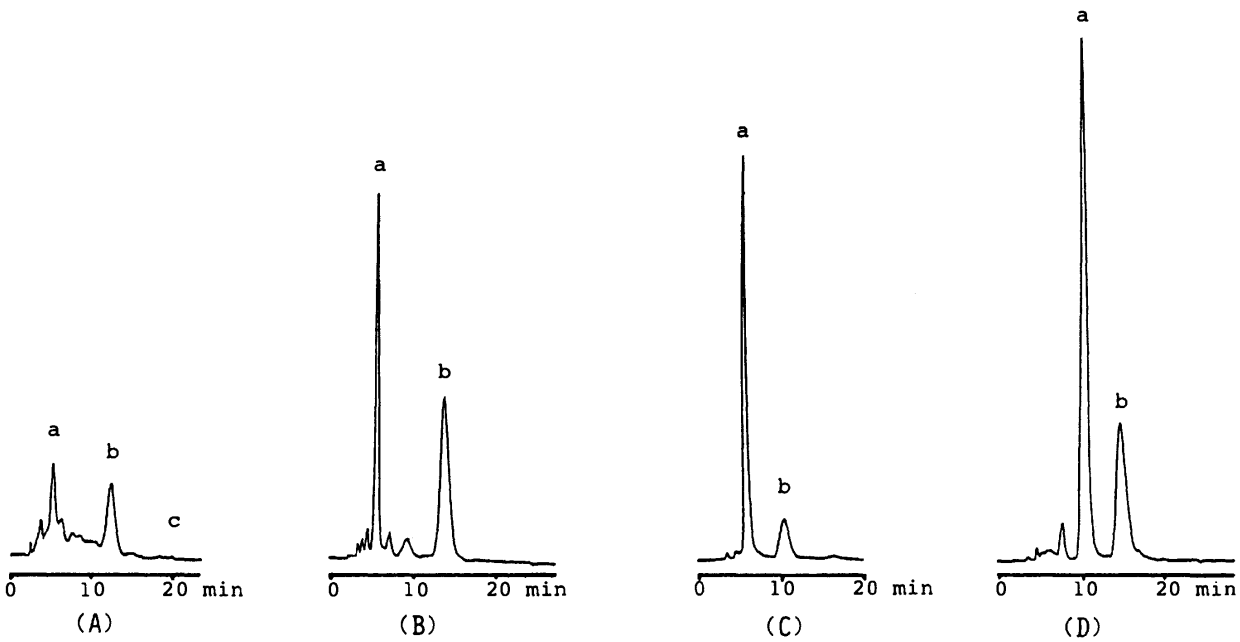

Fig. 4. HPLC profiles of crude products in cyclization of active esters related to GR.
The starting compounds are: (A), **5**; (B), **6**; (C), **7**; (D), **8**.
(a: cyclic monomer, b: cyclic dimer, c: cyclic trimer)

Table 1. Products of Cyclization of Penta- and Hexapeptide Active Esters[a]

Starting compounds	Yield(%)[b] of cyclic product	Ratios of cyclic peptides				
		Monomer	Dimer	Trimer	Tetramer	Pentamer
1	30	0	34[1409]	32[2115]	24[2820]	10[3524]
2	57	0	100[1409]	0	0	0
3	40	30[704]	46[1409]	21[2115]	3[2819]	0[3523][c]
4	48	100[704]	0	0	0	0
5	26	43[958]	57[1916]	0[2875][c]	0	0
6	38	45[958]	55[1916]	0	0	0
7	53	78[1027]	22[2053]	0	0	0
8	70	67[1027]	33[2053]	0	0	0

a) Numbers in brackets are mass numbers observed as the molecular ion peaks. b) The yield based on cyclic peptides separated from reaction mixture by HPLC. c) Small amount of the corresponding cyclic trimer or pentamer was separated using HPLC.

taining a L-Phe residue preceding Pro (**5**) yielded some cyclic products with higher molecular weights, though their amounts were negligible. The data indicated that the configurations of the constituent amino acids in the active esters and the lengths of the esters affect the course of cyclic polymerization. In both cases, the penta- and hexapeptide active esters, the configuration of the N-terminal amino acids affects cyclization. Esters with D-amino acids (**3**, **4**, **7**, **8**) clearly produce products of cyclic monomerization or cyclization at lower molecular weights.

Experimental

Synthesis of Boc-penta- and -hexapeptides was performed as manner described in our previous papers.[6,7]

Boc-Tyr(Bzl)-Val-Orn(Z)-Leu-D-Phe-Pro-OH. Yield, 79% from the corresponding benzyl ester: mp 181—184 °C; $[\alpha]_D^{20}$, −29.3° (*c* 1.0, DMF): Found: C, 64.80; H, 7.24: N, 8.95%. Calcd for $C_{59}H_{77}N_7O_{12}\cdot H_2O$: C, 64.76; H, 7.27; N, 8.96%.

Boc-D-Tyr(BzlCl$_2$)-Val-Orn(Z)-Leu-D-Phe-Pro-OH. Yield, 90% from the corresponding benzyl ester; mp 164—165 °C; $[\alpha]_D^{20}$, −14.5 (*c* 1.1, DMF); Found: C, 60.71; H, 6.63; N, 8.04%. Calcd for $C_{59}H_{75}N_7O_{12}Cl_2\cdot H_2O$: C, 60.92; H, 6.67; N, 8.43%. Cyclization via an active ester was performed in a similar manner to that described in our previous paper.[7] HPLC analysis was carried out using a Twincle system (Jasco) consisting of a Twincle pump, a VL-611 injector and a UVIDEC 100-III detector. A Finepak SIL C18 column (10 μm, 250×4.6 mm I.D., or 250×6.7 mm I.D., Jasco) was used: flow rate, 1 ml min^{-1}; solvent, methanol-water (9:1); monitoring wavelength, 220 nm. The peak area was recorded using a Chromatopac C-R3A integrator (Shimadzu Co.). Molecular weights of the cyclic products were determined by FAB mass spectrometry using a JEOL JMS-D300 mass spectrometer (in Toyo Jozo Co., Ltd.) and a JEOL JMS-HX110 mass spectrometer (in JEOL Ltd.), and/or secondary ion mass spectrometry using a Hitachi M-80 mass spectrometer (in Meijo Univ.).

We are grateful to Professor Makoto Suzuki and Associate Professor Ken-ichi Harada, Meijo University, for measurements of secondary ion mass spectrometry.

References

1) A. R. Battersby and L. C. Craig, *J. Am. Chem. Soc.*, **73**, 1887 (1951).

2) Amino acid residues with no prefix are of L-configuration unless otherwise noted. The abbreviations for amino acids and peptides are in accordance with the rules of IUPAC-IBU Commission of Biological Nomenclature. Abbreviations used are as follows: Boc, *t*-butoxycarbonyl; Z, benzyloxycarbonyl; Tos, tosyl; Bzl, benzyl: BzlCl$_2$, 2,4-dichlorobenzyl: -ONSu, hydroxysuccinimide ester; DMF, *N*,*N*-dimethylformamide.

3) R. Schwyzer and P. Sieber, *Helv. Chim. Acta*, **41**, 2186 (1958).

4) N. Izumiya, T. Kato, H. Aoyagi, M. Waki, and M. Kondo, "Synthetic Aspects of Biologically Active Cyclic-peptide—Gramicidin S and Tyrocidines" Kodansha, Tokyo, and Halsted Press, New York (1979), pp. 15—47.

5) a) G. G. Zharikova, S. P. Myaskovskaya, and A. B. Silaev, *Vesten. Mosk. Univ. Biol. Pochovoved.*, **27**, 110 (1972). b) S. P. Myaskovskaya, G. G. Zharikova, and A. B. Silaev, *ibid.*, **28**, 123, (1973).

6) M. Tamaki, *Bull. Chem. Soc. Jpn.*, **57**, 3210 (1984).

7) M. Tamaki, T. Okitsu, M. Araki, H. Sakamoto, M. Takimoto, and I. Muramatsu, *Bull. Chem. Soc. Jpn.*, **58**, 531 (1985).

8) Y. Minematsu, M. Waki, K. Suwa, T. Kato, and N. Izumiya, *Tetrahedron. Lett.*, **21**, 2179 (1980).

Regioselective Reaction of Oxiranes with *S*-Phenyl Thioesters Catalyzed by Quaternary Onium Salts or Crown Ether-Metal Salt Complexes

Takashi IIZAWA,* Akira GOTO, and Tadatomi NISHIKUBO
Department of Applied Chemistry, Faculty of Engineering, Kanagawa University, Rokkakubashi, Kanagawa-ku, Yokohama 221
(Received June 16, 1988)

Synopsis. Regioselective addition reactions of 2-substituted oxiranes with *S*-phenyl thioesters gave 2-aceyloxy-1-phenylthio derivatives in high yield using some 18-crown-6-metal complexes as well as tetrabutylammonium salts as a catalyst under relatively mild conditions.

The addition reaction of oxiranes with esters has attracted much attention in the field of polymer chemistry since two distinct functional groups are introduced into their molecules at the same time.[1] Since these substrates do not show a high reactivity, it is very important to select suitable catalysts for the reaction. Funahashi[2] previously undertook the reaction of oxiranes with esters using such bases as tertiary amines or potassium *t*-butoxide as a catalyst at high reaction temperatures. Recently, we found[3] that the reaction of a pendant epoxy group in a polymer with an active ester and thioester proceeded smoothly upon the addition of onium salts, which had much higher catalytic activities than the bases as a catalyst, under relatively mild conditions; crown ether-metal complexes were also available catalysts for this reaction.

We wish to report herein the identification of the addition products of 2-substituted oxiranes with *S*-phenyl thioesters, and to discuss the catalytic effect of crown ether-metal salt complexes on this reaction in comparison with that of tetrabutylammonium salt.

The addition reaction of 2-(phenoxymethyl)oxirane and 2-(methoxymethyl)oxirane with *S*-phenyl thiobenzoate and *S*-phenyl thioacetate was carried out in DMF using Bu_4NBr as a catalyst. The reactions did not occur without a catalyst; however, the addition of Bu_4NBr caused the reaction to proceed with high conversion, as shown in Table 1. The reaction could be expected to give two products, the corresponding 2-acyloxy-1-phenylthic derivatives (**1**) and 1-acyloxy-2-phenylthio derivatives (**2**), as shown in Scheme 1. However, the reaction of oxirane with *S*-phenyl thioester yielded only one product other than a very small amount of 2-hydroxy-3-(phenylthio) propyl ether (**3**). The reaction product agreed with **1** obtained from an acylation of **3**. **3** was also prepared from an addition reaction of the oxirane with thiophenol. Furthermore, it is easy to distinguish between **1** and **2**, which show very different ^1H NMR spectra.[4] The addition products of oxirane with *S*-phenyl thioester showed similar chemical shifts of methine and methylene protons to those of the known compounds **1**.[4a] These results strongly substantiated that the reaction of oxirane with *S*-phenyl ester proceeded regioselectively to give **1**.

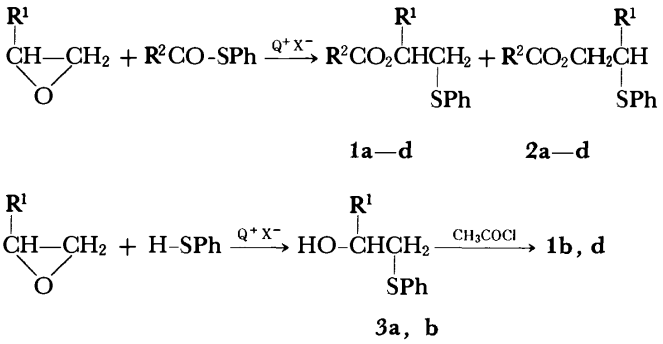

Q^-X^-: quaternary onium salt, crown ether-metal complex

1, 2a: R^1=$PhOCH_2$ R^2=Ph
b: R^1=$PhOCH_2$ R^2=Me
c: R^1=$MeOCH_2$ R^2=Ph
d: R^1=$MeOCH_2$ R^2=Me

3a: R^1=$PhOCH_2$
b: R^1=$MeOCH_2$

Scheme 1

The catalytic effect of crown ether-metal salt complexes on the addition reaction of 2-(phenoxymethyl) oxirane with *S*-phenyl thiobenzoate was investigated at 90 °C in diglyme, as shown in Table 2. Tertiary amines have been used as catalysts in the reaction of oxirane with ester;[2] however, tertiary amines, such as tributylamine and triethylamine, hardly showed any catalytic activity under these conditions. The reaction took place upon the addition of a mixture of 18-crown-

Table 1. Reaction of Oxiranes with *S*-Phenyl Thioester

Entry	Reagents		Reaction		Product	Yield[a] of **1**
	R^1	R^2	Temp / °C	Time / h		%
1	$PhOCH_2$	Ph	110	25	**1a**	71.0
2	$PhOCH_2$	Me	110	10	**1b**	75.9
3	$MeOCH_2$	Ph	110	50	**1c**	69.7
4	$MeOCH_2$	Me	110	10	**1d**	60.4

a) Isolated yield.

Table 2. Reaction of 2-(Phenoxymethyl)oxirane with *S*-Phenyl Thiobenzoate in Diglyme at 90 °C for 5 h

Entry	Catalyst	Yield %	Entry	Catalyst	Yield %
5	Et_3N	2.6	13	18-C-6/KI	69.1
6	Bu_3N	4.3	14	18-C-6/$KHSO_4$	0
7	AcOK	0	15	18-C-6/$KClO_4$	0
8	18-C-6[a)]	0	16	Bu_4NCl	91.0
9	18-C-6/AcOK	89.5	17	Bu_4NBr	70.7
10	18-C-6/KF	73.7	18	Bu_4NI	2.6
11	18-C-6/KCl	0.9	19	Bu_4NHSO_4	0
12	18-C-6/KBr	75.6	20	Bu_4NClO_4	0

a) 18-C-6: 18-crown-6.

6 and potassium salts as well as quaternary ammonium salt. Since neither 18-crown-6 nor potassium salt individually showed any catalytic activity, the 18-crown-6-metal salt complexes produced from the mixture worked as catalysts. The catalytic activity was markedly affected by the counter ions in the catalysts. The effect of a counter ion in tetrabutylammonium salt and 18-crown-6-potassium salt complex changed in the order; $HSO_4^- = ClO_4^- < I^- < Br^- < Cl^-$ and $AcO^- > Br^- > F^- > I^- > Cl^- > HSO_4^- = ClO_4^-$, respectively. The counter-ion effect was much different between the tetrabutylammonium salt and 18-crown-6-potassium salt complex. On the other hand, 18-crown-6-potassium acetate showed almost the highest catalytic activity of tetrabutylammonium salts and the crown ether-potassium salt complexes. These results suggest that 18-crown-6-potassium salt complexes are also suitable catalysts for an addition reaction of oxiranes with thioesters.

Experimental

General Procedure for Synthesis of 2-Acyloxy-3-(phenylthio)propyl Ethers (Table 1). 2-Benzoyloxy-3-(phenylthio)propyl Phenyl Ether (1a): The mixture of 2-(phenoxymethyl)oxirane (7.51 g, 50 mmol), *S*-phenyl thiobenzoate (10.70 g, 50 mmol), Bu_4NBr (1.61 g, 5 mmol), and dry DMF (50 ml) was stirred at 110 °C for 25 h. The conversion was 82.4%, measured by GLC. Ether (150 ml) was added to the reaction mixture, and the etheral solution was washed with water (50 ml×3), dried with $MgSO_4$, and evaporated in vacuo. The residue was recrystallized from hexane to afford **1a** (12.90 g, 71.0%); mp 39—40 °C; IR (KBr) 1720 cm^{-1} (C=O); ^1H NMR ($CDCl_3$) δ=3.35 (d, 2H, S-CH_2), 4.32 (d, 2h, O-CH_2), 5.36—5.70 (m, 1H), 6.80—8.10 (m, 15H). Found: C, 72.55; H, 5.80%. Calcd for $C_{22}H_{20}O_3S$: C, 72.50; H, 5.53%.

2-Acetoxy-3-(phenylthio)propyl Phenyl Ether (1b): Bp 190—195 °C/0.05 mmHg (1 mmHg≈133.322 Pa); IR (neat) 1740 cm^{-1} (C=O); ^1H NMR ($CDCl_3$) δ=1.98 (s, 3H), 3.28 (d, 2H, S-CH_2), 4.14 (d, 2H, O-CH_2), 5.10—5.40 (m, 1H), 6.76—7.56 (m, 10H). Found: C, 67.56; H, 6.27%. Calcd for $C_{17}H_{18}O_3S$: C, 67.52; H, 6.00%.

2-Benzoyloxy-3-(phenylthio)propyl Methyl Ether (1c): Viscous oil; IR (neat) 1720 cm^{-1} (C=O). ^1H NMR ($CDCl_3$) δ=3.34 (d, 2H, S-CH_2), 3.38 (s, 3H), 3.76 (d, 2H, O-CH_2), 5.24—5.56 (m, 1H), 7.10—8.20 (m, 10 H). Found: C, 67.82; H, 6.25%. Calcd for $C_{17}H_{18}O_3S$: C, 67.52; H, 6.00%.

2-Acetoxy-3-(phenylthio)propyl Methyl Ether (1d): Bp 96—100 °C/0.03 mmHg; IR (neat) 1740 cm^{-1} (C=O); ^1H NMR ($CDCl_3$) δ= 2.00 (s, 3H), 3.18 (d, 2H, S-CH_2), 3.34 (s, 3H), 3.60 (d, 2H, O-CH_2), 5.00—5.24 (m, 1H), 7.10—7.52 (m, 5H). Found: C, 60.02; H, 6.81%. Calcd for $C_{12}H_{16}O_3S$: C, 59.97; H, 6.71%.

3-Hydroxy-3-(phenylthio)propyl Phenyl Ether (3a): The mixture of 2-(phenoxymethyl)oxirane (15.02 g, 0.10 mol), thiophenol (11.02 g, 0.10 mol), Bu_4NBr (1.61 g, 5 mmol), and dry diglyme (50 ml) was stirred at 90 °C for 5 h. After the usual work-up, the residue was distilled under reduced pressure to give **3a** (20.32 g, 78.1%); bp 179—180 °C/0.03 mmHg; IR (neat) 3450 cm^{-1} (OH); ^1H NMR ($CDCl_3$) δ=2.76 (d, 1H, O-H), 3.16 (d, 2H, S-CH_2), 3.90—4.30 (m, 1H, CH), 4.02 (d, 2H, O-CH_2), 6.20—7.60 (m, 10H). Found: C, 69.20; H, 6.19%. Calcd for $C_{15}H_{16}OS$: C, 69.61; 6.20%.

3-Hydroxy-3-(phenylthio)propyl Methyl Ether (3b): Yield 67.2%; bp 110—112 °C/0.02 mmHg (lit,[5)] 103—104 °C/0.03 mmHg); IR (neat) 3450 cm^{-1} (OH); ^1H NMR ($CDCl_3$) δ=2.80 (d, 1H, O-H), 3.00 (d, 2H, S-CH_2), 3.08 (s, 3H, CH_3), 3.40 (d, 2H, O-CH_2), 3.70—4.10 (m, 1H, CH), 7.00—7.50 (m, 5H).

Synthesis of 1b from 3a: To a solution of **3a** (0.200 g, 73 mmol) in pyridine (5 ml) was added acetyl chloride (0.576 g, 73 mmol) at 5 °C. After allowing the mixture to stand at room temperature for 1 h, the mixture was poured into water, and extracted with ether. The etheral extract was washed with a dilute hydrochloric solution, dried, and evaporated in vacuo. The residue was chromatographed on silica gel, using benzene-ethyl acetate (10:1), to give **1b** (0.245 g, 95%) as a colorless viscous oil.

Synthesis of 1d from 3b: Yield 85.0%, after purification from chromatography on silica gel using hexane-ethyl acetate (7:3).

Reaction of 2-(Phenoxymethyl)oxirane with *S*-Phenyl Thiobenzoate (Table 2): A mixture of 2-(phenoxymethyl)-oxirane (10 mmol), *S*-phenyl thiobenzoate (10 mmol), catalyst (quaternary onium salt or potassium salt and 18-crown-6, 0.5 mmol), and dried diglyme (5 ml) was stirred at 90 °C under nitrogen flow. The amount of **1a** was monitored by GLC.

References

1) T. Nishikubo, T. Iizawa, E. Takahashi, and F. Nono, *Polym. J.*, **16**, 371 (1984); T. Nishikubo, T. Iizawa, E. Takahashi, and F. Nono, *Macromolecules*, **18**, 2131 (1985).

2) K. Funahashi, *Bull. Chem. Soc. Jpn.*, **52**, 1488 (1979).

3) T. Nishikubo, T. Iizawa, and S. Saita, *J. Polym. Sci., Polym. Chem. Ed.*, **24**, 1685 (1986); T. Nishikubo and S. Saita, *Makromol. Chem.*, **188**, 799 (1987).

4) M. S. Khan and L. N. Owen *J. Chem. Soc. C*, **1971**, 1448; A. Behzadi and L. N. Owen, *J. Chem. Soc., Perkin Trans. 1*, **1973**, 2733.

5) A. M. Kuliev, Z. A. Alizade, V. M. Farzaliev, and N. Yu. Lunkashu, *Azerb. Khim. Zh.*, **1971**, 44; *Chem. Abstr.*, **78**, 42947e (1973).

The Triflic Acid-Catalysed Deacylation and Decarboxylation of Polymethylbenzenecarbonyl Derivatives under Mild Conditions

Takashi KEUMI,* Toshio MORITA, Yoshihiro OZAWA, and Hidehiko KITAJIMA
Department of Applied Chemistry, Faculty of Engineering, Fukui University, Bunkyo, Fukui 910
(Received June 27, 1988)

Synopsis. Sterically hindered acylarenes are deacylated to arenes in good yields on heating in boiling 1,2-dichloroethane containing a catalytic amount of triflic acid and water. Hindered arenecarboxylic acids undergo decarboxylation under the same conditions to give arenes in high yields.

It is known that sterically hindered aromatic ketones and carboxylic acids can undergo protodeacylation or decarboxylation in the presence of concd sulfuric acid,[1] polyphosphoric acid,[2] or Friedel-Crafts catalysts.[3] However, the reaction of acylpolymethylbenzenes with these catalysts is accompanied by some side reactions, such as the sulfonation,[4,5] disproportionation,[6] or isomerization of alkyl groups in the substrates or products.[7,8] Olah and his co-workers reported that perfluororesin sulfonic acid, "Nafion-H," is an efficient catalyst for the deacylation of hindered aromatic ketones in hot toluene or anisole.[9] However, this procedure involves the problem of isolating the products from excess toluene or anisole. In addition, polymerized products result from the ketene formed during the deacetylation. We have previously reported on the transacylation between acylpolymethylbenzenes and some arenes in boiling trifluoroacetic acid (TFA).[10] In that paper, we described how the presence of a nucleophile in TFA accelerates the protodeacetylation rate of acetylpentamethylbenzene (AcPMB).

We wish to report now that the addition of a small amount of water to TFA increases the protodeacetylation rate of AcPMB and that, therefore, the deacylation of a variety of acylarenes to arenes can be selectively performed with a catalytic amount of triflic acid (TFSA) in boiling 1,2-dichloroethane (DCE) containing a small amount of water. The decarboxylation of arenecarboxylic acids with this system will be described.

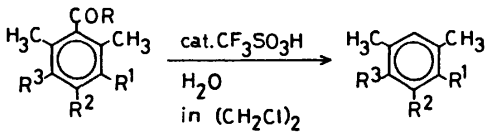

Scheme 1.

Results and Discussion

When AcPMB is heated in TFA under reflux, deacetylation proceeds to afford pentamethylbenzene (PMB). The apparent rate constant for the formation of PMB was determined in the presence of water. The rate

Table 1. First-Order Rate Constants for the Protodeacetylation of Acetylpentamethylbenzene (AcPMB) in Boiling TFA[a]

Run	Molar ratio H_2O/AcPMB	Rate constant $10^4k/s^{-1}$	r[b]
1[c]	0	2.05±0.004	
2	0.2	3.22	0.999
3	0.5	3.74	0.997
4	1	4.08	0.998
5	2	4.50	0.996
6	3	4.18	0.998

a) $[AcPMB]_0$=0.131 M in TFA. b) Correlation coefficient for the first-order rate plots (8 points). c) Quoted from Ref. 10.

Table 2. Protodeacetylation of Acetylpentamethylbenzene (AcPMB) to Pentamethylbenzene (PMB)[a]

Run	Acid	Molar ratio vs. AcPMB		Solvent	React. time	Yield of PMB	Recovery of AcPMB[b]
		Acid	H_2O		h	%	%
1	TFA[c]	100	—	—	2	40	60
2	TFA	100	0.3	—	1	71	30
3	TFA	100	0.6	—	1	75	27
4	TFA	100	1	—	1	76	20
5	TFA	100	5	—	1	99	1
6	TFA	100	11	—	1	97	1
7	TFA	5	2	DCE[d]	5	8	92
8	TFA	2	1	DCE	5	0	99
9	TFSA[e]	2	2	DCE	5	100	0
10	TFSA	0.5	2	DCE	5	100	0
11	TFSA	0.2	1	DCE	5	98	1
12	TFSA	0.5	—	DCE	5	56	17
13	TFSA	1.0	—	DCE	5	51	13

a) Carried out in boiling TFA or DCE. b) Determined by GLC. c) Trifluoroacetic acid. d) 1,2-Dichloroethane. e) Triflic acid.

constant obeys pseudo-first-order kinetics with respect to AcPMB in a solution with a large excess of TFA (more than a 50-fold excess) (Table 1). The results indicate that the addition of water into TFA promotes the deacetylation rate. The rate constant increased with the increase in the molar ratio of the added water. The effect of water was also confirmed in a preparative experiment. It can be seen from the results shown in Table 2 that the yield of PMB increases with the increase in the amount of water added. We found that TFA with a water content of ca. 15% works efficiently in the deacetylation of AcPMB. In order to save some of the TFA, the deacetylation was attempted in a DCE solution containing a small amount of water. The reaction with two equivalents of TFA in DCE did not occur at all, and the yield of PMB was only 8%, even with five equivalents of TFA. In contrast, the reaction using TFSA as an acid proceeded smoothly to give PMB in a quantitative yield. The deacetylation product can be obtained in a good yield even with a catalytic amount of TFSA. In the absence of water, though, the reaction was accompanied by some side reactions to result in a low yield of PMB and a low recovery of AcPMB.

A variety of pentamethylbenzenecarbonyl derivatives were subjected to deacylation or decarboxylation with TFSA in a DCE solution. The results are summarized in Table 3. Pentamethylbenzenecarbonyl derivatives, having not only alkanoyl but aroyl moieties, were deacylated to give PMB in satisfactory yields. The decarboxylation of pentamethylbenzoic acid was also efficiently performed under these conditions. However, in the case of ethyl pentamethylbenzoate, the yield of PMB was low and the starting ester was recovered.

Furthermore, various polymethylbenzenecarbonyl derivatives were reacted with catalytic amounts of TFSA in boiling DCE (Table 4).

As can be seen from the results listed in Table 4, the method works satisfactorily for sterically hindered alkyl aryl ketones, benzophenones, and benzoic acids, which have methyl groups at both the 2- and 6-positions. No side reactions have been observed.

Table 3. Protodeacylation and Decarboxylation of Pentamethylbenzenecarbonyl Derivatives (PMBC) with TFSA[a]

Run	Carbonyl group of PMBC	React. time	Yield of PMB[b]
		h	%
1	CH_3CO-	5	98
2	CH_3CH_2CO-	5	99
3	$CH_3CH_2CH_2CO$-	5	97
4	$(CH_3)_3CCO$-	5	99
5	$C_6H_5CH{=}CHCO$-	15	100
6	HOCO-	15	94
7	CH_3CH_2OCO-	15	18
8	*p*-$CH_3C_6H_4CO$-	5	91
9	*p*-ClC_6H_4CO-	15	90
10	*p*-FC_6H_4CO-	24	80
11	*p*-$CH_3OC_6H_4CO$-	24	93

a) Carried out with 0.5—2.0 equivalents of TFSA in boiling 1,2-dichloroethane containing ca. one equivalent of water. b) Determined by GLC.

Table 4. Protodeacylation and Decarboxylation of Polymethylbenzenecarbonyl Derivatives (POBC) with TFSA[a]

Run	Carbonyl group of POBC	Substituent of the benzene ring					React. time	Yield of methylbenzenes[b]
		2-	3-	4-	5-	6-position	h	%
1	CH_3CO-	CH_3	CH_3	H	CH_3	CH_3	5	95
2	CH_3CO-	CH_3	H	CH_3	CH_3	CH_3	5	100
3	CH_3CO-	CH_3	H	CH_3	H	CH_3	5	98
4	CH_3CO-	H	CH_3	CH_3	CH_3	CH_3	5	4
5	HOCO-	CH_3	CH_3	H	CH_3	CH_3	5	80
6	HOCO-	CH_3	H	CH_3	CH_3	CH_3	5	100
7	HOCO-	CH_3	H	CH_3	H	CH_3	10	100
8	HOCO-	H	CH_3	CH_3	CH_3	CH_3	5	0
9	C_6H_5CO-	CH_3	CH_3	H	CH_3	CH_3	24	90

a) Carried out with 0.5 equivalent of TFSA in boiling 1,2-dichloroethane containing ca. one equivalent of water. b) Determined by GLC.

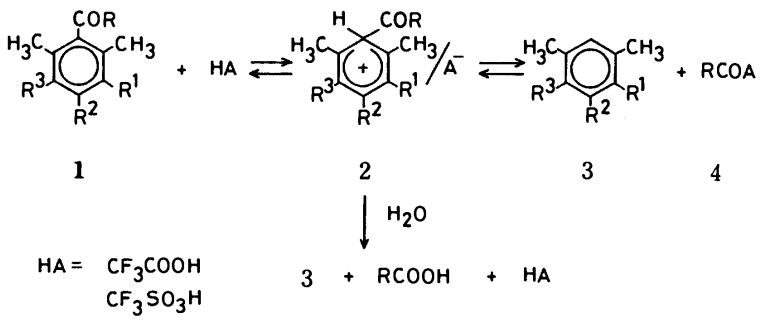

Scheme 2.

As regards the mechanism of the deacylation reaction, an ipso-protonated intermediate (**2**) at the ring C-atom attached to the acyl group may be assumed as has been reported before (Scheme 2).[10] In the absence of water, a conjugate base of the acids works as a nucleophile for the removal of the acyl group to give the hydrocarbon (**3**) and the mixed anhydride (**4**). The latter is known to acylate arenes in a TFA solution.[11,12] Thus in the deacetylation of AcPMB in boiling TFA, an equilibrium is reached with the formation of 40% of PMB.[10] When water is present in the solution, it works as a nucleophile to remove the acetyl group, thus giving PMB, TFA, and acetic acid. In the case of a stronger acid TFSA relative to TFA, the TFSA regenerated from a reaction of the intermediate **2** with water will work again for the ipso-protonation so that it may be enough in catalytic amount. Ethyl pentamethylbenzoate might be protonated at the alkoxyl oxygen to resist ipso-protonation to the ring carbon for the deethoxycarbonylation.

Experimental

Materials and Measurements: The acylpolymethylbenzenes were prepared from polymethylbenzenes and acyl chloride following the usual Friedel-Crafts reaction procedure. Commercial TFA (Peptide Institute) was used after distilling in the presence of a small amount of trifluoroacetic anhydride. The TFSA used was a commercial one (Aldrich). The GLC analyses were carried out on a Hitachi GC 163 Model gas chromatograph equipped with a hydrogen flame ionization detector and a stainless steel column (length 3 m, i.d., 3 mm) packed with 3% Dexil 300 GC on Chromosorb W. The product yields were calculated from the relative peak area with respect to the internal standard (dibenzofuran) on a System Instruments Chromatocorder 11 after calibration for each authentic compound.

Kinetic Studies: AcPMB (0.125 g, 0.657 mmol) was dissolved in TFA (5 ml) containing a given amount of water in a 10 ml flask. The mixture was immediately brought to reflux by immersing the reaction flask in an oil-bath maintained at 110 °C . After refluxing for a given period, the reaction mixture was quenched by pouring it into an excess of a cold 5% aqueous sodium carbonate solution; the resulting oily product was extracted with ether containing dibenzofuran (0.100 g) (as the internal standard for GLC analysis). The organic layer was washed with water and dried over anhydrous sodium sulfate. After the evaporation of the solvent, the residue was dissolved in benzene and then analyzed by means of GLC.

General Procedure for the Deacylation: The typical procedure described is for the reaction of AcPMB with TFSA: To a solution of AcPMB (0.114 g, 0.600 mmol) in 1,2-dichloroethane (3 ml) containing water (20 μl, 1.2 mmol) placed in a 30 ml flask, was added TFSA (0.045 g, 0.300 mmol) in DCE (2 ml) and the mixture was heated under reflux for 5 h. After that, the reaction mixture was poured into an excess of a cold 5% aqueous sodium carbonate solution and then extracted with ether (50 ml) containing dibenzofuran (0.100 g). The organic layer was washed with water and dried over anhydrous sodium sulfate. After the subsequent evaporation of the solvent under reduced pressure, the residue was analyzed by means of GLC.

References

1) W. M. Schubert and H. K. Latourette, *J. Am. Chem. Soc.*, **74**, 1829 (1952).
2) I. Agranat, Y. S. Shin, and Y. Bentor, *J. Am. Chem. Soc.*, **96**, 1259 (1974).
3) P. H. Gore and C. K. Thadani, *J. Chem. Soc. C*, **1966**, 1729.
4) J. A. Farooqi, P. H. Gore, E. F. Saad, D. N. Waters, and G. F. Moxon, *J. Chem. Soc., Perkin Trans. 2*, **1979**, 835.
5) P. H. Gore, A. M. G. Nassar, and E. F. Saad, *J. Chem. Soc., Perkin Trans. 2*, **1982**, 983.
6) G. Baddeley and A. G. Pendleton, *J. Chem. Soc.*, **1952**, 807.
7) R. H. Schlosberg and R. P. Woodbury, *J. Org. Chem.*, **37**, 2627 (1972).
8) T. Keumi, T. Morita, K. Korome, M. Ikeda, and H. Kitajima, *Nippon Kagaku Kaishi*, **1982**, 1785.
9) G. A. Olah, K. Laali, and A. K. Mehrotra, *J. Org. Chem.*, **48**, 4779 (1983).
10) T. Keumi, T. Morita, T. Shimada, N. Teshima, and H. Kitajima, *J. Chem. Soc., Perkin Trans. 2*, **1986**, 847.
11) T. Keumi, H. Saga, and H. Kitajima, *Bull. Chem. Soc. Jpn.*, **53**, 1638 (1980).
12) T. Keumi, K. Yoshimura, M. Shimada, and H. Kitajima, *Bull. Chem. Soc. Jpn.*, **61**, 455 (1988).

Synthesis of (±)-Hernandulcin by an Intramolecular Nitrile Oxide Cycloaddition Route from Farnesol

Guo-Chi ZHENG and Hiroshi KAKISAWA*
Department of Chemistry, University of Tsukuba, Tsukuba, Ibaraki 305
(Received June 28, 1988)

Synopsis. An intramolecular addition reaction of the nitrile oxide derived from (2*Z*, 6*E*)-farnesal oxime afforded an isoxazoline derivative, which was converted into hernandulcin, a sweet sesquiterpene of Verbenaceae plant.

Hernandulcin was found as a strongly sweet sesquiterpene from the Mexican plant *Lippia dulcis* Trev. (Verbenaceae) by Kinghorn[1] according to a classic book written in 1570—1576 by a Spanish physician, F. Hernandez, about natural history of ancient Mexico. Hernandez described a remarkably sweet plant known to the Aztec people by the name *Tzonpelic xihuitl* (literally 'sweet herb').[2] The structure and relative stereochemistry of this sesquiterpene **1** were proposed by Kinghorn[1] and the absolute configuration was determined by Mori et al. by a synthesis.[3] This report describes a convenient synthesis of (±)-hernandulcin from farnesol via an intramolecular nitrile oxide cycloaddition route.

Previously, the author reported that a nitrone **2** derived from (6*E*)-farnesal afforded a cycloaddition product **3** which was convertible into α-isobisabolol

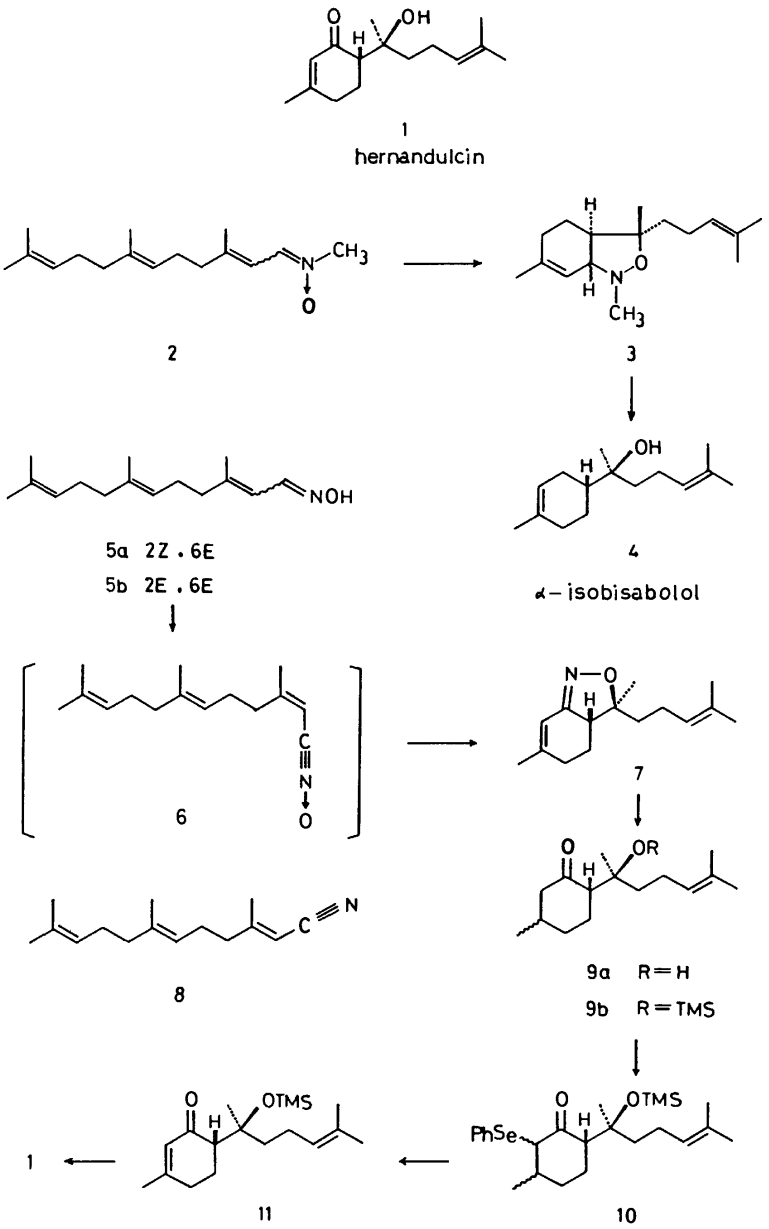

(**4**).[4] Although the relative stereochemistry of isoxazoline intermediate **3** was the same as that of hernandulcin, several attempts failed in converting the intermediate into hernandulcin. An isoxazoline derivative **7** was then made from farnesal oxime.[5] The reaction of (2*Z*,6*E*)-farnesal with hydroxylamine in pyridine afforded a mixture of (*E*)- and (*Z*)-oximes **5a** in a ratio of 4:1. Exposure of the mixture to aqueous sodium hypochlorite in dichloromethane with triethylamine as a catalyst at 0 °C resulted in the formation of a corresponding nitrile oxide (**6**), which was simultaneously cyclized by an intramolecular 1,3-dipolar cycloaddition to give an isoxazoline **7** in 83% yield. By means of the same reactions (2*E*, 6*E*)-farnesal oxime (**5b**) afforded the same isoxazoline **7** in poor yield (28%), besides 55% of nitrile derivative **8**. The stereochemistry of the isoxazoline **7** was assigned from the stereoselectivity of the cycloaddition of nitrile oxide. A catalytic hydrogenation of the isoxazoline in the presence of a deactivated Raney nickel afforded dihydrohernandulcin (**9a**) as a diastereomeric mixture.[6,7] The mixture of dihydro compounds was converted into a phenylseleno compound **10** after protecting the hydroxyl group with trimethyl silyl ether.[8] An oxidative elimination of the selenyl group by hydrogen peroxide[9] gave trimethylsilylhernandulcin in an overall yield 62% from the isoxazoline **7**. Removing the protecting group with dilute hydrogen fluoride[10] yielded hernandulcin (**1**) in quantitative yield.

Experimental

Proton magnetic resonance (^{1}H NMR) spectra were recorded on either a JEOL FX90Q spectrometer or a Bruker AM500 spectrometer with chemical shifts given in parts per million (δ) downfield from tetramethylsilane as an internal standard. Carbon magnetic resonance (^{13}C NMR) spectra were recorded at either 22.5 MHz on a JEOL EX 90 Q or 125 MHz on a Bruker AM 500 instrument. Infrared (IR) spectra were measured on a Hitachi 215 or a JASCO FT/IR-3 spectrophotometer. Mass spectra (MS) were obtained on a Hitachi RMU-6H GC/MS system using electrons of 70 eV ionization energy. Ultraviolet (UV) spectra were recorded on a Hitachi EPS-3T spectrophotometer. Elemental analyses were performed by the University of Tsukuba chemical analysis center. Gas chromatography data were obtained with a 063 Hitachi gas chromatograph by using a 1.7 m/3 mm i.d. glass column packed with 5% SE-30. Wako C-300 silica gel was used for flash column chromatography. Merck Kiesel gel 60 F-254 were used for analytical (0.25 mm) and preparative (0.5 mm) thin-layer chromatography.

(2*Z*,6*E*)-3,7,11-Trimethyl-2,6,10-dodecatrienal Oxime (5a). The (2*Z*,6*E*)-farnesal (2.61 g, 11.9 mmol, prepared by the procedure of Iwashita)[11] was dissolved in 100 ml pyridine and a recrystallized hydroxylamine hydrochloride (1.08 g, 15.5 mmol) was added. The reaction mixture was stirred for 10 min and the resulting mixture was poured into 200 ml of ether, washed with a saturated $CuSO_4$ solution and water, dried (Na_2SO_4), and concentrated to an odorous oil. The residue was purified by flash chromatography (SiO_2, hexane/ethyl acetate 9:1) to give **5a** (2.77 g, 99%). Though initially a mixture of the (*E*)-(80%) and (*Z*)-(20%) oximes, it gradually isomerized to only the (*E*)-form. The physical data of the (*E*)-oxime isomer are as follows: IR($CHCl_3$) 3560, 3250, 2900, 1635, and 1430 cm^{-1}; ^{1}H NMR ($CDCl_3$) δ= 1.60 (6H, s, CH_3×2), 1.68 (3H, s, CH_3), 1.86 (3H, br, s, CH_3), 1.86—2.19 (8H, m, CH_2CH_2, CH_2CH_2), 5.08 (2H, br, t), 5.90 (1H, d, J=10 Hz), 8.00 (1H, d, J=10 Hz), and 8.05 (1H, br, s); ^{13}C NMR ($CDCl_3$) δ=16.1 (q), 17.7 (q), 24.2 (q), 25.7 (q), 26.8 (t), 32.0 (t), 32.8 (t), 39.7 (t), 118.9 (d), 123.0 (d), 124.3 (d), 131.4 (s), 136.4 (s), 147.8 (s), and 148.7 (d); MS *m/z* (rel intensity %) 235 (M^+, 13), 217 (83), 202 (12), 135 (85), 120 (66), 110 (92), and 82 (100). The physical data of (*Z*)-isomer are as follows: ^{1}H NMR ($CDCl_3$) δ=1.60 (6H, s), 1.68 (6H, s), 1.86—2.19 (8H, m), 5.08 (2H, br, t), 6.50 (1H, br, d), and 7.26 (1H, br, d). Found: C, 76.70; H, 10.82; N, 6.01%. Calcd for $C_{15}H_{25}ON$: C, 76.54; H, 10.71; N, 5.95%.

(2*E*,6*E*)-3,7,11-Trimethyl-2,6,10-dodecatrienal Oxime (5b). The (2*E*,6*E*)-farnesal (4.71 g, 21.4 mmol, prepared by a procedure of Iwashita)[11] was dissolved in 150 ml of pyridine and a hydroxylamine hydrochloride(1.93 g, 27.8 mmol) was added. The reaction mixture was stirred for 10 min and then worked up, as described for (2*Z*, 6*E*)-farnesal oxime. Chromatography (SiO_2, hexane/ethyl acetate 8:2) provided a mixture of (*E*)-(80%) and (*Z*)-(20%) oximes (4.93 g, 98%), which gradually isomerized to only the (*E*)-form. The physical data of (*E*)-oxime are as follows: ^{1}H NMR ($CDCl_3$) δ=1.61 (6H, s, CH_3×2), 1.68 (3H, s, CH_3), 1.86 (3H, br, d, CH_3), 1.82—2.15 (8H, m, CH_2CH_2, CH_2CH_2), 5.10 (2H, br, t), 5.93 (1H, d, J=10 Hz), 8.07 (1H, d, J=10 Hz), and 8.42 (1H, br, s); ^{13}C NMR ($CDCl_3$) δ=16.0 (q), 17.2 (q), 17.6 (q), 25.7 (q), 26.3 (t), 26.8 (t), 39.8 (t), 40.1 (t), 118.0 (d), 123.4 (d), 124.4 (d), 130.2 (s), 134.1 (s), 147.7 (s), and 149.1 (d). The data of (*Z*)-oxime are as follows: ^{1}H NMR ($CDCl_3$) δ=1.61 (9H, s, CH_3×3), 1.68 (3H, s, CH_3), 1.82—2.15 (8H, m, CH_2CH_2, CH_2CH_2), 5.10 (2H, br, t), 6.52 (1H, d, J=9.5 Hz), and 7.35 (1H, d, J=9.5 Hz).

3,6-Dimethyl-1,3,3a,4,5,7a-hexahydro-3-(4-methyl-3-pentenyl)-2,1-benzisoxazole (7). To a vigorously stirred solution of the (2*Z*, 6*E*)-farnesal oxime (**5a**) (0.183 g, 0.78 mmol) in 30 ml of dichloromethane cooled to 0 °C was added 1 ml of commercial 11% aqueous sodium hypochlorite dropwise. After 1 h, TLC analysis revealed that the oxime had been consumed; stirring was stopped, the ice bath was removed, and the reaction mixture was allowed to stand overnight. The organic phase was separated and the aqueous phase was extracted with dichloromethane. The combined organic layers were dried over Na_2SO_4 and the solvent removed under reduced pressure. The resulting crude oil was chromatographed (Wakogel C-300, hexane/ethyl acetate 5:1) to provide 0.15 g (83%) of the isoxazoline as an oil. IR (film) 2971, 2929, 2858, 1718, 1650, 1447, 1378, 1110, 894, and 866 cm^{-1}; ^{1}H NMR ($CDCl_3$) δ=1.11 (3H, s), 1.61 (3H, s), 1.67 (3H, s), 1.85 (3H, s), 1.64—2.23 (8H, m), 2.85 (1H, dd, J=4.6, 13 Hz), 5.09 (1H, br, t), and 6.18 (1H, s); ^{13}C NMR ($CDCl_3$) δ=17.7 (q), 19.9 (q), 22.7 (t), 23.2 (t), 23.8 (q), 25.6 (q), 31.3 (t), 39.9 (t), 51.9 (d), 87.4 (s), 114.3 (d), 123.9 (d), 131.9 (s), 158.2 (s), and 158.4 (s); MS *m/z* 235, 234, 233 (M^+), 218, 217, 215, 203, 200, 192, 191, 188, 135, 133 (base), 105, and 101; Found: C, 77.32; H, 9.90; N, 6.09%. Calcd for $C_{15}H_{23}ON$: C, 77.20; H, 9.94; N, 6.00%.

The same reaction was repeated with oxime (**5b**). To a stirred solution of the (2*E*, 6*E*)-farnesal oxime (**5b**) (1.2 g, 5.1 mmol) in dichloromethane (200 ml) was added 11% aqueous sodium hypochlorite (8 ml) dropwise at 0 °C. After 1 h, chromatography of the reaction mixture on a Wakogel C-300 (CH_2Cl_2/CH_3OH 20:1) gave the less polar nitrile (**8**) (0.61 g, 55%) as an oil. IR ($CHCl_3$) 2950, 2900, 2840, 2270, 1615, 1428, 1375, 1344, 1290, and 1100 cm^{-1}; ^{1}H NMR ($CDCl_3$) δ=1.85 (6H, s), 1.67 (3H, s), 1.98 (3H, br, s), 2.00—2.30 (8H, m), 5.05 (2H, br, s), and 5.12 (1H, s); ^{13}C NMR ($CDCl_3$) δ=16.13 (q), 17.76 (q), 20.82 (q), 25.75 (q), 25.81 (t), 26.67 (t), 38.44 (t), 39.69 (t), 95.0 (d), 95.0 (s), 122.4 (d), 124.2 (d), 131.6 (s), 136.8 (s), and 160.6 (s); MS *m/z* 217 (M^+), 202, 175, 148, 146, 123, 122, 121, 108, 107, 106, 93, 91, 80 (base), 69, and 53. The more

polar compound (0.33 g, 28%) was identified as same isoxazoline as **7**.

2-(1-Hydroxy-1,5-dimethyl-4-hexenyl)-5-methylcyclohexanone (9a). A mixture of W-2 Raney nickel (0.4 g), which was deactivated prior to use by refluxing for 3 h with acetone, the isoxazoline **7** (0.4 g, 1.72 mmol), an acid solution made from 0.001 mol BCl_3 and 1 ml of methanol, and 100 ml of 5:1 MeOH/H_2O, was stirred under a hydrogen-filled balloon for 30 min. The reaction mixture was filtered and the filter was washed with MeOH. The combined filtrates were concentrated under reduced pressure. The residue was partitioned between ether and water. The organic phase was dried over Na_2SO_4 and concentrated to afford a crude oil (0.35 g, 85%), which was used without further purification for the next silylation step. An analytical sample was separated by preparative TLC. Spectral data were obtained with a mixture of two diastereomers (**9a**) in a ratio of 55:45. IR (film) 3600—3300, 2956, 2928, 2871, 1699, 1458, and 1420 cm^{-1}; ^1H NMR ($CDCl_3$) δ=1.02 and 1.20 (totally 3H, d, J=7.5 Hz), 1.18 (3H, s), 1.59 (3H, s), 1.67 (3H, s), 1.41—2.30 (11H, m), 2.38 (1H, dd), 3.95 (1H, s), and 5.08 (1H, br, t). ^{13}C NMR ($CDCl_3$) δ=17.7 (q), 22.1 (q), 22.3 (q), 23.8 (q), 25.7 (t), 28.5 (t), 34.1 (t), 35.4 (t), 40.6 (t), 51.6 (d), 56.9 (d), 73.0 (s), 124.6 (d), 131.5 (s), and 215.4 (s); MS m/z 238 (M^+), 223, 222, 221, 220 (base), 192, 191, 190, 189, 179, 178, 177, 162, 154, and 138. Found: C, 75.73; H, 10.89%. Calcd for $C_{15}H_{26}O_2$: C, 75.58; H, 11.00%.

2-(1-Trimethylsilyloxy-1,5-dimethyl-4-hexenyl)-5-methylcyclohexanone (9b). To a mixture of dry triethylamine (0.76 g, 7.56 mmol), crude tertiary alcohol **9a** (1.2 g, 5.04 mmol), 0.1 ml of DMSO and dry ether (40 ml) was added trimethylsilyl chloride (0.65 g, 6 mmol) in 10 min with stirring. After 30 min the reaction mixture was poured into ice water (50 ml). After being washed with water, the ethereal solution was dried over Na_2SO_4 and then concentrated under reduced pressure. The crude product was chromatographed on silica gel with hexane/ether 5:1 as eluent to yield 1.31 g (84%) of the title compound as a colorless oily diastereomeric mixture. IR (film) 2957, 2927, 2869, 1703, 1457, 1376, 1250, 1042, 840, and 754 cm^{-1}; ^1H NMR ($CDCl_3$) δ=0.10 and 0.11 (totally 9H, s), 0.92, 1.00 (totally 3H, d, J=7.5 Hz), 1.24 and 1.32 (totally 3H, s), 1.59 (3H, s), 1.69 (3H, s), 1.40—2.20 (11H, m), 2.28 (1H, m), and 5.08 (1H, br, s); MS m/z 295 (M^+−15), 285, 226, 220, 219, 203, 183, 175, 106 (base), 91, 79, and 78; Found: C, 69.84; H, 11.13%. Calcd for $C_{18}H_{34}O_2Si$: C, 69.61; H, 11.04%.

6-(1-Trimethylsilyloxy-1,5-dimethyl-4-hexenyl)-3-methyl-2-(phenylseleno)cyclohexanone (10). To a solution of diisopropylamine (0.043 g, 0.42 mmol) in 5 ml of dry THF, was added 0.35 ml of 1.36 M n-BuLi (1M=1mol dm^{-3}) in hexane under an argon atmosphere at −78 °C. After being stirred for 30 min at 0 °C, the LDA solution was chilled to −78 °C; then, a solution of **9b** (0.11 g, 0.35 mmol) in 5 ml of THF was added dropwise and the mixture was stirred for 30 min. A solution of benzeneselenenyl chloride (0.08 g, 0.42 mmol) in 3 ml of THF was added rapidly to the enolate solution. After 1.5 h, the reaction mixture was warmed to 0 °C and poured into a saturated $NaHCO_3$ solution (10 ml) and dichloromethane (20 ml). The organic layer was washed with water and saturated NaCl solution. After solvent removal, chromatography on SiO_2 (benzene) gave 0.127 g (78%) of **10** as a mixture of two diastereomers. ^1H NMR ($CDCl_3$) δ=0.11 and 0.12 (totally 9H, s), 1.15 (3H, d), 1.22 and 1.23 (totally 3H, s), 1.54 (3H, s), 1.58 (3H, s), 1.50—2.35 (10H, m), 3.17—3.80 (1H, m), 5.08 (1H, m), and 7.26—7.49 (5H, m); MS m/z 465 (M^+), 463, 450, 448, 376, 375, 373, 327, 326, 325 (base), 323, 310, 268, 252, 239, 226, 184, 165, 156, and 137. Found: C, 61.77; H, 8.40%. Calcd for $C_{24}H_{38}O_2SeSi$: C, 61.91; H, 8.23%.

6-(1-Trimethylsilyloxy-1,5-dimethyl-4-hexenyl)-3-methyl-2-cyclohexen-1-one (11). To a solution of 0.16 g (0.344 mmol) of a seleno compound **10** in 3 ml of dichloromethane containing 0.06 ml of pyridine was gradually added 0.1 g of 30% H_2O_2 and 0.1 ml of water at 0 °C. The reaction mixture was stirred vigorously at 25 °C for an additional 15 min and then poured into 40 ml of dichloromethane and 10 ml of a 20% $NaHCO_3$ solution. The aqueous layer was extrated with dichloromethane and the combined organic layers were washed with a 10% HCl solution, saturated NaCl and dried over Na_2SO_4. The organic phase was concentrated in vacuo to afford a residue, which was chromatographed on Wakogel C-300 (hexane/ether 4.5:1) to provide 0.1 g of **11** (95%). ^1H NMR ($CDCl_3$) δ=0.10 (9H, s), 1.47 (3H, s), 1.60 (3H, s), 1.65 (3H, s), 1.88 (3H, s), 1.60—2.50 (9H, m), 5.07 (1H, br, t), and 5.76 (1H, s); IR (film) 2965, 2930, 1652, 1210, 1124 cm^{-1}. Found: C, 70.18; H, 10.44%. Calcd for $C_{18}H_{32}O_2Si$: C, 70.07; H, 10.45%.

6-(1-Hydroxy-1,5-dimethyl-4-hexenyl)-3-methyl-2-cyclohexenone (1) (Hernandulcin). To a solution of acetonitrile (3 ml) containing 5% of 40% aqueous HF was added 0.079 g (0.26 mmol) of the silyl ether **11**. After 15 min dichloromethane and water were added. The organic phase was separated and evaporated to give pure hernandulcin (**1**) 0.061 g (100%). An analytical sample was obtained by chromatography on SiO_2 (hexane/ether 2:1). IR (film) 3470, 2969, 2935, 2870, 1650, 1215, 1126 and 1022 cm^{-1}. UV (c 0.0399, EtOH) λ_{max} 236 nm (13300); ^1H NMR ($CDCl_3$) δ=1.17 (3H, s), 1.47 (2H, ddd, J=8.4, 8.4, and 1.2 Hz), 1.62 (3H, s), 1.675 (1H, m), 1.677 (3H, s), 1.96 (3H, s), 2.02 (1H, m), 2.05 and 2.16 (2H, ddt, J=14.6, 7.2, and 8.4 Hz), 2.31 (1H, ddd, J=18.5, 5.0, and 2.5 Hz), 2.37 (1H, dm, J=13.0 Hz), 2.41 (1H, dd, J=14.1 and 14.5 Hz), 5.11 (1H, tm, J=7.2 Hz), 5.24 (1H, s), and 5.87 (1H, s); ^{13}C NMR ($CDCl_3$) δ= 17.7, 21.7, 23.7, 24.2, 25.2, 25.8, 31.4, 40.3, 52.3, 74.0, 124.6, 127.7, 131.6, 163.5, and 204.1; MS m/z 236 (M^+), 218, 110, 95, and 82 (base).

The authors are grateful to Kuraray Co., Ltd. for the kind provision of (2*E*,6*E*)-farnesol.

References

1) C. M. Compadre, J. M. Pezzuto, A. D. Kinghorn, and S. K. Kamath, *Science*, **227**, 417 (1985).

2) *Chem. Brit.*, 330 (1985); *Chem. and Eng. News*, January 28, 37 (1985).

3) K. Mori and M. Kato, *Tetrahedron Lett.*, **27**, 981 (1986); K. Mori and M. Kato, *Tetrahedron*, **42**, 5895 (1986).

4) T. Iwashita,T. Kusumi, and H. Kakisawa, *Chem. Lett.*, **1979**, 947.

5) The (2*E*, 6*E*)-farnesol was provided from Kuraray Co., Ltd., which was used without further purification. The (2*Z*, 6*E*)-farnesol was obtained by fractionation of a commercial farnesol with chromatography.

6) O. Tsuge, S. Kanemasa, N. Nakagawa, and H. Suga, *Bull. Chem. Soc. Jpn.*, **60**, 4091 (1987).

7) A. P. Kozikowski and P. D. Stein, *J. Org. Chem.*, **49**, 2302 (1984).

8) R. G. Visser, H. J. T. Bos, and L. Brandsma, *Recl. Trav. Chem. Pays-Bas*, **99**, 70 (1980).

9) D. L. J. Clive, *Tetrahedron*, **34**, 1049 (1978); H. J. Reich, J. M. Renga, and I. L. Reich, *J. Am. Chem. Soc.*, **97**, 5434 (1975).

10) R. F. Newton and D. P. Reynolds, *Tetrahedron Lett.*, **1979**, 3981.

11) T. Iwashita, Ph. D. Thesis, University of Tsukuba, **1980**.

The Reaction of Arylazo Aryl Sulfones with Carbon Monoxide and Nucleophiles Catalyzed by the Palladium(0) Complex[1)]

Nobumasa KAMIGATA,* Akira SATOH, Masato YOSHIDA, and Masayuki KAMEYAMA
Department of Chemistry, Faculty of Science, Tokyo Metropolitan University, Fukazawa, Setagaya-ku, Tokyo 158
(Received June 29, 1988)

Synopsis. The reaction of arylazo aryl sulfone (**1**) with carbon monoxide in the presence of the palladium(0) catalyst affords substituted benzoic acid in a good yield, together with minor yields of diaryl ketone and biaryl. The reactions of **1** with carbon monoxide and such nucleophiles as alcohols and amines under similar conditions give esters and amides, respectively.

Arylpalladium reagents obtained from aryl halides or arylmercurials have been utilized extensively for the arylation of olefins.[2)] Kikukawa et al. reported that arylpalladium species was also formed from arenediazonium salts[3)] or *N*-nitrosoacetanilide[4)] catalyzed by palladium complexes to arylate olefins in high yields. Recently, we reported the reaction of arylazo aryl sulfones with olefins catalyzed by the palladium(0) complex to give aryl olefins in a high yield, and a diarylpalladium(II) species was proposed as an intermediate.[5)] If such an intermediate participates in this reaction, the insertion of carbon monoxide into the carbon-metal σ-bond and the resulting carbonylated products can be expected, since a number of reactions of organometallics with carbon monoxide have been reported.[6)] We studied the reactions of arylazo aryl sulfone with carbon monoxide and nucleophiles catalyzed by the palladium(0) complex in order to clarify the formation of a diarylpalladium(II) intermediate by obtaining carbonylated products, and the results are described herein.

When carbon monoxide was passed through, with bubbling, into a solution of phenylazo *p*-tolyl sulfone (**1a**) in benzene and acetic acid, benzoic acid (35%), *p*-methylbenzoic acid (37%), *p*-methylbenzophenone (1%), and *p*-methylbiphenyl (6%) were obtained. Similarly, *p*-tolylazo phenyl sulfone (**1b**) afforded benzoic acid (42%), *p*-methylbenzoic acid (34%), 4-methylbenzophenone (1%), and *p*-methylbiphenyl (3%) under similar reaction conditions. When the two aryl groups of **1** are the same (**1c**: Ar=Ar′=Ph, **1d**: Ar=Ar′=*p*-Tol, and **1e**: Ar=Ar′=*p*-$MeOC_6H_4$), sole benzoic acid or substituted benzoic acid was formed in a good yield. The results are summarized in Table 1. It is of interest that almost equal amounts of benzoic acid and *p*-methylbenzoic acid were obtained, respectively, from the reactions of the azosulfone **1a** and **1b** with carbon monoxide catalyzed by the palladium(0) complex; these results suggest the formation of an intermediate, such as diarylpalladium(II), having an equal reactivity toward carbon monoxide, as we proposed previously.[5)]

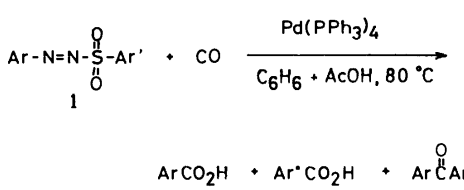

At first, we expected that diaryl ketone (ArCOAr′) would be formed as a major product; however, such a compound was obtained in a yield of only a few percent, and instead, carboxylic acid was formed in a good yield. The formation of benzoic acids may be attributed by the reaction of diarylpalladium(II) species with a carbon dioxide contaminated impurity in the carbon monoxide gas, similar to the reaction of a Grignard reagent and carbon dioxide. The reaction of **1c** with carbon dioxide was carried out in the presence of the palladium(0) complex under similar conditions. However no benzoic acid was detected in the reaction mixtures. Thus, the possibility of the formation of benzoic acids by the reaction of diarylpalladium(II) species with carbon dioxide can be excluded.

Then, we considered that the carboxylic acid was formed by the nucleophilic reaction of water, a contaminated impurity in carbon monoxide gas, and unremovable moisture in the reaction equipment, with the (arylcarbonyl)arylpalladium(II) species which had been formed by the insertion of carbon monoxide into the diarylpalladium(II) species. If this reaction path is real, the formation of esters or amides can be expected when the palladium(0)-catalyzed reaction of **1**

Table 1. Reaction of Arylazo Aryl Sulfone (**1**) with Carbon Monoxide Catalyzed by Tetrakis(triphenylphosphine)palladium(0)

	Ar and Ar′ in **1**		Products, Yield[a)]/%			
	Ar	Ar′	$ArCO_2H$	$Ar'CO_2H$	ArCOAr′	ArAr′
1a	Ph	*p*-Tol	35	37	1	6
1b	*p*-Tol	Ph	34	42	1	3
1c	Ph	Ph	76[b)]	—	2	5
1d	*p*-Tol	*p*-Tol	78[b)]	—	1	4
1e	*p*-$CH_3OC_6H_4$	*p*-$CH_3OC_6H_4$	72[b)]	—	1	5

a) The yields were determined by means of GC. b) This value includes the yield of $Ar'CO_2H$, since the products, $ArCO_2H$ and $Ar'CO_2H$, are identical when the Ar and Ar′ groups in **1** are the same.

is carried out in the presence of such nucleophiles as alcohols or amines. The reaction of **1c** catalyzed by the palladium(0) complex was carried out in benzene–methanol at 80 °C. As we expected, methyl benzoate was formed, although the yield was not so high; no benzoic acid was detected in this case. Similarly, the reaction of azosulfone **1** with such nucleophiles as ethanol, sodium methoxide, and amines under similar conditions gave the corresponding esters and amides in moderate yields. However, the reaction of **1c** with sodium acetate did not give acetylbenzoate or phenylbenzoate. The acetate ion may not have enough nucleophilicity to react with (arylcarbonyl)arylpalladium(II) species. The results are summarized in Table 2. These findings support our consideration of the formation of the diarylpalladium(II) species which is carbonylated by carbon monoxide to form arylcarbonyl aryl palladium(II) species and a subsequent reaction with nucleophiles to give the final product.

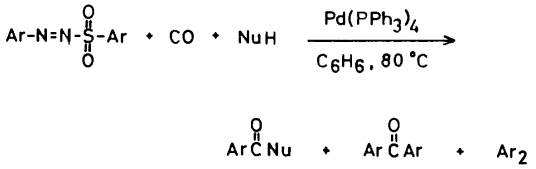

The palladium(II)-catalyzed reaction of arylazo aryl sulfones with carbon monoxide and nucleophiles is accounted for by Scheme 1, involving the oxidative addition of **1** to the palladium(0) catalyst to give the adduct **2**, which then extrudes nitrogen and sulfur dioxide to give the diarylpalladium(II) species (**3**). Carbon monoxide inserts into the palladium–carbon bond of the intermediate **3** to give (arylcarbonyl)arylpalladium(II) (**4**), which degrades to the corrsponding carboxylic acid derivatives and arylhydridopalladium(II) (**5**) upon the reaction with the nucleophiles. The reductive elimination of arene from **5** gives palladium(0), and thus the catalytic cycle is achieved.

The reason why the formation of benzophenone derivatives is minor may be attributed to the reaction of the (arylcarbonyl)arylpalladium(II) species with the nucleophiles to give benzoic acids or their esters and amides is faster than the reductive elimination of benzophenone derivatives from **4**,[7] (Eq. 1). The formation

Table 2. Reaction of Azosulfone (**1**) with Carbon Monoxide and Nucleophiles Catalyzed by Tetrakis(triphenylphosphine)-plladium(0)[a]

Azosulfone	Nucleophile	Product, Yield[b]/%	
1c	MeOH	$PhCO_2Me$	28
1c	EtOH	$PhCO_2Et$	35
1c	MeONa	$PhCO_2Me$	55
1d	MeONa	p-$CH_3C_6H_4CO_2Me$	54
1e	MeONa	p-$CH_3OC_6H_4CO_2Me$	50
1c	$PhNH_2$	PhCONHPh	59
1c	Et_2NH	$PhNEt_2$	57
1c	AcONa	$PhCO_2Ac$	0

a) Diaryl ketone (Ar_2CO; 1—2%) and biaryl (Ar_2; 4—10%) were formed in all cases. b) The yields were determined by means of GC.

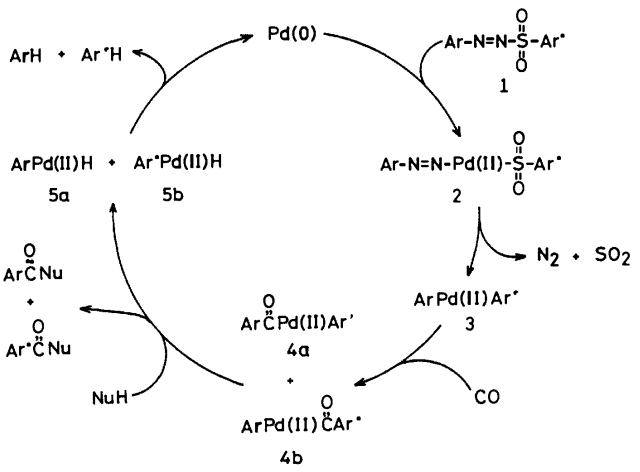

Scheme 1.

of biaryl may be accounted for by the reductive elimination from diarylpalladium(II) before which is carbonylated by carbon monoxide (Eq. 2).

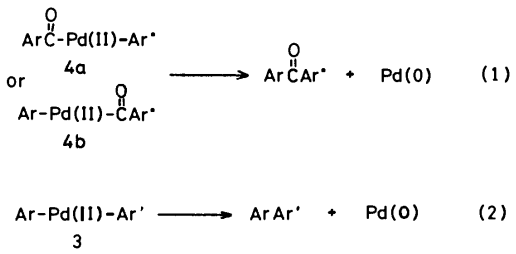

Experimental

Measurement. The melting points and boiling points are uncorrected. The infrared absorption spectra were determined on a Hitachi Model 260-10 spectrophotometer, using samples as either neat liquid or in KBr disks. The ^1H NMR spectra were recorded at 60 MHz by using a JNM-PMX 60 SI spectrometer, with tetramethylsilane as the internal standard in $CDCl_3$. The mass spectra were determined with a JEOL JMS-DX 300 mass spectrometer with the JEOL JMA-5000 Mass Data System at an ionizing voltage of 20—70 eV. The gas chromatography was carried out with Hitachi Models 163 and 263-30 gas chromatographs using a 1 m column packed with 10% SE-30. The gel-permeation chromatography was performed by using a JAI LC-08 liquid chromatograph with a JAIGEL column (20ϕ×600 mm×2, with chloroform as an eluent).

Materials. All the solvents were distilled and stored under nitrogen. Palladium chloride of Wako Chemicals was used without further purification. Tetrakis(triphenylphosphine)palladium(0) was prepared by the method described in the literature.[8] Phenylazo p-tolyl sulfone (**1a**) (mp 90—91 °C (90—91 °C)), p-tolylazo phenyl sulfone (**1b**) (mp 82—83 °C), phenylazo phenyl sulfone (**1c**) (mp 75—76 °C (76—77 °C)), p-tolylazo p-tolyl sulfone (**1d**) (mp 96—97 °C (96—97 °C)), and p-methoxyphenylazo p-methoxyphenyl sulfone (**1e**) (mp 111—112 °C) were prepared by the published procedures.[9]

General Procedure for the Reaction of Arylazo Aryl Sulfone with Carbon Monoxide Catalyzed by Tetrakis(triphenylphosphine)palladium(0). To a stirred solution containing arylazo aryl sulfone (2.0 mmol) and tetrakis(triphenylphosphine)palladium(0) (0.2 mmol) in 10.0 cm^3 of benzene–acetic acid (1 : 1) at 80 °C, carbon monoxide was introduced by bubbling for 2 h. The crude reaction mixture was then

concentrated and chromatographed on silica gel, using ethyl acetate as the eluent. The products were identified by comparing their retention times of GC and the IR, ^{1}H NMR, and mass spectra with those of authentic samples.

General Procedure for the Reaction of Arylazo Aryl Sulfone with Carbon Monoxide and Nucleophiles Catalyzed by the Palladium(0) Complex. a) To a stirred solution containing arylazo aryl sulfone (2.0 mmol), nucleophile (alcohol or amine, 2.0 cm^3), and tetrakis(triphenylphosphine)palladium(0) (0.2 mmol) in 10.0 cm^3 of benzene at 80 °C, carbon monoxide was introduced by bubbling for 2 h. b) To a stirred suspension containing arylazo aryl sulfone (2.0 mmol), nucleophile (sodium methoxide or sodium acetate, 10.0 mmol), and tetrakis(triphenylphosphine)palladium(0) (0.2 mmol) in 10.0 cm^3 of benzene at 80 °C, carbon monoxide was introduced by bubbling for 2 h. The crude reaction mixture was then concentrated and chromatographed on silica gel, using ethyl acetate as the eluent. The products were identified by comparing their retention times of GC and the IR, ^{1}H NMR, and mass spectra with those of authentic samples.

References

1) Reaction of Azo- and Azoxysulfones with Transition Metal Complexes. 4., Part 3: N. Kamigata, T. Fukushima, A. Satoh, and M. Kameyama, *Sulfur Lett.*, **7**, 181 (1988).

2) R. F. Heck, *Pure Appl. Chem.*, **50**, 691 (1978); R. F. Heck, *Acc. Chem. Res.*, **12**, 146 (1979); R. F. Heck, "Palladium Reagents in Organic Syntheses," Academic Press, New York (1985), Chap. 6.

3) K. Kikukawa and T. Matsuda, *Chem. Lett.*, **1977**, 159; K. Kikukawa, K. Nagira, N. Terao, F. Wada, and T. Matsuda, *Bull. Chem. Soc. Jpn.*, **52**, 2609 (1979); K. Kikukawa, K. Nagira, F. Wada, and T. Matsuda, *Tetrahedron*, **37**, 31 (1981); K. Kikukawa, K. Ikenaga, F. Wada, and T. Matsuda, *Chem. Lett.*, **1983**, 1337; K. Kikukawa, K. Kono, F. Wada, and T. Matsuda, *J. Org. Chem.*, **48**, 1333 (1983); K. Kikukawa, K. Ikenaga, F. Wada, and T. Matsuda, *Tetrahedron Lett.*, **25**, 5789 (1984); K. Ikenaga, K. Kikukawa, and T. Matsuda, *J. Chem. Soc., Perkin Trans. 1*, **1986**, 1959.

4) K. Kikukawa, M. Naritomi, G.-X. He, F. Wada, and T. Matsuda, *J. Org. Chem.*, **50**, 299 (1985).

5) N. Kamigata, T. Kondoh, M. Kameyama, and M. Kobayashi, *Chem. Lett.*, **1987**, 347; N. Kamigata, A. Satoh, T. Kondoh, and M. Kameyama, *Bull. Chem. Soc. Jpn.*, **61**, 3575 (1988).

6) H. Bahrmann, B. Cornils, C. D. Frohning, and A. Mullen, "New Syntheses with Carbon Monoxide," ed by J. Falbe, Springer-Verlag, New York (1980); "Organic Syntheses via Metal Carbonyls," Vol. 2, ed by I. Wender and P. Pino, John Wiley & Sons, New York (1977); R. F. Heck, "Organotransition Metal Chemistry," Academic Press, New York (1974); S. G. Davies, "Organotransition Metal Chemistry: Applications to Organic Synthesis," Pergamon Press, Oxford (1982).

7) At the present time, it is not clear why diaryl ketone was obtained only in small amounts, even when no nucleophile was added to the reaction media, since the formation of such a compound from the intermediate **4** as the major product has been reported: M. Tanaka, *Tetrahedron Lett.*, **1979**, 2601; J. W. Labadie and J. K. Stille, *J. Am. Chem. Soc.*, **105**, 6129 (1983).

8) D. R. Coulson, *Inorg. Synth.*, Coll. Vol. 13, 121 (1972).

9) A. Hantzsch and M. Singer, *Ber.*, **30**, 312 (1897); **31**, 636 (1898); M. Kojima, H. Minato, and M. Kobayashi, *Bull. Chem. Soc. Jpn.*, **45**, 2032 (1972).

Synthesis of Both the Enantiomers of Phoracantholide I, A Defensive Secretion of the Eucarypt Longicorn *(Phoracantha synonyma)*, Employing Microbial Asymmetric Reduction with Immobilized Baker's Yeast[1)]

Yoshinobu NAOSHIMA,* Hidenobu HASEGAWA,† Tadashi NISHIYAMA, and Akihiro NAKAMURA
Department of Biological Chemistry, Faculty of Science, Okayama University of Science, 1-1 Ridai-cho, Okayama 700
†Midori Kagaku Co., Ltd., 19-12 Kamiochiai, Shinjuku-ku, Tokyo 161
(Received July 19, 1988)

Synopsis. Highly optically pure (*R*)- and (*S*)-phoracantholide I were synthesized in relatively short steps starting from diethyl 3-oxoglutarate by means of a microbial asymmetric reduction of the intermediate keto acid with immobilized baker's yeast entrapped in gels of κ-carrageenan.

Since phoracantholide I (**1**), possessing a ten-membered lactone ring, has been isolated as a defensive secretion from the metasternal gland of the eucarypt longicorn, *Phoracantha synonyma*,[2)] several synthetic methods were reported for racemic **1**.[3)] The first synthesis of optically active **1** has recently been achieved by Kitahara et al. and the (*R*)-enantiomer was announced as the natural form of a defensive secretion of the insect.[4)] However, the method required multiple steps and the optical purity of synthesized enantiomers based on their GLC analyses with a chiral stationary phase was 89% e.e.

Recently we synthesized each enantiomer of 5-hexadecanolide and 4-dodecanolide with high optical purities via asymmetric reduction with immobilized baker's yeast (IBY).[5)] These are the pheromone of the oriental hornet and a defensive secretion of rove beetles. IBY, compared with free baker's yeast, has been found to have advantages in terms of the separation of products from the catalyst and of the reuse of the catalyst.[5,6)] In the expansion of the horizons of IBY in organic synthesis, we report herein a facile and short-step synthesis of the two enantiomers of **1** with highly optically pure forms.

Results and Discussion

First, diethyl 3-oxoglutarate (**2**) was alkylated regioselectively with *t*-butyl 7-bromoheptanoate and $Mg(OEt)_2$ to give the monoalkylated 3-oxoglutarate **3**, which was converted by a decarboxylative hydrolysis to the keto acid **4a** with a 78% yield from **2**. Compound **4a**, after treatment with an aqueous solution of KOH, was subjected to a microbial asymmetric reduction in an aqueous solution of KCl with the IBY entrapped by κ-carrageenan[5)] to give an optically pure alcohol (*S*)-**5a**. The optical purity of (*S*)-**5a** was determined to be 96% e.e. by HPLC analysis of the corresponding 3,5-dinitrophenylurethane (DNPU) derivative (*S*)-**5c**. Finally, (*S*)-**5a** was lactonized via the corresponding pyridinethiol ester (*S*)-**6** in the presence of $AgClO_4$ to give (*S*)-**1** with a 44% yield. For the synthesis of (*R*)-**1** reported as the natural form of **1**, the methyl ester (*S*)-**5b** was converted via a Mitsunobu inversion to (*R*)-**5a** with about 95% e.e. This was based on the HPLC analysis of a DNPU derivative (*R*)-**5c**. Lactonization of (*R*)-**5a**, as described above, gave the desired (*R*)-**1**. Thus highly optically pure (*R*)- and (*S*)-**1** were synthesized in seven and four steps, respectively, starting from **2**. The optical purity of the two enantiomers should be at least 95% e.e., because it was assumed that no apparent racemization at the chiral center of (*R*)- and (*S*)-**5a** occurred during their lactonization.

As shown in Table 1 the reuse of the IBY was achieved in two solvent systems, one of which is an aqueous KCl solution and the other an aqueous KCl solution containing ethyl acetate (EA). The reproducibility of both the chemical and optical yields was examined in each system. For the aqueous KCl solution system the first use of IBY catalyst gave a low chemical yield of (*S*)-**5a**, but after the 3rd use the yield was raised to 41%, a maximum yield of 46% being obtained after the 4th use. It is of interest that the

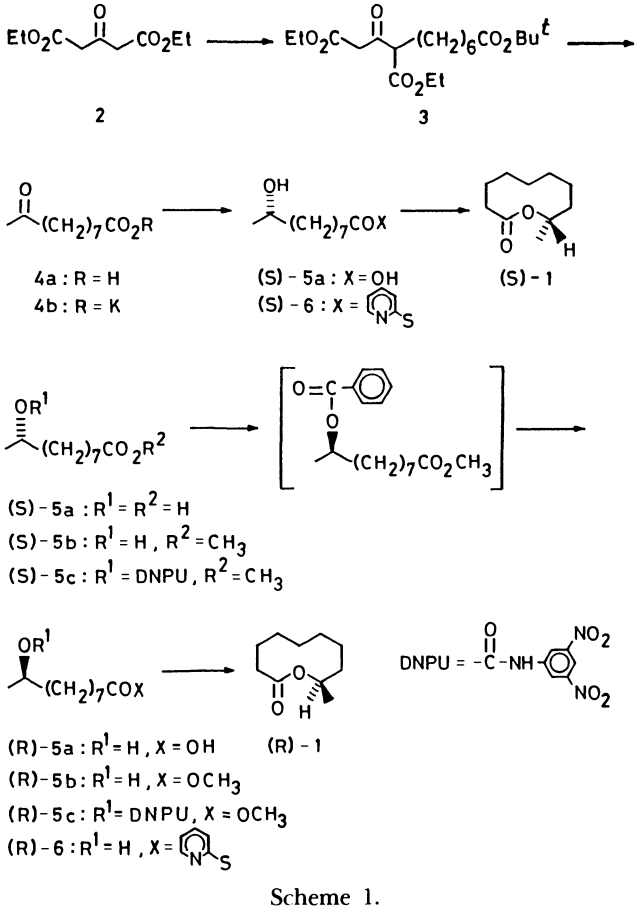

Scheme 1.

Table 1. Reuse of Immobilized Baker's Yeast in the Asymmetric Reduction of 9-Oxodecanoic Acid (**4a**)

Recycle number	Yieid of **5a** (%)		Optical purity of (*S*)-**5a** (% e.e.)	
	AK[a]	AKEA[b]	AK[a]	AKEA[b]
1	23	22	96	96
2	28	26	96	95
3	41	31	96	96
4	46	38	96	96
5	32	21	96	94
6	30	—	96	—
7	15	—	96	—

a) AK: 2% aqueous KCl solution. b) AKEA: 2% aqueous KCl solution containing ethyl acetate.

optical purity of the product (*S*)-**5a** remained almost constant, 96% e.e., throughout all the repetitive use of the catalyst. An EA-containing aqueous solution system with a carboxylic acid **4a** as the substrate also produced (*S*)-**5a**, and the optical purity was about the same as that observed for the aqueous solution system employing a potassium salt **4b**. Further, the trend of the chemical yield for EA-containing aqueous solution system was comparable with that obtained for aqueous solution system, the yield of **5a** attaining a maximum of 38% after the 4 th use.

It is noteworthy that (1) the IBY catalyst entrapped with κ-carrageenan can be stored in a 2% aqueous solution of KCl for six or more months at 0—5 °C, (2) the catalyst is reusable many times during the period, (3) the optical purity of the product is reproducible throughout all of the use of the catalyst, (4) the catalyst can be recovered and separated easily from the reaction mixture by simple filtration.

Experimental

General. IR spectra were determined on a Hitachi 260-10 spectrometer and on a Perkin Elmer 1720 Fourier transform IR spectrometer. ^{1}H and ^{13}C NMR spectra were obtained on a Hitachi R-24B spectrometer and on a Hitachi R-90H Fourier transform NMR spectrometer, respectively, in $CDCl_3$ solutions with tetramethylsilane as an internal standard. EI and CI mass spectra were recorded on a JEOL JMS-D300 mass spectrometer at 70 eV and 200 eV (isobutane), respectively, using a direct insertion probe. Optical rotations were measured on a Horiba SEPA-200 high sensitivity polarimeter. Column chromatography was carried out with 70—230 mesh silica gel (Merck Kieselgel 60 Art 7734).

Determination of the Optical Purities of (*R*)- and (*S*)-5a. (*R*)- and (*S*)-**5a** were converted via their methyl esters to (*R*)- and (*S*)-**5c** by treating with 3,5-dinitrophenyl isocyanate. HPLC analyses were carried out on a Gasukuro Kogyo model 576 liquid chromatograph equipped with a UV detector (254 nm). A Sumipax 2100 4X250 mm column (Sumitomo Chemical Co., Ltd., Osaka) was used with hexane: 1,2-dichloroethane:ethanol=100:20:1 (v/v, flow rate, 1 mL min^{-1}) as solvent. (*R*)- and (*S*)-**5c** were separable under these conditions and each showed two peaks. (*R*)-**5c**: R_t 12.4 min (2.5%) and 13.7 min (97.5%). (*S*)-**5c**: R_t 12.4 min (98%) and 13.7 min (2%). The optical purities of (*R*)- and (*S*)-**5a** were therefore 95% e.e. and 96% e.e.

9-*t*-Butyl Diethyl 2-Oxo-1,3,9-nonanetricarboxylate (3). Compound **3** was synthesized by alkylating diethyl 3-oxoglutarate (**2**, 20.2 g, 100 mmol) with *t*-butyl 7-bromoheptanoate (29.2 g, 110 mmol) in the presence of $Mg(OEt)_2$ according to the procedures described previously.[7] Purification by column chromatography on silica gel (hexane: ethyl acetate=3:1, v/v) gave **3** as a pale yellow viscous liquid (33.9 g, 88%). IR (neat) 1730, 1715 cm^{-1}. ^{1}H NMR δ=1.12—1.50 (21H, s at 1.43), 3.43 (2H, s), 3.55 (1H, t, *J*=7.2 Hz), 4.15 (4H, q, *J*=7 Hz). ^{13}C NMR δ=197.33, 172.82, 169.01, 166.44, 79.79. EIMS *m/z* (%) 330 (M^+ −56, 1), 313 (M^+ −73, 13), 202 (41), 156 (73), 57 (100). CIMS *m/z* (%) 387 [$(M+H)^+$, 41], 331 [$(M+H-56)^+$, 100].

9-Oxodecanoic Acid (4a). Monoalkylated 3-oxoglutarate **3** (19.3 g, 50 mmol) was heated in a 15% aqueous solution of NaOH (360 mL) under reflux for 15 h. The hydrolyzed mixture was acidified with concd HCl, saturated with NaCl and extracted with ether. Work-up of the ethereal solution gave a crude solid, which was recrystallized from petroleum ether to give **4a** as needles (8.28 g, 89%), mp 41—42 °C. IR (KBr) 3100, 1700 cm^{-1}. ^{1}H NMR δ=1.14—1.88 (10H, m), 2.15 (3H, s), 8.96 (1H, s). ^{13}C NMR δ=208.89, 179.09, 43.57. EIMS *m/z* (%) 186 (M^+, 2), 168 (M^+ −18, 6), 111 (20), 58 (70), 43 (100). CIMS *m/z* (%) 187 [$(M+H)^+$, 100]. Found: C, 64.38; H, 9.89%. Calcd for $C_{10}H_{18}O_3$: C, 64.69; H, 9.74%.

(*S*)-(+)-9-Hydroxydecanoic Acid [(*S*)-5a]. Use of Aqueous Solution System: According to the procedures described previously,[1,5] a mixture of the potassium salt **4b** derived from **4a** (1 g), baker's yeast (50 g) immobilized in carrageenan beads, and D-glucose (40 g) in a 2% aqueous solution of KCl (1000 mL) was shaken at 30 °C. Work-up of the reaction mixture gave crude (*S*)-**5a**, which was purified by column chromatography on silica gel (hexane:ethyl acetate=1:1, v/v) to give (*S*)-**5a** as a colorless liquid (465 mg, 46%), $[\alpha]_D^{22}$ +8.14° (*c* 0.41, chloroform). IR (neat) 3500, 1710 cm^{-1}. ^{1}H NMR δ=1.18 (3H, d, *J*=6 Hz), 1.12—1.86 (12H, m), 2.25 (4H, m), 3.72 (1H, m), 7.08 (2H, s). ^{13}C NMR δ=178.85, 68.08. EIMS *m/z* (%) 170 (M^+ −18, 1), 115 (17), 101 (41), 45 (100). CIMS *m/z* (%) 189 [$(M+H)^+$, 24], 171 [$(M+H-18)^+$, 100]. Found: C, 63.72; H, 10.91%. Calcd for $C_{10}H_{20}O_3$: C, 63.79; H, 10.71%.

Use of EA-Containing Aqueous Solution System: The same procedure was followed as described above except for using a 2% aqueous solution of KCl (1000 mL) containing ethyl acetate (10 mL) as solvent and the keto acid **4a** (1 g) itself as substrate.

(*S*)-(+)-Phoracantholide I [(*S*)-1]. To a solution of (*S*)-**5a** (160 mg, 0.85 mmol) in dry benzene (1 mL) were added triphenylphosphine (320 mg, 1.22 mmol) and dipyridyl disulfide (270 mg 1.22 mmol) under argon and the mixture was stirred for one hour at room temperature. The resulting pyridinethiol ester (*S*)-**6** was dissolved in dry benzene (50 mL) and the solution was added dropwise to a stirred suspension of $AgClO_4$ (1.13 g) in refluxing benzene (120 mL) under argon over period of 8 h with a motor-drive syringe (Micro Feeder JP-V, Furue Science, Tokyo). After the addition had been completed, the mixture was refluxed for an additional 15 min and cooled to room temperature. The precipitate was filtered off and washed with ether. The filtrate and washings were combined and concentrated in vacuo. The residue was purified by column chromatography on silica gel (hexane: ethyl acetate=10:1, v/v) followed by fractional distillation to give (*S*)-**1** (63 mg, 44%) with a characteristic odor, bp 65 °C (bath temperature)/3 mmHg (1 mmHg=133.32 Pa), $[\alpha]_D^{22}$ +38.38° (*c* 0.06, chloroform) [lit,[4] $[\alpha]_D^{22}$ +38.8° (*c* 0.68, chloroform)]. IR (neat) 1725 cm^{-1}. ^{1}H NMR δ=1.25 (3H, d, *J*=6 Hz), 4.72—5.51 (1H, m). EIMS *m/z* (%) 170 (M^+, 3), 152 (M^+ −18, 17), 126 (12), 111 (11), 98 (100), 84 (50), 69 (30), 54 (64), 40 (55). CIMS *m/z* (%) 171 [$(M+H)^+$, 100]. Found: C, 70.32; H, 10.63%. Calcd for $C_{10}H_{18}O_2$: C, 70.54; H, 10.66%.

(*R*)-(−)-9-Hydroxydecanoic Acid [(*R*)-5a]. Methyl ester (*S*)-**5b** (220 mg, 1.1 mmol) prepared from (*S*)-**5a** was dissolved in dry THF (15 mL) and the solution was stirred under ni-

trogen while triphenylphosphine (600 mg, 2.2 mmol) and benzoic acid (300 mg, 1.6 mmol) were added. To the stirred solution was slowly added diethyl azodicarboxylate (400 mg, 2.2 mmol) and the mixture was allowed to stir at room temperature overnight. After evaporation of the solvent in vacuo, the residue was chromatographed on silica-gel column. Elution with benzene gave a benzoate ester, a solution of which in THF (2 mL) was added dropwise over a 10-min period to a stirred and ice-cooled 1 mol dm^{-3} aqueous solution of KOH (2 mL) containing methanol (1.5 mL). After being stirred for 30 min at room temperature, the mixture was acidified with concd HCl to pH 1—2 under ice-cooling and extracted with dichloromethane. Work-up of the organic layer gave a crude product, which was purified by column chromatography on silica gel (hexane : ethyl acetate=2 : 1, v/v) followed by preparative TLC (hexane : ethyl acetate=1 : 1, v/v) to give (*R*)-**5a** as a colorless liquid (112 mg, 54% from (*S*)-**5a**), $[\alpha]_D^{22}$ −8.13° (*c* 0.11, chloroform). The IR, NMR, and CI mass spectra were identical with those of (*S*)-**5a**. Found: C, 63.66; H, 10.78%. Calcd for $C_{10}H_{20}O_3$: C, 63.79; H, 10.71%.

(*R*)-(−)-Phoracantholide I [(*R*)-1]. Lactonization of (*R*)-**5a** (94 mg, 0.5 mmol), as described for (*S*)-**5a**, gave (*R*)-**1** (28 mg, 33%), $[\alpha]_D^{22}$ −37.4° (*c* 0.02, chloroform) [lit,[4] $[\alpha]_D^{22}$ −35.1° (*c* 1.15, chloroform)]. (*R*)-**1** was identical in its spectral data with (*S*)-**1**. Found: C, 70.29; H, 10.81%. Calcd for $C_{10}H_{18}O_2$: C, 70.54; H, 10.66%.

We wish to thank Dr. Seiichiro Kawabe, Department of Fundamental Natural Science, Okayama University of Science, for his advice concerning the immobilization of baker's yeast. The present work was partially supported by the Agricultural Chemical Research Foundation and by a Grant-in-Aid for Scientific Research No. 63560135 from the Ministry of Education, Science and Culture.

References

1) A part of the present work has been reported as a preliminary communication: Y. Naoshima and H. Hasegawa, *Chem. Lett.*, **1987**, 2379.

2) B. P. Moore and W. V. Brown, *Aust. J. Chem.*, **29**, 1365 (1976).

3) H. Gerlach, P. Kunzler, and K. Oertle, *Helv. Chim. Acta*, **61**, 1226 (1978); N. Ono, H. Miyake, and A. Kaji, *J. Org. Chem.*, **49**, 4997 (1984) and references cited therein.

4) T. Kitahara, K. Koseki, and K. Mori, *Agric. Biol. Chem.*, **47**, 389 (1983).

5) Y. Naoshima, H. Hasegawa, and T. Saeki, *Agric. Biol. Chem.*, **51**, 3417 (1987).

6) T. Sakai, T. Nakamura, K. Fukuda, E. Amano, M. Utaka, and A. Takeda, *Bull. Chem. Soc. Jpn.*, **59**, 3185 (1986).

7) Y. Naoshima, H. Ozawa, H. Kondo, and S. Hayashi, *Agric. Biol. Chem.*, **47**, 1431 (1983) and references cited therein.

Synthesis of 10-(8-Aminooctyl)flavin and Its Use in Affinity Chromatography

Sabu KASAI,* Hideko NAKANO, Kazuya MAEDA,† and Kunio MATSUI††
Research Institute for Atomic Energy, Osaka City University, Sugimoto, Sumiyoshi-ku, Osaka 558
†General Education Course, Osaka City University, Sugimoto, Sumiyoshi-ku, Osaka 558
(Received July 23, 1988)

Synopsis. 7,8-Dimethyl-10-(8-aminooctyl)isoalloxazine was synthesized by coupling *N*-(8-aminooctyl)-4,5-dimethyl-1,2-benzenediamine with alloxan. The flavin was immobilized to epoxy activated gel to use for affinity chromatography. The gel was effective for purification of riboflavin-binding protein from egg white and flavokinase from rat liver.

10-(ω-Aminoalkyl)flavins (7,8-dimethylisoalloxazines) are readily bound covalently to many kinds of solid supports, for example, epoxy-, CNBr-, or *N*-hydroxysuccinimide-activated ones, with the alkylamino group. The immobilized flavin would be useful for affinity chromatography, technology using flavin-flavin binding protein complexes, study on flavoenzyme mechanism, preparation of flavoenzyme functioned materials, and others. The only example of such a flavin to be reported is 7,8-dimethyl-10-(2-aminoethyl)isoalloxazine. This was synthesized by reductive amination of 10-(formylmethyl)flavin, a periodate oxidation product of riboflavin, with sodium cyanotrihydroborate and ammonium chloride.[1] This synthetic route, however, is an unusual one for an (ω-aminoalkyl)flavin. In this report, we describe a more convenient synthetic method for this kind of flavin, as is shown in Scheme 1.

1-Chloro-2-nitro-4,5-dimethylbenzene (**1**) was coupled with 1,8-octanediamine to give 1-(8-aminooctylamino)-2-nitro-4,5-dimethylbenzene (**2**), which was catalytically hydrogenated with Raney's catalyst. Addition of strong acid was necessary to complete the reduction. The reduced compound **3** was coupled with alloxan in the usual way to give 7,8-dimethyl-10-(8-aminooctyl)isoalloxazine (**4**).

The epoxy-activated Cellulofine, a cellulose gel, was prepared and was bound with **4** as described by Sundberg and Porath.[2] The flavin content of the gel so prepared was approximately 17 μmol of the flavin/mL of the hydrated gel, and was relatively high compared with many kinds of flavin immobilized gel prepared by Merrill and McCormick (16.4—1.4 μmol mL^{-1}).[3]

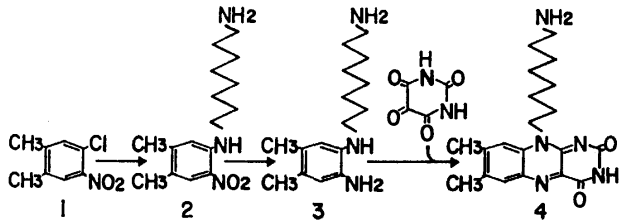

Scheme 1.

The flavin immobilized gel so obtained was used for affinity chromatography to show the high efficiency of the gel. Many kinds of flavin affinity chromatographic materials have already been prepared which have various features including ease or difficulty of preparation, high or low flavin content, high or low efficiency, etc.[4] An important factor is the position of immobilization of the flavin; for example, only gels immobilized at position 10 of flavin were effective for the purification of flavokinase from rat liver; gels immobilized at position 3 and 8 were negative.[3] Consequently, two proteins were chosen for purification; riboflavin-binding protein (RBP) from egg white, since this protein has been used for many studies and is easy to obtain, and flavokinase from rat liver, since the gel seems to be suitable for the purification of this protein as described above.

RBP, partially purified as described in the experimental section, was subjected to affinity chromatography and the elution pattern was shown in Fig. 1. RBP was bound to the gel and selectively eluted with a buffer containing 20 μM (M=mol dm^{-3}) riboflavin.

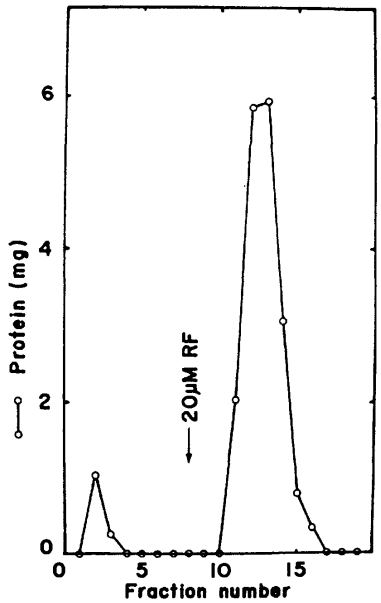

Fig. 1. Elution pattern for affinity chromatography of riboflavin-binding protein. Partially purified RBP was applied on a flavin-immobilized column and the column was washed. The bound RBP was eluted from the column with a phosphate buffer containing 20 μM riboflavin. The amount of protein in each fraction was determined according to Lowry et al.[7] and plotted.

†† Present address: Teikoku Women's University, Department of Home Economics, 6-173 Touda-cho, Moriguchi-shi, Osaka 570.

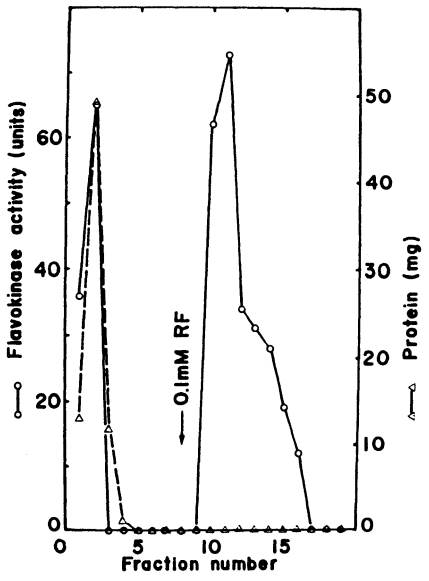

Fig. 2. Elution pattern for affinity chromatography of flavokinase from rat liver. A pooled sample from Sephadex G-75 chromatography was applied on an affinity chromatography and the column was washed. The bound flavokinase was eluted from the column with 100 μM riboflavin solution. The amount of protein (△) and flavokinase activity (○) in each fraction were plotted. Protein concentrations were determined according to Smith et al.[8]

The purified sample was analyzed by sodium dodecyl sulfate (SDS)-polyacrylamide gel electrophoresis and gave a single band (data not shown).

A crude extract of rat liver was fractionated with ammonium sulfate, and a 55 to 75% saturation fraction was chromatographed on a Sephadex G-75 column. Fractions containing flavokinase activity were collected and applied on the affinity column. Flavokinase with high specific activity was eluted with 0.1 mM riboflavin solution as shown in Fig. 2, though approximately 30% of the total eluted activity were found in the washings similarly to the affinity column reported by Merrill and McCormick.[5] Flavokinase binds irreversibly to fresh gel, so that a better yield was obtained after using several times.

These results indicate that the affinity column so prepared is effective for the purification of many proteins such as riboflavin carrier protein and flavokinase from many different origins.

Experimental

UV spectra were recorded on a Hitachi 320 recording spectrophotometer; 400 MHz ^{1}H NMR spectra were taken with a JEOL NMR spectrometer model JMM GX 400. Melting points were measured with a Yanaco MP micro melting point apparatus.

1-(8-Aminooctylamino)-2-nitro-4,5-dimethylbenzene (2). 1-Chloro-2-nitro-4,5-dimethylbenzene (**1**) was synthesized according to the procedure of Adams et al.[6] from 4,5-dimethyl-2-nitroaniline (Aldrich). A mixture consisting of 5.0 g of **1** and 25.0 g of 1,8-octanediamine was heated at 100 °C for 2 h and cooled to room temperature. The brown syrup obtained was then dissolved in 250 mL CH_2Cl_2 and washed five times with water. Anhydrous $MgSO_4$ was added to the organic phase and filtered off. The filtrate and washings were combined and evaporated in vacuo. The residue, dissolved in CH_2Cl_2, was applied on a silica-gel column (Wakogel C-200, 3 ×25 cm) and developed with a mixture of CH_2Cl_2 and methanol (8 : 2). Fractions from the second large red band were collected and evaporated. The syrupy residue was dissolved in a minimum amount of toluene and **2** was crystallized by gradually adding hexane. Fine orange crystals were filtered off, washed with hexane and dried over $CaCl_2$ in vacuo. Yield 7.0 g (88%): mp 68—70 °C; ^{1}H NMR ($CDCl_3$) (*exchangeable H) δ=1.34 (6H, m, CH_2), 1.44 (2H, m, CH_2), 1.51 (2H, m, CH_2), 1.71 (2H, m, CH_2), 2.17 (3H, s, CH_3), 2.27 (3H, s, CH_3), 2.62* (2H, s(broad), NH_2), 2.74 (2H, t, J=7 Hz, 8′CH_2), 3.26 (2H, td, J=5 and 7 Hz, 1′CH_2), 6.61 (1H, s, φ-H), 7.91 (1H, s, φ-H), 7.97* (1H, s(broad), NH). Found: C, 65.60; H, 9.20; N, 14.04%. Calcd for $C_{16}H_{27}N_3O_2$: C, 65.49; H, 9.28; N, 14.32%.

7,8-Dimethyl-10-(8-aminooctyl)isoalloxazine (4). 1.0 g of **2** was dissolved in 30 mL acetic acid and hydrogenated over 5% palladium on carbon (400 mg) at 100 °C under atmospheric pressure. When the color of the solution changed from orange-red to colorless (approximately 1 h later), 3 mL concentrated hydrochloric acid was added to the reaction mixture and hydrogenation was continued for a further 1 h. The catalyst was filtered off and washed with acetic acid. The combined filtrate and washings were evaporated and 30 mL water was added to the residue. The solution was evaporated to dryness to remove acetic acid. This procedure was repeated twice. The residue was dissolved in 30 mL water and DEAE-cellulose (OH^- form, suction dried weight, 20 g) was added to the solution and the suspension stirred gently for 10 min. The cellulose was filtered off and washed with water. The combined filtrate and washings were evaporated. Because the triamine so obtained was readily oxidized, it was subjected to the next reaction without isolation. The residue, dissolved in 30 mL methanol, was added to a hot solution of 0.5 g alloxan monohydrate and 10 g boric acid in 20 mL methanol. The solution was heated at 60 °C for 2 h and evaporated. The syrupy residue was crystallized from a solution of 2 g boric acid in 20 mL ethanol to yield 1.0 g (43%) of **4** as pentaborate. The crystals were dried over P_2O_5 at 150 °C overnight for elemental analysis: mp over 300 °C; ^{1}H NMR (DMSO-d_6) δ=1.32 (6H, m, CH_2), 1.47 (2H, m, CH_2), 1.57 (2H, m, CH_2), 1.71 (2H, m, CH_2), 2.40 (3H, s, CH_3), 2.52 (3H, s, CH_3), 2.75 (2H, m, 8′CH_2), 4.58 (2H, t, J=8 Hz, 1′CH_2), 7.81 (1H, s, φ -H), 7.90 (1H, s, φ-H), 8.06* (2H, s(broad), NH_2), 11.31* (1H, s, 3NH). UV (50 mM phosphate buffer pH 7.0) 223 nm (ε_{mM} 27.3), 266 (31.5), 368 (8.86), 443 (10.7); (6 M HCl) 265 (28.9), 392 (18.0), (0.1 M NaOH) 270 (36.3), 352 (10.3), 447 (10.8); Found: C, 41.71; H, 4.97; N, 12.43%. Calcd for $C_{20}H_{27}N_5O_2 \cdot 1.3H_2B_4O_7$: C, 41.86; H, 5.19; N, 12.20%.

Preparation of Flavin Immobilized Gel. Cellulose gel (Cellulofine, Chisso) was epoxy-activated using 1,4-butanediol diglycidyl ether according to Sundberg and Porath,[2] and allowed to react with **4**. 2.7 g of **4** was dissolved in a mixture of 50 mL of dioxane and 50 mL of 0.2 M carbonate buffer, pH 10.5, and 120 mL epoxy-activated Cellulofine gel (hydrated) was added to the solution. The slurry was stirred gently at 60 °C for 24 h. The yellow stained gel was filtered off and washed with hot water, dioxane, acetic acid and 20% NaCl solution repeatedly until greenish yellow fluorescence was not observed in the washings. Finally, the gel was washed with buffer for affinity chromatography. The nitrogen contents in the dried samples of modified and unmodified Cellulofine were 0.66 and 0.06% respectively. It was calculated from these data that the dry and hydrated gel contained approximately 86 μmol of flavin/g and 17 μmol of

flavin/mL respectively.

Affinity Chromatography. RBP from Egg White. RBP was partially purified from two eggs according to Nishina[9] before affinity chromatography; RBP was bound to 20 g DEAE-cellulose at pH 4.3 and then eluted with 0.1 M acetate buffer, pH 3.6. The collected fractions were rechromatographed on a Sephadex G-25 column (90×2.6 cm) using a glycine-HCl buffer (pH 3.15) to remove riboflavin. Protein was precipitated from the eluate by adding ammonium sulfate to 85% saturation. The precipitate was dialyzed against a 50 mM phosphate buffer (pH 7.0). The dialyzed sample (3 mL) was applied on a column of the flavin immobilized gel (15×1.0 cm), and the column was washed with the same buffer. RBP was eluted from the column with the phosphate buffer containing 20 μM riboflavin.

Flavokinase from Rat Liver. A buffer containing 0.1 M 3-morpholino-1-propanesulfonic acid (MOPS) and 0.1 mM $ZnSO_4$, pH 7.0 was used throughout. Flavokinase activity was determined as follows; each assay mixture was prepared adding 100 μL sample to 300 μL of a buffer containing 100 μM riboflavin, 1 mM ATP, 0.1 mM $ZnSO_4$, and 0.1 M MOPS, pH 8.0. After 30 min incubation at 37 °C, 50 μL of the mixture was assayed using HPLC; a Cosmosil 10C18 packed column (4.6×150 mm, Nacalai Tesque) and 50 mM phosphate buffer, pH 6.25, containing 0.5% pyridine, 9% ethanol, were used for separation. FMN synthesis was expressed in units of flavokinase activity; one unit produces 1 nmol FMN/h under the conditions described above.

Three rat livers (approximately 25 g) were homogenized in 75 mL buffer and the supernatant was fractionated by adding ammonium sulfate. A 55 to 75% saturation precipitate was dissolved in a small amount of buffer and applied on a Sephadex G-75 column (30×2.6 cm). After development, the fractions containing flavokinase activity were pooled and approximately one third of the volume was applied on the flavin affinity column (10×1.0 cm) again and the column was washed with the buffer. Fractions with high flavokinase activity were obtained by elution with the buffer containing 100 μM riboflavin.

The authors thank Mr. Junichi Goda for the elemental analyses.

References

1) T. Jones, R. Spencer, and C. Walsh, *Biochemistry*, **17**, 4011 (1978).

2) L. Sundberg and J. Porath, *J. Chromatogr.*, **90**, 87 (1974).

3) A. H. Merril and D. B. McCormick, *Anal. Biochem.*, **89**, 87 (1978).

4) A. H. Merrill and D. B. McCormick, "Methods Enzymol.," ed by D. B. McCormick and L. D. Wright, Academic Press, Inc., New York (1980), Vol. 66, pp. 338—345.

5) A. H. Merrill and D. B. McCormick, *J. Biol. Chem.*, **255**, 1335 (1980).

6) R. R. Adams, C. A. Weisel, and H. S. Mosher, *J. Am. Chem. Soc.*, **68**, 883 (1946).

7) O. H. Lowry, N. J. Rosebrough, A. L. Farr, and R. J. Randall, *J. Biol. Chem.*, **193**, 265 (1951).

8) P. K. Smith, R. I. Krohn, G. T. Hermanson, A. K. Mallia, F. H. Gartner, M. D. Provenzano, E. K. Fujimoto, N. M. Goeke, B. J. Olson, and D. C. Klenk, *Anal. Biochem.*, **150**, 76 (1985).

9) Y. Nishina, *Osaka-Daigaku Igaku Zasshi*, **29**, 261 (1977).

Synthetic Photochemistry. XLVII.[1] Formation and Degenerate Cope Rearrangement of 9-Dicyanomethylenebarbaralane

Guan Rong TIAN,† Shigeru SUGIYAMA, Akira MORI, and Hitoshi TAKESHITA*
Institute of Advanced Material Study, 86, Kyushu University, Kasuga-koen, Kasuga, Fukuoka 816
(Received August 3, 1988)

Synopsis. Photolysis of 2-dicyanomethylenehomobarrelene gave 9-dicyanomethylenebarbaralane, 5-dicyanomethylenetricyclo[4.3.0.0^{2,9}]nonadiene, and 1-dicyanomethyleneindan. Dicyanomethylenebarbaralane showed time-averaged NMR signals.

Recently, we synthesized several barbaralane derivatives[2] by a photolysis of 2-methylenehomobarrelenes[3] prepared from 1*H*-cyclohepta[*b*]furan-2-one derivatives and 2,3-bis(methoxycarbonyl)-7-oxanorbornadiene. In this paper we describe the synthesis of 9-dicyanomethylenebarbaralane (**1**)[4] from 2-dicyanomethylenehomobarrelene (**2**) and the time-averaged NMR spectrum of this internal Cope-rearrangement system.

Results and Discussion

When a chloroform solution of **2**, prepared by high-pressure cycloaddition-thermal cycloreversion procedure from 8,8-dicyanoheptafulvene (**3**) and 2,3-bis(methoxycarbonyl)-7-oxanorbornadiene (**4**),[3] was irradiated, three products (**1**,[4] **5**, and **6**[5]) were obtained in 18, 29, and 24% yields, respectively. These structures were determined by comparisons with the spectral data of the related compounds prepared previously.[3] The barbaralane derivative, **1**, revealed a time-averaged NMR spectra, as expected. A kinetic analysis of this intramolecular Cope rearrangement was carried out by measuring the half-height widths of NMR signals.[6] The kinetic parameters obtained are summarized in Table 1 together with those of related compounds, barbaralone (**7**)[4,7] and barbaralane (**8**).[4] In both toluene-d_8 and acetone-d_6, the rates of exchange were nearly equal and insensitive to the polarity of the solvent. This is consistent, together with other thermodynamic parameters, as the concerted rearrangement.[7-11]

The activation energy (E_a) of **1** was similar to that reported by Nakanishi for **7**.[7] A retardation of the

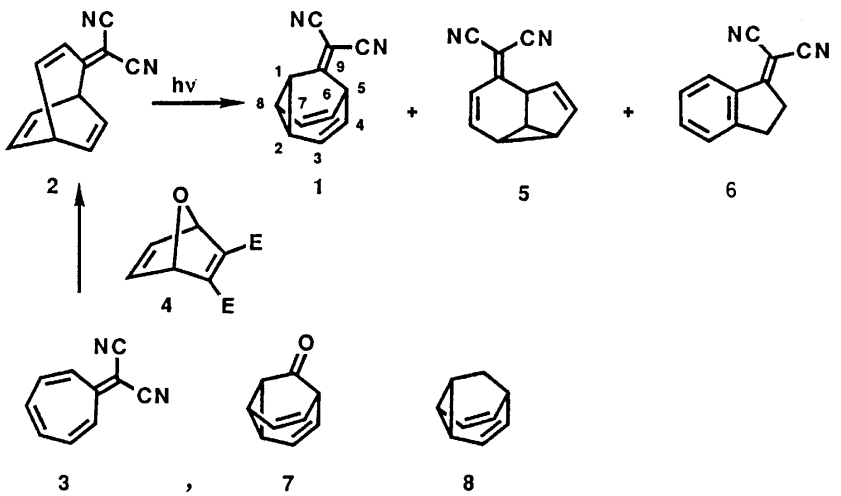

Scheme 1.

Table 1. Activation Parameters of Cope Rearrangement[a]

	E_a/kJ mol^{-1}	$\Delta H^{\neq}$/kJ mol^{-1}	$\Delta S^{\neq}$/J mol^{-1}K^{-1}	$\Delta G^{\neq}_{298}$/kJ mol^{-1}
7	33.9	31.4	−38.8	43.1[b]
	48.1±0.4	45.6±0.4	11.3±2.9	42.3±0.4[c]
1	45.0±1.5	42.6±1.5	−6.3±6.3	44.3±0.7[d]
	44.6±1.2	42.0±1.2	−6.5±4.9	44.0±0.5[e]
8	36.0	33.5	5.6	31.8[f]

a) Variable temperature ^{13}C NMR spectra were measured at 67.5 MHz in acetone-d_6 between −80 and 50 °C and in toluene-d_8 between −80 and 60 °C. See Experimental for the determination of activation parameters for **1**. b) In acetone-d_6.[4] c) In CS_2-CD_2Cl_2-acetone-d_6.[7] d) In acetone-d_6. e) In toluene-d_8. f) In CS_2.[4]

† On leave from Yanbian University, Yanji, Jilin, People's Republic of China.

rates of the degenerate Cope rearrangement for **1** and **7** may be another example of such that the electron-withdrawing carbonyl and dicyanomethylene groups strengthened the C_2-C_8 bond to raise the activation energy of the Cope rearrangement as has been already pointed out by Hoffmann and Stohrer.[12]

Experimental

Irradiation of 2. **a**) A $CHCl_3$ solution (2 cm^3) of **2** (320 mg) was irradiated for 4 h as previously described[3] to give **1** [colorless crystals, mp 142—143 °C, 31.3 mg, 18%. Found: C, 79.99; H, 4.24; N, 15.43%. Calcd for $C_{12}H_8N_2$: C, 79.88; H, 4.47; N, 15.54%. ^{1}H NMR δ[13]=3.68 (2H, tm, J=6.7 Hz), 4.46 (4H, tm, J=6.7 Hz), and 5.76 (2H, tt, J=6.7, 1.5 Hz). δ (toluene-d_8 at −90 °C)=1.58 (2H, br s), 2.30 (1H, br s), 3.36 (1H, br s), and 4.90 (4H, br s). δ (toluene-d_8 at 50 °C)=3.15 (2H, tm, J=5.9 Hz), 3.62 (4H, tm, J=5.9 Hz), and 5.11 (2H, tm, J=5.9 Hz). ^{13}C NMR at 60 °C δ=36.2 (2C), 76.6, 80.3 (br, 4C), 112.2 (2C), 121.2 (2C), and 178.9. IR ν: 2240 and 1585 cm^{-1}. UV (MeOH): 244.0 (ε 13400) and 300.0 nm (5600). MS m/z (%) 180 (M^+, 20), 153 (32), 115 (base), 63 (37), 51 (41), and 39 (32)], **5** [yellow crystals, mp 110—111 °C, 51 mg, 29%. Found: C, 80.13; H, 4.29; N, 15.52%. Calcd for $C_{12}H_8N_2$: C, 79.88; H, 4.47; N, 15.54%. ^{1}H NMR δ=2.14 (1H, td, J=7.5, 4.5 Hz), 2.52 (1H, td, J=7.5, 6.0 Hz), 2.96 (1H, dddd, J=7.5, 6.0, 2.5, 0.5 Hz), 4.12 (1H, ddm, J=7.5, 2.0 Hz), 5.36 (1H, dm, J=5.5 Hz), 5.89 (1H, ddd, J=5.5, 2.5, 1.5 Hz), 6.38 (1H, dd, J=10.0, 4.5 Hz), and 6.80 (1H, dd, J=10.0, 1.0 Hz). ^{13}C NMR δ=24.4, 30.9, 45.1, 48.1, 78.3, 112.0, 112.8, 125.4, 132.0, 133.8, 140.4, and 171.7. IR ν: 2210, 1595, and 1540 cm^{-1}. UV (MeOH): 242.0 (ε 5200 sh), 279.8 (7500), and 339.2 nm (10900). MS (%) 180 (M^+, 26), 153 (51), and 115 (base)], **6** [colorless crystals, mp 146—147 °C, 43 mg, 24%. Found: C, 79.77; H, 4.14; N, 15.37%. Calcd for $C_{12}H_8N_2$: C, 79.88; H, 4.47; N, 15.54%. ^{1}H NMR δ=3.1—3.4 (4H, m), 7.3—7.7 (3H, m), and 8.20 (1H, dm, J=7.5 Hz). ^{13}C NMR δ=29.6, 34.6, 78.0, 112.9, 113.5, 126.1, 126.2, 128.1, 135.1, 135.7, 154.0, and 179.2. IR ν: 2240 and 1575 cm^{-1}. UV (MeOH): 230.0 (ε 8300), 236.0 (7450), 255.4 (1850), 290.0 (11800 sh), 306.4 (15500), and 331.8 nm (17800). MS m/z (%) 180 (M^+, 63), 153 (47), 115 (base), 43 (68), and 39 (38)], and unreacted **2** (142.2 mg). **b**) An acetone-d_6 solution (1 cm^3) of **2** (143 mg) was irradiated to give **1** [16.9 mg, 15%], **5** [30.6 mg, 28%], **6** [26.7 mg, 24%], and unreacted **2** [32.8 mg].

Kinetics Measurements. A kinetic analysis was carried out by variable-temperature ^{13}C NMR measurements at 67.5 MHz (JEOL 270) in acetone-d_6 and toluene-d_8. The rate constants of the chemical exchange process were determined by broadened line widths of the exchangeable signals at the half height. Natural line widths were obtained from the signals of C-3 and C-7 around δ 121 in toluene and δ 122 in acetone. The temperature range was between −80 and 60 °C in toluene and between −80 and 50 °C in acetone.

References

1) Part. XLVI: G. R. Tian, A. Mori, N. Kato, and H. Takeshita, *Bull. Chem. Soc. Jpn.*, **62**, 506 (1989).
2) G. R. Tian, S. Sugiyama, A. Mori, H. Takeshita, M. Higashi, and H. Yamaguchi, *Chem. Lett.*, **1988**, 941.
3) G. R. Tian, S. Sugiyama, A. Mori, and H. Takeshita, *Bull. Chem. Soc. Jpn.*, **61**, 4397 (1988).
4) W. von E. Doering, B. M. Ferrier, E. T. Fossel, J. H. Hartenstein, M. Jones, Jr., G. Klumpp, R. M. Rubin, and M. Saunders, *Tetrahedron*, **23**, 3943 (1967).
5) D. M. W. Anderson, F. Bell, and J. L. Duncan, *J. Chem. Soc.*, **1961**, 470.
6) H. Günther, J. Runsink, H. Schmickler, and P. Schmitt, *J. Org. Chem.*, **50**, 289 (1985).
7) H. Nakanishi and O. Yamamoto, *Chem. Lett.*, **1975**, 513.
8) H. Nakanishi and O. Yamamoto, *Chem. Lett.*, **1973**, 1273.
9) H. Nakanishi and O. Yamamoto, *Tetrahedron Lett.*, **1974**, 1803.
10) H. Günther and J. Ulmen, *Tetrahedron*, **30**, 3781 (1974).
11) A. K. Cheng, F. A. L. Anet, J. Mioduski, and J. Meinwald, *J. Am. Chem. Soc.*, **96**, 2887 (1974).
12) R. Hoffmann and W.-D. Stohrer, *J. Am. Chem. Soc.*, **93**, 6941 (1971).
13) NMR spectra were measured in $CDCl_3$ solution unless otherwise specified.

A Mild, High-Yield Conversion of Thiols into Disulfides Using Disulfide Dication Salt: A New Redox System

Hisashi FUJIHARA, Ryouichi AKAISHI, and Naomichi FURUKAWA*
Department of Chemistry, University of Tsukuba, Tsukuba, Ibaraki 305
(Received August 3, 1988)

Synopsis. A new redox reaction of thiols with disulfide dication salt, 1,5-dithioniabicyclo[3.3.0]octane bis(trifluoromethanesulfonate), under mild conditions gave the corresponding disulfides in good yields together with 1,5-dithiacyclooctane.

The conversion of thiols into disulfides is an important phenomenon in chemical and biological redox reactions.[1,2] Numerous procedures are available for the oxidation of thiols to disulfides.[1] Meanwhile, the formation and the isolation of a few disulfide dications have been reported.[3,4] However, reactions using disulfide dication have not been well explored because of difficulties to obtain stable compounds. Recently, we succeeded in the preparation of the disulfide dication, 1,5-dithioniabicyclo[3.3.0]octane bis(trifluoromethanesulfonate) (**1**), as a remarkably stable crystalline salt which was first characterized by X-ray diffraction.[5] We found that the disulfide dication **1** acts both as an oxidizing agent and as an electrophile toward aromatics.[6] No synthetic application of this attractive organosulfur compound has been reported. We present here a new type of redox reaction of thiols with the disulfide dication salt **1** under mild conditions.

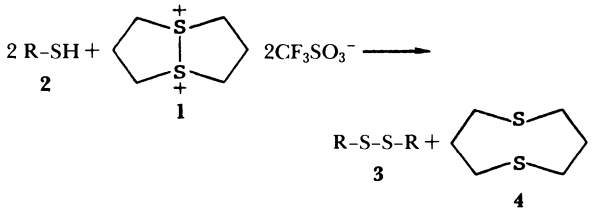

2a: n-C_4H_9, **2b**: *cyclo*-C_6H_{11}, **2c**: t-C_4H_9, **2d**: C_6H_5,

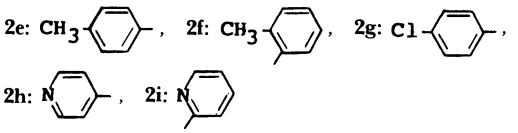

The disulfide dication salt **1** is a remarkably stable compound under dry conditions and can be easily prepared by the reaction of 1,5-dithiacyclooctane 1-oxide with trifluoromethanesulfonic anhydride. A redox reaction was carried out simply by stirring anhydrous acetonitrile solution of thiols (**2a—i**) and dication salt **1** under an Ar atmosphere at room temperature. Disulfides were completely consumed within a few hours, as determined by GLC or TLC. After the usual work-up procedure, the residue was purified by column chromatography to give the corresponding symmetrical disulfides (**3a—i**) in good yields, together with 1,5-dithiacyclooctane (**4**) as a reduction product. The results are summarized in Table 1. This method can be applied to the oxidation of a variety of alkane- (**2a—c**), arene- (**2d—g**), and heteroarenethiols (**2h** and **2i**).

Table 1. Oxidation of Thiols with Dication **1**[a]

R-SH	Yield/%		Mp or Bp/°C/mmHg[b] (lit)
	3	**4**	**3**
2a[c]	80	86	228—230/760(226/760)[8]
2b	82	95	120—123/0.6(138—141/1)[9]
2c	35	42	82—84/18(83—86/18)[9]
2d	86	84	60—61(61—62)[10]
2e	78	60	46(44—46)[10]
2f	73	83	36(36—38)[11]
2g	80	86	72(72—73)[12]
2h	86	80	d)
2i	83	84	57—58(57)[13]
2j	44	77	80(80—81)[14]

a) Time, 5 h. b) 1 mmHg≈133.322 Pa. c) At 0 °C. d) Determined by NMR with authentic compound.

2-Methyl-2-propanethiol (**2c**) can be oxidized to the corresponding disulfide in comparatively low yield, though in general the oxidation of **2c** is difficult. The oxidative cyclization of 1,2-bis(mercaptomethyl)benzene (**2j**) was performed using a high-dilution method and gave the corresponding cyclic disulfide **3j** and **4** (see Table 1). These were obtained together with polymeric products, due to an intermolecular oxidation of **2j**.

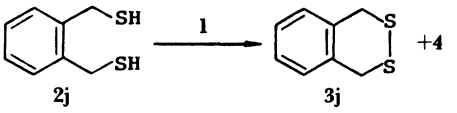

These results demonstrate that the disulfide dication **1** employed acts as an oxidant toward thiols. This redox reaction may proceed through an electron-transfer process between thiols and the dication **1**, since the oxidation potential of thiols is relatively lower than that of **4** as a precursor of **1**.[6] Another possibility, that involves the thiasulfonium cation intermediate, such as **5**, is also conceivable in the present reaction.

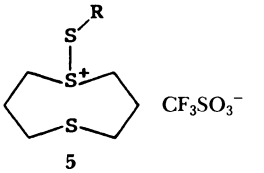

Thus, a new organosulfur compound, disulfide dication **1**, can be used for the oxidation of several thiols under mild conditions.

Experimental

The IR spectra were obtained on a JASCO A-3 spectrometer. ^{1}H NMR spectra were measured on a Hitachi R-600 FT-NMR spectrometer. All of the reactions were monitored by

gas chromatography (GLC) [Hitachi 163, using a 2% Silicon OV-1 Chromosorb W on SiO_2 (80—100 mesh) column] or thin-layer chromatography (TLC) [Wakogel B-5F].

Thiols, as shown in Table 1, were obtained from Wako Pure Chemicals. 1,2-Bis(mercaptomethyl)benzene was prepared from 1,2-bis(bromomethyl)benzene by a standard procedure.[7] 1,5-Dithiacyclooctane 1-oxide was prepared by a method given in the literature.[4] Other chemicals were of reagent grade.

Preparation of Disulfide Dication 1. To a stirred solution of 1,5-dithiacyclooctane 1-oxide (3.2 g, 19.5 mmol) in anhydrous dichloromethane (160 mL) was added dropwise a solution of trifluoromethanesulfonic anhydride (5.5 g, 19.5 mmol) in anhydrous dichloromethane (160 mL) at −20 °C. After the addition was complete, the mixture was stirred for 3 h, and the white precipitates were filtered and washed with anhydrous dichloromethane, giving salts **1** in 80% yield: mp 100—102 °C; ^{1}H NMR (CD_3CN) δ=2.2—2.7 (br s, 4H, CH_2) and 2.9—3.6 (br s, 8H, $^+SCH_2$). Calcd for $C_8H_{12}F_6O_6S_4$: C, 21.52; H, 2.70%. Found: C, 21.42; H, 2.71%.

Oxidation of Thiols with Dication 1. In a typical run, to a stirred solution of disulfide dication **1** (240 mg, 0.54 mmol) in anhydrous acetonitrile (5 mL) was added a solution of benzenethiol (118 mg, 1.08 mmol) in anhydrous acetonitrile (3 mL) under an Ar atmosphere at room temperature. The mixture was stirred at room temperature and the reaction was monitored by GLC. After the reaction was complete, the reaction mixture was treated with aqueous sodium hydrogencarbonate solution. The mixture was extracted with dichloromethane (5×20 mL). The extracts were dried with magnesium sulfate, and the solvent was evaporated under reduced pressure. The residue was purified with column chromatography on silica gel (eluent: hexane) to afford diphenyl disulfide. The oxidations of the other thiols were confirmed by the similar procedure. The yields of disulfides obtained are listed in Table 1. The purity of the isolated product was confirmed by GLC analysis: the IR and NMR spectra, and bp or mp, were in satisfactory agreement with values found in the literature.

Oxidation of 1,2-Bis(mercaptomethyl)benzene (2j). A solution of dication **1** (240 mg, 1.54 mmol) in anhydrous acetonitrile (20 mL) and 1,2-bis(mercaptomethyl)benzene (**2j**) (92 mg, 1.54 mmol) in anhydrous acetonitrile (20 mL) was added separately and simultaneously over 2 h to a vigorously stirred solution of anhydrous acetonitrile (10 mL). The mixture was stirred at room temperature for 8 h under an Ar atmosphere. The mixture was then treated as described above. Cyclic disulfide **3j** was obtained in 44% yield.

References

1) G. Capozzi and G. Modena, "The Chemistry of the Thiol Group," ed by S. Patai, John Wiley & Sons (1974), Chap. 17.

2) A. L. Fluharty, "The Chemistry of the Thiol Group," ed by S. Patai, John Wiley & Sons (1974), Chap. 13.

3) W. K. Musker, *Acc. Chem. Res.*, **13**, 200 (1980).

4) H. Fujihara, A. Kawada, and N. Furukawa, *J. Org. Chem.*, **52**, 4254 (1987).

5) H. Fujihara, R. Akaishi, and N. Furukawa, *J. Chem. Soc., Chem. Commun.*, **1987**, 930 For the X-ray data of **1**, see: F. Iwasaki, N. Toyoda, R. Akaishi, H. Fujihara, and N. Furukawa, *Bull. Chem. Soc. Jpn.*, **61**, 2563 (1988).

6) H. Fujihara, R. Akaishi, and N. Furukawa, *Chem. Lett.*, **1988**, 709.

7) G. G. Urquhart, J. W. Gates, and R. Connor, *Org. Synth.*, Coll. Vol. III, 363 (1955).

8) R. E. Stutz and R. L. Shriner, *J. Am. Chem. Soc.*, **55**, 1242 (1933).

9) K.-T. Liu and Y.-C. Tong, *Synthesis*, **1978**, 669.

10) E. Santaniello, F. Milani, and R. Casati, *Synthesis*, **1983**, 749.

11) T.-L. Ho, T. W. Hall, and C. M. Wong, *Synthesis*, **1974**, 872.

12) X. Huang and C.-C. Chan, *Synthesis*, **1982**, 1091.

13) W. Mackwald, W. Klemm, and H. Trabert, *Ber.*, **33**, 1559 (1900).

14) A. Lüttringhaus and K. Hägele, *Angew. Chem.*, **67**, 304 (1955).

Formation and Reaction of Oxazoles. Synthesis of *N*-Substituted 2-(Aminomethyl)oxazoles

Toshikazu IBATA* and Yasushi ISOGAMI
Institute of Chemistry, College of General Education, Osaka University, Toyonaka, Osaka 560
(Received August 13, 1988)

Synopsis. The BF_3-catalyzed reaction of substituted α-diazoacetophenones with chloroacetonitrile gave 5-aryl-2-chloromethyloxazoles (**3**) in high yields. Methyl *p*-nitrophenyldiazoacetate also yielded 2-(chloromethyl)-5-methoxy-4-(*p*-nitrophenyl)oxazole. The nucleophilic substitution of **3** with primary, secondary, and tertiary amines afforded the corresponding secondary amines, tertiary amines, and quaternary ammonium salts bearing a 2-oxazolylmethyl group.

The chemistry of oxazoles has strongly been interested in these two decades in connection with the synthesis of biologically active natural products containing oxazole ring system.[1] And also, the oxazoles having an (alkylamino)methyl group or an (dialkylamino)methyl group on C-2 have been paid attention because of their pharmaceutical properties.[2]

The authors have reported the general method of the synthesis of oxazoles through the BF_3-catalyzed reaction of α-diazo carbonyl compounds with nitrile.[3,4] We wish to report here the synthesis of *N*-alkyl-substituted 2-(aminomethyl)oxazole derivatives by the combination of the following two reactions: (i) the BF_3-catalyzed reaction of α-diazo carbonyl compounds with chloroacetonitrile to give 2-(chloromethyl)-oxazoles (**3**), (ii) the nucleophilic substitution reaction of **3** with amines.

Results and Discussion

Synthesis of 2-(Chloromethyl)oxazoles. The BF_3-catalyzed decomposition of substituted α-diazoacetophenones (**1**) in a chloroacetonitrile solution at −5 °C gave BF_3 salts of the corresponding 5-aryl-2-(chloromethyl)oxazoles (**3**) with evolution of nitrogen gas. The free 5-aryl-2-(chloromethyl)oxazoles (**3**) were obtained in high yields after neutralization with sodium hydrogencarbonate (Table 1). Structure of 3 was characterized on the basis of their spectroscopic data: The ^1H NMR signals of CH_2Cl and methine proton of oxazole-C-4 were observed at δ 4.65—4.72 and 7.3—7.5, respectively (Table 1). The yields of **3** are relatively lower than those of reactions of α-diazoacetophenones with acetonitrile.[3] This seems to be attributed to the low electron density on nitrogen atom of chloroacetonitrile.

The reaction of methyl *p*-nitrophenyldiazoacetate with chloroacetonitrile also gave 2-chloromethyl-5-methoxy-4-(*p*-nitrophenyl)oxazole (**3d**; R_1=CH_3O, R_2=*p*-$NO_2C_6H_4$) in moderate yield.

Nucleophilic Substitution Reaction of 2-(Chloromethyl)oxazoles with Amines. The 2-(chloromethyl)-oxazoles (**3**) are expected to have high reactivity toward nucleophilic reagents because they have structures similar to benzyl chloride. The reaction of 2-chloromethyl-5-(*p*-nitrophenyl)oxazole (**3a**: R_1=*p*-$NO_2C_6H_4$, R_2=H) with various primary, secondary, and tertiary amines was studied. The reactions were carried out in a benzene or an alcohol solution at room temperature or 40 °C using five molar equivalents of amines. Primary and secondary amines gave the corresponding secondary and tertiary amines (**4**), having a 2-oxazolylmethyl group in high yields. Aliphatic primary amines gave products **4a**—**4f** in quite high yields even in the case of bulky *t*-butylamine (Table 2). The ^1H NMR signals of CH_2-N group of these products were observed at δ 3.99—4.02.

2-Aminoethanol gave 2-[(2-hydroxyethylamino)-

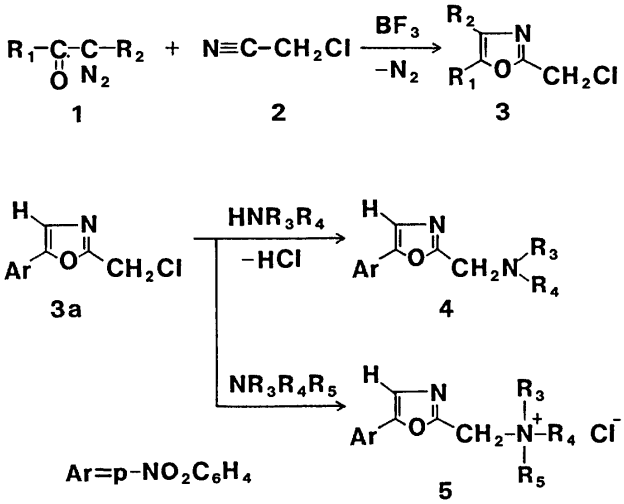

Table 1. Yields, Melting Points, and ^1H NMR Data of **3**

Run	R_1	R_2	Reaction temp/°C	Compd	Yield[a] %	Mp θ_m/°C	^1H NMR/δ CH_2-Cl	^1H NMR/δ C_4-H
a	*p*-$NO_2C_6H_4$	H	−5	**3a**	64	122—3	4.65	7.47
b	*m*-$NO_2C_6H_4$	H	−5	**3b**	64	80—1	4.72	7.49
c	C_6H_5	H	5	**3c**	84	74—5	4.65	7.30
d	CH_3O	*p*-$NO_2C_6H_4$	50	**3d**	45	163—4	4.55	—[b]

a) Yields were based on the diazo carbonyl compounds used. b) A singlet signal of OCH_3 was observed at δ 4.18.

Table 2. Yields, Melting Points, and ^{1}H NMR Data of **4**

Run	Amine	Reaction Cond. Temp/°C	Time/day	Product	Yield[a] %	Mp θ_m/°C	^{1}H NMR/δ[b] CH_2[c]	C_4-H
Reaction with primary amines[d]								
a	CH_3NH_2[e]	r.t.	4	**4a**	87	61—3	4.02	7.55
b	$CH_3CH_2NH_2$[f]	r.t.	2	**4b**	94	67—8	4.02	7.47
c	$CH_3CH_2CH_2NH_2$	r.t.	16	**4c**	96	[g]	4.01	7.48
d	$(CH_3)_2CHNH_2$	r.t.	5	**4d**	97	48—9	4.02	7.49
e	$(CH_3)_3CNH_2$	40	10	**4e**	99	40—2	3.99	7.48
f	CH_2=$CHCH_2NH_2$	r.t.	10	**4f**	95	40—1	4.02	7.47
g	$HOCH_2CH_2NH_2$	40	20	**4g**	95	Oil	4.05	7.48
h	$(CH_3)_2NCH_2CH_2NH_2$	r.t.	3	**4h**	ca. 80[h,i]	[g]	4.02	7.43
Reaction with secondary amines								
i	$(CH_3CH_2)_2NH$	r.t.	9	**4i**	98	Oil	3.92	7.50
j	Pyrrolidine	r.t.	1	**4j**	89	71—2	3.89	7.47
k	Piperidine	r.t.	1.5	**4k**	95	[g]	3.76	7.49
l	Morpholine	r.t.	1.5	**4l**	99	142—3	3.76	7.44
m	Piperazine	r.t.	1.8	**4m**	96	[g]	3.76	7.44
n	*N*-Methylpiperazine	r.t.	3	**4n**	93	116—9	3.79	7.43
o	$HOCH_2CH_2NHCH_3$	r.t.	5	**4o**	95[j]	Oil	3.92	7.51

a) Isolated yields on the basis of oxazoles used. b) Measured in $CDCl_3$. c) Methylene group attached to C_2 of oxazole ring. d) Reaction was carried out in a benzene solution otherwise cited. e) Methanol was used as a solvent. f) Ethanol was used as a solvent. g) Pure compound showing sharp melting point was not obtained. h) Reaction site was primary amine. i) Separation of the reaction product from starting amine was unsuccessful. j) Reaction site was secondary amine.

Table 3. Yields, Melting Points, and ^{1}H NMR Data of **5**

Run	Ar	Amine	Reaction time/day	Compd	Yield[a] %	Mp θ_m/°C	^{1}H NMR/δ[b] CH_2[c]	C_4-H
a	*p*-$NO_2C_6H_4$	$(CH_3CH_2)_3N$	100	**5a**	94	200—1	5.35	7.62
b	*p*-$NO_2C_6H_4$	1,4-Dimethylpiperazine[d]	12	**5b**	97	133—7	5.74	7.58
c	*p*-$NO_2C_6H_4$	DABCO[d]	1	**5c**	91	>300	4.94	8.18[e]

a) Isolated yields on the basis of oxazoles used. b) Measured in $CDCl_3$ unless otherwise noted. c) Methylene group attached to C_2 of oxazole ring. d) A 1 : 1-reaction product was obtained. e) Measured in DMSO-d_6 solution.

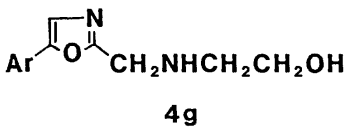

4g

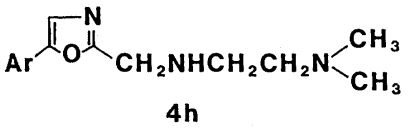

4h

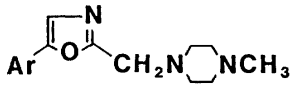

4n

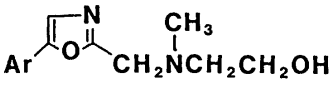

4o

Ar=p-$NO_2C_6H_4$

methyl]-5-(*p*-nitrophenyl)oxazole (**4g**) as a sole product, which was confirmed on the basis of its ^{1}H NMR spectrum. Chemical shift (δ 4.05) of CH_2-N group attached to oxazole ring of **4g** is quite similar to those of reaction products (δ 3.99—4.02) of other primary amines (Table 2). This indicates that the reaction site of 2-aminoethanol is not the hydroxyl group but the amino group as is predicted from the difference in nucleophilicities of amino and hydroxyl groups. Similarly, *N*,*N*-dimethylethylenediamine clarified not to react at the tertiary amine but to react at the primary amine to give secondary amine (**4h**).

Secondary amines also react with **3a** to yield the tertiary amines (**4**) in high yields (Table 2, Runs i—o). Diethylamine is shown to be less reactive than most primary amines listed in Table 2. However, cyclic secondary amines such as pyrrolidine, piperidine, morpholine, and piperazine are indicated to have higher reactivity than the usual primary amines. *N*-Methylpiperazine reacted with **3a** at the site of secondary amine to give tertiary amine (**4n**) which was characterized on the basis of ^{1}H NMR data. The chemical

Table 4. Results of the Elemental Anlysis of **3** and **4**

Compound	Found			Calcd			Molecular formula
	C	H	N	C	H	N	
3a	50.38	3.00	11.68	50.33	2.96	11.74	$C_{10}H_7N_2O_3Cl$
3b	50.45	2.95	11.75	50.33	2.96	11.74	$C_{10}H_7N_2O_3Cl$
3c	62.06	4.25	7.25	62.03	4.16	7.23	$C_{10}H_8NOCl$
3d	49.11	3.45	10.48	49.18	3.38	10.43	$C_{11}H_9N_2O_4Cl$
4d	59.77	5.76	15.88	59.76	5.79	16.08	$C_{13}H_{15}N_3O_3$
4l	57.91	5.18	14.47	58.12	5.28	14.53	$C_{14}H_{15}N_3O_4$

shifts of N-CH_3 of **4n** (δ 2.30) is quite similar to that of the starting *N*-methylpiperazine (δ 2.26), and CH_2 group attached to oxazole-C-2 of **4n** (δ 3.79) shows a signal in the same region as those of other cyclic secondary amines products (δ 3.76—3.89). 2-(Methylamino)ethanol also reacts at the nitrogen atom to give *N*-methyl-*N*-[[5-(*p*-nitrophenyl)-2-oxazolyl]-methyl]-2-hydroxyethylamine (**4o**) in 95% yield.

Tertiary amines such as triethylamine, 1,4-dimethylpiperazine, and 1,4-diazabicyclo[2.2.2]octane (DABCO) gave the corresponding quaternary ammonium chlorides (**5**) in high yields (Table 3). The reaction with triethylamine was very slow at room temperature. Although 1,4-dimethylpiperazine and DABCO have two reaction sites in each molecule, they afforded a 1 : 1-adduct even when half equivalent amount of amine was used.

Experimental

Melting points were measured with Yanagimoto Melting Point Apparatus and described without correction. The IR spectra were recorded on Hitachi Perkin Elmer Infrared Spectrometer model 983 in KBr mull. The ^1H NMR spectra were recorded in $CDCl_3$ solution at 90 MHz on a Varian Spectrometer model EM390 using TMS as an internal standard.

Materials. α-Diazoacetophenones were synthesized by the reaction of the corresponding acid chlorides with excess of diazomethane in the presence of triethylamine according to Newman's method.[5] Methyl *p*-nitrophenyldiazoacetate was synthesized by the diazo group transfer reaction reported by Regitz.[6] Chloroacetonitrile and amines were purified by distillation just before use.

General Procedure of the BF_3-Catalyzed Reaction of Diazo Carbonyl Compounds with Chloroacetonitrile. Diazo carbonyl compound (**1**; 5 mmol) was added in small portions to 20 ml of chloroacetonitrile containing BF_3 etherate (1.0 ml) at −5 °C or 0 °C under magnetic stirring. The reaction proceeded with vigorous evolution of nitrogen gas and gave a gray precipitate. After the N_2 evolution ceased, the reaction mixture was cooled to −15 °C to complete the precipitate formation. The precipitate (BF_3 salt of **3**) was separated by filtration, and was neutralized with saturated aqueous solution of $NaHCO_3$. Free 2-(chloromethyl)oxazole (**3**)[7] was extracted with ether (50 ml) twice. The oxazoles (**3**) were obtained from ether layer, after drying over anhydrous Na_2SO_4, evaporation of solvent. Analitical data of **3** were shown in Table 4.

General Procedure of the Nucleophilic Substitution of 3 with Amines. A benzene or an ethanol solution (only for methylamine and ethylamine) of 2.0 mmol of 2-chloromethyloxazole (**3a**) was treated with 10 mmol of amine at room temperature or 40 °C. The end point of the reaction was determined by the disappearance of the spot of **3a** in TLC. In the case of primary and secondary amine, solvent and excess amine were evaporated, and the residue was purified by recrystallization from benzene-hexane. The reaction products of tertiary amines were separated by filtration from benzene solution, washed with benzene, and recrystallized from dichloromethane.

References

1) J. M. Liesch and K. L. Rinehart, Jr., *J. Am. Chem. Soc.*, **99**, 1645 (1977); D. A. Evans, C. E. Sacks, W. A. Kleschick, and T. R. Taber, *ibid.*, **101**, 6789 (1979); A. I. Meyers and R. A. Amos, *ibid.*, **102**, 870 (1980); B. H. Lipshutz and R. W. Hungate, *J. Org. Chem.*, **46**, 1410 (1981); A. I. Meyers, J. P. Lawson, and D. R. Carver, *ibid.*, **46**, 3119 (1981); Y. Nagao, S. Yamada, and E. Fijita, *Tetrahedron Lett.*, **24**, 2291 (1983); C. Schregenberger and D. Seebach, *Tetrahedron Lett.*, **25**, 5881 (1984); M. J. Kukla and J. M. Fortunato, *J. Org. Chem.*, **49**, 5003 (1984).

2) Many patents have been issued on this subject as shown bellow; S. Inoue, K. Ohata, T. Tsutsui, and T. Nomura, *Jpn. Kokai Tokkyo Koho*, **79**, 30161 (*Chem Abstr.*, **91**, 56988z); **79**, 30162 (**91**, 56986x); **79**, 30163 (**91**, 74592v); **79**, 30164 (**91**, 74593w); **79**, 30165 (**91**, 74594x); **79**, 30166 (**91**, 74597a); **79**, 30169 (**91**, 56987y); **79**, 30170 (**91**, 91632a); **79**, 30186 (**91**, 39464h); **79**, 30191 (**91**, 91633b); **79**, 30192 (**91**, 39463g); etc.

3) T. Ibata and R. Sato, *Chem. Lett.*, **1978**, 1129; *Bull. Chem. Soc. Jpn.*, **52**, 3597 (1979).

4) T. Ibata, T. Yamashita, M. Kashiuchi, S. Nakano, and H. Nakawa, *Bull. Chem. Soc. Jpn.*, **57**, 2450 (1984).

5) M. S. Newman and P. F. Beal III, *J. Am. Chem. Soc.*, **71**, 1506 (1949).

6) M. Regitz, *Chem. Ber.*, **98**, 1210 (1965).

7) 2-Chloromethyloxazoles (**3**) are strongly skin irritating.

Reactivities of Stable Rotamers. XXVI. Some Bimolecular Elimination Reactions of 9-(2-Substituted 1-naphthyl)fluorene Rotamers[1]

Yoriko SONODA, Jiro TSUKAHARA, Nobuo NAKAMURA, and Michinori ŌKI*,†
Department of Chemistry, Faculty of Science, The University of Tokyo, Bunkyo-ku, Tokyo 113
(Received August 15, 1988)

Synopsis. Various elimination reactions which are believed to proceed with E_2-type mechanisms have been examined on 9-[2-(1,2-dibromoethyl)-1-naphthyl]fluorene and 9-[2-(1-hydroxy-2-trimethylsilylethyl)-1-naphthyl]fluorene rotamers. Generally, the reaction of the *sp* rotamers was faster than that of the *ap* by a factor of 2—9. The results are attributed to the steric effects that are operative in the *ap* form.

In the course of comparative study of the reactivities of rotational isomers of 9-arylfluorene series (1), we have noticed that S_N2 type reactions that occur over the fluorene ring (namely in *ap*-**1**) is much slower than the same type of reactions that occur in the other rotamer (*sp*-**1**) which does not suffer from steric hindrance at the reaction site.[2] The same was true for chromium(VI) oxide oxidation of alcohols and an aldehyde[3] due to the fact that the rate-limiting step in these reactions is the formation of bulky transition states.[4] Summarizing these results, we have concluded that a reaction that occurs over the fluorene ring (*ap*) with the space-demanding transition state is much slower than the counterpart (*sp*) in which the formation of the same transition state is less energy-requiring.

In contrast to these findings, addition reactions to a carbon-to-carbon[5] and a carbon-to-oxygen[3] double bonds did not show large differences in reactivities of the rotamers and we have explained the results by assuming that the least space-demanding hydrogen atom in the formyl or the vinyl group directs toward the fluorene ring in the transition states of the reactions.[5]

The transition state of the E_2-type elimination is assumed to be synchronous elongation, with assistance of a nucleophile and an electrophile, of the two bonds which connect the leaving groups to the two carbon frame, as well as the shortening of the carbon-to-carbon bond.[6] Thus the E_2-type eliminations will be candidates of demonstrating of a larger differences in the reactivities of rotamers than a mere addition reaction, because either a nucleophile or an electrophile must approach the group to be eliminated which is located over the fluorene ring in the *ap*-isomer whereas the steric effect will be small in the *sp*-isomer. Thus we have explored some E_2-type elimination reactions of the rotamers of the 9-arylfluorene series and wish to report the results in this paper.

There are varieties of elimination reactions reported in a paper which gives rise to *cis*-stilbene from *dl*-1,2-dibromo-1,2-diphenylethane with high stereospecificity.[7] These reactions may be assumed to proceed with the E_2 reaction mechanisms. We have examined these reactions, namely debromination from *ap*- and *sp*-rotamers (**2**) of 9-[2-(1,2-dibromoethyl)-1-naphthyl]-fluorene and compared the relative rates, k_{sp}/k_{ap}, with that in the reaction of which mechanism is thought to be different. The results are given in Table 1.

Debromination of **2** with zinc dust[8] proceeded smoothly at room temperature but the selectivity was very low as was expected from the behavior in the elimination from *dl*-1,2-dibromo-1,2-diphenylethane. The reaction must proceed via electron transfer from the metal as was discussed in the literature and is different from the bimolecular elimination.[7] Although sodium iodide is often used for debromination from 1,2-dibromoethane derivatives,[9] the reaction did not occur for the compounds in question below 50 °C, the temperature which is low enough to assure nonexistence of internal rotation of the compound.

Among the reagents that eliminate bromine from the dibromide listed in the literature, lithium tetrahydridoaluminate is one of those which give the highest stereoselectivity in the reaction.[7] Indeed, this reagent gave the highest k_{sp}/k_{ap} values of the reagents examined here, as are shown in Table 1. Interestingly, the selectivity was insensitive to the temperature of the reaction.

2 3

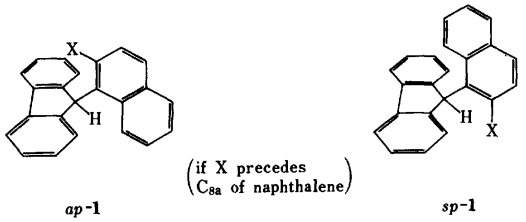

ap-**1** *sp*-**1**

Table 1. The Conditions and the Relative Rates of the Elimination Reactions of **2**

X	Y	Reagent	Temp/°C	k_{sp}/k_{ap}
Br	Br	Zn	Room temp	1.4
Br	Br	$LiAlH_4$	−15	8.6
Br	Br	$LiAlH_4$	0	8.8
Br	Br	$LiAlH_4$	40	8.7
Br	Br	Na_2Te	Room temp	3.1
OH	$Si(CH_3)_3$	H_2SO_4	15	2.6
OH	$Si(CH_3)_3$	H_2SO_4	0	2.5

† Present address: Department of Chemistry, Faculty of Science, Okayama University of Science, Ridaicho, Okayama 700.

Recently, Suzuki and Inouye described that sodium telluride gave the high stereospecificity in the elimination reactions of 1,2-dibromides.[10] Examination of this reagent with our rotamers revealed that, though the elimination in the *sp*-dibromo compound (**2**: X=Y=Br) was indeed faster than in the *ap*, the selectivity was not so high as that observed with the tetrahydridoaluminate reagent.

Another example of stereospecific elimination is Peterson reactions,[11] of which stereoselectivity was studied by Hudrlik and Peterson.[12] It is known that, if acid is used for the elimination from β-hydroxyalkylsilanes, the elimination takes place in the trans-fashion and, if the base is used, the reaction is cis-elimination. Since the compounds we examine, 9-arylfluorenes, carry acidic hydrogen at the 9-position, the strong base can cause isomerization.[2,3] We therefore concentrated our effort to the acidic trans-elimination, which should be compared with the debromination described in this paper. The results in Table **1** indicate that the Peterson reaction is modestly selective.

Summarizing the results, we notice that the steric effects in the *ap*-form of the 9-arylfluorene series are operative in various elimination reactions, relative to the *sp*-series. The results will mean that a nucleophile or an electrophile, which is larger than a hydrogen atom, must approach a leaving group at the α-position of the substituent of the naphthalene ring, which is over the fluorene ring, to make the reaction of the *ap*-form slower than that of the *sp*. The enhancement of the selectivity, though small, relative to the addition to the olefinic bond,[5] should be attributed to the fact that the nucleophile or the electrophile is larger than the hydrogen atom which is the main cause of steric interaction with the fluorene moiety in the case of addition reactions in the olefin and the aldehyde. Yet, the selectivity in the elimination reactions studied here is inferior to that of the S_N2 type reactions. We believe this is due to the fact that, while in the S_N2 reactions two bulky groups, a leaving group and a incoming group, approach the α-position of the substituent over the fluorene ring in the *ap* form, there is only one bulky group, the nucleophile or the electrophile, approaching the α-position of the substituent over the fluorene ring in the case of E_2-type reactions. Thus the steric effects in the E_2-reactions are less demanding than the S_N2 reactions.

Experimental

9-[2-(1,2-Dibromoethyl)-1-naphthyl]fluorene rotamers (**2**: X=Y=Br) were prepared according to the method described in the literature.[5]

9-[2-(1-Hydroxy-2-trimethylsilylethyl)-1-naphthyl]fluorene (2: X=OH, Y=Si(CH$_3$)$_3$). To a solution of 100.0 mg (0.313 mmol) of *ap*-9-(2-formyl-1-naphthyl)fluorene[3] in 10.0 mL of ether, was added 0.34 mL (0.34 mmol) of 1.0 mol L^{-1} solution of trimethylsilylmagnesium chloride in ether which was available from Aldrich Chemical Co. under a nitrogen atmosphere at once. The mixture was stirred for 80 min with vigorous refluxing and then decomposed with aqueous ammomium chloride. The ether layer was washed with aqueous sodium hydrogencarbonate and dried over magnesium sulfate. After evaporation of the solvent, the product was purified by preparative TLC on silica gel with a 5:7 hexane-dichloromethane eluent and then recrystallized from hexane to give the *ap* form of the desired product in 74% yield. The amount of the magnesium compound was crucial in obtaining the product in a good yield because the excess caused contamination with unidentified materials and the less caused recovery of the unreacted aldehyde. It was recrystallized from acetonitrile, mp 120.0—121.0 °C. Found: C, 81.87; H, 6.94%. Calcd for $C_{28}H_{28}OSi$: C, 82.30; H, 6.91%. ^{1}H NMR ($CDCl_3$) δ=−0.40 (9H, s), −0.05 (1H, app d, *J*=14.7 Hz), 0.76—0.91 (2H, m), 3.80 (1H, app d, *J*=11.5 Hz), 6.13 (1H, s), 7.14—7.95 (13H, m), 8.49—8.53 (1H, m).

The *sp*-form, mp 110.0—111.0 °C, was obtained much more easily than the *ap*-form: the usage of 1.0 mol of trimethylsilylmethylmsgnesium chloride per 1 mol of the aldehyde sufficed to give 93% yield of the product. It was recrystallized from methanol. Found: C, 82.29; H, 6.85%. Calcd for $C_{28}H_{28}OSi$: C, 82.30; H, 6.91%. ^{1}H NMR ($CDCl_3$) δ=0.08 (9H, s), 1.40—1.60 (2H, m), 1.97 (1H, br d, *J*=2.9 Hz), 5.70—5.80 (1H, m), 5.97 (1H, s), 6.38—8.00 (14H, m).

Elimination Reactions. Elimination reactions of **2** were carried out under the same conditions described for the competitive reactions below except that a single rotational isomer was submitted to the reaction conditions. It was confirmed that *ap*- or *sp*-9-(2-vinyl-1-naphthyl)fluorene (**3**)[5] was the exclusive product, the yield being over 95% in every case.

Competitive Debrominations. a) Debromination with Zinc. To a solution of 10.0 mg each of *sp*- and *ap*-**2** (X=Y=Br) in 30 mL of ether were added 3.0 mL of acetic acid and 30 mg of zinc dust and the whole was stirred for ca. 10 min at room temperature. The solid material was removed by filtration and the filtrate was washed with water and then with aqueous sodium hydrogencarbonate. After drying over magnesium sulfate, the solvent was evaporated and the residue was submitted to analysis.

b) Debromination with Lithium Tetrahydridoaluminate. To a solution of 10.0 mg each of *sp*- and *ap*-**2** (X=Y=Br) in 50 mL of tetrahydrofuran was added the specified amount of lithium tetrahydridoaluminate and the mixture was allowed to react for the time interval shown below. The reaction was quenched by cooling the mixture at −78 °C, water was added to the mixture at this temperature, and the temperature was allowed to rise to 0 °C. It was confirmed that the reaction was negligibly slow at −78 °C. Then dilute hydrochloric acid was added to the mixture which was extracted with ether. The ether extract was treated as above. The reaction temperature, the amount of the lithium tetrahydridoaluminate used, and the reaction period are given below.

Temperature/°C	Amount of $LiAlH_4$/mg	Period/min
ca. −15	30	30
0	25	30
40	20	4

c) Debromination with Telluride. A sodium telluride solution was prepared in the following way.[9,13] Tellurium (18 mg or 0.14 mmol) and 240 mg (1.56 mmol) of sodium hydroxymethanesulfinate dihydrate were added to 2 mL of 1 mol L^{-1} aqueous sodium hydroxide and 5 mL of dioxane and the mixture was stirred for ca. 10 min at 70 °C to give a dark red to purple solution. To this solution was added a solution of 10.0 mg each of *ap*- and *sp*-**2** (X=Y=Br) in 3.0 mL of dioxane and the mixture was stirred for 5—6 min at room temperature under a nitrogen atmosphere. The reaction was quenched by introducing air or adding water and ether to the reaction mixture. The formed tellurium was removed by decantation and the product was extracted with ether. The product was treated similarly as above.

Since debromination from 1,2-dibromoethane derivatives with a sulfinate was reported,[14] the dibromide was treated

with a sodium hydroxymethanesulfinate solution under the same conditions. However, no sign of formation of the olefin was detected.

Competitive Peterson Reaction. To a solution of 10.0 mg each of *sp*- and *ap*-rotamer of **2** (X=OH, Y=$Si(CH_3)_3$) in 30 mL of tetrahydrofuran was added 4 drops of concentrated sulfuric acid and the mixture was stirred for 15 min at 15 °C or for 30 min at 0 °C. The reaction was quenched by adding aqueous sodium hydrogencarbonate. The treatment of the mixture hereafter was the same with that described above.

Acquisition and Treatment of Data in Competitive Reactions. The reactions were quenched at less than 50% completion of the reaction, if both the isomers were counted, and the unreacted compounds were analyzed by ^1H NMR with the use of a JEOL GX270 NMR spectrometer. The relative rates (k_{rel}) were obtained by the following equation. The results shown in Table 1 are the averages of two to three runs.

$$k_{rel} = \frac{k_{ap}}{k_{sp}} = \frac{[\ln(a_0 - a)/a_0]_{sp}}{[\ln(a_0 - a)/a_0]_{ap}}$$

References

1) For Part XXV, see K. Moriyama, M. Nakamura, N. Nakamura, and M. Ōki, *Bull. Chem. Soc. Jpn.*, **62**, 485 (1989).

2) S. Murata, S. Kanno, Y. Tanabe, M. Nakamura, and M. Ōki, *Angew. Chem., Int. Ed. Engl.*, **20**, 606 (1981); *Bull. Chem. Soc. Jpn.*, **57**, 525 (1984).

3) M. Ōki and R. Saito, *Chem. Lett.*, **1981**, 649: R. Saito and M. Ōki, *Bull. Chem. Soc. Jpn.*, **55**, 3267 (1982).

4) K. B. Wiberg, "Oxidation by Chromic Acid and Chromyl Compounds," in "Oxidation in Organic Chemistry," Part A ed by K. B. Wiberg, Academic Press, New York (1965), pp. 142—178.

5) M. Ōki, J. Tsukahara, Y. Sonoda, K. Moriyama, and N. Nakamura, *Bull. Chem. Soc. Jpn.*, **61**, 4303 (1988).

6) R. A. Y. Jones, "Physical and Mechanistic Organic Chemistry," 2nd ed, Cambridge University Press, Cambridge (1984), pp. 175—195.

7) I. M. Mathai, K. Schug, and S. I. Miller, *J. Org. Chem.*, **35**, 1733 (1970).

8) W. M. Schubert, B. S. Rabinovitch, N. R. Larson, and V. A. Sims, *J. Am. Chem. Soc.*, **74**, 4590 (1952).

9) W. H. Perkin, *J. Chem. Soc.*, **24**, 37 (1871).

10) H. Suzuki and M. Inouye, *Chem. Lett.*, **1985**, 225.

11) D. J. Peterson, *J. Org. Chem.*, **33**, 780 (1968).

12) P. F. Hudrlik and D. Peterson, *J. Am. Chem. Soc.*, **97**, 1464 (1975).

13) L. Tschugaeff and W. Chlopin, *Ber.*, **47**, 1269 (1914).

14) R. Otto, *J. Prakt. Chem.*, **53**, 1 (1896): R. Otto and F. Stoffel, *Ber.*, **30**, 1799 (1897).

A Total Synthesis of (−)-Sacculatal

Hisahiro HAGIWARA* and Hisashi UDA
Chemical Research Institute of Non-aqueous Solutions, Tohoku University, Katahira, Sendai 980
(Received August 20, 1987)

Synopsis. The total synthesis of a tumor promoter, (−)-sacculatal (**1**), has been completed.

According to the recent study in chemical carcinogenesis, there are two successive stages, initiation and promotion, that are induced by chemical substances, initiater and promoter, respectively. Among them, control of the latter stage is much more important to prevent cancer because of its reversibility. (−)-Sacculatal (**1**), a diterpene dialdehyde isolated from the liverworts *Trichocoleopsis sacculata* and *Pellia endiviifolia* by Asakawa and his co-workers, was at first known as a constituent of pungent taste of liverworts.[1a] Later on, in connection with skin irritant property of these plants, (−)-sacculatal (**1**) was found to have tumor promoting activity by testing ornithine decarboxylase (ODC) activity, which was estimated as 1/100 active as 12-*O*-tetradecanoylphorbol 13-acetate.[1b] As a part of our program directed toward total syntheses of biologically active sacculatane type natural products,[3] we disclose herein our synthesis of natural (−)-sacculatal (**1**) starting from (4a*S*,5*S*,8a*S*)-(−)-5β,8aβ-dimethyl-5α-(4-methyl-3-pentenyl)-3,4,4a,-5,6,7,8,8a-octahydro-1(2*H*)-naphthalenone (**3**), an advanced common intermediate for sacculatane synthesis.[3b]

Results and Discussion

The (−)-ketone **3** {[α]$_D$ −8.2° (*c* 3.0 in MeOH); 80% enantiomeric excess} was formylated with ethyl formate in the presence of sodium hydride in benzene to give the keto aldehyde **4**, which was oxidized with 2,3-dichloro-5,6-dicyano-1,4-benzoquinone (DDQ) in dioxane to introduce an unsaturation furnishing the enone **5**. The formyl carbonyl group was selectively protected as an ethylene acetal to afford the acetal **6**. Although two intermediary aldehydes, **4** and **5**, were used without purification because of their instability, the overall yield of **6** from the ketone **3** was 69%. Finally, a protocol of Magnus[4] was employed in order to introduce a formyl group at the electronically less reactive and sterically congested C-1 position. Addition of methoxy(trimethylsilyl)methyllithium afforded in almost quantitatively the fragile single adduct **7** whose stereochemistry has not yet been determined. After extensive efforts to eliminate trimethylsilanol,

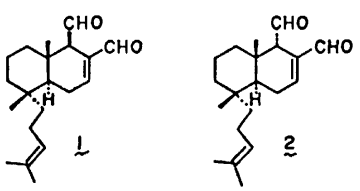

Fig. 1.

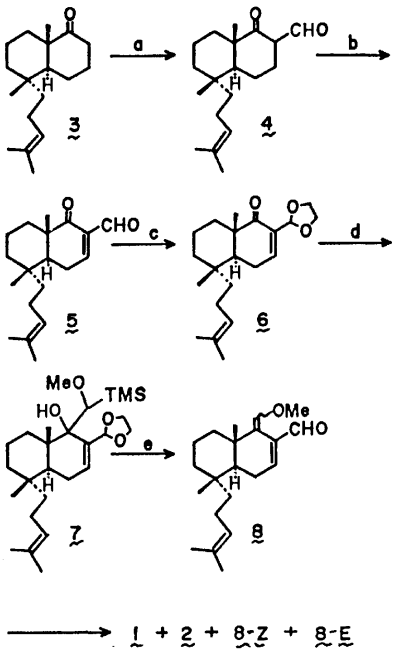

Scheme 1. Total synthesis of (−)-sacculatal (**1**). (a): HCO_2Et, NaH, benzene, (b): DDQ, dioxane, (c): Ethylene glycol, cat. *p*-TsOH, benzene, (d): $TMSCH_2OMe$, *s*-BuLi, THF, (e): Et_2O saturated with 46% aqueous HF.

treatment of the adduct **7** in ether saturated with 46% hydrogen fluoride[5] underwent facile deprotection of acetal and subsequent elimination of trimethylsilanol followed by slow hydrolysis of the resulting enol ethers **8** to afford (−)-sacculatal (**1**) (26%), isosacculatal (**2**) (16%), and the precursory enol ethers **8-Z** and **8-E** (20%). Attempts to eliminate trimethylsilanol with KH simply gave decomposition products. Isomerization of sacculatal (**1**) to isosacculatal (**2**) was unavoidable because of A$^{(1,2)}$ strain of formyl group at C-1β in addition to peri repulsion between proton at C-8β. The product which exhibited a singlet proton at δ 7.36 in ^{1}H NMR spectrum was assigned to be the (*E*)-enol ether **8-E**. The spectral data of synthetic (−)-sacculatal (**1**) (^{1}H NMR and IR), as well as the optical rotation and mp values {[α]$_D$ −30° (*c* 0.48, $CHCl_3$) (lit,[1a] [α]$_D$ −31.4° (*c* 3.5, $CHCl_3$)}; mp 65—66 °C (lit,[1a] mp 65—66 °C)], are identical with those of the natural sample.

In summary, we have completed the total synthesis of a tumor promoter, (−)-sacculatal (**1**).

Experimental

General. Melting point is uncorrected. Anhydrous solvents were distilled from sodium (benzene) or lithium aluminum hydride (tetrahydrofuran). All infrared spectra were obtained with a JASCO A-3 spectrophotometer for solutions

in carbon tetrachloride. ^{1}H NMR spectra were recorded with a JEOL PMX-60 SI (60 MHz) or FX-90Q (90 MHz) instrument. Chemical shifts were reported δ values relative to tetramethylsilane. Mass spectra were obtained with a JEOL JMS DX-300 mass spectrometer at 70 eV and relative intensities were reported. Optical rotations were recorded on a JASCO DIP-4S polarimeter for solutions in chloroform unless otherwise specified. Preparative medium-pressure liquid chromatographies (MPLC) were carried out on a JASCO PRC-50 system.

(4a*S*,5*S*,8a*S*)-(+)-5β,8aβ-Dimethyl-2-formyl-5α-(4-methyl-3-pentenyl)-3,4,4aα,5,6,7,8,8a-octahydro-1(2*H*)-naphthalenone (4). To a stirred slurry of sodium hydride (60%, 54 mg, 1.35 mmol) in anhydrous benzene (1 mL) were added a solution of the ketone **3** (51.8 mg, 0.198 mmol) in benzene (2 mL) and then ethyl formate (80 μL, 0.99 mmol). After stirring at room temperature for overnight under nitrogen, the resulting solution was poured into dil. HCl, and extracted with ether (30 mL×2). The combined extracts were washed with water and brine and dried. Evaporation of the solvents afforded the keto aldehyde **4** (67.4 mg), which was used soon for the next reaction without purification. The sample purified by MPLC exhibited $[\alpha]_D$ +22.3° (*c* 0.546, methanol); IR ν 1700, 1640, 1590, 1455 cm^{-1}; ^{1}H NMR (60 MHz) δ=0.88 (s, 3H), 1.23 (s, 3H), 1.6 (s, 3H), 1.7 (s, 3H), 1.0—2.5 (m, 16H), 5.09 (br t, 1H), 8.43 (d, *J*=4 Hz, 1H); MS *m/z* 290 (M^+, 9), 138 (19), 58 (41), 43 (100); Calcd for $C_{19}H_{30}O_2$: M, 290.22449. Found: *m/z* 290.22419.

(4a*S*,5*S*,8a*S*)-(+)-5β,8aβ-Dimethyl-2-formyl-5α-(4-methyl-3-pentenyl)-4a,5,6,7,8,8a-hexahydro-1(4*H*)-naphthalenone (5). To a solution of the crude keto aldehyde **4** (67.4 mg) in dioxane (3 mL) was added DDQ (freshly recrystallized from dichloromethane, 134 mg, 0.59 mmol) in one portion. The resulting solution was stirred for 1 h, and extracted with ether (30 mL×2). The combined organic layer was washed with water and brine. After evaporation of the solvents, the residue was passed through silica-gel short column with the aid of hexane/ethyl acetate. Evaporation of the solvents gave the enone **5** (162 mg), which was used without purification for the next reaction. The pure enone **5** after MPLC purification exhibited $[\alpha]_D$ +75.5° (*c* 0.249); IR ν 1705, 1680, 1620, 1450, 1380 cm^{-1}; ^{1}H NMR (90 MHz) δ=1.02 (s, 3H), 1.12 (s, 3H), 1.57 (s, 3H), 1.68 (s, 3H), 1.0—2.5 (m, 13H), 5.0 (br t, 1H), 7.92 (m, 1H), 10.0 (s, 1H); MS *m/z* 288 (M^+, 12), 273 (29), 245 (31), 189 (17), 175 (18), 162 (19), 150 (23), 137 (22), 109 (37), 69 (52), 58 (74), 43 (100); Calcd for $C_{19}H_{28}O_2$: M, 288.20891. Found: *m/z* 288.20891.

(4a*S*,5*S*,8a*S*)-(−)-5β,8aβ-Dimethyl-2-(1,3-dioxolan-2-yl)-5α-(4-methyl-3-pentenyl)-4aα,5,6,7,8,8a-hexahydro-1(4*H*)-naphthalenone (6). A solution of the crude enone **5** (162 mg) in anhydrous benzene (5 mL) in the presence of ethylene glycol (0.3 mL) and a catalytic amount of *p*-toluenesulfonic acid was refluxed for 30 min using a Dean-Stark water separator. After cooling to room temperature, the resulting solution was poured into aqueous $NaHCO_3$, and the product was extracted with ether (30 mL×2). Evaporation of the solvent followed by MPLC separation (silica gel, 4:1 hexane/ethyl acetate) afforded the enone acetal **6** (45 mg, 69% in overall 3 steps), which exhibited $[\alpha]_D$ −4.76° (*c* 0.315); IR ν 1680, 1620 cm^{-1}; ^{1}H NMR (60 MHz) δ=1.0 (s, 3H), 1.1 (s, 3H), 1.6 (s, 3H), 1.68 (s, 3H), 1.0—2.5 (m, 13H), 3.98 (br s, 4H), 5.02 (br t, 1H), 5.57 (s, 1H), 7.1 (t, *J*=4 Hz, 1H); MS *m/z* 332 (M^+, 64), 317 (56), 243 (33), 203 (30), 180 (37), 154 (37), 109 (68), 73 (100), 69 (70), 55 (34), 45 (45), 41 (66); Calcd for $C_{21}H_{32}O_3$: M, 332.23502. Found: *m/z* 332.23442.

(4a*S*,5*S*,8a*S*)-5β,8aβ-Dimethyl-2-(1,3-dioxolan-2-yl)-1-[methoxy(trimethylsilyl)methyl]-1,4,4aα,5,6,7,8,8a-octahydro-1-naphthalenol (7). To a stirred solution of methoxytrimethylsilylmethane (106 μL, 0.68 mmol) in anhydrous THF (1 mL) was added a hexane solution of *s*-BuLi (1.02 M†, 0.66 mL, 0.67 mmol) at −65 °C under nitrogen. After stirring for 30 min at −30 to −25 °C, a solution of the enone acetal **6** (45 mg, 0.136 mmol) in anhydrous THF (4 mL) was added. The resulting solution was stirred at −25 to 0 °C for 30 min and then at 0 °C for further 30 min. The reaction was quenched by addition of aqueous NH_4Cl and the product was extracted with ether (30 mL×2). Evaporation of the solvent left the trimethylsilyl alcohol **7**, an oil (77 mg), which was used without purification. IR ν 3500, 1385, 1250 cm^{-1}; ^{1}H NMR (60 MHz) δ=0.12 (s, 9H), 0.92 (s, 6H), 1.6 (s, 3H), 1.68 (s, 3H), 1.0—2.5 (m, 14H), 3.35 (s, 3H), 3.4 (s, 1H), 3.95 (m, 4H), 5.05 (br t, 1H), 5.37 (s, 1H), 6.67 (t, *J*=3 Hz, 1H).

(1*R*,4a*S*,5*S*,8a*R*)-(−)-5β,8aβ-Dimethyl-1β,2-diformyl-5α-(4-methyl-3-pentenyl)-1,4,4aα,5,6,7,8,8a-octahydronaphthalene [(−)-Sacculatal] (1), (1*S*,4a*S*,5*S*,8a*S*)-5β,8aβ-Dimethyl-1α,2-diformyl-5α-(4-methyl-3-pentenyl)-1,4,4aα,5,6,7,8,8a-octahydronaphthalene (Isosacculatal) (2), (4a*S*,5*S*,8a*S*)-5β,8aβ-Dimethyl-2-formyl-1*Z*-methoxymethylene-5α-(4-methyl-3-pentenyl)-1,4,4aα,5,6,7,8,8a-octahydronaphthalene (8-Z), and (4a*S*,5*S*,8a*S*)-5β,8aβ-Dimethyl-2-formyl-1*E*-methoxymethylene-5α-(4-methyl-3-pentenyl)-1,4,4aα,5,6,7,8,8a-octahydronaphthalene (8-E). A solution of the crude trimethylsilyl alcohol **7** (77 mg) in ether saturated with 46% aqueous hydrogen fluoride (5 mL) was stirred at room temperature for 6 h. The resulting solution was poured into cold aqueous $NaHCO_3$ and extracted with ether (30 mL×2). Evaporation of the solvent followed by MPLC separation of the residue (silica gel, 1:4 hexane/ethyl acetate) afforded (−)-sacculatal (**1**) (2.7 mg, 26.3%), isosacculatal (**2**) (1.6 mg, 15.6%) and a mixture of the enol ethers (**8-Z**) and (**8-E**) (2.1 mg, 19.6%) which were separated by repeated MPLC. (−)-Sacculatal (**1**) which crystallized spontaneously at −20 °C, exhibited mp 65—66 °C (lit,[1] mp 65—66 °C); $[\alpha]_D$ −30.1° (*c* 0.478) (lit,[1] −31.4°, *c* 3.5); IR ν 2700, 1725, 1685, 1640, 1385, 1240 cm^{-1}; ^{1}H NMR (90 MHz) δ=0.96 (s, 3H), 0.98 (s, 3H), 1.59 (s, 3H) 1.67 (s, 3H), 2.41 (m, 2H), 2.84 (br s, 1H), 1.0—2.0 (m, 11H), 5.05 (t, *J*=5 Hz, 1H), 7.11 (m, 1H), 9.46 (s, 1H), 9.49 (d, *J*=4.4 Hz, 1H); MS *m/z* 302 (M^+, 3), 274 (50), 259 (91), 231 (49), 121 (53), 91 (47), 69 (100), 55 (55), 41 (99); Calcd for $C_{20}H_{30}O_2$: M, 302.22453. Found: *m/z* 302.22263. Isosacculatal (**2**) exhibited IR ν 2700, 1685, 1650, 1450, 1380 cm^{-1}; ^{1}H NMR (90 MHz) δ=0.93 (s, 3H), 0.99 (s, 3H), 1.59 (s, 3H), 1.67 (s, 3H), 1.0—2.5 (m, 13H), 3.28 (br s, 1H), 5.04 (br t, 1H), 7.1 (m, 1H), 9.41 (s, 1H), 9.85 (d, *J*=2.6 Hz, 1H); MS *m/z* 302 (M^+, 18), 259 (34), 201 (38), 105 (47), 74 (64), 69 (70), 59 (100), 55 (51), 45 (58), 43 (54), 41 (94); Calcd for $C_{20}H_{30}O_2$: M, 302.22463. Found: *m/z* 302.22513. The enol ether (**8-Z**) exhibited IR ν 1700, 1640, 1605, 1220, 1130 cm^{-1}; ^{1}H NMR (90 MHz) δ=0.91 (s, 3H), 0.99 (s, 3H), 1.57 (s, 3H), 1.66 (s, 3H), 1.0—2.5 (m, 13H), 3.59 (s, 3H), 5.03 (br t, *J*=3.6 Hz, 1H), 5.97 (s, 1H), 6.53 (t, *J*=4 Hz, 1H), 9.65 (s, 1H); MS *m/z* 316 (M^+, 61), 302 (22), 301 (100), 199 (22), 163 (27), 145 (21), 119 (22), 109 (25), 105 (28), 91 (29), 81 (24), 69 (86), 55 (39), 41 (66); Calcd for $C_{21}H_{32}O_2$: M, 316.24013. Found *m/z* 316.24013. The enol ether (**8-E**) exhibited IR ν 2720, 1695, 1630, 1610, 1250, 1140 cm^{-1}; ^{1}H NMR (90 MHz) δ=0.91 (s, 3H), 1.05 (s, 3H), 1.59 (s, 3H), 1.67 (s, 3H), 1.0—2.5 (m, 13H), 3.64 (S, 3H), 5.06 (br t, *J*=3.6 Hz, 1H), 6.53 (m, 1H), 7.36 (s, 1H), 9.38 (s, 1H); mass spectrum *m/z* 316 (M^+, 52), 301 (82), 199 (22), 163 (23), 149 (54), 145 (21), 119 (23), 109 (32), 95 (27), 91 (34), 83 (22), 81 (26), 70 (23), 69 (100), 67 (21), 58 (54), 57 (35), 56 (21), 55 (56); Calcd for $C_{21}H_{32}O_2$: M, 316.24012. Found: *m/z* 316.24002.

We thank Professor Yoshinori Asakawa, Toku-

† 1 M=1 mol dm^{-3}.

shima Bunri University, for providing the spectral data of **1**.

References

1) a) Y. Asakawa, T. Takemoto, M. Toyota, and T. Aratani, *Tetrahedron Lett.*, **1977**, 1407; b) Y. Asakawa, *Latinoamer. Quim.*, **14**, 109, (1984); *idem*, *Farumashia*, **23**, 455 (1987).

2) S. Nakatsuka, T. Masuda, and T. Goto, *Tetrahedron Lett.*, **27**, 6245 (1986); **28**, 3671 (1987).

3) a) H. Hagiwara and H. Uda, *J. Chem. Soc., Chem. Commun.*, **1987**, 1333; b) **1988**, 815.

4) P. Magnus and G. Roy, *Organometallics*, **1**, 553 (1982).

5) C. R. Johnson and B. D. Tait, *J. Org. Chem.*, **52**, 281 (1987).

A Facile Reductive Removal of Bromine Atom(s) of 6,6-Dibromo- and 6-Bromopenicillanate Derivatives in a Pb/Al Bimetal System

Hideo TANAKA, Motoaki TANAKA, Akira NAKAI, Yasumi KATAYAMA, and Sigeru TORII*
Department of Applied Chemistry, Faculty of Engineering, Okayama University, Tushima-naka, Okayama 700
(Received September 1, 1988)

Synopsis. Reductive removal of the bromine atom(s) of 6,6-dibromo- and 6-bromopenicillanate 1-oxides has been performed successfully on treatment with aluminum metal in the presence of a catalytic amount of lead(II) bromide in methanol containing 1% aqueous hydrobromic acid. In a similar manner, 6,6-dibromopenicillanates and their 1,1-dioxides can be converted to the corresponding debromination products, respectively.

Since the discovery of the β-lactamase inhibitory properties of penicillanic acid 1,1-dioxide (sulbactam) **1a**,[1] its homologues, bearing the proper substituents at the β-C(2)-methyl group, have received much attention as potential β-lactamase inhibitors. Namely, the chloro, triazolyl, and tetrazolylthio substituted derivatives **1b** (BRL-2013),[2] **1c** (YTR-830),[3] and **1d**[4] have been proven to exhibit potent β-lactamase inhibitory activities. The syntheses of the penicillanic acid 1,1-dioxides **1** have been performed by the transformation of commercially accessible 6-aminopenicillanic acid (**2**). An inevitable task in the transformation (**2**→**1**) is the removal of the C(6)-amino moiety of **2**. The procedures available for this purpose have generally relied on the catalytic hydrogenation of 6-bromo- or 6,6-dibromopenicillanic acid derivatives **3**—**6**,[1c,5,6] derived from 6-aminopenicillanic acid **2**. Reductive debromination reactions with tributyltin hydride[7] or zinc[8] have also been utilized. However, most of these procedures suffer from one or more drawbacks: unsatisfactory yields of the hydrogenation products **7**—**10**, instability of protecting groups of C(3)-carboxylic acid (e.g., benzhydryl and allyl) under hydrogenolysis conditions and difficulty in removing the metal complexes generated in the zinc and tributyltin hydride reductions. Consequently, continuing efforts have been made to look for a new method for the reductive removal of the C(6)-bromine atom(s).

We have recently developed a new Pb/Al bimetal system, involving aluminum and a catalytic amount of lead salts, which acts as a powerful reductant for various synthetic purposes.[9] A new application of the Pb/Al bimetal system for the reductive debromination of the 6-bromo- and 6,6-dibromopenicillanates **3**—**6**, providing a simple and efficient route to the corresponding hydrogenation products **7**—**10**, respectively (Scheme 1), is described herein.

Reduction of 6,6-dibromopenicillanate 1-oxide **3a** (X^1=X^2=Br, Y=H, R=PMB) with aluminum and a catalytic amount of lead(II) bromide (0.1 equiv) was carried out at 30 °C in various media. Some of the examples are shown in Table 1. In aqueous media (Entries 3 and 4), the reduction of **3a** was completed in 1—2 h to afford 60—86% yields of the hydrogenation product **7a**, while in nonaqueous media, e.g., methanol and acetone, (Entries 1 and 2), only less than 24% yield of **7a** was obtained. Notably, addition of a small amount of 1% hydrobromic acid facilitates the hydrogenation of **3a**, affording up to 92% yield of **7a** (Entries 5—7). The reduction (**3a**—**7a**) can similarly be performed in a mixed solvent, e.g., MeOH/THF/aq HBr and MeOH/CH_2Cl_2/aq HBr (Entries 8 and 9).

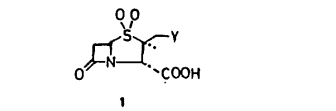

1

	Y		Reference
a	H	Sulbactam	1
b	Cl	BL-P 2013	2
c		YTR 830	3
d			4

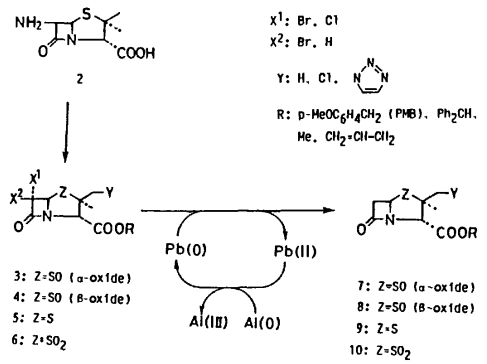

Scheme 1.

Table 1. Reduction of 6,6-Dibromopenicillanate 1α-Oxide **3a** with $PbBr_2$/Al[a]

Entry	Condition	Time / h	Yield of **7a**[b] / %
1	MeOH	3	23
2	Acetone	8	—(98)[c]
3	Acetone/H_2O(9/1)	1	60
4	MeOH/H_2O(9/1)	2	86
5	MeOH/aq 1% HBr(9/1)	2	92
6	MeOH/aq 1M NH_4Cl(9/1)	3	82
7	MeOH/aq 1M AcOH(9/1)	2	85
8	MeOH/CH_2Cl_2/aq 1% HBr (4/5/1)	3	95
9	MeOH/THF/aq 1% HBr(9/5/1)	3	87

a) Carried out with $PbBr_2$ (0.1 equiv) and Al(2.2 equiv) at 30°C. b) Isolated Yield. c) Recovered **3a**.

The presence of lead(II) bromide is essential for this purpose, since, in the absence of lead(II) bromide, most of the starting material **3a** is recovered intact (Table 2, Entry 2). This fact can be well understood by assuming that lead(0) generated by two-electron reduction of lead(II) on the aluminum surface[9] acts as a reductant in the reductive removal of the bromine atoms and thus generated lead(II) is again submitted to reduction with aluminum (Scheme 1). Satisfactory results were also obtained by use of lead(II) chloride or lead powder in combination with aluminum (Entries 3 and 4), while bismuth(III) chloride is less effective (Entry 5) and tin(II) bromide, titanium(IV) chloride, manganese(III) chloride, and chromium(III) chloride are not effective at all (Entries 6—9).

The Pb/Al bimetal system was successfully applied to the reduction of various halopenicillanate derivatives **3—6**. The conditions and results are summarized in Table 3. The reductive removal of bromine atoms of 6,6-dibromopenicillanate 1α-oxides **3** was performed in a methanolic mixed-solvent containing aqueous 1% hydrobromic acid to afford the penicillanate 1α-oxides **7** in 77—93% yields (Entries 1—3). Similarly, 6α-bromopenicillanate 1β-oxides **4**, 6,6-dibromopenicillanate **5**, and 6,6-dibromopenicillanate 1,1-dioxides **6** underwent the reductive debromination affording the hydrogenation products **8**, **9**, and **10**, respectively (Entries 4, 5, 7—12), in which, the substituents on the 2β-methyl group, e.g., chlorine and 1,2,3-triazolyl moiety, were retained intact. However, 6α-chloropenicillanate 1-oxide (**4c**) gave no appreciable amount of hydrogenation product **8c** (Entry 6).

The proper choice of the solvent for each compound **4—6** is significant. For example, when 6,6-dibromopenicillanate (**5a**) was treated with the aluminum and lead(II) bromide combination in methanol and aqueous 1% hydrobromic acid (9/1), the reaction was quite slow and, even after 15 h, afforded only 52% yield of penicillanate **9a** along with monobromo derivatives **5** (X^1=H; X^2=Br; and X^1=Br; X^2=H, 24%) (Entry 8). In contrast, when a small amount of acetone was added to this medium, the reaction was significantly accelerated and completed in 5 h to give **9** in 72% (Entry 7).

Another interesting observation is that the *p*-methoxybenzyl (PMB), benzhydryl, methyl, and allyl esters of 6-bromo- and 6,6-dibromopenicillanates **3—6** are successfully reduced to the corresponding penicillanates **7—10** without affecting the ester moieties, while the *p*-nitrobenzyl ester **6e** is completely resistant to the reductive debromination (Entry 13). The latter failure is probably ascribable to the fact that the nitrobenzyl moiety is susceptible to reduction to form a stable anion radical.[8b,c]

Table 2. Reduction of 6,6-Dibromopenicillanate 1α-Oxide **3a** with MX_n/Al[a]

Entry	Mx_n	Time	Yield/%[b]	
		h	**7a**	**3a**[c]
1	$PbBr_2$	3	92	—
2	None	4	—	98
3	$PbCl_2$[d]	6	82	—
4	Pb	4	79	—
5	$BiCl_3$	2	65	—
6	$SnBr_2$	5	—	92
7	$TiCl_4$	5	—	80
8	$MnCl_3$	5	—	93
9	$CrCl_3$	5	—	92

a) Carried out with MX_n (0.1 equiv) and Al(2.2 equiv) in MeOH/aq 1% HBr (9/1) at 30 °C. b) Isolated Yield. c) Recovered **3a**. d) aq 1% HCl was used in place of 1% HBr.

Experimental

Melting points were determined with a Thomas-Hoover capillary apparatus and are uncorrected. IR spectra were recorded on a JASCO IRA-1 grating spectrophotometer. ^{1}H NMR spectra were taken on a Hitachi R-24 (60 MHz) and a JEOL MX-100 spectrometers (100 MHz) using tetramethyl-

Table 3. Reductive Removal of Bromine Atom(s) of 6-Halo- or 6,6-Dihalopenicillanates[a]

Entry		Halopenicillanates				Solvent[c]	Time	Product	
		X^1	X^2	Y	R[b]		h	Yield/%[d]	
1	**3a**	Br	Br	H	PMB	A	3	**7a**	95
2	**3b**	Br	Br	H	$CHPh_2$	B	2	**7b**	93
3	**3c**	Br	Br	H	CH_3	A	4	**7c**	77
4	**4a**	Br	H	H	PMB	A	3	**8a**	80
5	**4b**	Br	H	H	$CHPh_2$	B	5	**8b**	82
6	**4c**	Cl	H	H	PMB	B	22	**8c**	—(92)[e]
7	**5a**	Br	Br	H	PMB	C	5	**9a**	72
8	**5a**	Br	Br	H	PMB	D	15	**9a**	52
9	**6a**	Br	Br	H	PMB	B	3	**10a**	91
10	**6b**	Br	Br	H	$CH_2CH{=}CH_2$	A	3	**10b**	94
11	**6c**	Br	Br	Cl	$CHPh_2$	A	5	**10c**	85
12	**6d**	Br	H	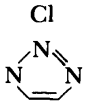	PMB	D	5	**10d**	86
13	**6e**	Br	Br	H	PNB	A	7	**10e**	—

a) Carried out with $PbBr_2$ (0.1 equiv) and Al (2.2 equiv) at 30 °C. b) PMB: *p*-methoxybenzyl; PNB: *p*-nitrobenzyl. c) A: MeOH/aq 1% HBr/CH_2Cl_2 (4/1/5); B: MeOH/aq 1% HBr/THF (9/1/5); C: MeOH/aq 1% HBr/acetone (8/1/1); D: MeOH/aq 1% HBr (9/1). d) Isolated yield. e) Recovered **4c**.

silane as an internal standard. Mass spectra were obtained on a JEOL JMS-DX303 spectrometer. Microanalyses were performed in our laboratory. 6-Bromo- and 6,6-dibromopenicillanates **3—6** were prepared from 6-aminopenicillanic acid **2** according to the procedures reported in the literatures.[1c,2,5,9]

Reductive Removal of Bromine Atom(s) of 6,6-Dibromo- and 6-Bromopenicillanates with $PbBr_2$-Al: To a stirred mixture of *p*-methoxybenzyl 6,6-dibromopenicillanate 1α-oxide **3a** (2 mmol), $PbBr_2$ (0.2 mmol) and finely cut aluminum foil (4.4 mmol) in methanol (4 ml) and dichloromethane (5 ml) was added aqueous 1% hydrobromic acid (1 ml). The stirring was continued at 30 °C until most of **3a** was consumed (3 h). The reaction mixture was diluted with EtOAc, washed with aqueous 5% hydrochloric acid followed by brine, dried, and concentrated to give penicillanate 1α-oxide **7a** (95%) as a light yellow foam. The analytical sample was obtained by a short silica-gel column with benzene-EtOAc (5 : 1) as an eluant: mp 103—103.5 °C; IR ($CHCl_3$) 1780 and 1745 cm^{-1}; ^1H NMR ($CDCl_3$) δ=1.25 (s, 3H, CH_3), 1.53 (s, 3H, CH_3), 3.10—3.70 (m, 2H, 6-H), 3.82 (s, 3H, OCH_3), 4.38 (s, 1H, 3-H), 4.50—4.65 (m, 1H, 5-H), 5.17 (s, 2H, OCH_2), 6.88 (d, J=9 Hz, 2H, aromatic H), and 7.33 (d, J=9 Hz, 2H, aromatic H); Found: C, 56.83; H, 5.70; N, 4.11%. Calcd for $C_{16}H_{19}NO_5S$: C, 56.96; H, 5.68; N, 4.15%.

In a similar manner, the following compounds were obtained.

Benzhydryl Penicillanate 1α-Oxide (7b): IR ($CHCl_3$) 1785 and 1745 cm^{-1}; ^1H NMR δ=1.09 (s, 3H, CH_3), 1.53 (s, 3H, CH_3), 3.27, 3.51 (AB-X, J_{AB}=14, J_{AX}= 2, J_{BX}=4 Hz, 2H, 6-H), 4.40 (s, 1H, 3-H), 4.48 (dd, J=2, 4 Hz, 1H, 5-H), 6.82 (s, 1H, $CHPh_2$), and 7.22 (s, 10H, aromatic H); HRMS, Found: m/z 406.1107. Calcd for $C_{21}H_{21}NO_4SNa$: M+Na, 406.1089.

Methyl Penicillanate 1α-Oxide (7c):[8b] IR (neat) 1770 and 1745 cm^{-1}; ^1H NMR δ=1.34 (s, 3H, CH_3), 1.58 (s, 3H, CH_3), 3.34, 3.58 (AB-X, J_{AB}=14, J_{AX}=2, J_{BX}=4 Hz, 2H, 6-H), 3.77 (s, 3H, CH_3), 4.36 (s, 1H, 3-H), and 5.07 (dd, J=2, 4 Hz, 5-H).

***p*-Methoxybenzyl Penicillanate 1β-Oxide (8a):** Mp 144—145 °C; IR ($CHCl_3$) 1780, 1735 cm^{-1}; ^1H NMR ($CDCl_3$) δ=1.07 (s, 3H, CH_3), 1.62 (s, 3H, CH_3), 3.30 (d, J=4 Hz, 2H, 6-H), 3.80 (s, 3H, OCH_3), 4.49 (s, 1H, 3-H), 4.89 (t, J=4 Hz, 1H, 5-H), 5.06, 5.21 (AB-q, J=11 Hz, 2H, OCH_2), 6.84 (d, J=8 Hz, 2H, aromatic H), and 7.27 (d, J=8 Hz, aromatic H); Found: C, 56.71; H, 5.76; N, 4.15%. Calcd for $C_{16}H_{19}NO_5S$: C, 56.96; H, 5.68; N, 4.04%.

Benzhydryl Penicillanate 1β-Oxide (8b): Mp 150—151.5 °C (lit,[8a] mp 145—148 °C); IR ($CHCl_3$) 1780 and 1740 cm^{-1}; ^1H NMR ($CDCl_3$) δ=0.94 (s, 3H, CH_3), 1.66 (s, 3H, CH_3), 3.30 (d, J=3 Hz, 2H, 6-H), 4.59 (s, 1H, 3-H), 4.86 (t, J=3 Hz, 1H, 5-H), 6.92 (s, 1H, $CHPh_2$), and 7.29 (s, 10H, aromatic H).

***p*-Methoxybenzyl Penicillanate (9a):** IR ($CHCl_3$) 1765 and 1740 cm^{-1}; ^1H NMR ($CDCl_3$) δ=1.36 (s, 3H, CH_3), 1.61 (s, 3H, CH_3), 3.04, 3.54 (AB-X, J_{AB}=14, J_{AX}=2, J_{BX}=4 Hz, 2H, 6-H), 3.80 (s, 3H, OCH_3), 4.46 (s, 1H, 3-H), 5.12 (s, 2H, OCH_2), 5.27 (dd, J=2, 4 Hz, 1H, 5-H), 6.94 (d, J=8 Hz, 2H, aromatic H), and 7.30 (d, 2H, J=8 Hz, aromatic H); HRMS, Found: m/z 344.0851. Calcd for $C_{16}H_{19}NO_4SNa$: M+Na, 344.0932.

***p*-Methoxybenzyl Penicillanate 1,1-Dioxide (10a):** IR ($CHCl_3$) 1785 and 1740 cm^{-1}; ^1H NMR ($CDCl_3$) δ=1.24 (s, 3H, CH_3), 1.51 (s, 3H, CH_3), 3.38 (d, J=4 Hz, 2H, 6-H) 3.77 (s, 3H, OCH_3), 4.33 (s, 1H, 3-H), 4.52 (t, J=4 Hz, 1H, 5-H), 5.03, 5.17 (AB-q, J=11 Hz, 2H, OCH_2), 6.80 (d, J=8 Hz, 2H, aromatic H), and 7.23 (d, J=8 Hz, 2H, aromatic H); HRMS, Found: m/z 376.0851. Calcd for $C_{16}H_{19}NO_6SNa$: M+Na, 376.0831.

Allyl Penicillanate 1,1-Dioxide (10b): Mp 82—84 °C; IR ($CHCl_3$) 1790 and 1745 cm^{-1}: ^1H NMR ($CDCl_3$) δ=1.41 (s, 3H, CH_3), 1.61 (s, 3H, CH_3), 3.47 (d, J=3 Hz, 2H, 6-H), 4.40 (s, 1H, 3-H), 4.61 (t, J=3 Hz, 1H, 5-H), 4.69 (d, J=6 Hz, 2H, OCH_2), and 5.15—6.30 (m, 3H, $CH{=}CH_2$); HRMS, Found: m/z 296.0562. Calcd for $C_{11}H_{15}NO_5SNa$: M+Na 296.0569.

Benzhydryl 2β-Chloromethyl-2α-methylpenam-3α-carboxylate 1,1-Dioxide (10c): IR ($CHCl_3$) 1795 and 1745 cm^{-1}; ^1H NMR δ=1.29 (s, 3H, CH_3), 3.48 (d, J=3 Hz, 2H, 6-H), 3.83, 4.01 (AB-q, J=12 Hz, 2H, CH_2Cl), 4.60 (t, J=3 Hz, 1H, 5-H), 4.67 (s, 1H, 3-H), 6.93 (s, 1H, $CHPh_2$), and 7.30 (s, 10H, aromatic H); HRMS, Found: m/z 456.0711. Calcd for $C_{21}H_{20}NO_5SClNa$: M+Na, 456.0648.

***p*-Methoxybenzyl 2α-Methyl-2β-[(triazol-1-yl)methyl]-penam-3α-carboxylate 1,1-Dioxide (10d):** IR($CHCl_3$) 1795 and 1745 cm^{-1}; ^1H NMR ($CDCl_3$) δ=1.20 (s, 3H, CH_3), 3.51 (d, J=3 Hz, 2H, 6-H), 3.81 (s, 3H, OCH_3) 4.57 (s, 1H, 3-H), 4.63 (t, J = 3 Hz, 1H, 5-H), 5.02 (s, 2H, CH_2N), 5.20 (s, 2H, OCH_2), 6.90 (d, J=9 Hz, 2H, aromatic H), 7.35 (d, J=9 Hz, 2H, aromatic H), 7.60 (s, 1H, aromatic H), and 7.74 (s, 1H, aromatic H); HRMS, Found: m/z 443.1001. Calcd for $C_{18}H_{20}N_4O_6SNa$: M+Na, 443.1001.

References

1) a) A. R. English, J. A. Retsema, A. E. Girard. J. E. Lynch, and W. E. Barth, *Antimicrob. Agents Chemother.*, **14**, 414 (1978); b) D. G. Brenner and J. R. Knowles, *Biochemistry*, **20**, 3680 (1981); c) R. A. Volkmann, R. D. Carroll, R. B. Drolet, M. L. Elliott, and B. S. Moore, *J. Org. Chem.*, **47**, 3344 (1982).

2) W. J. Gottstein, L. B. Crast, Jr., R. G. Graham, U. J. Hayner, and D. N. McGregor, *J. Med. Chem.*, **24**, 1531 (1981).

3) R. G. Micetich, S. N. Maiti, P. Spevak, T. W. Hall, S. Yamabe, N. Ishida, M. Tanaka, T. Yamazaki, A. Nakai, and K. Ogawa, *J. Med. Chem.*, **30**, 1469 (1987); L. Gutmann, M.-D. Kitzis, S. Yamabe, and J. F. Acar, *Antimicrob. Agents Chemother.*, **29**, 955 (1986); M. R. Jacobs, S. C. Aronoff, S. Johenning, D. M. Shlaes, and S. Yamabe, *ibid.*, **29**, 980 (1986).

4) H. Tanaka, M. Tanaka, A. Nakai, S. Yamada, N. Ishida, T. Otani, and S. Torii, *J. Antibiot.*, **41**, 579 (1988).

5) E. Evrard, M. Claesen, and H. Vanderhaeghe, *Nature (London)*, **201**, 1124 (1964); I. Ernest, J. Gosteli, and R. B. Woodward, *J. Am. Chem. Soc.*, **101**, 6301 (1979); D. D. Keith, J. Tengi, P. Rossman, L. Todaro, and M. Weigele, *Tetrahedron*, **39**, 2445 (1983).

6) J. P. Clayton, *J. Chem. Soc. C*, **1969**, 2123.

7) J. A. Aimetti, E. S. Hamanaka, D. A. Johnson, and M. S. Kellogg, *Tetrahedron Lett.*, **1979**, 4631; D. I. John, N. D. Tyrrell, and E. J. Thomas, *Tetrahedron*, **39**, 2477 (1983).

8) a) R. G. Micetich, S. N. Maiti, P. Spevak, M. Tanaka, T. Yamazaki, and K. Ogawa, *Synthesis*, **1986**, 292; b) R. G. Micetich, S. N. Maiti, M. Tanaka, T. Yamazaki, and K. Ogawa, *J. Org. Chem.*, **51**, 853 (1986); c) J. Brennan and F. H. S. Hussain, *Synthesis*, **1985**, 749; d) S. Ikeda, F. Sakamoto, R. Hirayama, Y. Takebe, M. Sotomura, and G. Tsukamoto, *Chem. Pharm. Bull.*, **36**, 218 (1988).

9) H. Tanaka, S. Yamashita, T. Hamatani, Y. Ikemoto, and S. Torii, *Synth. Commun.*, **17**, 789 (1987); H. Tanaka, S. Yamashita, Y. Ikemoto, and S. Torii, *Chem. Lett.*, **1987**, 673; H. Tanaka, S. Yamashita, and S. Torii, *Bull. Chem. Soc. Jpn.*, **60**, 1951 (1987); H. Tanaka, H. Dhimane, Y. Ikemoto, and S. Torii, *Chem. Express*, **2**, 487 (1987); S. Torii, H. Tanaka, S. Yamashita, M. Yamanoue, M. Taniguchi, and M. Sasaoka, *ibid.*, **2**, 615 (1987); H. Tanaka, S. Yamashita, Y. Katayama, and S. Torii, *ibid.*, **2**, 751 (1987); H. Tanaka, S. Yamashita, Y. Ikemoto, and S. Torii, *Tetrahedron Lett.*, **29**, 1721 (1988).

Catalytic Hydrogenation and Cracking of Anthracene over $MoCl_3$-LiCl-KCl and $NiCl_2$-LiCl-KCl Salts

Chunshan SONG, Tomohiro ONO, and Masakatsu NOMURA*
Department of Applied Chemistry, Faculty of Engineering, Osaka University, Yamada-oka 2-1, Suita, Osaka 565
(Received August 13, 1988)

Synopsis. The $MoCl_3$- and $NiCl_2$-LiCl-KCl salts, which are effective coal liquefaction catalysts, promoted the hydrogenation of anthracene (at 400 °C for 1 h with 9.8 MPa H_2) and afforded tetrahydro- and octahydro- as well as dihydroanthracene as major products. However, these catalysts did not remarkably enhance the ring-opening cracking reactions. A comparative examination suggested that the addition of LiCl-KCl to $MoCl_3$ and $NiCl_2$ suppressed their cracking ability and improved their hydrogenation selectivity.

Because of the complexity of coal structures and catalytic coal liquefaction reaction systems, hydrogenation and cracking reactions of polycyclic aromatic compounds have been taken as model test reactions for clarifying the effects of various catalysts for coal hydroliquefaction and upgrading of coal-derived products.[1-4] Recently, $MoCl_3$-LiCl-KCl and $NiCl_2$-LiCl-KCl salts have been found to be effective catalysts for the hydroliquefaction of brown, subbituminous and bituminous coals.[5,6] The most interesting features of these new catalysts are that they significantly promote oil production but do not remarkably enhance gas formation. This work was undertaken in order to develop a better understanding of their catalytic effects in promoting the hydrogenation and cracking of polycyclic aromatics.

Experimental

The synthesized and purified $MoCl_3$[5] and reagent grade $NiCl_2$, LiCl, and KCl were used in preparing $MoCl_3$-LiCl-KCl (molar composition, 12:51:37) and $NiCl_2$-LiCl-KCl (14:50:36) ternary salts and LiCl-KCl (58:42) binary salt.[5,6] The amounts of the salt catalysts used in the reactions, MCl_n-LiCl-KCl and MCl_n (MCl_n=$MoCl_3$, $NiCl_2$), were maintained at MCl_n/anthracene (3 g, 16.85 mmol)=0.3 (molar ratio). Hydrogenation was carried out in a 60-ml SUS-316 rocking autoclave at 400 °C for 1 h with an initial H_2 pressure of 9.8 MPa. The gaseous products were analyzed by GC. The liquid and solid products were analyzed quantitatively by GLC (Shimadzu GC-4C), with the aid of GC-MS (Hitachi RMU-6MG) analyses for product identification. The experimental and analytical procedures used in this work are similar to those described elsewhere.[2]

Results and Discussion

Hydrogenation and cracking of anthracene at 400 °C for 1 h produced various hydrocarbons. These prod-

Table 1. Results of Hydrogenation and Cracking of Anthracene

Run No. / Catalyst	1 None	2 LiCl-KCl	3[a] $MoCl_3$-LiCl-KCl	4[b] $NiCl_2$-LiCl-KCl	5 $MoCl_3$	6 $NiCl_2$
Products[c] (wt%)						
C_1—C_4	0.1	0.2	0.9	0.2	2.6	0.2
C_5—C_9	—	—	0.1	—	2.1	0.7
R_1-(C6H4)-R_2	—	—	0.9	—	1.1	—
R_1-(C10H6)-R_2 + (C10H7)-R	0.1	0.1	3.0	0.8	40.2	1.6
R_1-(C14H8)-R_2	0.2	0.1	0.6	0.1	1.8	0.1
(C14H12)[d] + (C14H13)-R	0.3	0.1	7.7	4.3	15.6	11.4
(C14H12)[e]	—	—	10.4	8.0	9.7	15.8
(C14H14)	14.9	15.8	44.9	41.0	6.4	37.3
(C14H14)	69.3	66.4	19.9	30.2	—	21.0
(C14H14)	14.4	13.8	6.4	12.1	2.4	7.6
(C14H14)[f]	—	—	2.1	1.6	8.7	4.0
Conversion	85.6	86.2	93.6	87.9	97.6	92.4

a, b) Molar contents of $MoCl_3$ (a) and $NiCl_2$ (b) are 12% and 14%, respectively. c) R, R_1 and R_2 mean alkyl groups or hydrogen. d) *unsym*-Octahydroanthracene. e) *sym*-Octahydroanthracene. f) *sym*-Octahydrophenanthrene.

ucts were grouped into 1) C_1—C_4 gases; 2) C_5—C_9 paraffins and cycloparaffins; 3) alkylbenzenes; 4) alkyltetralins and indans; 5) alkylnaphthalenes; 6) *unsym*-octahydro-, 7) *sym*-octahydro-, 8) tetrahydro-, and 9) dihydroanthracene; 10) anthracene; 11) isomerized tricyclic hydroaromatics (*sym*-octahydrophenanthrene). The results are given in Table 1. Among the 3-ring aromatics, anthracene is known to show a relatively high reactivity.[2,3] About 86% of anthracene was converted, even in a noncatalytic run. The run with LiCl-KCl (Run 2) alone, gave very similar results to those of a noncatalytic run. However, the major product in these runs was dihydroanthracene. The use of $MoCl_3$-LiCl-KCl (Run 3) and $NiCl_2$-LiCl-KCl (Run 4) considerably promoted the hydrogenation of anthracene and/or dihydroanthracene and increased the yield of tetrahydroanthracene. Moreover, the formation of *sym*- and *unsym*-octahydroanthracene was also enhanced by these catalysts; the yields of these products were somewhat higher with $MoCl_3$-LiCl-KCl (Run 3) than those with $NiCl_2$-LiCl-KCl (Run 4). The appearance of small amounts of bicyclic and monocyclic products in these runs (Runs 3, 4) indicates that ring-opening cracking reactions occurred, but only to a very limited degree, as can be seen from Table 1.

To examine the influence of the content of $MoCl_3$ and $NiCl_2$, runs with an increased content of MCl_n (25 mol%) in MCl_n-LiCl-KCl (MCl_n=$MoCl_3$, $NiCl_2$) at a constant mol ratio of MCl_n/anthracene (0.3) were also carried out. The results shown in Fig. 1 indicate that an increase in the molar content of $MoCl_3$ (from 12 to 25%, Fig. 1A) and $NiCl_2$ (from 14 to 25%, Fig. 1B) decreased the yield of tetrahydroanthracene and increased the yields of octahydroanthracene, without any remarkable increase of cracking products. These results suggest that increasing the content of $MoCl_3$ and $NiCl_2$ in $MoCl_3$- and $NiCl_2$-LiCl-KCl ternary salts could increase their hydrogenation activity without a remarkable change in the cracking ability. On the other hand, the runs with $MoCl_3$ and $NiCl_2$ alone converted more than 92% of the reactant, and produced more octahydroanthracene and hydrocracked products than their corresponding ternary salts (Table 1, Fig. 1). Especially in a run with $MoCl_3$, alone, dihydroanthracene disappeared and only a small amount of tetrahydroanthracene remained, whereas large quantities of products derived from extensive hydrogenation and cracking, such as *sym*- and *unsym*-octahydroanthracenes, bicyclic and monocyclic compounds and paraffins were formed (Table 1). It is worth while noting that in the catalytic runs of anthracene, *sym*-octahydrophenanthrene was also produced, as can be seen from Table 1. This is considered to be due to the isomerization of *sym*-octahydroanthracene, which is known to occur in the presence of Lewis acids, such as $ZnCl_2$ and $AlCl_3$.[2,3] The isomerization extent could be indicative of the relative Lewis acidity of the salt catalysts. As shown in Fig. 2, the yield of *sym*-octahydrophenanthrene increased as the molar content of MCl_n of MCl_n-LiCl-KCl increased, which appeared to be more remarkable with the $MoCl_3$-containing salts than with the $NiCl_2$-containing salts.

A comparison of the runs using $MoCl_3$- or $NiCl_2$-LiCl-KCl with runs using $MoCl_3$ or $NiCl_2$ (Table 1) indicates that the former promoted hydrogenation reactions and suppressed cracking reactions. This difference was most remarkable between $MoCl_3$-LiCl-KCl and $MoCl_3$ (Table 1, Fig. 1). Since the reactions were carried out at a constant MCl_n/anthracene ratio for both MCl_n-LiCl-KCl and MCl_n salt catalysts and LiCl-KCl showed essentially no catalytic effect, the comparative examination revealed that $MoCl_3$-LiCl-KCl and $NiCl_2$-LiCl-KCl have a lower cracking ability and a higher hydrogenation selectivity than their corresponding $MoCl_3$ and $NiCl_2$ single salts. This suggests that the addition of LiCl- KCl to $MoCl_3$ and $NiCl_2$ suppressed their cracking ability and improved

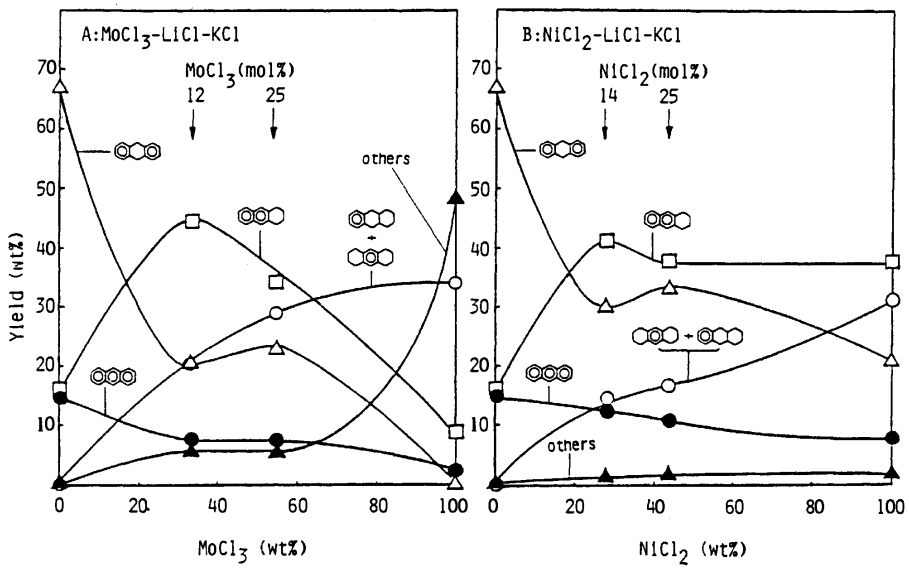

Fig. 1. The influence of MCl_n content in MCl_n-LiCl-KCl on hydrogenation of anthracene. Yields of octahydroanthracenes (○) include those of the isomerized octahydroanthracenes.

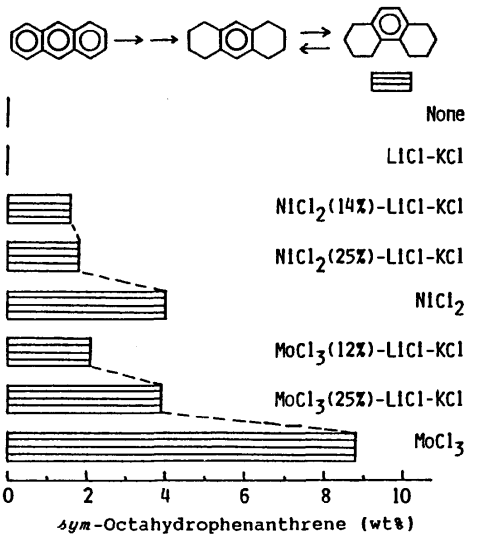

Fig. 2. Yield of *sym*-octahydrophenanthrene formed from hydrogenation of anthracene over MCl_n-LiCl-KCl. The number in the parenthesis indicates the molar content of MCl_n.

their hydrogenation selectivity.[7] This was probably because addition of LiCl-KCl to $MoCl_3$ or $NiCl_2$ led to the formation of some complex species[8] such as MCl_m^{n-} (M=Mo or Ni), which decreased the Lewis acidity of the catalyst. In addition, the hydrogenation of phenanthrene was also performed. Although it showed a lower reactivity, as is well-known,[2,3] the trend for difference between MCl_n-LiCl-KCl and MCl_n (MCl_n=$MoCl_3$, $NiCl_2$) appeared to be similar to that observed in the runs involving anthracene.

In our previous papers[5,6] we demonstrated that $MoCl_3$- and $NiCl_2$-LiCl-KCl salt catalysts greatly enhanced coal conversion with relatively low hydrogen consumption, and significantly increased yield of oil products, without any remarkable increase of C_1—C_4 gas yields. ^{1}H NMR analysis of the oil products revealed that the use of these catalysts increased the content of α- and β-methylene hydrogens present in hydroaromatic structures.[6] The present results show that these catalysts remarkably enhanced the production of partially hydrogenated aromatics without extensive cracking reactions, being consistent with the above-mentioned ^{1}H NMR analyses. Therefore, the results of this study provided a basis for assessing the extent of hydrogenation and cracking of polyaromatics occurring during coal hydroliquefaction using $MoCl_3$- and $NiCl_2$-based salt catalysts.

References

1) W. H. Wiser, S. Singh, S. A. Qader, and G. R. Hill, *Ind. Eng. Chem. Prod. Res. Dev.*, **9**, 350 (1970); A. V. Sapre and B. C. Gates, *Ind. Eng. Chem. Process Des. Dev.*, **20**, 68 (1981); D. H. Broderick, A. V. Sapre, B. C. Gates, H. Kwart, and G. C. A. Schuit, *J. Catal.*, **73**, 45 (1982); H. W. Haynes, J. F. Parcher, and N. E. Helmer, *Ind. Eng. Chem. Process Des. Dev.*, **22**, 401 (1983).

2) S. Kikkawa, M. Nomura, and K. Murase, *Sekiyu Gakkaishi*, **19**, 863 (1976); Y. Nakatsuji, T. Kubo, M. Nomura, and S. Kikkawa, *Bull. Chem. Soc. Jpn.*, **51**, 618 (1978); M. Miyake, H. Sakashita, M. Nomura, and S. Kikkawa, *Fuel*, **61**, 124 (1982); C. Song, K. Hanaoka, T. Ono, and M. Nomura, *Bull. Chem. Soc. Jpn.*, **61**, 3788 (1988).

3) S. S. Salim and A. T. Bell, *Fuel*, **63**, 469 (1984).

4) E. Ogata, K. Hatakeyama, and Y. Kamiya, *Chem. Lett.*, **1985**, 1913; J.-L. Lemberton and M. Guisnet, *Appl. Catal.*, **13**, 181 (1984).

5) C. Song, M. Nomura, and M. Miyake, *Fuel*, **65**, 922 (1986).

6) C. Song and M. Nomura, *Bull. Chem. Soc. Jpn.*, **59**, 3643 (1986); C. Song and M. Nomura, *Fuel*, **66**, 1225 (1987); C. Song, K. Hanaoka, and M. Nomura, *Energy Fuels*, **2**, 639 (1988).

7) Moreover, without LiCl-KCl, a part of $MoCl_3$ disproportionates (to form $MoCl_2$ and strongly Lewis acidic $MoCl_5$) and $NiCl_2$ is reduced at 400 °C, whereas the disproportionation of $MoCl_3$ and reduction of $NiCl_2$ are greatly suppressed by the addition of LiCl-KCl.[5]

8) For the formation of complex MCl_m^{n-}, see K. E. Johnson and J. R. Dickinson, "Advances In Molten Salt Chemistry," ed by J. Braunstein, G. Mamantov and G. P. Smith, Plenum Press, New York (1973), Vol. 2, p. 83; G. P. Smith and J. Brynestad, "Molten Salts," ed by G. Mamantov, Marcel Dekker, New York (1969), p.143; H. Kuhnel, *Angew. Chem., Int. Ed. Engl.*, **6**, 64 (1967).

Ab Initio Calculation for the Interaction Energy of He-He$^+$

Akira ICHIHARA* and Reikichi ITOH
Department of Chemistry, Faculty of Science and Engineering, Waseda University, 3-4-1 Ohkubo Shinjuku-Ku, Tokyo 160
(Received July 22, 1988)

Synopsis. Using an ab initio calculation with a configuration interaction (CI) treatment, the interaction energy of a He-He$^+$ system in the ground ($X^2\Sigma_u^+$) electronic state was calculated. For $X^2\Sigma_u^+He_2^+$ calculations, the Gaussian-type [6s3pld] basis set of Khan and Jordan was employed, and the effect of the basis set superposition error was estimated.

From a theoretical point of view, He_2^+ is a comparatively simple homonuclear ion, and there have been a number of reports in which the interaction energy of He_2^+ in the ground ($X^2\Sigma_u^+$) state has been calculated by the use of an ab initio MO method.[1-6] Recently Khan and Jordan utilized the multi-configuration self-consistent field (MC SCF) procedure to calculate the potential energy curve of $X^2\Sigma_u^+He_2^+$.[5] A contracted Gaussian-type [6s3pld] basis set was employed for their MC-SCF calculation. They determined the vibrational and rotational energy levels from the potential energy curve; the resulting spectroscopic constants were in excellent agreement with the experimental values. This result indicates that the [6s3pld] Gaussian set can give a significantly improved description of the potential energy curve of $X^2\Sigma_u^+He_2^+$.

On the other hand, we have calculated the interaction energies for the He-He[7] and He-H[8] systems in the ground and several electronic excited states. For these simple systems, the full CI treatment could be performed, and the basis set superposition error[9,10] was eliminated correctly from the interaction energies. Thus, it appears to be of interest to investigate the effect of the basis set superposition error on the interaction energy of $X^2\Sigma_u^+He_2^+$, itself calculated with the basis set of Khan and Jordan. In this paper we will report the results of full CI calculations of the interaction energy of $X^2\Sigma_u^+He_2^+$, and the basis set superposition error for these energies will be discussed. Our results concerning the vibrational and rotational energy levels will then be compared with the experimental and theoretical values.

Computational Details

In the CI treatment, $X^2\Sigma_u^+He_2^+$ is mainly described by a single configuration ($1\sigma_g^2 1\sigma_u$) for the whole range of internuclear distances calculated here; it has a dissociation limit, He($1s^2$) +He$^+$(1s), at an infinite separation. The results of full CI calculations for the interaction energy of $X^2\Sigma_u^+He_2^+$ were corrected in order to eliminate the basis set superposition error. We employed the function counterpoise method of Boys and Bernardi[9] to avoid this error. In this method, the He-He$^+$ interaction energy (E_{int}) is calculated using the difference between the full CI energy of $X^2\Sigma_u^+He_2^+$ ($E_{He_2^+}$) and an appropriate refference energy (E_{ref}):

$$E_{int}(R) = E_{He_2^+}(R) - E_{ref}(R), \quad (1)$$

where R is the internuclear distance of He-He$^+$. The reference energy is defined as the sum of the full CI energies of the He($1s^2$) and He$^+$(1s), with ghost orbitals at the expected location of the other atom:

$$E_{ref}(R) = E_{ghost}^{He(1s^2)}(R) + E_{ghost}^{He^+(1s)}(R) \quad (2)$$

The term "ghost" represents an atom with a zero nuclear charge and without any electrons.

Then the calculated interaction energy curve was interpolated in order to determine the vibrational and rotational energy levels of $X^2\Sigma_u^+He_2^+$. The vibrational analysis was given by the Störmer-Levy difference method, while the vibrational eigen functions were utilized to determine the rotational constants. The detailed procedure has been described elsewhere.[11,12] This method gives an accurate solution in a numerical form with a great number of mesh points and with the proper selection of position to make an initial guess from outside of the potential well.

In the present work, the spatial symmetry considered in the CI treatment of the $X^2\Sigma_u^+He_2^+$ is $D_{\infty h}$. The CI calculations contain 4562 configurations for the $^2\Sigma_u^+$ symmetry. The number of calculated interaction energy values was 18 points in the range of internuclear distances from 0.7 to 5.0 Å; the interpolated mesh width was taken to be 0.001 Å. The MO calculations were performed by using the graphical unitary group approach (GUGA) program of our group[7] and the HITAC M680 system of the Computer Center of the Institute for Molecular Science (IMS).

Results and Discussion

Table 1 indicates the interaction energies of $X^2\Sigma_u^+He_2^+$. The full CI energies of He($1s^2$) and He$^+$(1s) (E_{He}, E_{He^+}), without ghost orbitals, are −2.9016276 and −1.9998712 a.u. respectively. These energies are equal to $E_{ghost}^{He(1s^2)}$ and $E_{ghost}^{He^+(1s)}$ at the internuclear distance of R=5.0 Å. The basis set superposition error is evaluated by the use of $E_{ref}-E_{He}-E_{He^+}$ in Table 1. It can be seen from Table 1 that the basis set superposition error is less than 2.0×10^{-4} a.u. for the whole range of R values calculated and that it decreases rapidly as the internuclear separation is increased. In the present CI calculations, the interaction energy minimum was found to be −0.0902342 a.u. at R=1.080 Å. (The resulting dissociation energy (D_e) is 56.585 kcal mol^{-1}, while the D_e value calculated by Khan and Jordan is 56.52 kcal mol^{-1}.[5]) The basis set superposition error changes the energy well depth by only 0.06 percent. From these results, the basis set superposition error can be said to be negligible for $X^2\Sigma_u^+He_2^+$ in the range from 0.7 to 5.0 Å. On the other hand, it seems that the basis set superposition error can not be neglected in the strongly repulsive region.

Table 1. The He-He^+ Interaction Energies (E_{int}) in the $X^2\Sigma_u^+$ State

R/Å	$E_{He_2^+}$/a.u.[a]	E_{ref}/a.u.		E_{int}/a.u.
		E_{ref}	$E_{ref}(R)-E_{He(1s^2)}-E_{He^+(1s)}$	
0.7	−4.859992	−4.901645	−0.000146	0.041654
0.8	−4.935025	−4.901615	−0.000116	−0.033410
0.9	−4.972956	−4.901590	−0.000091	−0.071365
1.0	−4.988745	−4.901569	−0.000070	−0.087176
1.05	−4.991386	−4.901560	−0.000061	−0.089826
1.08	−4.991789	−4.901555	−0.000056	−0.090234
1.1	−4.991654	−4.901552	−0.000053	−0.090102
1.2	−4.987432	−4.901540	−0.000041	−0.085892
1.3	−4.979609	−4.901532	−0.000033	−0.078077
1.4	−4.970316	−4.901526	−0.000028	−0.068790
1.5	−4.960798	−4.901521	−0.000023	−0.059277
1.6	−4.951749	−4.901518	−0.000019	−0.050232
1.8	−4.936269	−4.901513	−0.000014	−0.034757
2.0	−4.924721	−4.901509	−0.000010	−0.023212
2.5	−4.909330	−4.901503	−0.000004	−0.007827
3.0	−4.904088	−4.901501	−0.000002	−0.002587
4.0	−4.901824	−4.901499	−0.000001	−0.000325
5.0	−4.901568	−4.901499	0.0	−0.000070

a) 1 a.u.=4.359814×10^{-18}J.

Table 2. Calculated Vibrational Energy Levels ($G(v)$) for $X^2\Sigma_u^+$ He_2^+

v	$\langle R\rangle$/Å	$G(v)$/cm^{-1}[a]	$G(v+1/2)$/cm^{-1}
0	1.096546	839.878	1627.108
1	1.128439	2466.986	1557.640
2	1.161817	4024.626	1490.595
3	1.198047	5515.221	1421.905
4	1.235369	6937.126	1351.234
5	1.275629	8288.360	1282.191
6	1.317454	9570.551	1208.296
7	1.361299	10778.847	1139.739
8	1.410699	11918.586	1068.203
9	1.464292	12986.789	998.855
10	1.519420	13985.644	930.631
11	1.585618	14916.275	852.483
12	1.652376	15768.758	794.190
13	1.722394	16562.948	710.226
14	1.825547	17273.174	614.392
15	1.942362	17887.566	516.692
16	2.074584	18404.258	452.057
17	2.198430	18856.315	366.460
18	2.440572	19222.775	253.959
19	2.716176	19476.734	188.738
20	3.054041	19665.472	105.743
21	3.864818	19771.215	—

a) 1 cm^{-1}=1.986481×10^{-23}J.

Table 3. Calculated Rotational Constants (B_v) for $X^2\Sigma_u^+$ He_2^+

v	$\langle 1/R^2\rangle$/$Å^{-2}$	B_v/cm^{-1}
0	0.842382	7.096153
1	0.815831	6.872489
2	0.789154	6.647765
3	0.760736	6.408374
4	0.733318	6.177407
5	0.704796	5.937140
6	0.677290	5.705432
7	0.650155	5.476849
8	0.619915	5.222110
9	0.588833	4.960278
10	0.559436	4.712640
11	0.525021	4.422731
12	0.493997	4.161388
13	0.464803	3.915460
14	0.421702	3.552381
15	0.379868	3.199975
16	0.338387	2.850543
17	0.307814	2.592998
18	0.250046	2.106366
19	0.202450	1.705421
20	0.161017	1.356393
21	0.094637	0.797214

Table 2 indicates the vibrational energy levels ($G(v)$[13]) of $X^2\Sigma_u^+He_2^+$ with the vibrational quantum number v. The difference in successive $G(v)$ values ($\Delta G(v+1/2)$[13]) and the mean values of R ($\langle R\rangle$) are also indicated in Table 2. In the present calculation, we obtained a $G(21)$ value about 41 cm^{-1} higher than the result calculated by Khan and Jordan.[5] The first four $G(v)$ values in Table 2 were then used in order to determine the vibrational constants ω_e and $\omega_e\chi_e$.[13] The resulting ω_e and $\omega_e\chi_e$ values are 1697.85 and 35.97 cm^{-1} respectively. These ω_e and $\omega_e\chi_e$ values are in significantly better agreement with both the experimental values (1698.5, 35.3 cm^{-1})[14] and the values calculated by Khan and Jordan (1697.4, 35.35 cm^{-1}).[5]

Table 3 indicates the rotational constants B_v[13] at each vibrational energy level, where the mean values of $1/R^2$ ($\langle 1/R^2\rangle$) are also indicated. It can be seen from Tables 2, 3 that the calculated $\langle 1/R^2\rangle$ values are always larger than the corresponding $1/\langle R\rangle^2$ values. The rotational constant, α_e[13]=0.2580 cm^{-1}, was obtained from the first four B_v values and from the equilibrium distance, R_e=1.080 Å (B_e=7.22214 cm^{-1}). Our α_e value is different from both the experimental value (0.224 cm^{-1})[14] and the value calculated by Khan and Jordan (0.224 cm^{-1}).[5] This discrepancy is mainly due to our smaller B_o value, i.e., to the smaller

$\langle 1/R^2 \rangle_{v=0}$ value.

It may be concluded from the results of this investigation that the basis set superposition error of the $X^2\Sigma_u^+ He_2^+$ system calculated by the use of [6s3pld] basis of Khan and Jordan is almost negligible in the range from 0.7 to 5.0 Å. The present interaction energy curve can give the vibrational energy levels. On the other hand, a rotational constant α_e larger than the experimental value was obtained.

We wish to thank Dr. Toshikazu Saitoh, Kazuhide Mori, and Kohtoku Sasagane for making their program code avaiable to us.

References

1) B. Liu, *Phys. Rev. Lett.*, **27**, 1251 (1971).
2) J. G. Maas, N. P. F. B. van Asselt, P. J. C. M. Nowak, J. Los, S. D. Peyerimhoff, and R. J. Buenker, *Chem. Phys.*, **17**, 217 (1976).
3) J. Wasilewski, V. Staemmler, and R. Jaquet, *Theoret. Chim. Acta*, **59**, 517 (1981).
4) K. K. Sunil, J. Lin, H. Siddiqui, P. E. Siska, K. D. Jordan, and R. Shepard, *J. Chem. Phys.*, **78**, 6190 (1983).
5) A. Khan and K. D. Jordan, *Chem. Phys. Lett.*, **128**, 368 (1986).
6) K. Balasubramanian, M. Z. Liao, and S. H. Lin, *Chem. Phys. Lett.*, **142**, 349 (1987).
7) A. Ichihara, K. Sasagane, T. Izaki, T. Miyazaki, and R. Itoh, *Bull. Chem. Soc. Jpn.*, **61**, 1014 (1988).
8) A. Ichihara, K. Sasagane, and R. Itoh, *Bull. Chem. Soc. Jpn.*, **61**, 3141 (1988).
9) S. F. Boys and F. Bernardi, *Mol. Phys.*, **19**, 553 (1970).
10) J. H. van Lenthe, J. G. C. M. van Duijneveldt-van de Rijdt, and F. B. van Duijneveldt, "Weakly Bonded systems," in "Advances in Chemical Physics, Volume LXIX, Ab Initio Methods in Quantum Chemistry, Part II," ed by K. P. Lawley, John Wiley and Sons, Chichester (1987), pp. 521—566.
11) T. Saitoh, K. Mori, and R. Itoh, *Chem. Phys.*, **60**, 161 (1981).
12) T. Saitoh, K. Mori, K. Sasagane, and R. Itoh, *Bull. Chem. Soc. Jpn.*, **56**, 2877 (1983).
13) G. Herzberg, "Spectra of Diatomic Molecules," Van Nostrand Reinhold, New York (1950), pp. 66—145.
14) K. P. Huber and G. Herzberg, "Constants of Diatomic Molecules," Van Nostrand Reinhold, New York (1979), pp. 298—299.

The Addition Effect of CH_3I on the Ignition of CH_4

Kazuo TAKAHASHI, Tadaaki INOMATA,* Takao MORIWAKI, and Satiko OKAZAKI
Department of Chemistry, Faculty of Science and Technology, Sophia University, Kioi-cho 7-1, Chiyoda-ku, Tokyo 102
(Received August 3, 1988)

Synopsis. Measurements and calculations of ignition delay times were performed in a mixture of CH_4-CH_3I-O_2-Ar in order to understand the characteristics of compouds including iodine during ignition. CH_3I accelerated the ignition of CH_4 more than CH_3Cl did, but less than CH_3Br did. The remarkably small bond-dissociation energies of CH_3I and HI, in comparison to these of other halomethanes, were the major cause of the characteristic behavior.

It is well-known that CH_4 is very difficult to ignite in relatively simple hydrocarbons and that all additives but permanent gases, which act only as diluents, promote the ignition.[1-8] The addition effects of CH_3Br and CH_3Cl[8] on the ignition of CH_4 have already been analyzed in experiments using shock tubes and by simulations based on an assumed reaction mechanism. CH_3Br was more effective as an ignition-promotor than CH_3Cl, although both of them promoted the ignition; the differences were accounted for by chemical kinetic reasons.

In this study, the addition effect of CH_3I on the ignition of CH_4 is investigated by the same method, and the action due to the difference in halogens is discussed.

Experimental

The ignition-delay times were measured in a mixture of CH_4 (2.0 mol%)-O_2 (4.0 mol%)-CH_3I (0.1 mol%)-Ar (93.9 mol%) at temperatures between 1500 and 2000 K and at pressures between 2.3 and 3.3 atm behind the shock wave. Analytical studies were performed by using the mechanism shown in Table 1, in addition to that of the CH_4-oxidation.[8] The details of the experiments and calculation are given in Ref.8. The measurements included an error of only a few %; the error due to the procedure of estimating the ignition-delay times was below 1 μs at 1800 K.

Results and Discussion

The measured ignition-delay times agree well with the calculated values (Fig.1). The promotion effect of CH_3I is larger than that of CH_3Cl, but somewhat smaller than that of CH_3Br. Table 1 includes ignition-delay times which calculated by simultaneously decreasing both forward and reverse rate constants concerning halogen species, one by one, to zero or to one-tenth of their both values at 1800 K. The time calculated by means of normal rate constants was 124 μs. The results indicate that the reactions which have large effects on the ignition are $R1_I$, $R4_I$, $R5_I$, and $R8_I$ (hereafter, a subscript will express the kind of halogen

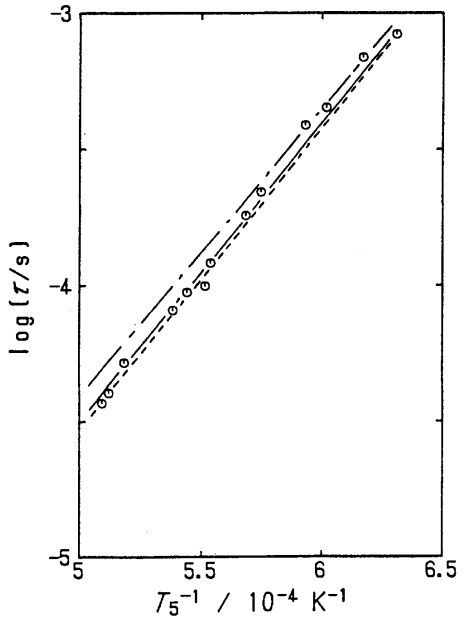

Fig. 1. Measured and calculated ignition delay times in CH_4-CH_3I-O_2-Ar. T_5 is temperature behind shock wave.
O: measured in CH_3I, ——: calculated in CH_3I, ----: calculated in CH_3Br,[8] — — —: calculated in CH_3Cl.[8]

Table 1. Reaction Mechanism, Rate Constants, and Calculated Ignition-Delay Times at 1800 K

	Reaction[a]	Ignition-delay time/10^{-6} s		k[b]			
		$k\times0$	$k\times0.1$	log A	n	E	Ref.
R1	$CH_3I=CH_3+I$	213	126	13.40	0.00	54.70	10
R2	$CH_3I+H=CH_3+HI$	125	126	14.54	0.00	4.50	9
R3	$CH_3I+I=CH_3+I_2$	125	125	14.30	0.00	19.80	9
R4	$CH_4+I=CH_3+HI$	143	139	14.70	0.00	33.90	9
R5	$HI+H=H_2+I$	122	123	13.52	0.00	0.00	9
R6	$I_2+H=HI+I$	124	125	14.39	0.00	0.00	9
R7	$I+I+M=I_2+M$	125	126	13.00	1.00	0.00	9
R8	$I+H+M=HI+M$	138	136	13.08	1.00	0.00	9

a) Reaction in which both forward and reverse rate constants are changed. The ignition-delay time calculated by the normal rate constants is 124 μs. b) Forward rate constants in the form $A\times T^n\exp(-E/RT)$, in cm^{-3}, mol, s, kcal, and K units.

in the corresponding reaction).

Although the thermal-decomposition reaction, $R1_I$, contributes most to the acceleration of an ignition like those of CH_3Cl and CH_3Br, each situation is different. When the forward and reverse rate constants of thermal decomposition, $R1_{Br}$ or $R1_{Cl}$, are changed by 10% in systems including CH_3Br or CH_3Cl, the ignition -delay time changes a small percentage, but it does not change at all in this case, and it only decreases about 1% with one-tenth of the $R1_I$. On the other hand, when both rate constants of thermal decomposition (R1) are zero, the ignition delay times are similar (about 220 μs) in the three halomethanes. The forward rate constant of $R1_I$ is two orders of magnitude larger than those of $R1_{Br}$ and $R1_{Cl}$, so the greater part of the CH_3I is decomposed in the early stage of the induction period, as is shown in Figs. 2 and 3. This means that the decomposition rate of CH_3I is very fast and that a small change in the decomposition rate does not affect the ignition-delay time.

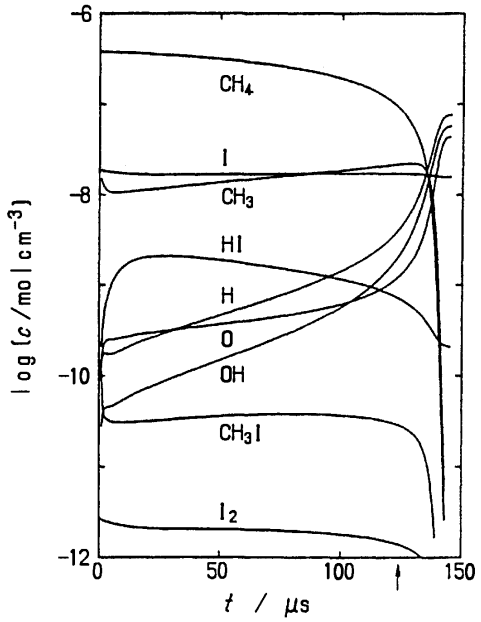

Fig. 2. Calculated concentration profiles at 1800 K. t is time after the arrival of shock wave. Arrow indicates the ignition-delay time.

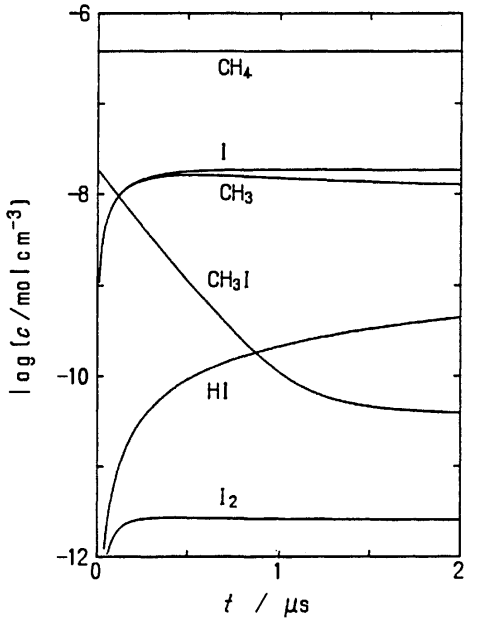

Fig. 3. Calculated concentration profiles at 1800 K in early stage of induction period.

The concentration profiles (Fig. 3) in the early stages of the induction period indicate that CH_3, which is importatnt in ignition, is generated from CH_3I, but not from CH_4. The concentration of iodine atoms reaches its maximum value 0.5 μs after the arrival of a shock wave and is the same as the decomposition value of CH_3I. The net reaction rate of $R1_I$ is very fast in the early stage of the induction period, but it is about 10^{-5} mol cm^{-3} s^{-1} during most of the induction period; this value is smaller by one or two orders than those of $R1_{Br}$ and $R1_{Cl}$. Therefore, $R1_I$ contributes significantly to the ignition only in the early stage. Since $R4_I$ proceeds in the forward direction and promotes the ignition, $R4_I$ has the possibility of making a chain with $R1_I$, in which the forward reaction is fast, and with $R2_I$, in which the reverse reaction is fast, just as in the case of CH_3Br addition.[8] However, the change of the forward and reverse rate constants of $R2_I$ has no effect on the calculated ignition-delay time (Table 1), and the net rate of $R1_I$ is slow through the greater part of the induction period. Therefore, the chain of $R1_I$, $R2_I$, and $R4_I$ is impossible. On the other hand, $R8_I$ proceeds in the reverse diretion and promotes the ignition. As a result, $R4_I$ forms a chain with $R8_I$, and their net reaction corresponds to the production of one H radical and one CH_3 radical from CH_4 in each chain. This net reaction is equivalent to that which is formed by $R1_{Br}$,

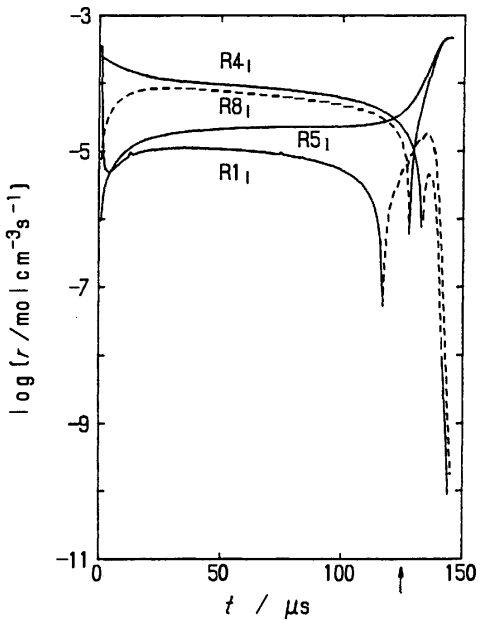

Fig. 4. Net reaction rates. t is time after the arrival of shock wave. Solid and dotted lines indicate that net reaction proceeds in the forward direction and in the reverse direction, respectively. Arrow indicates the ignition-delay time.

$R2_{Br}$, and $R4_{Br}$ when CH_3Br is used. However, the promotion effect of CH_3I is weaker than that of CH_3Br. As is apparent from Fig. 4, the net rate of $R4_I$ is nearly equal to the rate of $R8_I$ except for the early stage of the induction period, and the net rates of $R1_{Br}$, $R2_{Br}$, and $R4_{Br}$ previously reported are also equal to each other. However the net rate of $R2_{Br}$ controlling the rate of the chain formed in the CH_4-CH_3Br system is two times faster than that of $R8_I$ controlling the rate of chain formed when CH_3I is used; consequently, we infer that CH_3Br promotes the ignition better than CH_3I does.

Only $R5_I$ inhibits the ignition in the system involving CH_3I. When $R5_I$ or $R5_{Br}$ is deleted from the reaction mechanism in a system including CH_3I or CH_3Br, the calculated ignition-delay time becomes too short by 2 μs or 5 μs respectively. Although the forward reaction of $R5_I$ is fast and should greatly inhibit ignition, its reverse reaction is also fast, in spite of the low reverse rate constant, because iodine above 90% exists as iodine atoms, as is shown in Fig. 2. Therefore, the net rate of $R5_I$ is lower than that of $R2_I$ and $R8_I$ and has only a little effect on the inhibition of the ignition. In the system involving CH_3Br, the concentration of HBr is about three times that of Br atoms, and the rate constant of $R5_{Br}$ in the reverse direction is smaller by 2 orders than that in the forward direction, so the net rate of $R5_{Br}$ also becomes slow compared with those of other reactions which have a large effect on the ignition.

References

1) R. W. Crossley, E. A. Dorko, K. Scheller, and A. Burcat, *Combust. Flame*, **19**, 373 (1972).
2) E. A. Dorko, D. M. Bass, R. W. Crossley, and K. Scheller, *Combust. Flame*, **24**, 173 (1975).
3) A. Grillo and M. W. Slack, *Combust. Flame*, **27**, 377 (1976).
4) R. Ravikumar and K. A. Bhaskaran, *Combust. Flame*, **27**, 107 (1976).
5) E. K. Dabora, *Combust. Flame*, **24**, 181 (1975).
6) A. Burcat, *Combust. Flame*, **28**, 319 (1977).
7) T. Inomata, T. Moriwaki, and S. Okazaki, *Combust. Flame*, **62**, 183 (1985).
8) K. Takahashi, T. Inomata, T. Moriwaki, and S. Okazaki, *Bull. Chem. Soc. Jpn.*, **61**, 3307 (1988).
9) C. K. Westbrook and F. L. Dryer, *Proc. Energy Combust. Sci.*, **10**, 1 (1984).
10) G. Horrex and R. Lapage, *Discuss. Faraday Soc.*, **10**, 234 (1951).

Structure of a Cumulene Bearing Bulky Substituents. X-Ray Study of 1,1,4,4-Tetrakis(trimethylsilyl)butatriene

Yoshihiro MORIMOTO, Yoshiki HIGUCHI, Kuni WAKAMATSU,† Koichiro OSHIMA,† Kiitiro UTIMOTO,† and Noritake YASUOKA*

Basic Research Laboratory, Himeji Institute of Technology, Shosha 2167, Himeji 671-22

†Department of Industrial Chemistry, Faculty of Engineering, Kyoto University, Yoshida, Sakyoku, Kyoto 606

(Received August 8, 1988)

Synopsis. The structure of cumulene bearing bulky substituents, 1,1,4,4-tetrakis(trimethylsilyl)butatriene, has been determined by an X-ray diffraction method. The molecule is centrosymmetric, and the variation in carbon-carbon double bonds has been observed. The distance of the central C=C bond is 1.276(8) Å, whereas that of the terminal C=C bond is 1.319(6) Å. These bond lengths are very similar to the unsubstituted butatrienes and the influence of bulky trimethylsilyl groups is not recognized in this context. Some distortions have been observed in the bond angles concerning the trimethylsilyl groups; the overcrowded environment of the central C=C bond seems to make this less reactive.

Cumulene is a very reactive molecule and it is important to know more details about the molecular structure in order to correlate its reactivety with structure. The trimethylsilyl group is an important substituent in synthetic chemistry because it gives an overcrowded environment to unsaturated compounds. Differences in the reactivity between 1,1,4,4-tetrakis(trimethylsilyl)butatriene (**1**) and other butatrienes have been reported. The hydrogenation of **1** with Rh-C or Pd-C gives $(Me_3Si)_2CH\text{-}CH{=}CH\text{-}CH(SiMe_3)_2$ and the hydrogenation of 1,4-diphenylbutatriene provides 1,4-diphenyl-1,3-butadiene.[1] Here, we wish to describe the molecular structure of 1,1,4,4-tetrakis(trimethylsilyl)butatriene and to discuss the effect of bulky substituents on the cumulene structure.

Experimental

A tetrahydrofuran solution of bis(trimethylsilyl)butadiyne (1.0 mmol) was added to a solution of $(Me_3Si)_3MnMgMe$ (2.0 mmol) at 0 °C.[2] The resulting mixture was stirred at 0 °C for 1 h, then 30 min at 25 °C. A workup and purification by preparative thin-layer chromatography on silica gel gave 1,1,4,4-tetrakis(trimethylsilyl)butatriene (0.11 g)[3] in 33% yield and was subjected to X-ray structure analysis. Pale-yellow crystals were obtained from a benzene solution. The specimen was sealed by immersion in collodion to prevent any sublimation. The unit cell parameters were determined from 25 Bragg angles, carefully measured on a Rigaku four-circle diffractometer. Graphite monochromatized Cu$K\alpha$ radiation was used. Crystal data: $C_{16}H_{36}Si_4$, FW=340.78, crystal size 0.2×0.15×0.15 mm^3, triclinic, space group $P\bar{1}$; Z=1; a=11.075(2), b=12.035(2), c=6.501(1) Å, α=97.67(2), β=94.38(2), and γ=134.37(1)°. D_c=0.95 g cm^{-3}. μ(Cu$K\alpha$)=21.41 cm^{-1}. The intensity data were collected by a θ-2θ scan method at 24 °C. A total of 1727 reflections were obtained up to sin θ/λ<0.56 Å^{-1}, of which 1613 reflections were non-zero and used for the subsequent structure analysis. No absorption correction was performed. The structure was solved by the direct method with use of the computer program MULTAN,[4] and refined by block-diagonl least-squares method. Each weighting factor was assigned to twenty levels of the observed structure factors, divided according to their magnitude, in order to minimize any residuals in each region. Hydrogen atoms were located on a difference map and were included in the refinement. the final discrepancy indices, R and R_w, for 1613 non-zero reflections were 0.042 and 0.043, respectively. The calculation was carried out by a NEC PC-9801 computer using the UNICS computer program system[5] modified by Profs. Y. Katsube and N. Tanaka. The atomic scattering factors were taken from Ref. 6. The final atomic parameters are listed in Table 1, whereas the anisotropic thermal parameters and complete tables of the observed and calculated structure factors are kept as Document No. 8855 by the Editor of the Bulletin of the Chemical Society of Japan.

Results and Discussion

The molecular structure is shown in Fig. 1. A linear molecule lies on the center of symmetry in the crystal, and four trimethylsilyl groups are located in a staggered form. The effect of the bulkiness of the trimeth-

Table 1. Atomic Positional and Equivalent Isotropic Thermal Parameters of 1,1,4,4-Tetrakis(trimethylsilyl)butatriene

Atom	x	y	z	B_{eq}/B_{iso}
Si(1)	0.4395(1)	0.7272(1)	0.4142(1)	5.8
Si(2)	0.1633(1)	0.3403(1)	0.1487(2)	6.2
C(1)	0.3681(3)	0.5298(3)	0.3494(5)	5.5
C(2)	0.4587(4)	0.5123(3)	0.4537(5)	5.9
C(3)	0.6525(5)	0.8823(4)	0.6124(6)	8.4
C(4)	0.4638(5)	0.7977(5)	0.1709(6)	8.8
C(5)	0.2736(5)	0.7010(5)	0.5256(6)	8.7
C(6)	0.0433(6)	0.3726(5)	0.0075(9)	13.5
C(7)	0.2207(6)	0.2668(6)	−0.0438(7)	10.4
C(8)	0.0218(5)	0.1900(5)	0.3011(8)	11.3
H(31)	0.644(3)	0.847(3)	0.728(4)	3.1
H(32)	0.736(4)	0.896(3)	0.570(4)	4.7
H(33)	0.682(5)	0.977(4)	0.635(6)	9.2
H(41)	0.533(5)	0.809(4)	0.105(6)	9.0
H(42)	0.370(5)	0.736(4)	0.077(6)	8.9
H(43)	0.493(5)	0.883(5)	0.193(6)	9.6
H(51)	0.253(4)	0.659(4)	0.648(5)	6.9
H(52)	0.176(4)	0.635(4)	0.429(5)	7.7
H(53)	0.310(5)	0.790(5)	0.569(6)	10.6
H(61)	−0.035(5)	0.291(4)	−0.078(6)	8.1
H(62)	0.031(6)	0.416(6)	0.081(7)	13.5
H(63)	0.086(5)	0.430(5)	−0.094(7)	11.3
H(71)	0.292(5)	0.265(4)	0.013(6)	8.2
H(72)	0.131(6)	0.181(6)	−0.146(7)	13.3
H(73)	0.256(4)	0.336(4)	−0.122(5)	6.0
H(81)	0.077(6)	0.162(5)	0.360(7)	11.6
H(82)	−0.072(5)	0.095(4)	0.200(6)	8.6
H(83)	−0.022(6)	0.223(6)	0.348(7)	13.3

$B_{eq}=(4/3)(B_{11}a^2+B_{22}b^2+B_{33}c^2+B_{12}ab\cos(\gamma)+B_{13}ac\cos(\beta)+B_{23}bc\cos(\alpha))$.

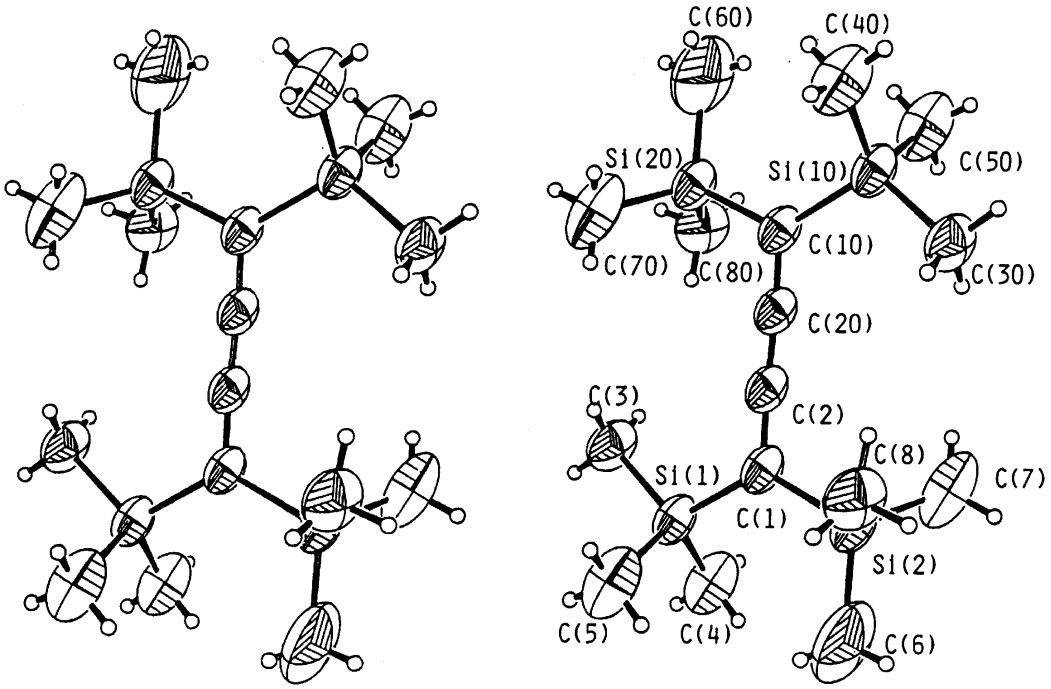

Fig. 1. Molecular structure (ORTEP drawing) of 1,1,4,4-tetrakis(trimethylsilyl)butatriene with atomic numbering scheme. The molecule is centrosymmetric. C(10) is related to C(1) by a center of symmetry and so on.

Table 2. Intramolecular Distances and Bond Angles in 1,1,4,4-Tetrakis(trimethylsilyl)butatriene

Intramolecular distances (l/Å)		Bond angles (θ/°)	
Si(1)-C(1)	1.872(4)	C(1)-Si(1)-C(3)	110.7(2)
Si(1)-C(3)	1.856(5)	C(1)-Si(1)-C(4)	110.1(3)
Si(1)-C(4)	1.844(6)	C(1)-Si(1)-C(5)	109.0(3)
Si(1)-C(5)	1.858(6)	C(3)-Si(1)-C(4)	108.1(3)
Si(2)-C(1)	1.889(4)	C(3)-Si(1)-C(5)	109.4(3)
Si(2)-C(6)	1.843(7)	C(4)-Si(1)-C(5)	109.5(3)
Si(2)-C(7)	1.834(7)	C(1)-Si(2)-C(6)	112.3(3)
Si(2)-C(8)	1.860(6)	C(1)-Si(2)-C(7)	109.1(3)
C(1)-C(2)	1.319(6)	C(1)-Si(2)-C(8)	106.9(3)
C(2)-C(20)	1.276(8)	C(6)-Si(2)-C(7)	110.1(4)
		C(6)-Si(2)-C(8)	108.1(3)
C(2)···C(3)	3.251(6)	C(7)-Si(2)-C(8)	110.3(3)
		Si(1)-C(1)-Si(2)	125.2(3)
		Si(1)-C(1)-C(2)	120.4(3)
		Si(2)-C(1)-C(2)	114.3(3)

ylsilyl groups is reflected on the bond angles around the C(1) atom. As can be seen from Table 2, which summarizes the interatomic distances and the angles in the molecule, the angle of C(2)-C(1)-Si(1) is larger than that of C(2)-C(1)-Si(2). This is due to the repulsion of C(2) and C(3), the latter being forced to lie on the plane through C(2), C(1), and Si(1) because of the overcrowded trimethylsilyl groups. The C(1)-C(2) double bond is seemingly buried by these groups and should be less reactive. The structure of tetrakis(trimethylsilyl)ethylene at −70 °C was reported by Sakurai and his co-workers.[7] The effect of bulky substituents has been observed on the molecular structure. The C=C bond length is 1.368(3) Å, significantly longer than the usual double bond. Furthermore, substituted ethylene is no longer planar, the dihedral angle between two Si-C-Si plane being 29.5°. It is reasonable that the effect of bulky trimethylsilyl groups on the present molecule is less remarkable than the tetrakis(trimethylsilyl)ethylene, because two bis(trimethylsilyl) groups are located at a greater distance in the former molecule than in the latter. In fact, a treatment of **1** with 1M HCl (1M=1 mol dm^{-3}) in THF at 25 °C provides $Me_3SiC{\equiv}C{-}CH{=}C(SiMe_3)_2$ quantitatively. Meanwhile, tetrakis(trimethylsilyl)ethylene was quite stable and was recovered unchanged under the same conditions.

The varieties observed in the C=C bond lengths in substituted cumelenes have been discussed by Irngartinger and his co-workers.[8] They recognized that a clear difference exists between cumulenes with

Table 3. The Variation in C=C Bond Lengths in Butatriene

Compound	X (l/Å)	Y (l/Å)	Technique	Ref.
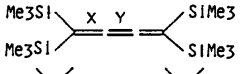	1.319(6)	1.276(8)	X-Ray	This work
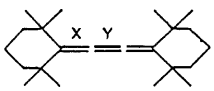	1.332	1.261	X-Ray	9
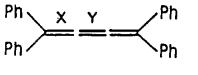	1.345(3)	1.246(3)	X-Ray	10
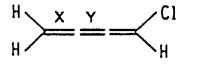	1.326(5)	1.260(10)	Electron diffraction	11
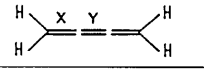	1.318(5)	1.283(5)	Electron diffraction	12

an even number and those with an odd number of double bonds: that is, the terminal double bonds in the former are somewhat shorter than those in the latter. We summarize in Table 3 the C=C bond lentgths observed in substituted butatrienes. The longer terminal double bond in tetraphenylbutatriene may be attributed to conjugation with the phenyl group, whereas the bond lengths observed in the present molecule is very similar to those in unsubstituted butatriene.

The authors wish to thank to Professors Yukiteru Katsube and Nobuo Tanaka for their kind permission to use their computer programs. They are also indebted to Dr. Yukio Morimoto for his invaluable assistance in performing computations.

References

1) T. Kusumoto and T. Hiyama, *Tetrahedron Lett.*, **28**, 1811 (1987).

2) J. Hibino, S. Nakatsukasa, K. Fugami, S. Matsubara, K. Oshima, and H. Naozaki, *J. Am. Chem. Soc.*, **107**, 6416 (1985).

3) T. Kusumoto and T. Hiyama, *Tetrahedron Lett.*, **28**, 1807 (1987).

4) P. Main, S. E. Hull, L. Lessinger, G. Germain, J-P. Declercq, and M. M. Woolfson, A System of Computer Programs for the Automatic Solution of Crystal Structures from X-ray diffraction Data, MULTAN, University of York, (1980).

5) T. Ashida, (1979). HBLS V, the Universal Crystallographic Computing System-Osaka, P.53. The Computation Center, Osaka University.

6) "International Table for X-Ray Crystallography," ed by J. A. Ibers and W. C. Hamiltom, Kynoch Press, Birmingham, U. K.(1974), Vol. IV, p. 72.

7) H. Sakurai, Y. Nakadaira, H. Tobita, T. Ito, K. Toriumi, and H. Ito, *J. Am. Chem. Soc.*, **104**, 300 (1982).

8) H. Irngartinger and W. Goetzmann, *Angew. Chem.*, **98**, 359 (1986).

9) H. Irngartinger and H-U. Jaeger, *Angew. Chem.*, **88**, 615 (1976).

10) Z. Berkovitch-Yellin and L. Leiserowitz, *Acta Crystallogr., Sect. B*, **33**, 3657 (1977).

11) A. Almenningen, G. Gundersen, A. Borg, M. Granberg, and F. Karlsson, *Acta Chem. Scand., Ser. A*, **29**, 395 (1975).

12) A. Almenningen, O. Bastiansen, and M. Traetteberg, *Acta Chem. Scand.*, **15**, 1557 (1961).

Activation of Dinitrogen over Various Raney Type Metal Catalysts

Yoichi OGATA, Ken-ichi AIKA,* and Takaharu ONISHI
Research Laboratory of Resources Utilization, Tokyo Institute of Technology, 4259 Nagatsuta, Midori-ku, Yokohama 227
(Received August 26, 1988)

Synopsis. Raney Ni, Rh, Re, and Ir adsorbed molecular nitrogen which was stable up to about 300 K. Raney Fe, Co, Ni, Ru, Rh, Ir, and Pt adsorbed atomic nitrogen which was desorbed around 700 or 800 K. The XPS spectra of atomically adsorbed nitrogen was observed on Co, Ni, and Ru samples. While the per-weight activity of Raney Ru for isotopic equilibration of N_2 is much higher than that of 5% Ru-K/AC, those of other Raney metals are lower than those of 5% metal-K/AC.

Supported Ru catalysts are known to be promoted with metallic potassium,[1,2] however, Raney Ru, which has no potassium promoter, was found to be as active as potassium-promoted Ru catalysts.[3] Thus, other transition metals of Raney-type catalysts might be active without a potassium promoter. The adsorption characteristics and the activity of isotopic equilibration (IE) reaction of the N_2 are compared for various Raney catalysts.

Experimental

Raney catalysts were prepared by leaching metal-Al alloys (weight ratio; 1/1) with a 5 M of KOH solution at 373 K for 2 h.[4] The weight of the leached sample was estimated to be that of the starting transition metal (normally 1 g), thereby neglecting the weight of remaining Al (ca. 10%). After the sealing water was evacuated in the reactor at room temperature for 10 h the sample was dryed under circulating He at 523 K with a liquid-nitrogen trap for 5 h, and then evacuated at 523 K for 2 h. After the BET surface area was measured by N_2 at 77 K, the sample was stabilized under a N_2 atmosphere at 623 K for 40 to 50 h. This treatment caused N_2 adsorption and sintering of the sample. After evacuation at 623 K (here, ca. one third of N_2 was still irreversibly adsorbed in the case of Ru sample) H_2 chemisorption (273 K) and the BET area (77 K) were again measured. The rate of the IE reaction of N_2 was measured this time at 473 to 773 K. Another series of samples were sealed in glass tubes after N_2 adsorption at 623 K, and were then transfered into the XPS spectrometer.

Results

Characterization of Various Raney Metal. Most of the metal-Al alloys were leached smoothly, except for the Fe sample (10 h for the leaching). The resultant solution of the Fe sample was dark greenish, which suggested that a part of the Fe was dissolved. The leached Raney Fe was treated exceptionally with H_2 at 723 K for 100 h since the surface might have been oxidized. The BET surface area of all the samples measured before N_2 uptake are shown in Table 1. The leached samples have a high surface area (27 to 142 m^2g^{-1}), except for Pd (5 m^2g^{-1}) and Fe (14 m^2g^{-1}), compared to the starting alloy (ca. 1 m^2g^{-1}). The surface area (Table 1) was decreased by sintering during the N_2 treatment at 623 K, except for the Fe sample, in which case nitride formation was suggested.[1]

The metallic atom percentage on the surface was calculated by assuming the relation: (number of H chemisorbed)/(number of surface metal estimated by BET area)[5] (Table 1). The metallic atom percentage on the surface was also measured by XPS, assuming the molar ratio Me/(Me+Al); see Table 1. The XPS results show that Al remained on the surface, except for Raney Re. The surface metallic atom percentage measured by H_2 chemisorption is generally lower than that measured by XPS. Several reasons have been suggested: 1) The surface dencity of Al atoms is lower than that of Ru, because oxidized Al requires a wider space for the counter anion (oxygen); 2) irreversibly adsorbed nitrogen might partly remain; and 3) a part of the surface transition metal, such as Fe or Re, is oxidized. An XPS study showed that about 20% of Re and 70% of Fe were oxidized; however, other samples were all metallic. The residual Al was metallic (Al_{2s}=117.5 eV) over Rh, Pt, and Ir samples, though, it was almost oxidized (Al_{2s}=119.0 eV) over other sam-

Table 1. Characterization of Various Transition Metal Raney Catalysts

Raney catalyst sample	BET before N_2 uptake[a]	BET after N_2 uptake[a]	N_2 uptake[a]	H_2 ads.[b]	Surf. metal atom% by ads.[c]	Surf. metal atom% by XPS[d]
	m^2g^{-1}	m^2g^{-1}	$ml\,g^{-1}$	$ml\,g^{-1}$		
R-Fe[e]	14.0	46.6	2.0	0.23	2	53
R-Co	—	22.7	5.2	0.57	9	52
R-Ni	82.7	63.0	7.0	3.8	21	37
R-Ru	98.4	51.4	9.4	6.0	51	79
R-Rh	141.7	31.5	—	1.6	21	60
R-Pd	5.0	0.8	Neg	—[f]	—	47
R-Re	83.6	11.1	Neg	1.10	34	100
R-Ir	41.2	22.3	0.5	0.98	18	44
R-Pt	26.7	6.8	Neg	1.50	96	57

a) With 400 Torr N_2 (1 Torr≈133.322 Pa) at 623 K for 40 h. b) Measured at 273 K. c) Calculated using H_2 ads. and BET area by the method in Ref. 5, p. 296. d) M/(M+Al). e) Sample after H_2 reduction at 723 K for 100 h. f) Calculation was not carried out for Raney Pd because of the excess hydrogen dissolution to Pd metal phase.

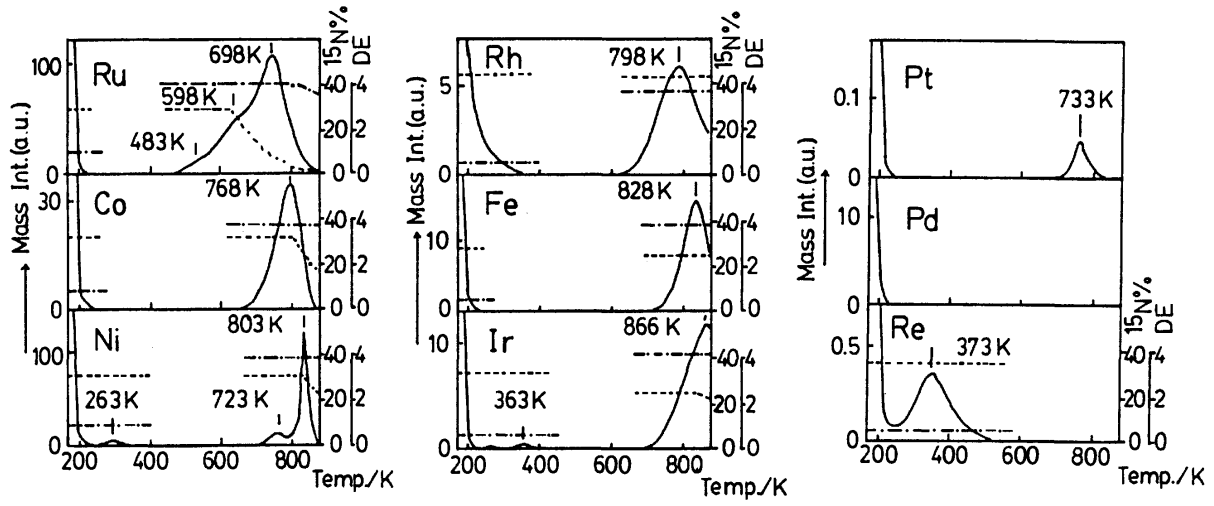

Fig. 1. TPD spectra of adsorbed nitrogen after some extent of isotopic randomization over various Raney type metals. The kind of metal is shown in the figures. ——; total nitrogen ($^{28}N_2+^{29}N_2+^{30}N_2$), ·····; $^{15}N\%$ ($^{29}N_2/2+^{30}N_2$), -·-·-; DE in the text.

ples (Co, Ni, Ru, and Pd).

TPD Study Using ^{15}N Isotope. About one half of the gas-phase nitrogen ($^{28}N_2$) was replaced with $^{30}N_2$ at 573 K. At this point the IE reaction was carried out at 573 K in order to supply an isotopic mixture of surface nitrogen until the degree of equilibration (D.E.) reached approximately unity.

$$\text{D.E.} = (^{29}N_2)^2(^{28}N_2)^{-1}(^{30}N_2)^{-1} \quad (1)$$

An adequate value of D.E. could not be obtained for Pd, Re, and Pt, because of the low activity. The adsorbed nitrogen was quenched and the gas-phase nitrogen was evacuated at 77 K for 3 h; then, a TPD run was carried out to 873 K at a rate of 4 K min^{-1}.

In Fig. 1, the solid lines indicate the total amount of all isotopes of nitrogen during TPD, and the dots and lines show the value of D.E. If no isotopic randomization in N_2 molecule occurs during the desorption (i.e., molecular adsorption), the value of D.E. of the desorbing gas should be kept unchanged from the initial D.E. (ca. 1.0). If isotopic randomization occurs (i.e., atomic adsorption), the value of D.E. should reach about 4.0. Therefore, peaks below 195 K were all assigned to the molecular species (γ-type) because of the low D.E. value (ca. 1.0). Molecular species which were stable at around room temperature (α-type) were observed on Ni, Re, Ir, and probably on Rh catalyst. Peaks above 500 K were all assigned to atomic species since the D.E. values were near 4. It is interesting that Pt, Ir, and Rh samples have β-type, despite the fact that these metals are known to be poor catalysts for N_2 activation, and that there has been no report concerning atomic adsorbed nitrogen from N_2.[1]

The $^{15}N\%$ of the desorbing gas is also shown as dotted lines in Fig. 1. If pre-adsorbed nitrogen (containing ^{14}N) is completely mixed during the IE reaction at 573 K, the $^{15}N\%$ should be constant during a TPD run. However, the value becomes lower at high temperature for Ru, Co, and Ni samples. This means that some pre-adsorbed nitrogen did not take part in the IE reaction at 573 K, and that the atomic nitrogen was adsorbed at various heats of adsorption (surface heterogeneity).

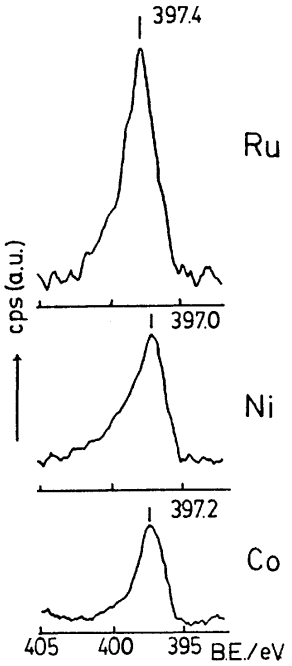

Fig. 2. XPS spectra of N_{1s} region of adsorbed nitrogen on Raney Ru, Ni, and Co.

XPS Spectra of Adsorbed Nitrogen. Only Ru, Ni, and Co samples showed XPS spectra of nitrogen (Fig. 2). The binding energies are 397.4 for Ru, 397.0 for Ni, and 397.2 eV for Co sample, respectively. Since the binding energy of AlN is 396.7 eV, these spectra have been identified to be adsorbed nitrogen on transition metals. Since molecularlly adsorbed nitrogen was evacuated in the XPS chamber at room temperature, the observed XPS spectra should correspond to atomic nitrogen (β-type) for Ru, Ni,[6] and Co catalysts. The relative XPS intensities of nitrogen against metal are 0.07 for Ru, 0.05 for Ni, 0.04 for Co sample, respec-

Table 2. Kinetic Data of Isotopic Equilibration Reaction over Raney Catalysts

Catalyst	10^4×TOF[a]	10^{-16}×Activity[a]		Act. energy		Desorption temp[d]
	10^4×molec. s^{-1} $site^{-1}$	10^{-16}×molec. min^{-1} g^{-1}		kcal mol^{-1}		K
R-Fe	0.0031	0.023	(4.6)[e]	33	(35)[f]	828
R-Co	0.035	0.64	(1.5)[e]	40	(38)[f]	768
R-Ni	0.0014	0.17	(0.35)[e]	34	(31)[f]	723
R-Ru	88.2 (24.1)[b]	17000	(503)[e]	27	(23)[f]	483
R-Rh	0.0088	0.45	(1.2)[e]	21	(25)[f]	798
R-Pd	0.000[c]	—	—	—	—	—
R-Re	0.000[c]	—	(1.3)[e]	—	(40)[f]	—
R-Ir	0.0147	0.46	(0.75)[e]	15	(26)[f]	866
R-Pt	0.000[c]	—	—	—	—	733

a) At 588 K under 150 Torr. b) TOF over 5% Ru-K/AC.[4] c) Rate is not measurable even at 773 K. d) The lowest peak temperature for the desorption of β-nitrogen. e) 10^{-16}×Activity over 5% Me-K/AC.[2] f) Activation energy over 5% Me-K/AC.[2]

tively. These values are lower than the surface metallic atom percentages listed in Table 1, probably because of an overestimation of the bulk metal by XPS.

Isotopic Equilibration Reaction of Dinitrogen. The rates of the IE reaction were observable at a temperature where the β-type started to be desorbed. Kinetic data of the reaction are shown on Table 2. The activities are rearranged as TOF in which the number of sites is based on H_2 chemisorption. The activities of all the catalysts were stable during runs for several days at 473 to 773 K.

Discussion

TPD of Adsorbed Nitrogen and TOF of IE Reaction. Molecularly adsorbed nitrogen (α-type) was found at around room temperature on Raney Ni, Re, Ir, and probably on Rh catalysts. Molecularly adsorbed nitrogen has been also observed by ir on Ni-SiO_2 (2202 cm^{-1}), Rh-SiO_2 (2236 cm^{-1}), and Ir (2185 cm^{-1}).[1]

Atomically adsorbed nitrogen should be related with an IE reaction. The desorption peak temperature of the β-type nitrogen is compared with the TOF of an IE reaction at 588 K in Table 2. Raney Ru, which has the lowest desorption temperature, is extraordinarily active. Since the desorption process is one of the steps in the IE reaction, the above two data should be related to each other. The surprizing thing is the activity difference among the catalysts. Only Raney Ni and Ru have multiple TPD peaks for atomic nitrogen. All of the other samples give sharp and single TPD spectra of the β-type. Raney Ni and Ru seem to have multiple active sites. The β-type species must be the intermediate for the IE reaction. The activation energy of IE reaction is equal to that of the adsorption step when the coverage is low and is equal to that of desorption step when the coverage is high. Among Fe, Co, Ni, and Ru on which nitrogen coverage seems to be high (see the mass intensity in Fig. 1), Ru gives the lowest activation energy (Table 2). Rh and Ir give low activation energies, probably, because the coverages are low. Of course, the activation energy data is not decisive in explaining the extraordinal activeness of Raney Ru. It is suggested that a relatively high concentration of the special active site is formed.[3]

Comparison of the Activity of Raney Metal with That of Potassium Promoted Metals. Activity data of potassium promoted metals on AC (Me-K/AC) are only available for comparing the activity of various metal catalysts.[2] The activity is, however, described on the bases of catalyst weight, shown in Table 2. The per-weight activity over Raney Ru is quite high (17000×10^{16} molec. min^{-1} g^{-1}), compared to that (503×10^{16} molec. min^{-1} g^{-1}) over 5%Ru-K/AC.[2,4] The major reason is that Raney Ru has 6% dispersion, i.e., (0.06 g-surface Ru) (g-catalyst)$^{-1}$, and that the 5%Ru/AC has only 12.7% dispersion i.e., (0.0064 g-surface Ru) (g-catalyst)$^{-1}$. Thus, if the two catalysts have the same TOF, the per-weight activity of Raney catalyst must be about ten-times higher than that of 5% Me-K/AC. In this respect, the TOFs of Raney Co, Ni, Rh, and Ir seem to be less than one tenth of those of 5% Me-K/AC. This is because these Raney catalysts have an even lower per-weight activity than Me-K/AC catalysts (Table 2).

Inactiveness of Fe and Re. Fe and Re single crystals have been reported to be quite active for ammonia synthesis.[7] XPS results showed that our Fe and Re samples were partly oxidized because the Raney-type catalyst is prepared in water. This must be the reason why the activities of these samples are low.

References

1) A. Ozaki and K. Aika, "Catalytic Activation of Dinitrogen" in "Catalysis-Science and Technology," ed by J. R. Anderson and M. Boudart, Springer-Verlag, Berlin-New York (1981), Vol. 1, p. 87.

2) K. Urabe, A. Ohya, and A. Ozaki, *J. Catal.*, **54**, 436 (1978).

3) Y. Ogata, K. Aika, and T. Onishi, *J. Catal.*, **112**, 469 (1988).

4) K. Urabe, K. Aika, and A. Ozaki, *J. Catal.*, **32**, 108 (1974); **38**, 430 (1975).

5) J. R. Anderson, "Structure of Metallic Catalysts," Academic Press, New York (1975).

6) M. Grunze, C. R. Brundle, and D. Tomanek, *Surf. Sci.*, **119**, 133 (1982).

7) G. Ertl, S. B. Lee, and M. Weiss, *Surf. Sci.*, **114**, 515, 527 (1982); N. D. Spencer, R. C. Schoonmaker, and G. A. Somorjai, *J. Catal.*, **74**, 129 (1982).

Acid-Catalyzed Oxidation of Oxiranes with Dimethyl Sulfoxide Giving α-Hydroxy Ketones

Tadakazu TSUJI
Department of Chemistry, Japan Women's University, Mejirodai, Bunkyo-ku, Tokyo 112
(Received June 14, 1988)

Synopsis. The reaction of various oxiranes with dimethyl sulfoxide in the presence of Molecular Sieve 4A and acid afforded the corresponding α-hydroxy ketones. The molecular sieve was found to accelerate the reaction.

It has previously been reported that the boron trifluoride induced dimethyl sulfoxide (DMSO) oxidation of some oxiranes gave α-hydroxy ketones.[1] Subsequently, the proposed intermediacy of (2-hydroxyalkoxy)sulfonium salts has been prepared by Swern and co-workers as a stable form by the treatment of oxiranes with excess DMSO in the presence of an equimolar amount of acid (i.e., CF_3CO_2H, HBF_4, and CH_3SO_3H).[2,3] However, they reported that the thermolysis of the intermediate alkoxysulfonium salt from 1,2-epoxycyclohexane gave a complex mixture without giving any predominant products.[3] They also described that the reaction of the salts from 2-phenyloxirane and 2,3-dimethyloxirane in DMSO-d_6 at 100 °C for 1 h resulted in an exclusive formation of phenylethanal and 2-butanone, respectively.[2,3] We found that the treatment of a DMSO solution of 2-phenyloxirane (**1a**) at 100 °C in the presence of a catalytic amount of alkoxysulfonium salt (**2a**), which was generated in situ from DMSO, **1a** and CF_3CO_2H, gave the expected 2-hydroxy-1-phenylethanone (**3a**). This finding led us to investigate the reactions of oxiranes with DMSO and acid giving α-hydroxy ketones via the alkoxysulfonium salts. The present paper deals with reactions of the various types of oxiranes with DMSO in the presence of an appropriate acid as catalyst.

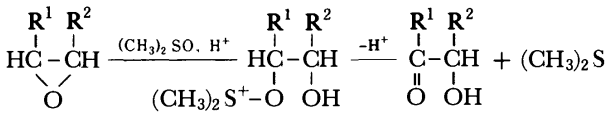

1 **2** **3**

	R^1	R^2
a	C_6H_5	H
b	C_6H_5	C_6H_5
c	C_2H_5	H
d	C_6H_{13}	H
e	CH_3	CH_3
f	-(CH_2)-	
g	-$(CH_2)_{10}$-	

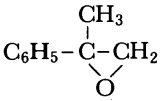

1h

Results and Discussion

The acid-catalyzed DMSO oxidation of 2-phenyloxirane (**1a**) in the presence of molecular sieve was examined in a ^1H NMR sealed tube. The solution of **1a** (0.5 mmol) in DMSO or DMSO-d_6 (2.5 mmol) showed the NMR signals which are assignable to the starting material. Upon the addition of CF_3CO_2H (0.025 mmol) and Molecular Sieve 4A (20 mg) at room temperature, three signal sets appeared: a methylene doublet at δ 3.90 and a methine triplet at δ 5.70 along with a pair of singlet of two nonequivalent *S*-methyl groups at δ 3.35 and 3.50. The new spectral sets observed are consistent with those of the reported (2-hydroxyalkoxy)sulfonium salt **2a**.[3] The molar ratio of **1a** : **2a** was calculated to be about 25 : 1, by a comparison of the signal magnitude of methylene protons of **1a** (δ 2.80 and 3.15) with that of *S*-methyl protons of **2a**. Upon heating the mixture at 100 °C, the signals of oxirane ring protons gradually disappeared and were replaced by three sets of signals: a singlet at δ 4.98 and two multiplets at δ 7.33—7.75 and 7.91—8.71. By a comparison with the spectrum of authentic sample **3a**,[1] the singlet and two multiplets could be assigned to the methylene and aromatic protons of **3a**. The simultaneous appearance of the other additional sets of signals, two multiplets at δ 3.0—3.8 and 4.4—4.8, and a singlet at δ 7.1, were observed. These are assigned to the methylene, methine, and aromatic proton signals[4] of the polymer of **1a** (**4**), which was isolated from the mixture after work-up. In addition, the formation of dimethyl sulfide was found in the NMR spectra (δ 2.00, singlet). No formation of 1,2-diol nor aldehyde was observed in a reaction mixture by NMR and GC-MS analysis, but a trace amount of the dimer of **1a** was detected by GC-MS. The dimer was assumed to be in a mixture of 2,5-diphenyl-1,4-dioxane and 2-benzyl-4-phenyl-1,3-dioxolane by NMR.[5] The relation between the used amount of CF_3CO_2H and the yields of **3a** and **4** in this reaction (100 °C, 7 and 14 h with molecular sieve) was examined, and the results are shown in Table 1. The yields of both compounds were calculated by an integration of their methylene signals using the aromatic proton signals as an internal standard. As shown in the table, the yield of **3a** reached its maximum value, 68.5% in a concentration of 0.05 equimolar amount of acid (Run 3). The yield of polymer **4** was 28.3% in this run. The use of a large amount of acid resulted in a decrease in the formation of **3a**. However, a longer time was required for completion at a lower content of CF_3CO_2H amount. In one run using 0.05 equivalent of CF_3CO_2H without a molecular sieve (Run 4), the reaction rate was slower than that in the presence of a molecular sieve (Run 3).

Meanwhile, the correlation between the amount of DMSO (2—9 equivalents) and the yield of **3a** was examined in the presence of a molecular sieve and 0.05 equivalent of CF_3CO_2H at 100 °C for 7 h. As a result, it was found that the use of a 5 equivalent amount of DMSO is optimum to yield **3a**.

Subsequently, the catalytic efficacy of other acids

Table 1. Reaction of 2-Phenyloxirane (**1a**) with DMSO in the Presence of CF_3CO_2H[a]

Run	CF_3CO_2H/equiv	React. time/h	Products and yields/%[b]		
			3a	**4**	**1a**
1	0.03	7	18.5	7.6	72.3
2	0.04	7	50.8	19.6	27.1
3	0.05	7	68.5	28.3	0
4[c]	0.05	7	49.1	20.3	27.5
5	0.1	7	53	43.4	0
6	0.15	7	36.8	60	0
7	0.03	14	35.5	14.3	46.9
8	0.04	14	70.5	27	0

a) Reaction of **1a** (0.5 mmol) was conducted with DMSO (5 equiv) in the presence of CF_3CO_2H at 100 °C. All runs except Run 4 was carried out in the presence of Molecular Sieve 4A (20 mg). b) Determined by ^1H NMR. c) Molecular Sieve 4A was not added.

Table 2. Acid-Catalyzed Oxidation of Oxiranes with DMSO

Run	Compd., mmol	Acid, mmol	DMSO/ mmol	Mol. Sieve 4A/g	React. time/h	α-Hydroxy ketone (Isolated yield/%)	Other products (Isolated yield/%)
1	**1a**, 100	CF_3CO_2H, 5	500	4	20	**3a**(62.1)	Polymer **4**(8.4), **1a**(1.1)
2	**1b**, 100	CF_3CO_2H, 10	500	4	9	**3b**(57.2)	1,2-Diphenylethanone (7.9), Dimer of **1b**[a] (trace)
3	**1b**, 100	CF_3CO_2H, 10	500	0	9	**3b**(49.3)	1,2-Diphenylethanone (7.1), Dimer of **1b** (trace), **1b**(6.6)
4	**1c**, 30	$HBF_4.Me_2O$, 1.5	150	0.75	10	**3c**(51.4)	
5	**1d**, 50	$HBF_4.Me_2O$, 2	250	1.25	14	**3d**(74.6)	**1d**(10.9)
6	**1e**, 30	$HBF_4.Me_2O$, 1.5	150	0.75	10	**3e**(44.4)	
7	**1f**, 50	$HBF_4.Me_2O$, 2	250	1.25	5	**3f**(88)[b]	Cyclohexanone(0.8)
8	**1g**, 33	$HBF_4.Me_2O$, 1.65	165	0.825	9	**3g**(19.9)	Cyclododecanone(50)
9	**1h**, 50	CF_3CO_2H, 1	250	1.25	10	—	2-Phenylpropanal(44)

a) Detected by GC-MS.[6] b) A mixture of monomer and dimer.[1]

were examined by the NMR technique. A reaction of **1a** with DMSO in the presence of either $HBF_4 \cdot Me_2O$ (0.05 equivalent) or CH_3SO_3H (0.1 equivalent) at 100 °C for 10 h gave **3a** in modest yield, 30.1 and 25.2%, respectively.

The preparative experiment was carried out by the reaction of oxiranes with 5 equivalent DMSO in the presence of Molecular Sieve 4A and a catalytic amount of acid at 100 °C. The reaction conditions and results are given in Table 2. When Runs 2 and 3 were compared, it seemed likely that the use of a molecular sieve promotes the reaction of *trans*-2,3-diphenyloxirane (**1b**). The similar effect of a molecular sieve is demonstrated in Table 1, in a reaction of 2-phenyloxirane (**1a**). Thus, the other runs in Table 2 were performed in the presence of a molecular sieve. Compounds **3a** and **3b** were synthesized by the use of CF_3CO_2H as acid, while the preparation of other α-hydroxy ketones, **3c—3g**, were accomplished by the use of 0.04—0.05 equivalents of $HBF_4 \cdot Me_2O$, but not by CF_3CO_2H and CH_3SO_3H. No formation of isomeric 2-hydroxy aldehyde was observed in the oxidation of **1c** or **1d**. The reaction of 1,2-epoxycyclododecane (**1g**) gave a mixture of 2-hydroxycyclododecanone (**3g**) and cyclododecanone in yields of 19.9 and 50%, respectively. The modest yield of **3g** may be due to the steric hindrance of a bulky cycloalkyl group against the attack of DMSO on the oxonium salt of **1g**. 2-Methyl-2-phenyloxirane (**1h**) afforded 2-phenylpropanal exclusively in 44% yield. The GC-MS analysis of the crude product suggested the presence of a trace amount of 2-hydroxy aldehyde.

Swern and co-workers have reported that a treatment of the intermediate salt **2a** from 2-phenyloxirane **1a** with a base gave **3a**, but other salts prepared from other oxiranes decomposed by the action of base to a mixture of simple ketones, 1,2-diols or other products without giving α-hydroxy ketones.[3] In contrast, various α-hydroxy ketones were now obtained by the acid-catalyzed oxidation of oxiranes via salts **2**.

The present method for the preparation of α-hydroxy ketones has synthetic utility. The reaction pathway involving the formation of (2-hydroxyalkoxy)sulfonium salts **2** and the elimination of dimethyl sulfide from **2** giving **3** are under way.

Experimental

^1H NMR spectra were obtained using a JEOL JNM-PMX 60 spectrometer (60 MHz). TMS was used as an internal

standard. GC-MS was performed on a JEOL JMX-DX 300 spectrometer at 70 eV.

NMR Monitoring Experiment for Oxidation of 2-Phenyloxirane (1a) with DMSO. Compound **1a** (0.5 mmol), DMSO-d_6 or DMSO (2.5 mmol) containing DSS as an NMR internal standard, Molecular Sieve 4A (20 mg) and CF_3CO_2H (0.025 mmol) were introduced into NMR tube in this order. The tube was sealed after the atmosphere was displaced by CO_2, and the NMR spectrum was then measured. The molar ratios of the reactants and yields of the products were calculated by integrating the NMR signals using the aromatic signals as an internal standard.

General Procedure for Preparation of α-Hydroxy Ketones by DMSO Oxidation of Oxiranes. Oxirane, anhydrous DMSO, Molecular Sieve 4A (beads size) and acid were placed in a sealed tube, and a stream of dry CO_2 was passed through the apparatus in order to displace the air. The vessel was sealed and the reaction mixture was heated at 100 °C. After completion of the reaction, the reaction mixture was poured into ice water and extracted with CH_2Cl_2. The CH_2Cl_2 solution and the aqueous solution were separately evaporated in vacuum. The residues were purified by recrystallization or distillation in vacuo. The products were identified by comparisons with authentic samples (mp, IR and /or ^{1}H NMR spectra).

2-Hydroxy-1-phenylethanone (3a): Bp 105—110 °C/7 mmHg (1 mmHg≈133.322 Pa); mp 74—75 °C (lit,[2] 75 °C); IR (KBr) 3400 (OH) and 1690 cm^{-1} (C=O); ^{1}H NMR (DMSO-d_6) δ=4.98 (2H, s, CH_2), 7.33—7.75 (2H, m, arom) and 7.91—8.71 (3H, m, arom).

***dl*-2-Hydroxy-1,2-diphenylethanone (3b):** Mp 130—131 °C (lit,[7] 129 °C); ^{1}H NMR ($CDCl_3$) δ=3.46 (1H, s, OH), 6.15 (1H, s, CH) and 7.23—8.05 (10H, m, arom); CI-MS M$^+$+1, 213.

1-Hydroxy-2-butanone (3c): Bp 110—113 °C/100 mmHg (lit,[8] 79—80 °C/30 mmHg); IR (KBr) 3400 (OH) and 1710 cm^{-1} (C=O); EI-MS M$^+$, 88.

1-Hydroxy-2-octanone (3d): Oil; bp 74—78 °C/6 mmHg (lit,[9] 70—76 °C/6 mmHg); IR (KBr) 3400 (OH) and 1710 cm^{-1} (C=O); ^{1}H NMR ($CDCl_3$) δ=0.93 (3H, d, CH_3), 1.32—2.33 (8H, m, CH_2), 2.67 (2H, t, CH_2CO), and 4.22 (2H, s, CH_2OH); CI-MS M$^+$+1, 145.

2-Hydroxybutanone (3e): Oil; bp 98-105 °C/100 mmHg (lit,[10] 148 °C); IR (KBr) 3420 (OH) and 1710 cm^{-1} (C=O); CI-MS M$^+$+1, 89.

2-Hydroxycyclohexanone (3f): Bp 82—85 °C/13 mmHg (lit,[1] 83—85 °C/13 mm); Compound **3f** was readily dimerized to 1,4-dioxane derivative.[1]

2-Hydroxycyclododecanone (3g): Bp 114—116 °C/6 mmHg; mp 75—77 °C (lit,[11] 78—79 °C); ^{1}H NMR ($CDCl_3$) δ=1.38—2.25 (18H, m, -$(CH_2)_9$-), 2.83 (2H, m, CH_2CO) and 4.42 (1H, s, CH); CI-MS M$^+$+1, 198.

Cyclododecanone: Bp 73—81 °C/8 mmHg; mp 60—61 °C (lit,[12] 60.7 °C); CI-MS M$^+$+1, 183.

2-Phenylpropanal: Bp 125—128 °C/96 mmHg (lit,[13] 202—205 °C).

References

1) T. Cohen and T. Tsuji, *J. Org. Chem.*, **26**, 1681 (1961).
2) M. A. Khuddus and D. Swern, *J. Am. Chem. Soc.*, **95**, 8393 (1973).
3) T. M. Santosusso and D. Swern, *J. Org. Chem.*, **40**, 2764 (1975).
4) Z. Jedlinski, J. Kasperczyk, A. Dworak, and B. Matuszewska, *Makromol. Chem.*, **183**, 587 (1982).
5) R. Velichkova and R. Tsevi, *J. Polym. Sci. Part A: Polym. Chem.*, **24**, 3399 (1986).
6) The structure of **8** was not determined.
7) R. Adams and C. S. Marvel, *Org. Synth.*, Coll. Vol. **1**, 94.
8) M. Sommelet, *Bull. Soc. Chim. Fr.*, **9**, [iv], 35 (1911).
9) T. Tsuji, *Tetrahedron Lett.*, **1966**, 2413.
10) O. Daniel and E. Stephan, *Ber.*, **40**, 4338 (1907).
11) M. Stoll and A. Rouve, *Helv. Chim. Acta*, **30**, 1822 (1947); S. Torii, T. Inokuchi, and R. Oi, *J. Org. Chem.*, **47**, 47 (1982).
12) G. A. Olah, M. Arvaghi, and Y.D. Vanker, *J. Org. Chem.*, **45**, 3531 (1980).
13) S. N. Danilov and E. D. Venus-Danilova, *Ber.*, **60**, 1062 (1927).

Asymmetric Radical Reaction in the Coordination Sphere. IV.[1] Ruthenium(II)-Catalyzed Asymmetric Addition of Sulfonyl Chloride to 1-Phenylpropene

Masayuki KAMEYAMA and Nobumasa KAMIGATA*
Department of Chemistry, Faculty of Science, Tokyo Metropolitan University, Fukazawa, Setagaya-ku, Tokyo 158
(Received June 23, 1988)

Synopsis. The asymmetric addition of methane- and *p*-toluenesulfonyl chloride to 1-phenylpropene catalyzed by $Ru_2Cl_4[(-)\text{-diop}]_3$ affords optically active 1 : 1 adducts, (+)-(1*R*,2*RS*)-1-chloro-2-methylsulfonyl-1-phenylpropane (**2**) and (+)-(1*R*,2*RS*)-1-chloro-1-phenyl-2-tosylpropane (**3**), with about 13—19%ee. Similarly, (−)-(1*S*,2*RS*)-**2** and (−)-(1*S*,2*RS*)-**3** were obtained when $Ru_2Cl_4[(+)\text{-diop}]_3$ was employed. A enantiolace differentiation is considered to occur in the chlorine atom transferring step from the ruthenium(III) species to the carbon radical in the coordination sphere.

Polyhaloalkanes and sulfonyl chlorides reacted with olefins in the presence of transition metal complexes such as $RuCl_2(PPh_3)_3$ to give 1 : 1 adducts in high yields.[2,3] It is considered that these reactions proceed by a radical redox mechanism and the intermediate radicals are restricted in the coordination sphere of the metal complexes. We assume that the resulting radical complexes closely resemble carbene-metal complexes. The asymmetric addition of alkyl diazoacetates to olefins catalyzed by copper-chiral ligands complexes is known to form optically active cyclopropanes and in which reaction involves a carbenoid intermediate.[4] An asymmetric addition of bromotrichloromethane to styrene catalyzed by a rhodium complex with a chiral ligand has also been reported.[5] Thus, an asymmetric induction is expected in the reaction of sulfonyl chlorides with olefins which proceeds by a radical intermediate in the coordination sphere. We recently found that alkane- and arenesulfonyl chlorides,[6] trichloromethanesulfonyl chloride, and carbon tetrachloride[1] reacted with olefins in the presence of a catalytic amount of ruthenium(II) complex with chiral ligand, $Ru_2Cl_4[(+)\text{-diop}]_3$ ((+)-**1**) or $Ru_2Cl_4[(-)\text{-diop}]_3$ ((−)-**1**), to give optically active adducts with about 10—40% ee. However, we have only observed an asymmetric induction to a benzylic carbon bonding to a chlorine atom since terminal olefins, such as styrene, were used in these addition reactions. An asymmetric induction to the β-position of olefins, bonding to the sulfonyl group, may also be possible by using internal olefins. Here, we report on the asymmetric addition of methane- and *p*-toluenesulfonyl chloride to *trans*- and *cis*-1-phenylpropene catalyzed by the ruthenium(II) complex with chiral ligand **1**.

The addition of methanesulfonyl chloride with 1-phenylpropene was carried out in the presence of the ruthenium(II)-DIOP complex **1** as a catalyst. When $Ru_2Cl_4[(-)\text{-diop}]_3$ ((−)-**1**) was used as a catalyst, the reaction of methanesulfonyl chloride with *trans*-1-phenylpropene at 100 °C for 24 h in a degassed sealed tube gave a 1 : 1 adduct (**2**) in 47% yield. Adduct **2** showed a specific rotation $[\alpha]_D$ +4.7° (*c* 5.3, $CHCl_3$). In

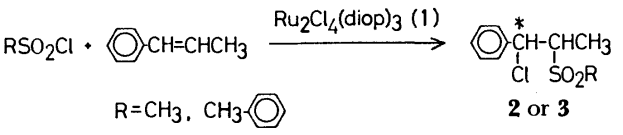

a similar manner, the reaction of methanesulfonyl chloride with *trans*-1-phenylpropene catalyzed by $Ru_2Cl_4[(+)\text{-diop}]_3$ ((+)-**1**) was carried out; 1 : 1 adduct (**2**) was formed in 47% yield and showed $[\alpha]_D$ −4.9° (*c* 6.0, $CHCl_3$). Methanesulfonyl chloride reacted with *cis*-1-phenylpropene by using (−)-**1** as a catalyst to give adduct **2**, which showed $[\alpha]_D$ +4.2° (*c* 11, $CHCl_3$). Adduct **2** showed the same positive optical rotation as product **2**, which formed in the reaction of *trans*-1-phenylpropene.

In order to examine an asymmetric induction to a β-carbon of 1-phenylpropene bonding to the methanesulfonyl group, the adduct (+)-**2** ($[\alpha]_D$ +4.7° (*c* 5.3, $CHCl_3$)) was reduced by lithium aluminum hydride to afford 2-methylsulfonyl-1-phenylpropane, which was an optically inactive compound.[7] This means that an asymmetric induction did not occur in the β-position. In other words, the methanesulfonyl radical, generated by an interaction of the ruthenium(II)-DIOP complex **1**, was not interacted with effectively by the chiral ligands in the addition step to the olefin.

The reaction of *p*-toluenesulfonyl chloride with *trans*- and *cis*-1-phenylpropene was also carried out with (+)-**1** or (−)-**1** as a chiral catalyst, in a similar way, to give 1 : 1 adducts (**3**). The results are summarized in Table 1.

The enantiomeric excess and absolute configuration of products **2** and **3** in the present reactions were estimated by making comparison with optically pure compounds, which were prepared by a similar procedure to that mentioned in our previous report.[5] Starting from commercially available, optically pure (+)-(*S*)- and (−)-(*R*)-mandelic acid, (+)-(*R*)-**2** or (+)-(*R*)-**3** and (−)-(*S*)-**2** or (−)-(*S*)-**3** were synthesized with retention, respectively.

The ruthenium(II)-catalyzed asymmetric addition can be explained by the following process involving a radical redox mechanism in the coordination sphere of the ruthenium(II) complexes[8] (Scheme 1). Methanesulfonyl chloride is activated by the ruthenium(II) complex **1** to give a methanesulfonyl radical confined in the coordination sphere of the ruthenium(III) complex (**4**). Then, the confined sulfonyl radical intermediate **4** reacts with 1-phenylpropene without any effect of the chiral ligands to form a 1-phenyl-2-(methylsulfonyl)propyl radical confined in the ruthenium(III) species (**5**). The carbon radical in **5** abstracts the chlo-

Table 1. Reaction of Sulfonyl Chloride with 1-Phenylpropene

R	$PhCH=CHCH_3$	DIOP	Product	Chemical yield/%	$[\alpha]_D$/° (*c*, in $CHCl_3$)	Optical yield/%ee[a]	Absolute configuration
CH_3	Trans	(−)	**2**	47	+4.7 (5.3)	15 (12)	R
CH_3	Trans	(+)	**2**	47	−4.9 (6.0)	14 (12)	S
CH_3	Cis	(−)	**2**	29	+4.2 (11)	14 (11)	R
CH_3	Cis	(+)	**2**	30	−4.5 (11)	13 (11)	S
p-$CH_3C_6H_4$	Trans	(−)	**3**	91	+9.0 (13)	19	R
p-$CH_3C_6H_4$	Trans	(+)	**3**	85	−8.0 (10)	16	S
p-$CH_3C_6H_4$	Cis	(−)	**3**	89	+7.8 (11)	16	R
p-$CH_3C_6H_4$	Trans	(+)	**3**	83	−9.3 (11)	19	S

a) Optical yields were estimated by optically pure compounds and ^1H NMR with $E(hfc)_3$ in parentheses.

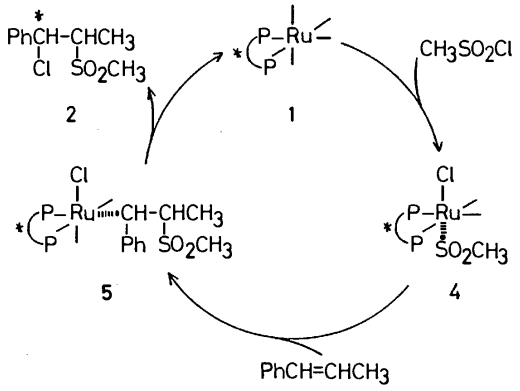

Scheme 1.

rine atom from the ruthenium(III) species containing chiral ligands to give adduct **2** and regenerates the ruthenium(II) complex, **1**. Since 1-phenylpropene is not coordinated as strongly as the sulfonyl radical coordinated to the ruthenium(III) complex (such as **4**), an asymmetric induction does not occur in the intermolecular addition of **4** to the olefin. However, an asymmetric induction occurs in the chlorine atom abstracting step by a carbon radical effected by the chiral ligand, since the carbon radical is coordinated with the ruthenium complex as **5**. The same products were formed in both reactions of *trans*- and *cis*-1-phenylpropene. This means that the sulfonyl radical, generated by a homolytic cleavage of sulfonyl chloride with the ruthenium complex, added to the olefin and a free rotation took place around the carbon-carbon bond in intermediate **5**.

Experimental

Measurement. The infrared absorption spectra were determined on a Hitachi Model 260-10 spectrophotometer with samples as neat liquids. The proton magnetic resonance spectra were recorded at 60 MHz by using a JNM-PMX 60 SI spectrometer with Me_4Si as an internal standard in $CDCl_3$. Optical rotations were measured with a JASCO DIP-140 polarimeter. The gel-permeation liquid chromatography was performed by using a JAI LC-08 liquid chromatograph with a JAIGEL-1H column (20ϕ×600 mm×2, chloroform as an eluent). Mass spectra were determined with a JEOL JMX-DX 300 mass spectrometer with JEOL JMX 5000 Mass Data System at ionizing voltages of 20—70 eV.

Materials. The ruthenium(II) complexes, such as Ru_2Cl_4-[(−)-diop]$_3$ ((−)-**1**) and Ru_2Cl_4[(+)-diop]$_3$ ((+)-**1**), were prepared by methods described in the literature.[9] Methanesulfonyl chloride, *trans*-1-phenylpropene (Wako Chemicals), and *cis*-1-phenylpropene (ICN Pharmaceuticals) were purified by distillation under nitrogen prior to use. *p*-Toluenesulfonyl chloride (Nacalai Tesque) was purified by recrystallization from hexane prior to use.

General Procedure for the Reaction of Sulfonyl Chloride with Olefin. A solution containing 1.0 mmol of sulfonyl chloride, 1.5 mmol of 1-phenylpropene, and 0.01mmol of **1** in 2.0 cm^3 of benzene was degassed and heated in a sealed tube at 100 °C for 24 h. The reaction mixture was chromatographed on Florisil (4:1 (v/v) hexane-ethyl acetate as an eluent) to remove any ruthenium complexes. Purification by gel-permeation liquid chromatography using chloroform as an eluent gave 1:1 adducts (**2** and **3**). The products were identified by their infrared absorption spectra, proton magnetic resonance spectra, mass spectra, and high-resolution mass spectra. The physical and spectral data of the compounds (**2** and **3**) are as follows.

(+)-(1*R*,2*RS*)-1-Chloro-2-methylsulfonyl-1-phenylpropane (2): $[\alpha]_D$ +4.8° (*c* 7.7, $CHCl_3$); IR (neat) 1300, 1145, and 1130 cm^{-1}; ^1H NMR ($CDCl_3$) δ=1.45 (3H, d, *J*=7.0 Hz), 2.60 (3H, s), 3.00—3.70 (1H, m), 5.51 (1H, d, *J*=3.0 Hz), and 7.23 (5H, s); MS *m/z* (rel intensity) 232 (M^+; 3), 197 (9), 196 (18), 156 (13), 155 (100); HRMS, Found: *m/z* 232.0343. Calcd for $C_{10}H_{13}O_2SCl$: M, 232.0325.

(−)-(1*S*,2*RS*)-1-Chloro-2-methylsulfonyl-1-phenylpropane (2): $[\alpha]_D$ −4.9° (*c* 6.0, $CHCl_3$); IR (neat) 1300, 1145, and 1130 cm^{-1}; ^1H NMR ($CDCl_3$) δ=1.49 (3H, d, *J*=7.0 Hz), 2.70 (3H, s), 3.13—3.90 (1H, m), 5.63 (1H, d, *J*=3.0 Hz), and 7.31 (5H, s); MS *m/z* (rel intensity) 232 (M^+; 2), 197 (11), 196 (49), 156 (9), 155 (100); HRMS, Found: *m/z* 232.0342. Calcd for $C_{10}H_{13}O_2SCl$: M, 232.0325.

(+)-(1*R*,2*RS*)-1-Chloro-1-phenyl-2-tosylpropane (3): $[\alpha]_D$ +9.0° (*c* 13, $CHCl_3$); IR (neat) 1320, 1300, and 1145 cm^{-1}; ^1H NMR ($CDCl_3$) δ=1.40 (3H, d, *J*=7.2 Hz), 2.37 (3H, s), 3.39 and 3.45 (1H, qd, *J*=7.2 and 3.0 Hz), 5.60 (1H, d, *J*=3.0 Hz), 7.20 (5H, s), and 7.21 and 7.63 (4H, ABq, *J*=8.4 Hz); MS *m/z* (rel intensity) 308 (M^+; 1), 273 (5), 272 (11), 209 (24), 157 (100), and 155 (100); HRMS, Found: *m/z* 308.0631. Calcd for $C_{16}H_{17}O_2SCl$: M, 308.0638.

(−)-(1*S*,2*RS*)-1-Chloro-1-phenyl-2-tosylpropane (3): $[\alpha]_D$ −8.1° (*c* 7.3, $CHCl_3$); IR (neat) 1320, 1305, and 1145 cm^{-1}; ^1H NMR ($CDCl_3$) δ=1.39 (3H, d, *J*=7.2 Hz), 2.33 (3H, s), 3.40 and 3.45 (1H, qd, *J*=7.2 and 3.0 Hz), 5.58 (1H, d, *J*=3.0 Hz), 7.13 (5H, s), and 7.14 and 7.60 (4H, ABq, *J*=8.4 Hz); MS *m/z* (rel intensity) 308 (M^+; 1). 273 (13), 272 (28), 209 (33), 157 (100), and 155 (100); HRMS, Found: *m/z* 308.0589. Calcd for $C_{16}H_{17}O_2SCl$: M, 308.0638.

Preparation of Optically Pure 1-Chloro-2-methylsulfonyl-1-phenylpropane and 1-Chloro-1-phenyl-2-tosylpropane. Starting from commercially available optically pure (+)-(*S*)-mandelic acid, (+)-(1*R*,2*RS*)-**2**, and (+)-(1*R*,2*RS*)-**3** were pre-

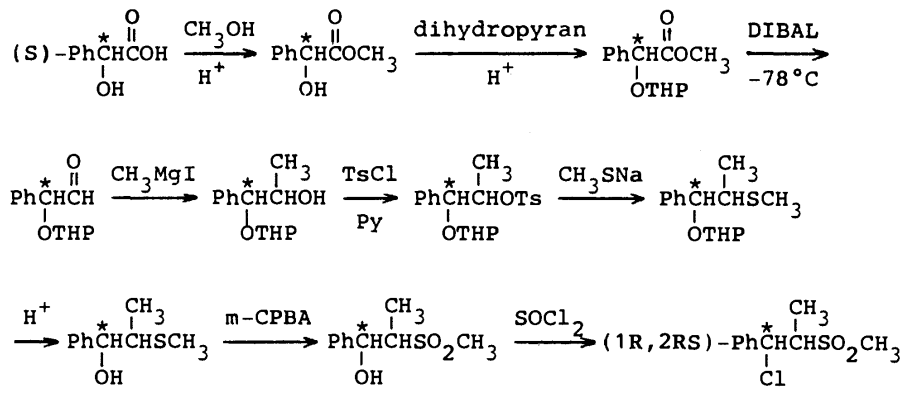

Scheme 2.

pared by the similar procedures described in our previous paper,[6] respectively, as shown in the following scheme. Similarly, (−)-(1*S*,2*RS*)-**2** and (−)-(1*S*,2*RS*)-**3** were prepared from (−)-(*R*)-mandelic acid.

The physical and spectral data of the authentic opically pure compounds **2** and **3** are as follows.

(+)-(1*R*,2*RS*)-1-Chloro-2-methylsulfonyl-1-phenylpropane (2): $[\alpha]_D$ +31° (*c* 1.1, $CHCl_3$); IR (neat) 1300, 1140, and 1130 cm^{-1}; ^1H NMR ($CDCl_3$) δ=1.56 (3H, d, *J*=6.6 Hz), 2.80 (3H, s), 3.10—3.50 (1H, m), 5.44 (0.5H, d, *J*=6.6 Hz), 5.70 (0.5H, d, *J*=3.0 Hz), and 7.41 (5H, s); MS *m/z* (rel intensity) 232 (M^+; 3), 197 (9), 196 (18), and 155 (100); HRMS, Found: *m/z* 232.0322. Calcd for $C_{10}H_{13}O_2SCl$: M, 232.0325.

(−)-(1*S*,2*RS*)-1-Chloro-2-methylsulfonyl-1-phenylpropane (2): $[\alpha]_D$ −34° (*c* 1.8, $CHCl_3$); IR (neat) 1300, 1140, and 1130 cm^{-1}; ^1H NMR ($CDCl_3$) δ=1.55 (3H, d, *J*=6.8 Hz), 3.09 (3H, s), 3.30—3.60 (1H, m), 5.43 (0.5H, d, *J*=6.6 Hz), 5.69 (0.5H, d, *J*=3.0 Hz), and 7.37 (5H, s); MS *m/z* (rel intensity) 232 (M^+; 1), 197 (2), 196 (2), 155 (34), and 154 (100); HRMS, Found: *m/z* 232.0318. Calcd for $C_{10}H_{13}O_2SCl$: M, 232.0325.

(+)-(1*R*,2*RS*)-1-Chloro-1-phenyl-2-tosylpropane (3): $[\alpha]_D$ +48° (*c* 4.5, $CHCl_3$); IR (neat) 1320, 1300, and 1150 cm^{-1}; ^1H NMR ($CDCl_3$) δ=1.40 (3H, d, *J*=7.2 Hz), 2.41 (3H, s), 3.41 and 3.46 (1H, qd, *J*=7.2 and 3.0 Hz), 5.63 (1H, d, *J*=3.0 Hz), 7.20 (5H, s), and 7.22 and 7.68 (4H, ABq, *J*=8.4 Hz); MS *m/z* (rel intensity) 308 (M^+; 1), 272 (5), 271 (15), 233 (14), 209 (29), 158 (15), and 157 (100); HRMS, Found: *m/z* 308.0658. Calcd for $C_{16}H_{17}O_2SCl$: M, 308.0638.

(−)-(1*S*,2*RS*)-1-Chloro-1-phenyl-2-tosylpropane (3): $[\alpha]_D$ −50° (*c* 1.4, $CHCl_3$); IR (neat) 1320, 1300, and 1150 cm^{-1}; ^1H NMR ($CDCl_3$) δ=1.25 (1.5H, d, *J*=7.2 Hz), 1.42 (1.5H, d, *J*=7.2 Hz), 2.44 (3H, s), 3.30—3.90 (1H, m), 5.50—7.70 (1H, m), 7.36 (5H, s), and 7.34 and 7.74 (4H, ABq, *J*=8.4 Hz); MS *m/z* (rel intensity) 308 (M^+; 1), 273 (1), 272 (4), 209 (9), 158 (14), and 157 (100); HRMS, Found: *m/z* 308.0641. Calcd for $C_{16}H_{17}O_2SCl$: M, 308.0638.

Reduction of (−)-(1*S*,2*RS*)-2 by Lithium Aluminum Hydride. To a stirred suspension of 210 mg (5.5 mmol) of lithium aluminum hydride in 5 cm^3 of dry tetrahydrofuran was added dropwise 250 mg (1.1 mmol) of (−)-(1*S*,2*RS*)-**2** in 10 cm^3 of dry tetrahydrofuran at room temperature under nitrogen. After the addition was completed, the mixture was refluxed for an additional 12 h, then cooled in an ice bath, and treated with water and then with 5% sulfuric acid. Ether was added to the mixture and the ethereal layer was separated and dried over magnesium sulfate. The solvent was evaporated to give 132 mg (61%) of 2-methylsulfonyl-1-phenylpropane; $[\alpha]_D$ 0° (*c* 6.6, $CHCl_3$); IR (neat) 1300 and 1140 cm^{-1}; ^1H NMR ($CDCl_3$) δ=1.31 (3H, d, *J*=6.0 Hz), 2.76 (3H, s), 2.90—3.60 (3H, m), and 7.22 (5H, s); MS *m/z* 198 (M^+).

References

1) For Part 3, see: M. Kameyama and N. Kamigata, *Bull. Chem. Soc. Jpn.*, **60**, 3687 (1987).

2) H. Matsumoto, T. Nakano, and Y. Nagai, *Tetrahedron Lett.*, **1973**, 5147; H. Matsumoto, T. Nikaido, and Y. Nagai, *J. Org. Chem.*, **41**, 396 (1976); H. Nagashima, H. Wakamatsu, and K. Itoh, *J. Chem. Soc., Chem. Commun.*, **1984**, 652; D. Belluš, *Pure Appl. Chem.*, **57**, 1827 (1985).

3) N. Kamigata, H. Sawada, and M. Kobayashi, *J. Org. Chem.*, **48**, 3793 (1983); N. Kamigata, H. Sawada, N. Suzuki, and M. Kobayashi, *Phosphorus and Sulfur*, **19**, 199 (1984).

4) H. Nozaki, S. Moriuti, H. Takaya, and R. Noyori, *Tetrahedron Lett.*, **1966**, 5239.

5) S. Murai, R. Sugise, and N. Sonoda, *Angew. Chem., Int. Ed. Engl.*, **20**, 475 (1981).

6) M. Kameyama, N. Kamigata, and M. Kobayashi, *J. Org. Chem.*, **52**, 3312 (1987).

7) The reduction of (+)-**2** with lithium aluminum deuteride was also carried out and quenched with deuterium oxide (99.8 atom% D) to give 2-methylsulfonyl-1-phenylpropane-1-*d*. The α-hydrogen of sulfonyl group in (+)-**2** was not found to be abstracted by lithium aluminum deuteride under the conditions since the α-hydrogen was not converted by deuterium. Thus, we confirmed that there was no racemization at C-2 during the reduction.

8) Davis et al. proposed a similar mechanism on the addition of polyhaloalkanes to alkenes catalyzed by $RuCl_2(PPh_3)_3$; W. J. Bland, R. Davis, and J. L. A.Durrant, *J. Organomet. Chem.*, **267**, C45 (1984).

9) B. R. James, D. K. Wang, and R. F. Voight, *J. Chem. Soc., Chem. Commun.*, **1975**, 574.

The Preparation and Structure of the Copper(II) Chloride Complex of 5,5′-Carbonylbis[1,3-dimethyl-3,4,5,6-tetrahydro-1,3,5-triazin-2(1*H*)-one]

Toichi EBISUNO,* Michiaki TAKIMOTO, Miyuki TAKAHASHI,† and Ryuichi SHIBA†
Department of Chemistry, Faculty of Science, Toho University, Miyama 2-2-1, Funabashi, Chiba 274
†Department of Applied Science, Faculty of Technology, Tokyo Denki University, Kanda, Chiyoda-ku, Tokyo 101
(Received August 2, 1988)

Synopsis. A new 1,3-dimethylurea-formaldehyde condensate like a crown compound with two rings, 5,5′-carbonylbis[1,3-dimethyl-3,4,5,6-tetrahydro-1,3,5-triazin-2(1*H*)-one], was prepared. The molecular structure of the complex with the condensate and copper(II) chloride (1 : 1) was determined by means of X-ray analysis. The copper(II) ion was coordinated intermolecularly between two oxygen atoms (O(2) and O(2)′ in the adjacent molecule).

The previous papers[1,2] reported that the addition of 1,3-dimethylurea-formaldehyde condensates, such as 1,3,5,7-tetramethyltetrahydro-1,3,5,7-tetrazocine-2,6-(1*H*,3*H*)-dione and bis(1,3-dimethylureido)methane, changed the absorption spectrum of a solution of the metal salts of phenol into that of free phenol. An apparent specific interaction between these condensates and the metal ions was suggested.

A new 1,3-dimethylurea-formaldehyde condensate like a crown compound with two rings, 5,5′-carbonylbis[1,3-dimethyl-3,4,5,6-tetrahydro-1,3,5-triazin-2(1*H*)-one] (CDTTO), was prepared, and the molecular structure of the complex with CDTTO and copper(II) chloride (1 : 1) was determined by means of X-ray analysis in order to elucidate the coordination between the CDTTO and copper(II) chloride.

Experimental

Preparation of a Complex with 5,5′-Carbonylbis[1,3-dimethyl-3,4,5,6-tetrahydro-1,3,5-triazin-2(1*H*)-one] and Copper(II) Chloride. One mole of 1,3-bis(methoxymethyl)-urea, two moles of 1-methoxymethyl-1,3-dimethylurea, and a small amount of *p*-toluenesulfonic acid as an acid catalyst were dissolved in DMF. The solution was then heated at 110 °C in an oil bath for 30 min. After the DMF has distilled away, the crystals deposited (CDTTO) were recrystallized from EtOH (Yield, 76%). Elemental analysis: Found, C, 46.45; H, 7.11; N, 29.47%; Calcd for $C_{11}H_{20}N_6O_3$, C, 46.47; H, 7.09; N, 29.56%. ^{1}H NMR (DMSO-d_6): δ=4.58 (8H, s, -C$\underline{H}_2$-), 2.74 (12H, s, -C$\underline{H}_3$): ^{13}C NMR (DMSO-d_6): δ=160.43 (O=$\underline{C}$<), 150.79 (O=$\underline{C}$<), 61.74 (-$\underline{C}$H$_2$-), 31.98 (-$\underline{C}$H$_3$). MS (FD): m/z=284 (M^+).

Equimolecular quantities of CDTTO and copper(II) chloride were dissolved in distilled water, after which the solution was stirred for 30 min at room tempersture. After the evaporation of the solvent, the deposited crystals were recrystallized from EtOH. The copper content in the complex with CDTTO and copper(II) chloride was determined by atomic absorption analysis. CDTTO : Cu=1.01 : 1.

X-Ray Analysis. A brown, transparent crystal with dimensions of ca. 0.2×0.2×0.2 mm^3 was mounted on a Rigaku AFC-6S automated diffractometer. The systematic absences of (h00) reflections for h odd and (0k0) for k odd led to the space group of $P2_12_12$. The intensity data were measured by means of the ω-2θ scan mode (scan speed 4° min^{-1} in ω) up to 2θ of 60° by using graphite-monochromated Mo $K\alpha$ radiation (λ=0.7107 Å). Lorentz and polarization corrections were made, but no correction for absorption. Among the 1495 reflections measured, 1351 reflections with $|F_o|>3\sigma(|F_o|)$ were used for the structure determination.

Crystal Data. $C_{11}H_{20}N_6O_3\cdot CuCl_2$. F.W.=418.77, orthorhombic, space group $P2_12_12$, a=12.772(2), b=10.850(4), c=6.004(1) Å, V=832.1 Å^3, Z=2, D_c=1.67 g·cm^{-3} μ (Mo $K\alpha$)=16.6 cm^{-1}.

The structure was solved by the direct method (MULTAN78[3]). The positions of the H atoms were determined from a difference Fourier map. The structure was refined anisotropically for non-H atoms and isotropically for H atoms by a block-diagonal least-squares method. The final discrepancy factors were R=0.056 and R_w=0.085 (w=unit wt), and $(\Delta/\sigma)_{max}$ in the final refinement cycle was 0.110 for non-H atoms. The scattering factors were taken from Ref. 4. The calculations were carried out on a HITAC M-680H computer at the Computer Center of The University of Tokyo, using the local version of UNICS III.[5]

Results and Discussion

The final atomic and equivalent isotropic thermal parameters, as defined by Hamilton,[6] are listed in Table 1.[7] The selected bond lengths and bond angles, and also some interatomic distances, are shown in Table 2. A perspective view of the complex along the b-axis, with atomic numbering, is shown in Fig. 1. The carbonyl group of C(1)-O(1) and Cu^{2+} are on the two-fold rotation axis. The four atoms of C(1), O(1), N(1), and N(1)′ lie on the same plane. The least-squares plane formed by the seven atoms of O(2), C(2), C(3), C(4), N(1), N(2), and N(3) intercepts another least-squares plane formed by seven symmetric atoms (O(2)′, C(2)′, C(3)′, C(4)′, N(1)′, N(2)′, and N(3)′) at

Table 1. Final Atomic Parameters (Positional ×10^4) and Equivalent Isotropic Thermal Parameters (B_{eq}×10), with Their Estimated Standard Deviations in Parentheses

Atom	x	y	z	B_{eq}/Å^2
Cu	0	0	2203(3)	23(1)
Cl	290(2)	1902(2)	1035(6)	39(1)
O(1)	5000(0)	0	6048(14)	38(4)
O(2)	1388(4)	−253(6)	3468(11)	29(3)
N(1)	4343(5)	761(7)	2775(13)	13(3)
N(2)	2665(6)	1112(8)	4366(14)	29(3)
N(3)	2823(4)	−150(8)	1200(12)	25(3)
C(1)	5000(0)	0	4028(18)	22(4)
C(2)	3710(7)	1636(8)	3991(19)	28(4)
C(3)	3858(6)	350(10)	678(15)	31(3)
C(4)	2258(6)	235(7)	3007(15)	22(3)
C(5)	2006(8)	1741(11)	5978(19)	39(5)
C(6)	2400(8)	−1030(10)	−402(18)	31(4)

Table 2. Selected Bond Lengths and Bond Angles, with Their Estimated Standard Deviations in Parentheses

Bond length	l/Å	Bond angle	ϕ/°
O(1)-C(1)	1.213(3)	O(1)-C(1)-N(1)	122.6(5)
C(1)-N(1)	1.397(9)	C(1)-N(1)-C(2)	116.9(8)
N(1)-C(2)	1.445(12)	C(1)-N(1)-C(3)	122.3(8)
N(1)-C(3)	1.473(12)	C(2)-N(1)-C(3)	113.3(7)
C(2)-N(2)	1.468(10)	N(1)-C(2)-N(2)	109.4(7)
C(3)-N(3)	1.463(9)	N(1)-C(3)-N(3)	108.0(7)
N(2)-C(4)	1.357(12)	C(2)-N(2)-C(4)	121.9(8)
N(2)-C(5)	1.453(14)	C(2)-N(2)-C(5)	116.5(8)
N(3)-C(4)	1.368(11)	C(4)-N(2)-C(5)	120.5(8)
N(3)-C(6)	1.459(13)	C(3)-N(3)-C(4)	122.2(8)
C(4)-O(2)	1.261(9)	C(3)-N(3)-C(6)	115.8(7)
Cu-Cl	2.211(3)	C(4)-N(3)-C(6)	121.8(7)
Cu-O(2)	1.948(6)	N(2)-C(4)-O(2)	120.0(8)
		N(3)-C(4)-O(2)	120.7(8)
		N(2)-C(4)-N(3)	119.3(7)
		N(1)-C(1)-N(1)′	114.8(8)
		Cl-Cu-Cl′	143.0(1)
		Cl-Cu-O(2)	98.3(2)
		Cl-Cu-O(2)″[a]	95.9(2)
		O(2)-Cu-O(2)″[a]	134.1(3)

a) O(2)″ is the O(2)′ atom in the adjacent molecule.

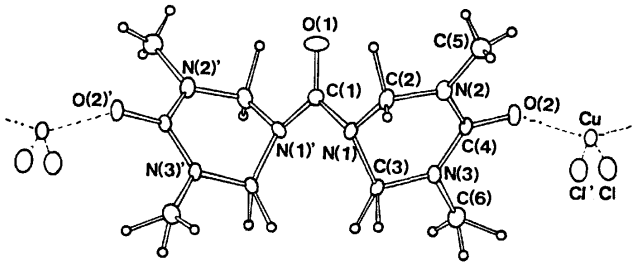

Fig. 1. A view of the molecular structure of the complex with 5,5′-carbonylbis[1,3-dimethyl-3,4,5,6-tetrahydro-1,3,5-triazin-2(1*H*)-one] and copper(II) chloride with the numbering scheme.

the angle of 148°. The Cu^{2+} ion is not located between the two ring structures of 1,3-dimethyl-3,4,5,6-tetrahydro-1,3,5-triazin-2(1*H*)-one in the same molecule; it coordinates intermolecularly to two oxygen atoms (O(2) and O(2)′ in the adjacent molecule).

The observed interatomic distance of Cu-O(2) (1.948 Å) was shorter than that of 2.71—2.75 Å of Cu-O in the complex with 1,4,10,13-tetraoxa-7,16-diazacyclooctadecane and copper(II) chloride.[8] Furthermore, it was shorter than the value of 2.12 Å which was estimated by considering the van der Waals radius of the oxygen atom and the ionic radius of Cu^{2+}. These results suggest a strong interaction between Cu^{2+} and O(2).

The bond lengths for the carbonyl groups of C(1)-O(1) and C(4)-O(2) were 1.213 and 1.216 Å respectively. While C(1)-O(1) has a strong double-bond character, C(4)-O(2) is intermediate between single and double bonds. The resonated structures of $N\text{-}\overset{\displaystyle O^-}{\overset{|}{C}}\text{=}N^+$ and $N^+\text{=}\overset{\displaystyle O^-}{\overset{|}{C}}\text{-}N$ make a larger contribution to N(2)-C(4)O(2)-N(3) than to N(1)′-C(1)O(1)-N(1), partly because of the effect of the two methyl groups and partly because of the stabilization of the anionic structure of O(2) by the coordination to Cu^{2+}.

We wish to thank Professor Hayao Kobayashi for his kind support in the data collection on the Rigaku AFC-6S diffractometer at Toho University and in the computation and Dr. Minoru Takada for his atomic absorption analyses.

References

1) T. Ebisuno, M. Takimoto, M. Takahashi, and R. Shiba, *Bull. Chem. Soc. Jpn.*, **61**, 2191 (1988).

2) T. Ebisuno, M. Takimoto, M. Takahashi, and R. Shiba, *Bull. Chem. Soc. Jpn.*, **61**, 4441 (1988).

3) P. Main, S. E. Hull, L. Lessinger, G. Germain, J. P. Declercq, and M. M. Woolfson, MULTAN 78. "A System of Computer Programs for the Automatic Solution of Crystal Structures from X-Ray Diffraction Data," Universities of York, England, and Louvain, Belgium (1978).

4) "International Tables for X-Ray Crystallography," Kynoch Press, Birmingham (1974), Vol. IV.

5) T. Sakurai and K. Kobayashi, *Rikagaku Kenkyusho Hokoku*, **55**, 69 (1979).

6) W. C. Hamilton, *Acta Crystallogr.*, **12**, 609 (1959).

7) The coordinates and isotropic thermal parameters of H atoms, the anisotropic thermal parameters of non-H atoms, and the F_o—F_c tables have been deposited as Document No. 8857 at the Office of the Editor.

8) M. Herceg and R. Weiss, *Acta Crystallogr., Sect. B*, **29**, 542 (1973).

 © 1989 The Chemical Society of Japan Bull. Chem. Soc. Jpn., 62, 653—656 (1989)

The High-Temperature Reaction of Iron with Sulfur Dioxide

Ken-ichiro OTA,* Hiroyuki SUGIMOTO,†,†† and Kazuo FUEKI†,†††
Department of Energy Engineering, Faculty of Engineering, Yokohama National University, Tokiwadai, Hodogaya-ku, Yokohama-shi 240
†Department of Industrial Chemistry, Faculty of Engineering, University of Tokyo, Hongo, Bunkyo-ku, Tokyo 113
(Received July 11, 1988)

The reaction of Fe with SO_2 has been studied in the temperature range from 923 K to 1123 K and in the pressure range from 1.3 kPa to 101 kPa. The reaction obeyed the parabolic law except for the initial period, and the rate constant was equal to that in O_2. In the scale, Fe_3O_4, FeO, and FeS were found as the reaction products. Among them, FeS was formed only in the initial period of the reaction and stayed at the scale/metal interface. The constant amount of sulfide in the scale became larger at higher temperatures or at lower SO_2 pressures. The sulfide formation in the initial period of the reaction might cause the increase in the corrosion of Fe at low pressures of SO_2 and cause the difference from the corrosion by O_2.

The corrosion of metals by SO_2 gas causes severe problems in the combustion processes of fossil fuels containing sulfur and also in thermochemical hydrogen production, where high-concentration SO_2 is utilized at high temperatures.

Several reports on the high temperature corrosion of Fe in SO_2 have been published.[1-5] Baukloh and Valena[1] studied the corrosion of Fe in 101 kPa SO_2 and found that the reaction started at 473 K and obeyed the parabolic law between 673—1273 K. Chretien and Broglin,[2] however, observed a deviation from the parabolic law in the initial period between 773 and 1073 K. Flatley and Birks[3] studied the reaction in the temperature range of 773—1273 K and the SO_2 pressure range of 0.25—20 kPa. The reaction obeyed the linear law in the initial period and the parabolic law in the latter period. The same tendency was reported by Kurokawa[5] at 1073 K. According to Flatley and Birks,[3] the parabolic rate constant reached a maximum value at a SO_2 pressure of 2 kPa at 1073 K. When the SO_2 pressure was increased beyond 2 kPa, however, the parabolic rate constant decreased until it reached that in pure oxygen.

Three kinds of iron compounds, FeS, FeO, and Fe_3O_4, were found in the scale.[3-5] FeS always appeared at the metal/scale interface, and its existence promoted the falling of the scale during thermal cycles. Therefore, it is important to elucidate the mechanism of FeS formation in a scale. According to Rahmel,[6] FeS is formed as a result of the inward penetration of SO_2 through micropores in the scale as well as by the diffusion of sulfur from the gas/scale interface to the scale/metal interface. Ross et al.[7,8] studied the reaction between mild steel and sulfur and speculated that FeS is formed in the initial period of the reaction where the reaction rate is high. However, they presented no supporting experimental result. Gilewicz-Wolter[9] studied the corrosion of Fe in SO_2 of 101 kPa at 1073 K using a radio-isotope ^{35}S and found that FeS was formed along the cracks in the scale, mostly in the initial stage of the reaction.

These works carried out previously have thus not yielded a clear interpretation of the mechanism of FeS formation in SO_2. The present paper aims to evaluate the formation of FeS during the reaction between Fe and SO_2 by means of a chemical analysis in order to elucidate the mechanism of the formation of FeS around 1073 K.

Experimental

(1) Specimen. A pure iron sheet supplied by the Nippon Steel Corp. was used as the sample. Table 1 shows the result of the chemical analysis of the impurities. The sheet was cut into rectangular specimens 10×10×0.8 mm; they were polished with No. 1000 SiC polishing paper, washed with soap and water, rinsed in alcohol, and dried.

(2) Reaction-Rate Measurement. A finished and weighed specimen was suspended in the room-temperature region of a mulite reaction tube; then the entire system was evacuated, and SO_2 gas was introduced. The specimen was lowered to the reaction zone, the temperature of which was controlled to within 2 K. In order to react the iron specimen with SO_2, SO_2 gas was circulated by means of a magnetic piston pump. After the predetermined time of reaction, the specimen was taken out of the reaction tube and the weight change was determined.

(3) Analysis of Scale. The reaction products were examined by the X-ray diffraction methods. The cross-sections of the reacted specimens were studied by EPMA as well as with an optical microscope.

Table 1. Results of Chemical Analysis of Iron

Component	wt%	Component	wt%
C	0.003	Si	<0.01
Mn	<0.01	P	0.002
S	0.004	Ti	<0.001
N	0.0013	O	0.0020
Al	0.001		

†† Present address: Hitachi, Ltd., Kuji-cho, Hitachi-shi, Ibaragi 319-12.
††† Present address: Tokyo University of Science, Yamazaki, Noda-shi, Chiba 278.

In order to know the sulfide growth, the total amount of sulfur in the scale was chemically analyzed by the following method. A reacted specimen was dissolved in a HCl (1 M§)–Br_2 (0.01 M) solution in order to oxidize the sulfide ions to sulfate ions. After the filtation, the solution was passed through cation-exchange resin (Dow Chemical 50W-X8) and the Fe ions were removed. Then $BaSO_4$ was precipitated by adding a $BaCl_2$ solution to the solution. The amounts of sulfur were calculated from the weight of the $BaSO_4$ precipitate.

Results and Discussion

Figure 1 shows a parabolic plot of the weight increase in Fe at the SO_2 pressure of 101 kPa. The temperature range was from 923 K to 1123 K. Clearly, the reaction obeys the parabolic rate law except for the very initial period. In order to compare with the oxidation reaction, the oxidation of Fe in 101 kPa O_2 was carried out at 1073 K. The oxidation reaction obeyed the parabolic rate law from the initial period. The parabolic rate constants for oxidations in SO_2 and in O_2 were the same (6.6×10^{-8} g^2 cm^{-4} s^{-1}); the only difference appeared in the initial period. These results agree well with those of Baukloh[1] and Flatley.[3]

By the observations of the cross-sections of specimens reacted with SO_2 in 101 kPa at 1073 K utilizing a optical microscope, the scale was found to be composed of a monolayer at the very initial period of the reaction and to become double layers after a 1-h reaction. The inner layer or the layer at the metal/scale interface showed a lamellar structure, as has been shown in previous papers.[3–5]

After Fe was oxidized in 101 kPa SO_2 at 1073 K for 16 h, the products were examined by the X-ray diffraction methods. X-Ray diffraction obtained by gradual sectioning from the surface revealed that the scale had a layer structure of Fe_3O_4/FeO/FeO–FeS. When the scale was peeled off from the base metal and ground to a powder, however, only FeO was detected. This result indicates that FeO is the major oxide for this sample and that Fe_3O_4 exists only on the surface of the scale.

Figure 2 shows the Arrhenius plots of the parabolic rate constants for Fe in 101 kPa SO_2. The parabolic rate constants for oxidation in pure O_2[10,11] (B, C) and in S_2[12] (A) are also shown for the sake of comparison. A linear relation is observed for SO_2 reaction. The rates are very close to the oxidation rate in O_2.

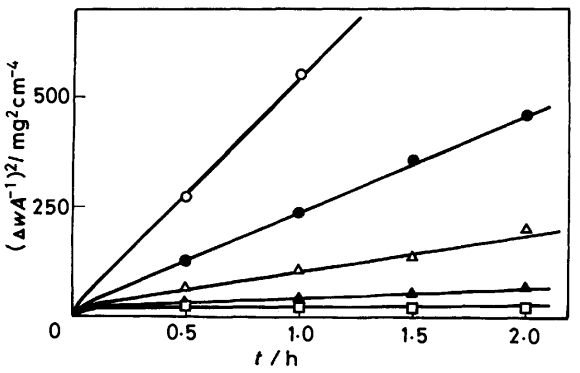

Fig. 1. Parabolic plot of reaction of Fe in SO_2 (101 kPa).
○: 1123 K, ●: 1073 K, △: 1023 K, ▲: 973 K, □: 923 K.

§ 1 M=1 mol dm^{-3}.

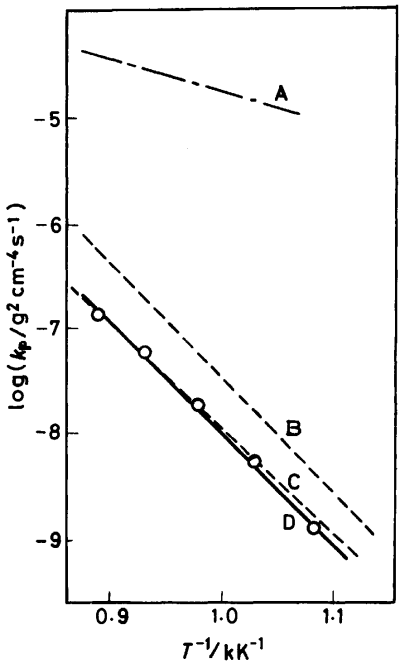

Fig. 2. Arrhenius plot of parabolic rate constant.
A: Sulfidation in S_2.[12] B: Oxidation in O_2.[10] C: Oxidation in O_2.[11] D: This work.

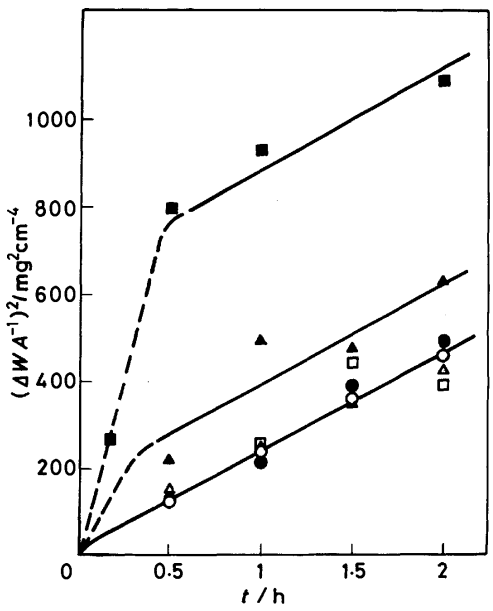

Fig. 3. Parabolic plot of reaction of Fe in SO_2 at 1073 K.
■: 1.3 kPa, ▲: 2.1 kPa, △: 13 kPa, □: 25 kPa, ●: 51 kPa, ○: 101 kPa.

Compared to the sulfidation rate (A), the absolute value and the slope of line are both different. This shows that the reaction of Fe in 101 kPa SO_2 might be fundamentally the same as that in pure O_2, including the rate determining step.

Figure 3 shows the parabolic plot of the weight increase in Fe in SO_2 gas at 1073 K. The SO_2 pressures are 1.3, 2.1, 13, 25, 51, and 101 kPa respectively. The low SO_2 pressure was controlled by the temperature of the cold spot in the reaction system utilizing a Dry Ice–ethanol mixture. The reacted amounts are almost the same when the SO_2 pressure is between 13 and 101 kPa. At lower SO_2 pressures, the reacted amounts increase. However, the difference appears only at the initial period (less than 0.5 h). After a 1-h reaction the parabolic rate constants do not depend on the SO_2 pressure; that is, the rate is equal to that in O_2. The corrosion reaction that is characteristic of SO_2 gas might take place only in the initial period of the reaction.

Figure 4 shows the results of EPMA analysis for the cross-sections of specimens reacted in 101 kPa SO_2 at 1073 K for 10 min, 1.5 h, and 8 h respectively. In this figure, l denotes the scale thickness, and 0, the metal/scale interface. The scale/gas interface is the point where the oxygen concentration diminishes to zero. The sulfide is formed near the metal/scale interface. It appears from these results that the oxide thickness increased during the reaction, while sulfide did not grow.

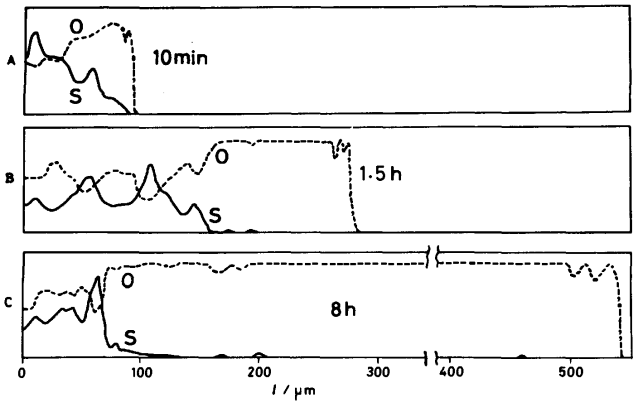

Fig. 4. Distribution of sulfur and oxygen in the scales reacted 10 min, 1.5 h and 8 h in SO_2 (101 kPa) at 1073 K.

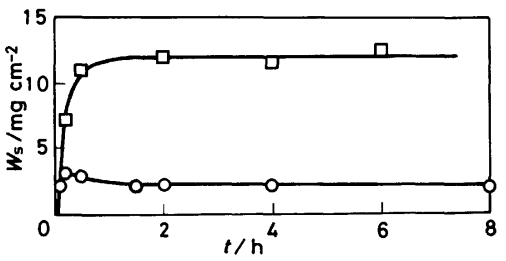

Fig. 5. Change of the total sulfur weight in the scale during the reaction of Fe in SO_2 at 1073 K.
□: 1.3 kPa, ○: 101 kPa.

Figure 5 shows the amounts of sulfur (W_s) in a scale, as obtained by chemical analysis. The total amounts of sulfur are constant after the reaction times of 5 min and 1 h under SO_2 pressures of 101 and 1.3 kPa respectively. These results indicate that the sulfide is formed only in the initial period of the reaction. The constant amount of sulfur in 101 kPa SO_2 was smaller than that in 1.3 kPa SO_2. The difference in the reactions in the initial period shown in Fig. 3 might be explained by the sulfide formation. At low SO_2 pressures a large amount of sulfide formation takes place during the initial period, thus leading to the increase in the total amount reacted. However, once the formation of sulfide ceases, only the oxidation reaction proceeds. At this stage there is no significant difference in the reaction rates (parabolic rate constants).

Figure 6 shows the dependence of the constant

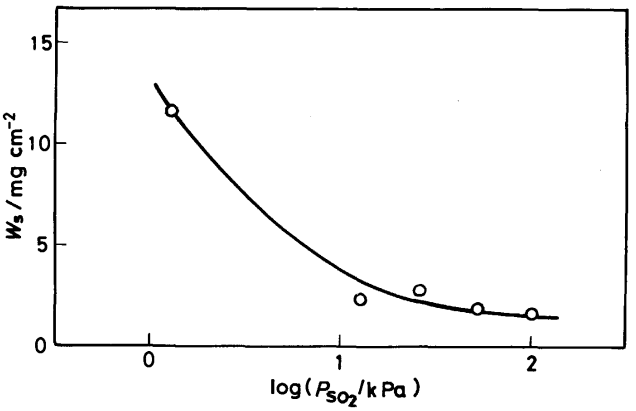

Fig. 6. Dependence of the constant sulfur amount in the scale on SO_2 pressure during the reaction of Fe in SO_2 at 1073 K.

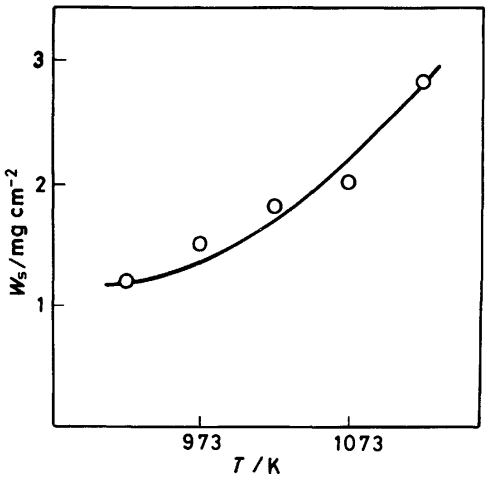

Fig. 7. Dependence of the constant sulfur amount in the scale on temperature during the reaction of Fe in SO_2 (101 kPa).

sulfur amount in the scale on the SO_2 pressure. The amount of sulfur increases at lower SO_2 pressures. Figure 7 shows the dependence of the constant sulfur amount in the scale on the temperature. The sulfur amount increases with the rise in the reaction temperature.

FeS is thermochemically unstable in a SO_2 atmosphere.[5] In order to study the reaction of FeS on Fe with SO_2 and confirm a stable phase, Fe was sulfided for 20 min in pure H_2S at 1073 K and then reacted with SO_2 of 101 kPa for 20 h at 1073 K. It was found that, after the reaction, the sulfide scale was covered with the oxides, FeO and Fe_3O_4. Another experiment was carried out using a single crystal of FeS. It was reacted with SO_2 of 101 kPa at 1073 K. By means of an X-ray diffraction study, only Fe_3O_4 was found as the reaction product. From this result, Fe_3O_4 was found to be a stable compound in 101 kPa SO_2 at 1073 K.

In order to know whether sulfur diffuses inward through the oxide scale, Fe was oxidized for 10 and 30 min in pure O_2 at 1073 K and then reacted with SO_2 of 101 kPa for 20 h. In both cases, no sulfide was detected by the chemical analysis. The sulfide formed after oxidation might be less than 1/20 of that without preoxidation, considering the limits of the analysis. According to Gilewicz-Wolter,[9] sulfur does not diffuse through the scale after Fe is reacted with SO_2 for 3 h at 1073 K. Watanabe and Ohira[13] reported that sulfide was not formed at 1023 K during the reaction of SO_2 and Fe, which was covered with a thick oxide film formed by the preoxidation for 4 h in pure O_2 at 1023 K. The present study has shown that a thin oxide film formed by only a 10-min preoxidation is able to suppress the sulfur diffusion throughout the scale. From these results it is concluded that sulfur cannot diffuse easily through a dense oxide scale. Thus, the FeS at the scale/metal interface is not formed as a result of the penetration of sulfur through the oxide layer. FeS might, however, be formed by the direct reaction between Fe and sulfur in the initial period of the reaction, as has been proposed by Chattergie[4] and Kurokawa.[5]

References

1) W. Baukloh and I. Valena, *Korrosion u. Metallshutz*, **5**, 9 (1939).
2) A. Chretien and J. Broglin, *Proc. Int. Congr. Pure Appl. Chem.*, **5**, 705 (1947).
3) T. Flatley and N. Birks, *J. Iron Steel Inst.*, **209**, 523 (1971).
4) B. Chatterjee and A. J. Dowell, *Corr. Sci.*, **15**, 639 (1975).
5) K. Kurokawa, T. Narita, and K. Nishida, *Boshoku Gijutu*, **30**, 396 (1981).
6) A. Rahmel, *Corr. Sci.*, **13**, 125 (1973).
7) T. K. Ross, A. J. MacNab, and B. E. Leyland, *J. Inst. Fuel*, **33**, 540 (1960).
8) T. K. Ross, *Corr. Sci.*, **5**, 327 (1965).
9) J. Gilewicz-Wolter, *Oxid. Met.*, **11**, 81 (1977).
10) K. Haufe, "Reaktionen in und an Festen Stoffen," Springer-Verlag (1966), p. 721.
11) M. H. Davies, M. H. Simnad, and C. E. Birchenall, *J. Met.*, **3**, 889 (1951).
12) L. Czerski, S. Mrowec, and T. Werber, *J. Electrochem. Soc.*, **109**, 273 (1962).
13) A. Watanabe and G. Ohira, *Imono*, **42**, 14 (1970).

The Meaning of the Equilibrium Spreading Pressure of Fatty Acid Being Relatively Soluble in an Underlying Subphase

Makio IWAHASHI,* Kimiyo IIDUKA,†,†† Takashi WATANABE,†,††† and Tsutomu SEIMIYA†
Department of Chemistry, School of Hygienic Sciences, Kitasato University, Sagamihara, Kanagawa-ken 228
†Department of Chemistry, Faculty of Sciences, Tokyo Metropolitan University, Setagaya-ku, Tokyo 158
(Received July 15, 1988)

The spreading pressure of a lipid monolayer in equilibrium with its crystal placed at the air/water interface is a thermodynamical property—i.e., the equilibrium spreading pressure (ESP). It is, however, quite likely that the apparently constant spreading pressure of a lipid with a relatively large desorption rate into the underlying subphase is not a thermodynamical property but merely a steady-state one. Mutual comparisons were, therefore, carried out for the rate constants of the six possible processes associated with the spreading pressure of tetradecanoic acid, whose monolayer has a relatively large desorption rate into the underlying subphase; it was found that monolayer formation from its crystal was predominant and that the desorption from the monolayer little affected the spreading pressure, even at high temperatures. Consequently, the apparently constant spreading pressure for the tetradecanoic acid can be regarded as the ESP even at high temperatures, in which the dissolution of the monolayer into the subphase occurs very rapidly.

Many lipids spread spontaneously when placed in a solid or liquid form at the air/water interface, thus giving monolayers in apparent equilibrium with the excess bulk lipid phase. The corresponding surface pressure (Π) of the monolayer is generally known as the equilibrium spreading pressure (ESP). The ESP is, in principle, useful for obtaining thermodynamic information on the crystal-monolayer transition; monolayer experiments carried out beyond the pressure of ESP are thought to be thermodynamically invalid. However, it appears to be doubtful that the apparently constant spreading pressure for the lipid, which has a relatively large desorption rate into the underlying subphase, is a true equilibrium property; that is, it seems quite likely that the apparent constancy of the spreading pressure is attributable not to the genuine ESP, but to a steady-state caused by the monolayer material being lost from the interface by desorption.

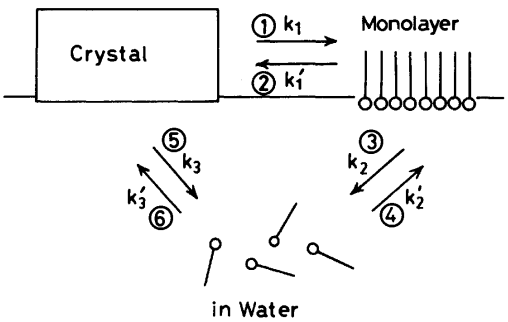

Fig. 1. General mode for the monolayer spreading process.

Six processes (see Fig. 1) are, in general, possible in accounting for the spreading of a relatively soluble and nonvolatile lipid crystal: (1) a monolayer formation by the spreading of the lipid from its crystal; (2) the re-binding of the molecule in the monolayer to the crystal; (3) the dissolving of the monolayer into the underlying subphase; (4) the adsorption from the subphase to the monolayer; (5) the dissolution of lipid molecules from its crystal into the subphase; and (6) the adsorption from the subphase to the crystal.

In the present study we investigated the above processes for tetradecanoic acid, which has a relatively large desorption rate into the underlying water, and discussed kinetically the meaning of the ESP by comparing the rate constants for the above processes with one another.

Experimental

The sample of tetradecanoic acid (purity: 99.7%; Applied Science Co., Ltd.) was further purified by repeated slow crystallizations overnight from hexane. Needle-like (small) and plate-like (large) crystals formed from the hexane solution were both freed of the solvent by being pumped out for a week on a vacuum line. The crystallographic forms were determined for the two types of crystals with a X-ray diffraction instrument (Rigaku Denki Model Geigerflex RAD-1A). The needle-like and plate-like crystals were A-super-type and C-type forms respectively.[1] The purest grade hexane from the Wako Co., Ltd. (Tokyo), was redistilled two times before being used for the preparation of the above crystal samples and as the spreading solvent in the monolayer-desorption experiment. The subphase solution consisted of triply distilled water whose pH has been adjusted to 2 with twice-distilled HCl.

The spreading pressure of the crystal was measured by the Wilhelmy plate method, using the apparatus shown in Fig. 2 and under temperatures (constant to ±0.01 K) over the range of 290—318 K and at almost a 100% humidity. A Wilhelmy

†† Present address: Gyosei International School UK., Milton Keynes, MK15 9JX, U. K.

††† Present address: Lion Co., Ltd., Hirai, Edogawa-ku, Tokyo 132.

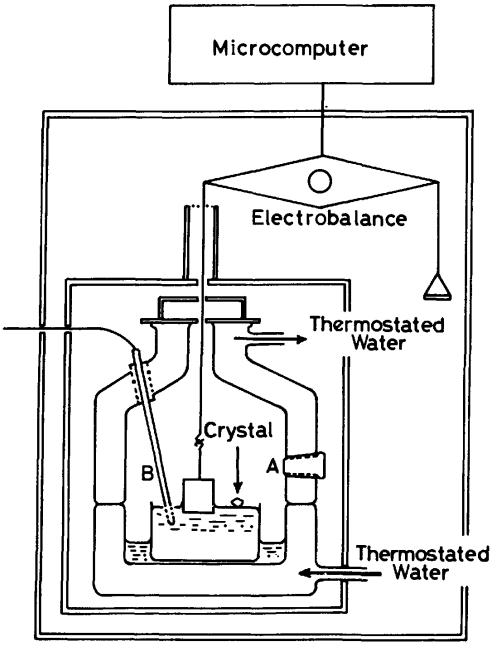

Fig. 2. Schematic representation of apparatus for measurement of surface pressure. A denotes a hole though which samples are introduced onto clean water surface and B, an IC-thermometer.

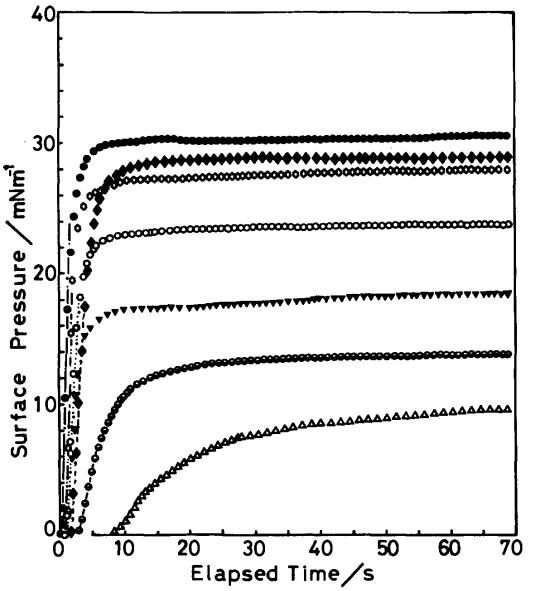

Fig. 3. Time dependences of spreading pressure of tetradecanoic acid crystal on the water surface at various temperatures. Diamond denotes plate-like crystal and other symbols needle-like crystal. △: T=292.1 K, ○: 296.1 K, ▽: 303.1 K, ○: 308.1 K, □: 313.1 K, ● and ◆: 318.1 K.

plate was connected to an electrobalance (Shimadzu Model TGA-31), whose output was in turn connected to a digital multimeter (Hewlett-Packard Model 3478A) and a personal computer (NEC Model PC-8001MKII). Needle-like crystals (or a single crystal of a plate-like form) were introduced onto the clean surface through the hole A (shown in Fig. 2); the surface pressure was recorded every half-second. The sensitivity of the balance was ±0.01 mN m^{-1}, and the reproducibility was ±0.1 mN m^{-1}. A constant surface pressure was obtained 5—10 min after the crystal has been placed onto the water surface; the constancy of the pressure for the plate-like crystal did not change for 120 h, while that for the needle-like crystals varied somewhat with the time. The constant values thus obtained were taken as the apparent ESP (see Table 1).

For desorption experiments on the monolayer at constant surface pressures, we used a Langmuir glass trough (600 mm× 109 mm×57 mm) whose surface has been treated with dimethyldichlorosilane in order to make it hydrophobic. Two glass pipes were set on the bottom of the trough for temperature control (±0.1 K). The surface pressure was also observed by the Wilhelmy plate method. After spreading a monolayer and evaporating the spreading solvent, compression was carried out to a surface pressure below about 0.3 mN m^{-1} of the apparent ESP so as to avoid spontaneous monolayer collapse. This pressure was maintained constant within 0.1 mN m^{-1} by further manually decreasing the area. This area decrease was measured as a function of the time.

Scanning electron micrographic observation (SEM) for the plate-like crystals used in the spreading-pressure experiments was carried out with a JOEL JXA-840 scanning electron microscope.

Results and Discussion

Figure 3 shows the time dependence of the spreading pressure of the tetradecanoic acid crystal introduced at the air/water interface. After a retardation time, the surface pressure Π increased rapidly for a few seconds, followed by a gradual increase before it reached a constant value. The yield point was dependent on the crystal type or on the temperature. In the case of the needle-like crystal at a higher temperature (318.1 K), we could not recognize the retardation time. The yield point was defined as time zero for the spreading process of the molecules from the crystal.

In the six processes illustrated in Fig. 1, the contributions of Processes (4) and (6), i.e., the k_2' and k_3' terms, to the whole system appear to be negligibly small because of the extremely small concentration of the tetradecanoic acid in the water,[2] especially at the initial stage. Furthermore, the k_3 (the desorption constant from the crystal into water) in Process (5) is thought to be smaller than the k_2 (the desorption constant from monolayer into water) in Process (3), for the molecules in the crystal are more ordered and are combined more tightly with one another than the molecules in the monolayer.

Spreading Process. Assuming the first-order mode for every process, the rate equation for the monolayer formation (spreading) is given by:

$$d\Gamma/dt = k_1C - (k_1' + k_2)\Gamma \quad (1)$$

where Γ is the amount of molecules in the monolayer; t, the elapsed time after the yield point of the spreading pressure; C, the amount of crystal directly in contact with the water; k_1, the rate constant for the spreading process of the molecules from the crystal to form the monolayer (Process (1)), and k_1', the rate constant for the re-binding of the molecules to the crystal (Process (2)).

In the initial stage of the spreading from the crystal, the molecular density in the monolayer is so small that Γ can be almost zero. Consequently, Eq. 1 is expressed as:

$$d\Gamma/dt = k_1C \quad (2)$$

In the temperature range of 290—318 K in our experiment, the monolayer of tetradecanoic acid is in the liquid-expanded state.[3,4] For the liquid-expanded film, Langmuir proposed the following equation:[3]

$$(\Pi - \Pi_0)(A - A_0) = RT \quad (3)$$

where Π is the surface pressure (mN m^{-1}): Π_0, the characteristic surface pressure of the film material ($\Pi_0 = -11.2$ mN m^{-1} for tetradecanoic acid[5]); A, the occupied area per mole (m^2 mol^{-1}) of the film material; A_0, the excluded area per mole (m^2 mol^{-1}); R, the gas constant and T, the absolute temperature.

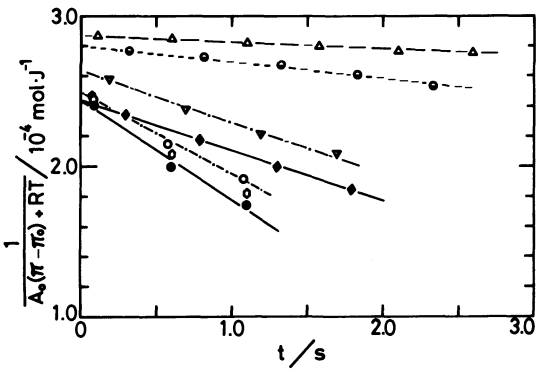

Fig. 4. $1/[A(\Pi-\Pi_0)+RT]$-t relationships for tetradecanoic acid monolayers on 0.01 M HCl at various temperatures. Diamond denotes plate-like crystal and other symbols needle-like crystal. △: T=292.1 K, ○: 296.1 K, ▽: 303.1 K, ○: 308.1 K, □: 313.1 K, ● and ◆: 318.1 K.

Many theoretical equations[6-9] of the state for liquid-expanded monolayers have been proposed; Smith[9] compared the equations with the experimental data for fatty acids and concluded that Langmuir's equation described the experimental data better than any other equation in spite of the variation in Π_0. Consequently, by using Langmuir's equation and by defining $\Gamma = A_T/A$, where A_T is the area of the trough (m^2) containing the subphase solution, we obtain:

$$\Gamma = A_T(\Pi - \Pi_0)/[A_0(\Pi - \Pi_0) + RT] \quad (4)$$

wherefrom we obtain:

$$d\Gamma/dt = (d\Gamma/d\Pi)(d\Pi/dt) = \{A_TRT/[A_0(\Pi - \Pi_0)+RT]^2\}(d\Pi/dt). \quad (5)$$

The substitution of Eq. 2 in Eq. 5 and subsequent integration yield:

$$\{1/[A_0(\Pi - \Pi_0) + RT]\} = -(A_0k_1C/A_TRT)t + 1/(RT - A_0\Pi_0). \quad (6)$$

Figure 4 shows the relationship between $\{1/[A_0(\Pi - \Pi_0) + RT]\}$ and t at various constant temperatures. Good linearities are observed. The slopes for these lines give us k_1C values by the use of A_T=59.17×10^{-4} m^2 and A_0=6022×[12.0+0.178(T−273.15)] m^2 mol^{-1} for the tetradecanoic acid monolayer.[5] The k_1C values thus obtained are listed in Table 1.

The surface pressure, especially at the initial spreading process of the film, is thought to be associated with the number of acid molecules, which are directly in contact with the water, in the crystal. Consequently, we can evaluate the k_1 value only if we know the actual amount of molecules, C.

Figure 5 shows the relationship between the k_1C and the amount of crystal placed on the water surface at 318.1 K. The k_1C value for the needle-like crystals (circle) is always larger than that for the plate-like crystal (square). This may be attributable to the fact that the needle-like crystals have many sharp points[10] at the ends of the crystal, as is shown in the SEM

Table 1. ESP, k_1, k_2, and k_1' Values for the Needle-Like Crystal at Various Temperatures

T	ESP	k_1C	k_1	k_2	k_1'
K	mN m^{-1}	mol·s^{-1}	s^{-1}	s^{-1}	s^{-1}
292.1	14.0	9.96×10^{-10}	13.8	1.2×10^{-5}	2.0×10^{-2}
296.1	16.7	1.81×10^{-9}	25.1	1.8×10^{-5}	5.6×10^{-2}
303.1	20.4	6.15×10^{-9}	85.2	2.8×10^{-5}	19.2×10^{-2}
308.1	24.3	8.08×10^{-9}	112	5.9×10^{-5}	25.3×10^{-2}
313.1	27.0	8.45×10^{-9}	117	33.8×10^{-5}	26.3×10^{-2}
318.1	30.9	8.88×10^{-9}	123	74.0×10^{-5}	27.7×10^{-2}
		5.25×10^{-9}[a]	72.8[a]		

a) These values are for a plate-like crystal.

photograph **A** in Fig. 6, rather than to the difference in the crystallographic forms. The k_1C for the plate-like crystal is independent of the crystal size, while that for the needle-like crystals is also independent of their amounts. Consequently, the number of molecules which are directly in contact with the water seems to be restricted and to be almost constant, regardless of the size or amount of the crystal placed onto the water surface: there is never a time when all the crystal is in contact with the water. In fact, as is shown in the SEM photograph **B** in Fig. 6, the surface of the plate-like crystal used for the spreading-pressure experiment was found to be corroded only partially, even after the crystal has stood on the water surface for 7 days at 318.1 K.

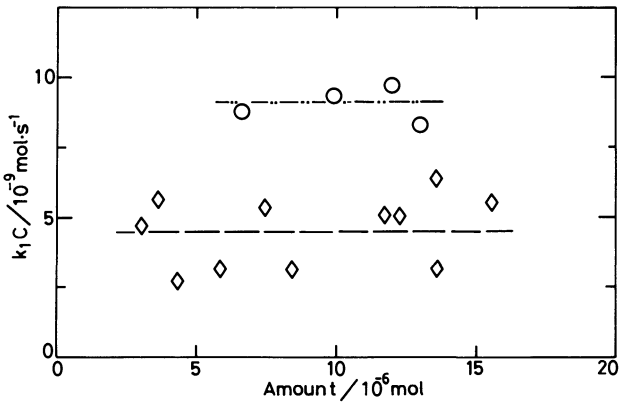

Fig. 5. Relationship between k_1C and amount of crystals placed on water surface at 318.1 K. Circles denote needle-like crystals; diamonds, plate-like crystals.

Although it is essential to know the amount of the molecules, C, directly in contact with the water in the initial stage of the spreading process, the estimation of the genuine amount is impracticable at the present time. Accordingly, a rough approximation was carried out as follows.

C is assumed to be the amount of the molecules in the outermost molecular layer of the crystal facing the underlying water, disregarding the fact that only a part of the crystal surface is directly in contact with the water. The area of the plate-like crystal used in our experiment was determined to be in the range of 7.83—26.7 mm^2 by means of photographic observations. The amount of C for the 7.83 mm^2-sized crystal was estimated to be 7.22×10^{-11} mol by using the cross-section of the 18 Å^2/molecule for the fatty-acid molecule. The k_1 values thus obtained from this C amount at various temperatures are listed in Table 1. Although the ESP increases linearly with the temperature, the k_1 increases in an S-shape. The rapid increase in the k_1 value between 296 and 308 K seems to due not only to the increase in its genuine value, but also to the increase in the wettability of the crystal to water-that is, the increase in the amount of C which is directly in contact with the water. The k_1 value at low temperatures is, therefore, probably smaller than the genuine value because water has a low wettability against the crystal surface because of the higher surface tension of water at low temperatures. The magnitude of k_1 is, however, sufficiently large in comparison with the other rate constants which will be mentioned below.

Desorption Process. In order to estimate the rate constant k_2 in the process of dissolving tetradecanoic acid from its monolayer (Process (3)), desorption

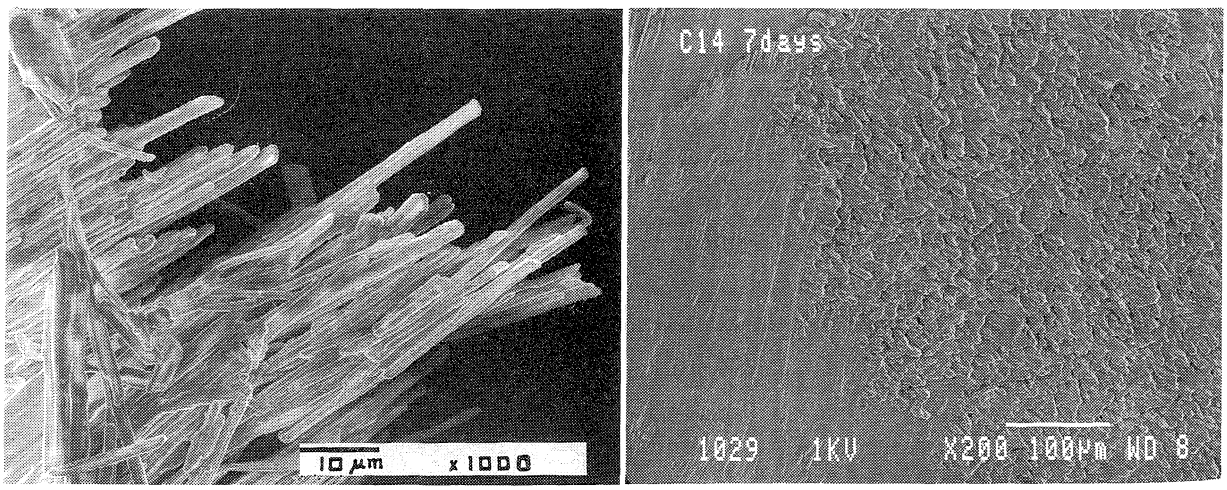

Fig. 6. Photograph **A** represents the needle-like crystals which have sharp ends. Photograph **B** represents a plate-like crystal which was kept for standing on water surface for 7 days at 318.1 K. Only right side of the crystal is corroded.

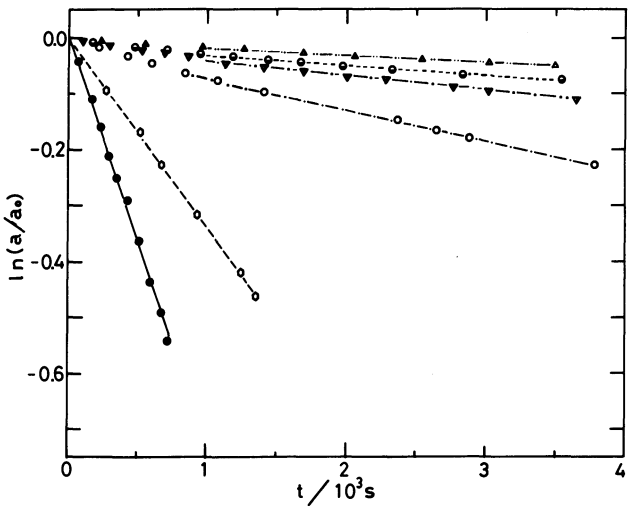

Fig. 7. Desorption performance of tetradecanoic acid from its monolayer into subphase of 0.01 M HCl under 0.3 mN m^{-1} below ESP values at various temperatures. △: T=292.1 K, ◒: 296.1 K, ▼: 303.1 K, ○: 308.1 K, ⬡: 313.1 K, and ●: 318.1 K.

experiments on the tetradecanoic acid monolayer were carried out under the conditions of constant surface pressures and at various temperatures. In Fig. 7, the logarithm of the relative area, $\ln(a/a_0)$, is plotted against t, in which a_0 is the initial area of the monolayer immediately after the monolayer had been compressed to a desired surface pressure, and a, the area of the monolayer at time t. The desorption curve for an experiment at a low temperature has two parts: a curved part at the beginning and a linear one for a higher value of t, as has also been reported by Ter Minassian-Saraga.[10] That is to say, the first desorption stage (shown as a curved part) is diffusion-controlled, while the second one (shown as a linear part) is steady-state. At lower temperatures the steady-state commences at t=ca. 15 min, while at higher temperatures it appears to begin immediately. The rate constant k_2 of the dissolving process was consequently obtained from the $\ln(a/a_0)$ vs. t relationship in the steady-state; it also is listed in Table 1. The k_2 value is found to increase very rapidly with the temperature above 308 K.

Re-binding Process. Next we must consider the re-binding process of the film molecule to the crystal (Process (2)). The variation in the surface concentration of the acid molecules, $d\Gamma/dt$, expressed by Eq. 1, is zero after the spreading pressure becomes constant:

$$d\Gamma/dt = k_1C - (k_1' + k_2)\Gamma_s = 0 \quad (7)$$

where Γ_s is the saturated amount of molecules in the monolayer possessing the area of A_T. Consequently, k_1' is expressed as:

$$k_1' = (k_1C/\Gamma_s) - k_2. \quad (8)$$

The Γ_s value for an insoluble monolayer is, in general, obtainable as the inverse of the molar area of the monolayer at the ESP in its Π–A relationship. The Γ_s for the tetradecanoic acid monolayer at 318.1 K could not be, however, obtained from its Π–A relationship because of the rapid dissolving of the monolayer into the underlying subphase solution. Therefore, by substituting the values of A_t, A_0, Π (ESP), and Π_0 into Eq. 4, the Γ_s value was obtained. For example, the Γ_s value thus obtained at 318.1 K was 3.19×10^{-8} mol, the molecular area being 30.8 Å^2/molecule. This value is reasonable for the acid monolayer at that temperature. On the other hand, the value of C, 7.22×10^{-11} moles, used for the evaluation of the k_1 value seems to be too small compared with this Γ_s value. The C value is, however, the molar amount of the acid in the outermost molecular layer of its crystal directly in contact with the water surface. Even if the outermost layer is desorbed from the crystal into the monolayer, the next layer will appear continuously.

The k_1' value obtained from k_1C, k_2, and Γ_s is also listed in Table 1. When comparing these rate constants with one another, the k_1 is found to be much larger than k_2 at various temperatures. Therefore, the constant spreading pressure, even at high temperatures, at which the monolayer dissolves into the subphase very rapidly, can be regarded as a property in the equilibrium state, namely, the ESP.

The authors wish to express their thanks to Professor Koichi Kobayashi and Mr. Akira Yoshida of Musashi Institute of Technology for their technical help in performing the SEM observations. The present work was supported by a Grant-in-Aid for Scientific Research from the Ministry of Education.

References

1) M. Gotoh, *J. Jpn. Oil Chem. Soc.*, **36**, 909 (1987).
2) A. W. Ralston and C. W. Hoerr, *J. Org. Chem.*, **7**, 546 (1942); K. Motomura, A. Shibata, M. Nakamura, and R. Matuura, *J. Colloid Interface Sci.*, **29**, 623 (1969).
3) I. Langmuir, *J. Chem. Phys.*, **1**, 756 (1933).
4) N. K. Adam and G. Jessop, *Proc. R. Soc. London, Ser. A*, **112**, 362 (1926).
5) M. Nakagaki, "Surface and Colloid States," Tokyo Kagaku Doujin (1968), p. 68.
6) G. Jura and W. D. Harkins, *J. Chem. Phys.*, **12**, 113 (1944).
7) R. Mittleman and R. C. Palmer, *Trans. Faraday Soc.*, **38**, 506 (1942).
8) D. G. Hedge, *J. Colloid Sci.*, **12**, 417 (1957).
9) T. Smith, *J. Colloid Interface Sci.*, **23**, 27 (1967).
10) M. Iwahashi, N. Maehara, Y. Kaneko, T. Seimiya, S. R. Middleton, N. R. Pallas, and B. A. Pethica, *J. Chem. Soc., Faraday Trans. 1*, **81**, 973 (1985).
11) L. Ter Minassian-Saraga, *J. Colloid Sci.*, **11**, 398 (1956); *J. Chim. Phys.*, **52**, 181 (1955); L. Saraga, *Compt. Rend.*, **233**, 135 (1951).

Formulation and Enumeration of Five-Center Organic Reactions

Shinsaku FUJITA
Research Laboratories, Ashigara, Fuji Photo Film Co., Ltd.,
Minami-Ashigara, Kanagawa-ken 250-01
(Received July 30, 1988)

Five-center organic reactions are formulated in the form of pentagonal reaction-center graphs (RCC's) that are subgraphs of imaginary transition structures. This formulation is based on the concept of a charge space that affords rational representations of coordinate bonds. Pólya's theorem is applied to the enumeration of these RCG's, in which the obligatory minimum valencies of vertices restrict the mode of substitution.

The enumeration of reaction types is important for any computer manipulation of organic reactions. In previous papers,[1] we have reported on the enumeration of generic reaction types in the form of the counting of reaction graphs (RG's) that are defined as subgraphs of imaginary transition structures (ITS's).[1b,c] Thus, we have enumerated pentagonal RG's, which represent five-center organic reactions, such as 1,3-dipolar additions and cheletropic reactions.[1c] However, the enumeration of RG's has disregarded the variation of atoms that occupy the vertices of the RG's and has, thus, been limited within the counting of modes of bond-switchings. For an effective manipulation of organic reactions, it is necessary to count more specific reaction types that define the variation of the atoms as well as the modes of bond-switching. This can be accomplished by counting the reaction-center graphs (RCG's) of the pentagonal class. In a continuation of the enumeration of hexagonal RCG's,[1n] this paper will discuss that of pentagonal RCG's.

A Charge Space for Representing Coordinate Bonds in the Imaginary Transition Structure Approach. In an enumeration of such five-center organic reactions, one of the most troublesome problems is in the treatment of coordinate bonds (Scheme 1). Although many approaches have been devoted to this problem, none of them have ever resulted in a comprehensive solution. For example, Ugi et al.[2] have expressed reactions (1a) and (1b) with graphs (**7** and **10**, respectively) in the most abstract fashion (Scheme 2). They have ascribed the two graphs (**7** and **10**) to irreducible reaction matrices (R-matrices) that are presumed to represent five-membered cyclic processes. However, expression (**7**) disregards the presence of a coordinate bond, which is in turn replaced by lone pairs on the terminal atoms. In other words, graph (**7**) and the corresponding R-matrix indicate an acyclic process in their strict sense. Although they had intended to classify **7** and **10** into the same class, this classification requires the presupposition of an implicit invariant bond. If the implicit invariant bond is neglected, just as the graph (**7**) indicates, there would be no good reason to classify reactions **7** and **10** into the same class.

Hendrickson's representations for five-center reactions[3] are equivalent to the formulas (**7** and **10**) in an abstract fashion. Hence, his method has the same drawback as that mentioned as above, although it claims that both of the two formulas represent pericyclic five-center reactions. Vladutz[4] has presented a participating charge with a special symbol placed on an atom. Zefirov et al.[5] have treated a charge as an independent node (vertex). These methods permit an ionic representation as well as the covalent one, where both of the two representations are legitimately alternative forms and, in other words, are not integrated. Brandt el al.[6] have adopted Ugi's R matirices along with the same representation of charges as Vladutz's one. Although these approaches have described the appearance and disappearance of charges, they have paid little attention to the difficulty concerned with coordinate bonds and the dual character of a bond (i.e. the covalent vs. ionic character). Dubois et al.[7] have reported the concept of chromatic transfographs,

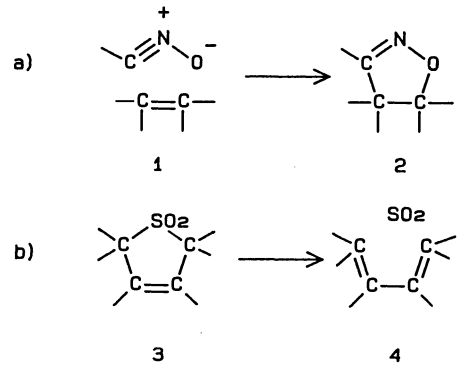

Scheme 1.

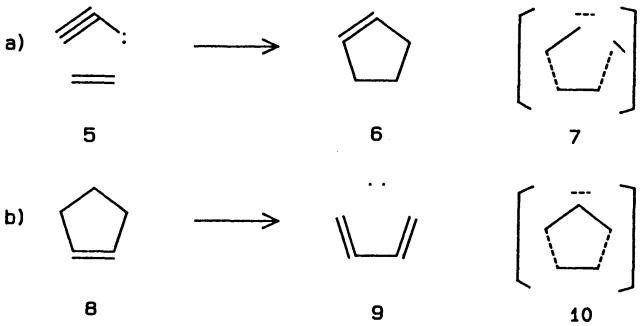

Scheme 2.

which also pays no attention to charges and abnormal valencies.

In order to settle the problem, the ITS approach has introduced a charge space that is attached to a synthesis space (Scheme 3).[1h] The synthesis space contains all nodes that represent atoms or groups participating in a reaction. The charge space consists of charges that are regarded as independent nodes. These nodes (atoms and charges) are linked by par-bonds (——), in-bonds (-⊖-), and out-bonds (-⊣⊢-) in accord with any structural changes during a reaction. The resulting structural formula is called a *full ITS* or an *ITS with charges.* The concept of charge space thus allows us to described a 1,3-dipolar reaction (Scheme 1a) in light of a full ITS (**11**). This type of representation is an integrated representation of covalent and ionic characters (Scheme 3). Thus, the ionic representation (e.g. N^+–O^-) of a coordinate bond and the covalent counterpart (e.g. N=O) are interconvertible to one another via the full ITS (e.g. **11**).

The corresponding ITS (**12**) is obtained by projecting to an ITS (P_{its}), which is a deletion of interspace bonds[8] and of charges and a simultaneous attachment of the intraspace bonds[9] to the respective edges. A corresponding ionic representation (**15**) can be generated by projecting to an ionic ITS (P_{ion}) that deletes the bonds of a charge space.

The graphic representations collected in Scheme 3 may be unfamiliar to organic chemists who used to discuss organic reactions in terms of the usual reaction diagrams. To convert an ITS representation into a reaction diagram, projections to the starting stage and to the product stage (PS and PP) are introduced. The PS operation represents a deletion of all in-bonds. This operation regenerates the starting stage. The PP operation, on the other hand, represents a deletion of all out-bonds, the operation of which creates the product stage.

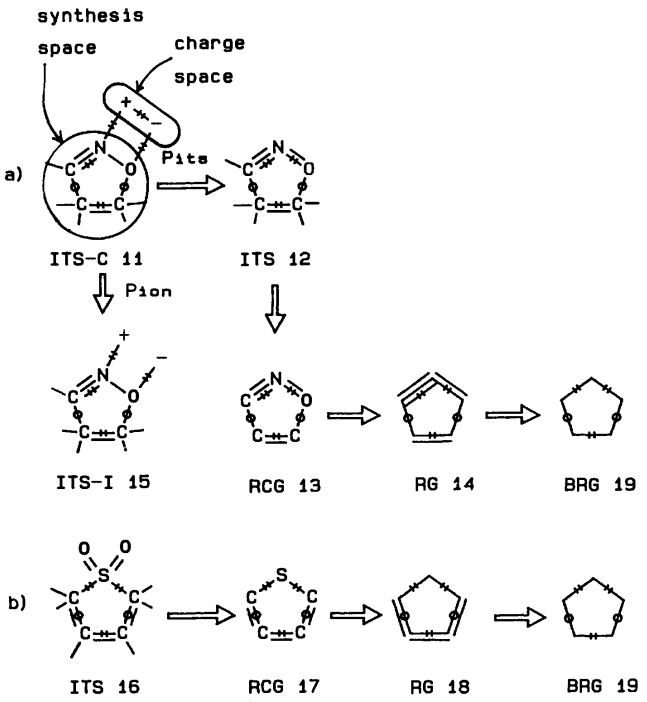

Scheme 3.

In the enumeration procedures of the ITS approach, the covalent representation of a bond is preferred rather than the ionic one.[1c] This methodology can be rationalized by the indroduction of a charge space and by the defining of the P_{its} and P_{ion} operations.[1h] The preference of the covalent character has an advantage in that this overcomes an apparent difference provided by the dual representation of the bond character. Note, for example, that though the ionic repesentation ($N^+(=O)$–O^-) of a nitro group indicates the unequality of the two oxygen atoms in the literal sense, the covalent representation ($N(=O)_2$) equalifies them.

In light of the ITS's extended in this section, a general treatment of five-center reactions is available. As shown in Scheme 3, reaction (1b) is represented by an ITS (**16**) in the usual fashion, since it contains no charge space. Reactions (1a) and (1b) (Scheme 1) produce the corresponding RCG's (**13** and **17**) and RG's (**14** and **18**). The latter pair affords a common basic reaction graph (BRG **19**), which logically indicates that the two reactions belong to the same category of pentagonal class.[10]

Enumeration of Pentagonal RCG's. The present method that enumerates RCG's consists of the following steps:[11,12] (1) finding the permutation group of a parent RG, (2) considering the obligatory minimum valency (OMV) of each vertex (node), (3) obtaining the corresponding cycle index, and (4) substituting the variables of the cycle index by appropriate atom-figure inventories to afford an RCG-counting polynomial as a generating function.

Table 1 lists parent RG's of the pentagonal class.[1c] There are no self-reaction pairs[13] in this series. Each of the RG's has one vertex to which two out-bonds (or two in-bonds) are incident. We call this a valency-changed position (or vertex) because of its chemical meaning. For simplicity of discussions, we suppose that an atom Q always occupies the valency-changed position of each parent RG (Table 1). Several examples for atoms Q are collected in Table 2. The expressions of expanded valencies listed in Table 2 have a sound basis by means of a charge space. The present approach is capable of producing both the covalent representation and the ionic one with the appropriate projections (Scheme 3). The ITS approach permits a quinquivalent nitrogen, a quadrivalent oxygen and so on in the level of ITS's projected from full ITS's.

Positions other than a valency-changed atom undergo ordinary interconversions in which one in-bond and one out-bond are attached to each of the positions.

Table 1. Parent Reaction Graphs of Pentagonal Class That Have 0 to 5 Single Par-Bonds and Are Occupied by an Atom Q[a-c]

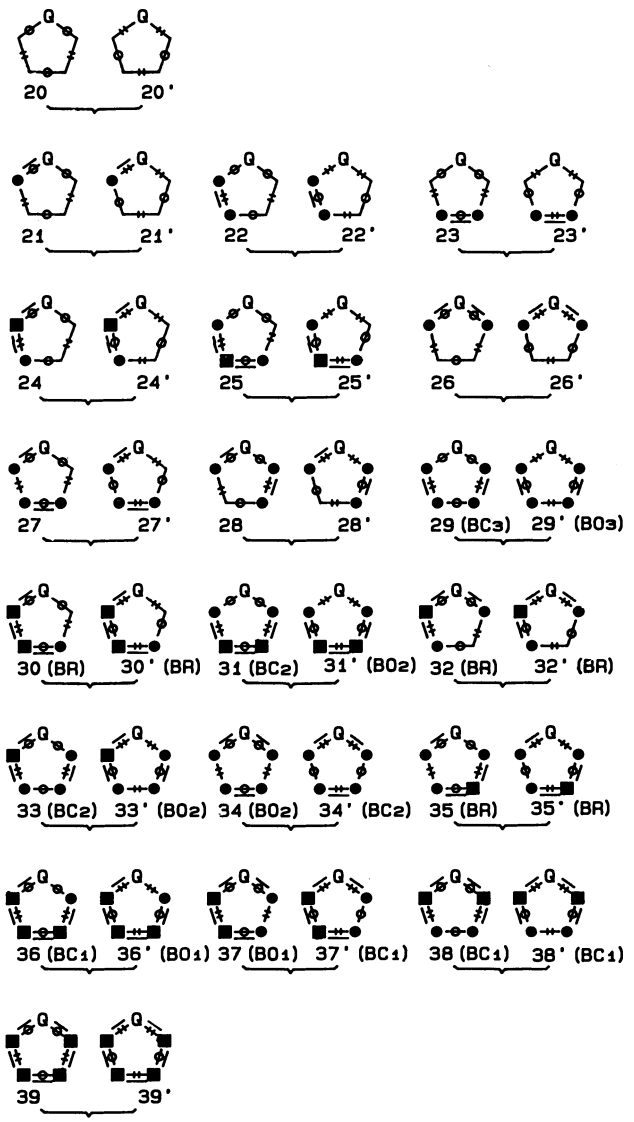

a) The positions marked by ■, ●, and none have minimum valencies of v=3, 2, and 1, respectively. b) Each couple linked with a brace is a reaction pair (an RG pair). There are no self-reaction pairs. c) BO_p is a bridge of ring opening of order p. BC_q is a bridge of ring closure of order q. BR is a bridge of rearrangement.

Their obligtory minimum valencies (OMV) are v=1 (unmarked), v=2 (marked with ●), or v=3 (marked with ■) in accord with the substitution of par-bonds. The unmarked positions are substituted by any atoms that have a valency of larger than 1. We choose carbon, hydrogen, oxygen, and nitrogen atoms as substituents in order to simplify the following discussions. Any position marked with ● (v=2) is capable of taking C, N, or O, but incapable of taking a hydrogen atom. Each position of v=3 (■) is capable of having C or N as a substituent.

Table 2. Atoms (Q) Capable of Valency Change

Atom (Q)[a]	Chemical meaning
	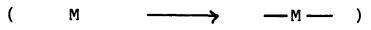
	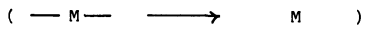
	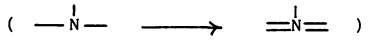
	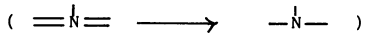
	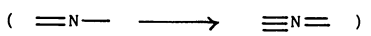
	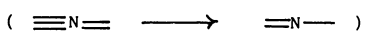
	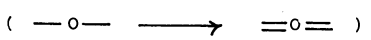
	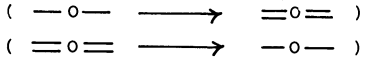

a) The symbol (M) indicates a metal.

Table 3. Cycle Indices for the Parent RG's of Pentagonal Class Preoccupied by an Atom Q

RG[a]	Symmetry	Cycle index[b]	Eq.
20,20'	C_2	G: $(1/2)(c_1^4+c_2^2)$	1
21,21'	C_1	G: $b_1c_1^3$	2
22,22'	C_1	G: $b_1^2c_1^2$	3
23,23'	C_2	G: $(1/2)(b_1^2c_1^2+b_2c_2)$	4
24,24'	C_1	G: $a_1b_1c_1^2$	5
25,25'	C_1	G: $a_1b_1^2c^1$	6
26,26'	C_2	G: $(1/2)(b_1^2c_1^2+b_2c_2)$	7
27,27'	C_1	G: $b_1^3c_1$	8
28,28'	C_1	G: $b_1^3c_1$	9
29,29'	C_2	G: $(1/2)(b_1^4+b_2^2)$	10
30,30'	C_1	G: $a_1^2b_1c_1$	11
31,31'	C_2	G: $(1/2)(a_1^2b_1^2+a_2b_2)$	12
32,32'	C_1	G: $a_1b_1^2c_1$	13
33,33'	C_1	G: $a_1b_1^3$	14
34,34'	C_2	G: $(1/2)(b_1^4+b_2^2)$	15
35,35'	C_1	G: $a_1b_1^3$	16
36,36'	C_1	G: $a_1^3b_1$	17
37,37'	C_1	G: $a_1^2b_1^2$	18
38,38'	C_2	G: $(1/2)(a_1^2b_1^2+a_2b_2)$	19
39,39'	C_2	G: $(1/2)(a_1^4+a_2^2)$	20

a) The parent RG's are collected in Table 1. b) G: a cycle index for counting RCG's.

The OMV requires an extension of Pólya's theorem, in which positions of different OMV's take different atom-figure inventories.[1n] Table 3 summarizes the cycle indices corresponding to the parent RG's of Table 1, where variables a_r, b_r, and c_r are assigned to the vertices marked by ■, ●, and none, respectively.[14]

If the variables of the cycle indices (Table 3) are substituted by atom-figure inventories (Eqs. 21 to 23), RCG-counting polynomials are obtained as generating functions:[15]

$$a_r = 1 + u^r, \tag{21}$$

$$b_r = 1 + u^r + v^r, \tag{22}$$

and

$$c_r = 1 + u^r + v^r + w^r. \tag{23}$$

Table 4. Enumeration of Pentagonal RCG's with an Atom Q

Parent RG			**20**	**21**	**22**	**23**	**24**	**25**	**26**	**27**	**28**	**29**	**30**	**31**	**32**	**33**	**34**	**35**	**36**	**37**	**38**	**39**
			20′	**21′**	**22′**	**23′**	**24′**	**25′**	**26′**	**27′**	**28′**	**29′**	**30′**	**31′**	**32′**	**33′**	**34′**	**35′**	**36′**	**37′**	**38′**	**39′**
i	j	k	Number of RCG's																			
0	0	0	1	1	1	1	1	1	1	1	1	1	1	1	1	1	1	1	1	1	1	1
1	0	0	2	4	4	2	4	4	2	4	4	2	4	2	4	4	2	4	4	4	2	4
0	1	0	2	4	4	2	3	3	2	4	4	2	2	1	3	3	2	3	1	2	1	0
2	0	0	4	6	6	4	6	6	4	6	6	4	6	4	6	6	4	6	6	6	4	6
1	1	0	6	12	12	6	9	9	6	12	12	6	6	3	9	9	6	9	3	6	3	0
0	2	0	4	6	6	4	3	3	4	6	6	4	1	1	3	3	4	3	0	1	1	0
3	0	0	2	4	4	2	4	4	2	4	4	2	4	2	4	4	2	4	4	4	2	4
2	1	0	6	12	12	6	9	9	6	12	12	6	6	3	9	9	6	9	3	6	3	0
1	2	0	6	12	12	6	6	6	6	12	12	6	2	1	6	6	6	6	0	2	1	0
0	3	0	2	4	4	2	1	1	2	4	4	2	0	0	1	1	2	1	0	0	0	0
4	0	0	1	1	1	1	1	1	1	1	1	1	1	1	1	1	1	1	1	1	1	1
3	1	0	2	4	4	2	3	3	2	4	4	2	2	1	3	3	2	3	1	2	1	0
2	2	0	4	6	6	4	3	3	4	6	6	4	1	1	3	3	4	3	0	1	1	0
1	3	0	2	4	4	2	1	1	2	4	4	2	0	0	1	1	2	1	0	0	0	0
0	4	0	1	1	1	1	0	0	1	1	1	1	0	0	0	0	1	0	0	0	0	0
0	0	1	2	3	2	1	2	1	1	1	1	0	1	0	1	0	0	0	0	0	0	0
1	0	1	6	9	6	3	6	3	3	3	3	0	3	0	3	0	0	0	0	0	0	0
0	1	1	6	9	6	3	4	2	3	3	3	0	1	0	2	0	0	0	0	0	0	0
2	0	1	6	9	6	3	6	3	3	3	3	0	3	0	3	0	0	0	0	0	0	0
1	1	1	12	18	12	6	8	2	6	6	6	0	2	0	4	0	0	0	0	0	0	0
0	2	1	6	9	6	3	2	1	3	3	3	0	0	0	1	0	0	0	0	0	0	0
3	0	1	2	3	2	1	2	1	1	1	1	0	1	0	1	0	0	0	0	0	0	0
2	1	1	6	9	6	3	4	2	3	3	3	0	1	0	2	0	0	0	0	0	0	0
1	2	1	6	9	6	3	2	1	3	3	3	0	0	0	1	0	0	0	0	0	0	0
0	3	1	2	3	2	1	0	0	1	1	1	0	0	0	0	0	0	0	0	0	0	0
0	0	2	2	3	1	1	1	0	1	0	0	0	0	0	0	0	0	0	0	0	0	0
1	0	2	3	6	1	1	2	0	1	0	0	0	0	0	0	0	0	0	0	0	0	0
0	1	2	3	6	1	1	1	0	1	0	0	0	0	0	0	0	0	0	0	0	0	0
2	0	2	2	3	0	1	1	0	1	0	0	0	0	0	0	0	0	0	0	0	0	0
1	1	2	3	6	0	1	1	0	1	0	0	0	0	0	0	0	0	0	0	0	0	0
0	2	2	2	3	0	1	0	0	1	0	0	0	0	0	0	0	0	0	0	0	0	0
0	0	3	2	1	0	0	0	0	0	0	0	0	0	0	0	0	0	0	0	0	0	0
1	0	3	2	1	0	0	0	0	0	0	0	0	0	0	0	0	0	0	0	0	0	0
0	1	3	2	1	0	0	0	0	0	0	0	0	0	0	0	0	0	0	0	0	0	0
0	0	4	1	0	0	0	0	0	0	0	0	0	0	0	0	0	0	0	0	0	0	0

Table 5. RCG Isomers with N_2O Based on **36**, **37**, and **38**

Parent RG	RCG with N_2O
36	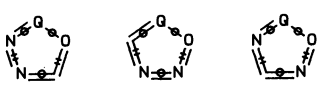
37	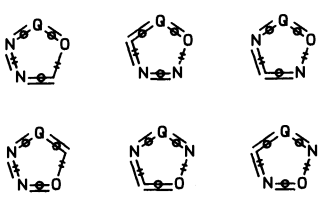
38	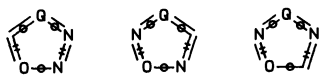

Equation 21 is an atom-figure inventory for counting the modes of C and N substitution, where a variable for C is not expressed explicitly. Equation 22 enumerates the modes of C, N, and O substitution. The modes of C, N, O, and H substitution are counted by Eq. 23. The coefficients of the RCG-counting polynomial series are collected in Table 4, in which each column is in accord with a given parent RG, each line indicates the powers (i, j, and k) and their intersection is the coefficient of the $u^i v^j w^k$. This value is the number of RCG isomers with i nitrogens, j oxygens, and k hydrogens ($N_iO_jH_k$).

Table 5 shows RCG isomers derived form parent RG's (**36**, **37**, and **38**) by N_2O substitution. The number of RCG isomers from **36** is 3, which is found at column **36** and line i=2, j=1, and k=0 in Table 4. The number of RCG isomers derived from **37** and **38** are also listed in Table 4.

Table 6 collects parent RG's in which a pentagonal basic reaction graph (BRG **19**) has one double par-bond and two single par-bonds. One Q atom preoc-

Table 6. Parent Reaction Graphs of Pentagonal Class That Have One Double Par-Bond and Two Single Par-Bonds and Are Occupied by an Atom Q[a-c]

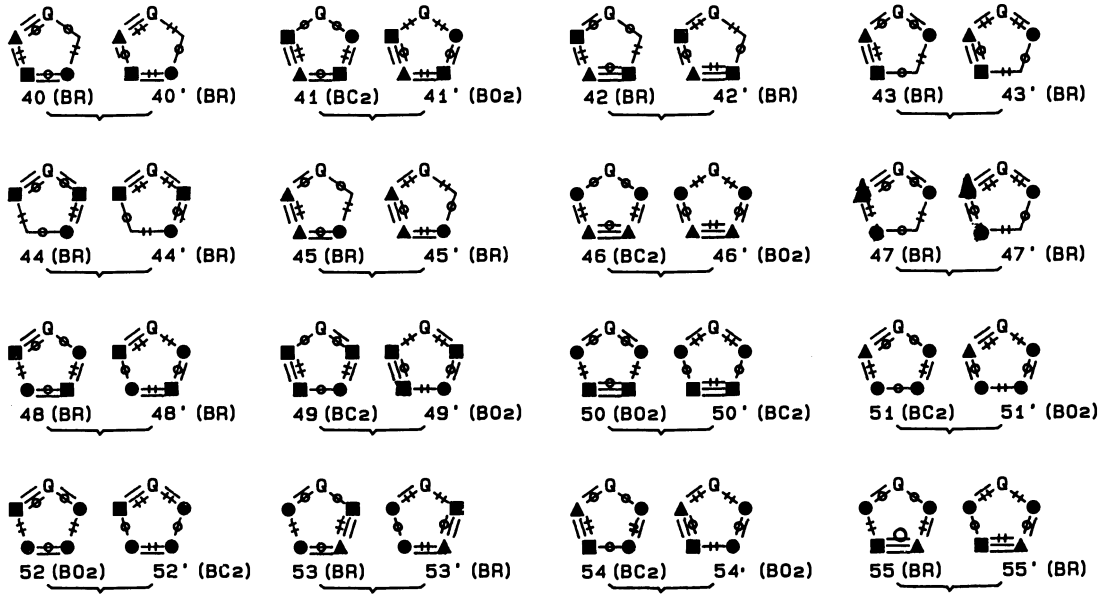

a) The positions marked by ▲, ■, ●, and none have minimum valencies of v=4, 3, 2, and 1, respectively. b) Each couple linked with a brace is a reaction pair (an RG pair). c) BO_p is a bridge of ring opening of order p. BC_q is a bridge of ring closure of order q. BR is a bridge of rearrangement.

Table 7. Cycle Indices for the Parent RG's of Pentagonal Class Preoccupied by an Atom Q

RG[a]	Symmetry	Cycle index[b]	Eq.
40,40′	C_1	G: $a_1b_1c_1$	24
41,41′	C_1	G: $a_1^2b_1$	25
42,42′	C_1	G: $a_1^2c_1$	26
43,43′	C_1	G: $a_1b_1c_1$	27
44,44′	C_1	G: $a_1^2b_1c_1$	28
45,45′	C_1	G: b_1c_1	29
46,46′	C_1	G: b_1^2	30
47,47′	C_1	G: $b_1^2c_1$	31
48,48′	C_1	G: $a_1^2b_1^2$	32
49,49′	C_1	G: $a_1^3b_1$	33
50,50′	C_2	G: $(1/2)(a_1^2b_1^2+a_2b_2)$	34
51,51′	C_1	G: b_1^3	35
52,52′	C_1	G: $a_1b_1^3$	36
53,53′	C_1	G: $a_1b_1^2$	37
54,54′	C_1	G: $a_1b_1^2$	38
55,35′	C_1	G: $a_1b_1^2$	39

a) The parent RG's are collected in Table 6. b) G: a cycle index for counting RCG's.

cupies the valency-changed position of each of the RG's. The other positions are discriminated by their OMV's (i.e. ▲ for v=4, ■ for v=3, ● for v=2, and none for v=1).

Table 7 summarizes the cycle indices corresponding to the respective RG's of Table 6. Each of the cycle indices contains variables selected from a_r (for v=3), b_r (for v=2), and c_r (for v=1). The position marked by ▲ can be substituted only by a carbon atom and, hence, takes no variables in the present treatment. If the

Table 8. RCG Isomers with One Oxygen on **34′**, **50′**, and **52′**

Parent RG	RCG isomers
34′	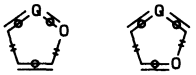
50′	
52′	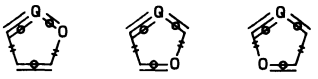

variables (a_r, b_r, and c_r) of each cycle index (Table 7) are substituted by the atom figure inventories (Eqs. 21 to 23), the corresponding RCG-counting polynomial is obtained as a generating function for each case. The coefficient of the term $u^iw^jw^w$ in the RCG-counting polynomial indicates the number of RCG isomers having $N_iO_jH_k$.

Table 8 compares the RG's (**34′**, **50′**, and **52′**) substituted by one oxygen. The number of isomeric RCG's based on each of the RG's emerges as the coefficient of term v in an RCG-counting polynomial derived from Eq. 15, 34, or 36.

Conclusion

Five-center organic reactions are formulated in the form of pentagonal reaction-center graphs (RCG's). These RCG's are enumerated by extending Pólya's theorem, so that different variables are assigened to the vertices of each parent reaction graph (RG) in accord with the obligatory minimum valencies of the vertices.

References

1) a) S. Fujita, *J. Chem. Inf. Comput. Sci.*, **26**, 205 (1986). See also *Chem. Eng. New. (Sept. 29)*, 75 (1986). b) S. Fujita, *J. Chem. Inf. Comput. Sci.*, **26**, 221 (1986). c) S. Fujita, *J. Chem. Inf. Comput. Sci.*, **26**, 224 (1986). d) S. Fujita, *J. Chem. Inf. Comput. Sci.*, **26**, 231 (1986). e) S. Fujita, *J. Chem. Inf. Comput. Sci.*, **26**, 238 (1986). f) S. Fujita, *J. Chem. Inf. Comput. Sci.*, **27**, 99 (1987). g) S. Fujita, *J. Chem. Inf. Comput. Sci.*, **27**, 104 (1987). h) S. Fujita, *J. Chem. Inf. Comput. Sci.*, **27**, 111 (1987). i) S. Fujita, *J. Chem. Inf. Comput. Sci.*, **27**, 115 (1987). j) S. Fujita, *J. Chem. Inf. Comput. Sci.*, **27**, 120 (1987). k) S. Fujita, *J. Chem. Inf. Comput. Sci.*, **28**, 1 (1988). l) S. Fujita, *J. Chem. Inf. Comput. Sci.*, **28**, 78 (1988). m) S. Fujita, *J. Chem. Soc., Perkin Trans. 2*, **1988**, 598. n) S. Fujita, *Bull. Chem. Soc. Jpn.*, **61**, 4189 (1988).

2) J. Bauer, R. Herges, E. Fontain, and I. Ugi, *Chimia*, **39**, 43 (1985).

3) J. B. Hendrickson, *Angew. Chem., Int. Ed. Engl.*, **13**, 47 (1974).

4) G. Vladutz, "Modern Approaches to Chemical Reaction Searching," ed by P. Willet, Gower Publishing, England (1986), Chap. 15.

5) a) N. S. Zefirov and S. S. Tratch, *Zhur. Org. Khim.*, **20**, 1121 (1984); b) N. S. Zefirov, S. S. Tratch, and G. A. Gamziani, *Zhur. Org. Khim.*, **22**, 1341 (1986).

6) a) J. Brandt and K. Stadler, "Modern Approaches to Chemical Reaction Searching," ed by Gower Publishing Co., Ltd., England (1986), Chap. 16. b) J. Brandt, J. Bauer, R. M. Frank, A. von Scholley, *Chem. Scripta*, **18**, 53 (1981).

7) a) J.-E. Dubois, G. Sicouri, and R. Ricchiottino, "Modern approaches to Chemical Reaction Seaching," Gower Publishing, ed by P. Willet, England (1986), Chap. 17. b) G. Sicouri, Y. Sobel, R. Picchiottino, and J.-E. Dubois, *C. R. Acad. Sc. Paris*, **299**, 523 (1984).

8) An interspace bond is defined as a linkage between a synthesis space and a charge space. See Ref. 1h.

9) An intraspace bond is defined as a bond which links two nodes of the same space. See Ref. 1h.

10) The RCG's, RG's, and BRG's represent the levels of a reaction hierarchy in ascending order of generality.

11) For the enumeration of organic compounds, see a) D. H. Rouvray, *Chem. Soc. Rev.*, **3**, 355 (1974). b) "Chemical Applications of Graph Theory," ed by A. T. Balaban, Academic Press, London (1976). c) N. L. Biggs, E. K. Lloyd, and R. J. Wilson, "Graph Theory 1736—1936," Clarendon Press, Oxford (1976), Chap. 4.

12) a) G. Pólya, *Acta Math.*, **68**, 145 (1937). b) G. Pólya, R. E. Tarjan, and D. R. Woods, "Notes on Introductory Combinatorics," Birkhaeuser Boston Inc. (1983), Chapt 6. c) C. L. Liu, "Introduction to Combinatorial Mathematics," McGraw-Hill (1969).

13) A. reaction pair is a pair of RG's that are interconvertible by an exchange operation between in-bonds and out-bonds. A self reaction pair is an RG that is invariant in the operation.

14) For the derivation of cycle indices, see Ref. 1n. It should be noted that, since variables a_r, b_r, and c_r are assigned in accord with OMV's, unequivalent vertices can take the same variable.

15) The substitution of carbon atoms is presumed implicitly in all cases.

Study of Conformers of 2,2′-, 3,3′-, and 4,4′-Dimethylbiphenyls in the Phosphorescent Triplet States by Electron Spin Resonance and Phosphorescence

Katsumi TANIGAKI,† Noriyuki TAGUCHI, Mikio YAGI, and Jiro HIGUCHI*
Department of Physical Chemistry, Faculty of Engineering, Yokohama National University, Tokiwadai, Hodogaya-ku, Yokohama 240
(Received August 13, 1988)

For the phosphorescent triplet (T_1) states of symmetrically-substituted dimethylbiphenyls, the relationship between the twisting angle of the two aromatic rings and the zero-field splitting parameters is discussed in terms of the ESR spectra. Two sets of ESR spectra observed for 2,2′- and 3,3′-dimethylbiphenyls (2DMBP and 3DMBP) are precisely assigned to the corresponding s-cis or s-trans conformer. The results clarify the inadequate assignment of the spectra of these molecular species in the previous literature. The lifetime obtained for the s-cis conformer is different from that of the s-trans one for both 2DMBP and 3DMBP. Examining the T_1–T_1 energy transfer from one conformer to the other, the relative locations for the T_1 states of s-cis and s-trans conformers are obtained, even if phosphorescence measurements do not provide each isolated spectrum: E_T (*s-cis*-3DMBP)<E_T(*s-trans*-3DMBP) and E_T(*s-cis*-2DMBP)>E_T(*s-trans*-2DMBP).

The geometry of biphenyl (BP) has been discussed under different conditions. In the ground (G) state BP is a nonplanar molecule and its twisting angle between the two phenyl rings is 20—40° in the vapor phase and in solutions,[1,2] while it is zero (or nearly zero) in a crystal.[3,4] In the lowest excited triplet (T_1) state, however, BP has been clarified to be planar[5,6] by the phosphorescence and T_n←G absorption measurements[7] as well as photochemical quenching data.[6] Several theoretical calculations[8–10] have supported the coplanar structure between two phenyl rings of BP in its T_1 state.

In the T_1 states, s-cis and s-trans conformers have been detected by ESR for some of biphenyl derivatives and their related molecules. For the ESR spectra of 2,2′-bipyridine (BPY), the s-cis and s-trans conformers are detectable.[11–13] However, their twisting angles (θ's) between the two aromatic rings are nearly zero, and one of the zero-field splitting (ZFS) parameters, D, is almost the same for both conformers.[11–13] As a result, the influence of any deviation from a coplanar structure upon the ZFS parameters could not be experimentally obtained. On the other hand, the dimethylbiphenyls (DMBP's)†† are actually suitable examples in examining such an influence, since θ is expected to be changed without any large affection of the electronic structures upon the positions of the methyl substituents. Fourteen years ago, Scheve and Wagner[14] studied the ESR of the T_1 states of methyl-substituted biphenyls and found two sets of conformers for some of the DMBP's, although their assignment to the conformation is still uncertain. Their result is distinctly contradictory to the theoretical prediction that the D value decreases with increasing θ. Under these circumstances, we tried to reexamine the ESR of the symmetrically-substituted DMBP's.

In the present paper, we report on the ESR and phosphorescence of symmetrically-substituted DMBP's. For 2DMBP and 3DMBP, two sets of observed ESR spectra have been assigned to the corresponding s-cis and s-trans conformers using a stretched poly(vinyl alcohol) (PVA) film as a host. The spectra obtained for 2DMBP are remarkably different from those reported by Scheve and Wagner.[14] The relationship between the ZFS parameters and θ of the conformers will be discussed.

The ESR spectra observed in the T_1 states of DMBP's are interpreted by the following spin Hamiltonian:

$$\begin{aligned}\mathscr{H} &= g\mu_B \boldsymbol{B}\cdot\boldsymbol{S} + \boldsymbol{S}\cdot\boldsymbol{D}\cdot\boldsymbol{S} \\ &= g\mu_B \boldsymbol{B}\cdot\boldsymbol{S} - XS_x^2 - YS_y^2 - ZS_z^2 \quad (S=1) \\ &= g\mu_B \boldsymbol{B}\cdot\boldsymbol{S} + D[S_z^2 - (1/3)S^2] + E[S_x^2 - S_y^2]:\end{aligned}$$

where $\boldsymbol{D}(x,y,z)$ is the ZFS tensor with principal values ($-X$, $-Y$, and $-Z$) and principal axes (x,y,z). D and E denote the ZFS parameters and are related to ($-X$,$-Y$,

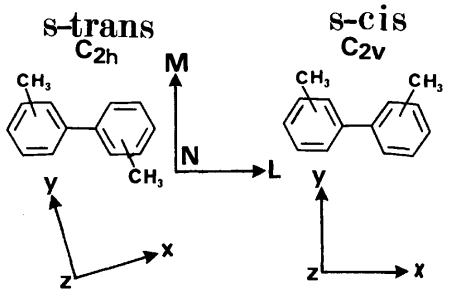

Fig. 1. Molecular structures and coordinate systems for DMBP's: Molecular axes (L,M,N), $\boldsymbol{D}$ tensor axes (x,y,z).

† Permanent address: Fundamental Research Laboratories, NEC Corporation, 1-1, Miyazaki 4-chome, Miyamae-ku, Kawasaki 213.

†† In the present paper, 2,2′-, 3,3′- and 4,4′-dimethylbiphenyls are abbreviated as 2DMBP, 3DMBP, and 4DMBP, respectively.

$-Z$) by $D=(-3/2)Z$ and $E=(-1/2)(X-Y)$. The other symbols have their usual meanings. The anisotropy of the g tensor is neglected since the observed ESR spectra could be reasonably analyzed with the isotropic g_e for free electrons.

For the planar conformation of DMBP's in their T_1 states, the principal axes of $\boldsymbol{D}(x,y,z)$ and the molecular axes (L,M,N) are taken to be as shown in Fig. 1. For $\boldsymbol{D}(x,y,z)$, the x-axis is relatively close to the longest direction of the molecule, the y-axis is perpendicular to it in the molecular plane and the z-axis is normal to the molecular plane. For the molecules treated here, L is parallel to the central C–C bond that connects two of the same aromatic rings, M is perpendicular to it in the molecular plane, and N is normal to the molecular plane. For a stretched PVA film, s is the stretched direction, c is perpendicular to it in the film plane, and n is normal to the film plane.

Experimental

4,4′-Dimethylbiphenyl (Tokyo Kasei) was purified two times by recrystallization from its ethanol solution. 3DMBP (Tokyo Kasei) was distilled under reduced pressure (bp=114—115 °C/400 Pa). 2DMBP (Tokyo Kasei) was distilled under reduced pressure (bp=90 °C/153 Pa) and was further purified with a silicagel (Kanto Chemicals C-200) column using hexane as an elutant (more than five times). Three unremovable impurities still remained after only distillation. Two of them could be easily removed by column purification, though the other was very difficult to remove. At least four column purifications were required in order to obtain pure 2DMBP, which is sufficient for ESR and phosphorescence measurements. Hexane was the best elutant among the solvents studied. The solvents suitable for a rigid glass medium, ethanol (Wako S.S.G.) and methylcyclohexane (Dotite Spectrosol), were used without further purification after being carefully checked for the absence of an extraneous ESR and phosphorescence signals prior to use.

The purity of 2DMBP and 3DMBP was checked by gas chromatography (GC) with a Shimadzu GC-4A apparatus using a Shimadzu SE-30 column. They exhibited a single peak after purification (more than 99.95%). No impurities were spectroscopically detected for 4DMBP and BP by phosphorescence and ESR measurements.

The PVA films containing 2DMBP, 3DMBP, or 4DMBP were prepared following the same method as described previously.[15] The PVA sample films were prepared by the diffusion method using methanol solutions.[16] The standard concentrations of the 4DMBP, 3DMBP, and 2DMBP solutions used were 1.0×10^{-3}, 8.9×10^{-4}, and 8.3×10^{-3} mol dm^{-3}, respectively. The concentrations of the sample solutions for 3DMBP and 2DMBP were chosen in order to obtain the nearly equal intensities of spectra between s-cis and s-trans conformers. The PVA films obtained were stretched at 80 °C with Shibayama SS-60 film stretcher. The films, thus obtained, have about 200% of stretch in the stretched direction s.

Sample-cooling was controlled by the penetration rate of a quartz tube (5 mm o.d.) into liquid nitrogen from rapid cooling to 0.042 mm s^{-1}. For the magnetophotoselection experiments, a Glan-Thompson polarizer was placed between the Xe-Hg lamp and the sample cavity.

The ESR and phosphorescence spectra were measured at 77 K in the same way as reported previously.[13]

Results

The ESR spectrum of $\Delta M_S=\pm1$ transitions for the T_1 state of 4DMBP was measured in an ethanol glass, as shown in Fig. 2a. For the assignment of the observed signals to the corresponding magnetic principal axes of $\boldsymbol{D}(x,y,z)$, we measured the ESR spectra using a stretched PVA film as a host. According to the general relationships concerning the orientation of planar guest molecules in the stretched PVA films,[15,16] the assignment of the observed signals is straightforward, as shown in Figs. 2b ($\boldsymbol{B}//\boldsymbol{s}$) and 2c ($\boldsymbol{B}//\boldsymbol{n}$). As a result, we can reasonably assign all of the observed signals, as indicated in Fig. 2a.

For 3DMBP, the ESR of $\Delta M_S=\pm1$ transitions was measured in an ethanol glass. As shown in Fig. 2d, we clearly observed two sets of spectra, which are ascribed

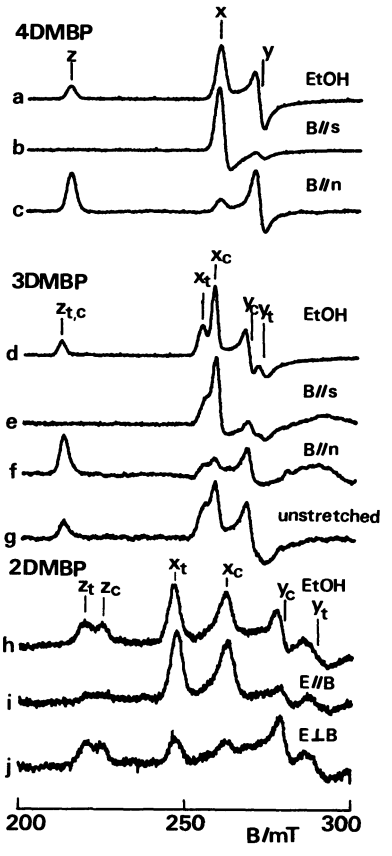

Fig. 2. ESR spectra of the low field $\Delta M_S=\pm1$ transitions for the T_1 state of 4DMBP in ethanol (a) and in PVA films [$\boldsymbol{B}//\boldsymbol{s}$ (b) and $\boldsymbol{B}//\boldsymbol{n}$ (c)], 3DMBP in ethanol (d) and in PVA films [$\boldsymbol{B}//\boldsymbol{s}$ (e), $\boldsymbol{B}//\boldsymbol{n}$ (f) and unstretched (g)], and 2DMBP in ethanol with no polarization (h) and in ethanol with $\boldsymbol{E}//\boldsymbol{B}$ (i) and $\boldsymbol{E}\perp\boldsymbol{B}$ (j).

to the s-cis and s-trans conformers. The spectra resembled those reported by Scheve and Wagner.[14] As in the case of 4DMBP, the observed signals were reasonably assigned to the corresponding magnetic principal axes of $\boldsymbol{D}(x,y,z)$ using a stretched PVA film as a host,[15,16] as shown in Figs. 2e and 2f.

In a randomly oriented rigid glass, the assignment of two sets of spectra to the corresponding s-cis and s-trans conformers is generally impossible. Here, we tried to assign the observed two sets of spectra to the corresponding conformers with the help of the orientation of guest molecules in stretched PVA films.[11] For the s-cis conformer with symmetry C_{2v}, the principal x-axis is parallel to L ($x//L$), while that of the s-trans one with symmetry C_{2h} should deviate from L to some extents. When $\boldsymbol{B}$ is applied parallel to s ($\boldsymbol{B}//s$), the intensity of the x-signal for the s-cis conformer would be more enhanced than that for the s-trans one. For 3DMBP, the relative intensity of the x-signal at 260 mT to that at 256 mT was enhanced in stretched PVA films with $\boldsymbol{B}//s$ [Fig. 2e], compared with that in unstretched PVA films [Fig. 2g]. As a result, a set of signals belonging to the x-signal at 260 mT was assigned to the s-cis conformer, and the other set of signals belonging to the x-signal at 256 mT was assigned to the s-trans one. The assignment carried out in this work disagrees with that by Scheve and Wagner,[14] possibly because of their unreasonable postulation that the larger anisotropic electron distribution in the molecular plane is for the s-cis conformer.

For 2DMBP, two sets of ESR spectra were also observed in an ethanol glass as shown in Fig. 2h. However, these obtained spectra were markedly different from those reported by Scheve and Wagner.[14] Furthermore, no dependence of cooling rate on the relative intensity between the two sets of spectra was found in our experiments (see, Experimental section), which is also contradictory to their report.[14] ^{1}H NMR and GC measurements supported that 2DMBP used here is extremely pure (more than 99.95%). In their ESR measurements, therefore, some impurities might be incorporated and their assignment on the basis of the cooling rate dependence seems to be meaningless.

We tried to assign the two sets of spectra to the corresponding s-cis or s-trans conformer, and each signal to the principal axes of $\boldsymbol{D}(x,y,z)$ using the stretched PVA film method. However, 2DMBP was tremendously difficult to incorporate into PVA films to obtain an ESR spectrum with sufficient intensity, even if a high concentration of 1.0×10^{-2} mol dm^{-3} was adopted. For the assignment of the principal axes of $\mathbf{D}(x,y,z)$, therefore, we used the magnetophotoselection method.[17] The main excitation path for 2DMBP is associated with the absorption of a strong band centered at around 250 nm, which shows mainly a long-axis polarization.[18] Therefore, the transition moment of 2DMBP at the wavelength of the exciting light used in this experiment is considered to be parallel (or nearly parallel) to L. If the electric vector of the exciting light ($\boldsymbol{E}$) is parallel to $\boldsymbol{B}$ ($\boldsymbol{E}//\boldsymbol{B}$), the x-signals would be more enhanced than the other signals and be easily distinguishable from the others. As shown in Figs. 2i and 2j, the signals at 249 mT and 264 mT were more enhanced than the others with $\boldsymbol{E}//\boldsymbol{B}$, indicating that these two signals are x-signals. The two sets of outer signals are assigned to the z-signals, since the character of the T_1 states of 2DMBP should not be largely different from that of BP because of the D values of ca. 0.1 cm^{-1} and the lifetimes of 2—4 s. The assignment of these two sets of spectra to the s-cis and s-trans conformers will be described in the following paragraph.

The ZFS parameters and the lifetimes obtained in the present work are listed in Table 1, including the D^* values obtained from the B_{min} signals. The D values are considered to be closely related to the twisting angle between two aromatic rings. From this table, the $|D|$ values for the s-cis and s-trans conformers of 3DMBP are almost identical within the resolution of our experiments and are close to that of 4DMBP. This

Table 1. ZFS Parameters, Lifetimes, τ, and 0-0 Energies of the $T_1\rightarrow G$ Transitions, $\nu_{0\text{-}0}$ for BP and DMBP's in the T_1 States

Molecule	Host	$\lvert X\rvert$	$\lvert Y\rvert$	$\lvert Z\rvert$	$\lvert D\rvert$	$\lvert E\rvert$	$D^{*a)}$	$\tau^{b)}$	$\nu_{0\text{-}0}$
		cm^{-1}	cm^{-1}	cm^{-1}	cm^{-1}	cm^{-1}	cm^{-1}	s	cm^{-1}
BP	EtOH	0.0406	0.0331	0.0738	0.1107	0.0037	0.1109	4.4	23010
s-trans-2DMBP	EtOH	0.0472	0.0192	0.0664	0.0996	0.0140	0.1010[c)]	4.6	>24390[d)]
s-cis-2DMBP	EtOH	0.0374	0.0259	0.0633	0.0950	0.0058	0.1010[c)]	2.0	
s-trans-3DMBP	EtOH	0.0415	0.0296	0.0714	0.1070	0.0060	0.1068[c)]	4.5	22670[e)]
s-cis-3DMBP	EtOH	0.0391	0.0322	0.0714	0.1071	0.0035	0.1068[c)]	4.2	
s-trans-3DMBP	PVA	0.0410	0.0304	0.0711	0.1067	0.0055	0.1061[c)]	3.6	—
s-cis-3DMBP	PVA	0.0391	0.0319	0.0711	0.1067	0.0036	0.1061[c)]	2.7	—
4DMBP	EtOH	0.0391	0.0315	0.0708	0.1061	0.0038	0.1059	4.4	22540
4DMBP	PVA	0.0390	0.0312	0.0707	0.1058	0.0039	0.1056	4.2	—

a) Obtained from the observed resonance field of the $\Delta M_S=\pm2$ transition with Kottis-Lefebvre's correction.[23] b) Obtained from the x-signals of $\Delta M_S=\pm1$ transitions. c) Could not be isolated for each conformer. d) Phosphorescence was broad with no vibronic structures. e) Phosphorescence could not be isolated for each conformer.

implies that the twisting angle of the T_1 state of 3DMBP is nearly the same and possibly zero for both s-cis and s-trans conformers. On the other hand, one of the $|D|$ values observed for 2DMBP was especially small among those for the other DMBP's and BP, while the $|D|$ value of the other species is slightly smaller than those for the other DMBP's and BP. The twisting angle of the *s-cis*-2DMBP is considered to deviate substantially from zero due to the large repulsion between the two methyl substituents, though its deviation of *s-trans*-2DMBP would be small. From this consideration, the different features of one ESR spectrum from that of the others lead us to its assignment to the s-cis conformer.

The $|E|$ values for the s-cis conformers were smaller than those for the s-trans ones for both 3DMBP and 2DMBP. For a planar conformation, if the coordinate system is chosen to be in the same direction of the molecular axes (*L,M,N*), the nonzero off-diagonal elements of the ***D*** tensor appear only for the s-trans conformers with C_{2h}, while all of the off-diagonal elements are zero for the s-cis ones with C_{2v} from the viewpoint of their symmetries.[11] From this consideration, the $|E|$ value for the s-cis conformers should be smaller than that for the s-trans ones if the electron spin distribution is not much different from each other. The tendency of the $|E|$ values observed for 3DMBP would be simply explained by this analysis. For a discussion concerning 2DMBP with a nonplanar conformation in the T_1 state, a similar relationship is also valid, although further studies of other 2,2′-disubstituted biphenyls are required.

The lifetimes in the T_1 states of DMBP's were obtained from the decay of the low-field *x*-signals of the ESR spectra. All decay's were exponential over at least three times the lifetimes (within experimental error). For 3DMBP, the lifetime of the s-cis conformer (4.2 s) was different from that of the s-trans one (4.5 s). Although the difference was very small, it was beyond the experimental error. For 2DMBP, the lifetime of the s-cis conformer (2.2 s) was almost half of that of the s-trans one (4.6 s). The difference was quite large. Considering that the T_1 lifetimes of DMBP's except *s-cis*-2DMBP are very close to that of BP, the twisting angle of only *s-cis*-2DMBP would deviate to a great extent from zero, due to a steric hindrance between the two methyl groups.

The phosphorescence spectra for DMBP's were measured in ethanol at 77 K, as shown in Fig. 3. Especially for 2DMBP, the phosphorescence spectrum was very broad and did not show any vibronic structure. We could not isolate the phosphorescene of s-cis and s-trans conformers for both 2DMBP and 3DMBP. From the edge of the high-energy region, as well as the 0-0 bands of the phosphorescence, we estimated the locations of the T_1 states (E_T) for DMBP's and BP in the order of E_T(2DMBP)>E_T(BP)>E_T(3DMBP)~E_T(4DMBP).

The lifetimes for DMBP's in the T_1 states were also measured from the decay of phosphorescence. BP and 4DMBP showed the same lifetimes as those obtained by ESR (within experimental error). The decay of 3DMBP was almost single exponential at any wavelength monitored; however, it could not be discussed in detail because of the overlapping of the two types of phosphorescence with very close lifetimes of s-cis and s-trans conformers. On the other hand, 2DMBP showed a nonexponential decay because of the coexistence of the conformers with appreciably different lifetimes.

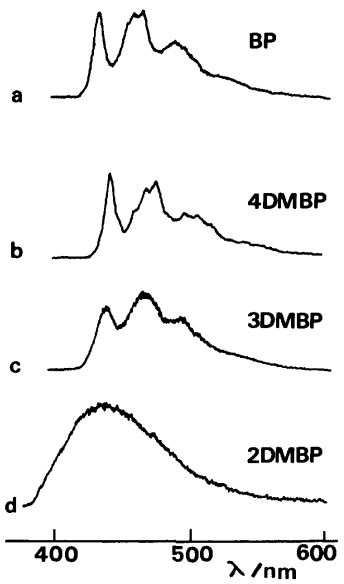

Fig. 3. Phosphorescence spectra of BP (a), 4DMBP (b), 3DMBP (c), and 2DMBP (e) in ethanol at 77 K.

Discussion

An important question to be argued concerns the state, from which the s-cis and s-trans conformers detected in the T_1 states are formed. There are two possibilities: one is that these conformers are formed from the two species in the G states trapped in a rigid medium prior to excitation; the other is that they are formed in the excited states, S_1 and/or T_1, through the conformational change after excitation, even if a species with only one conformation is trapped in a rigid medium. Information related to this problem is provided by the dependence of the excitation wavelength and the kind of rigid media upon the ESR signal intensity ratio between the s-cis and s-trans conformers.

For 3DMBP the ESR spectra were measured in ethanol with various filter combinations. The results are shown in Figs. 4a—4c. The intensity of the ESR signal for the s-trans conformer relative to that for the s-cis one decreased under lower energy excitation. This indicates that two kinds of species with different

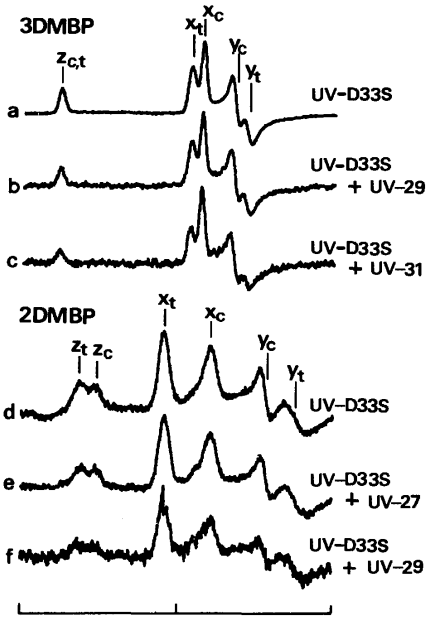

Fig. 4. ESR spectra of the low field $\Delta M_S=\pm 1$ transitions for the T_1 state of 3DMBP in ethanol with UV-D33S (a), UV-D33S+UV-29 (b) and UV-D33S+UV-31 (c) excitation, and for 2DMBP in ethanol with UV-D33S (d), UV-D33S+UV-27 (e) and UV-D33S+UV-29 (f) excitation. The filters used, UV-D33S, UV-27, UV-29, and UV-31, cut off the shorter wavelength region and have transmittances of 50% at $\lambda\approx 255$, 270, 290, and 310 nm, respectively. The UV-D33S filter also cuts off the longer wavelength region and has a transmittance of 50% at $\lambda=$ 385 nm.

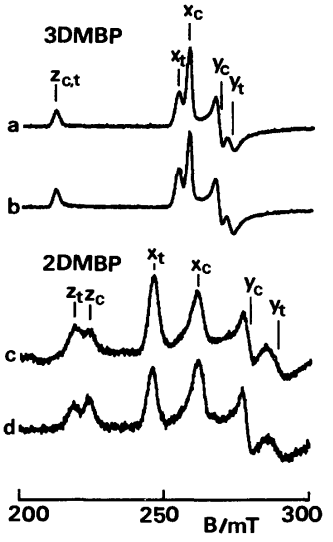

Fig. 5. ESR spectra of the low field $\Delta M_S=\pm 1$ transitions for the T_1 state of 3DMBP in ethanol (a) and methylyclohexane (b), and 2DMBP in ethanol (c) and methylcyclohexane (d).

absorption characteristics exist in the frozen media prior to excitation. The s-cis conformer arises from a species with longer wavelength absorption than the other, from which the s-trans conformer arises. The ESR spectra observed for 3DMBP were independent of the kind of frozen media, ethanol or methylcyclohexane, as shown in Figs. 5a and 5b, although two kinds of species with different conformations exist.

For 2DMBP, the dependence of the ESR spectra on the kind of frozen media was also studied using ethanol and methylcyclohexane, as shown in Figs. 5c and 5d. The intensity ratio of the ESR signal of the s-cis conformer to that of the s-trans one was distinctly influenced by the rigid media. This phenomenon shows the existence of two kinds of species trapped in the frozen media: that is, the s-cis and s-trans conformers are independently formed from the two kinds of species in their G states. No excitation wavelength dependence on the signal intensity ratio between the s-cis and s-trans conformers was observed, as shown in Figs. 4d—4f. This shows that the two species trapped in the frozen media are scarcely different from each other in their absorption characteristics.

The phosphorescence spectra measured in this study did not give any information on the relative locations for the T_1 levels of the s-cis and s-trans conformers. The relative locations of the T_1 levels could be compared using the T_1–T_1 energy transfer from one conformer to the other, as has widely been admitted.[19–22] Regarding the ESR signal intensity ratio, the contribution of the energy transfer from the lowest singlet state of one conformer to that of the other is considered to be small owing to the relatively shorter lifetimes of the S_1 states than those of the T_1 states.

Figures 6a—6c show the ESR spectra of the low-field $\Delta M_S=\pm 1$ transitions for 3DMBP in ethanol with concentrations of 5.4×10^{-2} to 8.9×10^{-5} mol dm^{-3}. The signal intensity ratio of the s-cis conformer to that of the s-trans one increased as the concentration of the samples increased. This indicates that the absorbed energy transfers from the T_1 level of the *s-trans*-3DMBP to that of *s-cis*-3DMBP. Thus, we can conclude that E_T(*s-trans*-3DMBP) locates higher in energy than E_T(*s-cis*-3DMBP).

For 2DMBP, the ESR spectra of the low-field $\Delta M_S=\pm 1$ transitions were measured in ethanol, changing the concentration of 2DMBP from 8.3×10^{-2} to 8.3×10^{-5} mol dm^{-3}, as shown in Figs. 6d—6f. In this case the opposite trend to that for 3DMBP was obtained. As a result, we concluded that E_T(*s-trans*-2DMBP) locates lower in energy than E_T(*s-cis*-2DMBP).

Ortho methyl substituents were found to impede a coplanar conformation of the two aromatic rings, even in the T_1 state (especially for the s-cis conformer). D values and lifetimes were closely related to the twisting angle between the two phenyl rings. The results indicated that the $|D|$ value decreases with increasing the deviation of the twisting angles between the two

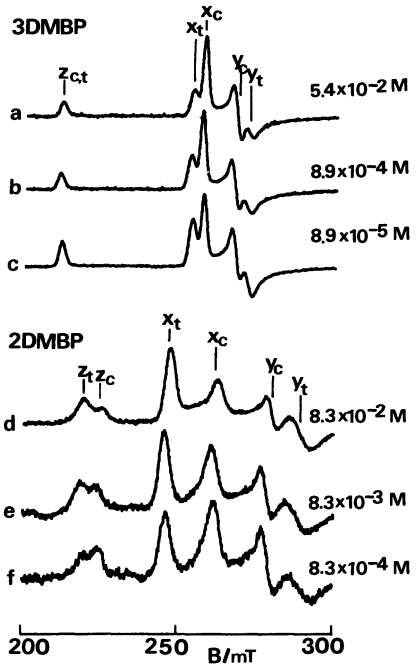

Fig. 6. ESR spectra of the low field $\Delta M_S=\pm 1$ transitions for T_1 state of 3DMBP in ethanol of 5.4×10^{-2} mol dm^{-3} (a), 8.9×10^{-4} mol dm^{-3} (b), and 8.9×10^{-5} mol dm^{-3} (c), and for 2DMBP in ethanol of 8.3×10^{-2} mol dm^{-3} (d), 8.3×10^{-3} mol dm^{-3} (e), and 8.3×10^{-4} mol dm^{-3} (f). 1 M=1 mol dm^{-3}.

aromatic rings from zero, as was seen for *s-trans*-3,3′-dimethyl-2,2′-bipyridine.[11] This is quite the same conclusion as that deduced from a theoretical consideration on the spin delocalization in a biphenyl molecule. It should be noted here that in ESR spectroscopy the influence of methyl substitution in BP appears only for a change in the twisting angle. Further studies of other substituted biphenyls would systematically clarify the relationship between ZFS parameters and conformation, especially for the twisting angle.

This work was supported by a Grant-in-Aid for Scientific Research No. 61430002 from the Ministry of Education, Science and Culture. One of us, K. Tanigaki, wishes to thank NEC Corporation for a leave of absence during the term of this research.

References

1) O. Bastiansen and M. Traetteberg, *Tetrahedron*, **17**, 147 (1962).
2) H. Suzuki, *Bull. Chem. Soc. Jpn.*, **32**, 1340 (1959).
3) J. Trotter, *Acta Crystallogr.*, **14**, 1135 (1961).
4) A. Hargreaves and S. H. Rizvi, *Acta Crystallogr.*, **15**, 365 (1962).
5) J. Mispelter, *Chem. Phys. Lett.*, **10**, 539 (1971).
6) P. J. Wagner, *J. Am. Chem. Soc.*, **89**, 2820 (1967).
7) E. C. Lim and Y. H. Li, *J. Chem. Phys.*, **52**, 6416 (1970).
8) A. Imamura and R. Hoffmann, *J. Am. Chem. Soc.*, **90**, 5379 (1968).
9) M. K. Orloff and J. S. Brinen, *J. Chem. Phys.*, **47**, 3999 (1967).
10) A. Golebiewski and A. Parczewski, *Z. Naturforsh., Teil A*, **25**, 1710 (1970).
11) J. Higuchi, M. Yagi, T. Iwaki, M. Bunden, K. Tanigaki, and T. Ito, *Bull. Chem. Soc. Jpn.*, **53**, 890 (1980).
12) T. Ito and J. Higuchi, *Chem. Lett.*, **1974**, 1519.
13) M. Yagi, K. Makiguchi, A. Ohnuki, K. Suzuki, J. Higuchi, and S. Nagase, *Bull. Chem. Soc. Jpn.*, **58**, 252 (1985).
14) B. J. Scheve and P. J. Wagner, *Chem. Phys. Lett.*, **25**, 324 (1974).
15) T. Ito, J. Higuchi, and T. Hoshi, *Chem. Phys. Lett.*, **35**, 141 (1975).
16) J. Higuchi, T. Ito, M. Yagi, M. Minagawa, M. Bunden, and T. Hoshi, *Chem. Phys. Lett.*, **46**, 477 (1977).
17) M. A. El-Sayed and S. Siegel, *J. Chem. Phys.*, **44**, 1416 (1966).
18) L. O. Edwards and W. T. Simpson, *J. Chem. Phys.*, **53**, 4237 (1970).
19) A. Terenin and V. Ermolaev, *Trans. Faraday Soc.*, **52**, 1042 (1956).
20) N. Nakashima, Y. Kume, and N. Mataga, *J. Phys. Chem.*, **79**, 1788 (1975).
21) A. Kira and J. K. Thomas, *J. Phys. Chem.*, **78**, 196 (1974).
22) R. G. Bennett, R. P. Schwenker, and R. E. Kellogg, *J. Chem. Phys.*, **41**, 3040 (1964).
23) P. Kottis and R. Lefebvre, *J. Chem. Phys.*, **39**, 393 (1963).

γ-Radiolysis of 1-Substituted 5-Fluorouracil Derivatives

Tokuyuki KURODA,* Koji HISAMURA, Ikuo MATSUKUMA, Hiroshi NISHIKAWA, and Nobuhiro NAKAMIZO
Pharmaceutical Research Laboratories, Kyowa Hakko Kogyo Co. Ltd., Shimotogari, Nagaizumi-cho, Sunto-gun, Shizuoka 411
(Received August 26, 1988)

A new concept, "Radiation-Induced Drug (RID)", was proposed as a novel type of drugs for cancer therapy. To test the usefulness of this concept, 5-fluorouracil (5-FU) derivatives having various types of substituents at the 1-position were prepared and the γ-radiolyses of their aqueous solutions were studied. The compounds having sulfonyl and thioureido groups as the substituents produced efficiently 5-FU with high G values upon γ-irradiation. The medium effects on the radiolyses revealed that the above two substituents were removed mainly with HO· and hydrated electrons e^-_{eq}.

It has long been recognized that a serious problem in cancer chemotherapy is the lack of site-selectivity in drug action for tumor cells.[1-3] The drugs usually manifest severe side effects on normal cells.[1-3] In the radiotherapy, tumor cells often resist against γ-radiation, and also most of solid tumors are known to have a low sensitivity to γ-radiation.[3-6] However, there is the possibility that these defects in the cancer therapies may be removed by developing a novel type of drugs which we call "Radiation-Induced Drug (RID)". We define the RID as that the drug itself is pharmaceutically inactive both for cancer and normal cells, but it produces an active drug specifically for cancer cells upon γ-irradiation. Since γ-ray can be irradiated selectively on cancer cells, the RID is supposed to become an anticancer drug with minimal toxicity for normal cells. We have thought that the RID may be prepared by the chemical modification of a drug which is known to be active for cancer cells. This approach consists in the conversion of the active drug to its functionalized derivative from which the functional group can be removed by γ-radiolysis to reproduce the active drug.

The previous work has shown that the chemically active species in the radiotherapy are the species generated by the γ-radiolysis of water.[7] Such species are shown in Eq. 1 with the G values of their formation.

$$\underset{\text{G value}}{H_2O} \xrightarrow{\gamma\text{-ray}} \underset{2.6}{e^-_{aq}}, \quad \underset{2.6}{HO\cdot}, \quad \underset{0.7}{H\cdot}, \quad \underset{0.65}{H_2O_2}, \quad \underset{0.4}{H_2} \qquad (1)$$

With this background we have initiated to search candidate compounds for the RID. In this investigation, we chose 5-fluorouracil (5-FU, 5-fluoro-2,4(1*H*, 3*H*)-pyrimidinedione) as a base active drug of the RID and synthesized its derivatives having various substituents at the 1-position. We then studied the γ-radiolysis of aqueous solutions of these compounds. A special attention was focused on what kinds of the reactive species play an important role in the γ-ray radiolysis of the aqueous solutions of the RID candidate compounds. The results are described in this paper.

Results and Discussion

Synthesis of 5-FU Derivatives. Twenty-five 5-FU derivatives (Table 1) which have various substituents at the 1-position were synthesized according to the routes outlined in Scheme 1. The detailed synthetic procedures and the structure confirmation of the compounds are described in the Experimental section.

Chemically Reactive Species Generated by the γ-Radiolysis of Water. The reactive species generated by the γ-radiolyses of water (Eq. 1) may be classified into two types: the reductive species such as hydrated electron (e^-_{aq}), H· and H_2, and the oxidative species such as HO· and H_2O_2. In this investigation, we confined our attention specifically to the reactivities of three reactive species, e^-_{aq}, HO· and H·, toward the RID candidate compounds because of the large G values of the formation of these reactive species. We then attempted to examine the way to discriminate the predominant reactive species from other species.

The rate constants for the reactions of these reactive species with molecules closely related to this investiga-

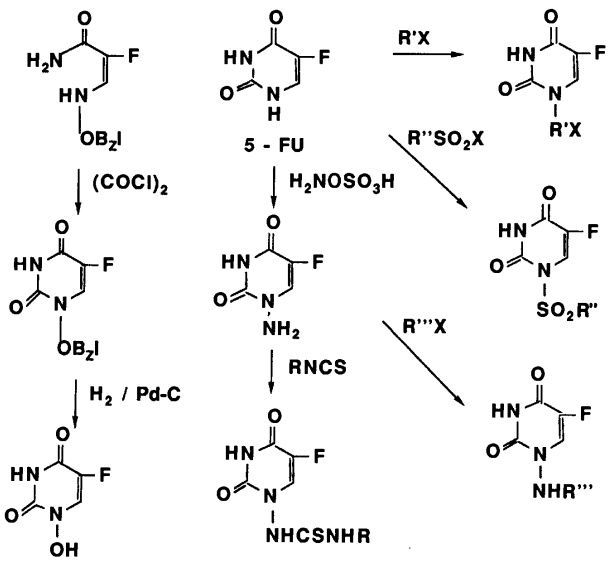

Scheme 1.

Table 1. *G* Values for the Formation of 5-FU upon γ-Irradiations of Aqueous Solutions of 1-Substituted 5-FU Derivatives

	Compound	*G*(5-FU)		
	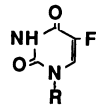	e^-_{aq}[a]	H·[b]	HO·[c]
1	R = $-SO_2N(CH_3)_2$	0.75	0.02	0.14
2	R = $-SO_2CH{=}CHPh$	0.82	0.22	0.69
3	R = $-CO_2CH_2CCl_3$		Hydrolysis	
4	R = $-CO_2CH_2$–	0.05	0.10	0.11
5	R = $-COSCH_2$–	Trace	Trace	Trace
6	R = $-NH_2 \cdot HCl$	—	—	—
7	R =	0.35	0.11	Trace
8	R = $-N(COCH_3)_2$	0.34	Trace	Trace
9	R = $-N(COPh)_2$	0.60	Trace	Trace
10	R =	Trace	Trace	Trace
11	R = $-NHSO_2$–	0.41	Trace	0.15
12	R = $-NHCO_2CH_2CCl_3$	0.11	0.05	0.04
13	R = $-NHCSNHCO_2Et$	1.00	1.14	0.40
14	R = $-NHCSNHPh$	0.59	0.89	0.15
15	R = $-NHCSNHBu^t$	0.40	1.11	0.20
16	R = $-NHCSNHCH_2Ph$	0.49	0.82	0.17
17	R = $-NHCONHPh$	Trace	Trace	Trace
18	R = $-NHCONHBu^t$	Trace	Trace	Trace
19	R = $-NHSO_2N(CH_3)_2$	0.07 (>NH) 0.64 (>N–NH_2)	Trace	Trace
20	R = $-CH(CH_3)$–	—	—	—
21	R = $-CH($– $)_2$	Trace	Trace	Trace
22	R = $-C(CH_3)_2$–		Hydrolysis	
23	R = $-OH$	—	—	—
24	R = $-OCH_2Ph$	0.48	Trace	Trace
25	R = $-OSO_2$–	0.24	Trace	Trace
26	R = $-OCO$–	0.31	Trace	Trace

a) γ-Irradiations were carried out in 1 vol% methanol-water solutions. b) γ-Irradiations were carried out in 1 vol% methanol-water solutions containing 0.05 M H_2SO_4. c) γ-Irradiations were carried out in 1 vol% acetonitrile-water solutions saturated with N_2O gas.

tion have already been reported. The typical data are shown in Eqs. 2—7.[7,8] The other data have shown that the rate constants for the reactions of e^-_{aq} and HO· with organic compounds lie in the region of 10^8—10^{11}.[9-12]

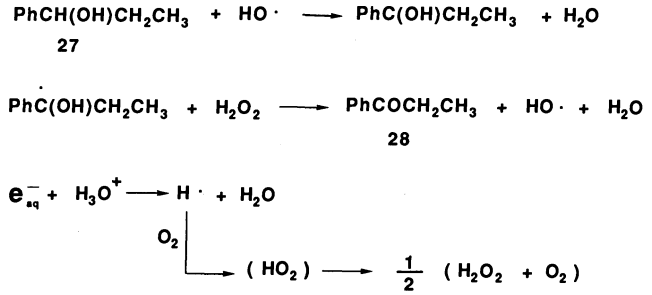

Scheme 2.

$$k(CH_3OH + HO\cdot \longrightarrow \dot{C}H_2OH + H_2O) = 4.8\times10^8 \quad (2)$$

$$k(CH_3OH + e^-_{aq}) < 10^4 \quad (3)$$

$$k(CH_3CN + HO\cdot \longrightarrow \cdot CH_2CN + H_2O) = 5.5\times10^6 \quad (4)$$

$$k(CH_3CN + e^-_{aq}) = 2.5\times10^7 \quad (5)$$

$$k(e^-_{aq} + H_3O^+ \longrightarrow H\cdot + H_2O) = 2.4\times10^{10} \quad (6)$$

$$k(e^-_{aq} + N_2O \longrightarrow HO\cdot + HO^- + N_2) = 8.7\times10^9 \quad (7)$$

These data indicate that methanol reacts with HO· much faster than with e^-_{aq}. Therefore, it is reasonable to assume that in the γ-radiolysis of an aqueous solution, the HO· species can be quenched effectively by adding methanol to the reaction mixture. On the other hand, acetonitrile reacts rather slowly and at comparable rates with both HO· and e^-_{aq}. Hence, even if acetonitrile is added to the reaction mixture, no selective quenching of both the reactive species can be expected. This presumption was confirmed by the following experiments.

Previously, Yamamoto et al. have reported that the γ-ray radiolysis of an aqueous solution of 1-phenyl-1-propanol (**27**) gives 1-phenyl-1-propanone (**28**) via the pathways shown in Scheme 2.[13]

By examining the solvent effects on this reaction, we found that the *G* value for the formation of **28** was affected to a small extent by adding acetonitrile, but to a great extent by adding methanol to the reaction system. The results are shown in Fig. 1. The addition of 1 vol% methanol caused the significant decrease in the *G* value for the formation of **28**; the *G* value decreased from 1.17 to 0.24. However, the addition of 1 vol% of acetonitrile caused no appreciable change in the *G* value; the *G* value changed from 1.17 to 1.14. These results strongly suggest that the reactive species would be quenched in accord with the pathways indicated in Eqs. 2—7.

From these quenching experiments, we made the following assumption about the reactive species in the γ-radiolysis: (1) e^-_{aq} is the principal reactive species in the reactions in 1 vol% methanol aqueous solution, (2) H· is that in the reaction in 0.05 M (M=mol dm^{-3}) H_2SO_4 solution in 1 vol% methanol aqueous solution,

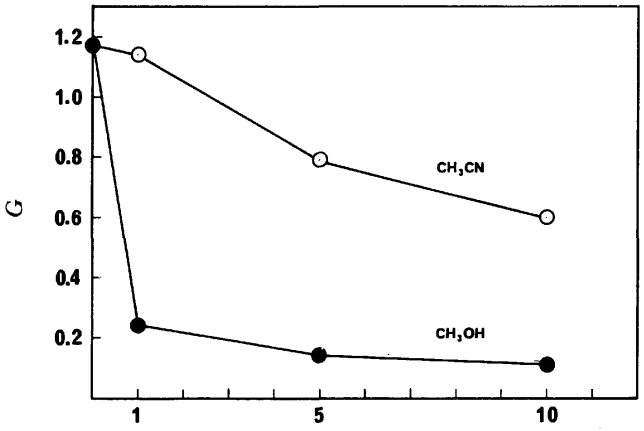

Fig. 1. Effects of added organic solvents on the G values for the formation of **28** in the γ-radiolysis of the aqueous solution of **27**.

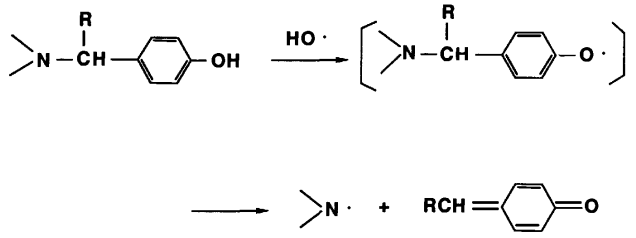

Scheme 3.

(3) HO· is that in the reaction in N_2O saturated 1 vol% acetonitrile aqueous solution.

γ-Radiolyses of 5-FU Derivatives. The γ-radiolyses of 5-FU derivatives were carried out under the conditions described in the preceding section and the G values for the formation of 5-FU were measured. The results are summarized in Table 1. The efficiency of the γ-radiolyses of the compounds are discussed separately according to types of bonds that are cleaved.

(1) N-C Bond Cleavage: We expected at the outset of this study that **20** and **21** may be cleaved to 5-FU via the routes shown in Scheme 3 (N represents the nitrogen at the 1-position of 5-FU). But, this type of the reaction was found not to occur appreciably. We also found that **22**, which has no hydrogen at the α carbon of the substituent, was unstable under the reaction conditions and gave 5-FU along with 2-(4-hydroxyphenyl)-2-propanol by sponthaneous hydrolysis.

For the γ-radiolysis of compound **3**, we expected that the reaction with e^-_{aq} may occur to produce 5-FU. However, this compound was also unstable under the reaction conditions and gave 5-FU by spontaneous hydrolysis.

(2) N-O Bond Cleavage: Compounds **24**, **25**, and **26** produced 5-FU mainly by the reaction with e^-_{aq} upon γ-irradiation, but the efficiency of this reaction

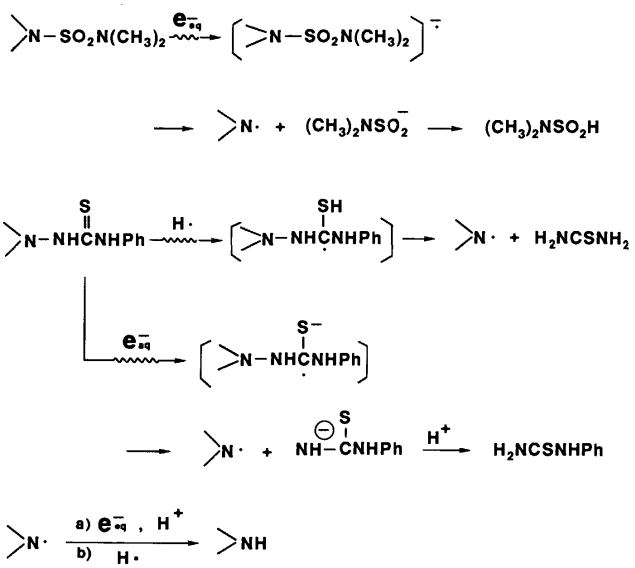

Scheme 4.

was low.

(3) N-S Bond Cleavage: The *N*-sulfonyl compounds, **1** and **2**, were cleaved efficiently to produce 5-FU upon γ-irradiation. The medium effects on this reaction showed that the radiolysis was promoted mainly with e^-_{aq} and partly with HO·.

(4) N-N Bond Cleavage: The *N*-imido compounds, **7** and *N*-diacylamino compounds **8**, **9** were cleaved relatively efficiently to produce 5-FU mainly with e^-_{aq} upon γ-irradiation. However, we found that among all the compounds examined, the compounds having thioureido substituents such as **13—16** were efficiently cleaved to produce 5-FU upon γ-irradiation, although ureido substituents were insensitive to the γ-radiolysis. The high sensitivity of the thioureido substituents to the γ-radiolysis is due to the fact that these substituents are highly reactive toward two reductive species e^-_{aq} and H· as well as the oxidative species HO·. It should be pointed out here that the results for compounds **1** and **19** show that the N-S bond is much more sensitive than the N-N bond to the γ-radiolysis.

Mechanistic Implication. The results so far obtained indicate that 5-FU derivatives having sulfonyl or thioureido groups at the 1-position efficiently produce 5-FU upon γ-irradiation of their aqueous solutions, and they would become good candidates for the RID. The results also indicate that the sulfonyl and thioureido substituents of 5-FU derivatives are eliminated mainly with reductive species such as e^-_{aq} and H·. The plausible mechanisms for the γ-radiolysis of these sulfur-containing compounds are presented in Scheme 4.

The sulfonyl and thioureido groups have a relatively high electron-accepting ability. In addition, the radical anions of these group produced by electron

transfer become good leaving groups as their anions, and hence these groups are cleaved efficiently upon γ-irradiation.

The usefulness of the concept of RID and the mechanistic details of their γ-radiolysis are now under investigation, and will be reported in subsequent papers.

Experimental

Melting points were determined with a Büchi 510 capillary melting point apparatus and are uncorrected. ^{1}H NMR spectra were recorded on a JEOL JNM-PMX 60 spectrometer using Me_4Si as an internal standard. IR spectra were obtained on a Shimadzu IR-400 spectrometer. Mass spectra were recorded on a JEOL JMS-D300 mass spectrometer. Column chromatography was performed on silica gel (silica gel 60, Merck). The purity of compounds was checked by TLC on silica-gel plates (silica gel 60, F_{254}, Merck). Elementary analyses were performed by an Yanagimoto CHN Corder MT-3, and the errors were within ±0.4% of calculated values. γ-Irradiations were carried out by ^{137}Cs source at the National Institute of Genetics. HPLC analyses were performed on a Shimadzu LC-3A, using a 25 cm×4 mm i.d. stainless steel column packed with RP-18 chemically bonded silica gel (Lichrosorb, 10 μm, Merck).

Preparation of Materials. 1-(Dimethylaminosulfonyl)-5-fluorouracil (1). To a solution of 5-FU (200 mg, 1.54 mmol) in 2 cm^3 of *N,N*-dimethylacetamide were added *N,N*-dimethylsulfamoyl chloride (342 mg, 2.38 mmol) and triethylamine (0.5 cm^3). The mixture was stirred at room temperature for 6 h, acidified to pH 3.0 with 1 M HCl, and filtered. The filtrate was concentrated, and the residue was chromatographed on silica gel with $CHCl_3$–acetone (15:1) to give 280 mg (77%) of **1**; mp 211—212 °C. IR (KBr) 1700, 1670, 1330, 1170 cm^{-1}; ^{1}H NMR (DMSO-d_6) δ=3.16 (6H, s), 8.42 (1H, d, *J*=6.0 Hz), 12.46 (1H, bs); MS *m/z* 237 (M$^+$). Found: C, 30.61; H, 3.35; N, 17.49%. Calcd for $C_6H_8N_3O_4FS$: C, 30.38; H, 3.40; N, 17.72%.

5-Fluoro-1-(2-phenylethenesulfonyl)uracil (2). A mixture of 5-FU (200 mg, 1.54 mmol), 2-phenylethenesulfonyl chloride (467 mg, 2.31 mmol) and triethylamine (2 cm^3) in *N,N*-dimethylacetamide (2 cm^3) was stirred at room temperature for 2.5 h. Water (8 cm^3) and 1 M HCl (2 cm^3) were added and then the mixture was extracted three times with 20 cm^3 portions of $CHCl_3$. The organic layer was washed with water, dried (Na_2SO_4) and concentrated. The residue was chromatographed on silica gel with $CHCl_3$–acetone (30:1) to give **2** (270 mg, 59%) as colorless crystals; mp 180—182 °C. IR (KBr) 1700, 1670, 1330, 1170 cm^{-1}; ^{1}H NMR (DMSO-d_6) δ=7.26—8.08 (7H, m), 8.19 (1H, d, *J*=6.6 Hz), 12.24 (1H, bs); MS *m/z* 296 (M$^+$). Found: C, 48.48; H, 3.11; N, 9.51%. Calcd for $C_{12}H_9N_2O_4FS$: C, 48.65; H, 3.06; N, 9.46%.

5-Fluoro-1-(2,2,2-trichloroethoxycarbonyl)uracil (3). To a solution of 5-FU (156 mg, 1.20 mmol) in 2.2 cm^3 of DMF were added 1,1,1-trichloroethoxycarbonyl chloride (386 mg, 1.82 mmol) and triethylamine (170 mg, 1.68 mmol). The mixture was stirred under ice-cooling for 1.5 h and filtered. The filtrate was concentrated. The residue was dissolved in a small amount of DMF and poured into water to give **3** (176 mg, 48%) as white crystals; mp 164—166 °C. IR (KBr) 1800 and 1680 cm^{-1}; ^{1}H NMR (DMSO-d_6) δ=5.14 (2H, s), 8.22 (1H, d, *J*=7.2 Hz), 11.22 (1H, bs); MS *m/z* 304 (M$^+$). Found: C, 27.37; H, 1.39; N, 9.34%. Calcd for $C_7H_4N_2O_4Cl_3F$: C, 27.52; H, 1.32; N, 9.17%.

5-Fluoro-1-(4-methoxybenzyloxycarbonyl)uracil (4). A mixture of trichloromethyl chloroformate (0.3 cm^3) and active carbon (200 mg) in $ClCH_2CH_2Cl$ (10 cm^3) was stirred at room temperature for 30 min, and cooled to 5 °C. A solution of 4-methoxybenzyl alcohol (350 mg, 4 mmol) and triethylamine (610 mg, 6 mmol) in 2 cm^3 of $ClCH_2CH_2Cl$ was then added dropwise, and stirred at room temperature for 3.5 h. The precipitate was filtered off and the filtrate was concentrated. The residue was dissolved in a small amount of DMF, and then 5-FU (260 mg, 2 mmol) and triethylamine (0.4 cm^3) were added to this solution. After stirring for 6 h, the mixture was poured into water and extracted with $CHCl_3$. The organic layer was washed with aqueous NaCl solution, dried (Na_2SO_4) and concentrated to give crystals, which were recrystallized from $CHCl_3$–hexane to afford pure **4** (120 mg, 20%); mp 162.5—163.5 °C. IR (KBr) 1700, 1680 cm^{-1}; ^{1}H NMR (DMSO-d_6) δ=3.76 (3H, s), 4.76 (2H, s), 6.94—7.34 (4H, m), 8.18 (1H, d, *J*=6.8 Hz), 11.84 (1H, bs); MS *m/z* 294 (M$^+$). Found: C, 52.83; H, 3.91; N, 9.47%. Calcd for $C_{13}H_{11}N_2O_5F$: C, 53.07; H, 3.77; N, 9.52%.

5-Fluoro-1-[(4-methoxybenzylthio)carbonyl]uracil (5). A mixture of trichloromethyl chloroformate (0.3 cm^3) and active carbon (200 mg) in dioxane (12 cm^3) was stirred at room temperature for 30 min and cooled to 5 °C. A solution of 4-methoxyphenylmethanethiol (460 mg, 3 mmol) and triethylamine (610 mg, 6 mmol) in dioxane (2 cm^3) was added dropwise and stirred at room temperature for 3 h. The precipitate was filtered off and the filtrate was evaporated. The residue was dissolved in a small amount of DMF and then 5-FU (260 mg, 2 mmol) and triethylamine (0.4 cm^3) were added. After stirring for 1.75 h, the mixture was poured into water. The deposited solid was recrystallized from AcOEt–acetone to give **5** (430 mg, 74%); mp 197—198 °C. IR (KBr) 1735, 1700 cm^{-1}; ^{1}H NMR (DMSO-d_6) δ=3.68 (3H, s), 4.12 (2H, s), 6.86—7.30 (4H, m), 8.36 (1H, d, *J*=7.2 Hz), 12.30 (1H, bs); MS *m/z* 310 (M$^+$). Found: C, 50.20; H, 3.44; N, 9.26%. Calcd for $C_{13}H_{11}N_2O_4FS$; C, 50.32; H, 3.57; N, 9.03%.

1-(Benzylideneamino)-5-fluorouracil. To a solution of 5-FU (50 g, 0.38 mol) and KOH (112 g, 1.71 mol) in water (600 cm^3) was added an aqueous solution (200 cm^3) containing hydroxylamine-*O*-sulfonic acid (6.44 g, 1.16 mol) below 10 °C. The mixture was stirred for 4 h at room temperature and acidified to pH 3 with 5 M HCl. A solution of benzaldehyde (40 g, 0.38 mol) in ether (300 cm^3) was then added, and the resulting mixture was stirred at room temperature for 4 h. The precipitated solid was filtered, washed with water and dried to give 74.7 g of crude product which was then stirred in 750 cm^3 of dioxane at 60 °C for 30 min and cooled. The precipated white crystals were filtered to give 47.5 g (64%) of 1-(benzylideneamino)-5-fluorouracil; mp 229—231 °C. TLC (AcOEt) R_f 0.60; IR (KBr) 1722, 1650, 1605, 1565 cm^{-1}; ^{1}H NMR (DMSO-d_6) δ=7.39—8.04 (6H, m), 8.67 (1H, s), 11.31 (1H, bs).

1-Amino-5-fluorouracil Hydrochloride (6). Hydrogen gas was bubbled into a solution of 1-benzylideneamino-5-fluorouracil (20 g, 0.086 mol) in CH_3OH (200 cm^3) containing 0.5 M HCl (200 cm^3) and 10% Pd–C (2.0 g) with stirring at room temperature for 9 h. The mixture was filtered, and the filtrate was concentrated to dryness and triturated with

ether to give amorphous **6** (15.1 g, 97%). IR (KBr) 1735, 1660 cm^{-1}; ^1H NMR (DMSO-d_6) δ=5.47 (2H, bs), 7.76 (1H, d, J=5.6 Hz); MS m/z 181 (M^+). Found: C, 26.21; H, 2.71; N, 23.02%. Calcd for $C_4H_5N_3O_2ClF$: C, 26.46; H, 2.78; N, 23.15%.

5-Fluoro-1-succinimidouracil (7). To a solution of **6** (1.0 g, 5.5 mmol) in 20 cm^3 of DMF were added succinyl dichloride (0.67 cm^3, 6.1 mmol) and triethylamine (3.1 cm^3, 22 mmol) under ice-cooling. The mixture was stirred at room temperature for 15 h, and filtered. The filtrate was concentrated, poured into water, and extracted with AcOEt. The organic layer was washed with aqueous NaCl solution, dried (Na_2SO_4) and concentrated. The residue was chromatographed on silica gel with AcOEt–hexane (1:1) to give **7** (500 mg, 42.5%); mp 204—206.5 °C. IR (KBr) 1755, 1735, 1700 cm^{-1}; ^1H NMR (DMSO-d_6) δ=2.97 (4H, s), 7.40 (1H, d, J=5.4 Hz), 11.44 (1H, bs); MS m/z 227 (M^+). Found: C, 42.48; H, 2.69; N, 18.73%. Calcd for $C_8H_6N_3O_4F$: C, 42.30; H, 2.66; N, 18.50%.

1-(Diacetylamino)-5-fluorouracil (8). Acetyl chloride (1.73 g, 22 mmol) was added to a solution of **6** (1.0 g, 5.5 mmol) in DMF (10 cm^3) and pyridine (20 cm^3) under ice-bath cooling. The mixture was stirred at room temperature for 3 h and filtered. The filtrate was concentrated, poured into water (40 cm^3) and then extracted with AcOEt. The extract was washed with water, dried (Na_2SO_4) and evaporated. The residue was recrystallized from AcOEt to give **8** (420 mg, 33%); mp 154.5—156.0 °C. TLC (AcOEt) R_f 0.58; IR (KBr) 1760, 1745, 1700, 1680 cm^{-1}; ^1H NMR (DMSO-d_6) δ=2.29 (6H, s), 8.06 (1H, d, J=6.2 Hz), 11.33 (1H, bs); MS m/z 229 (M^+). Found: C, 41.79; H, 3.65; N, 18.46%. Calcd for $C_8H_8N_3O_4F$: C, 41.93; H, 3.52; N, 18.34%.

1-(Dibenzoylamino)-5-fluorouracil (9). Benzoyl chloride (1.15 g, 8.22 mmol) was added to a solution of **6** (500 mg, 2.75 mmol) in 10 cm^3 of pyridine under ice-cooling. The mixture was stirred at room temperature overnight and filtered. The filtrate was concentrated, poured into water (200 cm^3), and extracted with AcOEt. The extracts was washed with water, dried (Na_2SO_4) and concentrated. The residue was chromatographed on silica gel with AcOEt–hexane (1:1) to give **9** (535 mg, 55%); mp 168.5—170 °C. TLC (AcOEt–hexane (1:2) R_f 0.35; IR (KBr) 1760, 1700 cm^{-1}; ^1H NMR (DMSO-d_6) δ=6.79—7.85 (11H, m), 9.24 (1H, bs); MS m/z 353 (M^+). Found: C, 60.92; H, 3.38; N, 11.63%. Calcd for $C_{18}H_{12}N_3O_4F$; C, 61.19; H, 3.42; N, 11.89%.

5-Fluoro-1-phthalimidouracil (10). Phthaloyl dichloride (1.40 g, 6.9 mmol) was added to a solution of **6** (1.0 g, 5.5 mmol) in *N,N*-dimethylacetamide (20 cm^3) and pyridine (20 cm^3) under ice-bath cooling. The mixture was stirred at room temperature for 1 h, concentrated to dryness, poured into water (50 cm^3), and then extracted with AcOEt. The extracts was washed with water, dried (Na_2SO_4) and concentrated. The residue was chromatographed on silica gel with $CHCl_3$–MeOH (20:1). Recrystallization of the crude product from AcOEt–hexane gave pure **10** (300 mg, 20%) as white crystals; mp 248.0—249.5 °C. TLC (AcOEt) R_f 0.65; IR (KBr) 1760, 1740, 1700 cm^{-1}; ^1H NMR (DMSO-d_6) δ=7.79—8.36 (4H, m), 8.23 (1H, d, J=6.0 Hz), 10.57 (1H, bs); MS m/z 275 (M^+). Found: C, 52.51; H, 2.28; N, 15.34%. Calcd for $C_{12}H_6N_3O_4F$: C, 52.37; H, 2.20; N, 15.27%.

1-(4-Chlorobenzenesulfonamide)-5-fluorouracil (11). To a solution of **6** (2.0 g, 11.0 mmol) in 20 cm^3 of pyridine and 40 cm^3 of *N,N*-dimethylacetamide was added 4-chlorobenzenesulfonyl chloride (2.79 g, 13.2 mmol). The mixture was stirred at room temperature for 3.5 h, concentrated to dryness, poured into water (50 cm^3), and then extracted with AcOEt. The extract was washed with water, dried (Na_2SO_4) and concentrated. The residue was chromatographed on silica gel with $CHCl_3$–MeOH (9:1) to give **11** (1.31 g, 37%); mp 254—255.5 °C. TLC (AcOEt) R_f 0.57; IR (KBr) 1745, 1700, 1680, 1370, 1170 cm^{-1}; ^1H NMR (DMSO-d_6) δ=7.55—8.25 (5H, m), 11.02 (1H, br), 11.81 (1H, br); MS m/z 319 (M^+). Found: C, 37.39; H, 2.10; N, 13.36%. Calcd for $C_{10}H_7N_3O_4ClFS$: C, 37.57; H, 2.21; N, 13.14%.

5-Fluoro-1-(2,2,2-trichloroethoxycarbonylamino)uracil (12). 2,2,2-Trichloroethyl chloroformate (2.90 g, 13.7 mmol) was added to a solution of **6** (1.0 g, 5.5 mmol) in *N,N*-dimethylacetamide (20 cm^3) and pyridine (20 cm^3) under ice-bath cooling. The mixture was stirred at room temperature overnight, concentrated to dryness, poured into water (50 cm^3), and then extracted with AcOEt. The extract was washed with water, dried (Na_2SO_4) and concentrated. The residue was chromatographed on silica gel with $CHCl_3$–MeOH (20:1) to give **12** (1.06 g, 60.3%); mp 226.5—227.0 °C. TLC (AcOEt) R_f 0.80; IR (KBr) 1735, 1680 cm^{-1}; ^1H NMR (DMSO-d_6) δ=4.73—5.02 (2H, m), 7.73—8.13 (1H, m), 9.39 (2H, bs); MS m/z 319 (M^+). Found: C, 26.51; H, 1.58; N, 13.27%. Calcd for $C_7H_5N_3O_4Cl_3F$: C, 26.24; H, 1.57; N, 13.11%.

1-[*N'*-(Ethoxycarbonyl)thioureido]-5-fluorouracil (13). To a solution of **6** (500 mg, 2.75 mmol) in 20 cm^3 of pyridine was added ethoxycarbonyl isothiocyanate (397 mg, 3.03 mmol). The mixture was stirred at room temperature for 4 h, concentrated, poured into water (50 cm^3) and then extracted with AcOEt. The extract was washed with aqueous NaCl solution, dried (Na_2SO_4) and concentrated to give **13** (547 mg, 72%) as white crystals; mp 188—189 °C. IR (KBr) 1735, 1695, 1520 cm^{-1}; ^1H NMR (DMSO-d_6) δ=1.25 (3H, t, J=7.3 Hz), 4.21 (2H, q, J=7.2 Hz), 7.90 (1H, d, J=5.8 Hz), 11.31 (3H, bs); MS m/z 276 (M^+). Found: C, 34.51; H, 3.02; N, 20.49%. Calcd for $C_8H_9N_4O_4FS$: C, 34.78; H, 3.28; N, 20.28%.

5-Fluoro-1-[*N'*-(phenyl)thioureido]uracil (14). From **6** (2.75 mmol) and phenyl isothiocyanate (3.03 mmol), **14** was obtained in a 98% yield in a similar manner as described for **13**; mp 188—189 °C. TLC ($CHCl_3$–MeOH (4:1)) R_f 0.50; IR (KBr) 1740, 1690, 1540 cm^{-1}; ^1H NMR (DMSO-d_6) δ=7.02—7.66 (5H, m), 7.89 (1H, d, J=5.2 Hz), 10.12 (2H, br), 11.12 (1H, bs); MS m/z 280 (M^+). Found: C, 47.29; H, 3.08; N, 20.24%. Calcd for $C_{11}H_9N_4O_2FS$: C, 47.14; H, 3.24; N, 19.99%.

1-[*N'*-(*t*-Butyl)thioureido]-5-fluorouracil (15). From **6** (2.75 mmol) and *t*-butyl isothiocyanate (3.03 mmol), **15** was obtained in a 79% yield in a similar manner as described for **13**; mp 201—202 °C. TLC ($CHCl_3$–MeOH (4:1)) R_f 0.52; IR (KBr) 1720, 1680, 1525 cm^{-1}; ^1H NMR (DMSO-d_6) δ=1.44 (9H, s), 7.79 (1H, bs), 7.84 (1H, d, J=5.8 Hz), 9.14 (1H, bs), 11.06 (1H, bs). MS m/z 260 (M^+). Found: C, 41.70; H, 5.31; N, 21.38%. Calcd for $C_9H_{13}N_4O_2FS$: C, 41.53; H, 5.03; N, 21.53%.

1-[*N'*-(Benzyl)thioureido]-5-fluorouracil (16). From **6** (2.75 mmol) and benzyl isothiocyanate (3.03 mmol), **16** was obtained in a 84% yield in a similar manner as above; mp 163—165 °C. TLC ($CHCl_3$–MeOH (4:1)) R_f 0.48; IR (KBr) 1740, 1680, 1555 cm^{-1}; ^1H NMR (DMSO-d_6) δ=4.68 (2H, d, J=5.4 Hz), 7.00—7.42 (3H, m), 7.82 (1H, d, J=5.2 Hz), 8.72

(1H, t, J=5.7 Hz), 9.69 (1H, bs); MS m/z 294 (M^+). Found: C, 49.18; H, 3.93; N, 19.17%. Calcd for $C_{12}H_{11}N_4O_2FS$: C, 48.97; H, 3.77; N, 19.04%.

5-Fluoro-1-(*N'*-phenylureido)uracil (17). From **6** (2.75 mmol) and phenyl isocyanate (3.02 mmol), **17** was obtained in a 22% yield; mp 258—260 °C. IR (KBr) 1740, 1680 cm^{-1}; ^1H NMR (DMSO-d_6) δ=6.78—7.63 (5H, m), 7.90 (1H, d, J=5.8 Hz), 8.62 (1H, bs), 9.12 (1H, bs), 11.27 (1H, bs); MS m/z 264 (M^+). Found: C, 49.79; H, 3.21; N, 21.13%. Calcd for $C_{11}H_9N_4O_3F$: C, 50.00; H, 3.43; N, 21.21%.

1-(*N'*-*t*-Butylureido)-5-fluorouracil (18). To a solution of **6** (1.0 g, 5.51 mmol) in pyridine (40 cm^3) was added *t*-butyl isocyanate (600 mg, 6.06 mmol) and the mixture was stirred at room temperature for 10 h. Work-up of the reaction mixture in the similar manner as above gave **18** in a 45% yield as white crystals; mp 238 °C. TLC (AcOEt) R_f 0.20; IR (KBr) 1740, 1690 cm^{-1}; ^1H NMR (DMSO-d_6) δ=1.25 (9H, s), 6.33 (1H, bs), 7.71 and 7.80 (1H, d, J=6.0 Hz, 5.2 Hz), 7.96 (1H, bs), 11.09 (1H, bs); MS m/z 244 (M^+). Found: C, 44.44; H, 5.48; N, 22.84%. Calcd for $C_9H_{13}N_4O_3F$: C, 44.26; H, 5.37; N, 22.94%.

1-(*N,N*-Dimethylsulfamoylamino)-5-fluorouracil (19). To a solution of **6** (1.0 g, 5.51 mmol) and triethylamine (5 cm^3) in DMF (25 cm^3) was added *N,N*-dimethylsulfamoyl chloride (1.22 g, 8.50 mmol). The mixture was stirred at room temperature for 5 h, and filtered. The filtrate was concentrated, poured into water and extracted with AcOEt. The extract was washed with aqueous NaCl solution, dried (Na_2SO_4), and concentrated. The residue was recrystallized from acetone to give **19** (690 mg, 50%); mp 187—189 °C. TLC (AcOEt) R_f 0.60; IR (KBr) 1710, 1680, 1380, 1180 cm^{-1}; ^1H NMR (DMSO-d_6) δ=3.40 (6H, s), 8.00 (1H, d, J=6.0 Hz), 11.01 (1H, br), 11.47 (1H, br); MS m/z 252 (M^+). Found: C, 28.35; H, 3.57; N, 21.93%. Calcd for $C_6H_9N_4O_4FS$: C, 28.57; H, 3.60; N, 22.21%.

1-[4-(Tetrahydropyranyloxy)phenyl]ethanol. A mixture of *p*-hydroxylbenzaldehyde (2.4 g), 3,4-dihydro-2*H*-pyran (20 cm^3) and pyridine *p*-toluenesulfonate (0.7 g) was stirred at room temperature for 15 h, concentrated and poured into water (200 cm^3), and then extracted with $CHCl_3$. The chloroform layer was washed with aqueous NaCl solution, dried (Na_2SO_4) and concentrated. The residue was chromatographed on silica gel with $CHCl_3$–acetone (40:1) to give 2.2 g (54.3%) of 4-(tetrahydro-2-pyranyloxy)benzaldehyde; TLC ($CHCl_3$–acetone (20:1)) R_f 0.80. The protected aldehyde thus obtained was dissolved into ether (10 cm^3), and the ether solution was added to a solution of CH_3Li (2.12 mmol) in ether over 5 min. The resulting mixture was refluxed for 1 h, cooled, and poured into water (100 cm^3). The ether layer was separated, washed with an aqueous NaCl solution, dried (Na_2SO_4) and concentrated. The residue was chromatographed on silica gel with $CHCl_3$–acetone (40:1) to give 1.28 g (54%) of 1-[4-(tetrahydropyranyloxy)phenyl]ethanol. IR (KBr) 3410, 2950, 1620, 1520 cm^{-1}; ^1H NMR ($CDCl_3$) δ=1.39 (3H, d, J=6.4 Hz), 1.10—2.24 (6H, m), 2.71 (1H, bs), 3.26—4.15 (2H, m), 4.74 (1H, q, J=6.4 Hz), 5.22—5.46 (1H, m), 6.94 and 7.18 (4H, ABq, J=8.8 Hz).

5-Fluoro-1-[1-(4-hydroxyphenyl)ethyl]uracil (20). To a solution of 1-[4-(tetrahydropyranyloxy)phenyl]ethanol (435 mg) in $ClCH_2CH_2Cl$ (30 cm^3) was added thionyl chloride (1 cm^3). The mixture was stirred at room temperature for 30 min and concentrated. The residue was dissolved into acetonitrile (10 cm^3), and 2,4-*O*-bis(trimethylsilyl)-5-fluorouracil (1.5 g) and $SnCl_4$ (0.06 cm^3) was then added to the solution. The mixture was stirred at room temperature for 1 h, and 5% aqueous $NaHCO_3$ solution (20 cm^3) was added and the reacting mixture was extracted with AcOEt. The organic layer was washed with an aqueous NaCl solution, dried (Na_2SO_4) and concentrated. The residue was chromatographed on silica gel with $CHCl_3$–acetone (30:1) to give 330 mg (67%) of amorphous **20**. TLC ($CHCl_3$–acetone (4:1)) R_f 0.20; IR (KBr) 1700, 1680 cm^{-1}; ^1H NMR (DMSO-d_6) δ=1.61 (3H, d, J=7.0 Hz), 5.68 (1H, q, J=7.5 Hz), 6.76—7.18 (4H, m), 7.88 (1H, d, J=6.1 Hz), 9.46 (1H, bs), 11.78 (1H, bs); MS m/z 250 (M^+). Found: C, 57.43; H, 4.29; N, 11.02%. Calcd for $C_{12}H_{11}N_2O_3F$: C, 57.60; H, 4.43; N, 11.20%.

Bis(4-acetoxyphenyl)methyl Bromide. Acetic anhydride (6 cm^3) was added to a solution of bis(4-hydroxyphenyl)methanol (1.0 g, 5 mmol) in pyridine (20 cm^3) and stirred at room temperature for 15 h. The mixture was concentrated, poured into water, and extracted with AcOEt. The organic layer was washed successively with 5% aqueous $NaHCO_3$ and aqueous NaCl solution, dried (Na_2SO_4), and concentrated. The residue was chromatographed on silica gel with $CHCl_3$–MeOH (20:1) to give 1.22 g (26%) of bis(4-acetoxyphenyl)-methane; mp 66—68 °C. IR (KBr) 1745, 1200 cm^{-1}; ^1H NMR (DMSO-d_6) δ=2.19 (6H, s), 3.88 (2H, s), 6.94 and 7.16 (8H, ABq, J=8.4 Hz). To a solution of bis(4-acetoxyphenyl)-methane (90 mg, 3.16 mmol) in CCl_4 (30 cm^3) was added *N*-bromosuccinimide (0.63 g) and catalytic amount of AIBN. After refluxing for 1 h, the reaction mixture was concentrated. The residue was chromatographed on silica gel with $CHCl_3$–acetone (40:1) to give 0.73 g (64%) of bis(4-acetoxyphenyl)methyl bromide. TLC ($CHCl_3$–actone (20:1)) R_f 0.7; ^1H NMR ($CDCl_3$) δ=2.27 (6H, s), 5.36 (1H, s), 7.06 and 7.35 (8H, ABq, J=8.8 Hz).

1-[Bis(4-hydroxyphenyl)methyl]-5-fluorouracil (21). To a solution of bis(4-acetoxyphenyl)methyl bromide (0.63 g, 1.74 mmol) and 2,4-*O*-bis(trimethylsilyl)-5-fluorouracil (0.98 g) in acetonitrile (20 cm^3) was added $SnCl_4$ (0.2 cm^3) and the mixture was stirred for 1.2 h. After adding 5% aqueous $NaHCO_3$ solution (20 cm^3), the reaction mixture was extracted with AcOEt. The AcOEt layer was washed with aqueous NaCl solution, dried (Na_2SO_4) and concentrated. The residue was chromatographed on silica gel with $CHCl_3$–acetone (30:1) to give 0.5 g of 1-[bis(4-acetoxyphenyl)methyl]-5-fluorouracil. IR (KBr) 1760, 1705, 1670, 1380, 1245, 1205 cm^{-1}; ^1H NMR (DMSO-d_6) δ=2.25 (6H, s), 6.92 (1H, bs), 7.16 and 7.25 (4H, ABq, J=9.0 Hz), 7.63 (1H, d, J=6.8 Hz), 11.93 (1H, bs). 1-[Bis(4-acetoxyphenyl)methyl]-5-fluorouracil (0.32 g, 0.78 mmol) in ethanol was dissolved in aqueous 1 M NaOH solution. The solution was acidified to pH 3.8 with dil HCl and extracted with AcOEt. The organic layer was washed with aqueous NaCl solution, dried (Na_2SO_4), and concentrated to give solids. The solids was triturated with ether to afford 250 mg (68%) of amorphous **23**. TLC ($CHCl_3$–acetone (4:1)) R_f 0.10; IR (KBr) 1700, 1680 cm^{-1}; ^1H NMR (DMSO-d_6) δ=6.53—7.20 (9H, m), 7.45 (1H, d, J=6.8 Hz), 9.68 (2H, bs), 11.69 (1H, bs); MS m/z 328 (M^+). Found: C, 62.45; H, 4.18; N, 8.38%. Calcd for $C_{17}H_{13}N_2O_4F$: C, 62.20; H, 3.99; N, 8.53%.

2-[4-(Tetrahydropyranyloxy)phenyl]-2-propanol. Pyridine *p*-toluenesulfonate (10.7 g) was added to a solution of methyl *p*-hydroxybenzoate (2.13 g) and 3,4-dihydro-2*H*-pyran (20 cm^3) in acetone (20 cm^3). The mixture was stirred

at room temperature for 15 h, concentrated, poured into water, and then extracted with $CHCl_3$. The organic layer was washed with aqueous NaCl solution, dried (Na_2SO_4) and concentrated. The residue was chromatographed on silica gel with hexane–AcOEt (15:1) to give 3.34 g (100%) of methyl 4-(tetrahydropyranyloxy)benzoate, which was dissolved in ether (30 cm^3). To this ether solution was added CH_3Li (60 mmol) in ether over 10 min. The reaction mixture was refluxed for 1 h, diluted with water (10 cm^3) and then extracted with AcOEt. The organic layer was washed with aqueous NaCl solution, dried (Na_2SO_4) and concentrated to afford 2.64 g of 2-[4-(tetrahydropyranyloxy)phenyl]-2-propanol. TLC ($CHCl_3$–acetone (4:1)) R_f 0.80; ^1H NMR ($CDCl_3+D_2O$) δ=1.50 (6H, s), 1.16—2.10 (6H, m), 3.27—4.08 (2H, m), 5.24—5.43 (1H, m), 6.92 and 7.31 (4H, ABq, J=8.7 Hz).

5-Fluoro-1-[1-(4-hydroxyphenyl)-1-methylethyl]uracil (22). To a solution of 2-[4-(tetrahydropyranyloxy)phenyl]-2-propanol (2.1 g) and 2,4-*O*-bis(trimethylsilyl)-5-fluorouracil (10.0 g) in acetonitrile (50 cm^3) was added $SnCl_4$ (1 cm^3) at −20 °C. The mixture was stirred at the same temperature for 30 min, and then 5% aqueous $NaHCO_3$ (20 cm^3) was added and was extracted with AcOEt. The organic layer was washed with aqueous NaCl solution, dried (Na_2SO_4) and concentrated. The residue was chromatographed on silica gel with $CHCl_3$–acetone (30:1) to give 330 mg (14%) of **22**; mp 270—272 °C. TLC ($CHCl_3$–acetone (4:1) R_f 0.12; IR (KBr) 1710, 1660 cm^{-1}; ^1H NMR (DMSO-d_6) δ=1.74 (6H, s), 6.67—7.03 (4H, m), 8.07 (1H, d, J=8.4 Hz), 9.23 (1H, bs), 11.43 (1H, d, J=5.0 Hz); MS m/z 264 (M^+). Found: C, 58.88; H, 4.86; N, 10.83%. Calcd for $C_{13}H_{13}N_2O_3F$: C, 59.09; H, 4.96; N, 10.60%.

5-Fluoro-1-hydroxyuracil (23). Hydrogen gas was introduced at room temperature into a solution of **24** (500 mg, 2.1 mmol) in ethanol–water (8:2) containing 10% Pd–C (50 mg) for 1.3 h and the catalyst was filtered off. The filtrate was concentrated and the residue was triturated with ether to give 220 mg (72%) of **23**; mp 208 °C (decomp). TLC ($CHCl_3$–MeOH–AcOH (40:5:1)) R_f 0.22; IR (KBr) 3450, 1710, 1670 cm^{-1}; ^1H NMR (DMSO-d_6) δ=8.33 (1H, d, J=7.0 Hz), 11.28 (2H, bs); MS m/z 146 (M^+). Found: C, 32.61; H, 2.21; N, 18.93%. Calcd for $C_4H_3N_2O_3F$: C, 32.85; H, 2.07; N, 19.15%.

1-Benzyloxy-5-fluorouracil (24). A mixture of 3-benzyloxyamino-2-fluoroacrylamide (5.3 g, 25 mmol) and oxalyl dichloride (7.2 g, 57 mmol) in CH_2Cl_2 (220 cm^3) was refluxed for 27 h and then concentrated. The residue was chromatographed on silica gel with $CHCl_3$–MeOH (100:1) to give 1.55 g (26%) of **24**; mp 184—185 °C. IR (KBr) 1725, 1695 cm^{-1}; ^1H NMR (DMSO-d_6) δ=5.10 (2H, s), 6.98—7.79 (6H, m), 11.91 (1H, bs); MS m/z 236 (M^+). Found: C, 55.77; H, 3.60; N, 11.72%. Calcd for $C_{11}H_9N_2O_3F$: C, 55.94; H, 3.84; N, 11.86%.

1-(4-Chlorophenylsulfonyloxy)-5-fluorouracil (25). To a solution of **23** (300 mg, 2.05 mmol) in pyridine (5 cm^3) was added 4-chlorobenzenesulfonyl chloride. The mixture was stirred at room temperature for 15 min, concentrated, diluted with water, and then extracted with AcOEt. The organic layer was successively washed with 0.1 M NaOH and aqueous NaCl solution, dried (Na_2SO_4) and concentrated. The residue was chromatographed on silica gel with $CHCl_3$–MeOH (4:1) to give 220 mg (33%) of **25**; mp>300 °C. TLC ($CHCl_3$–MeOH (4:1)) R_f 0.63; IR (KBr) 1720, 1640 cm^{-1}, ^1H NMR (DMSO-d_6) δ=7.72—7.98 (4H, m), 8.47 (1H, d, J=6.0 Hz), 11.07 (1H, bs); MS m/z 320 (M^+). Found: C, 37.63; H, 1.71; N, 8.53%. Calcd for $C_{10}H_6N_2O_5ClFS$: C, 37.45; H, 1.89; N, 8.74%.

1-(4-Chlorobenzyloxy)-5-fluorouracil (26). To a solution of **23** (500 mg, 3.42 mmol) in pyridine (10 cm^3) was added 4-chlorobenzoyl chloride (0.46 cm^3, 3.60 mmol). The mixture was stirred at room temperature for 30 min, concentrated, diluted with water (70 cm^3) and then extracted with AcOEt. The organic layer was washed with aqueous NaCl solution, dried (Na_2SO_4) and concentrated. The residue was chromatographed on silica gel with $CHCl_3$–MeOH (4:1). The crude product obtained by evaporation of the solvent was diluted with tetrahydrofuran, and then the insoluble matter was filtered off. The filtrate was concentrated and the residue was triturated with ether to give 350 mg (36%) of **26**; mp 201—203 °C. TLC ($CHCl_3$–MeOH (4:1)) R_f 0.68; IR (KBr) 1780, 1710 cm^{-1}; ^1H NMR (DMSO-d_6) δ=7.69—8.09 (4H, m), 8.67 (1H, d, J=6.0 Hz), 10.68 (1H, bs); MS m/z 284 (M^+). Found: C, 46.27; H, 2.30; N, 9.89%. Calcd for $C_{11}H_6N_2O_4ClF$: C, 46.42; H, 2.12; N, 9.84%.

γ-Radiolysis of 1-Phenyl-1-propanol (27). Stock solutions of **27** were prepared by dissolving it in deionized distilled water or in 1%, 5%, and 10% (v/v) aqueous acetonitrile or methanol in concentration of 200 μg cm^{-3}. The each solution was deaerated with N_2 bubbling for 20 min. An approximately 2 cm^3 of the solution was put into a 5 mmϕ Pyrex glass tube under N_2 and irradiated for 100 Gy (3.15 Gy min^{-1}) with the γ-ray of ^{137}Cs at room temperature (ca. 20 °C). The irradiated mixture was subjected to HPLC to analyze **28**. The conditions of the HPLC analyses were as follows: Column; Lichrosorb RP-18, Mobile phase; aqueous 30% (v/v) methanol solution, Detection; UV, 254 nm.

General Procedure for γ-Radiolysis of 5-Fluorouracil Derivatives. Three kinds of sample solutions of 5-fluorouracil derivatives were prepared by dissolving them in the following three deaerated solvents in concentration of 50 μg cm^{-3}; (a) deaerated aqueous 1% methanol (v/v) solution, (b) 0.1 M H_2SO_4 deaerated solution in aqueous 1% methanol (v/v), (c) deaerated aqueous 1% acetonitrile (v/v) solution saturated with N_2O gas.

Each sample solution was irradiated with γ-ray in the same manner as the γ-radiolysis of **27**. After irradiation, the amount of 5-FU produced by the radiolysis was analyzed by HPLC. The conditions of the HPLC were as follows: Column; Lichrosorb RP-18, Mobile phase; 0.02 M KH_2PO_4–0.02 M K_2HPO_4–2% CH_3CN, Detection; UV, 270 nm.

The authors wish to express their thanks to Professor Yoshio Otsuji of University of Osaka Prefecture for his useful comments and helpful discussions.

References

1) D. R. Friend and G. W. Chang, *J. Med. Chem.*, **28**, 51 (1985).

2) P. K. Chakravarty, P. L. Carl, M. J. Weber, and J. A. Katzenellenbogen, *J. Med. Chem.*, **26**, 633 (1983).

3) F. Kawamura, *Rinsho Hoshasen*, **26**, 815 (1981).

4) H. Asakawa, J. Watarai, and T. Hoshino, *Jpn. J. Cancer Chemother.*, **11**, 1225 (1984).

5) Y. Tanaka, *Igaku no Ayumi*, **131**, 284 (1984).
6) T. L. Phillips and T. H. Wasserman, *Cancer Treatment Reports*, **68**, 291 (1984).
7) M. Kondo and Y. Shinozaki, "Hoshasen Kagaku" in "Kiso Genshiryoku Koza," Corona Co. Ltd., Tokyo (1980), Vol. 7, Chap. 8.
8) N. Anbar and P. Neta, *Int. J. Appl. Radiat. Isotopes*, **18**, 493 (1967); M. Simic, *Biochem. Biophys. Res. Commun.*, **50**, 364 (1973).
9) E. J. Hart, S. Gordon, and J. K. Thomas, *J. Phys. Chem.*, **68**, 1271 (1964).
10) M. Anbar and E. J. Hart, *J. Phys. Chem.*, **69**, 271 (1965).
11) G. I. Grossweiner, *Radiation Res. Rev.*, **2**, 345 (1970).
12) G. E. Adams and B. D. Michael, *Trans. Faraday Soc.*, **63**, 1171 (1967).
13) M. Yamanoto, T. Tanii, N. Nakano, and M. Matsui, *Radioisotopes*, **30**, 258 (1981).

Proton and Carbon-13 NMR Study of 1,1,4,4-Tetraphenyl- and 1,4-Diphenyl-1,3-butadiene Dianions in Solution. The Charge Distributions, Structural Features and Rotational Barriers of Phenyl Groups

Yukihiro YOKOYAMA, Yutaka TAKAKURA, Takeshi SAWASAKI, and Kensuke TAKAHASHI*
Department of Applied Chemistry, Nagoya Institute of Technology,
Gokiso-cho, Showa-ku, Nagoya 466
(Received September 1, 1988)

The dicarbanions (**1** and **2**) produced from 1,1,4,4-tetraphenyl- and 1,4-diphenylbutadienes (**1a** and **2a**) were investigated by means of the ^1H and ^{13}C NMR techniques. Large upfield shifts of the proton and carbon signals caused by the conversion of the hydrocarbons into the dianions were observed. Such shifts were used for evaluating the excess charge distributions in the dianions. From the coupling constants obtained it is concluded that the configuration of the central bond of the anion is the trans one for **1** but the cis one for **2**. Thermodynamical parameters were obtained for the restricted rotation of the phenyl group of the lithium salt of **2**.

Butadiene is the simplest hydrocarbon among the acyclic unsaturated conjugate ones. The dianions derived from the butadienes are, therefore, one of the interesting objectives from their electronic and structural view points. There have been many NMR studies concerning carbanions with odd carbon skeletons, such as allyl, pentadienyl, or heptatrienyl carbanions.[1] Little work, however, has been reported on the NMR parameters of the acyclic carbanions with even carbon skeletons. A ^1H NMR study of 1,1,4,4-tetraphenylbutadiene dianion (**1**) was reported in our previous paper.[2] Recently, we have observed the NMR spectra of the dianions (**2**) produced from 1,4-diphenylbutadiene.[3] We therefore wish to report on the structures and behaviors of these dianions, evaluated from their ^1H and ^{13}C NMR data.

Experimental

The starting materials, **1a** and **2a**, were commercially available and were used without further purification. The solvents used for the preparation of the anionic sample solutions, THF, THF-d_8, and DME, were refluxed upon sodium metal, distilled, degassed, and finally kept on a sodium-potassium alloy. The starting hydrocarbon, **1a** or **2a**, was sublimed, degassed under vacuum, and then dissolved in dried and degassed solvents. The solution was in contact with freshly cut alkali metal flakes (lithium, sodium, or potassium) at room temperature in a hand-made reaction container under vacuum. Immediately after contact, the solution showed a deep-purple color. This colored solution sometimes did not give any narrow ^1H NMR signals, except for very broad ones which were ascribed to a contamination of some anionic radical species. Consequently, the solution was kept in its vessel with stirring for a day or two longer at room temperature so that the reaction would come to completion. Then, the resulting solution was filtered and sealed in an NMR tube and a glass ampule with a breakable seal. All NMR samples were prepared to be 0.1—0.3 mol dm^{-3} solutions sealed in 5 or 10 mm o.d. NMR tubes.

All of the NMR spectra were measured on a Varian XL-200 Fourier transform NMR spectrometer. Variable-temperature spectra were measured in the range from +50 to −95 °C. The proton and carbon-13 NMR chemical shifts were evaluated from the solvent peak used as an internal reference and then converted to δ_H and δ_C values from TMS, by taking δ_H 1.79 (1.75) and δ_C 26.4 (25.4) for THF (THF-d_8), and δ_H 3.28 and δ_C 58.8 for DME.

In order to obtain chemical evidence that the anionic species are dicarbanions, the sodium salt of **2** in THF was quenched by deuterium oxide. The quenched products consist of two isomers. A major component was shown to have a structure consistent with *cis*-1,4-dideutero-1,4-diphenyl-2-butene, C_6H_5-CHD-CH=CH-CHD-C_6H_5; yield ca. 80%; its NMR data were δ_C(CHD)=33.2, $^1J_{CD}$=19.5, δ_H(CHD)=3.48 broad, δ_H(CH)=5.70, doublet (J=5.1 and $J_{\beta\beta'}$=11.4). Another minor component was shown to have a structure consistent with *trans*-3,4-dideutero-1,4-diphenyl-1-butene, C_6H_5-CH=CH-CHD-CHD-C_6H_5: yield ca. 20%; its NMR data were δ_H(C_1H)=6.41, doublet (J=15.9); δ_H(C_2H)=6.23, d-d (J=15.9, 6.6); δ_H(C_3HD)=2.49, d-d (J=6.6, 8) broad; δ_H(C_4HD)=2.75, doublet (J=8 broad).

Results and Discussion

NMR Chemical Shifts and Excess Charge Distributions. The NMR parameters obtained for the anionic species and their precursors are summarized in Tables 1 and 2. Typical examples of the ^{13}C NMR spectra are also shown in Figs. 1 and 2.

All of the ^1H chemical shifts of the dianions are shielded by about 0.2 to 3.4 ppm, as compared with those of the corresponding precursors. This tendency of the upfield shift changes is consistent with the general trend observed in other carbanions.[1] However, it should be pointed out here that the β-proton-chemical-shift change of **2** is significantly large and characteristic. For example, the upfield shift changes of the lithium salt of **2** are about 3.4 and 1.7 ppm for α- and β-protons. While those of pentadienyllithium (as a typical odd-carbon carbanion) are about 2.0, 0.0, and 1.9 ppm for α-, β-, and γ-protons respectively.[4] The upfield shift changes are clearly alternative for the example of odd-carbon carbanions. **2** (as an example of even-carbon

Table 1. Proton NMR Data of The Carbanions and Their Precursors at 200 MHz and 23 °C

Compd/metal/solvent	Chemical shifts δ/ppm					Couplings/Hz	
	H_o	H_m	H_p	H_α	H_β	$J_{\alpha\beta}$	$J_{\beta\beta'}$
1/Na/THF-d_8	7.23	6.70	5.96	—	5.99	—	15.4[a]
2/Li/THF-d_8	6.03[b]	6.38[b]	5.33	3.61	4.95	12.2	7.7
2/Li/THF-d_8[c]	5.92	6.21	5.22	3.66	4.91	d)	d)
	5.96	6.38					
2/Na/THF-d_8	5.94	6.18	5.18	3.79	4.96	11.6	9.4
	5.96	6.37					
1a/THF	(7.43	—	7.08)	—	6.79	—	d)
1a/$CDCl_3$	(7.45	—	7.15)	—	6.79	—	11.1[a]
2a/THF	7.44	7.28	7.17	7.01	6.68	15.5	10.6
2a/$CDCl_3$	7.41	7.30	7.21	6.92	6.64	15.7	10.3

a) Measured from the ^{13}C satellite spectrum at 300 MHz. b) Broad. c) Measured at −60 °C. d) Not available.

Table 2. C-13 Chemical Shifts (δ) of the Carbanions and Their Precursors in ppm

Compd/metal/solvent	Assignment[a]					
	C_i	C_o	C_m	C_p	C_α	C_β
1/Na/THF	145.12	121.94(152)	128.67(151)	112.33(158)	87.31	109.21(139)
2/Li/THF	146.65	118.53(149)	128.45(149)	104.86(157)	65.74(146)	97.42(146)
		110.60(149)				
2/Na/THF	146.03	118.32(153)	129.56(146)	103.01(157)	67.73(b)	98.06(146)
		109.69(149)	128.00(148)			
2/K/DME	144.50	118.23(b)	130.05(b)	103.10(b)	b)	100.59(b)
		108.60(b)	128.07(b)			
1a/THF	143.40	129.74(160[b])	131.47(159[b])	128.4[b](158[b])	145.13	126.61(154)
	140.91	128.36(158[b])	128.93(160[b])	128.17(160[b])		
2a/THF	138.51	127.18(158[b])	129.35(159[b])	128.21(160)	130.22(158[b])	133.66(156)
2a/DME	138.43	127.15(b)	129.36(160)	128.23(161)	130.12(b)	133.66(156)

a) The values in parentheses are the $^1J_{CH}$ in Hz. b) With large error or not available because of overlapping or low intensity of the signal.

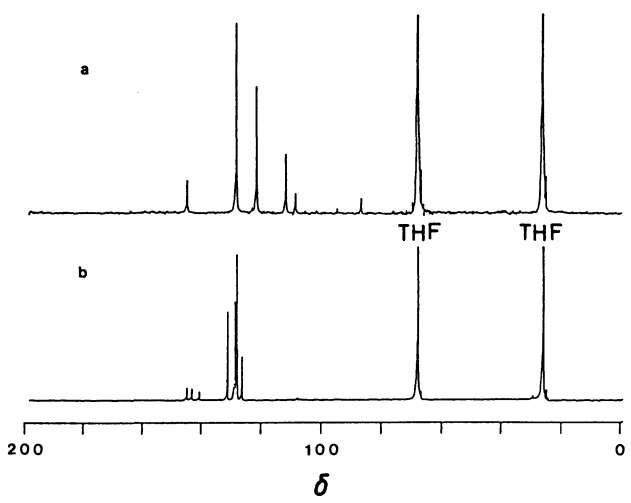

Fig. 1. ^{13}C NMR spectra of **1** and **1a** in THF. (a) The sodium salt of **1** and (b) **1a**.

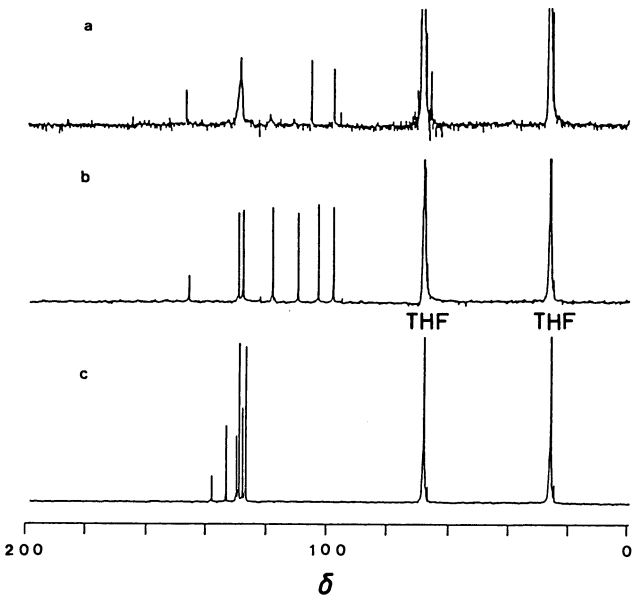

Fig. 2. ^{13}C NMR spectra of **2** and **2a** in THF. (a) The lithium salt of **2**, (b) the sodium salt of **2**, and (c) **2a**.

carbanions), however, cannot have such alternation of the shift changes because of its symmetrical even-carbon skeleton. It is also noted that the aromatic proton shifts of **2** are in order of meta, ortho, and para positions from low to high field in the same manner as phenylmethanide ion,[5] while those of **1** are in the order of ortho, meta, and para positions as well as those of 1,1,4,4-tetraphenylbutane-1,4-diide (**3**) and 1,1,2,2-tetraphenylethanediide ions (**4**).[6] This distinc-

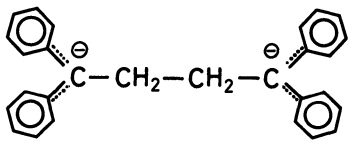

3

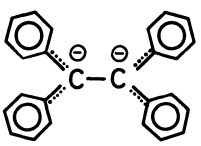

4

tion between the two casses can be explained in terms of several reasons. One is due to the number of phenyl groups available to delocalization of excess charge, as is pointed out before.[6c] This is because the former dianion has one phenyl group, but the latter has two phenyl groups on the α-carbon, which is an anionic center.

The large upfield shifts of the carbon signals caused by the conversion of hydrocarbons into dianions as well as those of the proton signals are transpired from the data given in Table 2. It is well-known that for delocalized carbanions, carbon-13 shift changes have been used as empirical guides to the distribution of electron densities within the carbanions.[1,7] Because the change are much larger in magnitude than those observed in the ^1H chemical shifts and are less sensitive to other effects than to changes in the electron density. The excess charges on carbons in the carbanions are obtained from a comparison of the chemical shifts between the carbanions and their neutral precursors. The differences of the chemical shifts are extremely large, for example 58—64 ppm at α-carbon, 17—36 ppm at β-carbon, and 30—47 ppm at the total sum of the phenyl carbons, as shown in Table 2. An estimation of the charges on the carbon atoms is made by using an empirical equation proposed by Fraenkel et al.[8] and a factor (160 ppm/electron) presented by Spiesecke and Schneider.[9] The experimentally evaluated values are presented in Table 3. As for the dianion **2**, in comparison with the total excess charges on a phenyl ring, the value of the lithium salt (0.265) is smaller than the values of the sodium and potassium salts (0.283 and 0.296 respectively). However, the excess charge of **1** is estimated to be 0.189 per phenyl ring. This value is smaller than even the smallest one of **2** (0.265). On the other hand, the excess charges on the α- and β-carbon atoms increase from potassium to lithium salts. Furthermore, excess charge on the β-carbon is estimated to be 0.207—0.227 for **2**, though for **1** it is almost one half of **2**. These facts can be explained on the basis of the following: the relative decrease of the charge on the α- of β-carbon atom is consistent with a large delocalization of the charge into phenyl rings. Therefore, the total excess charges on the carbon atoms of dianions **1** and **2** are evaluated to be about 1.7—1.8e from Table 3. It must be pointed out here that the excess charges on the β-carbon of **2** is the second largest next to the α-carbon of **2**. This is one of the characteristic points of the dianion of **2**. This situation will be related to the structural features described later.

Structural Features of the Dianions in Solution. As shown in Table 1, the values of $J_{\alpha\beta}$ and $J_{\beta\beta'}$ of the neutral precursor (**2a**) agree with the previous data reported by Bothner-By and Harris.[10] Consequently, this confirms that **2a** has a certain configuration of trans, trans geometry. Further, the values of $J_{\beta\beta'}$ of **1a** and **2a** have an approximately average value between the typical magnitudes of the s-trans geometries with respect to the rotation about the central bond. In the dianions, on the other hand, $J_{\beta\beta'}$ of **1** and **2** were about 15 and 8 Hz, respectively. These values suggest that the configuration around the central bond of the anion is trans for **1**, but cis for **2**. The situations are quite different for the two carbanions, **1** and **2**. This can be explained as follows: Two phenyl groups attached to the C_α of **1** will have a greater repulsion than the α-carbon moiety of **2** due to steric effects. Another fact must be noted, that the $J_{\beta\beta'}$ value of the sodium salt of **2** is almost similar to that of the lithium salt. Therefore, the cis configuration of **2** is one of its characteristic structural features. The results obtained here regarding the THF solution are consistent with a theoretical prediction[11] and an X-ray analysis of the dianion in the solid state.[12] The *cis*-butene-like skeleton of **2**, thus determined, can surround the counter-cations. This situation is related to the fact that the excess charge is concentrated, especially on both the α- and β-carbons in the dianion **2**, as stated in the former section. From the large excess charge on C_α and C_β it is considered that the two carbons are expected to be in the proximity of the counter cations. As described in the experimental section, the main quenched product of **2** has the cis configuration in the central bond, which is assigned from its coupling constant of 11.4 Hz, as compared with the value of 2-butene.[13] Therefore, it is concluded that the configuration of **2** is held as it is when it is quenched by D_2O.

Table 3. Comparison of Charge Distributions of **1** and **2** in Unit of the Absolute Value of the Charge of an Electron

Anion/metal/solvent	q_i	q_o	q_m	q_p	q_{ring}	q_α	q_β
1/Na/THF	−0.019	0.044	0.010	0.100	0.189	0.361	0.109
2/Li/THF	−0.051	0.079[a]	0.006	0.146	0.265	0.403	0.227
2/Na/THF	−0.047	0.082[a]	0.004[a]	0.158	0.283	0.391	0.223
2/K/DME	−0.037	0.086[a]	0.002[a]	0.157	0.296	b)	0.207

a) Average values of two positions. b) Not available.

Equivalency or Nonequivalency of Ortho or Meta Positions in the Phenyl Groups of the Dianions. The chemical shifts of two ortho or meta carbons in a phenyl ring of **1** are equivalent, but those of **2** are nonequivalent, as is shown in Figs. 1a and 2b. Additionally, coalescence of meta carbon lines and broadening of ortho carbon resonances were observed for the lithium salt of **2** at room temperature, as shown in Fig. 2a. The appearance of the nonequivalency in the sodium and potassium salts was attributed to the higher rotational barrier about the C_α and C_i bond, as compared with the case of lithium salt (Figs. 2a and 2b). This fact can be interpreted on the basis of the effect of the counter cations.[14] The nonequivalency was caused by a conjugative interaction between C_i and C_α. This situation is similar to the nonequivalency observed in 1-phenylethanide (**5**) and 2,5-diphenylhexane 2,5-diide (**6**) ions.[6c,14,15] This is due to the fact

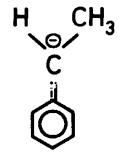

5

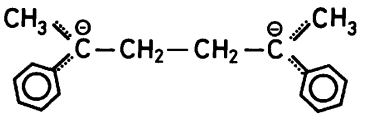

6

that both a phenyl ring and a butadiene skeleton prefer to take their positions on a plane because of a strong $p\pi$–$p\pi$ interaction. However, in the neutral molecule **2a** there is a free rotation around the bond between the phenyl ring and its adjacent carbon; however, in the case of **2** the rotation is restricted in its NMR time scale. On the other hand, the two phenyl rings connected to the α-carbon of **1** cannot be coplanar due to their steric hindrance as well as those of the neutral precursor **1a**.[15] As is shown in Fig. 1, however, the ^{13}C spectra of **1** showed an equivalency of the four ortho or meta carbons in the two geminal phenyl rings, while there are two C_i, C_o, C_m, and C_p signals in **1a**. These facts suggest that there is a free rotation about the C_i and C_α bond in **1** and **1a**, while the rotation around the bond between the C_α and C_β atoms is forbidden in **1a** but allowded in **1** at room temperature.

Temperature Dependency of the Chemical Shifts of 2. It was pointed out before that in the ^{13}C NMR spectrum of the lithium salt of **2** (Fig. 2a) coalescence of the C_m signals and broadening of the C_o signals were observed at room temperature. These phenomena can be explained by the restricted rotation of the phenyl group around the C_i–C_α bond. The temperature-dependent ^{13}C chemical shifts are shown in Figs. 3a and 3b. As shown in the figures the C_m and C_β shifts are almost constant in the temperature range studied, while the C_i, C_o, and C_p shifts move towards a lower field by about 1—2 ppm in magnitude when the temperature is raised; the C_α shift, however, moves towards a higher field by about 2 ppm. This tendency

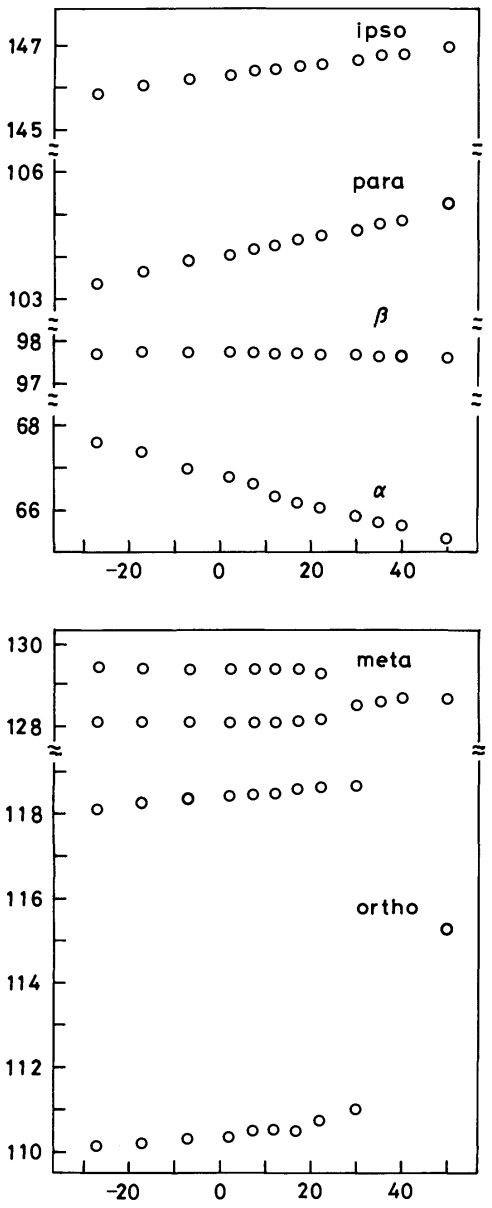

Fig. 3. ^{13}C chemical shifts (ordinate in ppm) of **2** in THF-d_8 as a function of temperature (abscissa in °C) at 50.3 MHz.

can be explained by an excess charge on the C_α which increases with increasing temperature. This means that the $p\pi$–$p\pi$ interaction between the C_α and C_i decreases with increasing temperature. This is consistent with the fact that the phenyl ring can rotate at higher temperature, faster than that of the NMR time scale. In the sodium salt of **2**, on the other hand, the spectrum does not change its line shape in the temperature range from −70 to 60 °C. Therefore, the activation free-energy change will be larger than 68 kJ mol^{-1} by using an equation given by Sandström[16] and the chemical-shift difference of 78.5 Hz. Therefore, it must be said that the barrier of phenyl rotation of **2** is strongly affected by a counterion whose tendency is similar to that stated by Worsfold and Brownstein.[14]

Table 4. Thermodynamical Parameters for the Hindered Rotation of the Phenyl Group of the Lithium Salt of **2**

Site	E_a/kJ mol^{-1}	log A	ΔH^*/kJ mol^{-1}	ΔS^*/J K^{-1} mol^{-1}
Ortho	62.7±1.2	13.0±0.3	60.3±1.1	−3.0±4.0
Meta	61.6±1.4	12.7±0.3	59.2±1.4	−10.0±5.0

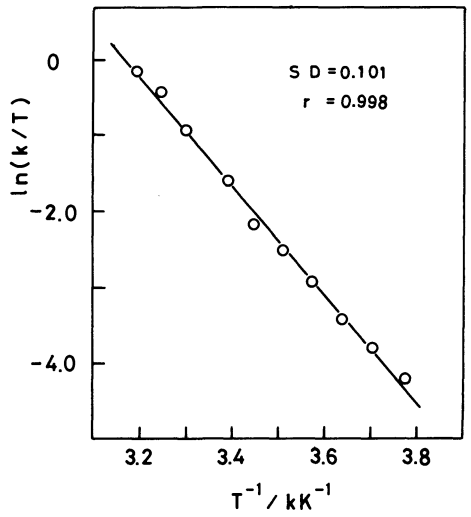

Fig. 4. An Eyring plot for the rotation of phenyl groups of the lithium salt of **2** in THF-d_8.

In the lithium salt of **2**, ^{13}C NMR analyses were carried out for both the ortho and meta carbon signals as an AX-spin system. The parameters used for the DNMR analyses are $\Delta\delta$ (ortho)=405; $\Delta\delta$ (meta)=64.3 Hz; T_2*=0.134 s. The kinetic parameters have been determined by visual fittings of the calculated line shapes with the experimental ones. The thermodynamic parameters were obtained by the Arrhenius and Eyring plots of the rate constants with inverse temperatures, one of which is shown in Fig. 4. The parameters, thus determined, are given in Table 4. The parameters independently obtained for both the ortho and meta carbons are consistent with each other within the experimental errors. The values are compared with those reported for similar substituted phenylmethanide ions.[14,17-20] The barrier of the phenyl rotation of **2** is larger than those observed for diphenylmethanide ions.[21,22]

The authors wish to thank Messrs. Katsuhiko Kushida and Hajime Katoh (Varian Instruments Ltd.) for their kindness in measuring several ^{1}H spectra at 300 MHz. This work was partly supported by a Grant-in-Aid for Scientific Research (1988), No. 63540336, from the Ministry of Education, Science and Culture.

References

1) E. H. O'BVrien, "Comprehensive Carbanion Chemistry," ed. by E. Buncel and T. Durst, Elsvier, New York (1980), Vol. 5A, p. 271.

2) M. Ushio, M. Takaki, K. Takahashi, and R. Asami, *Bull. Chem. Soc. Jpn.*, **44**, 2559 (1971).

3) Y. Yokoyama and K. Takahashi, *Chem. Lett.*, **1987**, 589.

4) R. B. Bates, D. W. Gosselink, and J. A. Kaczynski, *Tetrahedron Lett.*, **1967**, 205.

5) V. R. Sandel and H. H. Freedman, *J. Am. Chem. Soc.*, **85**, 2328 (1962).

6) a) K. Takahashi and R. Asami, *Bull. Chem. Soc. Jpn.*, **41**, 231 (1968); b) K. Takahashi, Y. Inoue, and R. Asami, *ibid*, **3**, 349 (1971); c) K. Takahashi, M. Takaki, and R. Asami, *J. Phys. Chem.*, **75**, 1062 (1971).

7) K. Takahashi, K. Yamada, K. Wakata, and R. Asami, *Org. Magn. Reson.*, **6**, 62 (1974).

8) G. Fraenkel, R. E. Carter, A. McLachlan, and J. H. R. Richard, *J. Am. Chem. Soc.*, **82**, 5846 (1960).

9) H. Spiesecke and W. G. Schneider, *Tetrahedron Lett.*, **1961**, 468.

10) A. A. Bothner- By and R. K. Harris, *J. Am. Chem. Soc.*, **87**, 3451 (1965).

11) R. Hoffmann and R. A. Olofson, *J. Am. Chem. Soc.*, **88**, 943 (1966).

12) D. Wilhelm, T. Clark, P. von R. Schleyer, H. Dietrich, and W. Mahdi, *J. Organomet. Chem.*, **280**, C6 (1985).

13) R. K. Harris and B. R. Howes, *J. Mol. Spectr.*, **28**, 191 (1968).

14) S. Brownstein and D. J. Worsfold, *Can. J. Chem.*, **50**, 1246 (1972).

15) K. Takahashi, M. Takaki, and R. Asami, *Org. Magn. Reson.*, **3**, 539 (1971).

16) J. Sandström, "Dynamic NMR Spectroscopy," Academic Press, London (1982), p. 96.

17) V. R. Sandel, S. V. McKinley, and H. H. Freedman, *J. Am. Chem. Soc.*, **90**, 495 (1969).

18) K. Matsuzaki, Y. Schinohara, and T. Kasai, *Macromol. Chem.*, **181**, 1923 (1980).

19) G. Fraenkel, J. G. Russell, and Y-H. Chen, *J. Am. Chem. Soc.*, **95**, 3208 (1973).

20) G. Fraenkel and J.M. Geckle, *J. Am. Chem. Soc.*, **102**, 2869 (1980).

21) C. H. Bushweller, J. S. Sturges, M. Cipullo, S. Hoogasin, M. W. Gabriel, and S. Bank, *Tetrahedron Lett.*, **1978**, 1359.

22) G. A. Olah and M. I. Watkins, *Proc. Natl. Acad. Sci. U.S.A.*, **77**, 703 (1980).

Electrochemical Preparation and Characterization of the Radical Salts of (Phthalocyaninato)nickel, $NiPc(SbF_6)_{0.5}$, and $NiPc(AsF_6)_{0.5}$

Kyuya YAKUSHI,*,† Hideo YAMAKADO, Michiko YOSHITAKE, Nobuhiro KOSUGI, Haruo KURODA, Tadashi SUGANO,†† Minoru KINOSHITA,†† Atsushi KAWAMOTO,††† and Jiro TANAKA†††

Department of Chemistry, Faculty of Science, the University of Tokyo, Hongo, Tokyo 113

††Institute for Solid State Physics, the University of Tokyo, Roppongi, Tokyo 106

†††Department of Chemistry, Faculty of Science, Nagoya University, Furocho, Chikusa-ku, Nagoya 464

(Received September 5, 1988)

The single crystals of $NiPc(SbF_6)_{0.5}$ and $NiPc(AsF_6)_{0.5}$ were prepared by means of an electrochemical method. The electrical, magnetic, optical, and structural properties of these crystals were examined. These crystals are isostructural to each other, and exhibit a metallic behavior at least above 200 K. The g-values of the ESR signals remarkably depend upon temperature. By the aid of the low temperature experiments of XANES and reflectance spectrum, the temperature dependence is explained by the model based on the interaction between the small amount of local spins on the Ni atoms and the conduction electrons on the ligand chain. In addition, a sample dependence was found on the ESR properties of the crystals of $NiPc(AsF_6)_{0.5}$. This is attributed to the sample dependence of the concentration of the local spins on Ni atoms. From these considerations, we concluded that the ligand part is mainly oxidized in these partially oxidized salts, in other words the conduction electrons are located on the ligand chain. The bandwidth of the conduction band was estimated to be about 1 eV.

The one-dimensional metals based on the metal phthalocyanine (MPc) or metal tetrabenzoporphyrin (MTBP) are unique materials which may be able to involve two conduction pathways in the same metal macrocycle column.[1] These pathways are possibly composed of the π-orbital of the ligand and the d_{z^2}-orbital of the central metal, first because the molecules are stacking with the overlapping mode of a metal-over-metal type,[2] secondly because the highest occupied molecular orbital (HOME) of a phth alocyanine (Pc) does not mix with the d_{z^2}-orbital of the central metal due to the symmetry restriction, thirdly because their orbital energies are quite close.[3-5] The excitonic superconducting mechanism is theoretically proposed in the materials which involve this kind of composite energy bands that are weakely coupled and proximately located to each other.[6] Therefore, it is of great importance to elucidate which orbitals are contributing to make the conduction bands. The research group at Northwestern University extensively studied the partially oxidized salts of metal phthalocyanine (MPc) and metal tetrabenzoporphyrin (MTBP).[1,2,7-14] As for the iodine complex (NiPcI) of NiPc, the conduction band is formed from the highest occupied molecular orbital (HOMO, a_{1u}) of the Pc ligand, and the d-orbital is not involved in the conduction band.[2] On the other hand, the conduction electrons of CoPcI are located on the metal chain in the Pc column.[10] Furthermore, the unpaired electrons of the iodine complex (NiTBPI) of NiTBP exhibit that they are located partly at the ligand site and partly at the Ni site.[1] Martinsen et al. interpreted this phenomenon by considering that the conduction band is composed of $a_{1g}(3d_{z^2})$-band along the metal chain and the $a_{1u}(\pi)$-band along the ligand chain.[1] We prepared the analogous complexes, $NiPc(SbF_6)_{0.5}$ and $NiPc(AsF_6)_{0.5}$, by the use of the electrochemical oxidation of NiPc, and found that the ESR behavior of $NiPc(SbF_6)_{0.5}$ is quite similar to that of NiTBPI.[15,16] Later on, we found a strong sample dependence on the ESR property of $NiPc(AsF_6)_{0.5}$. Lookig at this phenomenon through the eyes of ESR, some crystals of $NiPc(AsF_6)_{0.5}$ behave like NiPcI, someone like CoPcI, and the others like NiTBPI. We are interested in whether the conduction band of $NiPc(SbF_6)_{0.5}$ is really composed of the π-and d_{z^2}-orbitals, and whether the sample dependence of $NiPc(AsF_6)_{0.5}$ is the intrinsic property. In this paper, we present the experimental results on the temperature dependence of the ESR property, XANES and reflectance spectrum of $NiPc(SbF_6)_{0.5}$, and characterize the magnetically different $NiPc(AsF_6)_{0.5}$ by means of EPMA, X-ray diffraction, and reflectance spectrum.

Experimental

The finely powdered NiPc was refluxed in the pyridine solution and was filtrated to remove CoPc. This procedure was repeated over ten times and then the filtrated NiPc powder was sublimed in vacuum for four times. The contamination by the magnetic impurity was less than 10^{-4} spins per a NiPc molecule which was estimated with the aid of ESR at low temperature. The ESR signal of this impurity, probably Co^{2+} species, was not attributed to CoPc, since the ESR pattern due to the hyperfine splitting was entirely different from that of CoPc.[17] $(n\text{-}Bu)_4NSbF_6$ and $(n\text{-}Bu)_4NAsF_6$ which were used as electrolytes for the electrochemical oxidation were prepared by mixing the equimolar aqueous solutions of $(n\text{-}Bu)_4NBr$ and $NaSbF_6$ or $KAsF_6$. The precipitated $(n\text{-}Bu)_4NSbF_6$ and $(n\text{-}Bu)_4NAsF_6$ were recrystallized from the methanol solution for three times. 1-chloronaphthalene was refluxed with CaH_2 and purified by vacuum distillation. The radical salts of NiPc were prepared by the method of electrochemical crystallization at 120±2 °C under the Ar

† Present address: Institute for Molecular Science, Myodaiji-cho, Okazaki, Aichi 444.

atmosphere. The concentrations of the electrolyte and NiPc were 2.5×10^{-3} and 3×10^{-4} mol l^{-1}, respectively. The crystals were grown for about two weeks with a galvanostatic mode of 2 μA.

The chemical analysis of Ni, Sb, and As were conducted with the aid of ICP atomic emission spectroscopy. Several single crystals (ca. 10 μg) were dissolved in concd H_2SO_4, then decomposed in concd HNO_3 and diluted with pure water. The emission lines, 231.6, 206.8, and 193.6 nm were used for the detection of Ni, Sb, and As. The intensities of these emission lines were measured simultaneously by using Jarrel-Ash, Model Plasma Atomcomp MK-II. The atomic ratios were Sb/Ni=0.48±0.04 for NiPc-SbF_6 and As/Ni=0.50±0.02 for NiPc-AsF_6. The sample dependence of the atomic ratio between Ni and As of the single crystal was measured by means of EPMA using JEOL superprobe 733. The Ni foil and the single crystal of GaAs were used as the standard materials of Ni and As atoms. EPMA were performed at seven points on each crystal of 0.03 mm×0.03 mm×0.3 mm by the use of the electron beam of 1 μm diameter.

ESR was measured on a needle-like single crystal or a bundle of single crystals using JEOL JES-FE1XG combined with an Air Products LTR-3-110 continuous flow type liquid He cryostat. The needle-like crystals over 10 were aligned in the Pyrex capillary. Li-TCNQ was used as the standard sample to determine the g-value. The intensity of the ESR signal was calculated by the numerical double integration, and this intensity was transformed to the spin susceptibility by the comparison with the intensity of the ESR signal of violanthrone for which the static susceptibility had been measured.

For the experiment of X-ray diffraction, we used the needle-like crystal of $NiPc(AsF_6)_{0.5}$ developing along the c-axis, the typical dimension of which was 0.05 mm×0.05 mm×0.5 mm. The 2296 reflections were collected using Rigaku four-circle automated diffractometer. The X-ray source was the Cu $K\alpha$ radiation monochromatized with a graphite plate. We selected 1940 reflections which are three times larger than the standard deviations estimated from the counting errors. The absorption correction was made with a program ACACA written by Prewitt. The structure was solved by the heavy atom method and was refined by the block-diagonal least-squares method with the anisotropic temperature factors for Ni, N, C, As, and F atoms and the isotropic temperature factors for H atoms. The possible space group was *Pncm* or *Pnc*2 from the systematic absence. At first the structure was analyzed assuming the space group, *Pncm*. However, the final R-value was 0.12, and the temperature factors of F atoms were too large. This means that F atoms are neither located on the mirror plane nor two-fold axis. Thus, the structure was analyzed in the non-centrosymmetric space group, *Pnc*2. The final R-value was 0.065.

The X-ray absorption spectrum near the Ni K-edge was measured using the EXAFS facilities at the beam line 10B of the Photon Factory in the National Laboratory for High Energy Physics (KEK-PF).[18] The single crystal of the dimension, 0.15 mm×0.15 mm×2 mm, was used for measuring the transmission spectrum. This crystal was fixed with vacuum grease onto the round mask which was made from stainless steel with the thickness of 0.1 mm, and had a rectangular diaphragm of 0.1 mm×1 mm. Polarized spectra were measured with the X-ray polarization parallel, 45°, and perpendicular to the long axis of the crystal. The CTi cryocooler, Model 20, was used for cooling the sample crystal.

The polarized reflectance spectra of single crystals were measured at room temperature and 80 K using the micro-spectro-reflectometer which was designed and constructed in our laboratory (Chemistry Department, the University of Tokyo).[19]

Temperature dependence of the electrical resistivity was measured by the low-frequency AC four-probe method. The electrical contact to the 10 μm gold wires was made with carbon paint. The cooling rate of the crystal was about 0.5 K min^{-1}.

Results and Discussion

$NiPc(SbF_6)_{0.5}$. The chemical ratio between NiPc and SbF_6 is consistent with the crystal structure which we have published in the previous paper.[15] The crystal belongs to the orthorhombic system, the space group being *Pnc*2. The lattice constants are a=14.113(1) Å, b=28.710(2) Å, c=6.441(2) Å, and Z=2. The crystal structure is essentially the same as that of $NiPc(AsF_6)_{0.5}$, the structural details of which will be described in the next section. NiPc is stacking metal-over-metal with the planes of molecules normal to the stacking axis. Successive molecules are staggered by 41.0°. The unit cell contains two molecular columns. The counter anions, SbF_6^-, are located on the same plane of NiPc, so that NiPc is pushed away by 0.2 Å from the stacking axis. Therefore, the metal chain of NiPc is aligned zigzag along the c-axis. Unlike the disordered arrangement of I_3^- in the NiPcI crystal,[2] SbF_6^- is three dimensionally ordered in this material. However, they are probably thermally fluctuating since the temperature factors of anion is larger by a factor of 5—10 than those of NiPc.[15]

The electrical conductivity is 10—200 S cm^{-1} at room temperature and gradually increases on lowering temperature down to 250 K. At lower temperature, however, the resistivity jumps take place at various temperatures, which are not reproducible in the heating or cooling processes. Therefore, the intrinsic behavior of the electrical resistivity in the low temperature region is unidentified at present. Since these resistivity jumps are sometimes observed in the one-dimensional materials, this phenomenon indicates the one-dimensional electric conduction in this material.

The angle dependence of the g-value at room temperature was showm in Fig. 1. The principal values are $g_{/\!/}$=1.994 and $g_{\perp}$=2.030, where // and ⊥ denote the geometrical relation between the c-axis of the crystal and the static magnetic field. These axes just coincide with the principal axes of the NiPc molecule. The principal values of NiPc molecule are

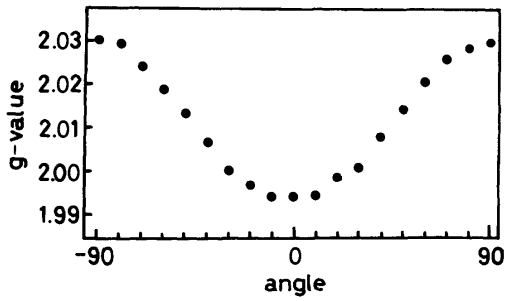

Fig. 1. Angular dependence of the g-value of $NiPc(SbF_6)_{0.5}$. The c-axis is parallel to the static magnetic field when the angle is 0°.

$g_{/\!/}$=2.113 and $g_\perp$=2.292 for metal-oxidized species, $Ni^{3+}Pc^{2-}$, and $g_{/\!/} \sim g_\perp$=2.003 for ligand-oxidized species, $Ni^{2+}Pc^{-}$.[20] Therefore the unpaired electrons of $NiPc(SbF_6)_{0.5}$ has an intermediate character between the metal-oxidized $Ni^{3+}Pc^{2-}$ and the ligand-oxidized $Ni^{2+}Pc^{-}$. This character of the unpaired electrons show a contrast to the π-character of NiPcI, in which the principal values are $g_{/\!/}$=2.0075, $g_\perp$=2.0007.[2] Martinsen et al. found the intermediate g-values ($g_{/\!/}$=2.060 and $g_\perp$=2.018) in NiTBPI, and attributed them to the rapid transfer of the unpaired electron between a ligand and a central metal.[1] Therefore, a similar situation is possibly realized in $NiPc(SbF_6)_{0.5}$. The relation, $g_{/\!/} > g_\perp$, which is reverse to the usual square planar d^7 complex with a low spin configuration, was explained on the basis of the back charge transfer from triiodide ion. In this sense, the contrary relation, $g_{/\!/} < g_\perp$, in this crystal is consistent with their interpretation, because this material does not contain triiodide ions. At the same time, the angular dependence of the g-value indicates that the ESR signal is originated from the $Ni^{3+}Pc^{2-}$ species in the crystal, and suggests that the d-hole configuration of $Ni^{3+}Pc^{2-}$ is $(d_{x^2-y^2})^2(d_{z^2})^1$.[21]

The temperature dependence of ESR were conducted on ca. 20 single crystals aligned in the glass capillary so that the needle axes (//c) were perpendicular to the static magnetic field. The temperature dependence of $g_\perp$, a linewidth, and a doubly integrated intensity were displayed in Figs. 2b—2d. With the decrease of temperature,the linewidth and $g_\perp$ remarkably increase and the intensity slightly decreases. The increase of the linewidth is closely related to the increase of $g_\perp$ which is the measure of the contribution of d-orbital which brings about the fast relaxation due to the large spin-orbit coupling constant. The temperature-dependent spin susceptibility was divided into two components, one of which comes from the metal chain and the other from the ligand chain using the following equation.[22]

$$\chi_{Ni}(T) = [(g_{obs} - g_{Pc})/(g_{Ni} - g_{Pc})]\chi_{obs}(T)$$
$$\chi_{Pc}(T) = [(g_{Ni} - g_{obs})/(g_{Ni} - g_{Pc})]\chi_{obs}(T)$$

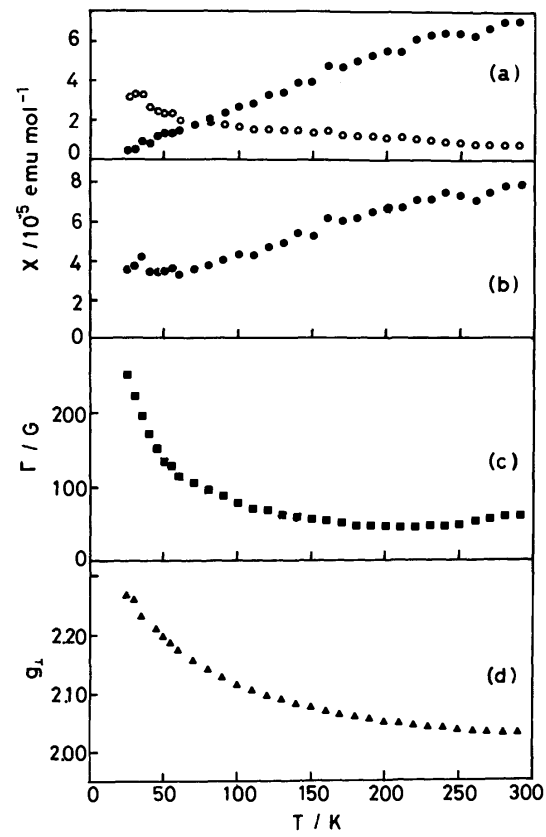

Fig. 2. Temperature dependence of the ESR signal (H⊥c) of $NiPc(SbF_6)_{0.5}$. (a) Spin susceptibilities of the Ni chain (open circle) and the Pc chain (solid circle), (b) observed spin susceptibility, (c) linewidth, and (d) g-value.

These results are drawn by solid and open circles in Fig. 2a. In this process, we tentatively used g_{Ni}=2.292 and g_{Pc}=2.003 which were reported by Bobrovskii and Sidorov in the oleum solution of NiPc.[20] The $g_\perp$ of $NiPc(SbF_6)_{0.5}$ is in-between those of $Ni^{3+}Pc^{2-}$ and $Ni^{2+}Pc^{-}$, but the $g_{/\!/}$ is smaller than both of them. It is well-known that the g-values of the transition metal atoms coordinated with a square planar mode are very sensitive to the axial coordination by the solvent molecule. In fact as we will mention in the next section, the $g_\perp$-value of some crystals of $NiPc(AsF_6)_{0.5}$ is larger than $g_\perp$=2.292 of $Ni^{3+}Pc^{2-}$. Therefore, the larger values than 2.292 should be taken as the standard g-value of a metal-oxidized species. Taking this situation into account, the contribution of $\chi_{Ni}(T)$ is overestimated in this analysis, but we believe that the qualitative trend on temperature dependence is reliable. At low temperature, $\chi_{Ni}(T)$ increases and overwhelms $\chi_{Pc}(T)$ which is dominant at room temperature.

Martinsen et al. studied the structure and properties of NiTBPI, which exhibits quite similar ESR properties to that of $NiPc(SbF_6)_{0.5}$.[2] They qualitatively interpreted the d-character of the unpaired electrons using the

band model composed of the two conduction bands, one of which derived from the HOMO of the ligand (a_{1u}-band) and the other from the $3d_{z^2}$ orbital of a Ni atom (a_{1g}-band). They regarded the a_{1g}-band as the origin of the d-character. The conduction electrons in the a_{1u} and a_{1g} bands exchange with each other faster than the microwave frequency. In this model a considerable amount of charge carriers are located on the conducting Ni chain as well as on the conducting Pc chain. However, it is not easy to explain the temperature dependence of the g-value by this model. For example, the contribution of $\chi_{Pc}(T)$ is dominant at room temperature, but it is reverse at low temperature as shown in Fig. 2a. To explain this behavior based on the Pauli paramagnetism of the two tight-binding bands, we have to shift the relative position of these band centers depending upon the temperature so as to adjust the density of state at the Fermi level of each band. This requires the temperature dependent band filling factor, namely the degrees of oxidation at the Ni and ligand sites. Another possible interpretation is based on the model in which the conduction electrons are located mainly on the ligands and they exchange rapidly with a small amount of localized electrons on the Ni sites. This is the extreme case where the bandwidth of the d-band is much narrower than that of π-band. In this model, the increase of $\chi_{Ni}(T)$ is attributed to the Curie law, and the decrease of $\chi_{Pc}(T)$ is related to a narrow energy gap in the conduction band, which will be discussed again in the next section. Assuming the Curie law as to $\chi_{Ni}(T)$, the spin concentration at the Ni site with $S=1/2$ was estimated to be 4×10^{-3} spins per a NiPc. Therefore, the ligand site is predominantly oxidized, so that the temperature dependent degree of oxidation at the ligand site is not necessary in this model. These two models can be distinguished from the temperature dependence of the numbers of charge carriers on each chain. If the degree of oxidation on each chain does change at low temperature, we have to adopt the former model, while the latter model will be appropriate if not. The temperature dependence of the d-holes at the Ni site is examined with the X-ray absorption spectrum of 1s→3d transition, and the change of the degree of oxidation at Pc site at low temperature is checked by the intensity of the Q-band.

The X-ray absorption spectrum of the electron quadrupole transition, 1s→3d, provides the information on the bulk property of the vacant d-orbitals. The spectra (1) and (2) shown in Fig. 3 are the X-ray absorption spectra near the K-edge on the powdered samples of $NiPc(SbF_6)_{0.5}$ and NiPc, respectively. As for the 1s→3d transition at 8321.5 eV, no significant difference was found between them. The spectra (3), (4), and (5) in Fig. 3 are the polarized absortion spectra of the 1s→3d quadrupole transition of the single crystal of $NiPc(SbF_6)_{0.5}$. The selection rule of the

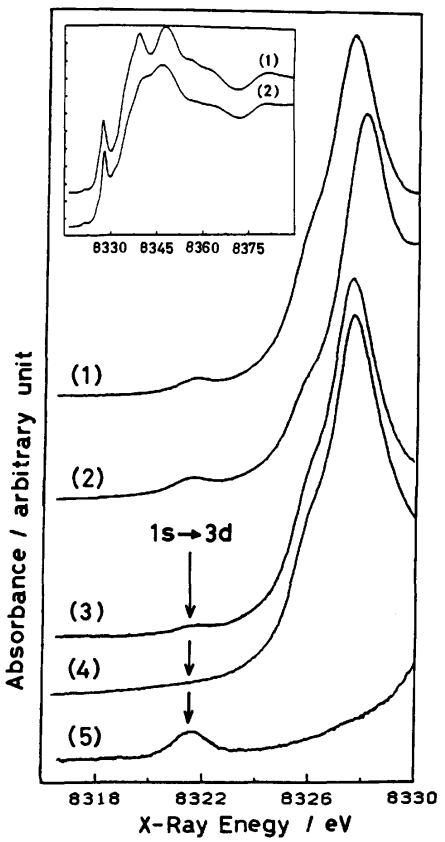

Fig. 3. X-Ray absorption spectra of the powdered samples of (1) $(NiPc)_2SbF_6$ and (2) NiPc, and (3—5) the single crystals of $NiPc(SbF_6)_{0.5}$. A weak absorption band at about 8321.5 eV is the 1s→3d electric quadrupole transition, and the absorption band at about 8328 eV is the electric dipole 1s→π^* transition. (3) The electric vector makes an angle of 45° with the c-axis in the polarization plane. (4) The electric vector of the incident light is parallel to the c-axis. (5) The polarization plane of the incident light is perpendicular to the c-axis.

quadrupole transition is determined by the relative direction between the one-dimensional Ni chain and the polarization plane (the plane of vibration of electric field).[23] The selection rule of the 1s to 3d transition is listed in Table 1. If this absorption band is a single component, this transition is assigned to the 1s→$3d_{x^2-y^2}$ from the selection rule and the theoretical study of the NiPc free molecule.[5] This experimental result apparently indicates that the d-orbitals except $3d_{x^2-y^2}$ is fully occupied as expected in the second model. However, the interpretation of this spectrum is not simple, because CoPc and FePc also exhibited a single absorption band for the 1s→3d transition,[24] although they have respectively the electronic configurations of $(3d)^7$ and $(3d)^6$. Therefore, we cannot preclude the possibility that 1s→3d band of $NiPc(SbF_6)_{0.5}$ is attributed to the superposition of the 1s→$3d_{x^2-y^2}$ transition and the other 1s→3d transition. This case is consistent with the first model (two-band model). If

Table 1. Selection Rule of Quadrupole Transition

(1) E⊥c: When the c-axis of the crystal is perpendicular to the polarization plane, a quadrupole transition is allowed only from 1s to $3d_{x^2-y^2}$ and to $3d_{xy}$. (2) E//c: When the electric vector is parallel to the c-axis, quadrupole transition is allowed from 1s to $3d_{xy}$ and $3d_{yz}$. (3) $\angle(E,c)=45°$: When the c-axis makes an angle of 45° against the electric field vector in the polarization plane, the transition from 1s to $3d_{z^2}$ and $3d_{x^2-y^2}$ is allowed.

	$d_{x^2-y^2}$	d_{z^2}	d_{xy}	d_{xz}	d_{yz}	Experimental
(1)	O	×	O	×	×	Observed
(2)	×	×	×	O	O	Not observed
(3)	O	O	×	×	×	Observed

O: allowed transition, ×: forbidden transition.

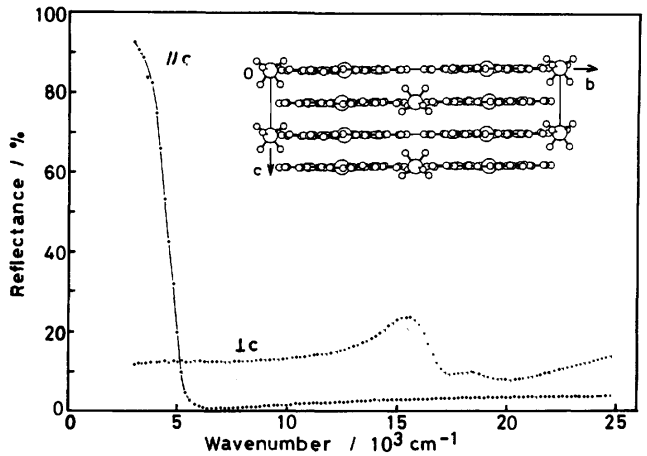

Fig. 4. Polarized reflectance spectrum of the single crystal of $(NiPc)_2SbF_6$. The inset shows the crystal structure of $(NiPc)_2SbF_6$.

this is the case, the candidate of this vacant d-orbital is $3d_{z^2}$ or $3d_{xy}$ from the selection rule shown in Table 1, and then the $1s\rightarrow 3d_{z^2}$ or $1s\rightarrow 3d_{xy}$ transition should change significantly at low temperature accompanying the change of the degree of oxidation at the Ni site. However, no significant change was detected in the 50 K spectra of the powdered sample and the single crystal. This result supports the second model, that is, the majority of carriers are located on the ligand chain and a small amount of unpaired electrons are localized at the Ni site. The d-character of the ESR signal is attributable to the rapid exchange between these local spins at the Ni site and the migrating spins on the ligand chain. Figure 4 shows the polarized reflectance spectrum of the single crystal of $NiPc(SbF_6)_{0.5}$. In the ⊥c spectrum, the intramolecular transition (Q-band) of a neutral NiPc was observed at 15400 cm^{-1}. Figure 5 shows the comparison of the ⊥c spectra at room temperature and 80 K. In this spectrum, weak shoulders showed up around 13000 and 23000 cm^{-1}. These weak dispersions are tentatively assigned to the intramolecular transitions of $Ni^{2+}Pc^-$ cation radical

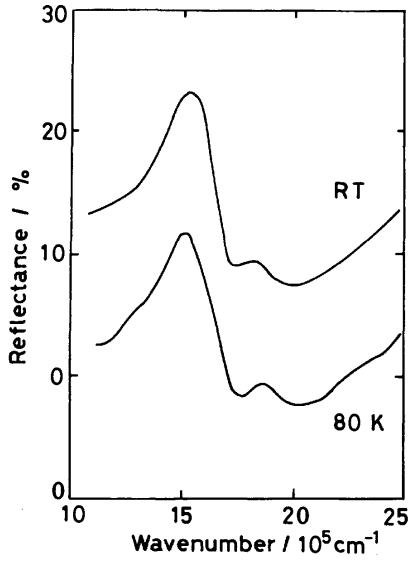

Fig. 5. Reflectance spectrum of the Q-band measured at 80 K and room temperature.

from the comparison of the solution spectra of Li^+Pc^-[25] and $Co^{2+}Pc^-$,[26] the ligands of which are oxidized. Since the transition probability of the intramolecular transitions of NiPc cation radicals are small, we consider that these shoulders are faded away at room temperature. The reflectivity of the Q-band of $NiPc(SbF_6)_{0.5}$ is considerably smaller than that of NiPcI.[8] This result is reasonable, since the degree of oxidation $NiPc(SbF_6)_{0.5}$ is larger than that of NiPcI. Thus, the intensity of the Q-band reflects the degree of oxidation at the ligand site. Although a considerable increase of the d-character is expected at 80 K from the g-value of the ESR signal, the reflectivity of the Q-band does not change significantly. This result supports again the second case that the majority of carriers are located on the π-band in the whole temperature range.

We analyzed the reflectance curve of the //c spectrum using the Drude model, and obtained the plasma frequency and the relaxation time. The plasma frequency, $\hbar\omega_P$, was estimated to be 0.86 eV, the relaxation time, $(0.8—1.2)\times10^{-14}$ s, and dielectric constant, 2.1. The bandwidth, $4t$, was calculated using the following equation,

$$4t = \{V_m(\hbar\omega_P)^2\}/\{4e^2c^2\sin(k_fc)\}$$

where V_m is the volume of $(NiPc)(SbF_6)_{0.5}$, c the interplanar distance between the adjacent phthalocyanines, e the unit charge of an electron, and k_f the Fermi wavevector. Since the majority of carrier is located on the ligand chain, the width of the π-band, 4t is estimated to be 1.1 eV from the values, $V_m=6.524\times10^{-22}$ cm^3, $\hbar\omega_p=0.86$ eV, $c=3.22\times10^{-8}$ cm, and $k_fc=3\pi/4$. In the analogous materials like H_2PcI, NiPcI, and CuPcI, the conduction bands are made up of π-orbitals

of ligands. The bandwidth of these materials are 0.84,[2] 1.3,[12] and 1.4 eV[14] for NiPcI, H_2PcI, and CuPcI, respectively. The bandwidth, 1.1 eV, of $NiPc(SbF_6)_{0.5}$ falls in the range of these materials with π-conduction bands. We briefly comment on the relaxation time of conduction electrons which is the measure of the strength of the electron-phonon interaction. Although the ambiguity of the relaxation time is much larger than that of plasma frequency in the curve-fitting analysis, the following discussion is qualitatively reliable. The relaxation time is comparable with the corresponding values, 0.7×10^{-14} s for NiPcI and 0.9×10^{-14} s for H_2PcI, and 1.4×10^{-14} s for CuPcI[14] but significantly longer than the room-temperature values of other organic metals, 0.4×10^{-14} s for TTF-TCNQ,[27] 0.2×10^{-14} s for $TTF\text{-}I_{0.71}$,[28] 0.3×10^{-14} s for $(TMTSF)_2PF_6$,[29] 0.4×10^{-14} s for $(TMTSF)_2ClO_4$,[30] 0.3×10^{-14} s for $(DMtTSF)_2ReO_4$.[31] These results suggest that the conduction electron on the phthalocyanine ring is interacting weakly with the lattice phonon.

$NiPc(AsF_6)_{0.5}$. In contrast to $NiPc(SbF_6)_{0.5}$, we found a strong sample dependence on the magnetic property of $NiPc(AsF_6)_{0.5}$. To characterize these magnetically different crystals, we selected 90 crystals which were larger than 0.05 mm×0.05 mm×6 mm, and measured the ESR signal on each crystal under the condition that the needle axis is perpendicular to the static magnetic field. Figure 6 shows the distribution of the ESR patterns which was classified by the linewidth. The ESR signal is sometimes composed of two or three components with different linewidths. These mixtures are indicated by the dotted histograms. As shown in this figure, the linewidth of the ESR signal is almost continuously distributed from about 1 G to over 100 G (1 G=10^{-4} T). F denotes the sample which is ESR silent probably due to the too broad linewidth. The typical examples of the ESR pattern is shown in Fig. 7. The different types of crystals, i.e. types A and D, were usually found in the same batch. We consider that the sample dependence is not attributed to the contamination of the magnetic impurities because the samples are prepared from the same starting materials as what was used for the preparation of $NiPc(SbF_6)_{0.5}$ which does not show such a sample dependence. The temperature dependence of the magnetic susceptibility, linewidth and g-value of the typical types of crystals were measured on the single crystals of the types A and B and the aligned crystals of the types D and E. The results are shown in Fig. 8.

It is well-known that the electrochemical oxidation of BEDT-TTF (bis(ethylenedithio)tetrathiafulvalene) produces the crystals which have many chemical compositions and a variety of polymorphs with the same composition.[32] In these crystals of BEDT-TTF, the physical properties are quite different from each other. In order to examine whether these ESR patterns

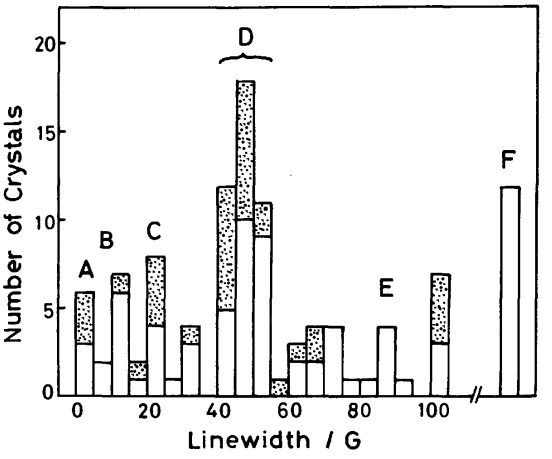

Fig. 6. Histogram of the sample dependence of the ESR signal of $NiPc(AsF_6)_{0.5}$ classified by the linewidth. The open rectangles denote the number of crystals with a single component and dotted ones stands for the ones which exhibit two or three components.

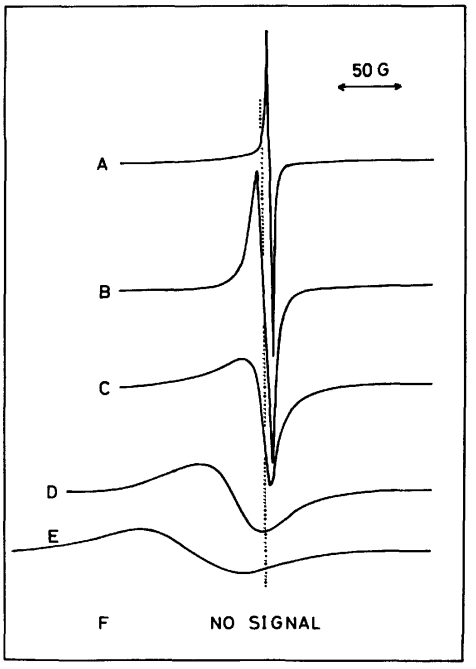

Fig. 7. Line shape of the ESR signal of the typical crystals of $NiPc(AsF_6)_{0.5}$. The symbols, A—F, correspond to those written in Fig. 6.

comes from the different chemical compositions or the polymorphism, we conducted the elementary analysis on each crystals with the aid of EPMA. The results shown in Table 2 indicates that all these crystals have essentially the same chemical composition, 2:1 for Ni:As within the experimental error.

The oscillation and Weissenberg photographs indicated that these crystals belonged to the same orthorhombic system with the space group, *Pncm* or *Pnc*2. The lattice constants of the types A, B, D, and E

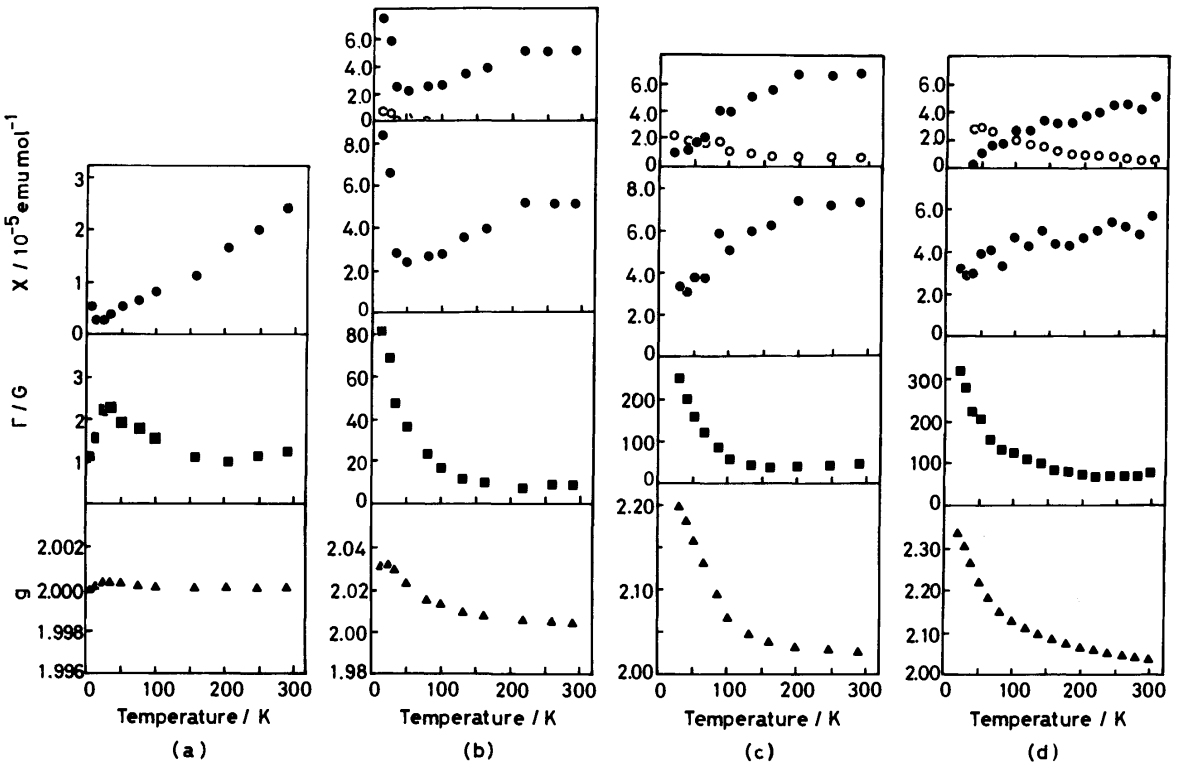

Fig. 8. Divided spin susceptibilities (top panel, solid circle for the Pc chain and open circle for the Ni chain), observed spin susceptibility (second from the top, solid circle), linewidth (second from the bottom, square), and g-value (bottom, triangle) of the ESR signal of the (a) type A, (b) type B, (c) type D, and (d) type E crystals of $NiPc(AsF_6)_{0.5}$. Except the type A crystal, the spin susceptibility is calibrated to the absolute value.

Table 2. Elementary Analysis of Ni and As of $NiPc-AsF_6$ Salts by the Method of EPMA

	A	B	D	E
As/Ni	0.48	0.43	0.49	0.51
σ	0.04	0.07	0.02	0.02

Table 3. Lattice Constants of $NiPc(AsF_6)_{0.5}$ and $NiPc(SbF_6)_{0.5}$

	a	b	c
$NiPc(AsF_6)_{0.5}$			
A	14.015(1)	28.485(2)	6.466(3)
B	14.11(2)	28.37(3)	6.462(3)
E	14.018(1)	28.485(2)	6.468(4)
F	14.027(4)	28.495(11)	6.447(6)
$NiPc(SbF_6)_{0.5}$[a)]	14.113(1)	28.710(2)	6.441(2)

a) See Ref. 14.

were determined using a four-circle diffractometer on the crystals of $NiPc(AsF_6)_{0.5}$. The results are shown in Table 3 together with that of $NiPc(SbF_6)_{0.5}$. The lattice constants agreed with each other except that of the type B crystal. We consider that this small difference comes from the poor quality of the crystal B, which is reflected on the 10 times larger standard deviations. The crystal structure analysis was conducted on the type A crystal which exhibits most different magnetic behavior from that of $NiPc(SbF_6)_{0.5}$. The final atomic coordinates are shown in Table 4. Figure 9 illustrates the molecular arrangement in the crystal of $NiPc(AsF_6)_{0.5}$. The NiPc molecules are slightly zigzag stacking along the c-axis. The shift of the central Ni atom from the axis (0.5, 0.25, z) is 0.21 Å, which is the same value as that of $NiPc(SbF_6)_{0.5}$. The neighboring NiPc is staggered by 40.4° around the stacking axis. The crystal structure is almost exactly the same as that of $NiPc(SbF_6)_{0.5}$.[33] The temperature factors of AsF_6^- is considerably larger than those of NiPc. The root-mean-square displacement of the As atom is 0.23, 0.19, and 0.45Å along the a-, b-, and c-axes, respectively. Since the c-component of the temperature factor of As is also large, AsF_6^- is not only orientationally disordered, but also positionally fluctuated along the c-axis. Therefore, the molecular structure of AsF_6^- is determined to be heavily distorted as shown in Fig. 9a. This kind of distortion was also observed on SbF_6^- in the crystal of $NiPc(SbF_6)_{0.5}$.[15] Incidentally the equivalent isotropic temperature factors of SbF_6^- were 7.8 for Sb and 14.9, 15.2, and 25.9 for F atoms. No significant difference was found in the molecular structure of NiPc between this complex and $NiPc(SbF_6)_{0.5}$. We consider that the structure of the type A crystal is essentially the same as

Table 4. Fractional Atomic Coordinates ($\times 10^4$) and Equivalent Temperature Factors ($B_{eq}=(4/3)\sum_{ij}\beta_{ij}a_ja_i$)

Atom	X	Y	Z	B_{eq}	Atom	X	Y	Z	B_{eq}
Ni1	5123(1)	2456(1)	57(8)	1.8	C24	5910(7)	1043(4)	32(44)	2.4
N2	6355(6)	2734(3)	22(33)	1.9	C25	5227(8)	1427(3)	108(40)	2.4
N3	5694(5)	1849(3)	80(34)	1.9	C26	3687(7)	1704(4)	168(37)	2.1
N4	3893(6)	2176(3)	10(34)	2.0	C27	2662(7)	1626(4)	64(40)	2.3
N5	4555(5)	3058(3)	16(33)	1.8	C28	2125(9)	1213(4)	219(44)	3.2
N6	7376(6)	2047(3)	226(31)	2.1	C29	1142(9)	1274(5)	−51(55)	4.1
N7	4296(6)	1350(3)	−25(35)	2.5	C30	718(8)	1712(5)	118(56)	4.2
N8	2868(6)	2864(3)	11(35)	2.4	C31	1261(8)	2125(5)	−148(43)	3.2
N9	5951(6)	3563(3)	−7(34)	2.1	C32	2250(7)	2065(4)	70(42)	2.5
C10	6560(7)	3207(3)	146(37)	2.0	C33	3028(7)	2405(4)	92(43)	2.3
C11	7594(7)	3281(4)	143(37)	2.2	C34	3594(7)	3159(4)	26(38)	2.2
C12	8144(8)	3684(4)	−29(48)	3.1	C35	3443(7)	3670(4)	30(42)	2.3
C13	9125(8)	3625(4)	35(56)	4.4	C36	2617(8)	3937(4)	59(47)	3.3
C14	9534(8)	3180(4)	117(56)	4.0	C37	2739(10)	4424(4)	9(60)	4.5
C15	8983(8)	2778(4)	−173(40)	2.7	C38	3646(10)	4624(4)	153(62)	4.4
C16	8001(7)	2844(3)	72(44)	2.2	C39	4483(9)	4355(4)	247(44)	3.1
C17	7215(6)	2506(4)	71(43)	2.1	C40	4337(7)	3870(4)	51(41)	2.4
C18	6651(7)	1751(3)	102(41)	2.2	C41	5027(8)	3490(3)	103(41)	2.2
C19	6814(7)	1240(4)	−4(43)	2.5	As42	10000	5000	5000	7.6
C20	7625(8)	968(4)	10(51)	3.5	F43	9799(30)	5336(7)	−2059(31)	22.8
C21	7522(10)	486(4)	243(52)	3.9	F44	11029(8)	5240(4)	−530(63)	19.0
C22	6601(10)	288(4)	102(55)	4.7	F45	9552(8)	5425(4)	1559(27)	8.9
C23	5784(9)	557(4)	238(47)	3.2					

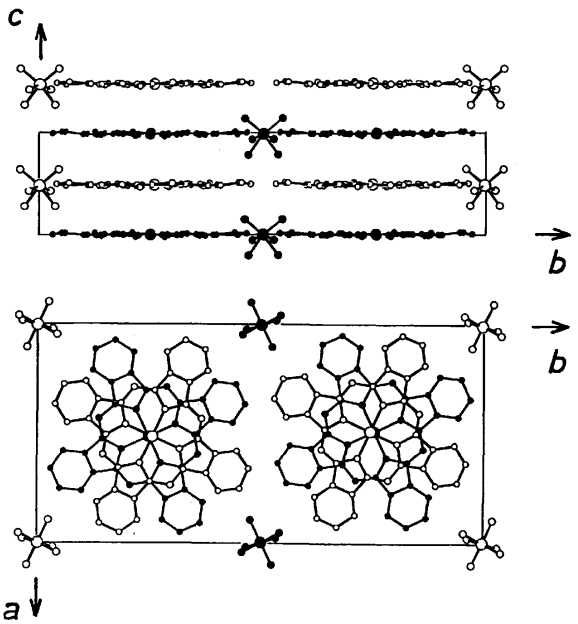

Fig. 9. Crystal structure of $NiPc(AsF_6)_{0.5}$. (a) Side view and (b) top view of NiPc columns.

those of the other types of crystals and of $NiPc(SbF_6)_{0.5}$. The anisotropic temperature factors and F_o-F_c data are deposited as Document No. 8856 at the office of the Editor of Bull. Chem. Soc. Jpn.

The electrical conductivities of the crystals of types C and F exhibited metallic behavior at least down to 200 K. The temperature dependence of the resistivity of these crystals was exactly the same with each other. Due to the resistivity jumps, the intrinsic electrical properties in the low temperature region could not be revealed.

The reflectance spectra of the crystals, C and F, were measured at room temperature. The spectrum of the type C crystal was shown in Fig. 10. These crystals exhibited a typical metallic reflection spectrum with a one-dimensional nature along the c-axis. The reflectivity curve around the plasma edge was analyzed by the use of Drude model. The plasma frequencies and the relaxation times were obtained to be 0.89 eV and 1×10^{-14} s for the type C crystal and 0.91 eV and 0.9×10^{-14} s for the type F crystal. The bandwidth of the tight binding band of these crystals were estimated to be 1.2 eV for both types. The $\perp c$ spectrum was drawn by a dotted line. The dispersions around 15000 cm^{-1} are the Q-band of the neutral NiPc. No significant difference was found between the spectra of the types C and F in the Q-band region. If we use the two-band model, the degree of oxidation at the Ni site of the type F is different from that of the type C. However, the plasma edge and the Q-band of the type C were almost exactly the same as those of the type F. This result is quite similar to the temperature independent property on the Q-band of $NiPc(SbF_6)_{0.5}$.

The crystal structure, electrical conductivity, and reflectance spectrum of $NiPc(AsF_6)_{0.5}$ are essentially the same as those of $NiPc(SbF_6)_{0.5}$. The temperature dependence of g-values and the linewidths of some $NiPc(AsF_6)_{0.5}$ quite resemble those of $NiPc(SbF_6)_{0.5}$, and $NiPc(SbF_6)_{0.5}$ is situated between the types D and E comparing the ESR property of $NiPc(SbF_6)_{0.5}$ with those of $NiPc(AsF_6)_{0.5}$ shown in Fig. 8. Thus, the magnetic

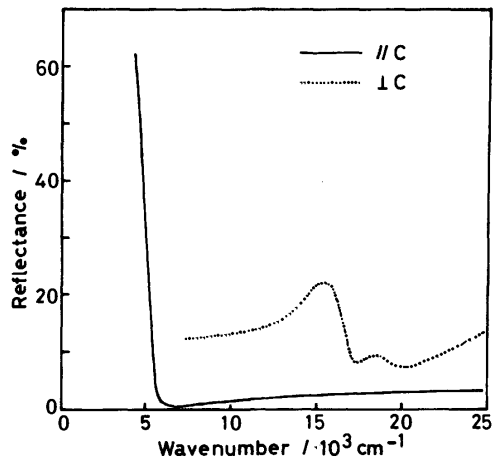

Fig. 10. Polarized reflectance spectrum of the single crystal of $NiPc(AsF_6)_{0.5}$.

properties of $NiPc(AsF_6)_{0.5}$ should be explained on the same basis as $NiPc(SbF_6)_{0.5}$. The spin susceptibilities of these types were divided into the contribution from the Ni chain, $\chi_{Ni}(T)$, and that from the Pc chain, $\chi_{Pc}(T)$, applying the same method as described before. The results are shown in the top panels od Fig. 8. As shown in these figures, $\chi_{Ni}(T)$ increases upon cooling like Curie law. Analyzing the temperature dependence of $\chi_{Ni}(T)$ by the use of the Curie law, the spin concentrations at the Ni site were estimated to be 2×10^{-4}, 3×10^{-3}, 4×10^{-3} spins per a NiPc for the types B, D, and E. These concentrations are reasonable for the localized spins at i.e. the defect sites. Furthermore, the chemical compositions, lattice parameters, electrical conductivities, and reflectance spectra of $NiPc(AsF_6)_{0.5}$ are sample independent. Therefore, these results support that the oxidation takes place mainly at the ligand site so that the conduction electrons are located on the ligand chain, from the same reason as the temperature independent bulk properties of $NiPc(SbF_6)_{0.5}$. Thus the sample dependence of the ESR properties of $NiPc(AsF_6)_{0.5}$ is understandable from the sample dependent concentration of the local spins at the Ni site. That is to say, the concentration of the local spins at the Ni site increases in order of A, B, C, D, E, and F, and the ESR property of the sample A is mostly reflecting the conduction electrons in the Pc chain. This interpretation is consistent with the fact that the behavior of $\chi(T)$ in the crystal A is qualitatively the same as those of $\chi_{Pc}(T)$ of other crystals, B, D, E, of $NiPc(AsF_6)_{0.5}$, and the concentration of the local spins increases from B to E. Unfortunately, the absolute value of the spin susceptibility of the type A crystal could not be obtained, since the number of crystals in this class was very small. The local spins on the lattice defect seem to be located not only at the Ni site but also at the ligand site. The local spins with narrow linewidth are characterized from the sharp rise at low temperature, and they are found in the crystals of types A and B as shown in the top panels of Figs. 8a and 8b. The broader linewidth of the type B crystal is probably attributed to the exchange interaction with the local spins at the Ni sites. We consider that the rise-up of the ESR intensity below 20 K in the crystals of the types A and B is probably related to the low concentration of the local spins at Ni site. When the concentration of the local spins at Ni sites becomes higher like the crystals of the types D and E, the ESR signal of the local spins at the ligand sites are probably hidden by the exchange interaction with the local spins at Ni sites through the conduction electrons on the ligand chain.

The magnetic properties of $NiPc(AsF_6)_{0.5}$ and $NiPc(SbF_6)_{0.5}$ are different from those of NiPcI, although the one-dimensional structure of the NiPc column is the same among them. This different property is connected with the higher degree of oxidation in $NiPc(AsF_6)_{0.5}$ and $NiPc(SbF_6)_{0.5}$ than in NiPcI, and also with the near orbital energy between the $3d_{z^2}$ orbital of the Ni atom and the HOMO (a_{1u}) of the ligand.[5] However, it is not clear at present why such a heavy sample dependence takes place only in the crystals of $NiPc(AsF_6)_{0.5}$, since the different point between $NiPc(AsF_6)_{0.5}$ and $NiPc(SbF_6)_{0.5}$ is only the anion size. If we adopt the model that the conduction electrons are located mainly on the Pc chain, the spin susceptibility on the Pc chain, $\chi_{Pc}(T)$, cannot be the Pauli paramagnetism, since $\chi_{Pc}(T)$ decreases upon the decrease of temperature. We consider that the number of conduction electrons decreases on lowering temperature due to the existence or growing-up of a narrow energy gap. The origin of this narrow gap is either the Peierls instability or the strong electron-electron Coulomb interaction. In the organic metals, the electron-electron Coulomb interaction is estimated from the enhancement of the spin susceptibility as compared with the Pauli paramagnetic susceptibility calculated from the transfer integrals which is obtained from the optical spectrum.[34] The spin susceptibility, $\chi_{Pc}(T)$, was roughly estimated from the flat region of $\chi_{Pc}(T)$. They are 8×10^{-5} emu mol^{-1} at room temperature for $NiPc(SbF_6)_{0.5}$ and $(5-7)\times10^{-5}$ emu mol^{-1} at room temperature for the crystals of types B, D, and E. The Pauli paramagnetic susceptibility (χ_{Pauli}) was calculated to be 5×10^{-5} emu mol^{-1} for all the crystals of $NiPc(AsF_6)_{0.5}$ and $NiPc(SbF_6)_{0.5}$. Therefore, the enhancement factor, $\chi_{s,obs}/\chi_{Pauli}$, is significantly smaller than the corresponding values, 3.0 for TTF-TCNQ and 3.3 for $TMTSF(PF_6)_{0.5}$.[34] Therefore, the Coulomb interaction on the Pc chain is considered to be weak, so that Peierls distortion may be one of the candidates for the energy gap.

The crystals of $NiPc(SbF_6)_{0.5}$ and $NiPc(AsF_6)_{0.5}$ belong to the orthorhombic system, wheres the crystals of NiPcI and $NiPc(ClO_4)_{0.39-0.47}$ to the tetragonal

system. This structural difference comes from the shape and the position of the counter anions. In the case of the NiPcI crystal, the periodicity of the linear I_3^- does not coincide with that of NiPc, so that the I_3^- is only ordered one-dimentionally along the stacking axis. The tetrahedral ClO_4^- is located at the interstitial position of the molecular layers of NiPc with the site occupancy of about 0.5. Therefore, in both crystals the counter anions are positionally disordered. On the other hand, the SbF_6^- and AsF_6^- are located at the same plane as the molecular layer of NiPc. This location of the anion brings about the two zigzag chains in the unit cell. Thus the unit cell contains two channels for accommodating the counter anions, so that these anions are three-dimensionally ordered. The difference of the periodic potential may affect the electronic conduction along the one-dimensional NiPc column at low temperature. According to Martinsen et al., the electrical conductivity of NiPcI exhibits an extrinsic peak around 20—30 K, and the Peierls instability is suppressed by the random potential.[8] From this viewpoint, it is interesting to examine the low temperature behavior of the electrical resistivity of $NiPc(SbF_6)_{0.5}$ and $NiPc(AsF_6)_{0.5}$. Unfortunately, the electrical conductivity of these material in the low temperature region is unidentified at present because of the occurrence of frequent resistivity jumps.

We acknowledge Professor Hiroki Haraguchi in the Chemistry Department of the University of Tokyo for conducting the ICP atomic emission spectroscopy. We thank Professor Akimasa Masuda, Dr. Hiroshi Shimizu, and Dr. Kazuya Takahashi in the Chemistry Department of the University of Tokyo for the assistance of the elementary analysis by the method of EPMA. We acknowledge Dr. Kosuke Ueyama, in Kuroda Solid Surface Project, in JRDC, for making a micro-diaphragm to eliminate the stray X-ray. This research was supported by the Ciba-Geigy Foundation for the Promotion of Science (Grant 104269 to K. Y.).

References

1) J. Martinsen, L. J. Pace, T. E. Phillips, B. M. Hoffman, and J. A. Ibers, *J. Am. Chem. Soc.*, **104**, 83 (1982).

2) C. J. Schramm, R. P. Scaringe, D. R. Stojakovic, B. M. Hoffman, J. A. Ibers, and T. J. Marks, *J. Am. Chem. Soc.*, **102**, 6702 (1980).

3) A. M. Schaffer, M. Gouterman, and E. R. Davidson, *Theor. Chim. Acta*, **30**, 9 (1973).

4) M.-H. Whangbo and K. R. Stewart, *Isr. J. Chem.*, **23**, 133 (1983).

5) F. W. Kutzler and D. E. Ellis, *J. Chem. Phys.*, **84**, 1033 (1986).

6) W. A. Little, *J. Phys. (Paris) Colloq.*, **1983**, C3-819.

7) T. E. Phillips, R. D. Scaringe, B. M. Hoffman, and J. A. Ibers, *J. Am. Chem. Soc.*, **102**, 3435 (1980).

8) J. Martinsen, S. M. Palmer, J. Tanaka, R. L. Greene, and B. M. Hoffman, *Phys. Rev. B*, **30**, 6269 (1984).

9) S. M. Palmer, J. L. Stanton, N. K. Jaggi, B. M. Hoffman, J. A. Ibers , and L. H. Schwartz, *Inorg. Chem.*, **24**, 2040 (1985).

10) J. Martinsen, J. L. Stanton, R. L. Greene, J. Tanaka, B. M. Hoffman, and J. A. Ibers, *J. Am. Chem. Soc.*, **107**, 6915 (1985).

11) T. Inabe, S. Nakamura, W. B. Liang, T. J. Marks, R. L. Burton, C. R. Kannewurf, and K. Imaeda, *J. Am. Chem. Soc.*, **107**, 7224 (1985).

12) T. Inabe, T. J. Marks, R. L. Burton, J. W. Lyding, W. J. McCarthy, C. R. Kannewurf, G. M. Reisner, and F. H. Herbstein, *Solid State Commun.*, **54**, 501 (1985).

13) M. Almeida, M. G. Kanatzidis, L. M. Tonge, T. J. Marks, H. O. Maracy, W. J. McCarthy, and C. R. Kannewurf, *Solid State Commun.*, **63**, 457 (1987).

14) M. Y. Ogawa, J. Martinsen, S. M. Palmer, J. L. Stanton, J. Tanaka, R. L. Greene, B. M. Hoffman, and J. A. Ibers, *J. Am. Chem. Soc.*, **109**, 1115 (1987).

15) K. Yakushi, M. Sakuda, H. Kuroda, A. Kawamoto, and J. Tanaka, *Chem. Lett.*, **1986**, 1161.

16) K. Yakushi, M. Sakuda, I. Hamada, H. Kuroda, A. Kawamoto, J. Tanaka, T. Sugano, and M, Kinoshita, *Synthetic Metals*, **19**, 769 (1987).

17) J. M. Assour and W. K. Kahn, *J. Am. Chem. Soc.*, **87**, 207 (1965).

18) H. Oyanagi, T. Matsushita, M. Ito, and H. Kuroda, *KEK Report*, **83**, 30 (1984).

19) K. Yakushi, M. Iguchi, and H. Kuroda, *Bull. Chem. Soc. Jpn.*, **52**, 3180 (1979).

20) A. P. Bobrovskii and A. N. Sidorov, *J. Struct. Chem. (Engl. Transl.)*, **17**, 50 (1976).

21) J. S. Griffith, *Discuss. Faraday Soc.*, **26**, 81 (1958).

22) Y. Tomkiewicz, A. R. Taranko, and J. B. Torrance, *Phys. Rev.*, **36**, 751 (1976).

23) J. E. Hahn, R. A. Scott, K. O. Hodgson, S. Doniach, S. R, Desjardins, and E. I. Solomon, *Chem. Phys. Lett.*, **88**, 595 (1982).

24) These results are probably attributable to the different orbital relaxation effects on the 1s to 3d excited states.

25) P. Turek, J.-J. Andre, A. Giraudeau, and J. Simon, *Chem. Phys. Lett.*, **134**, 471 (1987).

26) P. C. Minor, M. Gouterman, and A. B. P. Lever, *Inorg. Chem.*, **24**, 1894 (1985).

27) Y. Cao, K. Yakushi, and H. Kuroda, *Solid State Commun.*, **35**, 739 (1980).

28) Y. Cao, K. Yakushi, and H. Kuroda, *Solid State Commun.*, **35**, 601 (1980).

29) C. S. Jacobsen, D. B. Tanner, and K. Bechgaard, *Phys. Rev. B*, **28**, 7019 (1983).

30) K. Kikuchi, I. Ikemoto, K. Yakushi, H. Kuroda, and K. Kobayashi, *Solid State Commun.*, **42**, 433 (1982).

31) K. Kikuchi, K. Yakushi, H. Kuroda, I. Ikemoto, and K. Kobayashi, *Mol. Cryst. Liq. Cryst.*, **125**, 345 (1985).

32) R. P. Shibaeva, V. F. Kaminshii, and E. B. Yagubskii, *Mol. Cryst. Liq. Cryst.*, **119**, 361 (1985).

33) We revised the lattice constants and the space group of $NiPc(AsF_6)_{0.5}$, since the weak reflections (hkl) with $k=2n+1$ were missing in the data collection of the previous paper.

34) C. S. Jacobsen, *J. Phys. C*, **19**, 5643 (1986).

 © 1989 The Chemical Society of Japan Bull. Chem. Soc. Jpn., 62, 697—700 (1989)

The State of Polarization of Light Scattered by Anisotropic Spheroids

Yoh SANO
National Institute of Agrobiological Resources, Tsukuba Science City, Ibaraki 305
(Received September 12, 1988)

Using the light scattering theory of Rayleigh-Gans, theoretical expressions were derived for the state of polarization of light scattered by anisotropic spheroids in the case of linearly polarized incident light whose electric vector is inclined by ψ to the scattering plane. The azimuth of the ellipse of the light scattered is a function of the two scattering angles, θ and ψ, only and the scattered light is linearly polarized for linearly polarized incident light. The degree of polarization of the scattered light, which is defined as the ratio of the polarized component to the intensity of the scattered light, depends on the intrinsic anisotropy, p_m; the relative refractive index of the spheroid to the solvent, m, and θ, together with the ψ angle. The degree of polarization varies from 1.0 to 0, depending strongly on p_m, p, and m. It has been suggested that the determination of the degree of polarization as a function of ψ and θ provides good information about the optically intrinsic anisotropy of the spheroid.

For most proteins and nucleoproteins in water or dilute salt solutions, the anisotropy is too small to affect the angular distribution of light scattering. Only in the case of positively birefringent and anisometric particles is there likely to be any influence of the anisotropy on the angular distribution of light scattering.[1,2] Bovine serum albumin in a native state is known to be somewhat asymmetrical and to possess an intrinsic anisotropy.[3,4] The appreciable intrinsic anisotropy parameter of bovine serum albumin has been experimentally determined.[3]

The light scattered by optically anisotropic scatterers is partially polarized and contains some unpolarized component. In the cases of optically isotropic and anisometric particles[5,6] and also optically anisotropic spheres,[7] the state of polarization of scattered light has already been calculated on the basis of the Rayleigh[8]–Gans[9] theory, which will henceforth be referred to as the Rayleigh–Gans theory of spheroids (RGS theory) in order to avoid confusion with the well-known Rayleigh–Gans (RG) theory of scattering, which involves the restrictive assumption that the refractive index of the particle is close to that of the surrounding medium. However, to the author's knowledge, no theory exists for taking into consideration the optically anisotropic effect on the light scattered by spheroids.

In the present paper, the effect of the intrinsic optical anisotropy on the state of polarization of light scattered by spheroids such as bovine serum albumin is discussed on the basis of the RGS theory by examining a set of parameters: the degree of polarization, ellipticity, azimuth, and handedness of the ellipse of the polarized component of the scattered light.

Theory

General Consideration. Let us consider the light scattered by a small, optically anisotropic and spheroidal particle whose symmetrical center is situated in the center of the scattering cell. We will consider the effect of the anisotropy on the optical polarizability, that is, the intrinsic (structural) anisotropy. The intrinsic anisotropy occurs when the dispersed phase (the material composing the particle) itself has optical anisotropy.[10] If the dispersed spheroid is optically uniaxial, the excess polarizability, which is the difference between the polarizabilities of the particle and the medium, can be expressed by a spheroid, i.e., $(\alpha_a,\alpha_b,\alpha_b)$, while the optical anisotropy is given by this ratio:

$$p_g = \alpha_a/\alpha_b. \tag{1}$$

In the following discussion, it is reasonable to assume that the direction of the principal polarizability of the spheroid is in agreement with that of the symmetry a-axis of the spheroid.

If the principal refractive indices divided by the refractive index of the solvent n_0 are (m_a,m_b,m_b), the intrinsic (structural) anisotropy p_m is defined by:

$$p_m = (m_a^2 - 1)/(m_b^2 - 1), \tag{2}$$

and the mean relative refractive index m is defined by reference to the equation of the index ellipsoid:

$$1/(m^2 - 1) = [1/(m_a^2 - 1) + 2/(m_b^2 - 1)]/3. \tag{3}$$

Scattering Matrix. All possible states of scattered light can easily be analyzed by using the Stokes parameters and the Mueller or scattering matrix, which depends only on the characteristics of the scattering medium.

If the particle is sufficiently small compared to the wavelength of light, the scattering matrix $\boldsymbol{M}$ for a randomly oriented spheroid is given by the RGS theory with the help of the matrix element:[11]

$$\boldsymbol{M} = \begin{vmatrix} S_{11} & S_{12} & 0 & 0 \\ S_{12} & S_{22} & 0 & 0 \\ 0 & 0 & S_{33} & 0 \\ 0 & 0 & 0 & S_{44} \end{vmatrix}, \tag{4}$$

where the matrix elements, S_{11}, S_{12}, S_{22}, S_{33}, and S_{44}, are given for the optically anisotropic spheroid

$$\begin{aligned} S_{11} &= F_1(1 + \cos^2\theta) + F_2, \\ S_{12} &= F_1(\cos^2\theta - 1), \\ S_{22} &= F_1(\cos^2\theta + 1), \\ S_{33} &= 2F_1\cos\theta, \\ S_{44} &= 2(F_1 - F_2)\cos\theta, \end{aligned} \tag{5}$$

where:

$$\begin{aligned} F_1 &= F_0(p_g^2 + 3p_g + 7/2), \\ F_2 &= F_0(p_g - 1)^2, \\ F_0 &= (x^6/135p^4)\{(m^2 - 1)(1 + 2p_m)/ \\ &\quad [3p_m + (m^2 - 1)(1 + 2p_m)L_b]\}^2. \end{aligned} \tag{6}$$

The x is the size parameter defined by:

$$x = 2\pi a/\lambda, \tag{7}$$

where λ is the wavelength of light in the medium. The anisometry, i.e., the form anisotropy, is expressed by the axial ratio of the spheroid:

$$p = a/b, \tag{8}$$

while the shape parameter L_b in the b-direction is only a function of axial ratio p, as has been shown in a previous paper.[10]

A particle of isotropic material has the same relative refractive index m in all directions of an electric vector of light, independent of the particle form. Therefore, in the case of the anisometric particle made of the isotropic phase (p_m=1), we obtain:

$$\begin{aligned} F_1 &= (A^2 + 2AB/3 + 2B^2/15)/2, \\ F_2 &= 2B^2/15, \\ p_g &= 1 + B/A. \end{aligned} \tag{9}$$

These results agree with those obtained in a previous paper.[5] Here, A and B are functions of m, and the axial ratio p as defined by Eq. 15 in Ref. 5.

State of Polarization of the Scattered Light. The scattered light is, in general, partially polarized, and behaves as an incoherent sum of the polarized, I_p, and the unpolarized, I_u, components, which are defined in terms of time averages of the electric-field components of an electromagnetic wave. To give a complete description of a partially elliptically polarized beam of scattered light, we should state the intensities associated with both polarized and unpolarized components, and also give the full specifications of the polarization ellipse.

If we consider a linearly polarized incident light whose electric vector makes an angle ψ with the scattering plane, we can calculate each parameter of partially polarized scattered light with the help of the Stokes parameters and the scattering matrix as follows:

$$\begin{aligned} I_p &= I_p^\circ(1 - \cos^2\psi\sin^2\theta), \\ I &= I_p^\circ(1 - \cos^2\psi\sin^2\theta) + I_u, \\ I_p^\circ &= 2F_1,\ I_u = 2F_2, \\ \eta &= 0. \end{aligned} \tag{10}$$

The I_u term is contributed only by the F_2 term, showing the optical anisotropy analogously to the cases of an optically isotropic spheroid and an optically anisotropic sphere.

The ellipticity η of the polarized component of scattered light is always equal to 0, which means that the polarized component for an anisotropic spheroid is linearly polarized in the case of linearly polarized incident light.

The azimuth, ζ, of the linearly polarized component of the scattered light is given by:

$$\tan\zeta = \tan\psi/\cos\theta, \tag{11}$$

and is only a function of ψ and θ, it is independent of m, p, x, and p_m in the case of an anisotropic spheroid. The ζ has the same sign as ψ for the forward scattering ($0<\theta<90°$), while it has the opposite sign for the backward scatterig($90°<\theta<180°$).

The degree of polarization, P, defined as the ratio of the intensity of the polarized portion to the intensity, is given by Eq. 10:

$$\begin{aligned} P_\psi(\theta) &= (1 - \sin^2\theta\cos^2\psi)/[(1 - \sin^2\theta\cos^2\psi) + (F_2/F_1)], \\ F_2/F_1 &= (p_g - 1)^2/(p_g^2 + 3p_g + 7/2), \end{aligned} \tag{12}$$

and depends on p, p_m, m, θ, and ψ. In the case of isotropic spherical particles (p_m=1), the $P_\psi(\theta)$ is always equal to 1 over the entire range of θ. For an anisotropic sphere ($p_m \neq 1$, p=1) and an optically isotropic (p_m=1, $p \neq 1$) or anisotropic ($p_m \neq 1$, $p \neq 1$) spheroid, the $P_\psi(\theta)$ is smaller than 1.0, but it is independent of x, as far as RGS theory holds.

Numerical Results and Discussion

Variation of the Intensity of the Scattered Light. The numerical calculations were made with an ACOS 850/20 Computer at the Computer Center of the Ministry of Agriculture and Forestry. Figure 1 shows the variation in the intensities of the scattered light for the unpolarized component I_u and the maximum of the polarized component I_p° as a function of the intrinsic anisotropy p_m for m=1.20. The I_u depends strongly on the p_m value. Here, the quantity I is called the "intensity" of the scattered light, but it is a dimensionless quantity which is equal to the Rayleigh ratio

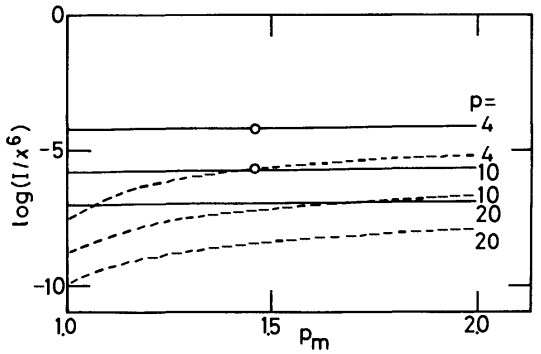

Fig. 1. Variation of $\log(I_u/x^6)$ (dotted lines) and $\log(I_p{}^\circ/x^6)$ (solid lines) with the intrinsic anisotropy $p_m>1$ for $m=1.20$. Open circles show bovine serum albumin molecule.

per particle multiplied by k^2 (where $k=2\pi/\lambda$) and is usually expressed by i.

Bovine serum albumin in a native state is a globular protein, and its overall molecular shape may be represented as a prolate spheroid whose major semiaxis and minor semiaxis are 7.1 and 1.7 nm respectively.[4] The intrinsic anisotropy parameter of bovine serum albumin is calculated to be $p_m=1.46$ with the refractive index increment and the scattering ratio at a scattering angle of 90°.[3] For such a spheroidal particle, it is reasonable to assume that the direction of the principal polarizability of the spheroid is in agreement with that of the symmetry a-axis of the spheroid; therefore, it is satisfactory to think of the case of $m_a>m_b$, i.e., the values of $p_m>1$, and also to think about the values of $p_m<2.0$.

Variation in the Degree of Polarization. The degree of polarization at $\theta=90°$, as given by Eq. 12, is:

$$P_\psi(90) = \sin^2\psi/(\sin^2\psi + F_2/F_1). \quad (13)$$

Figure 2 shows the variation in $P_\psi(90)$ with the intrinsic anisotropy p_m and ψ, especially in cases in which the ψ is from 1° to 20°.

Figure 3 shows the variation in $P_\psi(90)$ with $\pm\psi$. The $P_\psi(90)$ increases monotonously from 0 to almost 1 with the increase in $|\psi|$, its value becomes smaller, however, as the p_m deviates from the isotropic materials ($p_m=1$).

Determination of Parameter Values. The scattering ratio is defined by the ratio of the intensity scattered at $\theta=90°$ for the incident light vibrating perpendicular to and parallel to the plane of observation. The scattering ratio is of the same numerical value as the depolarization ratio, which is defined by the ratio of the intensity of the parallel component to the perpendicular component of the scattered light for an unpolarized incident beam, when the orientation of the particle is assumed to be completely random. However, the latter has an experimental disadvantage, for perfectly unpolarized incident light is rather difficult to obtain.

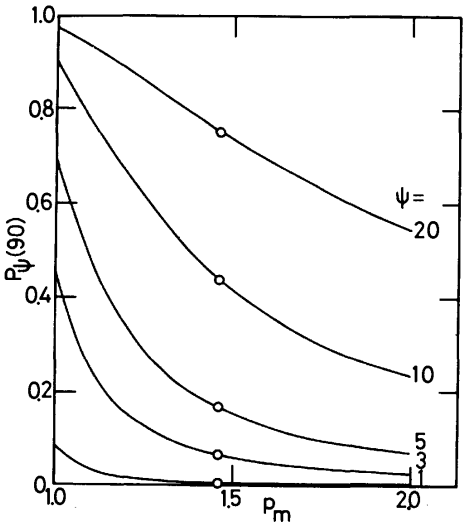

Fig. 2. Variation of the degree of polarization at $\theta=90°$, $P_\psi(90)$, with the intrinsic anisotropy $p_m>1$ and $m=1.20$ and $p=4$ for various values of ψ(degree). Open circles show bovine serum albumin molecule.

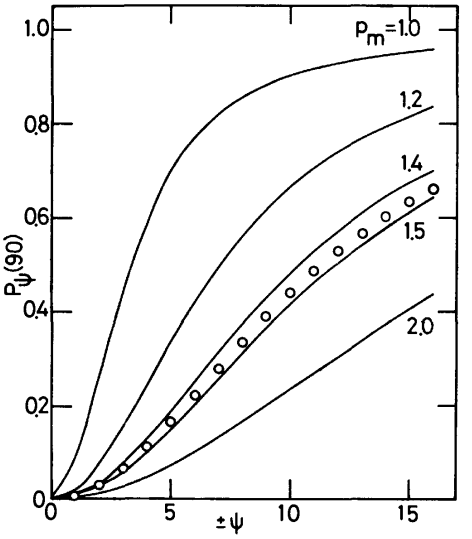

Fig. 3. Variation of the degree of polarization at $\theta=90°$, $P_\psi(90)$, with ψ(degree) and $m=1.20$ and $p=4$ for various values of $p_m>1$. Open circles show bovine serum albumin molecule.

The degree of polarization can also be measured by rotating the polarizer, similar to the case of the scattering ratio. Although only the two special cases of parallel to ($\psi=0$) and perpendicular to ($\psi=90°$) the scatterring plane are discussed in the case of the scattering ratio, the degree of polarization can be mainly used for small ψ values, as is shown in Figs. 2 and 3. The degree of polarization depends strongly on the intrinsic anisotropy p_m, and it is independent of x. If we measure the $P_\psi(90)$ value, the intrinsic (structual) anisotropy can be determined directly from the curvefitting method to the theoretical values.

Knowledge about p_m and m gives information regarding the refractive index of both the a- and b-axes of the spheroid if the refractive index of the solvent is known.

In conjunction with the knowledge of the intrinsic anisotropy p_m, the value of x is obtained from the intensities, I, I_p, and I_u, and the knowledge of x immediately gives information on the molecular weight if the partial specific volume is known.

The theory presented in this paper can be efficiently applied to relatively small p_m values, as is shown in Fig. 3.

This work was supported in part by a Grant-in-Aid (Bio Media Program) from the Ministry of Agriculture, Forestry, and Fisheries (BMP 89-IV-1-1).

References

1) P. Horn, H. Benoit, and G. Oster, *J. Chim. Phys.*, **48**, 550 (1951).
2) E. P. Geiduschek, *J. Polym. Sci.*, **13**, 408 (1953).
3) Y. Sano, *J. Colloid Interface Sci.*, **124**, 403 (1988).
4) M. Nakagaki and Y. Sano, *Bull. Chem. Soc. Jpn.*, **45**, 2100 (1972).
5) Y. Sano and M. Nakagaki, *J. Colloid Interface Sci.*, **105**, 348 (1985).
6) Y. Sano and M. Nakagaki, *Bull. Chem. Soc. Jpn.*, **59**, 3023 (1986).
7) Y. Sano, *Bull. Chem. Soc. Jpn.*, **61**, 3667 (1988).
8) L. Rayleigh, *Phil. Mag.*, **44**, 28 (1897).
9) R. Gans, *Ann. Phys. (Leipzig)*, **37**, 881 (1912); **62**, 331 (1920).
10) Y. Sano and M. Nakagaki, *J. Phys. Chem.*, **88**, 95 (1984).
11) H. C. Van de Hulst, "Light Scattering by Small Particles," Wiley, New York (1957).

 © 1989 The Chemical Society of Japan Bull. Chem. Soc. Jpn., 62, 701—708 (1989)

Parametrized Equations-of-Motion Method at the (1p-1h)+(2h-2p) Level and Its Application to Linear Polyenes

Tai-ichi SHIBUYA,* Tadashi FUNADA,# and Susumu NARITA
Department of Chemistry, Faculty of Textile Science and Technology,
Shinshu University, Ueda, Nagano-ken 386
(Received September 24, 1988)

The previously proposed idea of parametrizing the equations-of-motion method [*Int. J. Quantum Chem.*, **18**, 205 (1980)] has been worked out for the $\pi\rightarrow\pi^*$ transitions of linear polyenes. The excitation operator consists of not only 1p-1h creation and annihilation operators but also 2p-2h creation and annihilation operators. [*Bull. Chem. Soc. Jpn.*, **61**, 1103 (1988)]. The proposed scheme accounts for the effect of $\sigma\rightarrow\sigma^*$ mixings in contrast with the traditional pi-electron theories. In the present work, the two-center Coulomb integrals are evaluated by $1/R$, and all the one-center integrals on the C atom are assumed to be the same. Values of the three parameters (a, b, ζ) introduced in the scheme are so determined that the computed excitation energies of ethylene and *s-trans*-butadiene fit the observed values. The scheme has been applied to a series of all-s-trans linear polyenes through dodecahexaene. Some notable results are: (1) The $\sigma\rightarrow\sigma^*$ mixings play a significant role in lowering the excitation energies of the allowed transition to 1^1Bu; (2) the 2^1Ag state is of Ag^- type and almost free from this effect; (3) double excitations (2p-2h states) are dominant in the 2^1Ag state but practically negligible in the 1^1Bu state.

The basic idea of the equations-of-motion (EOM) method employed here is to find an excitation operator $O_\lambda^\dagger$ which creates an excited state $|\lambda>$ by its action on the ground state $|0>$:

$$|\lambda> = O_\lambda^\dagger |0> \qquad (\text{and } O_\lambda|0> = 0). \tag{1}$$

The operater $O_\lambda^\dagger$ is constructed as a linear combination of creation and annihilation operators of particle-hole pairs and their products. The coefficients of the linear combination are determined in such a way that the excitation operator $O_\lambda^\dagger$ satisfies an equation which is formally the same as the equation of motion for a boson creation operator:

$$[H, O_\lambda^\dagger]\,|0> = \omega_\lambda O_\lambda^\dagger|0>. \tag{2}$$

Certain molecular integrals appearing in the traditional configuration interaction (CI) calculations for the ground and excited states are eliminated in the EOM calculations because Eq. 2 is set up directly for the difference between the two states.[1]

In a previous publication,[2] we proposed a way to parametrize the EOM for the $\pi\rightarrow\pi^*$ transition in conjugated molecules. Emphasis was then laid on the treatment of the effect of $\sigma\rightarrow\sigma^*$ mixings. This effect, called the sigma-dynamical screening,[3] was expected to make a significant contribution to lowering of the singlet transition energies.[2-4] The traditional pi-electron theories like the PPP method do not explicitly account for this type fo sigma-electron screenings. In the PPP calculations on conjugated hydrocarbons, the one-center integral γ_{00} is set equal to 11 eV instead of 17 eV as evaluated by the Slater 2p orbital with the effective nuclear charge Z^*=3.18.[5] The discrepancy was analyzed by Orloff and Sinanoglu[6] from the view point of sigma-pi electron correlations.

The proposed semiempirical scheme is constructed on the EOM initially written for the STO-basis "Hartree-Fock" orbitals. In the final form of the scheme, however, the SCF orbitals are computed only for pi-orbitals; sigma-electrons are assumed to be localized in separate bonds (C-C and C-H). Excitation energies for $\sigma\rightarrow\sigma^*$ are all set equal to an adjustable parameter a which is expected to be around 1. Hereafter, Hartree's atomic units are employed unless otherwise specified. The one-center integrals needed in this scheme are all for the 2p orbitals of the C atom and set equal to one parameter $\gamma_{00}=(93/256)\zeta$ whose value is expected to be around 0.6 (i.e. 17 eV) (or ζ=1.6) as evaluated from the Slater orbitals. The two-center integrals γ_{pq} are all set equal to $1/R_{pq}$ which is the leading term in the expansion of γ_{pq} when the Slater orbitals are used. The resonance integrals β_{pq} are set to be $-bS_{pq}/R_{pq}$, where S_{pq} are the overlap integrals evaluated with the Slater orbitals, and b is an adjustable parameter which is expected to be around 1. Values of these parameters (a, b, ζ) are determined in such a way that the calculated transition energies fit the observed values for the N→T, V transitions of ethylene and butadiene.

Low-lying excited states of conjugated molecules are usually well described as linear combinations of singly excited configurations. However, the 2^1Ag state of linear polyenes is the well-known exception where doubly excited configurations are thought to be more important.[7] Thus, in the present study, we employ the (1p-1h) plus (2p-2h) EOM[8] which may also be termed as the 2nd higher RPA.[1b] The proposed scheme is applied to all-trans linear polyenes through dodecahexaene.

The EOM method employed in the present work is closely related to the propagator methods. A recent review article[9] gives ample references on these methods.

Present address: Yashiro High School, Koshoku, Nagano-ken 387.

1. Summary of the (1p-1h)+(2p-2h) EOM[8]

The following form is assumed for the excitation operator:

$$O^{\dagger}(\lambda SM) = \sum_{m\gamma}\{Y_{m\gamma}(\lambda S)C_{m\gamma}^{\dagger}(SM) - Z_{m\gamma}(\lambda S)C_{m\gamma}(\overline{SM})\} + \sum_{(m\gamma,n\delta)}\{Y^{(2)}_{(m\gamma,n\delta)}(\lambda S)\Gamma_{(m\gamma,n\delta)}^{\dagger}(SM) - Z^{(2)}_{(m\gamma,n\delta)}(\lambda S)\Gamma_{(m\gamma,n\delta)}(\overline{SM})\}. \quad (3)$$

In this expression, $C_{m\gamma}^{\dagger}(SM)$ and $C_{m\gamma}(\overline{SM})$ are the creation and annihilation operator of particle-hole (1p-1h) pairs (m, γ),[1a] and $\Gamma_{(m\gamma,n\delta)}^{\dagger}(SM)$ and $\Gamma_{(m\gamma,n\delta)}(\overline{SM})$ are the creation and annihilation operators of 2p-2h states $(m\gamma, n\delta)$.[1b,8] They produce excited states with spin symmetry (S, M) by their action on the closed-shell ground state $|0\rangle$. Hereafter, m and n refer to unoccupied (particle state) orbitals, and γ and δ to occupied (hole state) orbitals. They are assumed to be the Hartree-Fock (HF) orbitals. The $\Gamma_{(m\gamma,n\delta)}^{\dagger}$ listed in Table 1 are "orthonormal" in a sense that the 2p-2h states created by these operators acting on the Hartree-Fock ground state $|HF\rangle$ are orthonormal.

With this excitation operator $O^{\dagger}(\lambda)$, Eq. 2 approximately leads[8] to

$$\begin{bmatrix} \mathscr{A} & \mathscr{B} & \mathscr{A}^{\circ(1,2)} & 0 \\ -\mathscr{B} & -\mathscr{A} & 0 & -\mathscr{A}^{\circ(1,2)} \\ \mathscr{A}^{\circ(2,1)} & 0 & A^{\circ(2,2)} & 0 \\ 0 & -\mathscr{A}^{\circ(2,1)} & 0 & -A^{\circ(2,2)} \end{bmatrix} \begin{bmatrix} \mathscr{Y} \\ \mathscr{Z} \\ Y^{(2)} \\ Z^{(2)} \end{bmatrix} = \omega \begin{bmatrix} \mathscr{Y} \\ \mathscr{Z} \\ Y^{(2)} \\ Z^{(2)} \end{bmatrix}. \quad (4)$$

In this matrix equation,

$$\mathscr{Y}_{m\gamma} = g_{m\gamma}Y_{m\gamma};\ \mathscr{Z}_{m\gamma} = g_{m\gamma}Z_{m\gamma}, \quad (5)$$

$$g_{m\gamma} = (1 + \rho_{\gamma\gamma} - \rho_{mm})^{1/2}, \quad (6)$$

$$\mathscr{A}_{m\gamma,n\delta}(S) = \delta_{mn}\delta_{\gamma\delta}(\varepsilon_m - \varepsilon_\gamma) + \{-[(mn\,|\,\gamma\delta) + \delta_{mn}T_{\gamma\delta} - \delta_{\gamma\delta}T_{mn}] + (\delta_{S0})2(m\gamma\,|\,n\delta)\}/(g_{m\gamma}g_{n\delta}), \quad (7a)$$

$$\mathscr{B}_{m\gamma,n\delta}(S) = \{-(-1)^S[(m\delta\,|\,n\gamma) - S_{m\gamma,n\delta}] + (\delta_{S0})2(m\gamma\,|\,n\delta)\}/(g_{m\gamma}g_{n\delta}), \quad (7b)$$

$$S_{m\gamma,n\delta} = -\sum_{p\mu}[(m\delta\,|\,p\mu)C_{p\mu,n\gamma}(0) + (n\gamma\,|\,p\mu)C_{p\mu,m\delta}(0)], \quad (8a)$$

$$T_{mn} = (1/2)\sum_{\nu}S_{m\nu,n\nu};\ T_{\gamma\delta} = -(1/2)\sum_{p}S_{p\gamma,p\delta}, \quad (8b)$$

$$\rho_{mn} = (1/2)\sum_{p\mu\nu}\sum_{S=0,1}C'_{mv,p\mu}(S)C_{nv,p\mu}(S), \quad (9a)$$

$$\rho_{\gamma\delta} = -(1/2)\sum_{pq\mu}\sum_{S=0,1}C'_{q\gamma,p\mu}(S)C_{q\delta,p\mu}(S), \quad (9b)$$

where

$$C'(0) = [3C(0) + C(1)]/4;\ C'(1) = [C(0) + 3C(1)]/4 \quad (10)$$

and

$$C_{m\gamma,n\delta}(S) = -[-(-1)^S(m\delta\,|\,n\gamma) + (\delta_{S0})2(m\gamma\,|\,n\delta)]/(\varepsilon_m + \varepsilon_n - \varepsilon_\gamma - \varepsilon_\delta). \quad (11)$$

Hereafter, p and q refer to unoccupied orbitals and μ and ν to occupied orbitals. In these expressions, ε_k is the HF orbital energy and $(ij|kl)$ is the two-electron molecular integral:

$$(ij\,|\,kl) = \int[i(1)j(1)](1/r_{12})[k(2)l(2)]\,d\upsilon_1 d\upsilon_2. \quad (12)$$

In Eq. 4,

$$\mathscr{A}^{\circ(2,1)} = \tilde{\mathscr{A}}^{\circ(1,2)}, \quad (13a)$$

$$\mathscr{A}^{\circ(1,2)}{}_{m'\gamma':(m\gamma,n\delta)}(S) = A^{\circ(1,2)}{}_{m'\gamma':(m\gamma,n\delta)}(S)/g_{m'\gamma'}, \quad (13b)$$

Table 1. The "Orthonormal" 2p-2h Creation Operators $\Gamma_{(m\gamma,n\delta)}^{\dagger}(SM)$

$S=M=0$	
$\Gamma_{(m\gamma,m\gamma)}^{\dagger} = C_{m\gamma}^{\dagger}(00)C_{m\gamma}^{\dagger}(00)$	
$\Gamma_{(m\gamma,n\gamma)}^{\dagger} = \sqrt{2}C_{m\gamma}^{\dagger}(00)C_{n\gamma}^{\dagger}(00)$	$(m\neq n)$
$\Gamma_{(m\gamma,m\delta)}^{\dagger} = \sqrt{2}C_{m\gamma}^{\dagger}(00)C_{m\delta}^{\dagger}(00)$	$(\gamma\neq\delta)$
$\Gamma_{(m\gamma,n\delta)_1}^{\dagger} = C_{m\gamma}^{\dagger}(00)C_{n\delta}^{\dagger}(00) + C_{m\delta}^{\dagger}(00)C_{n\gamma}^{\dagger}(00)$	$(m\neq n, \gamma\neq\delta)$
$\Gamma_{(m\gamma,n\delta)_2}^{\dagger} = (1/\sqrt{3})[C_{m\gamma}^{\dagger}(00)C_{n\delta}^{\dagger}(00) - C_{m\delta}^{\dagger}(00)C_{n\gamma}^{\dagger}(00)]$	$(m\neq n, \gamma\neq\delta)$
$S=1, M=0$	
$\Gamma_{(m\gamma,n\gamma)}^{\dagger} = (1/\sqrt{2})[C_{m\gamma}^{\dagger}(10)C_{n\gamma}^{\dagger}(00) - C_{n\gamma}^{\dagger}(10)C_{m\gamma}^{\dagger}(00)]$	$(m\neq n)$
$\Gamma_{(m\gamma,m\delta)}^{\dagger} = (1/\sqrt{2})[C_{m\gamma}^{\dagger}(10)C_{m\delta}^{\dagger}(00) - C_{m\delta}^{\dagger}(10)C_{m\gamma}^{\dagger}(00)]$	$(\gamma\neq\delta)$
$\Gamma_{(m\gamma,n\delta)_1}^{\dagger} = (1/2)[C_{m\gamma}^{\dagger}(10)C_{n\delta}^{\dagger}(00) - C_{n\delta}^{\dagger}(10)C_{m\gamma}^{\dagger}(00)] + [C_{m\delta}^{\dagger}(10)C_{n\gamma}^{\dagger}(00) - C_{n\gamma}^{\dagger}(10)C_{m\delta}^{\dagger}(00)]$	$(m\neq n, \gamma\neq\delta)$
$\Gamma_{(m\gamma,n\delta)_2}^{\dagger} = (1/2)[C_{m\gamma}^{\dagger}(10)C_{n\delta}^{\dagger}(00) - C_{n\delta}^{\dagger}(10)C_{m\gamma}^{\dagger}(00) - C_{m\delta}^{\dagger}(10)C_{n\gamma}^{\dagger}(00) + C_{n\gamma}^{\dagger}(10)C_{m\delta}^{\dagger}(00)]$	$(m\neq n, \gamma\neq\delta)$
$\Gamma_{(m\gamma,n\delta)_3}^{\dagger} = (1/\sqrt{2})[C_{m\gamma}^{\dagger}(10)C_{n\delta}^{\dagger}(00) + C_{n\delta}^{\dagger}(10)C_{m\gamma}^{\dagger}(00)]$	$(m\neq n, \gamma\neq\delta)$

and $A^{\circ(1,2)}$ and $A^{\circ(2,2)}$ are defined by

$$A^{\circ(1,2)}{}_{m'\gamma':(m\gamma,n\delta)}(S) \equiv <HF|[C_{m'\gamma'}(S0), H, \Gamma_{(m\gamma,n\delta)}{}^{\dagger}(S0)]|HF>, \tag{14a}$$

$$A^{\circ(2,2)}{}_{(m'\gamma',n'\delta'):(m\gamma,n\delta)}(S) \equiv <HF|[\Gamma_{(m'\gamma',n'\delta')}(S0), H, \Gamma_{(m\gamma,n\delta)}{}^{\dagger}(S0)]|HF>, \tag{14b}$$

where $|HF>$ is the HF ground state (i.e. the noncorrelated part of $|0>$.) Referring to Table 1, we can readily obtain these elements from their primitive ones

$$\begin{aligned} A^{\circ(1,2)}{}_{m'\gamma':m\gamma,n\delta}(S) &\equiv <HF|[C_{m'\gamma'}(S0), H, C_{m\gamma}{}^{+}(S0)C_{n\delta}{}^{+}(00)]|HF> \\ &= \sqrt{2}\{\delta_{\gamma\gamma'}[(mm'|n\delta) - (nm'|m\delta)/2] \\ &+ \delta_{\delta\gamma'}[\delta_{s0}(nm'|m\gamma) - (mm'|n\gamma)/2] \\ &- \delta_{mm'}[(\gamma\gamma'|n\delta) - (\delta\gamma'|n\gamma)/2] \\ &-\delta_{nm'}[\delta_{s0}(\delta\gamma'|m\gamma) - (\gamma\gamma'|m\delta)/2]\}; \end{aligned} \tag{15}$$

$$\begin{aligned} A^{\circ(2,2)}{}_{m'\gamma',n'\delta':m\gamma,n\delta}(S) &\equiv <HF|[(C_{m'\gamma'}{}^{+}(S0)C_{n'\delta'}{}^{+}(00))^{\dagger}, \\ &\qquad H, C_{m\gamma}{}^{+}(S0)C_{n\delta}{}^{+}(00)]|HF> \\ &= \{(\varepsilon_m + \varepsilon_n - \varepsilon_\gamma - \varepsilon_\delta)[(\delta_{mm'}\delta_{nn'}\delta_{\gamma\gamma'}\delta_{\delta\delta'} \\ &- \delta_{mm'}\delta_{nn'}\delta_{\delta\gamma'}\delta_{\gamma\delta'}/2 - \delta_{nm'}\delta_{mn'}\delta_{\gamma\gamma'}\delta_{\delta\delta'}/2) \\ &+ (\delta_{s0})\delta_{nm'}\delta_{mn'}\delta_{\delta\gamma'}\delta_{\gamma\delta'}] \\ &+ (\delta_{mm'}\delta_{nn'} - \delta_{nm'}\delta_{mn'}/2)(\gamma\gamma'|\delta\delta') \\ &+ ((\delta_{s0})\delta_{nm'}\delta_{mn'} - \delta_{mm'}\delta_{nn'}/2)(\delta\gamma'|\gamma\delta') \\ &+ (\delta_{\gamma\gamma'}\delta_{\delta\delta'} - \delta_{\delta\gamma'}\delta_{\gamma\delta'}/2)(mm'|nn') \\ &+ ((\delta_{s0})\delta_{\delta\gamma'}\delta_{\gamma\delta'} - \delta_{\gamma\gamma'}\delta_{\delta\delta'}/2)(mn'|nm')\} \\ &+ \{[\delta_{mm'}\delta_{\gamma\gamma'}2(n'\delta'|n\delta) - (\delta_{mm'}\delta_{\gamma\delta'}(n'\gamma'|n\delta) \\ &+ \delta_{mn'}\delta_{\gamma\gamma'}(m'\delta'|n\delta) + \delta_{nm'}\delta_{\gamma\gamma'}(n'\delta'|m\delta) \\ &+ \delta_{mm'}\delta_{\delta\gamma'}(n'\delta'|n\gamma)) + (1/2)(\delta_{mm'}\delta_{\delta\delta'}(n'\gamma'|n\gamma) \\ &+ \delta_{nn'}\delta_{\delta\gamma'}(m'\delta'|m\delta) + \delta_{nm'}\delta_{\gamma\delta'}(n'\gamma'|m\delta) \\ &+ \delta_{mn'}\delta_{\delta\gamma'}(m'\delta'|n\gamma))] + (\delta_{s0})[2(\delta_{nm'}\delta_{\delta\gamma'}(n'\delta'|m\gamma) \\ &+ \delta_{mn'}\delta_{\gamma\delta'}(m'\gamma'|n\delta) + \delta_{nn'}\delta_{\delta\delta'}(m'\gamma'|m\gamma)) \\ &- (\delta_{nn'}\delta_{\delta\gamma'}(m'\delta'|m\gamma) + \delta_{nm'}\delta_{\delta\delta'}(n'\gamma'|m\gamma) \\ &+ \delta_{mn'}\delta_{\delta\delta'}(m'\gamma'|n\gamma) + \delta_{nn'}\delta_{\gamma\delta'}(m'\gamma'|m\delta))]\} \\ &+ \{[- (\delta_{mm'}\delta_{\delta\delta'}(nn'|\gamma\gamma') + \delta_{nn'}\delta_{\gamma\gamma'}(mm'|\delta\delta') \\ &+ \delta_{mm'}\delta_{\gamma\gamma'}(nn'|\delta\delta') + \delta_{nn'}\delta_{\delta\delta'}(mm'|\gamma\gamma')) \\ &+ (1/2)(\delta_{mm'}\delta_{\gamma\delta'}(nn'|\delta\gamma') + (\delta_{mn'}\delta_{\gamma\gamma'}(nm'|\delta\delta') \\ &+ \delta_{nm'}\delta_{\gamma\gamma'}(mn'|\delta\delta') + \delta_{mm'}\delta_{\delta\gamma'}(nn'|\gamma\delta') \\ &+ \delta_{nn'}\delta_{\delta\gamma'}(mm'|\gamma\delta') + \delta_{nm'}\delta_{\delta\delta'}(mn'|\gamma\gamma') \\ &+ \delta_{mn'}\delta_{\delta\delta'}(nm'|\gamma\gamma') + \delta_{nn'}\delta_{\gamma\delta'}(mm'|\delta\gamma'))] \\ &+ (\delta_{s0})[- (\delta_{nm'}\delta_{\gamma\delta'}(mn'|\delta\gamma') + \delta_{mn'}\delta_{\delta\gamma'}(nm'|\gamma\delta') \\ &+ \delta_{nm'}\delta_{\delta\gamma'}(mn'|\gamma\delta') + \delta_{mn'}\delta_{\gamma\delta'}(nm'|\delta\gamma'))]\}. \end{aligned} \tag{16}$$

In solving Eq. 4, we split it into two equations. By doing so, the order of the matrix to be diagonalized is reduced to half. They are written as follows:

$$\begin{bmatrix} \mathscr{A} - \mathscr{B} & \mathscr{A}^{\circ(1,2)} \\ \mathscr{A}^{\circ(2,1)} & A^{\circ(2,2)} \end{bmatrix} \begin{bmatrix} \mathscr{A} + \mathscr{B} & \mathscr{A}^{\circ(1,2)} \\ \mathscr{A}^{\circ(2,1)} & A^{\circ(2,2)} \end{bmatrix} \begin{bmatrix} \mathscr{Y} + \mathscr{X} \\ Y^{(2)} + Z^{(2)} \end{bmatrix} = \omega^2 \begin{bmatrix} \mathscr{Y} + \mathscr{X} \\ Y^{(2)} + Z^{(2)} \end{bmatrix}; \tag{17a}$$

$$\begin{bmatrix} \mathscr{A} + \mathscr{B} & A^{\circ(1,2)} \\ \mathscr{A}^{\circ(2,1)} & A^{\circ(2,2)} \end{bmatrix} \begin{bmatrix} \mathscr{A} - \mathscr{B} & A^{\circ(1,2)} \\ \mathscr{A}^{\circ(2,1)} & A^{\circ(2,2)} \end{bmatrix} \begin{bmatrix} \mathscr{Y} - \mathscr{X} \\ Y^{(2)} - Z^{(2)} \end{bmatrix} = \omega^2 \begin{bmatrix} \mathscr{Y} - \mathscr{X} \\ Y^{(2)} - Z^{(2)} \end{bmatrix}. \tag{17b}$$

Note that the eigenvalues in these equations are ω^2.

The transition dipole moment is given by

$$\boldsymbol{D}_\lambda \equiv - <0|(\boldsymbol{r})_{op}|\lambda> = (\delta_{s0})\sqrt{2}\Sigma_{m\gamma}\{\mathscr{Y}_{m\gamma}(\lambda 0) + \mathscr{X}_{m\gamma}(\lambda 0)\}(g_{m\gamma}\boldsymbol{d}^{\circ}{}_{m\gamma}), \tag{18}$$

where

$$\boldsymbol{d}^{\circ}{}_{m\gamma} \equiv \int m(r)\boldsymbol{r}\gamma(r)\mathrm{d}^3r. \tag{19}$$

Note that terms of $Y^{(2)}$ and $Z^{(2)}$ vanish in deriving the last expression of Eq. 18.[8] The oscillator strength is written

$$f_\lambda = (2/3)\omega_\lambda|\boldsymbol{D}_\lambda|^2. \tag{20}$$

It is important to note that the result in Eq. 18 has been derived on the assumption of the normalization condition $<\lambda|\lambda>=1$ or equivalently

$$\Sigma_{m\gamma}\{|\mathscr{Y}_{m\gamma}(\lambda S)|^2 - |\mathscr{X}_{m\gamma}(\lambda S)|^2\} + \Sigma_{(m\gamma,n\delta)}\{|Y^{(2)}{}_{(m\gamma,n\delta)}(\lambda S)|^2 - |Z^{(2)}{}_{(m\gamma,n\delta)}(\lambda S)|^2\} = 1. \tag{21}$$

Thus, $\boldsymbol{D}_\lambda$ is indirectly affected by $Y^{(2)}$ and $Z^{(2)}$ through this normalization condition. Normalization of the eigenvectors of the reduced Eqs. 17a,b must be handled with great care so that they satisfy Eq. 21.[10]

2. Effective EOM for the $\pi \rightarrow \pi^*$ Transitions

Previously[2,3] an effective EOM for the $\pi \rightarrow \pi^*$ transitions was derived by partitioning the (1p-1h) EOM into the $\Pi \equiv (\pi^*, \pi)$ and $\Sigma \equiv (\sigma^*, \sigma)$ parts. The assumption of the zero differential overlaps between pi- and sigma-orbitals leads[4] to

$$\mathscr{A}_{\sigma^*\sigma,\pi^*\pi}(S) = \mathscr{B}_{\sigma^*\sigma,\pi^*\pi}(S) = (\delta_{s0})2(\sigma^*\sigma|\pi^*\pi)/(g_{\sigma^*\sigma}g_{\pi^*\pi}). \tag{22}$$

We shall later let $g_{\sigma^*\sigma}=1$. It was then shown[2] that the effect of the Σ part on the EOM for the Π part was to reduce the integral $(m\gamma|n\delta)$ in $\mathscr{A}$ and $\mathscr{B}$, Eq. 7, as follows:

$$(m\gamma|n\delta) \rightarrow (m\gamma|n\delta)'' = (m\gamma|n\delta) - \frac{a}{a^2 - \omega_\lambda{}^2} G_{m\gamma,n\delta}, \tag{23}$$

where

$$G_{m\gamma,n\delta} = 4\Sigma_{\sigma^*\sigma}(m\gamma|\sigma^*\sigma)(n\delta|\sigma^*\sigma). \tag{24}$$

Henceforth, m and n refer to the π^*-orbitals, and γ and

δ to the π-orbitals. In deriving Eq. 23, we have set all the diagonal elements $\mathscr{A}_{\sigma^*\sigma,\sigma^*\sigma}$ equal to one adjustable parameter a which is expected to be around 1 (in Hartree a.u.). In order to calculate G in Eq. 24, we construct sigma-orbitals by linear combinations of sp^2 hybrids for carbon and 1s orbitals for hydrogen. Employing the approximation of complete neglect of differential overlaps between sigma-AO's and the approximation that all the charge densities of sigma-AO's be 1 and the bond orders be 1 for bonded sigma-AO's and 0 otherwise, we have

$$G_{m\gamma,n\delta} = \sum_{\eta}^{\text{sigma-bonds}} [m\gamma|\eta][n\delta|\eta], \tag{25}$$

where, for a sigma-bond (η) formed by sigma-AO's u and v,

$$[m\gamma|\eta][n\delta|\eta] \equiv [(m\gamma|uu) - (m\gamma|vv)][(n\delta|uu) - (n\delta|vv)]. \tag{26}$$

In dealing with the 2p-2h states, we shall consider only those of pi-electrons and ignore any 2p-2h states in which sigma-electrons are involved. Then, our effective EOM for pi-electrons takes the same form as Eq. 4 or 17 with m and n referring to the π^*-orbitals and γ and δ to the π-orbitals. Only the difference is that the integral $(m\gamma|n\delta)$ in Eq. 7 should be replaced by $(m\gamma|n\delta)''$ given in Eq. 23. In computing the S, T, and ρ in Eqs. 8a—9b, however, note that the summations of p and q run over both π^* and σ^*, and the summations of μ and ν run over both π and σ. Therefore, if these summations are restricted to running over only π- and π^*-orbitals in the effective EOM for the $\pi\rightarrow\pi^*$ transitions, one must add to these S, T, and ρ the following correction terms S', T', and ρ', respectively, due to correlations with sigma-electrons. As is shown in Appendix A, they are written as

$$S'_{m\gamma,n\delta} = (1/2)[(a + \varepsilon_m - \varepsilon_\delta)^{-1} + (a + \varepsilon_n - \varepsilon_\gamma)^{-1}]G_{m\delta,n\gamma}, \tag{27}$$

$$T'_{mn} = (1/2)\sum_{\pi} S'_{m\pi,n\pi}; T'_{\gamma\delta} = -(1/2)\sum_{\pi^*} S'_{\pi^*\gamma,\pi^*\delta}, \tag{28}$$

$$\rho'_{mm} = (1/2)\sum_{\pi} G_{m\pi,m\pi}/(a + \varepsilon_m - \varepsilon_\pi)^2; \tag{29a}$$

$$\rho'_{\gamma\gamma} = -(1/2)\sum_{\pi^*} G_{\pi^*\gamma,\pi^*\gamma}/(a + \varepsilon_{\pi^*} - \varepsilon_\gamma)^2. \tag{29b}$$

When Eq. 4 or 17, with the replacement of Eq. 23, is solved for pi-electrons, the normalization condition in Eq. 21 is satisfied for the amplitudes of pi-electrons. Then, the norm $\langle\lambda|\lambda\rangle$ becomes greater than 1 due to contributions from the amplitudes of sigma-electrons. As is shown in Appendix B, we have

$$N_\lambda^2 \equiv \langle\lambda|\lambda\rangle \cong 1 + (\delta_{s0})\frac{4a\omega_\lambda}{(a^2 - \omega_\lambda^2)^2}\sum_{\pi_1^*\pi_1}\sum_{\pi_2^*\pi_2}(G_{\pi_1^*\pi_1,\pi_2^*\pi_2}/[g_{\pi_1^*\pi_1}g_{\pi_2^*\pi_2}]) \times \{\mathscr{Y}_{\pi_1^*\pi_1}(\lambda) + \mathscr{X}_{\pi_1^*\pi_1}(\lambda)\}\{\mathscr{Y}_{\pi_2^*\pi_2}(\lambda) + \mathscr{X}_{\pi_2^*\pi_2}(\lambda)\}. \tag{30}$$

Thus, the transition dipole moment in Eq. 18 should be written as

$$\boldsymbol{D}_\lambda = (\delta_{s0})N_\lambda^{-1}\sqrt{2}\sum_{m\gamma}\{\mathscr{Y}_{m\gamma}(\lambda 0) + \mathscr{X}_{m\gamma}(\lambda 0)\}(g_{m\gamma}\boldsymbol{d}^{\circ}_{m\gamma}). \tag{31}$$

3. Parametrization

A parameter a has been already introduced as an averaged energy for the $\sigma\rightarrow\sigma^*$ excitations. In evaluating the two-electron integrals, we have been employing the zero-differential overlap (ZDO) approximation. For these integrals, we only have the following types:

$$(ij|kl) = \sum_p C^{(i)}{}_p C^{(j)}{}_p C^{(k)}{}_p C^{(l)}{}_p \gamma_{pp} + \sum_p \sum_{(q\neq p)} \sum_q C^{(i)}{}_p C^{(j)}{}_p C^{(k)}{}_q C^{(l)}{}_q \gamma_{pq}; \tag{32a}$$

$$(ij|u_q u_q) = C^{(i)}{}_q C^{(j)}{}_q \gamma'_{qu_q} + \sum_{p(\neq q)} C^{(i)}{}_p C^{(j)}{}_p \gamma'_{pu_q}, \tag{32b}$$

where i, j, k, and l refer to π and/or π^* MO's and u_q is a sigma-AO at atom q. The coefficients $C^{(k)}{}_p$ are of the SCF pi-MO k. We set

$$\gamma_{pp} = \gamma'_{pu_p} = \gamma_{00} \equiv (93/256)\zeta; \tag{33a}$$

$$\gamma_{pq} = \gamma'_{pu_q} = 1/R_{pq} \quad (p \neq q), \tag{33b}$$

where R_{pq} is the distance between atoms p and q.

Now, the SCF-MO's for pi-electrons are obtained according to the usual procedure.[11] The coefficients of the LCAO-MO's and the orbital energies satisfy the equations

$$\sum_s F_{rs} C^{(i)}{}_s = \varepsilon_i C^{(i)}{}_r, \tag{34}$$

where the Fock matrix elements are, in the ZDO approximation,

$$F_{rr} = H_{rr} + (1/2)P_{rr}\gamma_{rr} + \sum_{s(\neq r)} P_{ss}\gamma_{rs}; \tag{35a}$$

$$F_{rs} = H_{rs} - (1/2)P_{rs}\gamma_{rs} \quad (r \neq s), \tag{35b}$$

and

$$P_{rs} \equiv 2\sum_i^{occ} C^{(i)}{}_r C^{(i)}{}_s. \tag{36}$$

The diagonal elements H_{rr} of the core Hamiltonian operator are approximated as

$$H_{rr} = U_{rr} - \sum_{s(\neq r)} \gamma_{rs}, \tag{37}$$

where the one-center terms U_{rr} are all the same (U_0) for carbon atoms. We set

$$U_{rr} = U_0 = -0.4101 \text{ (the negative of I.P. for C(2p))}, \tag{38}$$

although any other value of U_0 suffices for the present purpose as we need only the orbital coefficients and

the orbital energy differences rather than the absolute values of ε_k. The off-diagonal core matrix elements H_{rs} are approximated to be the resonance integrals. Here we employ Ohno's proposal[12] that

$$\beta_{rs} = (\gamma_{rs} - 2/R_{rs})S_{rs}. \tag{39}$$

We therefore set

$$H_{rs} = \beta_{rs} = -bS_{rs}/R_{rs}, \tag{40}$$

where b is an adjustable parameter whose value is expected to be around 1 and S_{rs} is the overlap integral

$$S_{rs} = [1 + \rho + (2/5)\rho^2 + (1/15)\rho^3]\exp(-\rho); \quad \rho \equiv \zeta R_{rs}. \tag{41}$$

Note that the simple replacement of γ_{rs} by $1/R_{rs}$ in Ohno's formula corresponds to letting b=1 in Eq. 40.

4. Application to Linear Polyenes

The effective EOM with adjustable parameters described in the preceding sections is now applied to the $\pi \rightarrow \pi^*$ transitions of all-*s*-trans linear polyenes.

(i) Determination of the Values of a, b, and ζ. Values of the parameters a, b, and ζ are determined in such a way that the computed transition energies fit the observed values for the N→T, V transitions of ethylene and butadience. The assignment of 4.6 eV to the N→T and 7.6 eV to the N→V of ethylene is well established.[13] On the other hand, the ordering of the lowest excited states of *s-trans*-butadiene has been a subject of considerable controversy.[7,13-21] In the present work, we employ the assignment proposed by Doering in his electron impact study,[20a] i.e., 5.9 eV for the optically allowed ^{1}Bu state and 5.8 eV for the 2^1Ag state. The value for the ^{1}Bu state seems well established both in UV spectral[19] and electron impact[20] studies.

These four values are used to determine values of the three parameters a, b, and ζ in the vicinity of a=1, b=1, and ζ=1.6. An optimized set of values has been obtained as a=1.10, b=1.05, and ζ=1.65. With these parameter values, we obtain 4.21 eV, 6.65 eV for the T, V states of ethylene, and 5.72 eV, 5.83 eV for the ^{1}Bu, 2^1Ag states of butadiene, respectively.

(ii) Computational Details. Input data of molecular geometries are as follows. The planar shape with the C_{2h} symmetry (D_{2h} for ethylene) is assumed for all the polyene molecules. For ethylene, *s-trans*-butadiene, and *s-trans*-hexatriene, the following experimental data[22] are used: R(C=C)=1.337 Å, R(C–H)=1.103 Å, and ∠HCH=116.2° for ethylene, R(C=C)=1.3405 Å, R(C–C)=1.463 Å, R(C–H)=1.090 Å (averaged), and ∠CCC=123.3° for butadiene, and R(C=C)=1.337 Å at both ends and 1.367 Å at center, R(C–C)=1.457 Å, ∠CCC=121.7° (outer), and 124.4° (inner) for hexatriene. The angular conformation of the CH_2 group at both ends of butadiene and hexatriene is assumed to be the same as that of ethylene. All the ∠CCH's, except at both ends, are assumed to be the same, and R(C–H)= 1.09 Å is assumed for all the C–H bonds. For longer polyenes, we set R(C=C)=1.367 Å (but 1.337 Å at both ends), R(C–C)=1.457 Å, R(C–H)=1.09 Å and ∠HCH= ∠CCH=∠CCC=120°.

With these molecular geometries and a given set of parameters a, b, and ζ, the SCF-MO's for pi-electrons are obtained by solving the secular equations of Eq. 34. Then, the matrices $\mathscr{A}$, $\mathscr{B}$, $\mathscr{A}^{\circ(1,2)}$, and $A^{\circ(2,2)}$ are constructed including the S', T', and ρ' described in Section 2, and Eq. 17a or 17b is solved for ω. For each singlet transition, the molecular integrals $(m\gamma|n\delta)$ of $\mathscr{A}$ and $\mathscr{B}$ are replaced by the reduced quantities $(m\gamma|n\delta)''$ with the previously obtained eigenvalue of ω, and Eq. 17a or 17b with these new $\mathscr{A}$ and $\mathscr{B}$ is solved to give final results for the singlet transition. As mentioned above, great care is needed in normalization of the eigenvectors in this case.[10]

(iii) Results. The transition energies computed with the parameter values (a=1.10, b=1.05, and ζ=1.65) are listed in Table 2. The weight of (2p-2h) components, i.e. the value of the second term in Eq. 21, is also given in parentheses for each transition. For the allowed transitions, 1^1Ag→1^1Bu, the oscillator strengths are given in square brackets. Due to the correction of Eq. 23, i.e. the sigma-dynamical screening effect, the transition energy for the 1^1Bu state was reduced by 1.56 eV for ethylene, 1.16 eV for butadiene, 1.05 eV for hexatriene, 1.03 eV for octatetraene, 1.00 eV for decapentaene, and 1.00 eV for dodecahexaene. Such reduction was negligibly small for the 2^1Ag states: 0.02 eV for butadiene, 0.01 eV for hexatriene, 0.003 eV for octatetraene, and so forth. All of these 2^1Ag states were of A_g^- type. The observed values for ^{1}Bu listed in Table 2 are all taken from Table 2 of Ref. 7. They agree very well with those more recently given by Leopold et al.,[23] i.e., 5.74 eV for butadiene, 4.93 eV for hexatriene, and 4.41 eV for octatetraene. Ramasesha and Soos[24a] gave values of the oscillator strength per site by their "exact" PPP calculations. They are 0.169 for hexatriene, 0.164 for octatetraene, and 0.159 for decapentaene, which may be compared with our values 0.193, 0.184, and 0.180, respectively. The oscillator strength f is plotted against the number of double bonds in Fig. 1. The f value of the s-trans linear polyene with 11 double bonds is that of β-carotene which was deduced from its absorption intensities in various organic solvents[25] using the dielectric theory proposed by Shibuya.[26] The transition energies for 1^3Bu, 1^3Ag, 1^1Bu, and 2^1Ag are plotted in Fig. 2.

5. Discussion

The numerical results presented in the preceding Section appear fairly reasonable as a whole. As is seen

Table 2. Computed Transition Energies (in eV) to the Low-Lying Valence States of All-s-Trans Linear Polyenes

	^{3}Bu	(obsd)	^{3}Ag	(obsd)	^{1}Bu	(obsd)[a]	2^1Ag	(obsd)[a]
Butadiene	3.44 (0.05)	3.2[b]	4.61 (0.01)	4.95[b]	5.72 (0.007) [0.85]	5.91	5.83 (0.73)	
Hexatriene	2.88 (0.08)	2.7[c]	4.04 (0.06)	4.2[c]	4.93 (0.02) [1.16]	4.93	4.89 (0.77)	
Octatetraene	2.58 (0.11)	2.1[d]	3.48 (0.08)	3.6[d]	4.42 (0.02) [1.47]	4.40	4.21 (0.79)	3.97
Decapentaene	2.41 (0.13)		3.11 (0.10)		4.08 (0.03) [1.80]	4.02	3.86 (0.81)	3.48
Dodecahexaene	2.32 (0.14)		2.85 (0.12)		3.83 (0.029) [2.137]	3.65	3.67 (0.82)	2.91

Values in parentheses are the weights of (2p–2h) components, and values in square brackets are the oscillator strengths. a) All taken from the review article of Hudson et al.[7] b) From Doering.[20a] c) R. McDiarmid, A. Sabljic, and J. P. Doering, *J. Am. Chem. Soc.*, **107**, 826 (1985). d) M. Allan, L. Neuhaus, and E. Haselbach, *Helv. Chim. Acta*, **67**, 1776 (1984).

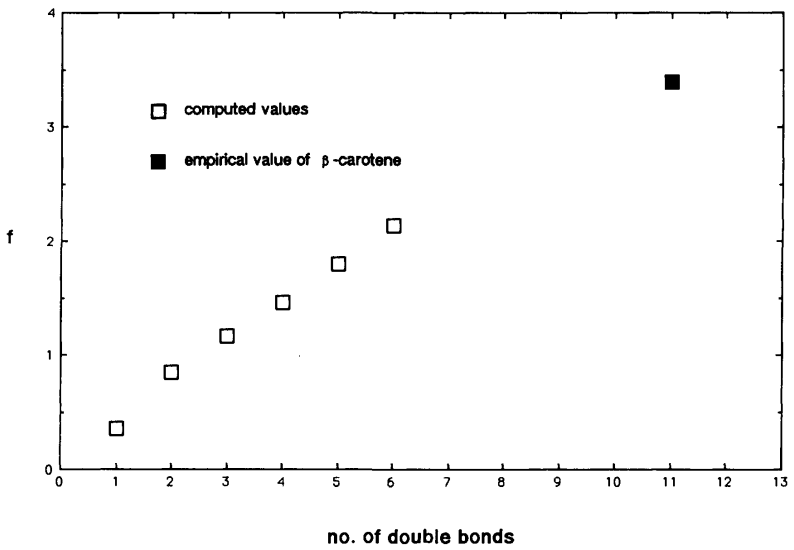

Fig. 1. The oscillator strength (f) of the 1^1Bu transition of all-s-trans linear polyenes against the number of double bonds. The empirical value of β-carotene was deduced from its absorption intensities in various organic solvents[25] using the dielectric theory.[26]

in Fig. 1, the plot of the calculated oscillator strengths well extrapolates to the "empirical" value of β-carotene. The computed transition energies of the allowed ^{1}Bu states are all in excellent agreement with experiment. The 2^1Ag states, which mostly lie below the allowed ^{1}Bu states, were found to be essentially dominated by the 2p-2h states. This agrees with the widely accepted notion.[7] Figure 2 indicates that these transition energies converge to certain finite values as the number of double bonds increases.

We have tried to see whether a pure pi-electron EOM scheme is possibly constructed. This means that not only the sigma-dynamical screening Eq. 23 is omitted but also the correction terms S', T', and ρ' are ignored. In this case we would have only two parameters b and ζ. This, however, was not successful: The EOM became instable for the triplet transitions. The inclusion of the correction terms S' and T' was

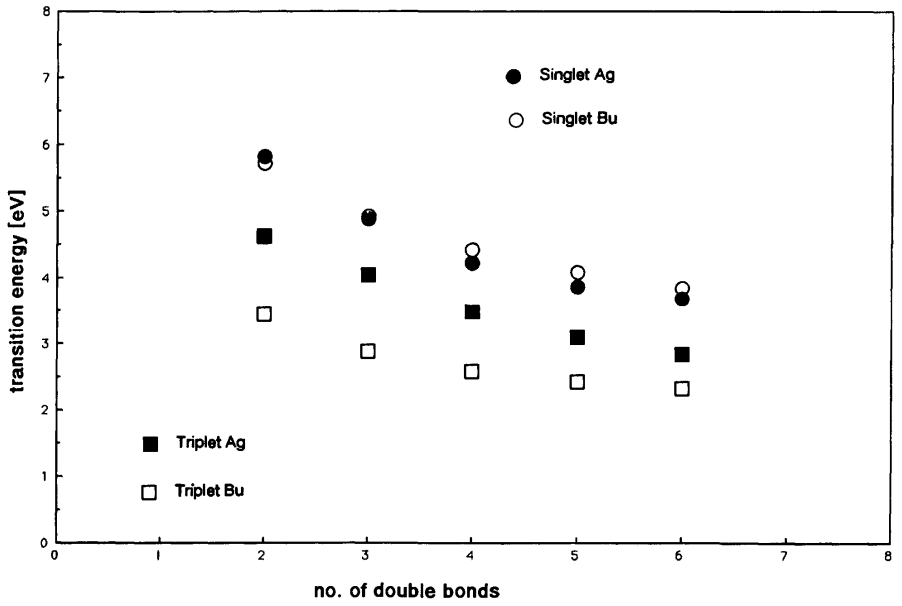

Fig. 2. Calculated transition energies for the four lowest excited valence states (1^3Bu, 1^3Ag, 1^1Bu, 2^1Ag) of all-s-trans linear polyenes against the number of double bonds.

essential. Parametrization at the RPA level would also fail, as the RPA fails for the triplet transitions already in its non-empirical treatment.[1)]

Great interest in polyacetylene $(CH)_x$ as an electronic material has stimulated some recent investigations of the low-lying excitations in linear polyenes.[24,27-29)] Gutsev et al.[27)] employed the Discrete Variational Xα method, but all the other investigators[24,28-29)] employed schemes in the framework of the PPP approximation. Hemley et al.[30)] employed an extended PPP-CI theory to analyze the absorption spectra of the $1A_g \rightarrow 1^1B_u$ transition of jet-cooled hexatriene.[23b)]

Application of the present scheme to nonlinear conjugated hydrocarbons is straightforward,and such a study is currently in progress.

Appendix A: The Correction Terms S', T', and ρ'

From Eq. 8a, we have

$$S'_{m\gamma,n\delta} = -\sum_{\sigma^*\sigma}[(m\delta|\sigma^*\sigma)C_{\sigma^*\sigma,n\gamma}(0) + (n\gamma|\sigma^*\sigma)C_{\sigma^*\sigma,m\delta}(0)], \quad (A\cdot1)$$

where m and n refer to the π^*-orbitals and γ and δ to the π-orbitals. Note that in the summation of Eq. 8a, the terms for $(p,\mu)=(\pi^*, \sigma)$ and (σ^*, π) vanish due to the symmetry or to the ZDO approximation between the pi- and sigma-orbitals. Using Eq. 11, we have

$$C_{\sigma^*\sigma,n\gamma}(0) = -2(\sigma^*\sigma|n\gamma)/(\varepsilon_n - \varepsilon_\gamma + a), \quad (A\cdot2)$$

and a similar expression for $C_{\sigma^*\sigma,m\delta}(0)$. In deriving Eq. A. 2, we have let all the $\varepsilon_{\sigma^*}-\varepsilon_\sigma=a$ according to the approximation introduced in Section 2, and $(\sigma^*\gamma|n\sigma)=0$ due to the ZDO approximation. Substituting these expressions in Eq. A. 1 and using the G defined by Eq. 24, we obtain

$$S'_{m\gamma,n\delta} = (1/2)[(\varepsilon_m - \varepsilon_\delta + a)^{-1} + (\varepsilon_n - \varepsilon_\gamma + a)^{-1}]G_{m\delta,n\gamma}. \quad (A\cdot3)$$

To derive T', first note that $S_{m\sigma,n\sigma}=S_{\sigma^*\gamma,\sigma^*\delta}=0$ due to the ZDO approximation. Then, from Eq. 8b together with the result Eq. A. 3, we have

$$T'_{mn} = (1/2)\sum_\pi S'_{m\pi,n\pi};\ T'_{\gamma\delta} = -(1/2)\sum_{\pi^*} S'_{\pi^*\gamma,\pi^*\delta}. \quad (A\cdot4)$$

The derivation of ρ' is more complicated. Substituting Eq. 10 together with Eq. 11 into Eq. 9a, we obtain

$$\rho_{mm} = (1/2)\sum_{p\mu\nu}[3(p\mu|m\nu)^2 - 2(p\mu|m\nu)(p\nu|m\mu) + (p\nu|m\mu)^2]/(\varepsilon_p + \varepsilon_m - \varepsilon_\mu - \varepsilon_\nu)^2 \quad (A\cdot5)$$

where m refers to the π^*-orbitals, but p to both π^* and σ^*, and μ and ν to both π and σ. We note that the terms in the summation of Eq. A. 5 vanish due to the ZDO approximation if both μ and ν are σ. Similarly, the terms with $\mu\nu=\sigma\pi$ or $\pi\sigma$ are nonvanishing only if $p=\sigma^*$. Therefore,

$$\rho'_{mm} = (1/2)\sum_\pi\sum_{\sigma^*\sigma} 4(\sigma^*\sigma|m\pi)^2/(\varepsilon_m - \varepsilon_\pi + \varepsilon_{\sigma^*} - \varepsilon_\sigma)^2. \quad (A\cdot6)$$

Letting all the $\varepsilon_{\sigma^*}-\varepsilon_\sigma=a$, we obtain Eq. 29a. The expression of $\rho'_{\gamma\gamma}$ in Eq. 29b is derived in a similar manner.

Appendix B: The Normalization Constant N_λ^{-1} in Eq. 30

Originally the normalization condition $\langle\lambda|\lambda\rangle=1$ was assumed as in Eq. 21. For the effective EOM for pi-electrons, however, the summations in Eq. 21 run over the 1p-1h and 2p-2h states of pi-electrons only. Thus, $N_\lambda^2=\langle\lambda|\lambda\rangle$ differs from 1 and becomes greater than 1 due to the contribution

from the terms of sigma-electrons. In our model, the mixing of $\sigma \rightarrow \sigma^*$ is considered only at the level of 1p-1h states. Therefore,

$$N_\lambda^2 - 1 = \sum_{\sigma^*\sigma} \{ |\mathcal{Y}_{\sigma^*\sigma}(\lambda)|^2 - |\mathcal{X}_{\sigma^*\sigma}(\lambda)|^2 \}$$
$$\equiv [\mathcal{Y}_\Sigma(\lambda) \; -\mathcal{X}_\Sigma(\lambda)] \begin{bmatrix} \mathcal{Y}_\Sigma(\lambda) \\ \mathcal{X}_\Sigma(\lambda) \end{bmatrix}. \quad \text{(B.1)}$$

As was shown earlier,[3]

$$\begin{bmatrix} \mathcal{Y}_\Sigma(\lambda) \\ \mathcal{X}_\Sigma(\lambda) \end{bmatrix} =$$
$$- \begin{bmatrix} (\mathcal{A}_{\Sigma\Sigma} - \omega_\lambda) & \mathcal{B}_{\Sigma\Sigma} \\ -\mathcal{B}_{\Sigma\Sigma} & -(\mathcal{A}_{\Sigma\Sigma} + \omega_\lambda) \end{bmatrix}^{-1} \begin{bmatrix} \mathcal{B}_{\Sigma\Pi} & \mathcal{A}_{\Sigma\Pi} \\ -\mathcal{A}_{\Sigma\Pi} & -\mathcal{B}_{\Sigma\Pi} \end{bmatrix} \begin{bmatrix} \mathcal{Y}_\Pi(\lambda) \\ \mathcal{X}_\Pi(\lambda) \end{bmatrix}. \quad \text{(B.2)}$$

Letting $\mathcal{B}_{\Sigma\Sigma}=0$ and using Eq. 22, we have

$$\begin{bmatrix} \mathcal{Y}_\Sigma(\lambda) \\ \mathcal{X}_\Sigma(\lambda) \end{bmatrix} = \begin{bmatrix} -(\mathcal{A}_{\Sigma\Sigma} - \omega_\lambda)^{-1} \mathcal{A}_{\Sigma\Pi} \{\mathcal{Y}_\Pi(\lambda) + \mathcal{X}_\Pi(\lambda)\} \\ (\mathcal{A}_{\Sigma\Sigma} + \omega_\lambda)^{-1} \mathcal{A}_{\Sigma\Pi} \{\mathcal{Y}_\Pi(\lambda) + \mathcal{X}_\Pi(\lambda)\} \end{bmatrix}. \quad \text{(B.3)}$$

So that,

$$N_\lambda^2 - 1 = |(\mathcal{A}_{\Sigma\Sigma} - \omega_\lambda)^{-1} \mathcal{A}_{\Sigma\Pi} \{\mathcal{Y}_\Pi(\lambda) + \mathcal{X}_\Pi(\lambda)\}|^2$$
$$- |(\mathcal{A}_{\Sigma\Sigma} + \omega_\lambda)^{-1} \mathcal{A}_{\Sigma\Pi} \{\mathcal{Y}_\Pi(\lambda) + \mathcal{X}_\Pi(\lambda)\}|^2$$
$$= \left[\frac{1}{(a - \omega_\lambda)^2} - \frac{1}{(a + \omega_\lambda)^2} \right] \sum_{\pi_1^*\pi_1} \sum_{\pi_2^*\pi_2} \sum_{\sigma^*\sigma}$$
$$\{\mathcal{Y}_{\pi_1^*\pi_1}(\lambda) + \mathcal{X}_{\pi_1^*\pi_1}(\lambda)\} \mathcal{A}_{\pi_1^*\pi_1, \sigma^*\sigma}(S)$$
$$\times \mathcal{A}_{\sigma^*\sigma, \pi_2^*\pi_2}(S) \{\mathcal{Y}_{\pi_2^*\pi_2}(\lambda) + \mathcal{X}_{\pi_2^*\pi_2}(\lambda)\} \quad \text{(B·4)}$$

In deriving the last expression, we have let $\mathcal{A}_{\sigma^*\sigma,\sigma^*\sigma}=a$ and all the off-diagonal elements of $\mathcal{A}_{\Sigma\Sigma}$ be 0. Now, referring to Eqs. 22 and 24 and letting $g_{\sigma^*\sigma}=1$, we obtain

$$N_\lambda^2 - 1 = (\delta_{s0}) \frac{4a\omega_\lambda}{(a^2 - \omega_\lambda^2)^2} \sum_{\pi_1^*\pi_1} \sum_{\pi_2^*\pi_2}$$
$$(G_{\pi_1^*\pi_1, \pi_2^*\pi_2} / [g_{\pi_1^*\pi_1} g_{\pi_2^*\pi_2}]) \{\mathcal{Y}_{\pi_1^*\pi_1}(\lambda) + \mathcal{X}_{\pi_1^*\pi_1}(\lambda)\}$$
$$\times \{\mathcal{Y}_{\pi_2^*\pi_2}(\lambda) + \mathcal{X}_{\pi_2^*\pi_2}(\lambda)\}. \quad \text{(B·5)}$$

Computations were carried out using facilities of the Computer Centers both at Shinshu University and the University of Tokyo. This work was supported by a Grant-in-Aid for Scientific Research from the Ministry of Education.

References

1) a) T. Shibuya and V. McKoy, *Phys. Rev. A*, **2**, 2208 (1970); b) T. Shibuya, J. Rose, and V. McKoy, *J. Chem. Phys.*, **58**, 500 (1973).

2) T. Shibuya and T. Funada, *Int. J. Quantum Chem.*, **XVIII**, 205 (1980).

3) T. Shibuya, Y. J. I'Haya, and V. McKoy, *Int. J. Quantum Chem.*, **IX**, 505 (1975).

4) T. Shibuya and T. Funada, *Chem. Phys. Lett.*, **70**, 199 (1980).

5) R. G. Parr, "Quantum Theory of Molecular Electronic Structure," Benjamin Inc., New York (1964).

6) M. K. Orloff and O. Sinanoglu, *J. Chem. Phys.*, **43**, 49 (1965).

7) See, e,g., B. S. Hudson, B. E. Kohler, and K. Schulten, "Excited States," Vol. 6, ed by E. C. Lim, Academic Press, New York (1982), pp. 1—95.

8) T. Shibuya, T, Funada, and H. Gotoh, *Bull. Chem. Soc. Jpn.*, **61**, 1103 (1988).

9) J. Oddershede, *Adv. Chem. Phys.*, **69**, 201 (1987).

10) S. Narita, S. Kumei, and T. Shibuya, to be published.

11) See, e.g., J. A. Pople and D. L. Beveridge, "Approximate Molecular Orbital Theory," McGraw-Hill Inc., New York (1970).

12) K. Ohno, *Theoret. Chim. Acta*, **2**, 219 (1964).

13) See, e.g., R. S. Mulliken and W. C. Ermler, "Polyatomic Molecules: Results of ab initio calculations," Academic Press, New York (1981).

14) a) K. Schulten, I. Ohmine, and M. Karplus, *J. Chem. Phys.*, **64**, 4422 (1976); b) A. C. Lasaga, R. J. Aerni, and M. Karplus, *ibid.*, **73**, 5230 (1980).

15) R. P. Hosteny, T. H. Dunning, Jr., R. R. Gilman, A. Pipano, and I. Shavitt, *J. Chem. Phys.*, **62**, 4764 (1975).

16) R. J. Buenker, S. Shih, and S. D. Peyerimhoff, *Chem. Phys. Lett.*, **44**, 385 (1976).

17) Y. S. Lee, K. F. Freed, and H. Sun, *J. Chem. Phys.*, **79**, 3862 (1983).

18) M. Aoyagi, Y. Osamura, and S. Iwata, *J. Chem. Phys.*, **83**, 1140 (1985).

19) K. K. Innes and R. McDiarmid, *J. Chem. Phys.*, **68**, 2007 (1978).

20) a) J. P. Doering, *J. Chem. Phys.*, **70**, 3902 (1979); b) J. P. Doering and R. McDiarmid, *idid.*, **73**, 3617 (1980); **75**, 500 (1981); c) R. McDiarmid and J. P. Doering, *Chem. Phys. Lett.*, **88**, 602 (1982).

21) R. McDiarmid, a) *J. Chem. Phys.*, **79**, 9 (1983); b) *Int. J. Quantum Chem.*, **XXIX**, 875 (1986).

22) "Kagaku Benran, Kiso-hen II", 2nd ed, ed. by the Chemical Society of Japan, Maruzen, Tokyo (1975), Chap. 11.

23) a) D. G. Leopold, V. Vaida, and M. F. Granville, *J. Chem. Phys.* **81**, 4210 (1984); b) D. G. Leopold, R. D. Pendley, J. L. Roebber, R. J. Hemley, and V. Vaida, *ibid.*, **81**, 4218 (1984).

24) S. Ramasesha and Z. G. Soos, a) *J. Chem. Phys.*, **80**, 3278 (1984); b) *Synth. Met.*, **9**, 283 (1984); c) Z. G. Soos and S. Ramasesha, *Chem. Phys. Lett.*, **101**, 34 (1983).

25) T. Shibuya and K. Terai, unpublished

26) T. Shibuya, *J. Chem. Phys.*, **78**, 5175 (1983).

27) G. L. Gutsev, A. I. Boldyrev, and A. A. Ovchinnikov, *Int. J. Quantum Chem.*, **XXX**, 647 (1986).

28) M. Baldo, R. Pucci, and P. Tomasello, *Int. J. Quantum Chem.*, **XXIII**, 1111 (1983).

29) P. Tavan and K. Schulten, *J. Chem. Phys.*, **85**, 6602 (1986).

30) R. J. Hemley, A. C. Lasaga, V. Vaida, and M. Karplus, *J. Phys. Chem.*, **92**, 945 (1988).

Electrochemistry of Tris(β-diketonato)ruthenium(III) Complexes at Platinum Electrodes in Nonaqueous Solutions and Substituent Effects on Their Reversible Half-Wave Potentials[1,2]

Akira ENDO, Yoshimasa HOSHINO, Keigo HIRAKATA, Yasushi TAKEUCHI, Kunio SHIMIZU, Yuriko FURUSHIMA, Haruko IKEUCHI, and Gen P. SATÔ*
Department of Chemistry, Faculty of Science and Technology, Sophia University, 7-1 Kioicho, Chiyoda-ku, Tokyo 102
(Received September 10, 1988)

The one-electron oxidation and reduction processes at platinum electrodes of a series of β-substituted and γ-substituted tris(β-diketonato)ruthenium(III) complexes are studied in acetonitrile, *N*,*N*-dimethylformamide, and nitromethane solutions, each containing 0.1 mol dm^{-3} $(C_2H_5)_4NClO_4$ at 25 °C. Syntheses of three new γ-substituted derivatives are described. Attempts to isolate the immediate product of the one-electron oxidation of [Ru(acac)$_3$] in acetonitrile failed; bis(acetonitrile)bis(acetylacetonato)ruthenium(III) was obtained instead. Diffusion coefficients of the complexes in the acetonitrile medium are presented. The reversible half-wave potentials for the oxidation and the reduction in the acetonitrile medium depended linearly on the sum of the Hammett constants of the substituents (σ_p for the β-substituents and σ_m for the γ-substituents). Analysis of the dependence of the half-wave potentials on several kinds of substituent parameters suggests that the inductive effect is operative at both the β-positions and the γ-position, while the resonance effect is operative only at the β-positions.

Electrochemical properties of tris(β-diketonato)complexes involving many kinds of metals (e.g., cobalt(III),[3-7] chromium(III),[4,5,8,9] europium(III),[5] cerium(III),[5,6] iron(III),[4-6,9-12] manganese(III),[4-6,13] ruthenium(III),[14-18] and osmium(III)[15]) have been studied in various solvents. Most of these complexes undergo simple one-electron reduction and/or one-electron oxidation. In some cases, the reversible half-wave potentials for the reduction have been found to be linearly correlated with σ_p, σ_m, and σ^*, where σ_p and σ_m are the Hammett constants for para and meta positions, respectively, and σ^* is Taft's polar substituent constant.

Reduction processes of some tris(β-diketonato)ruthenium(III) complexes to the corresponding ruthenium(II) complexes have been studied in acetonitrile (AN)[14-18] and in *N*,*N*-dimethylformamide (DMF).[15] Linear relationships between the half-wave potentials and the sum of the Hammett constants were also reported.[15,18] These complexes, however, were all β-substituted complexes with one exception, and only a few quantitative analyses of oxidation processes to the ruthenium(IV) state have been reported.[14,16,19-21]

This paper deals with the electrochemical reduction and oxidation processes at platinum electrodes of a series of both β-substituted and γ-substituted tris(β-diketonato)ruthenium(III) complexes in AN, DMF, and nitromethane (NM). The electrochemistry in AN is studied in detail, since the potential window of AN, particularly its anodic limit for platinum electrodes, is wider than those of the other solvents. Substituent effects on the half-wave potentials for both the oxidation and the reduction are examined in terms of σ_p and σ_m. The diffusion coefficients of the complexes in AN are presented together with the partial molar volumes of a few related complexes.

Experimental

Preparation of the Ruthenium(III) Complexes.** All the tris(β-diketonato)ruthenium(III) complexes except **12**, **13**, and **14** were synthesized according to the "ruthenium blue solution" method.[22,23] The three halogenated complexes were prepared by the direct substitution at the γ-positions of the ligands of **9**. In the cases of **12** and **13**, a chloroform solution of *N*-bromosuccinimide (Wako Pure Chemical Ltd.) or *N*-chlorosuccinimide (Aldrich Chemical Company Inc.) was added to **9** dissolved in chloroform. In the case of **14**, a benzene solution of *N*-iodosuccinimide (Fluka AG) was added to a benzene solution of **9**, because preliminary experiments indicated that extended refluxing in chloroform led to complete decomposition of all the complex species. The amount-of-substance ratio of the *N*-halosuccinimide to **9** was 4.5 for **12**, 3.0 for **13**, and 9.0 for **14**. Too large an excess of the succinimide resulted in the decomposition of the product in the cases of **12** and **13**. *N*-Bromosuccinimide immediately reacted with **9** to give **13**. However, **12** was obtained by allowing the mixture to stand overnight, and **14** was obtained by refluxing the mixture for ca. 2 h. The solution containing the product was passed through a column of Merck Aluminiumoxid 90 (in the case of **12**, it was necessary to evaporate off the solvent and to extract the residue with benzene before the chromatographic separation). The eluent was evaporated to dryness. The residue was recrystallized from ethanol, and the crystals were dried under a vacuum. Interestingly, when the benzene solution of iodine monochloride was introduced to the benzene solution of **9**, the γ-chloro complex, not the γ-iodo complex, was produced immediately with ca. 100% yield, although this

** The ligand symbols are given in Table 1; the complexes are numbered as indicated there.

Table 1. Ligand Symbols[a] and Numbers for the Complexes

Number	Complex	[O=CR-CR′-CR″=O]⁻ R	R′	R″
β-Substituted complexes				
1	[Ru(fhfa)$_3$]	CF_3	H	CF_3
2	[Ru(fhoa)$_3$]	CF_3	H	C_4H_3O[a]
3	[Ru(bhfa)$_3$]	CF_3	H	C_6H_5
4	[Ru(fhsa)$_3$]	CF_3	H	C_4H_3S[a]
5	[Ru(fhma)$_3$]	CF_3	H	CH_3
6	[Ru(fhpa)$_3$]	CF_3	H	$C(CH_3)_3$
7	[Ru(bhba)$_3$]	C_6H_5	H	C_6H_5
8	[Ru(bhma)$_3$]	C_6H_5	H	CH_3
9	[Ru(acac)$_3$]	CH_3	H	CH_3
10	[Ru(mhpa)$_3$]	CH_3	H	$C(CH_3)_3$
11	[Ru(phpa)$_3$]	$C(CH_3)_3$	H	$C(CH_3)_3$
γ-Substituted complexes				
12	[Ru(mClma)$_3$]	CH_3	Cl	CH_3
13	[Ru(mBrma)$_3$]	CH_3	Br	CH_3
14	[Ru(mIma)$_3$]	CH_3	I	CH_3
15	[Ru(mbma)$_3$]	CH_3	C_6H_5	CH_3
16	[Ru(mmma)$_3$]	CH_3	CH_3	CH_3
17	[Ru(mema)$_3$]	CH_3	C_2H_5	CH_3
Mixed-ligand complexes				
18	[Ru(acac)$_2$(bhfa)][20,35]			
19	[Ru(acac)$_2$(fhfa)][20]			
20	[Ru(acac)$_2$(mClma)]			

a) These provisional symbols (except the usual "acac") are constructed as follows: the first and the penultimate letters represent R and R″; the middle R′; the last "a" means a derivative of acetylacetone; "b" stands for phenyl, "e" for ethyl, "f" for trifluoromethyl, "h" for hydrogen, "m" for methyl, "o" for 2-furyl, "p" for *t*-butyl, and "s" for 2-thienyl.

compound is known to be an iodination reagent in chloroform or in acetate buffer.[24] When a small amount of chloro-, bromo-, or iodosuccinimide was added to **9**, a mixture of the mixed-ligand complexes [Ru(acac)$_n$(mXma)$_{3-n}$] (X=Cl, Br, I) was formed. These mixed-ligand complexes may be separated by column chromatography. Actually, **20** was obtained in this way.

The three γ-halogenated complexes are new compounds. They are readily soluble in benzene and chloroform giving reddish blue solutions; they are sparingly soluble in acetonitrile and acetone. Their elemental analyses and other characteristics are as follows. **12** Found: Ru, 20.1; C, 37.1; H, 3.6%. Calcd for $RuC_{15}H_{18}O_6Cl_3$: Ru, 20.1; C, 35.9; H, 3.6%. **13** Found: Ru, 14.9; C, 27.3; H, 2.7%. Calcd for $RuC_{15}H_{18}O_6Br_3$: Ru, 15.9; C, 28.4; H, 2.9%. **14** Found: Ru, 12.0; C, 23.5; H, 2.3%. Calcd for $RuC_{15}H_{18}O_6I_3$: Ru, 13.0; C, 23.3; H, 2.3%. UV (AN; λ_{max}/nm with log [ε/mol^{-1} dm^3 cm^{-1}] in the parentheses): **12** 563 (3.36), 362 (3.95), 287 (4.15); **13** 556 (3.39), 363 (3.94). 291 (4.09); **14** 563 (3.44), 367 (3.92), 291 (4.08). ^{1}H NMR (C_6D_6): **12** δ=−8.31; **13**, δ=−7.79; **14**, δ=−7.16. Magneton number (μ_{eff}/μ_B): **12** 1.79; **13** 1.76; **14** 1.73.

All the complexes have optical isomers, and those complexes with three asymmetrical ligands have geometrical isomers. The samples used in the present experiment were mixtures of the isomers as prepared. No differences in the electrochemical behavior of the geometrical isomers were discernible.

Other Chemicals. Tris(acetylacetonato)iron(III) and tris-(acetylacetonato)cobalt(III) were purified by sublimating the samples purchased from Dojindo Laboratories under a reduced pressure at ca. 180 °C and ca. 200 °C, respectively. The sample of [Fe(phpa)$_3$] was prepared according to Hammond et al.[25] and purified by sublimation at ca. 200 °C; the same procedure was used for preparing [Fe(mbma)$_3$], except that the ligand was dissolved in ethanol instead of methanol and the sample was purified by recrystallization from benzene–petroleum ether.

Tetraethylammonium perchlorate (TEAP), tetrabutylammonium perchlorate (TBAP), and tetrabutylammonium tetrafluoroborate ((TBA)BF_4) used as supporting electrolytes were of special polarographic grade purchased from Nakarai Chemicals, Ltd. Silver perchlorate was prepared by dissolving silver oxide in perchloric acid (this silver oxide was obtained by adding a sodium hydroxide solution to a silver nitrate solution). The mixture was evaporated to dryness. The anhydrous salt was obtained by drying the residue under vacuum at room temperature for ca. 24 h, and then at 50 °C for a few days. The purification method of acetonitrile[26] was slightly modified: the third distillation with calcium hydride was carried out under argon atmosphere by means of a Widmer-type distilling column (ca. 100 cm long). *N*,*N*-Dimethylformamide was spectral reagent grade (Dojindo Laboratories, Dotite Spectrosol). Nitromethane was purified according to the literature method.[27] The other chemicals were of guaranteed reagent grade.

Measurement. Two kinds of platinum test electrodes were used in the voltammetric experiments. One was a platinum disk electrode (PtDE) of 1.99 mm diameter embedded in glass, which was used for the cyclic and normal pulse voltammetry. The other was a rotating platinum disk electrode (RPtDE) of 1.96 mm diameter embedded in poly(tetrafluoroethylene). Both electrodes were polished with aluminium oxide (particle size, ca. 0.03 μm).

A platinum gauze electrode was used as the working electrode for controlled potential electrolysis. An MCI AS01 hanging mercury electrode (Mitsubishi Chemical Industries, Ltd.) was used for the chronoamperometric determination of diffusion coefficients. In all the experiments, a spiral of platinum wire or a sheet of platinum was used as an auxiliary electrode.

Silver–silver ion reference electrodes were used for all the solvents: a spiral of silver wire was immersed in the respective solvent containing 0.1 mol dm^{-3} $AgClO_4$. The $AgClO_4$ solution was freshly prepared at each experiment. The reference electrode was placed in a compartment of an H-type cell with a G4 glass frit plug. It was connected to the test solution through a bridge filled with 0.1 mol dm^{-3} TEAP, TBAP, or (TBA)BF_4 solution of the needed solvent. All the potential values in this report are referred to these electrodes.

The concentration of the supporting electrolyte was 0.1 mol dm^{-3}. All the electrochemical measurements were carried out at (25.0±0.1) °C. Deoxygenation of the solutions was carried out with argon gas which had been passed through a series of two washing bottles containing the needed solvent kept at 25 °C. A Fuso Polarograph Model 312 was used for normal pulse voltammetry. For cyclic voltammetry, a Fuso Potential Scanning Unit Model 321 was attached to this instrument. When the voltammetry was performed with RPtDE, a Nikko Keisoku Motor Speed Controller SC-5 was used.

The reversible half-wave potentials ($E^{1}_{1/2}$) were determined from the normal pulse or hydrodynamic voltammograms by means of the conventional logarithmic plot method (natural logarithm was used) in Nernstian cases. In quasi-reversible cases, the reversible half-wave potentials were obtained by extrapolating the plots of $E+(RT/nF)\ln(I/(I_d-I))$ against E.[28]

Controlled potential electrolysis was carried out by using either the Polarograph Model 312 with a Fuso Coulometer Model 343 or a controlled potential electrolyzer with digital coulometer[29] constructed in this laboratory. The computerized data acquisition-processing system used for the chronoamperometric determination of diffusion coefficients was described elsewhere.[30]

The partial molar volumes were determined as follows. The densities (d) of acetonitrile solutions containing the complex to be studied at different molalities (m) were measured by means of a digital density meter (Anton Paar, DMA 60 with a DMA 602 cell). The cell temperature was controlled within ±0.003 °C. The density meter was calibrated with nitrogen and ultrapure deionized water at the beginning and the end of each day's measurements. When $(1+mM)/d$, where M is the molar mass of the complex, is plotted against m, the slope of the tangent of this curve at m gives the partial molar volume at m. In the present experiment, the plot was linear in every case, and the partial molar volume at infinite dilution was determined as the slope of the linear least squares regression.

Results and Discussion

The Reduction Process in AN. Each ruthenium(III) complex gave a well-defined reduction step on the normal pulse polarogram and a pair of cathodic and anodic peaks on the cyclic voltammogram in 0.1 mol dm^{-3} TEAP–acetonitrile solution. In some cases, the reduction step was followed by a second step, which was partly covered by the final discharge of the base solution. Only the first steps will be discussed.

In every case, the limiting current of the first reduction step of the normal pulse voltammogram was diffusion controlled as indicated by the inversely proportional dependence of the limiting current on the square root of the sampling time. The logarithmic plot of the step was a straight line with a reciprocal slope near the Nernstian value for a one-electron step (RT/F=25.7 mV at 25 °C), except in the cases of **10**, **11**, **16**, and **17**, which had the most negative half-wave potentials. The logarithmic plots of these four complexes were curved, indicating that their reduction processes were quasi-reversible at the platinum electrode, whereas their reduction processes were Nernstian at mercury electrodes. The peak separations of the cyclic voltammograms (ΔE_p) reflected this situation. These data are presented in Table 2. The reversible half-wave potentials of the reduction at PtDE for all the complexes were in good agreement with those observed at a dropping mercury electrode.

At RPtDE, all the complexes except the above-mentioned four complexes showed Nernstian steps over the rotation frequency range between 400 min^{-1} and 3600 min^{-1}. The limiting currents were convective-diffusion-controlled. The voltammograms of **10** and **11** showed Nernstian steps only at lower rotation frequencies. The reduction steps of **16** and **17** were poorly reproducible even at lower rotation frequencies.

The Reduction Processes in DMF and NM. The following five complexes were examined: **1**, **5**, **8**, **9**, and **11**. In 0.1 mol dm^{-3} TEAP–DMF solution, **5** and **8** gave Nernstian reduction steps at PtDE, as indicated by the ΔE_p values (Table 3) and the reciprocal slopes of the logarithmic plots of the normal pulse voltammograms (not listed). However, the reduction processes of **9** and **11** were quasi-reversible at PtDE, although Patterson and Holm[15] reported that the reductions at a platinum electrode were Nernstian in DMF. The data for **1** in DMF were obtained from the quasi-reversible oxidation step observed with a test solution containing K[Ru(fhfa)$_3$], because **1** was quickly reduced to the ruthenate(II).

In 0.1 mol dm^{-3} TEAP–NM solution, **1**, **5**, and **8** showed quasi-reversible reduction steps at PtDE, while no reduction steps of **9** and **11** were observed within the potential window of this medium.

The reversibility of the reduction processes of the tris(β-diketonato)ruthenium(III) complexes depended on both the kind of solvent and the electrode material. Nevertheless, the relative values of $E^{1}_{1/2}$ in each solvent (the values referred to **8** are given in Table 4) were almost independent of the kind of solvent. The

Table 2. Electrochemical Data of β-Diketonatoruthenium(III) Complexes[a,b]

Complex	$\Sigma\sigma_{pmp}$	Ru^{IV}/Ru^{III}			Ru^{III}/Ru^{II}			$10^{10}D$	r_S
		ΔE_p/mV	s/mV	$E^r_{1/2}$/V	ΔE_p/mV	s/mV	$E^r_{1/2}$/V	$m^2\,s^{-1}$	nm
β-Substituted complexes									
1	+3.24	no	no	no	68	27.7	+0.36	11.8	0.510
2	+1.89	73	25.8	+1.22	65	25.1	−0.32	10.9	0.552
3	+1.59	75	qr	+1.21	67	29.3	−0.33	11.0	0.547
4	+1.59	69	25.3	+1.28	67	25.5	−0.33	10.8	0.558
5	+1.11	72	qr	+1.31	69	27.9	−0.45	15.0	0.401
6	+1.02	260	qr	+1.27[c]	60	26.5	−0.53	12.6	0.478
7	−0.06	59	25.8	+0.68	65	26.9	−0.88	7.8	0.772
8	−0.54	60	26.1	+0.66	64	26.5	−1.02	10.7	0.563
9	−1.02	61	25.8	+0.63	68	29.6	−1.14	14.5	0.415
10	−1.11	67	25.3	+0.60	78	qr	−1.21	11.7	0.515
11	−1.20	59	26.0	+0.46	80	qr	−1.44	11.6	0.519
γ-Substituted complexes									
12	+0.09	74	26.1	+0.80	65	25.6	−0.82	12.6	0.478
13	+0.15	70	24.6	+0.79	65	25.6	−0.81	12.2	0.494
14	+0.03	65	25.4	+0.73	65	25.8	−0.84	12.3	0.490
15	−0.84	59	25.5	+0.53	60	28.4	−1.21	10.4	0.579
16	−1.23	67	27.6	+0.35	67	qr	−1.30	13.2	0.456
17	−1.23	65	27.6	+0.35	80	qr	−1.34	12.4	0.486
Mixed-ligand complexes									
18[20]	−0.15	61	27.7	+0.84	65	26.9	−0.85		
19[20]	+0.40	70	25.1	+1.05	66	26.0	−0.61		
20	−0.65	68	28.1	+0.68	71	27.9	−1.03		

a) $E^r_{1/2}$, reversible half-wave potential vs. Ag/0.1 mol dm^{-3} $AgClO_4$ in AN; ΔE_p, cyclic voltammetric peak separation; D, diffusion coefficient; s, the absolute value of the reciprocal slope of the natural logarithmic plot; r_S, the Stokes radius calculated from the D value; no, not observed; qr, quasi-reversible. b) 1 mol m^{-3} in 0.1 mol dm^{-3} TEAP-AN at 25°C, PtDE. c) The values previously reported[2a,21] are revised.

Table 3. Peak Separations (ΔE_p) and Reversible Half-Wave Potentials ($E^r_{1/2}$)[a] for Ru^{IV}/Ru^{III} and Ru^{III}/Ru^{II} Steps of Some Tris(β-diketonato)ruthenium(III) Complexes at PtDE in DMF and NM Containing 0.1 mol dm^{-3} TEAP at 25°C

Solvent	DMF				NM			
	Ru^{IV}/Ru^{III}		Ru^{III}/Ru^{II}		Ru^{IV}/Ru^{III}		Ru^{III}/Ru^{II}	
Complex[b]	ΔE_p/mV	$E^r_{1/2}$/V	ΔE_p/mV	$E^r_{1/2}$/V	ΔE_p/mV	$E^r_{1/2}$/V	ΔE_p/mV	$E^r_{1/2}$/V
1	c)	c)	141[d]	+0.27[d]	c)	c)	85	−0.17
5	c)	c)	69	−0.54	c)	c)	92	−0.95
8	100	+0.56	67	−1.14	65	+0.14	78	−1.49
9	84	+0.53	100	−1.29	86	+0.16	c)	c)
11	102	+0.40	84	−1.56	79	−0.09	c)	c)

a) Against Ag/0.1 mol dm^{-3} $AgClO_4$ in the respective solvent. b) Concentration, 1 mol m^{-3}. c) Not observed. d) $K[Ru^{II}(fhfa)_3]$ was used (see text).

Table 4. Relative Reversible Half-Wave Potentials ($\Delta E^r_{1/2}$)[a] for Ru^{IV}/Ru^{III} and Ru^{III}/Ru^{II} Steps in AN, DMF, and NM Containing 0.1 mol dm^{-3} TEAP at 25°C

Complex	$\Delta E^r_{1/2}(Ru^{IV}/Ru^{III})$/V			$\Delta E^r_{1/2}(Ru^{III}/Ru^{II})$/V		
	AN	DMF	NM	AN	DMF	NM
1	b)	b)	b)	1.38	1.41	1.32
5	0.65	b)	b)	0.57	0.60	0.54
9	−0.03	−0.03	+0.02	−0.12	−0.15	b)
11	−0.20	−0.16	−0.23	−0.42	−0.42	b)

a) Referred to the $E^r_{1/2}$ value of $[Ru(bhma)_3]$ (**8**) in each medium. b) Not observed.

solvent effects on the reversible half-wave potential for the reduction appear to be small, in spite of the difference in the donor numbers of these solvents.

Oxidation Process in AN. A well-defined oxidation step was observed at both PtDE and RPtDE, and the cyclic voltammogram at PtDE exhibited a corresponding pair of anodic and cathodic peaks for each complex, except in the case of **1**, which showed no oxidation step within the potential window. In most cases, this step was followed by an ill-defined, irreversible second oxidation step, which will not be discussed.

The first steps were diffusion controlled. Comparison of their diffusion currents to those of the first reduction steps indicated that they were one-electron steps. These steps were Nernstian, except for the three complexes with the most positive half-wave potentials, i.e., **3**, **5**, and **6**. The oxidation steps of these three complexes were quasi-reversible. The $E^{I}_{1/2}$ values and the reciprocal slopes are presented in Table 2 together with the cyclic voltammetric ΔE_p values.

The constant potential coulometry of **8**, **9**, **11**, and **15** in AN confirmed that the steps were of the one-electron oxidation process to the corresponding ruthenium(IV) species and that the ruthenium(IV) complexes were stable and could be electrolytically reduced to the original ruthenium(III) species in a quantitative way.

In some other cases, however, the oxidation process was accompanied by slow subsequent reactions. When **3** was electrolyzed at +1.5 V in 0.1 mol dm^{-3} TEAP–AN, the anodic diffusion current decreased only slightly with the progress of the electrolysis, and the reduction step of $[Ru^{IV}(bhfa)_3]^+$ did not appear. Instead, new steps appeared at more negative potentials. Similar phenomena were observed when the supporting electrolyte was (TBA)BF_4 or TBAP. These facts show that the most part of $[Ru^{IV}(bhfa)_3]^+$ was reduced back to **3** by some species, whose oxidation product(s) produced the new reduction steps. Such regenerative reduction of the ruthenium(IV) species was observed also in the cases of **2**, **5**, and **6**. The oxidized forms of the complexes with $E^{I}_{1/2}(Ru^{IV}/Ru^{III})$ values more positive than +1.2 V catalyzed the oxidation of some unidentified species. These catalytic oxidation processes were fast enough to be observed in the controlled potential electrolysis, but they were too slow to affect the voltammetric current–voltage curves.

Since the oxidized forms of those complexes with less positive half-wave potentials (**9**, **11**, **15**, etc.) were stable in the acetonitrile solution, as mentioned above, attempts were made to isolate the ruthenium(IV) species. A blue solution which was obtained by the electrolytic oxidation of **9** in the $NaClO_4$–AN solution was evaporated under a reduced pressure. The residue was extracted with benzene. A blue solid was obtained when the benzene extract was evaporated. These operations were carried out under an argon atmosphere, and care was taken to exclude moisture as far as possible.

This blue solid was $[Ru^{III}(acac)_2(CH_3CN)_2](ClO_4)$ as indicated by the elemental analyses: Found: C,33.5; H, 4.0; N, 5.7% (Calcd for $RuC_{14}H_{20}N_2O_8Cl$: C, 35.0; H, 4.2; N, 5.7%), although the UV-vis spectrum of its $NaClO_4$–AN solution (λ_{max}/nm=285, 322, 580) was almost the same as that of the original solution from which it had been separated (λ_{max}/nm=280, 323, 560). This compound in the AN medium showed a reversible reduction step with $E^{I}_{1/2}$=−0.24 V, which agreed well with the half-wave potential of the oxidation step of $[Ru^{II}(acac)_2(CH_3CN)_2]$.[31] Its other characteristics are as follows: IR (KBr) 1095 cm^{-1} (ClO_4^-), 2300 cm^{-1} (CH_3CN). Magneton number, 1.75.

In this way, $[Ru^{IV}(acac)_3]^+$ was converted to the bis(acetonitrile) complex in the course of isolation. Attempts at isolating the oxidized products of **11** and **15**, which were also found to be stable in the acetonitrile solution, have so far led to recovering the original ruthenium(III) complexes. It appears that these tris(β-diketonato)ruthenium(IV) species were stable only in the presence of acetonitrile, and that their isolation would be very difficult, if not impossible, although a number of mononuclear ruthenium(IV) species with O^{2-}, halide ions, pyridine, or other organic ligands have been isolated.[19,32]

Oxidation Processes in DMF and NM. Five complexes, **1**, **5**, **8**, **9**, and **11**, were examined in these media. Among them, **8**, **9**, and **11** showed quasi-reversible one-electron oxidation steps (Table 3). The oxidation steps of the complexes with trifluoromethyl substituents lay beyond the positive ends of the potential windows of these media. Here again, the relative values of $E^{I}_{1/2}$ were roughly the same in the three solvents (Table 4).

Diffusion Coefficients and Partial Molar Volumes. The values of the diffusion coefficients of the tris(β-diketonato)ruthenium(III) complexes were evaluated approximately on the basis of the Levich equation from both the oxidation and the reduction limiting currents at the RPtDE, with the following values for 0.1 mol dm^{-3} TEAP–AN solution at 25 °C: density, 0.7901 g cm^{-3} and viscosity, 3.627×10^{-3} g cm^{-1} s^{-1}. For each complex, the value of the diffusion coefficient calculated from the oxidation limiting current agreed well with that calculated from the reduction limiting current. These values are listed in Table 2.

In order to establish the validity of these values, a more accurate value of the diffusion coefficient of **9** was determined by means of the chronoamperometric method with hanging mercury drop electrode[33] at several potentials in the cathodic diffusion current region. The average value obtained from four independent data sets (each consisting of at least six

Table 5. Partial Molar Volumes of Some Tris(β-diketonato) Complexes in Acetonitrile

t/°C	V_m/cm³ mol⁻¹				
	[Fe(acac)₃]	[Fe(mbma)₃]	[Fe(phpa)₃]	[Co(acac)₃]	[Ru(acac)₃]
15	272.2			257.4	264.1
20	274.3				
25	275.0		585.2	259.9	261.6
30	283.3				
35	269.0	457.8	590.3	259.5	269.8
Average[a]	274.2±1.3	457.8±1.0	588.2±2.5	258.0±0.6	263.4±1.2
N	18	4	7	12	12
V_c[b]	261[36]		571[37]	253[38]	251[39]

a) Calculated from the pooled N measurements over all the temperature; the uncertainty is the standard deviation.
b) Molar volume of crystal/cm³ mol⁻¹.

chronoamperograms) was (14.4±0.3)×10⁻¹⁰ m² s⁻¹ at 95% confidence level. The agreement between this value and the value in Table 2 is satisfactory.

The complexes with more bulky ligands seem to have smaller diffusion coefficients. Table 2 includes the Stokes radii calculated from the D values on the basis of the Einstein-Stokes relation. The partial molar volume (V_m) of **9** in AN (not containing the supporting electrolyte) was determined and is presented in Table 5 together with the values for some other tris(β-diketonato) complexes. The averages were calculated by pooling the data over all the temperatures, because the variations of V_m with temperature were within the experimental errors. It is seen that the V_m values are slightly larger than the molar volumes of the crystals.

The radius of a sphere having the same volume as the V_m/L value (L is the Avogadro constant) of **9** is 0.471 nm, and the radius calculated on the basis of the molar volume of the crystal is 0.463 nm. The Stokes radius of **9** is smaller than these values. Such a "negative effect" is reported in the cases of tetraalkylammonium perchlorate, and other bulky polyatomic ions.[34]

Substituent Effect on $E^r_{1/2}$. The values of $E^r_{1/2}$(Ru^{III}/Ru^{II}) and $E^r_{1/2}$(Ru^{IV}/Ru^{III}) in AN are listed in Table 2; the data for some mixed ligand complexes are also included. The values depended on the substituents of the ligands: with the increase in the number and/or the strength of electron-withdrawing substituents, both $E^r_{1/2}$(Ru^{III}/Ru^{II}) and $E^r_{1/2}$(Ru^{IV}/Ru^{III}) became more positive. Patterson and Holm[15] investigated the substituent effect on $E^r_{1/2}$(Ru^{III}/Ru^{II}) at platinum electrode in DMF of a series of β-substituted tris(β-diketonato)ruthenium(III) complexes, which included eight of the present ones. They found linear relationships between $E^r_{1/2}$(Ru^{III}/Ru^{II}) and the sums of Hammett constants or Taft constants. We have also reported a similar linear relationship for the reduction at mercury electrodes in AN.[18]

A more detailed study of the substituent effect is feasible now that quite a number of the β-substituted and γ-substituted derivatives have become available. Here, the effect of the substituents at the β- and γ-positions on the reversible half-wave potentials for the reduction and the oxidation is examined in terms of the following combinations of σ_m, and σ_p, where σ_m and σ_p are the Hammett constants for the meta and the para positions of the specified substituents.

$$\Sigma\sigma_{mmm} = 3[\sigma_m(R) + \sigma_m(R') + \sigma_m(R'')] \quad (1)$$

$$\Sigma\sigma_{mpm} = 3[\sigma_m(R) + \sigma_p(R') + \sigma_m(R'')] \quad (2)$$

$$\Sigma\sigma_{pmp} = 3[\sigma_p(R) + \sigma_m(R') + \sigma_p(R'')] \quad (3)$$

$$\Sigma\sigma_{ppp} = 3[\sigma_p(R) + \sigma_p(R') + \sigma_p(R'')] \quad (4)$$

Linear regression lines are drawn through the plots of $E^r_{1/2}$(Ru^{III}/Ru^{II}) and $E^r_{1/2}$(Ru^{IV}/Ru^{III}) against these parameters (the plots against $\Sigma\sigma_{pmp}$ are presented in Fig. 1). The plots against $\Sigma\sigma_{mpm}$ and $\Sigma\sigma_{pmp}$ fit to straight lines better than the others, mainly because the points for the γ-substituted complexes tend to deviate from the regression line for the β-subsituted complexes if $\Sigma\sigma_{mmm}$ or $\Sigma\sigma_{ppp}$ is taken as the parameter.

Whether $\Sigma\sigma_{mpm}$ or $\Sigma\sigma_{pmp}$ is more reasonable, however, cannot be decided by the fitness of the regressions. A more detailed piece of information is obtained when the relationships of $E^r_{1/2}$ with Taft's inductive substituent constant σ_I and the resonance substituent constant σ_R^0 are examined, because σ_p is a parameter which pertains to both the inductive and resonance effects.

When the $E^r_{1/2}$ values are plotted against $\Sigma\sigma_I$, two pairs of straight lines can be drawn: one for the β-substituted complexes and the other for the γ-substituted complexes (Fig. 2). This fact indicates that the inductive effect of the substituent strongly affects $E^r_{1/2}$ both at the β-position and at the γ-position. But, the slopes of the lines for the γ-substituents is smaller than those for the β-substituents, probably reflecting the γ-position's remoteness from the ruthenium atom.

When $E^r_{1/2}$ is plotted against $\Sigma\sigma_R^0$ (Fig. 3), an evident linear correlation is found only for the β-substituted complexes, while the points for the γ-substituted complexes are scattered. This fact

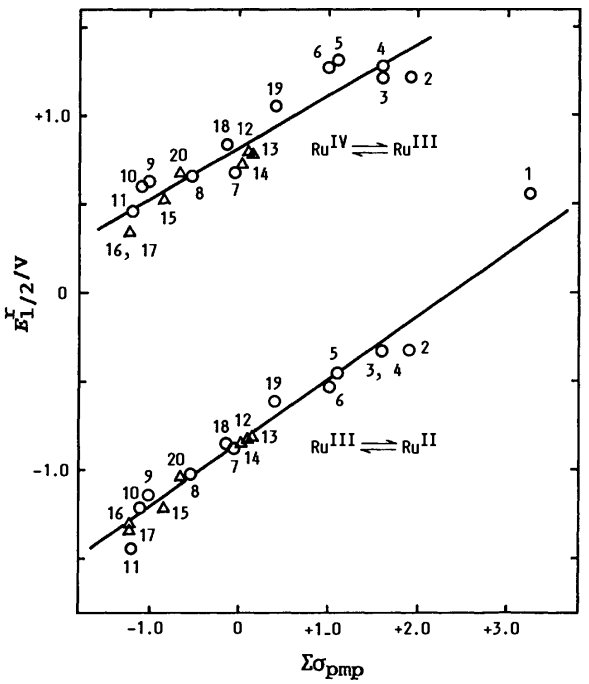

Fig. 1. Plots of $E^{I}_{1/2}$ against $\Sigma\sigma_{pmp}$.
Slope(Ru^{IV}/Ru^{III})=0.293 V, correlation coefficient-(Ru^{IV}/Ru^{III})=0.949; slope(Ru^{III}/Ru^{II})=0.354 V, correlation coefficient(Ru^{III}/Ru^{II})=0.988.
O: β-Substituted complexes, Δ: γ-substituted complexes.

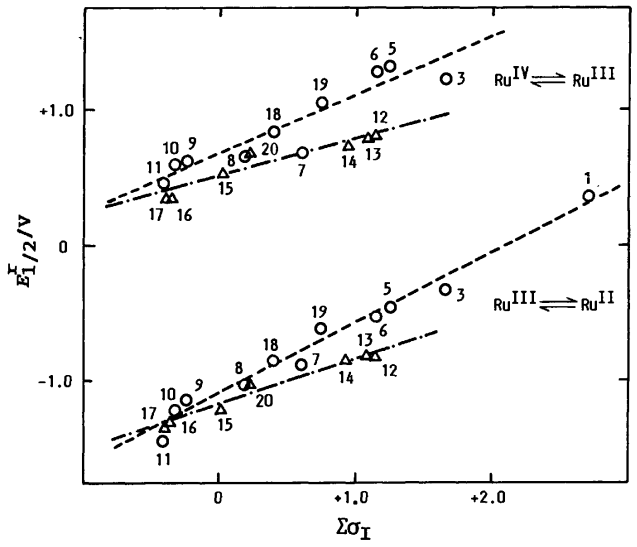

Fig. 2. Plots of $E^{I}_{1/2}$ against $\Sigma\sigma_{I}$.
---O---: β-Substituted complexes; slope(Ru^{IV}/Ru^{III})=0.407 V, correlation coefficient(Ru^{IV}/Ru^{III})=0.922; slope(Ru^{III}/Ru^{II})=0.523 V, correlation coefficient(Ru^{III}/Ru^{II})=0.988.
-·-Δ-·-: γ-Substituted complexes; slope(Ru^{IV}/Ru^{III})=0.280 V, correlation coefficient(Ru^{IV}/Ru^{III})=0.955; slope(Ru^{III}/Ru^{II})=0.345 V, correlation coefficient(Ru^{III}/Ru^{II})=0.986.

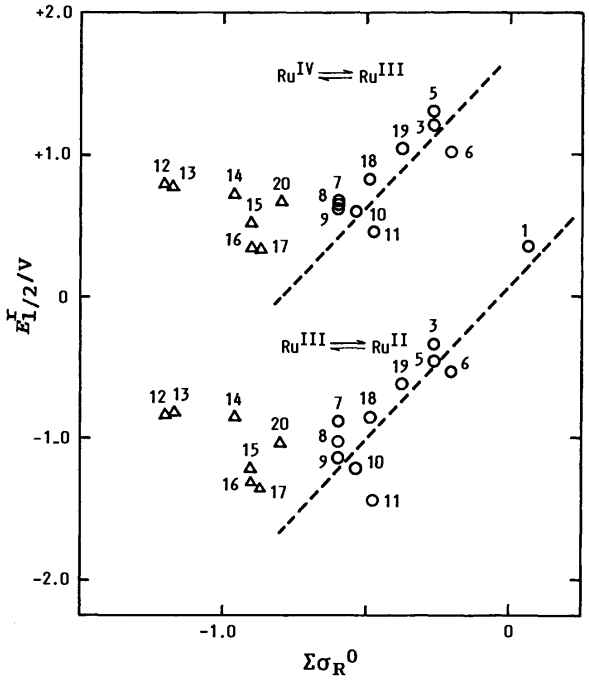

Fig. 3. Plots of $E^{I}_{1/2}$ against $\Sigma\sigma_{R}{}^{0}$.
---O---: β-Substituted complexes, Δ: γ-substituted complexes.

indicates that the resonance effect plays a less decisive role when the substituent is at the γ-position. In other words, the effect of the substituent at the γ-position is predominantly inductive, whereas the substituents at the β-positions exert both inductive and resoance effects. It is, therefore, $\Sigma\sigma_{pmp}$ that describes the substituent effects more reasonably than the other combinations of σ_p and σ_m. The same tendency has been observed in chromium(III) and cobalt(III) systems. In the case of tris(β-diketonato)chromium(III) complexes, Handy and Lindvedt[8] and Tsiamis et al.[9] established linear dependence of $E^{I}_{1/2}(Cr^{III}/Cr^{II})$ on $\Sigma\sigma_{pmp}$. With β-substituted tris(β-diketonato)cobalt-(III) complexes, the regression of the half-wave potential on $\Sigma\sigma_p$ was better than that on $\Sigma\sigma_m$.[3]

The substituent effects in β-diketonato ruthenium-(III) complexes have been explained qualitatively in terms of the influence of the substituents on the electron densities in the dπ orbitals.[15] The above-mentioned tendency has been accounted for by the idea that the β-substituents perturb the electron density on the ligating oxygen atoms rather than on the central atom.[8] Quantitative explanation is difficult, however, in the case of β-diketonato ruthenium-(III) complexes, which are paramagnetic, since no information about the electronic state is available directly from the UV-vis spectra, and the molecular orbital calculations are not easy.

The authors thank Makiko Ikai, Shinji Arai, and Noriko Mihara for their experimental assistance and

Dr. Yuichi Satsu for his helpful discussions. Dr. Kazuko Tanaka, The Institute of Physical and Chemical Research, kindly permitted the use of the digital density meter of her laboratory. Mrs. Nakako Tokita's assistance in the elemental analyses is gratefully acknowledged. Thanks are also due to Dr. F. Scott Howell, Sophia University, for correcting the manuscript. This work was partially supported by Grants-in-Aid for Scientific Research Nos. 547045 and 58740287 from the Ministry of Education, Science and Culture.

References

1) A part of A. Endo's Doctoral Thesis, Sophia University, Tokyo, Japan, 1986.

2) Preliminary notes have been published: a) Y. Takeuchi, A. Endo, K. Shimizu, and G. P. Satô, *J. Electroanal. Chem.*, **185**, 185 (1985). b) A. Endo, K. Shimizu, and G. P. Satô, *Chem. Lett.*, **1985**, 581.

3) A. D. Jannakoudakis, C. Tsiamis, P. D. Jannakoudakis, and E. Theodoridou, *J. Electroanal. Chem.*, **184**, 123 (1985).

4) A. M. Bond, R. L. Martin, and A. F. Masters, *Inorg. Chem.*, **14**, 1432 (1975).

5) G. Gritzner, H. Murauer, and V. Gutmann, *J. Electroanal. Chem.*, **101**, 177 (1979).

6) O. Sock, P. Lemoine, and M. Gross, *Electrochim. Acta*, **26**, 99 (1981).

7) C. Tsiamis, S. Cambanis, and C. Hadjikostas, *Inorg. Chem.*, **26**, 26 (1987).

8) R. F. Handy and R. L. Lintvedt, *Inorg. Chem.*, **13**, 893 (1974).

9) C. Tsiamis, C. C. Hadjikostas, S. Karageorgiou, and G. Manoussakis, *Inorg. Chim. Acta*, **143**, 17 (1988).

10) K. Shimizu, K. Morinaga, and K. Nakano, *Nippon Kagaku Zasshi*, **90**, 564 (1969).

11) R. W. Murray and L. K. Hiller, Jr., *Anal. Chem.*, **39**, 1221 (1967).

12) M. K. Kalinowski and A. Cmiel, *Inorg. Chim. Acta*, **49**, 179 (1981).

13) G. Gritzner, H. Murauer, and V. Gutmann, *J. Electroanal. Chem.*, **101**, 185 (1979).

14) G. W. Everett, Jr., and R. R. Horn, *J. Am. Chem. Soc.*, **96**, 2087 (1974).

15) G. S. Patterson and R. H. Holm, *Inorg. Chem.*, **11**, 2285 (1972).

16) N. A. Lewis and B. K. P. Sishta, *J. Chem. Soc., Chem. Commun.*, **1984**, 1428.

17) A. Endo, M. Watanabe, S. Hayashi, K. Shimizu, and G. P. Satô, *Bull. Chem. Soc. Jpn.*, **51**, 800 (1978).

18) A. Endo, *Bull. Chem. Soc. Jpn.*, **56**, 2733 (1983).

19) B. A. Moyer and T. J. Meyer, *Inorg. Chem.*, **20**, 436 (1981).

20) Y. Hoshino, A. Endo, K. Shimizu, and G. P. Satô, *J. Electroanal. Chem.*, **246**, 225 (1988).

21) Y. Satsu, A. Endo, K. Shimizu, G. P. Satô, K. Ono, I. Watanabe, and S. Ikeda, *Chem. Lett.*, **1986**, 585.

22) A. Endo, K. Shimizu, G. P. Satô, and M. Mukaida, *Chem. Lett.*, **1984**, 437.

23) A. Endo, M. Kajitani, M. Mukaida, K. Shimizu, and G. P. Satô, *Inorg. Chim. Acta*, **150**, 25 (1988).

24) J. P. Collman, R. A. Moss, H. Maltz, and C. C. Heindel, *J. Am. Chem. Soc.*, **83**, 531 (1961).

25) G. S. Hammond, D. C. Nonhebel, and C.-H. S. Wu, *Inorg. Chem.*, **2**, 73 (1963).

26) G. A. Forcier and J. W. Olver, *Anal. Chem.*, **37**, 1447 (1965).

27) J. A. Riddick and E. E. Toops, Jr., "Organic Solvents," 2nd ed., in "Techniques of Organic Chemistry," ed by A. Weissberger, Interscience Publishers, Inc., (1955), Vol. 7, p. 431.

28) R. Tamamushi and G. P. Satô, "Application of Polarography and Related Electrochemical Methods to the Study of Labile Complexes in Solution," in "Progress in Polarography," ed by P. Zuman, L. Meites, and I. M. Kolthoff, Vol. 3, Wiley-Interscience, New York (1971), p. 16.

29) S. Hayashi, K. Shimizu, and G. P. Satô, 21st Annual Meeting on Polarography and Electroanalytical Chemistry, Kyoto, November 1975, Abstr., *Rev. Polarogr. (Kyoto)*, **21**, 13 (1975).

30) Gen P. Satô, K. Shimizu, H. Ikeuchi, A. Endo, Y. Shirai, and S. Fujiwara, *Asahi Garasu Kogyogijutsu Shoreikai Kenkyuhokoku*, **43**, 115 (1983).

31) T. Kobayashi, Y. Nishina, K. Shimizu, and G. P. Satô, *Chem. Lett.*, **1988**, 1137.

32) For example: a) T. Ishiyama, *Bull. Chem. Soc. Jpn.*, **44**, 1571 (1971); b) F. L. Phillips and A. C. Skapski, *J. Chem. Soc., Dolton Trans.*, **1976**, 1448; c) K. W. Given, B. M. Mattson, and L. H. Pignolet, *Inorg. Chem.*, **15**, 3152 (1976); d) B. M. Mattson and L. H. Pignolet, *Inorg. Chem.*, **16**, 488 (1977); e) B. A. Moyer and T. J. Meyer, *J. Am. Chem. Soc.*, **100**, 3601 (1978); f) G. L. Miessler and L. H. Pignolet, *Inorg. Chem.*, **18**, 210 (1979); g) I. W. Nowell, *J. Chem. Soc., Chem. Commun.*, **1979**, 547; h) H. Nagashima, T. Ohshima, and K. Itoh, *Chem. Lett.*, **1984**, 789; i) K. Aoyagi, Y. Yukawa, K. Shimizu, M. Mukaida, T. Takeuchi, and H. Kakihana, *Bull. Chem. Soc. Jpn.*, **59**, 1493 (1986). For a brief review, see A. Endo, *Kagaku To Kogyo*, **38**, 143 (1985).

33) H. Ikeuchi, Y. Fujita, K. Iwai, and G. P. Satô, *Bull. Chem. Soc. Jpn.*, **49**, 1883 (1976).

34) T. Fujinaga and I. Sakamoto, *J. Electroanal. Chem.*, **67**, 201 (1976); **73**, 235 (1976).

35) Y. Hoshino, Y. Yukawa, A. Endo, K. Shimizu, and G. P. Satô, *Chem. Lett.*, **1987**, 845.

36) J. Iball and C. H. Morgan, *Acta Crystallogr.*, **23**, 239 (1967).

37) I. A. Baidina, P. A. Stabnikov, V. I. Alekseev, I. K. Igumenov, and S. V. Borisov, *Zh. Strukt. Khim.*, **27**, 102 (1986).

38) B. Morosin and J. R. Brathovde, *Acta Crystallogr.*, **17**, 705 (1964).

39) G. Kung-Jou Chao, R. L. Sime, and R. J. Sime, *Acta Crystallogr., Sect. B*, **29**, 2845 (1973).

Catalysis by Heteropoly Compounds. XII.[1] Absorption Properties of 12-Tungstophosphoric Acid and Its Salts

Toshio OKUHARA,* Shin TATEMATSU,† Kwan Young LEE, and Makoto MISONO*
Department of Synthetic Chemistry, Faculty of Engineering, The University of Tokyo, Hongo, Bunkyo-ku, Tokyo 113
(Received September 19, 1988)

The absorption of organic molecules into the bulk of $H_3PW_{12}O_{40}$ and its salts was studied. Polar (or basic) molecules, such as alcohols and amines, were readily absorbed into $H_3PW_{12}O_{40}$, but nonpolar hydrocarbons were not absorbed. The absorption depended not only on the polarity but also on the molecular size. The diffusion coefficients of the absorption of C_1—C_4 alcohols were of similar magnitudes, and were much smaller than that of the intracrystalline diffusion of methanol in ZSM-5. The amounts of absorbed molecules in $H_3PW_{12}O_{40}$ tended to be in discrete values: that is, integral multiples of the number of protons (3, 6, etc.). This fact indicates that these polar molecules are protonated and form stable secondary structures throughout the bulk. It was confirmed in the case of methanol or ethanol that the transition between the states of 6 and 9 molecules/anion took place through the pressure changes. The absorptivity was greatly suppressed by the substitution of Cs^+ for more than two H^+, while the Na salts showed an absorptivity similar to that of $H_3PW_{12}O_{40}$.

We previously reported that the important characteristic of solid heteropoly acids, such as $H_3PW_{12}O_{40}$, is that these compounds absorb readily polar molecules, such as alcohols and amines, but not nonpolar hydrocarbons.[2-4] This property discriminates molecules by the difference in the polarity. This is different from zeolites which recognize molecular size.

Due to the absorptivity, some reactions proceed very rapidly in the bulk. This state has been called the "pseudoliquid phase".[3-6] The pseudoliquid phase brings about peculiar activity patterns[6,7] and selectivities in the reactions of alcohols and ethers.[8-11] We recently reported unusual pressure dependencies of the rate and selectivity of ethanol dehydration over $H_3PW_{12}O_{40}$, and explained the phenomenon in terms of changes in the number of ethanol molecules absorbed in the pseudoliquid phase.[12] Thus, the pseudoliquid phase behavior is essential for understanding the catalysis of heteropoly compounds.

The absorption of alcohols has already been studied by us,[2] Niiyama et al.,[13] and Moffat et al.[14] However, the factors determining the absorption rate, the amount, and the diffusion coefficient in the pseudoliquid phase have not been fully elucidated and the transition process between two pseudoliquid phases[15] has not been examined in detail. In this study, the rates of absorption as well as the amounts were systematically measured for various molecules over $H_3PW_{12}O_{40}$ under controlled conditions. It was also attempted to control the absorptivity of $H_3PW_{12}O_{40}$ by the substitution of Na^+ or Cs^+ for H^+.

Experimental

Catalysts and Materials. $H_3PW_{12}O_{40}$ (Nippon Inorganic Colour and Chemical Co., Ltd.) was recrystallized from water after purification by extraction with diethyl ether.[6] The salts of Na and Cs were prepared from Na_2CO_3 and Cs_2CO_3 by a previously described method.[6,10] The amount of water of crystallization was measured with a thermogravimeter (Shimadzu TG-30) which was connected to a vacuum system. The surface area was measured by the BET method using N_2-gas adsorption after the samples were pretreated at 130 °C in He. Pyridine, alcohols (C_1—C_4), and amines (C_3—C_4) were degassed by a freeze-thaw cycle; water contained as an impurity was removed by Molecular Sieve 3A. Ethers (C_2—C_6) were used after being degassed by a freeze-thaw cycle.

Apparatus and Procedure. Absorption and desorption of molecules were followed by a quartz spring balance (sensitivity; 14 mg mm^{-1}) which was connected to a vacuum system. The heteropoly compounds (about 1.0 g) were exposed to the vapor of the molecules at 28 °C and at a desired pressure after being evacuated at 130 °C for 1 h. We call the saturated amount of absorption obtained in the presence of the vapor the "amount of saturated absorption". The number of molecules held in heteropoly compounds after evacuation at 28 °C is called the "amount of irreversible absorption".

If absorption occurs into a particle with a radius, r, Eq. 1 can be used for large t,[16,17] where Q_t and Q_∞ are the amounts of absorption at time t and at equilibrium, respectively:

$$Q_t/Q_\infty = 1 - (6/\pi^2)\exp(-D\pi^2 t/r^2). \quad (1)$$

Here, D is the diffusion coefficient in a particle of $H_3PW_{12}O_{40}$. The concentration of molecule at the surface of the $H_3PW_{12}O_{40}$ particle is assumed to be constant during the absorption. We estimated r to be about 1000 Å from the surface area (5.0 m$^2\cdot$g^{-1}) and the density (5.8 g$\cdot$cm^{-3}) of $H_3PW_{12}O_{40}$.[18] From Eq. 1, the slope of a straight line in a plot of $\ln(1-Q_t/Q_\infty)$ against t gives D. This plot was compared with another one, $Q_t/Q_\infty=6(D/\pi r^2)^{1/2}t^{1/2}$, which is suitable for small t.[17] As a result, the former was confirmed to be adequate for our data.

In order to follow rapid changes in the amounts of absorption by the pressure jump of methanol or ethanol, a

† Present address: Asahi Glass Co., Ltd., Hazawa-cho, Kanagawa-ku, Yokohama 221.

thermogravimeter connected to the vacuum system was used. About 50 mg of $H_3PW_{12}O_{40}$ was pretreated in vacuo at 130 °C for 1 h. Methanol and ethanol were introduced at 45 and 60 °C, respectively. The pressures were changed by controlling the temperature of the liquid of the alcohols in a Pyrex tube container connected to the system. It was confirmed that no reaction took place under these conditions.

Results

Rate of Absorption into $H_3PW_{12}O_{40}$. Typical time courses of the absorption of methanol and diethyl ether are shown in Fig. 1. The ordinate is the amount of absorption in the unit of the number of molecules per polyanion, $PW_{12}O_{40}^{3-}$ (averaged over whole bulk). In the case of methanol, the initial rate of absorption, which is defined as the amount absorbed in the initial 10 min, appeared to be slightly dependent on the pressure; however, the amount of saturated absorption showed two discrete values: about 6 molecules/anion at the pressure of 15—30 Torr (1 Torr=133.3 Pa) and about 12 molecules/anion at 60—100 Torr. As discussed previously,[2] these amounts correspond to more than 50 surface layers. Therefore, it is obvious that the uptake is not the adsorption but the absorption. In accordance with this idea, the expansion of the sample volume was observed.

The absorption of diethyl ether was slow at a pressure lower than 70 Torr (Fig. 1b). However, at higher pressures (160—350 Torr), the absorption reached very rapidly about 6 molecules/anion. The presence of a similar critical pressure has previously been observed for acetone.[2]

In Table 1, the initial rates of absorption as well as the amounts of absorption are summarized. In spite of the great difference in the pressure introduced, the variation of the initial rates was within an order of magnitude for alcohols and amines. As for the alcohols, the rates in the pressure range of 20—30 Torr were in the following order: methanol≈ethanol >1-propanol>2-propanol.

Figure 2 shows a plot of $\ln(1-Q_t/Q_\infty)$ against t for

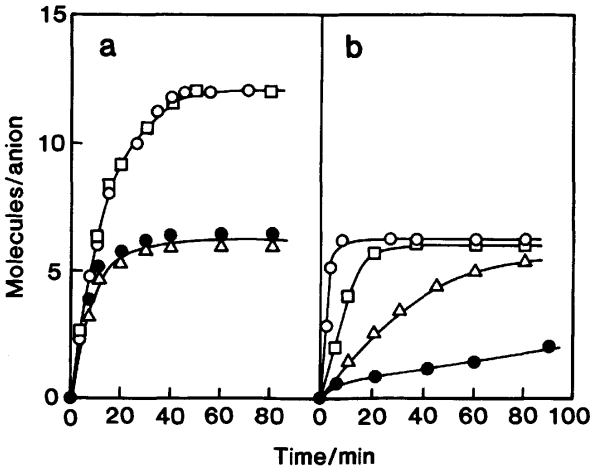

Fig. 1. Typical time course of absorption in $H_3PW_{12}O_{40}$ at 28 °C.
a) Methanol at 15 Torr (△), 30 Torr (●), 60 Torr (□), and 100 Torr (○). b) Diethyl ether at 70 Torr (●), 160 Torr (△), 200 Torr (□), and 350 Torr (○).

Table 1. Rate and Amount of Absorption of Molecule into $H_3PW_{12}O_{40}$

Molecule	(pK_a)	Size[a]	μ[b]	P[c]	Rate[d]	Absorption amount[e]	
						S[f]	I[g]
CH_3OH	(−2.0)	20	1.71	30(20)	5.2	6.0	3.1 (26)
				100(68)	6.5	12.0	3.1 (26)
C_2H_5OH	(−3.0)	25	1.73	30(43)	5.5	14.1	6.1 (64)
				50(71)	6.5	14.5	6.2 (65)
n-C_3H_7OH	(−3.0)	30	1.73	20(80)	3.8	14.0	6.2 (78)
i-C_3H_7OH	(−3.2)	31	1.67	30(57)	3.1	12.1	6.1 (76)
n-C_4H_9OH	(−3.8)	35	1.81	4(50)	2.0	5.4	2.8 (41)
$(CH_3)_2O$	(−3.8)	30	1.30	760(15)	1.6	4.0	2.6 (33)
$(C_2H_5)_2O$	(−3.6)	37	1.17	350(59)	6.2	6.3	5.8 (89)
$(n$-$C_3H_7)_2O$	(−4.3)	45	1.20	30(52)	1.1	4.9	4.6 (86)
1,4-Dioxane	(−2.9)	33	1.40	30(76)	2.2	8.3	4.8 (66)
n-$C_3H_7NH_2$	(10.7)	32	1.34	30(9)	3.1	12.0	7.0 (89)
				150(43)	9.6	17.5	8.4 (105)
i-$C_3H_7NH_2$	(10.6)	33	—	30(5)	4.1	9.5	6.9 (86)
				300(46)	7.5	14.8	7.9 (97)
n-$C_4H_9NH_2$	(10.8)	35	1.32	30(28)	6.0	15.2	8.6 (125)
				50(47)	8.0	17.7	8.8 (137)
C_5H_5N	(5.2)	31	2.32	15(62)	4.0	8.5	6.0 (78)
C_6H_6[h]		34	0	65(43)	—	0.50	0.10(1.4)
C_2H_4[h]		16	0	60(0.13)	—	0.04	0.03(0.2)

a) Cross section/Å^2. b) Dipole moment, Debye. c) Introduced at 28 °C; Torr. The figures in parentheses are the relative pressure/%. d) The initial absorption rate; number of molecules (anion·10 min)$^{-1}$. e) Number of molecule anion^{-1}. f) Saturated amount. g) Irreversible amount. The figures in parentheses are the number of surface layer (see text). h) Ref. 2.

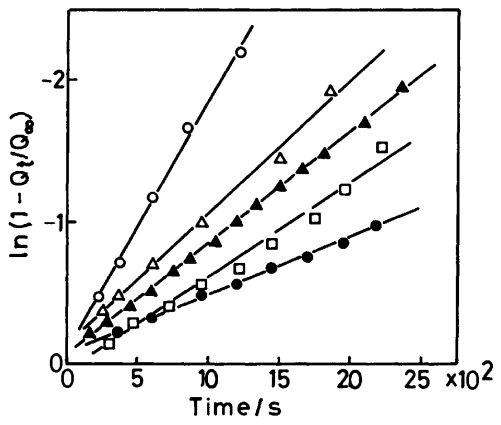

Fig. 2. Plots of $\ln(1-Q_t/Q_\infty)$ vs. t for various polar molecules into $H_3PW_{12}O_{40}$ at 28°C.
(○) Methanol at 30 Torr, (△) ethanol at 30 Torr, (□) 1-propanol at 20 Torr, (●) 2-propanol at 30 Torr, and (▲) 1-propanamine at 30 Torr.

Table 2. Diffusion Coefficients of Molecules into $H_3PW_{12}O_{40}$ at 28°C

Molecule	Pressure / Torr	Q_∞[a]	Diffusion coefficient, D / 10^{-14} cm²·s⁻¹
CH_3OH	15	6.0	1.75
	30	6.0	1.80
	100	12.0	1.20
C_2H_5OH	5	6.0	1.38
	10	6.0	1.60
	30	14.1	1.03
	50	14.5	1.00
n-C_3H_7OH	20	14.0	0.63
i-C_3H_7OH	30	12.1	0.42
n-C_4H_9OH	4	5.4	0.86
$(C_2H_5)_2O$	160	6.0	0.43
	200	6.0	2.00
1,4-Dioxane	30	8.3	1.12
n-$C_3H_7NH_2$	30	12.0	0.88
	150	17.5	0.68
i-$C_3H_7NH_2$	30	9.5	0.48
	300	14.8	0.42
n-$C_4H_9NH_2$	30	15.2	0.96
	50	17.7	0.83
Pyridine	15	8.5	0.66

a) Amount of saturated absorption; number of molecule·anion⁻¹.

alcohols and amines (see Eq. 1). All of the curves could be fitted by straight lines. The diffusion coefficients, D, which were calculated from the slopes of the curves, are summarized in Table 2. In the case of the alcohols, the D in the pressure range from 20 to 30 Torr was in the following order: methanol> ethanol>1-propanol>2-propanol. For a comparison, the data reported for the intracrystalline diffusion of various molecules for zeolites are given in Table 3.[19-24]

In Fig. 3, the pressure dependencies of the initial absorption rates and the diffusion coefficients are shown for methanol and 1-propanamine, where the abscissa is the relative pressure, which is the ratio of the pressure introduced to the saturated vapor pressure at 28°C multiplied by 100. It was found that the pressure dependence of the absorption rate was different in these molecules; when the relative pressure increased from 10 to 60%, the absorption rate of 1-propanamine increased by a factor of about 3. However, the increase in the rate for methanol was small. The initial absorption rate tended to be nearly constant for each molecule at higher relative pressures (>40%).

Amounts of Absorption. The influence of the pressure on the amounts of absorption is shown in

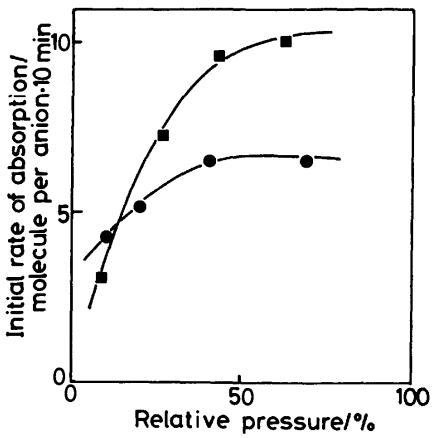

Fig. 3. Changes of the initial absorption rates as a function of the relative pressure.
●: Methanol, ■: 1-propanamine.

Table 3. Diffusion Coefficients of Molecules into Zeolites

Molecules/Zeolite	Temperature / °C	D / cm²·s⁻¹	Ref.
CH_3OH/H-ZSM-5	30	2.6×10^{-11}	19
$(CH_3)_2O$/H-ZSM-5	30	7.5×10^{-11}	19
C_2H_5OH/Zeolite-T	150	1.0×10^{-11}	20
C_2H_6/H-ZSM-5	25	7.0×10^{-11}	21
C_3H_8/H-ZSM-5	25	1.3×10^{-11}	22
n-C_4H_{10}/Ca-A	75	6.0×10^{-14}	22
C_6H_6/H-ZSM-5	20	8.6×10^{-11}	19
C_6H_{12}/H-ZSM-5	73	5.2×10^{-14}	23
C_6H_{12}/H-ZSM-5	80	2.2×10^{-14}	24
p-C_8H_{10}/H-ZSM-5	80	2.2×10^{-12}	24

Fig. 4. For methanol, the amounts of saturated absorption were about 6 and 12 molecules in the relative pressure of 10—80%. The amount of irreversible absorption was 3 molecules/anion in this pressure range. On the other hand, the amount of irreversible absorption of ethanol and diethyl ether was about 6 molecules/anion. As summarized in Table 1, the amounts of irreversible absorption of alcohols and ethers often showed values close to 3 and 6 molecules per anion, respectively. The ratios of the amount of irreversible absorption to that of monolayer adsorption are shown in parentheses in Table 1. Hereafter, this ratio is called the "number of surface layers".

The transition between the different absorption states can be seen in Figs. 5 and 6. The state of 6 molecules of methanol per anion, which was obtained at a pressure of 20 Torr, did not change upon the pressure increase to 55 Torr (Fig. 5). By a further increase to 70 Torr, the number of molecules increased to 9 molecules/anion. This state (9 molecules/anion) remained unchanged until the pressure was decreased to 20 Torr, inducing a change of the state to 6 molecules/anion. Figure 6 shows a similar behavior for ethanol. The transition between 6 and 9 molecules/anion took place reversibly through a pressure change from 45 to 3.5 Torr.

The absorption properties of acidic salts of Na and Cs were measured by using ethanol as a probe molecule; they are summarized in Table 4. The uptakes of ethanol for Na and Cs salts are shown in Fig. 7 in units of "number of surface layer" as a function of the cation content. The "number of surface layer" was estimated from the cross section of ethanol (25 Å^2) and the surface area of these salts.[25] As can be seen in Fig. 7, the numbers of surface layers for Na salts were about 60

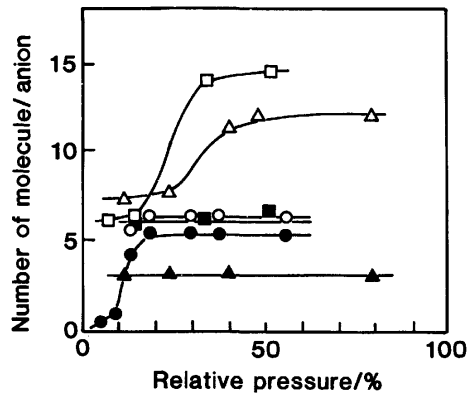

Fig. 4. Pressure dependence of the amounts of absorption into $H_3PW_{12}O_{40}$ at 28°C.
Saturated amount: (□) ethanol, (△) methanol, (○) diethyl ether.
Irreversible amount: (■) ethanol, (▲) methanol, (●) diethyl ether.

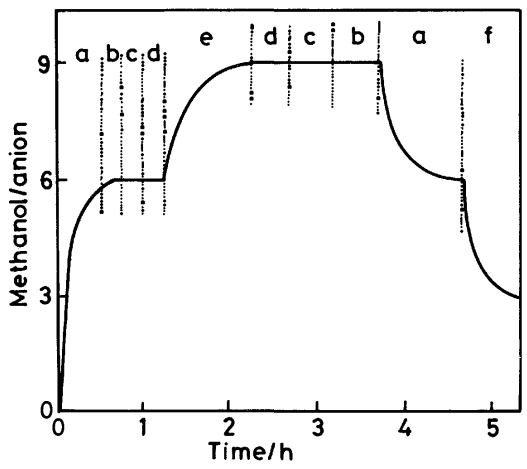

Fig. 5. Changes of absorption amount in $H_3PW_{12}O_{40}$ by the pressure jump of methanol at 45°C.
(a) 20 Torr, (b) 30 Torr, (c) 40 Torr, (d) 55 Torr, (e) 70 Torr, (f) 0 Torr.

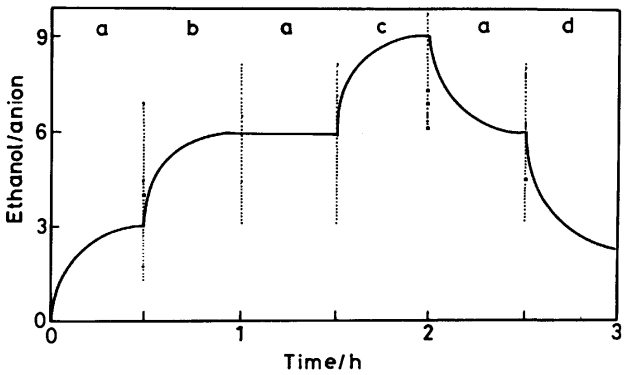

Fig. 6. Changes of absorption amount in $H_3PW_{12}O_{40}$ by the pressure jump of ethanol at 60°C.
(a) 3.5 Torr, (b) 13 Torr, (c) 45 Torr, (d) 0 Torr.

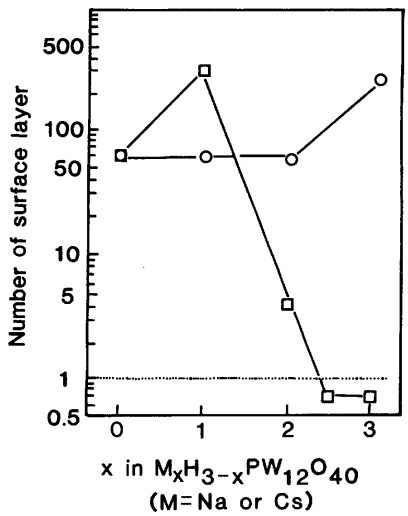

Fig. 7. Uptakes of ethanol into Na and Cs salts of $H_3PW_{12}O_{40}$ at 28°C. (○) Na, (□) Cs.
The samples were pretreated at 150°C. The pressure of ethanol was 30 Torr.

Table 4. Rate and Amount of Uptake of Ethanol for Na and Cs Salts

	$Na_xH_{3-x}PW_{12}O_{40}$				$Cs_xH_{3-x}PW_{12}O_{40}$			
	$x=0$	1	2	3	1	2	2.5	3
Rate[a]	6.5	5.5	4.5	2.5	5.5	3.0	4.0	4.0
Uptakes[b]	6.2	4.3	2.9	2.2	3.1	1.9	1.8	1.7
Surface area[c]	5.0	3.7	2.5	0.8	0.5	21	114	176

a) Initial rate for absorption, molecules (anion·10 min)$^{-1}$. b) Irreversible amount. c) $m^2\ g^{-1}$ (after pretreatment at 130 °C). Ethanol (30 Torr) was added at 28 °C.

and 143 in $0 \leq x \leq 2$ and at $x=3$, respectively. On the other hand, this number changed greatly from 322 to 0.5 as x varied from 1 to 3 for Cs salts.

Discussion

Factors Determining the Absorption. The uptakes of benzene, ethylene (Table 1), and other hydrocarbons were nearly equal to or less than the amount of monolayer;[2] the numbers of surface layers were less than 1. This shows that these hydrocarbons are not absorbed. On the other hand, the numbers of surface layers for alcohols, ethers, and amines were greater than 26, indicating that these polar molecules are absorbed into the bulk of $H_3PW_{12}O_{40}$. Due to a large uptake, an increase in the sample temperature was always observed. Since $H_3PW_{12}O_{40}$ is a strong acid, an acid–base interaction must be the driving force of the absorption of basic (or polar) molecules.

The basicity may be expressed by pK_a of the protonated molecules (conjugate acid), where K_a is the dissociation constant of protonated molecules; $BH^+ + H_2O \rightleftarrows B + H_3^+O$ (B; base). Then, the molecules can be classified into three groups by their pK_a values. The first group consists of alcohols and ethers, of which the pK_a values are between −2.0 and −4.3. The molecules in the second group are amines having pK_a's of about 10, which are much more strongly basic. The third is the group of hydrocarbons. While the values of pK_a of hydrocarbons are not clear, these molecules must be much less basic than alcohols and ethers. In the gas phase, oxygenated compounds like alcohol and ether are generally more basic than olefins.[26]

The polarity of molecule also appears to be relevant to the absorption. The polarity may be represented by the dipole moment. As shown in Table 1, alcohol, ether, and amine have large dipole moments (e.g., about 1.7 (alcohols), 1.2 (ethers), 1.3 (amines), and 2.2 (C_5H_5N) in the unit of Debye),[27] but it is zero for ethylene and benzene. Generally, hydrocarbons have very small dipole moments. Therefore, it is concluded that either the basicity or polarity of molecules is important regarding absorption. Since these molecules tend to form hydrogen bonding, whether the hydrogen bonding is formed with $H_3PW_{12}O_{40}$ or not may be a key factor for absorption.

Rate of Absorption. As shown in Fig. 3, the initial absorption rate had a nearly constant value at the relative pressure higher than about 40%. When the initial rates measured at the relative pressure higher than 40% were plotted against the molecular size, correlations for polar molecules were obtained as shown in Fig. 8. The initial rates of alcohols greatly decreased as the molecular size increased (20 Å^2 (methanol)—35 Å^2 (1-butanol)). However, the initial rates for propanamines and 1-butanamine were distinctly higher than those of alcohols in spite of their greater molecular size. This difference is probably due to the large difference in the pK_a values of alcohols ($-2 \leq pK_a \leq -3.8$) and amines ($pK_a \approx 10$). It may therefore be stated that the rate is primarily determined by the basicity (or polarity) and secondarily by the molecular size.

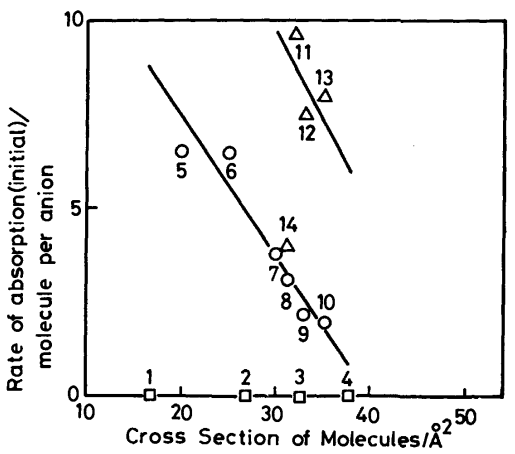

Fig. 8. Initial rates of absorption of various molecules by $H_3PW_{12}O_{40}$ vs. molecular size.
1. Ethylene (0.13), 2. dichloromethane (27), 3. benzene (43), 4. toluene (91), 5. methanol (68), 6. ethanol (71), 7. 1-propanol (80), 8. 2-propanol (57), 9. 1,4-dioxane (76), 10. 1-butanol (50), 11. 1-propanamine (43), 12. 2-propanamine (46), 13. 1-butanamine (47), 14. pyridine (62).
The figures in parentheses are the relative pressure.

As shown in Table 2, the diffusion coefficients for alcohols tended to become lower as the molecular size increased (from methanol to 2-propanol). This trend is the same as the initial rates. Since the diffusion coefficient is regarded as being the rate constant of absorption, the rate of absorption would be proportional to the product of the diffusion coefficient and the concentration of the molecule at the surface. There-

fore, the difference in the initial rate for alcohols may mainly be ascribable to a difference in the diffusion coefficient. Although the diffusion coefficients of the amines were not so great (Table 2), the initial rates were high (Fig. 8). The higher initial rates for the amines are probably brought about by the higher concentrations of amines on the surface as compared with those of alcohols, while the concentration at the surface during the absorption is not yet known.

The diffusion coefficient for the hydrocarbons into the pore of ZSM-5 zeolite varied from 10^{-11} to 10^{-14} $cm^2 \cdot s^{-1}$ depending on the molecules (Table 3). This great difference in D is called the molecular sieve effect.[17] In the case of $H_3PW_{12}O_{40}$, the difference between hydrocarbons and polar molecules was very large. But, the diffusion coefficients of alcohols and amines into the bulk of $H_3PW_{12}O_{40}$ showed similar values, about $0.42—1.80\times10^{-14}$ $cm^2 \cdot s^{-1}$ (at 30 Torr). The uptake of $H_3PW_{12}O_{40}$ is not diffusion into pores,[3] but absorption into the bulk between the polyanions. Therefore, it may meet a much greater resistance than the diffusion of molecules into the micropores of zeolite.

It is clear that the absorptivity of $H_3PW_{12}O_{40}$ was greatly suppressed by the substitution of Cs^+ for H^+, while the absorptivity varied little upon substitution of Na^+ for H^+ (Fig. 7). Since the acidity decreased upon substitution of Na^+ for H^+,[6] the decrease in the rate of ethanol absorption as the content of Na^+ increased (Table 4) also suggests the importance of the acidity of heteropoly compounds (basicity of molecules).

Transition between Pseudoliquid Phases. As for the absorption of polar molecules, there are at least two states which differ in the number of absorbed molecules. The states of 6 and 9 molecules/anion existed (Figs. 5 and 6) and each state was stable within a certain range of pressure. We reported for the dehydration of 2-propanol over $H_3PW_{12}O_{40}$ that there were at least two pseudoliquid phases differing in the catalytic activity.[15] At 80 °C, the number of 2-propanol absorbed was 3 molecules/anion for the high-activity state and 8—9 molecules/anion for the low-activity states. Their transitions brought about unusual pressure dependencies of the activity.[15]

It is noted that the amounts of alcohol, ether, and pyridine were nearly integral multiples (1, 2, and 3) of the number of protons present in the bulk of $H_3PW_{12}O_{40}$. These numbers indicate that these molecules are homogeneously absorbed and that the stable forms are probably, e.g., $CH_3OH_2^+$, $(C_2H_5OH)_2H^+$, and $(Py)_2H^+$. IR and gravimetric measurements have previously suggested that pyridinium ion in dimer species, $(Py)_2H^+$ existed.[2] Recently, ^1H and ^{13}C solid-state NMR of ethanol absorbed on $H_3PW_{12}O_{40}$ have been measured.[28] ^1H NMR spectra of $H_3PW_{12}O_{40}\cdot6C_2H_5OH$ resembled those of protonated ethanol in superacid,[29] suggesting that this species is $(C_2H_5OH)_2H^+$.[28] Furthermore, the infrared spectra of $H_3PW_{12}O_{40}\cdot6C_2H_5OH$ also supported the presence of $(C_2H_5OH)_2H^+$ in the bulk.[30] Although the exact structure of a compound having 6 molecules/anion is unknown yet, for example, the structure of $H_3PW_{12}O_{40}\cdot6C_2H_5OH$ may be similar to that of $H_3PW_{12}O_{40}\cdot6H_2O$, of which the structure was determined by X-ray diffraction,[31] since the XRD patterns were similar.

Summary

1. For absorption, the basicity or polarity of molecules was important. The rate of absorption depended on the molecular size as well as basicity.

2. In the absorption state (i.e., pseudoliquid phase), the numbers of molecules were integral multiples of the number of protons; the amount of irreversible absorption of methanol was equal to the number of H^+; those of ethanol, diethyl ether, and propanols were twice the number.

3. In the presence of gas-phase methanol or ethanol, the transition between different pseudoliquid phases takes place reversibly, depending on the pressure ranges.

4. The absorptivity of $H_3PW_{12}O_{40}$ can be controlled by the formation of acidic salts of Cs.

The present work was supported in part by a Grant-in-Aid for Scientific Research No. 62470070 from the Ministry of Education, Science and Culture and by Asahi Glass Foundation.

References

1) Part XI: N. Mizuno and M. Misono, *J. Phys. Chem.*, in press.

2) M. Misono, N. Mizuno, K. Katamura, A. Kasai, Y. Konishi, K. Sakata, T. Okuhara, and Y. Yoneda, *Bull. Chem. Soc. Jpn.*, **55**, 400 (1982).

3) M. Misono, K. Sakata, Y. Yoneda, and W. Y. Lee, Proc. 7th Intern. Congr. Catal., Tokyo, 1980, Kodansha (Tokyo)-Elsevier (Amsterdam), 1981, p. 1047.

4) M. Misono, *Catal. Rev.*, **29**, 269 (1987).

5) T. Okuhara, T. Hashimoto, M. Misono, Y. Yoneda, H. Niiyama, Y. Saito, and E. Echigoya, *Chem. Lett.*, **1983**, 573.

6) T. Okuhara, A. Kasai, N. Hayakawa, Y. Yoneda, and M. Misono, *J. Catal.*, **83**, 121 (1983).

7) Y. Saito and H. Niiyama, *J. Catal.*, **106**, 329 (1987).

8) T. Okuhara, A. Kasai, N. Hayakawa, M. Misono, and Y. Yoneda, *Chem. Lett.*, **1981**, 391.

9) T. Okuhara, T. Hibi, K. Takahashi, S. Tatematsu, and M. Misono, *J. Chem. Soc., Chem. Commun.*, **1984**, 697.

10) T. Hibi, K. Takahashi, T. Okuhara, M. Misono, and Y. Yoneda, *Appl. Catal.*, **24**, 69 (1986).

11) T. Baba, J. Sakai, H. Watanabe, and Y. Ono, *Bull. Chem. Soc. Jpn.*, **55**, 2555 (1982).

12) M. Misono, T. Okuhara, T. Ichiki, T. Arai, and Y. Kanda, *J. Am. Chem. Soc.*, **109**, 5535 (1987).

13) Y. Saito, H. Niiyama, and E. Echigoya, *Nippon Kagaku Kaishi*, **1984**, 391.
14) J. G. Highfield and J. B. Moffat, *J. Catal.*, **95**, 108 (1985).
15) K. Takahashi, T. Okuhara, and M. Misono, *Chem. Lett.*, **1985**, 841.
16) J. Crank, "The Mathematics of Diffusion," Clarendon Press, Oxford (1957), p. 89.
17) R. M. Barrer, "Zeolite-Science and Technology," ed. by F. R. Ribeiro et al., Martinus Nijhoff Publishers (1984), p. 261.
18) W. Pier and A. Weiss, Landolt-Bornstein Neue Series III/7f (1977).
19) P. Wu and Y. H. Ma, Proc. 6th Intern. Zeolite Conf., Reno, 1984, Butterworths, p. 251.
20) R. L. Gorring, *J. Catal.*, **31**, 13 (1973).
21) M. Bulow, H. Schlodder, L. V. C. Rees, and R. E. Richards, Proc. 7th Intern. Zeolite Conf., Tokyo, 1986, Kodansha, Elsevier, p. 579.
22) R. M. Barrer and D. J. Clarke, *J. Chem. Soc., Faraday Trans. 1*, **70**, 535 (1974).
23) H. Chon, B. J. Ahn, and S. E. Park, Proc. 8th Intern. Congr. Catal., Berlin, 1984, Verlag Chemie, Weinheim, IV-555.
24) C. Wu, G. Qin, and Y. Xie, Proc. 7th Intern. Zeolite Conf., Tokyo, 1986, Kodansha, Elsevier, p. 481.
25) N. Hayakawa, T. Okuhara, M. Misono, and Y. Yoneda, *Nippon Kagaku Kaishi*, **1982**, 356.
26) D. H. Ave and M. T. Bowers, "Gas Phase Ion Chemistry," ed. by M. T. Bowers, Academic Press, New York (1979), Vol. 2, Chap. 9.
27) B. Starch, "Landolt-Bornstein Tables," New Series, II/4 Springer (1967); A. L. McClellan, "Tables of Experimental Dipole Moments," W. H. Freeman and Company, San Francisco and London (1963).
28) Y. Kanda, K. Y. Lee, S. Nakata, S. Asaoka, and M. Misono, *Chem. Lett.*, **1988**, 139.
29) G. A. Olah, J. Sommer, and E. Namanworth, *J. Am. Chem. Soc.*, **89**, 3576 (1967).
30) K. Y. Lee, N. Mizuno, T. Okuhara, and M. Misono, *Bull. Chem. Soc. Jpn.*, in press.
31) G. M. Brown, M. R. Neo-Spiret, W. R. Busing, and H. A. Levy, *Acta Crystallogr., Sect. B*, **33**, 1038 (1977).

Cobalt(III) Complexes with Quadridentate Ligands. VIII.[1] The Preparation and Properties of Cis-β_1 and β_2-Isomers of the Thiosalicylato-(quadridentate amine)cobalt(III) Complexes

Yoshihisa YAMAMOTO,* Kayoko YOSHII, Eiko TOYOTA, and Kazuko KONNO
Faculty of Pharmaceutical Sciences, Higashi Nippon Gakuen University,
Ishikari-Tobetsu, Hokkaido 061-02
(Received May 2, 1988)

cis-β_1 and β_2-Thiosalicylato(quadridentate amine)cobalt(III) complexes, *cis*-β_1, β_2-[Co(thiosal)L]X·nH$_2$O (L: trien (2,2,2-tet), 3,2,3-tet; X: Cl, NO_3), have been prepared from a reaction mixture of [$CoCl_2$L]Cl·nH$_2$O (L: trien, 3,2,3-tet), Ag_2O, thiosalicylic acid (*o*-mercaptobenzoic acid), and 28% aqueous ammonia. Two geometrical isomers (cis-β_1 and β_2) of their complexes were separated by Dowex 50W-X2 column chromatography. The isomerization between the cis-β_1 and β_2-isomers is reversible in water at 40 °C. The IR spectra of these complexes showed four or five absorption bands in the 990—1100 cm^{-1} region and four absorption bands in the 3000—3300 cm^{-1} region. This indicates that these complexes assume the cis-β-form. Their cis-β_1 and β_2 configurations have been established by their absorption and NMR spectra. The *cis*-β_1 and β_2-thiosalicylato(trien)cobalt(III) complexes have been tentatively assigned to the *RR,SS* diastereoisomer by their ^{1}H NMR spectra. The color of solid state materials, solubilities in alcohols, isomerization at 40 °C, reaction in 60% nitric acid, absorption spectra, and chemical shift of Co–S–C carbon of the coordinated thiosalicylato ligand for the title complexes are different from those of the corresponding *cis*-β_1 and β_2-salicylato(quadridentate amine)cobalt(III) complexes, *cis*-β_1, β_2-[Co(sal)L]Cl·nH$_2$O (L: trien, 2,3,2-tet, 3,2,3-tet, 3,3,3-tet), reported previously.

Previous papers[2,3] have been concerned with the preparation, properties, and NMR spectra of *cis*-β_1 and β_2-salicylato(quadridentate amine)cobalt(III) chloride hydrates, *cis*-β_1, β_2-[Co(sal)L]Cl·nH$_2$O (L: trien, 2,3,2-tet, 3,2,3-tet, 3,3,3-tet).

Many investigations[4–10] of the metal complexes with thiosalicylato (*o*-mercaptobenzoato) ligand have been concerned with the stability, formation constants, and potentiometric studies. However, the preparation of thiosalicylato metal complexes has not yet been described, except for Rh(thiosal)$_2$,[11] Ni(thiosal)$_2$,[12] [Pt(bpy)(thiosal)],[13] and (PPh_4)[Mn(thiosal)$_2$(HIm)][14] (HIm: imidazole). Little is known of the preparation and physical and general properties for octahedral thiosalicylato metal complexes, in contrast with those of octahedral salicylato cobalt complexes and the related complexes.[1–3,15–18] The present paper deals with the preparation and properties of *cis*-β_1 and β_2-thiosalicylato(quadridentate amine)cobalt(III) complexes, *cis*-β_1, β_2-[Co(thiosal)L]Cl·nH$_2$O (L: trien, 3,2,3-tet), and deals with the assignments of the configuration of cis-β_1 and β_2-isomers on their IR, NMR, and absorption spectra.

Experimental

Measurements. The electric conductivities in aqueous solutions were determined by the use of a conductometric meter, CM-30 (Shimadzu), at room temperature. The magnetic susceptibilities were measured by Faraday's method using a magnetic balance (Shimadzu) at room temperature. The IR spectra were recorded in potassium bromide disks with a 270—30 spectrophotometer (Hitachi). The visible absorption spectra were recorded with a Shimadzu UV-210 recording spectrophotometer. The NMR spectra were recorded with an FX90Q apparatus (JEOL) for ^{1}H NMR and an FX-60 apparatus (JEOL) for ^{13}C NMR. The melting points were measured on a MP-500D apparatus (Yanako).

Preparation of Complexes. *cis*-α-Dichloro(triethylenetetramine)cobalt(III) Chloride (1) and *trans*-Dichloro(4,7-diazadecane-1,10-diamine)cobalt(III) Chloride Hydrate (2): These complexes were prepared by the methods of Sargeson[19] and Bosnich.[20]

***cis*-β_1-Thiosalicylato(triethylenetetramine)cobalt(III) Chloride Hydrate (3) and β_2-Thiosalicylato(triethylenetetramine)-cobalt(III) Chloride Trihydrate (4):** Complex **1** (5.0 g, 16.05 mmol) was added to moistend fresh Ag_2O, which was made from silver nitrate (5.5 g, 32.10 mmol) and potassium hydroxide (1.80 g, 32.10 mmol). The mixture was stirred for several minutes at room temperature; to the mixture was added 20 cm^3 of water and kept for about 30 min at 60 °C. The precipitated silver chloride was filtered off. Then, thiosalicylic acid (2.5 g, 16.2 mmol) and 3 cm^3 of 28% aqueous ammonia were added to the solution. From the reaction mixture, complexes **3** and **4** were obtained according to the following methods 1—3.

Method 1: The reaction mixture was stirred at 50 °C for 6 h; it was then concentrated on a rotary evaporator and dried. Yield: 6.38 g for *cis*-β-[Co(thiosal)trien]Cl·nH$_2$O. *cis*-β-[Co(thiosal)trien]Cl·nH$_2$O of 0.8 g was dissolved in 2 cm^3 of water, and the solution was injected onto a column of ion-exchange resin (Dowex 50W-X2, ϕ2.5×30 cm). Upon elution with 0.1 mol dm^{-3} NaCl, the effluent of the first russet band of complex **4** and that of the second russet band of complex **3** was collected and concentrated, respectively. The separated NaCl was removed. The purification for complexes **3** and **4** was recrystallized from water–acetone. Yields: 2.61 g (39.5%) for **3**, 2.30 g (32.0%) for **4**.

Method 2: The reaction mixture was stirred at 40 °C for 3 h, and allowed to remain one night in an icebox; then the precipitated complex **3** was filtered and recrystallized. To the filtrate was added ethanol; the mixture was allowed to remain one night. The precipitated complex **4** was filtered

and recrystallized from water-acetone. Yields: 1.0 g (15.2%) for **3**, 2.6 g (36.1%) for **4**.

Method 3: The reaction mixture was stirred at 60 °C for 6 h, and concentrated on a rotary evaporator. A little water was added to the reaction mixture, and the separated complex **3** filtered and recrystallized from water-acetone. To the filtrate was added ethanol. The separated complex **4** was filtered, and recrystallized from water-acetone. Yields: 3.2 g (48.5 %) for **3**, 0.9 g (13.6%) for **4**. Color: dark russet for **3** and violet russet for **4**. Found **3**: C, 38.30; H, 6.07; N, 13.43; Cl, 9.12%. Calcd for $CoC_{13}H_{24}N_4O_3SCl$ (MW 410.81) C, 38.01; H, 5.89; N, 13.64; Cl, 8.63%. Found **4**: C, 34.93; H, 6.43; N, 12.89; Cl, 8.53%. Calcd for $CoC_{13}H_{28}N_4O_5SCl$ (MW 446.84) C, 34.94; H, 6.32; N, 12.54; Cl, 7.93%. Mp: 241 °C for **3**, 233 °C for **4**. Λ=130 for **3** and 118 S cm^2 mol^{-1} for **4** in water. IR spectra: 994, 1034, 1054, 1078, 1094 cm^{-1}, and 3040, 3112, 3204, 3272 cm^{-1} for **3**, 1000, 1034, 1056, 1066, 1080 cm^{-1}, and 3070, 3116, 3200, 3280 cm^{-1} for **4**.

Complexes **3** and **4** did not isomerize to **4** and **3**, respectively, in water or aqueous ammonia (pH≒10) at 20 °C after for 24 h, though **3** and **4** did isomerize to **4** and **3**, respectively, in water at 40 °C after for 24 h.

***cis*-β_1 and β_2-Thiosalicylato(4,7-diazadecane-1,10-diamine)-cobalt(III) Chloride Hydrate (cis-β_1 (5), β_2 (6)):** Complex **2** (5.8 g, 16.2 mmol) was added to moistend fresh Ag_2O, which was made from silver nitrate (5.5 g, 32.1 mmol) and potassium hydroxide (1.8 g, 32.1 mmol). The mixture was stirred for several minutes at room temperature before adding 20 cm^3 of water. The mixture was left for about 30 min at 60 °C. The precipitated silver chloride was filtered off. Then, thiosalicylic acid (2.5 g, 16.2 mmol) and 3 cm^3 of 28% aqueous ammonia were added to the solution. From the reaction mixtures, complexes **5** and **6** were obtained according to the methods described in 1—2.

Method 1: The reaction mixture was stirred at 40 °C for 6 h, and concentrated on a rotary evaporator. The concentrated solution was injected on a column chromatograph on alumina. Upon elution with ethanol, the first green band was collected and concentrated on a rotary evaporator. The solution was cooled in an icebox; separated complex **5** was filtered and recrystallized. The filtrate was concentrated and dried. The dried product (0.8 g) was dissolved in 2 cm^3 of water. This solution was injected onto a column of ion-exchange resin (Dowex 50W-X2, ϕ2.5× 30 cm). On elution with 0.1 mol dm^{-3} NaCl, the effluent of the first green band of complex **6** and that of the second green band of complex **5** was collected and concentrated, respectively. The separated NaCl was removed. Complex **5** was recrystallized from water-methanol (1 : 7) and complex **6** was recrystallized from ethanol. Yields: 3.3 g (46.5%) for **5**, 0.8 g (11.3%) for **6**.

Method 2: The reaction mixture was stirred at 50 °C at 6 h and then concentrated on a rotary evaporator. The concentrated solution was injected onto a column chromatograph on alumina on elution with ethanol; the green band was collected and concentrated on a rotary evaporator. The solution was allowed to remain one night in an icebox. The precipitated complex **5** was filtered. From the filtrate of **5**, separation of **5** and **6** was achieved by a column of ion-exchange resin of the method 1. Yields: 3.45 g (48.5%) for **5**, 0.21 g (3.0%) for **6**. Color: greenish gray for **5** and **6**. Found **5**: C, 41.18; H, 6.67; N, 12.82; Cl, 8.11%. Found **6**: C, 41.15; H, 6.63; N, 13.01; Cl, 8.36%. Calcd for $CoC_{15}H_{28}N_4O_3SCl$ (MW 438.86) C, 41.05; H, 6.43; N, 12.77; Cl, 8.08%. Mp: 234 °C for **5** and **6**. Λ=105 for **5** and 110 S cm^2 mol^{-1} for **6** in water. IR spectra: 1018, 1036, 1052, 1067 cm^{-1}, and 3060, 3120, 3200, 3276 cm^{-1} for **5**, 1014, 1038, 1056, 1088 cm^{-1}, and 3084, 3160, 3192, 3260 cm^{-1} for **6**. Complexes **5** and **6** isomerize to **6** and **5**, respectively in water at 40 °C after for 24 h.

***cis*-β_1-Thiosalicylato(triethylenetetramine)cobalt(III) Nitrate Hydrate (7) and *cis*-β_2-Thiosalicylato(triethylenetetramine)cobalt(III) Nitrate Dihydrate (8):** Complexes **7** and **8** were prepared from the reaction mixture of silver nitrate (0.20 g, 1.20 mmol) and **3** (0.49 g, 1.19 mmol) or **4** (0.53 g, 1.19 mmol) in water, respectively. They were recrystallized from water-acetone and were unstable in 1.8 mol dm^{-3} and 3.6 mol dm^{-3} D_2SO_4 solution. Yields: 0.22 g (42.3%) for **7**, 0.25 g (46.3%) for **8**. Color: grayish russet for **7** and **8**. Found **7**: C, 35.87; H, 5.72; N, 16.27%. Calcd for $CoC_{13}H_{24}N_5O_6S$ (MW 437.37) C, 35.70; H, 5.53; N, 16.01%. Found **8**: C, 34.49; H, 6.02; N, 15.32%. Calcd for $CoC_{13}H_{26}N_5O_7S$ (MW 455.38) C, 34.29; H, 5.76; N, 15.38%. Mp: 230 °C for **7**, 227 °C for **8**. Λ=107 for **7** and 103 S cm^2 mol^{-1} for **8** in water. IR spectra: 999, 1035, 1068, 1088 cm^{-1}, and 3115, 3145, 3210, 3255 cm^{-1} for **7**, 990, 1035, 1065, 1077 cm^{-1}, and 3105, 3160, 3190, 3240 cm^{-1} for **8**. Absorption spectra: 294 nm (ε=12000),415 sh, 533 (250), and 580 (235) for **7**, 295 nm (ε=12500) and 570 (315) for **8** in water.

Results and Discussion

***cis*-β_1 and β_2-Thiosalicylato(quadridentate amine)-cobalt(III) Chloride Hydrates:** Abbreviations of the thiosalicylato(quadridentate amine)cobalt(III) complexes studied in this paper are listed in Table 1. Octahedral thiosalicylato(quadridentate amine)cobalt-(III) complexes exist in three isomeric forms of cis-α, cis-β_1, and cis-β_2, as shown in Fig. 1. A mixture of *cis*-β_1 and β_2-thiosalicylato(quadridentate amine)cobalt-(III) chloride hydrates has been obtained from a reaction mixture of complex **1** or **2**, Ag_2O, thiosalicylic acid and 28% aqueous ammonia. Two geometrical isomers (cis-β_1 (**3** and **5**) and cis-β_2 (**4** and **6**)) of their complexes were separated by Dowex 50W-X2 column chromatography. The *cis*-β_1 and β_2-thiosalicylato(trien)-cobalt(III) nitrate hydrate (**7** and **8**) have been prepared from the reaction mixture of silver nitrate and the

Table 1. The Abbreviations of the Thiosalicylato(quadridentate amine)-cobalt(III) Complexes

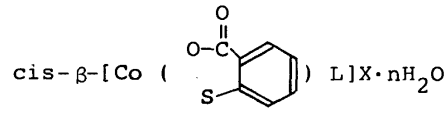

Complex No.	3	4	5	6	7	8
Form	β_1	β_2	β_1	β_2	β_1	β_2
L	trien	trien	3,2,3-tet	3,2,3-tet	trien	trien
X	Cl	Cl	Cl	Cl	NO_3	NO_3
n	1	3	1	1	1	2

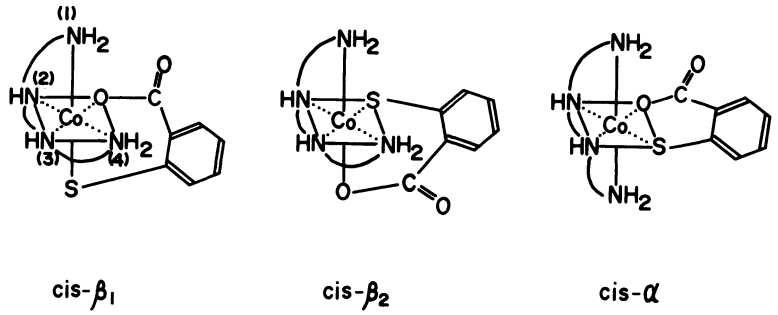

Fig. 1. The cis-α, β_1, and β_2 configurations of thiosalicylato(quadridentate amine)cobalt(III) complexes.

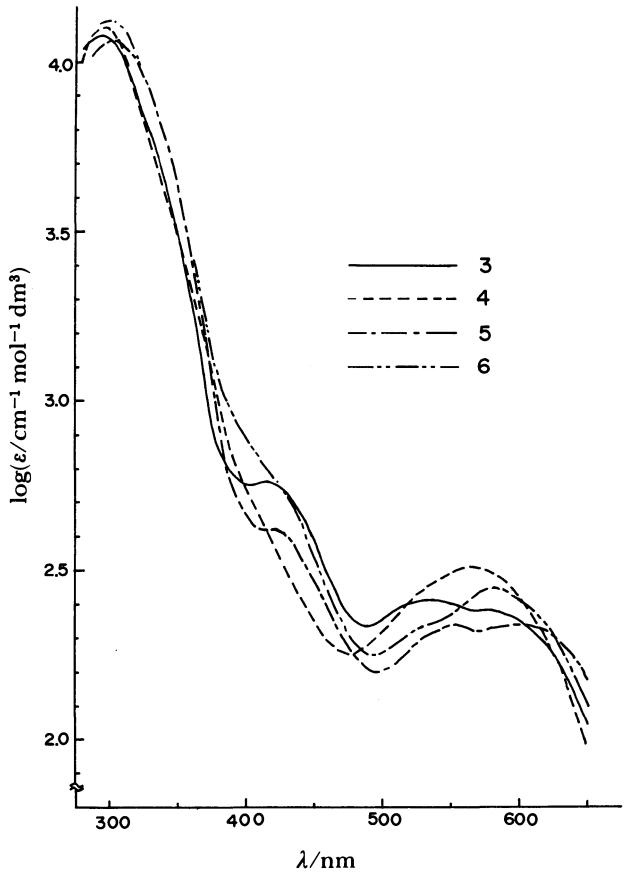

Fig. 2. The absorption spectra of complexes **3**—**6** in water.
3: *cis*-β_1-[Co(thiosal)trien]Cl·H_2O. **4**: *cis*-β_2-[Co(thiosal)trien]Cl·$3H_2O$. **5**: *cis*-β_1-[Co(thiosal)3,2,3-tet]Cl·H_2O. **6**: *cis*-β_2-[Co(thiosal)3,2,3-tet]Cl·H_2O.

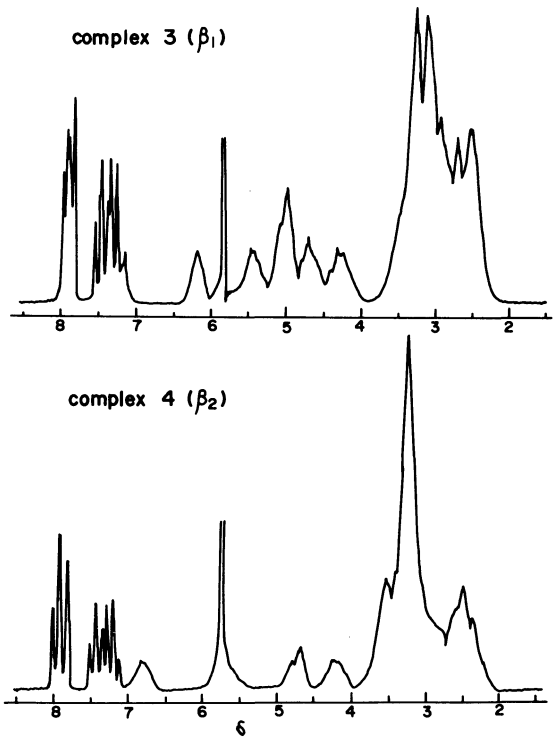

Fig. 3. The ^{1}H NMR spectra of complexes **3** and **4** in 1.8 mol dm^{-3} D_2SO_4.
3: *cis*-β_1-[Co(thiosal)trien]Cl·H_2O. **4**: *cis*-β_2-[Co(thiosal)trien]Cl·$3H_2O$.

corresponding chloride complexes (**3** and **4**). Complex **3** is soluble in water, and complexes **4**—**6** are very soluble in water. Complexes **3**—**6** are very soluble in methanol and DMSO, and soluble in ethanol but insoluble in the other common organic solvents, such as acetone and ether. The isomerization between **3** and **4** or **5** and **6** was reversible in water at 40 °C. Complexes **3** and **4** were diamagnetic, indicated by the magnetic susceptibility. The electric conductivities for **3**—**6** in aqueous solutions were 103—130 S cm^2 mol^{-1}.

The absorption spectra of **3**—**6** were measured in water, as shown in Fig. 2. The absorption bands at around 300 nm of **3**—**6** were assigned to the charge transfer band for the S–Co(III) bond.[21–23] The absorption bands at the 570—590 nm region for **4** and **6** are assigned to the first absorption band,[23] and those at 530—560 and 580—600 nm regions for **3** and **5** can be assigned to the split first absorption band.[24–26]

The ^{1}H NMR spectra of **3**—**6** were measured in 1.8 mol dm^{-3} D_2SO_4, as shown in Fig. 3. The signals at δ 2.1—3.8 and 3.6—6.8 of **3**—**6** were assigned to the methylene protons and amine protons of the coordinated quadridentate amine ligand respectively, and the lowest field signals at δ 7.0—8.1 were assigned to the coordinated thiosalicylato protons.[13] The signals of

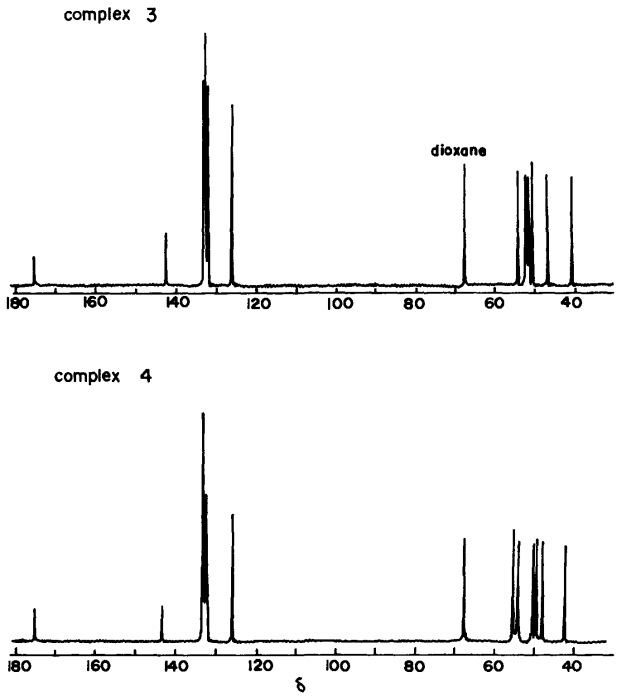

Fig. 4. The ^{13}C NMR spectra of complexes **3** and **4** in water.
3: *cis*-β_1-[Co(thiosal)trien]Cl·H_2O. **4**: *cis*-β_2-[Co(thiosal)trien]Cl·$3H_2O$.

the center, NH_2- side, and NH- side methylene protons and of the primary and secondary amine protons of **3**—**6** have been assigned by comparisons with those of *cis*-β_1- and β_2-salicylato(quadridentate amine)cobalt(III) chloride hydrate, *cis*-β_1, β_2-[Co(sal)L]Cl·nH_2O (L: trien (β_1:**9**, β_2:**10**); 3,2,3-tet (β_2:**11**)),[2,3] and collected in Table 2. The signals of the primary and secondary amine protons of **3** and **4** disappeared in heavy water.

The ^{13}C NMR spectra of **3**—**6** were measured in D_2O, as shown in Fig. 4 and Table 2. There have been observed 6—8 signals for the quadridentate amine ligands and 5—7 signals for the thiosalicylato ligand. The chemical shifts of the coordinated thiosalicylato ligand in **3**—**6** and of thiosalicylic acid have been assigned by comparisons with those of the coordinated salicylato ligand in **9**—**11**[2,3] and salicylic acid,[17] respectively. On the other hand, the chemical shifts of the coordinated quadridentate amine ligands are difficult to assign to the individual carbon atoms; however, regions of the chemical shifts of the center, NH_2- side, and NH- side methylene carbons are around δ 21—28, 37—48, and 49—57, respectively, and their regions are close to those of **9**—**11**,[2,3] as shown in Table 2.

A distinction between **3** and **4** or **5** and **6** was found in the IR, NMR, and absorption spectra. The IR spectra of **3**—**6** showed four absorption bands in the NH stretching region (3000—3300 cm^{-1}) and four or five absorption bands in the NH_2 twisting region (990—1100 cm^{-1}), as shown in Experimental section. The ^{13}C NMR spectra of **3**—**6** showed 6—8 signals for the quadridentate amine ligands. They indicate that these complexes assume the cis-β-form.[2,27] In the ^1H NMR spectra, the methylene proton signals for the trien ligand in **4** can be divided into two groups of the NH_2- side methylene protons at δ 2.1—2.7 and NH- side methylene protons at δ 2.7—3.5 regions, as shown in Fig. 3. However, those of **3** could not be divided into two groups. One proton in the NH_2- side methylene protons for **4** overlapps to the NH- side methylene protons, since the intensity ratio of both methylene proton signals is 3:9. Also, the chemical shift (δ 3.45—4.0) of the proton signal of the N(1)H_2 group of **4** is at a higher field than that (δ 4.28) of **3**, i.e., the N(1)H_2 group of **4** is considered to be at a position trans[2] to the carboxyl oxygen of the coordinated thiosalicylato ligand, which is more electronegative than the thiolato sulfur. In addition, the spectrum of **4** showed five peaks with an intensity ratio of 2:1:1:1:1 for the amine protons, while that of **3** showed five peaks with an intensity ratio of 1:1:2:1:1, as shown in Fig. 2 and Table 2. These properties of **4** and **3** are similar to those of **10** and **9**,[2] respectively, as shown in Table 2. Thus, complexes **4** and **3** have been assigned to the cis-β_2 and β_1-isomers, respectively. On the other hand, complexes **5** and **6** could not be assigned from the ^1H NMR spectra, but they can be assigned from results of the absorption spectra. For instance, complexes **3**—**6** give the first absorption band at nearly the same position, but the first absorption band of **5** differs remarkably from that of **6**, and the absorption bands of **5** and **6** are very close to those of **3** and **4**, respectively, as shown in Fig. 2. Also, the elution order of **5** and **6** is similar to that of **3** and **4**, respectively. Then, complexes **5** and **6** are assigned to the cis-β_1 and β_2-isomers, respectively.

Buckingham and Sargeson have been concerned with the ^1H NMR, absorption spectra, and X-ray diffraction of the diastereoisomers of *cis*-β_1 and β_2-glycinato(trien)cobalt(III) complexes,[28,29] *cis*-β_1, β_2-[Co(gly)trien]$^{2+}$ ions, (β_1-*RR,SS*: **12a**, β_1-*RS,SR*: **12b**; β_2-*RR,SS*: **13a**, β_2-*RS,SR*: **13b**). The difference ($\Delta\delta$:0.5) of the chemical shifts for the N(1)H_2 protons in the ^1H NMR spectra of β_1 (**12**) and β_2 (**13**) is bigger than that ($\Delta\delta$:0) of **12a** and **12b** or of **13a** and **13b**. The first absorption bands of **12a** and **13a** are close to those of **12b** and **13b**, respectively. If the same relation holds in **3** and **4**, the difference ($\Delta\delta$:0.7) of the chemical shift for the N(1)H_2 protons of **3** and **4** is close to that of cis-β_1 (**12**) and β_2 (**13**). The first absorption band of **3** differs remarkably from that of **4**, i.e., complexes **3** and **4** could not be assigned to the diastereoisomers, and have been assigned to the cis-β_1 and β_2-isomers, respectively. Next, the differences of the chemical shifts of the both N(2)H and N(3)H protons of **12a** and **12b** which are in positions trans of O atom and N atom

Table 2. ^{1}H, ^{13}C NMR, and Absorption Spectra of Complexes **3**—**6** and **9**—**11**

^{1}H Complex No. (isomer)	x,y,z	$NH_2(CH_2)_xNH(CH_2)_yNH(CH_2)_zNH_2$ δ: Center methylene protons	NH_2- side methylene protons [Center+NH_2-+NH-]	NH- side methylene protons [NH-+$N(1)H_2$]	$N(1)H_2$	$N(4)H_2$ [$N(1)H_2$+$N(4)H_2$]	N(3)H N(2)H [N(3)H+N(2)H]	Thiosalicylato δ	solvent	Absorption bands in water λ/nm (ε/cm^{-1} mol^{-1} dm^3)			
3(β_1)	2,2,2		2.20—3.75(12H)	4.28(1H)	4.70(1H)	4.96(2H)	5.45(1H) 6.20(1H)	7.1—8.1(4H)	1	295	417sh	533	580
			2.20—3.80(12H)	4.20(1H)	4.60(1H)	4.86(2H)	5.20(1H) 6.10(1H)	a)	2	(12000)		(260)	(240)
			2.30—3.55(12H)					7.1—7.9(4H)	3				
4(β_2)	2,2,2		2.12—2.70(3H)	2.70—3.45(9H)	3.45—4.00(2H)	4.20(1H) 4.70(1H)	a) 6.80(1H)	7.0—8.1(4H)	1	295			568
			2.25—2.75(3H)	[2.75—3.82(11H)]		4.12(1H) 4.58(1H)	5.67(1H) 6.67(1H)	a)	2	(12700)			(320)
			2.20—2.77(3H)	2.77—3.60(9H)				7.1—7.9(4H)	3				
5(β_1)	3,2,3		[1.50—2.60(10H)]	[2.60—3.70(7H)]		[3.4—4.5(3H)]	[5.70(2H)]	7.1—8.1(4H)	1	302	415sh	555	603
			[1.50—2.58(10H)]	[2.58—3.65(7H)]		[3.8—4.5(3H)]	[5.58(2H)]	a)	2	(11800)		(220)	(220)
6(β_2)	3,2,3		[1.30—2.61(10H)]	[2.61—3.60(7H)]		[3.90(2H)] 4.28(1H)	[5.50(2H)]	7.1—8.1(4H)	1	300		535sh[b]	588
			[1.40—2.60(10H)]	[2.60—3.55(7H)]		[3.75(2H)] 4.26(1H)	[5.28(2H)]	a)	2	(13200)			(280)
9(β_1)[c]	2,2,2		2.39—3.76(12H)	4.34(1H)	4.57(1H)	4.81(1H) 5.23(1H)	6.20(1H) 6.51(1H)	6.7—8.0(4H)	1		331 (2960)	530 (270)	
10(β_2)[c]	2,2,2		2.38—2.80(3H)	2.80—3.80(9H)	4.34(2H)	4.76(1H) 5.21(1H)	6.07(1H) [6.5—8.0(5H)]		1		333 (3050)	520 (270)	
11(β_2)[d]	3,2,3	1.44—1.97(4H)	1.97—2.40(3H)	2.40—3.20(9H)	3.32(1H)	4.14(1H) 4.71(2H)	5.12(1H) 6.31(1H)	6.6—8.0(4H)	1		335 (2420)	533 (217)	

^{13}C	$NH_2(CH_2)_xNH(CH_2)_yNH(CH_2)_zNH_2$ δ: Center methylene carbon		NH_2- side methylene carbon		NH- side methylene carbon				δ: C-1	C-2	C-3	C-4	C-5	C-6	C-7
3 (β_1)			40.4	46.8	50.3	51.3	52.0	53.9	125.7	142.4	125.7	133.0	131.7	132.6	175.2
4 (β_2)			41.8	47.6	49.0	49.8	53.5	54.9	125.5	143.3	125.5	133.0	132.1	133.0	175.6
5 (β_1)	21.7	26.2	37.0	38.3	44.6	46.1	47.4	51.7	126.1	143.1	125.8	133.2	132.0	132.9	175.2
6 (β_2)[e]	24.2	27.2	38.7	39.1	48.9	49.8	53.0	56.4	125.6	143.0	125.6	133.2	131.8	133.2	174.7
9 (β_1)[c]			43.6	45.8	51.9	52.1	53.9	56.9	118.6	167.8	117.4	134.3	124.2	132.4	174.6
10 (β_2)[c]			42.0	47.5	48.3	49.7	52.1	52.7	118.1	168.2	117.1	134.5	124.3	132.3	174.1
11 (β_2)[d]	21.9	27.2	37.0	38.5	45.2	47.6	48.3	52.9	117.1	168.2	116.6	134.4	124.4	132.2	174.1
L′									128.4	140.6	126.3	134.3	132.7	133.8	170.7
L[f]									113.8	162.7	118.0	136.6	120.2	131.5	173.6

Solvent and standard: ^{1}H NMR: 1) 1.8 mol dm^{-3} D_2SO_4, 2) 3.6 mol dm^{-3} D_2SO_4, 3) D_2O, internal DSS (δ=0); ^{13}C NMR: **3**—**6**, **9**—**11**: D_2O, internal dioxane (δ=67.4): L′: thiosalicylic acid, L″: salicylic acid: MeOH-d_4 (δ=49.8). a) This signal overlapped with each solvent. b) Very week shoulder. c) Ref. 2. d) Ref. 3. e) This spectrum has small spectrum of **5**, because of isomerism in the measurement. f) Ref. 17.

are 0.8 and 0 ppm, respectively, while those of **13a** and **13b** which are in positions trans of N atom and N atom are 0.15 and 0.25 ppm, respectively. In the case of **3** and **4**, the differences of the chemical shifts of both the NH protons of **3** and **4** which are in positions trans S atom and N atom are 0.8 and 1.0 ppm, respectively. They are very close to that of **12a**. Thus, complexes **3** and **4** are tentatively assigned to the *cis*-β_1-*RR,SS*- and *cis*-β_2-*RR,SS*-[Co(thiosal)trien]Cl·nH$_2$O, respectively.

In the complexes **3—6**, the melting point and solubility of **3** and **4** are almost similar to those of **5** and **6**. However, the color of the solid state, formation ratio, and first absorption band of **3** and **4** are different from those of **5** and **6**, i.e., the formation ratio of **3** and **4** is ca. 4:3 at 50 °C but that of **5** and **6** is ca. 16:1 at 50 °C. The ε of the first absorption band of **3** and **4** is larger than that of **5** and **6**, respectively and their first absorption band shifts from 530—580 nm to 550—600 nm. These results are similar to those of **9—11**, and the related complexes, *cis*-β_1, β_2-[Co(sal)L]Cl·nH$_2$O (L: 2,3,2-tet (β_1: **14**, β_2: **15**), 3,3,3-tet (β_2:**16**)), i.e., it is attributable to the center methylenes of the quadridentate ligands.[3]

***cis*-β_1 and β_2-Thiosalicylato(trien)cobalt(III) Complexes (3 and 4) and *cis*-β_1 and β_2-Salicylato(trien)-cobalt(III) Complexes (9 and 10):** The color of the solid state, solubilities in alcohols, formation ratio, isomerization, absorption and ^{13}C NMR spectra, and reaction in 60% nitric acid for **3** and **4** are different from those for **9** and **10**.[2] The color of **3** and **4** is dark russet and violet russet, respectively, but that of **9** and **10** is russet. The formation ratios of **3** and **4** are ca. 3:7 at 40 °C, ca. 4:3 at 50 °C and ca. 4:1 at 60 °C, i.e., the yield for **3** increases with a rise in reaction temperature. The formation ratio of **9** and **10** is ca. 1:20 at 50 °C. The isomerization between **3** and **4** is reversible in water at 40 °C, but isomerization between **9** and **10** is irreversible in water, i.e., complex **10** does not isomerize to **9** at 40 °C after for 24 h. The first absorption band of **3** showed at 533 and 580 nm, but that of **9** showed at 530 nm. The chemical shift (δ ca. 143) of C-2 carbon of the coordinated thiosalicylato ligand in **3** and **4** differs remarkably from that (δ ca. 168) of **9** and **10**. It can be affected by the electronic effect of the S atom of the coordinated thiosalicylato ligand. The paramagnetic 5-nitrothiosalicylato(trien)-cobalt(III) complexes could not be prepared from a reaction mixture of **3** or **4** and 60% nitric acid, while the paramagnetic *cis*-β_1 and β_2-5-nitrosalicylato(trien)-cobalt(III) complexes, *cis*-β_1,β_2-[Co(5-NO$_2$sal)trien]Cl·NO$_3$·2H$_2$O, were obtained from the reaction mixture of **9** or **10** and 60% nitric acid, reported previously.[18] These properties can be attributed to differences of the electronic effect and atomic radius of S and O atoms, and of the stability between the Co–S and Co–O bonds of coordinated ligands.

Some properties for complexes **3—6** and **9—11** are listed in Table 2 and Experimental section.

References

1) Part VII: E. Toyota, Y. Yamamoto, and Y. Yamamoto, *Bull. Chem. Soc. Jpn.*, **61**, 3175 (1988).

2) Y. Yamamoto and E. Toyota, *Bull. Chem. Soc. Jpn.*, **52**, 2540 (1979).

3) Y. Yamamoto, H. Kudo, and E. Toyota, *Bull. Chem. Soc. Jpn.*, **56**, 1051 (1983).

4) P. V. Khadikar and S. N. Kakkar, *J. Indian Chem. Soc.*, **53**, 548 (1976).

5) A. Vanni and P. G. Daniele, *Ann. Chim. (Rome)*, **65**, 239 (1975).

6) V. Kumari, R. C. Sharma, and G. K. Chaturvedi, *J. Indian Chem. Soc.*, **52**, 84 (1975).

7) N. S. Al-Niaimi and B. M. Al-Saadi, *J. Inorg. Nucl. Chem.*, **36**, 1617 (1974).

8) R. Sarin and K. N. Munshi, *J. Indian Chem. Soc.*, **50**, 307 (1973).

9) M. V. Reddy and P. K. Bhattacharya, *J. Inorg. Nucl. Chem.*, **32**, 2321 (1970).

10) A. N. Kumar and H. L. Nigam, *Indian J. Chem.*, **11**, 472 (1966).

11) A. G. Maiorova, L. A. Nazarova, and G. N. Amel'yanova, *Zh. Neorg. Khim.*, **18**, 1866 (1973).

12) L. A. Ezhova, V. N. Mikhailova, and V. V. Solomentsev, *Deposited Doc.*, **1981**, 7; *Chem. Abstr.*, **98**, 171902y (1983).

13) L. Kumar, K. H. Puthraya, and T. S. Srivastava, *Inorg. Chim. Acta*, **86**, 173 (1984).

14) J. S. Bashkin, J. C. Huffman, and G. Christou, *J. Am. Chem. Soc.*, **108**, 5038 (1986).

15) G. T. Morgan and J. D. M. Smith, *J. Chem. Soc.*, **1956**, 1922.

16) Y. Yamamoto, M. Mori, H. Yoneda, S. Misumi, and K. Ito, *Bull. Chem. Soc. Jpn.*, **42**, 984 (1969).

17) Y. Yamamoto, *Bull. Chem. Soc. Jpn.*, **51**, 2894 (1978).

18) Y. Yamamoto, E. Toyota, and N, Mitsudera, *Bull. Chem. Soc. Jpn.*, **53**, 3517 (1980).

19) A. M. Sargeson and G. H. Searle, *Inorg. Chem.*, **6**, 787 (1967).

20) B. Bosnich, J. M. Harrowfield, and H. Boucher, *Inorg. Chem.*, **14**, 815 (1975).

21) M. J. Heeg, R. C. Elder, and E. Deutsch, *Inorg. Chem.*, **18**, 2036 (1979).

22) M. H. Dickman, R. J. Doedens, and E. Deutsch, *Inorg. Chem.*, **19**, 945 (1980).

23) M. Kojima and J. Fujita, *Bull. Chem. Soc. Jpn.*, **56**, 2958 (1983).

24) N. Matsuoka, J. Hidaka, and Y. Shimura, *Bull. Chem. Soc. Jpn.*, **40**, 1868 (1967).

25) H. Yamatera, *Bull. Chem. Soc. Jpn.*, **31**, 95 (1958).

26) Y. Yamamoto and N. Shinya, *Bull. Chem. Soc. Jpn.*, **60**, 1186 (1987).

27) D. A. Buckingham and D. Jones, *Inorg. Chem.*, **4**, 1387 (1965).

28) D. A. Buckingham, P. J. Cresswell, R. J. Dellaca, M. Dwyer, G. J. Gainsford, L. G. Marzilli, I. E. Maxwell, W. T. Robinson, A. M. Sargeson, and K. R. Turnbull, *J. Am. Chem. Soc.*, **96**, 1713 (1974).

29) D. A. Buckingham, M. Dwyer, G. J. Gainsford, V. Janson Ho, L. G. Marzilli, W. T. Robinson, A. M. Sargeson, and K. R. Turnbull, *Inorg. Chem.*, **14**, 1739 (1975).

Photochemical Generation of Sn(III) in Hydrochloric Acid Solutions

Nobuyoshi SHINOHARA* and Makoto INOUE
Department of Chemistry, Yokohama City University, Seto, Kanazawa-ku, Yokohama 236
(Received June 7, 1988)

In the flash photolysis of Sn(II) in a deaerated hydrochloric acid solution, Sn(III) was produced. Sn(III) has an absorption maximum at 280 nm in a 1 mol dm^{-3} hydrochloric acid solution. In the flash photolysis of a deaerated Sn(IV) solution, intermediates of Sn(III) and Cl_2^- were produced. Transient absorption spectra of intermediates generated by the flashed Sn(IV) solutions were measured under various concentrations of dissolved oxygen. Since Sn(III) reacts with oxygen very rapidly, only Cl_2^- was confirmed in the oxygen-saturated Sn(IV) solution. In the flash photolysis of Sn(IV) solutions containing Sn(II), the yield of Sn(III) increased with an increase of the added Sn(II), due to the generation of Sn(III) by the reaction of Cl_2^- with Sn(II). It was found that only Sn(III) was produced in the irradiation of 5.0×10^{-4} mol dm^{-3} Sn(IV) solution containing Sn(II) at concentrations of more than ca. 7×10^{-5} mol dm^{-3}. The reaction rate constant for the reaction of Sn(II) with Cl_2^- was estimated to be 8.9×10^8 mol^{-1} dm^3 s^{-1}. The mechanisms for the photochemical generation of Sn(III) are discussed.

Flash photolysis and pulse radiolysis have proved to be very useful in the generation and characterization of metal ions in unusual valency states. The species formed include the metal ions known to be formed as intermediates in thermal reactions. However, they are poorly characterized beause of their instability and difficulty to form novel valency states in other ways. Though the chemical properties and behavior of these species have been investigated, much still remains to be studied.[1,2]

The stable oxidation states of non-transition elements usually differ by two units in their mononuclear compounds. Most oxidation-reduction reactions of such elements involve either a two-equivalent change with the direct formation of a stable oxidation state or successive one-equivalent steps. In the latter case, an unstable intermediate oxidation state of non-transition metal is produced, which may show some of the characteristics of a free radical. In Sn(II)-Sn(IV) redox chemistry, unstable Sn(III) is assumed to be an intermediate.[3-6] Only a few studies of the intermediate oxidation state, Sn(III), have been carried out briefly regarding radiation chemistry.[7-9] In a previous paper, we reported on the photochemical generation of Sn(III) from tin ions in deaerated aqueous hydrochloric acid solutions.[10] In the present paper we give more details regarding Sn(III) generated upon the irradiation of tin ions in hydrochloric acid solutions.

Experimental

Sn(II) solutions used for flash photolysis were obtained by adding $SnCl_2$ to a deaerated solution of hydrochloric acid. The deaerations were carried out by bubbling with oxygen-free nitrogen obtained through a tube containing heated cupper metal pieces. All preparations of Sn(II) solutions should be carried out with adequate safety precautions. Mixed gases were prepared by mixing pure oxygen and nitrogen. The oxygen content in the mixture was determined gas chromatographically. Sn(IV) solutions containing dissolved oxygen at the desired concentration were obtained by bubbling with the mixed gas. Sn(IV) solutions were prepared by the oxidation of Sn(II) with oxygen. All of the chemicals were of chemically pure grade. Pure water obtained from a Millipore Super-Q system was used for the preparation of samples. A flash photolysis apparatus was the same as that used previously.[10] The main flash lamps dissipated 450 J max. at 15 kV with a flash duration of 10 μs. Solutions for flash photolysis were taken in a quartz cell with a 10-cm path length. Transient absorption changes were recorded on a Textronix 7633 oscilloscope.

Results and Discussion

Photolysis of Sn(II) Solutions. In our previous paper we reported on the absorption spectrum of Sn(III) obtained by using a flash photolysis technique.[10] The spectrum is shown in Fig. 1 together with the absorption spectra of Sn(II) and Sn(IV), measured in a 1 mol dm^{-3} hydrochloric acid solution.

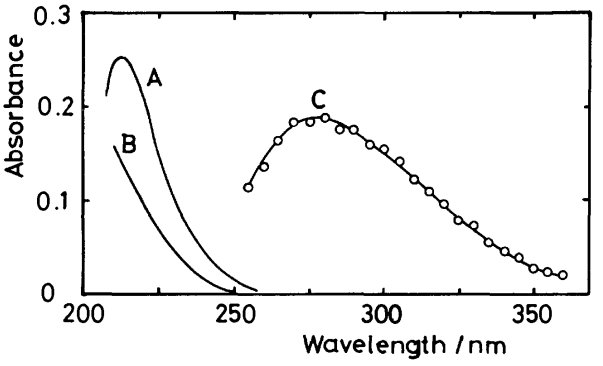

Fig. 1. Absorption spectra of Sn(II), Sn(III), and Sn(IV) in 1 mol dm^{-3} hydrochloric acid solutions. A: 1.0×10^{-5} mol dm^{-3} Sn(II), B: 4.0×10^{-5} mol dm^{-3} Sn(IV), C: Sn(III) obtained in the flash photolysis of 1.0×10^{-4} mol dm^{-3} Sn(II) in the deaerated solution.

Under our experimental conditions, these tin ions exist in chloro complex forms.[11-13] The Sn(II) hydrochloric acid solution, subjected to a flash, showed a transient absorption maximum at 280 nm, which was attributed to the generation of Sn(III), as shown in Reaction (1).

$$Sn(II) + H^+ \xrightarrow{h\nu} Sn(III) + H \quad (1)$$

The resulting H atoms produced H_2 by Reaction (2). However, since Sn(II) can be oxidized by oxygen very easily, the Sn(II) solution usually contains a small amount of Sn(IV) as an impurity. Therefore, some of H atoms react with Sn(IV) very rapidly, according to Reaction (3).[14]

$$H + H \rightarrow H_2 \quad (2)$$
$$Sn(IV) + H \rightarrow Sn(III) + H^+ \quad (3)$$

Photolysis of Sn(IV) solutions. Typical oscillograms obtained by flashing oxygenated Sn(IV) solutions are given in Fig. 2. When the Sn(IV) solution containing a small amount of dissolved oxygen was flashed, there was a fast decay after a rapid increase (within the flash) in absorbance (oscillogram A in Fig. 2). However, the fast decay step could not be observed in the flash photolysis of the oxygen-saturated Sn(IV) solution ($[O_2]=1.38\times10^{-3}$ mol dm^{-3}) (oscillogram B in Fig. 2). Oxygen has a large effect upon the reaction course. Then, flash photolysis was carried out in Sn(IV) solutions under various concentrations of dissolved oxygen, and the obtained absorption spectra are given in Fig. 3. The transient absorption spectrum obtained in the deaerated Sn(IV) solution shows a discernible shoulder at the shorter-wavelength side of the main absorption band at 340 nm. The absorbance near 280 nm decreased with increasing the concentration of dissolved oxygen. The absorption spectrum in an aerated solution is close to that in an oxygen-saturated solution. This fact shows that the amount of oxygen in an aerated solution is sufficient to scavenge the Sn(III) formed by photolysis. The spectrum obtained in the oxygen-saturated solution has an absorption maximum at 340 nm which is attributed to Cl_2^-.[15-18] The difference between the spectrum obtained in the oxygen-free solution and the spectrum obtained in the oxygen-saturated solution (Fig. 3) is similar to the spectrum of Sn(III) in Fig. 1. This suggests that Sn(III) are produced in a flashed Sn(IV) solution. Thus, the reactions in the flashed Sn(IV) solution can be explained by Eqs. 4 and 5, where Sn(IV)-Cl denotes chloro complexes.

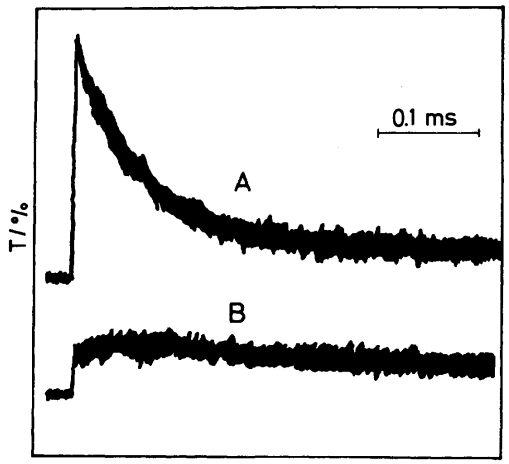

Fig. 2. Oscilloscope traces showing changes in absorption measured at 280 nm after the flash of 5.0×10^{-4} mol dm^{-3} Sn(IV) in 1 mol dm^{-3} hydrochloric acid solutions in the presence of dissolved oxygen.
Concentrations of dissolved oxgen A: 8.83×10^{-5} mol dm^{-3}, B: 1.38×10^{-3} mol dm^{-3}.

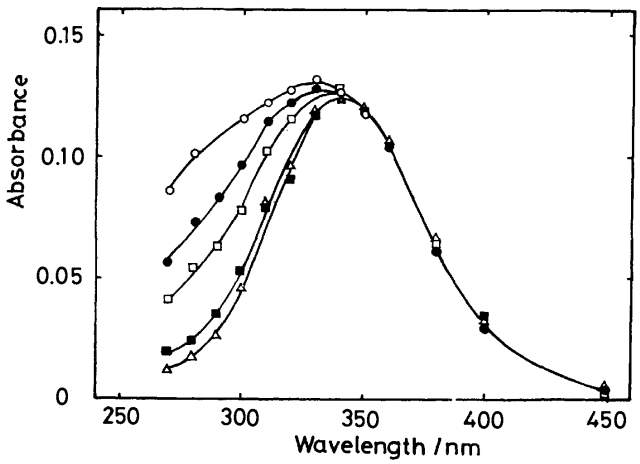

Fig. 3. Transient absorption spectra obtained in the flash photolysis of Sn((IV) solutions in the presence of various concentration of oxygen at 30 μs after the flash.
Concentrations of oxygen; ○: 0, ●: 8.83×10^{-5}, □: 1.60×10^{-4}, ■: 2.84×10^{-4} (aerated), △ 1.38×10^{-3} mol dm^{-3} (oxygen-saturated).

$$Sn(IV)\text{-}Cl \xrightarrow{h\nu} Sn(III) + Cl \quad (4)$$
$$Cl + Cl^- \longrightarrow Cl_2^- \quad (5)$$

The resulting Cl_2^- disappears by Reaction (6), where the rate constant was estimated to be $2k_6=9.7\times10^9$ mol^{-1} dm^3 s^{-1}, as shown in our previous paper.[10]

$$Cl_2^- + Cl_2^- \rightarrow Cl_3^- + Cl^- \quad (6)$$

Sn(III) reacts very rapidly with oxygen; the rate constant k_7 was obtained to be 1.7×10^8 mol dm^3 s^{-1}.

$$Sn(III) + O_2 + H^+ \rightarrow Sn(IV) + HO_2 \quad (7)$$

Photolysis of Sn(IV) Solutions Containing Sn(II). The effect of Sn(II) on the generation of Sn(III) in

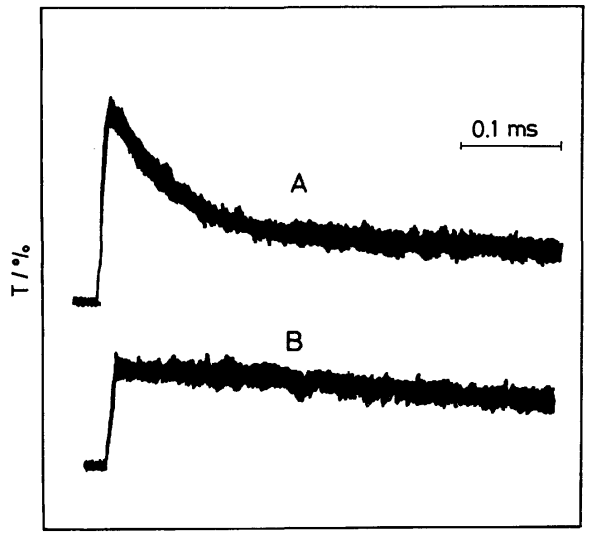

Fig. 4. Oscilloscope traces showing changes in absortion measurd at 350 nm after the flash of 5.0×10^{-4} mol dm^{-3} Sn(IV) containing Sn(II) in the deaerated 1 mol dm^{-3} hydrochloric acid solutions. Concentration of Sn(II); A: 1.7×10^{-5} mol dm^{-3}, B: 8.9×10^{-5} mol dm^{-3}.

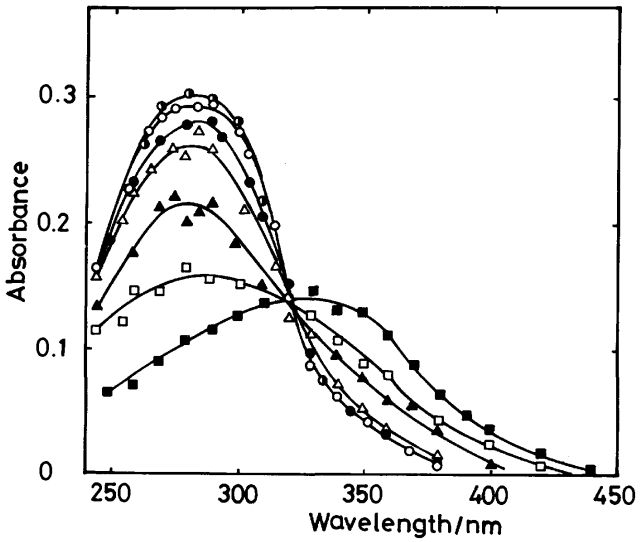

Fig. 5. Transient absorption spectra obtained in the flash photolysis of 5.0×10^{-4} mol dm^{-3} Sn(IV) solutions with various concentration of Sn(II) in deaerated 1 mol dm^{-3} hydrochloric acid solutions. Absorbance were measured 30 μs after the flash. Concentrations of Sn(II); ■: 0, □: 1.7×10^{-5}, ▲: 3.0×10^{-5}, △: 5.0×10^{-5}, ●: 6.9×10^{-5}, ○: 8.9×10^{-5}, ◑: 1.3×10^{-4} mol dm^{-3}.

flash photolysis of a deaerated Sn(IV) solution was studied. Figure 4 shows typical oscillograms obtained in the flash photolysis of Sn(IV) solutions containing Sn(II). Oscillogram A had a fast decay species which did not appear in oscillogram B, measured in a solution containing Sn(II) at a higher concentration. The fast decay is attributed to the reaction of Cl_2^- with

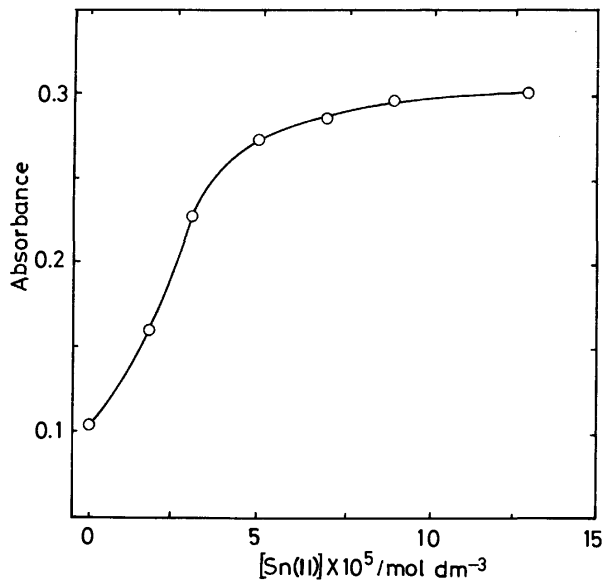

Fig. 6. The dependence of the yields of Sn(III) as a function of the Sn(II) concentration in the deaerated 1 mol dm^{-3} hydrochloric acid solution. The yields are expressed as the absorbances measured at 280 nm 30 μs after the flash. The concentration of Sn(IV) was kept at constant, 5.0×10^{-4} mol dm^{-3}.

Sn(II). The transient absorption spectra obtained in the flash photolysis of Sn(IV) with Sn(II) at various concentrations are shown in Fig. 5. An increase in Sn(II) caused a decrease in the absorbance at 340 nm, followed by an increase in the absorbance at 280 nm. The dependence of the yields of Sn(III) is shown as a function of the Sn(II) concentration in Fig. 6. The yield increases rapidly with an increase in the concentration of the Sn(II), but gradually at higher Sn(II) concentration (> ca. 7×10^{-5} mol dm^{-3}). A pronounced effect on the transient absorption spectrum is caused by the presence of the added Sn(II).

The obtained results can be explained in terms of the following reaction sequence:

$$Sn(II) + H^+ \xrightarrow{h\nu} Sn(III) + H \quad (1)$$

$$Sn(IV) + H \rightarrow Sn(III) + H^+ \quad (3)$$

$$Sn(IV)\text{-}Cl \xrightarrow{h\nu} Sn(III) + Cl \quad (4)$$

$$Cl + Cl^- \rightarrow Cl_2^- \quad (5)$$

$$Sn(II) + Cl_2^- \rightarrow Sn(III) + 2Cl^- \quad (8)$$

An H atom can react rapidly with Sn(IV) to give Sn(III), as already described. The reaction is completed very fast within the flash. The lack of an absorption maximum at 340 nm in the flashed Sn(IV) solution containing Sn(II) at a higher concentration (Fig. 5) can be attributed to the reaction of Cl_2^- with the added Sn(II) (Eq. 8). The rate constant k_8 was estimated to be 8.9×10^8 mol^{-1} dm^3 s^{-1} from a kinetic plot of the curve A in Fig. 4. The Sn(III) yield increases rapidly with increasing Sn(II) concentration,

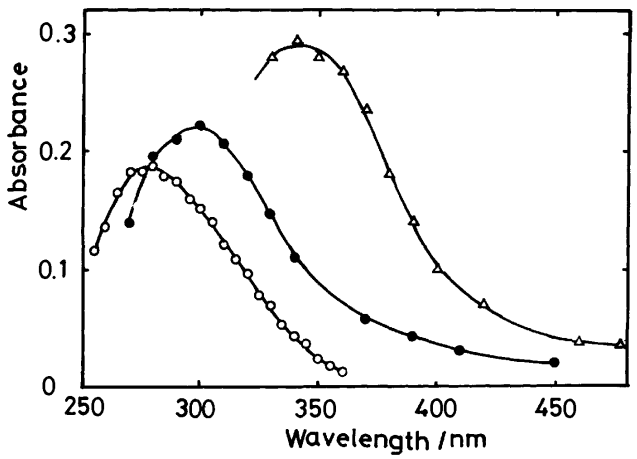

Fig. 7. Transient absorption spectra of Sn(III) obtained in the flash photolysis of 1.0×10^{-4} mol dm^{-3} Sn(II) in 1 mol dm^{-3} acidic solutions.
O: Hydrochloric acid, ●: hydrobromic acid, △: hydroiodic acid.

as shown in Fig. 6. The rapid increase is attributed to the Sn(III) formed by Reactions (1) and (8). Since the Sn(IV) concentration is held constant at 5.0×10^{-4}mol dm^{-3}, the Cl_2^- yield from Reactions (4) and (5) is kept constant. Therefore, the Sn(III) yield from Reaction (8) is also kept constant in the high Sn(II) concentration region (> ca. 7×10^{-5} mol dm^{-3}), in which all the Cl_2^- react with Sn(II). For this reason, a slight increase in the Sn(III) yield in such a concentration region is attributed to the only contribution arising from Reaction (1). Thus, the Sn(III) species can be produced efficiently in the photolysis of an Sn(II)–Sn(IV) mixture.

The transient absorption spectra obtained in the flash photolysis of Sn(II) in hydrobromic and hydroiodic acid solutions are shown in Fig. 7. The spectrum of Sn(III) obtained in a hydrochloric acid solution is also shown for comparison. The spectrum might be attributed to bromo and iodo complex formations of Sn(III), which have the absorption maxima at 300 and 340 nm, respectively.

References

1) D. Meyerstein, *Acc. Chem. Res.*, **11**, 43 (1978).
2) R. M. Sellers, *J. Chem. Educ.*, **58**, 114 (1981).
3) W. C. E. Higginson, R. T. Leigh, and R. Nightingale, *J. Chem. Soc.*, **1962**, 435.
4) D. J. Drye, W. C. E. Higginson, and P. Knowles, *J. Chem. Soc.*, **1962**, 1137.
5) E. A. M. Wetton and W. C. E. Higginson, *J. Chem. Soc.*, **1965**, 5890.
6) A. E. Shilov and A. A. Shteinman, *Kinet. Katal.*, **14**, 149 (1973).
7) M. Malszczak and Cz. Stradowski, *Radiochem. Radioanal. Lett.*, **49**, 81 (1981).
8) B. G. Ershov and A. I. Aleksandrov, *Radiat. Phys. Chem.*, **10**, 327 (1977).
9) K.-D. Asmus, M. Bonifacic, P. Toffel, P. O'Neill, D. Schulte-Frohlinde, and S. Steenken, *J. Chem. Soc., Faraday Trans. 1*, **74**, 1820 (1978).
10) N. Shinohara, K. Mori, and M. Inoue, *Chem. Lett.*, **1986**, 661.
11) P. N. Schatz, P. J. Stephens, G. N. Henning, and A. J. McCaffery, *Inorg. Chem.*, **7**, 1246 (1968).
12) R. S. Tobias and Z. Z. Hugus, Jr., *J. Phys. Chem.*, **65**, 2165 (1961).
13) S. W. Rabideau and R. H. Moore, *J. Phys. Chem.*, **65**, 371 (1961).
14) J. W. Boyle, S. Weiner, and C. J. Hochanadel, *J. Phys. Chem.*, **63**, 892 (1959).
15) L. I. Grossweiner and M. S. Matheson, *J. Phys. Chem.*, **61**, 1089 (1957).
16) M. Anbar and J. K. Thomas, *J. Phys. Chem.*, **68**, 3829 (1964).
17) M. E. Langmuir and E. Hayon, *J. Phys. Chem.*, **71**, 3808 (1967).
18) G. G. Jayson, B. J. Parsons, and A. J. Swallow, *J. Chem. Soc., Faraday Trans. 1*, **69**, 1597 (1973).

 © 1989 The Chemical Society of Japan Bull. Chem. Soc. Jpn., 62, 734—737 (1989) [Vol. 62, No. 3

Photochemical Reactions of the Oxoperoxovanadium(V) Complex in an Acidic Aqueous Solution

Nobuyoshi SHINOHARA* and Yayoi NAKAMURA
Department of Chemistry, Yokohama City University, Seto, Kanazawa-ku, Yokohama 236
(Received July 5, 1988)

The photochemical decomposition of oxoperoxovanadium(V), $VO(O_2)^+$, was studied in perchloric acid media. It was found that the irradiation of $VO(O_2)^+$ solutions with 313, 365, and 436 nm exciting light resulted in the photoreduction of the complex, and gave VO^{2+}, with an evolution of oxygen. The overall reaction is: $4VO(O_2)^+ + 4H^+ \longrightarrow 4VO^{2+} + 3O_2 + 2H_2O$. The photochemical reaction mechanism is also discussed.

A large number of papers have been published on various aspects of the solution chemistry of peroxovanadium(V) complexes. There have been a large number of interesting kinetic studies of the formation,[1-8] decomposition,[9,10] and substrate reactions[11-15] of peroxo vanadium complexes. Further, vanadium compounds have been used as catalysts for the oxidation of olefins by H_2O_2 or ROOH.[16,17] The mechanisms of the redox reactions of peroxo vanadium compounds are generally complicated and cannot be interpreted by simple redox reactions between $VO(O_2)^+$, VO_2^+, VO^{2+}, and H_2O_2. Short-lived transients must often be assumed, particularly radical species arising from the reduction or oxidation of H_2O_2.

Information about the photochemical reactions of vanadium compounds is relatively scanty. The present study of the photolysis of the oxoperoxovanadium(V) complex in an acidic aqueous solution is an attempt to elucidate the mechanism of the photochemical reaction of the peroxo complex.

Experimental

All the chemicals used were of an analytical grade. Pure water obtained from a Millipore Super-Q system was used for the preparation of the samples. Sodium metavanadate (Soekawa Chemicals, >99% in purity) was used as the source of VO_2^+. Solutions of $VO(O_2)^+$ were prepared by adding the required amount of a standardized solution of hydrogen peroxide to a VO_2^+ solution. The equilibrium ($VO_2^+ + H_2O_2 \rightleftarrows VO(O_2)^+ + H_2O$) was thoroughly investigated.[1,9,12] The rate of the decomposition of $VO(O_2)^+$ is sufficiently slow so that photochemical reactions can be studied. The changes in the concentrations of $VO(O_2)^+$ and VO^{2+} were followed by means of absorption spectrophotometry using a Shimadzu MPS-2000 spectrophotometer. The $VO(O_2)^+$ solution was irradiated with a high- or ultrahigh-pressure mercury lamp. The monochromatic light (313, 365, and 436 nm) was obtained by the combination of solution and glass filters. The incident-light intensities were measured by the use of the tris(oxalato)ferrate(III) ion as the actinometer.[18] The oxygen evolution was measured polarographically with a Clarke-type electrode attached to a Yellow Springs Instruments Oxygen Monitor. A cell equipped with the oxygen electrode was used as the reaction vessel. The cell was thermostated at 25±0.1 °C. The reactant solution was deaerated in the reaction vessel with pure nitrogen gas in order to keep the evolved oxygen in solution as completely as possible. The oxygen dissolved initially had no influence on the photochemical reactions of $VO(O_2)^+$.

Results

Figure 1 shows the absorption spectra of oxoperoxovanadium(V), bisoxovanadium(V), and oxovanadium(IV) in 1 mol dm^{-3} perchloric acid solutions: These substances exist as $VO(O_2)^+$, VO_2^+, and VO^{2+} respectively. The absorption maxima of these vanadium compounds are as follows: $VO(O_2)^+$: absorption maxima at 285 nm (ε=486 mol^{-1} dm^3 cm^{-1}) and 456 nm (ε=281 mol^{-1} dm^3 cm^{-1}); VO_2^+: two shoulders at 260 and 330 nm; VO^{2+}: two shoulders at 240 and 640 nm and absorption maximum at 764 nm (ε=17.4 mol^{-1} dm^3 cm^{-1}).

The acidic solutions of $VO(O_2)^+$ underwent the spectral changes upon irradiation (Fig. 2). The absorbance at 456 nm decreased with an increase in the irradiation time, and a new absorption appeared at 764 nm, with an isosbestic point at about 660 nm which was due to the formation of VO^{2+}. In Fig. 3, the amounts of the decomposed $VO(O_2)^+$ and of the generated VO^{2+} upon irradiation with 366 nm light are plotted against the irradiation time. The changes in the concentration of $VO(O_2)^+$ and VO^{2+} were measured spectrophotometrically at 456 and 764 nm respectively. The amount of VO^{2+} generated increased

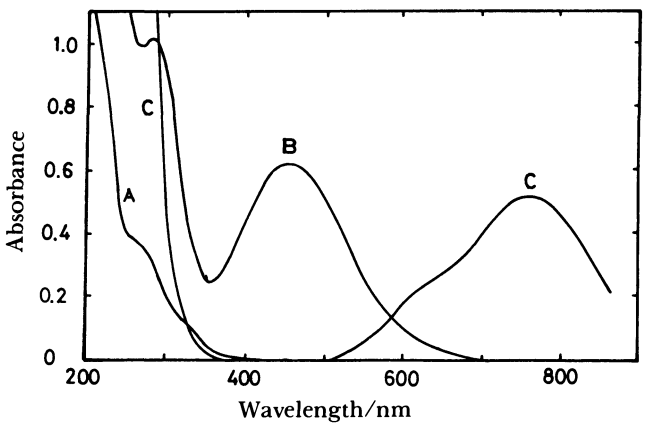

Fig. 1. Absorption spectra of VO_2^+, $VO(O_2)^+$, and VO^{2+} in 1 mol dm^{-3} perchloric acid solutions: A: 4.50×10^{-4} mol dm^{-3} VO_2^+, B: 2.20×10^{-3} mol dm^{-3} $VO(O_2)^+$, C: 3.00×10^{-2} mol dm^{-3} VO^{2+}.

Table 1. Yields of Decomposed $VO(O_2)^+$ and Produced VO^{2+} and Oxygen[a]

	$-[VO(O_2)^+]$[b]	$[VO^{2+}]$	$[O_2]$
	10^4/mol dm^{-3}	10^4/mol dm^{-3}	10^4/mol dm^{-3}
$VO(O_2)^+$[c]	2.20	2.07	1.41
$VO(O_2)^+$[c] + 2-PrOH[d]	2.12	2.10	0.93

a) Irradiation time: 20 min, wavelength for irradiation: 366 nm. $-[VO(O_2)^+]$ and $[VO^{2+}]$ were obtained with the same irradiated solutions as were used for the determination of the evolved oxygen. A 5-cm cell was used for the spectrometrical determination of VO^{2+}, the extinction coefficient of which was small. b) Determined for the disappearance of $[VO(O_2)]^+$. c) $[VO(O_2)^+]=1.8\times10^{-3}$ mol dm^{-3}. d) [2-PrOH]=0.25 mol dm^{-3}.

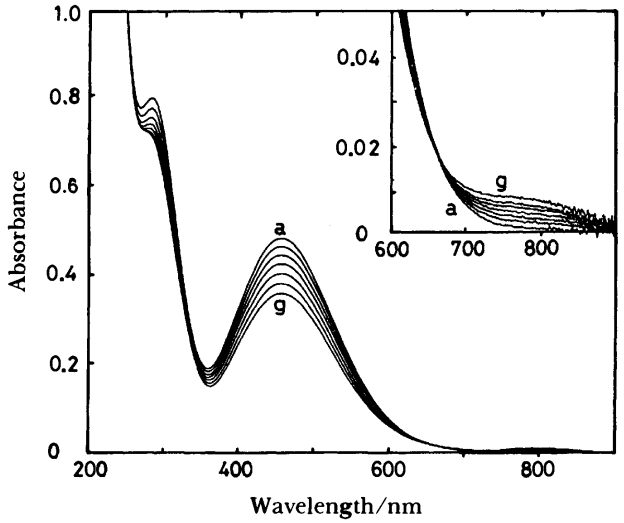

Fig. 2. Absorption spectra changes induced by 366 nm photolysis of $VO(O_2)^+$: Photolysis times for curves a—g respectively are 0, 10, 20, 30, 40, 50, and 60 min. The insert shows the enlarged spectra.

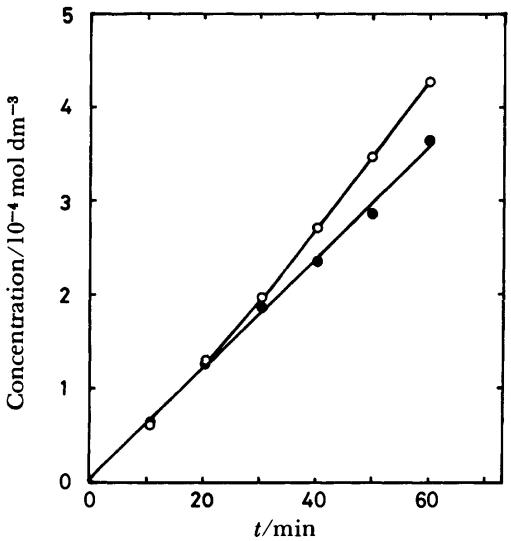

Fig. 3. Decomposition of $VO(O_2)^+$ (○) and generation of VO^{2+} (●) as a function of time upon 366 nm irradiation of 1.8×10^{-3} mol dm^{-3} $VO(O_2)^+$ in 1 mol dm^{-3} perchloric acid solution.

linearly with the increase in the irradiation time. The amount of $VO(O_2)^+$ decomposed was initially equal to that of the generated VO^{2+}. However, the former

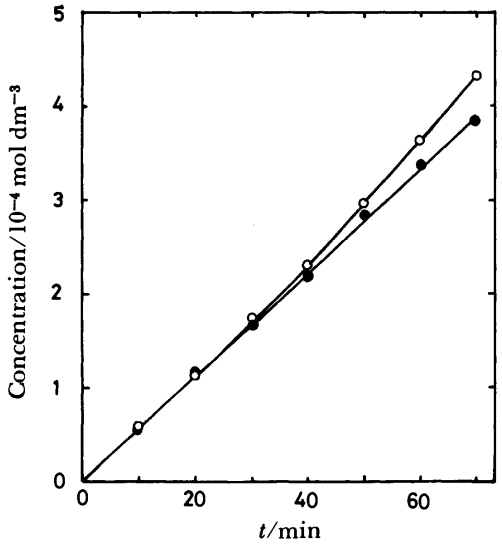

Fig. 4. Decomposed $VO(O_2)^+$ (○) and generated VO^{2+} (●) as a function of time upon 366 nm irradiation of 1.8×10^{-3} mol dm^{-3} containing 0.25 mol dm^{-3} 2-propanol in perchloric acid solution.

became larger than the latter with the increase in the irradiation time. The decomposition of $VO(O_2)^+$ was accompanied by the evolution of oxygen. The photolysis of $VO(O_2)^+$ gave 4 mol of VO^{2+} and 3 mol of O_2 per 4 mol of the complex decomposed at the initial stage. The quantum yields for the decomposition of the complex at 313, 366, and 436 nm were 0.010, 0.0038, and 0.0015 respectively.

$VO(O_2)^+$ solutions containing 2-propanol were irradiated in a 1 mol dm^{-3} percloric acid solution. The amount of $VO(O_2)^+$ decomposed by irradiation with a 366 nm light is plotted against the irradiation time in Fig. 4. The quantity of VO^{2+} resulting increased linearly with the irradiation period. The yields of VO^{2+} were the same in both the presence and absence of 2-propanol, within the limits of experimental error. The photolysis of $VO(O_2)^+$ in the presence of 2-propanol gave 2 mol of VO^{2+} and 1 mol of O_2 per 2 mol of the decomposed $VO(O_2)^+$, as is shown in Table 1.

Discussion

Photolysis of $VO(O_2)^+$. The quantum yields for the photochemical disappearance of $VO(O_2)^+$ in 1 mol dm^{-3} perchloric acid solutions increased with the in-

crease in the energy of the exciting light; this suggests that the photodecomposition occurs into the tail of the ultraviolet band. The irradiation of an acidic solution of $VO(O_2)^+$ gave rise to complicated reactions which eventually led to 4 mol of VO^{2+} for 4 mol of $VO(O_2)^+$ decomposed, with the evolution of 3 mol of oxygen. These results suggest the following overall reaction:

$$4VO(O_2)^+ + 4H^+ \xrightarrow{h\nu} 4VO^{2+} + 3O_2 + 2H_2O \quad (2)$$

We propose the following scheme to explain our results:

$$VO(O_2)^+ \xrightarrow{h\nu} [O=V^{IV}-O-O\cdot^+]^* \quad (3)$$

$$[O=V^{IV}-O-O\cdot^+]^* + H^+ \longrightarrow VO^{2+} + HO_2 \quad (4)$$

$$VO(O_2)^+ + HO_2 + H^+ \longrightarrow VO^{2+} + O_2 + H_2O_2 \quad (5)$$

$$VO^{2+} + H_2O_2 \longrightarrow VO_2^+ + OH + H^+ \quad (6)$$

$$VO(O_2)^+ + OH \longrightarrow VO_2^+ + HO_2 \quad (7)$$

$$VO_2^+ + H_2O_2 \longrightarrow VO(O_2)^+ + H_2O \quad (8)$$

It seems reasonable to conclude that the primary photochemistry responsible for Reaction (2) is electron transfer from O_2^{2-} to V^V (Eq. 3). This conclusion is reached for the following reasons: (1) the products of the photolysis of $VO(O_2)^+$ were VO^{2+} and O_2; the electron transfer from O_2^{2-} to V^V occured later to give VO^{2+} and O_2; (2) vanadium(IV) compounds were obtained in the photolysis of VO_2^+,[19] alkoxy vanadium(V) chelates,[20] and $VO(acac)_2Cl$[21]; (3) vanadium(IV) is the most stable oxidation state of vanadium under ordinary conditions. This intermediate $O=V^{IV}-O-O\cdot^+$ may be presumed to be very unstable. Thus, we assume that the first step is a cleavage of a V-O bond, affording formally the hyperoxovanadium(IV) complex (Eq. 3) in a manner similar to that previously reported in the photolysis of the diperoxo(porphyrinato)molybdenum(VI) complex.[22] The next step will be the departure of HO_2, providing VO^{2+} (Eq. 4). The resulting HO_2 will react with $VO(O_2)^+$ to generate H_2O_2, as is shown in Eq. 5. Rush and Bielki[23] have investigated the kinetics of the reaction of HO_2 with $VO(O_2)^+$ using a pulse radiolysis technique; they showed that HO_2 reduces $VO(O_2)^+$ to VO^{2+} according to Eq. 5 ($k_5=2.8\times10^5$ mol^{-1} dm^3 s^{-1}). The resulting H_2O_2 in Eq. 5 will react with VO^{2+} ($k_6=6.3$ mol^{-1} dm^3 s^{-1} [2]) as well as Fe(II) (Fenton's reagent) to give VO_2^+ and OH radicals. Samuni et al.[2] have reported that the oxidation of VO^{2+} to VO_2^+ by H_2O_2 is accompanied by a generation of $VO(O_2)^+$, even in the absence of an excess of H_2O_2 (Eq. 8). Working at $[H_2O_2]<[VO^{2+}]$ results in the appearance of $VO(O_2)^+$ even before all the VO^{2+} has been oxidized to VO_2^+.[1] That is, Reaction (6) is rapidly followed by Reaction (8) ($k_6=6.3$ mol^{-1} dm^3 s^{-1},[2] $k_8=2.96\times10^4$ mol^{-1} dm^{3}s^{-1} [10]). $VO(O_2)^+$ and VO^{2+} compete for the OH radicals formed by Eq. 6 (Eqs. 7 and 9):

$$VO^{2+} + OH \longrightarrow VO_2^+ + H^+ \quad (9)$$

Since $VO(O_2)^+$ is in excess relative to VO^{2+} under our present experimental conditions, the OH radicals react predominantly through Reaction (7) ($k_7=2.1\times10^{10}$ mol^{-1} dm^3 s^{-1}, $k_9=6.4\times10^8$ mol^{-1} dm^3 s^{-1} [2]). The HO_2 generated by Reaction (7) goes to Reaction (5). Thus, the overall reaction (2) can be explained by assuming Reactions (3)—(8).

As is shown in Fig. 3, the amount of the decomposed $VO(O_2)^+$ was equal to that of the VO^{2+} generated at the initial stage. However, the former became larger than the latter during a prolonged irradiation time. The difference was attributed to the thermal decomposition catalyzed with VO^{2+}. The thermal decomposition was investigated by Gardes-Alberyt et et al.[10]; they found the decomposition products to be VO_2^+ and O_2. At the initial stage, the thermal decomposition can be neglected. The amount of the decrease in the absorption at 285 nm in Fig. 2 became smaller with the increase in the irradiation time; this phenomenon is attributed to the generation of VO_2^+ by the thermal decomposition for the larger extinction coefficient of VO_2^+ ($\varepsilon=697$ mol^{-1} dm^3 cm^{-1}) compared to that of $VO(O_2)^+$ ($\varepsilon=468$ mol^{-1} dm^3 cm^{-1}). However, the amount of VO_2^+ generated at the initial stage is negligibly small.

Effect of 2-Propanol on the Photolysis of $VO(O_2)^+$. The assumption stated above was checked by the addition of an excess of 2-propanol to the reaction mixture. In such a case, OH radicals will react with 2-propanol ($k_{10}=2.0\times10^9$ mol^{-1} dm^3 s^{-1} [26]) to yield 2-propanol radicals, according to:

$$(CH_3)_2CHOH + OH \longrightarrow (CH_3)_2COH + H_2O \quad (10)$$

The 2-propanol radicals react with a number of metal ions and complex ions very rapidly; their rate constants were also measured.[27] The resulting 2-propanol radicals react thus with VO_2^+:

$$(CH_3)_2COH + VO_2^+ + H^+ \longrightarrow VO^{2+} + (CH_3)_2CO + H_2O \quad (11)$$

or

$$(CH_3)_2COH + O_2 \longrightarrow (CH_3)_2C(OH)O_2\cdot \quad (12)$$

$$VO_2^+ + (CH_3)_2C(OH)O_2\cdot + H^+ \longrightarrow VO^{2+} + (CH_3)_2CO + O_2 + H_2O \quad (13)$$

Reaction (11) (or Reactions (12) ($k_{12}=4.5\times10^9$ mol^{-1} dm^3 s^{-1} [28]) and (13)) can be supported by the facts that VO_2^+ was not detected at the initial stage of the photolysis and that ketone (acetone) as an oxidation product was detected in the irradiated solutions.[29] Thus, when Reactions (3)—(6), (10), and (11) (or (12)

and (13) instead of (11)) are assumed as the photochemical reaction mechanism in the presence of 2-propanol, the overall reaction can be written as follows:

$$2VO(O_2)^+ + (CH_3)_2CHOH + 2H^+ \xrightarrow{h\nu} 2VO^{2+} + (CH_3)_2CO + O_2 + 2H_2O \quad (14)$$

The results given in Table 1 can be explained satisfactorily in terms of Reaction (14).

It may be concluded that the photochemical decomposition reactions of $VO(O_2)^+$ in acidic aqueous solution occur according to the scheme presented above.

References

1) M. Orhanovic and R. G. Wilkins, *J. Am. Chem. Soc.*, **89**, 278 (1967).

2) A. Samuni, D. Meisel, and G. Czapski, *J. Chem. Soc., Dalton Trans.*, **1972**, 1273.

3) H. B. Brooks and F. Sicilio, *Inorg. Chem.*, **10**, 2530 (1971).

4) S. Funahashi, K. Haraguchi, and M. Tanaka, *Inorg. Chem.*, **16**, 1349 (1977).

5) S. Funahashi, T. Midorikawa, and M. Tanaka, *Inorg. Chem.*, **19**, 91 (1980).

6) S. Funahashi, K. Ishihara, and M. Tanaka, *Inorg. Chem.*, **20**, 51 (1981).

7) S. Funahashi, S. Funada, M. Inamo, R. Kurita, and M. Tanaka, *Inorg. Chem.*, **21**, 2202 (1982).

8) K. Wieghardt, *Inorg. Chem.*, **17**, 57 (1978).

9) G. A. Dean, *Can. J. Chem.*, **39**, 1174 (1961).

10) M. Gardes-Alberyt, C. Ferradini, and J. Pucheault, *J. Chem. Soc., Dalton Trans.*, **1975**, 2075.

11) A. Samuni and G. Czapski, *Isr. J. Chem.*, **8**, 563 (1970).

12) F. Secco, *Inorg. Chem.*, **19**, 2722 (1980).

13) R. Thompson, *Inorg. Chem.*, **21**, 859 (1982).

14) R. Thompson, *Inorg. Chem.*, **22**, 584 (1983).

15) H. Minoun, L. Saussine, E. Daire, M. Postel, J. Fischer, and R. Weiss, *J. Am. Chem. Soc.*, **105**, 3101 (1983).

16) R. A. Sheldon and J. K. Kochi, "Metal-Catalyzed Oxidations of Organic Compounds," Academic Press, New York (1981); pp. 48—97.

17) J. E. Lyons, "Aspects of Homogeneous Catalysis," ed by R. Ugo, D. Reidel, Dordrecht (1977), pp. 1—125.

18) C. G. Hatchard and C. A. Parker, *Proc. R. Soc. London, Ser. A*, **235**, 518 (1956).

19) B. G. Jeliazkowa, S. Nakamura, and H. Fukutomi, *Bull. Chem. Soc. Jpn.*, **48**, 347 (1975).

20) S. M. Aliwi and C. H. Bamford, *J. Chem. Soc., Faraday Trans. 1*, **73**, 776 (1977).

21) S. M. Aliwi and C. H. Bamford, *J. Chem. Soc., Faraday Trans. 1*, **70**, 2092 (1974).

22) H. J. Ledon and M. Bonnet, *J. Am. Chem. Soc.*, **103**, 6209 (1981).

23) J. D. Rush and B. H. J. Bielski, *J. Phys. Chem.*, **89**, 1524 (1985).

24) A. Samuni, *J. Phys. Chem.*, **76**, 2207 (1972).

25) The rate constant between $VO(O_2)^+$ and the OH radical (k_7) was evaluated by the use of the value (k_9=6.4×10^8 mol^{-1} dm^3 s^{-1}) obtained by Samuni et al. (Ref. 2).

26) R. L. Willson, C. L. Greenstock, G. E. Adams, R. Wagenman, and C. M. Dorfman, *Int. J. Radiat. Phys. Chem.*, **3**, 211 (1971).

27) A. Ross and P. Neta, "Rate Constants for the Reactions of Aliphatic Carbon-centered Radicals in Aqueous Solution," NSRDS, National Bureau of Standards, 70 (1982).

28) J. Butler, G. G. Jayson, and A. J. Swallow, *J. Chem. Soc., Faraday Trans. 1*, **70**, 1394 (1974).

29) Ketone was detected as its 2,4-dinitrophenylhydrazone (G. R. A. Johnson and G. Scholes, *Analyst*, **79**, 217 (1954)).

Preparation of μ-Cyano Dinuclear Chromium(III) Complexes $M^I[F(en \text{ or } tn)_2Cr(NC)Cr(CN)_5]$ from the Doubly Complexed Salts of the Form $M^I[CrF(H_2O)(en \text{ or } tn)_2][Cr(Cn)_6]$

Makoto JOHDA, Masatatsu SUZUKI, and Akira UEHARA*
Department of Chemistry, Faculty of Science, Kanazawa University, Kanazawa 920
(Received July 30, 1988)

Preparation of the μ-cyano dinuclear complexes $M^I[F(en \text{ or } tn)_2Cr(NC)Cr(CN)_5]\cdot nH_2O$ from the double complexes $M^I[CrF(H_2O)(en \text{ or } tn)_2][Cr(CN)_6]\cdot nH_2O$ was carried out both in the solid state and in solution, where M^I is Li^+, Na^+, K^+, or Rb^+ ion; en and tn stand for 1,2-ethanediamine and 1,3-propanediamine, respectively. The desired μ-cyano dinuclear complexes were successfully obtained in solution, but the mixture of di- and trinuclear complexes was formed along with unknown polymeric species in the solid state. The electronic spectra of the dinuclear complexes exhibited a small but clear band due to spin-forbidden transition ($^4A_{2g}\rightarrow{}^2E_g$). Magnetic moments of the dinuclear complexes were 3.4—3.5 μ_B at ambient temperatures and 2.2—2.4 μ_B at 80 K, which are substantially smaller than the spin-only value (3.87 B.M.). The J values for the dinuclear complexes were estimated to be −19—−20 cm^{-1}, indicating that an antiferromagnetic superexchange interaction is exerted between two chromium(III) ions through μ-CN group, but the magnitude of the interaction is smaller than that of the μ-oxo complexes (J=−450 cm^{-1}) and comparable to that of the μ-hydroxo complexes (J=−23 cm^{-1}) reported previously.

Several magnetic studies have declared that a superexchange interaction is exerted in the dinuclear chromium(III) complexes containing μ-hydroxo,[1-10] μ-oxo,[1,11-15] and μ-alkoxo[16,17] groups: e.g., $[(NH_3)_5Cr(OH)Cr(NH_3)_5]Br_5$[5,6] and $[(NH_3)_5Cr(O)Cr(NH_3)_5]Br_4$[11] give the magnetic moments of 3.44 (294.5 K) and 1.29 μ_B (294.7 K) respectively, which are considerably lower magnetic moments than that expected from the spin-only value for the chromium(III) ion. The J values for the μ-hydroxo[5,6] and μ-oxo[11] complexes have been evaluated as −23 and −450 cm^{-1}, respectively. Earnshaw and Lewis[1] have pointed out from magnetic studies on the analogues of the above dinuclear complexes that the degree of metal–metal interaction depends upon the nature of the bridging group and markedly upon the M–L–M′ bond angle: The greater the bonding ability of the bridging groups and the larger the M–L–M′ bond angle is, the stronger the metal–metal interaction becomes (M and M′ are the same or different metal ions, and L is the bridging ligand). From this point of view, the dinuclear chromium(III) complexes containing a single μ-cyano group are another interesting candidates for examining magnetic interaction between two metal ions because Cr(III)–CN–Cr(III) is linear. Unfortunately, although polymeric μ-cyano complexes have been reported,[18,19] any dinuclear chromium(III) complex with a single μ-cyano group has not been known except for $K[F(en)_2Cr(NC)Cr(CN)_5]$ reported by Ribas et al.[20,21] Very recently, we derived the same complex from $K[CrF(H_2O)(en)_2][Cr(CN)_6]$ in solution, and found that our complex exhibits astonishingly different physicochemical properties from that reported previously.[20,21] For example, the magnetic moments of our complex were 3.40 μ_B at 300 K and 2.22 μ_B at 80 K, whereas those of the previous complex were 3.79 μ_B at 293.5 K and 3.51 μ_B at 77 K.[20] Thus, we suspected that the previous complex is not a dinuclear complex, but simply a doubly complexed salt $K[CrF(H_2O)(en)_2][Cr(CN)_6]$.

Therefore, the present paper was undertaken (1) to prepare a series of the dinuclear chromium(III) complexes with a single μ-cyano group $M^I[F(en \text{ or } tn)_2Cr(NC)Cr(CN)_5]$ from the double complexes $M^I[CrF(H_2O)(en \text{ or } tn)_2][Cr(CN)_6]$, where M^I is Li^+, Na^+, K^+, or Rb^+; en and tn stand for 1,2-ethanediamine and 1,3-propanediamine, respectively, and (2) to examine physicochemical properties of the complexes especially from the view point of a superexchange interaction exerted between two chromium(III) ions through a μ-cyano group.

Experimental

Preparation of the Starting Materials for Obtaining Double Complexes. $K_3[Cr(CN)_6]$[22] and *trans*-$[CrF(H_2O)(en)_2](ClO_4)_2$[23a] were prepared by the same methods as those described in the literature.

trans-$[CrF(H_2O)(tn)_2](ClO_4)_2$ was obtained from *trans*-$[CrF_2(py)_4]ClO_4$ (py: pyridine)[24] as follows: *trans*-$[CrF_2(py)_4]ClO_4$ (20 mmol) and 1,3-propanediamine (40 mmol) were dissolved in 2-methoxyethanol (80 cm^3). The solution was refluxed for 1 h and cooled to room temperature. Products thus obtained were collected by filtration, washed with ethanol and ether, and air-dried. Purification of the products was carried out by dissolving them in water and adding a mixture of ethanol and ether (1:1) to the solution.

Preparation of Double Complexes. ***trans*-$K[CrF(H_2O)(en \text{ or } tn)_2][Cr(CN)_6]\cdot H_2O$.** *trans*-$[CrF(H_2O)(en \text{ or } tn)_2](ClO_4)_2$ (25 mmol) was dissolved in ice-cooled water (100 cm^3), to which $K_3[Cr(CN)_6]$ (25 mmol) was added with stirring. After several minutes, the $KClO_4$ which formed was removed by filtration. To the filtrate was added ethanol (100 cm^3) to give products, which were collected by filtration, washed with ethanol and ether, and air-dried. The products were purified by dissolving them in a minimum amount of ice-cooled

Table 1. Analytical Data and Molar Conductivities (Λ) of the Double and the Dinuclear Complexes Obtained

Complex	C(%) Found	C(%) Calcd	H(%) Found	H(%) Calcd	N(%) Found	N(%) Calcd	Λ/Ω^{-1} cm^2 cm^{-1}
Double complexes							
trans-Li[CrF(H_2O)(en)$_2$][Cr(CN)$_6$]·2H_2O	26.05	26.09	4.89	4.38	30.36	30.43	285
trans-Na[CrF(H_2O)(en)$_2$][Cr(CN)$_6$]·H_2O	26.29	26.21	4.53	4.40	30.65	30.56	272
trans-K[CrF(H_2O)(en)$_2$][Cr(CN)$_6$]·H_2O	25.84	25.32	4.05	4.25	29.82	29.52	282
trans-Rb[CrF(H_2O)(en)$_2$][Cr(CN)$_6$]·H_2O	23.21	23.06	3.92	3.87	27.01	26.89	311
trans-K[CrF(H_2O)(tn)$_2$][Cr(CN)$_6$]·H_2O	28.71	28.68	4.85	4.81	27.76	27.88	341
Dinuclear complexes							
Li[F(en)$_2$Cr(NC)Cr(CN)$_5$]·4.5H_2O	24.61	24.65	5.19	5.17	28.93	28.74	95
Na[F(en)$_2$Cr(NC)Cr(CN)$_5$]·1.5H_2O	26.85	26.73	4.37	4.26	31.31	31.17	123
K[F(en)$_2$Cr(NC)Cr(CN)$_5$]·1.5H_2O	25.92	25.83	4.21	4.11	30.26	30.12	130
Rb[F(en)$_2$Cr(NC)Cr(CN)$_5$]·1.5H_2O	23.49	23.47	3.88	3.74	27.38	27.37	112
K[F(tn)$_2$Cr(NC)Cr(CN)$_5$]·1.5H_2O	29.38	29.21	4.66	4.70	28.56	28.38	102

water and adding ethanol to the solution.

***trans*-Li[CrF(H_2O)(en)$_2$][Cr(CN)$_6$]·2H_2O and *trans*-Na[CrF(H_2O)(en)$_2$][Cr(CN)$_6$]·H_2O.** K_3[Cr(CN)$_6$] (25 mmol) was dissolved in a minimum amount of water (100 cm^3) and thereto excess $LiClO_4$ or $NaClO_4$ (125 mmol) was added. The solution was stirred for 5 min. The $KClO_4$ thus formed was filtered off. To the filtrate, *trans*-[CrF(H_2O)(en)$_2$](ClO_4)$_2$ (25 mmol) was added. The solution was once filtered and thereto ethanol (100 cm^3) was added with stirring to produce precipitates. The precipitates were collected by filtration, washed with ethanol and acetone, and air-dried. Purification was carried out in a manner similar to that of *trans*-K[CrF(H_2O)(en)$_2$][Cr(CN)$_6$]·H_2O.

***trans*-Rb[CrF(H_2O)en$_2$][Cr(CN)$_6$]·H_2O.** K_3[Cr(CN)$_6$] (25 mmol) was added to a solution of *trans*-[CrF(H_2O)(en)$_2$](ClO_4)$_2$ (25 mmol) in ice-cooled water (100 cm^3). The solution was allowed to stand for several minutes to precipitate $KClO_4$. After the $KClO_4$ was removed out by filtration, RbCl (50 mmol) was added to the filtrate. To the resulting solution, ethanol (100 cm^3) was added with stirring to produce precipitates. The precipitates were collected by filtration, washed with ethanol and acetone, and air-dried. Purfication was carried out by the same method as that of *trans*-K[CrF(H_2O)(en)$_2$][Cr(CN)$_6$]·H_2O.

Preparation of Dinuclear Complexes from Double Complexes in Water. The double complexes *trans*-M^I[CrF(H_2O)(en)$_2$][Cr(CN)$_6$]·*n*H_2O (M^I: Li^+, Na^+, K^+, or Rb^+) (5.0 g) were dissolved in a minimum amount of water (10 cm^3) and the resulting solution was warmed for 30 min at 45—50 °C. The solution was once filtered and the filtrate was cooled at 0 °C to produce crude dinuclear complexes. The crude complexes were recrystallized from water. K[F(tn)$_2$Cr(NC)Cr(CN)$_5$]·1.5 H_2O was similarly prepared except that *trans*-K[CrF(H_2O)(tn)$_2$][Cr(CN)$_6$]·H_2O was used in place of M[CrF(H_2O)(en)$_2$][Cr(CN)$_6$]·*n*H_2O.

The double complexes are in general pink in color, while the dinuclear complexes are orange. The analytical data of the complexes obtained are summarized in Table 1 together with the molar conductivities measured in water of the complexes.

Spectral Measurements. The IR spectra of samples were measured by a KBr-disk method with a Jasco Model A-3 infrared spectrophotometer. Visible and UV spectra in water were measured with a Jasco UVIDEC-505 UV/VIS recording digital spectrophotometer. The spectra in the solid state were measured by a diffuse reflectance methed with a Jasco UVIDEC-410 UV/VIS spectrophotometer equipped with a Jasco Model TIS-241 reflectance attachment.

Molar Conductivity Measurements. Molar conductivities of the complexes were measured in water at 25 °C on a Toa CM-20S conductivity meter at a concentration of 10^{-3} mol dm^{-3}.

Magnetic Measurements. The effective magnetic moments of samples were evaluated from magnetic susceptibilities measured by Gouy method at room temperature. Hg[Co(NCS)$_4$] was employed as a susceptibility standard in all cases. Variable-temperature(78—300 K) magnetic susceptibilities were monitored on a Shimadzu torsion magnetometer MB-2 which was calibrated with Hg[Co(NCS)$_4$]. Diamagnetic correction was made by using Pascal's constants.

TG and DTA Measurements. The TG and DTA measurements for samples were carried out with a Seiko TA Station SSC 5000 system under a constant flow of nitrogen (100 cm^3 min^{-1}), sample weight being in the range of 10—20 mg. Heating rate was 2.0 °C min^{-1}. Heating processes were also observed by using a Chyo 100-L thermobalance.

Results

For clarification of the following discussion, the double complexes *trans*-M^I[CrF(H_2O)(en or tn)$_2$][Cr(CN)$_6$] and the dinuclear complexes M^I[F(en or tn)$_2$Cr(NC)Cr(CN)$_5$]will be simply abbreviated as M(en or tn)[Cr][Cr] and M(en or tn)[Cr–Cr]. The first and second products stand for the products formed at the temperature of the first and second plateaus during the thermal reactions of the double complexes, respectively.

Molar Conductivities. The values for molar conductivities of the complexes are given in the last column of Table 1. The values of the double and the dinuclear comlexes are in the range of 272—341 and 95—130 Ω^{-1}cm^2 mol^{-1}, indicating that the double and the dinuclear complexes are 2:1 and 1:1 electrolytes, respectively.[25]

Thermal Reactions of the Double Complexes in the Solid State. The thermal reactions of the double complexes were observed in the solid state by means of TG and DTA methods. As an example, Fig.1 shows the TG and DTA curves of *trans*-K[CrF(H_2O)(en)$_2$]-[Cr(CN)$_6$]·H_2O and *trans*-K[CrF(H_2O)(tn)$_2$][Cr(CN)$_6$]·H_2O. The TG curve of the complex K(en)[Cr][Cr] shows two steps of the mass losses at 25—162 °C. The first mass loss starts at about 25 °C endothermically. Then, a break point appears at about 52 °C, after which a smooth plateau is obtained at 52—110 °C. The second mass loss takes place at 110—162 °C, the second plateau being obtained at 162—210 °C. The first and second mass losses correspond to the losses of one mole of lattice water (Found: 3.8%; Calcd: 3.8%), and one mole of coordinated water (Found: 3.7%; Calcd: 3.8%). The original pink color remained unchanged at the first plateau and changed to orange at the second plateau. Similar TG and DTA patterns can be seen for the complex K(tn)[Cr][Cr]. The complex turned in color from the original pink to orange at the second plateau. The color change is due to the formation of the dinuclear complex K(en or tn)[Cr–Cr] along with minor polynuclear species as mentioned later. Table 2 lists up the temperatures and enthalpy changes (ΔH) for the evolution of lattice and coordinated waters of the double complexes. The ΔH's for the evolution of coordinated waters are greater than those for those of lattice water for all the double complexes.

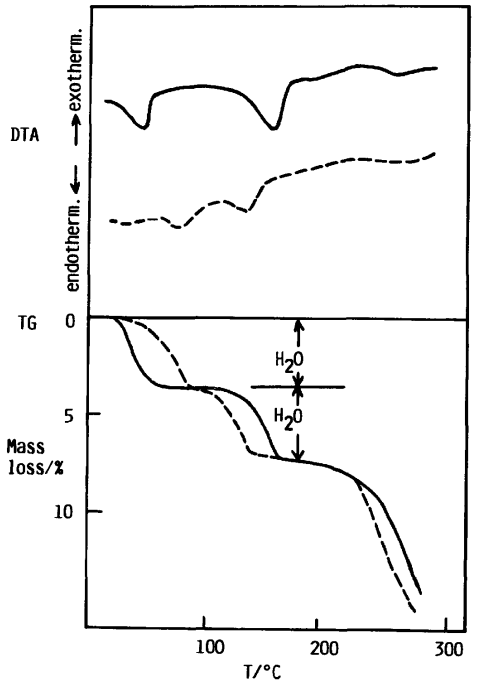

Fig. 1. TG and DTA curves of *trans*-K[CrF(H_2O)-(en)$_2$][Cr(CN)$_6$]·H_2O (——) and *trans*-K[CrF(H_2O)-(tn)$_2$][Cr(CN)$_6$]·H_2O (------).

IR Spectra. Table 3 summarizes the IR data due to CN stretching vibration. As seen from the table, all the double complexes give a single peak at 2130—2138 cm^{-1}, which is assignable to the terminal CN stretching vibration of $[Cr(CN)_6]^{3-}$ (2135 cm^{-1}). On the other hand, the dinuclear complexes indicate two peaks at 2130—2138 and 2160—2170 cm^{-1}; the former is due to the terminal CN stretching and the latter is attributable to the bridging CN stretching vibration.[26] The first products show only terminal-CN stretching band, whereas the second products, both terminal- and bridging-CN stretching bands.

Electronic Spectra. The electronic spectral data of the double and the dinuclear complexes in water are listed in Table 4 together with those of the reference complexes *trans*-[CrF(H_2O)(en or tn)$_2$](ClO_4)$_2$ and K_3[Cr(CN)$_6$]. On the other hand, the electronic spectral data in the solid state are summarized in Table 5 which also includes the data of the second products obtained by heating the double complexes M(en or tn)[Cr][Cr]. Figure 2 shows the electronic spectra in water of *trans*-[CrF(H_2O)(en)$_2$](ClO_4)$_2$, K_3[Cr(CN)$_6$], the double complex K(en)[Cr][Cr] and the dinuclear complex K(en)[Cr–Cr]. The spectrum of the double complex K(en)[Cr][Cr] exhibits four bands at 505, 451, 376, and 307 nm. The bands at 505 and 451 nm are due to the components of the first band of the cationic moiety *trans*-[CrF(H_2O)-(en)$_2$]$^{2+}$. The band at 376 nm may be the mixture of the second band (370 nm) of *trans*-[CrF(H_2O)(en)$_2$]$^{2+}$ and the first band (377 nm) of $[Cr(CN)_6]^{3-}$. The last band at 307 nm is assignable to the second band of $[Cr(CN)_6]^{3-}$. On the other hand, in the spectrum of the dinuclear complex K(en)[Cr–Cr], three bands can be seen at 677, 492, and 372 nm; the small but clear band at 677 nm (ε=≈5) comes from spin-forbidden transition ($^4A_{2g}\rightarrow$

Table 2. Temperatures and Enthalpy Changes (ΔH) for the Evolution of Lattice and Coordinated Waters of the Double Complexes *trans*-M^{I}[CrF(H_2O)(en or tn)$_2$][Cr(CN)$_6$]·nH_2O

Complex	Lattice water		Coordinated water	
	Temperature/°C	ΔH/kJ mol^{-1}	Temperature/°C	ΔH/kJ mol^{-1}
trans-Li[CrF(H_2O)(en)$_2$][Cr(CN)$_6$]·2H_2O	40—116	40.7	116—166	51.5
trans-Na[CrF(H_2O)(en)$_2$][Cr(CN)$_6$]·H_2O	20— 70	41.1	115—165	52.7
trans-K[CrF(H_2O)(en)$_2$][Cr(CN)$_6$]·H_2O	25— 52	38.6	130—162	73.7
trans-Rb[CrF(H_2O)(en)$_2$][Cr(CN)$_6$]·H_2O	40— 90	43.0	117—150	55.4
trans-K[CrF(H_2O)(tn)$_2$][Cr(CN)$_6$]·H_2O	30— 90	51.8	95—146	68.2

Table 3. IR Spectral Data (cm^{-1}) Due to the CN-Stretching Vibration (ν_{CN})

Compound[a]	Terminal-CN bands	Bridging-CN bands
$K_3[Cr(CN)_6]$	2135	—
trans-$Li[CrF(H_2O)(en)_2][Cr(CN)_6]\cdot 2H_2O$	2138	—
first product	2138	—
second product	2138	2167
$Li[F(en)_2Cr(NC)Cr(CN)_5]\cdot 4.5H_2O$	2138	2166
trans-$Na[CrF(H_2O)(en)_2][Cr(CN)_6]\cdot H_2O$	2133	—
first product	2135	—
second product	2133	2162
$Na[F(en)_2Cr(NC)Cr(CN)_5]\cdot 1.5H_2O$	2133	2160
trans-$K[CrF(H_2O)(en)_2][Cr(CN)_6]\cdot H_2O$	2130	—
first product	2130	—
second product	2130	2165
$K[F(en)_2Cr(NC)Cr(CN)_5]\cdot 1.5H_2O$	2130	2165
trans-$Rb[CrF(H_2O)(en)_2][Cr(CN)_6]\cdot H_2O$	2130	—
first product	2130	—
second product	2128	2162
$Rb[F(en)_2Cr(NC)Cr(CN)_5]\cdot 1.5H_2O$	2130	2170
trans-$K[CrF(H_2O)(tn)_2][Cr(CN)_6]\cdot H_2O$	2134	—
first product	2134	—
second product	2134	2165
$K[F(tn)_2Cr(NC)Cr(CN)_5]\cdot 1.5H_2O$	2132	2166

a) The first and second products are the products obtained at the first and second plateaus during the thermal reactions of the double complexes, respectively.

Table 4. Electronic Spectral Data in Water

Complex	λ_{max}/nm (ε/mol^{-1} dm^3 cm^{-1})[a]			
Reference complex				
trans-$[CrF(H_2O)(en)_2](ClO_4)_2$[23a]	520(24.2)	458(25.6)	370(31.2)	
trans-$[CrF(H_2O)(tn)_2](ClO_4)_2$[23b]	533(20.9)	460(22.4)	375(37.8)	
$K_3[Cr(CN)_6]$[22]			377(85.9)	307(59.5)
Double complex				
trans-$Li[CrF(H_2O)(en)_2][Cr(CN)_6]\cdot 2H_2O$	515sh(28)	452sh(32)	377(121)	307(77)
trans-$Na[CrF(H_2O)(en)_2][Cr(CN)_6]\cdot H_2O$	513sh(39)	451sh(41)	377(135)	307(94)
trans-$K[CrF(H_2O)(en)_2][Cr(CN)_6]\cdot H_2O$	505sh(33)	451sh(37)	376(128)	307(82)
trans-$Rb[CrF(H_2O)(en)_2][Cr(CN)_6]\cdot H_2O$	510sh(31)	450sh(36)	377(129)	307(86)
trans-$K[CrF(H_2O)(tn)_2][Cr(CN)_6]\cdot H_2O$	530sh(27)	453sh(30)	376(128)	307(66)
Dinuclear complex				
$Li[F(en)_2Cr(CN)Cr(CN)_5]\cdot 4.5H_2O$	677(≈5)[b]	490(50)	370(155)	
$Na[F(en)_2Cr(CN)Cr(CN)_5]\cdot 1.5H_2O$	677(≈5)[b]	490(46)	371(150)	
$K[F(en)_2Cr(CN)Cr(CN)_5]\cdot 1.5H_2O$	677(≈5)[b]	492(46)	372(147)	
$Rb[F(en)_2Cr(CN)Cr(CN)_5]\cdot 1.5H_2O$	677(≈5)[b]	491(49)	371(156)	
$K[F(tn)_2Cr(CN)Cr(CN)_5]\cdot 1.5H_2O$	677(≈5)[b]	499(43)	370(154)	

a) Measured in water. b) Spin-forbidden transition ($^4A_{2g}\rightarrow{}^2E_g$).

^2E_g).[27-29] Other two bands at 492 and 372 may be due to spin-allowed transition $^4A_{2g}\rightarrow{}^4T_{2g}$ and $^4A_{2g}\rightarrow{}^4T_{1g}$, respectively.

Figure 3 illustrates the electronic spectra in the solid state of the double complex K(en)[Cr][Cr], of the dinuclear complex K(en)[Cr–Cr], and of the second product obtained by heating the double complex K(en)[Cr][Cr]. The spectrum of the double complex gives five bands at 665, 520, 460 (sh), 380, and 307 nm (Table 5). The bands at 520 and 460 nm are due to the components of the first band of *trans*-$[CrF(H_2O)(en)_2]^{2+}$; the band at 380 nm is assignable to the mixture of the second band of *trans*-$[CrF(H_2O)(en)_2]^{2+}$ plus the first band of $[Cr(CN)_6]^{3-}$; and the band at 307 nm is the second band of $[Cr(CN)_6]^{3-}$. A tiny band can be seen at 665 nm, which may be due to spin-forbidden transition. The spectrum of the second product obtained by heating the double complex

Table 5. Electronic Spectral Data in the Solid State

Compound	λ_{max}/nm					
trans-Li[CrF(H_2O)(en)$_2$][Cr(CN)$_6$]·2H_2O	*665w	520		456	374	307
Second product[a]	*677w		490		374	
Li[F(en)$_2$Cr(NC)Cr(CN)$_5$]·4.5H_2O	*677s		494		374	
trans-Na[CrF(H_2O)(en)$_2$][Cr(CN)$_6$]·H_2O	*665w	520		460sh	379	309
Second product[b]	*677w		488		378	
Na[F(en)$_2$Cr(NC)Cr(CN)$_5$]·1.5H_2O	*677s		497		380	
trans-K[CrF(H_2O)(en)$_2$][Cr(CN)$_6$]·H_2O	*665w	520		460sh	380	307
Second product[c]	*677w		490		378	
K[F(en)$_2$Cr(NC)Cr(CN)$_5$]·1.5H_2O	*675s		490		370	
trans-Rb[CrF(H_2O)(en)$_2$][Cr(CN)$_6$]·H_2O	*665w	525		460sh	380	310
Second product[d]	*677w		490		378	
Rb[F(en)$_2$Cr(NC)Cr(CN)$_5$]·1.5H_2O	*680s		500		380	
trans-K[CrF(H_2O)(tn)$_2$][Cr(CN)$_6$]·H_2O	*668w	530	470		378	309
Second product[e]	*676w		499		374	
K[F(en)$_2$Cr(NC)Cr(CN)$_5$]·1.5H_2O	*678s		500		374	

* Spin-forbidden transition ($^4A_{2g} \rightarrow {}^2E_g$): w=week, s=strong. a to e): The products obtained by heating the corresponding double complexes in air bath for 2 h: a) at 175 °C, b) at 175 °C, c) at 165 °C, d) at 165 °C, and e) at 150 °C.

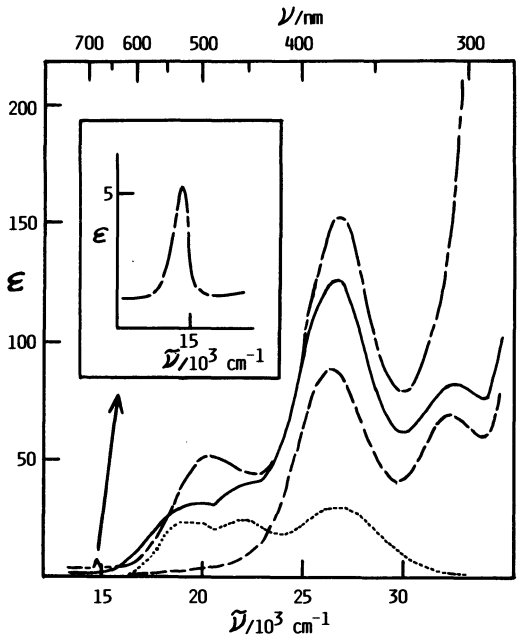

Fig. 2. Electronic spectra in water of *trans*-[CrF(H_2O)(en)$_2$](ClO_4)$_2$ (------), K_3[Cr(CN)$_6$] (———), *trans*-K[CrF(H_2O)(en)$_2$][Cr(CN)$_6$]·H_2O (———), and K[F(en)$_2$Cr(NC)Cr(CN)$_5$]·1.5H_2O (———).

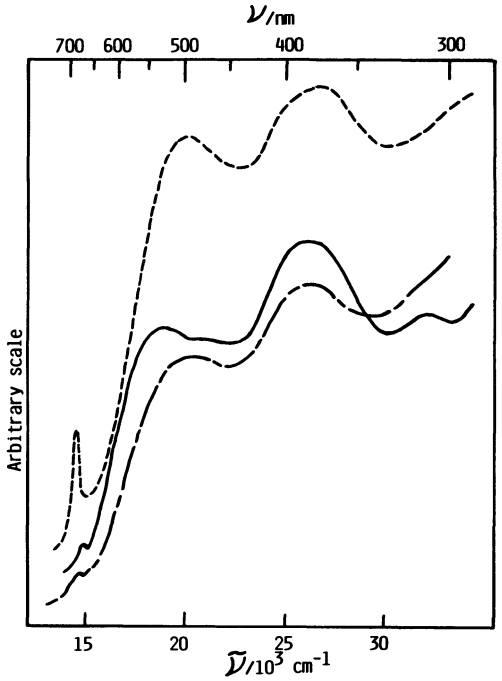

Fig. 3. Electronic spectra in the solid state of *trans*-K[CrF(H_2O)(en)$_2$][Cr(CN)$_6$]·H_2O (———), the product obtained by heating the double complex (———), and K[F(en)$_2$Cr(CN)Cr(CN)$_5$]·1.5H_2) (-----).

K(en)[Cr][Cr] is very similar to that of the dinuclear complex, but the spin-forbidden band at 677 nm is much smaller than that of the dinuclear complex. This implies that the product contains some species other than the dinuclear species (vide infra).

Magnetic Properties. Table 6 summarizes the effective magnetic moments (μ_{eff}) of the double complexes, of the second products obtained by heating the double complexes, and of the dinuclear complexes. As seen from the table, the μ_{eff}'s per a Cr(III) ion of all the double complexes are 3.81—3.89 B.M. at ambient temperatures, whereas those of the second products obtained by heating the double complexes are 3.40—3.67 B.M., and those of the dinuclear complexes are 3.31—3.47 B.M. In both cases of the second products and of the dinuclear complexes, the μ_{eff}'s are obviously reduced from the spin-only value and so it is

Table 6. Effective Magnetic Moment μ_{eff}, per a Chromium(III) Ion of Double Complexes, of Their Second Products by Heating Double Complexes, and of Dinuclear Complexes

Complex	μ_{eff}/B.M.	Temp/K
Double complex		
trans-Li[CrF(H_2O)(en)$_2$][Cr(CN)$_6$]·2H_2O	3.89	290
Second product[a]	3.42	289
trans-Na[CrF(H_2O)(en)$_2$][Cr(CN)$_6$]·2H_2O	3.81	298
Second product[b]	3.41	290
trans-K[CrF(H_2O)(en)$_2$][Cr(CN)$_6$]·2H_2O	3.85	295
Second product[c]	3.43	300
	2.96	80
trans-Rb[CrF(H_2O)(en)$_2$][Cr(CN)$_6$]·2H_2O	3.89	292
Second product[d]	3.49	298
trans-K[CrF(H_2O)(tn)$_2$][Cr(CN)$_6$]·2H_2O	3.84	289
Second product[e]	3.40	290
Dinuclear complex		
Li[F(en)$_2$Cr(NC)Cr(CN)$_5$]·4.5H_2O	3.47	290
Na[F(en)$_2$Cr(NC)Cr(CN)$_5$]·1.5H_2O	3.31	286
K[F(en)$_2$Cr(NC)Cr(CN)$_5$]·1.5H_2O	3.40	300
	2.22	80
Rb[F(en)$_2$Cr(NC)Cr(CN)$_5$]·1.5H_2O	3.45	300
	2.28	80
K[F(tn)$_2$Cr(NC)Cr(CN)$_5$]·1.5H_2O	3.43	300
	2.44	80

a) Obtained by heating *trans*-Li[CrF(H_2O)(en)$_2$][Cr(CN)$_6$]·2H_2O at 175 °C for 2 h. b) Obtained by heating *trans*-Na[CrF(H_2O)(en)$_2$][Cr(CN)$_6$]·2.5H_2O at 175 °C for 2 h. c) Obtained by heating *trans*-K[CrF(H_2O)(en)$_2$][Cr(CN)$_6$]·H_2O at 165 °C for 2 h. d) Obtained by heating *trans*-Rb[CrF(H_2O)(en)$_2$][Cr(CN)$_6$]·H_2O at 165 °C for 2 h. e) Obtained by heating *trans*-K[CrF(H_2O)(tn)$_2$][Cr(CN)$_6$]·H_2O at 150 °C for 2 h.

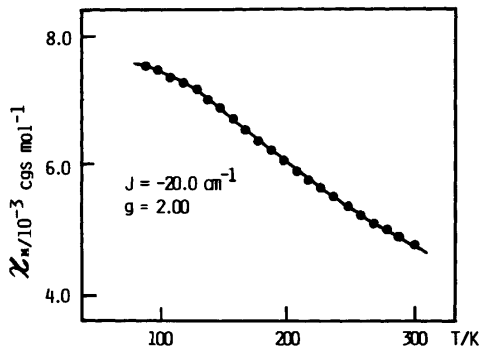

Fig. 4. Temperature dependence of magnetic susceptibilities of K[F(en)$_2$Cr(CN)Cr(CN)$_5$]·1.5H_2O.

conceivable that certain metal–metal interaction is exerted through the CN bridge.

The measurements of the magnetic susceptibilities in the temperature range of 80—300 K, however, indicated different results between the second product and the dinuclear complexes. The results were analyzed with the spin–spin interaction Hamiltonian, $H=-2JS_1\cdot S_2$. The molar susceptibility (χ_M) of an $S_1=S_2=3/2$ exchange coupling dimer is given by the following equation:

$$\chi_M = \frac{N\beta^2 g^2}{3\kappa T}\cdot\frac{3x^{10}+15x^6+42}{x^{12}+3x^{10}+5x^6+7}$$

where $x=\exp(-J/\kappa T)$ and the symbols have their usual meanings. The experimental values are well-interpreted in terms of the above equation as can be seen in Fig. 4. The solid line is a calculated curve by using the following parameters, $J=-20.0$ cm^{-1} and $g=2.00$ for K(en)[Cr–Cr], indicating that an antiferromagnetic interaction is effected in the dinuclear complex. Such antiferromagnetic interaction was also observed in another dinuclear complex: $J=-19.0$ cm^{-1} and $g=2.00$ for Rb(en)[Cr–Cr].

On the other hand, the magnetic properties of second product obtained by heating the double complex K(en)[Cr][Cr] were not explained by the above equation. This may be due to the presence of impure species (vide infra).

Discussion

Preparation of Dinuclear Complexes. Ribas et al. reported that the dinuclear complex K[F(en)$_2$Cr(NC)-Cr(CN)$_5$]·2H_2O is obtained by mixing *trans*-[CrF-(H_2O)(en)$_2$](ClO_4)$_2$ with K_3[Cr(CN)$_6$] in water-ice bath.[20,21] Our reexamination of the procedures always gave the pink double complex K[CrF(H_2O)-(en)$_2$][Cr(CN)$_6$]·H_2O. On the other hand, we obtained the dinuclear complexes M(en or tn)[Cr–Cr] by heating the corresponding double complexes in water at 45—50 °C for about 30 min. Our dinuclear complexes are orange in color and have magnetic moments of 3.4—3.7 μ_B at room temperatures and 2.2—2.4 μ_B at 80 K, whereas the previously reported complex is pink in color and has magnetic moments of 3.79 μ_B at 293.5 K and 3.51 μ_B at 77.0 K. It seems reasonable to consider that the previous complex is not a dinuclear complex, but the double complex K[CrF-(H_2O)(en)$_2$][Cr(CN)$_6$]·H_2O.

Products Obtained by Heating the Double Complexes in the Solid State. The pinkish double complexes M(en or tn)[Cr][Cr], upon heating, evolved first lattice waters and then coordinated waters to convert into orange products (second products). From the results of TG and DTA analyses, the second products are seemingly conceivable to be dinuclear complexes. However, minute examination of the orange products revealed that the products are the mixture of di- and trinuclear complexes along with unknown polymeric species. This suggests that the thermal deaquation-anation of the double complexes in the solid state does not give pure dinuclear complexes.

Configuration of the Dinuclear Complexes. Two geometrical isomers (cis and trans) are possible for the dinuclear complexes $K[CrF(en \text{ or } tn)_2Cr(NC)Cr(CN)_5]$ with respect to the positions of F^- ion and $-(NC)Cr(CN)_5$ moiety. It is difficult to accurately decide the geometrical configurations from electronic spectral data because both isomers are expected to give a similar spectrum to each other. In fact, it has been reported that both *cis*- and *trans*-$[CrF(NH_3)(en)_2]^{2+}$ exhibit close band maxima except for ε values because they have the same core ($CrFN_5$) and hence the same symmetry (C_{4v}).[30,31] However, we tentatively conclude that the dinuclear complexes in the present study are trans-configuration provided that trans-to-cis isomerization were not involved in the preparative procedures. Possibility of the isomerization can be completely discarded in the case of the tn complex because $[CrX_2(tn)_2]^+$ has been found to undergo cis-to-trans isomerization, but not trans-to-cis isomerization.[32] Comparison of the λ_{max}'s and ε's in Table 4 implies that both en and tn dinuclear complexes give essentially similar spectra except that the λ_{max}'s of the tn complex appear at longer wavelengths than those of the en complexes, which arises from the difference in ligand field strength of en and tn. Therefore, it seems reasonable to consider that the en dinuclear complexes also have trans-configuration.

Financial support from the Ministry of Education, Science and Culture Grant-in-Aid for Scientific Research (No. 62470040) is acknowledged.

References

1) A. Earnshaw and J. Lewis, *J. Chem. Soc.*, **1961**, 396.
2) H. Kobayashi, T. Haseda, and E. Kanbe, *J. Phys. Soc. Jpn.*, **15**, 1646(1960).
3) T. Morishita, K. Hori, E. Kyuno, and R. Tsuchiya, *Bull. Chem. Soc. Jpn.*, **38**, 1276 (1965).
4) J. T. Veal, D. Y. Jeter, J. C. Hempel, R. P. Eckberg, W. E. Hatfield, and D. J. Hodgson, *Inorg. Chem.*, **12**, 2928 (1973).
5) S. J. Cline, J. Glerup, D. J. Hodgson, G. S. Jensen, and E. Pedersen, *Inorg. Chem.*, **20**, 2229 (1981).
6) M. Thompson and R. E. Connick, *Inorg. Chem.*, **20**, 2279 (1981).
7) R. P. Scaringe, W. E. Hatfield, and D. J. Hodgson, *Inorg. Chem.*, **16**, 1600 (1977).
8) W. E. Hatfield, J. J. Macdougall, and R. E. Shepherd, *Inorg. Chem.*, **20**, 4216 (1981).
9) H. Riesen and H. U. Gudel, *Inorg. Chem.*, **25**, 3566 (1986); **26**, 2347 (1987).
10) H. Riesen, C. Reber, H. U. Gudel, and K. Wieghardt, *Inorg. Chem.*, **26**, 2747 (1987).
11) E. Pedersen, *Acta Chem. Scand.*, **26**, 333 (1972).
12) M. Divaira and F. Mani, *Inorg. Chem.*, **23**, 409 (1984).
13) D. J. Liston and B. O. West, *Inorg. Chem.*, **24**, 1568 (1985).
14) M. D. Vaira and F. Mani, *Inorg. Chem.*, **23**, 409 (1984).
15) R. Rancashire and T. D. Smith, *J. Chem. Soc., Dalton Trans.*, **1982**, 693.
16) F. A. Cotton and G. G. Stanley, *Inorg. Chem.*, **16**, 2668 (1977).
17) H. R. Fischer, D. J. Hodgson, and E. Pedersen, *Inorg. Chem.*, **23**, 4755 (1984).
18) J. E. House and J. C. Bailar, Jr., *Inorg. Chem.*, **8**, 672 (1969).
19) A. Uehara, S. Terabe, and R. Tsuchiya, *Inorg. Chem.*, **22**, 2864 (1983).
20) J. Ribas, J. Casabo, M. Monfort, M. L. Alvareg, and J. M. Coronas, *J. Inorg. Nucl. Chem.*, **42**, 707 (1980).
21) M. Monfort, M. Serra, A. Escuer, and J. Ribas, *Thermochim. Acta*, **69**, 397 (1983).
22) W. B. Schaap, R. Krishnamurthy, D. K. Wakefield, and W. F. Coleman, "Coordination Chemistry," S. Kirschner, Ed., Plenum Press, New York, N. Y. (1969), p. 177.
23) a) J. W. Vaughn, O. J. Stvan, Jr., and V. E. Magnuson, *Inorg. Chem.*, **7**, 736 (1968); b) J. M. DeJovime, W. R. Mason, and J. W. Vaughn, *Inorg. Chem.*, **13**, 66 (1974).
24) J. Glerup, J. Josephsen, K. Michelsen, E. Pedersen, and C. E. Schäffer, *Acta Chem. Scand.*, **24**, 247 (1970).
25) W. J. Geary, *Coord. Chem. Rev.*, **7**, 81 (1971).
26) K. Nakamoto, "Infrared and Raman Spectra of Inorganic and Coordination Compounds," 3rd ed., John Wiley & Sons, Inc. (1978), pp. 259—267.
27) S. Decurtins and H. U. Gudel, *Inorg. Chem.*, **21**, 3598 (1982).
28) C. Reber, H. U. Gudel, L. Spiccia, and W. Marty, *Inorg. Chem.*, **26**, 3186 (1987).
29) T. Schonherr, *Inorg. Chem.*, **25**, 171 (1986).
30) C. F. C. Wong and A. D. Kirk, *Can. J. Chem.*, **53**, 3388 (1975).
31) J. W. Vaughn, *Inorg. Chem.*, **20**, 2397 (1981).
32) R. Tsuchiya, A. Uehara, and T. Yoshikuni, *Inorg. Chem.*, **21**, 590 (1982).

Studies on Mixed Chelates. XVII. Crystal Structure and Spectral Properties of Mixed Nickel(II) Nitrate Complexes Containing 1,2-Dipiperidinoethane and β-Diketonate Ligands

Yutaka FUKUDA,* Chiori FUJITA, Hiroshi MIYAMAE,† Hiroko NAKAGAWA,†† and Kozo SONE
Department of Chemistry, Faculty of Science, Ochanomizu University, Bunkyo-ku, Tokyo 112
†Faculty of Science, Josai University, Keyakidai, Sakado, Saitama 350-02
††Faculty of Pharmaceutical Science, Josai University, Keyakidai, Sakado, Saitama 350-02
(Received August 5, 1988)

Several new mixed nickel(II) nitrate complexes with 1,2-dipiperidinoethane (dipe) and β-diketonate ions (dike), [Ni(NO_3)(dike)(dipe)], have been obtained and characterized. The crystal structure of one of them, [Ni(NO_3)(acac)(dipe)], was determined by X-ray crystallography. The crystal is monoclinic with the space group *Cc*, $Z=4$, $a=9.0517(4)$, $b=21.932(1)$, $c=9.8814(6)$ Å, $\beta=88.151°$. Block-diagonal least-squares refinements have led to a final R value of 0.036 for 2471 reflections. It was confirmed that the nitrate ion in the octahedral complex acts as a bidentate ligand and that the conformation of the piperidine ring in dipe is a chair form. The spectral behaviors of these complexes in various organic solvents are discussed in comparison with those of similar complexes with other *N,N'*-alkylated ethylenediamine ligands (diam). It was concluded that, in a solvent with low polarity, the complexes are dissolved unchanged; in a more polar solvent, however, dissociation of NO_3^- takes place, producing solvated or unsolvated cationic species ([Ni(dike)(diam)(Solvent)$_2$]$^+$ (Oh) or [Ni(dike)(diam)]$^+$ (Square Planar)) according to the donor and acceptor properties of the solvent.

1,2-Dipiperidinoethane ($(CH_2)_5N(CH_2)_2N(CH_2)_5$;dipe) is a potential bidentate ligand which has not been thoroughly studied so far.[1] The chelate ring structure of dipe is similar to that of *N,N,N',N'*-tetramethylethylenediamine (tmen), but the bulky groups $-(CH_2)_5-$ on the N-donor atoms hinder the coordination of this ligand to the central metal ion, and also that of other ligands in the coordination sphere. Therefore, dipe is expected to be a weaker ligand than tmen.

We have reported the mixed nickel(II) complexes with various kinds of *N,N'*-alkylated ethylenediamines (diam) and β-diketonate ions (dike), many of which show remarkable chromotropic behaviors in the solid state or solutions.[2] While continuing this series of studies, we recently obtained several kinds of Ni(II) nitrates containing both dipe and dike, in which the nitrate ion acts as a bidentate ligand. In addition to the results regarding their IR and electronic spectra, as well as their electric conductivities in organic solvents, we have determined the crystal structure of [Ni(NO_3)(acac)(dipe)] in order to understand the mode of the nitrate coordination and the conformation of the dipe ligand. The structural results and a spectral comparison of the dipe complexes with similar mixed ligand complexes containing tmen and related ligands are discussed in this paper.[3–9]

Experimental

Materials. Nickel(II) nitrate hexahydrate, tmen, *N,N,N'*-triethylethylenediamine (Et3en), and *N,N,N',N'*-tetraethylethylenediamine (teen) (Wako Pure Chemical Co.), dipe (Aldrich), and all of dikeH (Dojindo Laboratory) were purchased and used without further purification. All solvents used for physical measurements were Guaranteed Reagent or Spectro grade; hygroscopic solvents were dried by conventional methods.[10]

General Preparation of Solid Complexes: [Ni(NO_3)(dike)(diam)] (dike:acetylacetonate (acac), benzoylacetonate (bzac), dibenzoylmethanate (dibm), dipivaloylmethanate (dipm), trifluoroacetylacetonate (tfac), and hexafluoroacetylacetonate (hfac) ions; diam:teen, Et3en, tmen, and dipe). To an ethanolic solution of $Ni(NO_3)_2\cdot 6H_2O$ (10 mmol in 30 ml of ethanol (EtOH)) a mixture of an appropriate β-diketone and KOH (10 mmol each) dissolved in 20 ml of EtOH is added; then, diam (10 mmol in 10 ml of EtOH) is dropped into it with vigorous stirring. After completing the reaction, the deep-green solution is filtered (to separate the precipitate of KNO_3) and dried up in a rotary evaporator. The crude crystals obtained are dissolved in hot 1,2-dichloroethane (DCE) and filtered; the solution is kept in a freezer for several days. The obtained complex is recrystallized again from hot DCE. [Ni(NO_3)(hfac)(dipe)] could not be obtained in this way, but a non-charged chelate [Ni(hfac)$_2$(dipe)] was formed instead. The dipm mixed complex was obtained as a hydrate, [Ni(NO_3)(dipm)(dipe)-(H_2O)], in a small quantity, though it was rather unstable in solution and decomposed gradually to a mixture of the noncharged chelate [Ni(dipm)$_2$(dipe)] and an unknown green paste.[9]

Physical Measurements. The methods used in the measurements of IR and electronic spectra (solid and solution), magnetic susceptibilities, TG-DTA curves, and electric conductivities in solution are the same as those reported before.[11]

Determination of the Crystal Structure of [Ni(NO_3)(acac)(dipe)]. The crystal used for X-ray work was grown from a DCE solution. Crystal data are as follows: $NiC_{17}H_{31}N_3O_5$; M. W. 416.2; monoclinic; $a=9.0517(4)$, $b=21.932(1)$, $c=9.8814(6)$ Å, $\beta=88.151(4)°$; $U=1960.6(2)$ Å^3; $D_x=1.41$ g cm^{-3}; $Z=4$; space group *Cc*; μ (Mo $K\alpha$) $=1.02$ mm^{-1}. The intensity data were collected on a Rigaku automated four-circle diffractometer AFC-5 with the θ–2θ scan technique, scan range $(1.1+(1/2)\tan\theta)°$ and scan speed 3° min^{-1} in θ. Dimensions of the crystal used for the data collection were 0.38×0.34×0.21 mm. A total of 3036 independent reflections

Table 1. Analytical Data, Color, and Magnetic Moments of the Complexes Obtained

Complex	Color	C%[a]	H%[a]	N%[a]	μ_{eff}/BM
[Ni(NO3)(dipe)(acac)]	Deep blue	49.02 (49.07)	7.70 (7.51)	10.06 (10.10)	3.23
[Ni(NO3)(dipe)(tfac)]	Blue	43.47 (43.43)	6.18 (6.00)	9.11 (8.94)	3.10
[Ni(NO3)(dipe)(bzac)]	Green	55.21 (55.26)	7.18 (6.96)	8.73 (8.29)	3.25
[Ni(NO3)(dipe)(dipm)(H2O)]	Green	54.86 (54.86)	9.01 (8.75)	8.30 (8.11)	—
[Ni(dipe)(dipm)2]	Blue	64.62 (65.70)	10.31 (11.10)	4.46 (4.98)	—
[Ni(dipe)(hfac)2]	Yellow green	39.33 (39.49)	3.95 (3.92)	3.81 (4.19)	—
[Ni(NO3)(Et3en)(acac)]	Deep blue	42.55 (42.89)	7.69 (7.48)	11.41 (11.54)	3.29

a) Calculated values in parentheses.

were measured ($2°<2\theta<60°$), using graphite monochromated Mo $K\alpha$ radiation, of which 2471 reflections were $|F_o|>3\sigma(|F_o|)$. Corrections for Lorentz and polarization factors were made, but not for absorption. The structure was solved by the heavy-atom method using the UNICS-III program system.[12] A refinement was carried out by block-diagonal least-squares. Atomic scattering factors were taken from "International Tables for X-ray Crystallography".[13] The R and R_w values converged to 0.036 and 0.036, respectively. Computations were performed on FACOM M-360R and M-360 computers at the Computer Center of Josai University.

Results and Discussion

Solid Complexes. In Table 1, analytical data and some properties of the solid complexes obtained in this study, [Ni(NO3)(dike)(dipe)], are listed. The complexes containing hfac or dipm seem to have a tendency to be converted into the non-charged octahedral complexes, [Ni(dike)2(dipe)]. We could thus obtain only a small amount of a monohydrate, [Ni(NO3)(dipm)(dipe)(H2O)], and two noncharged complexes, [Ni(dipm)2(dipe)] and [Ni(hfac)2(dipe)], for these ligands. In the same table, the data on another nitrate complex with Et3en are also given, which is similar in appearance and properties to those of the complexes of tmen and teen reported earlier.[3-5] From the colors and magnetic moments of the complexes, it can be seen that all these complexes have an octahedral geometry. There is a simple and very useful criterion for the coordination mode of NO_3 from the IR spectra, devised by Lever et al.[14] The key region is 1700—1800 cm^{-1}, where a weak combination band of the NO_3^- ion in a complex compound appears. This band is often split in two; when the splitting is small ($\Delta\tilde{\nu}_{NO_3}$=20—25 cm^{-1}), the NO_3^- ion is a monodentate ligand, but when it is larger, the ion is a bidentate ligand.[15,16] The IR data of the anhydrous complexes in this region are given in Table 2. All of the anhydrous nitrate complexes obtained here have a rather large splitting of this band ($\Delta\tilde{\nu}_{NO_3}$=45—50 cm^{-1}), showing that the NO_3^- ions in these anhydrous complexes act as bidentate ligands.[17] There is only one exception; the monohydrate [Ni(NO3)(dipm)(dipe)(H2O)] shows a small splitting ($\Delta\tilde{\nu}_{NO_3}$=18 cm^{-1}), which indicates that NO_3^- in it is a monodentate ligand.[18]

The difference between the C=O and C=C stretching frequencies of dike ($\Delta\tilde{\nu}_{dike}=\tilde{\nu}_{C=O}-\tilde{\nu}_{C=C}$) is also a characteristic value. As reported earlier,[3,4] this difference notably decreases in going from as octahedral (high-spin) Ni(II) complex to a square planar (low-spin) 4-coordinate one, indicating that, as the Ni-O(dike) bonds become stronger, the C=O bonds become weaker, and the C=C bonds become stronger.[20] This view is also supported by the bond distances of C=O and C=C of acac in its complexes with different coordination numbers.[21,22] The IR data are consistent with this view; the values of $\Delta\tilde{\nu}_{dike}$ observed in the range of 1600—1500 cm^{-1} ($\Delta\tilde{\nu}_{dike}$=78—115 cm^{-1}; cf. Table 2) are similer to those of the octahedral complexes studied before, confirming the octahedral structure of the new complexes.

Structure of [Ni(NO3)(acac)(dipe)]. As stated above, evidences for the bidentate coordination of NO_3^- in the complexes studied can be obtained form IR spectra, and electronic spectral data and conductivity data in solution (vide infra) are also consistent with this view. We have now determined the crystal structure of [Ni(NO3)(acac)(dipe)] to understand how such coordination takes place. The final atomic

Table 2. IR Data of the Nitrate Complexes[a]

	Complex	$\tilde{\nu}_{NO_3}$		$\Delta\tilde{\nu}_{NO_3}$	$\tilde{\nu}_{dike}$		$\Delta\tilde{\nu}_{dike}$
					$\tilde{\nu}_{C=O}$	$\tilde{\nu}_{C=C}$	
[I]	$[Ni(NO_3)(acac)(dipe)]$	1772	1723	49	1600	1517	83
[II]	$[Ni(NO_3)(acac)(teen)]$[b]	1772	1727	45	1603	1518	85
[III]	$[Ni(NO_3)(acac)(tmen)]$[c]	1771	1725	46	1608	1519	89
[IV]	$[Ni(NO_3)(acac)(Et_3en)]$	1768	1718	50	1592	1514	78
[V]	$[Ni(NO_3)(tfac)(dipe)]$	1773	1726	47	1635	1520	115
[VI]	$[Ni(NO_3)(bzac)(dipe)]$	1773	1728	45	1598	1510	88
[VII]	$[Ni(NO_3)(dipm)(dipe)(H_2O)]$	1763	1745	18	—[d]	—[d]	—[d]

a) The bands observed in the ranges of 1500—1650 cm^{-1} and 1700—1800 cm^{-1} are given. b) Ref. 5. c) Refs. 3 and 4. d) Assignment could not be done exclusively.

Table 3. Final Atomic Coordinates ($\times10^4$ except $\times10^5$ for Ni) of the Non-Hydrogen Atoms and Their Thermal Parameters Given by the Equivalent Temperature Factors ($Å^2$) (Estimated Standard Deviations in Parentheses)

Atom	X	Y	Z	B_{eqv}
Ni	1496(9)	16562(2)	327(8)	2.20(1)
N(0)	2798(4)	1887(2)	622(4)	3.48(9)
O(N1)	1878(3)	1691(1)	1500(3)	3.59(8)
O(N2)	2280(3)	2047(1)	−505(3)	3.55(8)
O(N3)	4108(3)	1931(2)	836(4)	5.78(12)
O(1)	1074(3)	830(1)	−374(3)	3.25(7)
O(2)	−691(3)	1661(1)	−1815(2)	3.07(7)
C(1)	2204(6)	33(2)	−1603(5)	4.14(12)
C(2)	1232(4)	595(2)	−1536(4)	2.70(9)
C(3)	614(4)	805(2)	−2699(4)	2.95(9)
C(4)	−300(4)	1317(2)	−2795(3)	2.46(8)
C(5)	−888(5)	1480(2)	−4141(4)	3.91(12)
N(1)	−1628(3)	1287(1)	1121(3)	2.20(7)
N(2)	−779(3)	2519(1)	518(3)	2.37(7)
C(B1)	−2402(4)	1812(2)	1788(4)	2.87(9)
C(B2)	−2335(4)	2364(2)	889(4)	2.98(10)
C(A1)	−2617(4)	946(2)	213(4)	3.09(10)
C(A2)	−3826(5)	580(2)	962(5)	4.17(13)
C(A3)	−3188(6)	167(2)	2024(5)	4.54(13)
C(A4)	−2223(5)	518(2)	2945(4)	3.96(12)
C(A5)	−1039(4)	861(2)	2142(4)	3.05(10)
C(C1)	−34(4)	2830(2)	1649(4)	2.78(9)
C(C2)	−581(5)	3473(2)	1950(4)	3.31(10)
C(C3)	−524(5)	3871(2)	694(5)	3.72(11)
C(C4)	−1279(5)	3558(2)	−448(4)	3.71(11)
C(C5)	−694(5)	2921(2)	−686(4)	3.25(11)

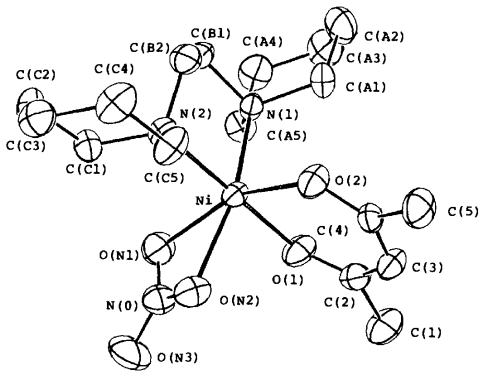

Fig. 1. Molecular structure of the complex $[Ni(NO_3)(acac)(dipe)]$ with atom numbering projected on the O(N1)-O(1)-N(1) plane.

parameters and their estimated standard deviations are listed in Table 3, and the bond distances and angles are shown in Table 4 (numbering scheme indicated in Fig. 1). Figure 2 shows the crystal structure projected on (10$\bar{1}$) plane.

From the X-ray results, it is noted that (1) the NO_3^- is really a bidentate ligand, which is coordinated to the Ni(II) ion with the two bonds, Ni-O(N1) and Ni-O(N2) of nearly the same length. The bite angle, ($\angle$O(N1)-Ni-O(N2)=60.13°), is rather narrow; such a value is not so rare among the data on the bidentate nitrates.[23] The Ni-O(NO_3) bonds are remarkably longer than Ni-O(acac), explaining the easy cleavage of Ni-O(NO_3) bonds in some solvents (DMSO or CH_3NO_2; vide infra). The terminal N(O)-O(N3) bond length is shorter than the other two N-O bonds because both of the O atoms of the latter bonds are coordinated to the central metal ion. It is now quite obvious that this complex and also the nitrate complexes $[Ni(NO_3)(dike)(diam)]$ of other diam and dike with similar properties are octahedral complexes with the bidentate NO_3^- ligand, in agreement with the expectation from Lever's criterion. The crystallographic data of this compound are the first evidence for a bidentate coordination mode of NO_3^- in Ni(II) complexes. (2) The bond distances between Ni(II) and the acac ligand, and those in this ligand itself, are nearly the same as those reported for another octahedral Ni(II) complex, $[Ni(acac)_2(py)_2]$ (py=pyridine).[24] Although there is no crystal data for the planar $[Ni(acac)(dipe)]^+$ (vide infra), the preliminary X-ray data for the dinuclear Ni(II) complex, $[(tmen)Ni(1)(tetraketonate)Ni(2)(tmen)(H_2O)_2]^{2+}$, in which the coordination sphere of Ni(1) is square planar and that of Ni(2) is octahedral, indicate that the coordinate bonds in the square planar arrangement are much shorter than those in the octahedral species.[25] (3) Both piperidine rings in dipe are in the chair conformation, and the three bidentate ligands, i.e. dipe, acac, and NO_3^-, are placed so as to minimize the interligand

Table 4. Bond Distances (Å) and Angles in the Complex [Ni(NO_3)(acac)(dipe)] (Estimated Standard Deviations in Parentheses)

Distance			
Ni-O(N1)	2.168(3)	N(1)-C(B1)	1.490(5)
Ni-O(N2)	2.161(3)	N(1)-C(A1)	1.489(5)
Ni-O(1)	2.030(3)	N(1)-C(A5)	1.485(5)
Ni-O(2)	2.001(3)	N(2)-C(B2)	1.483(5)
Ni-N(1)	2.070(3)	N(2)-C(C1)	1.489(5)
Ni-N(2)	2.118(3)	N(2)-C(C5)	1.482(5)
N(0)-O(N1)	1.259(5)	C(B1)-C(B2)	1.501(6)
N(0)-O(N2)	1.272(5)	C(A1)-C(A2)	1.529(6)
N(0)-O(N3)	1.214(6)	C(A2)-C(A3)	1.515(7)
O(1)-C(2)	1.262(5)	C(A3)-C(A4)	1.495(7)
O(2)-C(4)	1.269(5)	C(A4)-C(A5)	1.514(6)
C(1)-C(2)	1.515(6)	C(C1)-C(C2)	1.522(6)
C(2)-C(3)	1.374(5)	C(C2)-C(C3)	1.517(6)
C(3)-C(4)	1.399(5)	C(C3)-C(C4)	1.503(7)
C(4)-C(5)	1.492(6)	C(C4)-C(C5)	1.510(6)
Angle			
O(N1)-Ni-O(N2)	59.6(1)	O(N1)-N(0)-O(N2)	116.3(3)
O(N1)-Ni-O(1)	82.1(1)	O(N1)-N(0)-O(N3)	122.3(4)
O(N1)-Ni-O(2)	156.0(1)	O(N2)-N(0)-O(N3)	121.4(4)
O(N1)-Ni-N(1)	103.4(1)	O(1)-C(2)-C(1)	114.9(4)
O(N1)-Ni-N(2)	96.2(1)	O(1)-C(2)-C(3)	125.9(4)
O(N2)-Ni-O(1)	87.0(1)	C(1)-C(2)-C(3)	119.2(4)
O(N2)-Ni-O(2)	97.8(1)	O(2)-C(4)-C(3)	125.2(3)
O(N2)-Ni-N(1)	162.7(1)	O(2)-C(4)-C(5)	116.1(3)
O(N2)-Ni-N(2)	92.6(1)	C(3)-C(4)-C(3)	118.8(4)
O(1)-Ni-O(2)	89.5(1)	C(2)-C(3)-C(4)	125.7(4)
O(1)-Ni-N(1)	93.6(1)	N(1)-C(B1)-C(B2)	110.6(3)
O(1)-Ni-N(2)	178.1(1)	N(2)-C(B2)-C(B1)	110.6(3)
O(2)-Ni-N(1)	99.4(1)	C(B1)-N(1)-C(A1)	111.7(3)
O(2)-Ni-N(2)	92.4(1)	C(B1)-N(1)-C(A5)	111.1(3)
N(1)-Ni-N(2)	86.3(1)	C(A1)-N(1)-C(A5)	109.3(3)
Ni-O(N1)-N(0)	91.6(2)	N(1)-C(A1)-C(A2)	114.0(3)
Ni-O(N2)-N(0)	91.5(2)	C(A1)-C(A2)-C(A3)	111.5(4)
Ni-O(1)-C(2)	125.4(2)	C(A2)-C(A3)-C(A4)	111.0(4)
Ni-O(2)-C(4)	126.0(1)	C(A3)-C(A4)-C(A5)	110.8(4)
Ni-N(1)-C(B1)	105.9(2)	C(A4)-C(A5)-N(1)	113.9(3)
Ni-N(1)-C(A1)	110.8(2)	C(B2)-N(2)-C(C1)	111.7(3)
Ni-N(1)-C(A5)	108.0(2)	C(B2)-N(2)-C(C5)	111.1(3)
Ni-N(2)-C(B2)	102.6(2)	C(C1)-N(2)-C(C5)	108.4(3)
Ni-N(2)-C(C1)	113.1(2)	N(2)-C(C1)-C(C2)	114.8(3)
Ni-N(2)-C(C5)	109.9(2)	C(C1)-C(C2)-C(C3)	111.8(4)
		C(C2)-C(C3)-C(C4)	110.4(4)
		C(C3)-C(C4)-C(C5)	111.9(4)
		C(C4)-C(C5)-N(2)	114.7(3)

repulsions. The chelate bite angles, ∠O(1)–Ni–O(2) (for acac) and ∠N(1)–Ni–N(2) (for dipe), are 89.48° and 85.87°, respectively.

Three tables for atomic coordinates of the H atoms (Table A), mean square displacement tensors of atoms (Table B), and structure factors (Table C) are deposited at the Chemical Society of Japan, Document No. 8858.

Electronic Spectra in Solution. Figure 3 shows the electronic spectra of [Ni(NO_3)(acac)(dipe)] in four kinds of organic solvents, i.e., DCE, CH_3NO_2, acetone, and DMSO. In Table 5, the spectral data for similar complexes are summarized. From these data, it can be seen that two kinds of spectral changes take place with changes in solvent polarity.

[I] The spectra in DCE, acetone and EtOH are nearly of the same pattern, showing two bands ($\tilde{\nu}_1$ and $\tilde{\nu}_2$; $\tilde{\nu}_1 < \tilde{\nu}_2$) which correspond to the octahedral structure of the complexes. The spectral shape is, however, somewhat anomalous, i.e., the values of the intensity ratio of the two bands ($R=\varepsilon(\tilde{\nu}_2)/\varepsilon(\tilde{\nu}_1)$) are nearly the same in these solvents and are about 2, whereas the same ratio for a typical octahedral complex (e.g., [Ni en_3]$^{2+}$) is nearly 1.[26] The same type of anomaly is also observed in the spectra of the solid nitrate complexes. This anomaly is probably related to the existence of a highly strained 4-membered chelate ring of NO_3^- in the coordination sphere (vide supra). On the other hand, in the case of DMSO solutions, the values of R are close to unity, so that the spectra look quite normal. The electric conductivity

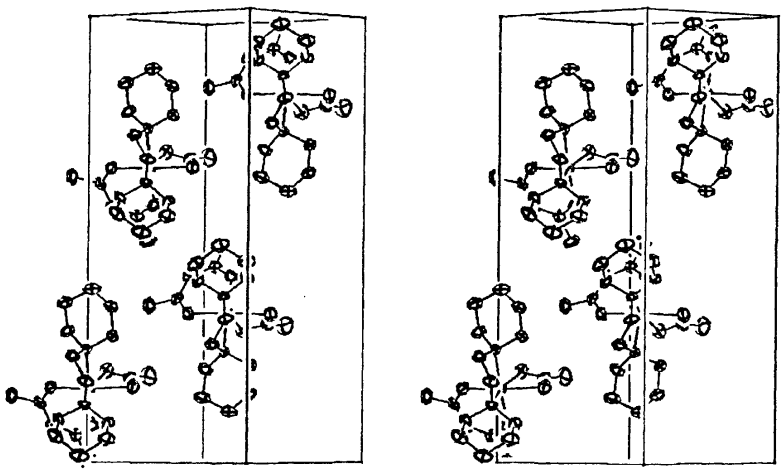

Fig. 2. Stereoscopic view of a unit cell projected on the (101) plane; horizontal [10$\bar{1}$], vertical b.

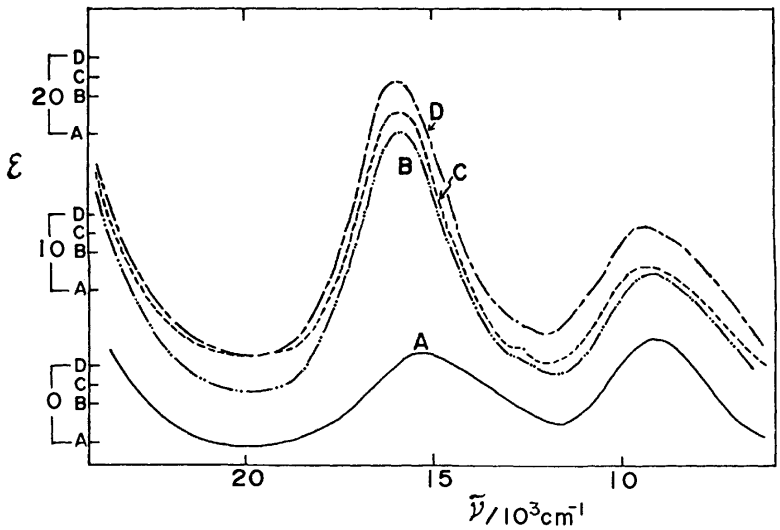

Fig. 3. Absorption spectra of [Ni(NO_3)(acac)(dipe)] in various solvents. Concn: 4×10^{-2} mol dm^{-3}, temp: ca. 20°C. A=DMSO, B=acetone, C=CH_3NO_2, D=DCE.

data shown in Table 6 indicate now that the complex species in DCE or acetone are non-charged ones, while those in DMSO are 1:1 electrolytes.

These results lead to the conclusion that, in a solvent such as DCE (DN=0, AN=16.7)[28] or acetone (DN=17.0, AN=12.5) which have a relatively low polarity, the complex structure in the solid state remains unchanged, i.e., the species in the solution is the non-charged complex [Ni(NO_3)(acac)(diam)]:

[Ni(NO_3)(acac)(diam)]⟶[Ni(NO_3)(acac)(diam)]
(Solid) Blue/Green, Oh ($R\approx2$)

When the complex is dissolved in DMSO (DN=29.8, AN=19.3) which is a more polar solvent, however, it dissociates the NO_3^- ion to form the solvated cations [Ni(acac)(diam)(Solvent)$_2$]$^+$:

[Ni(NO_3)(acac)(diam)] ⟷ [Ni(acac)(diam)(Solvent)$_2$]$^+$ + NO_3^-
Blue/Green, Oh ($R\approx2$) Blue, Oh ($R\approx1$) (1)

This equilibrium is strongly shifted to the right hand side in DMSO; the strain in the coordination sphere is thereby lost, and the spectrum of the solution looks quite normal.

[II] Although the occurrence of the spectral change (I) was already indicated in our former studies,[2-5] there is another kind of spectral change (II) which we have overlooked hitherto. This change occurs in CH_3NO_2 solutions where, according to the conductivity data (Table 6), partial dissociation of the complexes occurs, which increases in the following order of diam:

Table 5. Absorption Spectra of the Complexes [Ni(NO_3)(dike)(diam)] in Solid State and in Various Solvents ($\tilde{\nu}_{max}/10^3$ cm^{-1}, ε_{max} in Parentheses, Concn: 4×10^{-2} mol dm^{-3}, Temp: ca. 20 °C)

Complex	Solid	DCE	CH_3NO_2	Acetone	DMSO
[Ni(NO_3)(acac)(dipe)]	9.80	9.25(9.1)	9.37(8.6)	9.26(8.7)	9.18(6.7)
	16.13	15.92(19.0)	15.95(18.7)	15.87(17.8)	15.34(5.8)
			20(sh)[a,b]		
[Ni(NO_3)(acac)(teen)]	9.00	9.09(8.9)	9.09(7.0)	9.07(8.8)	8.94(4.9)
	15.75	15.75(20.6)	15.68(16.5)	15.69(19.6)	15.15(4.9)
			20.09(20.4)		
[Ni(NO_3)(acac)(tmen)]	9.68	9.60(9.7)	9.55(9.3)	9.55(9.5)	9.49(6.8)
	16.54	16.29(19.6)	16.26(19.5)	16.26(18.8)	15.80(5.2)
			20.0(sh)[b]		
[Ni(NO_3)(acac)(Et_3en)]	9.80	9.58(9.8)	9.54(9.3)	9.53(10.9)	9.34(4.7)
	16.67	16.39(21.9)	16.34(20.9)	16.31(21.8)	15.72(4.2)
			20.0(sh)[b]		
[Ni(NO_3)(tfac)(dipe)]	9.52	9.31(17.1)	9.47(9.9)	9.29(8.8)	9.11(5.8)
	16.25	15.98(28.4)	15.83(20.9)	15.85(18.1)	15.13(6.9)
[Ni(NO_3)(bzac)(dipe)]	8.94	9.31(9.1)	9.34(9.0)	9.29(9.5)	9.01(6.3)
	15.64	15.92(19.6)	15.85(20.2)	15.88(18.8)	15.20(5.5)
			20(sh)[b]		

a) sh=shoulder. b) This band is very weak at room temperature (see Ref. 29).

Table 6. Molar Conductivity Data of the Complexes [Ni(NO_3)(dike)(diam)] in Various Organic Solutions (Λ_M/S cm^2 mol^{-1}, Concn: 2×10^{-2} mol dm^{-3}, Temp: 25±0.1 °C)

[A] [Ni(NO_3)(dike)(dipe)]				
dike	DCE	CH_3NO_2	Acetone	DMSO
tfac	0.02	6.80	1.65	32.97
bzac	0.03	3.77	0.91	41.06
acac	0.05	5.06	0.93	30.46

[B] [Ni(NO_3)(acac)(diam)]				
diam	DCE	CH_3NO_2	Acetone	DMSO
dipe	0.05	5.06	0.93	30.46
teen	0.30	33.77	2.01	33.84
tmen	0.04	4.73	1.29	36.99
Et_3en	0.06	6.26	1.45	34.31
Ref.[a]	20.89	100.6	137.8	39.10
	(10—24)	(75—95)	(100—140)	(ca. 35)

a) The values for [Ni(acac)(tmen)]ClO_4, i.e., a typical 1:1 electrolyte, in the respective solvents, and standard values for an 1:1 electrolyte in parentheses.[27]

teen ≫ Et_3en > dipe ~ tmen.

The values of R in these solutions do not change so much from 2; however, a new band appears at ca. 20×10^3 cm^{-1}, which can be assigned to the unsolvated square planar chelate cation [Ni(dike)(diam)]$^+$.[2-5] This change can, thus, be ascribed to the change:

$$[Ni(NO_3)(acac)(diam)] \rightleftarrows [Ni(acac)(diam)]^+ + NO_3^- \quad (2)$$

Blue/Green, Oh ($R\approx2$) Red, square planar

In this case, the solvent (CH_3NO_2) is a very weak donor, but a relatively strong acceptor (DN=2.7, AN=20.5). Since the coordination of NO_3^- in the complex is weak (vide supra), a part of the NO_3^- ions can be solvated and dissociated from the complex by interaction with this acceptor solvent. On the other hand, the solvent molecules will not coordinate effectively to Ni(II) to form an octahedral species, as those in Eq. 1, owing to their poor donor ability, so that the "naked"square planar cation newly appears in solution.

Figure 4 shows the absorption spectra of four kinds of [Ni(NO_3)(acac)(diam)] in CH_3NO_2. It can be seen that the relative intensity of the band at ca. 20×10^3 cm^{-1}, which is an approximate measure for the formation of the square planar species in this solvent, decreases in the order of diam

$$\text{teen} \gg Et_3\text{en} > \text{tmen} \gtrsim \text{dipe}^{29)} \quad (3)$$

for this series of complexes, which is nearly in parallel with the expectation from the conductivity data. It is easy to understand that the free movements of the ethyl groups on the N-donor atoms of teen will strongly destabilize the octahedral chelate by their steric hindrance, so that the equilibrium in Eq. 2 will be shifted strongly to the right-hand side. This destabilizing effect will decrease in the order teen>Et_3en> tmen, with the decrease in size and number of the alkyl groups. The piperidino groups of dipe are very bulky, but their free movements (and especially those toward the axial sites) are strongly restricted by their rigid ring structure.[1] Therefore, the complex [Ni(NO_3)(acac)-(dipe)] will be much more stable than the corresponding complexes with teen or Et_3en, and comparable to that of tmen (or even more than that, if the decreased ligand field strength (l.f.s.) of dipe (vide infra) is taken into account), with respect to the equilibrium of Eq. 2. The above-mentioned ligand order will, thus, come about.

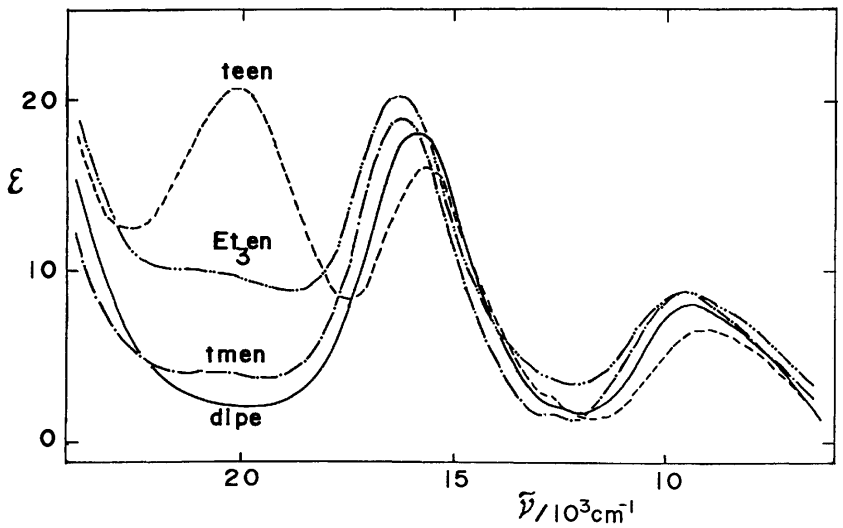

Fig. 4. Absorption spectra of [Ni(NO_3)(acac)(diam)] (diam=teen, Et_3en, dipe, and tmen) in CH_3NO_2. Concn: 4×10^{-2} mol dm^{-3}, temp: ca. 20 °C.

The spectra of these nitrate complexes in CH_3NO_2 show concentration and temperature dependence, especially in the vicinity of the band of the square planar species. In each case, a gradual increase of the square planar species takes place at lower concentrations and at higher temperatures, showing that the nitrate dissociation is favored by dilution and heating, and confirming the existence of the equilibrium shown in Eq. 2. Quantitative aspects of this equilibrium, and also those of the equilibria observed in EtOH solutions,[30] are now under study.

Finally, it may be pointed out that the differences among the l.f.s. of the diamines used in this study can be estimated from the values of $\tilde{\nu}_1$ of the octahedral nitrate complexes in DCE. Although such differences are not large, the data in Table 5 indicate that the order of decreasing l.f.s. of the diamines is:

$$\text{tmen} > \text{Et}_3\text{en} > \text{dipe} > \text{teen}. \quad (4)$$

It is generally conceivable that a ligand with a strong donor property will tend to form a square planar complex with Ni(II), and to shift the solution equilibrium between a square planar complex and an octahedral one to the side of the former. The order of Eq. 4, however, dose not coincide with that of Eq. 3, indicating that the steric hindrance of the bulky substituent groups on the N-donor atoms is important in determining the equilibrium.

The authors are grateful to the Ministry of Education, Science and Culture for support of this work through a Grant-in-Aid for Scientific Research (Grant No. 63540475).

References

1) Part XVI: Y. Fukuda, M. Cho, and K. Sone, *Bull. Chem. Soc. Jpn.*, **62**, 51 (1989).

2) K. Sone and Y. Fukuda, "Inorganic Thermochromism" ("Inorganic Chemistry Concepts", Vol. 10), Springer, Heildelberg (1987).

3) Y. Fukuda and K. Sone, *J. Inorg. Nucl. Chem.*, **34**, 2315 (1972).

4) Y. Fukuda and K. Sone, *J. Inorg. Nucl. Chem.*, **37**, 455 (1975).

5) Y. Fukuda, R. Morishita, and K. Sone, *Bull. Chem. Soc. Jpn.*, **49**, 1017 (1976).

6) N. T. Nga, Y. Fukuda, and K. Sone, *Bull. Chem. Soc. Jpn.*, **50**, 154 (1977).

7) N. Hoshino, Y. Fukuda, and K. Sone, *Chem. Lett.*, **1979**, 437.

8) N. Hoshino, Y. Fukuda, and K. Sone, *Trans. Metal Chem.*, **4**, 183 (1979).

9) Y. Saito, T. Takeuchi, Y. Fukuda, and K. Sone, *Bull. Chem. Soc. Jpn.*, **54**, 196 (1981).

10) For example, J. A. Riddick and W. B. Bunger, "Organic Solvents" ("Techniques of Chemistry", Vol. 11), 3rd ed., Wiley-Interscience, New York (1970).

11) Y. Fukuda, M. Yasuhira, and K. Sone, *Bull. Chem. Soc. Jpn.*, **58**, 3523 (1985).

12) T. Sakurai and K. Kobayashi, UNICS-III, *Rikagaku Kenkyusho Hokoku*, **55**, 69 (1979).

13) "International Tables for X-Ray Crystallography," Kynoch Press, Birmingham (1974), Vol. IV.

14) A. B. P. Lever, E. Montovani, and B. S. Ramaswamy, *Can. J. Chem.*, **49**, 1957 (1971).

15) Y. Ihara, Y. Fukuda, and K. Sone, *Bull. Chem. Soc. Jpn.*, **59**, 1825 (1986).

16) Y. Ihara, Y. Fukuda, and K. Sone, *Inorg. Chem.*, **26**, 3745 (1987).

17) The fact that the IR spectra of the complexes [Ni(NO_3)(dike)(tmen)] and [Ni(NO_3)(dike)(teen)] indicate

the existence of bidentate NO_3^- was already pointed out in our former studies.[3-6]

18) Whether this ion is cis or trans to H_2O is still an open question.

19) K. Nakamoto, "Infrared and Raman Spectra of Inorganic and Coordination Compounds," 3rd ed., John-Wiley & Sons, New York (1978).

20) It is interesting to note that the directions of these changes are in complete harmony with the bond length variation rule proposed by Gutmann. cf. V. Gutmann, "The Donor-Acceptor Approach to Molecular Interactions," Plenum, New York (1978), Chap.1.

21) P. A. Tucker, *Acta Crystallogr., Sect. B*, **37**, 1113 (1981).

22) P. A. Tucker, *Acta Crystallogr., Sect. C*, **40**, 620 (1984).

23) A. F. Wells, "Structural Inorganic Chemistry," 5th ed., Oxford, New York (1984).

24) R. C. Eider, *Inorg. Chem.*, **7**, 2316 (1968).

25) K. Mafune, M. Konno, Y. Fukuda, and K. Sone, XXXVIIth Symposium on Coordination Chemistry (The Chemical Society of Japan), Tokyo, October 1987, Abstract 1A01 (p. 2).

26) A. B. P. Lever, "Inorganic Electronic Spectroscopy," Elsevier, Amsterdam (1968).

27) W. J. Geary, *Coord. Chem. Rev.*, **7**, 81 (1971).

28) DN and AN are donor number and acceptor number of the solvent, respectively; cf. Ref. 20.

29) In the case of the acac-dipe complex, this band is nearly imperceptible on the curve in Fig. 4. However, an analysis of the absorption curve indicates its existence. Upon heating the solution to ca. 40 °C, or upon diluting it to 4×10^{-3} mol dm^{-3}, it appears as a clear hump, with an intensity which is apparently comparable to that of the tmen complex under the same conditions. Therefore, the positions of tmen and dipe in this order are quite near, as indicated by the conductivity data (cf. Table 6).

30) In EtOH solutions of the complex, it seems that the equilibria of (Eq. 1) and (Eq. 2) take place at the same time, i.e., there is a partial ionization of NO_3^- (cf. Table 6), but the cations formed are an equilibrium mixture of $[Ni(dike)(diam)(EtOH)_2]^+$ and $[Ni(dike)(diam)]^+$. The proportion of the latter ion in this mixture decreases again in the order of teen $\gg$ Et_3en $>$ tmen $\approx$ dipe.

 © 1989 The Chemical Society of Japan Bull. Chem. Soc. Jpn., 62, 753—759 (1989)

Base-Catalyzed Isomerization and Racemization Reactions of $[Co(L_1)(L_2)]^+$-Type Complexes (L_1=Iminodiacetato or *N*-Methyliminodiacetato and L_2=3-Azapentane-1,5-diamine or 3-Methyl-3-azapentane-1,5-diamine)

Hiroshi KAWAGUCHI,* Masato SHIMIZU, Tomoharu AMA, and Takaji YASUI
Department of Chemistry, Faculty of Science, Kochi University, Akebono-cho, Kochi 780
(Received August 12, 1988)

The isomerization and racemization reactions of the $[Co(ida)(dien)]^+$ and $[Co(ida)(mdien)]^+$ systems were studied in an aqueous solution. The main isomerization path of the $[Co(ida)(dien)]^+$ system was *u-fac*⇌*mer*⇌*s-fac* and the rate law for each of the processes could be described as $R=k[\text{complex}][OH^-]$. In the $[Co(ida)(mdien)]^+$ system, there was an additional isomerization path of *u-fac*⟶*s-fac*. The equilibrium mole ratio of three isomers was *u-fac*:*mer*:*s-fac*=25:19:56% for $[Co(ida)(dien)]^+$ and *u-fac*:*mer*:*s-fac*=3:3:94% for $[Co(ida)(mdien)]^+$. In the isomerization of $(+)^{CD}_{564}$-*u-fac*-$[Co(mida)(mdien)]^+$, $(+)^{CD}_{582}$-*mer* isomer was stereoselectively produced. The racemization mechanisms of *mer*-$[Co(ida)(dien)]^+$ and *mer*-$[Co(mida)(dien)]^+$ are also discussed.

As part of a study of the structure-reactivity pattern in octahedral complexes, our attention was drawn to cobalt(III) complexes containing two terdentate ligands such as dien, ida, and their analogs.[1] This type complex provides three possible geometrical isomers; *s-fac*, *u-fac*, and *mer* (Fig. 1). Each isomer of $[Co(dien)_2]^{3+}$ isomerized in water at high temperature (82 °C), giving a mixture of all three isomers. The isomerization reaction was thought to proceed through three intramolecular paths; *u-fac*⇌*mer*, *mer*⇌*s-fac*, and *s-fac*⇌*u-fac*.[2] We previously studied the isomerization reactions of the $[Co(ida)_2]^-$ and $[Co(ida)(mida)]^-$ systems and found that the reactions proceeded through two intramolecular paths, as shown in Scheme 1. All of the reactions are base-catalyzed and probably involve conjugate base intermediates.[3] The isomers of $[Co(mida)_2]^-$, which have no N–H proton to deprotonate, did not isomerize under the same conditions as those for the isomers of $[Co(ida)_2]^-$.[4] The isomers of $[Co(edma)_2]^+$ also isomerized to other ones in a basic aqueous solution; however, the main reaction paths are quite different from those of the $[Co(ida)_2]^-$ system.[5]

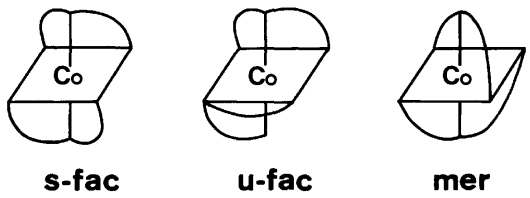

Fig. 1. Three geometrical isomers of the [Co(L)(L′)] type complex, where L and L′ are symmetrical terdentate ligands.

u-fac ⇌ mer ⇌ s-fac

Scheme 1.

Recently, we presented preliminary results concerning the reactivities of the $[Co(ida)(dien)]^+$, $[Co(ida)(mdien)]^+$, $[Co(mida)(dien)]^+$, and $[Co(mida)(mdien)]^+$ complexes.[6] In this paper, we describe a detailed study of the isomerization reaction of those complexes. In addition, we also report on rate data regarding racemization for the *mer* isomers of $[Co(ida)(dien)]^+$ and $[Co(mida)(dien)]^+$.

Experimental

Complexes and Reagents. The complexes examined here were prepared according to the methods described in previous papers.[7] They are *u-fac*-$[Co(ida)(dien)]Cl\cdot 0.5H_2O$, *mer*-$[Co(ida)(dien)]Cl\cdot H_2O$, *s-fac*-$[Co(ida)(dien)]Cl\cdot 0.5H_2O$, *u-fac*-$[Co(ida)(mdien)]Cl\cdot 1.5H_2O$, *mer*-$[Co(ida)(mdien)]Cl\cdot 2H_2O$, *u-fac*-$[Co(mida)(dien)]Cl\cdot 1.5H_2O$, *mer*-$[Co(mida)(dien)]Cl\cdot 1.5H_2O$, *u-fac*-$[Co(mida)(mdien)]Cl\cdot 3H_2O$, *mer*-$[Co(mida)(mdien)]Cl\cdot 2H_2O$, $(+)^{CD}_{538}$-*u-fac*-$[Co(ida)(dien)]Cl\cdot 2H_2O$ ($\Delta\varepsilon_{538}$=+2.014), $(-)^{CD}_{550}$-*u-fac*-$[Co(ida)(mdien)]Cl\cdot 1.5H_2O$ ($\Delta\varepsilon_{550}$=−1.804), $(+)^{CD}_{544}$-*u-fac*-$[Co(mida)(dien)]Cl\cdot 0.5H_2O$ ($\Delta\varepsilon_{544}$=+2.441), $(+)^{CD}_{564}$-*u-fac*-$[Co(mida)(mdien)]Cl\cdot 3H_2O$ ($\Delta\varepsilon_{564}$=+1.658), $(+)^{CD}_{560}$-*mer*-$[Co(ida)(dien)]Cl\cdot 1.5H_2O$ ($\Delta\varepsilon_{560}$=+0.214), and $(-)^{CD}_{570}$-*mer*-$[Co(mida)(dien)]Cl\cdot 1.5H_2O$ ($\Delta\varepsilon_{570}$=−0.205).

All the chemicals used were of reagent grade, and the deionized water was degassed before use.

Isomerization. ***u-fac*-$[Co(ida)(dien)]^+$:** The following reaction conditions were set: complex concentration, 4.0×10^{-3} M (M=mol dm^{-3}); pH, 10.00±0.03, 10.30±0.03, and 10.60±0.03 (Na_2CO_3–$NaHCO_3$ buffer); ionic strength (*I*), 0.1 M ($NaClO_4$); temperature, 40.0±0.1 °C. The isomerization reaction was started by dissolving the isomer (540.20 mg) in 400 cm^3 of the buffer solution in a reaction vessel kept in a thermostated bath. The temperature and pH of the reaction solution were checked with a thermistor thermometer (TAKARA D221) and a pH meter (TOA TSC-10A), respectively. At prescribed time intervals, a constant volume (30.0 cm^3) of the reaction solution was taken out and acidified to pH 6 in order to stop the reaction, and then applied to a column (3.0 cm×60 cm) of SP-Sephadex C-25 (K^+ form) cation exchanger. On elution with 0.2 M KCl, two bands, el. 1 (*mer*) and el. 2 (*s-fac* and *u-fac*), were separated.

The two eluates were collected separately and concentrated to constant volumes (10 or 20 cm^3) and the amounts of the isomers were spectrophotometrically determined with a JASCO UVIDEC-670 spectrophotometer. The amounts of *u-fac* and *s-fac* were calculated from binary-curve analyses of the absorption spectrum of the concentrated el. 2 eluate. (In this curve analysis, the spectral data at 25 points in the visible region were used.) The analysis calculations were carried out on an NEC PC-9801F computer using the least-squares method. The isomerization reactions of *s-fac*- and *mer*-$[Co(ida)(dien)]^+$ were carried out by a procedure similar to that used for *u-fac* isomer.

The isomerization reactions for the $[Co(ida)(mdien)]^+$, $[Co(mida)(dien)]^+$, and $[Co(mida)(mdien)]^+$ systems were also conducted according to a similar method as described above.

CD Decrease of *u-fac* Isomers and Racemization of *mer* Isomers. The rates of CD decrease of optically active *u-fac* isomers were measured with a JASCO J-22 spectropolarimeter. A reaction vessel with a jacket and a water-jacket cell mounted in the cell compartment of the spectropolarimeter were thermostated at 40.0 °C with circulating water. The reaction was started by dissolving the complex in 20.0 cm^3 of a buffered solution in the reaction vessel. About 3 cm^3 of this solution was quickly transferred into the cell in order to record the decrease of the CD intensity. The reaction conditions were as follows: complex concentration, 5.0×10^{-3} M; pH, 10.30±0.05 (Na_2CO_3-$NaHCO_3$ buffer); *I*, 0.1 M ($NaClO_4$); temperature, 40.0±0.1 °C.

The racemization reactions of *mer*-$[Co(ida)(dien)]^+$ and *mer*-$[Co(mida)(dien)]^+$ were carried out by a procedure similar to that described above. The following reaction conditions were set: complex concentration, 5.02×10^{-3} M; pH, 4.2—6.0 (CH_3COOH-CH_3COONa buffer); *I*, 1.0 M ($NaNO_3$); temperature, 30—40 °C. The ionic product of water at the appropriate temperature was obtained from the literature[8] and the appropriate activity coefficient corrections for ionic strength were made using the same source. The hydroxide concentration could then be calculated. Plots of ln[CD intensity] vs. time gave a straight line over three half-lives, from which the pseudo-first-order rate constant k_{obsd} (s^{-1}) was obtained. Analyses of the kinetic data were carried out using the least-squares method. In each of the kinetic data analyses, the value of the standard deviation was within ±1% of the rate constant.

Results and Discussion

Isomerization of the $[Co(ida)(dien)]^+$ System. The isomerization reaction of *u-fac*-$[Co(ida)(dien)]^+$ was carried out under the conditions of pH 10.30 and I=0.1 M at 40.0 °C. Figure 2-a shows the concentration changes of the starting material and reaction products. A part of the numerical data are listed in Table 1.[9] In this reaction, *mer* was first formed and *s-fac* was subsequently formed. After about 25 h, the amount of *mer* began to decrease. The *s-fac* isomer gradually increased in its amount, and was a major product at the final stage of the reaction. Isomerization reactions using *mer* and *s-fac* as the starting materials were also carried out under the same conditions as used for *u-fac*. The results are shown in Figs. 2-b and 2-c and a part of the numerical data are listed in Table 1. The isomerization of *mer* proceeded rapidly, and *u-fac* and *s-fac* were formed simultaneously. The amount of *u-fac* formed was maximal about 30 h after the start of the reaction; it then gradually decreased. However, the isomerization of

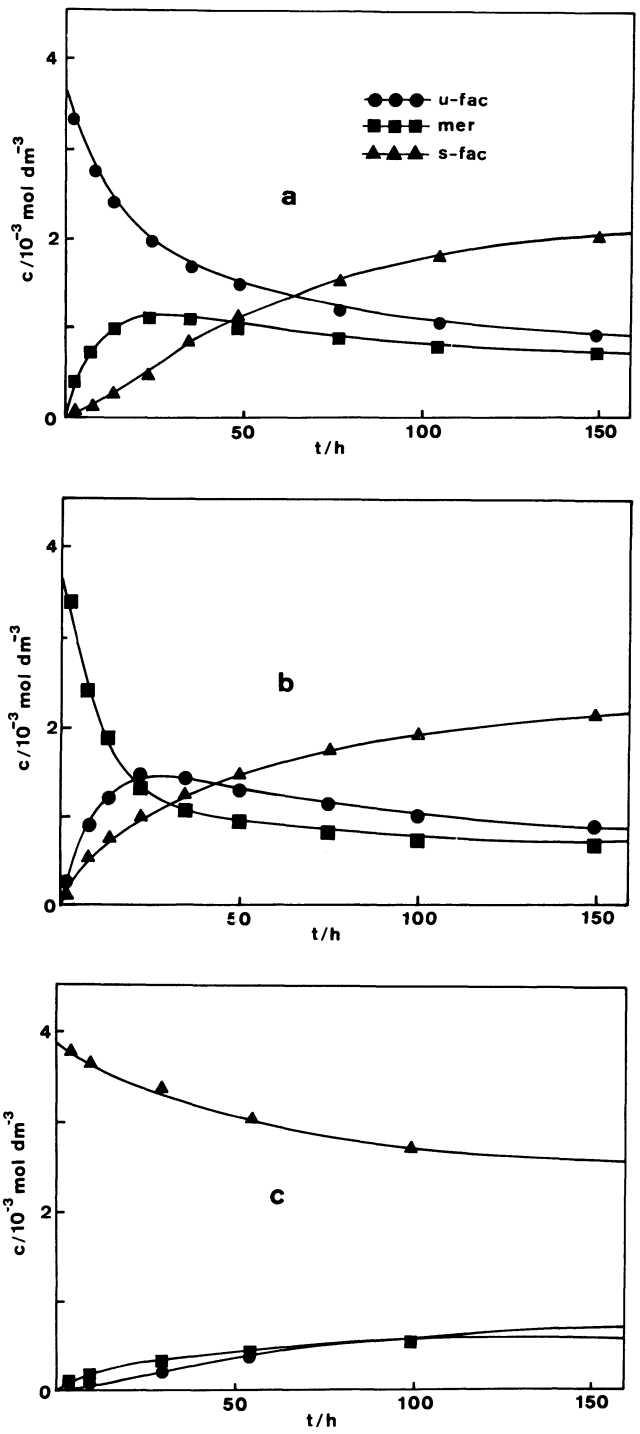

Fig. 2. The isomerization reaction of $[Co(ida)(dien)]^+$ in a basic aqueous solution (pH 10.30) at 40.0 °C. Starting isomers are *u-fac* (a), *mer* (b), and *s-fac* (c). Each of the lines is the curve calculated from the data at Table 2 by using Runge-Kutta method.

Table 1. Concentration Changes of the Starting Materials and Products in the Isomerization Reaction (40.0°C, pH 10.30)

(i) *u-fac*-[Co(ida)(dien)]+

t/h	Concn/10^{-3} mol dm^{-3}		
	u-fac	*mer*	*s-fac*
1.5	3.43	0.28	0.01
8.0	2.75	0.70	0.10
23.5	1.95	1.04	0.45
49.0	1.51	0.98	1.13
150.0	0.89	0.68	1.83

(ii) *mer*-[Co(ida)(dien)]+

t/h	Concn/10^{-3} mol dm^{-3}		
	u-fac	*mer*	*s-fac*
1.5	0.23	3.43	0.18
8.0	0.87	2.42	0.51
14.0	1.16	1.87	0.82
35.0	1.37	1.10	1.24
100.5	0.91	0.73	1.90

(iii) *s-fac*-[Co(ida)(dien)]+

t/h	Concn/10^{-3} mol dm^{-3}		
	u-fac	*mer*	*s-fac*
4.0	0.03	0.06	3.83
10.0	0.09	0.14	3.75
30.0	0.25	0.30	3.51
55.0	0.36	0.38	3.11
100.0	0.55	0.48	2.86

(iv) *u-fac*-[Co(ida)(mdien)]+

t/h	Concn/10^{-3} mol dm^{-3}			
	u-fac	*mer*	*s-fac*	pink
0.2	3.62	0.19	0.34	0.12
0.5	3.11	0.25	0.85	0.15
1.2	2.47	0.41	1.30	0.15
4.0	1.04	0.30	3.06	0.04
6.0	0.62	0.25	3.57	0

(v) *mer*-[Co(ida)(mdien)]+

t/h	Concn/10^{-3} mol dm^{-3}			
	u-fac	*mer*	*s-fac*	pink
0.2	0.16	3.11	0.33	0.14
0.5	0.49	2.12	0.98	0.24
1.2	0.79	1.00	1.75	0.29
3.5	0.57	0.31	2.83	0.16
5.0	0.44	0.20	3.13	0.12

(vi) *u-fac*-[Co(mida)(dien)]+

t/h	Concn/10^{-3} mol dm^{-3}		
	u-fac	*mer*	*s-fac*
1.0	2.81	0.92	0.09
4.0	1.52	1.75	0.10
6.0	1.21	1.77	0.10
12.0	1.08	1.49	0.04
24.0	1.00	1.05	0.05

(vii) *mer*-[Co(mida)(dien)]+

t/h	Concn/10^{-3} mol dm^{-3}		
	u-fac	*mer*	*s-fac*
1.0	0.58	3.42	0.22
2.0	0.82	2.92	0.10
8.0	1.22	2.10	0.07
13.0	1.08	1.55	0.04
24.0	0.90	1.06	0.10

(viii) *u-fac*-[Co(mida)(mdien)]+

t/min	Concn/10^{-3} mol dm^{-3}		
	u-fac	*mer*	*s-fac*
10	2.55	0.38	0.21
30	1.04	0.70	0.21
50	0.47	0.86	0.16
70	0.29	0.83	0.17
90	0.13	0.75	0.13

(ix) *mer*-[Co(mida)(mdien)]+

t/h	Concn/10^{-3} mol dm^{-3}		
	u-fac	*mer*	*s-fac*
0.5	0.10	3.25	0.17
2.0	0.14	2.44	0.46
6.0	0.11	1.25	0.87
14.0	0.31	0.38	1.10
25.0	0.35	0.14	1.12

s-fac (Fig. 2-c), of which the rate was very slow, produced *mer* at first and then *u-fac*. The amount of *u-fac* exceeded that of *mer* after about 70 h. The equilibrium mole ratio of the three isomers was *u-fac*:*mer*:*s-fac*=25:19:56%.

In the isomerization of the [Co(ida)(dien)]+ system, the reaction paths are described as Scheme 2. The rate constants (k_1'—k_6') were obtained on the basis of the following procedure. Tentative values of the rate constants, k_1'—k_6', were estimated from the initial rates and the equilibrium mole ratio of the three isomers. Curves of the concentration change of each isomer was obtained by Runge-Kutta method[10] using these tentative rate constants. The calculation of Runge-Kutta method was repeated using the modified

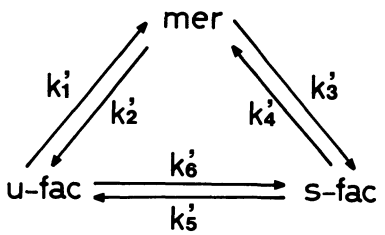

Scheme 2.

values of the rate constants until the difference between the calculated curves and the observed ones was minimized. The results are listed in Table 2 and the best-fit curves are shown in Fig. 2. The *u-fac*⇌*s-fac* change hardly occurs (Table 2). Thus, the main

Table 2. The Rate Constants for the Isomerization of the [Co(ida)(dien)]$^+$ and [Co(ida)(mdien)]$^+$ Systems (40.0 °C, I=0.1 M)

	[Co(ida)(dien)]$^+$						Co(ida)(mdien)]$^+$	
	pH[a] 10.00		pH[a] 10.30		pH[a] 10.60		pH[a] 10.30	
	k_n'[b]	k_n[c]	k_n'[b]	k_n[c]	k_n'[b]	k_n[c]	k_n'[b]	k_n[c]
u-fac ⟶ *mer* (1)	6.2	17	11	15	22	15	38	51
mer ⟶ *u-fac* (2)	8.0	22	14	19	28	19	83	112
mer ⟶ *s-fac* (3)	3.2	8.4	5.6	7.5	12	8.4	132	117
s-fac ⟶ *mer* (4)	1.0	2.8	1.8	2.5	6.0	4.0	2.1	2.8
s-fac ⟶ *u-fac* (5)	0	0	0	0	0	0	3.1	4.2
u-fac ⟶ *s-fac* (6)	0.5	1.4	0.9	1.2	1.9	1.2	101	135

a) Na_2CO_3–$NaHCO_3$ buffer. b) $\times 10^{-6}$ s^{-1}. c) $\times 10^{-3}$ M^{-1} s^{-1}.

isomerization paths of [Co(ida)(dien)]$^+$ system can be described as in Scheme 1, which is found in the isomerization reaction of the [Co(ida)$_2$]$^-$ system.

The isomerization reaction of the [Co(ida)(dien)]$^+$ system was also carried out under the conditions of pH 10.00 and 10.60 at 40.0 °C, and analyzed by the same method as described above. The pseudo-first-order rate constants (k_n') and second-order rate constants (k_n=k_n'/[OH$^-$]) are listed in Table 2. Judging from the constancy of k_n, the rate law for each isomerization path can be described as R=k_n[complex][OH$^-$]. It is probable that the isomerization of the [Co(ida)(dien)]$^+$ system proceeds through the conjugate base intermediate. In the isomerization reaction of the [Co(ida)-(dien)]$^+$ system, other species except for three geometrical isomers were little detected. This fact suggests that the ligand dissociation is not involved in the reaction; if such dissociation was involved, the reaction should provide hydrolysis products. Thus, the isomerization must involve only the intramolecular paths. We can consider two possibilities for the intramolecular rearrangement; twist proceeding through the trigonal prismatic transition state and bond rupture forming a five-coordinate intermediate and followed by rearrangement within the intermediate by a subsequent recoordination of the COO$^-$ group. The *mer*⇌*s-fac* change (in Scheme 2) can be sufficiently explained in terms of only the bond-rupture mechanism, whereas the *u-fac*⇌*mer* (and also *u-fac*⇌*s-fac*) change may be described by the mechanisms of both bond rupture and twist.

Isomerization of the [Co(ida)(mdien)]$^+$ System. The isomerization reactions using *u-fac*- and *mer*-[Co(ida)(mdien)]$^+$ as the starting materials were carried out under the conditions of pH 10.30 and I=0.1 M at 40.0 °C. The reaction rate was relatively faster in the [Co(ida)(mdien)]$^+$ system than in the [Co(ida)(dien)]$^+$ system. The concentration changes in the starting materials and products are shown in Figs. 3-a and 3-b. A part of the numerical data (five data points) are listed in Table 1.[9] In the isomerization reactions of both *u-fac* and *mer*, a small amount of pink by-product was formed together with the other isomers in the initial stage of the reactions. The pink by-product

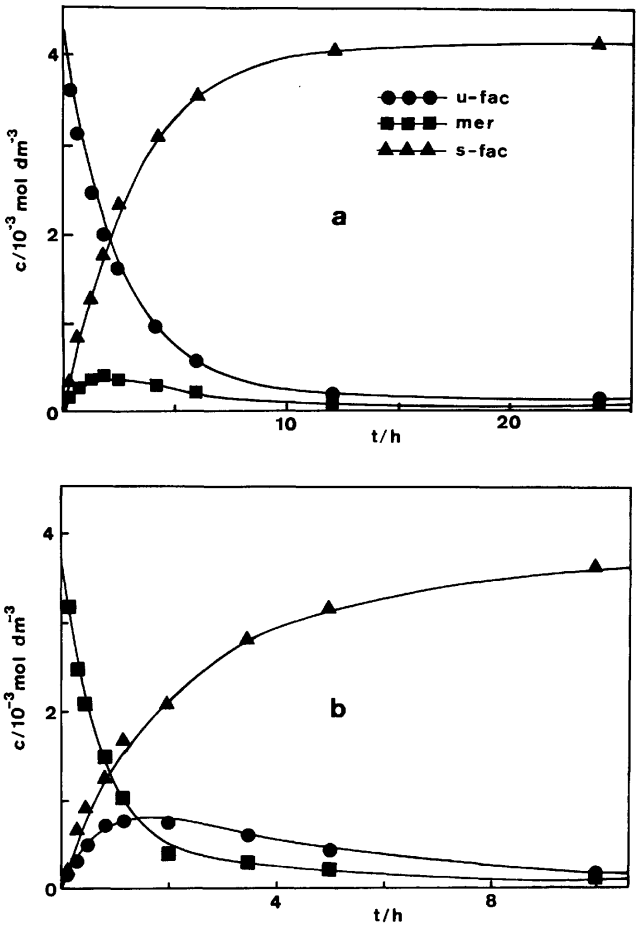

Fig. 3. The isomerization reaction of [Co(ida)(mdien)]$^+$ in a basic aqueous solution (pH 10.30) at 40.0 °C. Starting isomers are *u-fac* (a) and *mer* (b). Each of the lines is the curve calculated from the data in Table 2 by using Runge-Kutta method.

was eluted prior to the mixture of *u-fac* and *s-fac* but posterior to *mer* on SP-Sephadex column chromatograph. Therefore, the pink by-product must be +1 charged one. The pink by-product could not be isolated, because it was unstable and was formed only in a small amount. During the concentration of a solution containing the pink by-product under reduced pressure at 35—40 °C, the pink by-product changed to *s-fac*. The amount of the pink by-product was esti-

mated on the basis of the absorption spectrum of the *s-fac* formed from the pink by-product. The amount of the pink by-product was maximal about 30 min after the start of the reaction. It is likely that the pink by-product was a monoaqua species whose formation competes with isomerization in a bond-rupture process. No other species, except for three geometrical isomers and pink by-product, were detected in the isomerization reaction of the [Co(ida)(mdien)]+ system. At the final stage of the reaction, *s-fac* was the main product.

The base-catalyzed isomerization reaction of the [Co(ida)(mdien)]+ system was also analyzed by the Runge–Kutta method assuming Scheme 2. In this calculation, the formation of the pink by-product was neglected. The results are listed in Table 2, indicating that the reactions proceed through three intramolecular paths. The calculated curves of the concentration changes by Runge-Kutta method are shown in Fig. 3. It is worth noting that the *u-fac*⟶*s-fac* change occurs very easy in the [Co(ida)(mdien)]+ system but hardly in the [Co(ida)(dien)]+ system.

The *u-fac*⇌*mer* change can be explained in terms of both bond rupture and twist. However, the fact that the isomerization rate is faster in the mdien complex than in the dien complex (Tables 1 and 2) is not favorable to the twist mechanism, judging from the view point of the intramolecular steric factor. The equilibrium mole ratio of three isomers of [Co(ida)(mdien)]+ were *u-fac*:*mer*:*s-fac*=3:3:94%. The equilibrium further shifts to *s-fac* side compared with that of the [Co(ida)(dien)]+ system. Similarly, the equilibriums of [Co(ida)(mida)]− and [Co(dien)(mdien)]3+ systems shift more to *s-fac* side compared with those of the $[Co(ida)_2]^-$ and $[Co(dien)_2]^{3+}$ systems respectively.[2,3] These tendencies may be explained by the intramolecular steric repulsion.

Isomerization of the [Co(mida)(dien)]+ and [Co(mida)(mdien)]+ Systems. The isomerization reactions of the [Co(mida)(dien)]+ and [Co(mida)(mdien)]+ systems were studied under the conditions of pH 10.30 at 40.0 °C. A part of the numerical data are listed in Table 1. The *s-fac* isomer of [Co(mida)(dien)]+ was stable under the reaction conditions; other species, such as isomerization and/or hydrolysis products, were scarcely detected throughout a reaction of over 80 h. As shown in Table 1, the *u-fac*- and *mer*-[Co(mida)(dien)]+ interconverted each other accompanying the formation of unknown by-products with more than 2+ charge in a considerable amount. The *s-fac* isomer was scarcely formed in the isomerization reactions of *u-fac* and *mer*. In the isomerization of *mer*-[Co(mida)(mdien)]+, *u-fac* and *s-fac* were formed simultaneously, while in the isomerization of *u-fac*-[Co(mida)(mdien)]+, *mer* was mainly formed. The isomerization of *s-fac* was very slow. In these isomerization reactions, considerable amounts of unknown by-products with more than 2+ charge were formed. The isomerization reactions of the [Co(mida)(dien)]+ and [Co(mida)(mdien)]+ systems were complicated, so that the reaction processes could not be analyzed.

The CD Decrease of Optically Active *u-fac* Isomers. The rates of CD decrease of optically active *u-fac* isomers were measured under the conditions of pH 10.30 at 40.0 °C. In each case of [Co(ida)(dien)]+, [Co(ida)(mdien)]+, and [Co(mida)(dien)]+, the intensities of CD at two arbitrary wavelengths decreased in the same ratio, and the isocircular dichroism points lay on the base line. This fact indicates that no optically active products are formed. The rate constants of the CD decrease, k_{CD} (s^{-1}), for $(+)^{CD}_{538}$-*u-fac*-[Co(ida)(dien)]+ is $24\times10^{-6}\ s^{-1}$, which is larger than the sum of values of k_1' and k_6' (Table 2), probably indicating that racemization of *u-fac* itself occurs. The value of k_{CD} for $(-)^{CD}_{550}$-*u-fac*-[Co(ida)(mdien)]+ is $128\times10^{-6}\ s^{-1}$, which is nearly equal to the sum of the values of k_1' and k_6'. Therefore, the CD decrease of *u-fac*-[Co(ida)(mdien)]+ is attributed to the isomerization reaction. The rate of CD decrease for $(+)^{CD}_{544}$-*u-fac*-[Co(mida)(dien)]+ ($k_{CD}=84\times10^{-6}\ s^{-1}$) was also close to the rate of the decrease of the *u-fac* due to isomerization and decomposition.

For each of [Co(ida)(dien)]+, [Co(ida)(mdien)]+, and [Co(mida)(dien)]+, no optically active *mer* isomer was obtained from the isomerization reaction of optically active *u-fac* (as described above). However, this fact does not imply that the path of the *u-fac*⇌*mer* change is not stereoselective, because the racemizations of these *mer* are very fast under the present reaction conditions (vide post).

Figure 4 shows the CD spectral change of $(+)^{CD}_{564}$-*u-fac*-[Co(mida)(mdien)]+ with the passage of time under the conditions of pH 10.30 at 40.0 °C. The isocircular

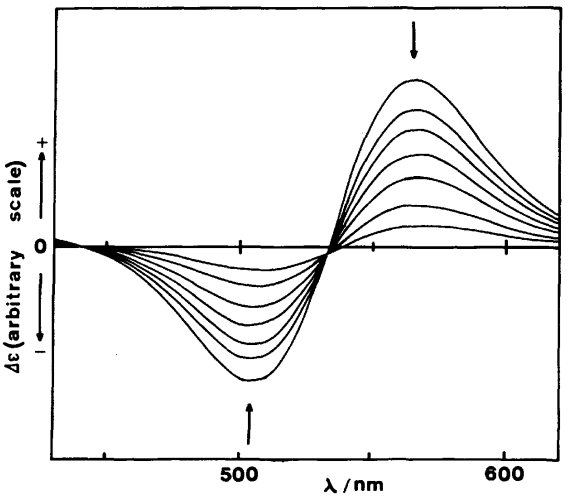

Fig. 4. The CD spectral change of $(+)^{CD}_{564}$-*u-fac*-[Co(mida)(mdien)]+ in a basic aqueous solution (pH 10.30) at 40.0 °C. Each of the curves was recorded at 2, 12, 19, 28, 39, 60, and 101 min, respectively.

dichroism points do not lie on the base line. This observation indicates the formation of an optically active product (*mer*). The reaction solution was acidified in order to stop the reaction 30 min after its start; then, optically active *mer* in the reaction solution was isolated by SP-Sephadex column chromatography. As shown in Fig. 5, the *mer* formed from $(+)^{CD}_{564}$-*u-fac* isomer is $(+)^{CD}_{582}$ form, and its optical purity is presumed to be considerably high, because its CD strength is comparable to that of pure $(-)^{CD}_{570}$-*mer*-[Co(mida)(dien)]$^+$. The absolute configuration of $(+)^{CD}_{564}$-*u-fac* has been determined to *ΛΔΛ*.[7a] The absolute configuration of $(+)^{CD}_{582}$-*mer* can be assigned to *λ*-spiral by a comparison of the CD spectral pattern with that of $(-)^{CD}_{570}$-*mer*-[Co(mida)(dien)]$^+$, the absolute configuration of which has been determined to be *δ*-spiral by the X-ray diffraction method.[12] The stereoselectivity in the *u-fac*⟶*mer* change (Scheme 3) may be attributed to the steric repulsion of two CH_3 groups in the isomerization process.

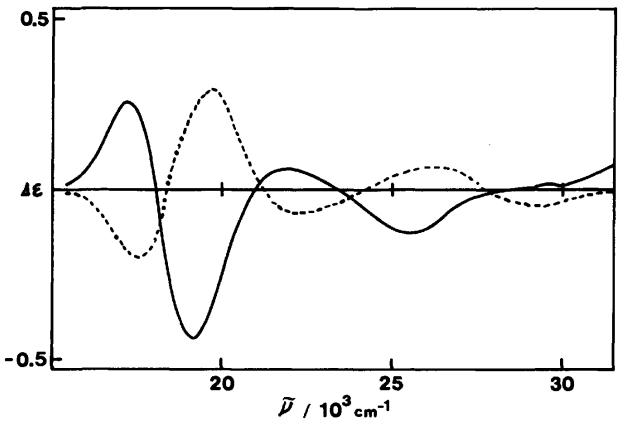

Fig. 5. CD spectral measured in 0.1 M HCl: $(-)^{CD}_{570}$-*mer*-[Co(mida)(dien)]$^+$ (·····) and $(+)^{CD}_{582}$-*mer*-[Co(mida))(mdien)]$^+$ (——) formed from $(+)^{CD}_{564}$-*u-fac* isomer.

Racemization of *mer*-[Co(ida)(dien)]$^+$ and *mer*-[Co(mida)(dien)]$^+$. Two *mer* isomers, *mer*-[Co(ida)(dien)]$^+$ and *mer*-[Co(mida)(dien)]$^+$, have been resolved into optically active ones; however, we have not yet been successful with *mer*-[Co(ida)(mdien)]$^+$. The enantiomer of these *mer* are designated by the *δ*- or *λ*-spiral configuration, due to the arrangement of the two trans N-H groups in *mer*-[Co(ida)(dien)]$^+$ or due to the arrangement of the trans N-H and N-CH_3 groups in *mer*-[Co(mida)(dien)]$^+$; the absolute configurations of $(-)^{CD}_{570}$-*mer*-[Co(mida)(dien)]$^+$ and $(-)^{CD}_{560}$-*mer*-[Co(ida)-(dien)]$^+$ are assigned to the *δ*-spiral configuration.[12] The CD spectra of $(+)^{CD}_{560}$-*mer*-[Co(ida)(dien)]$^+$ and $(-)^{CD}_{570}$-*mer*-[Co(mida)(dien)]$^+$ changed with time in an acetate buffer solution (pH 4.20—6.00 at 30—40 °C). The isocircular dichroism points lay on the base line and the values of the CD intensities at various wavelengths decreased in the same ratio. The absorption spectra did not change during a CD measurement, indicating that no isomerization and/or hydrolysis oc-

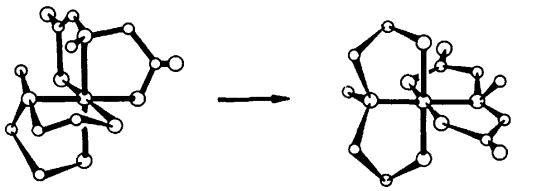

Scheme 3.

Table 3. Rate Constants and Activation Parameters for Racemization of $(+)^{CD}_{560}$-*mer*-[Co(ida)(dien)]$^+$ and $(-)^{CD}_{570}$-*mer*-[Co(mida)(dien)]$^+$ Ions (I=1.0 M)

(i) $(+)^{CD}_{560}$-*mer*-[Co(ida)(dien)]$^+$					
T / °C	pH[a]	k_{rac}' / 10^{-4} s^{-1}	k_{rac} / 10^4 M^{-1} s^{-1}	ΔH^* / kJ mol^{-1}	ΔS^* / J K^{-1} mol^{-1}
30.0	5.10	1.28	5.30	72.7±6.5	85.3±21.1
30.0	5.37	2.34	5.21		
30.0	5.70	5.03	5.23		
30.0	6.00	9.38	4.89		
35.0	5.11	2.87	8.13		
40.0	5.06	6.19	14.0		
(ii) $(-)^{CD}_{570}$-*mer*-[Co(mida)(dien)]$^+$					
T / °C	pH[a]	k_{rac}' / 10^{-4} s^{-1}	k_{rac} / 10^4 M^{-1} s^{-1}	ΔH^* / kJ mol^{-1}	ΔS^* / J K^{-1} mol^{-1}
30.0	4.20	1.60	52.6	59.7±1.3	61.4±4.3
30.0	4.41	2.63	53.3		
30.0	4.75	5.55	51.4		
30.0	5.34	21.9	52.2		
35.0	4.20	3.40	78.3		
40.0	4.20	7.15	117		

a) CH_3COOH-CH_3COONa buffer.

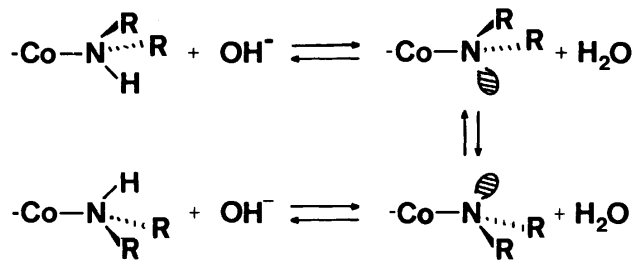

Scheme 4.

curred. Therefore, the CD decreases can be due to racemizations of *mer*, themselves. The progress of the racemization was followed by monitoring the decrease of the CD intensity at 560 nm for *mer*-[Co(ida)(dien)]+ and at 570 nm for *mer*-[Co(mida)(dien)]+. Kinetic data are summarized in Table 3. The values of the racemization rate constant k_{rac} ($=k_{rac}'/[OH^-]$) for *mer*-[Co(ida)-(dien)]+ at 30.0 °C are essentially constant, so that the rate law is described as $R=k_{rac}$[complex][OH^-]. Activation energies E_a were calculated by a least-squares method of the Arrhenius plots of k_{rac}. The activation parameters calculated for the two complexes are given in Table 3. The racemization rate of *mer*-[Co(mida)-(dien)]+ is about one order faster than that of *mer*-[Co(ida)(dien)]+, and the activation enthalpy of the former is smaller than that of the latter. It seemes likely that the electron-donative CH_3 group exerts a trans effect in *mer*-[Co(mida)(dien)]+, enhancing the racemization rate. A similar trans effect (enhancing of the racemization rate) was observed in the racemization of *mer*-[Co(edma)(mdien)]2+.[13]

All of the racemization data for the present complexes can be explained according to the mechanism shown in Scheme 4, proposed for the racemizations of *mer*-[Co(dien)$_2$]3+ [14] and *mer*-[Co(edma)(dien)]2+.[13] This proposal can be supported by the fact that optically active *mer*-[Co(mida)(mdien)]+ did not racemize, even in a weakly basic aqueous solution.

The racemization rates for *mer*-type complexes increase in the order of [Co(dien)$_2$]3+<[Co(edma)-(dien)]2+<[Co(ida)(dien)]+. The difference in the racemization rates may be attributed to the electronic property of the chelates. The electronegative carbonyl group decreases the electron density on the secondary amine nitrogen center, in which inversion occurs. Consequently, the pre-equilibrium of Scheme 4 displaces to the deprotonated form and the racemization rate increases.

References

1) Abbreviations used: dien, 3-azapentane-1,5-diamine; ida, iminodiacetate dianion; mdien, 3-methyl-3-azapentane-1,5-diamine; mida, *N*-methyliminodiacetate dianion; edma, ethylenediamine-*N*-acetate anion.

2) G. H. Searle, F. R. Keene, and S. F. Lincoln, *Inorg. Chem.*, **17**, 2362 (1978).

3) H. Kawaguchi, T. Ama, and T. Yasui, *Bull. Chem. Soc. Jpn.*, **57**, 2422 (1984).

4) In a basic solution, *u-fac*-[Co(mida)$_2$]$^-$ decomposed with the decomposition of one ligand per two complex ions and the reduction of cobalt(III) to cobalt(II). T. Ama, H. Kawaguchi, and T. Yasui, *Chem. Lett.*, **1981**, 323.

5) H. Kawaguchi, R. Niiyama, T. Ama, and T. Yasui, *Bull. Chem. Soc. Jpn.*, **60**, 3953 (1987).

6) M. Shimizu, T. Hosogi, T. Ama, H. Kawaguchi, and T. Yasui, presented at the 37th Symposium on Coordination Chemistry, Tokyo (Ocyanomizu), October, 1987, Abstr., No. 2CP25.

7) a) T. Yasui, K. Okamoto, J. Hidaka, T. Ama, and H. Kawaguchi, *Bull. Chem. Soc. Jpn.*, **60**, 2573 (1987). b) J. I. Legg and D. W. Cooke, *Inorg. Chem.*, **5**, 594 (1966). c) N. Koine, T. Tanigaki, J. Hidaka, and Y. Shimura, *Chem. Lett.*, **1980**, 871.

8) H. S. Harned and W. J. Harmer, *J. Am. Chem. Soc.*, **55**, 2194, (1933).

9) The total concentrations at various reaction times do not agree one another. The reason may be attributed to the experimental errors.

10) T. Kunii, A. Nakamura, and F. Ito, "Suuchi-keisan to Puroguramingu," Kyoritsu Syuppan, Tokyo (1970), p. 53.

11) Unpublished results. The preparation of the complexes: T. Yasui, T. Shikiji, N. Koine, T. Ama, and H. Kawaguchi, *Bull. Chem. Soc. Jpn.*, **60**, 595 (1987).

12) K. Okamoto, T. Yasui, and J. Hidaka, *Chem. Lett.*, **1987**, 551.

13) H. Kawaguchi, H. Fukaki, T. Ama, T. Yasui, K. Okamoto, and J. Hidaka, *Bull. Chem. Soc. Jpn.*, **61**, 2359 (1988).

14) G. H. Searle and F. R. Keene, *Inorg. Chem.*, **11**, 1006 (1972).

Crystal Structures of [VO(sal-L-ala)(OCH$_3$)(CH$_3$OH)] (sal-L-ala= *N*-salicylidene-L-alaninate) and {[VO(sal-L-ala)]$_2$O}$_2$·2CH$_2$Cl$_2$, and the Catalytic Activity of These and Related Complexes on Asymmetric Oxidation of Methyl Phenyl Sulfide with *t*-Butyl Hydroperoxide

Kiyohiko NAKAJIMA, Masaaki KOJIMA,† Koshiro TORIUMI, Kazuo SAITO,†† and Junnosuke FUJITA†,*
Institute for Molecular Science, Okazaki National Research Institutes, Myodaiji, Okazaki 444
†Department of Chemistry, Faculty of Science, Nagoya University, Chikusa-ku, Nagoya 464-01
††Faculty of Science, International Christian University, Osawa, Mitaka 181
(Received October 24, 1988)

A reddish brown oxovanadium(V) complex, [V^{V}O(sal-L-ala)(OCH$_3$)(CH$_3$OH)] (**2a**, sal-L-ala=*N*-salicylidene-L-alaninate) was formed by dissolving [V^{IV}O(sal-L-ala)(H$_2$O)] (**1a**) in methanol. Treatment of **2a** with wet dichloromethane yielded deep blue crystals of {[V^{V}O(sal-L-ala)]$_2$O}$_2$·2CH$_2$Cl$_2$ (**3a**). The structures of **2a** and **3a** have been determined by X-ray analyses. Crystal data are: [VO(sal-L-ala)(OCH$_3$)(CH$_3$OH)] (**2a**), monoclinic, *C*2, *a*=19.621(6), *b*=6.734(1), *c*=12.059(4) Å, *β*=117.72(2)° and *Z*=4. {[VO(sal-L-ala)]$_2$O}$_2$·2CH$_2$Cl$_2$ (**3a**), orthorhombic, $P2_12_12_1$, *a*=19.938(4), *b*=23.854(5), *c*=11.526(2) Å, and *Z*=4. In **2a**, the tridentate sal-L-ala ligand and a methoxide ion occupy the basal positions, and form distorted octahedral geometry around the vanadium(V) ion together with one methanol molecule (V–O distance: 2.384(4) Å) and the oxide ion of oxovanadium(V). The tetranuclear complex (**3a**) consists of two *μ*-oxo dinuclear vanadium(V) complexes, and each vanadium(V) ion has a distorted octahedral coordination. The Schiff base coordinates equatorially to each vanadium(V) ion, of which one axial site is occupied by O^{2-} and the other is weakly linked to the carboxylate O atom of a nearby Schiff base (V–O distance: 2.34—2.56 Å). Octahedral coordination on each vanadium(V) is achieved by sharing an equatorial O^{2-} ligand. The brown complexes, [VO(sal-L-aa)(OCH$_3$)(CH$_3$OH)] (**2**, sal-L-aa=*N*-salicylidene L-amino carboxylate) catalyze the oxidation of methyl phenyl sulfide with *t*-butyl hydroperoxide in dichloromethane at 4 °C to give (*R*)-methyl phenyl sulfoxide with optical yields (e.e.) of 8—14%.

In a previous paper,[1] we reported that optically active tetradentate Schiff base–oxovanadium(IV) complexes catalyze asymmetric oxidation of sulfides into the corresponding sulfoxides with organic hydroperoxides. However, neither the mechanism nor the characterization of useful precursors was discussed in detail. Recently, we found that the oxovanadium(V) complex with a tridentate $^{-}$O–N–O^{-}-type ligand, [V^{V}O(dipic)(OOBu^{t})(H$_2$O)] (H$_2$dipic=2,6-pyridinedicarboxylic acid, HOOBu^{t}=*t*-butyl hydroperoxide)[2] catalyzes a similar reaction very efficiently.[3] Thus, it seems interesting to examine catalytic activity of oxovanadium(V) complexes with optically active, tridentate $^{-}$O–N–O^{-}-type Schiff base ligands.

This paper deals with the preparation and characterization of oxovanadium(V) complexes with *N*-salicylidene L-amino carboxylates, X-ray crystal structure analysis of the L-alanine derivatives, and their catalytic activity on asymmetric oxidation of methyl phenyl sulfide with *t*-butyl hydroperoxide.

Experimental

Synthesis. [V^{V}O(sal-L-aa)(OCH$_3$)(CH$_3$OH)] (2) (L-aa=L-ala, L-phe, L-val, and L-leu). These complexes were prepared by a method similar to that of Gillard et al.[4] The procedure is described for the L-ala derivative. The other three complexes were prepared by similar procedures. [V^{IV}O(sal-L-ala)(H$_2$O)][5] (**1a**) (2.11 g, 7.65 mmol) was dissolved in methanol (50 cm^3) to give a reddish brown solution. The solvent was evaporated slowly in a refrigerator to yield brown crystals of [V^{V}O(sal-L-ala)(OCH$_3$)(CH$_3$OH)] (**2a**), which were collected by filtration and air dried. Yield: 1.4 g (57%). Found: C, 44.67; H, 5.02; N, 4.36%. Calcd for C$_{12}$H$_{16}$NO$_6$V: C, 44.87; H, 5.02; N, 4.36%. Found: C, 54.12; H, 4.62; N, 3.72%. Calcd for [VO(sal-L-phe)(OCH$_3$)(CH$_3$OH)]=C$_{18}$H$_{20}$NO$_6$V (**2b**): C, 54.41; H, 5.07; N, 3.52%. Found: C, 47.89; H, 5.21; N, 4.27%. Calcd for [VO(sal-L-val)(OCH$_3$)(CH$_3$OH)]=C$_{14}$H$_{20}$NO$_6$V (**2c**): C, 48.14; H, 5.77; N, 4.01%. Found: C, 49.13; H, 5.60; N, 4.06%. Calcd for [VO(sal-L-leu)(OCH$_3$)(CH$_3$OH)]=C$_{15}$H$_{22}$NO$_6$V (**2d**): C, 49.59; H, 6.10; N, 3.86%.

{[VO(sal-L-ala)]$_2$O}$_2$·2CH$_2$Cl$_2$ (3a). Complex **2a** (1.4 g, 4.4 mmol) was dissolved in wet dichloromethane (30 cm^3), and the dark blue solution was evaporated to ca. 5 cm^3. The concentrate was allowed to stand in a refrigerator to yield dark blue crystals of **3a**. Yield: 0.9 g (66%).

Crystal Structure Analysis of 2a and 3a. Crystals of [V^{V}O(sal-L-ala)(OCH$_3$)(CH$_3$OH)] (**2a**) and {[V^{V}O(sal-L-ala)]$_2$O}$_2$·2CH$_2$Cl$_2$ (**3a**) were grown by slow evaporation, respectively, from methanol and dichloromethane solutions at room temperature. Crystal data and experimental details are listed in Table 1. A reddish brown prism of **2a** was coated first with paraffin and then with epoxy resin to avoid intensity changes during the data collection. The crystals of **3a** deteriorated when removed from the mother liquor, presumably owing to loss of the solvent of crystallization. A dark blue prism of **3a** was coated with epoxy resin. Intensity data for **2a** and **3a** were collected on a Rigaku AFC-5 and a Rigaku AFC-5R four-circle diffractometer, respectively, by use of graphite monochromatized Mo *Kα* radiation (*λ*= 0.71073 Å). Lattice constants were determined by least-squares calculations based on 2*θ* values ($22<2\theta<32°$) of 36 reflections for **2a**, and 30 2*θ* values ($20<2\theta<26°$) for **3a**. The

Table 1. Crystal Data and Experimental Details

Complex	2a	3a
Formula	$VC_{12}H_{16}NO_6$	$V_4C_{40}H_{36}N_4O_{18}\cdot 2CH_2Cl_2$
Formula weight	321.2	1234.4
Crystal system	Monoclinic	Orthorhombic
Space group	$C2$	$P2_12_12_1$
a/Å	19.621(6)	19.938(4)
b/Å	6.734(1)	23.854(5)
c/Å	12.059(4)	11.526(2)
β/°	117.72(2)	
Z	4	4
V/Å^3	1410.5(8)	5482(2)
D_x/g cm^{-3}	1.51	1.50
μ(Mo $K\alpha$)/cm^{-1}	5.11	5.11
Crystal color	Reddish brown	Dark blue
Crystal habit	Prismatic	Prismatic
Crystal size/mm^3	0.1×0.2×0.3	0.2×0.2×0.35
Scan type	θ-2θ	θ-2θ
$2\theta_{max}$/°	55	50
Reflcns measd	$\pm h$, $\pm k$, $+l$	$+h$, $+l$, $+k$
No. of reflcns measd	3413	5614
No. of reflcns obsd [$\|F_o\|>3\sigma(\|F_o\|)$]	1892	2557
R	0.046	0.088
R_w	0.041	0.111
Weighting scheme	$w=[\sigma_{count}^2+(0.015\|F_o\|)^2]^{-1}$	$w=[\sigma_{count}^2+(0.020\|F_o\|)^2]^{-1}$

structures were solved by the direct method (MULTAN 78)[6] and refined by the block-diagonal least-squares method for **2a**, and by the full-matrix least-squares method for **3a**. The absolute configuration of the structures was assigned on the basis of the known configuration of the L-alanine moiety. The reason for the rather high R-value of **3a** (R=0.088, R_w=0.111) will be discussed later. Atomic scattering factors and anomalous scattering corrections were taken from Ref. 7. The final atomic parameters are listed in Table 2. All the calculations were carried out on a HITAC M-680 computer at the Computer Center of Institute for Molecular Science using the Universal Crystallographic Computation Program System UNICS-III[8] for **2a** and RADIEL[9] for **3a**. Lists of observed and calculated structure factors, anisotropic thermal parameters for nonhydrogen atoms, and the coordinates of hydrogen atoms, and the ORTEP drawings of crystal structures are deposited at the office of the Chemical Society of Japan (Document No. 8861).

Reactions. Reaction of 3a with Organic Hydroperoxide. To a dichloromethane solution of **3a** was added ten times molar quantity of 1-methyl-1-phenylethyl hydroperoxide (73%). The color of the solution changed immediately from deep blue to reddish brown. Hexane was added to this solution slowly, and the mixture was allowed to stand in a refrigerator to yield brown crystals (**4a**). Complex **4a** is unstable both in solution and in the solid state. When *t*-butyl hydroperoxide was used instead of 1-methyl-1-phenylethyl hydroperoxide, a similar color change occurred but the product was not isolated because of its high solubility in common organic solvents.

Oxidation of Methyl Phenyl Sulfide by *t*-Butyl Hydroperoxide with a Catalytic Amount of 2. To a dichloromethane solution (10 cm^3) of **2** (0.1 mmol) were added methyl phenyl sulfide (1.0 mmol) and *t*-butyl hydroperoxide (80%, 1.0 mmol), and the mixture was kept at 4 °C. After 5.5—8 h, the solvent was removed under reduced pressure, and the residue was extracted with diethyl ether. The solvent was evaporated off, and methyl phenyl sulfoxide was isolated from the resulting oil. It was purified by column chromatography on silica gel (ϕ 1.0 cm×10 cm, eluent: ethyl acetate–cyclohexane (1:1 (v/v)). The enantiomeric excess (e.e.) was determined on the basis of the reported optical rotation of the pure enantiomer.[10]

Spectroscopic Measurements. ^{1}H NMR spectra were recorded on a JEOL GX-400 spectrometer using TMS as an internal reference. Optical rotations were measured with a JASCO DIP 4 polarimeter. Absorption spectra were recorded on a Hitachi U-3400 spectrophotometer.

Results and Discussion

Characterization and X-Ray Analysis of the Complexes. [V^{V}O(sal-L-ala)(OCH$_3$)(CH$_3$OH)]: The bluish-gray oxovanadium(IV) complexes (**1**) with the general formula of VO(sal-aa)(H_2O) were prepared by Theriot et al. and characterized as a square pyramidal complex with an aqua ligand at the basal site.[5] Recently, this structure was confirmed by X-ray analysis on the L-alanine derivative.[11] Gillard et al.[4] obtained brown complexes (**2**) from methanol solutions of the bluish-gray complexes (**1**) (Scheme 1). They assigned **2** to monomeric oxovanadium(V) species with the formula [V^{V}O(sal-aa)(OCH$_3$)(CH$_3$OH)], the oxidizing agent being suggested to be atmospheric oxygen. The assignment was confirmed by the present X-ray structure determination on [V^{V}O(sal-L-ala)(OCH$_3$)(CH$_3$OH)] (**2a**). Complex **2a** was prepared from [V^{IV}O(sal-L-ala)-(H_2O)] by a method similar to that of Gillard et al.[4] without any particular oxidizing agent.

Figure 1 shows a perspective view of **2a**. Selected bond distances and angles are listed in Tables 3 and 4.

Table 2. Atomic Coordinates ($\times 10^4$; for V of **2a** $\times 10^5$) and Equivalent Isotropic Temperature Factors for **2a** and **3a**[a)]

Atom	x	y	z	B/Å^2	Atom	x	y	z	B/Å^2
	(a) [VO(sal-L-ala)(OCH_3)(CH_3OH)] (**2a**)				Cl(21)	6490(12)	3775(12)	5655(22)	19.6
V(1)	17357(4)	0(19)	23234(8)	3.2	Cl(22)	6577(15)	4125(18)	7937(25)	27.2
O(1)	1860(2)	840(5)	3627(3)	4.7	Cl(31)	7163(44)	5148(26)	5280(86)	18.5
O(2)	2749(2)	−210(6)	2618(3)	4.0	Cl(32)	7552(47)	4088(54)	6830(78)	34.7
O(3)	669(2)	−865(4)	1640(3)	3.6	Cl(41)	7678(49)	4765(68)	9805(77)	29.5
O(4)	1445(2)	2187(5)	1392(3)	4.3	Cl(42)	8135(30)	4622(25)	7570(44)	19.2
O(5)	−190(2)	−3149(5)	1489(3)	4.7	C(10)	1009(11)	6813(10)	3131(21)	2.8
O(6)	1499(2)	−1642(6)	426(3)	4.1	C(11)	591(14)	6321(12)	3338(24)	5.0
N(1)	1843(2)	−2996(5)	2853(3)	2.8	C(12)	939(16)	5900(13)	4238(30)	7.4
C(1)	3273(2)	−1639(8)	2908(4)	3.2	C(13)	92(13)	5546(11)	2188(23)	4.1
C(2)	3981(3)	−1230(9)	2936(5)	4.6	C(14)	−28(15)	5186(13)	1176(28)	6.2
C(3)	4511(3)	−2695(9)	3184(5)	5.1	C(15)	−375(15)	4668(12)	1380(24)	5.3
C(4)	4367(3)	−4659(11)	3390(5)	5.3	C(16)	−441(21)	4307(17)	456(37)	9.7
C(5)	3684(3)	−5068(11)	3381(4)	4.2	C(17)	−199(16)	4456(14)	−530(29)	6.6
C(6)	3126(3)	−3605(7)	3151(4)	3.2	C(18)	116(15)	4917(13)	−837(27)	5.9
C(7)	2414(3)	−4160(7)	3135(4)	3.1	C(19)	265(13)	5361(12)	21(24)	4.6
C(8)	1190(3)	−3685(10)	4127(5)	5.4	C(20)	1060(15)	8243(12)	1561(24)	4.6
C(9)	1137(3)	−3817(7)	2834(5)	3.3	C(21)	1661(13)	8352(11)	2206(22)	4.0
C(10)	473(3)	−2569(7)	1911(4)	3.1	C(22)	1996(16)	8880(14)	1722(30)	7.2
C(11)	1027(3)	2609(9)	105(6)	5.8	C(23)	2463(12)	7769(10)	3075(21)	3.7
C(12)	1965(3)	−2015(11)	−155(6)	6.2	C(24)	2784(13)	7260(12)	3153(23)	4.4
					C(25)	3094(15)	7072(13)	4114(28)	6.4
	(b) {[VO(sal-L-ala)]$_2$O}$_2$·2CH_2Cl_2 (**3a**)				C(26)	3442(15)	6565(14)	4348(29)	6.8
V(11)	1087(2)	6293(2)	825(4)	3.6	C(27)	3449(15)	6201(13)	3471(26)	5.3
V(21)	1910(2)	7381(2)	667(4)	3.8	C(28)	3192(12)	6295(11)	2462(24)	4.4
V(31)	−464(2)	8025(2)	2763(4)	3.9	C(29)	2872(13)	6837(11)	2325(24)	4.5
V(41)	375(2)	7727(2)	5253(4)	4.1	C(30)	−118(11)	7240(10)	1024(20)	2.8
O(1)	1461(7)	6823(7)	−82(13)	3.7	C(31)	−617(13)	7589(12)	364(22)	5.0
O(2)	168(7)	8038(7)	3868(13)	4.3	C(32)	−287(14)	7853(12)	−858(26)	5.8
O(11)	1697(8)	5897(7)	1085(14)	4.6	C(33)	−1353(12)	8364(10)	770(22)	3.6
O(12)	1293(7)	6842(7)	2080(14)	3.7	C(34)	−1604(12)	8788(11)	1462(22)	3.8
O(13)	1116(8)	7187(7)	3821(13)	4.1	C(35)	−2203(14)	9026(12)	1035(24)	4.9
O(14)	581(10)	5842(7)	−86(14)	5.1	C(36)	−2463(15)	9458(13)	1610(27)	6.3
O(21)	2283(9)	7714(7)	−370(16)	5.5	C(37)	−2080(16)	9658(13)	2801(28)	6.7
O(22)	1145(8)	7868(7)	759(14)	4.1	C(38)	−1524(11)	9432(10)	3099(20)	2.9
O(23)	501(9)	8493(7)	1695(15)	4.7	C(39)	−1298(12)	8974(10)	2438(20)	3.1
O(24)	2586(8)	6970(7)	1208(13)	4.6	C(40)	1729(16)	7900(12)	6148(25)	5.0
O(31)	−1104(9)	7709(8)	3311(14)	5.5	C(41)	1546(12)	7463(11)	6899(22)	4.0
O(32)	−72(7)	7376(7)	2029(12)	3.3	C(42)	2002(18)	6974(16)	6970(34)	9.2
O(33)	146(8)	6861(7)	490(14)	4.4	C(43)	564(13)	6891(11)	7207(23)	4.3
O(34)	−746(8)	8765(7)	2777(15)	4.6	C(44)	−115(13)	6668(11)	6985(23)	4.4
O(41)	−22(9)	8102(10)	6210(15)	6.4	C(45)	−426(15)	6288(13)	7793(26)	6.0
O(42)	1257(9)	8057(7)	5337(16)	5.2	C(46)	−1036(18)	6109(14)	7591(31)	7.5
O(43)	2272(10)	8090(8)	6009(18)	6.4	C(47)	−1347(18)	6173(16)	6414(32)	7.7
O(44)	−167(7)	7106(7)	5198(15)	4.6	C(48)	−1075(13)	6525(11)	5638(22)	4.2
N(11)	491(11)	5991(9)	2214(17)	4.6	C(49)	−447(12)	6773(10)	5945(20)	3.3
N(21)	2081(9)	7884(8)	2138(15)	3.4	C(1)	−175(28)	4448(22)	5110(49)	8.4
N(31)	−850(9)	8038(9)	1169(16)	4.0	C(2)	6478(30)	3564(25)	6968(61)	9.7
N(41)	854(9)	7261(9)	6555(15)	3.7	C(3)	7360(102)	4675(91)	5877(192)	14.7
Cl(11)	495(13)	4551(7)	5895(14)	14.5	C(4)	8164(51)	4518(45)	9293(94)	5.5
Cl(12)	−662(9)	4893(8)	4997(18)	12.4					

a) Equivalent isotropic temperature factors ($B_{eq}=4/3\{\sum_i\sum_j B_{ij}a_ia_j\}$) for noncarbon atoms, and isotropic temperature factors for carbon atoms.

The complex has a distorted octahedral coordination. The tridentate Schiff base ligand and a methoxide ion occupy the basal positions, and one methanol molecule (V–O distance: 2.384(4) Å) coordinates at the position trans to the oxo group. Thus the complex has a V^vO^{3+} core and the oxidizing agent should be atmospheric oxygen. Since oxidation of $V^{IV}O^{2+}$ is reported to form a *cis*-$V^vO_2^+$ core preferentially,[12] the present result is quite characteristic. The vanadyl V^v=O distance (1.579(3) Å) is almost the same as that (1.578(3) Å) in [V^{IV}O(sal-L-ala)(H_2O)] (**1a**).[11] The V=O bond length seems to be scarcely influenced by the oxidation of the vanadium ion. The vanadium(V) ion of **2a** deviates by 0.306 Å from the best least-squares equatorial plane towards the vanadyl O atom. In [V^vO(salen)ClO_4] (H_2salen=*N*,*N*′-disalicylideneethylenediamine), the

Table 3. Selected Bond Lengths (l/Å) for **2a** and **3a**

(a) [VO(sal-L-ala)(OCH_3)(CH_3OH)] (**2a**)

V(1)-O(1)	1.579(4)	N(1)-C(7)	1.277(6)
V(1)-O(2)	1.856(4)	N(1)-C(9)	1.482(7)
V(1)-O(3)	1.947(3)	C(1)-C(2)	1.401(8)
V(1)-O(4)	1.778(4)	C(2)-C(3)	1.362(8)
V(1)-O(6)	2.384(4)	C(3)-C(4)	1.399(10)
V(1)-N(1)	2.097(4)	C(4)-C(5)	1.364(9)
O(2)-C(1)	1.330(6)	C(5)-C(6)	1.401(8)
O(3)-C(10)	1.300(6)	C(6)-C(1)	1.415(7)
O(4)-C(11)	1.406(7)	C(6)-C(7)	1.437(8)
O(5)-C(10)	1.219(6)	C(8)-C(9)	1.515(9)
O(6)-C(12)	1.409(9)	C(9)-C(10)	1.514(6)

(b) {[VO(sal-L-ala)]$_2$O}$_2$·$2CH_2Cl_2$ (**3a**)

	$n=1$	$n=2$	$n=3$	$n=4$
V(n1)-O(n1)	1.571(17)	1.617(19)	1.611(18)	1.626(19)
V(n1)-O(n2)	1.994(17)	1.919(16)	1.931(16)	1.929(18)
V(n1)-O(n4)	1.810(18)	1.781(17)	1.852(17)	1.835(17)
V(n1)-N(n1)	2.120(21)	2.104(19)	1.992(19)	2.098(19)
O(n2)-C(n0)	1.34(3)	1.30(3)	1.21(3)	1.38(4)
O(n3)-C(n0)	1.22(3)	1.27(4)	1.21(3)	1.19(4)
O(n4)-C(n9)	1.32(3)	1.44(3)	1.27(3)	1.30(3)
N(n1)-C(n1)	1.53(3)	1.40(3)	1.49(3)	1.52(3)
N(n1)-C(n3)	1.33(3)	1.35(3)	1.35(3)	1.30(3)
C(n0)-C(n1)	1.46(4)	1.43(4)	1.51(4)	1.40(4)
C(n1)-C(n2)	1.60(4)	1.53(4)	1.68(4)	1.48(5)
C(n3)-C(n4)	1.47(4)	1.38(4)	1.38(4)	1.48(4)
C(n4)-C(n5)	1.44(4)	1.35(4)	1.41(4)	1.44(4)
C(n5)-C(n6)	1.38(5)	1.42(5)	1.33(4)	1.31(5)
C(n6)-C(n7)	1.29(5)	1.33(5)	1.64(5)	1.50(5)
C(n7)-C(n8)	1.32(5)	1.29(4)	1.28(4)	1.34(5)
C(n8)-C(n9)	1.48(4)	1.45(4)	1.41(3)	1.43(4)

V(11)-O(1)	1.802(16)	V(21)-O(1)	1.821(16)
V(31)-O(2)	1.791(15)	V(41)-O(2)	1.809(16)
V(11)-O(33)	2.344(17)	V(21)-O(12)	2.412(16)
V(31)-O(23)	2.542(18)	V(41)-O(13)	2.562(16)

Table 4. Selected Bond Angles (ϕ/°) for **2a** and **3a**

(a) [VO(sal-L-ala)(OCH_3)(CH_3OH)] (**2a**)

O(1)-V(1)-O(2)	100.4(2)	O(2)-V(1)-N(1)	85.5(2)
O(1)-V(1)-O(3)	99.6(2)	O(3)-V(1)-O(4)	90.8(2)
O(1)-V(1)-O(4)	100.8(2)	O(3)-V(1)-O(6)	76.3(2)
O(1)-V(1)-O(6)	172.9(2)	O(3)-V(1)-N(1)	77.1(1)
O(1)-V(1)-N(1)	95.4(2)	O(4)-V(1)-O(6)	85.2(2)
O(2)-V(1)-O(3)	154.5(2)	O(4)-V(1)-N(1)	161.2(1)
O(2)-V(1)-O(4)	100.6(2)	O(6)-V(1)-N(1)	78.1(2)
O(2)-V(1)-O(6)	82.0(2)		

(b) {[VO(sal-L-ala)]$_2$O}$_2$·$2CH_2Cl_2$ (**3a**)

	$n=1$	$n=2$	$n=3$	$n=4$
O(n1)-V(n1)-O(1)	102.3(8)	103.6(8)	—	—
O(n1)-V(n1)-O(2)	—	—	106.6(8)	105.1(9)
O(n1)-V(n1)-O(n2)	95.6(8)	96.3(8)	96.7(8)	100.6(9)
O(n1)-V(n1)-O(n4)	100.6(9)	100.4(9)	101.6(8)	100.5(9)
O(n1)-V(n1)-N(n1)	94.9(8)	104.0(8)	93.6(9)	91.7(9)
O(1)-V(n1)-O(n2)	82.8(7)	94.5(7)	—	—
O(2)-V(n1)-O(n2)	—	—	92.3(7)	94.9(7)
O(1)-V(n1)-O(n4)	108.1(8)	97.8(8)	—	—
O(2)-V(n1)-O(n4)	—	—	101.0(7)	99.5(7)
O(n2)-V(n1)-N(n1)	77.9(7)	74.9(7)	76.4(7)	76.4(7)
O(n4)-V(n1)-N(n1)	85.7(8)	84.8(8)	82.9(8)	82.3(7)
O(1)-V(n1)-N(n1)	155.3(8)	151.4(7)	—	—
O(2)-V(n1)-N(n1)	—	—	158.0(8)	162.4(8)
O(n2)-V(n1)-O(n4)	157.8(8)	156.3(8)	153.1(7)	150.3(8)
V(11)-O(1)-V(21)	116.2(8)	V(31)-O(2)-V(41)		141.4(10)

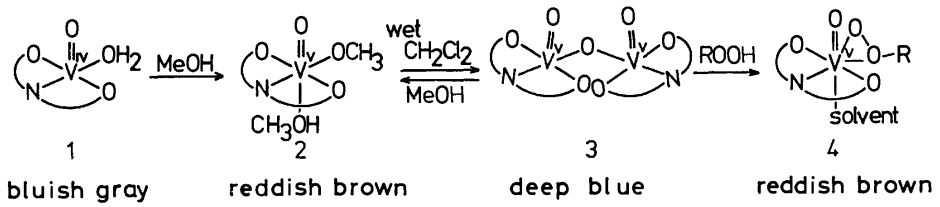

Scheme 1.

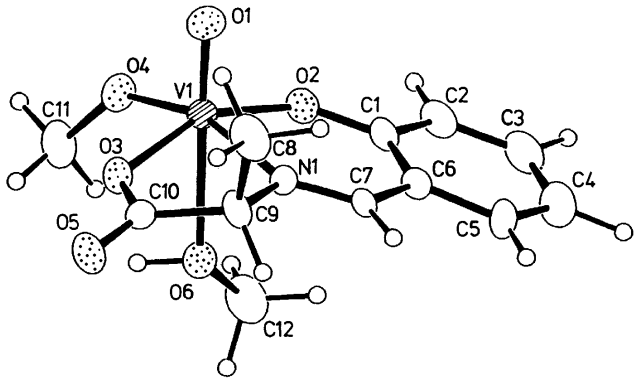

Fig. 1. ORTEP drawing and atom-numbering scheme for [V^{V}O(sal-L-ala)(OCH_3)(CH_3OH)] (**2a**). Vanadium and oxygen atoms are shown as shaded and dotted circles, respectively.

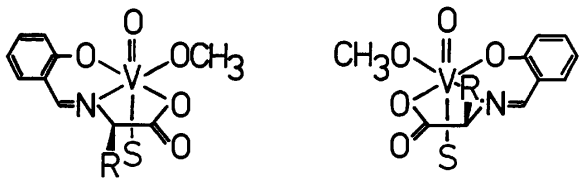

Fig. 2. Two possible geometrical isomers of [V^{V}O-(sal-L-aa)(OMe)(MeOH)], and S denotes a methanol molecule.

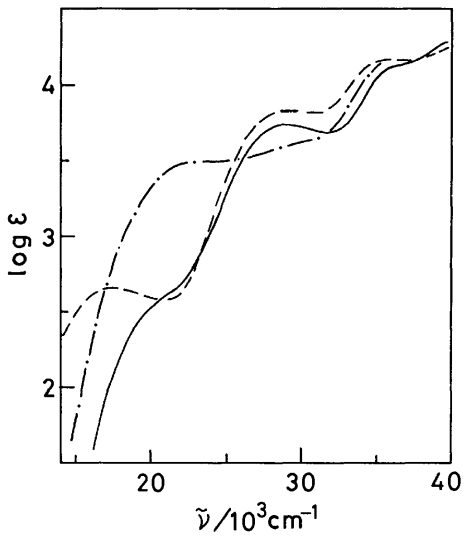

Fig. 3. Absorption spectra of [V^{V}O(sal-Lala)(OCH_3)-(CH_3OH)] (**2a**, ca. 1×10^{-3} mol dm^{-3} in the visible region and ca. 1×10^{-4} mol dm^{-3} in the UV region) in methanol (——), in wet dichloromethane (— — —) to form [VO(sal-L-ala)]$_2$O, and in wet dichloromethane in the presence of a large excess of *t*-butyl hydroperoxide (—·—) to form **4**.

vanadium atom is displaced towards the vanadyl O atom by 0.318 Å from the best salen N_2O_2 least-squares plane, and the V–O (perchlorate) length is relatively long (2.456(3) Å).[13] The vanadyl V^{V}=O distance of 1.576(3) Å in this complex is nearly the same as that of **2a**, but is shorter by 0.012 Å than the V^{IV}=O distance of [V^{IV}O(salen)].[14]

For the [VO(sal-L-aa)(OCH_3)(CH_3OH)] (**2**) complexes, two geometrical isomers are possible with respect to the mutual disposition of the substituent on L-aa and the V=O group (Fig. 2). The crystal of **2a** subjected to the present analysis contains the endo isomer. However, the ^{1}H NMR spectrum of complex **2a** in CD_3OD gives two doublet methyl signals due to the L-ala moiety at δ 1.60 and 1.73 in a relative ratio of 3:4, indicating the existence of two isomers. Since rapid isomerization between the two isomers is very unlikely, the complex obtained by the present synthesis will be a mixture of the two isomers. Attempts to separate the isomers by fractional crystallization were unsuccessful. Other methanolato complexes **2b—2d** were assigned to the same structure as **2a**, since the absorption spectra of these complexes are very similar to that of **2a** shown in Fig. 3.

[V^{V}O(sal-L-ala)]$_2$O·CH_2Cl_2: When the brown complex, **2a** was dissolved in wet dichloromethane, the color of the solution changed immediately from reddish brown to dark blue (Fig. 3), from which the dark blue crystals, **3a** were obtained (Scheme 1). Theriot et al.[15] obtained a green complex by a similar reaction and assigned it as a dimeric vanadium(IV) complex with the formula [V^{IV}O(sal-L-ala)(H_2O)]$_2$ on the basis of the data of magnetic susceptibility and molecular weight measurements, the carboxylate oxygen atoms being suggested to bridge the vanadium atoms. However, compound **3a** has the chemical composition of [VO(sal-L-ala)]$_2$O·CH_2Cl_2 and is ESR inactive both in the solid state and in frozen

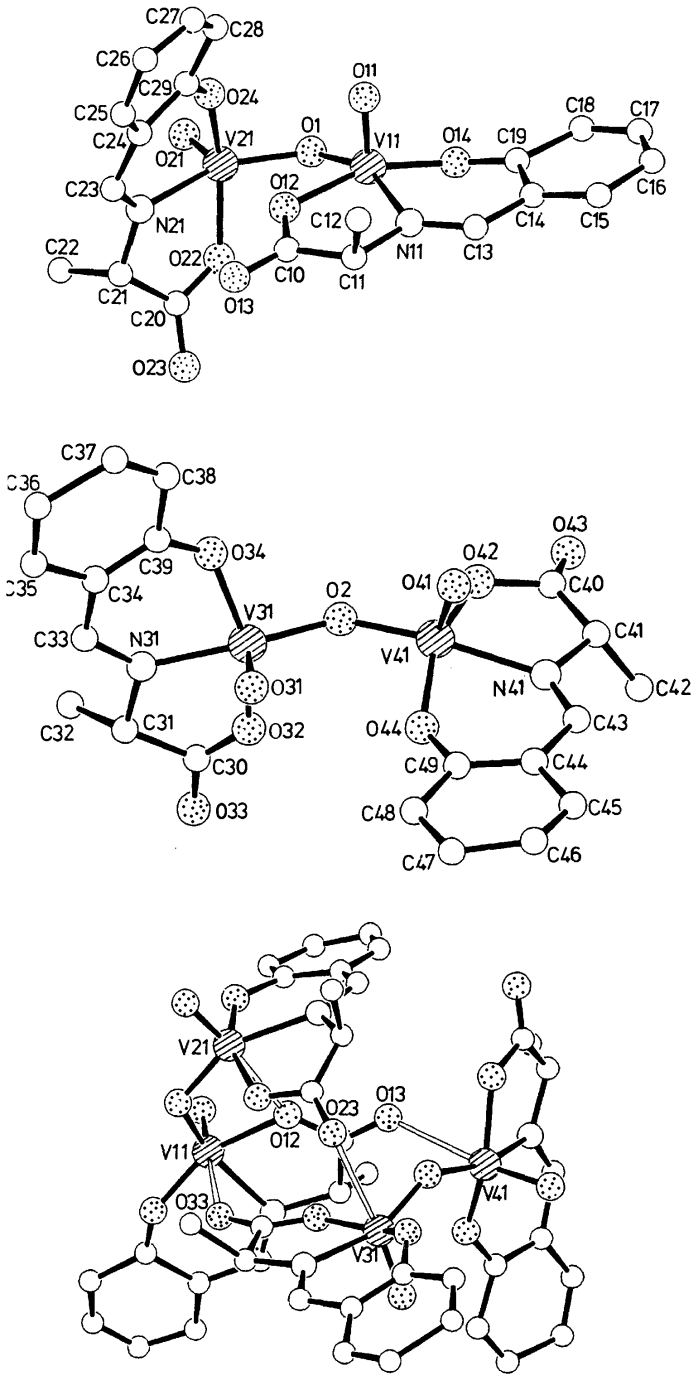

Fig. 4. ORTEP drawings and atom-numbering schemes for **3a-1** (endo form) (a), **3a-2** (exo form) (b), and the tetranuclear unit (**3a**) consisting of **3a-1** and **3a-2** (c). Vanadium and oxygen atoms are shown as shaded and dotted circles, respectively. Open rods indicate weak V–O bonds.

dichloromethane. These facts indicate that the oxidation state of vanadium is +5. The ^{1}H NMR spectrum of **3a** in CD_2Cl_2 exhibits two methyl doublets at δ 1.49 and 1.55 with the same intensity.

The X-ray analysis of **3a** disclosed that two isomeric dimers, **3a-1** and **3a-2** exist in a unit cell together with dichloromethane molecules (Fig. 4). Dimers **3a-1** and **3a-2** are close to each other to form a tetranuclear unit (Fig. 4(c)) and linked by weak bonds between vanadium atoms and carboxylate oxygen atoms of nearby Schiff bases with V–O distances of 2.344(17)—2.562(16) Å (Fig. 4(c)). The geometry around each vanadium atom can be described as a distorted octahedron. The tridentate Schiff base ligand coordinates in the basal plane. The vanadyl O atom occupies an axial site, and the carboxylate O atom of a nearby Schiff base ligand weakly coordinates at the site trans to the oxide ion. The octahedral coordination is completed by sharing an equatorial O^{2-} ligand. The two halves of each dimeric unit have the same geometrical configuration with respect to the disposition of the methyl and V=O groups; **3a-1** consists of two endo isomers while **3a-2** two exo isomers. Each V atom is displaced toward the vanadyl O atom by 0.291—0.363 Å from the equatorial plane. Close contact between O(31) and O(44) in **3a-2** is avoided by the large V(31)–O(2)–V(41) angle (141.4(10)°). In **3a-1**, there is no such close contact around the bridging group, and the V(11)–O(1)–V(21) angle is 116.2(8)°.

The dichloromethane molecules are highly disordered and are continuously distributed along the c-axis in a tunnel structure of the crystal. This structure should be responsible for the loss of solvent of crystallization and also for the large thermal parameters. Thus enough numbers of reflection data were not obtained to determine more accurate structure. An attempt of low temperature measurement was not effective.

Complex **3a** was formed by the treatment of **2a** with wet dichloromethane, but regenerated **2a** on treatment with methanol (Scheme 1). It is to be noted that **3a** is not formed when **2a** is dissolved in anhydrous dichloromethane. Thus the bridging oxygen atom seems to come from water in wet dichloromethane. Brown complex **4a** was obtained by the reaction of **3a** with 1-methyl-1-phenylethyl hydroperoxide in dichloromethane. The complex was unstable both in solution and in the solid state. When *t*-butyl hydroperoxide was used instead of 1-methyl-1-phenylethyl hydroperoxide, a similar color change occurred but the product was not isolated. Figure 3 shows the absorption spectrum of **3a** in the presence of a large excess of *t*-butyl hydroperoxide. Structure determination of **4a** was not achieved because of its instability. Organic peroxide complexes of vanadium(V) with dipic have been prepared and the structure of $[VO(dipic)(OOBu^t)(H_2O)]$ has been determined by the X-ray method.[2] This complex takes a pentagonal bipyramidal structure, the basal positions of which are occupied by two oxygen atoms of the peroxo group, and one nitrogen and two oxygen atoms of the dipic ligand. The peroxide ligand in the complex was

Table 5. Asymmetric Oxidation of Methyl Phenyl Sulfide to the Sulfoxide with *t*-Butyl Hydroperoxide by Complex Catalyst **2** (4°C)[a]

Entry	Complex catalyst	Time/h	Yield/%[b]	e.e./%[c]	Sulfoxide configuration
1	**2a**	8	50	4	*R*
2	**2b**	8	80	11	*R*
3	**2c**	6	78	14	*R*
4	**2d**	5.5	84	9	*R*

a) All reactions were performed as described in detail in Experimental. Molar ratio of complex catalyst: *t*-butyl hydroperoxide: methyl phenyl sulfide=1:10:10. b) Isolated yields, based on the sulfide. c) Based on the optical rotation of the pure enantiomer reported in Ref. 10.

reported to dissociate partially in a $(CD_3)_2CO$ solution by the NMR spectrum. Complex **4a** gives a reddish brown solution when dissolved in dichloromethane, but the color changed to violet brown within a few minutes at room temperature. The ^1H NMR spectrum of **4a** in CD_2Cl_2 shows a singlet methyl signal at δ 1.58 (6H) and multiplet phenyl signals at δ 7.25—7.56 (5H). These signals are identical with those of free 1-methyl-1-phenylethyl hydroperoxide in the same solvent. No signal attributable to the coordinated hydroperoxide was observed in the spectrum. The structure of complex **4a** remains unknown, but the complex seems to contain the peroxide coordinated to the vanadium(V) ion in a similar manner to the above dipic complex, and seems to release the peroxide rapidly on dissolution in dichloromethane. The peroxide complex will be formed only in the presence of a large excess of the peroxide.

The ^1H NMR spectrum of **4a** in CD_2Cl_2 changes within a few days at room temperature. Intensity of the methyl signal due to free 1-methyl-1-phenylethyl hydroperoxide at δ 1.58 becomes weaker and new signals grow gradually at δ 1.55, 2.12, and 2.58, which were assigned to the methyl groups of 2-phenyl-2-propanol, acetone, and acetophenone, respectively. In the absence of complex, such reductive decomposition of the hydroperoxide proceeds much more slowly.

Catalytic Activity of the Complexes. Table 5 shows the results of asymmetric oxidation of methyl phenyl sulfide with *t*-butyl hydroperoxide catalyzed by **2a—2d** in CH_2Cl_2. Dissolving **2** in wet dichloromethane yields a deep blue solution of **3**, and the color of the solution changes immediately to reddish brown on the addition of excess *t*-butyl hydroperoxide to form the peroxo complex **4** (Scheme 1 and Fig. 3). The activated peroxide in **4** will oxidize sulfides. For example, methyl phenyl sulfide is oxidized to the sulfoxide in CH_2Cl_2 with *t*-butyl hydroperoxide almost completely in 20 min at room temperature in the presence of a catalytic amount of **2a**. It was found that $[V^VO(dipic)(OOBu^t)(H_2O)]$ is also an excellent catalyst for the same oxidation in acetonitrile; the oxidation was completed in 10 min at room temperature.[3] On the other hand, the same reaction proceeds very slowly in dichloromethane with the oxovanadium(V) complexes containing tetradentate Schiff bases such as $[V^VO(sal\text{-}(RR)\text{-}chxn)X]$ ($H_2sal\text{-}(RR)$-chxn=(1*R*,2*R*)-*N*,*N*′-disalicylidene-1,2-cyclohexanediamine, X=ClO_4, Cl, NO_3), where the Schiff base occupies the four basal coordination sites.[16] Thus, sulfides seem to be oxidized easily only when the vanadium(V) ion can provide a basal coordination site for an organic peroxide. Since the ligand at the site trans to the vanadyl O atom is known to be replaced rapidly by another ligand, a sulfide (substrate) may coordinate at this apical site and be oxidized to the sulfoxide by the activated peroxide.

Recently, Colonna et al.[17] reported that oxidation of sulfides with *t*-butyl hydroperoxide in the presence of a catalytic amount of an oxovanadium complex containing sal-L-val led to racemic products, the characterization of the complex being not described. When **2** was used as the catalyst, however, (*R*)-methyl phenyl sulfoxide was obtained with an enantiomeric excess (e.e.) of 4—14% (Table 5). The e.e. seems to increase with a decrease in temperature. For example, at −30 °C the e.e. was 8% (*R*) for the same reaction with complex catalyst **2a**.

The present work was partially supported by a Grant-in-Aid for Scientific Research No. 61430013 from the Ministry of Education, Science and Culture.

References

1) K. Nakajima, M. Kojima, and J. Fujita, *Chem. Lett.*, **1986**, 1483.

2) H. Mimoun, P. Chaumette, M. Mignard, and L. Saussine, *Nouv. J. Chim.*, **7**, 467 (1983).

3) K. Nakajima, M. Kojima, and J. Fujita, unpublished results.

4) J. J. R. Frausto da Silva, R. Wootton, and R. D. Gillard, *J. Chem. Soc. A*, **1970**, 3369.

5) L. J. Theriot, G. O. Carlisle, and H. J. Hu, *J. Inorg. Nucl. Chem.*, **31**, 2841 (1969).

6) P. Main, S. E. Hull, L. Lessinger, G. Germain, J.-P. Declerco, and M. M. Woolfson, MULTAN 78 (1978). A System of Computer Programs for the Automatic Solution of Crystal Structures from X-ray Diffraction Data. Univs. of York, England and Louvain, Belgium.

7) International Tables for X-ray Crystallography (1974). Vol. IV. Birmingham: Kynoch Press. (Present Distributor Kluwer Academic Publishers, Dordrecht.)

8) T. Sakurai and K. Kobayashi, *Rikagaku Kenkyusho*

Hokoku, **55**, 69 (1979).

9) P. Coppens, T. N. Guru Row, P. Leung, E. D. Stevens, P. J. Becker, and Y. W. Yang, *Acta Crystallogr., Sect. A*, **35**, 63 (1979).

10) J. Jacobus and K. Mislow, *J. Am. Chem. Soc.*, **89**, 5228 (1967).

11) R. Hamalainen, U. Turpeinen, and M. Ahlgren, *Acta Crystallogr., Sect. C*, **41**, 1726 (1985).

12) K. Saito and Y. Sasaki, *Adv. Inorg. Bioinorg. Chem.*, **1**, 179 (1982).

13) J. A. Bonadies, W. M. Butler, V. L. Pecoraro, and C. J. Carrano, *Inorg. Chem.*, **26**, 1218 (1987).

14) P. E. Reiley, V. L. Pecoraro, C. J. Carrano, J. A. Bonadies, and K. N. Raymond, *Inorg. Chem.*, **25**, 154 (1986).

15) L. J. Theriot, G. O. Carlisle, and H. J. Hu, *J. Inorg. Nucl. Chem.*, **31**, 3303 (1969).

16) K. Nakajima, K. Kojima, M. Kojima, and J. Fujita, Symposium on Coordination Chemistry, 38th, Tokushima, 3AP05 (1988).

17) S. Colonna, A. Manfredi, M. Spadoni, L. Casella, and M. Gullotti, *J. Chem. Soc., Perkin Trans. 1*, **1987**, 71.

18) R. L. Farmer and F. L. Urbach, *Inorg. Chem.*, **9**, 2562 (1970).

19) H. C. Freeman, *Adv. Protein Chem.*, **22**, 257 (1967); C. J. Hawkins, "Absolute Configuration of Metal Complexes," Wiley-Interscience, New York (1971), pp. 94—99.

The Effect of pH and Counter Ion of Oxalate Ion on Photoreduction of Methylviologen

Hideyuki TAGAYA,* Hiroaki SAITO, Susumu SUDA, and Koji CHIBA*
Department of Applied Chemistry, Faculty of Engineering,
Yamagata University, Jonan, Yonezawa 992
(Received May 12,1988)

A higher formation of the methylviologen radical cation was observed at higher pH and when the counter ion of an oxalate ion was large in the continuous photolysis of deaerated solutions of methylviologen (MV^{2+})-oxalate ion ($C_2O_4^{2-}$). A dissociation of oxalic acid to the ion depended upon the pH at pH<7 and the dissociation constant of a MV^{2+}-$C_2O_4^{2-}$ complex depended on the pH at pH>10. The calculated absorbance of the MV^{2+}-$C_2O_4^{2-}$ complex at 350 nm, by using the dissociation constants of oxalic acid and the complex, agreed well with the observed absorbance. It was considered that the pH depedence of the MV^{+} formation resulted from the pH dependence of the concentration of the MV^{2+}-$C_2O_4^{2-}$ complex. The effect of a counter ion on the photoinduced electron transfer was explained in terms of the difference in the stability of the complex ion, in which smaller ions (Li^+, Na^+) tended to form more stable complexes than larger ions (NH_4^+, K^+).

Methylviologen (1,1′-dimethyl-4,4′-bipyridinum ion, MV^{2+}) has received considerable attention in recent years as being an efficient electron relay in the photocatalyzed reduction of water to hydrogen.[1] Therefore, reductions of MV^{2+} by various donors were carried out by many researchers.[2] On the other hand, an oxalate ion ($C_2O_4^{2-}$) has been used as a sacrificial electron donor.[3] The oxidation of the oxalate ion leads to the formation of $C_2O_4^{-}$, which undergoes rapid decomposition to CO_2 and CO_2^{-}. CO_2^{-} is well-known as a strong donor and gives CO_2 by donating an electron. Such a photoinduced irreversible electron transfer of carboxylic acid is known as the photo-Kolbe reaction.[4] In an electron acceptor–oxalate ion system it is expected that an electron-accepted molecule is stable for a long time because a back electron transfer from the electron-accepted molecule to $C_2O_4^{-}$ is minimized. Certainly it was reported that the continuous photolysis of a deaerated solution of MV^{2+}-$C_2O_4^{2-}$ generated MV^{+} which was stable for a long time.[5]

However, the study was carried out in an aqueous solution at neutral pH; no distinct discussion of the effect of the pH was presented. By elucidating the effect of the pH on the reaction, information on a reaction mechanism and most suitable conditions for a photoinduced electron transfer are given. Furthermore, the effect of a counter ion on a photoinduced electron transfer from an oxalate ion was scarcely mentioned. The photoinduced electron transfer from organic anions have been studied in relation to ion-pair phenomena.[6]

We undertook to investigate photoinduced electron transfer from anions.[7] In this work we carried out a continuous photolysis of the MV^{2+}-$C_2O_4^{2-}$ system and clarified the effects of the pH and counter ions of an oxalate ion on the yield of MV^{+} formation.

Experimental

Materials. Methylviologen dichloride (Nakarai) was used as received. $Li_2C_2O_4$, $Na_2C_2O_4$, $K_2C_2O_4$, and $(NH_4)_2C_2O_4$ were used without further purification. Aqueous solutions were prepared from distilled and deionized water and the pH was adjusted by the addition of KOH or NaOH to a $H_2C_2O_4$ solution.

Method. Aqueous solutions of MV^{2+} including oxalate ion were introduced into a 10 cm-long quarz cell jointed to a 2 mm quarz spectrophotometer cell. The concentrations of MV^{2+} and $C_2O_4^{2-}$ determined the concentration of the MV^{2+}-$C_2O_4^{2-}$ complex. In this study oxalate ions (0.1 M; 1 M=1 mol dm^{-3}) were in large excess to MV^{2+} (0.0025 M), in which about 70% of MV^{2+} formed a complex with the oxalate ions. Solutions for irradiation were thoroughly purged with Ar gas before irradiation, since MV^{+} reactions with O_2 to give MV^{2+} was well-known.[8] Irradiation was performed with a 500 W Xe lamp using an IRA-25S filter in which light longer than 300 nm was passed. Absorbance at 605 nm (extinction coefficient=1.37×10^4 M^{-1} cm^{-1})[9] due to the MV^{+} formed was monitored at determined time intervals.

Results and Discussion

The Effect of pH on the Yield of MV^{+}. The pH of MV^{2+}-$H_2C_2O_4$ solutions were adjusted by the addition of KOH (pH; 2.3—12.70); aqueous solutions of MV^{2+}-$H_2C_2O_4$ were irradiated for 5 h. The formation of MV^{+} depended upon the pH, as shown in Fig. 1. The production mechanism of the MV^{+} was complex because two MV^{2+} were reduced by one oxalate ion, despite one MV^{2+} formed complex with one oxalate ion (as described later). To avoid complexity we chose mild reaction conditions in which a small amount of MV^{2+} was reduced. It was expected in such conditions that MV^{2+} would be reduced linearly with the reaction time. However, the production rate of MV^{+} decreased with the reaction time over 2 h (Fig. 1). We must note here that the oxidation of an oxalate ion leads to the formation of two CO_2 which act as acid in an aqueous solution. Since the formation of MV^{+} was slow at low pH, lowering the pH might suppress the formation of MV^{+}. The concentration of CO_2 was calculated from the concentration of MV^{+} on the reaction at pH 7.2 for 5 h irradiation. The proton concentration, calculated

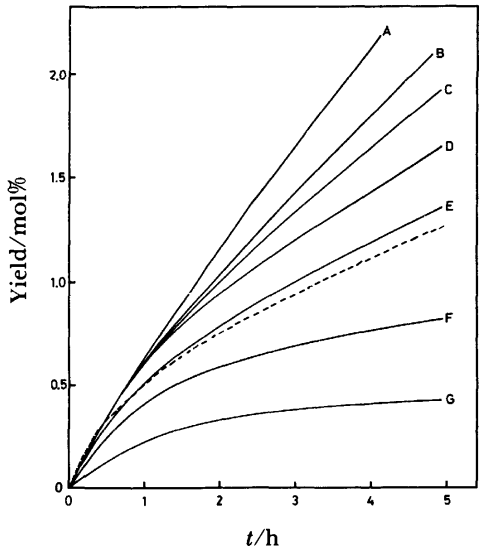

Fig. 1. The effect of pH on the yield of MV^+ in the irradiation of MV^{2+}-$K_2C_2O_4$ solutions. A; pH 12.70, B; 12.18, C; 10.61, D; 7.17, E; 5.60, F; 4.39, G; 3.0. The dotted line is the simulated curve.

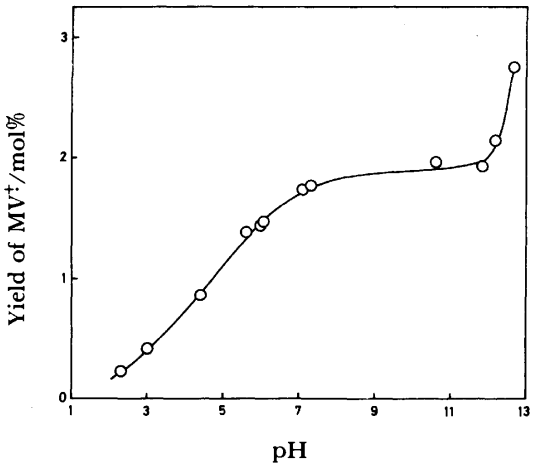

Fig. 2. The effect of pH on the yield of MV^+ in the irradiation of MV^{2+}-$K_2C_2O_4$ solutions for 5 h.

from the concentration of CO_2, reached 3×10^{-6} M, which could reduce the pH of the solution from 7.2 to 5.5 if all of the CO_2 was dissolved into the aqueous solution. The Ostwald solubility coefficient of CO_2 was 0.8280 at 25 °C, larger than 0.0341 of Argon gas.[10] However, The quantity of Argon present in the reaction vessel was larger by a factor of 10^4 than that of CO_2. This meant that a large amount of CO_2 was present as gas, indicating that the contribution of CO_2 to pH reduction was small. Certainly, the decrease of the production rate was observed not only at pH ca. 7, but also at low pH ca. 3, in which the proton concentration was an order of 10^{-3} M and CO_2, which evolved from an oxalate ion, could not change the pH of the solution. The decrease in the production rate with the reaction time could be explained in terms of the accumulation of MV^+. MV^+ possesses a strong absorption peak around 390 nm (extinction coefficient=4.2×10^4 M^{-1} cm^{-1} (1 M=1 mol dm^{-3}))[9] the extinction coefficient at 350 nm was 6000—7000 M^{-1} cm^{-1}. This value was fairly larger than 8.2 M^{-1} cm^{-1} of the MV^{2+}-$C_2O_4^{2-}$ complex at 350 nm (shown later). If the light intensity was reduced by the absorption of MV^+ which did not further react, a photoinduced electron transfer should be simply proportional to the absorption ratio of 8.2 [MV^{2+}-$C_2O_4^{2-}$] and 6500 [MV^+]+8.2 [MV^{2+}-$C_2O_4^{2-}$], in which the extinction coefficient of MV^+ was assumed to be 6500 M^{-1} cm^{-1} and the absorption by uncomplexed MV^{2+} was ignored. The dotted curve in Fig. 1 represents the calculated relationship between the reaction time and the yield of MV^+, considering the change of light intensity with the concentration of MV^+. The decrease in the production rate of MV^+ with the reaction time was well simulated. It was considered that the accumulation of MV^+ might suppress the photoinduced reaction, since MV^+ absorbed the light which was effective for the photoinduced reaction. Namely, MV^+ acted as a filter to reduce the light.

Higher yields of MV^+ were observed at higher pH's, as shown in Fig. 2, along with the yield of MV^+ for 5 h irradiation. An increase of the MV^+ yield at pH 2—5 and at above pH 11 was steep. It had already been reported that MV^{2+} was reduced to MV^+ in an alkaline aqueous solution in the absence of air without irradiation,[8b] and that the rate of MV^+ formation (R_i) obeyed the following rate law: $R_i=k_{obsd}[MV^{2+}]^2[OH^-]^2$: $k_{obsd}=0.12$ M^{-3} min^{-1} at 25 °C. We applied this rate law to our reaction conditions. The production of MV^+ was calculated as 0.02 mol% in the conditions at pH 12.7 for 5 h irradiation. The value was fairly small. We could not deny the possibility of the participation of OH^- in the high-pH region on the MV^{2+} reduction; however, the contribution of the reaction to MV^+ formation must be small.

The Effect of pH on the Absorption of MV^{2+}-Oxalate Solutions. It is well-known that MV^{2+} forms a complex with ionic and neutral species, such as $C_2O_4^{2-}$.[11] The absorption of a MV^{2+}-$C_2O_4^{2-}$ solution at $\lambda>300$ nm is larger than the absorption of MV^{2+} alone, despite the fact that $C_2O_4^{2-}$ possesses little absorption at wavelengths greater than 300 nm. This is because MV^{2+} forms a complex with $C_2O_4^{2-}$ and absorbs light when $\lambda>300$ nm.[5] To form the complex with an oxalate ion is one important ability of MV^{2+} on a photochemical reaction, since the complex has been believed to be a photoactive species.[5] The pH dependence of the absorption at 350 nm is shown in Fig. 3. The small change of the spectra in the pH range 7.0—10.0 is the same as which was reported.[5] However, at each oxalate ion concentration (0.02—0.1 M), the increase of the absorbance at pH 2—5 and at above pH 11 was steep. The pH dependence of absorption at

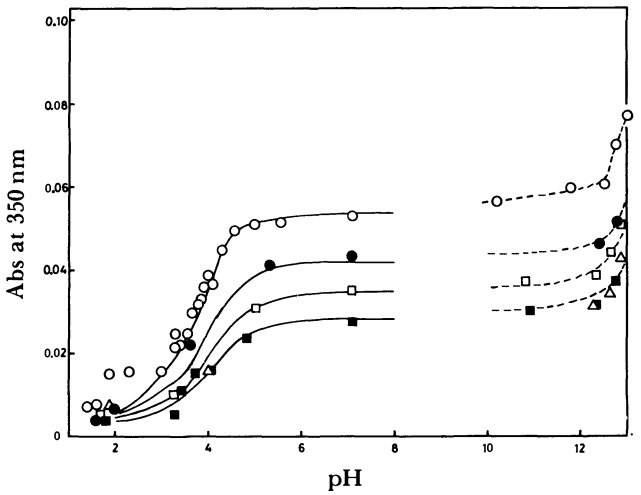

Fig. 3. The absorbance at 350 nm of MV^{2+}-$H_2C_2O_4$ solution whose pH was adjusted by the addition of KOH. Concentration of $H_2C_2O_4$ was 0.1 (○), 0.05 (●), 0.035 (□), 0.025 (■), and 0.02 (△) M and MV^{2+} was 0.01 M. The calculated absorbance by using the concentration of the MV^{2+}-$C_2O_4^{2-}$ complex and its ε_{350} was shown as the solid line.

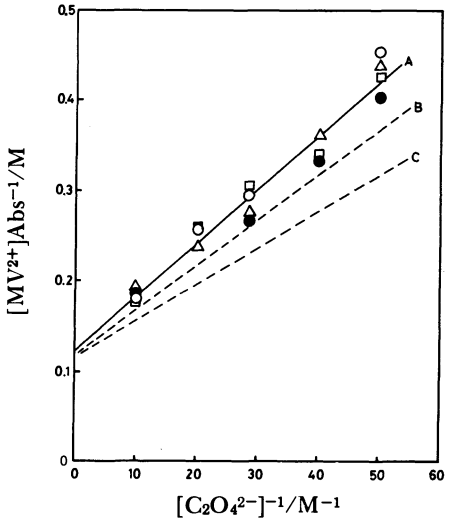

Fig. 4. The Benesi-Hildebrand analysis at 350 nm for the MV^{2+}-Li^+ (○), Na^+ (●), K^+ (△), or NH_4^+ (□) oxalate ion solutions. The pH was 7.1 (A), 12.35 (B), and 12.65 (C).

350 nm was similar with that of the $MV^{+\cdot}$ yield for 5 h irradiation. Since a complex with a 1:1 stoichiometry had already been clarified by a Job's plot,[5,12] the Benesi-Hildebrand analysis for a 1:1 donor-acceptor complex[13] was carried out for the absorbance of MV^{2+}-$M_2C_2O_4$ ($M=Li^+$, Na^+, K^+, or NH_4^+) solutions at 350 nm. Although Fig. 4 shows some scatter, an almost linear relation was observed and the effect of the counter ion on the spectra was small. Little effect of the counter ion on the spectra indicated that $M_2C_2O_4$ was completely dissociated into $C_2O_4^{2-}$ and 2 M^+ (Eq. 1 in the Scheme 1). A Benesi-Hildebrand analysis

$$M_2C_2O_4 \longrightarrow 2M^+ + C_2O_4^{2-} \quad (1)$$

$$C_2O_4^{2-} + H^+ \rightleftharpoons HC_2O_4^- \quad (2)$$

$$HC_2O_4^- + H^+ \rightleftharpoons H_2C_2O_4 \quad (3)$$

$$MV^{2+} + C_2O_4^{2-} \rightleftharpoons [MV^{2+}, C_2O_4^{2-}] \quad (4)$$

$$[MV^{2+}, C_2O_4^{2-}] \xrightarrow{h\nu} [MV^{+\cdot}, C_2O_4^{-}] \quad (5)$$

$$[MV^{+\cdot}, C_2O_4^{-}] \longrightarrow MV^{+\cdot} + C_2O_4^{-} \quad (6)$$

$$[MV^{+\cdot}, C_2O_4^{-}] \longrightarrow [MV^{2+}, C_2O_4^{2-}] \quad (7)$$

$$C_2O_4^{-} \longrightarrow CO_2^{-\cdot} + CO_2 \quad (8)$$

$$MV^{2+} + CO_2^{-\cdot} \longrightarrow MV^{+\cdot} + CO_2 \quad (9)$$

$$MV^{+\cdot} + C_2O_4^{-} \longrightarrow MV^{2+} + C_2O_4^{2-} \quad (10)$$

$$MV^{2+} + Cl^- \longrightarrow MV^{2+}Cl^- \quad (11)$$

$$MV^{2+}Cl^- + Cl^- \rightleftharpoons MV^{2+}(Cl^-)_2 \quad (12)$$

Scheme 1.

yielded K_3=20.4 M^{-1} and ε_{350}=8.2 $M^{-1}\,cm^{-1}$, which were almost identical to the reported values for K^+, 21 M^{-1} and 7.2 $M^{-1}\,cm^{-1}$, respectively.[5] The dissociation equilibrium constants of Eqs. 2 and 3 were reported as being 14500 and 17.5 $M^{-1}\,cm^{-1}$.[14] These values enabled us to calculate the concentration of $C_2O_4^{2-}$ in the reaction solution. The absorbance at 350 nm was calculated from the concentration of $C_2O_4^{2-}$, the values of K_3, ε_{350} of the complex and ε_{350} of uncomplexed MV^{2+} (ca. 0.9 $M^{-1}\,cm^{-1}$). The calculated absorbance (as shown in the solid line in Fig. 3) agreed very well with the observed value. This indicated that MV^{2+} could form the complex with only $C_2O_4^{2-}$ and that K_3 did not change in the pH range 2—8. Above pH 10, oxalate dissociates completely. This means that an increase in the amount of the oxalate ion was not the reason. And another reason was present for the increase in the absorbance at 350 nm and the yield of $MV^{+\cdot}$ with a pH in the high pH range. The Benesi-Hildebrand analysis was further applied for the absorbance at 350 nm in the high pH range as shown in Fig. 4. Here, lines B and C are best fit lines at pHs 12.35 and 12.65, respectively. Higher K_3s 23.3 and 28.5 M^{-1} than that in the lower pH range were obtained. This indicated that the increase of the formation of MV^+ with pH at above pH 10 might have resulted from an increase in the MV^{2+}-$C_2O_4^{2-}$ complex concentration, since the concentration of the MV^{2+}-$C_2O_4^{2-}$ complex increased with K_3.

The Effect of Ionic Strength and a Counter Cation on the Yield of $MV^{+\cdot}$. It was reported that modest concentrations (<0.5 M) of ions had a negligible effect on the yield of $MV^{+\cdot}$.[2c] However, in this study a

Table 1. The Effect of a Counter Ion of Oxalate Ion on the Yield of MV^+ after the Irradiation for 5 h

Counter ion of oxalate ion	pH	The yield of MV^+	Ion radius
		mol%	Å
Li^+	6.09	1.07	0.60
Na^+	6.00	1.22	0.95
Na^+	6.11	1.22	0.95
K^+	6.00	1.43	1.33
K^+	6.06	1.46	1.33
NH_4^+	6.49	1.71	1.43

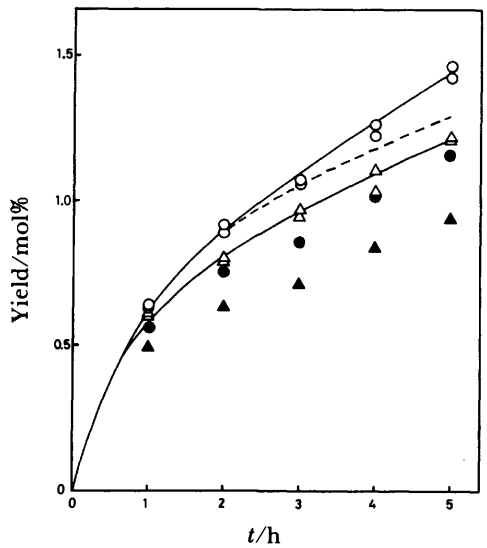

Fig. 5. The yields of MV^+ in the irradiation of the MV^{2+}–oxalate solutions. The pH was adjusted by using KOH (○, ●) or NaOH (△, ▲) with KCl (●, ▲) or without KCl (○, △). The dotted line was the results in which pH was adjusted by using the 1 : 1 mixture of NaOH and KOH solutions.

detrimental effect of an ionic strength on the yield MV^+ was observed, even at low ionic strength, upon the addition of KCl. The ion strength increased from 0.1 to 0.3, as shown in Fig. 5. The dissociation equilibrium constant of Eq. 12 in the scheme had been estimated from conductance measurements as being 0.1 M.[2b,15] The dissociation equilibrium constant of Eq. 11 was not reported; however, it was reported that the value was fairly larger than that of Eq. 12. If MV^{2+} existed as $MV^{2+}Cl^-$ initially, 3.4% of $MV^{2+}Cl^-$ could associate with Cl^- since initial concentration of MV^{2+} of our conditions was 0.0025 M. However, addition of KCl (0.2 M) increased the concentration of dichloride complex as large as 66.8%. The detrimental effect of anionic species, such as Cl^- on the yield of MV^+ might have resulted from the complex formation of MV^{2+} with Cl^-, which reduced the concentration of the photo active MV^{2+}–$C_2O_4^{2-}$ complex.

The yields of MV^+ in the solutions in which pH was adjusted by KOH were larger than that in the solutions in which pH was adjusted by NaOH as shown in Fig. 5. The yield of MV^+, in which a mixture of the KOH and NaOH solution was used as a pH moderator, was between them. MV^{2+}–$C_2O_4^{2-}$ solutions with other counter ions, Li^+ and NH_4^+ were also irradiated. The yield of MV^+ for 5 h irradiation increased with the ion radius of the counter ion (Table 1).

The effect of cationic species on photoinduced and electroinduced electron transfer from anions had been already discussed from the standpoint of a contact and loose ion pair.[6] For example, the rate constant of electron transfer from free biphenylide radical ions (B^-) to pyrene was $4.8\times10^{10}\ M^{-1}\ s^{-1}$; however, the rate constant from sodium biphenylide radical ions (B^-, Na^+) was $0.6\times10^{10}\ M^{-1}\ s^{-1}$.[6a] We have already reported that in electron transfer from the 9*H*-thioxanthene-9-one 10,10-dioxide (TO-SO_2) radical anion to diaryl disulfides, the order of the rate constant of electron transfer is as follows.[7a] $(TO\text{-}SO_2)^-$ is free radical anion.

$$(TO\text{-}SO_2)^- > (TO\text{-}SO_2)^-, K^+ > (TO\text{-}SO_2)^-, Na^+.$$

Smaller ions tended to form more stabilized ion pairs (contact ion pairs) since their charge densities were larger than those of larger ions. It was considered that a contact ion pair stabilized ion species and electron transfer from a cation contacted anion became slow compared to that from a solvent-separated ion or free ion. In the contact ion pair system, the ion contact was known to cause a blue shift in the absorption maximum;[16] however, we could not clarify the shift from the absorption of the MV^{2+}–$C_2O_4^{2-}$ complex since the absorption of uncomplexed MV^{2+} overlapped with that of the complex. The effect of a solvent-separated ion pair on a photoinduced electron transfer from a donor to MV^{2+} was reported by Mandell and Hoffman in the photo reduction of MV^{2+} using EDTA as the donor.[2c] They reported that EDTA formed ion pairs not only with MV^{2+} but also with $[Ru(bpy)_3]^{2+}$ and that electron transfer proceeded more easily than under conditions in which SO_4^{2-} was used instead of EDTA because SO_4^{2-} could not form any ion pairs.

$$[Ru(bpy)_3^{2+}\cdots EDTA\cdots MV^{2+}] \rightarrow$$

$$[Ru(bpy)_3^{3+}\cdots EDTA\cdots MV^{+}] \rightarrow [Ru(bpy)_3^{2+}\cdots EDTA_{ox}\cdots MV^{+}]$$

It was also reported that at high concentrations of MV^{2+} (>1 mM), MV^{2+} existed as an aggregate surrounded by $C_2O_4^{2-}$. In such aggregates, a participation of counter cation (M^+) with a MV^{2+}–$C_2O_4^{2-}$ aggregate was probable, although the spectroscopic effect of M^+ on the absorbance at 350 nm was not observed, as shown in Fig. 4. A possible sketch of the aggregate (dimer) of MV^{2+}–$C_2O_4^{2-}$ and participation of M^+ with the aggregate is as follows.

$$M^+$$
$$[C_2O_4^{2-}, MV^{2+}, C_2O_4^{2-}, MV^{2+}]$$
$$M^+$$

It was considered that smaller ions (Li^+, Na^+) tended to form more stable complexes with the MV^{2+}–$C_2O_4^{2-}$ aggregate than larger ions (K^+, NH_4^+) if the participation of M^+ with the aggregate occurred. It was also considered that a photoinduced electron transfer from the oxalate ion to MV^{2+} was more likely to occur in less stabilized complexes, such as the NH_4^+ or K^+ oxalate–MV^{2+} complex, than in a stabilized complex by the small ions, such as Li^+ or Na^+.

References

1) a) A. Harriman and A. Mills, *J. Chem. Soc., Faraday Trans. 2*, **77**, 2111 (1981). b) K. Kalyanasundaram, J. Kiwi, and M. Grätzel, *Helv. Chim. Acta*, **61**, 2720 (1978). c) E. Amouyal and B. Zilder, *Isr. J. Chem.*, **22**, 117 (1982). d) P. Brugger, P. Cuendet, and M. Grätzel, *J. Am. Chem. Soc.*, **103**, 2923 (1981). e) J. Kiwi and M. Grätzel, *J. Am. Chem. Soc.*, **101**, 7214 (1979). f) E. Borgarello, J. Kiwi, E. Pelizzetti, M. Visea, and M. Grätzel, *J. Am. Chem. Soc.*, **103**, 6324 (1981). g) A. Harriman, G. Porter, and M. Richoux, *J. Chem. Soc., Faraday Trans. 2*, **77**, 1175 (1981).

2) a) M. Z, Hoffman, D. R. Prasad, G. Jones II, and V. Malba, *J. Am. Chem. Soc.*, **105**, 6360 (1983). b) J. R. Barnett, A. S. Hopkins, and A. Ledwith, *J. Chem. Soc., Perkin Trans. 2*, **1973**, 80. c) K. Mandal and M. Z. Hoffman, *J. Phys. Chem.*, **88**, 185 (1984). d) *Idem, ibid.*, **88**, 5632 (1984). e) Y. Nishimura, H. Misawa, H. Sakuragi, and K. Tokumaru, Annual Symposium on Photochemistry, Sendai, August 1987, Abstr., No. B130. f) L. A. A. Oliveria and A. Hain, *J. Am. Chem. Soc.*, **104**, 3363 (1982). g) Q. G. Mulazzani, M. Verturi, and M. Z. Hoffman, *J. Phys. Chem.*, **89**, 722 (1985). h) N. Kitamura, Y. Kawanishi, and S. Tazuke, *Chem. Lett.*, **1983**, 1185.

3) a) M. Bliese, A. Launikonis, J. W. Loder, A. W. H. Man, and W. H. F. Sasse, *Aust. J. Chem.*, **36**, 1873 (1983). b) M. Chang, T. Saji, and A. J. Bard, *J. Am. Chem. Soc.*, **99**, 5399 (1977). c) I. Rubinstein and A. J. Bard, *ibid.*, **103**, 512 (1981).

4) a) B. Kraeuther and A. J. Bard, *J. Am. Chem. Soc.*, **100**, 2239 (1978). b) *Idem, ibid.*, **100**, 5985 (1978). c) *Idem, ibid.*, **99**, 7729 (1977). d) G. A. Epling and A. Lopes, *ibid.*, **99**, 2700 (1977). e) T. O. Meiggs, L. I. Grossmeiner, and S. I. Miller, *ibid.*, **94**, 7981 (1972). f) B. Kraeuther, C. D. Jaeger, and A. J. Brad, *ibid.*, **100**, 4903 (1978). g) H. Reiche, W. W. Dunn, and A. J. Bard, *J. Phys. Chem.*, **83**, 2248 (1979).

5) D. R. Prasad, M. Z. Hoffman, Q. R. Mulazzani, and M. A. J. Rodgers, *J. Am. Chem. Soc.*, **108**, 5135 (1986).

6) a) G. Rämme, M. Fisher, S. Claesson, and M. Szwarc, *Proc. R. Soc. London, Ser. A.*, **327**, 467 (1972). b) M. K. Kalinowski, *Chem. Phys. Lett.*, **7**, 55 (1970). c) A. Rains and M. Szwarc, *J. Am. Chem. Soc.*, **96**, 3008 (1974). d) B. Bockrath and L. M. Dorfman, *J. Phys. Chem.*, **77**, 2618 (1973).

7) a) H. Tagaya, T. Aruga, O, Ito, and M. Matsuda, *J. Am. Chem. Soc.*, **103**, 5484 (1981). b) H. Tagaya, T. Aruga, O. Ito, and M. Matsuda, ACS/CSJ Chemical Congress, Hawaii, April 1979, ORGN 219.

8) a) M. Verturi, Q. G. Mulazzani, and M. Z. Hoffman, *J. Phys. Chem.*, **88**, 912 (1984). b) V. Novakovic and M. Z. Hoffman, *J. Am. Chem. Soc.*, **109**, 2341 (1987).

9) T. Watanabe and K. Honda, *J. Phys. Chem.*, **86**, 2617 (1982).

10) R. Battino, *Chem. Rev.*, **66**, 395 (1966).

11) G. Jones II and M. B. Zisk, *J. Org. Chem.*, **51**, 947 (1986).

12) M. Onuki, H. Saito, S. Suda, H. Tagaya, and K. Chiba, Tohoku Regional Meeting of Chemical Society of Japan, Iwaki, October 1987, Abstr., No. 2P108.

13) H. A. Benesi and J. H. Hildebrand, *J. Am. Chem. Soc.*, **71**, 2703 (1949).

14) H. M. Dawson, C. R. Hoskins, and J. E. Smith, *J. Chem. Soc.*, **1929**, 1884.

15) T. W. Ebbesen, L. E. Manring, and K. S. Peters, *J. Am. Chem. Soc.*, **106**, 7400 (1984).

16) M. A. Fox, *Chem. Rev.*, **79** 253 (1979).

 © 1989 The Chemical Society of Japan Bull. Chem. Soc. Jpn., 62, 773—779 (1989)

Individuality of Amino Acid Residues in Protected Peptides.[1] Conformational and β-Sheet Structure-Disrupted Behaviors of Resin-Bound Peptides

Mitsuaki NARITA,* Shizuko ISOKAWA, Shinya HONDA, Hiroshi UMEYAMA, Hideaki KAKEI, and Satoshi OBANA

Department of Industrial Chemistry, Faculty of Technology, Tokyo University of Agriculture and Technology, Koganei 184

(Received July 18, 1988)

The conformational behavior of cross-linked polystyrene resin-bound peptides swollen in CH_2Cl_2 was analyzed using IR absorption spectroscopy. All of the resin-bound peptides easily aggregated with each other through intermolecular hydrogen bonding to form a β-sheet structure. The disruption of the β-sheet structure was further investigated by a solvent titration method in order to clarify the individuality of amino acid residues. At a pentapeptide level, the β-sheet structure was easily disrupted by the addition of a small amount of HFIP. On the other hand, at a larger peptide level, the disrupted behavior of the β-sheet structure was different from each other according to the amino acid composition. Based on the view that the secondary structure of globular proteins reflects the individuality of the 20 kinds of amino acid residues in proteins, we attempted to evaluate how easily the β-sheet structure of peptides is disrupted by HFIP using the average conformation values: $\langle P_\alpha \rangle$, $\langle P_\beta \rangle$, and $\langle P_c \rangle$. As a result, the β-sheet structure-disruption of peptides having a low potential for a β-sheet→helix transformation as well as for the randomness was difficult by adding increasing amounts of HFIP. On the other hand, that of the peptides having a $\langle P_c \rangle$ value larger than 0.85 and/or a high potential for the β-sheet→helix transformation proceeded smoothly upon adding increasing amounts of HFIP.

The 20 kinds of amino acid residues in proteins must reflect their individuality to form native three-dimensional structures of proteins. In order to predict the secondary structure of native globular proteins, Chou and Fasman determined the conformational parameters (P_α, P_β, and P_c) for the 20 kinds of amino acid residues on the basis of the three-dimensional structures of 15 kinds of proteins which were resolved by X-ray crystallography.[2] Thus, we have the view that parameters P_α, P_β, and P_c reflect the individuality of the 20 kinds of amino acid residues in proteins. In fact, in previous studies[3-6] we successfully applied the coil conformational parameters P_c to solubility predictions for protected peptides. The solubility-prediction method is based on the assumption that the larger P_c values of hydrophilic amino acid residues than those of hydrophobic ones reflect the tendency that the polar side-chain groups interact with their neighboring peptide bonds through hydrogen bonds, resulting in a disruption of helix and β-sheet structures.

In the solubility prediction, we also showed the usefulness of the average coil conformation value, $\langle P_c \rangle$, for estimating the potential of protected peptides for a β-sheet formation.[4,7,8] Furthermore, in a conformational transformation of protected peptides with an application of strong shear stress or with an increasing peptide chain length, we showed the usefulness of their average helix and β-sheet conformation values, $\langle P_\alpha \rangle$ and $\langle P_\beta \rangle$, for estimating their potential for the β-sheet→helix transformation.[8-10]

On the other hand, we found that the β-sheet structure of Boc–Val–Gly–Phe–Gly–Leu–Ile–Leu_2–OBzl in CH_2Cl_2 solution is easily disrupted by the addition of HFIP, a strong electron-acceptor solvent.[11]

In this paper, we demonstrate the usefulness of the $\langle P_\alpha \rangle$, $\langle P_\beta \rangle$, and $\langle P_c \rangle$ values for estimating the conformation of resin-bound peptides and the stability of their β-sheet structure, and discuss the individuality of amino acid residues included in protected peptides. The resin-bound peptides used in this study are shown in Fig. 1.

Boc-ValAlaValAla-Gly-OCH_2-Pam-resin A_1
Boc-(ValAlaValAla)$_2$-Ile-OCH_2-Pam-resin A_2
Boc-(ValAlaValAla)$_3$-Ile-OCH_2-Pam-resin A_3
Boc-ValIleValIle-Gly-OCH_2-Pam-resin B_1
Boc-(ValIleValIle)$_2$-Gly-OCH_2-Pam-resin B_2
Boc-(ValIleValIle)$_3$-Gly-OCH_2-Pam-resin B_3
Boc-ValGlyPheGlyLeuIleLeuLeu-Ala-OCH_2-Pam-resin C_1
Boc-(ValGlyPheGlyLeuIleLeuLeu)$_2$-Ala-OCH_2-Pam-resin C_2
Boc-(ValGlyPheGlyLeuIleLeuLeu)$_3$-Ala-OCH_2-Pam-resin C_3
Boc-GlnValGlu(OBzl)LeuGly-$NHCH_2$-resin D_1
Boc-GlnValGlyGlnValGlu(OBzl)LeuGly-$NHCH_2$-resin D_2
Boc-Glu(OBzl)AlaGlu(OBzl)Asp(OBzl)LeuGlnValGlyGlnValGlu(OBzl)LeuGly-$NHCH_2$-resin D_3

Fig. 1. The resin-bound peptides used in this study.

Table 1. Solid-Phase Peptide Synthesis Cycle for the Addition of One Oligopeptide[a]

Function	Solvent and/or reagent (amount)	Time/min	Number of application
1. Swelling	NMP[b] (30 ml)	10	1
2. Peptide	Tetra- or octapeptide (3.0 or 2.0 equiv) HOBt (3.0 or 2.0 equiv)	30	1
3. Coupling	DCC (3.0 or 2.0 equiv) in NMP[b] (5 ml)	3 days	1
4. Washing[c]	NMP, EtOH and CH_2Cl_2	5	3
5. Termination	Pyridine–acetic anhydride (Vol. ratio 1:1, 30 ml)	2 h	1
6. Washing[c]	CH_2Cl_2, EtOH, and CH_2Cl_2	5	3
7. Deprotection	TFA/CH_2Cl_2 (Vol. ratio 2:3, 30 ml)	2 h	1
8. Washing[c]	CH_2Cl_2, EtOH, and NMP	5	3
9. Neutralization	TEA (20 equiv) in NMP (20 ml)	10	2
10. Washing[c]	NMP, EtOH, CH_2Cl_2	5	3
11. Drying			

a) The resins used were 2.0 g, respectively. b) For assembly of the octapeptide (resin-bound peptides C_1—C_3), a mixture of NMP and CH_2Cl_2 (1:1, v/v) was used. c) Washing was carried out using each solvent.

Table 2. The Peptide Contents and Graft Ratios of the Resin-Bound Peptides

Resin-bound peptide	Peptide content[a]	Graft ratio[b]
A_1	133	1.4
A_2	89	1.0
A_3	66	0.77
B_1	116	1.3
B_2	50	0.58
B_3	34	0.40
C_1	83	0.95
C_2	56	0.68
C_3	48	0.61
D_1	106	1.2
D_2	97	1.1
D_3	79	1.0

a) $\mu mol\ g^{-1}$ of resin. The content does not include the terminated peptides. b) The ratio of grafted peptide to 100 styrene unit.

Experimental

Materials. Copoly(styrene/1% divinylbenzene) beads of 200—400 mesh, Bio-beads S-X1, were purchased from Bio-Rad Laboratories and used as polymer supports. Resin-bound peptides D_1, D_2, and D_3 were prepared before.[9] Other resin-bound peptides were prepared virtually using the cycle summarized in Table 1. The acid hydrolyses of resin-bound peptides A_1, A_2, A_3, B_1, B_2, and B_3 were carried out with propionic acid/12 M HCl (2:1, v/v; 1 M=1 mol dm^{-3})[12] for 10 days at 115 °C in evacuated and sealed tubes; those of resin-bound peptides C_1, C_2, and C_3, were carried out for 2 days at 115 °C. The amino acid composition of acid hydrolysates was determined using a Shimadzu HPLC LC-3A all amino acid analysis system. The peptide contents and graft ratios of the resin-bound peptides are shown in Table 2.

IR Measurements. The IR absorption spectra of resin-bound peptides were recorded at room temperature with a JEOL Model JIR-100 FT-IR spectrometer. IR measurements in the swollen state were performed by holding the samples between potassium bromide windows after resin-bound peptides were swollen overnight in CH_2Cl_2 or a mixture of HFIP and CH_2Cl_2.

Results

The Conformation of the Resin-Bound Peptides Swollen in CH_2Cl_2. The IR absorption spectra of the resin-bound peptides, except for D_1, D_2, and D_3, swollen in CH_2Cl_2 are presented in Figs. 2 and 3. They show significant spectral regions for conformational assignments (3500—3200 cm^{-1}, amide A; 1750—1600 cm^{-1}, amide I). All of the resin-bound peptides show strong bands around 3280 cm^{-1} in the amide A region and around 1630 cm^{-1} in the amide I region, assigned to a β-sheet structure.[10,13] This result is essentially the same as that of resin-bound peptides D_1, D_2, and D_3. Since the initial peptide contents of the resin-bound peptides were selected in order to obtain rational information for peptide chain interactions in solid-phase peptide synthesis, these results indicate that hydrogen bonding between pendant peptide chains do commonly occur in solid-phase peptide synthesis, as reported before.[9,10]

The Disruption of the β-Sheet Structure of the Resin-Bound Peptides by HFIP. The disruption of the β-sheet structure by HFIP was investigated using a solvent titration method.[14] It was monitored by a successive decrease in the intensity of the band around 1630 cm^{-1}, together with a successive addition of HFIP. Figure 4 shows the typical IR absorption spectra of resin-bound peptides A_1, A_3, B_1, and B_3 in a mixture of HFIP and CH_2Cl_2. Figures 5 and 6 illustrate the solvent-titration curves of resin-bound peptides A_1—A_3 and B_1—B_3, respectively, in CH_2Cl_2 using HFIP as a titrating solvent. The relative intensities shown in Figs. 5 and 6 as well as Figs. 7 and 8 were obtained using the band at 1603 cm^{-1} due to the aromatic ring of the resin support as a standard and were normalized to be 1.0 for each relative intensity in the absence of HFIP. In the case of resin-bound peptides A_1—A_3 and B_1, a successive addition of HFIP to CH_2Cl_2 induces a dramatic decrease in the strong band around 1630 cm^{-1} and an increase in the broad

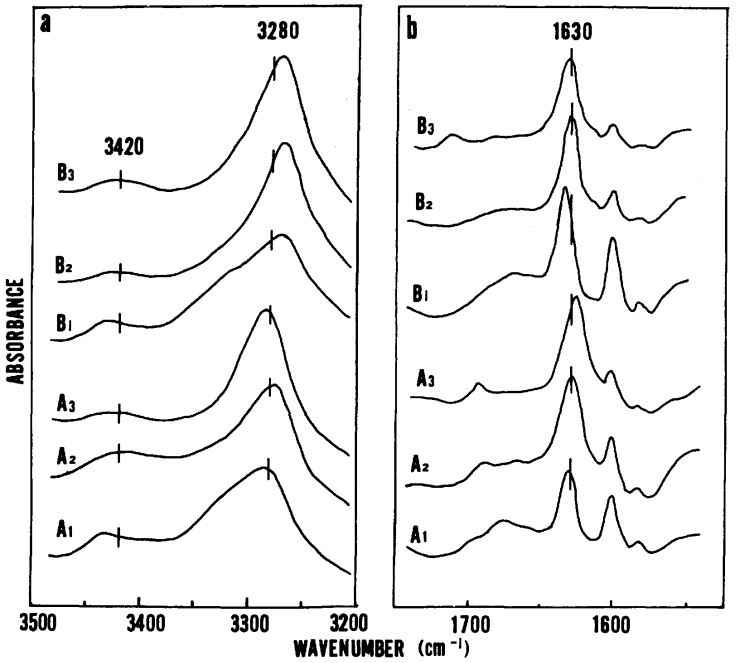

Fig. 2. IR absorption spectra (a) in the amide A and (b) in the amide I regions of the resin-bound peptides A_1—A_3 and B_1—B_3 swollen in CH_2Cl_2. The absorption band at 1603 cm^{-1} is due to aromatic rings of the polystyrene supports.

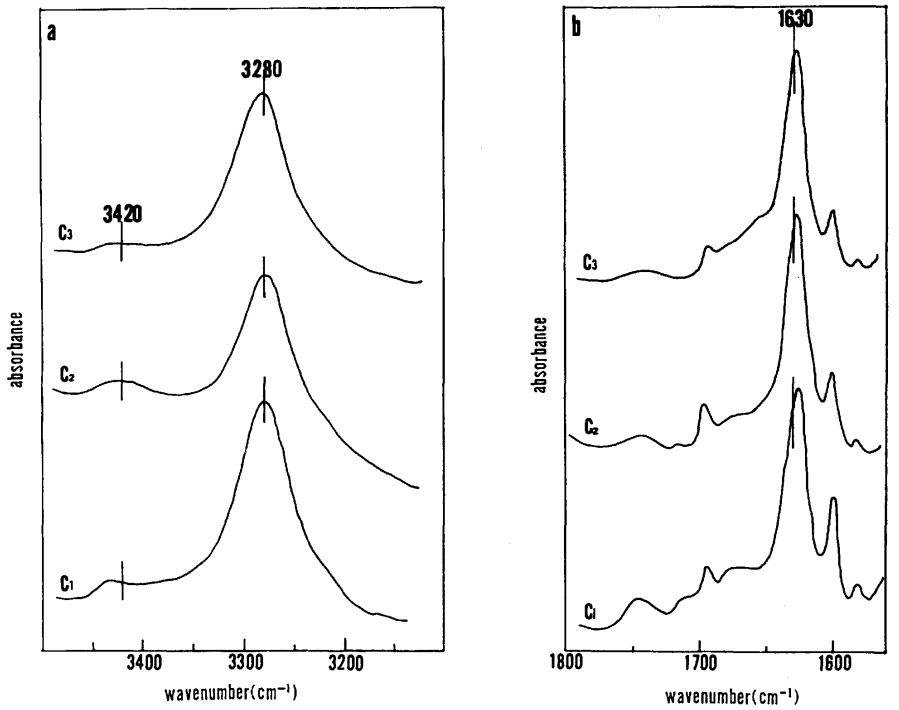

Fig. 3. IR absorption spectra (a) in the amide A and (b) in the amide I regions of the resin-bound peptides C_1—C_3 swollen in CH_2Cl_2.

band around 1655 cm^{-1}, indicating that the β-sheet aggregation of resin-bound peptides A_1—A_3 and B_1 is easily disrupted by increasing the amounts of HFIP. On the other hand, in the case of resin-bound peptides B_2 and B_3, the amide I carbonyl stretching band at 1632 cm^{-1} only shifts at 1637 cm^{-1} with broadening

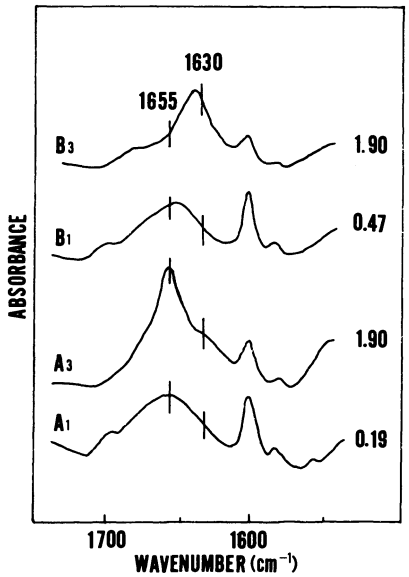

Fig. 4. Typical IR absorption spectra in the amide I region of the resin-bound peptides A_1, A_3, B_1, and B_3 swollen in HFIP–CH_2Cl_2. The numerals in Fig. 4 indicate concentrations of HFIP (M).

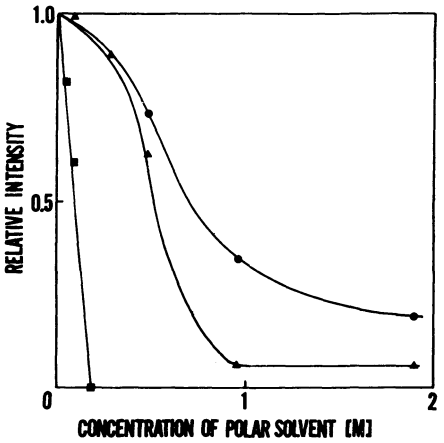

Fig. 5. The solvent-titration curves of the peptides A_1—A_3 in CH_2Cl_2 using HFIP as a titrating solvent. The peptide A_1, —■—; the peptide A_2, —▲—; the peptide A_3, —●—.

and a slight decrease in the intensity. This result strongly suggests that the β-sheet structure of the sequence of $(Val\text{-}Ile\text{-}Val\text{-}Ile)_n$ (n=2 and 3) is stable even in the presence of HFIP, although it is not clear why the band at 1632 cm^{-1} shifts at 1637 cm^{-1}. Figures 7 and 8 also present the solvent-titration curves of resin-bound peptides C_1—C_3 and D_1—D_3, respectively, in CH_2Cl_2 using HFIP as a titrating solvent. The result indicates that, regardless of an increasing peptide chain length, the β-sheet aggregation of resin-bound peptides C_1—C_3 and D_1—D_3 is easily disrupted by increasing the amounts of HFIP.

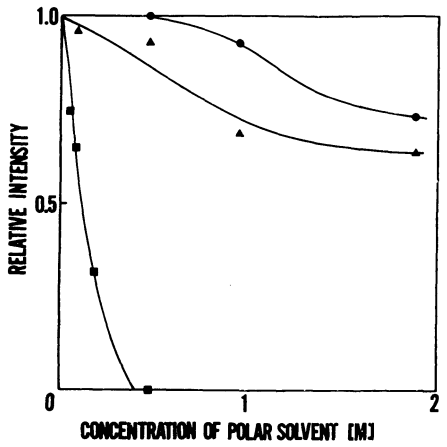

Fig. 6. The solvent-titration curves of the peptides B_1—B_3 in CH_2Cl_2 using HFIP as a titrating solvent. The peptide B_1, —■—; the peptide B_2, —▲—; the peptide B_3, —●—.

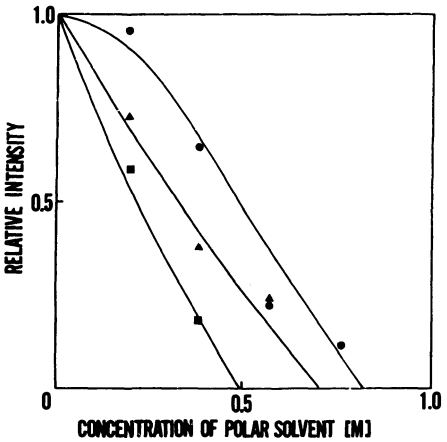

Fig. 7. The solvent-titration curves of the peptides C_1—C_3 in CH_2Cl_2 using HFIP as a titrating solvent. The peptide C_1, —■—; the peptide C_2, —▲—; the peptide C_3, —●—.

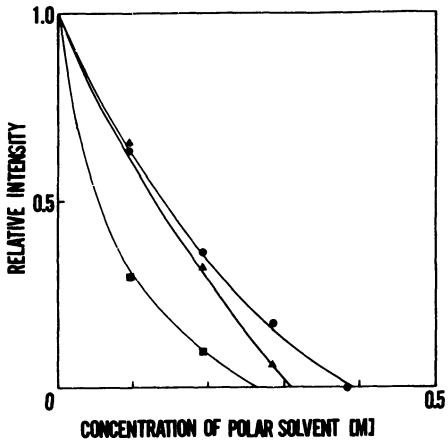

Fig. 8. The solvent-titration curves of the peptides D_1—D_3 in CH_2Cl_2 using HFIP as a titrating solvent. The peptide D_1, —■—; the peptide D_2, —▲—; the peptide D_3, —●—.

Discussion

The conformational behaviors of protected peptides must reflect the individuality of amino acid residues included in the peptides. We have the view that the conformational parameters, P_α, P_β, and P_c, for amino acid residues determined by Chou and Fasman[2] reflect the individuality of the 20 kinds of amino acid residues in proteins because the prediction method for the secondary structure of globular proteins using their $<P_\alpha>$ and $<P_\beta>$ values, proposed by Chou and Fasman,[15] is based on the three-dimensional structures of 15 kinds of proteins which are determined by X-ray crystallography.

In fact, the individuality of each amino acid residue reflected in the P_α, P_β, and P_c values is as follows. (1) The P_β values of the C^β-branched amino acid residues, that is, 1.60 of Ile, 1.20 of Thr, and 1.65 of Val are significantly larger than their P_α values, 1.00 of Ile, 0.82 of Thr, and 1.14 of Val, respectively. These values reflect the fact that the C^β-branched amino acid residues resist being included in a helical structure. (2) The values of P_α (0.53) and P_β (0.81) of the Gly residue are low and the P_c (1.50) value is extremely high. These values have been explained by the great freedom of the backbone dihedral angles, ϕ and ψ, of the Gly residue.[16] (3) The values of P_α (0.59) and P_β (0.62) of the Pro residue are low and P_c (1.59) is extremely high. These values clearly reflect the absence of an N–H bond of the Pro residue in the peptide bond.[17] (4) The P_c values of the hydrophilic amino acid residues (Arg, 1.04; Asn, 1.35; Asp, 1.20; Cys, 1.18; Gln, 0.86; Glu, 0.83; His, 1.06; Lys, 0.98; Ser, 1.32; Thr, 1.07; Tyr, 1.06) are larger than those of hydrophobic amino acid residues, except for the Pro residue, (Ala, 0.70; Ile, 0.66; Leu, 0.68; Met, 0.58; Phe, 0.71; Trp, 0.75; Val, 0.62) since the polar side-chain groups have a tendency to form hydrogen bonds with their neighboring peptide bonds, resulting in a disruption of the helical and β-sheet structures. (5) The P_c values of the hydrophilic amino acid residues having polar groups at their C^β atoms (Asn, 1.35; Asp, 1.20; Cys, 1.18; Ser, 1.32; Thr, 1.07) are larger than those of the other hydrophilic amino acid residues (Arg, 1.04; Gln, 0.86; Glu, 0.83; His, 1.06; Lys, 0.98; Tyr, 1.06). These values probably reflect the tendency that the former interacts more easily with the neighboring peptide bonds than the latter. (6) In the P_c values of the hydrophilic amino acid residues having polar groups at their C^β atoms, the P_c value of the Thr residue is the lowest due to the low freedom of the hydroxyl group. With respect to the P_c parameters for the 20 kinds of amino acid residues, our P_c parameters[3] used in this study are different from those obtained by Chou and Fasman.[2] Chou and Fasman determined them on the basis of data concerning 15 kinds of globular proteins, while we determined them on the basis of data concerning 29 kinds of globular proteins.

Table 3. The Average Conformation Values, $<P_\alpha>$, $<P_\beta>$, and $<P_c>$, of the Resin-Bound Peptides

Resin-bound peptide	$<P_\alpha>$	$<P_\beta>$	$<P_c>$
A_1—A_3	1.30	1.31	0.66
B_1—B_3	1.07	1.63	0.64
C_1—C_3	1.04	1.23	0.88
D_1	1.14	1.03	0.90
D_2	1.07	1.11	0.93
D_3	1.18	0.95	0.90

The $<P_\alpha>$, $<P_\beta>$, and $<P_c>$ values of the peptides A_1—A_3, B_1—B_3, and C_1—C_3 do not include their C-terminal amino acid residues.

Thus, the $<P_\alpha>$ and $<P_\beta>$ values of protected peptides must reflect their potential for helix and β-sheet formations, respectively, as much as their $<P_c>$ values reflect their potential for randomness. In Table 3, the average conformation $<P_\alpha>$, $<P_\beta>$, and $<P_c>$ values of the resin-bound peptides are summarized. The values of $<P_\alpha>$, $<P_\beta>$, and $<P_c>$ are necessarily determined, regardless of the amino acid sequence of the peptides.[15] They are only dependent on their amino acid composition.

With respect to the conformational behavior of resin-bound peptides, the fact that the resin-bound heptadecapeptide C_2 and pentacosapeptide C_3 swollen in CH_2Cl_2 have a β-sheet structure is quite different from that of H-Leu_n-Phe-resins (n=15 and 20), showing a helical structure in the swollen state in CH_2Cl_2.[10] Regardless of the increase in the peptide chain length, the amino acid sequence of peptides C_2 and C_3 has a high potential for a β-sheet formation, though a low potential for a helix formation, corresponding to the fact that their $<P_\alpha>$ and $<P_\beta>$ values are 1.04 and 1.23, respectively. In a conformational study of human hemoglobin α-chain fragments in the solid state,[8] we have shown that the potential of protected peptides for the β-sheet→helix transformation is clearly estimated using their $<P_\alpha>$ and $<P_\beta>$ values when the β-sheet→helix transformation occurs in the solid state under the application of shear stress. The conformational behavior of the resin-bound peptides C_1—C_3 indicates that the retention of the high potential for a β-sheet formation, regardless of an increase in the peptide chain length, can also be estimated using their $<P_\alpha>$ and $<P_\beta>$ values. Nevertheless, we should continuously make efforts to determine key sequences which dominate the peptide conformations, since the conformation of peptides is estimated to be essentially dependent on the key sequence. Concerning the sequence of peptides A_2 and A_3, its helical structure may be unstable due to repulsion between C^β-branched Ile and Val residues in the sequence of -Ile-Leu-Leu-Val-, as previously discussed in the sequence of

-Val-Ser-Thr-Val-,[8] as well as the great freedom of the backbone dihedral angles ϕ and ψ of two Gly residues.[15] Although $\langle R_\alpha \rangle$ and $\langle P_\beta \rangle$ values of protected peptides are necessarily determined regardless of the amino acid sequences of peptides and are only dependent on their amino acid compositions, they are still effective for estimating the potential for the β-sheet→helix transformation of peptides with increasing peptide chain length as well as with the application of shear stress.[8]

With regard to the β-sheet structure-disruption, Figs. 5—8 clearly show that, at a pentapeptide level, the β-sheet structure of resin-bound peptides is easily disrupted, regardless of their $\langle P_\alpha \rangle$, $\langle P_\beta \rangle$, and $\langle P_c \rangle$ values. This corresponds to the fact that protected peptides of a pentapeptide level have high solubility in highly polar solvents, regardless of their $\langle P_\alpha \rangle$, $\langle P_\beta \rangle$, and $\langle P_c \rangle$ values. In the case of peptides as long as or larger than an octapeptide, the β-sheet structure-disruption by HFIP is dependent on their $\langle P_\alpha \rangle$, $\langle P_\beta \rangle$, and $\langle P_c \rangle$ values. The $\langle P_\alpha \rangle$, $\langle P_\beta \rangle$, and $\langle P_c \rangle$ values of peptides A_2 and A_3 containing the Val and Ala residues are 1.30, 1.31, and 0.66, respectively, and their β-sheet structure is disrupted together with increasing amounts of HFIP (Fig. 5). On the other hand, the values of $\langle P_\alpha \rangle$, $\langle P_\beta \rangle$, and $\langle P_c \rangle$ of peptides B_2 and B_3 containing the Val and Ile residues are 1.07, 1.63, and 0.64, respectively, and their β-sheet structure-disruption is difficult, even with increasing amounts of HFIP (Fig. 6). As reflected in the $\langle P_\alpha \rangle$ and $\langle P_\beta \rangle$ values, peptides B_2 and B_3 have the sequence -(Val-Ile-Val-Ile)$_n$-, which can not form a helical structure due to the steric hindrance of side chains; however, peptides A_2 and A_3 have the sequence of -(Val-Ala-Val-Ala)$_n$- which can form a helical structure. Furthermore, the $\langle P_c \rangle$ values of both series of peptides are low, indicating that these peptides have a low potential for randomness. The result of the conformational behaviors of peptides A_2, A_3, B_2, and B_3 indicates that the β-sheet structure of a peptide having a high potential for a β-sheet→helix transformation, which is estimated from the $\langle P_\alpha \rangle$ and $\langle P_\beta \rangle$ values, can be disrupted by adding increasing amounts of HFIP. On the other hand, the β-sheet structure disruption of peptides is difficult when they have a low potential for a β-sheet→helix transformation, as well as for randomness. The $\langle P_\alpha \rangle$, $\langle P_\beta \rangle$, and $\langle P_c \rangle$ values of peptides C_1—C_3 are 1.04, 1.23, and 0.88, indicating a low potential for the β-sheet→helix transformation and a high potential for randomness; their β-sheet structure is disrupted regardless of an increase in peptide chain length (Fig. 7). The $\langle P_c \rangle$ values of peptides D_2 and D_3 are 0.93 and 0.90, respectively, and their β-sheet structure is also disrupted, regardless of any increase in the peptide chain length (Fig. 8). Peptide D_3 has been estimated to have a high potential for the β-sheet→helix transformation, while peptide D_2 has not been. Peptides D_2 and D_3 contain protected Asp and Glu residues and the use of the P_α, P_β, and P_c parameters of unprotected Asp and Glu residues for an evaluation of the $\langle P_\alpha \rangle$, $\langle P_\beta \rangle$, and $\langle P_c \rangle$ values of peptides D_2 and D_3 causes trouble. This is because side-chain protection clearly reduces the interaction of side chains with neighboring peptide bonds. Nevertheless, the $\langle P_\alpha \rangle$, $\langle P_\beta \rangle$, and $\langle P_c \rangle$ values of resin-bound peptides D_2 and D_3 are also useful for estimating the potential for their β-sheet structure-disruption.

The results in this paper strongly suggest the adequacy of the solubility prediction method for protected peptides using their $\langle P_c \rangle$ values, previously proposed by us.[3]

The authors wish to thank Central Glass Co., Ltd., Mitsubishi Kasei Co., Ltd., and Ajinomoto Co., Ltd., for the generous gift of reagents.

References

1) The abbreviations for amino acids are those recommended by the IUPAC-IUB Commission on Biochemical Nomenclature, *J. Biol. Chem.*, **247**, 977 (1972). Amino acid symbols except for Gly denote the L-configuration. Additional abbreviations used are the following: HFIP, 1,1,1,3,3,3-hexafluoro-2-propanol; Boc, *t*-butoxycarbonyl; OBzl, benzyl ester; Pam, phenylacetamidomethyl; NMP, *N*-methylpyrrolidone; HOBt, 1-hydroxy-1*H*-benzotriazole; DCC, dicyclohexylcarbodiimide; EtOH, ethanol; TFA, trifluoroacetic acid; TEA, triethylamine; IR, infrared.

2) P. Y. Chou and G. D. Fasman, *Biochemistry*, **13**, 211 (1974).

3) M. Narita, K. Ishikawa, J.-Y. Chen, and Y. Kim, *Int. J. Peptide Protein Res.*, **24**, 580 (1984).

4) M. Narita, J.-Y. Chen, Y. Sato, and Y. Kim, *Bull. Chem. Soc. Jpn.*, **58**, 2494 (1985).

5) M. Narita, T. Ogura, K. Sato, and S. Honda, *Bull. Chem. Soc. Jpn.*, **59**, 2433 (1986).

6) M. Narita, M. Doi, T. Nakai, and H. Takegahara, *Int. J. Peptide Protein Res.*, in press.

7) M. Narita, T. Ogura, K. Sato, and S. Honda, *Bull. Chem. Soc. Jpn.*, **59**, 2439, 2445 (1986).

8) M. Narita, M. Doi, and H. Takegahara, *Bull. Chem. Soc. Jpn.*, **60**, 2445 (1987).

9) M. Narita, S. Honda, H. Umeyama, and T. Ogura, *Bull. Chem. Soc. Jpn.*, **61**, 1201 (1988).

10) M. Narita, S. Isokawa, Y. Tomotake, and S. Nagasawa, *Polym. J.*, **15**, 25 (1983); M. Narita, Y. Tomotake, S. Isokawa, T. Matsuzawa, and T. Miyauchi, *Macromolecules*, **17**, 1903 (1984).

11) M. Narita, S. Honda, H. Umeyama, and S. Obana, *Bull. Chem. Soc. Jpn.*, **61**, 281 (1988); M. Narita, S. Honda, and S. Obana, *ibid.*, **62**, 342 (1989).

12) F. C. Westall, J. Scotchler, and A. B. Robinson, *J. Org. Chem.*, **37**, 3363 (1972).

13) T. Miyazawa and E. J. Blout, *J. Am. Chem. Soc.*, **83**, 712 (1961).

14) C. Toniolo, G. M. Bonora, M. Mutter, and F. Maser, *J. Chem. Soc., Chem. Commun.*, **1983**, 1298.

15) P. Y. Chou and G. D. Fasman, *Biochemistry*, **13**, 222

(1974).
16) M. Narita, M. Doi, K. Kudo, and Y. Terauchi, *Bull. Chem. Soc. Jpn.*, **59**, 3553 (1986).
17) M. Narita, T. Fukunaga, A. Wakabayashi, K. Ishikawa, and H. Nakano, *Int. J. Peptide Protein Res.*, **23**, 306 (1984); M. Narita, N. Ohkawa, S. Nagasawa, and S. Isokawa, *Int. J. Peptide Protein Res.*, **24**, 129 (1984); S. Isokawa, T. Asakura, and M. Narita, *Macromolecules*, **18**, 871 (1985); S. Isokawa, I. Tominaga, T. Asakura, and M. Narita, *ibid.*, **18**, 878 (1985).

The Electron Donor-Acceptor Interaction between Mixed Solvents and Its Influence on Their β-Sheet Structure-Disrupting Potential[1)]

Mitsuaki NARITA,* Hiroshi UMEYAMA, Shizuko ISOKAWA, Shinya HONDA, Chie SASAKI, and Hideaki KAKEI
Department of Industrial Chemistry, Faculty of Technology, Tokyo University of Agriculture and Technology, Koganei 184
(Received August 9, 1988)

Cross-linked polystyrene resin-bound peptides were useful for the investigation of the β-sheet structure-disrupting potential of mixed solvents although their β-sheet structure-disrupted behavior by mixed solvents was different from that of peptides free from a macromolecular protecting group due to the concentrating efficacy of a cross-linked resin. In mixed solvents, the electron-acceptor and -donor numbers (AN and DN) of organic solvents were one of the most important factors to estimate their β-sheet structure-disrupting potential. In a mixture of electron-acceptor solvents themselves or -donor solvents, the electron donor-acceptor interaction between solvents did not occur and electron-accepting or -donating property of each solvent was kept to disrupt the β-sheet aggregation in mixed solvents. On the other hand, in a mixture of electron-acceptor solvent and -donor solvent, the electron donor-acceptor interaction between solvents occurred predominantly to decrease the β-sheet structure-disrupting potential of mixed solvents. The present results clarify the criteria of the search for effective solvents in peptide and protein synthesis.

The β-sheet aggregation of peptides bound to a cross-linked polystyrene resin in the swollen state is one of the most serious obstacles in solid phase peptide synthesis.[2–6)] To elucidate the hydrogen-bonding behavior of resin-bound oligopeptides, we have investigated the conformational properties of oligo(Leu)s,[2)] human proinsulin C-peptide fragments,[3)] and a few of hydrophobic peptides[6)] which were bound to cross-linked polystyrene resins.

The β-sheet aggregation of peptides free from a macromolecular protecting group is also one of the most serious obstacles in classical peptide and protein synthesis since it causes the insolubility of peptide intermediates, protected peptides.[7–12)] In the study of the β-sheet structure-disruption of Boc–Val–Gly–Phe–Gly–Leu–Ile–Leu_2–OBzl in mixed solvents,[13)] we found that, in a mixture of organic solvents, their electron-acceptor and -donor numbers (AN and DN)[14)] were useful for estimating their solvating potential for peptide main chains, that is, their β-sheet structure-disrupting potential. As AN and DN of solvents were larger, their β-sheet structure-disrupting potential became higher. Moreover, on the basis of the results of the β-sheet structure-disruption of Boc–Val–Gly–Phe–Gly–Leu–Ile–Leu_2–OBzl in a three component solvent system, it could be concluded that the combination of electron-donor solvents themselves or -acceptor solvents was suitable in peptide and protein synthesis, but that of electron-donor solvent and -acceptor solvent was not effective due to the electron donor–acceptor interaction between them. The conclusion was obtained using Boc–Val–Gly–Phe–Gly–Leu–Ile–Leu_2–OBzl as a model peptide, which was a novel octapeptide to be soluble as a β-sheet structure in CH_2Cl_2. Thus, it is important to establish that the conclusion is generally available.

In this paper, we first demonstrate that the β-sheet structure-disruption of cross-linked polystyrene resin-bound peptides is more difficult than that of peptides free from a macromolecular protecting group due to the concentrating efficacy of a cross-linked resin. We next demonstrate the generality of the results of Boc–Val–Gly–Phe–Gly–Leu–Ile–Leu_2–OBzl and discussed the validity of AN and DN for the estimation of the electron donor-acceptor interaction between solvents as well as the hydrogen bonding interaction between a peptide and a solvent. The resin-bound peptides **1**—**5** used in this study are shown in Fig. 1.

Experimental

Materials. Copoly(styrene/1% divinylbenzene) beads of 200—400 mesh, Bio-Beads S-Xl, were purchased from Bio-Rad Laboratories. The resin-bound peptides except for **1b** and **1c** were prepared in previous papers,[3,6)] and the peptides **1b** and **1c** were also prepared by the method described previously.[6)] The graft ratios (grafted peptides per 100 styrene

Boc-ValGlyPheGlyLeuIleLeuLeu-Ala-OCH_2Pam-resin-a **1a**
Boc-ValGlyPheGlyLeuIleLeuLeu-Ala-OCH_2Pam-resin-b **1b**
Boc-ValGlyPheGlyLeuIleLeuLeu-Ala-OCH_2Pam-resin-c **1c**
Boc-ValAlaValAlaGly-OCH_2Pam-resin **2**
Boc-GlnValGlu(OBzl)LeuGly-$NHCH_2$-resin **3**
Boc-GlnValGlyGlnValGlu(OBzl)LeuGly-$NHCH_2$-resin **4**
Boc-Glu(OBzl)AlaGlu(OBzl)Asp(OBzl)LeuGlnValGlyGlnValGlu(OBzl)LeuGly-$NHCH_2$-resin **5**

Fig. 1. The resin-bound peptides **1**—**5** used in this study.

units) of the resin-bound peptides **1a—1c** are different with each other to be 0.95, 2.5, and 5.7%, respectively. Those of the resin-bound peptides **2—5** are 1.4, 1.2, 1.1, and 1.0%, respectively.

IR Measurements. The IR absorption spectra of resin-bound peptides were recorded at room temperature with a JEOL Model JIR-100 FT-IR spectrometer. IR measurements in the swollen state were performed by holding the samples between potassium bromide windows after resin-bound peptides were swollen overnight in various molar ratios of mixed solvents. The conformational analysis of the resin-bound peptides **1—5** was carried out using IR absorption spectroscopy as described in the previous papers.[3,6]

Results

The β-Sheet Structure-Disruption of Cross-Linked Polystyrene Resin-Bound Peptides by a Titrating Solvent. The β-sheet structure-disruption was investigated by a solvent-titration method.[15] It was monitored by the successive decrease in the intensity of the band around 1630 cm^{-1} due to the β-sheet structure together with the successive addition of a titrating solvent. Figure 2 shows the typical IR absorption spectra of the resin-bound peptide **1a** in a mixture of HFIP and CH_2Cl_2 at 0.19 M (1 M=1 mol dm^{-3}) and 0.38 M of HFIP. Figure 3 illustrates the solvent-titration curves of the resin-bound peptides **1a—1c**, which are different from each other in a peptide content, using HFIP and TFE as titrating solvents. Relative intensities in Fig. 3 as well as Figs. 4—10 were obtained using the band at 1603 cm^{-1} due to the aromatic ring of the resin support as a standard and were normalized to be 1.0 for each relative intensity in the absence of a titrating solvent. Figure 3 indicates that the more the loading amount of peptide chains on the matrices is, the more difficult the disruption of the β-sheet structure is. HFIP, a strong electron-acceptor solvent, has the high potential for the β-sheet structure disruption[13,16] and the β-sheet structure of the resin-bound peptides **1a—1c** swollen in CH_2Cl_2 is easily disrupted by adding increasing amounts of HFIP. However, in contrast with the fact that the β-sheet structure of Boc-Val-Gly-Phe-Gly-Leu-Ile-Leu_2-OBzl, which is free from a macromolecular protecting group, is completely disrupted at 0.19 M of HFIP,[13,16] that of the resin-bound peptides **1a—1c** is barely disrupted at the same concentration of HFIP. Moreover, the solvent-titration curves of the resin-bound peptides **1a—1c** with TFE show that the β-sheet structure of the resin-bound peptides **1a—1c** is incompletely disrupted even at 1.0 M of TFE, being in contrast with the fact that of Boc-Val-Gly-Phe-Gly-Leu-Ile-Leu_2-OBzl is completely disrupted below 1.0 M of TFE. The solvent-titration curves of the resin-bound peptide **1a** in CH_2Cl_2 using HMPA, DMSO, MeOH, and EtOH as titrating solvents (Fig. 4) are also quite different from those of Boc-Val-Gly-Phe-Gly-Leu-Ile-Leu_2-OBzl. The β-sheet structure of Boc-Val-Gly-Phe-Gly-Leu-Ile-Leu_2-OBzl in CH_2Cl_2, an electron-acceptor solvent, was easily disrupted by adding increasing amounts of strong electron-donor

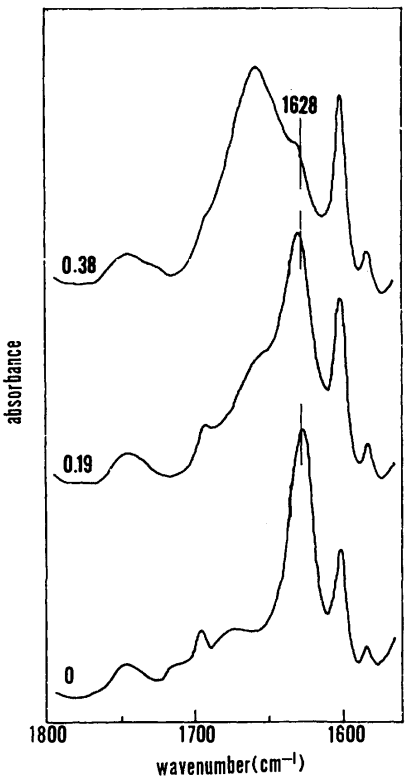

Fig. 2. Typical IR absorption spectra in the amide I region of the resin-bound peptides **1a** swollen in HFIP-CH_2Cl_2. The numerals in Fig. 2 indicate concentrations of HFIP (M).

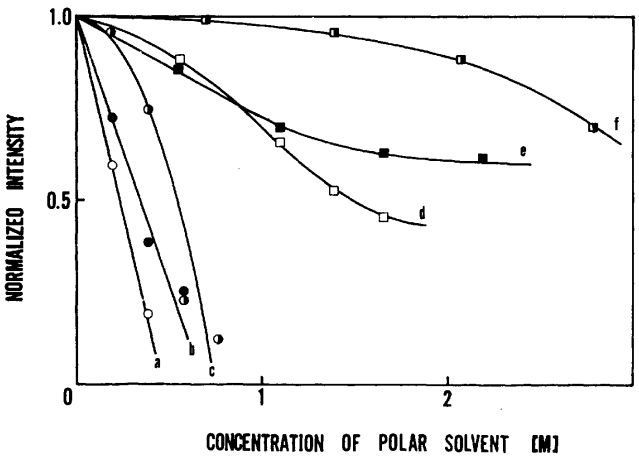

Fig. 3. The solvent-titration curves of the peptides **1a—1c** in CH_2Cl_2 using HFIP (a—c) and TFE (d—f) as titrating solvents. (a) and (d), the peptide **1a**; (b) and (e), the peptide **1b**; (c) and (f), the peptide **1c**. Relative intensities in Fig. 3 as well as Figs. 4—10 were obtained using the band at 1603 cm^{-1} due to the aromatic ring of the resin support as a standard and were normalized to be 1.0 for each relative intensity in the absence of a titrating solvent.

solvents, HMPA and DMSO, and -acceptor solvents, MeOH and EtOH, [13,17] while that of the resin-bound peptide **1a** could not be disrupted by the addition of these solvents. The solvent-titration curves in CH_2Cl_2 show that the larger the AN of titrating solvents is, the greater the β-sheet structure-disruption is, suggesting that AN of titrating solvents is the important factor to estimate their β-sheet structure-disrupting potential in CH_2Cl_2.

The Electron Donor-Acceptor Interaction between Mixed Solvents. Although the β-sheet structure-disruption of resin-bound peptides is more difficult than that of peptides free from a macromolecular protecting group, the fact that the β-sheet structure of resin-bound peptides is not disrupted in a mixture of electron-donor solvent and -acceptor solvent (Fig. 4) suggests that the electron donor-acceptor interaction occurs between mixed solvents. Thus, to certain the generality of the electron donor-acceptor interaction between electron-donor solvent and -acceptor solvent, the β-sheet structure-disruption of resin-bound peptides was examined using the peptides **2**—**5** having a variety of amino acid

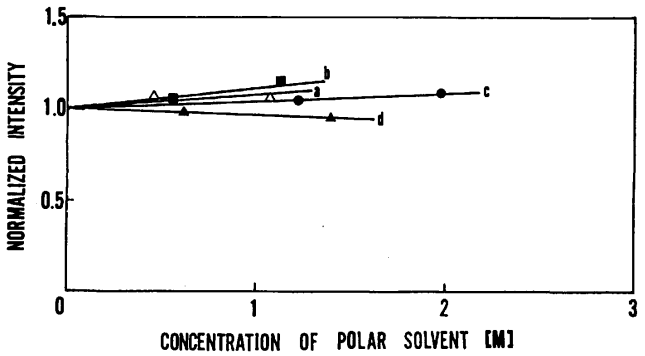

Fig. 4. The solvent-titration curves of the peptides **1a** in CH_2Cl_2 using HMPA (a), DMSO (b), MeOH (c), and EtOH (d) as titrating solvents.

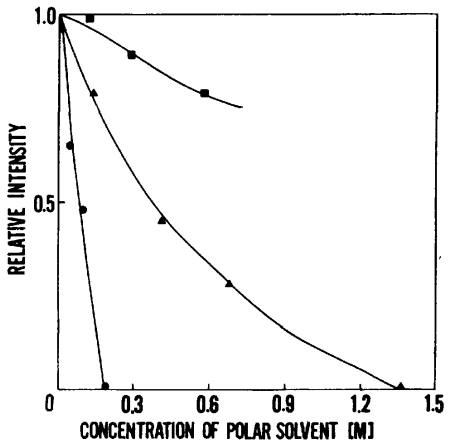

Fig. 5. The solvent-titration curves of the resin-bound peptide **2** in CH_2Cl_2 using HFIP (●), TFE (▲), and HMPA (■) as titrating solvents.

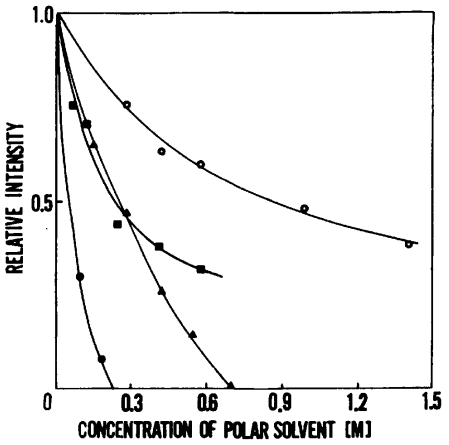

Fig. 6. The solvent-titration curves of the resin-bound peptide **3** in CH_2Cl_2 using HFIP (●), TFE (▲), HMPA (■), and DMSO (O) as titrating solvents.

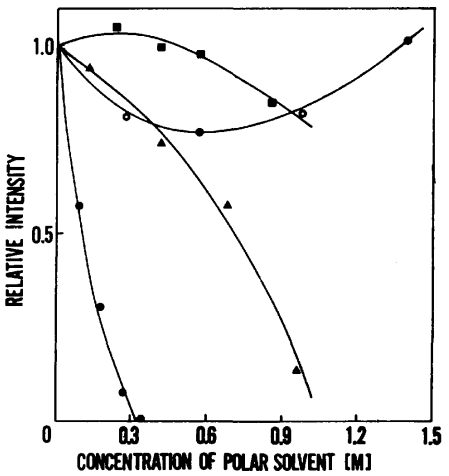

Fig. 7. The solvent-titration curves of the resin-bound peptide **4** in CH_2Cl_2 using HFIP (●), TFE (▲), HMPA (■), and DMSO (O) as titrating solvents.

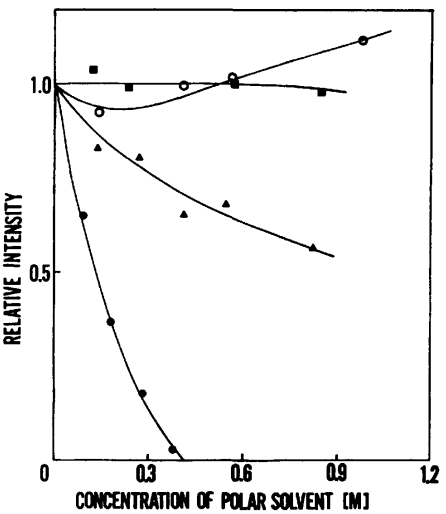

Fig. 8. The solvent-titration curves of the resin-bound peptide **5** in CH_2Cl_2 using HFIP (●), TFE (▲), HMPA (■), and DMSO (O) as titrating solvents.

sequences. It was monitored by the successive decrease in the intensity of the bands at 1632, 1630, 1628, and 1626 cm^{-1}, respectively. Figures 5—8 illustrate the solvent-titration curves of the resin-bound peptides **2—5** in CH_2Cl_2, an electron-acceptor solvent, using HFIP and TFE, electron-acceptor solvents, or DMSO and HMPA, electron-donor solvents, as, titrating solvents. The solvent titration curves in Figs. 5—8 also indicated that the combination of electron-acceptor solvents themselves effectively kept their β-sheet structure-disrupting potential and that of electron-donor solvent and -acceptor solvent did not, suggesting the electron donor-acceptor interaction between them. Furthermore, Figs. 5—8 exhibit that the β-sheet structure-disruption of peptides is strongly dependent on amino acid compositions and peptide chain lengths as discussed in the previous paper.[6]

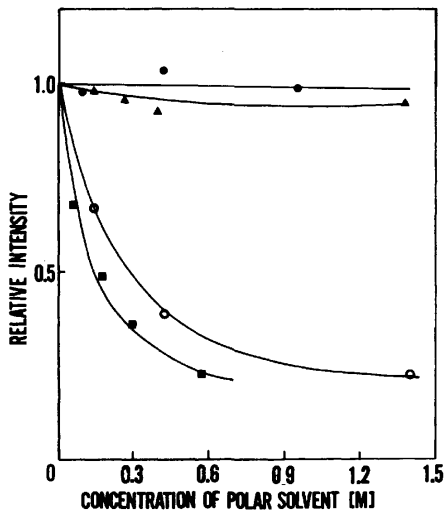

Fig. 9. The solvent-titration curves of the resin-bound peptide **2** in THF using HFIP (●), TFE (▲), HMPA (■), and DMSO (○) as titrating solvents.

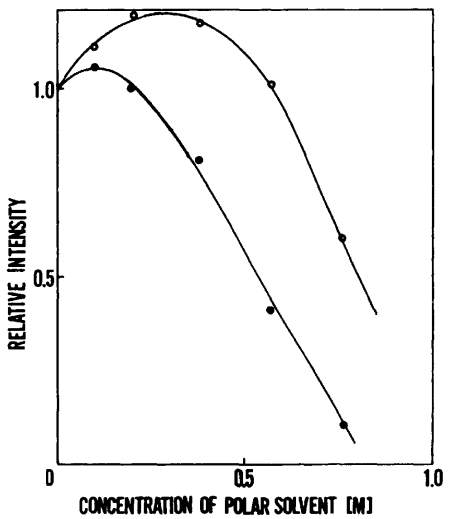

Fig. 10. The solvent-titration curves of the resin-bound peptide **4** in a mixture of CH_2Cl_2 and HMPA (●) and in that of CH_2Cl_2 and DMSO (○) using HFIP as a titrating solvent. Molar concentrations of HMPA and DMSO in CH_2Cl_2 were 0.17 M and 0.42 M, respectively.

Contrary to the results in an electron-acceptor solvent (Figs. 5—8), Fig. 9 illustrates the solvent titration curves of the resin-bound peptide **2** in an electron-donor solvent, THF. The results in Fig. 9 also indicate that the addition of heterogeneous electron-acceptor solvents (HFIP and TFE) decreases in their β-sheet structure-disrupting potential for peptides in THF, while that of homogeneous electron-donor solvents (HMPA and DMSO) does not influence on their β-sheet structure-disrupting potential. However, the β-sheet structure of Boc-(Val-Ala-Val-Ala)$_n$-Ile-OCH_2 Pam-resins (n=2 and 3)[6] in THF could little be disrupted by the successive addition of HMPA due to the low potential of HMPA for the β-sheet structure-disruption of the resin-bound nona- and tridecapeptides (not shown). The solvent titration curves in Fig. 10 illustrates the β-sheet structure-disruption of the peptide **4** in the three component solvent system. In a mixture of CH_2Cl_2 and HMPA or DMSO, the successive addition of HFIP changes the conformation of the resin-bound peptide **4**. The little increase in relative intensity together with the initial addition of HFIP denotes the increase in the β-sheet structure, also indicating the electron donor-acceptor interaction between HFIP and HMPA or HFIP and DMSO.

Discussion

Although peptides having a β-sheet structure in organic solvents usually could not be analyzed their conformation in solution due to their insolubility, anchoring of peptides to a cross-linked polystyrene-resin enabled their conformational analysis in various organic solvents in the swollen state. The solvent-titration curves of the resin-bound peptides **1a—1c** (Figs. 3 and 4) showed that their β-sheet-structure-disrupted behavior was quite different from that of Boc-Val-Gly-Phe-Gly-Leu-Ile-Leu_2-OBzl, which was free from a macromolecular protecting group, and strongly dependent on the loading amount of peptide chains on the matrices. The dependence on the loading amount clearly indicates that anchoring of a peptide to a cross-linked resin has a concentrating efficacy as pointed out before,[2,3] being contrary to the assumption that the high dilution principle would be achieved in solid-phase organic synthesis.[17]

The solvent-titration curves of the resin-bound peptides **1—5** (Figs. 3—10) also indicate that a mixture of heterogeneous solvents (combination of electron-acceptor solvent and -donor solvent) decreases in their β-sheet structure-disrupting potential due to the electron donor-acceptor interaction between them, while that of homogeneous solvents (Combination of electron-acceptor solvents themselves or -donor solvents) keeps electron-accepting or -donating property

Table 1. AN and DN of Organic Solvents Used in This Study[13,14]

Solvent	AN	DN
CH_2Cl_2	20.4	—
THF	8.0	20.0
HMPA	10.6	38.8
DMSO	19.3	29.8
HFIP	88	—
TFE	70	—
MeOH	41.3	19
EtOH	37.1	20

AN and DN of a peptide bond are not reported, but DN of *N*,*N*-dimethylacetamide is 27.8 and AN of formamide is 39.8.

of each solvent. Especially, the solvent-titration curves in Fig. 10 clearly show the electron donor–acceptor interaction between HFIP and HMPA or HFIP and DMSO. In the absence of HFIP, a small amount of HMPA or DMSO contributes solvation of peptide bonds and, by the initial addition of HFIP, the strong electron donor–acceptor interaction between HFIP and HMPA or HFIP and DMSO brings about to help the β-sheet formation of the resin-bound peptide **4**. By the further addition of HFIP, HFIP effectively solvates peptide bonds to disrupt the β-sheet aggregation. These conformational behaviors just correspond to those of Boc–Val–Gly–Phe–Gly–Leu–Ile–Leu_2–OBzl in a three component solvent system.[13] As discussed for the β-sheet structure-disruption of Boc–Val–Gly–Phe–Gly–Leu–Ile–Leu_2–OBzl in the three component solvent system,[13] the electron-accepting and -donating property of solvents indicated by AN and DN is one of the important factors to estimate their β-sheet structure-disrupting potential.

AN and DN of organic solvents used in this study were summarized in Table 1. AN of CH_2Cl_2 is 20.4, indicating that CH_2Cl_2 is a medium electron-acceptor solvent. DN of CH_2Cl_2 is not obtained, but is thought to be near zero since 1,2-dichloroethane is used as a standard for evaluation of DN of organic solvents.[14] In the medium electron-acceptor solvent, CH_2Cl_2, strong electron-acceptor solvents, HFIP and TFE, have a high potential for the β-sheet structure-disruption of the resin-bound peptides **1**—**5** having a variety of amino acid sequences (Figs. 3 and 5—8). On the other hand, strong electron-donor solvents, HMPA and DMSO, have no or little potential for their β-sheet structure-disruption (Figs. 4—8). These results clearly indicate that, in a mixture of homogeneous electron-acceptor solvents, electron donor–acceptor interaction does not occur and electron-accepting property of HFIP and TFE is kept to disrupt the β-sheet aggregation in CH_2Cl_2, while, in a mixture of heterogeneous solvents, electron donor–acceptor interaction occurs predominantly to lose electron-donating property of HMPA and DMSO for peptide N–H bonds.

Contrary to CH_2Cl_2, THF is a medium electron-donor solvent (DN, 20.0) and a weak electron-acceptor solvent (AN, 8.0). In THF, strong electron-donor solvents, HMPA and DMSO, have a high potential for the β-sheet structure-disruption of the resin-bound peptide **2**, while strong electron-acceptor solvents, HFIP and TFE, lose it. Namely, the electron donor–acceptor interaction does not occur in a mixture of homogeneous electron-donor solvents, and electron-donating property of HMPA and DMSO is kept to disrupt the β-sheet aggregation in THF, while, in a mixture of heterogeneous solvents, the electron donor–acceptor interaction occurs predominantly to lose electron-accepting property of HFIP and TFE for peptide C=O bonds. AN and DN of HMPA are 10.6 and 38.8, and those of DMSO, 19.3 and 29.8, respectively. These AN values suggest that the electron-donating property of HMPA and DMSO does not reduce in THF because the electron-accepting property of THF is smaller than that of HMPA and DMSO. HFIP has AN of 88 and strongly interacts with HMPA and DMSO through electron transfer, showing the solvent-titration curves presented in Fig. 10.

Conclusion

Cross-linked polystyrene resin-bound peptides were useful for the investigation of the β-sheet structure-disrupting potential of mixed solvents although their β-sheet structure-disruption by solvents was more difficult than that of peptides free from a macromolecular protecting group due to the concentrating efficacy of a cross-linked resin. As a results, the concentrating efficacy helped the observation of the electron donor–acceptor interaction between heterogeneous solvents which could not be observed for Boc–Val–Gly–Phe–Gly–Leu–Ile–Leu_2–OBzl. The β-sheet structure-disruption of resin-bound peptides having a variety of amino acid sequences indicates that the β-sheet structure disrupting potential of mixed solvents decreases in the case of the combination of heterogeneous solvents due to the electron donor–acceptor interaction. In peptide and protein synthesis, mixed solvents are commonly used in coupling reactions[18] since mixed solvents have a high solubilizing potential for large peptide intermediates probably due to the enhancement of solvation to peptide side chains by mixing. The results in this study clarify the criteria of the search for effective solvents in peptide and protein synthesis. The combination of homogeneous solvents should be selected in the direction that each solvent plays an important role in solvation of various kinds of peptide side-chains.

The authors wish to thank Central Glass Co., Ltd., Mitsubishi Kasei Co., Ltd., and Ajinomoto Co., Ltd., for the generous gift of reagents.

References

1) The abbreviations for amino acids are those recommended by the IUPAC-IUB Commission on Biochemical Nomenclature, *J. Biol. Chem.*, **247**, 977 (1972). Amino acid symbols except for Gly denote the L-configuration. Additional abbreviations used are the follwing: Boc, *t*-butoxycarbonyl; Pam, phenylacetamidomethyl; OBzl, benzyl ester; IR, infrared; HFIP, 1,1,1,3,3,3-hexafluoro-2-propanol; TFE, 2,2,2-trifluoroethanol; DMSO, dimethyl sulfoxide; HMPA, hexamethylphosphoric triamide; MeOH, methanol; EtOH, ethanol; THF, tetrahydrofuran.

2) M. Narita, S. Isokawa, Y. Tomotake, and S. Nagasawa, *Polym. J.*, **15**, 25 (1983); M. Narita, Y. Tomotake, S. Isokawa, T. Matsuzawa, and T. Miyauchi, *Macromolecules*, **17**, 1903 (1984).

3) M. Narita, S. Honda, H. Umeyama, and T. Ogura, *Bull. Chem. Soc. Jpn.*, **61**, 1201 (1988).

4) A. G. Ludwick, L. W. Jelinski, D. Live, A. Kintanar, and J. J. Dumais, *J. Am. Chem. Soc.*, **108**, 6493 (1986).

5) S. Isokawa, N. Kobayashi, R. Nagano, and M. Narita, *Makromol. Chem.*, **185**, 2065 (1984); M. Narita, S. Isokawa, T. Matsuzawa, and T. Miyauchi, *Macromolecules*, **18**, 1363 (1985); M. Narita, S. Isokawa, S. Nagasawa, and T. Ishijima, *Macromolecules*, **20**, 2306 (1987).

6) M. Narita, S. Isokawa, S. Honda, H. Umeyama, H. Kakei, and S. Obana, *Bull. Chem. Soc. Jpn.*, **62**, 773 (1989).

7) M. Narita, K. Ishikawa, J.-Y. Chen, and Y. Kim, *Int. J. Peptide Protein Res.*, **24**, 580 (1984).

8) M. Narita, T. Fukunaga, A. Wakabayashi, K. Ishikawa, and H. Nakano, *Int. J. Peptide Protein Res.*, **23**, 306 (1984).

9) M. Narita, J.-Y. Chen, H. Sato, and Y. Kim, *Bull. Chem. Soc. Jpn.*, **58**, 2494 (1985).

10) M. Narita, T. Ogura, K. Sato, and S. Honda, *Bull. Chem. Soc. Jpn.*, **59**, 2433, 2439, 2445 (1986).

11) M. Narita, M. Doi, and T. Nakai, *Bull. Chem. Soc. Jpn.*, **60**, 3255 (1988); M. Narita, M. Doi, and H. Takegahara, *ibid.*, **60**, 2445 (1987); M. Narita, M. Doi, T. Nakai, and H. Takegahara, *Int. J. Peptide Protein Res.*, in press.

12) M. Narita, M. Doi, H. Sugasawa, and K. Ishikawa, *Bull. Chem. Soc. Jpn.*, **58**, 1473 (1985).

13) M. Narita, S. Honda, and S. Obana, *Bull. Chem. Soc. Jpn.*, **62**, 342 (1989).

14) V. Gutmann, *Electrochim. Acta*, **21**, 661 (1976); U. Mayer, V. Gutmann, and W. Gerger, *Mh. Chem.*, **106**, 1235 (1975); V. Gutmann, "The Donor-Acceptor Approach to Molecular Interaction," Plenum Press, New York (1978).

15) C. Toniolo, G. M. Bonora, M. Mutter, and F. Maser, *J. Chem. Soc., Chem. Commun.*, **1983**, 1298.

16) M Narita, S. Honda, H. Umeyama, and S. Obana, *Bull. Chem. Soc. Jpn.*, **61**, 281 (1988).

17) J. I. Crowley and H. Rapoport, *Acc. Chem. Res.*, **9**, 135 (1976); V. K. Sarin, S. B. H. Kent, and R. B. Merrifield, *J. Am. Chem. Soc.*, **102**, 5463 (1980).

18) N. Fujii and H. Yajima, *J. Chem. Soc., Perkin Trans. 1*, **1981**, 789, 797, 804, 811, 819, 831.

The Zinc(II)-Catalyzed Henkel Reaction of Dipotassium 1,8-Naphthalenedicarboxylate in a Dispersion Medium

Koichi FUJISHIRO and Shuichi MITAMURA*
Chemicals Research Laboratory, R & D Laboratories-1,
Nippon Steel Co. 1618 Ida, Nakahara-ku, Kawasaki 211
(Received July 21, 1988)

The Henkel reaction of dipotassium 1,8-naphthalenedicarboxylate in naphthalene as a dispersion medium gave dipotassium 2,6-naphthalenedicarboxylate (**1**) in a higher yield and with a better reproducibility than the reaction without a dispersion medium . Catalysts, particularly zinc catalysts, were examined in detail. The anion moiety of zinc catalysts affected the reaction, and the halide anion was effective for the selective formation of **1**. The addition of potassium halide to the zinc catalysts also increased the yield of **1**. The catalytic activity of the halide anion increased in the order; $Cl^- < Br^- < I^-$. The activity of the zinc catalysts was also compared with that of cadmium catalysts.

2,6-Naphthalenedicarboxylic acid (**2**) has attracted attention because it is often used as a component of high-performance polymers. For example, poly(ethylene naphthalenedicarboxylate) is known for its heat resistance and high modulus.[1] We have been studying the preparation of **2** from 1,8-naphthalenedicarboxylic anhydride (**3**) (Scheme 1). The transformation of dipotassium 1,8-naphthalenedicarboxylate (**4**) into the 2,6-isomer (**1**) is well-known as the Henkel reaction, which is usually carried out by heating **4** under a pressure of carbon dioxide at 350—450 °C in the presence of a catalytic amount of cadmium salts or sometimes zinc salts.[2-7] The activity of the cadmium catalysts is much higher than that of the zinc catalysts. In order to produce **1** industrially, however, some practical problems must be overcome: (1) It is difficult to transport the starting material **4** and the reaction mixture because both of them are in the solid state during this process. (2) The powders of the reaction mixture stick together during the reaction, which leads to inefficient mixing and local superheating, resulting in a poor reproducibility of the reaction along with a low yield of **1**. (3) Cadmium salts are very toxic, though their catalytic activity is very high. We have focused our efforts on overcoming these problems. We have found that the addition of a dispersion medium such as naphthalene to the starting material obviates the problems, and improves both the reproducibility of the reaction and the yield of **1**. We have also found that the cadmium catalysts can be replaced by a combination of zinc(II) and the halide anion X^-, whose activity is as same as that of the cadmium catalysts. The roles of zinc(II) and X^- during the reaction are discussed on the basis of the effects of the anionic moiety of the zinc catalyst on the reaction and on the basis of thermal gravimetric analyses.

Experimental

All high-performance liquid chromatographies (HPLC) were taken on a Shimadzu LC-4A apparatus. All melting-points were measured with a Yanagimoto micro melting point apparatus and are uncorrected. The ^1H NMR spectra were taken on a JEOL JMN-FX90 spectrometer. The thermal gravimetric analyses were done with a Rigaku Denki TG-DTA apparatus.

Preparation of 4. According to the reported procedure,[2] **4** was prepared from 1,8-naphthalenedicarboxylic anhydride (**3**) and potassium hydroxide.

Henkel Reaction in a Dispersion Medium (General Procedure). The dipotassium salt **4** and the catalyst (1—12 mol% based on **4**) were mixed intimately in a glass ball mill. After drying in vacuo at 150 °C, 10 g of the mixed powder was put into a 200 cm^3 autoclave, which had been preheated at 100 °C, along with 30 g of a dispersion medium such as naphthalene. The autoclave was then filled with carbon dioxide to a pressure of 4.1 MPa. While the mixture in the autoclave was stirred at 100 °C, carbon dioxide was occasionally introduced into the autoclave until there was no pressure drop. The mixture was thereafter heated to 450 °C at the heating rate of 6 °C min^{-1} while being stirred; it was then maintained at 450 °C for 1 h. The pressure increased to 7.1 MPa. After the autoclave had been cooled, toluene (200 cm^3) and water (200 cm^3) was successively added to the reaction mixture; the mixture was then stirred at 60 °C for 0.5 h. The insoluble materials, which mainly consisted of carbonized materials, were separated by filtration. After the organic layer had been removed, the aqueous layer was washed with toluene (100 cm^3×2), and then subjected to the

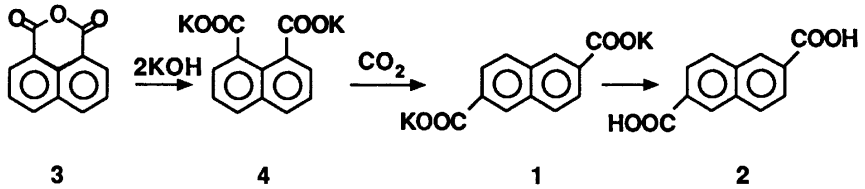

3 4 1 2

Scheme 1. Henkel process.

following product analysis.

Analysis of Products. Ten isomers of dipotassium naphthalenedicarboxylates can be obtained. Nine of them, potassium 2-naphthoate and tripotassium 2,3,6-naphthalenetricarboxylate were determined by HPLC using 1-naphthoic acid as the internal standard (column: Shimadzu Co.; Shimpack CLC ODS, and/or Japan Spectroscopic Co.; Finepak SIL C18S, eluent: a mixture of methanol and 0.2 wt% aqueous phosphoric acid solution). The yield of **1** is given by Eq. 1 (Eq. 2 is used in the case of a reaction using zinc naphthalate as the catalyst);

$$\text{Yield of } \mathbf{1}\,(\%) = 100\,A/R \quad (1)$$

$$\text{Yield of } \mathbf{1}\,(\%) = 100\,A/(R + C) \quad (2)$$

A/mol: Molar amount of **1** in the reaction mixture was determined by HPLC.

R/mol: Molar amount of **4**.

C/mol: Molar amount of zinc naphthalate.

Authentic Specimens. In order to analyze the products in the reaction mixture, a wide variety of naphthalenecarboxylic acids was prepared as follows. The 2,6-naphthalenedicarboxylic acid, 2,3-naphthalenedicarboxylic acid, 1,8-naphthalenedicarboxylic anhydride, 1-naphthoic acid, and 2-naphthoic acid were commercially available. Other dicarboxylic acids, such as the 1,2-, 1,3-, 1,4-, 1,5-, 1,6-, and 2,7-isomers, were prepared by the oxidation of the corresponding dimethylnaphthalenes with aqueous sodium dichromate.[9] The acid values were measured by titration in aqueous methanol with 0.1 mol dm^{-3} aqueous potassium hydroxide using 3,3-bis(4-hydroxyphenyl)phthalide as an indicator. The diacids prepared from dimethylnaphthalenes were esterified into the corresponding dimethyl esters by a usual procedure (catalyst: concd sulfuric acid) and were identified as follows.

1,2-Naphthalenedicarboxylic Acid: Acid value: 517.2. (Calcd for naphthalenedicarboxylic acid: 519.1). Dimethyl ester. Mp 83.5—84.8 °C (lit,[9] mp 84.0—85.0°C). ^{1}H NMR ($CDCl_3$) δ=3.96 (3H, s), 4.08 (3H, s), 7.5—7.7 (2H, m), 7.8—8.1 (4H, m).

1,3-Naphthalenedicarboxylic Acid: Acid value: 518.2. Dimethyl ester. Mp 101.5—102.5 °C (lit,[9] mp 104.5—105.0 °C. ^{1}H NMR ($CDCl_3$) δ=3.99 (3H, s), 4.08 (3H, s), 7.5—7.8 (2H, m), 7.9—8.0 (1H, m), 8.72 (2H, s), 8.93 (1H, d, J=8 Hz).

1,4-Naphthalenedicarboxylic Acid: Acid value: 517.5. Dimethyl ester. Mp 63.4—64.8 °C (lit,[9] mp 65.0—66.0 °C). ^{1}H NMR ($CDCl_3$) δ=4.00 (6H, s), 7.61 (2H, dd, J=10 Hz, 3 Hz), 8.05 (2H, s), 8.80 (2H, dd, J=10 Hz, 3 Hz).

1,5-Naphthalenedicarboxylic Acid: Acid value: 518.0. Dimethyl ester. Mp 119.0—119.5 °C (lit,[9] mp 119.0—120.0 °C). ^{1}H NMR ($CDCl_3$) δ=4.00 (6H, s), 7.61 (2H, t, J=8 Hz), 8.19 (2H, d, J=9 Hz), 9.11 (2H, d, J=9 Hz).

1,6-Naphthalenedicarboxylic Acid: Acid value: 518.4. Dimethyl ester. Mp 98.6—99.5 °C (lit,[9] mp 98.0—99.0 °C). ^{1}H NMR ($CDCl_3$) δ=3.98 (3H, s), 4.01 (3H, s), 7.54 (1H, dd, J=8 Hz, 8 Hz), 8.0—8.4 (3H, m), 8.61 (1H, d, J=2 Hz), 8.98 (1H, d, J=9 Hz).

2,7-Naphthalenedicarboxylic Acid: Acid value: 519.0. Dimethyl ester. Mp 136.5—137.3 °C (lit,[9] mp 136.5—137.0 °C). ^{1}H NMR ($CDCl_3$) δ=3.90 (6H, s), 7.7—8.2 (4H, m), 8.60 (2H, s).

2,3,6-Naphthalenetricarboxylic acid was isolated by sublimation from the reaction mixture as follows. The aqueous layer, which had been obtained from the reaction mixture as described in the general procedure, was concentrated in vacuo to give a slurry. The subsequent filtration of the slurry yielded **1** as colorless crystals. The filtrate was treated with active charcoal and acidified (pH less than 1) with concd hydrochloric acid to give precipitates of a mixture of naphthalenecarboxylic acids. The precipitates were filtered, washed with water, and dried. The esterification of the mixture of naphthalenecarboxylic acids with methanol was carried out in a usual procedure (catalyst; concd sulfuric acid, 130 °C, 0.61 MPa, 2 h). The esters were recrystalyzed from methanol to afford colorless crystals. The crystals were hydrolyzed with aqueous alkali, and then acidified with concd hydrochloric acid to give the corresponding acids. HPLC revealed that these acids were an isomeric mixture of naphthalenetricarboxylic acids and consisted mainly of the 2,3,6-isomer. The sublimation of the acids at 230 °C/133 Pa gave 2,3,6-naphthalenetricarboxylic acid 2,3-anhydride as colorless crystals. Found: C, 64.40; H, 2.41%. Calcd for $C_{13}H_6O_5$: C, 64.47; H, 2.50%. Trimethyl ester. Mp 123.0—125.0 °C (lit,[9] mp 125.0—126.0 °C). ^{1}H NMR ($CDCl_3$) δ=3.97 (6H, s), 4.00 (3H, s), 7.9—8.4 (4H, m), 8.64 (1H, s).

Thermal Gravimetric Analysis (TGA). A mixture (15 mg) of **4** and the catalyst was put into a platinum cell, and then heated to 520 °C at the rate of 10 °C min^{-1} in a stream of carbon dioxide.

Results and Discussion

Dispersion Mediums. The results of the Henkel reaction with and without a dispersion medium are summarized in Table 1. A mixture of zinc chloride and potassium iodide (8 mol% based on **4**, respectively) was used as the catalyst. Without a dispersion medium, the composition of the reaction mixture varied depending on the site in the autoclave. It was also found that **1** was obtained in a low yield and that the reproducibility of the reaction was very poor (Runs 1—3). On the other hand, the reaction in naphthalene as a dispersion medium gave **1** in a good yield (70 mol%), and the reproducibility was improved (Runs 4, 5). Using a specially designed autoclave equipped two windows in its wall, we were able to observe the reaction process and found that black powders of the crude products were dispersed uniformly in the liquid naphthalene. It should be also noted that the reaction gave almost the same products irrespective of whether or not **4** and the catalyst had been premixed before they were charged into liquid naphthalene. These results indicate that the liquid naphthalene promotes both heat and mass transfer in the reaction, so that the reproducibility of the reaction is improved along with the yield of **1**.

When biphenyl, a mixture of diphenyl ether and biphenyl, or phenanthrene was used as the dispersion medium, the yield of **1** was also improved (Runs 6—8).[10] On the other hand, the addition of methylnaphthalene or ethylbipenyl decreased the yield of **1** and gave more tarry materials (Runs 9, 10). Aromatic compounds with acidic hydrogens of the alkyl groups,

Table 1. Henkel Reaction in Various Dispersion Mediums

Run No.	Dispersion medium	Yields of products/mol%[a]			
		1	5	6	7
1	None	53.8	12.0	10.6	4.3
2	None	45.7	17.2	19.6	4.5
3	None	48.1	15.2	18.0	4.5
4	Naphthalene	69.1	2.5	3.0	2.4
5	Naphthalene	69.2	2.7	3.1	2.5
6	Biphenyl	62.6	3.3	2.5	2.5
7	Diphenyl ether+biphenyl[b]	60.4	2.8	2.5	3.3
8	Phenanthrene	61.3	4.8	9.0	3.3
9	Methylnaphthalene	44.6	1.1	10.5	0.4
10	Ethylbiphenyl[c]	21.3	21.3	34.0	0.8

4 was heated at 45 °C (c; 410 °C) for 1 h in the presence of $ZnCl_2$ (8 mol%) and KI (8 mol%). The initial pressure of CO_2 was 4.1 MPa at 100 °C. Thirty grams of the dispersion medium were used for each 10 g of the starting materials (**4** and the catalyst). a) **1**: dipotassium 2,6-naphthalenedicarboxylate, **5**: dipotassium naphthalenedicarboxylate except for **1**, **6**: potassium 2-naphthoate, **7**: tripotassium 2,3,6-naphthalenetricarboxylate. b) The molar ratio of diphenyl ether to biphenyl was 74/26.

Table 2. Zinc(II)-Catalyzed Henkel Reaction

Run No.	Catalyst	Yields of products/mol%[a]			
		1	5	6	7
11	ZnO	41.1	17.5	22.4	5.7
12	$ZnCO_3$	55.1	7.8	11.5	2.6
13	Zinc naphthalate[b]	57.1	4.6	8.2	4.5
14	$ZnCl_2$	62.3	4.0	7.7	4.7
15	ZnI_2	69.6	2.6	4.1	2.7
16	$ZnCl_2$+KCl	62.5	4.2	8.2	4.5
17	$ZnCl_2$+KBr	64.8	3.7	6.1	4.4
4	$ZnCl_2$+KI	69.1	2.5	3.0	2.4
18	Zinc naphthalate+KI[b]	70.3	2.4	5.1	2.4
19	ZnO+KI	45.8	20.7	16.1	3.7
20	$ZnCO_3$+KI	58.1	4.9	9.6	1.3

The reactions were carried out at 45 °C for 1 h in the presence of 8 mol% (b) 8.7 mol%) of the catalyst. The initial pressure of CO_2 was 4.1 MPa. Thirty grams of naphthalene were used for each 10 g of the starting materials (**4** and the catalyst). a) **1**: dipotassium 2,6-naphthalenedicarboxylate, **5**: dipotassium naphthalenedicarboxylate except for **1**, **6**: potassium 2-naphthoate, **7**: tripotassium 2,3,6-naphthalenetricarboxylate.

such as methylnaphthalene and ethylbiphenyl, seem to bring about the decarboxylation of both the starting material **4** and the products to lower the yield of **1**.

Catalysts. Zinc catalysts have rarely been used for the Henkel reaction because their catalytic activity was lower than that of cadmium catalysts.[2-6] From the standpoint of industrial production, however, it is desired to replace cadmium catalysts with zinc catalysts because of their toxicity and high price. Therefore, a wide variety of zinc compounds was examined as catalysts on this Henkel reaction.

Effects of the Anionic Moiety of the Zinc Catalysts: The results of the reactions with a wide variety of zinc compounds are shown in Table 2. The influence of the anionic moiety of the zinc catalysts on the yields of products was unexpecctedly large. Zinc halides were the most effective catalysts to yield **1** predominantly (Runs 14, 15), while zinc oxide (Run 11) or zinc carbonate (Run 12) gave **1** in a low yield. The addition of potassium halides to zinc chloride or zinc naphthalate catalyst (Runs 16—18, 4) was also effective in increasing the yield of **1**. The catalytic activity increased in the order;

$$Cl^- < Br^- < I^-$$

On the other hand, the addition of potassium iodide to zinc oxide (Run 19) or zinc carbonate (Run 20) hardly improved the yield of **1** at all.

Effects of the Amount of the Catalyst: The effects of the amounts of zinc naphthalate and potassium iodide are summarized in Table 3. It was found that the yield of **1** depended on both the amount of the zinc naphthalate and the molar ratio of the potassium iodide to the zinc naphthalate. When the amount of the zinc naphthalate was 1 mol%, regardless of the amount of potassium iodide, the reaction gave **1** in a low yield (Runs 21, 22). When the amount of the zinc naphthalate was over 4 mol%, the yield of **1** increased, whereas the yields of the isomers of **1** (**5**) and potas-

Table 3. Effects of the Amount of the Catalyst

Run No.	Amount of catalyst/mol%[a]		Yields of products/mol%[b]			
	Zinc naphthalate	KI	**1**	**5**	**6**	**7**
21	1.0	1.0	55.7	10.1	15.1	5.5
22	1.0	8.0	56.9	12.7	12.5	3.2
23	4.3	4.3	67.5	3.8	7.3	3.6
24	8.7	4.3	64.5	4.5	6.1	4.3
18	8.7	8.7	70.3	2.4	5.1	2.4
25	8.7	12.0	69.5	2.5	5.2	3.1

The reactions were carried out at 45 °C for 1 h. The initial pressure of CO_2 was 4.1 MPa. Thirty grams of naphthalene were used for each 10 g of the starting materals (**4** and the catalyst). a) The amounts of the catalyst were based on **4**. b) **1**: dipotassium 2,6-naphthalenedicarboxylate, **5**: dipotassium naphthalenedicarboxylate except for **1**, **6**: potassium 2-naphthoate, **7**: tripotassium 2,3,6-naphthalenetricarboxylate.

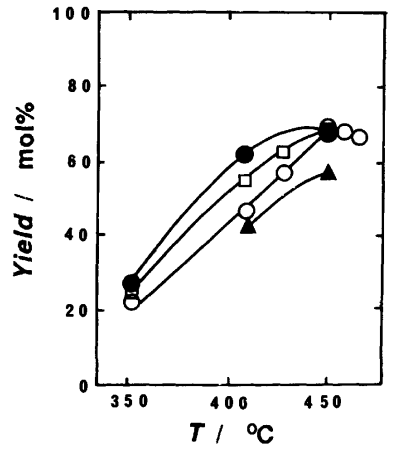

Fig. 1. Yields of **1** at different temperatures: **4** was heated at different temperatures for 1 h. The initial pressure of CO_2 was 4.1 MPa at 100 °C. Thirty grams of naphthalene were used for each 10 g of the starting materials (**4** and the catalyst). ○: zinc naphthalate (8.7 mol%)+KI (8.7 mol%), □: $ZnCl_2$ (8 mol%)+KI (8 mol%), ●: CdI_2 (8 mol%), ▲: CdO (8 mol%).

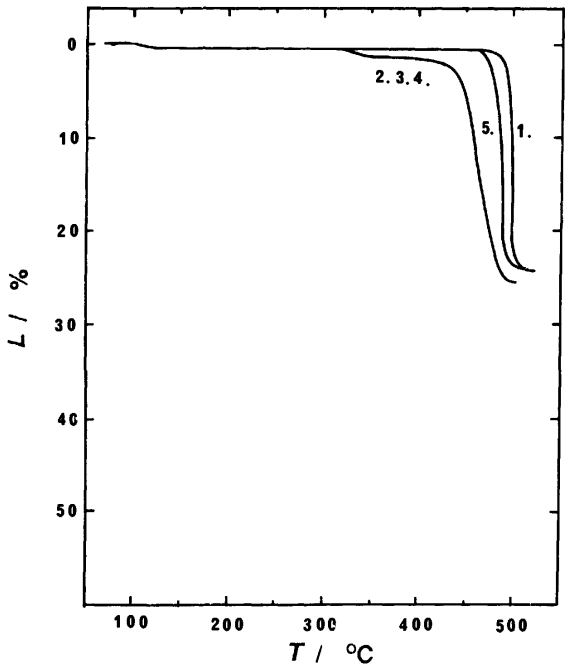

Fig. 2. Thermal gravimetric analyses for the starting materials in carbon dioxide stream: *L* is the weight loss of the starting material. 1: **4**, 2: **4**+$ZnCl_2$ (8 mol%)+KI (8 mol%), 3: **4**+zinc naphthalate (8.7 mol%)+KI (8.7 mol%), 4: **4**+zinc naphthalate (8.7 mol%), 5: **4**+ZnO (8 mol%)+KI (8 mol%).

sium 2-naphthoate (**6**) decreased. When the amount of the potassium iodide was used more than that of the zinc naphthalate, **1** was obtained in a satisfactory yield, i.e., 67—70 mol% (Runs 18, 23, and 25).

Comparison between Zinc and Cadmium Catalyst: The reaction using the zinc catalyst was carried out at different temperatures in order to compare the activity with that of the cadmium catalyst. The results are shown in Fig. 1. The activities of zinc catalysts having iodide anion (plots ○, □) were lower than that of the cadmium iodide (plot ●) below of the reaction temperature 430 °C, but almost the same as that at 450 °C.

The activity of the cadmium oxide (plot ▲) was lower than that of the cadmium iodide (plot ●), so the anionic moiety of the cadmium catalyst seems to play the same role as that of the zinc catalyst. Ogata et al. reported a similar observation that the increasing order of the catalytic activity was $CdCl_2 < CdBr_2 < CdI_2$ in the preparation of dipotassium terephthalate from dipotassium phthalate.[11]

We found that the cadmium catalyst could be replaced by a combination of zinc(II) and I^- catalyst whose activity was the same as that of the cadmium catalyst.

Thermal Gravimetric Analyses (TGA). TGA of **4** in the presence of various catalysts were carried out in order to examine the thermal behavior of **4** in its dependence on the kinds of the zinc catalysts. The results of TGA in a steam of carbon dioxide at an atmospheric pressure are shown in Fig. 2. In the presence of a catalytic amount of zinc chloride or zinc naphthalate (Line 2—4), **4** started to lose weight from 320 °C with foaming. The weight loss observed from 320 °C in TGA may be due to the decarboxylation of **4**.

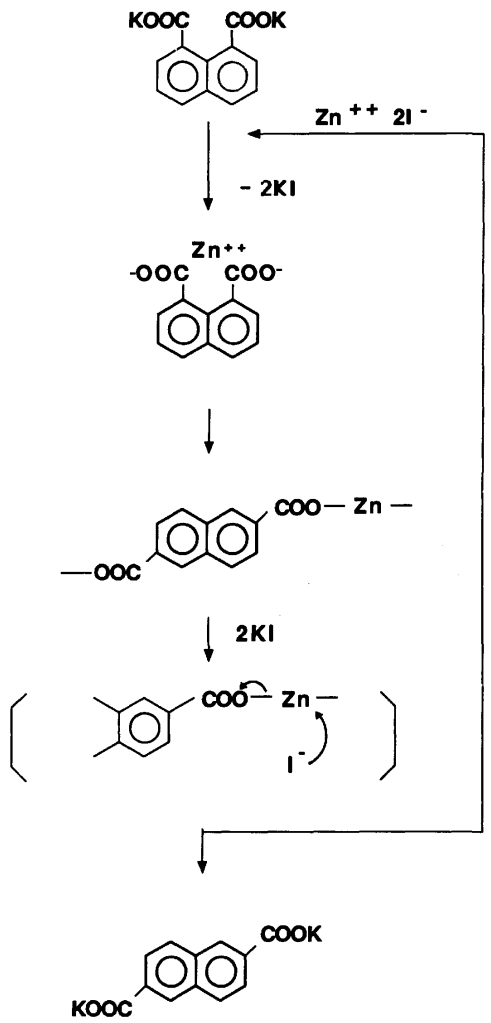

Scheme 2. Roles of the catalysts.

It should be noted that the Henkel reaction began to proceed at almost the same temperature. On the other hand, **4** without the catalyst (Line 1) or **4** with the catalytic amount of zinc oxide and potassium iodide (Line 5) started to lose weight over 450 °C. These results indicate that the zinc cation of zinc halide or zinc naphthalate can react with **4** and bring about the cleavage of the C–C bond between the carboxyl group and the naphthalene nucleus of **4**. In the case of zinc oxide, however, the affinity of the oxygen to the zinc is so strong that a little zinc oxide reacts with **4**.

Role of Catalysts: On the basis of our experimental findings, we propose the roles of the catalysts as shown in Scheme 2. The potassium cation of **4** is replaced by the zinc cation to form a zinc compound such as zinc naphthalate. The zinc cation of the zinc naphthalate loosens the C–C bond between the carboxyl group and the naphthalene nucleus and allows **4** to rearrange to give 2,6-isomer; then, the zinc cation is exchanged for the potassium cation. In this exchange reaction, the halide anion promotes the exchange rate.

References

1) a) T. Kuratsuji, S. Kawase, and T. Shima, Jpn. Tokkyo Koho 56-29006; *Chem. Abst.*, **83**, 61532k (1975). b) A. Shimozuma, T. Asai, M. Hosoi, H. Aoki, and M. Masuda, Jpn. Tokkyo Koho 56-46973 (1981); *Chem. Abst.*, **83**, 80723q (1975). c) S. Kumakawa, H. Yoshikawa, and I. Hamana, Jpn. Tokkyo Koho 57-2808 (1982); *Chem. Abst.*, **83**, 207467s (1975).

2) B. Raeck and H. Schirp, *Org. Synth.*, Coll. Vol. 5, 813 (1973).

3) E. McNelis, *J. Org. Chem.*, **30**, 1209 (1965).

4) J. Yamashita, K. Enomoto, H. Ebisawa, and S. Kato, *Yuki Gosei Kagaku Kyokai Shi*, **20**, 501 (1962).

5) K. Matsuoka, F. Kitao, and K. Konishi, *Kogyo Kagaku Zasshi*, **74**, 77 (1971).

6) J. Ratusky and R. Tykva, *J. Labelled Compd.*, **5**, 211 (1969).

7) Y. Dozen, *Bull. Chem. Soc. Jpn.*, **41**, 664 (1968).

8) J. Yamashita, K. Kurashima, and S. Kato, *Yuki Gosei Kagaku Kyokai Shi*, **20**, 277 (1962).

9) Y. Dozen, S. Fujishima, and H. Shingu, *Thermochim. Acta*, **25**, 209 (1978).

10) The reason why the reaction in naphthalene gave the best yield of **1** seems to be that some carboxylic groups of **4** are introduced into naphthalene as a dispersion medium to give naphthalenecarboxylic acid. We will discuss the transcarboxylation between carboxylic acid and naphthalene in the future.

11) Y. Ogata, M. Tsuchida, and A. Muramoto, *J. Am. Chem. Soc.*, **79**, 6005 (1957).

Physicochemical Stabilization of Lipid Microspheres by Coating with Polysaccharide Derivatives

Anders CARLSSON,† Toshinori SATO, and Junzo SUNAMOTO*,††
Department of Industrial Chemistry, Faculty of Engineering, Nagasaki University, Nagasaki 852
††Laboratory of Materials Science of Polymers and Artificial Cell Technology,
Department of Polymer Chemistry, Faculty of Engineering,
Kyoto University, Sakyo-ku, Yoshida Hommachi, Kyoto 606
(Received July 29, 1988)

A methodology to improve lipid microspheres (LM) as a carrier for lipophilic drugs and their physicochemical properties are described. The LM were prepared from glycerides, glycerol, and phospholipids. The method involves coating of the surface of the LM with a naturally occurring or chemically modified polysaccharide. Special emphasis will be made on cholesterol-bearing pullulan and amylopectin. This is the same approach as that adopted for the stabilization of liposomes. Turbidity measurement revealed that the coating effectively depressed the Ca^{2+}-induced aggregation of the LM. From fluorescence polarization measurements, it was concluded that the fluidity of the LM surface decreased with the polysaccharide coating. Furthermore, the coating effect was investigated by zeta-potential measurements. The coating reduced the negative zeta-potential of the LM to an apparently neutral value.

Lecithin emulsions, so-called lipid microspheres (LM) or microdroplets, have recently gained wide interest as a carrier for lipophilic drugs.[1-4] Liposomes are complementary to LM as a drug carrier system (DDS), especially for hydrophilic drugs. However, there are several advantages of LM over liposomes, such as a high colloidal stability, which makes it possible to store the emulsions for a long period (several months) at room temperature without any noticeable change in their physicochemical properties. Furthermore, they can be produced on an industrial scale, and maybe most importantly, LM can incorporate a relatively large amount of lipophilic substances. LM are oil-in-water emulsions where phospholipids are used as the emulsifying agent.[1] The oil phase can entirely consist of a substance with medicinal potency, such as methoxyflurane used as local anesthesia.[2] Alternatively, a neutral fat is used, e.g. soybean oil, in which lipophilic drugs are dissolved. Steroids[3] and prostaglandins[4] are examples of drugs which have been incorporated in LM and successfully employed in treatments of several diseases.

The methodology for using liposomes in DDS has been relatively well established, and their physicochemical properties and fate in biological systems also have been rather well characterized.[5,6] For liposomes, in addition, much effort have been made to improve their stability and cell-recognizability.[7] However, relatively few significant investigations have been made on LM.

Therefore, we investigated the colloidal stability of LM in the presence of salts and polysaccharides by turbidity measurements. The zeta-potential of the LM was determined by microelectrophoretic measurements in the presence and absence of the polysaccharides. Furthermore, an extensive fluorescence spectroscopic investigation was carried out. The spectral behavior and the fluorescence polarization of two different fluorophores encapsulated in the LM were monitored. The amphiphilic *N*-dansylhexadecylamine (DSHA) and the hydrophobic 1,6-diphenylhexatriene (DPH) were used as the fluorescent probes.

The employed polysaccharides were the same as those previously used for the stabilization of liposomes, namely cholesterol-bearing amylopectin and pullulan.[7] As a comparison, we also investigated the effects of unmodified dextran, amylopectin, and pullulan, respectively. In addition, we used ethyl(2-hydroxyethyl)cellulose (EHEC) which is a nonionic cellulose ether. EHEC is widely used, inter alia, as an emulsifier in foodstuffs and pharmaceutical formulations.[8]

Experimental

Materials. Lipid microspheres (LM) were kindly prepared by Dr. Kiyoshi Iwamoto, Eisai Co., Tsukuba, Japan.[9] One ml of an aqueous LM emulsion contained 100 mg of soybean oil, 12 mg of egg yolk phospholipids, and 25 mg of glycerol which makes the system isoosmotic in normal saline solution. The phospholipids employed (Asahi Chemical Industry Co., Japan) contained 67.0 mol% phosphatidylcholine, 18.6 mol% phosphatidylethanolamine, and 0.8 mol% lysolecithin. In addition, the phospholipids consisted of an unspecified amount of negatively charged lipids, such as phosphatidic acid and phosphatidylserine. The acid value was 17.1 mg/kg. The LM were sealed in glass ampoules under N_2 atmosphere and stored at 5 °C prior to use. All measurements were performed on LM diluted 1000 times (by volume) with water.

Pullulan-50 (M.W. 50000) and amylopectin-112 (M.W. 112000) were kind gifts from Hayashibara Biochemical Laboratories, Inc., Okayama, Japan. Dextran-40 (M.W. 40000) was purchased from Tokyo Kasei Co., Tokyo, and dextran-176 (M.W. 176000) from Nakarai Chemicals Ltd., Kyoto. Ethyl(2-hydroxyethyl)cellulose-146 (EHEC-146; M.W.

† On leave from Physical Chemistry 1, Chemical Center, Lund University, P.O.B. 124, S-221 00, Lund, Sweden.

146000 with 2,12-hydroxyethyl groups and 0.9 ethyl group per glucose unit) was kindly presented by Berol Kemi AB, Stenungsund, Sweden. Cholesterylpullulan (CHP) and cholesterylamylopectin (CHAp) were prepared according to the procedure described elsewhere.[10] CHP was synthesized from pullulan-61 (M.W. 61000) in Dojindo Laboratories, Kumamoto, Japan. This sample contained 1.0 cholesteryl group per 100 glucose units (analyzed by ^{1}H NMR) and is coded as CHP-61-1.0. Another CHP sample was synthesized in this laboratory (by the courtesy of K. Sakai) from pullulan-50 and contained 1.9 cholesteryl groups per 100 anhydroglucose units. This is coded as CHP-50-1.9. CHAp was synthesized from amylopectin-112 and it contained 1.8 cholesteryl groups per 100 glucose units and is coded as CHAp-112-1.8.

Both *N*-dansylhexadecylamine (DSHA) and 1,6-diphenyl-1,3,5-hexatriene (DPH) were the same as those used in previous studies.[11,12] All other reagents were of analytical grade and used without further purification. Membrane-filtrated water (Milli-Q, Millipore Corp., Bedford, USA) was used in all experiments and all glass wares were washed in dichromate-sulfuric acid and rinsed carefully with pure water.

Turbidity Measurements. An appropriate amount of electrolyte solution was added to a cuvette cell containing the LM emulsion diluted 1 : 1000 and preincubated at a given temperature (adjusted within ±0.5 °C). The turbidity (the optical density increase) was recorded at 600 nm as a function of time on a Hitachi 200-10 recording spectrophotometer, equipped with a thermoregulated cell compartment as previously described.[13] No stirring of the emulsion was performed. The results are presented as turbidity change $\Delta\tau$, calculated from $\tau_t-\tau_0$, where τ_t is the turbidity at time t and τ_0 is the turbidity of the LM emulsion at time zero without salt (τ_0 was typically 0.2 absorbance unit at λ=600 nm).

Zeta-Potential Measurements. Microelectrophoretic measurements were carried out on a Laser Zee Meter model 501 (PenKem, Inc., New York). In general, for charged particles, the zeta-potential ζ (V) is related to the electrophoretic mobility v ($m^2V^{-1}s^{-1}$) by the following equation:[14,15]

$$\zeta = v\eta/\{\varepsilon_r\varepsilon_0 f(\kappa, R)\} \quad (1)$$

where η is the viscosity of the medium, ε_r is the relative permittivity of the medium, ε_0 is the permittivity of free space, κ is the Debye-Hückel parameter, and R is the particle radius. For spherical particles at relatively low ionic strength, $f(\kappa, R)$=2/3 and thus Eq. 1 becomes the following:

$$\zeta = 3v\eta/(2\varepsilon_r\varepsilon_0) \quad (2)$$

In an aqueous solution at 20 °C Eq. 2 reduces to

$$\zeta = 2.126 \times 10^6 v \quad (3)$$

Actually, the instrument reads out ζ directly as calculated automatically from ζ=1.417×10^6 v, assuming that the measurement is carried out in an aqueous solution at 20 °C and that $f(\kappa, R)$ is unity. However, the latter assumption is only valid at relatively high ionic strength. In fact, we performed most of the measurements without salt or at low ionic strength (e.g. 5 mM $CaCl_2$). This means a transformation is necessary.[15]

The measurements of ζ were made on LM diluted 1 : 1000 over a temperature range of 20—24 °C. Since both ε_r and η are temperature dependent, the ζ-potential was corrected to 20 °C by the relation: $\zeta_{corr.}=\zeta_{meas.}[1-0.02(t-20)]$, where t (°C) is the actual temperature at which the measurement was made.

When polymer was added, the system was sonicated with a probe-type sonicator for 1 min (20 W) at 0 °C. The final polymer concentration in the cuvette cell was 0.1 wt%. This means that one can discard the effect of added polymer on the viscosity of the sample emulsion (cf. Eqs. 1 and 2). When salt was added, normally 3-4 measurements were made on a freshly prepared LM-salt sample and the whole procedure (from the addition of salt to the recording of ζ) was completed within 4 min.

Fluorescence and Fluorescence Polarization Measurements. The procedures were essentially the same as those previously adopted for the characterization of liposomes.[11-13,16,17] A small amount of the fluorescent probe dissolved in THF was added to the LM emulsion (diluted 1 : 1000), which also contained appropriate amounts of salt and/or polymer. The resulting mixture was then sonified on a Tomy UR-200P probe-type sonicator (20 W, duty 40 on the meter of the instrument) for 2 min at 60—70 °C under N_2 atmosphere. The final concentrations of DSHA and DPH in the LM were 1×10^{-6} M (M=mol dm^{-3}) and 2.5×10^{-8} M, respectively. The molar ratio of the fluorescent probe to the phospholipid was 1/15 for DSHA and 1/615 for DPH, respectively.

Spectral measurements were performed on a Hitachi 650-10S fluorescence spectrophotometer equipped with a thermoregulated cell compartment. Fluorescence polarizations were measured out on a Union Giken FS-501S fluorescence polarization spectrophotometer equipped with a thermoregulated cell compartment and a magnetic stirrer. A Sord Microcomputer M 200 Mark II system was combined with the instrument to control the measurement conditions and collect the data. DSHA was excited at 340 nm and its fluorescence was detected using a sharp cut-off filter Y-46 (Hoya Glass Works, Tokyo) to shut out the light of wavelengths less than 440 nm. DPH was excited at 360 nm and an L-39 filter was employed to cut the light below 370 nm. The degree of fluorescence polarization p was calculated by the following equation:[18]

$$p = (I_{VV} - C_f I_{VH})/(I_{VV} + C_f I_{VH}) \quad (4)$$

where I is the fluorescence intensity and subscripts V and H refer to the vertical and horizontal orientations of the excitation (first subscript) and analyzer (second) polarizers, respectively. The factor C_f ($=I_{HV}/I_{HH}$) corrects for artifacts arising from mismatched detectors.[19] All the I-values were taken as an average of at least 20 runs, with a gate time of 1 second. Before the computation of p, the intensity data were corrected by subtracting the intensity from a conventional LM emulsion. This was done in order to avoid artifacts arising from light scattering and fluorescent impurities which otherwise would yield a too high p-value.[19]

Table 1. Zeta-Potentials for LM at 20.0°C and Different Ca^{2+}- and Na^{+}-Ion Concentrations

	C_{salt}/mM	ζ/mV[a]
Without salt		−62.9±4.2
Ca^{2+}	0.5	−28.1±2.5
	1.0	−14.7±1.8
	2.0	−7.5±1.4
	3.0	0
Na^{+}	15	−29.4±2.9
	30	−20.7±1.5
	60	−9.4±1.3
	90	0

a) Average of at least 6 measurements. Error limits correspond to single standard deviations.

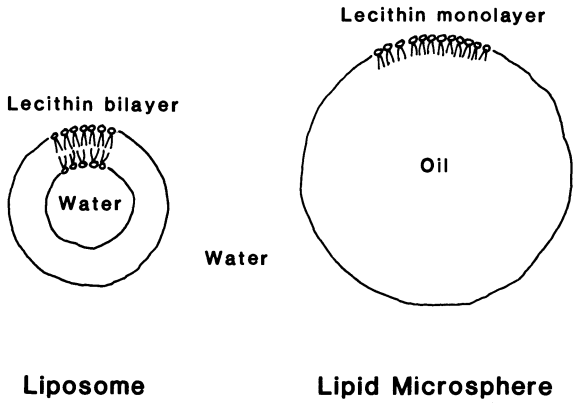

Fig. 1. Schematic representation of the structures of liposome and lipid microsphere.

Results and Discussion

As reported so far by Sunamoto and his co-workers,[7] liposomes can be effectively stabilized by coating the surface with a naturally occurring polysaccharide which bears cholesteryl groups in part. As we mentioned under Experimental the LM contain anionic lipids. Therefore, the surface of the LM employed in this work is negatively charged (Table 1), and the LM easily aggregate and are salted-out upon the addition of small amounts of electrolytes (Fig. 2). If one realizes the structural similarity of the LM surface, which is considered to be covered by a lipid monolayer, to that of liposomes as schematically represented in Fig. 1, it seems possible to also coat the LM with polymers in order to improve their structural stability. Therefore we investigated the colloidal stability of LM after coating the surface with different polysaccharides, particularly focusing on the effect of salt addition.

Due to the large particle size of the oil droplets and the difference in the refractive index between water and oil, the LM emulsion scatters light when irradiated. This feature was utilized to monitor the aggregation of LM in the presence of salt and different water-soluble polymers. Electrolytes were added up to the concentration corresponding to that under the physiological conditions. (In general, for mammalian the extra cellular fluid contains 145 mM Na^{+}, 5 mM K^{+}, 2.5—5 mM Ca^{2+}, and 1—2 mM Mg^{2+}.) The polymer concentration was arbitrarely chosen to be approximately

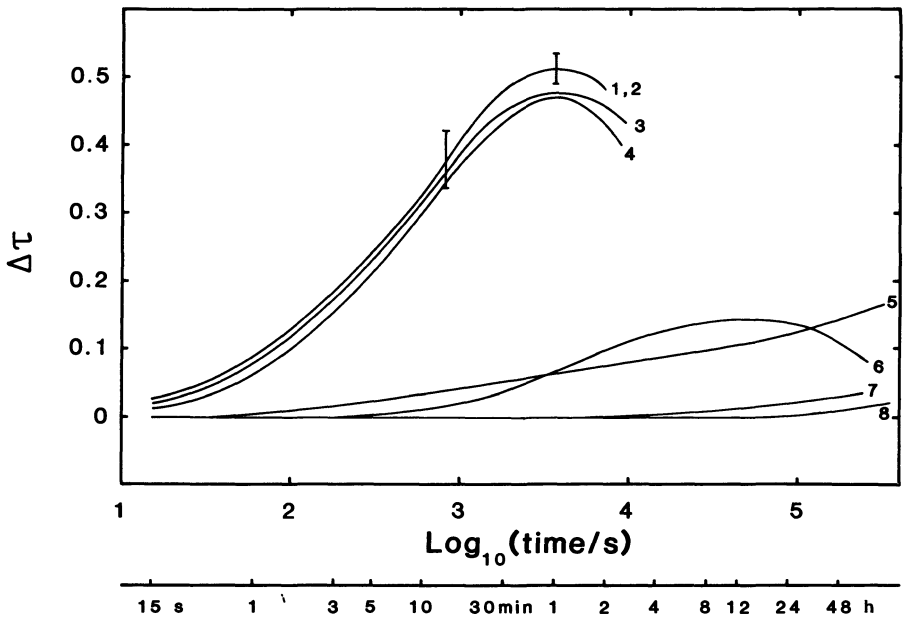

Fig. 2. Turbidity change ($\Delta\tau$) vs. time for LM (diluted 1:1000) after addition of 5 mM aqueous $CaCl_2$ at 37.0°C. 1: Without polysaccharide; 2: dextran-40 (0.96 mg ml^{-1}); 3: amylopectin-112 (0.95 mg ml^{-1}); 4: dextran-176 (0.95 mg ml^{-1}); 5: EHEC-146 (0.92 mg ml^{-1}); 6: pullulan-50 (0.95 mg ml^{-1}); 7: CHP-50-1.9 (0.87 mg ml^{-1}); 8: CHAp-112-1.8 (0.95 mg ml^{-1}).

0.9 mg per ml of LM emulsion (diluted 1:1000).

Presented in Fig. 2 are the turbidity measurements for LM in 5 mM aqueous $CaCl_2$ at 37 °C as a function of time. In the polymer-free system, a relatively rapid increase in the turbidity was observed, and after about 1 h $\Delta\tau$ reached its maximum. Due to precipitation of the LM aggregates, no further measurements were made after $\Delta\tau_{max}$. The same turbidity increase was recorded also at 25 °C. An almost clear solution was obtained if the samples were kept for 1—2 days in the presence of salts. Though not presented here, the effect of 150 mM Na^+-ion was less than that of 5 mM Ca^{2+}-ion. This was reflected through a slower increase in $\Delta\tau$ and a lower $\Delta\tau_{max}$. Even the addition of Na^+-ion caused a precipitation of the LM aggregates and led to a cleared supernatant. However, this was not observed until one week later. In the absence of salts, no significant change in turbidity was observed even after several months. These results suggest to us that we have to seriously consider the colloidal stability of LM in the blood stream when LM are employed as a carrier for lipophilic drugs, especially at higher concentrations.

However, if either CHAP-112-1.8, CHP-50-1.9, EHEC-146, or pullulan-50 was added to the LM before the addition of Ca^{2+}-ion, the aggregation behavior was dramatically altered (Fig. 2). This was reflected on the almost invariant $\Delta\tau$ values. Especially, the cholesterol-bearing polymers were superior in supressing the Ca^{2+}-induced aggregation, For example, the CHAP-112-1.8-coated LM showed no significant turbidity change even after 48 h. This means that these polysaccharides adsorb to the LM and effectively coat the surface, thereby largely preventing the salt-induced aggregation through steric stabilization.[20,21] The effect of pullulan-50 was noteworthy compared to the other three unmodified polysaccharides (amylopectin-112, dextran-40, and dextran-176). The three latter polymers completely lacked the ability to prevent LM aggregation. Even a three-fold increase in the concentration of amylopectin-112 did not significantly affect the result. Pullulan is a rather linear polymer and adsorbs more effectively to the LM surface than the other branched polymers.[13] The bulkyness of a branched polymer leads to a less surface coverage than that of a linear one.

Presented in Table 1 are the zeta-potential data for LM diluted 1:1000 at 20 °C as a function of the Ca^{2+}- and the Na^+-ion concentrations. The zeta-potential of the conventional LM employed in this work was approximately −63 mV. As expected, the addition of Na^+- or Ca^{2+}-ion led to a significant reduction in ζ, with the divalent cation substantially more effective than the monovalent,[22] as seen from the effective salt concentrations for to become zero. Thus, when the electrostatic double-layer repulsion is diminished, the colloidal particles can easily aggregate. No measurements were performed on systems in which both Ca^{2+}- and Na^+-ions were simultaneously present at the physiological concentration. If the Ca^{2+}-ion concentration is greater than 3% of the Na^+-ion concentration, the surface potential is solely determined by the Ca^{2+} ions.[22] Here, it should be pointed out that the obtained ζ-values probably are overestimated at the highest salt concentrations since $f(\kappa, R)$ in Eq. 1 appproaches unity at high ionic strength.[15] However, the measurements gave a qualitative picture of the changes of the surface potential upon the salt addition, and no efforts were made to correct the data.

Table 2. Zeta-Potentials for LM–Polysaccharide Systems[a] at 20.0 °C

Polymer	Concentration/mg ml^{-1}	ζ/mV
Dextran-40	1.00	−47.5
Dextran-176	1.01	−45.2
Pullulan-50	0.98	−32.6
EHEC-146	0.97	−13.5
CHP-61-1.0	0.98	−25.3
CHP-50-1.9	0.87	−18.8
CHAp-112-1.8	0.95	−11.3

a) The LM were diluted by water 1000 times (by vol.) prior to the addition of polysaccharide solution.

Table 2 presents the zeta-potentials of LM when various polysaccharide were added to the LM. The addition of all polymers caused a decrease in the zeta-potential. When a polymer adsorbs to the LM surface the charge density remains the same. However, due to the adsorbed polymer layer, the slipping plane is now moved to a point further out from the surface and therefore a lower ζ-potential is recorded. The effect of the two dextran derivatives was considerably less than that of the others. The results suggest that the coating efficiency by dextran is relatively low. In all cases in which the polymers were added, the addition of Ca^{2-}-ion to a concentration of 5 mM completely abolished the surface potential of the LM.

Clearly from the results the stability of the LM was largely affected by salts. The LM were especially sensitive to a divalent cation even at low concentration such as 5 mM Ca^{2+} (which is approximately the physiological concentration of the ion). The aggregation of the LM and the subsequent precipitation were directly observed as changes in the turbidity of the LM emulsions (Fig. 2).

The fluorescence polarization technique has frequently been used for the determination of the microviscosity of a molecular assembly, such as lipid bilayer membranes.[23] An important advantage of this technique is that the polarization data in terms of fluidity can be interpreted without further mathematical treatment. Presented in Fig. 3 are the p-values (as defined from Eq. 4) of DPH (top) and DSHA (bottom) in LM diluted 1:1000 as a function of temperature. Irrespective of the temperature, the p-

values of DPH in the hydrophobic core[23] of the LM were lower than those obtained in liposomal membranes.[12,16] This indicates that the fluidity of the interior core of the LM is higher compared to that of the lipid bilayers. Lipid bilayer membranes provide a more confined hydrophobic domain which leads to a more restricted motion of the fluorescent probe. The p-value of DPH in the LM decreased with an increase in the temperature, which indicates an increase in the fluidity of the interior core of the LM at higher temperatures. The fluorescence emission maximum (E_{max}) of DPH in the LM was 429 nm and constant over the range of 15—50 °C. The same emission maximum has been obtained when DPH was dissolved in both benzene and liposomes.[16,23] This indicates that DPH is locating in a very hydrophobic domain of the LM.

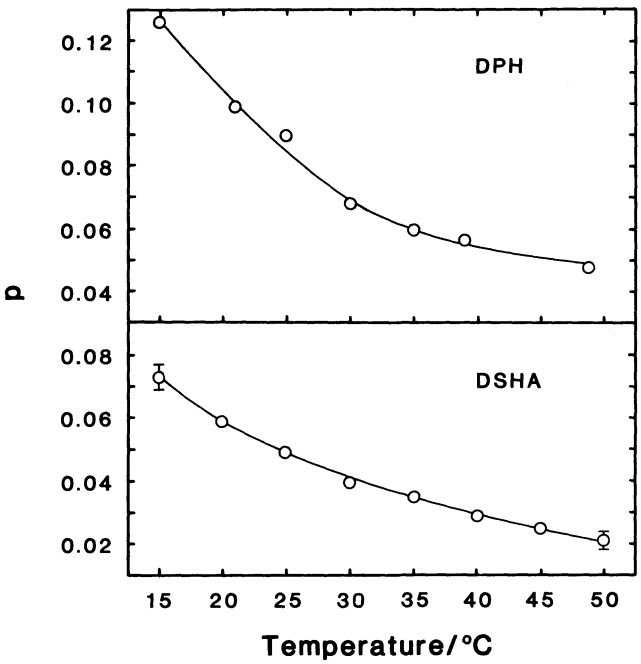

Fig. 3. Fluorescence polarization (p) of DPH (top) and DHSA (bottom) in LM (diluted 1:1000) as a function of temperature. The concentrations of DPH and DSHA in the LM were 2.5×10^{-8} M and 1×10^{-6} M, respectively.

The p-values of DSHA in LM (diluted 1:1000) as a function of temperature are given in Fig. 3 (bottom). DSHA is relatively amphiphilic and the dansyl moiety of DSHA is believed to locate in polar region close to the membrane surface in liposomal membranes.[11] Consequently, it is assumed that when DSHA is added to LM the polar dansyl group is in the region close to the microsphere-water interface and is surrounded by phospholipids. As for DPH, the p-value of DSHA also decreased on heating. This reflects that the fluidity of the phospholipid monolayer of the LM is also temperature dependent. The present data suggest either that the LM surface is more fluid compared with that of a liposomal surface, or that the probe is locating in a more fluid region close to the oil phase. For example, we obtained a p-value of 0.03 at 37 °C, while for egg L single-walled liposomes the p-value was 0.06 at the same temperature.[11] Over the temperature range studied, the emission maximum of DSHA was constant at 483 nm. This is 30—35 nm lower than that in single-walled liposomes,[11,12] and 7 nm lower than the value in water, where DSHA molecules self-aggregate.[11] This blue shift in E_{max} of DSHA in LM indicates that the probe is in a less polar environment compared with that in bilayer membranes of liposomes.

Emission maxima and p-values of DSHA at 37 °C are summarized in Table 3. The addition of Ca^{2+}- and Na^{+}-ions to concentrations of 5 and 150 mM, respectively, did not lead to any significant change in the p-value of DSHA. On the basis of this result, we did not investigate the salt effect on the DPH polarization.

Table 3. Fluorescence Emission Maxima and p-Values of DSHA (1×10^{-6} M) in LM (diluted 1:1000) at 37.0 °C

	Concentration		E_{max}/nm	p
	Salt/mM	Polymer/mg ml^{-1}		
No additives			483	0.031
Ca^{2+}	1		480	0.034
	5		479	0.029
	50		477	0.030
Na^{+}	150		480	0.029
Dextran-40		0.99		0.036
Dextran-176		1.00		0.032
Dextran-176+Ca^{2+}	5	1.00		0.030
Pullulan-50		1.01	482	0.038
Pullulan-50+Ca^{2+}	5	1.01	478	0.030
EHEC-146		1.0	478	0.041
EHEC-146+Ca^{2+}	5	1.0	478	0.038
CHP-61-1.0		1.00	482	0.046
CHP-61-1.0+Ca^{2+}	5	1.00	480	0.043
CHAp-112-1.8		1.00	478	0.057
CHAp-112-1.8+Ca^{2+}	5	1.00		0.061

However, a slight blue shift in E_{max} (3—6 nm) was observed when salts were present, probably because of the movement of the probe into a more hydrophobic domain upon the dehydration around the polar head group. The shift was more pronounced by adding 50 mM Ca^{2+}-ion. The addition of dextran-40 and -176, pullulan-50, and EHEC-146 showed no or little effect on the p-value of DSHA. However, the cholesterol-bearing polysaccharides (CHP-61-1.0 and CHAp-112-1.8) considerably increased the polarization of DSHA. Especially the addition of the latter one led to a two-fold increase in the p-value. This suggests that when these two polymers adsorb onto the LM surface, the cholesteryl group behaves as a hydrophobic anchor in the surface lipid layer. This would result in a lower fluidity of the surface of the LM. Though data are not shown, the difference in the p-values between the two groups of polymers was more pronounced at lower temperatures (15—30 °C). Even the addition of Ca^{2+} to a concentration of 5 mM to the LM-polymer samples did not significantly change the p-value.

After the addition of DSHA, the LM-EHEC-146 sample was sonicated under milder conditions (3 short flashes at 40 °C under N_2 atmosphere) in order to avoid phase separation during this procedure. Of the polymers employed in this work, EHEC-146 is the most hydrophobic one. This is evident from a lower critical solution temperature of an aqueous EHEC solution.[24] The change in the procedure for encapsulating the probe did not significantly alter the p-value of DSHA in a polymer-free LM sample (Fig. 3).

Judging from the results through the present investigation, we could conclude that the LM can effectively be coated by cholesterol-bearing polysaccharides similarly to liposomes. The coating of the LM surface with the polysaccharide derivatives led to a reduction of the divalent metal ion-induced aggregation of the LM. This is very promising for LM to be utilized as an improved carrier for lipophilic drug.

The stay of A. Carlsson in Japan was supported by a grant from the Swedish National Board for Technical Development. Comments on this work from Prof. Björn Lindman and Dr. Björn Bergenståhl are gratefully acknowledged. The instrument for microelectrophoretic measurements was kindly put at our disposal by Tsukuba Research Laboratories, Eisai Co. This research was financially supported by a Grant-in-Aid (No. 62850151) from the Ministry of Education, Science and Culture.

References

1) S. S. Davies, C. Washington, P. West, L. Illum, G. Liversidge, L. Sternson, and R. Kirsh, "Biological Approaches to the Controlled Delivery of Drugs," ed by R. L. Juliano, *Ann. N. Y. Acad. Sci.*, **507**, 75 (1987).

2) D. H. Haynes and A. F. Kirkpatrick, *Anesthesiology*, **63**, 490 (1985).

3) Y. Mizushima, T. Hamano, and K. Yokoyama, *Ann. Rheum. Dis.*, **41**, 263 (1982).

4) Y. Mizushima, A. Yanagawa, and K. Hoshi, *J. Pharm. Pharmacol.*, **35**, 666 (1983).

5) F. Szoka and D. Papahadjopoulos, *Ann. Rev. Biophys. Bioeng.*, **9**, 467 (1980).

6) P. Machy and L. Leserman, "Liposomes in Cell Biology and Pharmacology," John Libbey & Co., London (1987).

7) J. Sunamoto and K. Iwamoto, "CRC Critical Reviews in Therapeutic Drug Carrier Systems," **2**, 117 (1986).

8) G. K. Greminger and K. L. Krumel, "Handbook of Water-Soluble Gums and Resins," ed by R. L. Davidson, McGraw-Hill, New York (1980), Chap. 3.

9) The mean diameter of the LM used in this work was approximately 270 nm with a standard deviation of 60 nm (determined by a Coulter N4 Sub-micron Particle Analyzer, Coulter Electronics, Inc., Hialeah, Florida).

10) J. Sunamoto, T. Sato, M. Hirota, K. Fukushima, K. Hiratani, and K. Hara, *Biochim. Biophys. Acta*, **898**, 323 (1987).

11) K. Iwamoto and J. Sunamoto, *Bull. Chem. Soc. Jpn.*, **54**, 399 (1981).

12) K. Iwamoto, J. Sunamoto, K. Inoue, T. Endo, and S. Nojima, *Biochim. Biophys. Acta*, **691**, 44 (1982).

13) J. Sunamoto, K. Iwamoto, H. Kondo, and S. Shinkai, *J. Biochem.*, **88**, 1219 (1980).

14) E. G. Richards, "An Introduction to Physical Properties of Large Molecules in Solution," IUPAB Biophysics Series, Cambridge University Press (1980), Chap. 9.

15) P. Sennett and J. P. Olivier, *Ind. Eng. Chem.*, **57**, 33 (1965).

16) J. Sunamoto, K. Iwamoto, K. Inoue, T. Endo, and S. Nojima, *Biochim. Biophys. Acta*, **685**, 283 (1982).

17) K. Iwamoto and J. Sunamoto, *J. Biochem.*, **91**, 975 (1982).

18) E. N. Hudson, "Fluorescence Spectroscopy," ed by A. J. Pesce, C.-G. Rosén, and T. L. Pasby, Marcel Dekker, New York (1971), Chap. 4.

19) T. L. Pasby, in Ref. 18, Chap. 6.

20) W. Norde, "Microspheres and Drug Therapy. Pharmaceutical, Immunological and Medical Aspects," ed by S. S. Davies, L. Illum, J. G. McVie, and E. Tomlinson, Elsevier Science, Amsterdam (1984), Chap. 3.

21) B. Bergenståhl, "Gums and Stabilizers for the Food Industry 4," ed by G. O. Phillips, D. J. Wedlock, and P. B. Williams, IRL Press, Oxford, Washington D. C. (1988), p. 363.

22) J. N. Israelachvili, "Intermolecular and Surface Forces," Academic Press, London (1985), Chap. 12.

23) M. Shinitzky and Y. Barenholz, *Biochim. Biophys. Acta*, **515**, 367 (1978).

24) A 0.1% water-EHEC-146 solution has a cloud point of 75 °C. A. Carlsson, G. Karlström, B. Lindman, and O. Stenberg, *Colloid Polym. Sci.*, **266**, 1031 (1988).

Facile Synthesis of (2*S*,3*R*,4*R*)-2-Hydroxymethyl-3,4-pyrrolidinediol and 4-Acetamido-1,2,3-tri-*O*-acetyl-4-deoxy-L-xylopyranose from the Photoproduct of D-Mannose

Akira HOSAKA, Shuji ICHIKAWA, Hiroko SHINDO, and Tadashi SATO*
Department of Applied Chemistry, Waseda University,
Ookubo 3, Shinjuku-ku, Tokyo 160
(Received July 30, 1988)

Synthesis of (2*S*,3*R*,4*R*)-2-hydroxymethyl-3,4-pyrrolidinediol and 4-acetamido-1,2,3-tri-*O*-acetyl-4-deoxy-L-xylopyranose were attained in four steps from D-mannose, using iron(III)-catalyzed photoreaction as a key reaction.

In our previous papers,[1] we reported that UV irradiation of D-glucose (**1**) or D-mannose (**2**) in the presence of iron(III) chloride followed by acetylation gave 1,2,3-tri-*O*-acetyl-4-*O*-formyl-D-arabinopyranose (**4**), while D-galactose (**3**) gave 1,2,3-tri-*O*-acetyl-4-*O*-formyl-D-lyxopyranose (**5**) under the same conditions. The most characteristic point of the reaction is that the aldohexoses produce aldopentoses in which only C4 hydroxyl group is protected by formyl group.

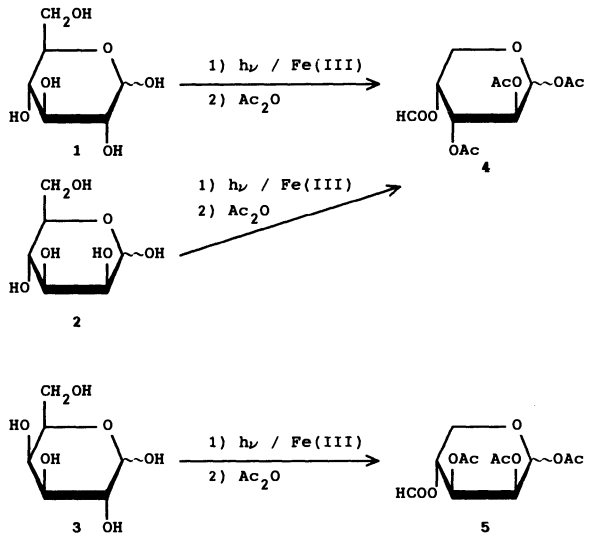

In order to explore the applicability of the photoproducts for synthetic purpose, we chose a pyrrolidine derivative and an amino sugar as the target compounds.

Some hydroxylated pyrrolidine derivatives have been known to possess glycosidase inhibition or immunoregulative activities.[2,3] In order to clarify the structure–bioactivity relationship, it is biologically important to prepare epimers of the bioactive molecules. Several stereoisomers of 2-hydroxymethyl-3,4-pyrrolidinediol have been synthesized.[2–6] We envisioned that (2*S*,3*R*,4*R*)-2-hydroxymethyl-3,4-pyrrolidinediol (**9**) could be synthesized quite easily by starting from our photoproduct.

In this paper we describe the facile synthesis of 4-acetamido-1,2,3-tri-*O*-acetyl-4-deoxy-L-xylopyranose (**8**) as well as **9**, using the photoproduct **4** as a key intermediate. The compounds **8** and **9** have been synthesized from 2-amino-2-deoxy-D-glucose in nine steps.[5]

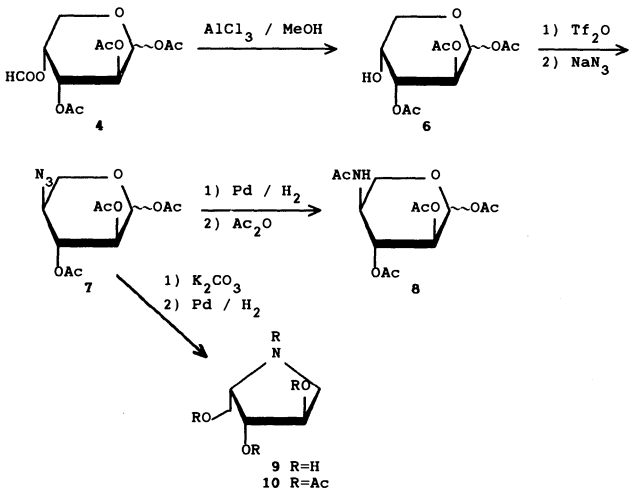

Although we have utilized iron(III) chloride as the catalyst for the selective photocleavage at C1–C2 bond of the carbohydrates, the reaction was accompanied by the formation of brown material, which adhered to the inside of the vessel, causing inconvenience for the large-scale preparation. We found that iron(III) trifluoromethanesulfonate (triflate) is superior to the chloride as shown below.

A pyridine solution of D-mannose (**2**) containing iron(III) triflate or iron(III) chloride was irradiated with a high-pressure mercury lamp in a Pyrex vessel while oxygen gas was bubbled through. After the irradiation for 8 h or 24 h, the products were isolated as acetates by treating the irradiated pyridine solution with acetic anhydride. The major product was an anomeric mixture of an aldopentose derivative **4**, along with the starting material as pentaacetate. The results are shown in Table 1. Evidently iron(III) triflate catalyzed the reaction more effectively than iron(III) chloride, and no solid material separated out during the irradiation under these conditions. In view of these results, we used 1/100 equiv of iron(III) triflate

Table 1. Catalytic Activities of Iron(III) Chloride and Iron(III) Triflate

Carbohydrate	Iron salt	Mole ratio to carbohydrate	Reaction time	Relative yield/%	
			h	Product	Starting material
D-Glucose	$FeCl_3$	1	24	**4** 45	55
	$Fe(OTf)_3$	1/100	8	**4** 44	56
D-Mannose	$FeCl_3$	1	24	**4** 17	83
	$Fe(OTf)_3$	1/100	8	**4** 57	43
D-Galactose	$FeCl_3$	1	24	**5** 40	60
	$Fe(OTf)_3$	1/100	8	**5** 56	44

for the large-scale preparation.

Treatment of the crude material, obtained from **2** through the irradiation and succeeding acetylation, with aluminium chloride in aqueous methanol[1] gave 1,2,3-tri-*O*-acetyl-D-arabinopyranose (**6**) in 24% overall yield from **2** after the purification on a silica-gel chromatography. Triflation of **6** with trifluoromethanesulfonic anhydride followed by treatment with sodium azide gave 1,2,3-tri-*O*-acetyl-4-azido-4-deoxy-L-xylopyranose (**7**) in 55% yield. It has been reported that no side reactions occur under these conditions.[7]

Catalytic hydrogenation of **7** followed by acetylation gave **8** in 27% yield. Deacetylation of **7** with potassium carbonate in methanol followed by catalytic hydrogenation gave **9** in 77% yield, after purification on an ion-exchange chromatography. Acetylation of **9** gave tetraacetate **10** in 55% yield. Treatment of the acetate with hydrochloric acid afforded the corresponding hydrochloride in 83% yield. The ^{13}C NMR spectrum of the hydrochloride was identical with that reported for its enantiomer.[6]

Experimental

General. Column chromatography was performed on Wakogel C-200 (Wako), and TLC was performed on Kieselgel 60 GF_{254} (Merck). ^1H NMR spectra (60 MHz) were recorded on a Hitachi R-24 spectrometer. ^1H NMR (90 MHz) and ^{13}C NMR spectra were measured on a Hitachi R-90H spectrometer, high-resolution mass spectra on a JEOL DX-300 mass spectrometer, IR spectra on a Shimadzu IR-400 spectrometer, and optical rotations on a JASCO DIP-4 polarimeter.

The irradiations were carried out using a high-pressure mercury lamp [Sen SL-2000 (2 kW)] at the temperature of running water.

1,2,3-Tri-*O*-acetyl-D-arabinopyranose (6). A pyridine solution (900 cm^3) of D-mannose (9 g, 50.0 mmol) and iron(III) triflate (252 mg, 5.01×10^{-1} mmol) was irradiated in a Pyrex vessel for 8 h while oxygen gas was bubbled through. Acetic anhydride (70 cm^3, 0.742 mmol) was added to the solution, and the solution was stirred for 14 h at room temp. The solution was concentrated under reduced pressure (35 °C) and the residue was partitioned between diethyl ether (100 cm^3) and brine (100 cm^3). After extraction of the aqueous layer with diethyl ether (100 $cm^3\times2$), the combined ether solution was dried over $MgSO_4$. The solvent was removed in vacuo, and the residue was dissolved in methanol (500 cm^3) containing aluminium chloride (410 mg, 3.07 mmol) and water (25 cm^3). After stirred for 36 h at room temp, the solution was concentrated in vacuo, and water (50 cm^3) was added. The mixture was shaken with dichloromethane, the extract was dried over $MgSO_4$, and the solvent was removed in vacuo. The residue was chromatographed (silica gel/Et_2O) to afford **6** (3.26 g, 24%) as a syrup (R_f=0.30, Et_2O).[1]

1,2,3-Tri-*O*-acetyl-4-azido-4-deoxy-L-xylopyranose (7). To a stirred solution of **6** (1.85 g, 6.70 mmol) in a mixture of dry dichloromethane (160 cm^3) and dry pyridine (0.81 cm^3) was added trifluoromethanesulfonic anhydride (1.24 cm^3, 7.37 mmol) dropwise at 0 °C under an atmosphere of nitrogen. After stirring for 1 h at 0 °C, the solution was poured into 100 cm^3 of ice-water. The organic layer was separated, and the aqueous layer was extracted with two 50 cm^3 portions of dichloromethane. The combined extract was dried over $MgSO_4$ and the solvent was removed to give a brown syrup. The crude triflate was dissolved in *N,N'*-dimethylformamide (80 cm^3), and sodium azide (435 mg, 6.70 mmol) and 15-crown-5 (1.33 cm^3, 6.70 mmol) were added to the solution. After stirred for 24 h at room temp, the solution was concentrated and the residue was partitioned between diethyl ether (30 cm^3) and water (30 cm^3). After extraction of the aqueous layer with diethyl ether (30 $cm^3\times2$), the combined extract was dried over $MgSO_4$. The solvent was evaporated and the residue was chromatographed (silica gel/Et_2O) to afford **7** (1.11 g, 55%, α/β=1/2) as a colorless syrup (R_f=0.74, Et_2O). IR (neat) ν_{max} 2110, 1750 cm^{-1}. ^1H NMR ($CDCl_3$) δ=2.00, 2.03, 2.08, 2.09, 2.11, 2.16 (9H, singlets, Ac), 3.39—4.14 (3H, m, H_4, H_5, $H_{5'}$), 4.88—5.45 (2H, m, H_2, H_3), 5.61 (1/3H, d, J=7.4 Hz, α-H_1), 6.19 (2/3H, d, J=3.5 Hz, β-H_1). ^{13}C NMR ($CDCl_3$), for α anomer, δ=58.48 (C_4), 63.94 (C_5), 70.10 (C_3), 72.93 (C_2), 92.14 (C_1); for β anomer, δ=59.09 (C_4), 61.56 (C_5), 69.49 (C_3), 70.43 (C_2), 89.34 (C_1).

4-Acetamido-1,2,3-tri-*O*-acetyl-4-deoxy-L-xylopyranose (8). A solution of **7** (660 mg, 2.19 mmol) in acetic acid (25 cm^3) was hydrogenated in the presence of 10% Pd-C (900 mg) under hydrogen (1 atm) for 2 h. The catalyst was filtered and the solvent was evaporated. To the residue dissolved in pyridine (30 cm^3) was added acetic anhydride (1.5 cm^3, 15.9 mol) and the mixture was stirred for 18 h at room temp. The solution was concentrated and the residue was partitioned between dichloromethane (15 cm^3) and brine (15 cm^3). After extraction of the aqueous layer with dichloromethane (15 $cm^3\times2$), the combined extract was dried over $MgSO_4$. The solvent was removed and the residue was chromatographed on silica gel (MeOH). A fraction corresponding to R_f 0.65 (MeOH) was β-8 (187 mg, 27%), a syrup, $[\alpha]_D^{23}$ −69° (*c* 3.56, MeOH). IR (neat) ν_{max}=3280, 2964, 1750, 1640, 1520 cm^{-1}. ^1H NMR ($CDCl_3$) δ=1.93 (3H, s, NAc), 2.01, 2.07, 2.13 (9H,

singlets, 3×OAc), 3.53—4.03 (3H, m, H_4, H_5, $H_{5'}$), 4.94—5.20 (2H, m, H_2, H_3), 5.96 (1H, bs, NHAc), 6.23 (1H, d, J=3.0 Hz, H_1). ^{13}C NMR ($CDCl_3$) δ=20.43, 20.73 (OAc-Me), 23.05 (NAc-Me), 49.88 (C_4), 62.11 (C_5), 69.27, 69.67 (C_2, C_3), 89.55 (C_1), 168.70, 169.31, 170.04 (OAc-CO), 171.69 (NAc-CO). HRMS, Found: m/z 318.1193. Calcd for $C_{13}H_{20}NO_8$: M+H, 318.1189.

(2*S*,3*R*,4*R*)-2-Hydroxymethyl-3,4-pyrrolidinediol (9). To a stirred solution of **7** (1.00 g, 3.32 mmol) in 10% aqueous methanol (10 cm^3) was added aqueous saturated potassium carbonate solution (0.5 cm^3) at 0 °C. After the solution was stirred for 15 min at 0 °C, acetic acid (25 cm^3) was added. The mixture was stirred under hydrogen (1 atm) with 10% Pd-C (1 g) for 3 days. After removal of the catalyst, the filtrate was concentrated to a volume of 1 cm^3. This solution was loaded onto an acid ion exchange column (Dowex 50X8-100, H^+ form). Acetic acid and inorganic substances were washed away with water and then the basic material was eluted from the column with 2.8% aqueous ammonium hydroxide. The solvent was removed from the eluate to give **9** (342 mg, 77%) as a syrup, ^{13}C NMR (D_2O with dioxane reference) δ=53.57 (C_5), 62.26 (CH_2OH), 64.06 (C_2), 69.30 (dioxane), 79.06, 79.33 (C_3, C_4). HRMS, Found: m/z 102.0568. Calcd for $C_4H_8NO_2$: M−CH_2OH, 102.0555.

Acetylation of **9** with pyridine-acetic anhydride gave acetate **10** in 55% yield as a syrup (R_f=0.50, MeOH: $CHCl_3$=1:15) after purification by column chromatography (silica gel/MeOH:$CHCl_3$=1:15). $[\alpha]_D^{24}$ −19° (c 4.37, MeOH). ^{1}H NMR ($CDCl_3$) δ=2.02—2.06 (12H, singlets), 3.24—3.45 (1H, m), 3.86—4.26 (4H, m), 5.18—5.30 (2H, m). ^{13}C NMR ($CDCl_3$) δ=20.52, 20.64, 20.82 (OAc-Me), 22.17 (NAc-Me), 50.25 (C_5), 55.28 (CH_2OH), 60.10 (C_2), 73.57, 74.12 (C_3, C_4), 169.46, 169.61, 169.77, 169.95 (CO). HRMS, Found: m/z 302.1231. Calcd for $C_{13}H_{20}NO_7$: M+H, 302.1240.

The hydrochloride of **9** was prepared by refluxing a solution of **10** (98 mg, 0.326 mmol) in methanol (2 cm^3) and aqueous HCl (4 mol dm^{-3}, 2 cm^3) for 16 h followed by concentration and purification through a column (Florigil/MeOH). The hydrochloride was obtained as powder (46 mg, 83%). ^{13}C NMR (D_2O with dioxane reference)[6] δ=53.32 (C_5), 60.09 (CH_2OH), 65.67 (C_2), 69.30 (dioxane), 77.14 (C_3, C_4).

References

1) S. Ichikawa, I. Tomita, A. Hosaka, and T. Sato, *Bull. Chem. Soc. Jpn.*, **61**, 513 (1988).

2) G. W. J. Fleet, S. J. Nicholas, P. W. Smith, S. V. Evans, L. E. Fellows, and R. J. Nash, *Tetrahedron Lett.*, **26**, 3127 (1985).

3) Fujisawa Pharmaceutical Co., Ltd., Jpn. Kokai, 61-171465; *Chem. Abstr.*, **106**, 50030n (1987).

4) N. Ikota and A. Hanaki, *Chem. Pharm. Bull.*, **36**, 1143 (1988).

5) H. Paulsen, J. Brüning, K. Propp, and K. Heyns, *Tetrahedron Lett.*, **1968**, 999.

6) D. W. C. Jones, R. J. Nash, E. A. Bell, and J. M. Williams, *Tetrahedron Lett.*, **26**, 3125 (1985).

7) K. C. Nicolaou, R. A. Daines, T. K. Chakraborty, and Y. Ogawa, *J. Am. Chem. Soc.*, **109**, 2821 (1987); K. C. Nicolaou, R. A. Daines, Y. Ogawa, and T. K. Chakraborty, *ibid.*, **110**, 4696 (1988).

Effects of Substituents and Solvents on the Electronic Spectra of 9,10-Dihydro-9,10-*o*-benzenoanthracene-1,4-diones: Intramolecular Charge Transfer

Nobuya KITAGUCHI†
Department of Chemistry, Faculty of Science, Kyoto University,
Kitashirakawa, Sakyo-ku, Kyoto 606
(Received August 2, 1988)

Electronic spectra of substituted 9,10-dihydro-9,10-*o*-benzenoanthracene-1,4-diones (triptycenequinones) in various solvents and that of benzo- and dibenzotriptycenequinones were investigated in this paper. Intramolecular charge-transfer (CT) bands ware observed in triptycenequinone system as a result of intramolecular interaction between benzene ring and benzoquinone moiety. Substituents on the benzene rings strongly affected the CT bands. Electron-donating groups gave absorption maxima at long wavelength. Naphthalene ring gave similar but stronger CT bands than benzene ring. Hammett σ^+ value of substituents gave good linear relationship with the energy of the CT bands. Calculations of reduced charge matrix of triptycenequinones by extended Hückel theory showed that the charge of aromatic ring(s) were transferred to benzoquinone moiety accompanying HOMO–LUMO excitation. Especially, absorption maxima of the methyl-substituted triptycenequinones gave good correlation with the amounts of charge transferred from benzene ring to benzoquinone moiety. These analysis confirmed clearly CT character of the absorption maxima of triptycenequinones. However, solvent effect of these CT bands maxima is not so clear as the substituent effect.

The problem of transannular π–π interaction among neighboring benzene rings in triptycene system is of increasing interest in organic chemistry.[1–10]

On the electronic state of triptycene, Bartlett explained its absorption spectrum by the cross-ring interaction as follows.[1,2]

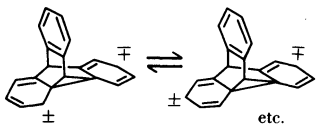

Structure **A**

Wit[3] prepared a variety of heterocyclic triptycenes and reported that the energy of their absorption maxima correlated to the energy calculated by Hückel MO including "through-space resonance" as follows. This fact suggests that "through-space" interactions may exist in triptycene system.

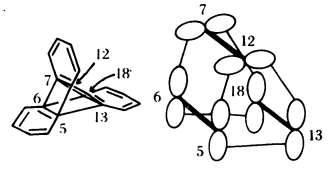

Structure **B**

Investigation of the intramolecular orbital interactions was reported to reveal differences in the nature of the interactions between the three benzene rings of triptycene based on electronic transmission spectroscopy.[4] It was also reported that the LUMO of triptycene is expected to have the significant contribution of the through-bond interaction, on the contrary to the HOMO which include the dominant through-space interaction.[5,6] 9,10-*o*-Benzenoanthracene-1,4,5,8-tetrone and 5,18:7,16:9,14-tri(*o*-benzeno)heptacen-1,4,6,8,10,13,15,17-octone derivatives were examined as electron acceptors in the intermolecular CT complex formation with 2-(1,3-dithiol-2-ylidene)-1,3-dithiole.[7] The properties of radical anions of triptycene bis- and tris-quinones have also been investigated.[8]

Furthermore, Murata observed charge-transfer (CT) transition for symmetry-forbidden CT interaction in methyl- or methoxy- substituted 9,10-*o*-benzenoanthracene-1,4-diones (triptycenequinones) (**1e—i**) using CH_2Cl_2 as a solvent.[9,10]

Thus, according to these previous results above, triptycene system itself has intramolecular through-space interaction between three benzene rings. It is interesting to investigate the change of such intramolecular interaction caused by introducing benzoquinone moiety into triptycene system and a variety of substituents into benzene rings.

In this paper, effect of substituents, (methyl, acetylamino, dichloro) on the absorption spectra of triptycenequinones (**1a—d**) as well as benzotriptycenequinone (**3**), dibenzotriptycenequinone (**4**) and non-aromatic analogue (**2**) will be reported together with solvent effect on substituted triptycenequinones **1a—d**. Some results of those quinones were discussed in view of charge flow induced by HOMO–LUMO excitation calculated with Extended Hückel Theory (EHT).

† Present address: Bio-science Laboratory, Life Science Laboratories, Asahi Chemical Industry Co., Ltd., Samejima 2-1, Fuji city, Shizuoka 416. A part of this work was done in this laboratory.

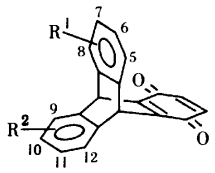

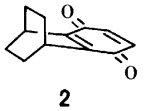

2

1a $R^1=R^2=H$
b $R^1=6\text{-}Me$, $R^2=H$
c $R^1=6\text{-}NHCOMe$, $R^2=H$
d $R^1=5\text{-}Cl$, $R^2=9\text{-}Cl$
e $R^1=5\text{-}Me$, $R^2=H$
f $R^1=5,8\text{-}Me_2$, $R^2=H$
g $R^1=6,7\text{-}Me_2$, $R^2=H$
h $R^1=5,8\text{-}(OMe)_2$, $R^2=H$
i $R^1=6,7\text{-}(OMe)_2$, $R^2=H$

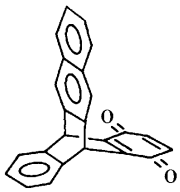

3

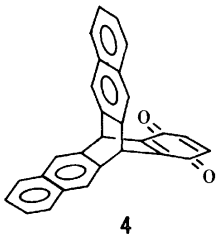

4

dichloro (**1d**), gave shorter absorption maximum than unsubstituted triptycenequinone (**1a**). So, these maxima can be regarded as the result of CT interaction between benzene ring and benzoquinone moiety (further analysis is given in the part of Discussion). Such maxima could not be observed by intermolecular interaction between **2** and benzene (Fig. 1). Intermolecular CT band of **2** and benzene appeared in the region of 280—300 nm (Fig. 2), far shorter wavelength than that of triptycenequinones. The 280—300 nm band of **2** in benzene is compatible to the reported CT band between 1,4-benzoquinone and benzene.[15] Furthermore, the absorption maxima of triptycenequinones are completely different from those observed in the electronic spectrum of cyclophanequinone **5**. The latter showed the CT band at 340 nm arising from interaction between benzene and 1,4-benzoquinone moieties.[16]

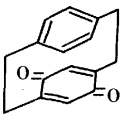

5

Result

1. Absorption Spectra of the Substituted Triptycenequinones. Figure 1 shows the absorption spectra (λ; wavelength, ε; absorptivity) of triptycenequinones **1a—d** in $CHCl_3$ and that of non aromatic derivative **2** in C_6H_6. The triptycenequinones have characteristic absorption maxima (ε; 190—360) in the region of 390—430 nm. Substitution with electron-donating groups, methyl (**1b**) or acetylamino (**1c**) group, gave absorption maxima at longer wavelength. To the contrary, substitution with electron-withdrawing group,

Consequently, it can be concluded that these absorption maxima of **1a—d** observed in the region of 390—430 nm are of characteristic in the triptycenequinone system, and that these bands are due to intramolecular CT interaction.

2. Solvent Dependency of the Absorption Maxima in Triptycenequinones 1a—d. To make clear CT character of the absorption maxima in triptycenequinone system, solvent dependency of absorption band of **1a** was examined in 14 solvents. Three solvents were used in the case of **1b—d**. The results are summarized in Tables 1 (**1a**) and 2 (**1b—d**). As a

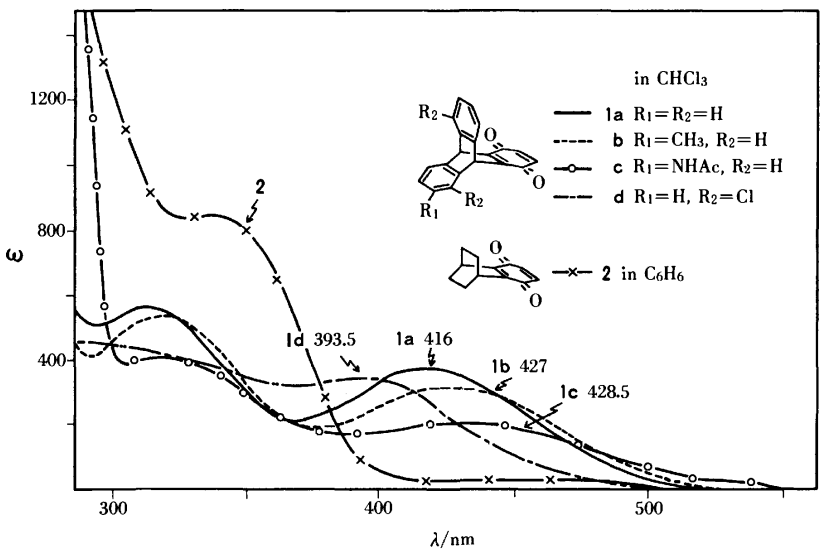

Fig. 1. Absorption spectra of **1a—d** in $CHCl_3$ and **2** in C_6H_6.

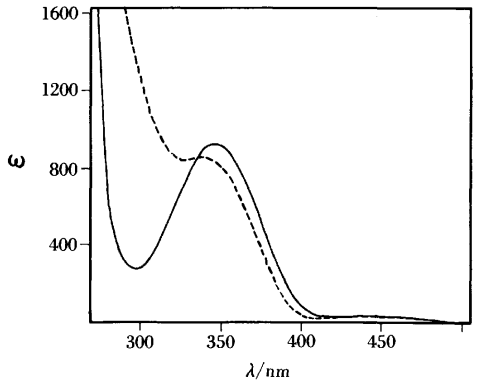

Fig. 2. Absorption spectra of **2** in $CHCl_3$ (solid line) and in C_6H_6 (dashed line).

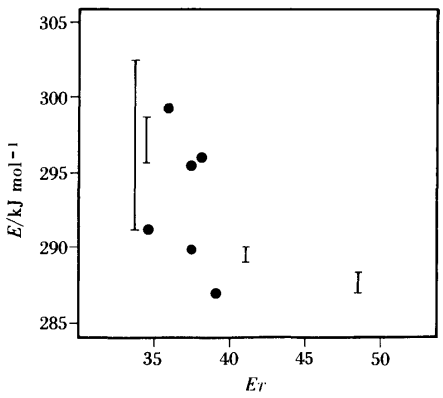

Fig. 3. Solvent dependency of the characteristic band of **1a**.

Table 1. Solvent Dependency of the Characteristic Bands of Triptycenequinone **1a**

Solvent	E_T	λ/nm (log ε)
$C_6H_5CH_3$	33.9	395—410 (shoulder)
C_6H_6	34.5	410 (2.50)
Et_2O	34.6	400.0—403.5
Dioxane	36.0	399.5
THF	37.4	404.5
C_6H_5Cl	37.5	412
$EtOCOCH_3$	38.1	403
$CHCl_3$	39.1	416 (2.56)
CH_2Cl_2	41.1	412—413
Acetone	42.2	403
DMF	43.8	404.0—406.5
CH_3CN	46.0	403—404 (2.50)
2-Propanol	48.6	414—416
Acetic acid	52.0[a]	407.5—410.0

a) Estimated from its Z value.

Table 2. Characteristic Bands of Substituted Triptycenequinones **1b—d**

Quinone	Solvent	Wavelength (nm)	log ε
1b	C_6H_6	421	2.47
	$CHCl_3$	427	2.50
	CH_3CN	412	2.45
1c	C_6H_6	428	2.29
	$CHCl_3$	428.5	2.28
	CH_3CN	423.5	2.29
1d	C_6H_6	—[a]	
	$CHCl_3$	393.5	2.54
	CH_3CN	381	2.51

a) Shoulder.

parameter of solvent polarity, Dimroth's E_T values[17,18] were adopted instead of Kosower's Z values by two reasons. Main reason is that Z values of some solvents have not been reported yet. The other reason is that E_T values are determined from intramolecular CT transition of diphenyl betaines **6**. Meanwhile, Z values are determined from closely-contacted interionic CT interaction between iodide anions and pyridium cations. Good linear correlation was obtained between E_T value and Z value (Z=1.259E_T+13.76).[18] In the case of the solvents whose E_T- and Z-values were both reported, analysis with Z values gave similar results as E_T values.

No clear solvent dependency can be recognized as given in Tables 1 and 2. However, among the solvents shown in Table 1, acetone, DMF, and acetonitrile are classified as "dissociating solvents" and acetic acid is classified as "associating solvent",[19-21] because these solvents affect excitation of compounds in a little different way from other solvents. When those dissociating and associating solvents are excluded, the energy of the absorption maximum (E) somehow tends to decrease with increase of solvent polarity E_T as given in Fig. 3. This tendency may support the CT character of the absorption maxima in triptycenequinone system.

Standing on another viewpoint, unclear solvent dependency of the absorption maxima can be speculated to be due to the following two reasons. One is that the charge separation of excited state in triptycenequinones is not so large as that in the compound (**6**) used for determination of E_T values. The other reason is that the character of n-π* transition of carbonyl group (blue shift when solvent polarity increases) might complex with the CT character (red shift when solvent polarity increases).

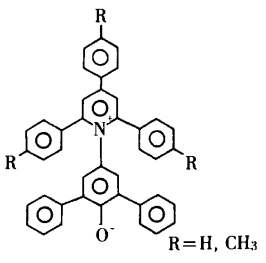

6

3. Absorption Spectra of Benzotriptycenequinone 3 and Dibenzotriptycenequinone 4. Naphthalene-ring-incorporated triptycenequinone analogues, benzotri-

ptycenequinone **3** and dibenzotriptycenequinone **4**, showed quite different spectra from that of a 1:1 mixture of **2** and naphthalene (Fig. 4) as in the case of benzene derivatives **1a—d**. The λ_{max}'s were 411—412 nm (ε= 468) in **3** and 400.5 nm (708) in **4**. The ε of the absorption maximum of **4** were larger than that of **3**, so it can be said that additional naphthalene ring may raise degree of intramolecular interaction. These absorption maxima in the region of 400—420 nm were very similar to those of **1a—d**, but had a little larger ε.

However, in the region of 470—550 nm, the quinones **3** and **4** have fairly strong absorption bands (ε's at 500 nm were ca. 100 and 160, respectively) compared with **1a—d**. The ε_A's—apparent absorptivity—of these absorption maxima of **3** and **4** did not depend on the concentration of these compounds. So, these 470—550 nm bands can be considered to come from *intramolecular* process.

Although a 1:1 mixture of **2** and naphthalene at low concentration showed no band arising from the intermolecular interaction between these two molecules ([**2**]=4.83×10^{-3} mol dm^{-3}, [naphthalene]=5.13×10^{-3} mol dm^{-3}), a highly concentrated 1:100 mixture of **2** and naphthalene ([**2**]=1.02×10^{-2} mol dm^{-3}, [naphthalene]=1.4 mol dm^{-3}) showed a weak band at 450 nm (Fig. 5). Based on these observations and the results of triptycenequinones described above, the strong and large absorption maxima of **3** and **4** in the region around 400—550 nm can be assigned to the intramolecular CT transition between naphthalene ring and benzoquinone moiety.

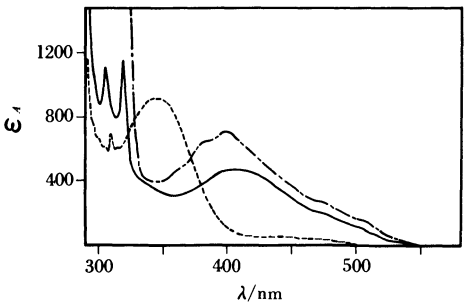

Fig. 4. Absorption spectra of **3** (——), **4** (— — — —), and 1:1 mixture of **2** and naphthalene (----) in $CHCl_3$. In the region of longer wavelength than 400 nm, [**2**]=4.83×10^{-3} mol dm^{-3}, and [naphthalene]=5.13×10^{-3} mol dm^{-3}. In the region of shorter wavelength than 400 nm, 4.83×10^{-4} mol dm^{-3} and 5.13×10^{-4} mol dm^{-3}, respectively.

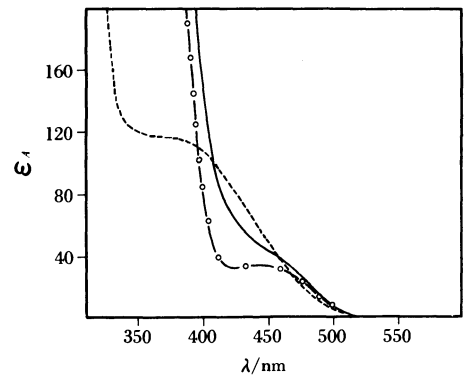

Fig. 5. Absorption spectra of 1:100 mixture of **2** (1.02×10^{-2} mol dm^{-3}) and naphthalene (1.4 mol dm^{-3}) (——), 1:100 mixture of 1,4-benzoquinone (1.02×10^{-2} mol dm^{-3}) and naphthalene (9.99×10^{-1} mol dm^{-3} (--------), and **2** itself (—O—O—). Solvent; $CHCl_3$.

4. Reduced Charge Calculations by EHT.[22,23] The calculation of the charges of each atom (reduced charge matrix, molecular orbital-atom) was carried out in HOMO and in LUMO of triptycenequinones **1a—d** by EHT in order to investigate more details on the absorption maxima.

The probable conformations of the triptycenequinones were calculated by molecular mechanics theory (see Experimental section), then reduced charge matrix were obtained by EHT calculation. As a result of these calculations, the overlap integrals and overlap populations between homoconjugative atoms (carbon atoms vicinal to bridgehead carbons) were found to be significant in these triptycenequinones. Reduced charge matrix in HOMO and in LUMO (one electron in each MO) and differences between these two MOs (Δ_{L-M}: LUMO minus HOMO, considered as S_0–S_1 excitation) are given in Table 3 in the case of unsubstituted triptycenequinone **1a**. In the case of other triptycenequinones (**1b—i**, **3**, **4**), only the summations of Δ_{L-M} in each moiety [$\sum$(moiety Δ_{L-H})] are tabulated in Table 4. Numbering of atoms are shown in the following structure. Here, [A] represents mainly-substituted aromatic ring, [B]; another aromatic ring, [Q]; benzoquinone moiety, and [BH]; bridgehead carbon atom.

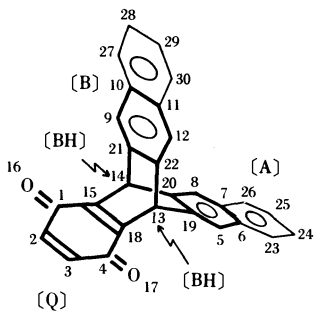

Structure **C**

As shown in Tables 3 and 4, $\sum(\Delta_{L-M})$ in each moiety are all negative in ring A and in sum of A and B (A+B), but all positive in ring Q, suggesting that HOMO-LUMO excitation in triptycenequinone system involves charge transfer from aromatic ring (ring A and/or B) to benzoquinone moiety (ring Q). That is, rings A and B can be considered as electron donor,

Table 3. Reduced Charge Matrix and Population Change Δ_{L-H} in **1a** Calculated by EHT

Moiety	Atom number	Reduced charge matrix		Population change Δ_{L-H}
		HOMO	LUMO	
A	20	0.0761	0.0223	−0.0538
	19	0.0738	0.0033	−0.0706
	5	0.0511	0.0059	−0.0452
	6	0.0332	0.0043	−0.0289
	7	0.0759	0.0069	−0.0690
	8	0.0042	0.0069	0.0027
	Σ(A)	0.3143	0.0496	−0.2647
B	22	0.0017	0.0057	0.0040
	21	0.0078	0.0139	0.0061
	9	0.0026	0.0086	0.0060
	10	0.0065	0.0043	−0.0022
	11	0.0009	0.0027	0.0018
	12	0.0075	0.0030	−0.0045
	Σ(B)	0.0270	0.0382	0.0112
BH	13	0.0662	0.0059	−0.0603
	14	0.0062	0.0297	0.0235
	Σ(BH)	0.0724	0.0356	−0.0368
Q	15	0.0718	0.1888	0.1170
	1	0.0151	0.2282	0.2131
	16	0.0210	0.0220	0.0010
	2	0.1121	0.0810	−0.0311
	3	0.0365	0.1099	0.0734
	17	0.1662	0.0442	−0.1220
	4	0.1522	0.1577	0.0055
	18	0.0060	0.0359	0.0299
	Σ(Q)	0.5809	0.8677	0.2868

Table 4. Summation of Population Change in Each Moiety Σ(moiety Δ_{L-H})[a] of Triptycenequinones

Quinone	Σ(moiety Δ_{L-H})				
	A	B	BH	Q	A+B
1a	−0.2647	0.0112	−0.0368	0.2868	−0.2535
1b[b]	−0.6640	0.0115	0.0167	0.6510	−0.6525
1c[b]	−0.2508	−0.1112	−0.0746	0.5011	−0.3620
1d	−0.2064	−0.0189	−0.0383	0.2558	−0.2253
1e	−0.2940	−0.0557	−0.0694	0.5357	−0.3497
1f	−0.3460	0.1036	0.0536	0.2008	−0.2424
1g	−0.7467	0.0100	0.0182	0.7639	−0.7367
1h	−0.1569	−0.0580	−0.0283	0.3340	−0.2149
1i	−0.0708	−0.1785	−0.0574	0.3498	−0.2493
3	−0.2783	−0.1307	−0.0422	0.4810	−0.4090
4	−0.2765	−0.1008	−0.0559	0.4324	−0.3772

a) Reduced net AO population was normalized to one electron occupation. b) Two of asymmetrical triptycenequinone derivatives (6-Me, **1b** and 6-NHCOCH$_3$, **1c**) were calculated as 7-Me and 7-NHCOCH$_3$ derivatives, respectively, for convenience sake.

and ring Q as electron acceptor, so charge is calculated to be transferred from mainly ring Q accompanying HOMO–LUMO excitation.

For comparison, reduced charge matrix of 9,10-dihydro-1,4-anthracenedione **7a** and its 6-methyl derivative **7b** were calculated by the same method as in the case of triptycenequinones. The results are summarized in Table 5. In both cases, sums of population change are all positive in ring A and "Bridge Head", and all negative in ring Q, as opposed to sterically rigid triptycenequinone system. So charge flow in

Table 5. Summation of Population Change in Each Moiety Σ(moiety Δ_{L-H})[a] of **7a, b**

Quinone	Σ(moiety Δ_{L-H})		
	A	BH	Q
7a	0.2804	0.2237	−0.5830
7b	0.3113	0.1808	−0.5651

a) Reduced net AO population was normalized to one electron occupation.

1a—i, **3**, and **4** can be considered as characteristic of these triptycenequinones.

More details are described in the part of "Discussion".

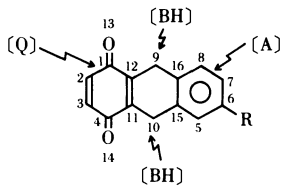

7a R=H
b R=CH_3

Discussion

Substituent effects and the CT character of absorption maxima in triptycenequinone system are analyzed using Hammett σ^+ constant and population change calculated by EHT as parameters.

The absorption maxima in triptycenequinone system could be analyzed quantitatively by the linear free energy relationship. When the positions 6, 7, 10, 11 of **1a—d** are assumed to be *p*-position and the positions 5,8,9,12 are *m*-position, the energy of these bands in three solvents (CH_3CN, $CHCl_3$, and C_6H_6) gave straight lines in Hammett plot using σ^+ values[24,25] (Fig. 6). Furthermore the absorption maxima of other triptycenequinones **1e—i**, obtained in CH_2Cl_2 previously by Murata et al.,[8,9] were analyzed with similar Hammett plot as shown in Table 6 and Fig. 7.

As shown in Figs. 6 and 7, clear linear correlation was obtained between energy of absorption maximum and σ^+, not σ. It suggests that benzene ring has a little cationic (electron-donating) character in the course of S_0–S_1 excitation, and then that these absorption maxima in triptycenequinones may reflect the presence of the charge-transfer electron transition from neighboring aromatic rings to 1,4-benzoquinone moiety.

This interpretation was also supported by EHT calculations of reduced charge. Sum of population change $\Sigma(\Delta_{L-H})$ in each moiety, benzene rings A and B, bridge head BH, and benzoquinone Q, are compared with energy of the absorption maxima in substituted triptycenequinones **1a—i**, **3**, and **4**. Population changes

Table 6. Energy of the Characteristic Bands[8,9] of Triptycenequinones **1a**, **b**, and **1e—i** in CH_2Cl_2 with Hammett Constant[a]

Quinone	E/kJ mol^{-1}	σ^+	σ
1a	288.3	0	0
1b	282.4	−0.26	−0.17
1e	287.9	−0.065	−0.069
1f	289.5	−0.13[b]	−0.138[b]
1g	273.2	−0.622[b]	−0.34[b]
1h	287.0	0.10[b]	0.23[b]
1i	253.6	−1.30[b]	0.536[b]

a) σ^+ values of **1c** and **1d** is −0.25 and 0.80, respectively.
b) Calculated as summation of σ or σ^+ values of single substituent.

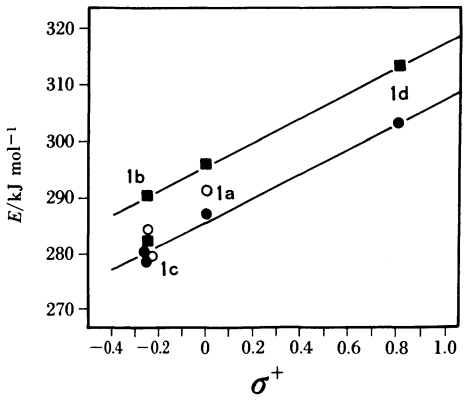

Fig. 6. Hammett plot: the energies of the absorption maxima in **1a—d** vs. σ^+ values. Closed circle; in $CHCl_3$. Closed square; in CH_3CN. Open circle; in C_6H_6.

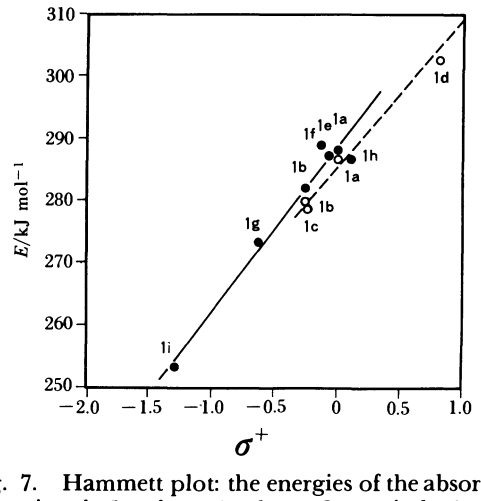

Fig. 7. Hammett plot: the energies of the absorption maxima in **1a—i** vs. σ^+ values. Open circle; **1a—d** in $CHCl_3$. Closed circle; **1a**, **1b**, and **1e—i** in CH_2Cl_2.[8,9]

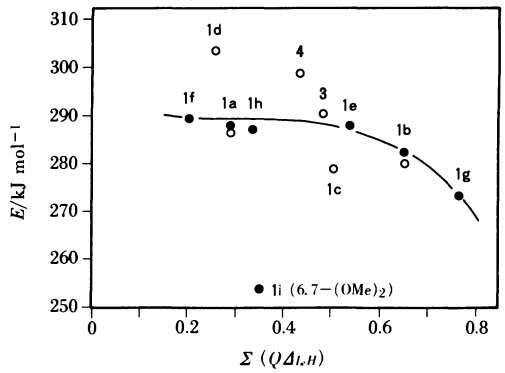

Fig. 8. A plot of sum of population change in moiety Q against absorption maximum energy. Open circle; **1a—d**, **3**, and **4** in $CHCl_3$. Closed circle; **1a**, **1b**, and **1e—i** in CH_2Cl_2.

in moiety Q[$\Sigma(Q\Delta_{L-H})$] are plotted against energy of the absorption maxima (Fig. 8). $\Sigma(Q\Delta_{L-H})$ shows good correlation to absorption maxima, especially in the case of methyl substituted triptycenequinones. Population change in moiety A and B [$\Sigma((A+B)\Delta_{L-H})$] gave similar results as $\Sigma(Q\Delta_{L-H})$.

Thus, analysis of S_0–S_1 transition by MO calculation strongly suggests that absorption maxima of triptycenequinones can be attributed to the charge transfer from benzene ring to quinone moiety, as well as analysis by Hammett plots. This charge transfer may be occurred mainly "through-space" because the quite different results were obtained by the calculation of **7a,b**, which can be considered to include much less "through-space" interaction than triptycenequinones because of their planar conformation.

The quite different population change of **7a,b** compared to triptycenequinones may result mainly from the difference of overlap integrals. The overlap populations between atomic orbitals of the carbon atoms adjacent to bridgehead carbons were much larger in triptycenequinones than in **7a,b**. Those in **7a,b** were almost zero. So, triptycenequinones may have much stronger through-space interaction than **7a,b**. Such difference was explicitly shown by the population change in bridgehead carbon atoms, which can interact with the benzoquinone moiety mainly by through-bond interaction. **7a,b** gave much larger $\Sigma(BH\Delta_{L-H})$ than triptycenequinones (Tables 4 and 5).

The summation of reduced charge of all atoms in benzoquinone moiety Q changed from 0.5809 to 0.8677 in **1a** and from 0.8603 to 0.2773 in **7a** through S_0–S_1 excitation. In the course of that excitation, population change of carbonyl groups was calculated to be 0.2131 for carbon atom and 0.0010 for oxygen atom in **1a**, and −0.2431 for C and −0.0436 for O in **7a**. So, the difference of population change $\Sigma(Q\Delta_{L-H})$ mainly came from the difference of the population change of carbonyl carbons. In the case of **7a,b**, the electron in S_0 state may exist mainly on the benzoquinone moiety, especially on carbonyl carbon atoms, and may diffuse into whole molecule by through-bond interaction in the course of excitation to S_1 state. Further, according to population change of carbonyl oxygen atoms described above, S_0–S_1 excitation of triptycenequinones might have somewhat π–π^* character, on the other hand, that of **7a,b** might have less π–π^* and more n–π^* character, because more electron on carbonyl oxygen atoms may diffuse in S_1 state in **7a,b** than in triptycenequinones. The cause of the different population change is still unclear and more investigation is required for exact explanation.

Based on good linear correlation between absorption maximum and σ^+ constant, the absorption maximum can be expected by Hammett plot such as Fig. 7. Furthermore, as far as methyl-substituted triptycenequinones, the absorption maximum may be expected also by such simple EHT calculation. However, neither $\Sigma(A\Delta_{L-H})$ nor $\Sigma(Q\Delta_{L-H})$ of 6,7-dimethoxy (**1i**), acetylamino (**1c**), chloro (**1d**), and dibenzo (**4**) derivatives gave clear correlation to the absorption maximum, compared with Hammett σ^+ constants. It is speculated as due to the effect of lone-pair electrons which is not perhaps involved sufficiently within this EHT calculation.

Experimental

Apparatus for Measurements. Electronic spectra were taken with a Shimadzu UV-200 spectrometer. ^{1}H NMR spectra were taken with a JEOL PS-100MHz spectrometer in suitable solvents using TMS as the internal standard.

Solvents. For absorption spectra measurements, solvents were dried with appropriate desiccant, and distilled.

Quinones. 1a—d, 3, 4 were prepared according to the previously reported method[1,10] with some modification. Corresponding anthracenes were synthesized (for **1b—d**) or purchased (for **1a**). Naphthacene (for **3**) and pentacene (for **4**) were synthesized as described later. All polyacenes were purified by recrystallization. Triptycenequinones were synthesized as follows. After Diels-Alder reaction of 1,4-benzoquinone and a polyacene, the adduct was precipitated with cooling to room temperature. The precipitate was recrystallized from benzene and then treated with HBr in acetic acid to give the corresponding hydroquinone. The hydroquinone was then oxidized to the corresponding triptycenequinone with potassium bromate in acetic acid. Detail conditions of Diels-Alder reaction were as follows [given as target compound, polyacene used (g), 1,4-benzoquinone used (g), solvent (ml), refluxing period, yield (g)]: **1a**, 10.8, 7.3, xylene 65, 3 h, 13.8; **1b**, 5.3, 3.6, xylene 65, 3 h, 5.9; **1c**, 2.1, 1.6, toluene 25, 3 h, 3.0; **1d**, 4.5, 2.1, xylene 30, 3.5 h, 2.8; **3**, 3.0, 1.4, xylene 25 (under N_2), 30 min, 2.1, 3.8; **4**, 1.9, 0.8, xylene 14 (under N_2), 20 min, 0.5.

The physical properties of **1a—d, 3, 4** were as follows.

1a: Yellow prisms recrystallized from $CHCl_3$, mp 289—294 °C (decomp) (lit, 292—296 °C). ^{1}H NMR ($CDCl_3$): δ=5.76 (s, 2H), 6.56 (s, 2H), 6.96—7.20 (m, 4H), 7.30—7.56 (m, 4H). IR (KBr): ν_{CO}=1655 cm^{-1}. UV ($CHCl_3$): λ_{max}= 416 nm (ε=357), 311 (513), 244 (16500).

1b: Yellow crystals from benzene, mp 165.2—168.4 °C (slightly decomp)(sealed tube). ^{1}H NMR ($CDCl_3$): δ=2.57 (s, 3H), 6.51 (s, 2H), 7.40 (s, 2H), 7.66 (m like d, 1H), 7.80—8.00 (m, 2H), 8.14 (s, 1H), 8.16—8.38 (m, 3H). IR (KBr): ν_{CO}=1660 cm^{-1}, $\nu_{C=C}$=1598 cm^{-1}. MS m/z=298 (M^+), 280 (M−CO). UV ($CHCl_3$): λ_{max}=427 nm (ε=316), 320 (526), 279 (3060), 261 (sh, 15100), 255 (15700). Found: C, 84.40; H, 4.81%. Calcd for $C_{21}H_{14}O_2$: C, 84.54; H, 4.73%.

1c: Orange yellow needles, mp 180.0—181.0 °C (decomp). ^{1}H NMR ($CDCl_3$): δ=2.10 (s, 3H), 5.66 (s, 2H), 6.50 (s, 2H), 6.87—7.03 (m, 3H), 7.1—7.4 (m, 4H, including NH), 7.60 (brs, 1H). IR (KBr): ν_{CO}=1652 cm^{-1} (broad), 1590, 1532, 1303. MS m/z=341 (M^+), 298 (M−Ac). UV ($CHCl_3$): λ_{max}=428.5 nm (ε=192), 321 (398), 257 (18400). Found: C, 77.28; H, 4.39; N, 3.88%. Calcd for $C_{22}H_{15}NO_3$: C, 77.41; H, 4.43; N, 4.10%.

1d: Yellow crystals from $CHCl_3$, mp at >240 °C slightly red and at 303—305 °C melted with decomposition (sealed tube). ^{1}H NMR ($CDCl_3$): δ=6.38 (s, 2H), 6.75 (s, 2H), 6.9—

7.3 (m, 4H), 7.3—7.6 (m like dd, 2H). IR (KBr): ν_{CO}= 1665 cm^{-1}, $\nu_{C=C}$=1590, 1570 cm^{-1}. MS m/z=354, 352 (M^+). UV ($CHCl_3$): λ_{max}=395.5 nm (ε=348), 298 (sh, 469), 278 (sh, 1000), 254.3 (14300). Found: C, 67.92; H, 2.79; Cl, 20.39%. Calcd for $C_{20}H_{10}O_2Cl_2$: C, 68.01; H, 2.85; Cl, 20.08%.

3: Orange yellow crystals, mp 210.5—211.0 °C (decomp) (sealed tube). ^{1}H NMR ($CDCl_3$): δ=5.86 (s, 2H), 6.58 (s, 2H), 7.0—7.2 (m, 2H), 7.4—7.6 (m, 4H), 7.6—7.8 (m, 2H), 7.78 (s, 2H). IR (KBr): ν_{CO}=1650 cm^{-1}, $\nu_{C=C}$=1585 cm^{-1}, ν=1305 cm^{-1}. MS m/z=335 (M+1), 334 (M^+). UV ($CHCl_3$) λ_{max}=411.5 nm (ε=460), 320.6 (1170), 306.8 (1120), 287.6 (4840), 262.5 (sh, 18900), 260 (19400), 243 (65600). Found: C, 86.13; H, 4.18%. Calcd for $C_{24}H_{14}O_2$: C, 86.21; H, 4.22%.

4: Orange crystals, mp 242—243 °C (sealed tube). ^{1}H NMR ($CDCl_3$): δ=5.92 (brs, 2H), 6.52 (s, 2H), 7.3—7.5 (m, 4H), 7.5—7.7 (m, 4H), 7.79 (s, 4H). IR (KBr): ν_{CO}=1655 cm^{-1}, $\nu_{C=C}$=1592 cm^{-1}, ν=1305 cm^{-1}. MS m/z=385 (M+1), 384 (M^+), 356, 355. UV ($CHCl_3$): λ_{max}=400.5 nm (ε=708). Found: C, 87.38; H, 4.22%. Calcd for $C_{28}H_{16}O_2$: C, 87.48; H, 4.20%.

2-Methylanthracene[11] and 1,5-Dichloroanthracene. 2-Methyl-9,10-anthraquinone and 1,5-dichloro-9,10-anthraquinone were reduced to the corresponding anthracenes with diborane in situ prepared by $NaBH_4$ and BF_3-etherate in diglyme. Crude substituted anthracene was purified by column chromatography on silica gel to give the mixture of the substituted anthracene and its 9,10-dihydro derivative. This mixture was oxidized with 1,4-benzoquinone (in the case of 2-methylanthracene) or chloranil (in the case of 1,5-dichloroanthracene) to give pure substituted anthracene.

2-Acethylaminoanthracene. 2-Amino-9,10-anthraquinone was reduced to 2-aminoanthracene in a similar manner as 6-methyl derivative. 2-Aminoanthracene obtained was acetylated with refluxing acetic anhydride to give 2-acetylaminoanthracene.

Naphthacene and Pentacene. 5,12-Naphthacenedione[12] and 6,13-pentacenedione[12] were prepared by condensation of $\alpha,\alpha,\alpha',\alpha'$-tetrabromo-*o*-xylene[13] and 1,4-naphthoquinone with NaI in dry *N,N*-dimethylformamide, and then reduced in a similar manner as in the case of substituted anthracenes.

5,6,7,8-Tetrahydro-5,8-ethano-1,4-naphthoquinone (2). Cyclohexadiene and 1,4-benzoquinone were condensed by Diels-Alder reaction. The adduct was rearranged to the corresponding hydroquinone, and then reduced with H_2/Pd-C. The hydroquinone was oxidized by $FeCl_3$. **2** was obtained as yellow crystals from hexane-benzene, mp 85.7—87.0 °C (sealed tube). ^{1}H NMR ($CDCl_3$): δ=1.2—1.6 (m, 4H), 1.6—1.9 (m, 4H), 3.34 (d, J=1 Hz, 2H), 6.71 (s, 2H). IR (KBr): ν_{CO}=1640 cm^{-1}, $\nu_{C=C}$=1585 cm^{-1}, ν=1303 cm^{-1}. MS m/z=188 (M^+), 186, 160 ($M-CH_2=CH_2$). UV ($CHCl_3$): λ_{max}=445 nm (ε=33), 348 (936), 254 (18000). Found: C, 76.41; H, 6.55%. Calcd for $C_{12}H_{12}O_2$: C, 76.57; H, 6.43%.

Purification of Quinones. In order to avoid the contamination with polyacenes, triptycenequinones **1a—d**, **3**, **4**, and nonaromatic quinone **2** were purified by column chromatography on silica gel twice and by recrystallization in a dark room.

EHT Calculations. A packaged soft for chemical calculations "CHEMLAB-II" supplied by MDL Inc. (U.S.A.) was used on VAX11/780, Digital Equipment Company. Molecular coordinates were calculated by "PRXBLD", one of suboptions in CHEMLAB-II, based on molecular mechanics. Extended Hückel calculations were carried out by "EHT" suboption.

The author wishes to express his grateful thanks to Professor Kazuhiro Maruyama for his guidance and invaluable discussions in this work. He is grateful to Dr. Yasuo Kubo for his helpful suggestions. He also thanks Dr. Tetsuo Otsuki, Dr. Yoshinori Naruta and Dr. Tatsuhisa Kato for fruitful discussion. The author wishes to thank Mr. Kazunori Toma for assistance of EHT calculations.

References

1) P. D. Bartlett, M. J. Ryan, and S. G. Cohen, *J. Am. Chem. Soc.*, **64**, 2649 (1942).
2) P. D. Bartlett and E. S. Lewis, *J. Am. Chem. Soc.*, **72**, 1005 (1950).
3) J. de Wit and H. Wynberg, *Tetrahedron*, **29**, 1379 (1973).
4) V. Balaji and K. D. Jordan, *Chem. Phys. Lett.*, **119**, 294 (1985).
5) S. Inagaki, T. Imai, and H. Kawata, *Chem. Lett.*, **1985**, 1191.
6) H. Iwamura and K. Makino, *J. Chem. Soc., Chem. Commun.*, **1978**, 720.
7) E. Lipczynska Kochany and H. Iwamura, *Chem. Lett.*, **1982**, 1075.
8) G. A. Russell and N. K. Suleman, *J. Am. Chem. Soc.*, **103**, 1560 (1981).
9) K. Yamamura, K. Nakasuji, I. Murata, and S. Inagaki, *J. Chem. Soc., Chem. Commun.*, **1982**, 396.
10) I. Murata, *Pure Appl. Chem.*, **55**, 323 (1983).
11) E. Clar, *Chem. Ber.*, **64**, 1676 (1931).
12) D. S. Bapt, B. C. Subba Rao, and M. K. Unni, *Tetrahedron Lett.*, **1960**, 15.
13) M. P. Cova, A. A. Deana, and K. Muth, *J. Am. Chem. Soc.*, **81**, 6459 (1959).
14) J. C. Bill and D. S. Tarbell, *Org. Synth.*, Coll. Vol. IV, 807 (1963).
15) L. J. Andrews and R. M. Keefer, *J. Am. Chem. Soc.*, **75**, 3776 (1953).
16) D. J. Cram and A. C. Day, *J. Org. Chem.*, **31**, 1227 (1966).
17) K. Dimroth, C. Reichardt, T. Siepmann, and F. Bohlmann, *Justus Liebigs Ann. Chem.*, **661**, 1 (1963).
18) K. Dimroth, C. Reichardt, and A. Schweig, *Justus Liebigs Ann. Chem.*, **669**, 95 (1963).
19) M. Senou and T. Arai, "Yuuki-kagaku-hannou Ni Okeru Youbaikouka," Sangyou Tosho, Tokyo (1975), Chap. 4.6—4.7.
20) E. M. Kosower, *J. Am. Chem. Soc.*, **80**, 3253, 3261, 3267 (1958).
21) C. Walling and P. J. Wagner, *J. Am. Chem. Soc.*, **86**, 3368 (1964).
22) R. Hoffmann, *J. Chem. Phys.*, **39**, 1397 (1963).
23) J. P. Lowe, "Quantum Chemistry," Academic Press, New York (1978), pp. 283—303.
24) S. L. Murov, "Handbook of Photochemistry," Marcel Dekker, Inc., New York (1973), Section 26, p. 200.
25) L. P. Hammett, "Physical Organic Chemistry," McGraw-Hill (1970), Chap. 11.

Stereoselective Synthesis of [1]Benzopyrano[4,3-*b*]pyrrol-4(3*H*)-ones through Cycloadditions of Azomethine Ylides with α,β-Unsaturated Esters

Kazunori UENO, Shuji KANEMASA,* and Otohiko TSUGE*
Institute of Advanced Material Study, and Department of Molecular Science and Technology, Interdisciplinary Graduate School of Engineering Sciences, Kyushu University, Kasugakoen, Kasuga 816
(Received August 3, 1988)

Cycloadditions of azomethine ylides generated from α-benzylideneamino nitriles bearing a hydroxyl or its *O*-protected moiety with α,β-unsaturated esters such as dimethyl maleate, fumarate, methyl acrylate, crotonate, methacrylate, and cinnamate lead stereoselectively to 3,3a-*trans*-3a,9b-*cis*-3a,9b-dihydro[1]benzopyrano[4,3-*b*]pyrrole-4(3*H*)-ones after subsequent lactonization.

The imines, bearing an electron-withdrawing substituent at the sp^3 carbon adjacent to the imine nitrogen, undergo a thermal imine–azomethine ylide tautomerism.[1] Since this tautomerism is catalyzed by a weak acid,[2] an intramolecular hydrogen bond to the nitrogen would accelerate such ylide generation. The replacement of the benzylidene moiety of α-benzylideneamino nitriles with a 2-hydroxybenzylideneamino group offers model compounds with which catalysis by an intramolecular hydrogen bond could be conveniently tested.

N-Unsubstituted azomethine ylides generated by the thermal tautomerism of *C*-aryl imines undergo stereo- and regioselective cycloadditions with α,β-unsaturated esters to produce cycloadducts, pyrrolidines or pyrrolines, in which the aryl and the ester groups are cis to each other. Therefore, the use of α-(2-hydroxybenzylideneamino) nitriles would lead to [1]benzopyrano[4,3-*b*]pyrrol-4(3*H*)-ones, which could be useful compounds for the synthesis of the hetero analogs of cannabinoids.[3]

The present article describes the generation of azomethine ylides from α-(arylmethyleneamino) nitriles bearing a hydroxy moiety or their *O*-protected derivatives. The ylides were utilized in stereoselective cycloadditions with α,β-unsaturated esters, followed by lactonization to give pyrrole ring-fused [1]benzopyrans.

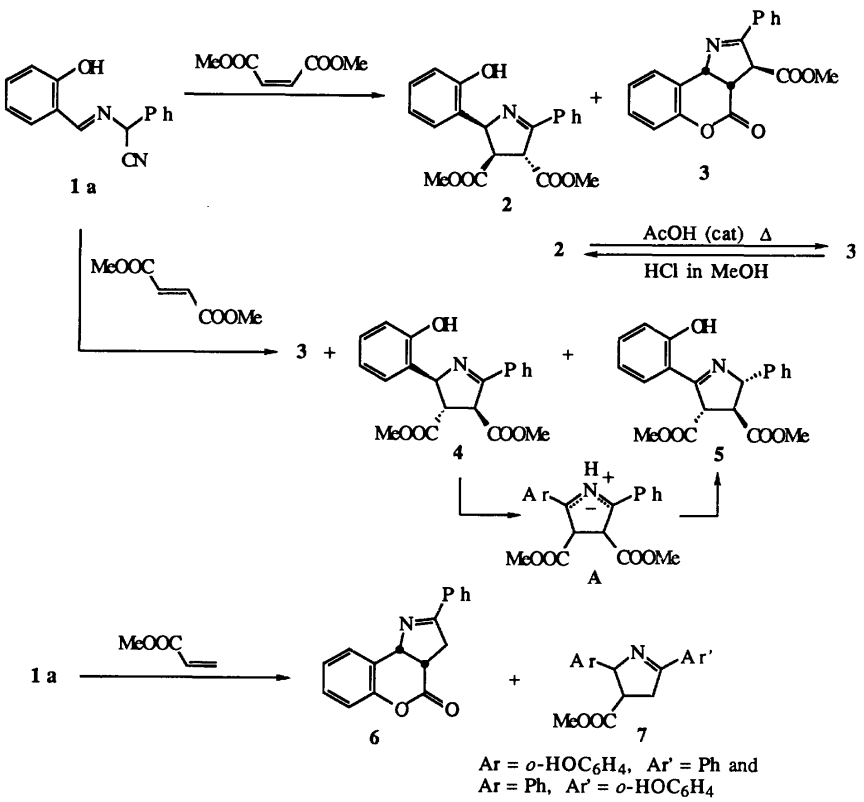

Scheme 1.

Results and Discussion

Among the *N*-unsubstituted azomethine ylides generated by a thermal tautomerism of α-benzylideneamino nitriles, the compounds bearing an aryl group on C_2 of the nitrile is one of the most reactive ylides toward α,β-unsaturated esters.[4] 2-(2-Hydroxybenzylidenamino)-2-phenylacetonitrile (**1a**) underwent a smooth and stereoselective cycloaddition with dimethyl maleate under reflux in toluene to give 4,5-*cis*-1-pyrroline **2** and its lactonized product **3** in a combined yield of 96% (Scheme 1).

The 3,4-trans geometry of **2** is due to epimerization through an imine–enamine tautomerism.[4] The 4,5-cis configuration of **2** was assigned on the basis of the strong shielding of the ester methyl protons on C_4 by the adjacent phenyl ring. The structures of **2** and **3** were confirmed by the facts that **2** could be quantitatively converted into **3** on heating with a catalytic amount of acetic acid, and that **3** underwent methanolysis giving **2** in 85% yield.

With dimethyl fumarate under similar conditions, the lactone **3** (31%) and an inseparable mixture of two isomeric 1-pyrrolines **4** and **5** (2:1, 62%) were obtained. The latter 1-pyrroline **5** must have been derived from **4**, presumably through a double-bond migration via an *N*-protonated azomethine ylide intermediate **A**. On the other hand the 4,5-cis stereoisomer **2** did not isomerize at all under comparable conditions.

The exclusive cis-selectivity achieved in the cycloaddition of **1a** with dimethyl maleate and the poor trans/cis ratio (2/1) observed in that with dimethyl fumarate correspond to the results previously observed in reactions of 2-(benzylideneamino)-2-phenylacetonitrile with both esters.[4]

In a reaction of **1a** with methyl acrylate, the expected lactone **8** was produced in 67% yield, together with an inseparable mixture (26%, 2:1) of two regioisomeric 1-pyrrolines **9**.

Similar stereoselectivities were observed in the reactions of 2-[(2-hydroxy-1-naphthyl)methylenamino]-2-phenylacetonitrile (**1b**) with dimethyl maleate and fumarate. Thus, lactone **6** was the sole product (91%) from the maleate, whereas a mixture of **6** (50%) and 1-pyrroline **7** (41%) was obtained from the fumarate (Scheme 2).

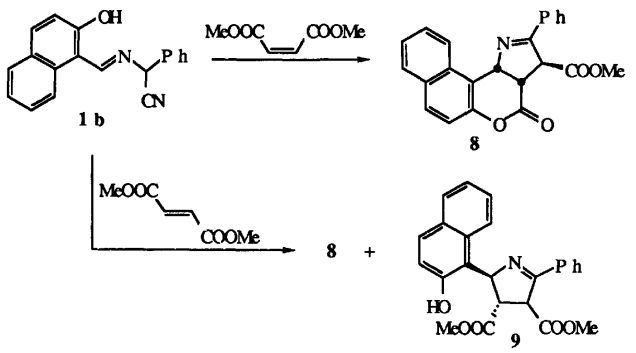

Scheme 2.

Thus, imines **1a** and **1b** can thermally generate, without *O*-protection, the corresponding *N*-unsubstituted azomethine ylides. These ylides undergo cycloadditions to several α,β-unsaturated esters producing 4,5-cis cycloadducts as exclusive or major isomers, which give lactones after spontaneous or acid-catalyzed lactonization. However, catalysis for ylide generation by an intramolecular hydrogen bond was unexpectedly insufficient, no remarkable rate acceleration of the ylide generation being observed. Accordingly, *O*-protected imines were employed in the following reactions.

O-Acetylation of **1a** gave imine **1c**. 4,5-*cis*-1-Pyrroline **10** (91%) or a mixture of **10** and 4,5-*trans*-1-pyrroline **11** (70% and 26%) was yielded from **1c** and dimethyl maleate or fumarate, respectively. The isomer ratio agrees with that obtained from 2-(benzylideneamino)-2-phenylacetonitrile and the fumarate.[4] The cis isomer **10** was converted into lactone **3** upon heating in toluene in the presence of a catalytic amount of *p*-toluenesulfonic acid (PTSA) in a moderate yield (60%).

(2-Hydroxybenzylideneamino)acetonitrile (**1d**) was found to be much less reactive than expected. Thus, the reactions of **1e** with *N*-methylmaleimide and dimethyl fumarate, under reflux in toluene for 14 h, gave unsatisfactory yields of the *N*-acetylated 6,6a-cis cycloadduct **12** (35%) and a mixture of two stereoisomeric cycloadducts, **13** (34%) and **14** (9%). The acetyl group migration from the phenolic oxygen atom to the pyrrolidine nitrogen atom occurred presumably through intramolecular aminolysis, since it is already known that the formation of 1-pyrrolines by the elimination of HCN is extremely slow in these systems.[4,5]

As *N*-unsubstituted (or *N*-protonated) azomethine ylides show only a limited reactivity toward the unsaturated esters, a higher degree of activation of ylides is needed. *N*-Lithiated azomethine ylides are our choice. A highly enhanced reactivity as well as an exclusive cis-selectivity in their cycloadditions was recently reported.[6,7]

The *O*-silyl derivative **1f**, readily prepared by the silylation of **1d** with chlorotrimethylsilane and triethylamine, generated the *N*-lithiated azomethine ylide upon a treatment with LDA in THF at −78 °C. The ylide smoothly underwent stereoselective cycloadditions to methyl acrylate, crotonate, and methacrylate at −78 °C. Though the unpurified reaction mixtures were shown to consist mostly of the *O*-silylated 4,5-*cis*-1-pyrrolines **15**—**17** by ^{1}H NMR, their purification by silica-gel chromatography brought about desilylation to give bicyclic *N*,*O*-acetals **18**—**20** as single stereo-

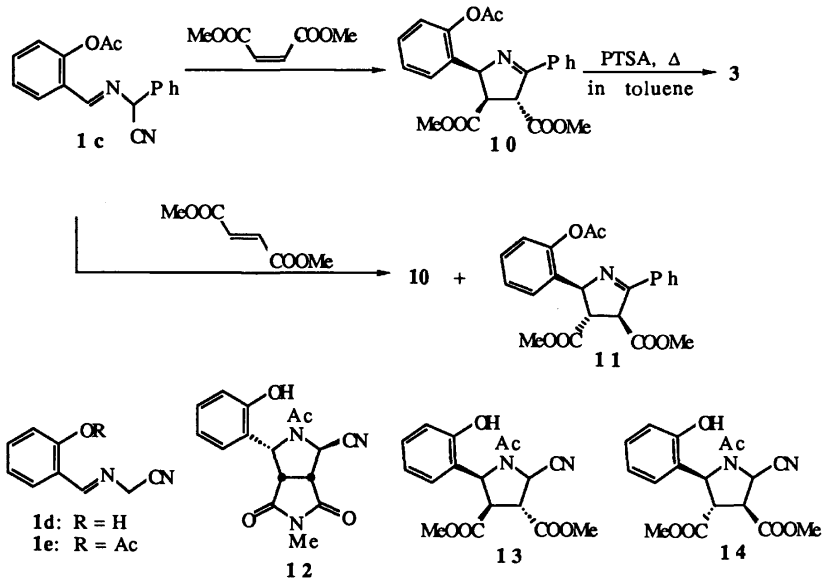

Scheme 3.

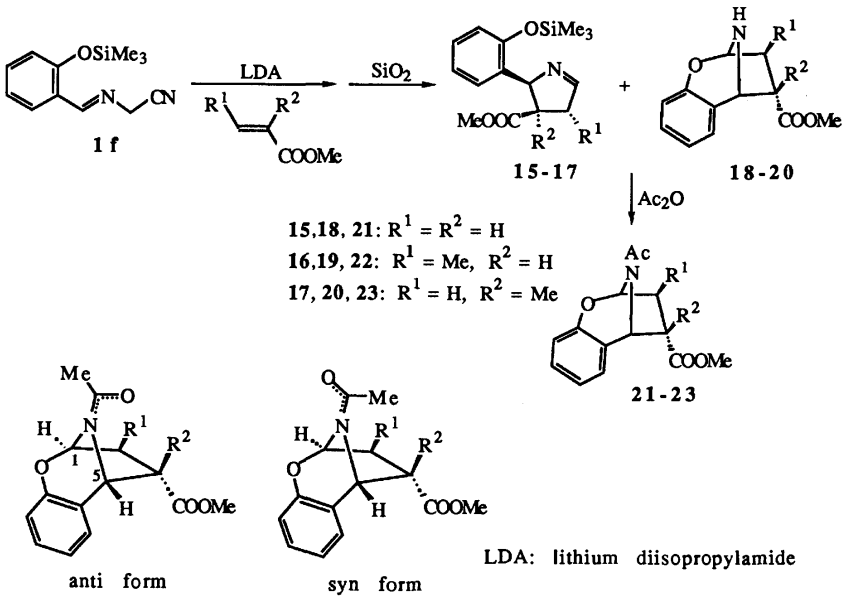

Scheme 4.

isomers in all cases (Scheme 4). Since they were too unstable to be further purified, their acetylation was carried out, leading to **21—23**.

Interestingly, these *N*-acetylated bicyclic *N,O*-acetals **21—23** exist as two isomeric forms in deuteriochloroform in 2:3 to 1:2 ratios. The major isomers, which show lower acetyl methyl protons, lower 5-Hs, and higher 1-Hs in their ^{1}H NMR spectra, were assigned as anti forms and, hence, the minor ones as syn forms. Ready formation of the bicyclic *N,O*-acetals **18—20** occurred probably because of the absence of substituents at C_2 of 1-pyrrolines **15—17**. Accordingly, methyl-substituted imine **1g** was employed in similar cycloadditions (Scheme 5).

With methyl crotonate and cinnamate, 4,5-*cis*-1-pyrrolines **24** and **26** were exclusively formed, however, the reaction with methyl methacrylate was rather nonstereoselective; a 3.5:1 mixture of 4,5-*cis*- **25** and 4,5-*trans*-1-pyrroline **27** was obtained.

Desilylation of **24** occurred easily on its chromatography over silica gel to give lactone **28** in 84% yield based on **1g**. The more stable **25** was only partly desilylated by a similar treatment, but was cleanly converted into **29** (78%) when **25** (as a mixture with **27**) was treated with cesium fluoride in THF. The desilylated derivative of the minor cycloadduct **27** was

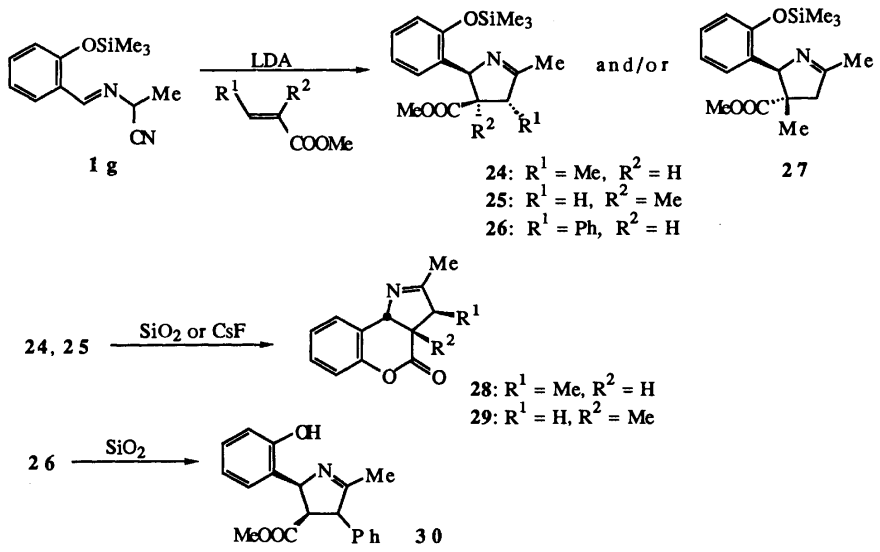

Scheme 5.

also separated.

A chromatographic treatment of the cinnamate adduct **26** resulted in a rather slow desilylation, giving a mixture of **26** and the desilylated product, 4,5-*cis*-1-pyrroline **30**. Smooth lactonization of **30** was not observed under various conditions since it was decomposed in all cases.

Experimental

General. Melting points were determined on a Yanagimoto melting-point apparatus and are uncorrected. IR spectra were taken with a JASCO IRA-1 or a JASCO A-702 spectrometer. ^{1}H NMR spectra were recorded on a Hitachi R-40 (90 MHz), a JEOL FX-100 (100 MHz), or a JEOL GSX-270 (270 MHz) instruments, and ^{13}C NMR on a JEOL FX-100 (25.05 MHz) or a JEOL GSX-270 spectrometer (67.94 MHz). Chemical shifts are expressed in parts per million downfield from tetramethylsilane as an internal standard. Mass spectra were measured with a JEOL-01SG-2 spectrometer at 70 eV of ionization energy. High-resolution mass spectra (HRMS) were obtained on the same instrument. Elemental analyses were performed on a Hitachi 026 CHN analyzer. Thin-layer chromatography (TLC) was accomplished on 0.2 mm precoated plates of silica gel 60 F-254 (Merck). Visualization was made with ultraviolet light (254 and 365 nm), iodine, molybdophosphoric acid (5% in ethanol), or *p*-anisaldehyde (5% in ethanol containing 5% of sulfuric acid). For preparative column chromatography, Wakogel C-200, C-300 (Wako), and Silicagel 60 (Merck) were employed. Flash chromatography was carried out on an Eyela EF-10 apparatus using a column (20×180 mm) packed with Silicagel 60 (Merck, size: 0.04—0.063 mm). Gas liquid chromatography (GLC) was accomplished on a Yanaco G-2800 gas chromatograph (Yanagimoto) with an ionization flame detector using a glass column (SE-30, 3×2000 mm) or a glass capillary column (Silicone GE, SE-30, 0.25×50000 mm). Micro vacuum distillation was carried out on a Sibata GTO-250R Kugelrohr distilling apparatus. Solvents were evaporated with a Tokyo Rikakikai rotary evaporator type-V at about 50 °C unless otherwise stated.

Materials and Solvents. 2-(2-Hydroxybenzylideneamino)-2-phenylacetonitrile (**1a**), 2-[(2-hydroxy-1-naphthyl)methyleneamino]-2-phenylacetonitrile (**1b**), 2-(2-acetoxybenzylideneamino)-2-phenylacetonitrile (**1c**), (2-hydroxybenzylideneamino)acetonitrile (**1d**), and (2-acetoxybenzylideneamino)-acetonitrile (**1e**) were prepared by condensations of the corresponding aldehydes with amino nitriles by an application of the reported methods.[4] **1a:** Colorless prisms (diethyl ether–hexane); mp 59—60 °C; IR (KBr) 3200—2400, 2240, and 1630 cm^{-1}; ^{1}H NMR ($CDCl_3$) δ=5.53 (1H, d, J=1.0 Hz, CH), 6.7—7.4 (9H, m, Ar), 8.47 (1H, d, J=1.0 Hz, CH=N), and 11.86 (1H, br s, OH); MS *m/z* (rel intensity, %) 236 (M^+, 2), 116 (base peak), and 89 (58). Found: C, 76.20; H, 5.12; N, 11.71%. Calcd for $C_{15}H_{12}N_2O$: C, 76.25; H, 5.12; N, 11.86%. **1b:** Colorless prisms (diethyl ether–hexane); mp 116—117 °C; IR (KBr) 3350, 2230, and 1630 cm^{-1}; ^{1}H NMR ($CDCl_3$) δ=4.84 (1H, s, CH), 7.0—8.3 (12H, m, Ar and CH=N), and 10.65 (1H, s, OH). Found: C, 79.66; H, 5.06; N, 9.58%. Calcd for $C_{19}H_{14}N_2O$: C, 79.70; H, 4.93; N, 9.78%. **1c:** Colorless liquid; IR (KBr) 2240, 1740, and 1630 cm^{-1}; ^{1}H NMR ($CDCl_3$) δ=2.20 (3H, s, Ac), 5.66 (1H, d, J=1.0 Hz, CH), 7.0—7.5 (8H, m, Ar), 7.82 (1H, m, Ar), and 8.55 (1H, d, J=1.0 Hz, CH=N). **1e:** Colorless liquid; IR (neat) 2250, 1765, and 1640 cm^{-1}; ^{1}H NMR ($CDCl_3$) δ=2.30 (3H, s, Ac), 4.52 (2H, t, J=1.5 Hz, CH_2), 6.7—7.8 (4H, Ar), and 8.43 (1H, t, J=1.5 Hz, CH=N). 2-[2-(Trimethylsilyloxy)benzylideneamino]-acetonitrile (**1f**) was prepared as follows: A solution of chlorotrimethylsilane (0.48 g, 4.1 mmol) in dry benzene (3 ml) was slowly added to a mixture of **1a** (0.56 g, 4 mmol) and triethylamine (0.45 g, 4.5 mmol) in benzene (10 ml). After stirring at room temperature for 1 h, the precipitate was removed off by filtration and the filtrate was subjected to vacuum distillation to give **1f** (0.66 g, 71%): Yellow liquid; bp 150 °C/133 Pa (bulb-to-bulb), IR (neat) 2220, 1640, 920, 840, and 760 cm^{-1}; ^{1}H NMR ($CDCl_3$) δ=0.30 (9H, s, $SiMe_3$), 4.63 (2H, d, J=2.0 Hz, CH_2) 6.8—7.9 (4H, m, Ar), and 8.90 (1H, t, J=2.0 Hz, CH=N); MS *m/z* (rel intensity, %) 232 (M^+, 8), 218

(17), 217 (base peak), 135 (38), 120 (25), 91 (23), and 77 (15). HRMS Found: *m/z* 232.1055. Calcd for $C_{12}H_{16}N_2OSi$: M, 232.1057. 2-[2-(Trimethylsilyloxy)benzylideneamino]propanenitrile (**1g**) was synthesized according to the following procedure: To a solution of freshly prepared LDA (10 mmol in THF (15 ml)) was added dropwise a solution of **1f** (1.6 g, 6.9 mmol) in THF (10 ml) at −78 °C. After 5 min, methyl iodide (1.56 g, 7.6 mmol) in THF (5 ml) was added. Stirring was continued at −78 °C for 3 h. The mixture was poured into saturated ammonium chloride and extracted with diethyl ether (20 ml×2). The combined extracts were dried over magnesium sulfate and evaporated in vacuo. The residue was assigned as 2-(2-hydroxybenzylideneamino)-propanenitrile: Pale yellow liquid; IR (neat) 3200—2400, 2250, and 1630 cm^{-1}; ^1H NMR ($CDCl_3$) δ=1.75 (3H, d, J=7.0 Hz, Me), 4.73 (1H, dq, J=7.0 and 2.0 Hz, CH), 6.9—7.5 (4H, m, Ar), 8.60 (1H, d, J=2.0 Hz, CH=N), and 12.20 (1H, br s, OH); MS *m/z* (rel intensity, %) 174 (M^+, 78), 173 (13), 160 (11), 159 (16), 120 (base peak), 106 (13), 102 (16), 91 (13), and 77 (23). HRMS Found: *m/z* 174.0790. Calcd for $C_{10}H_{10}N_2O$: M, 174.0790. To a mixture of this imine (2.25 g, 12.9 mmol) and chlorotrimethylsilane (1.72 g, 15.8 mmol) in dry benzene (35 ml) was added triethylamine (1.6 g, 15.8 mmol) in benzene (5 ml). After stirring at room temperature for 1 h, the precipitate was filtered off and the filtrate was distilled under reduced pressure to give **1g** (2.7 g, 85%): Yellow liquid; bp 180 °C/133 Pa (bulb-to-bulb); IR (neat) 2215, 1640, 920, 850, and 760 cm^{-1}; ^1H NMR ($CDCl_3$) δ=0.30 (9H, s, $SiMe_3$), 1.67 (3H, d, J=7.0 Hz, Me), 4.66 (1H, dq, J=7.0 and 1.5 Hz, CH), 6.8—7.9 (4H, m, Ar), and 8.90 (1H, d, J=1.5 Hz, CH=N).

Reaction of 1a with Dimethyl Maleate Leading to 2 and 3. A mixture of **1a** (0.146 g, 0.6 mmol) and dimethyl maleate (0.09 g, 0.6 mmol) in dry toluene (3 ml) was heated under reflux for 20 h. The toluene was evaporated in vacuo and the residue was chromatographed over silica gel by using chloroform as an eluent to give **3** (0.1 g, 50%) and then **2** (0.1 g, 46%). **2**: Colorless liquid; IR (neat) 3500—3050, 1740, and 1640 cm^{-1}; ^1H NMR ($CDCl_3$) δ=3.12 (3H, s, COOMe), 3.63 (3H, s, Me), 3.95 (1H, dd, J_{4-5}=7.0 and J_{4-3}=2.0 Hz, 4-H), 4.64 (1H, t, J_{3-4}=J_{3-5}=2.0 Hz, 3-H), 5.97 (1H, dd, J_{5-4}=7.0 and J_{5-3}=2.0 Hz, 5-H), 6.6—7.5 (7H, m, Ar), 7.85 (2H, m, Ar), and 8.40 (1H, br, OH); ^{13}C NMR ($CDCl_3$) δ=30.83 (d, 4-C), 53.00, 53.30 (each q, COOMe), 56.83 (d, 3-C), 75.12 (d, 5-C), 116.60, 119.71, 123.07, 128.25, 128.72, 128.91 (each d, Ar), 132.01 (s, Ar), 155.40 (s, Ar), 170.19 (s, 2-C), 170.30, and 171.78 (each s, COOMe); MS *m/z* (rel intensity, %) 353 (M^+, 40), 295 (15), 294 (78), 263 (20), 262 (base peak), 235 (35), 234 (11), 209 (31), 208 (15), 206 (13), 148 (24), 131 (21), 115 (24), 106 (11), 105 (21), 104 (15), 103 (18), 102 (9), 91 (10), 78 (30), and 77 (44). Found: C, 68.23; H, 5.32; N, 4.20%. Calcd for $C_{20}H_{19}NO_5$: C, 67.98; H, 5.42; N, 3.96%. **3**: Colorless liquid; IR (neat) 1750, 1735, 1610, 1490, and 1460 cm^{-1}; ^1H NMR ($CDCl_3$) δ=3.64 (3H, s, COOMe), 3.85 (1H, dd, J_{3a-9b}=7.0 and J_{3a-3}=2.0 Hz, 3a-H), 5.00 (1H, t, J_{3-3a}=J_{3-9b}=2.0 Hz, 3-H), 5.49 (1H, dd, J_{9b-3a}=7.0 and J_{9b-3}=2.0 Hz, 9b-H), and 6.9—7.9 (9H, m, Ar); ^{13}C NMR ($CDCl_3$) δ=46.47 (d, 3a-C), 53.00 (q, COOMe), 58.71 (d, 3-C), 70.12 (d, 9b-C), 117.23, 125.42, 128.83, 129.13, 130.25, 130.72 (each d, Ar), 131.83, 132.13 (each s, Ar), 150.72 (s, Ar), 167.54 (s, 2-C), 168.78, and 169.66 (each s, COO and COOMe); MS *m/z* (rel intensity, %) 321 (M^+, 21), 320 (base peak), 262 (13), 260 (36), 209 (39), and 105 (21). Found: C, 71.05; H, 4.74; N, 4.38%. Calcd for $C_{19}H_{15}NO_4$: C, 71.02; H, 4.71; N, 4.36%.

Acid-Catalyzed Cyclization of 2 Leading to 3 and Acid-Catalyzed Methanolysis of 3 into 2. Cyclization: A solution of **2** (0.1 g, 0.28 mmol) in toluene (3 ml) containing a catalytic amount of acetic acid was heated under reflux for 24 h. The mixture was evaporated to dryness in vacuo to give **3** (0.88 g, 98%). Methanolysis: A solution of **3** (0.084 g, 0.2 mmol) in methanol (10 ml) containing a catalytic amount of hydrochloric acid was heated under reflux for 1 h. The mixture was poured into ice water and extracted with chloroform (20 ml×2). The combined extracts were dried over magnesium sulfate and evaporated in vacuo to afford almost pure **2** (0.06 g, 85%).

Reaction of 1a with Dimethyl Fumarate Leading to 3—5. A mixture of **1a** (0.236 g, 1 mmol) and dimethyl fumarate (0.144 g, 1 mmol) in dry toluene (3 ml) was heated under reflux for 3.5 h. The solvent was evaporated in vacuo and the residue was chromatographed over silica gel by using chloroform to give **3** (0.1 g, 31%) and, then, an inseparable mixture of **4** and **5** (0.237 g, 62%). **4** and **5** (a 2:1 mixture (^1H NMR)): Colorless liquid; IR (neat) 3400—3100, 1740, 1640, 1495, and 1455 cm^{-1}; ^1H NMR ($CDCl_3$) one isomer: δ=3.53, 3.70 (each 3H, s, COOMe), 3.70 (1H, t, J_{4-3}=J_{4-5}=7.0 Hz, 4-H), 4.65 (1H, dd, J_{3-4}=7.0 and J_{3-5}=2.0 Hz, 3-H), 5.68 (1H, dd, J_{5-4}=7.0 and J_{5-3}=2.0 Hz, 5-H), 6.7—7.4 (7H, m, Ar), 7.70 (2H, m, Ar), and 9.00 (1H, br, OH); the other isomer: δ=3.58, 3.68 (each 3H, s, COOMe), 3.65 (1H, dd, J_{4-3}=7.5 and J_{4-5}=7.0 Hz, 4-H), 4.60 (1H, dd, J_{3-4}=7.5 and J_{3-5}=2.0 Hz, 3-H), 5.87 (1H, dd, J_{5-4}=7.0 and J_{5-3}=2.0 Hz, 5-H), 6.7—7.4 (7H, m, Ar), 7.70 (2H, m, Ar), and 8.20 (1H, m, OH); MS *m/z* (rel intensity, %) 353 (M^+, 50), 295 (15), 294 (71), 263 (20), 262 (base peak), 261 (13), 235 (41), 234 (13), 209 (30), 206 (18), 131 (31), 115 (28), 106 (13), 105 (20), 104 (20), 103 (20), 78 (32), and 77 (43). Found: C, 67.87; H, 5.46; N, 3.84%. Calcd for $C_{20}H_{19}NO_5$: C, 67.98; H, 5.42; N, 3.96%.

Reaction of 1a with Methyl Acrylate Leading to 6 and 7. A mixture of **1a** (0.4 g, 1.69 mmol) and methyl acrylate (0.36 g, 4.29 mmol) was heated under reflux in toluene (10 ml) for 28 h. The residue obtained by the evaporation of all the volatile materials in vacuo, was triturated with diethyl ether–hexane to give **6** (0.32 , 67%) as a colorless solid. The filtrate was evaporated and the residue chromatographed over silica gel with chloroform to afford **7** (0.14 g, 26%) as a 2:1 mixture of two isomers (^1H NMR). **6**: Colorless needles (benzene–hexane); mp 183—184 °C; IR (KBr) 1755, 1610, 1490, 1455, 1220, and 1195 cm^{-1}; ^1H NMR ($CDCl_3$) δ= 3.3—3.9 (3H, m, 3- and 3a-H), 5.36 (1H, dt, J_{9b-3a}=5.0 and J_{9b-3}= 3.0 Hz, 9b-H), and 7.0—7.9 (9H, m, Ar); ^{13}C NMR ($CDCl_3$) δ=40.94 (t and d, 3- and 3a-C), 70.12 (d, 9b-C), 117.24, 120.13, 125.24, 128.07, 128.77, 129.83, 130.25 (each d, Ar), 131.48, 133.24, 150.54 (each s, Ar), 169.12 (s, 2-C), and 172.60 (s, 4-C); MS *m/z* (rel intensity, %) 263 (M^+, 24), 209 (17), 208 (base peak), 160 (14), 132 (18), 131 (30), 115 (25), 105 (26), 104 (16), 103 (22), 102 (11), 89 (13), 77 (75), and 76 (19). Found: C, 77.48; H, 4.98; N, 5.43%. Calcd for $C_{17}H_{13}NO_2$: C, 77.55; H, 4.98; N, 5.32%. **7** (an inseparable 2:1 mixture of two regioisomers (^1H NMR)): Colorless liquid; IR (neat) 3400—2800, 1740, 1615, 1580, 1495, 1450, 1340, and 1250 cm^{-1}; ^1H NMR ($CDCl_3$) major isomer: δ=2.2—2.6 (1H, m, one of 4-H), 2.8—3.1 (1H, m, the other of 4-H), 3.63 (3H, s, COOMe), 4.27 (1H, dt, J_{3-4}=10.0 and J_{3-5}=2.0 Hz, 3-H), 5.60 (1H, dt, J_{5-4}=8.0 Hz and J_{5-3}=2.0 Hz, 5-H), 6.8—7.9 (9H, m, Ar), and 8.5—9.5 (1H, br, OH); minor isomer: δ=2.2—2.6

(1H, m, one of 4-H), 2.8—3.1 (3H, m, the other of 4-H), 3.53 (3H, s, COOMe), 4.16 (1H, m, 3-H), 5.36 (1H, dt, J_{5-4}=10.0 and J_{5-3}=2.0 Hz, 5-H), 6.8—7.9 (9H, m, Ar), and 8.5—9.5 (1H, br, OH); ^{13}C NMR ($CDCl_3$) major isomer: δ=35.71 (t, 3-C), 53.47 (q and d, COOMe and 4-C), 73.12 (d, 5-C), 169.42 (s, 2-C), 171.54 (s, COOMe); minor isomer: δ=36.12 (t, 3-C), 52.65 (q, COOMe), 53.47 (d, 4-C), 72.36 (d, 5-C), 169.95 (s, 2-C), 172.36 (s, COOMe); the other signals: δ=117.07, 119.71, 126.48, 127.89, 128.59, 128.89, 131.53, 131.54, 136.12, 156.25.

Reaction of 1b with Dimethyl Maleate Leading to 8. A solution of **1b** (0.278 g, 1 mmol) and dimethyl maleate (0.144 g, 1 mmol) in dry toluene (3 ml) was heated under reflux for 14 h. The mixture was evaporated in vacuo and the residue was chromatographed over silica gel by using chloroform to give **8** (0.36 g, 91%): Colorless needles (benzene-hexane); mp 203—204 °C; IR (KBr) 1755, 1730, 1625, 1510, 1430, 1305, 1270, 1220, and 1160 cm^{-1}; ^{1}H NMR ($CDCl_3$) δ=3.67 (3H, s, COOMe), 3.90 (1H, dd, J_{3a-11c}=8.0 and J_{3a-3}=1.5 Hz, 3a-H), 5.10 (1H, dd, J_{3-11a}=2.0 and J_{3-3a}=1.5 Hz, 3-H), 6.00 (1H, dd, J_{11c-3a}=8.0 and J_{11c-3}= 2.0 Hz, 11c-H), 7.0—8.0 (10H, m, Ar), and 8.25 (1H, m, Ar); ^{13}C NMR ($CDCl_3$) δ=46.03 (d, 3a-C), 52.89 (q, Me), 58.12 (d, 3-C), 67.34 (d, 11c-C), 112.19, 117.00, 124.05, 125.46, 127.58, 128.19, 128.40, 128.63, 130.92 (each d), 131.04, 131.51, 131.92, 148.19 (each d, Ar), 167.26 (s, 2-C), 168.62, and 169.43 (each s, COOMe and 4-C); MS *m/z* (rel intensity, %) 371 (M^+, 38), 312 (34), 284 (13), 258 (86), and 152 (base peak). Found: C, 74.45; H, 4.83; N, 3.77%. Calcd for $C_{23}H_{17}NO_4$: C, 74.38; H, 4.61; N, 3.77%.

Reaction of 1b with Dimethyl Fumarate Leading to 8 and 9. By a similar procedure, using **1b** (0.43 g, 1.5 mmol) and dimethyl fumarate (0.216 g, 1.5 mmol) in toluene (6 ml), after heating under reflux for 20 h and chromatography over silica gel with chloroform-ethyl acetate (49:1 v/v), **8** (0.28 g, 50%) and then **9** (0.28 g, 41%) were obtained, **9**: Colorless prisms (benzene-hexane); mp 188—189 °C; IR (KBr) 3500—2900, 1740, 1620, 1575, 1515, 1440, 1270, and 1210 cm^{-1}; ^{1}H NMR ($CDCl_3$) δ=3.60 (3H, s, COOMe), 3.80 (1H, dd, J_{4-5}=5.0 and J_{4-3}=2.0 Hz, 4-H), 4.70 (1H, dd, J_{3-4}=J_{3-5}= 2.0 Hz, 3-H), 6.32 (1H, dd, J_{5-4}=5.0 and J_{5-3}=2.0 Hz, 5-H), 7.0—8.0 (11H, m, Ar), and 10.00 (1H, br s, OH); MS *m/z* (rel intensity, %) 403 (M^+, 23), 344 (15), 313 (23), 312 (base peak), 285 (25), 284 (15), 259 (37), 258 (19), 256 (16), 228 (15), 181 (17), 153 (21), 128 (45), 127 (30), 115 (38), 105 (10), 104 (15), and 77 (27). Found: C, 71.71; H, 5.18; N, 3.72%. Calcd for $C_{24}H_{21}NO_5$: C, 71.45; H, 5.25; N, 3.47%.

Reaction of 1c with Dimethyl Maleate Leading to 10. A mixture of **1c** (0.278 g, 1 mmol) and dimethyl maleate (0.144 g, 1 mmol) was heated under reflux in toluene (1 ml) for 14 h. The mixture was evaporated in vacuo and the residue was chromatographed over silica gel by using chloroform-ethyl acetate (9:1 v/v) to give **10** (0.36 g, 91%): Colorless prisms (benzene-hexane); mp 96—97 °C; IR (KBr) 1765, 1730, 1620, 1570, 1430, 1200, and 1160 cm^{-1}; ^{1}H NMR ($CDCl_3$) δ=2.24 (3H, s, OAc), 3.06 (3H, s, 4-COOMe), 3.58 (3H, s, 3-COOMe), 3.86 (1H, dd, J_{4-5}=9.0 and J_{4-3}=3.0 Hz, 4-H), 4.80 (1H, dd, J_{3-4}=3.0 and J_{3-5}=1.5 Hz, 3-H), 5.95 (1H, dd, J_{5-4}=9.0 and J_{5-3}=1.5 Hz, 5-H), 7.0—7.4 (7H, m, ArH), and 7.90 (2H, m, Ar); MS *m/z* (rel intensity, %) 395 (M^+, 18), 294 (26), 262 (30), 261 (10), 208 (19), 131 (14), 115 (16), 105 (14), 77 (12), 76 (30), 51 (14), and 42 (base peak). Found: C, 67.11; H, 5.34; N, 3.75%. Calcd for $C_{22}H_{21}NO_6$: C, 66.87; H, 5.35; N, 3.54%.

refluxing for 8.5 h and the subsequent column chromatography over silica gel by using chloroform-ethyl acetate (9:1

This compound **10** (0.395 g, 1 mmol) and a catalytic amount of *p*-toluenesulfonic acid were heated under reflux in toluene (5 ml) for 13 h. The mixture was poured into water and extracted with dichloromethane (20 ml×2). The combined extracts were dried over magnesium sulfate and evaporated in vacuo. The residue was chromatographed over silica gel with chloroform to give **3** (0.193 g, 60%).

Reaction of 1c with Dimethyl Fumarate Leading to 10 and 11. By a similar procedure, using **1c** (0.278 g, 1 mmol) and dimethyl fumarate (0.144 g, 1 mmol) in toluene (1 ml), after v/v), a mixture of **10** and **11** (1:1 (^{1}H NMR), 0.208 g) and then **10** (0.17 g, 43%) were obtained. The yield of **10** was 69% and that of **11** was 26%. The latter product **11** could not be isolated in its pure form. **11**: ^{1}H NMR ($CDCl_3$): δ=2.20 (3H, s, OAc), 3.43 (1H, t, J_{4-3}=6.0 Hz, 4-H), 3.53 (3H, s, 3-COOMe), 3.65 (3H, s, 4-COOMe), 4.50 (1H, dd, J_{3-4}=6.0 and J_{3-5}=1.5 Hz, 3-H), 5.67 (1H, dd, J_{5-4}=6.0 and J_{5-3}=1.5 Hz, 5-H).

Reaction of 1e with *N*-Methylmaleimide Leading to 12. A solution of **1e** (0.404 g, 2 mmol) and *N*-methylmaleimide (0.222 g, 2 mmol) in dry toluene (15 ml) was heated under reflux for 14 h. The solvent was evaporated in vacuo and the residue was triturated with diethyl ether to give a colorless solid of **12** (0.057 g). The ether filtrate was evaporated and the residue was chromatographed over silica gel with chloroform-ethyl acetate (3:2 v/v) to afford another portion of **12** (0.16 g, total yield: 35%): **12**: Colorless prisms (acetonitrile): mp 239—240 °C; IR (KBr) 3100, 2225, 1790, 1710, and 1620 cm^{-1}; ^{1}H NMR ($CDCl_3$) δ=1.70 (3H, s, OAc), 2.65 (3H, s, NMe), 4.00 (1H, dd, J_{3a-6a}=10.0 and J_{3a-4}=2.0 Hz, 3a-H), 4.24 (1H, t, J_{6a-3a}=J_{6a-6}=10.0 Hz, 6a-H), 5.14 (1H, d, J_{4-3a}=2.0 Hz, 4-H), 5.38 (1H, d, J_{6-6a}=10.0 Hz, 6-H), 6.6—7.2 (4H, m, Ar), and 9.78 (1H, br s, OH); ^{13}C NMR ($CDCl_3$) δ=22.35 (q, NAc), 24.59 (NMe), 48.77 (d, 3a-C), 50.24 (d, 6a-C), 57.00 (d, 4-C), 63.24 (d, 6-C), 116.13 (d, Ar), 118.18 (s, CN), 119.42, 122.60 (each d, Ar), 130.18 (s, Ar), 131.60 (d, Ar), 154.19 (s, Ar), 169.48 (s, NAc), 173.54, and 175.60 (each s, CON); MS *m/z* (rel intensity, %) 313 (M^+, 19), 286 (8), 270 (38), and 160 (base peak). Found: C, 61.23; H, 4.90; N, 13.39%. Calcd for $C_{16}H_{15}N_3O_4$: C, 61.33, H, 4.83; N, 13.41%.

Reaction of 1e with Dimethyl Fumarate Leading to 13 and 14. A solution of **1e** (0.404 g, 2 mmol) and dimethyl fumarate (0.288 g, 2 mmol) in dry toluene (10 ml) was heated under reflux. When the mixture was cooled down to room temperature, a colorless solid of **13** (0.252 g, 34%) was precipitated. The filtrate was evaporated in vacuo and the residue was chromatographed over silica gel by using chloroform-ethyl acetate (3:1 v/v) to give **14** (0.06 g, 9%). **13**: Colorless prisms (acetonitrile); mp 222—223 °C; IR (KBr) 3600—3000, 2250, 1740, and 1620 cm^{-1}; ^{1}H NMR ($CDCl_3$) δ=1.64 (3H, s, NAc), 3.36 (3H, s, 4-COOMe), 3.70 (3H, s, 3-COOMe), 3.93 (2H, m, 3- and 4-H), 5.46 (1H, d, J_{2-3}=7.6 Hz, 2-H), 5.75 (1H, d, J_{5-4}=7.6 Hz, 5-H), 6.6—7.1 (4H, m, Ar), and 9.76 (1H, br s, OH); ^{13}C NMR ($CDCl_3$) δ=21.47 (q, NAc), 45.42 (d, 3-C), 47.83 (d, 4-C), 49.36 (d, 2-C), 51.77, 52.83 (each q, COOMe), 57.47 (d, 5-C), 115.42 (d, Ar), 116.48 (s, CN), 119.24 (d, Ar), 123.48 (s, Ar), 128.42, 129.54 (each d, Ar), 154.66 (s, Ar), 168.54, 168.83, and 169.19 (each s, COOMe and NAc); MS *m/z* (rel intensity, %) 346 (M^+, 51), 303 (42), 271 (28), 160 (73), and 42 (base peak); Found: C, 58.88; H, 5.29; N, 8.15%. Calcd for $C_{17}H_{18}N_2O_6$: C, 58.95; H,

5.24; N, 8.09%. **14**: Colorless prisms (acetonitrile); mp 194—195 °C; IR (KBr) 3270, 1750, 1730, 1635, and 1600 cm^{-1}; ^1H NMR ($CDCl_3$) δ=2.27 (3H, s, NAc), 3.46 (1H, dd, J_{3-4}=12.0 and J_{3-2}=9.0 Hz, 3-H), 3.62, 3.68 (each 3H, s, COOMe), 3.88 (1H, dd, J_{4-3}=12.0 and J_{4-5}=9.0 Hz, 4-H), 5.30 (1H, d, J_{2-3}=9.0 Hz, 2-H), 5.40 (1H, d, J_{5-4}=9.0 Hz, 5-H), 6.8—7.3 (4H, m, Ar), and 9.63 (1H, br s, OH); ^{13}C NMR ($CDCl_3$) δ=21.94 (q, NAc), 48.47 (d, 3-C), 50.12 (d, 4-C), 53.42 (d, 2-C), 53.71, 54.89 (each q, COOMe), 61.24 (d, 5-C), 116.83 (d, Ar), 117.89 (s, CN), 122.24 (d, Ar), 127.18 (s, Ar), 128.01, 130.83 (each d, Ar), 155.31 (s, Ar), 169.36, 170.00, and 171.66 (each s, COOMe and NAc); MS *m/z* (rel intensity, %) 346 (M^+, 26), 303 (11), 271 (12), 245 (10), 218 (12), 193 (31), 186 (21), 185 (17), 176 (27), 161 (18), 160 (30), 159 (13), 133 (17), 132 (13), 131 (22), 77 (18), and 43 (base peak). Found: C, 58.74; H, 5.20; N, 7.91%. Calcd for $C_{17}H_{18}N_2O_6$: C, 58.95; H, 5.24; N, 8.09%.

General Procedure for the Reaction of 1f with Olefins in the Presence of LDA Leading to 15—17 and 18—20. To a freshly prepared solution of LDA (1.6 mmol) in dry THF (5 ml) was slowly added a solution of **1f** (1.5 mmol) in THF (5 ml) at −78 °C. After 5 min, an olefin (1.5 mmol) in THF (5 ml) was added. The mixture was stirred at −78 °C for 5 h, poured into saturated aqueous ammonium chloride, and extracted with diethyl ether (20 ml×2). The combined extracts were dried over magnesium sulfate and evaporated in vacuo. The residue was chromatographed over silica gel by using chloroform to give an inseparable mixture of **15** and **18** or **17** and **20**. However **16** and **19** could be separated from each other.

15 and **18** (a 3:2 mixture (^1H NMR)): Yield 94%; ^1H NMR ($CDCl_3$) **15**: δ=0.30 (9H, s, $SiMe_3$), 2.3—2.6 (2H, m, 3-H), 3.15 (1H, m, 3-H), 5.75 (1H, d, J_{5-4}=9.0 Hz, 5-H), 6.6—7.2 (4H, m, Ar), and 7.80 (1H, br s, 2-H); **18**: δ=2.3—2.6 (3H, m, CH_2 and CH), 3.50 (3H, s, COOMe), 4.40 (1H, d, J=6.0 Hz, NCH), 5.50 (1H, d, J=4.0 Hz, OCHN), and 6.6—7.2 (4H, m, Ar).

16 (50%) and **19** (20%): **16**: Pale yellow liquid; IR (neat) 1730, 1635, 1595, 1450, 910, 840, 750 cm^{-1}; ^1H NMR ($CDCl_3$) δ=0.30 (9H, s, $SiMe_3$), 1.25 (3H, d, J_{Me-3}=7.5 Hz, 3-Me), 2.16 (3H, d, J=6.5 Hz, Me), 3.13 (3H, s, COOMe), 3.6—3.8 (2H, m, 3- and 4-H), 5.75 (1H, dd, J_{5-4}=8.0 Hz, J_{5-3}=2.0 Hz, 5-H), and 6.6—7.2 (4H, m, Ar); MS *m/z* (rel intensity, %) 319 (M^+, 23), 304 (19), 260 (33), 219 (31), 186 (29), 146 (19), 128 (50), 86 (13), 77 (10), 73 (30), and 44 (20). HRMS Found: *m/z* 319.1619. Calcd for $C_{17}H_{25}NO_3$: M, 319.1617. **19**: Colorless liquid; IR (neat) 3350, 2980, 1730, 1610, 1585, 1490, 1460, 1025, 910, and 760 cm^{-1}; ^1H NMR ($CDCl_3$) δ=1.16 (3H, d, J=7.0 Hz, Me), 2.1—2.7 (1H, br NH), 2.8—3.3 (2H, m, CH), 3.56 (3H, s, COOMe), 4.41 (1H, d, J=6.0 Hz, NCH), 5.10 (1H, s, OCHN), and 6.6—7.4 (4H, m, Ar); ^{13}C NMR ($CDCl_3$) δ=19.38 (Me), 42.08 (CHMe), 51.72 (COOMe), 58.64 (CHCOOMe), 60.44 (NCH), 93.90 (OCHN), 116.38, 119.36, 125.19, 126.45, 129.25, 151.41 (each Ar), and 171.37 (COOMe); MS *m/z* (rel intensity, %) 233 (M^+, 38), 175 (25), 174 (21), 85 (61), 83 (base peak), and 47 (29). HRMS Found: *m/z* 233.1049. Calcd for $C_{13}H_{15}NO_3$: M, 233.1047.

17 and **20** (**17**: 62%; **20**: 16% (^1H NMR)). Only **20** was isolated in a pure form): **17**: ^1H NMR ($CDCl_3$) δ=0.30 (9H, s, $SiMe_3$), 3.14 (3H, s, COOMe), and 7.70 (1H, d, J=2.0 Hz, 2-H). Other signals were overlapped with those of **20**. **20**: Colorless liquid; IR (neat) 3320, 2950, 1720, 1590, 1450, 1250, and 750 cm^{-1}; ^1H NMR ($CDCl_3$) δ=1.52 (3H, s, Me), 1.90 (1H, dd, J_{gem}=15.0 and J=4.0 Hz, one of CH_2), 2.95 (1H, d, J_{gem}=15.0 Hz, the other of CH_2), 3.0—3.3 (1H, br, NH), 3.46 (3H, s, COOMe), 3.95 (1H, s, NCH), 5.47 (1H, d, J=4.0 Hz, OCHN), and 6.6—7.3 (4H, m, Ar); ^{13}C NMR ($CDCl_3$) δ=25.80 (q, Me), 42.48 (t, CH_2), 51.79 (q, COOMe), 58.10 (s, *q*-C), 63.51 (d, NCH), 88.52 (OCHN), 116.35, 119.13, 125.45, 126.83, 129.08 (each d, Ar), 151.51 (s, Ar), and 174.77 (s, COOMe); MS *m/z* (rel intensity, %) 233 (M^+, 35), 175 (15), 174 (base peak), 172 (10), 133 (29), 132 (17), 131 (13), 112 (21), 105 (22), 104 (14), 91 (29), 84 (18), 82 (29), and 77 (21). HRMS Found: *m/z* 233.1049. Calcd for $C_{13}H_{15}NO_3$: M, 233.1049.

Acetylation of 18 Leading to 21. A mixture of **15** and **18** (2:1, 0.23 g) in acetic acid (1 ml) containing acetic anhydride (1 ml) was stirred at room temperature for 1 h. After the reaction was complete, ethanol (30 ml) was added. The mixture was evaporated in vacuo and the residue was triturated with diethyl ether to give a colorless solid of **21** (0.16 g, 71%): Colorless prisms (benzene-hexane); mp 129—130 °C; IR (KBr) 1725, 1640, 1475, 1400, 1200, 1170, 1020, 930, 890, and 745 cm^{-1}; ^1H NMR ($CDCl_3$) δ=2.13 (1/3×3H, s, Ac (syn)), 2.23 (2/3×3H s, Ac (anti)), 2.3—3.0 (2H, m, CH_2), 3.2—3.6 (1H, m, CH), 3.56 (3H, s, COOMe), 4.98 (1/3H, d, J=7.0 Hz, NCH (syn)), 5.49 (2/3H, d, J=6.5 Hz, NCH (anti)), 5.91 (2/3H, d, J=5.5 Hz, OCHN (anti)), 6.35 (1/3H, d, J=5.5 Hz, OCHN (syn)), and 6.6—7.3 (3H, m, Ar); MS *m/z* (rel intensity, %) 261 (M^+, 26), 202 (20), 160 (base peak), 132 (16), 131 (11), and 76 (13). Found: C, 64.64; H, 5.90; N, 5.31%. Calcd for $C_{14}H_{15}NO_4$:C, 64.36; H, 5.79; N, 5.36%.

Acetylation of 19 Leading to 22. A similar procedure using a mixture of **16** and **19** (3:1, 0.3 g) gave **22** (0.21 g, 73%): Colorless needles (benzene-hexane); IR (KBr) 1735, 1650, 1420, 1360, 1310, 1250, 1200, and 750 cm^{-1}; ^1H NMR ($CDCl_3$) δ=1.22 (3H, d, J=7.6 Hz, Me), 2.09 (2/5×3H, s, Ac (syn)), 2.20 (3/5×3H, s, Ac (anti)), 2.8—3.3 (2H, m, CH), 4.96 (2/5H, d, J=6.0 Hz, NCH (syn)), 5.44 (3/5H, br s, OCHN (anti)), 5.49 (3/5H, d, J=6.0 Hz, NCH (anti)), 5.94 (2/5H, br s, OCHN (syn)), and 6.7—7.2 (4H, m, Ar); MS *m/z* (rel intensity, %) 275 (M^+, 33), 216 (26), 175 (14), 174 (base peak), 132 (16), and 77 (15). Found: C, 65.44; H, 6.26; N, 4.90%. Calcd for $C_{15}H_{17}NO_4$: C, 65.44; H, 6.22; N, 5.09%.

Acetylation of 20 Leading to 23. A similar procedure using a mixture of **17** and **20** (4:1, 0.24 g) gave **23** (0.165 g, 73%): Colorless prisms (benzene-hexane); mp 137—138 °C; IR (KBr) 1725, 1650, 1410, 1290, 1200, 1160, 1120, and 750 cm^{-1}; ^1H NMR ($CDCl_3$) δ=1.44 (2/3×3H, s, Me (anti)), 1.50 (1/3×3H, s, Me (syn)), 2.10 (1/3×3H, s, Ac (syn)), 2.23 (2/3×3H, s, Ac (anti)), 2.8—3.3 (2H, m, CH_2), 3.50 (3H, s, COOMe), 4.50 (1/3H, s, NCH (syn)), 5.06 (2/3H, s, NCH (anti)), 5.92 (2/3H, d, J=6.0 Hz, OCHN (anti)), 6.35 (1/3H, d, J=6.0 Hz, OCHN (syn)), and 6.6—7.2 (4H, m, Ar); MS *m/z* (rel intensity, %) 275 (M^+, 20), 216 (30), 175 (10), 174 (66), 172 (16), 133 (17), 132 (25), 131 (14), 78 (13), and 77 (26). Found: C, 65.56; H, 6.47; N, 5.09%. Calcd for $C_{15}H_{17}NO_4$: C, 65.44; H, 6.22; N, 5.09%.

Reaction of 1g with Methyl Crotonate Leading to 24 and 28. To a solution of freshly prepared LDA (1.6 mmol) in THF (5 ml) was added at −78 °C a solution of **1g** (0.369 g, 1.5 mmol) in THF (5 ml). After the addition of methyl crotonate (0.16 g, 1.6 mmol in THF (5 ml)), the mixture was stirred at −78 °C for 1.5 h, poured into saturated aqueous ammonium chloride, and then extracted with diethyl ether (20 ml×2). The combined extracts were dried over magnesium sulfate and evaporated in vacuo. The residue was assigned as

24 on the basis of the following ^{1}H NMR spectrum ($CDCl_3$): δ=0.30 (9H, s, $SiMe_3$), 2.15 (3H, d, J_{Me-3}=6.5 Hz, 3-Me), 3.13 (3H, s, COOMe), 3.1—3.4 (1H, m, 3-H), 3.6—3.7 (1H, m, 4-H), 5.75 (1H, d, J_{5-4}=9.0 Hz, 5-H), and 6.7—7.2 (4H, m, Ar). It was chromatographed over silica gel by using chloroform as an eluent to give **28** (0.271 g, 84%): Colorless liquid; IR (neat) 2960, 1750, 1730, 1630, 1580, 1490, 1450, 1375, and 760 cm^{-1}; ^{1}H NMR ($CDCl_3$) δ=1.38 (3H, d, J_{Me-3}=7.0 Hz, 3-Me), 2.05 (3H, d, J=1.0 Hz, 2-Me), 3.08 (1H, dq, J_{3-Me}=7.0 and J_{3-Me}=1.0 Hz, 3-H), 3.73 (1H, d, J_{3a-9b}=8.0 Hz, 3a-H), 5.30 (1H, br d, J_{9b-3a}=8.0 Hz, 9b-H), and 6.7—7.7 (4H, m, Ar); ^{13}C NMR ($CDCl_3$) δ=15.98 (3-Me), 17.55 (2-Me), 48.64 (3a-C), 51.86 (3-C), 67.10 (9b-C), 116.93, 117.48, 125.09, 129.40, 129.56, 149.46, 168.59, and 178.28 (COO); MS *m/z* (rel intensity, %) 215 (M^+, 28), 174 (19), 146 (base peak), 131 (16), and 43 (21). HRMS Found: *m/z* 215.0933. Calcd for $C_{13}H_{13}NO_2$: M, 215.0933.

Reaction of 1g with Methyl Methacrylate Leading to 25, 27, and 29. A similar procedure using LDA (1.6 mmol) in THF (5 ml), **1g** (0.369 g, 1.5 mmol) in THF (5 ml), and methyl methacrylate (0.16 g, 1.6 mmol) in THF (5 ml), after column chromatography over silica gel with chloroform, gave **29** (0.16 g, 50%), and then an inseparable mixture of **25** and **27** (1:1 (^{1}H NMR), 0.17 g, 36%). The mixture of **25** and **27** (1:1, 0.17 g, 0.53 mmol) was stirred at room temperature for 1 h in the presence of cesium fluoride (10 mg) in THF (2 ml). After the reaction was completed, the mixture was poured into ice water and extracted with diethyl ether (20 ml). The extract was dried over magnesium sulfate and evaporated in vacuo. The residue was chromatographed over silica gel by using chloroform to give **29** (0.045 g, 79%) and **27** (0.06 g, 91%). **27**: Colorless prisms (benzene-hexane); mp 143—144 °C; IR (KBr) 3200—2800, 1730, 1640, 1590, 1450, 1370, 1110, and 750 cm^{-1}; ^{1}H NMR ($CDCl_3$) δ=1.43 (3H, s, 4-Me), 2.05 (3H, d, J_{Me-5}=2.0 Hz, 2-Me), 2.5—2.7 (2H, m, 3-H), 3.71 (3H, s, COOMe), 5.22 (1H, q, J=2.0 Hz, 5-H), and 6.8—7.2 (4H, m, Ar). Found: C, 69.39; H, 6.62; N, 5.32%. Calcd for $C_{14}H_{17}NO_3$: C, 69.48; H, 6.61; N, 5.40%. **29**: Colorless liquid; IR (neat) 1760, 1630, 1495, 1460, 1430, 1380, 1250, 1220, 1190, 1140, 1090, and 760 cm^{-1}; ^{1}H NMR ($CDCl_3$) δ=1.50 (3H, s, 3a-Me), 2.06 (3H, d, J_{Me-9b}=1.0 Hz, 2-Me), 2.70 (1H, d, J_{gem}=16.0 Hz, one of 3-H), 3.45 (1H, d, J_{gem}=16.0 Hz, the other of 3-H), 4.76 (1H, br s, 9b-H), and 6.7—7.7 (4H, m, Ar); ^{13}C NMR ($CDCl_3$) δ=20.23 (3a-Me), 22.54 (3-C), 48.94 (4-C), 51.84 (COOMe), 76.44 (9b-C), 117.11, 120.03, 129.94, 130.50, 150.42 (each Ar), and 175.73 (2C, COOMe and 4-C); MS *m/z* (rel intensity, %) 215 (M^+, 2), 213 (11), 146 (10), 100 (12), 94 (89), 85 (11), 83 (14), and 75 (base peak). HRMS Found: *m/z* 215.0934. Calcd for $C_{13}H_{13}NO_2$: M, 215.0933.

Reaction of 1g with Methyl Cinnamate Leading to 26 and 30. A similar procedure using LDA (1 mmol) in THF (3 ml), **1g** (0.246 g, 1 mmol) in THF (3 ml), and methyl cinnamate (0.162 g, 1 mmol) in THF (3 ml) gave **26** as a single product (by ^{1}H NMR). This crude product was chromatographed over silica gel with chloroform to give **26** (35%) and **30** (32%): **26**: Pale yellow liquid; IR (neat) 1735, 1650, 920, and 850 cm^{-1}; ^{1}H NMR ($CDCl_3$) δ=0.30 (9H, s, $SiMe_3$), 2.05 (3H, d, J_{Me-5}=2.0 Hz, 2-Me), 3.12 (3H, s, COOMe), 3.53 (1H, dd, J_{4-5}=9.0 and J_{4-3}=5.0 Hz, 4-H), 4.50 (1H, d, J_{3-4}=5.0 Hz, 3-H), 6.00 (1H, dd, J_{5-4}=9.0 and J_{5-Me}=2.0 Hz, 5-H), and 6.7—7.4 (9H, m, Ar); MS *m/z* (rel intensity, %) 381 (M^+, 10), 366 (3), 219 (15), 121 (13), and 86 (69). HRMS Found: *m/z* 381.1765. Calcd for $C_{22}H_{27}NO_3Si$: M, 381.1760. **30**: Pale yellow liquid; IR (neat) 3400—2800, 1730, and 1650 cm^{-1}; ^{1}H NMR ($CDCl_3$) δ=2.10 (3H, s, Me), 3.23 (3H, s, COOMe), 3.60 (1H, dd, J_{4-5}=9.0 and J_{4-3}=4.0 Hz, 4-H), 4.40 (1H, br s, 3-H), 5.90 (1H, br d, J_{5-4}=9.0 Hz, 5-H), and 6.7—7.5 (9H, m, Ar); MS *m/z* (rel intensity, %) 309 (M^+, 42), 251 (23), 250 (base peak), 236 (25), 147 (24), 84 (55), and 47 (18). HRMS Found: *m/z* 309.1347. Calcd for $C_{19}H_{19}NO_3$: M, 309.1363.

This work was financially supported by a Grant-in-Aid for Scientific Research (No. 63550652) from the Ministry of Education, Science and Culture.

References

1) As reviews: R. Grigg, *Chem. Soc. Rev.*, **16**, 89 (1987); R. Grigg, *Bull. Chim. Soc. Belg.*, **93**, 593 (1984).

2) R. Grigg and H. Q. N. Gunaratne, *J. Chem. Soc., Chem. Commun.*, **1982**, 384; R. Grigg, H. Q. N. Gunaratne, and V. Sridharan, *Tetrahedron*, **43**, 5887 (1987).

3) H. G. Pars, F. E. Granchelli, R. K. Razdan, and J. K. Keller, *J. Med. Chem.*, **19**, 445 (1976); R. K. Razdan, B. Z. Terris, G. R. Handrick, H. C. Dalzel, J. F. Howes, N. Plotnikoff, and P. Dodge, *ibid.*, **19**, 549 (1976); R. K. Razdan, "The Total Synthesis of Cannabinoids," in "The Total Synthesis of Natural Products," ed by J. ApSimon, A. Wiley-Interscience Publication, New York, Chichester, Brisbane, Toronto (1981), Vol. 4, Chap. 2, pp. 245—252.

4) O. Tsuge, K. Ueno, S. Kanemasa, and K. Yorozu, *Bull. Chem. Soc. Jpn.*, **59**, 1809 (1986).

5) O. Tsuge, S. Kanemasa, K. Yorozu, and K. Ueno, *Chem. Lett.*, **1985**, 1601.

6) O. Tsuge, S. Kanemasa, K. Yorozu, and K. Ueno, *Bull. Chem. Soc. Jpn.*, **60**, 3359 (1987).

7) O. Tsuge, S. Kanemasa, and M. Yoshioka, *J. Org. Chem.*, **53**, 1384 (1988); D. A. Barr, R. Grigg, H. Q. N. Gunaratne, J. Kemp, P. McMeekin, and V. Sridharan, *Tetrahedron*, **44**, 557 (1988).

Allylation of Quinones via Photoinduced Electron-Transfer Reactions from Allylstannanes

Kazuhiro MARUYAMA* and Hiroshi IMAHORI
Department of Chemistry, Faculty of Science, Kyoto University, Kyoto 606
(Received August 5, 1988)

Photochemical reactions of quinones with allylstannanes provided four types of products: adducts of allyl group to the carbonyl oxygens of quinones, adducts of allyl group to the olefinic carbons, adducts of allyl group to the carbonyl carbons, and hydroquinones. An electron-transfer mechanism was confirmed by ^{1}H-CIDNP (Chemically Induced Dynamic Nuclear Polarization) method. This study suggests that a) photoinduced electron transfer from allylstannanes to quinones produces the corresponding quinone anion radicals and tin cation radicals, b) the tin cation radicals cleave to give allyl radicals as well as tin cation, and c) the allyl radicals attack the quinone anion radicals resulting in the formation of final products, allylated quinones.

During the last decade the photostimulated electron-transfer reactions have been a topic in organic photochemistry.[1] One-electron transfer from donor to acceptor results in the formation of ion radical pair followed by the secondary reactions to produce final products. Efficacy of the secondary reactions, however, is controlled by the rate of back electron transfer. Many efforts to reduce the back electron transfer have been done so far. One of the way to solve this problem is the use of stabilized radical species generated by fragmentation of the cation radicals (Scheme 1). This process has been realized in the photooxidation of acid,[2] alcohol,[3] ether,[3] amine,[4] olefin,[5] silane,[6,7] stannane,[8-11] and so on[12] accompanied with the subsequent loss of a cation or a proton.

Mariano[6] and Mizuno[7] reported photoaddition reactions related to the allylsilane-iminium salt and allylsilane-cyano aromatics which were initiated by one-electron transfer and subsequent cleavage of silane cation radical to allyl radical and silane cation. However, only a few photochemical reactions of allyltin reagents have been reported.[8-11]

Allylation of quinones[13-15] is a major route for preparing isoprenoid quinones,[16] which play an important role in several metabolic sequences as well as being a key step in synthesis of antitumor-antibiotic quinonoid compounds.[17] It has been proved that allyl 4B metal compounds, allylsilane[14] and allylstannane,[15] are excellent reagents for direct introduction of allyl group to quinonoid nucleus. Thermal reactions of quinones with allylstannanes in the presence of a Lewis acid, especially BF_3, was of the most effective for allylation of quinones.[15] There have been a lot of reports on these thermal allylation of quinones, while by our knowledge one communication has appeared on photoallylation of quinones with allylsilane,[18] and no report on photoallylation of quinones with allylstannanes.

To explore the synthetic utility of the photochemistry of quinones with allylstannanes and to clarify the difference between thermal and photochemical reactions including the difference of reactivities between allylsilane and allylstannane, we have attempted to study the photochemistry of allylstannane-quinone systems. Now we will discuss the photochemistry of quinones with allylstannanes in this paper.

Results

Photochemical Reactions between Quinones and Allyltributylstannane. Photochemical reactions of a variety of quinones with allyltributylstannane were investigated. Irradiation of a benzene solution (25 ml) containing chloranil **1a** (1 mmol) and allyltributylstannane **2a** (2 mmol) with a high-pressure mercury lamp through an aqueous $CuSO_4$ filter ($h\nu$>315 nm) for 3 h under argon afforded a mixture of 4-allyloxy-

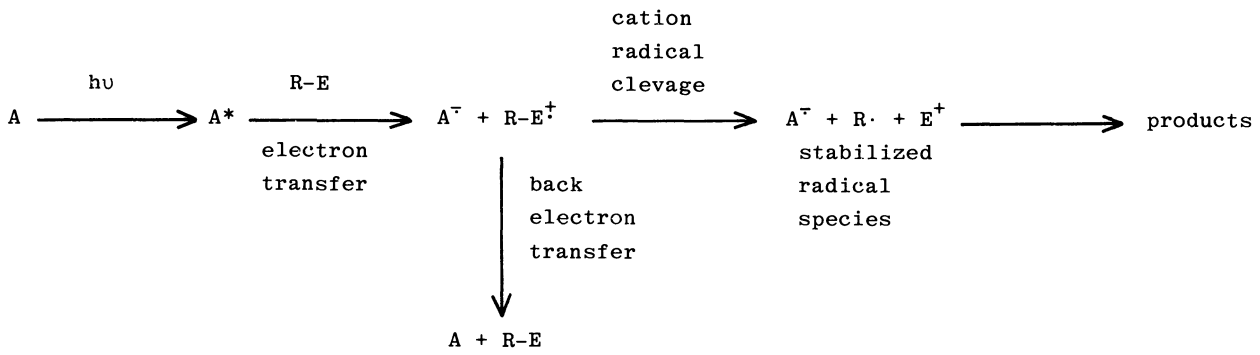

Scheme 1.

2,3,5,6-tetrachlorophenol **3a** (20%), 4-allyl-2,3,5,6-tetrachloro-4-hydroxy-2,5-cyclohexadien-1-one **7a** (20%), and 2,3,5,6-tetrachloro-1,4-benzenediol **8a** (50%). The yields of the respective products were based on the consumed quinone **1**. Likewise, **3a** (28%), **7a** (14%), and **8a** (12%) were obtained in acetonitrile (Run 2), but with different product distribution compared to the reaction in benzene. Structures of the products were readily assigned from the ^{1}H NMR, IR, mass spectroscopy, elemental analyses, suitable chemical transformations, and comparisons with those of structually related substances.[15] The IR spectrum of **3a** showed characteristic band due to hydroxyl group at 3430 cm^{-1}, while that of **7a** showed characteristic bands due to carbonyl and hydroxyl group at 1665 and 3400 cm^{-1}, respectively. In the mass spectrum of **3a** parent peaks appeared at *m/z* 286, 288, 290, 292, 294, indicating that one propene moiety had been incorporated into **1a**. In its ^{1}H NMR spectrum the α proton signal of allyl group in **3a** appeared at 4.53 as a doublet, while that of **7a** was at 2.97 as a doublet. Compound **3a** was compared with the authentic sample obtained by independent synthesis (see Experimental section). The results of photochemical reactions of quinones **1a—h** with allylstannane **2a** are summarized in Table 1. In the case of benzoquinone **1b** (Run 3), hydroquinone **8b** (52%) was major product besides yielding 4-(allyloxy)phenol **3b** (26%) and 2-allylhydroquinone **4b** (6%). On the other hand, naphthoquinone derivatives gave no 1,4-naphthalenediol (Runs 5—16). In the case of 2,3-dibromo-1,4-naphthoquinone **1c**, 2-allyl-3-bromo-1,4-naphthoquinone **5c** (29%) and 4-allyl-4-hydroxy-1(4*H*)-naphthalenone (designated to allyl quinol, hereafter) **7c** (28%) were obtained. The IR spectrum of **5c** showed characteristic bands due to carbonyl group at 1665 cm^{-1}, while that of **7c** showed those due to carbonyl and hydroxyl group at 1650 and 3360 cm^{-1}, respectively. In the mass

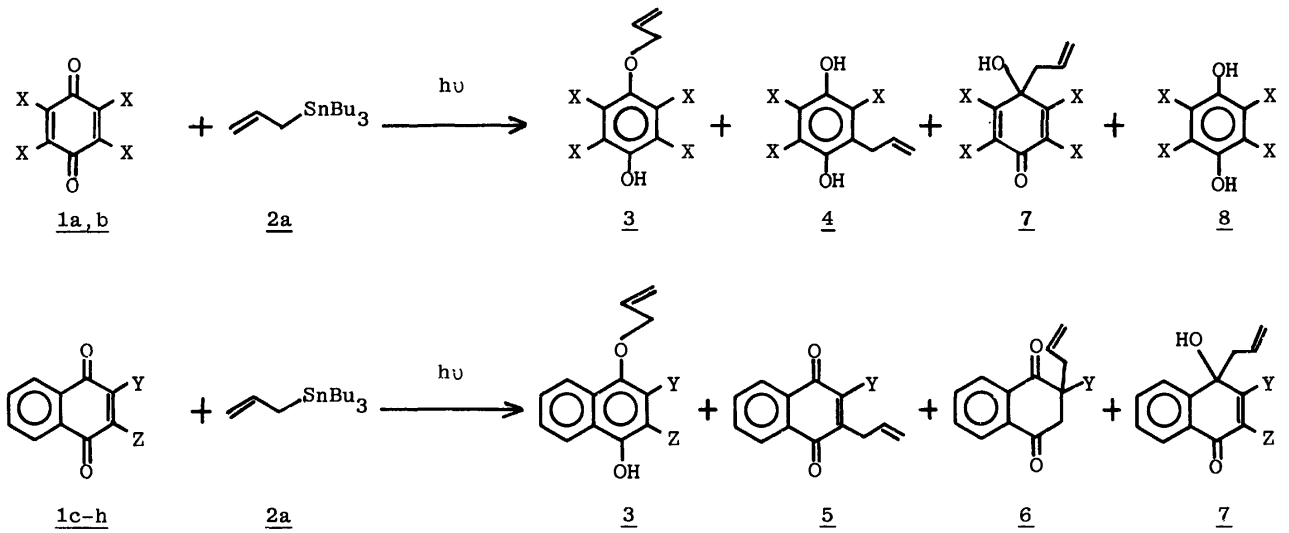

Scheme 2.

Table 1. Photochemical Reactions of Quinones **1** with Allyltributylstannane (**2a**)

Run	Quinone	Solvent	Conversion/%[a]	Products (yield/%)[b]
1	**1a**: X=Cl	C_6H_6	100	**3a**: X=Cl (20); **7a**: X=Cl (20); **8a**: X=Cl (50)
2	**1a**: X=Cl	CH_3CN	100	**3a**: X=Cl (28); **7a**: X=Cl (14); **8a**: X=Cl (12)
3	**1b**: X=H	C_6H_6	100	**3b**: X=H (26); **4b**: X=H (6); **8b**: X=H (52)
4	**1b**: X=H	CH_3CN	100	**3b**: X=H (23); **4b**: X=H (13); **8b**: X=H (57)
5	**1c**: Y=Z=Br	C_6H_6	75	**5c**: Y=Br (29); **7c**: Y=Z=Br (28)
6	**1c**: Y=Z=Br	CH_3CN	66	**5c**: Y=Br (47); **7c**: Y=Z=Br (32)
7	**1d**: Y=Z=Cl	C_6H_6	74	**5d**: Y=Cl (35); **7d**: Y=Z=Cl (15)
8	**1d**: Y=Z=Cl	CH_3CN	100	**5d**: Y=Cl (12); **7d**: Y=Z=Cl (26)
9	**1e**: Y=Br, Z=H	C_6H_6	81	**5c**: Y=Br (9); **5e**: Y=H (20)
10	**1e**: Y=Br, Z=H	CH_3CN	97	**5c**: Y=Br (15); **5e**: Y=H (15)
11	**1f**: Y=Z=H	C_6H_6	70	**3f**: Y=Z=H (21); **5e**: Y=H (14); **7f**: Y=Z=H (29)
12	**1f**: Y=Z=H	CH_3CN	98	**3f**: Y=Z=H (21); **5e**: Y=H (10); **7f**: Y=Z=H (11)
13	**1g**: Y=CH_3, Z=H	C_6H_6	78	**5g**: Y=CH_3 (38); **6g**: Y=CH_3 (28); **7g**: Y=H, Z=CH_3 (26)
14	**1g**: Y=CH_3, Z=H	CH_3CN	85	**5g**: Y=CH_3 (15); **6g**: Y=CH_3 (35); **7g**: Y=H, Z=CH_3 (32)
15	**1h**: Y=OCH_3, Z=H	C_6H_6	70	**5h**: Y=OCH_3 (53); **7h**: Y=OCH_3, Z=H (37)
16	**1h**: Y=OCH_3, Z=H	CH_3CN	50	**5h**: Y=OCH_3 (34); **7h**: Y=OCH_3, Z=H (56)

a) Irradiated for 3 h except Run 8 (35 h). b) Isolated yield based on a starting quinone consumed.

spectrum of **5c** parent peaks appeared at *m/z* 276, 278, indicating incorporation of one allyl group into **1c** and lose of one bromine atom from **1c**. In its ^{1}H NMR spectrum the α proton signal of allyl group in **5c** appeared at 3.66 as a doublet, while that of **7c** showed diastereotopic methylene at 2.70 (1H, dd, J=6, 13 Hz), 3.02 (1H, dd, J=6, 13 Hz). Similarly, 2,3-dichloro-1,4-naphthoquinone **1d** gave allyl quinone **5d** (35%) and allyl quinol **7d** (15%) (Run 7). 2-Bromo-1,4-naphthoquinone **1e**, however, gave no allyl quinol, but allyl quinones **5c** (9%) and **5e** (20%) were the products. Naphthoquinone **1f** gave all possible products, allyl ether **3f** (21%), allyl quinone **5e** (14%), and allyl quinol **7f** (29%). Reactions of unsymmetrical quinones, 2-methyl-1,4-naphthoquinone **1g** or 2-methoxy-1,4-naphthoquinone **1h**, gave allyl quinone **5g** (38%), 2-allyl-2,3-dihydro-1,4-naphthalenedione (abbreviated to allyl dione, hereafter) **6g** (28%), and allyl quinol **7g** (26%) (Run 13), or allyl quinone **5h** (53%) and allyl quinol **7h** (37%), respectively (Run 15). The ^{1}H NMR of allyl dione **6g** showed two pairs of diastereotopic methylene at δ 2.29 (1H, dd, J=7, 14 Hz), 2.61 (1H, dd, J=7, 14 Hz), 2.85 (1H, d, J=17 Hz), 3.10 (1H, d, J=17 Hz), and the ^{13}C NMR of **6g** showed carbonyl carbons at δ 196.0, 200.1. Surprisingly, in the cases of **1g** and **1h**, the corresponding allyl quinols **7g** and **7h**, were formed regioselectively.[19] Assignment of the regiochemistry was as follows. Since the ^{13}C NMR shift of β carbon in α,β-unsaturated ketone is characteristic, the signals appeared at δ 135.8 and 145.5 due to C2 and C3 may be assigned to 2-methyl-2-cyclohexen-1-one, while those appeared at δ 126.5 and 162.2 due to C2 and C3 to 3-methyl-2-cyclohexen-1-one, respectively. The ^{13}C NMR signals of **7g** due to C2 and C3 appeared at δ 129.9 and 147.1, respectively, which were determined by off-resonance decoupling of ^{13}C NMR spectroscopy and two dimensional ^{13}C–^{1}H shift correlation NMR spectroscopy. The structure of **7h** was assigned by comparison with the previously reported data.[15] Some of allyl quinols and allyl ethers were fairly unstable, and then after the hydroxyl group of them were acetylated the structure were confirmed (see Experimental section). In all cases, product distributions were quite dependent on solvents; benzene or acetonitrile, but there was no consistent inclinations.

Photochemical Reactions of 2,3-Dichloro-1,4-naphthoquinone with Prenyl (or Benzyl) Tin Reagents. The photochemical reactions of **1d** (1 mmol) with (3-methyl-2-butenyl)tributylstannane **2b** or benzyltributylstannane **2c** (2 mmol) were carried out in benzene (25 ml). As expected, three classes of products were obtained in both cases; compounds **9**, **10**, and **11**, which were also assigned by spectroscopic data and chemical transformation (see Experimental section). In the reaction of prenylstannane **2b**, prenyl ether **9b** (27%), prenyl quinone **10b** (27%), and prenyl quinol **11b** (19%) having α adduct structures were obtained exclusively[20] (Scheme 3). This method will provide a feasible route of isoprenoid quinones, which play an important role in biological electron transfer. Similarly, the photochemical reaction of **1d** with benzylstannane **2c** gave benzyl ether **9c** (26%), benzyl quinone **10c** (36%), and benzyl quinol **11c** (23%).

Mechanistic Aspects of the Reactions. To clarify the reaction mechanism, we have applied ^{1}H-CIDNP method to the photochemical reactions.[10] When a benzene-d_6 solution of **1d** ($\approx 10^{-2}$ mol dm^{-3}) and **2a** ($\approx 10^{-2}$ mol dm^{-3}) was irradiated (>330 nm) under argon, strong ^{1}H-CIDNP signals due to the allyl quinone **5d** and the by-product, 1,5-hexadiene **12a**, which were assigned by comparison with the authentic samples, were observed (Fig. 1). In acetonitrile-d_3 similar but weaker polarizations were observed. These polarizations are explained reasonably by the Kaptein's rule (See Ref. 21 for the polarization signals due to **5d** and **12a**). In the reaction of **1c** with **2a**, similar polarizations of allyl quinone **5c** and diene **12a** were observed in benzene-d_6, and furthermore in that of **1e** with **2a**, polarization signals due to allyl quinones **5c**,

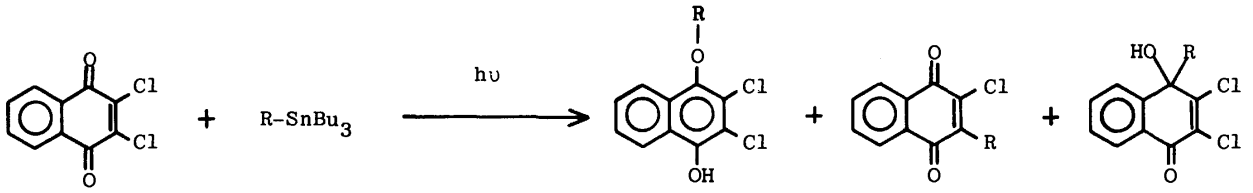

1d 2b,c 9 10 11

Stannane	Conversion/%[a]	Products (yield %)[b]		
2b: R=$CH_2CH=C(CH_3)_2$	73	**9b**: (27)	**10b**: (27)	**11b**: (19)
2c: R=CH_2Ph	84	**9c**: (26)	**10c**: (36)	**11c**: (23)

a) Irradiated for 3 h in benzene. b) Isolated yield based on a starting quinone consumed.

Scheme 3.

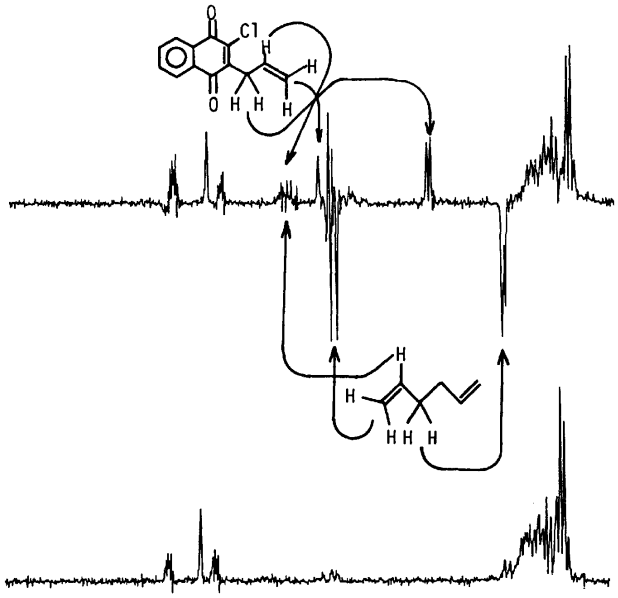

Fig. 1. ^{1}H NMR spectra (100 MHz) of a benzene-d_6 solution containing **1d** and **2a** in the dark (bottom) and during irradiation (top).

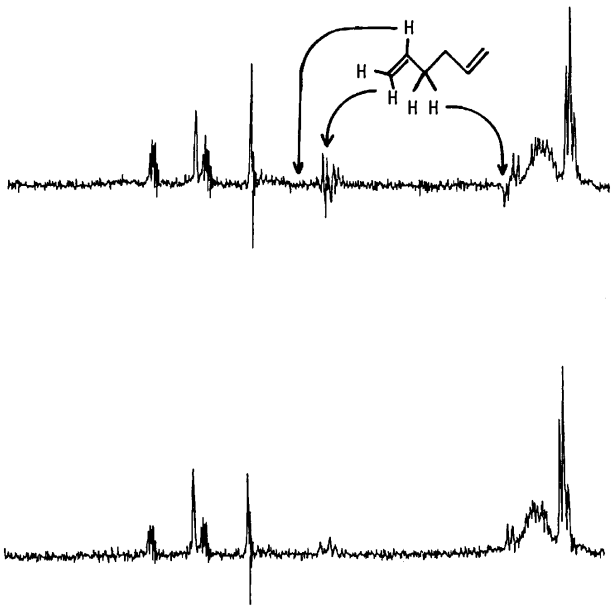

Fig. 2. ^{1}H NMR spectra (100 MHz) of a benzene-d_6 solution containing **1f** and **2a** in the dark (bottom) and during irradiation (top).

5e and diene **12a** were observed. But in the reactions of **1f** or **1g** with **2a**, only polarization signals due to **12a** were observed in benzene-d_6 (Fig. 2). None of the polarizations were observed in the reactions of **1b** or **1h** with **2a** in benzene-d_6. On the other hand in the reaction of **1a** with **2a**, the strongest polarizations due to both an adduct and diene **12a**, were observed in benzene-d_6, but the polarization due to the adduct could not be assigned to the final products, **3a**, **7a**, and

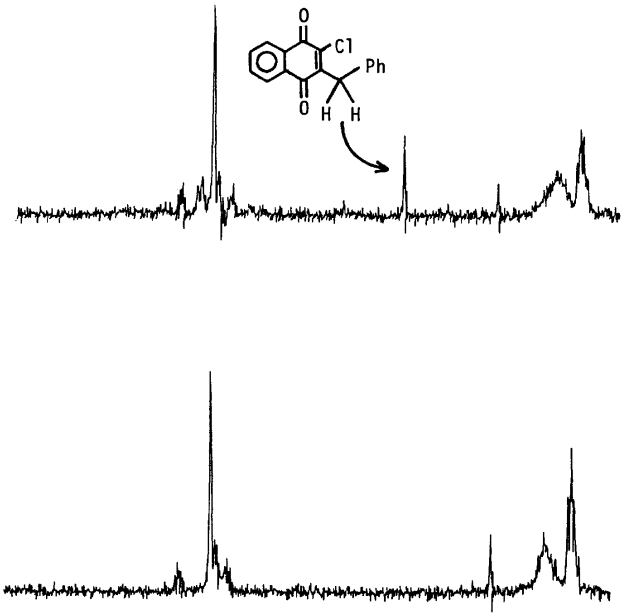

Fig. 3. ^{1}H NMR spectra (100 MHz) of a benzene-d_6 solution containing **1d** and **2c** in the dark (bottom) and during irradiation (top).

8a. In the reaction of **1d** with **2b**, ^{1}H NMR polarizations of allyl quinone **10b** were observed in benzene-d_6,[22] but polarizations based on other by-products; i.e, 2,7-dimethyl-2,6-octadiene, were not verified because of the complex signal derived from -SnBu$_3$ group. In the reaction of **1d** with **2c**, the polarization signals due to benzyl quinone **10c** were observed in benzene-d_6[23] (Fig. 3). In all of the CIDNP experiments, same pattern of polarization signals were observed in the reactions of both benzene-d_6 and acetonitrile-d_3 solution, but, in general, polarizations in benzene were stronger than that in acetonitrile.

Discussion

The free energy changes in electron-transfer process from a tin reagent to excited triplet quinone can be estimated by Rehm-Weller equation[24] (Eq. 1), where $E_{1/2}{}^{ox}$ and $E_{1/2_{red}}$ are redox potential of the electron donors and acceptors, respectively. $\Delta E_{0,0}$ is the excita-

$$\Delta G(\text{kcal mol}^{-1}) = 23.06(E_{1/2}^{ox} - E_{1/2}^{red} + C) - \Delta E_{0,0} \quad (1)$$

(1 cal = 4.184 J)

tion energy of **1**, and C represents the Coulomb term. We assume that the Coulomb term is too small to influence the present reactions. The reported or measured values of $E_{1/2}^{ox}$,[7] $E_{1/2}^{red}$,[25,26] and $\Delta E_{0,0}$[16b,27] were used for calculating the values of ΔG (see Table 2). The calculated values of ΔG were all negative, indicating that the electron transfer was possible.

Direct unambiguous evidences for electron-transfer

processes were obtained by CIDNP method. It is noteworthy that with some exceptions polarizations in the forward reaction path, but not in the reverse one, were observed. That is, polarizations due to both allyl quinone **5** and dimerization product of allyl radical **12a** were observed simultaneously in the reactions of **1c—e** with **2a**, whereas in many other photoinduced electron-transfer processes such as the reactions between quinones and 1,1-diarylethylenes[25] polarizations due to starting reactants based on the back electron transfer used to be observed. On the contrary, in the reactions of quinones **1f** or **1g**, only polarizations due to **12a** were observed, and in addition, no polarizations were observed in the reactions of quinones **1b** or **1h**. These quinones, i.e., **1b**, **1f—h**, have relatively low reduction potential. Therefore, an appreciable amount of polarizations would not be observed, because of the insufficient electron transfer in an unit time. This correlation between CIDNP polarizations and reduction potentials of quinones is another support of the electron-transfer processes in this system. Result of CIDNP in the reaction of **1a** with **2a** is interesting, polarizations of unstable adduct are quite strong and similar to those due to allyl quinones, but the adduct could not be isolated.[29]

In the reaction of **1d** with **2b**, polarizations due to prenyl quinone and possibly dimerization product of prenyl radical were observed similar to the reaction of **1d** with **2a**, but in the reaction of **1d** with **2c** only corresponding polarizations due to adduct **10c** were observed. But trace amount of 1,2-diphenylethane, dimerization product of benzyl radical, (GLC<1%) was detected in the photoproduct. Thus, the photochemical reactions of quinones with benzyltrialkylstannane as well as allyltrialkylstannane could proceed by electron-transfer mechanism.

On the basis of these findings, we propose an electron-transfer mechanism[30] shown in Scheme 4. This is analogous to the well-established mechanism for the iminium salt-allylsilane photochemical reaction.[6] Because of the strong oxidizing power of quinones and lower oxidation potential of allyl or benzylstannanes as compared to allylsilane, electron transfer easily occurs from tin reagent to excited triplet quinone,[31] producing the ion radical pair ($1^{\cdot-}$, $2^{\cdot+}$), but in nonpolar solvent the corresponding intermediate may be an exciplex.[32] Owing to the instability of $2^{\cdot+}$,[33] allyl or benzyl radical may cleave from the tin cation radical, forming triplet ion radical pair ($1^{\cdot-}$, R·, $SnBu_3^+$)^T subsequently. Attack of allyl or benzyl radical toward quinone anion radical $1^{\cdot-}$ followed by bonding with tin cation could give the corresponding intermediates, which lead to formation of the adducts **3—7**, **9—11** (Scheme 5). Quinone anion radical and allyl radical escaped from the solvent cage would give reduction product, hydroquinone **8**,[34] and the dimerization product **12** of allyl or benzyl radical.[35]

In the reactions of **1** with **2a**, conversion of reactions decreased as decrease of the reduction potential of quinones, suggesting the electron-transfer processes in the reactions. There is a tendency that allylations occur at almost all positions of quinones,[36] because spin densities of quinone anion radical are rather similar at all positions.[37,38] It is noteworthy, however, that allyl quinols **7g** and **7h** were formed regioselectively. Probably both steric hindrance of alkyl tin moiety against methyl group in **1g** and coordination of tin to the methoxyl group in **1h** affect the regioselective formation of **7g** and **7h**. In the reaction of **1d** with **2b**, it gave α adducts exclusively. The regioselectivity of the addition (α or γ addition) of allylic moiety may be influenced by steric hindrance between methyl groups in prenyl radical and func-

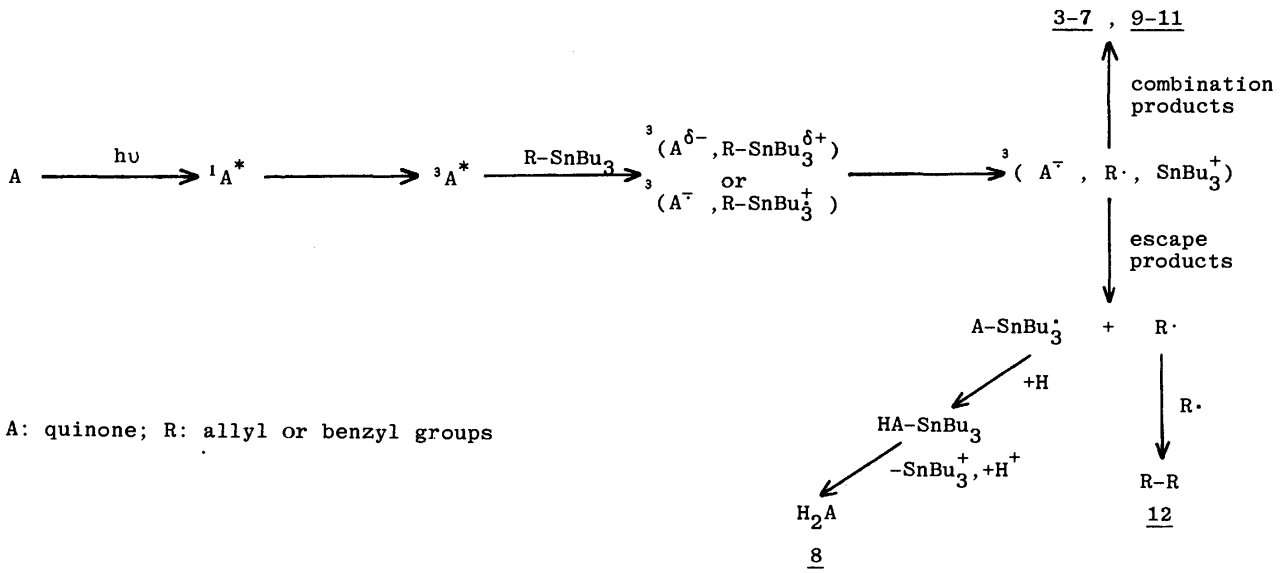

Scheme 4.

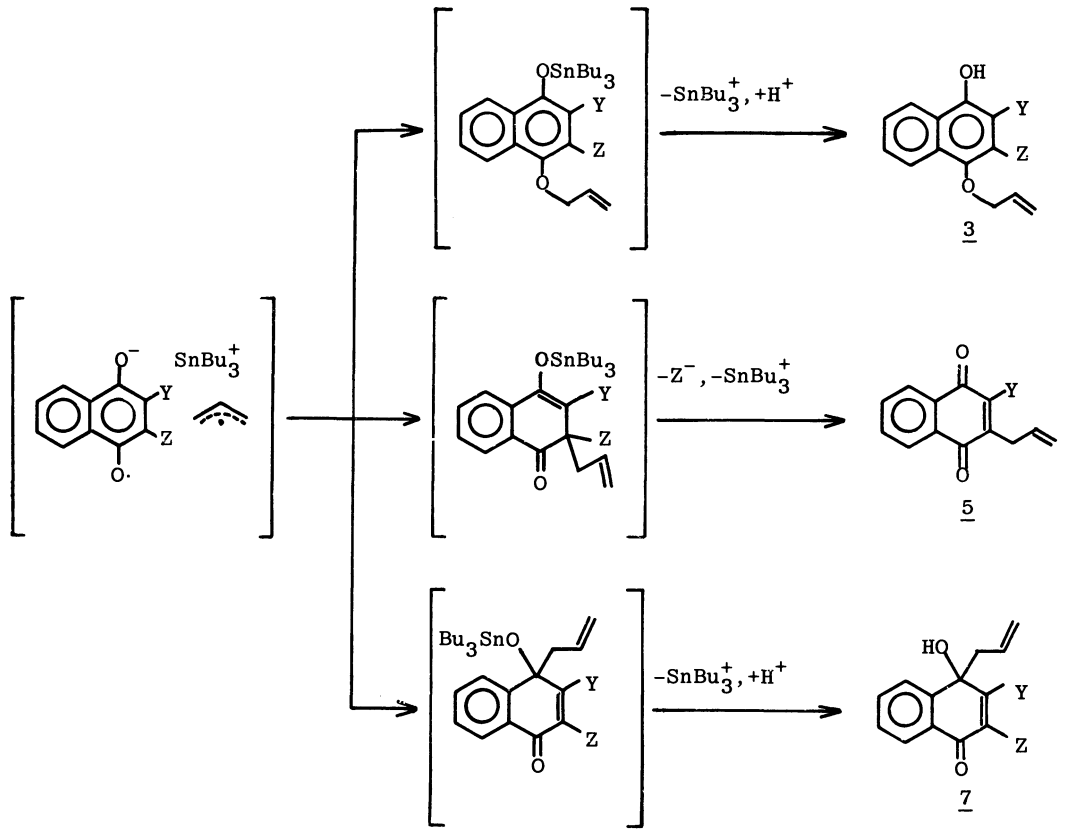

Scheme 5.

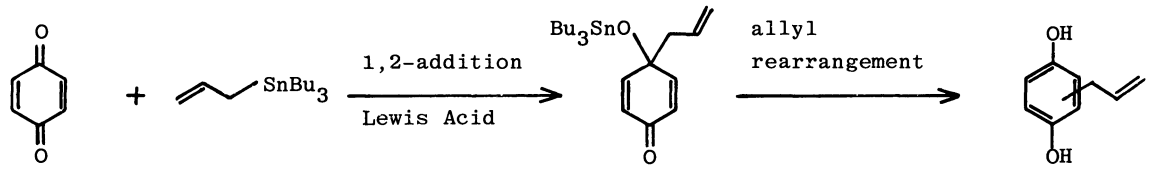

Scheme 6.

tional group in quinone.

Comparison of Other Related Reactions. In the thermal reactions allylation of quinones requires Lewis acids, e.g., BF_3, as catalyst, but in the photochemical reactions none of Lewis acids, of course, is required except with electronic activation of quinones. As the result of the mechanistic study of the thermal reaction between quinone and allyltin reagent in the presence of a Lewis acid, it was established that allylation of quinones proceeds via 1,2-addition followed by allyl rearrangement[15] (Scheme 6). Allyl quinol **7** obtained in the photoreaction of quinones with allylstannane is fairly stable once purified but gradually rearranges to give allyl quinone **5**. In fact, photoproduct **7d** could be transformed to **5d** in refluxing benzene for 2 days (75%), as reported previously.[15] On the contrary, **7d** underwent no photochemical reaction for 4 h, indicating that the same mechanism for the thermal allylation does not occur in the photoreaction.

Fujita et al.[18] reported that in the photochemical reactions of quinones with allylsilane **13**, [2π+2π] cyclobutane adducts were obtained as sole photoproduct (Scheme 7). To compare the difference in their reactivity between allylsilane and allylstannane, photo-CIDNP examination of quinone–allylsilane systems was carried out, but no polarizations were observed in the photochemical reactions of **1f** with **13** and even in the reaction of **1d** with **13**. This phenomena suggests that efficient electron transfer from **13** to quinones does not occur. Equation 1 allows us to estimate ΔG for photoinduced electron transfer from **13** to quinones **1** (Table 2). Much larger values of ΔG compared with the allylstannane–quinone systems, reflecting the higher oxidation potential of allylsilane, also support the inefficient electron-transfer process in the latter systems. Thus, in the reported photochemical reactions of allylsilane, only [2+2] cyclobutane adduct would be formed, while in those of allylstannane a variety of allylation

Table 2. Redox Potentials, Triplet Energies, and Free Energy Changes

Quinone	$E^{red}_{1/2}$ (Ag/Ag+)	E^T/kcal mol^{-1}	Stannane or silane	$E^{ox}_{1/2}$ (Ag/Ag+)	ΔG/kcal mol^{-1}
1a	−0.23[a]	62[c]	**2a**	+0.88[f]	−36.4
1b	−0.75[a]	53[d]	**2a**		−15.4
1c	−0.77[b]	—	**2a**		−18.0[h]
1d	−0.77[b]	56[e]	**2a**		−18.0
1d			**2b**	+0.58[f]	−24.9
1d			**2c**	+0.90[f]	−17.5
1d			**13**	+1.58[g]	− 1.8
1e	−0.86[b]	—	**2a**		−15.9[h]
1f	−0.95[a]	58[d]	**2a**		−15.8
1f			**13**		+ 0.3
1g	−1.11[b]	58[d]	**2a**		−12.1
1h	−1.15[b]	—	**2a**		− 9.2[h]

a) From Peover[26] and assumed that potential against Ag/Ag+ is 0.24 V lower than that measured against SCE.[28] b) From our work.[25] c) From Kasha.[27] d) From Ref. 16b. e) Determined by measurement of phosphorescence spectra. f) Measured in CH_3CN with Et_4NClO_4 as supporting electrolyte vs. Ag/Ag+. g) From Mizuno.[7] h) Assumed that the value of E^T is 56 kcal mol^{-1}.

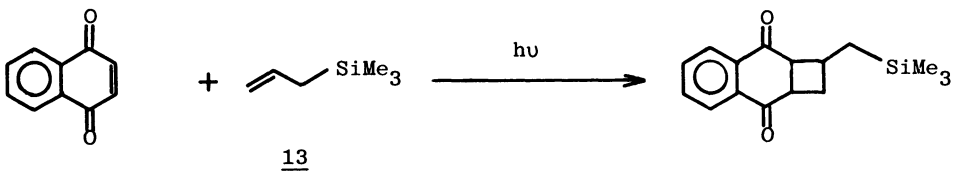

13

Scheme 7.

products of quinones could be produced via electron transfer including radical processes.

Experimental

General Procedures. All melting points were determined with a Yanagimoto micro melting point apparatus and uncorrected. Mass spectra were taken on a JEOL JMS-DX300 mass spectrometer. The electronic spectra were obtained by Shimadzu UV-200 spectrometer. ^{1}H NMR spectra were taken by using a JEOL JNM-PS-100 spectrometer or JEOL JNM-GX-400 spectrometer and chemical shifts were recorded in parts per million (ppm) on the δ scale from tetramethylsilane as an internal standard, while ^{13}C NMR spectra were taken by using JEOL JNM-GX-400 spectrometer. IR spectra were obtained by using a JASCO IRA-1 spectrometer on KBr pellets or liquid film on NaCl. Gas chromatography analyses were carried out by using JEOL-1100. Fluorescence and phosphorescence spectra were taken by using a Shimadzu RF-502A spectrometer. Elemental analyses were performed at the Micro Analytical Center of Kyoto University. Cyclic voltammetry was performed with a PAR Model 174. The working electrode was platinum wire. A Ag/Ag+ (0.1 M; 1 M=1 mol dm^{-3}) electrode was used as a reference electrode and 0.1 M tetraethylammonium perchlorate as supporting electrolyte.

In general, irradiation of a benzene or an acetonitrile solution (25 ml) containing quinone (1 mmol) and tin reagent (2 mmol) through an aqueous $CuSO_4$ and a Pyrex filter under argon are carried out at room temperature. After irradiation the reaction mixture is concentrated and separated by flash column chromatography on silica gel (Merck kiesel gel 60H), developing with hexane–benzene, benzene subsequently, and chloroform finally. The first band contains allylstannanes **2**, the second one contains allyl ether **3**, the third one contains allyl quinones **5** (**4**, **6**), the fourth one contains quinone **1**, the fifth one contains allyl quinol **7**, and the final one contains hydroquinone **8**.

Starting Materials. Chloranil **1a** benzoquinone **1b**, 2,3-dichloro-1,4-naphthoquinone **1d**, 1,4-naphthoquinone **1f**, and 2-methyl-1,4-naphthoquinone **1g** were commercially available and were purified by column chromatography, recrystallization, and sublimation. 2,3-Dibromo-1,4-naphthoquinone **1c**[39] and 2-bromo-1,4-naphthoquinone **1e**,[40] and 2-methoxy-1,4-naphthoquinone **1h**[41] were synthesized by the previous reported methods. Allyl and benzylstannanes **2a**—**c** were prepared by our previously reported method[42] and allyltrimethylsilane **13** was commercially available. Acetonitrile and benzene were used after distillation. Acetonitrile-d_3 and benzene-d_6 were commercially available and were used without further purification.

Physical Properties of the Products. 4-Allyloxy-2,3,5,6-tetrachlorophenol (**3a**): White plates from hexane–chloroform; mp 86.5—88.5 °C. MS; m/z 286, 288, 290, 292, 294 (M+). Found: C, 37.73; H, 1.99; Cl, 48.98%. Calcd for $C_9H_6O_2Cl_4$: C, 37.54; H, 2.10; Cl, 49.25%. IR (KBr); 3430 (OH) cm^{-1}. ^{1}H NMR ($CDCl_3$) δ=4.53 (2H, d, J=6 Hz), 5.3—5.6 (2H, m), 5.9—6.4 (2H, m). Compound **3a** was synthesized independently by the thermal allylation of the corresponding hydroquinone **8a** with K_2CO_3 and allyl bromide and the structure was confirmed.

4-(Allyloxy)phenol (3b): Colorless oil. High-resolution mass spectrum. Found: m/z 150.0685. Calcd for $C_9H_{10}O_2$: M, 150.0680. IR (NaCl); 3360 (OH) cm^{-1}. ^{1}H NMR ($CDCl_3$) δ=4.46 (2H, d, J=5 Hz), 5.1—5.5 (2H, m), 5.56 (1H, br-s),

5.8—6.2 (1H, m), 6.72 (4H, s).

4-Allyloxy-1-naphthol (3f): White needles from hexane–chloroform; mp 100—102 °C. MS; *m/z* 200 (M^+). Found: C, 77.94; H, 5.95%. Calcd for $C_{13}H_{12}O_2$: C, 77.98; H, 6.04%. IR (KBr); 3230 (OH) cm^{-1}. ^1H NMR ($CDCl_3$) δ=4.52 (2H, d, *J*=5 Hz), 5.2—5.6 (2H, m), 5.9—6.4 (1H, m), 6.46 (1H, d, *J*=8 Hz), 6.67 (1H, d, *J*=8 Hz), 7.01 (1H, br-s), 7.3—8.3 (4H, m).

2-Allyl-3-bromo-1,4-naphthoquinone (5c): Yellow crystals from hexane–chloroform; mp 46—49 °C. High-resolution mass spectrum. Found: *m/z* 275.9787. Calcd for $C_{13}H_9O_2{}^{79}Br$: M, 275.9786. Found: *m/z* 277.9765. Calcd for $C_{13}H_9O_2{}^{81}Br$: M, 277.9767. IR (KBr); 1665 (C=O) cm^{-1}. ^1H NMR ($CDCl_3$) δ=3.66 (2H, d, *J*=6 Hz), 5.1—5.5 (2H, m), 5.7—6.2 (1H, m), 7.84 (2H, m), 8.20 (2H, m).

2-Allyl-3-chloro-1,4-naphthoquinone (5d): Yellow needles from hexane–chloroform; mp 54—57 °C. High-resolution mass spectrum. Found: *m/z* 232.0293. Calcd for $C_{13}H_9O_2{}^{35}Cl$: M, 232.0291. Found: *m/z* 234.0256. Calcd for $C_{13}H_9O_2{}^{37}Cl$: M, 234.0261. IR (KBr); 1675 (C=O) cm^{-1}. ^1H NMR ($CDCl_3$) δ=3.62 (2H, d, *J*=6 Hz), 5.0—5.5 (2H, m), 5.7—6.3 (1H, m), 7.87 (2H, m), 8.23 (2H, m).

2-Allyl-3-methyl-1,4-naphthoquinone (5g): Yellow oil. High-resolution mass spectrum. Found: *m/z* 212.0838. Calcd for $C_{14}H_{12}O_2$: M, 212.0837. IR (NaCl); 1660 (C=O) cm^{-1}. ^1H NMR ($CDCl_3$) δ=2.17 (3H, s), 3.40 (2H, d, *J*=8 Hz), 5.0—5.1 (2H, m), 6.7—6.9 (1H, m), 7.6—7.8 (2H, m), 8.0—8.1 (2H, m).

2-Allyl-3-methoxy-1,4-naphthoquinone (5h): Yellow oil. High-resolution mass spectrum. Found: *m/z* 228.0784. Calcd for $C_{14}H_{12}O_3$: M, 228.0783. IR (NaCl); 1660 (C=O) cm^{-1}. ^1H NMR ($CDCl_3$) δ=3.33 (2H, d, *J*=7 Hz), 4.11 (3H, s), 4.9—5.3 (2H, m), 5.6—6.1 (1H, m), 7.5—7.7 (2H, m), 7.9—8.1 (2H, m).

2-Allyl-2,3-dihydro-2-methyl-1,4-naphthalenedione (6g): Yellow oil. High-resolution mass spectrum. Found: *m/z* 214.0989. Calcd for $C_{14}H_{14}O_2$: M, 214.0994. IR (NaCl); 1680 (C=O) cm^{-1}. ^1H NMR ($CDCl_3$) δ=1.30 (3H, s), 2.29 (1H, dd, *J*=7, 14 Hz), 2.61 (1H, dd, *J*=7, 14 Hz), 2.85 (1H, d, *J*=17 Hz), 3.10 (1H, d, *J*=17 Hz), 4.9—5.3 (2H, m), 5.6—6.1 (1H, m), 7.7—7.9 (2H, m), 8.0—8.2 (2H, m). ^{13}C NMR ($CDCl_3$) δ=23.5, 42.6, 48.4, 49.2, 119.2, 125.8, 127.2, 132.4, 133.5, 133.7, 134.1, 134.6, 196.0, 200.1.

4-Allyl-2,3,5,6-tetrachloro-4-hydroxy-2,5-cyclohexadien-1-one (7a): White needles from hexane–chloroform; mp 88—90.5 °C. MS; *m/z* 286, 288, 290, 292, 294 (M^+). Found: C, 37.56; H, 2.11; Cl, 49.03%. Calcd for $C_9H_6O_2Cl_4$: C, 37.54; H, 2.10; Cl, 49.25%. IR (KBr); 3400 (OH), 1665 (C=O) cm^{-1}. ^1H NMR ($CDCl_3$) δ=2.97 (2H, d, *J*=6 Hz), 4.41 (1H, br-s), 5.0—5.5 (3H, m).

4-Allyl-2,3-dibromo-4-hydroxy-1(4*H*)-naphthalenone (7c): White crystals from hexane–chloroform; mp 88—91 °C. MS; *m/z* 356, 358, 360 (M^+). IR (KBr); 3360 (OH), 1650 (C=O) cm^{-1}. ^1H NMR ($CDCl_3$) δ=2.70 (1H, dd, *J*=6, 13 Hz), 3.02 (1H, dd, *J*=6, 13 Hz), 3.60 (1H, br-s), 4.7—5.4 (3H, m), 7.4—8.2 (4H, m). The hydroxyl group of compound **7c** was acetylated by acetic anhydride and *N,N*-dimethylaniline and the structure was confirmed.

4-Acetoxy-4-allyl-2,3-dibromo-1(4*H*)-naphthalenone (14c): White crystals from hexane–chloroform; mp 90—92 °C. MS; *m/z* 398, 400, 402 (M^+). Found: C, 45.24; H, 3.10; Br, 39.80%. Calcd for $C_{15}H_{12}O_3Br_2$: C, 45.03; H, 3.02; Br, 39.95%. IR (KBr); 1730 (C=O), 1640 (C=O) cm^{-1}. ^1H NMR (CCl_4) δ=2.10 (3H, s), 2.68 (1H, dd, *J*=6, 13 Hz), 3.05 (1H, dd, *J*=6, 13 Hz), 4.8—5.2 (3H, m), 7.3—7.7 (3H, m), 8.18 (1H, m).

4-Allyl-2,3-dichloro-4-hydroxy-1(4*H*)-naphthalenone (7d): White crystals from hexane–chloroform; mp 86—88 °C. MS; *m/z* 269, 271, 273 ($M+1^+$). Found: C, 58.02; H, 3.66; Cl, 26.14%. Calcd for $C_{13}H_{10}O_2Cl_2$: C, 58.02; H, 3.75; Cl, 26.35%. IR (KBr); 3440 (OH), 1640 (C=O) cm^{-1}. ^1H NMR ($CDCl_3$) δ=2.78 (1H, dd, *J*=6, 14 Hz), 3.04 (1H, dd, *J*=6, 14 Hz), 3.48 (1H, br-s), 4.7—5.4 (3H, m), 7.4—8.2 (4H, m).

4-Allyl-4-hydroxy-1(4*H*)-naphthalenone (7f): Pale green oil. High-resolution mass spectrum. Found: *m/z* 200.0832. Calcd for $C_{13}H_{12}O_2$: M, 200.0837. IR (NaCl); 3400 (OH), 1660 (C=O) cm^{-1}. ^1H NMR ($CDCl_3$) δ=2.61 (2H, d, *J*=8 Hz), 4.25 (1H, br-s), 4.7—5.6 (3H, m), 6.21 (1H, d, *J*=10 Hz), 6.91 (1H, d, *J*=10 Hz), 7.2—8.3 (4H, m).

4-Allyl-4-hydroxy-2-methyl-1(4*H*)-naphthalenone (7g): Colorless oil. High-resolution mass spectrum. Found: *m/z* 214.0990. Calcd for $C_{14}H_{14}O_2$: M, 214.0994. IR (NaCl); 3440 (OH), 1680 (C=O) cm^{-1}. ^1H NMR ($CDCl_3$) δ=1.92 (3H, s), 2.62 (2H, m), 2.82 (1H, br-s), 4.94 (2H, m), 5.37 (1H, m), 6.70 (1H, s), 7.3—8.0 (4H, m). ^{13}C NMR ($CDCl_3$) δ=15.7, 47.9, 70.2, 119.6, 126.0, 126.3, 127.8, 129.9 (C_2), 131.3, 132.6, 134.6, 146.0, 147.1 (C_3), 185.0.

4-Allyl-4-hydroxy-3-methoxy-1(4*H*)-naphthalenone (7h): ^{13}C NMR ($CDCl_3$) δ=47.8 (t), 55.9 (q), 72.6 (s), 101.8 (d), 119.1 (t), 125.3 (d), 125.5 (d), 127.7 (d), 129.8 (s), 130.6 (d), 132.5 (d), 143.0 (s), 174.4 (s), 185.0 (s).

2,3-Dichloro-4-(3-methyl-2-butenyloxy)-1-naphthol (9b): Colorless oil. MS; *m/z* 296, 298, 300 (M^+). IR (NaCl); 3400 (OH , 1660 (C=O) cm^{-1}. ^1H NMR ($CDCl_3$) δ=1.70 (3H, s), 1.80 (3H, s), 5.60 (1H, m), 5.86 (1H, s), 7.3—7.6 (2H, m), 7.9—8.2 (2H, m). The hydroxyl group of compound **9b** was acetylated as in the case of **7c** and the structure was confirmed.

1-Acetoxy-2,3-dichloro-4-(3-methyl-2-butenyloxy)naphthalene (15b): Yellow crystals from hexane–chloroform; mp 70—72 °C. MS; *m/z* 338, 340, 342 (M^+). Found: C, 59.90; H, 4.66; Cl, 20.63%. Calcd for $C_{17}H_{16}O_3Cl_2$: C, 60.19; H, 4.75; Cl, 20.90%. IR (KBr); 1740 (C=O) cm^{-1}. ^1H NMR (CCl_4) δ=1.70 (3H, s), 1.80 (3H, s), 2.45 (3H, s), 4.64 (2H, d, *J*=7 Hz), 5.67 (1H, t, *J*=7 Hz), 7.4—7.8 (3H, m), 8.0—8.2 (1H, m).

4-Benzyloxy-2,3-dichloro-1-naphthol (9c): White crystals from hexane–chloroform; mp 142—144 °C. MS; *m/z* 318, 320, 322 (M^+). Found: C, 63.97; H, 3.79; Cl, 22.21%. Calcd for $C_{17}H_{12}O_2Cl_2$: C, 64.26; H, 4.02; Cl, 22.01%. IR (KBr); 3370 (OH) cm^{-1}. ^1H NMR ($CDCl_3$) δ=5.15 (2H, s), 6.15 (1H, br-s), 7.3—8.4 (9H, m).

2-Chloro-3-(3-methyl-2-butenyl)-1,4-naphthoquinone (10b): Yellow plates from hexane–chloroform; mp 81—83 °C. MS; *m/z* 260, 262 (M^+). Found: C, 68.98; H, 4.93; Cl, 13.78%. Calcd for $C_{15}H_{13}O_2Cl$: C, 69.10; H, 5.03; Cl, 13.60%. IR (KBr); 1660 (C=O) cm^{-1}. ^1H NMR ($CDCl_3$) δ=1.67 (3H, s), 1.80 (3H, s), 3.49 (2H, d, *J*=8 Hz), 5.09 (1H, m), 7.5—7.8 (2H, m), 7.9—8.2 (2H, m).

2-Benzyloxy-3-chloro-1,4-naphthoquinone (10c): Yellow crystals from hexane–chloroform; mp 120—122 °C. High-resolution mass spectrum. Found: *m/z* 282.0442. Calcd for $C_{17}H_{11}O_2{}^{35}Cl$: M, 282.0447. Found: *m/z* 284.0414. Calcd for $C_{17}H_{11}O_2{}^{37}Cl$: M, 284.0417. IR (KBr); 1670 (C=O) cm^{-1}. ^1H NMR ($CDCl_3$) δ=4.15 (2H, s), 6.9—8.3 (9H, m).

2,3-Dichloro-4-hydroxy-4-(3-methyl-2-butenyl)-1(4*H*)-naph-

thalenone (11b): Colorless oil. MS; *m/z* 296, 298, 300 (M^+). IR (NaCl); 3420 (OH), 1650 (C=O) cm^{-1}. ^1H NMR ($CDCl_3$) δ=1.21 (3H, s), 1.43 (3H, s), 2.60 (1H, dd, *J*=7, 12 Hz), 2.93 (1H, dd, *J*=7, 12 Hz), 3.87 (1H, br-s), 4.32 (1H, m), 7.2—8.1 (4H, m). The hydroxyl group of compound **11b** was acetylated as in the case of **7c** and the structure was confirmed.

4-Acetoxy-2,3-dichloro-4-(3-methyl-2-butenyl)-1(4*H*)-naphthalenone (16b): Colorless oil. MS; *m/z* 338, 340, 342 (M^+). Found: C, 60.06; H, 5.04; Cl, 20.61%. Calcd for $C_{17}H_{16}O_3Cl_2$: C, 60.19; H, 4.75; Cl, 20.90%. IR (NaCl); 1730 (C=O), 1650 (C=O) cm^{-1}. ^1H NMR (CCl_4) δ=1.23 (3H, s), 1.49 (3H, s), 2.08 (3H, s), 2.65 (1H, dd, *J*=14, 8 Hz), 2.99 (1H, dd, *J*=14, 8 Hz), 4.33 (1H, t, *J*=8 Hz), 7.3—7.7 (3H, m), 8.13 (1H, d, *J*=6 Hz).

4-Benzyl-2,3-dichloro-4-hydroxy-1(4*H*)-naphthalenone (11c): Colorless oil. MS; *m/z* 318, 320, 322 (M^+). IR (NaCl); 3420 (OH), 1670 (C=O) cm^{-1}. ^1H NMR ($CDCl_3$) δ=3.12 (1H, d, *J*=13 Hz), 3.43 (1H, d, *J*=13 Hz), 3.96 (1H, br-s), 6.3—6.5 (2H, m), 6.9—8.0 (7H, m). The hydroxyl group of compound **11c** was acetylated as in the case of **7c** and the structure was confirmed.

4-Acetoxy-4-benzyl-2,3-dichloro-1(4*H*)-naphthalenone (16c): Colorless oil. MS; *m/z* 360, 362, 364 (M^+). Found: C, 63.17; H, 3.61; Cl, 19.55%. Calcd for $C_{19}H_{14}O_3Cl_2$: C, 63.18; H, 3.91; Cl, 19.63%. IR (NaCl); 1740 (C=O), 1650 (C=O) cm^{-1}. ^1H NMR (CCl_4) δ=2.11 (3H, s), 3.22 (1H, d, *J*=12 Hz), 3.52 (1H, d, *J*=12 Hz), 6.3—6.5 (2H, m), 6.8—7.7 (6H, m), 7.91 (1H, d, *J*=6 Hz).

CIDNP Examinations. A typical CIDNP examination of the photochemical reaction was undertaken as follows: suitable amounts ($\approx 10^{-2}$ mol dm^{-3}) of quinone **1** and tin reagent **2** or silane reagent **13** were dissolved in benzene-d_6 or in acetonitrile-d_3 in a Pyrex NMR sample tube. The sample purged with argon for 2 min was irradiated at room temperature by a high-pressure Hg lamp through a glass filter (Toshiba UV-35) and the ^1H NMR signals were observed before, during, and after irradiation.

References

1) For a recent review summarizing results in this area see: S. L. Mattes and S. Farid, *Org. Photochem.*, **6**, 233 (1983); G. J. Kavarnos and N. J. Turro, *Chem. Rev.*, **86**, 401 (1986); J. Mattay, *Angew. Chem., Int. Ed. Engl.*, **26**, 825 (1987).

2) D. R. G. Brimage, R. S. Davidson, and P. R. Steiner, *J. Chem. Soc., Perkin Trans. 1*, **1973**, 526; R. S. Davidson and P. R. Steiner, *J. Chem. Soc., Perkin Trans. 2*, **1972**, 1357.

3) R. S. Davidson and S. P. Orton, *J. Chem. Soc., Chem. Commun.*, **1974**, 209; J. L. Stavinoha, E. Bay, A. A. Leone, and P. S. Mariano, *Tetrahedron Lett.*, **21**, 4581 (1980); P. S. Mariano, J. Stavinoha, and E. Bay, *Tetrahedron*, **37**, 3385 (1981).

4) S. G. Cohen, A. H. Parola, and G. H. Parsons, *Chem. Rev.*, **73**, 141 (1973); F. D. Lewis, *Acc. Chem. Res.*, **12**, 152 (1979).

5) D. R. Arnold, P. C. Wong, A. J. Maroulis, and T. S. Cameron, *Pure Appl. Chem.*, **52**, 2609 (1980).

6) P. S. Mariano, *Acc. Chem. Res.*, **16**, 130 (1983); R. M. Borg, R. O. Heuckeroth, A. J. Y. Lan, S. L. Quillen, and P. S. Mariano, *J. Am. Chem. Soc.*, **109**, 2728, 2738 (1987).

7) K. Mizuno, M. Ikeda, and Y. Otsuji, *Tetrahedron Lett.*, **26**, 461 (1985).

8) D. F. Eaton, *J. Am. Chem. Soc.*, **102**, 3280 (1980).

9) R. M. Borg and P. S. Mariano, *Tetrahedron Lett.*, **27**, 2821 (1986).

10) K. Maruyama, H. Imahori, A. Osuka, A. Takuwa, and H. Tagawa, *Chem. Lett.*, **1986**, 1719.

11) K. Mizuno, S. Toda, and Y. Otsuji, *Nippon Kagaku Kaishi*, **1987**, 1183; K. Mizuno, M. Yasueda, and Y. Otsuji, *Chem. Lett.*, **1988**, 229.

12) T. Y. Liang and G. B. Schuster, *J. Am. Chem. Soc.*, **109**, 7803 (1987).

13) L. F. Fieser, *J. Am. Chem. Soc.*, **61**, 2559 (1939); L. S. Hegedus and B. R. Evans, *ibid.*, **100**, 3461 (1978); S. Inoue, R. Yamaguchi, and K. Sato, *Bull. Chem. Soc. Jpn.*, **47**, 3098 (1974); C. D. Snyder and R. Rapoport, *J. Am. Chem. Soc.*, **96**, 8046 (1974).

14) A. Hosomi and H. Sakurai, *Tetrahedron Lett.*, **1977**, 4041.

15) K. Maruyama and Y. Naruta, *J. Org. Chem.*, **43**, 3796 (1978); Y. Naruta, *J. Am. Chem. Soc.*, **102**, 3774 (1980); Y. Naruta, *J. Org. Chem.*, **45**, 4097 (1980).

16) a) R. H. Thomson, "Naturally Occurring Quinones," 2nd ed., Academic Press, New York (1971). b) S. Patai, "The Chemistry of the Quinonoid Compounds," Parts 1 and 2, Wiley, New York (1974). c) R. A. Morton, "Biochemistry of Quinones," Academic Press, New York (1965).

17) H. Uno, *J. Org. Chem.*, **51**, 350 (1986).

18) M. Ochiai, M. Arimoto, and E. Fujita, *J. Chem. Soc., Chem. Commun.*, **1981**, 460.

19) Regioselective formation of allyl quinol **7h** was also observed in the thermal reaction of allylstannane in the presence of BF_3,[15] while reverse regioselective formation for **7g** was observed in the thermal reaction of allylsilane in the presence of $TiCl_4$.[14]

20) Similar exclusive formation of α adducts in the thermal reaction of **1h** with **2b** in the presence of BF_3 was observed.[15]

21) Electron transfer from **2a** to triplet quinone **1d** generates an ion pair in the triplet state (μ>0). *g*-Factor of allyl radical (*g*=2.0026) is lower than that of the quinone anion radical ($g \approx 2.004$-5; Δg<0). The products are generated by recombination of the radical ion (ε>0) or escape (ε<0). The sign of hyperfine coupling constant are calculated by McLachlan-Hückel MO and McConnell relationship. For example, Γne(-$\underline{CH_2}$-CH=CH_2)=$\mu \cdot \Delta g \cdot \varepsilon \cdot a$=+·−·+·−=+ for **5d** and Γne(-$\underline{CH_2}$-CH=CH_2)=+·−·−·−=− for **12a**. See, R. Kaptein, *J. Chem. Soc., Chem. Commun.*, **1971**, 732.

22) Γne(-$\underline{CH_2}$-CH=CMe_2)=+·−·+·−=+ for **10b**.

23) Γne(-$\underline{CH_2}$-Ph)=+·−·+·−=+ *for* **10c**.

24) D. Rehm and A. Weller, *Isr. J. Chem.*, **8**, 259 (1970).

25) K. Maruyama, T. Otsuki, and S. Tai, *J. Org. Chem.*, **50**, 52 (1985).

26) M. E. Peover, *J. Chem. Soc.*, **1962**, 4540.

27) M. Kasha, *Chem. Rev.*, **41**, 401 (1947).

28) M. P. Suh, W. Shin, H. Kim, and C. H. Koo, *Inorg. Chem.*, **26**, 1846 (1987).

29) Seemingly, the adduct could have structure (shown in Fig. 4), which would convert to give **3a** or **7a**.

30) Similar electron-transfer mechanism was proposed in the photochemical reactions between quinones and organotin compounds by ESR and CIDEP methods. S. Emori, D. Weri, and J. K. S. Wan, *Chem. Phys. Lett.*, **84**, 512 (1981); K. S. Chen, J. K. S. Wan, and J. K. Kochi, *J. Phys. Chem.*, **85**, 1726

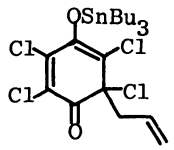

Fig. 4.

(1981).

31) It is said that $S_1 \rightarrow T_1$ process of quinones occurs with high efficiency (0.8—1.0),[16b] and no fluorescence spectra of quinones **1** were observed. Thus, this reaction proceeds via triplet state.

32) A mixture of **1d** and **2a** showed no charge-transfer (CT) band in the ground state. Accordingly, these reactions could not proceed via CT complex.

33) J. K. Kochi, "Organometallic Mechanisms and Catalysis," Academic Press, New York (1978); B. W. Walther, F. Williams, W. Lau, and J. K. Kochi, *Organometallics*, **2**, 688 (1983).

34) Quinone anion radical escaped from the solvent cage might be coordinated by tin cation.[30]

35) Eaton[8] and Mizuno[11] were reported that 1,2-diphenylethane and 1,5-hexadiene as by-product were produced from the corresponding tin reagents.

36) Productions of allyl ethers **3** which were not obtained in the thermal reactions (Scheme 6) support the involvement of radical processes.

37) A. Fairbourn and E. A. C. Lucken, *J. Chem. Soc.*, **1963**, 258; M. R. Das and G. K. Fraenkel, *J. Chem. Phys.*, **42**, 1350 (1965); P. D. Sullivivan and J. R. Bolton, *J. Am. Chem. Soc.*, **90**, 5366 (1968).

38) H. Fischer and K. H. Hellwege, "Landolt-Börnstein, Numerical Data and Functional Relationships in Science and Technology, New Series, Vol. 9, Magnetic Properties of Free Radicals," Springer-Verlag, Berlin-Heidelberg-New York (1980).

39) T. Zincke and M. Schmidt, *Chem. Ber.*, **27**, 2758 (1894).

40) S. N. Falling and H. Rapoport, *J. Org. Chem.*, **45**, 1260 (1980).

41) T. Otsuki, *Bull. Chem. Soc. Jpn.*, **47**, 3089 (1974).

42) Y. Naruta, Y. Nishigaichi, and K. Maruyama, *Chem. Lett.*, **1986**, 1857.

 © 1989 The Chemical Society of Japan Bull. Chem. Soc. Jpn., 62, 826—832 (1989) [Vol. 62, No. 3

Synthesis of Pyranoisoflavones from Pyronochalcones: Synthesis of Elongatin and Its Angular Isomer

Masao TSUKAYAMA,* Yasuhiko KAWAMURA, Hiroto TAMAKI, Tomoya KUBO, and Tokunaru HORIE
Department of Chemical Science and Technology, Faculty of Engineering,
The University of Tokushima, Minamijosanjima-cho, Tokushima 770
(Received August 6, 1988)

Elongatin (4′,5-dihydroxy-2′,5′-dimethoxy-2″,2″-dimethylpyrano[5″,6″-*g*]isoflavone) was synthesized by an oxidative rearrangement of the corresponding pyronochalcone [6-(1-oxo-3-phenyl-2-propenyl)-4-chromanone] with thallium(III) nitrate and a regioselective reduction of 7-(4-benzoyloxy-2,5-dimethoxyphenyl)-2,3-dihydro-2,2-dimethyl-5-tosyloxy-4*H*,6*H*-benzo[1,2-*b*:5,4-*b*′]dipyran-4,6-dione with sodium borohydride–palladium chloride, followed by dehydration of the resultant alcohol and hydrolysis. Its angular isomer (4′,5-dihydroxy-2′,5′-dimethoxy-2″,2″-dimethylpyrano[6″,5″-*h*]isoflavone) was also synthesized from the corresponding pyronochalcone in a similar manner.

A lot of natural isoflavones were synthesized by oxidative rearrangements of chalcones with thallium(III) nitrate (TTN).[1,2] Pyranoisoflavones (jamaicin and leiocarpin) containing an acid-labile group, such as a dimethylchromene ring, were directly synthesized from the corresponding pyranochalcones by this method.[3] We have also reported that pyranoisoflavones (elongatin and toxicarol isoflavone) of linear and angular phloroglucinol-types can be prepared by an oxidative rearrangement of the corresponding dihydropyranochalcones with TTN, followed by a dehydrogenation of the resultant dihydropyranoisoflavones.[4] Thus, the oxidative rearrangement of 2′-hydroxychalcones with TTN seems at present to be a more useful method for synthesizing natural linear and angular pyranoisoflavones (7-phenyl-2*H*,6*H*-benzo[1,2-*b*:5,4-*b*′]dipyran-6-ones and -4*H*,8*H*-benzo[1,2-*b*:3,4-*b*′]dipyran-4-ones). However, this method has not been applied hitherto to the synthesis of linear and angular pyronoisoflavones (2,3-dihydro-7-phenyl-4*H*,6*H*-benzo[1,2-*b*:5,4-*b*′]dipyran-4,6-diones and 8,9-dihydro-3-phenyl-4*H*,10*H*-benzo[1,2-*b*:3,4-*b*′]dipyran-4,10-diones) from the corresponding pyronochalcones [6-(1-oxo-3-phenyl-2-propenyl)-4-chromanones].

It is of much interest as a new pathway to extend this methodology to the synthesis of pyranoisoflavones from pyronochalcones with TTN; the subsequent regioselective reduction of the pyronoisoflavones, followed by dehydration of the resultant alcohols leads to the corresponding pyranoisoflavones. We report here on the synthesis of a linear pyranoisoflavone, elongatin (4′,5-dihydroxy-2′,5′-dimethoxy-2″,2″-dimethylpyrano[5″,6″-*g*]isoflavone)[5] (**1**) and its angular isomer (4′,5-dihydroxy-2′,5′-dimethoxy-2″,2″-dimethylpyrano[6″,5″-*h*]isoflavone)[4] (**2**)—systematic name 5-hydroxy-7-(4-hydroxy-2,5-dimethoxyphenyl)-2,2-dimethyl-2*H*,6*H*-benzo[1,2-*b*:5,4-*b*′]dipyran-6-one and 5-hydroxy-3-(4-hydroxy-2,5-dimethoxyphenyl)-8,8-dimethyl-4*H*,8*H*-benzo[1,2-*b*:3,4-*b*′]dipyran-4-one—by this method.

The condensation of 2,4,6-trihydroxyacetophenone with 3-methyl-2-butenoic acid in the presence of polyphosphoric acid (PPA) in dioxane afforded 8-acetylchromanone[6] (**3**) as a major product and 6-

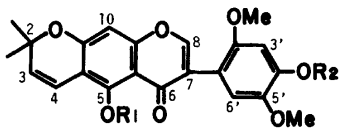

1 $R_1=R_2=H$
18 $R_1=R_2=Ts$
22 $R_1=Ts$, $R_2=PhCO$
23 $R_1=R_2=Ac$
24 $R_1=R_2=Me$

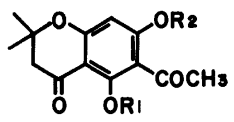

4 $R_1=R_2=H$
5 $R_1=H$, $R_2=Ts$
6 $R_1=Me$, $R_2=Ts$
7 $R_1=Me$, $R_2=H$

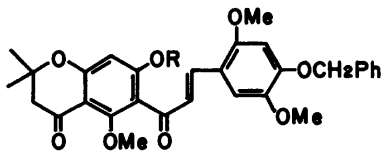

9 R=H
10 R=Ac

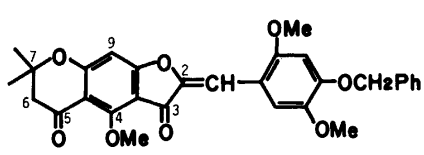

12

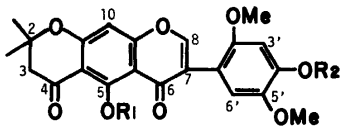

11 R_1=Me, R_2=$PhCH_2$
13 R_1=H, R_2=$PhCH_2$
14 R_1=R_2=H
15 R_1=R_2=Ts
19 R_1=H, R_2=PhCO
20 R_1=Ts, R_2=PhCO

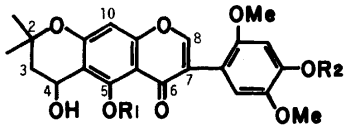

16 R_1=R_2=Ts
21 R_1=Ts, R_2=PhCO

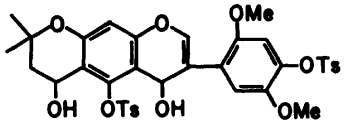

17

acetylchromanone (**4**) as a minor product. It was first found that chromanone (**3**) was easily isomerized to chromanone (**4**) with potassium carbonate in acetone; this method offers an efficient synthesis of the 6-acetylchromanone (**4**). Tosylation of **4**, and a successive methylation of the tosylate (**5**), followed by hydrolysis of the resultant methyl ether (**6**) afforded 7-hydroxy-5-methoxychromanone (**7**). Condensation of **7** with 4-benzyloxy-2,5-dimethoxybenzaldehyde[4] (**8**) in the presence of piperidine and pyridine in ethanol afforded chalcone (**9**), which was subsequently converted into acetate (**10**). The oxidative rearrangement of **10** with TTN in methanol, followed by cyclization of the resultant compound with diluted hydrochloric acid under reflux afforded a linear pyronoisoflavone (**11**) and a small amount of aurone (**12**). The ^1H NMR spectrum of **11** showed the presence of C_8-proton as a singlet at δ 7.67. A signal at δ 6.45 in the ^1H NMR spectrum of **12** is due to the benzylidene proton and is characteristic of an aurone system. Hydrogenolysis of **11** with palladium on charcoal afforded a mixture of the corresponding 4′-hydroxyisoflavone and 4′-hydroxyisoflavanone. However, the 5-hydroxypyronoisoflavone (**13**), which was prepared by demethylation of **11** with aluminum bromide in acetonitrile, was hydrogenolyzed with palladium on charcoal to give 4′,5-dihydroxypyronoisoflavone (**14**) in good yield. Compound **14** was easily converted into the ditosylate (**15**) with *p*-toluenesulfonyl chloride in acetone. We have reported that the carbonyl group in the chromanone ring of acetylchromanones is selectively reduced with sodium borohydride–palladium chloride to give the alcohols and that the subsequent dehydration affords the corresponding chromenes.[6] This method was applied to the synthesis of pyranoisoflavones from pyronoisoflavones. Compound **15** was reduced with sodium borohydride in the presence of palladium chloride in tetrahydrofuran–water to give the desired monoalcohol (**16**) and dialcohol (**17**). The monoalcohol (**16**) was easily dehydrated in the presence of *p*-toluenesulfonic acid to give linear pyranoisoflavone (**18**). Hydrolysis of **18** by a potassium hydroxide solution in boiling ethanol afforded linear pyranoisoflavone (elongatin) (**1**) and its isomeric angular pyranoisoflavone (**2**). This result shows that the tosyl group is not suitable for the protection of the hydroxyl group, since the hydrolysis of **18** is accompanied by a ring isomerization to its angular isomer (**2**). Therefore, a benzoyl group was tested for the protection of the hydroxyl group. Benzoylation of **14** with benzoyl chloride in acetone easily afforded 4′-benzoate (**19**), but did not yield 4′,5-dibenzoate. The 5-tosylate (**20**) of a 5-hydroxy compound (**19**) was selectively reduced with sodium borohydride in the presence of palladium chloride to give monoalcohol (**21**). Dehydration of compound **21** led to pyranoisoflavone (**22**), which was easily hydrolyzed with a potassium hydroxide solution without ring isomerization to give the desired linear pyranoisoflavone (elongatin) (**1**) in good yield. The physical properties of **1**, the diacetate (**23**), and the dimethyl ether (**24**) were identical with those of their authentic samples, prepared by a method described before,[4] respectively.

The partial benzylation of 2,4,6-trihydroxyacetophenone with benzyl chloride in the presence of potassium carbonate in hexamethylphosphoric triamide (HMPA) afforded 2,4-bis(benzyloxy)-6-hydroxyacetophenone (**25**) in good yield. This benzylation is superior to that in acetone[7] or *N*,*N*-dimethylformamide[8] since no *C*-benzylated compound is formed. Debenzylation of the methyl ether (**26**) of the 6-hydroxyacetophenone (**25**) with palladium on charcoal afforded 2,4-dihydroxy-6-methoxyacetophenone[9] (**27**). Condensation of **27** with 3-methyl-2-butenoyl chloride by a Friedel–Crafts reaction afforded 1-(3-acetyl-2,6-dihydroxy-4-methoxyphenyl)-3-methyl-2-buten-1-one (**28**) in good yield. The structure of **28** was determined by nuclear Overhauser effect (NOE) experiments at the C_5-proton: The integrated intensity of the signal at δ 5.85 for **28** increased up to 25% when the methoxyl

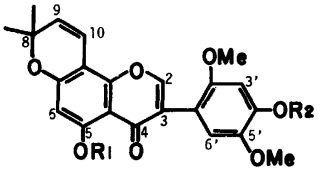

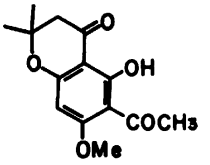

2 $R_1=R_2=H$
38 R_1=Ts, R_2=PhCO
39 $R_1=R_2$=Ac
40 R_1=H, R_2=Me
41 $R_1=R_2$=Me

25 $R_1=R_3=PhCH_2$, $R_2=R_4$=H
26 $R_1=R_3=PhCH_2$, R_2=H, R_4=Me
27 $R_1=R_2=R_3$=H, R_4=Me
28 $R_1=R_3$=H, $R_2=Me_2C$=CHCO
R_4=Me

29

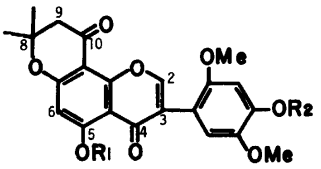

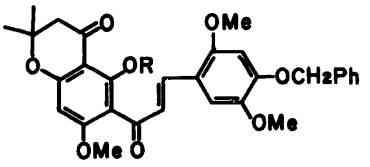

32 R_1=Me, $R_2=PhCH_2$
33 R_1=H, $R_2=PhCH_2$
34 $R_1=R_2$=H
35 R_1=H, R_2=PhCO
36 R_1=Ts, R_2=PhCO

30 R=H
31 R=Ac

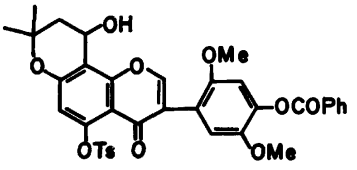

37

protons were saturated by double irradiation. The diketone (**28**) was easily converted into the 5-hydroxy-7-methoxychromanone (**29**) with a potassium hydroxide solution in methanol. Condensation of **29** with **8** afforded the chalcone (**30**), which was converted into acetate (**31**). An oxidative rearrangement of **31** with TTN under similar conditions to that of **11** afforded angular pyronoisoflavone (**32**), while the corresponding aurone was not obtained in this case. Demethylation of **32** and a subsequent debenzylation of the resultant 5-hydroxypyronoisoflavone (**33**) afforded 4′,5-dihydroxypyronoisoflavone (**34**). The partial benzoylation of **34** and tosylation of the resultant 4′-benzoate (**35**), followed by a reduction of the 5-tosylate (**36**) with sodium borohydride–palladium chloride, yielded quantitatively monoalcohol (**37**). Dehydration of **37** led to the pyranoisoflavone (**38**), which was easily hydrolyzed to give the desired angular pyranoisoflavone (**2**) in good yield. The physical properties of **2**, the diacetate (**39**), the 4′-methyl ether (toxicarol isoflavone) (**40**), and the dimethyl ether (**41**) were identical with those of their authentic samples prepared by the method described before,[4] respectively.

From the results described above, the selective reduction of the carbonyl group in the pyronoisoflavones and the subsequent dehydration are easier than the dehydrogenation of dihydropyranoisoflavones,[4] and therefore, this method is a facile synthesis of pyranoisoflavones.

Experimental

All the melting points are uncorrected. The UV spectra were taken in ethanol on a Hitachi 124 spectrophotometer. The ^1H NMR spectra were measured with a Hitachi R-20 spectrometer (60 MHz), using tetramethylsilane as an internal standard (δ, ppm). Column chromatography and thin-layer chromatography were carried out on Kieselgel 60 (70—230 mesh) and with Kieselgel 60 F-254 (Merck).

8-Acetyl-5,7-dihydroxy-2,2-dimethyl-4-chromanone (3) and 6-Acetyl-5,7-dihydroxy-2,2-dimethyl-4-chromanone (4). A mixture of 2,4,6-trihydroxyacetophenone (35.5 g) and 3-methyl-2-butenoic acid (28.7 g) in anhydrous dioxane (127 ml) was stirred in the presence of PPA (100 g) at 60 °C for 3 h. The reaction mixture was poured into ice-cold water and neutralized with a saturated K_2CO_3 solution to give precipitates. The resulting precipitates were recrystallized from MeOH–Me_2CO to give **3** (41 g, 77%) as colorless needles (R_f=0.38; hexane–EtOAc (4:1) on a silica-gel TLC plate): mp 158—160 °C; ^1H NMR ($CDCl_3$) δ=1.58 (6H, s, CH_3×2), 2.64 (3H, s, $COCH_3$), 2.79 (2H, s, $COCH_2$), 5.91 (1H, s, C_8–H), 12.65 and 14.30 (each 1H, s, OH).

Found: C, 62.26; H, 5.79%. Calcd for $C_{13}H_{14}O_5$: C, 62.39;

H, 5.64%.

The mother liquor was chromatographed over a silica-gel column with $CHCl_3$ to give **4** (2.11 g, 4%) as colorless needles (R_f=0.62): mp 148—150 °C; ^{1}H NMR ($CDCl_3$) δ=1.43 (6H, s, CH_3×2), 2.67 (3H, s, $COCH_3$), 2.70 (2H, s, $COCH_2$), 5.83 (1H, s, C_8–H), 14.10 and 14.40 (each 1H, s, OH).

Found: C, 62.41; H, 5.66%. Calcd for $C_{13}H_{14}O_5$: C, 62.39; H, 5.64%.

6-Acetyl-5,7-dihydroxy-2,2-dimethyl-4-chromanone (4). A mixture (14.9 g) of **3** and **4** was refluxed with stirring in the presence of K_2CO_3 (70 g) in anhydrous Me_2CO (500 ml) for 50 h. After removal of K_2CO_3 and the solvent, the residue was dissolved in EtOAc, washed with dil. HCl and water, and dried (Na_2SO_4). The resulting compound was recrystallized from MeOH–$CHCl_3$ to give **4** (13 g, 87%) as colorless needles; mp 148—150 °C.

6-Acetyl-5-hydroxy-2,2-dimethyl-7-tosyloxy-4-chromanone (5). A mixture of **4** (16.5 g), TsCl (14.1 g), and K_2CO_3 (46 g) in Me_2CO (450 ml) was refluxed with stirring for 1.5 h. After removal of K_2CO_3 and the solvent, the residue was dissolved in EtOAc, washed with dil. HCl and water, and dried (Na_2SO_4). The resulting compound was chromatographed over a silica-gel flash column with hexane–EtOAc (3:2) to give **5** (17 g, 64%) as colorless prisms: mp 105—106 °C (MeOH); ^{1}H NMR ($CDCl_3$) δ=1.46 (6H, s, CH_3×2), 2.38 (3H, s, $C_6H_4CH_3$), 2.45 (3H, s, $COCH_3$), 2.74 (2H, s, $COCH_2$), 6.38 (1H, s, C_8–H), 7.30 and 7.77 (each 2H, d, J=8.8 Hz, $C_6H_4CH_3$), 12.46 (1H, s, OH).

Found: C, 59.50; H, 5.00%. Calcd for $C_{20}H_{20}O_7S$: C, 59.39; H, 4.99%.

6-Acetyl-5-methoxy-2,2-dimethyl-7-tosyloxy-4-chromanone (6). A mixture of **5** (19.2 g), $(MeO)_2SO_2$ (11.4 ml), and K_2CO_3 (34 g) in Me_2CO (450 ml) was refluxed with stirring for 3.5 h. The reaction mixture was treated in the usual way, and the resulting compound was recrystallized from MeOH to give **6** (17.6 g, 88%) as colorless prisms: mp 110—111 °C; ^{1}H NMR ($CDCl_3$) δ=1.46 (6H, s, CH_3×2), 2.36 (3H, s, $C_6H_4CH_3$), 2.47 (3H, s, $COCH_3$), 2.69 (2H, s, $COCH_2$), 3.79 (3H, s, OCH_3), 6.72 (1H, s, C_8–H), 7.36 and 7.78 (each 2H, d, J=8.8 Hz, $C_6H_4CH_3$).

Found: C, 60.10; H, 5.26%. Calcd for $C_{21}H_{22}O_7S$: C, 60.28; H, 5.30%.

6-Acetyl-7-hydroxy-5-methoxy-2,2-dimethyl-4-chromanone (7). Compound **6** (11.0 g) was refluxed in the presence of K_2CO_3 (25 g) in MeOH (200 ml) with stirring for 1.5 h. The reaction mixture was poured into ice-cold water and acidified with HCl, and extracted with EtOAc, and dried (Na_2SO_4). The resulting compound was recrystallized from MeOH to give **7** (6.6 g, 95%) as colorless needles: mp 83—85 °C; ^{1}H NMR ($CDCl_3$) δ=1.46 (6H, s, CH_3×2), 2.66 (2H, s, $COCH_2$), 2.69 (3H, s, $COCH_3$), 3.92 (3H, s, OCH_3), 6.18 (1H, s, C_8–H), 13.70 (1H, s, OH).

Found: C, 63.61; H, 6.14%. Calcd for $C_{14}H_{16}O_5$: C, 63.63; H, 6.10%.

7-Hydroxy-5-methoxy-2,2-dimethyl-6-[1-oxo-3-(4-benzyloxy-2,5-dimethoxyphenyl)-2-propenyl]-4-chromanone (9). A mixture of **7** (2.64 g) and 4-benzyloxy-2,5-dimethoxybenzaldehyde[4] (**8**) (2.72 g) was refluxed with stirring in the presence of piperidine (2.8 ml) and pyridine (3.2 ml) in EtOH (150 ml) for 14 h. The reaction mixture was poured into ice-cold water and acidified with HCl. The resulting compound was recrystallized from MeOH to give **9** (1.62 g, 60%) as yellow needles: mp 167—169 °C; ^{1}H NMR ($CDCl_3$) δ=1.45 (6H, s, CH_3×2), 2.66 (2H, s, $COCH_2$), 3.78, 3.83, and 3.86 (each 3H, s, OCH_3), 5.19 (2H, s, $C_6H_5CH_2$), 6.22 (1H, s, C_8–H), 6.50 and 7.12 (each 1H, s, Arom-H), 7.36 (5H, s, C_6H_5), 7.77 and 8.20 (each 1H, d, J=16 Hz, CH=), 13.88 (1H, s, OH).

Found: C, 69.19; H, 5.74%. Calcd for $C_{30}H_{30}O_8$: C, 69.48; H, 5.83%.

Acetate 10. Compound **9** was converted into the acetate **10** as yellow needles by an acetic anhydride–sodium acetate method: mp 145—147 °C (MeOH); ^{1}H NMR ($CDCl_3$) δ=1.46 (6H, s, CH_3×2), 2.14 (3H, s, $COCH_3$), 2.68 (2H, s, $COCH_2$), 3.68, 3.79, and 3.82 (each 3H, s, OCH_3), 5.16 (2H, s, $C_6H_5CH_2$), 6.44 (1H, s, C_8–H), 6.53 and 7.00 (each 1H, s, Arom-H), 6.90 and 7.69 (each 1H, d, J=16 Hz, CH=), 7.33 (5H, s, $C_6H_5CH_2$).

Found: C, 68.40; H, 5.68%. Calcd for $C_{32}H_{32}O_9$: C, 68.55; H, 5.76%.

7-(4-Benzyloxy-2,5-dimethoxyphenyl)-2,3-dihydro-5-methoxy-2,2-dimethyl-4*H*,6*H*-benzo[1,2-*b*:5,4-*b'*]dipyran-4,6-dione (11) and 2-[(4-Benzyloxy-2,5-dimethoxyphenyl)methylene]-6,7-dihydro-4-methoxy-7,7-dimethyl-5*H*-furo[3,2-*g*][1]benzopyran-3(2*H*),5-dione (12). A mixture of **10** (3.55 g) and TTN (4.2 g) was stirred in MeOH (1.3 l) at 36—38 °C for 10 h, and then 10% HCl (70 ml) was added, and the mixture was refluxed for a further 3 h. After removal of the precipitates by filtration, the filtrate was concentrated to ca. 600 ml under reduced pressure and poured into a large amount of ice-cold water. The mixture was allowed to stand overnight at room temperature to give precipitates. The precipitates were recrystallized from MeOH to give **11** (2.30 g, 70%) as colorless needles: mp 164—165 °C; ^{1}H NMR ($CDCl_3$) δ=1.47 (6H, s, CH_3×2), 2.71 (2H, s, $COCH_2$), 3.62, 3.82, and 3.98 (each 3H, s, OCH_3), 5.14 (2H, s, $C_6H_5CH_2$), 6.57 (1H, s, C_{10}–H), 6.64 and 6.85 (each 1H, s, Arom-H), 7.35 (5H, bs, $C_6H_5CH_2$), 7.67 (1H, s, C_8–H).

Found: C, 69.89; H, 5.49%. Calcd for $C_{30}H_{28}O_8$: C, 69.75; H, 5.46%.

The mother liquor was chromatographed over a silica-gel column with $CHCl_3$–Me_2CO (50:1) to give the aurone **12** (40 mg, 1%) as pale yellow needles: mp 216—218 °C (MeOH); ^{1}H NMR ($CDCl_3$) δ=1.45 (6H, s, CH_3×2), 2.67 (2H, s, $COCH_2$), 3.72, 3.88, and 4.32 (each 3H, s, OCH_3), 5.16 (2H, s, $C_6H_5CH_2$), 6.37 (1H, s, C_9–H), 7.20 and 7.71 (each 1H, s, Arom-H), 6.45 (1H, s, C=CH), 7.34 (5H, s, $C_6H_5CH_2$).

Found: C, 69.63; H, 5.31%. Calcd for $C_{30}H_{28}O_8$: C, 69.75; H, 5.46%.

7-(4-Benzyloxy-2,5-dimethoxyphenyl)-2,3-dihydro-5-hydroxy-2,2-dimethyl-4*H*,6*H*-benzo[1,2-*b*:5,4-*b'*]dipyran-4,6-dione (13). A solution of anhydrous $AlBr_3$ (14.5 g) in MeCN (50 ml) was added to a solution of **11** (5.46 g) in MeCN (250 ml), and the mixture was stirred at 40 °C for 25 min. The reaction mixture was poured into a mixture of HCl and ice-cold water and then stirred at 55—60 °C for 20 min to give precipitates. The precipitates were recrystallized from MeOH–Me_2CO to give **13** (4.85 g, 91%) as pale-yellow needles: mp 173—174 °C; ^{1}H NMR ($CDCl_3$) δ=1.48 (6H, s, CH_3×2), 2.73 (2H, s, $COCH_2$), 3.63 and 3.82 (each 3H, s, OCH_3), 5.12 (2H, s, $C_6H_5CH_2$), 6.30 (1H, s, C_{10}–H), 6.57 and 6.84 (each 1H, s, Arom-H), 7.35 (5H, br, $C_6H_5CH_2$), 7.76 (1H, s, C_8–H), 14.62 (1H, s, OH).

Found: C, 69.56; H, 5.22%. Calcd for $C_{29}H_{26}O_8$: C, 69.31;

H, 5.22%.

2,3-Dihydro-5-hydroxy-7-(4-hydroxy-2,5-dimethoxyphenyl)-2,2-dimethyl-4*H*,6*H*-benzo[1,2-*b*:5,4-*b'*]dipyran-4,6-dione (14). Compound **13** (4.67 g) was hydrogenolyzed over 10% palladium on charcoal (2 g) in MeOH (350 ml) and EtOAc (350 ml). The resulting compound was recrystallized from MeOH to give **14** (3.51 g, 92%) as colorless needles: mp 192—194 °C; ^{1}H NMR ($CDCl_3$) δ=1.47 (6H, s, CH_3×2), 2.73 (2H, s, $COCH_2$), 3.70 and 3.82 (each 3H, s, OCH_3), 6.15 (1H, s, $C_{4'}$–OH), 6.31 (1H, s, C_{10}–H), 6.60 and 6.82 (each 1H, s, Arom-H), 7.81 (1H, s, C_8–H), 14.65 (1H, s, C_5–OH).

Found: C, 64.20; H, 4.97%. Calcd for $C_{22}H_{20}O_8$: C, 64.07; H, 4.90%.

2,3-Dihydro-7-[2,5-dimethoxy-4-(tosyloxy)phenyl]-2,2-dimethyl-5-tosyloxy-4*H*,6*H*-benzo[1,2-*b*:5,4-*b'*]dipyran-4,6-dione (15). A mixture of **14** (1.24 g), TsCl (2.0 g), and K_2CO_3 (4.2 g) was refluxed with stirring in Me_2CO (150 ml) for 6 h. The resulting compound was recrystallized from MeOH to give **15** (1.73 g, 80%) as colorless prisms: mp 152—154 °C; ^{1}H NMR ($CDCl_3$) δ=1.44 (6H, s, CH_3×2), 2.34 and 2.41 (each 3H, s, $C_6H_4CH_3$), 2.61 (2H, s, CH_2CO), 3.47 and 3.65 (each 3H, s, OCH_3), 6.73 (1H, s, Arom-H), 6.80 (2H, s, Arom-H×2), 7.1—7.9 (9H, m, $C_6H_4CH_3$×2 and C_8–H).

Found: C, 61.17; H, 4.40%. Calcd for $C_{36}H_{32}O_{12}S_2$: C, 61.36; H, 4.58%.

3,4-Dihydro-4-hydroxy-7-[2,5-dimethoxy-4-(tosyloxy)phenyl]-2,2-dimethyl-5-tosyloxy-2*H*,6*H*-benzo[1,2-*b*:5,4-*b'*]dipyran-6-one (16) and 3,4-Dihydro-4,6-dihydroxy-7-[2,5-dimethoxy-4-(tosyloxy)phenyl]-2,2-dimethyl-5-tosyloxy-2*H*,6*H*-benzo[1,2-*b*:5,4-*b'*]dipyran (17). A mixture of **15** (650 mg) and $PdCl_2$ (230 mg) was stirred in THF (70 ml) and water (14 ml), adding 180 mg each of $NaBH_4$ (360 mg) for two times, at 14—17 °C for 40 min, and then Me_2CO (5 ml) was added to the reaction mixture. After removal of the catalyst by filtration, water was added to the filtrate, and the solvent was removed under reduced pressure below 40 °C. The residue was extracted with EtOAc, washed with dil. HCl and brine, and dried (Na_2SO_4). The resulting compound was chromatographed over a silica-gel column with 1,2-dichloroethane–EtOAc–petroleum ether (50:2:1) to give the monoalcohol **16** (300 mg, 46%) as colorless needles (mp 204—206 °C; from Et_2O) and the dialcohol **17** (280 mg, 43%) as colorless needles (mp 194—196 °C; from Et_2O): ^{1}H NMR spectrum of **16**, ($CDCl_3$) δ=1.38 and 1.51 (each 3H, s, CH_3), 1.95—2.15 (2H, m, CH_2CHOH), 2.40 (6H, s, $C_6H_4CH_3$×2), 3.47 and 3.64 (each 3H, s, OCH_3), 5.07 (1H, t, J=5 Hz, CH_2CHOH), 6.74 (2H, s, Arom-H×2), 6.85 (1H, s, Arom-H), 7.1—8.0 (9H, m, $C_6H_4CH_3$×2 and C_8–H).

Found: C, 59.59; H, 4.51%. Calcd for $C_{36}H_{34}O_{12}S_2$: C, 59.83; H, 4.74%.

^{1}H NMR spectrum of **17**, ($CDCl_3$) δ=1.32 (6H, s, CH_3×2), 2.43 (8H, s, CH_2CHOH and $C_6H_4CH_3$×2), 3.35 and 3.57 (each 3H, s, OCH_3), 5.18 (1H, s, $CHOH$), 5.45 (1H, m, CH_2CHOH), 6.26, 6.45, and 6.47 (each 1H, s, Arom-H), 7.2—7.9 (8H, m, $C_6H_4CH_3$×2), 8.69 (1H, s, C_8–H).

Found: C, 59.71; H, 4.72%. Calcd for $C_{36}H_{36}O_{12}S_2$: C, 59.67; H, 5.01%.

7-[2,5-Dimethoxy-4-(tosyloxy)phenyl]-2,2-dimethyl-5-tosyloxy-2*H*,6*H*-benzo[1,2-*b*:5,4-*b'*]dipyran-6-one (18). Compound **16** (160 mg) was refluxed in toluene (30 ml) in the presence of TsOH·H_2O (20 mg) for 20 min. The resulting compound was recrystallized from MeOH–Me_2CO to give **18** (140 mg, 92%) as colorless prisms: mp 206—208 °C; ^{1}H NMR ($CDCl_3$) δ=1.42 (6H, s, CH_3×2), 2.40 and 2.43 (each 3H, s, $C_6H_4CH_3$), 3.49 and 3.67 (each 3H, s, OCH_3), 5.51 (1H, d, J=10 Hz, C_3–H), 6.31 (1H, d, J=10 Hz, C_4–H), 6.71, 6.77, and 6.90 (each 1H, s, Arom-H), 7.1—7.9 (9H, m, $C_6H_4CH_3$×2 and C_8–H).

Found: C, 61.17; H, 4.40%. Calcd for $C_{36}H_{32}O_{11}S_2$: C, 61.36; H, 4.58%.

Hydrolysis of 18. Compound **18** (143 mg) was refluxed in EtOH (150 ml) with a 20% KOH solution (12 ml) for 40 min. The resulting compound was separated by preparative TLC on silica gel with 1,2-dichloroethane–EtOAc–petroleum ether (50:2:3) to give linear pyranoisoflavone (elongatin) (**1**) and its angular isomer **2**.

7-(4-Benzoyloxy-2,5-dimethoxyphenyl)-2,3-dihydro-5-hydroxy-2,2-dimethyl-4*H*,6*H*-benzo[1,2-*b*:5,4-*b'*]dipyran-4,6-dione (19). A mixture of **14** (3.31 g), PhCOCl (1.2 ml), and K_2CO_3 (11.2 g) in Me_2CO (350 ml) was refluxed with stirring under an atmosphere of N_2 for 1 h. The resulting compound was recrystallized from MeOH to give **19** (3.53 g, 85%) as colorless needles: mp 240—242 °C; ^{1}H NMR ($CDCl_3$) δ=1.49 (6H, s, CH_3×2), 2.74 (2H, s, CH_2CO), 3.75 and 3.78 (each 3H, s, OCH_3), 6.36 (1H, s, C_{10}–H), 6.84 and 7.01 (each 1H, s, Arom-H), 7.4—8.3 (5H, m, C_6H_5CO), 7.87 (1H, s, C_8–H), 14.60 (1H, s, C_5–OH).

Found: C, 67.29; H, 4.74%. Calcd for $C_{29}H_{24}O_9$: C, 67.44; H, 4.68%.

7-(4-Benzoyloxy-2,5-dimethoxyphenyl)-2,3-dihydro-2,2-dimethyl-5-tosyloxy-4*H*,6*H*-benzo[1,2-*b*:5,4-*b'*]dipyran-4,6-dione (20). Tosylation of **19** (2.92 g) with TsCl (1.40 g) in Me_2CO (250 ml) and dioxane (150 ml) gave **20** (3.20 g, 84%) as colorless needles: mp 213—215 °C ($MeOH–Me_2CO$); ^{1}H NMR ($CDCl_3$) δ=1.46 (6H, s, CH_3×2), 2.38 (3H, s, $C_6H_4CH_3$), 2.67 (2H, s, CH_2CO), 3.73 and 3.76 (each 3H, s, OCH_3), 6.80 (1H, s, C_{10}–H), 6.87 and 7.00 (each 1H, s, Arom-H), 7.2—8.3 (9H, m, $C_6H_4CH_3$ and C_6H_5CO), 7.78 (1H, s, C_8–H).

Found: C, 64.21; H, 4.47%. Calcd for $C_{36}H_{30}O_{11}S$: C, 64.47; H, 4.52%.

7-(4-Benzoyloxy-2,5-dimethoxyphenyl)-3,4-dihydro-4-hydroxy-2,2-dimethyl-5-tosyloxy-2*H*,6*H*-benzo[1,2-*b*:5,4-*b'*]dipyran-6-one (21). A mixture of **20** (680 mg) and $PdCl_2$ (270 mg) in THF (200 ml) and water (40 ml) was stirred with adding $NaBH_4$ (380 mg) at 5—9 °C for 1 h. The reaction mixture was worked up by a method similar to that used for the preparation of **16** to give **21** (464 mg, 68%) as colorless needles: mp 174—176 °C (MeOH); ^{1}H NMR ($CDCl_3$) δ=1.42 and 1.55 (each 3H, s, CH_3), 2.07 (2H, m, CH_2CHOH), 2.42 (3H, s, $C_6H_4CH_3$), 3.74 and 3.76 (each 3H, s, OCH_3), 3.60 (1H, br, CH_2CHOH), 5.12 (1H, m, CH_2CHOH), 6.81 (2H, s, $C_{3'}$–H and C_{10}–H), 7.06 (1H, s, $C_{6'}$–H), 7.1—8.3 (9H, s, $C_6H_4CH_3$ and C_6H_5CO), 7.82 (1H, s, C_8–H).

Found: C, 63.98; H, 4.93%. Calcd for $C_{36}H_{32}O_{11}S$: C, 64.27; H, 4.80%.

7-(4-Benzoyloxy-2,5-dimethoxyphenyl)-2,2-dimethyl-5-tosyloxy-2*H*,6*H*-benzo[1,2-*b*:5,4-*b'*]dipyran-6-one (22). Dehydration of **21** (320 mg) with TsOH·H_2O (20 mg) gave **22** (280 mg, 90%) as colorless needles: mp 226—227 °C ($MeOH–Me_2CO$); UV λ_{max} nm (log ε) (EtOH) 263 (4.49), 294sh (4.32), 338sh (3.92); ^{1}H NMR ($CDCl_3$) δ=1.44 (6H, s, CH_3×2), 2.42 (3H, s, $C_6H_4CH_3$), 3.76 and 3.78 (each 3H, s, OCH_3), 5.59 (1H, d, J=10 Hz, C_3–H), 6.46 (1H, d, J=10 Hz, C_4–H), 6.76 (1H, s, C_{10}–H), 6.83 and 7.06 (each 1H, s, Arom-H), 7.1—8.3

(9H, m, $C_6\underline{H}_4CH_3$ and C_6H_5CO), 7.81 (1H, s, C_8–H).

Found: C, 65.97; H, 4.58%. Calcd for $C_{36}H_{30}O_{10}S$: C, 66.04; H, 4.63%.

5-Hydroxy-7-(4-hydroxy-2,5-dimethoxyphenyl)-2,2-dimethyl-2*H*,6*H*-benzo[1,2-*b*:5,4-*b'*]dipyran-6-one (Elongatin) (1). Hydrolysis of **22** (300 mg) with a 5% KOH solution in MeOH and dioxane gave **1** (151 mg, 83%) as colorless needles: mp 181—183 °C (MeOH) (lit,[4] mp 181—182 °C). Compound **1** was converted into the diacetate **23** (227—228 °C; lit,[4] mp 227—228 °C) and the dimethyl ether **24** (mp 132—134 °C; lit,[4] mp 132—134 °C), respectively.

2,4-Bis(benzyloxy)-6-hydroxyacetophenone (25). A mixture of 2,4,6-trihydroxyacetophenone (40 g), $PhCH_2Cl$ (58 ml), and K_2CO_3 (100 g) in HMPA (340 ml) was stirred under an atmosphere of N_2 at 90—93 °C for 70 min [monitered by silica-gel TLC with petroleum ether–1,2-dichloroethane (2:1), R_f=0.39]. After removal of K_2CO_3, the filtrate was poured into ice-cold water and acidified to pH 4 with dil. HCl, and then heated at 60—70 °C for 1 h to give white precipitates. The precipitates were recrystallized from MeOH–Me_2CO to give **25** (66.3 g, 80%): mp 100—102 °C (lit,[7] mp 98—100 °C, lit,[8] mp 96—98 °C).

Found: C, 75.68; H, 5.79%. Calcd for $C_{22}H_{20}O_7$: C, 75.84; H, 5.79%.

2,4-Bis(benzyloxy)-6-methoxyacetophenone (26). Methylation of **25** (30 g) with $(MeO)_2SO_2$ (20.4 g) gave **26** (28.4g, 91%) as colorless needles: mp 64—65 °C (MeOH–Me_2CO); ^{1}H NMR ($CDCl_3$) δ=2.43 (3H, s, $COCH_3$), 3.72 (3H, s, OCH_3), 4.99 (4H, s, $C_6H_5C\underline{H}_2$×2), 6.28 (2H, s, C_3–H and C_5–H), 7.30 and 7.33 (each 5H, s, $C_6\underline{H}_5CH_2$).

Found: C, 76.14; H, 5.97%. Calcd for $C_{23}H_{22}O_4$: C, 76.22; H, 6.12%.

2,4-Dihydroxy-6-methoxyacetophenone (27). Debenzylation of **26** (21.65g) with 10% palladium on charcoal (3 g) gave **27** (9.65 g, 89%) as colorless needles: mp 201—202 °C (MeOH) (lit,[9] mp 203—204 °C).

Found: C, 59.45; H, 5.30%. Calcd for $C_9H_{10}O_4$: C, 59.33; H, 5.53%.

1-(3-Acetyl-2,6-dihydroxy-4-methoxyphenyl)-3-methyl-2-buten-1-one (28). 3-Methyl-2-butenoyl chloride (7.8 g) in Et_2O (50 ml) was added, with stirring and cooling at 0 °C, to a solution of **27** (9.6 g) and $AlCl_3$ (4.9 g) in Et_2O (150 ml); the reaction mixture was then stirred for an additional 15 h. After removal of the ethereal layer, the residue was poured into a mixture of ice and HCl, and then warmed at 40 °C to give precipitates. The precipitates were recrystallized from EtOH to give **28** (12.4 g, 89%) as yellow needles: mp 117—119 °C; ^{1}H NMR ($CDCl_3$) δ=2.00 and 2.17 (each 3H, s, CH_3), 2.57 (3H, s, $COCH_3$), 3.86 (3H, s, OCH_3), 5.85 (1H, s, Arom-H), 7.12 (1H, m, CH=), 15.25 and 16.35 (each 1H, s, OH).

Found: C, 63.55; H, 5.96%. Calcd for $C_{14}H_{16}O_5$: C, 63.62; H, 6.10%.

6-Acetyl-5-hydroxy-7-methoxy-2,2-dimethyl-4-chromanone (29). A mixture of the diketone **28** (12.27 g) and 10% KOH solution (150 ml) in MeOH (350 ml) was stirred at room temperature for 3 h. The resulting compound was recrystallized from MeOH–H_2O to give **29** (11.43 g, 93%) as colorless needles: mp 116—117 °C; ^{1}H NMR ($CDCl_3$) δ=1.44 (6H, s, CH_3×2), 2.50 (3H, s, $COCH_3$), 2.70 (2H, s, $COCH_2$), 3.85 (3H, s, OCH_3), 5.95 (1H, s, Arom-H), 13.04 (1H, s, OH).

Found: C, 63.81; H, 6.11%. Calcd for $C_{14}H_{16}O_5$: C, 63.62; H, 6.10%.

5-Hydroxy-7-methoxy-2,2-dimethyl-6-[1-oxo-3-(4-benzyloxy-2,5-dimethoxyphenyl)-2-propenyl]-4-chromanone (30). Condensation of **29** (9.25 g) with **8** (9.53 g) gave **30** (9.80 g, 55%) as yellow needles: mp 148—150 °C (MeOH); ^{1}H NMR ($CDCl_3$) δ=1.47 (6H, s, CH_3×2), 2.70 (2H, s, $COCH_2$), 3.69, 3.80, and 3.85 (each 3H, s, OCH_3), 5.16 (2H, s, $C_6H_5C\underline{H}_2$), 6.00 (1H, s, C_8–H), 6.47 and 7.06 (each 1H, s, Arom-H), 6.94 and 7.76 (each 1H, d, J=16 Hz, CH=), 7.36 (5H, s, $C_6\underline{H}_5CH_2$), 12.35 (1H, s, OH).

Found: C, 69.25; H, 6.01%. Calcd for $C_{30}H_{30}O_8$: C, 69.48; H, 5.83%.

Acetate 31. Acetylation of 5-hydroxy compound **30** gave the acetate **31** as yellow needles: mp 167—169 °C (EtOH); ^{1}H NMR ($CDCl_3$) δ=1.47 (6H, s, CH_3×2), 2.20 (3H, s, $COCH_3$), 2.63 (2H, s, $COCH_2$), 3.70, 3.78, and 3.83 (each 3H, s, OCH_3), 5.15 (2H, s, $C_6H_5C\underline{H}_2$), 6.33 (1H, s, C_8–H), 6.47 and 6.98 (each 1H, s, Arom-H), 6.85 and 7.66 (each 1H, d, J=16 Hz, CH=), 7.35 (5H, s, $C_6\underline{H}_5CH_2$).

Found: C, 68.42; H, 5.69%. Calcd for $C_{32}H_{32}O_9$: C, 68.56; H, 5.75%.

3-(4-Benzyloxy-2,5-dimethoxyphenyl)-8,9-dihydro-5-methoxy-8,8-dimethyl-4*H*,10*H*-benzo[1,2-*b*:3,4-*b'*]dipyran-4,10-dione (32). The oxidative rearrangement of **31** (7.0 g) with TTN (6.4 g) and the subsequent cyclization gave **32** (4.91 g, 76%) as colorless needles: mp 204—206 °C (EtOAc); ^{1}H NMR ($CDCl_3$) δ=1.48 (6H, s, CH_3×2), 2.73 (2H, s, $COCH_2$), 3.59, 3.82, and 3.94 (each 3H, s, OCH_3), 5.16 (2H, s, $C_6H_5C\underline{H}_2$), 6.29 (1H, s, C_6–H), 6.56 and 6.97 (each 1H, s, Arom-H), 7.35 (5H, s, $C_6\underline{H}_5CH_2$), 7.92 (1H, s, C_2–H).

Found: C, 69.54; H, 5.29%. Calcd for $C_{30}H_{28}O_8$: C, 69.75; H, 5.47%.

3-(4-Benzyloxy-2,5-dimethoxyphenyl)-8,9-dihydro-5-hydroxy-8,8-dimethyl-4*H*,10*H*-benzo[1,2-*b*:3,4-*b'*]dipyran-4,10-dione (33). Demethylation of **32** (4.90 g) with $AlBr_3$ (15.2 g) gave **33** (4.65 g, 97%) as colorless needles: mp 186—188 °C (MeOH–EtOAc); ^{1}H NMR ($CDCl_3$) δ=1.46 (6H, s, CH_3×2), 2.71 (2H, s, $COCH_2$), 3.62 and 3.83 (each 3H, s, OCH_3), 5.15 (2H, s, $C_6H_5C\underline{H}_2$), 6.26 (1H, s, C_6–H), 6.57 and 6.90 (each 1H, s, Arom-H), 7.33 (5H, s, $C_6\underline{H}_5CH_2$), 8.06 (1H, s, C_2–H), 13.75 (1H, s, C_5–OH).

Found: C, 69.12; H, 5.40%. Calcd for $C_{29}H_{26}O_8$: C, 69.30; H, 5.23%.

8,9-Dihydro-5-hydroxy-3-(4-hydroxy-2,5-dimethoxyphenyl)-8,8-dimethyl-4*H*,10*H*-benzo[1,2-*b*:3,4-*b'*]dipyran-4,10-dione (34). Debenzylation of **33** (3.55 g) with 10% palladium on charcoal gave **34** (2.76 g, 95%) as colorless needles: mp 197—198 °C (MeOH–Me_2CO); ^{1}H NMR ($CDCl_3$) δ=1.50 (6H, s, CH_3×2), 2.72 (2H, s, $COCH_2$), 3.70 and 3.83 (each 3H, s, OCH_3), 5.95 (1H, s, $C_{4'}$–OH), 6.25 (1H, s, C_6–H), 6.60 and 6.86 (each 1H, s, Arom-H), 8.06 (1H, s, C_2–H), 10.93 (1H, s, C_5–OH).

Found: C, 64.05; H, 4.70%. Calcd for $C_{22}H_{20}O_8$: C, 64.07; H, 4.90%.

3-(4-Benzoyloxy-2,5-dimethoxyphenyl)-8,9-dihydro-5-hydroxy-8,8-dimethyl-4*H*,10*H*-benzo[1,2-*b*:3,4-*b'*]dipyran-4,10-dione (35). Benzoylation of **34** (310 mg) with PhCOCl (0.92 ml) gave **35** (380 mg, 97%) as colorless needles: mp 253—255 °C (MeOH–Me_2CO); ^{1}H NMR ($CDCl_3$) δ=1.50 (6H, s, CH_3×2), 2.70 (2H, s, $COCH_2$), 3.70 and 3.73 (each 3H, s, OCH_3), 6.23 (1H, s, C_6–H), 6.77 and 6.97 (each 1H, s, Arom-H), 7.3—8.2 (5H, m, C_6H_5CO), 8.06 (1H, s, C_2–H), 13.58 (1H, s, C_5–OH).

Found: C, 67.33; H, 4.51%. Calcd for $C_{29}H_{24}O_9$: C, 67.44;

H, 4.68%.

3-(4-Benzoyloxy-2,5-dimethoxyphenyl)-8,9-dihydro-8,8-dimethyl-5-tosyloxy-4*H*,10*H*-benzo[1,2-*b*:3,4-*b'*]dipyran-4,10-dione (36). Tosylation of **35** (710 mg) with TsCl gave **36** (820 mg, 89%) as colorless needles: mp 183—185 °C (Me_2CO); ^1H NMR ($CDCl_3$) δ=1.50 (6H, s, CH_3×2), 2.40 (3H, s, $C_6H_5C\underline{H}_3$), 2.76 (2H, s, $COCH_2$), 3.68 and 3.73 (each 3H, s, OCH_3), 6.75 (1H, s, C_6–H), 6.88 and 6.96 (each 1H, s, Arom-H), 7.1—8.2 (9H, m, C_6H_5CO and $C_6\underline{H}_4CH_3$), 7.91 (1H, s, C_2–H).

Found: C, 64.29; H, 4.49%. Calcd for $C_{36}H_{30}O_{11}S$: C, 64.47; H, 4.52%.

3-(4-Benzoyloxy-2,5-dimethoxyphenyl)-9,10-dihydro-10-hydroxy-8,8-dimethyl-5-tosyloxy-4*H*,8*H*-benzo[1,2-*b*:3,4-*b'*]dipyran-4-one (37). The selective reduction of **36** (780 mg) with $NaBH_4$ (460 mg) and $PdCl_2$ (310 mg) at 35—38 °C for 30 min gave **37** (712 mg, 91%) as colorless needles: mp 233—234 °C (Me_2CO–petroleum ether); ^1H NMR ($CDCl_3$) δ=1.41 and 1.46 (each 3H, s, CH_3), 2.08 (2H, d, J=4 Hz, $C\underline{H}_2$-CHOH), 2.38 (3H, s, $C_6H_4C\underline{H}_3$), 2.85 (1H, d, J=4 Hz, C_{10}–OH), 3.67 and 3.72 (each 3H, s, OCH_3), 5.07 (1H, t, J=4 Hz, $CH_2C\underline{H}OH$), 6.67, 6.75, and 6.96 (each 1H, s, Arom-H), 7.1—8.2 (9H, m, C_6H_5CO and $C_6\underline{H}_4CH_3$), 7.80 (1H, s, C_2–H).

Found: C, 64.00; H, 4.53%. Calcd for $C_{36}H_{32}O_{11}S$: C, 64.28; H, 4.80%.

3-(4-Benzoyloxy-2,5-dimethoxyphenyl)-8,8-dimethyl-5-tosyloxy-4*H*,8*H*-benzo[1,2-*b*:3,4-*b'*]dipyran-4-one (38). Dehydration of crude **37** (900 mg) gave **38** (510 mg, 67% yield based on **36**) as colorless needles: mp 215—217 °C (MeOH–Me_2CO); UV λ_{max} nm (log ε) (EtOH) 258 (4.59), 263 (4.59), 301 (4.15); ^1H NMR ($CDCl_3$) δ=1.46 (6H, s, CH_3×2), 2.39 (3H, s, $C_6H_4C\underline{H}_3$), 3.70 and 3.75 (each 3H, s, OCH_3), 5.65 (1H, d, J=10 Hz, C_9–H), 6.70 (1H, d, J=10 Hz, C_{10}–H), 6.67, 6.78, and 6.99 (each 1H, s, Arom-H), 7.1—8.2 (9H, m, C_6H_5CO and $C_6\underline{H}_4CH_3$), 7.80 (1H, s, C_2–H).

Found: C, 65.82; H, 4.63%. Calcd for $C_{36}H_{30}O_{10}S$: C, 66.04; H, 4.63%.

5-Hydroxy-3-(4-hydroxy-2,5-dimethoxyphenyl)-8,8-dimethyl-4*H*,8*H*-benzo[1,2-*b*:3,4-*b'*]dipyran-4-one (2). Hydrolysis of **38** (400 mg) gave **2** (180 mg, 74%) as yellow needles: mp 174—175 °C (MeOH–H_2O) (lit,[4] mp 173—175 °C). Diacetate **39** of **2**: mp 225—226 °C; lit,[4] mp 224—226 °C. 4′-Methyl ether (toxicarol isoflavone) (**40**): mp 219—220 °C; lit,[4] mp 219—220 °C. Dimethyl ether **41**: mp 178—180 °C; lit,[4] mp 179—180 °C.

References

1) L. Farkas, Á. Gottsegen, M. Nógrádi, and S. Antus, *J. Chem. Soc., Perkin Trans. 1*, **1974**, 305; P. M. Dewick, "The Flavonoids: Advances in Research," ed. by J. B. Harborne and T. J. Mabry, Chapman and Hall, London, 1982, pp. 535—640.

2) M. Nakayama, S. Hayashi, M. Tsukayama, T. Horie, and M. Masumura, *Chem. Lett.*, **1978**, 879; M. Tsukayama, T. Horie, K. Fujimoto, and M. Nakayama, *Chem. Pharm. Bull.*, **34**, 2369 (1986).

3) S. Antus, Á. Gottsegen, M. Nógrádi, and A. Gergely, *Chem. Ber.*, **112**, 3879 (1979).

4) M. Tsukayama, T. Horie, Y. Iguchi, and M. Nakayama, *Chem. Pharm. Bull.*, **36**, 952 (1988); M. Tsukayama, Y. Iguchi, T. Horie, M. Masumura, and M. Nakayama, *Heterocycles*, **22**, 709 (1984).

5) T. M. Smalberger, R. Vleggaar, and J. C. Weber, *Tetrahedron*, **31**, 2297 (1975).

6) M. Tsukayama, T. Sakamoto, T. Horie, M. Masumura, and M. Nakayama, *Heterocycles*, **16**, 955 (1981).

7) V. V. Sreerama Murti and T. R. Seshadri, *Proc. Ind. Acad. Sci.*, **29A**, 1 (1949).

8) M. Tsukayama, K. Fujimoto, T. Horie, M. Masumura, and M. Nakayama, *Bull. Chem. Soc. Jpn.*, **58**, 136 (1985).

9) V. B. Mahesh, S. Neelakantan, and T. R. Seshadri, *J. Sci. Ind. Research*, **15B**, 287 (1956).

Facile Construction of Optically Active 1,3-Diols. Synthesis of (2*S*,4*R*)-7-Octene-2,4-diol and *endo*-(1*S*,3*S*,5*R*)- and *exo*-(1*R*,3*S*,5*S*)-1,3-Dimethyl-2,9-dioxabicyclo[3.3.1]nonane

Hidenori CHIKASHITA,* Eiji KITTAKA, Yasunori KIMURA, and Kazuyoshi ITOH
Department of Applied Chemistry, Faculty of Engineering,
Kansai University, Suita, Osaka 564
(Received September 5, 1988)

A short and stereoselective asymmetric synthesis of (2*S*,4*R*)-7-octene-2,4-diol (a key intermediate in the Bartlett synthesis of nonactic acid) and two stereoisomers of a biologically active substance isolated from Norway spruce infested by ambrosia beetle, *endo*-(1*S*,3*S*,5*R*)- and *exo*-(1*R*,3*S*,5*S*)-1,3-dimethyl-2,9-dioxabicyclo-[3.3.1]nonane, was effectively accomplished in three and four reaction steps, respectively, by starting with easily obtainable (*S*)-1-(1,3-dithian-2-yl)-2-propanol by baker's yeast asymmetric reduction. The main strategy was based on a facile construction of optically active β-hydroxy ketones via alkylation of the dianion of (*S*)-1-(1,3-dithian-2-yl)-2-propanol with alkyl halides, followed by their stereoselective reductions.

A 1,3-dihydroxylated structure is often found on the backbone of natural products or important key intermediates for natural products synthesis (e.g., polyoxo and polyether natural products). The compounds, (2*S*,4*R*)-7-octene-2,4-diol (**1**) and 1,3-dimethyl-2,9-dioxabicyclo[3.3.1]nonane (**2**) are typical

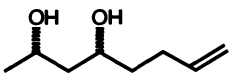

1

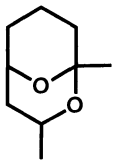

2

and simple examples. The former diol is known to be a key intermediate for the Bartlett synthesis of nonactic acid[1] and the latter bicyclic acetal, which is regarded to be potentially a 1,3-diol molecule, is a host-specific substance isolated from Norway spruce infested by the ambrosia beetle (*Trypodendron lineatum* Oliv.).[2] Although these compounds have already been synthesized in optically active forms by several groups,[3] some of these syntheses require lengthy reaction steps and are laborious in spite of their synthetic importances. In a preceding communication,[4] we showed the usefulness of (*S*)-1-(1,3-dithian-2-yl)-2-propanol (**3**) as a chiral building block for the synthesis of the Bartlett diol (**1**). In this paper, we would like to describe a short and efficient asymmetric synthesis of (2*S*,4*R*)-7-octene-2,4-diol (**1**) and two stereoisomers of **2**, *endo*-(1*S*,3*S*,5*R*)- and *exo*-(1*R*,3*S*,5*S*)-1,3-dimethyl-2,9-dioxabicyclo[3.3.1]nonane (**12** and **13**), which demonstrates the usefulness of **3** for the facile construction of this type of optically active 1,3-diols.

As outlined in Schemes 1 and 2, the present methodology comprises the alkylation of the dianion **4** with alkyl halides followed by the hydrolysis of the dithioacetal group and the subsequent 1,3-asymmetric induction by employing the stereoselective reduction of the resulting β-hydroxy ketones **6** and **9** leading to the corresponding 1,3-syn and 1,3-anti diols **1**, **10**, and **11**.

As shown in the previous communication[4] as well as in the literature,[5] optically active alcohol (*S*)-**3** was easily obtained by the baker's yeast asymmetric reduction of (1,3-dithian-2-yl)acetone in nearly quantitative yield with excellent optical purity (>99% ee). The transformation of (*S*)-**3** into the dianion **4** was

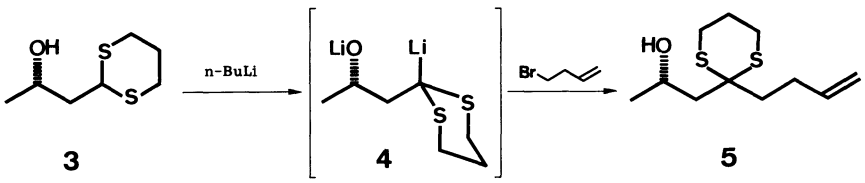

3 **4** **5**

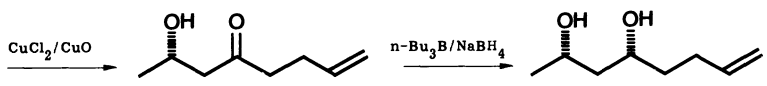

6 **1**

Scheme 1.

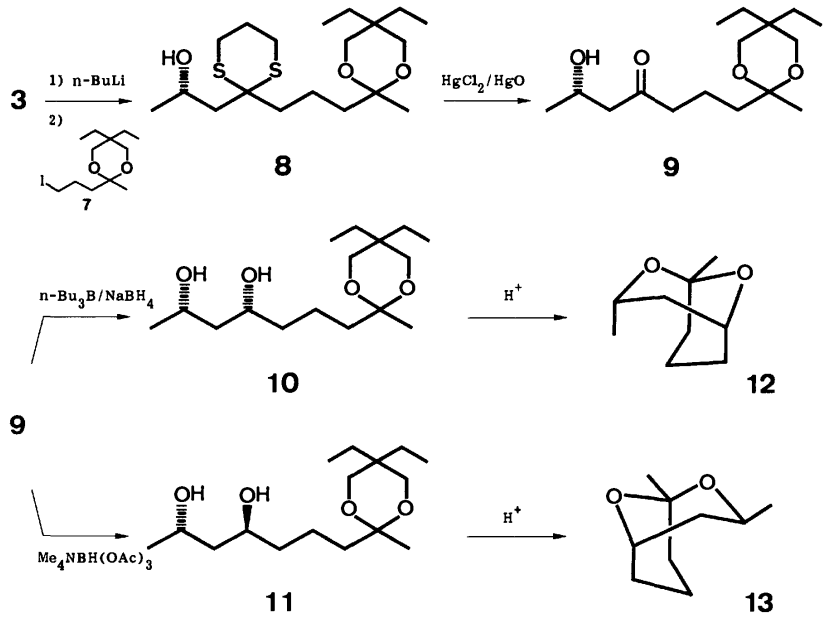

Scheme 2.

achieved by the reaction with 2.2 equiv. of *n*-BuLi in THF at −30—0 °C. When dianion **4** was treated with 1.1 equiv. of 4-bromo-1-butene in THF at −30—0 °C, the *C*-alkylation product (*S*)-**5** was obtained in high yield. (*S*)-**5** was then hydrolyzed with $CuCl_2/CuO$ in aqueous acetone[6] to give the optically active β-hydroxy ketone (*S*)-**6** in good yield without any evidence of dehydration. The stereoselective reduction of (*S*)-**6** to the syn-diol **1** was effectively accomplished using n-$Bu_3B/NaBH_4$[7] which produced the mixture of the Bartlett diol **1** and its C-4 epimer with high selectivity (syn:anti=97:3). They were cleanly separated by column chromatography on silica gel to give pure **1**.

We next tried the synthesis of *endo*-(1*S*,3*S*,5*R*)-**12** and *exo*-(1*R*,3*S*,5*S*)-**13** starting with the (*S*)-alcohol **3**, according to the following sequence (Scheme 2). The reaction of the dianion **4** with 1.1 equiv. of 2-(3-iodopropyl)-2-methyl-5,5-diethyl-1,3-dioxane (**7**) at −30—0 °C proceeded selectively to give (*S*)-**8** in high yield without the concomitant of *O*-alkylation product. In contrast to the case of a similar ethylene acetal analogue reported very recently,[8] the selective hydrolysis of the dithioacetal group in **8** could be easily achieved without the hydrolysis of the 2,2-diethyl-1,3-propanediyl acetal protecting group by the standard procedure using $HgCl_2/HgO$ in aqueous acetonitrile[9] to give the desired β-hydroxy ketone (*S*)-**9** in good yield. The reduction of (*S*)-**9** with n-$Bu_3B/NaBH_4$ satisfactorily provided the syn-diol **10** in excellent yield with high stereoselectivity (syn:anti=94:6), although the syn selective reduction of a similar ethylene acetal analogue has been reported ($Zn(BH_4)_2$: 9:1,[8] $NaBH_4/Et_2BOMe$: >99:1[30]). On the other hand, the anti-isomer **11** could be quantitatively obtained with excellent stereoselectivity (syn:anti=6:94) by reducing (*S*)-**9** with $Me_4NBH(OAc)_3$ in acetonitrile–acetic acid[10] in sharp contrast to the poor selectivity (1:2) on the reduction of an ethylene acetal analogue by $NaBH(OAc)_3$ in acetic acid or $NaBH_4/CeCl_3$ in methanol.[8] Although the isomers of *syn*-**10** and *anti*-**11** could be separated by silica-gel column chromatography, the crude diol mixture in both cases was available for use in the final cyclization stage without separation of the minor isomer or further purification. Thus, the acid-catalyzed cyclization of the crude mixtures was performed by means of a two-layer method with hexane–2 M H_2SO_4 (1 M=1 mol dm^{-3}) to produce *endo*-**12** and *exo*-**13** in good yields, respectively. These isomers were cleanly separated by the separable-TLC technique to obtain them as pure form, respectively.

In summary, (2*S*,4*R*)-**1**, *endo*-(1*S*,3*S*,5*R*)-**12**, and *exo*-(1*R*,3*S*,5*S*)-**13** of high chemical and enantiomeric purity were obtained in 75%, 61%, and 70% overall yield, respectively. Spectroscopic data of these compounds were in good agreement with reported values. Because of the ready availability of the starting alcohol (*S*)-**3**, high overall yields of products, and simplicity of the procedure, the method can be regarded as a general and useful one for the facile construction of this type of optically active 1,3-diols.

Experimental

Optical rotations were determined with a Union Digital PM-101 polarimeter. IR spectra were obtained on a JASCO A-202 spectrophotometer. ^1H NMR spectra were measured with JEOL JNM-GX400 spectrophotometer at 400 MHz with tetramethylsilane as an internal reference. Silica gel (Merck silica gel 60, 230—400 mesh ASTM) was used for

medium-pressure liquid chromatography (MPLC). Analytical and preparative TLC were carried out on Merck precoated silica gel plates (Merck silica gel 60 F_{254}).

Materials. The solvents were purified by the usual methods and were freshly distilled before use. (1,3-Dithian-2-yl)acetone was prepared from 4,4-dimethoxy-2-butanone and 1,3-propanedithiol according to the method in the literature.[11] 5-Iodo-2-pentanone was prepared by the halogen-exchange reaction of the corresponding chloride with NaI according to the method of Findlay et al.[12] Fresh baker's yeast (Oriental Yeast Co.) used was commercially available. The other reagents were supplied as high-grade commercial products and used without further purification.

(*S*)-(+)-1-(1,3-Dithian-2-yl)-2-propanol (3). The following modified procedure gave optically pure (*S*)-**3** in excellent yield.[5] Baker's yeast (200 g) was dispersed into a solution of sucrose (40 g) and $Na_4P_2O_7$ (10 g) in distilled water (600 ml), and then stirred for 1 h at 25 °C. To the fermenting mixture was added (1,3-dithian-2-yl)acetone (8 g, 45.4 mmol) and stirred at the same temperature for 1 day. An additional baker's yeast (100 g), sucrose (20 g), $Na_4P_2O_7$ (5 g), and distilled water (300 ml) were supplied and the stirring was continued for an additional day. Ethyl acetate (500 ml) was added to the reaction mixture and the mixture was stirred for 16 h. After filtration through a Celite pad, the filtrate was extracted with ethyl acetate and the extract was dried with $MgSO_4$. The solvent was removed by evaporation under reduced pressure and the residue was diluted with CH_2Cl_2. The solution was filtered through a silica-gel pad (Wakogel C-300) and the concentration of the filtrate in vacuo gave the almost TLC-pure (*S*)-**3** in quantitative yield (>99% ee by ^1H NMR analysis of the alcohol with the chiral shift reagent (+)-Eu(hfc)$_3$ and of the corresponding (+)-MTPA ester[13]). Distillation of this product gave pure (*S*)-**3** as a colorless oil (7.63 g, 94%); bp 135 °C/0.1 mmHg (lit,[5] 105 °C/0.05 mmHg; 1 mmHg≈133.322 Pa); $[\alpha]_D^{25}$ +25.1° (*c* 2.0, $CHCl_3$) (lit,[5] $[\alpha]_D^{20}$ +24.7° (*c* 2.0, $CHCl_3$)); IR (neat film) 3400, 2900, 1420, 1370, 1270, 1240, 1180, 1120, 1070, 1020, 940, 900, 860, 840, and 760 cm^{-1}; ^1H NMR ($CDCl_3$) δ=1.23 (d, 3H, *J*=6.1 Hz), 1.81—1.95 (m, 3H), 1.98 (br, 1H), 2.13 (m, 1H), 2.81—2.96 (m, 4H), 4.13 (m, 1H), and 4.24 (dd, 1H, *J*=8.5, 5.9 Hz).

(*S*)-(+)-2-(3-Butenyl)-2-(2-hydroxypropyl)-1,3-dithiane (5). A stirred solution of (*S*)-**3** (1.0 g, 5.6 mmol) in dry THF (8 ml) under nitrogen was cooled to −30 °C and 1.6 M solution of *n*-BuLi in hexane (8.4 ml, 13.4 mmol) was added dropwise. The mixture was stirred for 30 min at −30 °C and then for 3 h at 0 °C. The mixture was again cooled to −30 °C. 4-Bromo-1-butene (0.62 ml, 6.2 mmol) was slowly added to the solution and stirred for 1 h at −30 °C. After allowing to warm to 0 °C, the reaction mixture was stirred for additional 4 days in a refrigerator and then quenched by the addition of water. The aqueous mixture was extracted with benzene and the extract was washed successively with water, 7% aqueous KOH solution, and water. After drying the extract with $MgSO_4$, the solution was concentrated in vacuo and the residual oil was purified by MPLC (benzene/ethyl acetate 3:1 v/v) to give pure (*S*)-**5** as a colorless oil (1.18 g, 91%); $[\alpha]_D^{24}$ +25.5° (*c* 3.84, $CHCl_3$); IR (neat film) 3400, 3050, 2900, 1630, 1440, 1410, 1360, 1260, 1230, 1120, 1050, 980, 900, 860, and 780 cm^{-1}; ^1H NMR ($CDCl_3$) δ=1.20 (d, 3H, *J*=6.3 Hz), 1.88—2.22 (m, 6H), 2.33 (m, 2H), 2.81 (m, 2H), 2.97 (m, 2H), 3.50 (s, 1H), 4.16 (m, 1H), 5.00 (dq, 1H, *J*=10.1, 1.7 Hz), 5.07 (dq, 1H, *J*=17.1, 1.7 Hz), and 5.82 (m, 1H).

(*S*)-(+)-2-Hydroxy-7-octen-4-one (6). To a solution of (*S*)-**5** (800 mg, 3.44 mmol) in 99% aqueous acetone (34 ml) was added $CuCl_2$ (925 mg, 6.88 mmol) and CuO (1.09 g, 13.76 mmol). The mixture was stirred for 3 h at room temperature. It was filtered through a Celite pad and the Celite was washed with ether. The combined filtrate and washings were concentrated under reduced pressure and the residue was diluted again with ether (30 ml). The solution was thoroughly washed with 5% aqueous $NaHCO_3$ solution and dried with $MgSO_4$. After concentration in vacuo, MPLC purification of the residue (benzene–ethyl acetate 4:1 v/v) gave pure (*S*)-**6** as a colorless heavy oil (441 mg, 90%); $[\alpha]_D^{30}$ +59.3° (*c* 2.0, $CHCl_3$) (lit,[3d] $[\alpha]_D^{22}$ −57.2° (*c* 2.27, $CHCl_3$) for (*R*)-**6**); IR (neat film) 3450, 3100, 2975, 2925, 1710, 1640, 1410, 1380, 1280, 1110, 1070, 1040, 1000, 940, 920, 840, and 740 cm^{-1}; ^1H NMR ($CDCl_3$) δ=1.19 (d, 3H, *J*=6.3 Hz), 2.33 (q, 2H, *J*=7.3 Hz), 2.52 (d, 1H, *J*=17.5 Hz), 2.54 (t, 2H, *J*=7.3 Hz), 2.61 (dd, 1H, *J*=17.5, 3.4 Hz), 3.19 (br, 1H), 4.23 (m, 1H), 5.02 (m, 2H), and 5.80 (m, 1H).

(2*S*,4*R*)-(+)-7-Octene-2,4-diol (1). To a solution of (*S*)-**6** (200 mg, 1.41 mmol) in dry THF (3.5 ml) was added tributylborane (1.55 ml, 1.55 mmol) and then air (4.2 ml) was slowly bubbled into the solution. The mixture was stirred for 2 h at room temperature under nitrogen. After the mixture was cooled to −78 °C, $NaBH_4$ (59 mg, 1.55 mmol) was added and then stirred for 3 h at the same temperature. The reaction mixture was allowed to warm to room temperature and the mixture of 30% H_2O_2 (7 ml), buffer solution (pH 7, 14 ml), and methanol (21 ml) was then added. The solvent was removed by evaporation under reduced pressure and the residue was extracted with CH_2Cl_2. The extract was dried with $MgSO_4$ and the solvent was removed in vacuo to yield the almost pure mixture of *syn*-**1** and its C-4 epimer in 98% yield (syn:anti=97:3 by ^1H NMR analysis). MPLC purification (benzene/ethyl acetate 1:2 v/v) of the mixture gave pure *syn*-**1** (187 mg, 92%); $[\alpha]_D^{26}$ +18.5° (*c* 1.13, CCl_4) (lit,[1] $[\alpha]_D^{20}$ −18.3° (*c* 0.75, CCl_4) for the enantiomer of **1**); IR (neat film) 3400, 3100, 3000, 2950, 1650, 1440, 1380, 1330, 1130, 1080, 1000, 920, and 840 cm^{-1}; ^1H NMR ($CDCl_3$) δ=1.21 (d, 3H, *J*=6.1 Hz), 1.46—1.64 (m, 4H), 2.16 (m, 2H), 3.11 (s, 2H), 3.88 (m, 1H), 4.05 (m, 1H), 4.98 (dq, iH, *J*=10.0, 0.5 Hz), 5.05 (dq, 1H, *J*=17.1, 0.5 Hz), and 5.84 (m, 1H).

5,5-Diethyl-2-(3-iodopropyl)-2-methyl-1,3-dioxane (7). A mixture of 5-iodo-2-pentanone (21.2 g, 100 mmol), 2,2-diethyl-1,3-propanediol (26.4 g, 200 mmol), and *p*-toluenesulfonic acid monohydrate (1.90 g, 10 mmol) in benzene (247 ml) was refluxed in an apparatus equipped with a Dean–Stark trap for 15 h. After cooling to room temperature, 5% aqueous $NaHCO_3$ solution was added to the reaction mixture and then extracted with ether. The extract was washed with 0.1 M aqueous $Na_2S_2O_3$ solution and dried with $MgSO_4$. The solvent was removed by evaporation under reduced pressure and the residual pale yellow oil was distilled to yield pure **7** (23.7 g, 73%); bp 135 °C/0.1 mmHg; IR (neat film) 2900, 2850, 1440, 1360, 1280, 1240, 1220, 1180, 1160, 1100, 1040, 990, 920, 850, 780, 760, and 740 cm^{-1}; ^1H NMR ($CDCl_3$) δ=0.79 (t, 3H, *J*=7.8 Hz), 0.81 (t, 3H, *J*=7.8 Hz), 1.29 (q, 2H, *J*=7.8 Hz), 1.36 (s, 3H), 1.47 (q, 2H, *J*=7.8 Hz), 1.78 (m, 2H), 1.97 (m, 2H), 3.23 (t, 2H, *J*=6.8 Hz),

and 3.52, 3.54, 3.56, 3.59 (each s, 4H).

(+)-5,5-Diethyl-2-[(*S*)-6-hydroxy-4,4-(trimethylenedithio)-heptyl]-2-methyl-1,3-dioxane (8). To a cooled and stirred solution of (*S*)-**3** (5.17 g, 29 mmol) in dry THF at −30 °C under nitrogen, was added dropwise 1.6 M hexane solution of *n*-BuLi (41 ml, 65 mmol). After stirring for 30 min at −30 °C, the mixture was allowed to slowly warm to 0 °C and then stirred for 3 h. Iodide **7** (10.5 g, 32 mmol) was added dropwise to the resulting dianion solution cooled again to −30 °C and then stirring was continued for 2 h. The reaction mixture was allowed to warm to 0 °C and stood for 2 days at 0 °C in refrigerator. The mixture was then quenched by the addition of water and the aqueous mixture was extracted with benzene. The extract was successively washed with water, 7% aqueous KOH solution, and water and then dried with $MgSO_4$. The solvent was removed in vacuo to yield almost pure (*S*)-**8** in quantitative yield; $[\alpha]_D^{30}$ +12.7° (*c* 2.18, $CHCl_3$); IR (neat film) 3450, 2950, 1720, 1460, 1420, 1380, 1280, 1250, 1220, 1190, 1100, 1060, 1000, 930, 910, 870, 790, 760, and 740 cm^{-1}; ^1H NMR ($CDCl_3$) δ=0.79 (t, 3H, *J*=7.6 Hz), 0.81 (t, 3H, *J*=7.6 Hz), 1.20 (d, 3H, *J*=6.3 Hz), 1.31 (q, 2H, *J*=7.6 Hz), 1.36 (s, 3H), 1.47 (q, 2H, *J*=7.6 Hz), 1.68 (m, 4H), 1.86—2.08 (m, 5H), 2.33 (dd, 1H, *J*=15.4, 9.5 Hz), 2.79 (m, 2H), 2.98 (m, 2H), 3.50, 3.53 (each d, 2H, *J*=2.2 Hz), 3.55, 3.58 (each s, 3H), and 4.14 (m, 1H).

(+)-5,5-Diethyl-2-[(*S*)-6-hydroxy-4-oxoheptyl]-2-methyl-1,3-dioxane (9). To a stirred suspension of $HgCl_2$ (14.3 g, 52.8 mmol) and HgO (11.4 g, 52.8 mmol) in acetonitrile-water (4:1 v/v, 38 ml), a solution of (*S*)-**8** (9.04 g, 24 mmol) in acetonitrile-water (4:1 v/v, 230 ml) was added dropwise under nitrogen and then stirred for 4 h at room temperature. The reaction mixture was filtered through Celite and the Celite was washed with hexane-CH_2Cl_2 (1:1 v/v). 5 M aqueous ammonium acetate solution was added to the combined filtrate and washings and filtered again through Celite. The filtrate was washed with water and saturated aqueous NaCl solution. After drying with $MgSO_4$, the solvent was removed by evaporation under reduced pressure. The residual oil was purified by MPLC (benzene/ethyl acetate 1:1 v/v) to give pure (*S*)-**9** as a colorless heavy oil (5.71 g, 83%); $[\alpha]_D^{25}$ +32.9° (*c* 2.85, $CHCl_3$); IR (neat film) 3450, 3000, 1710, 1460, 1410, 1380, 1250, 1220, 1200, 1120, 1100, 1040, 1010, 940, 860, 790, 760, and 740 cm^{-1}; ^1H NMR ($CDCl_3$) δ=0.79 (t, 3H, *J*=7.6 Hz), 0.81 (t, 3H, *J*=7.6 Hz), 1.19 (d, 3H, *J*=6.3 Hz), 1.28 (q, 2H, *J*=7.6 Hz), 1.36 (s, 3H), 1.48 (q, 2H, *J*=7.6 Hz), 1.69 (m, 4H), 2.46 (t, 2H, *J*=7.1 Hz), 2.50 (dd, 1H, *J*=17.6, 9.0 Hz), 2.61 (dd, 1H, *J*=17.6, 2.9 Hz), 3.16 (d, 1H, *J*=3.2 Hz), 3.50, 3.53, 3.56, 3.59 (each s, 4H), and 4.22 (m, 1H).

(+)-5,5-Diethyl-2-[(4*R*,6*S*)-4,6-dihydroxyheptyl]-2-methyl-1,3-dioxane (10). To a solution of (*S*)-**9** (716 mg, 2.5 mmol) in dry THF (6.2 ml) was added tributylborane (2.75 ml, 2.75 mmol) and then air (7.5 ml) was slowly bubbled into the solution. The mixture was stirred for 3 h at room temperature under nitrogen. After cooling to −78 °C, $NaBH_4$ (104 mg, 2.75 mmol) was added and then stirred for 3 h at the same temperature. The reaction mixture was allowed to warm to room temperature and a mixture of 30% H_2O_2 (13 ml), buffer solution (pH 7, 23 ml), and methanol (38 ml) was then added. The solvent was removed by evaporation under reduced pressure and the residue was extracted with CH_2Cl_2. The extract was dried with $MgSO_4$ and the solvent was removed in vacuo to yield an almost pure diastereomeric mixture of **10** and **11** (707 mg, 98%, **10**:**11**=94:6 by ^1H NMR analysis). This mixture was used for the next cyclization without further purification. TLC purification (benzene/ethyl acetate 1:1 v/v) of a part of the mixture gave pure sample of *syn*-**10**; $[\alpha]_D^{26}$ +4.1° (*c*1.02, $CHCl_3$); IR (neat film) 3400, 2950, 1460, 1380, 1360, 1330, 1240, 1200, 1150, 1130, 1100, 1080, 1060, 1030, 970, 940, 870, 840, 800, 760, and 740 cm^{-1}; ^1H NMR ($CDCl_3$) δ=0.79 (t, 3H, *J*=7.6 Hz), 0.81 (t, 3H, *J*=7.6 Hz), 1.21 (d, 3H, *J*=6.1 Hz), 1.28 (q, 2H, *J*=7.6 Hz), 1.36 (s, 3H), 1.49 (m, 7H), 1.59 (dt, 1H, *J*=14.4, 2.6 Hz), 1.69 (m, 2H), 3.03 (bs, 1H), and 3.18 (bs, 1H), 3.51, 3.54, 3.57, 3.60 (each s, 4H), 3.88 (m, 1H), and 4.05 (m, 1H).

(1*S*,3*S*,5*R*)-(+)-1,3-Dimethyl-2,9-dioxabicyclo[3.3.1]nonane (12). The two-layer mixture of a solution of crude *syn*-**10** (515 mg, 1.79 mmol) in hexane (6.3 ml) and 2 M H_2SO_4 (1.5 ml) was vigorously stirred for 4 days at room temperature. Saturated aqueous $NaHCO_3$ solution was carefully added to the reaction mixture and the mixture was extracted with ethyl acetate. The organic layer was washed with saturated NaCl solution and dried with $MgSO_4$. After removal of the solvent by evaporation under reduced pressure, the pure *endo*-**12** was isolated from the residue by preparative TLC (CH_2Cl_2); 209 mg, 75%; $[\alpha]_D^{26}$ +31.1° (*c* 0.405, pentane) (lit,[3c] $[\alpha]_D^{20}$ +37.5° (*c* 5.4, pentane)); IR (neat film) 3450, 2950, 2850, 1460, 1380, 1280, 1240, 1200, 1160, 1120, 1080, 1050, 1020, 970, and 940 cm^{-1}; ^1H NMR ($CDCl_3$) δ=1.20 (d, 3H, *J*=6.3 Hz), 1.27 (s, 3H), 1.30—1.81 (m, 6H), 2.04—2.17 (m, 2H), 3.94 (m, 1H), and 4.27 (brm, 1H).

(+)-5,5-Diethyl-2-[(4*S*,6*S*)-4,6-dihydroxyheptyl]-2-methyl-1,3-dioxane (11). To a cooled and stirred solution of tetramethylammonium triacetoxyborohydride (4.62 g, 17.5 mmol) in a mixture of dry acetonitrile (14 ml) and acetic acid (14 ml) at −40 °C was added dropwise a solution of (*S*)-**9** (1.00 g, 3.5 mmol) in dry acetonitrile (3.5 ml) under nitrogen. After the mixture was stirred for 5 h at −20 °C, it was quenched by the addition of 0.5 M aqueous sodium potassium tartarate (Rochelle salt) (52 ml) with vigorous stirring and then stirred for further 30 min. The mixture was diluted with CH_2Cl_2 and washed with saturated aqueous $NaHCO_3$ solution. The organic layer was dried with Na_2SO_4 and concentrated in vacuo to yield an almost pure diastereomeric mixture of **11** and **10** in quantitative yield (**11**:**10**=94:6 by ^1H NMR analysis). This mixture was used for the next cyclization without further purification. TLC purification (benzene/ethyl acetate 1:1 v/v) of a part of the mixture gave pure sample of *anti*-**11**; $[\alpha]_D^{23}$ +8.7° (*c* 1.43, $CHCl_3$); IR (neat film) 3400, 3000, 1470, 1380, 1260, 1220, 1200, 1140, 1100, 1040, 1010, 940, 870, 840, 800, and 760 cm^{-1}; ^1H NMR ($CDCl_3$) δ=0.79 (t, 3H, *J*=7.6 Hz), 0.81 (t, 3H, *J*=7.6 Hz), 1.25 (m, 5H), 1.36 (s, 3H), 1.49—1.70 (m, 10H), 2.33 (bs, 1H), 2.40 (bs, 1H), 3.51, 3.54, 3.57, 3.60 (each s, 4H), 3.98 (m, 1H), and 4.17 (m, 1H).

(1*R*,3*S*,5*S*)-(−)-1,3-Dimethyl-2,9-dioxabicyclo[3.3.1]nonane (13). The two-layer mixture of a solution of crude *anti*-**11** (675 mg, 2.34 mmol) in hexane (8.2 ml) and 2 M H_2SO_4 (2 ml) was stirred for 3 days at room temperature. After a similar workup for *endo*-**12**, pure *exo*-**13** was isolated by preparative TLC (CH_2Cl_2); 307 mg, 84%; $[\alpha]_D^{24}$ −6.1° (*c* 0.212, pentane) (lit,[3c] $[\alpha]_D^{20}$ +4.7° (*c* 3.2, pentane) for the enantiomer of **13**); IR (neat film) 3500, 1470, 1460, 1420, 1380, 1260, 1160,

1100, 1020, 860, and 800 cm^{-1}; ^1H NMR ($CDCl_3$) δ=1.16 (d, 3H, J=6.1 Hz), 1.32 (s, 3H), 1.53—2.20 (m, 8H), 4.21 (brm, 1H), and 4.60 (m, 1H).

References

1) P. A. Bartlett, J. D. Meadows, and E. Ottow, *J. Am. Chem. Soc.*, **106**, 5304 (1984).

2) V. Heemann and W. Francke, *Naturwissenshaften*, **63**, 344 (1976); *Planta Med.*, **32**, 342 (1977) [*Chem. Abstr.*, **88**, 101563h (1978)].

3) For the synthesis of **1**: a) I. R. Silvermann, C. Edington, J. D. Elliott, and W. S. Johnson, *J. Org. Chem.*, **52**, 180 (1987); see also Refs. 1 and 3d. For the synthesis of **2**: b) H. Redlich, B. Schneider, and W. Franke, *Tetrahedron Lett.*, **21**, 3013 (1980); c) H. Redlich, B. Schneider, R. W. Hoffmann, and K. J. Geueke, *Liebigs Ann. Chem.*, **1983**, 393; d) T. Sato, T. Itoh, C. Hattori, and T. Fujisawa, *Chem. Lett.*, **1983**, 1391; e) T. Nakata, S. Nagao, S. Takao, T. Tanaka, and T. Oishi, *Tetrahedron Lett.*, **26**, 73 (1985); f) H. Ohta, K. Ozaki, and G. Tsuchihashi, *Chem. Lett.*, **1987**, 2225.

4) H. Chikashita, Y. Kimura, and K. Itoh, *Chem. Express*, **3**, 113 (1988).

5) D. Ghiringhelli, *Tetrahedron Lett.*, **24**, 287 (1983).

6) K. Narasaka, T. Sakashita, and T. Mukaiyama, *Bull. Chem. Soc. Jpn.*, **45**, 3724 (1972).

7) K. Narasaka and F.-C. Pai, *Tetrahedron*, **40**, 2233 (1984).

8) Parts of this work were presented at the 55th Annual Meeting of the Japan Chemical Society, October 1987, Fukuoka. After this, Ghiringhelli et al. reported a similar synthesis by basically the same strategy. They found that the ethylene acetal analogue of **9** can be hydrolyzed with a 4 M solution of mercury(II) perchlorate by controlling the pH with solid calcium carbonate. We found, however, the 2,2-diethyl-1,3-propanediyl acetal group in **9** is very stable under standard conditions ($HgCl_2$/HgO) for the hydrolysis of trimethylene dithioacetals: R. Bernardi and D. Ghiringhelli, *J. Org. Chem.*, **52**, 5021 (1987).

9) E. J. Corey and B. W. Erickson, *J. Org. Chem.*, **36**, 3553 (1971).

10) D. A. Evans and K. T. Chapman, *Tetrahedron Lett.*, **27**, 5939 (1986).

11) D. L. Coffen, K. C. Bank, and P. E. Garrett, *J. Org. Chem.*, **34**, 605 (1969).

12) J. A. Findlay and W. D. Mackay, *J. Chem. Soc. C*, **1970**, 2631.

13) J. A. Dale, D. L. Dull, and H. S. Mosher, *J. Org. Chem.*, **34**, 2543 (1969).

Synthesis and Reductive Desulfurization of Crown Ethers Containing Thiophene Subunit[1)]

Tyo SONE,* Kazuaki SATO, and Yoshihiro OHBA
Department of Applied Chemistry, Faculty of Engineering,
Yamagata University, Yonezawa 992
(Received September 13, 1988)

Crown ethers containing 3,4-thiophenediyl and 3,4-thiophenediylbis(methylene) subunits as a ring constituent were prepared starting from 2,5-bis(ethoxycarbonyl)-3,4-thiophenediol and 2,5-dichloro-3,4-bis(chloromethyl)thiophene, respectively. A Raney nickel desulfurization of the thiophene-containing crown ethers afforded crown ethers having two adjacent side chains, such as a methyl or ethoxycarbonylmethyl group. The extraction ability of these crown ethers towards alkali metal cations was also examined by the solvent extraction method.

In spite of much work, only a few crown ethers containing a thiophene subunit as part of the macrocyclic ring have appeared in the literature. The crown ethers so far prepared are restricted to those[2)] containing a 2,5-dimethyl-3,4-thiophenediylbis-(methylene) unit, thiacrown ethers[3)] containing a 2,5-thiophenediylbis(methylene) unit, crown esters[4)] derived from 2,5-thiophenedicarboxylic acid, and azacrown ethers[5)] derived from 2,5-thiophenedicarbaldehyde. None of the thiophene analogues (thienocrown ether) of benzocrown ether, in which thiophene nucleus is directly incorporated into the crown ether ring, has been synthesized. We report here on the syntheses of crown ethers **7** and **8** (3,4-thienocrown ether) containing a 3,4-thiophenediyl subunit and those (**12**, **13**) containing a 3,4-thiophenediylbis(methylene) subunit and their extraction ability towards alkali metal cations.

Recently, functionalized and substituted crown ethers received attention in view of the immobilization[6)] and modification of the properties of crown ethers.[7)] In this connection, we also report on the transformation of the thiophene-containing crown ethers into novel crown ethers having two adjacent methyl or ethoxycarbonylmethyl groups by a reductive desulfurization of the thiophene ring.

Results and Discussion

Synthesis. Thiophenediols, potential starting substances for the preparation of the thienocrown ethers, are unstable and easily decompose in air, although the corresponding dialkoxythiophenes are rather stable. This seems to be the principal reason for the lack of thienocrown ethers. It has been reported that 2,5-bis(ethoxycarbonyl)-3,4-thiophenediol (**1**), almost the only stable thiophenediol derivative available, reacts with 1,2-dibromoethane and bromochloromethane in the presence of a base to give 2,5-bis(ethoxycarbonyl)-

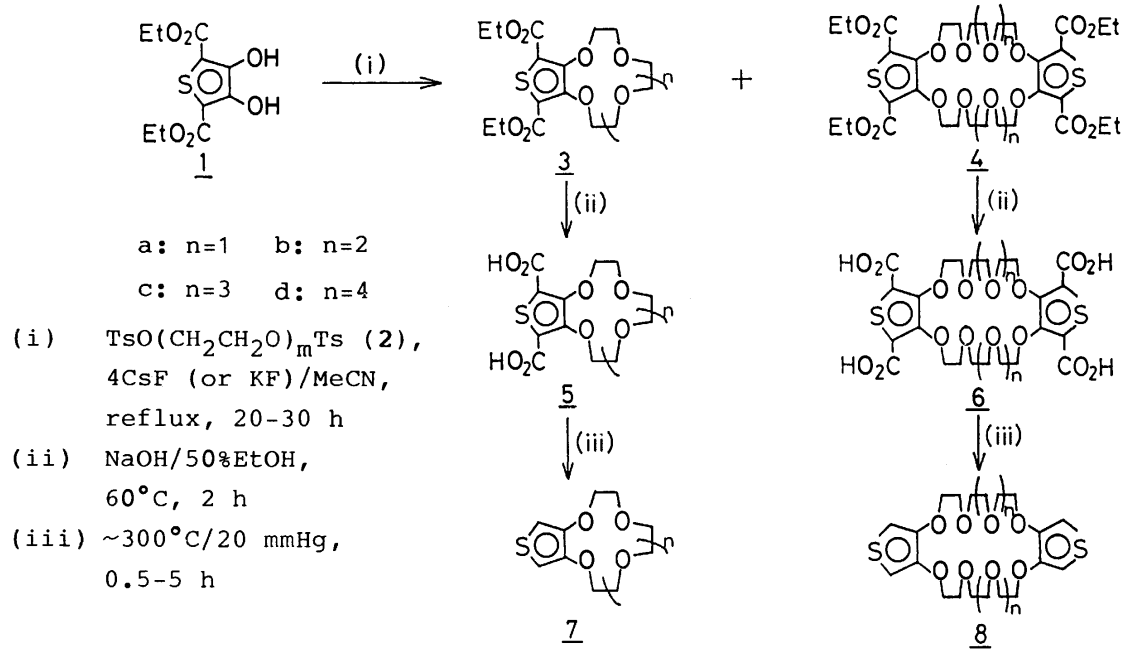

Scheme 1.

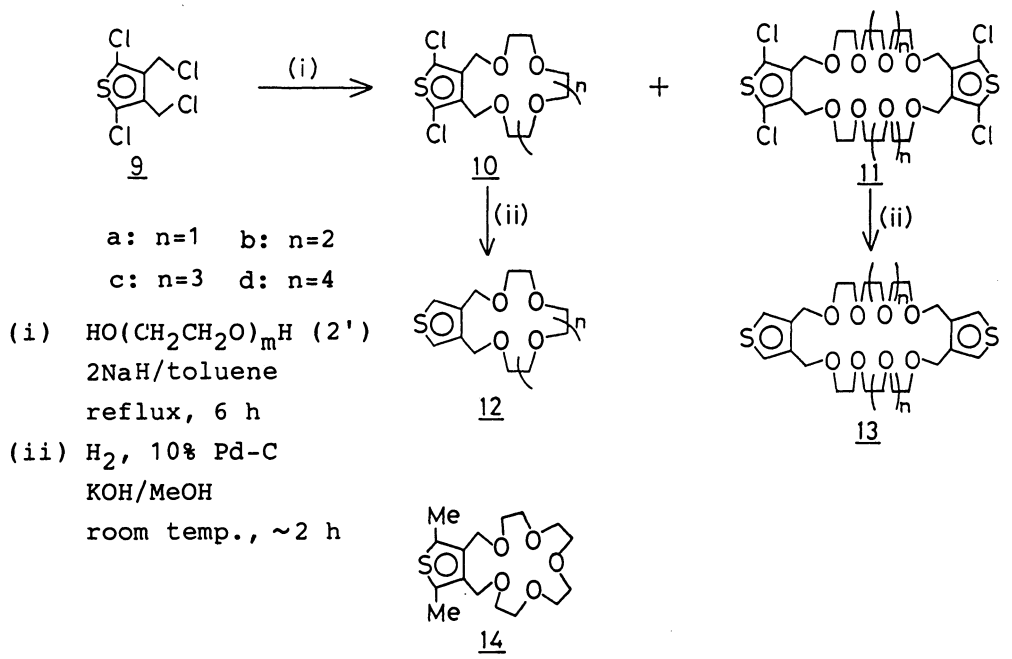

Scheme 2.

Table 1. Reaction of 2,5-Bis(ethoxycarbonyl)-3,4-thiophenediol (**1**) with Oligoethylene Glycol Ditosylates (**2**)

Reactant **2**	Base	Reaction time/h	Product	Yield/%[a]	Mp θ_m/°C
$m=3$	KF	30	**3a**	28	122—123
			4a	40	152—153
$m=4$	CsF	20	**3b**	44	66—67
			4b	2	94—95
$m=5$	CsF	25	**3c**	68	67—68
$m=6$	CsF	25	**3d**	56	41—42

a) Isolated yield based on **1** used.

3,4-ethylenedioxythiophene,[8] 2,5-bis(ethoxycarbonyl)-3,4-methylenedioxythiophene, and 6,8,14,16-tetrakis(ethoxycarbonyl)-2,4,10,12-tetraoxa-7,15-dithiatricyclo[11.3.0.0^{5,9}]hexadeca-1(16),5,8,13-tetraene,[9] respectively. The thienocrown ethers, **7** and **8**, were synthesized by the route outlined in Scheme 1. Namely, by the modification of the procedures described above, ethoxycarbonylthienocrown esters **3** (and, if any **4**) were first synthesized by the reaction of **1** and oligoethylene glycol ditosylates (**2**). The expected esters, **3** (and **4**), were obtained in relatively high yield, when **1** was reacted with **2** in refluxing MeCN for 25—30 h using CsF (KF for the synthesis of **3a**) as a base (Table 1). No satisfactory results were obtained by the use of other bases, such as NaH or EtONa, or a solvent, such as dioxane, even upon prolonged heating. Alkaline hydrolysis of **3** (or **4**) in 50% EtOH at 60 °C for 2 h gave the corresponding thienocrown acids, **5** (or **6**). It is interesting to note that the tetracarboxylic acid, **6a**, forms an adduct with four molecules of H_2O, which releases the H_2O upon heating under reduced pressure (130 °C/2 mmHg; 1 mmHg≈133.322 Pa) for 5 h. The thienocrown acids **5** (or **6**) underwent decarboxylation merely by heating at ca. 50 °C higher than their melting points under reduced pressure (20 mmHg) for 0.5—5 h to afford **7** and **8**.

The crown ethers, **12** and **13**, were synthesized as outlined in Scheme 2 in order to compare their physical properties with those of **7** and **8**. First, crown ethers **10** and/or **11**, containing a 2,5-dichloro-3,4-thiophenediylbis(methylene) unit, were prepared by the reaction of 2,5-dichloro-3,4-bis(chloromethyl)thiophene (**9**) with sodium or potassium oligoethylene glycolates according to Reinhoudt's method[2a] (Table 2). Early studies suggest that the chlorine atom(s) in chlorothiophene derivatives can be removed only with difficulty.[10] However, **10** and **11** were dechlorinated easily without any cleavage of the crown ether ring[11] by catalytic hydrogenation at room temperature in an atmospheric pressure hydrogenation apparatus; expected crown ethers **12** and **13** were obtained in good yields.

The structures of the new crown ethers were

Table 2. Reaction of 2,5-Dichloro-3,4-bis(chloromethyl)thiophene (**9**) with Oligoethylene Glycols (**2'**)

Reactant **2'**	Base	Reaction time/h	Product	Yield/%[a]	Mp θ_m/°C
$m=3$	NaH	6	**10a**	6	87—88
			11a	28	98—99
$m=4$	NaH	6	**10b**	43	47—48
			11b	6	77—79
$m=5$	NaH	6	**10c**	37	45—46
			11c	8	98—100
$m=6$	*t*-BuOK	6	**10d**	38	oil[b]
			11d	2	81—83

a) Isolated yield based on **9** used. b) Bp 180 °C (bath temp)/10^{-3} mmHg.

established by their elemental analyses and spectral data (MS, ^{1}H NMR, and IR).

Reductive Desulfurization. Considering the fact that thiophene ring is desulfurized by the action of Raney nickel with a complete saturation of the thiophene ring, the thiophene-containing crown ethers are potentially useful intermediates for the synthesis of crown ethers having two adjacent substituents on the macrocyclic ring. From this view, crown ethers **3**, **12**, and **13** were subjected to reductive desulfurization with Raney nickel, and found to proceed smoothly as expected. Namely, being stirred in refluxing EtOH with excess Raney nickel for 2 h, **3** yielded novel crown ethers **15** having two adjacent ethoxycarbonylmethyl groups. Similarly, novel crown ethers, **16** and **17**, having two adjacent methyl groups were obtained from **12** and **13**.

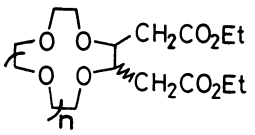

15

a: n=1
b: n=2
c: n=3
d: n=4

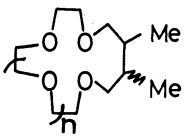

16

a: n=2
b: n=3
c: n=4

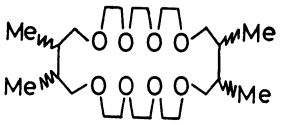

17

An NMR spectral study suggests that the desulfurized crown ethers consist of pairs of cis and trans isomers. For example, the ^{1}H NMR spectrum (200 MHz, $CDCl_3$) of **16a** shows, together with the complex absorptions ascribable to the oxymethylene protons of the crown ring, two doublets due to methyl protons at δ 0.85 and 0.88 with the coupling constants of 6.1 and 7.2 Hz, and a multiplet at δ ca. 2 due to the adjacent methine protons. ^{13}C NMR spectrum is consistent with the assignment; two peaks for the methyl carbons at δ 13.1 and 13.8 and two peaks for the methine carbons at δ 34.3 and 35.7 together with the peaks (δ 70.2, 70.4, 70.8, 70.9, 74.5, and 74.7) due to the methylene carbons.[12]

Table 3. Extraction of Alkali Metal Picrates with Thiophene-Containing Crown Ethers[a]

Crown compd	Extractability (%)				
	Li^+	Na^+	K^+	Rb^+	Cs^+
3a	1	1	5	5	4
3b	1	4	15	8	6
3c	4	9	36	29	23
3d	5	18	55	56	52
7a	0	2	1	1	1
7b	0(2)[b]	12(25)	24(52)	14(31)	4(14)
7c	2(2)	8(21)	93(94)	83(85)	66(68)
7d	4(5)	10(17)	72(86)	93(96)	99(98)
8a	1(1)	12(39)	33(61)	48(69)	73(78)
12a	1	0	3	2	1
12b	2	11	8	6	6
12c	2	10	36	34	31
12d	4	16	51	63	68
10b	1	18	10	9	8
14[c]	2	33	24	18	10
13a	3	12	45	47	60

a) Measured by Pedersen's method[13] at 25 °C: aqueous phase: [picric acid]=7×10^{-5} M (1 M=1 mol dm^{-3}), [MNO_3]=0.1 M; organic phase (CH_2Cl_2): [crown compd]=7×10^{-4} M. H_2O:CH_2Cl_2=1:1 (v/v). b) Figures in parentheses denote the values obtained for the corresponding benzo (or dibenzo) crown ethers which were prepared according to the literatures.[14] c) Prepared according to the literature.[2a]

It should be emphasized that the present results indicate the usefulness of the incorporation of a thiophene unit for the structural modification of a crown ring.

Extraction Ability. The extraction ability of the thiophene-containing crown ethers as well as the desulfurized crown ethers towards alkali metal cations was examined by Pedersen's extraction method.[13] Tables 3 and 4 summarize the results. The thienocrown ethers, **7** and **8**, and the corresponding benzocrown

Table 4. Extraction of Alkali Metal Picrates with the Desulfurized Crown Ethers[a)]

Crown compd	Extractability (%)				
	Li^+	Na^+	K^+	Rb^+	Cs^+
15a	1	2	2	1	1
15b	4	31	13	11	6
15c	7	37	95	82	51
15d	12	21	84	87	85
18-C-6	10	31	97	96	85
16a	2	14	14	8	6
16b	5	6	75	80	75
16c	4	8	39	48	67
17	2	4	26	19	21
17-C-5[b)]	1	11	10	5	4

a) Measured under similar conditions as described in the footnote in Table 3. b) Prepared according to the literature.[15)]

ethers are similar in selectivity, but the former shows a much higher K^+/Na^+ selectivity than the latter. On the other hand, the extraction ability of the thienocrown ethers are a little lower than that of benzocrown ethers; the thiophene unit with a sulfur atom in the position opposite to the crown ring weakens the coordination interaction between the crown oxygens and the metal cations.

Crown ethers **12** and **13**, having the 3,4-thiophenediylbis(methylene) unit(s), generally exhibit a lower extractability than that of the thienocrown ethers, **7** and **8**, with the same number of oxygens. This is probably due to the less symmetry arrangement of the donor oxygen[15)] and the non-coplanarity of the thiophene ring with the crown ether ring[2b)] in the molecules. Comparisons of a series of 17-crown-5 derivatives (the parent 17-crown-5,[15)] **10b**, **12b**, **14**, and **16a**) indicate that the extractability is not affected essentially by the incorporation of the thiophene unit in the crown ring, although the selectivity for Na^+ over K^+ somewhat increases. Crown ethers **7** and **12** exhibit a similar cation selectivity with a minor difference in that **12b** shows its highest extractability for Na^+, while **7b** for K^+.

Experimental

All the melting and boiling points are uncorrected. The ^1H NMR (90 MHz, TMS as an internal reference, $CDCl_3$ solution unless otherwise noted), MS (70 eV, unless otherwise noted), and UV spectra were obtained on Hitachi R-22, Hitachi R-90H, Hitachi RMU-6M, and Hitachi 228A spectrometers, respectively. TG/DTA curves were recorded with a Seiko Denshi Kogyo TG/DTA A30 Instrument with a heating rate of 10 °C min^{-1} under N_2 stream.

2,5-Bis(ethoxycarbonyl)-3,4-thiophenediol (**1**),[9)] 2,5-dichloro-3,4-bis(chloromethyl)thiophene (**9**),[16)] and oligoethylene glycol ditosylates (**2**)[15)] were prepared as described in the literature.

General Procedure for the Syntheses of 3 and 4 by the Reaction of 2,5-Bis(ethoxycarbonyl)-3,4-thiophenediol (1) with Oligoethylene Glycol Ditosylates (2). Under an N_2 atmosphere CsF (0.06 mol; KF for the synthesis of **3a**) was added to a solution of **1** (3.9 g, 0.015 mol) in dry MeCN (250 ml); the mixture was stirred for 1 h. To the resulting yellow suspension a solution of **2** (m=4—6; 0.015 mol) in dry MeCN (100 ml) was added and the mixture was refluxed with stirring for 25—30 h. The reaction mixture was filtered while hot and the precipitate was washed with MeCN (50 ml). Treatment of the precipitate with a dilute HCl solution yielded the recovered **1**. The filtrate and the washing were combined, the solvent evaporated to dryness, and the residual mass was extracted twice with $CHCl_3$ (100 ml, 50 ml). After removing the solvent from the $CHCl_3$ extracts, the residue was chromatographed (silica gel/AcOEt–hexane (2—4:1)) giving **3b—d** and, if any, **4** which were purified by recrystallization.

The crown ethers, **3a** and **4a**, were produced by the reaction of **1** with triethylene glycol ditosylate (**2**, m=3) using KF as a base. After removing the solvent from the $CHCl_3$ extracts, the residue was treated in hot MeOH (50 ml); **4a** was separated as a precipitate. The MeOH-soluble substances, after removing the MeOH, were chromatographed (silica gel/AcOEt–hexane (2:1), repeatedly to give **3a** and another crop of **4a**.

13,15-Bis(ethoxycarbonyl)-2,5,8,11-tetraoxa-14-thiabicyclo[10.3.0]pentadeca-1(15),12-diene (3a). White crystals (MeOH); ^1H NMR δ=1.37 (t, J=7.1 Hz, 6H, $CO_2CH_2\underline{CH_3}$), 3.7—4.4 (m, 12H, CH_2CH_2O), and 4.34 (q, J=7.1 Hz, 4H, $CO_2\underline{CH_2}CH_3$); MS m/z (rel intensity) 374 (M^+, 45). Found: C, 51.25; H, 6.03%. Calcd for $C_{16}H_{22}O_8S$: C, 51.33; H, 5.92%.

13,15,28,30-Tetrakis(ethoxycarbonyl)-2,5,8,11,17,20,23,26-octaoxa-14,29-dithiatricyclo[25.3.0.0^{12,16}]triaconta-1(30),12,15,27-tetraene (4a). White prisms (MeOH–$CHCl_3$); ^1H NMR δ=1.37 (t, J=7.1 Hz, 12H, $CO_2CH_2\underline{CH_3}$), 3.6—4.4 (m, 24H, CH_2CH_2O), and 4.33 (q, J=7.1 Hz, 8H, $CO_2\underline{CH_2}CH_3$); MS m/z 748 (M^+, 1). Found: C, 51.81; H, 5.93%. Calcd for $C_{32}H_{44}O_{16}S_2$: C, 51.33; H, 5.92%.

16,18-Bis(ethoxycarbonyl)-2,5,8,11,14-pentaoxa-17-thiabicyclo[13.3.0]octadeca-1(18),15-diene (3b). White plates (MeOH); ^1H NMR δ=1.37 (t, J=7.1 Hz, 6H, $CO_2CH_2\underline{CH_3}$), 3.7—4.4 (m, 16H, CH_2CH_2O), and 4.33 (q, J=7.1 Hz, 4H, $CO_2\underline{CH_2}CH_3$); MS m/z 418 (M^+, 56). Found: C, 51.60; H, 6.38%. Calcd for $C_{18}H_{26}O_9S$: C, 51.66; H, 6.26%.

16,18,34,36-Tetrakis(ethoxycarbonyl)-2,5,8,11,14,20,23,26,29,32-decaoxa-17,35-dithiatricyclo[31.3.0.0^{15,19}]hexatriaconta-1(36),15,18,33-tetraene (4b). White crystals (AcOEt); ^1H NMR δ=1.37 (t, J=7.1 Hz, 12H, $CO_2CH_2\underline{CH_3}$), 3.6—4.4 (m, 32H, CH_2CH_2O), and 4.33 (q, J=7.1 Hz, 8H, $CO_2\underline{CH_2}CH_3$); MS m/z 836 (M^+, 3). Found: C, 51.76; H, 6.38%. Calcd for $C_{36}H_{52}O_{18}S_2$: C, 51.66; H, 6.26%.

19,21-Bis(ethoxycarbonyl)-2,5,8,11,14,17-hexaoxa-20-thiabicyclo[16.3.0]heneicosa-1(21),18-diene (3c). White needles (MeOH); ^1H NMR δ=1.37 (t, J=7.1 Hz, 6H, $CO_2CH_2\underline{CH_3}$), 3.6—4.4 (m, 20H, CH_2CH_2O), and 4.33 (q, 4H, J=7.1 Hz, $CO_2\underline{CH_2}CH_3$); MS (20 eV) m/z 462 (M^+, 100). Found: C, 51.91; H, 6.62%. Calcd for $C_{20}H_{30}O_{10}S$: C, 51.94; H, 6.54%.

22,24-Bis(ethoxycarbonyl)-2,5,8,11,14,17,20-heptaoxa-23-thiabicyclo[19.3.0]tetracosa-1(24),21-diene (3d). White prisms (petroleum ether–AcOEt); ^1H NMR δ=1.37 (t, J=7.1 Hz, 6H, $CO_2CH_2\underline{CH_3}$), 3.6—4.4 (m, 24H, $CH_2\underline{CH_2}O$), and 4.33 (q, J=7.1 Hz, 4H, $CO_2\underline{CH_2}CH_3$); MS (20 eV) m/z 506 (M^+, 72). Found: C, 52.05; H, 6.88%. Calcd for $C_{22}H_{34}O_{11}S$: C, 52.16; H, 6.77%.

General Procedure for the Hydrolysis of 3 and 4. To a

solution of **3** (0.003 mol) in EtOH (15 ml) was added 5% NaOH solution (15 ml); the mixture was stirred at 60 °C for 2 h. After cooling the reaction mixture was acidified with HCl and stirred for ca. 30 min; then most of the EtOH was distilled off. Except for **3d**, the crystalline mass separated out upon ice-cooling, which was collected by filtration. It was dissolved in a minimum amount of hot H_2O; to the hot solution a few ml of 10% HCl solution was added. The contents were cooled and the white precipitate was collected by filtration and washed with a small amount of cold H_2O to afford pure dicarboxylic acid, **5**. By this procedure **4a** yielded the tetracarboxylic acid (**6a**), as the adduct with $4H_2O$, which, in turn, converted into the free acid upon heating at 130 °C under reduced pressure (2 mmHg) for 5 h. In the case of **3d**, the mixture was extracted with $CHCl_3$ after evaporating the EtOH. The extract was washed with H_2O and dried. Evaporation of the solvent gave **5d**.

2,5,8,11-Tetraoxa-14-thiabicyclo[10.3.0]pentadeca-1(15),12-diene-13,15-dicarboxylic Acid (5a). Yield, 76%. Colorless needles; mp 263—264 °C; MS (20 eV) *m/z* 318 (M^+, 10). Found: C, 45.01; H, 4.47%. Calcd for $C_{12}H_{14}O_8S$: C, 45.28; H, 4.43%.

2,5,8,11,14-Pentaoxa-17-thiabicyclo[13.3.0]octadeca-1(18),15-diene-16,18-dicarboxylic Acid (5b). Yield, 73%. Colorless needles, mp 244—245 °C; MS (20 eV) *m/z* 362 (M^+, 10). Found: C, 46.35; H, 5.18%. Calcd for $C_{14}H_{18}O_9S$: C, 46.41; H, 5.01%.

2,5,8,11,14,17-Hexaoxa-20-thiabicyclo[16.3.0]heneicosa-1(21),18-diene-19,21-dicarboxylic Acid (5c). Yield, 67%. Colorless needles, mp 191—192 °C; MS (20 eV) *m/z* 406 (M^+, 4). Found: C, 47.07; H, 5.51%. Calcd for $C_{16}H_{22}O_{10}S$: C, 47.29; H, 5.46%.

2,5,8,11,14,17,20-Heptaoxa-23-thiabicyclo[19.3.0]tetracosa-1(24),21-diene-22,24-dicarboxylic Acid (5d). Yield, 89%. White crystals (AcOEt), mp 146—147 °C; MS (20 eV) *m/z* 450 (M^+, 1). Found: C, 47.74; H, 5.90%. Calcd for $C_{18}H_{26}O_{11}S$: C, 47.99; H, 5.82%.

Attempted recrystallization of **5d** from H_2O yielded colorless needles, mp 81—83 °C, containing H_2O in the ratio **5d**:H_2O=1:1.6 (TG and ^1H NMR), which gradually released the H_2O on being left standing at room temperature for a few days.

2,5,8,11,17,20,23,26-Octaoxa-14,29-dithiatricyclo[25.3.0.$0^{12,16}$]triaconta-1(30),12,15,27-tetraene-13,15,28,30-tetracarboxylic Acid (6a). Yield, 74%. White powder, mp 250—251.5 °C; MS (20 eV) *m/z* 546 (M^+−90, 8). Found: C, 45.46; H, 4.39%. Calcd for $C_{24}H_{28}O_{16}S_2$: C, 45.28; H, 4.43%.

6a·4H₂O: Colorless needles, mp 257—258 °C. Found: C, 40.71; H, 5.02%. Calcd for $C_{24}H_{28}O_{16}S_2$ $4H_2O$: C, 40.68; H, 5.12%. TG/DTA data were given in the text.

General Procedure for the Syntheses of 7 and 8 by the Decarboxylation of 5 and 6. Crown ether **5** or **6** (0.003 mol) was placed in a small equipment for vacuum sublimation and heated at ca. 50 °C higher than its melting point under a pressure of 20 mmHg for 0.5 (for **5a** and **6a**), 3 (for **5b**—**c**), or 5 h (for **5d**). A dark-brown color developed concomitantly with the evolution of CO_2 gas. The residual mass was chromatographed (alumina/AcOEt) to give the desired crown ether, which was purified by recrystallization.

2,5,8,11-Tetraoxa-14-thiabicyclo[10.3.0]pentadeca-1(15),12-diene (7a). Yield, 69%. Colorless crystals (petroleum ether), mp 40—41.5 °C; ^1H NMR δ=3.6—4.3 (m, 12H, CH_2CH_2O) and 6.44 (s, 2H, Th-H); MS (20 eV) *m/z* 230 (M^+, 100). Found: C, 51.99; H, 6.25%. Calcd for $C_{10}H_{14}O_4S$: C, 52.16; H, 6.13%.

2,5,8,11,14-Pentaoxa-17-thiabicyclo[13.3.0]octadeca-1(18),15-diene (7b). Yield, 58%. Colorless needles (hexane–AcOEt), mp 71—72 °C; ^1H NMR δ=3.6—4.3 (m, 16H, CH_2CH_2O) and 6.26 (s, 2H, Th-H); MS (20 eV) *m/z* 274 (M^+, 95). Found: C, 52.45; H, 6.72%. Calcd for $C_{12}H_{18}O_5S$: C, 52.54; H, 6.61%.

2,5,8,11,14,17-Hexaoxa-20-thiabicyclo[16.3.0]heneicosa-1(21),18-diene (7c). Yield, 63%. Colorless needles (hexane–AcOEt), mp 89—90 °C; ^1H NMR δ=3.6—4.3 (m, 20H, CH_2CH_2O) and 6.19 (s, 2H, Th-H); MS (20 eV) *m/z* 318 (M^+, 66). Found: C, 52.67; H, 7.11%. Calcd for $C_{14}H_{22}O_6S$: C, 52.81; H, 6.97%.

2,5,8,11,14,17,20-Heptaoxa-23-thiabicyclo[19.3.0]tetracosa-1(24),21-diene (7d). Yield, 83%. Colorless crystals (hexane–AcOEt), mp 62—63 °C; ^1H NMR δ=3.5—4.3 (m, 24H, CH_2CH_2O) and 6.20 (s, 2H, Th-H); MS (20 eV) *m/z* 362 (M^+, 57). Found: C, 52.96 H, 7.46% Calcd for $C_{16}H_{26}O_7S$: C, 53.02; H, 7.23%.

2,5,8,11,17,20,23,26-Octaoxa-14,29-dithiatricyclo[25.3.0.$0^{12,16}$]triaconta-1(30),12,15,27-tetraene (8a). Yield, 51%. Colorless needles ($CHCl_3$–AcOEt), mp 140—141 °C; ^1H NMR δ=3.6—4.3 (24H, m, CH_2CH_2O) and 6.19 (s, 4H, Th-H); MS (20 eV) *m/z* 460 (M^+, 100). Found: C, 52.00; H, 6.17%. Calcd for $C_{20}H_{28}O_8S_2$: C, 52.16; H, 6.13%.

General Procedure for the Syntheses of 10 and 11 by the Reaction of 2,5-Dichloro-3,4-bis(chloromethyl)thiophene (9) and Oligoethylene Glycolate. Under an N_2 atmosphere NaH (for **2′**, *m*=3—5) or *t*-BuOK (for **2′**, *m*=6) (0.04 mol) was added to a solution of oligoethylene glycol (**2′**; 0.02 mol) in dry toluene (120 ml); the mixture was stirred at 60°C for 1 h. The mixture was then cooled to room temperature and a solution of **9** (5.0 g, 0.02 mol) in dry toluene (50 ml) was added at once to the mixture, which was then heated to reflux for 6 h. The precipitate formed was filtered and washed with a small amount of $CHCl_3$. The filtrate and washing were combined and evaporated. The residue was dissolved in $CHCl_3$ (50 ml), washed with H_2O, and dried. After removing the solvent, the crude products were chromatographed (alumina/hexane–dioxane (4:1)) to give **10**, together with **11**, which were purified by recrystallization.

15,17-Dichloro-3,6,9,12-tetraoxa-16-thiabiscyclo[12.3.0]heptadeca-1(17),14-diene (10a). White needles (hexane); ^1H NMR δ=3.66 (s, 4H, CH_2CH_2O), 3.72 (s, 8H, CH_2CH_2O), and 4.62 (s, 4H, $ThCH_2O$); MS (20 eV) *m/z* 326 (M^+, 32) and 328 (M^++2, 27). Found: C, 44.12; H, 5.04%. Calcd for $C_{12}H_{16}Cl_2O_4S$: C, 44.05; H, 4.93%.

15,17,32,34-Tetrachloro-3,6,9,12,20,23,26,29-octaoxa-16,33-dithiatricyclo[29.3.0.$0^{14,18}$]tetratriaconta-1(34),14,17,31-tetraene (11a). White needles (hexane); ^1H NMR δ=3.66 (s, 24H, CH_2CH_2O), and 4.59 (s, 8H, $ThCH_2O$); MS (20 eV) *m/z* 652 (M^+, 17) and 654 (M^++2, 20). Found: C, 44.07; H, 4.98%. Calcd for $C_{24}H_{32}Cl_4O_8S_2$: C, 44.05; H, 4.93%.

18,20-Dichloro-3,6,9,12,15-pentaoxa-19-thiabicyclo[15.3.0]-eicosa-1(20),17-diene (10b). White crystals (hexane); ^1H NMR (C_6D_6) δ=3.36, 3.50 (s, 8H each, CH_2CH_2O), and 4.53 (s, 4H, $ThCH_2O$); MS *m/z* 370 (M^+, 22) and 372 (M^++2, 12). Found: C, 45.30; H, 5.58%. Calcd for $C_{14}H_{20}Cl_2O_5S$: C, 45.29; H, 5.43%.

18,20,38,40-Tetrachloro-3,6,9,12,15,23,26,29,32,35-decaoxa-19,39-dithiatricyclo[35.3.0.$0^{17,21}$]tetraconta-1(40),17,20,37-tetraene (11b). White prisms (hexane); ^1H NMR (C_6D_6) δ=3.49 (s, 32H, CH_2CH_2O) and 4.56 (s, 8H, $ThCH_3O$); MS (20 eV) *m/z*

740 (M^+, 6) and 742 (M^++2, 8). Found: C, 45.20; H, 5.49%. Calcd for $C_{28}H_{40}Cl_4O_{10}S_2$: C, 45.29; H, 5.43%.

21,23-Dichloro-3,6,9,12,15,18-hexaoxa-22-thiabicyclo[18.3.0]-tricosa-1(23),20-diene (10c). Colorless plates (petroleum ether); ^{1}H NMR (C_6D_6) δ=3.3—3.6 (m, 20H, CH_2CH_2O) and 4.61 (4H, s, $ThCH_2O$); MS (20 eV) m/z 414 (M^+, 63) and 416 (M^++2, 48). Found: C, 46.23; H, 5.92%. Calcd for $C_{16}H_{24}Cl_2O_6S$: C, 46.27; H, 5.82%.

21,23,44,46-Tetrachloro-3,6,9,12,15,18,26,29,32,35,38,41-dodecaoxa-22,45-dithiatricyclo[41.3.0.0^{20,24}]hexatetraconta-1(46),20,23,43-tetraene (11c). Colorless needles (hexane); ^{1}H NMR δ=3.64 (br s, 40H, CH_2CH_2O) and 4.59 (s, 8H, $ThCH_2O$); MS (20 eV) δ= 828 (M^+, 3) and 830 (M^++2, 4). Found: C, 46.35; H, 5.98%. Calcd for $C_{32}H_{48}Cl_4O_{12}S_2$: C, 46.27; H, 5.82%.

24,26-Dichloro-3,6,9,12,15,18,21-heptaoxa-25-thiabicyclo-[21.3.0]hexacosa-1(26),23-diene (10d). Colorless viscous oil; ^{1}H NMR (C_6D_6) δ=3.4—3.7 (m, 24H, CH_2CH_2O) and 4.60 (s, 4H, $ThCH_2O$); MS (20 eV) m/z 458 (M^+, 22) and 460 (M^++2, 16). Found: C, 46.88; H, 6.29%. Calcd for $C_{18}H_{28}Cl_2O_7S$: C, 47.06; H, 6.14%.

24,26,50,52-Tetrachloro-3,6,9,12,15,18,21,29,32,35,38,41,44,47-tetradecaoxa-25,51-dithiatricyclo[47.3.0.0^{23,27}]dopentaconta-1(52),23,26,49-tetraene (11d). White crystals (hexane); ^{1}H NMR δ=3.65 (br s, 48H, CH_2CH_2O) and 4.59 (s, 8H, $ThCH_2O$); MS (20 eV) m/z 916 (M^+, 1) and 918 (M^++2, 2). Found: C, 47.04; H, 6.24%. Calcd for $C_{36}H_{56}Cl_4O_{14}S_2$: C, 47.06; H, 6.14%.

General Procedure for the Preparation of 12a—d and 13 by the Catalytic Dechlorination of 10a—d and 11. The reaction was conducted at room temperature by stirring a mixture of **10** or **11** (0.005 mol), KOH (1.5 g), 10% Pd-C (0.7 g), and MeOH (100 ml) in an atmospheric pressure hydrogenation apparatus. Within 1—2 h the calculated amounts of H_2 were consumed. The catalyst was filtered off and washed with $CHCl_3$ (50 ml). The filtrate was concentrated and water added to the residue. The products were extracted with the $CHCl_3$ washing. The extract was washed with H_2O, 5% HCl solution, and then H_2O, and dried. Evaporation of the solvent gave **12a—d** or **13** as an oil.

3,6,9,12-Tetraoxa-16-thiabicyclo[12,3,0]heptadeca-1(17),14-diene (12a). Yield, 83%. Colorless viscous oil; ^{1}H NMR (200 MHz) δ=3.67 (s, 4H, CH_2CH_2O), 3.74 (s, 8H, CH_2CH_2O), 4.74 (s, 4H, $ThCH_2O$), and 7.24 (s, 2H, Th-H); MS (20 eV) m/z 258 (M^+, 60). Found: C, 55.24; H, 7.11%. Calcd for $C_{12}H_{18}O_4S$: C, 55.79; H, 7.02%.

3,6,9,12,15-Pentaoxa-19-thiabicyclo[15.3.0]eicosa-1(20),17-diene (12b). Yield, 88%. Colorless viscous oil, bp 160 °C (bath)/5×10^{-3} mmHg. ^{1}H NMR (C_6D_6) δ=3.38, 3.52 (s each, 16H, CH_2CH_2O), 4.63 (s, 4H, $ThCH_2O$), and 7.07 (s, 2H, Th-H); MS (20 eV) m/z 302 (M^+ 100). Found: C, 55.39; H, 7.49%. Calcd for $C_{14}H_{22}O_5S$: C, 55.61; H, 7.33%.

3,6,9,12,15,18-Hexaoxa-22-thiabicyclo[18.3.0]tricosa-1(23),20-diene (12c). Yield, 81%. Colorless viscous oil, bp 160 °C (bath)/10^{-3} mmHg; ^{1}H NMR (C_6D_6) δ=3.49, 3.52 (s each, 20H, CH_2CH_2O), 4.58 (s, 4H, $ThCH_2O$), and 7.00 (2H, s, Th-H); MS (20 eV) m/z 346 (M^+, 94). Found: C, 54.78; H, 7.71%. Calcd for $C_{16}H_{26}O_6S$: C, 55.47; H, 7.56%.

3,6,9,12,15,18,21-Heptaoxa-25-thiabicyclo[21.3.0]hexacosa-1(26),23-diene (12d). Yield, 83%. Colorless viscous oil, bp 170—190 °C (bath)/10^{-3} mmHg; ^{1}H NMR (C_6D_6) δ=3.4—3.7 (m, 24H, CH_2CH_2O), 4.57 (s, 4H, $ThCH_2O$), and 7.03 (s, 2H, Th-H); MS (20 eV) m/z 390 (M^+, 90). Found: C, 54.98; H, 7.96%. Calcd for $C_{18}H_{30}O_7S$: C, 55.79; H, 7.02%.

3,6,9,12,20,23,26,29-Octaoxa-16,33-dithiatricyclo[29.3.0.0^{14,18}]tetratriaconta-1(34),14,17,31-tetraene (13a). Yield, 85%. Colorless viscous oil, bp 230 °C (bath)/10^{-3} mmHg; ^{1}H NMR (C_6D_6) δ=3.51, 3.47 (s each, 24H, CH_2CH_2O), 4.54 (s, 8H, $ThCH_2O$), and 7.02 (s, 4H, Th-H); MS (20 eV) m/z 516 (M^+, 20). Found: C, 55.59; H, 7.11%. Calcd for $C_{24}H_{36}O_8S_2$: C, 55.79; H, 7.02%.

Reductive Desulfurization of the Thiophene-Containing Crown Ethers (3a—d, 12b—d, and 13) with Raney Nickel. W-7 Raney nickel prepared from 15 g of the alloy was added to the solution of the crown ether (0.005 mol) in EtOH (50 ml); the mixture was stirred at the reflux temperature for 2 h. The reaction mixture was filtered and the nickel was washed with EtOH (10 ml). The filtrate and the washing were combined and evaporated. The residual oil was chromatographed (silica gel/hexane–dioxane (4:1) for **16** and **17**, silica gel/AcOEt–hexane (2—4:1) for **15**) giving the desulfurized crown ether.

2,3-Bis(ethoxycarbonylmethyl)-1,4,7,10-tetraoxacyclododecane (2,3-Bis(ethoxycarbonylmethyl)-12-crown-4) (15a). Yield, 53%. Colorless oil, bp 110 °C (bath)/10^{-3} mmHg; ^{1}H NMR δ=1.26 (t, J=7.1 Hz, 6H, $CH_2\underline{CH_3}$), 2.40 (d, J=5.3 Hz, 2H, $\underline{CH_2}CH$), 2.55 (d, J=8.1 Hz, 2H, $\underline{CH_2}CH$), 3.66, 3.71 (br s each, 12H, CH_2CH_2O), and 4.15 (q, J=7.1 Hz, $\underline{CH_2}CH_3$, overlapped with the $CH_2\underline{CH}$ peaks, 6H); MS (50 eV) m/z 348 (M^+, 41). Found: C, 54.41; H, 8.08%. Calcd for $C_{16}H_{28}O_8$: C, 55.16; H, 8.10%.

2,3-Bis(ethoxycarbonylmethyl)-1,4,7,10,13-pentaoxacyclopentadecane (2,3-Bis(ethoxycarbonylmethyl)-15-crown-5) (15b). Yield, 51%. Colorless oil, bp 125 °C (bath)/10^{-3} mmHg; ^{1}H NMR δ=1.26 (t, J=7.1 Hz, 6H, $CH_2\underline{CH_3}$), 2.37 (d, J=5.1 Hz, 2H, $\underline{CH_2}CH$), 2.51 (d, J=8.1 Hz, 2H, $\underline{CH_2}CH$), and 3.55—4.3 (m, 22H, CH_2CH_2O, $CH_2\underline{CH}$, and $\underline{CH_2}CH_3$ (4.15, q, J=7.1 Hz)); MS (50 eV) m/z 392 (M^+, 30). Found: C, 54.92; H, 8.41%. Calcd for $C_{18}H_{32}O_9$: C, 55.09; H, 8.22%.

2,3-Bis(ethoxycarbonylmethyl)-1,4,7,10,13,16-hexaoxacyclooctadecane (2,3-Bis(ethoxycarbonylmethyl)-18-crown-6) (15c). Yield, 55%. Colorless oil, bp 140 °C (bath)/10^{-3} mmHg; ^{1}H NMR δ=1.26 (t, J=7.1 Hz, 6H, $CH_2\underline{CH_3}$), 2.49 (d, J=4.5 Hz, 2H, $\underline{CH_2}CH$), 2.55 (d, J=6.1 Hz, 2H, $\underline{CH_2}CH$), and 3.45—4.3 (m, 26H, CH_2CH_2O, $CH_2\underline{CH}$, and $\underline{CH_2}CH_3$ (4.15, q, J=7.1 Hz)); MS (50 eV) m/z 436 (M^+, 60). Found: C, 54.67; H, 8.55%. Calcd for $C_{20}H_{36}O_{10}$: C, 55.03; H, 8.31%.

2,3-Bis(ethoxycarbonylmethyl)-1,4,7,10,13,16,19-heptaoxacycloheneicosane (2,3-Bis(ethoxycarbonylmethyl)-21-crown-7) (15d). Yield, 56%. Colorless oil, bp 150 °C (bath)/10^{-3} mmHg; ^{1}H NMR δ=1.26 (t, J=7.1 Hz, 6H, $CH_2\underline{CH_3}$), 2.49 (d, J=3.8 Hz, 2H, $\underline{CH_2}CH$), 2.55 (d, J=5.9 Hz, 2H, $\underline{CH_2}CH$), and 3.45—4.3 (m, 30H, CH_2CH_2O, $CH_2\underline{CH}$, and $\underline{CH_2}CH_3$ (4.15, q, J=7.1 Hz)); MS (50 eV) m/z 480 (M^+, 5). Found: C, 54.14; H, 8.53%. Calcd for $C_{22}H_{40}O_{11}$: C, 54.99; H, 8.39%.

15,16-Dimethyl-1,4,7,10,13-pentaoxacycloheptadecane (16a). Yield, 49%. Colorless oil, bp 100 °C (bath)/10^{-3} mmHg; ^{1}H NMR (200 MHz) δ=0.85, 0.88 (d, J=6.1 Hz, 7.2 Hz each, 6H, CH_3), 1.85—2.1 (m, 2H, $\underline{CH}CH_2O$), and 3.3—3.8 (m, 20H, CH_2CH_2O); MS (20 eV) m/z 276 (M^+, 8). Found: C, 60.13; H, 10.42%. Calcd for $C_{14}H_{28}O_5$: C, 60.84; H, 10.21%.

18,19-Dimethyl-1,4,7,10,13,16-hexaoxacycloeicosane (16b). Yield, 52%. Colorless oil, bp 120 °C (bath)/10^{-3} mmHg; ^{1}H NMR (200 MHz) δ=0.79, 0.89 (d, J=6.7 Hz, 6.8 Hz each, 6H, CH_3), 1.85—2.15 (m, 2H, $\underline{CH}CH_2O$), and 3.25—3.8 (m, 24H, CH_2CH_2O); MS (20 eV) m/z 320 (M^+, 1). Found: C, 59.33; H, 10.21%. Calcd for $C_{16}H_{32}O_6$: C, 59.98; H, 10.07%.

21,22-Dimethyl-1,4,7,10,13,16,19-heptaoxacyclotricosane (16c).

Yield, 52%. Colorless oil, bp 140—150 °C (bath)/10^{-3} mmHg; ^{1}H NMR (200 MHz) δ=0.80, 0.90 (d, J=6.8 Hz each, 6H, CH_3), 1.8—2.15 (m, 2H, $\underline{CH}CH_2O$), and 3.2—3.9 (m, 28H, CH_2CH_2O); MS (20 eV) m/z 364 (M^+, 1). Found: C, 58.37; H, 10.05%. Calcd for $C_{18}H_{36}O_7$: C, 59.32; H, 9.96%.

12,13,26,27-Tetramethyl-1,4,7,10,15,18,21,24-octaoxacyclooctacosane (17). Yield, 43%. Colorless oil, bp 170 °C (bath)/10^{-3} mmHg; ^{1}H NMR (200 MHz) δ=0.79, 0.89 (d, J=6.7 Hz, 6.8 Hz each, 12H, CH_3), 1.8—2.15 (m, 4H, $\underline{CH}CH_2O$), and 3.25—3.8 (m, 32H, CH_2CH_2O); MS (20 eV) m/z 464 (M^+, 1). Found: C, 61.23; H, 10.96%. Calcd for $C_{24}H_{48}O_8$: C, 62.04; H, 10.41%.

Solvent Extraction. Solvent extraction was carried out according to Pedersen's method.[13] The CH_2Cl_2 solution (5 ml) containing the crown ether (7×10^{-4} mol) and the aqueous solution (5 ml) containing the metal nitrate (1×10^{-1} mol) and picric acid (7×10^{-5} mol) were mixed and shaken for 10 min at 25 °C. The solution was equilibrated. Extraction of the picrate was followed by monitoring the absorbance of the aqueous solution at 354 nm.

The authors wish to thank Professor Kensuke Takahashi of Nagoya Institute of Technology for the ^{1}H (200 MHz) and ^{13}C NMR spectral measurements, and Messrs. Kohki Chiba, Shigeki Watanabe, Hideaki Kobayashi, Koichi Takahashi, Yoshikazu Inao, and Masahiro Wada for their assistance with some of experiments.

References

1) Presented at the Tohoku District Meetings of the Chemical Society of Japan, Yonezawa, October 1984, and Iwaki, October 1987.

2) a) D. N. Reinhoudt, R. T. Gray, C. J. Smit, Ms. I. Veenstra, *Tetrahedron*, **32**, 1161 (1976). b) D. N. Reinhoudt, R. T. Gray, F. de Jong, and C. J. Smit, *Tetrahedron*, **33**, 563 (1977). c) R. T. Gray, D. N. Reinhoudt, C. J. Smit, Ms. I. Veenstra, *Rec. Trav. Chim. Pays-Bas*, **95**, 258 (1976).

3) F. Vögtle and E. Weber, *Angew. Chem.*, **86**, 126 (1974); E. Weber and F. Vögtle, *Justus Liebigs Ann. Chem.*, **1976**, 891; A. Bhattacharjya and A. G. Hortmann, *J. Heterocycl. Chem.*, **15**, 1223 (1978).

4) J. S. Bradshaw, S. L. Baxter, J. D. Lamb, R. M. Izatt, and J. J. Christensen, *J. Am. Chem. Soc.*, **103**, 1821 (1981); K. T. Potts and M. J. Cipullo, *J. Org. Chem.*, **47**, 3038 (1982).

5) N. A. Bailey, M. M. Eddy, D. E. Fenton, and G. Jones, S. Moss, and A. Mukhopadhyay, *J. Chem. Soc., Chem. Commun.*, **1981**, 628; N. A. Bailey, M. M. Eddy, D. E. Fenton, S. Moss, and A. Mukhopadhyay, *J. Chem. Soc., Dalton Trans.*, **1984**, 2281.

6) For example, J. Smid and R. Sinta, "Topics in Current Chemistry," **121**, ed by F. Vögtle and E. Weber, Springer-Verlag (1984), pp. 105—156; G. W. Gokel and S. H. Korzeniowski, "Macrocyclic Polyether Syntheses," Springer-Verlag (1982), pp. 276—279.

7) For example, T. Mizuno, Y. Nakatsuji, S. Yanagida, and M. Okahara, *Bull. Chem. Soc. Jpn.*, **53**, 481 (1980); A. J. Bloodworth, D. J. Laphan, and R. A. Savva, *J. Chem. Soc., Chem. Commun.*, **1980**, 925.

8) V. N. Gogte, L. G. Shah, B. D. Tilak, K. N. Gadekar, and M. B. Sahasrabudhe, *Tetrahedron*, **23**, 2437 (1967).

9) F. Dallacker and V. Mues, *Ber.*, **108**, 569 (1975).

10) For example, M. G. Reinecke and P. Pedaja, "Thiophene and Its derivatives" Part 2, ed by S. Gronowitz, John-Wiley & Sons (1986), pp. 351—420; D. J. Zwanenburg and H. Wynberg, *J. Org. Chem.*, **34**, 340 (1969).

11) A case has been observed in which a crown ether ring is cleaved by catalytic hydrogenation; Y. Inoue, M. Ouchi, T. Nakazato, T. Matsuda, and T. Hakushi, *Chem. Lett.*, **1982**, 781.

12) The spectrum was measured in $CDCl_3$ solution using TMS as an internal reference on Varian XL-200 spectrometer with a frequency of 50.3 MHz. The peak assignments were made on the basis of the principle of substituent additivity as well as the off-resonance decoupled spectrum.

13) C. J. Pedersen, *Federation Proceeding*, **27**, 1305 (1968); S. Akabori, M. Ohtomi, M. Sato, and S. Ebina, *Bull. Chem. Soc. Jpn.*, **56**, 1455 (1983).

14) C. J. Pedersen, *J. Am. Chem. Soc.*, **89**, 7017 (1967); L. Mandolini and B. Masci, *J. Am. Chem. Soc.*, **106**, 168 (1984); D. N. Reinhoudt, F. de Jong, and H. P. M. Tomassen, *Tetrahedron Lett.*, **1979**, 2067.

15) M. Ouchi, Y. Inoue, T. Kanzaki, and T. Hakushi, *J. Org. Chem.*, **49**, 1408 (1984).

16) M. Winn and F. G. Bordwell, *J. Org. Chem.*, **32**, 1610 (1967).

Stereoselective β-*C*- and β-*S*-Glycosylation of 2-Deoxyribofuranose Derivatives Controlled by the 3-Hydroxy Protective Group

Yuh-ichiro ICHIKAWA, Hideki KUBOTA, Ken'ichi FUJITA, Tatsuo OKAUCHI, and Koichi NARASAKA*
Department of Chemistry, Faculty of Science, The University of Tokyo, Hongo, Bunkyo-ku, Tokyo 113
(Received September 29, 1988)

β-*C*-2-Deoxyribofuranosides and β-*S*-2-deoxyribofuranosides are prepared stereoselectively from 1-*O*-acetyl-5-*O*-benzyl-3-*O*-[2-(methylsulfinyl)ethyl]-2-deoxy-D-*erythro*-pentofuranose or the corresponding 3-*O*-(2-pyridylmethyl)pentofuranose *N*-oxide by the reaction with silyl enol ethers or trimethlsilyl sulfides in the presence of a Lewis acid.

Because of the potential utility in chemotherapeutic studies and in biochemical investigation of specific enzyme-catalyzed reactions, much effort has been devoted to preparing various types of glycoside derivatives.[1] One of the problems in the synthesis of glycoside derivatives is the stereoselective formation of β-glycoside linkages.

In the synthesis of ribofuranosides and xylo-type furanosides which have 2-α-hydroxyl group, the formation of β-glycoside linkage is generally controlled by using neighboring group participation of the adjacent 2-α-*O*-acyl group (so called the Baker's 1,2-trans rule).[2] On the other hand, there is no generally applicable method to obtain β-isomers stereoselectively in the case of the preparation of glycosides which possess no 2-α-hydroxyl group such as 2-deoxy-, 2-fluoro-, and 2-arabino-type glycosides.[1-3] The exceptional high β-selectivity has been reported only in the S_N2 type displacement of 2-deoxy-α-D-*erythro*-pentofuranosyl halide by purine derivatives or cyanide under basic conditions[4] and by silylated pyrimidine[5] and 5-(acetyl)thiouracil[6] derivatives under the modified Hilbert–Johnson conditions.[5]

In this paper, we wish to report the results on the stereocontrol in glycosylation reaction by neighboring group participation of a 3-α-*O*-substituent of 2-deoxy-D-*erythro*-pentofuranose (2-deoxyribofuranose) derivatives.[7] It was considered that when a suitable 3-*O*-subtituent was introduced instead of an acyl group for stabilizing the 1-cationic center in acid catalyzed glycosylation reactions, the stereoselection of the glycosylation would be controlled to give β-glycosides selectively. We, therefore, investigated *C*-glycosylation of 2-deoxyribofuranose derivatives with silyl enol ethers in the presence of a Lewis acid employing 1-*O*-acetyl-5-*O*-benzyl-2-deoxyribofuranoses which have various substituents on the 3-hydroxyl group.

Various 3-*O*-substituted 2-deoxyribofuranoses such as 3-*O*-substituted 1-*O*-acetyl-5-*O*-benzyl-2-deoxyribofuranoses **6a—e** and 1-*O*-acetyl-5-*O*-benzyl-3-*O*-[2-(alkylthio)ethyl]-2-deoxyribofuranose **6f—i** are prepared from methyl 2-deoxy-D-ribofuranoside, and the synthetic pathways are outlined in Schemes 1 and 2, respectively.

In these courses of the synthses, alkylation reaction reaction of the 3- or 5-hydroxy intermediates containing a silyl protective group (**3** and **7**) met some troubles in the conventional reaction conditions (NaH/DMF),

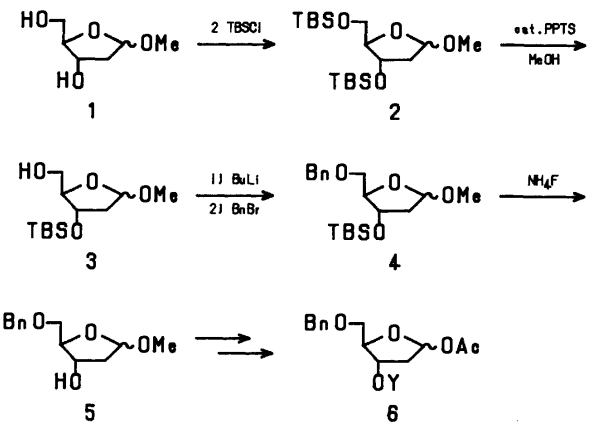

Scheme 1.

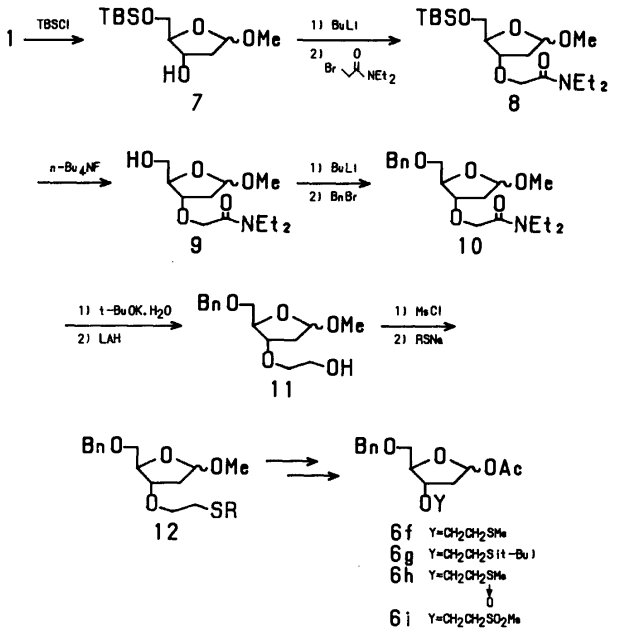

Scheme 2.

because of the migration of the silyl group and a low yield of the desired alkylated product. However, the alkylation was found to proceed even at room temperature affording the alkylated products in excellent yield, when the lithium alkoxides of **3** and **7** generated by treatment with *n*-BuLi or *t*-BuOLi were treated with bromides in the presence of sodium iodide and hexamethylphosphoric triamide (HMPA) in tetrahydrofuran (THF). This procedure appears to be of general utility in alkylation of other hydroxy compounds **5** and **9**.

At first, the reaction of 3-*O*-benzyl derivative **6a** with 1-trimethylsilyloxy-1-phenylethylene **13a** was examined at −78 °C in dichloromethane in the presence of $SnCl_4$,[8] and the α-*C*-glycoside **14a** was found to be produced in good selectivity (α-**14a**:β-**14a**=82:18). This result means that the introduction of such a group like benzyl group which would not tightly interact with the 1-cationic center results in the highly preferential formation of the α-glycoside.

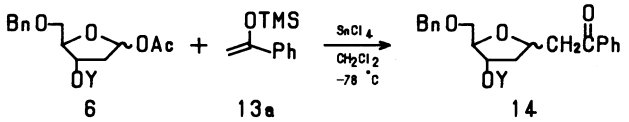

Table 1. Stereoselectivity of the Reaction of **6** and **13a**

6	Y	Yield of **14**/%	α : β
6a	CH_2Ph	92	82 : 18
6b	$CH_2OCH_2CH_2OMe$	83	75 : 25
6c	CH_2SMe	56	82 : 18
6d	$CH_2S(O)Me$	53	52 : 48
6e	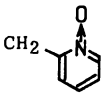	87	49 : 51
6f	CH_2CH_2SMe	46	42 : 58
6g	$CH_2CH_2SBu^t$	44	68 : 32
6h	$CH_2CH_2S(O)Me$	92	32 : 68
6i	$CH_2CH_2SO_2Me$	54	50 : 50

In order to find out the suitable substituent for the selective preparation of the β-isomer, effects of the 3-*O*-substituents on the stereoselectivity were examined using various 3-*O*-derivatives and the results are listed in Table 1. Among a variety of 3-substituents such as ethers, esters, and sulfides, 2-(alkylthio)ethyl group was found to afford slight excess amounts of the β-isomer. That is, by employing **6f** which has 2-(methylthio)-ethyl group, the corresponding *C*-glycosides **14f** were obtained in 46% yield in the ratio of α:β=42:58.

It was also noted that the reaction in a solvent which has little donor ability[9] such as dichloromethane or toluene exhibited higher selectivity as compared with a solvent having large donar property (for example, α:β=89:11 in acetonitrile). The ratio of the α-isomer to the β-isomer was not influenced by the kind of Lewis acids, namely $SnCl_4$,[8] trityl perchlorate,[10] and trimethylsilyl trifluoromethanesulfonate (TMSOTf).[11]

Then, 2-(methylthio)ethyl derivative **6f** was converted to the corresponding sulfoxide **6h** by considering that the participation by the sulfinyl group should be more efficient with respect to the electronic and steric effects. The sulfoxide **6h** actually reacted with the silyl enol ether **13a**, giving the β-*C*-glycoside β-**14h** predominantly (α-**14h**:β-**14h**=32:68) in an excellent yield. Reaction of an analogous *N*-oxide derivative **6e** having 2-pyridylmethyl group *N*-oxide as a 3-*O*-functionality, however, afforded almost equal amount of α- and β-isomers.

As the introduction of 3-*O*-methylsulfinyl group revealed to realize a good β-selectivity, the reactions of

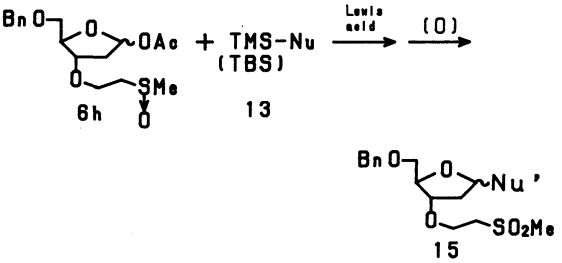

Table 2. Reaction of **6h** with Silyl Nucleophiles **13**

	Nucleophile	Lewis acid	**15**, Nu′	Yield **15**/%	α : β
13a		$SnCl_4$	CH_2COPh	92	32 : 68
13b		$SnCl_4$	CH_2COMe	82	22 : 78
13c		TMSOTf	CH_2COOCH_2Ph	86	9 : 91
13d	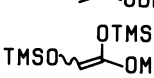	TMSOTf	CH(OH)COOMe	91	11 : 89
13e	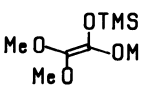	TMSOTf	$C(OMe)_2COOMe$	73	33 : 67
13f	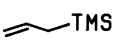	$SnCl_4$	$CH_2CH=CH_2$	50	87 : 13

6h with several silyl nucleophiles were examined using $SnCl_4$ or TMSOTf as a Lewis acid, and the results are summarized in Table 2.

The stereochemistry and the isomer ratio of these products are determined after conversion of the products to the corresponding sulfones **15**. The configuration of the major isomer of the *C*-glycosides **15c** was determined as the β-configuration by the transformation of **15c** into a lactone **16** by hydrogenolysis and successive treatment with acetic anhydride–pyridine.

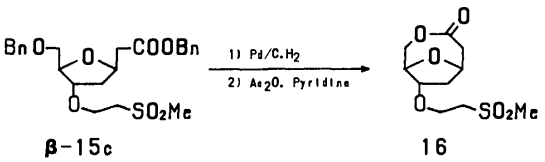

β-15c 16

Stereochemistry and isomer ratio of other products were determined by HPLC and by the comparison of their 400 MHz or 270 MHz ^1H NMR spectra with that of the above glycosides **15c**, in which the characteristic pattern of C-2 proton(s) appears as shown in Table 3.

The results in Table 2 clearly show that the stereoselectivity largely depends on the nucleophilicity of silyl nucleophiles. For example, allyltrimethylsilane, a weak nucleophile as compared with silyl enol ethers, affords the corresponding α-isomer predominantly. On the other hand, reaction with ketene silyl acetals **13c** and **13d**, gave the corresponding β-isomers **β-15c** and **β-15d** in about 90% selectivity.

Consequently, useful synthetic intermediates such as **15c** and **15d** for the synthesis of various *C*-nucleosides[12] were prepared in a highly β-selective manner by using the neighboring group participation of methylsulfinylethyl group on the 3-hydroxyl group. The 2-(methylsulfinyl)ethyl group was found to be easily removed after conversion to 2-(methylsulfonyl)-ethyl group by treatment with potassium *t*-butoxide in 1,2-dimethoxyethane at 0 °C.

Next, we applied this stereocontrol to prepare *S*-glycosides from 2-deoxyribofuranose. In the synthesis of *S*-glycosides, 2-(methylsulfinyl)ethyl group is not considered to be suitable because thioglycoside bond would be cleaved in the deprotecting process of the 2-(methylsulfinyl)ethyl group (oxidation followed by base treatment). 2-Pyridylmethyl group *N*-oxide was therefore chosen as a 3-*O*-protective group, and the reaction of **6e** with trimethlysilyl sulfides was tried in the presence of TMSOTf at −78 °C in dichloromethane, and the corresponding β-*S*-glycosides **β-17** were prepared predominantly as shown in the following table.

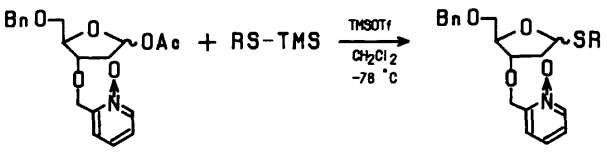

6e 17

Table 4. Reaction of **6e** with Trimethylsilyl Sulfides

17	R	Yield/%	α : β
17a	Et	83	16 : 84
17b	$PhCH_2$	77	25 : 75
17c	*i*-Pr	75	21 : 79
17d	t-Bu-	82	35 : 65

In these reactions, better selectivity was also observed by employing silyl sulfide having better nucleophilicity such as ethyl trimethylsilyl sulfide. The produced β-ethylthioglycoside **β-17a** isomerized by treatment with $SnCl_4$ at 0 °C, and quenching the reaction after cooling to −78 °C afforded an α-major mixture (α:β=75:25). Consequently, the β-selectivity of the above *S*-glycosylation reaction at −78 °C is indicated to be controlled kinetically.

Furthermore, when 3-*O*-benzyl derivative **6a** was

Table 3. ^1H NMR Data of C-2 Protons of the *C*-Glycosides **15**

Compound	NMR data	
15a-α	1.81 (ddd, *J*=4.2, 5.8, 13.4 Hz),	2.52 (td, *J*=6.7, 13.4 Hz)
15a-β	1.72 (ddd, *J*=6.1, 10.4, 13.5 Hz),	2.30 (ddd, *J*=1.1, 5.2, 13.5 Hz)
15b-α	1.69 (ddd, *J*=4.2, 6.3, 13.3 Hz),	2.41 (td, *J*=6.6, 13.3 Hz)
15b-β	1.62 (ddd, *J*=6.1, 10.4, 13.3 Hz),	a)
15c-α	1.78 (b)),	2.35 (td, *J*=6.8, 13.4 Hz)
15c-β	1.72 (ddd, *J*=6.4, 10.1, 13.4 Hz),	2.13 (dd, *J*=5.2, 13.4 Hz)
15c'-α	1.83 (ddd, *J*=3.7, 5.5, 13.4 Hz),	2.39 (td, *J*=6.8, 13.4 Hz)
15c'-β	1.71 (ddd, *J*=6.2, 10.3, 13.4 Hz),	2.19 (dd, *J*=5.6, 13.4 Hz)
15d'-α	1.82 (b)),	2.40 (td, *J*=6.4, 13.3 Hz)
15d'-β	1.72 (ddd, *J*=6.7, 11.0, 13.4 Hz),	2.16 (ddd, *J*=1.2, 5.1, 13.4 Hz)
15e-α	a)	2.35 (td, *J*=7.7, 13.7 Hz)
15e-β	a)	2.02 (ddd, *J*=1.4, 4.9, 13.7 Hz)
15f-α	1.80 (ddd, *J*=4.7, 7.1, 13.3 Hz),	2.43 (td, *J*=6.2, 13.3 Hz)
15f-β	a)	2.02 (ddd, *J*=1.2, 5.0, 13.3 Hz)

a) Overlapped with other signals(s). b) Poorly resolved.

employed in the reaction with ethyl trimethylsilyl sulfide under the same reaction conditions, the product was isolated as a 1:1 mixture of the α- and β-isomers, These results apparently show that the neighboring group participation from 3-*O*-functionality plays the efficient role to control the stereochemistry in acid catalyzed glycosylation reactions.

Experimental

General. The IR spectra were determined on a Hitachi Model 260-30 spectrometer. The ^{1}H NMR spectra were recorded with Hitachi R-24B, JEOL GX-270, and/or JEOL GX-400 spectrometers in $CDCl_3$ with tetramethylsilane as an internal standard, unless otherwise noted. The optical rotations were carried out on a JMN DIP-181 polarimeter. HPLC analyses were performed on μPorasil P/N 27477 S/N or Resolve 5μ-silica with Shimadzu LC-6A system. All reactions except for hydrolysis were carried out under an anhydrous argon atmosphere. The reaction mixtures and combined extracts were dried over Na_2SO_4, if necessary, and concentrated in vacuo by an evaporator at 30—40 °C. Purification of products was performed by column chromatography on silica gel (Wakogel C-200 or Merck, Art. 9385 Kieselgel 60, 230—400 mesh). Acetonitrile, dichloromethane, HMPA, and *N,N*-dimethylformamide (DMF) were distilled from CaH_2 and stored over Molecular Sieves. Tetrahydrofuran (THF) was freshly distilled from sodium benzophenone ketyl. Methanol was distilled with $Mg(OMe)_2$ and stored over Molecular Sieves. The 3-*O*-substituted 1-*O*-acetyl-5-*O*-benzyl-2-deoxy-D-ribofuranoses were prepared as their anomeric mixtures throughout the synthetic course, and the elemental analyses were carried out when samples were purified as each single isomer.

Methyl 5-*O*-*t*-Butyldimethylsilyl-2-deoxy-D-*erythro*-pentofuranoside (7). To a solution of methyl 2-deoxy-D-*erythro*-pentofuranoside[13] (**1**) (7.41 g, 50 mmol), triethylamine (6.37 g, 63 mmol), and 4-(dimethylamino)pyridine (DMAP) (cat. amount) in dichloromethane–DMF (10/1, v/v) (110 ml) was added *t*-butyldimethylsilyl chloride (7.91 g, 52 mmol) at 0 °C. After stirring at ambient temperature overnight, the mixture was quenched with pH 7 phosphate buffer and the organic layer was extracted with dichloromethane. The extract was washed with water and aqueous NaCl and dried. The dichloromethane solution was evaporated and the residue was purified by column chromatography (ethyl acetate:hexane=1:3, v/v) to give methyl 5-*O*-*t*-butyldimethylsilyl-2-deoxy-D-ribofuranoside (**7**) (10.81 g, 82%): α-isomer; $[\alpha]_D^{25}$ −87.1° (*c* 0.982, $CHCl_3$); IR(neat) 3400, 2920, 1100, 835, 780 cm^{-1}; ^{1}H NMR δ=0.05 (6H, s), 0.89 (9H, s), 1.73—2.43 (2H, m), 2.93 (1H, d, *J*=10.5 Hz), 3.40 (3H, s), 3.47—3.93 (2H, m), 3.93—4.43 (2H, m), 5.07 (1H, dd, *J*=1.5, 4.0 Hz); Found: C, 54.76; H, 10.13%. Calcd for $C_{12}H_{26}O_4Si$: C, 54.92; H, 9.99%. β-Isomer; $[\alpha]_D^{24.7}$ +85.8 (*c* 1.053, $CHCl_3$); IR(neat) 3400, 2920, 1100, 835, 780 cm^{-1}; ^{1}H NMR δ=0.08 (6H, s), 0.91 (9H, s), 1.83—2.37 (2H, m), 2.50 (1H, brs), 3.35 (3H, s), 3.47—4.37 (3H, m), 4.43 (1H, m), 5.07 (1H, dd, *J*=3.5, 5.5 Hz); Found: C, 54.66; H, 10.07%. Calcd for $C_{12}H_{26}O_4Si$: C, 54.92; H, 9.99%.

Alkylation of Hydroxy Compounds via Lithium Alkoxides: Methyl 5-*O*-*t*-Butyldimethylsilyl-2-deoxy-3-*O*-(diethylcarbamoyl)methyl-D-*erythro*-pentofuranoside (8). To a solution of monosilylated methyl furanoside (**7**) (17.92 g, 68.3 mmol) and NaI (10.2 g, 68 mmol) in THF (200 ml) was added slowly the solution of *n*-BuLi in hexane (45 ml, 68.2 mmol) at −78 °C, and the mixture was stirred at the same temperature for 30 min. After addition of HMPA (23.8 ml, 136 mmol) and freshly distilled *N,N*-diethy-l-bromoacetamide (11.6 ml, 81.9 mmol), the mixture was stirred at room temperature overnight. After addition of diethylamine (5 ml) and stirring for 1 h, pH 7 phosphate buffer was added, and the mixture was extracted with ether. The ether extract was washed with water and aqueous NaCl and dried. The ether solution was concentrated and the residue was purified by column chromatography (ethyl acetate:hexane=1:3—2:1, v/v) to give the alkylated silyl compound **8** (23.22 g, 91%): α-isomer; $[\alpha]_D^{26}$ +73.6° (*c* 1.09, $CHCl_3$); IR(neat) 2930, 1650, 1460, 1260, 1100, 840, 780 cm^{-1}; ^{1}H NMR δ=0.05 (6H, s), 0.88 (9H, s), 1.13 (6H, brt, *J*=7.0 Hz), 2.00—2.20 (2H, m), 3.32 (4H, q, *J*=7.0 Hz), 3.33 (3H, s), 3.53—3.75 (2H, m), 3.90—4.23 (2H, m), 4.10 (2H, s), 4.97 (1H, dd, *J*=2.8, 4.0 Hz); Found: C, 57.31; H, 10.01; N, 3.73%. Calcd for $C_{18}H_{37}NO_5Si$: C, 57.56; H, 9.93; N, 3.73%. β-Isomer; $[\alpha]_D^{22.6}$ −58.6° (*c* 0.517, $CHCl_3$); IR(neat) 2930, 1650, 1460, 1260, 1110, 840, 780 cm^{-1}; ^{1}H NMR δ=0.09 (6H, s), 0.90 (9H, s), 1.16 (6H, brt, *J*=7.0 Hz), 2.05—2.33 (2H, m), 3.05—3.80 (6H, m), 3.26 (3H, s), 3.80—4.28 (2H, m), 4.09 (2H, s), 5.03 (1H, t, *J*=4.2 Hz); Found: C, 57.32; H, 9.78; N, 3.76%. Calcd for $C_{18}H_{37}NO_5Si$: C, 57.56; H, 9.93; N, 3.73%.

Methyl 2-Deoxy-3-*O*-(diethylcarbamoyl)methyl-D-*erythro*-pentofuranoside (9). An 1 M-solution (1 M=1 mol dm^{-3}) of tetrabutylammonium fluoride in THF (6 ml, 6 mmol) was added to a solution of the above silyl compound **8** (1.88 g, 5.0 mmol) in THF (5 ml) at 0 °C and the mixture was stirred for 5 h at room temperature. Then the mixture was concentrated and purified by column chromatography (ethyl acetate:methanol=30:1—20:1, v/v) to give the hydroxy compound **9** (1.26 g, 96%): α-isomer; $[\alpha]_D^{26}$ +161.9° (*c* 1.461, $CHCl_3$); IR(neat) 3400, 2920, 1630, 1100 cm^{-1}; ^{1}H NMR (CCl_4) δ=0.95—1.40 (6H, m), 1.80—2.40 (2H, m), 3.10—4.15 (9H, m), 3.30 (3H, s), 4.07 (2H, s) 4.90 (1H, dd, *J*=2.0, 5.2 Hz). β-Isomer; $[\alpha]_D^{26}$ −33.9° (*c* 0.577, $CHCl_3$); IR(neat) 3400, 2920, 1630, 1100 cm^{-1}; ^{1}H NMR (CCl_4) δ=1.17 (6H, brt, *J*=7.0 Hz), 1.90—2.23 (2H, m), 2.70 (1H, br), 3.10—3.80 (6H, m), 3.25 (3H, s), 3.80—4.30 (2H, m), 4.07 (2H, s), 4.93 (1H, dd, *J*=2.5, 4.7 Hz).

Methyl 5-*O*-Benzyl-2-deoxy-3-*O*-(diethylcarbamoyl)methyl-D-*erythro*-pentofuranoside (10). Alkylation of methyl 2-deoxy-3-*O*-(diethylcarbamoyl)methyl-D-*erythro*-pentofuranoside (**9**) (1.20 g, 4.6 mmol) with benzyl bromide (0.94 g, 5.5 mmol) in the same manner as mentioned before gave the benzylated compound **10** (1.40 g, 87%): α-isomer; $[\alpha]_D^{24.5}$ + 90.6° (*c* 0.980, $CHCl_3$); IR(neat) 2940, 1650, 1370, 1210, 1110, 740, 700 cm^{-1}; ^{1}H NMR δ=1.10 (6H, t, *J*=7.0 Hz), 1.80—2.70 (2H, m), 3.05—3.70 (4H, m), 3.37 (3H, s), 3.60 (2H, d, *J*=6.0 Hz), 3.87—4.43 (2H, m), 4.10 (2H, s), 4.54 (2H, s), 5.03 (1H, dd, *J*=2.2, 4.7 Hz), 7.26 (5H, s); Found: C, 64.65; H, 8.50; N, 3.90%. Calcd for $C_{19}H_{29}NO_5$: C, 64.94; H, 8.32; N, 3.99% β-Isomer; $[\alpha]_D^{26}$ −57.0° (*c* 0.965, $CHCl_3$); IR(neat) 2940, 1650, 1370, 1210, 1110, 740, 700 cm^{-1}; ^{1}H NMR δ=1.10 (6H, t, *J*=7.0 Hz), 2.00—2.35 (2H, m), 2.90—3.60 (6H, m), 3.28 (3H, s), 4.07 (2H, s), 3.96—4.40 (2H, m), 4.52 (2H, s), 5.02 (1H, t, *J*=3.8 Hz), 7.26 (5H, s); Found: C, 64.78; H, 8.55; N, 3.76%. Calcd for $C_{19}H_{29}NO_5$: C, 64.94; H, 8.32; N, 3.99%.

Methyl 5-*O*-Benzyl-2-deoxy-3-*O*-(2-hydroxy)ethyl-D-*ery*-

thro-**pentofuranoside (11).** A slurry of the amide **10** (6.06 g 17.2 mmol), *t*-BuOK (12.76 g, 114 mmol), and water (0.62 ml, 34 mmol) in THF (170 ml) was stirred vigorously at room temperature overnight.[14] After addition of ice and water, the mixture was washed with ether. Aqueous layer was acidified with aqueous 2 M $KHSO_4$ and extracted with ether for five times. The ether extract was dried over $MgSO_4$ and evaporated to give the crude carboxylic acid.

To a suspension of lithium aluminum hydride (653 mg, 17.2 mmol) in THF (52 ml) was added dropwise a solution of the above carboxylic acid in THF (10 ml) at 0 °C, and the mixture was stirred at room temperature overnight. To this mixture was added carefully ethyl acetate followed by aqueous 30%-Rochelle salt, and the mixture was extracted with ether. The ether extract was dried and evaporated. Purification of the residue by column chromatography (ethyl acetate:hexane=2:1—1:0, v/v) gave the 2-hydroxyethyl compund **11** (4.15 g, 85%): α-isomer; $[\alpha]_D^{22.5}$ +94.6° (*c* 2.16, $CHCl_3$); IR(neat) 3450, 2900, 1450, 1360, 1200, 1100, 730, 690 cm^{-1}; ^1H NMR δ=1.90—2.25 (2H, m), 2.53 (1H, br), 3.20—4.40 (8H, m), 3.36 (3H, s), 4.52 (2H, s), 5.03 (1H, m), 7.25 (5H, s). β-Isomer; $[\alpha]_D^{22}$ −49.8° (*c* 0.765, $CHCl_3$); IR(neat) 3450, 2900, 1450, 1360, 1200, 1100, 730, 690 cm^{-1}; ^1H NMR δ=2.00—2.30 (2H, m), 2.55 (1H, br), 3.26 (3H, s), 3.30—3.80 (6H, m), 3.80—4.30 (2H, m), 4.52 (2H, s), 5.02 (1H, dd, *J*=2.6, 4.6 Hz), 7.27 (5H, s).

Methyl 5-*O*-Benzyl-2-deoxy-3-*O*-[(2-methylthio)ethyl]-D-*erythro*-pentofuranoside (12f). To a solution of the hydroxyethyl compound **11** (2.30 g, 8.2 mmol) and triethylamine (1.5 g, 14.7 mmol) in dichloromethane (30 ml) was added slowly methanesulfonyl chloride (1.4 g, 12.2 mmol) at 0 °C, and stirred at the same temperature for 30 min. After addition of pH 7 phosphate buffer, the mixture was extracted with ether. The ether extract was dried and evaporated to give the corresponding mesylate.

To a solution of dimethyl disulfide (1.62 ml, 18 mmol) in ethanol (10 ml) was added sodium borohydride (680 mg, 18 mmol) at 0 °C, and the above mesylate was added to the mixture and the resulting mixture was stirred at room temperature overnight. After evaporation of the solvent, followed by addition of water, the mixture was extracted with dichloromethane. The extract was dried and evaporated. The residue was purified by column chromatography (ethyl acetate:hexane=1:3, v/v) to afford 2-(methylthio)ethyl compound **12f** (1.71 g, 91%): α-isomer; $[\alpha]_D^{29}$ +106.7° (*c* 0.588, $CHCl_3$); IR(neat) 2900, 1445, 1360, 1200, 1100, 730, 690 cm^{-1}; ^1H NMR δ=1.95 (3H, s), 1.60—2.10 (2H, m), 2.48 (2H, t, *J*=7.0 Hz), 3.23 (3H, s), 3.30—4.16 (6H, m), 4.45 (2H, s), 4.91 (1H, dd, *J*=2.0, 5.6 Hz), 7.27 (5H, s); Found: C, 61.41; H, 7.84%. Calcd for $C_{16}H_{24}O_4S$: C, 61.51; H, 7.74%. β-Isomer; $[\alpha]_D^{29}$ −43.9° (*c* 1.154, $CHCl_3$); IR(neat) 2900, 1445, 1360, 1200, 1100, 730, 690 cm^{-1}; ^1H NMR δ=2.07 (3H, s), 1.70—2.30 (2H, m), 2.60 (2H, t, *J*=7.0 Hz), 3.26 (3H, s), 3.35—3.73 (4H, m), 3.80—4.30 (2H, m), 4.52 (2H, s), 5.00 (1H, dd, *J*=2.4, 4.4 Hz), 7.25 (5H, s); Found: C, 61.51; H, 7.78%. Calcd for $C_{16}H_{24}O_4S$: C, 61.51; H, 7.74%.

Methyl 5-*O*-Benzyl-2-deoxy-3-*O*-[(2-methylsulfinyl)ethyl]-D-*erythro*-pentofuranoside. To a solution of the methylthio compound **12f** (367 mg, 1.17 mmol) in methanol was added a solution of sodium periodate (265 mg, 1.23 mmol) in water (0.5 ml), and stirred at room temperature overnight. After separation of inorganic precipitates, the filtrate was diluted with dichloromethane and dried. Evaporation of the solution and purification by column chromatography (ethyl acetate:hexane:methanol=5:3:1, v/v/v) gave the methylsulfinyl compound (384 mg, 100%): α-isomer; IR(neat) 2900, 1450, 1360, 1100, 1050, 740, 700 cm^{-1}; ^1H NMR δ=2.00—2.50 (2H, m), 2.55 (3H, s), 2.80—3.10 (2H, m), 3.40 (3H, s), 3.50—3.70 (2H, m), 3.86 (2H, t, *J*=7.4 Hz), 3.95—4.40 (2H, m), 4.60 (2H, s), 5.05 (1H, dd, *J*=2.0, 5.0 Hz), 7.30 (5H, s). β-Isomer; IR(neat) 2900, 1450, 1360, 1100, 1050, 740, 700 cm^{-1}; ^1H NMR δ=1.90—2.40 (2H, m), 2.55 (3H, s), 2.70—3.10 (2H, m), 3.36 (3H, s), 3.40—3.70 (2H, m), 3.80 (2H, t, *J*=7.6 Hz), 3.97—4.35 (2H, m), 4.53 (2H, s), 5.01 (1H, dd, *J*=3.0, 4.6 Hz), 7.26 (5H, s).

1-*O*-Acetyl5-*O*-benzyl-2-deoxy-3-*O*-[(2-methylsulfinyl)-ethyl]-D-*erythro*-pentofuranose (6h). A vigorously stirred mixture of methyl 5-*O*-benzyl-2-deoxy-3-*O*-[(2-methylsulfinyl)ethyl]-D-*erythro*-pentofuranoside (**12f**) (1.47 g, 4.5 mmol) and Dowex 50-X8 (10 ml) in THF-water (2/1, v/v, 12 ml) was maintained at 45 °C for 5 h. After separation of the resin, the filtrate was extracted with dichloromethane. The extract was dried and evaporated to give a residue. To a solution of this residue, pyridine (0.36 ml, 4.5 mmol), and DMAP (67 mg 0.5 mmol) in dichloromethane (10 ml) was added acetic anhydride (0.64 ml, 6.8 mmol) at 0 °C. After stirring the mixture for 1 h at room temperature, the mixture was evaporated and purified by column chromatography (ethyl acetate:hexane:methanol=5:3:1, v/v/v) to give the desired acetate **6h** (1.30 g, 81%): IR(neat) 2900, 1735, 1370, 1240, 1100, 1050, 740, 700 cm^{-1}; ^1H NMR δ=1.93 (2/3×3H, s), 2.02 (1/3×3H, s), 2.10—2.45 (2H. m), 2.55 (2/3×3H, s), 2.58 (1/3×3H, s), 2.70—3.00 (2H, m), 3.51 (2H, d, *J*=5.0 Hz), 3.82 (2H, t, *J*=5.5 Hz), 3.93—4.37 (2H, m), 4.47 (1/3×2H, s), 4.52 (2/3×2H, m), 6.23 (1H, m), 7.26 (5H, s).

Methyl 3,5-Bis[*O*-(*t*-butyldimethylsilyl)]-2-deoxy-D-*erythro*-pentofuranoside (2). This compound was prepared from 2-deoxy-D-ribose by the same procedure used for the compound **7** except for using 2.6 equiv of *t*-butyldimethylsilyl chloride and 3.0 equiv of triethylamine in 87% yield. IR(neat) 2950, 1480, 1260, 1120, 840, 780 cm^{-1}; ^1H NMR δ=0.08 (12H, s), 0.88 (18H, s), 1.53—2.65 (2H, m), 3.33 (1/3×3H, s), 3.36 (2/3×3H, s), 3.50—4.10 (3H, m), 4.10—4.62 (1H, m), 4.85—5.18 (1H, m).

Methyl 3-*O*-*t*-Butyldimethylsilyl-2-deoxy-D-*erythro*-pentofuranoside (3). A solution of the disilyl compound **2** (25.6 g, 68 mmol) and pyridinium *p*-toluenesulfonate (1.58 g, 6.3 mmol) in methanol (80 ml) was stirred at room temperature for 1 d. After addition of aqueous Na_2CO_3, the reaction mixture was concentrated followed by extraction with dichloromethane. The extract was washed with water and then aqueous NaCl, dried, and evaporated. Separation of the residue by column chromatography (ethyl acetate:hexane=1:5—1:1, v/v) gave the recovered starting disilyl compound **2** (8.5 g, 33% recovered) and the desired 3-*O*-monosilylated compound **3** (9.75 g, 55%): α-isomer; IR(neat) 3400, 2930, 1460, 1250, 1100, 840, 790 cm^{-1}; ^1H NMR δ=0.05 (6H, s), 0.89 (9H, s), 1.73(1H, ddd, *J*=3.0, 6.0, 13.5 Hz), 2.27 (1H, ddd, *J*=5.5, 8.0, 13.5 Hz), 2.37 (1H, s), 3.27 (3H, s), 3.33—3.87 (3H, m), 4.13 (1H, dt, J_d=8.0 Hz, J_t=6.0 Hz), 4.83 (1H, dd, *J*=3.0, 5.5 Hz). β-Isomer; IR(neat) 3400, 2930, 1250, 1100, 840 cm^{-1}; ^1H NMR δ=0.07 (6H, s), 0.87 (9H, s), 1.67—2.23 (2H, m), 2.30 (1H, t, *J*=6.0 Hz), 3.28 (3H, s), 3.33—3.67 (2H, m), 3.80 (1H, m), 4.38 (1H, dt, J_d=4.0 Hz, J_t=6.0 Hz), 4.92 (1H, dd, *J*=2.5, 4.5 Hz).

Methyl 5-*O*-Benzyl-3-*O*-*t*-butyldimethylsilyl-2-deoxy-D-*ery*-

thro-pentofuranoside (**4**). According to the method for alkylation, the 3-*O*-monosilylated compound **3** was alkylated by benzyl bromide to the 5-*O*-benzyl-3-*O*-silyl derivative **4** in 92% yield: IR(neat) 2900, 1470, 1360, 1260, 1100, 840, 780, 700 cm^{-1}; ^1H NMR δ=0.05 (6H, s), 0.83 (9H, s), 1.50—2.62 (2H, m), 3.27 (1/2×3H, s), 3.33 (1/2×3H, s), 3.40—3.66 (2H, m), 3.70—4.45 (2H, m), 4.51 (2H, s), 4.80—5.10 (1H, m), 7.22 (5H, s).

Methyl 5-*O*-Benzyl-2-deoxy-D-*erythro*-pentofuranoside (5). Compound **5** was prepared from the above 5-*O*-benzyl-3-*O*-silyl compound **4** by the same procedure used for the compound **9** in 98% yield: IR(neat) 3450, 2900, 1100, 740, 700 cm^{-1}; ^1H NMR δ=1.80—2.14 (2H, m), 2.45—3.00 (1H, m), 3.27 (2/5×3H, s), 3.35 (3/5×3H, s), 3.30—3.60 (2H, m), 3.60—4.30 (2H, m), 4.44 (2H, brs), 4.75—4.98 (1H, m), 7.26 (5H, s).

Methyl 5-*O*-Benzyl-2-deoxy-3-*O*-(2-pyridylmethyl)-D-*erythro*-pentofuranoside *N*-Oxide. To a mixture of the methyl 5-*O*-benzyl-2-deoxyriboside **5** (480 mg, 2 mmol), sodium iodide (750 mg, 5 mmol), and *t*-butyl alcohol (296 mg, 4 mmol) in THF (7 ml) was added 60% sodium hydride (240 mg, 6 mmol), and the mixture was stirred for 1 h at room temperature. Then 2-(chloromethyl)pyridine *N*-oxide hydrochloride (558 mg, 3 mmol) was added to the mixture are the resulting mixture was stirred for 12 h at room temperature. After addition of pH 7 phosphate buffer, the organic compounds were extracted with the combined solvent (ether:ethanol=20:1, v/v). The extract was dried and evaporated. Purification of the residue by column chromatography (ethyl acetate:hexane:methanol=5:3:1, v/v/v) gave the titled compound (624 mg, 90%): IR(neat) 2920, 1500, 1435, 1360, 1250, 1100, 1050, 860, 770, 740, 700 cm^{-1}; ^1H NMR δ=2.00—2.33 (2H, m), 3.25 (2/5×3H, s), 3.33 (3/5×3H, s), 3.40—3.70 (2H, m), 3.90—4.45 (2H, m), 4.50 (2H, s), 4.69 (2H, s), 4.90—5.15 (1H, m), 6.95—7.70 (8H, m), 7.90—8.22 (1H, m).

1-*O*-Acetyl-5-*O*-benzyl-2-deoxy-3-*O*-(2-pyridylmethyl)-D-*erythro*-pentofuranose *N*-Oxide (6e). According to the procedure used for the compound **6h**, methyl 5-*O*-benzyl-2-deoxy-3-*O*-(2-pyridylmethyl)-D-*erythro*-pentofuranoside *N*-oxide was hydrolyzed then acetylated to give the 1-*O*-acetyl compound **6e** in 85% yield: IR(neat) 2900, 1730, 1480, 1420, 1360, 1230, 1100, 1000, 840, 760, 730, 690 cm^{-1}; ^1H NMR δ=1.93 (2/3×3H, s), 2.00 (1/3×3H, s), 2.10—2.50 (2H, m), 3.40—3.70 (2H, m), 4.10—4.60 (2H, m), 4.53 (2H, s), 4.73 (2H, s), 6.22—6.40 (1H, m), 6.90—7.60 (8H, m), 8.05—8.30 (1H, m).

Other 3-*O*-substituted 5-*O*-benzyl-2-deoxy-D-*erythro*-pentofuranosides listed in Table 1 were prepared by the essentially same procedure described above.

***C*-Glycosylation Reaction: Benzyl 5-*O*-Benzyl-2-deoxy-3-*O*-[(2-methylsulfonyl)ethyl]-D-*erythro*-pentofuranosylacetate (15c).** To a solution of methylsulfinyl compound (**6h**) (188 mg, 0.53 mmol) and 1-benzyloxy-1-(*t*-butyldimethylsilyloxy)ethylene (**13c**) (177 mg, 0.67 mmol) in dichloromethane (10 ml) was added a solution of TMSOTf (178 mg, 0.80 mmol) in dichloromethane (2 ml) slowly at −78 °C, and the mixture was stirred for 12 h at this temperature. The reaction mixture was quenched by addition of pH 7 phosphate buffer and the mixture was extracted with dichloromethane. The dichloromethane extract was dried and evaporated. After purification of the residue by column chromatography (ethyl acetate:hexane:methanol=5:3:1, v/v/v), the products were dissolved in methanol (10 ml) and oxidized by 10% H_2O_2 (10 ml) at room temperature in the presence of ammonium molybdate (VI) tetrahydrate (100 mg, 0.08 mmol) at room temperature. The reaction mixture was extracted with dichloromethane and dried, then followed by evaporation of the solvent. Purification of the residue by column chromatography (ethyl acetate:hexane=2:1, v/v) gave the mixture of the isomers of the *C*-glycoside **15c** (220 mg, 86%) (α:β=9:91): IR(neat) 2900, 1730, 1450, 1300, 1100, 740, 690 cm^{-1}; ^1H NMR δ=1.72 (9/10×1H, ddd, J=6.4, 10.1, 13.4 Hz), 1.78 (1/10×1H, m), 2.13 (9/10×1H, dd, J=5.2, 13.4 Hz), 2.39 (1/10×1H, td, J_t=6.8 Hz, J_d=13.4 Hz), 2.57 (1H, dd, J=6.5, 15.8 Hz), 2.72 (1H, dd, J=6.5, 15.8 Hz), 2.88 (1/10×3H, s), 2.92 (9/10×3H, s), 3.17 (2H, t, J=5.6 Hz), 3.38 (1H, dd, J=6.2, 10.2 Hz), 3.53 (1H, dd, J=4.3, 10.2 Hz), 3.82 (1H, dd, J=6.5, 11.7 Hz), 3.86 (1H, dd, J=5.6, 11.7 Hz), 3.96—4.01 (1H, m), 4.01—4.07 (1H, m), 4.37—4.48 (1H, m), 4.52 (2H, s), 5.13 (2H, s), 7.25—7.38 (10H, m).

The characteristic patterns of C-2 protons in NMR spectrum were summerized in Table 3 together with those of the other *C*-glycosides.

2-[5-*O*-Benzyl-2-deoxy-3-*O*-[(2-methylsulfonyl)ethyl]-D-*erythro*-pentofuranosyl]-1-phenylethanone (15a): IR(neat) 2920, 1680, 1600, 1450, 1310, 1130, 740, 695 cm^{-1}; ^1H NMR δ=1.50—2.50 (2H, m), 2.89 (1/3×3H, s), 2.96 (2/3× 3H, s), 3.00—3.26 (4H, m), 3.40—3.58 (2H, m), 3.77—4.44 (4H, m), 4.53 (2H, s), 4.55—4.85 (1H, m), 7.25—7.65 (8H, m), 7.90—8.10 (2H, m).

1-[5-*O*-Benzyl-2-deoxy-3-*O*-[(2-methylsulfonyl)ethyl]-D-*erythro*-pentofuranosyl]-2-propanone (15b): IR(neat) 2900, 1710, 1310, 1290, 1130, 1100, 740, 700 cm^{-1}; ^1H NMR δ=1.40—2.40 (2H, m), 2.16 (3H, s), 2.50—2.90 (1H, m), 2.92 (3H, s), 3.00—3.60 (4H, m), 3.70—4.10 (4H, m), 4.10—4.50 (1H, m), 4.51 (2H, s), 7.30 (5H, s).

Methyl 2-[5-*O*-Benzyl-2-deoxy-3-*O*-[(2-methylsulfonyl)-ethyl]-D-*erythro*-pentofuranosyl]glycolate (15d): IR(neat) 3470, 2900, 1735, 1120, 740, 700 cm^{-1}; ^1H NMR δ=1.60—2.45 (2H, m), 2.90 (3H, s), 3.00—3.65 (5H, m), 3.70—4.60 (9H, m), 4.50 (2H, s), 7.26 (5H, s).

Methyl 5-*O*-Benzyl-2-deoxy-3-*O*-[(2-methylsulfonyl)ethyl]-D-*erythro*-pentofuranosylacetate (15d'). To a solution of methyl 2-[5-*O*-benzyl-2-deoxy-3-*O*-[(2-methylsulfonyl)ethyl]-D-*erythro*-pentofuranosyl]glycolate (**15d**) (78 mg, 0.19 mmol), triethylamine (50 mg, 0.35 mmol), and DMAP (cat. amount) in anhydrous acetonitrile (3 ml) was added phenyl carbonochloridothioate (60 mg, 0.35 mmol) at 0°C and the solution was stirred at room temperature for 1 d. After addition of pH 7 phosphate buffer, the mixture was extracted with dichloromethane. The extract was dried and evaporated. The residue was purified by column chromatography (ethyl acetate:hexane=2:1, v/v) to give corresponding thiocarbonate (74 mg, 77%): ^1H NMR δ=1.75—2.40 (2H, m), 2.90 (3H, s), 3.00—3.60 (4H, m), 3.65—4.30 (6H, m), 4.48 (2H, s), 4.30—4.80 (1H, m), 5.56 (1H, dd, J=3.6 Hz, 8.0 Hz), 6.90—7.60 (5H, m), 7.25 (5H, s).

A solution of the thiocarbonate obtained above (74 mg, 0.146 mmol), tributyltin hydride (47 mg., 0.162 mmol), and azobisisobutyronitrile (cat. amount) in dry toluene (5 ml) was heated under reflux for 2 h. Evaporation of the mixture and purification of the residue by column chromatography (ethyl acetate:hexane=1:2, v/v) gave the deoxygenated compound (**15d'**) (42 mg, 75%): IR(neat) 2900, 1735, 1100, 745, 705 cm^{-1}; ^1H NMR δ=1.72 (9/10×1H, ddd, J=6.7, 11.0,

13.4 Hz), 1.82 (1/10×1H, m), 2.16 (9/10×1H, ddd, J=1.2, 5.1, 13.4 Hz), 2.40 (1/10×1H, td, J_t=6.4 Hz, J_d=13.3 Hz), 2.53 (1H, dd, J=6.1, 15.6 Hz), 2.67 (1H, dd, J=6.9, 15.6 Hz), 2.94 (1/10×3H, s), 2.96 (9/10×3H, s), 3.19 (2H, t, J=5.5 Hz), 3.41 (1H, dd, J=5.8, 10.0 Hz), 3.55 (1H, dd, J=4.6, 10.0 Hz), 3.68 (3H, s), 3.78—3.93 (2H, m), 3.97—4.18 (2H, m), 4.53 (2H, s), 7.27—7.42 (5H, m).

Methyl 2-[5-*O*-Benzyl-2-deoxy-3-*O*-[(2-methylsulfonyl)-ethyl]-D-*erythro*-pentofuranosyl]-2,2-dimethoxyacetate (15e): IR(neat) 2900, 1740, 1300, 1100, 735, 700 cm^{-1}; ^{1}H NMR δ=1.60—2.40 (2H, m), 2.85 (3H, s), 3.23 (2/5×6H, s), 3.33 (3/5×6H, s), 3.61 (3/5×3H, s), 3.71 (2/5×3H, s), 2.90—4.30 (9H, m), 4.43 (2H, s), 7.20 (5H, s).

3-[5-*O*-Benzyl-2-deoxy-3-*O*-[(2-methylsulfonyl)ethyl]-D-*erythro*-pentofuranosyl]-1-propene (15f): IR(neat) 2900, 1640, 1310, 1290, 1100, 740, 700 cm^{-1}; ^{1}H NMR δ=1.58—1.76 (1H, m), 1.96—2.50 (3H, m), 2.93 (3H, s), 3.18 (2H, t, J=5.4 Hz), 3.36—3.58 (2H, m), 3.77—3.92 (2H, m), 3.97—4.18 (3H, m), 4.55 (2H, s), 5.03—5.15 (2H, m), 5.72—5.88 (1H, m), 7.25—7.38 (5H, m).

(1*R*,6*R*,8*S*)-8-[(2-Methylsulfonyl)ethyl]-3,9-dioxabicyclo-[4.2.1]nonan-4-one (16). The dibenzyl *C*-glycoside **15c** (100 mg, 0.22 mmol) was hydrogenated with 10%-Pd/C (20 mg) in ethanol (1 ml) at 50 °C for 12 h. Separation of the catalyst and evaporation gave the corresponding hydroxy carboxylic acid **15c′** in quantitative yield: IR(neat) 3400, 2950, 1720, 1400, 1280, 1130, 1100, 960, 820, 740 cm^{-1}; ^{1}H NMR (CD_3OD) δ=1.71 (9/10×1H, ddd, J=6.2 10.3, 13.4 Hz), 1.83 (1/10×1H, m), 2.19 (9/10×1H, dd, J=5.6, 13.4 Hz), 2.39 (1/10×1H, m), 2.56 (2H, d, J=6.4 Hz), 3.02 (3H, s), 3.35 (2H, t, J=5.4 Hz), 3.51 (1H, dd, J=5.6, 11.5 Hz), 3.56 (1H, dd, J=5.1, 11.5 Hz), 3.82—3.94 (3H, m), 4.00—4.04 (1H, m), 4.42—4.57 (1H, m).

A solution of the above carboxylic acid **15c′** (33 mg, 0.12 mmol) and acetic anhydride (12 μl, 0.13 mmol) in anhydrous pyridine (12 ml) was heated under reflux for 12 h. The reaction mixture was condensed and purified by silica-gel preparative TLC (ethyl acetate) to give the lactone **16** (14 mg, 45%): IR (CH_2Cl_2) 1740, 1310, and 1100 cm^{-1}; ^{1}H NMR δ=2.15—2.30 (2H, m), 2.89 (1H, dd, J=5.1, 16.5 Hz), 2.98 (3H, s), 3.03 (1H, d, J=16.5 Hz), 3.19—3.24 (2H, m), 3.80—3.93 (2H, m), 4.28 (1H, dd, J=4.0, 13.6 Hz), 4.37 (1H, d, J=13.6 Hz), 4.40—4.45 (2H, m), 4.57—4.63 (1H, m).

S-Glycosilation reactions were performed with essentially the same procedure as the *C*-glycosylation reaction. The IR and NMR data of the *S*-glycosylation products listed in Table 3 are as follows:

Ethyl 5-*O*-Benzyl-2-deoxy-3-*O*-(2-pyridylmethyl)-1-thio-D-*erythro*-pentofuranoside *N*-Oxide (17a): IR(neat) 2850, 1500, 1440, 1360, 1230, 1100, 840, 760, 735, 690 cm^{-1}; ^{1}H NMR δ=1.30 (0.84×3H, t, J=7.5 Hz), 1.32 (0.16×3H, t, J=7.5 Hz), 2.07 (0.16×1H, m), 2.13 (0.84×1H, ddd, J=5.6, 8.6, 13.3 Hz), 2.43 (0.84×1H, ddd, J=3.4 6.0, 13.3 Hz), 2.60—2.80 (2.16H, m), 3.56 (1H, dd, J=6.0, 15.0 Hz), 3.66 (1H, dd, J=5.6, 15.0 Hz), 4.15—4.32 (2H, m), 4.57 (2H, s), 4.74 (1H, d, J=15.5 Hz), 4.82 (1H, d, J=15.5 Hz), 5.40 (0.84×1H, dd, J=6.0, 8.6 Hz), 5.53 (0.16×1H, dd, J=3.7, 7.6 Hz), 7.16—7.40 (7H, m), 7.49—7.63 (1H, m), 8.20 (1H, m).

Benzyl 5-*O*-Benzyl-2-deoxy-3-*O*-(2-pyridylmethyl)-1-thio-D-*erythro*-pentofuranoside *N*-Oxide (17b): IR(neat) 2870, 1485, 1425, 1240, 1085, 850, 760, 730, 690 cm^{-1}; ^{1}H NMR δ=2.02 (0.25×1H, td, J_t=3.0 Hz, J_d=14.2 Hz), 2.15 (0.75×1H, ddd, J=6.4, 7.8, 13.9 Hz), 2.37 (0.75×1H, ddd, J=2.9, 6.4, 13.9 Hz), 2.58 (0.25×1H, td, J_t=7.6 Hz, J_d=14.2 Hz), 3.59 (1H, dd, J=6.0, 13.5 Hz), 3.68 (1H, dd, J=5.0, 13.5 Hz), 3.82 (0.25×1H, d, J=13.5 Hz), 3.83 (0.75×1H, d, J=13.5 Hz), 3.93 (0.25×1H, d, J=13.5 Hz), 3.94 (0.75×1H, d, J=13.5 Hz), 4.13—4.47 (2H, m), 4.58 (2H, s), 4.75 (2H, s), 5.28 (0.75×1H, dd, J=6.4, 7.7 Hz), 5.37 (0.25×1H, dd, J=3.0, 7.6 Hz), 7.14—7.38 (12H, m), 7.45—7.63 (1H, m), 8.20 (1H, m).

Isopropyl 5-*O*-Benzyl-2-deoxy-3-*O*-(2-pyridylmethyl)-1-thio-D-*erythro*-pentofuranoside *N*-Oxide (17c): IR(neat) 2900, 1490, 1430, 1240, 1085, 850, 765, 740, 700 cm^{-1}; ^{1}H NMR δ=1.30 (6H, d, J=7.0 Hz), 1.95—2.18 (1H, m), 2.40—2.78 (1H, m), 3.18 (1H, m), 3.54 (1H, m), 3.66 (1H, m), 4.13—4.43 (2H, m), 4.58 (2H, s), 4.73 (1H, d, J=14.0 Hz), 4.82 (1H, d, J=14.0 Hz), 5.45 (0.79×1H, dd, J=6.2, 8.6 Hz), 5.58 (0.21×1H, dd, J=3.7, 8.1 Hz), 7.16—7.38 (7H, m), 7.48—7.55 (1H, m), 8.22 (1H, m).

4-*t*-Butylphenyl 5-*O*-Benzyl-2-deoxy-3-*O*-(2-pyridylmethyl)-1-thio-D-*erythro*-pentofuranoside *N*-Oxide (17d): IR(neat) 2950, 1420, 1240, 1100, 1080, 840, 760, 730, 690 cm^{-1}; ^{1}H NMR δ=1.29 (0.35×9H, s), 1.30 (0.65×9H, s), 2.10—2.32 (1H, m), 2.40—2.80 (1H, m), 3.56—3.68 (2H, m), 4.20—4.40 (2H, m), 4.48—4.65 (2H, m), 4.75—4.85 (2H, m), 5.58 (0.65×1H, dd, J=6.2, 9.0 Hz), 5.73 (0.35×1H, dd, J=3.1, 7.3 Hz), 7.15—7.35 (9H, m), 7.43—7.68 (3H, m), 8.18—8.33 (1H, m).

References

1) Reviews: S. Hanessian and A. G. Pernet, *Adv. Carbohydr. Chem. Biochem.*, **33**, 111 (1976); J. Goodchild, "The Biochemistry of Nucleoside Antibiotics," in "Topics in Antibiotic Chemistry," ed. by P. G. Sammes, John Wiley & Sons, New York (1982), Vol. 6, Part B; J. G. Buchanan and R. H. Wightman, "The Chemistry of Nucleoside Antibiotics," in "Topics in Antibiotic Chemistry," ed. by P. G. Sammes, John Wiley & Sons, New York (1982), Vol. 6, Part C; U. Hacksell and G. D. Daves, Jr., "The Chemistry and Biochemistry of *C*-Nucleosides and *C*-Arylglycosides," in "Progress in Medicinal Chemistry," ed. by G. P. Ellis and G. B. West, Elsevier Science Publishers B. V., Amsterdam (1985), Vol. 22.

2) Y. Mizuno, "The Organic Chemistry of Nucleic Acids," Elsevier Science Publishers B. V., Amsterbam (1986), Chap. 3.

3) W. Wierenga and H. I. Skulnick, *Carbohydr. Res.*, **90**, 41 (1981); N. B. Dyatkina, A. A. Krayevsky, and A. V. Azhayev, *Synthesis*, **1985**, 410; R. Noyori and M. Hayashi, *Chem. Lett.*, **1987**, 57; G. Gosselin, M.-C. Bergogne, J. De Rudder, E. De Clercq, and J. -L. Imbach, *J. Med. Chem.*, **30**, 982 (1987); A. D. Borthwick, S. Butt, K. Biggadike, A. M. Exall, S. M. Roberts, P. M. Youds, B. E. Kirk, B. R. Booth, J. M. Cameron, S. W. Cox, C. L. P. Marr, and M. D. Shill, *J. Chem. Soc., Chem. Commum.*, **1988**, 656; L. W. Hertel, J. S. Kroin, J. W. Misner, and J. M. Tustin, *J. Org. Chem.*, **53**, 2406 (1988).

4) A. Kolb, T. H. Dinh, and J. Igolen, *Bull. Soc. Chim. Fr.*, **1973**, 3447; Z. Kazimierczuk, H. B. Cottam, G. R. Revankar, and R. K. Robins, *J. Am. Chem. Soc.*, **106**, 6379 (1984); H. B. Cottam, Z. Kazimierczuk, S. Geary, P. A. McKernan, G. R. Revankar, and R. K. Robins, *J. Med, Chem.*, **28**, 1461 (1985); H. B. Cottam and R. K. Robins, *J. Heterocycl. Chem.*, **25**, 361 (1988); F. Seela, B. Westermann,

and U. Bindig, *J. Chem. Soc., Perkin Trans. 1*, **1988**, 697.

5) H. G. Howell, P. R. Brodfuehrer, S. P. Brundidge, D. A. Benigni, and C. Sapino, Jr., *J. Org. Chem.*, **53**, 85 (1988).

6) T. J. Bardos, M. P. Kotick, and C. Szantay, *Tetrahedron Lett.*, **1966**, 1759.

7) A part of the present work has been published in a preliminary form: K. Narasaka, Y. Ichikawa, and H. Kubota, *Chem. Lett.*, **1987**, 2139.

8) U. Niedballa and H. Vorbruggen, *J. Org. Chem.*, **39**, 3654 (1974).

9) V. Gutmann, "The Donar-Acceptor Approach to Molecular Interactions," Plenum Press, New York (1978).

10) T. Mukaiyama, S. Kobayashi, and S. Shoda, *Chem. Lett.*, **1984**, 1529 (1984).

11) H. Vorbruggen and K. Krolikiewicz, *Angew. Chem., Int. Ed. Engl.*, **14**, 421 (1975).

12) H. Ohrui, G. H. Jones, J. G Moffat, M. L. Maddox, A. T. Christensen, and S. K. Bryam, *J. Am. Chem. Soc.*, **97**, 4602 (1975); C. K. Chu, K. A. Watanabe, and J. J. Fox, *J. Heterocycl. Chem.*, **12**, 817 (1975); C. K. Chu, I. Wenpen, K. A. Watanabe, and J. J. Fox, *J. Org. Chem.*, **41**, 2793 (1976); G. Just and M. -I. Lim, *Can. J. Chem.*, **55**, 2993 (1977); R. Noyori, T. Sato, and Y. Hayakawa, *J. Am. Chem. Soc.*, **100**, 2561 (1978); Y. Ito, T. Shibata, M. Arita, H. Sawai, and M. Ohno, *ibid.*, **103**, 6739 (1981).

13) R. K. Ness, D. L. MacDonald, and H. G. Fletcher, Jr., *J. Org. Chem.*, **26**, 2895 (1961); J. J. Fox, N. C. Yung, I. Wenpen, and M. Hoffer, *J. Am. Chem. Soc.*, **83**, 4066 (1961).

14) P. G. Gassman, P. K. G. Hodgson, and R. J. Balchunis, *J. Am. Chem. Soc.*, **98**, 1275 (1976).

Formation of *N*-Tributylstannyl Heterocycle from Bis(tributyltin) Oxide and ω-Haloalkyl Isocyanate. One-Pot Convenient Synthesis of 2-Oxazolidinones and Tetrahydro-2*H*-1,3-oxazin-2-one

Ikuya SHIBATA,* Kenji NAKAMURA, Akio BABA, and Haruo MATSUDA
Department of Applied Chemistry, Faculty of Engineering, Osaka University,
2-1 Yamadaoka, Suita, Osaka 565
(Received September 30, 1988)

Novel types of compounds, *N*-tributylstannyl-2-oxazolidinone (**4a**) and tetrahydro-2*H*-1,3-oxazin-2-one (**4b**), are formed from the adduct of $(n\text{-Bu}_3\text{Sn})_2\text{O}$ (**1**) with ω-haloalkyl isocyanate (**2**), and the subsequent coupling reaction with alkyl halides gives a variety of *N*-substituted 2-oxazolidinones and tetrahydro-2-oxazinones in a one-pot procedure. Both the cyclization and the coupling reaction proceed quantitatively in the presence of HMPA which enhances the reactivity of the Sn–heteroatom bond by coordination.

Many organotin reagents have become widely used in organic synthesis.[1] Some important features of tin compounds are facile insertion of a heterocumulene such as an isocyanate toward a Sn–O bond,[2] and a great affinity toward a sulfur[3] or a halogen atom.[4]

We have reported the preparation of five- and six-membered heterocyclic compounds from the adduct of tributyltin ω-haloalkoxides ($n\text{-Bu}_3\text{SnO(CH}_2)_n\text{X}$) with a heterocumulene[5] (Scheme 1), in which a Lewis base plays an important role in the cyclization.

The coordination of a base toward the Sn atom increases the basicity of the adjacent heteroatom, which induces facile cyclization.

In connection with our interest in the use of this type of cyclization, we wish to report here a convenient method for the preparations of new compounds, *N*-tributylstannyl-2-oxazolidinone (**4a**) and tetrahydro-2*H*-1,3-oxazin-2-one (**4b**), by the cyclization of the adduct (**3**), generated from $(n\text{-Bu}_3\text{Sn})_2\text{O}$ (**1**) and ω-haloalkyl isocyanate (**2**). Furthermore, the preparation of a variety of *N*-substituted 2-oxazolidinones and tetrahydro-2-oxazinones by the subsequent coupling reaction could be achieved under mild and neutral conditions (Scheme 2).[6] 2-Oxazolidinones are an important class of heterocyclic compounds which have many biological uses.[7] In particular, the use of *N*-stannyl-2-oxazolidinones and tetrahydro-2-oxazinones in organic synthesis has never been reported, although the silylated analogue is widely known as a silylating agent.[8]

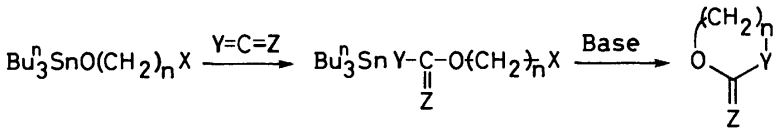

Scheme 1.

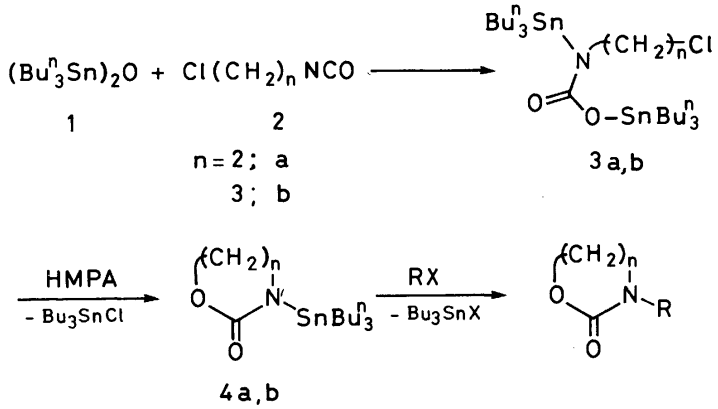

Scheme 2.

Results and Discussion

As shown in Scheme 2, *N*-tributylstannyl-2-oxazolidinone (**4a**) could be readily formed from the reaction of $(n\text{-Bu}_3\text{Sn})_2\text{O}$ (**1**) and 2-chloroethyl isocyanate (**2a**). At first, the isocyanate inserts into the Sn–O bond spontaneously to give *N*-stannylcarbamate (**3a**). This intermediate was indicated by the appearance of an IR absorption band at 1600 cm^{-1} in place of the NCO group (2280 cm^{-1}). ^1H NMR showed the multiplet peaks between δ 3.30 and 3.70 due to methylene groups adjacent the nitrogen and chloro atoms. To trap the intermediate **3a**, we tried the reaction with benzoyl chloride (Eq. 1). The *N*-acylation proceeded smoothly, and subsequent work-up gave the amide (**5**) in 98% yield, accompanied by decarboxylation.

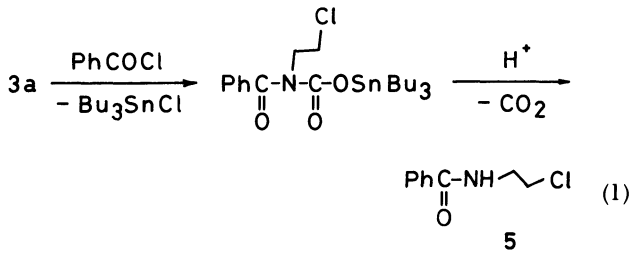

(1)

In the next stage, heating of **3a** induces the cyclization to give **4a**. IR band of the C=O group shifted to 1680 cm^{-1}, and ^1H NMR indicated the peaks of methylene groups adjacent to the nitrogen and chloro groups at δ 3.40—3.80 and 4.25—4.65, respectively. Moreover, GLC analysis showed the quantitative formation of the eliminated by-product, *n*-Bu_3SnCl.

The compound **4a** is so reactive that it was readily protonated to give 2-oxazolidinone (**6**) during work-up. Interestingly, the cyclization step is affected by additives (Table 1). Without any additives, the reaction hardly took place under the mild conditions (Entry 1), and elevated temperature (80 °C) was necessary to complete the cyclization (Entry 1, parentheses). Among the additives, the ones bearing a high coordinating ability toward a Sn atom are effective for the cyclization, and particularly, hexamethylphosphoric triamide (HMPA) was the most suitable one.[9] This coordination increases the basicity of the heteroatom adjacent to the Sn atom. Thus, the cyclization to form **4a** proceeded in high yield at room temperature in the presence of HMPA (Entry 6).

Table 1. Effect of Additive[a]

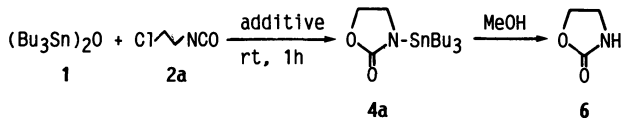

Entry	Additive	Yield of **6**/%[b]
1	—	tr (98)[c]
2	Et_3N	tr
3	Bu_3P	tr
4	DMF	73
5	Bu_3PO	62
6	HMPA	85

a) **1**; 5 mmol, **2a**; 5 mmol, additive 10 mmol. b) GLC yield. c) 80 °C, 1 h.

We next examined the coupling reactions of **4a** with organic halides. It is possible to carry out a one pot cyclization-coupling reaction by simply adding an acid chloride to the cyclization mixture. In this way, 3-benzoyl-2-oxazolidinone (**7**) was formed directly in 86% yield (Table 2, Entry 1). The acylation proceeded cleanly, affording the corresponding 3-acyl-2-oxazolidinones[10] (**7**—**13**). The yields are good or excellent, no side reactions were observed. Moreover, purification of the products was simple, and the by-product, *n*-Bu_3SnCl, could be removed completely by column chromatography using hexane as an eluent. With a half molar equivalent of oxalyl dichloride and adipoyl dichloride, bis(2-oxazolidinones) (**14**, **15**) were obtained, respectively (Entries 8 and 9).

Other organic halides also gave good yields. Similar to acid chlorides, the reactions with phosphoryl chlorides and a sulfonyl chloride proceeded spontaneously, and gave 3-phosphoryl- and 3-sulfonyl-2-oxazolidinones (**16**—**18**), respectively (Entries 10—12). With activated organic halides such as α-bromo carbonyl compounds, allyl and benzyl bromides, the coupling reactions proceeded at 80 °C to form **19**—**25** in high yields (Entries 13—19).

As in the cyclization reactions, HMPA was found to facilitate these coupling reactions, in contrast to the severe conditions previously reported for the alkylation of *N*-unsubstituted 2-oxazolidinone (**6**).[7a] For example, reaction of **4a** with cinnamyl bromide in the absence of HMPA at 80 °C for 1 h afforded only 31% of compound **22**; in the presence of HMPA, 73% yield was obtained (Entry 16). Apparently, HMPA enhances the reactivity of the Sn–N bond by coordination.

We next tried to prepare six-membered compounds, tetrahydro-2*H*-1,3-oxazin-2-one derivatives, by the analogous reactions using 3-chloropropyl isocyanate (**2b**) (Eq. 2).

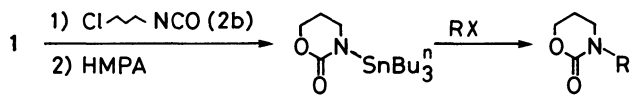

(2)

These results are shown in Table 3. Compared to the case of five-membered ring formation, the cyclization to form **4b** required severe conditions (80 °C, 1 h) for completion. Subsequent reaction with organic halides gave a variety of tetrahydro-2-oxazinone derivatives (**26**—**30**) in good yields.

Table 2. Synthesis of 2-Oxazolidinones

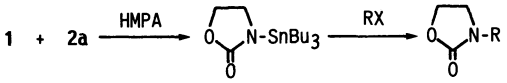

4a

Entry	RX	Conditions[a]	Product	Yield/%[a]
	RCOCl		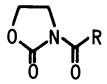	
1	R=Ph	rt, 10 min	**7**	86
2	Me	rt, 10 min	**8**	100
3	*i*-Pr	rt, 10 min	**9**	100
4	$PhCH_2$	rt, 10 min	**10**	94
5	$PhOCH_2$	rt, 10 min	**11**	99
6	PhCH=CH	rt, 10 min	**12**	88
7	$PhCH_2O$	rt, 10 min	**13**	100
	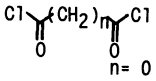		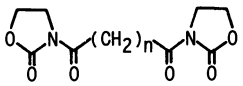	
8	n= 0	rt, 10 min	**14**	78[c]
9	4	rt, 10 min	**15**	84[c]
			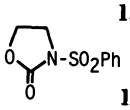	
10	$PhSO_2Cl$	rt, 10 min	**16**	80
			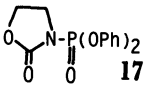	
11	$(PhO)_2PCl$	rt, 10 min	**17**	93
			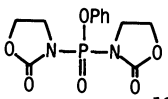	
12	$PhOPCl_2$	rt, 10 min	**18**	100[c]
			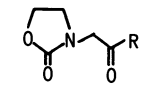	
13	R=Ph	80°C, 15 h	**19**	76
14	EtO	80°C, 15 h	**20**	78
	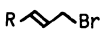		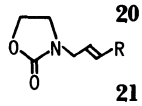	
15	R=H	80°C, 15 h	**21**	81
16	Ph	80°C, 15 h	**22**	73
			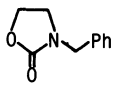	
17		80°C, 15 h	**23**	60
			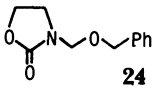	
18	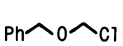	80°C, 15 h	**24**	90
			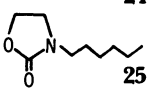	
19		80°C, 15 h	**25**	91

a) At the coupling reaction. b) Isolated yield. c) 0.5 equiv of RX was used.

Next, the preparation of 4,5-disubstituted 2-oxazolidinones was accomplished as follows. It is reported that iodine isocyanate (INCO) derived from silver cyanate and iodine, adds to an olefin in a stereospecific manner to produce 2-iodoethyl isocyanates[11] (Eq. 3).

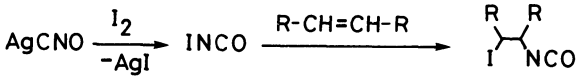

(3)

Employing these substrates, the preparation of 4,5-dialkyl-2-oxazolidinones could be achieved by the

Table 3. Synthesis of Tetrahydro-2-oxazinones

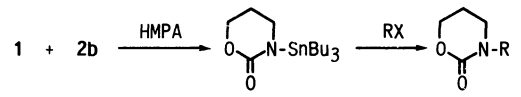

4b

Entry	RX	Condition[a]	Product	Yield/%[b]
1		rt, 10 min	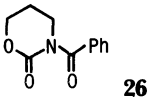 **26**	100
2		80 °C, 15 h	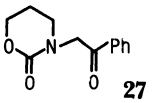 **27**	72
3	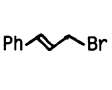	80 °C, 15 h	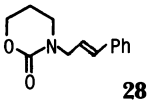 **28**	100
4	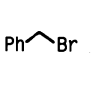	80 °C, 15 h	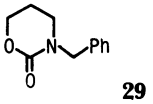 **29**	87
5	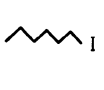	80 °C, 15 h	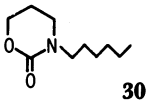 **30**	80

a) At the coupling reaction. b) Isolated yield.

Table 4. Synthesis of 2-Oxazolidinones from Olefins

Entry	Olefin	Product	Yield/%[a]
1		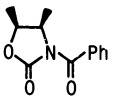 **31**	88
2		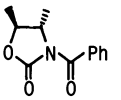 **32**	98
3		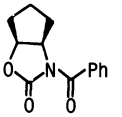 **33**	66
4		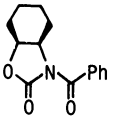 **34**	50
5		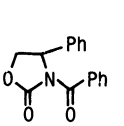 **35**	52

a) Isolated yield.

combination with our method (Table 4). For example, as shown in Eq. 4, *cis*-2-butene afforded *threo*-iodo isocyanate which reacted with **1** to give the adduct. Next, the cyclization to form *N*-stannyl-2-oxazolidinone proceeded via backside attack of the oxygen on the terminal alkyl iodide.[12] As a result, *cis*-4,5-dimethyl-2-oxazolidinone (**31**) was prepared in 88% overall yield (Entry 1).

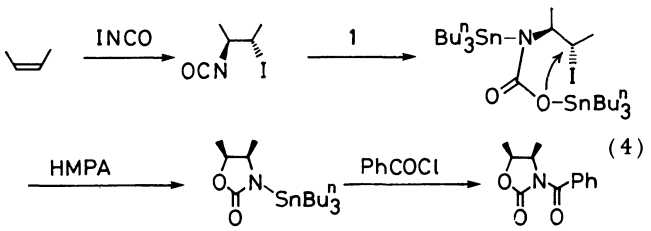

(4)

Similarly, the diastereoisomer, *trans*-dimethyl-2-oxazolidinone (**32**), was obtained from *trans*-2-butene (Entry 2).[13] Thus, 4,5-disubstituted 2-oxazolidinones could be easily prepared from olefins in a stereospecific manner by a one-pot reaction. The additional results obtained using other olefins are shown in Table 4.

In summary, we have demonstrated an effective and direct method for the preparation of 2-oxazolidinones and tetrahydro-2*H*-1,3-oxazin-2-ones by using organotin reagents. Our method provides several advantages in terms of mild and neutral conditions, high yields of products and operational convenience.

Experimental

Melting points were obtained by using a Yanaco Micromelting point apparatus and are uncorrected. IR spectra were recorded on a Hitachi 260-30 spectrometer using KBr pelletes or KRS-5 cells. ^{1}H NMR and ^{13}C NMR spectra were performed on Hitachi R-90HS spectrometer. Mass spectra were recorded on a Hitachi RMU-6E instrument. Analytical GLC was performed on Shimadzu GC-3B with TCD using a 2 m×3 mm glass column packed with Silicone OV-1 on uniport HP (5%, 60—80 mesh). Silica-gel column chromatography was used (Wakogel C-200).

Benzoyl-2-chloroethylamide (5). Under dry nitrogen, 0.53 g (5 mmol) of 2-chloroethyl isocyanate (**2a**) was added to 2.98 g (5 mmol) of bis(tributyltin) oxide (**1**). This process to form **3a** proceeded spontaneously. Next, to this solution was added 1.40 g (10 mmol) of PhCOCl at room temperature. After stirring for 10 min, the reaction mixture was chromatographed by silica-gel column, where decarboxylation occurred. Elusion with benzene gave the compound **5** which was purified by recrystallization from benzene–hexane (1:1): Mp 86—87 °C; MS *m/z* 183.5 (M^+); IR 1630 cm^{-1}; ^{1}H NMR ($CDCl_3$) δ=3.50—4.00 (m, 4H, CH_2), 6.35—6.85 (br, 1H, NH), 7.20—7.90 (m, 5H, phenyl). Calcd for $C_9H_{10}NOCl$: C, 58.86; H, 5.45; H, 7.63%. Found: C, 58.55; H, 5.41; N, 7.97%.

3-Benzoyl-2-oxazolidinone (7) (General Procedure for the Preparation of 2-Oxazolidinones): To the liquid of **3a** formed in situ was added 1.80 g (10 mmol) of HMPA. This mixture was stirred at 40 °C for 1 h, giving *N*-stannyl-2-oxazolidinone (**4a**) which was converted to **6** upon MeOH. Without HMPA, the cyclization required severe conditions (80 °C, 1 h). To this mixture containing **4a** was added 0.70 g (5 mmol) of benzoyl chloride at room temperature. After

10 min, the reaction mixture was chromatographed, and purified by recrystallization from benzene–hexane (1 : 1): mp 166—168 °C (lit,[14] mp 168 °C); IR (KBr) 1670, 1770 cm^{-1}; MS *m/z* 191 (M^+); ^1H NMR ($CDCl_3$) δ=3.80—4.35 (m, 2H, $C\underline{H}_2O$), 4.35—4.90 (m, 2H, $C\underline{H}_2N$), 7.10—8.00 (m, 5H, phenyl). The following compounds **8—18** were obtained in a similar manner by using suitable organic halides.

3-Acetyl-2-oxazolidinone (8): Mp 85 °C (lit,[7a] mp 87—87.5 °C); IR (KBr) 1690, 1780 cm^{-1}; MS *m/z* 129 (M^+); ^1H NMR ($CDCl_3$) δ=2.55 (s, 3H, $C\underline{H}_3$), 4.05 (t, *J*=8 Hz, 2H, $C\underline{H}_2N$), 4.45 (t, *J*=8 Hz, 2H, $C\underline{H}_2O$).

3-Isopropionyl-2-oxazolidinone (9): Wax, purified by Kugelrohr distillation at 100 °C/10^{-3} mmHg (1 mmHg= 133.322 Pa); IR (neat) 1700, 1780 cm^{-1}; MS *m/z* 157 (M^+); ^1H NMR ($CDCl_3$) δ=1.20 (d, *J*=7 Hz, 6H, $C\underline{H}_3$), 3.60—3.90 (m, 1H, $Me_2C\underline{H}$), 4.05 (dd, *J*=7 and 9 Hz, 2H, $C\underline{H}_2N$), 4.45 (dd, *J*=7 and 9 Hz, 2H, $C\underline{H}_2O$); Calcd for $C_7H_{11}NO_3$: C, 53.50; H, 7.01; N, 8.92%. Found: C, 53.38; H, 6.98; N, 9.04%.

3-Phenylacetyl-2-oxazolidinone (10): Mp 55—56 °C; IR (KBr) 1690, 1760 cm^{-1}; MS *m/z* 205 (M^+); ^1H NMR ($CDCl_3$) δ=3.95 (t, *J*=8 Hz, 2H, $C\underline{H}_2N$), 4.10—4.60 (m, 4H, $C\underline{H}_2O$ and $PhC\underline{H}_2$), 6.90—7.60 (m, 5H, phenyl); Calcd for $C_{11}H_{11}NO_3$: C, 64.39; H, 5.37; N, 6.83%. Found: C, 64.18; H, 5.07; N, 6.88%.

3-Phenoxyacetyl-2-oxazolidinone (11): Mp 93—95 °C; IR (KBr) 1720, 1790 cm^{-1}; MS *m/z* 221 (M^+); ^1H NMR ($CDCl_3$) δ=4.05 (t, *J*=8 Hz, 2H, $C\underline{H}_2N$), 4.50 (t, *J*=8 Hz, 2H, $C\underline{H}_2O$), 5.25 (s, 2H, $PhOCH_2$), 6.80—7.50 (m, 5H, phenyl); Calcd for $C_{11}H_{11}O_4N$: C, 59.72; H, 4.98; N, 6.33%. Found: C, 59.66; H, 4.93; N, 6.32%.

3-Cinnamoyl-2-oxazolidinone (12): Mp 148—149 °C; IR (KBr) 1620, 1770 cm^{-1}; MS *m/z* 217 (M^+); ^1H NMR ($CDCl_3$) δ=4.00—4.30 (m, 2H, $C\underline{H}_2N$), 4.30—4.60 (m, 2H, $C\underline{H}_2O$), 7.20—8.00 (m, 7H, phenyl and $C\underline{H}_2$=CH-Ph); Calcd for $C_{12}H_{11}NO_3$: C, 66.36; H, 5.07; N, 6.45%. Found: C, 66.24; H, 4.95; N, 6.55%.

3-Benzyloxycarbonyl-2-oxazolidinone (13): Mp 98—100 °C (lit,[7a] mp 101—102 °C); IR (KBr) 1800 cm^{-1}; MS *m/z* 221 (M^+); ^1H NMR ($CDCl_3$) δ=3.80—4.20 (m, 2H, $C\underline{H}_2N$), 4.30—4.60 (m, 2H, $C\underline{H}_2O$), 5.30 (s, 2H, $PhC\underline{H}_2$), 7.20—7.70 (m, 5H, phenyl).

3,3′-Oxalylbis(2-oxazolidinone) (14). The compounds **14** and **15** were prepared by using 0.5 equiv of acyl chlorides: mp 234—236 °C (lit,[7a] mp 238 °C); IR (KBr) 1710, 1790 cm^{-1}; MS *m/z* 228 (M^+); ^1H NMR ($CDCl_3$) δ=4.00—4.50 (m, 4H, $C\underline{H}_2N$), 4.50—4.90 (m, 4H, $C\underline{H}_2O$).

3,3′-Adipoylbis(2-oxazolidinone) (15): Mp 138 °C (lit,[7a] mp 138 °C); IR (KBr) 1710, 1780 cm^{-1}; MS *m/z* 284 (M^+); ^1H NMR ($CDCl_3$) δ=1.70—2.00 (m, 4H, $COCH_2C\underline{H}_2$), 2.96 (t, *J*=7 Hz, 4H, $COC\underline{H}_2$), 4.01 (t, *J*=7 Hz, 4H, $C\underline{H}_2N$), 4.32 (t, *J*=7 Hz, 4H, $C\underline{H}_2O$).

3-Phenylsulfonyl-2-oxazolidinone (16): Mp 136—138 °C (lit,[15] mp 130—135 °C); IR (KBr) 1770 cm^{-1}; MS *m/z* 227 (M^+); ^1H NMR ($CDCl_3$) δ=3.90—4.30 (m, 2H, $C\underline{H}_2N$), 4.30—4.60 (m, 2H, $C\underline{H}_2O$), 7.40—8.20 (m, 5H, phenyl).

3-Diphenyloxyphosphinyl-2-oxazolidinone (17): Mp 94—95 °C; IR (KBr) 1770 cm^{-1}; MS *m/z* 319 (M^+); ^1H NMR ($CDCl_3$) δ=3.84 (t, *J*=8 Hz, 2H, $C\underline{H}_2N$), 4.33 (t, *J*=8 Hz, 2H, $C\underline{H}_2O$), 7.20—7.40 (m, 10H, phenyl); Calcd for $C_{15}H_{14}NO_5P$: C, 56.43; H, 4.39; N, 4.39%. Found: C, 56.57; H, 4.44; N, 4.49%.

3,3′-Phenoxyphosphinylidenebis(2-oxazolidinone) (18). This compound was prepared by using 0.5 equiv of phenyl phosphorodichloridate: mp 158 °C; IR (KBr) 1770 cm^{-1}; MS *m/z* 312 (M^+); ^1H NMR ($CDCl_3$) δ=4.00—4.30 (m, 4H, $C\underline{H}_2N$), 4.40—4.70 (m, 4H, $C\underline{H}_2O$), 7.20—7.50 (m, 5H, phenyl); Calcd for $C_{12}H_{13}N_2O_6P$: C, 46.15; H, 4.17; N, 8.97%. Found: C, 45.99; H, 4.20; N, 8.89%.

3-Phenacyl-2-oxazolidinone (19). The coupling reaction of **4a** formed in situ with phenacyl bromide was performed at 80 °C for 15 h. The following compounds **20—25** were obtained in a similar manner using suitable organic halides: mp 105—108 °C; IR (KBr) 1700, 1750 cm^{-1}; MS *m/z* 205 (M^+): ^1H NMR ($CDCl_3$) δ=3.73 (dd, *J*=7 and 9 Hz, 2H, $C\underline{H}_2N$), 4.45 (dd, *J*=7 and 9 Hz, 2H, $C\underline{H}_2O$), 4.70 (s, 2H, $PhCOC\underline{H}_2$), 7.20—8.30 (m, 5H, phenyl); Calcd for $C_{11}H_{11}NO_3$; C, 64.38; H, 5.40; N, 6.83%. Found: C, 64.54; H, 5.29; N, 6.66%.

3-Ethoxycarbonylmethyl-2-oxazolidinone (20): Wax, purified by Kugelrohr distillation at 100 °C/10^{-3} mmHg; IR (neat) 1740, 1760 cm^{-1}; MS *m/z* 173 (M^+); ^1H NMR ($CDCl_3$) δ=1.29 (t, *J*=7 Hz, 3H, $C\underline{H}_3$), 3.70 (dd, *J*=7 and 9 Hz, 2H, $C\underline{H}_2N$), 4.02 (s, 2H, $C\underline{H}_2COOEt$), 4.10—4.50 (m, 4H, $C\underline{H}_2Me$ and $C\underline{H}_2O$); Calcd for $C_7H_{11}NO_4$: C, 48.55; H, 6.36; N, 8.09%. Found: C, 48.75; H, 6.47; N, 7.99%.

3-Allyl-2-oxazolidinone (21): Wax, purified by Kugelrohr distillation at 100 °C/10^{-3} mmHg (lit,[16] bp 123—125 °C/0.7 mmHg); IR (neat) 1750 cm^{-1}; MS *m/z* 127 (M^+); ^1H NMR ($CDCl_3$) δ=3.51 (dd, *J*=7 and 9 Hz, 2H, $C\underline{H}_2N$), 3.90 (d, *J*=6 Hz, 2H, $NC\underline{H}_2CH$=CH_2), 4.34 (dd, *J*=7 and 9 Hz, 2H, $C\underline{H}_2O$), 5.10—6.10 (m, 3H, $C\underline{H}$=$C\underline{H}_2$).

3-Cinnamyl-2-oxazolidinone (22): Mp 69 °C; IR (KBr) 1740 cm^{-1}; MS *m/z* 203 (M^+); ^1H NMR ($CDCl_3$) δ=3.62 (dd, *J*=7 and 9 Hz, 2H, $C\underline{H}_2N$), 4.08 (d, *J*=7 Hz, 2H, $CH_2C\underline{H}$=CHPh), 4.38 (dd, *J*=7 and 9 Hz, 2H, $C\underline{H}_2O$), 6.00—6.70 (m, 2H, $C\underline{H}$=$C\underline{H}$Ph), 7.20—7.60 (m, 5H, phenyl); Calcd for $C_{12}H_{13}NO_2$: C, 70.94; H, 6.40; N, 6.90%. Found: C, 70.78; H, 6.46; N, 6.66%.

3-Benzyl-2-oxazolidinone (23): Mp 77—78 °C (lit,[7a] mp 79—80 °C); IR (KBr) 1750 cm^{-1}; MS *m/z* 177 (M^+); ^1H NMR ($CDCl_3$) δ=3.40 (dd, *J*=7 and 9 Hz, 2H, $C\underline{H}_2N$), 4.28 (dd, *J*=7 and 9 Hz, 2H, $C\underline{H}_2O$), 4.41 (s, 2H, $PhC\underline{H}_2$), 7.40—7.60 (m, 5H, phenyl).

3-Benzyloxymethyl-2-oxazolidinone (24): Wax, purified by Kugelrohr distillation at 150 °C/10^{-3} mmHg; IR (neat) 1760 cm^{-1}; MS *m/z* 207 (M^+); ^1H NMR ($CDCl_3$) δ=3.62 (dd, *J*=7 and 9 Hz, 2H, $C\underline{H}_2N$), 4.25 (dd, *J*=7 and 9 Hz, $C\underline{H}_2O$), 4.56 (s, 2H, $C\underline{H}_2Ph$), 4.83 (s, 2H, $NC\underline{H}_2O$), 7.30—7.50 (m, 5H, phenyl); Calcd for $C_{11}H_{13}NO_3$:C, 63.77; H, 6.28; N, 6.76%. Found: C, 63.37; H, 6.41; N, 6.86%.

3-Hexyl-2-oxazolidinone (25): Wax, purified by Kugelrohr distillation at 100 °C/10^{-3} mmHg (lit,[7a] bp 176 °C/1 mmHg); IR (neat) 1740 cm^{-1}; MS *m/z* 171 (M^+); ^1H NMR ($CDCl_3$) δ=0.80—1.90 (m, 11H, $NCH_2C_5H_{11}$), 3.28 (t, *J*=7 Hz, 2H, $C\underline{H}_2C_5H_{11}$), 3.58 (dd, *J*=7 and 9 Hz, 2H, $C\underline{H}_2N$), 4.33 (dd, *J*=7 and 9 Hz, 2H, $C\underline{H}_2O$).

3-Benzoyltetrahydro-2*H*-1,3-oxazin-2-one (26) (General Procedure for the Preparation of Tetrahydro-2*H*-1,3-oxazin-2-ones). To a neat liquid of 2.98 g (5 mmol) of **1** was added 0.60 g (5 mmol) of 3-chloropropyl isocyanate (**2b**). After 10 min, 1.80 g (10 mmol) of HMPA was added to this reaction mixture, and heated at 80 °C for 1 h, where *N*-stannyltetrahydro-2*H*-1,3-oxazin-2-one (**4b**) was formed. Next, 0.70 g (5 mmol) of benzoyl chloride was added to this solution, and stirred at room temperature for 10 min. The product **26** was obtained by column chromatography: mp

87 °C; IR (KBr) 1680, 1720 cm^{-1}; MS *m/z* 205 (M^+); ^{1}H NMR ($CDCl_3$) δ=2.00—2.40 (m, 2H, $C\underline{H}_2$), 3.91 (t, *J*=6 Hz, 2H, $C\underline{H}_2N$), 4.43 (t, *J*=5 Hz, 2H, $C\underline{H}_2O$), 7.20—8.20 (m, 5H, phenyl); Calcd for $C_{11}H_{11}NO_3$: C, 64.39; H, 5.37; N, 6.83%. Found: C, 64.11; H, 5.43; N, 6.84%.

3-Phenacyltetrahydro-2*H*-1,3-oxazin-2-one (27). The coupling reaction of **4b** with organic halides to form **27—30** was performed at 80 °C for 15 h: mp 93 °C; IR (KBr) 1680, 1700 cm^{-1}; MS *m/z* 219 (M^+); ^{1}H NMR ($CDCl_3$) δ=2.16 (m, 2H, $C\underline{H}_2$), 3.43 (t, *J*=6 Hz, 2H, $C\underline{H}_2N$), 4.41 (t, *J*=5 Hz, $C\underline{H}_2O$), 4.82 (s, 2H, $PhCOC\underline{H}_2$), 7.20—8.00 (m, 5H, phenyl); Calcd for $C_{12}H_{13}NO_3$: C, 65.75; H, 5.94; N, 6.39%. Found: C, 65.55; H, 5.91; N, 6.45%.

3-Cinnamyltetrahydro-2*H*-1,3-oxazin-2-one (28): Wax, purified by Kugelrohr distillation at 150 °C/10^{-3} mmHg; IR (neat) 1690 cm^{-1}; MS *m/z* 217 (M^+); ^{1}H NMR ($CDCl_3$) δ=1.90—2.00 (m, 2H, $C\underline{H}_2$), 3.32 (t, *J*=6 Hz, 2H, $C\underline{H}_2N$), 4.11 (d, *J*=6 Hz, 2H, $C\underline{H}_2CH$=CHPh), 4.26 (t, *J*=5 Hz, 2H, $C\underline{H}_2O$), 6.00—6.70 (m, 2H, $C\underline{H}$=$C\underline{H}$Ph), 7.10—7.60 (m, 5H, phenyl); Calcd for $C_{13}H_{15}NO_2$: C, 71.89; H, 6.91; N, 6.45%. Found: C, 71.65; H, 7.08; N, 6.34%.

3-Benzyltetrahydro-2*H*-1,3-oxazin-2-one (29): Mp 35 °C; IR (KBr) 1690 cm^{-1}; MS *m/z* 191 (M^+); ^{1}H NMR ($CDCl_3$) δ=2.03 (m, 2H, $C\underline{H}_2$), 3.21 (t, *J*=6 Hz, 2H, $C\underline{H}_2N$), 4.25 (t, *J*=5 Hz, 2H, $C\underline{H}_2O$), 4.55 (s, 2H, $PhC\underline{H}_2$), 7.20—7.30 (m, 5H, phenyl); Calcd for $C_{11}H_{13}NO_2$: C, 69.11; H, 6.81; N, 7.33%. Found: C, 68.93; H, 6.83; N, 7.34%.

3-Hexyltetrahydro-2*H*-1,3-oxazin-2-one (30): Wax, purified by Kugelrohr distillation at 100 °C/10^{-3} mmHg; IR (neat) 1690 cm^{-1}; MS *m/z* 185 (M^+); ^{1}H NMR ($CDCl_3$) δ=0.80—1.90 (m, 11H, $NCH_2C_5\underline{H}_{11}$), 1.90—2.20 (m, 2H, $C\underline{H}_2$), 3.30 (m, 4H, $C\underline{H}_2N$ and $NC\underline{H}_2C_5H_{11}$), 4.23 (t, *J*=5 Hz, 2H, $C\underline{H}_2O$); Calcd for $C_{10}H_{19}NO_2$: C, 64.86; H, 10.27; N, 7.57%. Found: C, 64.97; H, 9.96; N, 7.68%.

3-Benzoyl-*cis*-4,5-dimethyl-2-oxazolidinone (31). *cis*-2-Butene (0.56 g, 10 mmol) was added to AgNCO (1.50 g, 10 mmol) in 5 ml of ether at −10 °C. The mixture was stirred vigorously while I_2 (2.54 g, 10 mmol) was added. Stirring was continued for 3 h. The slurry was filtered, and concentration of the solution gave a mobile brown liquid. To this liquid was added **1** (5.96 g, 10 mmol) at room temperature. After 10 min, HMPA (3.60 g, 20 mmol) was added to this reaction mixture, and heated at 40 °C for 1 h. Moreover, the addition of benzoyl chloride (1.40 g, 10 mmol) at room temperature and stirring for 10 min gave **31**. Mp 78 °C; IR (KBr) 1670, 1780 cm^{-1}; MS *m/z* 219 (M^+); ^{1}H NMR ($CDCl_3$) δ=1.39 (d, *J*=6.5 Hz, 3H, $NCHC\underline{H}_3$), 1.46 (d, *J*=6.5 Hz, 3H, $OCHC\underline{H}_3$), 4.50—5.00 (m, homodecoupling *J*=8 Hz, 2H, $C\underline{H}$), 7.20—7.90 (m, 5H, phenyl); ^{13}C NMR ($CDCl_3$) δ=13.2, 14.8, 54.9, 74.7, 127.9, 128.8, 132.2, 133.6, 153.0, 169.9; Calcd for $C_{12}H_{13}NO_3$: C, 65.75; H, 5.94; N, 6.39%. Found: C, 65.46; H, 5.94; N, 6.42%.

3-Benzoyl-*trans*-4,5-dimethyl-2-oxazolidinone (32): Mp 47 °C; IR (KBr) 1680, 1780 cm^{-1}; MS *m/z* 219 (M^+); ^{1}H NMR ($CDCl_3$) δ=1.46 (d, *J*=6 Hz, 3H, $NCHC\underline{H}_3$), 1.53 (d, *J*=6 Hz, 3H, $OCHC\underline{H}_3$), 4.00—4.50 (m, homodecoupling *J*=6 Hz, 2H, $C\underline{H}$), 7.20—7.90 (m, 5H, phenyl); ^{13}C NMR ($CDCl_3$) δ=17.8, 19.3, 58.2, 77.9, 128.0, 128.4, 129.2, 132.5, 162.7, 186.1; Calcd for $C_{12}H_{13}NO_3$: C, 65.75; H, 5.94; N, 6.39%. Found: C, 65.91; H, 6.03; N, 6.23%.

3-Benzoylhexahydro-2*H*-cyclopentoxazol-2-one (33): Mp 127 °C; IR (KBr) 1670, 1760 cm^{-1}; MS *m/z* 231 (M^+); ^{1}H NMR ($CDCl_3$) δ=1.80—2.30 (m, 6H, $(C\underline{H}_2)_3$), 4.80—5.20 (m, 2H, $C\underline{H}$), 7.20—7.80 (m, 5H, phenyl); Calcd for $C_{13}H_{13}NO_3$: C, 67.53; H, 5.63; N, 6.06%. Found: C, 67.20; H, 5.55; N, 6.08%.

3-Benzoylhexahydrobenzoxazol-2(3*H*)-one (34): Mp 112 °C (lit,[17] mp 114—115 °C); IR (KBr) 1670, 1690 cm^{-1}; MS *m/z* 245 (M^+); ^{1}H NMR ($CDCl_3$) δ=1.20—2.50 (m, 8H, $(C\underline{H}_2)_4$), 4.20—4.50 (m, 1H, $C\underline{H}N$), 4.50—4.80 (m, 1H, $C\underline{H}O$), 7.20—7.80 (m, 5H, phenyl).

3-Benzoyl-4-phenyl-2-oxazolidinone (35): Mp 167 °C; IR (KBr) 1680, 1790 cm^{-1}; MS *m/z* 267 (M^+); ^{1}H NMR ($CDCl_3$) δ=4.32 (dd, *J*=7 and 9 Hz, 1H, $C\underline{H}_2O$), 4.78 (t, 1H, *J*=9 Hz, $C\underline{H}_2O$), 5.64 (dd, *J*=7 and 9 Hz, 1H, $C\underline{H}N$), 7.20—7.80 (m, 10H, phenyl); Calcd for $C_{16}H_{13}NO_3$: C, 71.91; H, 4.87; N, 5.24%. Found: C, 71.80; H, 4.92; N, 5.19%.

This work was supported by the Grant-in-Aid for Scientific Research No. 62550613 from the Ministry of Education, Science and Culture.

References

1) For reviews see: A. K. Sawyer, "Organotin Compounds," Marcel Dekker New York (1971); E. Negishi "Organometallics in Organic Synthesis," Wiley, New York (1980), Vol. 1, p. 394; A. G. Davies and P. J. Smith, "Comprehensive Organometallic Chemistry," Pergamon, Oxford (1982), Vol. 2, p. 519; M. Pereyre, P. J. Quintard, and A. Rahm, "Tin in Organic Synthesis," Butterworth, London (1987).

2) A. J. Bloodworth and A. G. Davies, *J. Chem. Soc.*, **1965**, 5238; A. J. Bloodworth, A. G. Davies, and S. C. Vasishtha, *J. Chem. Soc. C*, **1967**, 1309.

3) S. Sakai, Y. Asai, Y. Kiyohara, K. Itoh, and Y. Ishii, *Organomet. Chem. Synth.*, **1**, 45 (1970); S. Sakai, Y. Fujimura, and Y. Ishii, *J. Organomet. Chem.*, **50**, 113 (1973); S. Sakai, H. Niimi, Y. Kobayashi, and Y. Ishii, *Bull. Chem. Soc. Jpn.*, **50**, 3271 (1977).

4) B. Delmond, J. C. Pommier, and J. Valade, *J. Organomet. Chem.*, **35**, 91 (1972); B. Delmond, J. C. Pommier, and J. Valade, *J. Organomet. Chem.*, **47**, 337 (1973).

5) A. Baba, H. Kishiki, I. Shibata, and H. Matsuda, *Organometallics*, **4**, 1329 (1985); A. Baba, I. Shibata, H. Kashiwagi, and H. Matsuda, *Bull. Chem. Soc. Jpn.*, **59**, 341 (1986); I. Shibata, A. Baba, and H. Matsuda, *Bull. Chem. Soc. Jpn.*, **59**, 4000 (1986).

6) A part of study on this cyclization-coupling reaction has been published as a communication: I. Shibata, A. Baba, and H. Matsuda, *J. Chem. Soc., Chem. Commun.*, **1986**, 1703.

7) For reviews see: a) M. E. Dyen, and D. Swern, *Chem. Rev.*, **67**, 197 (1967); b) V. A. Pankrotov, T. M. Frenkel, and A. M. Fainleib, *Usp. Khim. Zh. (Russ. Ed)*, **52**, 1018 (1983).

8) For example: C. Palomo, *Synthesis*, **1981**, 809; A. Arrieta and C. Palomo, *ibid.*, **1982**, 1050; J. M. Aizpurua, C. Palomo, and A. L. Palomo, *Can. J. Chem.*, **62**, 336 (1984). 336 (1984).

9) HMPA acts as an efficient ligand to organotin compounds bearing an electron withdrawing group. T. F. Bolles and R. S. Drago, *J. Am. Chem. Soc.*, **88**, 5730 (1966).

10) *N*-Acyl-2-oxazolidinones are known versatile key reagents in organic synthesis. For example; a) D. A. Evans, *Aldrichimica Acta*, **15**, 23 (1982). b) K. Narasaka, M. Inoue, and N. Okada, *Chem. Lett.*, **1986**, 1109.

11) A. Hassner, R. P. Hoblitt, C. Heathcock, J. E. Kropp,

and M. Lorber, *J. Am. Chem. Soc.*, **92**, 1326 (1970).

12) Sn–O bond has been reported to cause the backside attack toward the alkyl halides.[4]

13) The diastereoisomers, **31** and **32**, were confirmed by the coupling constant between the ring protons obtained by decoupling of the methyl protons. It has been reported that the value of cis isomer is larger than that of trans isomer: B. D. Harris, K. L. Bhat, and M. Joullie, *Tetrahedron Lett.*, **28**, 2837 (1987); D. J. Kempf, *J. Org. Chem.*, **51**, 3921, (1986).

14) O. Tsuge, T. Itoh, and K. Sakai, *Nippon Kagaku Zasshi*, **90**, 1031 (1969).

15) J. W. McFarland and R. W. Houser, *J. Org. Chem.*, **33**, 340 (1968).

16) J. S. Pierce, *J. Am. Chem. Soc.*, **50**, 241 (1928).

17) D. Ben-Ishai, *J. Am. Chem. Soc.*, **78**, 4962 (1956).

 © 1989 The Chemical Society of Japan Bull. Chem. Soc. Jpn., 62, 860—868 (1989) [Vol. 62, No. 3

New Synthesis of 2-Oxo-3-alkenylphosphonates and Hetero Diels–Alder Reactions with Vinyl Ethers Leading to 5-Substituted 2-Phosphinyl-2-cyclohexen-1-ones

Eiji WADA,* Shuji KANEMASA,* and Otohiko TSUGE
Institute of Advanced Material Study, and Department of Molecular Science and Technology,
Interdisciplinary Graduate School of Engineering Sciences,
Kyushu University, Kasugakoen, Kasuga 816
(Received October 1, 1988)

A new method of synthesizing phosphinyl-substituted enones, 2-oxo-3-alkenylphosphonates, is developed via the dianion of diethyl 2-oxopropylphosphonate. The enones serve as hetero dienes in thermal reactions with vinly ethers producing 2-alkoxy-6-(phosphinylmethyl)-3,4-dihydro-2*H*-pyrans. Acid-catalyzed cleavage of these cycloadducts is followed spontaneously by internal condensation furnishing 2-phosphinyl-2-cyclohexen-1-one derivatives.

It is well-known that a variety of α,β-unsaturated carbonyl compounds undergo thermal cycloadditions with electron-rich olefins such as vinyl ethers,[1] enamines,[2] or simple alkenes[3] producing dihydropyran skeletons. However no reaction example has been reported so far, to the best of our knowledge, of inverse electron-demand Diels–Alder cycloadditions[4] using readily enolizable hetero dienes such as 2-oxo-3-alkenyl ketones, 3-oxo-4-alkenoates, or 2-oxo-3-alkenyl sulfones.

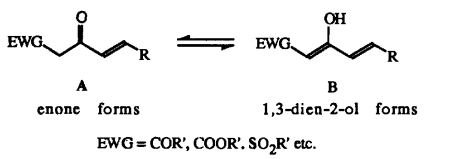

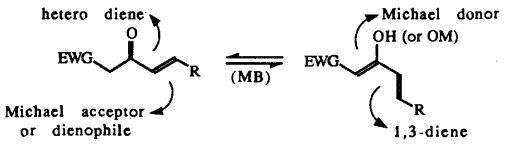

These hetero dienes with a general structure **A** undergo ready enolization into 1,3-dien-2-ols **B**. For example, methyl 3-oxo-4-pentenoate (**A**, EWG=COOMe, R=H) known as the Nazarov reagent[5] exists as a 1:1 mixture (^{1}H NMR) with enol form **B** in deuteriochloroform, and 5-hexene-2,4-dione (**A**, EWG=COMe, R=H) 1:19 (**A**:**B**) in deuteriobenzene.[6] In polar or protic medium, relative contribution of 1,3-dien-2-ols **B** must be increased. Only two examples of Diels–Alder cycloadditions of such enolized dienes **B** are known as intramolecular versions with simple olefin dienophiles.[7]

We became interested in this class of compounds as reagents in the study on Diels–Alder cycloadditions. They can be utilized as highly functionalized unsaturated molecules such as hetero dienes (enone), 1,3-dienes (1,3-dien-2-ol), and dienophiles,[8] and also as annulation reagents for six-membered ring formation via Michael type cyclizations.

To open the versatility of enone reagents of type **A**, we picked up 2-oxo-3-alkenylphosphonates (**A**, EWG=$(EtO)_2PO$). Their new synthetic method was developed and their thermal Diels–Alder reactions with electron-rich vinyl ethers were investigated. The details are presented herein.

Rsults and Discussion

Syntheses of 2-Oxo-3-alkenylphosphonates 4a—f. The known syntheses of 2-oxo-3-alkenylphosphonates consist of hydrolysis of 2-alken-1-ynylphosphonates,[9] acylation of anions of methylphosphonates,[10] and dehydration of 4-hydroxy-2-oxoalkylphosphonates.[11] As parent diethyl 2-oxo-3-butenylphosphonate (**4a**) could not be prepared[12] according to the acylation procedure reported in the literature,[10a] we needed another synthetic method of **4a**.[13]

Several examples are known for alkylations using dianion of diethyl 2-oxopropylphosphonate (**1**)[14] which is readily prepared from commercially available diethyl methylphosphonate. Therefore, we planned to open to new synthetic route of 2-oxo-3-alkenylphosphonates via the dianion of **1**.

The dianion **C**, generated according to the Grieco's method by treating **1** with sodium hydride and then butyllithium (both 1.1 equiv), was reacted with phenylthiomethyl iodide to give diethyl 2-oxo-4-(phenylthio)butylphosphonate (**2**) in 58% yield (Scheme 1). Oxidation of **2** with sodium periodate led to a quantitative yield of sulfoxide **3**. The sulfoxide **3** was then subjected, without further purification, to vacuum thermolysis (at 145 °C/13 Pa) in a Kugelrohr distilling apparatus to provide **4a** as mixture with diphenyl disulfide. A repeated distillation is enough to remove the disulfide and pure **4a** was obtained in 87% yield.

Another route to **4a** is even more general. When dianion **C** was treated with paraformaldehyde in THF in the presence of a catalytic amount of hexamethylphosphoric triamide (HMPA, 1 mol%), diethyl 4-hydroxy-2-oxobutylphosphonate (**5a**) was produced.[15] Dehydration of **5a** leading to the enone **4a** was

Table 1. Reactions of Dianion **C**[a] with Carbonyl Compounds Leading to 4-Hydroxy-2-oxoalkylphosphonates **5a—f** and 2-Oxo-3-alkenylphosphonates **4a—f**

Carbonyl compound	Condition[b]	Product (yield/%)[c]	Condition[d]	Product (yield/%)[c]
Paraformaldehyde	0 °C, 4 h[e]	**5a** (55)	0 °C, 20 min	**4a** (70)
MeCHO	−78 °C, 1 h	**5b** (72)	rt, 1 h	**4b** (89)
n-PrCHO	−78 °C, 30 min	**5c** (75)	0 °C, 1 h	**4c** (95)
PhCHO	−78 °C, 1 h	**5d** (83)	rt, 30 min	**4d** (88)[f]
p-MeOC$_6$H$_4$CHO	−78 °C, 30 min	**5e** (95)	rt, 1 h	**4e** (86)
MeCOMe	−78 °C, 1 h	**5f** (80)	80 °C, 2 h[g]	**4f** (91)

a) Dianion **C** was generated in THF by treating **1** with sodium hydride (1.1 equiv, rt, 30 min) and butyllithium (1.1 equiv, −30 to −40 °C, 30 min). b) 1.1 to 1.2 equivalent of a carbonyl compound was employed. c) Yields of isolated products. d) Triethylamine (3 equiv) was added at −30 to −50 °C to the mixture of **5** and methanesulfonyl chloride (1.2 equiv), and the mixture was stirred under conditions listed above. e) In the presence of HMPA (0.25 equiv). f) One-flask procedure without isolation of **5d** gave 80% yield of **4d** (based on **1**). g) Under reflux in benzene with *p*-TsOH (0.5 equiv).

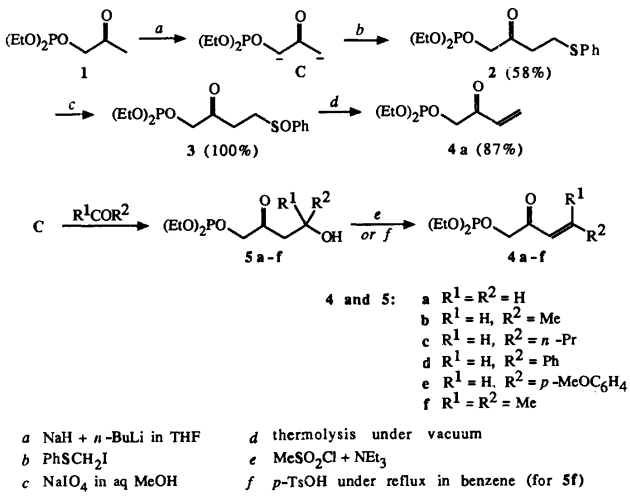

Scheme 1.

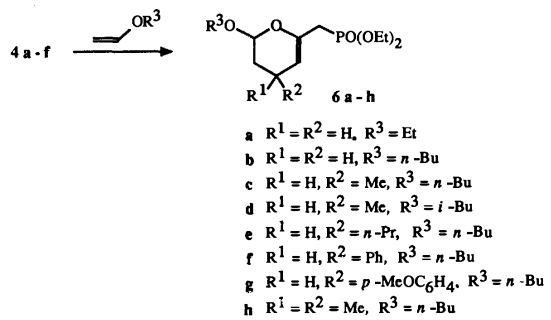

Scheme 2.

successfully carried out by a one-flask sequence of *O*-mesylation and *β*-elimination.[11]

Carbonyl compounds other than formaldehyde, such as aliphatic and aromatic aldehydes and acetone, could be employed in the condensation route with dianion **C** to give *β*-substituted derivatives **4b—f** in excellent yields (Scheme 1 and Table 1). Acid-catalyzed dehydration with *p*-toluenesulfonic acid (*p*-TsOH) was more effective for **5f**→**4f**.

Hetero Diels–Alder Reactions of 2-Oxo-3-alkenylphosphonates 4a—f with Vinyl Ethers. Thermally quite stable 2-oxo-3-alkenylphosphonates **4a—f** can undergo Diels–Alder cycloadditions as hetero dienes with vinyl ethers. Since their reactivity was not satisfactorily high, inexpensive vinyl ethers were employed in a large excess. The mixture of an enone **4a—f** and a vinyl ether in benzene was heated in a sealed tube at 85 °C for *β*-unsubstituted diene **4a**, or above 130 °C for other *β*-substituted dienes **4b—f**. In order to inhibit polymerization of vinyl ethers, a catalytic amount of *N*,*N*-diisopropylethylamine was added as a base.[16] According to these procedures, satisfactory yields of 2-alkoxy-6-(phosphinylmethyl)-3,4-dihydro-2*H*-pyrans **6a—h** were obtained (Scheme 2 and Table 2), while sterically hindered diene **4f** showed relatively decreased reactivity.

All these Diels–Alder reactions were regioselective like the previously observed examples,[1] however stereoselectivity was poor. The isolated products **6a—h** were always the mixtures of 2,4-trans and 2,4-cis isomers in 7:3 to 6:4 ratios (^{1}H NMR). However, stereoisomeric purity at the 2-position is not important in the present work because 2-alkoxy-3,4-dihydro-2*H*-pyrans **6a—h** are to be hydrolyzed in the following step.

Reactivity of 2-oxo-3-alkenylphosphonate **4a** as a hetero diene was comparable to that of 3-buten-2-one[17] or even higher, indicating that ready enolization of enones does not affect their activity as hetero dienes. Even *β*-aryl-substituted enones **4d—e**, whose dienol forms should be more highly stabilized than others, underwent smooth cycloadditions.

Acid-Hydrolysis and Subsequent Cyclization of the Diels–Alder Cycloadducts 6a—h. The hemiacetal moiety of 2-ethoxy-6-(diethoxyphosphorylmethyl)-3,4-dihydro-2*H*-pyran (**6a**) was readily hydrolyzed in 5 min at room temperature when treated with 4 M hydrochloric acid (1 M=1 mol dm^{-3}) in THF. The unpurified product was assigned to be almost pure 6-(diethylphosphoryl)-5-oxohexanal **D** (R^1=R^2=H in Scheme 3) on the basis of ^{1}H NMR spectrum: δ=1.33 (6H, t, J=7.0 Hz, OEt), 1.90 (2H, quint, J=7.0 Hz, 3-H), 2.50, 2.70 (each t, J=7.0 Hz, 2- and 4-H), 3.10

Table 2. Hetero Diels-Alder Reactions of **4a**—f with Vinyl Ethers and Subsequent Acid-Catalyzed Hydrolysis of the Cycloadducts **6a**—**h** Leading to 2-Phosphinyl-2-cyclohexen-1-ones **7a**—f

Heterodiene	Vinyl ether[a]	Condition[b]	Cycloadduct (yield/%)[c]	Condition[d]	Product (yield/%)[c]
4a	CH_2=CHOEt	85 °C, 18 h	**6a** (83)	rt, 5 min	**7a** (87)
4a	CH_2=CHOBu-*n*	85 °C, 20 h	**6b** (88)	rt, 5 min	**7a** (92)
4b	CH_2=CHOBu-*n*	130—135 °C, 48 h	**6c** (88)	rt, 5 min	**7b** (89)
4b	CH_2=CHOBu-*i*	130—135 °C, 48 h	**6d** (80)		
4c	CH_2=CHOBu-*n*	130—135 °C, 48 h	**6e** (75)	rt, 5 min	**7c** (85)
4d	CH_2=CHOBu-*n*	130—135 °C, 96 h	**6f** (66)	rt, 10 min	**7d** (79)
4e	CH_2=CHOBu-*n*	140—145 °C, 72 h	**6g** (81)	rt, 15 min	**7e** (84)
4f	CH_2=CHOBu-*n*	170—185 °C, 72 h	**6h** (57)[e]	rt, 10 min	**7f** (72)

a) Twenty equivalents of a vinyl ether were employed. b) All reactions were carried out in benzene in a sealed tube in the presence of a catalytic amount of *N,N*-diisopropylethylamine. c) Yields of isolated products. d) In THF with 4 M hydrochloric acid (2:1 v/v). e) 12% Yield of **4f** was recovered.

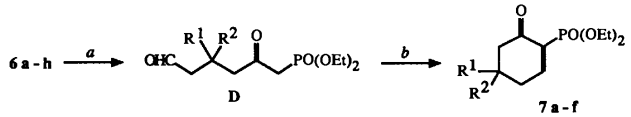

a $R^1 = R^2 = H$
b $R^1 = H$, $R^2 = Me$
c $R^1 = H$, $R^2 = n$-Pr
d $R^1 = H$, $R^2 = Ph$
e $R^1 = H$, $R^2 = p$-$MeOC_6H_4$
f $R^1 = R^2 = Me$

a 4M-HCl in THF at rt
b silica-gel chromatography

Scheme 3.

(2H, d J_{C-P}=22.5 Hz, 6-H), 4.20 (4H, dq J=7.0 and J_{C-P}=7.7 Hz, OEt), and 9.77 (1H, br s, CHO).

It was found that aldehyde **D** (R^1=R^2=H) underwent smooth cyclization leading to 2-(diethoxyphosphoryl)-2-cyclohexen-1-one (**7a**) in 87% yield on its attempted purification through column chromatography on silica gel. Presumably such a weak acid as silica gel is requisite in this facile cyclization since intermediate **D** (R^1=R^2=H) was found stable in 4 M hydrochloric acid as mentioned above. With a more diluted hydrochloric acid, the hydrolysis of **5a** becames slower and instead the acid-catalyzed cyclization of **D** is relatively accelerated, isolation of the intermediate aldehyde **D** in a pure form becoming more difficult.

Other 2-alkoxy-3,4-dihydro-2*H*-pyrans **4b**—**f** were hydrolyzed under similar conditions and crude reaction mixtures were subjected to silica-gel chromatoraphy to give 2-phosphinyl-2-cyclohexen-1-ones **7b**—**f** in satisfactory yields (Scheme 3 and Table 2).

Although acyclic vinylphosphonates bearing an acyl or ester moiety at the 1-position have been synthesized by the secondary amine-promoted condensation of phosphonates[18] or the β-elimination[19] of 1-sulfinyl phosphonates, synthetic example of 1-cycloalkenylphosphonates is quite limited.[20,21] The present reactions offer a high-yield and short step synthesis of 2-phosphinyl-2-cyclohexen-1-ones bearing a substituent at the 5-position.

Experimental

General. Melting points were determined on a Yanagimoto melting point apparatus and are uncorrected. IR spectra were taken with a JASCO IRA-1 or a JASCO A-702 spectrometer. ^{1}H NMR spectra were recorded on a Hitachi R-40 (90 MHz), a JEOL FX-100 (100 MHz), or a JEOL GSX-270 instrument (270 MHz), and ^{13}C NMR on a JEOL FX-100 (25.05 MHz) or a JEOL GSX-270 spectrometer (67.94 MHz). Chemical shifts are expressed in parts per million downfield from tetramethylsilane as an internal standard. Mass spectra and high resolution mass spectra were measured with a JEOL-01SG-2 spectrometer at 70 eV of ionization energy. Elemental analyses were performed on a Hitachi 026 CHN analyzer. For preparative column chromatography, Wakogel C-200, C-300 (Wako), and Silicagel 60 (Merck) were employed. Flash chromatography was carried out on an EYELA EF-10 apparatus using a column (20×180 mm) packed with Silicagel 60 (Merck, size: 0.04—0.063 mm). Gas liquid chromatography (GLC) was accomplished on a Yanaco G-2800 gas chromatograph (Yanagimoto) with an ionization flame detector using a glass column (SE-30, 3×2000 mm) or a glass capillary column (Silicone GE, SE-30, 0.25×50000 mm). Micro vacuum distillation was carried out on a Sibata GTO-250R Kugelrohr distilling apparatus. Solvents were evaporated with a Tokyo Rikakikai rotary evaporator type-V at about 50 °C unless otherwise stated.

Materials. Compounds **4d** and **5d** were previously prepared and characterized.[3] Though compounds **4a**, **4b**, **4f** are all known,[10a] refractive indexes, ^{1}H NMR spectra without coupling constants, and boiling points are the only reported data. Accordingly full data of these compounds are presented below. Triethylamine and dichloromethane were purified by distillation on potassium hydroxide and calcium hydride, respectively. Tetrahydrofuran (THF) was distilled on lithium aluminum hydride under nitrogen prior to use.

Diethyl 2-Oxo-4-(phenylthio)butylphosphonate (2). To a suspension of sodium hydride (60% in mineral oil, 0.93 g, 22 mol) in dry THF (60 ml) was added diethyl 2-oxopropylphosphonate (**1**, 3.88 g, 20 mmol) under nitrogen. After 30 min at room temperature, butyllithium (in hexane, 13 ml, 23 mmol) was added at −5 °C. The mixture was stirred at room temperature for 30 min and phenylthiomethyl iodide

(4.5 g, 18 mmol) was added. After stirring was continued at −10 to −5 °C for 2 h, the mixture was poured into ice-cold 3 M hydrochloric acid and then extracted with diethyl ether (30 ml×2). The combined extracts were dried over magnesium sulfate and evaporated in vacuo. The residue was chromatographed over silica gel by using hexane-ethyl acetate (1:2 v/v) to give **2** (3.32 g, 58%): Pale yellow liquid; IR (neat) 1710, 1580, 1475, 1440, 1250, 1050, 1015, 960, 800, 740, and 690 cm^{-1}; ^1H NMR ($CDCl_3$) δ=1.31 (6H, t, J=7.0 Hz, EtO), 2,95 (2H, t, J_{3-4}=6.9 Hz, 3-H), 3.07 (2H, d, J_{H-P}=22.7 Hz, 1-H), 3.14 (2H, t, J_{4-3}=6.9 Hz, 4-H), 4.12 (4H, quint, J=J_{H-P}=7.0 Hz, EtO), and 7.2—7.4 (5H, m, Ph); ^{13}C NMR ($CDCl_3$) δ=16.28 (d, J_{C-P}=5.9 Hz, EtO), 27.36 (4-C), 42.59 (d, J_{C-P}=127.1 Hz, 1-C), 43.58 (3-C), 62.66 (d, J_{C-P}=5.9 Hz, EtO), 126.39, 129.03, 129.63, 135.58 (each Ph), and 200.11 (d, J_{C-P}=5.9 Hz, CO); MS m/z (rel intensity, %) 316 (M^+, 31), 207 (base peak), 179 (40), 152 (26), 151 (44), 125 (39), 123 (35), 110 (21), 109 (35), and 97 (10). HRMS Found: m/z 316.0754. Calcd for $C_{14}H_{21}O_4PS$:M, 316.0897.

Oxidation of 2 with Sodium Periodate and Subsequent Thermolysis of 3 Leading to 4a. To a solution of **2** (1.8 g 5.69 mmol) in methanol (35 ml) was added aqueous sodium periodate (1.95 g, 9.1 mmol in 13 ml of water) at −10 to 0 °C. The mixture was stirred at 0 °C for 4 h and extracted with chloroform (25 ml). The extract was dried over magnesium sulfate and evaporated in vacuo. The crude sulfoxide **3** (1.9 g, 100%) was heated at 145 °C under vacuum (27 Pa) in a Kugelrohr distilling apparatus. The distillate (1.4 g) was purified by vacuum distillation to give **4a** (bp 130 °C/13 Pa, 1.13 g, 87%). The data of **4a** are presented below.

General Procedure for the Preparation of Diethyl 4-Hydroxy-2-oxoalkylphosphonates 5a—f. As a typical example the preparation of **5a** is described as follows: To the THF solution of dianion **C** freshly prepared from **1** (3.88 g, 20 mmol) according to the method mentioned above were added at −78 °C paraformaldehyde (0.6 g, 20 mmol) and hexamethylphosphoric triamide (HMPA, 0.1 ml). After stirred at 0 °C for 4 h, the mixture was acidified with 1 M hydrochloric acid. The THF was removed in vacuo and the aqueous residue was extracted with dichloromethane (40 ml×4). The combined extracts were dried over magensium sulfate and evaporated in vacuo. The crude product (4.6 g) was chromatographed over silica gel with ethyl acetate-methanol (99.5:0.5 to 96:4 v/v) to give **5a** (2.45 g, 55%). No HMPA was needed in the preparation of other derivatives **5b**—f; the reaction conditions and the results are summarized in Table 1. Eluents used in the chromatographic purification are as follows: **5b**, **5c**, and **5e**: ethyl acetate-methanol (95:5 v/v); **5d**: ethyl acetate; **5f**: ethyl acetate-methanol (98:2 v/v).

Diethyl 4-Hydroxy-2-oxobutylphosphonate (5a): Colorless liquid; IR (neat) 3400, 1710, 1240, 1020, and 800 cm^{-1}; ^1H NMR ($CDCl_3$) δ=1.32 (6H, t, J=7.0 Hz, EtO), 2.83 (2H, t, J_{3-4}=6.0 Hz, 3-H), 3.14 (2H, d, J_{H-P}=23.0 Hz, 1-H), 3.48 (1H, br s, OH), 3.48 (2H, t, J_{4-3}=6.0 Hz, 4-H), and 4.12 (4H, dq, J=7.0 and J_{H-P}=8.0 Hz, EtO); ^{13}C NMR ($CDCl_3$) δ=16.32 (qd, J_{C-P}=7.4 Hz, EtO), 42.65 (td, J_{C-P}=126.5 Hz, 1-C), 46.77 (t, 3-C), 57.47 (t, 4-C), 62.83 (td, J_{C-P}=5.9 Hz, EtO), and 202.30 (d, J_{C-P}=5.9 Hz, CO); MS m/z (rel intensity, %) 224 (M^+, 5), 194 (base peak), 179 (45), 152 (44), 151 (42), 125 (67), 123 (57), 109 (32), 108 (20), 97 (41), 81 (28), and 43 (28). HRMS Found: m/z 224.0808. Calcd for $C_8H_{17}O_5P$: M, 224.0813.

Diethyl 4-Hydroxy-2-oxopentylphosphonate (5b): Colorless liquid; IR (neat) 3400, 1710, 1245, 1050, 1020, 960, and 790 cm^{-1}; ^1H NMR ($CDCl_3$) δ=1.24 (3H, d, J_{5-4}=6.7 Hz, 5-H), 1.35 (6H, t, J=7.0 Hz, EtO), 2.76 (1H, d, J_{3-4}=6.4 Hz, one of 3-H), 2.74 (1H, d, J_{3-4}=5.5 Hz, the other of 3-H), 3.17 (2H, d, J_{H-P}=22.9 Hz, 1-H), 3.66 (1H, br d, J=4.0 Hz, OH), 4.16 (4H, dq, J=7.0 and J_{H-P}=8.1 Hz, EtO), and 4.0—4.3 (1H, m, 4-H); ^{13}C NMR ($CDCl_3$) δ=16.26 (dq, J_{C-P}=5.9 Hz, EtO), 22.76 (q, 5-C), 43.38 (dt, J_{C-P}=126.0 Hz, 1-C), 52.59 (t, 3-C), 62.60 (dt, J_{C-P}=5.9 Hz, EtO), 63.77 (d, 4-C), and 202.19 (d, J_{C-P}=5.9 Hz, CO); MS m/z (rel intensity, %) 238 (M^+, 3), 223 (25), 195 (27), 194 (base peak), 179 (31), 167 (21), 152 (34), 151 (22), 139 (20), 125 (44), 123 (33), 97 (25), 81 (21), and 43 (20). HRMS Found: m/z 238.0963. Calcd for $C_9H_{19}O_5P$: M, 238.0969.

Diethyl 4-Hydroxy-2-oxoheptylphosphonate (5c): Colorless liquid; IR (neat) 3400, 1710, 1395, 1250, 1050, 1020, 975, and 800 cm^{-1}; ^1H NMR ($CDCl_3$) δ=0.92 (3H, t, J_{7-6}=7.0 Hz, 7-H), 1.34 (6H, t, J=7.0 Hz, EtO), 1.3—1.6 (4H, m, 5- and 6-H), 2.70 (1H, dd, J_{gem}=17.2 and J_{3-4}=8.4 Hz, one of 3-H), 2.80 (1H, dd, J_{gem}=17.2 and J_{3-4}=3.7 Hz, the other of 3-H), 3.10 (1H, dd, J_{gem}=13.0 and J_{H-P}=22.7 Hz, one of 1-H), 3.19 (1H, dd, J_{gem}=13.0 and J_{H-P}=22.7 Hz, the other of 1-H), 3.35 (1H, br s, OH), 4.07 (1H, m, 4-H), and 4.15 (4H, dq, J=7.0 and J_{H-P}=8.1 Hz, EtO); ^{13}C NMR ($CDCl_3$) δ=13.98 (7-C), 16.33 (d, J_{C-P}=5.9 Hz, EtO), 18.68 (6-C), 38.89 (5-C), 43.09 (d, J_{C-P}=127.2 Hz, 1-C), 51.16 (3-C), 62.76 (d, J_{C-P}=6.9 Hz, EtO), 67.38 (4-C), and 202.89 (d, J_{C-P}=5.9 Hz, CO); MS m/z (rel intensity, %) 266 (M^+, 5), 222 (base peak), 195 (34), 194 (43), 179 (20), 139 (20), 125 (23), 123 (20), and 97 (13). HRMS Found: m/z 266.1320. Calcd for $C_{11}H_{23}O_5P$: M, 266.1320.

Diethyl 4-Hydroxy-4-(*p*-methoxyphenyl)-2-oxobutylphosphonate (5e): Colorless liquid; IR (neat) 3350, 1705, 1610, 1580, 1505, 1300, 1250, 1175, 1025, 960, 825, and 790 cm^{-1}; ^1H NMR ($CDCl_3$) δ=1.32 (6H, t, J=6.6 Hz, EtO), 2.92 (1H, dd, J_{gem}=17.2 and J_{3-4}=3.7 Hz, one of 3-H), 3.05 (1H, dd, J_{gem}=17.2 and J_{3-4}=8.8 Hz, the other of 3-H), 3.07 (1H, dd, J_{gem}=13.5 and J_{H-P}=22.7 Hz, one of 1-H), 3.16 (1H, dd, J_{gem}=13.5 and J_{H-P}=22.7 Hz, the other of 1-H), 3.65 (1H, br, OH), 4.12 (4H, m, EtO), 5.11 (1H, dd, J_{4-3}=8.8 and 3.7 Hz, 4-H), 6.86 (2H, dt, J=8.4 and 1.8 Hz, Ar), and 7.28 (2H, dt, J=8.4 and 1.8 Hz, Ar); ^{13}C NMR ($CDCl_3$) δ=16.30 (d, J_{C-P}=5.9 Hz, EtO), 43.11 (d, J_{C-P}=127.0 Hz, 1-C), 52.87 (3-C), 55.28 (*p*-MeO), 62.73 (d, J_{C-P}=6.9 Hz, EtO), 69.50 (4-C), 113.86, 126.97, 135.17, 159.10 (each Ar), and 201.98 (d, J_{C-P}=5.9 Hz, CO); MS m/z (rel intensity, %) 330 (M^+, 19), 195 (32), 194 (85), 167 (29), 161 (44), 152 (47), 150 (20), 139 (26), 137 (37), 136 (25), 135 (base peak), 125 (63), 123 (28), 109 (31), 96 (42), 80 (31), 76 (31), and 43 (33). HRMS Found: m/z 330.1235. Calcd for $C_{15}H_{23}O_6P$: M, 330.1231.

Diethyl 4-Hydroxy-4-methyl-2-oxopentylphosphonate (5f): Colorless liquid; IR (neat) 3400, 1705, 1470, 1440, 1380, 1350, 1320, 1240, 1155, 1040, 1020, 970, and 780 cm^{-1}; ^1H NMR ($CDCl_3$) δ=1.27 (6H, s, 5-H and 4-Me), 1.35 (6H, t, J=7.0 Hz, EtO), 2.82 (2H, s, 3-H), 3.14 (2H, d, J_{H-P}=22.7 Hz, 1-H), 3.70 (1H, br, OH), and 4.15 (4H, dq, J=7.0 and J_{H-P}=8.1 Hz, EtO); ^{13}C NMR ($CDCl_3$) δ=16.31 (d, J_{C-P}=5.9 Hz, EtO), 29.33 (5-and 4-Me), 43.83 (d, J_{C-P}=126.2 Hz, 1-C), 55.09 (3-C), 62.69 (d, J_{C-P}=5.9 Hz, EtO), 69.67 (4-C), and 203.55 (d, J_{C-P}=5.9 Hz, CO); MS m/z (rel intensity, %) 253 (M^++1, 5), 237 (91), 195 (25), 194 (94), 179 (47), 167 (49), 152 (49), 151 (36), 139 (77), 125 (81), 124 (22), 123 (77), 121 (41), 109 (37), 108 (20), 105

(22), 97 (63), 96 (43), 81 (61), 78 (24), 65 (33), 59 (73), 58 (21), and 43 (base peak). No analytical data was obtained because of the absence of parent ion peak and the hygroscopic nature.

General Procedure for the Dehydration of 5a—f Leading to 2-Oxo-3-alkenylphosphonates 4a—f. As a typical example the conversion of **5a** into **4a** is described as follows: To a solution of **5a** (5.15 g, 23 mmol) and methanesulfonyl chloride (3.16 g, 27.6 mmol) in dry dichloromethane (50 ml) was added dropwise triethylamine (6.91 g, 68.9 mmol) at −50 °C. After stirring at 0 °C for 20 min, the mixture was poured into ice water. The dichloromethane separated was washed with 1 M hydrochloric acid and water, dried over magnesium sulfate, and then evaporated in vacuo. The crude product (4.4 g) was subjected to vacuum distillation to give **4a** (3.3 g, 70%). Other compounds **5b—e** were similarly dehydrated under the reaction conditions listed in Table 1. Eluents used for the chromatographic purification of **4b—e** are as follows: **4b**: hexane–ethyl acetate (1:1 to 0:1 v/v); **4c**: ethyl acetate; **4d**: hexane–ethyl acetate (1:2 v/v); **4e**: hexane–ethyl acetate (1:4 to 0:1 v/v).

Diethyl 2-Oxo-3-butenylphosphonate (4a):[10a] Colorless liquid; bp 130 °C/13 Pa (bulb-to-bulb); IR (neat) 1670, 1610, 1240, 1020, and 800 cm^{-1}; ^1H NMR ($CDCl_3$) δ=1.32 (6H, t, J=7.0 Hz, EtO), 3.24 (2H, d, J_{H-P}=22.5 Hz, 1-H), 4.12 (4H, dd, J=7.0 and J_{H-P}=8.0 Hz, EtO), 5.90 (1H, dd, $J_{4-3(cis)}$=9.0 and J_{gem}=2.5 Hz, one of 4-H), 6.26 (1H, dd, $J_{4-3(trans)}$=17.5 and J_{gem}=2.5 Hz, the other of 4-H), and 6.50 (1H, dd, $J_{3-4(trans)}$=17.5 and $J_{4-3(cis)}$=9.0 Hz, 3-H); ^{13}C NMR ($CDCl_3$) δ=16.35 (qd, J_{C-P}=5.9 Hz, EtO), 39.88 (td, J_{C-P}=129.4 Hz, 1-C), 62.71 (td, J_{C-P}=5.9 Hz, EtO), 130.60 (t, 4-C), 136.42 (d, 3-C), and 192.04 (s, 2-C); MS m/z (rel intensity, %) 206 (M^+, 79), 179 (35), 178 (35), 161 (34), 151 (70), 134 (33), 133 (34), 125 (60), 123 (73), 109 (48), 97 (52), 96 (22), 81 (34), 70 (31), and 55 (base peak). HRMS Found: m/z 206.0698. Calcd for $C_8H_{15}O_4P$: M, 206.0707.

Diethyl (*E*)-2-Oxo-3-pentenylphosphonate (4b):[10a] Colorless liquid; bp 145—150 °C/20 Pa (bulb-to-bulb); IR (neat) 1660, 1625, 1440, 1290, 1245, 1050, 1020, 960, and 940 cm^{-1}; ^1H NMR ($CDCl_3$) δ=1.33 (6H, t, J=7.0 Hz, EtO), 1.94 (3H, br d, J_{5-4}=6.9 Hz, 5-H), 3.19 (2H, d, J_{H-P}=22.7 Hz, 1-H), 4.14 (4H, dq, J=7.0 and J_{H-P}=8.1 Hz, EtO), 6.26 (1H, br d, J_{3-4}=15.8 Hz, 3-H), and 6.96 (1H, br dq, J_{4-3}=15.8 and J_{4-5}=6.9 Hz, 4-H); ^{13}C NMR ($CDCl_3$) δ=16.31 (d, J_{C-P}=5.9 Hz, EtO), 18.37 (5-C), 40.06 (d, J_{C-P}=123.3 Hz, 1-C), 62.56 (d, J_{C-P}=5.9 Hz, EtO), 131.72 (3-C), 145.58 (4-C), and 191.10 (d, J_{C-P}=6.9 Hz, CO); MS m/z (rel intensity, %) 220 (M^+, 22), 125 (35), 97 (30), 69 (base peak), and 41 (49). HRMS Found: m/z 220.0863. Calcd for $C_9H_{17}O_4P$: M, 220.0863.

Diethyl (*E*)-2-Oxo-3-heptenylphosphonate (4c): Colorless liquid; bp 150 °C/27 Pa (bulb-to-bulb); IR (neat) 1690, 1665, 1625, 1250, 1055, 1025, 975, and 790 cm^{-1}; ^1H NMR ($CDCl_3$) δ=0.95 (3H, t, J_{7-6}=7.4 Hz, 7-H), 1.33 (6H, t, J=7.0 Hz, EtO), 1.52 (2H, sex, J_{6-5}=J_{6-7}=7.4 Hz, 6-H), 2.24 (2H, br q, J_{5-4}=J_{5-6}=7.4 Hz, 5-H), 3.21 (2H, d, J_{H-P}=22.7 Hz, 1-H), 4.14 (4H, dq, J=7.0 and J_{H-P}=8.1 Hz, EtO), 6.24 (1H, br d, J_{3-4}=15.8 Hz, 3-H), and 6.95 (1H, br dt, J_{4-3}=15.8 and J_{4-5}=7.4 Hz, 4-H); ^{13}C NMR ($CDCl_3$) δ=13.68 (7-C), 16.32 (d, J_{C-P}=6.8 Hz, EtO), 21.25 (6-C), 34.54 (5-C), 40.12 (d, J_{C-P}=128.1 Hz, 1-C), 62.52 (d, J_{C-P}=6.8 Hz, EtO), 130.22 (3-C), 150.25 (4-C), and 191.31 (d, J_{C-P}=5.9 Hz, CO); MS m/z (rel intensity, %) 248 (M^+, base peak), 220 (33), 179 (27), 152 (30), 151 (27), 125 (39), 123 (34), 110 (26), 97 (34), and 55 (33). HRMS Found: m/z 248.1191. Calcd for $C_{11}H_{21}O_4P$: M, 248.1176.

Diethyl (*E*)-4-(*p*-Methoxyphenyl)-2-oxo-3-butenylphosphonate (4e): Colorless prisms (diethyl ether–hexane); mp 53—54 °C; IR (KBr) 1675, 1640, 1595, 1295, 1250, 1175, 1075, 1050, 1025, 960, and 840 cm^{-1}; ^1H NMR ($CDCl_3$) δ=1.33 (6H, t, J=7.0 Hz, EtO), 3.30 (2H, d, J_{H-P}=22.7 Hz, 1-H), 3.84 (3H, s, *p*-MeO), 4.17 (4H, dq, J=7.0 and J_{H-P}=8.1 Hz EtO), 6.77 (1H, br d, J_{3-4}=16.1 Hz, 3-H), 6.91 (2H, br d, J=8.9 Hz, Ar), 7.53 (2H, br d, J=8.9 Hz, Ar), and 7.61 (1H, br d, J_{4-3}=16.1 Hz, 4-H); ^{13}C NMR ($CDCl_3$) δ=16.36 (d, J_{C-P}=5.9 Hz, EtO), 40.93 (d, J_{C-P}=128.1 Hz, 1-C), 55.42 (*p*-MeO), 62.58 (d, J_{C-P}=5.9 Hz, EtO), 114.50, 123.60, 126.88, 130.42, 144.60, 161.98 (Ar, 3- and 4-C), and 190.91 (d, J_{C-P}=5.9 Hz, CO); MS m/z (rel intensity, %) 312 (M^+, 24), 174 (56), 161 (base peak), and 133 (18). Found: C, 57.71; H, 7.01%. Calcd for $C_{15}H_{21}O_5P$: C, 57.69; H, 6.78%.

Diethyl 4-Methyl-2-oxo-3-pentenylphosphonate (4f).[10a] A solution of **5f** (1.008 g, 4 mmol) and *p*-toluenesulfonic acid monohydrate (0.38 g, 2 mmol) in benzene (30 ml) was heated under reflux for 2 h with continuous removal of water by the aid of a Dean-Stark trap. The mixture was evaporated in vacuo, the residue was washed with water, and extracted with dichloromethane (25 ml×2). The combined extracts were washed with saturated aqueous sodium hydrogencarbonate, dried over magnesium sulfate, and evaporated in vacuo. The residue was chromatographed over silica gel with dichloromethane–ethyl acetate (2:1 v/v) to give **4f** (0.85 g, 91%): Colorless liquid; bp 150 °C/27 Pa (bulb-to-bulb); IR (neat) 1680, 1620, 1445, 1390, 1250, 1025, 965, and 790 cm^{-1}; ^1H NMR ($CDCl_3$) δ=1.33 (6H, t, J=7.0 Hz, EtO), 1.92, 2.16 (each 3H, s, 5-H and 4-Me), 3.07 (2H, d, J_{H-P}=22.7 Hz, 1-H), 4.14 (4H, dq, J=7.0 and J_{H-P}=8.1 Hz, EtO), and 6.25 (1H, s, 3-H); ^{13}C NMR ($CDCl_3$) δ=16.32 (d, J_{C-P}=5.9 Hz, EtO), 21.02 (5-C), 27.79 (4-Me), 43.70 (d, J_{C-P}=127.2 Hz, 1-C), 62.42 (d, J_{C-P}=5.9 Hz, EtO), 123.93 (3-C), 158.04 (4-C), and 190.85 (d, J_{C-P}=5.9 Hz, 2-C); MS m/z (rel intensity, %) 234 (M^+, 17), 97 (23), 96 (61), 83 (base peak), 81 (34), 59 (66), and 58 (26).

Genral Procedure for the Hetero Diels-Alder Reaction of 4a—f Leading to 3,4-Dihydro-2*H*-pyrans 6a—h. As a typical procedure the reaction of **4a** with ethyl vinyl ether is described as follows: A mixture of **4a** (1.035 g, 5.02 mmol), ethyl vinyl ether (7.2 g, 100 mmol), and *N,N*-diisopropylethylamine (trace) in benzene (1 ml) was heated in a sealed tube at 85 °C for 18 h. The mixture was condensed in vacuo and the residue was chromatographed over silica gel by using ethyl acetate–methanol (1:0 to 98:2 v/v) to give **6a** (1.16 g, 83%). Other cycloadducts **6b—h** were similarly obtained under the reaction conditions listed in Table 2. Eluents used for the chromatographic purification are as follows: **6b**: hexane–ethyl acetate (1:2 to 0:1 v/v); **6c** and **6d**: dichloromethane–ethyl acetate (2:1 to 2:3 v/v); **6e** and **6h**: hexane–ethyl acetate (1:2 v/v); **6f**: hexane–ethyl acetate (2:3 v/v); **6g**: dichloromethane–ethyl acetate (3:1 v/v); No satisfactory analytical data were obtained because of the hygroscopic nature of **6a—h**. Analysis by HRMS was carried out for the stereochemically pure **6a, b**. The other compounds **6c—h** were characterized on the basis of spectral data and employed for the following reactions.

2-Ethoxy-6-[(diethoxyphosphoryl)methyl]-3,4-dihydro-2*H*-

pyran (6a): Colorless liquid; IR (neat) 1675, 1475, 1440, 1380, 1240, 1155, 1110, 1050, 1025, and 955 cm^{-1}; ^1H NMR (C_6D_6) δ=1.10 (6H, dt, J=7.0 and J_{H-P}=4.0 Hz EtO), 1.14 (3H, t, J=7.0 Hz, 2-EtO), 1.5—1.8 (3H, m, 3- and 4-H), 2.17 (1H, m, one of 3-H), 2.60 (2H, d, J_{H-P}=20.9 Hz, 6-CH_2P), 3.43 (1H, dq, J_{gem}=9.5 and J=7.0 Hz, 2-EtO), 3.9—4.1 (1H, m, 2-EtO), 4.13 (4H, dq, J=7.0 and J_{H-P}=8.1 Hz, EtO), 4.73 (1H, br q, J_{5-4}=J_{H-P}=4.4 Hz, 5-H), and 4.88 (1H, t, J_{2-3}=3.3 Hz, 2-H); ^{13}C NMR (C_6D_6) δ=15.33 (2-EtO), 16.53, 16.56 (each d, J_{C-P}=5.9 Hz, EtO), 17.32 (4-C), 26.58 (3-C), 32.94 (d, J_{C-P}=139.9 Hz, 6-CH_2P), 61.61, 61.81 (each d, J_{C-P}=5.9 Hz, EtO), 63.79 (2-EtO), 97.71 (2-C), 99.88 (d, J_{C-P}=9.8 Hz, 5-C), and 143.14 (d, J_{C-P}=10.8 Hz, 6-C); MS m/z (rel intensity, %) 278 (M^+, 45), 233 (37), 232 (base peak), 231 (49), 207 (30), 203 (65), 151 (33), 140 (30), 123 (24), 95 (42), 94 (61), and 72 (42). HRMS Found: m/z 278.1284. Calcd for $C_{12}H_{23}O_5P$: M, 278.1282.

2-Butoxy-6-[(diethoxyphosphoryl)methyl]-3,4-dihydro-2*H*-pyran (6b): Colorless liquid; IR (neat) 1675, 1445, 1390, 1360, 1250, 1120, 1030, 965, 840, 805, and 790 cm^{-1}; ^1H NMR (C_6D_6) δ=0.87 (3H, t, J=7.0 Hz, *n*-BuO), 1.10 (6H, dt, J=7.0 and J_{H-P}=4.4 Hz, EtO), 1.38 (2H, m, *n*-BuO), 1.55 (2H, m, *n*-BuO), 1.5—1.8 (3H, m, 3- and 4-H), 2.15 (1H, m, one 3-H), 2.62 (2H, d, J_{H-P}=20.9 Hz, 6-CH_2P), 3.41 (1H, dt, J_{gem}=9.5 and J=6.5 Hz, *n*-BuO), 3.9—4.1 (5H, m, EtO and *n*-BuO), 4.74 (1H, q, J_{5-4}=J_{H-P}=4.0 Hz, 5-H), and 4.89 (1H, t, J_{2-3}=3.4 Hz, 2-H); ^{13}C NMR (C_6D_6), δ=14.10 (*n*-BuO), 16.54, 16.57 (each d, J_{C-P}=5.9 Hz, EtO), 17.35 (d, J_{C-P}=2.1 Hz, 4-C), 19.73 (*n*-BuO), 26.59 (3-C), 32.18 (*n*-BuO), 32.96 (d, J_{C-P}=140.9 Hz, 6-CH_2P), 61.58, 61.77 (each d, J_{C-P}=5.9 Hz, EtO), 68.17 (*n*-BuO), 97.92 (2-C), 99.85 (d, J_{C-P}=9.6 Hz, 5-C), and 143.18 (d, J_{C-P}=10.8 Hz, 6-C); MS m/z (rel intensity, %) 306 (M^+, 28), 233 (29), 232 (base peak), 231 (34), 207 (26), 203 (55), 179 (26), 151 (32), 123 (23), 95 (28), 94 (55), and 56 (23). HRMS Found: m/z 306.1635. Calcd for $C_{14}H_{27}O_5P$: 306.1595.

2-Butoxy-6-[(diethoxyphosphoryl)methyl]-4-methyl-3,4-dihydro-2*H*-pyran (6c): A 34:66 mixture of cis and trans isomers (^{13}C NMR); Colorless liquid; IR (neat) 1675, 1450, 1390, 1370, 1325, 1295, 1250, 1120, 1050, 1020, 960, 830, and 770 cm^{-1}; ^1H NMR (C_6D_6) cis: δ=0.87 (3H, t, J=7.3 Hz, *n*-BuO), 0.92 (3H, d, J=6.6 Hz, 4-Me), 1.11 (6H, dt, J=7.0 and J_{H-P}=1.5 Hz, EtO), 1.2—1.7 (5H, m, 3-H and *n*-BuO), 1.83 (1H, dddd, J_{gem}=13.2, J_{3-4}=6.0, J_{3-2}=2.2, and J_{3-5}=1.0 Hz, one of 3-H), 2.19 (1H, m, 4-H), 2.57 (1H, dd, J_{gem}=15.0 and J_{H-P}=21.0 Hz, one of 6-CH_2P), 2.65 (1H, dd, J_{gem}=15.0 and J_{H-P}=21.0 Hz, the other of 6-CH_2P), 3.42 (1H, dt, J_{gem}=9.5 and J=6.8 Hz, *n*-BuO), 4.01 (4H, quint, J=J_{H-P}=7.0 Hz, EtO), 4.01 (1H, dt, J_{gem}=9.5 and J=6.8 Hz, *n*-BuO), 4.57 (1H, m, 5-H), and 4.86 (1H, dd, J_{2-3}=8.1 and 2.2 Hz, 2-H); trans: δ=0.87 (3H, t, J=7.0 Hz, *n*-BuO), 0.87 (3H, d, J=6.6 Hz, 4-Me), 1.10 (6H, br d, J=7.0 Hz, EtO), 1.2—1.7 (5H, m, 3-H and *n*-BuO), 1.7—1.9 (1H, m, one of 3-H), 2.52 (1H, m, 4-H), 2.5—2.7 (2H, m, 6-CH_2P), 3.3—3.4 (1H, m, *n*-BuO), 3.9—4.1 (5H, m, *n*-BuO and EtO), 4.65 (1H, m, 5-H), and 4.93 (1H, t, J_{2-3}=3.0 Hz, 2-H); ^{13}C NMR (C_6D_6) cis: δ=14.05 (*n*-BuO), 16.56 (d, J_{C-P}=5.9 Hz, EtO), 19.70 (*n*-BuO), 21.58 (d, J_{C-P}=2.9 Hz, 4-Me), 26.69 (d, J_{C-P}=2.0 Hz, 4-C), 32.20 (*n*-BuO), 32.69 (d, J_{C-P}=139.9 Hz, 6-CH_2P), 36.30 (3-C), 61.77 (d, J_{C-P}=5.9 Hz, EtO), 68.67 (*n*-BuO), 100.40 (2-C), 105.93 (d, J_{C-P}=9.8 Hz, 5-C), and 143.29 (d, J_{C-P}=10.8 Hz, 6-C); trans: δ=14.13 (*n*-BuO), 16.59 (d, J_{C-P}=5.9 Hz, EtO), 19.76 (*n*-BuO), 21.40 (d, J_{C-P}=2.9 Hz, 4-Me), 22.68 (d, J_{C-P}=2.0 Hz, 4-C), 32.22 (*n*-BuO), 32.89 (d, J_{C-P}=139.9 Hz, 6-CH_2P), 35.19 (3-C), 61.57 (d, J_{C-P}=5.9 Hz, EtO), 68.19 (*n*-BuO), 97.51 (2-C), 106.68 (d, J_{C-P}=9.8 Hz, 5-C), and 142.23 (d, J_{C-P}=10.8 Hz, 6-C); MS m/z (rel intensity, %) 320 (M^+, 34), 247 (35), 246 (86), 245 (36), 231 (91), 221 (74), 217 (29), 123 (40), 110 (25), 108 (base peak), 58 (22), and 57 (28).

6-[(Diethoxyphosphoryl)methyl]-2-isobutoxy-4-methyl-3,4-dihydro-2*H*-pyran (6d): A 38:62 mixture of cis and trans isomers (^{13}C NMR); Colorless liquid; IR (neat) 1675, 1450, 1390, 1365, 1250, 1120, 1050, 1020, 975, 895, 830, and 775 cm^{-1}; ^1H NMR (C_6D_6) cis: δ=0.92 (6H, d, J=7.0 Hz, *i*-BuO), 0.93 (3H, t, J=7.0 Hz, 4-Me), 1.11 (6H, dt, J=7.0 and J_{H-P}=1.5 Hz, EtO), 1.49 (1H, ddd, J_{gem}=13.2, J_{3-4}=9.2, and J_{3-2}=8.1 Hz, one of 3-H), 1.82 (1H, m, the other of 3-H), 1.88 (1H, m, *i*-BuO), 2.20 (1H, m, 4-H), 2.57, 2.65 (each 1H, dd, J_{gem}=13.5 and J_{H-P}=21.0 Hz, 6-CH_2P), 3.18, 3.81 (each 1H, dd, J_{gem}=9.5 and J=7.0 Hz, *i*-BuO), 4.01 (4H, dq, J=7.0 and J_{H-P}=8.1 Hz, EtO), 4.58 (1H, m, 5-H), and 4.85 (1H, dd, J_{2-3}=8.1 and 2.2 Hz, 2-H); trans: δ=0.88 (3H, d, J=7.0 Hz, 4-Me), 0.92, 0.94 (each 3H, d, J=7.0 Hz, (C_6D_6), 1.10 (6H, dt, J=7.0 and J_{H-P}=4.1 Hz, EtO), 1.26 (1H, ddd, J_{gem}=13.2, J_{3-4}=10.3, and J_{3-2}=2.9 Hz, one of 3-H), 1.76 (1H, m, the other of 3-H), 2.51 (1H, m, 4-H), 2.5—2.7 (2H, m, 6-CH_2P), 3.17, 3.84 (each 1H, dd, J_{gem}=9.5 and J=7.0 Hz, *i*-BuO), 4.65 (1H, m, 5-H), and 4.92 (1H, t, J_{2-3}=2.9 Hz, 2-H); ^{13}C NMR (C_6D_6) cis: δ=16.59 (d, J_{C-P}=5.9 Hz, EtO), 19.50, 19.54 (each *i*-BuO), 21.58 (d, J_{C-P}=2.9 Hz, 4-Me), 26.62 (d, J_{C-P}=2.0 Hz, 4-C), 28.91 (*i*-BuO), 32.83 (d, J_{C-P}=139.9 Hz, 6-CH_2P), 36.14 (3-C), 61.58 (d, J_{C-P}=5.9 Hz, EtO), 61.76 (d, J_{C-P}=6.9 Hz, EtO), 75.66 (*i*-BuO), 100.52 (2-C), 105.94 (d, J_{C-P}=9.8 Hz, 5-C), and 143.22 (d , J_{C-P}=9.8 Hz, 6-C); trans: δ=16.59 (d, J_{C-P}=5.9 Hz), 19.50, 19.54 (each *i*-BuO), 21.39 (d, J_{C-P}=2.9 Hz, 4-Me), 22.66 (d, J_{C-P}=2.0 Hz, 4-C), 28.91 (*i*-BuO), 32.83 (d, J_{C-P}=140.9 Hz, 6-CH_2P), 35.15 (3-C), 61.58 (d, J_{C-P}=5.9 Hz, EtO), 61.76 (d, J_{C-P}=6.9 Hz, EtO), 75.03 (*i*-BuO), 97.59 (2-C), 106.69 (d, J_{C-P}=9.8 Hz, 5-C), and 142.18 (d, J_{C-P}=9.8 Hz, 6-C).

2-Butoxy-6-[(diethoxyphosphoryl)methyl]-4-propyl-3,4-dihydro-2*H*-pyran (6e): A 35:65 mixture of cis and trans isomers (^{13}C NMR); Colorless liquid; IR (neat) 1670, 1250, 1120, 1055, 1020, and 965 cm^{-1}; ^1H NMR (C_6D_6) cis: δ=0.82 (3H, t, J=7.3 Hz, *n*-Pr), 0.88 (3H, t, J=7.3 Hz, *n*-BuO), 1.11 (6H, br t, J=7.0 Hz, EtO), 1.2—1.6 (9H, m, *n*-BuO, *n*-Pr, and 3-H), 1.88 (1H, dddd, J_{gem}=13.2, J_{3-4}=6.0, J_{3-2}=2.2, and J_{3-5}=1.0 Hz, one of 3-H), 2.14 (1H, m, 4-H), 2.59 (1H, dd, J_{gem}=13.5 and J_{H-P}=21.0 Hz, one of 6-CH_2P), 2.66 (1H, dd, J_{gem}=13.5 and J_{H-P}=21.0 Hz, the other of 6-CH_2P), 3.44 (1H, dt, J_{gem}=9.5 and J=7.2 Hz, *n*-BuO), 4.0—4.1 (5H, m, *n*-BuO, and EtO), 4.66 (1H, m, 3-H), and 4.88 (1H, dd, J_{2-3}=8.1 and 2.2 Hz, 2-H); trans: δ=0.82 (3H, t, J=7.3 Hz, *n*-Pr), 0.88 (3H, t, J=7.3 Hz, *n*-BuO), 1.10 (6H, br t, J=7.0 Hz, EtO), 1.8—1.9 (9H, m, *n*-BuO, *n*-Pr, and 3-H), 2.45 (1H, m, 4-H), 2.5—2.7 (2H, m, 6-CH_2P), 3.4—3.5 (1H, m, *n*-BuO), 3.9—4.1 (5H, m, *n*-BuO and EtO), 4.74 (1H, m, 5-H), and 4.97 (1H, dd, J_{2-3}=3.0 and 2.2 Hz, 2-H); ^{13}C NMR (C_6D_6) cis: δ=14.05 (*n*-BuO), 14.29 (*n*-Pr), 16.57 (d, J_{C-P}=5.9 Hz, EtO), 19.70 (*n*-BuO), 20.30, 31.68 (each *n*-Pr), 32.24 (*n*-BuO), 32.71 (d, J_{C-P}=139.9 Hz, 6-CH_2P), 34.50 (3-C), 38.54 (d, J_{C-P}=2.0 Hz, 4-C), 61.72 (d, J_{C-P}=6.9 Hz, EtO), 68.68 (*n*-BuO), 100.63 (2-C), 104.53 (d, J_{C-P}=9.8 Hz, 3-C), and 143.50 (d, J_{C-P}=10.8 Hz, 6-C); trans: δ=14.07 (*n*-BuO), 14.37 (*n*-Pr), 16.60 (d, J_{C-P}=5.9 Hz, EtO) , 19.77 (*n*-BuO), 20.10, 27.44 (each *n*-Pr),

32.21 (*n*-BuO), 32.97 (d, J_{C-P}=139.9 Hz, 6-CH_2P), 33.30 (3-C), 38.52 (d, J_{C-P}=2.9 Hz, 4-C), 61.57 (d, J_{C-P}=5.9 Hz, EtO), 68.23 (*n*-BuO), 97.62 (2-C), 105.16 (d, J_{C-P}=10.8 Hz, 5-C), and 142.38 (d, J_{C-P}=9.8 Hz, 6-C); MS *m/z* (rel intensity, %) 348 (M^+, 7), 246 (23), 231 (base peak), 221 (22), 136 (25), 123 (27), 108 (37), 58 (20), and 57 (33).

2-Butoxy-4-phenyl-6-[(diethoxyphosphoryl)methyl]-3,4-dihydro-2*H*-pyran (6f): A 23:77 mixture of cis and trans isomers (^{13}C NMR); Colorless liquid; IR (neat) 1670, 1600, 1250, 1125, 1050, 1025, 960, 755, and 695 cm^{-1}; ^1H NMR (C_6D_6) cis: δ=0.87 (3H, t, J=7.3 Hz, *n*-BuO), 1.14 (6H, dt, J=7.0 and J_{H-P}=1.1 Hz, EtO) 1.38 (2H, sex, J=7.3 Hz, *n*-BuO), 1.57 (2H, quint, J=7.3 Hz, *n*-BuO), 1.92 (1H, ddd, J_{gem}=13.2, J_{3-4}=10.6, and J_{3-2}=9.2 Hz, one of 3-H), 2.10 (1H, dddd, J_{gem}=13.2, J_{3-4}=6.0, J_{3-2}=1.8, and J_{3-5}=1.0 Hz, the other of 3-H), 2.5—2.8 (2H, m, 6-CH_2P), 3.3—3.5 (2H, m, 4-H and *n*-BuO), 3.9—4.1 (5H, m, EtO and *n*-BuO), 4.76 (1H, m, 5-H), 4.93 (1H, dd, J_{2-3}=9.2 and 1.8 Hz, 2-H), and 7.0—7.3 (5H, m, Ph); trans: δ=0.88 (3H, t, J=7.3 Hz, *n*-BuO), 1.09 (6H, t, J=7.0 Hz, EtO), 1.38 (2H, sex, J=7.3, *n*-BuO), 1.57 (2H, quint, J=7.3 Hz, *n*-BuO), 1.73 (1H, ddd, J_{gem}=13.2, J_{3-4}=10.6, and J_{3-2}=2.7 Hz, one of 3-H), 2.0—2.2 (1H, m, the other of 3-H), 2.5—2.8 (2H, m, 6-CH_2P), 3.75 (2H, m, 4-H and *n*-BuO), 3.9—4.1 (5H, m, EtO and *n*-BuO), 4.88 (1H, m, 5-H), 4.93 (1H, t, J_{2-3}=3.2 Hz, 2-H), and 7.0—7.3 (5H, m, Ph); ^{13}C NMR (C_6D_6) cis: δ=13.64 (*n*-BuO), 16.16, 16.21 (each d, J_{C-P}=5.9 Hz, EtO), 19.24, 31.76 (each *n*-BuO), 32.32 (d, J_{C-P}=139.9 Hz, 6-CH_2P), 37.29 (3-C), 38.20 (d, J_{C-P}=2.0 Hz, 4-C), 61.32, 61.43 (each d, J_{C-P}=6.9 Hz, EtO), 68.28 (*n*-BuO), 100.27 (2-C), 103.32 (d, J_{C-P}=9.8 Hz, 5-C), 126.32, 127.28, 128.33 (each Ar), 144.87 (d, J_{C-P}=10.8 Hz, 6-C), and 145.29 (Ar); trans: δ=14.11 (*n*-BuO), 16.53, 16.59 (each d, J_{C-P}=5.9 Hz, EtO), 19.73, 32.15 (each *n*-BuO), 32.94 (d, J_{C-P}=139.9 Hz, 6-CH_2P), 34.60 (d, J_{C-P}=2.0 Hz, 4-C), 36.26 (3-C), 61.59, 61.86 (each d, J_{C-P}=6.9 Hz, EtO), 68.38 (*n*-BuO), 97.30 (2-C), 103.97 (d, J_{C-P}=9.8 Hz, 5-C), 126.66, 127.97, 128.79 (each Ar), 143.75 (d, J_{C-P}=10.8 Hz, 6-C), and 145.92 (Ar); MS *m/z* (rel intensity, %) 382 (M^+, 2), 170 (32), 144 (23), 131 (21), 129 (34), 128 (36), 123 (34), 116 (31), 110 (21), 103 (23), 81 (26), 77 (21), and 30 (base peak).

2-Butoxy-4-(*p*-methoxyphenyl)-6-[(diethoxyphosphoryl)-methyl]-3,4-dihydro-2*H*-pyran (6g): A 26:74 mixture of cis and trans isomers (^{13}C NMR); Colorless liquid; IR (neat) 1675, 1610, 1510, 1460, 1445, 1370, 1250, 1030, 960, and 830 cm^{-1}; ^1H NMR (C_6D_6) cis: δ=0.87 (3H, t, J=7.3 Hz, *n*-BuO), 1.11 (6H, dt, J=7.0 and J_{H-P}=1.8 Hz, EtO), 1.36 (2H, sex, J=7.3 Hz, *n*-BuO), 1.56 (2H, quint, J=7.3 Hz, *n*-BuO), 1.94 (1H, ddd, J_{gem}=13.2, J_{3-4}=10.6, and J_{3-2}=9.2 Hz one of 3-H), 2.13 (1H, ddd, J_{gem}=13.2, J_{3-4}=6.0, and J_{3-2}=1.8 Hz, the other of 3-H), 2.62, 2.71 (each 1H, dd, J_{gem}=13.5 and J_{H-P}=21.6 Hz, 6-CH_2P), 3.35 (3H, s, *p*-MeO), 3.45, 4.03 (each 1H, dt, J_{gem}=9.5 and J=7.3 Hz, *n*-BuO), 3.4—3.5 (1H, m, 4-H), 4.02 (4H, dq, J=7.0 and J_{H-P}=8.1 Hz, EtO), 4.80 (1H, m, 5-H), 4.95 (1H, dd, J_{2-3}=9.2 and 1.8 Hz, 2-H), 6.81, and 7.14 (each 2H, dt, J=8.4 and 1.8 Hz, Ar); trans: δ=0.89 (3H, t, J=7.3 Hz, *n*-BuO), 1.11 (6H, dt, J=7.0 and J_{H-P}=1.8 Hz, EtO), 1.36 (2H, sex, J=7.3 Hz, *n*-BuO), 1.59 (2H, quint, J=7.3 Hz, *n*-BuO), 1.76 (1H, ddd, J_{gem}=13.2, J_{3-4}=10.6, and J_{3-2}=3.2 Hz, one of 3-H), 2.0—2.2 (1H, m, the other of 3-H), 2.5—2.8 (2H, m, 6-CH_2P), 3.4—4.5 (2H, m, 4-H and *n*-BuO), 3.78 (3H, s, *p*-MeO), 4.0—4.1 (5H, m, *n*-BuO, and EtO), 4.92 (1H, m, 5-H), 4.95 (1H, t, J_{2-3}=3.2 Hz, 2-H), 6.81, and 7.14 (each 2H, dt, J=8.4 and 1.8 Hz, Ar); ^{13}C NMR (C_6D_6) cis: δ=14.04 (*n*-BuO), 16.56, 16.59 (each d, J_{C-P}=5.9 Hz, EtO), 19.65, 32.18 (each *n*-BuO), 32.73 (d, J_{C-P}=138.9 Hz, 6-CH_2P), 37.88 (d, J_{C-P}=2.0 Hz, 4-C), 38.01 (3-C), 54.83 (*p*-MeO), 61.65, 61.82 (each d, J_{C-P}=6.9 Hz, EtO), 68.69 (*n*-BuO), 100.77 (2-C), 104.19 (d, J_{C-P}=10.8 Hz, 5-C), 114.27, 128.58 (each Ar), 137.20 (d, J_{C-P}=2.0 Hz, Ar), 145.07 (d, J_{C-P}=10.8 Hz, 6-C), and 158.93 (Ar); trans: δ=14.11 (*n*-BuO), 16.56, 16.62 (each d, J_{C-P}=5.9 Hz, EtO), 19.74, 32.20 (each *n*-BuO), 32.99 (d, J_{C-P}=139.9 Hz, 6-CH_2P), 33.89 (d, J_{C-P}=2.0 Hz, 4-C), 36.54 (3-C), 54.83 (*p*-MeO), 61.52, 61.76 (each d, J_{C-P}=5.9 Hz, EtO), 68.38 (*n*-BuO), 97.42 (2-C), 104.37 (d, J_{C-P}=9.8 Hz, 5-C), 114.34, 128.58 (each Ar), 137.89 (d, J_{C-P}=2.0 Hz, Ar), 143.66 (d, J_{C-P}=10.8 Hz, 6-C), and 158.93 (Ar); MS *m/z* (rel intensity, %) 412 (M^+, 8), 312 (34), 231 (88), 200 (36), 174 (28), 161 (41), 136 (21), 123 (27), 69 (54), and 30 (base peak).

2-Butoxy-4,4-dimethyl-6-[(diethoxyphosphoryl)methyl]-3,4-dihydro-2*H*-pyran (6h): Colorless liquid; IR (neat) 1670 1645, 1465, 1445, 1390, 1365, 1250, 1160, 1120, 1055, 1025, 960, and 795 cm^{-1}; ^1H NMR (C_6D_6) δ=0.85 (3H, t, J=7.0 Hz, *n*-BuO), 0.95, 1.03 (each 3H, s, 4-Me), 1.11 (6H, dt, J=7.0 and J_{H-P}=1.4 Hz, EtO), 1.2—1.8 (6H, m, *n*-BuO and 3-H), 2.56, 2.64 (each 1H, dd, J_{gem}=12.0 and J_{H-P}=20.0 Hz, 6-CH_2P), 3.43 (1H, dt, J_{gem}=9.5 and J=6.6 Hz, *n*-BuO), 4.02 (4H, dq, J=7.0 and J_{H-P}=8.1 Hz, EtO), 4.05 (1H, dt, J_{gem}=9.5 and J=6.6 Hz, *n*-BuO), 4.54 (1H, d, J_{H-P}=4.4 Hz, 5-H), and 4.94 (1H, dd, J_{2-3}=7.0 and 3.0 Hz, 2-H); ^{13}C NMR (C_6D_6) δ=14.07 (*n*-BuO), 16.59 (d, J_{C-P}=5.9 Hz, EtO), 19.71 (*n*-BuO), 29.88 (d, J_{C-P}=2.0 Hz, 4-C), 30.36 (d, J_{C-P}=2.9 Hz, 4-Me), 31.55 (d, J_{C-P}=3.9 Hz, 4-Me), 32.25 (*n*-BuO), 32.73 (d, J_{C-P}=139.9 Hz, 6-CH_2P), 41.83 (3-C), 61.63 (d, J_{C-P}=5.9 Hz, EtO), 68.78 (*n*-BuO), 98.93 (2-C), 110.64 (d, J_{C-P}=10.8 Hz, 5-C), and 141.79 (d, J_{C-P}=10.8 Hz, 6-C); MS *m/z* (rel intensity, %) 334 (M^+, 14), 245 (base peak), 235 (54), 123 (19), and 41 (23).

General Procedure for the Hydrolysis and Cyclization Sequence of 6a—h Leading to 2-Cyclohexen-1-ones 7a—f. As a typical procedure the conversion of **6a** into **7a** is described as follows: To a solution of **6a** (0.055 g, 0.198 mmol) in THF (4 ml) was added 4 M hydrochloric acid (2 ml). After stirring at room temperature for 5 min, the mixture was extracted with dichloromethane (15 ml×2). The combined extracts were dried over magesium sulfate and evaporated in vacuo. The residue was chromatographed over silica gel by using ethyl acetate-methanol (9:1 v/v) to give **7a** (0.04 g, 87%). Other compounds **6b—h** were similarly treated under the reaction conditions listed in Table 2. The purification of **7b—f** was carried out by silica-gel column chromatography using ethyl acetate-methanol: **7b**, **7c**, and **7e**: 9:1 v/v; **7d**: 98:2 v/v; **7f**: 19:1 v/v.

2-(Diethoxyphosphoryl)-2-cyclohexen-1-one (7a): Colorless liquid; IR (neat) 1675, 1600, 1345, 1245, 1160, 1060, 1025, and 965 cm^{-1}; ^1H NMR ($CDCl_3$) δ=1.33 (6H, dt, J=7.0 and J_{H-P}=0.8 Hz, EtO), 2.06 (2H, quint, J_{5-4}=J_{5-6}=6.6 Hz, 5-H), 2.50 (2H, t, J_{6-5}=6.6 Hz, 6-H), 2.54 (2H, dt, J_{4-5}=6.6 and J_{4-3}=4.1 Hz, 4-H), 4.17 (4H, m, EtO), and 7.92 (1H, dt, J_{3-4}=4.1 and J_{H-P}=21.3 Hz, 3-H); ^{13}C NMR ($CDCl_3$) δ=16.39 (d, J_{C-P}=5.9 Hz, EtO), 22.03 (5-C), 26.82 (d, J_{C-P}=14.7 Hz, 4-C), 38.48 (d, J_{C-P}=7.8 Hz, 6-C), 62.48 (d, J_{C-P}=5.9 Hz, EtO), 131.60 (d, J_{C-P}=181.9 Hz, 2-C), 163.37 (d, J_{C-P}=5.9 Hz, 3-C), and 196.05 (d, J_{C-P}=5.9 Hz, 1-C); MS *m/z* (rel intensity, %) 232 (M^+, 48), 204 (37), 177 (20), 176 (94), 159 (46), 149 (48), 148 (76), 132 (21), 127 (22), 123, (26), 121 (78), 120 (52), 106 (49), 95

(30), 94 (30), 91 (21), 81 (47), and 79 (26). HRMS Found: *m/z* 232.0859. Calcd for $C_{10}H_{17}O_4P$: M, 232.0863.

2-(Diethoxyphosphoryl)-5-methyl-2-cyclohexen-1-one (7b): Colorless liquid; IR (neat) 1675, 1600, 1360, 1340, 1240, 1155, 1095, 1050, 1020, 960, 790, 750, and 620 cm^{-1}; ^1H NMR ($CDCl_3$) δ=1.09 (3H, d, J=5.9 Hz, 5-Me), 1.32 (6H, dt, J=7.0 and J_{H-P}=0.7 Hz, EtO), 2.1—2.4 (3H, m, 4- and 5-H), 2.59 (2H, m, 6-H), 4.16 (4H, m, EtO), and 7.88 (1H, ddd, J_{3-4}=7.7, 2.2, and J_{H-P}=20.5 Hz, 3-H); ^{13}C NMR ($CDCl_3$) δ=16.37 (d, J_{C-P}=5.9 Hz, EtO), 20.59 (5-Me), 29.70 (5-C), 34.98 (d, J_{C-P}=14.7 Hz, 4-C), 46.58 (d, J_{C-P}=7.8 Hz, 6-C), 62.42, 62.46 (each d, J_{C-P}=5.9 Hz, EtO), 131.28 (d, J_{C-P}=182.9 Hz, 2-C), 162.69 (d, J_{C-P}=5.9 Hz, 3-C), and 196.29 (d, J_{C-P}=5.9 Hz, 1-C); MS *m/z* (rel intensity, %) 246 (M^+, 50), 231 (27), 203 (26), 176 (39), 175 (21), 173 (21), 149 (35), 148 (41), 121 (45), 120 (34), 91 (26), 81 (27), 79 (27), and 29 (base peak). HRMS Found: *m/z* 246.1065. Calcd for $C_{11}H_{19}O_4P$: M, 246.1019.

2-(Diethoxyphosphoryl)-5-propyl-2-cyclohexen-1-one (7c): Colorless liquid; IR (neat) 1675, 1600, 1345, 1240, 1050, 1025, 970, 790, and 755 cm^{-1}; ^1H NMR ($CDCl_3$) δ=0.87 (3H, t, J=6.2 Hz, *n*-Pr), 1.2—1.5 (4H, m, *n*-Pr), 1.27 (6H, dt, J=7.0 and J_{H-P}=0.7 Hz, EtO), 2.1—2.4 (3H, m, 4- and 5-H), 2.56 (2H, m, 6-H), 4.12 (4H, m, EtO), and 7.84 (1H, ddd, J_{3-4}=5.5, 2.2, and J_{H-P}=21.1 Hz, 3-H); ^{13}C NMR ($CDCl_3$) δ=13.98 (*n*-Pr), 16.37 (d, J_{C-P}=5.9 Hz, EtO), 19.50 (*n*-Pr), 33.31 (d, J_{C-P}=14.7 Hz, 4-C), 34.27, 37.72 (each *n*-Pr), 44.87 (d, J_{C-P}=7.8 Hz, 6-C), 62.45 (d, J_{C-P}=4.9 Hz, EtO), 131.41 (d, J_{C-P}=182.9 Hz, 2-C), 162.83 (d, J_{C-P}=5.9 Hz, 3-C), and 196.42 (d, J_{C-P}=5.9 Hz, 1-C); MS *m/z* (rel intensity, %) 274 (M^+, 3), 222 (base peak), 195 (32), 194 (37), 179 (23), 167 (24), 152 (24), 151 (20), 139 (33), 125 (35), 123 (44), 121 (25), 109 (23), 97 (30), and 81 (35). HRMS Found: *m/z* 274.1423. Calcd for $C_{13}H_{23}O_4P$: M, 274.1333.

2-(Diethoxyphosphoryl)-5-phenyl-2-cyclohexen-1-one (7d): Colorless liquid; IR (neat) 1680, 1600, 1500, 1450, 1390, 1365, 1345, 1250, 1215, 1100, 1060, 1025, 970, 790, 760, and 700 cm^{-1}; ^1H NMR ($CDCl_3$) δ=1.34 (6H, dt, J=7.0 and J_{H-P}=4.8 Hz, EtO), 2.6—2.9 (4H, m, 4- and 6-H), 3.37 (2H, m, 5-H), 4.20 (4H, m, EtO), 7.2—7.4 (5H, m, Ph), and 7.96 (1H, ddd, J_{3-4}=5.5, 2.6, and J_{H-P}=19.5 Hz, 3-H); ^{13}C NMR ($CDCl_3$) δ=16.39 (d, J_{C-P}=4.9 Hz, EtO), 34.58 (d, J_{C-P}=14.7 Hz, 4-C), 40.14 (5-C), 45.27 (d, J_{H-P}=7.8 Hz, 6-C), 62.54, 62.56 (each d, J_{C-P}=5.9 Hz, EtO), 126.59, 127.25, 128.89 (each Ph), 131.59 (d, J_{C-P}=18.4 Hz, 2-C), 142.23 (Ph), 162.18 (d, J_{C-P}=5.9 Hz, 3-C), and 195.57 (d, J_{C-P}=5.9 Hz, 1-C); MS *m/z* (rel intensity, %) 308 (M^+,7), 228 (82), 200 (51), 184 (22), 183 (base peak), 182 (29), 155 (31), and 67 (23). HRMS Found: *m/z* 308.1172. Calcd for $C_{16}H_{21}O_4P$: M, 308.1176.

2-(Diethoxyphosphoryl)-5-(*p*-methoxyphenyl)-2-cyclohexen-1-one (7e): Colorless liquid; IR (neat) 1675, 1610, 1510, 1250, 1180, 1060, 1025, 970, 835, 795, and 750 cm^{-1}; ^1H NMR ($CDCl_3$) δ=1.35 (6H, dt, J=7.3 and J_{H-P}=4.4 Hz, EtO), 2.5—2.9 (4H, m, 4- and 6-H), 3.30 (1H, m, 5-H), 3.80 (3H, s, *p*-MeO), 4.19 (4H, m, EtO), 6.88 (2H, dt, J=8.8 and 2.2 Hz, Ar), 7.15 (2H, dt, J=8.8 and 2.2 Hz, Ar), and 7.95 (1H, ddd, J_{3-4}=5.5, 2.2, and J_{H-P}=20.2 Hz, 3-H); ^{13}C NMR ($CDCl_3$) δ=16.40 (d, J_{C-P}=5.9 Hz, EtO), 34.88 (d, J_{C-P}=14.7 Hz, 4-C), 39.44 (5-C), 45.61 (d, J_{C-P}=7.9 Hz, 6-C), 55.30 (*p*-MeO), 62.53, 62.58 (each d, J_{C-P}=5.9 Hz, EtO), 114.24, 127.57 (each Ar), 131.55 (d, J_{C-P}=182.9 Hz, 2-C), 134.41, 158.71 (each Ar), 162.33 (d, J_{C-P}=5.9 Hz, 3-C), and 195.57 (d, J_{C-P}=5.9 Hz, 1-C); MS *m/z* (rel intensity, %) 338 (M^+, 79), 337 (21), 217 (27), 201 (28), 200 (45), 172 (22), 134 (base peak), 128 (26), 121 (54), 119 (30), 115 (28), 91 (37), 81 (34), and 77 (29). HRMS Found: *m/z* 338.1284. Calcd for $C_{17}H_{23}O_5P$: M, 338.1282.

2-(Diethoxyphosphoryl)-5,5-dimethyl-2-cyclohexen-1-one (7f): Colorless liquid; IR (neat) 1675, 1600, 1385, 1350, 1235, 1050, 1020, 965, 780, and 750 cm^{-1}; ^1H NMR ($CDCl_3$) δ=1.06 (6H, s, 5-Me), 1.32 (6H, t, J=7.0 Hz, EtO), 2.35 (2H, d, J_{H-P}=1.1 Hz, 6-H), 2.42 (1H, t, J_{4-3}=J_{H-P}=4.0 Hz, 4-H), 4.16 (4H, m, EtO), and 7.81 (1H, dt, J_{3-4}=4.0 and J_{H-P}=20.5 Hz, 3-H); ^{13}C NMR ($CDCl_3$) δ=16.37 (d, J_{C-P}=5.9 Hz, EtO), 28.13 (5-Me), 33.74 (5-C), 40.91 (d, J_{C-P}=15.7 Hz, 4-C), 52.14 (d, J_{C-P}=7.8 Hz, 6-C), 62.45 (d, J_{C-P}=5.9 Hz, EtO), 130.56 (d, J_{C-P}=182.9 Hz, 2-C), 161.66 (d, J_{C-P}=5.9 Hz, 3-C), and 196.26 (d, J_{C-P}=5.9 Hz, 1-C). MS *m/z* (rel intensity, %) 260 (M^+, 3), 176 (12), 149 (14), 121 (18), 81 (27), 79 (20), and 30 (base peak). HRMS Found: *m/z* 260.1179. Calcd for $C_{12}H_{21}O_4P$: M, 260.1176.

References

1) C. W. Smith, D. G. Norton, and S. A. Ballard, *J. Am. Chem. Soc.*, **73**, 5273 (1951); A. Belanger and P. Brassard, *Can. J. Chem.*, **53**, 195 (1975); K. B. Lipkowitz, S. Scarpone, B. P. Mundy, and W. G. Bornmann, *J. Org. Chem.*, **44**, 486 (1979); H. K. Hall, Jr., H. A. A. Rasoul, M. Gillard, M. Abdelkader, P. Nogues, and R. C. Sentman, *Tetrahedron Lett.*, **23**, 603 (1982); G. Berti, G. Catelani, F. Colonna, and L. Monti, *Tetrahedron*, **38**, 3067 (1982); R. R. Schmidt and M. Maier, *Tetrahedron Lett.*, **26**, 2065 (1985); R. A. John, V. Schmid, and H. Wyler, *Helv. Chim. Acta*, **70**, 600 (1987).

2) G. Stork and H. K. Landesman, *J. Am. Chem. Soc.*, **78**, 5129 (1956); R. N. Schut and T. M. H. Liu, *J. Org. Chem.*, **30**, 2845 (1965); I. Fleming and M. H. Karger, *J. Chem. Soc. (C)*, **1967**, 226; M. Moreno-Manas, E. Papell, R. Pleixats, J. Ribas, and A. Virgili, *J. Heterocycl. Chem.*, **23**, 413 (1986).

3) C. Fehr, J. Galindo, and G. Ohloff, *Helv. Chim. Acta*, **64**, 1247 (1981).

4) As a comprehensive review: G. Desimoni and G. Tacconi, *Chem. Rev.*, **75**, 651 (1975).

5) S. W. Pelletier, R. L. Chappell, and S. Prabhakar, *J. Am. Chem. Soc.*, **86**, 2038 (1964); G. Stork and R. N. Guthikonda, *Tetrahedron Lett.*, **1972**, 2755; G. Stork and R. N. Guthikonda, *J. Am. Chem. Soc.*, **94**, 5109 (1972); L. Pichat and J. P. Beacourt, *Synth.*, **1973**, 537; J. E. Ellis, J. S. Dutcher, and C. H. Heathcock, *Synth. Commun.*, **4**, 71 (1974); B. M. Trost and R. A. Kunz, *J. Org. Chem.*, **39**, 2648 (1974).

6) E. Wada, S. Kanemasa, and O. Tsuge, unpublished results.

7) K. J. Shea and E. Wada, *Tetrahedron Lett.*, **23**, 1523 (1982); G. A. Kraus and B. S. Fulton, *J. Org. Chem.*, **50**, 1782 (1985).

8) Methyl 3-oxo-4-pentenoate and 5-hexene-2,4-dione react with both electron-deficient and -rich olefins leading to cycloadducts in moderates yields (E. Wada, S. Kanemasa, and O. Tsuge, unpublished results).

9) G. Peiffer and P. Courbis, *Can. J. Chem.*, **52**, 2894 (1974).

10) a) F. Mathey and P. Savignac, *Tetrahedron*, **34**, 649 (1978); b) J. Motoyoshida, M. Miyajima, K. Hirakawa, and T. Kakurai, *J. Org. Chem.*, **50**, 1326 (1985).

11) O. Tsuge, S. Kanemasa, H. Suga, and N. Nakagawa, *Bull. Chem. Soc. Jpn.*, **60**, 2463 (1987).

12) Though the poor yield formation of **4a** was observed in the unpurified reaction mixture (^{1}H NMR), its isolation by vacuum distillation failed.

13) This compound **4a** is obtainable through the Raney Ni reduction of 3-[(diethoxyphosphoryl)methyl]-2-isoxazoline, prepared by cycloaddition of (diethoxyphophoryl)acetonitrile oxide to ethene, followed by dehydration (O. Tsuge, S. Kanemasa, N. Nakagawa, and H, Suga, unpublished results).

14) P. A. Grieco and C. S. S. Pogonowski, *J. Am. Chem. Soc.*, **95**, 3071 (1973); P. A. Grieco and R. S. Finkelhor, *J. Org. Chem.*, **38**, 2909 (1973); P. A. Grieco and C. S. Pogonowski, *Synthesis*, **1973**, 425.

15) The carbonyl addition takes place in the absence of HMPA but implacticably slow. The role of HMPA is not explained yet.

16) T. Cohen and J. R. Matz, *J. Am. Chem. Soc.*, **102**, 6900 (1980).

17) R. I. Longley, Jr. and W. S. Emerson, *J. Am. Chem. Soc.*, **72**, 3079 (1950); C. W. Smith, D. G. Norton, and S. A. Ballard, *ibid.*, **73**, 5267 (1951).

18) W. Lehnert, *Tetrahedron*, **30**, 301 (1974).

19) T. Minami, H. Suganuma, and T. Agawa, *Chem. Lett.*, **1978**, 285.

20) A synthetic example of 2-phosphinyl-2-cyclopenten-1-one has been recently presented (K. Watanabe, M. Hirotsuka, and T. Minami, 56th Annual Meeting of Japan Chemical Society (1988), Preprint II, p. 1210 (2-XII-B-09)).

21) As 2-phosphinyl-2-butenolides: T. Minami, Y. Kitajima, and T. Chikugo, *Chem. Lett.*, **1986**, 1229; T. Minami, K. Watanabe, T. Chikugo, and Y. Kitajima, *ibid.*, **1987**, 2369.

Cycloaddition vs. Michael Addition in the Metal Halide/Amine-Induced Reactions of α-(Alkylideneamino) Esters with Electron-Deficient Olefins

Shuji KANEMASA,* Manabu YOSHIOKA, and Otohiko TSUGE*
Institute of Advanced Material Study, and Department of Molecular Science and Technology,
Interdisciplinary Graduate School of Engineering Sciences,
Kyushu University, Kasugakoen, Kasuga 816
(Received October 1, 1988)

The lithiated intermediate derived from methyl 2-(benzylideneamino)propanoate and lithium bromide/triethylamine undergoes cycloaddition and Michael addition with methyl acrylate. 1,3-Dipole character of the intermediate is suggested on the basis of the product ratios obtained under a variety of conditions. The reaction mechanism via a four-centered transition state is proposed.

It was found that treatment of 2-(benzylideneamino)-alkanoates or -alkanamides PhCH=NCH(R)COY (Y= OMe, NHBu-*t*, or 1-pyrrolidinyl; R=H, Me, or *i*-Pr) with lithium bromide/triethylamine or 1,8-diazabicyclo[5.4.0]undec-7-ene (DBU) in tetrahydrofuran (THF) led to the generation of lithiated intermediates **A** (Eq. 1).[1] These species **A** showed high reactivity toward electron-deficient olefins and underwent highly stereo- and regioselective cycloadditions with α,β-unsaturated esters or ketones $R^1CH=C(R^2)COY'$ (Y'=COOMe, COOBu-*t*, COMe, or COAr) to produce stereochemically defined pyrrolidines.

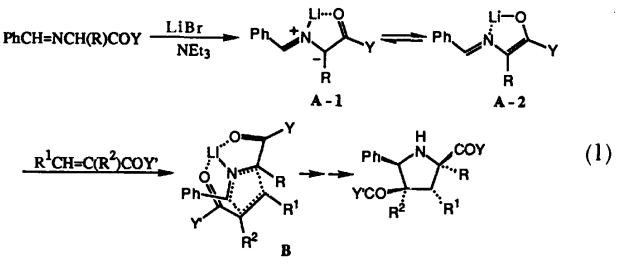

(1)

In the preceding paper,[1] we proposed two possible reaction mechanisms, concerted 1,3-dipolar cycloaddition of *N*-lithioazomethine ylide **A-1** and tandem Michael-imine addition of lithium enolate **A-2**. It was concluded that the high selectivity was due to the tight lithium chelation in the transition state, while specification of the reacting species was not made.

On the other hand, Michael additions with the imines of α-amino esters[2] or nitriles[3] are known. In some cases, metallic bases such as lithium diisopropylamide (LDA) and potassium *t*-butoxide were used as bases so that metalated intermediates like **A** must have been involved. Accordingly, metalated intermediates derived from the imines of α-amino esters can serve as both 1,3-dipoles and Michael donors, and probably the course of reactions depends upon the reaction conditions.

In the present article, the reaction of methyl 2-(benzylideneamino)propanoate with methyl acrylate has been investigated under various conditions employing metal halides/triethylamine or DBU. An alternative reaction mechanism leading to cycloaddition and Michael addition is presented.

Results and Discussion

An exception of the highly stereo- and regioselective cycloadditions of anions **A** depicted in Eq. 1 was the reaction of methyl 2-(benzylideneamino)propanoate (**1**) with methyl acrylate under identical conditions (with lithium bromide and triethylamine in THF at room temperature). A 5:1 mixture of cycloadduct **2** and Michael adduct **3** was produced (Scheme 1 and Entry 1 in Table 1). Therefore this reaction was investigated here under a variety of conditions. Analysis of the product ratio would help us to solve the factors which may be responsible for the determination of the reaction courses. The results are summarized in Table 1.

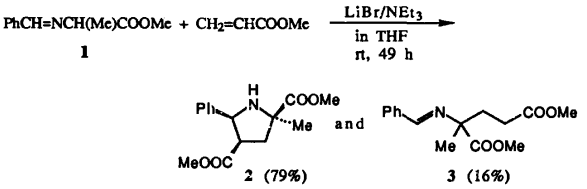

Scheme 1.

In most cases the reactions were carried out under the standard conditions using each 1.5 and 1.2 equivalent amounts of lithium bromide and triethylamine at room temperature in dry THF (5 ml for 1 mmol of imine **1**). The isomer ratio **2**:**3** remained unchanged (4—5:1) for several reaction times and temperatures (Entries 1—3 and 8). The comparable **2**:**3** ratio was observed even in the midst of reaction, indicating the kinetically controlled formation of both **2** and **3** (Entry 4). In fact compounds **2** and **3** were not interconverted with each other under these reaction conditions.[4]

A possible reaction mechanism was illustrated on the basis of the above results and the following observations (Fig. 1). Lithium bromide coordinates

with the imine nitrogen of **1** so that the α-hydrogen of **C** can be easily deprotonated with a weak base such as triethylamine to generate lithiated intermediate **D**.

As mentioned above, two intermediates **A-1** and **A-2** (R=Me, Y=OMe) were proposed in the preceding paper.[1] However the only structural difference between **A-1** and **A-2** comes from the relative covalency of the lithium–heteroatom bonds, indicating the existence of little, if any, energy barrier between them. We propose that anionic species **D** can be an intermediate which may exhibit properties both as *N*-lithiated azomethine ylide and as ester enolate.

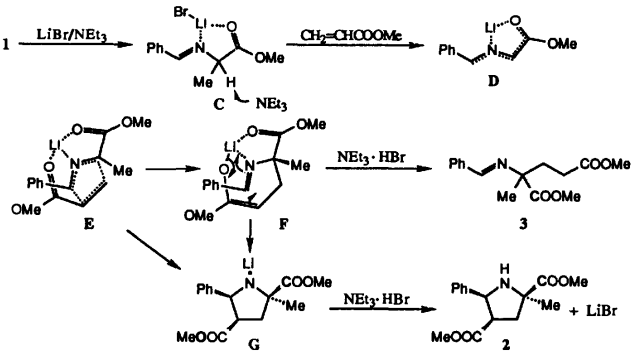

Fig. 1. Competitive formation of a cycloadduct **2** and a Michael adduct **3**.

Intermediate **D** would then be involved in the transition state **E** previously proposed for the lithium-chelated concerted cycloaddition.[1] Bond formation at the β-carbon of the acrylate precedes that at the α-carbon to give **F**. Quenching of **F** with a proton source, presumably triethylammonium bromide, leading to Michael adduct **3** competes with intramolecular cyclization producing cycloadduct lithium amide **G**.[5] Ready quenching of **G** with the ammonium salt produces cycloadduct **2**. The direct formation of **G** from **E** may also be involved.

In Entries 9—13, a catalytic amount of lithium bromide and/or triethylamine was employed. Both lithium bromide and triethylamine can be effectively recycled in the manner shown in Fig. 1. Since the step of deprotonation of **1** (**C**→**D**) is rate-determining as suggested by the rate acceleration upon using DBU (Entries 22—24), the catalyzed reactions were relatively decelerated. It is not surprising that no reaction took place in the absence of lithium bromide (Entry 13).

When either lithium bromide or triethylamine was used in moderate excess, the ratio of cycloaddition increased (Entries 14, 15). Presumably the excess lithium bromide or triethylamine reduces acidity of triethylammonium bromide by coordination.

Dilution with THF increased the amount of **2** (Entries 3 and 5—7). Since collapse of **F** into **3** is an

Table 1. LiBr/Amine-Induced Reactions of Imine **1** with Methyl Acrylate

Entry	LiBr	NEt_3	DBU	H_2O	Temperature	Time	Solvent[a]	Yield/%[b]	**2** : **3**[c]	Recovered **1**
		(equivalent)			°C	h		**2**+**3**		%
1	1.5	1.2			Room temp	49	THF	95	5 : 1	—
2	1.5	1.2			Room temp	3	THF	99	4 : 1	—
3	1.5	1.2			Room temp	1	THF	97	4 : 1	Trace
4	1.5	1.2			Room temp	10 min	THF	51	5 : 1	43
5	1.5	1.2			Room temp	15	THF (30 ml)	77	10 : 1	18
6	1.5	1.2			Room temp	2	THF (13 ml)	81	6 : 1	17
7	1.5	1.2			Room temp	2	THF (2.5 ml)	89	3 : 1	—
8	1.5	1.2			Reflux	1	THF	99	4 : 1	—
9	0.1	1.2			Room temp	1	THF	41	3.5 : 1	50
10	0.1	1.2			Room temp	14	THF	97	3 : 1	—
11	1.5	0.1			Room temp	3	THF	67	2.2 : 1	21
12	0.1	0.1			Room temp	48	THF	70	6 : 1	20
13	0	1.2			Room temp	20	THF	Trace	Trace	90
14	3.3	1.2			Room temp	1	THF	91	10 : 1	—
15	1.5	3.0			Room temp	1	THF	95	6 : 1	—
16	1.5	1.2		0.7	Room temp	1	THF	95	1.2 : 1	Trace
17	1.5	1.2		3	Room temp	1	THF	52	1 : 2	35
18	1.5[d]	1.2			Room temp	2	THF	95	2 : 1	—
19	1.5	1.2			Room temp	1	MeCN	79	1 : 1.4	—
20	1.5	1.2			Room temp	3	CH_2Cl_2	92	1 : 3.3	—
21	1.5	1.2			Room temp	3	Et_2O	44	2.5 : 1	50
22	1.5		1		Room temp	1 min	THF	96	1.8 : 1	—
23	1.5		1		Room temp	2	THF (50 ml)	99	10 : 1	—
24	1.5		0.1		Room temp	5 min	THF	98	1.8 : 1	—
25	1.5		1		−78	4.5	THF	98	1 : 5	—
26	1.5		1	1	−78	4.5	THF	83	1 : 5	14

a) Unless otherwise stated, 5 ml of solvent was used for 1 mmol of **1**. The amount in parenthesis indicates the volume of THF used for 1 mmol of **1**. b) Yield of isolated mixtures. c) Based on the ^1H NMR of an isolated mixture of **2** and **3**. d) Lithium iodide was used instead of LiBr.

intermolecular reaction and the dilution procedure disfavors this process, the relative rate of intramolecular process **F**→**G** was increased as a result. The effect of only catalytic amounts of lithium bromide and triethylamine (Entry 12) is similar to that of dilution.

Addition of water results in an increase of proton source; the Michael adduct formation increased (Entries 16, 17). It should be emphasized, however, that both anions **D** and **F** are quite stable toward water. Most of them can survive upon addition of 0.7 equivalent of water which corresponds to a large excess against **D** and **G**.[6]

When lithium bromide (Entry 11) or triethylamine (Entries 9, 10) was used in a large excess (tweleve- or fifteen-fold equivalents) in some catalyzed reactions, the **2**:**3** ratio was unexpectedly decreased. The large excess lithium bromide and triethylamine presumably collapse the lithium chelation **E** which is essential for the formation of **G**.

Replacement of THF by acetonitrile, dichloromethane, or diethyl ether favored the Michael addition (Entries 18—20). However the effect of polarity of solvent on **2**:**3** ratio remains ambiguous because all the reactions except in THF were carried out as suspension.

When DBU was employed as a stronger base, reactions were completed within 1 min at room temperature, indicating high acceleration of the deprotonation step leading to **D**. The decreased 2:3 ratio (1.8:1, Entry 21) is due to a relatively high concentration of intermediate **D** compared with the case employing triethylamine. No change of the **2**:**3** ratio in the DBU-catalyzed reaction (Entry 23) and predominant formation of the cycloadduct **2** in the ten-fold dilution reaction (Entry 22) are both comparable to the above results, Entries 9—11 and Entries 5, 6, respectively.

Deprotonation of **1** with lithium bromide and DBU occurred even at −78 °C, but the reaction with methyl acrylate at −78 °C unfortunately gave a low **2**:**3** ratio (Entry 24). Addition of water provided a similar result (Entry 25).

As discussed above, the **2**:**3** ratio is mainly determined by the relative rate of cyclization of **F** into **G**. On the other hand, route **E**→**F** competes with the direct cyclization route **E**→**G**. Substitution of the electropositive lithium metal in the intermediate **D** with a less positive one such as aluminum or magnesium is expected to increase the relative contribution of route **E**→**G**.

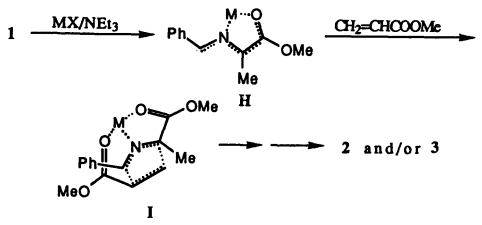

Scheme 2.

With an expectation to open the entry for similar metalated intermediates **H**, other metal halides (MX) were employed in the deprotonation step of imine **1** (Scheme 2). Thus **1** was treated with a variety of metal halides and triethylamine in dry THF in the presence of methyl acrylate. Since the resulting intermediates **H** certainly undergo chelation-controlled reactions with the acrylate via **I**, cycloadduct **2** and/or Michael adduct **3** are to be formed.

The results are summarized in Table 2. Quantitative recovery of the starting imine **1** in Entries 3 and 5 is due to the extremely poor solubility of sodium bromide and potassium iodide in THF. Use of sodium iodide generated intermediate **H** (M=Na) which led to preferred formation of Michael adduct **3** (Entry 4). Magnesium bromide diethyl etherate, zinc chloride, and ethylaluminum dichloride are also effective; the cycloadduct **2** was the only identified product as expected in all cases (Entries 6—10).

Michael additions occur regioselectively at the β-carbon of the olefins bearing an anion-stabilizing substituent. On the other hand, the regioselectivity of 1,3-dipolar cycloadditions with azomethine ylides

Table 2. Metal Halide/Triethylamine-Induced Reactions of Imine **1** with Methyl Acrylate[a]

Entry	Metal halide	(equivalent)	Triethylamine (equivalent)	Time/h	Yield/%[b]	**2** : **3**[c]	Recovered **1**
1	LiBr	1.5	1.2	3	99	4 1	—
2	NaBr	1.5	1.2	8	Trace		98
3	NaI	1.5	1.2	8	96	1 2.7	—
4	KI	1.5	1.2	8	Trace		98
5	$MgBr_2$[d]	1.5	1.2	7	99[e]	1 0	—
6	$MgBr_2$[d]	0.2	1.2	45	99[e]	1 0	—
7	ZnI_2	1.5	1.2	7	79	1 0	—
8	ZnI_2	0.1	1.2	68	39	1 0	—
9	Et_2AlCl	1.5	1.2	3	99[e]	1 0	—

a) All reactions were carried out in dry THF at room temperature. b) Yield of the isolated mixtures. c) Based on the ^1H NMR of an isolated mixture of **2** and **3**. d) Magnesium diethyl etherate was used. e) Unidentified isomers are contained in 5 to 8% (^1H NMR).

depends upon the orbital coefficients of frontier orbitals of both reagents.[7] Accordingly, examination of regioselectivity of the above reactions is an important clue by which the reaction mechanism is solved.

The lithium chelation-controlled cycloadditions of imines of α-amino esters and amides with electron-deficient olefins offer a few exceptional selectivities as shown below. Reaction of the lithium anion of **1** with methyl cinnamate gave two cycloadducts **4** and **4'** in a 2:1 ratio (Scheme 3 and Table 3). The major product **4** was assigned as a normal stereoisomer on the basis of the chemical shifts of 2-COOMe (δ=3.79), 4-COOMe (3.08), and 2-Me (1.19), while **4'** was its regioisomer (COOMe: 3.59 and 3.75; 2-Me: 1.74; 3-H: 3.31 as a doublet; 4-H: 3.75 as a doublet-doublet).

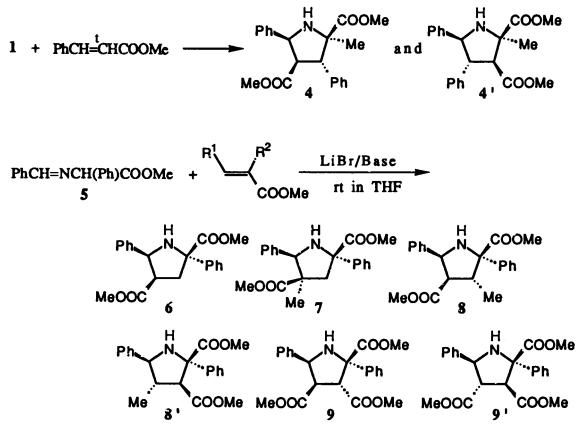

Scheme 3.

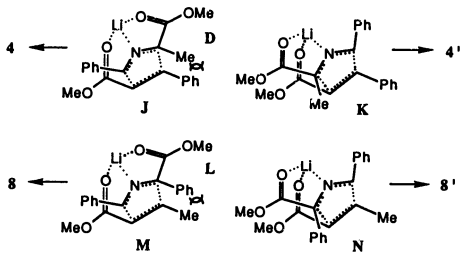

Fig. 2. Decreased regioselectivity by a steric repulsion.

Methyl 2-(benzylideneamino)phenylacetate (**5**) was reacted with several olefins in the presence of lithium bromide and triethylamine (Scheme 3 and Table 3). With methyl acrylate and methyl methacrylate normal regio- and stereoisomers **6** and **7** were obtained as single products. The reaction with methyl crotonate, however, gave two regioisomeric cycloadducts **8** and **8'** (1:6). It was quite surprising that abnormal regioisomer **8'** was the far major product. Structures of **8** and **8'** were also based on their ^{1}H NMR spectra: **8**: 4-COOMe: 3.21; 4-H: 3.02 as doublet-doublet; **8'**: 3-COOMe: 3.62; 3-H: 3.32 as a doublet.

In both approaches **J** and **M** leading to normal regioisomers **4** and **8**, respectively, serious steric repulsion exists between the methyl and phenyl substituents. Especially the repulsion in **M** should be more critical because the phenyl plane of **L** is forced out of the ylide triangle due to steric congestion caused by the adjacent methoxyl moiety.[8] Substitution by a phenyl moiety at the β-carbon of acrylate causes a decrease of the coefficient of the lowest unoccupied molecular orbital (LUMO) at this position. The reported atomic orbital coefficients (LUMO) are as follows:[9] methyl acrylate: C(C_α): 0.4286; C(C_β): −0.6194. Methyl cinnamate: C(C_α): 0.4717; C(C_β): −0.4248. This may be the reason why the regioisomeric approach **K** has participated in cycloaddition to give **4'**.

The unexpected regioselectivity giving **8'** as a far major regioisomer should be due to the serious steric repulsion in approach **M** which was already mentioned above. Predominant formation of **9'** in the reaction of **5** with dimethyl fumarate stems from a similar steric repulsion.

The above anomalous regiochemical consequences support the cycloaddition transition state, for example **E**, of anionic intermediate such as **D** or **H** first proposed in the present work.

Experimental

General. Melting points were determined on a Yanagimoto melting point apparatus and are uncorrected. IR spectra were taken with a JASCO IRA-1 or a JASCO A-702

Table 3. LiBr/Amine-Induced Reactions of Imine **1** or **5** with Electron-Deficient Olefins[a]

Entry	Imine	Olefin	LiBr (equivalent)	Amine (equivalent)	Time/h	Product	Yield/%[b]	Isomer ratio
1	**1**	Methyl crotonate	1.5	DBU 1	4	**4**+**4'**	60 (—)	**4**:**4'**=2:1[c]
2	**5**	Methyl acrylate	1.5	NEt_3 1.2	8	**6**	81 (8)	
3	**5**	Methyl methacrylate	1.5	NEt_3 1.2	15	**7**	46 (40)	
4	**5**	Methyl methacrylate	1.5	DBU 1	1	**7**	96 (—)	
5	**5**	Methyl crotonate	1.5	NEt_3 1.2	4	—	0 (100)	
6	**5**	Methyl crotonate	1.5	DBU 1	1	**8**+**8'**[d]	67 (—)	**8**:**8'**=1:6[e]
7	**5**	Dimethyl fumarate	1.5	DBU 1	3	**9**+**9'**[d]	82 (—)	**9**:**9'**=1:5[e]

a) All reactions were carried out in dry THF at room temperature. b) Yield of the isolated product(s). Yield of unreacted **5** is in parenthesis. c) Both isomers were separated from each other. The ratio was determined by ^{1}H NMR of the unpurified product. d) As an inseparable mixture. e) Based on ^{1}H NMR of the unpurified mixture.

spectrometer. ^{1}H NMR spectra were recorded on a Hitachi R-40 (90 MHz), a JEOL FX-100 (100 MHz), or a JEOL GSX-270 instrument (270 MHz), and ^{13}C NMR on a JEOL FX-100 (25.05 MHz) or a JEOL GSX-270 spectrometer (67.94 MHz). Chemical shifts are expressed in parts per million downfield from tetramethylsilane as an internal standard. Mass spectra and high resolution mass spectra (HRMS) were measured with a JEOL-01SG-2 spectrometer at 70 eV of ionization energy. Elemental analyses were performed on a Hitachi 026 CHN analyzer. For preparative column chromatography, Wakogel C-200, C-300 (Wako), and Silica gel 60 (Merck) were employed. Flash chromatography was carried out on an EYELA EF-10 apparatus using a column (20×180 mm) packed with Silica gel 60 (Merck, size: 0.04—0.063 mm). Gas liquid chromatography (GLC) was accomplished on a Yanaco G-2800 gas chromatograph (Yanagimoto) with an ionization flame detector using a glass column (SE-30, 3×2000 nm) or a glass capillary column (Silicone GE, SE-30, 0.25×50000 mm). Micro vacuum distillation was carried out on a Sibata GTO-250R Kugelrohr distilling apparatus.

General Procedures for Metal Halide/Amine-Induced Reactions of Imine 1[1] or 5[10] with Electron-Deficient Olefins. To a solution of imine **1** or **5** in dry THF (or other solvent) was added a metal halide under nitrogen. Addition of an olefin was followed and then an amine, both with the aid of a syringe. If necessary, an additive was added and the resulting mixture was stirred under the reaction conditions listed in Tables 1—3. After the reaction was over, the mixture was treated with saturated ammonium chloride and extracted with diethyl ether. The extract was dried over magnesium sulfate and evaporated in vacuo. The residue was subjected to ^{1}H NMR measurement to know the purity of products as well as the isomer ratio.

Dimethyl 2-(Benzylideneamino)-2-methylglutarate (3): This compound **3** decomposed so readily when chromatographed on silica gel that its separation from the mixture with **2**[1] was unsuccessful. **3**: Colorless liquid; IR (neat) 1730 (C=O) and 1630 (C=N) cm^{-1}; ^{1}H NMR ($CDCl_3$) δ=1.49 (3H, s, Me), 1.9—2.6 (4H, m, CH_2), 3.60, 3.69 (each 3H, s, COOMe), 7.3—7.4 (3H, m, Ph), 7.7—7.8 (2H, m, Ph), and 8.24 (1H, s, CH=N); MS *m/z* (rel intensity, %) 278 (M^++1, 2), 219 (17), 218 (base peak), 158 (47), 131 (19), 130 (19), 104 (34), 98 (53), 90 (28), and 89 (19). No HRMS was obtainable due to the lack of M^+.

Dimethyl 2-Methyl-*t*-3,*c*-5-diphenylpyrrolidine-*r*-2,*c*-4-dicarboxylate (4): The mixture of **4** and **4′** was chromatographed on silica gel by using hexane–ethyl acetate (5:1 v/v) to give **4** and then **4′**. **4**: Colorless prisms (chloroform–hexane); mp 84—85 °C; IR (KBr) 3330 (NH), 1735, and 1720 (each C=O) cm^{-1}; ^{1}H NMR ($CDCl_3$) δ=1.19 (3H, s, 2-Me), 3.06 (1H, br s, NH), 3.08 (3H, s, 4-COOMe), 3.79 (3H, s, 2-COOMe), 3.91 (1H, dd, J_{4-3}=10.6 and J_{4-5}=9.5 Hz, 4-H), 4.20 (1H, d, J_{3-4}=10.6 Hz, 3-H), 4.90 (1H, d, J_{5-4}=9.5 Hz, 5-H), 7.2—7.4 (8H, m, Ph), and 7.44 (2H, d, Ph); ^{13}C NMR ($CDCl_3$) δ=21.22 (2-Me), 51.32, 52.44 (each COOMe), 54.44, 54.98 (3- and 4-C), 62.81 (5-C), 68.87 (2-C), 127.30, 127.38, 127.77, 128.19, 128.28, 128.64, 137.22, 140.34 (each Ph), 171.69, and 175.50 (each COOMe); MS *m/z* (rel intensity, %) 353 (M^+, 1), 295 (18), 294 (83), 234 (31), 192 (16), 191 (base peak), 132 (13), 131 (92), 130 (17), 115 (18), 103 (11), 91 (17), 90 (16), and 77 (10). Found: C, 71.18; H, 6.55; N, 4.00%. Calcd for $C_{21}H_{23}NO_4$: C, 71.37; H, 6.56; N, 3.96%.

Dimethyl 2-Methyl-*t*-4,*c*-5-diphenylpyrrolidine-*r*-2,*c*-3-dicarboxylate (4′): Colorless needles (chloroform–hexane); mp 108—109 °C; IR (KBr) 3360 (NH), 1735, and 1717 (C=O) cm^{-1}; ^{1}H NMR ($CDCl_3$) δ=1.74 (3H, s, 2-Me), 3.03 (1H, br s, NH), 3.31 (1H, d, J_{3-4}=12.1 Hz, 3-H), 3.59 (3H, s, 3-COOMe), 3.63 (1H, dd, J_{4-3}=12.1 and J_{4-5}=10.6 Hz, 4-H), 3.75 (3H, s, 2-COOMe), 4.31 (1H, d, J_{5-4}=10.6 Hz, 5-H), and 7.1—7.3 (10H, m, Ph); ^{13}C NMR ($CDCl_3$) δ=27.37 (2-Me), 51.98, 52.76 (each COOMe), 57.33 (3-C), 63.18 (4-C), 67.87, 69.12 (2- and 5-C), 127.05, 127.27, 127.61, 127.71, 128.43, 128.51, 138.02, 140.13 (each Ph), 171.77, and 175.19 (each COOMe); MS *m/z* (rel intensity, %) 294 (M^+—COOMe, 28), 192 (11), 191 (87), 132 (13), 131 (base peak), 130 (23), 129 (17), 128 (10), 115 (16), 91 (17), 90 (17), and 77 (10). Found: C, 71.35; H, 6.61; N, 4.02%. Calcd for $C_{21}H_{23}NO_4$: C, 71.37; H, 6.56; N, 3.96%.

Dimethyl 2,*c*-5-Diphenylpyrrolidine-*r*-2,*c*-4-dicarboxylate (6): Colorless needles (chloroform–hexane); mp 104—105 °C; IR (KBr) 3360 (NH), 1735, and 1730 (C=O) cm^{-1}; ^{1}H NMR ($CDCl_3$) δ=2.61 (1H, dd, J_{gem}=13.2 and J_{3-4}=7.0 Hz, one of 3-H), 3.15 (1H, dd, J_{gem}=13.2 and J_{3-4}=5.9 Hz, the other of 3-H), 3.22 (3H, s, 4-COOMe), 3.23 (1H, ddd, J_{4-5}=7.3 and J_{4-3}=7.0 and 5.9 Hz, 4-H), 3.48 (1H, br s, NH), 3.75 (3H, s, 2-COOMe), 4.57 (1H, d, J_{5-4}=7.3 Hz, 5-H), 7.3—7.4 (8H, m, Ph), and 7.74 (2H, d, Ph); ^{13}C NMR ($CDCl_3$) δ=40.99 (3-C), 50.32 (4-C), 51.16, 52.81 (each COOMe), 64.74 (5-C), 71.83 (2-C), 126.33, 126.75, 127.48, 127.64, 128.23, 128.33, 139.22, 143.08 (each Ph), 173.05, and 174.48 (each COOMe); MS *m/z* (rel intensity, %) 281 (20), 280 (M^+—COOMe, base peak), 220 (27), 193 (27), 115 (17), 104 (11), and 76 (11). Found: C, 70.86; H, 6.30; N, 4.02%. Calcd for $C_{20}H_{21}NO_4$: C, 70.78; H, 6.24; N, 4.13%.

Dimethyl *t*-4-Methyl-2,*c*-5-diphenylpyrrolidine-*r*-2,4-dicarboxylate (7): Colorless prisms (chloroform–hexane); mp 114—115 °C; IR (KBr) 3360 (NH), 1720, and 1710 (C=O) cm^{-1}; ^{1}H NMR ($CDCl_3$) δ=1.24 (3H, s, 4-Me), 2.31 (1H, d, J_{gem}=13.6 Hz, one of 3-H), 3.31 (3H, s, 4-COOMe), 3.37 (1H, d, J_{gem}=13.6 Hz, the other of 3-H), 3.76 (3H, s, 2-COOMe), 3.82 (1H, br s, NH), 4.02 (1H, s, 5-H), 7.2—7.4 (8H, m, Ph), and 7.76 (2H, d, Ph); ^{13}C NMR ($CDCl_3$) δ=21.28 (4-Me), 50.83 (3-C), 51.33, 52.84 (each COOMe), 56.34 (4-C), 71.30 (2-C), 73.33 (5-C), 126.45, 126.48, 127.32, 128.07, 128.28, 128.35, 137.45, 144.59 (each Ph), 175.01, and 175.27 (each COOMe); MS *m/z* (rel intensity, %) 353 (M^+, 1), 294 (18), 293 (87), 252 (40), 233 (30), 194 (19), 193 (base peak), 129 (11), 115 (13), 104 (14), 91 (18), 90 (15), 89 (11), 77 (15), and 44 (10). Found: C, 71.52; H, 6.56; N, 4.08%. Calcd for $C_{21}H_{23}NO_4$: C, 71.37; H, 6.56; N, 4.08%.

Dimethyl *t*-3-Methyl-2,*c*-5-diphenylpyrrolidine-*r*-2,*c*-4-dicarboxylate (8) + Dimethyl *t*-4-Methyl-2,*c*-5-diphenylpyrrolidine-*r*-2,*c*-3-dicarboxylate (8′): An inseparable mixture of **8** and **8′** (1:6 by ^{1}H NMR) was obtained after column chromatographic purification of the crude reaction mixture on silica gel with chloroform. Spectral data were obtained as a mixture. **8**: ^{1}H NMR ($CDCl_3$) δ=0.82 (3H, d, J_{Me-3}=6.6 Hz, 3-Me), 3.02 (1H, dd, J_{4-3}=10.2 and J_{4-5}=9.2 Hz, 4-H), 3.21 (3H, s, 4-COOMe), 3.40 (2H, m, 3-H and NH), 3.78 (3H, s, 2-COOMe), 5.01 (1H, d, J_{5-4}=9.2 Hz, 5-H), and 7.3—7.5 (10H, m, Ph); ^{13}C NMR ($CDCl_3$) δ=15.35 (3-Me), 41.11 (3-C), 51.14, 52.47 (each COOMe), 55.72 (4-C), 62.53 (5-C), 74.25 (2-C), 126.62, 127.17, 127.56, 128.07, 128.13, 128.69, 140.79, 142.00 (each Ph), 171.41, and 174.00 (each COOMe). **8′**:

^{1}H NMR ($CDCl_3$) δ=0.89 (3H, d, J_{Me-4}=6.6 Hz, 4-Me), 2.53 (1H, tq, J_{4-3}=J_{4-5}=9.5 and J_{4-Me}=6.6 Hz, 4-H), 3.32 (1H, d, J_{3-4}=9.5 Hz, 3-H), 3.40 (1H, br s, NH), 3.61 (1H, d, J_{5-4}=9.5 Hz, 5-H), 3.62 (3H, s, 4-COOMe), 3.78 (3H, s, 2-COOMe), 7.3—7.5 (8H, m, Ph), and 7.81 (2H, d, Ph); ^{13}C NMR ($CDCl_3$) δ=15.55 (4-Me), 49.00 (4-C), 52.18, 52.91 (each COOMe), 64.25 (3-C), 69.07 (5-C), 74.25 (2-C), 127.08, 127.34, 127.63. 127.87, 128.25, 128.69, 140.23, 142.93 (each Ph), 173.11, and 173.93 (each COOMe).

Trimethyl 2,*c*-5-Diphenylpyrrolidine-*r*-2,*t*-3,*c*-4-tricarboxylate (9) + Trimethyl 2,*c*-5-Diphenylpyrrolidine-*r*-2,*c*-3,*t*-4-tricarboxylate (9′): An inseparable mixture of **9** and **9′** (1 : 5 by ^{1}H NMR) was obtained after column chromatographic purification of the crude reaction mixture on silica gel with chloroform. Spectral data were obtained as a mixture. **9**: ^{1}H NMR ($CDCl_3$) δ=3.25, 3.34 (each 3H, s, 3- and 4-COOMe), 3.6—3.9 (2H, m, 4-H and NH), 3.80 (3H, s, 2-COOMe), 4.54 (1H, d, J_{3-4}=7.3 Hz, 3-H), 5.15 (1H, d, J_{5-4}=8.0 Hz, 5-H), 7.2—7.6 (8H, m, Ph), and 7.85 (2H, d, Ph); ^{13}C NMR ($CDCl_3$) δ=52.40, 52.67, 52.76 (each COOMe), 54.47 (4-C), 61.90 (3-C), 67.95 (5-C), 74.67 (2-C), 126.79, 126.88, 127.67, 127.83, 128.68, 129.00, 139.78, 139.89 (each Ph), 171.05, 171.36, and 173.30 (each COOMe). **9′**: ^{1}H NMR ($CDCl_3$) δ=3.47 (1H, dd, J_{4-5}=9.2 and J_{4-3}=8.4 Hz, 4-H), 3.51, 3.65 (each 3H, s, 3- and 4-COOMe), 3.73 (1H, br s, NH), 3.78 (3H, s, 2-COOMe), 4.09 (1H, d, J_{3-4}=8.4 Hz, 3-H), 4.31 (1H, d, J_{5-4}=9.2 Hz, 5-H), 7.3—7.5 (8H, m, Ph), and 7.80 (2H, d, Ph); ^{13}C NMR ($CDCl_3$) δ=52.11, 52.51, 53.03 (each COOMe), 57.18 (4-C), 59.60 (3-C), 64.98 (5-C), 74.97 (2-C), 127.11, 127.99, 128.07, 128.19, 128.38, 128.78, 139.54, 140.95 (each COOMe), 171.82, 172.33, and 173.08 (each COOMe).

The present work was financially supported by a Grant-in-Aid for Scientific Research (No. 63550652) from the Ministry of Education, Science and Culture.

References

1) O. Tsuge, S. Kanemasa, and M. Yoshioka, *J. Org. Chem.*, **53**, 1384 (1988).

2) G. Stork, A. Y. W. Leong, and A. M. Touzin, *J. Org. Chem.*, **41**, 3491 (1976); P. Bey and J. P. Vevert, *Tetrahedron Lett.*, **1977**, 1455; J. F. Fitt and H. W. Gschwend, *J. Org. Chem.*, **42**, 2639 (1977).

3) O. Tsuge, K. Ueno, S. Kanemasa, and K. Yorozu, *Bull. Chem. Soc. Jpn.*, **60**, 3347 (1987).

4) Some examples of base-induced cyclization of the imines of glutamates producing pyrrolidine-2,4-dicarboxylates: R. Grigg and J. Kemp, *J. Chem. Soc., Chem. Commun.*, **1978**, 109; R. Grigg, J. Kemp, J. Malone, and A. Tangthongkum, *ibid.*, **1980**, 648.

5) A. stereoselective Michael addition is the only reaction observed between the camphor imine of *t*-butyl glycinate and methyl crotonate, indicating the contribution of route **E**→**F**→**3** (S. Kanemasa, A. Tatsukawa, and O. Tsuge, unpublished result).

6) Since quench of **D** with triethylammonium bromide reproduces imine **1**, lithium bromide, and triethylamine, reversible formation of anion **D** may start again. On the contrary, **F** is quenched in an irreversible manner.

7) K. N. Houk, J. Sims, R. E. Duke, Jr., R. W. Strozier, and J. K. George, *J. Am. Chem. Soc.*, **95**, 7287 (1973); K. N. Houk, J. Sims, C. R. Watts, and L. J. Luskus, *ibid.*, **95**, 7301 (1973); K. N. Houk, *Acc. Chem. Res.*, **8**, 361 (1975).

8) Such steric repulsion has been previously discussed: O. Tsuge, K. Ueno, S. Kanemasa, and K. Yorozu, *Bull. Chem. Soc. Jpn.*, **59**, 1809 (1986).

9) G. Surpateanu and A. L.-Combier, *Heterocycles*, **22**, 2079 (1984).

10) R. Grigg, H. Q. N. Gunaratne, and J. Kemp, *J. Chem. Soc., Perkin Trans. 1*, **1984**, 41.

 © 1989 The Chemical Society of Japan Bull. Chem. Soc. Jpn., 62, 875—879 (1989)

Stereochemical Control in Microbial Reduction. 8. Stereochemical Control in Microbial Reduction of β-Keto Esters

Kaoru NAKAMURA,* Yasushi KAWAI,† Shinzaburo OKA,† and Atsuyoshi OHNO†
Department of Chemistry, Shiga University of Medical Science, Seta, Ohtsu 520-21
†Institute for Chemical Research, Kyoto Unversity, Uji, Kyoto 611
(Received October 7, 1988)

Stereochemistry of the reduction of β-keto esters with bakers' yeast is controlled by the addition of a certain α,β-unsaturated carbonyl compound (or its reduced form). Glucose also exerts the same effect. The additives tend to shift the stereochemistry of the reduction toward the production of D-hydroxy ester. Namely, methyl 3-oxopentanoate and ethyl 3-oxo-6-heptenoate were reduced to the corresponding D-hydroxy esters with excellent stereoselectivities and chemical yields. The enones are supposed to inhibit the enzymes that produce the L-hydroxy ester, whereas glucose plays a role to activate the enzymes that produce the D-hydroxy ester.

Since chiral alcohols are versatile and convenient building blocks in the syntheses of biologically important compounds, asymmetric reduction of ketones has been studied quite extensively.[1] Namely, the reduction mediated by a microbe has been a promising candidate to synthesize chiral alcohols in an excellent stereoselectivity and the research in this field has been expanded tremendously within recent one or two decade(s).[2] In most cases so far reported, the results are satisfactory with high chemical yields and high stereoselectivity. However, it should be emphasized that there was a lot of examples that afforded unsatisfactory results; low chemical yields and/or low stereoselectivities. Usually, almost all of these results are discarded unreported.

At the same time, a microbe does not necessarily afford the compound of desired configuration for further use in syntheses. In this case, we have to control or reverse the stereochemistry of the reduction. There are several methods to improve or control the stereoselectivity of the reduction. The first and most common method is to screen microbes to find a suitable one for a particular purpose.[3–5] This is a purely biological method and the result can not be predicted on the basis of chemistry. The second is the modification of the substrate.[6–8] In most cases in this category, steric bulk of two substituents on the carbonyl group is differentiated so that the enzyme (or enzymes) can recognize the *re*- and *si*-faces of the substrate easily, and the results are more or less chemically predictable. The third and brand-new method reported from our laboratory is to modify the reaction conditions.[9,10] Immobilization of a microbe into a hydrophobic network of a polymer is a typical example in this category. It has been reported that there is a relationship between the hydrophobicity of medium in the vicinity of microbe and the preferability to the configuration in the product hydroxy ester.[9,10]

In this paper, we would like to report the fourth method: the addition of a third reagent to the reaction system affects the stereochemical course of the reduction and the stereoselectivity can be improved up to satisfactory levels.[11]

Results and Discussion

There are two possibilities for an unsatisfactory stereoselectivity. One of them is the case in which only one dehydrogenase is responsible for the reduction of a substrate and the structure of the substrate is not suitable to exert its enantio- (or diastereo)-facial difference in the pocket of the enzyme. A low stereoselectivity seen in the reduction with an isolated dehydrogenase is the extreme of this category.[12,14] The other is the case in which two or more dehydrogenases are operating simultaneously but some enzymes produce the (*R*)-alcohol while others contribute to produce the (*S*)-alcohol, although each reduction proceeds with a high stereoselectivity.[15] There is a good chance to obtain a racemic mixture from a microbial reduction system. If the low stereoselectivity observed in a microbial reduction is due to the latter situation, there is a chance for a chemist to improve the stereoselectivity: inhibition or activation of an appropriate enzyme (or enzymes) will result in higher stereoselectivity. Based on the concept mentioned above, we looked for an inhibitor and an activator for particular enzymes responsible for the reduction of β-keto esters with bakers' yeast.

Two different states of bakers' yeast were employed as the microbe. One is the raw bakers' yeast (RBY) and the other is the dry bakers' yeast (DBY). Although the effect of the additive is much larger for RBY than for DBY, the activity of RBY changes from a lot to another and sometimes the stereoselectivity of reduction deviates up to 10% from a run to another when the specificity is relatively low. The activity of RBY also decreases on storage and it is difficult to confirm the reproducibility in stereoselectivity of the reduction with RBY. Therefore, we employed the result from DBY to discuss fundamental trends of the reduction, but RBY is recommended for practical purpose,

Table 1. Effect of the Amount of Bakers' Yeast on the Reduction of Methyl 3-Oxopentanoate[a]

Yeast/g	Configuration	e.e./%[b]	Chem. yield/%[c]
RBY (1)	*R* (D)	54	19
RBY (2)	*R*	51	37
RBY (3)	*R*	44	33
RBY (5)	*R*	33	35
DBY (1)	*R*	10	50
DBY (2)	*R*	7	41
DBY (4)	*R*	12	46

a) Substrate, 1 mmol; Water 20 ml. b) Reproducibility in the reaction with RBY and DBY are about 10% and 1%, respectively. c) Reproducibility in the reaction with RBY and DBY are about 5% and 1%, respectively.

because the latter affords a better stereoselectivity, an enantiomer excess (e.e.).

As listed in Table 1, the relative amount of DBY against the substrate does not affect the stereoselectivity of the reduction meaningfully, whereas that of RBY results in decreases in e.e. Thus, it seems probable that DBY and RBY are different in levels of various enzymes. In other words, plural enzymes are operating in the reduction system and the effect of an additive can be expected for this system.

The effect of α,β-unsaturated carbonyl and hydroxy compounds on the e.e. of product was studied in the reduction of methyl 3-oxopentanote with DBY and the results are summarized in Table 2. The bakers' yeast was preincubated for 30 min in the presence of an

Table 2. Reduction of Methyl 3-Oxopentanoate with Bakers' Yeast in the Presence of Carbonyl or Hydroxy Compound[a]

Additive	Yeast	Configuration	e.e./%[b]	Chem. yield/%[c]
	DBY	*R* (D)	68	51
	RBY	*R*	89	22
	DBY	*R*	61	71
	RBY	*R*	78	50
	DBY	*R*	60	68
	RBY	*R*	89	67
	DBY	*R*	44	67
	RBY	*R*	66	68
	DBY	*R*	44	63
	RBY	*R*	68	63
	DBY	*R*	39	61
	RBY	*R*	66	34
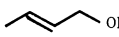	DBY	*R*	23	67
	RBY	*R*	35	31
	DBY	*R*	22	58
	RBY	*R*	61	58
	DBY	*R*	21	67
	RBY	*R*	35	36
	DBY	*R*	16	59
	RBY	*R*	31	30
	DBY	*R*	16	51
	RBY	*R*	41	48
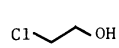	DBY	*R*	13	66
	RBY	*R*	25	31
None	DBY	*R*	12	46
	RBY	*R*	37	38
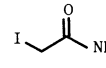	DBY	*R*	4	24
	RBY	*R*	20	34

a) DBY, 4 g (or RBY, 2 g); water, 20 ml; substrate, 1 mmol; additive, 0.5 mmol. b) The reproducibilities in the reduction with RBY are about 2% at >80% e.e., 5% at >50% e.e., and 10% at <50% e.e., respectively. Those with DBY are about <1%. c) The reproducibilities in the reduction with RBY and DBY are about 5% and 1%, respectively.

Table 3. Effect of Glucose on the Stereochemistry of the Reduction of Methyl 3-Oxopentanoate with Dry Bakers' Yeast[a)]

DBY/g	Glucose/g	Configuration	e.e./%	Chem. yield/%
2	0	*R* (D)	7	41
2	1	*R*	23	43
4	0	*R*	12	46
4	1	*R*	31	61

a) Substrate, 1 mmol; water, 20 ml.

additive (or additives), then a substrate was added to the reduction system. It should be mentioned that e.e. of methyl 3-hydroxypentanoate obtained from the reduction without an additive is only 12%, which means that the enzyme(s) which affords the D-product (D-enzyme) and that (those) which affords the L-product (L-enzyme) are nearly equally active for this substrate. In contrast, the addition of methyl vinyl ketone or 2-cyclohexen-1-one improves the stereoselectivity up to 60—70% e.e. Allyl alcohol exerts the same effect, but the substitution of one methyl group on any carbon of allyl alcohol decreases the effect sharply as seen in the reductions in the presence of *trans*-2-buten-1-ol, 3-buten-1-ol, and 2-methyl-2-propen-1-ol. Propargyl alcohol is ineffective either. Thus, molecular shape plays a crucial role in exerting the effect on stereochemistry of the reduction. Acrylic acid and its methyl ester are also effective, though the effect is a little bit smaller than those of ketones. It is interesting to note that the specificity decreases in the presence of iodoacetamide, which indicates that this compound shifts the stereoselectivity toward the L-side. The results from the reduction with RBY is also listed in Table 2 for comparison.

In the presence of glucose, the energy-gaining and NAD(P)H-producing glycolysis system of yeast is stimulated. Consequently, the dehydrogenase-levels are distorted in yeast and the change in the stereoselectivity of the reduction can be expected. The results from the addition of glucose to the reduction system are summarized in Table 3. Indeed, it is recognized that the addition of glucose improves both the chemical yield and the stereoselectivity toward the D-side.

In order to elucidate the mechanism for the shift of stereochemistry on addition of an α,β-unsaturated carbonyl compound or its corresponding alcohol and of glucose, the kinetics of the reduction were followed in the presence or absence of these additives. The results plotted in Fig. 1 clearly show that glucose accelerates and methyl vinyl ketone retards the reduction in comparison to that without the additive. Since both glucose and methyl vinyl ketone are the additives that increase the yield of the *R* (D)-product, there is no doubt that the former *activates* the D-enzyme(s) (along the glycolysis cycle), whereas the latter *inhibits* the L-enzyme(s). The improvement of the specificity toward the D-side is not due to

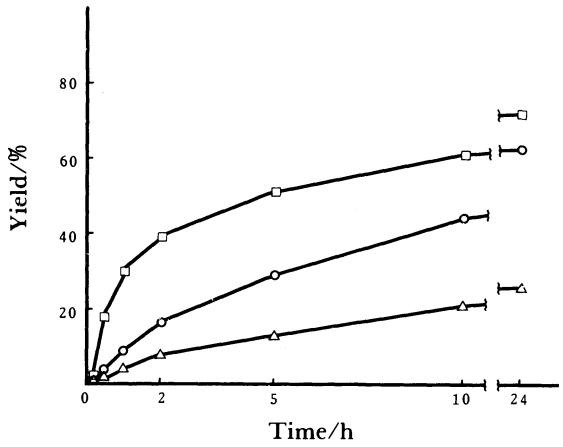

Fig. 1. Plots of the chemical yields of methyl 3-hydroxypentanoate against reaction time for the reduction of methyl 3-oxopentanoate with DBY in the presence of glucose (—□—□—) or methyl vinyl ketone (—△—△—), or absence of an additive (—○—○—).

decomposition of the *S* (L)-product.

We believe that the hydroxy compounds employed as inhibitors are once oxidized in yeast by the dehydrogenase system, than the resulted aldehyde is again trapped by an enzyme(s) in the reducing system. Since all the additives so far exerted the efficient inhibitory effect are good Michael acceptors, it is conceivable that the attack on the double bond in the α,β-unsaturated carbonyl compound by a nucleophile at the vicinity of the reaction center of dehydrogenase takes place faster than the process to reduce the substrate.[16)] It is not clear at present why these compounds do not inhibit the D-enzyme(s). Probably, the D- and L-enzymes locate in different sites in yeast so that the D-enzyme does not find a chance to encounter with these inhibitors. Another alkylating agent, 2-chloroethanol, did not work effectively.

For practical purpose, a composite use of glucose and an enone in the reduction with RBY will afford the most favorable result. This idea has been tested for various β-keto esters and the results are summarized in Table 4. It is obvious that the present method is quite useful in obtaining the D-hydroxy esters. Although the reduction of ethyl acetoacetate did not result in the reversion of configuration, it should be noted that, unlike other β-keto esters, the stereoselectivity of the

Table 4. Stereochemical Results for the Reductions of Various β-Keto Esters with Raw Bakers' Yeast[a]

Substrate	Reaction condition[b]	Configuration	e.e./%[c]	Chem. yield/%[d]
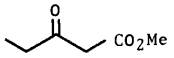	A	*R* (D)	59	54
	B	*R*	98	10
	B′	*R*	90	70
	C	*R*	98	37
	C′	*R*	96	56
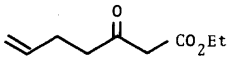	A	*R* (D)	64	77
	B	*R*	99	8
	B′	*R*	98	61
	C	*R*	97	37
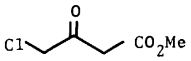	A	*S* (D)	52	74
	B	*S*	94	22
	C	*S*	78	74
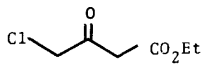	A	*S* (D)	43	62
	B	*S*	68	20
	C	*S*	85	42
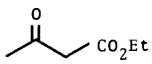	A	*S* (L)	77	66
	B′	*S*	47	66
	C′	*S*	40	68

a) RBY, 2 g; water, 20 ml; substrate, 1 mmol; glucose, 2 g. b) A, without an enone; B, with 1 mmol of methyl vinyl ketone; B′, with 0.5 mmol of methyl vinyl ketone; C, with 1 mmol of allyl alcohol; C′, with 0.5 mmol of allyl alcohol. c) The reproducibilities are about 1% at >95% e.e., 2% at >80% e.e., and 5% at >50% e.e. d) The reproducibilities are about 5%.

reduction of this substrate without additives is quite high in the L-side. The present method is not effective enough to shift the e.e. more than 40% toward the D-side. More effective device is awaited for a versatile reversion of configuration.

Experimental

Instruments. ^{1}H NMR spectra were recorded on a Varian VXR-200 spectrometer in $CDCl_3$ with Me_4Si as an internal standard. Gas chromatograms were recorded on a YANACO G-2800 gas chromatograph. HPLC was performed on a Hitachi 655 liquid chromatography with Wakosil 5SIL (4.6×150 mm) column and an IRICA 852-III spectrophotometer. Optical rotation was measured with a Perkin-Elmer 241 polarimeter.

Materials. Methyl 3-oxopentanoate, methyl and ethyl 4-chloro-3-oxobutanoates, and (*R*)-(+)-α-methoxy-α-(trifluoromethyl)phenylacetic acid (MTPA) were purchased from Aldrich Chemical Co. Ethyl 3-oxo-6-heptenoate was prepared according to the literature procedure.[17] Raw bakers' yeast (pressed bakers' yeast; RBY) and dry bakers' yeast DBY) were purchased from Oriental Yeast Co. and stored in a refrigerator. Other reagents were purchased from Nacalai Tesque Co.

Reduction of β-Keto Ester. In general, an appropriate amount of an additive was added to a suspension composed of 4 g of dry bakers' yeast and 20 ml of water. The whole mixture was stirred for 30 min at 30 °C. Then, 1 mmol of a substrate was added to the mixture and the stirring was continued at the same temperature. After 1 day, Hyflo-super cel and ethyl acetate was added to the suspension and the resulted mixture was filtered. The celite was washed with ethyl acetate and the combined filtrate was extracted with ethyl acetate. The organic portion was washed with water and brine, dried over anhydrous sodium sulfate, concentrated under reduced pressure, and the residue was subjected to preparative gas chromatography (PEG, 1.5 m, 130—170 °C), giving the corresponding hydroxy ester.

Determination of the Optical Purity. To a stirred mixture of 0.03 mmol of a β-hydroxy ester and 1 ml of benzene, were added 1.5 mmol of pyridine and 0.2 mmol of (*R*)−(+)−α-methoxy-α-(trifluoromethyl)phenylacetyl chloride in this order and the mixture was stirred overnight. Ethyl acetate and water were added to the mixture and the layers were separated. The organic portion was washed with 1 M hydrochloric acid (1 M=1 mol dm^{-3}), saturated aqueous sodium carbonate, and brine, then dried over anhydrous sodium sulfate and concentrated to give the corresponding (*R*)-MTPA ester in more than 90% yield.

The enantiomer excess in the hydroxy ester was determined by GLC (OV 1701, 25 m, 200 °C; ethyl 3-hydroxybutanoate and methyl 3-hydroxypentanoate) and HPLC (hexane/ethyl acetate=30/1; methyl and ethyl 4-chloro-3-hydroxybutanoate, and ethyl 3-hydroxy-6-heptenoate) analyses of the corresponding (*R*)-MTPA ester.

Kinetics of the Reduction. To a suspension containing 2 g of DBY in 20 ml of water 1 mmol of methyl 3-oxopentanoate was added and the whole suspension was stirred at room temperature. After appropriate time intervals, 2 ml aliquots were taken out from the suspension and poured into 5 ml of ethyl acetate containing ethyl succinate (an internal standard for GLC). The organic materials were extracted and subjected to GLC (PEG, 1 m, 100 °C). The experiment with glucose (2 g, 11 mmol) or methyl vinyl ketone (70 mg, 1 mmol) was also run in the same way as mentioned above by adding these additives to the suspension of DBY in water 30 min before the addition of

methyl vinyl ketone. The results are plotted in Fig. 1.

The authors wish to thank the Ministry of Education, Japan for financial support for this research by the Grants Nos. 62216011 and 63303002.

References

1) For a review; J. D. Morrison and H. S. Mosher, "Asymmetric Organic Reactions," Prentice-Hall, London (1971).

2) For reviews; C. J. Sih and C.-H. Chen, *Angew. Chem., Int. Ed. Engl.*, **23**, 570 (1984): J. B. Jones, *Tetrahedron*, **42**, 3351 (1986).

3) B. Wipf, E. Kupfer, R. Bertazzi, and H. G. W. Lenenberger, *Helv. Chim. Acta*, **66**, 485 (1983).

4) D. Zeebach, M. F. Zuger, F. Giovannini, B. Sonnleitner, and A. Fiechter, *Angew. Chem., Int. Ed. Engl.*, **23**, 151 (1984).

5) R. Bernardi, R. Cardillo, and D. Ghiringhell, *J. Chem. Soc., Chem. Commun.*, **1984**, 460.

6) K. Nakamura, K. Ushio, S. Oka, and A. Ohno, *Tetrahedron Lett.*, **25**, 3979 (1984).

7) T. Fujisawa, T. Itoh, and T. Sato, *Tetrahedron Lett.*, **25**, 5083 (1984).

8) C. Fuganti, P. Casati, and M. Carmeno, *Tetrahedron Lett.*, **26**, 101 (1985).

9) K. Nakamura, M. Higaki, K. Ushio, S. Oka, and A. Ohno, *Tetrahedron Lett.*, **26**, 4123 (1985).

10) K. Nakamura, K. Inoue, K. Ushio, S. Oka, and A. Ohno, *J. Org. Chem.*, **53**, 2589 (1988).

11) Preliminary communication: K. Nakamura, K. Inoue, K. Ushio, S. Oka, and A. Ohno, *Chem. Lett.*, **1987**, 679.

12) J. B. Jones and J. F. Beck, "Asymmetric Syntheses and Resolution Using Enzymes" in "Application of Biological Systems in Organic Chemistry," ed by J. B. Jones, C. J. Sih, and D. Perlman, John Wiley and Sons, New York, N. Y. (1976), pp. 107—401.

13) J. B. Jones and H. M. Schwartz, *Can. J. Chem.*, **59**, 1574 (1981).

14) L. K. P. Lam, I. A. Gair, and J. B. Jones, *J. Org. Chem.*, **53**, 1611 (1988).

15) W-R. Shieh, A. S. Gopalan, and C. J. Sih, *J. Am. Chem. Soc.*, **107**, 2993 (1985).

16) C. Wills, *Nature (London)*, **261**, 26 (1976).

17) M. Hirama and M. Uei, *J. Am. Chem. Soc.*, **104**, 4251 (1982).

Isolation of Four 2,3,5,6,11,11b-Hexahydro-3-oxo-1*H*-indolizino[8,7-*b*]indole-5-carboxylic Acids from *Clerodendron Trichotomum* Thunb and Properties of Their Derivatives

Hajime IRIKAWA,* Yasuhiro TOYODA, Hiroaki KUMAGAI, and Yasuaki OKUMURA
Department of Chemistry, Faculty of Science, Shizuoka University, Ohya, Shizuoka 422
(Received October 12, 1988)

Four 2,3,5,6,11,11b-hexahydro-3-oxo-1*H*-indolizino[8,7-*b*]indole-5-carboxylic acids, plausible precursors of trichotomine, were isolated as the methyl esters from *Clerodendron trichotomum* Thunb, and the structures elucidated on the basis of their spectral and chemical evidences. The existence of two pairs of the C-11b epimers in the above plant were supported by the methoxide-catalyzed equilibrations of the compounds having the substituent on C-11b. Blue pigments were formed from the isolated compounds.

A blue pigment, trichotomine (**1**), was isolated from the fruits of *Clerodendron trichotomum* Thunb and the structure was elucidated by Iwadare et al.[1] The synthesis of **1** was reported by three groups.[2–4] Iwadare et al. prepared trichotomine dimethyl ester (**2**) by the autoxidation of **3**.[2] Kapadia and Rao synthesized **1** by one-pot reaction of L-tryptophan and 2-oxoglutaric acid, and suggested the intermediacy of **4**, formed from **5a** and/or **5b**, in the biosynthesis of **1**.[3] Since the skeleton of L-tryptophan with intact steric configuration is present in **1**, we attempted to search the extracts of the above plant for the substances supposed to be biosynthetic precursors of **1** in the lights of ultraviolet absorptions and color reactions with Ehrlich's reagent. Preliminary results of this study have been published in two communications.[5,6]

Isolation and Structure of 5a,b and 6a,b. The extracts were chromatographed on TSK gel G-3000s and then on Sephadex LH-20 to give four acidic compounds **5a,b** and **6a,b**, which showed characteristic blue sports on TLC with Ehrlich's reagent. On treatment with ethereal diazomethane, **5a,b** and **6a,b** afforded the dimethyl esters **7a,b** and the monomethyl esters **8a,b**, respectively.

The structures of **7a** and **7b** were deduced from the spectral data, and confirmed by the synthesis. Reaction of L-tryptophan methyl ester hydrochloride and dimethyl 2-oxoglutarate in methanol gave **7a** and **7b**, which were identical with the natural specimens of **7a** and **7b** by spectroscopic (IR, ^{1}H NMR, MS, and CD) and TLC comparisons, respectively. The diester **7b** was also prepared as follows. In a manner similar to that of Kapadia and Rao,[3] a mixture of L-tryptophan and 2-oxoglutaric acid in water was kept under nitrogen atmosphere at room temperature for two weeks to give **9a**, which was treated with ethereal diazomethane to afford the trimethyl ester **9b**. On treatment with 8 wt% hydrogen chloride–methanol, **9b** underwent cyclization to **7b**.

The stereochemical relationship of the two methoxycarbonyl groups in **7b** was determined in the following way. Reduction of **7b** with sodium borohydride in methanol–tetrahydrofuran gave the diol **10**, which afforded the ether **11** on treatment with *p*-toluenesulfonyl chloride in pyridine. Formation of **11** can be rationalized by tosylation of the hydroxymethyl group on C-5, followed by an intramolecular nucleophilic attack on the tosyloxymethyl carbon with the oxygen of the hydroxymethyl group on C-11b. Thus, formation of **11** indicates that the two methoxycarbonyl groups in **7b** bear 1,3-cis relationship to each other.

On treatment with sodium methoxide in methanol, the natural **7a** gave a mixture of **7a** and the antipode of **7b** in a ratio of 1:9, since the CD spectrum of the epimerization products was almost identical with that of the antipode of **7b** prepared from D-tryptophan methyl ester hydrochloride and dimethyl 2-oxoglutarate.

Accordingly, the structures of **7a** and **7b** were confirmed as shown in Fig. 1 including absolute configurations.

The structures of **8a** and **8b** were deduced from the spectral data, and confirmed by the synthesis.

Reaction of L-tryptophan methyl ester and 2-oxoglutaric acid in refluxing benzene afforded **8a** and **8b**[7] which were identical with the natural specimens of **8a** and **8b** in every respect of spectroscopic (IR, ^{1}H NMR, MS, and CD) and TLC comparisons, respectively. On treatment with sodium methoxide in methanol, **8a** underwent epimerization at C-5 to an epimer, which was identical with the antipode of **8b** prepared from D-tryptophan methyl ester and 2-oxoglutaric acid ($[\alpha]_D$, IR, ^{1}H NMR, and CD). The absolute configurations of the C-11b proton in **8a** and **8b** were supported by comparison of the CD spectra with those of yohimbane and pseudo-yohimbane, respectively.[8]

Accordingly, the structures of **8a** and **8b** were confirmed as shown in Fig. 1 including the absolute configurations.

Methoxide-Catalyzed Equilibrations. Tendency of epimerization at C-5 observed in **7a** and **8a** caused us to study on the methoxide-catalyzed equilibrations of the 11b-substituted derivatives of **8a** and **8b**.[6]

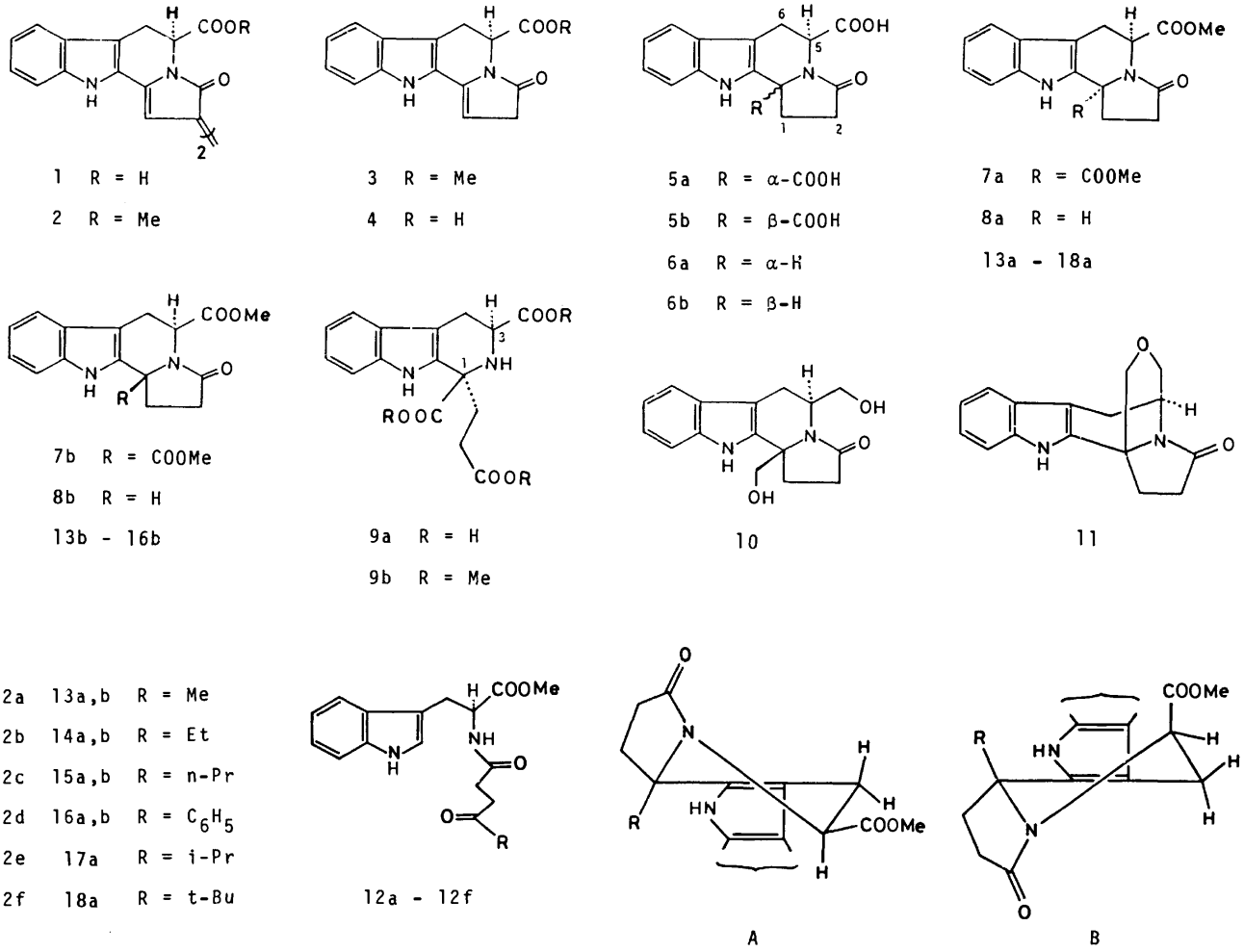

Fig. 1.

Table 1. ^{1}H and ^{13}C NMR Spectral Data (δ-values), and Equilibrations at C-5 (%)

Compound	5-H		OMe		C-5		C-11b		Ratio[a]	
	a[b]	b[c]	a	b	a	b	a	b	a	b
7 R=COOMe	4.39	5.48	3.83[d]	3.59	53.7	49.2	66.7	63.9	10	90
8 R=H	4.12	5.34	3.82	3.63	54.7	49.5	56.3	52.5	<1	>99
13 R=Me	4.09	5.40	3.79	3.66	52.2	48.7	61.9	59.8	19	81
14 R=Et	4.07	5.39	3.83	3.68	52.1	48.9	64.9	63.1	35	65
15 R=*n*-Pr	4.10	5.37	3.82	3.69	52.2	48.9	64.6	62.9	30	70
16 R=C_6H_5	3.88	5.23	3.74	2.89	52.1	48.3	68.1	64.4	46	54
17 R=*i*-Pr	4.15		3.81		51.8		67.7		100	0
18 R=*t*-Bu	4.51		3.78		53.9		70.5		100	0

a) Equilibration ratios determined by HPLC. b) Double doublet, J=10.0—11.1 and 5.1—5.8 Hz. c) Double doublet, J=6.6—8.1 and 1.5—2.1 Hz. d) Assignment may by interchangeable with the singlet at δ=3.87.

The amides **12a—12f** were prepared from L-tryptophan methyl ester and the corresponding 4-oxo carboxylic acids. On treatment with 13 wt% hydrogen chloride–methanol, **12a—12d** afforded **13a** and **13b** (in a ratio of 1:2), **14a** and **14b** (2:1), **15a** and **15b** (2:1), **16a** and **16b** (>20:1), respectively.[9] Cyclization of **12e** and **12f** under similar conditions yielded predominantly **17a** and **18a**, respectively. The stereoselective formation of **17a** and **18a** seems to be due to the interaction between the methoxycarbonyl group and the bulky R group (R=*i*-Pr or *t*-Bu) in the cyclization intermediates, respectively.[10]

The conformations of the compounds described above were analyzed as follows. As shown in Table 1, the ^{1}H NMR spectra of **7a**, **8a**, and **13a—18a** showed the signals at δ=3.88—4.51 (dd, $J_{5\alpha,6\beta}$=10.0—11.1 and $J_{5\alpha,6\alpha}$=5.1—5.8 Hz), which suggested the axial orientations of the C-5 proton in these compounds. On the

other hand, the double doublet signals in **7b**, **8b**, and **13b—16b** were observed at δ=5.23—5.48 ($J_{5\alpha,6\alpha}$=6.6—8.1 and $J_{5\alpha,6\beta}$=1.5—2.1 Hz), indicating the equatorial orientations of the C-5 proton in these compounds.[11] The proton signals of the methoxycarbonyl group in **7b**, **8b**, and **13b—15b** were observed at δ=3.59—3.69, while that in **16b** appeared at δ=2.89 because of the magnetic anisotropic effect of the phenyl group on C-11b, being in line with the 1,3-cis relationship of the two substituents on C-5 and -11b in **16b**.[12]

As shown in Table 1, the ^{13}C NMR signals for C-5 and -11b in **7a**, **8a**, and **13a—16a** appeared at lower field than those in the corresponding **7b**, **8b**, and **13b—16b**. This trend is also in agreement with the above-mentioned orientations of the methoxycarbonyl group in these compounds.[13,14] The ^{1}H and ^{13}C NMR characteristics are similar to those of the 1,3-disubstituted 1,2,3,4-tetrahydro-β-carbolines (^{1}H NMR signals of C-3 and -4 protons and ^{13}C NMR signals of C-1 and -3).[12,14,15]

Therefore, assuming that the indolizinone ring is cis-fused,[16] the conformer **A** was assigned to **7a**, **8a**, and **13a—18a**, and the conformer **B** to **7b**, **8b**, and **13b—16b**.

The methoxide-catalyzed equilibrations of the above-mentioned compounds were examined as follows. Each of the compounds **7a,b**, **8a,b**, **13a,b—16a,b**, **17a**, and **18a** was dissolved in 0.1 mol dm^{-3} methanolic sodium methoxide, and let stand at room temperature for a few days until the equilibrium was reached. The ratios of a pair of epimers were determined by HPLC, and the results were shown in Table 1.[9]

The unsubstituted **8a** is thermodynamically more unstable than **8b**, and exists to the extent of less than 1%. Compound **8a** seems to be destabilized by the interaction between the amide carbonyl group and the methoxycarbonyl group on C-5 as shown in the conformer **A** (R=H). Epimerization at C-5 in **7b**, and **13b—16b** seems to be affected by another interaction between the substituent on C-11b and the methoxycarbonyl group on C-5 as shown in the conformer **B**. No epimerization isomers of **17a** and **18a** were detected either by ^{1}H NMR or HPLC. Similar epimerization trend was reported in tetrahydro-β-carboline derivatives.[15]

The equilibration experiments excluded the possibility of the epimerization at C-5 in **5a,b** and **6a,b** during the isolation procedure, and supported the existence of two pairs of **5a,b** and **6a,b** in the above plant.

Oxidative Dimerization. Autoxidation of indole compounds gave various products via 3*H*-indol-3-yl hydroperoxides.[17] The coloration of **8b** above its melting point resulted from the formation of **2**, which might proceed via the 3*H*-indol-3-yl hydroperoxide from **8b**.[18] Treatment of **8b** with *N*-bromosuccinimide in *t*-butyl alcohol gave **2** in one-pot reaction; **2** might be produced through **3** derived from **8b** via the corresponding 3-bromo-3*H*-indole. Trichotomine **1** was formed from **7b** by hydrolysis with potassium hydroxide in aqueous methanol, followed by autoxidation in aqueous acetic acid. These results suggested that **5a,b** and **6a,b** were plausible precursors of trichotomine **1**.

In general, indole compounds are stable against autoxidation when the indole nitrogen atom bears a protecting group. Therefore, we examined the oxidative dimerization of **19**, the acetate of **3**.

Acetylation of **8a** and **8b** with acetic anhydride and pyridine gave **20a** and **20b**, respectively. On electrolysis in methanol containing tetrabutylammonium tetrafluoroborate as a supporting electrolyte, both **20a** and **20b** afforded the methoxy lactam **21**, which was formed probably by addition of methanol to an intermediate **22**.[19] The ^{1}H NMR signals of the C-5 proton in **21** (δ=5.37, dd, J=7.2 and 0.9 Hz) indicated the β-orientation of the methoxyl group on C-11b. Treatment of **21** with formic acid yielded **19** after a loss of methanol. On aeration of a solution of **19** in butyl alcohol, **19** underwent oxidative dimerization to trichotomine dimethyl ester diacetate (**23**).[1]

Isolation of **5a** and **5b** shows the involvement of 2-oxo acid, 2-oxoglutaric acid, in the biosynthetic pathway of trichotomine **1** [L-tryptophan→**9a** and /or an epimer at C-1→**5a** and/or **5b**→(**6a** and/or **6b**)→**4**→**1**]; this indicates another example of G. Hahn's proposal.[3] The formation of **1** from **4** and of **23** from **19** might be another type of well-known oxidative dimerization of indoxyl to indigo.[20]

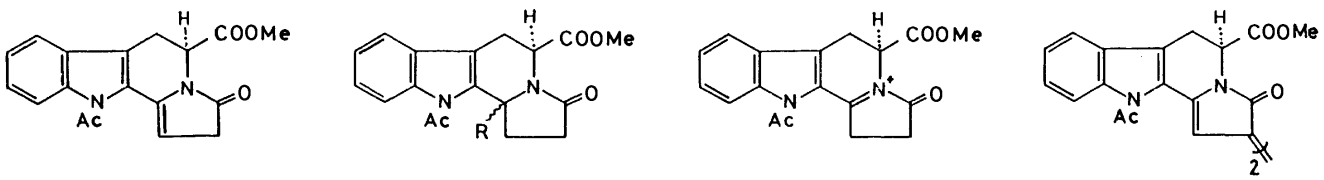

19 20a R = α-H 20b R = β-H 21 R = β-OMe 22 23

Fig. 2.

Experimental

All melting points were determined on a Yanagimoto micro melting point apparatus and are uncorrected. IR spectra were recorded on a Hitachi EPI-G$_3$. ^{1}H NMR spectra were obtained on a Varian EM-390 (90 MHz) or a JNM-GSX-400 (400 MHz), and ^{13}C NMR spectra on a JNM-PFT-60 (15 MHz) or a JNM-GSX-400 (100 MHz), using $CDCl_3$ as solvent, unless otherwise stated. UV spectra were measured on a JASCO UVIDEC-510 and CD spectra on a JASCO J-500A, using MeOH as solvent. Mass spectra were obtained on a Hitachi M-52 or M-80 at an ionization energy of 70 eV. Optical rotations were measured on a Union PM-101. Analytical TLC was carried out on silica-gel plates (Kieselgel 60 F_{254}, E. Merk). HPLC were performed on a JASCO Trirotor apparatus using a 4.6×250 mm Fine SIL-5 column with $CHCl_3$–hexane (3:2) at 1.3 ml min^{-1} flow rate.

Isolation. The blue fruits of the plant *Clerodendron trichotomum* Thunb (30 kg) were collected in October and immersed in EtOH (75 l) at room temperature for 2 weeks and then filtered. The combined filtrates were concentrated under reduced pressure to ca. 12 l. The remaining aqueous solution (3 l) was washed with AcOEt (3 l×3), and then roughly separated by column chromatography on TSK-gel G-3000s (900 g) using a gradient solution of H_2O–EtOH to give 4 fractions: fraction 1, H_2O 1 l; fraction 2, H_2O–EtOH (4:1) 1 l; fraction 3, H_2O–EtOH (3:2) 1 l; fraction 4, H_2O–EtOH (2:3) 1 l. In the same way, the remaining aqueous solution was separated to 4 fractions. The eluates of fraction 2, 3, and 4 were concentrated under reduced pressure, respectively. Analytical TLC of the residues of fraction 2, 3, and 4 (*n*-BuOH–AcOH–H_2O, 4:1:1) showed the blue spots of **5a** (R_f 0.40), **5b** (R_f 0.52), and **6a,b** (R_f 0.63) with Ehrlich's reagent, respectively. The residue of fraction 2 was further separated by column chromatography on Sephadex LH-20 using MeOH as eluent to give an acidic compound **5a**. To a solution of **5a** in MeOH was added an ethereal solution of CH_2N_2. The mixture was allowed to stand at room temperature overnight, and evaporated to leave an oil, which was purified by column chromatography on SiO_2 using MeOH–$CHCl_3$ (3:100) to give the diester **7a** as a colorless oil (8 mg): IR($CHCl_3$) 3450, 1740, and 1705 cm^{-1}; ^{1}H NMR δ=2.1—3.0 (4H, m, C_1-2H, C_2-2H), 2.99 (1H, dd, J=15.9 and 5.4 Hz, C_6-H), 3.34 (1H, dd, J=15.9 and 10.5 Hz, C_6-H), 3.83 (3H, s, OMe), 3.87 (3H, s OMe), 4.39 (1H, dd, J=10.5 and 5.4 Hz, C_5-H), 7.0—7.6 (4H, m, aromatic protons), and 8.25 (1H, br s, NH); MS *m/z* (rel intensity) 342 (M$^+$; 3), 283 (100), and 223 (29); CD $[\theta]_{295}$ −1600, $[\theta]_{291}$ −800, $[\theta]_{286}$ −3200, $[\theta]_{259}$ 0, $[\theta]_{236}$ +38000, $[\theta]_{225}$ 0, and $[\theta]_{218}$ −48000. Found: *m/z* 342.1234. Calcd for $C_{18}H_{18}N_2O_5$: M, 342.1214.

According to essentially the same procedure as described above, fraction 3 afforded **7b** as crystals (76 mg): mp 189—190 °C; IR($CHCl_3$) 3450, 1741, and 1696 cm^{-1}; ^{1}H NMR δ=1.9—3.0 (4H, m, C_1-2H, C_2-2H), 3.06 (1H, dd, J=16.2 and 6.6 Hz, C_6-H), 3.31 (1H, dd, J=16.2 and 1.8 Hz, C_6-H), 3.59 (3H, s, OMe), 3.81 (3H, s, OMe), 5.48 (1H, dd, J=6.6 and 1.8 Hz, C_5-H), 7.0—7.6 (4H, m, aromatic protons), and 8.53 (1H, br s, NH); MS *m/z* (rel intensity) 342 (M$^+$; 14), 283 (100), and 223 (31); CD $[\theta]_{295}$ +900, $[\theta]_{290}$ 0, $[\theta]_{270}$ +4000, $[\theta]_{259}$ 0, $[\theta]_{238}$ −19000, $[\theta]_{231}$ 0, and $[\theta]_{221}$ +81000.

According to essentially the same procedure as described above, fraction 4 gave a mixture of **8a** and **8b**, which was separated by column chromatography on SiO_2 (MeOH–$CHCl_3$, 3:100). **8a** (as an oil, 9 mg): IR(film) 3300, 1740, and 1677 cm^{-1}; ^{1}H NMR δ=2.0—2.7 (4H, m, C_1-2H, C_2-2H), 2.98 (1H, ddd, J=15.9, 5.1, and 1.8 Hz, C_6-H), 3.35 (1H, ddd, J=15.9, 10.2, and 2.1 Hz, C_6-H), 3.82 (3H, s, OMe), 4.12 (1H, dd, J=10.2 and 5.1 Hz, C_5-H), 5.05 (1H, m, C_{11b}-H), 7.0—7.6 (4H, m, aromatic protons), and 8.02 (1H, br s, NH); MS *m/z* (rel intersity) 284 (M$^+$; 90), 225 (100), and 223 (60). **8b** (as an oil, 29 mg): IR(film) 3260, 1740, and 1671 cm^{-1}; ^{1}H NMR δ=1.7—2.9 (4H, m, C_1-2H, C_2-2H), 3.10 (1H, ddd, J=15.9, 7.2 and 2.1 Hz, C_6-H), 3.44 (1H, dt, J=15.9 and 1.5 Hz, C_6-H), 3.63 (3H, s, OMe), 5.16 (1H, m, C_{11b}-H), 5.34 (1H, dd, J=7.2 and 1.5 Hz, C_5-H), 7.0—7.6 (4H, m, aromatic protons), and 8.31 (1H, br s, NH); MS *m/z* (rel intensity) 284 (M$^+$; 100), 225 (60), and 223 (62).

Synthesis of 7a and 7b. A mixture of L-tryptophan methyl ester hydrochloride (1.27 g, 5.0 mmol) and dimethyl 2-oxoglutarate (1.22 g, 7.0 mmol) in MeOH (15 ml) was refluxed for 24 h. The solution was concentrated under reduced pressure to ca. 4 ml,† and allowed to stand at 4 °C overnight to give the crystals of **7b** (0.52 g). The mother liquor was concentrated under reduced pressure to leave an oil, which was dissolved in $CHCl_3$. From the solution, the starting L-tryptophan methyl ester hydrochloride (0.12 g) was recovered by filtration. The filtrate was separated by column chromatography (SiO_2–$CHCl_3$) to give **7b** (0.45 g, total amount of **7b**, 0.97 g, 57%) and **7a** (as an oil, 0.15 g, 10%), which were identical with natural **7a** and **7b** by spectroscopic (IR, ^{1}H NMR, MS, and CD) and TLC comparisons, respectively. **7a**: $[\alpha]_D$ −37° (*c* 0.54, MeOH); UV 220 (ε 27400), 276 (7490), 282 (7810), and 291 nm (6380); ^{13}C NMR δ=22.6 (C-6), 29.4 (C-1*), 30.2 (C-2*), 52.5 (OMe), 53.3 (OMe), 53.7 (C-5), 66.7 (C-11b), 110.1 (C-6a), 111.5 (C-10), 118.7 (C-7), 120.1 (C-8), 123.1 (C-9), 126.1 (C-6b), 130.1 (C-11a), 136.8 (C-10a), 170.2 (-COO-), 171.3 (-COO-), and 175.2 (C-3). **7b**: $[\alpha]_D$ +110° (*c* 0.219, MeOH); UV 222 (ε 37600), 273 (8390), 280 (8350), and 290 nm (6550); ^{13}C NMR δ=24.0 (C-6), 30.8 (C-2), 34.0 (C-1), 49.2 (C-5), 52.3 (OMe), 52.8 (OMe), 63.9 (C-11b), 105.8 (C-6a), 111.4 (C-10), 118.5 (C-7), 119.7 (C-8), 122.6 (C-9), 126.0 (C-6b), 130.7 (C-11a), 137.0 (C-10a), 170.8 (-COO-), 172.2 (-COO-), and 174.9 (C-3). Anal. ($C_{18}H_{18}N_2O_5$) C, H, N.

Preparation of 9b. A mixture of L-tryptophan (4.0 g, 20 mmol) and 2-oxoglutaric acid (3.4 g, 23 mmol) in H_2O (250 ml) was allowed to stand at room temperature for 2 weeks under nitrogen atmosphere. The precipitate of the crude **9a** (1.4 g) was collected. To a solution of **9a** (0.80 g) in MeOH (30 ml) was added an ethereal solution of CH_2N_2. The solution was allowed to stand at room temperature for 4 h, and evaporated to leave an oil, which was crystallized from MeOH to give **9b** (0.49 g): mp 142.0—142.5 °C; $[\alpha]_D$ −41° (*c* 0.285, MeOH); UV 222 (ε 35300), 276 (sh, 8910), 283 (9580), and 291 nm (8090); IR(Nujol) 3420, 3330, 1753, and 1726 cm^{-1}; ^{1}H NMR δ=2.1—2.9 (4H, m), 2.74 (1H, dd, J=15.3 and 9.6 Hz), 3.11 (1H, dd, J=15.3 and 4.8 Hz), 3.60 (3H, s), 3.77 (3H, s,), 3.83 (3H, s), 3.6—3.8 (1H, m), 7.0—7.5 (4H, m), and 8.28 (1H, br s); ^{13}C NMR δ=25.8, 29.5, 34.3,

† HPLC analysis of this solution showed the presence of **7a** and **7b** in a ratio of 1:5. *Asterisks indicate that assignments are not unambiguous.

51.6, 52.3, 53.1, 61.4, 108.9, 111.2, 118.4, 119.6, 122.5, 126.5, 131,5, 136.1, 172.7, and 173.7; MS *m/z* 374 (M^+); CD $[\theta]_{298}$ +700, $[\theta]_{295}$ 0, $[\theta]_{291}$ −2600, $[\theta]_{288}$ −1200, $[\theta]_{283}$ −2600, $[\theta]_{267}$ −1300, $[\theta]_{235}$ −36600, $[\theta]_{227}$ 0, and $[\theta]_{219}$ +45200. Anal. ($C_{19}H_{22}N_2O_6$) C, H, N.

Cyclization of 9b to 7b. A solution of **9b** (43 mg) in 8 wt% HCl-MeOH (5 ml) was refluxed for 1 h. The solution was concentrated under reduced pressure to leave an oil, which was crystallized with $CHCl_3$-hexane to give **7b** (25 mg, 64%), which was identical with that obtained above by IR and TLC comparisons.

$NaBH_4$ Reduction of 7b. A mixture of **7b** (1.0 g, 2.9 mmol) and $NaBH_4$ (0.4 g, 11 mmol) in MeOH-THF (4—16 ml) was stirred at room temperature for 1 h, and then concentrated under reduced pressure. The residue was partitioned between H_2O and $CHCl_3$. The organic layer was dried over Na_2SO_4, and evaporated under reduced pressure to give **10** (0.58 g, 69%): mp 226—227 °C (from acetone-diisopropyl ether); $[\alpha]_D$ +138° (*c* 0.208, MeOH); UV 223 (ε 37400), 273 (7940), 278 (8090), 281 (8070), and 289 nm (6570); IR(Nujol) 3380, 3290, and 1664 cm^{-1}; ^1H NMR(CD_3OD) δ=1.9—3.1 (6H, m), 3.54 (1H, dd, *J*=10.8 and 8.4 Hz), 3.70 (1H, d, *J*=11.7 Hz), 3.72 (1H, dd, *J*=10.8 and 7.5 Hz), 3.92 (1H, d, *J*=11.7 Hz), 4.9 (1H, m), and 6.8—7.5 (4H, m); ^{13}C NMR (pyridine-d_5) δ=22.2, 31.5, 32.0, 49.7, 63.6, 64.1, 69.5, 104.9, 111.8, 118.8, 119.5, 121.9, 127.9, 135.9, 137.7, and 175.5; MS *m/z* 286 (M^+). Anal. ($C_{16}H_{18}N_2O_3$) C, H, N.

Formation of 11. A mixture of **10** (300 mg, 1.1 mmol) and *p*-toluenesulfonyl chloride (300 mg, 1.6 mmol) in pyridine (3 ml) was kept at 60 °C for 30 h. The solution was concentrated under reduced pressure to leave an oil, which was dissolved in $CHCl_3$. The solution was successively washed with dilute HCl, H_2O, and aqueous $NaHCO_3$, and then dried over Na_2SO_4. Evaporation of the solvent under reduced pressure gave an oil, which was crystallized from $CHCl_3$-hexane to yield **11** (96 mg, 34%): mp>300 °C (from EtOH); UV 224 (28800), 274 (sh 7210), 279 (sh 7430), 281 (7450), and 289 nm (6050); IR(Nujol) 3250, 1671, and 1649 cm^{-1}; ^1H NMR (pyridine-d_5) δ=1.7—2.8 (4H, m), 2.88 (1H, d, *J*=16.2 Hz), 3.39 (1H, ddd, *J*=16.2, 6.9, and 0.9 Hz), 3.48 (1H, d, *J*=10.5 Hz), 3.71 (1H, dd, *J*=11.4 and 2.7 Hz), 3.90 (1H, d, *J*=10.5 Hz), 3.99 (1H, dd, *J*=11.4 and 0.9 Hz), 4.60 (1H, dd, *J*=6.9 and 2.7 Hz), 7.2—7.7 (4H, m), and 8.70 (1H, br s); ^{13}C NMR (pyridine-d_5) δ=25.0, 25.6, 30.0, 46.1, 59.2, 72.2, 73.4, 110.5, 112.0, 118.5, 119.5, 121.7, 127.6, 135.1, 137.2, and 172.1; MS *m/z* 268 (M^+). Anal. ($C_{16}H_{16}N_2O_2$) C, H, N.

Epimerization of 7a. A solution of the natural **7a** (4 mg) in 0.1 mol dm^{-3} methanolic NaOMe (0.2 ml) was allowed to stand at room temperature overnight. After addition of AcOH (2 drops), the solution was concentrated under reduced pressure. The residue was partitioned between aqueous $NaHCO_3$ and $CHCl_3$. The organic layer was dried over Na_2SO_4, and concentrated under reduced pressure to give a mixture of **7a** and the antipode of **7b** in a ratio of 1:9 (by HPLC). CD of the reaction products $[\theta]_{238}$ +17000, $[\theta]_{231}$ 0, and $[\theta]_{221}$ −67000.

Antipode of 7b. According to essentially the same procedure as described above, the reaction of D-tryptophan methyl ester hydrochloride and dimethyl 2-oxoglutarate in MeOH yielded the antipode of **7b**: $[\alpha]_D$ −107° (*c* 0.205, MeOH); CD $[\theta]_{295}$ −1100, $[\theta]_{291}$ 0, $[\theta]_{286}$ −2200, $[\theta]_{284}$ −2000, $[\theta]_{270}$ −4300, $[\theta]_{259}$ 0, $[\theta]_{238}$ +18000, $[\theta]_{231}$ 0, and $[\theta]_{221}$ −78000.

Synthesis of 8a and 8b. According to the literature,[7] L-tryptophan methyl ester (4.36 g, 20 mmol) was dissolved in benzene (400 ml), and 2-oxoglutaric acid (3.5 g, 24 mmol) was added in small portions to the refluxing solution. After addition, reflux was continued for 19 h. The solution was washed with aqueous $NaHCO_3$, dried over Na_2SO_4, and then concentrated under reduced pressure to ca. 20 ml[††] to yield the crystals of **8b**[7] (2.94 g). The mother liquor was concentrated under reduced pressure to leave an oil, which was separated by column chromatography on SiO_2. Elution with $CHCl_3$ gave **8b** (0.62 g, total amount of **8b**, 3.56 g, 64%) and **8a** (0.94 g, 12%), which were identical with the natural **8b** and **8a** by spectroscopic (IR, ^1H NMR, MS, and CD), and TLC comparisons, respectively. **8a:** mp 109—111 °C (from $CHCl_3$); $[\alpha]_D$ −110° (*c* 0.218, MeOH); ^{13}C NMR δ=22.8 (C-6), 24.3 (C-1), 30.1 (C-2), 52.5 (OMe), 54.7 (C-5), 56.3 (C-11b), 108.0 (C-6a), 111.3, (C-10), 118.2 (C-7), 119.8 (C-8), 122.2 (C-9), 126.5 (C-6b), 133.3 (C-11a), 136.5 (C-10a), 170.2 (-COO-), and 175.9 (C-3); CD $[\theta]_{294}$ +2400, $[\theta]_{289}$ +100, $[\theta]_{285}$ +2700. $[\theta]_{282}$ +2400, $[\theta]_{269}$ +6100, $[\theta]_{246}$ +2700, $[\theta]_{231}$ +15700, $[\theta]_{226}$ 0, and $[\theta]_{218}$ −42300. Anal. ($C_{16}H_{16}N_2O_3 \cdot CHCl_3$) C, H, N. Found: *m/z* 284.1174. Calcd for $C_{16}H_{16}N_2O_3$: M, 284.1159. **8b:** mp 202—203 °C (from $CHCl_3$-hexane); $[\alpha]_D$ +187° (*c* 0.214, MeOH); ^{13}C NMR δ=23.7 (C-6), 26.3 (C-1), 31.6 (C-2), 49.5 (C-5), 52.5 (C-11b and OMe), 105.0 (C-6a), 111.1 (C-10), 118.3 (C-7), 119.7 (C-8), 122.1 (C-9), 126.6 (C-6b), 132.6 (C-11a), 136.5 (C-10a), 171.1 (-COO-), and 173.9 (C-3); CD $[\theta]_{295}$ −400, $[\theta]_{293}$ 0, $[\theta]_{289}$ +1600, $[\theta]_{286}$ 0, $[\theta]_{285}$ −200, $[\theta]_{284}$ 0, $[\theta]_{282}$ +400, $[\theta]_{280}$ 0, $[\theta]_{232}$ −22000, $[\theta]_{227}$ 0, and $[\theta]_{215}$ +61000.

Epimerization of 8a. A solution of **8a** (170 mg) in 0.1 mol dm^{-3} methanolic NaOMe (2 ml) was allowed to stand at room temperature for 2 h. After addition of AcOH (0.1 ml), the solution was worked up as described above to give an epimer almost quantitatively, which was identical with the antipode of **8b** prepared as described below ($[\alpha]_D$, IR, ^1H NMR, and CD).

Antipode of 8b. According to essentially the same procedure as described above, the reaction of D-tryptophan methyl ester and 2-oxoglutaric acid in benzene yielded the antipode of **8a** and the antipode of **8b**. Antipode of **8a:** $[\alpha]_D$ +112° (*c* 0.203, MeOH). Antipode of **8b:** $[\alpha]_D$ −186° (*c* 0.205, MeOH); CD $[\theta]_{295}$ +600, $[\theta]_{292}$ 0, $[\theta]_{289}$ −1700, $[\theta]_{285}$ −300, $[\theta]_{282}$ −800, $[\theta]_{278}$ 0, $[\theta]_{232}$ +23000, $[\theta]_{226}$ 0, and $[\theta]_{215}$ −61000.

Preparation of 12a. A solution of L-tryptophan methyl ester (2.18 g, 10 mmol) and 5-methyl-2(3*H*)-furanone (1.20 g, 12 mmol) in benzene (30 ml) was allowed to stand at room temperature for 22 h to give **12a** (2.86 g, 91%): mp 139—140 °C (from MeOH); IR(Nujol) 3360, 1753, 1701, and 1654 cm^{-1}; MS *m/z* 316 (M^+); Anal. ($C_{17}H_{20}N_2O_4$) C, H, N.

Preparation of the Amides 12b—12f. 1) A typical procedure is described for the preparation of **12b**. To a solution of L-tryptophan methyl ester (2.18 g, 10 mmol) and 4-oxohexanoic acid[21] (1.30 g, 10 mmol) in CH_2Cl_2 (60 ml) was added a solution of dicyclohexylcarbodiimide (2.06 g, 10 mmol) in CH_2Cl_2 (40 ml). The reaction mixture was stirred at room temperature for 7 h. AcOH (3 drops) was added to the reaction mixture, and the *N,N'*-dicyclohexylurea which precipitated was removed by filtration. The filtrate was concentrated under reduced pressure to leave an oil, which was crystallized from benzene to give the crude **12b**.

†† HPLC analysis of this solution showed the presence of **8a** and **8b** in a ratio of 1:3.

Recrystallization from MeOH afforded the colorless crystals of **12b** (2.70 g, 82%): mp 129—130 °C; IR(Nujol) 3280, 1753, 1708, and 1654 cm^{-1}; MS *m/z* 330 (M^+); Anal. ($C_{18}H_{22}N_2O_4$) C, H, N.

2) The amide **12c** was prepared using 4-oxoheptanoic acid.[22] **12c** (77%): mp 89—90 °C; IR(Nujol) 3390, 1739, 1720, and 1660 cm^{-1}; MS *m/z* 344 (M^+); Anal. ($C_{19}H_{24}N_2O_4$) C, H, N.

3) The amide **12d** was prepared using 3-benzoylpropanoic acid. **12d** (84%): mp 101—102 °C; IR(Nujol) 3310, 1739, and 1660 cm^{-1}; MS *m/z* 378 (M^+); Anal. ($C_{22}H_{22}N_2O_4$) C, H, N.

4) The amide **12e** was prepared using 5-methyl-4-oxohexanoic acid.[23] **12e** (88%): mp 128—129 °C; IR(Nujol) 3280, 1740, 1715, and 1660 cm^{-1}; MS *m/z* 344 (M^+); Anal. ($C_{19}H_{24}N_2O_4$) C, H, N.

5) The amide **12f** was prepared using 5,5-dimethyl-4-oxohexanoic acid.[23] **12f** (86%): mp 160—161 °C; IR(Nujol) 3270, 1740, 1709, and 1661 cm^{-1}; MS *m/z* 358 (M^+); Anal. ($C_{20}H_{26}N_2O_4$) C, H, N.

Cyclization of the Amides 12a—12f. 1) A typical procedure is described for the cyclization of the amide **12a**. A solution of **12a** (158 mg, 0.50 mmol) in 13 wt% hydrogen chloride-MeOH (10 ml) was allowed to stand at room temperature for 20 h. The solution was concentrated under reduced pressure. The residue was partitioned between aqueous $NaHCO_3$ and $CHCl_3$. The organic layer was dried over Na_2SO_4. Evaporation of the solvent under reduced pressure gave a mixture of **13a** and **13b** (ratio determined by HPLC, 1:2) almost quantitatively, which were separated after column chromatography (SiO_2-$CHCl_3$). **13a**: mp 247—248 °C (from MeOH); IR($CHCl_3$) 3460, 1740, and 1691 cm^{-1}; ^1H NMR δ=1.70 (3H, s), 2.1—2.8 (4H, m), 2.95 (1H, dd, *J*=15.9 and 5.1 Hz), 3.33 (1H, dd, *J*=15.9 and 10.8 Hz), 3.79 (3H, s), 4.09 (1H. dd, *J*=10.8 and 5.1 Hz), 7.0—7.6 (4H, m), and 8.33 (1H, br s); ^{13}C NMR δ=22.7, 27.0, 29.7, 32.1, 52.2, 52.4, 61.9, 107.1, 111.3, 118.3, 119.8, 122.2, 126.5, 136.4, 137.2, 170.7, and 176.6; MS *m/z* 298 (M^+) and 283; Anal. ($C_{17}H_{18}N_2O_3$) C, H, N. **13b**: mp 218—219 °C (from $CHCl_3$-hexane); IR($CHCl_3$) 3460, 1745, and 1683 cm^{-1}; ^1H NMR δ=1.58 (3H, s), 2.0—2.8 (4H, m), 2.98, (1H, dd, *J*=15.9 and 7.8 Hz), 3.57 (1H, dd, *J*=15.9 and 1.5 Hz), 3.66 (3H, s), 5.40 (1H, dd, *J*=7.8 and 1.5 Hz), 7.0—7.5 (4H, m), and 8.33 (1H, br s); ^{13}C NMR δ=21.8, 25.9, 30.6, 34.7, 48.7, 52.4, 59.8, 103.6, 111.1, 118.6, 119.6, 122.1, 126.5, 136.4, 136.7, 171.7, and 174.2; MS *m/z* 298 (M^+) and 283; Anal. ($C_{17}H_{18}N_2O_3$) C, H, N.

2) Cyclization of the amide **12b** gave a mixture of **14a** and **14b** (ratio, 2:1) almost quantitatively. **14a**: mp 246—247 °C (from MeOH); IR($CHCl_3$) 3460, 1748, and 1693 cm^{-1}; ^1H NMR δ=1.12 (3H, t, *J*=7.5 Hz), 1.98 (2H, q, *J*=7.5 Hz), 2.0—2.7 (4H, m), 2.96 (1H, dd, *J*=15.9 and 5.1 Hz), 3.34 (1H, dd, *J*=15.9 and 10.8 Hz), 3.83 (3H, s), 4.07 (1H, dd, *J*=10.8 and 5.1 Hz), 7.0—7.6 (4H, m), and 8.00 (1H, br s); ^{13}C NMR δ=8.1, 22.6, 28.2, 29.9, 31.9, 52.1, 52.4, 64.9, 106.9, 111.2, 118.2, 119.7, 122.1, 126.5, 136.4, 137.8, 170.6, and 176.6; MS *m/z* 312 (M^+) and 283; Anal. ($C_{18}H_{20}N_2O_3$) C, H, N. **14b**: mp 191—192 °C (from MeOH); IR($CHCl_3$) 3460, 1744, and 1681 cm^{-1}; ^1H NMR δ=1.08 (3H, t, *J*=7.2 Hz), 1.83, (2H, q, *J*=7.2 Hz), 2.0—2.9 (4H, m), 3.04 (1H, dd, *J*=16.2 and 8.1 Hz), 3.51 (1H, dd, *J*=16.2 and 2.1 Hz), 3.68 (3H, s), 5.39 (1H, dd *J*=8.1 and 2.1 Hz), 7.0—7.6 (4H, m), and 8.15 (1H, br s); ^{13}C NMR δ=8.5, 21.4, 30.3, 31.0, 33.7, 48.9, 52.3, 63.1, 104.1, 111.0, 118.6, 119.8, 122.2, 126.5, 136.2, 137.1, 171.8, and 174.7; MS *m/z* 312 (M^+) and 283; Anal. ($C_{18}H_{20}N_2O_3$) C, H, N.

3) Cyclization of the amide **12c** gave a mixture of **15a** and **15b** (ratio, 2:1). **15a** (54%): $[\alpha]_D$ −148° (*c* 0.119, MeOH): IR($CHCl_3$) 3450, 1742, and 1688 cm^{-1}; ^1H NMR δ=0.96 (3H, t, *J*=6.6 Hz), 1.3—2.0 (4H, m), 2.0—2.7 (4H, m), 2.96 (1H, dd, *J*=16.0 and 5.1 Hz), 3.34 (1H, dd, *J*=16.0 and 10.7 Hz), 3.82 (3H, s), 4.10 (1H, dd, *J*=10.7 and 5.1 Hz), 7.0—7.6 (4H, m), and 8.30 (1H, br s); ^{13}C NMR δ=14.3, 17.2, 22.6, 29.1, 29.9, 41.8, 52.2, 64.6, 107.0, 111.2, 118.2, 119.7, 122.1, 126.5, 136.3, 137.6, 170.6, and 176.5; MS *m/z* 326 and 283. Found: *m/z* 326.1612. Calcd for $C_{19}H_{22}N_2O_3$: M, 326.1628. **15b** (20%): mp 244—245°C (from $CHCl_3$-hexane); $[\alpha]_D$ +105° (*c* 0.124, MeOH); IR($CHCl_3$) 3450, 1740, and 1677 cm^{-1}; ^1H NMR δ=0.91 (3H, t, *J*=6.6 Hz), 1.2—2.0 (4H, m), 2.0—2.8 (4H, m), 3.03 (1H, dd, *J*=15.9 and 8.1 Hz), 3.51 (1H, dd, *J*=15.9 and 2.1 Hz), 3.69 (3H, s), 5.37 (1H, dd, *J*=8.1 and 2.1 Hz). 7.0—7.6 (4H, m), and 8.03 (1H, br s); ^{13}C NMR δ=14.3, 17.4, 21.4, 31.0, 43.3, 48.9, 52.4, 62.9, 103.8, 111.0, 118.5, 119.6, 122.1, 126.4, 136.2, 137.2, 171.7, and 174.7; MS *m/z* 326 (M^+) and 283; Anal. ($C_{19}H_{22}N_2O_3$) C, H, N.

4) Cyclization of the amide **12d** gave a mixture of **16a** and **16b** (ratio, >20:1). **16a** (82%): mp 236—237 °C (from MeOH); IR($CHCl_3$) 3450, 3270, 1735, and 1690 cm^{-1}; ^1H NMR δ=2.1—2.7 (4H, m), 2.87 (1H, dd, *J*=15.6 and 5.1 Hz), 3.42 (1H, dd, *J*=15.6 and 11.1 Hz), 3.74 (3H, s), 3.88 (1H, dd, *J*=11.1 and 5.1 Hz), 7.0—7.6 (9H, m), and 8.97 (1H, br s); ^{13}C NMR δ=22.2, 30.1, 34.1, 52.1, 52.4, 68.1, 109.6, 111.4, 118.5, 119.8, 122.6, 126.4, 126.5, 128.1, 128.7, 134.2, 136.5, 142.9, 170.4, and 177.0; MS *m/z* 360 (M^+) and 283; Anal. ($C_{22}H_{20}N_2O_3$) C, H, N. **16b** (3%): mp 265—266 °C (from $CHCl_3$-hexane); IR($CHCl_3$) 3450, 1745, and 1684 cm^{-1}; ^1H NMR δ=2.4—3.2 (4H, m), 2.89 (3H, s), 3.00 (1H, dd, *J*=15.6 and 7.8 Hz), 3.50 (1H, dd, *J*=15.6 and 1.8 Hz), 5.23 (1H, dd, *J*=7.8 and 1.8 Hz), 7.0—7.7 (9H, m), and 8.25 (1H, br s); ^{13}C NMR δ=20.7, 31.1, 34.3, 48.3, 51.7, 64.4, 107.5, 111.1, 118.9, 120.0, 122.6, 126.4, 127.1, 128.2, 128.7, 134.0, 136.4, 143.0, 170.4, and 173.8; MS *m/z* 360 (M^+) and 283; Anal. ($C_{22}H_{20}N_2O_3$) C, H, N.

5) Cyclization of the amide **12e** gave **17a** (80%): $[\alpha]_D$ −80° (*c* 0.201, MeOH); IR($CHCl_3$) 3460, 1742, and 1689 cm^{-1}; ^1H NMR δ=1.09 (3H, d, *J*=7.1 Hz), 1.17 (3H, d, *J*=7.1 Hz), 2.0—2.6 (5H, m), 2.96 (1H, dd, *J*=15.9 and 5.4 Hz), 3.37 (1H, dd, *J*=15.9 and 10.8 Hz), 3.81 (3H, s), 4.15 (1H, dd, *J*=10.8 and 5.4 Hz), 7.0—7.6 (4H, m), and 8.27 (1H, br s); ^{13}C NMR δ=17.2, 22.4, 24.5, 29.8, 35.5, 51.8, 52.4, 67.7, 108.0, 111.2, 118.3, 119.8, 122.3, 126.5, 136.2, 137.2, 170.6, and 176.8; MS *m/z* 326 and 283. Found: *m/z* 326.1642. Calcd for $C_{19}H_{22}N_2O_3$: M, 326.1629.

6) Cyclization of the amide **12f** gave **18a** (79%): mp 231—232 °C (from benzene); $[\alpha]_D$ −90° (*c* 0.201, MeOH); IR ($CHCl_3$) 3460, 1740, and 1685 cm^{-1}; ^1H NMR δ=1.16 (9H, s), 2.0—2.7 (4H, m), 2.98 (1H, dd, *J*=16.0 and 5.8 Hz), 3.31 (1H, dd, *J*=16.0 and 10.0 Hz), 3.78 (3H, s), 4.51 (1H, dd, *J*=10.0 and 5.8 Hz), 7.0—7.6 (4H, m), and 8.20 (1H, br s); ^{13}C NMR δ=22.2, 27.1, 28.0, 30.0, 39.6, 52.3, 53.9, 70.5, 109.0, 111.2, 118.2, 119.6, 122.2, 126.3, 135.5, 136.4, 171.1, and 177.9; MS *m/z* 283 (M^+ −57). Anal. ($C_{20}H_{24}N_2O_3$) C, H, N.

Methoxide-Catalyzed Equilibration. Each compound **7a,b**, **8a,b**, **13a,b**—**16a,b**, **17a**, and **18a** (0.1 mmol) was dissolved in 0.1 mol dm^{-3} methanolic NaOMe (3 ml). Each solution was kept at room temperature for a few days until the equilibrium was reached. After addition of AcOH (2 drops), each solution was worked up as described above to give a

residue, which was analyzed by HPLC. The results were summarized in Table 1.

***N*-Bromosuccinimide (NBS) Oxidation of 8b.** A mixture of **8b** (57 mg, 0.20 mmol) and NBS (53 mg, 0.30 mmol) in *t*-BuOH (30 ml) was stirred at 26—32 °C for 2 days. The resulting blue solution was concentrated under reduced pressure to give a residue, which was dissolved in AcOEt. The solution was washed with water, dried over Na_2SO_4, and evaporated under reduced pressure. Separation of the residue by column chromatography (SiO_2–$CHCl_3$) afforded **2** (6 mg, 11%), which was identical with that synthesized following the procedure of Iwadare et al.[2] (IR, ^1H NMR, CD, and TLC).

Conversion of 7b into 1. A solution of **7b** (103 mg, 0.30 mmol) and KOH (45 mg, 0.80 mmol) in H_2O–MeOH (0.8—8 ml) was allowed to stand at 26—30 °C for 22 h to give crystals of the potassium salt of **5b** (90 mg, 77%): IR(Nujol) 1676, 1640, and 1609 cm^{-1}; ^1H NMR (D_2O) δ=1.98 (1H, m), 2.44 (1H, m), 2.63 (1H, m), 2.84 (1H, dd, J=15.8 and 7.3 Hz), 2.98 (1H, m), 3.19 (1H, dd, J=15.8 and 1.5 Hz), 4.96 (1H, dd, J=7.3 and 1.5 Hz), 7.14 (1H, t, J=8.0 Hz), 7.22 (1H, t, J=8.0 Hz), 7.46 (1H, d, J=8.0 Hz), and 7.54 (1H, d, J=8.0 Hz); ^{13}C NMR (D_2O) δ=26.4, 34.4, 36.3, 55.5, 70.1, 107.5, 114.2, 121.1, 121.9, 124.4, 128.7, 137.6, 139.1, 179.3, 180.1, and 181.1.

A solution of the potassium salt of **5b** (30 mg) in H_2O–AcOH (3—0.2 ml) was stirred at 24—29 °C for 4 days to give a dark blue precipitate (13 mg). Analytical TLC of the precipitate (*n*-BuOH–AcOH–H_2O, 4:1:1) showed the presence of a blue spot (R_f 0.88) corresponding to trichotomine **1**. To a solution of the precipitate (13 mg) in MeOH (10 ml) was added an ethereal solution of CH_2N_2. The mixture was allowed to stand at 24 °C for 2 h, and evaporated. Separation of the blue residue by column chromatography (SiO_2–$CHCl_3$) gave **2** (0.3 mg), which was identical with the authentic sample[2] (^1H NMR and TLC).

Acetylation of 8a. A solution of **8a** (202 mg, 0.50 mmol) in acetic anhydride–pyridine (5—8 ml) was heated at 88—93 °C for 15 h. The solution was concentrated under reduced pressure to give an oil, which was purified by column chromatography (SiO_2–$CHCl_3$), and crystallized from MeOH to give **20a** (102 mg, 63%): mp 261—263 °C; $[\alpha]_D$ −314° (*c* 0.042, MeOH); UV 204 (ε 27900), 241 (18100), 264 (11700), 291 (6160), and 299 nm (6160); IR(Nujol) 1742, 1703, and 1682 cm^{-1}; ^1H NMR δ=1.8—2.9 (4H, m), 2.80, (3H, s), 2.91 (1H, ddd, J=16.8, 4.8 and 2.4 Hz), 3.28 (1H, ddd, J=16.8, 10.8, and 2.7 Hz), 3.88 (3H, s), 3.99 (1H, dd, J=10.8 and 4.8 Hz), 5.48 (1H, m), and 7,2—7.8 (4H, m); ^{13}C NMR δ=23.3, 25.3, 26.9, 29.8, 52.5, 53.9, 58.8, 114.0, 117.1, 119.2, 123.5, 124.9, 129.6, 135.3, 137.0, 168.7, 169.7, and 175.4; MS *m/z* 326 (M^+), 283, 225, and 223; CD $[\theta]_{288}$ −11300, $[\theta]_{282}$ −10800, $[\theta]_{252}$ −42700, $[\theta]_{242}$ 0, $[\theta]_{226}$ +55600, $[\theta]_{210}$ 0; Anal. ($C_{18}H_{18}N_2O_4$) C, H, N.

Acetylation of 8b. A solution of **8b** (284 mg) in acetic anhydride–pyridine (5—7 ml) was heated at 90 °C for 8 h, and work up as described above to give **20b** (257 mg, 79%): mp 183—184 °C (from MeOH); $[\alpha]_D$ +277° (*c* 0.205, MeOH); UV 204 (ε 24000), 241 (16100), 263 (10100), 290 (5090), and 299 nm (5020); IR(Nujol) 1745, 1716, and 1697 cm^{-1}; ^1H NMR δ=1.6—3.2 (5H, m), 2.79 (3H, s), 3.41 (1H, dt, J=16.5 and 1.5 Hz), 3.67 (3H, s), 5.39 (1H, dd, J=7.2 and 1.2 Hz), 5.50 (1H, m), and 7.2—7.8 (4H, m), ^{13}C NMR δ=23.7, 27.1, 31.0, 48.4, 52.6, 55.0, 114.0, 119.1, 123.2, 124.7, 129.5, 135.1, 135.5, 168.6, 170.6, and 173.9; MS *m/z* 326 (M^+), 283, 225, and 223; CD $[\theta]_{256}$ +28700, $[\theta]_{242}$ 0, and $[\theta]_{227}$ −36400; Anal. ($C_{18}H_{18}N_2O_4$) C, H, N.

Electrolysis of 20a and 20b. A mixture of **20a** (65 mg, 0.20 mmol), tetrabutylammonium tetrafluoroborate (330 mg) and MeOH (80 ml) was placed in a beaker-type undivided cell, and glassy carbon rods were used as an anode and a cathode, respectively.[24] After electrolysis at constant potential of 1.3 V vs. SCE (electricity: ca. 5.5 F mol^{-1} (1F=96480 C)), the electrolytic solution was concentrated under reduced pressure to give a residue, which was dissolved in benzene. The solution was washed with H_2O and with brine, and then dried over Na_2SO_4. Evaporation of the solvent under reduced pressure gave an oil, which was purified by column chromatography (SiO_2–$CHCl_3$) to afford **21** (as an oil, 47 mg, 66%): IR($CHCl_3$) 1744 and 1708 cm^{-1}; ^1H NMR δ=2.2—3.5 (4H, m), 2.80 (3H, s), 2.89 (1H, dd, J=16.2 and 7.2 Hz), 3.32 (3H, s), 3.53 (1H, dd, J=16.2 and 0.9 Hz), 3.70 (3H, s), 5.37 (1H, dd, J=7.2 and 0.9 Hz), and 7.2—7.8 (4H, m); MS *m/z* 356 (M^+), 325, 283, 282, and 223. Found: *m/z* 356.1387. Calcd for $C_{19}H_{20}N_2O_5$: M, 356.1371.

Under similar conditions to those described above, **20b** (65 mg, 0.20 mmol) was electrolyzed to give **21** (43 mg, 61%), which was identical with that obtained from **20a** by ^1H NMR and TLC comparisons.

Formation of 19. A solution of **21** (49 mg, 0.14 mmol) in 99% HCOOH–$CHCl_3$ (0.3—2.7 ml) was kept at 15 °C for 1 h. The solution was washed with aqueous $NaHCO_3$, and dried over Na_2SO_4. Evaporation of the solvent under reduced pressure gave an oil, which was purified by column chromatography (SiO_2–$CHCl_3$) to yield **19** (as an oil, 37 mg, 82%): IR($CHCl_3$) 1748, 1710, and 1641 cm^{-1}; ^1H NMR δ=2.77 (3H, s), 3.12 (1H, dd, J=16.8 and 6.9 Hz), 3.35 (2H, m), 3.66 (3H, s), 3.67 (1H, dd, J=16.8 and 1.2 Hz), 5.22 (1H, dd, J=6.9 and 1.2 Hz), 5.71 (1H, t, J=3.0 Hz), 7.2—7.8 (3H, m), and 7.90 (1H, m); MS *m/z* 324 (M^+), 282, and 223. Found: *m/z* 324.1105. Calcd for $C_{18}H_{16}N_2O_4$: M, 324.1109.

Air Oxidation of 19. According to Iwadare's method,[2] air was bublled with capillary tubing through a solution of **19** (37 mg) in *n*-BuOH (50 ml) kept at 66—76 °C for 19 h. The blue solution was concentrated under reduced pressure. The residue was separated by column chromatography (SiO_2–$CHCl_3$) to give **23** (8 mg, 22%), which was identical with that synthesized following the procedure of Iwadare et al.[1,2] (IR, ^1H NMR, and TLC). **23**: ^{13}C NMR δ=24.8, 27.0, 48.5, 53.0, 102.7, 115.1, 120.2, 123.2, 124.0, 126.8, 127.5, 128.0, 128.9, 136.2, 139.3, 168.1, 169.8, and 170.4; CD $[\theta]_{427}$ −12000, $[\theta]_{407}$ 0, $[\theta]_{364}$ +55000, $[\theta]_{345}$ 0, and $[\theta]_{326}$ −38400.

We would like to thank Dr. Hiroshi Sakurai of Meijo University for obtaining the mass spectra.

References

1) S. Iwadare, Y. Shizuri, K. Sasaki, and Y. Hirata, *Tetrahedron*, **30**, 4105 (1974).

2) S. Iwadare, Y. Shizuri, K. Yamada, and Y. Hirata, *Tetrahedron*, **34**, 1457 (1978).

3) G. J. Kapadia and R. E. Rao, *Tetrahedron Lett.*, **1977**, 975, and references cited therein.

4) G. Palmisano, B. Danieli, G. Lesma, and R. Riva, *J. Org. Chem.*, **50**, 3322, (1985).

5) Y. Toyoda, H. Kumagai, H. Irikawa, and Y.

Okumura, *Chem. Lett.*, **1982**, 903.
6) H. Irikawa and Y. Okumura, *Chem Lett.*, **1983**, 1055.
7) D. Soerens, J. Sandrin, F. Ungemach, P. Mokry, G. S. Wu, E. Yamanaka, L. Hutchins, M. DiPierro, and J. M. Cook, *J. Org. Chem.*, **44**, 535 (1979).
8) L. Bartlett, N. J. Dastoor, J. Hrbek jr., W. Klyne, H. Schmid, and G. Snatzke, *Helv. Chim. Acta*, **54**, 1238 (1971).
9) The figures of the products show the relative configurations of the methoxycarbonyl group on C-5 and the substituent on C-11b because of the epimerization at C-5.
10) F. Ungemach, M. DiPierro, R. Weber, and J. M. Cook, *J. Org. Chem.*, **46**, 164 (1981).
11) B. E. Maryanoff, D. F. McComsey, and B. A. Duhl-Emswiler, *J. Org. Chem.*, **48**, 5062 (1983).
12) F. Hamaguchi, T. Nagasaka, and S. Ohki, *Yakugaku Zasshi*, **94**, 351 (1974).
13) N. K. Wilson and J. B. Stothers, "Topics in Stereochemistry," ed by E. L. Eliel and N. L. Allinger, J. Wiley & Sons, New York (1974), Vol. 8, p. 26.
14) F. Ungemach, D. Soerens, R. Weber, M. DiPierro, O. Campos, P. Mokry, J. M. Cook, and J. V. Silverton, *J. Am. Chem. Soc.*, **102**, 6976 (1980).
15) K. T. D. DeSilva, D. King, and G. N. Smith, *J. Chem. Soc., Chem. Commun.*, **1971**, 908.
16) E. Wenkert, S. Garratt, and K. G. Dave, *Can. J. Chem.*, **42**, 489 (1964).
17) S. McLean and G. I. Dmitrienko, *Can. J. Chem.*, **49**, 3642 (1971), and references cited therein.
18) H. Irikawa and Y. Okumura, *Bull. Chem. Soc. Jpn.*, **60**, 3797 (1987).
19) T. Shono, H. Hamaguchi, and Y. Matsumura, *J. Am. Chem. Soc.*, **97**, 4264 (1975).
20) G. A. Russell and G. Kaupp, *J. Am. Chem. Soc.*, **91**, 3851 (1969).
21) M. C. Kloetzel, *J. Am. Chem. Soc.*, **70**, 3571 (1948).
22) A. S. Perlin and C. B. Purves, *Can. J. Chem.*, **31**, 227 (1953).
23) P. W. Ford, *Aust. J. Chem.*, **27**, 2525 (1974).
24) T. Shono, Y. Matsumura, and K. Tsubata, *Org. Synth.*, Vol. 63, 206 (1984).

Synthesis of $Ba_2YCu_3O_{7-\delta}$ Superconductor through Organometallic Route

Shin-ichi HIRANO,* Takashi HAYASHI, Masashi MIURA, and Hiroyuki TOMONAGA
Department of Applied Chemistry, Faculty of Engineering, Nagoya University,
Furo-cho, Chikusa-ku, Nagoya 464
(Received June 30, 1988)

The chemical synthesis of a high-T_c $Ba_2YCu_3O_{7-\delta}$ superconductor was investigated through the organometallic route, using Ba metal, $Y(OPr^i)_3$, and Cu-alkoxides or Cu-acetylacetonate as starting materials. Chemically homogeneous submicron powders of single phase $Ba_2YCu_3O_{7-\delta}$ were successfully prepared at 750 °C by controlled partial hydrolysis of metal alkoxides. The utilization of ozone for favorable decomposition of $Ba_2YCu_3O_{7-\delta}$ precursors was found to have a remarkable effect on suppressing the formation of $BaCO_3$ and lowering the formation temperature of $Ba_2YCu_3O_{7-\delta}$ to about 650 °C. The single phase $Ba_2YCu_3O_{7-\delta}$ ceramics exhibited superconductivity at approximately 83 K (T_c end).

Recently, intensive studies on the preparation of high-T_c $Ba_2YCu_3O_{7-\delta}$ superconductor have been performed.[1] The superconducting $Ba_2YCu_3O_{7-\delta}$ compound has been usually prepared by the conventional solid-state reaction between Y_2O_3, $BaCO_3$, and CuO and sintering at 950 °C, followed by slow cooling in the range of 350—650 °C. It is, however, difficult to prepare chemically homogeneous, highly pure fine particles by the solid state reaction and to control the particle size and morphology suitable for the fabrication of dense ceramics on sintering. Therefore, the alternative chemical routes such as coprecipitation of nitrates with oxalate[2,3] and citrate,[4] pyrolysis of organic acid salts,[5,6] and spray pyrolysis of nitrate solution[7] have currently received particular attention. These procedures may allow the synthesis of more chemically homogeneous fine particles. Although the chemical route affords highly pure and homogeneous particles and more controllable processing, there are some difficulties: non-uniform and incomplete precipitation, contamination by precipitating agents, and heterogeneous segregation due to the difference in decomposition temperatures of organic acid salts. Furthermore, another unavoidable problem encountered in the chemical route is the formation of $BaCO_3$ during calcination of the powder precursors, resulting easily in heterogeneous phase separation and, thereby, the formation of secondary phases such as $BaCuO_2$, Y_2O_3, Y_2BaCuO_5, etc. In particular, pyrolytic process of organic acid salts involves easier formation of $BaCO_3$.

The sol-gel method using alkoxides generally offers possibility of formation of films and fibers by controlling the solution viscosity as well as of high homogeneity, high purity, and lower temperature processing.

In a preceding work,[8] we reported the preparation of $Ba_2YCu_3O_{7-\delta}$ superconductor through an organometallic route with metal alkoxides and acetylacetonates. The preliminary experiments were tried to select organometallic compound and metal alkoxide as starting materials and appropriate solvent to prepare homogeneous solution. However, the calcination conditions to prepare $Ba_2YCu_3O_{7-\delta}$ powders at temperatures as low as possible have not fully optimized and the influence of firing atmosphere on the formation of $Ba_2YCu_3O_{7-\delta}$ compound has not been clarified. The present paper describes the selection of Cu-compound and solvent, a newly developed preparation process of chemically homogeneous solution, and calcination conditions to prepare fine powders of orthorhombic $Ba_2YCu_3O_{7-\delta}$ compound at temperatures as low as possible.

Experimental

The use of cupric organometallic compounds as starting materials is limited due to low solubility in common organic solvents. In the present work, $Cu(OEt)_2$, $Cu(OC_2H_4OEt)_2$, $Cu(acac)_2$, and $Cu(C_{17}H_{35}COO)_2$ with chemical-pure grade were examined as the source of Cu-compounds. The solubility of each Cu-compound in various organic solvents is compared in Table 1. $Cu(OEt)_2$ was found to be insoluble in organic solvents except amine and acetylacetone which tend to form readily coordination compounds with Cu-compounds. $Cu(C_{17}H_{35}COO)_2$ was soluble in toluene, pyridine, and acetylacetone, while these solvents were not suitable for $Y(OPr^i)_3$ and $Ba(OPr^i)_2$. $Cu(acac)_2$ was soluble in 2-methoxy-and 2-ethoxyethanol. $Cu(OC_2H_4OEt)_2$ was soluble in 2-ethoxyethanol, THF, and amine solvents. Thus, $Cu(acac)_2$ and $Cu(OC_2H_4OEt)_2$ were selected as starting materials. 2-Methoxy- and 2-ethoxyethanol were the most suitable solvents among common organic solvents for these starting materials.

Figure 1 shows the flowchart for chemical processing of $Ba_2YCu_3O_{7-\delta}$ superconductors through the organometallic route. $Y(OPr^i)_3$ (purity 99.9%) and high-pure Ba metal (purity 99.99%), which are soluble in common organic solvents, were used as starting materials.

The starting materials were dissolved in absolute 2-ethoxyethanol in the stoichiometric composition of Ba:Y:Cu=2:1:3. The initial concentration of alkoxides was 0.005 mol l^{-1}. The solution was stirred in dry nitrogen and heated at 40 °C for 12 h. Then, the solution was hydrolyzed by slow addition of desired amount of water diluted with solvent (1:10 volume ratio). The molar ratio of water to the sum of Ba-, Y-, and Cu-alkoxides was 1/4 and 1 (the theoretically required amount). After stirring and heating for several hours, the solution was evaporated with stirring

Table 1. Solubility of Cupric Organometallic Compounds[a]

Solvents	$Cu(Sta)_2$	$Cu(OEt)_2$	$Cu(OR)_2$[b]	$Cu(acac)_2$
Hexane	—	×	—	—
Toluene	○	×	—	—
Triethylamine	—	×	—	—
Diethylamine	—	○	○	—
Diisopropylamine	—	×	—	—
Ethylene glycol dimethyl ether	×	—	×	×
Tetrahydrofuran	—	×	○	—
Pyridine	○	—	—	—
2-Methoxyethanol	×	—	×	○
1-Propanol	—	×	—	—
2-Propanol	×	×	—	×
Ethanol	—	×	—	×
Acetylacetone	○	○	—	×
2-Ethoxyethanol	—	—	○	○
Diethylene glycol	—	—	—	×
Methanol	—	—	×	—
2-Aminoethanol	—	○	—	—
Ethylene glycol	—	—	—	—
Hexamethyldisiloxane	×	—	—	—
Dimethyl sulfoxide	×	×	—	—
N,N-Dimethylformamide	×	×	—	—

a) ○; soluble, ×; insoluble or sparingly soluble. b) $R=C_2H_4OC_2H_5$.

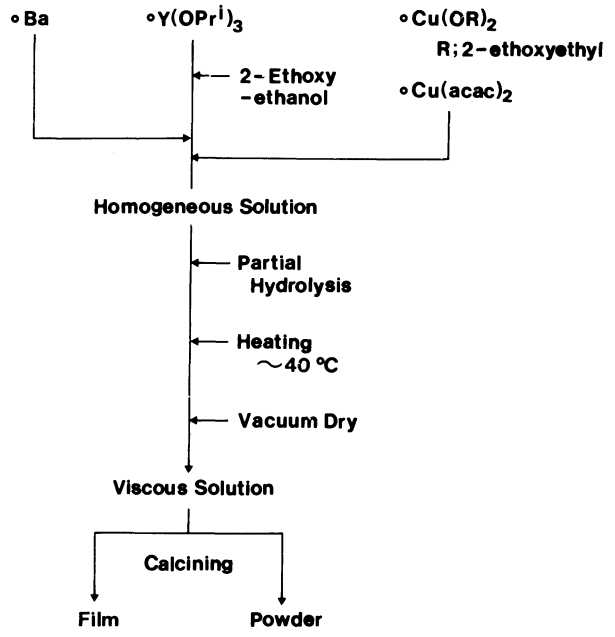

Fig. 1. The flowchart for chemical processing of $Ba_2YCu_3O_{7-\delta}$ through organometallic route.

under vacuum at about 40 °C to give an amorphous powder precursor. The powder was calcined in flowing O_2 or O_2/O_3 (3000 ppm O_3) mixture at the temperatures range between 650 and 950 °C for 24 h. The calcined powder was die-pressed and sintered in flowing O_2 at temperatures up to 920 °C, followed by annealing at temperatures between 450 and 550 °C. Thin film was also prepared on the substrates from concentrated solution with controlled viscosity by a dip-coating method.

The specimens were characterized by the X-ray powder diffraction method. DTA-TG analysis was performed at a heating rate of 10 °C min^{-1}. The dc resistivity of the specimens was measured by the four probe method with indium contact electrodes. The magnetization was measured by the vibrating sample magnetometry.

Results and Discussion

Figure 2 shows DTA-TG curves of as-prepared specimens by the hydrolysis of Y-, Ba-, and Cu-alkoxides. Two exothermic peaks with gradual weight loss were observed for all the specimens at 200—300 and 400—500°C; the second peak corresponds to thermal decomposition and oxidation of organic groups. In the specimens prepared by the hydrolysis of metal alkoxides, less-noticeable weight loss was observed above 600 °C, while a large weight loss was observed above 800 °C for the specimen prepared without water addition (no-hydrolysis). The large weight loss corresponds to the decomposition of $BaCO_3$ formed during heating by the reaction of barium compound with carbonaceous residue from organic groups.

Also, when $Cu(acac)_2$ was used as a starting material insterd of $Cu(OC_2H_4OEt)_2$, more remarkable exothermic peak associated with large weight loss was observed, which corresponds to the thermal decomposition and the oxidation of organic groups. The fact indicates the formation of coordination compounds between $Cu(acac)_2$ and 2-ethoxyethanol, and/or a partially exchange reaction of acac groups of $Cu(acac)_2$ with the solvent.

Figure 3 shows the X-ray powder diffraction patterns of the powders calcined at 850 °C for 12 h, 900 °C for 7 h, and 920 °C for 5 h, followed by the annealing at 450—550 °C in O_2 flow. In the powders prepared by the hydrolysis of metal alkoxides with the

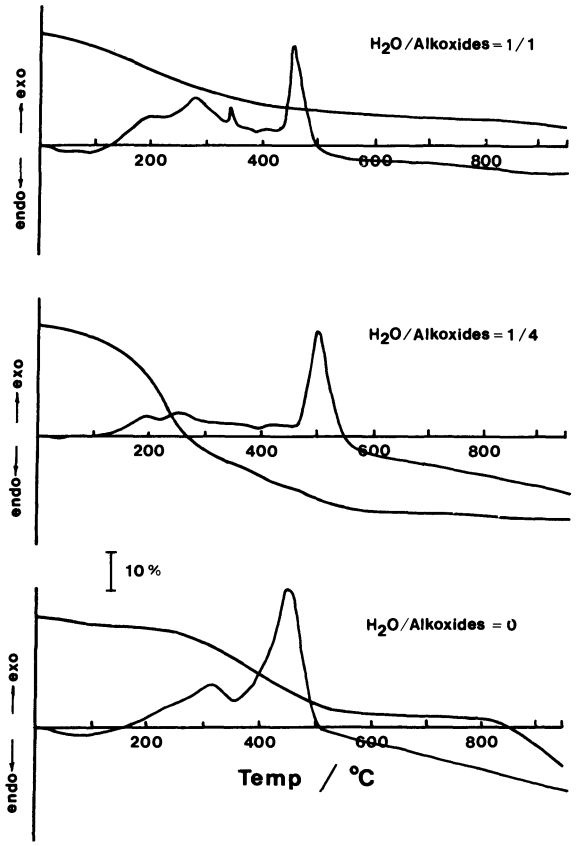

Fig. 2. DTA-TG curves of as-prepared specimens by the hydrolysis of Y-, Ba-, Cu-alkoxides.

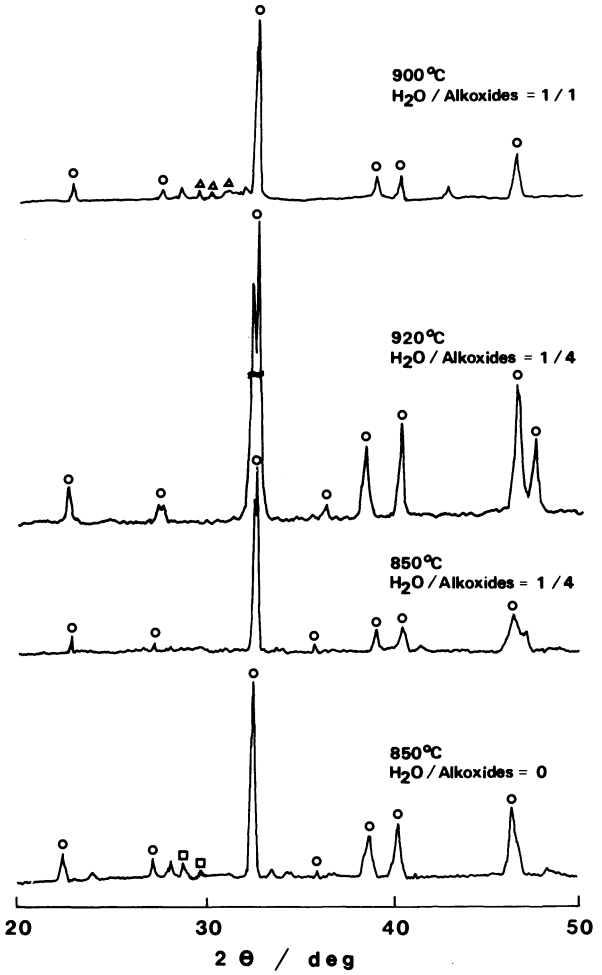

Fig. 3. X-Ray powder diffraction patterns of $Ba_2YCu_3O_{7-\delta}$ powders calcined at 850°C for 12 h, 900 °C for 7 h and 920°C for 5 h.
O: $Ba_2YCu_3O_{7-\delta}$ △: Y_2BaCuO_5, □: $BaCuO_2$.

equivalent amount of water, $BaCuO_2$ and Y_2BaCuO_5 were formed together with $Ba_2YCu_3O_{7-\delta}$. On the other hand, chemically homogeneous submicron powders of single phase $Ba_2YCu_3O_{7-\delta}$ were prepared at 850 °C by the controlled partial hydrolysis of metal alkoxides with addition of water less than the equivalent amount.

Figure 4 shows the X-ray powder diffraction patterns of the powders prepared by the calcination of partially hydrolyzed precursors at various temperatures for 12 h. The as-prepared powders were amorphous. $Ba_2YCu_3O_{7-\delta}$ compound formed at 750 °C was of single phase, and its crystallinity was further improved by heat treatment at 850 °C. Furthermore, by flowing O_2/O_3 mixture during the thermal decomposition of organic groups of the precursors, $Ba_2YCu_3O_{7-\delta}$ compound was prepared at the temperature as low as 650 °C. The importance of the utilization of O_3 gas was indicated by suppressed formation of $BaCO_3$. The addition of O_3 results in the direct formation of $Ba_2YCu_3O_{7-\delta}$ compound without any formation of intermediate phases such as $BaCuO_2$ and Y_2BaCuO_5. The carbon content in calcined powders, for example, in pure O_2 flow was 2.24%, which was drastically decreased to 0.94% by flowing O_2/O_3 mixture.

Figure 5 shows the SEM photograph of $Ba_2YCu_3O_{7-\delta}$ powders calcined at 850 °C. The resulting powders were chemically homogeneous, less agglomerated submicron particles, which can be ultrasonically dispersed homogeneously in organic solvents.

Figure 6 shows the dc resistivity of $Ba_2YCu_3O_{7-\delta}$ sintered at 920°C as a function of temperature. The superconducting transition starts at approximately 90 K and the resistance becomes zero at about 83 K. The superconducting-state magnetization, $Ms(H)$, of the fine powders determined by a magnetic balance, is shown at 85 K in Fig. 7. The hysteresis caused by the trap of magnetic flux exists in the $Ms(H)$ curves between the increase and the decrease of the magnetic field (H). The lower critical field H_{c1} was about 0.2 kOe at 85 K and the susceptibility was about −0.016 emu g^{-1}.

Figure 8 shows the fracture surface of the $Ba_2YCu_3O_{7-\delta}$ sintered body. The microstructure consisted of uniform grains of 2—3 μm, and no abnormal grain

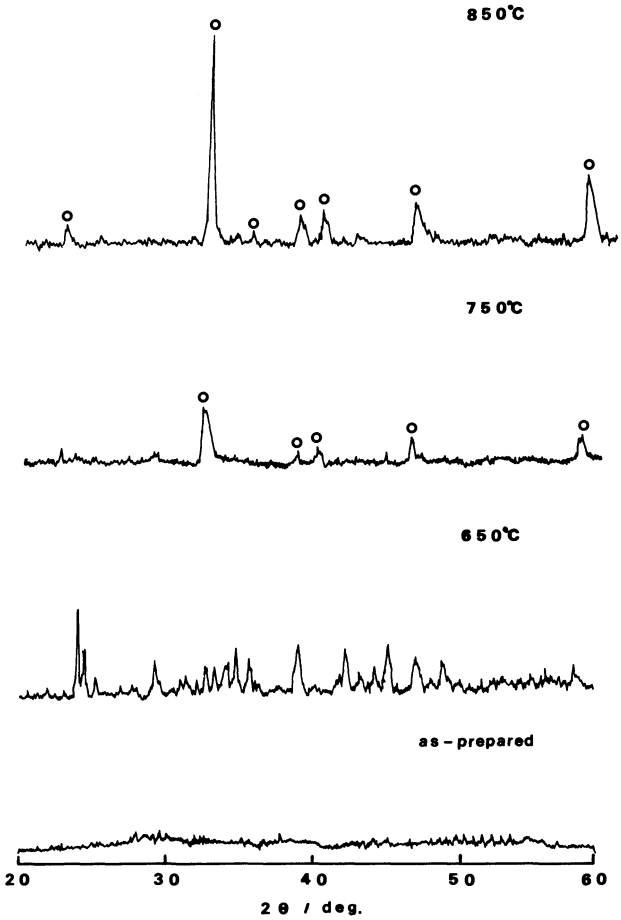

Fig. 4. X-Ray powder diffraction patterns of the powders prepared by the calcination of partially hydrolyzed precursors at various temperatures for 12 h.
O: $Ba_2YCu_3O_{7-\delta}$.

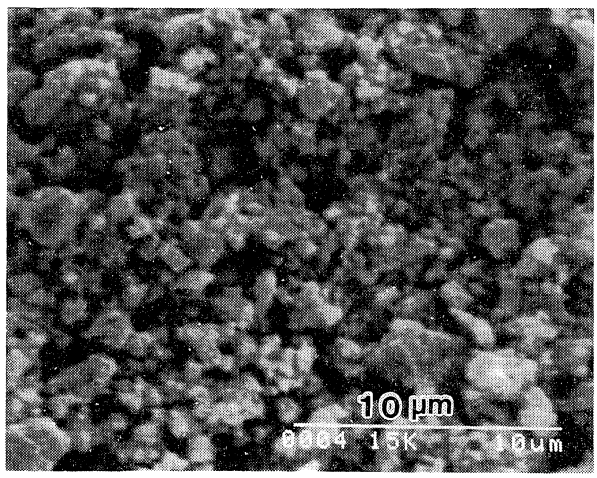

Fig. 5. SEM photograph of $Ba_2YCu_3O_{7-\delta}$ powders calcined at 850°C.

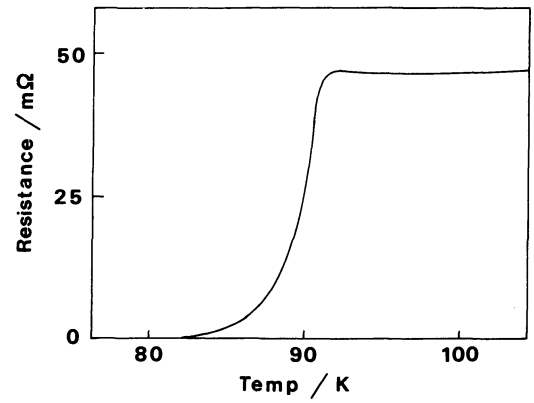

Fig. 6. DC resistivity of $Ba_2YCu_3O_{7-\delta}$ body sintered at 920°C as a function of temperature.

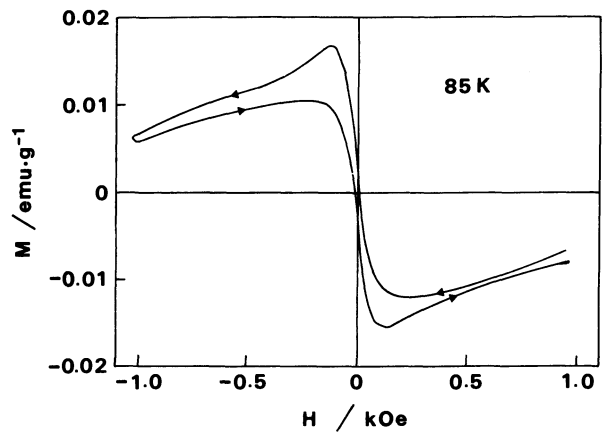

Fig. 7. Magnetization vs. magnetic field for $Ba_2YCu_3O_{7-\delta}$ calcined powder.

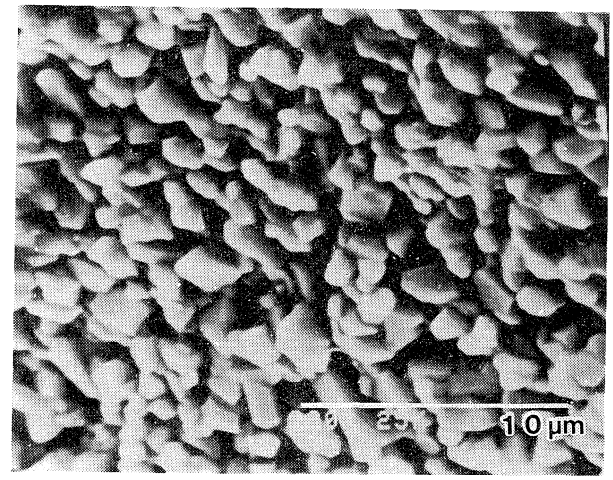

Fig. 8. Fracture surface of the $Ba_2YCu_3O_{7-\delta}$ sintered body.

growth was observed. No significant difference of properties was recognized for the powders or sintered bodies prepared from $Cu(OC_2H_4OEt)_2$ and $Cu(acac)_2$ in a flow of O_2/O_3 mixture.

The further research is in progress to synthesize the epitaxially grown films with c-axis orientation and the fibers of $Ba_2YCu_3O_{7-\delta}$ at lower temperature, on which

details will be reported elsewhere.

Conclusion

The synthesis of high-T_c $Ba_2YCu_3O_{7-\delta}$ superconductor in the relatively low temperature range was investigated through organometallic route, using Ba metal, $Y(OPr^i)_3$, and $Cu(OC_2H_4OEt)_2$ or Cu-acetylacetonate as starting materials by use of appropriate solvent.

1) Chemically homogeneous submicron powders of single phase $Ba_2YCu_3O_{7-\delta}$ was successfully prepared at 750 °C by controlled partial hydrolysis of alkoxides.

2) Utilization of O_2/O_3 mixture for the decomposition of the $Ba_2YCu_3O_{7-\delta}$ precursors showed a remarkable effect on suppressing the formation of $BaCO_3$ and lowering the formation temperature of $Ba_2YCu_3O_{7-\delta}$ to 650 °C.

3) It was confirmed by dc resistivity and magnetic susceptibility measurements that the single phase $Ba_2YCu_3O_{7-\delta}$ ceramics thus formed exhibit superconductivity at about 83 K (T_c end).

References

1) D. R. Clarke, *Advanced Ceramic Materials*, **2**, 273 (1987).

2) M. Hirabayashi, H. Ihara, N. Terada, K. Senzaki, K. Hayashi, S. Waki, K. Murata, M. Tokumoto, and Y. Kimura, *Jpn. J. Appl. Phys.*, **26**, L454 (1987).

3) N. Yamamoto, Y. Oka, Y. Tomii, H. Kitaguchi, J. Takada, A. Osaka, Y. Miura, and M. Kiyama, Proceedings of the Annual Fall Meeting of the Japan Society of Powder and Metallurgy, 1987, 36.

4) B. Dunn, C. T. Chu, L-W. Zhou, J. R. Cooper, and G. Gruner, *Advanced Ceramics Materials*, **2**, 343 (1987).

5) T. Kumagai, H. Yokota, K. Kawaguchi, W. Kondo, and S. Mizuta, *Chem. Lett.*, **1987**, 1645.

6) H. Nasu, *J. Ceram. Soc. Jpn.*, **96**, 710 (1988).

7) R. L. Henry, H. Lessoff, E. M. Swiggard, and S. B. Oudri, *J. Cryst. Growth*, **85**, 615 (1987).

8) S. Hirano, T. Hayashi, R. H. Baney, M. Miura, and H. Tomonaga, *Chem. Lett.*, **1988**, 665.

The Removal of Nitrogen Monoxide by the Dry Iron(II) Complex Immobilized on Chelate Resin. The Preparation and Characterization of the Complex

Naoki TOSHIMA,* Hiroyuki ASANUMA, and Hidefumi HIRAI†
Department of Industrial Chemistry, Faculty of Engineering,
The University of Tokyo, Hongo, Bunkyo-ku, Tokyo 113
(Received September 1, 1988)

A new dry-type adsorbent for nitrogen monoxide was successfully prepared from an iron(II) salt and a chelate resin containing iminodiacetic acid moieties. The capability of adsorbing nitrogen monoxide depended greatly on the method of preparation. The very active adsorbent was prepared by mixing 31.4 mmol of iron(II) sulfate and a commercial chelate resin containing 21.0 mmol of iminodiacetic acid moieties; the mixture was dried after the solid parts had been washed with methanol. The resulting solid adsorbent could adsorb more than 99% of the nitrogen monoxide from 6 dm^3 of nitrogen gas containing 1000 ppm of nitrogen monoxide within 25 min. This high capability for adsorbing nitrogen monoxide was derived from the increase in the surface area (43.1 $m^2 g^{-1}$) of the resin-immobilized iron(II) complex upon washing with methanol. The mechanism for the increase in the surface area is also discussed.

The atmosphere has been fairly well improved by the recent high technologies for protecting the environment. The concentration of nitrogen monoxide (NO), which is a source of pollution such as photochemical smog in the atmosphere has, however, not decreased in the past decade. Therefore, advanced technology for the removal of NO is strongly desired. At the present time, the catalytic reduction of NO into nitrogen by a gaseous reducing agent like ammonia is practically adopted, especially for such statistic sources as heavy oil and coal boilers.[1-3] Other methods under investigation involve the absorption of NO by molten salts, where the catalytic reduction proceeds partially,[4] and the absorption of NO by an aqueous solution of iron(II)–ethylenediaminetetraacetic acid (Fe(II)–EDTA), which can form a complex with NO.[5-8] Since an aqueous solution of Fe(II)–EDTA absorbs NO and desorbs it reversibly, this method has potential for use as an absorbent for recovering NO; i.e., the absorbed NO can be used again as a resource for nitrogen industries. However, this solution involves Fe(II) ions, which are easily oxidized into inactive Fe(III) ions by the contaminated oxygen. A reducing agent is necessary to avoid this deactivation of the complex in this system. Moreover, the recovery of the complex from the solution is difficult because of the homogeneity of the solution.

The immobilization of a metal complex, in general, offers the following advantages:[9] 1) the protection of the active site of the metal complex; 2) an increase in the activity by the polymer effect, and 3) easier handling because of the solidification of the complex by using a polymer support. Some polymer complexes have been investigated in order to apply them to catalysts and to the absorbents of carbon monoxide and ethylene.[10-13] Since, however, few studies have been reported on the application of a polymer complex for the removal of NO, it is significant to investigate an absorbent composed of the polymer complex with the above advantages. We have successfully prepared an aqueous dispersion by mixing an aqueous solution of Fe(II) ions with a chelate resin involving iminodiacetic acid moieties instead of EDTA in order to achieve easier handling and higher stability than the aqueous solution of Fe(II)–EDTA.[14,15] The resulting dispersions can absorb NO effectively, even at a low concentration, and can desorb NO reversibly upon heating at a higher concentration. The chelate resin-immobilized Fe(II) complex (CR–Fe(II)) can easily be recovered from the dispersions by filtration. Moreover, it has a higher durability against oxygen than Fe(II)–EDTA, the usual absorbent of NO, since the central atom of Fe(II) can be protected by polymer matrices.

We have examined the preparation of the dry-type, water-free chelate resin-immobilized Fe(II) complexes in order to develop more active and stable absorbents. Dry-type absorbents have been expected to have the following advantages: 1) contamination with the solvent vapor can be avoided in the recovery of NO; 2) much of the heat loss can be avoided when the adsorbed NO is recovered by heating, and 3) the handling of the adsorbent is easy enough to be applied to the moving sources of NO. To the best of our knowledge, nothing has yet been reported about the dry-type adsorbent of NO except for the active carbon[16] and the active carbon fiber-supported FeOOH.[17] Since the adsorption by these adsorbents is mainly based on a physical interaction between NO molecules and the adsorbents, they are not usually used for the removal of NO at extremely low concentrations. Now, we have successfully prepared a dry-type adsorbent of NO composed of the polymer complex.[18] In the present paper, the preparation and characterization of the

† Present address: Department of Industrial Chemistry, Faculty of Engineering, Science University of Tokyo, Kagurazaka, Shinjuku-ku, Tokyo 162.

polymer complex and its capability of adsorbing NO are reported.

Experimental

Materials. A commercial chelate resin (Diaion CR-10; mean diameter of the particles, 0.5 mm) purchased from Mitsubishi Chemical Industry, Ltd., was used in a swollen state, as it was, or in a dry state by drying after washing with a large amount of methanol since the commercial resin is swollen with water. One gram of the swollen resin was determined by pH titration to contain 0.98 mmol of iminodiacetic acid moieties. One gram of the resin dried in vacuo, on the other hand, has 2.78 mmol of the moieties. A mass of the chelate resin in a dry or a swollen state containing 21.0 mmol of iminodiacetic acid moieties was used at one time for the preparation of each adsorbent.

The reagent-grade solvents were used without further purification.

The iron(II) sulfate 7 hydrate and the Fe(II) chloride n hydrate (the n was determined to be 4.59 by the 1,10-phenanthroline method[19]) were used without further purification.

The gases of NO and nitrogen mixed at designed NO concentration were purchased from Takachiho Shoji, Ltd., and were used without further purification.

Preparation of the Adsorbent. 1) Preparation of the Aqueous Dispersions of the Chelate Resin-Immobilized Iron(II) Complex: The chelate resin containing 21.0 mmol of iminodiacetic acid moieties (21.4 g in a swollen state or 7.53 g in a dry state) and 31.4 mmol of Fe(II) salts were stirred in 50 cm^3 of water under nitrogen for 24 h to immobilize any Fe(II) ions on the resin. We will hereafter call the resulting aqueous mixture the "aqueous dispersion."

2) Preparation of Dry Adsorbent by Washing: The supernatant of the aqueous dispersion prepared as above was removed by decantation. After the solid part of the aqueous dispersion had been washed with 50 cm^3 of another solvent (a washing solvent) 4 times, drying it at 50 °C in vacuo gave a dry-type solid adsorbent.

3) Preparation without Washing: A solid adsorbent was prepared only by evacuating water from the aqueous dispersion at 50 °C in vacuo.

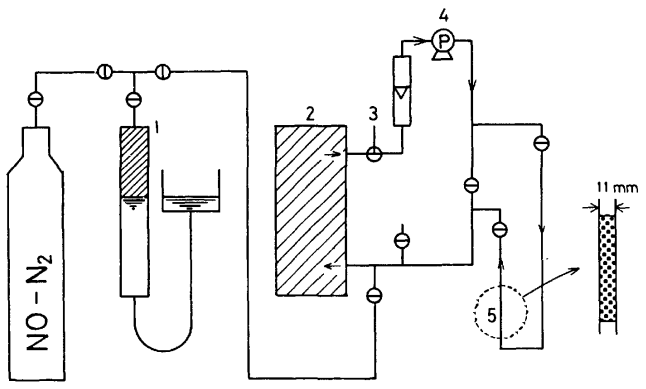

Fig. 1. Schematic diagram of gas adsorption apparatus. 1. Gas burette. 2. Gas holder. 3. Sampling outlet. 4. A gas-circulating pump. 5. An adsorbent column.

Adsorption of NO. The adsorption experiments of NO were carried out by using the closed circulation system illustrated in Fig. 1. After putting an adsorbent in a column of 1 l ϕ, 6 dm^3 of nitrogen containing 1000 ppm (or 980 ppm) of NO (the total amount of NO was 0.246 mmol) was introduced into this apparatus at room temperature, after which the sample gas was circulated through the column at the rate of 1.6 $dm^3\ min^{-1}$. Changes in the NO concentration in nitrogen were traced by sampling the mixed gas in a 100 mm-cell and measuring the absorbance at 226.5 nm.

Measurement of the Spectrum of the Adsorbent. The electronic spectra of the solid complexes were measured with a Hitachi model 340 spectrophotometer equipped with an integrated reflection apparatus. The ESR spectra were measured with a JEOL PE-1X ESR spectrometer. The chelate resin-Fe(II)-NO complex for the spectroscopic measurement was prepared by placing the solid adsorbent in contact with pure NO at 1 atm for 24 h.

Measurement of the Specific Surface Area. The BET surface area of the dry-type adsorbent was measured from the amount of adsorbed nitrogen at 77 K with a Micromeritics Instrument Co., Ltd., model 2200A rapid surface-area analyzer. The sample was completely dried by heating the sample at 90 °C for 40 min under a nitrogen stream before the measurement.

Electron Microscopy and X-Ray Microanalysis. Scanning electron microscopy (SEM) and X-ray microanalysis (EPMA) on the resin of the adsorbents were carried out by the use of a Hitachi model X-650 micro-scanning X-ray analyzer, the resolution of the X-ray image of which is around 100 Å. The sample beads were cut with a stainless steel cutter and then coated with gold so that cross-sections of the beads were irradiated by an electron beam. The distributions of Fe and S atoms were evaluated by the intensity of the characteristic X-ray.

Measurement of the Immobilized Iron(II) Ions on the Resin. The concentration of Fe(II) ions in the supernatant of the aqueous dispersion was measured by the 1,10-phenanthroline method.[19] The amount of immobilized Fe(II) ions was calculated from the discrepancy in the amount of initially charged Fe(II) ions and that of Fe(II) ions remaining in the supernatant after the immobilization. The amount of immobilized Fe(II) ions was 16.2 mmol when 7.53 g of the chelate resin containing 21.0 mmol of iminodiacetic acid moieties and 8.72 g of $FeSO_4$ was used.

Results

Preparation of the Adsorbent and Its Capability to Adsorb NO. The supernatant of the adsorbent dispersions prepared from Fe(II) sulfate and the chelate resin had a light green color due to the dissolution of Fe(II) sulfate. The light greenish color of the aqueous solution gradually diminished due to the immobilization of the dissolved Fe(II) ions onto the resin through ion-exchange. In contrast, the chelate resin (solid part) acquired a light green color by the immobilization. The immobilization completed within a few hours. The amount of immobilized Fe(II) ions was found to be 16.2 mmol. The solvent-free adsorbent prepared only by removing the water

from the aqueous dispersion in vacuo adsorbed any scarcely NO in spite of the immobilization of the Fe(II) ions on the resin, as is shown by open circles in Fig. 2. In contrast, the adsorbent prepared by drying after the immobilizing resin has been washed 4 times with 50 cm^3 of a "washing solvent" had the capability of adsorbing NO. Especially, the adsorbent prepared by washing with methanol shows so high a capability that almost all the NO in the system was adsorbed within 25 min, as is illustrated by the closed circles in Fig. 2.[20]

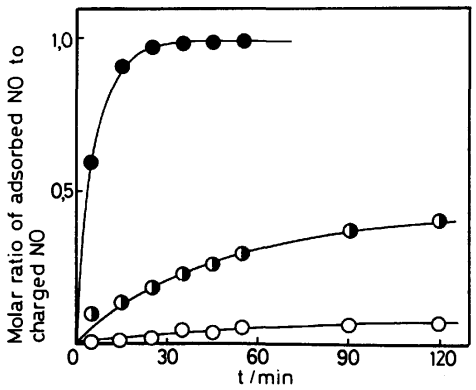

Fig. 2. Adsorption curves for NO by the chelate resin-immobilized adsorbent prepared by drying after washing with methanol (●), water (◑), and without washing (○). These adsorbents were prepared from 21.4 g of chelate resin and 8.72 g (31.4 mmol) of $FeSO_4 \cdot 7H_2O$. Adsorption experiment was carried out by circulating 6 dm^3 of nitrogen containing 1000 ppm of NO at room temperature at the rate of 1.6 $dm^3\ min^{-1}$.

Figure 3 reveals the adsorption curves of NO by the adsorbent prepared from Fe(II) chloride instead of sulfate according to the same method as was used with the sulfate. The adsorbent prepared from Fe(II) chloride by washing with methanol also shows as high a capability for the adsorption of NO as that of the adsorbent from the sulfate. The adsorbents obtained from chloride without washing or by washing with water, however, have a higher capability than the corresponding adsorbents prepared from the sulfate illustrated in Fig. 2.

A freeze-dried absorbent was also prepared by freeze-drying after the solid part of the aqueous dispersion had been washed with water. However, it has almost the same capability as the adsorbent dried at 50 °C in vacuo, as is shown in Fig. 4. Table 1 compares the amount of NO adsorbed by the dry-type adsorbent, the original chelate resin itself, the powder of the Fe(II) sulfate, and that of Fe(II) chloride. This table clearly

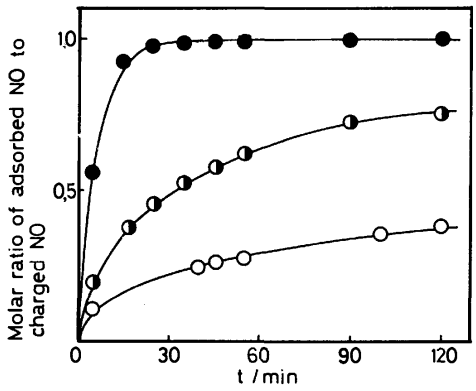

Fig. 3. Adsorption curves for NO by the CR-Fe(II) complex prepared from 31.4 mmol of $FeCl_2$ and 21.4 g of chelate resin by drying after washing with methanol (●), water (◑), and without washing (○). The adsorbent was contacted with 6 dm^3 of nitrogen containing 1000 ppm of NO at room temperature at the rate of 1.6 $dm^3\ min^{-1}$.

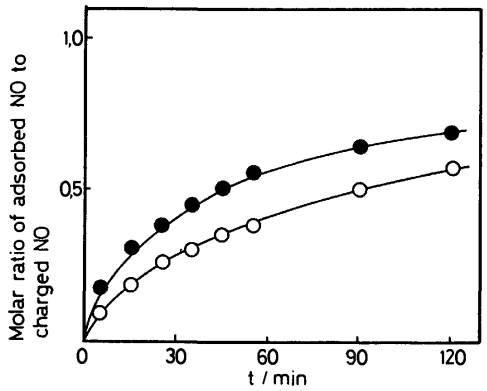

Fig. 4. Effect of the drying temperature on the adsorption of NO. The adsorbents were prepared by drying at 50 °C (○) and by freeze-drying (●) after washing the CR-Fe(II) complex with water. The adsorbent was contacted with 6 dm^3 of nitrogen containing 1000 ppm of NO at room temperature at the rate of 1.6 $dm^3\ min^{-1}$.

Table 1. Adsorption of NO by the Dry-Type CR-Fe(II) Adsorbent and Its Starting Materials

Material	Amount/g	Amount of adsorbed NO[a]/mmol
Chelate resin[b]	7.53	0.0
$FeCl_2 \cdot 4.59H_2O$	6.56 (31.4 mmol)	0.0
$FeSO_4 \cdot 7H_2O$	8.72 (31.4 mmol)	0.0
CR-Fe(II)[c]	9.02	0.246

a) Adsorption experiments were carried out by placing the material in contact with 6 dm^3 of nitrogen containing 1000 ppm of NO. The initially charged amount of NO was 0.246 mmol. b) The commercial chelate resin dried after having been washed with ethanol. c) A dry-type chelate resin-Fe(II) adsorbent prepared by drying after washing with methanol. See text for details.

Table 2. Effects of Solvents for the Immobilization of Iron(II) Ions on the Adsorbing Capability for NO[a]

Solvent	Molar ratio of adsorbed NO to charged NO	
	In 15 min	At equilibrium[b]
Water	0.170	>0.425
Methanol	0.173	>0.536
Ethanol	0.443	0.921
2-Propanol	0.263	>0.794
Acetone	0.139	>0.502
Acetonitrile	0.111	>0.464
Chloroform[c]	0.023	0.026

a) Adsorbents were prepared from 50 cm^3 of a solvent, 31.4 mmol of $FeCl_2$, and 21.4 g of the chelate resin swollen with water. b) When the equilibrium was not attained within 180 min, the ratio of the adsorbed NO at this time is shown in this column. c) The adsorbent was prepared from chloroform, $FeCl_2$, and dried chelate resin which had previously been washed with ethanol.

indicates that the adsorption of NO does not take place only by means of each starting material, but the adsorbent resulting from mixing the starting materials does.

The preparation of adsorbent dispersions was examined from 21.4 g of water-swollen chelate resin, 31.4 mmol of $FeCl_2$, and 50·cm^3 portions of various organic solvents. The color of the supernatant became light green in each system and then gradually faded through the immobilization of the Fe(II) on the resin, which showed the light green color in contrast. In this system, the supernatant is actually composed of the organic solvent and water derived from the water-swollen resin. The ratio of water to the organic solvent is calculated to be 0.27 (v/v), because 21.4 g of the chelate resin contains 13.4 g of water. The adsorbent was prepared by removing the solvent from the above dispersion in vacuo at 50 °C. The amounts of NO adsorbed by these adsorbents are listed in Table 2; the table shows not very high adsorbing capabilities in this method except for the adsorbent prepared with ethanol.

In order to avoid the effect of water in the solvent, the adsorbent dispersion was prepared from ethanol (the solvent used for immobilization), the dried chelate resin, and $FeCl_2$, which is soluble in ethanol. The ethanol solution of $FeCl_2$ offered a brownish color, although the aqueous solution was light green. The immobilization of Fe(II) scarcely proceeded, since, though the resin was colored a little brownish, no fading in the color of the supernatant was observed. The removal of the ethanol by the adsorbent dispersions gave the resin-immobilized Fe(II) complex and a large amount of $FeCl_2$ salts which were not immobilized on the resin. The adsorbing capability of the adsorbent prepared by the above method is illustrated with closed circles in Fig. 5; it is not so high as that given by the washing method. The adsorbent prepared by using chloroform as a solvent scarcely adsorbs any NO at all, as is shown by the open circles in the same figure. In this system, the Fe(II) ions could

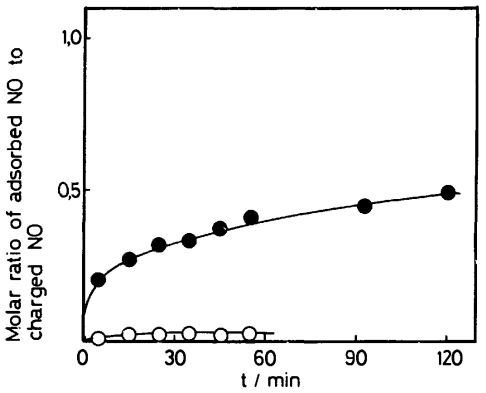

Fig. 5. Effect of the solvent used for immobilization of Fe(II) ions on the adsorbing capability for NO. The adsorbents were prepared from 7.53 g of the dried chelate resin, 31.4 mmol of $FeCl_2$, and ethanol (●) or chloroform (○) for immobilization of Fe(II) ions on the resin. See text for details.

not be immobilized on the resin because $FeCl_2$ does not dissolve in chloroform. These results indicate that chloroform is not an appropriate solvent for the immobilization of Fe(II) on the resin.

Among the methods examined, the method to prepare the most effective adsorbent has turned out to be the use of water as a solvent for the immobilization, followed by drying under a vacumm after washing the swollen CR–Fe(II) complex with methanol (vide infra).

Adsorbing Capability for NO and Specific Surface Area of the Dry-Type Chelate Resin-Iron(II) Complex Prepared by Washing with a Solvent. We have shown in the previous paragraph that the adsorbent prepared by drying after washing the swollen CR–Fe(II) complex with methanol has the highest adsorbing capability for NO among those examined. Table 3 indicates the effect of the washing solvent on the capability for adsorbing NO. An obvious difference in the adsorption rate of NO is observed in the solvent used for washing the swollen CR–Fe(II), but there is

no significant difference in its appearance. The adsorbent prepared by using methanol or ethanol adsorbs NO at the initial rate of 1.54×10^{-2} mmol min^{-1}. The adsorption rate, however, slightly decreases in the case of acetone. A significant decrease in the adsorption rate is observed in the case of water and chloroform, which is immiscible with water. Table 3 also shows the specific surface area ($A/m^2\,g^{-1}$) of each adsorbent, as measured by the BET method, which clearly demonstrates that the adsorption rate is in reasonable linear relationship with the specific surface area.

The above results show the best method of preparation to be as follows: 1) the immobilization of the Fe(II) ion on the resin has to be carried out in water, and 2) the drying of the CR-Fe(II) dispersion

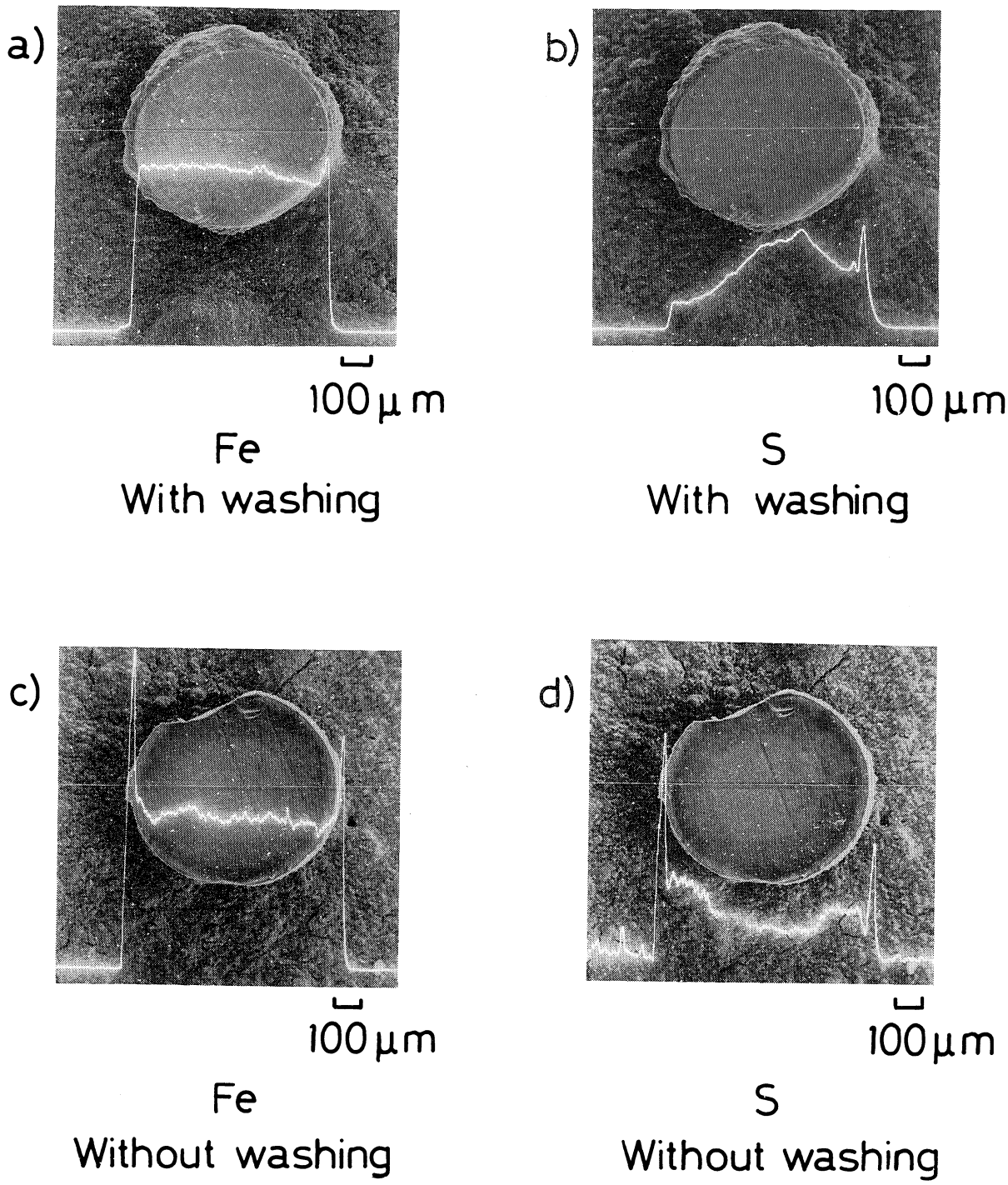

Fig. 6. SEM photographs and EPMA data of the cross-section of the dry adsorbents prepared from $FeSO_4$ and the chelate resin with washing with ethanol (a, b) or without washing (c, d).

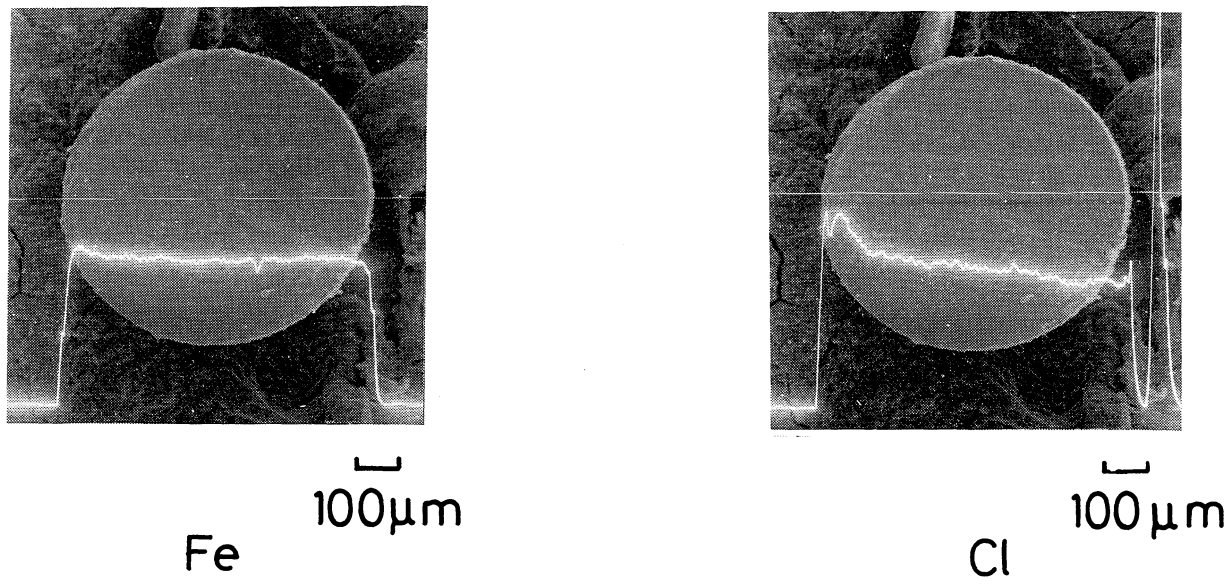

Fig. 7. SEM photograph of the cross section of the adsorbent prepared from $FeCl_2$ and the chelate resin without washing and its EPMA traces for Fe and Cl.

had better to be carried out after washing the resin with an organic solvent miscible with water, especially with methanol. Moreover, the effect of the washing has turned out to be an increase in the surface area of the adsorbent.

Analysis of the Adsorbent with Electron Microscopy and X-Ray Microanalysis. The distribution of the immobilized Fe(II) salts on the resin beads was analyzed by means of SEM and EPMA. Figure 6 shows SEM photographs of the dry-type adsorbent prepared by drying after washing with ethanol and by drying without washing. The waveline refers to the distributions of Fe and S atoms along the corresponding white straight lines on the cross-sections of the beads. The height of the waveline refers to the density of each atom. For both adsorbents, Fe atoms are homogeneously distributed inside the resin. For the adsorbent without washing, however, the density of Fe atoms is higher on the outer surface than inside the bead, while, for the adsorbent with washing, it is uniformly distributed not only inside the beads, but also on the surface. A low distribution of S atoms is observed both inside and on the surface of the bead. For the adsorbent without washing, however, many S atoms are located near the surface of the bead. These analyses indicate that the $FeSO_4$ is attached to the outer surface of the bead without washing. For the adsorbent prepared from $FeCl_2$, a homogeneous distribution of Fe atoms inside and on the outer surface was observed, as is depicted in Fig. 7.

The above facts clearly indicate that the residual powder of $FeSO_4$, which is not immobilized on the resin, is attached to the outer surface of the resin beads and that it suppresses the diffusion of NO molecules into the inside of the resin, resulting in a low capability for adsorbing NO. On the contrary, the adsorbent with $FeCl_2$ without washing has a sufficient adsorbing capability for NO. This fact also coincides with the results of the EPMA, which show the delocalized distribution of Fe atoms.

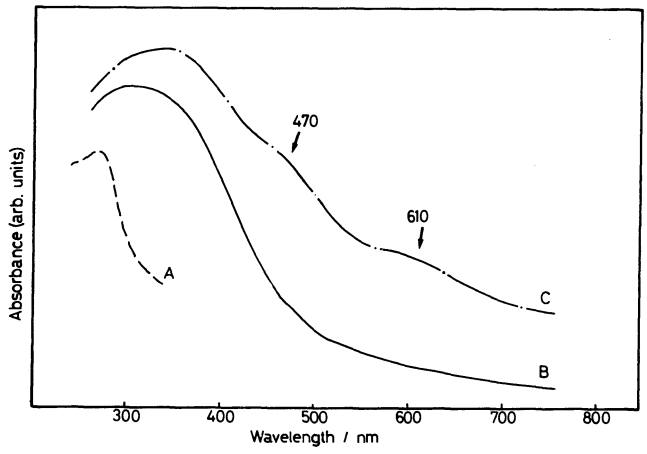

Fig. 8. Electronic spectra of the NO adsorbent and the related materials. A(——): chelate resin, B(—): CR-Fe(II), and C(—·—): CR-Fe(II)-NO.

Spectra of the Adsorbent. The water-swollen chelate resin before the immobilization of Fe(II) ions is white and has its maximum peak in its electronic spectrum at 280 nm due to the benzene chromophore of the matrices, as is shown by the broken line in Fig. 8. The color of the resin changes from white to light green upon the immobilization of the Fe(II) ions; also, a new peak appears around 300 nm. The exposure of the CR-Fe(II) complex to pure NO rapidly change its color from light green to brown, and new shoulder peaks appear in its electronic spectrum at 470 and

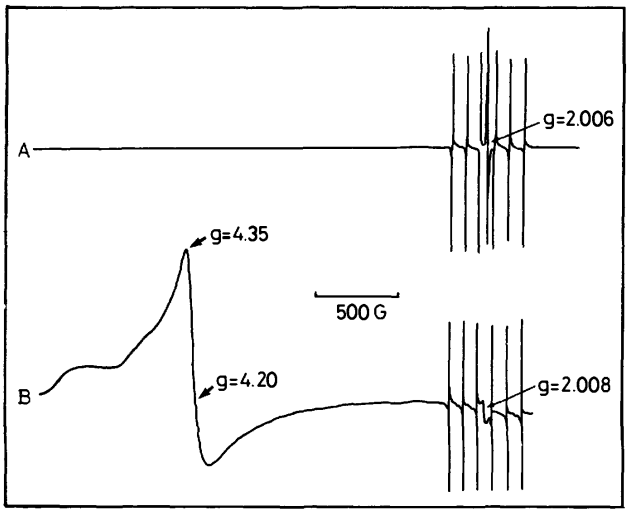

Fig. 9. ESR spectra of chelate resin (A) and CR-Fe(II) complex before the exposure with NO gas (B). Six signals in the same magnitude are derived from a Mn^{2+} marker.

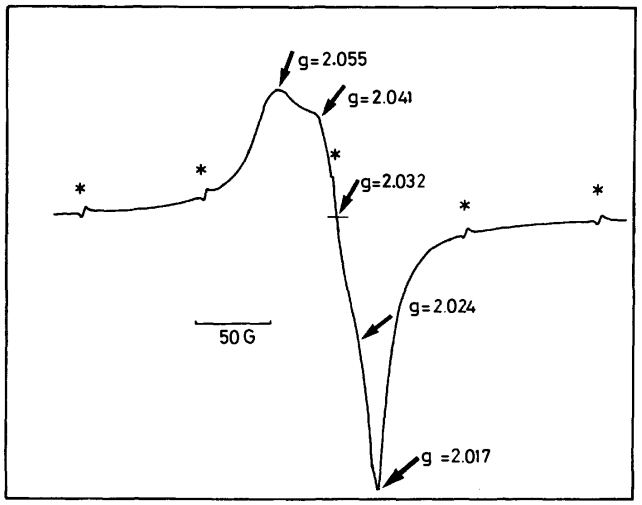

Fig. 10. ESR spectrum of CR-Fe(II)-NO complex at central magnetic field. Five weak signals with asterisks are derived from a Mn^{2+} marker.

610 nm. A similar change has been observed in the case of the absorption of NO by an aqueous solution of the Fe(II)-EDTA complex.[6]

In the ESR spectrum, the dried commercial resin before the immobilization of Fe(II) ions has a sharp signal at g=2.006 assigned to the organic radical, while no signals are observed at low magnetic fileds, as is illustrated in A of Fig. 9. The six sharp signals in Fig. 9 are derived from a manganese marker (S=5/2). By the immobilization of the Fe(II) ions on the resin, the sharp signal at g=2.006 disappears and broad new signals, probably due to the contaminated Fe(III), appear at g=4.20,[21] as is shown in B of Fig. 9. A new, unsymmetrical, strong, broad signal with unresolved shoulders appears upon the exposure to NO as is

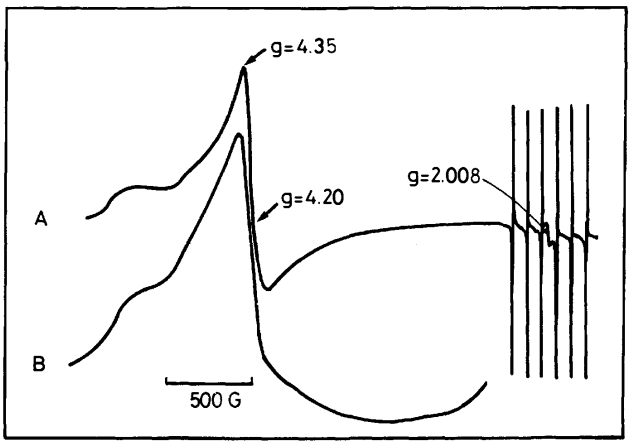

Fig. 11. ESR spectra of CR-Fe(II) (A) and CR-Fe(II)-NO (B) at low magnetic field. Six signals at central magnetic field are derived from a Mn^{2+} marker. The spectrum B in the central magnetic field region is shown in Fig. 10 and omitted in this Figure.

shown in Fig. 10. The g values at the maximum and minimum of the signal were 2.055 and 2.017 respectively. In this case, the signal at g=4.20 does not change, as is shown in Fig. 11.

Discussion

Coordination of Nitrogen Monoxide. The appearance of a new band in the electronic spectrum by the immobilization of Fe(II) ions indicates the coordination of Fe(II) ions to the IDA moieties in the chelate resin. Upon the adsorption of NO new shoulder peaks appear at 470 nm and 610 nm; this is similar to the change in the spectrum observed with an aqueous solution of Fe(II)-EDTA or Fe(II) salts.[6] This change is reported to be due to the coordination of an NO molecule on the Fe(II) ion.[6] Thus, the adsorption of NO by the present dry-type adsorbent proceeds by the coordination of an NO molecule with the Fe(II) ion in the resin complex.

The ESR signals around g=2.03 appearing upon the contact of the adsorbent with an NO gas are commonly observed in the case of Fe(II)-NO complexes derived from an NO molecule with a free electron.[22] This fact also strongly supports the idea that the adsorption of NO by the present adsorbent proceeds by means of the coordination of NO on the Fe(II) ion. Moreover, the appearance of the signal at around g=2.03, not in the lower magnetic field, indicates the formation of a low-spin (S=1/2) Fe(II)-NO complex.[22] In general, there are two types of Fe(II)-NO complexes. One is a low-spin state (S=1/2), and the other, a high-spin state (S=3/2). When a ligand field is strong enough, a low-spin complex is known to be formed. In the present system, since the IDA moieties in the chelate resin work as strong ligands, the low-spin complexes of Fe(II)-NO are thought to be produced.

Preparation of a Dry-Type Adsorbent with a High Capability for Adsorbing NO upon Washing. From the results of EPMA, the Fe atoms in the adsorbent prepared with washing seem to be distributed homogeneously both inside and on the surface of the resin beads. On the contrary, in the case of the adsorbent prepared without washing, more Fe atoms are distributed on the surface than on the inside of the resin. A similar result is also observed in the distribution of S atoms. These results indicate that the Fe(II) ions which cannot be immobilized on the resin are attached on the surface of the resin beads as $FeSO_4$. This $FeSO_4$ attached on the surface suppresses the diffusion of NO molecules into the resin inside.

The capability for adsorbing NO, especially the adsorption rate of the adsorbent prepared by washing, coincides well with the specific surface area, as is shown in the right column in Table 3. Figure 12 shows the plots of the adsorption rate of NO against the specific surface area. The adsorption rate linearly increases with an increase in the surface area until 24 $m^2 g^{-1}$. This fact clearly demonstrates that the increase in the surface area contributes directly to the increase in the adsorption rate. Over a surface area of 24 $m^2 g^{-1}$, the adsorption rate is so fast that the adsorption apparatus used in this experiment cannot follow the increase in the adsorption rate while keeping a constant rate at 1.54×10^{-2} mmol min^{-1}.

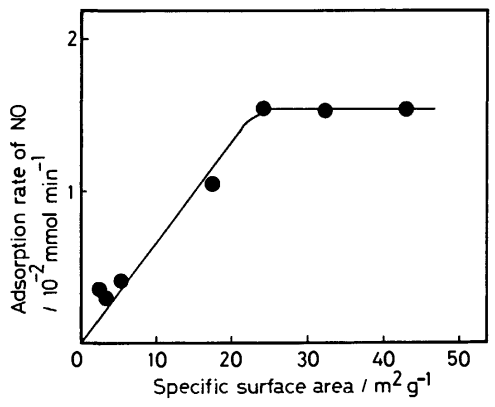

Fig. 12. Correlation of the specific surface area with the adsorption rate of NO by various CR-Fe(II) adsorbents.

The increase in the specific surface area upon washing with an organic solvent can be explained as follows. The chelate resin swells well in water and exists in a rubber state. When the solvent (water) in the resin in the rubber state is exchanged with an organic solvent miscible with water, many microgels will be generated through a phenomenon similar to the "reprecipitation" of the polymer by the addition of a poor solvent to the polymer solution, since the freeze-dried adsorbent from water has a low porosity. The resin is transformed from the rubber state into a glassy state during the exchange of the solvent because of the poor swelling in the organic solvent.[23,24] In this glassy state, the shrinkage of the resin during the drying of the resin is suppressed by the low mobility of the polymer. Consequently, the surface area increases due to the remaining of the pores produced by drying the resin after the exchange of the solvent. On the contrary, the resin swollen in water shrinks during the evacuation of the solvent in the resin, for the polymer chains have a high mobility in the rubber state. In

Table 3. Effects of the Washing Solvents on the Adsorption Rate of NO and the Specific Surface Area of the Adsorbent

Solvent	Adsorption rate[a]/ 10^{-2} mmol min^{-1}	Ratio of adsorbed NO[b]	Specific surface area[c]/$m^2 g^{-1}$
Chloroform	0.36	0.789	2.3
Water	0.30	>0.425	3.2
Acetone	1.04	0.933	17.1
Ethanol[d]	1.54	0.997	31.1
Methanol[d]	1.54	0.997	43.1

a) The adsorption rates were evaluated from the amount of NO adsorbed in 15 min. b) Molar ratio of adsorbed NO to charged NO at equilibrium. c) Measured by a BET method. d) No difference in the adsorption of NO between the two adsorbents could be observed because the adsorption occurred too fast.

Table 4. Effects of the Washing Solvents on the Specific Surface Area of the Chelate Resin-Immobilized Fe(II) Complex

Solvent	Solubility parameter $\delta^{a)}/10^3$ $(J m^3)^{1/2}$	Specific surface area[b]/$m^2 g^{-1}$
Chloroform	19.0	2.3
Water	47.9	3.2
Acetone	20.3	17.1
2-Propanol	23.5	31.7
Ethanol	26.0	31.1
Methanol	29.7	43.1

a) Quoted from Ref. 25. b) Measured by a BET method.

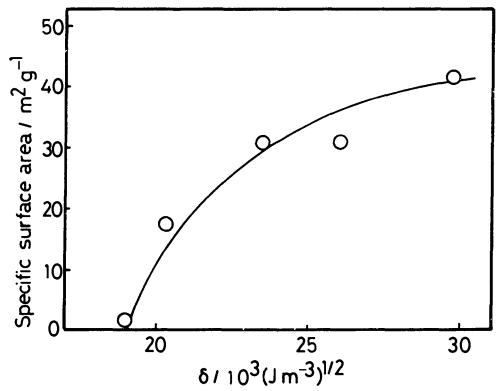

Fig. 13. Relationship between the specific surface area and the solubility parameter (δ) of the solvent used for washing the water-swollen CR-Fe(II) complex.

fact, the adsorbent prepared by washing with the organic solvent is lower in apparent density than that prepared by washing with water.

The surface area increases with the increase in the solubility parameter δ[25] in the order of: acetone, ethanol, and methanol, as is shown in Table 4. The date are plotted in Fig. 13. This parameter δ corresponds to the square root of the cohesive energy density ($(E/V)^{1/2}$).[25] If the solubility parameters δ of two solvents are close to each other, it indicates that their mutual miscibility is high.[25] The adsorbent prepared by chloroform, whose δ is apart from that of water, has a small surface area. On the contrary, the maximum porosity is obtained by the use of methanol, whose δ is close to that of water. These facts indicate that mutual miscibility with water contributes to the surface area (porosity) of the adsorbent. Probably, the solvent with a δ close to that of water, like methanol, will be able to penetrate into the inner portions of the resin and be exchanged with water to make pores through "reprecipitation."

The dry-type resin-immobilized Fe(II) complexes prepared from $FeSO_4$ without washing cannot adsorb NO, while those from $FeCl_2$ can adsorb NO even without washing. From the results of EPMA, $FeCl_2$ seemed not so much attached on the outer surface of the resin as was observed in the case of $FeSO_4$. This phenomenon is probably connected with the crystallinity of the Fe(II) salts. For $FeSO_4$, an excess amount of the salt can form crystals easily and can cause it to attach itself on the surface, resulting in a suppression of the adsorption of NO. On the contrary, since the excess amount of $FeCl_2$ is not attached on the surface, the adsorption of NO takes place.

Concerning the adsorbent prepared by using a hydrophilic organic solvent and a water-swollen resin without the washing treatment, though the immobilization of Fe(II) ions took place, its adsorbing capability for NO was as low as that when using water without washing, except when ethanol was used as the hydrophilic solvent. In these systems, since the solvents used has boiling points lower than that of water, the organic solvent was first removed from the water-mixed solvent by evaporation. Consequently, these adsorbents prepared from the water-mixed solvent were the same as that dried directly from water without an organic solvent. In the case of ethanol, however, the evaporation of an azeotropic mixture of ethanol and water actually proceeded resulting in an adsorbent different from that prepared from only water.

In the case of the adsorbent prepared by using ethanol and the dried chelate resin, the immobilization of Fe(II) ions does not proceed even for $FeCl_2$, which is soluble in ethanol. Since the immobilization of Fe(II) ions occurs by means an ion-exchange with sodium ions in water, the ion-exchange does not proceed smoothly in ethanol, which is not a good electrolyte.

Conclusion

1) The dry-type adsorbent was prepared from 21.4 g of chelate resin (containing 21.0 mmol of iminodiacetic acid moieties) and 31.4 mmol of $FeSO_4$ by drying after the water-swollen CR-Fe(II) complex had been washed with methanol. The resulting adsorbent adsorbed almost all the NO from 6 dm^3 of nitrogen containing 1000 ppm of NO within 25 min.

2) The high adsorbing capability for NO obtained by washing with an organic solvent is derived from the increase in the specific surface area. The surface area greatly depends on the kind of washing solvent used. The maximum porosity (43.1 $m^2 g^{-1}$) was obtained by using methanol, whose solubility parameter δ was close to that of water. On the contrary, no increase in the surface area was observed with chloroform, whose δ is far from that of water. Thus, it is clarified that the mutual miscibility with water greatly contributes to the increase in the surface area.

3) The adsorbent after the contact with an NO gas exhibits the two shoulder peaks at 470 nm and 610 nm in the electronic spectra. A similar appearance of the peaks is observed with an aqueous solution of a Fe(II)-NO complex. Thus, the adsorption of NO by the present dry adsorbent proceeds through the coordination of NO on Fe(II). Moreover, the CR-Fe(II) complex after the adsorption of NO has signals centered at g=2.03 in the ESR spectrum, which is characteristic of the low spin Fe(II)-NO complex. This fact also supports the idea that the adsorption proceeds through the coordination of the NO on the Fe(II) ion in the resin.

The authors wish to express their thanks to Dr. Eisuke Ogata of the Department of Reaction Chemistry, The University of Tokyo, for his technical advice on measuring the specific surface area.

References

1) S. Kasaoka, E. Sasaoka, and S. Nakashima, *Nenryo Kyokai Shi*, **63**, 54(1984).
2) T. Inui, T. Otowa, M. Kawata, and Y. Takegami, *Nenryo Kyokai Shi*, **62**, 762 (1983).
3) I. Mochida, K. Suetsugu, H. Fujitsu, and K. Takeshita, *J. Catal.*, **77**, 519 (1982).
4) T. Shikada, T. Oba, K. Fujimoto, and H. Tominaga, *Ind. Eng. Chem., Prod. Res. Rev.*, **23**, 417 (1984).
5) M. Teramoto, S. Hiramine, Y. Shimada, Y. Sugimoto, and H. Teranishi, *J. Chem. Eng. Jpn.*, **11**, 450 (1978).
6) K. Ogura and T. Ozeki, *Denki Kagaku*, **51**, 762 (1983).
7) Y. Hishinuma, R. Kaji, H. Akimoto, F. Nakajima, T. Mori, T. Kamo, Y. Arikawa, and S. Nozawa, *Bull. Chem. Soc. Jpn.*, **52**, 2863 (1979).
8) E. Sada, H. Kumazawa, and H. Machida, *Ind. Eng. Chem. Res.*, **26**, 2016 (1987).
9) H. Hirai and N. Toshima, "Tailored Metal Catalysts" ed. by Y. Iwasawa, D. Reidel Publishing Company (1986), p. 87; "Kobunshi Sakutai Shokubai (Macromolecular Complex Catalysts)," ed. by H. Hirai and N. Toshima, Japan Scientific Societies Press, Tokyo (1982).
10) H. Hirai, S. Hara, and M. Komiyama, *Bull. Chem. Soc. Jpn.*, **59**, 109 (1986).
11) H. Hirai, S. Hara, and M. Komiyama, *Bull. Chem. Soc. Jpn.*, **59**, 1051 (1986).
12) H. Hirai, S. Hara, and M. Komiyama, *Bull. Chem. Soc. Jpn.*, **60**, 385 (1987).
13) H. Hirai, K. Wada, and M. Komiyama, *Bull. Chem. Soc. Jpn.*, **59**, 1043 (1986)
14) H. Hirai, H. Asanuma, and N. Toshima, *Chem. Lett.*, **1985**, 655.
15) H. Hirai, H. Asanuma, and N. Toshima. *Chem. Lett.*, **1985**, 1921.
16) S. N. Ganz, *Zh. Prikl. Khim.*, **31**, 138 (1958).
17) K. Kaneko, S. Ozeki, and K. Inouye, *Nippon Kagaku Kaishi*, **1985**, 1351.
18) N. Toshima, H. Asanuma, and H. Hirai, *Chem. Lett.*, **1986**, 667.
19) Japanese Industrial Standard (JIS) K1010.
20) The adsorption of NO with Fe(II) ion in the present case has been revealed to occur through 1:1 complex formation; the details will be published in the near future: H. Asanuma and N. Toshima,to be published.
21) N. P. Evmiridis, *Inorg. Chem.*, **25**, 4362 (1986).
22) C. C. McDonald, W. D. Phillips, and H. F. Mower, *J. Am. Chem. Soc.*, **87**, 3319 (1965).
23) P. P. Wieczorek, B. N. Kolarz, and H. Galina, *Angew. Makromol. Chem.*, **126**, 39 (1984).
24) W. L. Sederel and G. J. Dejong, *J. Appl. Polym. Sci.*, **17**, 2815 (1973).
25) H. Burrell, "Polymer Handbook," ed. by J. Brandrup and E. H. Immergut, A Wiley-Interscience Publication (1974), Chap. 4, p. 337.

 © 1989 The Chemical Society of Japan Bull. Chem. Soc. Jpn., 62, 903—907 (1989)

Preparation and Characterization of Hydrogen Molybdenum Bronzes, H_xMoO_3

Noriyuki SOTANI,* Kazuo EDA, Masayasu SADAMATU,† and Sadao TAKAGI†
College of Liberal Arts, Kobe University, Tsurukabuto, Nada, Kobe 657
†Department of Chemistry, Kinki University, Kowakae, Higashi-osaka 577
(Received September 9, 1988)

Hydrogen molybdenum bronzes, H_xMoO_3, of Type-I (x=0.21), Type-III (x=1.55), and Type-IV (x=1.90) were prepared by the Glemser's method. Type-II (x=0.91) was obtained from Type-III by standing in air for 120 days. The bronzes with low hydrogen contents were stable, but those with high contents were not so stable. All these bronzes have been studied by X-ray diffraction, IR spectroscopy, and TG-DTA. Bronzes with high hydrogen contents were changed upon heating in air, successively, to those with low hydrogen contents by the evolution of H_2.

Hydrogen molybdenum bronzes, H_xMoO_3 ($0<x\leqq2$), are obtained from MoO_3 by reduction in an acidic media[1,2] and hydrogen spillover.[3] Recently, Birtill and Dickens[4] have confirmed four distinct phases in the range $0<x\leqq2$ and their ranges of homogeneity with the approximate limit: Type-I (blue, orthorhombic), $0.23<x<0.4$; Type-II (blue, monoclinic), $0.85<x<1.04$; Type-III (red, monoclinic), $1.55<x<1.72$ and Type-IV (green, monoclinic), $x=2$. Among these phases, Type-I has been characterized by many authors using X-ray diffraction,[4] neutron diffraction,[5] thermal decomposition,[6-8] IR,[9-11] and NMR.[12,13] The catalytic activity for 1-butene isomerization on Type-I was also studied and the effect of hydrogen atoms on catalytic activity has been confirmed.[9] On the other hand, there are several reports on Type-III studied by NMR.[12-14] Its catalytic activity for hydrogenation reaction has been reported.[15,16] However, Type-II and Type-IV have not been characterized completely because of instability.

The authors have studied[6-8] precisely the thermal decomposition of Type-I by vacuum heating and have discussed its decomposition mechanism. We also attempted to study other phases of bronzes. However, it was very difficult to prepare all types of bronze and to isolate them. The purpose of this work was to prepare all phases of hydrogen molybdenum bronzes and to characterize them by X-ray diffraction, IR spectroscopy, and TG-DTA.

Experimental

Preparation of Hydrogen Molybdenum Bronzes. All phases of hydrogen bronzes were obtained by the Glemser's method.[1]

Type-I. 30 g of MoO_3 was suspended in a 2—3 M (mol l^{-1}) HCl aqueous solution at 0—10 °C. 5 g of Zn powder was divided into several portions; about 1 g of Zn powder was introduced every after nascent hydrogen was stopped to generate. When all the Zn powder was consumed the sample was filtrated, and washed with 2—3 M HCl and then water. The sample was blue and the X-ray result was identical with that of Birtill and Dickens.[4] The hydrogen content was determined to be x=0.21 by chemical analysis.[17] Type-I was very stable, even after standing in air for more than six months.

Type-II. It was very difficult to isolate only one phase of Type-II by the Glemser's method.[1] Type-II was obtained from Type-III by standing in air for at least 120 days. The color was blue and the X-ray result was identical to that of Birtill and Dickens.[4] The hydrogen content was x=0.91. This was stable for more than two months.

Type-III. Type-III was prepared from MoO_3 or Type-I by repeating from three to five runs of the same method described above. The color was red and the X-ray result was identical to that of Birtill and Dickens.[4] The hydrogen content was x=1.55. This was stable for about 10 days (Fig. 1). According to X-ray results, Type-II appeared after Type-III had stood in air for at least 11 days; it increased gradually. Type-III was completely transformed to Type-II by 120 days.

Type-IV. Type-IV was prepared from Type-III by repeating one to two runs of the same method. The sample

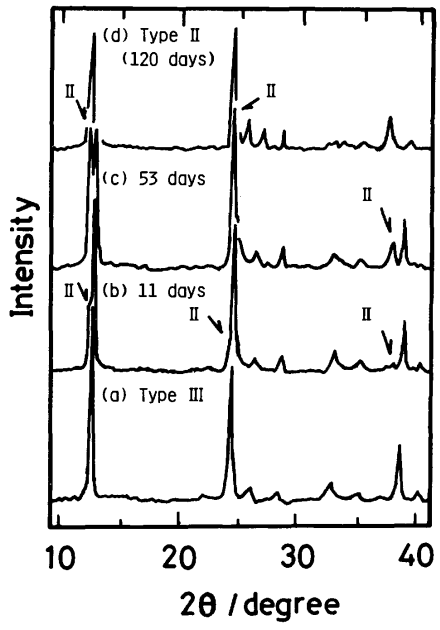

Fig. 1. Changes of X-ray diffraction patterns of Type III by standing in air. (a): Type III (immediately after filtration), (b): stood for 11 days, (c): stood for 53 days, and (d): Type II (stood for 120 days).

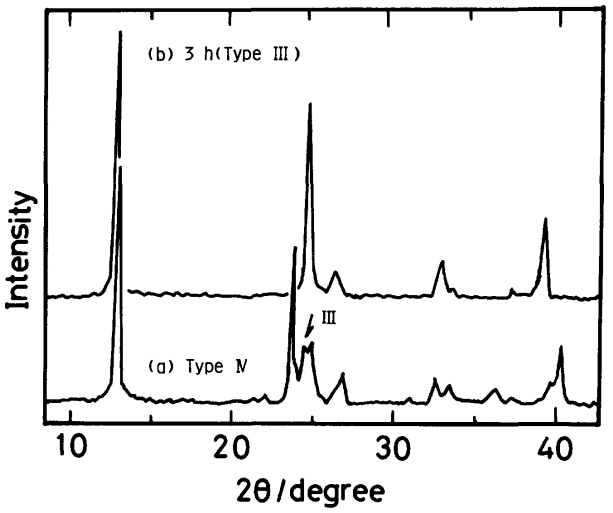

Fig. 2. Changes of X-ray diffraction patterns of Type IV by standing in air. (a): Type IV (immediately after filtration) and (b): stood for 3 h (Type III).

began to decompose immediately after being washed with water and completely transformed to Type-III within three hours (Fig. 2).* However, it kept the Type-IV phase when it was filtrated by a suction filter without washing. Type-IV was green in color and the X-ray result was identical to that of Birtill and Dickens.[4] The hydrogen content was x=1.90. When this sample was left standing in a 2—3 M HCl aqueous solution it kept its monoclinic structure and green color for about seven days.

Characterization of Hydrogen Molybdenum Bronzes. Samples were observed and identified by a powder X-ray diffraction method. IR spectra were obtained by using JASCO 701G and SIMADZU FTIR-4000 spectrophotometers. TG-DTA curves were carried out on a MAC SCIENCE TG-DTA 2000 with a heating rate of 10 K min^{-1}.

The hydrogen contents of hydrogen bronzes were determined chemically by the Choain and Marion's method.[17]

Results and Discussion

Figure 3 shows the IR absorption bands at 1001, 855, 677, 590, 436, and 370 cm^{-1} for Type-I, at 956 and 501 cm^{-1} for Type-II, and at 950, 615, and 450 cm^{-1} for Type-III. The spectrum of Type-IV is nearly the same to that of Type-III. MoO_3 shows bands at 992, 877, 819, 614, 375, and 304 cm^{-1}. By the insertion of hydrogen atoms into the MoO_3 layers, the band at 992 cm^{-1} in MoO_3 shifted to 1001 cm^{-1} in Type-I. The bands at 877 and 819 cm^{-1} decreased in intensity. A small band at 855 cm^{-1} in Type-I with x=0.21 remained, but Type-I with x=0.34 showed no detectable band in this region. The band in this region appeared and gradually increased,[10,11] when Type-I was heated in vacuo. This suggests that the band at 855 cm^{-1} may have been due to a residual MoO_3 framework which is not completely reduced to Type-I. This leads to the conclusion that the insertion of hydrogen atoms causes a rearrangement of octahedron

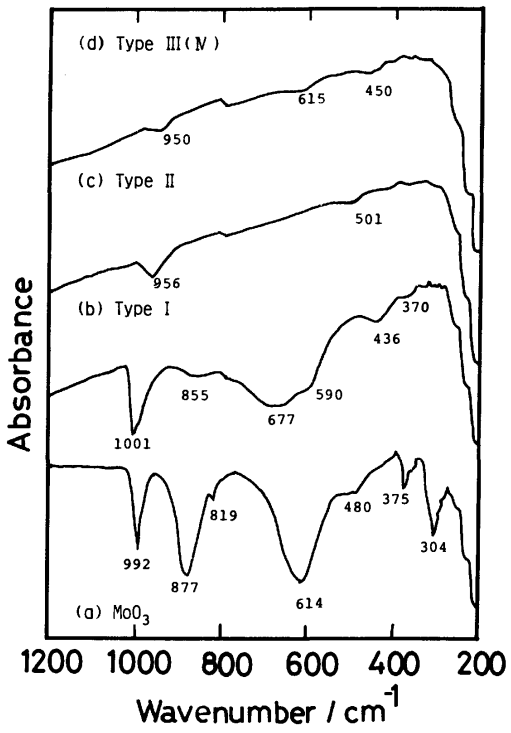

Fig. 3. IR spectra of hydrogen molybdenum bronzes.

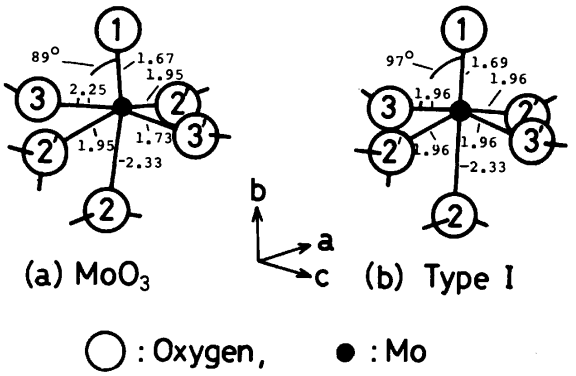

Fig. 4. Schematic model of coordination of oxygen atoms around the molybdenum atom. Unit of numerals is Å.

from the MoO_3 structure to the structure of Type-I (Fig. 4). Berrclough et al.[19] have assigned the band at 992 cm^{-1} to Mo=O(1), that at 877 cm^{-1} to Mo–O(3,3′)–Mo, and that at 819 cm^{-1} to Mo–O(2′)–Mo in MoO_3. On the other hand, Py and Maschke[20] have interpreted the experimental results of MoO_3 by using a modification of the intralayer force constants proposed by Beattie et al.[21] According to their calculation,[20] bands at 877 and 819 cm^{-1} in MoO_3 can be assigned to Mo–O(3,3′)–Mo and the band at 614 cm^{-1}, to Mo–O(2′)–Mo.

According to Kihlborg,[18] a schematic model of the oxygen atoms around a molybdenum atom is shown

in Fig. 4. The bond length in MoO_3 of Mo–O(2′), Mo–O(3), and Mo–O(3′) is 1.95, 2.25, and 1.73 Å, respectively. By insertion of atomic hydrogen into MoO_3, the bond length of Mo–O(3) is shortened to 1.96 Å and that of Mo–O(3′) is lengthened to 1.96 Å. The bond length of Mo–O(2′) and Mo–O(3,3′) become equal in Type-I. The bond length of Mo=O(1) is lengthened from 1.67 Å in MoO_3 to 1.69 Å in Type-I. The bond angle of O(1)–Mo–O(3) changes from 87° in MoO_3 to 97° in Type-I.

It has been reported[9,12,13] that a hydrogen atom connects with terminal oxygen (Mo=O(1)). This suggests that the bond strength of a doubly bonded terminal Mo=O(1) may be weakened; this may cause a shift to lower frequencies. In fact, a shift from 998 to 1001 cm^{-1} takes place. This result is not understandable in terms of the bond strength; other effects should possibly be considered. No large change in the bond length has been observed between MoO_3 and Type-I, while the bond angle of O(1)–Mo–O(3) changes upon the insertion of hydrogen atoms as mentioned above. The change of this bond angle may effect the stretching vibration of Mo=O(1). According to Py and Maschke,[20] the band at 614 cm^{-1} in MoO_3 has been assigned to Mo–O(2′)–Mo with a bond length of 1.95 Å. The bond length of Mo–O(2′,3,3′) in Type-I is 1.96 Å; this is very similar to that of Mo–O(2′)–Mo in MoO_3. Therefore, the band at 677 cm^{-1} in Type-I should be due to Mo–O(2′,3,3′)–Mo.

In the range of Mo–O stretching vibration, Type-II and Type-III(IV) show bands at 956 and 950 cm^{-1}, respectively. The band at 1001 cm^{-1} in Type-I shifts to lower frequencies. This is reasonable because Type-II and Type-III(IV) contain more hydrogen atoms than Type-I; a difference in the structure exists between Type-I (orthorhombic) and Type-II, Type-III, and Type-IV (monoclinic). These hydrogen atoms also attach to terminal oxygen and the bond strength of Mo=O(1) is weakened. The authors are studying by NMR the bahavior of hydrogen atoms in all phases. Considering the NMR results, a precise assignment of the band in Type-II and Type-III(IV) will be reported elsewhere.

Figure 5 shows TG-DTA curves of hydrogen molybdenum bronzes. [U] indicates an unwashed sample which was filtrated and immediately sucked dry. [W] indicates a sample washed with 2—3 M HCl, then washed with water and sucked dry. [U] of Type-I shows an exothermic peak at 263.6 °C and an endothermic peak at 709.4 °C. While [W] of Type-I shows the exothermic peak at 148.6 °C. The exothermic peak of [W] is lower than that of [U]. Each

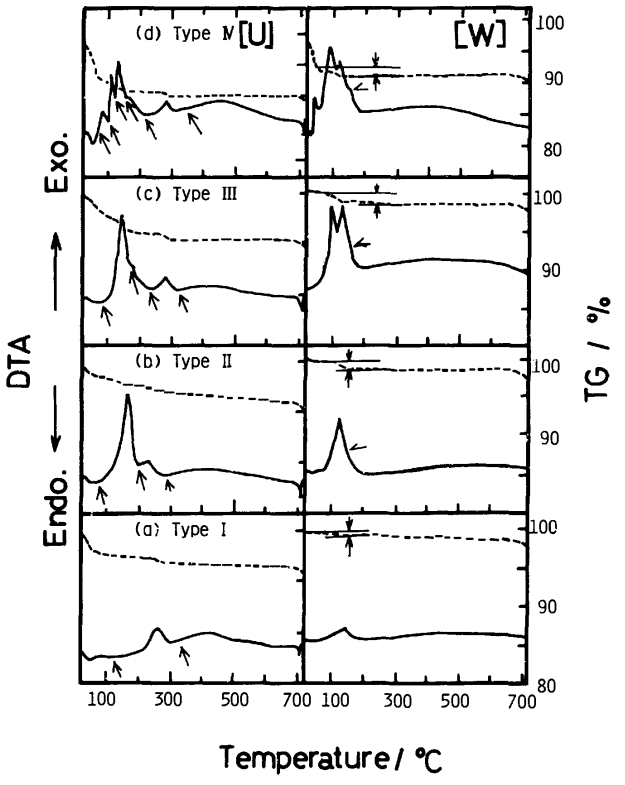

Fig. 5. TG-DTA curves of hydrogen molybdenum bronzes.
—: DTA, – – – –: TG; [U]: unwashed, and [W]: washed with water.

Table 1. Peak Temperature of DTA Curves and Composition of Bronze at Each Stage

Type	Peak temperature/°C [U]	[W]	Composition
I	709.4		MoO_3
	263.6 ----	148.6	----------
			Type I
II	712.1		MoO_3
	221.5 ----	156.6	----------
			Type I
	158.5 ----	130.0	----------
			Type II
III	712.8		MoO_3
	279.4 ----	151.1	----------
			Type I
	159.5 ----	131.4	----------
			Type II
	136.8 ----	99.3	----------
			Type III
IV	712.2		MoO_3
	275.2 (152.1) ----	151.9	----------
			Type I
	126.7 ----	123.0	----------
			Type II
	100.4 ----	91.0	----------
			Type III
	75.7 ----	47.2	----------
			Type IV

[U] of all phases of hydrogen bronzes show an endothermic peak at near 710 °C; [W] does not. Exothermic peaks of all phases of [U] arise at higher temperature than those of [W]. All peak temperatures are shown in Table 1. DTA curves of [U] give more distinct separate peaks than those of [W]. According to chemical analysis, [U] contains a small amount of residual Zn^{2+} and Cl^- ions, and [W], no residual ion. However, according to the X-ray results and chemical analysis, there are no difference in crystal structure and hydrogen contents between [U] and [W]. This suggests that the endothermic peak at near 710 °C and the exothermic peaks at higher temperature of [U] should be due to residual ions.

As has been reported[6,7] Type-I is decomposed by vacuum heating to the nonstoichiometric oxide with the rhombic MoO_3 structure by evolution of H_2O.

$$H_{0.30}MoO_3 \longrightarrow H_{0.21}MoO_{2.95}{}^{22)}$$

$$\longrightarrow H_{0.06}MoO_{2.88}{}^{23)} \longrightarrow MoO_{2.85}{}^{23)}$$

It is very important to know the decomposition of bronzes in air. As mentioned above, there are no differences in the crystal structure and hydrogen contents between [U] and [W]; however, [U] gives more distinct exothermic peaks than does [W]. Type-I treated at about 150 °C shows the original orthorhombic crystal structure, but that treated at about 330 °C shows the rhombic MoO_3 structure. The compositions of all phases heated at the temperature before and after exothermic peaks (marked by arrows (⟶) in Fig. 5) are shown in Table 1. This result suggests that the hydrogen molybdenum bronze changes successively from a bronze with a higher hydrogen content to one with a lower hydrogen content upon heating: Type-IV⟶Type-III⟶Type-II⟶Type-I⟶MoO_3.

The weight loss of samples can be calculated from TG curves. [U] gives a clear phase separation, though it contains a small amount of residual Zn^{2+} and Cl^- ions. It is therefore not reasonable to obtain gravimetric results. The total weight losses are obtained from the TG results of [W] by substracting the adsorbed water molecules (Table 2). Under vacuum heating, the decomposition of Type-I takes place by an evolution of H_2O. Usually, the decomposition of a bronze can occur by the following two ways.

$$H_xMoO_3 \longrightarrow \frac{x}{2} H_2 + MoO_3 \quad (1)$$

and

$$H_xMoO_3 \longrightarrow \frac{x}{2} H_2O + MoO_{3-x/2} \quad (2)$$

The weight loss can be lead to the conclusion if the decomposition should proceed by Eq. 1 or 2. Since the hydrogen contents of Type-I, Type-II, Type-III, and Type-IV were determined to be x=0.21, 0.91, 1.55, and 1.90, respectively, the theoretical weight losses were calculated from the above equations (Table 2). Comparing these results, the observed weight loss from TG is very close to the theoretical weight loss calculated from Eq. 1. This means that the bronzes decompose upon heating in air by the evolution of H_2. DTA and X-ray results also support the idea that the decomposition of bronzes change from a higher hydrogen content to a lower hydrogen content. It is therefore reasonable to conclude that the bronzes decompose in air through Eq. 1 as follows:

Table 2. Weight Loss of Bronzes

x	Weight loss/%		
	H_2	H_2O	Observed
0.21	0.15	1.31	0.40
0.91	0.63	5.65	0.89
1.55	1.06	9.59	1.38
1.90	1.30	11.73	1.29

$$\text{Type IV} \xrightarrow[\text{ca. 47 °C}]{H_2\uparrow} \text{Type III} \xrightarrow[\text{ca. 91—99 °C}]{H_2\uparrow} \text{Type II}$$

$$\xrightarrow[\text{ca. 123—131 °C}]{H_2\uparrow} \text{Type I} \xrightarrow[\text{ca. 149—157 °C}]{H_2\uparrow} MoO_3$$

Precise thermal studies are in progress.

References

1) O. Glemser and G. Lutz, *Z. Anorg. Allg. Chem.*, **264**, 17 (1951).

2) R. Schöllhorn, R. Kuhlman, and J. O. Besenhard, *Mat. Res. Bull.*, **11**, 83 (1976).

3) G. C. Bond and J. B. P. Tripathi, *Trans. Faraday Soc.*, **72**, 933 (1976).

4) J. J. Birtill and P. G. Dickens, *Mat. Res. Bull.*, **13**, 311 (1978).

5) P. G. Dickens, J. J. Birtill, and C. J. Wright, *J. Solid State Chem.*, **28**, 185 (1979).

6) N. Sotani, M. Kunitomo, and M. Hasegawa, *Chem. Lett.*, **1983**, 647.

7) N. Sotani, N. Yoshida, Y. Kawamoto, S. Kishimoto, and M. Hasegawa, *Bull. Chem. Soc. Jpn.*, **57**, 3032 (1984).

8) N. Sotani, Y. Kawamoto, and M. Inui, *Mat. Res. Bull.*, **18**, 797 (1983).

9) F. A. Schröder and Weitzel, *Z. Anorg. Allg. Chem.*, **435**, 247 (1977).

10) N. Sotani, N. Yoshida, Y. Yosioka, and S. Kishimoto, *Bull. Chem. Soc. Jpn.*, **58**, 1626 (1985).

11) T. Ohno, H. Miyata, F. Hatayama, and N. Sotani, *Bull. Chem. Soc. Jpn.*, **60**, 3435 (1987).

12) R. C. T. Slade, T. K. Halstead, and P. G. Dickens, *J. Solid State Chem.*, **34**, 183 (1980).

13) Cl. Ritter, W. Müller-Warmuth, and R. Schöllhorn, *J.*

Chem. Phys., **83**, 6130 (1985).
14) R. E. Tayler, M. M. Silva Crawfrd, and B. C. Gerstein, *J. Catal.*, **62**, 401 (1980).
15) P. A. Sermon and G. C. Bond, *J. Chem. Soc., Faraday Trans. 1*, **76**, 889 (1980).
16) J. P. Marcq, X. Wispenninckx, G. Poncelet, D. Krevis, and J. J. Fripiat, *J. Catal.*, **73**, 309 (1982).
17) C. Choain and F. Marion, *Bull. Soc. Chim. Fr.*, **1963**, 212.
18) L. Kihlborg, *Arkiv Kem.*, **21**, 357 (1963).
19) C. G. Berrclough, J. Lewis, and R. S. Nyholm, *J. Chem. Soc.*, **1959**, 3552.
20) M. A. Py and K. Mashk, *Physica*, **105B**, 370 (1981).
21) I. R. Beattie, N. Cheetham, M. Gardner, and D. E. Rogers, *J. Chem. Soc. A*, **1971**, 2240.
22) Type I, orthorhombic bronze, with the lowest hydrogen content.
23) Isomorphous with the rhombic MoO_3 structure.

Dielectric Dispersion and Intermolecular Association for 28 Pure Liquid Alcohols. The Position Dependence of Hydroxyl Group in the Hydrocarbon Chain

Toshiomi SHINOMIYA†
School of Pharmaceutical Sciences, Kitasato University,
Shirokane, Minato-ku, Tokyo 108
(Received September 10, 1988)

The dielectric constants and losses of 28 linear alcohols, 1-alkanol (n=3—10), 2-alkanol (n=3—10), 3-alkanol (n=5—10), 4-alkanol (n=7—10), and 5-alkanol (n=9 and 10), have been measured at the frequencies from 1.35 to 4500 MHz at 15, 25, and 35 °C. The Kirkwood-Fröhlich equation was modified so that it could be applied to each dispersion region calculated. The concentration C_1 of linear hydrogen-bonded chain polymers, which primary dispersion originates, was evaluated by means of this modified equation. The C_1 decreases as the hydroxyl group approaches the center of a molecule, except for propanols and butanols, and also decreases with increasing temperature. For isomeric decanols, for example, the percentages of C_1 ($C_1 \times 100/C_0$) against alcohol gross stoichiometric concentration C_0 at 15, 25, and 35 °C are about 71, 63, and 53% for 1-decanol, 52,40,and 29% for 2-decanol, 22, 17, and 12% for 3-decanol, 11, 7, and 6% for 4-decanol, and 8, 6, and 5% for 5-decanol, respectively. The thermodynamic parameters, ΔF^*, ΔH^*, and ΔS^*, were obtained for dipole relaxation and viscous flow. The $\Delta F\tau^*$ decreases, although the $\Delta H\tau^*$ and $\Delta S\tau^*$ increase, as the hydroxyl group approaches the center of a molecule. The $\Delta F\eta^*$ increases linealy with the molecular volume, irrespective of the position of the hydroxyl group.

The liquid structure of alcohols has been the subject of many investigations because of its having a possible hydrogen bonding between adjacent molecules. Studies of the dielectric relaxation processes[1-3] have estimated the existence of monomers and hydrogen-bonded molecular species in pure liquid alcohols. The magnitude of the primary dispersion is usually much greater than that of the higher dispersion. Its relaxation time is long and strongly temperature dependent. Therefore, this process is considered to be attributed to the characteristic of linear hydrogen-bonded chain polymers.[2-4] A clear detailed molecular model has, however, still not been realized. It is interesting to investigate relationship between the magnitude of primary dispersion and molecular geometry. In isomeric alcohols, the magnitude of dispersion may depend on the positions of the hydroxyl and methyl groups in a chain. It is considered that any difference in their dielectric behaviors must be due entirely to a difference in the extent of intermolecular association, since these isomers have approximately the same dipole moment and the same molecular volume. The formation of a linear hydrogen-bonded chain polymer changes according to the amount of shielding of the hydroxyl group and/or to the steric hindrance of the alkyl group. In the present study, therefore, 28 pure alcohols were selected to investigate the influences due to the position of the hydroxyl group in a chain.

Wide-range measurements indicated two or three different dispersion regions at low temperature and room temperature.[2-6] No theory can satisfactorily interpret the co-existence of the two or three dispersion regions observed. Experimental data concerning the dielectric dispersion for water and liquid alcohols have usually been analyzed by means of Kirkwood-Fröhlich theory,[7-9] which was developed on the basis of a single relaxation process. This theory can not interpret the large value of the Kirkwood correlation factor. Although this equation is still used to obtain information concerning the configuration for neighboring dipole moments, there are doubtful problems in the application of this equation to data of the dielectric dispersion for liquid alcohols. Their equation was, therefore, modified; then the concentration of the primary dispersion region was calculated.

Experimental

Purification of Materials. The commercial alcohols were fractionally distilled under reduced pressure at a very high reflux ratio. About 80% of the middle fraction was distilled again by the same method. Two distillation systems were used, one consisting of a 1 m adiabatic column packed with glass-helix packings and the other consisting of a 60 cm adiabatic column with a Teflon spinning band with a rotation speed variable from 1000 to 6000 rpm. Both systems have 200—300 theoretical plates. A Molecular Sieve of 3A or 5A was used as a drying agent. The middle portion was finally distilled in a grease-free apparatus under reduced pressure before use.

Apparatus. The dielectric constants and losses were measured by making use of the following three types of apparatus over the frequency range from 1.35 to 4500 MHz.

Low Frequency Range: A Boonton Radio RX meter (Type 250A) was used for measurements at frequencies of 1.35, 6.3, 17, 30, and 45 MHz. An adaptor (GR 900-QNP) and a T-type adaptor (which is joined to an inductor) were put between a cell and a terminal of RX meter's bridge. The necessary corrections of coaxial transmission line were made

† Present address: 207-52, Shirahata kami-cho, Kanagawa-ku, Yokohama 221.

according to the transmission line formulas by the use of the terminations (Type GR 900-W50, GR 900-W200, and GR 900-WO4) and the reference air lines (Type GR 900-LZ) as standard equipments. Two dielectric cells were carefully made of a GR Precision Inner-Conductor Rod, an Outer-Conductor Tube, and a GR 900-BT connector. The temperature of the cell was kept constant within ±0.1 °C of the specified values by circulation of water from a thermostat through a jacket around the cell.

Middle Frequency Range: Measurements at frequencies 60, 80, 100, 150, 200, 250, 300, 400, and 480 MHz were made with a Hewlet-Packard VHF Bridge which comprised a VHF Signal Generator (Model 608C), a VHF Detector (Model 417A), a VHF Bridge (Model 803A), an SWR meter (415E), and a frequency counter. This apparatus was described in detail by Komooka.[10] The frequencies of the RX meter and VHF Bridge were controlled to be within ±0.01% of the specified values.

High Frequency Range: A General Radio Precision Slotted Line (Type 900-LB) was used for measurements at frequencies of 600, 750, 1000, 1400, 2000, 3000, and 4500 MHz. This equipment has a slotted section of 9/16-inch and is a precision coaxial transmission line with a characteristic impedance of 50.0 ohm±0.1%. The signal sources were a Modulating Power Supply (Type 1264-B) and a VHF Oscillator (Type 1362), a Modulating Power Supply (Type 1264-B) and a Lockable Oscillator (Type 1218-BV), and a HP Signal Generator (Type 8616A). The line was fitted with a movable carriage which provides a mount for a detector diode, a tuning stub, an adjustable probe, and a Type 874 output connector which was connected with an SWR meter (415E). Two cells were identical to those used in the measurement of the low-frequency range described above.

Calculation of Dielectric Parameters. In general, the dielectric constant ε' and loss ε'' are described by

$$\varepsilon_j' = \varepsilon_\infty + \sum_{i=1}^{n}\left(\frac{\varepsilon_{i-1}-\varepsilon_i}{2}\left(1-\frac{\sinh\theta_i}{\cosh\theta_i+\sin\left(\frac{\pi}{2}h_i\right)}\right)\right)$$

and

$$\varepsilon_j'' = \sum_{i=1}^{n}\left(\frac{\varepsilon_{i-1}-\varepsilon_i}{2}\left(\frac{\cos\left(\frac{\pi}{2}h_i\right)}{\cosh\theta_i+\sin\left(\frac{\pi}{2}h_i\right)}\right)\right),$$

where ε_∞ is the limiting high-frequency dielectric constant. $\theta_i=(1-h_i)\ln(f_j/fr_i)$. h_i is constant, $0\leqq h_i<1$. When $0<h_i<1$, the dispersion is a Cole–Cole like, depressed-center semicircular arc. In the limit $h_i=0$, it reduces to a Debye-like, semicircular arc. $\varepsilon_{i-1}-\varepsilon_i$ is a magnitude and fr_i is a relaxation frequency of the i-th dispersion. ε_j' and ε_j'' are experimental values at frequency f_j. The dielectric parameters were calculated by the equations with the least-squares method.

Results and Discussion

Dielectric Relaxation. The Cole–Cole plots are shown in Fig. 1 for isomeric pentanols and in Fig. 2 for isomeric decanols, respectively. Primary dispersion is quantitatively described by a Debye-like semicircular arc, though it is also evident that the data

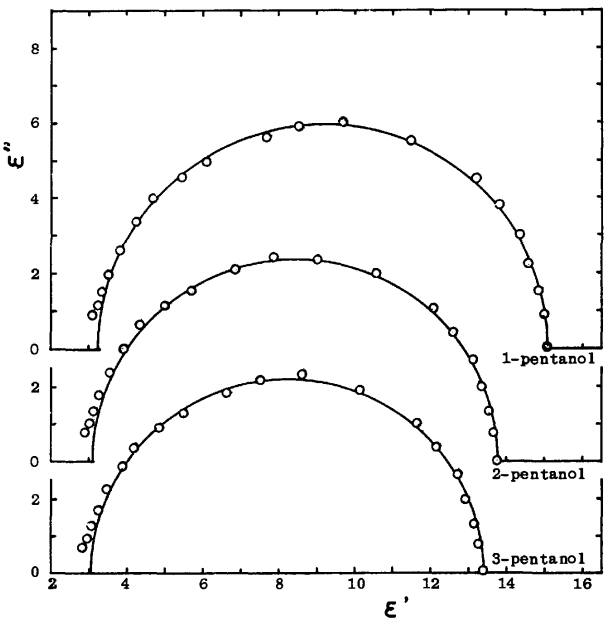

Fig. 1. Cole–Cole plots for isomeric pentanols at 25 °C.

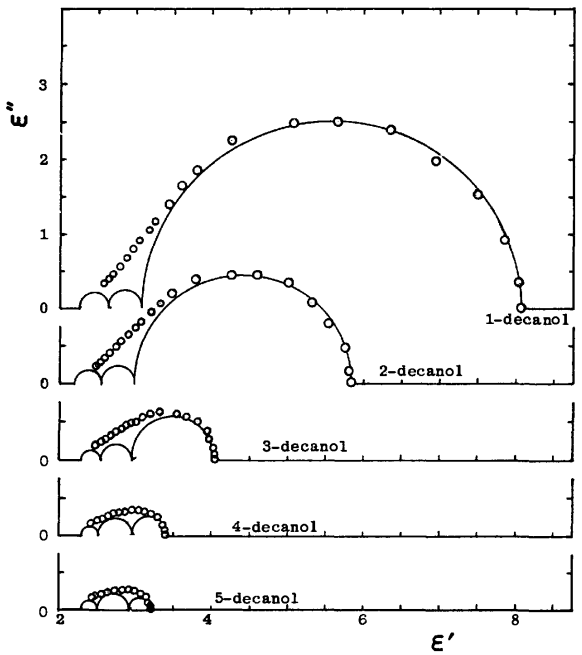

Fig. 2. Cole–Cole plots for isomeric decanols at 25 °C, together with calculated behavior for the three dispersion regions.

can not be satisfactorily fitted in the high-frequency region of the dispersion. At first glance it looks as if the Cole–Cole plots can be grouped into three dispersion types. The first one is best described by several overlapping Debye-like semicircular arcs, $\varepsilon^*-\varepsilon_\infty=(\varepsilon_0-\varepsilon_\infty)/(1+i\omega\tau)$, such as isomeric pentanols in Fig. 1 and 1-decanol in Fig. 2. The second one by Davidson–Cole skewed arc, $\varepsilon^*-\varepsilon_\infty=(\varepsilon_0-\varepsilon_\infty)/(1+(i\omega\tau))^\beta$,

Table 1. Dielectric Parameters, Refractive Indices, Densities, and Viscosities

Compound	ε_0	ε_1	fr / MHz	n_D	d / g cm^{-3}	$\eta\times10^3$ / N s m^{-2}
			15°C			
1-Propanol	21.77	3.78	322	1.3878	0.8075	2.52
1-Butanol	18.81	3.56	204	1.4015	0.8132	3.40
1-Pentanol	16.24	3.39	142	1.4120	0.8185	4.71
1-Hexanol	14.18	3.28	104	1.4201	0.8219	6.31
1-Heptanol	12.48	3.20	80.0	1.4262	0.8252	8.48
1-Octanol	10.98	3.12	65.8	1.4314	0.8282	11.04
1-Nonanol	9.80	3.08	55.0	1.4357	0.8306	14.17
1-Decanol	8.78	3.03	48.2	1.4392	0.8328	17.84
2-Propanol	20.99	3.53	273	1.3807	0.7890	2.85
2-Butanol	18.42	3.29	169	1.3994	0.8105	4.65
2-Pentanol	15.46	3.16	120	1.4087	0.8131	5.27
2-Hexanol	12.51	3.06	94.5	1.4171	0.8173	6.61
2-Heptanol	10.48	3.00	74.5	1.4233	0.8195	8.41
2-Octanol	8.84	2.98	62.0	1.4284	0.8233	10.84
2-Nonanol	7.53	2.90	53.1	1.4329	0.8261	13.80
2-Decanol	6.59	2.86	46.7	1.4366	0.8285	17.26
3-Pentanol	15.38	3.02	105	1.4128	0.8240	8.35
3-Hexanol	11.35	2.99	84.6	1.4186	0.8227	8.80
3-Heptanol	7.72	2.95	80.7	1.4243	0.8243	9.17
3-Octanol	5.92	2.93	73.2	1.4289	0.8264	10.82
3-Nonanol	4.75	2.87	67.1	1.4332	0.8287	13.27
3-Decanol	4.22	2.79	58.4	1.4366	0.8302	16.46
4-Heptanol	6.58	2.98	86.4	1.4223	0.8209	9.23
4-Octanol	4.35	2.88	93.8	1.4271	0.8226	11.10
4-Nonanol	3.66	2.76	88.3	1.4314	0.8250	13.48
4-Decanol	3.36	2.71	76.7	1.4352	0.8272	16.27
5-Nonanol	3.48	2.78	94.1	1.4315	0.8252	14.98
5-Decanol	3.16	2.68	86.3	1.4350	0.8272	18.13
			25°C			
1-Propanol	20.44	3.64	474	1.3833	0.7991	1.95
1-Butanol	17.54	3.44	314	1.3973	0.8057	2.59
1-Pentanol	15.10	3.37	223	1.4082	0.8115	3.51
1-Hexanol	13.12	3.27	169	1.4162	0.8148	4.57
1-Heptanol	11.53	3.23	133	1.4225	0.8186	5.97
1-Octanol	10.11	3.19	112	1.4276	0.8214	7.63
1-Nonanol	9.00	3.17	94.5	1.4319	0.8241	9.59
1-Decanol	8.03	3.10	84.3	1.4352	0.8260	11.74
2-Propanol	19.41	3.43	438	1.3753	0.7808	2.08
2-Butanol	16.72	3.28	301	1.3950	0.8025	3.10
2-Pentanol	13.78	3.23	226	1.4044	0.8053	3.46
2-Hexanol	11.06	3.16	179	1.4129	0.8096	4.22
2-Heptanol	9.25	3.11	144	1.4191	0.8131	5.33
2-Octanol	7.80	3.11	116	1.4245	0.8160	6.75
2-Nonanol	6.66	3.06	104	1.4290	0.8190	8.43
2-Decanol	5.82	2.99	94.1	1.4326	0.8212	10.42
3-Pentanol	13.38	3.20	218	1.4081	0.8155	4.69
3-Hexanol	9.66	3.17	180	1.4143	0.8144	4.90
3-Heptanol	6.71	3.15	169	1.4202	0.8160	5.38
3-Octanol	5.35	3.13	146	1.4250	0.8188	6.47
3-Nonanol	4.49	3.06	127	1.4293	0.8213	8.00
3-Decanol	4.05	2.96	113	1.4329	0.8229	9.80
4-Heptanol	5.85	3.16	172	1.4182	0.8120	5.47
4-Octanol	4.24	3.13	204	1.4232	0.8153	6.74

Table 1. (Continued)

Compound	ε_0	ε_1	fr / MHz	n_D	d / g cm^{-3}	$\eta\times10^3$ / N s m^{-2}
4-Nonanol	3.69	3.09	175	1.4275	0.8179	8.16
4-Decanol	3.42	3.00	141	1.4314	0.8202	9.82
5-Nonanol	3.54	2.99	200	1.4277	0.8181	8.95
5-Decanol	3.24	2.91	161	1.4312	0.8201	10.84
			35 °C			
1-Propanol	19.17	3.46	699	1.3792	0.7914	1.54
1-Butanol	16.38	3.40	470	1.3934	0.7979	2.00
1-Pentanol	14.04	3.36	351	1.4042	0.8039	2.63
1-Hexanol	12.11	3.35	276	1.4124	0.8080	3.40
1-Heptanol	10.57	3.33	217	1.4186	0.8117	4.34
1-Octanol	9.27	3.37	186	1.4239	0.8149	5.46
1-Nonanol	8.22	3.23	162	1.4282	0.8171	6.69
1-Decanol	7.33	3.25	144	1.4317	0.8195	8.11
2-Propanol	17.91	3.35	682	1.3708	0.7722	1.54
2-Butanol	15.09	3.28	507	1.3909	0.7938	2.15
2-Pentanol	12.28	3.28	400	1.4002	0.7969	2.35
2-Hexanol	9.76	3.25	340	1.4088	0.8018	2.89
2-Heptanol	8.20	3.27	283	1.4157	0.8054	3.57
2-Octanol	7.03	3.25	248	1.4205	0.8084	4.46
2-Nonanol	5.95	3.27	218	1.4249	0.8115	5.57
2-Decanol	5.30	3.23	193	1.4286	0.8143	6.78
3-Pentanol	11.61	3.27	429	1.4037	0.8067	2.82
3-Hexanol	8.24	3.25	389	1.4098	0.8061	3.05
3-Heptanol	6.03	3.24	392	1.4158	0.8085	3.49
3-Octanol	5.01	3.22	362	1.4208	0.8112	4.20
3-Nonanol	4.33	3.17	323	1.4252	0.8138	5.20
3-Decanol	3.98	3.17	295	1.4286	0.8157	6.30
4-Heptanol	5.41	3.25	412	1.4139	0.8050	3.50
4-Octanol	4.20	3.25	463	1.4191	0.8078	4.37
4-Nonanol	3.72	3.15	439	1.4235	0.8104	5.27
4-Decanol	3.45	3.10	404	1.4274	0.8130	6.33
5-Nonanol	3.59	3.08	513	1.4235	0.8106	5.71
5-Decanol	3.31	3.01	543	1.4272	0.8129	6.88

such as 3-decanol in Fig. 2. The third one by Cole–Cole depressed-center semicircular arc, $\varepsilon^*-\varepsilon_0=(\varepsilon_0-\varepsilon_\infty)/(1+(i\omega\tau)^\alpha)$, such as 5-decanol in Fig. 2. ε^* is the complex dielectric constant, ε_0 and ε_∞ are the limiting low- and high-frequency dielectric constants, ω is the angular frequency, τ the relaxation time, and α and β are parameters, $0<\alpha$ or $\beta<1$. However, the loci of these compounds are temperature dependent and will change probably from a Debye type to a Davidson–Cole type or a Cole–Cole type by a decrease in the magnitude of the primary dispersion region in comparison with those of other dispersion regions. We assumed, therefore, that the dielectric absorption for each compound was the sum of several overlapping Debye-like dispersion regions. The dielectric parameters of the primary dispersion calculated are listed in Table 1, together with refractive indices, densities, and with viscosities.

The magnitude, $(\varepsilon_0-\varepsilon_1)T/C_0$, of primary dispersion region is plotted in Fig. 3 against the alcohol gross concentration C_0. T is the absolute temperature. Figure 3 shows that the curves from 1-propanol to 1-decanol and from 2-propanol to 2-decanol indicate a maximum at about 11 mol dm^{-3}, in the vicinity of butanols, respectively. The dielectric properties of higher alcohols (at lower alcohol concentration than the maximum) are often different with those of lower alcohols (such as propanols and butanols). For higher alcohols, the value of the magnitude decreases with decreasing alcohol concentration and becomes extremely small as the hydroxyl group approaches the center of a molecule. The magnitude of 5-decanol is 13 K mol^{-1} dm^3, being about 5% of that of 1-decanol. These isomers differ remarkably from each other in the average value of magnitude per one hydroxyl group. The difference leads us to anticipate that the magni-

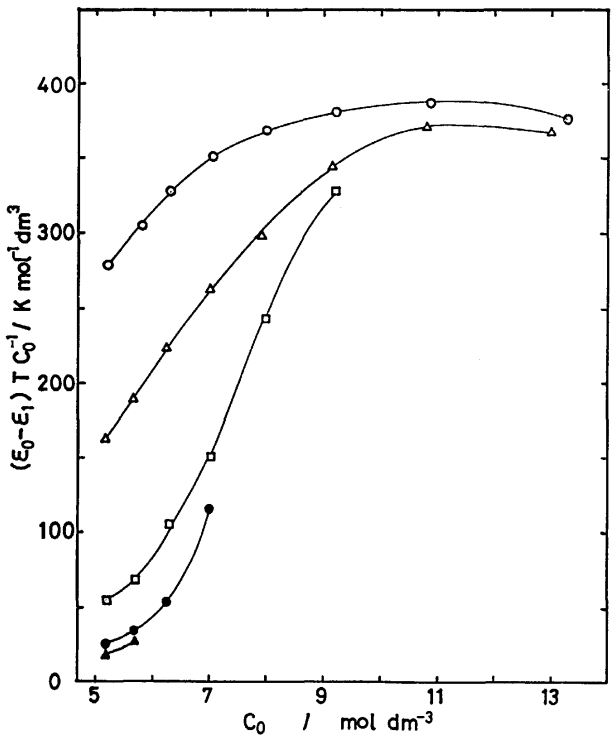

Fig. 3. The magnitude of primary dispersion region as a function of alcohol gross concentration C_0 at 25 °C.
○: 1-propanol-1-decanol, △: 2-propanol-2-decanol, □: 3-pentanol-3-decanol, ●: 4-heptanol-4-decanol, ▲: 5-nonanol and 5-decanol.

tude is intimately related to the extent of hydrogen bonding and to the existence of a nonpolar cyclic polymer. It is desired to examine the equilibrium between linear chain polymers and nonpolar cyclic polymers.

Concentration of Primary Dispersion Region. Experimental data concerning the dielectric dispersion have usually been analyzed by means of the Kirkwood-Fröhlich equation:[8,9]

$$\varepsilon_0 - n_D^2 = \frac{3\varepsilon_0}{2\varepsilon_0 + n_D^2} = \left(\frac{n_D^2+2}{3}\right)^2 \frac{4\pi N_0 \mu_0^2}{3kT} g, \quad (1)$$

where n_D is the refractive index, N_0 the number of molecule per unit volume, and μ_0 the dipole moment of the molecule in vacuum. From Eq. 1, in which 1.05 n_D^2 was used in place of n_D^2,[11] the Kirkwood correlation factors g were calculated to be 3.14, 3.19, 3.15, 3.07, 2.97, 2.83, 2.70, and 2.56 at 25 °C for pure normal alcohols from propyl through decyl, respectively. These g factors are much greater than 2.39 obtained by Oster and Kirkwood[8,12] for a model of an infinite hydrogen-bonded chain of alcohol molecules with free rotation about the hydrogen bonds. For isomeric decanols at 25 °C, the respective g factors are 2.56 for 1-decanol, 1.77 for 2-decanol, 1.00 for 3-decanol, 0.70 for 4-decanol, and 0.62 for 5-decanol. The observation that the g factor is less than unity has been interpreted as being due to an antiparallel alignment of near-neighbor dipole moments. The g factor increases with decreasing temperature and becomes 4.7 for an infinitely long chain of 6-methyl-3-heptanol at a very low temperature.[11] The large values of the g factor can not be interpreted satisfactorily for liquid alcohols. Dannhauser[13] proposed a partial hindrance of the rotation in place of the free rotation about the hydrogen bonds described in the Kirkwood model.[8] We believe that the large value of the g factor is attributed to the value of 1.05 n_D^2 which is usually less than the limiting high-frequency dielectric constant and that a concentration factor should be introduced instead of the molecular volume into the Kirkwood-Fröhlich equation[8,9] in the same manner that the existence of a nonpolar cyclic polymer is considered when the g factor is less than unity. If their equation is applied to the data of liquid alcohols, we must take care concerning the following four points: 1) The dispersion of liquid alcohols can be resolved into some overlapping relaxation processes; 2) therefore, the choice of n_D^2 must be corrected for each dispersion region calculated; 3) alcohol molecules must be assigned to each dispersion region; and 4) if nonpolar cyclic polymers exist, their concentrations must be neglected in order to not contribute to the dispersion. According to the Kirkwood-Fröhlich theory, therefore, we propose that the cavity field G inside a spherical cavity with dielectric constant ε_i instead of the n_D^2 must be replaced by $G=3\varepsilon_0 E/(2\varepsilon_0+\varepsilon_i)$. E is the macroscopic field. The dipole moment μ in the Kirkwood equation can be expressed by making use of the vacuum moment μ_0 for a spherical molecule as follows: $\mu=(\varepsilon_i+2)\mu_0/3$. In order to apply the Kirkwood-Fröhlich equation to the some overlapping dispersion regions, this equation was modified as follows:

$$\varepsilon_{i-1} - \varepsilon_i = \frac{3\varepsilon_{i-1}}{2\varepsilon_{i-1}+\varepsilon_i}\left(\frac{\varepsilon_i+2}{3}\right)^2 \frac{4\pi N_A \mu_0^2}{3\times 10^3 kT} C_i g_i. \quad (2)$$

Where

$$C_0 = \sum_{i=1}^{k} C_i + C_{ring}, \quad (3)$$

$$g = 1, \text{ if } n = 1 \text{ and } g = 1 + Z\sum_{m=2}^{n} f(\cos^2\frac{\theta}{2})^{m-1}, \text{ if } n \geqq 2, \quad (4)$$

$$f = \frac{(\mu_H + \mu_R)(\mu_H + \mu_R\cos\theta)}{\mu_H^2 + \mu_R^2 + 2\mu_H\mu_R\cos\theta}.$$

In this equations, ε_{i-1} and ε_i are the limiting low- and high-frequency dielectric constants of the i-th dispersion, N_A Avogadro's number, C_0 the gross stoichiometric concentration in mol dm^{-3} of all alcohol molecules, C_i the alcohol concentration which the i-th

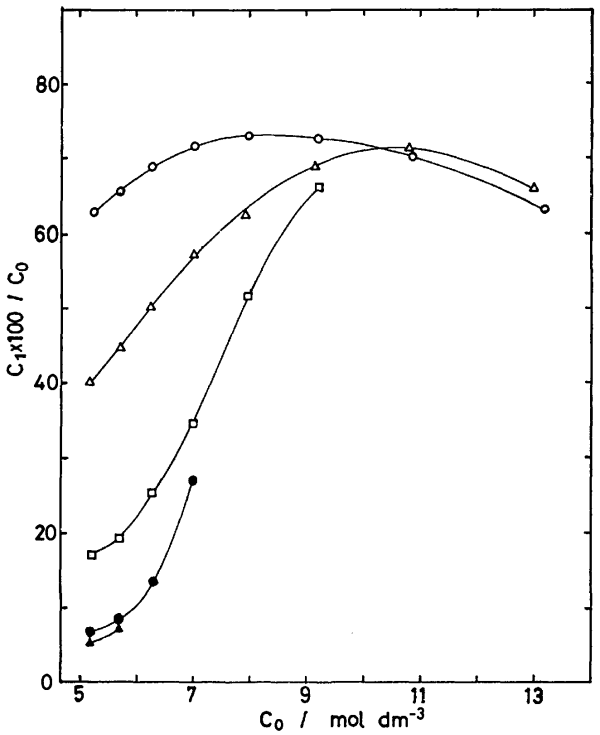

Fig. 4. The concentration (%) of primary dispersion region as a function of alcohol gross concentration C_0 at 25 °C.
○: 1-propanol-1-decanol, △: 2-propanol-2-decanol, □: 3-pentanol-3-decanol, ●: 4-heptanol-4-decanol, ▲: 5-nonanol and 5-decanol.

dispersion originates, C_{ring} that of a nonpolar cyclic polymer, and Z the coordination number. Additionally, μ_H and μ_R are the components of the dipole moment of alcohol molecule ROH along the O–H and O–R bonds, respectively, θ is the angle between O–H and O–R bonds, m represents m-th molecule, and n is the number of alcohol molecule in the linear chain polymer. It was assumed in Eqs. 2—4 that Z=2, μ_H=1.53 D, μ_R=1.20 D, μ_0=1.68 D, and θ=105° for the liquid alcohols investigated. The g_1 of the primary dispersion was calculated from Eq. 4, as being 1.87 if n=2, 2.31 if n=4, and 2.38 if n is greater than 6, respectively. If g_1 is assumed to be 2.38, the concentration of C_1 which the primary dispersion region originates can be calculated from Eq. 2 by making use of the experimental values of ε_0 and ε_1. The percentage of C_1, $C_1 \times 100/C_0$, against the gross stoichiometric concentration is shown in Fig. 4 at 25 °C. Figure 4 shows, for example, that the respective percentages of C_1 for isomeric decanols are 63% for 1-decanol, 40% for 2-decanol, 17% for 3-decanol, 7% for 4-decanol, and 6% for 5-decanol at 25 °C. Six percent of the gross concentration for 5-decanol is only associated with the formation of linear hydrogen-bonded chain polymers which the primary dispersion region originates. The other 94% for 5-decanol must exist as a monomer and some hydrogen-bonded short linear chains and nonpolar cyclic species. The C_1 generally decreases with increasing temperature. The percentages of C_1 for isomeric hexanols at 15, 25, and 35 °C are 76, 73, and 66% for 1-hexanol, 73, 62, and 53% for 2-hexanol, and 67, 52, and 41% for 3-hexanol, respectively. It may be that the depolymerization of linear hydrogen-bonded chain polymers occurs as the temperature increases.

Thermodynamic Parameters. The thermodynamic parameters, the free energy of activation ΔF^*, the heat of activation ΔH^*, and the entropy of activation ΔS^*, were calculated by the Eyring's equations,[14,15] which are described for dipole relaxation and for viscous flow as follows:

$$\tau = \frac{h}{kT}\exp\left(\frac{\Delta F\tau^*}{RT}\right) = \frac{h}{kT}\exp\left(-\frac{\Delta S\tau^*}{R}\right)\exp\left(\frac{\Delta H\tau^*}{RT}\right)$$

and

$$\eta = \frac{Nh}{V}\exp\left(\frac{\Delta F\eta^*}{RT}\right) = \frac{Nh}{V}\exp\left(-\frac{\Delta S\eta^*}{R}\right)\exp\left(\frac{\Delta H\eta^*}{RT}\right)$$

Here, τ is the relaxation time, h Planck's constant, RT the thermal energy, η the viscosity, and V is the molecular volume. ΔH^* and ΔS^* were calculated by the least-squares method in the temperature range 15—35 °C and ΔF^* was obtained at 25 °C. The thermodynamic parameters calculated are given in Table 2.

Table 2 shows that $\Delta H\tau^*$ increases with increasing alkyl chain length for normal alcohols and is nearly equal for secondary alcohols irrespective of length of alkyl chain, except for lower alcohols. $\Delta H\tau^*$ also increases as the hydroxyl group approaches the center of a molecule for isomeric alcohols, namely being expressed as 1-<2-<3-<4-<5-ol. $\Delta S\tau^*$ indicates the same tendency as the behavior of $\Delta H\tau^*$. $\Delta S\tau^*$ becomes large as the hydroxyl group approaches the center of a molecule. Therefore, it is noticeable that $\Delta F\tau^*$ increases with increasing alkyl chain length, being the same as that described for $\Delta H\tau^*$, but varies inversely as $\Delta H\tau^*$ in order to be a large value of $\Delta S\tau^*$ for isomeric alcohols, namely being expressed as 1->2->3->4->5-ol. It seems that the reorientation of a dipole moment of an alcohol molecule requires the rupture of hydrogen bondings and the rearrangement of some surrounding dipole moments, so that both $\Delta H\tau^*$ and $\Delta S\tau^*$ have large values. It is interesting that increases in $\Delta H\tau^*$ and $\Delta S\tau^*$ are strongly associated with the amount of shielding of the hydroxyl group in the hydrocarbon chain.

Table 2 shows that the $\Delta H\eta^*$ and $\Delta S\eta^*$ of normal alcohols increase with increasing alkyl chain length, being smaller than those of secondary alcohols. The $\Delta H\eta^*$ and $\Delta S\eta^*$ of secondary alcohols are nearly

Table 2. Thermodynamic Parameters, ΔF^*, ΔH^*, and ΔS^* for Temperature Dependence of Relaxation Times and Viscosities

Compound	Relaxation time			Viscosity		
	ΔF_τ^*	ΔH_τ^*	ΔS_τ^*	ΔF_η^*	ΔH_η^*	ΔS_η^*
	kJ mol^{-1}	kJ mol^{-1}	J K^{-1} mol^{-1}	kJ mol^{-1}	kJ mol^{-1}	J K^{-1} mol^{-1}
1-Propanol	18.9	26.1	23.9	14.6	17.4	9.2
1-Butanol	20.0	28.3	28.0	15.8	18.9	10.3
1-Pentanol	20.8	30.9	33.9	17.0	20.8	12.8
1-Hexanol	21.5	33.6	40.5	18.0	22.2	14.0
1-Heptanol	22.1	34.4	41.2	19.0	24.2	17.3
1-Octanol	22.5	35.9	44.7	19.9	25.4	18.4
1-Nonanol	22.9	37.4	48.6	20.7	27.1	21.6
1-Decanol	23.2	37.9	49.3	21.4	28.5	23.7
2-Propanol	19.1	31.3	40.8	14.9	21.8	23.3
2-Butanol	20.1	38.0	60.2	16.3	27.8	38.4
2-Pentanol	20.8	41.9	70.6	17.0	29.1	40.5
2-Hexanol	21.3	44.8	78.7	17.9	29.9	40.4
2-Heptanol	21.9	46.8	83.6	18.8	31.0	41.1
2-Octanol	22.3	48.6	88.2	19.6	32.1	42.0
2-Nonanol	22.6	49.6	90.6	20.4	32.9	41.7
2-Decanol	22.9	49.8	90.4	21.2	33.9	42.7
3-Pentanol	20.9	49.5	95.9	17.7	39.3	72.3
3-Hexanol	21.3	53.8	109	18.3	38.3	67.3
3-Heptanol	21.4	55.8	115	18.8	35.0	54.2
3-Octanol	21.6	56.4	117	19.5	34.2	49.4
3-Nonanol	21.9	55.4	112	20.3	33.9	45.8
3-Decanol	22.2	57.2	117	21.0	34.8	46.2
4-Heptanol	21.3	55.1	113	18.8	35.1	54.5
4-Octanol	21.0	56.4	119	19.6	33.8	47.5
4-Nonanol	21.2	56.6	119	20.3	34.0	45.9
4-Decanol	21.5	58.7	125	21.0	34.2	44.2
5-Nonanol	20.9	60.0	131	20.6	34.9	48.2
5-Decanol	21.1	65.1	148	21.3	35.1	46.5

equal, irrespective of the length of the alkyl chain and of the position of hydroxyl group, except for lower alcohols and some 3-alkanols. However, $\Delta F\eta^*$ increases with increasing alkyl chain length and is nearly equal for isomeric alcohols.

References

1) W. Dannhauser and L. W. Bahe, *J. Chem. Phys.*, **40**, 3058 (1964).
2) S. K. Garg and C. P. Smyth, *J. Phys. Chem.*, **69**, 1294 (1965).
3) W. Dannhauser, *J. Chem. Phys.*, **48**, 1918 (1968).
4) L. Glasser, J. Crossley, and C. P. Smyth, *J. Chem. Phys.*, **57**, 3977 (1972).
5) R. H. Cole and D. W. Davidson, *J. Chem. Phys.*, **20**, 1389 (1952).
6) A. Lebrum, *Ann. Phys.*, **10**, 16 (1955).
7) J. G. Kirkwood, *J. Chem. Phys.*, **7**, 911 (1939).
8) G. Oster and J. G. Kirkwood, *J. Chem. Phys.*, **11**, 175 (1943).
9) H. Fröhlich, "Theory of Dielectrics," Oxford University, New York, N. Y. (1958), 2nd ed.
10) H. Komooka, *Bull. Chem. Soc. Jpn.*, **45**, 1696 (1972).
11) W. Dannhauser, *J. Chem. Phys.*, **48**, 1911 (1968).
12) F. X. Hassion and R. H. Cole, *J. Chem. Phys.*, **23**, 1756 (1955).
13) W. Dannhauser, L. W. Bahe, R. Y. Lin, and A. F. Flueckinger, *J. Chem. Phys.*, **43**, 257 (1965).
14) S. Glasstone, K. J. Laidler, and H. Eyring, "The Theory of Rate Processes," McGraw-Hill Book Company, Inc., Ney York, N. Y. (1941), Chap. IX.
15) E. J. Hennelly, W. M. Heston, Jr., and C. P. Smyth, *J. Am. Chem. Soc.*, **70**, 4102 (1948).

Aryliminodimagnesium Reagents. XV.[1] Condensation with Nitrobenzene. Formation of Unsymmetrical Azobenzenes Favored by Long-Chain *p*-Alkoxy-Substituted Reagents

Masao Ōkubo,* Koji Matsuo, and Akira Yamauchi
Department of Chemistry, Faculty of Science and Engineering, Saga University, Honjō-machi, Saga 840
(Received September 28, 1988)

In the reaction of *p*-$MeC_6H_4N(MgBr)_2$ with *p*-alkoxynitrobenzene, no effect of alkoxyl chain length on the relative yields of azoxy and azo products was observed. In contrast, in the reaction of *p*-alkoxy-$C_6H_4N(MgBr)_2$ with *p*-nitrotoluene, C_{12}- and C_{18}-alkoxyl chains led to the corresponding unsymmetrical azobenzenes in unexpectedly high yields. This result, arising from efficient condensation and deoxygenation processes, was explained in terms of cooperation of reagent molecules through their aggregation assisted by a novel tying effect of their long chains.

The most important reaction of aryliminodimagnesium ($ArN(MgBr)_2$, IDMg) is the condensation with nitroarenes (Scheme 1). The *ONN* and *NNO* isomers of the unsymmetrical azoxyarene (**1**) are prepared by interchange of the substituents X and Y,[2] and the lack of interconversion of the isomers in the presence of IDMg is of significance for synthetic purposes. The reaction is applied to functionalization of azoxy- and azoarenes. If the compound **1** having a long chain alkyl or alkoxyl group (X or Y) is photoconverted into *o*-hydroxyazoarene,[3] it will be a useful chelating agent in micelle systems. The compound **2** having a long chain substituent will also be useful in micelle systems, by means of *Z–E* photoisomerization, as a probe for physicochemical studies.[4]

By use of molar excess of IDMg in the reaction with nitrobenzene (Scheme 1), the compound **1** is formed and successively deoxygenated to give **2**.[5] Single electron transfer (SET) from reagent to substrate is involved, and causes formation of minor coupling products: **3** frequently via oxidation of IDMg,[2,6] and **4** and **5** occasionally via reduction of nitroarene.[7] The coupling of nitroarene to give **4** is expected from the basic nature of IDMg because the coupling in basic medium[8] is well-known. The principal factor governing the relative yield of major and minor products is the relative SET efficiency estimated by oxidation and reduction potentials of reactants.[9,10] The precise mechanism remains to be studied.

In this study, the effect of the *p*-alkoxy (RO) chain length on the relative yield of **1** and **2** was examined using the combination of *p*-$ROC_6H_4NO_2$ with *p*-MeC_6H_4-IDMg (X=RO, Y=Me) and that of *p*-$MeC_6H_4NO_2$ with *p*-ROC_6H_4-IDMg (X=Me, Y=RO). Interestingly, "the long chain of the IDMg reagent was proved to be efficient for the formation of **2**." The reason for the variation of product yields will be discussed in this paper.

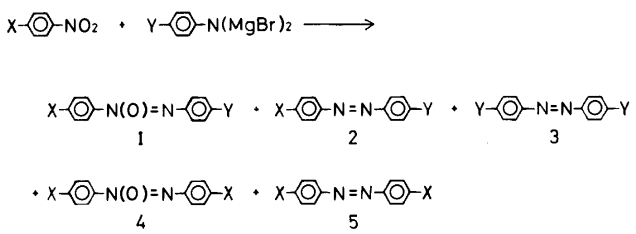

Scheme 1.

Results and Discussion

Product yields obtained by a typical treatment with 4.2 molar equivalents of IDMg (8.4 mmol in 50 ml THF at 55 °C for 3 h) are summarized in Table 1 (S1—S6 and R1—R10), which includes those affected by reaction conditions (R11—R14). Relative yields of **1**—**3** in the same combinations with S1 and R1[2] were reproduced.

The relative yield of **1**—**3** in S1—S6 (S-series) is essentially unaffected by the chain length of *p*-$ROC_6H_4NO_2$. The results of R1—R10 (R-series) using *p*-ROC_6H_4-IDMg are different from those of S-series, and are distinguished by two features. The first feature is the presence of *p,p'*-Me_2-azoxy- and -azobenzenes (**4** and **5**) in some cases of R-series (R1—R5, R7—R9), in contrast to the absence of the corresponding *p,p'*-$(MeO)_2$ products in S-series. The estimated relative SET efficiency in the combination of R1 is higher than that in S1,[2,9,10] and the electron-donating ability of *p*-ROC_6H_4-IDMg must be comparable to that of *p*-MeO reagent. Thus, the presence of **4** (or **5**) in R-series is ascribed to the rapid SET and not to any effect of chain length.

The second feature relates to the peculiar results of R6 and R10 among R-series. By use of the C_{12} and C_{18} alkoxy-substituted reagents, the yields of **2** are unusually elevated (at the expense of **1**) and concurrently the yields of **3**—**5** are reduced. The absense of **1** indicates its efficient deoxygenation to give **2**, and the appreciable yields of **3**—**5** arise usually from rapid SET.[2,10] It is thus recognized that the unusual reduction of the yields of **3** and **4** (or **5**) in R6 and R10, in spite of rapid SET (vide supra), accompanies the efficient formation of **2**. "The novel effect of reagent's chain length on the efficiency of condensation and deoxygenation processes"

Table 1. Yields of Products in the Reaction of Scheme 1

Run No.	X	Y	Yield/%[a]					Recovery/%
			1	2	3	4	5	
S1	CH_3O-	CH_3-	22.2	35.0	14.4	0	0	0
S2	n-$C_8H_{17}O$-	CH_3-	40.0	38.4	16.6	0	0	6.4
S3	n-$C_{10}H_{21}O$-	CH_3-	43.4	36.5	14.9	0	0	Trace
S4	n-$C_{12}H_{25}O$-	CH_3-	38.4	37.2	19.4	0	0	Trace
S5	n-$C_{18}H_{37}O$-	CH_3-	31.1	46.3	11.0	0	0	Trace
S6	n-$C_{22}H_{45}O$-	CH_3-	44.2	41.1	12.5	0	0	Trace
R1	CH_3-	CH_3O-	30.5	24.7	18.6	1.5	6.7	0
R2	CH_3-	n-$C_6H_{13}O$-	30.2	38.1	13.6	3.9	Trace	Trace
R3	CH_3-	n-$C_8H_{17}O$-	42.6	36.4	18.7	0	2.3	0
R4	CH_3-	n-$C_{10}H_{21}O$-	24.2	37.2	13.3	3.7	3.0	0
R5	CH_3-	n-$C_{11}H_{23}O$-	27.7	56.9	12.0	Trace	Trace	Trace
R6	CH_3-	n-$C_{12}H_{25}O$-	Trace	71.3	8.6	0	0	Trace
R7	CH_3-	n-$C_{13}H_{27}O$-	19.8	44.5	10.3	8.1	3.3	Trace
R8	CH_3-	n-$C_{15}H_{31}O$-	35.2	39.2	5.4	9.0	2.5	Trace
R9	CH_3-	n-$C_{17}H_{33}O$-	11.3	66.2	1.3	9.3	0	3.4
R10	CH_3-	n-$C_{18}H_{37}O$-	Trace	87.2	Trace	1.2	0	Trace
R11[b]	CH_3-	n-$C_{12}H_{25}O$-	1.9	33.4	7.0	0.7	0	33.5
R12[c]	CH_3-	n-$C_{12}H_{25}O$-	36.3	41.0	2.8	4.3	0	Trace
R13[d]	CH_3-	n-$C_{12}H_{25}O$-	37.9	37.9	3.2	5.4	1.4	0
R14[e]	CH_3-	n-$C_{12}H_{25}O$-	0	6.8	0	Trace	Trace	89.0

a) [IDMg]/[$ArNO_2$]=4.2, THF 50 ml, 55 °C, and 3 h. b) [IDMg]/[$ArNO_2$]=2.0. c) THF 200 ml. d) 55 °C and 0.5 h. e) Room temp and 10 min.

is discussed in what follows.

The conditions efficient for the two processes were reported. In the reaction with o-MeO- and o-halonitrobenzenes,[1] "normal addition" of them to a large molar excess of IDMg favors the condensation giving **1** and **2** (cf. Scheme 1), whereas "reverse addition" of a small molar excess of IDMg to the substrate favors, instead, the replacement of substituents leaving the nitro group unchanged. In order to deoxygenate azoxybenzenes to sufficient degree, the treatment with a 5-fold molar excess of the strongly electron-donating p-$MeOC_6H_4$-IDMg at 55 °C for 3 h[5,11] is needed. Even under these conditions, azoxybenzenes having a p-MeO-C_6H_4 group remote to the azoxy nitrogen (electronically resembling **1** formed in R-series) are sluggishly deoxygenated. The cited results reveal that high concentration in the proximity of nitro and/or azoxy groups is required for all the processes leading to **1** and **2**. At the usual concentrations (3—10 mmol in 50 ml THF), at least a part of IDMg molecules aggregate and "cooperate" for the condensation and also for the deoxygenation.

The aggregation arises from the equilibrium between monomeric and dimeric (or oligomeric) species of IDMg (Scheme 2a) resembling that in Grignard solution proposed early by Schlenk (Scheme 2b).[12] The deposition of IDMg crystals by cooling of the clear solution (of the concentration used in the previous[2,5] and present studies) to 0 °C is due to the formation of -Br···Mg< coordination bond, and indicates the presence of an equilibrium involving the bond formation and breaking, i.e., ligand exchange with

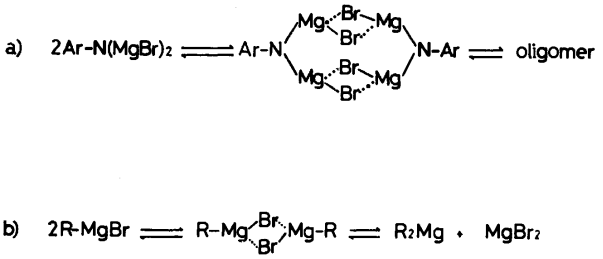

Scheme 2.

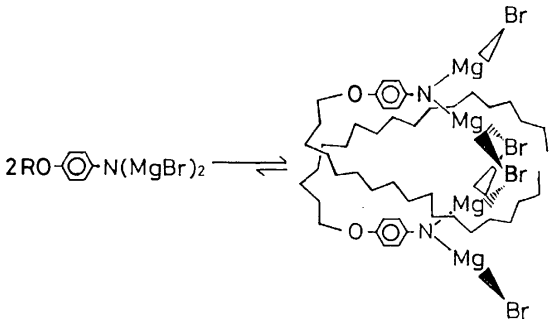

Fig. 1. Depiction of a Dimerized Species of p-n-$C_{18}H_{37}OC_6H_4$-IDMg.

THF molecule. Since a molecular model of p-alkoxyaniline shows that its C^{10} atom can locate close to the amino nitrogen of the same molecule, it is suggested that a long p-alkoxyl chain having more than eleven methylenes twists around the -$N(MgBr)_2$ group of the other molecule to tie the dimer (or oligomer); i.e., the dissociation is prevented and the

Table 2. Melting Points and ^1H NMR Data of Azoxyarenes
p-X-C_6H_4-N(O)=N-C_6H_4-Y-*p*

X	Y	Mp θ_m/°C	^1H NMR Data/δ
n-$C_6H_{13}O$-	CH_3-	102.5—103.5	8.20—7.90 (4H, m), 7.34—6.74 (4H, m), 3.96 (2H, t), 2.37 (3H, s), 2.00—0.60 (11H, m).
n-$C_8H_{17}O$-	CH_3-	88—89	8.34—7.97 (4H, m), 7.40—6.77 (4H, m), 3.95 (2H, t), 2.40 (3H, s), 2.10—0.67 (15H, m).
n-$C_{10}H_{21}O$-	CH_3-	85—86	8.34—7.95 (4H, m), 7.32—6.85 (4H, m), 3.94 (2H, t), 2.37 (3H, s), 2.10—0.62 (19H, m).
n-$C_{12}H_{25}O$-	CH_3-	85.5—86	8.20—7.84 (4H, m), 7.24—6.70 (4H, m), 3.92 (2H, t), 2.38 (3H, s), 2.10—0.67 (23H, m).
n-$C_{18}H_{37}O$-	CH_3-	83—83.5	8.30—7.94 (4H, m), 7.34—6.77 (4H, m), 3.98 (2H, t), 2.38 (3H, s), 1.94—0.64 (35H, m).
n-$C_{22}H_{45}O$-	CH_3-	84.5—85.5	8.22—8.07 (4H, m), 7.24—6.91 (4H, m), 3.99 (2H, t), 2.40 (3H, s), 1.84—0.86 (43H, m).
CH_3-	*n*-$C_6H_{13}O$-	70—71	8.30 and 6.97 (4H, ABq, J=9.5Hz), 8.17 and 7.27 (4H, ABq, J=8.8Hz), 4.02 (2H, t), 2.44 (3H, s), 1.86—0.87 (11H, m).
CH_3-	*n*-$C_8H_{17}O$-	61—62	8.29 and 6.96 (4H, ABq, J=9.2Hz), 8.16 and 7.27 (4H, ABq, J=8.5Hz), 4.02 (2H, t), 2.43 (3H, s), 1.86—0.87 (15H, m).
CH_3-	*n*-$C_{10}H_{21}O$-	54.5—55	8.29 and 6.95 (4H, ABq, J=9.2Hz), 8.16 and 7.25 (4H, ABq, J=8.5Hz), 3.99 (2H, t), 2.41 (3H, s), 1.81—0.86 (19H, m).
CH_3-	*n*-$C_{11}H_{23}O$-	65—66	8.28 and 6.93 (4H, ABq, J=9.5Hz), 8.15 and 7.24 (4H, ABq, J=8.8Hz), 3.98 (2H, t), 2.41 (3H, s), 1.83—0.85 (21H, m).
CH_3-	*n*-$C_{12}H_{25}O$-	56.5—57	8.29 and 6.93 (4H, ABq, J=9.2Hz), 8.15 and 7.23 (4H, ABq, J=8.5Hz), 3.97 (2H, t), 2.39 (3H, s), 1.82—0.85 (23H, m).
CH_3-	*n*-$C_{13}H_{27}O$-	66—67	8.29 and 6.97 (4H, ABq, J=9.5Hz), 8.17 and 7.28 (4H, ABq, J=8.8Hz), 4.03 (2H, t), 2.44 (3H, s), 1.86—0.85 (25H, m).
CH_3-	*n*-$C_{15}H_{31}O$-	77.5—73	8.29 and 6.97 (4H, ABq, J=9.3Hz), 8.17 and 7.27 (4H, ABq, J=8.8Hz), 4.02 (2H, t), 2.44 (3H, s), 1.86—0.85 (29H, m).
CH_3-	*n*-$C_{17}H_{35}O$-	74.5—75	8.29 and 6.96 (4H, ABq, J=9.3Hz), 8.17 and 7.27 (4H, ABq, J=8.8Hz), 4.02 (2H, t), 2.44 (3H, s), 1.86—0.85 (33H, m).
CH_3-	*n*-$C_{18}H_{37}O$-	—[a]	8.30 and 6.97 (4H, ABq, J=9.2Hz), 8.17 and 7.28 (4H, ABq, J=8.5Hz), 4.03 (2H, t), 2.44 (3H, s), 1.83—0.85 (35H, m).

a) Undetermined.

self-aggregation is assisted. Figure 1 shows a tentative depiction of a dimeric aggregate tied by the *p*-octadecyloxyl group causing an ideal cooperation responsible for the high yield of **2** in R10. The cooperation will be initiated by efficient binding of nitroarene molecule with the IDMg aggregate through the coordination of nitro (and/or azoxy) oxygen to Mg atoms.

The effect of even-numbered chains (R6, R10) is somewhat different from that of odd-numbered ones (R5, R7—R9) probably due to different conformations more or less favoring the twist. Another mode of twist, i.e., that of a reagent's long chain around a substrate molecule seems possible, but may be excluded by the notable formation of **4** in R7—R9 (probably arising from a dissociation, after SET, of σ-complex formed at the initial stage of reaction[10]). The twist of substrate's long chain around a reagent molecule is excluded by the lack of chain length effect in S-series. Physical evidence for IDMg aggregation was difficultly obtained by means of the expected shift of n-π^* elecronic absorption band or ^1H NMR signal. An advanced measurement of ^{14}N and/or ^{15}N NMR spectra, which may be hopeful, remains to be carried out. However, the suggestion of IDMg cooperation and some previous observations (vide infra) are supported, as shown below, by the variation of the yields of C_{12}-substituted **1** and **2** in R11—R14, the reaction conditions being changed from that of R6.

The use of 2.0 molar equivalents of reagent in R11 leads expectedly[2] to the fair amount of recovery (34%), but the suggestion is supported by the still much higher yield (33%) of **2** than that (2%) of **1**. Fair yields of **1** at the expense of **2** were obtained by use of four-fold volume of solvent (200 ml, R12) and by use of shorter time of heating (0.5 h, R13; the mixture is the same with R6). The result of R12 indicates the effect of reduced population of dimer (or oligomer) due to left-hand side shift of the equilibrium of Scheme 2a by dilution. The result of R13 supports a previous observation,[5] i.e., sluggish deoxygenation of **1** compared to its formation. In spite of the great amount of recovery (89%) in R14 due to quite a low conversion after stirring (the mixture is the same with R6) for 10 min at room temperature,[2] a low yield (7%) of **2** is still accompanied by an undetectable amount of **1**.

As discussed above, the major factor (relative SET efficiency), governing a variety of both Grignard and IDMg reactions,[10] was modified by the effect of cooperation of reagent molecules as one of the minor factors. The effect evokes a similar cooperation proposed from structures and behavior of intermediates

of Grignard addition to benzil and benzophenone,[14] and the unified view of reactions of the two magnesium reagents[10] will be elaborated. The other minor factor, based on the effect of coordination of substrate's oxygen to reagent's Mg,[10,13] was disclosed owing to the mild electron-donating ability of IDMg.[9] The major and minor factors, determining the product yields, will be utilized for mechanistic and synthetic studies.

Experimental

Materials and Procedures. The *p*-alkoxynitrobenzenes were prepared by treatment of dried potassium *p*-nitrophenolate with appropriate alkyl bromides in refluxing cyclopentanone.[15] The *p*-alkoxyanilines were prepared in yields higher than 80% by the reduction of the corresponding nitrobenzenes by zinc powder in refluxing ethanol.[16] Longer times of refluxing are needed for efficient reduction of nitrobenzenes having longer alkoxyl chains: 1 h for C_6 and C_8, 2 h for C_{10} and C_{11}, 3 h for C_{12} and C_{13}, 4 h for C_{15}, and 5 h for C_{17} and C_{18}. By heating C_6 nitrobenzene for 3 h, some decomposition leading to 38% yield was observed. Some attempts to reduce *p*-$C_8H_{17}O$-nitrobenzene by use of $NaBH_2S_3$[17] gave poor results.

A preparation of IDMg reagents from the corresponding anilines and their reaction with nitrobenzenes were carried out according to the reported procedures.[2] The products were separated by column and thin-layer chromatographies on silica gel (Wako Gel C-200 and C-300 and Merck Kieselguhr 60G). In Table 2, the melting points (uncorrected) and ^1H NMR data of **1** (obtained in S2—S6 and R2—R10) are summarized. The other products are known.

The authors thank Miss Takae Ura for the preparation of *p*-octyloxyaniline and the reaction of its IDMg reagent. A part of this work was financially supported by Grants-in-Aid for Scientific Research (Nos. 60470026 and 63540405).

References

1) Part XIV: M. Ōkubo, Y. Inatomi, N. Taniguchi, and K. Imamura, *Bull. Chem. Soc. Jpn.*, **61**, 3581 (1988).
2) M. Ōkubo, T. Takahashi, and K. Koga, *Bull. Chem. Soc. Jpn.*, **56**, 199 (1983).
3) M. Ōkubo, H. Hyakutake, and N. Taniguchi, *Bull. Chem. Soc. Jpn.*, **61**, 3005 (1988).
4) For example; S. Shinkai, *Pure Appl. Chem.*, **59**, 425 (1987).
5) M. Ōkubo and K. Koga, *Bull. Chem. Soc. Jpn.*, **56**, 203 (1983).
6) M. Ōkubo, S. Yoshida, Y. Egami, K. Matsuo, and S. Nagase, *Bull. Chem. Soc. Jpn.*, **60**, 1741 (1987).
7) M. Ōkubo, M. Tokisada, and T. Gondo, *Nippon Kagaku Kaishi*, **1985**, 303.
8) For example; H. W. Galbraith, E. F. Degering, and E. F. Hitch, *J. Am. Chem. Soc.*, **73**, 1323 (1951); and the literatures cited therein.
9) M. Ōkubo, T. Tsutsumi, A. Ichimura, and T. Kitagawa, *Bull. Chem. Soc. Jpn.*, **57**, 2679 (1984).
10) M. Ōkubo, T. Tsutsumi, and K. Matsuo, *Bull. Chem. Soc. Jpn.*, **60**, 2085 (1987).
11) M. Ōkubo, C. Sugimori, M. Tokisada, and T. Tsutsumi, *Bull. Chem. Soc. Jpn.*, **59**, 1644 (1986).
12) W. Schlenk and W. Schlenk, Jr., *Chem. Ber.*, **64**, 739 (1931); W. Walker and E. C. Ashby, *J. Am. Chem. Soc.*, **91**, 3845 (1969).
13) M. Ōkubo, *Bull. Chem. Soc. Jpn.*, **58**, 1644 (1985).
14) K. Maruyama and T. Katagiri, *J. Am. Chem. Soc.*, **108**, 6263 (1986); K. Maruyama, J. Hayami, and T. Katagiri, *Chem. Lett.*, **1986**, 601.
15) C. Weygand and R. Gabler, *J. Prakt. Chem.*, **155**, 332 (1940).
16) W. E. Kuhn, *Org. Synth.*, Coll. Vol., **2**, 447 (1943).
17) J. M. Lalancette, A. Freche, and R. Monteux, *Can. J. Chem.*, **46**, 2754 (1968).

Quadrupole Coupling Constants in the Symmetric Tetrasubstituted Germanes

Toshie HARAZONO, Katsumi TANAKA, and Yoshito TAKEUCHI*
Department of Chemistry, The College of Arts and Sciences, The University of Tokyo, Komaba, Meguro-ku, Tokyo 153
(Received June 21, 1988)

Synopsis. The quadrupole coupling constants in the symmetric tetrasubstituted germanes, GeR_4 (R=CH_3, C_2H_5, n-C_3H_7, n-C_4H_9, Cl, and Br) were obtained by measuring the ^{73}Ge spin-lattice relaxation times (T_1) and the reorientational correlation times (τ_c) of the chloroform solutions. Quadrupole coupling constants of GeR_4 were in the range of 0.72 MHz (R=n-C_4H_9) to 1.51 MHz (R=CH_3), and these decreased slightly as the molecular radius increased.

Very little had been reported on the relaxation mechanism of ^{73}Ge nuclei (I=9/2)[1,2] when we[3] started to study this subject. Since then we analyzed the relaxation mechanism of ^{73}Ge in such symmetrical tetrasubstituted germanes as GeR_4 (R=H, CH_3, C_2H_5, n-C_3H_7, n-C_4H_9, Cl, Br, and I).[4-6] We demonstrated that the spin-lattice relaxation of ^{73}Ge in all compounds investigated and the spin-spin relaxation of ^{73}Ge in compounds except GeH_4, $GeCl_4$, $GeBr_4$, and GeI_4 occur solely via the quadrupole relaxation mechanism. The spin-spin relaxation of ^{73}Ge in GeH_4, $GeCl_4$, $GeBr_4$, and GeI_4 were found to occur via a combination of quadrupole and scalar coupling relaxation mechanisms.

During this investigation we noticed that very few quadrupole coupling constants have so far been reported for organogermanium compounds.[1] The quadrupole coupling constants in the crystal or powder states are generally obtained from Mössbauer or NQR (nuclear quadrupole resonance) spectra. If electric field gradients occur at the central germanium nuclei, and if correlation times are obtainable in the symmetric tetrasubstituted germanes mentioned above, the quadrupole coupling constants of ^{73}Ge in the liquid state can be estimated from the relaxation times and the correlation times. In this paper we describe our attempts along this line.

Experimental

Preparation of Compounds. Tetraalkylgermanes were prepared by the procedures described in the literature.[7] $GeCl_4$, guaranteed reagent grade, was purchased from Sumitomo Metal and Mines Co., Ltd. $GeBr_4$ (bp 82—83 °C/32 mmHg; 1 mmHg≈133.322 Pa) was synthesized by the procedures described in the literature.[8] The purity of the compounds were confirmed by ^1H NMR spectra (Varian EM-390) and/or GLC (Shimadzu GC-3BT). GeR_4 were dissolved in $CDCl_3$ (50% v/v). The solution was taken in an egg shaped cell and degassed by the freeze-thaw method.

Germanium-73 NMR Spectra. The ^{73}Ge NMR spectra were recorded by JEOL FX-90Q equipped with a low frequency insert NM-IT10LF at 3.10 MHz. T_1 was determined by the inversion-recovery method. The error in T_1 thus determined was estimated to be about or less than 5%. Other conditions of the measurements have been described in previous papers.[5,6]

Measurement of Viscosity. For the measurement of viscosity of GeR_4, the sample was dissolved in $CHCl_3$ (50% v/v). The procedure of the measurement has been described in the previous papers.[5,6]

Estimation of Molecular Radius. The radius of GeR_4 (R=alkyl) is defined as the distance between the germanium nucleus and the terminal hydrogen atom plus van der Waals radius of terminal hydrogen atom. The germanium-hydrogen distance was obtained from the structure of the alkylgermanes optimized by the molecular mechanics calculations[9] while for GeR_4 (R=halogen) the reported values for germanium-halogen distance were used.[10,11]

Results and Discussion

Origin of Relaxation. It is generally accepted that if electric field gradients occur at the nucleus site, the quadrupole relaxation times, T_1 and T_2, of nuclei with nuclear spin $I>1/2$ are related to the reorientational correlation time τ_c at the extreme-narrowing limit as given below:[12]

$$\pi\Delta\nu_{1/2} = \frac{1}{T_1} = \frac{1}{T_2} = \frac{3\pi^2}{10}\,\frac{2I+3}{I^2(2I-1)} \times \left(\frac{e^2Qq}{h}\right)^2\left(1+\frac{\zeta^2}{3}\right)\tau_c \qquad (1)$$

where e^2Qq/h is quadrupole coupling constant and ζ is asymmetry parameter.

Since tetrasubstituted germanes of the type GeR_4 have tetrahedral symmetry, the electric field gradient at the germanium nuclei must be zero, which is expected to make the relaxation time of germanium nuclei infinitely long. The fact is, however, that the relaxation time is finite.

Some authors have proposed a theory to account for the quadrupole relaxation of symmetric molecules. Brown and Colpa suggested that the quadrupole relaxation occurs by the vibration and/or rotation,[13] while Osten and Jameson attributed the effect to the collision among molecules.[14] The electric field gradient generated at the germanium nuclei of symmetric tetrasubstituted germanes is averaged to zero but it has a non vanishing mean square, i.e., $(e^2Qq/h)^2\neq 0$.[14] Osten and Jameson calculated the relaxation rate of neat $GeCl_4$ at 300 K by using the collision model as $1/T_1=2\ s^{-1}$ comparable with the observed rate ($1.2\ s^{-1}$).[2] Sekatsis et al. suggested that the non-zero electric field gradient is induced by the deformation of the molecular orbitals during molecular collisions.[1] Tarasov et al.[2] suggested that the quadrupole relaxation of $GeCl_4$ and $GeBr_4$ was affected by the vibrationally-induced electric field gradients. We have also shown in previous papers[3-6] that T_1 of ^{73}Ge compounds investigated are predominantly governed by the quadrupole relaxation mechanism. If the reorientational correlation time can, for instance, be determined from the viscosity

Table 1. The Values of the Concentration, Density, Viscosity, and Radius of Tetrasubstituted Germanes

Compd	Concn	ρ (30 °C)	η (30 °C)	r
	mol dm^{-3}		cP[a]	Å
$GeMe_4$	3.67	1.26	0.537	3.75
$GeEt_4$	2.63	1.21	0.573	5.11
$GePr_4$	1.95	1.20	0.720	5.83
$GeBu_4$	1.55	1.19	0.910	6.90
$GeCl_4$	4.37	1.67	0.586	3.89
$GeBr_4$	4.02	2.29	0.986	4.24

a) 1 P=0.1 Pa s.

Table 2. The Values of T_1(IR), and τ_c, and e^2Qq/h of Tetrasubstituted Germanes

Compd	T_1(IR)	τ_c(30 °C)	e^2Qq/h
	ms	10^{-11} s	MHz
$GeMe_4$	290	0.69	1.51
$GeEt_4$	220	2.2	0.97
$GePr_4$	100	4.5	1.00
$GeBu_4$	80	10.9	0.72
$GeCl_4$	280	0.78	1.45
$GeBr_4$	160	1.8	1.25

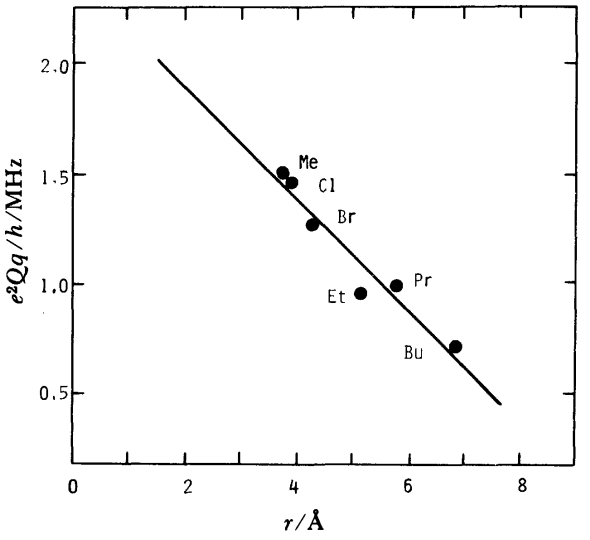

Fig. 1. Plot of e^2Qq/h. vs. radius of GeR_4.

data, it is tempting to employ Eq. 1 as a means to estimate the quadrupole coupling constants of organogermanium compounds in solution. Some authors have interpreted the quadrupole relaxation data associated with highly symmetric nuclei, such as $^{55}Mn(CNR)_6^{+ \text{ or } 2+}$, (R=*i*-$C_3H_7$ and *t*-C_4H_9),[15] aqueous tetrahedral oxoacid anions MO_4^{X-} (M=^{51}V, ^{53}Cr, ^{97}Mo, ^{183}W, ^{55}Mn, ^{99}Tc, ^{185}Re, ^{189}Os, X=1, 2, 3),[16,17] and chloride ion[18–20] and halide ions[21] by Eq. 1.

At the moment, we believe that Eq. 1 may be extended to the assessment of the quadrupole coupling constants of highly symmeteric molecules as has previously been done by several investigators[15–21] mentioned above.

Quadrupole Coupling Constants. We estimated the quadrupole coupling constants of GeR_4 with the aid of Eq. 1. The values of the concentration, density (ρ), viscosity (η), and radius (r) of tetrasubstituted germanes are shown in Table 1. The correlation time, τ_c is given by Eq. 2,[22]

$$\tau_c = 4\pi r^3 \eta f / 3kT \quad (2)$$

where k is the Boltzmann constant, T the absolute temperature, and f a microviscosity which is described in the previous papers.[5,6,22] The mean radius of solvent molecule $CHCl_3$ was estimated as 3.13 Å.

The quadrupole coupling constants for GeR_4 were found in the range of 0.72 to 1.7 MHz as shown in Table 2. For $Ge(CH_3)_4$ and $Ge(C_4H_9)_4$ in $CDCl_3$, the values of quadrupole coupling constants have been reported as 1.7 and 1.1 MHz, respectively,[1] in which τ_c was calculated from dipole–dipole interaction of CH_3 group. This discrepancy of the quadrupole coupling constants may be due to the different methods of determining τ_c values.

Since the relaxation rate is proportional to the correlation time and to the square of the quadrupole coupling constant, it is interesting to determine which of the two mainly determines the relaxation rate.

We found that the difference of relaxation rate is mainly governed by the correlation time rather than by the quadrupole coupling constant from the data for GeR_4 shown in Table 2.

A linear relationship exists between ln τ_c and the molecular radius as shown in the previous paper.[6] On the other hand, the value of quadrupole coupling constant slightly decreases as the molecular radius increases. In Fig. 1 a plot of the quadrupole coupling constants vs. molecular radius, r is given. The larger is the radius, the smaller is the quadrupole coupling constant. It seems that in symmetrical germanium compounds investigated the smaller complex molecule will be instantaniously distorted by the molecular vibrations and rotations, or collisions. On the other hand, for octahedral manganese isocyanide complexes, the differences in the line widths were attributed to variable values of quadrupole coupling constants under the assumption that the correlation time is essentially independent on the shape and size of similar molecules.[15] Indeed, Nielson et al. showed that wider half widths were observed for the complexes with larger ligands whereas molecules with large complex ligands tend to distort due to vibrational and rotational movements.[15]

The authors wish to thank Professor Hiroshi Watanabe, Department of Chemistry, the College of Arts and Sciences, the University of Tokyo for his help in the measurement of viscosity, Professor Isao Ando and Woo-Sik Jung, The Tokyo Institute of Technology, for valuable discussions. Thanks are also due to ASAI Germanium Research Institute and the Ministry of Education for financial support.

References

1) I. P. Sekatsis, É. É. Liepin'sh, I. A. Zitsmane, and É. Lukevits, *Zh. Obshch.*, **53**, 2064 (1983).
2) V. P. Tarasov, V. I. Privalov, S. G. Drobyshev, and Yu. A. Busleav, *Dokl. Akad. Nauk SSSR*, **272**, 1176 (1983).
3) Y. Takeuchi, T. Harazono, and N. Kakimoto, *Inorg. Chem.*, **23**, 3835 (1984).
4) T. Harazono, K. Tanaka, Y. Takeuchi, and N. Kakimoto, *Chem. Lett.*, **1986**, 1841.
5) T. Harazono, K. Tanaka, and Y. Takeuchi, *Inorg. Chem.*, **26**, 1894 (1987).
6) T. Harazono, K. Tanaka, Y. Takeuchi, and H. Fukutomi, *Inorg. Chem.*, **26**, 3851 (1987).
7) D. L. Tabern, W. R. Orndorff, and L. M. Lewis, *J. Am. Chem. Soc.*, **47**, 2039 (1925).
8) A. W. Laubengayer and P. L. Brandt, *J. Am. Chem. Soc.*, **54**, 621 (1932).
9) Y. Takeuchi, M. Shimoda, K. Tanaka, S. Tomoda, K. Ogawa, and H. Suzuki, *J. Chem. Soc., Perkin Trans. 2*, **1988**, 7.
10) F. Glockling, "The Chemistry of Germanium," Academic Press, New York (1969).
11) E. G. Rochow and E. W. Abel, "The Chemistry of Germanium, Tin and Lead," Pergamon Press, Oxford (1975).
12) A. Abragam, "The Principles of Nuclear Magnetism," Oxford University Press, (1961), Chap. 8.
13) R. J. C. Brown and J. P. Colpa, *J. Chem. Phys.*, **77**, 1501 (1982).
14) H. J. Osten and C. J. Jameson, *Mol. Phys.*, **57**, 553 (1986).
15) R. M. Nielson and S. Wherland, *Inorg. Chem.*, **24**, 3458 (1985).
16) R. G. Kidd, *J. Magn. Reson.*, **45**, 88 (1981).
17) E. Haid, D. Kohnlein, G. Kossler, O. Lutz, and W. Schich, *J. Magn. Reson.*, **55**, 145 (1983).
18) H. A. Berman and T. R. Stengle, *J. Phys. Chem.*, **79**, 1001 (1975).
19) H. A. Berman, H. J. C. Yeh, and T. R. Stengle, *J. Phys. Chem.*, **79**, 2551 (1975).
20) M. Yudasaka, T. Sugawara, H. Iwamura, and T. Fujiyama, *Bull. Chem. Soc. Jpn.*, **54**, 1933 (1981).
21) H. Wennerstrom, B. Lindman, and S. Forsen, *J. Phys. Chem.*, **75**, 2936 (1971).
22) A. Gierer and K. Wirtz, *Z. Naturforsch*, **A8**, 532 (1953).

Prediction of Soil Sorption Coefficients of Hydrophobic Organic Pollutants by Adsorbability Index

Shoichi OKOUCHI* and Hisayoshi SAEGUSA
Chemistry Laboratory, College of Engineering, Hosei University,
Koganei, Tokyo 184
(Received August 31, 1988)

Synopsis. The adsorbability index proposed by Abe et al. to predict the activated carbon adsorption of organic compounds from aqueous solution was well correlated with the soil sorption coefficients of polycyclic aromatic hydrocarbons (PAHs), alkylbenzenes, chlorobenzenes, chlorinated alkanes and alkenes, heterocyclic and substituted PAHs, and halogenated phenols. The adsorbability index was also found to be well correlated with the first-order molecular connectivity index and the total molecular surface areas of these compounds.

The adsorbability index, AI, has recently been proposed by Abe et al.[1] from a quantitative structure–activity relationship analysis based on the molecular refraction to predict the activated carbon adsorption of 157 compounds from aqueous solutions (Freundlich adsorption constant: K). Their results indicated the good linear relationship between $\log K$ and AI with the correlation coefficient, r, of 0.986. Then, we investigated whether the adsorbability index was applicable to predict the soil sorption as well as the activated carbon adsorption. As a quantitative measure of the soil adsorption a soil sorption coefficient, K_{om},[2–15] has been used, which is defined as the ratio between the concentrations of a given chemical sorbed by the soil and dissolved in the soil water normalized to the total organic carbon content of the soil. The soil sorption coefficient, K_{om}, is also one of the important parameters to describe the environmental fate of chemicals. Besides the experimental determination of K_{om}, the values of K_{om} can be estimated from the water solubility[4,7,8,11,13–15] or 1-octanol/water partition coefficient,[4,7–11] but the estimation needs their accurate data.

Recently, Sabljić[2] showed the first-order molecular connectivity index, χ, as a good structure parameter that described most adequately a relationship between the molecular structure of 72 hydrophobic organic compounds and their adsorption by soil. Furthermore, he indicated that χ was well correlated with the total molecular surface areas, TSA, of the compounds. Then, attempts were made to determine a relationship between AI and TSA of the 72 hydrophobic organic compounds reported by Sabljić,[2] which included polycyclic aromatic hydrocarbons (PAHs), alkylbenzenes, chlorobenzenes, chlorinated alkanes and alkenes, heterocyclic and substituted PAHs, and halogenated phenols.

Results and Discussion

The adsorbability index, AI, of a given molecule can be readily calculated from Eq. 1[1] by adding the values of A and I shown in Table 1,

$$\mathrm{AI} = \Sigma A + \Sigma I \tag{1}$$

where A and I indicate the factors of the respective increasing and decreasing adsorbabilities of the atom or functional group in the molecule onto the activated carbon from aqueous solution.

The AI values calculated from Eq. 1 are shown in Table 2 for the 72 hydrophobic organic compounds.[2] The AI values in Table 2 are obtained by only the A values, since the I values can be ingnored for the compounds used in this work. The logarithm of K_{om} was expressed by the following regression equation:

$$\log K_{om} = 0.62\,\mathrm{AI} + 0.16 \quad (r = 0.967,\ s = 0.341), \tag{2}$$

where s is the standard deviation. The graphical representation of this fit is given in Fig. 1. This led to the conclusion that the adsorbability index gave good prediction of the soil sorption coefficients as well as

Table 1. Adsorbability Index (AI)[a]

	A			I
C	0.26	Aliphatic		
H	0.12	-OH	(alcohols)	−0.53
N	0.26	-O-	(ethers)	−0.36
O	0.17	-CHO	(aldehydes)	−0.25
S	0.54	N	(amines)	−0.58
Cl	0.59	-COOR	(esters)	−0.28
Br	0.86	>C=O	(ketones)	−0.30
NO_2	0.21	-COOH	(fatty acids)	−0.03
-C=C-	0.19	Aromatics		
Iso	−0.12	-OH, -O-, N, -COOR, >C=O, -COOH		0
Tert.	−0.32	α-Amino acids		−1.55
Cyclo	−0.28			

a) Ref. 1.

Table 2. Values of the Soil Sorption Coefficients (K_{om}), the Adsorbability Indexes (AI) of the 72 Hydrophobic Organic Compounds

Compound	log K_{om}[a]	AI[b]	(log K_{om}) Error(%)[c]	(TSA) Error(%)[d]
Dibenz(*a*,*h*)anthracene	6.31	9.49	3.6	−5.9
3-Methylcholanthrene	6.25	9.09	6.7	−4.8
Dibenzo(*a*,*i*)carbazole	6.14	8.92	6.7	−9.4
2,3,4,5,6,2′,5′-Heptachlorobiphenyl	5.95	8.75	5.5	5.6
Naphthacene	5.81	7.83	13.2	−6.5
DDT[e]	5.38	8.81	−5.2	8.9
7,12-Dimethylbenz(*a*)athracene	5.37	8.83	−5.6	−0.9
2,4,5,2′,4′,5′-Hexachlorobiphenyl	5.34	8.28	0.2	4.8
6-Aminochrysene	5.21	8.21	−1.4	−4.9
2,3,4,2′,3′,4′-Hexachlorobiphenyl	5.05	8.28	−5.5	4.8
Pyrene	4.92	6.88	9.5	−11.2
9-Methylanthracene	4.81	6.67	10.1	−3.6
DDE[f]	4.70	8.29	−13.5	5.1
2,5,2′,5′-Tetrachlorobiphenyl	4.67	7.34	−1.5	2.8
2,4,5,2′,5′-Pentachlorobiphenyl	4.63	7.81	−8.7	3.9
2,3,4,2′,5′-Pentachlorobiphenyl	4.50	7.81	−11.9	3.9
Aldrin	4.45	8.00	−15.8	6.5
2-Aminoanthracene	4.45	6.55	4.6	−5.3
Anthracene	4.42	6.17	9.3	−7.4
2,4,4′-Trichlorobiphenyl	4.38	6.87	−1.5	1.7
Phenanthrene	4.36	6.22	7.3	−8.1
Acridine	4.22	6.05	6.7	−7.9
Dibenzothiophene	4.05	5.76	7.3	−5.6
2-Methylnaphthalene	3.93	5.01	16.4	−3.8
2,4′-Dichlorobiphenyl	3.90	6.40	−6.5	0.3
Pentachlorophenyl	3.73	5.37	5.9	3.4
2,2′-Dichlorobiphenyl	3.68	6.40	−12.9	0.3
Hexachlorobenzene	3.59	5.67	−3.0	3.6
3,4,5-Trichlorophenyl	3.56	4.43	17.9	0.1
Pentachlorobenzene	3.50	5.20	2.7	2.2
Butylbenzene	3.39	4.85	6.0	7.0
1,2,3-Trichlorobenzene	3.37	4.26	16.4	−1.5
2,4,5-Trichlorophenol	3.36	4.43	13.0	0.1
2,3,4,6-Tetrachlorophenol	3.35	4.90	4.0	1.9
1-Naphthol	3.33	4.68	7.5	−6.9
2-Chlorobiphenyl	3.23	5.93	−19.5	−1.2
Hexachlorocyclohexane	3.21	6.08	−23.2	10.7
1,2,3,5-Tetrachlorobenzene	3.20	4.73	2.8	0.6
1,2,4,5-Tetramethylbenzene	3.12	4.85	−2.1	7.8
Naphthalene	3.11	4.51	4.4	−8.8
2,4,6-Trichlorophenol	3.02	4.43	3.2	0.1
1,3,5-Trichlorobenzene	2.85	4.26	1.1	−1.5
1,3,5-Trimethylbenzene	2.82	4.35	−1.9	4.8
1,2,3-Trimethylbenzene	2.80	4.35	−2.7	4.8
2,4-Dichlorophenol	2.75	3.96	4.3	−2.1
1,2,4-Trichlorobenzene	2.70	4.26	−4.4	−1.5
2,3-Dichlorophenol	2.65	3.96	0.7	−2.1
Bromobenzene	2.60	3.59	7.7	−6.6
1,4-Dimethylbenzene	2.52	3.85	−1.7	1.0
1,4-Dichlorobenzene	2.40	3.79	−5.2	−4.0
Toluene	2.39	3.35	5.8	−4.2
Tetrachloroethene	2.32	3.07	10.5	1.8
1,2-Dichlorobenzene	2.26	3.79	−11.7	−4.0
1,3-Dimethylbenzene	2.26	3.85	−13.4	1.0
1,3-Dichlorobenzene	2.23	3.79	−13.2	−4.0
4-Bromophenol	2.17	3.76	−15.5	−4.5
1,2-Dibromo-3-chloropropane	2.11	3.69	−16.7	7.9
Chlorobenzene	2.10	3.32	−6.3	−7.2
1,1,1-Trichloroethane	2.02	2.65	10.2	6.8
Trichloroethene	2.00	2.60	10.9	−0.8
Ethylbenzene	1.98	3.85	−29.4	0.6
Benzene	1.92	2.85	−1.0	−11.4
1,1,2-Trichloroethane	1.87	2.65	3.0	4.8

Table 2. (Continued)

Compound	log K_{om}[a]	AI[b]	(log K_{om}) Error(%)[c]	(TSA) Error(%)[d]
Tetrachloromethane	1.85	2.62	3.0	4.1
1,1,2,2-Tetrachloroethane	1.66	3.12	−27.0	7.9
Trichloromethane	1.65	2.15	9.0	−0.5
1,2-Dibromoethene	1.65	2.67	−10.7	1.2
1,2-Dibromoethane	1.56	2.72	−19.1	0.7
Dichloromethane	1.44	1.68	16.1	−7.2
1,2-Dichloropropane	1.43	2.68	−28.1	7.5
1,3-Dichloropropane	1.42	1.90	5.2	7.1
1,2-Dichloroethane	1.28	2.18	−18.8	0.5

a) Ref. 2. b) Calcd from Eq. 1. c) Error(%)={1−(log $K_{om\,calcd}$ from Eq. 2)/(log K_{om})}×100. d) Error(%)={1−(TSA_{calcd} from Eq. 4)/(TSA)}×100. e) 1,1-Bis(4-chlorophenyl)-2,2,2-trichloroethane. f) 2,2-Bis(4-chlorophenyl)-1,1-dichloroethylene.

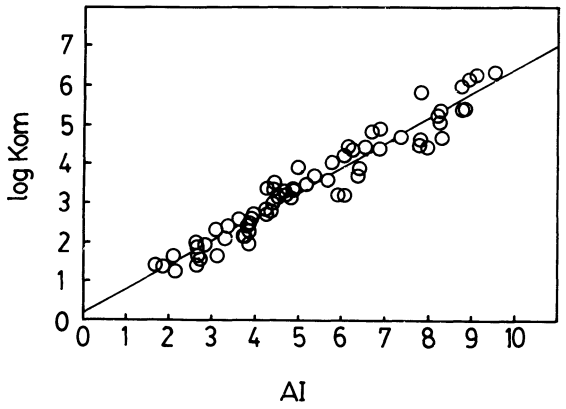

Fig. 1. Relationship between log K_{om} and adsorbability index, AI.

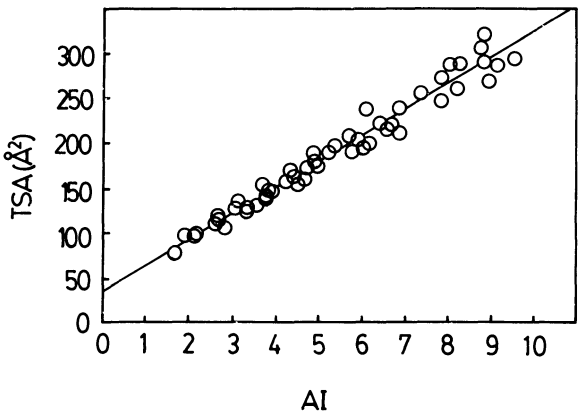

Fig. 2. Relationship between total molecular surface areas, TSA, and adsorbability index, AI.

the first-order connectivity index (χ) as shown by Eq. 3.[2]

$$\log K_{om} = 0.53\chi + 0.54 \quad (3)$$
$$(r = 0.976,\ s = 0.298)$$

Therefore, the adsorbability index for prediction of the activated carbon adsorption was also found to be effective for prediction of the soil adsorption coefficient.

On the other hand, the regression analysis showed that the relationships between AI, TSA, and χ were expressed as the following linear functions:

$$TSA = 29.4AI + 35.3 \quad (4)$$
$$(r = 0.985,\ s = 10.9)$$

$$\chi = 1.16AI - 0.68 \quad (5)$$
$$(r = 0.988,\ s = 0.377)$$

$$TSA = 24.1\chi + 58.5 \quad (6)$$
$$(r = 0.956,\ s = 19.4),$$

The AI index was well correlated with both TSA and χ. The correlation of TSA with AI (Eq. 4) was superior to that of TSA with χ (Eq. 6) reported by Sabljić.[2] Figure 2 shows the relationship between TSA and AI according to Eq. 4. The adsorbability index was found to be a parameter that strongly depends on the total molecular surface areas.

References

1) I. Abe, H. Tatsumoto, and T. Hirashima, *Suishitsuodaku Kenkyu*, **9**, 153 (1986).
2) A. Sabljić, *Environ. Sci. Technol.*, **21**, 358 (1987).
3) A. Sabljić, *J. Agric. Food Chem.*, **32**, 243 (1984).
4) C. T. Chiou, P. E. Porter, and D. W. Schmedding, *Environ. Sci. Technol.*, **17**, 227 (1983).
5) R. Koch, *Toxicol. Environ. Chem.*, **6**, 87 (1983).
6) E. E. Kenaga, *Ecotoxicol. Environ. Saf.*, **4**, 26 (1980).
7) S. W. Karickhoff, D. S. Brown, and T. A. Scott, *Water Res.*, **13**, 241 (1979).
8) G. G. Briggs, *J. Agric. Food Chem.*, **29**, 1050 (1981).
9) K. Schellenberg, C. Leuenberg, and R. P. Schwarzenbach, *Environ. Sci. Technol.*, **18**, 652 (1984).
10) R. P. Schwarzenbach and J. Westall, *Environ. Sci. Technol.*, **15**, 1360 (1981).
11) J. C. Means, S. G. Wood, J. J. Hassett, and W. L. Barnwart, *Environ. Sci. Technol.*, **16**, 93 (1982).
12) H. M. Seip, J. Alstad, G. E. Carlberg. K. Martinsen, and P. Skaane, *Sci. Total Environ.*, **50**, 87 (1986).
13) W. L. Banwart, J. J. Hassett, S. G. Wood, and J. C. Means, *Soil Sci.*, **133**, 42 (1982).
14) R. P. Wijayaratne and J. C. Means, *Mar. Environ. Res.*, **11**, 77 (1984).
15) C. T. Chiou, L. J. Peters, and V. H. Freed, *Science*, **206**, 381 (1979).

Rotational Lattice Vibrations of [$^1H_4$]- and [$^2H_4$]Pyrazine Crystals

Toshikazu HIEIDA, Masayoshi MAEHARA, Yoshinori NIBU, Hiroko SHIMADA,* and Ryoichi SHIMADA†

Department of Chemistry, Faculty of Science, Fukuoka University, Nanakuma, Jonan-ku, Fukuoka 814-01

†Department of Chemistry, Faculty of Science, Kyushu University 33, Hakozaki, Higashi-ku, Fukuoka 812

(Received September 8, 1988)

Synopsis. Low-frequency Raman bands of the [$^1H_4$]- and [$^2H_4$]pyrazine crystals were studied at various temperatures between 4.2 and 300 K. All six rotational lattice vibrations were identified based on the isotopic factor (the ratio of the vibrational frequency of the [$^1H_4$]- and [$^2H_4$]pyrazine crystals) of the individual vibrations. Classification of the rotational lattice vibrations into symmetry species was made through the polarization measurement of the Raman bands in single crystals.

The rotational lattice vibrations of pyrazine crystal were first studied by Ito and Shigeoka.[1] They observed five low-frequency Raman bands due to the rotational lattice vibrations and gave assignments for these bands on the basis of the normal coordinate calculation assuming intermolecular force constants of the pyrazine crystal. Their calculation indicated that the lowest vibrational frequency of the rotational lattice vibration would be about 20 cm^{-1} and they considered that the Raman band due to this lattice vibration could not be observed under their experimental conditions. Pasquier et al. also observed the low-frequency Raman bands of pyrazine crystal and determined the six rotational lattice vibrations based on the normal coordinate calculation,[2] although their assignments given for some bands are different from those given by Ito et al.

In this work the low-frequency Raman bands of the [$^1H_4$]- and [$^2H_4$]pyrazine crystals are reinvestigated and the assignments of the six rotational lattice vibrations are discussed based on the isotopic factor and the polarization behavior of the bands.

Experimental

Material. [$^2H_4$]Pyrazine was synthesized by exchange reaction of [$^1H_4$]pyrazine with D_2O using palladium asbestos as a catalyst.[3] The isotopic purity of the product was confirmed by nuclear magnetic resonance measurement. The samples were purified by repeated vacuum distillations.

Optical Measurements. Low-frequency Raman bands of the pyrazine crystals were observed with a SPEX 1402 doublemonochromator at 4.2 K and with a JEOL 400T laser Raman spectrophotometer at various temperatures between 77 and 300 K. The polarization behavior of the Raman bands was observed in the following way. It is known that the pyrazine crystal grows along the b axis and the crystal is twinned on the cleavage (101) plane.[4] A well-grown single crystal obtained by the Bridgman method was cut along the cleavage plane, which will be referred to as bc′ plane, where the c′ axis is inclined counterclockwise by 57.6° from the c axis in the ac plane, and was sealed in a small rectangular glass cell with the bc′ plane attaching to the cell face. The crystal in the cell was excited with the 514.5 nm beam from an Ar^+ ion laser. The power of the laser beam was adjusted low enough because of high sublimation property of the pyrazine crystal. The propagation direction of the excitation light beam was set to be parallel to the c′ axis or perpendicular to the bc′ plane. In this alignment the a′a′, bb, c′c′, a′b, and bc′ polarized Raman spectra were obtained by the back scattering method, where the a′ axis is taken to be perpendicular to the c′ axis in the ac plane and the first and second letters refer to the polarization directions of the excitation and scattering lights, respectively.

Results and Discussion

Pyrazine crystallizes in the orthorhombic space group P_{mnn} (D_{2h}^{12}) with two molecules in the unit cell.[4] The six rotational lattice vibrations are distributed among the four symmetry species: $1A_g+1B_{3g}+2B_{1g}+2B_{2g}$. The rotational modes of the molecule around the z axis give rise to the A_g and B_{3g} lattice vibrations and the rotational modes around the x and y axes give rise to the B_{1g} and B_{2g} lattice vibrations as shown in Table 1.[1] The x axis is taken to be perpendicular to the molecular plane and the y and z axes in the plane with the z axis passing through the nitrogen atoms.

The Raman spectra of the [$^1H_4$]- and [$^2H_4$]pyrazine crystals in the low-frequency region observed at 4.2 K are shown in Fig. 1. Seven Raman bands were clearly observed and their frequencies are given in Fig. 1 and Table 2. In this table the frequencies and assignments of the rotational lattice vibrations of the [$^1H_4$]pyrazine crystal determined by Ito et al.[1] and Pasquier et al.[2] are also given. The Raman band at 56 cm^{-1} observed by Ito et al. at 4.2 K resolved into two bands at 57 and 58 cm^{-1} and a weak additional Raman band was clearly observed at 116 cm^{-1}. No bands could be observed in the low frequency region around 20 cm^{-1} contrary to the prediction given by Ito et al. The observed Raman bands can be ascribed to the rotational lattice vibrations, if the isotopic factor of the bands ($\tilde{\nu}[^1H_4]/\tilde{\nu}[^2H_4]$) is equal to the value of $\{I_r[^2H_4]/I_r[^1H_4]\}^{1/2}$, where $\tilde{\nu}$ is the Raman frequency and I_r is the moment of inertia of the molecule about the axis r(=x, y, z). Using the values of the moments of inertia of the

Table 1. Raman Active Rotational Lattice Vibrations of Pyrazine Single Crystal

Symmetry species	Raman active polarization	Rotational modes about molecular axes
A_g	aa, bb, cc	R_z
B_{1g}	ab	R_x, R_y
B_{2g}	ac	R_x, R_y
B_{3g}	bc	R_z

Table 2. Rotational Lattice Vibrations of [$^1H_4$]- and [$^2H_4$]Pyrazine Crystals

[$^1H_4$]Pyrazine						[$^2H_4$]Pyrazine					
Ito[a]		Pasquier[b]	This work			This work			Isotopic factors		Assignments
$\tilde{\nu}$/cm^{-1}		$\tilde{\nu}$/cm^{-1}	$\tilde{\nu}$/cm^{-1}		Pol	$\tilde{\nu}$/cm^{-1}		Pol	$\tilde{\nu}[^1H_4]/\tilde{\nu}[^2H_4]$		
4.2 K	293 K	298 K	4.2 K	300 K		4.2 K	300 K		4.2 K	300 K	
		43	57	46	a'b, bc'	54	44	a'b, bc'	1.06	1.05	B_{1g} R_x, R_y
56	42	44	58	47	a'a', c'c'	55	45	a'a', c'c'	1.05	1.04	B_{2g} R_x, R_y
97	80	92	88	72	a'b, bc'	84	69	a'b, bc'	1.05	1.04	B_{1g} R_x, R_y
86	68	70	98	78	a'a', c'c'	93	74	a'a', c'c'	1.05	1.05	B_{2g} R_x, R_y
			116	93	a'a', bb, c'c'	105	85	a'a', bb, c'c'	1.11	1.09	A_g overtone
126	97	103	128	104	a'a', bb, c'c'	116	94	a'a', bb, c'c'	1.10	1.11	A_g R_z
134	109	109	136	115	a'b, bc'	125	104	a'b, bc'	1.09	1.11	B_{3g} R_z

a) See Ref. 1. b) See Ref. 2.

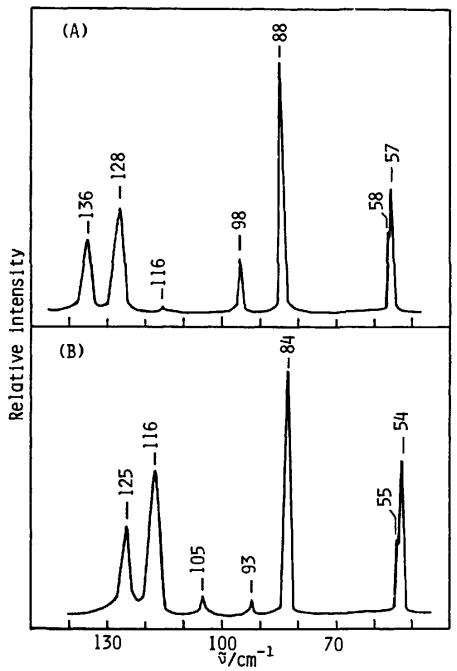

Fig. 1. The Raman spectra of the [$^1H_4$]- (A) and [$^2H_4$]pyrazine (B) crystals in the low-frequency region observed at 4.2 K.

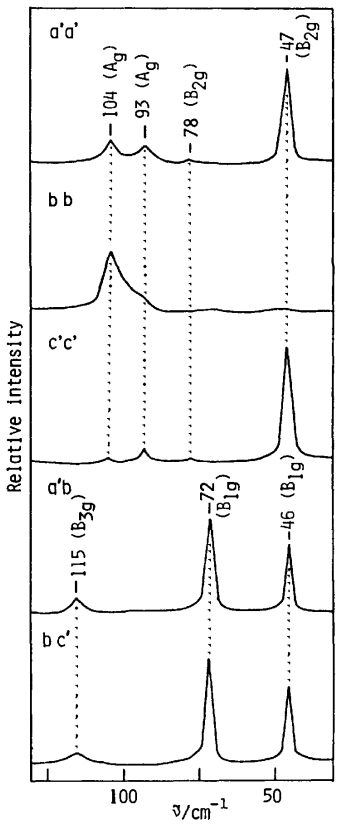

Fig. 2. The polarized Raman spectra of the [$^1H_4$]-pyrazine single crystal in the low-frequency region observed at 300 K.

[$^1H_4$]- and [$^2H_4$]pyrazine molecules calculated based on the molecular structure determined by Wheatley,[4] the isotopic factors were calculated to be 1.069, 1.036, and 1.105 for the rotational lattice vibrations about the x, y, and z axes, respectively.

The structures of the Raman spectra observed at various temperatures between 300 and 77 K are the same as that observed at 4.2 K except for the band width, which increases with increasing temperature. This indicates that no apparent phase transition takes place between 300 and 4.2 K. The polarized Raman spectra of the [$^1H_4$]pyrazine single crystal observed at 300 K are given in Fig. 2. According to Table 1, the lattice vibrations belonging to the symmetry species A_g will be observed in the aa, bb, and cc spectra and those belonging to the B_{1g}, B_{2g}, and B_{3g} species in the ab, ac, and bc spectra, respectively. The a'a' and c'c' spectra include the aa, cc, and ac spectra, while the a'b and bc' spectra include the ab and bc spectra because the a' and c' axes are in the ac plane. Therefore, the Raman bands observed in the bb spectrum should be assigned to the A_g species, those in the a'a' and c'c' spectra to the A_g or B_{2g} species, and those in the a'b and bc' spectra to the B_{1g} or B_{3g} species. The band at 115 cm^{-1}, whose isotopic factor is 1.11, was observed in the a'b and bc' spectra and the band at 104 cm^{-1} giving the isotopic factor of 1.11 was observed in the a'a', bb, and c'c' spectra. Therefore, these bands were assigned to the rotational lattice vibrations of the B_{3g} and A_g species about the molecular z axis, respectively. The

lowest wavenumber band could not resolve into doublet at 300 K. However, careful observation showed that the frequency of the bands observed in the a'a' and c'c' spectra was 47 cm^{-1} and that observed in the a'b and bc' spectra was 46 cm^{-1}. This observation indicates that the 47 and 46 cm^{-1} bands should be assigned to the vibrations belonging to the different symmetry species. The 46 and 47 cm^{-1} bands correspond to the 57 and 58 cm^{-1} bands observed at 4.2 K, respectively. The observed isotopic factors of the bands at 46, 47, 72, and 78 cm^{-1} ranges between 1.06 and 1.04 and thus these bands are to be assigned to the rotational modes about the molecular x and y axes. The 72 cm^{-1} band showed the a'b and bc' polarization and the 78 cm^{-1} band the a'a' and c'c' polarization behavior. Therefore, the 46 and 72 cm^{-1} bands were assigned to the B_{1g} species and the 47 and 78 cm^{-1} bands to the B_{2g} species although Ito et al. and Pasquier et al. gave different assignments for the 72 and 78 cm^{-1} bands as shown in Table 2. The band at 93 cm^{-1} showing the a'a', bb, and c'c' polarization behavior and giving the isotopic factor of 1.09 was assigned to the overtone vibration of the 46 and/or 47 cm^{-1} bands although Pasquier et al. assigned this band to the B_{1g} vibration. These assignments are given in Table 2.

The polarization behavior of the Raman bands of the [$^2H_4$]pyrazine crystal is exactly the same as that of the [$^1H_4$]pyrazine crystal. The assignments for the low-frequency Raman bands of the [$^2H_4$]pyrazine crystal are also given in Table 2. We believe that the polarization behavior of the Raman bands in single crystals gives clear and definite experimental justification for the vibrational assignments and the six rotational lattice vibrations of the [$^1H_4$]- and [$^2H_4$]-pyrazine crystals determined in this work are quite reasonable. The isotopic factors measured for the individual bands also confirm the reliability of the assignments.

The tetramethylpyrazine crystal hydrates quite easily with moisture in the air and the Raman bands due to the hydrated crystal were observed in the intramolecular and lattice vibrations.[5] In order to study the effect of hydration on the intramolecular and lattice vibrations of the pyrazine crystal, the Raman spectra of wet pyrazine crystal prepared by adding water to the pyrazine crystal were observed, but no distinct change of the spectral structure and vibrational frequencies were observed untill the pyrazine crystal deliquesces by water.

References

1) M. Ito and T. Shigeoka, *J. Chem. Phys.*, **44**, 1001 (1966).
2) B. Pasquier, D. Bougeard, N. le Calve, and R. Romain, *Mol. Cryst. Liq. Cryst.*, **32**, 17 (1976).
3) H.-H. Perkampus and E. Baumgarten, *Spectrochim. Acta*, **19**, 1473 (1963).
4) P. J. Wheatley, *Acta Crystallogr.*, **10**, 182 (1957).
5) M. Maehara, T. Hieida, Y. Nibu, H. Shimada, and R. Shimada, *Bull. Chem. Soc. Jpn.*, **61**, 2579 (1988).

The Ultraviolet Spectrum of Ozone Produced in the γ-Irradiated Liquid Nitrogen Containing a Small Amount of Oxygen

Hirotomo HASE,* Guangchuan JIN,† and Takenobu HIGASHIMURA
Research Reactor Institute, Kyoto University, Kumatori-cho, Sennan-gun, Osaka 590-04
†Jilin City Radiation Chemistry Research Institute, Jilin City, P. R. China
(Received September 16, 1988)

Synopsis. The ultraviolet spectrum observed in γ-irradiated liquid nitrogen containing a small amount of oxygen has been ascribed to ozone. The εG value was obtained. The dose rate effect on the yield of ozone was observed. The value of $\varepsilon_m G$ was inversely proportional to the square root of the dose rate. This allowed us to discuss the formation mechanism of ozone in liquid nitrogen.

It is well-known that ozone is produced in irradiated liquid nitrogen containing a small amount of oxygen and that the decomposition of such ozone sometimes leads to incidental explosions during the irradiation with γ-rays[1] electron beams[2] or reactor radiation.[3] The yield of ozone as a function of oxygen concentration in γ-irradiated liquid nitrogen has been measured by an indirect method.[4]

Although the optical absorption spectrum of gaseous ozone was previously reported,[5,6] there is no report of the ultraviolet absorption spectrum of ozone produced in γ-irradiated liquid nitrogen as far as we are aware. In the ultraviolet region there often appear the absorption bands due to ionic species or radicals when organic substances are irradiated in liquid nitrogen. So, if one uses the same cryostat for both irradiation and optical measurement, it becomes indispensable to distinguish the ultraviolet spectrum of the species from that of ozone.

In this study we report the ultraviolet spectrum of ozone produced in γ-irradiated liquid nitrogen. We also discuss the formation mechanism of ozone in connection with the effect of dose rate on the yield of ozone.

Experimental

Liquid nitrogen supplied by the Osaka Sanso Co. was used. Oxygen concentration in liquid nitrogen was measured by a zirconia type oxygen gas sensor and a gas chromatography. Although the concentration of oxygen in liquid nitrogen stored in a 3000 dm^3 storage tank was about 0.3 ppm, it amounted to 160±30 ppm after liquid nitrogen was transferred in air from a 5 dm^3 container to an optical cryostat. This nitrogen in the cryostat was used for both γ-irradiation and optical absorption measurement. Nitrogen gas evaporated inside the cryostat was released into atmosphere after passing through silicon oil in a gas wash bottle which was attached to the cryostat. This device prevented the outside air being dissolved in liquid nitrogen.

Liquid nitrogen was irradiated by γ-rays with various dose rates (163 Gy h^{-1}—1602 Gy h^{-1}). The total dose was always 801 Gy. Optical absorption measurements were carried out with a Shimadzu double beam spectrophotometer. Optical absorption spectra were recorded in the ultraviolet region of 210 nm$<\lambda<$320 nm and in the absorbance region of $0<A<4$.

Results and Discussion

The ultraviolet spectrum of liquid nitrogen recorded after the γ-irradiation with the dose rate of 1602 Gy h^{-1} is shown in Fig. 1(A), where ε is the molar absorption coefficient ($dm^3\ mol^{-1}\ cm^{-1}$) and G is the G-value (molecules formed/100 eV absorbed). The spectrum shows the wavelength of the absorption maximum (λ_{max}) of 255 nm, the half-height width ($W_{1/2}$) of 6.6×10^3 cm^{-1} and a vibrational band structure near the absorption maximum.

The apparent absorption intensity of the spectrum increased as the amount of liquid nitrogen in the cryostat decreased owing to the natural evaporation. The reciprocal plots of the absorption intensity against the evaporation time after the irradiation were linear for an extended period of time, e.g. 4 hours. This can be explained on the assumption that liquid nitrogen in the cryostat evaporates at a constant rate and that the species responsible for the absorption does not evaporate together with nitrogen, being dissolved in the remaining liquid nitrogen.

After liquid nitrogen in the cryostat was completely evaporated, the absorption measurement was again carried out in order to see if there is any absorption due to the residual gas inside the cryostat. The absorption

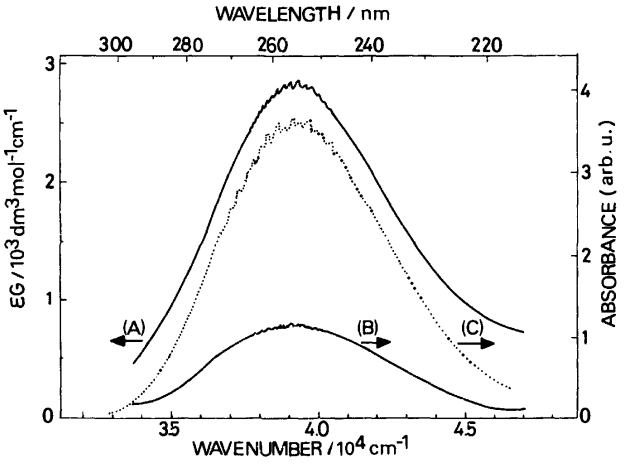

Fig. 1. The ultraviolet absorption spectra of ozone: (A) observed in γ-irradiated liquid nitrogen containing 160 ppm oxygen, (B) observed after liquid nitrogen was completely evaporated, and (C) reported spectrum of gaseous ozone (Ref. 5). The γ-irradiation was carried out at the dose rate of 1602 Gy h^{-1}. The total dose was 801 Gy.

spectrum thus recorded is shown in Fig. 1(B). The values of λ_{max} and $W_{1/2}$ of spectrum (B) were the same as those of spectrum (A). Opening the frange of the cryostat, we could smell irritatingly. The smell was characteristic of ozone. The ultraviolet spectrum of ozone at 300 K which was reported previously by other authors[6] is shown in Fig. 1(C), where the Hartley band structure is clearly seen near the absorption maximum. The values of λ_{max} and $W_{1/2}$ of spectra (A) and (B) were almost the same as those of spectrum (C). From these observations, we ascribe spectra (A) and (B) to ozone formed by γ-irradiation of liquid nitrogen containing the small amount of oxygen. The value of ε at $\lambda=\lambda_{max}$, ε_m, reported for ozone at 300 K[6] is 2900 $dm^3\,mol^{-1}\,cm^{-1}$. If we use this value for the present case, we obtain the G-value of ozone, $G(O_3)=1.0$ for the dose rate of 1602 Gy h^{-1}. It is reported, however, that the value of ε depends on temperature at temperatures higher than 300 K.[7] If this is also true at 77 K, the calculated $G(O_3)$ is not correct. Instead, if the empirical relationship between the value of ε and temperature[7] is extrapolated to 77 K, the value of ε becomes about 3500 $dm^3\,mol^{-1}\,cm^{-1}$ at 77 K so that $G(O_3)=0.83$ is obtained. Matumoto et al.[4] used the method of the stoichiometric reaction between ozone and nitrogen monoxide in order to determine $G(O_3)$. According to their results, one can estimate $G(O_3)=6.0$ under the conditions of the oxygen concentration of 160 ppm and the γ-dose rate of 1.1×10^4 Gy h^{-1}. Their value is much larger than ours. This may partly due to an enhanced reaction of oxygen atom with the quartz wall of the cryostat in our case. However, the discrepancy between the reported $G(O_3)$ and ours cannot be elucidated by the present knowledge.

A dose rate effect on the yield of ozone was observed. This is demonstrated in Fig. 2. It is seen from Fig. 2 that the plots of log ($\varepsilon_m G$) against log (dD_a/dt), where dD_a/dt is the dose rate, gave a straight line with the gradient of $-1/2$.

It was reported that N_3^+ ion is one of the major radiolytic products of nitrogen gas and that N_3^+ ion reacts with O_2 to give rise to oxygen atom.[8,9] On this basis, we put forward the following reaction mechanism for the formation of ozone in the γ-irradiated liquid nitrogen containing a small amount of oxygen:

$$N_2 \longrightarrow N_3^+ \quad (1)$$

$$N_3^+ + e^- \longrightarrow \text{neutralization} \quad (2)$$

$$N_3^+ + O_2 \longrightarrow O + NO^+ + N_2 \quad (3)$$

$$O + O_2 + N_2 \longrightarrow O_3 + N_2 \quad (4)$$

$$O + \text{wall} \longrightarrow 1/2O_2 + \text{wall} \quad (5)$$

The formation rate of N_3^+ ion is given by $\{G(N_3^+)/100N_0\}(dD_a/dt)$, where $G(N_3^+)$ is the G-value of N_3^+ ion, N_0 the Avogadro constant and dD_a/dt is the dose rate in the unit of eV $dm^{-3}\,s^{-1}$. During γ-irradiation the steady-state conditions of $d[N_3^+]/dt=d[e^-]/dt=d[O]/dt=0$ must be satisfied, where $[N_3^+]$, $[e^-]$, and $[O]$ are the concentration of N_3^+ ion, the excess electron, and oxygen atom. The rate constants of the Reactions 2 and 3, k_2 and k_3, are in the ranges of 10^{-6} and 10^{-10} $cm^3\,s^{-1}$ respectively.[10,11] The values of $\{G(N_3^+)/100N_0\}(dD_a/dt)$ and $[O]$ are in the ranges of 10^{-7} mol $dm^{-3}\,s^{-1}$ and 10^{-3} mol dm^{-3}, respectively in the present case. These values result in $\{G(N_3^+)/100N_0\}(dD_a/dt)\gg\{k_2[O^2]\}$.[2] Under this condition we obtain

$$G(O_3) = \{G(N_3^+)\}^{1/2} f([O_2],k_2,k_3,k_4,k_5)(dD_a/dt)^{-1/2}, \quad (6)$$

where k_4 and k_5 are the rate constants of the Reactions 4 and 5, respectively and $f([O_2],k_2,k_3,k_4,k_5)$ is given by

$$f = (100N_0)^{1/2} k_3 k_4 [O_2]^2 / \{(2k_2)^{1/2}(k_4[O_2] + k_5)\}. \quad (7)$$

Equation 6 shows that the yield of ozone is inversely proportional to the square root of the dose rate. Thus the observed dependence of log ($\varepsilon_m G$) on log (dD_a/dt) is explained by the proposed mechanism.

Matumoto et al.[4] investigated the effect of oxygen concentration on the yield of ozone in liquid nitrogen and proposed a mechanism for the formation of ozone in liquid nitrogen. According to their mechanism, the excited state of nitrogen molecule undergoes the reaction with oxygen molecule to produce oxygen atom. However, they did not discuss the mechanism in detail, since they did not investigate other effects e.g. the dose rate effect.

It may be instructive to mention the following. If the excited nitrogen molecules react with themselves or with other transient species which concentration is proportional to that of the excited nitrogen molecules and if the reaction is competitive to the reaction with oxygen molecule, one can obtain an equation which is essentially the same as Eq. 6. In this context it is beyond our present knowledge whether N_3^+ ion or an excited state of nitrogen is responsible for the formation of ozone in liquid nitrogen.

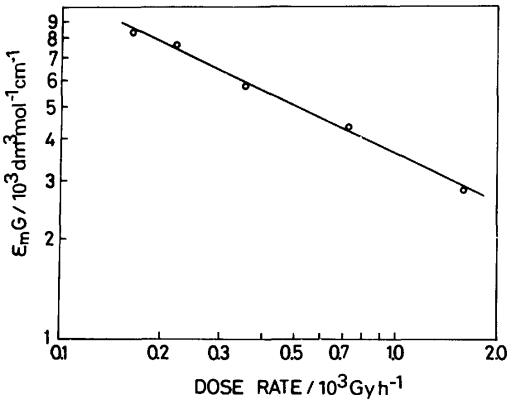

Fig. 2. Effect of the dose rate on $\varepsilon_m G$ of ozone produced in liquid nitrogen. The total dose was 801 Gy.

The authors are greatly indebted to Prof. Kenji Fueki, Nagoya University, for his valuable suggestions. The authors are greatful toi Messrs. Kenzo Kawamoto, Hisao Kodaka, and Kiyomi Miyata of Research Reactor Institute, Kyoto University for the measurement of oxygen concentration in liquid nitrogen.

References

1) Z. Kuri, *Genshiryoku Kogyo*, **7**, 30 (1961).
2) M. Takehisa, K. Yoshida, W. Kawakami, T. Seguchi, R. Tanaka, H. Watanabe, T. Watanuki, and E. Kikuchi, JAERI-M6363 (in Japanese), (1976).
3) C. W. Chen and R. G. Struss, *Cryogenics*, **131**, (1969).
4) A. Matsumoto, R. Yugeta, H. Karasawa, and S. Sato, *Bull. Chem. Soc. Jpn.*, **51**, 2838 (1978).
5) E. C. Y. Inn and Y. Tanaka, *J. Opt. Soc. Am.*, **43**, 870 (1953).
6) J. W. Simons, R. J. Paur, H. A. Webster III, and E. J. Bair, *J. Chem. Phys.*, **59**, 1203 (1973).
7) D. C. Astholz, A. E. Croce, and J. Troe, *J. Phys. Chem.*, **86**, 696 (1982).
8) J. L. McCrumb and P. Warneck, *J. Chem. Phys.*, **66**, 5416 (1977).
9) D. Smith, N. G. Adams, and T. M. Miller, *J. Chem. Phys.*, **69**, 308 (1978).
10) W. H. Kasher and M. A. Biondi, *Phys. Rev.*, **137**, 317 (1965).
11) D. B. Dunkin, F. C. Fehsenfeld, A. L. Schmelfekopf, and E. E. Ferguson, *J. Chem. Phys.*, **54**, 3817 (1971).

Inversion at the Sulfur Atom in Bis(diethyl sulfide)-(1,1,2,2-tetraacetylethane-*C,O'*)platinum(II)

Shinsaku YAMAZAKI* and Tomoharu AMA†
Chemistry Laboratory, Kochi Gakuen College, 292 Asahi tenjin-cho, Kochi 780
†Department of Chemistry, Faculty of Science, Kochi University,
2-5-1 Akebono-cho, Kochi 780
(Received May 9, 1988)

Synopsis. Variable temperature ^{1}H NMR suggests that the metal-carbon bonded Pt(II) complex of 1,1,2,2-tetraacetylethane(dahd=3,4-diacetyl-2,4-hexadiene-2,5-diol), [Pt(dahd-C^3,O')(SEt_2)$_2$] undergoes two distinct rearrangements at the sulfides, one of which is accompanied by an anomalous dissociation process. From a comparison of the estimated kinetic parameters for inversion, an arrangement of the two sulfides in planar geometry is proposed.

A number of studies concerning internal exchange processes of pyramidal sulfur have been done on Pt(II) and Pt(IV) complexes with symmetry.[1-6] ^{1}H NMR spectral change of methylene hydrogens from the AB(ABCD) to the A_2 spin system in *trans*-[MCl_2{S-(CH_2SiMe_3)$_2$}$_2$] (M=Pd, Pt),[3] [MCl_2{S(Ph)(CH_2SiMe_3)}$_2$] (M=Pd, Pt),[3] *cis*-[$PtCl_2(SEt_2)_2$][6] has been sufficiently explained by the inversion process on the assumption of fast M-S and S-C bond rotations. Still, sulfur inversion in a Pt(II) complex with low symmetry is relatively elusive.

The authors have recently prepared several anomalous 1,1,2,2-tetraacetylethane Pd(II) and Pt(II) complexes, in which the ligand links a metal with the (*C,O'*)-chelate; [M(dahd-C^3,O')L_2]{M=Pd, L_2=1,10-phen;[7] M=Pt, L=SEt_2, PMe_2Ph, L_2=2,9-R_2-1,10-phen (R=H, Me)}.[8] They have formerly been characterized by means of ^{1}H, ^{13}C NMR {^1J(^{195}Pt-C^3)=489 Hz} and Fast Atom Bombardment Mass Spectroscopy (M^+=572).[8] Of them, ^{13}C NMR of [Pt(dahd-C^3,O')(SEt_2)$_2$] at the ambient temperature unexpectedly shows an absence of ^{195}Pt satellites in resonances due to one SEt_2. These findings led us to investigate the rearrangement dynamics of pyramidal sulfides arranged unsymmetrically in square planar geometry, one of which may possibly proceed via some dissociation.

This note will deal with the inversion processes of two distinct sulfides in [Pt(dahd-C^3,O')(SEt_2)$_2$], as studied by variable-temperature ^{1}H NMR; moreover, from a comparison of the activation parameter of inversion, an arrangement of the sulfides will also be discussed.

Results and Discussion

^{1}H NMR pattern of [Pt(dahd-C^3,O')(SEt_2)$_2$] in $CDCl_3$ changes with the temperature, as is shown in Fig. 1. The changes are remarkable in resonances due to methylene hydrogen of SEt_2 (δ 2.4—3.3). Throughout the temperature change, two distinct resonance patterns (S^1, S^2) were obtained. This finding is, as expected, consistent with no mutual exchange of the sulfides. The signals arising from S^1 show a quartet with no ^{195}Pt satellite at 308 K, consistent with its ^{13}C NMR. On the other hand, the resonances arising from S^2 obviously show the ^{195}Pt satellite {J(^{195}Pt-H)=28.8Hz}, though the coupling constant is relatively small compared with those of 46.4 and 37.2 Hz

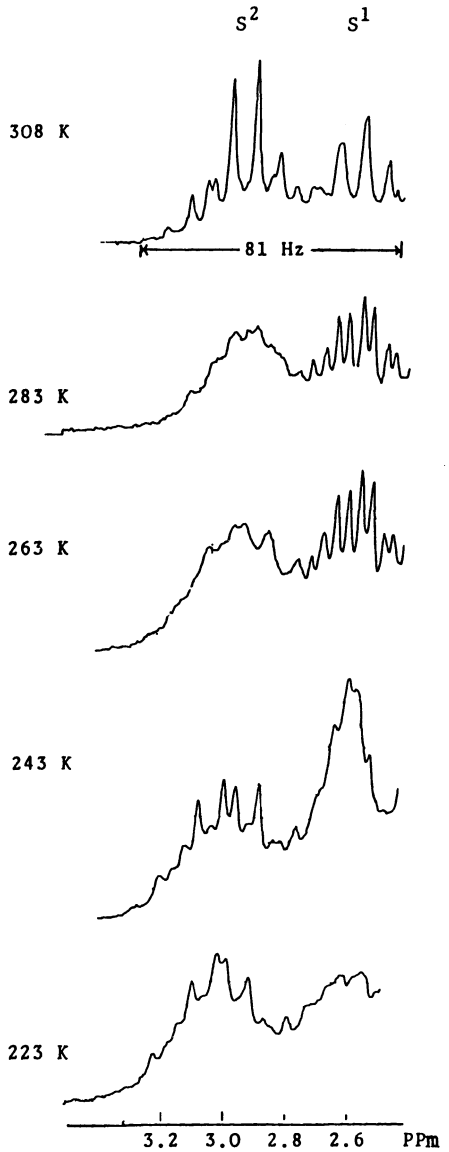

Fig. 1. Variable temperature ^{1}H NMR (resonances due to methylene proton of SEt_2) of Pt(dahd-C^3,O')(SEt_2)$_2$ in $CDCl_3$. The spectra were recorded using Hitachi R-90H FT NMR (90.04 MHz) operating Fourier transform mode. Deviation of temperature control was ±2%±1° on the centigrade temperature scale.

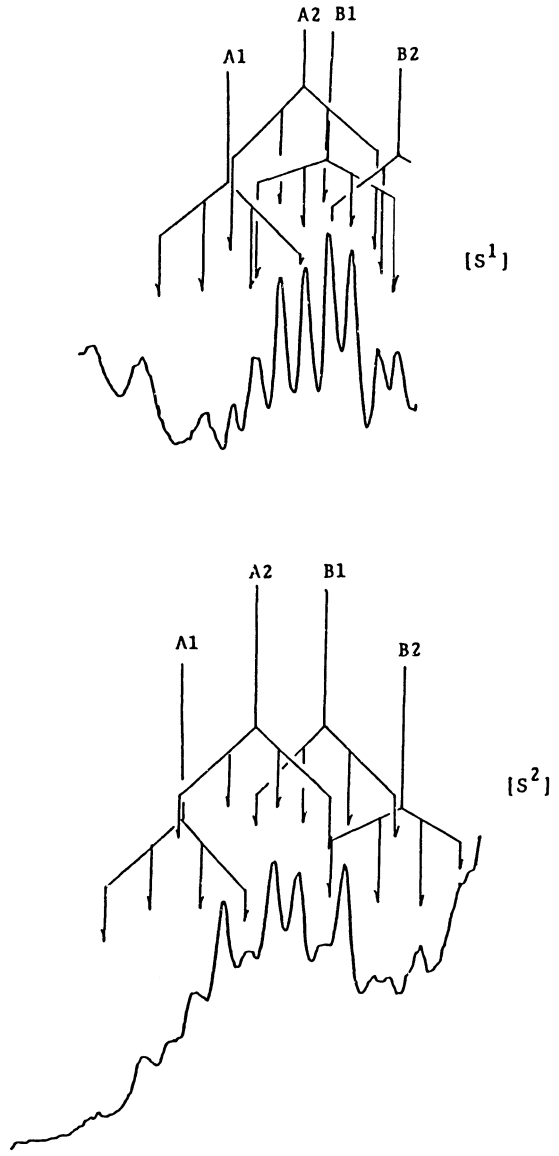

Fig. 2. AB part of ABM_3 spin system assigned to methylene hydrogen at; S^1 at 263 K and S^2 at 243 K.

found for *cis*- and *trans*-$[PtCl_2(SEt_2)_2]$[6] respectively over the coalescence temperature.

The resonances due to S^2 at 283 K are very close to coalescence, but below 283 K the resonaces separate. At 243 K, four predominant quartets could be discerned with $J(H,H')=7.2$ Hz, although the complete analysis of $J(^{195}Pt-H)$ could not be performed. However the spectrum is in good agreement with the simulated lines of ABM_3 spin system with $J_{AB}=11.7$ and $J_{AM}=J_{BM}=7.2$ Hz. A spin-system change, $ABM_3 \rightleftarrows A_2M_3$, thus arising from S^2 corresponds to an averaging process of two pairs of methylene hydrogen. This mutual exchange of methylene hydrogen cannot be explained by rotation about the Pt-S and S-C bonds. The only process causing such an exchange is inversion at the pyramidal sulfur atom. The effect of inversion is shown in Fig. 3 as a preferred conformation, [A] or [B]. The symmetry plane bisecting the pyramidal sulfide ligand for both conformations is in coplanar with the coordination plane where the two conformations are enantiometrically related and where the methylene protons between the two groups are indistinguishable magnetically. The [B] conformation is obtained by the inversion of S^2 in [A] together with a 180° rotation about the Pt-S^2 bond and 120° rotation about the S^2-C bond; the net effect is a mutual exchange of methylene hydrogen. Concerning the so-called hindered rotation, no firm spectral evidence has been obtained in the Pt(II) and Pd(II) complexes so far

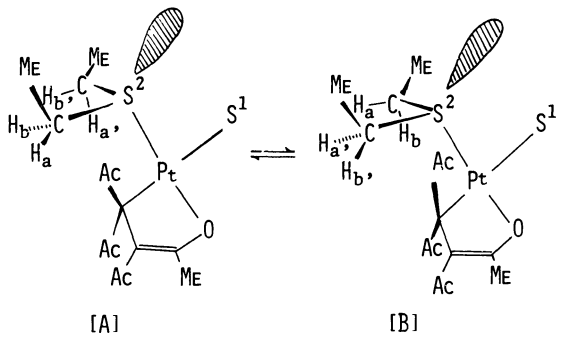

Fig. 3. A conformation [B] is obtained by inversion at S^2 in [A] together with 180° rotation about Pt-S bond and 120° rotation about S-C bond.

Table 1. Variable-Temperature ^1H NMR Data

T/K	$\Delta\nu$/Hz[a]		J_{AB}/Hz[b]		ΔG^*/kJ·mol^{-1}[c]		k/s^{-1}[d]	
	S^1	S^2	S^1	S^2	S^1	S^2	S^1	S^2
308					67.7			
	}[T_c]				|		}21.7(±0.4)	
283		[T_c]			62.0	65.8(±0.1)		45.0(±0.2)
263	9.70(±0.2)		11.3(±0.5)					
243		20.1(±0.1)		11.7(±0.1)				

a) Spacing estimated by $\sqrt{(A1-B2)(A2-B1)}$, where A1, A2, B1, and B2 are the chemical shifts due to the ABM_3 spin system observed for methylene hydrogen in the order of low-field resonances. b) Coupling constant $J_{H,H}$ within the methylene group. c) Calculated by the use of $\Delta G^*/RT_c=22.96+\ln(T_c/\Delta\nu)$, where ΔG^* is the activation parameter for the inversion of sulfide at the coalescence temperature; R. J. Abraham and P. Loftus, "Proton and Carbon-13 NMR spectroscopy-An Integrated Approach," Heydon and Son (1978). d) Inversion rate calculated by the use of $k=RT_c/Nh \exp(-\Delta G^*/RT_c)$. e) Coalescence may exist between 283—308 K, and its ΔG^* was arbitrarily estimated, with 283 K as its lower limit and 308 K as its upper limit. f) Coalescence temperature.

studied even at 213 K,[3] which can be assumed to be fast. In the present case also, the rotation about Pt–S^2 bond is tentatively presumed to be fast in the NMR time scale. The activation parameter for the inversion process at S^2 was thus estimated to be $\Delta G^*(T_c=283\ K)=65.8\ kJ\cdot mol^{-1}$ and k (inversion rate at T_c)$=45.0\ s^{-1}$. These activation parameters obtained for [Pt(dahd-C^3,O')(SEt_2)$_2$] are comparable with those of $\Delta G^*=70.3\ kJ\cdot mol^{-1}$ and $k=64.7\ s^{-1}$ ($T_c=333$ K) found for *cis*-[$PtCl_2(SEt_2)_2$] and those of $58.2\ kJ\cdot mol^{-1}$ and $k=36.4\ s^{-1}$ ($T_c=274$ K) for its trans form.

On the other hand, low-temperature ^1H NMR (resonances arising from S^1Et_2) shows an analogous and more explicit spectral change, while its ^{13}C NMR at the ambient temperature exhibits no ^{195}Pt satellites. The coalescence temperature is in the vicinity of 300 K. The resonances at 263 K, which seem to be two quartets overlapping, are, however, assigned to the AB part of the ABM_3 spin system; the spectrum accords well with lines simulated using the five-spin system with $J_{AB}=11.3$ and $J_{AM}=J_{BM}=7.2$ Hz. We could not, unfortunately, obtain precise information whether or not ^{195}Pt–H coupling exists at that temperature. The spin system change thus arising from S^1, $ABM_3 \rightleftarrows A_2M_3$, corresponds to an averaging process of methylene hydrogen and can also be explained only by an inversion process. However, this inversion cannot proceed intramolecularly, because the lack of ^{195}Pt–H and ^{195}Pt–C couplings indicates a bond breakage of the sulfide, S^1. In fact, on the addition of the free ligand SEt_2 into [Pt(dahd-C^3,O')(SEt_2)$_2$], only the broad resonances arising from S^1, whose spectrum is close to the coalescence temperature, became a sharp and single quartet with an increase in the intensity, while its chemical shift did not change. For the spectral change with the temperature due to S^1, T_c has not definitely been fixed. The activation free energy was arbitrarily estimated at the two temperatures, 283 and 308 K, to be 62.0 and $67.7\ kJ\cdot mol^{-1}$ respectively. Although such a rough estimation for ΔG^* gives a fair deviation, the inversion rates k thus derived at both temperatures eventually approach $21.7\ s^{-1}$, unaccompanied by any significant deviations. Accordingly, the inversion rate of S^1 estimated at 283 K can be compared with that of S^2, which unexpectedly results in one half of the rate of S^2. As has been established formerly,[8] S^1 in [Pt(dahd-C^3,O')(SEt_2)$_2$] is readily displaced by PPh_3 to give [Pt(dahd-C^3,O')(PPh_3)(S^2Et_2)], in which PPh_3 is arranged trans to C^3\{$J(^{31}P-C^3)=60$ Hz\}. By accounting for the trans labilizing effect: C(3)(from $acac^-$)> O(from $acac^-$),[8,9] S^1 undergoing rearrangement via a bond breakage should be arranged trans to C(3) from the $dahd^{2-}$. If an analogous intramolecular rearrangement can be presumed, the inversion of S^1 should proceed much faster than that of S^2. In contrast to this expectation, the inversion rate of S^1, accompanied by bond dissociation, is comparatively much slower than that of S^2. It is most likely that the rearrangement of S^1 proceeds via an intermolecular pathway.[10]

One of the present authors (S. Y.) wishes to thank Yasuko Tanaka (Applied Engineering Center, Hitachi, Ltd., Ibaragi) for obtaining the NMR spectra.

References

1) P. Haake and P. C. Turley, *Inorg. Nucl. Chem. Lett.*, **2**, 173 (1966).
2) E. W. Abel, A. R. Khan, K. Kite, K. G. Orrel, and V. Sik, *J. Chem. Soc., Dalton Trans.*, **1980**, 1175.
3) E. W. Abel, G. W. Farrow, K. G. Orrel, and V. Sik, *J. Chem. Soc., Dalton Trans.*, **1977**, 42.
4) P. Woodward, L. F. Dahl, E. W. Abel, and B. G. Grosse, *J. Am. Chem. Soc.*, **87**, 5251 (1965).
5) P. Haake and P. C. Turley, *J. Am. Chem. Soc.*, **89**, 4611 (1967).
6) P. C. Turley and P. Haake, *J. Am. Chem. Soc.*, **89**, 4617 (1967).
7) S. Yamazaki, *Polyhedron*, **5**, 1183 (1986).
8) S. Yamazaki, T. Ama, and Z. Taira, *Polyhedron*, **7**, 353 (1988).
9) A. Yamamoto, "Organometallic Chemistry-Principle and Applications," Syokabo, Tokyo (1986); F. Basolo and R. G. Pearson, "Mechanism of Inorganic Reactions," 2nd ed., John Wiley, New York (1967); T. Ito, T. Kiriyama, Y. Nakamura, and A. Yamamoto, *Bull. Chem. Soc. Jpn.*, **49**, 3257 (1976).
10) J. B. Lambert, *Topics Stereochem.*, **6**, 19 (1971).

XPS Study of Binuclear Mo(V) Complexes with Di-μ-oxo, μ-Oxo-μ-sulfido, and Di-μ-sulfido Bridges

Hideaki TAKAHASHI,† Takashi SHIBAHARA,†† and Yoshihisa YAMAMOTO*
Faculty of Pharmaceutical Sciences, Higashi Nippon Gakuen University, Ishikari-Tobetsu, Hokkaido 061-02
†Faculty of Engineering, Hokkaido University, Sapporo 060
††Department of Chemistry, Okayama University of Science, 1-1 Ridai-cho, Okayama 700
(Received August 4, 1988)

Synopsis. X-Ray photoelectron spectroscopy (XPS) was applied to three binuclear molybdenum(V) complexes of di-μ-oxo-, μ-oxo-μ-sulfido-, and di-μ-sulfido-bis[(cysteinato)-oxomolybdate(V)]$^{2-}$, $[Mo_2(\mu\text{-}O)_x(\mu\text{-}S)_yO_2(cys)_2]^{2-}$ (x=2, y=0; x=y=1; and x=0, y=2), and the electronic state for Mo atom of the $(\mu\text{-}O)_2$ bridge, $(\mu\text{-}O, \mu\text{-}S)$ bridge and $(\mu\text{-}S)_2$ bridge complexes was studied. It has been found that the binding energy of the Mo $3d_{5/2,3/2}$ peaks shifts to a lower value by at most 0.5 eV with increasing the number of μ-S bridges from 0 to 2. On the other hand, those of O 1s, C 1s, N 1s, and S 2s peaks are not significantly affected by bridge substitution. The change in the electronic state of Mo atoms is discussed in terms of the low electronegativity of the S atom.

The structures of binuclear molybdenum(V)–cysteine complexes with oxo and sulfide bridges, $[Mo_2(\mu\text{-}X)(\mu\text{-}Y)O_2(cys)_2]^{2-}$ (X,Y=O or S, cys: $SCH_2CH(NH_2)CO_2$), have been examined though X-ray analyses (Fig. 1) by several investigators, Knox et al.[1] have determined the structure of $Na_2[Mo_2(\mu\text{-}O)_2O_2(cys)_2]\cdot 2H_2O$ (abbreviation: $(\mu\text{-}O)_2$ bridge), Brown et al.[2] have dealt with

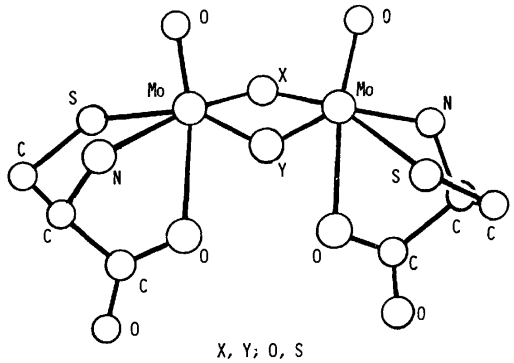

Fig. 1. The structure of $[Mo_2(\mu\text{-}X)(\mu\text{-}Y)O_2(cys)_2]^{2-}$.

$Na_2[Mo_2(\mu\text{-}S)_2O_2(cys)_2]\cdot 5H_2O$ (abbreviation: $(\mu\text{-}S)_2$ bridge), and Shibahara et al.[3] have elucidated the structure of $Ca[Mo_2(\mu\text{-}O)(\mu\text{-}S)O_2(cys)_2]\cdot 3H_2O$ (abbreviation: $(\mu\text{-}O)(\mu\text{-}S)$ bridge). A comparison of data between $(\mu\text{-}O)_2$ and $(\mu\text{-}S)_2$ bridge complexes for the structure allows us to recognize that a complex with a $(\mu\text{-}S)_2$ bridge has longer distances between Mo–Mo and Mo–O_{cys}, and a shorter distance between Mo–O_t than does a complex with a $(\mu\text{-}O)_2$ bridge. This may be due to a difference in the electronic state of Mo atoms between these two complexes.

The present paper deals with the electronic state of the $(\mu\text{-}O)_2$ bridge, the $(\mu\text{-}O)(\mu\text{-}S)$ bridge and $(\mu\text{-}S)_2$ bridge complexes by XPS measurements.

Experimental

Preparation of Complexes. $Na_2[Mo_2(\mu\text{-}O)(\mu\text{-}O)O_2(cys)_2]\cdot 5H_2O$, $Na_2[Mo_2(\mu\text{-}O)(\mu\text{-}S)O_2(cys)_2]\cdot 4H_2O$ and $Na_2[Mo_2(\mu\text{-}S)(\mu\text{-}S)O_2(cys)_2]\cdot 5H_2O$ were prepared according to published procedures.[4]

Measurements. XPS measurements were carried out in a vacuum of around 1.3×10^{-7} Pa with irradiation of Mg $K\alpha$ X-rays ($h\nu$=1253.6 eV) to the sample mounted on a holder with Au-mesh, using a VG ESCA 3 electron spectrometer. The binding energes (E_B) of all peaks was corrected by taking the kinetic energy ($=h\nu-E_B$) of the Na KLL Auger peak to be 990.0 eV, in order to avoid any ambiguity in accurately determining the value of E_B of broad C 1s peaks.

Results and Discussion

In spectra for $Na_2[Mo_2(\mu\text{-}O)(\mu\text{-}O)O_2(cys)_2]\cdot 5H_2O$, $Na_2[Mo_2(\mu\text{-}O)(\mu\text{-}S)O_2(cys)_2]\cdot 4H_2O$, and $Na_2[Mo_2(\mu\text{-}S)(\mu\text{-}S)O_2(cys)_2]\cdot 5H_2O$, there appeared to be O 1s, C 1s, N 1s, S 2p, S 2s, Mo $3d_{5/2}$, Mo $3d_{3/2}$, Mo $3p_{3/2}$, and Mo $3p_{1/2}$ ESCA-peaks and O(KLL), and Na(KLL) Auger-peaks. The binding energy (E_B) and the full width at half

Table 1. Binding Energy (E_B)[a] and Full Width at Half Maximum (FWHM)[b] of Peaks Obtained for Binuclear Molybdenum(V)–Cysteine Complexes

Complex		C 1s	O 1s	S 2p	N 1s	Mo 3d		Mo 3p	
						5/2	3/2	3/2	1/2
$Na_2[Mo_2(\mu\text{-}O)(\mu\text{-}O)O_2(cys)_2]\cdot 5H_2O$	E_B (eV)	285.2	531.5	162.4	400.0	231.3	234.4	397.2	414.7
	FWHM (eV)	3.4	2.7	2.8	2.5	3.0	2.4	3.4	3.3
$Na_2[Mo_2(\mu\text{-}O)(\mu\text{-}S)O_2(cys)_2]\cdot 4H_2O$	E_B (eV)	285.2	531.6	162.4	400.2	231.2	234.4	396.9	414.5
	FWHM (eV)	3.2	2.6	2.7	2.6	3.0	2.2	3.8	3.4
$Na_2[Mo_2(\mu\text{-}S)(\mu\text{-}S)O_2(cys)_2]\cdot 5H_2O$	E_B (eV)	285.4	531.6	162.3	400.1	230.8	233.9	396.6	414.3
	FWHM (eV)	3.3	2.6	2.6	2.7	2.8	2.0	3.7	3.4

a) The value of E_B for all peaks was corrected by using the kinetic energy of Na KLL Auger peak to be 990.0 eV.
b) The value of FWHM for N 1s, Mo $3d_{5/2}$, Mo $3d_{3/2}$, and Mo $3p_{3/2}$ was obtained by a peak deconvolution with computer analysis.

maximum (FWHM) of the ESCA-peaks are shown in Table 1. All of the examined complexes have relatively broad C 1s peaks, because of a difference in E_B of C 1s between hydrocarbon and carbonyl group in the cysteine ligand. Each complex shows relatively sharp peaks of N 1s, O 1s, and S 2p; these peaks have similar values of E_B and FWHM. This suggests that the O and S atoms included in a different functional group have similar electronic states, and that the electronic states of N, O, and S atoms are not significantly affected by bridge substitution.

The binding energy of Mo $3d_{5/2}$ and Mo $3d_{3/2}$ peaks for the $(\mu\text{-S})_2$ complex is lower by about 0.4 and 0.5 eV than those for the $(\mu\text{-O})(\mu\text{-S})$ and $(\mu\text{-O})_2$ complexes, respectively, and Mo $3p_{3/2,1/2}$ peaks also show about 0.3 eV of chemical shift to the lower binding energy side by substituting $(\mu\text{-S})_2$ for a $(\mu\text{-O})_2$ bridge.[5] This strongly suggests that the electron density for Mo atoms in a $(\mu\text{-S})_2$ complex is higher than that in $(\mu\text{-O})(\mu\text{-S})$ and $(\mu\text{-O})_2$ complexes. The lower electronegativity of the S atom, compared with that of the O atom, could make the electron density for Mo atoms higher, leading to an enhancement of the covalent bonding characteristics of the bridge.

Recently, similar effects of the S atom have been reported for other type of complexes. Ikari et al.[6] examined $[M_2(\mu\text{-X})(\mu\text{-Y})O_2(edta)]^{2-}$ complexes (M: Mo or W; X, Y: O or S) by XPS. They reported that E_B of Mo $3d_{5/2}$ peak for the $(\mu\text{-O})(\mu\text{-S})$ complexes is lower by 1.2 eV than that for the $(\mu\text{-O})_2$ complex, and that W $4f_{7/2}$ peak shifts 1.1 eV lower by substituting $(\mu\text{-S})_2$ bridge for $(\mu\text{-O})_2$ bridge. Shibahara et al.[7] showed a decrease of ca. 2 eV in E_B of the Mo $3d_{5/2}$ peak by replacing O-bridge with S-bridge for $[Mo_3O_{4-n}S_n(NCS)_9]^{5-}$ (n=0—3). Ansari et al.[8] reported that E_B of W $4d_{5/2}$ for $[W_2O_2(\mu\text{-S})_2(S_2CNEt_2)_2]$ is higher by 0.5 eV than that for $[W_2S_2(\mu\text{-S})_2(S_2CNEt_2)_2]$. The chemical shift of the Mo 3d peak observed in this investigation by the bridge substitution seems to be smaller than that reported for the other type of complexes stated above. Thus, the electronic state of the central metal atoms can be appreciably affected by the electronic effect, steric effect, coordination number or configuration of the coordinated ligands in complexes.

References

1) J. R. Knox and C. K. Prout, *Acta Crystallogr., Sect. B*, **25**, 1857 (1969).

2) D. H. Brown and J. A. D. Jeffreys, *J. Chem. Soc., Dalton Trans.*, **1973**, 732.

3) T. Shibahara, H. Kuroya, K. Matsumoto, and S. Ooi, *Bull. Chem. Soc. Jpn.*, **60**, 2277 (1987).

4) V. R. Ott, D. S. Swieter, and F. A. Schultz, *Inorg. Chem.*, **16**, 2538 (1977), and references therein.

5) The lower chemical shift in Mo $3p_{3/2,1/2}$ peaks compared with that in Mo $3d_{5/2,3/2}$ peaks may be due to a less effect of charge density change for Mo atom on E_B of the more inner orbital of Mo.

6) S. Ikari, Y. Sasaki, and T. Ito, *Inorg. Chem.*, in press.

7) T. Shibahara, H. Tsuru, and H. Kuroya, *Inorg. Chim. Acta*, **150**, 167 (1988). The following values (eV) of E_B of Mo $3d_{5/2}$ were obtained: $[Mo_3(\mu_3\text{-O})(\mu\text{-O})_3(NCS)_9]^{5-}$, 231.8; $[Mo_3(\mu_3\text{-S})(\mu\text{-O})_3(NCS)_9]^{5-}$, 229.8; $[Mo_3(\mu_3\text{-S})(\mu\text{-O})_2(\mu\text{-S})(NCS)_9]^{5-}$, 229.6; $[Mo_3(\mu_3\text{-S})(\mu\text{-O})(\mu\text{-S})_2(NCS)_9]^{5-}$, 229.5; $[Mo_3(\mu_3\text{-S})(\mu\text{-S})_3(NCS)_8(H_2O)]^{4-}$, 229.2.

8) M. A. Ansari, J. Chandrasekaran, and S. Sarkar, *Bull. Chem. Soc. Jpn.*, **61**, 2265 (1988).

Synthesis of Heterobinuclear Cu(II)Ni(II) Complexes with Bis(tetraazamacrocycle)

Katsura MOCHIZUKI* and Yumiko ENDOH
Department of Chemistry, Yokohama City University, Yokohama 236
(Received September 7, 1988)

Synopsis. A new series of heterobinuclear Cu(II)Ni(II) complexes with bis(tetraazamacrocycle), i.e., 7,7′-polymethylenebis[2,12-dimethyl-3,7,11,17-tetraazabicyclo[11.3.1]heptadeca-1(17),2,11,13,15-pentaene]copper(II)nickel(II) perchlorates with polymethylene bridges with a length of 2—6-C, were synthesized by a template reaction.

Metal–metal interactions of homobinuclear Cu(II)-Cu(II)[1-4] and Ni(II)Ni(II)[3-6] complexes with bis(tetraazamacrocycle) have been actively studied by means of the ESR spectroscopical,[1-4] magnetical,[1] and electrochemical methods.[2-6] Recently we synthesized the Ni(II)Ni(II) complexes with several ligands, 7,7′-polymethylenebis[2,12-dimethyl-3,7,11,17-tetraazabicyclo[11.3.1]heptadeca-1(17),2,11,13,15-pentaene](polymethylene = ethylene (L^2), trimethylene (L^3), tetramethylene (L^4), pentamethylene (L^5), and hexamethylene (L^6)), in which two of the same tetraazamacrocycles are linked by polymethylene bridges of various lengths.[6] Our electrochemical study of the Ni(II)Ni(II) complexes revealed that the metal–metel interaction operates when the polymethylene bridge is shorter than that of tetramethylene.[6]

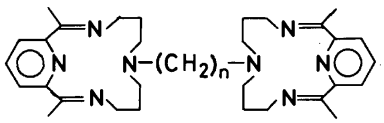

L^2 : n = 2
L^3 : n = 3
L^4 : n = 4
L^5 : n = 5
L^6 : n = 6

In order to investigate the metal–metal interaction of two different metals, a series of heterobinuclear complexes with L^2—L^6 is required. To the best of our knowledge, however, no such heterobinuclear complex has yet been synthesized except for one compound, $[Cu^{II}Ni^{II}(bis(cyclam))]^{4+}$,[4] which was prepared by the addition of Ni(II) and Cu(II) ions to an aqueous solution of a presynthesized ligand, bis(cyclam), i.e., by a complexation reaction.

In this paper we will describe the synthesis of a series of heterobinuclear Cu(II)Ni(II) complexes with L^2—L^6 by the use of a template reaction; this is the first example of the preparation of heterobinuclear complexes with bis(tetraazamacrocycle) by a template reaction.

In seeking for the proper reaction conditions for the preparation of heterobinuclear Cu(II)Ni(II) complexes, the following characteristic results were obtained. (1) When *N,N,N′,N′*-tetrakis(3-aminopropyl)-1,4-butanediamine, hereafter termed a branched polyamine, was added to a solution containing both Cu(II) and Ni(II) ions and 2,6-diacetylpyridine, the mixture immediately turned blue, indicating that the Cu(II) ion is more favorable for the template reaction than the Ni(II) ion. In fact, after the mixture had been kept at 60 °C for 6 h, the homobinuclear Cu(II)Cu(II)[1] complex was isolated as the major product, and the Cu(II)Ni(II) and Ni(II)Ni(II)[6] complexes, as minor ones. (2) When the template reaction was performed without the Cu(II) ion under the conditions used for the preparation of Cu(II)Ni(II) complexes (see Experimental), the expected monomacrocyclic Ni(II) complex, formed by the template reaction on a single side of the branched polyamine, could not be obtained, but the bismacrocyclic Ni(II)Ni(II) complex was. These results suggest that it is difficult to stop the second cyclization reaction and/or to isolate the monocyclic Ni(II) complex. (3) When a solution including equimolar amounts of the Ni(II)Ni(II) complex and the Cu(II) ion was heated at 50 °C for 3 h, no changes occurred, suggesting that the Ni(II) ion in the complex is not replaced by the Cu(II) ion. On the basis of these results, the procedures described in the experimental section were employed for the preparation of Cu(II)-Ni(II) complexes.

Because the template reaction always afforded a mixture of Cu(II)Cu(II),[1] Cu(II)Ni(II), and Ni(II)-Ni(II)[6] complexes, its products should be separated by column chromatography of SP-Sephadex C-25 ion-exchange resin, followed by elution with an aqueous solution of 0.5 mol dm^{-3} NaCl. In every instance of chromatography, the blue Cu(II)Cu(II) complex was eluted first, the reddish-violet Cu(II)Ni(II) complex second, and the orange Ni(II)Ni(II) complex last. This clear separation of the three bands indicates that the second band is not a mixture of the Cu(II)Cu(II) and Ni(II)Ni(II) complexes.

In fact, the complexes isolated from the second band, the Cu(II)Ni(II) complexes, were characterized as follows.

In the IR spectra, all the complexes show distinct bands at about 1620 ($\nu_{C=N}$) and 1580 cm^{-1} (the skeletal vibration of pyridine), but no bands corresponding to $\nu_{C=O}$ and the vibrations of the free amines, indicating a formation of the cyclic ligand by the condensation of diacetylpyridine with branched polyamines.

The presence of Cu(II) and Ni(II) ions in a ratio of 1:1 was determined by polarography. The complexes were decomposed with H_2O_2–H_2SO_4; the subsequent solutions, containing a NH_3–NH_4^+ buffer (pH 10),

showed three waves, at −0.02, −0.32, and −0.87 V vs. Hg-pool, which were assigned to the Cu^{II}/Cu^{I}, Cu^{I}/Cu^{0}, and Ni^{II}/Ni^{0} couples respectively. By a comparison of these wave heights with those of a standard solution containing both Cu(II) and Ni(II) ions, the amounts of the metals were determined (see the elemental analyses in Experimental).

The absorption spectra and differential pulse polarograms (DP) show that the products have two macrocycles of Cu(II) and Ni(II) complexes in the same molecule. Figure 1 shows the absorption spectrum of $[Cu^{II}Ni^{II}(L^4)]^{4+}$ in an aqueous solution; it is practically equal to the sum of the spectrum of $[Ni^{II}_2(L^4)]^{4+}$ and that of $[Cu^{II}_2(L^4)]^{4+}$. The same conclusion was also obtained by differential pulse polarography. Figure 2 shows the DP observed in the oxidation of $[Cu^{II}Ni^{II}(L^4)]^{4+}$ in acetonitrile. The peak of the Ni^{II}/Ni^{III} couple (ca. 1.2 V) is symmetrical, suggesting that the electrode process is quasi-reversible;

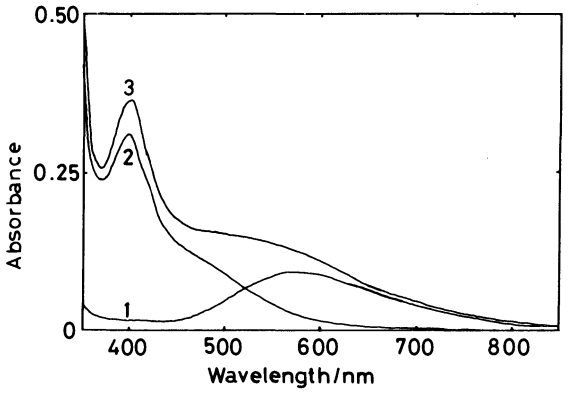

Fig. 1. Absorption spectra of the aqueous solution of $[MM'(L^4)]^{4+}$: 2×10^{-4} mol dm^{-3} M=M'=Cu(II) (1), 2×10^{-4} mol dm^{-3} M=M'=Ni(II) (2), 4×10^{-4} mol dm^{-3} M=Cu(II) and M'=Ni(II) (3). T=25 °C.

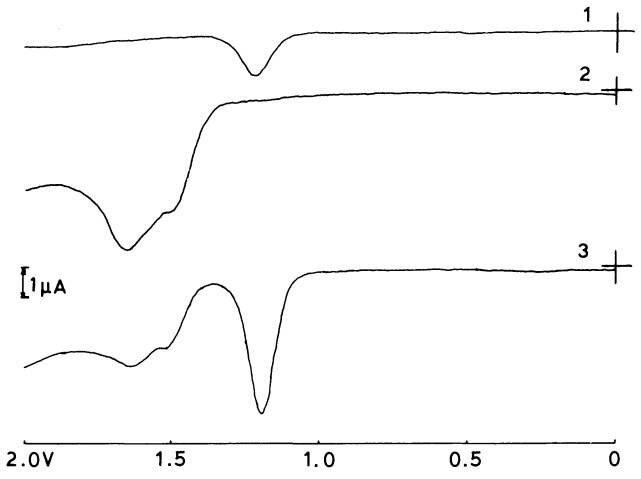

Fig. 2. Differential pulse polarograms (scan rate: 1 mV s^{-1}; pulse amplitude: 10 mV) of $[MM'(L^4)]^{4+}$ in acetonitrile: M=M'=Ni(II) (1), M=M'=Cu(II) (2), M=Cu(II) and M'=Ni(II) (3). V vs. $Ag-Ag^+$ (0.01 mol dm^{-3} $AgNO_3$). Glassy carbon electrode.[11] T= 25 °C.

also, it is well-separated from that of the Cu^{II}/Cu^{III} couple. The DP of $[Cu^{II}Ni^{II}(L^4)]^{4+}$ is again equal to the sum of the DP of $[Cu^{II}_2(L^4)]^{4+}$ and that of $[Ni^{II}_2(L^4)]^{4+}$. Similar results in the absorption spectra and DPs were obtained for the other binuclear complexes prepared herewith.

Thus, the desired heterobinuclear Cu(II)Ni(II) complexes were successfully obtained.[7]

Experimental

Materials. A typical procedure for the preparation of the heterobinuclear complexes was as follows.

2,6-Diacetylpyridine (3.26 g, 0.02 mol) and nickel(II) acetate tetrahydrate (2.49 g, 0.01 mol) were dissolved in 200 cm^3 of ethanol-water (1:1, v/v). To this solution we then added 100 cm^3 of ethanol-water (1:1, v/v) containing *N,N,N',N'*-tetrakis(3-aminopropyl)-1,4-butanediamine (3.22 g, 0.0102 mol) which had been neutralized with acetic acid just before the addition. After the solution had then been stirred for 3.5 h at 60 °C, 100 cm^3 of an ethanol-water (1:1, v/v) solution containing copper(II) acetate monohydrate (2.00 g, 0.01 mol) was added. The mixture was stirred for 4.5 h at 60 °C, left to stand at room temperature for 1 h, evaporated to half of its original volume, and then filtered. To the filtrate we added a saturated aqueous sodium perchlorate solution to obtain dark brown precipitates. The precipitates were suspended in a small amount of water and then the suspension was passed through a column of Cl-form anion-exchange resin (Amberlite IRA410, ϕ=30 mm, l=300 mm) to exchange the counter ions. The resulting clear solution was chromatographed with a cation-exchange column (SP-Sephadex C-25, ϕ=30 mm, l=1250 mm), with 0.5 mol dm^{-3} sodium chloride solution as the eluant, to give three well-separated bands. The first, blue-violet band and the third, reddish-yellow one were assigned to the homobinuclear Cu(II)Cu(II)[1] and Ni(II)Ni(II)[6] complexes respectively by comparison with authentic samples. The second, dark-reddish-purple eluate was concentrated to ca. 20 cm^3. The sodium chloride then precipitated by the addition of ethanol to the solution was filtered off. The same procedure was repeated five times in order to remove all the sodium chloride. The residue thus obtained was dissolved in a minimum amount of water, to which was added a saturated aqueous sodium perchlorate solution to yield microcrystalline precipitates. After dissolving the precipitates in a small amount of hot water, the addition of a small amount of $HClO_4$ gave crystals, which were then washed well with water and dried over P_2O_5 in a vacuum. The absence of chloride ions in the complex was checked by the use of $AgNO_3$.

The physical data of the new compounds are given below. $[Cu^{II}Ni^{II}(L^4)](ClO_4)_4\cdot2H_2O$: Yield: 8%.[8] Found: C, 36.28; H, 4.49; N, 9.91; Cu, 5.5; Ni, 5.1%. Calcd for $C_{34}H_{50}N_8CuNiCl_4O_{16}\cdot2H_2O$: C, 36.24; H, 4.83; N, 9.94; Cu, 5.64; Ni, 5.21%. IR (KBr): 1619 (C=N) and 1580 cm^{-1} (py).

The hexamethylene, pentamethylene, and trimethylene derivatives were prepared by the same procedure except that for using *N,N,N',N'*-tetrakis(3-aminopropyl)-1,6-hexanediamine, *N,N,N',N'*-tetrakis(3-aminopropyl)-1,5-pentanediamine, and *N,N,N',N'*-tetrakis(3-aminopropyl)-1,3-propanediamine were used instead of *N,N,N',N'*-tetrakis(3-aminopropyl)-1,4-butanediamine. In the case of ethylene derivative (*N,N,N'N'*-tetrakis(3-aminopropyl)-1,2-ethanediamine), however, a longer reaction time (8 and 9 h after the addition of the Ni(II) and Cu(II) ions respectively) was required, because only small amounts of macrocyclic products were obtained under the conditions described

above.

$[Cu^{II}Ni^{II}(L^6)](ClO_4)_4 \cdot 2H_2O$: Yield: 10%.[8] Found: C, 37.53; H, 4.72; N, 9.65; Cu, 5.8; Ni, 4.8%. Calcd for $C_{36}H_{54}N_8CuNiCl_4O_{16} \cdot 2H_2O$: C, 37.44; H, 5.06; N, 9.70; Cu, 5.50; Ni, 5.08%. IR (KBr): 1615 (C=N) and 1575 cm^{-1} (py).

$[Cu^{II}Ni^{II}(L^5)](ClO_4)_4 \cdot 2H_2O$: Yield: 8%.[8] Found: C, 36.51; H, 4.64; N, 9.58; Cu, 5.8; Ni, 5.1%. Calcd for $C_{35}H_{52}N_8CuNiCl_4O_{16} \cdot 2H_2O$: C, 36.85; H, 4.95; N, 9.82; Cu, 5.57; Ni, 5.14%. IR (KBr): 1615 (C=N) and 1575 cm^{-1} (py).

$[Cu^{II}Ni^{II}(L^3)](ClO_4)_4 \cdot 2H_2O$: Yield: 8%.[8] Found: C, 35.63; H, 4.44; N, 10.04; Cu, 5.3; Ni, 4.9%. Calcd for $C_{33}H_{48}N_8CuNiCl_4O_{16} \cdot 2H_2O$: C, 35.62; H, 4.71; N, 10.07; Cu, 5.71; Ni, 5.27%. IR (KBr): 1620 (C=N) and 1580 cm^{-1} (py).

$[Cu^{II}Ni^{II}(L^2)](ClO_4)_4$: Yield 27%.[8,9] Found: C, 36.19; H, 4.29; N, 10.38; Cu, 5.5; Ni, 5.1%. Calcd for $C_{32}H_{46}N_8CuNiCl_4O_{16}$: C, 36.16; H, 4.36; N, 10.54; Cu, 5.78; Ni, 5.34%. IR (KBr): 1615 (C=N) and 1585 cm^{-1} (py).

Measurements. The infrared and visible absorption spectra were measured with Hitachi 260-10 and Hitachi 340 spectrophotometers respectively. The electrochemical measurements were performed according to the method described in our previous paper.[10]

The present work was partially supported by a Grant-in-Aid for Scientific Research (No. 62740352) from the Ministry of Education, Science and Culture.

References

1) I. Murase, K. Hamada, and S. Kida, *Inorg. Chim. Acta*, **54**, L171 (1981); I. Murase, K. Hamada, S. Ueno, and S. Kida, *Synth. React. Inorg. Met.-Org. Chem.*, **13**, 191 (1983); I. Murase, S. Ueno, and S. Kida, *Inorg. Chim. Acta*, **111**, 57 (1986).

2) M. Ciampolini, M. Micheloni, N. Nardi, F. Vizza, A. Buttafava, L. Fabbrizzi, and A. Perotti, *J. Chem. Soc., Chem. Commun.*, **1984**, 998; L. Fabbrizzi, F. Forlini, A. Perotti, and B. Seghi, *Inorg. Chem.*, **23**, 807 (1984); A. Buttafava, L. Fabbrizzi, A. Perotti, A. Poggi, and B. Seghi, *Inorg. Chem.*, **23**, 3917 (1984).

3) R. Schneider, A. Riesen, and T. A. Kaden, *Helv. Chim. Acta*, **68**, 53 (1985).

4) L. Fabbrizzi, L. Montagna, A. Poggi, T. A. Kaden, and L. Siegfried, *Inorg. Chem.*, **25**, 2671 (1986); L. Fabbrizi, L. Montagna, A. Poggi, T. A. Kaden, and L. C. Siegfried, *J. Chem. Soc., Dalton Trans.*, **1987**, 2631.

5) E. K. Barefield, D. Chueng, D. G. Van Derveer, and F. J. Wagner, *J. Chem. Soc., Chem. Commun.*, **1981**, 302.

6) K. Mochizuki and A. Iijima, 37th Annual Meeting on Coordination Chemistry, Tokyo, October 1987, Abstr., No. 2CP07; K. Mochizuki, *Bull. Chem. Soc. Jpn.*, **61**, 1023 (1988).

7) The product ratios of the Cu(II)Cu(II):Cu(II)Ni(II):Ni(II)Ni(II) complexes were as follows: 0.30:1:0.18 (L^2); 0.12:1:1.1(L^3); 0.23:1:1.0(L^4); 0.48:1:1.2(L^5); 0.28:1:1.4(L^6). If there is no difference in reactivity between Cu(II) and Ni(II) ions, the product ratio can be expected to be 1:2:1. However, the experimental results did not agree with this surmise.

8) The overall yield (isolated after recrystallization) is calculated by assuming that the reaction gave the Cu(II)-Ni(II) complex only.

9) The conditions employed for the preparation of the complexes with L^3—L^6 gave only small amounts of the macrocyclic products. Prolonging the reaction time considerably increased the yield of $[Cu^{II}Ni^{II}(L^2)]^{4+}$. These results might be explained as indicating that the electrostatic repulsion between two metal ions which are located close to each other during the reactions is serious in the case of the ethylene derivatives, thus retarding the template reaction.

10) K. Mochizuki and M. Fujimoto, *Bull. Chem. Soc. Jpn.*, **58**, 1520 (1985).

11) Similar results were obtained with the Pt-electrode.

Preparation of Bismuth Sulfide Thin Films by Solution Pyrolysis of Bismuth Dithiocarbamate Complexes

Ryoki NOMURA,* Kouichi KANAYA, and Haruo MATSUDA
Department of Applied Chemistry, Faculty of Engineering,
Osaka University, Yamada-Oka, Suita, Osaka 565
(Received October 8, 1988)

Synopsis. Solution pyrolysis of $Bi(S_2CNRR')_3$ in *p*-xylene or chloroform on a glass substrate at 350 °C under Ar atmosphere gave polycrystalline and low resistive (10^2 Ω cm in dark) bismuth sulfide thin films which showed large photoelectric effect.

Bismuth sulfide (Bi_2S_3) is the direct band gap material with E_g of 1.3 eV[1] and useful for photodiode arrays or photovoltaics.[2,3] Preparation of photoconducting Bi_2S_3 thin layers has so far been limited to the physical methods such as vacuum evaporation[4] or sintering.[5] However, to develop the chemical thin film process has been considered to be indispensable to produce large area chalcogenide layers in low cost.[6,7] Thus, some chemical processes such as dip-dry method,[2] chemical liquid deposition (CLD)[7,8] and solution-gas interface technique[9] have already examined, but they generally supplied highly resistive and amorphous Bi_2S_3 films. Recently, we have reported the preparation of several polycrystalline oxide or sulfide thin films via a "solution pyrolysis" technique (printing method) using organometallics[10] and/or metal dithiocarbamate complexes.[11] The printing method is the most convenient procedure for the preparation of thin layers,[11] however, the method remains unemployable state yet bacause of a lack of suitable precursor compounds for Bi_2S_3 layers. Therefore we attempted to prepare Bi_2S_3 films via the solution pyrolysis using bismuth dithiocarbamate complexes ($Bi(S_2CNRR')_3$) on the basis of their thermal analysis data.

Experimental

General. Characterization of the obtained bismuth sulfide films were performed with a Rigaku Rota-flex X-ray diffractometer (Cu $K\alpha$, 40 kV), a Shimadzu ESCA 650B, a Hitachi S-405 type scanning electron microscope (SEM), and a Shimadzu UV-200S spectrophotometer. Resistivity was measured by means of four probe method using a Tycoon 841 type apparatus. Thermal analysis of the bismuth dithiocarbamate complexes was done with a SEIKO TG/DTA 20 type thermal analyzer. Commercial bismuth(III) oxide (Mitsuwa, purity >99.9%) was used without purification. Other reagents and solvents were used after distillation.

Preparation of $Bi(S_2CNRR')_3$. Preparation of $Bi(S_2CNRR')_3$ was conducted with the procedure reported previously.[12] Into a suspension of Bi_2O_3 (6 mmol) in methanol (20 ml), carbon disulfide (50 mmol), and amines (40 mmol) were added dropwise in this order. The mixture was stirred for 19—48 h at room temperature and the resulting yellow precipitates were recrystallized from methanol or chloroform. **$Bi(S_2CNEt_2)_3$**: Mp 194—196 °C (lit,[13] 194—195 °C); IR (KBr) 1490 cm^{-1}. **$Bi(S_2CNBu^n_2)_3$**: Mp 98—99 °C; IR (KBr) 1480 cm^{-1}; Found: C, 39.42; H, 6.60; N, 5.11; S, 23.42%. Calcd for $C_{27}H_{54}BiN_3S_6$: C, 39.45; H, 6.62; Bi, 25.42; N, 5.11; S, 23.40%. **$Bi(S_2CNHex^n_2)_3$**: Mp 80—81 °C; IR (KBr) 1480 cm^{-1}; Found: C, 45.31; H, 8.24; N, 4.38; S, 20.10%. Calcd for $C_{36}H_{78}BiN_3S_6$: C, 45.30; H, 8.24; Bi, 21.90; N, 4.40; S, 20.16%. **$Bi(S_2CNHBu^i)_3$**: Mp 140 °C (decomp); IR (KBr) 1510 cm^{-1}; Found: C, 27.47; H, 4.45; N, 6.26; S, 29.03%. Calcd for $C_{15}H_{30}BiN_3S_6$: C, 27.55; H, 4.63; Bi, 31.96; N, 6.43; S, 29.43%.

Preparation of Bismuth Sulfide Films by Solution Pyrolysis Method. A detailed technique for the solution pyrolysis was reported previously.[10,11] About a 100 μl of 10 wt-% solution of $Bi(S_2CNRR')_3$ in the prescribed solvent was dropped onto a glass substrate (IWAKI Code 2926 WSLID-P, 76×26 mm) and spread over the whole surface by tipping. Thus the substrate was heated in a quartz tube under Ar atmosphere. A heating sequence was as follows: 1) 100 °C for 1 h, 2) cooling to room temperature, 3) 250—350 °C for 1 h. Chloroform and *p*-xylene were selected as the solvents for $Bi(S_2CNEt_2)_3$ and for $Bi(S_2CNBu^n_2)_3$ and $Bi(S_2CNHex^n_2)_3$, respectively.

Results and Discussion

We first investigated on the thermal properties of $(BiS_2CNRR')_3$, in order to optimize the process for

Table 1. Thermal Analysis Data of Bismuth Dithiocarbamate[a]

Compound	TG			DTA
	Weight loss		%-weight loss (calcd)[b]	
	Start/°C	End/°C		Endothermic peak[c]/°C
$Bi(S_2CNEt_2)_3$	248	350	60.0 (60.7)	192, 328
$Bi(S_2CNBu^n_2)_3$	262	348	67.5 (68.7)	99, 317
$Bi(S_2CNHex^n_2)_3$	266	346	76.0 (72.9)	79, 313
$Bi(S_2CNHBu^i)_3$	100	218	55.6 (60.7)	146

a) Conditions: instrument, SEIKO TG/DTA 20; N_2 flow; heating program, 10 °C min^{-1}, rt—500 °C. b) Values of total %-weight loss are presented. Calcd means the weight loss to give Bi_2S_3 and is indicated in the parentheses. c) Underlined temperatures showed the melting points.

preparation of Bi_2S_3 films, and the results are summarized in Table 1. It was found that the $Bi(S_2CNRR')_3$ employed here decomposed with endotherms. Three dialkyl derivatives decomposed at around 310—330 °C and gave Bi_2S_3 powders quantitatively till 350 °C. While $Bi(S_2CNHBu^i)_3$ decomposed at ca. 150 °C and also gave Bi_2S_3 powders. Although $Bi(S_2CNHBu^i)_3$ seemed to be a more suitable precursor for the preparation of Bi_2S_3 only from its decomposition temperature, it decomposed with a significant degree of vaporization, and its solubility was too low to use in the solution pyrolysis. Therefore, we investigated to prepare Bi_2S_3 films using the dialkyldithiocarbamate complexes.

If the solution on the substrate was directly heated at the pyrolysis temperatures (250—350 °C), only Bi_2S_3 powders deposited and no film was obtained. While, a "preheating" at 100 °C for 1 h which preceded the calcination was found to be effective to inhibit the formation of powders and the two step heating process gave smooth and homogeneous thin layers. In the following discussion, the term "temperature" will indicate the second step temperature.

The X-ray diffraction patterns of the obtained films are displayed in Fig. 1. The intensities of the diffraction peaks increased with temperature rising from 250 to 350 °C. The Bi_2S_3 films obtained from $Bi(S_2CNBu^n_2)_3$ at 350 °C possessed the polycrystalline texture as shown in Fig. 2. The surface morphology of this film rather resembled the vacuum-evaporated Bi_2S_3 films[9] than those obtained by CLD method.[7a] Observation by ESCA on the surface and the cross sectional composition indicated that the film was the stoichiometric Bi_2S_3.

Generally, it is well-known that the Bi_2S_3 films prepared by the chemical process show high resistivity (10^6—10^{13} Ω cm) and low sensitivity of the photoelectric response.[2,3,7] In contrast, the Bi_2S_3 films obtained by the solution pyrolysis of $Bi(S_2CNRR')$ in this study possessed relatively low resistivity (10^{2-3} Ω cm in dark) as shown in Table 2. It is obvious that the degree of the photoelectric effect increases with an increase of the crystallinity. The specimen prepared from $Bi(S_2CNBu_2)_3$ at 350 °C showed the largest photoelectric response and the difference of the dark and the light resistivities was found to be more than two orders of magnitude. In addition, optical band gap energy $(E_g)_{opt}$ of this sample was also estimated to be 1.40 eV by UV-visible spectrometry, which was lower than those of the Bi_2S_3 films obtained by other chemical method (1.47—1.65 eV)[3,5] and slight larger than the value for single crystal (1.3 eV).[1]

Thus, polycrystalline and low resistive Bi_2S_3 thin films can be conveniently prepared from bismuth

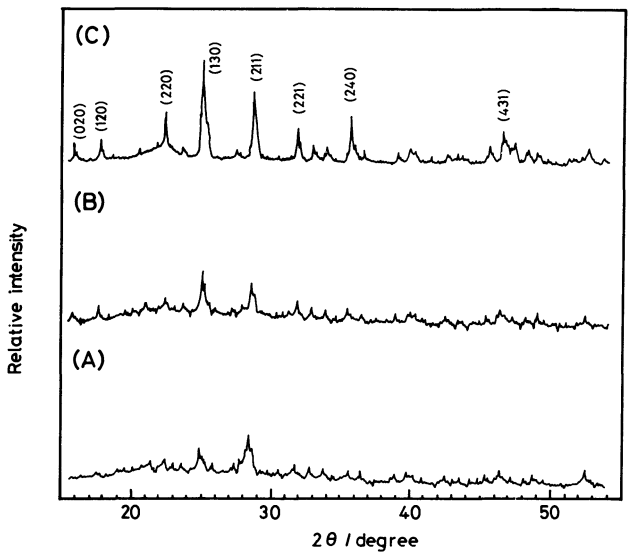

Fig. 1. Typical X-ray diffraction patterns of as-deposited bismuth sulfide thin films obtained by solution pyrolysis of $Bi(S_2CNBu^n_2)_3$ at 250 °C (A), 300 °C (B), and 350 °C (C), under Ar atmosphere for 1 h.

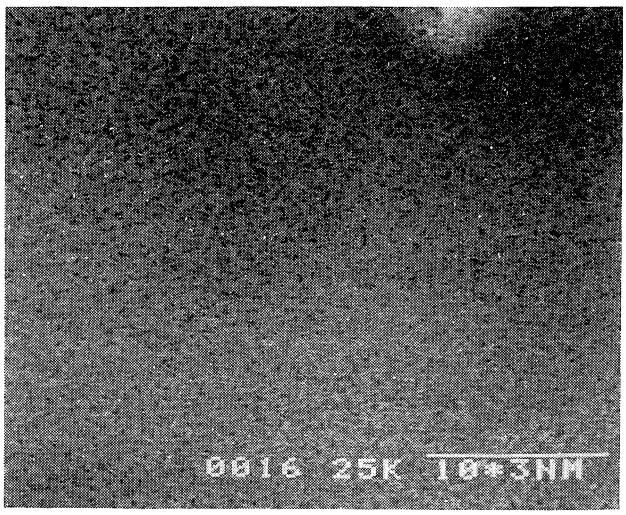

Fig. 2. Surface profile of as deposited Bi_2S_3 films from $Bi(S_2CNBu^n_2)_3$ at 350 °C. The measure bar indicates 10 μm.

Table 2. Resistivity of Bi_2S_3 Thin Films Prepared from $Bi(S_2CNR_2)_3$

Precursor $Bi(S_2CNR_2)_3$ R=	T/°C	Resistivity[a]/Ω cm		Thickness[b]/nm
		Dark	Light[c]	
Et	350	3.1×10^3	3.2×10^2	870
Bu^n	300	2.3×10^3	3.7×10^2	200
	350	2.6×10^3	1.0×10^1	250
Hex^n	350	8.2×10^2	4.1×10^2	200

a) Four probe method. b) SEM cross section. c) Under irradiation of a 60 W tungsten lump (distance from the specimen, 30 cm).

dithiocarbamate complexes by solution pyrolysis at 350 °C under Ar atmosphere. In addtion, preparation of Bi_2S_3 films is now feasible under the innert atmosphere such as Ar without the use of the hazardous sulfuration reagents such as H_2S and CS_2 which are necessary in other chemical process to maintain the Bi_2S_3 stoichiometry.[2,3,7,8]

References

1) J. Black, E. M. Conwell, L. Seigle, and C. W. Spencer, *J. Phys. Chem. Solids*, **2**, 240 (1957).

2) B. B. Nayak, H. N. Acharya, G. B. Mitra, and B. K. Mathur, *Thin Solid Films*, **105**, 17 (1983).

3) S. H. Pawar, P. N. Bhosale, M. D. Uplane, and S. Tanhankar, *Thin Solid Films*, **110**, 165 (1983).

4) A. Lopez-Otero, *Thin Solid Films*, **49**, 3 (1978); C. Ghosh and B. P. Vorma, *ibid.*, **60**, 61 (1979); J. George and M. K. Radhakrishnan, *J. Phys. D*, **14**, 899 (1981); P. A. Krishna Moorthy and G. K. Shrivakumar, *Thin Solid Films*, **121**, 151 (1984).

5) M. J. Chokalingam, K. N. Rao, N. Rangarajar, and C. V. Suryanarayan, *J. Phys. D*, **3**, 1641 (1970).

6) N. Croitoru and S. Jakobson, *Thin Solid Films*, **56**, L5 (1979).

7) a) P. Pramanik and R. N. Bhattachrya, *J. Electrochem. Soc.*, **127**, 2087 (1980); b) R. N. Bhattacharya and P. Pramanik, *ibid.*, **129**, 332 (1982); c) S. Biswas, A. Mondal, D. Mukherjee, and P. Pramanik, *ibid.*, **133**, 48 (1986).

8) B. B. Nayak, S. K. Singh, and B. S. Acharya, *Phys. Stat. Solidi (A)*, **105**, 455 (1988).

9) P. Pramanik and S. Bhattachrya, *J. Mater. Sci. Lett.*, **6**, 1105 (1987).

10) R. Nomura, S.-J. Inazawa, H. Matsuda, and S. Saeki, *Polyhedron*, **6**, 507 (1987); R. Nomura, A. Moritake, K. Kanaya, and H. Matsuda, *Thin Solid Films*, in press.

11) R. Nomura, K. Kanaya, and H. Matsuda, *Chem. Lett.*, **1988**, 1849.

12) R. Nomura, A. Takabe, and H. Matsuda, *Polyhedron*, **6**, 411 (1987).

13) G. E. Manoussakis and P. Karayannidis, *Inorg. Nucl. Chem. Lett.*, **6**, 71 (1970).

Asymmetric Hydrogenation Using Diphenylphosphinite Derivatives of Carbohydrates as the Chiral Ligand of Rhodium Catalysts

Mitsuji YAMASHITA,* Manabu NAOI, Hiroyuki IMOTO, and Tatsuo OSHIKAWA
Department of Applied Chemistry, Faculty of Engineering, Shizuoka University, Hamamatsu 432
(Received March 26, 1988)

Synopsis. Diphenylphosphinite derivatives of carbohydrates (L-rhamnose, D-mannitol, and cellulose), which have asymmetric centers on the skeletons were synthesized. Asymmetric hydrogenations of prochiral substrates using rhodium catalysts with the prepared chiral phosphinite ligand were carried out to obtain chiral substances in 8—78% optical yield.

Monosaccharides have several chiral carbon atoms in their skeletons, however, their applications to homogeneous asymmetric hydrogenation are found only in several papers.[1-6] Cellulose, which widely exists in nature, is one of the most important naturally occurring resources and will work as a functional polymer, however, the investigation to apply the chirality to asymmetric induction are very much limited. As the result, the application of a bisphosphinite of cellulose to a chiral ligand for the rhodium catalyst was reported.[7]

In our preceding paper we reported the asymmetric hydrogenation of prochiral unsaturated acid derivatives to afford the corresponding saturated acid derivatives in an optical yields up to 100%, where methyl 2,3-*O*-isopropylidene-4-*O*-(diphenylphosphino)-α-L-rhamnopyranoside was revealed to be a good ligand for di-μ-chloro-bis(cyclooctadiene)dirhodium(I) catalyst.[6b] In this note we tried to clarify the efficiency of asymmetric hydrogenation catalysts in comparison with the preparative methods for the catalyst as well as the structure to spread the utility of carbohydrate ligands for asymmetric inductions.

Results and Discussion

Synthesis of Carbohydrate Ligands. Methyl 2,3-*O*-isopropylidene-4-*O*-(diphenylphosphino)-α-L-rhamnopyranoside (**1**) was prepared by the reaction of the anion of methyl 2,3-*O*-isopropylidene-α-L-rhamnopyranoside with diphenylphosphinous chloride in ether, compound **1** thus prepared being agreed with that reported.[6b] 1,2:5,6-Di-*O*-isopropylidene-3,4-di-*O*-(diphenylphosphino)-D-mannitol (**2**) was prepared from 1,2:5,6-di-*O*-isopropylidene-D-mannitol by an action of diphenylphosphinous chloride in the presence of triethylamine (Eq. 1). 2,3,6-Tri-*O*-(diphenylphosphino)cellulose (**3**) was prepared from cellulose and diphenylphosphinous chloride in the presence of pyridine (Eq. 2).

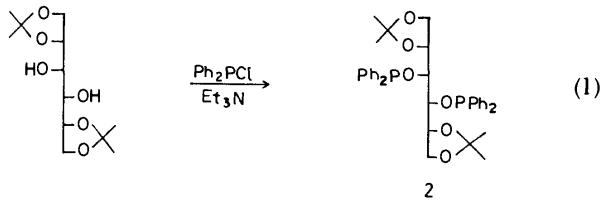

(1)

2

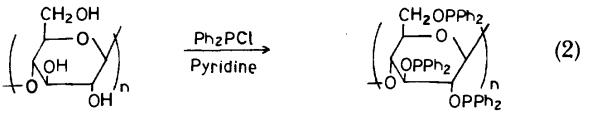

(2)

3

Preparation of Cationic Rhodium(I) Perchlorate Catalyst 4. Rhodium(I) perchlorate catalyst **4** was prepared by the reaction of di-μ-chloro-bis(cyclooctadiene)dirhodium(I) with ligand **1** and sodium perchlorate (Eq. 3).

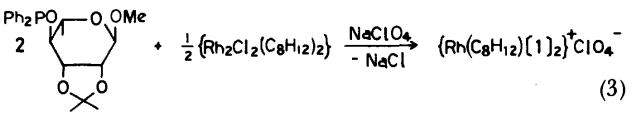

(3)

1 4

Asymmetric Hydrogenation of Prochiral Substrates. Asymmetric hydrogenation of prochiral substrates such as (*Z*)-α-acetylaminocinnamic acid, methyl (*Z*)-α-acetylaminocinnamate, (*Z*)-α-benzoylaminocinnamic acid, itaconic acid, dimethyl itaconate, tiglic acid, and acetophenone was carried out. The hydrogenation using rhodium(I) perchlorate catalyst **4** proceeded in 100% chemical yield for such a substrate as (*Z*)-α-acetylaminocinnamic acid to afford *N*-acetylphenylalanine ethyl ester. The optical yield was 54% with *R* configuration, being improved in optical yield over the previous work.[6b] The results are shown in Table 1. The complex was effective enough for the asymmetric hydrogenation, however, the chemical yields were not improved.

The asymmetric hydrogenation of prochiral olefins using di-μ-chloro-bis(cyclooctadiene)dirhodium(I) and mannitol **2** or cellulose **3** gave the results summarized in Table 2.

These results suggest that the cellulose ligand seems not to bring about a good asymmetric induction enough toward prochiral olefins owing mainly to its poor coordinating power to the rhodium catalyst because of its bulkiness, which cancels the merit of cellulose ligand in the hydrogenation procedure. Asymmetric hydrogenation of prochiral olefins with rhodium(I) catalysts having a cyclic carbohydrate ligand was expected to proceed excellently, because the tetrahydropyran ring has more rigid conformation

Table 1. Asymmetric Hydrogenation of Prochiral Substrates with $\{Rh(C_8H_{12})[1]_2\}^+ClO_4^-$ (4)[a]

Substrate	Product	Chemical yield/%	$[\alpha]_D$/° (Solvent)	Optical yield/%[b]	(Configuration)
(*Z*)-α-Acetylaminocinnamic acid	*N*-Acetylphenylalanine ethyl ester[c]	100	−7.4 (*c* 0.85, EtOH)	54	(*R*)
Methyl (*Z*)-α-acetylaminocinnamate	*N*-Acetylphenylalanine methyl ester	50	−6.8 (*c* 1.02, MeOH)	32	(*R*)
(*Z*)-α-Benzoylaminocinnamic acid	*N*-Benzoylphenylalanine	53	+12.5 (*c* 0.28, MeOH)	31	(*R*)
Itaconic acid	Methylsuccinic acid	50	−13.3 (*c* 0.84, EtOH)	78	(*S*)
Dimethyl itaconate	Dimethyl methylsuccinate	96	−4.5 (*c* 0.96, EtOH)	73	(*S*)
Tiglic acid	2-Methylbutyric acid	60	+1.5 (*c* 0.77, EtOH)	8	(*R*)
Acetophenone	1-Phenylethanol	21	+19.4 (*c* 0.33, CH_2Cl_2)	37	(*R*)

a) The ratio of the substrate to the Rh complex was 25:1. All hydrogenations were carried out in 2 ml of benzene–ethanol (1:1) for 24 h at room temperature under atmospheric pressure of hydrogen in the presence of Et_3N (0.04 ml). b) Calculated on the basis of reported values of specific rotation for the optically pure compouds: (*S*)-*N*-acetylphenylalanine ethyl ester,[9] (*S*)-*N*-acetylphenylalanine methyl ester,[9] (*S*)-*N*-acetylphenylalanine,[10] (*S*)-*N*-benzoylphenylalanine,[11] (*R*)-methylsuccinic acid,[1] dimethyl (*R*)-methylsuccinate,[12] (*S*)-2-methylbutyric acid,[13] and (*S*)-1-phenylethanol.[14] c) Ethyl esterification proceeded at the deionization process of the catalyst with Dowex 50W (H^+).

Table 2. Asymmetric Hydrogenation of Prochiral Olefins with $[Rh(C_8H_{12})Cl]_2$ and Ligand **2** or **3**[a]

Substrate	Ligand	Product	Chemical yield/%	$[\alpha]_D$/° (Solvent)	Optical yield/%[b]	(Configuration)
(*Z*)-α-Acetylaminocinnamic acid[c]	**3**	*N*-Acetylphenylalanine	100	−3.8 (*c* 0.32, EtOH)	8.2	(*R*)
Methyl (*Z*)-α-acetylaminocinnamate[c]	**3**	*N*-Acetylphenylalanine methyl ester	100	+3.4 (*c* 1.39, MeOH)	16	(*S*)
(*Z*)-α-Benzoylaminocinnamic acid[c]	**3**	*N*-Benzoylphenylalanine	43	−3.6 (*c* 0.73, MeOH)	9.0	(*S*)
Itaconic acid	**2**	Methylsuccinic acid	50	−13.3 (*c* 0.84, EtOH)	78	(*S*)
Dimethyl itaconate[c,d]	**3**	Dimethyl methylsuccinate	100	+2.3 (*c* 1.00, EtOH)	38	(*R*)
Dimethyl itaconate	**2**	Dimethyl methylsuccinate	50	−1.2 (*c* 0.50, EtOH)	20	(*S*)

a) The ratio of the ligand to the Rh complex was 4:1. The reaction conditions were the same as that of Table 1 except otherwise noted. b) Calculated on the basis of the reported values of specific rotation for the optically pure compounds in Table 1. c) Conducted in 4 ml of the solvent. d) Conducted at 30°C under 50 atm of hydrogen.

than cyclohexane ring.[7] Ligands with less rigid and/or less soluble framework in solvents did not afford any good results in the asymmetric hydrogenation.

Experimental

Measurements. ^1H NMR spectra were measured on a Hitachi R-24B (60 MHz) spectrometer with tetramethylsilane as an internal standard, mass spectra were measured on a Hitachi RMU 7MG GC-MS spectometer, and IR spectra on a Japan Spectroscopic Co., Ltd. A-3 infrared spectrophotometer. Optical rotations were measured on Japan Spectroscopic Co., Ltd. DIP-4 digital polarimeter. Melting and boiling points were uncorrected.

Materials. The following materials were synthesized according to reported methods: di-μ-chloro-bis(cyclooctadiene)dirhodium(I),[6a] methyl 2,3-*O*-isopropylidene-α-L-rhamnopyranoside,[6a] and 1,2:5,6-di-*O*-isopropylidene-D-mannitol.[8]

Synthesis of (Cyclooctadiene)bis[methyl 2,3-*O*-isopropylidene-4-*O*-(diphenylphosphino)-α-L-rhamnopyranoside]rhodium(I) Perchlorate (4). To a mixture of di-μ-chloro-bis(cyclooctadiene)dirhodium(I) (0.30 g) in dichloromethane (6 ml) and sodium perchlorate (0.15 g) in water (6 ml) was added methyl rhamnopyranoside **1** (1.0 g). The mixture was stirred for 5 h at room temperature. The reaction mixture was washed with water (6 ml×3) and the organic layer was dried over anhydrous sodium sulfate. Concentration of the solvent up to 2 ml followed by addition of cyclohexane (30 ml) gave precipitates (0.18 g), which was filtered off. Concentration of the mother liquid up to 2 ml followed by addition of hexane (20 ml) gave the cationic rhodium catast (**4**, 0.13 g) in 13% yield, mp 135 °C.

^1H NMR ($CDCl_3$) δ=1.0—1.7 (m, 18H, $2C(CH_3)_2$, $2CHCH_3$), 2.0—2.4 (m, 8H, C_4H_8), 3.4—4.3 (m, 8H, $2C_{2,3,4,5}$-H), 4.4—5.0 (m, 4H, C_4H_4), 5.35 (s, 2H, $2C_1$-H), 7.1—8.2 (m, 20H, 4Ph).

Synthesis of 1,2:5,6-Di-*O*-isopropylidene-3,4-di-*O*-(diphenylphosphino)-D-mannitol (2). Reaction of 1,2:5,6-di-*O*-isopropylidene-D-mannitol (0.50 g, 1.9 mmol) with diphenylphosphinous chloride (0.42 g) (0.92 mmol) in the presence of triethylamine (2 ml) for 48 h at room temperature followed

by filtration and evaporation gave **2** (0.50 g) in 44% yield.

^{1}H NMR ($CDCl_3$) δ=1.25, 1.35 (2s, 12H, $2C(CH_3)_2$), 3.5—4.3 (m, 8H, $2CH_2CHCH$), 7.0—8.2 (m, 20H, 4Ph); Found: C, 46.11; H, 6.23%. Calcd for $C_{36}H_{40}O_6P_2$: C, 46.46; H, 6.39%.

Synthesis of 2,3,6-Tri-*O*-(diphenylphosphino)cellulose (3). Reaction of cellulose (1.0 g) with diphenylphosphinous chloride (3.7 g) in pyridine (30 ml) for 8 d at room temperature followed by washing the reaction mixture with ethanol, separation of the product by successive centrifuging and decantation, and evaporation of the solvent in vacuo gave **3** (1.8 g) in 43% yield.

IR ν_{max} (neat, cm^{-1}) 1440 (P-Ph), 1020 (P-O-C), but no OH absorption.

Asymmetric Hydrogenation of *N*-Acetylaminocinnamic Acid with Cationic Rhodium(I) Perchlorate Catalyst 4. Asymmetric hydrogenation of *N*-acetylaminocinnamic acid (1.0 g) was carried out in dried benzene–ethanol (1:1 v/v, 2 ml) in the presence of rhodium catalyst **4** (21.8 mg, 0.82 mmol) and triethylamine (0.04 ml) for 24 h at room temperature under hydrogen atmosphere. Removal of the rhodium catalyst from the reaction mixture with ion-exchange resince Dowex 50 W (H^+ form, 10 g), where ethyl esterification proceeded quantitatively, followed by decolorization with active charcoal and evaporation of the solvent in vacuo afforded *N*-acetylphenylalanine ethyl ester (0.12 g) in 100% conversion. The structure of the product was confirmed by ^{1}H NMR,[6a] $[\alpha]_D^{13}$=−7.4° (*c* 0.85, EtOH), optical yield 54% with *R* configuration [lit,[9] for (*S*)-*N*-acetylphenylalanine ethyl ester $[\alpha]_D^{20}$=+13.8° (*c* 2.0, 95% EtOH)].

Asymmetric Hydrogenation of *N*-Acetylaminocinnamic Acid with Di-μ-chloro-bis(cyclooctadiene)dirhodium(I) and Cellulose 3. Asymmetric hydrogenation of *N*-acetylaminocinnamic acid (1.0 g) was carried out in dried benzene–ethanol (1:1 v/v, 4 ml) in the presence of di-μ-chloro-bis(cyclooctadiene)dirhodium(I) (1.0 mg, 0.020 mmol), cellulose **3** (29 mg), and triethylamine (0.04 ml) for 24 h at 30 °C under 50 atm of hydrogen in autoclave. Removal of the rhodium catalyst from the reaction mixture by filtration followed by decolorization with active charcoal and evaporation of the solvent in vacuo afforded *N*-acetylphenylalanine (0.077 g) in 100% conversion. The structure of the product was confirmed by ^{1}H NMR,[6b] $[\alpha]_D^{12}$=−3.8° (*c* 0.32, EtOH), optical yield 8.2% with *R* configuration [lit[10] for (*S*)-*N*-acetylphenylanine $[\alpha]_D^{26}$=+46.0° (*c* 2.0, EtOH)].

References

1) T. Iwami, T. Yoshida, and M. Sato, *Nippon Kagaku Kaishi*, **1976**, 1652.
2) W. R. Cullen and Y. Sugi, *Tetrahedron Lett.*, **1978**, 1635.
3) Y. Sugi and W. R. Cullen, *Chem. Lett.*, **1979**, 39.
4) T. H. Johnson and G. Rangerjan, *J. Org. Chem.*, **45**, 62 (1980).
5) D. Lafont, D. Sinou, and G. Descotes, *J. Organomet. Chem.*, **169**, 87 (1979).
6) a) M. Yamashita, K. Hiramatsu, M. Yamada, N. Suzuki, and S. Inokawa, *Bull. Chem. Soc. Jpn.*, **55**, 2917 (1982); b) M. Yamashita, M. Kobayashi, M. Sugiura, K. Tsunekawa, T. Oshikawa, S. Inokawa, and H. Yamamoto, *ibid.*, **59**, 175 (1986).
7) Y. Kawabata, M. Tanaka, and I. Ogata, *Chem. Lett.*, **1976**, 1213.
8) E. Baer and H. O. L. Fischer, *J. Biol. Chem.*, **128**, 463 (1939); *Chem. Abstr.*, **33**, 7276 (1939).
9) G. Schiavon, S. Zecchin, and G. Pilloni, *J. Organomet. Chem.*, **121**, 261 (1976).
10) T. P. Dang, J. C. Poulin, and H. B. Kagan, *J. Organomet. Chem.*, **91**, 105 (1975).
11) M. D. Fryzuk and B. Bosnich, *J. Am. Chem. Soc.*, **99**, 6262 (1977).
12) R. Rossi, P. Diversi, and G. Ingrosso, *Gazz. Chem. Ital.*, **98**, 1391 (1968).
13) Y. Asahina and T. Shimizu, *Nippon Yakugaku Kaishi*, **479**, 1 (1922).
14) A. Levi, G. Modena, and G. Scorrano, *J. Chem. Soc., Chem. Commun.*, **1975**, 6.

Hydrolysis of Spiro Derivatives that Undergo No Shrinkage on Polymerization

Hirotaka TAGOSHI† and Takeshi ENDO*
Research Laboratory of Resources Utilization, Tokyo Institute of Technology, Nagatsuta-cho, Midori-ku, Yokohama 227
†Oita Research Laboratory, Showa Denko K. K., 2 Nakanosu, Oita-shi 870-01
(Received June 4, 1988)

Synopsis. Acid-catalyzed hydrolyses of spiroorthoeters (**1**, **2a**, **2b**, and **2c**) and spiroorthocarbonates (**3** and **4**) were carried out to give the corresponding ring-opening reaction products. The ring-cleavage modes of these spiro derivatives depended on the structure of intermediate cations.

Cationic ring-opening polymerization of spiroorthoesters (SOE)[1,2] and spiroorthocarbonates (SOC),[3-6] which undergo no shrinkage in volume on polymerization, affords the poly(ester–ether)s and poly(carbonate–ether)s, respectively. Radical ring-opening polymerization, and polyaddition of unsaturated spiroorthoesters (USOE)[7] or spiroorthocarbonates (USOC)[8] have been reported. Although, each of SOE, SOC, USOE, and USOC is rather labile to moisture, there is few report on the hydrolysis of them, i.e. hydrolysis of cyclic dialkoxy orthoesters by Deslongchamps and et al.[13] and that of benzospiroorthoesters via dialkoxycarbocation intermediate by McClelland and Moreau.[14]

In this paper, we describe hydrolyses of some spiro derivatives in order to demonstrate the stability of these spiro monomers to water, and to clear the ring-cleavage mode of USOE and USOC.

Results and Discussion

As indicated in Scheme 1, there are two possible modes (a and b) of decomposition of intermediates (**6a** and **6b**) producing hydroxy esters **7a**, **7b**, and lactone **8** in hydrolysis of SOE. Actually, the mixture of **7a** and **7b** was obtained by the hydrolysis of SOE **1**, but **8** not at all. This result shows that the reaction proceeds via mode a only and further lactonization of the produced hydroxy esters does not occur.

In the hydrolysis of USOE **2**, there are two possible initial intermediates **9** and **13**. The former may give hydroxy ester **12**, and the latter, ester **16** via mode a (Scheme 2). The exclusive formation of **12** (Table 1) suggests that the intermediate **9** is more stable than **13** because of conjugate structure of cation.

There are two possible modes of decomposition of intermediate **11** which eventually affords **12** via mode a or lactone **17** and hydroxyacetone **18** via mode b. The hydrolysis of **2a** produced immediately corresponding **12a** accompanied by large amount of **17a**. **12a** can give the lactone under the similar conditions, but this

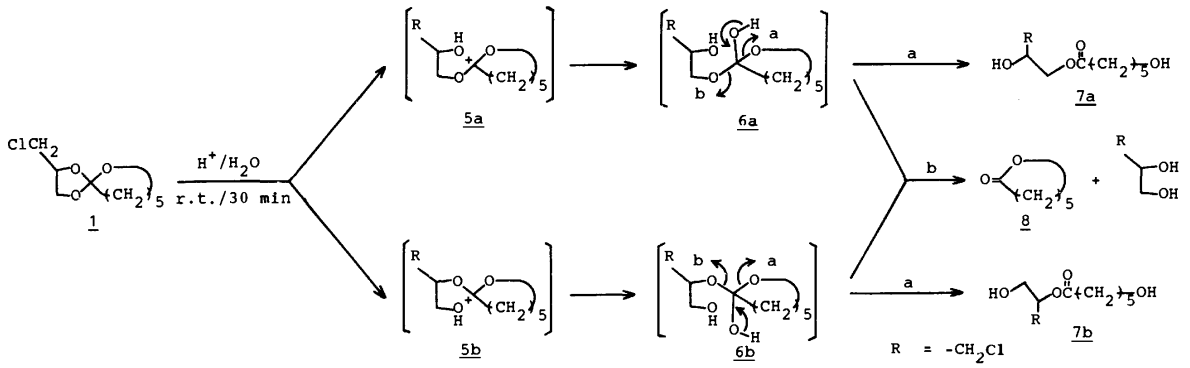

Scheme 1.

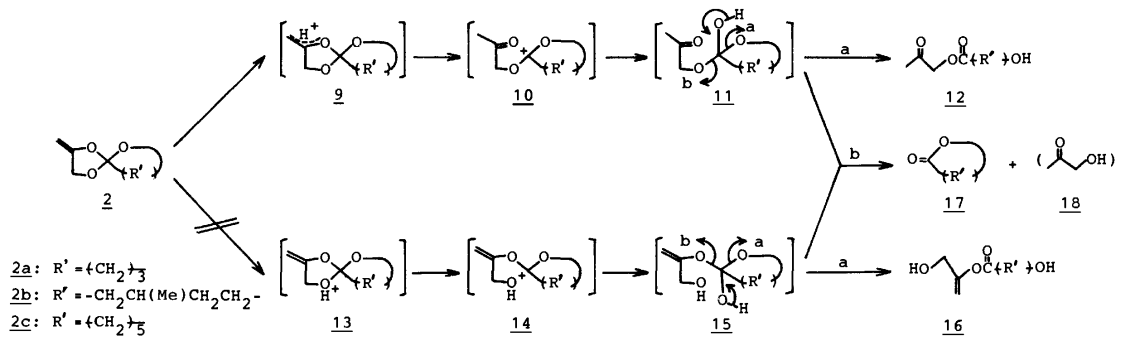

Scheme 2.

Table 1. Acid-Catalyzed Hydrolysis of Unsaturated Spiroorthoesters[a)]

Unsaturated spiroorthoester	Reaction time	Products[b)]			
		Hydroxy ester	Yield/%	Lactone	Yield/%
2a	10 min	$CH_3CCH_2OC(CH_2)_3OH$ (O, O) **12a**	15	**17a**	57
2b	60 min	$CH_3CCH_2OCCH_2CHCH_2CH_2OH$ (O, O, Me) **12b**	74		Trace
	20 h		0	**17b**	100
2c	20 h	$CH_3CCH_2OC(CH_2)_3OH$ (O, O) **12c**	63	**17c**	0

a) Hydrolysis proceeded in THF/H_2O (4/1 in volume) at ambient temperature. b) Isolated yield.

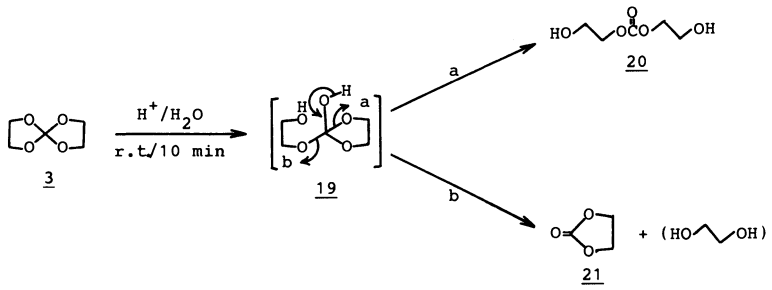

Scheme 3.

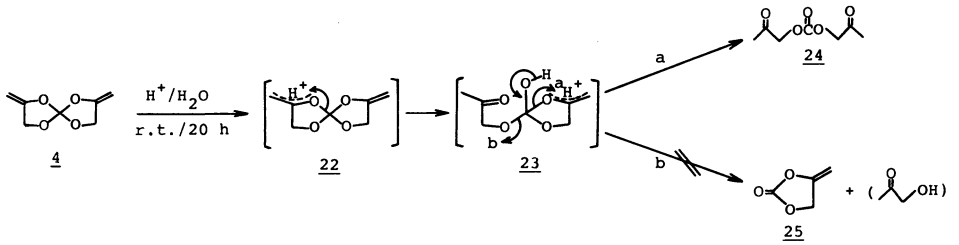

Scheme 4.

process is relatively slow.[15)] Therefore, the hydrolysis of **2a** proceeds via both modes a and b. The hydrolysis of **2b** initially (60 min) gave the corresponding hydroxy ester **12b**, but finally (20 h) lactone **17b** quantitatively. Meanwhile, the hydrolysis of **2c** produced only **12c**. In conclusion, the mode of the hydrolysis of USOE including subsequent lactonization depends upon the structure (possibly upon the ring size) of spiro derivatives.

The hydrolysis of SOC **3** was completed in 10 min to give **20** and **21** in 24% and 56% yields, respectively (Scheme 3). This behavior of **3** is very similar to that of SOE (Scheme 1). The less selectivity in this hydrolysis is in good accordance with the results of cationic ring-opening polymerization of **3** which afforded a mixture of poly(ether-carbonate) and polyether with the elimination of **21**.[3)]

In contrast to **3** USOC **4** having bidenticle exomethylene groups was hydrolyzed to give only **24** via mode a. As shown in Shceme 4, decomposition of intermediate **23** take place via protonation of vinyl ether group followed by ring cleavage.

Experimental

Preparation of Spiroorthoester Derivatives. SOE **1** and USOEs (**2a**, **2b**, and **2c**) were prepared by the method reported earlier.[7,16)]

2b: colorless liquid; bp 52—54 °C/0.4 mmHg (1 mmHg= 133.322 Pa); IR (neat) 1693 (C=C), 1284, 1188, 1168, 1141, 1115, 1068, 1041, and 1018 cm^{-1}; ^1H NMR ($CDCl_3$) δ=4.7—4.3 (3H, m), 4.0—3.7 (3H, m), 2.1— 1.8 (2H, m), 1.0—1.7 (3H, m), and 0.99 (3H, d, J=6.3 Hz); ^{13}C NMR ($CDCl_3$) δ=155.3, (121.2*), 120.8, 79.7, (79.2*), (66.5*), 65.3, (64.5*), 64.4, 39.6, 32.8, (28.0*), 27.9, and 21.7 (*: chemical shift of

minor isomer); Anal. ($C_9H_{14}O_3$) C, H.

Preparation of Spiroorthocarbonate Derivatives. The preparation of **3**[17] and **4**[11] was carried out according to the procedure reported previously.

Hydrolysis (General Procedure). A solution of spiro derivative and a few drops of aq HCl (6 mol dm^{-3}) in THF or THF-H_2O were stirred at ambient temperature. The reaction was monitored by GC. The reaction mixture was quenched by adding a few drops of saturated aq $NaHCO_3$, dried over $MgSO_4$, and evaporated.

7a and 7b: separated by silica gel preparative TLC (ethyl acetate as eluent); quantitative yield; IR (neat) 3400 and 2940 cm^{-1}; ^1H NMR ($CDCl_3$) δ=4.23 (2H, d, J=7 Hz)*, 4.22 (2H, d, J=6 Hz)*, 4.08 (1H, m) 3.68 (2H, t, J=7 Hz), 3.64 (2H, d, J=6 Hz), 3.12 (1H, br s, -OH), 2.40 (2H, t, J=7 Hz)**, 2.32 (2H, t, J=7 Hz)**, 1.92 (1H, br s, -OH), and 1.2—1.8 (6H, m) (*, **: chemical shift of **7a** or **7b**). **12a**: colorless liquid, 15%; bp 125 °C/0.55 mmHg (Kugelrohr); IR (neat) 3400 and 1725 cm^{-1}; ^1H NMR ($CDCl_3$) δ=4.68 (2H, s), 3.68 (2H, t, J=6 Hz), 2.73 (1H, br s), 2.56 (2H, t, J=7 Hz), 2.17 (3H, s), and 1.91 (2H, tt, J=7 Hz, 6 Hz); ^{13}C NMR ($CDCl_3$) δ=202.0, 173.1, 68.2, 61.4, 30.4, 27.6, and 26.0; HRMS Found: m/z 160.0730. Calcd for $C_7H_{12}O_4$: M, 160.0735. **12b**: colorless liquid; bp 150 °C/0.15 mmHg (Kugelrohr); IR (neat) 3450 and 1730 cm^{-1}; ^1H NMR ($CDCl_3$) δ=4.68 (2H, s), 3.69 (2H, t, J=6.6 Hz), 2.6—2.0 (4H, m), 2.17 (3H, s), 1.59 (2H, m), and 1.02 (3H, d, J=6.5 Hz); ^{13}C NMR ($CDCl_3$) δ=201.7, 172.4, 68.1, 60.3, 41.2, 39.2, 27.1, 26.1, and 20.0; HRMS Found: m/z 188.10343. Calcd for $C_9H_{16}O_4$: M, 188.10485. **12c**: colorless liquid; bp 140 °C/0.09 mmHg (Kugelrohr); IR (neat) 3400 and 1730 cm^{-1}; ^1H NMR ($CDCl_3$) δ=4.67 (2H, s), 3.64 (2H, t, J=6 Hz), 2.46 (2H, t, J=7 Hz), 2.17 (3H, s), 2.13 (1H, s), and 1.9—1.2 (6H, m); ^{13}C NMR ($CDCl_3$) δ=201.8, 173.0, 68.1, 62.4, 33.7, 32.2, 26.0, 25.2, and 24.5; HRMS Found: m/z 188.10537. Calcd for $C_9H_{16}O_4$: M, 188.10485. **20**: separated by silica-gel preparative TLC (hexane/ethyl acetate=2/8 in volume as eluent); colorless oil, 24%; bp 135 °C/0.12 mmHg (Kugelrohr); IR (neat) 3350 and 1740 cm^{-1}; ^1H NMR ($CDCl_3$) δ=4.30 (4H, m), 3.83 (4H, m), and 3.73 (2H, br s, -OH). **24**: colorless needle (recrystallized from CCl_4), 96%; mp 71—71.5 °C; IR (KBr) 1766 and 1728 cm^{-1}; ^1H NMR ($CDCl_3$) δ=4.71 (4H, s) and 2.21 (6H, s); ^{13}C NMR ($CDCl_3$) δ=201.1, 154.4, 71.3, and 26.0; Anal. ($C_7H_{10}O_5$) C, H.

References

1) K. Bodenbenner, *Justus Liebigs Ann. Chem.*, **625**, 183 (1959).

2) W. J. Bailey, R. L. Sun, H. Katsuki, T. Endo, H. Iwama, R. Tsushima, K. Saigo, and M. M. Bitritto, *ACS, Symp. Ser.*, **59**, 38 (1977).

3) S. Sakai, T. Fujinami, and S. Sakurai, *J. Polym. Sci., Polym. Lett. Ed.*, **11**, 631 (1973).

4) T. Endo and W. J. Bailey, *Makromol. Chem.*, **176**, 2897 (1975).

5) W. J. Bailey and T. Endo, *J. Polym. Sci., Polym. Chem. Ed.*, **14**, 1735 (1976).

6) T. Endo, H. Katsuki, and W. J. Bailey, *Makromol. Chem.*, **177**, 3231 (1976).

7) T. Endo, M. Okawara, and W. J. Bailey, *J. Polym. Sci., Polym. Chem. Ed.*, **19**, 1283 (1981).

8) T. Endo and W. J. Bailey, *J. Polym. Sci., Polym. Chem. Ed.*, **13**, 2525 (1975).

9) H. Fukuda, M. Hirota, T. Endo, M. Okawara, and W. J. Bailey, *J. Polym. Sci., Polym. Chem. Ed.*, **20**, 2935 (1982).

10) U. S. Etlis, F. N. Shomina, A. B. Bulovyatova, L. A. Tsareva, and E. G. Pomerantseva, *Polym. Sci., U. S. S. R.*, **25**, 857 (1983).

11) H. Tagoshi and T. Endo, *J. Polym. Sci., Part A; Polym. Chem.*, in press.

12) H. Tagoshi and T. Endo, *Chem. Lett.*, **1987**, 2363.

13) P. Deslongchamps, R. Chenevert, R. J. Taillefer, C. Moreau, and J. K. Saunders, *Can. J. Chem.*, **53**, 1601 (1975).

14) R. A. McClelland and C. Moreau, *Can J. Chem.*, **63**, 2673 (1985).

15) R. A. McClelland and M. Alibhai, *Can. J. Chem.*, **59**, 1169 (1981).

16) T. Endo and W. J. Bailey, *J. Polym. Sci., Polym. Lett. Ed.*, **18**, 25 (1980).

17) T. Endo and M. Okawara, *Synthesis*, **1984**, 837.

Low-Temperature Coal Liquefaction in Basic Nitrogen Compounds

Hideyuki TAGAYA,* Akira SAITO, and Koji CHIBA*
Department of Applied Chemistry, Faculty of Engineering,
Yamagata University, Jonan, Yonezawa 992
(Received August 1, 1988)

Synopsis. A high conversion (75%) of Taiheiyo coal was attained using indole at 300 °C. Morpholine and tetrahydroquinoline were also effective solvents although quinoline, aniline, and triethylamine were not effective as well as tetralin and 1-methylnaphthalene. Extraordinarily high SRC yields and their molecular weight distributions suggested the presence of a solvent dimer and hydrogen donation.

We have already reported that the conversion exceeded 80% when the Taiheiyo coal was liquefied at 300 °C for 10 h using butylamine as a solvent.[1] The presence of low molecular weight compounds in coal has been proven by the fact that coal solubilization was proceeded by mild alkylation.[2a] It was suggested that the substitution reaction of butylamine with hydroxyl groups of coal contributed to the rupture of non covalent bonds, such as hydrogen bonds between coal molecules. The undesirable condensation or polymerization reactions of coal fragments can be avoided by liquefaction at low temperatures,[3] and the chemical structures of liquefaction products which were obtained at mild conditions provide important information about coal structure.[2]

We examined the coal-liquefaction reaction with basic nitrogen compounds other than butylamine to obtain information about a liquefaction mechanism at low temperature.

Experimental

Coal Samples and Solvents. Four coals were used in this study. Analyses of these coals are given in Table 1. The coals were ground so as to pass through a 100 mesh (149 m) screen and dried at 107 °C in a nitrogen atmosphere. Reagent-grade tetralin was used after distillation under reduced pressure. Various solvents were reagent grade.

Coal Liquefaction Procedure. Coal (6 g) and solvent (18 g) were placed in a 100 ml magnetically stirred autoclave and pressurized to 3 MPa with nitrogen. Materials remaining in the autoclave after liquefaction were extracted with benzene. Any benzene-insoluble material was further extracted with tetrahydrofuran (THF). Conversion to a THF-extractable material was calculated according to the following equation:

conversion (wt%, daf basis) = 100 × (weight of coal charged−weight of THF-insoluble material)/weight of daf coal

The liquefaction solvent was recovered from the benzene extract by vacuum distillation at 240 °C and 933 Pa. The distillation residue was weighed as a solvent-refined coal (SRC):

SRC yield (wt%, daf coal basis) = 100 × weight of SRC/weight of daf coal

Analysis of SRC. For the measurement of molecular weight distributions of SRC, gel permeation chromatography (GPC) was used. In the GPC measurement, THF was used as the liquid phase and a refractometer and a UV detector (254 nm) were used for monitoring the effluents from the columns.

Results and Discussion

The conversion of Taiheiyo coal at 300 °C are shown in Fig. 1. We already reported that tetralin scarcely donated hydrogen to coal at 300 °C.[1] Tetralin seems to act only as a diluent. Furthermore, conversions using 1-methylnaphthalene, quinoline, aniline, and triethylamine as solvents were almost the same with that using tetralin. However, higher conversions than these were obtained when indole was used as the solvent. The conversion reached to 75% for a liquefaction of 10 h. Conversions using tetrahydroquinoline and morpholine were also higher than that using tetralin, although they were lower than that using indole.

The liquefaction of subbituminous coal (Wyodak coal) using indole and a high conversion of the coal (62% at 375 °C, 20 min) have already been reported by Padrick and Lockwood, although the reaction temperature was higher than 300 °C.[4] When butylamine was used as the liquefaction solvent, coal conversion depended upon the hydroxyl oxygen content of coal,[1] as shown in Table 2. The conversion tended to increase, generally, with an increase in the hydroxyl content of coal in the case of butylamine. We tried to liquefy different kinds of coal using indole. The

Table 1. Analyses of Coals (wt%)

Coal	Ultimate analysis[a]				Proximate analysis			
	C	H	N	O_{diff} (OH)[b]	ash	mois	FC	VM
Yallourn	67.5	5.7	0.6	26.2 (7.2)	2.2	13.2	41.0	43 .6
Taiheiyo	77.5	6.4	1.0	15.1 (6.8)	15.1	4.7	35.3	44.9
Wandoan	77.6	6.2	0.8	15.4 (7.3)	7.3	9.2	38.6	44.9
Miike	82.2	6.2	1.0	10.6 (3.6)	9.5	2.2	44.4	43.9

a) daf coal basis. b) Content of hydroxyl oxygen.[1]

Table 2. Conversion of Coal and SRC Yield in the Liquefaction Using Basic Nitrogen Compound at 300 °C for 1 h

Solvent	Coal			
	Yallourn	Taiheiyo	Wandoan	Miike
Tetralin	4.8	5.7	4.8	9.1
Indole	29.8	23.5	24.9	25.5
Butylamine[1]	24.0	34.7	24.6	16.3

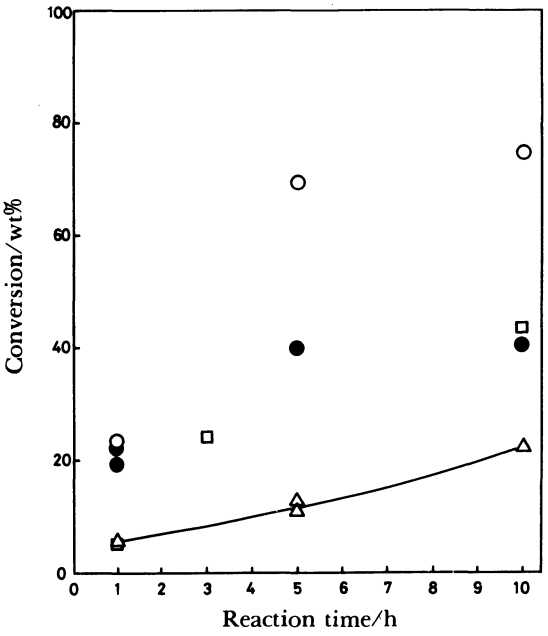

Fig. 1. Conversion of Taiheiyo coal using tetralin (△), indole (○), tetrahydroquinoline (●), and morpholine (□).

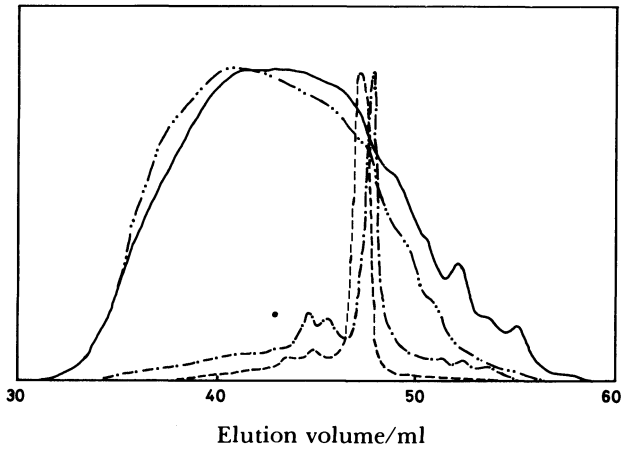

Fig. 2. Molecular distributions of Taiheiyo coal SRCs measured by a GPC UV detector. Solvents were tetralin (————), indole (— — — —), tetrahydroquinoline (— — — —), morpholine (— · — · —).

results are also given in Table 2. Coal conversions using indole at 300 °C for 1 h liquefaction were in the range from 23—30% and scarcely affected by coal rank. Indole was a more effective solvent than butylamine for Miike coal liquefaction, whose hydroxyl content was the smallest in four coals. This fact indicated that the liquefaction mechanism in indole was different from that in butylamine.

SRC yields using indole were higher than the conversions and exceeded 100% when Taiheiyo coal was liquefied for 5 and 10 h; the yields were 120 and 177%, respectively. The extraordinarily large SRC yields indicate the presence of an incorporation reaction of indole to coal or the oligomerization of indole. The molecular weight distributions of the SRCs are shown in Fig. 2. The SRCs were obtained in the liquefaction of Taiheiyo coal at 300 °C using tetralin, indole, tetrahydroquinoline, and morpholine; the yields (reaction time and conversion) were 3.0 (1 h, 5.7%), 90.3 (1 h, 23.5%), 95.5 (10 h, 40.4%), and 86.3% (10 h, 43.6%), respectively. Smooth molecular weight distributions were observed when tetralin and morpholine were used as the solvents and the same with that when butylamine was used.[1] However, clear peaks which did not arise from the solvents themselves were observed when indole and tetrahydroquinoline were used.

Padrick and Lockwood reported the presence of a new peak in the product distribution of coal using indole, and concluded that the peak could be assigned as a complex between two indole molecules and one coal molecule with a molecular weight of 400.[4] However, we could not believe the above mechanism since the liquefaction products of coal had a wide range molecular weights.

It had already been reported that the heating of indole with sulfur produced an indole dimer.[5] We tried a reaction of indole and sulfur and confirmed that the elution volume of the dimer corresponded with that of the peak in Fig. 2. Furthermore, from the mass spectroscopy of the SRC the presence of the indole dimer was confirmed; its molecular weight was 232. This indicated that two indoles dimerized, evolving two hydrogen. The dimerization was also supported from the H/C values of the SRCs. The H/C of SRC in indole was 0.86; this value was fairly smaller than 1.15 in tetralin and also than 0.88 of indole itself. We could not determine the structure of indole dimer;[6] however, the presence of a dimer suggested that indole donated hydrogen to coal and dimerized. The same mechanism should be applied to liquefaction using tetrahydroquinoline. The presence of biquinoline in the reaction products under liquefaction conditions had already been reported.[7] The peak in Fig. 2 must be due to biquinoline.

To clarify the mechanism, the hydrogen donor ability of indole was measured using anthracene as a

hydrogen acceptor.[8] When indole (3 g) and anthracene (3 g) was reacted at 300 °C for 1 h, 6% of the anthracene was hydrogenated to dihydroanthracene, although no anthracene was hydrogenated when tetralin was reacted with anthracene at 300 °C for 1 h.[8b] ESR studies of Petrakis and Grandy indicated that the radical concentration increased from low temperatures at 300 °C.[9] It is suggested that coal fragmentation at low-temperature occurred. It was considered that some part of the coal fragmented even at 300 °C and that the fragments were stabilized by the hydrogen donation of indole.

We already confirmed that the hydrogen donor ability of butylamine was not so large.[1] The molecular weight distribution of SRC in morpholine was smooth (Fig. 2) as with that in butylamine. An incorporation reaction in preference to dimerization was suggested because the SRC yields were larger than coal conversion and no dimer was observed by GPC and mass spectroscopy analysis. The same liquefaction mechanism as that in butylamine was considered.

In the low-temperature liquefaction of coal using butylamine, it was suggested that the substitution reaction of butylamine with hydroxyl groups in coal caused the rupture of noncovalent bonds in coal.[1] The same liquefaction mechanism was suggested in liquefaction using morpholine as a solvent. Furthermore, Mayo et al. carried out extractions and reactions of coals below 100 °C and proposed that pyridine and several amines cleaved some of the coal network to a soluble material.[10] This study suggested that the hydrogen donor abilities of basic nitrogen compounds, like indole and tetrahydroquinoline, were higher at low temperatures (like 300 °C) than expected. It was considered that at low temperature, coal solubility was attained by the complex actions of basic nitrogen compounds expressed above, such as a disruption of noncovalent bonds between coal molecules by a substitution reaction and hydrogen donation to coal fragments.

The authors would like to express their gratitude to Mr. Jouji Sugai for his technical assistance.

References

1) H. Tagaya, J. Sugai, M. Onuki, and K. Chiba, *Energy Fuels*, **1**, 397 (1987).

2) a) M. Miyake and N. Nomura, *Kagaku To Kogyo*, **41**, 186 (1988). b) M. Iso, Y. Lee, K. Sato, T. Shirahase, and S. Omi, *Fuel*, **67**, 19 (1988).

3) E. C. Moroni, *Prepr. Pap. Am. Chem. Soc., Div. Fuel Chem.*, **31**(**4**), 1 (1986).

4) a) T. D. Padrick and S. J. Lockwood, *Prepr. Pap. Am. Chem. Soc., Div. Fuel Chem.*, **29**(**1**), 153 (1984). b) *idem, ibid.*, **29**(**5**), 92 (1984).

5) W. Carpentar, M. S. Grant, and H. R. Snyder, *J. Am. Chem. Soc.*, **82**, 2739 (1960).

6) H. F. Hodson and G. F. Smith, *J. Chem. Soc.*, **1957**, 3544.

7) K. Ouchi, A. Hirota, and H. Ito, *Fuel Processing Technology*, **1**, 21 (1977).

8) a) K. Chiba, H. Tagaya, and N. Saito, *Energy Fuels*, **1**, 338 (1987). b) H. Tagaya, K. Katsuma, Y. Shibazaki, and K. Chiba, *Fuel*, **67**, 786 (1988).

9) L. Petrakis and D. W. Grandy, *Anal. Chem.*, **50**, 303 (1978).

10) a) F. R. Mayo, J. S. Zevely, and L. A. Pavelka, *Fuel*, **67**, 595 (1988). b) F. R. Mayo, D. H. Buchanan, L. A. Pavelka, and A. S. Hirschon, *ibid.*, **67**, 600 (1988). c) F. R. Mayo, L. A. Pavelka, J. S. Zevely, and A. S. Hirschon, *ibid.*, **67**, 607 (1988).

A Simple Synthesis of (±)-*cis*-(6-Methyltetrahydro-2-pyranyl)acetic Acid, a Constituent of Civet

Kazuhiro KOBAYASHI* and Hiroshi SUGINOME
Organic Synthesis Division, Faculty of Engineering, Hokkaido University, Sapporo 060
(Received August 12, 1988)

Synopsis. The title compound was synthesized stereoselectively starting with readily available 5-hexanolide in a 47% overall yield.

cis-(6-Methyltetrahydro-2-pyranyl)acetic acid (**5**) was isolated as a minor constituent of civet, which is utilized in perfumery, by Mauer et al. in 1979.[1] Since then, several synthetic methods for the preparation of **5** have been reported.[2] We now wish to report a more simple synthesis of **5**, which involves a stereoselective reduction of the cyclic acetal **3**.

t-Butyl (2-methoxy-6-methyltetrahydro-2-pyranyl)-acetate (**3**) was prepared from the reaction of 5-hexanolide with the lithium enolate of *t*-butyl acetate[3] followed by the subsequent treatment of the cyclic hemiacetal **2** with methanol and trimethyl orthoformate in dichloromethane in the presence of a catalytic amount of *p*-toluenesulfonic acid. The magnesium enolate of *t*-butyl acetate[4] also could be used for the preparation of **2**. Although the yield was slightly reduced, the reaction proceeded under milder conditions. In each case **3** was obtained in stereochemically pure form. The stereochemistry of **3** was determined on the basis of the reported ^{1}H NMR examination.[5]

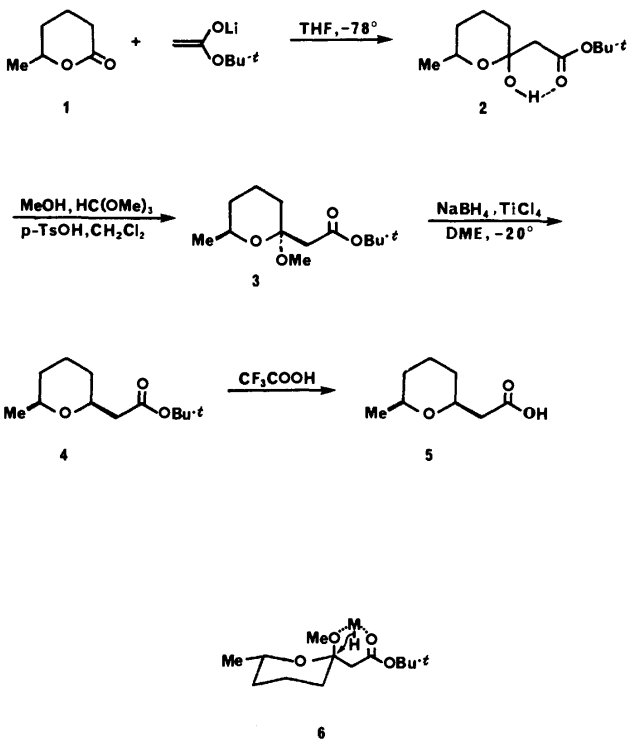

The sodium borohydride reduction of **3** to **4** was found to be feasible using titanium tetrachloride as a catalyst. Thus, **3** was allowed to react with 1 equivalent of sodium borohydride in the presence of 1.5 equivalent of the catalyst in 1,2-dimethoxyethane at −20 °C, and the reduced product **4** was produced stereoselectively in an 80% isolated yield. The reaction occurred immediately and cleanly, and the ester moiety was not affected under the present conditions.[6] The use of excess sodium borohydride or the catalyst, prolonged reaction time, and elevated reaction temperature led to complicated mixture of products arising from the reduction of the ester moiety. 1,2-Dimethoxyethane was essential for the reaction, and the use of diethyl ether, THF, benzene, and dichloromethane was not effective. The use of lithium aluminum hydride instead of sodium borohydride was also ineffective.

The specific formation of **4** in the reduction of **3** may be explained in terms of the involvement of the intermediate **6**.[7]

The ester cleavage of **4** was carried out in trifluoroacetic acid to give **5** in a 79% yield. Since the present method is operationally simple and highly selective, it offers advantages over the porevious methods for the preparation of **5**.[2]

Experimental

The IR spectra were recorded on a Hitachi 285 spectrometer. The ^{1}H NMR spectra were recorded on a Hitachi R-90B spectrometer in $CDCl_3$ with tetramethylsilane as an internal standard. The high and low resolution mass spectra were determined with a JEOL JMS-D300 spectrometer. Thin-layer chromatography was performed using Merck Silica Gel 60 GF_{254}. All solvents were dried over appropriate agents and distilled under nitrogen prior to use. All reactions were carried out in a nitrogen atmosphere.

***t*-Butyl (2-Hydroxy-6-methyltetrahydro-2-pyranyl)acetate (2).** To a stirred solution of lithium diisopropylamide (LDA) (10 mmol), which was prepared by the treatment of diisopropylamine (1.0 g, 10 mmol) with butyllithium (10 mmol, 1.5 M† in hexane solution) in THF (20 ml) at −78 °C, was added *t*-butyl acetate (1.2 g, 10 mmol). After stirring for 20 min at the same temperature 5-hexanolide[2c] (1.1 g, 10 mmol) was added to the reaction mixture and it was stirred for additional 4 h. The resulting mixture was quenched by adding aqueous ammonium chloride and extracted with ether three times. The combined extract was washed with brine, dried over anhydrous magnesium sulfate, and evaporated to give a crude **2** (2.2 g), which was not further purified and used in the next step. Compound **2** was alternatively prepared as follows. Diisopropylamine (4.1 g, 40 mmol) was added to an ethereal solution (30 ml) of ethylmagnesium bromide (20 mmol) at 0 °C and the mixture was stirred for 1 h at the same temperature. To the resulting turbid solution were successively added *t*-butyl acetate (1.2 g,

† 1 M=1 mol dm^{-3}.

10 mmol) and 5-hexanolide (1.1 g, 10 mmol), and the mixture was stirred for additional 30 min. The resulting mixture was quenched by adding aqueous ammonium chloride and extracted with ether three times. The combined extract was dried over anhydrous magnesium sulfate, and concentrated in vacuo. The resulting crude product was not further purified and used in the next step.

***t*-Butyl (2-Methoxy-6-methyltetrahydro-2-pyranyl)acetate (3).** A solution of the crude **2** (2.2 g), trimethyl orthoformate (2 ml), methanol (1 ml), and *p*-toluenesulfonic acid (95 mg, 0.5 mmol) in dichloromethane (20 ml) was stirred at room temperature overnight. The resulting mixture was washed with aqueous sodium hydrogencarbonate and dried over anhydrous sodium sulfate. Evaporation of the solvent gave a crude oil which was distilled using Kugelrohr to afford **3** (1.8 g, 75% from **1**). Bp 110 °C (bath temperature)/0.1 Torr[††]; IR (neat) 1725 cm^{-1}; ^1H NMR δ=1.12 (d, J=6.2 Hz, 3H), 1.45 and 1.3—2.0 (s and m, combined 15H), 2.38 (d, J=13.4 Hz, 1H), 2.67 (d, J=13.4 Hz, 1H), 3.25 (s, 3H), 3.4—3.8 (m, 1H); MS, m/z (rel intensity) 244 (M^+, 0.2), 213 (6.2), 119 (95.8), 57 (100). Found: m/z 244.1666. Calcd for $C_{13}H_{24}O_4$: M, 244.1675.

***t*-Butyl *cis*-(6-Methyltetrahydro-2-pyranyl)acetate (4).** To a stirred suspension of sodium borohydride (0.19 g, 5 mmol) and **3** (1.2 g, 5 mmol) in 1,2-dimethoxyethane (20 ml) was added dropwise titanium tetrachloride (0.43 g, 7.5 mmol) at −20 °C. An exothermic reaction immediately occurred and the suspension turned to a green solution, which was poured into aqueous ammonium chloride and extracted with ether three times. The combined extract was washed with brine, dried over anhydrous sodium sulfate, and concentrated in vacuo. Distillation of the residue gave **4** (0.86 g, 80%). Bp 95 °C (bath temperature)/0.2 Torr; IR (neat) 1725 cm^{-1}; ^1H NMR δ=1.14 (d, J=6.2 Hz, 3H), 1.44 and 1.3—1.9 (s and m, combined 15H), 2.25 (dd, J=14.8, 6.2 Hz, 1H), 2.47 (dd, J=14.8, 6.8 Hz, 1H), 3.3—3.9 (m, 2H); MS, m/z (rel intensity) 214 (M^+, 0.1), 199 (0.8), 99 (84), 57 (100). Found: 214.1573. Calcd for $C_{12}H_{22}O_3$: M, 214.1569.

***cis*-(6-Methyltetrahydro-2-pyranyl)acetic Acid (5).** To a solution of **4** (0.21 g, 1 mmol) in dichloromethane (4 ml) was added trifluoroacetic acid (0.2 ml), and the mixture was stirred at room temperature overnight. Evaporation of the solvent gave a crude solid which was recrystallized from petroleum ether to afford **5** (0.13 g, 79%). Mp 51—52 °C (lit,[2a] 50—52 °C).

[††] 1 Torr=133.322 Pa.

References

1) B. Mauer, A. Grieder, and W. Thommen, *Helv. Chim. Acta*, **62**, 44 (1979).

2) a) D. Seebach and M. Pohmakotr, *Helv. Chim. Acta*, **62**, 843 (1979). b) B. Mauer and W. Thommen, *ibid.*, **62**, 1096 (1979). c) S. V. Ley, B. Lygo, H. Molines, and J. A. Motton, *J. Chem. Soc., Chem. Commun.*, **1982**, 1251. d) Y. Kim and B. P. Mundy, *J. Org. Chem.*, **47**, 3556 (1982). e) H. A. Bates and P.-N. Deng, *ibid.*, **48**, 4479 (1983). f) Y. Masaki, Y. Serizawa, K. Nagata, and K. Kaji, *Chem. Lett.*, **1983**, 1601. g) M. F. Semmelhack and C. Bodurow, *J. Am. Chem. Soc.*, **106**, 1496 (1984). h) T. Gallagher, *J. Chem. Soc., Chem. Commun.*, **1984**, 1554. i) L. Coppi, A. Ricci, and M. Taddei, *J. Org. Chem.*, **53**, 911 (1988).

3) A. J. Dugan, M. A. Adams, P. J. Bryne, and J. Meinwald, *Tetrahedron Lett.*, **1978**, 4323.

4) T. Hiyama and K. Kobayashi, *Tetrahedron Lett.*, **23**, 1597 (1982); K. Kobayashi and H. Suginome, *Bull. Chem. Soc. Jpn.*, **59**, 1635 (1986); T. Hiyama, K. Kobayashi, and K. Nishide, *ibid.*, **60**, 2127 (1987).

5) T. Nakata, S. Takano, M. Fukui, T, Tanaka, and T. Oishi, *Tetrahedron Lett.*, **24**, 3837 (1983).

6) The reduction of carboxylic esters to ethers with mixed anhydride has been well known: J. R. Dias and G. R. Pettit, *J. Org. Chem.*, **36**, 3485 (1971).

7) P. C. Loewen, W. W. Zajac, Jr., and R. K. Brown, *Can. J. Chem.*, **47**, 4059 (1969).

Effect of the Particle Size of Catalyst Metal on the Stereochemistry of Hydrogenation

Yasuhisa SENDA,*,† Kazuhito KOBAYASHI, Shin-ichi KAMIYAMA, Jun-ichi ISHIYAMA, Shin IMAIZUMI, Akifumi UENO,†† and Yoshihiro SUGI†††
Department of Engineering Science, Tohoku University, Aoba, Sendai 980
††Toyohashi University of Technology, Tenpakucho, Toyohashi 440
†††National Chemical Laboratory for Industry, Tsukuba, Ibaraki 305
(Received August 20, 1988)

Synopsis. Particle size of the metal catalysts controlled the stereoselectivity in the hydrogenation of methylenecyclohexanes. No effect of particle size, on the contrary, was observed in the hydrogenation of substituted 3-methylenetetrahydropyran and 5-methylene-1,3-dioxane which contain oxygen atom/atoms in the molecule.

Explanations of the stereochemistry in catalytic hydrogenation have been dominated by ideas concerning the manner in which a given unsaturated compound may best be fitted onto a planar surface from which hydrogen is abstracted; cis addition is the consequences.[1] However, the effect of the steric interaction of substrates with the metallic surface on the product distribution is still complicated.

In order to investigate the correlation between the stereochemistry of hydrogenation and the interaction of the substrate with the catalyst surface, 1-*t*-butyl-4-methylenecyclohexane (**1**), 3,3,5-trimethyl-1-methylenecyclohexane (**2**), 2-*t*-butyl-5-methylenetetrahydropyran (**3**), and 2-*t*-butyl-5-methylene-1,3-dioxane (**4**) were hydrogenated over several transition metal catalysts whose particle sizes of the metal were controlled.

Results and Discussion

The catalysts used in the present study were a Rh and Os colloid in a matrix of poly(*N*-vinylpyrrolidone), and highly dispersed Rh on a SiO_2 surface. Two types of Rh colloid were prepared by the method of Hirai (one type is tentatively named colloid A and the other is colloid B).[2] The average particle diameter of colloid A was reported to be 9 Å and that of colloid B to be 20 Å. The observed particle size of the latter was 27 Å by electron microscope at a magnification of 200000. Two types of Os colloid were similarly prepared as Rh. These Os colloids were highly dispersed and the particle sizes were distributed in very narrow ranges. The average particle diameters of these two types of colloid were 30 Å (colloid A) and 40 Å (colloid B). Three types of Rh supported on SiO_2 were also used as the catalysts. These were 1.0, 4.7, and 14.2% Rh on SiO_2, the average particle sizes of which are 14, 28, and 48 Å, respectively.[3] In some cases, a small amount of endo-cyclic olefins, which were derived by the double bond migration of the original substrates, appeared during the hydrogenation (see Table 1). since the rate of hydrogenation of these endo-cyclic olefins is very slow compared with the original substrates (the apparent rate of hydrogenation of endo-cyclic olefins was less than 1/10 of that of the oiriginal substrates), the appearance of these isomerized olefins with the progress of the reaction seemed to have little influence

Table 1. The Product Distribution of Hydrogenation of Substituted Methylenecyclohexanes, -tetrahydropyran, and -dioxane

Catalyst	Average diameter (Å)	(axial methyl isomer in saturated product (%)) (1)	(2)	(3)	(4)
Rh colloid A	9	58(14)[a]	50(9)	96(0)	98(3)
Rh colloid B	27	80(12)	83(6)	97(0)	98(3)
Rh black		90(4)	84(6)	94(0)	98(1)
Os colloid A	30	73(2)	88(1)	97(0)	98(1)
Os colloid B	40	74(2)	93(1)	97(0)	95(1)
Os black		91(2)	89(1)	92(*t*)[b]	92(*t*)
1.0% Rh/SiO_2	14	65(12)	65(7)	94(0)	95(1)
4.7% Rh/SiO_2	28	71(12)	69(8)	95(0)	96(2)
14.2% Rh/SiO_2	48	78(13)	77(10)	95(0)	96(1)

a) Values in parentheses are olefins which are derived by the double bond migration of the original substrates.
b) Trace.

† Present address: Department of Chemistry, Yamagata University, Yamagata 990.

on the epimeric ratios of the saturated products from the original substrates in the early stage of the reaction. The product distribution of the hydrogenation is summarized in Table 1.

The stereochemistry of the hydrogenation of **1** depended on the particle size of the catalyst metal. The ratios of the axial methyl product to the equatorial tend to decrease in the order; black catalyst, colloid B, colloid A on Rh catalyst and those eventually approached unity. A similar trend was observed with Os colloid catalyst. This means that a decrease in the average particle size of the metal colloid gives a decrease in the ratio of the axial methyl isomer. The hydrogenation of **2** also showed the same trend as that of **1**.

Siegel and his co-workers discussed the hydrogenation of cyclic olefins in terms of Horiuti–Polanyi mechanism and proposed that the change in the product-controlling step coincides with a change in the ratio of the products.[4] The distribution of stereoisomeric products will depend upon which of the elementary reactions is product-controlling because the geometry and/or composition of the several possible transition states differ from one another. When the product-controlling step is the adsorption of the substrate on the catalyst or the first hydrogen transfer from the catalyst to the adsorbed species, the stereochemistry of the reaction is controlled by the interaction between the substrate and the catalyst surface.

Since it has been known that the hydrogenation of **1** over noble metal black catalysts always gave cis product,[5] the stereochemistry of the product is considered to be determined by the steric interaction between the substrate and the catalyst surface. Taking into account the average particle size of the catalyst metal together with the product distribution obtained in the present study, the geometries of the adsorption states on the catalyst are illustrated as in Fig. 1, in which the stereochemical correlation of the substrate with the catalyst is imagined. The product distribution leads to the tentative conclusion that (1) the compressional stress of the axial and the equatorial side of a six-membered ring is not very different on the catalyst whose particle size is rather small, so that the attack of hydrogen from either the axial or the equatorial side is roughly equal. This results in the low stereoselectivity of hydrogenation. (2) It is clear from the drawings that the difference of the compressional stress between the axial and the equatorial side increases with increasing particle size of the catalyst metal, so that the adsorption of the substrate becomes easier from the equatorial side than from the axial side. An extremely high axial methyl selectivity is responsible for the overwhelmingly equatorial addition of hydrogen on the metal black catalyst whose particle size of the metal is considered to be macroscopically infinite.

Of particular interest are the results for **3** and **4** which contain the oxygen atom/atoms in the molecule. The compounds containing a polar substituent or atom such as an oxygen or a nitrogen near a reducible double bond are known to exert special directing effect. Presumably, some type of attractive interaction has bound the polar group or atom to the catalyst surface during the hydrogenation so as to enforce the addition of hydrogen from the same side.[6] On the other hand, when the polar atom and the unsaturated group are placed at an appropriate position in the molecule, the directing effect is no longer predominant. For instance, the stereochemistry of the hyrogenation of 2-substituted 5-methylene-1,3-dioxanes over Group VIII transition metal black catalysts made a sharp contrast with that of 4-substituted 1-methylenecyclohexanes. A high cis selectivity was observed in the former, while the latter exhibited a wide variety of diastereomeric product distribution depending on the catalyst metals.[7,8] If the directing effect of the oxygen atom operates, hydrogens should be incorporated from the axial side to give the equatorial methyl isomer. Hydrogen, however, transfers stereoselectively to the unsaturated bond from the opposite side of oxygen lone pairs (Scheme 1). Such high stereoselectivity was interpreted in terms of the presence of the intramolecular interaction between the n orbital of the oxygen atom and the π_{cc} orbital in these compounds.[7,8] In the present study, **3** and **4** gave more than 92% cis product irrespective of the characteristics of the catalysts. This strongly supports that the product distribution of the hydrogenation of these compounds is not controlled

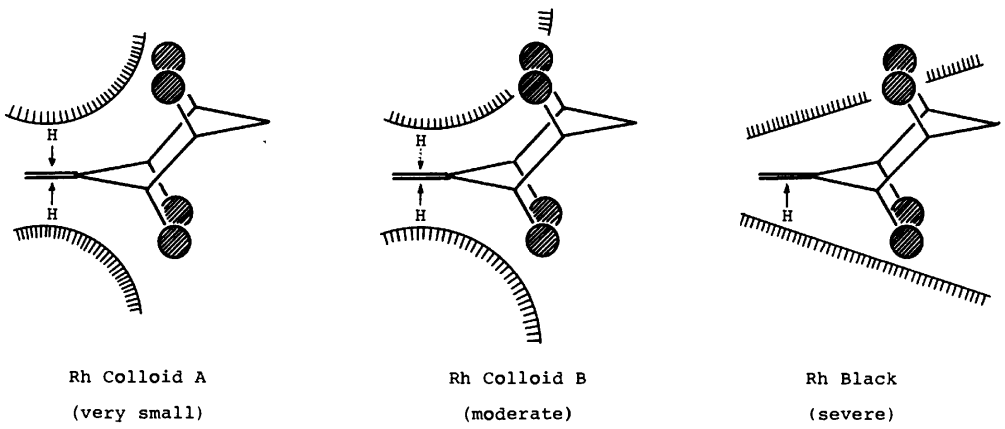

Fig. 1. Steric hindrance to adsorption.

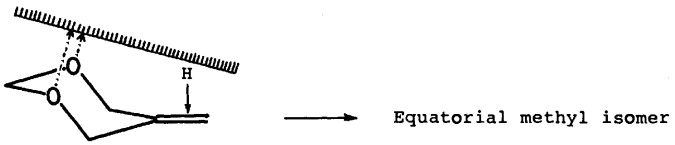

Directing effect of oxygen

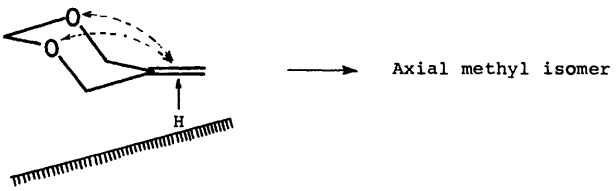

Intramolecular $n_O-\pi_{CC}$ interaction

Scheme 1.

by the particle size of the catalyst at all. In other words, the stereochemistry of the hydrogenation seems not to be determined by the steric and/or directing effect, but by the intramolecular orbital interaction.

Experimental

Materials. Compound **3**[8] was prepared by the Wittig reaction[9] of 6-*t*-butyltetrahydropyran-3-one which was obtained by the pyridinium dichromate oxidation of 6-*t*-butyltetrahydropyran-3-ol.[10] Compound **4** has been previously reported.[11]

Catalysts. Rh colloids were prepared by the method of Hirai et al.[2] Os colloid A: OsO_4 (8.5 mg) and poly(*N*-vinylpyrrolidone) (150 mg) were separately dissolved in two portions of methanol (22.5 ml for each). Both solutions were combined and refluxed. After refluxing for 30 min, a methanol solution (5 ml) of sodium hydroxide (6.7 mg) was added dropwise to the solution under reflux, resulting in rapid color change of the solution to dark brown, which corresponded to the formation of Os particles. After further refluxing for 10 min, a dark brown solution of colloid A was obtained. Os Colloid B: OsO_4 (8.5 mg) and poly(*N*-vinylpyrrolidone) (150 mg) were separately dissolved in two portions of ethanol (22.5 ml for each). Both solutions were combined and refluxed. After refluxing for 3 h, a dark brown solution of colloid B was obtained.

Catalytic Hydrogenation. The substrate (0.5 mmol) was stirred in a hydrogen atmosphare in 5 ml methanol (colloid A and black catalysts) or ethanol (colloid B and silica supported catalysts) at room temperature over a weighed catalyst (colloid: substrate/catalyst; 120—250 mol/g-atom, black catalyst: 5 mg, silica supported catalyst: 50 mg). The reaction was followed gas chromatographically by analyzing aliquots of the reaction mixture at appropriate time intervals.

References

1) R. P. Linstead, W. F. Doering, S. B. Davis, P. Levine, and R. R. Whetstone, *J. Am. Chem. Soc.*, **64**, 1985 (1942).
2) H. Hirai, Y. Nakao, and N. Toshima, *Chem. Lett.*, **1978**, 545.
3) H. Arakawa, K. Takeuchi, T. Matsuzaki, and Y. Sugi, *Chem. Lett.*, **1984**, 1607.
4) S. Siegel and B. Dmukovsky, *J. Am. Chem. Soc.*, **84**, 3132 (1962); and the references cited therein.
5) S. Mitsui, K. Gohke, H. Saito, A. Nanbu, and Y. Senda, *Tetrahedron*, **29**, 1525 (1973).
6) M. C. Dart and H. B. Henbest, *J. Chem. Soc.*, **1960**, 3563; C. P. Rader, G. E. Wicks, Jr., R. L. Young, Jr., and H. S. Aaron, *J. Org. Chem.*, **29**, 2252 (1964); T. J. Howard, *Chem. Ind.*, **1963**, 1899; T. J. Howard and B. Morley, *Chem. Ind.*, **1967**, 73; S. Mitsui, Y. Senda, and H. Saito, *Bull. Chem. Soc. Jpn.*, **39**, 694 (1966); S. Mitsui, M. Ito, A. Nanbu, and Y. Senda, *J. Catal.*, **36**, 119 (1975).
7) J-I. Ishiyama, Y. Senda, and S. Imaizumi, *J. Chem. Soc., Perkin Trans. 2*, **1982**, 71; Y. Senda, A. Ohno, J-I. Ishiyama, S. Imaizumi, and S. Kamiyama, *Bull. Chem. Soc. Jpn.*, **60**, 613 (1987).
8) J-I. Ishiyama, S. Kamiyama, Y. Senda, and S. Imaizumi, *Chem. Ind.*, **1988**, 466.
9) R. Greenwald, M. Chaycovsky, and E. J. Corey, *J. Org. Chem.*, **35**, 2654 (1970).
10) C. Anselmi, G. Berti, G. Catelani, L. Lecce, and L. Monti, *Tetrahedron*, **33**, 2271 (1977).
11) E. L. Eliel and N. C. Knoeber, *J. Am. Chem. Soc.*, **92**, 3444 (1970).

A Practical Method for Optical Resolution of 1,1′-Binaphthyl-2,2′-dicarboxylic Acid via 1-Phenylethylamides

Shuichi Ôi, Yutaka Matsuzaka, Junzo Yamashita,† and Sotaro Miyano*
Department of Biochemistry and Engineering, Faculty of Engineering, Tohoku University, Aramaki-Aoba, Sendai 980
†Chemical Research Laboratory, Tokyo Medical College, 1-1, 6-Chome, Shinjuku-ku, Tokyo 160
(Received September 9, 1988)

Synopsis. Both enantiomers of 1,1′-binaphthyl-2,2′-dicarboxylic acid (100% ee's by HPLC) were conveniently obtained in high yields (ca. 80% of the theory) via fractional crystallization of the (*S*)-1-phenylethylamide diastereomers of the racemic acid followed by treatment with thionyl chloride and then alkaline hydrolysis.

Since Kuhn and Albrecht first resolved 1,1′-binaphthyl-2,2′-dicarboxylic acid **1** in 1928,[1] optically active **1** has been widely utilized for the preparation of various axially chiral binaphthyl derivatives.[2,3] Recently increasing attention has been centered on **1** as it has become to be known that **1** shows characteristic features not only as chiral host for selective inclusion of enantiomeric alcohols[4] but also as chiral stationary phase for direct discrimination of various enantiomers.[5] The enantiomers of **1** have conventionally been obtained by means of an optical resolution through its quinine salt. But the procedure is rather tedious, and efficiency of resolution was low.[2,6] Quite recently Suda and his co-workers have reported an improved optical resolution of **1**, while it still requires to use highly toxic brucine as the resolving agent.[7]

In this paper, we report another practical method for optical resolution of **1** in substantial quantities via 1-phenylethylamide diastereomers (Scheme 1). Treatment of (a*RS*)-**1**[8] with dicyclohexylcarbodiimide (DCC) gave acid anhydride(s),[9] which in turn allowed to react with ca. 1.2 equiv of (*S*)-1-phenylethylamine to give the pair of the diastereomeric mono amides ((a*R*,*S*)- and (a*S*,*S*)-**2**) in quantitative yield. Upon trying various solvents, we have eventually found that acetonitrile is the specific medium to crystallize (a*S*,*S*)-**2** from the mixture. The (a*S*,*S*)-**2** was obtained as fine crystals of a 1:1 clathrate with acetonitrile; the yield amounted to 86% based on one of the enantiomers of **1** with more than 99% diastereomeric excess (de) as evidenced by HPLC. The filtrate was recrystallized twice from ethanol to give the (a*R*,*S*)-counterpart as a 1:1 clathrate with ethanol in a 81% yield and here again in essentially diastereomerically pure state.

The amide bond of **2** was intact by treatment with aqueous sodium hydroxide or sulfuric acid. Eventually, diastereomeric **2** was first treated with thionyl chloride to give the nitrile **3** (the von Brawn reaction),[10] which was then hydrolyzed to the free diacid ((a*R*)- or (a*S*)-**1**) without any appreciable racemization nevertheless rather severe reaction conditions.

Although the resolution method disclosed here requires amides formation followed by regeneration of the free acids, the procedure is operationally simple and straightforward, and applicable to obtain substantial quantities of optically pure **1**, using rather inexpensive enantiomeric 1-phenylethylamine as the resolving agent. Another merit of the procedure is that diastereomeric purity of **2** is readily checked by HPLC to ensure the obtention of enantiomerically pure **1**.[11]

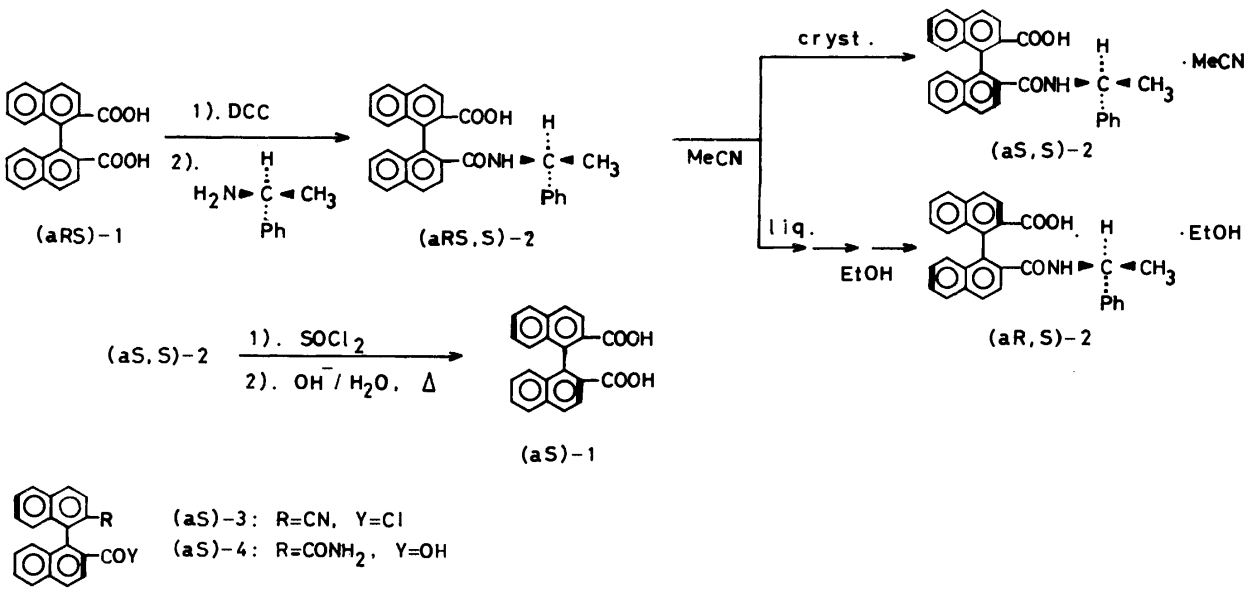

Scheme 1.

Experimental

Instruments. HPLC measurements were carried out on a JASCO TRIROTAR-III equipped with a JASCO UVIDEC-100-III ultraviolet detector (254 nm). IR spectra were measured on a Shimadzu IR-430 grating spectrophotometer. ^{1}H NMR spectra were recorded on a JEOL JNM-FX 60 instrument with tetramethylsilane as an internal standard. Optical rotations were recorded on a Union PM-101 automatic digital polarimeter in a 1-cm cell at 23—25 °C. Melting points were measured on a Yamato MP-21 apparatus and are uncorrected.

Materials. (a*RS*)-**1** was obtained according to the literature procedure;[2,12] mp 271—272.5 °C; IR (KBr) 3500—2300, 1690, 1280, 1240, and 1130 cm^{-1}; ^{1}H NMR (DMSO-d_6) δ=12.2 (2H, br, s, -COOH) and 6.6—8.2 (12H, m, ArH). (*S*)-1-Phenylethylamine ([α]$_D$=−38.0 ° (*c* 2, ethanol)) and DCC were used as purchased. Thionyl chloride and recrystallization solvents (acetonitrile and ethanol) were distilled before use.

Preparation and Separation of Diastereomeric Amides from (*S*)-1-Phenylethylamine and (a*RS*)-1. To a stirred solution of (a*RS*)-**1** (15.0 g, 43.8 mmol) in THF (150 ml) was added a solution of DCC (9.04 g, 43.8 mmol) in THF (100 ml) at room temperature for 1 h under a nitrogen atmosphere. The mixture was stirred for another 2 h at that temperature, and then heated at reflux for 4 h. After triethylamine (5 ml) and (*S*)-1-phenylethylamine (6.37 g, 52.6 mmol) were added to the hot mixture, it was refluxed for 3 h. The mixture was allowed to cool to room temperature, precipitated *N,N'*-dicyclohexylurea was filtered off, and the solids were rinsed with small portions of THF. The solvent was removed from the filtrate under reduced pressure, and the residue was dissolved in 200 ml of chloroform. The solution was washed with concd HCl (200 ml×2) and then with water (200 ml×4), dried over $MgSO_4$ in the presence of activated charcoal. After filtration, the solvent was evaporated in vacuo to give crude (a*RS,S*)-**2**.

The (a*RS,S*)-**2**, which was contaminated with a small amount of *N,N'*-dicyclohexylurea, was directly dissolved in 1000 ml of acetonitrile, and then 700 ml of the solvent was distilled off under atmospheric pressure. The remaining solution was kept overnight at 4 °C to give 9.14 g (85.8% yield, >99% de by HPLC[13]) of (a*S,S*)-**2** clathrated with 1 mol of acetonitrile; mp 190.5—192 °C; [α]$_D$=−123.3 ° (*c* 1.04, chloroform); IR (KBr) 3500—2500, 3260, 1703, 1595, and 1565 cm^{-1}; ^{1}H NMR (DMSO-d_6) δ=0.99 (3H, d, -CH$_3$), 2.05 (3H, s, acetonitrile), 4.6 (1H, m, CH), and 6.3—8.5 (18H, m, NH and ArH). Found: C, 79.27; H, 5.67; N, 5.29%. Calcd for $C_{30}H_{23}NO_3 \cdot C_2H_3N$: C, 78.99; H, 5.39; N, 5.76%.

The solvent of the mother liquor from the above crystallization was removed under reduced pressure. The residue was dissolved in 260 ml of ethanol with warming, and then 150 ml of which was distilled off under atmospheric pressure. The remaining solution was kept overnight at 4 °C. The precipitated crystals were recovered by filtration (9.12 g), and were again dissolved in 250 ml of ethanol. The solvent was distilled (108 ml) until just prior to causing cloudiness of the solution. The solution was kept overnight at 4 °C to give 8.68 g (80.6% yield, >99% de by HPLC) of (a*R,S*)-**2**; mp 260—261 °C; [α]$_D$=+183.2 ° (*c* 1.01, chloroform); ^{1}H NMR (DMSO-d_6) δ=0.79 (3H, d, -CH$_3$), 1.0 (3H, t, ethanol -CH$_3$), 3.4 (2H, q, ethanol -CH$_2$-), 4.6 (1H, m, CH), 6.6—8.2 (17H, m, ArH), and 8.3 (1H, d, NH). Found: C, 78.25; H, 6.09; N, 2.91%. Calcd for $C_{30}H_{23}NO_3 \cdot C_2H_6O$: C, 78.19; H, 5.95; N, 2.85%.

Regeneration of Axially Homochiral (a*S*)-1. To the 9.14 g (18.8 mmol) of (a*S,S*)-**2** were added 100 ml of thionyl chloride and one drop of DMF, and the mixture was refluxed for 3 h. The excess of thionyl chloride was distilled out, and the residue was dried at 70 °C under vacuum to give (a*S*)-**3**, which was substantiated by IR as methyl ester by treatment with methanol; IR (KBr) 2200 and 1715 cm^{-1}. The crude (a*S*)-**3** was directly dissolved in 130 ml of ethanol with warming, and 10 g of KOH in 30 ml of water was added and then refluxed for 5 h to give amide (a*S*)-**4** as evidenced by IR; (KBr) 3500—2500, 3400, 1700, and 1640 cm^{-1}. After volatiles were removed under reduced pressure, the residue was suspended in a solution of 50 g of NaOH in 400 ml of water and heated at reflux; the mixture became almost clear solution after 10-h heating, and the reaction was continued for another 30 h to ensure complete hydrolysis, while almost all the hydrolysis seemed to be completed by 20-h heating. After cooling to room temperature, 200 ml of water was added and washed with ether (200 ml×2) to remove nonacidic compounds. The aqueous solution was acidified with concd HCl and the precipitate was extracted with ethyl acetate (150 ml×3). The combined organic layer was dried over $MgSO_4$ in the presence of activated charcoal. After filtration, the solvent was evaporated in vacuo and recrystallization from toluene gave 5.84 g (91% yield) of (a*S*)-**1**, which was of essentially 100% ee as evidenced by HPLC; a small sample of the acid was converted to the bis(butylamide) and subjected to HPLC analysis on a chiral stationary phase as reported before;[14] mp 165—167 °C;[15] [α]$_{546}$=−126.2 ° (*c* 1.05, 0.1 mol dm^{-3} NaOH) (lit,[7] [α]$_{546}$=−127 ° (*c* 1.0, 0.1 mol dm^{-3} NaOH)).

(a*R*)-2: Similar treatment of 8.68 g (17.7 mmol) of (a*R,S*)-**2** gave 5.69 g (94% yield, 100% ee by HPLC) of (a*R*)-**1**.

References

1) R. Kuhn and O. Albrecht, *Justus Liebigs Ann. Chem.*, **465**, 282 (1928).

2) D. M. Hall and E. E. Turner, *J. Chem. Soc.*, **1955**, 1242.

3) S. Miyano, H. Inagawa, S. Handa, and H. Hashimoto, *Chem. Ind., (London)*, **1985**, 236, and references cited therein.

4) S. Kanoh, Y. Hongoh, S. Katoh, M. Motoi, and H. Suda, *J. Chem. Soc., Chem. Commun.*, **1988**, 405.

5) S. Ôi, M. Shijo, J. Yamashita, and S. Miyano, *Chem. Lett.*, **1988**, 1545.

6) Cf., N. Maigrot and J. P. Mazaleyrat, *Synthesis*, **1985**, 317.

7) S. Kanoh, Y. Hongoh, M. Motoi, and H. Suda, *Bull. Chem. Soc. Jpn.*, **61**, 1032 (1988).

8) The subscript "a" refers to axial chirality.

9) The sample showed MS peak at M/e 324 corresponding to the molecular ion of monomeric anhydride, which does not exclude the possibility of the presence of polymeric anhydrides via intermolecular dehydration.

10) W. R. Vaughan and R. D. Carlson, *J. Am. Chem. Soc.*, **84**, 769 (1962); cf., F. X. Webster, J. G. Millar, and R. M. Silverstein, *Tetrahedron Lett.*, **27**, 4941 (1986).

11) Merits and demerits of optical resolution via covalent diastereomers: J. Jacques, A. Collet, and S. H. Wilen, "Enantiomers, Racemates and Resolutions", John Wiley and Sons., Inc., New York, N. Y. (1981).

12) S. Miyano, M. Tobita, S. Suzuki, Y. Nishikawa, and H. Hashimoto, *Chem. Lett.*, **1980**, 1027; E. Weber, I. Csöregh, B. Stenstand, and M. Czugler, *J. Am. Chem. Soc.*, **106**, 3297 (1984).

13) The acid was converted to methyl ester by treatment with diazomethane and subjected to HPLC on silica-gel column (hexane-2-propanol (1%)).

14) J. Yamashita, T. Numakura, H. Kita, T. Suzuki, S. Ôi, S. Miyano, H. Hashimoto, and N. Takai, *J. Chromatogr.*, **403**, 275 (1987).

15) Melting points of the samples of axially chiral **1** substantially differ from literature to literature; see for example, Ref. 7.

Sommelet-Hauser Rearrangement of Oxygen and Sulfur Containing Heteroaromatic Sulfonium Ylides

Makoto YAMAMOTO,* Madoka KAKINUMA, Shigeo KOHMOTO, and Kazutoshi YAMADA
Department of Industrial Chemistry, Faculty of Engineering, Chiba University,
1-33 Yayoi-cho, Chiba-shi 260
(Received September 16, 1988)

Synopsis. A Sommelet-Hauser rearrangement of sulfonium ylides of 4*H*-pyran-4-ones, furan, and thiophenes are discussed. The sulfonium halides which were prepared from excess dimethyl sulfide with corresponding halides were treated with NaH or NaOR in a polar solvent to give moderate to good yields of rearranged products.

Allyl and arylsulfonium ylides undergo an orbital-symmetry allowed [2.3] sigmatropic rearrangement, commonly known as the Sommelet-Hauser rearrangement.[1] The Sommelet-Hauser rearrangement of acyclic sulfonium ylides[1] and its aromatic analogues[2] can be widely quoted. However, the rearrangement of heteroaromatic ylides has been sparsely reported.[3]

We wish to report here on the Sommelet-Hauser rearrangement of 4-pyranones, furan and thiophene derivatives. Many methods for the preparation of a sulfonium ylide are known, such as sulfonium salt-base,[4] carbene insertion,[5] and nitrene addition.[6] We prepared the sulfonium ylides via the sulfonium salt-base, which we found to be a simple method.

In general, a Sommelet-Hauser rearrangements of heteroaromatic compounds were carried out by treating the substrates in an inert atmosphere with an excess of dimethyl sulfide, followed by treatment with a base (MeONa-MeOH, EtONa-EtOH, or NaH). Following this procedure, 2,6-dimethyl-3-methylthiomethyl-4*H*-pyran-4-one (**2a**) was obtained in 92% yield from 2-bromomethyl-6-methyl-4*H*-pyran-4-one (**1a**).[7] In this reaction none of the [1.2] rearranged product was detected. Compound **2a** was also prepared by treating the sulfonium salt of **1a** with sodium hydride in refluxing THF or dioxane in 84 and 55% yields, respectively.

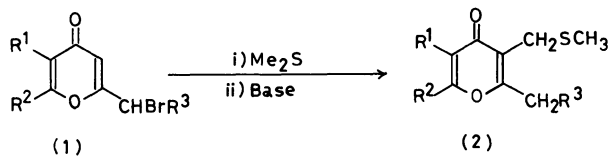

(1) (2)

a: $R^1=R^3=H$, $R^2=Me$
b: $R^1=R^3=H$, $R^2=Ph$
c: $R^1=OCH_2Ph$, $R^2=R^3=H$
d: $R^1=H$, $R^2=Me$, $R^3=CH_2CH_2CH_3$

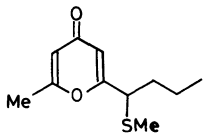

(3)

The halopyrans, **1b** and **1c**, gave the corresponding rerranged products, **2b** and **2c**, in 87 and 73% yields, respectively. In contrast, a treatment of the branched bromide **1d** gave only 3% of the desired product **2d**, together with 52% of 2-methyl-6-(1-methylthiomethyl)-4*H*-pyran-4-one (**3**).

2-(Chloromethyl)furan (**4**) gave **5** in 34% yield. However, the sulfonium salt of **4** and the rearranged product **5** were unstable and easily decomposed to a black tar.

3-(Bromomethyl)thiophene (**6**) afforded rearranged product **7** in 67% yield. Compound **7** was also

Table 1. Spectral Data of the Rearranged Products

Compound	IR/cm^{-1}	^{1}H NMR (δ) S-CH_3	C_2-CH_3	C_3-CH_2-S	MS Found (m/z)	Calcd (M)
2a	1670	2.19	2.29	3.38	C; 58.60%	58.68%[a]
	1600				H; 6.52	6.56
	1185					
2b	1650	2.18	2.50	3.63	246.3240	246.3246
	1615				($C_{14}H_{14}O_2S$)	
	1170					
2c	1635	2.07	2.17	3.37	276.3500	276.3514
	1615				($C_{15}H_{16}O_3S$)	
	1185					
5	1625	1.92	2.23	3.37	142.0451	142.0451
	1515				($C_7H_{10}OS$)	
	1180					
7	3100	2.00	2.20	3.73	158.0224	158.0244
	1250				($C_7H_{10}S_2$)	
11	1680	1.88	2.43	3.72	208.0739	208.0739
	1470				($C_{11}H_{12}S_2$)	

a) Elemental analysis data was listed for compound **2a**.

obtained in 60% yield when the sulfonium bromide of **6** was treated with sodium ethoxide in ethanol at room temperature and in 22% yield when the same reaction was carried out at 0 °C. Interestingly, the reaction in refluxing ethanol gave 24% of the ethyl ether **8** in addition to 12% of **7**. A similar result was obtained in the case of sodium methoxide in refluxing methanol (**7**: 19%, **9**: 19%). The mechanisms for the formation of **8** and **9** are sitll not clear.

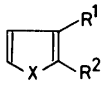

(4): R^1=H, R^2=CH_2Cl, X=O

(5): R^1=CH_2SCH_3, R^2=CH_3, X=O

(6): R^1=CH_2Br, R^2=H, X=S

(7): R^1=CH_3, R^2=CH_2SCH_3, X=S

(8): R^1=$CH_2OCH_2CH_3$, R^2=CH_2SCH_3, X=S

(9): R^1=CH_2OCH_3, R^2=CH_2SCH_3, X=S

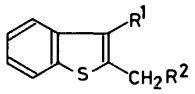

(10): R^1=H, R^2=Br

(11): R^1=CH_2SCH_3, R^2=H

The sulfonium bromide of 2-(bromomethyl)benzo[*b*]thiophene (**10**)[8] gave the desired product **11** in 57% yield.

We have thus demonstrated that the heteroaromatic ylides undergo an efficient Sommelet–Hauser rearrangement. Moreover, the methylene of a newly formed methylthiomethyl group can be used as a d^1-synthon. Applications of the aforementioned synthetic potentialities of this reaction are presently being studied in the laboratory. Results will be communicated separately.

Experimental

2,6-Dimethyl-3-methylthiomethyl-4*H*-pyran-4-one (2a): A mixture of **1a** (2.03 g, 10 mmol) in 5 ml of chloroform and excess dimethyl sulfide (3.72 g, 60 mmol) was stirred overnight at room temperture under nitrogen. The resulting precipitate was collected by filtration and, without further purification, the precipitate was added to an equimolar amount of sodium methoxide in 20 ml of methanol. The mixture was heated to reflux for 2 h, cooled, neutralized with diluted hydrochloric acid and worked up as usual to give a crude product which was purified by silica-gel column chromatography using benzene–ethyl acetate (2:1) as an eluent to give colorless plates of **2a** (1.69 g, 92%), mp 56—58 °C (from benzene–hexane=1:3).

Sulfonium bromide of **1a** (1.02 g, 5 mmol) was treated with sodium hydride (132 mg, 5.5 mmol) in refluxing THF (15 ml) or in refluxing dioxane (12 ml) for 2 h under nitrogen to give **2a** in 773 mg (84%) or 506 mg (55%), respectively. Similarly, rearranged products **2b** (87%; mp 77—78 °C), and **2c** (73%; pale yellow liquid) were obtained. Spectral data are listed in Table 1.

Attempted Rearrangement of the Branched Sulfonium Ylide: A mixture of **1d** (2.31 g, 9.43 mmol) prepared from 2-butyl-6-methyl-4*H*-pyran-4-one[9] and excess dimethyl sulfide (1.84 g, 13.0 mmol) in chloroform (8 ml) was treated according to the procedure mentioned above; the products were purified similarly to give **2d** (52 mg, 3%) and **3** (975 mg, 52%). ^{1}H NMR of **2d** (CCl_4, δ): 0.92 (t, 3H), 1.20—1.87 (m, 4H), 2.00 (s, 3H), 2.25 (s, 3H), 2.60 (t, 2H), 3.60 (s, 2H) and 5.40 (s, 1H). ^{1}H NMR of **3** ($CDCl_3$, δ): 0.97 (t, 3H), 1.10—1.80 (m, 4H), 2.00 (s, 3H), 2.25 (s, 3H), 3.34 (t, 1H) and 5.90 (s, 2H). MS of **3**: Found: *m/z* 212.0876, Calcd as $C_{11}H_{16}O_2S$: M, 212.0870. *m/z* 212 (M^+, 100), 141 (33), 85 (90) and 43 (60).

3-Methylthiomethyl-2-methylfuran (5): A mixture of 2-(chloromethyl)furan (**4**; 816 mg, 7.0 mmol) and dimethyl sulfide (1.28 g, 21 mmol) was kept at room temperature overnight. The resulting brown paste was stirred with sodium ethoxide (7.7 mmol) in ethanol (40 ml) at 0 °C for 3.5 h. The reaction mixture was quenched with water (12 ml), extracted with ether, dried over anhydrous magnesium sulfate, concentrated, and purified by silica-gel column chromatography with hexane to give **5** (338 mg, 34%) as a colorless oil. The spectral data are listed in Table 1.

3-Methyl-2-(methylthiomethyl)thiophene (7): 3-(Bromomethyl)thiophene (**6**; 1.04 g, 5.9 mmol), which was prepared from 3-methylthiphene with NBS and benzoyl peroxide in refluxing benzene,[7] was mixed with dimethyl sulfide (733 mg, 11.8 mmol) the mixture was kept overnight at room temperature. The resulting brown paste was washed several times with ether and dried to give a crude sulfonium bromide (959 mg, 68%). This sulfonium bromide in THF (25 ml) was treated with sodium hydride (106 mg, 4.4 mmol) with stirring at room temperature for 22 h. The reaction mixture was quenched with water, extracted with ether, dried, concentrated and purified by silica-gel column chromatography with hexane to give **7** (628 mg, 67%) as a colorless oil. The sulfonium bromide of **6** (720 mg) was treated with sodium ethoxide in refluxing ethanol (20 ml) for 2 h to give **7** (57 mg, 12%) and 3-ethoxymethyl-2-(methylthiomethyl)thiophene (**8**; 146 mg, 24%). IR (neat) of **8**: 3100, 2990, and 1090 cm^{-1}. ^{1}H NMR (CCl_4, δ) of **8**: 1.20 (t, 3H, J=7.0 Hz), 2.04 (s, 3H), 3.45 (q, 2H, J=7.0 Hz), 3.82 (s, 2H), 4.41 (s, 2H), 6.88 (d, 1H, J=5.2 Hz) and 7.07 (d, 1H, J=5.2 Hz). MS of **8**: Found: *m/z* 202.0474, Calcd as $C_9H_{14}OS_2$: M, 202.0474. ^{13}C NMR ($CDCl_3$, δ) of **8**: 14.96 (q), 15.45 (q), 30.27 (t), 65.64 (t), 65.74 (t), 123.3 (d), 128.8 (d), 136.2 (s), and 138.4 (s).

The sulfonium bromide of **6** (720 mg) was also treated with sodium methoxide in refluxing methanol (20 ml) for 2 h to give **7** (90 mg, 19%) and 3-methoxymethyl-2-(methylthiomethyl)thiophene (**9**; 108 mg, 19%). ^{1}H NMR (CCl_4, δ) of **9**: 2.04 (s, 3H), 3.30 (s, 3H), 3.82 (s, 2H), 4.38 (s, 2H), 6.88 (d, 1H, J=5.0 Hz) and 7.08 (d, 1H, J=5.0 Hz).

2-Methyl-3-(methylthiomethyl)benzo[*b*]thiophene (11): A solution of 2-(bromomethyl)benzo[*b*]thiophene (**10**)[8] (2.37 g, 10.4 mmol) in chloroform (1 ml) was added to dimethyl sulfide (1.97 g, 31.7 mmol); the mixture was kept overnight at room temperature. The resulting white precipitate was filtered, washed several times with ether, dried to give crude sufonum bromide of mp 132—133 °C (2.45 g, 81%). To a solution of this sulfonium bromide (941 mg, 3.33 mmol) in THF (15 ml) was added sodium hydride (184 mg, 3.5 mmol) the mixture was heated to reflux for 5 h. The reaction mixture was quenched with 1 M-hydrochloric acid (1M=1 mol dm^{-3}), extracted with benzene, dried, concentrated and purified by silica-gel column chromatography with benzene–ethyl acetate (9:1) to give **11** (365 mg, 57%) as yelow paste. Spectral data are listed in Table 1.

References

1) B. M. Trost and L. S. Melvin, Jr., "Sulfur Ylides," Academic Press (1975).

2) A. Padwa and J. R. Gasdaska, *J. Org. Chem.*, **51**, 2857 (1986). S. J. Campbell and D. Darwish, *Can. J. Chem.*, **54**, 193 (1976).

3) M. Hori, T. Kataoka, H. Shimizu, S. Ohno, and K. Narita, *J. Chem. Soc., Chem. Commun.*, **1981**, 364. M. Hori, T. Kataoka, H. Shimizu, and O. Komatsu, *J. Chem. Soc., Chem. Commun.*, **1985**, 883.

4) G. B. Payne, *J. Org. Chem.*, **32**, 3351 (1967). B. M. Trost and H. C. Arndt, *ibid.*, **38**, 3140 (1973). M. G. Ahmed and R. W. Alder, *Chem. Comm.*, **1969**, 1329. R. M. Acheson and D. R. Harrison, *ibid.*, **1969**, 724. E. Vedejs, M. J. Arco, D. W. Powell, J. M. Renga, and S. P. Singer, *J. Org. Chem.*, **43**, 4831 (1978).

5) W. Ando, *Acc. Chem. Res.*, **10**, 179 (1977).

6) H. Sashida and T. Tsuchiya, *Heterocycles*, **22**, 1303 (1984).

7) M. Yamamoto, S. Iwasa, K. Takatsuki, and K. Yamada, *J. Org. Chem.*, **51**, 346 (1986).

8) Y. Matsuki and B. Chihli, *Nippon Kagaku Zasshi*, **87**, 186 (1966).

9) Compound **1d** was prepared from 2,6-dimethyl-4*H*-pyran-4-one by the procedure described in; M. Yamamoto and N. Sugiyama, *Bull. Chem. Soc. Jpn.*, **48**, 508 (1975).

Production of L-Tryptophan from γ-Glutamaldehydic Acid

Hirozumi ETO,* Chikahiko EGUCHI, and Teruhiko KAGAWA
Central Research Laboratories, Ajinomoto Co., Inc. 1-1,
Suzuki-cho, Kawasaki-ku, Kawasaki 210
(Received September 17,1988)

Synopsis. Labile γ-glutamaldehydic acid (**1**) was first converted to tryptophan via its phenylhydrazone; no racemization occurred during the reaction. The stability of **1** was shown to be remarkably enhanced in the presence of additives.

The production of L-tryptophan (L-Trp) has been extensively investigated after its positive effects as a feed additive became recognized.[1] We focused our attention on obtaining L-Trp by a combination of a fermentation and chemical synthesis. Practical synthetic methods for the production of L-Trp generally require an optical resolution of the racemic form, followed by the racemization of D-Trp.[2] Our process dose not necessitate these steps since optically active starting material prepared by fermentation is used.

γ-Glutamaldehydic acid (GAA, **1**) and its cyclic imine form, 3,4-dihydro-2*H*-pyrrole-2-carboxylic acid, were known to be labile intermediates in the biosynthesis of proline from glutamic acid.[3-5] GAA (**1**) was likely to be a suitable starting material of the nonprotected L-Trp synthesis by a Fischer indole formation. GAA (**1**), however, has neither been isolated in a pure form nor has it been used as a useful synthetic intermediate, probably because of its instability. The stability of **1** depended on its concentration; 30% of **1** in a 50-mM neutral solution (1 M=1 mol dm^{-3}) was reported to decompose within 1 hour.[6] On the other hand, none of these changes were observed in a 1-mM solution.[6] In the course of our practical research toward the establishment of a production method for L-Trp, 1) the possibility of chemical conversion of **1** to Trp, 2) the stereochemistry during the reaction, and 3) the way for preservation of **1** in neutral solution, were investigated.

In order to mimic the combination of biosynthesis of **1** and chemical conversion of it to Trp, GAA (**1**) was conveniently generated by the acidic hydrolysis of GAA dimethyl acetal (**5**), because L-**1** was not currently available by a fermentative production.[8] Since the phenylhydrazone (**6**) did not quantitatively precipitate due to its solubility, phenylhydrazone formation and indole synthesis were carried out consecutively. *N*-Ac-GAA (**3**) and GAA-hydantoin (**4**) were reported to afford the corresponding protected Trp in good yield under mild reaction conditions: [0.1 M HCl, reflux, 1 equiv of phenylhydrazine].[9] Meanwhile, for the case of **1**, Trp was provided in poor yield under the same conditions as mentioned above. The yield was shown to depend on the acidity and the amount of phenylhydrazine (Table 1). When 15 equiv of phenylhydrzine and 0.45 M (1 M=1 mol dm^{-3}) sulfuric acid was used, the result was remarkably improved (85% yield). GAA (**1**) in a

Table 1. Synthesis of Trp from **5** under Various Conditions

$PhNHNH_2 \cdot HCl$ (equiv to **1**)	H_2SO_4/M	Yield/%
1.0	0.05	17
1.0	0.45	27
7.0	0.45	62
15.0	0.45	85

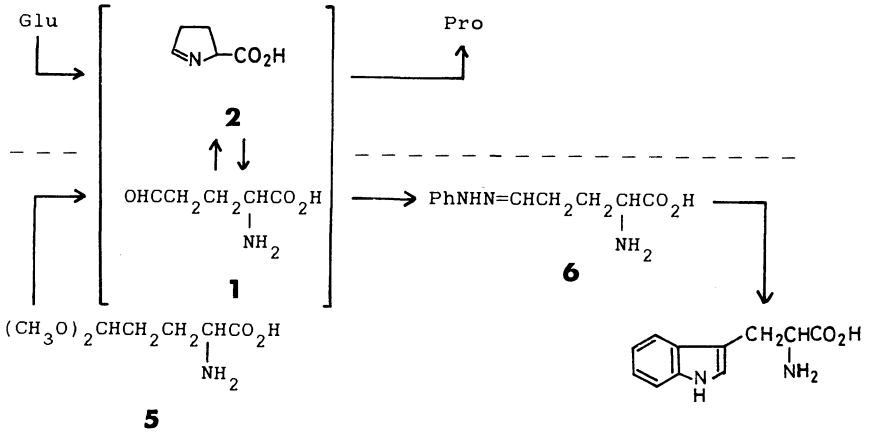

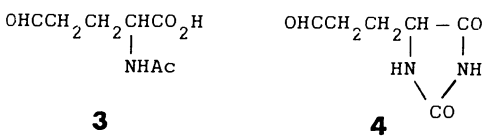

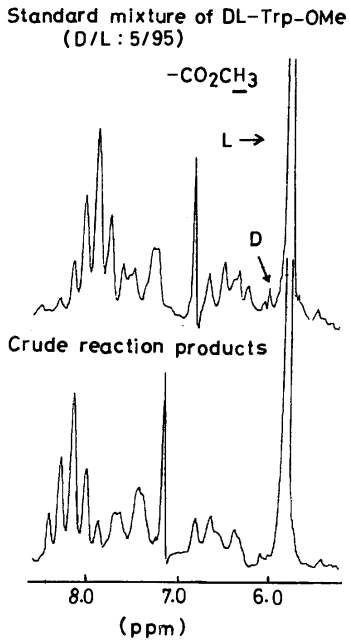

Fig. 1. ^1H NMR spectrum of standard mixture of DL-Trp-OMe (D/L: 5/95) and crude reaction products after adding chiral shift reagent.

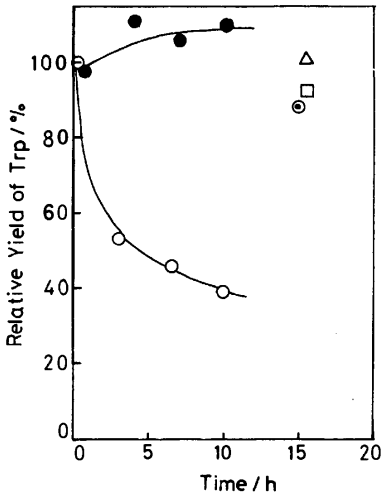

Fig. 2. Stabilizing effect of additives to solution of **1**. ● $PhNHNH_2 \cdot HCl$, △ $NaHSO_3$, □ $NH_2OH \cdot HCl$, ⊙ $H_2NCONHNH_2$, ○ none.

neutral solution provided the same results (85% yield) under optimum reaction conditions.

The previously mentioned successful observation suggested that L-**1** in a fermentation broth was able to be effectively converted to L-Trp. We therefore investigated whether isomerization took place during the course of the reaction. Optically active **5** was prepared by enzymatic deacylation of racemic *N*-acetyl-**5**. Compound L-**5** was subjected to the aforementioned Trp synthesis followed by esterification. The optical purity of the obtained L-Trp methyl ester (L-Trp-OMe) was examined by ^1H NMR using a chiral shift reagent. The ^1H NMR spectra of the reaction products were compared to the spectra of a mixture (95:5) of L- and D-Trp-OMe in the presence of tris[3-(trifluoromethylhydroxymethylene)-*d*-camphorato]europium(III).[10] Since no signal corresponding to D-Trp-OMe was detected in the reaction product (Fig. 1), it was concluded that isomerization did not occur during the reactions.

Since an accumulation of **1** in the fermentation broth with a high concentration is desired in order to produce L-Trp on an industrial scale, we investigated the enhancement of the stability of **1** in a neutral environment.

When a 230-mM solution of **1** (pH 7) was left at 31 °C for several hours, followed by treatment with phenylhydrazine in acidic solution, Trp formation at an appropriate time decreased linearly with a time (Fig. 2). Meanwhile, reagents which generally react with aldehydes such as phenylhydrazine, sodium hydrogensulfite, hydroxylamine, and semicarbazide were added to a neutral solution of **1** before left standing, in order to form a stable adduct. As expected, no substantial decrease in Trp formation was observed, even after 15 hours. This meant that **1** could be preserved under standard fermentation conditions (pH 7, 31 °C). A stable form was exhibited to have the same chemical reactivity as **1** from the Trp synthesis.

These results strongly indicate the possibility of accumulating L-**1** by fermentation without decomposition and conversion to L-Trp. This process is highly straightforward and practically attractive. Further, progress in the fermentative production of L-**1** and its conversion to L-Trp will be reproted elsewhere.[8]

Experimental

High performance liquid chromatography (HPLC) was obtained with a Hitachi 635 fitted with a 500 mm×2.1 mm column containing Hitachi cation resin #2610. The eluent was a phosphate buffer (0.1 M KH_2PO_4: 0.1 M Na_2HPO_4= 16:1) at a flow rate of 0.5 ml min^{-1}. The temperature was 52 °C and detection was at 274 nm. IR and NMR spectra were recorded on a JASCO Infrared Spectrometer Model IR-S and Varian NMR Spectrometer XL-100A, respectively. The optical rotation was determined on a JASCO Digital Polarimeter DIP-140. Melting points are uncorrected. Racemic GAA dimethyl acetal (**5**) was prepared according to the procedure reported by Okuda.[7] Aminoacylase derived from *Aspergillus oryzae* was purchased from Amano Pharmaceutical Co.

Trp (general procedure). **Method A.** To the solution of phenylhydrazine hydrochloride (2.46 g, 17.0 mmol) in 0.9 M sulfuric acid (6 ml) was added **5** (201 mg, 1.1 mmol) in water (6 ml) dropwise under reflux. The reaction was carried out for 1 hour and analyzed by HPLC (85% yield). **Method B.** To a cooled solution of 1 M hydrochloric acid (10 ml) in an ice bath was added **5** (201 mg, 1.1 mmol). The mixture was stirred for 30 minutes and neutralized to pH 7 by adding 1 M aq. sodium hydroxide solution. This solution was added to a refluxing solution of phenylhydrazine hydrochloride (2.45 g, 17.0 mmol) in 0.9 M sulfuric acid (15 ml). The reaction mixture was refluxed for 1 hour and analyzed by HPLC (85% yield).

L-γ-Glutamaldehydic Acid Dimethyl Acetal (L-5). To a solution of **5** (3.39 g, 1.9 mmol) in 0.44 M aq. sodium hydroxide (50 ml) was added acetic anhydride (2.5 g,

25 mmol) while keeping the pH at 9 by the occasional addition of aq. sodium hydroxide at room temperature. The mixture was stirred for 1 hour and lyophilized after the pH was adjusted to 7. The residue was dissolved in water (80 ml) and 10 mM cobalt(II) chloride solution (4 ml) and amino-acylase (198.5 mg) were added. The enzymic reaction was carried out for 92 hours at 37 °C and the pH was kept in the range of 7.5 to 8.0. Inorganic salts were removed by adding a cation-exchange resin (IRC-50) and an anion-exchange resin (IR-45). The solvent was evaporated under reduced pressure and the residue (1.2 g) in water (400 ml) was charged to a sirotherm resin (supplied by Japan Sirotherm Co., Inc.) (80 ml) in column in order to remove any unreacted *N*-acetylated **3**. The column was washed with water (250 ml) at 0 °C and then eluted with water (300 ml) at 80 °C. The eluent was lyophilized and the residue was recrystallized from water (1 ml) and ethanol (1 ml) and diethyl ether (2 ml) to afford 93.3 mg (0.53 mmol) of L-**5**. $[\alpha]_D^{25}$ −1.07 (*c* 0.93, water).

L-Trp-OMe. L-**5** (93.3 mg, 0.3 mmol) was converted to L-Trp as previously described. The resultant solution was adjusted to pH 9.5 and washed with benzene and diethyl ether to remove phenylhydrazine. The aqueous phase was neutralized and concentrated to dryness. The residue was dissolved in methanol (20 ml) and esterified by bubbling HCl gas for 1.5 hours at room temperature. The solvent was removed and the residue, dissolved in chloroform, was washed with aq. sodium hydrogencarbonate, water and dried to give L-Trp-OMe (46.5 mg, 0.21 mmol).

Determination of Optical Purity of L-Trp-OMe. The Kainosho method was used.[10]

Stability of γ-Glutamaldehydic Acid (1). GAA dimethyl acetal (**5**, 280 mg, 1.58 mmol) was treated with 1 M HCl (7 ml) at 5 °C overnight. The mixture was allowed to warm to room temperature and then neutralized by adding aq. sodium hydroxide. To this solution of **1** was added equimolar amounts of reagents ($PhNHNH_2 \cdot HCl$, $NaHSO_3$, $NH_2OH \cdot HCl$, $H_2NCONHNH_2 \cdot HCl$). The pH was then adjusted to 7 and the volume adjusted to 10 ml. The mixture was left at 31 °C for an appropriate time and then converted to tryptophan using optimum reaction conditions. The yield of tryptophan was compared to the yield when nothing was added to a solution of **1**.

References

1) S. Ariyoshi, "Aminosan Siryo Gaku," Chikusan Syuppansha, Tokyo (1983), p. 144.

2) K. Toi, "Aminosan Kogyo, Gosei to Riyo," ed by T. Kaneko, Y. Izumi, I. Chibata, and T. Itoh, Koudansha Scientific, Tokyo (1973), p. 214.

3) H. J. Vogel and B. D. Davis, *J. Am. Chem. Soc.*, **74**, 109 (1952).

4) H. J. Strecker, *J. Biol. Chem.*, **235**, 2045 (1960); V. A. Mezland and W. E. Knox, *Anal. Biochem.*, **74**, 430 (1976); D. J. Hayzer, R. V. Krishna, and R. Margraff, *Anal. Biochem.*, **96**, 94 (1979).

5) G. Y. Wu and S. Seifter, *Anal. Biochem.*, **67**, 413. (1975); M. Tanaka, T. Kishi, and S. Kinoshita, *Nippon Nogei Kagaku Kaishi*, **34**, 972 (1960).

6) I. Williams and L. Frank, *Anal. Biochem.*, **64**, 85 (1975).

7) T. Okuda, *Bull. Chem. Soc. Jpn.*, **30**, 358 (1957).

8) Fermentative production of L-**1** will be reported soon. H. Morioka, K. Miwa, H. Eto, C. Eguchi, and S. Nakamori, *Agric. Biol. Chem.*, in press.

9) Y. Komachiya, K. Suzuki, T. Yamada, H. Miyayashiki, and S. Sakurai, *Nippon Kagaku Kaishi*, **86**, 856 (1965); F. Masumi, H. Takeuchi, S. Kondo, K. Suzuki, and S. Yamada, *Chem. Pharm. Bull.*, **30**, 3831 (1982); K. Izawa, *Yuki Gosei Kagaku Kyokai Shi*, **46**, 218 (1988).

10) K. Ajisaka, M. Kamisaku, and M. Kainisho, *Chem. Lett.*, **1972**, 857.

Preparation of Nickel Complexes with η^2-Coordinated Fluorinated Ketones from Dialkylnickel Complexes

Yong-Joo KIM, Kohtaro OSAKADA, and Akio YAMAMOTO*
Research Laboratory of Resources Utilization, Tokyo Institute of Technology,
4259 Nagatsuta, Midori-ku, Yokohama 227
(Received September 17, 1988)

Synopsis. Reactions of hexafluoroacetone and 2,2,2-trifluoroacetophenone with dialkylnickel complexes cause extrusion of the alkyl ligands to give nickel complexes having an η^2-coordinated ketone and an auxiliary ligand such as bpy (2,2′-bipyridine) or dpe (1,2-bis(diphenylphosphino)ethane).

In comparison to a rich variety of η^2-olefin-coordinated transition metal complexes,[1] examples of η^2-ketone-coordinated transition metal complexes are still scarce.[2-5] We report here preparation and characterization of new ketone-coordinated nickel complexes derived from dialkylnickel complexes by reactions with fluorinated ketones.

Ketones with electron-withdrawing groups may cause two types of reactions with transition metal alkyls or hydrides. One is insertion of the carbonyl group in ketones into a metal–alkyl or metal–hydrogen bond to give transition metal alkoxides and the other is ketone coordination which induces reductive elimination of transition metal alkyls or hydrides. A similar effect of olefins with electron-withdrawing groups to promote reductive elimination of dialkylnickel complexes is well known.[6]

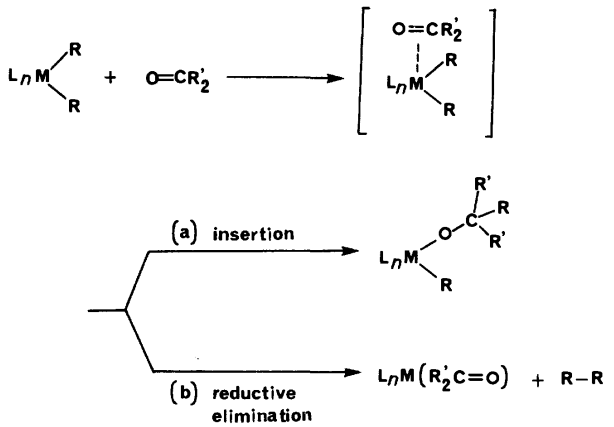

In our previous communication we have observed facile insertion of the carbonyl group in hexafluoroacetone and 2,2,2-trifluoroacetophenone into a metal–hydrogen bond of cobalt, ruthenium and rhodium hydride complexes to give stable alkoxides of these late transition metals.[7]

In the course of our recent study on the chemistry of nickel and palladium alkoxide complexes,[8] we examined reactions of fluorinated ketones with dialkyl nickel(II) complexes. We observed extrusion of the alkyl groups and formation of nickel complexes with the fluorinated ketones bonded in a side-on manner to the nickel center. Some of the ketone-coordinated nickel complexes prepared in the present study by treatment of dialkylnickel complexes with the fluorinated ketones have been previously prepared by displacement of olefin or tertiary phosphine ligands coordinated to Ni(0) center.[2-5] The present method provides an alternative route to the ketone-coordinated complexes, which have attracted less attention than the olefin-coordinated complexes.

Results and Discussion

Dialkylnickel complexes, $NiMe_2(bpy)$, $NiEt_2(bpy)$, and $NiMe_2(dpe)$ (dpe=1,2-bis(diphenylphosphino)-ethane), react smoothly with hexafluoroacetone to give $Ni(\eta^2\text{-}(CF_3)_2CO)(bpy)$ **1** and $Ni(\eta^2\text{-}(CF_3)_2CO)(dpe)$ **3**. The reaction of $NiMe_2(dpe)$ with the fluorinated ketone gives mixtures of CH_4 and C_2H_6 as gaseous products, while similar reactions of $NiR_2(bpy)$ (R=Me, Et) give reductive elimination products R–R exclusively. Complexes **1** and **3** have been prepared from reactions of the ketone with $Ni(cod)_2$ (bis(1,5-cyclooctadiene)-nickel) in the presence of the auxiliary ligands, bpy and dpe, respectively.[4] The products obtained in the present study show the IR spectra almost identical to those in the literature.[4] A similar reaction of $NiEt_2(bpy)$ with 2,2,2-trifluoroacetophenone gives a nickel–ketone complex $Ni(\eta^2\text{-}CF_3COPh)(bpy)$ **2** with

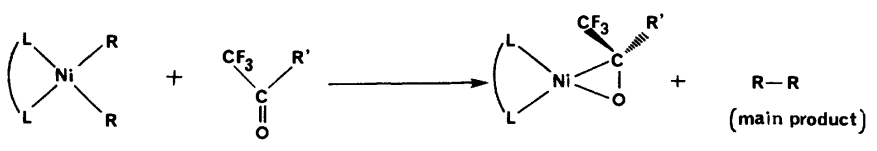

R = Me, Et.

1 L⌣L = bpy, R′ = CF_3;

2 L⌣L = bpy, R′ = Ph;

3 L⌣L = dpe, R′ = CF_3;

4 L⌣L = dpe, R′ = Ph.

Table 1. Reactions of Fluoro Ketones with Dialkylnickel Complexes

NiR_2L_2 (mmol)	Fluoro ketone (mmol)	Conditions[a]		Products (Yield/%)[b]	
		Temp	Time		
$NiMe_2$(bpy) (0.36)	CF_3COCF_3 (0.36)	25 °C	1 h	C_2H_6 (92)	**1** (62)
$NiEt_2$(bpy) (0.40)	CF_3COCF_3 (0.40)	25 °C	1 h	C_2H_6 (2), C_4H_{10} (85)	**1** (77)
$NiEt_2$(bpy) (0.42)	CF_3COPh (0.42)	40 °C	1 h	C_4H_{10} (86)	**2** (63)
$NiMe_2$(dpe) (0.40)	CF_3COCF_3 (1.00)	40 °C	10 h	CH_4 (23), C_2H_6 (42)	**3** (53)
$NiMe_2$(dpe) (0.42)	CF_3COPh (2.00)	50 °C	18 h	CH_4, C_2H_6[c]	**4** (23)

a) Reactions were carried out in THF under reduced pressure. b) Yields by GC for gaseous products. c) The formation was confirmed by GC, but the yields were not measured.

evolution of C_4H_{10}. Conversion of $NiMe_2$(dpe) to Ni(η^2-CF_3COPh)(dpe) **4** requires more severe conditions. Stirring a THF solution of $NiMe_2$(dpe) with CF_3COPh for 18 h at 50 °C gave **4** in a 23% yield. Complex **4** can be independently prepared by reactions of the CF_3COPh-coordinated nickel complex with bipyridine ligand, **2**, with an equimolar amount of dpe in a higher yield. In

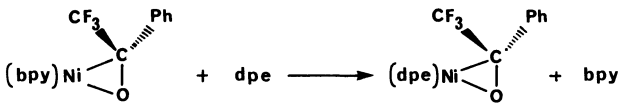

2 4

general, dpe coordinates to a nickel center more tightly than bpy, and $NiMe_2$(bpy) undergoes a facile ligand exchange with dpe to give $NiMe_2$(dpe).[9] Products of these reactions are summarized in Table 1.

New complexes **2** and **4** obtained in these reactions were characterized by IR and NMR spectroscopy and elemental analysis as well as chemical reactions. IR spectrum of **2** shows a ν(C–F) band at 1140 cm^{-1} and a ν(C–O) band at 1080 cm^{-1}, the latter band being shifted by ca. 650 cm^{-1} lower than that of the uncoordinated ketone. ^1H NMR spectrum of **2** shows signals only in the aromatic hydrogen region, indicating the absence of alkyl ligand in the complex. Complex **2** reacts with an equimolar amount of I_2 to give 2,2,2-trifluoroacetophenone (83%) and NiI_2(bpy).

The ^1H NMR of complex **4** shows signals due to hydrogens of dpe ligand and of the phenyl group in the coordinated ketone. $^{31}P\{^1H\}$ NMR spectrum shows two doublet signals, each of which is split into a quartet due to coupling with three fluorine atoms (see Experimental). $^{13}C\{^1H\}$ NMR spectrum of **4** shows signals due to the carbonyl carbon atom at δ=79.42 as a doublet of quartets by coupling with three fluorine and one phosphorus nuclei. The low value of the chemical shift of the signal and the low frequency of the ν(C–O) vibration in the IR spectrum suggest that complex **4** may be better formulated as a σ-bonded Ni(II) oxametallacycle (**A**) rather than a π-bonded Ni(0) complex (**B**).[10] These spectroscopic features indicate that complex **4** has a square planar coordination with a carbon, an oxygen, and two phosphorus ligating atoms around the nickel center.[11]

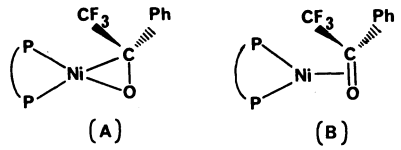

(A) (B)

Experimental

All manipulations were carried out under nitrogen or argon atmosphere. Dialkylnickel complexes were prepared by the methods in the literature.[12,13] Hexafluoroacetone was purchased from PCR Inc. and introduced to the reaction flask by means of a vacuum line technique.[14] 2,2,2-Trifluoroacetophenone was purchased from Tokyo Kasei Co., Ltd.

Preparation of the Complexes 1, 2, and 3. To a THF (3 cm^3) solution of diethyl(bipyridine)nickel (110 mg, 0.40 mmol), hexafluoroacetone (66 mg, 0.40 mmol) was added at room temperature. Complex **1** was immediately precipitated as a red solid which was filtered, washed with hexane several times, and dried in vacuo (113 mg, 77%).

Complexes **2** and **3** were prepared analogously.

Complex 2: Mp 147—150 °C (decomp); ^1H NMR (CD_3COCD_3) δ=7.7—8.9 (m, $C_{10}H_{10}N_2$ and C_6H_5); ^{19}F NMR 12.6 ppm (downfield from external CF_3COOH, s). Found: C 54.7; H 3.1; N 6.9%. Calcd for $C_{17}H_{13}F_3N_2ONi$: C 54.2; H 3.4; N 7.4%.

Preparation of 4. A toluene (5 cm^3) solution of **2** (180 mg, 0.47 mmol) and dpe (90 mg, 0.47 mmol) was stirred for 1 h at room temperature to cause precipitation of a yellow solid of **4**, which was filtered and recrystallized from THF (52%).

Complex **4** was also obtained in a lower yield from the reaction of 2,2,2-trifluoroacetophenone with $NiMe_2$(dpe) at 50 °C for 18 h.

Complex 4: Mp 153—156 °C (decomp); ^1H NMR (C_6D_6) δ=1.6—2.1 (4H, m, CH_2) and 7.0—8.3 (25H, m, C_6H_5); ^{31}P NMR (CD_2Cl_2) 58.16 ppm (downfield from external PPh_3 qd, J_{P-F}=4 Hz, J_{P-P}=51 Hz) and 51.56 ppm (qd, J_{P-F}=13 Hz, J_{P-P}=51 Hz); ^{19}F NMR (CD_2Cl_2) 12.8 ppm (downfield from external CF_3COOH, dd); ^{13}C NMR (CD_2Cl_2) δ=28.51 (dd, CH_2, J_{P-C}=18, 11 Hz), 24.40 (dd, CH_2, J_{P-C}=29, 11 Hz) 79.42 (qd, CO, J_{P-C}=27 Hz, J_{C-F}=33 Hz), and 117.10 (q, CF_3, J_{C-F}=292 Hz). Found: C 64.4; H 4.5%. Calcd for $C_{34}H_{29}F_3OP_2Ni$: C 64.7; H 4.6%.

This work was financially supported by a Grant-in-Aid for Scientific Research from the Ministry of

Education, Science and Culture (No. 63470079). The authors are grateful to Toyo Stauffer Chemical Co. for their kind donation of $AlMe_3$ and $AlEt_2(OEt)$.

References

1) P. W. Jolly and G. Wilke, "The Organic Chemistry of Nickel," Academic Press, New York (1974), Vol. 1, Chap. 5; P. W. Jolly, "Nickel Alkene and Alkyne Complexes," in "Comprehensive Organometallic Chemistry," Vol. 6, ed. by G. Wilkinson, F. G. A. Stone, and E. Abel, Pergamon Press, Oxford (1982); A. Yamamoto, "Organotransition Metal Chemistry," John Wiley, New York (1986).

2) S. D. Ittel, *J. Organomet. Chem.*, **137**, 223 (1977).

3) T. T. Tsou, J. C. Huffman, and J. K. Kochi, *Inorg. Chem.*, **18**, 2311 (1979).

4) J. Browning, C. S. Cundy, M. Green, and F. G. A. Stone, *J. Chem. Soc. A*, **1969**, 20.

5) R. Countryman and B. R. Penfold, *J. Chem. Soc., Chem. Commun.*, **1971**, 1598.

6) T. Yamamoto, A. Yamamoto, and S. Ikeda, *J. Am. Chem. Soc.*, **93**, 3350 and 3360 (1971); P. Binger, J. H. Doyle, C. Krüger, and Y. H. Tsay, *Z. Naturforsch.*, **34B**, 1289 (1979); K. Tatsumi, A. Nakamura, S. Komiya, A. Yamamoto, and T. Yamamoto, *J. Am. Chem. Soc.*, **106**, 8181 (1984).

7) Y. Hayashi, S. Komiya, T. Yamamoto, and A. Yamamoto, *Chem. Lett.*, **1984**, 1363.

8) Y.-J. Kim, K. Osakada, K. Sugita, T. Yamamoto, and A. Yamamoto, *Organometallics*, **7**, 2182 (1988).

9) T. Kohara, T. Yamamoto, and A. Yamamoto, *J. Organomet. Chem.*, **192**, 265 (1980).

10) A. Yamamoto, "Organotransition Metal Chemistry," John Wiley, New York (1986), p. 60.

11) A. previous study of X-ray crystallography on $Ni(\eta^2\text{-}(CF_3)_2CO)(PPh_3)_2$ has revealed a pseudo square planar configuration with an angle of 6.9 ° between the C=O bond of the ketone and the coordination plane. See Ref. 5.

12) T. Saito, Y. Uchida, A. Misono, A. Yamamoto, K. Morifuji, and S. Ikeda, *J. Am. Chem. Soc.*, **88**, 5193 (1966).

13) T. Yamamoto, M. Takamatsu, and A. Yamamoto, *Bull. Chem. Soc. Jpn.*, **50**, 1318 (1977).

14) D. F. Shriver, "The Manipulation of Air-Sensitive Compounds," McGraw Hill, New York (1969).

Reaction of Triarylchloroallenes with Nucleophiles under Solvolytic Conditions

Tsugio KITAMURA,* Sumiya MIYAKE, Shinjiro KOBAYASHI, and Hiroshi TANIGUCHI*
Department of Applied Chemistry, Faculty of Engineering, Kyushu University 36,
Hakozaki, Fukuoka 812
(Received September 24, 1988)

Synopsis. Solvolytic reactions of triarylchloroallenes in the presence of thiocyanate and *O*-ethyl dithiocarbonate anions gave the corresponding allenyl derivatives, while the reaction in the presence of cyanate anion afforded the corresponding propargyl derivative. These results are interpreted in terms of a steric factor of the nucleophiles.

Since allenyl cations were first suggested in solvolysis by Jacobs and Fenton,[1] much work has been done about the chemistry of allenyl cations; especially Schiavelli and co-workers have revealed intervention of the allenyl cations in their detail mechanistic studies.[2] One of the most interesting features is an ambident character of allenyl cations, which can provide allenyl and/or propargyl derivatives. However, most works on solvolysis of allenyl halides indicate that nucleophiles attack on the γ-position of the resulting allenyl cations unless bulky substituents are present on the γ-position.[3]

On the other hand, we have studied photolysis of arylvinyl halides and disclosed that the photogenerated vinyl cations react with various nucleophiles to give substituted ethylenes and heterocyclic compounds.[4] This successful vinylic substitution led us to examine the reaction of the extended unsaturated carbenium ions, allenyl cations. Here we report a high regioselectivity depending on nucleophiles in the reaction of triarylchloroallenes under solvolytic conditions.

Results and Discussion

1,3,3-Triphenylchloroallene (**1a**) solvolyses under mild conditions: the half-life period $t_{1/2}$=1.0 h at 26.1 °C in 70:30 acetone water (v/v).[3] The solvolysis was carried out in the presence of KSCN, KS_2COEt, and KNCO in a similar manner as conducted by Schiavelli and co-workers.[3] In contrast to the reported results,[3] solvolytic reaction of chloroallenes **1a—c** with potassium thiocyanate gave allenyl thiocyanates **2a—c** in high yields. In the IR spectra of **2a—c** were observed a sharp absorption of the thiocyanato group at 2150 cm^{-1} and a weak absorption of the allenyl bond at 1920—1930 cm^{-1}, but the latter was obscured by overlapping with aromatic ring absorptions. The strong evidence for the allenyl structure was obtained from the ^{13}C NMR spectra. The allenyl carbons of triphenylallenyl thiocyanate (**1a**) resonated at 207 ppm for the β carbon, and at 99 and 118 ppm for γ and α carbons, respectively.[5] The carbon of thiocyanato group resonated at 110 ppm.[6] Similar substitution at the α carbon observed in the presence of potassium *O*-ethyl dithiocarbonate as a nucleophile. Solvolytic reaction of chloroallenes **1a** and **1b** led to formation of the corresponding allenyl *O*-ethyl dithiocarbonates **3a** and **3b** in 73 and 57% yield, respectively.

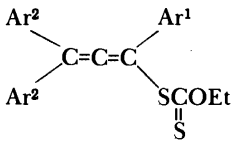

3a: 73%
3b: 57%

However, when potassium cyanate was used as a nucleophile, the cyanate anion attacked on the γ-position to give propargyl derivatives **4**. The IR spectrum of the crude product showed the absorpotion at 3340—2700 and 1700—1645 cm^{-1}, which were assignable to propargylcarbamic acids **5**. However, the compounds **5** could not be isolated because of their instability. Instead, propargyl amines **4** were isolated after treatment of the crude product with an alkaline solution.

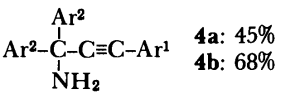

4a: 45%
4b: 68%

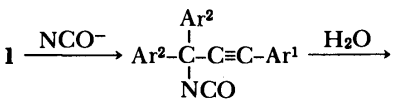

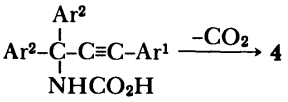

5

These results indicate that the reaction manner can be controlled by choice of nucleophiles. From the kinetic[3] and theoretical[7] studies, it is predicted that

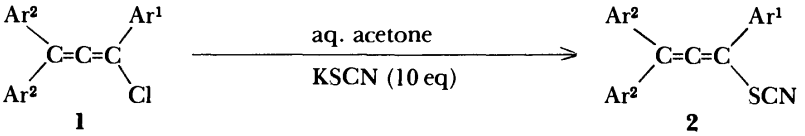

a: Ar^1=Ar^2=Ph
b: Ar^1=Ph, Ar^2=*p*-MeC_6H_4
c: Ar^1=*n*-Bu, Ar^2=Ph

2a: 98%
2b: 88%
2c: 72%

nucleophiles react at the propargyl position of the allenyl cation. However, when the γ-position bears a sterically hindered substituent a nucleophile should attack on the allenyl position.[8] Such a steric factor may be operative for a bulky nucleophile. Among the nucleophiles used in this study, thiocyanate and *O*-ethyl dithiocarboate anions are greater in size than cyanate anion because sulfur atom has much larger van der Waals radius than nitrogen or oxygen atom does.[9] The larger nucleophile prefers to attack the allenyl position which has less steric congestion, while the smaller nucleophile prefers the propargyl position which is more reactive than the allenyl position.[3,7] Thus, a high regioselectivity of nucleophiles toward triarylallenyl cations can be explained in terms of the capacity and reactivity of the reacting position and the size of the nucleophiles.

Experimental

Chloroallene 1. Chloroallenes **1** were prepared according to the method prepared by Jacobs and Fenton,[1] from the corresponding propargyl alcohols.[1,3]

Solvolytic Reaction of Chloroallenes 1 in the Presence of Nucleophiles (KSCN, KS_2COEt, and KNCO). To a solution (100—200 ml) of 70:30 acetone-water (v/v) were added chloroallene **1** (1 mmol) and a nucleophile (10 mmol; KSCN, KS_2COEt, or KNCO) and the mixture was stirred for 12—48 h at 25 °C. The reaction mixture was poured into water and the products were extracted with ether. The organic layer was washed with water, saturated sodium chloride solution, and then dried over anhydrous sodium sulfate. After evaporation of the ether, the products were separated by column chromatography on silica gel or alumina using ether–hexane eluent. In the case of potassium cyanate, the crude product obtained by extraction with ether was refluxed for 12 h in a solution of sodium hydroxide (5 mmol) in ethanol (20 ml), benzene (10 ml), and water (20 ml). The product was extracted with ether–benzene and separated by column chromatography on silica gel.

The products obtained are as follows. 1,3,3-Triphenylallenyl thiocyanate (**2a**): mp 115—116 °C (benzene–hexane); ^{1}H NMR ($CDCl_3$) δ=7.20—7.60 (m, ArH); ^{13}C NMR ($CDCl_3$) δ=98.60 (C-3), 110.06 (SCN), 118.01 (C-1), 126.72, 128.95, 129.13, 131.83, 134.12 (aromatic carbons), and 206.90 (C-2); IR (Nujol) 2150 (m, SCN) and 1920 cm^{-1} (m). Found: C, 80.74; H, 4.65; N, 4.20%. Calcd for $C_{22}H_{15}NS$: C, 81.20; H, 4.65; N, 4.30%. 3,3-Bis(*p*-methylphenyl)-1-phenylallenyl thiocyanate (**2b**): Mp 114—115 °C (benzene–hexane); ^{1}H NMR ($CDCl_3$) δ=2.37 (s, Me) and 7.05—7.63 (m, ArH); IR (Nujol) 2150 (m, SCN) and 1920 cm^{-1} (m). Found: C, 81.40; H, 5.41; N, 3.98%. Calcd for $C_{24}H_{19}NS$: C, 81.55; H, 5.42; N, 3.96%. 1-Butyl-3,3-diphenylallenyl thiocyanate (**2c**): Oil; ^{1}H NMR ($CDCl_3$) δ=0.80—2.73 (m, *n*-Bu) and 7.10—7.70 (m, ArH); IR (neat) 2150 (s, SCN) and 1930 cm^{-1} (m). Found: C, 78.55; H, 6.32; N, 4.62%. Calcd for $C_{20}H_{19}NS$: C, 78.65; H, 6.27; N, 4.59%. 1,3,3-Triphenylallenyl *O*-ethyl dithiocarbonate (**3a**): Oil; ^{1}H NMR ($CDCl_3$) δ=1.12 (t, *J*=7 Hz, Me), 4.47 (q, *J*=7 Hz, CH_2), and 6.75—7.70 (m, ArH); ^{13}C NMR ($CDCl_3$) δ=13.35 ($OCH_2\underline{C}H_3$), 70.12 ($O\underline{C}H_2CH_3$), 102.24 (C-3), 112.95 (C-1), 126.65, 128.06, 128.37, 128.72, 129.01, 129.66, 134.13, 134.77 (aromatic carbons), 211.01, and 211.31 (C-2 and C=S); IR (neat) 1930 (w), 1220, 1100, and 1030 cm^{-1} (S_2CO). 3,3-Bis(*p*-methylphenyl)-1-phenylallenyl *O*-ethyl dithiocarbonate (**3b**): Oil; ^{1}H NMR (CCl_4) δ= 1.12 (t, *J*=7 Hz, Me), 2.31 (s, Me), 4.44 (q, *J*=7 Hz, CH_2), and 6.55—7.62 (m, ArH); IR (neat) 1920 (m), 1230, 1115, and 1040 cm^{-1} (S_2CO). **3a** and **b** were not satisfied with their elemental analyses because of their instability. 3-Amino-1,3,3-triphenylpropyne (**4a**): mp 90—91 °C (EtOH–benzene); ^{1}H NMR ($CDCl_3$) δ=2.25 (s, NH_2) and 7.13—7.78 (m, ArH); ^{13}C NMR ($CDCl_3$) δ=59.06 (C-3), 85.12 (C-2). 95.18 (C-1), 123.24, 126.42, 127.30 128.36, 131.71, and 146.19 (aromatic carbons); IR (Nujol) 3370, 3300 (NH_2), and 2200 cm^{-1} (w, C≡C). Found: C, 88.69; H, 6.22; N, 4.92%. Calcd for $C_{21}H_{17}N$: C, 89.01; H, 6.05; N, 4.94%. 3-Amino-3,3-bis(*p*-methylphenyl)-1-phenylpropyne (**4b**): Mp 101—103 °C (EtOH–benzene); ^{1}H NMR (CCl_4) δ=2.18 (s, NH_2), 2.29 (s, Me), and 6.99—7.64 (m, ArH); IR (Nujol) 3300 and 3350 cm^{-1} (NH_2). Found: C, 88.54; H, 6.58; N, 4.65%. Calcd for $C_{23}H_{21}N$: C, 88.71; H, 6.80; N, 4.50%.

References

1) T. L. Jacobs and D. M. Fenton, *J. Org. Chem.*, **30**, 1808 (1965).

2) P. J. Stang, Z. Rappoport, M. Hanack, and L. R. Subramanian, "Vinyl Cations," Academic Press (1979), pp. 246—270, and references cited therein.

3) M. D. Schiavelli, S. C. Hixon, H. W. Moran, and C. J. Boswell, *J. Am. Chem. Soc.*, **93**, 6989 (1971).

4) T. Kitamura, M. Murakami, S. Kobayashi, and H. Taniguchi, *Tetrahedron Lett.*, **27**, 3885 (1986); T. Kitamura, S. Kobayashi, and H. Taniguchi, *J. Org. Chem.*, **49**, 4755 (1984); T. Kitamura, S. Kobayashi, and H. Taniguchi, *Chem. Lett.*, **1984**, 1523; T. Kitamura, S. Kobayashi, and H. Taniguchi, *Tetrahedron Lett.*, **1979**, 1619.

5) J. W. Munson, "The Chemistry of Ketenes, Allenes and Related Compounds," ed by S. Patai, John Willey & Sons (1980), Chap. 5.

6) E. Breitmaier and W. Voelter, "Carbon-13 NMR Spectroscopy," VCH (1987), p. 245.

7) H. Mayr and R. Scheider, *Chem. Ber.*, **115**, 3470 (1982).

8) M. D. Schiavelli, R. P. Gilbert, W. A. Boynton, and C. J. Boswell, *J. Am. Chem. Soc.*, **94**, 5061 (1972).

9) L. Pauling, "The Nature of the Chemical Bond," 3rd ed., Cornell Univ. Press (1960).

1,1′-(1,32-Dotriacontanediyl)bis[2-acetyl-*sn*-glycero(3)phosphocholine]: A Long Persisting Agonist as a Potential Antihypertension Agent

Kiyoshi YAMAUCHI,* Mitsuyoshi HIHARA, Masayoshi KINOSHITA, Masahiro WATANABE,†
Takao KONDO,† and Shigeki KUWAHARA†
Department of Applied Chemistry, Osaka City University, Sumiyoshi-ku, Osaka 558
†Research Division, the Green Cross Corporation, Hirakawa 573
(Received October 28, 1988)

Synopsis. A dimer of platelet activating factor (PAF), 1,1′-(1,32-dotriacontanediyl)bis[2-acetyl-*sn*-glycero(3)phosphocholine] (**7**), was synthesized and examined for platelet aggregation and antihypertension activities. The compound **7** showed both activities with the maximum levels of 1/50—1/100-fold of those of PAF, but the antihypertension effect of **7** persisted much longer and appeared with time lag of 1—3 min. The unique expression of the activities was discussed in conjunction with the molecular structure.

1-Alkyl-2-acetyl-*sn*-glycero(3)phosphocholine (alkyl: C_nH_{2n+1}, n=16 and 18) is released from IgE-sensitized basophiles. The lipids are potent platelet activating factor (PAF)[1,2] and serve as chemical mediators in physiological processes such as anaphylaxis and inflammation.[3] Various agonists have been synthesized to reveal the following structural features for the biological activity;[4] (a) a long chain-alkyl ether linkage at the *sn*-1-O atom,[5,6] (b) short chain acylation (C_{2-4}) at the *sn*-2-O atom,[7,8] and (c) a quaternary ammonium residue as small as $(CH_3)_3N^+$ of the phosphorylcholine moiety at the *sn*-3 position.[9,10] In this paper we wish to report preparation and biological activities (platelet activation and antihypertension) of a new agonist of PAF, 1,1′-(1,32-dotriacontanediyl)bis[2-acetyl-*sn*-glycero(3)phosphocholine] (**7**). The bis(glycerophospholipid) may be considered as a dimeric version of PAF.

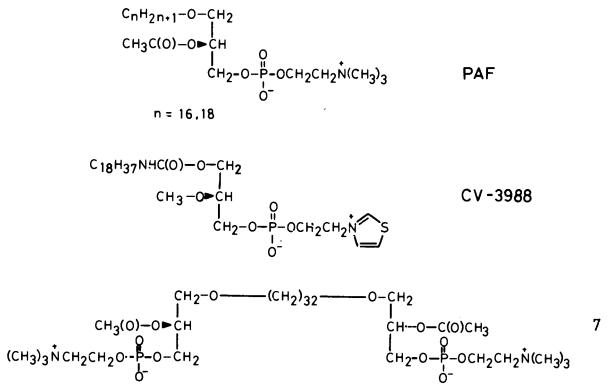

Experimental

Synthesis. 2,3-Isopropylidene-*sn*-glycerol (**1**), after conversion into the sodium alkoxide, was heated with 1,32-dibromodotriacontane in decane at 140 °C. The resulting **2** was transformed via **3** and **4** into **5** by a series of usual reactions including acid catalyzed deisopropylidenation, tritylation and acetylation in an overall yield of 73%. Removal of the trityl groups of **5** required considerable experimentation since the acetyl group at the *sn*-2-O position tended to rearrange into the *sn*-3-O position.[11] A treatment of a benzene–ethyl acetate solution of **5** with 25% hydrogen bromide–acetic acid at 0 °C for 50 s was satisfactory to generate **6**, which was isolated by means of Sephadex LH-20 gel column chromatography. A subsequent treatment of **6** with 2-bromoethyl phosphorodichloridate in the presence of triethylamine at room temperature overnight and a reaction of the resulting phosphate with trimethylamine in *N*,*N*-dimethylformamide at 55 °C for 4 d provided **7**, which was isolated and purified by a combination of silica-gel and Sephadex LH-20 gel column chromatographies: 400 MHz ^{1}H NMR ($CDCl_3$–CD_3OD, 2:1 v/v; 7.26 ppm-singlet of $CHCl_3$ as an internal standard) δ 1.14 [coherent peak, 60H, $(CH_2)_{30}$], 2.45 (s, 6H, 2×*sn*-2-CH); IR (KBr) 1735 (C=O), 1240 and 1095 (P-O-C) cm^{-1}. Table 1 lists physical constants of **2**—**7**.

Biological Assays. (i) **Platelet Aggregation.** A 9:1 volumetric mixture of male New Zealand white rabbit blood and 3.8% trisodium citrate was centrifuged at 1100 rpm for

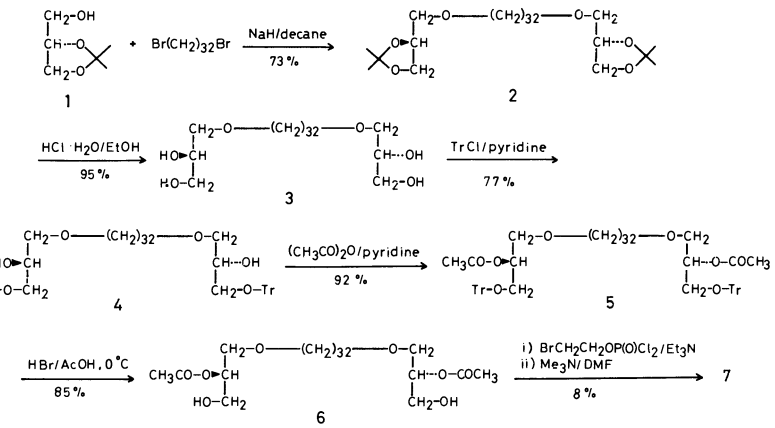

10 min at room temperature. The upper layer, platelet-rich plasma (PRP), was collected. Then, the residual blood sample was centrifuged at 3000 rpm for 10 min at 4 °C to provide platelet-poor plasma (PPP). Platelet count in PRP was measured by Systemax Platelet Counter PL-100, and adjusted to 5×10^8/ml by appropriate dilution with PPP. Platelet aggregation was initiated by adding 30 μl of **7** in a 0.025 M (1 M=1 mol dm^{-3}) tris-HCl buffer (pH 7) containing 0.13 M NaCl into 270 μl of PRP. The assay was conducted according to the turbidimetric procedure of Born and Cross.[13] In the experiment to know the effect of *rac*-3-[*N*-(octadecyl)carbamoyloxy]-2-methoxypropyl 2-(3-thiazolino)-ethyl phosphate (CV-3988)[12] on test compound-induced platelet aggregation, PRP was pretreated with 100 μM of CV-3988 for 3 min. Typical results are displayed in Fig. 1.

(ii) Antihypertension. Wister male rats (weight, 254—276 g) were anesthetized with sodium pentobarbitol (60 mg/kg, i.p.). Appropriate amounts of **7** dissolved in saline or PAF in 0.05 M tris-HCl–0.15 M NaCl buffer (pH 7) was then injected intravenously, and the blood pressure in jugular vein was measured for 15 min by the use of a pressure-transducer, a Nippon Hatsuden model RMP-6018. The results are shown in Fig. 2.

Results and Discussion

It was found that dimerization of PAF into **7** resulted in modifying the platelet aggregation and antihypertension activities in a unique manner; e.g., although the maximum levels of both activities of **7** were 1/50—1/100-fold of those of PAF (Fig. 1a and 1b; Fig. 2) and appeared to be dose-dependent in the examined range (10^{-1}—1 μM for platelet aggregation and 10—100 μg/kg of rat for antihypertension), the antihypertension effect was exhibited with time lag of

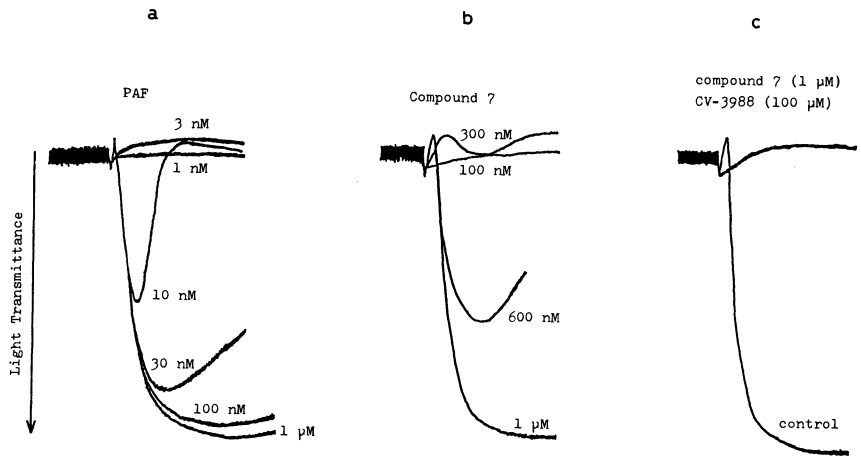

Fig. 1. Typical patterns of PAF- and compound **7**-induced rabbit platelet aggregation (a and b), and inhibitory effect (c) of CV-3988 on the compound **7**-induced aggregation.

Table 1. Physicochemical Results[a]

Compound	Purification	Yield %	Mp/°C	$[\alpha]_D^{25}$	Silica-gel TLC, R_f	C and H analysis FAB mass spectrum
2	Silica-gel column[b]	73	69—72	−6.9° (*c* 1.3, chloroform)	0.37[h]	*m/z* 711 (M+1) (Calcd for $C_{44}H_{86}O_6$, 710).
3	Recrystal. (chloroform)	95	112—117	−2.8° (*c* 1.5, chloroform)	0.35[i]	Calcd for $C_{38}H_{78}O_6$: C, 72.33; H, 12.46%. Found: C, 71.90; H, 12.53%.
4	Silica-gel column[c]	77	g)	+2.6° (*c* 1.25, chloroform	0.39[j]	*m/z* 1115 (M+1) (Calcd for $C_{76}H_{106}O_6$, 1114).
5	Silica-gel column[f]	92	g)	+11.7° (*c* 1.7, chloroform	0.61[j]	*m/z* 1199 (M+1) (Calcd for $C_{80}H_{110}O_8$, 1198).
6	Sephadex LH-20 gel column[d]	85	77—79	−3.5° (*c* 3.5, chloroform)	0.23[k]	*m/z* 715 (M+1) (Calcd for $C_{42}H_{82}O_8$, 714).
7	Silica-gel column,[e] then Sephadex LH-20	8	241—244	−3° (*c* 0.3, chloroform–methanol, 2:1 v/v)	0.40[l]	*m/z* 1045 (M+1) (Calcd for $C_{52}H_{106}O_{14}N_2P_2$, 1044)

a) Silica-gel column support, Merck 7734, 70—230 mesh; Silica gel TLC, precoated sheet, Merck Art. 5735; matrix used in the FAB mass spectra, 3-mercapto-1,2-propanediol-glycerol, 1:1 v/v. b) Hexane–ethyl acetate–triethylamine in gradually changing from 70:4:1 to 40:4:1 v/v. c) Hexane–ethyl acetate in gradually changing from 13:1 to 3:1 v/v. d) Chloroform–methanol, 2:1 v/v. e) Chloroform–acetone–methanol–concd ammonia in gradually changing from 8:6:6:1 to 8:6:6:3 v/v. f) Hexane–ethyl acetate, 7:1 v/v. g) A compound to melt at room temperature. h) Hexane–ethyl acetate, 5:1 v/v. i) Chloroform–methanol, 8:1 v/v. j) Hexane–ethyl acetate, 3:1 v/v. k) Chloroform–ethyl acetate, 1:1 v/v. l) Chloroform–acetone–methanol–concd ammonia, 4:2:6:3 v/v.

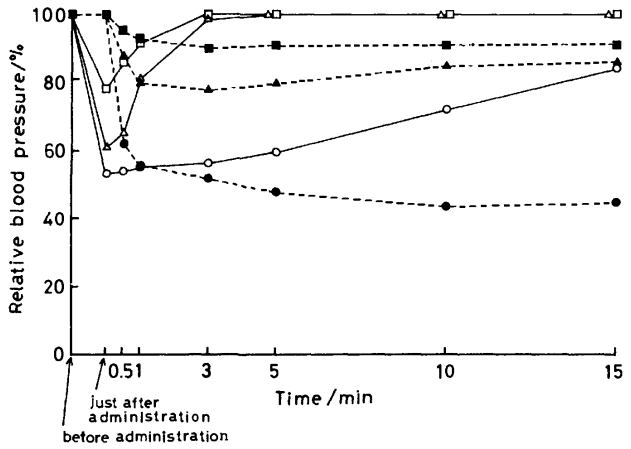

Fig. 2. Time course of antihypertension effects of compound **7**, 100 μg/kg (●), 30 μg/kg (▲), 10 μg/kg (■), PAF, 1.0 μg/kg (○), 0.3 μg/kg (△), and 0.1 μg/kg (□) in rats. Each point represents the mean of three animals.

1—3 min and seemed to persist for a period much longer than PAF (Fig. 2). By contrast, the effect of PAF was transient and became inactive rapidly within a few minutes after administration. The integrated biological activity over the effective time, though examined only qualitatively, may thus be comparabale with or surpass that of PAF. A mechanism of the PAF-effect has not been understood well.[12,14–16] The compound **7**, however, was seemed to act on platelets in a manner similar to PAF because (i) **7** resembled with PAF in aggregation pattern and (ii) the activity of **7** was inhibited competitively by an antagonist of PAF, CV-3988[14] (typical aggregations: Fig. 1a—c). The decreased magnitudes in the biological activities of **7** may be attributed to conformational or steric effect of the 1,32-dotriacontanediyl residue and/or the increased polarity due to two phosphorylcholine residues. Such a structural modulation would result in slow metabolism leading to long duration of the activities, and the time lag as well, which might be ascribed to slow accommodation of **7** to PAF-receptors on platelets.

References

1) C. A. Demopoulos, R. N. Pinckard, and D. J. Hanahan, *J. Biol. Chem.*, **254**, 9355 (1979).
2) J. Benveniste, M. Tence, P. Varenne, J. Bidault, C. Boullet, and J. Polonsky, *C. R. Acad. Sci. Paris, Ser. D*, **289**, 1037 (1979).
3) R. N. Pinckard, L. M. McManus, and D. J. Hanahan, "Adv. Inflam, Res.," ed by G. Weissmann, Raven Press, New York (1982), Vol. 4, pp. 147—180.
4) M. Shiraiwa, K. Fujita, H. Yoshiwara, S. Kobayashi, and M. Ohno, *Yuki Gosei Kagaku Kyokai Shi*, **45**, 369 (1987).
5) D. J. Hanahan, P. G. Munder, K. Satouchi, L. M. McManus, and R. N. Pinckard, *Biochem. Biophys. Res. Commun.*, **99**, 183 (1981).
6) G. Hirth, H. Saroka, W. Bannwarth, and R. Barner, *Helv. Chim. Acta*, **66**, 1210 (1983).
7) P. Harvary, J. M. Cassal, G. Hirth, R. Baener, and H. R. Baumgartner in INSERM Symposium 23, Platelet Activating Factor and Structually Related Ether Lipids, ed by J. Benveniste and B. Arnoux, Elsevier, Amsterdam, 1983, p. 57.
8) J. J. Godfroid, F. Heymans, E. Michel, C. Redeuilh, E. Steiner, and J. Benveniste, *FEBS Lett.*, **116**, 161 (1980).
9) K. Satouchi, R. N. Pinckard, L. M. McManus, and D. J. Hanahan, *J. Biol. Chem.*, **256**, 4425 (1981).
10) M. Ohno, K. Fujita, H. Nakai, S. Kobayashi, K. Inoue, and S. Inoue, *Chem. Pharm. Bull.*, **33**, 572 (1982).
11) A. Pluckthun and E. A. Dennis, *Biochemistry*, **21**, 1743 (1982).
12) Z. Terashita, Y. Imura, and K. Nishikawa, *Biochem. Pharmacol.*, **34**, 1491 (1985).
13) G. V. R. Born and M. J. Cross, *J. Physiol.*, **168**, 178 (1963).
14) S. Hwang, C. Lee, M. J. Cheah, and T. Y. Chan, *Biochemistry*, **22**, 4756 (1983).
15) P. Inarrea, J. G. Gambronero, M. Neito, and M. S. Crespo, *Eur. J. Pharmacol.*, **105**, 309 (1984).
16) F. H. Valone, E. Coles, V. R. Reinhold, and E. J. Goetzl, *J. Immunol.*, **129**, 1637 (1982).

Active Sites of a Reduced Molybdena-Alumina Catalyst. A Transient Study of Hydrodenitrogenation of Carbazole and Acridine

Masatoshi NAGAI* and Takashi MASUNAGA†
Department of Chemical Engineering, Tokyo University of Agriculture and Technology, Koganei, Tokyo 184
(Received October 7, 1988)

Synopsis. A response study of the hydrodenitrogenation of acridine and carbazole on a reduced MoO_3/Al_2O_3 catalyst was performed at 300 °C and 10.1 MPa total pressure. Acridine was strongly adsorbed on the acidic sites of the catalyst surface for hydrogenation, while carbazole was weakly adsorbed not only on the same sites as acridine, but also on the terminal oxygen anion sites in the presence of strong bases.

Molybdena–alumina catalysts have been extensively investigated in an effort to understand the nature of their catalytically active sites for hydrogenation and hydrogenolysis. The chemisorption of NO,[1] oxygen,[2] and pyridine[3,4] has been applied to reduced and sulfided molybdena–alumina catalysts at reduced pressure. The chemisorptions were correlated with the hydrogenation activity and coordinatively unsaturated sites (Lewis acid sites) of the pretreated molybdena surface.

However, hydrodenitrogenation (HDN), hydrogenolysis of a carbon–nitrogen bond of polynuclear aromatic nitrogen compounds, proceeds at high pressure and high reaction temperature.[5–7] The nature of the active sites for HDN should be determined under these reaction conditions. Our recent poisoning studies at 10.1 MPa of the total pressure revealed that both hydrogenation and denitrogenation sites exist on the surface of the molybdenum catalysts.[6,7] The active sites of a sulfided $NiMo/Al_2O_3$ catalyst for hydrogenation were correlatable with the gas-phase basicity of the nitrogen compound,[8] which was proportional to their proton affinity; therefore, hydrogenation takes place on the Brönsted acid sites of molybdenum atoms of the catalyst. Furthermore, the active sites of the catalysts for denitrogenation were related with the gas-phase acidity of the sulfur and oxygen compound;[9] therefore, denitrogenation occurs on the terminal oxygen anion sites which exist on the reduced catalyst as well as desulfurization.[7,9]

A polynuclear nitrogen compound contains two types of nitrogen compounds: a basic (acridine) and nonbasic (carbazole) polynuclear aromatic nitrogen compound. The non-basic nitrogen compound becomes the basic nitrogen compound during hydrogenation. This observation suggested that the adsorption sites of a reduced molybdenum catalyst were different for the two typical nitrogen compounds.

In this work, a transient response study of the HDN of these two typical nitrogen compounds has been applied in order to facilitate an understanding of the nature of the active sites of a reduced Mo/Al_2O_3 catalyst for the HDN of carbazole and acridine at 300 °C and 10.1 MPa.

Experimental

The reagents, the catalyst, and the reactor used in this study are shown elsewhere.[6] Two grams of the 12.5% MoO_3/Al_2O_3 catalyst were placed in the reactor during a typical series of experiments. The catalyst was oxidized in air at 450 °C for more than 24 h and then reduced in hydrogen for 4 h at 400 °C before a run. After reduction, the reactor was cooled to the desired temperature by a flowing hydrogen stream. A solution containing a mixture of 0.013 mol L^{-1} of carbazole and 0.013 mol L^{-1} of acridine in xylene was injected at 20 ml h^{-1}. A steady state was usually reached within 3 h. The reaction products, having higher boiling points than xylene, were analyzed by F.I.D. gas chromatography (Dexsil 400, 2.5%). The lower boiling point products, such as NH_3 and any light cracking products, were not determined because the amounts formed during reactions were negligible.

Results and Discussion

In previous studies,[6,7] acridine was easily hydrogenated to produce perhydroacridine and octahydroacridine on the Brönsted acid sites. The major denitrogenated compound was dicyclohexylmethane by the C–N scission of perhydroacridine on the terminal oxygen anion sites. Carbazole was difficult to hydrogenate to tetrahydrocarbazole. Other hydrogenated carbazole compounds were barely formed at any of the other reaction temperatures. The major denitrogenated product was 1,1′-bicyclohexyl together with 2-ethylbicyclo[4.4.0]decane and hexylcyclohexane.

The transient experiment provided two different aspects for the HDN of acridine and carbazole with different basicities. The HDN of acridine on the reduced Mo/Al_2O_3 catalyst at 300 °C and 10.1 MPa in the presence and absence of carbazole is shown in Fig. 1. A transient response occurred during the first 2.5 h; the HDN reaction then reached a steady state. The addition of carbazole increased the amount of octahydroacridine formed and decreased both dicyclohexylmethane and benzylcyclohexane amounts. This result showed that the addition of carbazole hindered the hydrogenation of octahydroacridine to perhydroacridine. This result suggested that carbazole was adsorbed and hydrogenated on the same active site as both acridine and octahydroacridine.

The concentration of perhydroacridine initially jumped for the first 2.5 h upon the addition of carbazole and, then, gradually decreased again to its initial concentration before the addition of carbazole. This implied that the addition of carbazole expelled

† Present address: Kumon Publishing Co., Misakicho 3-6-9, Chiyoda-ku, Tokyo 101.

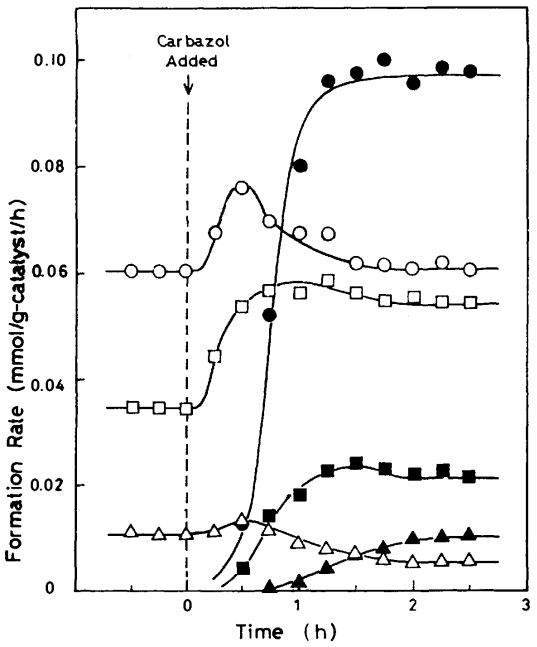

Fig. 1. The addition of carbazole to the HDN of acridine on the reduced Mo/Al_2O_3 catalyst at 300 °C and 10.1 MPa total pressure. Key: □, 1,2,3,4,4a,9,9a,10-octahydroacridine; ○, perhydroacridine; △, dicyclohexylmethane; ●, carbazole; ■, 1,2,3,4-tetrahydrocarbazole; ▲, 1,1′-bicyclohexyl.

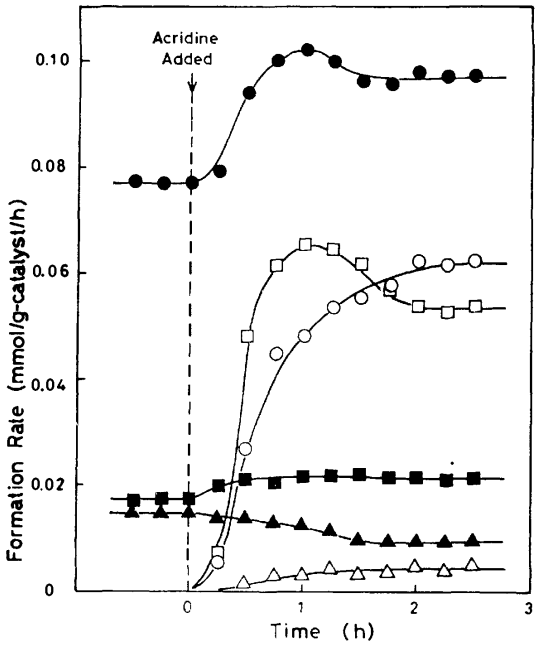

Fig. 2. The addition of acridine to the HDN of carbazole on the reduced Mo/Al_2O_3 catalyst at 300 °C and 10.1 MPa total pressure. The symbols are the same as those in Fig. 1.

the perhydroacridine adsorbed from the active site of the catalyst. The amount of perhydroacridine adsorbed was calculated as being 11.8 μmol g^{-1} on the basis of the area of the increased perhydroacridine. This observation indicated that carbazole was also adsorbed on the same active site where perhydroacridine was adsorbed. Since perhydroacridine was adsorbed on the terminal oxygen anion sites, carbazole was competitively adsorbed on the same anion sites as perhydroacridine as well as on the Brönsted acid sites.

On the other hand, for the addition of acridine to carbazole HDN, there was no similar observation to that when perhydroacridine was desorbed by the addition of carbazole. Figure 2 shows that the addition of acridine to carbazole HDN decreased 1,1′-bicyclohexyl and then 5.7 μmol g^{-1} of both carbazole and tetrahydrocarbazole were released to the solution from the catalyst surface in 2.5 h. The addition of acridine appears to have inhibited the hydrogenations of tetrahydrocarbazole to perhydrocarbazole. In addition, 5.8 mol g^{-1} of both acridine and the hydrogenated compounds were adsorbed on the catalyst's surface. The adsorbed amount of acridine hydrogenated compounds was almost equal to the released amount of the carbazole hydrogenated compounds. Therefore, acridine was adsorbed and hydrogenated on the Brönsted sites of the catalyst, but not adsorbed on the anion sites. Acridine is also competitively hydrogenated with the resulting hydrogenated acridine compounds on the same sites. On the other hand, carbazole is actually a very weak base, but carbazole turns to a basic compound during the reaction; therfore carbazole is weakly adsorbed on the same sites as acridine, and even adsorbed on the terminal oxygen anion sites in the presence of a stong base.

Estimating the amount of denitrogenation sites on which perhydroacridine and carbazole were adsorbed found that the 12.5 wt% MoO_3 catalyst (N_2 BET surface area: 188 $m^2 g^{-1}$) contains 5.16×10^{18} Mo molecules/m^2. The amount of perhydroacridine (11.8 μmol/g-cat) released from denitrogenation sites corresponds to 3.7×10^{16} molecules/m^2. The number is two orders of magnitude smaller than the total molybdenum available on the catalyst. It could be estimated that 0.72% of the molybdenum sites have become active sites.

Suarez et al.[4] studied the adsorption of pyridine on reduced Mo/Al_2O_3 (7.48 wt% Mo, BET 211 $m^2 g^{-1}$) at 400 °C. The amount of adsorbed pyridine (Lewis acid site) was 0.18×10^{18} molecules/m^2 when the catalyst was exposed for 6 h. When the value was converted to that on the 12.5 wt% Mo/Al_2O_3, it was 0.3×10^{18} Mo molecules/m^2, which was three times that obtained in this study. They reported that adsorbed pyridine (Brönsted acid site) barely exists on the surface of the reduced catalyst. Furthermore, Segawa and Hall[2] found that the Brönsted acidity could be eliminated by a reduction of the catalyst; Lewis acid sites were present on both the molybdenum and alumina portions of the catalyst's surface. The reduced catalyst held many Lewis acid sites, but rarely Brönsted acid sites under reduced pressure. Thus, there was a great gap between the results of our study at high hydrogen pressure and that of the adsorption experiment under reduced pressure. The acidity and number of active sites on the surface of the Mo/Al_2O_3 catalyst during the reaction would be expected to be different from those measured

under vacuum. It is suggested that molybdenum Lewis acid sites turned to Brönsted sites at high hydrogen pressure.

References

1) E. A. Lombardo, M. Lo. Jacono, and W. K. Hall, *J. Catal.*, **64**, 15 (1980).
2) N. K. Nag, *J. Catal.*, **92**, 432 (1985).
3) K. Segawa and K. Hall, *J. Catal.*, **76**, 133 (1982); **77**, 221 (1983).
4) W. Suarez, J. A. Dumesic, and C. G. Hill, Jr., *J. Catal.*, **94**, 408 (1985).
5) F. Glola and V. Lee, *Ind. Eng. Chem. Process Des. Dev.*, **25**, 918 (1986).
6) M. Nagai, T. Masunaga, and N. Hana-oka, *Energy & Fuels*, **2**, 645 (1988).
7) M. Nagai, T. Masunaga, and N. Hana-oka, *J. Catal.*, **101**, 284 (1986).
8) M. Nagai, T. Satoh, and A. Aiba, *J. Catal.*, **97**, 52 (1986).
9) M. Nagai and T. Ogino, *Preprints of Petrol. Chem. Div., ACS*, **32**, 286 (1987).

A Conductometric Study on the Phenylglyoxylic Acid-Strychnine Complex

Yasuzo SAKAI, Kenichi SATO, Ikuko ITO, and Fujio TAKAHASHI*
Department of Applied Chemistry, Faculty of Engineering, Utsunomiya University, Utsunomiya 321
(Received June 27, 1988)

In order to elucidate the mechanism by which phenylglyoxylic acid (PGA) is reduced electrochemically in the presence of strychnine (SC) to form mandelic acid (MA), which exhibits an optically active property, conductometric studies were carried out. The formation of a 1 : 1 complex between PGA (or MA) and SC was suggested from the results that equimolar mixture of PGA (or MA) and SC showed a maximum decrease of conductivity. Equilibrium constants of the 1 : 1 complex of PGA-SC or MA-SC were determined from the results of conductivity measurements at various temperatures. The thermodynamic data were calculated. ΔH and ΔS were found to be +22 kJ mol^{-1} and +1.1×10^2 J K^{-1} mol^{-1} for both the PGA-SC complex and MA-SC complex.

There have been many papers concerning asymmetric electrochemical reaction occurring in the presence of optically active substances such as alkaloids used as inductors.[1-6] It is known that phenylglyoxylic acid (PGA) is reduced electrochemically under the influence of strychnine (SC) to form mandelic acid (MA), which exhibits a dextrorotatory property.[1,2] However, the reaction mechanism remains unclear at present. Therefore, we presumed that PGA might combine with SC to form a complex, which was adsorbed onto the surface of the electrode,[7] and reduced to form the MA-SC complex. For the first step towards verifying our presumption, in this paper, we present the results of conductometric studies to determine equilibrium constants, and then calculate thermodynamic data for complexes of PGA-SC and MA-SC. On the basis of these results, we speculate about a possible formation of the complex for the asymmetric electrochemical reduction.

Theoretical

Let K be an equilibrium constant, if PGA or MA reacts with SC to form a 1 : 1 complex. Also let concentrations of free PGA (or MA), free SC and 1 : 1 complex be [P], [S], and [PS], and total concentrations of PGA (or MA) and SC be P_T and S_T, then,

$$\mathrm{P} + \mathrm{S} \rightleftarrows \mathrm{PS}, \tag{1}$$

$$K = \frac{[\mathrm{PS}]}{[\mathrm{P}]\,[\mathrm{S}]}, \tag{2}$$

$$P_T = [\mathrm{P}] + [\mathrm{PS}], \tag{3}$$

$$S_T = [\mathrm{S}] + [\mathrm{PS}], \tag{4}$$

In the case of an equimolar mixture, we define a ratio of [PS] to C as α,

$$\alpha = \frac{[\mathrm{PS}]}{C}, \tag{5}$$

where

$$P_T = S_T = C. \tag{6}$$

From Eqs. 2—6, the following equation was derived.

$$\frac{\alpha}{(1-\alpha)^2} = KC. \tag{7}$$

From plots of $\alpha/(1-\alpha)^2$ against C, we may obtain a straight line, the slope of which is equal to K.

The value of α will be obtained by the measurement of conductivity as follows:

Let the conductivity of each individual solution of PGA (or MA) and SC, and the conductivity of mixture of PGA (or MA) and SC be κ_P, κ_S, κ_{PS}, and their molar conductivities be Λ_P, Λ_S, Λ_{PS}, then

$$\kappa_P = P_T\Lambda_P, \tag{8}$$

$$\kappa_S = S_T\Lambda_S, \tag{9}$$

$$\kappa_{PS} = [\mathrm{P}]\Lambda_P + [\mathrm{S}]\Lambda_S + [\mathrm{PS}]\Lambda_{PS}. \tag{10}$$

Eq. 10 is acceptable at very low concentrations of PGA (or MA) and SC, unless other species of complex may exist in the solution. The difference of conductivity, $\Delta\kappa$, is

$$\Delta\kappa = (\kappa_P + \kappa_S) - \kappa_{PS}. \tag{11}$$

The 1 : 1 complex may exhibit less ionic property, because a carboxyl group of PGA (or MA) and a heterocyclic nitrogen (not an indolizine nitrogen) of SC are locked inside the complex by the formation of an ionic bond. Therefore, it is reasonable to assume that

$$\Lambda_{PS} \ll \Lambda_P \text{ or } \Lambda_{PS} \ll \Lambda_S. \tag{12}$$

If we neglect Λ_{PS}, then, the following equation is introduced from Eqs. 5 and 8—12.

$$\frac{\Delta\kappa}{\kappa_P + \kappa_S} = \alpha. \tag{13}$$

The values of α are determined at every concentration of equimolar mixtures of PGA (or MA) and SC by Eq. 13 from the measurement of conductivity. Then, we can obtain K from the slope at zero with respect to concentration on plots of $\alpha/(1-\alpha)^2$ against C according to Eq. 7. If a 1 : 1 complex exists in the mixture, a maximum difference of $\Delta\kappa$ must appear at $P_T = S_T$ in relation between the molar ratio and $\Delta\kappa$, when

P_T+S_T=constant. This can be demonstrated by the derivation in the same manner as Jop's consecutive variation method,[8] except that absorption is replaced by conductivity. This modified Jop's method is valuable for the determination of the equilibrium constants of molecular complexes, which is obtained by ionic bond formation with conductivity change and without absorption change.

Experimental

PGA, MA, and SC sulfate used were commercially available reagent grade. SC sulfate was used in place of free SC, which is less soluble in water. These compounds were dissolved in deionized water to prepare a 1—60 mol dm^{-3} solution.

The conductivities were measured with a TOA conductometer CM-30ET at 20—35 °C

Results and Discussion

The sample solutions were prepared with various concentrations of individual solution of PGA, MA, and SC, and those of equimolar mixture of PGA (or MA) and SC. The conductivities were measured at 20—35 °C. The results are shown in Figs. 1 and 2.

In order to verify the presence of a 1 : 1 complex, sample solutions were prepared with various molar

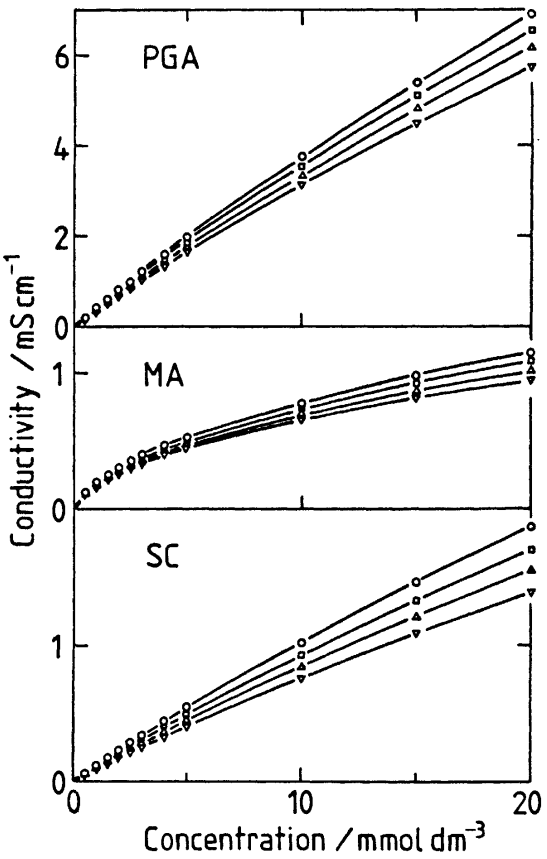

Fig. 1. The conductivities of individual solution of PGA, MA, or SC. —▽—: 20 °C, —△—: 25 °C, —□—: 30 °C, and —○—: 35 °C.

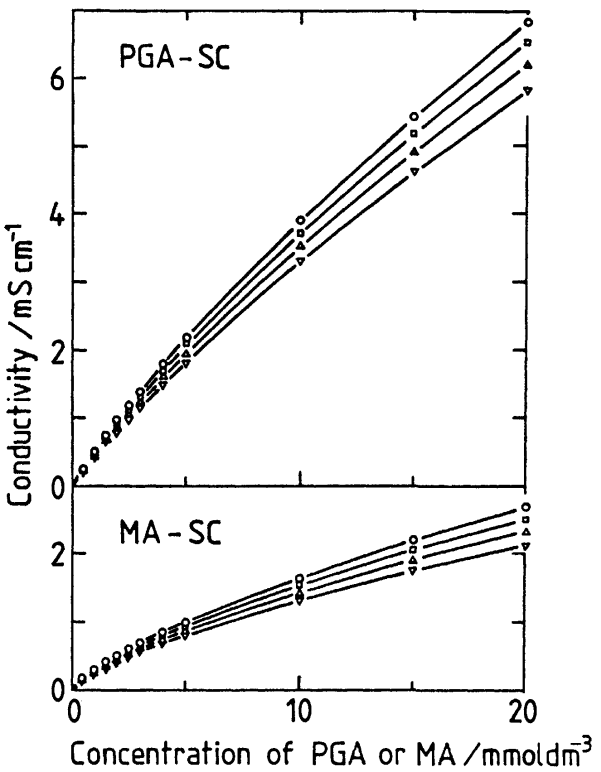

Fig. 2. The conductivities of equimolar mixture of PGA and SC, or MA and SC. The same symbols as those in Fig. 1 are used.

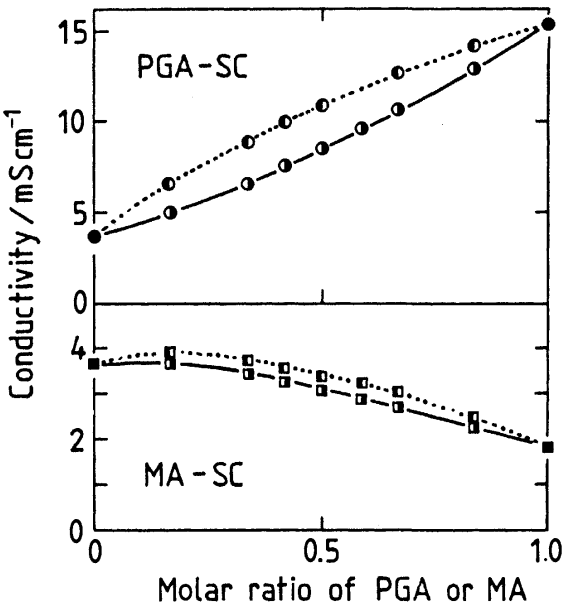

Fig. 3. Plots of conductivity against molar ratio on PGA-SC and MA-SC systems (25 °C). Total concentrations of PGA (or MA) and SC were maintained at 60 mmol dm^{-3}. Solid lines; conductivity of mixture of PGA (or MA) and SC at each molar ratio. Dotted lines; sum of conductivities of individual solution of PGA (or MA) and SC at corresponding concentration.

ratio of PGA (or MA) and SC under the conditions that the total concentration of the two components was kept constant, and these conductivites were measured at 25 °C. We have many data on the relation between conductivity and molar ratio. In order to avoid duplication we present here only two plots at 60 mmol dm^{-3} of total concentration as typical results in Fig. 3.

In Fig. 3, plots on solid lines show the conductivity of a mixture of PGA (or MA) and SC at each molar ratio, and plots on dotted lines show the sum of conductivities of individual solution of PGA (or MA) and SC at the corresponding concentration. The sum of conductivities was calculated from the data in Fig. 1. The gaps between the solid lines and dotted lines are equal to $\Delta\kappa$s. It was found that the maximum gap ($\Delta\kappa$) was obtained at a molar ratio of 0.5.

It must be considered that SC sulfate might be dissociated into SC and sulfate ion completely at infinite dilution in water. The same consideration is applied in the case of a mixture of PGA (or MA) and SC, when the conductivity of the sulfate portion may be offset by the subtraction of the mixture from the sum of indvidual solutions.

This consideration sustains our presumption of the presence of a 1 : 1 complex in the mixture of PGA (or MA) and SC. The conductivity of the mixture was smaller than the sum of the conductivities of the individual solution of PGA (or MA) and SC. This is because the concentrations of free carboxyl group and free base decrease on the formation of an ionic bond.

The values of α were calculated by Eq. 13 and in turn those of $\alpha/(1-\alpha)^2$ were obtained. Plots of $\alpha/(1-\alpha)^2$ against concentration of PGA (or MA) are shown in Fig. 4. This indicates that Eq. 7 is effective at very low the concentrations. The slopes, which should be equal to the equilibrium constant, K, were determined at zero extrapolation on every curve in Fig. 4. It was found, on the other hand, that plots according to Kohlrausch's equation, $\Lambda=\Lambda_\infty-A\sqrt{C}$, with the data in Figs. 1 and 2 fell on straight lines in lower regions of concentration of individuals and mixtrues of PGA and SC as shown in Fig. 5. The values of α in the case of the PGA-SC mixture in the region of very low concentration were recalculated by using values obtained from the straight lines in Fig. 5. The dotted lines in Fig. 4 in the case of the PGA-SC mixtures were obtained by using values, α from Fig. 5. Equilibrium constants, K, were determined from the slopes at every temperature. In the case of MA solutions, no straight line is obtained from the Kohlrausch plots (Fig. 6). This is because MA is a weak acid. Therefore, we made slopes in Fig. 4 in the case of MA-SC mixture by a rough estimate. The values of K are summarized in Table 1, larger error in the case of MA-SC than PGA-SC should be considered in Table 1.

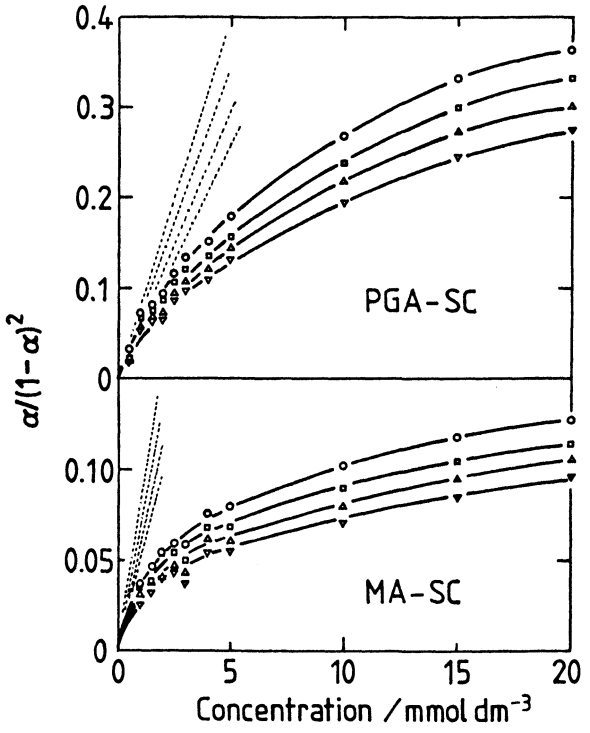

Fig. 4. Plots of $\alpha/(1-\alpha)^2$ against concentration of PGA (or MA). The same symbols as those in Fig. 1. are used. Dotted lines show the slopes of each curve at the zero concentration.

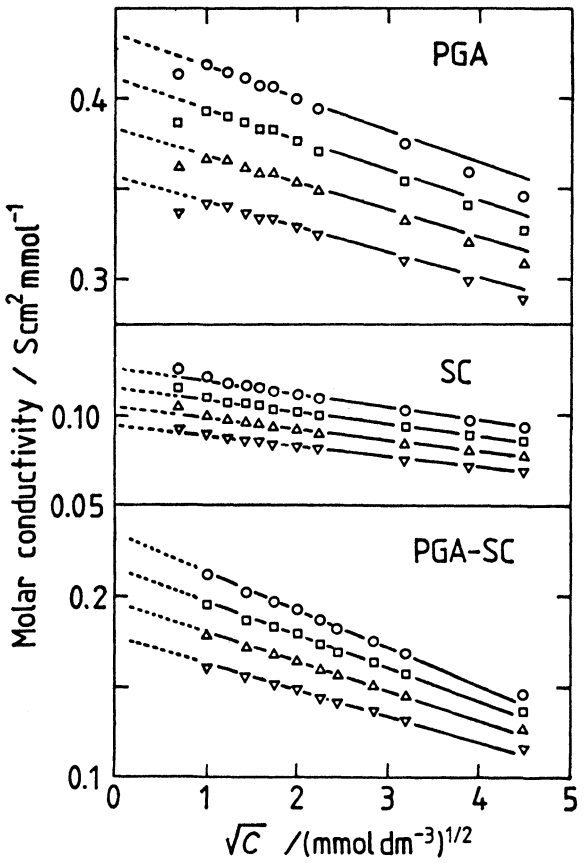

Fig. 5. Plots according to Kohlrausch's equation on PGA, SC, and PGA-SC solutions. The same symbols as those in Fig. 1 are used.

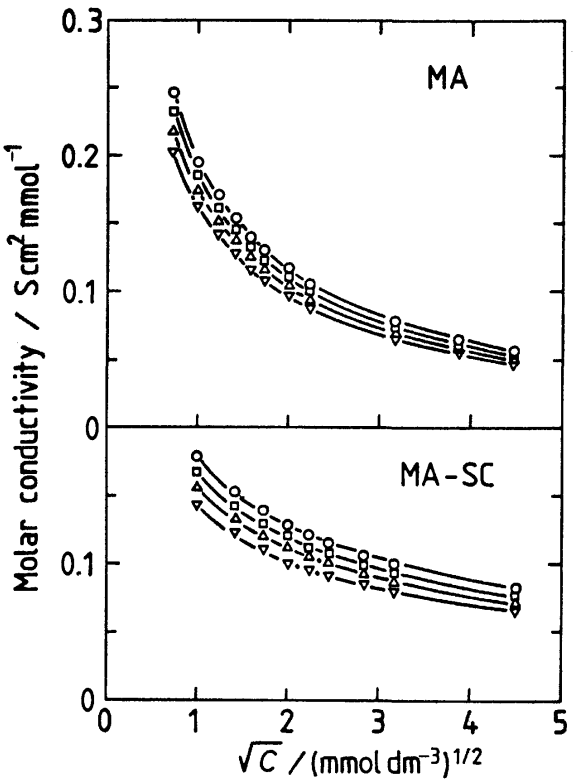

Fig. 6. Plots according to Kohlrausch's equation on MA and MA-SC solutions. The same symbols as those in Fig. 1 are used.

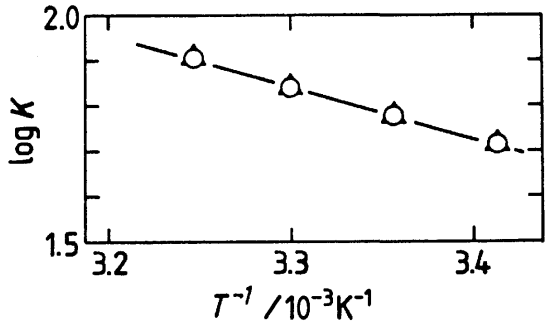

Fig. 7. Plots of $\log K$ against $1/T$ on PGA-SC and MA-SC systems. —○—: PGA-SC system and —△—: MA-SC system.

From plots of $\log K$ against $1/T$, we obtained straight lines as shown in Fig. 7. Thermodynamic data, ΔH and ΔS, were calculated with slopes in Fig. 7 by the equation, $\ln K=(-\Delta H/R)\ (1/T)+(\Delta S/R)$, as shown in Table 1.

Positive values of ΔH and ΔS suggest the existence of hydrophobic interaction in the process of 1 : 1 complex formation in aqueous solution. It is plausible that a phenyl group of PGA (or MA) may contact with a hydrophobic group supposed to be a benzene ring of SC by excluding water molecules from hydrated PGA (or MA) and hydrated SC.

Table 1. Equilibrium Constants and Thermodynamic Data for Both PGA-SC and MA-SC Systems. The Same Data Were Obtained on Both Systems as in Table 1

Equilibrium constant/$dm^3\,mol^{-1}$	52±5 (293 k) 60±5 (298 K) 69±5 (303 K) 80±5 (308 K)
$\Delta H°/J\,mol^{-1}$	$+2.2\times10^4$
$\Delta S°/J\,K^{-1}\,mol^{-1}$	$+1.1\times10^2$

The values of ΔH and ΔS show almost no difference in both the PGA-SC complex and the MA-SC complex. It seems that the difference of molecular structure between PGA and MA may change little with the ratio of complex formation.

The equilibrium constant of the PGA-SC complex is consistent with that of the MA-SC complex in the region of 20—35 °C. Therefore, it is possible that the PGA in the PGA-SC complex is replaced by MA to form the MA-SC complex. As the PGA-SC complex is reduced to form the MA-SC complex on the surface of the electrode, the following process must be repeated:

$$\text{PGA} + \text{SC} \rightleftarrows \text{PGA-SC} \xrightarrow{2H^+,\,2e} \text{MA-SC} \rightleftarrows \text{MA} + \text{SC}. \quad (14)$$

References

1) M. Jubault, E. Raoult, and D. Peltier, *Electrochim. Acta*, **19**, 865 (1974).
2) M. Jubault, *J. Chem. Soc., Chem. Commun.*, **1980**, 953.
3) E. Raoult, M. Jubault, and D. Peltier, *Electrochim. Acta*, **24**, 1219 (1979).
4) J. Kopilov, E. Kariv, and L. L. Miller, *J. Am. Chem. Soc.*, **99**, 3450 (1977).
5) K. Köster and H. Wendt, *J. Electroanal. Chem.*, **138**, 209 (1982).
6) K. Köster, H. Wendt, and A. Lebouc, *J. Electroanal. Chem.*, **157**, 89 (1983).
7) R. Bennes, M. Jubault, M. Privat, and P. Vanel, *Electrochim. Acta*, **26**, 1079 (1981).
8) "Jikken Kagaku Koza zoku 7," ed by Nippon Kagaku Kai, (1966), p. 196.

 © 1989 The Chemical Society of Japan Bull. Chem. Soc. Jpn., 62, 979—984 (1989)

A Theoretical Study of the Ionized State of Polymers with the Localized Molecular Orbital Method

Akira IMAMURA,* Kehong YE, and Masahiro TAKETOSHI
Department of Chemistry, Faculty of Science, Hiroshima University, Higashisenda-machi, Hiroshima 730
(Received August 1, 1988)

A localized molecular orbital method for the investigation of the ionized state of polymers is presented. It is based on the Crystal Orbital Method(CO). By performing a super-cell method and Edmiston and Ruedenberg's LMO method, the Bloch function was transformed into a nearly completely localized Wannier function. Furthermore, the calculation of the configuration interaction was introduced to obtain more reasonable results. The present method was applied to polyacetylene (PA), polyethylene (PE), and polypropylene (PP). Ionization potentials of these polymers were calculated and compared with experimental and other theoretical results. All the calculations were performed using the CNDO/S approximation.

Interest in the theoretical studies of organic polymers has grown considerably in recent years. As the result of the remarkable development of computers, it has become possible to investigate the electronic structure of huge molecules or complicated systems which could not be treated before. Consequently, many theoretical methods have been proposed, and many calculated results have been reported. Most of these calculations, however, have been carried out on the ground state of polymers. Not many attempts have been done to investigate the ionized state of polymers. We carried out this study for the following two main reasons. One is that suitable theory has not yet been established. The second reason is the lack of precise experimental values, which makes the comparison between experimental and theoretical results defficult, sometimes even impossible.

It is known that, for the species in which the interaction between segments is very weak, the exciton model is useful, while for the species in which the interaction is very strong, the crystal orbital method provides a good description. However, for the species in which the interaction is between the above two, the theory seems not to be established. Therefore, the purpose of this study is to present a theoretical method for the investigation of the ionized state of polymers. In our method, by using a super-cell method[1] and Edmiston and Ruedenberg's LMO method[2,3] a nearly completely localized Wannier function can be obtained from Bloch's function. We can calculate the ionization potential from this Wannier function directly or after carrying out the configuration interaction procedure. We applied the method to polyacetylene, polyethylene, and polypropylene. The results seem to be in somewhat good agreement with the experimental values.

Method of Calculations

In the tight-binding approximation, one electron-crystal orbital for a linear-periodic polymer is given by Bloch's function as follows:[4]

$$\psi_{ks}(\boldsymbol{r}) = (1/N)^{1/2} \sum_{j=1}^{N} \sum_{t=1}^{n} C_{ks,jt} \chi_t \{\boldsymbol{T}^j(\boldsymbol{r} - \boldsymbol{r}_t - j\boldsymbol{a})\} \quad (1)$$

$$C_{ks,jt} = \exp(ikj) C_{ks,t} \quad (2)$$

$$k = 2\pi p/N \quad (p = 0, 1, 2 \cdots\cdots N-1) \quad (3)$$

where j denotes a cell in the polymer; t, an atomic orbital in the j-th cell; $\boldsymbol{r}_t$, its vector from the center of a segment; $\boldsymbol{T}$, the rotational operator around the helical axis, and $\boldsymbol{a}$, the unit vector of the translational symmetry which is paralled to the helical axis. N and n specify the total number of cells and the number of atomic orbitals in an unit cell, while the s value, ranging from 1 to n, indicates an energy band. $C_{ks,jt}$ can be rewritten as Eq. 2; here i denotes the imaginary number. The k value in Eq. 3 corresponds to the wavenumber vector defined by the solid state physics.

A localized molecular orbital (LMO) can be obtained in several ways. In the case of polymers, the Wannier transformation is well known. The Wannier function has a particular property: if the overlap integrals between neighbouring segments are very small, the MO coefficients, C_k's, do not depend on the wavenumber vector, k. That is, the MOs obtained are localized in a certain segment. However, in general, a nearly completely localized molecular orbital can not be expected by using the Wannier transformation only. Therefore, in order to get a well-localized molecular orbital for polymers, we considered two procedures before the Wannier transformation. One is called the super-cell method, and second, a modification of the Edmiston and Ruedenberg's LMO procedure which was performed for the wave function of super cells in each wavenumber vector. By performing these two procedures, the overlap integrals between corresponding localized orbitals in neighbouring segments become very small; that is, well-localized MOs can be expected with the two procedures, followed by the Wannier transformation.

The details of the super-cell method can be found in Ref. 1. Here we will give just a simple outline. It assumed that, in a linea-periodic polymer system, several units can be considered as big units, named "super cells", if the relation between such a super cell and the

unit cells satisfies the following equations:

$$k' = mk - 2\pi j \quad (j: \text{integer}) \tag{4}$$

$$C_{k's,t}(l) = C_{ks,t} \exp\{i(l-1)k\} \tag{5}$$

where k' and $C_{k's,t}$ denote the wave vector and the MO coefficient of the super cell, while k and $C_{ks,t}$ are those of the unit cells. The integer j in Eq. 4 must be chosen so that the value of k is in the range of the first Brillouin zone (0—2 π); l indicates the l-th cell in the super cell.

After the super cells were created, as has been mentioned above, we treated the super cell thus obtained in each wavenumber vector with the modification of the Edmiston and Ruedenberg's energy-localized MO method. In general, however, the wave functions of polymers are complex; so in this procedure we completed the LMO by considering three kinds of transformations, which will be described in detail below.

1. Orthogonal transformation:

$$\begin{pmatrix} u_1 \\ u_2 \end{pmatrix} = \begin{pmatrix} \cos\gamma & \sin\gamma \\ -\sin\gamma & \cos\gamma \end{pmatrix} \begin{pmatrix} \psi_1 \\ \psi_2 \end{pmatrix} \tag{6}$$

where u_1, u_2, and ψ_1, ψ_2 are the complex functions. After the transformation, the sum of the diagonal elements is given by the following equations:

$$D(u) = D(\psi) + A_{12} + (A_{12}+B_{12})^{1/2} \cos 4(\gamma-\alpha) \tag{7}$$

$$2A_{12} = [\psi_1^*\psi_2 + \psi_1\psi_2^* | \psi_1^*\psi_2 + \psi_1\psi_2^*] - [\psi_1\psi_1^* - \psi_2\psi_2^* | \psi_1\psi_1^* - \psi_2\psi_2^*] \tag{8}$$

$$B_{12} = [\psi_1\psi_1^* - \psi_2\psi_2^* | \psi_1^*\psi_2 + \psi_1\psi_2^*] \tag{9}$$

$$\tan 4\alpha = -B_{12}/A_{12} \tag{10}$$

In Eq. 7, when the value of $\gamma=\alpha+(n\pi/2)$, $D(u)$ reaches a maximum. By placing the Bloch function, Eq. 1, into Eqs. 8 and 9 and by using the periodic boundary condition and the CNDO/S[5] approximation, Eqs. 8 and 9 can be rewritten as follows:

$$2A_{k,12} = 1/N \sum_{t=1}^{n}\sum_{u=1}^{n} \{(C_{k1,t}^* C_{k2,t} + C_{k1,t} C_{k2,t}^*)(C_{k1,u}^* C_{k2,u} + C_{k1,u} C_{k2,u}^*) - (C_{k1,t}^* C_{k1,t} - C_{k2,t} C_{k2,t}^*)(C_{k1,u} C_{k1,u}^* - C_{k2,u} C_{k2,u}^*)\} \sum_{j=1}^{N} \gamma_{tu}^{0j} \tag{11}$$

$$B_{k,12} = 1/N \sum_{t=1}^{n}\sum_{u=1}^{n} (C_{k1,t} C_{k1,t}^* - C_{k2,t} C_{k2,t}^*)(C_{k1,u}^* C_{k2,u} + C_{k1,u} C_{k2,u}^*) \sum_{j=1}^{N} \gamma_{tu}^{0j} \tag{12}$$

$$\gamma_{tu}^{0j} = [\chi_t \chi_t | \chi_u(\boldsymbol{T}^j\boldsymbol{r} - j\boldsymbol{a}) \chi_u(\boldsymbol{T}^j\boldsymbol{r} - j\boldsymbol{a})] \tag{13}$$

2. Transformation between the real part of one MO and the imaginary part of the other MO:

$$\begin{pmatrix} u_1 \\ u_2 \end{pmatrix} = \begin{pmatrix} \cos\gamma & i\sin\gamma \\ i\sin\gamma & \cos\gamma \end{pmatrix} \begin{pmatrix} \psi_1 \\ \psi_2 \end{pmatrix} \tag{14}$$

In this case, the sum of the diagonal elements has the following forms:

$$D(u) = D(\psi) + A_{12} + (A_{12}+B_{12})^{1/2} \cos 4(\gamma-\alpha) \tag{15}$$

$$2A_{12} = [\psi_1^*\psi_2 - \psi_1\psi_2^* | \psi_1^*\psi_2 - \psi_1\psi_2^*] - [\psi_1\psi_1^* - \psi_2\psi_2^* | \psi_1\psi_1^* - \psi_2\psi_2^*] \tag{16}$$

$$B_{12} = [\psi_1\psi_1^* - \psi_2\psi_2^* | \psi_1^*\psi_2 - \psi_1\psi_2^*] i \tag{17}$$

$$\tan 4\alpha = -B_{12}/A_{12} \tag{18}$$

By using the same procedures as in Transformation 1, Eqs. 16 and 17 become:

$$2A_{k,12} = -1/N \sum_{t=1}^{n}\sum_{u=1}^{n} \{(C_{k1,t}^* C_{k2,t} - C_{k1,t} C_{k2,t}^*)(C_{k1,u}^* C_{k2,u} - C_{k1,u} C_{k2,u}^*) + (C_{k1,t} C_{k1,t}^* - C_{k2,t} C_{k2,t}^*)(C_{k1,u} C_{k1,u}^* - C_{k2,u} C_{k2,u}^*)\} \sum_{j=1}^{N} \gamma_{tu}^{0j} \tag{19}$$

$$B_{k,12} = i/N \sum_{t=1}^{n}\sum_{u=1}^{n} (C_{k1,t} C_{k1,t}^* - C_{k2,t} C_{k2,t}^*)(C_{k1,u}^* C_{k2,u} - C_{k1,u} C_{k2,u}^*) \sum_{j=1}^{N} \gamma_{tu}^{0j} \tag{20}$$

Well-localized MOs can be obtained by carrying out the above two transformations iteratively for every wavenumber vector. Finally, to rearrange the MO coefficients to similar types for all k values, a third transformation will be performed.

3. Transformation between real part and imaginary part in the same MO:

$$u_1 = \{a(a^2+b^2)^{1/2} - ib(a^2+b^2)^{1/2}\}\psi_1 \tag{21}$$

The LMO of the super cell completely obtained can be expressed in the following form:

$$\psi_{ks}(\boldsymbol{r}) = (1/N)^{1/2} \sum_{j=1}^{N}\sum_{t=1}^{n} \exp(ikj) C_{ks,t}(\text{LMO}) \chi_t(\boldsymbol{T}^j\boldsymbol{r} - j\boldsymbol{a}) \tag{22}$$

Using the above formula, we can derive the Wannier function easily. It is well-known that the Wannier function[6] is described as follows:

$$a_s(\boldsymbol{r}-l) = (1/N)^{1/2} \sum_{k} \exp(-ikl)\psi_{ks}(\boldsymbol{r}) \tag{23}$$

where l is the l-th segment of the Wannier function. By inserting Eq. 22 into Eq. 23, we obtain:

$$a_s(\boldsymbol{r}-l) = \sum_{j=1}^{N}\sum_{t=1}^{n} A_{ls,jt} \chi_t(\boldsymbol{T}^j\boldsymbol{r} - j\boldsymbol{a}) \tag{24}$$

$$A_{ls,jt} = (1/N) \sum_{k} \exp\{ik(j-l)\} C_{ks,t}(\text{LMO}) \tag{25}$$

In order to calculate the ionization potential from the Wannier function, four kinds of calculation models were considered; the ionization was assumed to arise from the central cell of the Wannier function. Next, we will give an outline for each model.

Model 1. The ionization energy is calculated from the above-obtained Wannier function directly:

$$I.P = E(M) - E(M^+) = H_{m0} + \sum_{l=1}^{N}\sum_{s=1}^{n} (2J_{ls,m0} - K_{ls,m0}) \tag{26}$$

where M corresponds to the ground state, and M^+ to the ionized state.

$$H_{m0} = [a_m(\boldsymbol{r}_1) | \hat{h} | a_m(\boldsymbol{r}_1)] \tag{27}$$

$$J_{ls,m0} = [a_s(\boldsymbol{r}_1 - l) a_m(\boldsymbol{r}_2) | 1/r_{12} | a_s(\boldsymbol{r}_1 - l) a_m(\boldsymbol{r}_2)] \tag{28}$$

$$K_{ls,m0} = [a_s(\boldsymbol{r}_1 - l) a_m(\boldsymbol{r}_2) | 1/r_{12} | a_m(\boldsymbol{r}_1) a_s(\boldsymbol{r}_2 - l)] \tag{29}$$

Using the Wannier function, the one electron term in Eq. 26 becomes:

$$H_{m0} = \sum_{tt'}\sum_{jj'} A_{m0,jt}^* A_{m0,j't'} [\chi_t(\boldsymbol{T}^j\boldsymbol{r} - j\boldsymbol{a}) | \hat{h} | \chi_{t'}(\boldsymbol{T}^{j'}\boldsymbol{r} - j'\boldsymbol{a})] \tag{30}$$

while the two electron term is:

$$\sum_l \sum_s (2J_{ls,m0}-K_{ls,m0}) = 2\sum_{tt'}\sum_{jj'} A^*_{m0,j't'}A_{m0,j't'}\gamma^{jj'}_{tt'} \sum_l \sum_s A^*_{js,jt}A_{ls,jt} - \sum_{tt'}\sum_{jj'} A^*_{m0,j't'}A_{m0,jt}\gamma^{jj'}_{tt'} \sum_l \sum_s A^*_{js,jt}A_{ls,j't'} \quad (31)$$

Model 2. In order to get even more reliable results, that is, results more comparable with the experimental values, in this model we introduced a configuration interaction treatment and carried it out in a unit cell of the polymer.

In the present work, a complete singly excited configuration interation (SECI) was considered. The elements of matrix for SECI can be simply expressed in the following way:

Diagonal elements:

$$H_{kk}=-\{h_{kk}+\sum_i (2J_{ik}-K_{ik})\} \quad (32)$$

Non-diagonal elements:

$$H_{kl}=-h_{kl}-\sum_i \{2(kl|ii)-(ki|ii)\}-(kl|kk)-(kl|ll) \quad (33)$$

Using the Wannier function and the parameters of the CNDO/S approximation, the ionization potential can be obtained by diagonalizing the above matrix.

Model 3. It is known that, in the CI calculation, the more configurations interact, the better results can be obtained. In this case, therefore, we extended the above CI calculation to a super cell. The CI matrix in this model is similar to that in Model 2.

Model 4. Generally speaking, ionization can be considered as arising from a rather localized state. However, due to some disagreements between the theoretical and experimental results, a question arises: is the excitation of a polymer limited in a particular space or does it arise from a more extended space? In other words, can the ionized state move along the polymer chain or not? In an attemp to answer this question, in this model, based on the concept of exciton, we change the above CI matrix into a new hermit matrix by using the following equation, which satisfies the periodic boundary condition.

$$H^{(0,0)}_{tu}=H^{(0,0)}_{tu}+\sum_{m=1} \cos mk(H^{(0,m)}_{tu}+H^{(0,-m)}_{tu}) + i\sum_{m=1} \sin mk(H^{(0,m)}_{tu}-H^{(0,-m)}_{tu}) \quad (34)$$

Also, the ionization potential of a polymer can be obtained by diagonalizing the new matrix.

Results and Discussion

We applied the present method to polyacetylene, polyethylene, and polypropylene. The structures of these polymers are shown in Fig. 1. The ionization potentials were calculated by using the four models of calculation described in the previous section.

In order to compare the polymers, first we calculate the ionization energies of some small molecules. These molecules can be considered as oligomers of the corresponding polymers. The results are shown in Table 1. The values obtained seem to be in good agreement with the experimental results. This means that the present method is suitable for investigating the ionized state of oligomers; consequently, it may also be suitable for polymers. From ethane to isobutane, as the number of carbons in the molecule increases, the corresponding values decrease. Table 1 shows that the ionization energies of alkenes are lower than those of corresponding alkanes because of the existence of a double bond in the molecules. This

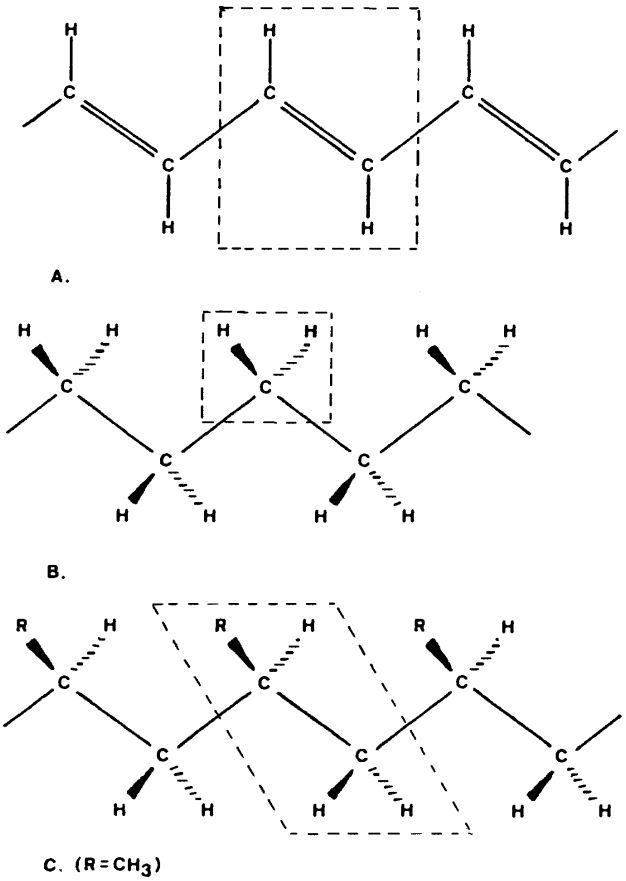

Fig. 1. Structures of *all-trans*-polyacetylene (A), polyethylene (B), and polypropylene (C). Unit cells are surrounded by broken lines.

Table 1. Ionization Energies of Some Small Molecules (eV)

Molecule	Symmetry	This work	Experiment
Ethane	Ag	14.898	12.1
	Eg	14.196	13.6
	Eu	19.167	15.4
Propane	A1	13.778	12.1
	B2	13.579	12.7
	A2	15.914	13.5
Isobutane	E	12.923	11.4
	A1	12.923	12.1
	A2	13.243	12.8
Ethylene	B3u	10.796	10.5
Butadiene	Bg	9.369	9.03
	Au	12.696	11.46

suggests that the ionization energy of polyacetylene is smaller than that of polyethylene. In fact, this is true, as can be seen from Tables 4 and 7. Consequently, the CNDO/S parameters are adequately reliable for the calculation of the ionization energies of the polymers under consideration.

Polyacetylene (PA). First, the MO's coefficient will be considered. The results are listed in Tables 2 and 3. These tables show that the molecular orbitals obtained are quite localized on the central cell. With the number of unit cells contained in a super cell increased from 3 to 4, the MO's coefficients undergo a little change, but not a very large one. For example, in the case of C-C (π), the difference is about 0.0003. We can expect that such a small difference would not affect the values of the ionization potential. Also, this means that, in our calculation for PA, taking the number of unit cells in a super cell as 3 or 4 is sufficient.

Next, let us compare our results with those obtained by experiments and other theoretical calculations.[7-10] The results are shown in Table 4. Peak 1 corresponds to the C-C π bonding orbital; the value given by Model 1 is larger than the others. The reason for this disagreement can be understood as follows. π-electrons, generally, are considered as moving in a broad space. However, in this method they are described as localized upon a particular bond. This may produce the disagreement. Peaks 2 and 3 in Model 1 also give very large values; these ionization arise from C-H bonds. The most probable explanation may be that these ionization arise from a more delocalized space instead of a localized one; that is, ionization occurs not just in a limited bond, but in a broader space extending to the neighboring bonds. The results would be improved if the CI procedure is introduced. In fact, this can be seen by comparing Model 1 with Models 2—4. For Peak 2, the result obtained from Model 4 is rather good, while the value given by Model 2 is desirable for Peak 3. This also means that the delocalized space in Peak 2 is broader than that in Peak 3. Finally, Peaks 4 and 5 are related to the C-C σ orbitals; the results of Model 1 are in good agreement with the experimental values and some other theoretical ones.

Polyethylene (PE). The MO's coefficients of PE

Table 2. Square of MO Coefficients
C-H Bonding Orbital (PA)

		4 Units[a]	3 Units[a]
Central cell-1	C S	0.16279	0.16380
	C Py	0.34784	0.34692
	C Pz	0.00000	0.00001
	H S	0.48558	0.48553
Central cell-2	C S	0.00030	0.00029
	C Py	0.00060	0.00061
	C Pz	0.00003	0.00003
	H S	0.00092	0.00092
1st cell-1	C S	0.00015	0.00013
	C Py	0.00000	0.00000
	C Pz	0.00002	0.00002
	H S	0.00003	0.00003
1st cell-2	C S	0.00003	0.00003
	C Py	0.00001	0.00001
	C Pz	0.00004	0.00004
	H S	0.00000	0.00000

a) Number of unit cells in a super cell.

Table 3. Square of MO Coefficients
C-C(π) Bonding Orbital (PA)

		4 Units[a]	3 Units[a]
Central cell	C Px	0.47406	0.47433
	C Px	0.47386	0.47331
1st cell	C Px	0.01299	0.01285
	C Px	0.01068	0.01059
2nd cell	C Px	0.00054	0.00047
	C Px	0.00132	0.00119

a) Number of unit cells in a super cell.

Table 4. Ionization Energies of Polyacetylene (eV)

	Peak 1	Peak 2	Peak 3	Peak 4	Peak 5
Model 1	12.26	22.30	22.30	24.54	26.08
Model 2	12.27	16.17	19.73	24.10	30.58
Model 3	10.03	14.07	16.73	20.37	26.82
Model 4	11.18	13.32	16.04	24.73	30.08
Band Model	8.02	14.66	15.00	22.05	29.58
XPS[a]	4.84	12.25	19.96	25.40	27.82
VEH[b]	7.26	13.30	20.68	26.03	31.65
MNDO[c]	4.7				
ab initio[d]	6.19				

a) From the X-ray-photoelectron spectroscopy (XPS) data of M. Kitani. b) From the XPS theoretical spectrum obtained by using the valence effective hamiltonian (VEH) calculation by Bredas et al. c) By Tripathy et al. d) Calculation for the model molecule C_8H_{10} reported by Kirtman.

Table 5. Square of MO Coefficients
C-H Bonding Orbital (PE)

		4 Units[a]	3 Units[a]
Central cell	C S	0.12337	0.12157
	C Px	0.12953	0.13159
	C Py	0.25152	0.25152
	C Pz	0.00000	0.00000
	H S	0.49278	0.49269
	H S	0.00000	0.00000
1st cell	C S	0.00011	0.00007
	C Px	0.00007	0.00011
	C Py	0.00036	0.00036
	C Pz	0.00006	0.00000
	H S	0.00053	0.00053
	H S	0.00001	0.00001
2nd cell	C S	0.00013	0.00002
	C Px	0.00004	0.00000
	C Py	0.00002	0.00002
	C Pz	0.00000	0.00000
	H S	0.00002	0.00002
	H S	0.00000	0.00000

a) Number of unit cells in a super cell.

Table 6. Square of MO Coefficients C-C Bonding Orbital (PE)

		4 Units[a]	3 Units[a]
	C S	0.12425	0.12646
	C Px	0.12302	0.12097
	C Py	0.00000	0.00000
	C Pz	0.25147	0.25145
	H S	0.00000	0.00000
	H S	0.00000	0.00000
Central cell			
	C S	0.12429	0.12649
	C Px	0.12306	0.12101
	C Py	0.00000	0.00000
	C Pz	0.25143	0.25145
	H S	0.00000	0.00000
	H S	0.00000	0.00000
	C S	0.00002	0.00001
	C Px	0.00041	0.00018
	C Py	0.00000	0.00000
	C Pz	0.00024	0.00024
	H S	0.00001	0.00002
	H S	0.00001	0.00002
1st cell			
	C S	0.00025	0.00011
	C Px	0.00015	0.00034
	C Py	0.00000	0.00000
	C Pz	0.00005	0.00004
	H S	0.00000	0.00003
	H S	0.00000	0.00003

a) Number of unit cells in a super cell.

Table 7. Ionization Energies of Polyethylene (eV)

	Peak 1	Peak 2	Peak 3
Model 1	21.74	21.74	22.85
Model 2	17.91	18.44	26.03
Model 3	14.15	17.34	26.29
Model 4	10.62	20.54	25.94
Band Model	11.37	14.39	23.72
ESCA[a]	8.3	18.7	23.5
CNDO/2[b]	13	20	30
Extended Huckel[c]	11.9		
ab initio[d]	13.2		

a) By Delhalle et al. b) By Wood et al.; results for the model molecule $C_{36}H_{74}$. c) By Delhalle et al. d) By Teramae et al.; the STO-3G basis set was used.

Table 8. Square of MO Coefficients C-H Bonding Orbtal (PP)

		3 Units[a]
	C S	0.11815
	C Px	0.25203
Central cell	C Py	0.13442
	C Pz	0.00000
	H S	0.49273
	H S	0.00000
	C S	0.00001
	C Px	0.00000
1st cell	C Py	0.00004
	C Pz	0.00003
	H S	0.00000
	H S	0.00005

a) Number of unit cells in a super cell.

Table 9. Square of MO Coefficients C-C Bonding Orbital (PP)

		3 Units[a]
	C S	0.12811
	C Px	0.00002
	C Py	0.12192
	C Pz	0.24871
	H S	0.00000
Central cell		
	C S	0.12975
	C Px	0.00001
	C Py	0.11935
	C Pz	0.24875
	H S	0.00001
	H S	0.00000
	C S	0.00025
	C Px	0.00000
	C Py	0.00015
	C Pz	0.00007
	H S	0.00001
1st cell		
	C S	0.00003
	C Px	0.00000
	C Py	0.00021
	C Pz	0.00021
	H S	0.00002
	H S	0.00002

a) Number of unit cells in a super cell.

are shown in Tables 5 and 6. Table 5 shows the MO's of the C-H bonding orbital, and Table 6, those of the C-C bond. We can see that the MO coefficients are localized completely on the central cell and are almost independent of the numbers of unit cell, contained in a super cell. Therefore, taking 3 or 4 unit cells for a super cell is enough for our treatment.

Next, it is interesting to compare our results with other theoretical and experimental ones.[11-13] The results are shown in Table 7. First, let us examine Peak 1, which is obtained from the ionization that arise from one C-H bond. The value given by Model 1 is very large, even greater than the result of CNDO/2. This may suggest that the ionization arises from a more delocalized space, similar to Peaks 2 and 3 in PA discussed above. On the other hand, Model 4 gives a reasonable result. This may be due to the fact that CI was taken into account. From Model 2 to Model 4, as the space of configuration interaction is extended, the results seem to be improved greatly. Next, as for Peak 2, the value from Model 1 seems greater than the others, but not very large, and it is degenerate when compared with Peak 1. The results given by Models 2 and 3 show a very good agreement with the ESCA's, while Model 4 gives an overestimated value. Finally, in the case of Peak 3, Model 1 gives a very good result. This may imply that, for the high-energy region, an ionized state can be well described by a localized model.

Table 10. Ionization Energies of Polypropylene (eV)

	Peak 1	Peak 2	Peak 3	Peak 4	Peak 5
Model 1	21.49	21.51	21.59	21.60	22.20
Model 2	15.07	16.33	17.63	18.11	18.97
Model 3	9.80	13.41	13.85	14.45	16.68
Model 4	7.69	9.89	12.83	15.95	19.01
Band model	7.51	11.80	13.17	13.69	17.78

Polypropylene (PP). Some of the Mo's coefficients of PP are given in Tables 8 and 9. In this case, we just consider the super cell that contains only 3 unit cells. From these tables, we can see that, as with PA and PE, the molecular orbitals are well localized. For PP, unfortunately, we can not find any related experimental results at present. Therefore, our results are shown in Table 10 just with those obtained by the use of the Band model. The values given by Model 1 also seem to be too large, especially in Peak 1 to Peak 3, they were improved by introducing the CI calculation from Model 2 to Model 4. Therefore, it seems that the general tendency of the ionization of PP is the same as those of PA and PE.

Conclusion

The present method seems to be applicable to the investigation of the ionized state of one-dimensional periodic polymers such as PE and PA. The localized model (Model 1) described ionizations from the high-energy region quite well, but failed to explain those from the low-energy region. By introducing the models including configuration interaction (Model 2 to Model 4), the results of ionization from the low-energy region were improved and became comparable with the experimental values. Therefore, we concluded that, in the high-energy region, ionizations arise from a rather localized space, so Model 1 is suitable. In the low-energy region, especially in the first ionization potential, ionization occurs from a more delocalized space; here, Model 4 is excellent, In the middle region, ionized states can be well described by Models 2 and 3.

We are very grateful to Dr. Kazuhiko Seki for his useful discussions. All the calculations were performed in the Information Processing Center of Hiroshima University, to which we express our gratitude.

References

1) A. Imamura, S. Suhai, and J. Ladik, *J. Chem. Phys.*, **76**, 6067 (1982).
2) C. Edmiston and K. Ruedenberg, *Rev. Mod. Phys.*, **35**, 457 (1963).
3) C. Trindle and O. Sinanoglu, *J. Chem. Phys.*, **49**, 65 (1968).
4) H. Fujita and A. Imamura, *J. Chem. Phys.*, **53**, 4555 (1970).
5) J. Del Bene and H. H. Jaffe, *J. Chem. Phys.*, **48**, 1807 (1968).
6) G. H. Wannier, *Phys. Rev.*, **52**, 191 (1937).
7) M. Kitani, from Ref. 33 of Ref. 8.
8) J. L. Bredas, R. R. Chance, S. Silbey, G. Nicolas, and Ph. Durand, *J. Chem. Phys.*, **75**, 255 (1981).
9) S. K. Tripathy, D. Kichen, and M. A. Druy, *Macromolecules*, **16**, 190 (1980).
10) B. Kirtman, W. B. Nilsson, and W. E. Palke, *Solid State Commun.*, **46**, 791 (1983).
11) J. Delhalle, J. M. Andre, S. Delhalle, J. J. Pireaux, R. Caudano, and J. J. Verbist, *J. Chem. Phys.*, **60**, 595 (1974).
12) M. H. Wood, R. Lavery, I. H. Hillier, and M. Barber, *Faraday Discuss. Chem. Soc.*, **60**, 173 (1976).
13) H. Teramae, T. Yamabe, and A. Imamura, *Theor. Chim. Acta*, **64**, 1 (1983).

 © 1989 The Chemical Society of Japan Bull. Chem. Soc. Jpn., 62, 985—992 (1989)

Solubilities and Dissolution States of a Series of Symmetrical Tetraalkylammonium Salts in Water

Haruo NAKAYAMA,* Hiromi KUWATA, Norikazu YAMAMOTO, Yutaka AKAGI, and Hiroshi MATSUI†
Division of Materials Science and Chemical Engineering, Faculty of Engineering, Yokohama National University, Tokiwadai, Hodogaya-ku, Yokohama 240
†The Radio Isotope Center, Yokohama National University, Tokiwadai, Hodogaya-ku, Yokohama 240
(Received August 26, 1988)

The solubilities of a series of symmetrical tetraalkylammonium salts, R_4NX ($R=CH_3$—n-C_8H_{17}, including i-C_4H_9 and i-C_5H_{11}; X=Cl, Br, I, NO_3, and ClO_4), in water have been determined over the temperature range between 5 and 45 °C. The solubilities of these salts were found to be strongly dependent upon both the chain length of R of the R_4N^+ cation and upon the partial molar volume of the X^- anion. It has been concluded that these solubilities are closely related with the stability of a "cage-like" water structure, which is presumably formed around the R_4N^+ cation in the solution. A thermodynamic interpretation of the solubility of the R_4NX salts was made by using some thermodynamic properties obtained by a differential scanning calorimetry, together with the enthalpy of the solution calculated from the temperature dependence of the solubility.

It has been pointed out that one of the most important factors which contributes to the stability of a tetraalkylammonium cation in an aqueous solution is the formation of a "cage-like" or "clathrate-like" water structure around its nonpolarizable moieties.[1] This explanation is closely related to a phenomenon in which many tetrabutylammonium salts (or tetraisopentylammonium salts) form unique hydrates having a large number of moles of water.[2] Single-crystal X-ray examinations[3-5] by Jeffrey and his coworkers on these hydrates showed that the central N atom lies at a common vertex of four large polyhedra, which are either tetrakaidecahedra or pentakaidecahedra; each of the four alkyl chains extends into one of the polyhedral cages. Furthermore, other experimental results[6] suggest that such short alkyl chains as $R=C_2H_5$ and $R=n$-C_3H_7 are stably accommodated within a pentagonal dodecahedron. Thus, a "cage-like" water structure around R_4N^+ cations with $R=C_2H_5$—n-C_4H_9, and i-C_5H_{11}, is expected to be fairly stable and to contribute to the elevation of the solubilities in water.

The effect of an anion X^- on the solubility of a R_4NX salt has not been fully discussed. However, the most important effect of an anion X^- on the dissolution state of the R_4NX salts in water may be considered to be a deformative or destructive effect on the "cage-like" water structure around the R_4N^+ cation, owing to the large molar volume of the anion. This consideration comes from the fact that the melting points of the hydrates formed by a series of salts $(n\text{-}C_4H_9)_4NX$ with X=F, Cl, Br, IO_3, NO_3, and ClO_3 decrease almost linearly with increasing the partial molar volume of the X^- anion.[7]

In this study, in order to determine whether the above-mentioned effects of both R_4N^+ cations and X^- anions on the solubilities of the R_4NX salts are generally adequate, the solubilities of various R_4NX salts in water have been measured, especially for salts whose solubility data are not available in literature. Furthermore, some attempts were made at a thermodynamic interpretation of these solubility data.

Experimental

Materials. Most of the symmetrical tetraalkylammonium salts, R_4NX, used were prepared from the corresponding tetraalkylammonium iodides, R_4NI. The iodides with $R=CH_3$—n-C_3H_7 were purchased from Tokyo Kasei Kogyo Co., Ltd. and purified by repeated recrystallization from pure water. The iodides with $R=n$-C_4H_9—n-C_8H_{17}, i-C_4H_9, and i-C_5H_{11}, were sythesized and purified by the same procedure previously reported.[8] Aqueous solutions of all the chlorides and the bromides having $R=i$-C_5H_{11}, n-C_6H_{13}, and n-C_8H_{17} were prepared by neutralizing each tetraalkylammonium hydroxide solution with either a HCl or HBr solution. The hydroxide solution was obtained by treating the tetraalkylammonium iodide with freshly prepared silver hydroxide in water with vigorous shaking, followed by filtration of silver iodide in a CO_2-free atmosphere.[9] Tetraalkylammonium nitrates were obtained by reacting each R_4NI with silver nitrate either in water (for $R=CH_3$—n-C_4H_9) or in acetone-water mixture (for $R=n$-C_5H_{11}—n-C_8H_{17}), followed by filtration of silver iodide and evaporation of the solvent using a rotary evaporator. These nitrates, except for $(n\text{-}C_8H_{17})_4NNO_3$, were purified by recrystallization from water and $(n\text{-}C_8H_{17})_4NNO_3$ from diethyl ether. Tetraalkylammonium perchlorates, R_4NClO_4, with $R=CH_3$—n-C_3H_7 were purchased from Tokyo Kasei Kogyo Co., Ltd. Since the solubilities of tetraalkylammonium perchlorates with long alkyl chains ($R=n$-C_4H_9—n-C_8H_{17}) were quite low, these solubilities were determined by measuring the radioactivity of ^{36}Cl-labeled perchlorates, $R_4N^*ClO_4$. Two radioactive perchlorates with $R=n$-C_4H_9 and n-C_5H_{11} were obtained in the following manner: nonradioactive perchlorate, which was obtained as a precipitate by mixing an aqueous R_4NCl solution with an aqueous solution of $NaClO_4$ and purified by repeated recrystallization from water, was dissolved in hot water containing a small amount of radioactive K^*ClO_4. The radioactive perchlorate solid was then obtained by cooling the solution. The other two radioactive perchlorates, $(n\text{-}C_6H_{13})_4N^*ClO_4$ and $(n\text{-}C_8H_{17})_4N^*ClO_4$, were obtained by the neutralization of each nonradioactive hydroxide solution, which was prepared by the same procedure as men-

tioned above, with an aqueous solution of $HClO_4$ containing a small amount of K^*ClO_4.

Procedure. The solubilities were determined in the following manner. In a measuring cell (3-cm diameter and 10-cm high) immersed in a constant-temperature bath, each salt was saturated in 10—20 cm^3 of water by vigorous stirring with a magnetic stirrer for 5—30 h. It took more than 20 h until a saturation equilibrium was attained for a sparingly soluble salt like $(n\text{-}C_8H_{17})_4NClO_4$. Then, a given amount of each saturated solution was withdrawn and analyzed by one of the methods listed below according to the magnitude of the solubility values and the types of cations and anions of the samples: (1) determination of the water content using the Karl Fischer titration method; (2) evaporation of water to dryness; (3) titration of either $(n\text{-}C_4H_9)_4N^+$ cation or $(i\text{-}C_5H_{11})_4N^+$ cation with a sodium tetraphenylborate solution;[7] (4) colorimetric determination of the ClO_4^- ion by Methylene Blue-ClO_4^- complex formation;[10] (5) potentiometry using an electrode responding to I^- ion; and (6) an efficiency tracing technique applied to a radioactive ^{36}Cl atom. The Karl Fischer titration was carried out on a MK-II apparatus manufactured by Kyoto Electronics Manufacturing Co. The radioactivity was measured using the TRI-CARB 460C Automatic Liquid Scintillation System manufactured by Packard Instrument Co., Inc. in the same manner as described in the previous papers.[11,12]

The melting points and transition temperatures as well as enthalpies of melting and of transitions were measured using a differential scanning calorimeter, DSC 10 with SSC 580 thermal controller manufactured by Seiko Instruments and Electronics Ltd.

Results and Discussion

(1) Solubilities of a Series of Tetraalkylammonium Salts in Water at 25 °C. The measured solubilities of a series of tetraalkylammonium salts, R_4NX, in water at 25 °C are summarized in Table 1, together with those available in the literature.[8,13-16] For both chlorides and bromides, the solubilities of those with R=$i\text{-}C_5H_{11}$, $n\text{-}C_6H_{13}$, and $n\text{-}C_8H_{17}$, were newly measured in this study. The solubilities of $(i\text{-}C_5H_{11})_4NCl$ and of $(i\text{-}C_5H_{11})_4NBr$ are considerably low compared, for example, with those of $(n\text{-}C_5H_{11})_4NCl$ and of $(n\text{-}C_5H_{11})_4NBr$ since the solid phase which is in equilibrium with a saturated aqueous solution at 25 °C is a clathrate hydrate, $(i\text{-}C_5H_{11})_4NCl(ca.\ 39)H_2O$ and $(i\text{-}C_5H_{11})_4NBr(ca.\ 39)H_2O$,[8] respectively. Three systems, $(n\text{-}C_6H_{13})_4NCl\text{-}H_2O$, $(n\text{-}C_6H_{13})_4NBr\text{-}H_2O$, and $(n\text{-}C_8H_{17})_4NCl\text{-}H_2O$, become a two-liquid phase equilibrium at 25 °C, in which a fairly dilute aqueous solution is in equilibrium with a fairly concentrated solution. The concentrations of both phases are also listed in Table 1. The solubilities of the iodides reported in Table 1 are somewhat different from those reported earlier: 0.0622 $mol \cdot kg^{-1}$ for $(n\text{-}C_4H_9)_4NI$;[17] 2.50×10^{-3} $mol \cdot kg^{-1}$ for $(n\text{-}C_5H_{11})_4NI$.[17]

The solubilities of all the nitrates, R_4NNO_3, were determined for the first time. In all cases, a solid phase was found to be anhydrous through the Karl Fischer titration method. It is interesting to note that the solubilities of nitrates with R=CH_3—$n\text{-}C_4H_9$ are quite high, whereas those of nitrates with R longer than C_5 are quite low. As a result, the solubility of $(n\text{-}C_4H_9)_4NNO_3$ is about 700-times that of $(n\text{-}C_5H_{11})_4NNO_3$. The reason for this will be discussed below.

The solubilities of perchlorates with R=CH_3—$n\text{-}C_4H_9$ are in good agreement with those reported earlier: 0.0747,[15] 0.075,[18] and 0.0753[19] $mol \cdot kg^{-1}$ for $(CH_3)_4NClO_4$; 0.232[15] and 0.217[18] $mol \cdot kg^{-1}$ for $(C_2H_5)_4NClO_4$; 0.0204[18] and 0.0197[19] $mol \cdot kg^{-1}$ for $(n\text{-}C_3H_7)_4NClO_4$; 0.0100[20] and 0.0103[19] $mol \cdot kg^{-1}$ for $(n\text{-}C_4H_9)_4NClO_4$. However, the values reported by Deno et al.,[18] 6.7×10^{-4} $mol \cdot kg^{-1}$ for $(n\text{-}C_5H_{11})_4NClO_4$ and 4.4×10^{-4} $mol \cdot kg^{-1}$ for $(n\text{-}C_6H_{13})_4NClO_4$, are fairly different from our values listed in Table 1. Our values seem to be more exact since a radio tracer technique is appropriate for a determination of such low solubility. The solid phase, which was in equilibrium with the saturated aqueous solution and analyzed by the Karl Fischer titration method, was shown to be anhydrous in all cases. In Table 1, it should be noted that the solubilities of $(i\text{-}C_4H_9)_4NClO_4$ and of $(i\text{-}C_5H_{11})_4NClO_4$

Table 1. Solubilities of Symmetrical Tetraalkylammonium Salts, R_4NX, in Water at 25 °C (in $mol \cdot kg^{-1}$)

R	X				
	Cl	Br	I	NO_3	ClO_4
CH_3	19.06[13]	6.35[14]	0.272[14]	7.12	0.0748
C_2H_5	9.47[13]	14.74[15]	1.75[16]	17.92	0.225
$n\text{-}C_3H_7$	19.00[8]	10.73[8]	0.626[8]	12.42	0.0198
$n\text{-}C_4H_9$	20.53[8]	21.48[8]	0.0658	29.92	0.0106
$i\text{-}C_4H_9$	—	—	—	—	0.0691
$n\text{-}C_5H_{11}$	40.20[8]	0.232[8]	1.80×10^{-3}	0.0428	4.11×10^{-4}
$i\text{-}C_5H_{11}$	0.201[a]	0.095[a]	8.63×10^{-3}	—	1.46×10^{-3}
$n\text{-}C_6H_{13}$	0.088[b] / 6.17	0.019[b] / 9.04	4.5×10^{-4}	7.86×10^{-3}	7.64×10^{-5}
$n\text{-}C_8H_{17}$	5.7×10^{-4}[b] / 15.45	9.0×10^{-5}	8.0×10^{-5}	5.58×10^{-5}	4.31×10^{-6}

This work, except where indicated

a) Solid phase is a clathrate hydrate. b) Two-liquid phase system.

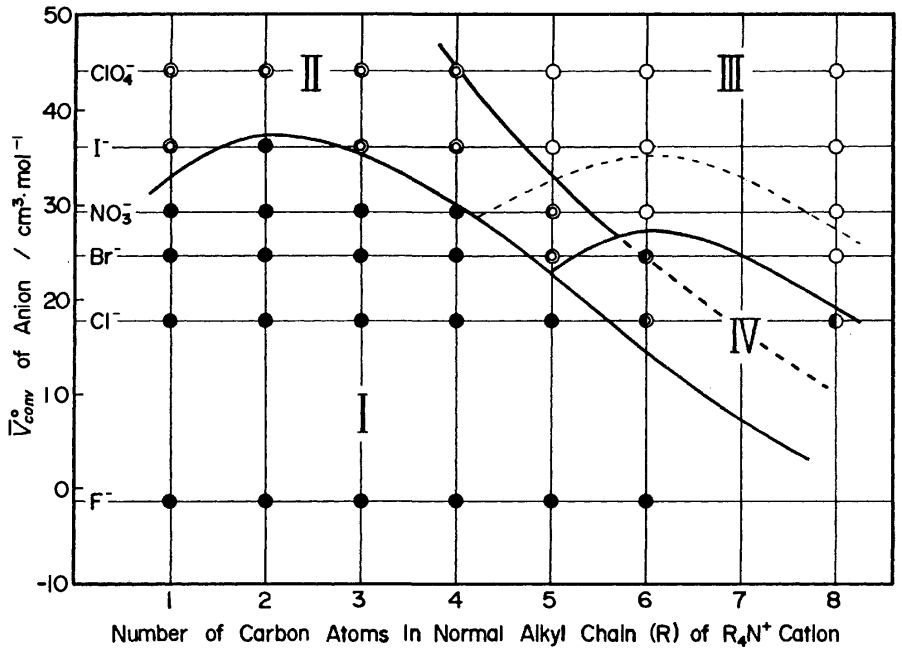

Fig. 1. The relationship between the solubilities of a series of symmetrical tetraalkylammonium salt, R_4NX, in water at 25 °C and the number of carbon atoms in a normal alkyl chain R of the R_4N^+ cation and a conventional partial molar volume of the anion X^- at 25 °C, $\bar{V}^\circ_{conv}$. The solubility of the R_4NX salt is divided into three ranges: ●: higher than 1.0 mol·kg^{-1}; ◎: 0.01—1.0 mol·kg^{-1}; ○: lower than 0.01 mol·kg^{-1}. Three marks ●, ◎, and ○ form the region I, II, and III in this order. The region IV represents a liquid-liquid equilibrium. Precise explanation about the simbols is given in the text.

are about 6.5-times and 3.6-times higher than that of $(n\text{-}C_4H_9)_4NClO_4$ and of $(n\text{-}C_5H_{11})_4NClO_4$, respectively.

The effect of the alkyl chain, R, of the R_4N^+ cation and of the type of the X^- anion on the solubilities of the R_4NX salts in water will be discussed in the following manner. The solubility values are tentatively classified into three concentration ranges: higher than 1.0 mol·kg^{-1}; 0.01—1.0 mol·kg^{-1}; and less than 0.01 mol·kg^{-1}. Using notations ●, ◎, and ○, in this order, all the solubilities of the R_4NX salts, including some fluorides,[8] are represented in Fig. 1. The ordinate of this figure is a conventional partial molar anionic volume at 25 °C, $\bar{V}^\circ_{conv}$, and the abscissa is the number of carbon atoms of a normal alkyl chain R of the R_4N^+ cation. The conventional partial molar anionic volume, i.e., a partial molar anionic volume at infinite dilution based on the assumption that the partial molar volume of a hydrogen ion at infinite dilution is equal to 0, are used as an indication of the effective volume of an anion in a saturated aqueous solution. The values of $\bar{V}^\circ_{conv}$ for the anions discussed in this study are taken from the literature.[21] Symbols ◐ and ◐ in Fig. 1 represent a liquid-liquid phase equilibrium: the mark ◐ indicates a system in which a fairly concentrated solution (in the range of ●, defined above) is in equilibrium with a fairly dilute solution (in the range of ◎); similarly, ◐ indicates a liquid-liquid equilibrium in which the concentration of a dilute solution phase is in the range of ○. It is interesting to note that each symbol (●, ◎, ○, and ◐+◐) gathers within a limited area and forms four domains (I—IV) as shown in Fig. 1. This figure clearly demonstrates the following: (1) that the solubilities of a variety of R_4NX salts in water can be interpreted in terms of two factors, i.e., the chain length of R of the R_4N^+ cation and the molar volume of the X^- anion; (2) as a general trend, the solubility decreases with increasing both the chain length of R and the anionic volume; and (3) the two liquid phase region (IV) appears between region I and III (or II) when the chain length of R becomes fairly long. At 60 °C, for example, domain IV extends to the region shown by a thin dotted line. Tetrahexylammonium salts are most liable to be in a liquid-liquid equilibrium. This would be, at least partly, due to the fact that, for the same kind of anion, the melting points of tetrahexylammonium salts are lower than those both of tetrapentylammonium salts and of tetraoctylammonium salts, as shown below (Table 3).

In Fig. 2, the logarithm of the solubilities (m_{sat}) at 25 °C, given in Table 1, is plotted against the conventional partial molar anionic volumes, $\bar{V}^\circ_{conv}$, for a series of salts having the same R_4N^+ cations. The mark in parenthesis indicates the concentration of a water-rich

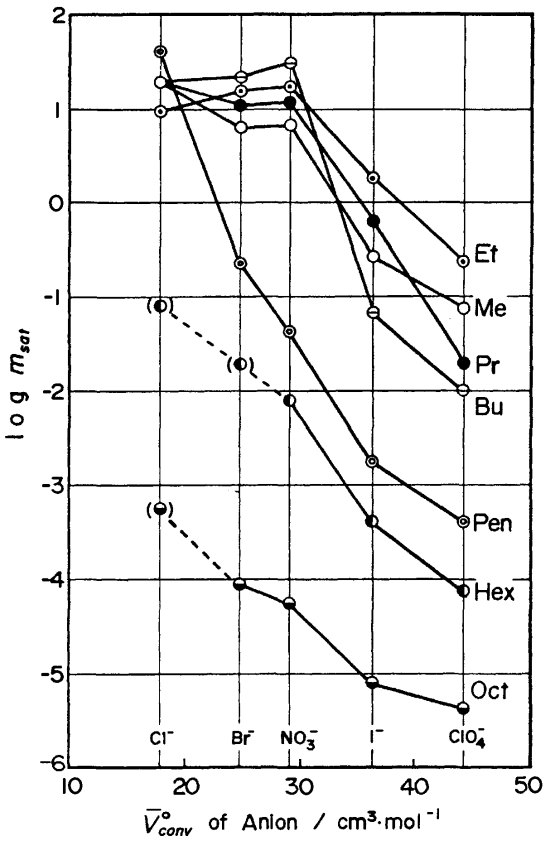

Fig. 2. The relations between the logarithm of the solubilities, m_{sat} (in molality), of a series of R_4NX salts at 25 °C and the conventional partial molar volume of the X^- anion, $\bar{V}^{\circ}_{conv}$. ○: R=CH_3; ⊙: R=C_2H_5; ●: R=n-C_3H_7; ○: R=n-C_4H_9; ◎: R=n-C_5H_{11}; ◐: R=n-C_6H_{13}; ◒: R=n-C_8H_{17}. The symbol in parenthesis represents the concentration of a water-rich phase in a liquid-liquid equilibrium.

phase in a liquid-liquid equilibrium. Generally, as can be seen for tetrahexylammonium and tetraoctylammonium salts, the solubilities of the R_4NX salts decrease with increasing the $\bar{V}^{\circ}_{conv}$. However, it is noteworthy to point out that (1) the solubilities of tetraethylammonium and tetrapropylammonium salts, except for $(C_2H_5)_4NCl$ and $(n\text{-}C_3H_7)_4NClO_4$, are higher than those of tetramethylammonium salts, in consistent with the observation that the "cage-like" water structure (may be pentagonal dodecahedron) around C_2H_5 and n-C_3H_7 group is more stable than that around a CH_3 group. This is verified by the relationship between the melting points of a series of clathrate-like hydrates of $(n\text{-}C_4H_9)_4NOOCR'$ and the chain length of the R′ group.[6] (2) The solubilities of three tetrabutylammonium salts, $(n\text{-}C_4H_9)_4NCl$, $(n\text{-}C_4H_9)_4NBr$, $(n\text{-}C_4H_9)_4NNO_3$, and of $(n\text{-}C_5H_{11})_4NCl$, are extremely high as compared with the values expected from a monotonous relation between log m_{sat} vs. $\bar{V}^{\circ}_{conv}$, in perfect coincidence with the fact that all of these salts can form a stable clathrate-like hydrate.[7,8] In conclusion, the high solubility of R_4NX salts always corresponds to the ability of a clathrate-like hydrate formation. This suggests that the formation of a stable "cage-like" water structure around the R_4N^+ cation greatly contributes to the high solubility of the R_4NX salt.

In Fig. 3, log m_{sat} is plotted against the number of carbon atoms in a normal alkyl chain R in the R_4N^+ cation for a series of salts with voluminous anions NO_3^-, I^-, and ClO_4^-, respectively. Except for $(n\text{-}C_4H_9)_4NNO_3$, whose solubility is remarkably high, all the other salts cannot form a clathrate-like hydrate;[7]

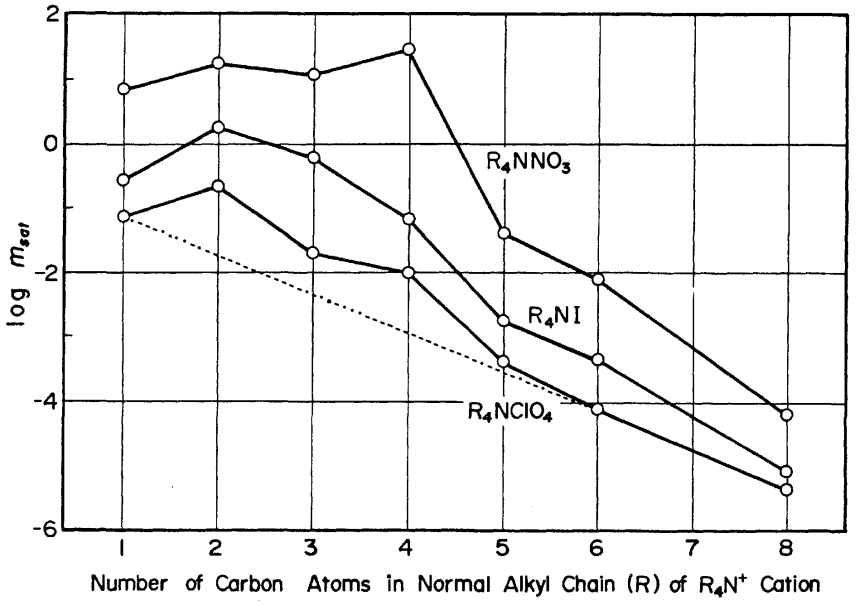

Fig. 3. The relations between the logarithm of the solubilities of a series of R_4NX salts at 25 °C, m_{sat} (in molality), and the number of carbon atoms in a normal alkyl chain R of the R_4N^+ cation. The points corresponding to the salts with the same anions (X=NO_3, I, and ClO_4) are connected by a full line. A dotted line is explained in the text.

Table 2. Solubilities of Symmetrical Tetraalkylammonium Salts, R_4NX, in Water at Various Temperatures

Salt	Solubility m_{sat}/mol·kg^{-1}			
	5 °C	15 °C	35 °C	45 °C
$(i\text{-}C_5H_{11})_4NI$	—	7.60×10^{-3}	1.02×10^{-2}	1.26×10^{-2}
$(n\text{-}C_6H_{13})_4NI$	4.5×10^{-4}	4.1×10^{-4}	6.9×10^{-4}	9.0×10^{-4}
$(CH_3)_4NNO_3$	5.68	6.42	7.92	—
$(C_2H_5)_4NNO_3$	14.71	16.21	19.92	—
$(n\text{-}C_3H_7)_4NNO_3$	8.58	10.42	14.94	—
$(n\text{-}C_4H_9)_4NNO_3$	16.39	22.83	35.75	—
$(n\text{-}C_5H_{11})_4NNO_3$	4.21×10^{-2}	4.11×10^{-2}	4.85×10^{-2}	—
$(n\text{-}C_6H_{13})_4NNO_3$	6.84×10^{-3}	7.34×10^{-3}	—	—
$(n\text{-}C_8H_{17})_4NNO_3$	5.16×10^{-5}	5.46×10^{-5}	6.44×10^{-5}	—
$(CH_3)_4NClO_4$	3.60×10^{-2}	5.17×10^{-2}	0.111	0.148
$(C_2H_5)_4NClO_4$	0.121	0.164	0.318	0.452
$(n\text{-}C_3H_7)_4NClO_4$	1.43×10^{-2}	1.67×10^{-2}	2.59×10^{-2}	3.24×10^{-2}
$(n\text{-}C_4H_9)_4NClO_4$	1.01×10^{-2}	9.95×10^{-3}	1.15×10^{-2}	1.31×10^{-2}
$(i\text{-}C_4H_9)_4NClO_4$	4.51×10^{-2}	5.15×10^{-2}	7.71×10^{-2}	8.74×10^{-2}
$(n\text{-}C_5H_{11})_4NClO_4$	2.59×10^{-4}	3.04×10^{-4}	5.50×10^{-4}	7.66×10^{-4}
$(i\text{-}C_5H_{11})_4NClO_4$	1.37×10^{-3}	1.43×10^{-3}	1.77×10^{-3}	2.25×10^{-3}
$(n\text{-}C_6H_{13})_4NClO_4$	4.85×10^{-5}	5.92×10^{-5}	9.23×10^{-5}	1.40×10^{-4}
$(n\text{-}C_8H_{17})_4NClO_4$	3.27×10^{-6}	3.91×10^{-6}	6.13×10^{-6}	8.01×10^{-6}

i.e., in these solutions a voluminous anion seems to prevent the formation of a stable "cage-like" water structure around the R_4N^+ cation. For the perchlorates, a dotted line is drawn by connecting the point corresponding to R=CH_3 with the points to R=n-C_6H_{13} and n-C_8H_{17}. Generally, for a sparingly soluble salt solution, log m_{sat} is approximately proportional to $\mu_s-\mu^\circ$ divided by $2.303RT$, where μ_s is the chemical potential of a solid salt and μ° is the standard chemical potential of the salt dissolved in water at a hypothetical concentration of 1 mol·kg^{-1}. If a specific phenomenon such as the formation of a "cage-like" water structure around the R_4N^+ cation does not occur, log m_{sat} will change monotonously upon increasing the number of carbon atoms in R, since both μ_s and μ° are expected to change monotonously with the chain length of R. However, the points corresponding to R=C_2H_5, n-C_3H_7, and n-C_4H_9, deviate remarkably from the dotted line. This clearly indicates that the formation of a "cage-like" water structure around such cations as $(C_2H_5)_4N^+$, $(n\text{-}C_3H_7)_4N^+$, and $(n\text{-}C_4H_9)_4N^+$ contributes to the elevation of their solubility. A similar discussion can essentially be made for the behavior of the other two lines for R_4NI and R_4NNO_3 in Fig. 3.

(2) Temperature Dependence of the Solubilities of Symmetrical Tetraalkylammonium Salts in Water. The solubilities of a few tetraalkylammonium iodides and of various nitrates and perchlorates over the temperature range 5—45 °C are listed in Table 2. The values at 25 °C are omitted from this table since they are already listed in Table 1. The solid phases of all the salts were found to be anhydrous from Karl Fischer titration. The system $(n\text{-}C_6H_{13})_4NNO_3$-$H_2O$ became a liquid-liquid equilibrium at temperatures higher than 28.9 °C. In Fig. 4, the logarithm of the solubilities (expressed in molality, m_{sat}) is plotted against the

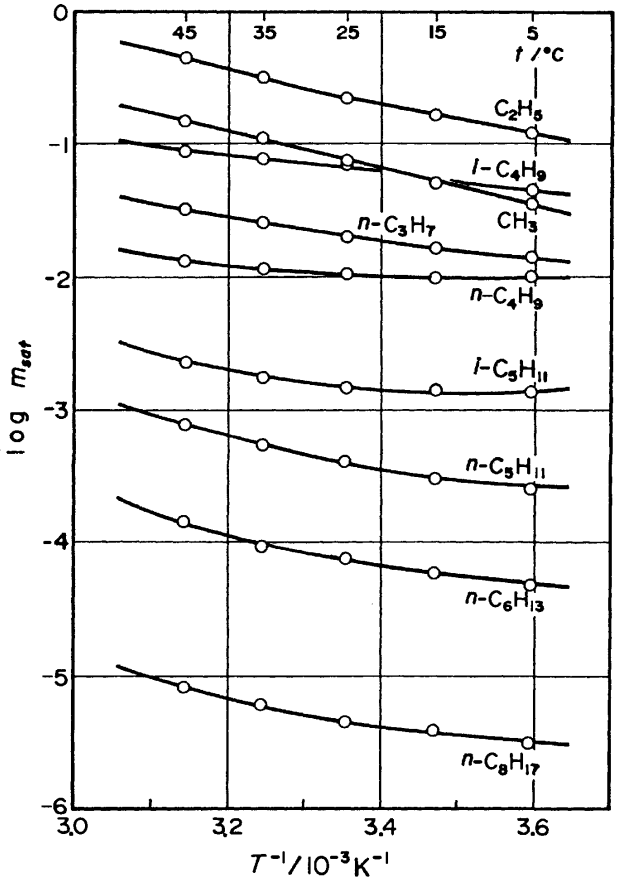

Fig. 4. Temperature dependence of the solubilities of a series of tetraalkylammonium perchlorates, R_4NClO_4, in water. The logarithm of the solubility, m_{sat} (in molality), is plotted against the reciprocal of the absolute temperature. The alkyl group R is shown by each line. The temperature expressed in ordinary Celsius units is shown on the upper side of the figure.

reciprocal of the absolute temperature for a series of tetraalkylammonium perchlorates. A similar plot for the nitrates shows an analogous behavior. This figure clearly indicates that (1) a pronouncely high solubility of tetraethylammonium perchlorate, found at 25 °C as shown in Table 1, is also the case for those at all the temperatures examined; and (2) the slopes $-\partial \log m_{sat}/\partial(1/T)$ for the perchlorates with R=n-C_3H_7, n-C_4H_9, i-C_4H_9, and i-C_5H_{11} at low temperatures are relatively small as compared with those of the other perchlorates, indicating that the enthalpies of solution of these four perchlorates are somewhat small. This may be due to the evolution of heat owing to the formation of a stable "cage-like" water structure around cations like $(n\text{-}C_3H_7)_4N^+$, $(i\text{-}C_4H_9)_4N^+$, $(n\text{-}C_4H_9)_4N^+$, and $(i\text{-}C_5H_{11})_4N^+$ over the temperature range studied. It is interesting to note that this behavior is not eminent for $(C_2H_5)_4NClO_4$ notwithstanding a stable "cage-like" water structure around the $(C_2H_5)_4N^+$ cation is expected as mentioned above. Precise discussion will be impossible since for such a very soluble salt an activity should be used instead of the solubility itself.

(3) Thermodynamic Analysis of the Solubilities of Symmetrical Tetraalkylammonium Salts in Water. If we use a hypothetical liquid supercooled below its melting point as the standard state, the chemical potential of a solid substance at T, μ_2^s, is given by

$$\mu_2^s = \mu_2^l + RT\ln a_2, \quad (1)$$

where μ_2^l is the chemical potential of the standard state, a_2 is the activity of the solute, and R is the gas constant. The quantity $RT\ln a_2$ can be expressed by[22]

$$RT\ln a_2 = -\Delta H_m^F(1-T/T_m) + \Delta C_p(T_m-T) + T\Delta C_p\ln(T/T_m), \quad (2)$$

in which ΔC_p ($=C_p^l-C_p^s$) is the difference of the molar heat capacities between liquid and solid state, and ΔH_m^F is the molar enthalpy of melting at the melting point, T_m.

Under equilibrium conditions between a solid and a saturated aqueous solution,

$$\mu_2^s = \mu_2 = \bar{H}_2 - T\bar{S}_2, \quad (3)$$

where $\bar{H}_2$ and $\bar{S}_2$ are partial molar enthalpy and entropy of a solute, respectively, in a saturated solution. Thus, from Eqs. 1 and 3, together with the relation $\mu_2^l = H_2^l - TS_2^l$, we may write

$$(\bar{H}_2 - H_2^l) - T(\bar{S}_2 - S_2^l) = RT\ln a_2. \quad (4)$$

The enthalpy term in Eq. 4 can be written as

$$\bar{H}_2 - H_2^l = \Delta H_s(\text{sat}) - \Delta H_m^F + \Delta C_p(T_m - T) \quad (5)$$

The term $\Delta H_s(\text{sat})$ ($=\bar{H}_2-H_2^s$) represents the molar enthalpy of solution of a solid substance in a saturated solution.

The entropy term in Eq. 4 may be expressed by[23]

$$\bar{S}_2 - S_2^l = -R\{\nu_+\ln(X_+^{sat}/X_+^l) + \nu_-\ln(X_-^{sat}/X_-^l)\} + S_2^E, \quad (6)$$

where X_+^{sat} and X_-^{sat} is the mole fraction of the cation and the anion, respectively, in a saturated solution, and similarly, X_+^l and X_-^l in a hypothetical melt of a solute. The ν_+ and ν_- are the number of moles of cations and anions, respectively, when one mole of a solute dissociates in the solution. S_2^E is the excess entropy of the solution and Eq. 6 may be regarded as the definition of S_2^E.

By inserting $X_+^{sat}=(\nu_+\cdot m_{sat})/(M+\nu\cdot m_{sat})$, $X_-^{sat}=(\nu_-\cdot$

Table 3. Melting Point (t_m), Transition Temperature (t_{tr}), Enthalpy of Melting (ΔH_m^F), and of Transition(ΔH_{tr}) of Symmetrical Tetraalkylammonium Salts

Salts	t_m / °C	ΔH_m^F / kJ·mol^{-1}	t_{tr} / °C	ΔH_{tr} / kJ·mol^{-1}
$(n\text{-}C_3H_7)_4NNO_3$	>250	—	57.6	8.97
$(n\text{-}C_3H_7)_4NClO_4$	241.0(237—239[18])	14.2	171.0	11.2
			173.5	4.47
$(n\text{-}C_4H_9)_4NI$	146.0(145—147[8])	9.18	116.0	27.1
$(n\text{-}C_4H_9)_4NNO_3$	116.1	15.6	89.1	0.21
$(n\text{-}C_4H_9)_4NClO_4$	214.5(207—209[18])	12.3	56.0	3.10
$(n\text{-}C_5H_{11})_4NI$	134.0(134—135[8])	38.2	121.0	15.2
$(n\text{-}C_5H_{11})_4NNO_3$	110.5	29.4	82.5	11.5
$(n\text{-}C_5H_{11})_4NClO_4$	116.0(110—116[18])	36.1	88.9	16.3
$(i\text{-}C_5H_{11})_4NI$	147.5(146—147[8])	16.0	118.0	23.9
$(i\text{-}C_5H_{11})_4NClO_4$	113.0	22.4	98.0	6.60
$(n\text{-}C_6H_{13})_4NI$	102.5(103—104[8])	17.7	67.5	28.8
			76.0	5.76
$(n\text{-}C_6H_{13})_4NNO_3$	62.0	17.0	44.0	24.8
$(n\text{-}C_6H_{13})_4NClO_4$	104.0(105—106[18])	16.8	58.5	23.3
			81.5	5.88
			93.0	2.02
$(n\text{-}C_8H_{17})_4NCl$	18—19	22.6	—	—
$(n\text{-}C_8H_{17})_4NI$	128.0	48.7	81.5	3.54
$(n\text{-}C_8H_{17})_4NNO_3$	110.5	41.0	101.0	2.33
$(n\text{-}C_8H_{17})_4NClO_4$	134.0	46.5	70.0	4.68

$m_{sat})/(M+\nu\cdot m_{sat})$, $X_+^l=\nu_+/\nu$, and $X_-^l=\nu_-/\nu$ into Eq. 6, we can get

$$\bar{S}_2-S_2^l=-\nu R\ln\{(\nu\cdot m_{sat})/(M+\nu\cdot m_{sat})\}+S_2^E, \quad (7)$$

where $\nu=\nu_++\nu_-$, M=55.51, and m_{sat} is the solubility expressed in molality. Thus, from Eqs. 2, 4, 5, and 7, the following relation is obtained:

$$-\nu RT\ln\{(\nu\cdot m_{sat})/(M+\nu\cdot m_{sat})\}=$$
$$\Delta H_s(sat)-\Delta H_m^F(T/T_m)-T\Delta C_p\ln(T/T_m)-TS_2^E. \quad (8)$$

Furthermore, since most of the symmetrical tetraalkylammonium salts discussed here have transition temperatures (as shown later, Table 3) between room temperature and their melting points, the term $-\sum_{tr}\Delta H_{tr}(T/T_{tr})$ should be added to the right side of Eq. 8, where ΔH_{tr} is the molar enthalpy of a transition at a transition temperature, T_{tr}, and summation is carried out with respect to all the transitions when a solid has more than one transition point between T and T_m. Then Eq. 8 becomes,

$$-\nu RT\ln\{(\nu\cdot m_{sat})/(M+\nu\cdot m_{sat})\}=$$
$$\Delta H_s(sat)-\Delta H_m^F(T/T_m)-\sum_{tr}\Delta H_{tr}(T/T_{tr})-T\Delta C_p\ln(T/T_m)-TS_2^E. \quad (9)$$

In the following discussion, the term containing ΔC_p is omitted for the following reasons: (1) precise information about the values of ΔC_p is not available and (2) the melting points (Table 3) of the salts discussed here are lower than 150 °C, except for $(n\text{-}C_3H_7)_4NClO_4$ and $(n\text{-}C_4H_9)_4NClO_4$, so that the quantity of $\ln(T/T_m)$ is smaller than 0.41 at T=298.15 K. Thus, we use the following equation:

$$-\nu RT\ln\{(\nu\cdot m_{sat})/(M+\nu\cdot m_{sat})\}=$$
$$\Delta H_s(sat)-\{\Delta H_m^F(T/T_m)+\sum_{tr}\Delta H_{tr}(T/T_{tr})\}-TS_2^E. \quad (10)$$

The melting points, transition temperatures, the enthalpy of melting, and the enthalpy of transition which are determined by differential scanning calorimetry are listed in Table 3, together with some of the melting points reported in the literature. The errors inherent in the determination of the enthalpies of melting and transition are of the order of 5—10 per cent, since calibration of the apparatus was carried out at the melting point of In alone (156.6 °C, and ΔH_m^F=3.3 kJ·mol^{-1}). No transition temperatures and enthalpy data had been reported earlier. For the salts whose ΔH_s(sat) data are available, each term in Eq. 10 at 298.15 K can be calculated from the data given in Tables 1—3; these are listed in Table 4. The ΔH_s(sat) values in Table 4 are either the values obtained by Krishnan et al.[24] or values calculated from the relation $\Delta H_s(sat)=-2R\partial\ln m_{sat}/\partial(1/T)$ using the data shown in Tables 1 and 2. This calculation is reasonable, at least to a first approximation, since this relation was only applied to sparingly soluble salts. The values obtained by Krishnan et al.[24] are based upon the enthalpies of solution in propylene carbonate and the enthalpy of transfer from propylene carbonate to water. Therefore, these values are not exactly equal to the enthalpy of solution of the solid salt at its saturation concentration. However, we use these values as approximate values of ΔH_s(sat) since there are no data available and the other terms listed in Table 4, especially the one containing ΔH_m^F and ΔH_{tr}, are not so accurate.

It is interesting to note that, for the most iodides and perchlorates, the quantity ΔH_s(sat) is almost compensated for by the quantity $\Delta H_m^F(T/T_m)+\sum_{tr}\Delta H_{tr}(T/T_{tr})$, resulting in a large positive value of the $-\nu RT\ln\{(\nu\cdot m_{sat})/(M+\nu\cdot m_{sat})\}$ term corresponds roughly to a large negative value of the excess entropy TS_2^E. In case of the nitrates, not only the values of the ΔH_s(sat) term are generally smaller than the term $\Delta H_m^F(T/T_m)+\sum_{tr}\Delta H_{tr}(T/T_{tr})$, but also the term $-\nu RT\ln\{(\nu\cdot m_{sat})/(M+\nu\cdot m_{sat})\}$ is rather small compared with those of iodides

Table 4. Each Term in Eq. 10 and Calculated Values of Excess Entropy at 298.15 K for Some Symmetrical Tetraalkylammonium Salts

Salt	(A)[a]	ΔH_s(sat)	(B)[b]	S_2^E	S_2^E/n
	kJ·mol^{-1}			J·K^{-1}·mol^{-1}	
$(n\text{-}C_3H_7)_4NClO_4$	35.8	27.2[24]	18.7	−92	−7.7
$(n\text{-}C_4H_9)_4NI$	29.8	17.7[24]	27.3	−132	−8.3
$(n\text{-}C_4H_9)_4NClO_4$	39.0	10.8[24]	10.3	−129	−8.1
$(n\text{-}C_5H_{11})_4NI$	47.8	34.5[24]	39.5	−177	−8.9
$(n\text{-}C_5H_{11})_4NNO_3$	32.1	13.0	32.5	−173	−8.7
$(n\text{-}C_5H_{11})_4NClO_4$	55.4	43.0[24]	41.1	−180	−9.0
$(i\text{-}C_5H_{11})_4NI$	40.3	17.4	29.5	−176	−8.8
$(i\text{-}C_5H_{11})_4NClO_4$	48.8	14.4	22.6	−191	−9.6
$(n\text{-}C_6H_{13})_4NI$	55.2	38.3	44.1	−205	−8.5
$(n\text{-}C_6H_{13})_4NNO_3$	40.5	10.5	38.5	−230	−9.6
$(n\text{-}C_6H_{13})_4NClO_4$	63.5	33.7	40.7	−237	−9.9
$(n\text{-}C_8H_{17})_4NNO_3$	65.0	15.5	33.8	−280	−8.8
$(n\text{-}C_8H_{17})_4NClO_4$	77.8	36.6	38.1	−266	−8.3

a) (A)$=-\nu RT\ln\{(\nu\cdot m_{sat})/(M+\nu\cdot m_{sat})\}$. b) (B)$=\Delta H_m^F(T/T_m)+\sum_{tr}\Delta H_{tr}(T/T_{tr})$.

and perchlorates with the same type of cation because of relatively high solubility of the nitrates (Table 1). Eventually, this situation also results in a large negative excess entropy. The values of S_2^E calculated from Eq. 10 are also listed in Table 4. It is interesting to note that (1) the S_2^E becomes more negative upon increasing the number of carbon atoms of the R_4N^+ cation and (2) for the same kind of cation S_2^E has almost a similar value, irrespective of the kind of anion. This result suggests that the value of S_2^E is mainly determined by the number of carbon atoms of the R_4N^+ cation. Tentatively, if we calculate the excess entropy per mole of carbon atoms, S_2^E/n, n being the total number of carbon atoms of the R_4N^+ cation, this value has almost a similar value ranging from -8 to -10 $J \cdot mol^{-1} \cdot K^{-1}$ for all the salts examined here. This value is also listed in the last column of Table 4. The simple average of S_2^E/n is -8.8 $J \cdot mol^{-1} \cdot K^{-1}$. Although a quantitative discussion about the behavior of the excess entropy is impossible at present, the behavior of S_2^E (or of S_2^E/n) found in this study will undoubtedly reflect a restricted motion of the carbon chain of the R_4N^+ cation in the solution due to the water networks surrounding the R_4N^+ cation. Unfortunately, it is impossible to discuss the relation between a "cage-like" water structure and the excess entropy defined here, since S_2^E cannot be calculated (for the reasons mentioned below) for many tetraalkylammonium salts to which the existence of a stable "cage-like" water structure in its aqueous solution is expected. The reasons are: (1) a value for ΔH_s(sat) is not available in the literature and its estimation from the temperature dependence of the solubility is inadequate because of the high solubility of the salt concerned, and (2) in general, such a salt has a fairly high melting point and sometimes gradually decomposes at high temperatures, so that accurate values of T_m and ΔH_m^F (and T_{tr} and ΔH_{tr}) cannot be obtained by thermal analyses.

The present work was partially supported by a Grant-in-Aid for Scientific Research (No. 60470006) from the Ministry of Education, Science and Culture.

References

1) H. S. Frank and W-Y. Wen, *Discuss. Faraday Soc.*, **24**, 133 (1957).
2) D. L. Fowler, W. V. Loebenstein, D. B. Pall, and C. A. Kraus, *J. Am. Chem. Soc.*, **62**, 1140 (1940).
3) R. K. McMullan, M. Bonamico, and G. A. Jeffrey, *J. Chem. Phys.*, **39**, 3295 (1963).
4) M. Bonamico, G. A. Jeffrey, and R. K. McMullan, *J. Chem. Phys.*, **37**, 2219 (1962).
5) D. Feil and G. A. Jeffrey, *J. Chem. Phys.*, **35**, 1863 (1961).
6) H. Nakayama and S. Torigata, *Bull. Chem. Soc. Jpn.*, **57**, 171 (1984).
7) H. Nakayama, *Bull. Chem. Soc. Jpn.*, **56**, 877 (1983).
8) H. Nakayama, *Bull. Chem. Soc. Jpn.*, **54**, 3717 (1981).
9) H. Nakayama, *Bull. Chem. Soc. Jpn.*, **60**, 2319 (1987).
10) I. Iwasaki, S. Utsumi, and C. Kang, *Bull. Chem. Soc. Jpn.*, **36**, 325 (1963).
11) H. Matsui and H. Nakayama, *Bull. Chem. Soc. Jpn.*, **57**, 2663 (1984).
12) H. Nakayama, K. Tsunakawa, M. Kanō, and H. Matsui, *Bull. Chem. Soc. Jpn.*, **60**, 1585 (1987).
13) S. Lindenbaum and G. E. Boyd, *J. Phys. Chem.*, **68**, 911 (1964).
14) B. J. Levin, *Aust. J. Chem.*, **18**, 1161 (1965).
15) A. Giacomelli and R. Menicagli, *Ann. Chim.*, **59**, 860 (1969).
16) C. J. Peddle and W. E. S. Turner, *J. Chem. Soc.*, **103**, 1202 (1913).
17) F. Frank and D. L. Clarke, *J. Phys. Chem.*, **71**, 1155 (1967).
18) N. C. Deno and H. E. Berkheimer, *J. Org. Chem.*, **28**, 2143 (1963).
19) C. L. de Ligny, D. Bax, M. Alfenaar, and M. G. L. Elferink, *Recl. Trav. Chim. Pays-Bas*, **88**, 1183 (1969).
20) J. Steigman and J. Dobrow, *J. Phys. Chem.*, **72**, 3424 (1968).
21) F. J. Millero, "The Partial Molal Volumes of Electrolytes in Aqueous Solutions," in "Water and Aqueous Solutions," ed by R. A. Horne, Wiley-Interscience, London (1972), Chap. 13, pp. 519—595.
22) J. H. Hildebrand and R. L. Scott, "Regular Solutions," Prentice-Hall Inc., Englewood Cliffs, New Jersey (1962).
23) H. Nakayama, *Bull. Chem. Soc. Jpn.*, **44**, 1709 (1971).
24) C. V. Krishnan and H. Friedman, *J. Phys. Chem.*, **73**, 3934 (1969).

 © 1989 The Chemical Society of Japan Bull. Chem. Soc. Jpn., 62, 993—998 (1989)

A Least-Squares Method for Computing Rate Constants of Reversible, First-Order, Triangular Network Reactions and Its Application to the Intermolecular Rearrangements of Acetylacetonatobis(4,4,4-trifluoro-1-phenyl-1,3-butanedionato)ruthenium(III)

Yoshimasa HOSHINO, Ryouta TAKAHASHI, Kunio SHIMIZU, Gen P. SATÔ,* and Koichi AOKI†
Department of Chemistry, Faculty of Science, Sophia University, Kioicho, Chiyoda-ku, Tokyo 102
†Department of Electronic Chemistry, Graduate School at Nagatsuta, Tokyo Institute of Technology, Midori-ku, Yokohama 227
(Received August 31, 1988)

A useful method for computing the rate constants of reversible, first-order, triangular network reactions ($\mathbf{B}_1 \rightleftarrows \mathbf{B}_2$, $\mathbf{B}_2 \rightleftarrows \mathbf{B}_3$, $\mathbf{B}_3 \rightleftarrows \mathbf{B}_1$) is developed. It gives the best-fit set of the rate constants from the experimental data of the equilibrium constants and the mole fraction-time curves through an iterative least-squares method. This type of reaction can be classified into three categories for different shapes of the mole fraction-time curves. The method was successfully applied to determining the rate constants of the rearrangement reactions among the three isomers of [Ru(acac)(tfpb)$_2$] (acac$^-$=acetylacetonate ion, tfpb$^-$=4,4,4-trifluoro-1-phenyl-1,3-butanedionate ion) in *N,N*-dimethylformamide at 90 °C. The direct conversion between the *de,fc*-bis(tfpb) isomer and the *cf,ed*-bis(tfpb) isomer was forbidden. The twist mechanisms are incompatible with this fact.

The simplest network reaction is a first-order reversible reaction of three components with a triangular scheme, exemplified by isomerization of butene[1] and cobalt complexes.[2,3] A theory of the triangular network reaction has been fully developed by Wei and Prater.[1] Numerical methods for determining rate constants have been presented in a detailed review.[4] Since the differential equations for the kinetics is linear, the solution is composed of a sum of exponential terms.[5] In order to evaluate rate constants from experimental data through combinations of exponential functions, it is necessary to linearize the equation. The numerical method of Wei and Prater[1] is essentially based on the linearization around the equilibrium. Consequently, a number of accurate data points near the equilibrium are required for the determination of rate constants. Such data are difficult to obtain when the experimental precision is limited by the presence of side reactions or for other reasons; besides, a sufficient number of such data are rarely available if the reaction is very slow. Furthermore, this numerical method does not give the absolute values of the rate constants, but only their ratios. It is desirable to explore a technique that gives the absolute values of rate constants making use of all the experimental points.

This report is devoted to development of a numerical technique based on nonlinear regression and to the evaluation of the rate constants of the triangular network of a set of the isomers of β-diketonato-ruthenium(III) complexes.

Theoretical

Figure 1 illustrates the reaction scheme of the triangular network, where k_{ij} is the rate constant of the reaction $\mathbf{B}_i \rightarrow \mathbf{B}_j$. We denote the mole fraction of species $\mathbf{B}_j$ by x_j. Then kinetic equations for the triangular reaction are

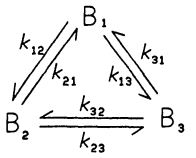

Fig. 1. Model of the triangular network reversible reaction. The equilibrium constants are defined in Eq. 5.

$$dx_1/dt = -(k_{12}+k_{13})x_1 + k_{21}x_2 + k_{31}x_3 \quad (1)$$
$$dx_2/dt = k_{12}x_1 - (k_{21}+k_{23})x_2 + k_{32}x_3 \quad (2)$$
$$dx_3/dt = k_{13}x_1 + k_{23}x_2 - (k_{31}+k_{32})x_3, \quad (3)$$

where t is the time since the beginning of the reaction. The initial conditions are given by

$$t=0: x_1=x_1^0,\ x_2=x_2^0,\ x_3=x_3^0. \quad (4)$$

Here x_j^0 is the initial mole fractions of species $\mathbf{B}_j$. We define the following three equilibrium constants:

$$K_{12} = x_2^e/x_1^e = k_{12}/k_{21}$$
$$K_{23} = x_3^e/x_2^e = k_{23}/k_{32} \quad (5)$$
$$K_{31} = x_1^e/x_3^e = k_{31}/k_{13}.$$

The superscript e means the equilibrium. An alternative form of Eq. 5 is

$$x_1^e = (1+K_{12}+1/K_{31})^{-1}$$
$$x_2^e = (1+K_{23}+1/K_{12})^{-1} \quad (6)$$
$$x_3^e = (1+K_{31}+1/K_{23})^{-1}.$$

Obviously only two of the three equilibrium constants are independent because $K_{12}K_{23}K_{31}=1$. Hence the following relation holds:

$$k_{12}k_{23}k_{31} = k_{13}k_{32}k_{21}, \quad (7)$$

The initial problem of Eqs. 1—4 can be solved by means of a conventional method, e.g., the Laplace transformation, although it is cumbersome to elim-

inate two of the three dependent variables. The solution is expressed by

$$x_j = x_j^e + r_j e^{-pt} + s_j e^{-qt}, \quad (j=1, 2, 3) \tag{8}$$

with

$$p = \{\alpha - (\alpha^2 - 4\beta)^{1/2}\}/2 \tag{9}$$

$$q = \{\alpha + (\alpha^2 - 4\beta)^{1/2}\}/2 \tag{10}$$

$$r_j = (x_j^0 p - \kappa_j + \lambda_j/p)/(p-q) \tag{11}$$

$$s_j = (x_j^0 q - \kappa_j + \lambda_j/q)/(q-p),$$

where

$$\kappa_1 = x_1^0(k_{21}+k_{23}+k_{32}+k_{31}) + x_2^0 k_{21} + x_3^0 k_{31} \tag{12a}$$

$$\kappa_2 = x_1^0 k_{12} + x_2^0(k_{12}+k_{13}+k_{31}+k_{32}) + x_3^0 k_{32} \tag{12b}$$

$$\kappa_3 = x_1^0 k_{13} + x_2^0 k_{23} + x_3^0(k_{12}+k_{21}+k_{23}+k_{13}) \tag{12c}$$

$$\lambda_1 = k_{31}k_{21} + k_{23}k_{31} + k_{32}k_{21} \tag{13a}$$

$$\lambda_2 = k_{12}k_{32} + k_{31}k_{12} + k_{13}k_{32} \tag{13b}$$

$$\lambda_3 = k_{23}k_{13} + k_{12}k_{23} + k_{21}k_{13} \tag{13c}$$

$$\alpha = k_{12}+k_{21}+k_{23}+k_{32}+k_{31}+k_{13} \tag{14}$$

$$\beta = k_{12}k_{23}/x_3^e + k_{23}k_{31}/x_1^e + k_{31}k_{12}/x_2^e. \tag{15}$$

A characteristic of Eq. 8 is that the arguments of the exponential are common to the three species. A set of these equations are essentially the same as Wei and Prater's matrix expression.[2]

Examples of the x_j-t curves calculated for the case where $K_{12}=K_{23}=K_{31}$, $x_1^0=1$, and $x_2^0=x_3^0=0$ are shown in Fig. 2. Here the three sets of the curves represent the following typecal cases:

(A) When the values of k_{ij} is comparative (the solid curves), x_2 and x_3 increase monotonically at the sacrifice of x_1 and then approach the equilibrium values. The rate of the decrease of x_1 is almost the same as the sum of the rates of the increase of x_2 and x_3. A special case is that all the values of k_{ij} are the same. Then Eq. 8 reduces to

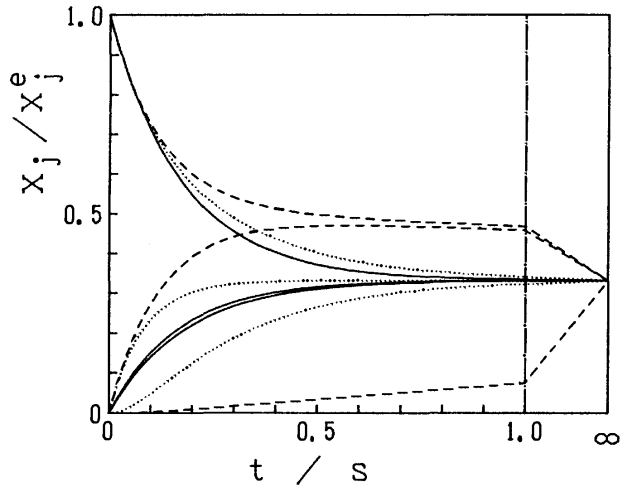

Fig. 2. Variations of x_j (j=1,2,3) with time at K_1=K_2=K_3=1 calculated from Eqs. 8—15 for (k_{12}, k_{23}, k_{31})=(2.0, 2.0, 1.8)(——), (4.0, 4.0, 0.0)(·····) and (4.0, 0.2, 0.0)(-----). The initial conditions are x_1^0=1.0, x_2^0=0, and x_3^0=0.

$$x_j = 1/3 + (x_j^0 - 1/3)\exp[-3k_{ij}t]. \tag{16}$$

Then the overall relaxation time is $1/(3k_{ij})$.

(B) When both k_{12} and k_{23} are large and k_{31} is small (the dotted curves), $\mathbf{B}_3$ is generated through $\mathbf{B}_2$ without direct supply from $\mathbf{B}_1$. The increase of x_3 is slower than that of x_2. Since x_3 increases very slowly at the beginning, the curve for x_3 is a sigmoid. In an extreme case where $k_{31}=k_{13}=0$, the network reduces to a two-step consecutive reaction.

(C) When k_{12} is large and both k_{23} and k_{31} are small (the dashed curves), $\alpha^2 \gg 4\beta$ or $q \gg p$. Then the mole fractions vary mainly with $\exp(-\alpha t)$ or $\exp[-(k_{12}+k_{21})]$. In this case, x_1 and x_2 converge before reaching the equilibrium value.

Let us explore a technique of determining the rate constants from a set of experimental x_j curves. It is assumed that the equilibrium constants are known in advance. Then the unknown parameters are k_{12}, k_{23}, and k_{31}. It is possible to use any other three independent parameters composed of adequate combinations of k_{12}, k_{23}, and k_{31}: for example (α, β, κ_1) or (p, q, r_1). Choice of the independent parameters is important for successful curve fitting. We chose (p, q, r_1), because this set is directly connected with the shape of the x_j-t curves.

A convenient numerical technique of curve fitting is the least squares method.[6] Since Eq. 8 is nonlinear with respect to p, q, and r_1, it has to be linearized. The Taylor expansion of Eq. 8 is carried out around a set of tentative values of p', q', and r_j'. Retaining only the linear terms, one has

$$x_j = x_j^e + (x_j^0 - x_j^e)e^{-q't} - (e^{-p't} - e^{-q't})r_j + r_j' te^{-p't}(p-p') - (x_j^0 - x_j^e + r_j')te^{-q't}(q-q'). \tag{17}$$

The sum of squares of the differences between Eq. 17 and the experimental values for each x_j-t curve is $\sum(x_j - x_{jn})^2$, where x_{jn} is the value of x_j at the n-th experimental point. The minimum condition for the total sum of squares of a set of three x_j-t curves is give by Eq. 18 (note that the adjustable parameters are p, q, r_1, r_2, and r_3).

$$\sum_{j=1}^{3}[\partial\sum_n(x_j - x_{jn})^2/\partial p + \partial\sum_n(x_j - x_{jn})^2/\partial q + \partial\sum_n(x_j - x_{jn})^2/\partial r_j] = 0. \tag{18}$$

The values of p, q, r_1, r_2, and r_3 that minimize the total sum of squares for a given set of p', q', r_1', r_2', and r_3' are determined by solving Eq. 18. These values are inserted into Eq. 17 in place of p', q', r_1', r_2', and r_3'. By solving the resultant equation, a new set of p, q, r_1, r_2, and r_3 that gives a better fitting will be obtained. This procedure is repeated until the values of these parameters converge. The convergence naturally depends on how the values of the first set of p', q', r_1', r_2', and r_3' are close to the final values; too unrealistic initial values may result in divergence. A method of determining the initial values will be described in

Results and Discussion. Equation 18 is rewritten as

$$\mathrm{D}\begin{pmatrix} p \\ q \\ r_1 \\ r_2 \\ r_3 \end{pmatrix} = \mathrm{F}\begin{pmatrix} p' \\ q' \\ r_1' \\ r_2' \\ r_3' \end{pmatrix} \quad (19)$$

Here D is a symmetric square matrix with five columns. The element of D at the h-th column and the m-th line is given by $\sum_n \sum_j a_h a_m$ (j=1,2,3; h=1,2,···,5; m=1,2,···,5), where

$$\begin{aligned} a_1 &= -r_j' t_n \exp(-p' t_n) \\ a_2 &= -\{x_j^0 - x_j^e - r_j'\} t_n \exp(-q' t_n) \\ a_3 &= a_4 = a_5 = \exp(-p' t_n) - \exp(-q' t_n) \end{aligned} \quad (20)$$

and F is a diagonal matrix the element of which at the m-th column, b_m (m=1,2,···,5) is given by

$$b_m = \sum_{j=1}^{3} \sum_n [x_j^e + r_j' \exp(-p' t_n) - x_{jn} + \{x_j^0 - x_j^e - r_j'\} \exp(-q' t_n)] a_m. \quad (21)$$

Equation 19 is the simultaneous equation for p, q, r_1, r_2, and r_3. Its solution and the iteration can be executed on a personal computer. An example of estimation of the initial values of p', q', r_1', r_2', and r_3' is given below.

Experimental

Chemicals. The following three geometrical isomers of acetylacetonatobis(4,4,4-trifluoro-1-phenyl-1,3-butanedionato)ruthenium(III) were prepared and isolated according to the procedure described previously:[7] *ab*-acetylacetonato-*de*,*fc*-bis(4,4,4-trifluoro-1-phenyl-1,3-butanedionato)ruthenium(III) (**B**$_1$), *ab*-acetylacetonato-*cf*,*de*-bis(4,4,4-trifluoro-1-phenyl-1,3-butanedionato)ruthenium(III) (**B**$_2$), and *ab*-acetylacetonato-*cf*,*ed*-bis(4,4,4-trifluoro-1-phenyl-1,3-butanedionato)ruthenium(III) (**B**$_3$). Deionized water (Barnstead, NANOpure) was used, and the other solvents were of liquid-chromatographic grade unless otherwise stated.

Chromatography. High-pressure liquid chromatography was conducted on a Toyo Soda CCPM liquid chromatograph with a Toyo Soda UV-8000 ultraviolet-visible detector operating at 304 nm. The three isomers were separated on a silanised silica gel column (250 mm length, 4 mm internal diameter; Merck LiChrosorb RP-18, particle size 5 μm) by a mixture or methanol-water-acetonitrile (8:3:2 by volume) at a flow rate of 1 cm^3 min^{-1}. Retention time were 19 min for **B**$_3$, 20 min for **B**$_2$, and 23 min for **B**$_1$.

The peak area (defined as the product of the peak hight and the half-peak width) was proportional to the amount of each isomer. The mole fractions of the isomers in the reaction mixtures were determined by means of calibration curves drawn for a standard series of mixtures prepared gravimetrically from the isolated samples of the isomers.

Kinetic Measurement. Each of the isomers (**B**$_1$, 3.87×10^{-5} mol; **B**$_2$, 4.02×10^{-5} mol; **B**$_3$, 2.29×10^{-5} mol) was dissolved in 50 cm^3 of *N*,*N*-dimethylformamide (DMF) of the spectrophotometric grade (Dojindo Laboratories, Dotite Spectrosol). Forty five 0.1 cm^3 aliquots of each solution were transferred into glass tubes of 1.5 mm internal diameter. After the contents were deoxygenated by passing argon through a glass capillary for 1 min, the tubes were sealed in a flame and mounted on a holder. During these operations, the solutions were cooled with ice-water. The reaction was started by immersing the holder with 135 tubes into an oil bath (Thomas Kagaku Thermostatic Oil Bath, T-201) maintained at (90±0.1) °C. Three tubes, one for each starting isomer, were removed from the oil bath at certain time intervals and immediately quenched in ice-water. Each tube was then cut open, and a 2 mm^3 portion of its content was injected into the chromatograph.

The mole fractions of the three isomers under equilibrium conditions were determined in a similar manner when the reaction mixtures were allowed to stand at 90 °C until no further change was detected (2—3 days).

No indication of any side reactions was observed.

Results and Discussion

The three equilibrium constants are presented in Table 1. They were independent of the starting species and are not far from the statistical values (4:1:2).

Figures 3a, 3b, and 3c show variations of x_j with the time when starting species are **B**$_1$, **B**$_2$, and **B**$_3$, respectively. Evidently, the reactions **B**$_1$→**B**$_3$ and **B**$_3$→**B**$_1$ are slower than the other reactions, and the reaction **B**$_2$→**B**$_3$ is slower than the reaction **B**$_2$→**B**$_1$. The curves in Fig. 3a are essentially similar to the dotted curves in Fig. 2, suggesting that the reaction belongs to case (B).

The initial values of parameters p', q', r_1', r_2', and r_3' were determined as follows. If $q \gg p$, plot of $\ln(x_{jn} - x_j^e)$ against t_n at long times should fall on a straight line, of which slope and intercept give approximate values of p and r_j, respectively. The plots for the three curves with x_j^0=1 in Figs. 3a, 3b, and 3c are straight lines (Fig. 4), although their slopes are not quite the same. We took the slope of the line corresponding to Fig. 3a (circles in Fig. 4) as the initial value of p' and its intercepts as the initial value of r_1'. The initial value of q' was set to be twice the initial value of p' and r_2'=r_3'=0 (there was no particular reason for this choice). The values of p, q, r_1, r_2, r_3 for the data of Fig. 3a were successfully determined by inserting these initial values into Eqs. 19—21 and executing the iteration.

The same procedure was applied to the data of Figs. 3b and 3c. Values of the five parameters thus obtained are listed in Table 2. From these values, three sets of κ_j were calculated by means of the following equation:

Table 1. Equilibrium Constants[a)]

Starting species	$K_{12}=x_2^e/x_1^e$	$K_{23}=x_3^e/x_2^e$	$K_{31}=x_1^e/x_3^e$	Number of runs
B$_1$	1.820 (0.059)	0.677 (0.018)	0.813 (0.014)	3
B$_2$	1.799 (0.086)	0.665 (0.044)	0.839 (0.037)	4
B$_3$	1.823 (0.054)	0.694 (0.044)	0.792 (0.027)	2
Average	1.811 (0.064)	0.675 (0.034)	0.820 (0.032)	

a) Values in the parentheses are standard deviations.

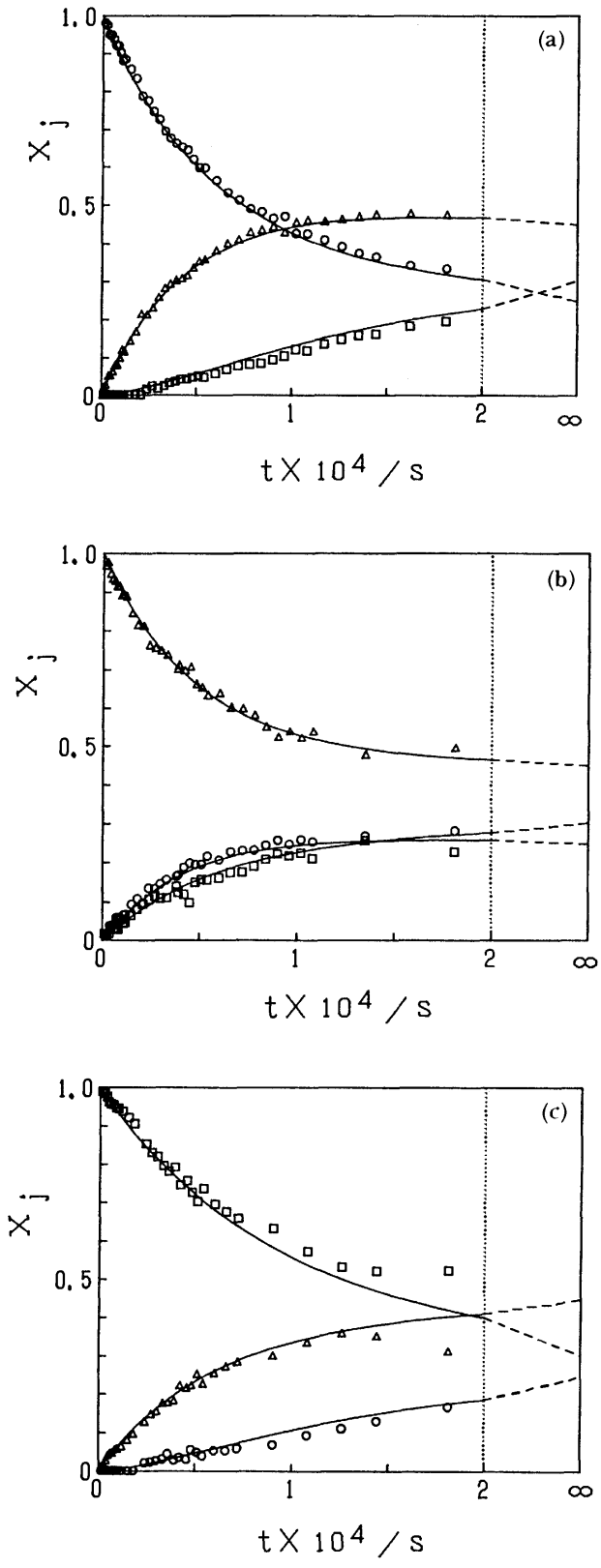

Fig. 3. Variations of mole fractions, x_j (j=1,2,3), for $\mathbf{B}_1$(○), $\mathbf{B}_2$(△), and $\mathbf{B}_3$(□) with time. Starting species are $\mathbf{B}_1$(a), $\mathbf{B}_2$(b), and $\mathbf{B}_3$(c). Solid lines are simulated curves calculated from Eqs. 8—15 at the following values: K_{12}=1.811, K_{23}=0.675, K_{31}=0.820, k_{12}=1.228×10^{-4} s^{-1}, k_{23}=0.476×10^{-4} s^{-1}, and k_{31}=0.027×10^{-4} s^{-1}.

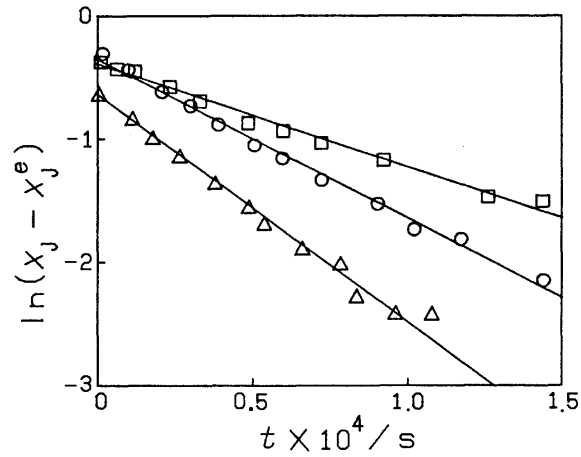

Fig. 4. Logarithmic plots of deviation of the mole fraction from the equilibrium against the time. Symbols ○, △, and □ correspond respectively to data ○ in Fig. 3a, data △ in Fig. 3b, and data □ in Fig. 3c.

Table 2. Auxiliary Kinetic Parameters Required for Determination of k_{ij}

Starting species	$p\times10^4$ / s^{-1}	$q\times10^4$ / s^{-1}	r_1	r_2	r_3
$\mathbf{B}_1$	0.863	2.116	0.333	0.177	−0.510
$\mathbf{B}_2$	0.681	2.266	0.078	0.066	−0.144
$\mathbf{B}_3$	0.584	2.875	−0.286	−0.236	0.522

Table 3. Linearly Combined Rate Constants, κ_j

Starting species	$\kappa_1\times10^4$ / s^{-1}	$\kappa_2\times10^4$ / s^{-1}	$\kappa_3\times10^4$ / s^{-1}
$\mathbf{B}_1$	1.805	1.171	0.002
$\mathbf{B}_2$	0.685	1.803	0.459
$\mathbf{B}_3$	0.058	0.750	2.650

$$\kappa_j = x_j^0(p+q) - pr_j - q(x_j^0 - x_j^e - r_j), \qquad (22)$$

which has been derived from Eq. 11 by eliminating λ_j. The values of κ_j are listed in Table 3. Since κ_j is the linear combinations of k_{12}, k_{23}, and k_{31} (Eq. 12), the rate constants can be immediately estimated: κ_2 for $\mathbf{B}_1$ (1.2×10^{-4} s^{-1}) is $x_1^0k_{12}$, while κ_1 for $\mathbf{B}_2$ (0.68×10^{-4} s^{-1}) is $x_2^0k_{21}$, and so forth. However, the k values obtained in this way are not consistent. For example, the calculated values of k_{12} and k_{21} do not satisfy k_{12}/k_{21}=1.811 (=K_{12}). There are nine known values for κ_j from which three k's are to be determined. This redundancy can be effectively utilized for increasing the precision of the computation in the following way.

Let us consider a three-dimensional space (k_{12}, k_{23}, k_{31}). Each κ_j value is represented as a plane in this space. The most probable values of k_{12}, k_{23}, and k_{31} will be given by the coordinates of the center of the polyhedron defined by the nine κ_j planes. The center is the point where the total sum of squares of the distances between that point and the nine planes is a

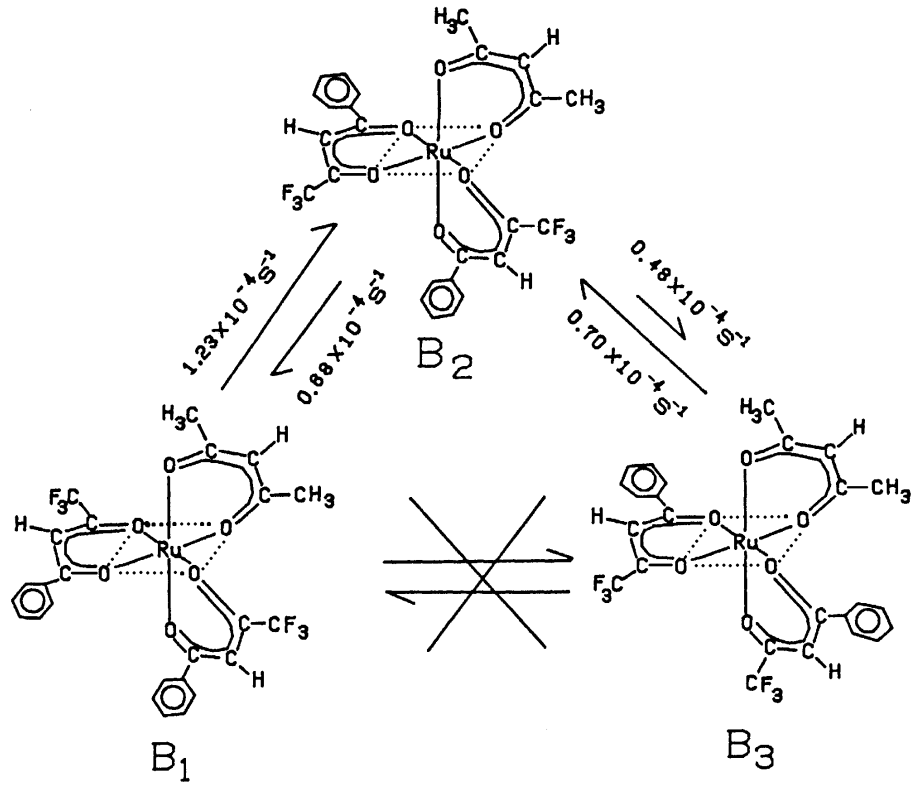

Fig. 5. Kinetic parameters for the isomerization of [Ru(acac)(tfpb)].

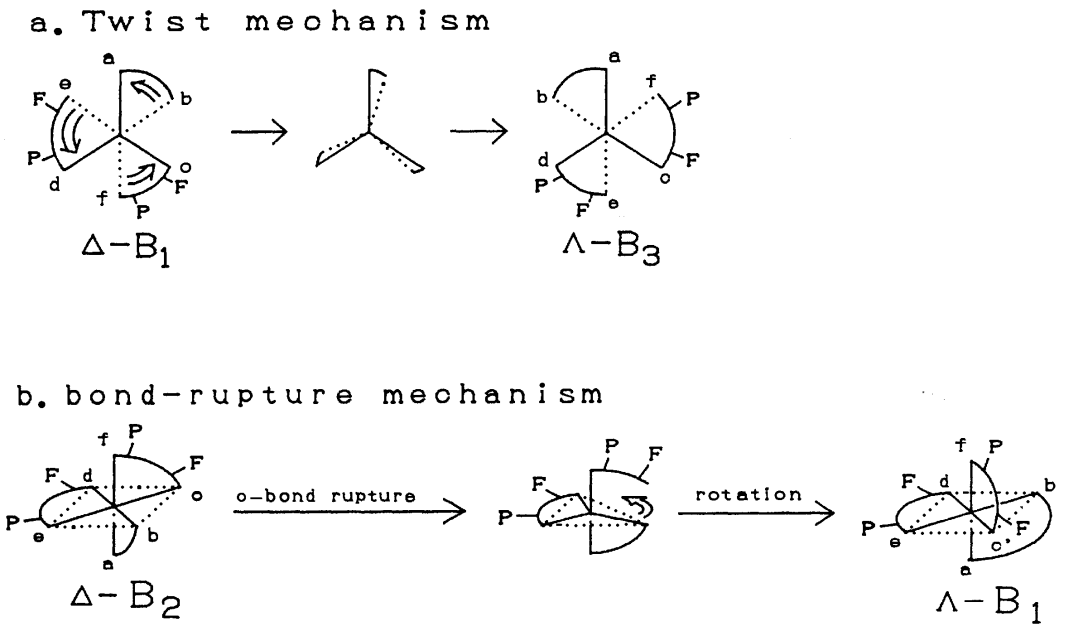

Fig. 6. Examples of twist mechanism (a) and bond-rupture mechanism (b).

minimum. This least squares method leads to the following values: $k_{12}=1.22_8\times10^{-4}$ s^{-1}, $k_{23}=0.47_6\times10^{-4}$ s^{-1}, and $k_{31}=0.02_7\times10^{-4}$ s^{-1}. The standard deviation is $0.05_3\times10^{-4}$ s^{-1}. The curves in Fig. 3 are calculated from Eq. 8 with these k values. They are in good agreement with the experimental data. The deviation of the points from the calculated curves for $t>$ca. 1.5×10^4 s is attributable to experimental errors. Noteworthy is the fact that the direct conversion between **B**$_1$ and **B**$_3$ was forbidden. Isomerization reactions of octahedral tris-chelate complexes are generally interpreted in terms of two basic pathways: twist mechanisms and bond-rupture mechanisms.[8] The twist mechanisms are not compatible with this fact because

the rotation around two of the possible four axes allows the conversion between $\mathbf{B}_1$ and $\mathbf{B}_3$ (for example, Fig. 6a). On the contrary, certain types of bond-rupture pathways[9] (for example, Fig. 6b) are in accord with the absence of the direct conversion between $\mathbf{B}_1$ and $\mathbf{B}_3$. More detailed discussion will be presented in a subsequent paper.

The technique of determining the rate constants presented above has the following advantages: 1) absolute values of the rate constants can be obtained; 2) all the experimental points, not only those near the equilibrium, are effectively utilized; 3) the rate constants are determined consistently from all the available data; 4) the requirement of the precision of the data is not too strict.

The authors' thanks are due to Dr. S. F. Howell, Sophia University, for correcting the manuscript.

References

1) J. Wei and C. D. Prater, "Advances in Catalysis," Academic Press Inc., New York (1962), Vol. 13.

2) M. Watabe, S. Kawaai, and S. Yoshikawa, *Bull. Chem. Soc. Jpn.*, **49**, 1845 (1976).

3) M. Watabe, M. Zama, and S. Yoshikawa, *Bull. Chem. Soc. Jpn.*, **51**, 1354 (1978).

4) M. Boudart, "Kinetics of Chemical Processes," Prentice-Hall Inc., Englewood Cliffs, New Jersey (1968).

5) F. H. Raven, "Mathematics of Engeneering Systems," McGraw-Hill, New York (1966), Chap. 3.

6) S. L. S. Jacoby, J. S. Kowalik, and J. T. Pizzo, "Iterative Methods for Nonlinear Optimization Problems," Prentice-Hall Inc., Englewood Cliffs, New Jersey (1972).

7) Y. Hoshino, Y. Yukawa, A. Endo, K. Shimizu, and G. P. Satô, *Chem. Lett.*, **1987**, 845.

8) J. G. Gordon, II, and R. H. Holm, *J. Am. Chem. Soc.*, **92**, 5319 (1970).

9) E. L. Muetterties, *J. Am. Chem. Soc.*, **90**, 5097 (1968).

 © 1989 The Chemical Society of Japan Bull. Chem. Soc. Jpn., 62, 999—1003 (1989)

Stabilities in Water and Transfer Activity Coefficients from Water to Nonaqueous Solvents of Benzo-18-crown-6-Metal Ion Complexes

Yasuyuki TAKEDA,* Rie KOHNO, Yoshihiro KUDO, and Naoaki FUKADA
Department of Chemistry, Faculty of Science, Chiba University, Yayoi-cho, Chiba 260
(Received September 5, 1988)

Formation constants in water of 1 : 1 benzo-18-crown-6 (B18C6)-metal ion complexes and the B18C6 solubility in water were determined at 25 °C by conductometry or potentiometry with ion-selective electrodes and spectrophotometry, respectively. The selectivity sequences of B18C6 for metal ions in water are $Pb^{2+} > Ba^{2+} > Sr^{2+} > Ag^+ > K^+ > Tl^+ > Na^+ > Rb^+$. In each case of alkali and alkaline earth metal ions, the more closely a metal ion fits into the B18C6 cavity, the more stable is the B18C6-metal ion complex. Although the solvation power of water for an alkali metal ion is not the largest of all solvents, the formation constant of a given B18C6-alkali metal ion complex in water is by far the smallest of all solvents. The transfer activity coefficients (γ) from water to nonaqueous solvents of the B18C6-metal ion complexes were then calculated from the formation constants of the B18C6 complexes, γ values of B18C6 (obtained from solubilities of B18C6), and γ values of the uncomplexed metal ions. The γ value of B18C6 is larger than those of B18C6-alkali metal ion complexes. This shows that when B18C6 forms a complex with an alkali metal ion, the B18C6 complex becomes more soluble in nonaqueous solvents than in water, compared with uncomplexed B18C6.

The formation constants in water and transfer activity coefficients from water to nonaqueous solvents of crown ether-metal ion complexes provide valuable information on effects of water on the stabilities and aspects of hydration of crown ether complexes, respectively, where the transfer activity coefficients of the crown ether complexes are calculated by using the formation constants of the crown ether complexes. The formation constants[1] in water and the transfer activity coefficients[2-4] from water to nonaqueous solvents of 18-crown-6 (18C6)- and dibenzo-18-crown-6 (DB18C6)-metal ion complexes have been reported. However, no data on the stabilities of benzo-18-crown-6 (B18C6)-metal ion complexes in water[1] have been reported.

In this study, the formation constants in water and the transfer activity coefficients from water to nonaqueous solvents of B18C6-metal ion complexes were determined at 25 °C. Effects on the stabilities in water and the aspects of hydration of the B18C6-metal ion complexes are discussed in detail.

Experimental

Materials. Benzo-18-crown-6 was prepared according to a method of Pedersen.[5] The product was recrystallized four times from hexane and dried in a vacuum oven at room temperature. Its purity was checked by melting point (mp 44—45 °C), elemental analysis, NMR, and conductometry.

Extremely pure NaCl, KCl, RbCl, CsCl, $Sr(NO_3)_2$, $Ba(NO_3)_2$, and analytical grade $TlNO_3$ were obtained from Merck Japan Ltd. They were used without further purification. Analytical grade $AgNO_3$ and $Pb(NO_3)_2$ were purchased from Wako Pure Chemicals Ltd. The purities of $AgNO_3$ and $Pb(NO_3)_2$ were determined by means of KCl and EDTA titration, respectively. The conductivity of water was less than $4\times10^{-7}\ \Omega^{-1}\ cm^{-1}$.

Apparatus and Procedure. The conductance measurements were made on a Fuso conductivity apparatus (model 362B) in a water bath thermostated at 25±0.005 °C. Two cells with cell constants of 0.05823 and 0.08135 cm^{-1} were used. The experimental procedure to obtain the formation constants of B18C6-metal ion complexes was almost the same as that described in a previous paper.[6]

The emf measurements were carried out with a Denki Kagaku Keiki ion meter apparatus (model IOC-10) in a water bath thermostated at 25±0.05 °C. For Na^+ and K^+, a Horiba 1512A-06T Na^+-selective electrode and a Toko Kagaku 1200 K^+-selective electrode were used, respectively. The Denki Kagaku Keiki 7080 Ag^+-selective electrode and the 7180 Pb^{2+}-selective electrode were used for Ag^+ and Pb^{2+}, respectively. Horiba 2535A-06T (Ag|AgCl electrode) and Denki Kagaku Keiki 4083 (Ag|AgCl electrode) were used as references for Na^+, K^+ measurements, and for Ag^+, Pb^{2+} measurements, respectively. Experiments for obtaining the formation constants of B18C6-metal ion complexes were performed according to the method of Frensdorff.[7]

Solubility of B18C6. A B18C6 suspension in water was stirred at 25±0.02 °C for 3 days; then, the solution saturated with B18C6 was filtered under nitrogen. The B18C6 concentration of the aqueous solution was determined spectrophotometrically (at 273 nm). The solubility of B18C6 in water (average of seven measurements) at 25 °C was 0.94±0.02 M (1 M=1 mol dm^{-3}).

Results and Discussion

The analysis of conductometric data for obtaining the formation constants (K_{ML}) of complexes of B18C6 with K^+, Rb^+, Tl^+, Sr^{2+}, and Ba^{2+} was the same as that described elsewhere.[6] Here, $K_{ML}=[ML^{m+}]/[M^{m+}][L]$; M^{m+} and L are a metal ion and a crown ether, respectively. The analysis of potentiometric data for obtaining K_{ML} values of complexes of B18C6 with Na^+, K^+, Ag^+, and Pb^{2+} was the same as that described by Frensdorff.[7] In this study, it is assumed that the association between a cation and an anion is negligible and that B18C6 forms a 1 : 1 complex with a metal ion. The log K_{ML} values are compiled in Table 1.

Stability Constants. It can be seen from Table 1 that the selectivity sequence of B18C6 for alkali metal ions

Table 1. $\log(K_{ML}/mol^{-1}dm^3)$ Values at 25 °C

	Ionic radius (Å)[a]	18C6	B18C6						DB18C6
		H_2O	AN[b]	PC[c]	CH_3OH	H_2O	DMF	DMSO	H_2O
Na^+	1.02	0.8_0[d]	4.9[k]	5.3[k]	4.5[k]	1.38±0.02[n]	2.5[k]	—	1.1_6[q]
		0.8_2[e,f]			4.0_3[l]				1.1[r]
					4.35[m]				
K^+	1.38	2.0_3[d]	5.3[k]	5.4[k]	5.7[k]	1.744±0.004[o]	3.6[k]	2.8[k]	1.6_7[q]
		2.04_7[e]			5.2_7[l]	1.79±0.02[n]			1.6[r]
		2.0_6[g]			5.05[m]				
		2.03_4[h]							
Rb^+	1.49	1.5_6[d]	4.4[k]	4.5[k]	5.1[k]	1.15±0.02[o]	3.2[k]	2.6[k]	1.0_8[q]
					4.6_2[l]				
Cs^+	1.70	0.9_9[d]	3.8[k]	3.6[k]	4.1[k]	(0.88)[p]	2.8[k]	2.4[k]	0.8_3[q]
		0.9_8[e]			3.6_6[l]				
		0.8[g]							
Ag^+	1.15	1.5_0[d]	—	—	—	1.83±0.02[n]	—	—	1.4_1[q]
		1.6[g]							1.5[r]
Tl^+	1.50	2.2_7[d]	—	—	—	1.68±0.01[o]	—	—	1.5_0[q]
		2.2[i]							1.5[r]
Sr^{2+}	1.13	2.7_2[d]	—	—	4.92[l]	2.41±0.01[o]	—	—	1.0_0[q]
		2.8[j]							
Ba^{2+}	1.36	3.8_7[d]	—	—	5.35[l]	2.90±0.02[o]	—	—	$\sim 1.9_5$[q]
Pb^{2+}	1.19	4.2_7[d]	—	—	—	3.19±0.02[n]	—	—	1.8_8[q]
		4.4[i]							

a) R. D. Shannon and C. T. Prewitt, *Acta Crystallogr., Sect. B*, **25**, 925 (1969). b) Acetonitrile. c) Propylene carbonate. d) Ref. 8, calorimetry. e) Ref. 9, ion exchange membrane. f) Ref. 10, NMR. g) Ref. 7, potentiometry. h) Ref. 11, conductometry. i) Ref. 12, potentiometry. j) Ref. 13, potentiometry. k) Ref. 14, conductometry. l) Ref. 15, spectrophotometry. m) Ref. 16, potentiometry. n) This study, ion selective electrode. o) This study, conductometry. p) Estimated value from $\log K_{ML}$ values of 18C6 and DB18C6 complexes in H_2O; $\{(0.99+0.98+0.8)/3+0.83\}/2 \simeq 0.88$. q) Ref. 17, spectrophotometry. r) Ref. 2, solubility.

in H_2O is $K^+ > Na^+ > Rb^+$ ($> Cs^+$). The selectivity tendency in H_2O of B18C6 for alkali metal ions other than Na^+ agrees completely with those of 18-crown-6 (18C6) and dibenzo-18-crown-6 (DB18C6); namely, the more closely the metal ion fits into the B18C6 cavity (18C6 cavity radius: 1.38 Å[18]), the more stable is the B18C6-metal ion complex (size-fit concept). A similar selectivity trend of 18C6, B18C6, and DB18C6 for K^+, Rb^+, and Cs^+ was observed in nonaqueous solvents.[14] The sodium ion-selective tendency of B18C6 in H_2O is consistent with that of DB18C6, but is different from that of 18C6. This may be attributed largely to the higher ligand-ring rigidity of B18C6 caused by the benzo group, compared with 18C6. It has been reported that a complexation reaction of Na^+ with a flexible crown ether causes a large ligand-ring conformational change, resulting in a great entropy-destabilization of the Na^+ complex.[14] The K_{ML} (K^+)/K_{ML} (Na^+) ratio of B18C6 varies somewhat with the solvent, in comparison with DB18C6; however, the $K_{ML}(K^+)/K_{ML}(Na^+)$ ratio of 18C6 varies greatly. Kolthoff and Chantooni, Jr.[2] reported that, from the K_{ML} (K^+)/K_{ML} (Na^+) ratios of 18C6 and DB18C6, the conformation of L in ML^+ seemed to be more affected by the solvent when L is 18C6 than when it is DB18C6. It, thus, appears from this that the conformation of B18C6 in ML^+ is somewhat greater, and is less affected by the solvent, compared with DB18C6 and 18C6, respectively.

A K^+ ion fits most nicely into the B18C6 cavity, whereas the size of a Ag^+ ion is smaller than that of the B18C6 cavity; though the Gibbs-free energy of hydration ($\Delta G_h°$) of Ag^+ is smaller than that of K^+ (Table 3), the B18C6 forms a slightly more stable complex with Ag^+ than K^+ in water (Table 1). Although the ionic sizes of Tl^+ and Rb^+ are almost the same and $\Delta G_h°$ of Tl^+ is slightly smaller than that of Rb^+, the Tl^+-B18C6 complex is more stable than the Rb^+-B18C6 complex in water.

From Table 1, the $\log K_{ML}$ value of a B18C6-Ba^{2+} complex in water is larger than that of a B18C6-Sr^{2+} complex; this tendency is entirely consistent with the size-fit concept. The same is true for the cases of 18C6 and DB18C6. A Pb^{2+} ion has a less suitable size for the B18C6 cavity than does a Ba^{2+} ion; though $\Delta G_h°$ of Ba^{2+} is larger than that of Pb^{2+} (Table 3), the Pb^{2+}-B18C6 complex is somewhat more stable than the Ba^{2+}-B18C6 complex in water. The unexpected behavior of B18C6 complexes with Ag^+, Tl^+, and Pb^{2+} may be ascribed to different binding forms of Ag^+, Tl^+, and Pb^{2+} with ether oxygen atoms of B18C6 from those of s-block metal ions.

Ba^{2+} and K^+ are nearly identical in size; though $\Delta G_h°$ of Ba^{2+} is very much smaller than that of K^+ (Table 3), Ba^{2+} forms a more stable complex with B18C6 than K^+ in water. The ionic radii of Sr^{2+} and Pb^{2+} are approx-

imately equal to that of Ag^+; though ΔG_h° of Sr^{2+} and Pb^{2+} are very much smaller than that of Ag^+, Sr^{2+}- and Pb^{2+}-B18C6 complexes are more stable than a Ag^+-B18C6 complex in water. The same trend is found for 18C6 and DB18C6, except for the cases of Sr^{2+}- and Ag^+-DB18C6 complexes (Table 1).

On account of the higher basicity of an aliphatic ether oxygen atom compared with an aromatic ether oxygen atom, it can be expected that the stabilities of the complexes of a given metal ion with the three crown ethers in water decrease in the order 18C6> B18C6> DB18C6. The data on water given in Table 1 are consistent with this expectation, except for the cases of Na^+ and Ag^+. For each case of Na^+ and Ag^+, the B18C6 complex is more stable than the DB18C6 complex in water, which is in accord with the expectation; however, the stability sequence of the 18C6 complex among these three crown ether complexes is unexpected. On account of the smaller size of the metal ion compared with the 18C6 cavity-size and the higher ligand-ring flexibility of 18C6, the metal ion with higher charge density may cause a large conformational change upon complexation. Thus, the 18C6 complex is entropy-destabilized, resulting in the unexpected stability sequence.

Although the solvation power of water for an alkali metal ion (i.e., relative solubility of the alkali metal ion), which is derived from the data on transfer activity coefficients of the alkali metal ion,[2] is the third largest of all the solvents listed in Table 1, the log K_{ML} value of a given B18C6-alkali metal ion complex in water is by far the smallest of all the solvents. The same tendency was observed for the cases of 18C6- and DB18C6-alkali metal-ion systems.[14] It appears from this finding that the hydrogen bonds between ether oxygen atoms of the crown ether and water molecules cause the much lower stability of the crown ether-alkali metal ion complex in water than all the other solvents.

Benzo-18-crown-6 forms much more unstable complexes with Sr^{2+} and Ba^{2+} in water than in methanol (Table 1). The much stronger solvation of Ba^{2+} in water than in methanol[20] is probably responsible for the much lower stability of the Ba^{2+} complex in water than in methanol.

Transfer Activity Coefficient. The logarithm of the transfer activity coefficient ($\log {}^{s_1}\gamma^{s_2}(ML^{m+})$[21]) of a B18C6-metal ion complex between solvent s_1 and solvent s_2 is calculated as follows:

$$\log {}^{s_1}\gamma^{s_2}(ML^{m+}) = (\log K_{ML})_{s_1} - (\log K_{ML})_{s_2} + \log {}^{s_1}\gamma^{s_2}(L) + \log {}^{s_1}\gamma^{s_2}(M^{m+}), \quad (1)$$

where ${}^{s_1}\gamma^{s_2}(L)$[21] and ${}^{s_1}\gamma^{s_2}(M^{m+})$[21] refer to the transfer activity coefficients of B18C6 and a metal ion between solvent s_1 and solvent s_2, respectively. Further, $(\log K_{ML})_s$ denotes the $\log K_{ML}$ value in solvent s. When $\log {}^{s_1}\gamma^{s_2}(ML^{m+})$ is positive, it can be considered that the complex, ML^{m+}, undergoes stronger solvation in s_1 than in s_2. The transfer activity coefficient values of ML^{m+}, M^{m+}, and L when s_1=H_2O are compiled in Table 2.

$\log {}^{H_2O}\gamma^s(L)$ values of benzo-15-crown-5 (B15C5) at 25 °C are −1.24, −1.04, and −0.56, when s=CH_3CN (AN), propylene carbonate (PC), and methanol, respectively.[26] In each case of s=AN and PC, the $\log {}^{H_2O}\gamma^s(L)$ value of B18C6 is larger than that of B15C5; the $\log {}^{H_2O}\gamma^{CH_3OH}(L)$ value of B18C6 is slightly greater than that of B15C5. This shows that, from B15C5 to B18C6, the crown ether is more soluble in water than in the nonaqueous solvents. The size of B18C6 is larger than that of B15C5 by an ether oxygen atom and an ethylene group. Thus, the additional hydrogen bonding between the added ether oxygen atom of B18C6 and water may be responsible for the higher $\log {}^{H_2O}\gamma^s(L)$ values of B18C6 compared with B15C5. The $\log {}^{H_2O}\gamma^s(L)$ value of B18C6 is larger than the corresponding $\log {}^{H_2O}\gamma^s(L)$ value of DB18C6; $\log {}^{H_2O}\gamma^{CH_3OH}$ (18C6) is greater than $\log {}^{H_2O}\gamma^{CH_3OH}$(B18C6) (Table 2). This reveals that with more benzo groups, the crown ether is more soluble in nonaqueous sol-

Table 2. Transfer Activity Coefficients at 25 °C

s=	CH_3CN		Propylene carbonate		CH_3OH			DMF		DMSO	
$\log {}^{H_2O}\gamma^s(M^{m+})$											
Na^+ [2]	2.3		2.9_4		1.4			−1.7		−2.5	
K^+ [2]	1.3		1.5_4		1.7			−1.8		−2.2	
Rb^+ [2]	1.1		1.2_2		1.7			−1.9		−2.0	
Cs^+ [2]	0.8		0.9_4		1.6			−1.7		−2.3	
Ba^{2+} [22]	—		—		3.2			—		—	
$\log {}^{H_2O}\gamma^s(L)$	B18C6	DB18C6[2]	B18C6	DB18C6[2]	18C6[3]	B18C6	DB18C6	B18C6	DB18C6[2]	B18C6	DB18C6[2]
	0.53	−3.5	−0.41	-2.9_1	1.6_6	−0.49	-1.8_5[2]	−0.50	-3.4_5	−0.47	-3.3_9
$\log {}^{H_2O}\gamma^s(ML^{m+})$											
Na^+	−0.7	-5.0_5	−1.4	-4.0_5	-0.4_4	−2.2	-3.7_5[2]	−3.3	-6.8_5	−3.3[23]	-6.6_5
K^+	−1.7	-5.4_5	−2.5	-4.9_0	-0.6_4	−2.7	-3.5_5[2]	−4.2	—	−3.7	-6.4_5
Rb^+	−1.6	—	−2.5	—	—	−2.7	—	−4.5	—	−3.9	—
Cs^+	−1.6	—	−2.2	—	—	−2.1	—	−4.1	—	−4.3	—
Ba^{2+}	—	—	—	—	1.7_6	0.2_6[24]	-0.9_5[3]	—	—	—	—

vents than in water. This is due to the lipophilicity of the benzo group.

Generally, $\log {}^{H_2O}\gamma^s$ values of B18C6-K^+ and -Rb^+ complexes for a given solvent s are approximately equal; but, $\log {}^{H_2O}\gamma^s$ values of B18C6-K^+ and -Rb^+ complexes are somewhat different from those of B18C6-Na^+ and -Cs^+ complexes. This indicates that the nature of solute-solvent interactions of the B18C6-K^+ and -Rb^+ complexes is almost the same; however, this is different from the nature of the solute-solvent interactions of the B18C6-Na^+ and -Cs^+ complexes. This reflects the fact that both K^+ and Rb^+ have more suitable sizes for the B18C6 cavity than do Na^+ and Cs^+.

The $\log {}^{H_2O}\gamma^s(M^{m+})$ value is larger than the corresponding $\log {}^{H_2O}\gamma^s(ML^{m+})$ value of B18C6. This shows that when a M^{m+} ion forms a complex with B18C6, the M^{m+} ion complexed with B18C6 becomes less soluble in water than in nonaqueous solvents, compared with the free M^{m+} ion; namely, B18C6 plays a role in enhancing the lipophilicity of the M^{m+} ion. When s=AN, PC, DMF, and DMSO, $\log {}^{H_2O}\gamma^s(ML^+)$ value of a given alkali metal ion decreases in the order B18C6>DB18C6 (3.7—4.4, 2.4—2.7, 3.6, and 2.7—3.4 units, respectively); the $\log {}^{H_2O}\gamma^{CH_3OH}(ML^{m+})$ value sequence of a given metal ion is 18C6>B18C6>DB18C6 (the differences: 1.5—2.1 and 0.8—1.6 units, respectively). Similar differences are observed for the cases of free 18C6, B18C6, and DB18C6. It can be concluded from this finding that the more the number of benzo groups is, the more hydrophobic (lipophilic) the crown ether-M^{m+} complex is, regardless of a variety of the metal ions. This may be ascribed largely to the hydrophobic entropy effect[3] caused by the enforcement of a hydrogen-bonded structure of water against the benzo group.

For a given solvent s, $\log {}^{H_2O}\gamma^s$(B18C6) is larger than $\log {}^{H_2O}\gamma^s$ of B18C6-alkali metal-ion complexes; the same is true for the cases of 18C6 and DB18C6. This shows that when B18C6 forms a complex with an alkali metal ion, the B18C6 complex becomes more soluble in nonaqueous solvents than in water, compared with uncomplexed B18C6. Chantooni, Jr. and Kolthoff[3] have reported that upon the complexation of a crown ether with a M^{m+} ion, hydrogen bonding to the ether oxygen atoms is greatly decreased as a result of ionic M^{m+}-O bonding. The considerably reduced strength of hydrogen bonding between ether oxygen atoms and water may cause an enforcement of the hydrogen-bonded structure of water for a bulky crown ether complex, resulting in a higher hydrophobicity of the complex, compared with an uncomplexed crown ether. The solvation power of DMF and DMSO for an alkali metal ion is greater than that of water.[27] When s=DMF and DMSO, both the effect of the reduced strength of hydrogen bonding and the stronger interaction between the complexed alkali metal ion and solvents may be responsible for the result, $\log {}^{H_2O}\gamma^s(L) > \log {}^{H_2O}\gamma^s(ML^+)$. Although water has a stronger solvation power for an alkali metal ion than do acetonitrile, propylene carbonate, and methanol,[27] $\log {}^{H_2O}\gamma^s(L)$ is larger than the corresponding $\log {}^{H_2O}\gamma^s(ML^+)$. The solvation power of water for an alkali metal ion is not so large as that of DMF or DMSO.[27] Thus, the superiority of the effect of reduced strength of hydrogen bonding between ether oxygen atoms and water over the effect of the stronger solvation power of water may result in $\log {}^{H_2O}\gamma^s(L) > \log {}^{H_2O}\gamma^s(ML^+)$. The above discussion is supported by a large difference in $\log {}^{H_2O}\gamma^s(L) - \log {}^{H_2O}\gamma^s(ML^+)$ for the same alkali metal ion and crown ether between a group of AN, PC, CH_3OH and that of DMF, DMSO.

$\log {}^{H_2O}\gamma^{CH_3OH}$ of a B18C6-Ba^{2+} complex is larger than that of a free B18C6. The same is true for the cases of 18C6 and DB18C6. This is different from the cases of alkali metal ions, which is due to a difference in the charge density between Ba^{2+} and M^+. Since Ba^{2+} is much more strongly solvated in water than in methanol, compared with an alkali metal ion (log ${}^{H_2O}\gamma^{CH_3OH}(Ba^{2+})=3.2$ in Table 2), the effect of a very much stronger interaction with water of the Ba^{2+} ion in the crown ether complex than with methanol probably surpasses the effect of the reduced strength of hydrogen bonding between ether oxygen atoms and water, resulting in $\log {}^{H_2O}\gamma^{CH_3OH}(BaL^{2+}) > \log {}^{H_2O}\gamma^{CH_3OH}(L)$.

These data on the transfer activity coefficients strongly support the conclusion in the preceding section that the unexpected lowest stability of the crown ether-metal ion complex in water of all the solvents can be attributed to the very strong hydrogen bonding between the ether oxygen atoms of the uncomplexed crown ether and water molecules.

Although the solvation power of water for an alkali metal ion is the third largest of all the solvents listed in Table 2,[27] that of water for a B18C6-alkali metal ion complex is the smallest. The same tendency is found for 18C6- and DB18C6-alkali metal ion complexes. This can probably be ascribed to the above-mentioned effect produced by the greatly reduced strength of hydrogen bonding between ether oxygen atoms and water on a bulky crown ether-alkali metal ion complex.

From Table 2, a B18C6-Ba^{2+} complex is slightly more soluble in water than in methanol; the reverse is

Table 3. Gibbs Free Energy of Hydration ($\Delta G_h°$) of Metal Ions at 25 °C[19]

Ion	$-\Delta G_h°$/kJ mol^{-1}
Na^+	411.3
K^+	338
Rb^+	320
Cs^+	297
Ag^+	479.1
Tl^+	343
Sr^{2+}	1447
Ba^{2+}	1318
Pb^{2+}	1497

true for the B18C6-alkali metal ion complexes. The very much stronger interaction of Ba^{2+} with water than with methanol, compared with the cases of alkali metal ions, may be responsible for the slightly higher solubility of the B18C6-Ba^{2+} complex in water than in methanol.

References

1) R. M. Izatt, J. S. Bradshaw, S. A. Nielsen, J. D. Lamb, and J. J. Christensen, *Chem. Rev.*, **85**, 271 (1985).

2) I. M. Kolthoff and M. K. Chantooni, Jr., *Anal. Chem.*, **52**, 1039 (1980).

3) M. K. Chantooni, Jr. and I. M. Kolthoff, *Proc. Natl. Acad. Sci. U.S.A.*, **78**, 7245 (1981).

4) M. H. Abraham and H. C. Ling, *Tetrahedron Lett.*, **23**, 469 (1982).

5) C. J. Pedersen, *J. Am. Chem. Soc.*, **89**, 7017 (1967).

6) Y. Takeda, H. Yano, M. Ishibashi, and H. Isozumi, *Bull. Chem. Soc. Jpn.*, **53**, 72 (1980).

7) H. K. Frensdorff, *J. Am. Chem. Soc.*, **93**, 600 (1971).

8) R. M. Izatt, R. E. Terry, B. L. Haymore, L. D. Hansen, N. K. Dalley, A. G. Avondet, and J. J. Christensen, *J. Am. Chem. Soc.*, **98**, 7620 (1976).

9) H. Høiland, J. A. Ringseth, and T. S. Brun, *J. Solution Chem.*, **8**, 779 (1979).

10) J. D. Lin and A. I. Popov, *J. Am. Chem. Soc.*, **103**, 3773 (1981).

11) Y. Takeda and O. Arima, *Bull. Chem. Soc. Jpn.*, **58**, 3403 (1985).

12) M. Kodama and E. Kimura, *Bull. Chem. Soc. Jpn.*, **49**, 2465 (1976).

13) G. Anderegg, *Helv. Chim. Acta*, **64**, 1790 (1981).

14) Y. Takeda, Y. Ohyagi, and S. Akabori, *Bull. Chem. Soc. Jpn.*, **57**, 3381 (1984).

15) G. Ercolani, L. Mandolini, and B. Masci, *J. Am. Chem. Soc.*, **103**, 7484 (1981).

16) D. E. Fenton, D. Parkin, and R. F. Newton, *J. Chem. Soc., Perkin Trans. 1*, **1981**, 449.

17) E. Shchori, N. Nae, and J. Jagur-Grodzinski, *J. Chem. Soc., Dalton Trans.*, **1975**, 2381.

18) "Progress in Macrocyclic Chemistry," ed by R. M. Izatt and J. J. Christensen, John Wiley and Sons, New York (1981), Vol. 2.

19) H. L. Friedman and C. V. Krishnan, "Water," ed by F. Franks, Plenum, New York (1973), Vol. 3, p. 55.

20) From $\log {}^{H_2O}\gamma^{CH_3OH}(Ba^{2+})$ value (=3.2) in Table 2, Ba^{2+} undergoes much stronger solvation in water than in methanol.

21) ${}^{s_1}\gamma^{s_2}(X)=[X]_{s_1}/[X]_{s_2}$, X being ML^{m+}, L, or M^{m+}.

22) G. R. Hedwig, D. A. Owensby, and A. J. Parker, *J. Am. Chem. Soc.*, **97**, 3888 (1975).

23) $\log {}^{H_2O}\gamma^{DMSO}$ (B18C6·Na^+) was calculated by using $\log K_{ML}$ value (1.70)[25] in 99% aqueous DMSO at 25 °C.

24) $\log {}^{H_2O}\gamma^{CH_3OH}$(B18C6·$Ba^{2+}$) was calculated by using $\log K_{ML}$ value (5.35)[15] in methanol at 25 °C.

25) L. Mandolini and B. Masci, *J. Am. Chem. Soc.*, **106**, 168 (1984).

26) Y. Takeda and T. Kumazawa, *Bull. Chem. Soc. Jpn.*, **61**, 655 (1988).

27) Y. Takeda, *Bull. Chem. Soc. Jpn.*, **54**, 3133 (1981).

Photocatalytic Decomposition of 2-Ethoxyethanol on Titanium Dioxide

Sadamu YAMAGATA,* Ryo BABA, and Akira FUJISHIMA
Department of Synthetic Chemistry, Faculty of Engineering, University of Tokyo, Hongo, Bunkyo-ku, Tokyo 113
(Received September 13, 1988)

The reaction mechanism of the photocatalytic oxidation of 2-ethoxyethanol (Ethyl Cellosolve, $EtOCH_2CH_2OH$) on TiO_2 powder was investigated by gas chromatography-mass spectrometry (GC-MS), infrared (IR) spectroscopy, and electron spin resonance (ESR) with spin trapping technique. Irradiation of TiO_2 powder with UV light in the presence of $EtOCH_2CH_2OH$ under air led to the formation of ethyl formate, ethanol, acetaldehyde and carbon dioxide. The main product, ethyl formate was different from the product through the reaction pathway proposed before for primary alcohols. It was also different from the product of electrolysis on Pt. Reaction mechanism is proposed based on IR and ESR studies.

There have been many studies on the photocatalytic reactions of organic substances on illuminated semiconductor powders.[1] However, detailed mechanisms of the reactions have not been well understood so far. Therefore, this work was undertaken to investigate the reaction mechanism of photocatalytic oxidation of an organic substance on TiO_2 powder, using mainly IR spectroscopy. There have been many studies on the IR spectra of surface species on TiO_2[2-5] but studies on the photocatalytic reactions of organic substances on TiO_2 powder by IR spectroscopy are relatively few. Filimonov reported the IR spectra of the adsorbed species produced by the photocatalytic reaction of some alcohols and alkanes on TiO_2.[6] Kawai et al. studied the photocatalytic hydrogen evolution from various alcohols and water adsorbed on Pt/TiO_2 and proposed that two processes are involved in the reaction based on an IR study.[7] One was a direct reaction of alcohols with the photoproduced hole in the valence band and the other was the $\cdot OH$ formation from the reaction of the hole with an adsorbed H_2O on the photocatalyst.

The organic substance we employed was 2-ethoxyethanol ($EtOCH_2CH_2OH$) which is widely used as an organic solvent. In order to keep the environment clean and safe it is usually necessary to remove from the air the volatile organic solvents such as $EtOCH_2CH_2OH$ exhausted from manufacturing plants. A photocatalytic reaction is in principle available to treat poisonous chemical species such as CN^- in an aqueous solution[8] or stinking molecules in the air, though the reaction mechanism is not clear yet. From a practical point of view it is quite promising to employ photocatalysis for the treatment of $EtOCH_2CH_2OH$.

Furthermore, we are interested in the oxidative reaction of alkoxyethanols such as $EtOCH_2CH_2OH$ because they have two functional groups, i.e. alcoholic hydroxyl (-OH) and etheric oxy (-O-) groups. It is quite interesting from the viewpoint of organic chemistry to get information as to which group is oxidized first by the photocatalyst. For example, Nishimoto et al. investigated the photocatalytic degradation and polymerization of poly(oxyethylene) on TiO_2 powder in aqueous solution and concluded that both functional groups, alcoholic hydroxyl and etheric oxy, were oxidizable depending on the surface condition of TiO_2.[9] Ross et al. reported that 2-methoxyethanol, a homologous compound of $EtOCH_2CH_2OH$, was oxidized on a platinum and a carbon electrode through the electron transfer at the etheric oxy group rather than the hydroxyl group.[10] Sugawara studied the oxidation of a series of alkoxyethanols on a Pt electrode.[11] The oxidations of alkoxyethanol by pyrolysis[12] and permanganate[13] have also been studied. These investigations on the decomposition of alkoxyethanols showed that the reaction products were different depending on the oxidation processes. The photocatalytic reaction of 1,1-diphenylethylene on the illuminated TiO_2 powder was reported to give products different from those of the electrolysis on Pt.[14] Taking these into consideration the photocatalytic oxidation of $EtOCH_2CH_2OH$ on semiconductor powders seems quite interesting in terms of its reaction pathway and products.

In this study the photocatalytic oxidation of $EtOCH_2CH_2OH$ on TiO_2 powder was investigated, using GC-MS, IR spectroscopy, and ESR with a spin trapping method.

Experimental

Materials. TiO_2 (Nippon Aerosil, P-25) was used as a photocatalyst without pretreatments. Photoirradiation on CdS (Wako Chemicals), ZnS (Wako Chemicals), Al_2O_3 (Wako Chemicals), SnO_2 (Furuuchi Chemicals), and MnO_2 (Kanto Chemicals) powders were carried out for references. All organic reactants in the present experiments were reagent grade (Tokyo Kasei).

Products Analysis. Reaction products in the gas/solid reaction were sampled from a circulating system (volume 800 ml). This system had a fan to vaporize the organic liquid and to circulate the sample gas. It was also equipped with a Pyrex glass reactor with a flat bottom (area 50 cm^2) to support the photocatalyst. The catalyst powder (0.5 g) was evenly spread over the transparent bottom of the reactor and was irradiated from beneath with a 500 W high-pressure mercury lamp. The concentration of the organic substance in the gas phase was about 3000 ppm. Reaction products in the gas phase were analyzed periodically by the gas chroma-

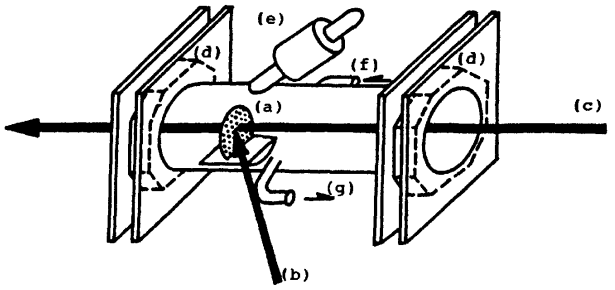

Fig. 1. The IR cell used for the simultaneous IR measurement and GC analysis; (a): TiO_2 pellet; (b): UV light for excitation; (c): IR for monitor; (d): NaCl plate; (e): tube for gas sampling; (f): gas inlet; (g): gas outlet.

tography (Hitachi 163; column: PEG 4000 for organic gases and silica gel for CO_2).

In order to identify the products by GC-MS, photocatalytic reaction of TiO_2 slurry in liquid $EtOCH_2CH_2OH$ was carried out because a gas/solid reaction in the present system did not supply a sufficient amount of the products for a qualitative analysis by GC-MS. The TiO_2 powder (500 mg) dispersed in a given 2-alkoxyethanol (5 ml) saturated with air was irradiated for 5 h in a flask which was installed with an internal high-pressure Hg lamp. The products in liquid phase were collected by distillation and then analyzed by GC-MS (Shimadzu QP1000 with a 30 m OV101 column).

IR Studies. The measurement of IR transmittance of the adsorbed species on the photocatalyst was performed with self-supporting TiO_2 disks. The TiO_2 powder was exposed overnight to the air which was saturated with the organic compound in the dark at room temperature and then the powder (50 mg) was pressed into a disk of 20 mm in diameter and about 0.1 mm in thickness. The IR spectrum was recorded after periodic UV-irradiation with a 500 W Xe-lamp through a water filter to reduce the heating effect. The IR spectrum of liquid $EtOCH_2CH_2OH$ was also recorded by a liquid film method using NaCl plates. A cell was used to analyze the gas phase which is shown in Fig. 1. The cell was first evacuated slowly after the TiO_2 disk which was adsorbed with $EtOCH_2CH_2OH$ was placed inside, and then an air saturated with $EtOCH_2CH_2OH$ was introduced into the cell. An inlet and an outlet of the cell were closed with screw cocks and then the IR measurement and the gas phase analysis were carried out after periodical UV-irradiation under the atmospheric pressure.

ESR Studies. Spin trapping method for an ESR measurement was applied to the present system. The experimental procedure was previously mentioned.[15] 5,5-Dimethyl-4,5-dihydro-3*H*-pyrrole *N*-oxide (DMPO) was used as a spin trapping reagent.

Results

Products Analysis. The gas chromatography analysis of the products in gas/solid reaction showed four peaks, three of which had the same retention times with those of acetaldehyde, ethyl formate, and ethanol, respectively, but the fourth peak which had a longer retention time than $EtOCH_2CH_2OH$ has not been identified yet. This substance was different from ethyl-

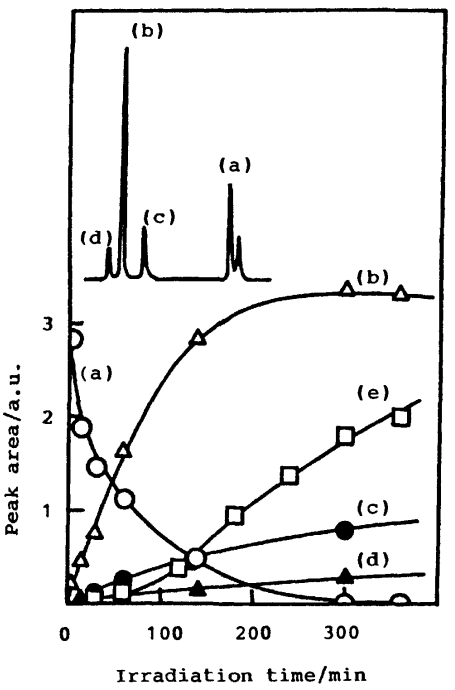

Fig. 2. Gas chromatogram of the reaction products and the time profile of each product in gas/solid reaction of $EtOCH_2CH_2OH$ on the TiO_2 powder. (a): $EtOCH_2CH_2OH$; (b): ethyl formate; (c): ethanol; (d): acetaldehyde; (e): carbon dioxide.

ene glycol and was supposed to be such an ether as produced from $EtOCH_2CH_2OH$ by photoreaction in the presence of $TiCl_4$.[16] Carbon dioxide was also detected in a separate experiment. Figure 2 shows the gas chromatogram of the products and the time profile of each product.

CdS and ZnS also gave the same products upon irradiation but were found to be less active than TiO_2. SnO_2, and Al_2O_3 powders did not photocatalyze the decomposition of $EtOCH_2CH_2OH$ because of their large bandgap energies compared with the UV light employed.

Decomposition of $EtOCH_2CH_2OH$ did not occur either when the catalyst was illuminated with a light of a longer wavelength than the bandgap of TiO_2 or when the system temperature was raised up to 353 K in the dark. In the absence of molecular oxygen, photoirradiation caused the reduction of TiO_2 and turned its color blue, and the amount of detected products was insignificant. When the sample gas was flowed over an oxidizing agent, e.g. MnO_2 powder, in the dark, the same gaschromatogram was obtained as when the UV-irradiated photocatalysts were employed. These results suggest that the reaction on the illuminated TiO_2 proceeded through a photocatalytic oxidation involving molecular oxygen in gas phase upon the bandgap illumination of the TiO_2.

A qualitative analysis of the products in liquid/solid reaction by GC-MS showed only one peak, mass spectrum of which agreed well with that of ethyl for-

mate,[17] in addition to the out-of-scale $EtOCH_2CH_2OH$ peak which was in contrast to the results in the gas/solid experiment. There have been some reports mentioning that chemisorbed species react at low pressure gas/solid reactions while physisorbed species become important at high pressure of gas/solid and liquid/solid reactions.[18,19] In our conditions the pressure of $EtOCH_2CH_2OH$ is high enough and the physisorbed molecules react as in the case of liquid/solid phase. Therefore, the difference in the products was ascribed to the surface concentration of $EtOCH_2CH_2OH$ on TiO_2. $EtOCH_2CH_2OH$ is oxidized much easier than ethyl formate in the present conditions, which leads to the production of only ethyl formate under high concentration of $EtOCH_2CH_2OH$.

Alkyl formate is produced from alkoxyethanol by the dissociation of the C-C bond between the two oxygen atoms followed by the subsequent oxidation of one of these carbon atoms. Indeed, when 2-methoxyethanol, 2-isopropoxyethanol, or 2-butoxyethanol was used as a reactant, it was found by GC-MS that the corresponding formate was produced in each case. This result suggests that the C-C bond between the two oxygen atoms of alkoxyethanol is photocatalytically dissociated on the illuminated TiO_2 surface.

IR Studies. Adsorption of $EtOCH_2CH_2OH$ on TiO_2 in the Dark: Infrared spectra of bare TiO_2 (a), liquid $EtOCH_2CH_2OH$ (b), $EtOCH_2CH_2OH$ adsorbed on TiO_2 (c), and ethyl formate adsorbed on TiO_2 (d) are shown in Fig. 3. Bare TiO_2 has broad bands at 650—1100, 1500—1700, and 3000—3600 cm^{-1}, which are assigned to H_2O and OH groups on TiO_2. A comparison of the IR spectrum of $EtOCH_2CH_2OH$ in liquid phase with that of adsorbed $EtOCH_2CH_2OH$ on TiO_2 powder shows that the absorption band of $EtOCH_2CH_2OH$ at 1380 cm^{-1} decreased in intensity more than the bands at 1360 and 1450 cm^{-1} after the adsorption of $EtOCH_2CH_2OH$ onto TiO_2. The decrease of the band at 1380 cm^{-1} indicates that this

Table 1. IR Bands Assignment of Adsorbate on the TiO_2 Surface

IR bands/cm^{-1}	1570, 1360	1440	1730	
Surface species	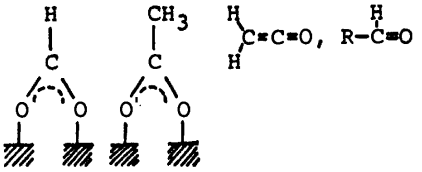			
	formate	acetate	ketene	aldehyde
References	20	20	21	25

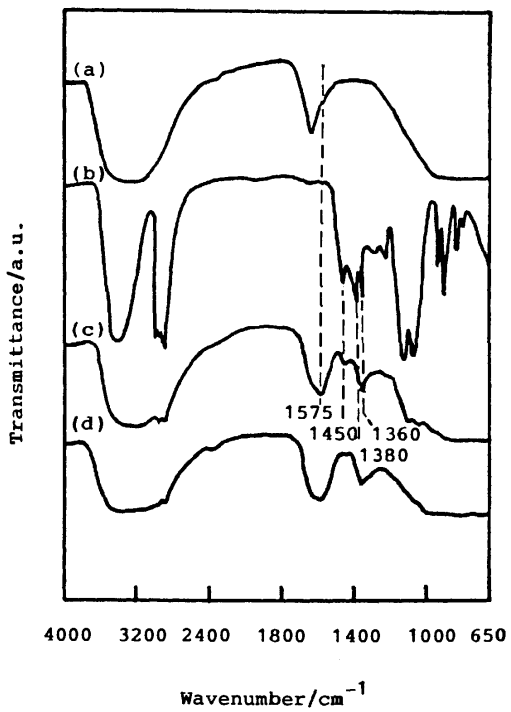

Fig. 3. Infrared spectra of bare TiO_2 (a), liquid phase $EtOCH_2CH_2OH$ (b), $EtOCH_2CH_2OH$ adsorbed on TiO_2 (c), and ethyl formate adsorbed on TiO_2 (d).

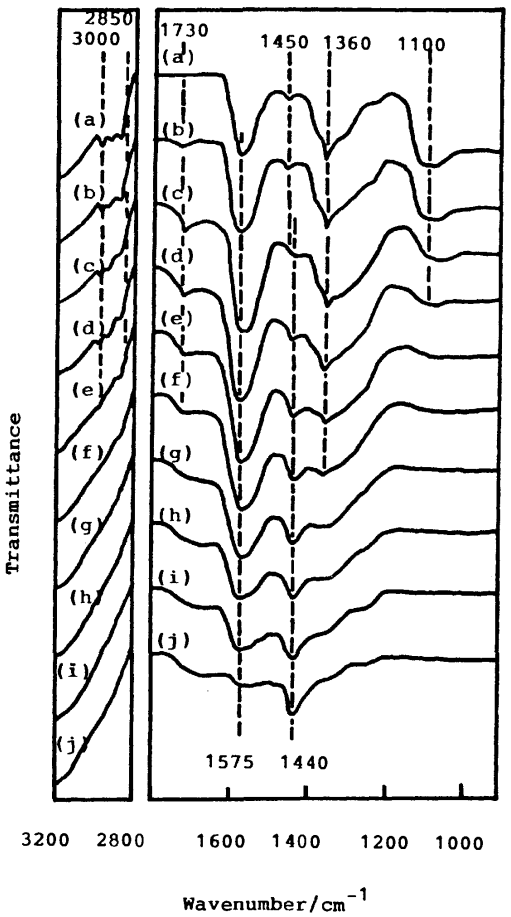

Fig. 4. The time profile of the IR spectrum of adsorbed species upon UV irradiation. Each curve shows the spectrum after the following minutes of UV irradiation (a) 0; (b) 5; (c) 10; (d) 20; (e) 40; (f) 60; (g) 90; (h) 120; (i) 150; (j) 240. The spectra were recorded with the reference of untreated TiO_2 for the wavenumbers from 650—1800 cm^{-1}.

band is due to -OH in $EtOCH_2CH_2OH$, because alcohols are reported to be adsorbed onto TiO_2 forming alkoxides, i.e. losing their -OH groups.[20] It is worth noting that the new band appearing at 1575 cm^{-1} is different from that of the surface formate species reported by Nakajima et al.[20] (Table 1). This band was ascribed to the surface complex produced from the adsorbed $EtOCH_2CH_2OH$ and oxygen species (Fig. 7 (**VI**)), which will be discussed later.

Time Dependence of IR Spectrum of the Adsorbed Species on TiO_2 Powder upon UV Irradiation: The IR spectrum of $EtOCH_2CH_2OH$ adsorbed on the TiO_2 disk showed a time dependence upon UV-irradiation as shown in Fig. 4. That is, the irradiation of the disk with UV light for the first 20 minutes caused an increase in the band intensity at 1575 and 1360 cm^{-1} and a decrease in the band intensity at 1100, 1450, and 2850—3000 cm^{-1}. In addition, new bands appeared, which are at 1440 and 1730 cm^{-1}. A prolonged UV-irradiation caused the band at 1440 cm^{-1} to increase, and the bands, at 1730, 1575, and 1360 cm^{-1} to decrease.

The band at 1440 cm^{-1} was assigned to the surface acetate species[20] (Table 1). The other band at 1530 cm^{-1} due to the surface acetate species reported by Nakajima et al. was obscured by a strong band at around 1575 cm^{-1}. The stable adsorption of the acetate species was reported[20,21] and was also evidenced in the present study by the existence of the band at 1440 cm^{-1} even after 240 minutes of UV-irradiation.

The band at around 1730 cm^{-1} is assigned to the physisorbed ethyl formate (Fig. 7 (**VII**)) which will be further photocatalytically oxidized to ethanol, acetaldehyde, and acetate as will be discussed below.

Simultaneous Measurement of an Adsorbed Species and a Gas-Phase Product: The time profiles of the intensity of the IR band at 1575 cm^{-1} and that of the amount of ethyl formate in gas phase analyzed by GC during UV-irradiation are shown in Fig. 5. The maxima occurred at 40 minutes and 25 minutes of UV-irradiation for the IR absorbance at 1575 cm^{-1} and for the amount of produced ethyl formate in the gas phase, respectively. This result suggests that the surface species which has IR band at 1575 cm^{-1} may be different from ethyl formate because the maxima are different.

Radical Detection by Spin Trapping Method: Figure 6 shows the ESR spectrum observed after 20 seconds of UV-irradiation of the TiO_2 slurry in $EtOCH_2CH_2OH$ with DMPO. The hyperfine splitting constants (a_N=14.6 G and a_H=20.6 G; 1 G=10^{-4} T) indicate that a carbon-centered radical[22] was produced by the photocatalytic reaction of $EtOCH_2CH_2OH$ on TiO_2.

Discussion

Based on the experimental results we propose a reaction mechanism of the photocatalytic decomposition of $EtOCH_2CH_2OH$ on TiO_2 as shown in Fig. 7 and the details of it will be discussed in this section.

Reaction Products. The formation of ethyl formate from $EtOCH_2CH_2OH$ on the photoexcited TiO_2 powder is interpreted through the dehydration and the subsequent oxidation of the double bond according to the oxidation mechanism proposed by Djeghri and Teichner.[23] They have studied the photocatalytic oxidation of primary, secondary, and tertiary alcohols on TiO_2 and concluded that there are two oxidation pathways; one is a direct oxidation which produces aldehydes and ketones from primary and secondary alcohols, respectively. The other is dehydration of alcohols into alkenes which are oxidized at the double bond, forming carbon dioxide and aldehydes or ketones with less carbon atoms than the original alcohols. Applying their reaction mechanisms to the photocatalytic oxidation of $EtOCH_2CH_2OH$ on the illuminated TiO_2 powder, ethoxyacetaldehyde (through direct oxidation) and ethyl formate (through dehydra-

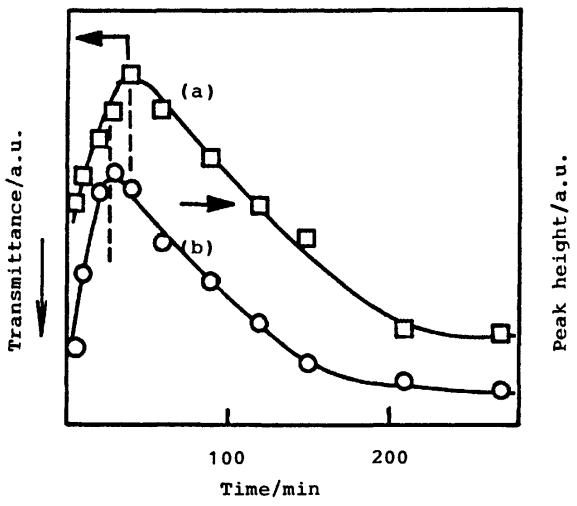

Fig. 5. The time profiles of the IR transmittance at 1575 cm^{-1} (a) and the peak height of ethyl formate in gas chromatogram (b).

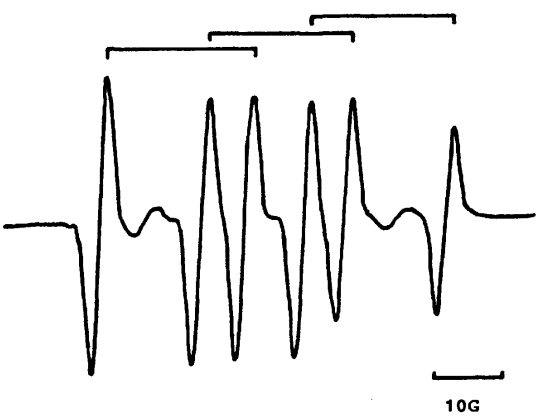

Fig. 6. ESR spectrum of the spin adduct obtained after 20 second UV irradiation of TiO_2 slurry in $EtOCH_2CH_2OH$ with DMPO.

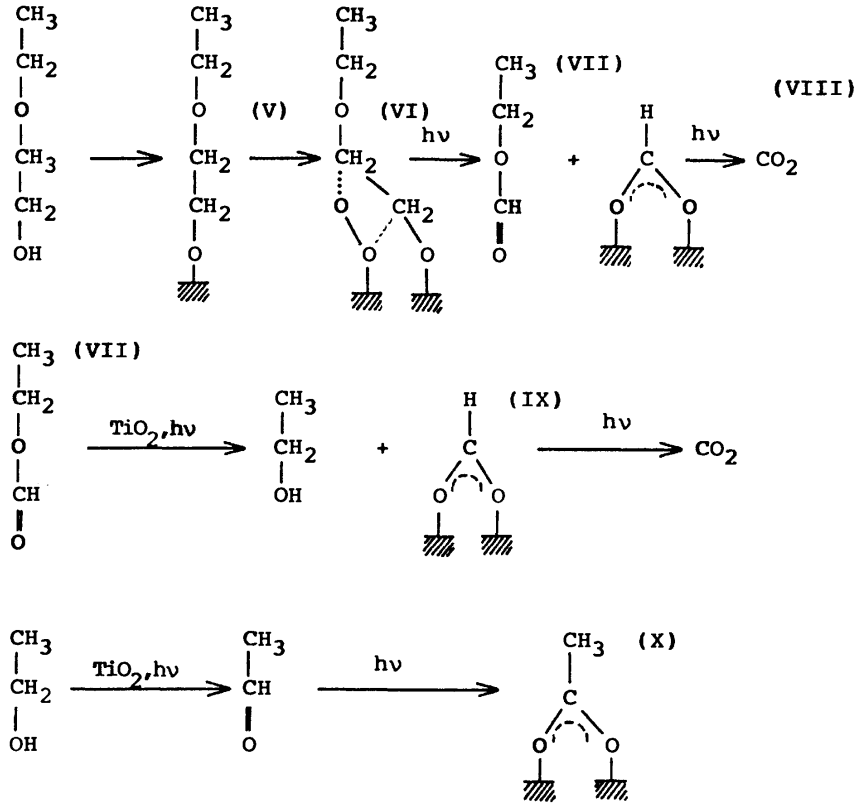

Fig. 7. The reaction scheme of the photocatalytic oxidation of $EtOCH_2CH_2OH$ on TiO_2.

tion-oxidation) are expected to be reaction products. However, only ethyl formate was detected in the present experiment, even though $EtOCH_2CH_2OH$, a primary alcohol, might tend to be oxdized directly into ethoxyacetaldehyde.

No production of ethoxyacetaldehyde may be ascribed to the molecular structure of $EtOCH_2CH_2OH$, i.e., the configuration of the oxygen atom at the β-position of the carbon atom which has the alcoholic -OH. Indeed, the indirect oxidation of alkoxyethanol was previously reported by Sugawara on a Pt electrode.[11] He investigated the electrochemical oxidation of a series of alkoxyethanols and proposed the following mechanism: Discharge occurs at an alcoholic oxygen which is followed by the fission of the C-C bond between the two oxygen atoms, producing a cation **I** and a formaldehyde **II**. This path corresponds to the step between **VI** and **VII** in Fig. 7. The cation **I** is then subjected to the C-O bond fission, producing an alcohol **III** and a formaldehyde **IV**.

$$ROCH_2CH_2OH \xrightarrow{-e,\,-H^+} ROCH_2CH_2O\cdot \xrightarrow{-e} \overset{+}{R}OCH_2\ (\mathbf{I}) \xrightarrow{+H_2O,\,-H^+} ROH\ (\mathbf{III}) + H_2CO\ (\mathbf{II}) \qquad + H_2CO\ (\mathbf{IV})$$

Scheme 1.

Our experimental results indicate that the first two steps of Scheme 1 occurred on the irradiated TiO_2 surface. The subsequent C-O bond fission, however, did not occur. Instead, oxidation of the carbon atom of **I** took place, yielding ethyl formate.

Adsorption of $EtOCH_2CH_2OH$ on TiO_2 in the Dark. We assigned the IR bands at 1575 and 1360 cm^{-1} which appeared after the adsorption of $EtOCH_2CH_2OH$ on TiO_2, to the surface species produced from adsorbed $EtOCH_2CH_2OH$ and oxygen species on TiO_2 (Fig. 7 (**VI**)). Although these bands are in good accordance with those at 1560 and 1360 cm^{-1} of the formate species on TiO_2 prepared from 2-propanol and oxygen at 523 K,[20] it is concluded that the adsorption of $EtOCH_2CH_2OH$ onto TiO_2 surface at room temperature in the dark did not produce the surface formate species. This is because raising the temperature of the TiO_2 powder with $EtOCH_2CH_2OH$ up to 353 K did not release any decomposed products which would be formed along with the surface formate species. In our experimental conditions molecular oxygen was adsorbed on the TiO_2 surface before the introduction of $EtOCH_2CH_2OH$. Molecular oxygen is reported to accept an electron from TiO_2, producing surface O_2^- which is stable at room temperature and can react with organic substances when they are introduced at higher temperatures.[24] Taking this into consideration we propose that the preadsorbed oxygen molecule accepts an electron from TiO_2 and reacts with $EtOCH_2$-

CH_2OH to form a surface formate-like species (Fig. 7 (**VI**)) which has IR bands at 1575 and 1360 cm^{-1}.

Surface Species on TiO_2 during the UV-Irradiation. The UV-irradiation caused an increase in intensity of the band at 1575 cm^{-1} (Figs. 4, 5). We assigned this band to the surface formate species (Fig. 7 (**VIII**)) for the following two reasons: (1) the bands at around 2850—3000 cm^{-1} due to $-CH_3$, and $-CH_2-$ disappeared while the band at 1575 cm^{-1} increased upon irradiation (Fig. 4). This result indicates that the species which has band at 1575 cm^{-1} produced upon UV-irradiation is neither adsorbed $EtOCH_2CH_2OH$ nor ethyl formate on TiO_2 because both of them have the IR bands at 2850—3000 cm^{-1} (Fig. 3 (c),(d)), (2) the simultaneous measurement of the intensity of the IR transmittance at 1575 cm^{-1} and the amount ot ethyl formate in gas phase (Fig. 5) showed that the production of ethyl formate precedes the surface species. This result can be interpreted as follows; surface formate species is produced from the C_1-species which is formed concomitantly with ethyl formate through the C-C cleavage.

Gonzalez et al. assigned the IR band at 1730 cm^{-1} to a surface ketene species (Table 1), which was produced by the thermal reaction of acetic acid on TiO_2.[21] This surface ketene species was produced by the dehydrogenation of a surface acetate species, which indicated that the ketene species was in a more oxidized state than the acetate species. In our experiment the band at 1730 cm^{-1} appeared only in the early stage of the illumination and it did not increase in intensity upon the prolonged UV-irradiation, which was in contrast to the progressive increase of the band at 1440 cm^{-1} with irradiation time. From this result, it is reasonable to assign the band at 1730 cm^{-1} not to the ketene species but to a precursor of an acetate species. Since free aldehyde has an IR band at around 1730—1740 cm^{-1} due to C=O stretching,[25] the formation of physisorbed aldehyde may be responsible for the IR band at 1730 cm^{-1}. When ethyl formate (Fig. 3 (d)) or acetaldehyde was adsorbed on TiO_2 in the dark, the band due to C=O was shifted to lower wavenumbers because aldehyde was chemisorbed on TiO_2. But carboxylate species such as formates and acetates were reported by Gonzalez et al. to have a dislodging effect on oxygen species bound to Ti^{4+},[21] which allowed aldehyde to physisorb onto the TiO_2 surface. Hence, we concluded that the band at 1730 cm^{-1} was due to the physisorbed ethyl formate (Fig. 7 (**VII**)) which has a formyl group in it.

Based on the results from the IR studies and products analysis we propose a reaction pathway for the photocatalytic oxidation of $EtOCH_2CH_2OH$ on TiO_2 surface, as shown in Fig. 7; $EtOCH_2CH_2OH$ is adsorbed on TiO_2 to yield surface alkoxide **V** and then reacts with the adsorbed O_2^- to produce formate-like species **VI** which has a strong IR band at 1575 and 1360 cm^{-1}. This surface species decomposes upon UV irradiation into ethyl formate **VII** in gas phase and the surface formate species on TiO_2 **VIII**. The surface formate species is oxidized further to CO_2. Further, the ethyl formate is oxidized photocatalyticaly to ethanol, acetaldehyde, and acetate species when the surface concentration of $EtOCH_2CH_2OH$ is low.

Intermediate Radical Species. The ESR experiment revealed that carbon-centered radical was produced from $EtOCH_2CH_2OH$ on TiO_2 upon UV-irradiation. Assuming that the electron transfer from the alcoholic OH of the adsorbed $EtOCH_2CH_2OH$ takes place in the primary step of the reaction, analogous to the case of Pt electrode, the photocatalytically produced radical **XI** will be converted to 2-ethoxy-1-hydroxyethyl radical **XII** or ethoxymethyl radical (**XIII**) by the subsequent β fragmentation, as shown in Scheme 2. This process corresponds to the step between **VI** and **VII** in Fig. 7.

$$EtOCH_2CH_2\dot{O}\overset{+}{H}\ (\mathbf{XI}) \begin{cases} \nearrow\ EtOCH_2\dot{C}HOH\ (\mathbf{XII}) + H^+ \\ \searrow\ EtOCH_2\dot{C}\ (\mathbf{XII}) + H_2CO + H^+ \end{cases}$$

Scheme 2.

Both of the radicals (**XII** and **XIII**) are carbon-centered. The former corresponds to the intermediate in the direct oxidation and the latter corresponds to the intermediate in the indirect oxidation.[23] From the reaction product, ethyl formate, a radical species **XIII** is supposed to be produced in the present experiment. We have already reported that alcohols with an α-hydrogen does not give a high concentration of spin adducts with DMPO in the irradiated TiO_2 suspension of alcohol. This is because the intermediate radicals immediately inject another electron into the conduction band of TiO_2, inducing a current doubling phenomenon.[15] Although $EtOCH_2CH_2OH$ is an alcohol with α-hydrogens and hence can bring about a current doubling,[26] $EtOCH_2CH_2OH$ gave experimentally a rather high concentration of a spin adduct in comparison with methanol or ethanol. The radical species **XIII** is more stable than those produced from methanol , ethanol, and 2-propanol.

Conclusion

The photocatalytic reaction of $EtOCH_2CH_2OH$ on TiO_2 powder gives ethyl formate as the primary product. The reaction product is different from the one expected from the reaction mechanism proposed for primary alcohol before. Base on our experimental results, we conclude that $EtOCH_2CH_2OH$ adsorbs on TiO_2 and reacts with the adsorbed O_2^- on the TiO_2 surface to produce a surface formate-like species . This surface species is photocatalytically oxidized to give ethyl formate and surface formate species. The former is further oxidized to ethanol, acetaldehyde, and acetate species by prolonged UV-irradiation. The photocatalytic oxidation of $EtOCH_2CH_2OH$ on TiO_2 is another example in which the products are different

from those from the electrolysis on a Pt electrode.[14]

Mr. Haru Sakashita of Faculty of Engineering, University of Tokyo is acknowledged for GC-MS analysis.

References

1) M. A. Fox, *Acc. Chem. Res.*, **16**, 314 (1983).
2) D. J. C. Yates, *J. Phys. Chem.*, **65**, 746 (1961).
3) M. L. Hair, "Infrared Spectroscopy in Surface Science," Marcel Dekker, Inc., New York (1967).
4) K. Tanaka and J. M. White, *J. Phys. Chem.*, **86**, 4708 (1982) and references therein.
5) G. Busca, H. Saussey, O. Saur, J. C. Lavalley, and V. N. Lorenzelli, *Appl. Catal.*, **14**, 245 (1985).
6) V. N. Filimonov, *Kinet. Catal.*, **7**, 512 (1966).
7) M. Kawai, T. Kawai, S. Naito, and K. Tamaru, *Chem. Phys. Lett.*, **110**, 58 (1984).
8) S. N. Frank and A. J. Bard, *J. Am. Chem. Soc.*, **99**, 303 (1977).
9) S. Nishimoto, B. Ohtani, H. Shirai, S. Adzuma, and T. Kagiya, *Polym. Commun.*, **26**, 292 (1985)
10) S. D. Ross, J. E. Barry, M. Finkelstein, and E. J. Rudd, *J. Am. Chem. Soc.*, **95**, 2193 (1973).
11) M. Sugawara, *Bull. Yamagata Univ., Eng.*, **16**, 43 (1980).
12) C. Bruneau, N. Soyer, A. Brault, and M. Kerfanto, *Ind. Eng. Chem. Prod. Res. Dev.*, **21**, 74 (1982).
13) R. Gopalan and G. R. R. Sankar, *J. Indian Chem. Soc.*, **55**, 1011 (1978).
14) M. A. Fox, C-C. Chen, K. H. Park, and J. N. Younathan, Am. Chem. Soc. Symposium Series, **278**, 69 (1973).
15) S. Yamagata, S. Nakabayashi, K. M. Sancier, and A. Fujishima, *Bull. Chem. Soc. Jpn.*, **61**, 3429 (1988).
16) T. Sato, K. Takahashi, and S. Ichikawa, *Nippon Kagaku Kaishi*, **1984**, 119.
17) "Registry of Mass Spectral Data," ed by E. Stenhagen, S. Abrahamsson, and F. W. Melafferty, John Wiley and Sons, New York (1974), Vol. 1, p. 29.
18) P. R. Harvey, R. Rudham, and S. Ward, *J. Chem. Soc., Faraday Trans. 1*, **79**, 2975 (1983).
19) J. Cunningham and B. K. Hondnett, *J. Chem. Soc., Faraday Trans. 1*, **77**, 2777 (1981)
20) T. Nakajima, H. Miyata, and Y. Kubokawa, *Bull. Chem. Soc. Jpn.*, **55**, 609 (1982).
21) F. Gonzalez, G. Munuera, and J. A. Prieto, *J. Chem. Soc., Faraday Trans. 1*, **74**, 1517 (1978).
22) E. G. Janzen and J. I-P. Liu, *J. Mag. Res.*, **9**, 510 (1973).
23) N. Djeghri and S. J. Teichner, *J. Catal.*, **62**, 99 (1980).
24) M. Akimoto and E. Echigoya, *J. Chem. Soc., Faraday Trans. 1*, **73**, 193 (1977).
25) L. J. Bellamy, "The Infra-red Spectra of Complex Molecules," John Wiley and Sons, New York (1975).
26) S. Yamagata and A. Fujishima, unpublished data.

Novel Ferroelectric Liquid Crystals Derived from Normal Alkyl Esters of (*R*)-3-Hydroxybutanoic Acid. The Correlation between Molecular Structure and Mesomorphic Properties

Jun NAKAUCHI,* Keiichi SAKASHITA, Yoshitaka KAGEYAMA, Seiji HAYASHI, and Kenji MORI†
Tokyo Research Laboratory, Mitsubishi Rayon Co., Ltd., Noborito, Tama-ku, Kawasaki, Kanagawa 214
†Department of Agricaltural Chemistry, The University of Tokyo, Yayoi 1-1-1, Bunkyo-ku, Tokyo 113
(Received Sepetmber 16, 1988)

The following series of novel ferroelectric liquid crystals, derived from normal alkyl esters of (*R*)-3-hydroxybutanoic acid, have been synthesized, and several factors determining their mesomorphic properties have been investigated:

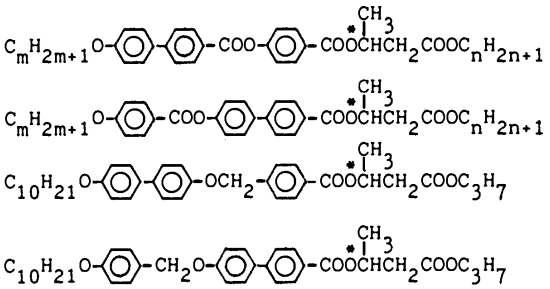

The smectic polymorphism for these compounds with three aromatic rings is strongly affected by the position and kind of the linkage groups in the core. The effects of the lengths of the two terminal chains (*m*,*n*) and the linkage groups in the core on the thermal stability of the smectic A and chiral smectic C phases have been discussed from the structural points of view.

Very many compounds with a chiral smectic C(Sm*C) phase have been synthesized since the invention of high-speed switching devices based on these compounds' ferroelectric properties.[1] Their common structural features are a rigid core consisting of at least two aromatic rings and two terminal chains at the ends of the core, one of which contains at least one chiral group.

There have been many studies of the effects of molecular structure of the core and the length of the achiral terminal chain on the mesomorphic properties of the liquid crystals.[2] However, the correlation between the molecular structure and the mesomorphic properties still remains insufficiently understood. Especially, there have been few investigations of the effect of the length of terminal chain at the chiral part on the mesomorphic properties because of the limited number of chiral reagents used in experiments.

Systematic investigations of the effect of the lengths of the two terminal chains on the mesomorphic properties have been made by Goodby and Gray employing homologues of the normal alkyl esters of 4′-alkoxy-1-biphenylcarboxylic acids. They have shown that the SmC phase appears when both the terminal chains have an appropriate chain length,[3] although these compounds do not have chiral groups in their molecular structures.

We have selected normal alkyl esters of (*R*)-3-hydroxybutanoic acid as chiral reagents and have synthesized novel ferroelectric liquid crystals with three aromatic rings in the core. Their general molecular structures are as follows:

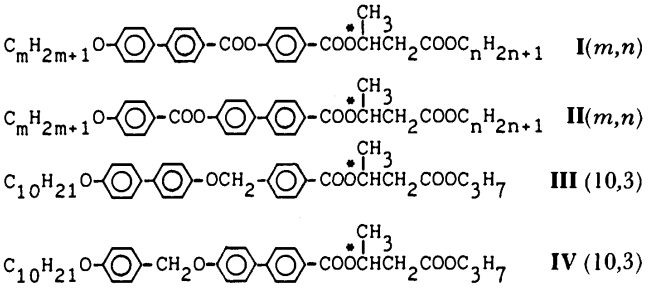

One of these compounds **I**(8,2) has already been synthesized and its ferroelectric property reported by Taniguchi et al.;[4] however, no systematic investigations of the mesomorphic properties of the homologous series have yet been done.

In the present paper, we discuss the effect of the lengths of two terminal chains and of the position and kind of the linkage groups in the core on the thermal stability of the mesophase.

Experimental

Preparation of Materials. The homologous series, **I**(*m*,*n*) and **II**(*m*,*n*), and the analogues, **III**(10,3) and **IV**(10,3), were synthesized by Scheme 1.

In order to obtain highly optically pure reagents, poly-((*R*)-3-hydroxybutanoic acid) (PHB) (Imperial Chemical Industry Co., Ltd.) was chosen as the starting material. The normal alkyl esters of (*R*)-3-hydroxybutanoic acid were eas-

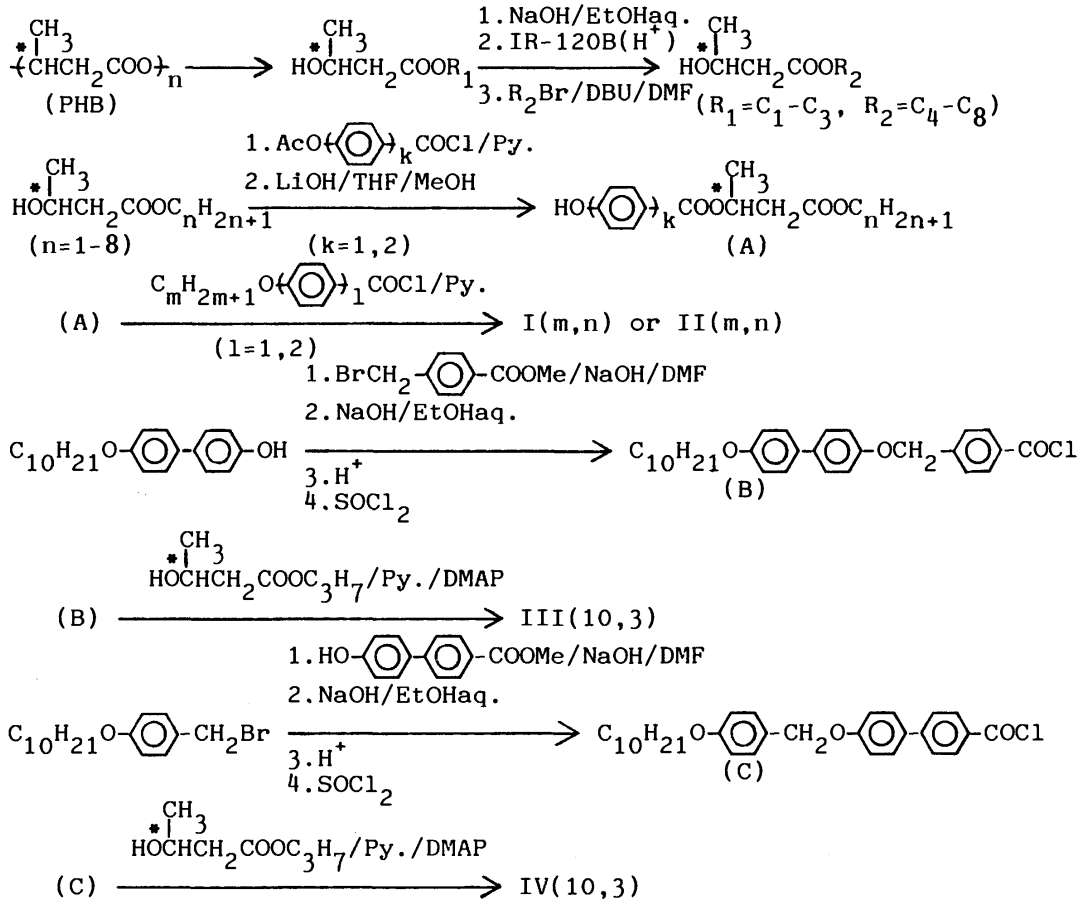

Scheme 1.

ily prepared by the following method. The lower alkyl (R_1: methyl, ethyl, propyl) esters of (*R*)-3-hydroxybutanoic acid were synthesized by the alkolysis of PHB in the corresponding dry alcohols, using conc. H_2SO_4 as the catalyst. Sugai et al. reported that the optical purity of ethyl (*R*)-3-hydroxybutanoate synthesized by a similar method was 100% e.e. ($[\alpha]_D^{21}=-43.4°$ in $CHCl_3$).[5] The specific rotation $[\alpha]_D^{23}$ of the ethyl (*R*)-3-hydroxybutanoate prepared by our method was −44.7°; therefore, its optical purity was estimated to be 100% e.e. The higher alkyl (R_2: butyl, pentyl, octyl) esters of (*R*)-3-hydroxybutanoic acid were prepared by an esterification reaction of (*R*)-3-hydroxybutanoic acid obtained by the hydrolysis of the ethyl (*R*)-3-hydroxybutanoate with the corresponding alkyl bromides in *N*,*N*-dimethylformamide (DMF), using 1,8-diazabicyclo[5.4.0.]-7-undecene (DBU) as the catalyst. The esters of 4-hydroxybenzoic acid or 4′-hydroxy-1-biphenylcarboxylic acid with the normal alkyl esters of (*R*)-3-hydroxybutanoic acid were prepared by reacting 4-acetoxybenzoyl chloride or 4′-acetoxy-1-biphenylcarbonyl chloride with normal alkyl (*R*)-3-hydroxybutanoates in dry pyridine, followed by the hydrolysis of acetoxyl group selectively in a mixed solvent of tetrahydrofuran (THF) and methanol containing equimolar 1 mol dm^{-3} LiOH. The homologous series, **I**(*m*,*n*) and **II**(*m*,*n*), were synthesized by esterifying the (A) compounds with the corresponding 4-alkoxybenzoyl chlorides or 4′-alkoxy-1-biphenylcarbonyl chlorides in dry pyridine. Compounds **III**(10,3) and **IV**(10,3) were prepared by reacting propyl (*R*)-3-hydroxybutanoate with Compounds **B** and **C** respectively in dry pyridine containing 10 wt% 4-dimethylaminopyridine (DMAP). All the final products were purified by silica-gel column chromatography, followed by two recrystallizations from ethanol.

Their elementary analysis data are listed in Table 1.

Measurement of Thermal Properties. The mesophase was identified using a Nikon polarizing microscope equipped with a Mettler FP-52 heating stage. the transition temperatures were measured using a Daini Seikosha SSC-560 differential scanning calorimeter (DSC) at a scanning rate of 2.5 °C min^{-1} under N_2 atomosphere.

Results and Discussion

The melting points and the mesomorphic transition temperatures for the homologous series, **I**(*m*,*n*) and **II**(*m*,*n*), are summarized in Table 2. The mesomorphic trends of **I**(*m*,3) and **II**(*m*,3) are shown in Figs. 1 and 2. As can be seen in the figures, both of the series show the phase sequence of isotropic(Iso)-smectic A(SmA)-chiral smectic C(Sm*C)-unidentified smectic phase(Sm3)-crystal(Cryst). The Sm3 phase for **I**(*m*,3) appears monotropically below the Sm*C in the homologues with shorter alkoxyl chains (*m*=7—11). This phase shows a broken and banded focal-conic fan texture or a pseudo-homeotropic or schlieren texture which resembles photomicrographs of the reference sample reported by Gray and Goodby.[6] The transi-

Table 1. Elemental Analyses for the I(m,n), II(m,n), III(10,3), and IV(10,3) Homologous Series

Homologous series	Carbon No. (m,n)	Calcd (%)		Found (%)	
		C	H	C	H
I(m,n)	(7,3)	72.83	7.19	72.97	7.25
	(8,3)	73.15	7.37	72.87	7.53
	(9,3)	73.44	7.53	73.55	7.30
	(10,3)	73.73	7.69	74.01	7.82
	(11,3)	74.00	7.84	74.12	7.85
	(12,3)	74.26	7.99	74.26	8.25
	(14,3)	74.74	8.26	74.75	8.12
	(16,3)	75.19	8.51	75.14	8.59
	(10,1)	73.15	7.37	73.18	7.54
	(10,2)	73.44	7.53	73.58	7.66
	(10,4)	74.00	7.84	73.86	7.86
	(10,5)	74.26	7.99	74.48	7.99
	(10,8)	74.97	8.39	75.14	8.63
II(m,n)	(7,3)	72.83	7.19	72.82	7.24
	(8,3)	73.15	7.37	73.00	7.40
	(9,3)	73.44	7.53	73.61	7.67
	(10,3)	73.73	7.69	73.66	7.72
	(12,3)	74.26	7.99	74.44	7.98
	(14,3)	74.74	8.26	74.97	8.48
	(16,3)	75.19	8.51	75.46	8.72
	(10,2)	73.44	7.53	73.66	7.59
	(10,4)	74.00	7.84	74.08	8.03
	(10,6)	74.50	8.13	74.23	8.25
	(10,7)	74.74	8.26	74.68	8.34
	(10,8)	74.97	8.39	75.12	8.44
III(10,3)	(10,3)	75.48	8.22	75.87	8.44
IV(10,3)	(10,3)	75.48	8.22	75.23	8.42

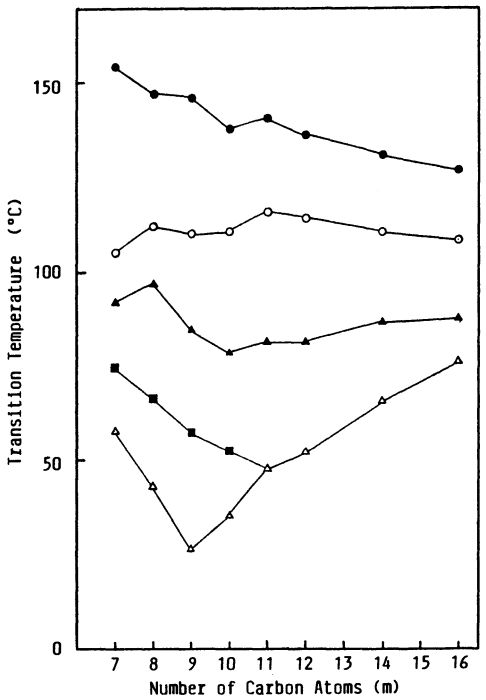

Fig. 1. Plots of transition temperatures against the number of carbon atoms (m) in the alkoxyl chain of homologous series I (m,3): mp (—▲—); Iso-SmA (—●—); SmA-Sm*C (—○—); Sm*C-Sm3 (—■—); Sm3-Cryst (—△—).

Table 2. Phase-Transition Temperatures for the I(m,n) and II(m,n) Homologous Series

Homologous series	Carbon No. (m,n)	Phase-transition temperatures(°C)[a]				
		Mp	Sm4-Sm3	Sm3-Sm*C	Sm*C-SmA	SmA-Iso
I(m,n)	(7,3)	91.8	—	(74.9)[b]	105.0	154.3
	(8,3)	96.8	—	(66.6)	112.0	147.0
	(9,3)	84.5	—	(57.1)	110.0	146.1
	(10,3)	78.6	—	(52.5)	110.5	137.9
	(11,3)	81.2	—	—	115.9	140.6
	(12,3)	81.3	—	—	114.1	136.1
	(14,3)	86.3	—	—	110.5	130.1
	(16,3)	87.2	—	—	108.2	126.9
	(10,1)	78.5	(64.0)	102.8	120.0	155.7
	(10,2)	88.1	—	(58.0)	120.0	146.1
	(10,4)	68.0	—	(50.2)	111.1	136.5
	(10,5)	70.9	—	(49.2)	95.9	129.6
	(10,8)	74.5	—	—	83.5	123.7
II(m,n)	(7,3)	68.7	—	(30.7)	(57.8)	127.6
	(8,3)	77.7	—	—	(67.5)	131.5
	(9,3)	92.2	—	—	(80.0)	129.2
	(10,3)	85.8	—	(56.6)	(84.0)	126.5
	(12,3)	77.2	—	—	93.0	122.8
	(14,3)	72.1	—	(49.3)	96.1	118.7
	(16,3)	72.2	—	—	96.5	116.0
	(10,2)	75.8	—	(58.9)	82.9	131.0
	(10,4)	63.9	—	(53.9)	65.5	124.0
	(10,6)	72.2	—	(44.3)	(64.6)	110.5
	(10,7)	76.3	—	(46.3)	(62.5)	110.5
	(10,8)	76.3	—	(46.1)	(63.9)	110.9

a) Mp; melting point, Sm3, Sm4; unidentified smectic phase, Sm*C; chiral smectic C, SmA; smectic A, Iso; isotropic liquid. b) ( ); monotropic transition.

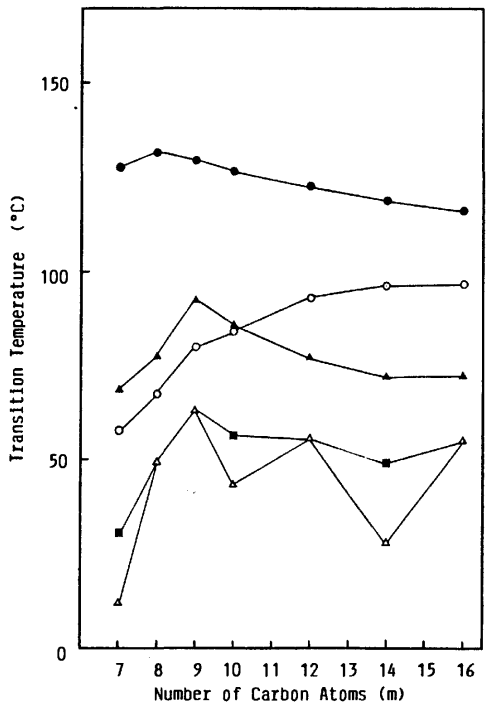

Fig. 2. Plots of transition temperatures against the number of carbon atoms (m) in the alkoxyl chain of homologous series **II** (m,3): mp (—▲—); Iso-SmA (—●—); SmA-Sm*C (—○—); Sm*C-Sm3 (—■—); Sm3-Cryst (—△—).

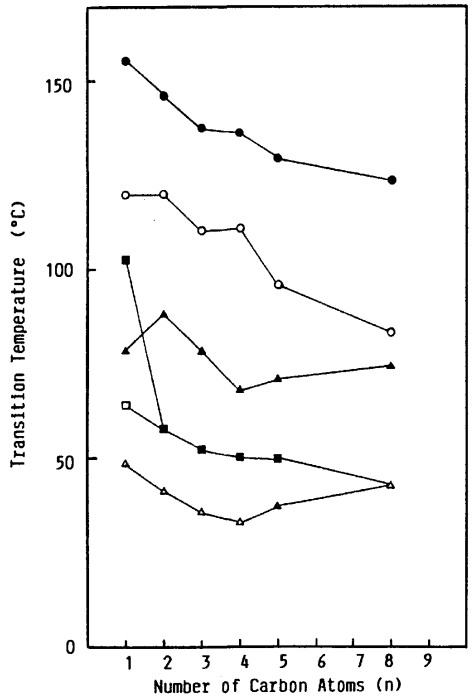

Fig. 3. Plots of transition temperatures against the number of carbon atoms (n) in the alkyl ester chain of homologous series **I** (10,n): mp (—▲—); Iso-SmA (—●—); SmA-Sm*C (—○—); Sm*C-Sm3 (—■—); Sm3-Sm4 (—□—); Sm3,Sm4-Cryst(—△—).

tion enthalpies measured by DSC are about 0.86—1.5 kJ mol^{-1}. On the other hand, the Sm3 phase for **II**(m,3) appears monotropically below the Sm*C in the homologues with heptyloxyl, decyloxyl, and tetradecyloxyl chains and shows a focal-conic fan texture or a homeotropic texture formed from the broken focal-conic fan or the schlieren textures of the Sm*C phase, respectively. Moreover, the transition bars across the backs of the fans are observed at the transition from the Sm3 phase to the Sm*C. The transition enthalpies are about 1.5—4.5 kJ mol^{-1}. From these findings, we speculate that the Sm3 phases of **I**(m,3) and **II**(m,3) may be chiral smectic I(Sm*I) and smectic B(SmB), respectively; however, more detailed study by the X-ray diffraction method and the misibility test will be necessary for the assignment of these phases.

The Iso-SmA transition temperaturs for **I**(m,3) and **II**(m,3) show normal trends, that is, an odd-even alternation and a gentle falling as the series ascend. On the other hand, the SmA-Sm*C transition temperatures show significantly different features. The Sm*C phase for **I**(m,3) appears enantiotropically, and the SmA-Sm*C transition temperatures do not change very much in respect to the length of the terminal alkoxyl chain, whereas the Sm*C phase for **II**(m,3) appears monotropically in the region of the shorter alkoxyl chains (m=7—10) and becomes enantiotropic in the region of the longer alkoxyl chains (m=12—16). Their transition temperatures gradually increase with the length of the terminal alkoxyl chain, leading to the decrease in the temperature range of the SmA phase.

There are some characteristic features in the phase transition from the Sm*C phase to the Sm3 phase for **I**(m, 3) and **II**(m, 3). The Sm*C-Sm3 transition for **I**(m,3) appears as a monotropic transition in the homologues with shorter alkoxyl chains (m=7—10), and the transition temperatures decrease with the length of the terminal alkoxyl chain. On the other hand, the Sm*C-Sm3 transition for **II**(m,3) appears as a monotropic one, and the transition temperatures seem to increase with the length of the terminal alkoxyl chain in the region of the shorter chains and to slightly decrease in the region of the longer chains. However, the correlation between the molecular structure and these Sm3 phases cannot be found at this stage because the assignment of these phases has not yet been accomplished.

Figures 3 and 4 present the mesomorphic trends of the homologous series, **I**(10,n) and **II**(10,n). These homologous series show phase sequences similar to those of the corresponding homologous series **I**(m,3) and **II**(m,3). The Sm3 phases again appear monotropically in all the homologues except **I**(10,8). All the Sm3 phases for **I**(10,n) and **II**(10,n) except that for **I**(10,1) exhibit a texture similar to those of the **I**(m,3) and **II**(m,3); therefore, the Sm3 phases of **I**(10,n) and **II**(10,n) may be Sm*I and SmB, respectively. The Sm3 phase of the **I**(10,1) homologue shows a broken focal-

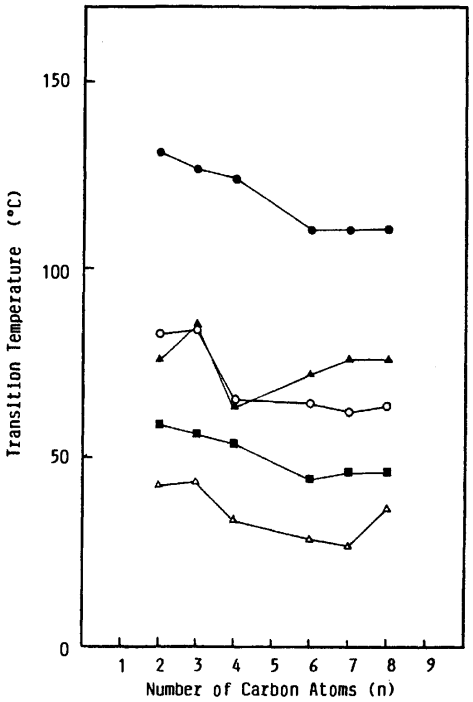

Fig. 4. Plots of transition temperatures against the number of carbon atoms (n) in the alkyl ester chain of homologous series **II** (10,n): mp(—▲—); Iso-SmA (—●—); SmA-Sm*C (—○—); Sm*C-Sm3 (—■—); Sm3-Cryst (—△—).

conic fan whose back is "L"-shaped and which has highly coloured patches or pseudo-homeotropic textures. The transition enthalpy is too small to be estimated from the DSC chart. From these findings, we speculate that this phase may be chiral smectic F(Sm*F); however, more detailed studies employing the X-ray diffraction method will be necessary for the assignment of this phase.

The effects of the terminal chain length for the chiral part on the thermal stability of the mesophase are a little different from those of the other terminal alkoxyl chain. The Iso-SmA transition temperatures for **I**(10,n) and **II**(10,n) show a gentle falling with the terminal chain length (n), although the odd-even alternation is not clear. The SmA-Sm*C transition temperatures for **I**(10,n) and **II**(10,n) also decrease with the terminal chain length (n), unlike those of the corresponding homologous series, **I**(m,3) and **II**(m,3) where the other terminal chain varies. This tendency probably means that the thermal stability of the Sm*C phase is reduced as the difference in length between the two terminal chains is small. Such a tendency has also been reported by Goodby and Gray in the homologous series of n-alkyl esters of 4-alkoxy-1-biphenylcarboxylic acids, in which the SmC phase has been observed only with the alkoxyl chain from hexyloxyl to tetradecyloxyl and with the alkyl ester chains from propyl to decyl. However, in comparison with the homologous series of the normal alkyl esters of 4-alkoxy-1-biphenyl carboxylic acids, there are some differences in

Table 3. Phase Sequence and Transition Temperature

Analogues	Phase sequence and transition temperature (°C)
I(10,3)	Cryst $\xrightarrow{78.6}$ Sm*C $\underset{}{\overset{110.5}{\rightleftharpoons}}$ SmA $\underset{}{\overset{137.9}{\rightleftharpoons}}$ Iso 35.6 ↖ Sm3 ↙ 52.5
II(10,3)	Cryst $\xrightarrow{85.8}$ SmA $\underset{}{\overset{126.5}{\rightleftharpoons}}$ Iso 43.4 ↖ Sm3 $\xleftarrow{56.6}$ Sm*C ↙ 84.0
III(10,3)	Cryst $\xrightarrow{85.4}$ Sm2 $\underset{}{\overset{110.5}{\rightleftharpoons}}$ Sm*C $\underset{}{\overset{127.0}{\rightleftharpoons}}$ Iso 35.6 ↖ Sm3 ↙ 85.4
IV(10,3)	Cryst $\xrightarrow{90.0}$ SmA $\underset{}{\overset{93.6}{\rightleftharpoons}}$ Iso 72.6 ↖ Sm*C ↙ 84.0

the effects of the terminal chains on the thermal stability of the Sm*C phase for the homologous series, **I**(m,n) and **II**(m,n), with three aromatic rings in the core. According to McMillan,[7] de Jeu,[8] and Patel and Goodby,[9] the thermal stability of the Sm*C phase is strongly affected by the polar groups in the core. In the cases of **I**(m,n) and **II**(m,n), the only structural difference between them is the position of -COO- linkage in the core. This means that the effects of the terminal chain length on the thermal stability of Sm*C phase are quite different only if the position of the linkage group is changed in the core.

To investigate the effects of the linkage groups in the core with three aromatic rings on the mesomorphic properties in more detail, the mesomorphic properties of two further analogues with the same terminal chains will be examined (Table 3).

In comparison with **I**(10,3) and **II**(10,3), the **III**(10,3) and **IV**(10,3) analogues with a $-CH_2O-$ linkage in the core have the phase sequences of Iso-Sm*C-Sm2-Sm3-Cryst and of Iso-SmA-Sm*C-Cryst, respectively. The Sm2 phase of **III**(10,3) shows a broken-fan or a schlieren texture under a polarizing microscope, and the transition enthalpy is 1.4 kJ mol^{-1}; therefore, this phase may be Sm*I. The microscopic texture of the Sm2 phase changes slightly at the Sm2-Sm3 transition and turns into another broken-banded fan or schlieren texture in the Sm3 phase, and the transition enthalpy is 2.1 kJ mol^{-1}; however, this phase cannot be speculated on at this stage. As is evident from these results, the smectic polymorphism for the homologous series with three aromatic rings in the core is strongly influenced by the position and kind of the linkage groups in the core.

There are also some characteristic tendencies for the mesomorphic transition temperatures among these four analogues. The Iso-SmA or Iso-Sm*C transition are in the order of: **I**(10,3)>**II**(10,3)≈**III**(10,3)>**IV**(10,3). As is to be expected from Gray's report,[2] the thermal stability of the smectic phase depends on the rigidity and planarity of the central linkage in the core. Con-

traty to the -COO- linkage, the $-CH_2O-$ linkage has no double-bond character; therefore, the Iso-Sm*C and Iso-SmA transition temperatures for **III**(10,3) and **IV**(10,3) should be lower than those for **I**(10,3) and **II**(10,3). Judging from the data, this speculation seems to be valid; however, the Iso-SmA transition temperature for **II**(10,3) (126.5 °C), is almost the same as the Iso-Sm*C transition temperature for **III**(10,3) (127.0 °C), and the difference in the Iso-smectic transition temperature between **I**(10,3) and **II**(10,3) is only 11.4 °C, whereas that between **III**(10,3) and **IV**(10,3) is 33.4 °C. These facts cannot be explained only by the difference in the flexibility of the linkage groups. In the core moiety containing three aromatic rings, the biphenyl ring is known greatly to enhance the thermal stability of the smectic phase because of its lath-like shape. On the other hand, the chiral part with a protruding 1-methyl branch in the molecule significantly reduces the thermal stability of the smectic phase. If the biphenyl ring is connected to the chiral part with 1-methyl branch through the -COO- linkage, as is **II**(10,3) and **IV**(10,3), they could not form a parallel arrangement with one another because of the steric hindrance of the 1-methyl branch. In the cases of **I**(10,3) and **III**(10,3), the biphenyl ring is connected to the chiral part through the $-COO-C_6H_4-COO-$ or the $-OCH_2-C_6H_4-COO-$ linkage. In these two analogues, the biphenyl rings could be packed parallel with one another more easily than those in **II**(10,3) and **IV**(10,3), because the effect of the protruding 1-methyl branch on the packing of the biphenyl ring is diluted through the linkage groups, thus leading to Iso-smectic transition temperatures higher than the corresponding analogues **II**(10,3) and **IV**(10,3). Additionally, compared with the biphenyl ring in **I**(10,3), that in **III**(10,3) is connected to the $-C_6H_4-COO^{*}CH(CH_3)-CH_2COOC_3H_7$ through the $-OCH_2-$ linkage, which is more flexible than the -COO- linkage, so that the biphenyl ring in **III**(10,3) could form the parallel arrangement most easily in the smectic phase, with the result that **III**(10,3) has a comparatively higher Iso-Sm*C transition temperature among these four analogues.

The authors would like to thank Dr. Hiroshi Sato for his hearty encouragement throughout this work and also to thank Dr. Toshio Yoshihara for his useful suggestions. The authors also wish to thank Mr. Teruyuki Yamada, Mr. Shigeo Kamimura, Mr. Yoshihiro Sako, and Mrs. Mioko Uematsu for their assistance in the experiments.

References

1) N. A. Clark and S. T. Lagerwall, *Appl. Phys. Lett.*, **36**, 899 (1980).
2) G. W. Gray, "Advances in Liquid Crystals," ed by G. H. Brown, Academic press, New York, San Francisco, London (1976), Vol. 2, p. 1.
3) J. W. Goodby and G. W. Gray, *Mol. Cryst. Liq. Cryst.*, **48**, 127 (1978).
4) H. Taniguchi, M. Ozaki, and K. Yoshino, *Jpn. J. Appl. Phys.*, **26**, Suppl. 26-2 101 (1987).
5) T. Sugai, M. Fujita, and K. Mori, *Nippon Kagaku Kaishi*, **1983**, 1315.
6) G. W. Gray and J. W. Goodby, "Smectic Liquid Crystals—Textures and Structures," Leonard Hill, Glasgow and London (1984).
7) W. L. McMillan, *Phys. Rev. A*, **8**, 1921 (1973).
8) W. H. de Jeu, *J. Phys. (Paris)*, **38**, 1265 (1977).
9) J. S. Patel and J. W. Goodby, *Mol. Cryst. Liq. Cryst.*, **144**, 117 (1987).

 © 1989 The Chemical Society of Japan Bull. Chem. Soc. Jpn., 62, 1017—1022 (1989)

The Preparation of Monodispersed α-Iron(III) Oxide Particles from 2,2′-Bipyridineiron(II) Complex

Shuichi HAMADA,* Yoshiyuki KUDO, and Takanobu MATSUMOTO
Department of Applied Chemistry, Faculty of Science, and Institute of Colloid and Interface Science, Science University of Tokyo, Kagurazaka, Shinjuku-ku, Tokyo 162
(Received September 26, 1988)

Monodispersed α-iron(III) oxide (hematite) particles were produced from an iron(II) chloride/2,2′-bipyridine system in the presence of potassium nitrate at elevated temperatures, 90—100 °C. An aqueous solution of 2,2′-bipyridineiron(II) complex directly gave spherical hematite particles (0.35 μm in size with a relative standard deviation of 0.09) under the conditions of 1.0×10^{-3} mol dm^{-3} $FeCl_2$, 3.0×10^{-3} mol dm^{-3} 2.2′-bipyridine, 6.0×10^{-3} mol dm^{-3} HCl, and 5.0×10^{-2} mol dm^{-3} KNO_3 at 100 °C for 8 h. The oxidation of iron(II) ions would be slower than the dissociation of the complex and precipitation during the course of aging. The hematite particles grew through the polynuclear layers mechanism. Iron(II) sulfate/2,2′-bipyridine mixed solutions were also capable of yielding monodispersed particles, though they were a mixture of hematite and α-iron(III) hydroxide oxide (goethite). The points of zero charge (PZC) of these particles were estimated as pH 7.7 and 7.5 for those obtained from the iron(II) chloride and sulfate/2,2′-bipyridine systems, respectively.

The preparation and characterization of monodispersed particles of metal oxide and hydrous oxide have been extensively studied by forced hydrolyses.[1-8] Monodispersed α-iron(III) oxide (hematite) particles have been prepared by aging acidified iron(III) salt solutions at elevated temperatures through the conversion of β-iron(III) hydroxide oxide, β-FeOOH, previously deposited.[2,4,5] On the other hand, an iron(III) chloride/glycine system directly gave monodispersed hematite particles through forced hydrolysis.[9,10] In the latter case, the glycinatoiron(III) complex acts as a soluble reservoir for hydroxoiron(III) complexes at higher temperatures.

In the present work, monodispersed iron(III) oxide and hydroxide oxide particles were prepared by the forced hydrolysis of 2,2′-bipyridineiron(II) complex solutions in the presence of potassium nitrate as an oxidizing agent. Furthermore, the growth process and surface characterization of the monodispersed particles are discussed.

Experimental

Materials. All of the reagents used in this work were of guaranteed grade and employed without further purification. A small amount of iron(III) species in iron(II) chloride and sulfate solutions was reduced with iron of 99.9% in purity (≈200 mesh) and corresponding acid. An aliquot of the iron(II) salt solution was passed through a column charged with an H-type cation-exchange resin (Amberlite IR 120B). Then a concentration of acid, thus replaced, was titrated in order to determine the total number of moles of iron(II) and acid. The concentration of the iron(II) species was determined spectrophotometrically with 2,2′-bipyridine. All of the solutions were previously filtered through a Membrane filter (0.2 μm in pore size) and then deoxygenated by bubbling nitrogen before use.

Procedures. A mixed solution of iron(II) salt, 2,2′-bipyridine, corresponding acid, and potassium nitrate was tightly sealed in a screw-capped glass tube at specified concentrations and then aged at 100±1 and and 90±1 °C for 8—72 h in a thermostatted air oven. The produced particles were centrifuged at 1160 g and washed repeatedly with doubly distilled water using ultrasonic equipment. The morphology and size of the particles were observed with a scanning electron microscope (model ALPHA-10S). The particles were identified using an X-ray diffractometer (model Geigerflex RAD IIIA).

The mixed solution was also aged at 100±0.5 °C for 14 h in an oil bath in order to study the growth process of monodispersed hematite particles from the concentration changes of the iron species remaining in the solution. The aged solution was quenched to room temperature at regular intervals and centrifuged to remove precipitates, followed by filtration through a Membrane filter (0.1 μm in pore size). The total concentration of the iron(II) and (III) species was determined spectrophotometrically with 2,2′-bipyridine after reducing the iron(III) species to iron(II) with hydroxylamine hydrochloride. The concentration of the iron(II) species was separately determined after masking the iron(III) ions with sodium ethylenediaminetetraacetate.

A specific surface area was measured using a modified BET analyzer (model SA1000). The surface charge density of the particles was determined by ordinary potentiometric titration as follows: a sample of 0.40 g was suspended in 50.0 cm^3 of 4.00×10^{-3} mol dm^{-3} potassium hydroxide solution. The suspension was titrated very slowly (≈30 h) with 5.00×10^{-3} mol dm^{-3} nitric acid at 25±0.1 °C under an ionic strength of 0.10 mol dm^{-3} (KNO_3) in a nitrogen atmosphere.

A surface analysis was carried out in order to identify the species adsorbed on the surface of particles using an X-ray photoelectron spectroscope (XPS), model ESCALAB Mk II.

Results

Formation of Monodispersed Hematite Particles from Iron(II) Chloride/2,2′-Bipyridine System. Figure 1 shows the concentration domain of iron(II) chloride and hydrochloric acid for making iron(III) oxide particles by forced hydrolysis at 100±1 °C for 24 h under fixed concentration ratios of [bpy]/[$FeCl_2$]=3.0 and [KNO_3]/[$FeCl_2$]=50, respectively. Monodispersed spherical particles were directly produced under a

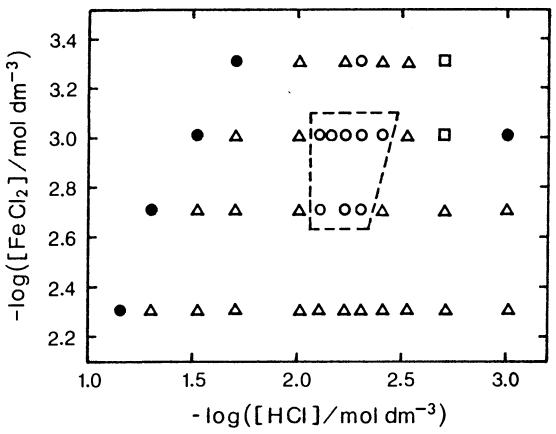

Fig. 1. Concentration domain of $FeCl_2$ and HCl for making hematite particles by forced hydrolysis at 100°C for 24 h. Conditions: [bpy]/[$FeCl_2$]=3.0, [KNO_3]/[$FeCl_2$]=50. Symbols: ○; spherical, □; flower-like, △; irregular, ●; no precipitation. A dashed line indicates the composition range for monodispersed spherical particles.

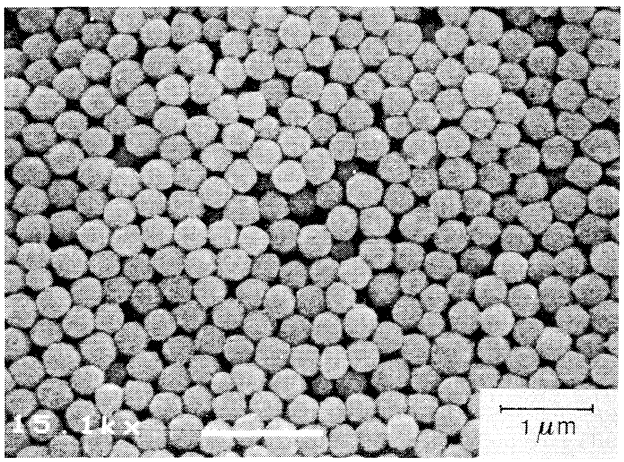

Fig. 2. Scanning electron micrograph of monodispersed spherical hematite particles prepared by forced hydrolysis at 100°C for 8 h. Conditions: [$FeCl_2$]=1.0×10^{-3}, [bpy]=3.0×10^{-3}, [HCl]=6.0×10^{-3}, [KNO_3]=5.0×10^{-2} mol dm^{-3}.

limited set of conditions (indicated by ○). No particles were observed, even after aging for 72 h, in the region indicated by ●.

Figure 2 shows an example of monodispersed spherical particles obtained at 100±1 °C for 8 h under the conditions given in the figure (an initial pH 2.2 and a final pH 2.3). The average size of these particles was estimated as being 0.35 μm, with a relative standard deviation of 0.09. The spherical particles would be polycrystals or aggregates of well-crystallized fine hematite[11] particles, judging from X-ray powder diffractometry and their morphology. On the other hand, flower-like particles (Fig. 3) were produced under the conditions shown by □, which consisted of mixtures of α-iron(III) hydroxide oxide (goethite)[12] and hematite.

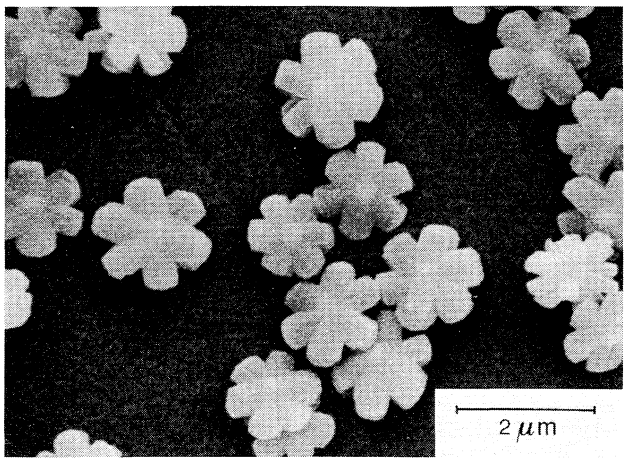

Fig. 3. Scanning electron micrograph of flower-like partilces obtained at 100°C for 24 h. Conditions; [$FeCl_2$]=5.0×10^{-4}, [bpy]=1.5×10^{-3}, [HCl]=2.0×10^{-3}, [KNO_3]=2.5×10^{-2} mol dm^{-3}.

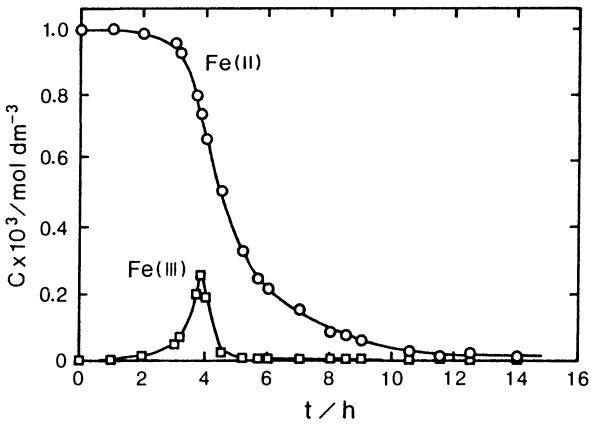

Fig. 4. Concentration changes in Fe(II) and (III) species in supernatant solution during forced hydrolysis at 100°C in 2,2′-bipyridine/iron(II) chloride system. Conditions: [$FeCl_2$]=1.0×10^{-3}, [bpy]=3.0×10^{-3}, [HCl]=6.0×10^{-3}, [KNO_3]=5.0×10^{-2} mol dm^{-3}.

Concentration Change in Iron Species during Growth of Monodispersed Spherical Hematite Particles in Iron(II) Chloride/2,2′-Bipyridine System. The concentrations of iron species in a supernatant solution were determined at 100±0.5 °C for 14 h in order to elucidate the growth process of monodispersed hematite particles under the conditions given in Fig. 2. Figure 4 shows the concentration changes in both the iron(II) and iron(III) species as a function of the aging time. The concentration of iron(II) species decreased after 1.7 h, as the release and oxidation of iron(II) ions were enhanced. However, the iron(III) species steeply increased up to a maximum value, 2.5×10^{-4} mol dm^{-3}, at 3.8 h and then drastically decreased. At the same time, the particles were generated, following a rapid decrease in the total iron concentration. The concentration of iron(III) species reached a critical supersaturation for spontaneous and rapid nucleation at 3.8 h,

followed by a negligibly small concentration of iron (III) species after 4.5 h. The oxidation of iron(II) to the trivalent state, in general, takes place slowly in the presence of nitrate ions, even in a neutral solution.[13] Thus, this process would be a rate-determining step during the growth of hematite particles after iron(II) ions have been released through the dissociation of the 2,2′-bipyridineiron(II) complex.

It has been confirmed that hydroxoiron(III) complexes act as the precursors of iron(III) oxide particles.[14,15] An appropriate supersaturation of hydroxoiron(III) complexes should be maintained in order to produce monodispersed particles[16,17] without secondary nucleation. Thus, the conditions given in the present work would satisfy the above criteria.

Growth Process of Spherical Hematite Particles. The growth process of the spherical hematite particles was examined by following the total concentration of iron species in the supernatant solution during the course of aging (Fig. 4). The reaction degree, α, is defined as

$$\alpha=(C_0-C)/(C_0-C_f), \quad (1)$$

where C_0, C_f, and C are the initial and final concentrations of the iron species, and that at reaction time t, respectively.

Nielsen[18] has proposed that a change in the reaction degree, $d\alpha/dt$, can be expressed by the following equation for the growth of particles through a polynuclear layers mechanism as:

$$d\alpha/dt=KC^{(m+2)/3}\alpha^{2/3}, \quad (2)$$

where the parameters, K and m, stand for the apparent rate constant under the given conditions and the exponent of the concentration dependence for the surface nucleation, respectively.

Parameters m and K[19] were numerically estimated as being 3.53 and 8.53×10^5 by a least-squares method using logarithmic values of $d\alpha/dt$, C, and α. Figure 5 shows the results calculated from Eq. 2 by the Runge-Kutta method using the parameters obtained above. The values, thus obtained (solid curve), agreed well with those observed in a rather wide range of the reaction degree from around 0.1 to 0.9. Similar numerical treatments were also made for the mononuclear layer and diffusion mechanisms. However, calculated values for both the mechanisms did not fit with the experimental ones. Thus, the monodispersed spherical hematite particles would grow through the polynuclear layers mechanism in the iron(II) chloride system, though they were polycrystals or aggregates.

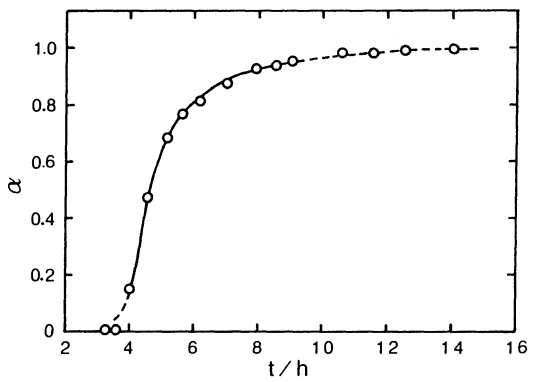

Fig. 5. Change in reaction degree during forced hydrolysis at 100 °C. Conditions: $[FeCl_2]=1.0\times10^{-3}$, $[bpy]=3.0\times10^{-3}$, $[HCl]=6.0\times10^{-3}$, $[KNO_3]=5.0\times10^{-2}$ mol dm^{-3}.

Precipitation of Iron(III) Hydrous Oxide Particles from Iron(II) Sulfate/2,2′-Bipyridine System. Mixed solutions were aged at 100±1 °C for 24 h under the fixed conditions of 5.0×10^{-3} mol dm^{-3} iron(II) sulfate and $[KNO_3]/[FeSO_4]$ ratio of 50, varying concentrations of sulfuric acid from 1.0×10^{-3} to 1.0×10^{-1} mol dm^{-3} and 2,2′-bipyridine from 5.0×10^{-3} to 2.0×10^{-2} mol dm^{-3}.

Spherical particles of a reasonably narrow size distribution were obtained only in a narrow composition range of sulfuric acid from 4.0×10^{-3} to 5.0×10^{-3} mol dm^{-3} (an initial pH 2.2—2.3) and $[bpy]/[FeSO_4]$ ratios between 2.7 and 3.3. Figure 6 shows an example of the particles comprising a mixtures of hematite and goethite, in contrast to the particles obtained in the iron(II) chloride system. Their average size was estimated as being 2.9 μm with a relative standard deviation of 0.12, much larger than those obtained in the chloride system.

Sulfate ions, in general, promote the polymerization of hydroxometal complexes, while the condensation reaction is much slower than the former.[20] Thus, hydroxoiron(III) complexes easily generate the goethite partly framed by -OH- bridges with the aid of sulfate ions, which lead to coprecipitated larger particles.

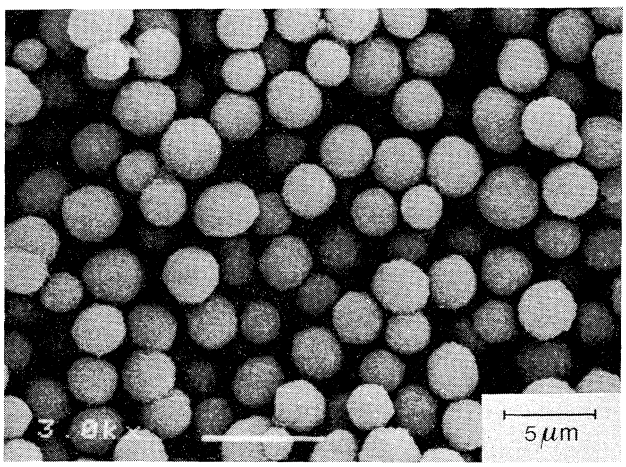

Fig. 6. Scanning electron micrograph of spherical particles obtained from 2,2′-bipyridine/iron(II) sulfate mixed solution at 100 °C for 8 h. Conditions: $[FeSO_4]=5.0\times10^{-3}$, $[bpy]=1.5\times10^{-2}$, $[H_2SO_4]=5.0\times10^{-3}$, $[KNO_3]=2.5\times10^{-1}$ mol dm^{-3}.

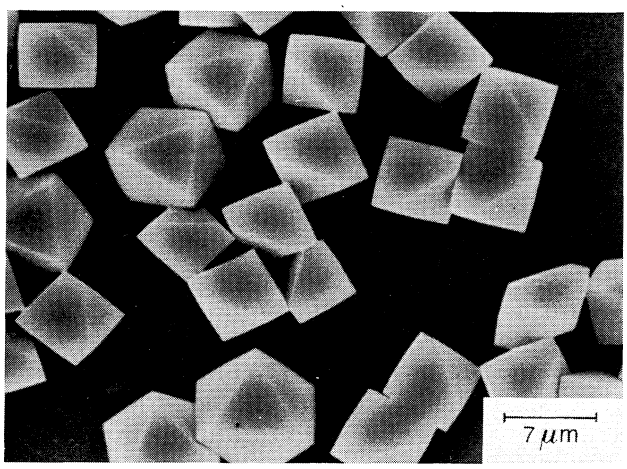

Fig. 7. Scanning electron micrograph of hydronium jarosite particles produced from 2,2′-bipyridine/iron (II) sulfate mixed solution at 100 °C for 72 h. Conditions: $[FeCl_2]=5.0\times10^{-3}$, $[bpy]=5.0\times10^{-3}$, $[H_2SO_4]=7.1\times10^{-2}$, $[KNO_3]=2.0\times10^{-1}$ mol dm^{-3}.

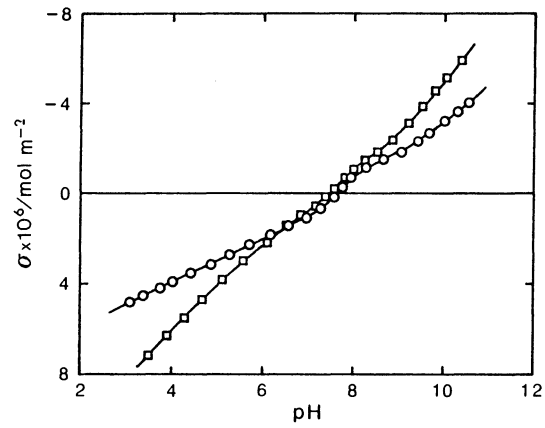

Fig. 8. Surface charge densities of spherical particles at 25 °C and I=0.1 mol dm^{-3}. Symbols: O; hematite particles obtained from iron(II) chloride system, □; mixed particles of hematite and goethite obtained from iron(II) sulfate system.

On the other hand, well-crystallized particles (Fig. 7) were created at rather higher sulfuric acid concentrations (from 5.0×10^{-2} to 7.1×10^{-2} mol dm^{-3}, an initial pH 1.1—1.2), independently of the [bpy]/[$FeSO_4$] ratio. They were identified as hydronium jarosite, $Fe_3(SO_4)_2(OH)_5\cdot2H_2O$,[21,22] by X-ray powder diffractometry, in analogy with that reported.[1] According to the formation constant and enthalpy change of protonation of 2,2′-bipyridine,[23,24] iron(II) ions would hardly form a complex with this ligand in such a low pH range (1.1—1.2). However, iron(II) ions can easily produce the sulfato complex in the presence of a large amount of sulfate ions due to their affinity.[25] Thus, these complex ions generate hydronium jarosite, independently of the [bpy]/[$FeSO_4$] ratio.

Spherical particles of reasonably narrow size distribution were also obtained at 90±1 °C under the same conditions given in Fig. 6, of which the average size was 2.0 μm with a relative standard deviation of 0.11. The composition of these particles varied depending on the duration of aging. Only goethite precipitated as spherical particles at 90±1 °C, while the particles changed to a mixture of goethite and hematite by prolonged aging for 120 h.

Goethite is irreversibly converted to hematite through topotatic dehydration due to similar oxygen stackings in their crystal structure.[26] However, the goethite scarcely changes to hematite in a solution after the former has been deposited, even though -O- bridge is more stable than -OH- bridge.[27,28] Thus, the hematite that becomes incorporated with the goethite would be directly generated during the prolonged aging at 90 °C and not through the conversion of the previously deposited goethite.

Surface Characterization of Monodispersed Spherical Particles. Surface charge densities of the particles were determined by an ordinary potentiometric titration for those obtained from the iron(II) chloride and sulfate systems. The particles were washed twenty times with doubly distilled water using ultrasonic equipment. Then they were further treated with a 1.0×10^{-4} mol dm^{-3} potassium hydroxide solution, followed by washing again twenty times with doubly distilled water. Figure 8 shows the surface charge densities of the particles as a function of pH.

The points of zero charge (PZC) were estimated as being of almost the identical pH (7.7 and 7.5) for particles prepared from the iron(II) chloride and sulfate systems, respectively. However, the PZC of the particles made from the latter was apparently found to be as low as pH 3.7 if the alkali-treatment had not been carried out, whereas that of the particles prepared from the former was approximately the same pH (7.5).

It has been reported that sulfate ions are strongly adsorbed on the surfaces of goethite particles, depending on the pH.[29] The sulfate ions would be easily replaced by hydroxide ions in an alkaline solution. Actually, the titration on the particles (the sulfate system) indicated much lower pH values, especially during the early stage of titration, as a result of the consumption of hydroxide ions. Thus, the value of PZC was apparently found to be as low as pH 3.7. According to the XPS, sulfur was detected from the surface of these particles, in contrast with those prepared from the iron(II) chloride system. A trace amount of sulfur was still detectable, even after these particles had been alkali-treated, as mentioned above, and by etching them with Ar^+ ions for 10 min in the XPS instrument. This result indicated that sulfate ions were also internally included, not only on the surfaces of the particles.

Discussion

Hydroxoiron(III) complexes have been proposed to serve as the precursors of iron(III) oxide.[15] An

enthalpy change for the formation of 2,2′-bipyridineiron(II) complex has been determined as −105—−131 kJ mol^{-1}.[23,30,31] Thus, this complex should dissociate at elevated temperatures. Figure 9 shows the absorption spectra of the 2,2′-bipyridineiron(II) complex at different temperatures. The intensity of the spectra markedly decreased with increasing temperature. These facts confirmed the above consideration.

A direct oxidation of 2,2′-bipyridineiron(II) complex is unlikely because the formal oxidation-reduction potential, $E^{0\prime}$, of the $[Fe(bpy)_3]^{3+}/[Fe(bpy)_3]^{2+}$ couple (+1.120 V)[32] is much larger than that of the Fe(II)/Fe(III) couple (+0.74 V in 0.2 mol dm^{-3} HNO_3).[33] Furthermore, 2,2′-bipyridineiron(III) species would quickly oxidize iron(II) ions (a rate constant, k=2.7×10^4 l mol^{-1} s^{-1} at 25 °C),[34] even if the direct oxidation of 2,2′-bipyridineiron(II) took place.

The stability of 2,2′-bipyridine, itself, was examined under the conditions given in this work using its own absorption band from 250 to 300 nm. A solution contained 1.5×10^{-2} mol dm^{-3} 2,2′-bipyridine, 5.0×10^{-3} mol dm^{-3} sulfuric acid, and 2.5×10^{-1} mol dm^{-3} potassium nitrate was heat-treated at 100 °C for 24 h. Little change in the intensity of the absorption band indicated that 2,2′-bipyridine scarcely decomposed under these conditions.

These facts clearly indicated that the iron(II) ions were released by only the dissociation of the complex, not by the degradation of the ligand at higher temperatures. Then, iron(II) ions were oxidized to the trivalent state by coexisting nitrate ions, followed by forced hydrolysis. Thus, the 2,2′-bipyridineiron (II) complex acted as a soluble reservoir of hydroxoiron(III) complexes for the iron(III) oxide and hydroxide oxide particles.

Monodispersed spherical particles were obtained at almost the same pH range (2.2—2.4) in both the iron (II) chloride and sulfate systems. Hydroxoiron(III) complexes should be controlled at a suitable supersaturation for making monodispersed oxide particles by adjusting the iron(II) salt concentration and pH of the starting solution. The kind of anions present also affect the shape, size, and chemical composition of the particles.[3-6] As mentioned above, the optimum conditions were limited to within a relatively narrow range.

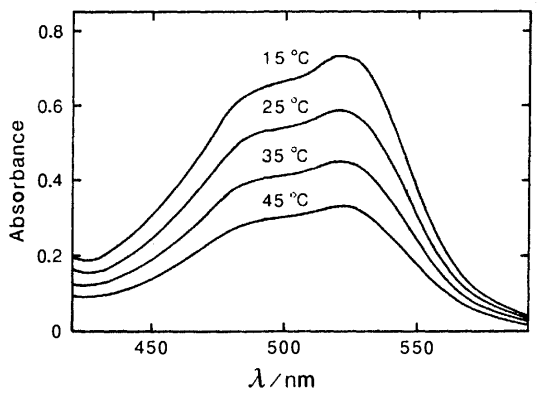

Fig. 9. Spectra of 2,2′-bipyridineiron(II) complex solution at different temperatures. Conditions: $[FeSO_4]$=1.6×10^{-4}, [bpy]=4.8×10^{-4}, $[H_2SO_4]$=5.0×10^{-3} mol dm^{-3}.

Table 1. Effect of Potassium Nitrate Concentration on Formation of Hematite Particles at 100°C[a]

Sample	$\frac{[KNO_3]}{[FeCl_2]}$	d / μm	RSD[b]	Morphology
A	5			Irregular
B	10	1.11	0.21	Spherical
C	25	0.61	0.16	Spherical
D	50	0.39	0.14	Spherical
E	100	0.32	0.17	Spherical

a) $[FeCl_2]$=1.0×10^{-3}, [bpy]=3.0×10^{-3}, [HCl]=6.0×10^{-3} mol dm^{-3}; aging time: 94 h (A), 24 h (B—E). b) Relative standard deviation.

The oxidation rate of iron(II) ions is also an important factor for making monodispersed particles. One effect of the oxidant concentration on the morphology and size of the particles was examined by varying the concentration ratio, $[KNO_3]/[FeCl_2]$, from 5 to 100. As shown in Table 1, spherical particles of the narrowest size distribution could be obtained at a concentration ratio of 50 under these experimental conditions, whereas the average size normally decreased from 1.11 to 0.32 μm owing to a rapid oxidation of iron(II) species as the concentration ratio increased from 10 to 100. Thus, this concentration ratio of 50 was taken in the present work.

Nitrate ions, in general, scarcely coordinate with iron(III) ions, so that they hardly affect the nucleation and growth rates by surface complexation but by oxidation. On the other hand, much faster oxidation makes longer nucleation periods, leading to polydispersed particles.

The concentration ratio of 2,2′-bipyridine to iron(II) ions was also sensitive for making monodispersed particles, especially in the iron(II) sulfate system. It is well known that 2,2′-bipyridine coordinates with iron(II) ion at a molar ratio of 3 : 1. Therefore, the stability of this complex would be greatly dependent on the ratio, [bpy]/[Fe(II)], and the pH of the solution.

References

1) E. Matijević, R. S. Sapieszko, and J. B. Melville, *J. Colloid Interface Sci.*, **50**, 567 (1975).
2) E. Matijević and P. Scheiner. *J. Colloid Interface Sci.*, **63**, 509 (1978).
3) E. Matijević, *Acc. Chem. Res.*, **14**, 22, (1981).
4) S. Hamada and E. Matijević, *J. Colloid Interface Sci.*, **84**, 274 (1981).
5) S. Hamada and E. Matijević, *J. Chem. Soc., Faraday Trans. 1*, **78**, 2147 (1982).
6) E. Matijević, *Ann. Rev. Mater. Sci.*, **15**, 483 (1985).
7) S. Hamada, K. Bando, and Y. Kudo, *Bull. Chem. Soc.*

Jpn., **59**, 2063 (1986).
8) S. Hamada, Y. Kudo, J. Okada, and H. Kano, *J. Colloid Interface Sci.*, **118**, 356 (1987).
9) S. Hamada, T. Hanami, and Y. Kudo, *Nippon Kagaku Kaishi*, **1984**, 1065.
10) S. Hamada, S. Niizeki, and Y. Kudo, *Bull. Chem. Soc. Jpn.*, **59**, 3443 (1986).
11) V. Kastalsky and M. F. Wescott, *Aust. J. Chem.*, **21**, 1061 (1968).
12) M. A. Peacock, *Trans. Roy. Soc. Canada IV*, **36**, 116, (1942).
13) T. Sugimoto and E. Matijević, *J. Colloid Interface Sci.*, **74**, 227 (1980).
14) R. T. Atkinson, A. M. Posner, and J. P. Quirk, *Clays Clay Minerals*, **25**, 49 (1977).
15) C. M. Flynn, Jr., *Chem. Rev.*, **84**, 31 (1984).
16) V. K. La Mer, *Ind. Eng. Chem.*, **44**, 1270 (1952).
17) T. Sugimoto, *Hyomen*, **22**, 177 (1984).
18) A. E. Nielsen, "Kinetics of Precipitation," Pergamon Press, Oxford (1964), p. 29.
19) The dimension of K is $dm^6 mol^{-2} h^{-1}$ assuming that m equals 4.
20) J. Dousma and P. L. Bruyn, *J. Colloid Interface Sci.*, **64**, 154 (1978).
21) J. D. H. Donnay and H. M. Ondic, "Crystal Data Determinative Tables," 3rd ed., U. S. Dept. of Commerce, Washington D.C., 1973, Vol. 2, p. 238.
22) J. D. Dana and E. S. Dana, "The System of Mineralogy," 7th ed., John Willey, New York (1951), Vol. 2, p. 555.
23) R. L. Davies and K. W. Dunning, *J. Chem. Soc. (London)*, **1965**, 4168.
24) D. D. Perrin and S. Sharma, *J. Inorg. Nucl. Chem.*, **28**, 1271 (1966).
25) R. L. S. Willix, *Trans. Faraday Soc.*, **59**, 1315 (1963).
26) E. J. Fasiska, *Corros. Sci.*, **7**, 833 (1967).
27) A. L. Mackay, "Reactivity of Solid," ed. by J. H. De Boer, Elsevier, Amsterdam (1961), p. 571.
28) J. C. Bailar, Jr. and D. H. Busch, "The Chemistry of the Coordination Compound," Reinhold, New York (1956), p. 448.
29) R. L. Parfitt and R. St. C. Smart, *J. Chem. Soc., Faraday Trans. 1*, **73**, 796 (1977).
30) G. Anderegg, *Helv. Chim. Acta*, **46**, 2813 (1963).
31) G. Biswas, S. Aditya, and S. C. Lahiri, *Thermochim. Acta*, **19**, 55 (1977).
32) S. Kotrlý and L. Šůcha, "Handbook of Chemical Equilibria in Analytical Chemistry," Ellis Horwood, West Sussex (1985), p. 230.
33) G. Charlot, M. A. Collumeau, and M. J. C. Marchon, "Selected Constants: Oxidation-Reduction Potentials of Inorganic Substances in Aqueous Solution," Butterworths, London (1971), p. 20.
34) M. H. Ford-Smlth and N. Sutin, *J. Am. Chem. Soc.*, **83**, 1830 (1961).

Charge-Transfer Rates in Thin Polyelectrolyte Films Incorporating a Redox Molecule with Two Separate Electroactive Centers Having Different Redox Potentials. An Alizarine Red S-Cationic Perfluoropolymer Film System

Takeo OHSAKA, Youko TAKAHIRA, Osamu HATOZAKI, and Noboru OYAMA*
Department of Applied Chemistry for Resources, Tokyo University of Agriculture and Technology, Koganei, Tokyo 184
(Received October 13, 1988)

The diffusion coefficients for the charge-transport processes through 9,10-dihydro-3,4-dihydroxy-9,10-dioxo-2-anthracenesulfonate (Alizarine Red S, **1**)-incorporating cationic perfluoropolymer (CPFP) polyelectrolyte films on electrodes undergoing oxidation or reduction of two separate electroactive centers with different redox potentials, i.e., the two-electron reduction of **1** to 3,4,9,10-tetrahydroxy-2-anthracenesulfonate (**2**) and the two-electron oxidations of **2** to **1** and **1** to 3,4,9,10-tetrahydro-3,4,9,10-tetraoxo-2-anthracenesulfonate (**3**) were measured by potential-step chronoamperometry and chronocoulometry. The apparent diffusion coefficients for **1** to **2**, **2** to **1**, and **1** to **3** processes where the first two processes are reversible and the **1** to **3** process is irreversible, represented as $D_{app}^{rev}(1\rightarrow2)$, $D_{app}^{rev}(2\rightarrow1)$ and D_{app}^{irrrev} $(1\rightarrow3)$, respectively, decreased with increasing the concentration (C_{film}) of **1** (or **2**) in the CPFP film, and for a given C_{film} they were found to be in the following order: $D_s' \gg D_{app}^{rev}(1\rightarrow2) \sim D_{app}^{rev}(2\rightarrow1) > D_{app}^{irrev}(1\rightarrow3)$, where D_s' represents the diffusion coefficients corresponding to the diffusion of supporting electrolyte ions coupled to electron transfer and molecular motion of reactant itself. It became apparent that the difference in $D_{app}^{rev}(1\rightarrow2)$ (or $D_{app}^{rev}(2\rightarrow1)$) and D_{app}^{irrev} $(1\rightarrow3)$ can be attributed to different contributions of electron exchange between electroactive centers to the overall charge-transport rates. The results demonstrate that the contributions from molecular motion of reactant itself and electron exchange between reactants to the overall charge-transport rates can be estimated depending upon which redox center is employed in an electrochemical measurement of diffusional rates.

Charge transport through thin films (thicknesses are typically ca. 10^{-6}—10^{-3} cm) of redox polymers with electroactive mobile reactants or fixed sites, which are coated on electrode surfaces and are well-swollen with solvent/electrolyte, has been a subject of much interest in recent years.[1-20] The mechanisms of charge transport are generally reasonably well-understood, but in any particular case it is often difficult to determine the rate-determining step, especially in the case[2a,3,4f,5,6a,9,12,14,15,17] where the electroactive reactants incorporated in films are not part of the polymeric structure or permanently attached to functional groups present in the films. In this case, the diffusion of electroactive reactants within the polymeric matrix can include contributions from both molecular motion[1b,2a-c,3a,b,d,e,g,4b,c,f,g,5,9,12,14,15] and electron exchange between adjacent pairs of the oxidized and reduced reactants.[1a,b,2c-e,3b,c,f,g,4a,d,e,5g-i,12,21,22] The diffusion is also usually accompanied by migration of electrolyte ions to maintain electroneutrality, motion of solvent and segmental motion of polymeric chain. Thus, it has been generally known that the rates of charge transport, which has been proved to be treated in many cases[1-5,7a,8a,9a,b,12-15,17-20] as a Fickian diffusion process, depend on the polymer matrix, the electroactive reactant incorporated into it, the concentration of the reactant, the supporting electrolyte and its concentration, pH of solution, solvent, etc.

A variety of redox polymer film systems have been ever used as models for the fundamental elucidation of charge-transfer process within thin films on electrodes.[1-9,12,14,15,17-20] Among these, a system, where a molecule with two separate electroactive centers having different redox potentials is incorporated in a polyelectrolyte film on electrodes, is of particular interest as originally pointed out by Tsou and Anson,[3f] because one could obtain new information on charge transport that is not obtained or is different from that obtained for cases where a kind of redox species is incorporated in a film or two kinds of redox species are simultaneously incorporated in it. Tsou and Anson have measured the diffusion coefficients of the hetero-binuclear metal complex $(NH_3)_5RuC_5H_4N$-$CH_2NHC(=O)$-$CpFeCp$ (C_5H_4N=4-pyridyl, Cp=cyclopentadienide or substituted cyclopentadienide) within Nafion coatings in all three of its possible redox states (i.e., $Ru^{II}LFe^{II}$, $Ru^{III}LFe^{II}$, $Ru^{III}LFe^{III}$) and have explained successfully possible origins of the differences of the diffusional rates corresponding to these three oxidation states and their concentration dependences on the basis of intermolecular electron self-exchange, single-file diffusion and electrostatic cross linking. More recently, we[23] also have reported the preliminary results concerning the charge-transport rates for the oxidation and reduction of the two separate electroactive centers-containing molecule/thin polymer film system, i.e., 9,10-dihydro-3,4-dihydroxy-9,10-dioxo-2-anthracenesulfonate (which is often called Alizarine Red S dye and is abbreviated as ARS in this paper)-incorporating perfluoropolymer (CPFP) film system. ARS contains two separate electroactive centers, i.e., 3,4-dihydroxy and 9,10-dioxo groups, and the electrode reactions of 3,4-dihydroxy and 9,10-dioxo groups are irreversible and reversible, respectively.[23,24] Thus, if the electron exchange between electroactive centers contributes significantly

to the overall charge-transport rates, we could observe different charge-transport rates for the oxidation (or reduction) process of these two kinds of the electroactive centers. This is the first reason why we chose ARS as an electroactive molecule to be incorporated in films. The electroinactive functional group (i.e., SO_3^- group) serves as a counter anion site of the fixed cationic quaternized ammonio groups of CPFP and the net charge on ARS does not change before and after the oxidation or reduction of the electroactive centers. This is another reason for using ARS. In a previous paper,[23] it has been suggested that the contributions from molecular motion of reactant itself and electron exchange between reactants to the overall charge-transport rates can be estimated depending upon which redox center is employed in an electrochemical measurement of diffusional rates.

In this study, in addition to the fundamental redox behavior of ARS incorporated in CPFP films, we examined in more detail the charge-transport process within ARS-incorporating CPFP films undergoing oxidation or reduction of 3,4-dihydroxy and 9,10-dioxo groups, e.g., the dependences of the diffusional charge-transport rates on the concentration of ARS in films and the differences between these rates and the diffusional rates corresponding to the physical diffusion of counter ions which is necessarily, for charge neutrality, coupled to electron transfer (i.e., the homogeneous oxidation-reduction reaction of the electroactive groups in the CPFP films). The results obtained are reported in this paper.

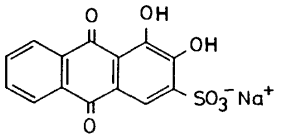

Alizarine Red S

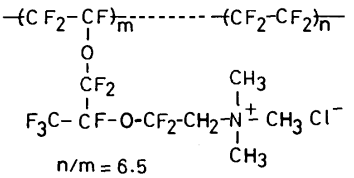

n/m = 6.5

CPFP

Experimental

Materials. 9,10-Dihydro-3,4-dihydroxy-9,10-dioxo-2-anthracenesulfonate (abbreviated as ARS) of reagent grade was obtained from Wako Pure Chemical Industries, Ltd., and was recrystallized three times from H_2O-C_2H_5OH mixture (volume ratio=1 : 1), then dried at 100 °C. A stock solution of cationic perfluoropolymer (abbreviated as CPFP) was prepared as described previously.[25] The concentration of CPFP stock solution (solvent: H_2O-C_2H_5OH-2-propanol (volume ratio=1 : 1 : 1)) was 10.5 mg ml^{-1}. $[Co(tpy)_2]Cl_2 \cdot 2H_2O$ (tpy: 2,2′ : 6′,2″-terpyridine) was prepared and purified according to the literature.[26] NaI was of reagent grade (Tokyo Kasei Co., Ltd.). Basal-plane pyrolytic graphite (BPG, Union Carbide Co.) and In-Sn oxide conducting glass (ITO, Matsuzaki Shinku Co.) were used as working electrodes. Unless otherwise noted, the areas of BPG and ITO electrodes used were 0.19 and 0.25 cm^2, respectively. A platinum wire was used as a counter electrode. The supporting electrolyte solutions were 0.2 M (1 M=1 mol dm^{-3}) CF_3COONa, prepared from CF_3COOH (Aldrich) and NaOH, adjusted to the desired pH's with CF_3COOH, NaOH and/or the commonly used buffer solutions: citric acid/Na_2HPO_4 buffer solutions (at pH 3, 5, and 7), $Na_2B_4O_7$/HCl buffer solution (pH 9) and Na_2HPO_4/NaOH buffer solution (pH 11). Aqueous solutions were prepared from doubly distilled water. Other chemicals were of reagent grade and were used as received.

Apparatus and Procedures. A standard three-electrode, electrochemical cell was used for all the electrochemical experiments. The electrode assembly consisted of an uncoated or a CPFP film-coated BPG (or ITO) as the working electrode, a sodium chloride saturated calomel electrode (SSCE) as the reference electrode, and a platinum wire as the counter electrode.

For cyclic voltammetry (CV), potential-step chronoamperometry (PSCA) and potential-step chronocoulometry (PSCC), a homemade instrument was employed. Positive feedback circuitry was employed to compensate the resistances associated with the polymer films as much as possible. PSCA and PSCC data (i.e., current-time responses and charge-time responses) were monitored and stored on a Nicolet digital oscilloscope (model 3091). These data were then transferred to the laboratory's minicomputer (NEC, PC-9801VE), where calculation was performed, and then graphically presented on an X-Y recorder (Graphtec Co.). Rotating-disk voltammograms were obtained with standard, previously described procedures and apparatus.[27]

The preparation of CPFP film-coated electrodes and the measurement of the film thickness (typically 1.0 μm) were carried out by the same procedure as before.[25] The CPFP film-coated electrodes were equilibrated with 0.01—0.1 mM solutions (pH 1.0) (containing 0.2 M CF_3COONa) of ARS in order to achieve the incorporation of desired quantities of ARS into the films. During the incorporation of several hours, the electrode potential was repeatedly cycled between −0.6 and 0.2V vs. SSCE, and simultaneously the solution was stirred. The quantity (Γ) of ARS incorporated into the CPFP films on the electrodes was estimated (in mol cm^{-2}) by measuring the area of cyclic voltammograms for the oxidation of ARS obtained at slow potential scan rates (1—5 mV s^{-1}). In this case, the electrode potential was held at −0.6 V vs. SSCE for ca. 5—20 min and then the potential was scanned from −0.6 to 0.2 V vs. SSCE. The concentration (in mol cm^{-3}) of the incorporated ARS was calculated from the Γ value thus obtained using the measured film thickness. All experiments were run under a nitrogen atmosphere at laboratory temperature (25±1 °C). The potentials were measured and are quoted with respect to the SSCE.

Results

Incorporation of ARS into CPFP Films Coated on Electrodes. Figure 1 shows typical cyclic voltammograms demonstrating the incorporation of ARS into the CPFP film (thickness: 1.0 μm) coated on an ITO electrode in a 0.2 M CF_3COONa aqueous solution (pH 1.0) containing 0.1 mM ARS. The incorporation of ARS by anion exchange with Cl^- ions, which are initially present in the film as the counteranions of the fixed cationic quaternized ammonio groups, continued for about 90 min (Fig. 1B). No further increases

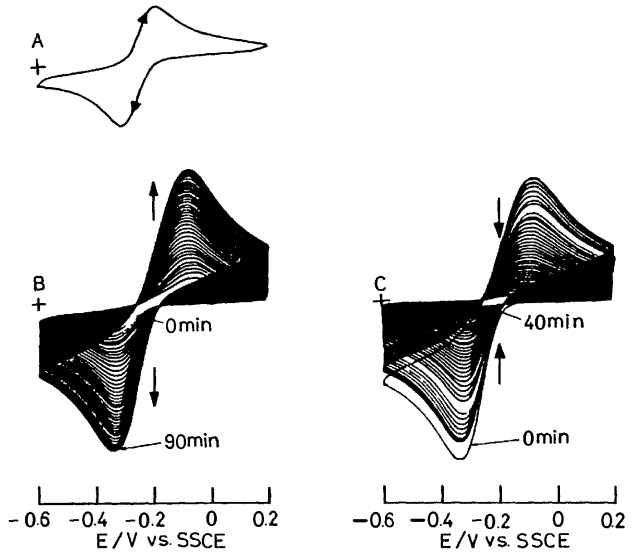

Fig. 1. (A) Cyclic voltammogram of ARS at an uncoated ITO electrode in 0.2 M CF_3COONa solution (pH 1.0) containing 0.1mM ARS. (B) Cyclic voltammograms demonstrating the incorporation of ARS into the CPFP film coated on an ITO electrode in the same solution as used in A. Thickness of the CPFP film: 1.0 μm. Volume concentration of the quaternized ammonium site in the CPFP film: 1.7 M. (C) Cyclic voltammograms obtained when the electrode used in B was transferred to a 0.2 M CF_3COONa solution (pH 1.0). Immersion time is indicated on the voltammograms. In every case, scan rate was 50 mVs^{-1} and electrode area was 0.25 cm^2.

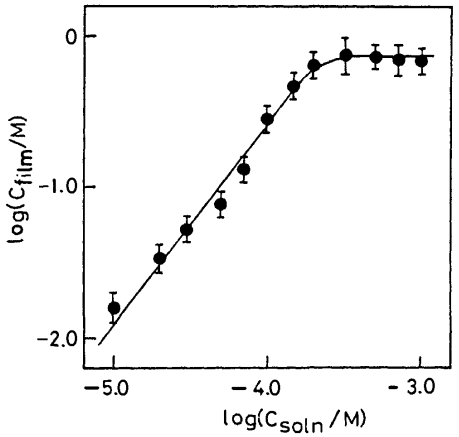

Fig. 2. Equilibrium distribution curve of ARS in the bulk of 0.2 M CF_3COONa solutions (pH 1.0) and in the CPFP films (thickness: 1.0 μm) coated on electrodes. C_{soln} and C_{film} refer to the concentrations of ARS in the bulk of CF_3COONa solution and the CPFP film, respectively.

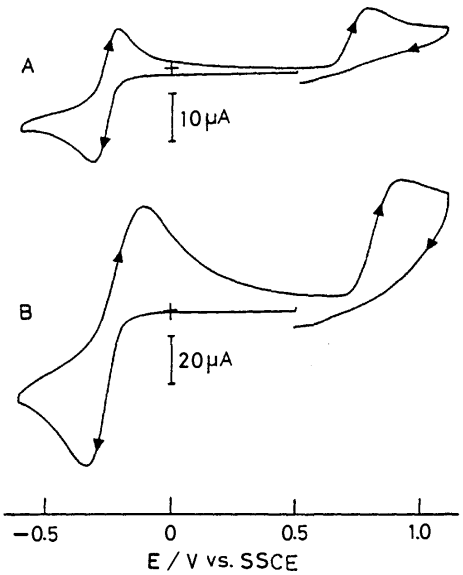

Fig. 3. (A) Cyclic voltammogram of ARS at an uncoated ITO electrode in 0.2 M CF_3COONa solution (pH 1.0) containing 0.1 mM ARS. Scan rate: 20 mVs^{-1}. (B) Cyclic voltammogram of ARS confined in the CPFP film (thickness: 1.0 μm) coated on ITO electrode in the same solution as used in A. Scan rate: 50 mVs^{-1}. In both cases, the electrode areas were 0.22 cm^2.

in peak current were observed with scanning time longer than 90 min. The peak current at the coated electrode was about 2.5 times that at an uncoated electrode (Fig. 1A), and the concentration of the incorporated ARS was 0.46 M. This indicates that the quantity of the incorporated ARS corresponds to ca. 27% of the total amount (1.7 M)[25] of the quaternized ammonium site in the CPFP film. When the CPFP-coated electrode was removed from the incorporating solution and replaced in the pure supporting electrolyte, the ARS anions leached gradually from the CPFP film, and thus the peak current decreased with scanning time. After about 40 min, most of the ARS anions were lost from the film (Fig. 1C). However, the steady-state currents shown in Fig. 1B remained substantially unchanged in the incorporating solution containing 0.1 mM ARS for a period of several hours, even when the electrode was rotated at rotation rates of 100—4900 rpm in the hydrodynamic voltammetric experiments using rotating-disk electrodes (as mentioned below).

The equilibrium distribution curve for ARS partitioned into the CPFP film from 0.2 M CF_3COONa solution (pH 1.0) is shown in Fig. 2, where the logarithm of the concentration (C_{film}) of ARS incorporated into the films is plotted against the logarithm of the concentration (C_{soln}) of ARS in the incorporating solutions over the concentration range 10^{-5} to 10^{-3} M. It is apparent from this figure along with Fig. 1 that ARS is incorporated and concentrated into CPFP film on electrode. The C_{film} vs. C_{soln} plot is almost linear at $C_{soln}<0.14$ mM and the equilibrium distribution coefficients, defined as C_{film}/C_{soln}, are estimated to be (1—3) $\times 10^3$ at $C_{soln}=10^{-5}$—10^{-4} M.

Cyclic Voltammetry of ARS in Solution and CPFP Film. The cyclic voltammetric behavior of ARS confined in CPFP film was found to be essentially the

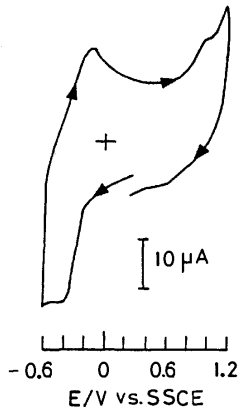

Fig. 4. Cyclic voltammogram for ARS confined in the CPFP film (thickness: 1.0 μm) coated on ITO electrode in 0.2 M CF_3COONa (pH 1.0) containing 0.025 mM ARS. Scan rate: 10 Vs^{-1}.

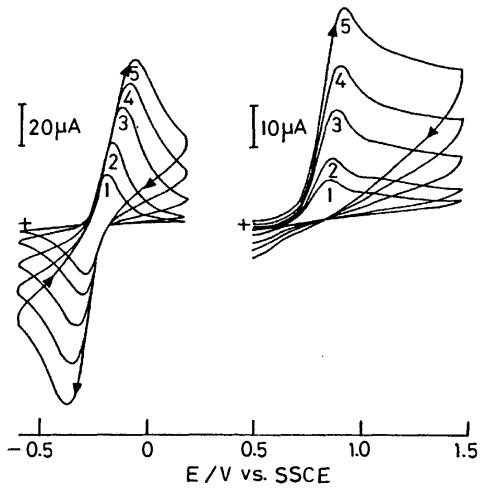

Fig. 5. Cyclic voltammograms of ARS confined in the CPFP film coated on ITO electrode in 0.2 M CF_3COONa solution containing 0.1 mM ARS at various potential scan rates. Concentration of ARS in the CPFP film (thickness: 1.0 μm): 0.46M. Electrode area: 0.25 cm^2. Scan rates: (1) 10, (2) 20, (3) 50, (4) 100, and (5) 200 mVs^{-1}.

same as dissolved in solution, as shown in Fig. 3. That is to say, the reversible and irreversible redox responses can be observed at ca. −0.27 and ca. 0.8 V vs. SSCE, which correspond to the oxidation-reduction reaction of 9,10-dioxo group and the oxidation of 3,4-dihydroxy group, respectively. The data in Fig. 3 were obtained with ITO electrodes. Almost similar results were also obtained with BPG electrodes, but in this case an adsorption of ARS on uncoated BPG electrode substrates was observed. The reversibility of the electrode reactions of 9,10-dioxo and 3,4-dihydroxy groups seemed essentially unchanged on the time scale (ca. 1—40 ms) of the potential-step experiments from which the diffusion coefficients for the diffusional charge-transport processes were obtained (mentioned below), as seen from the cyclic voltammograms shown in Fig. 3 and obtained at a scan rate of 10 Vs^{-1} (Fig. 4). The time scale of 10 Vs^{-1} at CV approximately corresponds to ca. 1 ms at PSCA and PSCC.[28] Plots of the peak currents (i_p) for the oxidation and/or reduction of 9,10-dioxo and 3,4-dihydroxy groups of ARS incorporated in the CPFP film against the square root of potential scan rate, $v^{1/2}$, were nearly linear in the range of v from 10 to 200 mVs^{-1} (as shown typically in Figs. 5 and 6), indicating that charge transport through the CPFP film is apparently diffusional and obeys Fick's law.[28]

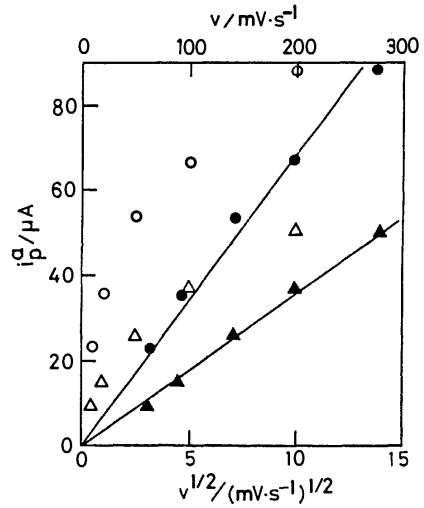

Fig. 6. Dependences of the anodic peak currents, i_p^a, for the oxidations of ARS confined in the CPFP film upon potential scan rate, v. The plots correspond to the data used in Fig. 5. (○, △): i_p^a vs. v plots, (●, ▲): i_p^a vs. $v^{1/2}$ plots. (○, ●): oxidation of **2** to **1**, (△, ▲): oxidation of **1** to **3**.

The formal redox potentials ($E^{o\prime}$) (estimated as the average of the anodic and cathodic peak potentials) for the oxidation-reduction reaction of the 9,10-dioxo group of ARS in both solution and CPFP film shifted to negative potentials with increasing pH, and the slope of the $E^{o\prime}$ vs. pH plot was about −56 mV/pH. Thus, protons and electrons were found to take part in the electrode reaction in a 1/1 ratio. On the basis of the above-mentioned and previously reported results,[23,24] the mechanism of the electrode reaction of ARS confined in the CPFP film on electrodes can be represented as follows.

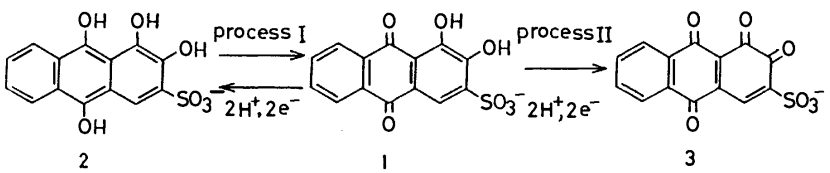

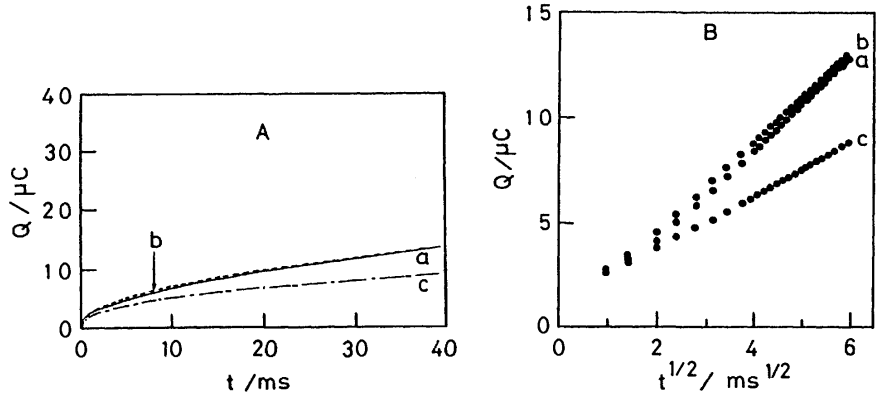

Fig. 7. (A) Typical potential-step chronocoulometric responses for (a) the reduction of **1** to **2**, and the oxidations of (b) **2** to **1** and (c) **1** to **3** of ARS confined in the CPFP film coated on ITO electrode (0.25 cm^2) in 0.2 M CF_3COONa solution (pH 1.0) containing 0.01 mM ARS. Concentration of ARS in the CPFP film (thickness: 1.0 μm): 35 mM. The electrode potentials were stepped from (a) 0.2 to −0.6, (b) −0.6 to 0.2, and (c) 0.2 to 1.3 V vs. SSCE. (B) Chronocoulometric Cottrell plots for the data in A.

Potential-Step Chronoamperometry and Chronocoulometry. Figure 7A shows typical potential-step chronocoulometric responses for an ITO/CPFP, ARS electrode where the electrode potentials were stepped from (a) 0.2 to −0.6, (b) −0.6 to 0.2, and (c) 0.2 to 1.3 V vs. SSCE. Responses a and b correspond to process I and response c corresponds to process II. The chronocoulometric Cottrell plots (i.e., Q vs. $t^{1/2}$ plots) are shown in Fig. 7B. The data gave almost linear Q-$t^{1/2}$ plots in the examined range of t from ca. 1 to 40 ms, and thus the slopes of these plots yielded the apparent diffusion coefficients (D_{app}) for the diffusion-like charge-transport processes within the films. The D_{app} values were also obtained by potential-step chronoamperometry. The results thus obtained are summarized in Fig. 8 and Table 1. In this paper, for convenience, we will represent D_{app}'s for the reversible process I and the irreversible process II as D_{app}^{rev} and D_{app}^{irrev}, respectively. It should be noted that the D_{app} values changed slightly from one electrode to another, even when the experimental conditions (e.g., C_{film} and step-potential in PSCA and PSCC experiments) were the same. For this reason, the values of D_{app}^{rev}, D_{app}^{irrev}, and κD_s (D_s: diffusion coefficients for I^- and $[Co(tpy)_2]^{2+}$ in CPFP films, κ: partition coefficient, mentioned below)

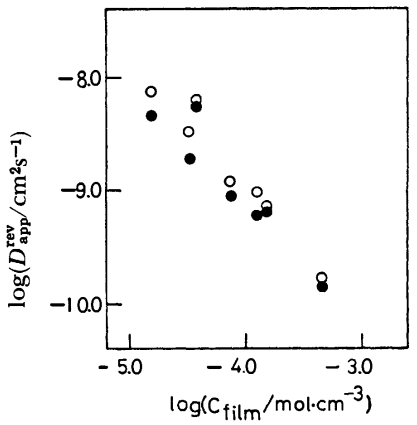

Fig. 8. Dependence of D_{app}^{rev} on C_{film}. CPFP film thickness: 1.0 μm. Supporting electrolyte: 0.2 M CF_3COONa (pH 1.0). (○): oxidation of **2** to **1**; (●) reduction of **1** to **2**.

at a given C_{film}, summarized in Table 1, were obtained at the same electrode. From Fig. 8 and Table 1, we can see that D_{app}^{rev} and D_{app}^{irrev} decrease with increasing C_{film} and that $D_{app}^{rev} > D_{app}^{irrev}$ for a given C_{film}.[35]

Rotating-Disk Voltammetry. In order to estimate the diffusion coefficients coresponding to the diffusion of supporting electrolyte ions which is necessarily, for

Table 1. Comparison of D_{app}'s for ARS with κD_s's for $[Co(tpy)_2]^{2+}$ and I^- [a,b]

C_{film}/M	D_{app}^{rev}/cm^2s^{-1} [c]	D_{app}^{irrev}/cm^2s^{-1} [c]	κD_s/cm^2s^{-1}	
			$[Co(tpy)_2]^{2+}$ [d]	I^- [d]
0.035	$(5.6\pm0.5)\times10^{-9}$(Red) $(5.7\pm0.5)\times10^{-9}$(Ox)	$(2.0\pm0.2)\times10^{-9}$(Ox)	$(3.7\pm0.6)\times10^{-8}$	$(6.3\pm0.5)\times10^{-6}$
0.46	$(1.5\pm0.2)\times10^{-10}$(Red) $(1.6\pm0.1)\times10^{-10}$(Ox)	$(6.1\pm0.1)\times10^{-11}$(Ox)	$(2.6\pm0.4)\times10^{-8}$	$(1.2\pm0.1)\times10^{-6}$

a) Supporting electrolyte: 0.2 M CF_3COONa (pH 1.0). CPFP film thickness: 1.0 μm. b) See the text for the definition of C_{film}, D_{app}^{rev}, D_{app}^{irrev}, and κD_s. c) Ox: oxidation process, Red: reduction process. d) The D_{soln} values of $[Co(tpy)_2]^{2+}$ and I^- in 0.2 M CF_3COONa solutions (pH 1.0) were estimated to be $(3.8\pm0.2)\times10^{-6}$ and $(2.4\pm0.2)\times10^{-5}$ cm^2s^{-1}, respectively.

charge neutrality, coupled to electron transfer (i.e., redox reactions of electroactive groups of ARS), the redox ions, which are electroactive in such a potential region (ca. 0—0.7 V vs. SSCE) that the redox response of ARS is not substantially observed, are required owing to electroinactivity (under the experimental conditions employed in this study) of the supporting electrolyte ions used (Na^+ and CF_3COO^-). For this purpose, I^- and $[Co(tpy)_2]^{2+}$ were chosen. Figure 9 shows typical steady-state current-potential curves for the oxidation of I^- at both bare and CPFP film-coated rotating BPG disk electrodes in a 0.2M CF_3COONa solution (pH 1.0) containing 0.01 mM ARS and 0.5 mM NaI. In this case, the CPFP film-coated electrode was previously equilibrated with a 0.01 mM ARS solution containing no I^-, and then the hydrodynamic voltammetric experiments were conducted. Note that the oxidation of I^- is not thermodynamically mediated by ARS incorporated in the CPFP film, as seen from the comparison of formal redox potentials ($E^{\circ\prime}$'s) of ARS and I_2/I^- couple, i.e., the $E^{\circ\prime}$'s of ARS (for process I) and I_2/I^- couple are −0.27 and 0.44 V vs. SSCE, respectively, in 0.2 M CF_3COONa aqueous solution (pH 1.0). The oxidation of I^- might be mediated by the I_2/I^- couple present within the CPFP film, since it is an anion-exchanging film and thus the trapping of I^- in the film is possible. However, this possibility may be ignored from the following fact. After the above-mentioned rotating-disk voltammetric experiments, the electrode was transferred into a 0.2 M CF_3COONa solution (pH 1.0) containing no ARS and I^- and the cyclic voltammetric response was examined as soon as possible. Consequently, we observed a well-defined redox response of ARS, but no redox response corresponding to I_2/I^- couple was obtained. Thus, the observed anodic currents correspond to the oxidation of I^- ions that penetrate the ARS-containing CPFP films to reach the electrode surface. Figure 10A shows the Levich plots[29] of limiting current, i_{lim} vs. (rotation rate, ω)$^{1/2}$ obtained from the steady-state current-potential curves such as those shown in Fig. 9. The deviations of the limiting currents with CPFP-coated electrodes from the straight line obtained with a bare BPG electrode reflect the different diffusion rates of I^- ion in the bulk of the solution and the swollen, ARS-containing CPFP films.

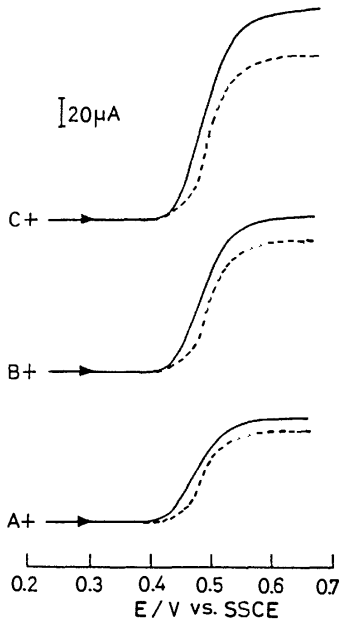

Fig. 9. Typical steady-state current-potential curves for the oxidation of iodide ion at uncoated and ARS-containing CPFP film-coated BPG disk electrodes. (——): at an uncoated BPG electrode in 0.2 M CF_3COONa solution (pH 1.0) containing 0.5 mM NaI; (----): at an ARS-containing CPFP film-coated BPG electrode in 0.2 M CF_3COONa solution (pH 1.0) containing 0.01 mM ARS and 0.5 mM NaI. Concentration of ARS in the CPFP film (thickness: 1.0 μm): 35 mM. Electrode areas: 0.19 cm^2. Potential scan rate: 2 mVs^{-1}. Electrode rotation rate: (A) 400, (B) 900, (C) 1600 rpm.

The quantitative analysis of this problem was made according to the Koutecky-Levich equation as described previously:[28,30]

$$\frac{1}{i_{lim}} = \frac{1}{i_{Lev}} + \frac{1}{i_s} \tag{1}$$

with

$$i_{Lev} = 0.62\, nFAD_{soln}^{2/3}\, \nu^{-1/6}\, C_{soln}\, \omega^{1/2} \tag{2}$$

$$i_s = nFA\kappa C_{soln} D_s \phi^{-1} \tag{3}$$

where i_{Lev} is the Levich current,[29] i_s is the "permeation current"[7c,28,31,32] of I^- ion through the CPFP film, D_{soln} is the diffusion coefficient of I^- ion in a bulk solution, D_s is the diffusion coefficient of I^- ion in the film, ν is the kinematic viscosity of the solution, C_{soln} is the bulk concentration of I^- ion, ϕ is the film thickness, and κ is the partition coefficient of I^- ion between in the film and in the bulk of the solution. The Koutecky-Levich plots of i_{lim}^{-1} vs. $\omega^{-1/2}$ for the data of Fig. 10A were linear, as expected from Eq. 1, and the slopes matched that at a bare electrode (Fig. 10B). Thus, from the data shown in Fig. 10B, the values of D_{soln} and κD_s for I^- ion were estimated (Table 1).

The values of D_{soln} and κD_s for $[Co(tpy)_2]^{2+}$ ion ($E^{\circ\prime}$ of $[Co(tpy)_2]^{2+/3+}$ couple=0.035 V vs. SSCE in 0.2 M CF_3COONa solution (pH 1.0)) were also estimated according to the same way as mentioned above (Table 1). We can see that the diffusion rates of I^- and $[Co(tpy)_2]^{2+}$ ions in the swollen CPFP film of a given C_{film} are different and that they change with C_{film}.

Discussion

Dependence of D_{app}^{rev} on C_{film}. The decrease of apparent diffusion coefficients (D_{app}) for charge-transport processes within electroactive films with increasing the concentration (C_{film}) of electroactive species confined in the films has been previously

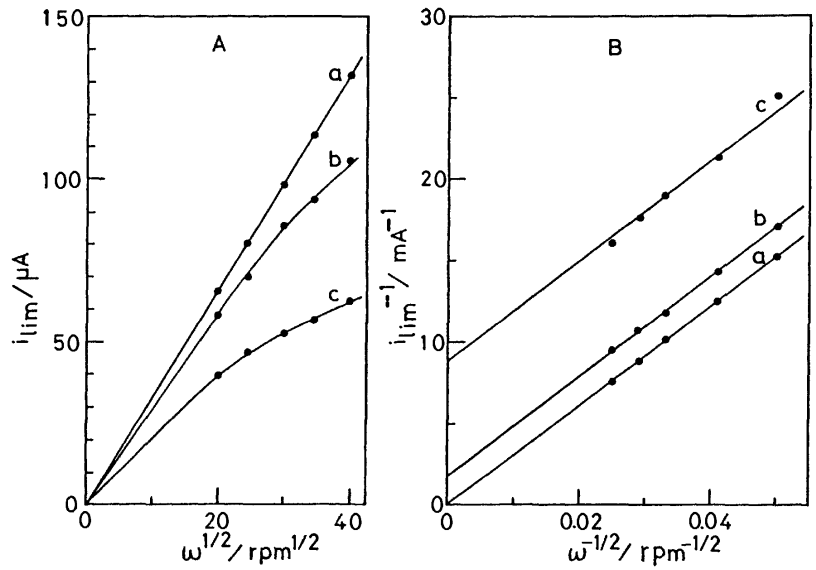

Fig. 10. (A) Levich plots of limiting current, i_{lim}, vs. (rotation rate, ω)$^{1/2}$ for the oxidation of iodide ion at (a) uncoated and (b,c) ARS-containing CPFP film-coated BPG electrodes. (B) Koutecky-Levich plots of i_{lim}^{-1} vs. $\omega^{-1/2}$ for the data used in A. Solution compositions: (a) 0.2 M CF_3COONa (pH 1.0)+0.5 mM NaI; (b) 0.2 M CF_3COONa (pH 1.0)+0.5 mM NaI+0.01 mM ARS; (c) 0.2 M CF_3COONa (pH 1.0)+0.5 mM NaI+0.1 mM ARS. Other experimental conditions are the same as in Fig. 9.

observed in many cases[3,5a-f,j] where multiply-charged electroactive species are electrostatically confined in oppositely charged polymer films. In these cases, the decrease of D_{app} with increasing C_{film} has been explained in terms of an electrostatic cross-linking of the polymer film[2,3,4b-c-f,g,5a-f,j-25] and a single-file diffusion.[3c-f,33,34] That is to say, an increase of the electrostatic cross linking with increasing C_{film} causes a decrease in the diffusion rate of electroactive species itself as well as decreases in the rates of the charge-compensating counterion motion which is necessarily coupled to electron transfer, the motion of solvent and/or the segmental motion of the polymeric chain. Also, the diffusion species which must move between more or less fixed sites within a polymeric matrix are considered to have their rate of motion limited by the decreasing availability of sites as C_{film} of diffusing species increases ("single-file diffusion effect"[34]). These result in the decrease of the overall rate of the charge transport with an increase in C_{film}.

However, the same explanation seems not to be straightforwardly applicable to the case of the ARS-CPFP film system examined in this study (though the decrease of D_{app}^{rev} with increasing C_{film} was observed (Fig. 8), because ARS bears only a single negative charge as SO_3^- group and thus replacing Cl^- anions initially present in the film by ARS anions can not be expected to produce a cross linking based on an electrostatic interaction alone. A possible explanation for the result obtained is that a hydrophobic interaction between the aromatic ring of ARS and the large fluorocarbon component of the CPFP coating as well as an electrostatic interaction between the SO_3^- group and the cationic quaternized ammonio group in the film concurrently contribute to the trapping of ARS anion in the film and such a combined interaction operates in the same manner as an electrostatic interaction[3,5a-f,j] between multiply-charged species and oppositely charged polyelectrolyte films. A similar hydrophobic interaction has been realized in the incorporation of electroactive compounds into polyelectrolyte films on electrode surfaces.[3c,h,33,36] A relatively high concentration of ARS anions into the CPFP coating (shown in Figs. 1 and 2), which is almost comparable to that of multiply-charged species into polyelectrolyte films by electrostatic interactions,[3,5a-f,j] may support this explanation.

Differences in Rates of Various Diffusional Processes and Their Physical Significance. Prior to considering differences in rates of various diffusional processes, it seems to be useful in developing the discussion to mention some reasons for use of ARS as an electroactive species incorporated in the CPFP film on electrodes: (i) ARS contains two separate electroactive centers with different $E^{\circ\prime}$'s and different reversibility of their electrode reactions, (ii) the electroinactive functional group (i.e., SO_3^- group) other than the electroactive ones (i.e., 3,4-dihydroxy and 9,10-dioxo groups) serves as a counteranion site of the fixed cationic quaternized ammonio groups in the CPFP film domain, and (iii) the net charge on ARS does not change before and after the oxidation or reduction of

the electroactive centers.

As can be seen from Table 1, the diffusion coefficients for processes I and II and for the physical diffusion of I^- and $[Co(tpy)_2]^{2+}$ in the film are in the following order: $\kappa D_s \gg D_{app}^{rev}$ (1→2)~D_{app}^{rev} (2→1)>D_{app}^{irrev}(1→3), where D_{app}^{rev} (1→2), D_{app}^{rev} (2→1), and D_{app}^{irrev} (1→3) correspond to **1** to **2**, **2** to **1**, **1** to **3** processes, respectively. The diffusion coefficients (D_s') for the diffusion of supporting electrolyte ions used (Na^+ and CF_3COO^-) in the CPFP film have been unknown. The diffusion coefficients (D_s) of I^- and $[Co(tpy)_2]^{2+}$ in the ARS-containing CPFP film were estimated by hydrodynamic voltammetry using rotating disk electrodes. These ions were chosen based on the fact that they are electroactive in the potential region where the redox response of ARS is not substantially observed. The mean ionic diameters (a) of Na^+ and CF_3COO^- ions can be assumed to be between those of I^- and $[Co(tpy)_2]^{2+}$ ions: a's of I^-, Na^+, CF_3COO^- and $[Co(tpy)_2]^{2+}$ are roughly considered to be ca. 3, 4.5, 5, and >6 Å, respectively.[37] Thus, D_s's for I^- and $[Co(tpy)_2]^{2+}$ ions were obtained as a rough measure of D_s''s for Na^+ and CF_3COO^- ions. Based on these considerations and the obtained values of κD_s, D_{app}^{rev}, and D_{app}^{irrev}, it can be expected that $D_s' \gg D_{app}^{rev} > D_{app}^{irrev}$. This suggests that the rate of the charge transport in the film is not substantially controlled by motion of the counterion (supporting electrolyte ion) in the polymer matrix which is coupled to electron transfer and molecular motion of ARS itself undergoing electrolysis.

The different values of D_{app}^{rev} and D_{app}^{irrev} seem to be instructive in understanding the charge transport mechanism as pointed out in a previous paper.[23] In general, the D_{app} value can include contributions from both molecular motion (physical diffusion of reactant in film) and electron exchange between reactants, which will be represented as D_o and D_{ex} (in units of $cm^2 s^{-1}$), respectively:[2d,e,3b,c,f,4c,d,5h,21-23]

$$D_{app} = D_o + D_{ex} \quad (4)$$

According to Dahms and Ruff,[21,22] D_{ex} is expressed by Eq. 5.

$$D_{ex} = (\pi/4)\, k_{ex} \delta^2 C \quad (5)$$

where k_{ex} is the second-order electron-exchange rate constant for the redox couple, δ is the distance between the reactants when the electron transfer occurs, and C is the concentration of reactants (the sum of the concentrations of the oxidized and reduced forms of the redox couple). In **1** to **2** and **1** to **3** processes, the contribution (D_o) from molecular motion should be the same, because the same molecule takes part in both processes. Thus, based on Eq.4 the difference in D_{app}^{rev} (1→2) and D_{app}^{irrev} (1→3) at a given C_{film} may be considered to originate from that in D_{ex}'s. As can be readily seen from Eq.5, the degree of the contribution from electron exchange to the overall charge-transport rate depends on the electron self-exchange rate constant between electroactive reactants, i.e., homogeneous electron self-exchange rate constant (k_{ex}): The larger k_{ex} is, the larger is D_{ex}, and thus the larger is the contribution of electron exchange. Alternatively, k_{ex} can be correlated to the heterogeneous electron-transfer rate constant (k°)[38], i.e., in a qualitative sense to the reversibility of the electrode reaction: For the redox system with large k_{ex}, the k° value is large. As seen from Fig. 3, process I is reversible, while process II is irreversible. Thus, the k° value for process I should be larger than that for process II. Based on these considerations, the difference in D_{app}'s for processes I and II can be attributed to different contributions of electron exchange between electroactive centers to the overall charge-transport rates.

This work was partially supported by a Grant-in-Aid for Scientific Research on Priority Area of "Dynamic Interactions and Electronic Processes of Macromolecular Complexes" No. 62612504, for N. Oyama, from the Ministry of Education, Science and Culture.

References

1) a) F. B. Kaufman and E. M. Engler, *J. Am. Chem. Soc.*, **101**, 547 (1979). b) F. B. Kaufman, A. H. Schroeder, and J. Q. Chamber, *ibid.*, **102**, 483 (1980).

2) a) I. Rubinstein and A. J. Bard, *J. Am. Chem. Soc.*, **103**, 5007 (1981). b) P. J. Peerce and A. J. Bard, *J. Electroanal. Chem.*, **122**, 97 (1980). c) P. J. Peerce and A. J. Bard, *J. Electroanal. Chem.*, **114**, 89 (1980). d) H. S. White, J. Leddy, and A. J. Bard, *J. Am. Chem. Soc.*, **104**, 4811 (1982). e) C. R. Martin, I. Rubinstein, and A. J. Bard, *ibid.*, **104**, 4817 (1982).

3) a) N. Oyama and F. C. Anson, *J. Electrochem. Soc.*, **127**, 640 (1980). b) D. A. Buttry and F. C. Anson, *J. Electroanal. Chem.*, **130**, 333 (1981). c) D. A. Buttry and F. C. Anson, *J. Am. Chem. Soc.*, **105**, 685 (1983). d) F. C. Anson, T. Ohsaka, and J. M. Savéant, *J. Phys. Chem.*, **87**, 640 (1983). e) D. D. Montgomery and F. C. Anson, *J. Am. Chem. Soc.*, **107**, 3431 (1985). f) Y. M. Tsou and F. C. Anson, *J. Phys. Chem.*, **89**, 3818 (1985). g) D. A. Buttry, J. M. Savéant, and F. C. Anson, *ibid.*, **88**, 3086 (1984). h) Y. M. Tsou and F. C. Anson, *J. Electrochem. Soc.*, **131**, 595 (1984). i) N. Oyama and F. C. Anson, *Anal. Chem.*, **52**, 1192 (1980).

4) a) R. Nowak, F. A. Schultz, M. Umana, R. Lam, and R. W. Murray, *Anal. Chem.*, **52**, 315 (1980). b) P. Daum, J. R. Lenhard, D. Rolison, and R. W. Murray, *J. Am. Chem. Soc.*, **102**, 4649 (1980). c) J. Facci and R. W. Murray, *J. Phys. Chem.*, **85**, 2870 (1981). d) J. Facci, R. H. Schmehl, and R. W. Murray, *J. Am. Chem. Soc.*, **104**, 4959 (1982). e) R. Schmehl and R. W. Murray, *J. Electroanal. Chem.*, **152**, 97 (1983). f) J. Facci and R. W. Murray, *ibid.*, **124**, 339 (1981). g) K. Kuo and R. W. Murray, *ibid.*, **131**, 37 (1982). h) B. J. Feldman and R. W. Murray, *Inorg. Chem.*, **26**, 1702 (1987).

5) a) N. Oyama, T. Ohsaka, M. Kaneko, K. Sato, and H. Matsuda, *J. Am. Chem. Soc.*, **105**, 6003 (1983). b) N. Oyama, T. Ohsaka, and T. Ushirogouchi, *J. Phys. Chem.*, **88**, 5274 (1984). c) T. Ohsaka, H. Yamamoto, M. Kaneko, A. Yamada, M. Nakamura, S. Nakamura, and N. Oyama, *Bull. Chem. Soc. Jpn.*, **57**, 1844 (1984). d) T. Ohsaka, K. Sato, H. Matsuda, and N. Oyama, *J. Electrochem. Soc.*, **132**, 1871

(1985). e) T. Ohsaka, T. Ushirogouchi, and N. Oyama, *Bull. Chem. Soc. Jpn.*, **58**, 3252 (1985). f) T. Ohsaka, T. Okajima, and N. Oyama, *J. Electroanal. Chem.*, **215**, 191 (1986). g) K. Chiba, T. Ohsaka, and N. Oyama, *ibid.*, **217**, 239 (1987). h) N. Oyama, T. Ohsaka, H. Yamamoto, and M. Kaneko, *J. Phys. Chem.*, **90**, 3850 (1986). i) T. Ohsaka, H. Yamamoto, and N. Oyama, *ibid.*, **91**, 3775 (1987). j) N. Oyama, T. Ohsaka, K. Chiba, and K. Takahashi, *Bull. Chem. Soc. Jpn.*, **61**, 1095 (1988).

6) a) D. C. Bookbinder, J. A. Bruce, R. N. Dominey, N. S. Lewis, and M. S. Wrighton, *Proc. Natl. Acad. Sci. U. S. A.*, **77**, 6280 (1980). b) D. J. Harrison, K. A. Daube, and M. S. Wrighton, *J. Electroanal. Chem.*, **163**, 93 (1984).

7) a) C. P. Andrieux and J. M. Savéant, *J. Electroanal. Chem.*, **111**, 377 (1980). b) C. P. Andrieux, J. M. Dumas-Bouchiat, and J. M. Savéant, *ibid.*, **131**, 1(1982). c) C. P. Andrieux and J. M. Savéant, *ibid.*, **142**, 1 (1982).

8) a) E. Laviron, *J. Electroanal. Chem.*, **112**, 1 (1980). b) K. M. O'connell, E. Waldner, L. Roullier, and E. Laviron, *ibid.*, **162**, 77 (1984).

9) a) M. Majda and L. R. Faulkner, *J. Electroanal. Chem.*, **137**, 149 (1982). b) M. Majda and L. R. Faulkner, *ibid.*, **169**, 77 (1984).

10) A. N. K. Lau, L. L. Miller, and B. Zinger, *J. Am. Chem. Soc.*, **105**, 5278 (1983).

11) W. T. Yap, R. A. Durst, E. A. Blubaugh, and D. D. Blubaugh, *J. Electroanal. Chem.*, **144**, 69 (1983).

12) a) K. Doblhofer, H. Braun, and R. Lange, *J. Electroanal. Chem.*, **206**, 93 (1986). b) R. Lange and K. Doblhofer, *ibid.*, **237**, 13 (1987).

13) G. Inzelt, J. Q. Chambers, J. F. Kinstle, and R. W. Day, *J. Am. Chem. Soc.*, **106**, 3396 (1984).

14) I. Rubinstein, *J. Electroanal. Chem.*, **188**, 227 (1985).

15) M. W. Espenscheid and C. R. Martin, *J. Electroanal. Chem.*, **188**, 73 (1985).

16) W. J. Albery, M. G. Boutelle, P. J. Golby, and A. R. Hillman, *J. Electroanal. Chem.*, **133**, 135 (1982).

17) B. Lindholm, M. Sharp, and R. D. Armstrong, *J. Electroanal. Chem.*, **235**, 169 (1987).

18) C. J. Miller and M. Majada, *J. Am. Chem. Soc.*, **108**, 3118 (1986).

19) O. Haas and B. Sandmeier, *J. Phys. Chem.*, **91**, 5072 (1987).

20) C. M. Elliott and J. G. Redepenning, *J. Electroanal. Chem.*, **181**, 137 (1984).

21) a) I. Ruff, *Electrochim. Acta*, **15**, 1059 (1970). b) I. Ruff and V. Friedrich, *J. Phys. Chem.*, **75**, 3297 (1971). c) I. Ruff and V. Friedrich, *J. Phys. Chem.*, **76**, 2954 (1972).

22) H. Dahms, *J. Phys. Chem.*, **72**, 362 (1968).

23) T. Ohsaka, Y. Takahira, S. Nakamura, and N. Oyama, *J. Electroanal. Chem.*, **247**, 339 (1988).

24) H. E. Zittel and T. M. Florence, *Anal. Chem.*, **39**, 320 (1967).

25) N. Oyama, T. Ohsaka, and T. Okajima, *Anal. Chem.*, **58**, 979 (1986).

26) R. Hogg and R. G. Wilkins, *J. Chem. Soc.*, **1962**, 341.

27) T. Ohsaka, T. Hirokawa, H. Miyamoto, and N. Oyama, *Anal. Chem.*, **59**, 1758 (1987).

28) For example, A. J. Bard and L. R. Faulkner, "Electrochemical Methods, Fundamentals and Applications," Wiley, New York (1980).

29) V. G. Levich, "Physicochemical Hydrodynamics," Prentice-Hall, Englewood Cliffs, NJ. (1962).

30) J. Koutecky and V. G. Levich, *Zh. Fiz. Khim.*, **32**, 1565 (1956).

31) D. A. Gough and J. K. Leypoldts, *Anal. Chem.*, **51**, 439 (1979).

32) N. Oyama, Y. Ohnuki, T. Ohsaka, and H. Matsuda, *Nippon Kagaku Kaishi*, **1983**, 949.

33) N. Oyama, T. Ohsaka, T. Ushirogouchi, S. Sanpei, and S. Nakamura, *Bull. Chem. Soc. Jpn.*, **61**, 3103 (1988).

34) K. Heckmann, "Biomembranes," ed by A. L. Manson, Plenum Press, New York (1972), Vol. 3, p. 127.

35) Preliminary experiments revealed that the D_{app} values obtained at pH 1 and 5 were almost the same within experimental error.

36) N. Oyama, T. Ohsaka, K. Sato, and H. Yamamoto, *Anal. Chem.*, **55**, 1429 (1983).

37) J. Kielland *J. Am. Chem. Soc.*, **59**, 1675 (1937).

38) For example, R. A. Marcus, *Electrochim. Acta*, **13**, 995 (1968).

Physicochemical Properties of α,ω-Type Surfactant in Aqueous Solution. Bis(triethylammonium) 1,20-Eicosanediyl Disulfate

Kenji IKEDA,* Motoharu ISHIKAWA, Masaaki YASUDA, Kunio ESUMI, Kenjiro MEGURO, William BINANA-LIMBELE,† and Raoul ZANA†
Department of Applied Chemistry, Institute of Colloid and Interface Science, Science University of Tokyo, Kagurazaka, Shinjuku-ku, Tokyo 162
†CNRS, Institut C. Sadron (C.R.M.-E.A.H.P.), 6 rue Boussingault, 67083 Strasboug-Cedex, France
(Received October 24, 1988)

The physicochemical properties of the α,ω-type (bolaform) surfactant, bis(triethylammonium) 1,20-eicosanediyl disulfate (α,ω $C_{20}N_2Et_6$), in aqueous solution have been investigated by means of surface tension, electrical conductivity, dye solubilization and time-resolved fluorescence quenching. The critical micelle concentration of α,ω $C_{20}N_2Et_6$ was 1—1.3×10^{-3} mol dm^{-3}. The micelle ionization degree of the surfactant was larger than a conventional surfactant having the same head group. From surface tension measurements, the molecular area of α,ω $C_{20}N_2Et_6$ at the air-water interface was found to be about twice as large as that of a normal type surfactant, such as sodium dodecyl sulfate (SDS). This reveals that α,ω $C_{20}N_2Et_6$ probably forms vertical looping ("wicket-like" conformation) at the air-water interface. By time-resolved fluorescence quenching measurements, the aggregation number of α,ω $C_{20}N_2Et_6$ micelle was found to be strongly dependent on the concentration, but only slightly dependent on the temperature. At low concentrations the aggregation number is close to half that corresponding to a normal type surfactant having a chain length that is that of the bolaform. The solubilizing power of a micellar solution of α,ω $C_{20}N_2Et_6$ toward Orange OT was 7.6×10^{-3} mol of dye per mol of surfactant, that is, a value smaller than that of SDS.

α,ω-Type (bolaform) surfactnts have hydrophilic head groups at both ends of the hydrophobic alkyl chain. Interest in bolaform surfactants has increased steadily in recent years from the stand points of both fundamental investigations and applications.[1-14] The investigations of α,ω-type surfactants in aqueous solutions have shown the following. First, the propensity of micelle formation of the α,ω-type surfactants is generally lower, the size of their micelles is smaller,[8,9,11-13] and their cmc is generally higher than that of single head surfactants of comparable chain length.[7-9] Second, the α,ω-type surfactants have been shown to adopt a folded, wicket-like, conformation at the air-water interface.[6,8] Third, it was suggested that these surfactants may exist in a predominantly folded conformation in micelles.[9c] As regards to the last point, a study for providing direct evidence on the conformation of these surfactants in micellar solutions, performed by using ^{13}C and ^{14}N NMR relaxation techniques,[13] suggested that bolaform surfactant chains adopt a predominantly stretched form in micelles. Recently, we have reported on the properties of α,ω-type cationic surfactant.[12,13] However, there have been a few reports about other types α,ω surfactant, i.e. the anionic or nonionic type.

In this study, as one of the systematic investigations with α,ω-type surfactants, the physicochemical properties of the anionic surfactant bis(triethylammonium) 1,20-eicosanediyl disulfate in aqueous solution have been investigated by means of surface tension, electrical conductivity, dye solubilization and time-resolved fluorescence.

Experimental

Materials. Bis(triethyl ammonium) 1,20-eicosanediyl disulfate was synthesized by using eicosanedioic acid (Okamura Oil Mill Ltd.) as the starting material via 1,20-eicosanediol. Eicosanedioic acid was reduced to 1,20-eicosanediol by using borane-THF complex (Aldrich Chem. Co.). The diol was recrystallized twice from benzene and dried for 48 h under vacuum. Its purity was confirmed by IR spectroscopy. The diol was reacted with chlorosulfuric acid to give 1,20-eicosanedisulfonic acid which was neutralized with triethylamine. The bolaform was recrystallized three times from an acetone-ethanol mixture and three times from an ethyl acetate-ethanol mixture; it was then washed twice with diethyl ether and dried for more than 72 h under vacuum. The white crystalline product was found to be more than 99% pure by elemental analysis, isotachophoresis (IP-3A: Shimadzu Co., Ltd.), NMR, and surface tension. *N*-Phenylbenzoylacetamide (BZAA), ammonium 8-anilino-1-naphthalenesulfonate (ANS) (Wako Pure Chemical Industries. Ltd.) and benzoylacetone (BZA) (Tokyo Kasei Co.) were used without further purification. Yellow OB and Orange OT (Tokyo Kasei Co., recrystallized twice from ethanol) were used as dyes.

Measurements and Methods. The surface tensions of aqueous surfactant solutions were measured by a Wilhelmy-type surface tensiometer (Shimadzu ST-1) at 25 °C. The establishment of equilibrium was checked by repeated measurements in 5-minute intervals. The electrical conductivity of the solution was measured by means of a conductivity meter (Model CM-30ET Toa Denpa Co.) at 25±0.1 °C. The fluorescence and UV spectra of each sample were measured with a fluorescence spectrophotometer (Hitachi 650-10S) and a UV spectrophotometer (Hitachi 220A). The emission and excitation slits were set at 10 nm for ANS and at 1 nm for pyrene. Pyrene and ANS were excited at 335 and 365 nm, respectively. The concentrations of these probes were kept at 5.0×10^{-5} mol dm^{-3} for ANS and 1.6×10^{-6} mol dm^{-3} for pyrene. The emission intensity was measured from 350 to 600 nm.

The solubilization measurements of water-insouble dyes

were carried out as follows. After an excess amount of water-insoluble dye was added to the surfactant solutions, the solutions were shaken for 48 h in order to reach a solubilization equilibrium. After centrifugation (5000 rpm, 30 min) of these suspensions, the supernatant solutions were taken, and diluted by ethanol. The optical density of the solution at each absorption maximum was measured with a UV spectrophotometer; the dye concentration was determined from calibration curves.

Prior to fluorescence measurements the solutions were bubbled with argon for about 20 min for deoxygenation. The fluorescence decay experiments were performed with the same photon-counting apparatus as in our previous studies,[15] modified by the use of an amplifier and single-channel analyzer (Ortec, type 590), which ensured rejection of multiphoton events and, thus, permitted a higher count rate. The measurements were performed at concentrations of 0.05, 0.1, 0.197, 0.296, 0.302 mol dm^{-3}. The fluorescence decay curves were determined at low pyrene concentration (generally around 10^{-5} mol dm^{-3}) in the absence and in the presence of the quencher *N*-dodecylpyridinium chloride (DPCl) at a concentration such that the [DPCl]/[micelle] molar concentration ratio, *R*, was around 1. The decay curves were computer-fitted to Eqs. 1 and 2 in both absence and presence of the DPCl:

$$I = I(0)\exp(-t/\tau_0) \quad (1)$$

and

$$I = I(0)\exp[-A_2 t - A_3(1-\exp(-A_4 t))], \quad (2)$$

respectively, after convolution with a lamp curve, using a nonlinear weighted least-squares procedure. The fitting yielded τ_0, fluorescence lifetime of micelle-solubilized pyrene in the absence of quencher and constants A_2, A_3, and A_4. In general, it was found that $\tau_0 > A_2^{-1}$. This result indicated that the quencher was not completely immobile on the fluorescence timescale. However, the use of the full expressions of A_2, A_3, and A_4 values in such a situation[16] yielded $A_3 = R$ because of the high concentration of quencher used in the experiments in view of the small aggregation number of the bolaform micelles. The aggregation number *N* was obtained from

$$N = R(C - \text{cmc})/[\text{DPCl}], \quad (3)$$

where *C* is the concentration of the surfactant and cmc its critical micelle concentration

The aggregation number of α,ω $C_{20}N_2Et_6$ micelles was also determined by the static fluorescence quenching method.[26] The quenching of the fluorescence emission (at 372 nm) of micelle-solubilized pyrene by *N*-hexadecylpyridinium chloride (CPCl) was measured at increasing contents of quencher and constant concentration of pyrene (1×10^{-5} mol dm^{-3}) and surfactant. The slope of the line obtained by plotting $\ln I_0/I$ (where *I* and I_0 are the fluorescence intensities with and without a quencher) versus the quencher concentration yields the micelle aggregation number.

Results and Discussion

Surface Tension. Figure 1 shows a plot of the equilibrium surface tension, γ, versus the log of the concentration *C* (in molarity) of an α,ω $C_{20}N_2Et_6$ aqueous solution. The γ_{cmc} value of α,ω $C_{20}N_2Et_6$ was

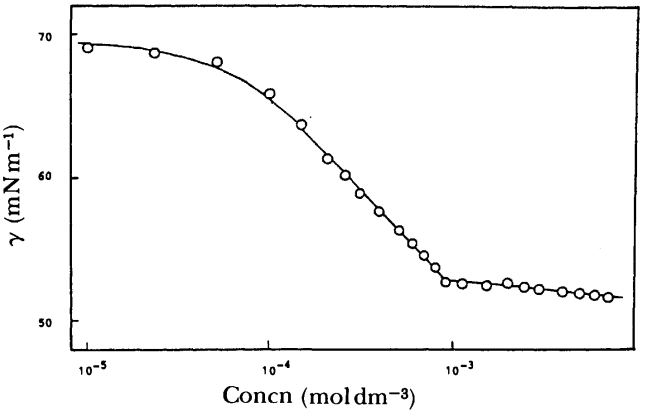

Fig. 1. Plot of surface tension, γ, against log concentration

slightly higher than those for the corresponding normal-type surfactants, i.e., alkyl hydrogensulfate. Figure 1 shows that the break in the γ vs. log *C* curve at the cmc is nearly as sharp as for normal-type surfactants such as sodium dodecyl sulfate (SDS). However, there appears to be a small decrease of γ upon increasing *C* at above 3×10^{-3} mol dm^{-3}. The critical micelle concentration of α,ω $C_{20}N_2Et_6$ from the surface tension was 1.0×10^{-3} mol dm^{-3}. Surface area calculations were based on the Gibbs adsorption equation,

$$\Gamma = -(1/nRT)(\partial\gamma/\partial \ln a), \quad (4)$$

where γ, Γ, and *a* denote the surface tension in mN m^{-1}, the surface excess in mol cm^{-2}, and the activity of the surfactant, respectively. The factor $n=3$ in the denominator is applicable for a 2:1 electrolyte with no added salt; and for a dilute solution *a* is substituted for by the concentration, *C*. In Eq. 5, where N_A is Avogadro's number,

$$A = 10^{16}/\Gamma N_A \quad (5)$$

gives the surface area *A* in Å^2 per molecule. The surface area was calculated from γ vs. log *C* plots. α,ω $C_{20}N_2Et_6$ had a surface area of 66.1 Å^2/molecule, which is very close to twice the value of 33.0 Å^2/molecule for SDS obtained by other workers.[17] Therefore, α,ω $C_{20}N_2Et_6$ seems to form vertical looping, "wicket-like" conformation, at the air-water interface. This picture is consistent with that suggested by other reports.[2,6,8]

Conductivity. The variations of the conductivity κ with concentration *C*, and of the equivalent conductivity *Λ* with the square root of the concentration expressed in equivalent per liter $(2C)^{1/2}$ are shown in Fig. 2. Each plot shows a sharp break at a concentration corresponding to the critical micelle concentration (cmc): 1.3×10^{-3} mol dm^{-3} from the κ-plot and 1.25×10^{-3} mol dm^{-3} from the *Λ*-plot. The slope of the *Λ* vs. $(2C)^{1/2}$ plot is close to the limiting slope expected for a 2:1 electrolyte in the range 3×10^{-4}—10^{-3} mol dm^{-3} (below 3×10^{-4} mol dm^{-3}, the error on κ is too large for meaningful calculations of *Λ*-values.) The

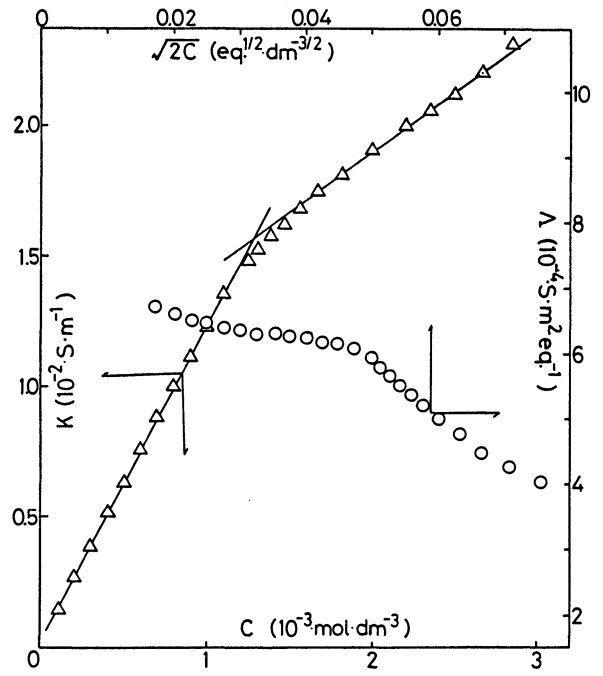

Fig. 2. Electrical conductivity-concentration of α,ω $C_{20}N_2Et_6$ (△) and equivalent conductivity-(concentration)$^{1/2}$ (○) curves.

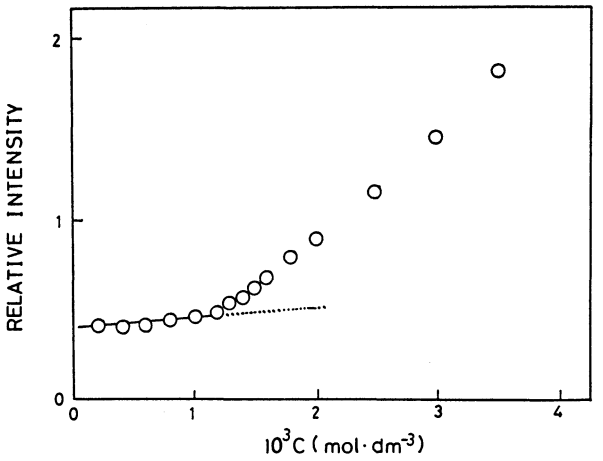

Fig. 3. Variation of the intensity of fluorescence of ANS as a function of α,ω $C_{20}N_2Et_6$ concentration.

micelle ionization degree, α=0.38, was obtained as the ratio of the slopes of the κ vs. C plots above and below cmc. This value is slightly larger than that of SDS micelles: 0.32, obtained as part of this work from the κ vs. C plot for this surfactant.

Solubilization of Dyes. The solubilization properties of aqueous solutions of α,ω $C_{20}N_2Et_6$ were studied by using ANS, BZA, BZAA, pyrene, Yellow OB, and Orange OT. The absorption and fluorescence spectra of organic compounds solubilized in micelles provide information about micellar properties. ANS is an indicator for the determination of the cmc of a surfactant because the quantum yield of this fluorescence probe is much higher in a nonpolar medium than in a

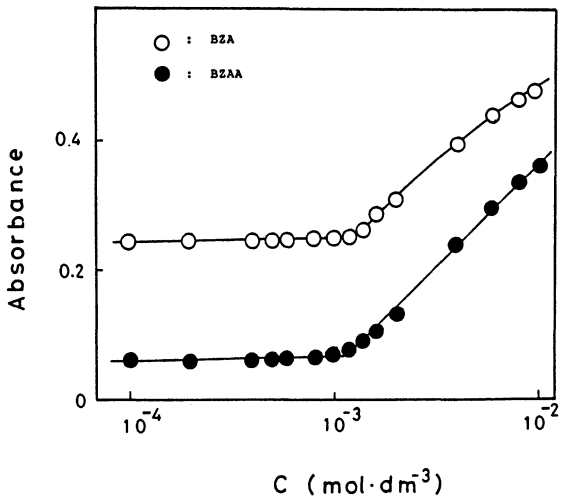

Fig. 4. UV absorbance of BZA and BZAA as a function of α,ω $C_{20}N_2Et_6$ concentration.

Table 1. cmc of α,ω $C_{20}N_2Et_6$ at 25 °C

Method	10^3cmc/mol dm^{-3}
Surface tension	1.0
Equivalent conductivity	1.3
Solubilization (ANS)	1.25
(BZA)	1.2
(BZAA)	1.2

polar solvent like water.[8,18,19] Figure 3 shows that the fluorescence intensity of ANS increased steadily at C above 1.25×10^{-3} mol dm^{-3}, which can be considered as the cmc of α,ω $C_{20}N_2Et_6$. This cmc value agrees with those obtained by electrical conductivity and surface tension.

The keto-enol tautomerisms of BZAA and BZA were also used to probe for micelle formation. The keto-form structure is predominant when the probe is in water. The change from a keto-form to an enol-form structure occurs when the polarity of the probe environment is decreased.[20] The cmc value (1.2×10^{-3} mol dm^{-3}) determined from the change of the probe absorbance, associated with this conformational transition (Fig. 4) agrees with those from other methods. All the cmc values obtained by several methods are listed in Table 1.

The fluorescence probe pyrene was used to investigate the polarity of α,ω $C_{20}N_2Et_6$ micelles. The ratio I_1/I_3 of the intensities of the first and third vibronic peaks of pyrene increases upon going from aliphatic to polar solvents and can be used as an indicator of the effective local polarity of the pyrene solubilization site in the micelles.[21] Figure 5 shows that I_1/I_3 decreases with an increasing α,ω $C_{20}N_2Et_6$ concentration from a value above 1.8 below cmc to a value of 1.42 at a concentration of 0.1 mol dm^{-3}, well above cmc. This last value is well above that found with normal-type surfactants, such as SDS, and indicates that pyrene senses

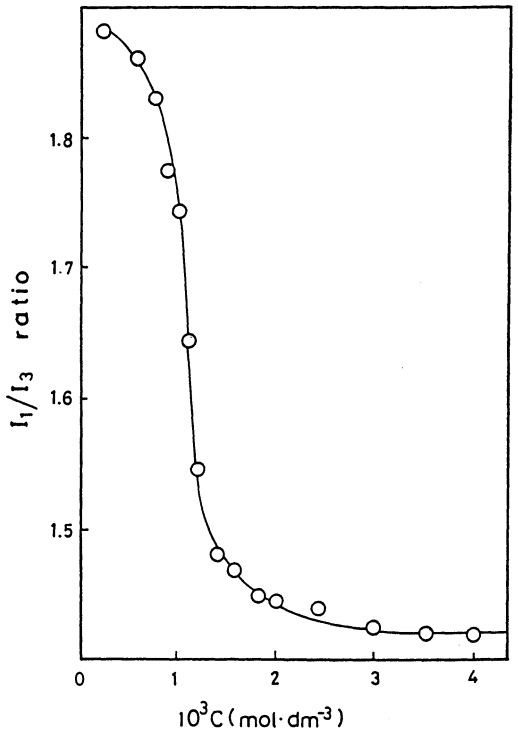

Fig. 5. Variation of the I_1/I_3 intensity ratio for pyrene in aqueous solutions of α,ω $C_{20}N_2Et_6$ as a function of the surfactant concentration.

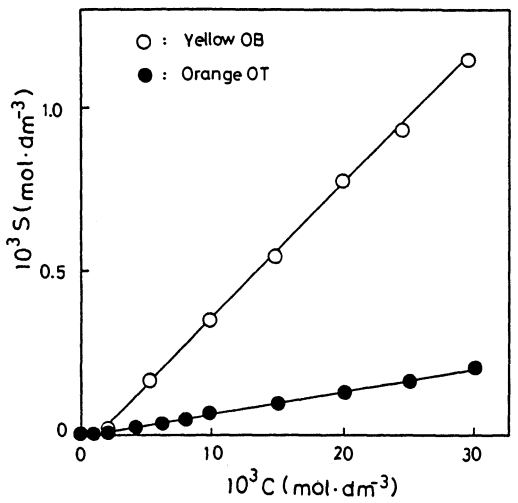

Fig. 6. Solubility of Yellow OB and Orange OT in α,ω $C_{20}N_2Et_6$ solutions as a function of concentration.

a fairly polar environment in α,ω $C_{20}N_2Et_6$ micelles. These micelles may not be as well organized as a normal-type surfactant micelle and allow somewhat more extensive pyrene-water contacts in the micelle palisade layer where pyrene preferentially resides.[21]

The molar concentrations of Yellow OB and Orange OT solubilized in α,ω $C_{20}N_2Et_6$ solutions are plotted against the surfactant concentration in Fig. 6. The solubilities of Yellow OB and Orange OT increased rapidly and linearly above the cmc. The slope of the line yields the number of moles of solubilized dye per

Table 2. Aggregation Number of α, ω $C_{20}N_2Et_6$ Micelles as a Function of Temperature and Concentration

T	C/mol dm^{-3}				
°C	0.05	0.1	0.197	0.296	0.302
25	20±2	29±3	39	—	44
30	19	—	—	—	—
35	—	—	39	—	—
40	18.5	—	39	46	48
50	17±2	—	37	—	47

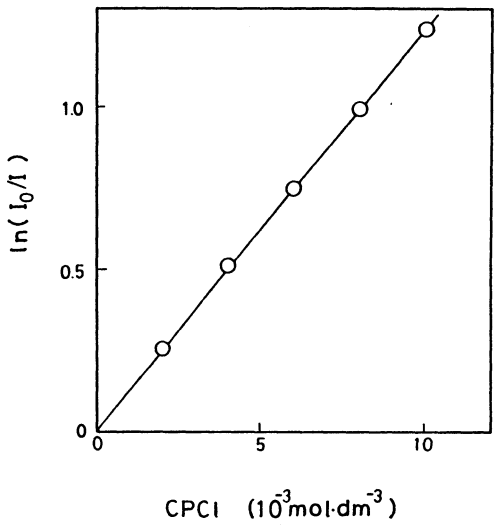

Fig. 7. Variation of $\ln I_0/I$ with the CPCl concentration in a 2×10^{-2} mol dm^{-3} solution of α,ω $C_{20}N_2Et_6$.

mole of micellar surfactant, i.e., the solubilizing power. For α,ω $C_{20}N_2Et_6$ micelles, the solubilizing power was 4.49×10^{-2} and 7.64×10^{-3} mol of dye per mol of surfactant for Yellow OB and Orange OT, respectively. The value for Orange OT was smaller than that of the conventional surfactant micelles such as SDS: 9.90×10^{-3} for Orange OT. If the solubilizing power is expressed in moles of solubilized dye per mole of surfactant head groups, the value of α,ω $C_{20}N_2Et_6$ then appears to be much smaller than that of SDS. However, the solubilizing power of different surfactants should be compared at a constant solubilizing volume, which is proportional to the alkyl chain length, that is the number of carbon atoms, to the third power. The solubilizing power of α,ω $C_{20}N_2Et_6$ expressed in moles of dye per mole of surfactant head groups was thus found to be 6.6×10^3 when corrected by the factor $(12/10)^3$, that is a little smaller than for SDS.

Aggregation Number. Table 2 lists the values of the micelle aggregation number, N, at several temperatures and surfactant concentrations, obtained from time-resolved fluorescence quenching experiments. Static fluorescence quenching experiments using pyrene as probe and *N*-hexadecyl pyridinium chloride (CPCl) as quencher yielded a linear $\ln I_0/I$ vs. quencher concentration plot (see Fig. 7) from which the value $N=15$ was obtained by using Eq. 3 in Ref. 22,

at $C=2\times10^{-2}$ mol dm^{-3} (25 °C), in good agreement with the results in Table 2. The aggregation number greatly increased with concentration. This increase is somewhat comparable to that found for SDS, where N increases from 65 to 110 when the concentration goes from 0.1 to 0.6 mol dm^{-3}.[23] Notice that a 0.3 mol dm^{-3} α,ω-type surfactant corresponds to 0.6 mol dm^{-3} of a classical surfactant with an alkyl chain equal to half that of the α,ω-type surfactant. Studies with another bolaform surfactant, 1,20-bis(triethylammonio)eicosane dibromide, referred to as $C_{20}Et_6$, have yielded an aggregation number which showed only little dependence on the concentration.[25] This difference with α,ω $C_{20}N_2Et_6$ may be due to the fact that the head-group size in $C_{20}Et_6$ is much larger than in α,ω $C_{20}N_2Et_6$. It will, thus, form small micelles and will have a lesser tendency to grow upon increasing concentration since its stacking parameter[24] (volume/surface area per head group × alkyl chain length) is smaller. On the other hand, it is noteworthy that $C_{20}Et_6$ and α,ω $C_{20}N_2Et_6$ have nearly the same aggregation numbers at low concentration: 17—20, and that these values are close to that calculated with the oil drop model for a classical surfactant with a 10 carbon atom alkyl chain. Finally, Table 2 shows that the aggregation number of α,ω $C_{20}N_2Et_6$ in an aqueous solution depends little on the temperature in comparison with normal type surfactants. Dodecyltrimethylammonium chloride (DTAC), dodecyltrimethylammonium bromide (DTAB), and SDS show a linear, or nearly linear, decrease of N upon increasing temperature.[26-28] For normal-type surfactants, the larger the value of N at low temperature, the steeper the decrease of N upon increasing the temperature.

One last point must be made. From the analysis of the pyrene fluorescence decay curve in presence of DPCl, we have been able to extract the rate constant k^- for the exit of the quencher dodecylpyridinium ion from α,ω $C_{20}N_2Et_6$ micelles. Although these values are fairly inaccurate, because of the small magnitude of k^- with respect to the quantity A_4, they all turned out to be in the range $1-2\times10^5$ s^{-1}. The residence time of the probe in the bolaform micelle is, thus, 5 to 10 μs. This value is comparable to that for other surfactants having the same chain length.[29]

The authors are grateful to Okamura Oil Mill Ltd. for the gift of a number of eicosanedioic acids.

References

1) P. H. Elworthy, *J. Pharm. Pharmacol.*, **11**, 557 (1959).
2) P. H. Elworthy, *J. Pharm. Pharmacol.*, **11**, 624 (1959).
3) T. L. Broadwater and D. F. Evans, *J. Phys. Chem.*, **73**, 164 (1969).
4) O. D. Bonner and S. Kim, *J. Phys. Chem.*, **73**, 1367 (1969).
5) M. Ueno, T. Hikota, T. Mitama, and K. Meguro, *J. Am. Oil Chem. Soc.*, **49**, 250 (1974).
6) F. M. Menger and S. Wrenn, *J. Phys. Chem.*, **78**, 1387 (1974).
7) M. Ueno, S. Yamamoto and K. Meguro, *J. Am. Oil Chem. Soc.*, **51**, 373 (1974).
8) K. Meguro, K. Ikeda, A. Otsuji, M. Taya, M. Yasuda, and K. Esumi, *J. Colloid Interface Sci.*, **118**, 372 (1987); K. Ikeda, K. Esumi, K. Meguro, W. Binana-Limbele, R. Zana, and B. Lindman, *J. Colloid Interface Sci.*, in press.
9) a) S. Yiv, K. M. Kale, J. Lang, and R. Zana, *J. Phys. Chem.*, **80**, 2651 (1976); b) S. Yiv and R. Zana, *J. Colloid Interface Sci.*, **77**, 449 (1980); c) R. Zana and S. Yiv, *ibid.*, **77**, 456 (1980).
10) A. Cipiciani, M. Fracassini, R. Germani, G. Savelli, and C. A. Bunton, *J. Chem. Soc., Perkin Trans. 2*, **1987**, 547.
11) D. C. Mackenzie, C. A. Bunton, D. F. Nicoli, and G. Savelli, *J. Phys. Chem.*, **91**, 5709 (1987).
12) K. Ikeda, K. Meguro, A. Khan, and B. Lindman, *J. Colloid Interface Sci.*, in press.
13) T. Wong, K. Ikeda, K. Meguro, U. Ollson, O. Söderman, and B. Lindman, *J. Phys. Chem.*, in press.
14) R. Zana, Y. Muto, K. Esumi, and K. Meguro, *J. Colloid Interface Sci.*, **123**, 502 (1988).
15) P. Lianos, J. Lang, and R. Zana, *J. Phys. Chem.*, **86**, 1019 and 4809 (1982); P. Lianos, J. Lang, and R. Zana, *J. Colloid Interface Sci.*, **91**, 276 (1983); P. Lianos and R. Zana, *J. Phys. Chem.*, **88**, 1098 (1984).
16) M. Tachiya, *Chem. Phys. Lett.*, **33**, 289 (1975); M. Tachiya, *J. Phys. Chem.*, **76**, 340 (1982); P. Infelta, *Chem. Phys. Lett.*, **61**, 88 (1979); J. Dederen, M. Auwerauer, and F. C. Schryver, *Chem. Phys. Lett.*, **68**, 451 (1979).
17) G. Nilsson, *J. Phys. Chem.*, **61**, 1135 (1957).
18) H. C. Chiang and A. Lukton, *J. Phys. Chem.*, **79**, 1935 (1975).
19) K. S. Birdi, H. N. Singh, and S. U. Dalsager, *J. Phys. Chem.*, **83**, 2733 (1979).
20) T. Suzuki, K. Esumi, and K. Meguro, *J. Colloid Interface Sci.*, **93**, 205 (1983).
21) R. Zana, "Surfactant Solutions: New Methods of Investigation," ed by R. Zana, M. Dekker Inc., New-York (1987), Chap. 5.
22) N. J. Turro and A. Yekta, *J. Am. Chem. Soc.*, **100**, 5951 (1978).
23) R. Zana, J. Lang, and A. Maliaris, unpublished results.
24) J. Israelachvili, D. J. Mitchell, and B. Ninham, *J. Chem. Soc., Faraday Trans. 2*, **72**, 1525 (1976).
25) K. Ikeda, M. Yasuda, M. Ishikawa, K. Esumi, K. Meguro, W. Binana-Limbele, and R. Zana, to be submitted.
26) A. Malliaris, J. Le Moiggne, J. Sturm, and R. Zana, *J. Phys. Chem.*, **89**, 2705 (1985).
27) E. Roelants, E. Gelade, J. Smid, and F. C. Schryver, *J. Colloid Interface Sci.*, **107**, 335 (1985).
28) M. Jones and J. Piercy, *J. Chem. Soc., Faraday Trans. 1*, **68**, 1839 (1972).
29) J. Lang and R. Zana, "Surfactant Solutions: New Methods of Investigation," ed by R. Zana, M. Dekker Inc., New-York (1987), Chap. 8.

 © 1989 The Chemical Society of Japan Bull. Chem. Soc. Jpn., 62, 1037—1041 (1989)

Interaction between Disodium 1,14-Tetradecanediyl Disulfate and Sodium Dodecyl Sulfate or Poly(oxyethylene) Nonyl Phenyl Ether on Alumina

Kunio ESUMI,* Yuki ASANO, Yuichi SAKAMOTO, and Kenjiro MEGURO
Department of Applied Chemistry, Institute of Colloid and Interface Science, Science University of Tokyo, Kagurazaka, Shinjuku-ku,Tokyo 162
(Received October 25, 1988)

The interactions between disodium 1,14-tetradecanediyl disulfate ($\alpha,\omega C_{14}$) and sodium dodecyl sulfate (SDS) or poly(oxyethylene) nonyl phenyl ether (NP 7.5) on α-alumina have been studied by measuring the zeta potential, the mean particle size, the amounts of surfactants adsorbed, and the fluorescence spectra of pyrene. When $\alpha,\omega C_{14}$, SDS, or NP 7.5 as a second additive is added to alumina previously flocculated by the addition of SDS or $\alpha,\omega C_{14}$, as a first additive, the flocculated alumina redisperses in the $\alpha,\omega C_{14}$-SDS and $\alpha,\omega C_{14}$-NP 7.5 systems. For the $\alpha,\omega C_{14}$-SDS and $\alpha,\omega C_{14}$-NP 7.5 systems, the redispersion of alumina proceeds in such a manner that the hydrophobic parts of SDS or NP 7.5 are in contact with the $\alpha,\omega C_{14}$-coated alumina and the hydrophilic polar groups direct out to aqueous solution, resulting in the formation of mixed bilayers on the alumina, while for the $\alpha,\omega C_{14}$-SDS system the adsorption of SDS on the $\alpha,\omega C_{14}$-coated alumina is not enough to attain the redispersion of alumina. The measurement of the ratio I_1/I_3 of intensities of the first and third vibrionic bands of the pyrene monomer fluorescence spectra indicates that pyrene is solubilized in a much lower polar site for the $\alpha,\omega C_{14}$-SDS mixed bilayer than for the mixed bilayer of $\alpha,\omega C_{14}$-NP 7.5.

Recently, we have studied the properties of mixed bilayers[1-3] of surfactants formed on monodispersed ferric hydro sols and on alumina by measuring the zeta potential, the mean particle size, the amounts of surfactants adsorbed, and the fluorescence spectra of pyrene. The formation of the mixed bilayers depends on the combination of surfactants used: the mixed bilayers are more preferentially formed for anionic hydrocarbon-nonionic hydrocarbon surfactants than for anionic fluorocarbon-anionic hydrocarbon surfactants. All of the studies of the mixed bilayers have been limited to combinations of conventional surfactants consisting of a straight-hydrocarbon chain or a fluorocarbon chain and one hydrophilic group.

A bolaform surfactant is composed of a hydrocarbon chain with one ionic or polar head group attached at each of its two ends. Ionic bolaform surfactants show several important differences from conventional surfactants with the same head group.[4-8] The bolaform surfactants have been reported to take a folded, wicket-like conformation at the air-water interface.[5,8] Zana et al.[9] have reported the mixed micellization in mixtures of α,ω-bis(trimethylammonio)alkane dibromide and alkyltrimethylammonium bromide, and they have found that the mixed micellization depends on the matching of the hydrocarbon chain length between bolaform and conventional surfactants, and on their concentrations. This study would lead the possibility of the formation of a mixed bilayer between bolaform and conventional surfactants on particle surfaces.

This work will extend the above approach to the solid/aqueous solution interface. In this paper, the interactions between disodium tetradecanediyl disulfate ($\alpha,\omega C_{14}$) and sodium dodecyl sulfate (SDS) or poly(oxyethylene) nonyl phenyl ether (NP7.5) will be studied through the redispersion behavior of alumina by measuring the zeta potential, the mean particle size of alumina, the amounts of surfactants adsorbed, and the fluorescence spectra of pyrene.

Experimental

Materials. The disodium 1,14-tetradecanediyl disulfate was synthesized as follows. Tetradecanedioic acid supplied by the Tokyo Kasei Co. was reduced to 1,14-tetradecanediol with borane-THF complexes following the esterization of the diol with chlorosulfuric acid. The product was then neutralized by the addition of sodium hydrogencarbonate. The final product was recrystallized twice with mixtures of 2-propanol-water and then with diethyl ether. Sodium dodecyl sulfate was also synthesized and purified. Poly(oxyethylene) nonyl phenyl ether with average oxyethylene chains of 7.5 was obtained from the Nikko Chemicals Co., Ltd., and was used without further purification.

The water used in all experiments was purified by passing it through a Mill-Q system (Nihon Millipore Co.) until its specific conductivity fell below $10^{-7}\ \Omega^{-1}\ cm^{-1}$.

The alumina used was α-alumina of a 99.995% purity supplied by Showa Denko K.K. The specific surface area and the average particle diameter of the alumina were 10.1 $m^2\ g^{-1}$ and 500 nm respectively.

Procedure. As the alumina had an isoelectric point of pH 9.0, the alumina flocculated upon the addition of anionic surfactants at pH 3.5, where the alumina showed an appropriate positive zeta potential value. Then, a second surfactant, different from the first one, was added to the flocculated alumina. After the mixture had reached an adsorption equilibrium, the interaction between first and second surfactants on the alumina was characterized by measuring the zeta potentials and the particle size of the alumina. The zeta potential of alumina was measured using an electrophoresis apparatus (Pen Kem, Laser Zee 500). The particle size of alumina was measured using photocorrelation spectroscopy (Autosizer, Malvern Co.). Further, after the centrifugation of the suspension, the concentrations of all the surfactants except NP7.5 in the supernatant were determined by means of an isotachophoresis method. The concentration of NP7.5, which has an absorption band at 275 nm, was determined by means of a UV spectrophotometer. The amounts

of surfactants adsorbed on the alumina were determined from the difference in the concentration before and after the adsorption.

For the measurement of the fluorescence spectra, the suspension was added to a flask in which pyrene dissolved in ethanol had first been introduced, after which the solvent had been allowed to evaporate. The steady-state emission spectra of the suspensions were obtained using a Hitachi 650-10S fluorescence spectrophotometer. The concentration of pyrene ranged from 1×10^{-6} to 1×10^{-7} mol dm^{-3}. The excitation wavelength of pyrene was at 335 nm.

In order to keep the ionic strength constant, all the measurements were carried out at 25 °C in 10 mmol dm^{-3} sodium nitrate. Nitric acid was used to adjust the pH of the suspension.

Results and Discussion

Figure 1 shows the adsorption isotherms of SDS and $\alpha,\omega C_{14}$ on the alumina. The amounts of SDS and $\alpha,\omega C_{14}$ adsorbed increased at first gradually and then sharply, following a plateau level. This adsorption behavior has been reported by many workers.[10-13]

In order to study the dispersion state of the alumina upon the addition of SDS or $\alpha,\omega C_{14}$, the zeta potentials and the mean particle sizes of the alumina were measured.

Figure 2 shows that the zeta potentials of the alumina decrease with the concentration of both SDS and $\alpha,\omega C_{14}$, then they are reversed, the zeta potential of the alumina upon the addition of SDS being much smaller than that upon the addition of $\alpha,\omega C_{14}$. The mean particle size measurement suggests that the alumina is flocculated by the addition of $\alpha,\omega C_{14}$ above 0.5 mmol dm^{-3} and that it is not redispersed anywhere in the whole concentration region studied, whereas the alumina is flocculated and then redispersed with an increase in the concentration of the SDS additive. By the addition of $\alpha,\omega C_{14}$, the alumina might be covered with $\alpha,\omega C_{14}$ molecules orienting their hydrocarbon chains toward the aqueous solution, resulting in the hydrophobic surface of the alumina and flocculation. This mechanism may be supported by the view that α,ω surfactants generally adopt a folded, wicket-like conformation at an air-water interface.[5,8] On the other hand, SDS molecules are adsorbed on the alumina, orienting their hydrophobic chains toward the aqueous solution, and with an increase in the concentration the bilayer of SDS[14] on the alumina is formed, resulting in a redispersion of the alumina. In this study, it is found that the optimum flocculation con-

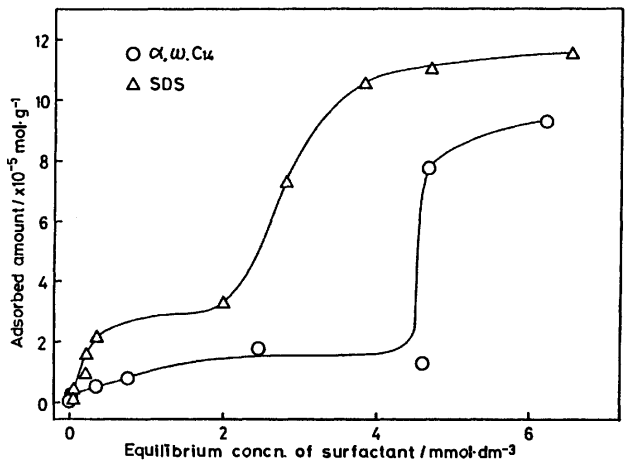

Fig. 1. Adsorption isotherms of SDS and α,ω C_{14} on alumina at 25 °C.

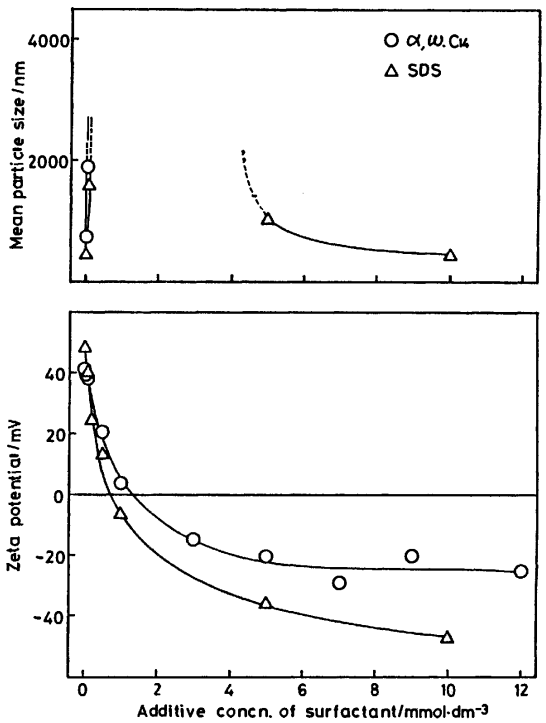

Fig. 2. Changes in mean particle size and zeta potential of alumina with additive concentration of SDS or $\alpha,\omega C_{14}$.

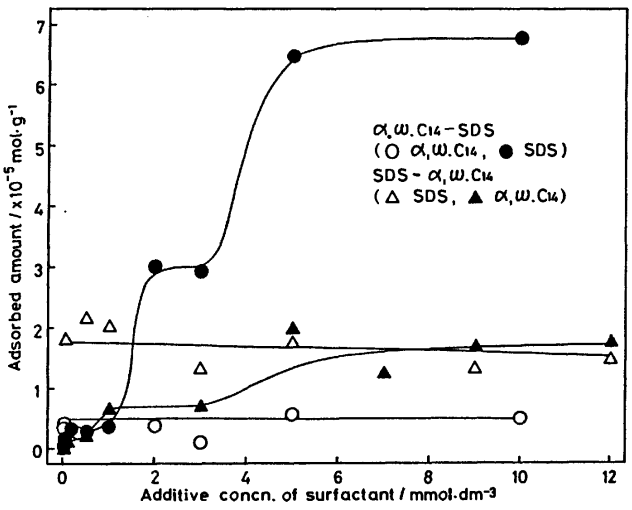

Fig. 3. Amount adsorbed of SDS and α,ω C_{14} on alumina with additive concentration of anionic surfactant for SDS-$\alpha,\omega C_{14}$ and $\alpha,\omega C_{14}$-SDS systems.

centrations of SDS and $\alpha,\omega C_{14}$ for the alumina are about 1 mmol dm^{-3}.

In order to elucidate the interaction between $\alpha,\omega C_{14}$ and SDS or NP7.5 on the alumina, SDS, $\alpha,\omega C_{14}$ or NP7.5 was added to alumina which had been flocculated by the addition of SDS or $\alpha,\omega C_{14}$ at its optimum flocculation concentration.

Figure 3 shows the amounts of SDS and $\alpha,\omega C_{14}$ adsorbed on the alumina for the SDS-$\alpha,\omega C_{14}$ and $\alpha,\omega C_{14}$-SDS systems. Here, the SDS-$\alpha,\omega C_{14}$ system means that in which the alumina is flocculated by the addition of 1 mmol dm^{-3} SDS as a first additive and then $\alpha,\omega C_{14}$ as a second additive to the flocculated alumina. The other systems are studied by the same procedure as the SDS-$\alpha,\omega C_{14}$ system. In the SDS-$\alpha,\omega C_{14}$ system, it is clear that the amount of SDS adsorbed is nearly constant after the addition of $\alpha,\omega C_{14}$, while the amount of $\alpha,\omega C_{14}$ adsorbed is relatively small. This result may imply that the hydrophobicity of the hydrocarbon chain of $\alpha,\omega C_{14}$ is not strong enough to form hydrophobic bonding between SDS and $\alpha,\omega C_{14}$. On the contrary, in the $\alpha,\omega C_{14}$-SDS system, the amount of $\alpha,\omega C_{14}$ adsorbed is almost constant, while the amount of SDS adsorbed increases gradually with the concentration of the SDS additive, suggesting that, with the concentration of the SDS additive, SDS is adsorbed on the hydrocarbon chains of $\alpha,\omega C_{14}$ covering on the alumina, resulting in the formation of a mixed bilayer between SDS and $\alpha,\omega C_{14}$. These differences in adsorption behavior between $\alpha,\omega C_{14}$ and SDS as the second additive may be supported by the fact that the surface activity of a bolaform surfactant[9] is considerably smaller than that of alkyl hydrogensulfate because of the lower hydrophobicity of the bolaform surfactant.

Figure 4 shows that the amount of $\alpha,\omega C_{14}$ adsorbed on the alumina is nearly constant, even after the addition of various concentrations of NP7.5, while the amount of NP7.5 adsorbed increases with an increase in the concentration of the NP7.5 additive. These results imply that with an increase in the concentration of the NP7.5 additive, the $\alpha,\omega C_{14}$ adsorbing on the alumina is not replaced by NP7.5, but a subsequent adsorption of NP7.5 forms mixed bilayers of $\alpha,\omega C_{14}$-NP7.5 on the alumina. This mixed bilayer is probably formed in such a manner that the hydrophobic parts of NP7.5 are in contact with the $\alpha,\omega C_{14}$-coated alumina and the hydrophilic polar groups, i.e., oxyethylene chains, directed out toward the aqueous solution.

Furthermore, in order to characterize the properties of layers adsorbed between $\alpha,\omega C_{14}$ and SDS or NP7.5, pyrene fluorescence experiments were carried out. The pyrene fluorescence fine structure has been found to be remarkably dependent on the solvent: the intensity ratio of I_1/I_3 (I_1, first vibrionic, and I_3 third vibrionic bands at 373 and 383 nm respectively) is sensitive to the solvent polarity.[15] Typically, the I_1/I_3 ratio for pyrene

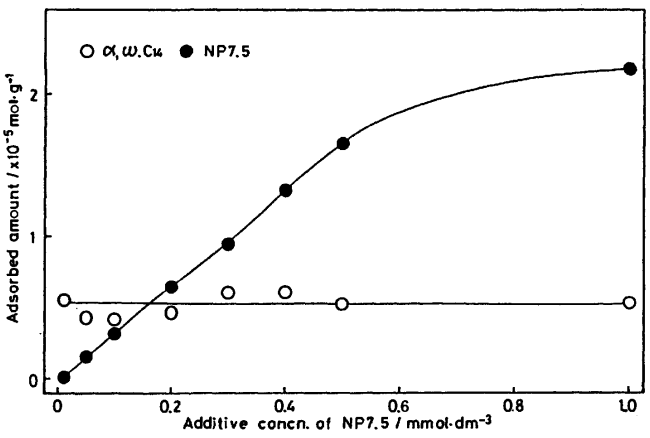

Fig. 4. Amount adsorbed of α,ω C_{14} and NP7.5 on alumina with additive concentration of NP7.5.

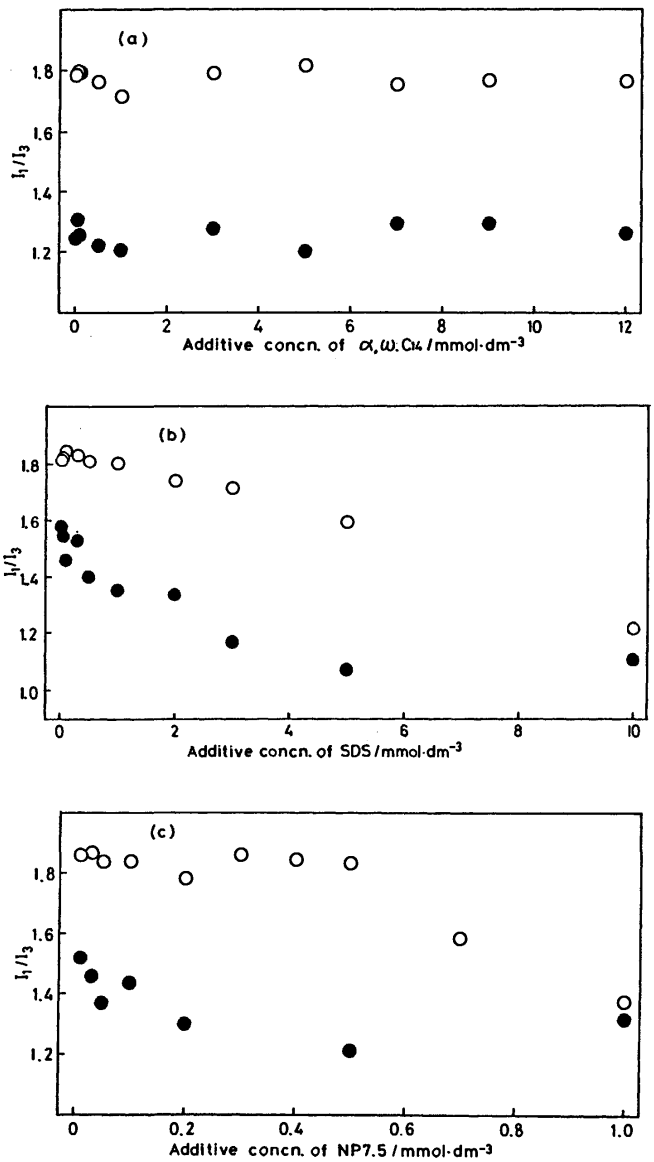

Fig. 5. Changes in I_1/I_3 value of pyrene for(a) SDS-α,ω C_{14}, (b) α,ω C_{14}-SDS, and (c) α,ω C_{14}-NP7.5 systems: open mark, in supernatant; closed mark, in suspension.

changes from 1.8 in water to 0.6 in hydrocarbon media.[16] This fluorescence technique, when applied to an aqueous system[17-20] containing solid particles, has given useful information on the microenvironmental properties of surfactants adsorbed on particles. Figures 5(a) and (b) show the changes in the I_1/I_3 values of pyrene for the SDS-$\alpha,\omega C_{14}$ and $\alpha,\omega C_{14}$-SDS systems. It may be seen that in the SDS-$\alpha,\omega C_{14}$ system, the I_1/I_3 values of the suspension are nearly constant, i.e., 1.2—1.3, even after the addition of various concentrations of $\alpha,\omega C_{14}$ while the I_1/I_3 values of the supernatant range from 1.8 to 1.7. This result indicates that the pyrene is located in hydrocarbon chain of SDS adsorbed on the alumina, for the I_1/I_3 values are very close to that in the SDS micelles. On the other hand, in the $\alpha,\omega C_{14}$-SDS system, the I_1/I_3 values of the suspension decreased from 1.6 to about 1.1 with an increase in the concentration of the SDS additive, while the I_1/I_3 values of the supernatant decreased gradually, reaching about 1.2 at the concentration of the SDS additive, 10 mmol dm^{-3}. This result can be interpreted by the view that pyrene, solubilized in hydrocarbon chains of $\alpha,\omega C_{14}$ adsorbed on the alumina, becomes located at the hydrocarbon chains of SDS, taking into consideration the fact that the I_1/I_3 values of pyrene are about 1.6 for $\alpha,\omega C_{14}$ micelles[8] and about 1.1—1.2 for SDS micelles. It is noteworthy that, on the redispersion state of alumina, the I_1/I_3 values of the suspension are much lower than that of the supernatant, indicating that the mixed bilayer of $\alpha,\omega C_{14}$ and SDS formed on the alumina is much more compact than in the case of the micelle in an aqueous solution.

Figure 5(c) shows that,in the $\alpha,\omega C_{14}$-NP7.5 system, the I_1/I_3 values of pyrene for the suspension decrease with the concentration of the NP7.5 additive until they reach a constant value (1.3), while those for the supernatant also decrease. Above 0.2 mmol dm^{-3} of NP7.5, the mixed bilayer of $\alpha,\omega C_{14}$-NP7.5 begins to be formed, but the amount of NP7.5 adsorbed is not enough to obtain a redispersion state of the alumina below 1 mmol dm^{-3} of NP7.5. In the redispersion state of alumina, the I_1/I_3 values of the suspension are not very different from those of the supernatant, suggesting that the compactness in the mixed bilayer and the mixed micelle is almost the same. The comparison with the I_1/I_3 values for the bilayers shows that the I_1/I_3 value for the $\alpha,\omega C_{14}$-SDS bilayer is lower than that for mixed bilayer of $\alpha,\omega C_{14}$-NP7.5, indicating that the pyrene is solubilized in much a lower polar site for the former than for the latter.

In order to ensure a dispersion state of the alumina for the three systems, the zeta potential and the mean particle size of the alumina were measured. Figure 6 shows that, in the $\alpha,\omega C_{14}$-SDS system, the zeta potential of the alumina decreases with an increase in the concentration of the SDS additive, reaching about −50 mV, while above the concentration of 5 mmol dm^{-3}, the mean particle size is detectable by the Auto-

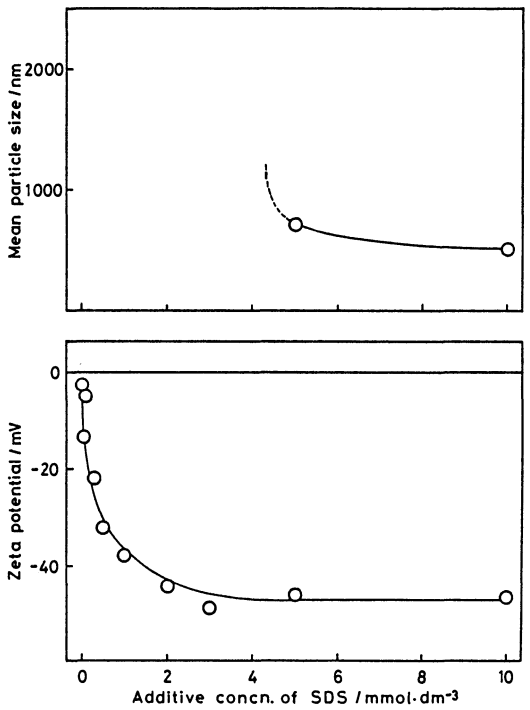

Fig. 6. Changes in zeta potential and mean particle size of alumina with additive concentration of SDS for $\alpha,\omega C_{14}$-SDS system.

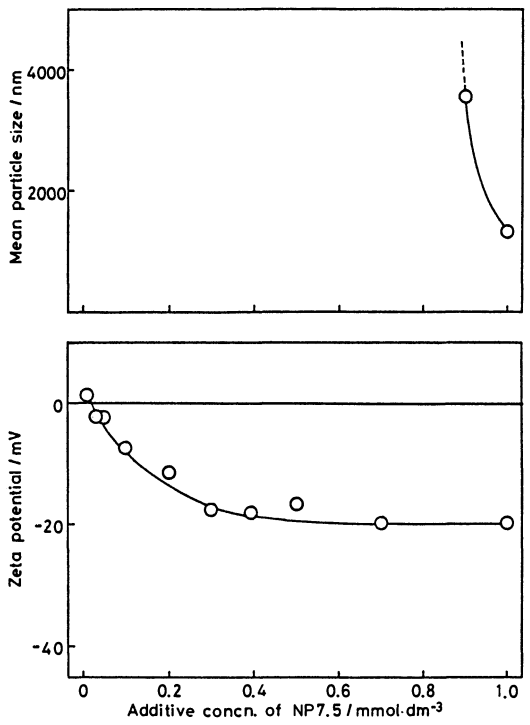

Fig. 7. Changes in zeta potential and mean particle size of alumina with additive concentration of NP7.5 for $\alpha,\omega C_{14}$-NP7.5 system.

sizer. The redispersion state of the alumina is found to be achieved by the concentration of the SDS additive above 5 mmol dm^{-3}. However, although not shown in the figure, in the SDS-$\alpha,\omega C_{14}$ system, the mean parti-

cle size of the alumina could not be measured because of the flocculated alumina, and the zeta potential value of the alumina was not significantly changed. Figure 7 demonstrates that,in the $\alpha,\omega C_{14}$-NP7.5 system, the mean particle size of the alumina decreases with the concentration of the NP7.5 additive, while the zeta potential also decreases. The reason why the zeta potential value is negative, although NP7.5, which is a nonionic surfactant, is adsorbed on the $\alpha,\omega C_{14}$-covered alumina, can not be explained at the present time. It is found that the redispersion state of the alumina can be attained by the addition of more than 1 mmol dm^{-3} of NP7.5.

Thus, these changes in the zeta potential and the mean particle size of the alumina are well correlated with those in the amounts of surfactants adsorbed and in the I_1/I_3 values for the three systems.

This study shows that the alumina previously flocculated by the addition of $\alpha,\omega C_{14}$ redisperses upon the addition of SDS and NP7.5 due to the formation of mixed bilayers of $\alpha,\omega C_{14}$-SDS and $\alpha,\omega C_{14}$-NP7.5 on the alumina, while the alumina previously flocculated by the addition of SDS hardly redisperses upon the addition of $\alpha,\omega C_{14}$ judging from the measurements of the zeta potential, the mean particle size of alumina, and the amounts of surfactants adsorbed. From the measurement of the I_1/I_3 ratio of pyrene, it is found that pyrene is solubilized in a much lower polar site of the $\alpha,\omega C_{14}$-SDS mixed bilayer than in the mixed bilayer of $\alpha,\omega C_{14}$-NP7.5.

References

1) K. Esumi, Y. Ono, M. Ishizuka, and K. Meguro, *Colloids Surf.*, **32**, 139 (1988).

2) K. Esumi, Y. Sakamoto, K. Yoshikawa, and K. Meguro, *Bull. Chem. Soc. Jpn.*, **61**, 1475 (1988).

3) K. Esumi, Y. Sakamoto, and K. Meguro, *Colloid Polym. Sci.*, in press.

4) M. Ueno, T. Hikota, T. Mitama, and K. Meguro, *J. Am. Oil Chem.*, **49**, 250 (1972).

5) F. M. Menger and S. Wrenn, *J. Phys. Chem.*, **78**, 1387 (1974).

6) S. Yiv and R. Zana, *J. Colloid Interface Sci.*, **77**, 449 (1980).

7) R. Zana, S. Yiv, and K. M. Kale, *J. Colloid Interface Sci.*, **77**, 456 (1980).

8) K. Meguro, K. Ikeda, A. Otsuji, M. Taya, M. Yasuda, and K. Esumi, *J. Colloid Interface Sci.*, **118**, 372 (1987).

9) R. Zana, Y. Muto, K. Esumi, and K. Meguro, *J. Colloid Interface Sci.*, **123**, 502 (1988).

10) P. Somasundaran and D. W. Fuerstenau, *J. Phys. Chem.*, **70**, 90 (1966).

11) J. F. Scamehorn, R. S. Schechter, and W. H. Wade, *J. Colloid Interface Sci.*, **85**, 463 (1982).

12) M. J. Rosen and Y. Nakamura, *J. Phys. Chem.*, **81**, 873 (1977).

13) K. Esumi, K. Yamada, T. Sugawara, and K. Meguro, *Bull. Chem. Soc. Jpn.*, **59**, 697 (1986).

14) K. Meguro, *Kogyo Kagaku Zasshi*, **58**, 905 (1955).

15) A. Nakajima, *Bull. Chem. Soc. Jpn.*, **44**, 3272 (1971).

16) K. Kalyanasundaram and J. K. Thomas, *J. Am. Chem. Soc.*, **99**, 2039 (1977).

17) P. Chandar, P. Somasundaran, and N. J. Turro, *J. Colloid Interface Sci.*, **117**,31 (1987).

18) P. Levitz, H. Van Damme, and D. Keravis, *J. Phys. Chem.*, **88**, 2228 (1984).

19) T. Nakamura and J. K. Thomas, *Langmuir*, **3** ,234 (1987).

20) K. Esumi and K. Meguro, *J. Colloid Interface Sci.*, in press.

Photocatalytic Hydrogen Evolution from Aqueous Solutions of Sodium Sulfite Using Platinum-Loaded $CdS_{1-x}Se_x$ Mixed Crystal Powder

Toshio UCHIHARA,† Hirohisa ABE, Michio MATSUMURA, and Hiroshi TSUBOMURA*
Laboratory for Chemical Conversion of Solar Energy and Department of Chemistry, Faculty of Engineering Science, Osaka University, Toyonaka, Osaka 560
(Received November 10, 1988)

The $CdS_{1-x}Se_x$ mixed-crystal powder was prepared for the purpose to reduce the band gap of CdS and expand the effective wavelength region of the photocatalyst. Hydrogen evolution was observed from an aqueous solution of 1 M sodium sulfite by use of the mixed-crystal photocatalyst loaded with platinum under illumination at wavelengths longer than 520 nm, where neither the platinum-loaded CdS nor CdSe photocatalyst is active. However, when the mixed-crystal catalysts were illuminated at wavelengths longer than 390 nm or with an AM 1 solar simulator, the rate of the hydrogen evolution was lower than that of CdS. The energy levels of the electronic bands in the mixed-crystals have been clarified from the results of the electrochemical studies, and the fact that the mixed-crystal powder has lower photocatalytic activity than CdS powder has been ascribed to the downward shift of the conduction band edge. These findings are useful in designing photocatalysts for hydrogen production.

Photocatalytic hydrogen evolution on semiconductor particles has been attracting much attention in view of solar energy utilization.[1] Among various semiconductor materials most frequently studied, cadmium sulfide (CdS) is known to have a spectral response in the visible region.[2-8] For the purpose of solar energy utilization, however, semiconductors having smaller band gaps are more suitable because they can convert light energy in a wider spectral region. As a candidate we may take up cadmium selenide (CdSe) because its band gap (1.7 eV) is smaller than that of CdS (2.4 eV) and its physical and chemical properties are similar to those of CdS. It is known, however, that CdSe does not cause hydrogen evolution.[9] We have therefore undertaken to study the photocatalytic properties of the $CdS_{1-x}Se_x$ mixed-crystal powder for the purpose of obtaining efficient photocatalysts working under sun light. The results were analyzed based on the electrochemical measurements of the $CdS_{1-x}Se_x$ sinter electrodes.

The photoelectrochemical properties of the $CdS_{1-x}Se_x$ mixed-crystal electrodes have been reported by some groups.[10-14] Kawai et al.[15] studied the photocatalytic hydrogen evolution from aqueous solutions containing ethanol or formic acid on $CdS_{1-x}Se_x$ powder and concluded that the photocatalytic activity was mainly determined by the energy value of the valence band and the transport property of the photogenerated carriers in the mixed crystal. In this paper, we will emphasize the importance of the height of the conduction band energy for the hydrogen evolution based on our results on the electrochemical measurements.

Experimental

The $CdS_{1-x}Se_x$ powder was prepared by grinding CdS and CdSe powders purchased from Fruuchi Chem. Co., Ltd. in an agate mortar and, then, heating at 750 °C for 20 h under a nitrogen atmosphere in an electric furnace. The ratio of S and Se in the powder was controlled by changing the quantities of the CdS and CdSe powders. The preparation of the $Cd_{1-x}Zn_xSe$ powder from CdSe and ZnSe powders was also attempted in a similar manner. The semiconductor powder thus prepared was loaded with 3 wt% platinum powder by shaking the semiconductor powder and platinum powder in a glass flask.[4] The X-ray diffraction (XRD) patterns of the powder specimens were obtained with a Shimadzu VD-1 diffractometer using the Cu $K\alpha$ radiation. The diffuse reflection spectra were obtained with a Shimadzu UV-360 spectrophotometer equipped with an integrating sphere.

Photocatalytic hydrogen evolution was studied in a 100 ml glass flask containing 30 ml of an aqueous solution of 1 M (M=mol dm^{-3}) sodium sulfite and 300 mg photocatalyst. The pH of the solution was adjusted to 8.0 by addition of boric acid and sodium hydroxide. After the air in the flask was evacuated, the suspension was illuminated with a 500 W xenon lamp combined with a Toshiba L-39 or VO-52 cut-off glass filter, or with an AM 1 (100 mW cm^{-2}) solar simulator (Wacom Co., Ltd.). Hydrogen was the only gaseous product and its amount was determined from the pressure in the glass flask and the total volume of the flask plus the vacuum line used for the pressure measurements.

The sintered disks of CdS, CdSe, ZnSe, and the mixed-crystal materials were prepared by pressure-sintering at 850 °C, applying a pressure of 1.25×10^7 Pa for 10 h under a nitrogen atmosphere. The densities of CdS and CdSe sintered disks prepared by this method were 96 and 89% of the single crystals, respectively, being considerably higher than those obtained by sintering under ambient pressure. The electrodic properties of these disks were studied in a three-electrode cell having such a semiconductor electrode, a platinum counter electrode, and a saturated calomel electrode (SCE). The potential of the semiconductor electrode was controlled with a potentiostat (Nikkokeisoku, NPGS-301). The intensity of incident light was measured with a thermopile (Eppley Lab.).

Results and Discussion

1. Photocatalytic Activity of the $CdS_{1-x}Se_x$ Powder. The XRD pattern of the mixture of CdS and CdSe

† On leave of absence from Department of Chemistry, College of Science, University of the Ryukyus, Nishihara, Okinawa 903-01.

powders without heat treatment consists of diffraction peaks of pure CdS and CdSe powders as seen in Fig. 1a. By heating it at 750 °C for 2 h, the peaks due to CdS and CdSe become weak and new peaks appear at intermediate positions between the corresponding peaks of CdS and CdSe (Fig. 1b). Only the new peaks are observed after heating for 20 h (Fig. 1c), and the positions of the new peaks change continuously with the mole fraction of CdSe (X). These results indicate that homogeneous crystalline particles are formed by heating for a time longer than 20 h at 750 °C. After the heat treatment, the particle size increased to about 3 μm from the original size of the CdS and CdSe particles, about 1 μm.

The reflection spectra of the mixed crystal specimens also changed continuously from that of CdS to that of CdSe along with the fraction X. The reflection spectra were analyzed according to the Kubelka-Munk's equation,[16]

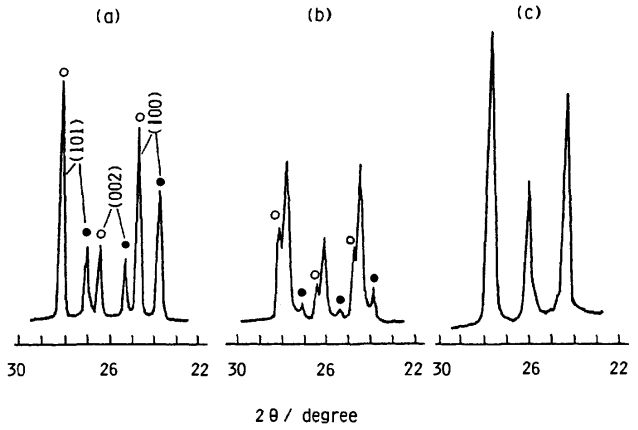

Fig. 1. XRD patterns for the CdS-CdSe mixed powder containing 40 wt% CdSe, before heat treatment (a) and after heat treatment at 750 °C for 2 h (b) and 20 h (c). Open and closed circles denote the peaks assigned to CdS and CdSe, respectively.

$$f(R_d) = \alpha/S = (1-R_d)^2/2R_d \quad (1)$$

where R_d is the relative diffuse reflectance, α the absorption coefficient, and S the coefficient of light diffusion. The $f(R_d)$ calculated is plotted against wavelength in Fig. 2. The $f(R_d)$ value of pure CdS and CdSe powders at the wavelengths corresponding to their band gap energy of 2.4 and 1.7 eV are 4.0 and 3.7 (denoted by points A and B in Fig. 2). Accordingly, the band gaps of the $CdS_{1-x}Se_x$ mixed-crystal specimens are determined from the wavelengths corresponding to the intersections of the curves of the $CdS_{1-x}Se_x$ specimens with the straight line passing through A and B as shown in Fig. 2. The band gaps thus obtained are plotted against X in Fig. 3.

The $CdS_{1-x}Se_x$ mixed-crystal powder was loaded with 3 wt% platinum, and the photocatalyzed hydrogen evolution from an aqueous solution of 1 M sodium sulfite at pH 8.0 was measured under illumination with a 500 W xenon lamp combined with a glass filter. In the solution of sodium sulfite, the platinized CdS photocatalyst was stable[17] and generated hydrogen with quantum efficiencies higher than 20% under illumination at wavelengths shorter than 500 nm.[4,18] When light in the region shorter than 520 nm was eliminated with a cut-off glass filter (VO-52), hydrogen did not evolve on CdS because CdS does not absorb light in the region longer than 520 nm. The CdSe photocatalyst did not evolve hydrogen from the same solution in spite of the fact that it does absorb light in this region. Nevertheless, the $CdS_{1-x}Se_x$ mixed-crystal powder caused hydrogen evolution, the rate showing a plateau at X values from about 0.1 to 0.3 as indicated by the solid line in Fig. 4. As shown by the broken line, higher rates of hydrogen evolution were obtained when the cut-off wavelength was lowered to 390 nm by use of a L-39 glass filter, where pure CdS showed the highest rate. Similar results were

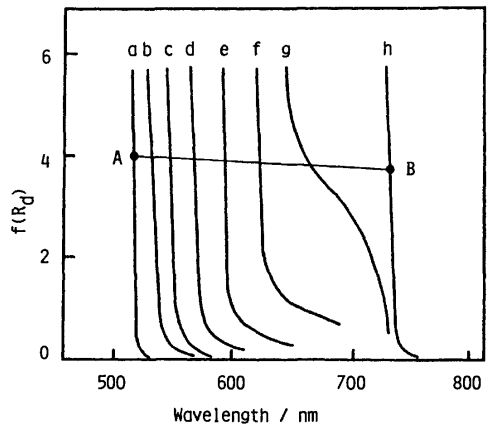

Fig. 2. Wavelength dependence of $f(R_d)$ for the $CdS_{1-x}Se_x$ mixed-crystal powder with various X values. The X values are 0 (a), 0.04 (b), 0.08 (c), 0.16 (d), 0.34 (e), 0.53 (f), 0.75 (g), and 1.0 (h), respectively.

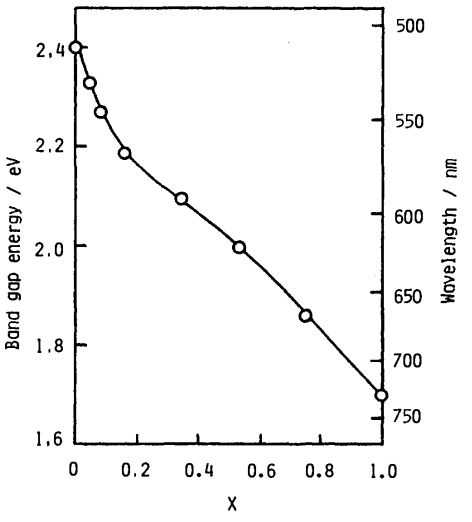

Fig. 3. The band gaps of $CdS_{1-x}Se_x$ mixed-crystals as a function of X estimated from the data of Fig. 2.

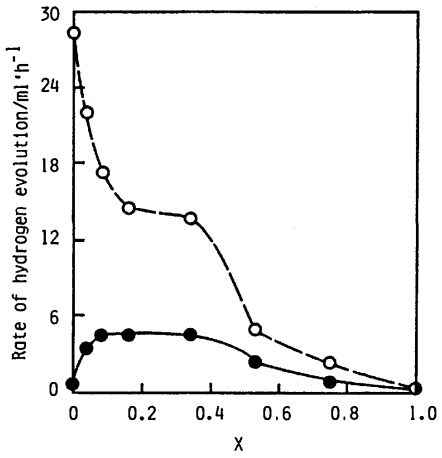

Fig. 4. The Rate of the photocatalytic hydrogen evolution from an aqueous solution of 1 M sodium sulfite (pH 8.0) by use of the $CdS_{1-x}Se_x$ mixed-crystal powder as a function of X. Illumination was made through cut-off glass filters, Toshiba L-39 (○) and VO-52 (●), which showed 50% transparency at 390 and 520 nm, respectively.

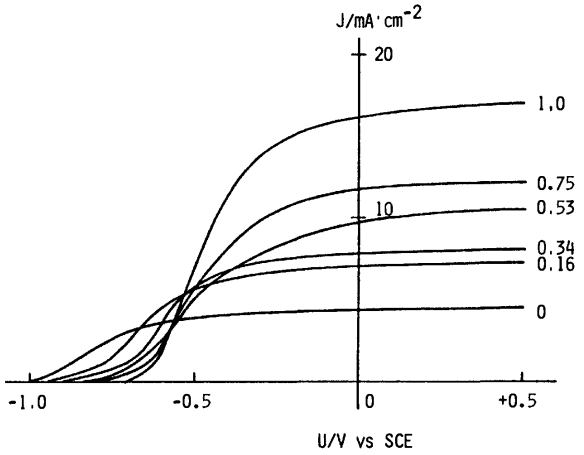

Fig. 5. The J-U curves for the $CdS_{1-x}Se_x$ sinter electrodes in a solution of 1 M sodium sulfite (pH 8.0). Illumination was carried out with an AM 1 solar simulator. The numbers on curves denote X.

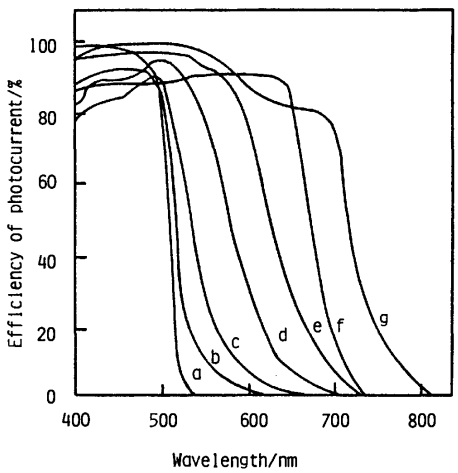

Fig. 6. The photocurrent quantum efficiency spectra for the $CdS_{1-x}Se_x$ sinter electrodes in an aqueous solution of 1 M sodium sulfite under anodic polarization (at +0.5 V vs. SCE) for X values 0 (a), 0.08 (b), 0.16 (c), 0.34 (d), 0.53 (e), 0.75 (f), and 1.0 (g).

obtained when AM 1 solar simulator was used, the pure CdS photocatalyst having the highest activity for hydrogen evolution. Thus, the trial to enhance the reaction efficiency under sun light by use of $CdS_{1-x}Se_x$ mixed-crystals was unsuccessful, although the effective region of wavelengths was expanded.

2. Photoelectrochemical Measurements of the $CdS_{1-x}Se_x$ Sinter Electrodes. For the further understanding of the photocatalyst properties, photoelectrochemical measurements were carried out by use of the $CdS_{1-x}Se_x$ mixed-crystal sinter electrodes, which were prepared by the pressure-sintering of mixed CdS-CdSe powder at 850 °C. The XRD pattern and the reflection spectra revealed that the sintered disks have a homogeneous mixed-crystal structure. Under simulated AM 1 illumination for the electrodes containing various amounts of Se in a solution of 1 M sodium sulfite, the saturated photocurrent density increased with the fraction of Se as shown in Fig. 5. This is explained well on account of the matching of band gaps of the mixed-crystal electrodes with the AM 1 spectrum. Another remarkable feature observed is that the photocurrents start at more positive potentials as the Se fraction increases.

In the absence of sulfite ions in the solution, the photocurrents due to the dissolution of the electrodes rose up from more positive potentials and decayed during illumination for all cases of the $CdS_{1-x}Se_x$ electrodes. That the onset potentials of the photocurrents are more negative in the presence of sulfite ions indicates that sulfite ions react well with positive holes photogenerated in the valence band of the mixed-crystal electrodes and prevent the electrode from corroding. The photocurrents measured in the solution of 1 M sodium sulfite were stable when the electrodes were illuminated at potentials more negative than the onset potential of the photoanodic dissolution currents.

The action spectra for the photocurrents of the mixed-crystal electrodes measured in aqueous solutions of 1 M sodium sulfite under anodic polarization are shown in Fig. 6. The photocurrents rise up at wavelengths corresponding to the band gaps obtained from the reflection spectra. The photocurrent quantum efficiencies of all specimens having various Se fractions showed nearly the same saturation values at short wavelengths, 80 to 95% without correction of the light losses due to the reflection on the electrode surface and the cell window.

The Mott-Schottky plots of the pure CdS sinter electrodes measured in an aqueous solution of 1 M sodium sulfite at 1 kHz gave straight lines and the flat band

potential was deteremined to be −1.01 V vs. SCE, nearly in agreement with the onset potential of the photocurrents. On the other hand, for the case of the $CdS_{1-x}Se_x$ electrodes having X values larger than 0.2, the Mott-Schottky plots did not show straight lines probably because they were porous, so that no flat band potential was determined by this method. So, we used the onset potential of the photocurrents of the $CdS_{1-x}Se_x$ electrodes in the 1 M sodium sulfite solution as a measure of the flat band potentials of the electrodes. It is conceivable that the difference between the Fermi level and the bottom of the conduction band is negligibly small for this case, because the semiconductors are rather highly doped. The solid line in Fig. 7 shows the position of the conduction band thus determined against the X value. The position of the valence band determined by subtracting the band gap energy from the energy level of the conduction band is also shown by the broken line in the figure. The results indicate that the conduction band energy goes down and the valence band energy goes up as the Se fraction increases in the mixed-crystal electrodes. The fact mentioned above that all the $CdS_{1-x}Se_x$ electrodes are fairly well stabilized by sulfite ions in the solution shows that the reactivity of the photogenerated holes in the valence band with sulfite ions is not spoiled by the upward shift of the valence band of the mixed crystal with increasing Se fraction.

When the CdSe electrode was short-circuited with a Pt electrode and illuminated in an aqueous solution of 1 M sodium sulfite, practically no photocurrent was observed. This is explained by taking into account the fact that the conduction band of CdSe is very close to the hydrogen evolution potential (Fig. 7). The bands

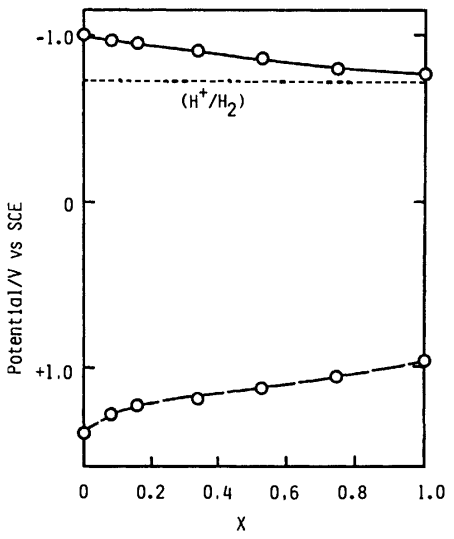

Fig. 7. The estimated energy levels of the conduction band of the $CdS_{1-x}Se_x$ mixed-crystal (solid line) and those of the valence band (broken line) as a function of X in an aqueous solution of 1 M sodium sulfite. The dotted line represents the potential for the hydrogen evolution in the same solution.

are therefore flattened under illumination, leading to very rapid recombination of the photogenerated electrons and holes. This result is in harmony with the inactivity of the CdSe photocatalyst for the hydrogen evolution (Fig. 4). On the other hand, for the case of a CdS electrode connected to a Pt electrode, electron-hole separation occurs efficiently and a photocurrent of 2.3 mA cm^{-2} is observed under AM 1 (100 mW cm^{-2}) illumination.

The highest quantum efficiency of the photocatalytic reaction on Pt-loaded CdS photocatalyst measured in our previous work was about 35%.[18] The efficiency limitation most probably arises from insufficient band bending of the photocatalyst at the working condition.[18] The downward shift of the conduction band by the incorporation of Se into the photocatalyst further weakens the band bending and lowers the efficiency of the photocatalytic reaction. This unfavorable effect caused by the incorporation of Se overcomes the positive effect of expanding the available wavelength region of the photocatalyst and makes the photocatalyst less active under illumination with the solar simulator or the similar light sources.

Kawai et al.[15] observed the lowering of the activity of the $CdS_{1-x}Se_x$ photocatalysts with the increase of X for the hydrogen evolution from aqueous solutions of alcohols. They attributed the reason for this to the upward shift of the valence band, disregarding the change of the energy level of the conduction band. Our results reveal that the energy level of the conduction band is largely changed by the incorporation of Se and this is the main reason for the lowering of the efficiency of the hydrogen evolution.

Noufi et al.[10] and Fujishima et al.[12] reported that the flat band potential of the $CdS_{1-x}Se_x$ mixed crystal electrodes determined from the onset potentials of the photocurrents became the maximum at an intermediate X values between 0.1 to 0.5 in alkaline solutions with and without sulfide ions. However, in our experiments, no maximum was observed for the flat band potential. This is consistent with the result that the band position changes linearly with the electronegativity of the elements of which the semiconductor is made.[19]

3. Characterization of CdSe-ZnSe Mixed Powders. Based on the above consideration, it is expected that the reaction efficiency under sun light may be enhanced if one can find a mixed crystal having a higher conduction band. It has been reported that the conduction band energy of ZnS is much higher than that of CdS and its photocatalytic activity is high under illumination in UV region.[20] From the results obtained so far, it is expected that the conduction band energy will move upward by incorporating a small amount of ZnSe (E_g 2.7 eV) into CdSe. However, the CdSe-ZnSe mixed-powder prepared by us showed very poor photocatalytic activity for the hydrogen production in an aqueous solution of 1 M sodium sulfite.

The reflection spectra of the CdSe-ZnSe mixed-powder samples heat-treated at 750 °C for 20 h showed that CdSe and ZnSe diffuse into each other to some extent. However, the spectra showed more broad tailing at the reflection edge than those of the $CdS_{1-x}Se_x$ powder. The XRD patterns of the heat-treated CdSe-ZnSe mixed powder showed new peaks ascribable to the CdSe-ZnSe mixed phase. They were broader than those of the $CdS_{1-x}Se_x$ mixed-crystal powder. These results suggest that the inhomogeneity of the CdSe-ZnSe mixed powder was not well removed by the heat treatment. The sintered disks of the mixture of CdSe and ZnSe powders prepared by pressure-sintering showed no photocurrents in a photoelectrochemical cell. These results can be explained by assuming that the mixed crystals have too many defect states, causing rapid recombination of the photogenerated carriers.

References

1) For example, "Energy Resouces through Photochemistry and Catalysis," ed by M. Grätzel, Academic Press, New York (1983); "Homogeneous and Heterogeneous Photocatalysis," ed by E. Pelizzetti and N. Serpone, D. Reidel Publishing, Dordrecht (1986).

2) J. R. Darwent and G. Porter, *J. Chem. Soc., Chem. Commun.*, **1981**, 145.

3) J. R. Harbour, R. Wolkow, and M. L. Hair, *J. Phys. Chem.*, **85**, 4026 (1981).

4) M. Matsumura, S. Furukawa, Y. Saho, and H. Tsubomura, *J. Phys. Chem.*, **89**, 1327 (1985).

5) N. Bühler, K. Meier, and J.-F. Reber, *J. Phys. Chem.*, **88**, 3261 (1984).

6) H. Harada, T. Sakata, and T. Ueda, *J. Am. Chem. Soc.*, **107**, 1773 (1985).

7) D. H. M. W. Thewissen, A. H. A, Tinnemans, M. Eeuwhorst-Reinten, K. Timmer, and A. Mackor, *Nouv. J. Chim.*, **7**, 191 (1983).

8) N. Serpone, E. Borgarello, and M. Grätzel, *J. Chem. Soc., Chem. Commun.*, **1984**, 342.

9) M. Fujii, T. Kawai, and S. Kawai, *Chem. Phys. Lett.*, **106**, 517 (1984).

10) R. N. Noufi, P. A. Kohl, and A. J. Bard, *J. Electrochem. Soc.*, **125**, 375 (1978).

11) T. Inoue, A. Fujishima, and K. Honda, *Denki Kagaku*, **48**, 294 (1980).

12) A. Fujishima, T. Inoue, and K. Honda, *Denki Kagaku*, **48**, 299 (1980).

13) H. H. Streckert, Jiu-ru Tong, M. K. Carpenter, A. B. Ellis, *J. Electrochem. Soc.*, **129**, 772 (1982).

14) R. O. Loutfy and D. S. Ng, *Solar Energy Mat.*, **11**, 319 (1984).

15) S. Kambe, M. Fujii, T. Kawai S. Kawai, and F. Nakahara, *Chem. Phys. Lett.*, **109**, 105 (1984).

16) "Shinjikkenkagakukouza," ed by The Chemical Society of Japan, Maruzen, Tokyo (1976), Vol. 4, p. 395.

17) M. Matsumura, H. Ohnishi, K. Hanafusa, and H. Tsubomura, *Bull. Chem. Soc. Jpn.*, **60**, 2001 (1987).

18) M. Matsumura, T. Uchihara, K. Hanafusa, and H. Tsubomura, *J. Electrochem. Soc.*, in press; "Photoelectrochemistry and Electrosynthesis on Semiconducting Materials," ed. by D. S. Ginley et al., p. 59, The Electrochem. Soc. Softbound Proceeding Series (1988).

19) J.-L. Sculfort and J. Gautron, *J. Chem. Phys.*, **80**, 3762 (1984).

20) S. Yanagida, T. Azuma, H. Kawakami, H. Kizumoto, and H. Sakurai, *J. Chem. Soc., Chem. Commun.*, **1984**, 21.

 © 1989 The Chemical Society of Japan Bull. Chem. Soc. Jpn., 62, 1047—1052 (1989)

Thermodynamic Study on the Extraction of Cobalt Complex with 8-Quinolinol into 1,1,2,2-Tetrachloroethane

Etsu YAMADA,* Eiichiro NAKAYAMA,† and Masanori SATO††
Center for Waste Water Treatment, Kyoto Institute of Technology, Sakyo-ku, Kyoto 606
†Research Center for Instrumental Analysis, Faculty of Science, Kyoto University, Sakyo-ku, Kyoto 606
††Faculty of Textile Science, Kyoto Institute of Technology, Sakyo-ku, Kyoto 606
(Received May 27, 1988)

The extraction behavior of cobalt(II) into 1,1,2,2-tetrachloroethane (TCE) with 8-quinolinol (HQ) from an aqueous solution in the presence of various inorganic anions (X^-) such as perchlorate, nitrate, and chloride ions was studied themodynamically. The extraction equation can be written as

$$2Co^{2+} + 6HQ_{(o)} + X^- \rightleftarrows Co_2Q_3(HQ)_3{}^+{}_{(o)} + X^-_{(o)} + 3H^+$$

The ion-pair of the binuclear complex (complex ion-pair) dissociates to a complex cation and an inorganic anion in the organic phase. The extraction constant increases in proportion to the radius of the counter anion. Changes in the enthalpy and entropy are negative for the overall extraction of cobalt with 8-quinolinol. These thermodynamic parameters were compared with those of zinc and cadmium. The temperature effect on the extraction behavior of cobalt with 8-quinolinol was also investigated in a chloroform system for comparison.

In recent years a number of studies have been carried out concerning the various factors affecting the solvent extraction of a metal chelate. However, only a few thermodynamic studies have been carried out.[1-5] Nakayama[6,7] studied the effect of temperature on the extraction of 8-quinolinol itself and copper, zinc and cadmium chelate of 8-quinolinol into TCE. Yamada et al.[8] clarified the mechanism of a synergistic solvent extraction of metal diphenylcarbazonate using thermodynamic data. It is thought that thermodynamic data provide valuable information regarding extraction mechanisms.

The extraction behavior of cobalt with 8-quinolinol into chloroform has been studied by several investigators.[9-13] It was reported that the species extracted into chloroform is the self-adduct, such as $CoQ_2(HQ)_2$[9,10] or CoQ_2HQ.[11,12] While Sekido et al.[13] found that an ion-pair complex containing a large anion, such as perchlorate, $Co_2Q_3(HQ)_3X$, is extracted below pH 5.1.

In this study, the temperature effects on the extraction behavior of cobalt with 8-quinolinol were investigated in both TCE and chloroform systems.

Experimental

Reagents. 8-Quinolinol was recrystallized twice from ethanol. Cobalt chloride ($CoCl_2 \cdot 6H_2O$) was used to prepare a stock solution of cobalt. A ^{60}Co solution (1 mCi) was obtained from the Japan Radio-isotope Association. Sodium Salts of perchlorate, nitrate and chloride as well as other chemicals were all of analytical grade.

Apparatus. Extraction was carried out in a cylindrical glass tube with a magnetic stirrer in a Yamato BH-71 water bath regulated at a temperature of ±0.05 °C. The cobalt concentration in the aqueous phase was determined by a Rigaku Denki energy dispersive X-ray fluorescence spectrometer Ultra-trace system according to a previously reported method.[14] In the case of $[Co]_{init.} = 10^{-8}$ M ($[Co]_{init.}$ is the initial concentration of cobalt in the aqueous phase, 1M=1 mol dm^{-3}), the concentration of cobalt was determined by measuring the γ-radio-activity of aliquots of both phases with a Packard Auto-Gamma 5100 single-channel pulse-height analyzer. For pH measurements, a Philips PW 9422 pH meter was used.

Extraction Procedure. A 30 ml portion of a buffered cobalt solution was stirred with a 10 ml portion of the 8-quinolinol solution of organic solvent standing in a constant-temperature bath for 30 min (a time period required to attain equilibrium). The initial aqueous solution was adjusted to the desired pH with a small amount of an acetic acid-acetate buffer solution, and to an ionic strength of 0.1 with sodium perchlorate, sodium nitrate or sodium chloride.

After stirring, the pH of the aqueous phase measured in situ was taken as the equilibrium pH. After phase separation, the concentration of cobalt in the aqueous phase was determined by an X-ray fluorescence spectrometer after concentrating cobalt as a diethyldithiocarbamate (DDTC) complex on a Millipore filter. Measurements were carried out by using a Mo anode and a Ge secondary target under excitation conditions of 35 kV-30 mA. The data-accumulation time was usually 100 s and the Co $K\alpha$ line intensity was used throughout the analytical calculations. The equilibrium concentration of cobalt in the organic phase was calculated from the aqueous equilibrium concentration and the initial concentration. The volume of the aqueous phases was corrected for temperature with values of the water density in the Smithsonian tables. The volumes of the organic phases were corrected for temperature using an experimentally determined density function. The density of TCE at any desired temperature employed could be obtained using the formula $1.597 - 1.562 \times 10^{-3}(t-20)$, where t is the temperature in degrees centigrade.

Results and Discussion

Extraction of Cobalt into TCE with 8-Quinolinol in the Presence of Various Inorganic Anions. All investigations were carried out below pH 6.0, because the species containing no anion, $Co_2Q_4(HQ)_2$, may be extracted in higher pH ranges.[13]

Plots of log D vs. pH at 25 °C in the presence of perchlorate, nitrate and chloride ions are shown in Fig. 1. The slopes of 1.5 indicate that the ratios Co : Q^- are 2 : 3, since the predominant species of cobalt in the aqueous phase is considered to be Co^{2+}. The order of the distribution ratios is ClO_4^->NO_3^-> Cl^-. In Figs. 2—4 the relationship between log D vs. log$[HQ]_o$ at various temperatures is shown for perchlorate, nitrate and chloride ions, respectively. In a perchlorate system, the slopes are 3 up to 70 °C. In a nitrate system, the slopes are 3 up to 55 °C. At 70 °C the slope is nearly down to 2. In a chloride system, the slopes change from 3 to nearly 2 above 55 °C. These facts suggest that the extracted species is 1 : 3 chelate at room temperatures and 1 : 2 chelate at sufficiently high temperatures for the nitrate and chloride systems. The effects of the concentration of the inorganic anions (ClO_4^-, NO_3^-, and Cl^-) on the distribution of cobalt in TCE were examined. Here, the ionic strength of the aqueous phase was adjusted to 0.1 with sodium sulfate. All of the plots of log D vs. log$[X^-]$ indicate a slope of nearly 0.5. This suggests that the ratios Co : X^- are 2 : 1.

From the slope analysis stated above, the extracted species is considered to be $Co_2Q_3(HQ)_3X$. In addition, the plots of log D vs. log$[Co]_{aq}$ are constant in the cobalt concentration range from 10^{-6} M to 10^{-4} M. This is generally accepted as being evidence for the existence of a mononuclear complex in the organic phase. However, our analysis of the results suggests

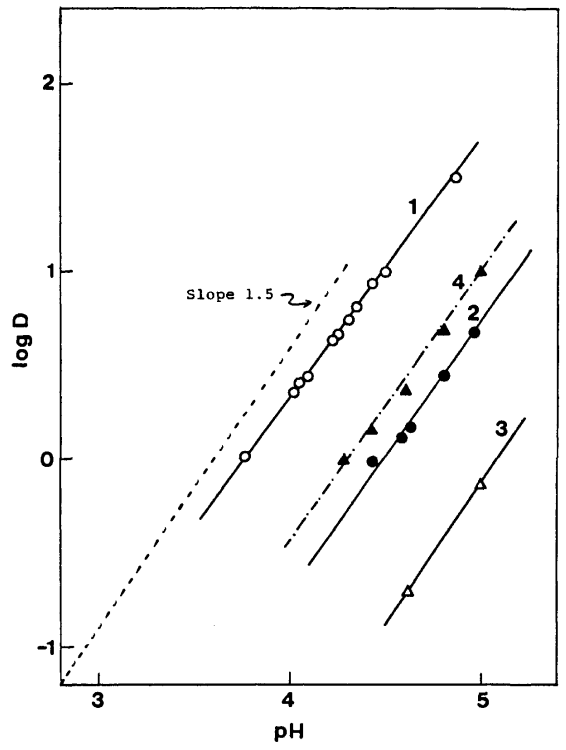

Fig. 1. Effect of pH on the distribution ratio of cobalt between TCE and water in the presence of various inorganic anions at 25 °C.
$[Co]_{init.}$=5 ppm, 0.09 M salts+0.01 M(AcOH-AcO-Na buffer), $[HQ]_o=10^{-2}$M 1; $NaClO_4$, 2; $NaNO_3$, 3; NaCl, $[HQ]_o=2.1\times10^{-2}$ M 4; NaCl.

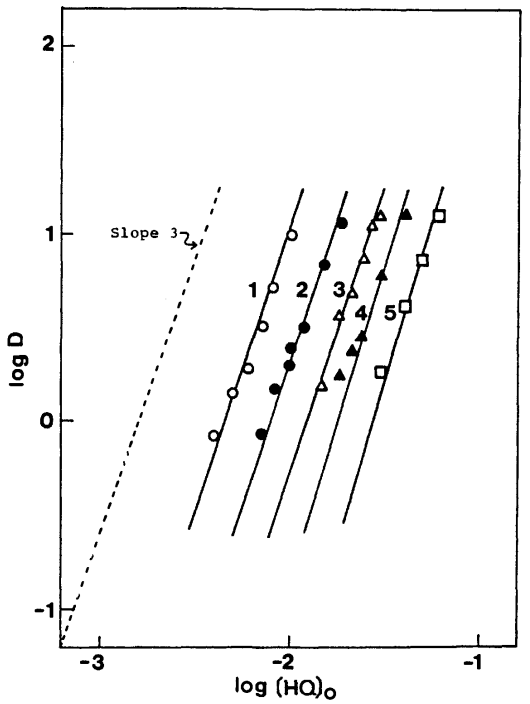

Fig. 2. Effect of 8-quinolinol concentration on the distribution ratio of cobalt between TCE and water in the presence of perchlorate.
pH 4.05, 1; 10 °C 2; 25 °C 3; 40 °C 4; 50 °C 5; 70 °C.

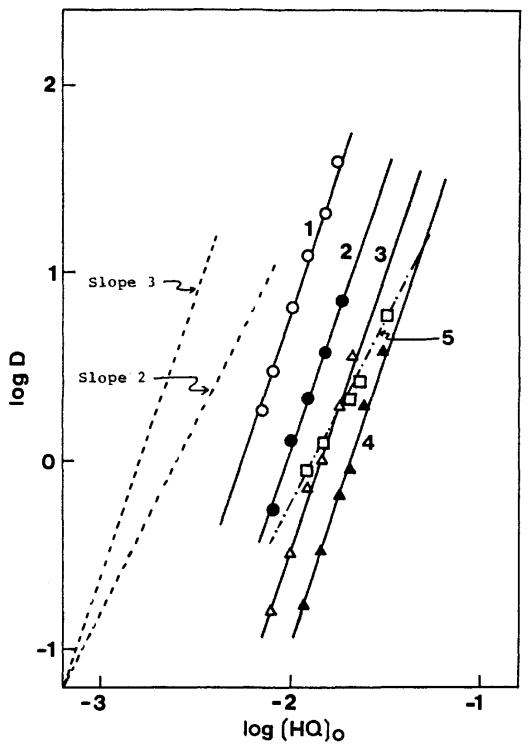

Fig. 3. Effect of 8-quinolinol concentration on the distribution ratio of cobalt between TCE and water in the presence of nitrate.
pH 4.6, 1; 10 °C 2; 25 °C 3; 40 °C 4; 55 °C 5; 70 °C.

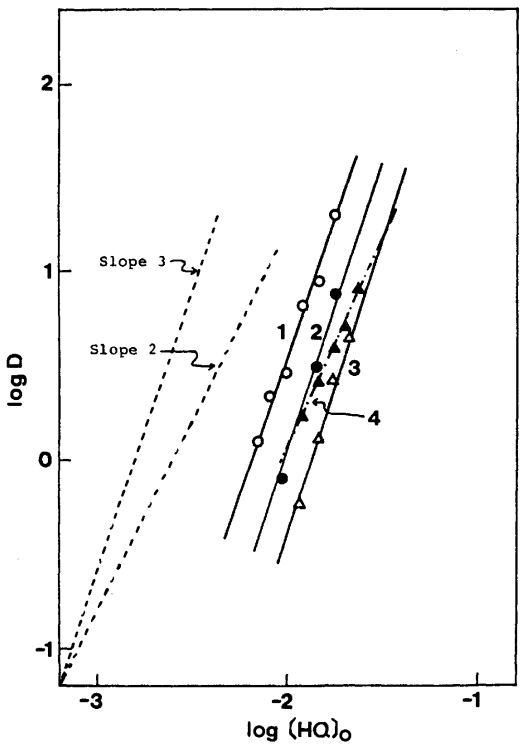

Fig. 4. Effect of 8-quinolinol concentration on the distribution ratio of cobalt between TCE and water in the presence of chloride.
pH 5.0, 1; 10°C 2; 25°C 3; 40°C 4; 55°C.

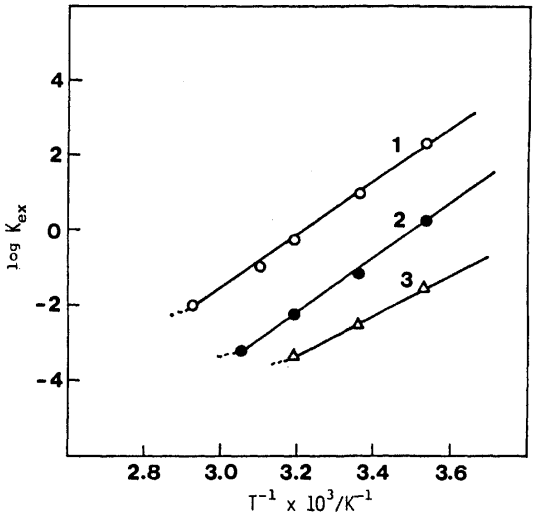

Fig. 5. Temperature effect on the extraction constants of cobalt between TCE and water.
1; $NaClO_4$ system, 2; $NaNO_3$ system, 3; NaCl system.

that the binuclear complex of cobalt dissociates in TCE in a way similar to the case of cadmium and zinc, as previously stated.[6,7]

Therefore, the extraction equation can be given as

$$2Co^{2+} + 6HQ_{(o)} + X^- \rightleftharpoons Co_2Q_3(HQ)_{3(o)}^{+} + X^-_{(o)} + 3H^+. \quad (1)$$

where o refers to the species in the organic phase. The extraction constant is

$$K_{ex} = \frac{[Co_2Q_3(HQ)_3^+]_o\,[X^-]_o\,[H^+]^3}{[Co^{2+}]^2\,[HQ]_o^6\,[X^-]}. \quad (2)$$

To maintain electrical neutrality in the organic phase, $[Co_2Q_3(HQ)_3^+]_o = [X^-]_o$, Eq. 2 can be transformed into

$$K_{ex} = \frac{[Co_2Q_3(HQ)_3^+]_o^2\,[H^+]^3}{[Co^{2+}]^2\,[HQ]_o^6\,[X^-]}. \quad (3)$$

The distribution ratio, D, can be given as

$$D = 2K_{ex}^{1/2}[HQ]_o^3[H^+]^{-3/2}[X^-]^{1/2}. \quad (4)$$

This equation means that plots of $\log D$ vs. $\log[HQ]_o$ show a slope of 3; plots of $\log D$ vs. pH show a slope of 1.5; and plots of $\log D$ vs. $\log[X^-]$ show a slope of 0.5. Thus, the assumption that the ion-pair of the binuclear complex would dissociate in the organic phase agrees well with the experimental results. It is, therefore, apparent that the extraction mechanism of cobalt with 8-quinolinol into TCE is similar to those of cadmium and zinc. The dissociation of an ion-associated complex in an organic solvent whose dielectric constant is relatively large, such as nitrobenzene (34.8), has already reported. However, the dielectric constant of TCE is 8.2 (at 20 °C). In order to certify the dissociation of the binuclear complex in TCE, the conductivities of the extract of zinc into TCE were measured. The results of conductivity measurements support the assumption that the ion-pair of the binuclear complex dissociates into a complex cation and an inorganic anion in TCE.[15] It has already been reported that many compounds, for example triarylmethyl chloride, dissociate in chlorinated ethanes such as 1,2-dichloroethane and TCE whose dielectric constants are not very large.[16,17]

Plots of $\log K_{ex}$ vs. $1/T$ in the presence of perchlorate, nitrate and chloride are shown in Fig. 5. The distribution ratios decrease remarkably with an increase in the temperature for each anion. This trend is more remarkable for a larger anion, such as perchlorate. The slopes of $\log K_{ex}$ vs. $1/T$ plots become gentle for smaller anions, such as chloride. Changes in the slope of $\log K_{ex}$ vs. $1/T$ suggest that the extracted species in high-temperature ranges are different from those in low-temperature ranges. This is supported by the fact that the slopes of plots of $\log D$ vs. $\log[HQ]_o$ become smaller than 3 at high temperatures, especially for the smaller anions as stated above. At high temperatures, the extraction of anhydrous chelate CoQ_2 may occur in a manner similar to zinc extraction with 2-methyl-8-quinolinol.[15] In a perchlorate system, the extractable ion-associated compound is formed even at high temperatures because the ionic redius of perchlorate is fairly large.

The value of the enthalpy change, ΔH, was calculated from the slope. The value of the entropy change, ΔS was calculated from the corresponding ΔH and K_{ex}

values. The results are listed in Table 1. The data show that the extraction of the complex ion-pair is an exothermic reaction. Extraction in the perchlorate system is mainly enthalpy controlled, resulting in a positive $\log K_{ex}$ value. In nitrate and chloride systems, negative enthalpy changes are canceled by large negative entropy changes, resulting in negative $\log K_{ex}$ values. In a nitrate system, the contribution of the entropy is larger than that in a perchlorate system. Plots of ΔG and ΔH of ion-pair extraction of cobalt vs. ΔG and ΔH of hydration of perchlorate, nitrate and chloride ions are shown in Fig. 6. These indicate that the dehydration of perchlorate, nitrate and chloride ions plays an important role in ion-pair extraction. These thermodynamic parameters were compared with those of zinc and cadmium, since the extraction mechanism of cobalt is similar to those of zinc and cadmium. The ΔH values of the extraction of cobalt, zinc and cadmium are listed in Table 2.[7] In perchlorate and nitrate systems, the larger the size of metal ion, the more exothermic is the ion-pair extraction (Co^{2+} 0.72 Å, Zn^{2+} 0.74 Å, Cd^{2+} 0.97 Å[19]). In a chloride system, ΔH values for all metal ions are almost the same.

Extraction of Cobalt into Chloroform with 8-Quinolinol in the Presence of Perchlorate Ion. The extraction behavior of cobalt with 8-quinolinol into chloroform was studied at various temperatures for a comparison with that in the TCE system. The concentration ratio of perchlorate to metal ion in chloroform was 0.5. Plots of $\log D(1+D)$ vs. pH are shown in Fig. 7. Here, the slopes are 3. The distribution decreases with a rise in temperature, which is similar to the case of TCE. Plots of $\log D(1+D)$ vs. $\log [HQ]_o$ are straight lines with slopes of 6. Plots of log D vs. $\log [Co]_{aq}$ give a straight line with a slope of 1 in the vicinity of $[Co]_{init.}=10^{-4}$—10^{-5} M. These results suggest that the extracted binuclear complex of cobalt would almost associate in chloroform, unlike the case in the TCE system. This is probably attributable to the fact that the dielectric constant of chloroform (4.9) is lower than that of TCE. Nevertheless, the dissociation of a com-

Table 1. Thermodynamic Values for Extraction of Co(II) with 8-Quinolinol into TCE in the Presence of Various Anions at 25 °C

System	$\log K_{ex}$	ΔG	ΔH	ΔS
		kJ mol^{-1}	kJ mol^{-1}	J K^{-1} mol^{-1}
$NaClO_4$	0.98	−5.59	−137	−441
$NaNO_3$	−1.22	6.96	−135	−476
NaCl	−2.50	14.3	−101	−387

Table 2. ΔH(kJ mol^{-1}) Values for Extraction of Cobalt, Zinc, and Cadmium Chelates with 8-Quinolinol into TCE

System	Co	Zn[7]	Cd[7]
$NaClO_4$	−137	−153	−169
$NaNO_3$	−135	−151	—
NaCl	−101	−95.4	−108

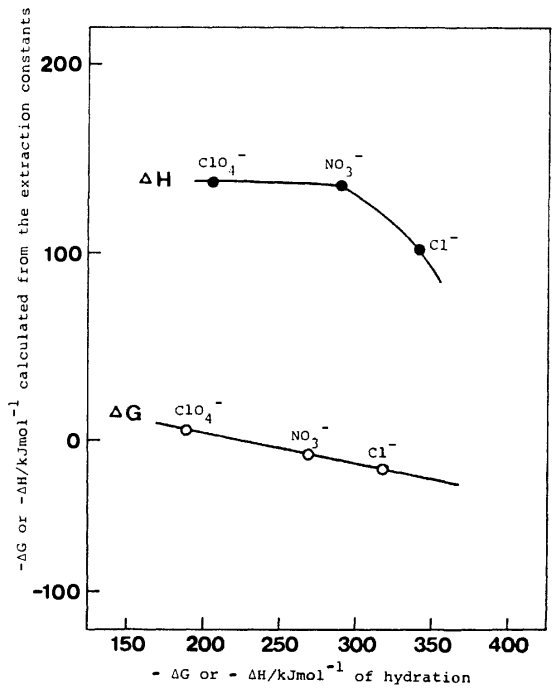

Fig. 6. Relationship between thermodynamic parameters for extraction of cobalt chelates with 8-quinolinol into TCE in the presence of various inorganic anions and hydration energies of those anions.

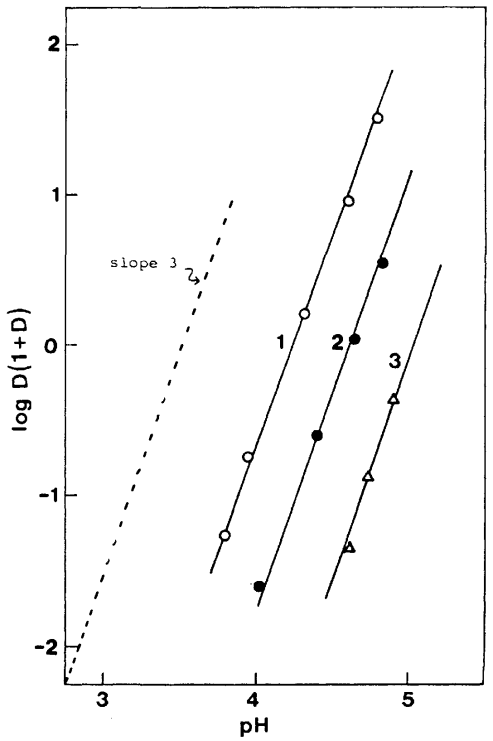

Fig. 7. Effect of pH on the distribution ratio of cobalt between chloroform and water in the presence of perchlorate.
1; 10 °C 2; 25 °C 3; 40 °C.

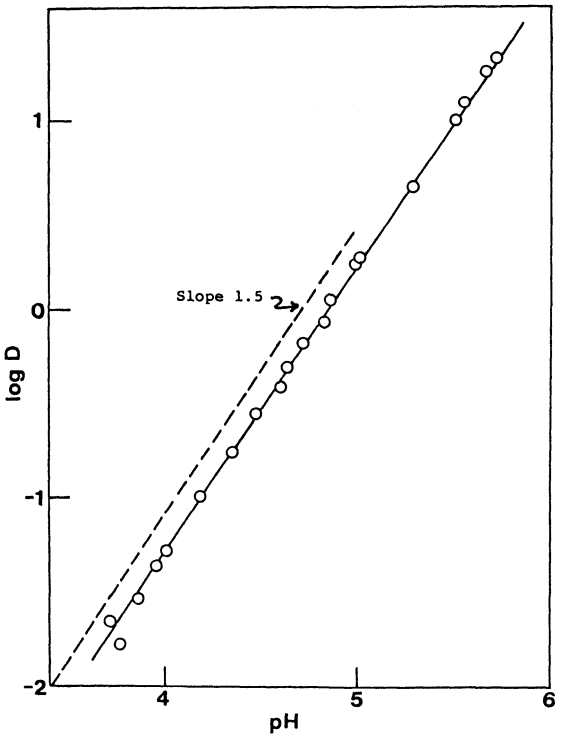

Fig. 8. Effect of pH on the distribution ratio of cobalt between chloroform and water in the presence of perchlorate ion in the case of low $[Co]_{init.}$. $[Co]_{init.}=10^{-8}$ M, $[HQ]_o=10^{-2}$ M, 0.09 M $NaClO_4$ +0.01 M AcOH-AcONa buffer, temp=20°C.

plex ion-pair is expected, even in a chloroform system when $[Co]_{init.}$ is sufficiently low. Figure 8 shows the plots of log$D$ vs. pH in the case of $[Co]_{init.}=10^{-8}$ M. This experiment was conducted by using ^{60}Co as a cobalt tracer. The slope of 1.5 indicates that cobalt is extracted into chloroform by a similar mechanism occurring in the TCE system. Sekido et al. suggested that cobalt is extracted into chloroform as a monomeric complex of 8-quinolinol when $[Co]_{init.}$ is lower than 10^{-6} M from the fact that the log D values are independent of $[Co]_{init.}$ in this concentration range.[13] Our result, however, demonstrates that the dissociation of the complex ion-pair is more likely than the extraction of the monomeric complex.

When $[Co]_{init.}$ is more than 10^{-5} M, the extraction equation can be written as

$$2Co^{2+}+6HQ_{(o)}+ClO_4^- \rightleftharpoons Co_2Q_3(HQ)_3(ClO_4^-)_{(o)}+3H^+. \quad (5)$$

The extraction constant is given by

$$K_{ex}=\frac{[Co_2Q_3(HQ)_3(ClO_4^-)]_o[H^+]^3}{[Co^{2+}]^2[HQ]_o^6[ClO_4^-]}. \quad (6)$$

The distribution ratio, D, is represented by

$$D=2K_{ex}[Co^{2+}][HQ]_o^6[H^+]^{-3}[ClO_4^-]. \quad (7)$$

Since $[Co^{2+}]=[Co]_{init.}/(1+D)$, Eq. 7 can be transformed to

$$D(1+D)=2K_{ex}[Co]_{init.}[HQ]_o^6[H^+]^{-3}[ClO_4^-]. \quad (8)$$

The logK_{ex} values are 4.04, 2.85, and 1.61 at 10, 25, and 40°C, respectively. The logK_{ex} value at 25°C agrees with the value given by Sekido et al.[13] (2.60). Thermodynamic data at 25°C are $\Delta G=-16.3$ kJ mol^{-1}, $\Delta H=-137$ kJ mol^{-1} and $\Delta S=-405$ J K^{-1} mol^{-1}. The values of enthalpy and entropy changes for chloroform are negative, similar to those for ion-pair extraction.

Comparing the extraction mechanism of cobalt 8-quinolinol complex into TCE with that into chloroform, the extracted binuclear complex of cobalt almost dissociates in TCE, while it almost associates in chloroform. Accordingly, it is considered that the difference in the thermodynamic parameters between TCE and chloroform systems would depend on the difference in the thermodynamic parameters of the distribution of 8-quinolinol and its cobalt complex and of the dissociation of the extracted binuclear cobalt complex in TCE. The values of logK_{DR}, ΔH, and ΔS for the distribution of 8-quinolinol are 2.64, −5.02 kJ mol^{-1}, and 33.5 J K^{-1} mol^{-1} for TCE[6] and 2.63, −9.02 kJ mol^{-1}, and 20.0 J K^{-1} mol^{-1} for chloroform,[4] respectively. The difference in the ΔH values for the distribution constant between TCE and chloroform is small. Moreover, the difference in ΔH values for the distribution of binuclear cobalt complex between TCE and chloroform systems may be small because the distribution species of cobalt for TCE is similar to that for chloroform.[15] Then, since the ΔH values for the extraction constant have almost the same values for both solvents, the ΔH value for the dissociation of an extracted binuclear cobalt complex in TCE would not be so large.

This work was supported in part by a Grant-in-Aid for Scientific Research Nos. 58740256 and 59740275 from the Ministry of Education, Science and Culture.

References

1) F. F. Dyer and G. K. Schweitzer, *Anal. Chim. Acta*, **23**, 1 (1960).
2) G. K. Schweitzer and G. R. Coe, *Anal. Chim. Acta*, **24**, 311 (1961).
3) H. E. Hellwege and G. K. Schweitzer, *Anal. Chim. Acta*, **28**, 236 (1963).
4) J. G. Mason and I. Lipshitz, *Talanta*, **18**, 1111 (1971).
5) G. R. Choppin, A. T. Kandil, H. F. Aly, and M. Raieh, *J. Inorg. Nucl. Chem.*, **37**, 229 (1975).
6) E. Nakayama, *Memoirs of the Faculty of Science, Kyoto University, Series A of Physics, Astrophysics, Geophysics and Chemistry*, **35**, 203 (1977).
7) E. Nakayama, *Memoirs of the Faculty of Science, Kyoto University, Series A of Physics, Astrophysics, Geophysics and Chemistry*, **35**, 210 (1977).
8) E. Yamada, E. Nakayama, T. Kuwamoto, and T. Fujinaga, *Bull. Chem. Soc. Jpn.*, **55**, 3155 (1982).
9) J. Stary, *Anal. Chim. Acta*, **28**, 132 (1963).
10) N. M. Kuz'min and Yu. A Zolotov, *Zh. Neorg. Khim.*,

11, 2316 (1966).
11) S. Ôki, *Anal. Chim. Acta*, **50**, 465 (1970).
12) H. Akaiwa, H. Kawamoto, and T. Saito, *Nippon Kagaku Zasshi*, **92**, 1156 (1971).
13) E. Sekido and K. Fujita, *Bull. Chem. Soc. Jpn.*, **49**, 3073 (1976).
14) E. Yamada and M. Sato, *Bunseki Kagaku*, **32**, 654 (1983).
15) E. Nakayama, Y. Sohrin, K. Isshiki, H. Karatani, and E. Yamada, *Bull. Chem. Soc. Jpn.*, submitted.
16) "Charlot Yobai no Kagakuhanno to Heiko," translated by T. Fujinaga and M. Sato, Maruzen, Tokyo (1975) pp. 192—196; {G. Charlot and B. Tremillon: "Les Reactions Chimiques Dansles Solvants et les Sels Fondus," Gauthier-Villars & Cie, Paris (1963)}.
17) A. G. Evans, A. Price, and J. H. Thomas, *Trans. Faraday Soc.*, **52**, 332 (1956).
18) S. Motomizu, K. Toei, and T. Iwachido, *Bull. Chem. Soc. Jpn.*, **42**, 1006 (1969).
19) "Sakukeisei Hanno," ed by M. Tanaka, Maruzen, Tokyo (1974).

 © 1989 The Chemical Society of Japan Bull. Chem. Soc. Jpn., 62, 1053—1056 (1989)

Inversion and Deuteration at the Chiral Nitrogen Centers of [Co(acac or ox)$_2$(Me-en or Me$_3$en)]$^{+or-}$ (acac=2,4-Pentanedionate Ion; ox=Oxalate Ion; Me-en=*N*-Methylethylenediamine, Me$_3$en=*N,N,N'*-Trimethylethylenediamine)

Guilin MA, Tomomi HIBINO, Masaaki KOJIMA, and Junnosuke FUJITA*
Department of Chemistry, Faculty of Science, Nagoya University, Chikusa-ku, Nagoya 464-01
(Received July 15, 1988)

The rates of the base-catalyzed proton exchange (deuteration, k_D) and isomerization (epimerization, k_{ep}) at the chiral amine nitrogen centers of [Co(acac or ox)$_2$(Me-en or Me$_3$en)]$^{+or-}$ in aqueous solutions were measured at 34.0 °C, and the results were compared with one another and with those of related complexes. The deuteration rate is affected more by the nature of coexisting ligands than the overall charge on the complex. The uninegative ox complexes have larger k_D values than the unipositive acac complexes. The k_{ep} values of the ox complexes are ca. 10^4 times as large as those of the acac complexes. For both ox and acac complexes, the complexes with Me$_3$en have larger k_D and k_{ep} values than the complexes with Me-en. The deuteration rates are ca. 10^4—10^5 and ca. 10^2 times greater than the inversion rates for the acac and ox complexes, respectively.

In a previous paper,[1] we reported that the rates of OH^--catalyzed isomerization (epimerization, k_{ep}) and proton exchange (deuteration, k_D) at the chiral nitrogen center of [Co(acac)$_2$(Me-en)]$^+$ are unusually slow, the rates being ca. 10^4 times as small as those of [Co(NH$_3$)$_4$(Me-en)]$^{3+}$.[2] The rates of the same reactions of the sarcosinate ion (sar) in [Co(sar)(Hbg)$_2$]$^{2+}$ (Hbg: biguanide=NH$_2$C(=NH)NHC(=NH)NH$_2$)[3] are also ca. 10^3—10^4 times as small as those of [Co(sar)(NH$_3$)$_4$]$^{2+}$.[4] These results suggest that the rates are largely affected by the nature of coexisting ligands, although deuteration rates at the coordinated amine nitrogen centers are known to increase with an increasing positive charge on the complex.[5] Thus it is interesting to compare the rates of [Co(acac)$_2$(diamine)]$^+$ with those of [Co(ox)$_2$(diamine)]$^-$; both complexes belong to the CoO_4N_2-type, but they have charge of different signs.

In this paper, we report the rates of epimerization and deuteration at chiral nitrogen centers of [Co(acac or ox)$_2$(Me-en or Me$_3$en)]$^{+or-}$. The paper also describes the preparation and some properties of oxalato complexes with related diamines.

Experimental

[Co(acac)$_2$(Me$_3$en)]ClO$_4$ (Me$_3$en=*N,N,N'*-trimethylethylenediamine) was prepared and separated into the two isomers, *Λ*(*R*)*Δ*(*S*) and *Λ*(*S*)*Δ*(*R*), as described previously.[6] Absorption and ^{1}H NMR spectra were measured on a Hitachi 323 spectrophotometer and a Hitachi R-90H spectrometer, respectively.

Λ(R)Δ(S)-Na[Co(ox)$_2$(Me-en)]·H$_2$O, Λ(S)Δ(R)-Na[Co(ox)$_2$(Me-en)]·H$_2$O, Na[Co(ox)$_2$(*N,N*-Me$_2$en)]·0.5NaCl·0.5H$_2$O (*N,N*-Me$_2$en=*N,N*-Dimethylethylenediamine), Λ(RR)Δ(SS)-Na[Co(ox)$_2$(*N,N'*-Me$_2$en)]·2H$_2$O (*N,N'*-Me$_2$en=*N,N'*-Dimethylethylenediamine), Λ(RS)Δ(SR)-Na[Co(ox)$_2$(*N,N'*-Me$_2$en)]·2H$_2$O, and Λ(SS)Δ(RR)-Na[Co(ox)$_2$(*N,N'*-Me$_2$en)]. These complexes were prepared by a similar method to that for Na[Co(ox)$_2$(en)] (en=ethylenediamine).[7] Yield: 20—50%. For Me-en and *N,N'*-Me$_2$en complexes, the complexes were epimerized in dil Na_2CO_3 solution (pH 8—9) for 30 min at room temperature, and then the isomers were separated by Dowex 1×8 column chromatography (eluent: 0.05 mol dm^{-3} NaCl-0.01 mol dm^{-3} HCl). Anal. ($C_7H_{12}N_2CoNaO_9$=*Λ*(*R*)*Δ*(*S*)- and *Λ*(*S*)*Δ*(*R*)-Na[Co(ox)$_2$(Me-en)]·H$_2$O) C,H,N. ($C_8H_{13}N_2Cl_{0.5}CoNa_{1.5}O_{8.5}$=Na[Co(ox)$_2$(*N,N*-Me$_2$en)]·0.5NaCl·0.5H$_2$O) C,H,N. ($C_8H_{16}N_2CoNaO_{10}$=*Λ*(*RR*)*Δ*(*SS*)- and *Λ*(*RS*)*Δ*(*SR*)-Na[Co(ox)$_2$(*N,N'*-Me$_2$en)]·2H$_2$O) C,H,N. ($C_8H_{12}N_2CoNaO_8$=*Λ*(*SS*)*Δ*(*RR*)-Na[Co(ox)$_2$(*N,N'*-Me$_2$en)]) C,H,N.

Λ(R)Δ(S)-Na[Co(ox)$_2$(Me$_3$en)]·H$_2$O and Λ(S)Δ(R)-Na[Co(ox)$_2$(Me$_3$en)]·3H$_2$O. To an aqueous solution (80 cm^3) of K$_3$[Co(ox)$_3$]·3H$_2$O (3.7 g, 9.4 mmol) was added an aqueous solution (20 cm^3) of Me$_3$en (1.35 g, 11.3 mmol). The mixture was stirred for 25 h at room temperature and then filtered. The purple filtrate was diluted with water (1 dm^3), and applied on a column (ϕ2.6 cm×20 cm) of Dowex 1×8 (200—400 mesh). By elution with 0.15 mol dm^{-3} NaCl, a purple, a pink (probably a cobalt(II)-ox complex), and a green ([Co(ox)$_3$]$^{3-}$) band developed in this order. From the purple eluate the complex (a mixture of the two isomers) was isolated as the sodium salt. Yield: 2.6 g (73%). The complex was epimerized and separated into the two isomers, *Λ*(*R*)*Δ*(*S*) and *Λ*(*S*)*Δ*(*R*), in the ratio of 5.2 : 1 by the same method as for the Me-en complex. Anal. ($C_9H_{16}N_2CoNaO_9$=*Λ*(*R*)*Δ*(*S*)-Na[Co(ox)$_2$(Me$_3$en)]·H$_2$O) C,H,N. ($C_9H_{20}N_2CoNaO_{11}$=*Λ*(*S*)*Δ*(*R*)-Na[Co(ox)$_2$(Me$_3$en)]·3H$_2$O) C,H,N.

Na[Co(ox)$_2$(Me$_4$en)]·4H$_2$O (Me$_4$en=*N,N,N',N'*-Tetramethylethylenediamine). This complex was prepared by a method similar to that described for the Me$_3$en complex in a yield of 37% (violet crystals). Anal. ($C_{10}H_{24}N_2CoNaO_{12}$) C,H,N.

Deuteration Studies. The rates of deuteration at the chiral nitrogen centers of [Co(ox)$_2$(Me-en)]$^-$, [Co(ox)$_2$(Me$_3$en)]$^-$, and [Co(acac)$_2$(Me$_3$en)]$^+$ were followed by monitoring N-CH$_3$ signal changes in the ^{1}H NMR spectra as described previously.[1] [Co(acac)$_2$(Me$_3$en)]ClO$_4$ was converted into the more soluble chloride with a Dowex 1×8 anion exchanger in the chloride form. The rates for [Co(ox)$_2$(Me-en)]$^-$ and [Co(acac)$_2$(Me$_3$en)]$^+$ were measured in a phosphate buffer (pD 5.7—7.1) at 34.0 °C, while that for [Co(ox)$_2$(Me$_3$en)]$^-$ in a phthalate buffer (pD 4.3—6.5) at 34.0 °C. The empirical formula, pD=pH meter reading+0.4, was used to calculate

$[OD^-]$.[8]

Epimerization Studies. The rates of epimerization for $[Co(ox)_2(Me\text{-}en)]^-$, $[Co(ox)_2(Me_3en)]^-$, and $[Co(acac)_2(Me_3en)]^+$ in aqueous solutions at 34.0 °C were followed by the same method as that described previously.[1,9] It involves separation of two isomers of the complexes by a high-performance liquid chromatographic method, and analysis of chromatograms changed with reaction time.

Results and Discussion

Two, three, and two isomers (racemic pairs of diastereomers) are possible for $[Co(ox)_2(Me\text{-}en)]^-$, $[Co(ox)_2(N,N'\text{-}Me_2en)]^-$, and $[Co(ox)_2(Me_3en)]^-$, respectively (Fig. 1). All these isomers were separated by Dowex 1×8 column chromatography under acidic conditions. The aqueous solutions should be kept acidic to avoid isomerization (inversion at the chiral nitrogen centers, vide infra). The structures of the complexes were assigned on the basis of the ^1H NMR spectra taking magnetic anisotropy of the carboxyl group into consideration; a complex which shows a doublet attributable to the *N*-methyl group at a higher magnetic field is assigned to the $\Lambda(S)\Delta(R)$-isomer (Table 1).

The distributions of the isomers at equilibrium (34 °C) were analyzed by the reversed-phase high-performance liquid chromatographic technique, and the results are given in Table 1. Table 1 also gives the absorption spectral data for the complexes. Both distributions of the isomers and positions of the d-d absorption bands seem to be related with the steric crowding involved in the isomers. For example, the $\Lambda(S)\Delta(R)$-isomer of $[Co(ox)_2(Me\text{-}en)]^-$, in which the *N*-methyl group is situated over one of the ox ligands and larger steric crowding will be involved than the $\Lambda(R)\Delta(S)$-isomer, is formed less and exhibits the d-d absorption bands at lower energy than the $\Lambda(R)\Delta(S)$-isomer (Fig. 1 and Table 1). The $[Co(ox)_2(Me_4en)]^-$ complex exhibits the d-d absorption bands at the lowest energy in the present complexes (Table 1). The low ligand field strength of the Me_4en ligand was also reported for $[Co(acac)_2(Me_4en)]^+$ and was ascribed to the steric crowding which occurs in the complex.[6,10]

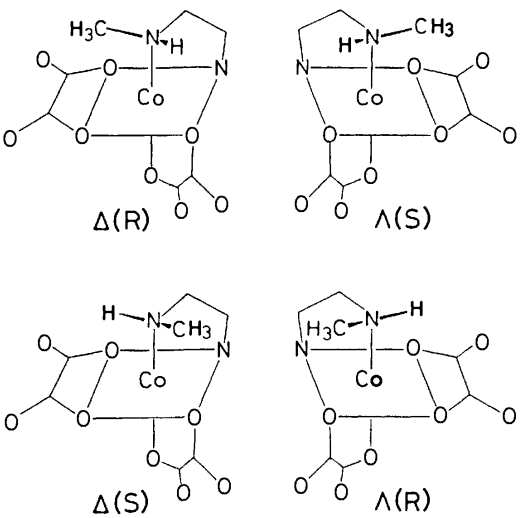

Fig. 1. The four possible isomers of $[Co(ox)_2(Me\text{-}en)]^-$.

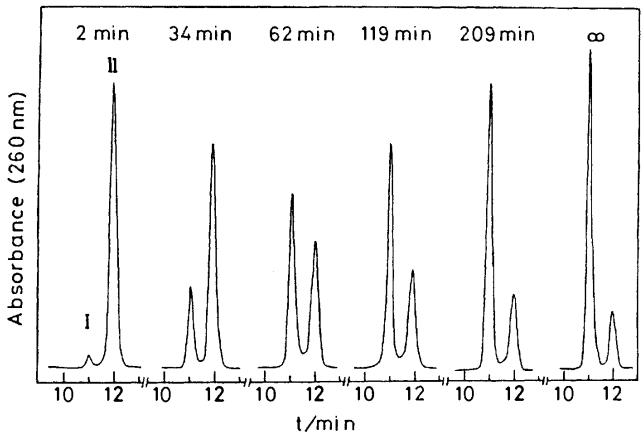

Fig. 2. Change in the elution curve during the epimerization of $\Lambda(S)\Delta(R)$-$[Co(ox)_2(Me_3en)]^-$ at pH 6.03 and 34.0 °C (I: $\Lambda(R)\Delta(S)$ isomer, II: $\Lambda(S)\Delta(R)$ isomer). Chromatographic conditions: column, JASCO Finepack SIL C_{18}, ϕ 0.46 cm×25 cm; eluent, 5×10^{-3} mol dm^{-3} Bu_4NCl in CH_3CN-H_2O (11:89 v/v); flow rate, 2.0 cm^3 min^{-1}; UV detection, 260 nm.

Table 1. ^1H NMR and Absorption Spectral Data for $[Co(ox)_2L]^-$ and the Distributions of the Isomers at Equilibrium (34 °C)

L	Assignment	^1H NMR (δ)		Absorption (d-d bands)	Relative
		CH_3	$NH(CH_3)$	$\tilde{\nu}_{max}/10^3$ cm^{-1} (log ε)	abundance/%
en				18.52 (2.11) 26.11 (2.31)[c]	
Me-en	$\Lambda(R)\Delta(S)$	2.25d	5.50[a]	18.35 (2.12) 25.91 (2.31)[d]	68
	$\Lambda(S)\Delta(R)$	1.87d	5.92[a]	18.32 (2.11) 25.84 (2.31)[d]	32
N,N'-Me_2en	$\Lambda(RR)\Delta(SS)$	2.20d	5.83[a]	18.18 (2.12) 25.71 (2.32)[d]	58
	$\Lambda(RS)\Delta(SR)$	2.23d, 1.80d	5.96, 6.22[a]	18.15 (2.11) 25.64 (2.31)[d]	33
	$\Lambda(SS)\Delta(RR)$	1.84d	6.29[a]	18.12 (2.10) 25.64 (2.31)[d]	9
N,N-Me_2en		2.36s, 1.88s[b]		17.89 (2.11) 25.45 (2.29)[c]	
Me_3en	$\Lambda(R)\Delta(S)$	2.33s, 2.19d, 1.86s	5.96[a]	17.73 (2.12) 25.25 (2.32)[d]	82
	$\Lambda(S)\Delta(R)$	2.35s, 1.82d, 1.86s	6.45[a]	17.70 (2.06) 25.19 (2.26)[d]	18
Me_4en		2.33s, 1.87s[b]		17.30 (2.13) 24.63 (2.31)[c]	

a) In D_2O-DCl. b) In D_2O. c) In H_2O. d) In 10^{-2} mol dm^{-3} HCl.

Table 2. A Comparison of Data for the Deuteration and Inversion at Chiral Nitrogen Centers of [Co(ox)$_2$L]$^-$ (L=Me-en, Me$_3$en) and [Co(acac)$_2$L]$^+$ at 34.0 °C

Complex	Isomer	k_D/M^{-1} s^{-1} [b]	k_{ep}/M^{-1} s^{-1}	(k_1 or k_{-1})/M^{-1} s^{-1}	k_D/(k_1 or k_{-1})
[Co(ox)$_2$(Me-en)]$^-$	$\Lambda(R)\Lambda(S)$	2.2×10^4	8.4×10^2	k_{-1}: 2.7×10^2	8.1×10
	$\Lambda(S)\Lambda(R)$	1.8×10^5		k_1: 5.7×10^2	3.2×10^2
[Co(ox)$_2$(Me$_3$en)]$^-$	$\Lambda(R)\Lambda(S)$	1.2×10^5	1.2×10^4	k_{-1}: 2.1×10^3	5.7×10
	$\Lambda(S)\Lambda(R)$	8.1×10^5		k_1: 9.9×10^3	8.2×10
[Co(acac)$_2$(Me-en)]$^+$ [a]	$\Lambda(R)\Lambda(S)$	[c]	1.3×10^{-1}	k_{-1}: 5.9×10^{-2}	
	$\Lambda(S)\Lambda(R)$	8.9×10^3		k_1: 7.1×10^{-2}	1.3×10^5
[Co(acac)$_2$(Me$_3$en)]$^+$	$\Lambda(R)\Lambda(S)$	2.4×10^3	1.0	k_{-1}: 3.4×10^{-1}	7.1×10^3
	$\Lambda(S)\Lambda(R)$	1.1×10^4		k_1: 6.6×10^{-1}	1.7×10^4

a) From Ref. 1. b) 1M=1 mol dm^{-3}. c) The data could not be obtained because of the overlapping of the N-CH$_3$ and C-CH$_3$ signals.

Kinetic studies of reversible isomerization (epimerization) between the two isomers of [Co(ox)$_2$(Me-en)]$^-$, [Co(ox)$_2$(Me$_3$en)]$^-$, and [Co(acac)$_2$(Me$_3$en)]$^+$ were performed in aqueous solutions at 34.0 °C by observing the change in chromatograms with reaction time. Figure 2 shows a typical set of elution curves obtained at intervals after $\Lambda(S)\Lambda(R)$-[Co(ox)$_2$(Me$_3$en)]$^-$ had been dissolved in water at pH 6.03 and 34.0 °C. The pseudo-first-order rate constant, $k_{ep(obsd)}$ was obtained by the method described previously.[1,9] The $k_{ep(obsd)}$/[OH$^-$] ($=k_{ep}$) values are constant at 34.0 °C in the pH range 5.7—6.7 indicating that the reaction is first order in [OH$^-$]. Thus, the rate law was the same as that for racemization (epimerization) of other chiral amine complexes, $R=k_{ep}$[complex][OH$^-$].[11] The runs starting from either of the isomers gave the same result within the experimental error. From these observations, the reaction can be expressed as

$$\Lambda(S)\Lambda(R) \underset{k_{-1}}{\overset{k_1}{\rightleftharpoons}} \Lambda(R)\Lambda(S)$$

The forward and reverse second-order rate constants, k_1 and k_{-1}, were obtained from k_{ep} ($k_{ep}=k_1+k_{-1}$) and the equilibrium constant ($K_{eq}=k_1/k_{-1}$) as given in Table 2.

The rates of deuteration at chiral amine nitrogen centers of [Co(ox)$_2$(Me-en)]$^-$, [Co(ox)$_2$(Me$_3$en)]$^-$, and [Co(acac)$_2$(Me$_3$en)]$^+$ were followed by monitoring siganl changes in the ^{1}H NMR spectra. From the changes, the pseudo-first-order rate constants for deuteration, $k_{D(obsd)}$ were obtained by a method similar to that for epimerization. The rate law for the deuteration reaction was the same as that obtained previously for other amine complexes, $R=k_D$[complex][OD$^-$].[11] The k_D values are given in Table 2.

In the deuteration reactions, the term in [OD$^-$] is interpreted as removal of H$^+$ from the coordinated amine to leave a pyramidal center.[4,11] The pyramidal nitrogen center is followed by formation of a trigonal planar amide which leads to the inversion of the nitrogen center (epimerization of the complex).[4,11] Thus the k_{ep} values will be related to both the rate of deuteration and the stability of the trigonal planar amide in the transition state. The k_D values for the $\Lambda(S)\Lambda(R)$ isomers of the present complexes are ca. 5—8 times as large as those for the $\Lambda(R)\Lambda(S)$ isomers. The rate differences can be attributed to a difference in steric effect between the isomers. As is seen in Fig. 1 the secondary amine hydrogen in the $\Lambda(R)\Lambda(S)$ isomer, which is situated over one of the ox ligands, will be more effectively hindered by the ox ring from atacking of OH$^-$ than the hydrogen in the $\Lambda(S)\Lambda(R)$ isomer. The same interpretation is given for the rate difference between the isomers of [Co(acac)$_2$(Me$_3$en)]$^+$.

For both ox and acac complexes, the complexes with Me$_3$en have larger k_D values than the complexes with Me-en. The result seems to be related with a difference in electron density on the secondary amine hydrogen atoms as suggested in the ^{1}H NMR spectra. For example, as one goes from $\Lambda(S)\Lambda(R)$-[Co(ox)$_2$(Me-en)]$^-$ to $\Lambda(S)\Lambda(R)$-[Co(ox)$_2$(Me$_3$en)]$^-$, the amine proton signal (N<u>H</u>(CH$_3$)) is shifted from δ 5.92 to 6.45, suggesting a decrease in electron density at the hydrogen atom in line with the increase in k_D value (Tables 1 and 2). The k_{ep} values for the Me$_3$en complexes are also larger than those for the Me-en complexes.

It is known that deuteration rates increase with an increasing positive charge on the complex (ca. 10-fold for each unit of charge).[5] Thus the unipositive acac complexes are expected to give larger k_D values than the uninegative ox complexes. However, the inverse has been found. The difference in k_{ep} values between the ox and acac complexes is much more pronounced; the k_{ep} values for the ox complexes are ca. 10^4 times as large as those for the corresponding acac complexes. Kawaguchi et al.[3] reported that [Co(sar)(Hbg)$_2$]$^{2+}$ also gives much smaller k_D (ca. 10^4 mol^{-1} dm^3 s^{-1} at 39.6 °C) and k_{rac} ($=k_{ep}$, 13.8 mol^{-1} dm^3 s^{-1} at 35.0 °C) values than those (k_D=1.2 ×10^8 mol^{-1} dm^3 s^{-1} and k_{rac}=3.3×10^4 mol^{-1} dm^3 s^{-1} at 33.3 °C) of the corresponding ammine complex [Co(sar)(NH$_3$)$_4$]$^{2+}$.[4] These results suggest that the reactivity of coordinated secondary amine nitrogen center is affected more by the kind of coexisting ligands than the overall charge on the complex. The reason for the small rates of the acac and Hbg complexes remains unknown. However, it is worth noting that both acac and Hbg ligands form a chelate ring with delocalized π-electrons.

The $k_D/(k_1$ or $k_{-1})$ ratios (retention ratios) for $[Co(acac)_2(Me\text{-}en$ or $Me_3en)]^+$ (ca. 10^4—10^5) are similar to that for $[Co(NH_3)_4(Me\text{-}en)]^{3+}$ (2.5×10^5 at 34.3 °C),[2] and the values imply that the configuration about the chiral nitrogen atom (pyramidal configuration) is retained most of the time that the proton is off the quarternary N site. On the other hand, the retention ratios for $[Co(ox)_2(Me\text{-}en$ or $Me_3en)]^-$ (ca. 10^2) and $[Co(sar)(Hbg)_2]^{2+}$ (10^2—10^3) are small. The smaller retention ratios may result from an increased stabilization of the trigonal planar amide in the transition state.[2,12] However, the factors governing the retention ratio for the above complexes are not clear at the moment. More kinetic data will be needed to elucidate the effect of coexisting ligands on the reactivity of coordinated amine nitrogen center.

The present work was supported by a Grant-in-Aid for Scientific Research No. 61430013 from the Ministry of Education, Science and Culture.

References

1) M. Kojima, T. Hibino, Y. Ouyang, and J. Fujita, *Inorg. Chim. Acta*, **117**, 1 (1986).

2) D. A. Buckingham, L. G. Marzilli, and A. M. Sargeson, *J. Am. Chem. Soc.*, **89**, 825 (1967).

3) H. Kawaguchi, M. Natsuki, T. Ama, and T. Yasui, *Bull. Chem. Soc. Jpn.*, **59**, 31 (1986).

4) B. Halpern, A. M. Sargeson, and K. R. Turnbull, *J. Am. Chem. Soc.*, **88**, 4630 (1966).

5) J. W. Palmer and F. Basolo, *J. Phys. Chem.*, **64**, 778 (1960); F. Basolo, J. W. Palmer, and R. G. Pearson, *J. Am. Chem. Soc.*, **82**, 1073 (1960).

6) Y. Ouyang, M. Kojima, and J. Fujita, *Bull. Chem. Soc. Jpn.*, **57**, 3574 (1984).

7) F. P. Dwyer, I. K. Reid, and F. L. Garvan, *J. Am. Chem. Soc.*, **83**, 1285 (1961).

8) P. K. Glasoe and F. A. Long, *J. Phys. Chem.*, **64**, 188 (1964).

9) K. Nakajima, M. Kojima, M. Fujita, and J. Fujita, *J. Chromatogr.*, **301**, 241 (1984); K. Nakajima, M. Kojima, and J. Fujita, *ibid.*, **362**, 281 (1986); K. Nakajima, M. Kojima, and J. Fujita, *Bull. Chem. Soc. Jpn.*, **59**, 3505 (1986).

10) R. J. York, W. D. Bonds, Jr., B. P. Cotsoradis, and R. D. Archer, *Inorg. Chem.*, **8**, 789 (1969).

11) W. G. Jackson and A. M. Sargeson, "Rearrangement in Coordination Complexes," in "Rearrangements in Ground and Excited States," ed by P. de Mayo, Academic Press, New York (1980), Vol. 2, p. 273, and references therein.

12) J. B. Goddard and F. Basolo, *Inorg. Chem.*, **8**, 2223 (1969).

Structure and Properties of Chloro(*N,N*-diethylglycinato)copper(II)

Yasuhiko YUKAWA,* Shin NAKAGOME,† Hiromitsu YAMAGUCHI,† Yoshie INOMATA,† and Toshio TAKEUCHI†
Division of Chemistry, General Education Department, Niigata University, 8050, Ikarashi Nino-cho, Niigata 950-21
†Department of Natural Sciences, Faculty of Science and Technology, Sophia University, 7-1, Kioi-cho, Chiyoda-ku, Tokyo 102
(Received August 18, 1988)

An X-ray diffraction study of the title complex has been carried out, along with spectroscopic measurements and thermal analyses. The crystal is orthorhombic, space group $P2_12_12_1$, Z=4, a=9.978(2), b=12.624(3), c=7.129(1) Å, U=898.0(3) Å^3. Block-diagonal least-squares refinements have led to the final R value of 0.032. The structure consists of a one-dimensional polymer chain bridged by a carboxylato group of an *N,N*-diethylglycinato ligand. One oxygen atom in the carboxylato group is coordinated to two copper atoms, and the other is coordinated to one of these two copper atoms. This is the same bridging form as in aquachloro(4-hydroxy-L-prolinato)copper(II). The copper atom reveals a distorted five-coordination: the copper atom is surrounded by three carboxylato oxygen atoms, one nitrogen atom, and one chlorine atom. The infrared spectra of the title complex and of aquachloro(4-hydroxy-L-prolinato)copper(II) both show the characteristic pattern at the peaks assigned to the vibrations of the carboxylato group. The peaks can be an indicator of the bridging form.

The amino acids with a pyrrolidine ring, 4-hydroxy-L-proline (Hhpro) and L-proline (Hpro) (their anion ligands abbreviate to hpro and pro, respectively), have slightly different structural features from other α-amino acids. Some interesting properties of their metal complexes are reported. To give an example, the solution of Cu^{II} complex with an L-amino acid, in general, exhibits a negative circular dichroism (CD) band at near 600 nm, and that of a D-amino acid has a positive one. But those of L-pro and L-hpro both exhibit a positive CD band at near 600 nm.[1,2] Another example is as follows. The four possible isomers, *Λ-fac, Λ-fac, Δ-mer*, and *Λ-mer*, are all obtained in the tris amino acid complexes of Co^{III} with L-alanine, L-valine and L-leucine. However, in the L-pro complex only three isomers can be isolated, and *Λ*-mer isomer can not be obtained.[3] These facts are based on the characteristic structures of Hhpro and Hpro. Therefore studies about syntheses, properties, and structures of some metal complexes with Hhpro and Hpro have been carried out in our group.[4-8]

A complex was prepared from $CuCl_2$ and Hhpro ([CuCl(hpro)(H_2O)]),[5] and its crystal structure was discussed.[8] In this work, a complex was prepared from $CuCl_2$ and *N,N*-diethylglycine (Hdeg; the anion ligand abbreviates to deg); its structure was determined and its spectroscopic data and thermal behavior were investigated, in order to compare the results with those of [CuCl(hpro)(H_2O)]. The aim of this study is to confirm whether the interesting bridging form existing in [CuCl(hpro)(H_2O)] is characteristic for amino acid ligands having a pyrrolidine ring (e.g. hpro), or whether it can also be formed by other *N*-substituted amino acids like Hdeg.

Experimental

Preparation of Chloro(*N,N*-diethylglycinato)copper(II). To an ethanol solution (100 cm^3) of 1.53 g (0.01 mol) of sodium *N,N*-diethylglycinate, 1.34 g (0.01 mol) of dichlorocopper(II) was added. As $CuCl_2$ was dissolved, sodium chloride was precipitated. As soon as $CuCl_2$ was dissolved completely, centrifugation of the solution was carried out until NaCl was removed. Dark blue crystals were obtained from the solution by keeping it at room temperature for several days. The crystals were recrystallized from methanol. Found: C, 31.53; N, 5.97; H, 5.22%. Calcd for $CuCl(C_6H_{12}NO_2)$: C, 31.44; N, 5.97; H, 5.28%.

X-Ray Measurements and Structure Determination. The crystal data are as follows. The crystal is orthorhombic, space group $P2_12_12_1$, Z=4, a=9.978(2), b=12.624(3), c=7.129(1) Å, U=898.0(3) Å^3, D_m=1.67 g cm^{-3}, D_m=1.70 g cm^{-3}, μ(Mo $K\alpha$)=27.7 cm^{-1}. The size of the crystal used for the measurement was 0.15×0.16×0.14 mm^3. The reflection intensities were collected by the ω-2θ scan technique (measured range 3—60° (2θ); scan width 1.30° (θ); scan speed 4° min^{-1} (θ)) on a Rigaku AFC-6A automated four-circle X-ray diffractometer with graphite-monochromated Mo $K\alpha$ radiation. The measured reflections were 1598, of which 1255 ($|F_o|>3\sigma(|F_o|)$) were used for the structure refinement. The intensities were corrected for Lorentz and polarization factors, but not for absorption and extinction.

The structure was solved by a heavy-atom method. The positions of the copper and chlorine atoms were deduced on a three-dimensional Patterson map; other atoms were located by successive Fourier syntheses. Their positional, isotropic and then anisotropic thermal parameters (except for hydrogen atoms) were refined by the block-diagonal least-squares method. Isotropic temperature factors for hydrogen atoms of -CH_3 in -CH_2CH_3 were assumed to be 4.0 Å^2. All the calculations were carried out on a HITAC M-680H computer at the Computer Center of The University of Tokyo, using the local version of the UNICS program.[9] The atomic scattering factors were taken from Ref. 10. The final R value was 0.032 and R_w was 0.038.[11]

The Other Measurements. The simultaneous thermogravimetric (TG) and differential thermal (DTA) analyses were carried out with a Rigaku Denki "Thermoflex" M-8075 using a sample weighing about 7.8 mg; the heating rate was 5 °C min^{-1} in air; α-alumina was used as the reference.

The infrared spectra of the sample were obtained by means

of a Hitachi 295 type infrared spectrophotometer, using Nujol mull and KBr disks.

Visible and ultraviolet spectra were measured on a Hitachi U-3200 Spectrophotometer.

The magnetic moment was obtained for the solid sample by the Gouy method at room temperature, using Hg[Co(SCN)$_4$] as a calibration standard.

Results and Discussion

The final atomic parameters are listed in Table 1, the interatomic distances in Table 2, and the bond angles in Table 3.[12] The perspective drawing of the complex and the numbering scheme of the atoms are shown in Fig. 1.

Table 1. Final Positional Parameters ($\times10^5$ for Cu and $\times10^4$ for the Other Non-Hydrogen Atoms) and Equivalent Isotropic Temperature Factors (B_{eq}/Å^2), with the Estimated Standard Deviations in Parentheses

Atom	x	y	z	B_{eq}[a]
Cu	19430(5)	38573(4)	28463(7)	2.02
Cl	1828(1)	2325(1)	1390(2)	3.46
O(1)	2239(3)	4935(3)	4756(4)	2.73
O(2)	1230(3)	5844(2)	6984(4)	2.63
N	1(3)	3908(3)	3755(5)	2.11
C(1)	1209(4)	5244(3)	5605(6)	2.14
C(2)	−136(4)	4882(4)	4855(6)	2.60
C(3)	−978(4)	3874(4)	2170(7)	2.91
C(4)	−739(5)	4713(4)	710(8)	3.94
C(5)	−244(5)	2968(4)	4972(7)	3.20
C(6)	748(5)	2837(4)	6528(8)	4.08

a) The equivalent isotropic temperature factors were computed using the following expression: $B_{eq}=4/3(B_{11}a^2+B_{22}b^2+B_{33}c^2)$.

Table 2. Interatomic Distances (l/Å) with the Estimated Standard Deviations in Parentheses

Cu-Cl	2.199(1)	C(1)-C(2)	1.515(6)
Cu-O(1)	1.947(4)	C(3)-C(4)	1.504(8)
Cu-O(1)^{I}	2.801(4)	C(5)-C(6)	1.496(8)
Cu-O(2)^{I}	1.961(3)	N-C(2)	1.465(6)
Cu-N	2.044(3)	N-C(3)	1.494(6)
C(1)-O(1)	1.254(5)	N-C(5)	1.490(6)
C(1)-O(2)	1.241(6)		

Key to symmetry operation: I. 0.5−x, 1.0−y, −0.5+z.

Table 3. Bond Angles (ϕ/°) with the Estimated Standard Deviations in Parentheses

Cl-Cu-O(1)	162.4(1)	O(1)-C(1)-O(2)	124.0(4)
Cl-Cu-O(1)^{I}	97.05(8)	O(1)-C(1)-C(2)	117.5(4)
Cl-Cu-O(2)^{I}	94.00(9)	O(2)-C(1)-C(2)	118.6(4)
Cl-Cu-N	97.3(1)	C(1)-C(2)-N	111.1(3)
O(1)-Cu-O(1)^{I}	97.2(1)	C(2)-N-Cu	106.5(3)
O(1)-Cu-O(2)^{I}	86.8(1)	C(3)-N-Cu	112.3(3)
O(1)-Cu-N	84.3(1)	C(5)-N-Cu	108.4(3)
N-Cu-O(1)^{I}	120.6(1)	C(4)-C(3)-N	113.6(4)
N-Cu-O(2)^{I}	167.1(1)	C(6)-C(5)-N	114.2(4)
O(1)^{I}-Cu-O(2)^{I}	51.5(1)	Cu-O(1)-Cu^{II}	167.0(2)
Cu-O(1)-C(1)	115.5(3)		

Key to symmetry operations: I. 0.5−x, 1.0−y, −0.5+z; II. 0.5−x, 1.0−y, 0.5+z.

The structure of the complex consists of a one-dimensional polymer chain bridged by only one carboxylato group of deg. One carboxylato oxygen atom of the deg is coordinated to two copper atoms to form an oxygen bridge, and the other is coordinated to one of these two copper atoms. Therefore the carboxylato group forms a four-membered chelate ring. It is the same bridging form as that of the hpro in [CuCl(hpro)(H$_2$O)] forms.[8]

The copper atom is surrounded by five atoms: three carboxylato oxygen atoms, one nitrogen atom, and one chlorine atom. The coordination type can not be assigned to a typical five-coordination polyhedron, a trigonal-bipyramid or a square-pyramid. It may be an extremely distorted tetrahedron, if the whole of the carboxylato group (forming the four-membered chelate ring) is regarded as an unidentate ligand.

The bond length of Cu-Cl, 2.199(1) Å, is a common value as a bond of Cu-Cl(terminal), which is different from Cu-Cl in [CuCl(hpro)(H$_2$O)]. The other bond lengths are common values except for Cu-O(1)^{I}, 2.801(4) Å. The rather long distance of Cu-O(1)^{I}, however, is not very surprising as discussed previously.[8]

In this complex, one of the two types of the chelate rings, the four-membered ring formed by Cu, O(1)^{I}, C(1)^{I}, and O(2)^{I}, is a fairly flat plane: the deviations from the least-squares plane are: Cu^{II} (0.007 Å), O(1)^{I}

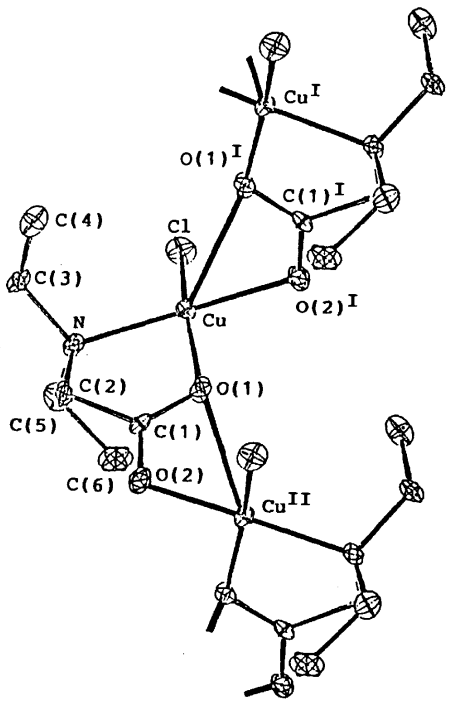

Fig. 1. The perspective drawing of [CoCl(deg)] and the numbering scheme of the atoms. Thermal ellipsoids are drawn at 30% probability level.
Key to symmetry operations: I. 0.5−x, 1.0−y, −0.5+z; II. 0.5−x, 1.0−y, 0.5+z.

(−0.013 Å), C(1)^{I} (0.028 Å), O(1)^{I} (−0.022 Å). The other, five-membered ring formed by Cu, O(1), C(1), C(2), and N, is slightly distorted; C(2) and N deviate from the plane formed by the five atoms in opposite directions. The distortion is not found in [CuCl(hpro)(H_2O)].[8] The difference of the five-membered chelate ring between [CuCl(hpro)(H_2O)] and [CuCl(deg)] is likely to be based on the difference of the positions of N and C(2) in each amino acid ligand. In hpro, N and C(2) belong to a pyrrolidine ring. On the other hand, N and C(2) in deg can be shifted more easily than those of hpro. The N and C(2) in deg, may deviate from the above mean plane in order to avoid the steric hindrance by ethyl groups connected to the nitrogen atom. The ethyl groups may also play a role of preventing coordination of a solvent molecule.

The projection of the structure along the c axis is given in Fig. 2. The polymer chains arrange in parallel with the c axis. There is no hydrogen bond, since the complex does not have any hydrogen donors, different from [CuCl(hpro)(H_2O)]: in [CuCl(hpro)(H_2O)], there are two types of hydrogen bonds, inter- and intrachain hydrogen bonds, between the water oxygen and chlorine atoms.

The structure of [CuCl(deg)] has the same bridging form as that of [CuCl(hpro)(H_2O)], though the coordination environment of the copper atom and the formation of the hydrogen bonds are different, as mentioned above. The bond lengths of Cu-N in [CuCl(deg)] and in [CuCl(hpro)(H_2O)] are 2.044(3) Å and 2.024(5) Å, respectively. Both of them are slightly longer than that common for Cu-N. It is suggested that the interesting bridge is formed when the nitrogen atom in an amino acid ligand makes the longer bond to the metal, because of steric hyndrance due to *N*-substituted groups. The coordination number of a metal or hydrogen bonding is not a principal cause of the formation of the bridging.

The magnetic moment of [CuCl(deg)] is 1.86 B.M. This is close to the value of [CuCl(hpro)(H_2O)], 1.89 B.M. The value is a little lower than those of the common octahedral copper(II) complexes, but the apparent Cu-Cu interaction is not considered. The result is supported by Cu-Cu atomic distances: 4.72 Å in [CuCl(deg)], and 4.46 Å in [CuCl(hpro)(H_2O)].

Infrared spectra of [CuCl(deg)] and [CuCl(hpro)(H_2O)] are shown in Fig. 3. There is a characteristic large split peak around 1600 cm^{-1} in both complexes, and near 1400 cm^{-1} a slightly split peak (in [CuCl(hpro)(H_2O)]) or a peak with a shoulder (in [CuCl(deg)]). These peaks are assigned to COO^- antisymmetric and symmetric stretching vibrations, respectively. The shapes of the peaks reflect the coordination form of the carboxylato group. Therefore the peaks can be an indicator of this coordination type, without reference to whether the amino acids have a pyrrolidine ring or not. The bis-chelate complex, [Cu(deg)$_2$(H_2O)$_2$], has the peak at 1617 cm^{-1} (COO^- antisymmetric). This agrees well with the higher frequency peak of the COO^- antisymmetric split peaks of [CuCl(deg)]. Moreover, the COO^- symmetric vibration of [Cu(deg)$_2$(H_2O)$_2$] has the same frequency (1381 cm^{-1}) as that of [CuCl(deg)].[13] These similarities are also found for [Cu(hpro)$_2$] and [CuCl(hpro)(H_2O)]: [Cu(hpro)$_2$] has the peaks at 1592 cm^{-1} and 1407 cm^{-1} and they agree with the higher frequency peaks between the respective corresponding split peaks of [CuCl(hpro)(H_2O)]. Therefore, in the interesting carboxylato bridging, the COO^- anti- and symmetric vibrations which are also shown in the normal amino acid chelate are kept and the new vibrations are added.

The electronic spectrum of the methanol solution

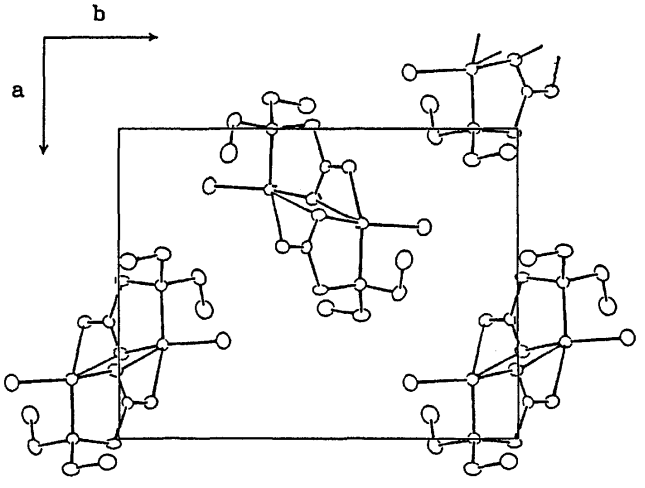

Fig. 2. The projection of the structure along the c axis.

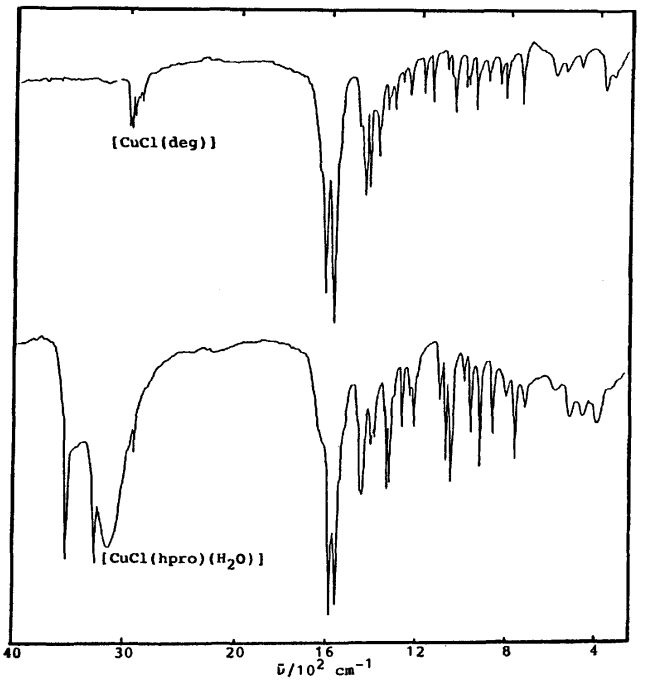

Fig. 3. Infrared spectra of [CuCl(deg)] and [CuCl(hpro)(H_2O)].

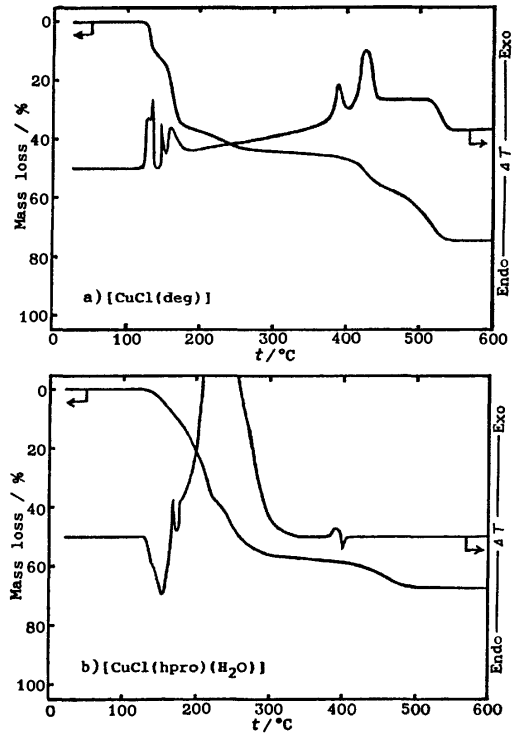

Fig. 4. The thermogravimetric and differential thermal analysis curves of [CoCl(deg)] and [CuCl(hpro)(H_2O)].

(756 nm ($\log\{\varepsilon/mol^{-1}\,dm^3\,cm^{-1}\}$=1.87), 266 nm (3.74)) is different from the powder diffuse reflection spectrum (609 nm (shoulder ca. 750 nm))[14] in [CuCl(deg)], which is similar to that observed in [CuCl(hpro)(H_2O)]. The deg complex is also likely to change into a six-coordinated Cu^{II} complex cation in the solution. The peak in the methanol solution, 756 nm, is closer to that in the powder diffuse reflection spectrum in [CuCl(hpro)(H_2O)] rather than to the corresponding peak of the electronic spectrum in [CuCl(hpro)(H_2O)]. The fact may indicate that the coordination polyhedron is not a typical shape, i.e. an elongate-octahedral symmetry due to coordination of solvent molecules along the axis normal to the molecular plane, but a widely different shape from an octahedron. The effect of the difference in solvent could not be checked, because the deg complex is hydrolyzed in the aqueous solution.

The results of the simultaneous TG and DTA of [CuCl(deg)] and of [CuCl(hpro)(H_2O)] are shown in Fig. 4. In the former, the decomposition began at about 130 °C, with some exothermic peaks on the DTA, and beyond 540 °C, black ash was obtained. In [CuCl(hpro)(H_2O)], after the elimination of water molecules (endothermic reaction), the decomposition began immediately and the black ash was obtained at the final stage. Both complexes change into CuO in the last place, but the process of the decomposition of each amino acid is different. It appears that the deg in [CuCl(deg)] decomposes through some steps, but in [CuCl(hpro)(H_2O)] the hpro decomposes at once. The difference may be based on the difference of the structure of the amino acid: the deg has two flexible ethyl groups, while the hpro has a rigid pyrrolidine ring.

The authors wish to express their thanks to Professor Akira Ouchi of The University of Tokyo and Associate Professor Mamoru Shimoi of Tohoku University for X-ray diffractometer measurements. They gratefully acknowledge the assistance on the structure-analysis calculations given by Mr. Kimitake Aoyagi of Sophia University. Thanks are due to Associate Professor Yoshio Masuda of Niigata University for TG and DTA measurements. They would also like to thank Dr. F. S. Howell of Sophia University for correcting this manuscript.

References

1) T. Yasui, J. Hidaka, and Y. Shimura, *J. Am. Chem. Soc.*, **87**, 2762 (1965).

2) T. Yasui, *Bull. Chem. Soc. Jpn.*, **38**, 1746 (1965).

3) R. G. Denning and T. S. Piper, *Inorg. Chem.*, **5**, 1056 (1966).

4) Y. Yukawa, Y. Inomata, T. Takeuchi, M. Shimoi, and A. Ouchi, *Bull. Chem. Soc. Jpn.*, **55**, 3135 (1982).

5) Y. Inomata, T. Takeuchi, and T. Moriwaki, *Inorg. Chim. Acta*, **68**, 187 (1983).

6) Y. Yukawa, Y. Inomata, and T. Takeuchi, *Bull. Chem. Soc. Jpn.*, **56**, 2125 (1983).

7) Y. Yukawa, N. Yasukawa, Y. Inomata, and T. Takeuchi, *Bull. Chem. Soc. Jpn.*, **58**, 1591 (1985).

8) S. Itoh, Y. Yukawa, Y. Inomata, and T. Takeuchi, *Bull. Chem. Soc. Jpn.*, **60**, 899 (1987).

9) "Universal Crystallographic Computation Program System (UNICS)," ed by T. Sakurai, Crystallographic Society of Japan, Tokyo (1967).

10) "International Tables for X-Ray Crystallography," Kynoch Press, Birmingham (1974), Vol. IV.

11) $R=\sum||F_o|-|F_c||/\sum|F_o|$; $R_w=[\sum\omega(|F_o|-|F_c|)^2/\sum\omega|F_o|^2]^{1/2}$, where $\omega=1/[\{\sigma(|F_o|)\}^2+(F_{weight}\times|F_o|)^2]$, F_{weight}= 0.025.

12) The final thermal parameters, the final positional parameters including hydrogen atoms, the final F_o-F_c table, some bond lengths for hydrogen atoms, and several least-squares planes are deposited as Document No. 8863 at the Office of the Editor of the Bulletin of the Chemical Society of Japan.

13) Y. Inomata, Y. Kato, Y. Yukawa, and T. Takeuchi, the 50th National Meeting of the Chemical Society of Japan, Tokyo, April 1985, Abstr. 1K03.

14) The reflection spectrum data reported at the 52th National Meeting of the Chemical Society of Japan, Kyoto, April 1986, Abstr. 4K27, was 626 nm, as measured by a Hitachi 624 digital spectrophotometer. In this work, the data were remeasured.

The Solubility of (Biphenyl, Naphthalene)-(Benzene, Cyclohexane, 1-Octanol) Binary Mixtures in Water

Isao SANEMASA,* Masaya KUMAMARU, Kazunari ISHIBASHI, and Toshio DEGUCHI
Department of Chemistry, Faculty of Science, Kumamoto University, Kurokami 2-39-1, Kumamoto 860
(Received August 23, 1988)

The solubility in water at 25 °C of binary mixed solutes, combinations of biphenyl and naphthalene with benzene, cyclohexane, and 1-octanol, was measured using a shake-flask method. As a function of biphenyl or naphthalene mole fraction, activity coefficients of biphenyl and naphthalene in benzene, cyclohexane, and 1-octanol, and those of benzene in biphenyl-benzene and naphthalene-benzene binary systems have been determined.

The solubility of hydrocarbons in water is still an important physicochemical property, and a large number of data have been accumulated. Most of the available data are concerned with the solubility of pure compounds, and there are only a few reports concerning the aqueous solubility of mixed solutes. For a better understanding of natural environment, it is essential to study mixed solute systems, since mixed organic compounds rather than a single solute is what we encounter in reality, e.g., spilled oil on water surface.

The study of aqueous solubility of binary organic solutes is also important in considering partition of an organic solute between aqueous and organic phases. The partition coefficient of a chemical is thought to be a measure of its relative hydrophobicity and considered to be a significant factor of bioaccumulation: the chemical with a large partition coefficient is likely to be accumulated into fish body.[1-3]

The object of this work is to determine activity coefficients of biphenyl and naphthalene in benzene, cyclohexane, 1-octanol, and water by measuring the solubility of these solid solutes in water.

Experimental

Materials. Deionized redistilled water was used throughout this work. Biphenyl, naphthalene, benzene, cyclohexane, and 1-octanol were of analytical reagent grade and used without further purification.

Apparatus and Procedures. Aqueous solutions saturated with binary solute mixtures were prepared in a glass vessel consisting of two parts. The upper part (300 cm^3 capacity) and the lower part (200 cm^3 capacity) were connected by a ground glass joint with stopcock. A side-arm with a stopcock was attached to the lower bottle at 2 cm above the bottom. The binary solute mixture (20—30 cm^3) was placed with 100 cm^3 of water in the lower bottle and the vessel was immersed up to above the stopcock of the joint in a water bath thermostated at 25.0±0.1 °C. The stopcock was closed and the contents were stirred for at least 24 h by a Teflon-coated magnet in the bottom. The vessel was then allowed to stand for at least 24 h without stirring and taken out of the bath. The upper part of the vessel was lightly evacuated through a stopcock attached to the top of the vessel. The top stopcock was closed, then the middle one with the joint was temporarily opened to reduce pressure inside the lower bottle, and air was carefully introduced into the bottle through the side arm by operating its stopcock to remove any solute droplets present inside the side arm. Then, the vessel was immersed again in the bath and stood for 24 h. A portion of the aqueous solution was withdrawn via the side arm, weighed, and extracted with cyclohexane.

The UV absorption of the extract was examined for biphenyl, naphthalene, and benzene at 247.5, 285, and 254 nm, respectively, on a Hitachi 100-50 spectrophotometer. The absorbance of benzene at 285 nm is practically negligible, while that of naphthalene at 254 nm cannot be neglected. Correction for naphthalene absorbance was made on benzene measurements; the contribution of naphthalene amounted to 3—20% depending on the relative concentration of naphthalene and benzene in the cyclohexane extract.

Because of a relatively high solubility of benzene in comparison with biphenyl, the absorbance of benzene at 247.5 nm is very strong, and hence, biphenyl cannot be determined directly on the cyclohexane extract. We overcame this problem by making use of the fact that in the presence of β-cyclodextrin the volatilization rate of benzene from aqueous into gaseous phase is much larger than that of biphenyl: Biphenyl forms more stable 1:1 complex with β-cyclodextrin than benzene does.[4] A 20 cm^3 portion of the aqueous solution containing biphenyl and benzene was taken into a cylindrical test tube (100 cm^3), to which 5 cm^3 of β-cyclodextrin (10^{-2} mol dm^{-3}) was added. The test tube was immersed in a water bath at 25.0±0.1 °C, and nitrogen was bubbled in the solution through a sintered glass ball at a rate of 500 cm^3 min^{-1} for 30 min. The content was diluted with water to 80 cm^3, and extracted with cyclohexane. Under the N_2 bubbling condition, 98.0% of benzene present initially was driven out of the solution, while 62.0% of biphenyl remained in the solution.

The absorbance of biphenyl at 254 nm cannot be neglected, and its correction was made on benzene measurements: the contribution of biphenyl was in 3—30% range.

Results and Discussion

Solubility in water of benzene, biphenyl, and naphthalene in binary mixtures was measured at 25 °C, but that of cyclohexane and 1-octanol was not measured. The results are shown in Figs. 1 and 2 as a function of biphenyl or naphthalene mole fraction. These solubility data were treated by the curve-fitting method as follows:

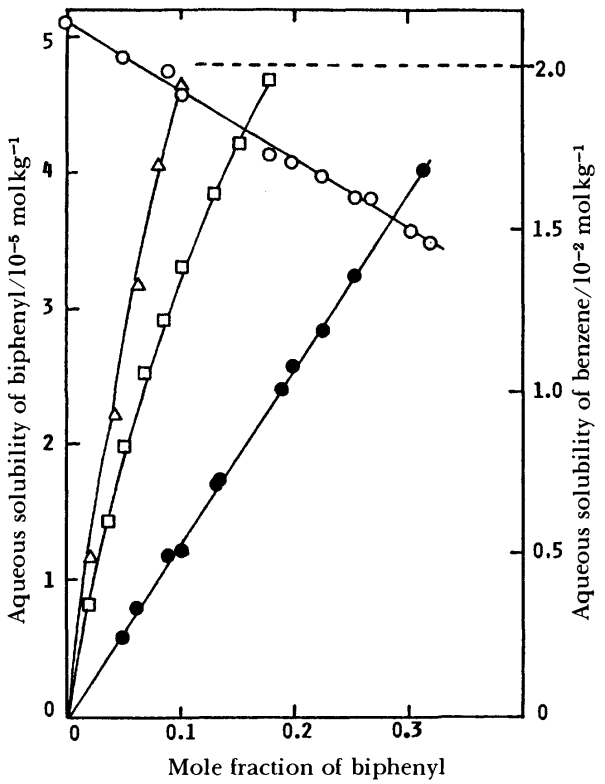

Fig. 1. Biphenyl-(benzene, cyclohexane, 1-octanol) binary systems at 25 °C. Aqueous solubility of biphenyl; ●: benzene system, □: cyclohexane system, △: 1-octanol system. Aqueous solubility of benzene; ○: biphenyl-benzene system. The dotted horizontal line shows the aqueous solubility of biphenyl determined at 25 °C for the solid solute.

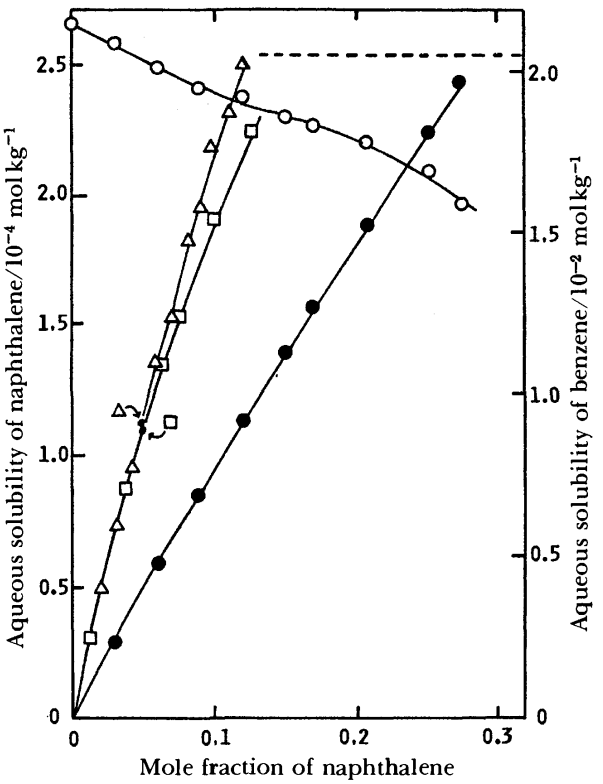

Fig. 2. Naphthalene-(benzene, cyclohexane, 1-octanol) binary systems at 25 °C. Aqueous solubility of naphthalene; ●: benzene system, □: cyclohexane system, △: 1-octanol system. Aqueous solubility of benzene; ○: naphthalene-benzene system. The dotted horizontal line shows the aqueous solubility of naphthalene determined at 25 °C for the solid solute.

benzene solubility;

$5.55\times10^{3}X_w=-2.15X_o+2.14$
(biphenyl-benzene system),

biphenyl solubility;

$5.55\times10^{6}X_w=12.8X_o-0.015$
(biphenyl-benzene system),
$5.55\times10^{6}X_w=-90.44X_o^2+41.45X_o+0.07327$
(biphenyl-cyclohexane system),
$5.55\times10^{6}X_w=-150.4X_o^2+60.98X_o-0.007946$
(biphenyl-1-octanol system),

naphthalene solubility;

$5.55\times10^{5}X_w=-3.812X_o^2+9.884X_o-0.0001182$
(naphthalene-benzene system),
$5.55\times10^{5}X_w=-57.10X_o^2+24.92X_o+0.001489$
(naphthalene-cyclohexane system),
$5.55\times10^{5}X_w=-33.27X_o^2+24.90X_o+0.0003351$
(naphthalene-1-octanol system),

where X_w is the aqueous solubility in mole fraction and X_o is mole fraction of biphenyl or naphthalene in the binary system. The results are summarized in Tables 1 and 2.

From equilibrium thermodynamics, the activity of a given solute is equal in both phases, then,

$$X_w\gamma_w=X_o\gamma_o, \quad (1)$$

where γ_w and γ_o are activity coefficients of a solute in the aqueous and the organic solvent phases, respectively. According to the literature,[5-8] the biphenyl-benzene system shows very small positive deviation from Raoult's law. It is, however, difficult to discriminate this small deviation from solubility measurements, because a relatively large error is unavoidable in solubility measurements. The X_w vs. X_o plots being linear, we assume this system as an ideal one: the γ_o values for benzene and biphenyl in the binary system are taken to be unity. From the reciprocal slope of the straight line, activity coefficients of biphenyl and benzene in water at 25 °C are evaluated to be 4.33×10^{5} and 2.58×10^{3}, respectively. Using these values as γ_w, the activity coefficient of biphenyl in the binary system with cyclohexane or 1-octanol and that of benzene in the binary system with naphthalene can be determined at any composition, X_o, with the aid of Eq. 1. The results are given in Table 2.

On the other hand, though there is a report from vapor pressure measurements of benzene to support that naphthalene forms an ideal solution with benzene,[9] it seems reasonable to consider from the data

on the solubility of naphthalene in benzene[10,11] that this system is not ideal, but exhibits more positive deviation from Raoult's law in comparison with the biphenyl-benzene system. We, therefore, determined γ_w for naphthalene from the equation,[12]

$$\ln(X_w\gamma_w) = \ln(f_s/f_l) = \Delta H_f(T_m^{-1} - T^{-1})R^{-1}, \quad (3)$$

where f_s and f_l are the fugacity of pure solid naphthalene and its supercooled liquid, ΔH_f is the heat of fusion of naphthalene, T_m is the melting temperature, T is the temperature of the system, and R is the gas constant. The data are available in the literature,[13] ΔH_f=18.979 kJ mol^{-1} and T_m=353.43 K, then, the activity coefficient of naphthalene in water is evaluated to be 6.68×10^4 at 25 °C using 4.52×10^{-6} as X_w. Using this value, activity coefficients of naphthalene in benzene, cyclohexane, and 1-octanol are determined from Eq. 1. The results are given in Tables 1 and 2.

The activity coefficient of a solute in binary mixtures has been usually determined by measuring vapor pressure of the constituent solute. In the system, however, where a solid solute is concerned, as in the pres-

Table 1. (Biphenyl, Naphthalene)-Benzene Binary Mixed Solute Solutions, the Aqueous Solubility at 25 °C and the Activity Coefficient in the Binary Mixtures

X_o[a]	Aqueous solubility		Activity coefficient[c]	
	Biphenyl	Benzene[b]	Naphthalene	Benzene
	10^{-5} mol kg^{-1} or Naphthalene 10^{-4} mol kg^{-1}	10^{-2} mol kg^{-1}		
Biphenyl-benzene system				
0		2.14		
0.01	0.113	2.12		
0.05	0.625	2.03		
0.1	1.27	1.92		
0.15	1.91	1.82		
0.2	2.55	1.71		
0.25	3.19	1.60		
0.3	3.83	1.50		
0.35	4.47	1.39		
	4.75[d]	1.40[d]		
Naphthalene-benzene system				
0		2.14		1.00
0.01	0.0983	2.12	1.18	1.00
0.025	0.245	2.09	1.18	1.00
0.05	0.485	2.03	1.16	0.999
0.075	0.720	1.97	1.15	0.995
0.1	0.950	1.93	1.14	1.00
0.125	1.18	1.90	1.13	1.01
0.15	1.40	1.86	1.12	1.02
0.175	1.61	1.82	1.10	1.03
0.2	1.82	1.79	1.09	1.05
0.225	2.03	1.75	1.08	1.06
0.25	2.23	1.68	1.07	1.05
0.275	2.43	1.59	1.06	1.02
	2.52[d]	1.60[d]		

a) Mole fraction of biphenyl or naphthalene in benzene. b) Aqueous solubility of benzene in the naphthalene-benzene system at a given X_o was estimated from the solubility curve shown in Fig. 2. c) The biphenyl-benzene system is assumed to be ideal. d) These values were obtained in the excess of the solid solute, that is, the biphenyl or naphthalene phase appears separated from the organic liquid phase.

Table 2. (Biphenyl, Naphthalene)-(Cyclohexane, 1-Octanol) Binary Mixed Solute Solutions, the Aqueous Solubility at 25 °C and the Activity Coefficient of Biphenyl or Naphthalene in the Binary Mixtures

X_o[a]	Aqueous solubility[b]		Activity coefficient[b]
	Biphenyl	Naphthalene	
	10^{-5} mol kg^{-1}	10^{-4} mol kg^{-1}	
Biphenyl-cyclohexane system			
0.01	0.479		3.73
0.025	1.05		3.27
0.05	1.92		2.99
0.075	2.67		2.77
0.1	3.31		2.58
0.125	3.84		2.39
0.15	4.26		2.21
0.175	4.56		2.03
0.25	4.75		1.48
	4.77[c]		
Biphenyl-1-octanol system			
0.01	0.587(0.776)		4.57(4.54)
0.02	1.15(1.50)		4.48(4.41)
0.03	1.69(2.17)		4.37(4.27)
0.04	2.19(2.78)		4.26(4.12)
0.05	2.67(3.34)		4.15(3.97)
0.06	3.10(3.85)		4.03(3.82)
0.07	3.52(4.30)		3.92(3.67)
0.08	3.91(4.70)		3.80(3.52)
0.09	4.26		3.68
0.1	4.59		3.57
	4.72[c]		
Naphthalene-cyclohexane system			
0.01		0.245	2.94
0.025		0.589	2.83
0.05		1.10	2.64
0.075		1.55	2.48
0.1		1.92	2.30
0.125		2.22	2.13
		2.50[c]	
Naphthalene-1-octanol system			
0.01		0.246(0.325)	2.95(2.94)
0.02		0.485(0.636)	2.91(2.88)
0.03		0.717(0.934)	2.87(2.83)
0.04		0.943(1.22)	2.83(2.78)
0.05		1.16(1.49)	2.78(2.73)
0.06		1.37(1.75)	2.75(2.67)
0.07		1.58(1.99)	2.71(2.62)
0.08		1.78(2.23)	2.67(2.57)
0.09		1.97(2.45)	2.63(2.52)
0.1		2.16	2.59
		2.51[c]	

a) Mole fraction of biphenyl or naphthalene in cyclohexane or 1-octanol. b) The aqueous solubility and the activity coefficient of biphenyl or naphthalene shown in the parentheses are those correspond to X_o^*, mole fraction of biphenyl or naphthalene in 1-octanol saturated with water. c) See footnote. d) In Table 1.

ent cases, the vapor pressure of the solid solute is too low to be accurately measured, and hence, only that of the solvent is measured. Then, the activity coefficient of the other less volatile component is estimated indirectly by means of the Gibbs-Duhem transformation. In contrast to this, the present approach gives direct information concerning the solid solute. There is, however, inevitable disadvantage in the present method that the system is not binary in a strict sense but ternary, because water itself participates more or less in the system. This seems not to be a serious problem when benzene or cyclohexane is used as a constituent component of binary systems.[14,15] This is, however, not the case for 1-octanol because the solubility of water in 1-octanol is very high.

The solubility of water in 1-octanol is reported to be 0.25 mole fraction at 25 °C.[16] This water content being considered, the mole fraction of a solute in water-free 1-octanol, X_o, should be corrected: $X_o = X_o^*/(0.75+0.25X_o^*)$,[17] where X_o^* refers to the mole fraction in water-saturated 1-octanol. Activity coeficients, corrected for water in 1-octanol, are given in Table 2.

The 1-octanol/water partition coefficient, $K_{o/w}$, is commonly defined as follows:

$$K_{o/w} = C_o/C_w = \gamma_w^* \bar{V}_w^*/(\gamma_o^* \bar{V}_o^*), \quad (4)$$

where C_o and C_w denote the molar concentration of a solute in 1-octanol saturated with water and that in water saturated with 1-octanol, respectively. The activity coefficient of a solute in water saturated with 1-octanol, γ_w^*, can be made equal to γ_w, and the partial molar volume of water saturated with 1-octanol, $\bar{V}_w^*$, can also be made equal to the molar volume of water,[18] because the solubility of 1-octanol in water is low. Using 0.018 $dm^3 mol^{-1}$ as $\bar{V}_w$ and 0.12 $dm^3 mol^{-1}$ as $\bar{V}_o^*$,[18] log $K_{o/w}$ values are found to be 4.1 for biphenyl and 3.5 for naphthalene. Here we used γ_o^* of 4.74 for biphenyl and 2.96 for naphthalene, which are estimated at infinite dilution of X_o^*, that is, $(\gamma_o^*)_{X_o^* \to 0}$. These log $K_{o/w}$ values obtained are comparable with those in the literature, 4.09 (biphenyl) and 3.36 (naphthalene).[18]

The authors wish to thank the Ministry of Education, Science and Culture for a financial support, a Grant-in-Aid for Scientific Research (No. 62540445).

References

1) H. Watarai, M. Tanaka, and N. Suzuki, *Anal. Chem.*, **54**, 702 (1982).
2) J. E. Garst, *J. Pharm. Sci.*, **73**, 1623 (1984).
3) A. Opperhuizen, P. Serné, and J. M. D. Van der Steen, *Environ. Sci. Technol.*, **22**, 286 (1988).
4) I. Sanemasa and Y. Akamine, *Bull. Chem. Soc. Jpn.*, **60**, 2059 (1987). I. Sanemasa, unpublished data.
5) H. Tompa, *J. Chem. phys.*, **16**, 292 (1948).
6) J. H. Baxendale, B. V. Enüstün, and J. Stern, *Phil. Trans.*, **A243**, 169 (1951).
7) D. H. Everett and M. F. Penney, *Proc. R. Soc. London, Ser. A*, **212**, 164 (1952).
8) S. H. Maron and A. C. Lowell, *J. Macromol. Sci., Phys.*, **3**, 123 (1969).
9) N. Campbell, *Can. J. Res.*, **B19**, 143 (1941).
10) E. L. Heric and C. D. Posey, *J. Chem. Eng. Data*, **9**, 35 (1964).
11) P. B. Choi, C. P. Williams, K. G. Buehring, and E. McLaughlin, *J. Chem. Eng. Data*, **30**, 403 (1985).
12) K. Shinoda, "Yôeki to Yôkaido," Maruzen, Tokyo (1974), Chap. 8.
13) H. E. Lundager Madsen, *J. Crystal Growth*, **85**, 377 (1987).
14) G. Arich, I. Kikic, and P. Alessi, *Chem. Eng. Sci.*, **30**, 187 (1975).
15) Considering the mole fraction solubility of water in benzene, 0.0026, we get an equation (see Ref. 17, below), $X_o = X_o^*/(0.9974+0.0026\ X_o^*)$, where X_o^* refers to the solute mole fraction in water-saturated benzene. The difference between X_o and X_o^* is small.
16) G. T. Hefter, "IUPAC Solubility Data Series, Vol. 15," ed by A. F. M. Barton, Pergamon, Oxford (1984), pp. 364—367 (1-octanol).
17) This relation is drawn by combining three equations: $X_o = n_2/(n_1+n_2)$, $X_o^* = n_2/(n_1+n_2+n_3)$, and $X_3 = n_3/(n_1+n_3) = 0.25$, where subscripts 1, 2, and 3 refer to 1-octanol, solute, and water, respectively.
18) C. T. Chiou, D. W. Schmedding, and M. Manes, *Environ. Sci. Technol.*, **16**, 4 (1982).

 © 1989 The Chemical Society of Japan Bull. Chem. Soc. Jpn., 62, 1065—1069 (1989)

Stereoselective Isomerization Reaction of (Iminodiacetato)-(ethylenediamine-*N*-acetato)cobalt(III), [Co(ida)-(edma)], in a Basic Aqueous Solution

Hiroshi KAWAGUCHI,* Hideko MIYAMOTO, Tomoharu AMA, and Takaji YASUI
Department of Chemistry, Faculty of Science, Kochi University, Akebono-cho, Kochi 780
(Received August 29, 1988)

Isomerization reactions among four geometrical isomers (pink, violet, brown, and light-brown) of [Co(ida)(edma)] were studied in a basic aqueous solution. In a reaction of $(-)^{CD}_{554}$-pink, three isomers of $(+)^{CD}_{563}$-violet, $(+)^{CD}_{565}$-brown (with a low optical purity), and racemic light-brown formed simultaneously. The major products in reactions of $(+)^{CD}_{563}$-violet and $(+)^{CD}_{565}$-brown were $(+)^{CD}_{565}$-brown and $(+)^{CD}_{563}$-violet, respectively. Light-brown mainly isomerized to brown at a rapid rate. Moreover, it was found that $(+)^{CD}_{563}$-violet racemized at a considerable rate. These stereoselective reactions are discussed in connection with those for $[Co(edma)_2]^+$ and $[Co(ida)_2]^-$.

Over the last few years we have been investigating the structure-reactivity pattern of octahedral complexes, particularly the isomerization of the bis(terdentate)cobalt(III) complexes. In previous papers,[1,2] we reported the preparation and characterization of four geometrical isomers of [Co(ida)(edma)] (Fig. 1),[3] and also a determination of the absolute configurations of the three isomers containing facially coordinated ligands. The possible configurations and CD signs for the three isomers are shown in Table 1. We describe here the isomerization reaction of the [Co(ida)(edma)] system, which is discussed on the basis of the previous studies on the related complexes, $[Co(ida)_2]^-$[4] and $[Co(edma)_2]^+$.[5]

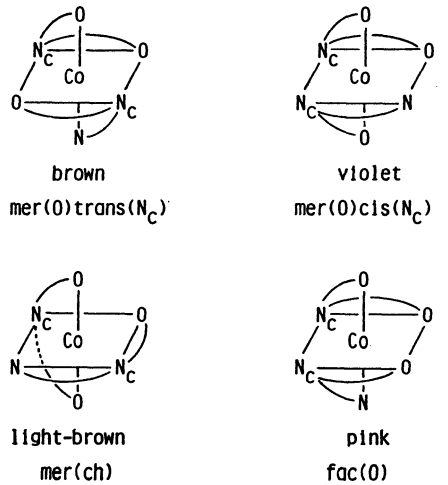

Fig. 1. Four geometrical isomers of [Co(ida)(edma)]. N_c denotes a central nitrogen.

Table 1. Possible Configurations and CD Signs of [Co(ida)(edma)]

Geometrical isomer	Possible configuration and CD sign	
mer(O)trans(N_c) (brown)	$(+)^{CD}_{565}$-$\Lambda\Lambda(S)$	$(-)^{CD}_{565}$-$\Delta\Delta(R)$
mer(O)cis(N_c) (violet)	$(+)^{CD}_{563}$-$\Lambda\Delta\Lambda(S)$	$(-)^{CD}_{563}$-$\Delta\Lambda\Delta(R)$
fac(O) (pink)	$(+)^{CD}_{554}$-$\Lambda\Delta\Lambda(S)$	$(-)^{CD}_{554}$-$\Delta\Lambda\Delta(R)$

Experimental

Complexes and Reagents. The complexes examined here were prepared and optically resolved according to methods described in our previous papers.[1,2] They are $(+)^{CD}_{565}$-*mer(O)trans*(N_c)-[Co(ida)(edma)] (abbreviation: $(+)^{CD}_{565}$-brown), $(+)^{CD}_{563}$-*mer(O)cis*(N_c)-[Co(ida)(edma)]·H_2O ($(+)^{CD}_{563}$-violet), $(-)^{CD}_{554}$-*fac(O)*-[Co(ida)(edma)] ($(-)^{CD}_{554}$-pink), and *mer(ch)*-[Co(ida)(edma)]·H_2O (light-brown). All the chemicals used were of a reagent grade, and the deionized water was degassed before use.

Isomerization. $(+)^{CD}_{563}$-Violet Isomer: This isomer (0.2211 g) was dissolved in 100.0 cm^3 of water in a reaction vessel kept in a thermostated bath at 40.0 °C. The reaction was started by stirring 100.0 cm^3 of a buffer solution [Na_2CO_3(0.5606 g)-$NaHCO_3$(0.2241 g)] previously kept at 40.0 °C into the reaction vessel. The reaction conditions were as follows: Complex concentration, 3.4×10^{-3} M (M= mol dm^{-3}); pH, 10.30±0.03; temperature, 40.0±0.1 °C. The temperature and pH of the reaction solution were checked with a thermistor thermometer (Takara D221) and a pH meter (Toa TSC-10A), respectively, throughout the kinetic run. At a prescribed time, the reaction solution was acidified to pH 5 in order to stop the reaction. (Such kinetic runs with different reaction times were carried out repeatedly.) The acidified solution was concentrated under reduced pressure at 35—40 °C and then applied to a column (3.0 cm×80 cm) of Sephadex G-10 in order to remove salts.[6] The eluate containing the isomers of [Co(ida)(edma)] was concentrated again and chromatographed on a column (3.7 cm×80 cm) of QAE-Sephadex A-25 [$Sb_2(d\text{-tart})_2^{2-}$ form] using water as an eluent; three bands of el 1 [$(+)^{CD}_{565}$-brown and violet], el 2 [$(-)^{CD}_{565}$-brown and light brown], and el 3 [pink]. The three eluates were collected separately and concentrated to appropriate constant volumes. The amount and optical purity of each isomer were determined from absorption and CD data measured by a Hitachi 557 spectrophotometer and a JASCO J-22 spectropolarimeter, respectively. The amounts of the two isomers and the optical purity of violet in el 1 were estimated from binary-curve analyses of the absorption and CD spectra. The amounts of the two isomers in el 2 were also estimated by a procedure similar to that described above.

In these curve analyses, the spectral data at 20 points in the visible region were used; the analyses were carried out on an NEC PC-9801F computer using a least-squares method.

$(+)^{CD}_{565}$-Brown, $(-)^{CD}_{554}$-Pink, and Light-Brown Isomers: The isomerization reaction of $(+)^{CD}_{565}$-brown was carried out by a procedure similar to that used for $(+)^{CD}_{563}$-violet. The reaction conditions were the same as those in the case of $(+)^{CD}_{563}$-violet.

The solubility of $(-)^{CD}_{554}$-pink was low. Thus, the saturated solution (180 cm^3) of $(-)^{CD}_{554}$-pink, which was obtained by stirring the powder of the isomer in water at 40.0 °C for 10 min, and a buffer solution (20 cm^3) containing 0.5653 g of Na_2CO_3 and 0.2241 g of $NaHCO_3$ were prepared for the isomerization reaction. The procedure of the reaction was the same as that in the case of $(+)^{CD}_{563}$-violet. The reaction conditions were as follows: Complex concentration, 2.8×10^{-3} M (It was determined from the absorption data at the start of the reaction.); pH, 10.30±0.02; temperature, 40.0±0.1 °C.

The isomerization study of light-brown could not be carried out sufficiently, since the preparation of the isomer was very difficult. Only one isomerization run using light-brown as a starting material was carried out on a small scale (1/4 of the scale for violet), and the isomer proportions at one hour after the start of the reaction were determined by a procedure similar to that in the case of $(+)^{CD}_{563}$-violet.

In weak acidic and neutral solutions at room temperature, the absorption and CD spectral changes of each isomer were not observed for about one day. Therefore, progress of the isomerization and/or racemization reaction during such procedures as chromatographic separation and concentration under reduced pressure should be negligible.

Results and Discussion

Base-Catalyzed Isomerization Reaction. $(-)^{CD}_{554}$-Pink Isomer: The isomerization reaction of $(-)^{CD}_{554}$-pink was followed over a period of 12 h under the conditions of pH 10.30 and 40.0 °C. Figure 2 shows the changes in the proportions of the starting material and reaction products. A part of the numerical data are listed in Table 2, together with the enantiomer excess percentage of each isomer. The isomerization reaction of pink is faster than the reactions of violet and brown. The half-life period (with regard to the decrease in pink) is about 40 min under the conditions described above. In this reaction, three products — $(+)^{CD}_{563}$-violet, $(+)^{CD}_{565}$-brown, and racemic light-brown — were simultaneously formed. Throughout the reaction, no other products were detected by the present experimental method. The brown isomer increased in amount with the passage of time and was a major species after a prolonged reaction time. The concentrations of light-brown and violet were maximal at about 45 min and about 4 h after the reaction start, respectively; thereafter, they decreased. At longer reaction times (>ca. 4 h), the amount of light-brown was almost negligible.

As shown in Table 2, $(-)^{CD}_{554}$-pink (starting material) retained a high optical purity until about 2 h; at that time most of the pink had already isomerized to other isomers. This fact probably indicates that the racemization of $(-)^{CD}_{554}$-pink, itself, is negligible. During the initial stage of the reaction, $(+)^{CD}_{563}$-violet formed from $(-)^{CD}_{554}$-pink retained an optical purity of about 100%. The isomerization path of $(-)^{CD}_{554}$-pink → $(+)^{CD}_{563}$-violet

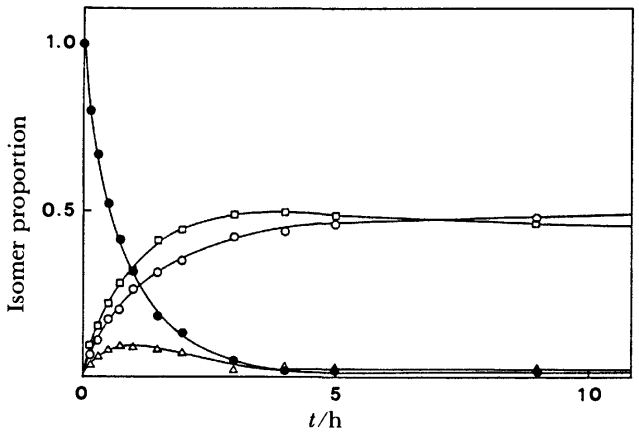

Fig. 2. The changes of the isomer proportions in the isomerization reaction of $(-)^{CD}_{554}$-pink (40.0 °C, pH 10.30); pink (-●—●-), violet(-□—□-), brown (-○—○-), and light-brown (-△—△-).

Table 2. The Proportions and Optical Purities of the Starting Materials and Products in the Isomerization Rreaction (40.0 °C, pH 10.30)

(i) $(-)^{CD}_{554}$-pink

t	Isomer proportion (optical purity/%)			
min	$(-)^{CD}_{554}$-pink	$(+)^{CD}_{565}$-brown	$(+)^{CD}_{563}$-violet	light-brown
10	0.800(100)	0.060(14)	0.095(100)	0.045
30	0.561(100)	0.156(9)	0.205(100)	0.078
60	0.336(100)	0.250(10)	0.322(87)	0.092
120	0.133(92)	0.351(10)	0.446(61)	0.072
240	0.031(50)	0.434(12)	0.498(49)	0.037

(ii) $(+)^{CD}_{563}$-violet

t	Isomer proportion (optical purity/%)			
h	$(+)^{CD}_{563}$-violet	$(+)^{CD}_{565}$-brown	$(-)^{CD}_{554}$-pink	light-brown
1	0.935(92)	0.019(71)	0.020(100)	0.026
3	0.853(53)	0.078(50)	0.029(65)	0.039
5	0.803(46)	0.131(28)	0.026(53)	0.039
8	0.697(21)	0.242(24)	0.026(25)	0.035
13	0.617(8)	0.326(14)	0.024(13)	0.033
24	0.456(0)	0.496(8)	0.021(3)	0.027

(iii) $(+)^{CD}_{565}$-brown

t	Isomer proportion (optical purity/%)			
h	$(+)^{CD}_{565}$-brown	$(+)^{CD}_{563}$-violet	$(-)^{CD}_{554}$-pink	light-brown
2	0.967(98)	0.014(70)	0.007(25)	0.038
5	0.921(94)	0.053(22)	0.010(17)	0.016
8	0.887(89)	0.083(16)	0.011(15)	0.019
13	0.848(83)	0.122(9)	0.013(14)	0.017
30	0.790(79)	0.181(0)	0.015(0)	0.014

(iv) light-brown[a)]

t	Isomer proportion			
h	light-brown	brown	violet	pink
1	0.167	0.685	0.118	0.030

a) Reaction conditions; pH 10.28 and 40.0 °C.

change is thus highly stereoselective. However, the optical purity of the formed $(+)^{CD}_{563}$-violet decreased with the passage of time. The $(+)^{CD}_{565}$-brown formed in the same reaction showed a low optical purity (ca. 10 %). Moreover, the value of the optical purity was nearly constant throughout the present reaction (12 h). Accordingly, it is thought that $(-)^{CD}_{554}$-pink isomerizes to $(+)^{CD}_{565}$- and $(-)^{CD}_{565}$-brown with a constant ratio (55 : 45%).

In an isomerization reaction among three geometrical isomers of $[Co(ida)_2]^-$, the reaction scheme was found to be *u-fac* ⇄ *mer* ⇄ *s-fac*.[4] However, in the $[Co(edma)_2]^+$ system, the isomerization from the *fac*-type isomers to the *mer* isomer was not observed. Isomerization among *fac*-type isomers of $[Co(edma)_2]^+$ accompanies inversion at one of two secondary nitrogen (sec-N) centers of the coordinated edma ligands. The inversion is thought to be caused by a coordination-site exchange between the sec-N and carboxylato oxygen of a coordinated edma ligand.[5] If [Co(ida)(edma)] has a reactivity that is similar to those of both $[Co(ida)_2]^-$ and $[Co(edma)_2]^+$, the reaction paths shown in Scheme 1 should be expected for the isomerization of $(-)^{CD}_{554}$-pink: Three paths from $(-)^{CD}_{554}$-pink to $(+)^{CD}_{563}$-violet, $(+)^{CD}_{565}$-brown, and $(-)^{CD}_{565}$-brown are proposed by considering the isomerization mechanism for the $[Co(edma)_2]^+$ system (coordination-site exchange between the sec-N and O of the coordinated ida or edma ligand), and the $(-)^{CD}_{554}$-pink → light-brown path is proposed on the basis of the assumption that the reaction proceeds by a process similar to that for the $[Co(ida)_2]^-$ system. The experimental results described above, namely the simultaneous formation of $(+)^{CD}_{563}$-violet, approximately racemic brown, and light-brown are well explained with the simultaneous occurence of four paths in Scheme 1. The light-brown obtained in this isomerization reaction was racemate. This does not mean that the $(-)^{CD}_{554}$-pink → light-brown change is not stereoselective. Even though the change is stereoselective, the optically active light-brown formed from $(-)^{CD}_{554}$-pink must racemize very rapidly under the present reaction conditions, judging from the racemization rates of *mer*-[Co(ida)(dien)]$^+$,[7] *mer*-[Co(edma)(dien)]$^{2+}$,[8] and *mer*-$[Co(dien)_2]^{3+}$.[9] The decrease of the optical purities in $(+)^{CD}_{563}$-violet and $(-)^{CD}_{554}$-pink with the passage of time are explained in the later section.

$(+)^{CD}_{563}$-Violet Isomer: The isomerization reaction using $(+)^{CD}_{563}$-violet as a starting material was also carried out in a carbonate buffer (pH 10.30) at 40 °C, and a part of the data are listed in Table 2. In the initial stage of the reaction, three products — $(+)^{CD}_{565}$-brown, $(-)^{CD}_{554}$-pink, and light-brown (racemate) — were formed. The amounts of pink and light-brown little increased even though the reaction was allowed to proceed for a long time, indicating that the subsequent isomerizations from these isomers to brown and/or violet occurred. While, brown increased in its amount with the passage of time and was a major species in the final stage of the reaction.

As shown in Table 2, the optical purity of the starting material — $(+)^{CD}_{563}$-violet — decreased more rapidly compared with the rate of its concentration decrease. This fact means that $(+)^{CD}_{563}$-violet, itself, racemized at a considerable rate. $(-)^{CD}_{554}$-Pink and $(+)^{CD}_{565}$-brown, which were formed from $(+)^{CD}_{563}$-violet, showed optical purities of about 100 and about 70%, respectively, during the initial stage of the reaction. These two isomerization paths are, thus, stereoselective. However, the optical purities of these two products decreased with the passage of time. The results may be attributed to a rapid

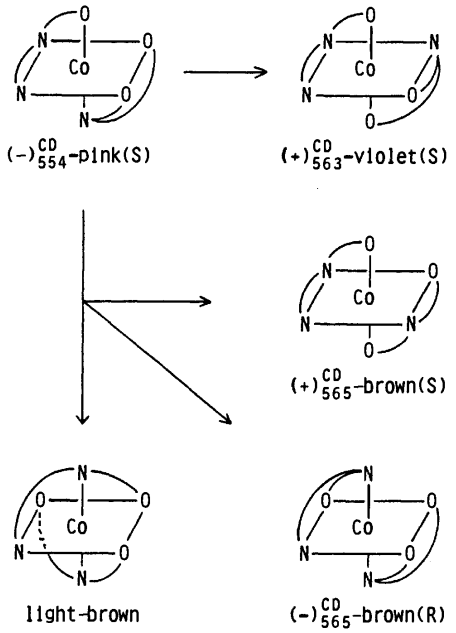

Scheme 1.

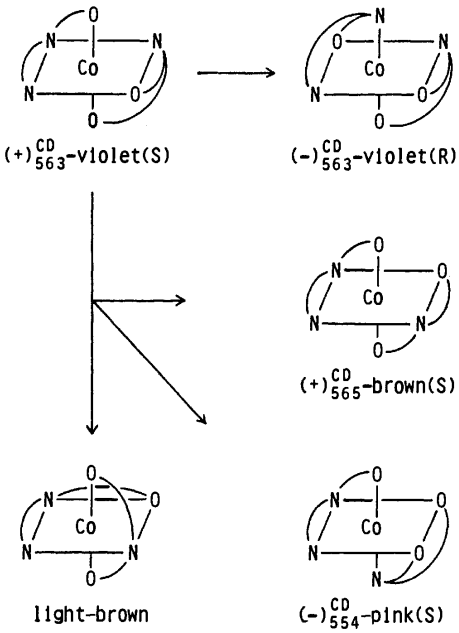

Scheme 2.

racemization of the starting material; $(-)^{CD}_{563}$-violet formed in the racemization of the starting material [$(+)^{CD}_{563}$-violet] produces $(+)^{CD}_{554}$-pink and $(-)^{CD}_{565}$-brown.

The isomerization of $(+)^{CD}_{563}$-violet can also be explained in a manner similar to that in the isomerization of $(-)^{CD}_{554}$-pink. If the isomerization due to the mechanism proposed for the $[Co(edma)_2]^+$ system occurs in $(+)^{CD}_{563}$-violet, three isomers — $(-)^{CD}_{563}$-violet, $(+)^{CD}_{565}$-brown and $(-)^{CD}_{554}$-pink — must be formed, as shown in Scheme 2. This proposal is consistent with the experimental results except for the minor formation of $(-)^{CD}_{554}$-pink. In the $[Co(edma)_2]^+$ system, it is found that the inversion at the sec-N center trans to the ligating nitrogen [*trans*(*N*)-sec-N] occurs slowly and that the inversion at the *trans*(*O*)-sec-N center occurs rapidly.[5] If such phenomenon as observed in the $[Co(edma)_2]^+$ system is expected to occur in the reaction of $(+)^{CD}_{563}$-violet, the experimental results, namely, the fast racemization of $(+)^{CD}_{563}$-violet and the minor formation of $(-)^{CD}_{554}$-pink, can be rationalized: The $(+)^{CD}_{563}$-violet → $(-)^{CD}_{563}$-violet change (racemization) accompanies the inversion at *trans*(*O*)-sec-N center, therefore, its rate is fast, and the $(+)^{CD}_{563}$-violet → $(-)^{CD}_{554}$-pink change accompanying the inversion at *trans*(*N*)-sec-N center occurs slowly. The formation rate of brown from $(+)^{CD}_{563}$-violet is relatively faster than that of pink in the same reaction, even though the $(+)^{CD}_{563}$-violet → $(+)^{CD}_{565}$-brown change accompanies an inversion at *trans*(*N*)-sec-N center. This fact may be ascribed to additional isomerization paths, such as $(+)^{CD}_{563}$-violet → $(-)^{CD}_{554}$-pink → $(+)^{CD}_{565}$-brown and $(+)^{CD}_{563}$-violet → light-brown → brown.

$(+)^{CD}_{563}$-Violet isomerized to racemic light-brown in a small amount. This indicates the existence of isomerization due to a mechanism similar to that in the $[Co(ida)_2]^-$ system, even though it is a minor path in the isomerization of $(+)^{CD}_{563}$-violet.

$(+)^{CD}_{565}$-Brown Isomer: The isomerization reaction of $(+)^{CD}_{565}$-brown proceeded slowly. The major product was $(+)^{CD}_{563}$-violet, of which the optical purity was high during the initial stage of the reaction (Table 2). $(-)^{CD}_{554}$-Pink with low optical purity and light-brown were also formed in a small amount; their amounts did not increase with time. This result can be rationalized using the same idea as used for the isomerization of $(+)^{CD}_{563}$-violet. If the isomerization of $(+)^{CD}_{565}$-brown proceeds on the mechanism of the coordination-site exchange between the sec-N and O of the edma or ida ligand, three products of $(+)^{CD}_{563}$-violet and $(-)^{CD}_{554}$- and $(+)^{CD}_{554}$-pink may be formed (Scheme 3). Two sec-N atoms in brown are located at the trans positions to each other [*trans*(*N*)-sec-N]; therefore, the isomerization of brown is expected to be slow. This expectation coincides with the present experimental result. The formation of light-brown can be explained by assuming an isomerization path similar to that proposed for the $[Co(ida)_2]^-$ system, even though it is a minor path in this reaction.

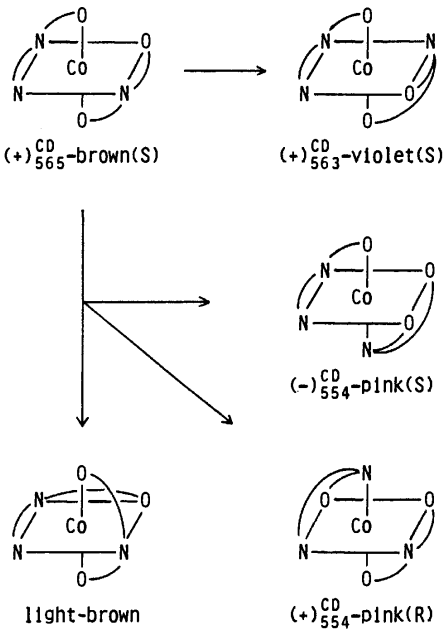

Scheme 3.

Light-Brown Isomer: The isomerization study of light-brown was not sufficient, since the preparation of its isomer was very difficult. The absorption spectrum of light-brown changed more rapidly, compared with the spectral changes of other isomers. From this spectral change, the formations of brown (major) and violet (minor) were presumed. Light-brown was allowed to react for one hour under the conditions of pH 10.28 at 40.0 °C; the proportions of the starting material and products in the reaction solution were chromatographically obtained. As shown in Table 2, the major product was brown (83% of the total amount of the products) one hour after the reaction started.

In the previous section it was described that $(+)^{CD}_{565}$-brown with a very low optical purity was obtained in the isomerization reaction of $(-)^{CD}_{554}$-pink. The result has been explained by the occurrence of two different N-O displacement processes (Scheme 1). The formation of racemic brown from $(-)^{CD}_{554}$-pink was also expected through the successive path of $(-)^{CD}_{554}$-pink → light-brown → brown (with a rapid rate). This path is similar to the isomerization process in the $[Co(ida)_2]^-$ system. It may be sure that the pink → light-brown → brown change contributes to the isomerization of pink to a considerable extent.

References

1) T. Ama, H. Kawaguchi, and T. Yasui, *Bull. Chem. Soc. Jpn.*, **59**, 1471 (1986).

2) T. Ama, R. Niiyama, H. Kawaguchi, and T. Yasui, *Bull. Chem. Soc. Jpn.*, **60**, 119 (1987).

3) Abbreviations used: ida, iminodiacetate dianion; edma, ethylenediamine-*N*-acetate monoanion; dien, 3-azapentane-1,5-diamine.

4) H. Kawaguchi, T. Ama, and T. Yasui, *Bull. Chem.*

Soc. Jpn., **57**, 2422 (1984).

5) H. Kawaguchi, R. Niiyama, T. Ama, and T. Yasui, *Bull. Chem. Soc. Jpn.*, **60**, 3953 (1987).

6) The removal of the salts makes it easy to separate the isomers on a QAE-Sephadex column.

7) H. Kawaguchi, M. Shimizu, T. Ama, and T. Yasui, *Bull. Chem. Soc. Jpn.*, **62**, 753 (1989).

8) H. Kawaguchi, H. Fukaki, T. Ama, T. Yasui, K. Okamoto, and J. Hidaka, *Bull. Chem. Soc. Jpn.*, **61**, 2359 (1988).

9) G. H. Searle and F. R. Keene, *Inorg. Chem.*, **11**, 1006 (1972).

Structures of Three Diastereomers of *trans*(*N*-Ph, *N*-Ph)-2,4-Pentanedionatobis-(*N*-phenylethylenediamine)cobalt(III) and of One Diastereomer of *trans*(*N*-Ph, *N*-Ph)-Oxalatobis(*N*-phenylethylene-diamine)cobalt(III) Complex Cations

Toshiaki AKAGAWA, Guilin MA,† Nahomi SUZUKI, Shigeru OHBA, Yue OUYANG,† Masaaki KOJIMA,† Junnosuke FUJITA,† and Yoshihiko SAITO*

Departmet of Chemistry, Faculty of Science and Technology, Keio University, 3-14-1, Hiyoshi, Kohoku-ku, Yokohama 223
†Department of Chemistry, Faculty of Science, Nagoya University, Chikusa-ku, Nagoya 464

(Received September 13, 1988)

The molecular structures of three racemic pairs of diastereomers, *ΔRR*(*ΔSS*)-, *ΔSR*(*ΔRS*)-, and *ΔSS*(*ΔRR*)-*trans*(*N*-Ph, *N*-Ph)-[Co(pd)(Ph-en)$_2$]$^{2+}$ and of one racemic pair of diastereomers, *ΔSS*(*ΔRR*)-*trans*(*N*-Ph, *N*-Ph)-[Co(ox) (Ph-en)$_2$]$^+$ (pd=2,4-pentanedionate ion, ox=oxalate ion, Ph-en=*N*-phenylethylenediamine) were determined by the single-crystal X-ray diffraction method in order to study the intramolecular interactions between π-systems in the ligands. For the *ΔSS*(*ΔRR*)-isomer of [Co(pd)(Ph-en)$_2$]$^{2+}$, three kinds of crystal structures **3a**, **3b**, and **3c** were investigated. The crystal data and final R values are: *ΔRR*(*ΔSS*)-[Co(pd)(Ph-en)$_2$](ClO$_4$)$_2$·H$_2$O (**1**), orthorhombic, *Pbca*, a=32.472(9), b=11.120(3), c=15.303(4) Å, V=5526(3) Å^3, Z=8, R=0.065 for 2113 observed unique reflections. *ΔSR*(*ΔRS*)-[Co(pd)(Ph-en)$_2$](ClO$_4$)$_2$ (**2**), orthorhombic, $P2_12_12_1$, a=19.440(8), b=16.406(8), c=8.407(3) Å, V=2681(2) Å^3, Z=4, R=0.038 for 2205 reflections. *ΔSS*(*ΔRR*)-[Co(pd)(Ph-en)$_2$]-Cl$_2$·H$_2$O (**3a**), monoclinic, $P2_1/c$, a=12.475(3), b=11.590(2), c=19.054(4) Å, β=117.18(2)°, V=2450.6(9) Å^3, Z=4, R=0.035 for 2164 reflections. *ΔSS*(*ΔRR*)-[Co(pd)(Ph-en)$_2$](ClO$_4$)Cl·H$_2$O (**3b**), triclinic, $P\bar{1}$, a=11.847(5), b=13.584(4), c=8.367(2) Å, α=103.57(2), β=91.85(3), γ=84.25(3)°, V=1302.1(8) Å^3, Z=2, R=0.087 for 1374 reflections. *ΔSS*(*ΔRR*)-[Co(pd)(Ph-en)$_2$](ClO$_4$)Cl (**3c**), triclinic, $P\bar{1}$, a=11.660(5), b=14.028(3), c=8.308(7) Å, α=108.00(8), β=101.57(9), γ=92.47(13)°, V=1258(3) Å^3, Z=2, R=0.052 for 1118 reflections. *ΔSS*(*ΔRR*)-[Co(ox)(Ph-en)$_2$] Br·6H$_2$O (**4**), orthorhombic, $Pna2_1$, a=15.804(1), b=15.646(1), c=10.428(2) Å, V=2578.5(4) Å^3, Z=4, R=0.065 for 1496 reflectios. The numbers of phenyl rings of the Ph-en ligands that overlap with the pd π system in the complex cation are 0, 1, and 2 for **1**, **2**, and **3** respectively. The ox ligand of **4** is ill-sandwiched by the two phenyl rings, whereas the pd ligand is well-sandwiched in **3a**. The arrangements of the phenyl groups relative to the pd differ slightly from one another in the crystals of **3a**, **3b**, and **3c**. The dihedral angles between the pd (or ox) and phenyl rings range from 25 to 35°.

Three isomers of *trans*(*N*-Ph, *N*-Ph)-[Co(pd)(Ph-en)$_2$]$^{2+}$ were prepared and characterized.[1] Their absorption spectra are different from each other, although the structures differ simply in the absolute configurations of the coordinated secondary N atoms. The greater the number of Ph rings placed over the pd chelate ring, the lower the energy of the first absorption band.[1] X-Ray crystal structure analyses have been done to verify their relative configurations, as assigned on the basis of the ^{1}H NMR spectra, and to investigate the intramolecular interaction of the π systems. The *ΔSS*(*ΔRR*)-*trans*(*N*-Ph,*N*-Ph)-[Co(ox)(Ph-en)$_2$]$^+$ complex has also been prepared and its structure examined in order to compare the results with those for the pd complexes.

Experimental

Preparation of [Co(ox)(Ph-en)$_2$]Br·6H$_2$O. The procedure was carried out under an atmosphere of nitrogen until the complex was formed. To a deaerated solution (180 cm^3) of K$_3$[Co(ox)$_3$]·3H$_2$O (2.8 g, 7.1 mmol) in dimethyl sulfoxide-water (4:5 v/v) we added deaerated *N*-phenylethylenediamine (1 g, 7.34 mmol). The mixture was warmed at 30 °C for 3 h. The resulting dark purple solution was diluted with water (1500 cm^3) and placed in a column (ϕ2.8 cm ×20 cm) of Dowex 1×8 (Cl$^-$ form) to remove the anionic species. The column was then washed with water, and the red effluent was placed in a column (ϕ2.8 cm×20 cm) of Dowex 50W×8 (Na$^+$ form). By elution with 0.6 mol dm^{-3} NaBr-0.01 mol dm^{-3} HBr, two red bands and a brown band developed in this order, the brown one remaining at the top of the column. The eluate containing the fastest-moving red band (main band) was collected and evaporated to dryness under reduced pressure. The residue was shaken with methanol to extract the complex, and the solvent was removed under reduced pressure. The residue was dissolved in a small amount of 0.01 mol dm^{-3} HBr and then allowed to stand overnight in a refrigerator. The red crystals were collected by filtration and washed with water and then methanol. Yield: 0.93 g (23%). UV-VIS spectrum (0.01 mol dm^{-3} HBr) 18.55 (log ε 2.32), 28.59 (4.72), and 42.72×10^3 cm^{-1} (4.87).

The slower-moving red band seemed to contain another isomer (racemic pair of the diastereomers) of [Co(ox)(Ph-en)$_2$]$^+$. The complex was not isolated, however, since it was unstable and the amount was very small. The complex showed the first absorption band at 18870 cm^{-1}. The abundance of the first band relative to that of the second band was ca. 30:1 when the two isomers were assumed to have the same molar absorption coefficient.

Crystal-Structure Determination. Crystals of **1**, **2**, and **3** were grown from acetone-HCl and HClO$_4$ mixtures to avoid epimerization.[1] Compound **4** was recrystallized from water. The experimental conditions and refinement information are listed in Table 1. The intensities were measured using graphite monochromatized Mo$K\alpha$ radiation (λ=0.71073 Å) on an automated Rigaku four-circle diffractometer AFC-5. The θ-2θ scan technique was employed at a scan rate of 6° min^{-1} in θ. The lattice constants were determined from

Table 1. Crystal Data, Experimental Conditions, and Refinement Details

	(1) *ΔRR*(*ΔSS*)-[Co(pd)-(Ph-en)$_2$]-(ClO_4)$_2$·H_2O	(2) *ΔSR*(*ΔRS*)-[Co(pd)-(Ph-en)$_2$](ClO_4)$_2$	(3) *ΔSS*(*ΔRR*)-[Co(pd)(Ph-en)$_2$]			(4) *ΔSS*(*ΔRR*)-[Co(ox)(Ph-en)$_2$]Br·$6H_2O$
			(a) Cl_2·H_2O	(b) (ClO_4)Cl·H_2O	(c) (ClO_4)Cl	
Formula weight	647.4	629.3	519.4	583.4	565.3	607.3
Space group and Z	*Pbca*, 8	$P2_12_12_1$, 4	$P2_1/c$, 4	$P\bar{1}$, 2	$P\bar{1}$, 2	$Pna2_1$, 4
D_m and D_x/Mg m^{-3}	1.55(1), 1.56	1.56(1), 1.56	1.41(1), 1.41	1.49(1), 1.49	1.49(1), 1.49	1.50(2), 1.56
μ(Mo $K\alpha$)/mm^{-1}	0.870	0.896	0.940	0.912	0.935	2.22
Color and shape of crystals	Brown-red prisms	Brown prisms	Green prisms	Brown prisms	Brown prisms	Orange-red prisms
Size of specimen/mm^3	0.20×0.20×0.40	0.18×0.18×0.60	0.12×0.25×0.28	0.20×0.20×0.25	0.05×0.10×0.20	0.20×0.36×0.50
$2\theta_{max}$/°	45	55	50	40	40	55
Range of h, k, and l	$0\leqq h\leqq 34$ $0\leqq k\leqq 11$ $0\leqq l\leqq 16$	$0\leqq h\leqq 25$ $0\leqq k\leqq 21$ $0\leqq l\leqq 10$	$0\leqq h\leqq 14$ $0\leqq k\leqq 13$ $-22\leqq l\leqq 22$	$-11\leqq h\leqq 11$ $-13\leqq k\leqq 13$ $-8\leqq l\leqq 0$	$-11\leqq h\leqq 11$ $-13\leqq k\leqq 13$ $0\leqq l\leqq 8$	$0\leqq h\leqq 20$ $0\leqq k\leqq 20$ $0\leqq l\leqq 13$
Systematic absences	*hk*0, *h* odd; 0*kl*, *k* odd; *h*0*l*, *l* odd	*h*00, *h* odd 0*k*0, *k* odd; 00*l*, *l* odd	*h*0*l*, *l* odd; 0*k*0, *k* odd	None	None	*h*0*l*, *h* odd; 0*kl*, *k*+*l* odd
Possible space groups	*Pbca*	$P2_12_12_1$	$P2_1/c$	*P*1 or $P\bar{1}$	*P*1 or $P\bar{1}$	$Pna2_1$ or *Pnam*
Variation in standard reflections $\sum(\lvert F_o\rvert/\lvert F_o\rvert_{initial})/n$	1.00—1.01 n=5	0.99—1.00 n=5	0.99—1.00 n=4	0.99—1.00 n=4	0.95—1.02 n=3	0.99—1.01 n=5
Number of reflections measured	4206	3475	4528	2789	2557	3127
Number of reflections observed [$\lvert F_o\rvert>3\sigma(\lvert F_o\rvert)$]	2113	2205	2276	1567	1228	1496
Transmission factor, A	0.584—0.825	0.718—0.792	0.779—0.904	0.836—0.870	No absorption correction	0.441—0.648
Number of unique reflections	2113	2205	2164	1374	1118	1469
Final R value	0.065	0.038	0.035	0.087	0.052	0.065
$(\Delta/\sigma)_{max}$ for nonhydrogen atoms	0.15	0.42	0.42	0.32	0.27	0.25
$\Delta\rho$/e Å^{-3}	−0.65, 0.68	−0.26, 0.32	−0.25, 0.37	−0.62, 0.72	−0.33, 0.37	−0.96, 0.32

Table 2. Fractional Coordinates (×10^4, ×10^5 for Co) and Equivalent Isotropic Thermal Parameters (×10)

Atom	x	y	z	$10B_{eq}$/Å^2	Atom	x	y	z	$10B_{eq}$/Å^2
1 Co	12899(4)	24007(13)	50373(10)	21	C(11)	1496(3)	−2096(10)	3679(8)	33
Cl(1)	613(1)	5193(3)	2554(2)	35	C(12)	1117(4)	−1917(11)	4079(9)	41
Cl(2)	2492(1)	995(3)	2309(2)	49	C(13)	1080(3)	−1006(10)	4666(8)	33
O(1)	761(2)	2442(7)	5529(5)	28	C(14)	1969(3)	3758(12)	4378(8)	39
O(2)	1120(2)	1868(6)	3919(4)	26	C(15)	1583(4)	4417(11)	4070(8)	37
O(11)	1015(3)	5669(10)	2702(8)	80	C(16)	1084(3)	4999(10)	5229(7)	23
O(12)	578(3)	5007(9)	1641(6)	60	C(17)	662(3)	5139(11)	5333(8)	33
O(13)	595(4)	4075(9)	3006(7)	80	C(18)	530(5)	5958(12)	5967(10)	62
O(14)	321(3)	6010(10)	2820(7)	82	C(19)	789(5)	6635(12)	6440(9)	52
O(21)	2646(4)	−74(13)	2619(8)	117	C(20)	1216(4)	6494(12)	6309(9)	49
O(22)	2309(4)	847(12)	1496(7)	97	C(21)	1358(4)	5661(12)	5704(8)	42
O(23)	2225(5)	1516(15)	2858(9)	150	O(W1)	2604(3)	1679(10)	5517(7)	70
O(24)	2831(4)	1765(14)	2115(11)	140					
N(1)	1499(3)	2889(8)	6187(6)	28	**2** Co	5458(4)	12719(4)	4949(9)	20
N(2)	1343(2)	716(8)	5491(5)	22	Cl(1)	3098(1)	12(1)	620(2)	32
N(3)	1840(2)	2463(8)	4536(6)	27	Cl(2)	471(1)	4242(1)	−1644(2)	36
N(4)	1220(2)	4103(8)	4588(6)	25	O(1)	−154(2)	1916(2)	−416(5)	28
C(1)	51(3)	2160(12)	5705(9)	42	O(2)	301(2)	1501(2)	2629(4)	25
C(2)	438(3)	2064(10)	5182(8)	30	O(11)	2747(3)	619(3)	−252(6)	53
C(3)	409(3)	1604(11)	4324(8)	35	O(12)	3316(3)	336(3)	2112(6)	54
C(4)	745(3)	1539(10)	3760(7)	24	O(13)	2642(3)	−652(4)	903(8)	74
C(5)	685(4)	1002(13)	2862(8)	44	O(14)	3677(3)	−291(4)	−203(6)	64
C(6)	1509(4)	1839(11)	6782(8)	35	O(21)	241(3)	3841(3)	−231(5)	53
C(7)	1629(3)	758(11)	6244(8)	33	O(22)	343(3)	5073(3)	−1539(7)	71
C(8)	1406(3)	−269(10)	4882(7)	25	O(23)	87(4)	3949(4)	−2979(7)	83
C(9)	1792(4)	−471(11)	4501(9)	39	O(24)	1142(3)	4060(4)	−1888(9)	85
C(10)	1830(4)	−1395(12)	3920(9)	43	N(1)	832(3)	1091(3)	−1716(6)	33

Table 2. (Continued)

Atom	x	y	z	$10B_{eq}$/Å^2
N(2)	1177(2)	2246(3)	423(6)	26
N(3)	1250(2)	540(3)	1292(6)	25
N(4)	−68(2)	287(3)	574(6)	23
C(1)	−1118(3)	2771(4)	−622(11)	47
C(2)	−601(3)	2337(3)	338(8)	28
C(3)	−606(3)	2398(4)	1984(8)	33
C(4)	−179(3)	1982(4)	3024(7)	28
C(5)	−276(4)	2076(5)	4796(8)	47
C(6)	1140(3)	1855(4)	−2319(8)	33
C(7)	1619(3)	2168(4)	−1042(8)	31
C(8)	1556(3)	2485(4)	1852(7)	25
C(9)	2149(3)	2084(4)	2288(8)	29
C(10)	2483(3)	2307(4)	3696(9)	39
C(11)	2224(4)	2925(4)	4597(9)	47
C(12)	1639(4)	3326(4)	4147(9)	46
C(13)	1300(3)	3104(4)	2756(9)	36
C(14)	1036(3)	−326(4)	1065(8)	30
C(15)	292(3)	−352(4)	1513(8)	33
C(16)	−788(3)	400(4)	1017(8)	27
C(17)	−1002(3)	333(4)	2597(9)	36
C(18)	−1684(4)	455(4)	2962(10)	49
C(19)	−2160(3)	654(5)	1807(12)	58
C(20)	−1936(4)	735(5)	226(11)	55
C(21)	−1266(3)	594(4)	−151(9)	37
3a Co	14243(5)	24661(6)	46879(3)	21
Cl(1)	1614(1)	−673(1)	7052(1)	48
Cl(2)	1895(1)	5876(1)	5601(1)	44
O(1)	2027(2)	1000(3)	5112(2)	25
O(2)	2861(3)	3023(3)	4709(2)	28
N(1)	−62(3)	1969(3)	4697(2)	27
N(2)	1904(3)	3113(3)	5778(2)	25
N(3)	676(3)	3931(3)	4221(2)	29
N(4)	882(3)	1943(3)	3563(2)	24
C(1)	3377(5)	−531(4)	5655(3)	43
C(2)	3103(4)	663(4)	5315(2)	28
C(3)	3973(4)	1316(4)	5232(3)	31
C(4)	3828(4)	2418(5)	4953(2)	31
C(5)	4844(5)	3052(5)	4904(4)	55
C(6)	176(4)	1855(4)	5531(3)	31
C(7)	860(4)	2922(4)	5952(3)	31
C(8)	3087(4)	2795(4)	6410(2)	24
C(9)	4052(4)	3492(4)	6547(3)	30
C(10)	5185(4)	3222(5)	7147(3)	39
C(11)	5340(4)	2277(4)	7619(3)	42
C(12)	4374(5)	1583(4)	7479(3)	41
C(13)	3235(4)	1832(4)	6871(3)	31
C(14)	−72(5)	3790(4)	3351(3)	39
C(15)	613(5)	3013(4)	3070(3)	36
C(16)	1631(4)	1113(4)	3424(2)	24
C(17)	2468(4)	1422(5)	3172(3)	39
C(18)	3169(5)	601(6)	3065(3)	53
C(19)	3048(5)	−527(6)	3213(3)	57
C(20)	2216(5)	−874(5)	3468(3)	42
C(21)	1496(4)	−37(4)	3563(3)	33
O(W)1[a]	−1491(6)	1155(6)	1339(4)	69
O(W)2	−2197(21)	704(21)	1203(13)	45
O(W)3	−1545(23)	1511(24)	1192(15)	61
3b Co	31068(21)	21976(19)	31008(34)	40
Cl(1)	6786(5)	2737(4)	7046(7)	62
O(1)	2128(8)	2361(8)	4852(13)	44
O(2)	2226(8)	3126(8)	2051(13)	41
O(11)	6433(17)	2342(12)	8298(21)	126
O(12)	6080(15)	2576(18)	5739(23)	168
O(13)	6814(29)	3745(12)	7595(24)	229
O(14)	7777(14)	2334(25)	6566(34)	229

Atom	x	y	z	$10B_{eq}$/Å^2
N(1)	4021(11)	1232(10)	4094(20)	59
N(2)	2313(11)	1030(10)	1775(20)	56
N(3)	4172(12)	2053(11)	1336(18)	58
N(4)	4018(10)	3357(10)	4304(16)	39
C(1)	552(17)	2892(16)	6584(27)	73
C(2)	1182(13)	2952(12)	5082(21)	41
C(3)	766(13)	3557(12)	4030(20)	38
C(4)	1277(13)	3593(12)	2637(21)	37
C(5)	767(16)	4287(14)	1584(25)	60
C(6)	3585(19)	247(17)	3633(29)	87
C(7)	2779(20)	147(18)	2360(31)	98
C(8)	1100(14)	1141(12)	1654(21)	43
C(9)	687(15)	1476(14)	351(24)	56
C(10)	−539(19)	1663(17)	224(29)	86
C(11)	−1190(17)	1515(15)	1281(26)	68
C(12)	−879(18)	1153(17)	2545(28)	82
C(13)	354(17)	981(15)	2764(26)	73
C(14)	5084(17)	2761(15)	1823(26)	72
C(15)	4544(15)	3729(13)	3022(23)	54
C(16)	3466(13)	4163(12)	5589(21)	38
C(17)	2917(14)	5032(13)	5198(22)	46
C(18)	2436(15)	5775(13)	6500(23)	53
C(19)	2497(15)	5685(14)	8074(24)	57
C(20)	3031(17)	4810(15)	8439(26)	70
C(21)	3576(15)	3973(13)	7139(23)	52
Cl(2)A[b]	3766(16)	−19(15)	−1667(26)	33
Cl(2)B	3249(22)	500(20)	−2290(34)	29
Cl(2)C	3126(21)	1246(19)	−2087(33)	28
Cl(2)D	3827(20)	377(18)	−2090(31)	23
Cl(2)E	3880(46)	−140(42)	−1267(73)	31
Cl(2)F	3958(46)	1511(41)	−2321(71)	29
Cl(2)G	3621(56)	−921(50)	−3046(86)	33
Cl(2)H	2836(83)	962(73)	−1962(127)	31
Cl(2)I	3799(27)	−197(25)	−1019(42)	22
3c Co	31756(15)	28726(14)	15216(23)	21
Cl(1)	3908(3)	7855(3)	2479(5)	47
Cl(2)	6122(3)	5182(3)	3246(4)	40
O(1)	1890(6)	2510(6)	−449(9)	28
O(2)	2537(6)	2115(5)	2705(9)	24
O(11)	2980(8)	7351(8)	2835(13)	69
O(12)	4929(10)	7891(12)	3678(18)	140
O(13)	4098(11)	7391(10)	839(14)	111
O(14)	3690(14)	8830(8)	2597(19)	136
N(1)	3810(8)	3777(7)	393(12)	28
N(2)	2484(8)	4079(7)	2789(12)	25
N(3)	4588(7)	3233(7)	3452(11)	23
N(4)	4014(7)	1694(7)	463(12)	25
C(1)	41(11)	1811(10)	−2293(17)	40
C(2)	952(10)	1957(9)	−556(15)	26
C(3)	729(10)	1495(9)	577(15)	26
C(4)	1510(10)	1591(9)	2126(16)	30
C(5)	1209(11)	1044(10)	3303(17)	44
C(6)	3092(10)	4617(9)	516(15)	29
C(7)	2887(10)	4977(9)	2265(15)	29
C(8)	1225(10)	3983(8)	2759(15)	24
C(9)	880(10)	3772(9)	4113(15)	29
C(10)	−311(12)	3663(10)	4142(18)	50
C(11)	−1143(12)	3737(10)	2750(18)	47
C(12)	−816(12)	3926(10)	1456(19)	51
C(13)	356(11)	4069(9)	1372(16)	35
C(14)	5498(10)	2603(9)	2953(16)	33
C(15)	4909(11)	1569(9)	1926(16)	36
C(16)	3339(11)	760(9)	−748(16)	33
C(17)	3124(10)	598(9)	−2499(16)	35
C(18)	2479(11)	−324(9)	−3641(16)	38

Table 2. (Continued)

Atom	*x*	*y*	*z*	$10B_{eq}$/Å^2	Atom	*x*	*y*	*z*	$10B_{eq}$/Å^2
C(19)	2100(11)	−1029(10)	−3035(17)	42	N(4)	1245(8)	1580(9)	−785(13)	17
C(20)	2286(11)	−882(10)	−1277(17)	40	C(1)	1898(10)	3896(10)	−381(17)	16
C(21)	2931(10)	30(9)	−100(16)	33	C(2)	1193(11)	3609(12)	450(18)	28
					C(3)	1782(11)	437(11)	515(19)	27
4 Br	893(2)	1229(2)	3597(4)	75	C(4)	1011(10)	795(10)	−43(21)	21
Co	22072(12)	21607(13)	0[c]	13	C(5)	3873(10)	2415(10)	225(15)	15
O(1)	3199(6)	2662(6)	745(10)	14	C(6)	3736(12)	1770(11)	−886(19)	26
O(2)	2933(6)	1575(6)	−1083(11)	15	C(7)	3046(10)	914(10)	1786(17)	15
O(3)	4580(7)	2674(8)	489(13)	37	C(8)	3263(11)	1276(12)	2954(20)	28
O(4)	4322(7)	1457(8)	−1540(14)	31	C(9)	4056(14)	1106(13)	3464(26)	43
O(W1)	711(7)	2879(8)	7288(12)	29	C(10)	4583(12)	516(13)	2901(21)	35
O(W2)	966(9)	3170(10)	4730(13)	47	C(11)	4347(12)	145(11)	1858(20)	28
O(W3)	4009(9)	3990(9)	2366(16)	47	C(12)	3568(11)	323(12)	1246(19)	26
O(W4)	3242(10)	360(9)	−3196(17)	55	C(13)	2850(11)	3298(10)	−2074(17)	21
O(W5)	2258(10)	3918(10)	3208(14)	52	C(14)	3526(10)	3813(10)	−1785(17)	19
O(W6)	1497(9)	646(9)	−3382(15)	46	C(15)	4199(11)	3865(13)	−2655(18)	25
N(1)	2123(7)	3168(8)	−1191(13)	13	C(16)	4180(11)	3470(14)	−3705(23)	37
N(2)	1481(8)	2820(9)	1149(13)	17	C(17)	3536(14)	2975(13)	−4077(19)	38
N(3)	2253(9)	1153(8)	1226(13)	19	C(18)	2797(13)	2886(12)	−3207(19)	33

a) Population parameters of disordered H_2O: O(W1), 0.6; and O(W2) and O(W3), 0.2. b) Population parameters of disordered Cl^-: A, 0.20; B, C and D, 0.15; E and F, 0.07; G, 0.06; H, 0.04, and I, 0.11. c) This parameter was used to define the origin of the unit cell along *z* and is listed without e.s.d.

Table 3. Bond Lengths(Å) and Bond Angles(°)

	1	**2**	**3a**		**4**
Bond length (Å)					
Co-O(1)	1.876(7)	1.885(4)	1.884(3)	Co-O(1)	1.917(10)
Co-O(2)	1.893(6)	1.894(4)	1.888(4)	Co-O(2)	1.852(10)
Co-N(1)	1.962(9)	1.963(5)	1.949(4)	Co-N(1)	2.011(13)
Co-N(2)	2.005(9)	2.016(5)	2.025(4)	Co-N(2)	1.954(13)
Co-N(3)	1.945(7)	1.940(5)	1.946(3)	Co-N(3)	2.031(13)
Co-N(4)	2.027(9)	2.010(5)	2.023(4)	Co-N(4)	1.951(13)
O(1)-C(2)	1.248(12)	1.278(7)	1.277(5)	O(1)-C(5)	1.256(18)
O(2)-C(4)	1.295(12)	1.266(7)	1.285(6)	O(2)-C(6)	1.321(21)
N(1)-C(6)	1.481(15)	1.479(8)	1.483(7)	O(3)-C(5)	1.220(19)
N(2)-C(7)	1.481(13)	1.507(8)	1.500(7)	O(4)-C(6)	1.250(23)
N(2)-C(8)	1.453(14)	1.463(8)	1.463(5)	N(1)-C(1)	1.462(21)
N(3)-C(14)	1.519(16)	1.493(8)	1.494(6)	N(1)-C(13)	1.486(21)
N(4)-C(15)	1.463(15)	1.487(8)	1.498(6)	N(2)-C(2)	1.504(23)
N(4)-C(16)	1.466(14)	1.460(7)	1.447(7)	N(3)-C(3)	1.536(22)
C(1)-C(2)	1.494(15)	1.473(9)	1.500(6)	N(3)-C(7)	1.432(21)
C(2)-C(3)	1.412(17)	1.387(10)	1.390(8)	N(4)-C(4)	1.498(22)
C(3)-C(4)	1.393(15)	1.385(9)	1.363(7)	C(1)-C(2)	1.481(24)
C(4)-C(5)	1.511(17)	1.509(9)	1.504(9)	C(3)-C(4)	1.462(25)
C(6)-C(7)	1.508(17)	1.511(9)	1.508(6)	C(5)-C(6)	1.552(24)
C(8)-C(9)	1.401(16)	1.377(9)	1.372(7)	C(7)-C(8)	1.386(27)
C(8)-C(13)	1.379(15)	1.363(9)	1.380(7)	C(7)-C(12)	1.361(24)
C(9)-C(10)	1.364(19)	1.399(10)	1.388(6)	C(8)-C(9)	1.387(29)
C(10)-C(11)	1.386(17)	1.362(10)	1.374(8)	C(9)-C(10)	1.375(30)
C(11)-C(12)	1.389(17)	1.367(11)	1.370(8)	C(10)-C(11)	1.288(29)
C(12)-C(13)	1.359(17)	1.391(10)	1.393(6)	C(11)-C(12)	1.414(26)
C(14)-C(15)	1.527(17)	1.495(8)	1.499(9)	C(13)-C(14)	1.372(23)
C(16)-C(17)	1.388(14)	1.396(10)	1.381(8)	C(13)-C(18)	1.349(26)
C(16)-C(21)	1.365(17)	1.389(9)	1.384(7)	C(14)-C(15)	1.400(25)
C(17)-C(18)	1.398(19)	1.376(10)	1.369(9)	C(15)-C(16)	1.258(30)
C(18)-C(19)	1.341(21)	1.380(12)	1.360(10)	C(16)-C(17)	1.336(29)
C(19)-C(20)	1.410(21)	1.405(13)	1.391(10)	C(17)-C(18)	1.485(29)
C(20)-C(21)	1.388(19)	1.360(10)	1.389(8)		
Bond angle(°)					
O(1)-Co-O(2)	95.9(3)	95.3(2)	96.3(2)	O(1)-Co-O(2)	86.7(4)
O(1)-Co-N(1)	87.2(3)	84.5(2)	85.7(2)	O(1)-Co-N(1)	89.1(5)
O(1)-Co-N(2)	87.9(3)	89.0(2)	91.2(1)	O(1)-Co-N(2)	90.9(5)
O(1)-Co-N(3)	176.5(3)	175.1(2)	175.5(1)	O(1)-Co-N(3)	91.9(5)

Table 3. (Continued)

	1	2	3a		4
O(1)-Co-N(4)	90.6(3)	92.0(2)	93.4(1)	O(1)-Co-N(4)	176.0(5)
O(2)-Co-N(1)	176.2(3)	176.7(2)	176.8(2)	O(2)-Co-N(1)	93.0(5)
O(2)-Co-N(2)	92.6(3)	91.4(2)	91.1(2)	O(2)-Co-N(2)	177.4(5)
O(2)-Co-N(3)	85.5(3)	88.5(2)	87.9(2)	O(2)-Co-N(3)	88.7(5)
O(2)-Co-N(4)	87.3(3)	88.8(2)	88.8(2)	O(2)-Co-N(4)	89.8(5)
N(1)-Co-N(2)	85.3(4)	85.3(2)	86.4(2)	N(1)-Co-N(2)	85.8(5)
N(1)-Co-N(3)	91.5(3)	91.9(2)	90.1(2)	N(1)-Co-N(3)	178.1(5)
N(1)-Co-N(4)	94.8(4)	94.5(2)	93.5(2)	N(1)-Co-N(4)	93.1(5)
N(2)-Co-N(3)	95.2(3)	94.1(2)	90.1(1)	N(2)-Co-N(3)	92.6(5)
N(2)-Co-N(4)	178.5(4)	178.9(2)	175.4(2)	N(2)-Co-N(4)	92.6(6)
N(3)-Co-N(4)	86.3(3)	84.8(2)	85.3(1)	N(3)-Co-N(4)	86.0(5)
Co-O(1)-C(2)	126.2(7)	126.3(4)	124.3(3)	Co-O(1)-C(5)	113.1(10)
Co-O(2)-C(4)	122.2(6)	123.9(4)	123.1(3)	Co-O(2)-C(6)	112.7(11)
Co-N(1)-C(6)	109.9(7)	108.1(4)	108.1(3)	Co-N(1)-C(1)	105.7(10)
Co-N(2)-C(7)	107.1(6)	107.7(4)	107.0(3)	Co-N(1)-C(13)	116.0(10)
Co-N(2)-C(8)	119.6(6)	119.6(4)	117.7(3)	C(1)-N(1)-C(13)	116.1(12)
C(7)-N(2)-C(8)	115.8(8)	114.0(4)	115.6(4)	Co-N(2)-C(2)	108.3(10)
Co-N(3)-C(14)	110.5(7)	110.4(3)	109.7(3)	Co-N(3)-C(3)	104.2(10)
Co-N(4)-C(15)	108.5(7)	107.8(3)	106.7(3)	Co-N(3)-C(7)	119.4(10)
Co-N(4)-C(16)	116.2(7)	118.4(4)	117.5(3)	C(3)-N(3)-C(7)	115.5(12)
C(15)-N(4)-C(16)	116.3(9)	113.9(5)	114.4(4)	Co-N(4)-C(4)	110.9(10)
O(1)-C(2)-C(1)	117.1(10)	117.0(6)	114.4(4)	N(1)-C(1)-C(2)	106.5(13)
O(1)-C(2)-C(3)	125.0(10)	122.6(6)	124.5(4)	N(2)-C(2)-C(1)	107.7(14)
C(1)-C(2)-C(3)	117.9(9)	120.5(6)	121.1(4)	N(3)-C(3)-C(4)	108.5(14)
C(2)-C(3)-C(4)	122.9(10)	126.1(6)	125.7(5)	N(4)-C(4)-C(3)	108.3(13)
O(2)-C(4)-C(3)	127.3(10)	125.7(6)	126.0(5)	O(1)-C(5)-O(3)	125.2(15)
O(2)-C(4)-C(5)	113.8(9)	114.5(5)	112.9(5)	O(1)-C(5)-C(6)	113.8(14)
C(3)-C(4)-C(5)	118.9(9)	119.8(6)	121.1(5)	O(3)-C(5)-C(6)	120.8(14)
N(1)-C(6)-C(7)	107.4(10)	107.1(5)	106.5(4)	O(2)-C(6)-O(4)	122.4(16)
N(2)-C(7)-C(6)	106.7(9)	105.0(5)	109.9(4)	O(2)-C(6)-C(5)	113.6(15)
N(2)-C(8)-C(9)	120.9(10)	120.8(5)	118.4(4)	O(4)-C(6)-C(5)	124.0(16)
N(2)-C(8)-C(13)	119.6(9)	118.3(5)	121.3(4)	N(3)-C(7)-C(8)	117.9(15)
C(9)-C(8)-C(13)	119.5(10)	120.9(6)	120.3(4)	N(3)-C(7)-C12)	122.6(16)
				C(8)-C(7)-C(12)	119.4(16)
C(8)-C(9)-C(10)	118.2(11)	119.3(6)	119.9(4)	C(7)-C(8)-C(9)	118.8(18)
C(9)-C(10)-C(11)	121.8(12)	119.6(6)	120.3(5)	C(8)-C(9)-C(10)	120.8(21)
C(10)-C(11)-C(12)	119.7(11)	120.8(7)	119.5(4)	C(9)-C(10)-C(11)	119.2(19)
C(11)-C(12)-C(13)	118.5(11)	120.1(7)	120.8(5)	C(10)-C(11)-C(12)	123.0(18)
C(8)-C(13)-C(12)	122.2(10)	119.4(6)	119.1(4)	C(7)-C(12)-C(11)	118.3(17)
N(3)-C(14)-C(15)	106.1(9)	105.3(5)	107.0(4)	N(1)-C(13)-C(14)	123.1(15)
N(4)-C(15)-C(14)	112.3(9)	107.5(5)	105.9(5)	N(1)-C(13)-C(18)	115.4(15)
N(4)-C(16)-C(17)	116.8(9)	121.2(6)	123.0(5)	C(14)-C(13)-C(18)	121.4(17)
N(4)-C(16)-C(21)	121.8(9)	119.3(6)	117.4(5)	C(13)-C(14)-C(15)	118.9(16)
C(17)-C(16)-C(21)	121.5(10)	119.4(6)	119.6(5)	C(14)-C(15)-C(16)	121.2(19)
C(16)-C(17)-C(18)	117.1(11)	119.2(6)	120.5(6)	C(15)-C(16)-C(17)	123.8(20)
C(17)-C(18)-C(19)	123.2(14)	121.6(7)	119.9(6)	C(16)-C(17)-C(18)	118.4(18)
C(18)-C(19)-C(20)	118.5(13)	118.7(7)	121.4(7)	C(13)-C(18)-C(17)	116.2(18)
C(19)-C(20)-C(21)	119.7(13)	120.1(8)	118.3(6)		
C(16)-C(21)-C(20)	119.9(12)	121.0(7)	120.3(5)		

15—34 2θ values ($20<2\theta<30°$). Absorption corrections were made except for the small crystal of **3c**. The positions of the heavy atoms were determined from the Patterson function, while the other nonhydrogen atoms were located by means of Fourier syntheses and were refined anisotropically. The ratios of the number of H atoms located by the difference synthesis are **1** 24/31, **2** 24/31, **3a** 30/31, **3b** 16/31, **3c** 27/31, and **4** 12/24. The other H atoms were calculated and refined isotropically. The function, $\sum w||F_o|-|F_c||^2$, was minimized with $w^{-1}=\sigma^2(|F_o|)+(0.015|F_o|)^2$ by the block-diagonal least-squares method. Complex neutral-atom scattering factors were used.[2] The calculations were carried out on a FACOM M380R computer at Keio University using the computation program system UNICS-III.[3] The final atomic parameters are listed in Table 2, and the bond lengths and bond angles within the complex cations, in Table 3.[4] The following points are worth mentioning. The structure of **1** is difficult to solve because the Co and two Cl atoms lie nearly on the glide planes, as shown in Fig. 1. The statistics of the intensity data showed that *hkl* with *h* or *l* odd is weak, suggesting pseudo translational symmetries of *a*/2 and *c*/2. The positions of the heavy atoms were determined by direct methods with MULTAN78[5] using a single overall scale factor in the normalization. The coordinated N and O atoms were deduced by means of Fourier synthesis utilizing the Co-ligand vectors found in the Patterson function. The

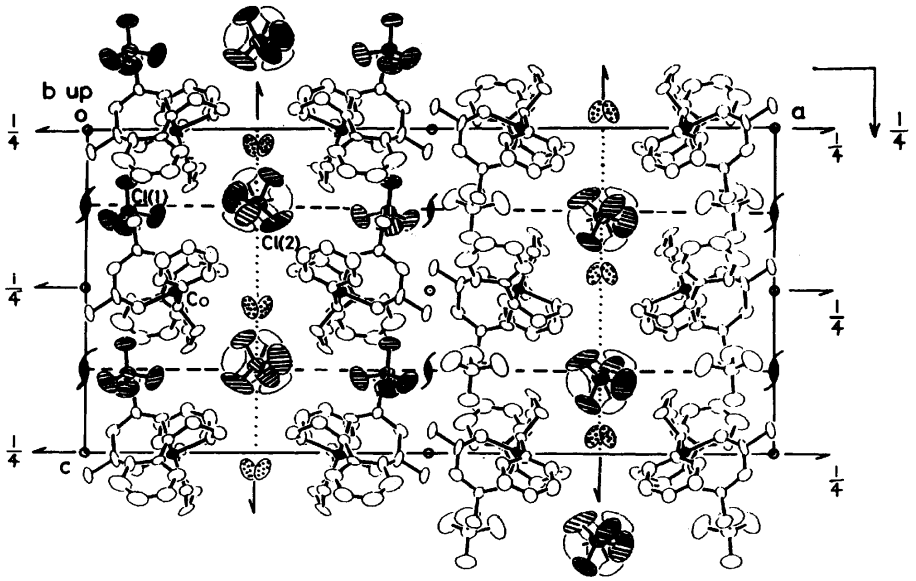

Fig. 1. A projection of the crystal structure of **1** along *b*.

space group of **2** is $P2_12_12_1$, indicating spontaneous resolution. The absolute structure was determined by anomalous-scattering techniques. The enantiomeric structure converged to R=0.0387 and wR=0.0449, slightly larger than the values of 0.0380 and 0.0441 for the adopted structure. In **3a**, the water molecules are disordered. The population parameters of three possible positions of O(W) were estimated by the trial-and-error method in such a way that the isotropic thermal parameter took nearly equal values. The Cl^- ion and water molecules in **3b** are disordered. The difference synthesis gave nine positions with peak heights greater than 1.0 e Å^{-3}. Since the disordered water molecules can not be distinguished from the disordered Cl^- ions, those peaks were tentatively assumed to be Cl^- ions and their population parameters were estimated by the trial-and-error method. The relatively large R value of **3b**, 0.087, may be attributed to this disorder. As the crystal of **3c** was too small to collect sufficient number of reflections, the carbon atoms were refined isotropically. The systematic absences of **4** indicated that the space group was $Pna2_1$ (No. 33) or the $ac\bar{b}$ setting of *Pnma* (No. 62). Since Z=4 and the complex cation has no mirror plane and no inversion center, the space group was determined to be $Pna2_1$.

Table 4. Short Intramolecular Distances (Å)

1	
C(17)···O(1)	3.031(14)
2	
C(16)···O(1)	3.026(7)
C(17)···C(4)	3.163(9)
C(21)···C(2)	3.165(8)
3a	
C(8)···O(1)	3.034(5)
C(9)···C(4)	3.174(7)
C(13)···C(2)	3.195(7)
C(16)···O(1)	3.026(6)
C(21)···C(2)	3.115(6)
4	
C(7)···C(5)	3.142(23)
C(12)···C(6)	3.184(27)
C(13)···C(5)	3.205(23)
C(13)···C(6)	3.035(24)
C(14)···C(5)	3.079(23)
C(18)···O(2)	3.026(22)

Results and Discussion

The atomic parameters of **1**, **3**, and **4** in Table 2 were selected to represent the absolute configuration *Δ* for convenience of comparison with **2**. The bond lengths and bond angles within the complex cations are listed in Table 3, while the short intramolecular distances and hydrogen bonds are listed in Tables 4 and 5 and

Table 5. Hydrogen Bonds (Distances in Å)

A···H-B (symmetry code)		A···B	A···H	H-B
1				
O(12)···H(N2)-N(2)	(i)	3.149(12)	2.22(9)	0.98(9)
O(22)···H(N1)1-N(1)	(i)	3.019(15)	2.17(8)	0.92(8)
2				
O(12)···H(N1)2-N(1)	(ii)	3.032(7)	2.05(7)	1.11(6)
O(14)···H(N3)2-N(3)	(iii)	2.979(7)	2.17(7)	0.85(7)
O(22)···H(N1)1-N(1)	(iv)	3.186(8)	2.12(5)	1.14(5)
3a				
Cl(1)···H(N4)-N(4)	(v)	3.146(4)	2.17(4)	0.98(4)
O(W)2···H(N3)2-N(3)	(vi)	3.14(3)	2.25(7)	1.01(6)
3b				
Cl(2)G···H(N1)2-N(1)	(vii)	2.92(7)	1.93(15)	0.98(14)
Cl(2)I···H(N3)2-N(3)	(vii)	3.27(3)	2.34(13)	1.04(12)
3c				
Cl(2)···H(N2)-N(2)	(vii)	3.19(1)	2.14(10)	1.07(11)
O(13)···H(N4)-N(4)	(viii)	3.04(2)	2.16(12)	0.96(12)
4				
O(W1)···H(N1)-N(1)	(ix)	2.77(2)	1.98(15)	0.80(15)

Symmetry code: (i) x, 1/2−y, z−1/2, (ii) 1/2−x, −y, z+1/2, (iii) 1/2−x, −y, z−1/2, (iv) −x, y+1/2, −z−1/2, (v) −x,−y, 1−z, (vi) −x, y−1/2, 1/2−z, (vii) 1−x, −y, −z, (viii) 1−x, 1−y, −z, (ix) x, y, z+1.

perspective drawings of the complex cations are presented in Fig. 2. The combinations of two asymmetric N atoms of the $[Co(pd)(Ph\text{-}en)_2]^{2+}$ complexes agree with the assignments based on the ^1H NMR spectra:[1] **1** *ΔRR*, **2** *ΔSR*, and **3** *ΔSS*. Only one of the diastereomers was isolated for the $[Co(ox)(Ph\text{-}en)_2]^+$ complex, the **4** *ΔSS* isomer. The two Ph-en ligands in the pd complexes take the lel ob conformation, which breaks the twofold symmetry of the *ΔRR* and *ΔSS* isomers. For the ox complex **4**, however, the Ph-en ligands take ob_2 configuration, which retains a twofold symmetry. The difference in the structures may be attributed to the difference in the O-Co-O chelate angles, 95.3(2)—96.3(2)° and 86.7(4)° for pd and ox respectively. The pd complexes are isomerized in a neutral aqueous solution with this equilibrium distribution ratio; *ΔRR*(*ΔSS*): *ΔSR*(*ΔRS*): *ΔSS*(*ΔRR*)=5 : 78 : 17 at 20 °C.[1] The N-Ph bonds in the most stable isomers **2** and **4** take a conformation equatorial to the en chelate ring. The Co atom lies almost on the pd or ox plane in each complex, in contrast to the bent Co-pd chelate ring in $(+)^{GD}_{531}$-$[Co(pd)(RR\text{-}chxn)(edpp)](ClO_4)_2$.[6] The dihedral angles between the pd or ox chelate ring and phenyl groups range from 25 to 35° (see Table 6). There are no significantly close contacts between the phenyl groups and methyl groups of pd. Comparing

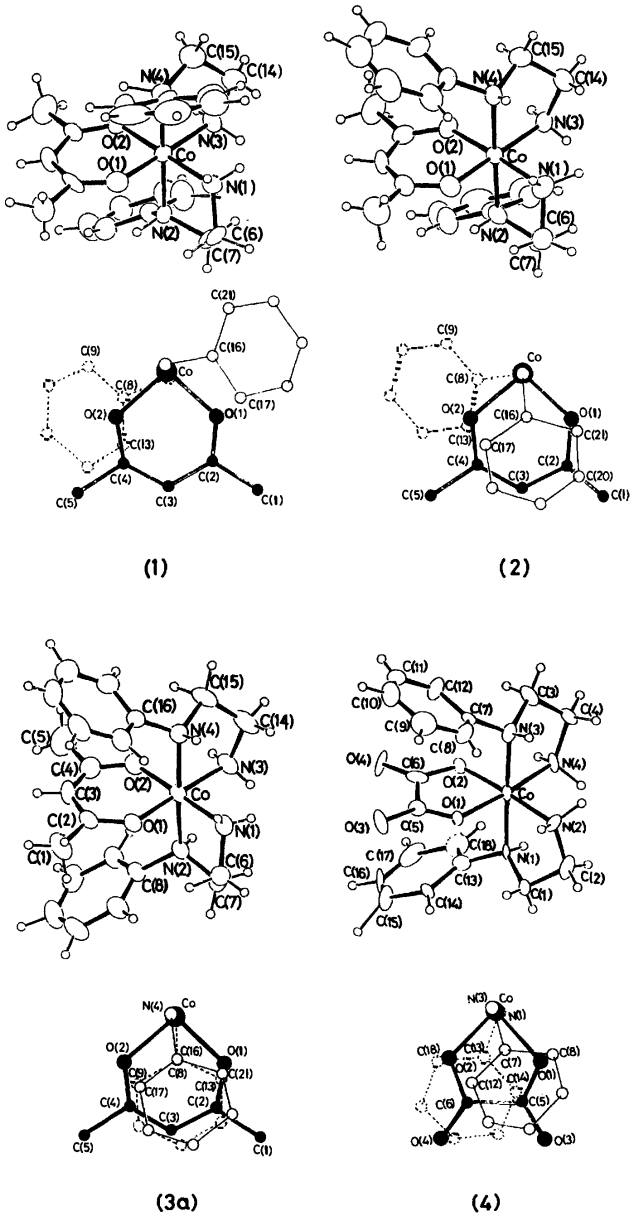

Fig. 2. Molecular structures, and projections of the Ph rings on the least squares plane through the pd or ox ligand for **1**, **2**, **3a**, and **4**. The Ph rings above and below the projection plane are drawn with solid and broken lines, respectively.

Table 6. Dihedral Angles (°) between the pd or ox Chelate Ring and Ph Rings Involving C(8) and C(16) Atoms

	C(8)	C(16)
1	25.6	27.9
2	28.7	29.8
3a	30.7	28.7
3b	27.5	33.5
3c	28.4	35.3
4	24.5	30.7

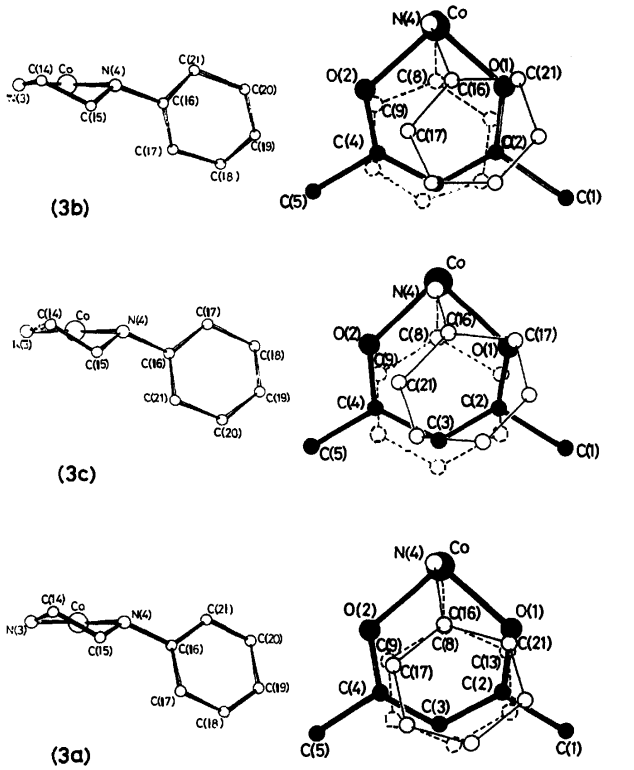

Fig. 3. Comparison of the Ph-en chelate ring conformations in *ΔSS*-$[Co(pd)(Ph\text{-}en)_2]^{2+}$ ions of **3b**, **3c**, and **3a**. The left half shows a projection along the line through the Co atom and the midpoint of the N(3)-N(4) axis. The right half shows a projection of the Ph rings on the pd chelate ring. The projections are arranged in a sequence that vividly illustrates the smooth change in the Ph-en chelate ring conformation in different crystal field.

the projections of the Ph rings to the least-squares plane through the pd in **3a** with that through the ox in **4** (see Fig. 2), the Ph rings of **3a** may be seen to overlap more with the pd π system than in **4**. However, the flexibility of the Ph-en chelate ring was revealed by the difference in the structures of **3a**, **3b**, and **3c**, as is shown in Fig. 3. The orientation of one of the Ph groups to the pd ligand alters with a different conformation of the five-membered chelate ring. After all, the orientation of the Ph group is altered along with the chelate-ring conformation of the Ph-en ligand, which is itself primarily determined by the coordination geometry around the Co atom. Molecular packing stabilization is a secondary condition, while the minor conditions are the intramolecular interactions between the π systems. The difference in the energy of the first absorption band of the three diastereomers of the pd complex[1] could not be explained by the structural data; no significant differences in the Co-N and Co-O bond lengths are observed among these diastereomers (see Table 3). The Co-N(HPh) bond distance is longer than the Co-N(H_2) distance by 0.06—0.07(1) Å, which corresponds to the fact that the ligand-field strength of Ph-en is weaker than that of en.[7]

References

1) Y. Ouyang, M. Kojima, and J. Fujita, *Bull. Chem. Soc. Jpn.*, **58**, 2705 (1985).

2) "International Tables for X-Ray Crystallography," Birmingham, Kynoch Press (1974), Vol. IV. (Present distributor D. Reidel, Dordrecht.)

3) T. Sakurai and K. Kobayashi, *Rikagaku Kenkyusho Hokoku*, **55**, 69 (1979).

4) Tables of the coordinates of hydrogen atoms, the anisotropic thermal parameters of the nonhydrogen atoms, and the observed and calculated structure factors are kept as Document No. 8859 at the Chemical Society of Japan.

5) P. Main, S. E. Hull, L. Lessinger, G. Germain, J.-P. Declercq, and M. M. Woolfson, MULTAN78. A system of Computer Programs for the Automatic Solution of Crystal Structures from X-ray Diffraction Data, Univs. of York, England, and Louvain, Belgium (1978).

6) M. Takata, K. Kashiwabara, H. Ito, T. Ito, and J. Fujita, *Bull. Chem. Soc. Jpn.*, **58**, 2247 (1985).

7) Y. Ouyang, M. Kojima, and J. Fujita, *Bull. Chem. Soc. Jpn.*, **57**, 3574 (1984).

Preparation and Crystal Structure of New Gold(I) Complexes Linked to Pyrimidines

Takashi AMAGAI, T. Ken MIYAMOTO,* Hikaru ICHIDA, and Yukiyoshi SASAKI
Department of Chemistry, Faculty of Science, The University of Tokyo, Hongo, Bunkyo-ku, Tokyo 113
(Received October 4, 1988)

Two new gold(I) complexes linked to pyrimidines, (5-fluoro-2′-deoxyuridinato-N^3)(triphenylphosphine)-gold(I) (**1**) and [5-fluoro-1-(tetrahydro-2-furanyl)-2,4(1*H*,3*H*)-pyrimidinedionato-N^3](triphenylphosphine)gold(I) (**2**) were synthesized and characterized by ^{31}P, ^1H NMR and IR spectra. The structure of **2** was determined by an X-ray diffraction method. A linear, two-coordination around gold(I) has been shown. In order to estimate the possible alteration of **1** and **2** in vivo, several factors such as the effect of pH, and reactions with thiol, thiophenol, and imidazole were examined.

For a long time, gold(0) have been used as anti-rheumatoid drugs.[1] Recent progress in medicinal chemistry has led to a new finding that auranofin [(2,3,4,6-tetra-*O*-acetyl-1-thio-β-D-glucopyranosato-*S*)-(triethylphosphine)gold(I)] has not only antirheumatoid but anticancer activities.[2,3] Other gold(I) phosphine complexes, e.g. [bis[1,2-bis(diphenylphosphino)-ethane]gold(I) chloride] also show anticancer activities.[4] In these gold(I) compounds, a lot of thiolate or chloride complexes have been investigated extensively;[5] however, antitumor activities of gold(I) complexes containing nitrogen ligands have been not well-characterized.

Organic derivatives of 5-fluorouracil have been widely known as anticancer drugs. They contain nitrogen atoms, which can coordinate to metal atoms. By using these ligands, we have successfully synthesized new compounds.

In this paper, the preparation and crystal structure of these compounds are described. Additionally, the reactions of the complexes to thiol and imidazole are also mentioned.

Experimental

Materials. Chloro(triphenylphosphine)gold(I) were prepared by the literature method,[5] and further recrystallized from tetrahydrofuran (THF). Two pyrimidines, e.g., 5-fluoro-2′-deoxyuridine (5FdUrd) and 5-fluoro-1-(tetrahydro-2-furanyl)-2,4(1*H*,3*H*)-pyrimidinedione (tegafur) were offered by Mitsui Pharmaceutical Inc. Reagent grade solvents were used without further purification.

Measurements. Elemental analysis were carried out by analytical technicians in this department. ^{31}P NMR spectra at 36.4 MHz were recorded with a JEOL FX90Q in 10 mm-tubes using a 85% H_3PO_4 solution as an external reference. ^1H NMR spectra at 60 MHz were obtained with a Hitachi R24B in 5 mm-tubes. IR spectra were measured with a Hitachi 260-30.

Preparation of (5-Fluoro-2′-deoxyuridinato-N^3)(triphenylphosphine)gold(I) (1). All procedures were performed under an Ar atmosphere. Chloro(triphenylphosphine)-gold(I) 1.87 g (3.78 mmol), 5FdUrd 1.94 g (7.89 mmol) and KOH 0.43 g (7.66 mmol) were dissolved in H_2O (30 ml)/THF (30 ml). The solution was stirred at 50—60 °C; then the product was obtained as precipitation by evaporation of THF. The solid was filtered off and recrystallized from THF with addition of diethyl ether. (2.23 g; 83.8% yield) Calcd for $C_{27}H_{25}N_2O_5AuFP$ (M.W.=704.45): C, 46.04; H, 3.58; N, 3.98%. Found: C, 45.87; H, 3.79; N, 3.81%.

Preparation of [5-Fluoro-1-(tetrahydro-2-furanyl)-2,4-(1*H*, 3*H*)-pyrimidinedionato-N^3](triphenylphosphine)gold(I) (2). The complex was prepared by the same procedure as that of **1**. From chloro(triphenylphosphine)gold(I) 3.06 g (6.19 mmol), tegafur 2.98 g (14.9 mmol) and KOH 0.74 g (13.2 mmol), 2.53 g of **2** were obtained. (62.1% yield) Calcd for $C_{26}H_{23}N_2O_3AuFP$ (M.W.=658.42): C, 47.43; H, 3.52; N, 4.25%. Found: C, 47.05; H, 3.55; N, 3.96%.

Crystal Structure Determination. X-Ray diffraction intensities were measured on a Rigaku automated four-circle diffractometer with Mo $K\alpha$ radiation at room temperature. Calculations were carried out with UNICS3 programs on a HITAC M-680H/M-682H computer at the Computer Centre of the University of Tokyo.[7]

Crystal dimensions were 0.6×0.15×0.15 mm. Intensities were collected for $4° \leqq 2\theta \leqq 55°$ by the ω-2θ scan technique. Independent 2722 points were collected and 2470 reflections with $F_o \leqq 2.5\sigma(F_o)$ were used for calculation. The position of the Au atom was determined by the heavy-atom method. Other atoms, except for H atoms, were located from subsequent Fourier syntheses. The positional and thermal parameters were refined by a block-diagonal least-squares method. The final R-value was 0.076.

Crystallographic data of **2** are as follows: Formula $C_{26}H_{23}N_2O_3AuFP$ (F.W.=658.42), monoclinic, space group $P2_1/n$, a=10.200(2) Å, b=26.115(5) Å, c=9.344(2) Å, β=102.05(3)°, V=2434 Å^3, D_x=1.797 g cm^{-3}, Z=4, μ=61.34 cm^{-1}. The atomic parameters are listed in Table 1. The complete F_o-F_c data are deposited as Document No. 8866 at the Office of the Editor of Bull. Chem. Soc. Jpn.

Examination of the Chemical Stability. A. Effect of pH. Since each complex has an extremely low solubility in H_2O, reactions were performed in two-layer solvents ($CHCl_3$-H_2O). A solution of each complex (0.2 mmol) in $CHCl_3$ (10 ml) was added to excess hydrochloric acid (pH=2, 40 ml), excess amount of aqueous KOH (pH=12, 40 ml) or 10 ml of distilled H_2O (pH=6). The solution was shaken vigorously for ten minutes in a separatory funnel. The organic layer was separated. The organic solution was evaporated to dryness and the residue was characterized by the ^1H NMR and IR spectra.

B. Reaction of 1 and 2 with Methanethiol, *p*-Toluenethiol, or Imidazole. Ethanethiol (0.4 mmol), *p*-toluenethiol (0.4 mmol), or imidazole (0.4 mmol) was added to a chloro-

form solution (10 ml) containing each complex (0.2 mmol). The solution was shaken vigorously for 10 minutes. Unreacted methanethiol, *p*-toluenethiol or imidazole was extracted into the aqueous KOH phase as potassium salts. The products in $CHCl_3$ were isolated by evaporation and characterized by the ^1H NMR and IR spectra.

Results and Discussion

Preparation and Characterization of 1 and 2. Compound **1** was obtained as a powdery solid, while **2** was obtained as colorless transparent pillar crystals. We also tried to prepare analogous (triethylphosphine)gold(I) derivatives; however, preparations of the products were unsuccessful under the present exprimental conditions.

Table 1. Positional Parameters ($\times 10^3$) and Isotropic Temperature Factors for Non-Hydrogen Atoms in **2**

Atom	*x*	*y*	*z*	B_{eq}/Å
Au	476.7(1)	376.5(1)	594.6(1)	4.0
P	332.3(6)	317.8(2)	642.3(7)	3.6
F	860(2)	519(1)	705(2)	8.3
O(1)	487(2)	429(1)	305(2)	6.6
O(2)	708(2)	440(1)	775(2)	6.3
O(3)	700(3)	545(1)	182(2)	8.8
N(1)	654(2)	486(1)	359(2)	4.6
N(2)	593(2)	434(1)	540(2)	3.5
C(1)	395(2)	343(1)	936(3)	5.2
C(2)	404(3)	332(1)	1088(3)	6.9
C(3)	368(3)	287(1)	1134(3)	5.6
C(4)	312(3)	249(1)	1033(3)	5.9
C(5)	301(3)	258(1)	880(3)	4.9
C(6)	344(2)	305(1)	837(2)	3.5
C(7)	74(3)	351(1)	660(3)	5.6
C(8)	−54(3)	370(1)	601(3)	5.7
C(9)	−88(3)	381(1)	450(3)	5.7
C(10)	3(3)	373(1)	360(3)	6.9
C(11)	130(3)	352(1)	420(2)	4.9
C(12)	162(2)	342(1)	567(3)	3.9
C(13)	235(3)	228(1)	497(3)	5.6
C(14)	256(3)	178(1)	444(3)	5.7
C(15)	382(3)	159(1)	453(3)	5.9
C(16)	492(3)	188(1)	518(3)	4.5
C(17)	480(3)	238(1)	568(2)	4.6
C(18)	347(2)	255(1)	559(2)	3.3
C(19)	575(2)	449(1)	399(2)	4.0
C(20)	693(2)	455(1)	647(3)	3.8
C(21)	770(2)	495(1)	602(3)	4.7
C(22)	752(2)	511(1)	459(3)	4.1
C(23)	631(3)	500(1)	196(3)	6.6
C(24)	685(3)	458(1)	111(3)	6.3
C(25)	825(3)	477(1)	112(4)	6.8
C(26)	803(4)	535(1)	99(4)	9.2

Coordination of 5-fluorouracil derivatives to gold(I) in **1** and **2** was confirmed by the ^{31}P, ^1H NMR and IR spectra.

^{31}P NMR of **1** (δ 31.7 in $CDCl_3$-THF) and **2** (δ 31.8 $CDCl_3$), proved to be upfield shifts, compared with that of chloro(triphenylphosphine)gold(I) (δ 33.4 in $CDCl_3$). The ^{31}P upfield shifts were also observed for other (triethylphosphine)gold(I)-(nitrogen ligand) compounds.[8,9] Thus, ^{31}P shifts imply that the nitrogen atom links to the gold(I) atom.

^1H NMR spectral data of **1** and **2** are summarized in Table 2. For **1**, the peak of pyrimidine H(6) proton shows an upfield shift, compared to that of free 5FdUrd, and overlaps with that of fifteen phenyl protons. While, for **2**, the peak of pyrimidine H(6) proton also shows an upfield shift compared with that of free tegafur, it does not overlap with fifteen phenyl protons. ^1H NMR results suggest again that those upfield shifts are caused by a coordination of the pyrimidines.

IR data of **1** and **2** are shown in Table 3. Characteristic absorption bands due to C=O were found in the range 1530—1660 cm^{-1} in these compounds. The C=O absorption peaks shift to a lower frequency than those of the free 5FdUrd or tegafur in the range 1650—1720 cm^{-1}. These results mean that the C=O bonds increase the single-bond character by the coordination, i.e., a part of bond electrons of C=O move toward nitrogen-gold(I) link.

Structure of 2. The molecular structure of **2** is illustrated in Fig. 1 by the use of ORTEP program.[10] Selected bond lengths and angles are listed in Table 4. Au(I) has almost a linear coordination. The lengths of Au-N and Au-P, and the angle of P-Au-N, agree with those of (phthalimidate)(triethylphosphine)gold(I) and (adeninate)(triethylphosphine)gold(I).[8,9] A deformation of ligands resulting through coordination is not found, except that the N(2) atom is slightly pulled toward the Au(I) atom; also, tetrahydrofuranyl moiety rotates around C(23)-N(1) bond. This rotation is

Table 3. IR Data for **1**, **2**, 5FdUrd, and Tegafur (KBr Disk)

Compound	ν/cm^{-1}
5FdUrd	3400, 1720, 1690, 1480, 1360, 1270, 1140, 1040
1	3400, 1650, 1600, 1520, 1430, 1100, 690, 540
tegafur	3040, 1720, 1690, 1650, 1470, 1400, 1270, 1070
2	3050, 1650, 1610, 1530, 1430, 1260, 1100, 700

Table 2. ^1H NMR Data for **1**, **2**, 5FdUrd, and Tegafur

Compound	δ			Solvent	Internal reference
	Phenyl protons	Pyrimidine proton	Other protons		
5FdUrd		8.10(1H; d)	2.35(2H, m), 4.00(1H, m), 4.35(2H, m), 6.30(1H, m)	D_2O	DSS
1	7.3 7.6(16H; m)		2.15(2H, m), 3.70(5H, m), 4.35(1H, m), 6.20(1H, m)	$CDCl_3$	TMS
tegafur		7.70(1H; d)	1.90(2H, m), 2.10(2H, m), 4.00(2H, m), 5.80(1H, m)	$CDCl_3$	TMS
2	7.3 7.5(15H; m)	7.20(1H; d)	2.00(4H, m), 4.00(2H, m), 5.95(1H, m)	DMSO-d_6	TMS

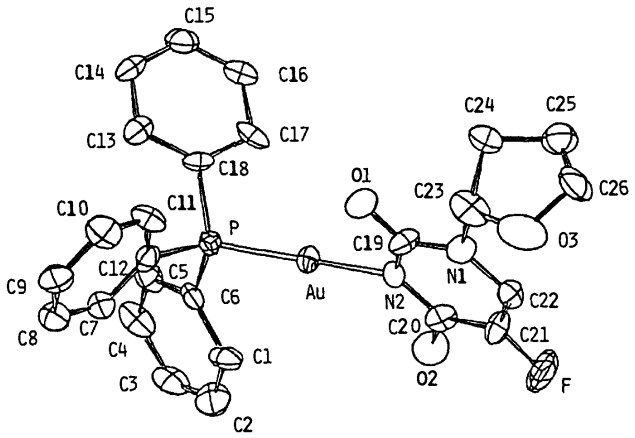

Fig. 1. Molecular structure of **2** showing the numbering system.

Table 4. Selected Bond Lengths (l/Å) and Angles (ϕ/°)

Bond length (l/Å)			
Au-P	2.235(7)	Au-N(2)	2.042(24)
P-C(6)	1.829(20)	F-C(21)	1.339(30)
O(1)-C(19)	1.233(27)	O(2)-C(20)	1.237(34)
O(3)-C(23)	1.390(39)	O(3)-C(26)	1.454(52)
N(1)-C(19)	1.360(34)	N(1)-C(22)	1.382(30)
N(1)-C(23)	1.536(34)	N(2)-C(19)	1.350(27)
N(2)-C(20)	1.389(30)	C(13)-C(14)	1.428(38)
C(13)-C(18)	1.364(35)	C(14)-C(15)	1.364(43)
C(15)-C(16)	1.385(39)	C(16)-C(17)	1.401(37)
C(17)-C(18)	1.413(37)	C(20)-C(21)	1.422(36)
C(21)-C(22)	1.375(39)	C(23)-C(24)	1.523(41)
C(24)-C(25)	1.510(44)	C(25)-C(26)	1.532(37)

Bond angle (ϕ/°)	
P-Au-N(2)	174.5(6)
Au-P-C(6)	114.5(8)
Au-N(2)-C(19)	119.3(16)
Au-N(2)-C(20)	119.3(17)
C(23)-O(3)-C(26)	109.6(24)
C(19)-N(1)-C(22)	122.5(20)
C(19)-N(1)-C(23)	117.7(18)
C(22)-N(1)-C(23)	119.8(23)
C(19)-N(2)-C(20)	121.3(23)
N(1)-C(19)-N(2)	120.5(19)
N(2)-C(20)-C(21)	116.5(24)
C(20)-C(21)-C(22)	122.7(21)
N(1)-C(22)-C(21)	116.4(22)
O(3)-C(23)-C(24)	108.3(26)
C(23)-C(24)-C(25)	101.8(22)
C(24)-C(25)-C(26)	101.6(25)
C(3)-C(26)-C(25)	104.2(28)

caused by stacking of the bulky triphenylphosphine group in the crystal. Substituent fluorine has only little effect on the molecular structure of pyrimidine skeleton.[11]

Examination of the Chemical Stability of 1 and 2. Compound **1** was stable against neutral or alkaline solutions (pH=12; aqueous KOH), but under acidic conditions (pH=2; hydrochloric acid), **1** was transformed to chloro(triphenylphosphine)gold(I). Compound **2** was stable under the above conditions. The instability of **1** is attributable to the existance of hydroxyl groups in **1**; polar hydroxyl groups may accelerate the reactions by hydrogen bond or proton affinity.

Both **1** and **2** reacted with methanethiol, *p*-toluenethiol or imidazole. In each case, the corresponding phosphine thiolate gold(I) complexes or phosphine imidazolato gold(I) complex were formed. These facts suggest that **1** and **2** have a possibility to react with a protein containing a cysteine or histidine residue in vivo.

Antitumor Activity. Preliminary antitumor antimal tests against Mouse Leukemia L1210 were carried out using female CDF_1 mice. While **2** showed comparable activity to tegafur, compound **1**, however, indicated an enhanced activity, compared with 5FdUrd. Further animal tests by use of Lymphocytic Leukemia P388 are in progress.

This work was supported in part by Grand-in-Aid for Cancer Research from the Ministry of Health and Welfare of Japan. Thanks are also given to Mr. Shizuo Shimada (Institute of Biological Sciences, Mitsui Pharmaceuticals Inc.) for the antitumor activity test against L1210 Leukemia.

References

1) D. H. Brown and W. E. Smith, *Chem. Soc. Rev.*, **9**, 217 (1980).
2) A. G. Gilman, L. S. Goodman, T. W. Rall, and F. Murad, "The Pharmacological Basis of Therapeutics," 7th ed., Macmillan Publishing Co., Inc., New York (1985), pp. 704—707.
3) T. M. Simon, D. H. Kunishima, G. J. Vilbert, and A. Lorber, *Cancer Res.*, **41**, 94 (1981).
4) S. J. B.-Price, C. K. Millabelli, R. K. Johnson, M. R. Mattern, F. L. McCabe, L. F. Faucette, C.-M. Sung, S.-M. Mong, P. J. Sadtler, and S. T. Crooke, *Cancer Res.*, **46**, 5486 (1986).
5) C. K. Mirabelli, R. K. Johnson, D. T. Hill, L. F. Faucette, G. R. Girard, G. Y. Kuo, C. M. Sung, and S. T. Crooke, *J. Med. Chem.*, **29**, 218 (1986).
6) M. L. Malvano, *Reak. Accad. Nazl. Lincei*, **17**, 857 (1908).
7) T. Sakurai and K. Kobayashi, *Rep. Inst. Phys. and Chem. Res.*, **55**, 69 (1979).
8) S. J. B.-Price, M. J. DiMaltino, D. T. Hill, R. Kuroda, M. A. Mazid, and P. J. Sadtler, *Inorg. Chem.*, **24**, 3425 (1985).
9) Y. Rosopulos, U. Nagel, and W. Beck, *Chem. Ber.*, **118**, 931 (1985).
10) C. K. Johnson, ORTEP Report ORNL-3794 Oak Ridge National Laboratory, Tennessee, U.S.A. (1965).
11) H. M. Verdegaal, F. B. Martens, and C. Romers, *J. Chem. Soc., Perkin Trans. 2*, **1979**, 833.

 © 1989 The Chemical Society of Japan Bull. Chem. Soc. Jpn., 62, 1081—1085 (1989)

Activation of Aromatic Carbon-Hydrogen Bonds by Palladium(II) Acetate-Dialkyl Sulfide Systems. Formation and Characterization of Novel Diphenyltripalladium(II) Complexes

Yoshio FUCHITA, Katsuma HIRAKI,* Yasuko KAMOGAWA, Miho SUENAGA, Kazutaka TOHGOH, and Yuzo FUJIWARA†

Department of Industrial Chemistry, Faculty of Engineering, Nagasaki University, Bunkyo-machi, Nagasaki 852
†Department of Applied Chemistry, Faculty of Engineering, Kyushu University, Hakozaki, Higashiku, Fukuoka 812
(Received October 24, 1988)

Palladium(II) acetate reacts with benzene in the presence of dialkyl sulfides at 70 °C to afford novel diphenyltripalladium(II) complexes of $[(R^1SR^2)PhPd(\mu\text{-}MeCO_2)_2Pd(\mu\text{-}MeCO_2)_2PdPh(R^1SR^2)]$ (**1a**; R^1=Bu^t, R^2=CH_2Bu^t: **1b**; R^1=R^2=Bu^t: **1c**; R^1=R^2=Pr^i: **1d**; R^1=R^2=Et). Adducts, $[Pd(MeCO_2)_2(Bu^tSCH_2Bu^t)_2]$ and $[Pd(MeCO_2)_2(SPr^i_2)_2]$, prepared by the reactions of palladium(II) acetate and the corresponding dialkyl sulfides in benzene at 5—10 °C, change to **1a** and **1c**, respectively, on heating in benzene at 70 °C. In contrast, reactions of palladium(II) acetate with toluene or thiophene in the presence of diisopropyl sulfide afford no isolable tolyl- or thienyl-palladium species, but coupling products, i.e. bitolyls or bithienyls, are detected by GLC analysis. Treatment of **1b** with styrene produces *trans*-stilbene, whereas **1c** reacts with carbon monoxide as well as carbon dioxide to yield benzoic acid. When palladium(II) acetate and *t*-butyl phenethyl sulfide are heated at 80 °C in benzene, an adduct $[Pd(MeCO_2)_2(Bu^tSCH_2CH_2Ph)_2]$ is formed, in sharp contrast with the case of benzyl *t*-butyl sulfide, which gives a cyclopalladated complex under the same reaction conditions.

Although the metallations of arenes with non-transition metal compounds such as thallium[1] and mercury compounds[2] are well-known, the activation of arene C-H bonds by transition metals is a subject undergoing current research in organometallic chemistry. Up to date, mainly two types of the preparations of σ-aryl complexes directly from arenes and transition metal compounds have been reported. The first type is the oxidative addition of arene C-H bonds to coordinatively unsaturated species which are photochemically generated from dihydridometal complexes such as $[W(\eta^5\text{-}C_5H_5)_2H_2]$[3] and $[M(\eta^5\text{-}C_5Me_5)H_2(PMe_3)]$ (M=Rh,[4] Ir[5]) or thermally generated from $[M(2\text{-naphthyl})H(Me_2PCH_2CH_2PMe_2)_2]$ (M=Fe, Ru).[6] The second type is electrophilic substitution of arenes by metal complexes such as $AuCl_3$,[7] H_2PtCl_6,[8] and [Rh(octaethylporphyrinato)Cl]-Ag salt.[9]

It was proposed that σ-arylpalladium(II) complexes were formed in the arylation of olefins,[10] or carbonylation[11] and carboxylation[12] of arenes by palladium(II) acetate, but such the complex had never been isolated. Previously, we reported preliminary results about novel diphenyltripalladium(II) complexes isolated from palladium(II) acetate-dialkyl sulfide systems in benzene.[13] Here, we wish to report both the details of the C-H bond activation of arenes by the same systems and by a few additional ones and characterization of the resulting diphenyltripalladium(II) complexes.

Results and Discussion

Reactions of Palladium(II) Acetate with Dialkyl Sulfides in Benzene. Palladium(II) acetate reacted with *t*-butyl neopentyl sulfide in benzene at 70 °C to give yellow-brown crystals of **1a** and biphenyl (70% yield). The IR spectrum of **1a** showed newly a ν(C-H) frequency of the aromatic ring at 3040 cm^{-1}, together with the bands due to bridging acetato ligands at 1570, 1555, 1410, and 1395 cm^{-1}. The NMR data (^{1}H and ^{13}C; see below) of **1a** in C_6D_6 confirmed the presence of phenyl groups as well as acetato and *t*-butyl neopentyl sulfide ligands. The molecular weight was determined to be 1055 by osmometry in benzene at 42 °C (Calcd for $C_{38}H_{62}O_8Pd_3S_2$: M, 1030.28). On the basis of these results and elemental analysis, **1a** was assigned as diphenyltripalladium(II) complex with four μ-acetato ligands, $[(Bu^tSCH_2Bu^t)PhPd(\mu\text{-}MeCO_2)_2Pd(\mu\text{-}MeCO_2)_2PdPh(Bu^tSCH_2Bu^t)]$. The ^{1}H NMR spectrum of **1a** exhibited the phenyl proton signals at δ 8.14 (d), 8.05 (d), and 6.95—7.5 (m). In addition, the acetatomethyl protons appeared as four singlets at δ 1.63 (3H), 1.73 (3H), 1.84 (3H), and 1.93 (3H), whereas the methyl protons of the sulfide moieties resonated as three singlets at δ 1.31 (18H, $CH_2C\underline{Me}_3$), 1.39 (9H, $SC\underline{Me}_3$), and 1.46 (9H, $SC\underline{Me}_3$). These data indicated that **1a** consisted of two geometrical isomers, *al-* and *ak*-diphenyl types (Scheme 1) in a population ratio of 1 : 1. In the $^{13}C\{^1H\}$ NMR spectrum,[14] signals due to the two isomers were observed almost separately.

Complex **1a** reacted with lithium chloride in acetone to give an adduct $[PdCl_2(Bu^tSCH_2Bu^t)_2]$ (**2**) but not a phenylpalladium species. However, biphenyl was detected in 70% yield based on **1a** by GLC analysis of the reaction mixture. In contrast, when **1a** was treated with triethylphosphine and lithium bromide in acetone, both *trans*-$[PdBr_2(PEt_3)_2]$ (**3**) and *trans*-$[PdBr(Ph)(PEt_3)_2]$ (**4**) were isolated in 61% and 14% yields, respectively. These results confirmed that **1a** contained phenylpalladium moieties as well as '$Pd(MeCO_2)_2$' moiety. The formation of trinuclear palladium(II) complexes containing four μ-acetato ligands has been found in $[Pd_3(\eta^3\text{-allyl})_2(\mu\text{-}MeCO_2)_4]$,[15]

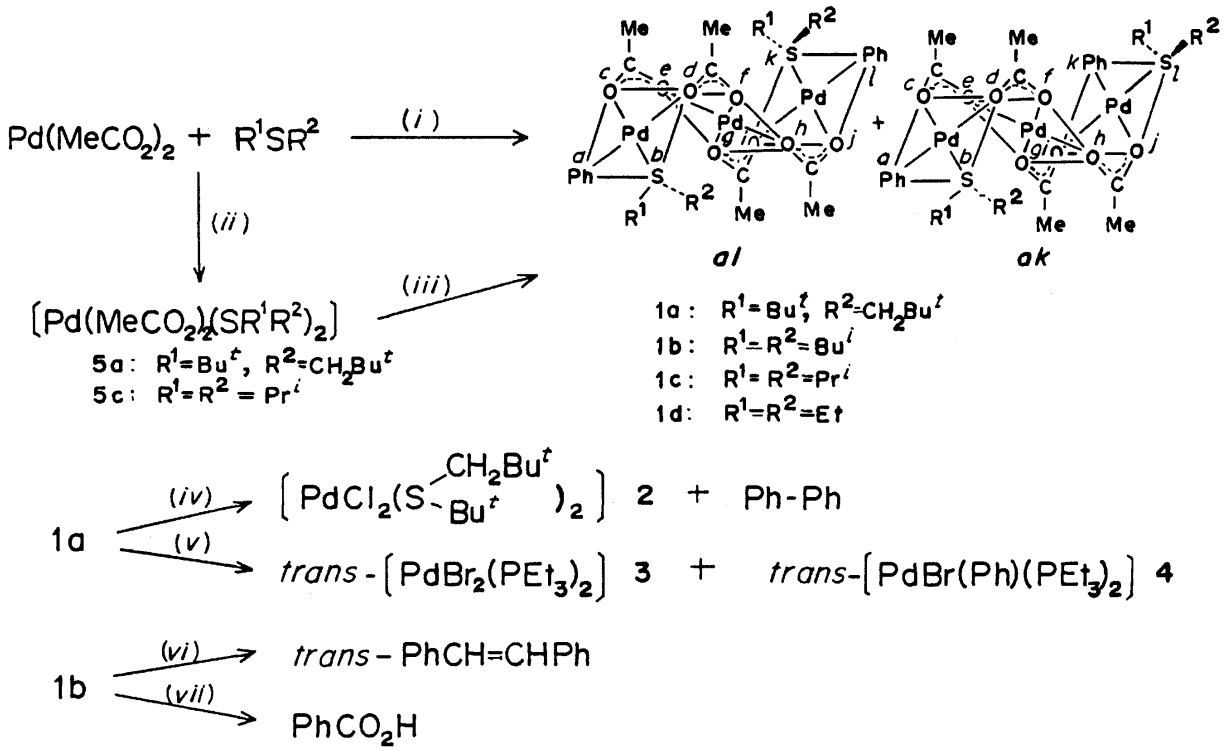

Scheme 1. Reactions of palladium(II) acetate with dialkyl sulfides in benzene and the reactivities of complexes **1a** and **1b**. (i) Benzene, 70 °C. (ii) Benzene, 5—10 °C. (iii) Benzene, 70 °C. (iv) LiCl. (v) PEt_3, LiBr. (vi) $PhCH{=}CH_2$. (vii) CO or CO_2.

Table 1. Yields, Melting Points, IR, and Analytical Data of the Complexes

Complex	Yield %	Mp[a] θ_m/°C	IR/cm^{-1} ν(CH aromatic)	IR/cm^{-1} ν(COO)	Found (Calcd)(%) C	Found (Calcd)(%) H
1a	29 45[b]	139	3040	1570, 1555 1410, 1395	43.62(44.30)	5.94(6.07)
1b	37	152	3030	1570, 1550 1415, 1390	42.81(43.14)	5.81(5.83)
1c	27 29[c]	140	3020	1570, 1550 1400, 1375	40.67(40.62)	5.34(5.33)
1d	9	141	3030	1580, 1550 1410, 1375	37.32(37.77)	4.66(4.76)
2	41	205	—	—	42.94(43.42)	8.08(8.10)
3	61	135	—	—	28.38(28.68)	6.04(6.02)
4	19	104	3030	—	42.96(43.26)	6.92(7.06)
5a	19	128	—	1620, 1300	48.40(48.47)	8.39(8.50)
5c	53	108	—	1610, 1275	41.27(41.69)	7.50(7.43)
7	20	123	3060 3030	1620, 1300	54.96(54.85)	6.74(6.90)

a) With decomposition. b) Yield from **5a**. c) Yield from **5c**.

$[Pd_3(CH_2CMe_2CH_2NMe_2)_2(\mu\text{-}MeCO_2)_4]$,[16] and $[Pd_3(CH_2C_6H_4NMe_2\text{-}o)_2(\mu\text{-}MeCO_2)_4]$,[17] which were produced by the reactions of palladium(II) acetate with monoolefins, *N,N*-dimethylneopentylamine, and *N,N*-dimethyl-*o*-toluidine, respectively.

It is also found that when palladium(II) acetate was treated with benzene at 70 °C for 2 h in the presence of each of diisobutyl, diisopropyl, and diethyl sulfides, the corresponding diphenyltripalladium(II) complexes $[(R^1SR^2)PhPd(\mu\text{-}MeCO_2)_2Pd(\mu\text{-}MeCO_2)_2PdPh(R^1SR^2)]$ (**1b**, $R^1{=}R^2{=}Bu^i$; **1c**, $R^1{=}R^2{=}Pr^i$; **1d**, $R^1{=}R^2{=}Et$) were obtained with the formation of biphenyl in 12, 22, and 39% yields, respectively. The complexes **1b—1d** were characterized by means of elemental analyses (Table 1) and spectroscopic data (Tables 1 and 2). Complexes **1b—1d** were also composed of two isomers *al*- and *ak*-diphenyl types in population ratios of about 1 : 0.8.

Complexes **1a—1d** were fairly stable in solid state, but decomposed gradually in solution to give metallic palladium. Any good single crystal suitable for X-ray structural analysis could not be obtained owing to their instability in solution. It should be noted that

Table 2. ^1H NMR Data of the Complexes[a]

Complex	CH_3	CH_2	CH	CH_3COO	Aromatic
1a[b]	1.31s	3.5br	—	1.63s, 1.74s	8.14d,[c] 8.05d[c]
	1.39s, 1.46s			1.84s, 1.93s	7.3m
1b[b]	0.87d[c]	2.78d[d]	2.03n[d]	1.66s, 1.78s	7.94d[c]
		2.86d[d]		1.80s, 1.92s	7.1m
1c[b]	1.30d[d]	—	3.22h[d]	1.62s 1.69s	7.97d[c]
	1.49d[d]			1.79s, 1.86s	7.05m
1d[b]	1.15br	2.65br	—	1.59s, 1.75s	8.08d,[c] 8.16d[c]
				1.96s	7.1m
2	1.14s, 1.41s	2.8br	—	—	—
3	1.06q[e]	2.01[f]	—	—	—
4	1.07q[e]	1.58[f]	—	—	6.89t,[e] 6.97t[e]
					7.21d[e]
5a	1.24s, 1.49s	2.35br	—	1.89s	—
5c	1.57d[g]	—	3.04h[g]	1.87s	—
7	1.55s	2.6br	—	1.94s	7.3m
		3.4br			

a) δ value in $CDCl_3$, unless noted elsewhere: s=singlet, d=doublet, t=triplet, q=quintet, h=heptet, n=nonet, m=multiplet, br=broad. b) In C_6D_6. c) $^3J_{HH}$=8 Hz. d) $^3J_{HH}$=6 Hz. e) $^3J_{HH}$=8 Hz. $^{3+5}J_{PH}$=8 Hz. f) Triple quartet with intensity ratio of 1:2:4:6:6:6:4:2:1. $^3J_{HH}$=8 Hz. $^{2+4}J_{PH}$=4 Hz. g) $^3J_{HH}$=7 Hz.

the benzene molecule was directly activated by palladium(II) acetate in the presence of dialkyl sulfides to give the diphenyltripalladium(II) complexes of **1a**—**1d**.

When di-*t*-butyl sulfide or tetrahydrothiophene was heated in benzene at 70 °C for 2 h with palladium(II) acetate, the corresponding diphenyltripalladium(II) complex like **1** could not be isolated in both cases. However, biphenyl was detected in 19% (in the case of SBu^t_2) and 40% yields [in the case of $S(CH_2)_4$] based on palladium(II) acetate by GLC analysis of the reaction mixtures. When palladium(II) acetate was treated with benzene at 70 °C for 2 h in the absence of dialkyl sulfide, no biphenyl was detected. Taking these facts into consideration, it seemed likely that benzene was also activated in the cases of di-*t*-butyl sulfide and tetrahydrothiophene.

The reactions of palladium(II) acetate with *t*-butyl neopentyl sulfide and diisopropyl sulfide, carried out in benzene at 5—10 °C, produced mononuclear addition complexes, $[Pd(MeCO_2)_2(Bu^tSCH_2Bu^t)_2]$ (**5a**) and $[Pd(MeCO_2)_2(SPr^i_2)_2]$ (**5c**), respectively. Complex **5a** was heated in benzene at 70 °C for 2 h to give yellow-brown crystals, which was ascribed to the diphenyltripalladium(II) complex **1a**, but not to a binuclear palladium(II) species such as $[(Bu^tSCH_2Bu^t)PhPd(\mu\text{-}MeCO_2)_2PdPh(Bu^tSCH_2Bu^t)]$. Similarly, **5c** was converted to **1c** under the same conditions.

Reactivity of the Diphenyltripalladium(II) Complex $[(Bu^i_2S)PhPd(\mu\text{-}MeCO_2)_2Pd(\mu\text{-}MeCO_2)_2PdPh(SBu^i_2)]$ (1b). The complex **1b** reacted with styrene in THF at room temperature to produce *trans*-stilbene in 94% yield. When carbon monoxide was bubbled through a THF solution of **1b** at room temperature and the reaction mixture was treated with sodium hydrogencarbonate and hydrochloric acid, benzoic acid was obtained in 64% yield by GLC analysis. Benzoic acid was also produced in 9% yield (GLC analysis) by treating **1b** with 4.4×10^6 Pa of carbon dioxide in a THF-$MeCO_2H$ (4:1) mixed solvent in an autoclave at 60 °C. Furthermore, very small amount of phenol was obtained by treating **1b** with pressurized mixture of dioxygen and carbon monoxide.[18]

It was reported that benzene was carbonylated with carbon monoxide (1.52×10^6 Pa) and was also carboxylated with carbon dioxide (3.04×10^6 Pa) in the presence of palladium(II) acetate to give benzoic acid in 26% and 13% yield, respectively.[11,12] The facts that *trans*-stilbene and benzoic acid were obtained from **1b** are important in elucidating the mechanisms for the arylation of alkenes[10] and carbonylation[11] as well as carboxylation of arenes[12] by palladium(II) acetate.

Reaction of Palladium(II) Acetate with Dialkyl Sulifde in Toluene or in Thiophene. Treatment of palladium(II) acetate with diisobutyl sulfide in toluene at 80 °C for 2 h gave only an intractable oil. However, GLC analysis of the reaction mixture revealed the presence of bitolyls composed of six isomers [2,2′:(2,3′+2,4′):3,3′:3,4′:4,4′=6:6:22:45:21] in 25% yield based on palladium(II) acetate. The above reaction carried out in thiophene also afforded an intractable oil, but bithienyls consisting of three isomers [2,2′:(2,3′+3,3′)=9:1] were detected in 25% yield based on palladium(II) acetate by GLC analysis. On the other hand, no coupling product was detected in a toluene or thiophene solution heated only with palladium(II) acetate at 80 °C for 2 h. In consideration of these facts, it seemed likely that tolyl- and thienylpalladium species were formed during the reactions as intermediates, and that diisobutyl sulfide enhanced the coupling reactions of aromatic compounds.

Reactions of Palladium(II) Acetate with Phenyl-Substituted Dialkyl Sulfides, $Ph(CH_2)_nSBu^t$ (n=1,2) in Benzene. It is interesting to investigate whether palladium(II) acetate could activate the C-H bond of benzene intermolecularly even in the presence of phenyl-substituted dialkyl sulfides or activate the ortho C-H bond of the phenyl group in the sulfides intramolecularly. The reaction of benzyl *t*-butyl sulfide with palladium(II) acetate in benzene at 80 °C afforded a cyclopalladated complex $[\{Pd(\mu\text{-}MeCO_2)(C_6H_4CH_2SBu^t\text{-}C^1,S)\}_2]$ (**6**), whose IR and ^1H NMR spectra were identical with those of the authentic sample.[19] In contrast, *t*-butyl phenethyl sulfide afforded only an adduct, $[Pd(MeCO_2)_2(Bu^tSCH_2CH_2Ph)_2]$ (**7**) under the same reaction conditions. Prolonged heating of **7** in benzene at 50 °C for 20 h gave neither a cyclopalladated species nor a phenylpalladium one, but only **7** was recovered from the reaction mixture. Up to date, there has been only one report concerning the formation of six-membered cyclopalladated complexes of sulfur ligands.[20,21] In these cases, the sulfur-containing six-membered cyclopalladated structures were reinforced by the double chelations or a five-membered C-S or C-N chelate.[20] It seemed likely that *t*-butyl phenethyl sulfide was also hard to be cyclopalladated and form a simple six-membered palladacycle $Pd\text{-}C_6H_4CH_2CH_2\text{-}SBu^t\text{-}C^1,S$.

Experimental

t-Butyl neopentyl sulfide,[22] benzyl *t*-butyl sulfide,[23] and *t*-butyl phenethyl sulfide[24] were prepared according to the literatures. Diisobutyl, diisopropyl, diethyl, and di-*t*-butyl sulfides and tetrahydrothiophene were commercial samples. Gas chromatographic analyses were made with a Shimadzu GC-4B gas chromatograph using helium as a carrier gas on columns of Apieson Grease L and Silicone OV-17. Identification of the reaction products was performed by coinjection with authentic samples on the columns and by a Nichiden-Varian TE-600 gas chromatograph-mass spectrometer. For determination of yields, the following internal standards were used: naphthalene for biphenyls, bitolyls, and bithienyls, and hexamethylbenzene for benzoic acid. Other procedures were as described previously.[25]

Preperations of $[(R^1SR^2)PhPd(\mu\text{-}MeCO_2)_2Pd(\mu\text{-}MeCO_2)_2\text{-}PdPh(R^1SR^2)]$ (1a; R^1=Bu^t, R^2=CH_2Bu^t: 1b; R^1=R^2=Bu^i: 1c; R^1=R^2=Pr^i: 1d; R^1=R^2=Et). A mixture containing palladium(II) acetate (250 mg, 1.11 mmol) and *t*-butyl neopentyl sulfide (119 mg, 0.742 mmol) in 10 cm^3 of benzene was heated at 70 °C for 90 min. After filtration, the filtrate was concentrated under reduced pressure and diluted with hexane to give 79 mg of **1a** as beige crystals. Complexes **1b**, **1c**, and **1d** were prepared similarly.

Reation of 1a with Lithium Chloride. Lithium chloride (103 mg, 2.43 mmol) in water (2 cm^3) was added to an acetone solution (15 cm^3) of **1a** (250 mg, 0.243 mmol), and the resulting mixture was stirred at room temperature for 6 h. After the mixture was evaporated to dryness, the residue was extracted with benzene. The extract was diluted with hexane to give 50 mg of $[PdCl_2(Bu^tSCH_2Bu^t)_2]$ (**2**) as a yellow powder.

Reaction of 1a with Triethylphosphine and Lithium Bromide-Water (1/1). Triethylphosphine (124 mg, 1.05 mmol) in acetone (5 cm^3) was added to **1a** (150 mg, 0.146 mmol) in acetone (15 cm^3), and the mixture was stirred at room temperature for 4 h. To the resulting yellow solution, lithium bromide-water (1/1) (507 mg, 5.84 mmol) was added. Stirring was further continued for 20 h, and then the mixture was evaporated to dryness. The residue was chromatographed on a silica-gel column (200 mesh, 1.8×16 cm). A yellow fraction eluted by benzene was collected and evaporated to dryness to give 44 mg of *trans*-$[PdBr_2(PEt_3)_2]$ (**3**). Another yellow fraction eluted by CH_2Cl_2/Et_2O (3/1) afforded 28 mg of *trans*-$[PdBr(Ph)(PEt_3)_2]$ (**4**).

Reactions of Palladium(II) Acetate with Di-*t*-butyl Sulfide or Tetrahydrothiophene in Benzene. A mixture containing palladium(II) acetate (250 mg, 1.11 mmol) and di-*t*-butyl sulfide (108 mg, 0.738 mmol) or tetrahydrothiophene (65 mg, 0.738 mmol) in benzene (15 cm^3) was heated at 70 °C for 2 h. After the reaction mixture was filtered, the filtrate was concentrated under reduced pressure and diluted with hexane to give only dark brown oil in both cases.

Preparation of the Adduct $[Pd(MeCO_2)_2(SR^1R^2)_2]$ (5a; R^1=Bu^t, R^2=CH_2Bu^t: 5c; R^1=R^2=Pr^i). A benzene solution (5 cm^3) of *t*-butyl neopentyl sulfide (857 mg, 5.34 mmol) was added to a benzene solution (10 cm^3) of palladium(II) acetate (400 mg, 1.78 mmol) at 5—10 °C. After stirring for 4 h at 10 °C, the resulting yellow solution was concentrated under reduced pressure and diluted with hexane to yield 180 mg of **5a**. Similarly, **5c** was prepared.

Reactions of 5a or 5c with Benzene. A benzene solution (10 cm^3) of **5a** (150 mg, 0.275 mmol) was heated at 70 °C for 2 h and then filtered. The filtrate was concentrated under reduced pressure and diluted with hexane to afford 43 mg of **1a**. Complex **5c** was similarly converted to **1c**.

Reactions of 1b with Styrene, Carbon Monoxide, or Carbon Dioxide. (i) **With Styrene.** Styrene (44 mg, 0.42 mmol) was added to a THF solution (10 cm^3) of **1b** (200 mg, 0.200 mmol), and the resulting mixture was stirred at room temperature for 1 h. The mixture was filtered to remove the precipitated palladium black, and the filtrate was chromatographed on a silica-gel column (200 mesh, 1.8×30 cm). A fraction eluted by benzene/hexane (1/1) was collected and evaporated to dryness to give 68 mg of *trans*-stilbene as white crystals, whose IR, mp, and ^1H NMR spectrum were identical with those of the authentic sample.

(ii) **With Carbon Monoxide.** Carbon monoxide was bubbled through a THF solution (30 cm^3) of **1b** (100 mg, 0.100 mmol) for 3 h at room temperature. Precipitated palladium black was filtered, and the filtrate was added to a saturated sodium hydrogencarbonate solution (10 cm^3). Then, diethyl ether (15 cm^3) was added. The water layer was separated and acidified with concentrated HCl and the organic product was extracted with diethyl ether (15 cm^3). The ethereal layer was dried by Na_2SO_4 and after evaporation of the solvent, the product was analyzed and identified as benzoic acid by GLC analysis (64% based on **1b**), mp, and IR.

(iii) **With Carbon Dioxide.** In a 200-cm^3 autoclave was placed a 100-cm^3 beaker containing **1b** (213 mg, 0.213 mmol), THF (20 cm^3), and acetic acid (5 cm^3). The autoclave was closed, flushed with carbon dioxide, and pressurized to 4.4×10^6 Pa. The mixture was heated at 60 °C with stirring for 20 h. The resulting mixture was filtered and the filtrate

was similarly treated as described in (ii). The organic products detected by GLC analysis were benzoic acid (9% yield) and biphenyl (1% yield).

Reactions of Palladium(II) Acetate with Diisobutyl Sulfide in Toluene or Thiophene. A mixture containig palladium(II) acetate (150 mg, 0.668 mmol) and diisobutyl sulfide (65 mg, 0.445 mmol) in 10 cm^3 of toluene or thiophene was heated at 70 °C for 2 h, and then filtered. The filtrate was concentrated under reduced pressure and diluted with hexane to give dark brown oil in both cases.

Reactions of Palladium(II) Acetate with Phenyl-Substituted Dialkyl Sulfides $Ph(CH_2)_nSBu^t$ (n=1,2) in Benzene. (i) With $PhCH_2SBu^t$. A mixture containing palladium(II) acetate (150 mg, 0.670 mmol) and benzyl *t*-butyl sulfide (145 mg, 0.804 mmol) in benzene (10 cm^3) was heated at 80 °C for 4 h, and then filtered. The filtrate was diluted with hexane to afford 50 mg of $[\{Pd(\mu\text{-}MeCO_2)(C_6H_4CH_2SBu^t\text{-}C^1, S)\}_2]$ (**6**) as a yellow powder.

(ii) With $PhCH_2CH_2SBu^t$. A mixture containing palladium(II) acetate (200 mg, 0.890 mmol) and *t*-butyl phenethyl sulfide (380 mg, 1.96 mmol) in benzene (20 cm^3) was heated at 80 °C for 4 h, and then filtered. The filtrate was diluted with hexane to give 110 mg of $[Pd(MeCO_2)_2(Bu^tSCH_2CH_2Ph)_2]$ (**7**) as yellow crystals.

The authors wish to thank the Asahi Glass Foundation for Industrial Technology for financial support to this study and acknowledge Mrs. Hisako Mazume for her technical assistance.

References

1) A. Mckillop, J. D. Hunt, M. J. Zelesko, J. S. Fowler, E. C. Taylor, G. McGillivary, and F. Kienzle, *J. Am. Chem. Soc.*, **93**, 4841 (1971).

2) W. Kitching, *Organomet. Chem. Rev.*, **3**, 35 (1968).

3) M. Berry, K. Elmitt, and M. L. H. Green, *J. Chem. Soc., Dalton Trans.*, **1979**, 1950.

4) W. D. Jones and F. J. Feher, *J. Am. Chem. Soc.*, **106**, 1650 (1984).

5) A. H. Janowicz and R. G. Bergman, *J. Am. Chem. Soc.*, **105**, 3929 (1983).

6) C. A. Tolman, S. D. Ittel, A. D. English, and J. P. Jesson, *J. Am. Chem. Soc.*, **101**, 1742 (1979).

7) M. S. Kharasch and T. M. Beck, *J. Am. Chem. Soc.*, **56**, 2057 (1934).

8) G. B. Shul'pin, A. E. Shilov, A. N. Kitagorodskii, and J. V. Z. Krevor, *J. Organomet. Chem.*, **201**, 319 (1980).

9) Y. Aoyama, T. Yoshida, K. Sakurai, and H. Ogoshi, *Organometallics*, **5**, 168 (1986).

10) I. Moritani and Y. Fujiwara, *J. Am. Chem. Soc.*, **91**, 7166 (1969).

11) Y. Fujiwara, T. Kawaguchi, and H. Taniguchi, *J. Chem. Soc., Chem. Commun.*, **1980**, 220.

12) Y. Fujiwara, I. Kawata, H. Sugimoto, and H. Taniguchi, *J. Organomet. Chem.*, **256**, C35 (1983).

13) Y. Fuchita, K. Hiraki, Y. Kamogawa, and M. Suenaga, *J. Chem. Soc., Chem. Commun.*, **1987**, 941.

14) **1a**: $^{13}C\{^1H\}$ NMR (C_6D_6) δ 22.6, 23.4, 23.9, and 24.0 ($\underline{C}H_3CO_2$), δ 29.4, 29.7, 29.9, and 30.0 ($C\underline{C}H_3$), δ 31.7 ($CH_2\underline{C}Me_3$), δ 45.3 and 45.4 ($\underline{C}H_2$), δ 50.4 and 50.5 ($S\underline{C}Me_3$), δ 124.0 (*p*-C of Ph), δ 127.0 and 127.5 (*m*-C of Ph), δ 128.6 and 129.0 (*o*-C of Ph), and δ 140.3 and 140.7 (*i*-C of Ph).

15) R. G. Brown, R. V. Chaudhari, and J. M. Davidson, *J. Chem. Soc., Dalton Trans.*, **1977**, 176.

16) Y. Fuchita, K. Hiraki, and Y. Matsumoto, *J. Organomet. Chem.*, **280**, C51 (1985).

17) M. Pfeffer, E. Wehman, and G. van Koten, *J. Organomet. Chem.*, **282**, 127 (1985).

18) T. Jintoku, Y. Fujiwara, and H. Taniguchi, unpublished result.

19) Y. Fuchita, K. Hiraki, T. Yamaguchi, and T. Maruta, *J. Chem. Soc., Dalton Trans.*, **1981**, 2405.

20) R. A. Holton and R. V. Nelson, *J. Organomet. Chem.*, **201**, C35 (1980).

21) I. Omae, "Organometallic Intramolecular-Coordination Compounds," Elsevier, Amsterdam (1986), Chap. 6.

22) R. Davies and J. Hudec, *J. Chem. Soc., Perkin Trans. 2*, **1975**, 1395.

23) A. C. Cope, D. E. Morrison, and L. Field, *J. Am. Chem. Soc.*, **72**, 59 (1950).

24) K. Yamagishi, *Nippon Kagaku Zasshi*, **80**, 1361 (1959).

25) Y. Fuchita, M. Nakashima, K. Hiraki, M. Kawatani, and K. Ohnuma, *J. Chem. Soc., Dalton Trans.*, **1988**, 785.

Reaction of 1,4,2-Dithiazolium and 1,3-Dithiolium Salts with Malononitrile

Katsumi YONEMOTO,* Isao SHIBUYA,* and Kazumasa HONDA
National Chemical Laboratory for Industry, Tsukuba, Ibaraki 305
(Received July 27, 1988)

The reaction of 5-substituted 3-phenyl-1,4,2-dithiazolium salts with malononitrile gave not only 5-dicyanomethylene-3-phenyl-1,4,2-dithiazole and an isothiazole derivative, but 4-amino-5-cyano-2-(1-cyano-2-dialkylamino-2-mercaptovinyl)-6-phenylpyrimidines (**6**) and a butadiene derivative, depending on substituents at C-5 and bases used. The structure of **6** was confirmed by X-ray crystallographic analysis of its methylated derivative. These results are well explained by assuming three possible fission modes of the initial adduct: liberation of substituents at C-5 (Path A), ring opening-ring closure reaction (Path B), and fragmentation of dithiazole ring (Path C). On the other hand, 2-dialkylamino-4,5-diphenyl-1,3-dithiolium salts were allowed to react with malononitrile to afford 2-amino-3-cyano-5,6-diphenyl-1,4-dithiin (**13**) and 4-amino-3-cyano-2-dicyanomethylene-5,6-diphenyl-2*H*-thiin (**14**) as well as 2-dicyanomethylene-4,5-diphenyl-1,3-dithiole (**12**). In a separate experiment, both **13** and **14** were formed by the reaction of **12** with malononitrile. This pathway can be interpreted in terms of considerable contribution of polar structure of **12** due to the push-pull effect of sulfur atoms and cyano groups. Furthermore, the reaction of 2-substituted 4-phenyl-1,3-dithiolium salts with malononitrile also gave 2-dicyanomethylene-4-phenyl-1,3-dithiole and thiophene derivatives.

Five-menbered heteroaromatic-cation compounds have attracted much attention on their reactivity to serve as versatile intermediates in organic synthesis.[1-3] In particular, it is well known that the reactions of 1,3-dithiolium cations (**2**)[3a,d] and 1,3-oxathiolium cations (**4**)[1b,3] with various kinds of nucleophiles lead to a wide range of heterocyclic compounds. The preparation of 1,4,2-dithiazolium cations (**1**) was recently established by three independent groups, and the reaction of **1** with a few nucleophiles was also reported.[4] We have shown in a previous paper that the reaction of **1** with various amino compounds can be classified into three types (Paths A, B, and C) depending on three possible fission modes (A, B, and C in Scheme 1) of the initial adduct (**D**), leading to 5-imino-1,4,2-dithiazole, 1,3,4-thiadiazole, and thiourea derivatives, respectively.[5] In our continuing investigation into the chemistry of **1**, we carried out the reaction of **1** with malononitrile, one of highly reactive methylene compounds, in the presence of various bases. For comparison, the behavior of 4-phenyl- and 4,5-diphenyl-1,3-dithiolium cations (**2** and **3**), carba-analogues of **1**, toward malononitrile was also examined, and some interesting information on their reactivity was obtained.

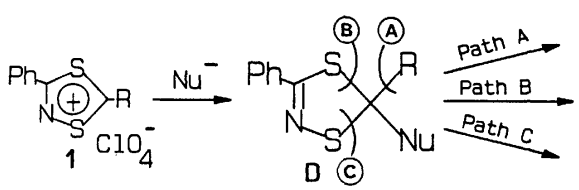

Scheme 1.

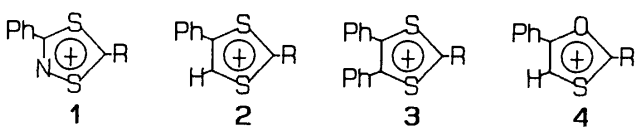

Results and Discussion

When 5-dimethylamino-3-phenyl-1,4,2-dithiazolium perchlorate (**1a**) was treated with malononitrile in the presence of Et_3N at room temperature, the reaction gave a yellow compound as the sole product (Entry 1 in Table 1). On the grounds of its elemental analysis and spectral data, i.e., mercapto, amino, and two cyano bands in IR spectrum, the signals attributable to dimethylamino and phenyl groups in ^1H NMR spectrum, and the molecular ion peak in mass spectrum, the pyrimidine derivative (**6a**) was proposed as the structure of this compound. The reaction of **1b** with malononitrile in the presence of Et_3N and γ-picoline also afforded this type of compound **6b** (Entries 2 and 3). Since the structure of the above products cannot be unequivocally determined from the present data, it was examined by X-ray crystallographic analysis of **7** which was obtained by methylation of **6b**. It proved the proposed pyrimidine structure; an ORTEP illustration of **7** is given in Fig. 1. It shows that the ring skeleton of starting material **1** is divided into sections

Table 1. The Reaction of 1,4,2-Dithiazolium Perchlorates **1** with Malononitrile

Entry	NR_2	Base (pK_a)	Solvent	Product (Yield/%)[a]
1	NMe_2	Et_3N (10.9)	CH_2Cl_2	**6a** (49)
2	NEt_2	Et_3N	THF	**6b** (83)
3	NEt_2	γ-Picoline (6.02)	CH_2Cl_2	**6b** (36)
4	NEt_2	NaH	EtOH	**8** (32)[b]
5	NEt_2	NaH	THF	**8** (67)[b]
6	NMe_2	Pyridine (5.19)	MeCN	**5a** (54)
7	Morpholino	γ-Picoline	MeCN	**5a** (27)
8	SMe	γ-Picoline	MeCN	**5a** (10)
9	Ph	Et_3N	MeCN	**9** (58)

a) Isolated yield. b) Combined yield of *Z*- and *E*-forms.

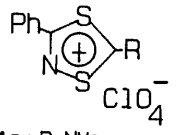

1a: R=NMe_2
1b: R=NEt_2
1c: R=morpholino
1d: R=SMe
1e: R=Ph

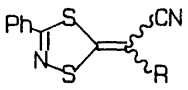

5a: R=CN
5b: R=SO_2Ph
5c: R=COPh

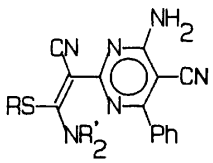

6a: R=H ; R'=Me
6b: R=H ; R'=Et
7 : R=Me; R'=Et

with elimination of one sulfur atom, into which two malononitrile molecules are consequently incorporated.

Detailed mechanism of the present reaction is not clear, but the formation of **6** is most likely rationalized by the pathway shown in Scheme 2. The initial adduct **D** formed by reaction of **1** with malononitrile undergoes ring opening (Path B) and subsequent ring closure leading to the intermediate **E**, which then brings about ring expansion with sulfur extrusion to give six-membered intermediate **F**; another malononitrile molecule attacks on C-2 position of **F** to afford intermediate adduct **G**, which then undergoes ring opening and ring closure to lead to the final products **6**.

The reaction of **1b** with malononitrile was carried out in NaH/THF or NaH/EtOH, i.e., EtONa/EtOH. In both cases, 2-amino-4-diethylamino-4-mercapto-1,1,3-tricyano-1,3-butadiene (**8**) was formed (Entries 4 and 5). On the other hand, in the case of using the combinations of **1** with relatively weak bases such as pyridine and γ-picoline (Entries 6—8), the reaction of **1** with malononitrile in MeCN at room temperature gave 5-dicyanomethylene-3-phenyl-1,4,2-dithiazole (**5a**). The formation of **8** and **5a** can be explained as follows. The initial adduct **D** (in Scheme 2) undergoes ring cleavage leading to intermediate **H** together with benzonitrile and sulfur (via Path C), which then reacts with another malononitrile to give **8**; **D** is alternatively converted into **5a** with liberation of dialkylamino or methylthio groups (via Path A).

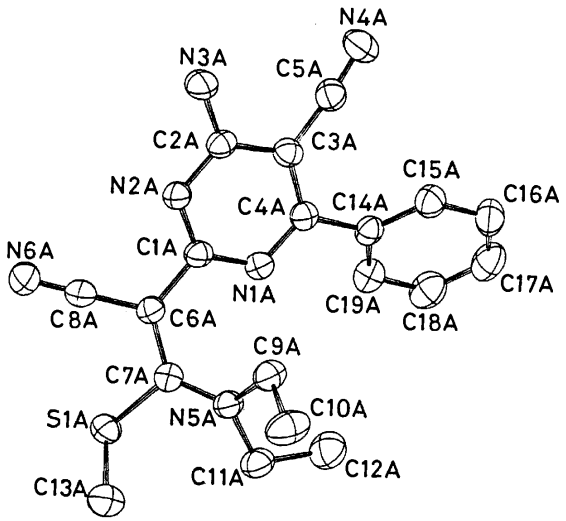

Fig. 1. Molecular structure[15] of **7** with the numbering system for the non-hydrogen atoms. Thermal ellipsoids are drawn at 40% probability.

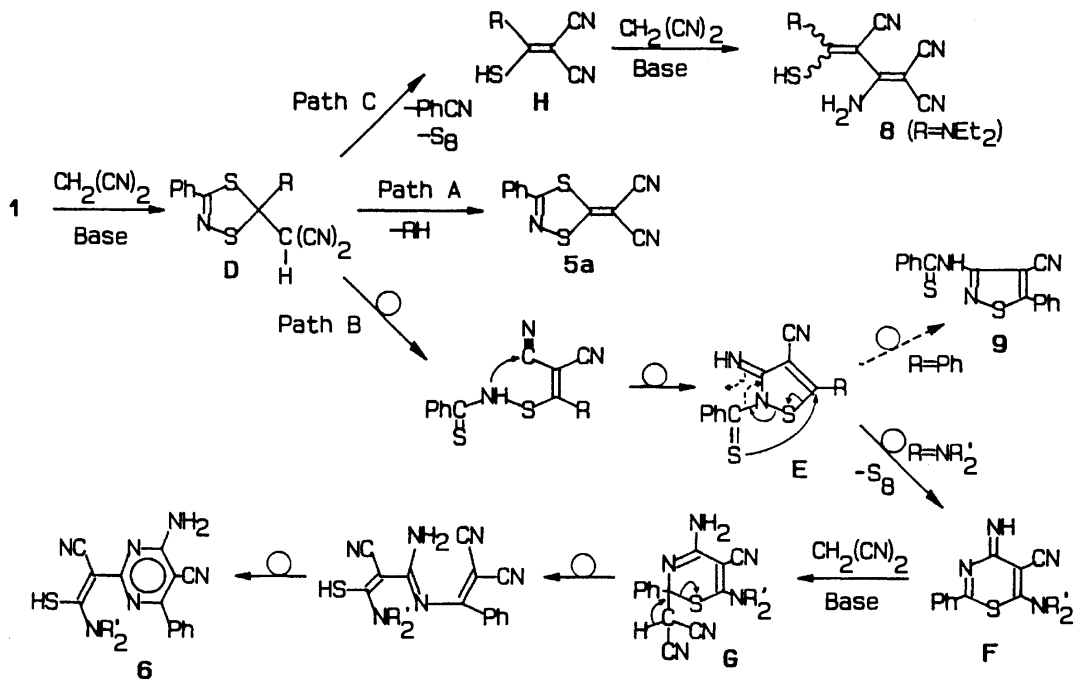

Scheme 2.

5-Phenyl form **1e** was allowed to react with malononitrile in the presence of Et_3N to give only 4-cyano-5-phenyl-3-(thiobenzoylamino)isothiazole (**9**) in 58% yield (Entry 9). The result was well explained in terms of [1,3]-shift of thiobenzoyl group in the intermediate **E** (in Path B).

From the above results, except the case of Entry 3, **5a** is preferentially formed (via Path A) in the presence of weaker bases such as pyridine and γ-picoline, whereas, in the presence of stronger bases such as Et_3N, NaH, and EtONa, the reaction undergoes ring opening (via Path B) or ring fragmentation (via Path C) resulting in the preferential formation of **6**, **8**, or **9**. In our previous work, a similar trend has been shown in the reaction of **1** with *p*-substituted aniline derivatives in the presence of various bases.[5]

On the other hand, the reactions of **1** with dimethyl malonate and Meldrum's acid in the presence of Et_3N have been reported, which lead to only 5-alkylidene-1,4,2-dithiazole derivatives (via Path A in Scheme 1).[4b,d] In order to examine generality of reaction courses corresponding to Path B (ring opening) or Path C (ring fragmentation), the reaction of **1a** with other active methylene compounds such as phenylsulfonylacetonitrile and benzoylacetonitrile in the presence of Et_3N was attempted; but the products other than 5-alkylidene-1,4,2-dithiazole derivatives **5b** and **5c** were not obtained.

In order to obtain additional information on the reactivity of five-membered heteroaromatic cations toward malononitrile, the reaction of 4-phenyl- and 4,5-diphenyl-1,3-dithiolium salts (**2** and **3**) bearing different substituents at C-2 position was carried out in the presence of different bases.[6] The results are presented in Tables 2 and 3, respectively.

The reaction of 2-diethylamino-4-phenyl-1,3-dithiolium perchlorate (**2a**) with malononitrile in the presence of γ-picoline (weak base) gave only 2-dicyanomethylene-4-phenyl-1,3-dithiole (**10**)[3d] (Entry 10), whereas, in the presence of Et_3N (strong base), **2a** afforded 3-amino-4-cyano-5-diethylamino-2-thiobenzoylthiophene (**11a**) (Entry 11). However, 2-dimethylamino form **2b** afforded only **10** (Entry 12) even under the same conditions as used in Entry 11. On the other hand, the sole formation of thiophene derivative **11b** by reaction of **2d** (Entry 14) is associated with the fact that phenyl group at C-2 has no leaving ability. Thus the reactivity of **2** seems to depend delicately on both substituents at C-2 position and bases used. The similar effects of base strength on reactivity have been observed in the reaction of 1,3-oxathiolium salts **4** with active methylene compounds; the reaction leads to 2-alkylidene-1,3-oxathioles (1,4-oxathiafulvenes) and open chain compounds which often undergo ring closure reaction to afford thiophene derivatives.[3b]

2-Morpholino- and 2-diethylamino-4,5-diphenyl-

Table 2. The Reaction of 4-Phenyl-1,3-dithiolium Perchlorates **2** with Malononitrile

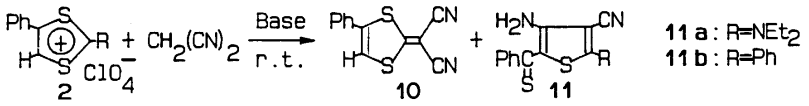

2 10 11

Entry	Dithiolium cation		Conditons	Product yield/%[a]	
	No.	R		**10**	**11**
10	**2a**	NEt_2	γ-Picoline/CH_2Cl_2/5h	62	—
11	**2a**	NEt_2	Et_3N/CH_2Cl_2/1h	Trace[b]	50
12	**2b**	NMe_2	Et_3N/CH_2Cl_2/1h	42	—
13	**2c**	Morpholino	γ-Picoline/MeCN/2h	88	—
14	**2d**	Ph	Et_3N/MeCN/0.5h	—	78

a) Isolated yield. b) Product **10** was detected only on TLC.

Table 3. The Reaction of 4,5-Diphenyl-1,3-dithiolium Perchlorates **3** with Malononitrile

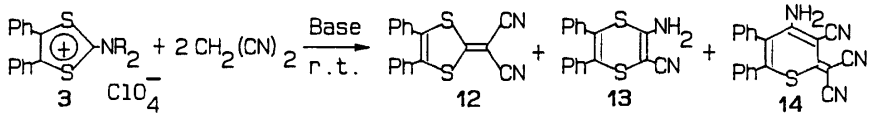

3 12 13 14

Entry	Dithiolium cation		Conditions	Product yield/%[a]		
	No.	NR_2		**12**	**13**	**14**
15	**3a**	Morpholino	Et_3N/MeCN/1.5h	42	17	6
16	**3b**	NEt_2	Et_3N/MeCN/1.5h	70	19	8
17	**3b**	NEt_2	Et_3N/MeCN/1d	—	45	19
18	**3b**	NEt_2	γ-Picoline/MeCN/1d	85	—	—
19	**3b**	NEt_2	NaH/THF/1h	50	Trace	Trace[b]

a) Isolated yield. b) Products **13** and **14** were detected only on TLC.

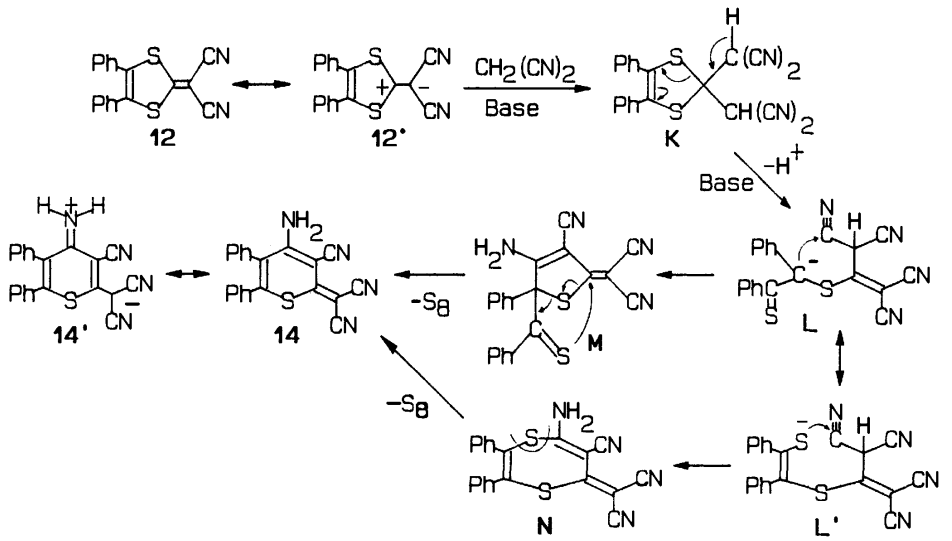

Scheme 3.

1,3-dithiolium perchlorates (**3a** and **3b**) were subjected to react with 2 equiv of malononitrile in the presence of Et_3N in MeCN at room temperature for 1.5 h to give three products (Entries 15 and 16). Their spectral data (IR, ^1H NMR, and MS) and elemental analyses suggested that the main product is the expected 2-dicyanomethylene-4,5-diphenyl-1,3-dithiole (**12**), and that the others are 2-amino-3-cyano-5,6-diphenyl-1,4-dithiin (**13**) and 4-amino-3-cyano-2-dicyanomethylene-5,6-diphenyl-2*H*-thiin (**14**). Characteristically, the ^1H NMR signals of two amino protons of **14** were magnetically unequivalent and broad, indicating large contribution of the polar structure **14'** as shown in Scheme 3.

The same reaction as in Entry 16, except prolonged standing (1 day), resulted in disappearance of **12** and improvement of yields of both **13** and **14**, the ratio of which was almost unchanged (Entry 17). In the case of using γ-picoline (weaker base) instead of Et_3N, neither **13** nor **14** was formed (Entry 18). Under the forced conditions, i.e., NaH/THF system (Entry 19), **12** was preferentially obtained in a short reaction time. Therefore, the formation of **13** and **14** is speculated to go via initially-formed **12**. In fact, the reaction of **12** with malononitrile under the same conditions as those used in Entry 17 gave **13** (42%) and **14** (26%) with no recovery of **12**.

These results are well explained by assuming considerable contribution of the polar structure **12'**, which takes the push-pull effect of two electron-donating sulfur atoms in hetero-ring and two electron-withdrawing cyano groups as shown in Scheme 3. Nucleophilic attack of malononitrile on C-2 position of **12'** leads to intermediate adduct **K** which then undergoes ring opening-ring closure reaction and subsequent rearrengement with sulfur extrusion to give **14** (via intermediates **L** and **M**). This pathway is similar to Path B in Scheme 2 and product **14** corresponds to intermediate **F**. Thus, the isolation of **14** seems to be an evidence for the transient existence of **F** in the proposed reaction pathway. On the other hand, we cannot exclude the possibility that intermediate **L'**, a tautomer of **L**, undergoes ring closure and sulfur extrusion via seven-membered intermediate **N** to give **14**. However, in the case of the reaction of **1**, the pathway similar to that via **L'** and **N** cannot be probable for Path B, because the corresponding seven-membered intermediate 1,4,2-dithiazepine derivative, aza-analogue of **N**, could not afford 1,3-thiazines **F** but 1,2-thiazines. A mechanism of the formation of **13** still remains uncertain.

In summary, the reaction of 1,4,2-dithiazolium salts **1** with malononitrile gave **5a** and **9** in similar manners to the reactions of 1,3-dithiolium salts **2** and **3** leading to **10**, **11**, and **12**,[3] whereas, via novel courses, **1** gave **6** and **8**, depending on substituents at C-5 position and bases used. It is known that the reaction manner of malononitrile to heteroaromatic cations is often different from that of other active methylene compounds.[2a,7] In this study, this tendency was shown again. Detailed studies on the behavior of fulvene-type compounds such as **5a**, **10**, and **12** toward various kinds of nucleophiles are currently under way.

Experimental

All the melting points were uncorrected. The ^1H NMR spectra were recorded on a HITACHI R-40 or a JEOL FX-90A spectrometer using TMS as an internal standard. The IR spectra were measured on a JASCO A-302 spectrometer using KBr disks. The low-resolution mass spectra were taken on a HEWLETT PACKARD 5995A spectrometer by electron impact ionizing technique at 70 eV.

1,4,2-Dithiazolium salts **1a**—**c**[4a] and **1b**,[4b] and 4-phenyl-1,3-dithiolium salts **2a**—**d**[8] were prepared according to the procedures in the literatures. The salt **1e** was prepared from dithiobenzoate in three steps utilizing the similar procedure

Table 4. Fractional Atomic Coordinates($\times 10^4$) and Equivalent Isotropic Thermal Parameters, with Estimated Standard Deviations in Parentheses

Atom	x	y	z	B_{eq}/Å^2
S1A	2267(1)	1141(1)	2940(1)	4.18(3)
N1A	4130(2)	3402(2)	3438(2)	3.50(8)
N2A	3094(2)	4327(2)	3908(2)	3.40(8)
N3A	3361(3)	5823(2)	4219(2)	4.50(10)
N4A	5325(2)	6399(3)	3941(3)	6.15(13)
N5A	3786(2)	1525(2)	3872(2)	3.56(8)
N6A	1217(2)	3149(3)	3347(3)	6.14(13)
C1A	3376(2)	3541(2)	3652(2)	3.23(9)
C2A	3629(2)	5028(2)	3990(2)	3.41(9)
C3A	4454(2)	4936(2)	3808(2)	3.50(9)
C4A	4672(2)	4095(2)	3524(2)	3.26(9)
C5A	4966(2)	5729(3)	3875(2)	4.21(11)
C6A	2796(2)	2771(2)	3555(2)	3.44(9)
C7A	3039(2)	1864(2)	3507(2)	3.33(9)
C8A	1916(3)	2972(2)	3447(3)	4.25(11)
C9A	4290(3)	1935(3)	4631(2)	4.19(11)
C10A	4530(4)	1251(4)	5321(3)	6.18(17)
C11A	4160(3)	741(3)	3523(3)	4.39(12)
C12A	5029(3)	930(4)	3363(4)	5.89(16)
C13A	2292(4)	184(3)	3639(4)	5.52(16)
C14A	5489(2)	3915(2)	3258(2)	3.55(9)
C15A	6238(2)	4335(3)	3637(3)	4.39(11)
C16A	6977(3)	4138(3)	3364(3)	5.44(14)
C17A	6976(3)	3532(4)	2723(3)	5.74(15)
C18A	6235(3)	3122(4)	2343(3)	5.45(15)
C19A	5500(3)	3300(3)	2618(3)	4.38(11)
S1B	−2457(1)	4370(1)	−876(1)	4.63(3)
N1B	−461(2)	2362(2)	305(2)	3.72(8)
N2B	−1572(2)	1342(2)	463(2)	3.49(8)
N3B	−1263(2)	−10(2)	1155(2)	4.57(10)
N4B	884(2)	−276(3)	1716(3)	6.18(12)
N5B	−1167(2)	3414(2)	−1245(2)	4.13(9)
N6B	−3359(3)	2680(3)	206(3)	6.23(13)
C1B	−1272(2)	2115(2)	197(2)	3.45(9)
C2B	−993(2)	747(2)	846(2)	3.42(9)
C3B	−122(2)	929(2)	938(2)	3.40(9)
C4B	120(2)	1765(2)	662(2)	3.36(9)
C5B	463(2)	279(3)	1367(3)	4.16(11)
C6B	−1908(2)	2767(2)	−219(2)	3.61(9)
C7B	−1759(2)	3433(2)	−770(2)	3.69(10)
C8B	−2722(3)	2724(3)	3(3)	4.37(11)
C9B	−735(3)	4235(4)	−1447(4)	5.95(16)
C10B	171(5)	4253(6)	−991(8)	10.09(35)
C11B	−845(3)	2553(3)	−1515(3)	4.58(12)
C12B	−852(4)	2537(5)	−2452(3)	6.13(17)
C13B	−2768(4)	4467(4)	−2002(3)	6.27(17)
C14B	1015(2)	2043(3)	794(2)	3.76(10)
C15B	1240(3)	2889(3)	1131(3)	5.86(15)
C16B	2091(4)	3132(4)	1302(4)	7.49(20)
C17B	2690(3)	2556(4)	1119(4)	6.92(18)
C18B	2467(3)	1735(4)	770(3)	5.89(16)
C19B	1637(3)	1471(3)	615(3)	4.87(13)

for **1a**—**c**.[9] 4,5-Diphenyl-1,3-dithiolium salts **3** were prepared from the reaction of dithiocarbamate and 2-bromo-2-phenylacetophenone in a similar manner to that described in Ref. 8. Other commercially available reagents and bases were used without any purification.

Reaction of 1,4,2-Dithiazolium Salts 1 with Malononitrile. 1,4,2-Dithiazolium perchlorates **1** (1 mmol) were added with stirring to the solution (6 ml) of malononitrile (2 mmol) and bases (2 mmol): the combinations of bases and solvents are listed in Table 1. The reaction mixture was stirred for 6 h at room temperature. In some cases, the products were recrystallized out and filtered off. The crude product was extracted with dichloromethane after addition of dil HCl. After the solvent was removed in vacuo, the residue was purified by column chromatography on silica gel and recrystallized from appropriate solvents. The yields of products are presented in Table 1.

5-Dicyanomethylene-3-phenyl-1,4,2-dithiazole (5a): Pale yellow powder. Mp 160.0—162.0 °C (CH_2Cl_2-hexane). ^{1}H NMR ($CDCl_3$) δ=7.5—7.7 (3H, m), 7.8—8.0 (2H, m). IR ν 2208, 1535, 1469, 1239 cm^{-1}. MS m/z (rel intensity) 243 (M^+, 29), 103(100). Found: C, 53.99; H, 2.10; N, 17.14; S, 26.25%. Calcd for $C_{11}H_5N_3S_2$: C, 54.30; H, 2.07; N, 17.27; S, 26.35%.

4-Amino-5-cyano-2-(1-cyano-2-dimethylamino-2-mercaptovinyl)-6-phenylpyrimidine (6a): Yellow powder. Mp 270.5—271.5 °C (DMF-water). ^{1}H NMR (DMF-d_7) δ=3.35 (6H, s), 7.5—7.7 (3H, m), 7.9—8.1 (2H, m). IR ν 3416, 3308, 3180, 2600(br), 2224, 2204, 1644, 1558 cm^{-1}. MS m/z (rel intensity) 322 (M^+, 63), 289 (21), 88 (100). Found: C, 59.39; H, 4.35; N, 25.68; S, 9.94%. Calcd for $C_{16}H_{14}N_6S$: C, 59.61; H, 4.38; N, 26.07; S, 9.94%.

4-Amino-5-cyano-2-(1-cyano-2-diethylamino-2-mercaptovinyl)-6-phenylpyrimidine (6b): Yellow powder. Mp 266.0—268.0 °C (DMF-water). ^{1}H NMR (DMSO-d_6) δ=1.25 (6H, t, J=7.2 Hz), 3.87 (4H, q, J=7.2 Hz), 7.6—7.8 (3H, m), 7.8—8.0 (2H, m). IR ν 3372, 3176, 2600, 2216, 2188, 1658, 1558 cm^{-1}. MS m/z (rel intensity) 350 (M^+, 26), 317 (8), 253 (86), 116 (31). Found: C, 61.58; H, 5.39; N, 24.16; S, 8.87%. Calcd for $C_{18}H_{18}N_6S$: C, 61.69; H, 5.18; N, 23.98; S, 9.15%.

(*Z*)- and (*E*)-2-Amino-4-diethylamino-4-mercapto-1,1,3-tricyano-1,3-butadiene (8): It is difficult to distingush between *Z*- and *E*-forms: a 3:2 isomeric mixture from comparison of the relative areas of ^{1}H NMR signals (diethylamino group). Yellow powder. Mp 178.5—179.5 °C (DMF-MeCN). ^{1}H NMR (DMSO-d_6) δ=1.18 (6H, t, J=7.2 Hz) and 3.46 (4H, q, J=7.2 Hz) for the major isomer, 1.32 (6H, t, J=7.2 Hz) and 3.86 (4H, q, J=7.2 Hz) for the minor isomer. IR ν 3412, 3192, 2226, 2196, 2136, 1652, 1566, 1444 cm^{-1}. MS m/z (rel intensity) 247 (M^+, 24), 230 (100), 175 (45). Found: C, 53.39; H, 4.92; N, 28.06; S, 12.96%. Calcd for $C_{11}H_{13}N_5S$: C, 53.42; H, 5.30; N, 28.32; S, 12.96%.

4-Cyano-5-phenyl-3-(thiobenzoylamino)isothiazole (9): Orange yellow powder. Mp 183.5—184.5 °C (CH_2Cl_2-ether). ^{1}H NMR ($CDCl_3$) δ=7.4—7.7 (8H, m), 7.8—8.0 (2H, m). IR ν 3176, 2224, 1543, 1443, 1418, 1386 cm^{-1}. MS m/z (rel intensity) 321 (M^+, 11), 320 (11), 121 (100). Found: C, 62.99; H, 3.43; N, 12.96; S, 19.91%. Calcd for $C_{18}H_{12}N_2SO$: C, 63.53; H, 3.45; N, 13.07; S, 19.95%.

Reaction of 1,4,2-Dithiazolium Salt 1a with Other Active Methylene Compounds. The salt **1a** (1 mmol) was added to stirred dichloromethane solution (6 ml) of active methylene compounds (1.5 mmol) and Et_3N (1.5 mmol). The reaction mixture was refluxed for 6 h. Subsequent work-up and purification were accomplished according to a similar procedure to the reaction of **1** with malononitrile.

5-[Cyano(phenylsulfonyl)methylene]-3-phenyl-1,4,2-dithiazole (5b): Yield 45%. Mp 201.5—203.0 °C (MeCN-$CHCl_3$). ^{1}H NMR ($CDCl_3$) δ=7.4—7.9 (8H, m), 8.0—8.2 (2H, m). MS m/z (rel intensity) 358 (M^+, 11), 135 (24). Found: C, 53.63; H, 2.77; N, 7.80; S, 26.83%. Calcd for $C_{16}H_{10}N_2S_3O_2$: C, 53.61; H, 2.81; N, 7.82; S, 26.83%.

5-(Benzoylcyanomethylene)-3-phenyl-1,4,2-dithiazole (5c):

Yield 56%. Mp 176.5—177.0 °C (DMF). ^{1}H NMR ($CDCl_3$) δ=7.6—7.8 (6H, m), 8.0—8.2 (4H, m). MS *m/z* (rel intensity) 322 (M^+, 11), 105 (51). Found: C, 63.26; H, 3.12; N, 8.64; S, 19.85%. Calcd for $C_{17}H_{10}N_2S_2O$: C, 63.33; H, 3.13; N, 8.69; S, 19.89%.

Methylation of 6b. To an ice-cooling suspension of sodium hydride (1.1 mmol) in abs tetrahydrofuran (4 ml) was added **6b** (1 mmol) to give a clear solution. Methyl iodide (3 mmol) was added to the mixture, which was stirred at room temperature for 1 h and then refluxed for 30 min. The mixture was quenched with dil HCl and the product was extracted with dichloromethane. The residue was purified by preparative TLC and recrystallized from dichloromethane-hexane to give **7** as yellow needles of mp 168.5—169.0 °C in 63% yield.

4-Amino-5-cyano-2-(1-cyano-2-diethylamino-2-methylthiovinyl)-6-phenylpyrimidine (7): ^{1}H NMR ($CDCl_3$) δ=1.26 (6H, t, *J*=7.7 Hz), 2.59 (3H, s), 3.67 (4H, q, *J*=7.7 Hz), 5.65 (2H, br. s), 7.4—7.6 (3H, m), 7.9—8.1 (2H, m). IR ν 3432, 3316, 3200, 2192, 1638, 1524, 1395 cm^{-1}. Found: C, 62.42; H, 5.50; N, 23.10; S, 8.65%. Calcd for $C_{19}H_{20}N_6S$: C, 62.61; H, 5.53; N, 23.06; S, 8.80%.

Reaction of 1,3-Dithiolium Salts 2 and 3 with Malononitrile. 1,3-Dithiolium salts **2** and **3** (1 mmol) were added to stirred solution (4 ml) of malononitrile (2 mmol) in the presence of bases (2 mmol) at room temperature. Other reaction conditions are listed in Tables 2 and 3. Subsequent work-up and purification were accomplished by a similar procedure to the reaction of **1**.

3-Amino-4-cyano-5-diethylamino-2-thiobenzoylthiophene (11a): Orange powder. Mp 245.0—246.0 °C (DMF-MeCN). ^{1}H NMR ($CDCl_3$) δ =1.30 (6H, t, *J*=7.2 Hz), 3.58 (4H, q, *J*=7.2 Hz), 7.3—7.4 (5H, br. s). IR ν 3332, 2196, 1602, 1553, 1499, 1458 cm^{-1}. MS *m/z* (rel intensity) 315 (M^+, 85), 243 (100), 121 (78). Found: C, 60.82; H, 5.36; N, 13.38; S, 20.37%. Calcd for $C_{16}H_{17}N_3S_2$: C, 60.92; H, 5.43; N, 13.32; S, 20.33%.

3-Amino-4-cyano-5-phenyl-2-thiobenzoylthiophene (11b): Orange powder. Mp 190.5—191.5 °C (MeCN-ether). ^{1}H NMR ($CDCl_3$) δ=7.3—7.6 (8H, m), 7.7—7.8 (2H, m), 8.3 (2H, br. s). IR ν 3372, 2208, 1602, 1422, 1334 cm^{-1}. MS *m/z* (rel intensity) 320 (M^+, 65), 319 (100), 287 (15), 243 (29), 121 (61). Found: C, 67.08; H, 3.75; N, 8.76%. Calcd for $C_{18}H_{12}N_2S_2$: C, 67.47; H, 3.77; N, 8.74%.

2-Dicyanomethylene-4,5-diphenyl-1,3-dithiole (12): Pale yellow powder. Mp 170.5—171.0 °C (CH_2Cl_2-MeCN). ^{1}H NMR ($CDCl_3$) δ=7.2—7.5 (10H, m). IR ν 2196, 1489, 1435, 1073 cm^{-1}. MS *m/z* (rel intensity) 318 (M^+, 100), 210 (48), 165 (86), 121 (51). Found: C, 67.73; H, 3.13; N, 8.84; S, 19.90%. Calcd for $C_{18}H_{10}N_2S_2$: C, 67.90; H, 3.17; N, 8.80; S, 20.14%.

2-Amino-3-cyano-5,6-diphenyl-1,4-dithiin (13): Yellow powder. Mp 191.0—192.0 °C (MeCN). ^{1}H NMR ($CDCl_3$) δ= 5.1 (2H, br. s) 7.0—7.2 (10H, m). IR ν 3384, 3260, 3176, 2188, 1618, 1542, 1440, 1310 cm^{-1}. MS *m/z* (rel intensity) 308 (M^+, 100), 276 (30), 242 (21), 178 (78), 121 (98). Found: C, 65.91; H, 3.93; N, 9.29%. Calcd for $C_{17}H_{12}N_2S_2$: C, 66.21; H, 3.92; N, 9.08%.

4-Amino-3-cyano-2-dicyanomethylene-5,6-diphenyl-2*H*-thiin (14): Yellow powder. Mp 258.5—260.0 °C (MeCN). ^{1}H NMR ($CDCl_3$) δ=5.8 (1H, br.), 6.7 (1H, br.), 7.0—7.5 (10H, m). IR ν 3432 (br.), 3332 (br.), 2204, 1635, 1441 cm^{-1}. MS *m/z* (rel intensity) 352 (M^+, 29), 178 (15), 121 (36), 55 (100). Found: C, 71.43; H, 3.40; N, 15.91; S, 9.12%. Calcd for $C_{21}H_{12}N_4S$; C, 71.57; H, 3.43; N, 15.90; S, 9.10%.

Reaction of 12 with Malononitrile. 2-Dicyanomethylene-4,5-diphenyl-1,3-dithiole **12** (1 mmol) was added to stirred acetonitrile solution (4 ml) of malononitrile (1 mmol) in the presence of Et_3N (1 mmol). The reaction mixture was stirred for 1 d at room temperature and worked up as described above to give **13** (42%) and **14** (26%).

Single-Crystal X-Ray Analysis of 7. Crystal data: $C_{19}H_{20}N_6S$; MW 364.48; monoclinic; space group $P2_1/c$; a=16.170 (4), b=14.822 (2), and c=16.276 (5) Å and β=101.27 (5)°; U=3826(1) Å^3; D_m=1.3 and D_c=1.27 g cm^{-3}, Z=8; μ(Mo $K\alpha$)= 1.85 cm^{-1}. Intensity data were collected on a Rigaku AFC-4 four-circle diffractometer by using graphite monochromated Mo $K\alpha$ radiation (λ=0.71069 Å) in the 2θ-ω scan mode with a scan width of $\Delta\omega$=(1.0+0.5 tan θ)° and a scan speed of 4.0° min^{-1} over the range of 2θ values of 2° up to 55°. Three standard reflections monitored every 50 reflections showed no significant X-ray damage or crystal decay. Intensities of 9446 reflections were measured and 4707 independent reflections ($|F_o|>3.0\,\sigma(|F_o|)$ were obtained and used for the analysis. The intensities were corrected for the Lorentz and polarization factors, but no correction were made for the absorption and extinction.

The structure was solved by MULTAN 78 program.[10] The positions of hydrogen atoms were obtained from the difference Fourier synthesis. Anisotropic thermal parameters and isotropic thermal parameters were assumed for non-hydrogen atoms and for hydrogen atoms, respectively. The structural parameters were refined by a full-matrix least-squares method to the final R value of 0.056 and the R_w=0.054 in conjunction with the weighting scheme of w=(40(sin θ/λ)^2−30 (sin θ/λ)+9)$^{-1}$. The atomic scattering factors for non-hydrogen atoms and for hydrogen atoms were taken from Refs. 11 and 12, respectively. All the computations were carried out on a FACOM M-380 and a M-780 computer using UNICS III system.[13] The final atomic parameters for non-hydrogen atoms are given in Table 4[14] and the molecular structure with the numbering system for non-hydrogen atoms is shown in Fig. 1.

The authors are grateful to Dr. Masayasu Kurahashi and Mrs. Midori Goto for helpful discussions with regard to the X-ray crystallographic analysis.

References

1) a) K. Hirai, H. Sugimoto, and T. Ishiba, *Yuki Gosei Kagaku Kyokai Shi*, **39**, 192 (1981). b) K. Hirai and T. Ishiba, *Chem. Pharm. Bull.*, **26**, 3017 (1978). c) I. Shibuya, *Nippon Kagaku Kaishi*, **1982**, 1518. d) *idem, ibid.*, **1979**, 389.

2) a) I. Shibuya, *Bull. Chem. Soc. Jpn.*, **52**, 1235 (1979). b) *idem, ibid.*, **57**, 605 (1984).

3) a) K. Hirai, T. Ishiba, and H. Sugimoto, *Chem. Pharm. Bull.*, **20**, 1711 (1972). b) K. Hirai and T. Ishiba, *ibid.*, **20**, 2384 (1972). c) *idem, Heterocycles*, **3**, 217 (1975). d) K. Hirai, *Tetrahedron Lett.*, **1971**, 1137.

4) a) I. Shibuya and K. Yonemoto, *Bull. Chem. Soc. Jpn.*, **59**, 2017 (1986). b) D. J. Greig, M. McPherson, R. M. Paton, and J. Crosby, *J. Chem. Soc., Chem. Commun.*, **1985**, 696. c) F. S. Y. Chan and M. P. Sammes, *ibid.*, **1985**, 1641. d) F. S. Y. Chan, M. P. Sammes, and R. L. Harlow, *J. Chem. Soc., Perkin Trans. 1*, **1988**, 899.

5) K. Yonemoto and I. Shibuya, *Bull. Chem. Soc. Jpn.*,

61, 4043 (1988).

6) Systematic studies on the reactivity of 2-piperidino-4-phenyl-1,3-dithiolium hydrogensulfate toward active methylene compounds including malononitrile in the presence of Et_3N have been reported to give 2-alkylidene-1,3-dithioles (1,4-dithiafulvenes).[3a-d] However, neither effect of substituents nor that of bases on reactivity has been examined. On the other hand, the behavior of 4,5-diphenyl-1,3-dithiolium salts toward nucleophiles remains almost unexplored.

7) a) I. Shibuya, *Bull. Chem. Soc. Jpn.*, **52**, 3767 (1979). b) *idem*, *Nippon Kagaku Kaishi*, **1986**, 780.

8) E. Campaigne and N. W. Jacobsen, *J. Org. Chem.*, **29**, 1703 (1964).

9) The details will be reported in a separate paper.

10) P. Main, S. E. Hull, L. Lessinger, G. Germain, J. P. Declercq, and M. M. Woolfson, MULTAN 78, "A System of Computer Programmes for the Automatic Solution of Crystal Structures from X-Ray Diffraction Data," University of York, York, England (1978).

11) "International Tables for X-Ray Crystallography," Kynoch Press, Birmingham (1974), Vol. 4.

12) R. F. Stewart, E. R. Davidson, and W. T. Simpson, *J. Chem. Phys.*, **42**, 3175 (1965).

13) T. Sakurai and K. Kobayashi, *Rep. Inst. Phys. Chem. Res.*, **55**, 69 (1978).

14) The lists of the coordinates and isotropic thermal parameters for hydrogen atoms, the anisotropic thermal parameters for non-hydrogen atoms, and the observed and calculated structure factors have been deposited at the Chemical Society of Japan as Document No. 8860.

15) C. K. Johnson, ORTEP II, Report ORNL-5138, Oak Ridge National Laboratory, Tennessee (1976).

 © 1989 The Chemical Society of Japan Bull. Chem. Soc. Jpn., 62, 1093—1096 (1989)

Rotational Isomerism in Fluorene Derivatives. XV.[1] Conformational Equilibria of 2-Substituted and 2,7-Disubstituted 9-(2′-Dimethylaminophenyl)-fluorene Derivatives and the Effects of Acid on Them

Akiko NISHIDA, Makoto TAKESHITA, Nobuaki KAWANO, Shizuo FUJISAKI, and Shoji KAJIGAESHI*
Department of Industrial Chemistry, Faculty of Engineering, Yamaguchi University, Tokiwadai, Ube 755
(Received July 29, 1988)

Several 9-(2′-dimethylaminophenyl)-9-fluorenols (**2**) and 9-(2′-dimethylaminophenyl)fluorenes (**3**), which had electron-attracting or electron-releasing groups at 2- or 2,7-positions of the fluorene ring, were synthesized. The conformational equilibria (anti⇄syn) of **2** and **3** in $CDCl_3$ lay near to their syn sides. However, the equilibria of **2** in DMSO-d_6 inclined to the anti side. By the addition of trifluoroacetic acid to the solution of **3** in $CDCl_3$, *anti*-**3** salts were formed and stabilized by the N-H···π interaction between the dimethylammonio group and the fluorene ring. In this case, the intensities of the N-H···π interaction were affected by the magnitudes of the π-electron density of the fluorene ring.

During the course of an investigation on the conformational equilibria (anti⇄syn)[2] in 9-(2′-substituted phenyl)fluorenes, we recently recognized the presence of the N-H···π interaction between the dimethylammonio group and the fluorene ring in the anti-form of ammonium trifluoroacetate of 9-(2′-dimethylaminophenyl)fluorene (**3a**).[3] In the present paper, we wish to report on the syntheses of several 2-substituted and 2,7-disubstituted 9-(2′-dimethylaminophenyl)fluorene derivatives having electron-attracting or releasing groups as substituents, and on the investigation of the effects of these substituents on their conformational equilibria in $CDCl_3$, DMSO-d_6, and trifluoroacetic acid.

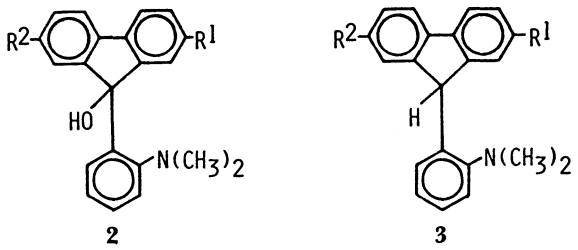

		R^1	R^2
2a,	**3a**	H	H
2b,	**3b**	Br	H
2c,	**3c**	Br	Br
2d,	**3d**	CH_3	H
2e,	**3e**	CH_3O	H
2f,	**3f**	CH_3O	CH_3O
	3g	OH	H
	3h	OH	OH

Scheme 1.

Results and Discussion

Preparation of 2-Substituted and 2,7-Disubstituted 9-(2′-Dimethylaminophenyl)fluorenes (3). The reaction of 2-substituted or 2,7-disubstituted fluorenones (**1**) with 2-dimethylaminophenylmagnesium bromide in ether gave the corresponding fluorenols (**2**) (**2b—2f** in Scheme 1). The reduction of **2b—2d** with hydrogen iodide in acetic acid in the presence of red phosphorus gave the desired fluorenes **3b—3d**. The same treatment of **2e** and **2f** with hydrogen iodide and red phosphorus

Table 1. Syntheses of 2-Substituted and 2,7-Disubstituted 9-(2′-Dimethylaminophenyl-9-fluorenols (**2**) and 2-Substituted and 2,7-Disubstituted 9-(2′-Dimethylaminophenyl)fluorenes (**3**)

Compd	R^1	R^2	Y	Mp	Yield	^{1}H NMR: δ/ppm					
						In $CDCl_3$					In DMSO-d_6
				θ_m/°C	%	$N(CH_3)_2$	R^1, R^2	Y	6′-H	Aromatics	$N(CH_3)_2$
2a[2]	H	H	OH	174—176	85	2.84s	—		6.36br.d	6.74—7.52m	1.96s
2b	Br	H	OH	160—161	50	2.94s	—		6.52br.d	6.80—7.90m	1.80s
2c	Br	Br	OH	262—263	51	2.94s	—		6.50br.d	6.80—7.70m	1.71s
2d	CH_3	H	OH	153—155	41	2.98s	2.36s		6.56br.d	6.90—7.80m	1.98s
2e	CH_3O	H	OH	195—196	59	2.84s	3.70s		6.28br.d	6.40—7.50m	2.03s
2f	CH_3O	CH_3O	OH	191—192	80	3.03s	3.81s		6.55br.d	6.70—7.60m	2.10s
3a[2]	H	H	H	122	69	2.86br.s	—	5.86br.s	6.34br.d	6.74—7.72m	
3b	Br	H	H	133—135	55	2.92br.s	—	5.96br.s	6.40br.d	6.80—7.90m	
3c	Br	Br	H	191—193	62	2.93br.s	—	5.98br.s	6.40br.d	6.80—8.00m	
3d	CH_3	H	H	—[a]	56	2.92br.s	2.36s	5.90br.s	6.44br.d	6.70—7.90m	
3e	CH_3O	H	H	86—87	27	2.92br.s	2.76s	5.84br.s	6.38br.d	6.60—7.80m	
3f	CH_3O	CH_3O	H	90—91	52	2.96br.s	3.79s	5.90br.s	6.49br.d	6.70—7.80m	

a) Light yellow liquid.

in acetic acid afforded a mixture of **3e** and 2-hydroxy compound (**3g**), and a mixture of **3f** and 2,7-dihydroxy compound (**3h**), respectively. Pure **3e** and **3f** were obtained by the treatment of each mixture with dimethyl sulfate in methanol. The mp's, yields, and NMR data of **2** and **3** are shown in Table 1.

Conformational Equilibria of 2 and 3 in $CDCl_3$. As shown in Table 1, dimethylamino protons and 6'-protons of **2b—2f** and **3b—3f** in $CDCl_3$ appeared at δ ca. 2.8—3.0 as singlets or broad singlets and at δ ca. 6.3—6.6 as broad doublets, respectively, as in the cases of **2a** and **3a**. For compound **2a** and **3a**, their conformational equilibria (anti⇄syn) have been investigated by the behavior of the chemical shifts of dimethylamino groups and 6'-protons, and these compounds have been confirmed to exist predominantly as the syn-form at room temperature.[3] From the similarity for the appearance of these chemical shifts as shown in the Table, it can be claimed that the equilibria of **2b—2f** and **3b—3f** are also inclined to the syn-form (Fig. 1).

DNMR spectra of **3b—3f** were observed in $CDCl_3$. However, the anti-signals were scarcely recognized at low temperature (−20 °C) because the equilibria lay close to the syn side. Furthermore, since **3b—3f** were almost insoluble in $CDCl_3$, the activation parameters of the internal rotation (anti⇄syn) of these compounds were not measured.

Conformational Equilibria of 2 in DMSO-d_6. We have already indicated the existence of intramolecular hydrogen bonding in **2a**[3] and 9-(2'-methoxyphenyl)-9-fluorenol[4] by the examination of their IR spectra in CCl_4 and their NMR spectra in $CDCl_3$ or DMSO-d_6. Accordingly, it was proved that the intramolecular hydrogen bonding between the hydrogen atom of the 9-hydroxyl group and the nitrogen atom of 2'-dimethylamino group stabilized the syn-form of **2** in $CDCl_3$ (Fig. 2).

In the compound **2a** in DMSO-d_6, particularly, the dimethylamino proton was observed at δ 1.96 as a singlet. That is, it could be noted that the equilibrium of the rotamer of **2a** lay near to the anti side.[3] The dimethylamino protons of **2b—2f** were similarly observed at δ 1.7—2.1 in DMSO-d_6. In these cases, intermolecular hydrogen bonding, which formed between the hydrogen atom of the 9-hydroxyl group and the oxygen atom of dimethyl sulfoxide, should stabilize the anti-form. Thus, the anti-form of **2** was exclusively predominant in DMSO-d_6 (Fig. 2).

As can be seen from Table 1, the chemical shifts of the dimethylamino protons in DMSO-d_6 were affected by the nature of the 2- or 2,7-substituents on the fluorene ring, and their increasing order of chemical shift was shown as follows; **2c<2b<2a<2d<2e<2f**. Each chemical shift was a specific values for compounds **2a—2f**, respectively. That is, these chemical shifts of **2** having stronger electron-attracting substituent appeared at higher magnetic field. In fact an electron-attracting substituent decreased the π-electron density of the fluorene ring. The repulsion between the fluorene ring and an unshared electron pair on the nitrogen atom in the dimethylamino group should be decreased. Thus, the magnitudes of the electron pair $\cdots$ π repulsive interaction in **2** can be given in the following order; **2c<2b<2a<2d<2e<2f**.

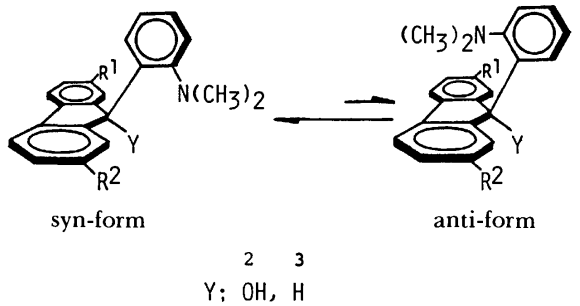

Fig. 1. Conformational equilibria between syn and anti forms of **2** and **3** in $CDCl_3$.

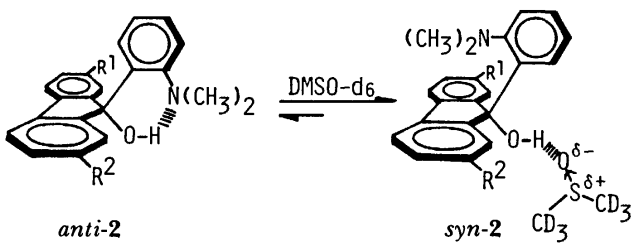

Fig. 2. Interconversion between syn and anti conformers of **2** in DMSO-d_6.

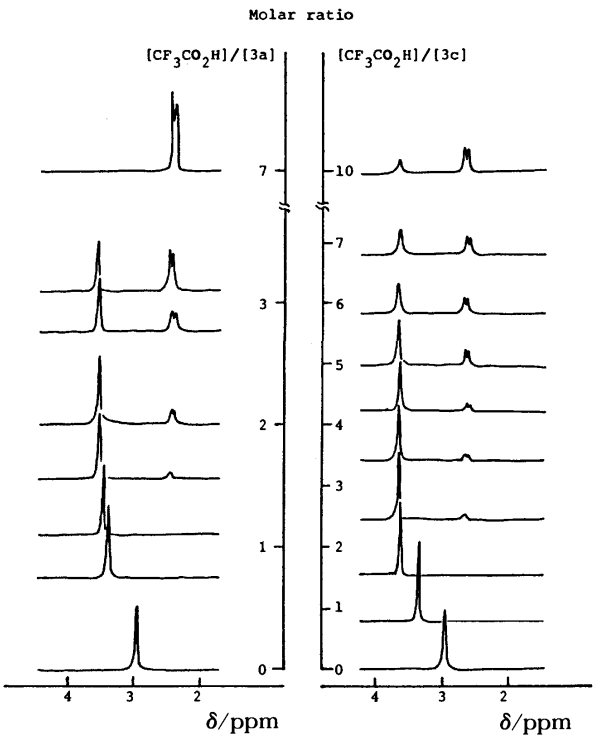

Fig. 3. Isomerization of **3a** and **3c** by addition of trifluoroacetic acid at 0 °C.

N-H···π Interaction of Ammonium Trifluoroacetates of 3. As shown in the previous paper,[3] we recognized that an N-H···π interaction between the dimethylammonio group and the fluorene ring stabilized the anti-form of **3a**-trifluoroacetate. Accordingly, it is interesting to investigate the influence of the π-density of the fluorene ring for the N-H···π interaction in **3**. In 2-substituted and 2,7-disubstituted 9-arylfluorene derivatives, the substituents should not affect the rotation about C(9)-C(Ar) bonds and the stabilization of the syn form. The electronic properties of these substituents change the π-density of the fluorene ring.

The variation of the ^{1}H NMR signals of the dimethylamino groups was followed upon addition of trifluoroacetic acid in $CDCl_3$ solution of **3b—3f**. For an example, the examination for **3c** was illustrated as compared with that of **3a** in Fig. 3.

The methyl signal (singlet) of *syn*-**3c** moved to a lower field on increasing the amount of acid added. When excess equivalent of acid was added ($[CF_3CO_2H]/[\mathbf{3c}]\approx3$), the methyl signal (doublet) of the anti-salt appeared. Further added acid ($[CF_3CO_2H]/[\mathbf{3c}]>10$) reversed the intensities of the anti- and syn-signals, and the syn-signal then almost disappeared. The methyl signal of **3a** in $CDCl_3$ also behaved in the similar manner on adding acid.[3] However, the anti-signal of the **3a**-salt has already appeared when $[CF_3CO_2H]/[\mathbf{3a}]\approx1.5$ (see Fig. 3).

Thus, the intensities of the two methyl signals (syn and anti) of the **3c**-salt changed more slowly compared with those of **3a**-salt. These experimental results should be attributed to the weaker N-H···π interaction in the **3c**-salt than in the **3a**-salt. Accordingly, the π-electron density of the fluorene ring of the **3c**-salt should be smaller than that of the **3a**-salt. This phenomenon can be understood from the fact that the electron-attracting property of bromine decreases the π-electron density of the fluorene ring in **3c**.

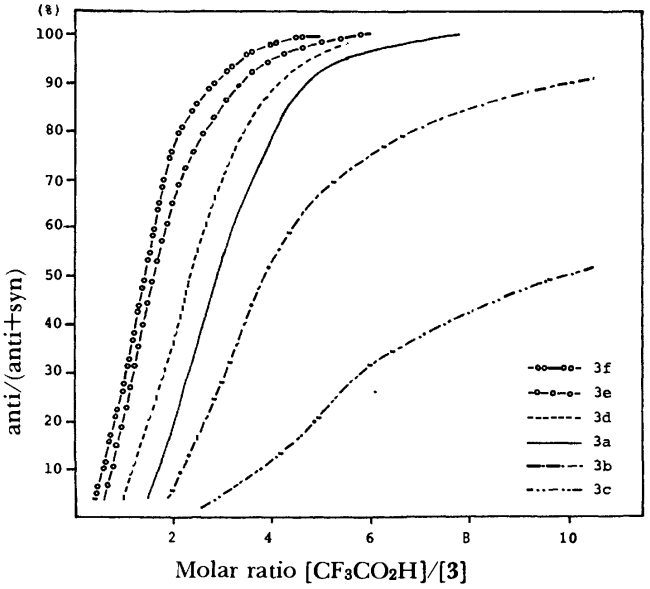

Fig. 4. Proportion of *anti*-**3** salt depend on the molar ratio of CF_3CO_2H vs. **3** ($[\mathbf{3}]/[CDCl_3]$=ca. 5×10^{-5} mol/0.4 ml).

On the other hand, in compound **3f**, the rate of variation of the conformational equilibria following the addition of trifluoroacetic acid was much faster than that of **3a**. The relationship between the variation of the conformational equilibria and the concentration of the acid in **3b—3f** are shown together with that in **3a** in Fig. 4.

It is apparent that the larger is the π-electron densities of the fluorene ring, the stronger is the N-H···π interaction; the magnitudes of the N-H···π interactions in *anti*-**3**-salts are given in the following order; **3f>3e>3d>3a>3b>3c**.

Experimental

^{1}H NMR spectra were recorded on a JEOL-MH-100 spectrometer with a JEOL model JES-VT-3 variable temperature controller. The chemical shifts are expressed in ppm, with tetramethylsilane as an internal standard. Mass spectra were recorded on a JEOL JMS-D spectrometer. The IR spectra were measured on a JASO IRA-1 spectrometer. All melting points are uncorrected.

2,7-Dibromo-9-(2′-dimethylaminophenyl)-9-fluorenol (2c). Typical Procedure. A solution of 2,7-dibromofluorenone (4.0 g, 12 mmol) in dry benzene was added to the Grignard reagent which was prepared from magnesium turnings (0.5 g, 12.5 mmol) and *o*-bromo-*N*,*N*-dimethylaniline (2.5 g, 12.5 mmol). The mixture was refluxed for 1 h. After cooling, the solution was poured into dil. hydrochloric acid. The solid precipitate was alkalized with sodium hydroxide solution and extracted with chloroform. The organic layer was dried with magnesium sulfate and distilled off in vacuo, leaving a residue which was recrystallized from chloroform to give **2c** as colorless prisms; yield 2.9 g (51%), mp 262—263 °C. Found: C, 54.90; H, 3.60; N, 3.05%. Calcd for $C_{21}H_{17}NOBr_2$: C, 54.93; H, 3.73; N, 3.05%.

2-Bromo-9-(2′-dimethylaminophenyl)-9-fluorenol (2b). Yield 50%; colorless crystals; mp 160—161 °C (from chloroform). Found: C, 66.21; H, 4.74; N, 3.52%. Calcd for $C_{21}H_{18}NOBr$: C, 66.33; H, 4.77; N, 3.68%.

2-Methyl-9-(2′-dimethylaminophenyl)-9-fluorenol (2d). Yield 41%; colorless needles; mp 153—155 °C (from chloroform). Found: C, 83.54; H, 6.75; N, 4.43%. Calcd for $C_{22}H_{21}NO$: C, 83.78; H, 6.71; N, 4.44%.

2-Methoxy-9-(2′-dimethylaminophenyl)-9-fluorenol (2e). Yield 59%; colorless crystals; mp 195—196 °C (from benzene). Found: C, 79.47; H, 6.18; N, 4.06%. Calcd for $C_{22}H_{21}NO_2$: C, 79.78; H, 6.39; N, 4.23%.

2,7-Dimethoxy-9-(2′-dimethylaminophenyl)-9-fluorenol (2f). Yield 80%; colorless crystals; mp 191—192 °C (from benzene). Found: C, 76.66; H, 6.53; N, 3.65%. Calcd for $C_{23}H_{23}NO_3$: C, 76.43; H, 6.41; N, 3.88%.

2,7-Dibromo-9-(2′-dimethylaminophenyl)fluorene (3c). Typical Procedure. To a solution of **2c** (1.4 g, 3mmol) in acetic acid (10 ml) was added red phosphorus (0.3 g, 10 mmol) and hydriodic acid (57%, 6.0 g, 50 mmol), and the mixture was refluxed for 4 h. After cooling, red phosphorus was filtered off and the solvent distilled off in vacuo. The

residue was alkalized by sodium hydroxide solution, extracted with benzene and the extract dried with magnesium sulfate. The solution was evaporated in vacuo, leaving a residue which was recrystallized from chloroform to give **3c** as colorless crystals; yield 0.8 g (62%), mp 191—193 °C. Found: C, 56.68; H, 3.78; N, 3.31%. Calcd for $C_{21}H_{17}NBr_2$: C, 56.91; H, 3.87; N, 3.16%.

2-Bromo-9-(2′-dimethylaminophenyl)fluorene (3b). Yield 55%; colorless crystals; mp 133—135 °C (from chloroform). Found: C, 69.11; H, 4.88; N, 3.94%. Calcd for $C_{21}H_{18}NBr$: C, 69.24; H, 4.98; N, 3.84%.

2-Methyl-9-(2′-dimethylaminophenyl)fluorene (3d). Yield 56%; oil; MS *m/z*: 219 (M^+).

2-Methoxy-9-(2′-dimethylaminophenyl)fluorene (3e). Hydriodic acid (57%, 6 g, 50 mmol) and red phosphrous (0.3 g, 10 mmol) were added to a solution of **2e** (1 g, 3 mmol) in acetic acid (20 ml) and refluxed for 3 h. The reaction mixture was concentrated in vacuo and the residue was treated with sodium hydrogensulfite. The solid precipitate was collected by filtration and dissolved in methanol. To the solution was added dimethyl sulfate (0.76 g, 6 mmol) and sodium hydroxide (0.36 g, 9 mmol), and the mixture was refluxed for 1 h. After cooling, the precipitate was washed with water and recrystallized from methanol to give **3e** as colorless crystals; yield 0.26 g (27%), mp 86—87 °C. Found: C, 83.89; H, 6.46; N, 4.37%. Calcd for $C_{22}H_{21}NO$: C, 83.78; H, 6.71; N, 4.44%.

2,7-Dimethoxy-9-(2′-dimethylaminophenyl)fluorene (3f). To a solution of **2f** (0.44 g, 1.2 mmol) in acetic acid (10 ml) was added hydriodic acid (57%,3 g, 25 mmol) and the mixture was refluxed for 2 h. The reaction mixture was worked up as described for the preparation of **3e**, to give **3f** as colorless crystals; yield 0.22 g (52%), mp 90—91 °C. Found: C, 80.17; H, 6.68; N, 4.12%. Calcd for $C_{23}H_{23}NO_2$: C, 79.97; H, 6.71; N, 4.05%.

The authors wish to thank Professor Masashi Tashiro, Institute of Advanced Material Study, Kyushu University, for the elemental analyses.

References

1) Part XIV of this series: A. Nishida, S. Shirakawa, S. Fujisaki, and S. Kajigaeshi, *Tec. Rep. Yamaguchi Univ.*, **4**, 145 (1988).

2) The conformations of 2-substituted and 2,7-disubstituted 9-(2′-dimethylaminophenyl)fluorenes were specified by the anti and syn nomenclature. The present IUPAC nomenclature of *ap* and *sp* for our systems is valid only when the fluorene ring is unsubstituted or symmetrically substituted. When unsymmetrically substituted a chiral center is created; the conformation must be specified in addition to the ±*sc*, ±*ac* nomenclature.

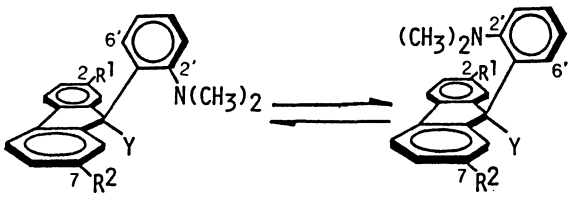

syn anti

3) A. Nishida, M. Takeshita, S. Fujisaki, and S. Kajigaeshi, *Nippon Kagaku Kaishi*, **1987**, 1791.

4) A. Nishida, S. Shiwaku, S. Fujisaki, and S. Kajigaeshi, *Nippon Kagaku Kaishi*, **1984**, 574.

Studies on Synthetic Ionophores. VIII.[1] Transport of Alkaline Earth Metal Ions by Polyether Carboxylic Acids through Liquid Membrane

Kazuo YAMAGUCHI, Hitoshi KUBONIWA, Nobuya MURAKAMI, Akira HIRAO, Seiichi NAKAHAMA,* and Noboru YAMAZAKI

Department of Polymer Chemistry, Tokyo Institute of Technology, 2-12-1 Ohokayama, Meguro-ku, Tokyo 152

(Received August 23, 1988)

Seven ω-hydroxy carboxylic acids bearing 2—5 ether oxygens with or without aromatic rings and five ω-alkoxy carboxylic acids bearing 2—6 ether oxygens with aromatic rings were employed as carriers for the active transport of alkaline earth metal ions as well as alkali metal ions through 1,2-dichloroethane or 1-hexanol as an organic liquid membrane. The relatively hydrophobic ω-hydroxy and ω-alkoxy carboxylic acids ($\log P>7$) exhibited a high M^{2+} transport ability and selectivity over M^+ through 1,2-dichloroethane, regardless of the number of ether oxygen. However, a marked selectivity among alkaline earth metal ions (Mg^{2+}, Ca^{2+}, Ba^{2+}) was not observed. The less hydrophobic carboxylic acids ($\log P<6$) did not transport Ba^{2+} through 1,2-dichloroethane. Ba^{2+} transport ability of the hydrophobic acids through 1-hexanol was lower than that through 1,2-dichloroethane. Linoleic acid in the presence of oligo- and polyethylene glycols showed efficient Ba^{2+} transport through 1,2-dichloroethane, although a long-chain fatty acid was not able to transport Ba^{2+} by itself.

Naturally occurring carboxylic acid ionophores have ether linkages in the framework and hydroxyl group at the other end. The ionophore forms a pseudo-cavity by head-to-tail hydrogen bonding between carboxyl and hydroxyl groups. When the ionophore forms a salt with a cation, the cation is trapped in the cavity and is coordinated with ether oxygen atoms of ionophores. The cation was thereby lipophilized and transported through biological and organic liquid membranes.[2] Each ionophore exhibits a particular ion selectivity. A few of the ionophores, such as lasalocid and A 23187, which are able to complex and transport divalent cations as well as monovalent ones, are called divalent polyether antibiotics.[2,3] Their backbones are considerably shorter than those of monovalent polyether antibiotics. Despite the short chain length, the coordination of two ionophore anions to M^{2+} makes the complex lipophilic.

We synthesized polyether carboxylic acids, the structures of which were analogous to the natural carboxylic ionophores (as mentioned above). These synthetic ionophores were employed for the transport of alkali metal ions through an organic liquid membrane in order to investigate the relationship between the primary structures of ionophores and the transport ability and selectivity.[1a,4] We report here the transport of alkaline earth metal ions by synthetic carboxylic ionophores with a variety of chain lengths, the carboxylic acid moiety at the terminal, and the structure at the other terminal. Although a few synthetic ionophores have already been reported for the transport of alkaline earth metal ions,[5] the purpose of this study is to use a series of our synthetic carboxylic ionophores for the transport of divalent ions as well as monovalent ones for a comparison. The cooperative transport of alkaline earth metal ions with carboxylic acid and polyether in separate molecules is also described.

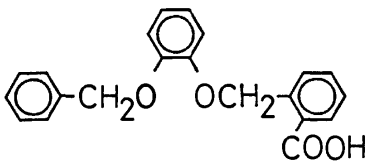

1

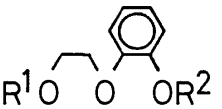

2; R^1=H, R^2=*o*-CH_2-C_6H_4-COOH
3; R^1=CH_3, R^2=*o*-CH_2-C_6H_4-COOH
4; R^1=$PhCH_2$, R^2=*o*-CH_2-C_6H_4-COOH

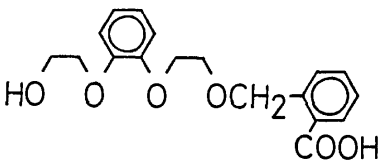

5

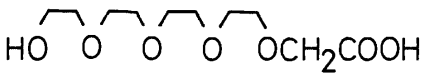

6

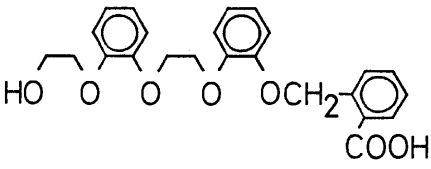

7

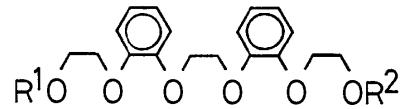

8; R^1=R^2=H
9; R^1=R^2=CH_3
10; R^1=H, R^2=*o*-CH_2-C_6H_4-COOH
11; R^1=CH_3, R^2=*o*-CH_2-C_6H_4-COOH
12; R^1=$PhCH_2$, R^2=*o*-CH_2-C_6H_4-COOH
13; R^1=H, R^2=*m*-CH_2-C_6H_4-COOH
14; R^1=H, R^2=*p*-CH_2-C_6H_4-COOH

Scheme 1. Polyether carboxylic acids.

Results and Discussion

Synthetic ionophores employed in this study are shown in the order of numbers of hydroxyl and ethereal oxygens in Scheme 1. Some of the compounds (**2**, **5**, **7**, **9**—**14**) have already been reported for the transport of alkali metal ions,[1a] and the rest of them (**1**, **3**, **4**, **6**, **8**) are newly synthesized for this study (as described in the experimental sections).

Transport of Alkaline Earth Metal Ions by Synthetic Carboxylic Ionophores. The stoichiometry of **10** and metal ions in chloroform was investigated (Fig. 1). It was revealed that at pH ca. 7, neither K^+ nor Ba^{2+} was incorporated into organic layer, but that at higher pH, 1 : 1 and 2 : 1 complexes of **10** were formed with K^+ and Ba^{2+}, respectively. Compound **10** containing one carboxyl group forms a neutral 1 : 1 complex of a potassium carboxylate, whereas divalent Ba^{2+} was complexed with two ionophore anions. This is consistent with the stoichiometry of complex for natural carboxylic ionophores.[3b,6] A 2 : 1 complex of ionophore and alkaline earth metal ion, where the cation is surrounded by two ionophore carboxylate molecules, is anticipated to be more hydrophobic than the corresponding 1 : 1 complex with alkali metal ion. This would result in an easy incorporation of M^{2+} into the organic layer, compared with M^+.

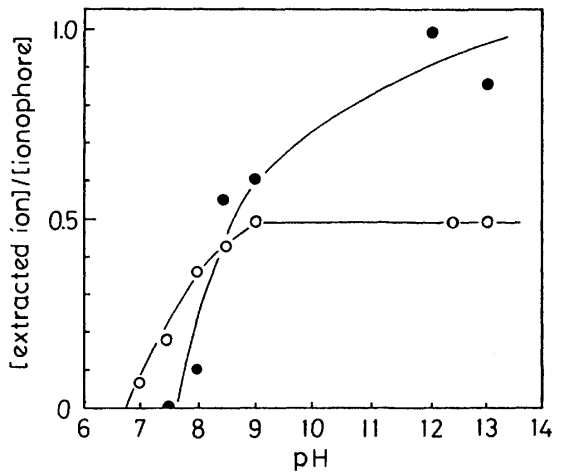

Fig. 1. Extracted amount of ions from aqueous solutions at various pH's to chloroform layer by **10**.
●: K^+, ○: Ba^{2+}

Table 1. Active Ion Transport by **10** and **7** through 1,2-Dichloroethane

Compound	Transported ion (%)[a]						
	Li^+	Na^+	K^+	Mg^{2+}	Ca^{2+}	Ba^{2+}	total
10	—	—	11	—	—	82	93
	—	3	—	—	—	94	97
	0	—	—	—	—	100	100
	—	—	17	—	74	—	91
	—	2	—	—	86	—	88
	0	—	—	—	99	—	99
	1	—	—	75	—	—	76
	—	—	—	—	45	48	93
	—	—	—	35	—	44	79
	0	—	—	41	45	—	86
7	—	—	8	—	—	91	99
	—	—	—	—	52	41	93

a) No ion is transported without ionophore.

The competitive transport of alkali and alkaline earth metal ions by **10** and **7** through 1,2-dichloroethane was carried out as shown in Table 1. Both ionophores exhibited K^+ selectivity among Li^+, Na^+, and K^+, as previously reported.[1a] Divalent cations (Ba^{2+}, Ca^{2+}, and Mg^{2+}) were transported in preference to monovalent cations. Among the divalent cations, little selectivity was observed.

Through a 1-hexanol membrane mono- and divalent ions were transported by **10** (Table 2). Compared with 1,2-dichloroethane the 1-hexanol membrane lowered the transport ability and the selectivity of the ionophore. From these results, it can be presumed that the ionophore functions only as an anionic ligand of the carboxylate in 1-hexanol, and that a cation in the salt is solvated by 1-hexanol molecules instead of ether oxygens of the ionophore.

Ionophores which have fewer ether oxygens or fewer aromatic rings than **10** were employed for Ba^{2+} transport through 1,2-dichloroethane. Table 3 shows the results together with the hydrophobicity parameter ($\log P$) of the ionophores.[1a] Compounds with $\log P$ of less than 6 (**6**, **2**, **5**, and **3**) did not transport Ba^{2+}. Ionophores with $\log P$ greater than 7 (**1**, **4**, **7**, **10**) transported Ba^{2+}, except for linoleic acid. Even **1**, bearing only two ether oxygens, has a high transport ability. In the case of ionophores with a low $\log P$ value, the salt complex formed at the interface is too hydrophilic to diffuse into the organic layer. Compounds, **6**, **2**, **5**,

Table 2. Active Ion Transport by **10** through 1-Hexanol

Transported ion (%)[a]				
Li^+	Na^+	K^+	Ba^{2+}	total
22(7)	—	—	38(0)	60(7)
—	17(9)	—	50(4)	67(13)
—	—	26(13)	38(0)	64(13)

a) Values in parentheses are transported ion without **10**.

Table 3. Ba^{2+} Transport through 1,2-Dichloroethane Using Various Ionophores

Ionophore	$\log P$	Transported Ba^{2+} (%)
6	−1.2	0
2	4.4	4
5	4.4	0
3	5.1	0
1	7.2	100
4	7.3	100
7	7.5	100
10	7.6	100
Linoleic acid	7.3	0

Table 4. Active Ion Transport Using Various Compounds

Compound	Liquid membrane	Transported ion (%)		
		K^+	Ca^{2+}	Ba^{2+}
10	1,2-Dichloroethane	—	—	100
		—	67	—
		49	—	—
11		—	75	—
12		—	—	98
		—	75	—
13		—	—	91
		0	—	—
14		—	—	89
		0	—	—
Linoleic acid		—	—	0
		0	—	—
10	1-Hexanol	—	—	68
13		—	—	66
14		—	—	60
Linoleic acid		—	—	67

and **3** ($\log P<6$) are not sufficiently hydrophobic to be an ion carrier. For more lipophilic compounds ($\log P>7$) two ether oxygens are sufficient for Ba^{2+} transport.

Ba^{2+} and Ca^{2+} were transported separately through 1,2-dichloroethane by **10** and its analogues (Table 4). For a comparison, K^+ transport was also carried out. Compounds **11** and **12**, hydroxyalkylated derivatives of **10**, revealed a comparable transport ability to **10**. Compounds **13** and **14**, *m*- and *p*-substituted isomers of **10**, were employed for Ba^{2+} transport. While neither **13** nor **14** transported K^+, both ionophores exhibited as high a transport ability for Ba^{2+} as **10**. A 2 : 1 complex of ionophore and M^{2+} seems to have a less rigid structure than the 1 : 1 complex does.[1b] In the 2 : 1 complex, ether oxygens of even *m*- and *p*-isomers are able to coordinate M^{2+} to be solubilized in the organic layer. These results show that if a ionophore has a carboxyl group and ether oxygens, the substituted position of the carboxyl group does not affect M^{2+} transport through 1,2-dichloroethane, in contrast to M^+ transport.

When 1-hexanol was used as a liquid membrane, linoleic acid had a similar transport ability to those of **10** and its isomers (Table 4). As mentioned above, the carboxylate anion of the ionophore interacts with the cation electrostatically and neither oxygens are very important for the transport of M^{2+}, compared to that of M^+. Water molecules are replaced out of the hydration sphere by 1-hexanol to solvate the divalent cation.

Transport of Alkaline Earth Metal Ions by Carboxylic Acids and Polyethers. As mentioned above, and reported previously,[1a] **10** exhibited the ability to transport monovalent ions through 1,2-dichloroethane, while its *m*- and *p*-substituted isomers, **13** and **14**, transported no alkali metal ion. On the other hand, divalent ions were transported by both **10** and its isomers. For alkaline earth metal ion transport, the relative position of the carboxyl group of ionophore to polyether linkages should not be important. It was expected that a simple carboxylic acid could transport M^{2+} in the presence of another polyether molecule. When a mixture of linoleic acid and diol **8**, each of which could not transport M^{2+}, was employed, 85% of Ba^{2+} was transported through 1,2-dichloroethane at 35 °C for 5 days. Under the same conditions, no K^+ was transported. A mixed system of carboxylic acid and ether was found to transport M^{2+} selectively. A mixture of diol **8** with various carboxylic acids as well as linoleic acid was applied to the transport of Ba^{2+}. The results are shown in Table 5. The hydrophobicity of the acids corresponds to the transport ability. Hydrophilic acids such as acetic, adipic, benzoic, hexanoic, and decanoic acids did not transport Ba^{2+}. A long-chain fatty acid such as lauric, myristic, palmitic, and linoleic acids transported Ba^{2+} in the presence of **8**. The transported amount of Ba^{2+} increased with an increase in the lipophilicity at acids. Unless the carboxylic acid was fully hydrophobic, the mixed system of carboxylic acid and **8** had no transport ability. Barium salts of hydrophilic carboxylic acids should be dissolved in an aqueous layer. Even if the salt is coordinated with polyether at the interface, the complex is not sufficiently hydrophobic to be incorporated into the organic layer. On the other hand, barium salts of lipophilic acids stayed mainly at interface, then, the replacement of water molecules out of the hydration sphere by the oxygens of **8** dissolved Ba^{2+} into the organic layer.

Table 5. Ba^{2+} Transport through 1,2-Dichloroethane Using Various Carboxylic Acids and **8**

Carboxylic acid	log *P*	Transported Ba^{2+} (%)
CH_3COOH	−0.2	0
$HOOC(CH_2)_4COOH$	0.7	0
PhCOOH	1.6	0
$CH_3(CH_2)_4COOH$	1.9	0
$CH_3(CH_2)_8COOH$	3.9	0
$CH_3(CH_2)_{10}COOH$	4.9	19
$CH_3(CH_2)_{12}COOH$	5.9	72
$CH_3(CH_2)_{14}COOH$	6.9	52
Linoleic acid	7.3	85

The effect of the polyether structure on ion transport was examined. Ba^{2+} transport by using linoleic acid together with various polyether compounds is shown in Table 6. Glycols and their derivatives were used as polyether. Ba^{2+} was not transported by ethylene glycol and the transported amount of Ba^{2+} increased with an increase in the oxyethylene units. Since a short-chain glycol is, itself, slightly soluble in an organic solvent, the coordinated glycol with Ba^{2+} of the salt is not sufficiently lipophilic to be incorporated into the organic layer. However, a stable complex of the salt with a long-chain glycol, such as tetraethylene glycol and polyethylene glycols, results in an increase in Ba^{2+} transport. Methyl ether derivatives (diglyme, tetraglyme, and **9**) exhibited a much lower transport ability

Table 6. Ba^{2+} Transport through 1,2-Dichloroethane by Linoleic Acid and Polyethers

Polyether	Transported Ba^{2+} (%)
Ethylene glycol	0
Diethylene glycol	38
Diglyme	22
Triethylene glycol	33
Tetraethylene glycol	75
Tetraglyme	9
Poly(ethylene glycol) (M_n=1000)	96
Poly(ethylene glycol) (M_n=7500)	95
8	85
9	2

than the corresponding glycols. The terminal hydroxy groups of the glycols seem to play an important role in the transport of Ba^{2+}.

Experimental

Methods. IR spectra were run with a Jasco IR-G spectrophotometer. ^1H NMR spectra were recorded with a JEOL JNM-PMX 60 instrument. UV spectra were recorded on a Hitachi 124 spectrophotometer. Mass spectra were obtained on a Hitachi M-80 mass spectrometer operating at 30 eV. Elemental analyses were performed on a Yanaco Model MT-3. Atomic absorption and flame spectrochemical analyses were performed with Hitachi 170—30 Atomic Absorption Spectrophotometer.

Materials. Unless stated otherwise reagent grade reactants and solvents were obtained from commercial suppliers and used without further purification.

Compound **1** was synthesized from 2-benzyloxyphenol[7] and with methyl 2-bromomethylbenzoate similar to synthesis of **7** previously reported.[1a]

2-[2-(2-Benzyloxyphenoxy)methyl]benzoic Acid (1). Yield (0.70 g, 48%). IR(KBr) 1685 cm^{-1} (C=O); ^1H NMR ($CDCl_3$) δ=5.2 (s, 2H, benzyl), 5.6 (s, 2H, benzyl), 6.9 (s, 4H, phenylene), 7.2—8.3 (m, 9H, phenyl and aromatic of toluic acid). Calcd for $C_{21}H_{18}O_4$: C, 75.43; H, 5.43%. Found: C, 75.60; H, 5.45%.

Compound **3** was prepared from **2** and methyl iodide and **4** was prepared from **2** and benzyl chloride by the same procedure as that for **11**.[1a]

2-[[2-(2-Methoxyethoxy)phenoxy]methyl]benzoic Acid (3). Yield (0.35 g, 75%). IR(KBr) 1715 cm^{-1} (C=O); ^1H NMR ($CDCl_3$) δ=3.45 (s, 3H, CH_3O), 3.83 (m, 2H, CH_2OMe), 4.20 (m, 2H, CH_2OAr), 5.51 (s, 2H, benzyl), 6.90 (s, 4H, phenylene), 7.3—8.1 (m, 4H, aromatic of toluic acid). High-resolution mass spectrum for $C_{17}H_{18}O_5$, Calcd 302.1154, Found 302.1116.

2-[[2-(2-Benzyloxyethoxy)phenoxy]methyl]benzoic Acid (4). Yield (0.13 g, 33%). IR(KBr) 1675 cm^{-1} (C=O); ^1H NMR ($CDCl_3$) δ=3.9 (m, 2H, CH_2), 4.3 (m, 2H, CH_2), 4.7 (s, 2H, benzyl), 5.6 (s, 2H, benzyl), 6.9 (s, 4H, phenylene), 7.3—8.3 (m, 8H, aromatic of toluic acid). Calcd for $C_{23}H_{22}O_5$: C, 73.00; H, 5.86%. Found: C, 72.54; H, 5.81%.

14-Hydroxy-3,6,9,12-tetraoxatetradecanoic Acid (6). Small pieces of Na (9.2 g, 0.4 mol) were by portions added to tetraethylene glycol (120 ml) (distilled under reduced pressure) under a nitrogen atmosphere. The mixture was heated at 100 °C for 6 h. Chloroacetic acid (18.9 g, 0.2 mol) in tetraethylene glycol (40 ml) was added dropwise to the alkoxide solution and the mixture was heated at 100 °C for 3 h. Excess of tetraethylene glycol was distilled under reduced pressure. To the residue was added concd HCl (100 ml) to form a white precipitate. The solid was removed by suction and the filtrate was evaporated under reduced pressure to remove water and HCl. The residue was distilled under vacuum to afford **6** (30 g, 60%). Bp 148—151 °C/1 mmHg (1 mmHg=133.322 Pa). IR(neat) 1740 cm^{-1} (C=O); ^1H NMR (CD_3OD) δ=3.65 (m, 16H, OCH_2COOH and CCH_2OC), 4.19 (t, 2H, CH_2OH, J=6 Hz). Calcd for $C_{10}H_{20}O_7$: C, 47.61; H, 7.99%. Found: C, 47.42; H, 8.27.

1,2-Bis[2-(2-methoxyethoxy)phenoxy]ethane (9). 1,2-Bis-[2-(2-hydroxyethoxy)phenoxy]ethane (3.4 g, 10 mmol) and 60% NaH (0.8 g, 20 mmol) in dry DMF (30 ml) were stirred at room temperature for 30 min. To this was added dropwise methyl iodide (2.9 g, 20 mmol) in dry DMF (20 ml); the mixture was stirred at room temperature for 2 h. DMF was removed in vacuo and the residue, dissolved in chloroform, was washed with water. The organic layer dried over sodium sulfate was evaporated and applied to a silica-gel column (chloroform/methanol=100/1) to afford 1,2-bis[2-(2-methoxyethoxy)phenoxy]ethane (2.9 g, 80%). ^1H NMR ($CDCl_3$) δ=3.40 (s, 6H, CH_3O), 3.73 (m, 4H, $OCH_2CH_2OCH_3$), 4.16 (m, 4H, $OCH_2CH_2OCH_3$), 4.38 (s, 4H, $ArOCH_2CH_2$), 6.90 (s, 8H, aromatic).

Stoichiometry of Complex of 10 and Metal ion in Chloroform. Chloroform saturated with water and water saturated with chloroform were used. A 10-ml chloroform solution of 5×10^{-5} mol of **10** and a 5-ml aqueous tris buffer solution (pH 7—9) containing $BaCl_2$ (0.05 M) or KCl (0.1 M) (1 M=1 mol dm^{-3}) in a 30-ml vial were vigorously shaken 60 times by hand. The vial was allowed to stand for 1 day in order to separate the organic layer from the aqueous layer. At higher pH, a metal hydroxide solution at an appropriate concentration was used instead of a tris buffer solution. A part of the organic layer (5 ml) was transferred to another 30-ml vial. To this was added a 5-ml HCl solution (0.2 M). The mixture was vigorously shaken 60 times by hand. The vial was allowed to stand for 1 day in order to separate the layers. The organic solution was diluted 100 times to determine the concentration of **10** by UV spectroscopy (273 nm). The aqueous solution was diluted 10 times to determine the concentration of K^+, or Ba^{2+} by flame spectrochemical analysis or atomic absorption analysis.

Ion Transport Experiment. Ion transport was carried out in U-type or H-type cells[4b] at 35±1 °C for 5 days with stirring at 200 rpm. Donor phase-I contains a 10-ml aqueous solution of an alkaline earth metal hydroxide (0.05 M). Acceptor phase -II contains a 10-ml aqueous solution of HCl (0.1 M) and an alkaline earth metal chloride (0.05 M). In the case of competitive ion transport, both the donor and acceptor phases also contain alkali or alkaline earth metal chlorides at the same concentration. Organic phase-III contains a 20-ml organic solution of a 10^{-4} mol carboxylic acid (and a 10^{-4} mol polyether). An aqueous solution at acceptor phase was diluted to an appropriate volume. The concentration of ions (10—100 ppm for M^+, 20—140 ppm for Ba^{2+} and Ca^{2+}, 1—20 ppm for Mg^{2+}) was determined to be c_0 and c_1 before and after the transport experiment by a flame spectrochemical analysis for alkali metal ions and by an atomic absorption analysis for alkaline earth metal ions. The transported ions (%) were calculated by $[(c_1-c_0)/c_0]\times100$.

References

1) a) Part VI: K. Yamaguchi, S. Negi, S. Kozakai, R. Nagano, H. Kuboniwa, A. Hirao, S. Nakahama, and N. Yamazaki, *Bull. Chem. Soc. Jpn.*, **61**, 2047 (1988); b) Part VII: H. Kuboniwa, K. Yamaguchi, S. Nakahama, K. Hori, and Y. Ohashi, *Chem. Lett.*, **1988**, 923.

2) R. Hilgenfeld and W. Saenger, "Topics in Current Chemistry 101. Host Guest Complex Chemistry II," ed by F. Vögtle, Springer-Verlag, Berlin (1982); pp. 1—82, and references cited therein.

3) a) H. Degani and H. L. Friedman, *Biochemistry*, **13**, 5022 (1974); b) D. R. Pfeiffer, P. W. Reed, and H. A. Lardy, *Biochemistry*, **13**, 4007 (1974).

4) a) N. Yamazaki, S. Nakahama, A. Hirao, and S. Negi, *Tetrahedron Lett.*, **1978**, 2429; b) N. Yamazaki, A. Hirao, and S. Nakahama, *J. Macromol. Sci.-Chem.*, **A13**, 321 (1979); c) H. Kuboniwa, K. Yamaguchi, A. Hirao, S. Nakahama, and N. Yamazaki, *Chem. Lett.*, **1982**, 1937; d) H. Kuboniwa, S. Nagami, K. Yamaguchi, A. Hirao, S. Nakahama, and N. Yamazaki, *J. Chem. Soc., Chem. Commun.*, **1985**, 1468.

5) a) M. J. Umen and A. Scarpa, *J. Med. Chem.*, **21**, 505 (1978); b) W. Wierenga, B. R. Evans, and J. A. Wolterson, *J. Am. Chem. Soc.*, **101**, 1334 (1979); c) K. Hiratani, H. Sugihara, K. Taguchi, and K. Iio, *Chem. Lett.*, **1983**, 1657; d) K. Taguchi, K. Hiratani, and H. Sugihara, *Chem. Lett.*, **1984**, 1457.

6) G. D. Smith and W. L. Duax, *J. Am. Chem. Soc.*, **98**, 1578 (1976).

7) W. L. Nelson, J. E. Wennerstrom, D. C. Dyer, and M. Engel, *J. Med. Chem.*, **20**, 880 (1977).

Efficient Synthetic Method for Differentially Protected Naturally Occurring Acyclic Polyamines

Masaaki IWATA* and Hiroyoshi KUZUHARA
RIKEN (The Institute of Physical and Chemical Research), Wako, Saitama 351-01
(Received August 25, 1988)

A new systematic route to threefold protected natural polyamines, spermidine, spermine, thermine, and thermospermine, was developed through alternate regioselective manipulation on the terminal primary amino groups, starting from *N,N*-phthaloyl-1,3-propanediamine hydrochloride (**3**). When **3** was tosylated at the amine terminal and the phthaloyl terminal was subjected to transformation to the formamido group followed by substitution at the tosyl terminal with, e.g., *N*-(4-bromobutyl)phthalimide, threefold protected spermidine was obtained in excellent yield. After hydrolysis of the formamido group to amine salt, a sequence of the reactions was satisfactorily repeated to afford various types of threefold protected natural tetramines.

Feasible synthetic methods for differentially protected natural acyclic polyamines play the crucial role in the total synthesis of polyamine conjugates[1] since the polyamine moiety has to be introduced regiospecifically at the proper step of the synthesis. In particular, in unsymmetrical natural polyamine-derived conjugates such as spermidine and thermospermine conjugates, the terminal primary amino groups have to be differentiated essentially for orientated introduction. In the literature survey, practical methods hitherto devised for discrimination of amino group have relied on (i) the reactivity difference in amino groups,[2] (ii) stoichiometric control of reactants in the level of triamine formation,[3] and (iii) the extension of differential protection generated in the level of diamine formation through the traditional way of stepwise synthesis.[4] Since the first method depends on the intrinsic nature of reactivity difference in amino groups of expensive spermidine as a starting material, it is inadequate for a large scale synthesis and for versatile synthetic utility.

We have recently found the novel transformation reaction[5] specific for *N,N:N′,N′*-diphthaloyl-1,3-propanediamine (**1**). In the transformation reaction *N,N*-phthaloyl-1,3-propanediamine hydrochloride (**3**) is readily obtained quantitatively passing through the fused heterocycle (**2**) prepared in high yield from **1**.[6]

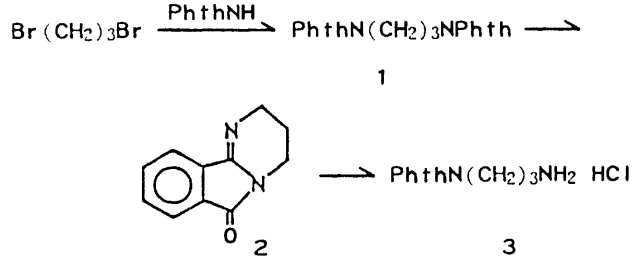

Since the transformation reaction indicates facile discrimination of the terminal primary amino groups in two steps, exemplification of synthetic feasibility of **3** was planned for molecular design of differentially protected polyamines, combining with another transformation reaction of phthalimides to formamides as follows;[7]

We set synthetic targets of threefold protected triamines (**C**) and tetramines (**F**) with the following types of functional groups;

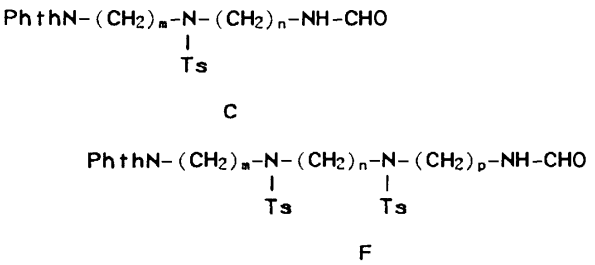

in which the primary amino groups at both ends are protected differently by the base- and hydrazine-sensitive phthaloyl group and by the acid-sensitive and reducible formyl group, respectively, and the secondary amino groups, by the photo-,[8] alkali metal- and HBr-sensitive tosyl group.[9]

The synthetic plan is shown in Scheme 1, which is characterized by alternate regioselective manipulation on the terminal primary amino groups in a systematic way as follows; to start with tosylation of **3** followed by the transformatlon of the phthalimido group to formamido group (**A**→**B**). Then, the tosylamino group at the other ω-terminus functioning as nucleophile reacts with ω-phthalimidated compounds, either **4**, **5**, or **6** (**B**→**C**). The formamido group is hydrolyzed to give ω-*N,N*-phthaloylated α,ω-diamine hydrochloride, which disposes the same functional groups as those of the starting **3** in a reversed order. Therefore, a series of the reactions will be repeated for construction of tetramines in a similar fashion, disposing the primary amino group outside in (**D**→**E**→**F**). Since there has been no report on nucleophilic reactivity of formamido nitrogen, **A** to **B** or **E** to **F** steps are crucial in the present plan in which the terminus of diamine **B** or **E**, bearing both tosylamino and formamido groups, reacts with ω-phthalimidated compound (**4**).

1) Stepwise Differential Manipulation at the Terminal Groups.

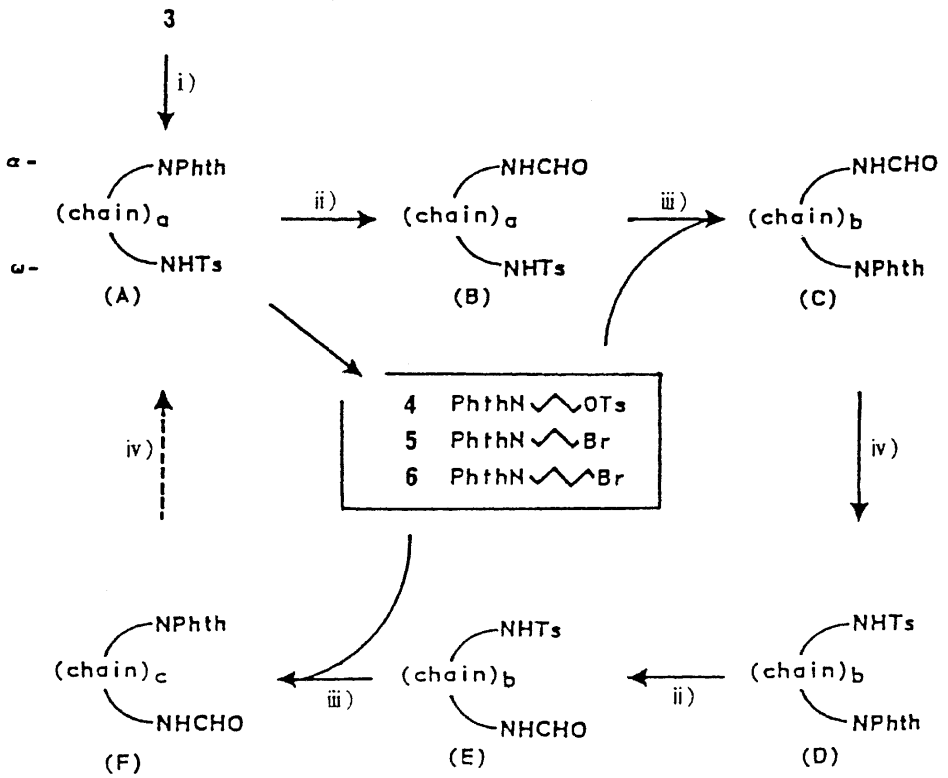

i) $TsCl/Py/NEt_3$, ii) N_2H_4 H_2O/DMF, iii) Cs_2CO_3/DMF, iv) 2M-HCl then i).

2) Correlation Diagram of the Methylene Chain Array with Nitrogen Content Involved in A through F Compounds.

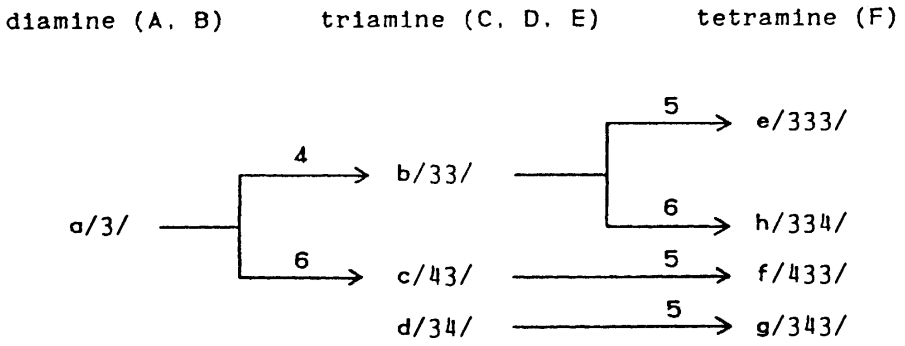

Scheme 1.

Results and Discussion

In the presence of triethylamine, **3** was tosylated with tosyl chloride in pyridine to give **Aa**,[10] which was treated with hydrazine hydrate in DMF to afford **Ba**. Alternatively, nitrosation of **Aa** followed by the rearrangement reaction in benzene gave **4**.[6,11] Condensation of **Ba** with **4** was best carried out by the use of cesium carbonate in DMF[6] to give the aimed threefold protected **Cb** exclusively. This reveals that the formamido nitrogen is far less reactive as nucleophile than the tosylamino nitrogen. Likewise, threefold protected spermidine (**Cc**) was obtained by the reaction of **Ba** with **6**. Hydrolysis of **C** in a mixed solvent of ethanol and 2 M HCl was completed at 75 °C for 3 h to yield the corresponding hydrochloride salts, which

were satisfactorily tosylated with tosyl chloride in pyridine in the presence of triethylamine to afford **D**. Since the present strategy is started with **3**, it is impossible to prepare **Dd** which bears the same functional groups at each primary amines in the opposite order to those of **Dc**. Therefore, **Dd** was supplied by the reaction of *N,N'*-ditosyl-1,4-butanediamine with **4**. All the **D** series of compounds were subjected to the transformation with hydrazine hydrate in DMF,[7] in the same way as **A** to **B** conversion, to afford **E** series. At this stage, we were ready to carry out the *N*-alkylation at the α-terminus with ω-phthalimidated compounds, **5** and **6**, to construct the second series of threefold protected natural tetramines (**F**). Symmetrical thermine derivative,[12a] **Fe**, was prepared by the reaction of **Eb** with **5** in DMF in the presence of cesium carbonate. Likewise, two isomers of unsymmetrical thermospermine derivatives,[12b] **Ff** and **Fh**, were prepared by the

Table 1. Product Yield(%) of Systematic Differential Protection of Amino Groups[a]

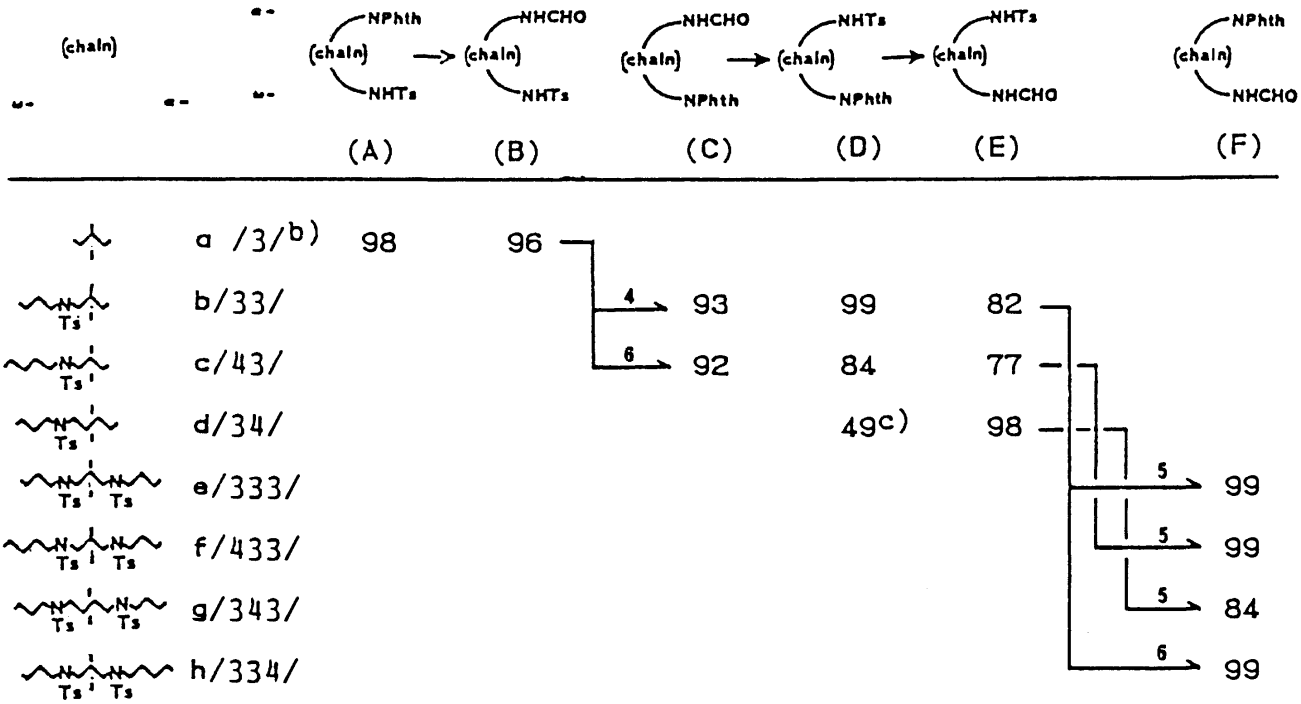

a) The transformation/substitution products are correlated by the arrow, the number on which corresponds to a electrophile employed in Scheme 1. b) the abbreviated chain symbol in the second column stands for the contiguous methylene chain blocks in Arabic numerals with default of nitrogen atoms between slant lines. In the first column, ω-terminus is placed at the left side and α-terminus, at the right side. These termini were arbitrarily chosen, independent of the nomenclature rule. c) **Dd**, obtained as by-product in the separate route (see Experimental).

Table 2. Chemical Shifts of Methylene Protons in ^{1}H NMR Spectra for Differentially Protected Polyamines, **B** through **F**.[a] (δ/ppm, in $CDCl_3$)

Compd		C1	C2	C3	C5	C6	C7	C8	C9	C10	C11	C12
Ba	3	3.40	1.70	2.96								
Cb	33	3.48	1.82	3.17	3.19	1.90	3.70					
Cc	43	3.44	1.77	3.16	3.14	1.56	1.66	3.66				
Db	33	3.67	1.84	3.15	3.15	1.84	3.10					
Dc	43	3.05	1.76	3.14	3.10	1.51	1.63	3.64				
Dd	34	3.78	1.87	3.15	3.04	1.71	1.60	2.99				
Eb	33	3.35	1.75	3.12	3.14	1.78	3.00					
Ec	43	3.03	1.78	3.13	3.08	1.55	1.55	3.31				
Ed	34	3.41	1.78	3.13	3.06	1.61	1.52	2.93				
Fe	333	3.43	1.82	3.16	3.12	1.88	3.15		3.16	1.94	3.71	
Ff	433	3.71	1.89	3.17	3.13	1.96	3.16		3.09	1.67	1.60	3.35
Fg	343	3.42	1.80	3.16	3.13	1.59	1.59	3.15		3.15	1.88	3.67
Fh	334	3.43	1.81	3.15	3.11	1.87	3.13		3.11	1.55	1.66	3.67

a) See Ref. 13 for the significance of abbreviated designation.

Table 3. Chemical Shifts of Miscellaneous Protons in ^{1}H NMR Spectra for Differentially Protected Polyamines, **B** through **F**.[a] (δ/ppm, in $CDCl_3$)

Compd	ArMe	NH-Ts	NH-CHO	CHO	ArHme	ArHs	PhthH
Ba 3	2.43	5.45	6.02	8.16	7.31	7.74	
Cb 33	2.42		6.37	8.21	7.29	7.65	7.73, 7.84
Cc 43	2.40		6.38	8.21	7.29	7.66	7.73, 7.84
Db 33	2.43	5.36			7.31	7.64, 7.76	7.72, 7.84
Dc 43	2.41, 2.43	5.35			7.29, 7.31	7.65, 7.77	7.72, 7.86
Dd 34	2.42, 2.43	5.15			7.30, 7.31	7.65, 7.75	7.73, 7.82
Eb 33	2.43	5.30	6.24	8.16	7.31, 7.32	7.65, 7.74	
Ec 43	2.43, 2.44	4.97	6.36	8.20	7.32, 7.33	7.67, 7.77	
Ed 34	2.43	5.37	5.80	8.18	7.31	7.65, 7.75	
Fe 333	2.42		6.45	8.20	7.31, 7.32	7.64, 7.66	7.75, 7.84
Ff 433	2.42, 2.43		6.17	8.17	7.31	7.65	7.73, 7.84
Fg 343	2.42, 2.43		6.41	8.19	7.30, 7.32	7.64, 7.67	7.73, 7.86
Fh 334	2.40, 2.43		6.42	8.20	7.29, 7.33	7.64, 7.66	7.72, 7.84

a) See Ref. 13 for the significance of abbreviated designation.

reaction of **Ec** with **5** and **Eb** with **6**, respectively. Threefold protected spermine derivative, **Fg**, was prepared from **Ed** and **5** as well. Relationshlp between starting materials and products are shown together with all the product yields in Table 1. Tables 2 and 3 are implicated to chemical shifts of all the protons in ^{1}H NMR spectra for **B** through **F** series of compounds.

In viewpoint of regioselectivity of the chain elongation and transformation and excellent product yields in each step, the present method for differential protection provides a new synthetic approach to polyamine conjugates. According to the present method, natural polyamines differentially modifiable at each terminus are supplied in a large scale from the cheap starting materials.

Experimental

General: The ^{1}H NMR spectra were recorded on JEOL GSX-500S (500 MHz) instrument with Me_4Si as an internal standard in $CDCl_3$ unless otherwise mentioned; chemical shifts (δ) and coupling constants (J) are in parts per million and hertz, respectively. Infrared spectra (IR) were obtained on a Shimadzu IR-27 apparatus. Merck sllica gel 60 (Art. 7734, 0.063—0.02) was used for column chromatography, and fragmented Merck precoated silica gel 60 F_{254} plates (Art. 5715, 20×20 cm), for thin layer chromatography (TLC). Product spots on TLC were detected either with UV-lamp or in an iodine vapor bath. The uncorrected melting points were measured in a bilayered coverglass (18 m/m, thickness 0.13—0.17 mm) with a micro melting point apparatus (Yanagimoto Seisakusho, Serial No. 2647).

Materials: *N,N*-Dimethylformamide (DMF) was dried over molecular sieves (Type A). Pyridine, triethylamine, tosyl chloride, hydrazine hydrate, anhydrous cesium carbonate, and sodium nitrite are purchased and employed without further purifIcation. The preparation of *N,N:N′,N′*-diphthaloyl-1,3-propanediamine (**1**) and its transformation to 3,4-dihydro-2*H*-pyrimido[2,1-*a*]isoindol-6-one (**2**) have been reported recently.[5] Hydrolysis of **2** to *N,N*-phthaloyl-1,3-propanediamine hydrochloride (**3**) and its tosylation to give *N,N*-phthaloyl-*N′*-tosyl-1,3-propanediamine (**Aa**) have been described in the preceding report.[6] ω-Phthalimidated electrophiles, **4**, **5**, and **6**, were prepared by the method in the preceding report.[6,11] N^1,N^1-Phthaloyl-4,N^8-ditosyl-4-azaoctane-1,8-diamine (**Dd**) was prepared as by-product in the following procedure; to a stirred mixture of Na-salt of *N,N′*-ditosyl-1,4-butanediamine[14] in DMF, **4** (2.6 mol equiv) in DMF was added dropwise at 80 °C. After workup, the residue was chromatographed on a silica-gel column to give *N,N′*-bis(3-phthalimidopropyl)-*N,N′*-ditosyl-1,4-butanediamine as a crystal in 44% yield[6] and **Dd** in 49% yield as viscous liquid; **Dd**, Found: C, 59.40; H, 5.71; N, 7.17; S, 10.71%. Calcd for $C_{29}H_{33}O_6N_3S_2$: C, 59.67; H, 5.70; N, 7.20; S, 10.99%. IR (KRS), ν 3290 (NH), 1770 and 1710 (CO), and 1330 and 1150 (SO_2) cm^{-1}.

General Procedure for Formation of Formamides (B and E) from Phthalimides (A and D): To a solution of phthalimide (**A** or **D**) in DMF, hydrazine hydrate (10 mol equiv) was added and the mixture was heated at 75 °C for more than 18 h. After removal of DMF under reduced pressure, the residue was chromatographed on a silica-gel column eluting with chloroform–methanol (9:1 v/v) to give formamide (**B** or **E**).

General Procedure for the Chain Elongation Reaction from ω-Formyl-α-*p*-toluenesulfonamides (B and E) to ω-Formyl-α-phthalimides (C and E): A mixture of formamidated *p*-toluenesulfonamide (**B** or **E**), one of appropriate ω-phthalimidated electrophile (**4**, **5**, or **6**) (1.1 mol equiv to **B** or **E**), and cesium carbonate (1.2 mol equiv) in DMF was stirred at ambient temperature for two days. The mixture was filtered through Celite, then the solvent was removed under reduced pressure. The residue was chromatographed on a silica-gel column eluting with chloroform–acetone (95:5 v/v) to give formamidated phthalimide (**C** or **F**).

General Procedure for Hydrolysis and Tosylation of α-Formy-ω-phthalimide (C) to Form α-Tosylamino-ω-phthalimide (D): To a solution of **C** in a small amount of ethanol, 2 M hydrochloric acid was added and heated at 80 °C for 4 h. The solvents were removed under reduced pressure and the residue was stirred with tosyl chloride (1.5 mol equiv to **C**) in pyridine containing a small amount of triethylamine at ambient temperature for 4 h. The solvents were evaporated under reduced pressure and the residue was chromatographed on a silica-gel column eluting with chloroform–acetone (9:1 v/v) to afford **D**.

N^1-Formyl-N^3-tosyl-1,3-propanediamine (Ba): viscous

liquid. Found: C, 51.55; H, 6.35; N, 10.94; S, 12.30%. Calcd for $C_{11}H_{16}O_3N_2S$: C, 51.54; H, 6.29; N, 10.93; S, 12.51%. IR (KRS) ν 3360, 3270 (NH), 1660, 1525, 1440 (C=O), 1320, 1150 (SO_2) cm^{-1}.

N^1-Formyl-N^7,N^7-phthaloyl-4-tosyl-4-azapheptane-1,7-diamine (Cb); mp 129—130 °C (spont. cryst.). Found: C, 59.32; H, 5.71; N, 9.53; S, 6.92%. Calcd for $C_{22}H_{25}O_5N_3S$: C, 59.58; H, 5.68; N, 9.48; S, 7.23%. IR (KBr) ν 3400 (NH), 1770, 1710 (C=O), 1670, 1520, 1435, (NHCHO), 1345, 1155 (SO_2) cm^{-1}.

N^7,N^7-Phthaloyl-N^1,4-ditosyl-4-azaheptane-1,7-diamine (Db); amorphous powder. Found: C, 59.05; H, 5.49; N, 7.17; S, 11.13%. Calcd for $C_{28}H_{31}O_6N_3S_2$: C, 59.03; H, 5.49; N, 7.38; S, 11.26%. IR (KBr) ν 3290 (NH), 1765, 1710 (C=O), 1330, 1155 (SO_2) cm^{-1}.

N^7-Formyl-N^1,4-ditosyl-4-azaheptane-1,7-diamine (Eb); viscous liquid. Found: C, 54.02; H, 6.35; N, 9.04; S, 13.74%. Calcd for $C_{21}H_{29}O_5N_3S_2$: C, 53.94; H, 6.25; N, 8.99; S, 13.72%. IR (KRS) ν 3380, 3290 (NH), 1670, 1520, 1450 (NHCHO), 1330, 1150 (SO_2) cm^{-1}.

N^1-Formyl-N^8,N^8-phthaloyl-4-tosyl-4-azaoctane-1,8-diamine (Cc); mp 103—104 °C (spont. cryst.). Found: C, 60.12; H, 6.01; N, 9.11; S, 6.88%. Calcd for $C_{23}H_{27}O_5N_3S$: C, 60.37; H, 5.95; N, 9.19; S, 7.01%. IR (KBr) ν 3320 (NH), 1770, 1700 (C=O), 1650, 1535 (NHCHO), 1340, 1160 (SO_2) cm^{-1}.

N^8,N^8-Phthaloyl-N^1,4-ditosyl-4-azaheptane-1,8-diamine (Dc); viscous liquid. Found: C, 59.89; H, 5.54; N, 7.04; S, 11.28%. Calcd for $C_{29}H_{33}O_6N_3S_2$: C, 59.67; H, 5.70; N, 7.20; S, 10.99%. IR (KRS) ν 3290 (NH), 1770, 1710 (C=O), 1330, 1160 (SO_2) cm^{-1}.

N^8-Formyl-N^1,4-ditosyl-4-azaheptane-1,8-diamine (Ec); viscous liquid. Found: C, 54.86; H, 6.49; N, 8.94; S, 13.04%. Calcd for $C_{22}H_{31}O_5N_3S_2$: C, 54.86; H, 6.49; N, 8.73; S, 13.32%. IR (KRS) ν 3370, 3290 (NH), 1665, 1525, 1450 (NHCHO), 1330, 1160 (SO_2) cm^{-1}.

N^1-Formyl-4,N^8-ditosyl-4-azaheptane-1,8-diamine (Ed); viscous liquid. Found: C, 54.67; H, 6.51; N, 8.70; S, 13.04%. Calcd for $C_{22}H_{31}O_5N_3S_2$: C, 54.86; H, 6.49; N, 8.73; S, 13.32%. IR (KRS) ν 3370, 3280 (NH), 1670, 1530, 1450 (NHCHO), 1325, 1155 (SO_2) cm^{-1}.

N^1-Formyl-N^{11},N^{11}-phthaloyl-4,8-ditosyl-4,8-diazaundecane-1,11-diamine (Fe); viscous liquid. Found: C, 58.98; H, 5.94; N, 8.47; S, 6.88%. Calcd for $C_{32}H_{38}O_7N_4S_2$: C, 58.69; H, 5.85; N, 8.56; S, 7.01%. IR (KRS) ν 3380 (NH), 1770, 1710 (C=O), 1670, 1520, 1425 (NHCHO), 1330, 1150 (SO_2) cm^{-1}.

N^{12}-Formyl-,N^1,N^1-phthaloyl-4,8-ditosyl-4,8-diazadodecane-1,12-diamine (Ff); viscous liquid. Found: C, 59.14; H, 6.10; N, 8.33; S, 9.84%. Calcd for $C_{33}H_{40}O_7N_4S_2$: C, 59.26; H, 6.03; N, 8.38; S, 9.59%. IR (KRS) ν 3390 (NH), 1770, 1710 (C=O), 1670, 1520, 1435 (NHCHO), 1335, 1157 (SO_2) cm^{-1}.

N^1-Formyl-N^{12},N^{12}-phthaloyl-4,9-ditosyl-4,9-diazadodecane-1,12-diamine (Fg); viscous liquid. Found: C, 59.48; H, 6.15; N, 8.64; S, 9.25%. Calcd for $C_{33}H_{40}O_7N_4S_2$: C, 59.26; H, 6.03; N, 8.38; S, 9.59%. IR (KRS) ν 3390 (NH), 1770, 1710 (C=O), 1670, 1520, 1432 (NHCHO), 1334, 1155 (SO_2) cm^{-1}.

N^1-Formyl-N^{12},N^{12}-phthaloyl-4,8-ditosyl-4,8-diazadodecane-1,12-diamine (Fh); viscous liquid. Found: C, 59.56; H, 6.12; N, 8.44; S, 9.42%. Calcd for $C_{33}H_{40}O_7N_4S_2$: C, 59.26; H, 6.03; N, 8.38; S, 9.59%. IR (KRS) ν 3390 (NH), 1770, 1710 (C=O), 1670, 1520, 1435 (NHCHO), 1330, 1153 (SO_2) cm^{-1}.

We are indebted to Dr. Hiroshi Yamazaki and his staff in RIKEN for performing elemental analyses and to Dr. Jun Uzawa and Mrs. Tamiko Chijimatsu in RIKEN for measurement of ^1H NMR spectra. M. I. is grateful to the Ministry of Education, Science and Culture for a financial support by a Grant-in-Aid for Scientific Research (No. 62540397).

References

1) B. Ganem, *Acc. Chem. Res.*, **15**, 290 (1982); H. H. Wasserman and J. S. Wu, *Heterocycles*, **17**, 581 (1982); G. B. Henderson, P. Ulrich, A. H. Fairlamb, and A. Cerami, *J. Chem. Soc., Chem. Commun.*, **1986**, 593.

2) K. Chantrapromma, J. S. McManis, and B. Ganem., *Tetrahedron Lett.*, **21**, 2475 (1980).

3) H. Yamamoto and K. Maruoka, *J. Am. Chem. Soc.*, **103**, 6133 (1981).

4) E. Waelchli-Schaer and C. H. Eugster, *Helv. Chim. Acta*, **61**, 928 (1978).

5) Presented in part at the 55th Annual Meeting of the Chemical Society of Japan, Fukuoka, October, 1987, Abstr. No. 1X12.

6) Presented in part at the 57th Annual Meeting of the Chemical Society of Japan, Sendai, September, 1988, Abstr. No. 1F433; M. Iwata and H. Kuzuhara, *Bull. Chem. Soc. Jpn.*, **62**, 198 (1989).

7) M. Iwata and H. Kuzuhara, *Chem. Lett.*, **1986**, 951.

8) T. Hamada, A. Nishida, and O. Yonemitsu, *J. Am. Chem. Soc.*, **108**, 140 (1986).

9) T. W. Greene, "Protective Groups in Organic Synthesis," John Wiley and Sons Inc., New York (1981).

10) The notation of the protected polyamines is comprised of the combination of the type of the terminal functional groups in capital letter with the type of the inside chain in small alphabet.

11) M. Iwata and H. Kuzuhara, *J. Chem. Soc., Chem. Commun.*, **1985**, 918; M. Iwata and H. Kuzuhara, *Chem. Lett.*, **1985**, 1941; **1986**, 369.

12) a) T. Ohshima, *Biochem. Biophys. Res. Commun.*, **63**, 1093 (1975). b) *Idem, J. Biol. Chem.*, **254**, 8720 (1979).

13) Cl- through C12-protons are the methylene protons at the position ordered by the nomenclature rule. ArMe-protons designate methyl protons attached to aromatic ring. ArHme-protons designate aromatic protons disposed at position ortho to the methyl group. ArHs-protons designate aromatic protons disposed at position ortho to the sulfonyl group.

14) M. Iwata and H. Kuzuhara, *Bull. Chem. Soc. Jpn.*, **55**, 2153 (1982).

 © 1989 The Chemical Society of Japan Bull. Chem. Soc. Jpn., 62, 1107—1110 (1989)

The Photoinduced Removal of Nitro Groups from Steroidal 6-Membered α,α′-Dinitro Cyclic Ketones[1)]

Hiroshi SUGINOME* and Yoshitaka KUROKAWA
Organic Synthesis Division, Department of Chemical Process Engineering,
Faculty of Engineering, Hokkaido University, Sapporo 060
(Received September 2, 1988)

2,4-Dinitro-5α- and 5β-cholestan-3-ones were prepared by dinitration of the parent 3-ones by a modified standard method. Spectroscopy indicated that in ethanol these α,α′-dinitro ketones exist in their enol forms. Photolysis of these dinitro ketones in ethanol gave diosphenols arising from the removal of their two nitro groups. On the basis of the results of the irradiation of hypothesized intermediate obtained by synthesis, we suggest the path likely to lead to the removal of the nitro groups.

In our previous paper,[2)] we reported the results of the photoreaction of several steroidal 6-membered cyclic α-nitro ketones in ethanol. The investigation disclosed that steroidal 6-membered cyclic α-nitro ketones, which exist in ethanol in their enol form, give the corresponding α-hydroxyimino ketones arising from a hydrogen abstraction by the excited nitro group and the corresponding α-diketone arising from the nitro-nitrite rearrangement, while irradiation of 6-membered cyclic α-nitro ketones, which exist in ethanol in their keto forms, gave the corresponding α-hydroxyimino ketones without any accompanying formation of the corresponding α-diketones. An anomalous formation of 5α-cholestane-2,3-dione was found when 2-nitro-5α-cholestan-3-one, which in ethanol exists exclusively in its enol form was photolyzed. We then suggested the probable paths for the formation of all these products in the photolysis.

In this paper, we wish to report the results of the photoreaction of two steroidal 6-membered cyclic α,α′-dinitro ketones, 2,4-dinitro-5α-cholestan-3-one (**3**) and its 5β-epimer (**5**).

Preparation of the α,α′-Dinitro Ketones 3 and 5. The α,α′-dinitro ketones **3** and **5** chosen for the present study were prepared by α,α′-dinitration of 5α-and 5β-cholestan-3-one (**1** and **2**) with alkyl nitrate and potassium *t*-butoxide in *t*-butyl alcohol.[3)]

We found that the potassium salts of 2,4-dinitro-5α-cholestan-3-one (**3**) and 2,4-dinitro-5β-cholestan-3-one (**5**) readily gave the corresponding α,α′-dinitro ketones **3** and **5** with no accompanying formation of α,ω-secosteroids when the *dried* potassium salts dissolved in glacial acetic acid were poured into a large volume of iced water instead of being treated with HCl in a diethyl ether suspension.[3)] On the other hand, we found that the above treatment of the potassium salts contaminated with water led to the formation of α,ω-dinitro secosteroids[3-5)] (e.g., **4**).

We also found that the α,α′-dinitro ketone **3** is readily hydrolysed to α,ω-dinitro alkanes when **3** is heated in acetic acid-water under reflux for 3 h, is passed through a silica-gel column,[4)] or is subjected to preparative TLC on silica gel.

The IR spectrum of α,α′-dinitro-5α-cholestan-3-one (**3**) in Nujol indicated that in the mull it exists in a keto form **3a**. Its ^{1}H NMR spectrum in $CDCl_3$, however, exhibited two doublets at δ 2.32 and 2.78 (J=16.6 Hz) and a doublet at δ 5.08 (J=11.2 Hz) assignable to the C-1 methylene and the 4β-H of the enol form, 2,4α-dinitro-5α-cholest-2-en-3-ol (**3b**). The IR spectrum of

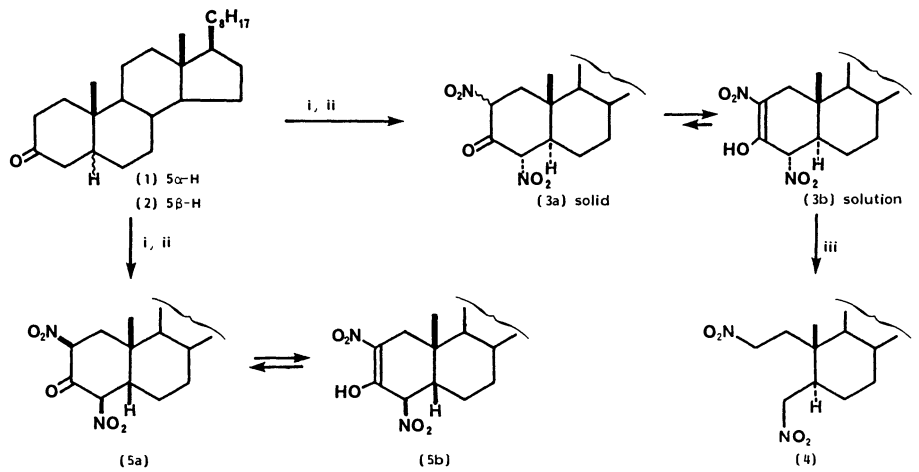

i) $CH_3CH_2CH_2ONO_2$–$(CH_3)_3COK$ ii) CH_3COOH iii) CH_3COOH–H_2O–reflux or SiO_2–H_3O^+

Scheme 1.

the solution ($CHCl_3$) and the UV spectra (hexane or ethanol) also indicated that in the solution it exists entirely in the enol form **3b**.

In contrast to the behavior of α,α'-dinitro-5α-cholestan-3-one (**3**), the IR spectrum of the 5β-epimer **5** in Nujol indicated that in the mull its keto and enol forms are in equilibrium. ^{1}H NMR spectrum of **5** in $CDCl_3$ exhibited a series of signals assignable both to the keto form, 2β,4β-dinitro-5β-cholestan-3-one (**5a**) and to the enol form, 2,4β-dinitro-5β-cholest-2-en-3-ol (**5b**). The ratio of the signal areas indicated that the ratio of the two forms was approximately 1 to 1 in $CDCl_3$ (see Experimental).

Photochemistry of α,α'-Dinitro-5α- and 5β-cholestan-3-ones (3 and 5). The photolysis of the two nitro ketones **3** and **5** was carried out in ethanol and in *t*-butyl alcohol under the conditions established for 6-membered cyclic α-nitro ketones reported in our previous paper.[2]

Photolysis of 2,4α-dinitro-5α-cholest-2-en-3-ol (**3b**) in ethanol with a Hanovia 450-W high-pressure mercury arc through a Pyrex filter in an atmosphere of nitrogen gave a product mixture from which a mixture of diosphenols, 3-hydroxy-5α-cholest-3-en-2-one **6** and its isomer **7**[2] was obtained in a 55% yield. Its purification by means of preparative TLC gave a 1 : 1 crystalline mixture of **6** and **7**. Essentially the same results were obtained when the photolysis was carried out in a less hydrogen-donating protic solvent, *t*-butyl alcohol.

Similar photolysis of an equilibrium mixture of 2β,4β-dinitro-5β-cholestan-3-one (**5a**) and 2,4β-dinitro-5β-cholest-2-en-3-ol (**5b**) gave a product in a 48% yield. Spectroscopy confirmed that the structure of the crystalline produt **8** was 3-hydroxy-5β-cholest-3-en-2-one (**8**). The diosphenol has been prepared by Sandmeier and Tamm only as a mixture of diosphenol **8** and 2-hydroxy-5β-cholest-1-en-3-one.[6]

The photochemistry of cyclic α,α'-dinitro ketones has never previously been reported.[7,8] Our present experiments show that the photolysis of α,α'-dinitro ketones in alcohol results in the efficient removal of the two nitro groups to give the corresponding α-diketones. Two probable paths leading to the α-diketones are outlined in Scheme 3. Thus, the first probable path would involve the removal of the 2-nitro group from an excited nitro ketone **A** through the species B, C, and D through a nitro nitrite rearrangement[8,9] to give 4-nitro-2,3-diketone **9** as in the case of the 6-membered cyclic α-nitro ketones reported in our previous paper.[2] A photoinduced homolysis of the C-N bond of 4-nitro-2,3-diketone **9** followed by the

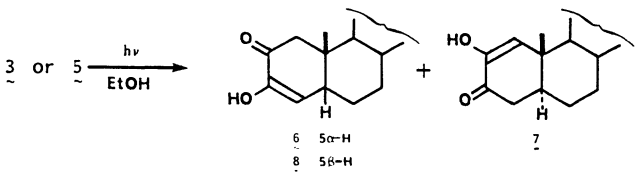

Scheme 2.

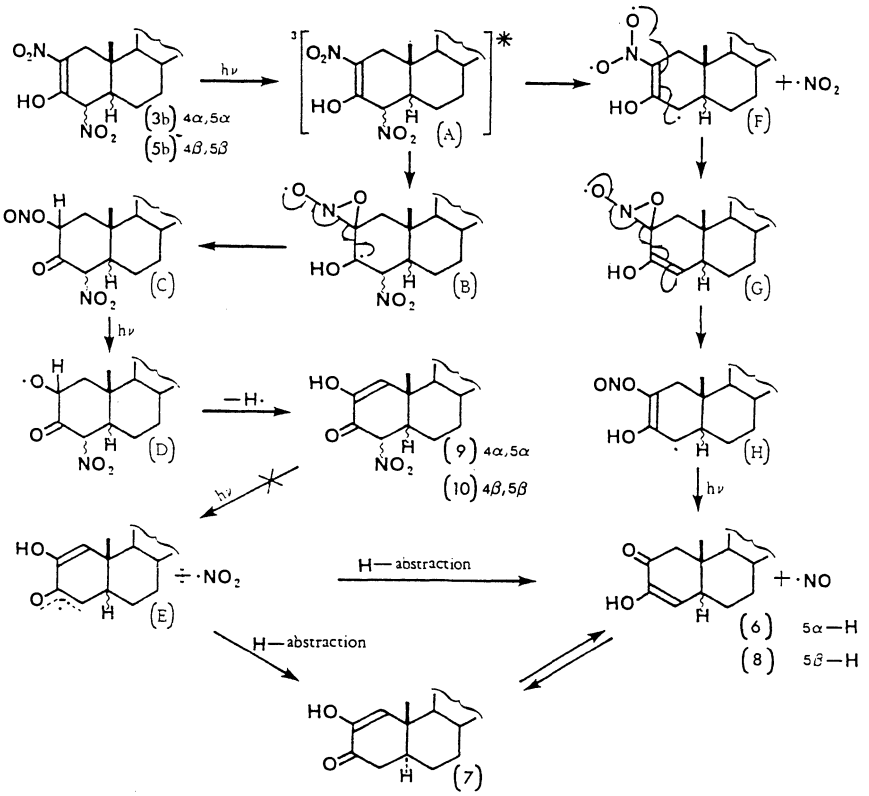

Scheme 3.

hydrogen abstraction from the solvent might then give the α-diketones **6**, **7**, and **8**.

A second possible path, on the other hand, would involve an initial homolysis of the C-N bond[10] of the 4-nitro group to give a nitrite radical **H** through an oxaziridine **G**. The homolysis of the C-N bond is considered to be especially facile since the generated species **F** is a stabilized allylic radical. In order to distinguish these two paths, we prepared 2-hydroxy-4α-nitro-5α-cholest-1-en-3-one **9** and carried out its photolysis.

Thus, nitration of 5α-cholestane-2,3-dione with butyl nitrate and potassium *t*-butoxide in THF gave mononitro-5α-cholestane-2,3-dione **9** in a 30% yield. The IR, NMR, and mass spectra confirmed that the structure was the desired 2-hydroxy-4α-nitro-5α-cholest-1-en-3-one (**9**). The IR spectra exhibited two bands at 1695 and 1648 cm^{-1} assignable to the α,β-unsaturated carbonyl group and a strong band at 1560 cm^{-1} due to the unconjugated nitro group. The ^1H NMR spectrum exhibited a singlet (1H) at δ 6.60 assignable to the proton attached to the C-1 and a doublet at δ 5.29 with J=13.55 Hz assignable to the 4β-proton.

We found that nitro ketone **9** is recovered unchanged when it is subjected to photolysis in ethanol for 3 h under the same conditions established for the photolysis of α,α'-dinitro ketone **3**. The result excludes the first path involving the intermediates **C** and **D** in the formation of α-diketones **6**, **7**, and **8**. The α-diketones are therefore very likely to be formed through intermediates **F**, **G**, and **H**, whose formations are triggered by the homolysis of the C_4-NO_2 bond.

Experimental

For the instruments used and the general procedure see Ref. 2.

Preparation of 2ξ,4α-Dinitro-5α-cholestan-3-one (3). Freshly sublimed potassium *t*-butoxide (4.0 g) was dissolved by heating in dry *t*-butyl alcohol (68 ml) in a nitrogen atmosphere. The solution was cooled to 19 °C and 5α-cholestan-3-one (**1**) (2.0 g) was dissolved in it. To the solution propyl nitrate (4 ml) was added over the course of 10 min and the solution was stirred for 20 h at 18—20 °C, after which the solution was poured into iced water. The separated potassium salt of dinitrocholestane was filtered off and dried. The yield of potassium salt was 2.468 g. The potassium salt was dissolved in glacial acetic acid and the solution was poured into iced water. The separated crystals of 2,3-dinitro-5α-cholestan-3-one (**3**) (2.3 g) were collected by filtration and recrystallized from ethyl alcohol. Mp 199—201 °C. IR (Nujol) 1737 (C=O) and 1558 cm^{-1} (NO_2); IR ($CHCl_3$) 1642 (C=C) and 1562 (4α-NO_2) and 1530 (br, 2-NO_2); (Found: C, 67.90; H, 9.37; N, 5.70%; Calcd for $C_{27}H_{44}N_2O_5$: C, 67.90; H, 9.31; N, 5.88%); UV (hexane), λ_{max} 308.5 nm (ε; 5790); (ethanol), 353 nm (ε; 8570); (ethanol and 1 equiv mol of sodium ethoxide), 345.5 nm (ε; 12170); ^1H NMR ($CDCl_3$), δ=0.67 (3H, s, 18-H), 0.87 (3H, s, 19-H), 2.32 (1H, d, J=16.60 Hz, 1-H), 2.78 (1H, d, J=16.60 Hz, 1-H), and 5.08 (1H, d, J=11.23 Hz, 4β-H); MS m/z (rel intensity) 476 (M^+, 87.8%), 430 (M^+-NO_2, 13.3), 322 (73.8), 321 (91.4), 69 (86.8), 57 (96.4), 55 (97.2), and 43 (100).

2,4-Dinitro-2,3-seco-*A*-nor-5α-cholestane (4). 2,4-Dinitro-5α-cholestan-3-one (**3a**) (50 mg) dissolved in glacial acetic acid (17 ml) and water (6 ml) was heated under reflux for 3 h. After the addition of hot water, the solution was extracted with dichloromethane three times. The combined solution was washed with water several times and dried over anhydrous sodium sulfate. The usual work-up gave a dinitro compound (63 mg), mp 165—169 °C. (lit,[5] 169—172 °C). UV, λ_{max} (EtOH) 277 nm (ε; 64); MS m/z (rel intensity) 450 (M^+, 23.8), 433 (M^+-NO_2, 9.8), 420 (19.8), 402 (15.5), 329 (18.3), and 55 (100%).

Preparation of 2,4-Dinitro-5β-cholestan-3-one (5a). Freshly sublimed potassium *t*-butoxide (3.0 g) was dissolved by heating in dry *t*-butyl alcohol (50 ml) in a nitrogen atmosphere. The solution was cooled to 20 °C and 5β-cholestan-3-one (**2**) (1.5 g) was added. To the solution, propyl nitrate (2 ml) was then added over a period of 10 min. More propyl nitrate (1 ml) was added after 30 min and the solution was stirred for 15 h at 16—20 °C. The solution was poured into iced water, and the mixture was made acidic (pH 3) with acetic acid. The orange colored precipitates were collected by filtration. The dried precipitates (2.0 g) were dissolved in glacial acetic acid (150 ml) and iced water (300 ml) was added to the solution. The colorless solid (1.83 g) was collected by filtration and dried. The dinitro ketone **5a** was recrystallized from ethanol to give crystals (698 mg, 37.2%), mp 177—179 °C. (Found: C, 68.03; H, 9.31; N, 5.85%. Calcd for $C_{27}H_{44}N_2O_5$: C, 68.03; H, 9.31; N, 5.88%); UV (EtOH) 353 nm (ε; 1060); IR (Nujol) 1751 (C=O) and 1655 (C=C) and 1548 (NO_2); ^1H NMR; the keto form, δ=0.66 (s, 18-H), 1.19 (s, 19-H), 5.33 (dd, J=12.4 and 5.12 Hz, 2α-H), and 5.58 (d, J=10.25 Hz, 4α-H), the enol form, 0.69 (s, 18-H), 1.26 (s, 19-H), 2.31 (d, J=17.09 Hz, 1-H), 3.08 (d, J=17.09 Hz, 1-H), and 5.71 (d, J=12.7 Hz, 4α-H); MS m/z (rel intensity) 476 (M^+, 18.7), 430 (M^+-NO_2, 31.9), 412 (19.5), 383 (36.4), 57 (100), and 55 (99.0%).

Photolysis of 2ξ,4α-Dinitro-5α-cholestan-3-one (3). (a) In Ethanol. α,α'-Dinitro ketone **3**, (300 mg, 0.63 mmol) in absolute ethanol (450 ml) was irradiated for 3 h with a Hanovia 450-W high-pressure mercury arc through a Pyrex filter in an atmosphere of dry nitrogen. Removal of the solvent under reduced pressure gave an oily residue (325 mg) which was subjected to preparative TLC with dichloromethane to give a mixture of diosphenols **6** and **7** (139 mg, 55.2%). This mixture was again purified by means of preparative TLC to give diosphenols (59 mg, 23.5%). This was recrystallized from methanol-water to give crystals of a 1 : 1 mixture of **6** and **7** (32 mg, 12%), mp 119—155 °C.

(b) In *t*-Butyl Alcohol. α,α'-Dinitro ketone **3** (300 mg) in dry *t*-butyl alcohol (350 ml) was similarly irradiated for 3 h. A similar work-up of the solution gave a mixture of diosphenols **6** and **7** (89 mg, 34.3%). This mixture was recrystallized from methanol to give crystals at a 1 : 1 mixture of **6** and **7** (26 mg, mp 129—155 °C).

Photolysis of 2,4-Dinitro-5β-cholestan-3-one (5). α,α'-Dinitro ketone **5**, (300 mg, 0.63 mmol) in absolute ethanol (400 ml) was irradiated for 6 h with a Hanovia 450-W high-pressure mercury arc through a Pyrex filter in an atmosphere of dry nitrogen. Removal of the solvent under a reduced pressure gave an oily residue (341 mg) which was subjected

to preparative TLC with dichloromethane to give diosphenol **8** (124 mg, 47.8%). This was recrystallized from diethyl ether-methanol to yield the specimens for analysis (74 mg), mp 157—162 °C. (Found: C, 80.94; H, 11.07%. Calcd for $C_{27}H_{44}O_2$: C, 81.00; H, 11.29%); IR (Nujol) 3528 and 2438 (OH), 1666 cm^{-1} (C=O); ^1H NMR (270 MHz) δ=0.64 (3H, s, 18-H), 1.11 (3H, s, 19-H), 2.23 (1H, d, J=16.6 Hz, 1β-H), 2.71 (1H, d, J=16.6 Hz, 1α-H), 5.75 (1H, d, J=2.93 Hz, 4-H) and 5.81 (1H, s, OH); MS, m/z (rel intensity) 400 (M^+, 100), 385 [$(M-Me)^+$, 7.9], 314 (38.9), 287 (37.7), 274 (18.3), 269 (18.3), 220 (15.4), 159 (25.0), 137 (43.5), 95 (42.1), 81 (38.0), 69 (36.8), 55 (47.7), and 43 (45.4).

Synthesis of 2-Hydroxy-4α-nitro-5α-cholest-1-en-3-one (9). To a solution of potassium *t*-butoxide (0.42 g) in THF (10 ml) at −40 °C, a solution of 5α-cholestane-2,3-dione[5] (0.5 g) in THF (10 ml) was added dropwise. To this solution, propyl nitrate (0.38 ml) was added and the temperature of the solution was then neutralized with glacial acetic acid and poured into iced water. The aqueous solution was extracted with diethyl ether. The organic layer was washed with water and dried over anhydrous Na_2SO_4. Evaporation of the solvent left a product (599 mg) which was recrystallized from methanol to give 4α-nitro-2-hydroxy-5α-cholest-1-en-3-one (**9**) (165 mg, 30 %), mp 157—161 °C. The specimen for analysis was obtained by recrystallization from methanol. Mp 159—161 °C. IR (Nujol) 3404 (OH), 1695 (C=O), 1648 (C=C), and 1560 cm^{-1} (NO_2); ^1H NMR (270 MHz) δ=0.69 (3H, s, 18-H), 1.13 (3H, s, 19-H), 5.29 (1H, d, J=13.55 Hz, 4β-H) and 6.60 (1H, s, 1-H); MS m/z (rel intensity) 445 (M^+, 9.8), 429 [$(M-O)^+$, 8.6], 415 [$(M-NO)^+$, 31.6], 398 [$(M-NO_2H)^+$, 100], 387 (27.9), and 137 (80%); UV (EtOH) λ_{max} 270 nm (ε; 7850); (Found; C, 72.46; H, 9.77; N, 2.90%. Calcd for $C_{27}H_{43}NO_4$; C, 72.77; H, 9.73; N, 3.14%).

Attempted Photolysis of 2-Hydroxy-4β-nitro-5α-cholest-1-en-3-one (9). Nitro enone **9** (50 mg) in absolute ethanol (50 ml) was irradiated through a Pyrex-filter in an atmosphere of nitrogen with a Hanovia 450-W Hg arc for 2 h. Removal of the ethanol gave an oil (47 mg). Examination of this oil by preparative TLC and ^1H NMR indicated that it was virtually the pure recovered starting material; this was confirmed by spectroscopy after purification.

References

1) Photoinduced Molecular Transformations. Part 102. Previous paper in this series; H. Suginome and Y. Kurokawa, *Bull. Chem. Soc. Jpn.*, **62**, 1343 (1989).

2) H. Suginome, Y. Kurokawa, and K. Orito, *Bull. Chem. Soc. Jpn.*, **61**, 4005 (1988).

3) H. Feuer, A. M. Hall, and R. S. Anderson, *J. Org. Chem.*, **36**, 140 (1971).

4) Y. Kobayashi, *Bull. Chem. Soc. Jpn.*, **46**, 3462 (1973).

5) D. J. Chadwick, W. R. T. Cottrell, and G. D. Meakins, *J. Chem. Soc., Perkin Trans. 1*, **1972**, 655.

6) R. Sandmeier and C. Tamm, *Helv. Chim. Acta*, **56**, 2238 (1973).

7) H. A. Morrison, "The Chemistry of Functional Groups" general ed by S. Patai; "The Chemistry of the Nitro and Nitroso groups, Part 1" ed by H. Feuer, Interscience Publ., New York (1969), pp. 165—213.

8) Y. L. Chow, "The Chemistry of Functional Groups" general ed by S. Patai; "The Chemistry of Amino, Nitroso, Nitro Compounds and Their Derivatives," ed by S. Patai, Wiley, New York (1982), pp. 181—290.

9) O. L. Chapman, P. G. Cleveland, and E. D. Hoganson, *J. Chem. Soc., Chem. Commun.*, **1966**, 101; G. W. Shaffer, *Can. J. Chem.*, **48**, 1984 (1970); J. T. Pinhey and E. Rizzardo, *Tetrahedron Lett.*, **1973**, 4057; I. Saito, M. Takami, and T. Matsuura, *Tetrahedron Lett.*, **1975**, 3155; R. G. Hunt and S. T. Reid, *J. Chem. Soc. Perkin Trems. 1*, **1977**, 2462; J. S. Cridland, P. J. Moles, S. T. Reid, and K. T. Taylor, *Tetrahdron Lett.*, **1976**, 4497; H. E. Zimmerman, L. C. Roberts, and R. R. Arnold, *J. Org. Chem.*, **42**, 621 (1977).

10) H. Suginome, K. Takakuwa, and K. Orito, *Chem. Lett.*, **1982**, 1357.

Inclusion Properties of Acyclic *p*-Substituted Phenol-Formaldehyde Oligomers

Tyo SONE,* Yoshihiro OHBA, and Hajime YAMAZAKI
Department of Applied Chemistry, Faculty of Engineering, Yamagata University, Yonezawa 992
(Received September 2, 1988)

Acyclic para-substituted phenol-formaldehyde oligomers (R=H, Me, *n*-Bu, *t*-Bu, and cyclohexyl; the number of phenol units=3—6) form host-guest complexes with various organic compounds. The inclusion property of the acyclic oligomers is greatly influenced by the *p*-substituents of phenol and the number of phenol units in the oligomers; for example, a) while the *t*-butyl tetramer is effective, the corresponding butyl tetramer has a poor ability for the complex formation, and b) the tetramers and pentamers are good hosts for organic compounds, forming 2:1 (host:guest) complexes in many cases.

Cyclic *p*-substituted phenol-formaldehyde oligomers with methylene bridges in positions ortho to the phenolic hydroxyl group, named "calixarene," are well-known to have the property of forming host-guest complexes with organic molecules.[1] The corresponding acyclic oligomers have also been found to form stable complexes, although only a few examples are available. For example, the trimer based on phenol (phenol trimer; **3e**) forms a complex with benzene;[2] the *p*-cresol tetramer (**4a**) forms complexes with $ClCH_2CH_2Cl$[3] or toluene;[4] the *p*-*t*-butylphenol tetramer (**4b**) forms a complex with cyclohexane.[5] It has been shown by X-ray analysis that the cyclic and acyclic oligomers are quite different from each other in conformation in the crystalline state[1,2] which plays an important role in the complex formation. This suggests that the inclusion property of acyclic oligomers differ from that of cyclic ones. There has, however, been no systematic study on the inclusion property of acyclic oligomers. We have investigated the subject and found that *p*-substituents of phenol and the number of phenol units in the oligomers have a striking effect on the inclusion property. The results will be reported.

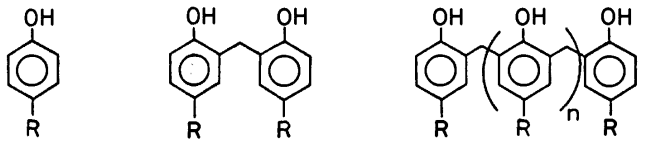

1 2 3: n=1 4: n=2 5: n=3 6: n=4

a: R=Me-
b: R=t-C_4H_9-
c: R=C_4H_9-
d: R=⬡-
e: R=H

Results and Discussion

Synthesis of Oligomers. In general, *p*-substituted phenol-formaldhyde oligomers are synthesized by the stepwise procedure[6,7] based on repeated hydroxymethylation-arylation reaction sequences on phenolic substrates. Except for the *p*-butylphenol tetramer (**4c**) and *p*-cyclohexylphenol tetramer (**4d**), all oligomers used in this study have been known. However, some of the oligomers could not be obtained in satisfactory yields by the reported procedures. Therefore, the synthetic routes were modified in such cases. For example, the tetramers **4a** and **4b** have been synthesized by the condensation of the bis(hydroxymethyl) dimer (**9a** or **9b**) with the corresponding phenol **1a** or **1b**. But **9b** could not be obtained in one step by the base-induced hydroxymethylation of *p*-*t*-butylphenol (**1b**) as described in the literature.[5] Such is also the case with the bis(hydroxymethyl) dimers **9c** and **9d**. The HCl-catalyzed condensation of **8b** with 10 molar equiv of **1b** gave the trimer **3b** in good yield. The NaOH-induced hydroxymethylation of **3b** with aq formaldehyde yielded the mono(hydroxymethyl) trimer **10b**, which was reacted with **1b** to afford **4b**. The tetramer **4d** was obtained by a similar method. On the other hand, the tetramer **4c** was synthesized by starting with 4-butyl-2-(hydroxymethyl)phenol (**7c**); the dimer **2c** which has been prepared by treating **7c** with excess *p*-butylphenol (**1c**) was hydroxymethylaled under basic conditions and the resultant bis(hydroxymethyl) dimer **9c** was again reacted with excess **1c** to afford **4c**. The phenol tetramer (**4e**) was easily produced by the debutylation of **4b** with $AlCl_3$, the procedure being analogous to that employed in the synthesis of unsubstituted calixarenes.[8] The synthetic pathway of the oligomers is illustrated in Scheme 1.

Inclusion Properties. Inclusion ability of oligomers toward organic molecules was examined by recrystallization of oligomers from various organic solvents. It was found that the oligomers had an ability to form complexes with a variety of molecules and that the complexation was dependent upon substituents in the *p*-position of phenol and the number of phenol units in the oligomers. While calixarene has been reported to form 1:2 (host:guest) or 1:1 complexes,[8-15] the corresponding acyclic oligomers form 2:1 complexes in many cases, suggesting that modes of host-guest association are quite different between

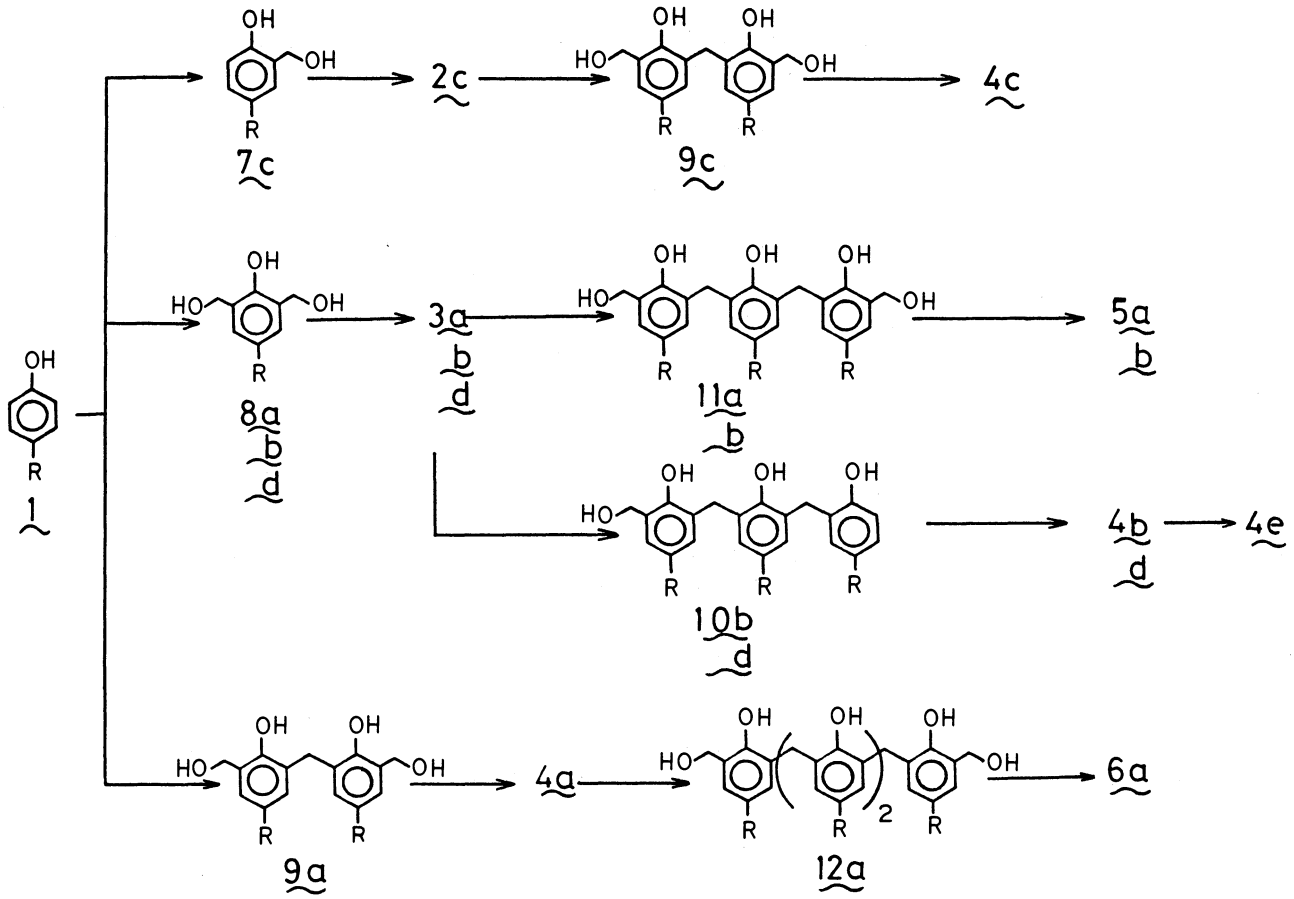

Scheme 1.

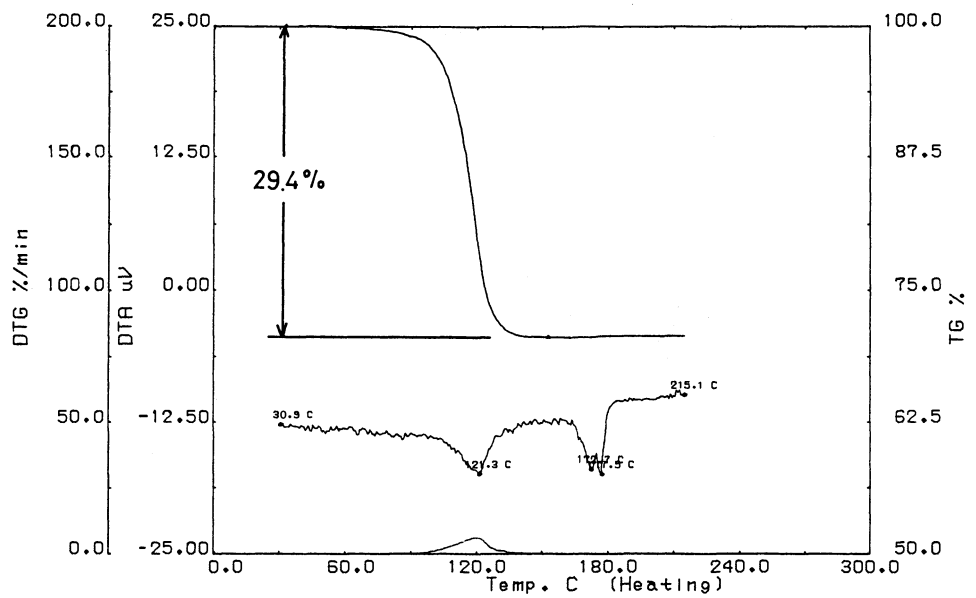

Fig. 1. TG-DTA curves of the complex of **4a** with 1,2-dibromoethane.

the cyclic and acyclic oligomers. The results are summarized in Tables 1 and 2.

The host-guest ratio was determined by ^{1}H NMR spectroscopy and thermogavimetry (TG). The TG-DTA (differential thermal analysis) patterns of a complex obtained from the tetramer **4a** and 1,2-dibromoethane are shown in Fig. 1 as an example. The TG curve indicates that the complex is stable up to 80 °C and the crystal morphology of the complex seems to change on heating. The weight loss corresponds accurately to the 1,2-dibromoethane content of the 1 : 1 complex of **4a** with 1,2-dibromoethane. The

stoichiometric ratio was ascertained by ^{1}H NMR integration as well as elemental analysis.

Table 1 shows that the inclusion properties of tetramers **4a—e** are greatly influenced by the *p*-substituent of phenol. The methyl-substituted tetramer **4a** forms host-guest compounds mainly with halogenated hydrocarbon compounds and not with aromatic compounds except for benzene. The unsubstituted tetramer **4e** is similar to **4a** in forming complexes with haloganated hydrocarbons but fails to form complexes with benzene. On the other hand, the *p*-*t*-butyl-substituted tetramer **4b** preferentially includes benzene and its alkyl derivatives. The host : guest molar ratios (2 : 1 and 1 : 1) suggest that different modes of complexation are expected between the benzene and toluene complexes. On the contrary, the butylphenol tetramer (**4c**) has a poor ability for the complex formation. The only difference between **4b** and **4c** is in the bulkiness of the butyl groups. These facts suggest that the linear and flexible butyl group at the *p*-position prevents the incorporation of the guest molecules into the crystalline lattice. The cyclohexyl-substituted tetramer **4d** differs from the others in forming complexes with ketones. Furthermore, **4d** gives a complex only with *o*-xylene among the isomeric xylenes.

Table 2 shows that the number of the phenol units also affects inclusion properties. The *p*-cresol (**4a**) and *t*-butylphenol tetramers (**4b**) and the corresponding pentamers (**5a** and **5b**) form efficiently complexes with many organic guests; the tetramer and the correspond-

Table 1. Molar Ratio and the Melting Points of the Complexes of **4a—4e**[a]

Guest (G)	Host (H)				
	4a	**4b**	**4c**	**4d**	**4e**
	H : G (°C)	H : G (°C)	H : G (°C)	H : G (°C)	H : G (°C)
None	(174—178)	(210—211)	(117—118)	(186—190)	(161—162)
Cyclohexane	—	1 : 2(105)	—	—	—
Benzene	2 : 1(172—175)	2 : 1(123—125)	—	—	—
Toluene	—	1 : 1(133—135)	—	2 : 1(186—190)	—
o-Xylene	—	2 : 1(151—153)	—	2 : 1(178—182)	—
m-Xylene	—	2 : 1(128—130)	—	—	—
p-Xylene	—	2 : 1(149—151)	—	—	—
Dioxane	1 : 1(142—143)	2 : 1(163—165)	—	—	2 : 1(147—149)
Acetone	—	—	+ (115—117)	2 : 1(167—172)	—
Methyl ethyl ketone	—	—	+ (115—117)	1 : 1(169—172)	—
Methanol	—	—	—	—	—
Ethanol	—	—	—	—	—
Dichloromethane	2 : 1(173—176)	—	—	—	2 : 1(161—162)
1,2-Dichloroethane	1 : 1(144—146)	+ (165—167)	—	2 : 1(172—176)	2 : 1(158—160)
1-Bromo-2-chloroethane	2 : 1(147—148)	—	—	1 : 1(167—170)	—
1,2-Dibromoethane	1 : 1(152—153)	+ (168—170)	—	1 : 1(172—177)	—
1,1,1-Trichloroethane	2 : 1(145—147)	2 : 1(109—110)	—	+ (165—169)	2 : 1(161—162)
Trichloroethylene	2 : 1(170—171)	—	—	—	—

a) —: host-guest complex does not form. +: host : guest ratio is not clear.

Table 2. Molar Ratio and the Melting Points of the Complexes of **3a**, **4a**, **5a**, **6a**, **3b**, **4b**, and **5b**[a]

Guest (G)	Host (H)						
	3a	**3b**	**4a**	**4b**	**5a**	**5b**	**6a**
	H : G (°C)	H : G (°C)	H : G (°C)	H : G (°C)	H : G (°C)	H : G (°C)	H : G (°C)
None	(214—215)	(221—222)	(174—178)	(210—211)	(127—128)	(218—219)	(215—216)
Benzene	+ (214—215)	+ (219—221)	2 : 1 (172—175)	2 : 1 (123—125)	2 : 1 (120—122)	2 : 1 (136—137)	2 : 1 (203—204)
Toluene	—	—	—	1 : 1 (133—135)	—	1 : 1 (139—141)	—
Acetone	—	—	—	—	—	1 : 1 (135—140)	—
Methanol	+ (214—215)	+ (224—227)	—	—	—	—	—
Ethanol	—	—	—	—	—	—	—
Dichloromethane	—	—	2 : 1 (173—176)	—	—	—	—
1,2-Dichloroethane	—	—	1 : 1 (144—146)	—	1 : 1 (119—120)	+ (135—136)	—

a)—: host-guest complex does not form. +: host : gest molar raio is not clear.

Table 3. Kinetic Data for the Thermal Dissociation of the Complexes of **4a**, **4b**, and **5a** with Benzene

Complex	Temp/°C	$k/10^{-4}\,s^{-1}$	E_a/kJ mol^{-1}	ln A
4a-benzene	116.4	1.174		
	121.8	2.178		
	126.6	3.950		
	134.3	11.07	165.9	42.1
4b-benzene	94.2	3.952		
	103.7	16.47		
	112.2	40.26		
	119.9	58.23	127.0	33.9
5a-benzene	94.7	8.953		
	98.1	17.14		
	102.4	25.25		
	111.7	57.00	123.7	33.1

ing pentamer include similar guests in each series. On the other hand, the trimers (**3a** and **3b**) exhibit almost no inclusion properties, and guests of the hexamer **6a** are rather limited. These results suggest that the molecular size of the trimers is not large enough to form lattice voids appropriate for the complex formation, whereas that of the hexamer is too large to form voids.

Besides the guests listed in the tables, the cresol tetramer (**4a**) forms complexes with chloroform (1 : 1), tetrahydrofuran (1 : 1), diethylamine, triethylamine (1 : 1), and chlorobenzene (2 : 1), but not with isopropyl alcohol, acetonitrile, cyclohexene, or aniline. None of the oligomers gave inclusion compounds with hexane or thiophene.

It should be noted that not a few molecules which possess no group to participate in hydrogen bonding are included by the oligomers; hydrogen bonding between hosts and guest molecules is not primarily responsible for complex formation. This makes a sharp contrast with the situation for many other phenolic hosts.[16-18]

Finally, in an attempt to estimate the thermal stability of host-guest complexes, some kinetic parameters for the dissociation of the complexes (host : guest=2 : 1) of **4a**, **4b**, and **5a** with benzene were obtained from their dissociation rates (Table 3). The thermal stability is dependent upon the substituents in the *p*-position or the size of the oligomers. For the tetramers methyl group is more favorable than *t*-butyl group for the formation of stable complex, whereas for the cresol oligomers the tetramer **4a** is more favorable than the pentamer **5a**.

Experimental

All melting points are uncorrected. NMR spectra were obtained on a Hitachi R-600 spectrometer at 60 MHz, using TMS as an internal reference. IR and mass (70 eV) spectra were recorded on a Hitachi EPI-S2 and a Hitachi UMU-6MG spectrometer, respectively. TG/DTA curves were recorded on a Seiko TG/DTA30 instrument with a heating rate of 10 °C min^{-1} under air stream.

The following oligomers were prepared according to the methods reported in literatures. **3a**: mp 214—215 °C (lit,[19] mp 215 °C). **4a**: mp 174—178 °C (lit,[5] mp 173 °C). **5a**: mp 127—128 °C (lit,[19] mp 130 °C). **6a**: mp 215—216 °C (lit,[19] 217 °C). **3b**: mp 221—222 °C (lit,[20] 220—221 °C). **5b**: mp 218—219 °C (lit,[20] 217—218 °C).

Synthesis of 2-[3-[3-(5-*t*-Butylsalicyl)-5-*t*-butylsalicyl]-5-*t*-butylsalicyl]-4-*t*-butylphenol (4b). Formalin (37%; 1.3 g, 16.1 mmol) was added with stirring over a period of 30 min to a mixture of **3b** (7.7 g, 16.1 mmol), 10% aqueous NaOH solution (30 ml), and methanol (30 ml) at 60 °C under an N_2 atmosphere. After stirring under reflux for 35 h, the reaction mixture was cooled to room temperature, acidified to pH 4 with 50% acetic acid, and extracted with chloroform. The organic layer was washed with water and dried over Na_2SO_4. The solvent was evaporated and the residue was chromatographed on silica gel (hexane/ethyl acetate=3/1) to give **10b** (2.7 g, 34%; mp 187—189 °C (lit,[5] mp 188.5—189 °C)), and **11b** (1.0 g, 12%; mp 143—145 °C (lit,[5] mp 140—145 °C)) together with unchanged **3b** (2.5 g, 33%).

A solution of **10b** (1.25 g, 2.48 mmol), *p*-*t*-butylphenol (**1b**; 20 g, 0.133 mol), and *p*-toluenesulfonic acid (45 mg) in benzene (30 ml) was stirred under reflux for 24 h; the water produced during the reaction was removed by azeotropic distillation using a Dean-Stark condenser. The benzene was evaporated and excess **1b** was removed by steam distillation. The residual mass was crystallized from cyclohexane to give the **4b**-cyclohexane complex (**4b**: cyclohexane=1 : 2) as a white powder (1.3 g, mp 105 °C (lit,[5] mp 105 °C)). This complex was heated at 80 °C under reduced pressure (1 mmHg; 1 mmHg=133.322 Pa) for 8 h to give cyclohexane-free **4b** as white powder (1.0 g, 64%; mp 210—211 °C (lit,[5] mp 212—213 °C)).

Synthesis of 2-[3-[3-(5-Butylsalicyl)-5-butylsalicyl]-5-butylsalicyl]-4-butylphenol (4c). To a mixture of *p*-butylphenol (**1c**; 10.0 g, 67 mmol) and formalin (5.4 g, 67 mmol) 10% aqueous NaOH solution (33 ml) was added with stirring under ice-cooling, and the reaction mixture was stirred at 50 °C for 6 h under an N_2 atmosphere. Then, another 5.4 g of formalin was added to the mixture, and the mixture was stirred for an additional 1 h. After being cooled to room temperature, the mixture was acidified with 50% acetic acid (pH 5) and extracted with benzene. After a usual work-up, the product was chromatographed on silica gel (Wako C-200; hexane/ethyl acetale=2/1) to give 4-butyl-2-(hydroxymethyl)phenol (**7c**; 2.0 g, 17%) and 4-butyl-2,6-bis(hydroxymethyl)phenol (**8c**; 7.5 g, 54%) together with unreacted **1c** (3.0 g, 30%).

7c: white plates; mp 79—80.5 °C; IR (KBr) 3450 (OH stretching) and 815 cm^{-1} (trisubstituted phenyl); ^{1}H NMR ($CDCl_3$) δ=0.92 (3H, t, J=5 Hz), 1.10—1.90 (4H, m), 2.30—2.75 (2H, m), 4.80 (2H, s), and 6.60—7.30 (3H, m); MS m/z 180 (M^+, 42%); Anal. ($C_{11}H_{16}O_2$) C, H.

8c: colorless prisms, mp 65—66 °C; IR (KBr) 3400, 3280 (OH stretching), and 880 cm^{-1} (tetrasubstituted phenyl); ^{1}H NMR ($CDCl_3$) δ=0.90 (3H, t, J=5 Hz), 1.10—1.95 (4H, m), 2.35—2.80 (2H, m), 3.80 (2H, s, OH), 4.40—5.00 (4H, m), 6.80 (2H, s), and 8.2 (1H, s, Ar-OH); MS m/z 210 (M^+, 34%); Anal. ($C_{12}H_{18}O_3$) C, H.

Hydrochloric acid (2 ml) was added to a mixture of **7c** (3.0 g, 17 mmol) and **1c** (7.7 g, 51 mmol), and the mixture was stirred at 110 °C for 6 h. After removing excess **1c** from the

reaction mixture by steam distillation, the residue was extracted with chloroform. A usual work-up gave a crude product, which was purified by medium-pressure column chromatography on silica gel (Kieselgel 60, 230—400 mesh; hexane/ethyl acetate=4/1) to give the *p*-butylphenol dimer (**2c**; 4.2 g, 79%).

2c: colorless powder; mp 66.5—67.0 °C; IR (KBr) 3250 (OH stretching) and 820 cm^{-1} (trisubstituted phenyl); ^1H NMR ($CDCl_3$) δ=0.90 (6H, t, J=5 Hz), 1.10—1.95 (8H, m), 2.30—2.75 (4H, m), 3.85 (2H, s), and 6.55—7.25 (6H, m); MS m/z (rel intensity) 314 (M^+, 100); Anal. ($C_{21}H_{28}O_2$) C, H.

To a mixture of **2c** (4.1 g, 13 mmol), 20% aqueous KOH solution (15 ml), and dioxane (20 ml), formalin (40 ml, 0.53 mol) was added over a period of 1 h under ice-cooling. The mixture was stirred at 60 °C for 20 h under an N_2 atmosphere. After being cooled to room temperature, the mixture was acidified with 50% acetic acid (pH 4) and extracted with benzene. After a usual work-up, the crude product was separated by medium-pressure liquid chromatography on silica gel (Kieselgel 60, 230—400 mesh; ethyl acetate/hexane=1/2) and recrystallized with chloroform-hexane to give the bis(hydroxymethyl) derivative (**9c**; 1.6 g, 33%) of **2c**.

9c: white powder; mp 123—124 °C; IR (KBr) 3375 (OH stretching) and 870 cm^{-1} (tetrasubstituted phenyl); ^1H NMR ($CDCl_3$) δ=0.90 (6H, t, J=5 Hz), 1.10—1.90 (8H, m), 2.00—2.80 (4H, m), 3.80 (2H, s), 4.70 (4H, s), and 6.60—7.30 (4H, m); MS m/z 372 (M^+, 14%); Anal. ($C_{23}H_{32}O_4$) C, H.

A mixture of **9c** (1.4 g, 3.7 mmol), **1c** (5.6 g, 37 mmol), and HCl (1 ml) was stirred at 100 °C for 3.5 h. Excess **1c** was removed by steam distillation and the residue was extracted with chloroform. After a usual work-up, the crude material was recrystallized from hexane to give **4c** (1.8 g, 75%).

4c: white powder; mp 117—118 °C; IR (KBr) 3250 (OH stretching), 875 (tetrasubstituted phenyl), and 820 cm^{-1} (trisubstituted phenyl); ^1H NMR ($CDCl_3$) δ=0.90 (12H, t, J=5 Hz), 1.10—2.00 (16H, m), 2.25—2.80 (8H, m), 3.80 (6H, s), and 6.75—7.30 (10H, m); MS m/z 636 (M^+, 76%); Anal. ($C_{43}H_{56}O_4$) C, H.

Synthesis of 2-[3-[3-(5-Cyclohexylsalicyl)-5-cyclohexylsalicyl]-5-cyclohexylsalicyl]-4-cyclohexylphenol (4d). A mixture of *p*-cyclohexylphenol (**1d**; 5.0 g, 28 mmol), 20% KOH (20 ml), and formalin (50 ml) was heated with stirring at 60 °C for 30 h under an N_2 atmosphere. The reaction mixture was cooled to room temperature, acidified to pH 5 with 10% aqueous HCl (50 ml), and extracted with chloroform (100 ml). After a usual work-up, the product was subjected to silica-gel column chromatography (hexane/ethyl acetate=2/1) to give 4-cyclohexyl-2,6-bis(hydroxymethyl)-phenol **8d** (5.7 g, 82%, mp 112—113 °C (lit,[21] 106—107 °C)).

A mixture of **8d** (2.7 g, 11.4 mmol), **1d** (10.0 g, 56.7 mmol), and HCl (2 ml) was stirred at 130 °C for 8 h. A work-up similar to the one described for the synthesis of **4c** from **9c** afforded the *p*-cyclohexylphenol trimer (**3d**), which was recrystallized from toluene to give pure **3d** (3.6 g, 57%).

3d: colorless needles; mp 186—188 °C; IR (KBr) 3300 (OH stretching), 865 (tetrasubstituted phenyl), and 810 cm^{-1} (trisubstituted phenyl); ^1H NMR ($CDCl_3$) δ=0.80—2.70 (33H, m), 3.90 (4H, s), and 6.60—7.30 (8H, m); MS m/z 552 (M^+, 21%); Anal. ($C_{38}H_{48}O_3$) C, H.

The hydroxymethyl derivative **10d** of **3d** was synthesized from **3d** in 33% yield in a similar manner as described for the synthesis of **10b** from **3b**.

10d: colorless needles; mp 156—157 °C; IR (KBr) 3280 (OH stretching), 865 (tetrasubstituted phenyl), and 815 cm^{-1} (trisubstituted phenyl); ^1H NMR ($CDCl_3$) δ=0.80—2.80 (33H, m), 3.80 (4H, s), 4.70 (2H, s), and 6.50—7.30 (7H, m); MS m/z 582 (M^+, 8%); Anal. ($C_{39}H_{50}O_4$) C, H.

A mixture of **10d** (1.2 g, 2.1 mmol), **1d** (4.0 g, 22.7 mmol), *p*-xylene (2 ml), and HCl (3 ml) was stirred at 130 °C for 12 h. After a usual work-up, the product was subjected to medium-pressure column chromatography on silica gel (Kieselgel 60, 230—400 mesh; hexane/ethyl acetate=5/1) to give **4d** (0.9 g, 58%).

4d: white powder; mp 179—182 °C; IR (KBr) 3250 (OH stretching), 870 (tetrasubstituted phenyl), and 815 cm^{-1} (trisubstituted phenyl); ^1H NMR ($CDCl_3$) δ=1.80—2.60 (44H, m), 3.85 (6H, s), and 6.60—7.30 (10H, m); MS m/z 740 (M^+, 0.1%); Anal. ($C_{51}H_{64}O_4$) C, H.

Synthesis of 2,2'-Methylenebis[6-(2-hydroxybenzyl)phenol] (4e). The procedure is a modification of the method used for the synthesis of calix[4]arene from *p-t*-butylcalix[4]arene.[8] Aluminum chloride (1.1 g, 8.2 mmol) was added to a solution of **4b** (1.0 g, 1.57 mmol) in toluene (50 ml), and the mixture was stirred at 50 °C for 2 h. The reaction mixture was cooled to 5 °C, and then dilute HCl (3%, 25 ml) was added to this mixture. A work-up and medium-pressure column chromatography (Kieselgel 60, 230—400 mesh, hexane/ethyl acetate=2/1) gave **4e** (0.42 g, 65%; mp 158—159 °C (lit,[2] mp 163 °C)).

Preparation of Inclusion Complex (General Procedure). The host oligomer (0.3 g) was dissolved in a minimum amount of organic solvent (guest) by heating and the solution was cooled to room temperature. The precipitates were filtrated, where necessary, washed with hexane, and dried at room temperature for 12 h. The guest-host ratio was determined by ^1H NMR (solvent $CDCl_3$) and/or TG measurements.

Kinetic Study. The weight decreasing rate of a complex was measured at four points using Al_2O_3 as an reference. The programmed temperature was raised at a rate of 10 °C min^{-1} up to each temperature. Based on the rate constants thus obtained, $\ln A$ and E_a values were calculated by the least-squares method. The results are shown in Table 3.

The authors are grateful to Professor Kenzo Matsuki and Mr. Takashi Endo for TG/DTA measurements. They also wish to thank Mr. Kazuaki Sato for elemental analyses and Mr. Kazuhiko Moriya and Miss Chikako Kobayashi for their assistance in some experiments.

References

1) For example, C. D. Gutsche, "Synthesis of Macrocycles," ed by R. M. Izatt and J. J. Christensen, John Wiley & Sons, New York (1987), p. 93.

2) G. Casiraghi, M. Cornia, G. Sartori, G. Casnati, V. Bocchi, and G. D. Andreetti, *Makromol. Chem.*, **183**, 2611 (1982).

3) R. F. Hunter, R. A. Morton, and A. T. Carpenter, *J. Chem. Soc.*, **1950**, 441.

4) E. Paulus and V. Böhmer, *Makromol. Chem.*, **185**, 1921 (1984).

5) B. Dhawan and C. D. Gutsche, *J. Org. Chem.*, **48**, 1536 (1983).

6) H. Kämmerer, W. Rausch, and H. Schweikert, *Makromol. Chem.*, **56**, 123 (1962); H. Kämmerer and W. Rausch, *ibid.*, **18/19**, 9 (1956); H. Kämmerer and W. Rausch, *ibid.*, **24**, 152 (1957).

7) B. T. Hayes and R. F. Hunter, *J. Appl. Chem.*, **8**, 743 (1958).

8) R. Ungaro, A. Pochini. G. D. Andreetti, and V. Sangermano, *J. Chem. Soc., Perkin Trans. 2*, **1984**, 1979.

9) V. Bocchi, D. Foina, A. Pochini, R. Ungaro, and G. D. Andreetti, *Tetrahedron*, **38**, 373 (1982).

10) C. D. Gutsche and L.-G. Lin, *Tetrahedron*, **42**, 1633 (1986).

11) R. Ungaro, A. Pochini, G. D. Andreetti, and P. Dominao, *J. Chem. Soc., Perkin Trans. 2*, **1985**, 197.

12) G. D. Andreetti, R. Ungaro, and A. Pochini, *J. Chem. Soc., Chem. Commun.*, **1979**, 1005.

13) G. D. Andreetti, R. Ungaro, and A. Pochini, *J. Chem. Soc., Chem. Commun.*, **1981**, 533.

14) M. Coruzzi, G. D. Andreetti, V. Bocchi, A. Pochini, and R. Ungaro, *J. Chem. Soc., Perkin Trans. 2*, **1982**, 1133.

15) G. D. Andreetti, A. Pochini, and R. Ungaro, *J. Chem. Soc., Perkin Trans. 2*, **1983**, 1773.

16) D. D. MacNicol, "Inclusion Compounds," ed by J. L. Atwood, J. E. D. Davies, and D. D. MacNicol, Academic Press, London (1984), Vol. 2, pp. 1—40.

17) F. Toda, K. Tanaka, T. Hyoda, and T. C. W. Mak, *Chem. Lett.*, **1988**, 107; F. Toda, K. Tanaka, M. C. Wong, and T. C. W. Mak, *ibid.*, **1987**, 2067; I. Goldberg, Z. Stein, K. Tanaka, and F. Toda, *J. Incl. Phenom.*, **6**, 15 (1988); I. Goldberg, Z. Stein, A. Kai, and F. Toda, *Chem. Lett.*, **1987**, 1617; F. Toda, Y. Takagi, H. Quan, F. Hai-fu, and T. C. W. Mak, *ibid.*, **1986**, 1913; F. Toda, K. Tanaka, and T. C. W. Mak, *ibid.*, **1984**, 2085; F. Toda, K. Tanaka, T. C. W. Mak, *ibid.*, **1983**, 1699; F. Toda, K. Tanaka, G. U. Daumas, and M. C. Sanchez, *ibid.*, **1983**, 1521.

18) J. E. Barry, M. Finkelstein, and S. D. Ross, *J. Org. Chem.*, **49**, 1669 (1984); J. E. Barry, N. E. Cipollini, M. Finkelstein, and S. D. Ross, *Tetrahedron*, **39**, 2151 (1983); J. E. Barry, N. E. Cipollini, M. Finkelstein, and S. D. Ross, *Tetrahedron*, **37**, 1699 (1981); J. E. Barry, M. Finkelstein, and S. D. Ross, *ibid.*, **32**, 223 (1976).

19) M. Imoto, I. Ijichi, and M. Kinoshita, *Makromol. Chem.*, **113**, 117 (1968).

20) G. Casiragi, M. Cornia, G. Ricci, G. Balduzzi, G. Casunati, and G. D. Andreetti, *Makromol. Chem.*, **184**, 1363 (1983).

21) A. Zinke, F. Hanus, E. Ziegler, F. Sperk, H. Troger, and E. Wienhardt, *J. Prakt. Chem.*, **152**, 126 (1939).

Synthesis of Salvilenone, a Diterpenoid Phenalenone of *Salvia miltiorrhiza*

Guo-Chi ZHENG and Hiroshi KAKISAWA*
Department of Chemistry, University of Tsukuba, Tsukuba, Ibaraki 305
(Received September 8, 1988)

Salvilenone **1**, a phenalenone diterpene isolated from the roots of *Salvia miltiorrhiza* Bunge, was synthesized in thirteen steps from resorcinol dimethyl ether. Dihydrophenalenol derivative **19**, a key intermediate, was treated with aqueous hydrobromic acid to give salvilenone accompanied by the formation of a hydroxy diketone **20**.

Salvilenone is a diterpenoid found in the roots of *Salvia miltiorrniza* Bunge. The dried root of this plant, Dan-shen, is a traditional medicine in China used for the treatment of blood difficulties, hemorrhages, miscarriages and viral hepatitis.[1,2] Recently, it is also used for the treatment of heart disease as a clinically important drug.[3]

The main constituents of this folk medicine were thoroughly studied to find many diterpenoid naphthoquinones and phenanthrenequinones possessing a norabietane carbon skeleton.[4] In the course of our studies on the minor constituents of Dan-shen, a bright yellow compound salvilenone was isolated in a trace amount, and the structure was determined to be a diterpenoide phenalenone **1** different from the known naphthoquinones and phenanthrenequinones of this medicine.[5] The low availability of this compound and scarce distribution of phenalenone derivatives in nature[6] prompted us to investigate its synthesis. The present paper describes in detail the synthesis of salvilenone.[7]

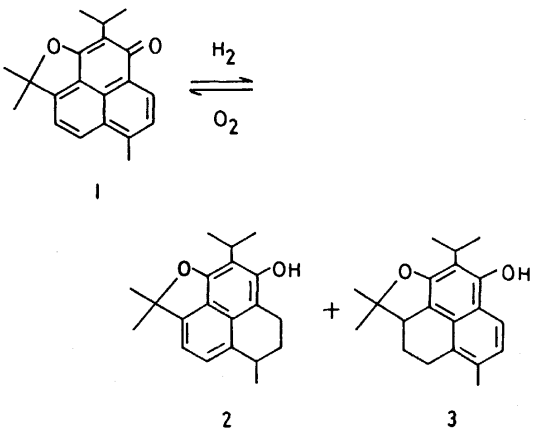

Scheme 1.

It was found in the course of the structural determination that on hydrogenation salvilenone **1** gave unstable products **2** and **3**, which were smoothly autooxidized to the original pigment.[5] On the basis of this observation, dihydrophenalenol derivative **3** was chosen as a key intermediate for the synthesis.

A dihydrophenalenone derivative **16a** was synthesized from resorcinol dimethyl ether (**4**) by an eleven step process.

The reaction of the dihydrophenalenone derivative **16a** with lithium acetylide-ethylenediamine complex proceeded smoothly to give an ethynyl derivative **17** in good yield.[9] Treatment of this ethynyl-substituted alcohol with mercury(II) sulfate and sulfuric acid at 55 °C under Rupe reaction conditions resulted in the formation of acetylphenalenone **18**[12] with concomitant demethylation in these mild conditions. This reaction confirmed the remarkably facile formation of phenalenone from a dihydrophenalenol as observed in the structural determination of salvilenone.

Because selective conversion of the acetyl group of

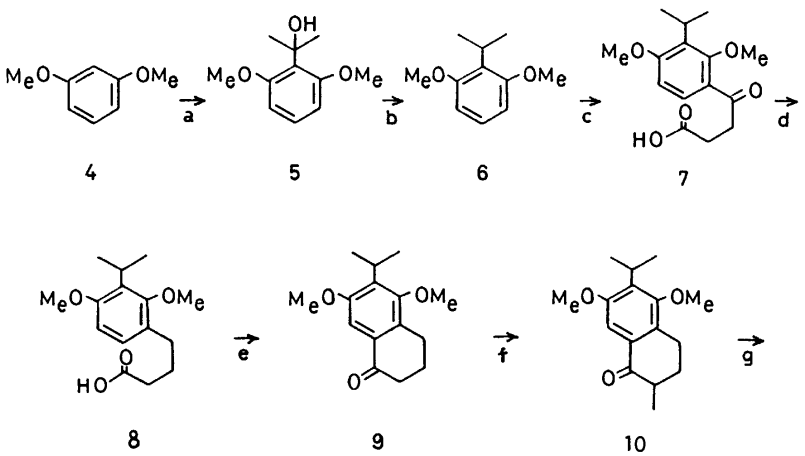

Scheme 2a.

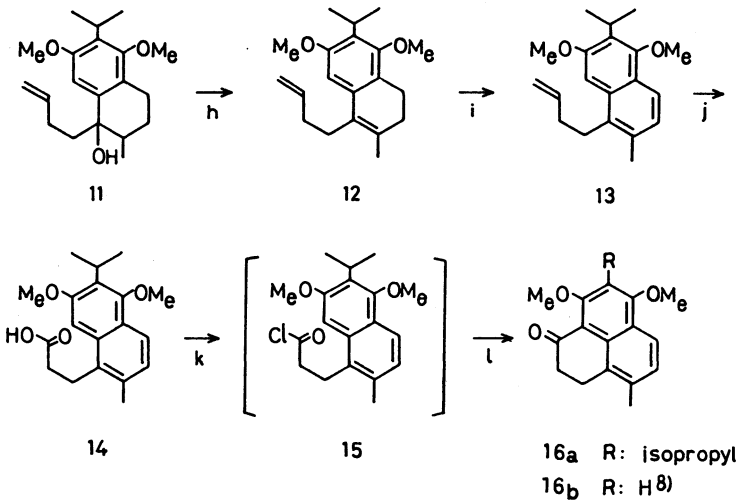

Reagents: a) *n*-BuLi, CH_3COCH_3, THF. b) PtO_2, HCl, AcOH. c) Succinic anhydride, $AlCl_3$, $PhNO_2$. d) H_2/Pd–C (10%), $HClO_4$, AcOH. e) PPA, CH_2Cl_2. f) MMC, CH_3I, DMF. g) CH_2=$CHCH_2CH_2MgBr$, ether. h) TsOH, PhH. i) DDQ, PhH. j) $KMnO_4$, KIO_4, Na_2CO_3, H_2O, dioxane. k) PCl_5, PhH. l) $SnCl_4$, PhH.

Scheme 2b.

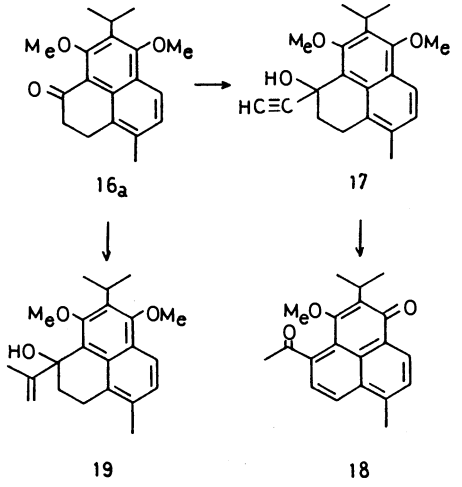

Scheme 3.

18 to an isopropenyl group was unsuccessful, isopropenyllithium[10] was allowed to react with dihydrophenalenone **16a** to obtain the intermediate **19**.

Treatment of the isopropenyl-substituted alcohol **19** with 47% aqueous hydrobromic acid[11] in boiling acetic acid for 48 h afforded salvilenone **1**, accompanied by the formation of a by-product hydroxy diketone **20**. Synthetic salvilenone **1** was identical with an authentic sample in ^{1}H NMR, ^{13}C NMR, IR spectra, and TLC. The structure of the by-product ($C_{20}H_{22}O_3$) was determined to be **20** by spectral analyses. The ^{1}H NMR spectrum showed the presence of two isopropyl groups, an aromatic methyl, and two adjacent aromatic protons. Two of three oxygen atoms of the by-product were considered to comprise two carbonyl groups from ^{13}C NMR signals at δ 193.2 and 197.7, and

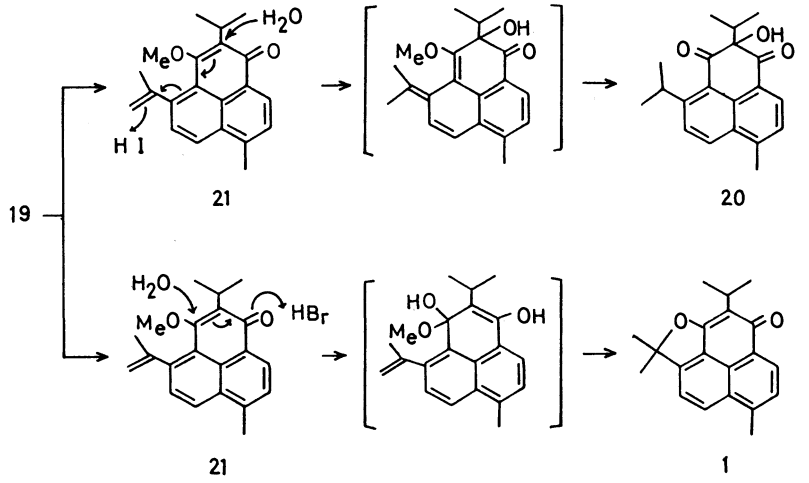

Scheme 4.

the remaining one was hydroxyl group from ^{1}H NMR signal at δ 9.67 and IR absorption at 3460 cm^{-1}. The presence of an asymmetric carbon atom was infered from the nonequivalence of the methyl groups in the two isopropyl groups in the NMR spectra [0.95 (3H, d), 0.97 (3H, d), 1.35 (3H, d), and 1.47 (3H, d)].

Although salvilenone **1** and the hydroxy diketone **20** were produced from the intermediate **19** by treatment with hydrobromic acid, on treating with hydriodic acid the intermediate **19** afforded the hydroxy diketone **20** as the sole product, and heating of **19** with iodine in carbon tetrachloride afforded a methoxyphenalenone **21**.[12] The hydroxy diketone **20** is considered to be produced from methoxyphenalenone **21**; protonation by hydriodic acid (a soft acid) may take place preferably at the isopropenyl terminal of **21** rather than at the carbonyl oxygen. Subsequent hydrolysis affords hydroxy diketone **20**. Salvilenone **1** is assumed to be produced by protonation at the carbonyl oxygen atom of the same intermediate **20** by rather hard acid, hydrobromic acid.

Experimental

Melting points were recorded on a Yamato capillary melting point apparatus. Proton magnetic resonance (^{1}H NMR) spectra were recorded on either a JEOL JNM-PMX60si or a JEOL FX90Q spectrometer or, where specified, on a Bruker AM500 spectrometer with chemical shifts given in parts per million (δ) downfield from tetramethylsilane as an internal standard. Deuteriochloroform was used as solvent unless otherwise noted. Carbon magnetic resonance (^{13}C NMR) spectra were recorded at 22.5 MHz on a JEOL EX90Q instrument. Infrared (IR) spectra were measured on a Hitachi 215 or a JASCO FT/IR-3 spectrophotometer. Mass spectra (MS) were obtained on a Hitachi RMU-6H GC/MS instrument at 70 eV. Elemental analyses were performed by the University of Tsukuba Chemical Analysis Center. Ultraviolet (UV) spectra were recorded on a Hitachi EPS-3T spectrophotometer. Gas chromatography (GLC) data were obtained with a 063 Hitachi gas chromatography (1.7 m/3 mm i.d. glass column packed with 5% SE-30). High-pressure liquid chromatography (HPLC) was carried out with a Waters ALC/GPC 202/401 instrument (1/4 in/1 ft column packed with RP-18). Wako C-300 silica gel was used for flash column chromatography. Merck Kieselgel 60 F_{254} Art 5744 (0.25 mm) and Merck Kiesel gel 60 F_{254} Art 5744 (0.5 mm) were used for analytical and preparative thin-layer chromatography.

1,3-Dimethoxy-2-(1-hydroxy-1-methylethyl)benzene (5). To a solution of resorcinol dimethyl ether **4** (3.2 g, 0.023 mol) in dry tetrahydrofuran, a solution of butyllithium in hexane (1.39 M, 20 ml, 0.028 mol; 1 M=1 mol dm^{-3}) was added dropwise and stirred under an argon atmosphere. After refluxing for 2 h, the solution was chilled to room temperature and a solution of dry acetone (1.6 g, 0.028 mol) in tetrahydrofuran was added dropwise. The mixture was heated under reflux for 3 h, cooled, and poured into ice water followed by extraction with ether. The organic layer was washed with water and then dried over sodium sulfate, evaporated under reduced pressure; distillation afforded a colorless oil **5** (2.9 g, 64%). Bp 120—124 °C/4Torr (1 Torr≈ 133.322 Pa). ^{1}H NMR ($CDCl_3$) δ=1.58 (6H, s, CH_3×2), 3.73 (6H, s, OCH_3×2), 4.95 (1H, brs, OH), 6.3—7.1 (3H, m, AB_2, ArH). Found: C, 67.47; H, 8.18%. Calcd for $C_{11}H_{16}O_3$: C, 67.32; H, 8.22%.

1,3-Dimethoxy-2-isopropylbenzene (6). A solution of **5** (0.64 g, 3.26 mmol), 3 M hydrochloric acid (0.1 ml), PtO_2 (0.05 g), and glacial acetic acid (20 ml) was stirred under H_2 for 3 h at room temperature. After filtration of the catalyst, the solution was evaporated under reduced pressure, and distillation of the residue afforded a colorless oil **6** (0.58 g, 99%). Bp 70—71 °C/0.5 Torr, IR ($CHCl_3$) 2940, 1580, 1450, and 1360 cm^{-1}; ^{1}H NMR (CCl_4) δ=1.25 (6H, d, J=8 Hz, CH_3×2), 3.60 [1H, sept, J=8 Hz, $(CH_3)_2\underline{CH}$], 3.85 (6H, s, OCH_3×2), and 6.2—7.2 (3H, m, AB_2, ArH). Found: C, 73.32; H, 8.94%. Calcd for $C_{11}H_{16}O_2$: C, 73.29; H, 8.94%.

4-(2,4-Dimethoxy-3-isopropylphenyl)-4-oxobutyric Acid (7). To a solution of **6** (1 g, 5.5 mmol) and succinic anhydride (0.55 g, 5.5 mmol) in dry nitrobenzene (50 ml), cooled in an iced water bath, a powdered anhydrous aluminum chloride (878 mg, 6.6 mmol) was added with stirring under an argon atmosphere. After stirring for 70 h at room temperature, the mixture was poured to ice water containing concentrated hydrochloric acid (10:1 v/v). The mixture was extracted with ether (5×50 ml), from which an acid product was obtained by the usual method as a solid (1.26 g, 82%). The crude product was recrystallized from benzene to give colorless plates, mp 91.5—93 °C; IR ($CHCl_3$) 2950, 1705, 1670, 1580, 1450, 1400, and 1360 cm^{-1}; ^{1}H NMR ($CDCl_3$) δ= 1.31 (6H, d, J=8 Hz, CH_3×2), 2.72 (2H, t, J=7 Hz, $COCH_2$), 3.26 (2H, t, J=7 Hz, -CH_2COO), 3.51 [1H, sept, J=8Hz, $(CH_3)_2CH$], 3.67 (3H, s, OCH_3), 3.82 (3H, s, OCH_3), 6.60 (1H, d, J=8.5 Hz, ArH), 7.46 (1H, d, J=8.5 Hz, ArH), and 12.65 (1H, s, COOH). Found: C, 64.04, H, 7.15%. Calcd for $C_{15}H_{20}O_5$: C, 64.27, H, 7.19%.

4-(2,4-Dimethoxy-3-isopropylphenyl)butanoic Acid (8). A mixture of acid **7** (0.42 g, 1.5 mmol), 10% Pd/carbon (0.07 g), and perchloric acid (70%, 0.1 ml) in acetic acid (20 ml) was stirred under H_2 at room temperature. After 70 h the solution was filtered. To the filtrate was added NaOAc (0.5 g) and the resulting gray ppt was filtered off. The neutralized filtrate was evaporated under reduced pressure to about 5 ml, water was added and the mixture thoroughly extracted with ether. The organic layer was washed with water and dried over magnesium sulfate. The solvent was evaporated to give yellow oil. Recrystallization from benzene/hexene afforded **8** (0.39 g, 97%) as bright yellow needles, mp 64—65.5 °C; IR (KBr) 2940, 1690, 1590, 1480, 1450, 1405, and 1335 cm^{-1}; ^{1}H NMR ($CDCl_3$) δ=1.34 (6H, d, J=7 Hz, CH_3×2), 1.7—2.8 (6H, m, $CH_2CH_2CH_2COO$), 3.45 [1H, sept, J=7 Hz, $CH(CH_3)_2$], 3.70 (3H, s, OCH_3), 3.79 (3H, s, OCH_3), 6.57 (1H, d, J=8.5 Hz, ArH), 6.96 (1H, d, J=8.5 Hz, ArH), and 10.35 (1H, brs, COOH). Found: C, 67.57; H, 8.30%. Calcd for $C_{15}H_{22}O_4$: C, 67.64; H, 8.32%.

5,7-Dimethoxy-6-isopropyl-α-tetralone (9). Phosphorus pentaoxide (3.8 g) was added to vigorously stirred phosphoric acid (3.1 g) at a temperature below 60 °C and the resulting mixture stirred for 5 h at 84 °C. A solution of **8** (0.32 g, 1.2 mmol) in dichloromethane (2 ml) was added to the polyphosphoric acid with vigorous stirring at 60—70 °C. After 30 min, the resulting reddish solution was cooled in an ice bath and 20 ml ice-water added. The mixture was extracted with three 30 ml portions of ether. The combined

ethereal extracts were successively washed with water, a 5% $NaHCO_3$ solution, water, and a saturated sodium chloride solution and dried over sodium sulfate. The ethereal solution was concentrated to afford a neutral oil. The oily mixture was distilled under reduced pressure to give **9** (0.28 g. 94%) as a colorless liquid (bp 135 °C/0.4 Torr). IR ($CHCl_3$) 2950, 1662, 1590, 1560, 1445, and 1405 cm^{-1}. ^1H NMR ($CDCl_3$) δ=1.32 (6H, d, J=7 Hz, CH_3×2), 1.90—2.93 (6H, m, $COCH_2CH_2CH_2$), 3.62 (1H, sept, J=7 Hz, CH), 3.68 (3H, s, OCH_3), 3.82 (3H, s, OCH_3), and 7.30 (1H, s, ArH). Found: C, 72.56; H, 8.20%. Calcd for $C_{15}H_{20}O_3$: C, 72.55; H, 8.11%.

5,7-Dimethoxy-6-isopropyl-2-methyl-α-tetralone (10). A solution of magnesium methoxide was prepared from magnesium (0.06 g) and 5 ml of anhydrous methanol. The bulk of the methanol was evaporated from the solution under reduced pressure with stirring at 50—55 °C. The anhydrous *N,N*-dimethylformamide (5 ml) was added. The resulting suspension was stirred vigorously while a stream of anhydrous carbon dioxide was passed into the reaction system. When the suspended magnesium methoxide changed into a clear solution, the flow of carbon dioxide was stopped. A solution of 0.15 g (0.6 mmol) of tetralone **9** in *N,N*-dimethylformamide (5 ml) was added and the reaction mixture refluxed for 2 h. The mixture was cooled to room temperature, and 0.34 g of iodomethane added dropwise. After the mixture was stirred for 10 h at 50 °C, it was poured into 1 M aqueous hydrochloric acid (10 ml) followed by extraction with ether. The combined organic extracts were washed with 5% aqueous $NaHCO_3$, saturated aqueous NaCl, and dried and finally evaporated to give a yellow oil. Distillation of this material gave 0.12 g of methyltetralone **10** as a colorless oil (74% 160 °C/0.3 Torr). IR ($CHCl_3$) 2930, 1665, 1590, 1450, 1410, 1360, and 1310 cm^{-1}. ^1H NMR ($CDCl_3$) δ=1.24 (3H, d, J=6.5 Hz, $COCHCH_3$), 1.37 (6H, d, J=7 Hz, CH_3×2), 1.78—3.20 (5H, m, CH_2CH_2CH), 3.51 [1H, sept, J=7 Hz, $(CH_3)_2\underline{CH}$], 3.70 (3H, s, OCH_3), 3.85 (3H, s, OCH_3), and 7.35 (1H, s, ArH). ^{13}C NMR ($CDCl_3$) δ=15.5(q), 20.8(q), 20.8(q), 22.6(t), 26.0(d), 31.3(t), 42.3(d), 55.4(q), 61.1(q), 104.9(d), 130.6(s), 131.5(s), 135.8(s), 155.8(s), 158.1(s), and 200.2(s); MS m/z 262 (M^+), 247 (M^+-CH_3), and 219 ($M^+-C_3H_7$). Found: C, 73.50; H, 8.41%. Calcd for $C_{16}H_{22}O_3$: C, 73.25; H, 8.45%. Further distillation of the residue afforded 0.009 g (5%) of 5,7-dimethoxy-2,2-dimethyl-6-isopropyl-α-tetralone as white needles (182—185 °C/0.3 Torr): ^1H NMR ($CDCl_3$) δ=1.20 (6H, s, CH_3×2), 1.32 (6H, d, J=8 Hz), 1.93 (2H, t, J=6 Hz, CH_2), 2.90 (2H, t, J=6 Hz, CH_2), 3.50 [1H, sept, J=8 Hz, $(CH_3)_2\underline{CH}$], 3.72 (3H, s, OCH_3), 3.83 (3H, s, OCH_3), and 7. 34 (1H, s, ArH); MS m/z 277 (M^++1), 276 (M^+), 261 (M^+-CH_3), and 246 (M^+-2CH_3). Found: C, 73.67; H, 8.89%. Calcd for $C_{17}H_{24}O_3$: C, 73.88; H, 8.75%.

1-(3-Butenyl)-5,7-dimethoxy-6-isopropyl-2-methyl-1,2,3,4-tetrahydro-1-naphthol (11). Magnesium metal shavings (0.24 g) were placed in a flask equipped with a reflux condenser and a dropping funnel. The system was flushed with nitrogen before addition of anhydrous ether (12 ml). The flask was cooled in an ice bath and a small volume of 4-bromo-1-butene was added to the stirred solution. Once the reaction had started, the remainder of the bromide (1 ml) in ether solution (2 ml) was added at below 20 °C. After 3 h the solution was cooled to 0 °C with ice bath, the α-methyl tetralone **10** (1 g, 3.8 mmol) in ether was added dropwise and the mixture was refluxed for 3 h. The reaction mixture was poured into ice cooled ammonium chloride solution and extracted with ether. The combined extracts were dried over anhydrous sodium sulfate. Evaporation of the solvent and flash chromatography of the residue on silica gel with 8:2 hexane/ethyl acetate afforded **11** as a pale yellow oil (1.03 g, 85%). IR ($CHCl_3$) 3580, 2920, 1595, 1565, 1440, 1400, and 1110 cm^{-1}; ^1H NMR ($CDCl_3$) δ=1.10 (3H, d, $COHCHCH_3$), 1.42 [6H, d, J=7.5 Hz, $CH(CH_3)_2$], 1.50—2.90 (8H, m, $CH_2CH_2CH_2CH_2$), 3.51 [1H, sept, J=7.5 Hz, $C\underline{H}(CH_3)_2$], 3.71 (3H, s, OCH_3), 3.79 (3H, s, OCH_3), 4.12 (1H, m, $CHCH_3$), 4.81—6.08 (3H, m, CH_2=CH), and 6.91, 7.00 (1H, ArH). Found: C, 75.44; H, 9.52%. Calcd for $C_{20}H_{30}O_3$: C, 75.43; H, 9.49%. Further elution affords 0.15 g of reduced product, 5,7-dimethoxy-6-isopropyl-2-methyl-1,2,3,4-tetrahydro-1-naphthol as colorless needles (8%). IR ($CHCl_3$) 3580, 2920, 1600, and 1565 cm^{-1}; ^1H NMR ($CDCl_3$) δ=1.10 (3H, d, $COHCHCH_3$), 1.31 (6H, d, J=7.5 Hz), 1.62 (1H, s, OH), 1.60—3.00 (4H, m, CH_2CH_2), 3.50 [1H, m, J=7.5 Hz $C\underline{H}(CH_3)_2$], 3.70 (3H, s, OCH_3), 3.76 (3H, s, OCH_3), 4.32 (1H, brs, $C\underline{H}OH$), and 6.78 (1H, s, ArH); MS m/z 265 (M^++1), 264 (M^+), 249 (M^+-CH_3), and 246 (M^+-H_2O). Found: C, 72.81; H, 9.32%. Calcd for $C_{16}H_{24}O_3$: C, 72.69; H, 9.15%.

1-(3-Butenyl)-5,7-dimethoxy-6-isopropyl-2-methyl-3,4-dihydronaphthalene (12). The alcohol **11** (0.739 g, 2.3 mmol) was added to 50 ml of dry benzene containing *p*-toluenesulfonic acid hydrate (0.24 g, 1 mmol) and calcium chloride (0.2 g). The solution was stirred at room temperature for 30 min. The mixture was filtered and the filtrate was washed with 20% aqueous $NaHSO_3$ and water until neutral, it was then dried over sodium sulfate. The solvent was evaporated under reduced pressure to give **12** as a yellow oil in 95% yield (0.65 g). This material was used directly for the next step without purification. An analytical sample was purified by chromatography: IR ($CHCl_3$) 2920, 1590, 1440, 1400, and 1310 cm^{-1}; ^1H NMR ($CDCl_3$) δ=1.31 [6H, d, J=8 Hz, $CH(CH_3)_2$], 1.88 (3H, brs, $=CCH_3$), 1.98—2.82 (8H, m, CH_2CH_2, CH_2CH_2), 3.60 [1H, sept, J=8 Hz, $CH(CH_3)_2$], 3.73 (3H, s, OCH_3), 3.81 (3H, s, OCH_3), 4.78—6.10 (3H, m, CH_2=CH), and 6.57 (1H, s, ArH); MS m/z (rel intensity, %) 301(24), 300(M^+, base), 286(9), 285(42), 247(8), 246(34), and 194(66). Found: C, 80.11; H, 9.18%. Calcd for $C_{20}H_{28}O_2$: C, 79.95; H, 9.39%.

1-(3-Butenyl)-5,7-dimethoxy-6-isopropyl-2-methylnaphthalene (13). A mixture of 2,3-dichloro-5,6-dicyano-*p*-benzoquinone (1 g, 4 mmol) and **12** (0.65 g, 2.2 mmol) in benzene (40 ml) was stirred for 15 h at room temperature under argon. The resulting solution was filtered through a column of Celite. Evaporation of the solvent afforded **13** as a bright yellow oil (0.6 g, 93%). The oil was used without further purification for the next reaction. The analytical sample was obtained by flash chromatography. IR ($CHCl_3$) 2930, 1615, 1590, and 1120 cm^{-1}; ^1H NMR ($CDCl_3$) δ=1.39 [6H, d, J=7.5 Hz, $CH(CH_3)_2$], 2.46 (3H, s , $ArCH_3$), 2.1—3.7 (5H, m, $CHCH_2CH_2$), 3.83 (3H, s, OCH_3), 3.87 (3H, s, OCH_3), 4.86—6.28 (3H, m, CH_2=CH), 6.98 (1H, s, ArH), and 7.06, 7.72 (2H , ABq, J=8 Hz, ArH). MS m/z (rel intensity) 299 (6), 298 (M^+, 23), 245 (18), 244 (base), 214 (4). Found: C, 80.55; H, 8.76%. Calcd for $C_{20}H_{26}O_2$: C, 80.49; H, 8.78%.

3-(5,7-Dimethoxy-6-isopropyl-2-methyl-1-naphthalene)-propionic Acid (14). To a solution of **13** (0.118 g, 0.4 mmol) in 40 ml of dioxane was added a mixed solution made from 0.52 g of KIO_4, 33.5 mg of $KMnO_4$, 16.8 mg of Na_2CO_3 and 20 ml of water. The mixture was stirred for 15 h at room

temperature. The excess reagent was decomposed by the addition of 5% aqueous H_2O_2 under ice cooling and most of the dioxane was evaporated, the residual solution was acidified with concentrated hydrochloric acid and extracted with dichloromethane. The organic layer was extracted three times with 5% sodium hydroxide solution. The combined alkaline extracts were acidified with concentrated hydrochloric acid and extracted thoroughly with ether. The organic layer was washed with water, dried over sodium sulfate, and evaporated to give an oil. Recrystallization from benzene/hexane afforded 0.101 g (80%) of **14** as white needles: mp 160—162 °C; IR (KBr) 3400—3500, 2950, 1700, and 1610 cm^{-1}; ^1H NMR ($CDCl_3$) δ=1.42 [6H, d, J=7.5 Hz, $CH(CH_3)_2$], 2.47 (3H, s, $ArCH_3$), 2.50—3.54 (4H, m, CH_2CH_2), 3.71 [1H, sept, J=7.5 Hz, $CH(CH_3)_2$], 3.84 (3H, s, OCH_3), 3.88 (3H, s, OCH_3), 7.09 (1H, s, ArH), 7.06, 7.73 (2H, ABq, J=8.5 Hz), and 10.23 (1H, brs, COOH). Found: C, 71.91; H, 7.63%; Calcd for $C_{19}H_{24}O_4$: C, 72.12; H, 7.64%.

7,9-Dimethoxy-8-isopropyl-4-methyl-1*H*-phenalen-1-one (16a). To a stirred suspension of phosphorus pentachloride (113 mg, 0.54 mmol) in dry benzene (2 ml), a solution of the propionic acid **14** (150 mg, 0.48 mmol) in benzene was added dropwise at room temperature under argon. When the vigorous reaction subsided, more benzene (2 ml) was added and the mixture warmed to 50—60 °C for 30 min. The clear solution was chilled in an ice bath and a solution of tin(IV) chloride (10 mg) in benzene (1 ml) was added dropwise with stirring while keeping the temperature below 5 °C. After being maintained for 2 h more at 5 °C, the dark solution was decomposed by the slow addition of 1 : 1 (v/v) hydrochloric acid/water (1 ml) while avoiding a rise in temperature above 15 °C. The clear red solution was separated and washed thoroughly with dilute hydrochloric acid, then water. Removal of benzene left a clear mobile oil which after chromatography (hexane/ethyl acetate 3 : 1) gave an oil (97 mg, 68%) of **16a**. IR ($CHCl_3$) 2950, 2850, 1670, 1605, and 1570 cm^{-1}; ^1H NMR ($CDCl_3$) δ=1.40 [6H, d, J=7.5 Hz, $CH(CH_3)_2$], 2.47 (3H, s, $ArCH_3$), 2.77—2.98 (2H, m, J=8 Hz, $ArCH_2$), 3.19—3.38 (2H, m, J=8 Hz, $COCH_2$), 3.68 [1H, sept, J=7.5 Hz, $CH(CH_3)_2$], 3.93 (6H, s, OCH_3×2), and 7.29, 7.86 (2H, ABq, J=8.5 Hz, ArH). MS m/z (rel intensity) 298 (M^+, 91), 284 (23), 283 (base), 281 (35), and 265 (52). Found: C, 76.24; H, 7.44%; Calcd for $C_{19}H_{22}O_3$: C, 76.48; H, 7.43%.

1-Ethynyl-7,9-dimethoxy-8-isopropyl-4-methyl-2,3-dihydro-1*H*-phenalen-1-ol (17). To a solution of lithium acetylide-ethylenediamine complex (0.138 g, 1.5 mmol) in anhydrous tetrahydrofuran (30 ml), a solution of **16a** (46 mg, 0.15 mmol) in dry tetrahydrofuran (10 ml) was added with stirring under an argon atmosphere. The reaction mixture was stirred for 18 h at room temperature. The mixture was poured into 5% ammonium chloride solution and extracted with ether. The combined ether extracts were washed with 2% HCl solution and water, dried over $MgSO_4$ and concentrated in vacuo. Purification of the residue by flash silica-gel chromatography gave white crystals **17** (46 mg, 92%). Mp: 123—126 °C; IR(CCl_4) 3480, 3300, 2950, 1600, 1485, 1440, and 1380 cm^{-1}. ^1H NMR ($CDCl_3$) δ=1.42 (3H, d, J=8.5 Hz, $CHCH_3$), 1.50 (3H, d, J=8.5 Hz, $CHCH_3$), 2.43 (3H, s, $ArCH_3$), 2.60 (1H, s, C≡CH), 2.00—3.35 (4H, m, CH_2CH_2), 3.50 [1H, m, J=8.5 Hz, $CH(CH_3)_2$], 3.93 (3H, s, OCH_3), 4.05 (3H, s, OCH_3), 6.38 (1H, s, OH), and 7.24, 7.75 (2H, ABq, J=9 Hz). MS m/z (rel intensity) 325 (7), 324 (M^+, 40), 307 (30), 306 (base), and 291 (23). Found: C, 77.93; H, 7.56%. Calcd for $C_{21}H_{24}O_3$: C, 77.75; H, 7.46%.

4-Acetyl-2-isopropyl-3-methoxy-7-methyl-1*H*-phenalen-1-one (18). To a solution of 1.4 ml of water, 0.16 ml of concentrated sulfuric acid and 0.1 ml of methanol, was added 1 mg of mercury(II) sulfate in 1 ml methanol. A solution of **17** (13 mg, 0.04 mmol) in 1 ml of MeOH was added to the solution at 50 °C with rapid stirring. The temperature was maintained at 50—55 °C throughout the reaction. After the reaction was completed (1 h), the reaction mixture was cooled to room temperature, 5 ml of water added and the product extracted with ether. The ether extract was washed with water and dried over anhydrous sodium sulfate. Evaporation of the solvent followed by chromatography on silica gel with hexane/ethyl acetate (8 : 2) afforded 8.2 mg (68%) of **18** as bright yellow orange needles. Mp: 114—116 °C; ^1H NMR ($CDCl_3$) δ=1.43 [6H, d, J=7 Hz, $CH(CH_3)_2$], 2.52 (3H, s, CH_3CO), 2.82 (3H, J=1 Hz, $ArCH_3$), 3.34 (1H, sept, J=7 Hz), 3.65 (3H, s, OCH_3), 7.33, 8.19 (2H, ABq, J=8.5 Hz), and 7.58, 8.49 (2H, ABq, J=7.7 Hz); MS m/z (rel intensity) 309 (14), 308 (M^+, 60), 294 (21), 293 (base), 279 (10), 278 (11), and 265 (48). Found: C, 77.65, H, 6.79%; Calcd for $C_{20}H_{20}O_3$: C, 77.90; H, 6.54%.

1-Isopropenyl-8-isopropyl-7,9-dimethoxy-4-methyl-2,3-dihydro-1*H*-phenalen-1-ol (19). A solution of isopropenyllithium in tetrahydrofuran was prepared by addition of butyllithium (0.8 M in hexane, 1 ml) to 2-bromopropene (0.1 ml) in 1 ml of dry tetrahydrofuran at −78 °C under argon followed by stirring for an additional 1 h at −78 °C. A ketone **16a** (85 mg, 0.29 mmol) in 0.5 ml tetrahydrofuran was added slowly to the stirred solution via a syringe. The reaction mixture was stirred for 2.5 h at −78 °C under argon, and the mixture was allowed to warm to 0 °C. Saturated aqueous sodium chloride was added to the reaction mixture, and the phases were separated. The aqueous phase was extracted with three 20 ml portions of ether. The combined organic phases were dried over anhydrous sodium sulfate and concentrated under vacuum to yield the crude product. Flash chromatography of the crude oil on silica gel with hexane/ether (8 : 1) afforded 87 mg (90%) of **19** as a pale yellow oil. IR ($CHCl_3$) 3430 and 1600 cm^{-1}; ^1H NMR ($CDCl_3$) δ=1.39 (3H, d, J=7.3 Hz), 1.49 (3H, d, J=7.3 Hz), 2.02 (3H, s, CH_3), 2.40 (3H, s, $ArCH_3$), 2.60—3.70 (4H, m, CH_2CH_2), 3.42 [1H, sept, J=7.3 Hz, $CH(CH_3)_2$], 3.77 (3H, s, OCH_3), 3.94 (3H, s, OCH_3), 4.89 (2H, brs, CH_2=), and 7.20, 7.76 (2H, ABq, J=8.7 Hz, ArH); ^{13}C NMR ($CDCl_3$) δ=18.5, 20.0, 22.6, 23.2, 24.1, 26.3, 34.1, 62.5, 63.0, 77.8, 114.0, 119.1, 125.5, 128.1, 128.6, 130.5, 131.3, 132.2, 132.8, 151.7, 153.8, 156.5; MS m/z (rel intensity) 340 (M^+, 33), 323 (26), 322 (63), 307 (18), 306 (7), 300 (29), and 299 (base). Found: C, 77.80; H, 8.34%; Calcd for $C_{22}H_{28}O_3$: C, 77.61; H, 8.29%.

9-Isopropyl-2,2,5-trimethylphenaleno[1,9-*bc*]furan-8(2*H*)-one (Salvilenone, 1) and 20. A mixture of alcohol **19** (30 mg, 0.088 mmol), acetic acid (4 ml), and 47% hydrobromic acid (1 ml) was heated under reflux for 48 h. The reaction mixture was evaporated in vacuo, and ether added to the residue. The ethereal solution was washed with 5% sodium carbonate solution and water, and dried over anhydrous sodium sulfate. The solvent was evaporated under reduced pressure. The residue was separated by preparative TLC (silica gel, was developed twice with 8 : 2 hexane/ethyl acetate) to give **1** (17 mg, 66%) and hydroxy diketone **20** (5.4 mg, 20%). Hydroxy diketone was recrystallized from hexane: mp 134—136 °C; IR 3460, 1712, and 1677 cm^{-1}. ^1H NMR ($CDCl_3$) δ=

0.95 (3H, d, J=6 Hz, $CHCH_3$), 0.97 (3H, d, J=6 Hz), 1.35 (3H, d, J=7 Hz), 1.47 (3H, d, J=7 Hz), 2.34 [1H, sept, J=6 Hz, $CH(CH_3)_2$], 2.80 (3H, s, $ArCH_3$), 4.10 [1H, sept, J=7 Hz, $ArCH(CH_3)_2$], 7.53 (1H, d, J=8 Hz, ABq), 7.79 (1H, d, J=9 Hz, ABq), 8.27 (1H, d, J=9 Hz, ABq), 8.35 (1H, d, J=8 Hz, ABq), and 9.67 (1H, brs, OH). MS m/z 311 (M^++1) 310 (M^+), 292 (M^+−18), and 267 (M^+−43); UV (EtOH): 208 (21080), 238 (44950), 325 nm (8060). ^{13}C NMR (125 MHz, $CDCl_3$) δ= 16.6(q), 17.0(q), 20.2(q), 23.3(q), 24.7(q), 29.3(d), 36.1(d), 101.6(s), 126.0(d), 126.7(s), 126.8(s), 127.2(d), 129.0(d), 129.7(d), 130.3(s), 131.8(s), 142.9(s), 152.8(s), 193.2(s), and 197.7(s). Found: C, 77.20; H, 7.16%; Calcd for $C_{20}H_{22}O_3$: C, 77.39; H, 7.14%.

2-Hydroxy-2,4-diisopropyl-7-methyl-1*H*-phenalene-1,3 (2*H*)-dione (20). A mixture of 7 mg of alcohol **19**, 2 ml of glacial acetic acid, and 1 ml of 50% hydriodic acid solution was heated under reflux for 35 h. The reaction mixture was concentrated in vacuo., and extracted with ether. The ether extracts were filtered through celite until the filtrate became clear. The combined filtrates were washed with 10% $NaHCO_3$ and water, dried, and concentrated. The residue was purified by chromatography on silica gel using hexane/ethyl acetate (7:3) as eluent to give 3.9 mg (59%) of a white solid, which was identical with the hydroxy diketone **20** obtained in the preceding experiment.

4-Isopropenyl-2-isopropyl-3-methoxy-7-methyl-1*H*-phenalen-1-one (21). A mixture of 7 mg (0.02 mmol) of alcohol **19** and iodine in 6 ml of carbon tetrachloride was stirred for 17 h at room temperature. The iodine was decomposed by addition of $Na_2S_2O_3$. After the precipitates were removed, the solution was washed with water, dried over sodium sulfate, and evaporated to give a yellow solid. Purification of the crude product by preparative TLC (hexane/ethyl acetate 6:49) gave 3.4 mg (54%) of **21** as an orange yellow solid. Mp 120—122 °C; ^1H NMR ($CDCl_3$) δ=1.42 [6H, d, J=7 Hz, $CH(CH_3)_2$], 2.01 (3H, s, $CH_3C{=}CH_2$), 2.81 (3H, s, $ArCH_3$), 3.44 [1H, sept, J=7 Hz, $CH(CH_3)_2$], 3.70 (3H, s, OCH_3), 5.1 (2H, m, $CH_3C{=}CH_2$), 7.27 (1H, d, J=9 Hz), 7.63 (1H, d, J=8 Hz), 8.12 (1H, d, J=9 Hz), and 8.48 (1H, d, J=8 Hz). MS m/z 360 (M^+). Found: C, 82.44; H, 7.33%. Calcd for $C_{21}H_{22}O_2$: C, 82.32; H, 7.23%.

References

1) Q. Zhou, "Advances in Chinese Materials Research," ed by H. M. Chang, H. W. Yeung, W. W. Tso, and A. Koo, 215, World Scientific Publishing Co., Singapore (1985).

2) H. Luo, B. Wu, Z. Yong, and Y. Jin, *Acta Pharm. Sinica*, **20**, 542 (1985).

3) C. W. Zhou, D. Y. Li, W. C. Gen, and T. G. Sheng, *Acta Pharm. Sinica*, **1979**, 277; Shanghai 201 Clinical Research Group on Dan-Shen, *Chinese Med. Comm.*, **37** (1978).

4) Y. Okumura, H. Kakisawa, M. Kato, and Y. Hirata, *Bull. Chem. Soc. Jpn.*, **34**, 895 (1961); K. Takiura, *Yakugaku Zashi*, **61**, 475, 482 (1941); H. Kakisawa, T. Hayashi, I. Okazaki, and M. Ohashi, *Tetrahedron Lett.*, **1968**, 3231; H. Kakisawa, T. Hayashi, and T. Yamazaki, *Tetrahedron Lett*, **1969**, 301.

5) T. Kusumi, T. Ooi, T. Hayashi, and H. Kakisawa, *Phytochemistry*, **24**, 2188 (1985).

6) R. G. Cook and J. M. Edwards, *Prog. Org. Nat. Prod.*, **40**, 153 (1981).

7) This paper has been partly presented as a preliminary communication; G. C. Zheng, T. Kojima, and H. Kakisawa, *Heterocycles*, **27**, 1341 (1988).

8) A cyclization of carboxylic acid **14** by polyphosphoric acid afforded a deisopropyl product **16b** as a major product. Although elimination of alkyl group on a benzene ring is a recognized feature in certain Friedel-Crafts reaction, very few cases of dealkylation have been recorded for the intramolecular ring closure reaction by polyphosphoric acid. K. Yamada, S. Takada, Y. Hayakawa, and Y. Hirata, *Bull. Chem. Soc. Jpn.*, **42**, 3011 (1969).

9) C. Schmidt, *Can. J. Chem.*, **54**, 2310 (1976).

10) R. C. Gadwood and R. M. Lett, *J. Org. Chem.*, **47**, 2268 (1982).

11) For a review, see M. V. Bhatt and S. U. Kulkarni, *Synthesis*, **1983**, 249.

12) Although isomeric structures **18'**, and **21'**, were also conceivable, the structures **18** and **21** were tentatively assigned based on the NMR data and mechanistic considerations.

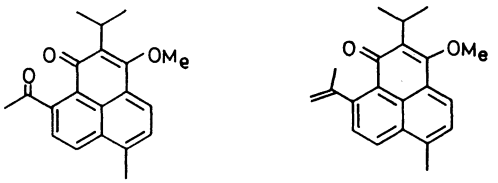

18' 21'

Scheme 5.

 © 1989 The Chemical Society of Japan Bull. Chem. Soc. Jpn., 62, 1123—1126 (1989)

Reduction of 2-Carboxy-4′-dimethylaminoazobenzene by *Bacillus* Diaphorase

Chizuko YATOME,* Toshihiko OGAWA, Toshihiko OGAWA, and Hideki HAYASHI
Department of Chemistry, Faculty of Engineering, Gifu University, Yanagido 1-1, Gifu 501-11
(Received September 14, 1988)

2-Carboxy-4′-dimethylaminoazobenzene (CDMAB) was reductively cleaved into its two component primary arylamines by *Bacillus* diaphorase together with NADH (pH 6.1, 25 °C). The reductive cleavage was found to proceed stoichiometrically by a spectrofluorometric assay of fluorescent *o*-aminobenzoic acid and a fluorescent product formed between *N*,*N*-dimethyl-*p*-phenylenediamine and fluorescamine. Parallel lines were obtained in Lineweaver-Burk plots of initial rate vs. CDMAB concentration for the reduction. This experimentally observed kinetic behavior is consistent with a reaction scheme in favor of the Ping Pong mechanism in which CDMAB is reduced by a reduced form of diaphorase. From a kinetic formula, the apparent K_m(CDMAB), K_m(NADH), and V_{max} values are 2.14×10^{-5} mol dm^{-3}, 7.35×10^{-5} mol dm^{-3}, and 1.8×10^{-7} mol dm^{-3} min^{-1} per mg of protein, respectively.

Most azo compounds are reduced into their parent primary arylamines by azoreductase in rat liver microsomes[1] and liver cytosol preparations.[2] Microbial reduction of water-soluble sulfonated azo compounds has been widely investigated, and it has been reported that microbial azoreductase was much more effective than liver microsomal azoreductase for a reduction of azo compounds.[3] However, there are few reports about the microbial reduction of slightly water-soluble and water-insoluble azo compounds.[4] As a part of studies on the microbiological treatment of wastewater containing various azo compounds, it is desirable to investigate on the microbial reduction (both in vivo and in vitro) of slightly water-soluble and water-insoluble azo compounds.

In this paper, the stoichiometry and kinetics of the enzymatic reduction of 2-carboxy-4′-dimethylaminoazobenzene by *Bacillus* diaphorase was followed.

Experimental

Chemicals. *Bacillus* diaphorase and NAD(P)H were purchased from Boehringer Mannheim GmbH and Wako Pure Chemical Industries, Ltd., respectively. These enzyme and chemicals were used without purification. The apparent specific activity of *Bacillus* diaphorase was about 15 units/mg (25 °C; with NADH and 2-(*p*-iodophenyl)-3-(*p*-nitrophenyl)-5-phenyltetrazolium chloride; pH 8.8). The prosthetic group of the enzyme was FMN. 2-Carboxy-4′-dimethylaminoazobenzene (CDMAB) was purchased from Nakarai Chemicals Ltd. and recrystallized from ethyl alcohol. The purity was verified by thin-layer chromatography using several systems.

Methods. Reduction of CDMAB by Diaphorase together with NADH: Suitable conditions for the reduction of CDMAB by diaphorase were examined as follows. A reaction mixture containing 0.5 cm^3 of 0.2 mmol dm^{-3} CDMAB aqueous solution, 0.02 cm^3 of 1 mg cm^{-3} diaphorase solution, and 0.5 cm^3 of 0.5 mmol dm^{-3} NADH solution in a final volume of 2 cm^3 of 0.07 mol dm^{-3} potassium phosphate buffer was incubated under an atmosphere of nitrogen in an ampule at a prescribed temperature (10—37 °C) and pH (5.5—7.5). The amount of protein was determeined by the method of Layne.[5] The reaction was terminated by addition of potassium hydroxide (0.1 mol dm^{-3}, 1 cm^3) and the residual CDMAB in the mixture was extracted with butyl alcohol. The disappearance of CDMAB was determined using a spectrophotometric assay based on the decrease in the absorbance of CDMAB at 435 nm (λ_{max} 435 nm in butyl alcohol saturated with water).

The azoreductase activity of diaphorase was determined as follows. A solution containing 19.8 to 72.8 nmol of CDMAB and 20 μg of diaphorase in 1.7 cm^3 of 0.07 mol dm^{-3} potassium phosphate buffer (pH 6.1) was placed in a spectrophotometric Thunberg cuvette. A solution containing 0.24 to 2.4 μmol of NADH in 0.3 cm^3 of 0.07 mol dm^{-3} potassium phosphate buffer was placed in the stopper of the Thunberg cuvette. Two solutions were bubbled independently with nitrogen gas for about 10 min. The reaction was initiated by mixing the two solutions. The mixture was incubated at 25 °C. The activity of diaphorase was determined in a spectrophotometer by recording the decrease in the absorbance of CDMAB at 430 nm (λ_{max} 430 nm in potassium phosphate buffer solution; pH 6.1) for 0—2 min and using the molar absorptivity of CDMAB (21.8 dm^3 mmol^{-1} cm^{-1}).

Assay of Reduction Products of CDMAB by Diaphorase: The products, *o*-aminobenzoic acid (*o*-ABA) and *N*,*N*-dimethyl-*p*-phenylenediamine (DMPA), were determined using a gas chromatographic-mass spectrometric (GC-MS) and a spectrofluorometric assay.

The reaction mixture was similar to that described above. The reaction (3 cm^3, pH 11) was terminated by addition of potassium hydroxide and the mixture was charged into a column of Extrelut 3 (purchased from Merck Co., Inc.) in an atmosphere of nitrogen and in the dark. Hexane (15 cm^3) was passed through the column after 10—15 min. Only one of the products, DMPA, was extracted into the hexane under these conditions with a recovery of about 90%. Then, 25 cm^3 of ether containing 0.1 cm^3 of acetic acid was passed through the column. Unreduced CDMAB was first extracted into the ether. Subsequently, the other product, *o*-ABA, was extracted into the ether with a recovery of about 100%.

The hexane of the extract containing DMPA was slowly removed by aspiration. To the residue (1), ethyl acetate and trifluoroacetic anhydride (TFAA) were added and the mixture was allowed to stand for 5 d at room temperature or for 6

h at 50 °C. Then 0.001 cm^3 was injected onto the GC-MS. On the other hand, the hexane extract containing DMPA was back extracted into 2 cm^3 of sodium acetate buffer (pH 4.0) and the upper hexane layer was carefully removed by aspiration in the dark. Fluorescamine solution (0.2 mg of fluorescamine in 1 cm^3 of acetone, 1 cm^3) was added to the aqueous phase with vigorous mixing. After 30 min, the fluorescence of the product formed between DMPA and fluorescamine was measured at 25 °C in a spectrofluorometer using excitation and emission wavelengths of 400 and 488 nm, respectively. A standard curve of DMPA was prepared by runs of the entire procedure with known amounts of authentic sample passed through the column of Extrelut 3.

The ether extract containing *o*-ABA was dehydrated by adding a few drops of 2,2-dimethoxypropane (DMP), and then the ether was evaporated under reduced pressure. To the residue (2), ethyl acetate and TFAA were added and 0.001 cm^3 was injected onto the GC-MS.[6] On the other hand, to the residue (2), 2 cm^3 of 0.07 mol dm^{-3} potassium phosphate buffer (pH 6.1) was added, and then the fluorescence of *o*-ABA was measured at 25 °C in a spectrofluorometer using excitation and emission wavelengths of 355 and 429 nm, respectively. A standard curve of *o*-ABA was prepared from the authentic sample subjected to the entire procedure.

Apparatus and Conditions: Visible spectra: a Hitachi Spectrophotometer Model 330 was used. Fluorescent spectra: a Hitachi Spectrofluorometer Model 650-10 was used. GC-MS: a Hitachi Mass Spectrometer Model M-52 was used; a 1 m×3 mm glass column was packed with Silicone OV-17 (2%) on Chromosorb WAW DMCS (80—100 mesh); samples were 0.001 cm^3. Operational conditions: column temperature 110—140 °C; carrier gas He; chamber voltage 20 eV.

Results and Discussion

Conditions for the Reduction of CDMAB by Diaphorase. The azoreductase activity of diaphorase was investigated using either NADH or NADPH as electron donor. Through the investigation it has been proved that the activity is supported favorably by NADH. Suitable conditions for the reduction of CDMAB by diaphorase together with NADH are as follows: (1) the optimum pH is 6.1; (2) the optimum temperature is 25 °C. The representative result is shown in Fig. 1.

Stoichiometry of the Reduction of CDMAB by Diaphorase together with NADH under Anaerobic Conditions. The stoichiometry of the reduction of CDMAB by diaphorase together with NADH was determined using a spectral assay based on the decrease in concentration of CDMAB and a spectrofluorometric assay based on the increase in amount of reduction products.

The magnitude of spectral change at 430 nm was initially proportional to the amount of NADH added. After addition of 250, 500, or 750 nmol of NADH to a solution containing 250 nmol of CDMAB, the spectral change (ΔA_{430}) was 0.17, 0.34, or 0.35, respectively. These results indicate that the reduction of 1 mol of CDMAB requires 2 mol of NADH under anaerobic conditions as reported by Huang et al.[2]

Reduction products were detected by GC-MS. The products were found having the same m/z (rel intensity) 215 (M^+; 26) and 146(100) with the TFA derivative of authentic *o*-ABA and the same m/z (rel intensity) 328 (M^+; 47), 231(45), and 162(100) with the TFA derivative of authentic DMPA. It has been confirmed from these results that CDMAB is reduced by diaphorase together with NADH to form two primary arylamines, *o*-ABA and DMPA.

The products, *o*-ABA and DMPA, in the reaction mixture could be simultaneously determined by spectrofluorometry since a satisfactory separation of the

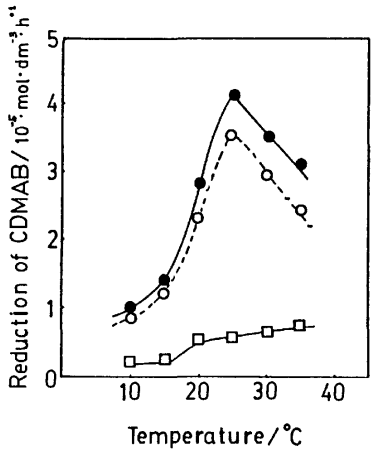

Fig. 1. Effect of temperature on reduction of CDMAB (5×10^{-5} mol dm^{-3}) by NADH (1.25×10^{-4} mol dm^{-3}) in the presence of diaphorase (10 $\mu g\,cm^{-3}$).
The reaction mixture containing CDMAB, NADH, and diaphorase was incubated under anaerobic conditions in an ampule at pH 6.1.
—●— total reduction, --○-- enzymatic reduction, —□— non-enzymatic reduction.

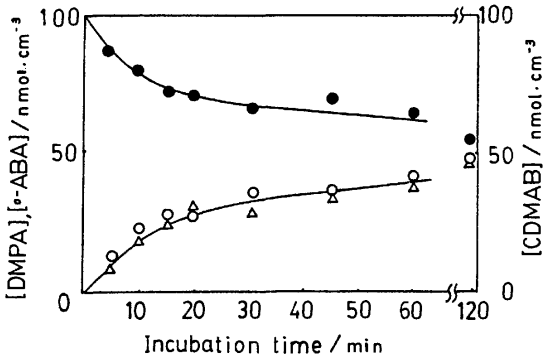

Fig. 2. Relationship between concentration of products (DMPA and *o*-ABA) and CDMAB on reduction of CDMAB (1.0×10^{-4} mol dm^{-3}) by NADH (1.0×10^{-4} mol dm^{-3}) in presence of diapholase (10 $\mu g\,cm^{-3}$).
The reaction mixture containing CDMAB, NADH, and diaphorase was incubated under anaerobic conditions in a Thunberg tube at 25 °C, pH 6.1.
—●— 2-carboxy-4′-dimethylaminoazobenzene (CDMAB), —○— *N,N*-dimethyl-*p*-phenylenediamine (DMPA), —△— *o*-aminobenzoic acid (*o*-ABA).

products was achieved using the column of Extrelut. The result is shown in Fig. 2. The expected stoichiometry for the reduction of the azo linkage of CDMAB by diaphorase together with NADH has been demonstrated. The reaction was completed within 120 min under the conditions adopted. Consequently these results indicate that *Bacillus* diaphorase consumes 2 mol of NADH as electron donor when 1 mol of CDMAB is reduced to *o*-ABA and DMPA under the present experimental conditions. The reduction of CDMAB by diaphorase is summarized as follows:

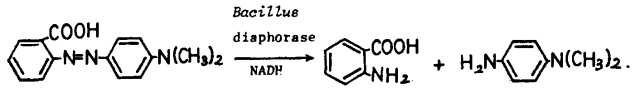

CDMAB *o*-ABA DMPA

Hydrazo intermediates are presumably formed in the reduction of azo compounds.[1,7] While CDMAB can be reduced to the hydrazo intermediate with sodium sulfite, at pH 5—8 CDMAB is known to be reduced to the amines via a four-electron reaction by electrode reaction.[8] The hydrazo intermediate was not detected in the present experiment.

Kinetic Studies. Under the conditions minimizing the non-enzymatic reduction (the non-enzymatic reaction was made not to occur during 2 min), the amounts of diaphorase used were selected so that the reaction rate was significant but small enough to remain linear for at least 2 to 3 min. Initial slopes of recorder tracings were taken as initial rates. Parallel lines were obtained in the Lineweaver-Burk plot of initial rate vs. CDMAB concentration at fixed enzyme and various NADH concentrations, as shown in Fig. 3. The result can be explained by the Ping Pong mechanism; Alberty,[9] suggested two kinds of mechanisms, Sequential and Ping Pong, as a result of inspection of double reciprocal plots of initial rate vs. substrate concentration (Lineweaver -Burk plot). In theory, lines in Lineweaver-Burk plots for the Ping Pong mechanism are parallel in contrast with the Sequential mechanism which exhibits converging lines. The feature of the Ping Pong mechanism is that the enzyme reacts with one of the substrates to form a complex, which in turn breaks down to yield a modified enzyme with dissociation of the product before the second substrate binds the enzyme. On the basis of the stoichiometry of reduction of CDMAB previously described, the result can therefore be summarized as the following reaction scheme, where E is the enzyme, diaphorase, and Eox and Ered are the oxidized and reduced forms of the enzyme, respectively:

$$\mathrm{Eox} + 2\mathrm{NADH} + 2\mathrm{H^+} \underset{k_{-1}}{\overset{k_{+1}}{\rightleftharpoons}} \mathrm{Eox\text{-}(NADH)_2\text{-}(H^+)_2},$$

$$\mathrm{Eox\text{-}(NADH)_2\text{-}(H^+)_2} \underset{k_{-2}}{\overset{k_{+2}}{\rightleftharpoons}} \mathrm{Ered} + 2\mathrm{NAD^+},$$

$$\mathrm{Ered} + \mathrm{CDMAB} \underset{k_{-3}}{\overset{k_{+3}}{\rightleftharpoons}} \mathrm{Ered\text{-}CDMAB},$$

$$\mathrm{Ered\text{-}CDMAB} \underset{k_{-4}}{\overset{k_{+4}}{\rightleftharpoons}} \mathrm{Eox} + \mathrm{DMPA} + o\text{-}\mathrm{ABA},$$

Eox: E-$(FMN)_2$, Ered: E-$(FMNH_2)_2$.

This mechanism leads to the following expression as for the Bi Bi Uni Uni Ping Pong mechanism using Cleland's nomenclature,[10] in which the initial reaction rate in a steady-state treatment depends on the square of the concentration, $[NADH]^2$, in the form[11,12]

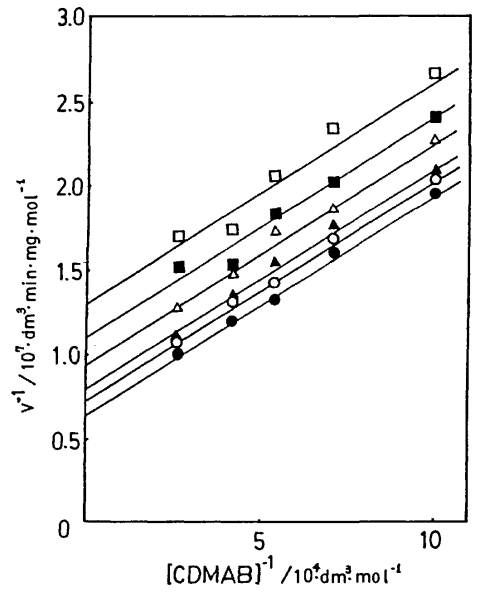

Fig. 3. Relationship between reciprocal intial reaction rate and reciprocal concentration of CDMAB (Lineweaver-Burk plots).
Concentration of diaphorase; 10 $\mu g\,cm^{-3}$. Concentration of NADH ($\times 10^{-5}$ mol dm^{-3}). —●— 120, —○— 60, —▲— 30, —△— 24, —■— 18, —□— 12.
The reaction mixture containing CDMAB, NADH and diaphorase was incubated under anaerobic conditions in a spectrophotometric Thunberg cuvette at 25°C, pH 6.1.

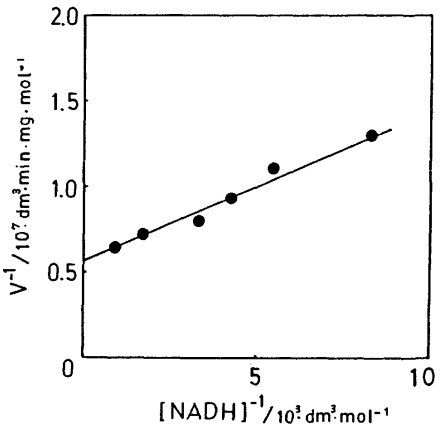

Fig. 4. Relationship between intercepts on the ordinate of Fig. 3 and reciprocal of concentration of NADH (Lineweaver-Burk plots).

$$\frac{V}{v} = 1 + \frac{K_m(\text{coen.})\,K'_m(\text{coen.})}{[\text{coen.}]^2} + \frac{2K_m(\text{coen.})}{[\text{coen.}]} + \frac{K_m(\text{dye})}{[\text{dye}]} \quad (1)$$

where

coen.: NADH, dye: CDMAB,

$$V = \frac{k'_{+2}\,k_{+2}\,k_{+4}}{k'_{+2}\,k_{+2} + k'_{+2}\,k_{+4} + k_{+2}\,k_{+4}}\,E_0\,,$$

$$K_m(\text{dye}) = \frac{k'_{+2}\,k_{+2}(k_{-3} + k_{+4})}{k_{+3}(k'_{+2}\,k_{+2} + k'_{+2}\,k_{+4} + k_{+2}\,k_{+4})}\,,$$

$$K_m(\text{coen.}) = \frac{k_{+2}\,k_{+4}(k_{-1} + k'_{+2})}{k_{+1}(k'_{+2}\,k_{+2} + k'_{+2}\,k_{+4} + k_{+2}\,k_{+4})}\,,$$

$$K'_m(\text{coen.}) = \frac{k'_{-1}}{k'_{+1}}\,.$$

The square term in Eq. 1 becomes negligible, provided [NADH] $\gg K_m$(NADH) or K'_m(NADH). Equation 1 may be rearranged to

$$\frac{V}{v} = 1 + \frac{2K_m(\text{coen.})}{[\text{coen.}]} + \frac{K_m(\text{dye})}{[\text{dye}]}\,. \quad (2)$$

Equation 2 predicts that a plot of v^{-1} vs. $[\text{NADH}]^{-1}$ will be linear. [NADH] under the present experimental conditions was varied in the range $12-120\times10^{-5}$ mol dm^{-3}. These conditions are higher than the tentative K_m(NADH) value, 7×10^{-5} mol dm^{-3}. In Fig. 4 data are presented to show that a secondary plot of the intercepts of the Lineweaver-Burk plots of Fig. 3 vs. NADH concentration gives a straight line. Equations 1 and 2 are in good agreement with the data in Figs. 3 and 4. Thus the experimental data suggest the correctness of the above reaction scheme that in the sequence of substrate binding and product release, CDMAB is reduced by a reduced form of the enzyme.

References

1) P. H. Hernandez, J. R. Gillette, and P. Mazel, *Biochem. Pharmacol.*, **16**, 1859 (1967).
2) M-T. Huang, G. T. Miwa, N. Cronheim, and A. Y. H. Lu, *J. Biol. Chem.*, **254**, 11223 (1979).
3) S. Nambara and T. Yamaha, *Yakugaku Zasshi*, **95**, 1302 (1975).
4) U. Meyer, G. Overney, and A. von Wattenwyl, *Textilveredlung*, **14**, 15 (1979).
5) E. Layne, "Methods in Enzymology," Academic Press, New York (1957), Vol. 3, pp. 447—454.
6) K. Hirano, K. Mori, N. Tsuboi, S. Kawai, and T. Ohno, *Chem. Pharm. Bull.*, **20**, 1412 (1972).
7) R. Gingell and R. Walker, *Xenobiotica*, **1**, 231 (1971).
8) T. M. Florence, *Aust. J. Chem.*, **18**, 609 (1965).
9) R. A. Alberty, *J. Am. Chem. Soc.*, **75**, 1928 (1953).
10) W. W. Cleland, *Biochim. Biophys. Acta*, **67**, 104 (1963).
11) E. L. King and C. Altman, *J. Phys. Chem.*, **60**, 1375 (1956).
12) T. Hashimoto, "Kouso-Hannou Sokudoron," Kyoritsu Shuppan, Tokyo (1971), Chap. 3.2, pp. 41—47.
13) M-T. Huang, G. T. Miwa, and A. Y. H. Lu, *J. Biol. Chem.*, **254**, 3930 (1979).

 © 1989 The Chemical Society of Japan Bull. Chem. Soc. Jpn., 62, 1127—1135 (1989)

Dehydrooligopeptides. XI. Facile Syntheses of Various Kinds of Dehydrodi- and tripeptides, and Dehydroenkephalins Containing ⊿Tyr Residue by Using *N*-Carboxydehydrotyrosine Anhydride[1)]

Chung-gi SHIN,* Takumi OBARA, Shuji TANIGUCHI, and Yasuchika YONEZAWA
Laboratory of Organic Chemistry, Faculty of Technology, Kanagawa University, Rokkakubashi, Kanagawa-ku, Yokohama 221
(Received September 17, 1988)

Several kinds of *N*-free and protected *N*-carboxydehydrotyrosine anhydride (⊿Tyr·NCA) derivatives, derived by both the cyclization of the corresponding *N*-benzyloxycarbonyldehydrotyrosine derivatives and the protection of the resulting ⊿NCA, were employed for a one-pot dehydrooligopeptide (DHP) synthesis. As a result, various kinds of DHPs with a wide variety of combinations of sequences could be synthesized in fairly good yields. In addition, by utilizing the obtained information, two kinds of leucine-dehydroenkephalins containing a ⊿Tyr[1] and both ⊿Tyr[1] and ⊿Phe[4] residues were also synthesized.

In a previous paper,[2)] we reported in detail the syntheses of various kinds of *N*,*O*-diprotected dehydrotyrosine (⊿Tyr) derivatives from mainly two routes. That is to say, the ⊿Tyr derivatives were derived by the condensation of *O*-protected *p*-hydroxybenzaldehyde with *N*-acyl-2-(diethoxyphosphinyl) glycine[3)] and by the reaction of *N*-carboxydehydrotyrosine anhydride (⊿Tyr·NCA), derived by the cyclization of *N*-benzyloxycarbonyl (Cbz)-dehydrotyrosine with $SOCl_2$, with methanol. On the other hand, recently, various modes of coupling of *N*-carboxy-α-dehydroamino acid anhydride (⊿NCA) with an amino (*N*-), carboxy (*C*-) or both two components of AA were carried out to give a number of dehydrooligopeptides (DHP) in fairly good yields.[4,5)] However, there has only been a few reports concerning a useful synthetic method for DHP containing a ⊿Tyr residue,[6)] although the hydrogenated one, namely L-tyrosine (Tyr) residue, is often an important bioactive site in opioid peptides, such as cholecystokinin-8.[7)]

In this paper we wish to report on convenient syntheses of various kinds of DHP containing (*Z*)-configurational ⊿Tyr residues blocked with available *N*- and *O*-protecting groups, such as Cbz, *t*-butoxycarbonyl (Boc), and methoxymethyl (MOM), by the so-called ⊿NCA method.[4,8–10)]

Moreover, in order to chemically modify naturally occurring peptides, leucine-enkephalin (Leu-Enk), as one of the numerous neuropeptides, was chosen and Tyr[1] or both Tyr[1] and phenylalanine (Phe[4]) residues were replaced by the corresponding ⊿Tyr and dehydrophenylalanine (⊿Phe) to obtain Δ^1 and $\Delta^{1,4}$-dehydroenkephalin derivatives (Δ^1Enk and $\Delta^{1,4}$Enk).[11)]

Results and Discussion

Syntheses of Dehydrodi- and tripeptides with ⊿Tyr Residue. We have already reported on the synthesis of (*Z*)-Cbz-(*O*-MOM)dehydrotyrosine [Cbz-⊿Tyr (MOM)-OH] (**1**), derived successively by the condensation of *p*-methoxymethoxy (MOMO) benzaldehyde with *N*-Cbz-2-(diethoxyphosphinyl)glycine methyl ester by the Schmidt method[3)] and the ester hydrolysis of (*Z*)-Cbz-⊿Tyr(MOM)-OMe. Futhermore, the facile conversion of **1** with $SOCl_2$ to (*Z*)-*N*-carboxy-(*O*-MOM)dehydrotyrosine anhydride [⊿Tyr(MOM)·NCA] (**2**) and subsequent deprotection with HCl to ⊿Tyr·NCA (**3**) was also reported[2)] (see Scheme 1).

In addition to the two compounds mentioned above (**2** and **3**), two more starting substrates were synthesized as follows. (*Z*)-*N*-Carboxy-(*O*-Boc)dehydrotyrosine anhydride [⊿Tyr(Boc)·NCA] (**4a**) was purely obtained in 70% yield by the selective acylation of a phenolic hydroxyl group alone of **3** with an equimolar di-*t*-butyl dicarbonate [$((CH_3)_3COCO)_2O$; $(Boc)_2O$] by the usual method.[2)] Moreover, a similar treatment of **3** with more than two moles of $(Boc)_2O$ was carried out to give (*Z*)-*N*-carboxy-*N*-Boc-(*O*-Boc)dehydrotyrosine anhydride [Boc-⊿Tyr(Boc)·NCA] (**4b**) as an unstable

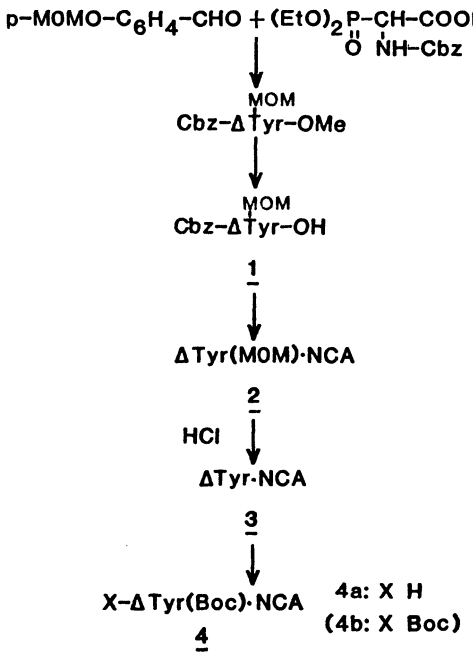

Scheme 1.

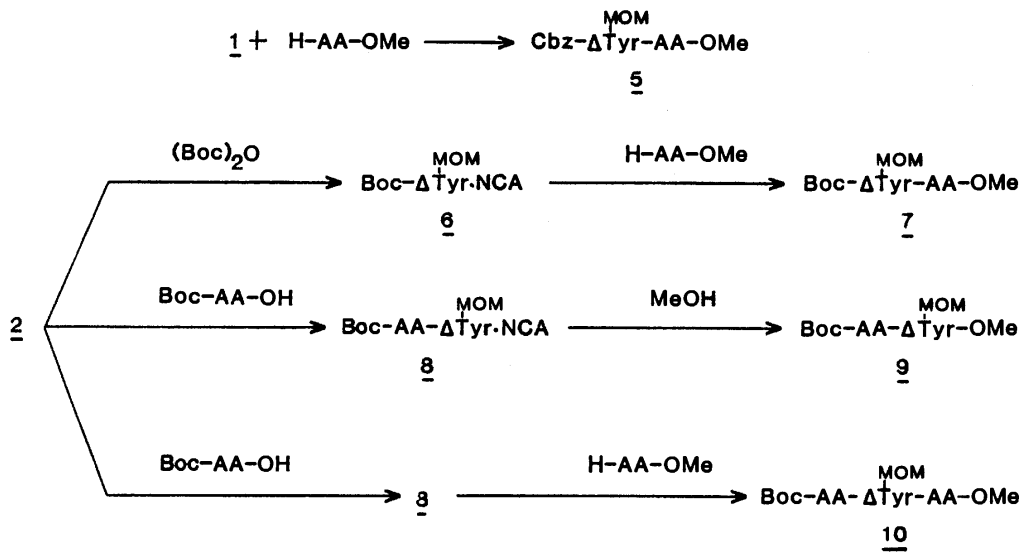

Scheme 2.

intermediate, although a pure isolation was unsuccessful. From the above results, in the case of the acylation of **3**, it can be seen that the side-chain phenolic hydroxyl group was more reactive than the ring imino group.

The four (*Z*)-*⊿*Tyr·NCA derivatives (**2**, **3**, **4a**, and **4b**) were subsequently subjected to the syntheses of numerous dehydrodi- and tripeptides by wide variety of combinations of appropriate AA and variously protected *⊿*Tyr residues, as illustrated in Schemes 2 and 3. Three more *N*-acyl-*⊿*Tyr·NCA intermediates were synthesized and then employed in situ to the synthesis of dehydrooligopeptides.

First, the stepwise elongation of **1** with L-*α*-amino acid methyl ester (H-AA-OMe) by using water-soluble [3-(dimethylamino)propyl]ethylcarbodiimide [C_2H_5-N=C=N-$(CH_2)_3$-N$(CH_3)_2$·HCl; WSC] was readily carried out to give Cbz-*⊿*Tyr(MOM)-AA-OMe (**5**) in a 75% yield.

On the other hand, by taking advantage of two highly reactive sites of compound **2**, three sorts of *⊿*^{1},*⊿*^{2}-dehydrotripeptides (**7** and **9**) and *⊿*^{2}-dehydrotripeptides (**10**)[11] containing a *⊿*Tyr(MOM) residue at N, C-termini and at the center could be readily synthesized.[11] In the case of the synthesis of Boc-*⊿*Tyr(MOM)-AA-OMe (**7**), the acylation of **2** with $(Boc)_2O$ was carried out as the first step to form the corresponding intermediate, *N*-Boc-(*O*-MOM)-dehydrotyrosine anhydride [Boc-*⊿*Tyr(MOM)·NCA] (**6**), which was subsequently treated in situ with H-AA-OMe as an *N*-component to give **7** in 56% yield.

Similarly, a one-pot synthesis of *⊿*^{2}-dehydrodipeptides (**9**) containing C-terminal *⊿*Tyr(MOM) residue was also worked up by the following successive reactions. The coupling of **2** with Boc-AA-OH as a *C*-component in the presence of pyridine by the dicyclohexylcarbodiimide (DCC) method and a subsequent reaction of the resulting intermediate Boc-AA-*⊿* Tyr(MOM)·NCA (**8**) with methanol were carried out to give Boc-AA-*⊿*Tyr(MOM)-OMe (**9**) in 71% yield. Consequently, as can be seen by a comparison with the structures of two compounds, **7** and **9**, they are apparently related to each other as a regioisomer.

Furthermore, in an analogous manner (as mentioned above), *⊿*^{2}-dehydrotripeptides (**10**) containing *⊿*Tyr(MOM) residue at the center were also readily synthesized in one-pot by the condensation of **2** with, in turn, Boc-AA-OH and H-AA-OMe. In this case too,

Table 1. The Yields and Melting Points of **5**

Compound No. Cbz-*⊿*AA-AA-OMe	Yield %	Mp[a] θ_m/°C	Formula	Found (Calcd)/% C	H	N
5a -*⊿*Tyr(MOM)-Gly-	77	103—105	$C_{22}H_{24}N_2O_7$	61.63 (61.67	5.66 5.65	6.55 6.54)
5b -*⊿*Tyr(MOM)-Ala-	80	Syrup	$C_{23}H_{26}N_2O_7$	62.75 (62.43	6.15 5.92	6.03 6.33)
5c -*⊿*Tyr(MOM)-Leu-	77	60—61	$C_{26}H_{31}N_2O_7$	64.20 (64.45	6.75 6.66	5.91 5.78)
5d -*⊿*Tyr(MOM)-Phe-	66	58—60	$C_{29}H_{30}N_2O_7$	67.01 (67.17	5.89 5.83	5.45 5.40)

a) Colorless needles from a mixture of ethyl acetate and hexane.

Table 2. The Spectral and Optical Data of **5**

Compound No.	IR, $\tilde{\nu}$/cm^{-1} in KBr			^{1}H NMR (δ, $CDCl_3$)		$[\alpha]_D^{24}$/°
	-NHCO-		-C=C-	Ar-CH=	α-H[a] (J/Hz)	(c 1, in MeOH)
5a	1665	1520	1625	6.64s	4.10d (5.5)	—
5b	1665	1520	1630	7.18s	4.61dq (6.8, 6.8)	6.6
5c	1660	1515	1625	6.88—7.74[b]	4.74dt (6.5, 7.0)	−22.3
5d	1670		1630	6.82—7.54[b]	4.91dt (8.0, 7.0)	−21.2

a) Proton on α-carbon of L-α-amino acid residue. b) Overlapped on phenyl protons.

Table 3. The Yields and Melting Points of **7** and **9**

Compound No. Boc-⊿AA-AA-OMe (**7**) Boc-AA-⊿AA-OMe (**9**)	Yield %	Mp[a] θ_m/°C	Formula	Found (Calcd)/%		
				C	H	N
7a -⊿Tyr(MOM)-Ala-	45	Syrup	$C_{20}H_{28}N_2O_7$	58.75 (58.81	7.02 6.91	6.81 6.86)
7b -⊿Tyr(MOM)-Val-	85	Syrup	$C_{22}H_{32}N_2O_7$	60.27 (60.53	7.66 7.39	6.67 6.42)
7c -⊿Tyr(MOM)-Ile-	50	Syrup	$C_{23}H_{34}N_2O_7$	61.12 (61.34	7.90 7.61	6.19 6.22)
7d -⊿Tyr(MOM)-Phe-	43	Syrup	$C_{26}H_{32}N_2O_7$	64.21 (64.45	6.92 6.66	5.72 5.78)
9a -Ala-⊿Tyr(MOM)-	67	101—103	$C_{20}H_{28}N_2O_7$	58.92 (58.81	6.98 6.91	6.79 6.86)
9b -Val-⊿Tyr(MOM)-	73	117—118	$C_{22}H_{32}N_2O_7$	60.72 (60.53	7.45 7.39	6.40 6.42)
9c -Ile-⊿Tyr(MOM)-	70	109—110	$C_{23}H_{34}N_2O_7$	61.31 (61.34	7.76 7.61	6.31 6.22)
9d -Phe-⊿Tyr(MOM)-	74	114—116	$C_{26}H_{32}N_2O_7$	64.71 (64.45	6.70 6.66	5.71 5.78)

a) Colorless needles from a mixture of ethyl acetate and hexane.

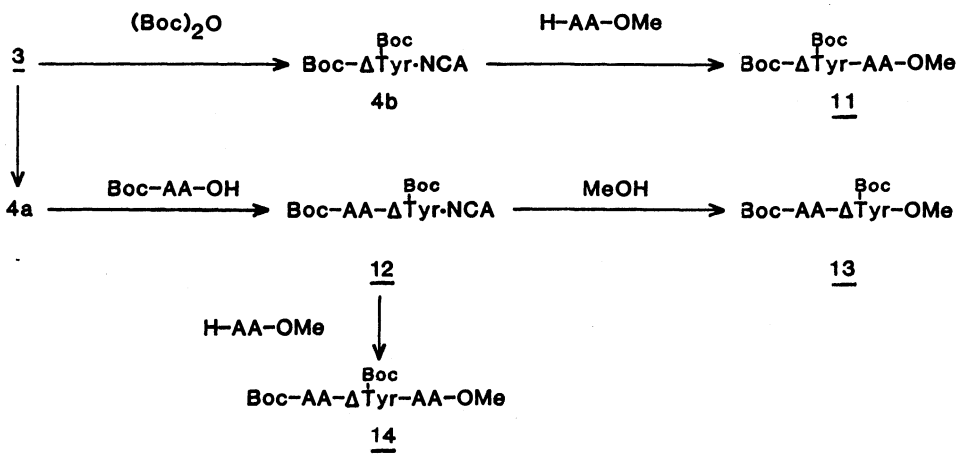

Scheme 3.

after forming the intermediate **8** in the first place, *N*-component subsequently coupled with the resulting **8** to give the expected Boc-AA-⊿Tyr(MOM)-AA-OMe (**10**) in 76% yield. As summarized in Tables 3 and 5, the yields of **7**, **9**, and **10**, thus obtained, were found to attain to 68%.

From the above results, these three synthetic procedures were further ascertained to be appreciably efficient for the synthesis of the diversified and complicating peptides containing polyfunctional α-dehydroamino and/or amino acid residues.

On the other hand, in order to obtain similar dehy-

dropeptides blocked with the same protecting group to the amino and side-chain hydroxyl groups, *N*- and *O*-unsubstituted *N*-carboxydehydrotyrosine anhydride (**3**) was successively acylated with more than two moles of $(Boc)_2O$ and coupled with H-AA-OMe in one-pot to give the desired Δ^1-dehydrodipeptide [Boc-ΔTyr-(Boc)-AA-OMe] (**11**) in 58% yield. In this case too, it is almost certain to initially form Boc-ΔTyr(Boc)·NCA (**4b**) (as mentioned earlier) and then to couple with *N*-component.

In addition, for the purpose of the stepwise elongation of the N- and both N- and C-terminal ΔTyr(Boc) moiety, compound **4a** was subjected to the *N*-acylation with *C*-component, followed by the coupling with *N*-component α-amino acid. In a similar manner as in the case of **2**, the acylation of **4a** with an appropriate Boc-AA-OH took place to yield an intermediate regarded as *N*-carboxy-*N*-Boc-acyl-(*O*-Boc)dehydrotyrosine anhydride [Boc-AA-ΔTyr(Boc)·NCA] (**12**), which was immediately reacted with methanol to give Δ^2-dehydrodipeptide [Boc-AA-ΔTyr(Boc)-OMe] (**13**) in 57% yield. Similarly, according to Scheme 3, **12** was

Table 4. The Spectral and Optical Data of **7** and **9**

Compound No.	IR, $\tilde{\nu}$/cm^{-1} in KBr			^{1}H NMR (δ, $CDCl_3$)		$[\alpha]_D^{27}$/°
	-NHCO-		-C=C-	Ar-CH=	α-H[a] (J/Hz)	(c 1, in MeOH)
7a	1605	1515	1630	7.17s	4.72dq (6.8, 6.8)	15.3
7b	1610	1520	1630	7.14s	4.74dd (5.1, 8.6)	−21.8
7c	1615	1525	1620	7.24s	4.71dd (6.0, 9.0)	−8.4
7d	1610		1635	6.72—7.68[b]	5.20m	−12.0
9a	1690	1510	1640	7.36s	4.41dq (7.0, 7.0)	3.6
9b	1670	1525	1645	7.24s	3.99dd (7.5, 9.0)	4.3
9c	1665	1525	1640	7.28s	4.05dd (6.2, 9.1)	90.9
9d	1670		1635	7.04—7.60[b]	4.68dt (7.0, 8.0)	0.2

a) Proton on α-carbon of L-α-amino acid residue. b) Overlapped on phenyl protons.

Table 5. The Yields and Melting Points of **10**

Compound No. Boc-AA-ΔAA-AA-OMe	Yield %	Mp[a] θ_m/°C	Formula	Found (Calcd)/%		
				C	H	N
10a -Gly-ΔTyr(MOM)-Ala-	88	123—124	$C_{22}H_{31}N_3O_8$	57.07 (56.76	6.79 6.71	8.95 9.01)
10b -Gly-ΔTyr(MOM)-Ser-	86	49—51	$C_{22}H_{31}N_3O_9$	54.82 (54.88	6.55 6.49	8.59 8.73)
10c -Val-ΔTyr(MOM)-Ile-	62	161—163	$C_{28}H_{43}N_3O_8$	61.25 (61.18	7.95 7.89	7.55) 7.65)
10d -Val-ΔTyr(MOM)-Pro-	67	64—65	$C_{27}H_{39}N_3O_8$	60.34 (60.77	7.33 7.37	7.80 7.88)

a) Colorless needles from ethyl acetate.

Table 6. The Spectral and Optical Data of **10**

Compound No.	IR, $\tilde{\nu}$/cm^{-1} in KBr			^{1}H NMR (δ, $CDCl_3$)			$[\alpha]_D^{22}$/°
	-NHCO-		-C=C-	Ar-CH=	α-H[a] (J/Hz)	α-H[a]	(c 1, in MeOH)
10a	1695	1515	1630	7.18s	3.86d (4.5)	4.52dq (6.3, 6.3)	−5.6
10b	1705	1520	1635	7.12s	3.90m	4.64m	1.7
10c	1660	1525	1640	7.20s	4.18m	4.65dd (4.2, 8.0)	17.0
10d	1680	1510	1640	7.40s	3.98m	4.48m	125.2

a) Proton on α-carbon of two L-α-amino acid residues.

Table 7. The Yields and Melting Points of **11** and **13**

Compound No. Boc-⊿AA-AA-OMe (**11**) Boc-AA-⊿AA-OMe (**13**)	Yield %	Mp[a] θ_m/°C	Formula	Found (Calcd)/% C	H	N
11a -⊿Tyr(Boc)-Gly-	50	Syrup	$C_{22}H_{30}N_2O_8$	58.35 (58.65	6.48 6.71	6.13 6.22)
11b -⊿Tyr(Boc)-Ala-	70	47—48	$C_{23}H_{32}N_2O_8$	59.21 (59.46	7.05 6.94	5.92 6.03)
11c -⊿Tyr(Boc)-Leu-	47	72—73	$C_{26}H_{38}N_2O_8$	61.35 (61.64	7.67 7.56	5.61 5.53)
11d -⊿Tyr(Boc)-Phe-	69	36—38	$C_{29}H_{36}N_2O_8$	64.61 (64.43	6.80 6.71	5.01 5.18)
13a -Gly-⊿Tyr(Boc)-	36	Syrup	$C_{22}H_{30}N_2O_8$	58.39 (58.65	6.39 6.71	6.02 6.22)
13b -Ala-⊿Tyr(Boc)-	70	Syrup	$C_{23}H_{32}N_2O_8$	59.82 (59.46	7.12 6.94	5.85 6.03)
13c -Leu-⊿Tyr(Boc)-	58	Syrup	$C_{26}H_{38}N_2O_8$	61.29 (61.64	7.31 7.56	5.18 5.53)
13d -Phe-⊿Tyr(Boc)-	63	64—65	$C_{29}H_{36}N_2O_8$	64.51 (64.43	6.78 6.71	5.10 5.18)

a) Colorless needles from a mixture of ethyl acetate and hexane.

Table 8. The Spectral and Optical Data of **11** and **13**

Compound No.	IR, $\tilde{\nu}$/cm^{-1} in KBr -NHCO-		-C=C-	^{1}H NMR (δ, $CDCl_3$) Ar-CH=	α-H[a] (*J*/Hz)	$[\alpha]_D^{23}$/° (*c* 1, in MeOH)
11a	1665	1510	1630	7.02s	4.10d (5.5)	—
11b	1670	1515	1635	7.05s	4.62dq (7.0, 7.0)	13.3
11c	1665	1510	1640	7.12s	4.68dt (7.0, 8.0)	−33.0
11d	1670	1510	1640	7.00—7.60[b]	4.90dt (5.0, 7.0)	−9.3
13a	1690	1510	1650	7.32s	3.86d (6.0)	—
13b	1690	1515	1650	7.34s	4.34dq (6.5, 7.0)	50.0
13c	1675	1515	1650	7.36s	4.30m	32.1
13d	1690	1510	1650	7.34s	4.56dt (7.0, 7.0)	11.4

a) Proton on α-carbon of L-α-amino acid residue. b) Overlapped on phenyl protons.

Table 9. The Yields and Melting Points of **14**

Compound No. Boc-AA-⊿AA-AA-OMe	Yield %	Mp θ_m/°C	Formula	Found (Calcd)/% C	H	N
14a -Gly-⊿Tyr(Boc)-Ser-	39	69—71	$C_{25}H_{35}N_3O_{10}$	55.92 (55.86	6.58 6.56	7.81 7.82)
14b -Gly-⊿Tyr(Boc)-Val-	30	113—115	$C_{27}H_{39}N_3O_9$	59.13 (59.00	7.25 7.15	7.60 7.65
14c -Val-⊿Tyr(Boc)-Ser-	18	Syrup	$C_{28}H_{41}N_3O_{10}$	58.22 (58.02	7.06 7.13	7.10 7.25)
14d -Val-⊿Tyr(Boc)-Val-	32	116—118	$C_{30}H_{45}N_3O_9$	60.76 (60.89	7.63 7.67	7.22 7.10)

coupled with H-AA-OMe in one-pot to give the expected Δ^2-dehydrotripeptide [Boc-AA-⊿Tyr(Boc)-AA-OMe] (**14**), although the yield was lower than 30%.

The yields, melting points, and spectral data (IR and ^{1}H NMR) of **7**, **9**, **10**, **11**, **13**, and **14**, are summarized in Tables 3—9, and 10.

In the IR spectra of all the new DHPs, thus obtained, the characteristic absorption bands of second-

Table 10. The Spectral and Optical Data of **14**

Compound No.	IR, $\tilde{\nu}$/cm^{-1} in KBr			^{1}H NMR (δ, $CDCl_3$)			$[\alpha]_D^{25}$/°
	-NHCO-		-C=C-	Ar-CH=	α-H[a] (J/Hz)	α-H[a]	(c 1, in MeOH)
14a	1675	1510	1630	7.05s	3.86d (9.8)	4.66m	−1.2
14b	1670	1515	1635	7.02s	3.75d (5.7)	4.43dd (6.0, 9.1)	−11.5
14c	1700	1510	1635	7.08s	3.88m	4.58m	15.4
14d	1690	1525	1640	7.03s	3.96dd (6.0, 8.2)	4.48dd (5.1, 8.5)	23.3

a) Proton on α-carbon of L-α-amino acid residues.

ary amide and carbon-carbon double bond functions appear at 1525—1510 and 1705—1605, and 1650—1620 cm^{-1} regions, respectively. Furthermore, in the ^{1}H NMR spectra, all of the olefin protons of the obtained DHPs shift at the δ 7.40—6.60 region as a singlet. Particularly, based on the chemical shifts of olefin protons, the configurations of the obtained Δ NCA and DHP could be tentatively confirmed to be (Z)-geometry, since the chemical shifts appeared at comparatively higher magnetic fields and the spectral patterns were quite similar to those of DHPs containing (Z)-α-dehydroamino acid (DHA) residues.[5]

From the above results and facts reported previously,[2,12] the selective protection of a hydroxyl group out of two functional groups (OH and NH) of ΔTyr·NCA was found to become feasible. Accordingly, in the case of obtaining various DHPs with a polyfunctional DHA residue as well as DHPs containing a ΔTyr residue protected by different protecting groups, the method developed here must be very effectively utilized. In addition, if α-amino acid and oligopeptide used as both the N- and C-components or segments are variously altered, even in the coupling of compound **2**, which is only one out of ΔTyr·NCAs, the further diversified types of DHP will be afforded. In fact, the various combinations of N- and C-components or moiety protected with the useful N- and O-protecting groups were already carried out to give the further wide variety of DHPs.[13]

Syntheses of Dehydroenkephalins. By utilizing the important N-terminal ΔTyr-Gly moiety, which was derived from Boc-ΔTyr(MOM)·NCA (**6**) and H-Gly-OMe by the ΔNCA method, the syntheses of two kinds of ΔEnk, e.g., Δ^1Enk and $\Delta^{1,4}$Enk, were tried, according to Scheme 4.

First of all, after an ester hydrolysis of the obtained Boc-ΔTyr (MOM)-Gly-OMe (**7e**) with 2 M LiOH, the resulting Boc-ΔTyr(MOM)-Gly-OH (**15**) was then coupled with H-Gly-L-Phe-L-Leu-OMe by the usual DCC method to give the expected Boc-ΔTyr (MOM)-Gly-Gly-Phe-Leu-OMe (**18**) in 45% yield. On the other hand, after preparation of Boc-Gly-(Z)-ΔPhe-L-Leu-OMe, derived by the one-pot reaction of N-carboxy dehydrophenylalanine anhydride (ΔPhe·NCA)[10] with in turn Boc-Gly-OH as an N-component and H-L-Leu-OMe as a C-component, and then conversion to H-Gly-(Z)-ΔPhe-L-Leu-OMe (**17**) by the N-deprotection with 4.5 M HCl, the fragment condensation of **15** with **17** was similarly worked up to give Boc-ΔTyr(MOM)-Gly-Gly-(Z)-ΔPhe-L-Leu-OMe (**19**) in 48% yield, according to Scheme 4.

In the ^{1}H NMR spectra of **18** and **19**, it was found that only the olefin protons of ΔTyr and ΔPhe residues could not be clearly assigned because of the overlap

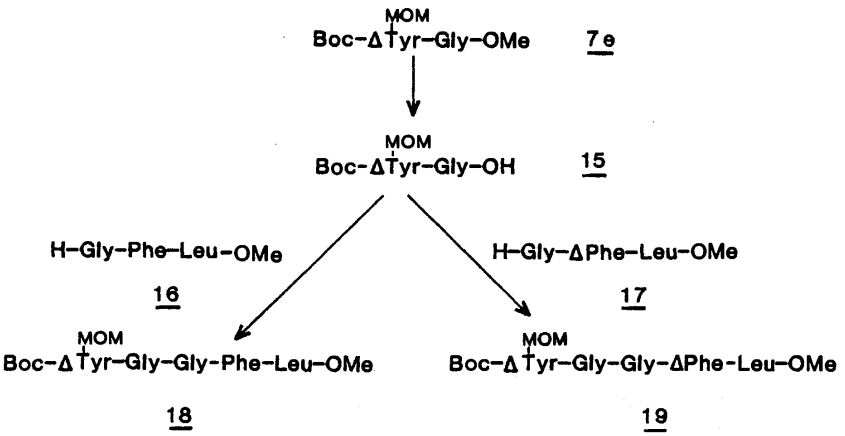

Scheme 4.

with the signals of aromatic ring and NH protons in the δ 7.34—6.86 region. At least, however, the appearance of a carbon-carbon double bond at about 1630 cm^{-1} in the IR spectra and the satisfactory elemental analyses indicated the formation of **18** and **19**.

Subsequently, in order to deprotect the protecting groups of the N-terminal ⊿Tyr residue, treatment of **18** with 2 M HCl/acetic acid in THF was carried out at room temperature for 1 h. After concentrating the reaction solution under reduced pressure, the obtained crude crystalline residue was gradually changed into a syrup during purification by the usual procedure to give *p*-hydroxyphenylpyruvoylpeptide. Unfortunately, an attempt to isolate the protecting group-free ⊿[1]Enk was unsuccessful. An enthusiastic deprotection of **18** and **19** is now under way.

In conclusion, the one-pot reactions of ⊿Tyr·NCA protected with various combination of *N*- and *O*-protecting groups were performed very smoothly. More interestingly, due to the considerable stability and reactivity of ⊿NCA, it is firmly believed that not only stepwise elongation and fragment condensation but also ring-opening polymerization to poly(α-dehydroamino acid) would be possible and diversify further the field of DHP chemistry.

Experimental

General. Melting points were determined with a Yamato micro melting-point apparatus model (MP-21) and were uncorrected. The IR spectra were recorded with a Hitachi EPI-G2 grating spectrometer. The ^1H NMR spectra were measured with a JEOL JMN PS-100 spectrometer in a $CDCl_3$ solution with tetramethylsilane as the internal standard. The specific rotations were measured in a 0.5-dm tube using a JASCO DIP-4 polarimeter (Japan Spectroscopic Co., Ltd.).

⊿Tyr(Boc)·NCA (4a) and Boc-⊿Tyr(Boc)·NCA (4b). A solution of **3** (0.50 g, 2.43 mmol) and $(Boc)_2O$ (0.53 g, 2.43 mmol) in the presence of pyridine (0.2 ml) in THF (2 ml) was stirred at room temperature for 5 h. After removing the solvent under reduced pressure, the residual syrup was crystallized by adding a small amount of hexane. The crude crystals were collected and then recrystallized from benzene to give **4a** as pale-yellow needles. Yield 70%, mp 167—170 °C (decompd). IR ν_{max}^{KBr} (cm^{-1}) 3280 (NH), 1830, 1780, (CO-O-CO), 1665 (C=C); ^1H NMR ($CDCl_3$) δ=11.48 (bs, 1H, NH), 7.40 (dd, 4H, *J*=9.0, 46.0 Hz, C_6H_4), 6.64 (s, 1H, -CH=), 1.48 [s, 9H, $-C(CH_3)_3$]. Found: C, 59.29; H, 5.07; N, 4.64%. Calcd for $C_{15}H_{15}NO_6$: C, 59.01; H, 4.95; N, 4.59%.

In a similar manner, the treatment of **3** with two molar $(Boc)_2O$ was worked up to give **4b**, which was immediately utilized to the next reaction, without isolation.

Cbz-⊿Tyr(MOM)-AA-OMe (5). A solution of an appropriate H-AA-OH·HCl (2.0 mmol) in dry CH_2Cl_2 (10 ml) in the presence of triethylamine (TEA) (0.2 ml, 2.0 mmol) was stirred at −10 °C for 30 min. To the solution, thus prepared, was added **1** (0.6 g, 1.50 mmol) and WSC (0.3 g, 1.56 mmol), and then the resulting solution was further stirred at −10 °C for 1 h. After stirring continuously at room temperature for 8 h, the reaction solution was concentrated under reduced pressure. The residual substance was dissolved in ethyl acetate (30 ml) and the resultant solution was washed successively with water, 10% citric acid, water, saturated $NaHCO_3$ aqueous solution, and then water, and finally dried over anhydrous Na_2SO_4. After removing the solvent under reduced pressure, the crystalline residue, thus obtained, was recrystallized from a mixture of ethyl acetate and hexane to give **5** as colorless needles. See Tables 1 and 2.

Boc-⊿Tyr(MOM)-AA-OMe (7). A solution of **2** (1.25 g, 5.0 mmol) and $(Boc)_2O$ (1.31 g, 6.0 mmol) in dry THF (10 ml) in the presence of pyridine (50 μl) was stirred at room temperature for 8 h. With stirring, to the solution, thus prepared, was added a solution of an appropriate H-AA-OMe·HCl (7.0 mmol) and TEA (0.7 ml, 7.0 mmol) in dry THF (10 ml). To the resulting solution was added *N*-methylmorpholine (NMM) (0.76 ml, 7 mmol) and then stirred continuously at room temperature for 2 h. After removing the solvent under reduced pressure, the residual syrup was dissolved in ethyl acetate (30 ml); the resultant solution was washed successively with chilled 10% citric acid, water, saturated $NaHCO_3$ aqueous solution, and then water, and finally dried over anhydrous Na_2SO_4. The concentration of the solution under reduced pressure gave a residual crude syrup, which was purified on a silica-gel column using a mixture of benzene and acetone (15:1 v/v) as an eluent to give **7** as colorless syrup. See Tables 3 and 4.

Boc-AA-⊿Tyr(MOM)-OMe (9). A solution of an appropriate Boc-AA-OH (6.0 mmol) and DCC (1.24 g, 5.0 mmol) in dry THF (10 ml) was stirred at −10 °C for 20 min; to the solution prepared was added **2** (1.25 g, 5.0 mmol) and pyridine (0.4 g, 5.0 mmol). After stirring at −10 °C for 2 h, the resulting solution was returned slowly to room temperature and then stirred continuously for 12 h. Finally, after treating further with MeOH (15 ml) and stirring for 2 h, to the reaction solution was added NMM (1.1 ml, 10 mmol). After removing THF and MeOH under reduced pressure, the residue was dissolved in ethyl acetate (10 ml); the *N,N'*-dicyclohexylurea separated out was then filtered off. The filtrate was diluted in ethyl acetate (20 ml) and the resultant solution was washed successively with 10% citric acid, saturated $NaHCO_3$ aqueous solution, water and then dried over anhydrous Na_2SO_4. After removing the solvent under reduced pressure, the crude residue was purified on a silica-gel column using a mixture of benzene and acetone (15:1 v/v) as an eluent. The main fraction was concentrated under reduced pressure to give a viscous syrup, which was crystallized with petroleum ether. Recrystallization from a mixture of ethyl acetate and hexane gave **9** as colorless needles. See Tables 3 and 4.

Boc-AA-⊿Tyr(MOM)-AA-OMe (10). To a solution of an appropriate Boc-AA-OH (6.0 mmol) in dry THF (10 ml) was added DCC (1.24 g, 6.0 mmol) at −10 °C and, after stirring for 20 min, further added **2** (1.25 g, 5.0 mmol) and pyridine (0.4 g, 5.0 mmol). After stirring continuously for 2 h, the resultant solution was returned slowly to room temperature and then stirred for 12 h. To the reaction solution was added a solution of another appropriate H-AA-OMe·HCl (7.0 mmol) and TEA (0.7 ml, 7.0 mmol) in THF (10 ml); the resulting solution was then treated with NMM (0.76 ml, 7 mmol). After stirring for 2 h, and then removing the solvent under reduced pressure, the residue was dissolved in chilled ethyl acetate (10 ml) and the *N,N'*-dicyclohexylurea separated out was filtered off. The filtrate was similarly worked up to give a crude syrup, which was purified on a

silica-gel column using a mixture of $CHCl_3$ and acetone (15:1 v/v) to give a viscous syrup. After being crystallized with petroleum ether, the formed crystals were collected and then recrystallized from a mixture of ethyl acetate and hexane to give **10** as colorless needles. See Tables 5 and 6.

Boc-⊿Tyr(Boc)-AA-OMe (11). A solution of **3** (1.0 g, 5.0 mmol) and $(Boc)_2O$ (3.27 g, 15.0 mmol) in THF (10 ml) in the presence of pyridine (5.0 ml) was stirred at room temperature for 8 h. To the resulting solution was added a solution of an appropriate H-AA-OMe·HCl (10.0 mmol) and TEA (1.0 g, 10.0 mmol) in THF (10 ml). After stirring at room temperature for 4 h, as in the case of the synthesis of **7**, the reaction solution was similarly worked up to give **11** as a colorless syrup or crystals. See Tables 7 and 8.

Boc-AA-⊿Tyr(Boc)-OMe (13). A solution of **3** (1.0 g, 5.0 mmol) and $(Boc)_2O$ (1.1 g, 5.0 mmol) in THF (10 ml) in the presence of pyridine (5.0 ml) was stirred until the spot of **3** disappeared on thin-layer chromatography. To the reaction solution, which was chilled to −10 °C, was added successively Boc-AA-OH (5.0 mmol), DCC (5.0 mmol) and pyridine (0.4 g, 5.0 mmol) and then stirred continuously for 1 h. The resulting solution of the intermediate (**12**) was returned to room temperature and stirred continuously for 12 h. Finally, as in the case of the synthesis of **9**, the reaction solution was treated with MeOH (10 ml) and then similarly worked up to give **13** as a colorless syrup or crystals. See Tables 7 and 8.

Boc-AA-⊿Tyr(Boc)-AA-OMe (14). In a similar manner, a solution of the intermediate (**12**) in THF (10 ml) was prepared. Finally, as in the case of the synthesis of **10**, the resulting solution was further treated with H-AA-OMe; then the reaction solution was similarly worked up to give **14** as a colorless syrup or crystals. See Tables 9 and 10.

Boc-⊿Tyr(MOM)-Gly-OH (15). To a solution of **7e** (5.0 g, 12.7 mmol) in THF (20 ml) was added 1 M LiOH (17.8 ml) drop by drop, with stirring, under cooling. After stirring for 1 h, the resulting solution was returned to room temperature and stirred continuously for 2 h. Chilled water (40 ml) was added to the reaction solution; then the aqueous layer was washed twice with diethyl ether (20 ml). The aqueous layer was further chilled and neutralized with chilled 0.5 M HCl and then made acidic to pH 3 with 10% citric acid. The acidic solution was extracted three times with ethyl acetate (30 ml). The combined extracts were washed with a saturated NaCl aqueous solution and then dried over anhydrous Na_2SO_4. Removal of the solvent under reduced pressure gave **15** as a colorless syrup. Yield 63%. IR ν_{max}^{KBr} (cm^{-1}) 1662, 1515 (CONH), 1630 (C=C). ^1H NMR (MeOH-d_4) δ=7.42 and 6.90 (d, 4H, J=9.5 Hz, C_6H_4-), 7.08 (s, 1H, -CH=), 5.09 (s, 2H, -O-CH_2-O-), 3.98 (s, 2H, -NH-CH_2-CO-), 3.38 (s, 3H, -CH_2OCH_3), 1.42 [s, 9H, -$C(CH_3)_3$]. Found: C, 56.64; H, 6.45; N, 7.19%. Calcd for $C_{18}H_{24}N_2O_7$: C, 56.83; H, 6.36; N, 7.37%.

HCl·H-Gly-⊿Phe-Leu-OMe (17). A solution of Boc-Gly-⊿Phe-Leu-OMe (0.3 g, 0.76 mmol) in 4.5 M HCl and ethyl acetate (20 ml) was stirred under cooling for 10 min. After removing the solvent under reduced pressure, the crude residue was dissolved in diethyl ether (20 ml) and the resulting solution was again concentrated. After adding a small amount of dry methanol and diethyl ether, the deposited crystals were collected. Yield 97%, mp 93—97 °C (decomp) IR ν_{max}^{KBr} (cm^{-1}) 3448 (NH_2), 1665, 1517 (CONH), 1635 (C=C). ^1H NMR (MeOH-d_4) δ=7.56—7.24 (m, 5H, C_6H_5), 7.09 (s, 1H, -CH=), 3.88 (s, 2H, -NH-CH_2-CO-), 3.72 (s, 3H, -CH_2OCH_3), 1.74 [m, 1H, -$CH(CH_3)_2$], 1.24 [m, 2H, -CH_2CH-$(CH_3)_2$], 0.98 [dd, 6H, J=7.3, 2.8 Hz, -$CH(CH_3)_2$]. $[\alpha]_D^{21}$ +39.3° (c 1.00, in MeOH). Found: C, 56.22; H, 6.90; N, 10.59%. Calcd for $C_{18}H_{26}N_3O_4Cl$: C, 56.32; H, 6.83; N, 10.95%.

Boc-⊿Tyr(MOM)-Gly-Gly-Phe-Leu-OMe (18). To a chilled solution of **15** (1.5 g, 4.0 mmol) in THF (20 ml) was added DCC (0.9 g, 4.4 mmol) and *N*-hydroxysuccinimide (0.5 g, 4.4 mmol). After stirring continuously for 30 min, a solution of **16** (1.7 g, 4.4 mmol) and TEA (0.5 ml, 4.9 mmol) in THF (10 ml) was added to the prepared solution; the combined solution was then further stirred under cooling for 2 h. The reaction solution was returned slowly to the room temperature for 24 h. The deposited *N,N'*-dicyclohexylurea were filtered off and the filtrate was concentrated under reduced pressure. The crude residue, thus obtained, was dissolved in ethyl acetate (70 ml) and the resulting solution was washed successively with 10% citric acid, saturated $NaHCO_3$ aqueous solution, and then saturated NaCl aqueous solution, and finally dried over anhydrous Na_2SO_4. After removing the solvent under reduced pressure, crude crystalline substance, thus obtained, was recrystallized from a mixture of ethyl acetate and hexane to give **18** as a pale yellow amorphous. Yield 65%, mp 65.5—67.5 °C. IR ν_{max}^{KBr} (cm^{-1}) 1662, 1630 (NHCO), 1630 (C=C). ^1H NMR (DMSO-d_6) δ=7.75 (bs, 1H, NH), 7.32—6.86 (m, 13H, -CH=, C_6H_5, C_6H_4, NH), 6.56 (bs, 1H, NH), 5.13 (s, 2H, -OCH_2O-), 3.94 (d, 2H, -NH-CH_2-CO-), 3.60 (s, 3H, -$COOCH_3$), 3.45 (s, 3H, -OCH_3), 1.42 [s, 9H, -$C(CH_3)_3$)], 0.88 [dd, 6H, J=7.3, 2.8 Hz, -$CH(CH_3)_2$]. $[\alpha]_D^{24}$ −5.11° (c 1.25, in MeOH). Found: C, 60.52; H, 6.93; N, 9.83%. Calcd for $C_{36}H_{49}N_5O_{10}$: C, 60.74; H, 6.94; N, 9.84%.

Boc-⊿Tyr(MOM)-Gly-Gly-⊿Phe-Leu-OMe (19). In a similar manner, the coupling of **15** and **17** was worked up to give colorless syrup, which was purified on a silica-gel column using a mixture of chloroform and acetone (20:1 v/v) as the eluent to give **19** as a colorless syrup. Yield 50%. IR ν_{max}^{KBr} (cm^{-1}) 1665, 1525 (NHCO), 1632 (C=C). ^1H NMR (DMSO-d_6) δ=8.72 (bs, 1H, NH), 8.09 (bs, 1H, NH), 7.86 (bs, 1H, NH), 7.34—6.86 (m, 12H, -CH=, C_6H_4, C_6H_5, NH), 4.13 (d, 2H, J=8.0 Hz, -NH-CH_2-CO-). 4.02 (d, 2H, J=8.0 Hz, -NH-CH_2-CO-), 5.08 (s, 2H, -OCH_2O-), 3.57 (s, 3H, -OCH_3), 3.40 (s, 3H, CH_3O-), 1.28 [s, 9H, -$C(CH_3)_3$], 0.86 [dd, 6H, J=6.3, 2.8 Hz, -$CH(CH_3)_2$]. $[\alpha]_D^{24}$ −10.5° (c 0.9, in MeOH). Found: C, 60.88; H, 6.55; N, 9.86%. Calcd for $C_{36}H_{47}N_5O_{10}$: C, 60.91; H, 6.67; N, 9.87%.

References

1) Part X. C. Shin, S. Morita, and Y. Yonezawa, *Bull. Chem. Soc. Jpn.*, **61**, 3265 (1988).

2) C. Shin, Y. Yonezawa, T. Obara, and H. Nishio, *Bull. Chem. Soc. Jpn.*, **61**, 885 (1988).

3) U. Schmidt, A. Lieberknecht, and J. Wild, *Synthesis*, **1984**, 53.

4) C. Shin and Y. Yonezawa, *Chem. Lett.*, **1985**, 519.

5) C. Shin, Y. Yonezawa, and M. Ikeda, *Bull. Chem. Soc. Jpn.*, **59**, 3573 (1986).

6) For example, Y. Shimohigashi and C. H. Stammer, *J. Chem. Soc., Perkin Trans. 1*, **1983**, 803.

7) For example, G. J. Dockray, R. A. Gregory, J. B. Hutchison, J. I. Harris, and M. J. Runswick, *Nature*, **274**, 711 (1978).

8) Y. Yonezawa, T. Yamada, and C. Shin, *Chem. Lett.*, **1982**, 1567.
9) C. Shin, T. Yamada, and Y. Yonezawa, *Tetrahedron Lett.*, **24**, 2175 (1983).
10) C. Shin, Y. Yonezawa, and T. Yamada, *Chem. Pharm. Bull.*, **32**, 3934 (1984).
11) Δ^{1}, $\Delta^{1,4}$, the position number of one or two double bonds of the DHA residues from the N-terminals in sequence.
12) C. Shin, Y, Yonezawa, and T. Obara, *Heterocycles*, **24**, 1561 (1986).
13) C. Shin, Y. Yonezawa, S. Honda, and K. Ogawa, the 55 Annual Meeting of Chemical Society of Japan, Fukuoka, October 1987. Reprint Vol. II, p. 759.

Superjacent and Subjacent Orbitals Participations for Kinetically-Controlled Cycloaddition Reactions of 2*H*-Cyclohepta[*b*]furan-2-ones and 8,8-Dicyanoheptafulvene to 2,3-Bis(methoxycarbonyl)-7-oxabicyclo[2.2.1]heptadiene

Guan Rong TIAN,† Shigeru SUGIYAMA,†† Akira MORI, Hitoshi TAKESHITA,* Miwako HIGASHI,††† and Hiroyuki YAMAGUCHI†††

Institute of Advanced Material Study, 86, Kyushu University, Kasuga-koen, Kasuga, Fukuoka 816
†††College of Technology, Ibaraki University, 4-12-1, Nakanarusawa, Hitachi 316

(Received September 28, 1988)

Thermal cycloaddition reactions of 2,3-bis(methoxycarbonyl)-7-oxabicyclo[2.2.1]heptadiene with 2*H*-cyclohepta[*b*]furan-2-ones and 8,8-dicyanoheptafulvene gave [4+2]adducts exclusively. This mode is different from the reported [8+2]adduct formations for 2*H*-cyclohepta[*b*]furan-2-ones with enamines and alkoxyethenes. A consideration of the superjacent and subjacent orbitals effects of the MO calculations gave a better result in favor of [4+2]adduct formation. Thermolysis of cycloadducts gave the methylene derivatives of homobarrelenes.

Recently, we investigated thermal cycloaddition reactions of 2*H*-cyclohepta[*b*]furan-2-ones (**1**) to 2,3-bis(methoxycarbonyl)-7-oxabicyclo[2.2.1]heptadiene (**2**) to give the [4+2]cycloadducts exclusively.[1] This was different from the previously-reported [8+2]cycloadducts formation in the thermal reactions of **1** with enamines[2] and alkoxyethenes.[3] Both reaction modes were explained by molecular orbital (MO) considerations involving not only a frontier molecular orbital approach but also the square of the sum of the products of the coefficients of interacting centers.[1,4] We have proposed that both the [4+2]cycloadducts for **1** and **2** and the [8+2]cycloadducts from **1** and enamines and alkoxyethenes were kinetically-controlled products. However, the above theoretical treatments were not always satisfactory to explain all the experimental results. This was the case for the more complicated molecules; such as substituted **1** and **2**.

Paddon-Row et al. have pointed out[4] the importance of superjacent orbital effects to explain the periselectivity for cycloaddition reactions of nonalternant 6,6-dimethylfulvene and cyclopentadiene, studied by Houk and Luskus.[5] In the case of 2*H*-cyclohepta[*b*]furan-2-ones, nonalternant aromatic compounds, we also found that better results to fit the experiments could be obtained when the calculation was extended to involve both interactions between a superjacent (NLU) and a highest occupied (HO) MOs and a subjacent (NHO) and a lowest unoccupied (LU) MOs. In this paper, we will describe these findings.

Results and Discussion

Cycloadditions of 1 and 2. When 2*H*-cyclohepta[*b*]-furan-2-one (**1a**) amd **2** were heated at 130 °C for 36 h in chlorobenzene, three products (**3a—5a**) were obtained together with 3,4-bis(methoxycarbonyl)furan (**6**). The ^{1}H and ^{13}C NMR spectra of **3a** showed an element of symmetry in a molecule and its structure was determined to be 2-oxatricyclo[6.2.2.0^{1,5}]dodeca-4,6,9,11-tetraen-3-one, a methylenehomobarrelene. Product **4a** was a bis(methoxycarbonyl) derivative of **3a**, a Diels-Alder adduct between **1a** and dimethyl butynedioate. Product **5a** was a [4+2]adduct and its stereochemistry was deduced from the coupling constant of the methine protons. No [8+2]cycloadduct was detected at all. Yields of products are summarized in Table 1.

Next, 3-methoxycarbonyl-2*H*-cyclohepta[*b*]furan-2-one (**1b**)[6] and **2** gave two [4+2]cycloadducts (**5b** and **7b**) and cycloreversed product **3b**. The reactions of **2** and 5-chloro-3-methoxycarbonyl (**1c**),[7] 5-methoxy-3-methoxycarbonyl (**1d**),[7] and 6-isopropyl-3-methoxycarbonyl (**1e**)[8] derivatives afforded similar products as shown in Scheme 1. The structures of these products were determined from comparison with the NMR data of the products from **1a** and **2**. In the case of **1e**, a single product (**5e**) was obtained in 8% yield. This low yield might be attributable to steric hindrance of the bulky isopropyl group at the reaction site. A reaction under 3000 bar afforded [4+2]adducts in improved yields; from **1b** and **2**, two [4+2]adducts (**5b** and **7b**) formed in 70% yield together with **3b** in 12% yield.

Table 1. Cycloaddition Products from **1** and **2**[a]

Substrate	Products (Yield/%)			
1a	**3a** (35)	**4a** (7)	**5a** (26)	—[b]
1b	**3b** (40)	—	**5b** (43)	**7b** (11)
	3b (12)[c]	—	**5b**+**7b** (70)[c]	
1c	**3c** (33)	**4c** (2)	**5c** (14)	**7c** (6)
1d	**3d** (50)	**4d** (3.6)	**5d** (34)	**7d** (12)
1e	—	—	**5e** (8)	—

a) Yields shown indicate amounts isolated based on consumed starting materials. b) Not isolated. c) Under 3000 bar.

† On leave from Yanbian University, Yanji, Jilin, People's Republic of China.

†† Present address: Department of Technology, Tokushima University, Tokushima 770.

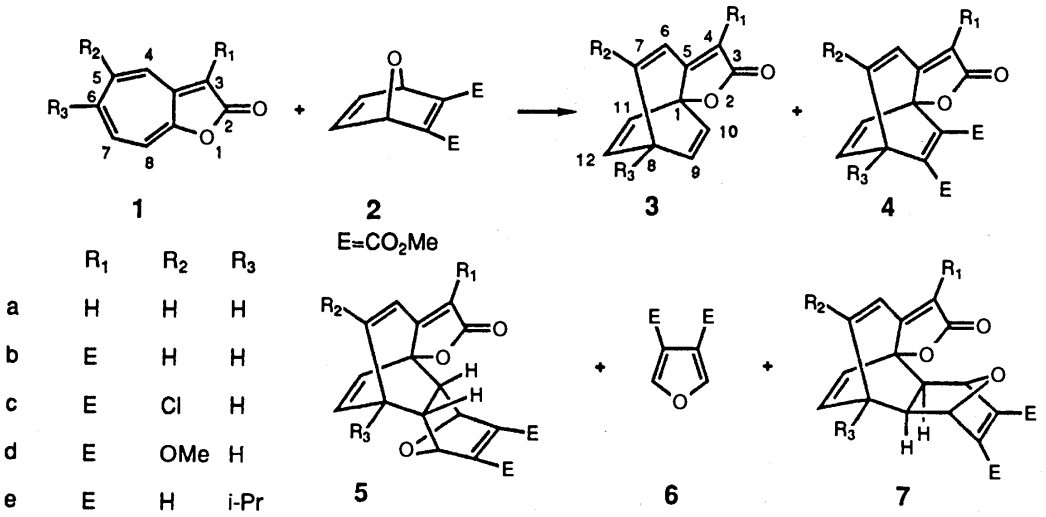

Scheme 1.

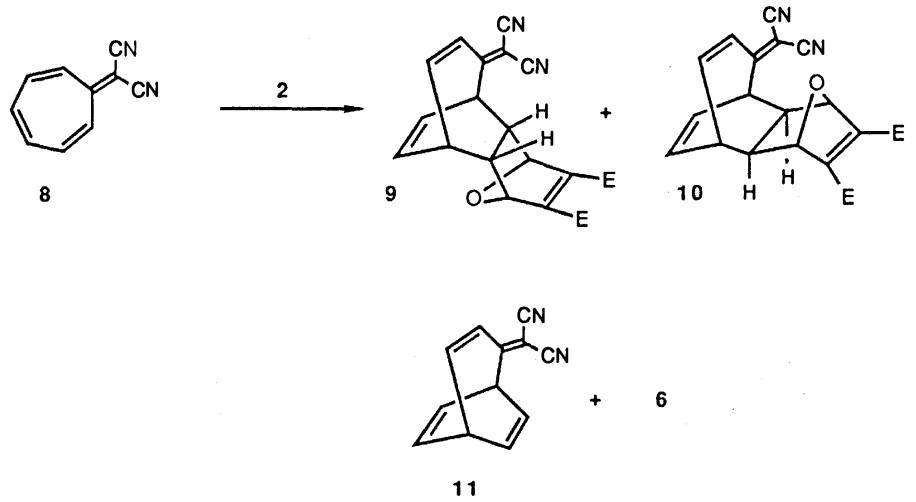

Scheme 2.

Similarly, the reaction of **2** and 8,8-dicyanoheptafulvene (**8**) gave [4+2]adducts (**9** and **10**) in 43 and 10% yields along with a cycloreversed 2-(dicyanomethylene)-homobarrelene (**11**). Yields of **9** and **10** increased to 76 and 13%, but that of **11** was 2.5% under 3000 bar. Thus, cycloreversions to **3** and **11** were suppressed under 3000 bar.

Pyrolysis of Adducts. Thermolyses of **5** and **9** in chlorobenzene gave methylenehomobarrelenes as summarized in Table 2. The chemical shifts of C_9 (δ 131.9—133.6) in **4** were high-field shifted by ca. 11—16 ppm than that of C_{10} (δ 145.0—147.8) and as well as the chemical shift of unsubstituted olefinic carbons, C_{11} and C_{12} (δ 131.0—135.4). From these observations, a methoxycarbonyl group at C_{10} took an out-of-plane conformation due to steric interactions with adjacent substituents.

Molecular Orbital Considerations. As mentioned above, no [8+2]adduct was isolated from the reactions of **1** and **2**. The molecular orbitals of **1** and **2** were calculated by the MNDO method together with (dimethylamino)ethene (**A**) and methoxyethene (**B**). From the energy separation between the frontier orbitals, the [8+2]adducts are preferred in the reactions between **2** and **1** (except for **1c**), whereas the [4+2]adducts are favored in the reactions of **1** with **A** and **B**. These are not in accord to the experimental observations.

Table 2. Thermolysis of **5** and **9** at 130 °C

Compound	Products yield/%		
	3	**6**	**11**
5a	54	54	
5b	57	57	
5c	70	70	
5d	55	55	
9		99	95

Namely, other than the reactions of 5-substituted **1c** and **1d**, the exclusive formation of [4+2]adducts from **1**

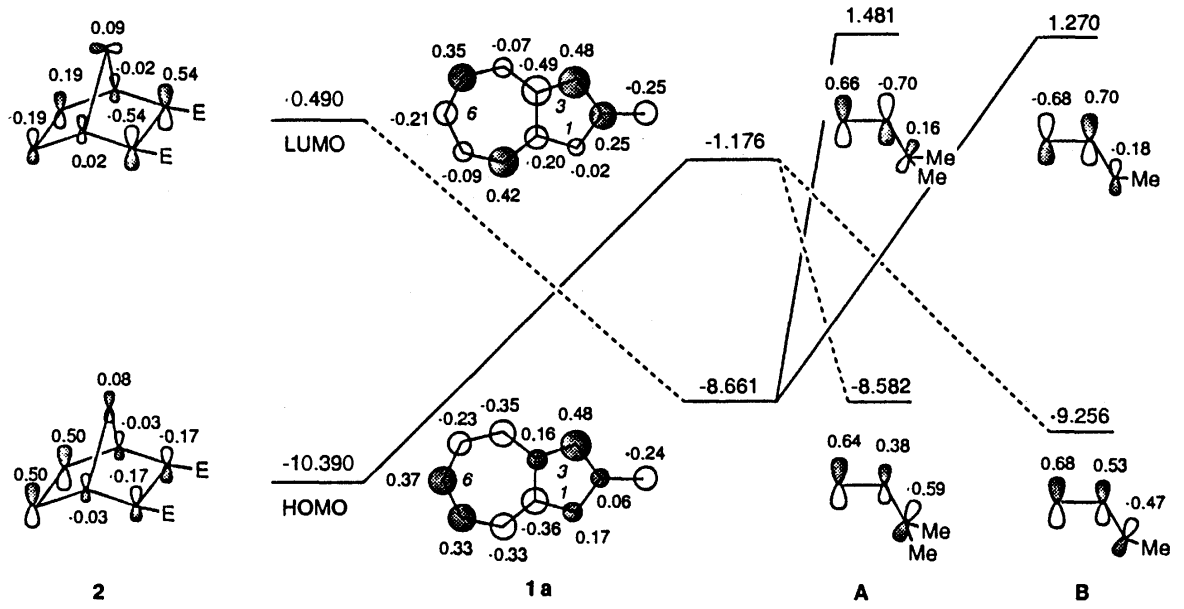

Fig. 1. HOMO-LUMO correlation diagrams of **1a** and olefins

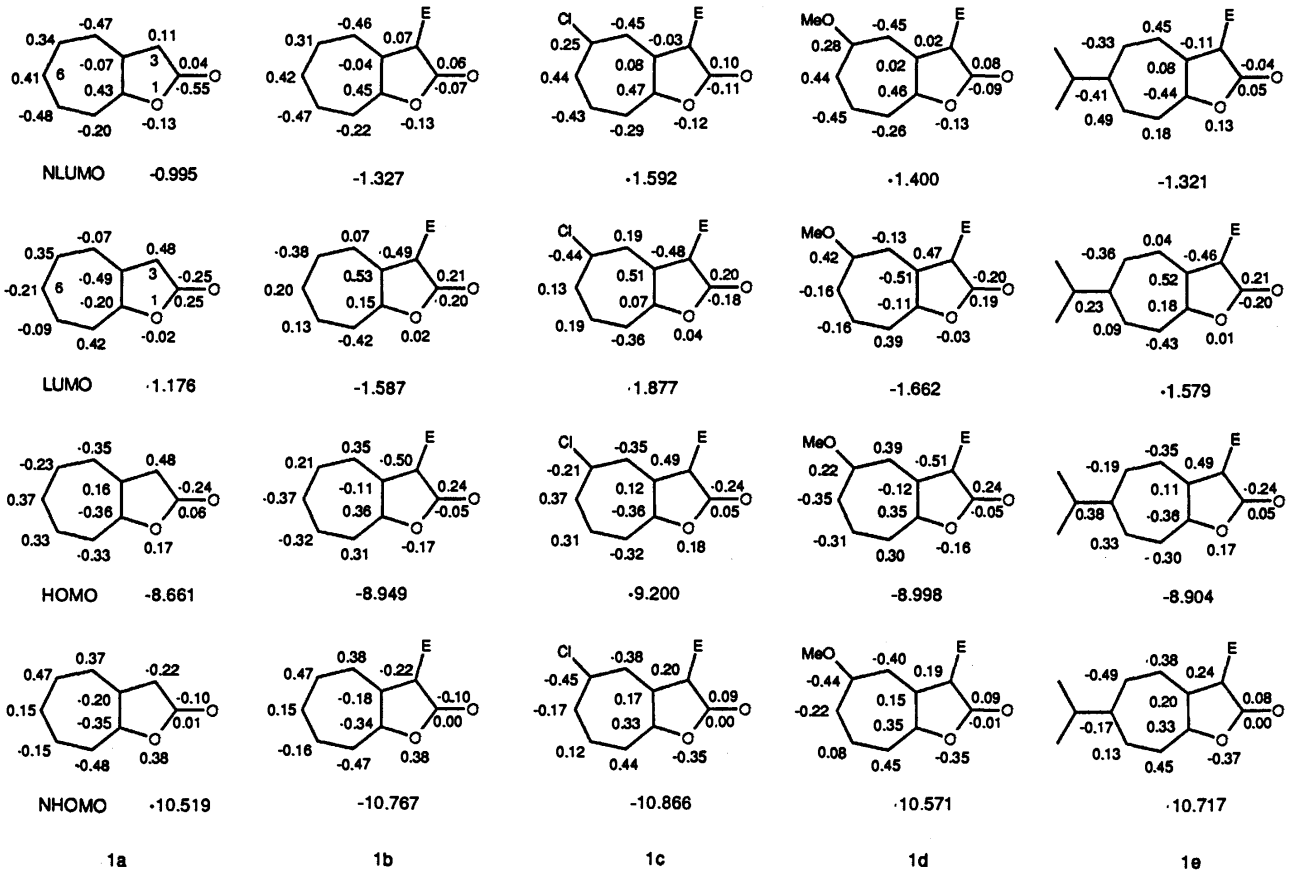

Fig. 2. Coefficients and energy levels of selected molecular orbitals of **1**.

and **2** is consistent with the prediction from the square of the sum of the products of the coefficients of interacting centers:[4] the HOMO(**2**)-LUMO(**1a**) interaction which expected the [4+2]adduct, is more favorable than the [8+2]adduct-forming HOMO(**1a**)-LUMO(**2**) interaction as shown in Fig. 1 and Table 3. In the same time, the antibonding interaction indicated to disfavor a formation of the [8+2]adduct. However, this treatment favored the formation of an [8+2]adduct between 5-substituted **1** and **2**, although it was not

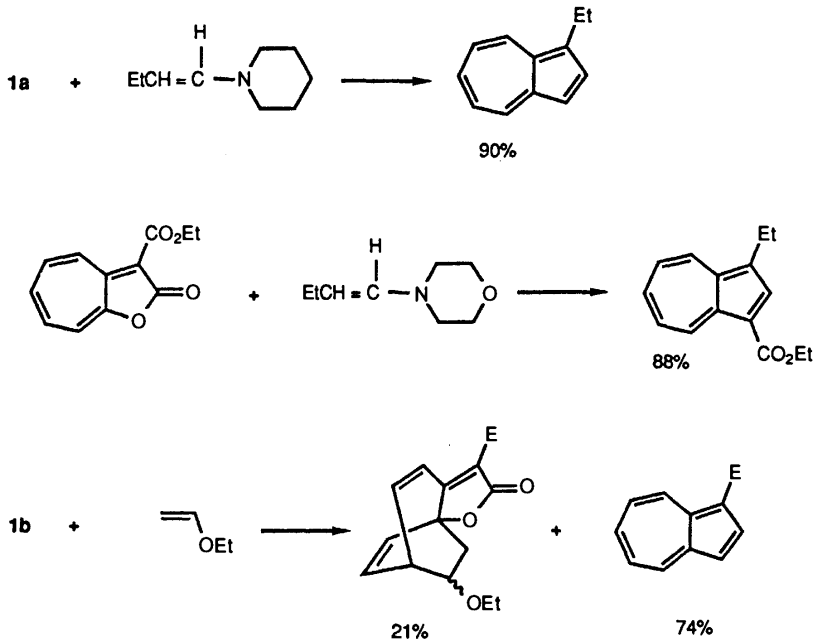

Scheme 3.

Table 3. Calculation of Stabilization Energy ($\times 10^4$)[a] between **1** and **2**

	Reaction mode	**1a**	**1b**	**1c**	**1d**	**1e**
HOMO(**2**)-LUMO(**1**)	[4+2]	46	35	12	21	48
LUMO(**2**)-HOMO(**1**)	[8+2]	31	32	30	31	31
HOMO(**2**)-NLUMO(**1**)	[4+2]	188	209	235	225	199
LUMO(**2**)-NHOMO(**1**)	[4+2]	9	8	9	12	9
[4+2]/[8+2]		243/31	252/32	256/30	258/31	256/31

a) See the Ref. 4.

Table 4. Calculation of Stabilization Energy between **1a** and **A** and **B**

	Reaction mode	**A**	**B**
HOMO(**A** or **B**)-LUMO(**1a**)	[4+2]	0.0058	0.0076
LUMO(**A** or **B**)-HOMO(**1a**)	[8+2]	0.0324	0.0340
HOMO(**A** or **B**)-NLUMO(**1a**)	[4+2]	0.0245	0.0314
LUMO(**A** or **B**)-NHOMO(**1a**)	[4+2]	0.0094	0.0100
[4+2]/[8+2]		397/324	490/340

consistent with the experimental results.

In order to provide a consistent explanation of the results, we took the participations of NLUMO and NHOMO of **1** into account since both pairs of LUMO(**1**) and NLUMO(**1**) and HOMO(**1**) and NHOMO(**1**) have the same pseudosymmetries at C_6 and C_{8a}[4] and the coefficients of the NLUMO(**1**) at these atoms are larger than those of LUMO(**1**). As shown in Table 3, the interaction between HOMO(**2**) and NLUMO(**1**) is the largest and it contributes 77—92% towards the total stabilization energy[4] for the [4+2]cycloaddition reaction. Thus, the formation of the [4+2]adduct could be explained.

On the other hand, the results of **1** and enamines and alkoxyethenes were reported to give rather complicated product distributions; the reactions of **1a** and 1-(1-pyrrolidinyl)-1-butene and 3-ethoxycarbonyl-2*H*-cyclohepta[*b*]furan-2-one and 1-morpholino-1-butene gave the [8+2]cycloadducts, 1-ethylazulene, and 1-ethyl-3-ethoxycarbonylazulene in 90 and 88% yields, respectively.[9] No [4+2]adduct formed.

Recently, Nozoe et al. reported the formation of a [8+2]cycloadduct by isolating 1-methoxycarbonylazulene in 74% yield together with an isomeric mixture of three [4+2]adducts in 21% yield, from **1b** and ethoxyethene to reveal two reaction modes.[3] There remained the problem of which cycloadduct is the kinetically-controlled product. From the HOMO-LUMO interactions, the formations of [8+2]adducts were expected, whereas an involvement of NLUMO and NHOMO effects would result in the formation of [4+2]adducts. The calculation of the stabilization energy between **1a** and **A** or **B** is shown in Table 4.

To make these points clear, a further study under high-pressure conditions should be desirable, where a formation of a kinetically-controlled product is expected to be predominant.

Experimental

Elemental analyses were performed by Miss S. Hirashima,

of the Institute of Advanced Material Study, Kyushu University. NMR spectra were measured with JEOL FX 100 Model and GSX 270 H Model spectrometers in $CDCl_3$ solution (unless otherwise specified); chemical shifts are expressed in the unit δ. Mass spectra were measured with a JEOL OlSG-2 spectrometer at 70 eV. IR spectra were taken as KBr disks or as liquid films inserted between NaCl plates using a Jasco IR-A 102 spectrometer. UV spectra were measured with a Hitachi U-3200 spectrophotometer.

Cycloadditions of 1 and 2. General Method. A chlorobenzene solution (1.5 cm^3) of **1** (0.2—1 mmol) and **2** (0.5—1.1 mmol) was heated at 130 °C for 36 h in a sealed ampule, purged with N_2. The mixture was chromatographed on a silica-gel column to give products.

3a: Colorless crystals, 35%; mp 116.5—117.5 °C. ^{1}H NMR δ=3.96 (1H, dtt, J=7.7, 6.6, 1.1 Hz), 5.70 (1H, s), 6.00 (1H, d, J=10.6 Hz), 6.35 (2H, dd, J=7.7, 1.1 Hz), 6.52 (2H, dd, J=7.7, 6.6 Hz), and 6.57 (1H, dd, J=10.6, 7.7 Hz); ^{13}C NMR δ=40.1, 87.8, 111.6, 118.7, 132.1 (2C), 133.0 (2C), 139.8, 158.2, and 173.5; IR 1760, 1620, 1350, 1105, 1025, 905, and 850 cm^{-1}; UV (MeOH) 259.4 (ε 10600) and 297.0 nm (5000); MS m/z (%) 170 (M^+, 10), 116 (62), 115 (base), 89 (29), and 63 (38).

Found: C, 77.03; H, 4.74%. Calcd for $C_{11}H_8O_2$: C, 76.73; H, 4.68%.

4a: Colorless crystals, 7%; mp 121—123 °C. ^{1}H NMR δ=3.78 (3H, s), 3.83 (3H, s), 4.51 (1H, dd, J=7.7, 7.0 Hz), 5.83 (1H, s), 6.15 (1H, d, J=10.6 Hz), 6.39 (1H, dd, J=7.7, 1.5 Hz), and 6.6 (2H, m); ^{13}C NMR δ=39.5, 52.8, 52.9, 86.4, 113.3, 119.9, 131.9, 132.7, 133.6, 138.2, 145.0, 155.6, 163.1, 163.9, and 171.7; IR 1765, 1720, 1435, 1330, and 1270 cm^{-1}; UV (MeOH) 219.2 (ε 9700), 248.0 (9750), and 293.0 nm (4200); MS m/z (%) 288 (M^+, 19), 229 (57), 228 (34), 197 (30), and 44 (base).

Found: C, 62.57; H, 4.19%. Calcd for $C_{15}H_{12}O_6$: C, 62.50; H, 4.20%.

5a: Colorless crystals, 26%; mp 137—139 °C. ^{1}H NMR δ=2.29 (1H, dd, J=8.1, 1.1 Hz), 2.53 (1H, dd, J=8.1, 1.1 Hz), 3.48 (1H, dd, J=8.8, 7.7 Hz), 3.81 (6H, s), 4.92 (1H, d, J=1.1 Hz), 5.47 (1H, d, J=1.1 Hz), 5.66 (1H, s), 6.09 (1H, d, J=8.4 Hz), 6.21 (1H, dd, J=8.4, 7.7 Hz), 6.33 (1H, d, J=10.6 Hz), and 6.67 (1H, dd, J=10.6, 8.8 Hz); ^{13}C NMR δ =39.4, 44.2, 49.3, 52.7, 52.8, 83.6, 85.5, 88.1, 111.4, 121.7, 130.0, 131.0, 144.2, 145.4, 145.5, 162.7, 162.9, 164.0, and 172.8; IR 1750, 1630, 1435, 1265, and 1210 cm^{-1}; UV (MeOH) 244.2 (ε 11500), 268.2 (10900), and 397.0 nm (1450).

Found: C, 63.95; H, 4.50%. Calcd for $C_{19}H_{16}O_7$: C, 64.04; H, 4.53%.

3b: Colorless crystals, 40%; mp 149—150 °C. ^{1}H NMR δ=3.87 (3H, s), 4.12 (1H, dttd, J=8.1, 6.2, 1.5, 1.1 Hz), 6.39 (2H, dd, J=7.3, 1.5 Hz), 6.65 (2H, dd, J=7.3, 6.2 Hz), 6.78 (1H, dd, J=10.7, 1.1 Hz), and 6.91 (1H, dd, J=10.7, 8.1 Hz); ^{13}C NMR δ=41.5, 52.2, 86.3, 112.2, 118.7, 132.9 (2C), 133.7 (2C), 145.8, 161.7, 162.7, and 168.6; IR 1770, 1710, 1610, 1430, 1260, and 1030 cm^{-1}; UV (MeOH) 212.4 (ε 5300), 276.4 (8900), and 319.0 nm (4600); MS m/z (%) 230 (M^+, base), 198 (46), 170 (39), 115 (85), 91 (69), and 44 (67).

Found: C, 67.67; H, 4.38%. Calcd for $C_{13}H_{10}O_4$: C, 67.82; H, 4.38%.

5b: Colorless crystals, 43%; mp 138.5—139.5 °C. ^{1}H NMR δ=2.32 (1H, dd, J=8.1, 1.1 Hz), 2.57 (1H, dd, J=8.1, 1.1 Hz), 3.62 (1H, dd, J=8.4, 7.3 Hz), 3.80 (3H, s), 3.82 (3H, s), 3.89 (3H, s), 4.95 (1H, d, J=1.5 Hz), 5.48 (1H, d, J=1.5 Hz), 6.10 (1H, dt, J=8.4, 1.1 Hz), 6.31 (1H, dd, J=8.4, 7.3 Hz), 7.00 (1H, dd, J=10.6, 8.4 Hz), and 7.16 (1H, d, J=10.6 Hz); ^{13}C NMR δ=40.3, 44.4, 49.6, 52.5, 52.7, 52.8, 83.6, 85.4, 86.3, 111.8, 121.6, 129.6, 132.2, 145.3, 145.7, 150.0, 162.0, 162.4, 162.8, 168.0, and 168.2; IR 1770, 1710, 1615, 1430, 1270, and 1210 cm^{-1}; UV (MeOH) 203.6 (ε 8350), 241.8 (7100), and 291.8 nm (10700).

Found: C, 60.91; H, 4.33%. Calcd for $C_{21}H_{18}O_9$: C, 60.87; H, 4.38%.

7b: Colorless crystals, 11%; mp 187—188 °C. ^{1}H NMR δ=2.58 (1H, dd, J=8.8, 5.9 Hz), 3.02 (1H, d, J=8.8 Hz), 3.73 (1H, dddm, J=8.4, 7.0, 5.9 Hz), 3.80 (3H, s), 3.81 (3H, s), 3.89 (3H, s), 4.74 (1H, d, J=1.1 Hz), 4.87 (1H, d, J=1.1 Hz), 6.22 (1H, dd, J=8.4, 0.7 Hz), 6.44 (1H, dd, J=8.4, 7.0 Hz), 6.73 (1H, dd, J=10.6, 8.4 Hz), and 7.41 (1H, d, J=10.6 Hz); ^{13}C NMR δ=38.3, 41.8, 52.1, 52.4, 52.5, 52.6, 79.1, 83.2, 87.4, 113.3, 125.9, 133.1, 135.1, 144.5, 145.4, 146.1, 161.5, 161.8, 162.5, 167.2, and 167.9; IR 1775, 1720, 1620, 1440, 1280, 1210, and 1035 cm^{-1}; UV (MeOH) 243.2 (ε 5900) and 295.8 nm (7600).

Found: C, 60.89; H, 4.40%. Calcd for $C_{21}H_{18}O_9$: C, 60.87; H, 4.38%.

3c: Colorless crystals, 33%; mp 148—149 °C. ^{1}H NMR δ=3.89 (3H, s), 4.26 (1H, tq, J=6.6, 1.5 Hz), 6.48 (2H, dd, J=7.7, 1.5 Hz), 6.72 (2H, dd, J=7.7, 6.6 Hz), and 6.95 (1H, d, J=1.5 Hz); ^{13}C NMR δ=50.5, 52.3, 85.3, 111.6, 115.8, 131.2 (2C), 134.6 (2C), 152.1, 161.5, 162.8, and 168.1; IR 1780, 1710, 1610, 1250, and 1035 cm^{-1}; UV (MeOH) 283.4 (ε 10500) and 321.4 nm (9400); MS m/z (%) 266 (M^++2, 11), 264 (M^+, 34), 229 (base), 197 (61), and 149 (36).

Found: C, 58.80; H, 3.42%. Calcd for $C_{13}H_9O_4Cl$: C, 59.00; H, 3.43%.

4c: Colorless crystals, 2%; mp 155—157 °C. ^{1}H NMR δ=3.83 (3H, s), 3.84 (3H, s), 3.90 (3H, s), 4.82 (1H, ddd, J=7.0, 1.8, 1.5 Hz), 6.51 (1H, dd, J=8.1, 1.5 Hz), 6.82 (1H, dd, J=8.1, 7.0 Hz), and 7.09 (1H, d, J=1.8 Hz); ^{13}C NMR δ=49.7, 52.6, 53.2 (2C), 84.0, 112.8, 117.0, 131.9, 132.8, 133.5, 145.8, 150.6, 160.4, 161.0, 162.2, 163.1, and 166.6; IR 1780, 1730, 1615, 1440, 1275, 1250, 1035, and 1025 cm^{-1}; UV (MeOH) 267.4 (ε 8600) and 322.6 nm (8200); MS m/z (%) 382 (M^++2, 14), 380 (M^+, 42), 349 (29), 323 (35), 321 (base), 292 (47), 289 (45), 277 (33), 207 (33), and 59 (75).

Found: C, 53.92; H, 3.58%. Calcd for $C_{17}H_{13}O_8Cl$: C, 53.63; H, 3.44%.

5c: Colorless crystals, 14%; mp 209—210 °C. ^{1}H NMR δ=2.36 (1H, dd, J=7.7, 1.1 Hz), 2.74 (1H, dd, J=7.7, 1.1 Hz), 3.77 (1H, dm, J=7.7 Hz), 3.81 (3H, s), 3.83 (3H, s), 3.90 (3H, s), 4.97 (1H, d, J=1.1 Hz), 5.47 (1H, d, J=1.1 Hz), 6.15 (1H, dm, J=8.8 Hz), 6.35 (1H, dd, J=8.8, 7.7 Hz), and 7.35 (1H, d, J=1.8 Hz); ^{13}C NMR δ=43.9, 49.5, 50.0, 52.4, 52.5, 52.7, 83.2, 84.8, 84.9, 110.9, 118.9, 129.7, 130.7, 145.0, 145.2, 155.5, 161.5, 162.0, 162.3, 166.7, and 167.2; IR 1775, 1720, 1610, 1438, 1260, and 1220 cm^{-1}; UV (MeOH) 242.6 (ε 8200) and 305.6 nm (13700).

Found: C, 56.29; H, 3.87%. Calcd for $C_{21}H_{17}O_9Cl$: C, 56.20; H, 3.82%.

7c: Colorless crystals, 6%; mp 155—156 °C. ^{1}H NMR δ=2.63 (1H, dd, J=8.8, 6.2 Hz), 3.00 (1H, d, J=8.8 Hz), 3.81 (3H, s), 3.83 (3H, s), 3.90 (3H, s), 3.9 (1H, m), 4.75 (1H, d, J=1.1 Hz), 5.06 (1H, d, J=1.1 Hz), 6.28 (1H, dd J=8.4, 0.7 Hz), 6.50 (1H, dd, J=8.4, 7.3 Hz), and 7.58 (1H, d, J=1.8 Hz); ^{13}C NMR δ=41.8, 48.4, 51.3, 52.4, 52.5, 52.6, 79.2, 82.4, 86.4, 112.6, 123.2, 132.8, 134.3, 145.3, 145.8, 150.2, 161.3, 161.7, 162.4, 165.6, and 167.4; IR 1775, 1720, 1620, 1440, 1335, 1270, 1250, and 1030 cm^{-1}; UV (MeOH) 240.0 (ε 7000) and 312.6

nm (11200).

Found: C, 56.26; H, 3.86%. Calcd for $C_{21}H_{17}O_9Cl$: C, 56.20; H, 3.82%.

3d: Colorless crystals, 50%; mp 136—137 °C. ^{1}H NMR δ=3.78 (3H, s), 3.87 (3H, s), 4.07 (1H, tdt, J=6.6, 2.6, 1.5 Hz), 6.06 (1H, d, J=2.6 Hz), 6.52 (2H, dd, J=7.4, 1.5 Hz), and 6.60 (2H, dd, J=7.4, 6.6 Hz); ^{13}C NMR δ=47.1, 53.1, 56.7, 85.7, 88.6, 106.0, 130.2 (2C), 136.5 (2C), 163.1, 169.1, 169.6, and 172.6; IR 1760, 1710, 1580, 1380, 1360, 1290, 1265, and 1035 cm^{-1}; UV (MeOH) 269.6 (ε 6300) and 344.2 nm (16250): MS m/z (%) 260 (M^+, base), 229 (39), 200 (35), 145 (35), 115 (38), 102 (37), 76 (30), and 65 (31).

Found: C, 64.81; H, 4.65%. Calcd for $C_{14}H_{12}O_5$: C, 64.61; H, 4.65%.

4d: Colorless crystals, 3.6%; mp 186—187 °C. ^{1}H NMR δ=3.80 (6H, s), 3.84 (3H, s), 3.87 (3H, s), 4.65 (1H, ddd, J=7.0, 2.2, 1.5 Hz), 6.19 (1H, d, J=2.2 Hz), 6.55 (1H, dd, J=7.7, 1.5 Hz), and 6.73 (1H, dd, J=7.7, 7.0 Hz); ^{13}C NMR δ=46.5, 52.6, 53.1 (2C), 56.7, 84.3, 89.6, 107.2, 131.0, 131.9, 135.4, 147.8, 162.5, 162.6, 163.5, 166.8, 167.7, and 170.9; IR 1780, 1730, 1690, 1440, 1285, and 1260 cm^{-1}; UV (MeOH) 208.8 (ε 17900), 263.6 (7900), and 348.4 nm (13900): MS m/z (%) 376 (M^+, 42), 317 (37), 288 (35), 285 (43), 203 (35), 119 (34), 93 (36), 76 (36), 59 (base), and 44 (60).

Found: C, 57.58; H, 4.30%. Calcd for $C_{18}H_{16}O_9$: C, 57.45; H, 4.29%.

5d: Colorless crystals, 34%; mp 232—233 °C. ^{1}H NMR δ=2.35 (1H, dd, J=8.1, 1.1 Hz), 2.61 (1H, dd, J=8.1, 1.5 Hz), 3.56 (1H, dm, J=6.6 Hz), 3.80 (3H, s), 3.82 (3H, s), 3.83 (3H, s), 3.88 (3H, s), 4.97 (1H, d, J=1.1 Hz), 5.47 (1H, d, J=1.1 Hz), 6.19 (1H, dt, J=8.8, 1.1 Hz), 6.26 (1H, dd, J=8.8, 6.6 Hz), and 6.50 (1H, d, J=2.2 Hz); ^{13}C NMR δ=43.4, 45.9, 50.2 (2C), 51.9, 52.6, 56.8, 83.2, 85.0, 85.1, 92.0, 105.2, 128.5, 132.5, 145.2, 145.6, 162.1, 162.5, 163.1, 168.5, 172.8, and 176.7; IR 1760, 1715, 1690, 1440, 1270, and 1235 cm^{-1}; UV (MeOH) 215.0 (ε 13500), 240.8 (10100), and 336.0 nm (18000).

Found: C, 59.33; H, 4.57%. Calcd for $C_{22}H_{20}O_{10}$: C, 59.46; H, 4.54%.

7d: Colorless crystals, 12%; mp 233—234 °C. ^{1}H NMR δ=2.59 (1H, dd, J=8.8, 7.0 Hz), 2.95 (1H, d, J=8.8 Hz), 3.65 (1H, tm, J=7.0 Hz), 3.81 (3H, s), 3.82 (3H, s), 3.84 (3H, s), 3.88 (3H, s), 4.78 (1H, d, J=1.1 Hz), 4.91 (1H, d, J=1.1 Hz), 6.33 (1H, dd, J=8.4, 1.5 Hz), 6.39 (1H, dd, J=8.4, 7.0 Hz), and 6.76 (1H, d, J=2.2 Hz); ^{13}C NMR δ=41.6, 44.7, 51.2, 51.8, 52.5 (2C), 56.8, 79.7, 82.3, 86.3, 96.6, 106.9, 131.6, 136.4, 145.2, 146.1, 161.8, 162.5, 162.9, 168.5, 171.3, and 173.4; IR 1760, 1710, 1695, 1440, and 1230 cm^{-1}; UV (MeOH) 219.2 (ε 12400) and 341.6 nm (16200).

Found: C, 59.27; H, 4.55%. Calcd for $C_{22}H_{20}O_{10}$: C, 59.46; H, 4.54%.

5e: Colorless crystals, 8%; mp 212 °C. ^{1}H NMR δ=1.17 (3H, d, J=6.6 Hz), 1.18 (3H, d, J=6.6 Hz), 2.17 (1H, sept, J=6.6 Hz), 2.34 (1H, d, J=8.1 Hz), 2.55 (1H, d, J=8.1 Hz), 3.80 (3H, s), 3.81 (3H, s), 3.89 (3H, s), 5.13 (1H, d, J=1.1 Hz), 5.49 (1H, d, J=1.1 Hz), 6.05 (1H, dd, J=9.2, 1.1 Hz), 6.10 (1H, dd, J=9.2, 1.1 Hz), 6.82 (1H, d, J=11.0 Hz), and 7.22 (1H, d, J=11.0 Hz); ^{13}C NMR δ=16.2, 18.4, 32.4, 47.6, 49.2, 50.5, 52.3, 52.4, 52.6, 80.5, 83.3, 85.8, 110.9, 121.3, 128.3, 136.3, 145.0, 146.0, 151.1, 161.8, 162.2, 162.6, 167.8, and 168.0; IR 1765, 1735, 1710, 1620, 1435, 1275, and 1225 cm^{-1}; UV (MeOH) 245.8 (ε 9800) and 294.0 nm (15600).

Found: C, 62.96; H, 5.32%. Calcd for $C_{24}H_{24}O_9$: C, 63.15; H, 5.30%.

Cycloaddition of 2 and 8. A chlorobenzene solution, (2 cm^3) of **8** (188 mg) and **2** (265 mg) was heated at 130 °C for 20 h in a sealed tube. The mixture was chromatographed on a silica-gel column to give 54 mg (47%) of **6**, 100 mg (43%) of **9**, 23 mg (10%) of **10**, 38.7 mg (42%) of **11**, and unreacted **8** (78.9 mg).

9: Colorless crystals, mp 164—165 °C; ^{1}H NMR δ=2.38 (1H, dm, J=7.7 Hz), 2.65 (1H, dd, J=7.7, 1.1 Hz), 3.51 (1H, ddm, J=8.1, 7.7 Hz), 3.82 (3H, s), 3.83 (3H, s), 4.17 (1H, dm, J=7.0 Hz), 4.93 (1H, d, J=1.1 Hz), 5.10 (1H, d, J=1.1 Hz), 6.09 (1H, dd, J=7.7, 7.0 Hz), 6.46 (1H, t, J=7.7 Hz), 6.52 (1H, dd, J=10.6, 2.2 Hz), and 7.02 (1H, dd, J=10.6, 8.1 Hz); ^{13}C NMR δ=40.0, 44.0, 46.1, 48.2, 52.5, 52.6, 81.1, 85.5, 86.4, 111.7, 112.8, 125.4, 126.3, 136.6, 144.9, 145.6, 152.0, 162.3, 162.7, and 169.4; IR 2250, 1730, 1610, 1440, 1290, 1255, and 1230 cm^{-1}. UV (MeOH) 243.4 (ε 8600) and 302.6 nm (16200).

Found: C, 65.97; H, 4.47; N, 7.47%. Calcd for $C_{20}H_{16}N_2O_5$: C, 65.93; H, 4.43; N, 7.69%.

10: Colorless crystals, mp 183—184 °C; ^{1}H NMR δ=2.63 (1H, dd, J=8.4, 5.8 Hz), 2.78 (1H, dd, J=8.4, 5.5 Hz), 3.64 (1H, td, J=8.0, 5.8 Hz), 3.81 (3H, s), 3.83 (3H, s), 4.27 (1H, dd, J=7.0, 5.5 Hz), 4.82 (2H, s), 6.16 (1H, dd, J=7.3, 7.0 Hz), 6.62 (1H, dd, J=8.0, 7.3 Hz), and 6.7—6.8 (2H, m); ^{13}C NMR δ=38.8, 44.9, 47.3, 48.0, 52.5, 52.6, 81.7, 82.6, 83.2, 111.8, 113.2, 129.2, 129.9, 140.4, 145.3, 146.0, 147.3, 162.4, 162.5, and 169.5; IR 2240, 1725, 1610, 1440, 1290, 1265, and 1230 cm^{-1}; UV (MeOH) 243.4 (ε 7900) and 307.2 nm (12600).

Found: C, 65.76; H, 4.45; N, 7.40%. Calcd for $C_{20}H_{16}N_2O_5$: C, 65.93; H, 4.43; N, 7.69%.

11: Colorless needles, mp 71—73 °C; ^{1}H NMR δ=3.98 (1H, dtm, J=8.4, 6.6 Hz), 4.68 (1H, tdd, J=6.6, 2.2, 1.5 Hz), 6.06 (1H, dd, J=10.6, 2.2 Hz), 6.36 (2H, td, J=6.6, 1.5 Hz), 6.84 (2H, td, J=6.6, 1.5 Hz), and 6.95 (1H, dd, J=10.6, 8.4 Hz); ^{13}C NMR δ=41.8, 46.8, 81.8, 111.6, 113.1, 122.3, 128.3 (2C), 140.2 (2C), 149.2, and 164.1; IR 2245, 1600, 1530, 1355, 1290, 930, and 897 cm^{-1}; UV (MeOH) 287.4 (ε 12700) and 390.6 nm (6200); MS m/z (%) 180 (M^+, 28), 153 (35), 115 (base), 76 (36), 75 (34), 63 (50), 62 (38), 51 (34), 50 (71), and 49 (33).

Found: C, 79.94; H, 4.49; N, 15.57%. Calcd for $C_{12}H_8N_2$: C, 79.98; H, 4.47; N, 15.54%.

Cycloadditions under 3000 bar. a) A chlorobenzene solution (2 cm^3) of **1b** (110 mg) and **2** (115 mg) was heated at 120 °C for 36 h. The mixture was purified to give 7.1 mg (11%) of **3b**, 5.7 mg (12%) of **6**, 78.6 mg (70%) of **5b** and **7b**, and unreacted **1b** (53 mg).

b) A chlorobenzene solution (1.5 cm^3) of **8** (153 mg) and **2** (353 mg) was heated at 120 °C to give 210.5 mg (76%) of **9**, 37 mg (13%) of **10**, 3.4 mg (2.5%) of **11**, and unreacted **8** (36.3 mg).

Thermolysis of 5 and 9. A chlorobenzene solution (1 cm^3) of **5** (40 mg) was heated at 130 °C for 24 h. The mixture was chromatographed to give the products. The results were summarized in Table 2.

References

1) G. R. Tian, S. Sugiyama, A. Mori, H. Takeshita, M. Higashi, and H. Yamaguchi, *Chem. Lett.*, **1988**, 941.

2) K. Takase and M. Yasunami, *Yuki Gosei Kagaku Kyokai Shi*, **39**, 1172 (1981).

3) P.-W. Yang, C.-P. Wu, T.-S. Huang, H. Wakabayashi, S. Ishikawa, H. Okae, and T. Nozoe, 55th National Meeting

of Chemical Society of Japan, Fukuoka, October 1987, Abstract, No. 3U31.

4) M. N. Paddon-Row, K. Gell, and R. N. Warrener, *Tetrahedron Lett.*, **1975**, 1975.

5) K. N. Houk and L. J. Luskus, *J. Org. Chem.*, **38**, 3836 (1973).

6) W. von E. Doering and C. F. Hiskey, *J. Am. Chem. Soc.*, **74**, 5688 (1952).

7) T. Nozoe, H. Takeshita, and K. Tajiri, *Bull. Chem. Soc. Jpn.*, **56**, 3679 (1983).

8) T. Sato, *Bull. Chem. Research Inst. Non-Aq. Solns., Tohoku Univ.*, **8**, 47 (1959).

9) M. Yasunami, Y. Kitamori, and K. Takase, Abstracts of 18th Symposium of Non-benzenoid Aromatic Compounds, No. A7-12, p. 51 (1985).

The Effect of Pressure on Sigmatropic Rearrangements of Seven-Membered Conjugated Systems. [3,3] and [1,9] Sigmatropies

Shigeru SUGIYAMA,* Akira MORI,† Nobuo KATO,† and Hitoshi TAKESHITA*,†
Department of Chemical Science and Technology, Faculty of Engineering, The University of Tokushima, Minamijosanjima-cho, Tokushima 770
†Institute of Advanced Material Study, 86, Kyushu University, Kasuga-koen, Kasuga, Fukuoka 816
(Received September 30, 1988)

The kinetic features of the [1,9] sigmatropy (with 2-benzyloxy-3-bromotropone) and the [3,3] sigmatropy (with 2-allyloxytropone and 2-[(3-methyl-2-butenyl)oxy]tropone) were investigated under various pressures (1 to 1600 bar). The activation volume of [1,9] sigmatropy was of the same order as those of [1,5] sigmatropy of cyclopentadienes. The activation volume of [3,3] sigmatropy of more sterically-hindered substrate was more negative than that of the unhindered one.

Studies of the sigmatropic rearrangement have attracted considerable interest. Its mechanistic aspects and applications to organic syntheses have been investigated continuously.[1] However, although it is recognized in general that the high-pressure technique is a powerful synthetic method, investigations of sigmatropies under high-pressure conditions still remain unexplored. The sigmatropies of troponoids are unique in view of their interesting π-electron arrangement. A tautomerism of 2-acetoxytropones has been known for a long time,[2] and a kinetic analysis for the process by means of ^{13}C NMR spectroscopy was carried out by Masamune et al., [3a] who proposed an ionic mechanism. Recently, we showed[4] that the migration of the acetyl group[3] of 2-acetoxytropones between their C-1 and C-2 is a concerted [1,9] sigmatropy (acetotropy) by the kinetic analysis using temperature-variable ^{13}C NMR spectroscopy. Consequently, the kinetic analysis of various sigmatropic rearrangements under high-pressure conditions should be worthwhile. Herein, we describe, in addition to our preliminary presentation[5] of [1,9] sigmatropy of 2-benzyloxy-3-bromotropone,[6] the effect of pressure on the [3,3] sigmatropy of troponoids. A determination of the activation volume is essential in order to evaluate the synthetic aspect of any pressure effect. Previously, such studies were limited to [1,5] sigmatropy of cyclopentadiene derivatives[7] and 2-alkoxypridine *N*-oxide[8] and [3,3] sigmatropy of benzenoids and acyclic compounds.[9]

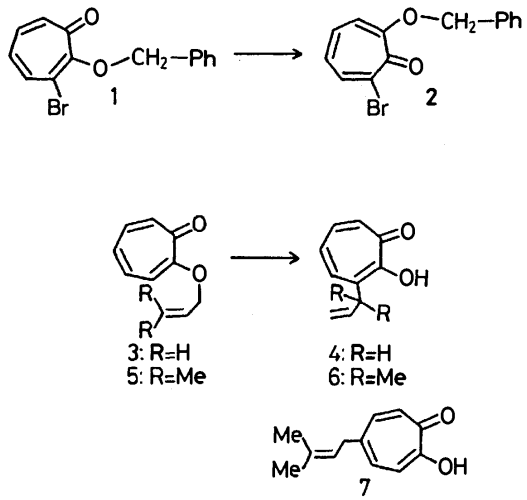

Scheme 1.

Results and Discussion

[1,9] Sigmatropy. The thermally-allowed [1,5] sigmatropies are well-known with cyclopentadienes. However, the next higher thermally-allowed electrocyclic systems, [1,9] process, are not so common. The concept of a [1,9] sigmatropy was introduced into troponoid chemistry by Harrison et al. when they observed a thermal rearrangement of 2-benzyloxy-3-bromotropone (**1**) to 7-benzyloxy-2-bromotropone (**2**).[6] Harrison et al. have also carried out a kinetic study of this rearrangement and expressed a view to favor a [1,9] process on the basis of the value of the activation energy (E_a).[6] However, it is known that E_a of sigmatropies varies from 27 to 210 kJ mol^{-1}, depending on the nature of the substrates.[10] Therefore, the conclusion drawn by Harrison deserves further investigation. We decided to examine the sigmatropy by means of a kinetic analysis. The results are summar-

Table 1. The Rate Constants (10^7k/s^{-1}) of the Rearrangement of **1** at Various Temperatures

Solv.	Temperature/°C			
	110	120	130	140
Cumene	1.17±0.16	2.94±0.16	4.91±0.16	25.1±0.1
1-Hexanol	4.22±0.07	10.0±0.3	26.6±0.4	49.3±0.3

Table 2. Activation parameters of the Rearrangement of **1** at 130 °C

Solv.	ΔH^*/kJ mol^{-1}	ΔS^*/J mol^{-1} K^{-1}	ΔG^*/kJ mol^{-1}
Cumene	128±4	−47±11	147±9
1-Hexanol	106±3	−92±7	143±5

Table 3. The Rate Constants of Each Rearrangement at Various Pressures

Material		Solv.	Pressure/bar				
			1	400	800	1200	1600
1[a]	$10^7k/s^{-1}$	IB	4.91±0.16	5.48±0.01	6.19±0.18	7.24±0.08	8.28±0.03
1[a]	$10^6k/s^{-1}$	HA	2.66±0.04	2.93±0.08	3.38±0.20	3.62±0.05	4.04±0.22
3[b]	$10^5k/s^{-1}$	BB	2.30±0.02	2.61±0.02	2.82±0.02	3.07±0.02	3.20±0.01
5[b]	$10^5k/s^{-1}$	BB	6.49±0.04	8.40±0.04	9.30±0.07	11.2±0.1	12.5 ±0.1

IB: cumene, HA: 1-hexanol, BB: bromobenzene.
a) At 130 °C, b) At 120 °C.

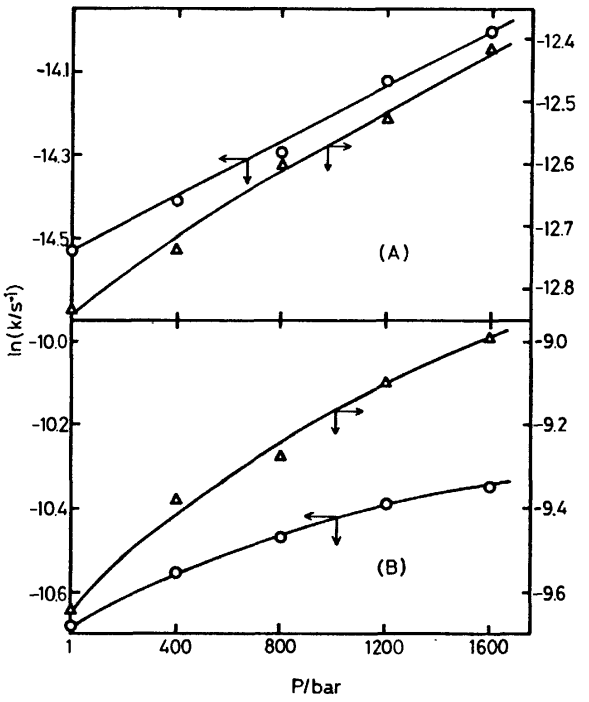

Fig. 1. Pressure dependence of $\ln k$.
(A): **1** at 130 °C, O; in cumene, Δ; in 1-hexanol. (B): O; **3** at 120 °C in bromobenzene, Δ; **5** at 120 °C in bromobenzene.

ized in Table 1. The activation parameters obtained at 130 °C are listed in Table 2.

Each activation parameter in both solvents, isopropylbenzene (cumene) and 1-hexanol, showed a similar tendency to those of a typical [1,5] sigmatropy operating within the range of temperature.[10] The activation entropies (ΔS^*) obtained at 130 °C were −47 and −92 J mol^{-1} K^{-1} in cumene and 1-hexanol, respectively. As a general tendency, the stronger the solvation, the more negative ΔS^* is expectable from the pressure effect on this rearrangement. This indicates a weak, but not negligible, contribution of a polarized structure in the transition state. The activation free energy (ΔG^*) remained nearly constant in both solvents as a result of the compensation effect between ΔS^* and the activation enthalpy (ΔH^*).[11] Then, we investigated the high-pressure kinetic analysis of this [1,9] sigmatropy of **1** to **2**.

In Table 3, the rate constants for the rearrangement of **1** to **2** at various pressures at 130 °C are listed. The activation volume (ΔV^*) was evaluated with Eq. 1 by using a linear function of $\ln k$ vs. pressure (P).

$$\Delta V^* = -RT(\partial \ln k/\partial P)_T, \quad (1)$$

The rates were accelerated with pressure; in cumene, the logarithm of the rate constants was linear to the pressure (correlation coefficient r: 0.998), but in 1-hexanol, it showed a curvature (Fig. 1 (A)). If one neglects the difference toward compressibility between the ground and transition states by assuming this rearrangement to be a unimolecular reaction, one reason of this behavior must be the contribution of a somewhat polarized transition state. This contribution may alter the degree of solvation in 1-hexanol under high pressure. Thus, from Eq. 1, ΔV^* were evaluated by a linear function in the case of cumene and a quadratic function in the case of 1-hexanol (tabulated in Table 4). The solvent effect on ΔV^* was very small and the above-mentioned solvation effect on the transition state was very weak. The rate constant at atmospheric pressure in 1-hexanol (dielectric constant ε=13.3 D) was five-times larger than that in cumene (ε=2.4 D). This magnitude of the rate enhancement is just similar to that of the Diels-Alder reaction of isoprene to maleic anhydride,[12] where the rate was about eight times larger in nitromethane (ε=38.6 D) than that in ethyl acetate (ε=6.06 D). These results show that the rearrangement of **1** to **2** is a concerted process, i.e., [1,9] sigmatropy. At the same time, the effect of pressure on [1,9] sigmatropy is similar to that of the other typical sigmatropy.

Consequently, from the temperature, pressure, and solvent effects, the present rearrangement is undoubtedly a concerted [1,9] sigmatropy.

[3,3] Sigmatropy. The Claisen rearrangement of tropolone derivatives has been a focus of attention. As early as in 1953, Sebe et al. carried out pioneering work, and reported some fundamental features.[13] However, Kitahara's studies on natural product syntheses, nootkatin and procerin,[14] have revealed a limitation of the process, i.e., the yields of the Claisen products, prenylated products, were only a few %. This was later explained by ourselves, i.e., the proto-Claisen thermolysates of the γ-substituted allyl ethers of tropolones cause another thermally-allowed fragmentation to tropolones and diene via the $[_s6_\pi + _s2_\pi + _s2_\sigma]$ electro-

cyclic reaction.[15] Intramolecular Diels-Alder reactions of the proto-products from the substituted troponyl allyl ethers found by Harrison et al.[16] and Schmid et al.[17] also constitute a limitation of the Claisen rearrangement. Nevertheless, the Claisen rearrangement of troponoids may be competitive with other electrocyclic reactions, and it is interesting from a theoretical point of view.

As a typical [3,3] sigmatropy, Claisen rearrangements of 2-allyloxytropone (**3**) to 3-allyltropolone (**4**) and 2-[(3-methyl-2-butenyl)oxy]tropone (**5**) to thermolysates (**6** and **7**) were carried out. Prior to high-pressure kinetics, authentic samples of thermolysates were prepared and isolated as 2-methoxytropone derivatives, i.e., 3-allyl-2-methoxytropone (**8**), 2-allyl-7-methoxytropone (**9**), 2-methoxy-3-(1,1-dimethyl-2-propenyl)tropone (**10**), 2-methoxy-7-(1,1-dimethyl-2-propenyl)tropone (**11**), and 2-methoxy-5-(3-methyl-2-butenyl)tropone (see Experimental). The rates of reactions under various pressures were measured by high-pressure liquid chromatography (HPLC) of the product mixture after treatment with ethereal diazomethane.

Table 3 shows the pressure effect on Claisen rearrangements of **3** and **5**. At 1 bar, the rate constant of **5** was three-times larger than that of **3**. This is predictable in terms of an electron-releasing effect of the methyl groups of **5**; however, the effect of this electronic character on the solvation term must be very small in this concerted reaction.[18] As shown in Fig. 1 (B), the acceleration with pressure was much larger in the case of **5** than **3**. By using a quadratic function of pressure to express this dependence $\Delta V^{\ddagger}$ was evaluated (listed in Table 4). Evidently, the rearrangement of **5**, being more sterically hindered at the reaction center, was more accelerated with pressure than that of **3**, being less hindered. There have been several discussions about a pressure effect on the steric hindrance to Menshutkin reaction.[19,20] Le Noble and Asano found that, by volume criterion, the transition state of Menshutkin reaction is more product-like as the reaction is more hindered. In other words, more hindered Menshutkin reactions tend to become more accelerated with pressure. This is consistent to a postulation by Hammond.[20] In order to explain the results, one has to consider the difference of the bulkiness of the reactant. That is, in order to cause a rearrangement, a reactant having a bulky substituent must be contracted

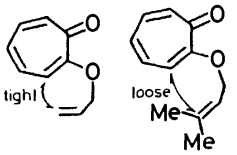

3 5

$|\Delta V^{\ddagger}| < |\Delta V^{\ddagger}|$

Scheme 2.

Table 4. The Activation Volumes of Each Rearrangement

Material	1	1	3	5
Solv.	IB	HA	BB	BB
$\Delta V^{\ddagger}$/cm^{3}mol^{-1}	−11.1±0.7	−10.1±0.5	−10.6±0.3	−18.2±1.0

IB: cumene, HA: 1-hexanol, BB: bromobenzene.

to a greater extent than that having a non-bulky one. As a result, the $\Delta V^{\ddagger}$ value for the more hindered rearrangement must be more negative (Scheme 2).

The Claisen rearrangement of **5** was much more accelerated with pressure than that of unsubstituted **3**, due to the contribution of two additional methyl groups. If there were more crowded substituents at the reaction center, the Claisen rearrangement might be more pressure-accelerated to give a more negative $\Delta V^{\ddagger}$ value than the ordinary [3,3] sigmatropy ($-18 < \Delta V^{\ddagger} < -7$).[9]

Experimental

Materials. Solvents were carefully purified by dehydration and distillation under N_2 atmosphere. All materials were prepared by the known procedures, and purified by silica-gel column chromatography. Recrystallizations for a solid sample were performed by using the solvents indicated in parentheses. The NMR spectra were measured in $CDCl_3$ solutions, and the chemical shifts were expressed in δ units with the internal standard, Me_4Si. The IR spectra were taken in $CHCl_3$ solutions.

Kinetic Measurements. The apparatus for kinetic runs was the same as used in our previous studies.[21] The reaction temperature was controlled within ±0.5 °C. The progress of the reaction was monitored by high-pressure liquid chromatography [Nippon Waters Model 244 apparatus] by the increase of product formations. In the case of Claisen rearrangements of **3** and **5**, tropolone derivatives were methylated with ethereal CH_2N_2 prior to analysis.

[1,9] Sigmatropy of 1 (Preparative). A cumene solution of **1** (mp 44—45 °C (from benzene-hexane) (lit,[6] 43—44 °C); 254 mg) was heated in a sealed tube at 150 °C for 24 h. The mixture was chromatographed on a silica-gel column to give the desired product:

2: Mp 94—95 °C (from benzene-hexane) (lit,[6] 96—97 °C).

Claisen Rearrangement of 3 (Preparative). Characterization of the Thermolysate (4) as its Methyl Ethers (8 and 9). A toluene solution of **3** (bp 60 °C/0.3 Torr (1 Torr=133.22 Pa)) (177 mg) was refluxed for 8 h. The mixture was then heated in vacuo to remove the solvent and the residue was chromatographed on a silica-gel column with benzene-EtOAc (1 : 1) to give **4** [colorless crystals, mp 42—43 °C (hexane-EtOAc) (lit,[22] 43—44 °C); 49.5 mg; 60%] and the recovered **3** (95.1 mg). The **4** was treated with ethereal diazomethane. Silica-gel column chromatography of the mixture with benzene-EtOAc (5 : 1) afforded methylated derivatives:

8: A pale yellow oil; 15 mg. Found: m/z 176.0836. Calcd for $C_{11}H_{12}O_2$: M, 176.0837; ^{1}H NMR δ=3.44 (2H, dt, J=6.6, 1.5 Hz), 3.91 (3H, s), 5.09 (1H, dtd, J=16.1, 1.5, 1.1 Hz), 5.10 (1H, dtd, J=11.0, 1.5, 1.1 Hz), 5.91 (1H, ddt. J=16.1, 11.0, 6.6 Hz), and 6.8—7.2 (4H, m). ^{13}C NMR δ=38.9, 58.9, 116.7, 129.7, 135.3, 135.4, 137.1, 137.7, 138.6, 163.9, and 181.8. IR ν; 1620, 1580, and 1275 cm^{-1}.

9: Colorless crystals, mp 48—49 °C (benzene-hexane);

35 mg. Found: C, 74.87; H, 6.79%. Calcd for $C_{11}H_{12}O_2$: C, 74.98; H, 6.86%. ^{1}H NMR δ=3.52 (2H, d, J=6.6 Hz), 3.93 (3H, s), 5.10 (1H, dm, J=9.9 Hz), 5.15 (1H, dm, J=17.0 Hz), 5.99 (1H, ddt, J=17.0, 9.9, 6.6 Hz), 6.74 (1H, br d, J=9.4 Hz), 6.84 (1H, br t, J=9.4 Hz), 7.01 (1H, br t, J=9.4 Hz), and 7.37 (1H, br d, J=9.4 Hz); ^{13}C NMR δ=39.8, 56.3, 112.1, 117.0, 127.1, 131.0, 135.8 (2C), 147.9, 164.0, and 179.3. IR ν: 1640, 1595, and 1275 cm^{-1}.

Claisen Rearrangement of 5 (Preparative). Characterization of the Thermolysates (6 and 7) as Methyl Ethers (10, 11, and 12). A toluene solution (20 cm^3) of **5**[23] (527 mg) was similarly refluxed for 17 h. The mixture was then heated in vacuo to remove the solvent, and the residue was chromatographed on a silica-gel column with benzene-EtOAc (1 : 1) to give **10** (89.2 mg; 19%), **11** (166.6 mg; 36%), **12** (130.2 mg; 28%), 2-methoxytropone (38.4 mg; 11%), and the recovered **5** (67.1 mg):

10: A pale yellow oil. Found: m/z 204.1148. Calcd for $C_{13}H_{16}O_2$: M, 204.1149. ^{1}H NMR δ=1.47 (6H, s), 3.80 (3H, s), 4.94 (1H, dd, J=17.6, 1.1 Hz), 4.99 (1H, dd, J=10.6, 1.1 Hz), 6.12 (1H, dd, J=17.6, 10.6 Hz), 6.82 (1H, ddd, J=11.7, 7.6, 1.8 Hz), 7.05 (1H, dd, J=12.1, 1.8 Hz), 7.15 (1H, ddd, J=12.1, 7.6, 7.1 Hz), and 7.28 (1H, br d, J=11.7 Hz); ^{13}C NMR δ=28.0 (2C), 43.5, 57.8, 109.6, 128.2, 134.2, 135.3, 136.9, 144.8, 148.5, 165.7, and 182.6. IR ν: 1630, 1605, and 1290 cm^{-1}.

11: Colorless crystals, mp 49—50 °C (benzene-hexane); Found: C, 76.21; H, 7.94%. Calcd for $C_{13}H_{16}O_2$: C, 76.44; H, 7.90%. ^{1}H NMR δ=1.49 (6H, s), 3.86 (3H. s), 5.01 (1H, dd, J=10.6, 1.1 Hz), 5.02 (1H, dd, J=17.6, 1.1 Hz), 6.16 (1H, dd, J=17.6, 10.6 Hz), 6.57 (1H, d, J=9.5 Hz), 6.75 (1H, br t, J=9.5 Hz), 6.91 (1H, br t, J=9.5 Hz), and 7.39 (1H, d, J=9.5 Hz). ^{13}C NMR δ=27.1 (2C), 44.1, 56.3, 110.1, 110.8, 125.9, 130.4, 133.5, 147.7, 153.1, 163.1, and 180.9. IR ν: 1625 and 1270 cm^{-1}.

12: A yellow oil, MS m/z, 204 (M^+). ^{1}H NMR δ=1.71 (3H, s), 1.76 (3H, s), 3.25 (2H, d, J=7.3 Hz), 3.92 (3H, s), 5.23 (1H, tm, J=7.3 Hz), 6.71 (1H, d, J=10.3 Hz), 6.92 (1H, br d, J=10.3 Hz), 7.11 (1H, dd, J=12.5, 1.8 Hz), and 7.20 (1H, d, J=12.5 Hz); ^{13}C NMR δ=17.9, 25.8, 37.6, 56.1, 113.1, 121.5, 130.5, 134.6, 136.7, 139.3, 141.9, 163.8, and 180.2. IR ν: 1630, 1570, and 1250 cm^{-1}.

The authors thank The Ministry of Education, Science and Culture for a Grant-in-Aid for Scientific Research to S. S. (Nos. 61740294 and 63740293).

References

1) Selected examples in the organic synthesis: J. S. Bindra and R. Bindra, "Creativity in Organic Syntheses," Academic Press, New York (1975); see also T. Shioiri and M. Shibasaki, "Organic Syntheses directed to Biologically Important Compounds," Kodansha, Tokyo (1985), p. 194.

2) An acetylation of hinokitiol is known to give only one acetate, while methyl and *p*-toluenesulfonyl derivatives of hinokitiol are known to exist as two isolable isomers. The same was true for many other substituted derivatives. For these phenomena, Dr. Masafumi Yasunami, Tohoku University, has pointed out that carboxylates of tropolones exist as an equilibrating mixture at the ordinary temperature. For hinikitiol acetate, see T. Nozoe, "Dai Yuki Kagaku (Comprehensive Organic Chemistry)," ed by M. Kotake, Asakura Shoten, Tokyo (1961), Vol. 13, p. 164.

3) a) S. Masamune, A. V. Kemp-Jones, J. Green, D. L. Rabenstein, M. Yasunami, K. Takase, and T. Nozoe, *J. Chem. Soc., Chem. Commun.*, **1973**, 283; b) V. I. Minkin, L. P. Olekhnovich, and Y. A. Zhdanov, *Acc. Chem. Res.*, **14**, 210 (1981).

4) H. Takeshita, A. Mori, H. Watanabe, T. Kusaba, S. Sugiyama, and M. Kodama, *Bull. Chem. Soc. Jpn.*, **60**, 4335 (1987).

5) S. Sugiyama, A. Mori, and H. Takeshita, *Chem. Lett.*, **1987**, 1247.

6) R. M. Harrison, J. D. Hobson, and A. W. Midgley, *J. Chem. Soc., Perkin Trans. 1*, **1976**, 2403.

7) E. M. Schulman, A. E. Merbach, M. Tutin, R. Weddinger, and W. J. le Noble, *J. Am. Chem. Soc.*, **105**, 3988 (1983).

8) W. J. le Noble and M. R. Daka, *J. Am. Chem. Soc.*, **100**, 5961 (1978).

9) C. Walling and M. Naiman, *J. Am. Chem. Soc.*, **84**, 2628 (1962); K. R. Brower, *ibid.*, **83**, 4370 (1961).

10) C. W. Spangler, *Chem. Rev.*, **76**, 187 (1976).

11) J. E. Leffer, *J. Org. Chem.*, **20**, 1202 (1955).

12) R. A. Grieger and C. A. Eckert, *Trans. Faraday Soc.*, **66**, 2579 (1970).

13) E. Sebe and S. Matsumoto, *Proc. Jpn. Acad.*, **29**, 207 (1953).

14) Y. Kitahara and M. Funamizu, *Bull. Chem. Soc. Jpn.*, **31**, 782 (1958); Y. Kitahara and T. Kato, *ibid.*, **37**, 895 (1964).

15) H. Takeshita, H. Mametsuka, and K. Uchida, *Chem. Lett.*, **1982**, 1061.

16) R. M. Harrison, J. D. Hobson, and M. M. Al Holly, *J. Chem. Soc. C*, **1971**, 3084; R. M. Harrison, J. D. Hobson, and A. W. Midgley, *J. Chem. Soc., Perkin Trans. 1*, **1973**, 1960.

17) A. Pride, J. Zindely, and H. Schmid, *Helv. Chim. Acta*, **57**, 1598 (1974).

18) H. Mametsuka, Ph. D. Thesis, Kyushu University, 1983; H. Takeshita, H. Mametsuka, and N. Matsuo, *Bull. Chem. Soc. Jpn.*, **55**, 1137 (1982).

19) W. J. le Noble and Y. Ogo, *Tetrahedron*, **26**, 4119 (1970), and the references cited therein.

20) W. J. le Noble and T. Asano, *J. Am. Chem. Soc.*, **97**, 1778 (1975).

21) S. Sugiyama and H. Takeshita, *Bull. Chem. Soc. Jpn.*, **60**, 977 (1987).

22) H. Takeshita, I. Kouno, and K. Miyake, *Kyushu Daigaku Seisan Kagaku Kenkyusho Hokoku*, **66**, 1 (1977).

23) In the preparation of **5**, a by-product, a colorless oil, was obtained in 4% yield. Its ^{1}H NMR indicated its structure to be 5-(3-methyl-2-butenyl)-2-[(3-methyl-2-butenyl)oxy]tropone. Since **5** was quite stable at the preparative condition (50 °C for 24 h), it must be formed directly from **5** and prenyl bromide.[18]

 © 1989 The Chemical Society of Japan Bull. Chem. Soc. Jpn., 62, 1147—1153 (1989)

Oxidation of 2,4-Di-*t*-butylphenol with Hydrogen Peroxide Catalyzed by Bis(ethylenediamine)copper(II) Complexes

Keiko KUSHIOKA,* Iwao TANIMOTO, and Kazuhiro MARUYAMA†
Department of Food Science, Faculty of Home Economics, Kyoto Women's University, Higashiyama-ku, Kyoto 605
†Department of Chemistry, Faculty of Science, Kyoto University, Sakyo-ku, Kyoto 606
(Received October 11, 1988)

2,4-Di-*t*-butylphenol (**1**) was efficiently oxidized with H_2O_2 in methanol in the presence of bis(ethylenediamine)copper(II) (Cu(II)$(en)_2$) complexes. Activity of the Cu(II) complexes was strongly dependent on the structure of the en ligands, as in the cases of the O_2 oxidation of phenol **1**.[1] In the H_2O_2 oxidation of **1**, ens having none of *N*-alkyl substituent were of the most efficient. By addition of H_2O_2, stable Cu(II)$(en)_2$ complexes exhibited a new absorption at 340 nm, which was assigned to Cu(II)-en-H_2O_2 (1 : 2 : 1) complexes. Furthermore, the rapid-scanning spectrophotometry proved that quadruple Cu(II)-en-phenol **1**-H_2O_2 (1 : 1 : 1 : 1) complexes were the key intermediate for the oxidation of **1**. The initial velocity can be summarized in the equation $v=k[H_2O_2]^1[\text{phenol } \mathbf{1}]^1[\text{Cu(II)}(en)_2]^1$. The oxidation mechanism of phenol **1** with H_2O_2 is proposed.

In the previous papers[1,2] reported on the autoxidation of phenols with molecular oxygen catalyzed by bis(*N*-alkylethylenediamine)copper(II) (abbreviated as Cu(II)(*N*-Ren)$_2$ (R=alkyl group) hereafter; the related complexes are also shown by the same type of abbreviation) complexes, we showed that the most active complexes were those derived from sterically overcrowded ens around the nitrogen atoms. This paper deals with the oxidation of 2,4-di-*t*-butylphenol (**1**) by hydrogen peroxide. Oxidation of phenols with hydrogen peroxide in the presence of Cu(II)-amine complexes has been scantly reported with exception of the hydroxylation of phenols.[3] Compared with molecular oxygen, hydrogen peroxide is a stronger oxidant and has a higher coordinating ability to copper(II). We have investigated Cu(II) complexes of a series of ens bearing *N*-alkyl or *C*-alkyl substituents to determine how the structure of en ligands affects the oxidation of phenol **1**. Only en and *C*-alkyl ens having none of *N*-alkyl substituent formed active Cu(II) complexes in this oxidation. Using such complexes, the initial stage of the oxidation was kinetically examined.

Results and Discussion

Phenol **1** was oxidized in methanol with hydrogen peroxide under a set of standard conditions (see Experimental section) except for minor deviations specified, if any. The oxidation of phenol **1** with hydrogen peroxide, as well as that with molecular oxygen,[1,2] afforded only 3,3′,5,5′-tetra-*t*-butyl-2,2′-dihydroxybiphenyl (**2**) and its oxidation product, i.e., 2,4,7,9-tetra-*t*-butyloxepino[2,3-*b*]benzofuran (**3**).

[I] Phenol Oxidation with Hydrogen Peroxide Catalyzed by Cu(II)(en)$_2$ Complexes. The results of the oxidation of phenol **1** with hydrogen peroxide in the presence of **stable** Cu(II)$(en)_2$ complexes are shown in Table 1, together with their stability constants.[4] In Tables 1 and 2, the relative oxidation activities of Cu(II)$(en)_2$ complexes are expressed as the percent yields of biphenol **2** for the first 10 min of oxidation, because the amount of benzofuran **3** produced during this period was negligible.

In the presence of the stable complexes, yields of biphenol **2** exceeded over 20% without exception, proving that hydrogen peroxide acted as a two-electron oxidant. Since oxidation was carried out under the conditions at hydrogen peroxide/phenol **1** (molar ratio) of 0.19, yields of **2** could not exceed over 19% if we would assume that one molecule of hydrogen peroxide oxidized only one molecule of phenol **1**. In

Table 1. Oxidation of Phenol **1** with Hydrogen Peroxide in the Presence of Cu(II)$(en)_2$ Complexes

Diamine R : CH_3	Product[a,b] **2**/%	Stability const. log K_T[4]
dl-H_2N-CHR-CHR-NH_2	22.5	21.21
H_2N-CH_2-CH_2-NH_2	21.1	20.13
meso-H_2N-CHR-CHR-NH_2	21.1	20.06
H_2N-CHR-CH_2-NH_2	21.8	20.06
H_2N-CR_2-CH_2-NH_2	20.5	19.58

a) Standard conditions. b) Benzofuran **3**: trace.

Table 2. Oxidation of Phenol **1** with Hydrogen Peroxide in the Presence of Cu(II)(*N*,*N*′-R_2en)$_2$ Complexes

(RNH-CH_2-)$_2$ R	CH_3OH Product[a-c] **2**/%	CH_3OH-H_2O (9 : 1) Product[b,d] **2**/%
CH_3	2.9	9.5
C_2H_5	2.4	7.7
n-C_3H_7	1.9	8.0
i-C_3H_7	1.8	8.5
n-C_4H_9	2.4	10.0
i-C_4H_9	3.6	11.9
s-C_4H_9	3.9	13.8
t-C_4H_9	2.6	2.9[e]

a) Standard conditions. b) Benzofuran **3**: trace. c) The yields of biphenol **2** increased little after the first 1 min of the oxidation. d) Standard conditions except for solvent. e) Absorption spectra showed the decomposition of the Cu(II)-complex by H_2O.

the absence of either copper(II) or en, phenol **1** was hardly oxidized to biphenol **2** under the same conditions (0.5—2.2%).

The copper(II) complexes of a series of *N,N'*-R_2ens were examined similarly (Table 2). All of the complexes were less active in the oxidation reactions. In the oxidation with molecular oxygen,[1] the less stable and tetrahedral copper(II) complexes which had alkyl branching on the carbon attached to nitrogen were the most active. The Cu(II) complexes could undergo facile coordination of phenolate anion and facile electron transfer from phenolate anion to Cu(II). Hydrogen peroxide of the high coordinating ability to Cu(II) complexes would expel diamine ligands or/and phenolate anion coordinated to Cu(II). Actually, addition of hydrogen peroxide to the concentrated methanolic solution of unstable Cu(II)(*N,N'*-(*t*-butyl)$_2$en)$_2$ complex resulted in the formation of a dark brown precipitate. The precipitate was proved to be peroxo-copper complexes with the luminol test (see Experimental section).

Too quick and exclusive replacement of diamine ligands or/and phenolate anion by hydrogen peroxide molecules in the less stable diamine complexes would block the oxidation of phenol **1**. This was confirmed by the reactions using 1:9 mixture of water and methanol as a solvent (Table 2), where yields of biphenol **2** increased by a factor of 3 to 5.[5] In the mixture, the hydrogen bond[6] between water and hydrogen peroxide would reduce concentration of hydrogen peroxide which is able to coordinate to copper complexes. Consequently, the succesive coordination of hydrogen peroxide to copper complexes would be retarded and the oxidation of phenol **1** would be facilitated. Furthermore, increase of concentration of phenol **1** in solution heightened yields of biphenol **2**, owing to impediment to the succesive coordination of hydrogen peroxide (Fig. 1). Those results indicate that the diamine complexes of copper(II) bearing both hydrogen peroxide and phenol **1** are indispensable for the oxidation of **1**.

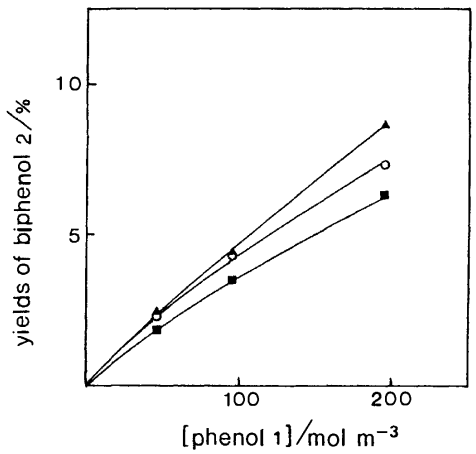

Fig. 1. Effect of phenol **1** concentration in oxidation of **1** in the presence of Cu(II)(*N,N'*-R_2en)$_2$ complexes. R: C_2H_5 ▲; *n*-C_3H_7 ■; *n*-C_4H_9 ○.

[II] The Mechanism of Oxidation of Phenol 1.

(1) Effect of en/Cu(II) Ratio. In methanolic solutions of copper(II) and ens, only 1:1 and 1:2 complexes were detected spectrophotometrically.[1] In the presence of copper(II) chloride and en, yields of biphenol **2** were affected by ratios of en to Cu(II) (Fig. 2). The maximum yield of biphenol **2** was achieved at en/Cu(II) ratio of 2/1. In the reaction at the higher ratio than 2/1, decrease of yields of **2** as well as appearance of an induction period was observed. On the other hand, in the mixtures of *N,N'*-R_2ens and Cu(II) which formed the less stable complexes, the maximum yield of **2** was achieved at the higher ratio than 2/1, but with no induction period. These observations suggest that Cu(II)(en)$_2$ complexes are the active catalysts. Excess en molecules surrounding the stable Cu(II)(en)$_2$ complex could impede the ligand exchange by hydrogen peroxide and/or phenol **1**, while, in the cases of the less stable complexes, presence of excess diamines surrounding Cu(II) may be advantageous for reproducing the active catalytic species.

(2) Spectral Studies. By addition of phenol **1**, a solution of less stable Cu(II)(*N,N'*-R_2en)$_2$ complexes exhibited a broad absorption at the region of 350—600 nm, whereas the spectrum of the stable Cu(II)(en)$_2$ complex was slightly changed by addition of **1** at 370—440 nm. Since in the latter case the absorbance at 410 nm increased with time, gradual coordination of phenol **1** to the stable Cu(II)(en)$_2$ complexes was substantiated. On the other hand, addition of hydrogen peroxide to a solution of the stable Cu(II)(en)$_2$ complexes exhibited absorption maximum at either 340 or

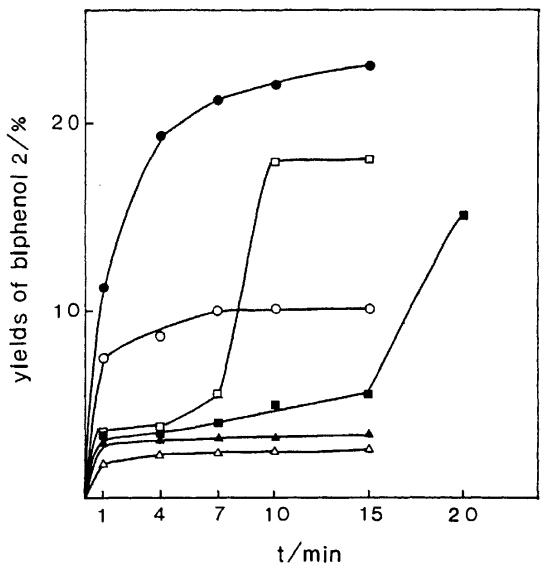

Fig. 2. Effect of en/Cu(II) ratio in oxidation of phenol **1**. en/Cu(II): 0.5 △; 1 ▲; 1.5 ○; 2 ●; 3 □; 4 ■; 2.43×10^{-3} mol of phenol **1**, 6.06×10^{-6} mol of $CuCl_2$ and 4.56×10^{-4} mol of H_2O_2 in 50 mL of methanol.

360—400 nm, which was depending on added amount of hydrogen peroxide. The absorption at 340 nm appeared at the relatively lower molar ratio of hydrogen peroxide in solution. However, examination by rapid-scanning spectrophotometry even at the higher molar ratio of hydrogen peroxide showed absorption (λ_{max} 340 nm) at the initial stage after mixing Cu(II)$(en)_2$ complex with hydrogen peroxide. Keeping the concentration of Cu(II)$(en)_2$ complex in solution at a constant, we added different amount of hydrogen peroxide and followed change of the absorbance at 340 nm by a stopped flow method. Initial increasing rate of the absorption at 340 nm was the first order with respect to initial concentrations of hydrogen peroxide (Fig. 3). Therefore, under our conditions the absorption at 340 nm was attributed to ternary Cu(II)-en-H_2O_2 (1:2:1) complexes, but not to hydroxo- or alkoxo-bridged copper(II) binuclear complexes which showed the characteristic absorption at 350—400 nm.[7] While, the absorption at 360—400 nm observed in the presence of the higher molar ratio of hydrogen peroxide would be formed via a complex showing the absorption at 340 nm. The similar broad absorption at around 360—400 nm was exhibited by addition of hydrogen peroxide to a solution of less stable Cu(II)-(N,N'-R_2en)$_2$ complexes. The absorption probably arise from Cu(II)-ens-H_2O_2 (1:1:2) complexes.

Then, applying rapid-scanning spectrophotometry, we examined appearence of an intermediate after mixing Cu(II)$(en)_2$ complex, phenol **1**, and hydrogen peroxide. By the addition of hydrogen peroxide, a solution of Cu(II)$(en)_2$-phenol **1** exhibited an absorption spectrum having maximum at 370 nm. The same spectrum appeared as well when a mixture of H_2O_2-phenol **1** was added to a solution of Cu(II)$(en)_2$ complex.[8] Thus, the absorption maximum at 370 nm could be attributed to a quadruple Cu(II)-en-H_2O_2-phenol **1** (1:1:1:1) complex. In order to examine the

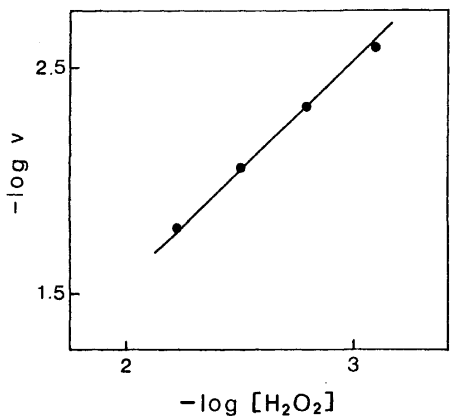

Fig. 3. Dependence of initial rate of the formation of the absorption at 340 nm on hydrogen peroxide concentration. $[CuCl_2]$=0.97 mol m^{-3}, [en]=1.94 mol m^{-3}, $[H_2O_2]$=0.76—6.06 mol m^{-3} in methanol, at 25°C.

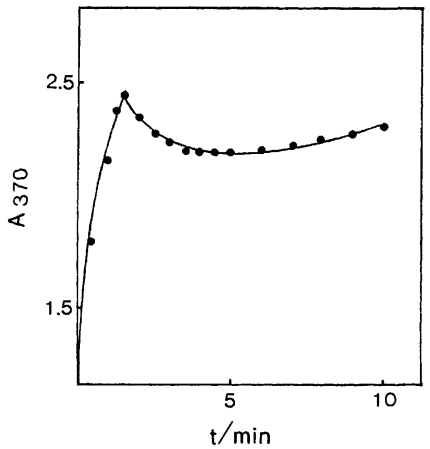

Fig. 4. Absorbance behavior at 370 nm indicating the formation of quadruple complex. 4.85×10^{-5} mol of $CuCl_2$, 9.7×10^{-5} mol of en, 2.43×10^{-3} mol of phenol **1** and 1.21×10^{-3} mol of H_2O_2 in 50 mL of methanol.

Table 3. Oxidation of Phenol **1** with Hydrogen Peroxide

$[H_2O_2]_{initial}$/mol m^{-3}	Biphenol **2**/%[a,b]
0.76	93
1.52	89
3.03	83
6.06	78

a) $[CuCl_2]$=0.121 mol m^{-3}, [en]=0.242 mol m^{-3} and [phenol **1**]=48.5 mol m^{-3}. The oxidation was carried out in methanol at 25°C for 7 min. b) Yields of biphenol **2** were estimated on the basis of hydrogen peroxide added, taking account of the experimental results that hydrogen peroxide acted as a two-electron oxidant (see Text).

formation and decay processes of the quadruple complex, the absorbance at 370 nm was traced (Fig. 4). As shown in Fig. 4, absorbance at 370 nm reached rapidly at a maximum, but falled then, and began to rise again gradually. This phenomenon indicates that besides of the quadruple Cu(II)-en-H_2O_2-phenol **1** complex the other species which has absorption at around 370 nm was accumulating in the solution with time. Actually, Cu(II)-en-biphenol **2** (reaction product)-H_2O_2 complex had absorption at around 370 nm. Thus, although exact trace of the quadruple Cu(II)-en-H_2O_2-phenol **1** complex was not carried out, it might be concluded that the quadruple complex was formed and reasonably stable.

On the other hand, addition of hydrogen peroxide to a solution containing unstable Cu(II)(N,N'-R_2en)$_2$ complexes and phenol **1** exhibited similarly the absorption at about 370 nm, but it disappeared within about 0.1 s. The instability of Cu(II)-N,N'-R_2en-H_2O_2-phenol **1** complexes might be responsible for less activity in the oxidation of **1**.

(3) Kinetic Studies. The kinetics were studied in the presence of the stable Cu(II)$(en)_2$ complex. The initial rate (v) of the reaction ([biphenol **2**]$_{initial}$/min^{-1})

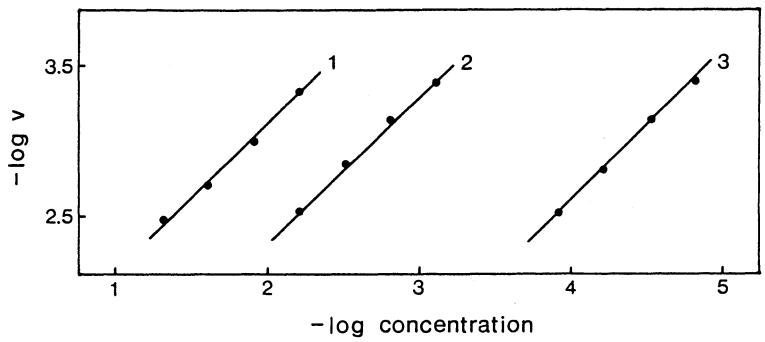

Fig. 5. Kinetic plots.
1: [phenol **1**]=6.06—48.5 mol m^{-3}, 2: [H_2O_2]=0.76—6.06 mol m^{-3}, 3: [Cu(II)-en]=1.52×10^{-2}—1.21×10^{-1} mol m^{-3}. Other conditions were as follows: [phenol **1**]=48.5 mol m^{-3}, [H_2O_2]=6.06 mol m^{-3} and [Cu(II)-en]=0.121 mol m^{-3} in methanol at 25 °C.

was determined. The initial rate increased linearly with concentration of hydrogen peroxide. From plots of log v against log [H_2O_2], the dependence on [H_2O_2] is of the first order. The dependence on [phenol **1**] and [Cu(II)(en)$_2$ complex] are also of the first order, respectively (Fig. 5). From those results, the following empirical rate expression was deduced.

$$v = k[H_2O_2]^1[\text{phenol } \mathbf{1}]^1[\text{Cu(II)(en)}_2 \text{ complex}]^1$$

Consequently, the kinetic results as well as spectral data indicate that under our conditions the oxidation of phenol **1** was not catalyzed by copper(II)-binuclear complexes.

The Cu(II)-en complex catalyzes decomposition of hydrogen peroxide.[9] Therefore, in the kinetic studies of the oxidation, we controlled conditions so that the oxidation of **1** can exclusively proceed (see Experimental section).

(4) Control Experiments. To determine whether free hydroxyl or hydroperoxyl radical which might be generated in our reactions could oxidize phenol **1** to biphenol **2**, first we attempted oxidation of **1** with free hydroxyl radical produced by photodecomposition of hydrogen peroxide.[10] After irradiation of the methanolic solution containing hydrogen peroxide and phenol **1** for 2 h, about 50% of hydrogen peroxide was decomposed. However, phenol **1** was wholly recovered and no oxidation product was detected by high performance liquid chromatography and by thin layer chromatography. Prior to the oxidation of **1**, hydroxyl radical would be quenched by methanol.[11]

Secondly, the decomposition of hydrogen peroxide catalyzed by Cu(II)(en)$_2$ complexes was studied in the absence of phenol **1**. The results are shown in Table 4, together with yields of biphenol **2** obtained in the studies of the oxidation of **1**. The less stable Cu(II)-(*N*,*N*′-R$_2$en)$_2$ complexes decomposed hydrogen peroxide efficiently, but were less active in the oxidation of **1**. In the stable Cu(II)(en)$_2$ complexes, yields of **2** exceeded considerably those expected to be produced by the decomposition products of hydrogen peroxide. While hydrogen peroxide in the presence of various metal ions (including copper(II)) or their complexes has been reported to oxidize 4-substituted phenols to hydroperoxidation products at the 4-position,[12] none of hydroperoxidation products was detected in the present studies.

Table 4. Decomposition of Hydrogen Peroxide Catalyzed by Cu(II)(en)$_2$ Complexes. Control Experiments

Diamine	Decomposition[a] H_2O_2/%	
less stable Cu(II)-complex		
$(CH_3NH\text{-}CH_2\rangle_2$	84	[7.7][b]
$(n\text{-}C_3H_7NH\text{-}CH_2\rangle_2$	80	[5.0]
$(n\text{-}C_4H_9NH\text{-}CH_2\rangle_2$	75	[6.4]
stable Cu(II)-complex		
$(dl\text{-}H_2N\text{-}CHCH_3\rangle_2$	33	[60]
$(H_2N\text{-}CH_2\rangle_2$	44	[56]
$(meso\text{-}H_2N\text{-}CHCH_3\rangle_2$	38	[56]

a) The decomposition of hydrogen peroxide was examined in the absence of **1**. The conditions were the same as those used in b), except for **1**. b) The yields of biphenol **2** in the oxidation of **1** under standard conditions.

In conclusion, under our conditions, phenol **1** was not oxidized with decomposition products of hydrogen peroxide, e.g., free hydroxyl or hydroperoxyl radical. Oxidation of **1** was achieved within the coordination sphere of the quadruple Cu(II)-en-H_2O_2-phenol **1** complex.

(5) The Mechanism of Oxidation of Phenol 1. The oxidation of phenol **1** was carried out within the coordination sphere of mononuclear Cu(II)-en-H_2O_2-phenol **1** complex and two molecules of **1** for each molecule of hydrogen peroxide was oxidized to biphenol **2**. The reaction sequence consisting with these results and kinetics as well as the spectral data is given in Scheme 1. Spectroscopic studies demonstrated similarly that under our conditions the quad-

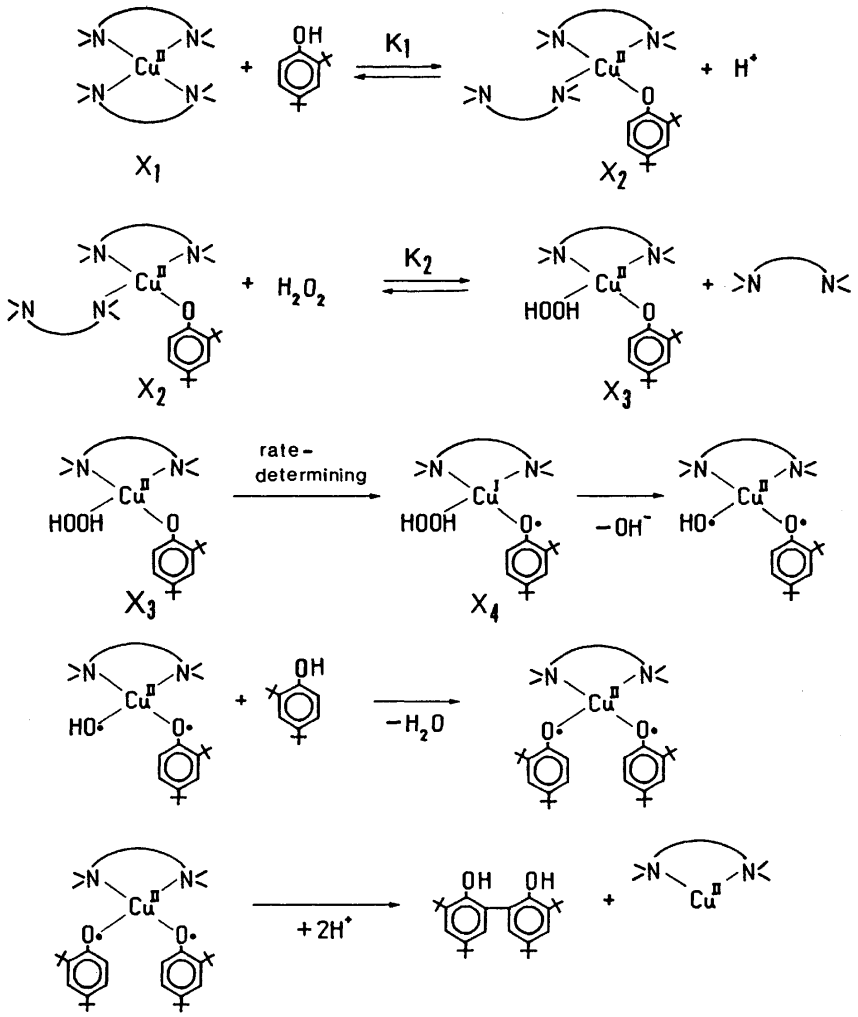

Scheme 1.

ruple complex $\mathbf{X_3}$ was produced via the coordination of **1** to Cu(II)-diamine complex $\mathbf{X_1}$. The formation of the quadruple complex $\mathbf{X_3}$ depended on the molar ratio of hydrogen peroxide to phenol **1**. A large excess of **1** would hinder coordination of hydrogen peroxide to Cu(II)-diamine-phenol **1** complex $\mathbf{X_2}$ and bring about an induction period into the whole sequence of reactions. On the contrary, for excess of hydrogen peroxide, yields of biphenol **2** were lowered with increasing concentration of hydrogen peroxide. Cu(II)-en-H_2O_2 (1 : 1 : 2) complex[9c] which is responsible for the decomposition of hydrogen peroxide would be formed in competition with the quadruple complex $\mathbf{X_3}$.

After forming the quadruple complex $\mathbf{X_3}$, phenolate anion would transfer an electron to hydrogen peroxide through copper.[13] The redox potential of Cu(II) complexes having two nitrogen donors is optimum for reduction of Cu(II).[9c] While, hydrogen peroxide is reduced with the generation of hydroxyl radical. The radical was not quenched by methanol because of the coordination with Cu(II) complex and oxidized another molecule of **1** by the participation of copper-(II). The whole process in which one molecule of hydrogen peroxide oxidized two molecules of **1** is consistent with the experimental results.

In the reaction, the reduction process of hydrogen peroxide of complex $\mathbf{X_4}$ might be rate-determining step, but this could be unlikely judging from redox potentials of both copper(II) complexes[14] and hydrogen peroxide. Then we assumed that complexes $\mathbf{X_1}$, $\mathbf{X_2}$, and $\mathbf{X_3}$ were in fast equilibrium and the process in which phenolate anion of the quadruple complex $\mathbf{X_3}$ transferred an electron to Cu(II) was the rate-determining step. By the assumptions a rate expression is deduced as follows,

$$v = k'[\text{complex } \mathbf{X_3}] \quad (1)$$

$$K_1 = [\text{complex } \mathbf{X_2}][H^+]/[\text{complex } \mathbf{X_1}][\text{phenol } \mathbf{1}]$$
$$K_2 = [\text{complex } \mathbf{X_3}][\text{en}]/[\text{complex } \mathbf{X_2}][H_2O_2]$$
$$K_1K_2 = [\text{complex } \mathbf{X_3}][H^+][\text{en}]/[\text{complex } \mathbf{X_1}][\text{phenol } \mathbf{1}][H_2O_2] \quad (2)$$

from Eqs. 1 and 2

$$v = k'K_1K_2[H_2O_2][\text{phenol } \mathbf{1}][\text{complex } \mathbf{X_1}]/[H^+][\text{en}] \quad (3)$$

Since all complexes in Scheme 1 were catalytic species,

they would be in low concentrations and in steady state. Then, $[H^+]$ and [en] which were mainly subjected to the respective concentrations of complexes $\mathbf{X_1}$ and $\mathbf{X_2}$ would be constant.

$$v = k''[H_2O_2][\text{phenol } \mathbf{1}][\text{complex } \mathbf{X_1}] \quad (4)$$

The rate expression (Eq. 4) consists with the foregoing empirical rate expression.

Experimental

GLC analyses were carried out on a JEOL Model JGC-20K equipped with 3% Apiezone L grease on Celite 545 NAW column. HPLC analyses were performed using methanol as a eluent on a Shimadzu Model LC-3A liquid chromatograph with Zorbax ODS column. Ultraviolet and visible spectra were taken using a Shimadzu UV-300 spectrophotometer. Stopped flow method and rapid scan technique were performed on an Otuka Denshi RA-401 stopped flow system equipped with RA-415 rapid scan system, gas driving device and RA-451 data processor. Temperature of a thermostat used in the kinetic measurement was controlled (±0.15 °C) by using a Komatsu-Yamato Coolnics CTR-220. Spectrophotometric determination of hydrogen peroxide was performed on a Shimadzu Model Double-Beam Spectrophotometer UV-140-02. The photoreactions were carried out on a Eichosha PIL-120, a low-pressure mercury lamp with quartz housing: $\Phi = 7.74\times10^{-5}$ (using a potassium tris(oxalato)ferrate(III) actinometer) in the decomposition reaction of hydrogen peroxide under the conditions used.

Materials. Anhydrous copper(II) chloride was prepared by heating the dihydrate in an oven at 100 °C for 20 h. Hydrogen peroxide (30%) was obtained from Santoku Kagaku Kogyo Co. and concentration was determined by iodometry before use. *dl*- And *meso*-2,3-butanediamine,[15] *N,N'*-dipropyl- and *N,N'*-dibutylethylenediamines (*N,N'*-(propyl)$_2$en and *N,N'*-(butyl)$_2$en)[16] and 3,3',5,5'-tetra-*t*-butyl-2,2'-dihydroxybiphenyl (**2**)[17] were prepared by procedures given in literatures.

Standard Conditions. Oxidation of 2,4-Di-*t*-butylphenol (1). Phenol **1** (2.43×10^{-3} mol) and the en (1.21×10^{-5} mol) were dissolved in methanol, and the volume was made up to 50 mL by adding methanol. Under a nitrogen atmosphere, anhydrous copper(II) chloride (6.06×10^{-6} mol) and hydrogen peroxide (4.56×10^{-4} mol) were added successively to the mixture and the oxidation was conducted at 25 °C for 10 min. The products were only biphenol **2** and its oxidation product, 2,4,7,9-tetra-*t*-butyloxepino[2,3-*b*]benzofuran (**3**).[1] The yields of product **2** were determined by GLC.

The Luminol Test. Addition of hydrogen peroxide (4.85×10^{-3} mol) to the methanolic solution (100 mL) containing anhydrous copper(II) chloride (9.7×10^{-5} mol) and *N,N'*-(*t*-butyl)$_2$en (1.94×10^{-4} mol) resulted in a precipitate, which was separated by centrifugation. The precipitate was thoroughly washed with methanol to remove free hydrogen peroxide and suspended in methanol. The suspension of the precipitate produced luminescence by addition of the luminol reagent.[18]

Effect of en/Cu(II) Ratio. In the presence of Cu(II)-en mixtures of various ratios, phenol **1** was oxidized under standard conditions.

Spectral Studies. Ultraviolet and Visible Absorption Spectra: In various combinations of phenol **1** (4.85×10^{-4} mol), biphenol **2** (2.43×10^{-4} mol), anhydrous copper(II) chloride (9.7×10^{-6} mol), the en (1.94×10^{-5} mol), and hydrogen peroxide (4.85×10^{-4}—7.6×10^{-6} mol), the absorption spectra of a methanolic solution (10 mL) of the mixture were taken using a spectrophotometer.

Rapid Scanning Spectra: Conditions were the same as those used in ultraviolet and visible absorption spectra, and the absorption spectra at 295—485 nm were obtained using a stopped flow system at 25 °C.

Formation Kinetics of the Absorption at 340 nm by Stopped-Flow Method: Concentrations of anhydrous copper(II) chloride (0.97 mol m^{-3}) and en (1.94 mol m^{-3}) were kept constant and concentration of hydrogen peroxide was varied from 0.76 mol m^{-3} to 6.06 mol m^{-3}. The change of the absorbance at 340 nm was followed by a stopped flow system at 25 °C. In every case, the result was accumulated about 10 times.

Absorbance Behavior at 370 nm: Phenol **1** (2.43×10^{-3} mol) and en (9.7×10^{-5} mol) were dissolved in 50 mL of methanol. Under a nitrogen atmosphere, anhydrous copper(II) chloride (4.85×10^{-5} mol) and hydrogen peroxide (1.21×10^{-3} mol) were added successively to the mixture at 25 °C. The sample was taken out of the reaction solution and the absorbance at 370 nm was measured on a spectrophotometer.

Kinetic Measurements. Bis(ethylenediamine)copper(II) complexes catalyzed both the oxidation of phenol **1** with hydrogen peroxide and the decomposition of hydrogen peroxide. For the purpose of carrying out the oxidation of **1** exclusively (Table 3), concentration of hydrogen peroxide was lowered from that under standard conditions by a factor of 2/3. Other conditions were the same as standard. The initial rate of the reaction ($[\text{product } \mathbf{2}]_{\text{initial}}/\text{min}^{-1}$) was determined by GLC.

Control Experiments. Photoreaction: Phenol **1** (1.21×10^{-2} mol) was dissolved in methanol, and the volume was made up to 250 mL by adding methanol. The solution was then placed in an inside-irradiation-type reaction flask equipped with a low-pressure mercury lamp. Under a nitrogen atmosphere, hydrogen peroxide (2.28×10^{-3} mol) was added to the solution and the irradiation was conducted at 30 °C for 2 h. The reaction mixture was analyzed by TLC (HPTLC-Fertigplatten Kieselgel 60 F_{254} Merck/benzene). Phenol **1** and biphenol **2** were determined by HPLC. The rate of decomposition of hydrogen peroxide was determined by iodometry.

Decomposition of Hydrogen Peroxide in the Absence of Phenol 1: Conditions were the same as those used in the oxidation, except for absence of **1**. The samples were taken out of the reaction solution and mixed with titanium(IV) chloride in 6 mol dm^{-3} HCl. The absorbance of titanium-H_2O_2 complex was measured at 450 nm on a spectrophotometer.[19]

References

1) K. Kushioka, *J. Org. Chem.*, **48**, 4948 (1983).
2) K. Kushioka, *J. Org. Chem.*, **49**, 4456 (1984).
3) W. Brackman and E. Havinga, *Rec. Trav. Chim.*, **74**, 1100, 1107 (1955); H. Gampp and A. D. Zuberbuhler, "Metal Ion in Biological Systems," ed by H. Sigel, Marcel Dekker, New York (1981), Vol. 12, pp. 162—165.

4) F. Basolo, Y. T. Chen, and R. K. Murmann, *J. Am. Chem. Soc.*, **76**, 956 (1954).

5) In the absence of phenol **1**, the decomposition of hydrogen peroxide in 1:9 mixture of water and methanol was reduced to one-half of that in methanol (Table 4).

6) R. C. Taylor and P. C. Cross, *J. Chem. Phys.*, **24**, 41 (1956); P. A. Giguere, O. Knop, and M. Falk, *Can. J. Chem.*, **36**, 883 (1958); S. A. Ukholin and M. Z. Pronina, *Issledovaniya Eksptl. Teoret. Fiz., Akad. Nauk S. S. S. R., Fiz. Inst. im. P. N. Lebedeva* **1959**, 244; *Chem. Abstr.*, **55**, 24229c (1961).

7) S. Kida, H. Okawa, and Y. Nishida, "Copper Coordination Chemistry: Biochemical and Inorganic Perspectives," ed by K. D. Karlin and J. Zubieta, Adenine Press, Guilderland, New York (1983), pp. 427—429; I. Murase, M. Hatano, M. Tanaka, S. Ueno, H. Okawa, and S. Kida, *Bull. Chem. Soc. Jpn.*, **55**, 2404 (1982); N. Oishi, M. Takeuchi, Y. Nishida, and S. Kida, *Polyhedron*, **3**, 157 (1984); T. Toki, M. Mikuriya, H. Okawa, I. Murase, and S. Kida, *Bull. Chem. Soc. Jpn.*, **57**, 2098 (1984).

8) Although hydrogen peroxide was expected to coordinate preferentially to Cu(II)-diamine complex, the absorption at 340 nm did not appear and the yields of biphenol **2** did not also affected.

9) a) H. Brintzinger and H. Erlenmeyer, *Helv. Chim. Acta*, **48**, 826 (1965); b) T. Kaden and H. Sigel, *ibid.*, **51**, 947 (1968); See also H. Sigel, *Angew. Chem.*, **81**, 161 (1969); c) V. S. Sharma and J. Schubert, *Inorg. Chem.*, **10**, 251 (1971).

10) A. J. Allmand and D. W. G. Style, *J. Chem. Soc.*, **1930**, 606; D. Richter, *ibid.*, **1934**, 1219; I. Loeff and G. Stein, *ibid.*, **1963**, 2623; K. Omura and T. Matsuura, *Tetrahedron*, **24**, 3475 (1968).

11) M. Anbar, D. Meyerstein, and P. Neta, *J. Chem. Soc. B*, **1966**, 742.

12) G. M. Coppinger, *J. Am. Chem. Soc.*, **79**, 2758 (1957); R. G. R. Bacon and L. C. Kuan, *Tetrahedron Lett.*, **1971**, 3397; Y. Hayashi, S. Shioi, M. Togami, and T. Sakan, *Chem. Lett.*, **1973**, 651.

13) W.W. Kaeding, *J. Org. Chem.*, **28**, 1063 (1963); R. G. R. Bacon and H. A. O. Hill, *Quart. Rev.*, **19**, 95 (1965); R. G. R. Bacon and A. R. Izzat, *J. Chem. Soc. C*, **1966**, 791.

14) B. R. James and R. J. P. Williams, *J. Chem. Soc.*, **1961**, 2007; W. G. Nigh, in W. S. Trahanovsky, "Oxidation of Organic Chemistry," Academic Press, New York (1973), Part B, Chap. 1, p. 1.

15) F. H. Dickey, W. Fickett, and H. J. Lucas, *J. Am. Chem. Soc.*, **74**, 944 (1952).

16) W. R. Boon, *J. Chem. Soc.*, **1947**, 307.

17) A. S. Hay and H. D. Becker, Ger. Patent 1900680 (1969); *Chem. Abstr.*, **71**, 91077k (1969).

18) R. D. Gillard and A. Spencer, *J. Chem. Soc. A*, **1970**, 1761.

19) W. C. Wolff, *Anal. Chem.*, **34**, 1328 (1962).

Induced Circular Dichroism Spectrum of α-Cyclodextrin Complex with Heptylviologen

Masato KODAKA* and Toshio FUKAYA
National Chemical Laboratory for Industry, Higashi, Tsukuba 305
(Received October 15, 1988)

The rotational strength of α-cyclodextrin (α-CDx) complex with heptylviologen (1,1′-diheptyl-4,4′-bipyridinium dibromide) was calculated by using the Kirkwood-Tinoco expression. The calculation shows that electric transition polarized along the long axis of heptylviologen gives negative induced circular dichroism (ICD) whereas the short-axis polarized transition gives positive ICD, when HV is axially included in α-CDx and the electric transition moment is located out of the cavity of α-CDx (above the narrower rim). From the comparison between the experimental and calculated results, it is concluded that the heptyl chain of heptylviologen is involved in the cavity while the pyridinium part is situated out of the cavity.

Induced circular dichroism (ICD) has been frequently used to determine the orientation of the aromatic molecule included in α-, β-, and γ-CDx's.[1-6] The theoretical calculation undertaken thus far is based on the expression developed by Kirkwood and Tinoco, and the agreement between the calculated and experimental results is fairly good.[1-4]

The calculation presented the general rule that the transition with an electric dipole moment parallel to the axis of CDx gives a positive ICD while the transition with an electric dipole moment perpendicular to the axis of CDx gives a negative ICD.[1-4] Although many experimental data have been analyzed using this rule, we must remember that this rule is applicable only when a chromophore is situated in the cavity of CDx. There has been no calculation dealing with the complex with the chromophore outside the cavity. For example, the complex between α-CDx and heptylviologen (4,4′-diheptyl-1,1′-bipyridinium dibromide; HV) gives negative ICD,[7] although HV seems to be axially included and the electric transition moment is expected to be parallel to the long axis of HV molecule. The observed ICD spectrum cannot be explained by the general rule described above. In the present study, therefore, the calculation is extended to the outside region of CDx.

Theoretical

The theoretical rotational strength of the transition from the ground state (0) to the excited state (a), R_{0a}, was calculated by the same method as that of Harata et al.,[1] using the following Kirkwood-Tinoco expression.[8]

$$R_{0a} = \pi \nu_a \mu_{0a}^2 \sum_j \frac{\nu_{0j}^2(\alpha_{33} - \alpha_{11})_j (\mathrm{GF})_j}{c(\nu_{0j}^2 - \nu_a^2)}$$

$$(\mathrm{GF})_j = \frac{1}{r_j^3}\left[\vec{e}_{0a} \cdot \vec{e}_j - \frac{3(\vec{e}_{0a} \cdot \vec{r}_j)(\vec{e}_j \cdot \vec{r}_j)}{r_j^2}\right]\vec{e}_{0a} \times \vec{e}_j \cdot \vec{r}_j$$

Here $\vec{e}_j$ is the unit vector in the direction of the symmetry axis of the bond j in α-CDx; $\vec{r}_j$ is the vector directed from the center of the chromophore (bipyridinium moiety) to the bond j in α-CDx; ν_{0j} is the frequency of the electric transitions of the bond j in α-CDx; $\vec{e}_{0a}$ is the unit vector in the direction of the electric dipole moment (μ_{0a}) of the transition from the ground state (0) to the excited state (a) in the chromo-

Table 1. The Frequency of the Electronic Transitions (ν_0) and Polarizability (α_{33}, α_{11}) of the Bonds in a Glucose Residue

Bond	$\nu_0 \times 10^{-15}/s^{-1}$	$\alpha_{33}/Å^3$	$\alpha_{11}/Å^3$
C-O	1.67	0.89	0.46
C-C	2.00	0.98	0.27

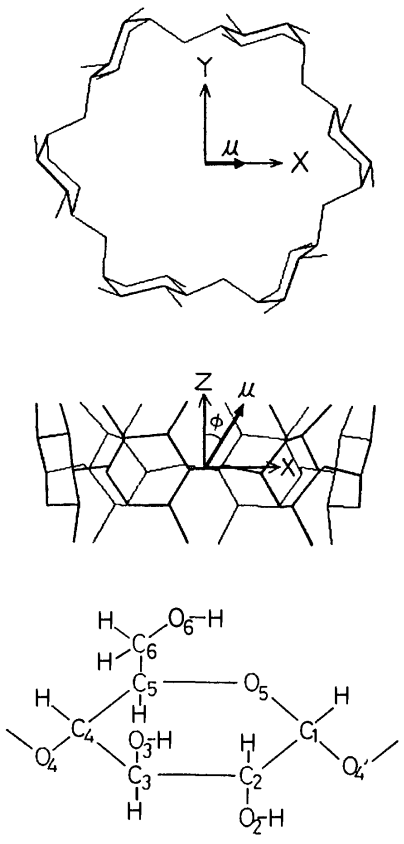

Fig. 1. The schematic drawing of α-CDx.

phore, and ν_a is its frequency; α_{33} and α_{11} are bond polarizability at zero frequency parallel and perpendicular, respectively, to the symmetry axis of the bond in α-CDx; c is the velocity of light.

The values of α_{33}, α_{11},[9,10] and ν_{0j}[1] are shown in Table 1. The assignment of the electronic transition of HV was undertaken by the CNDO/S-CI calculation. The electric transition moment was put at the center of the bipyridinium moiety. The geometry of α-CDx was derived from the X-ray data of the α-CDx-potassium acetate complex.[11] The axes of the coordinates were defined as shown in Fig. 1, where the origin of the coordinates was fixed on the plane determined by the six O_4 atoms. All the C_6-O_6 and O-H bonds were neglected owing to the flexibility. Furthermore, the effects of all the C-H bonds were neglected, for they may have isotropic polarizability.[12]

Results and Discussion

As the angle of twist (θ) around the central C-C bond of HV cannot be determined unequivocally, it seems to be appropriate that the CNDO/S-CI calculation is done at each point corresponding to the planar and angular conformations. In the case of biphenyl, the angle θ is about 42° in the gaseous phase,[13,14] while it is planar in the crystalline state.[15] On the other hand, in solution θ is 23°.[16] Taking into account these results about biphenyl, θ of HV is expected to be about 0—45°. And so we have undertaken the MO calculation about the three conformations (θ=0°, 22.5°, and 45°), with the central C-C bond length of HV fixed to 1.48 Å. For the pyridinium rings, all the C-N and C-C bond lengths and all the bond angles were assumed to be similar to those of benzene ring. The other bond lengths and bond angles were estimated from the standard values. In the CI calculations, 60 singly-excited configurations were taken into consideration. In Table 2 are summarized the calculated wavelengths and symmetries of the lower singlet states together with the oscillator strengths. The symmetries were determined on the assumption that HV has D_{2h} conformation for ϕ=0° and D_2 conformations for ϕ=22.5° and 45°. In the wavelength region under consideration, there can be seen three transitions. In these transitions, the $A_g \rightarrow B_{3u}$ (or $A \rightarrow B_3$) transition has the largest intensity, with its moment directed along the long axis of HV. On the other hand, the oscillator strength of the $A_g \rightarrow B_{2u}$ (or $A \rightarrow B_2$) transition is only ca. 40% of that of the $A_g \rightarrow B_{3u}$ (or $A \rightarrow B_3$) one, and the $A_g \rightarrow B_{1g}$ (or $A \rightarrow B_1$) transition is negligible as compared with the $A_g \rightarrow B_{3u}$ (or $A \rightarrow B_3$) transition. Experimentally HV has the absorption at 264 nm (D=38.4 debye^2), while the CNDO/S-CI calculation reproduced reasonable wavelengths and dipole strengths (the $A_g \rightarrow B_{3u}$ or the $A \rightarrow B_3$ transition); λ=266 nm and D=51.0 debye^2 at θ=0°, λ=261 nm and D=48.0 debye^2 at θ=22.5°, λ=250 nm and D=40.0 debye^2 at θ=45°; with the corresponding electric transition moments along the long axis of HV molecule.

In Fig. 2 is shown the dependence of the rotational strength of α-CDx-HV complex on the Z coordinates, with the X and Y coordinates fixed to be 0 Å. The electric transition moment is rotated in the X-Z plane by the angle ϕ as shown in Fig. 1. Inside the cavity of α-CDx, the large positive ICD is given at ϕ=0° (maximun; 36.3×10^{-40} cgs at Z=−0.5 Å) and the negative ICD at ϕ=90° (minimum; -17.7×10^{-40} cgs at Z=−0.6 Å). These results agree qualitatively with those for β-CDx complex obtained by Harata et al.[1] On the other hand, outside the cavity the sign of the ICD value is reversed, especially remarkably on the side of the primary hydroxyl groups (narrower rim) of α-CDx, with minimum at ϕ=0° (-19.6×10^{-40} cgs at

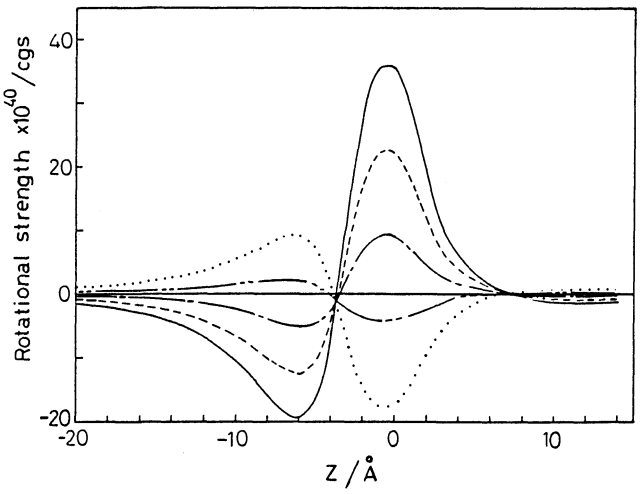

Fig. 2. The dependence of the calculated rotational strengths of α-CDx-HV complex on the Z coordinates (X=Y=0 Å). The directions of the electric transition moment(the angle ϕ) are 0° (——), 30° (----), 45° (-·-·-), 60° (— — —), 90° (·····).

Table 2. Calculated Wavelength (λ) and Oscillator Strength (f) of the Electronic Transitions of Heptylviologen

	θ=0°			θ=22.5°			θ=45°	
Type	λ	f	Type	λ	f	Type	λ	f
	nm			nm			nm	
$A_g \rightarrow B_{1g}$	294	0.00	$A \rightarrow B_1$	290	0.02	$A \rightarrow B_2$	280	0.29
$A_g \rightarrow B_{2u}$	286	0.36	$A \rightarrow B_2$	285	0.34	$A \rightarrow B_1$	279	0.06
$A_g \rightarrow B_{3u}$	266	0.90	$A \rightarrow B_3$	261	0.87	$A \rightarrow B_3$	250	0.75

Z=−6.1 Å) and maximum at ϕ=90° (9.2×10^{-40} cgs at Z=−6.4 Å). As shown in the previous report, methylviologen (1,1′-dimethyl-4,4′-bipyridinium dichloride) does not give ICD, while HV with hydrophobic alkyl chains gives negative ICD (R=-5.7×10^{-40} cgs) at 257 nm. It is suggested that in the case of HV the heptyl chain is included in the cavity of α-CDx and the bipyridinium part is placed outside the cavity.[7] This speculation is compatible with the calculated results shown in Fig. 2. Although there is a possibility that the $A_g\rightarrow B_{2u}$ (or $A\rightarrow B_2$) transition with the short-axis polarization may contribute to the positive rotational strength, the value must be about five times smaller than that due to the $A_g\rightarrow B_{3u}$ (or $A\rightarrow B_3$) transition in view of the results shown in Table 2 and Fig. 2. Consequently, the contribution from the $A_g\rightarrow B_{2u}$ (or $A\rightarrow B_2$) transition seems to be negligible.

Figures 3—5 show the rotational strength calculated with moving the position of the electric transition moment of HV in the X-Y plane, concerning the narrower rim region of α-CDx ($Z\leqq-4$ Å). In these figures, the left-hand figures indicate the rotational strength maps for the α-CDx-HV complex at various ϕ values. The maps are drawn on the rectangular region containing the X and Y-axes, the electric transition moment being parallel to the X-Z plane with a given rotation angle ϕ. The right-hand figures in Figs. 3—5 show the approximate negative ICD region (black region). When Z=−4.0 Å and ϕ=0° (Fig. 3 (a)), the negative region(black) is located in the centre of the map while the positive area (white) is far from the centre. As ϕ increases, the negative region shifts to the surroundings (Fig. 3 (b), (c)) and at last the central area becomes positive at ϕ=90° (Fig. 3 (d)). Similar tendencies are found in the case of Z=−6.0 Å and Z=−8.0 Å (Figs. 4 and 5). The rotational strength maps for Z=−6.0 Å and Z=−8.0 Å are relatively simple and resemble each other, whereas those for Z=−4.0 Å is more complicated (Fig. 3). Although the distribution of the positive area varies with the Z and ϕ values, it can be estimated qualitatively from Figs. 3—5 that the long axis of HV is nearly parallel to the axis of α-CDx, probably $0\leqq\phi<$ ca. 30°, and the centre of HV is not so

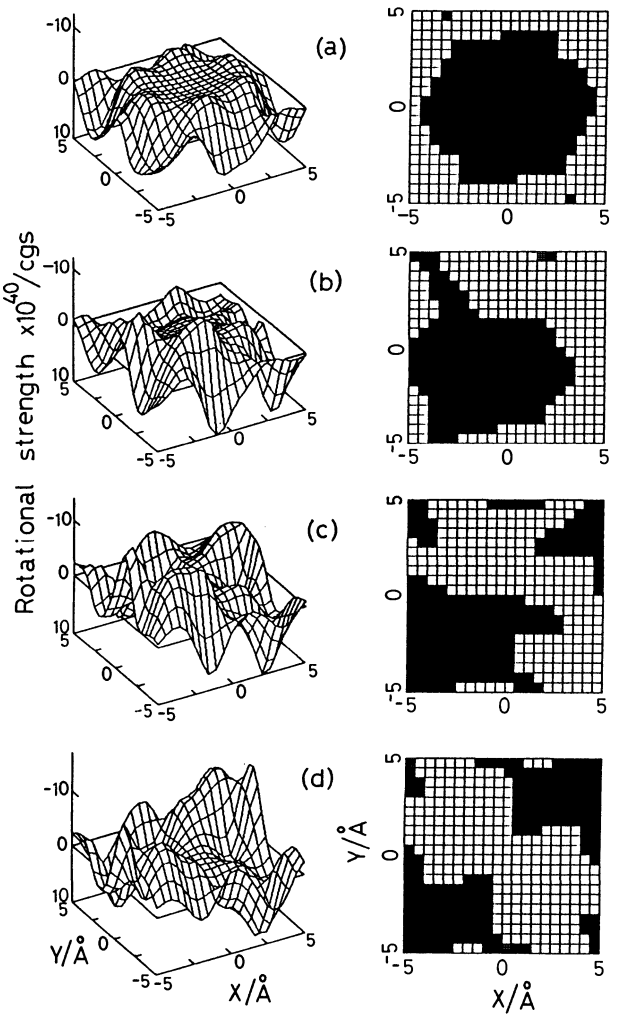

Fig. 3. The rotational strength maps for the α-CDx-HV complex at Z=−4.0 Å. (a) ϕ=0°, (b) ϕ=30°, (c) ϕ=60°, (d) ϕ=90°. The black area of the right-hand figures shows the approximate negative ICD region.

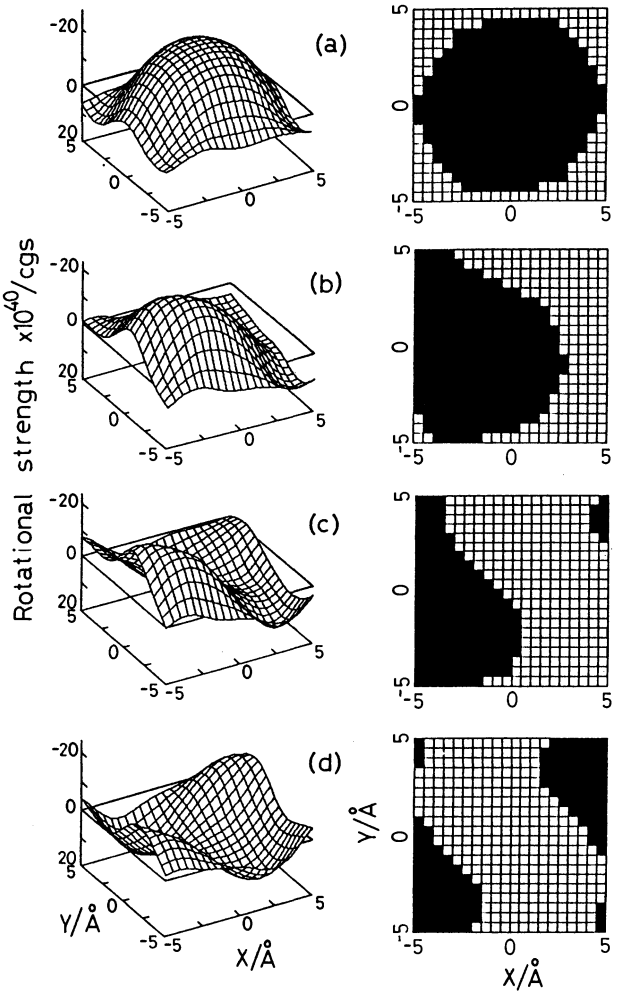

Fig. 4. Same as Fig. 3; Z=−6.0 Å.

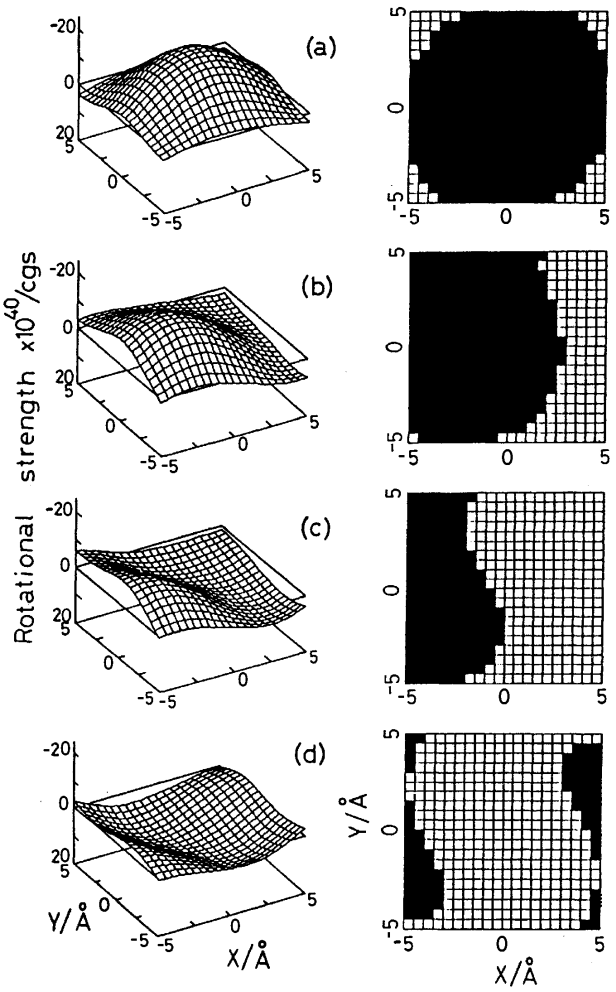

Fig. 5. Same as Fig. 3; Z=−8.0 Å.

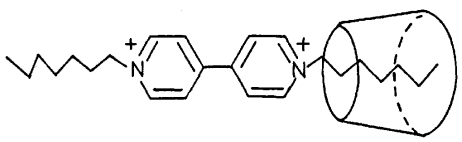

Fig. 6. The schematic drawing of α-CDx-HV complex.

far from the axis of α-CDx, perhaps within 4—5 Å.

From the calculation undertaken in the present study, it can be said qualitatively that when a chromophore is placed outside the cavity of CDx (especially above the narrower rim), the transition with an electric dipole moment nearly parallel to the axis of CDx gives a negative ICD and the transition with perpendicular polarization gives a positive ICD. This rule is quite the reverse of the general rule presented by Harata et al. for the chromophore included in the inner region of β-CDx.[1] The estimated structure of the α-CDx-HV complex is schematically depicted in Fig. 6.

Recently CDx derivatives which bear aromatic groups bound to the primary hydroxyl groups (narrower rim) have been studied by using CD spectra, as models of host-guest phenomena.[17-20] The findings obtained in the present study may be also useful for analyzing such CDx derivatives.

The authors wish to thank Dr. Kazutoshi Tanabe, National Chemical Laboratory for Industry, for his kind supply of the CNDO/S-CI program.

References

1) K. Harata and H. Uedaira, *Bull. Chem. Soc. Jpn.*, **48**, 375 (1975).
2) H. Shimizu, A. Kaito, and M. Hatano, *Bull. Chem. Soc. Jpn.*, **52**, 2678 (1979).
3) H. Shimizu, A. Kaito, and M. Hatano, *Bull. Chem. Soc. Jpn.*, **54**, 513 (1981).
4) H. Shimizu, A. Kaito, and M. Hatano, *J. Am. Chem. Soc.*, **104**, 7059 (1982).
5) N. Kobayashi, *J. Chem. Soc., Chem. Commun.*, **1988**, 918.
6) H. Yamaguchi, M. Higashi, and M. Oda, *Spectrochim. Acta*, **44A**, 547 (1988).
7) M. Kodaka and T. Fukaya, *Bull. Chem. Soc. Jpn.*, **59**, 2032 (1986).
8) I. Tinoco, Jr., *Adv. Chem. Phys.*, **4**, 113 (1962).
9) C. G. Le Fèvre and R. J. W. Le Fèvre *J. Chem. Soc.*, **1956**, 3549.
10) R. J. W. Le Fèvre, A. Sundaram, and R. K. Pierens, *J. Chem. Soc.*, **1963**, 479.
11) A. Hybl, R. E. Rundle, and D. E. Williams, *J. Am. Chem. Soc.*, **87**, 2779 (1965).
12) C. G. Le Fèvre and R. J. W. Le Fèvre, *Chem. Ind.*, **1955**, 1121.
13) O. Bastiansen and M. Treatterberg, *Tetrahedron*, **17**, 147 (1962).
14) A. Almenningen and O. Bastiansen, *K. Nor. Vidensk. Selsk. Skr.*, **1958**, 4.
15) J. Trotter, *Acta Crystallogr.*, **14**, 1135 (1961).
16) H. Suzuki, *Bull. Chem. Soc. Jpn.*, **32**, 1350 (1959).
17) A. Ueno, I. Suzuki, and T. Osa, *Chem. Pharm. Bull.*, **35**, 2151 (1987).
18) A. Ueno, F. Moriwaki, T. Osa, F. Hamada, and K. Murai, *Chem. Pharm. Bull.*, **34**, 438 (1986).
19) A. Ueno, F. Moriwaki, T. Matsue, and T. Osa, *Makromol. Chem., Rapid Commun.*, **6**, 231 (1985).
20) A. Ueno, F. Moriwaki, T. Osa, F. Hamada, and K. Murai, *J. Am. Chem. Soc.*, **110**, 4323 (1988).

Cyclohepta[*b*][1,4]benzothiazines and Their Diazine Analogues. 2. Formation and Properties of Cyclohepta[*b*]quinoxalines[1,2]

Kimio SHINDO,* Sumio ISHIKAWA, and Tetsuo NOZOE*,†
Department of Chemistry, Faculty of Science, Josai University, 1-1 Keyakidai, Sakado-shi, Saitama-ken 350-02
†Tokyo Research Laboratories, Kao Corporation, 2-1-3 Bunka, Sumida-ku, Tokyo 131
(Received October 17, 1988)

2-Chloro- or 2-methoxytropone reacts with *o*-phenylenediamine to give 2-(*o*-aminoanilino)tropone, which upon heating provides 6*H*-cyclohepta[*b*]quinoxaline (**10a**). Upon acidification, **10a** reversibly gives a green cation, **9a**. **10a** is easily converted, especially under basic conditions, into the oxidative dimer **16a**, which reproduces **9a** by reduction with Zn in acetic acid. The isopropyl derivatives of these compounds are prepared by the same method from 5-isopropyl-2-methoxytropone. The 5-methyl (**21a**) and 5,11-dimethyl derivatives **23** are made by the reaction of 2-chloro- or 2-methoxytropone with *N*-methyl- and *N,N'*-dimethyl-*o*-phenylenediamines. However, the methylation of **21a** with methyl fluorosulfate affords 5,11-dihydro-8,11-dimethyl-6*H*-cyclohepta[*b*]quinoxaline-5,6-sultone. H_2O_2 oxidation of **10a** mainly gives **16a** in addition to a small quantity of 6*H*-cyclohepta[*b*]quinoxalin-6-one. Compound **21a** is stable under basic conditions, but **23** rearranges under alkaline conditions to give, among other unidentified products, *N*-methyl-*N*-[*o*-(methylamino)phenyl]benzamide and 5,10-dihydro-5,10-dimethyl-2-phenazinecarbaldehyde. Reactions of title compounds with alkali and hydrogen peroxide are compared with those of *O*- and *S*-analogues.

One of the authors (T.N.) and his co-workers reported about thirty years ago that reactions of 5-nitroso- and 5-arylazotropolone (**1a,b**) with *o*-phenylenediamine (**2a**) gave quinoxaline derivatives (**3a,b**), which were considered to have quinonoid structures.[3] They subsequently found[4] that the reactions of 2-chloro- and 2-methoxytropone (**4a,b**) with **2a** afforded pale-violet crystals **A**, which, on catalytic reduction, produced **6a** and **7a** almost quantitatively.[4,5] They presumed that **A** was 5*H*-cyclohepta[*b*]quinoxaline (**5a**), which they named "benzo[*b*]tropazine."[4] However, they could not determine the position of the H-atom of **5a,b**, because NMR spectroscopy was not available at that time. Furthermore, they found that the reaction of 3-carboxytropolone (**4c**) with *o*-phenylenediamine (**2a**) and its methyl homologue (**2b**) produced **A** and its methyl derivative **B**, respectively. The former gave **6a** and **7a**, and the latter afforded their respective methyl derivatives (**6b** and **7b**) upon catalytic reduction. They attempted to purify the colored

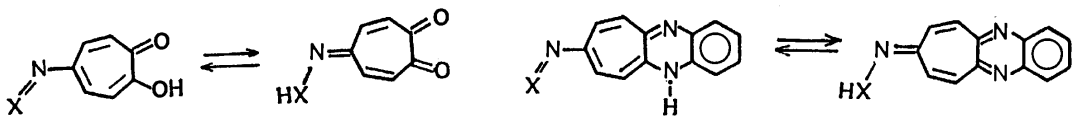

1a : X=O
b : X=NAr

3a : X=O
b : X=NAr

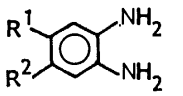

2	R^1	R^2
a	H	H
b	Me	H
c	Me	Me

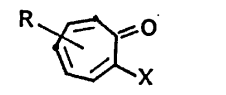

4	X	R
a	Cl	H
b	OMe	H
c	OH	3-COOH
d	OMe	5-i-Pr

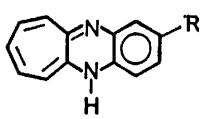

5a : R=H
b : R=Me

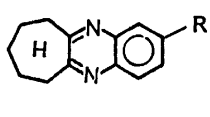

6a : R=H
b : R=Me

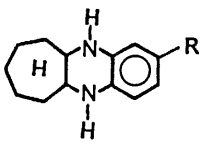

7a : R=H
b : R=Me

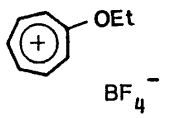

8

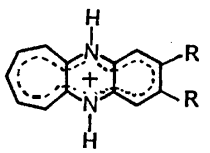

9a : R=H
c : R=Me

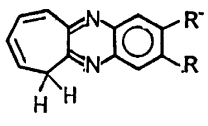

10a : R=H
c : R=Me

product **A** by using an alumina column chromatography and obtained colorless crystals **C** that were sparingly soluble in the usual organic solvents. They then considered that **C** was pure "benzo[*b*]tropazine" (**5a**).

In 1971, Fukunaga reported[5] that the reaction of ethoxytropylium tetrafluoroborate (**8**) with *o*-phenylenediamine (**2a**) and its dimethyl derivative (**2c**) gave greenish-black crystals **9a,c**, which upon basification produced neutral species **10a,c** that reverted to **9a,c** quantitatively upon acidification.[5] He believed that the structure of **10** was the quinoxaline form, and **9** existed as a resonance-stabilized (aromatic) peripheral 16 π electron system on the evidence of detailed NMR studies. He also recognized that **10** was easily dimerized oxidatively during alumina chromatography and suggested that the colorless product **C** obtained by Nozoe[4] was an oxidative dimer derived from **10a**; however, its structure was not studied.[5]

Recently, we reported in detail on cyclohepta[*b*]-[1,4]benzoxazine (**11**)[6] and its *S*-analogue (**12**);[7] we also reexamined previous studies on "benzo[*b*]tropazine"[4] because before-mentioned Fukunaga's research[5] has remained unpublished. In this report we wish to describe the detailed study on reactions of the reactive troponoids **4a,b,d** with *o*-phenylenediamine (**2a**) and its derivatives (**20a,b**).

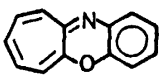

11

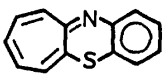

12

Results and Discussion

We first observed the reaction of **4a** with **2a** in EtOH by using time-dependent HPLC by the same method as in the case of the *S*-analogues.[8] It was found that

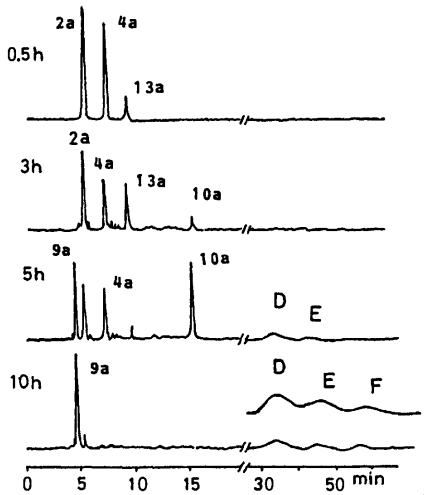

Fig. 1. Time-dependent HPLC chromatograms of the reaction mixture of **4a** with **2a** in EtOH at 80 °C.

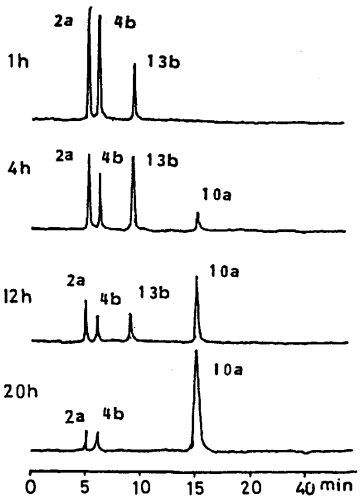

Fig. 2. Time-dependent HPLC chromatograms of the reaction mixture of **4b** with **2a** in EtOH at 80 °C.

2-(*o*-aminoanilino)tropone (**13a**) formed at an early stage of the reaction was gradually transformed into **10a** and highly polar **9a**. Finally, **13a** and **10a** almost disappeared; in addition to the main peak of polar **9a**, broad peaks with retention time (RT) 32 min (**D**), 44 min (**E**), and 57 min (**F**) appeared (see Fig. 1).

A similar reaction of **4b** with **2a** under nitrogen looked very simple chromatographically, giving **13a** and **10a** in good yields without the formation of **9a** and **D**, **E** (Fig. 2).

Compound **13a**, obtained as yellow needles, mp 183 °C, by the reaction of **4b** with **2a** in a sealed tube at 80 °C, was identified as 2-(*o*-aminoanilino)tropone on the basis of its IR, UV, NMR, and mass spectra, as well as elemental analysis; for assignments of the spectral signals, see the Experimental section. Upon further heating at 120 °C in a sealed tube, **13a** gave the dehydrated product as pale-yellow needles mp 69 °C, *m/z* 194 (M^+). This product was confirmed spectroscopically to exist in the quinoxaline form **10a**;[5] a methylene proton signal appeared at δ 3.59 (NMR), NH absorption was not seen in the IR and NMR spectra, and there was no absorption in the visible region.

Although the exitence of the tautomeric form **5a** ("benzo[*b*]tropazine") could not be detected spectroscopically, upon treatment of **10a** with MeOH-d_4 and a small amount of triethylamine at 40 °C, the H_2-6 signal gradually disappeared, presumably giving rise to the formation of deuterio compound **14** via "enamine" form **5a**.

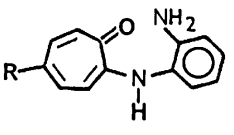

13a: R=H
b: R=i-Pr

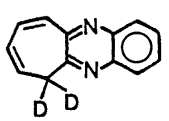

14

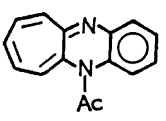

15

When **10a** (RT, 15 min) was heated in acetic anhydride containing a small amount of 1,4-diazabicyclo-[2.2.2]octane (Dabco) under nitrogen, we could observe (in the HPLC diagram) a new peak (RT, 12 min), having UV absorption maxima at 225, 253, and 385 nm and *m/z* 236 (M^+) corresponding to the *N*-acetyl derivative **15**; the exact structure of **15**, however, could not be confirmed because of its instability.

On acidification of both **13a** and **10a** were converted into a dark-green salt **9a**, which showed considerably long-wavelength absorption bands at 564, 616, 670, and 752 nm (log ε 3.01, 2.91, 2.83, and 2.34), in addition to the three intense absorption bands (449, 464, and 491 nm) in the visible region (Fig. 3). The ^{1}H NMR spectrum of **9a** consisted of five 2H signals and a 1H signal (at δ 6.04, t, *J*=9.5 Hz, H-8), indicating a symmetric structure. Neutralizing of **9a** with alkali under nitrogen gave **10a** quantitatively, however, an oxidative dimeric product **16a** was gradually formed by the same treatment under aerobic conditions. Compound **16a** was also formed when **10a** was passed through an alumina column[5] or underwent heating in EtOH (in this case, giving rise to two other products **E** and **F**, presumably oxidative oligomers of **10a** as well.) When **9a** and **10a** were (separately) treated with a base in open air, the former produced **16a** much faster than the latter, suggesting that **16a** was formed by the dimerization of radical **17**, that may be more readily derived from the diazinium form **9a** than from the 6*H*-cyclohepta[*b*]quinoxaline form **10a** (Scheme 1). Compound **16a** showed a UV spectrum similar to that of **10a**. The ^{1}H NMR spectrum of **16a** closely resembled that of **10a**, with the exception of the presence of a methine proton signal at δ 4.59 (instead of the H_2-6 signal of **10a** at δ 3.59), indicating also a symmetric structure. In the mass spectrum there are no fragment peaks between *m/z* 386 (M^+) and *m/z* 193 (M^+−193); we could therefore conclude that **16a** is the dehydro dimer (2H less in mass) of **10a**. Reduction of **16a** with Zn in AcOH was found to reproduce **9a** quantitatively. Heating of **16a** at 220 °C under vacuum gave **10a** and a reddish-brown substance, the latter being presumed a fulvalene derivative **19** on the basis of mass spectrometry [*m/z* 384 (M^+)] and UV spectrum; carbene **18** formed by disproportionation of radical **17** is suggested as the most likely intermediate to give **19** (Scheme 1). From the experimental evidence described so far, we now consider that colorless crystals **C**[4] must have been the dimer **16a**, as speculated by Fukunaga.[5] Further, the soluble, slightly colored substace used for the catalytic reduction[4] to give **6a** and **7a** was in fact pure **10a**, because our experimental results appear to be compatible with the Fukunaga's structures **9a** and **10a**[5] (except for their electronic structure).[9]

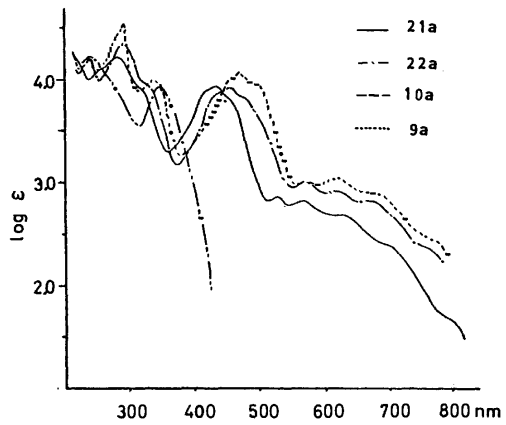

Fig. 3. Electronic spectra of some cyclohepta[*b*]quinoxalines in MeOH.

To make sure the characteristics of cyclohepta[*b*]-quinoxaline system, we also studied the isopropyl derivatives (**9b** and **10b**) prepared from 5-isopropyl-2-methoxytropone (**4d**) and **2a**, and we obtained a similar dimer **16b** reversibly from **9b**, as illustrated in Scheme 2.

We then tried to synthesize the *N*-methyl derivative **21a** (of **5a**), which can not take the tautomeric, qui-

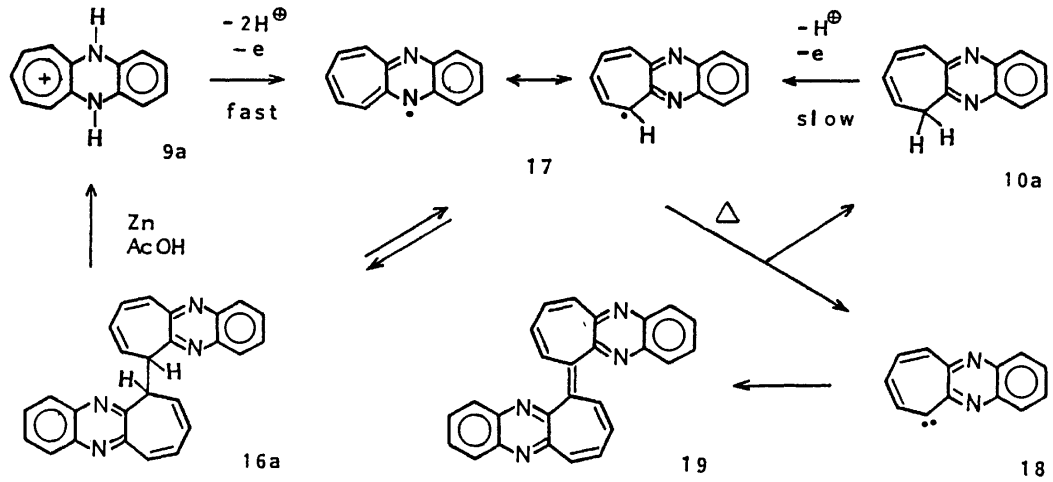

Scheme 1.

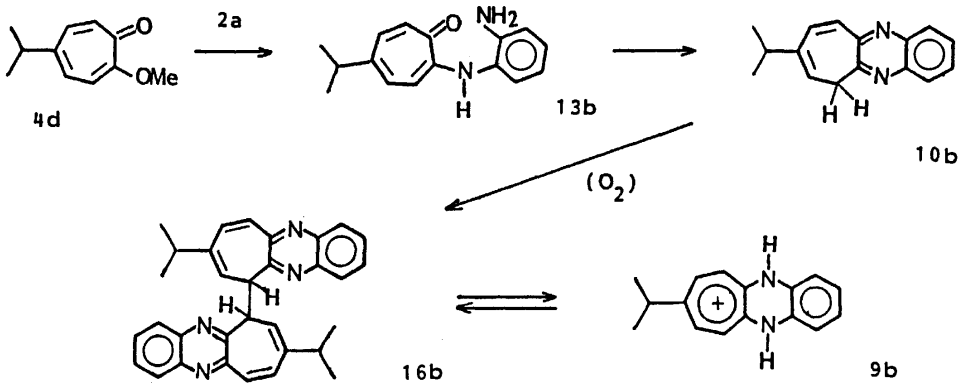

Scheme 2.

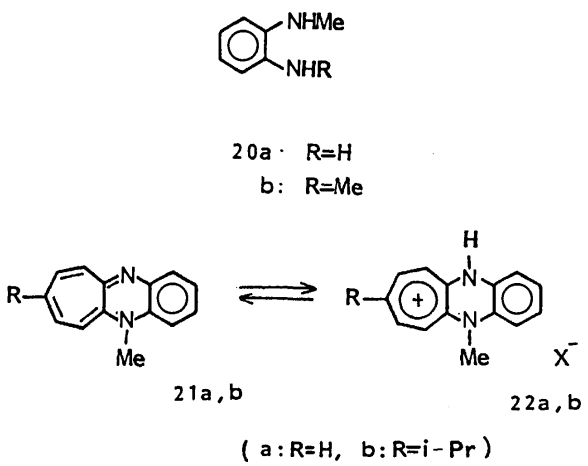

noxalo form, in order to compare its properties with those of the *O*- and *S*-analogues (**11**, **12**). Thus, *N*-methyl-5*H*-cyclohepta[*b*]quinoxaline (**21a**) was obtained as green needles having a low melting point (mp 68 °C), by the reaction of **4b** with *N*-methyl-*o*-phenylenediamine (**20a**). The structure of **21a** was established on the basis of the spectral data. It showed ^{1}H NMR signals at δ 2.67 (*N*-methyl), and at δ 4.47 (H-6) and 6.24 (H-4) due to two peri-protons; these were assigned on the basis of NOE experiment. It is worth noticing that the free *N*-methyl compound **21a** and its protonated cation **22a** have the same deep green color and are similar to **9a** in terms of the UV/VIS and ^{1}H NMR spectra, indicating that these compounds have a similar π-electron system.[9] We also prepared 8-isopropyl compound **21b** and its salt **22b** from methyl ether of γ-thujaplicin (5-isopropyltropolone).

N,N'-Dimethyl cation (**23**) was obtained as dark-greenish needles (chloride and BF_4^- salts) by heating **4a** or **4b** with *N,N'*-dimethyl-*o*-phenylenediamine (**20b**) at 120 °C in the presence of acid.[2] The long-wavelength absorptions at 578, 620, and 732 nm (log ε 3.07, 3.05, and 2.56) of **23** in MeOH are similar to those of **9a** and **22a** (Fig. 3). These bands disappear in alkali and exhibit only UV maxima of an unidentified conjugate base at 230, 250, 280, and 354 nm (they are restored upon acidification). The symmetrical structure of **23** was confirmed by the NMR spectrum, which showed two methyl signals at δ 3.10 (well-resolved), three signals at δ 6.25, 6.57, and 7.24 (ratio 2 : 1 : 2) due to the seven-membered ring protons, and signals of A_2 B_2 type at δ 6.71 and 6.95 due to benzene ring protons.

We then attempted to obtain compound **23** by the treatment of **21a** with "magic methyl," which, however, resulted in the formation of green needles **24**, mp 127—128.5 °C, which had a molecular composition of $C_{15}H_{14}N_2O_3S$ (gaining a methyl and an SO_3 groups) and showed characteristic IR absorptions (KBr) at 1340 and 1160 cm^{-1} (-SO_2-). This product exhibited visible absorption at 616, 676, and 680 nm in MeOH, but in hexane the longest-wavelength absorption was at 434 nm; the absorption maxima in MeOH shifted to slightly longer wavelengths in the presence of acid. ^{1}H NMR signals in benzene-d_6 appeared at δ 1.63 and 3.29 due to two methyl protons and at δ 3.33 due to a methine proton in addition to seven olefinic proton signals, thus showing that **24** would preferably exist in the form of the intramolecular conjugate base form, 5,10-dihydro-8,11-dimethyl-6*H*-cyclohepta[*b*]quinoxaline-5,6-sultone (**24b**) in nonpolar aprotic solvent. However, the H-6, H-1, and Me-8 proton signals of **24** shifted downfield (1 ppm) in CD_3CN from those in benzene-d_6 and the spectral pattern became rather similar to that of **21a**, thus indicating that **24** is more likely to exist in another tautomeric form **24a** predominantly in a polar solvent and in a solid as well. On the other hand, in acidic methanol, the spectrum of **24b** closely resembled those of cyclohepta[*b*]quinoxalinium salts **9a** and **22**, suggesting the cationic form **24c** in acid. It should be noted that methylation with magic methyl takes place at the seven-membered ring of **21a** to give **24**; this differs from the case of methylation of *O*- and *S*-analogues (**11** and **12**) with magic methyl,[8] and also from the result of methylation of **21a** with methyl iodide.[10] Although the mechanism of this unusual reaction has not been clarified yet, one of the possible pathways is shown in Scheme 3.

A comparison is now made between the reactivities of 5*H*-cyclohepta[*b*]quinoxaline (**21** and **23**) and those of *O*- and *S*-analogues (**11** and **12**) and their respective

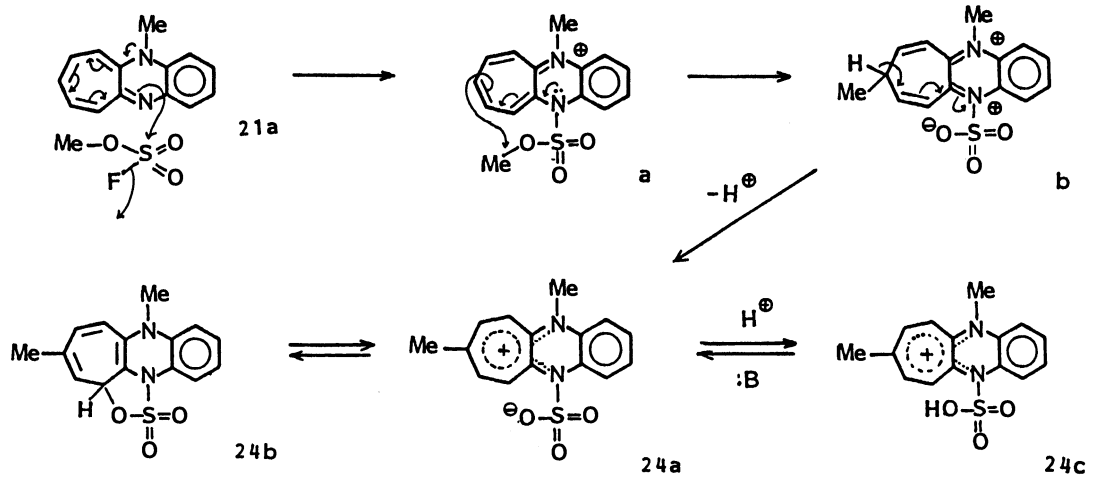

Scheme 3.

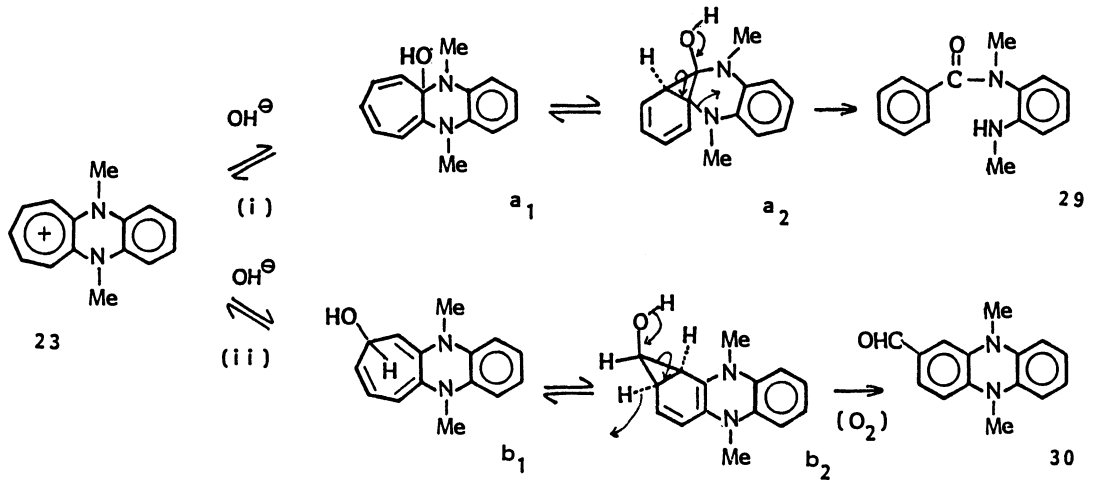

Scheme 4.

N-methylated cations (**25** and **26**). Facile ring opening by alkali and ring closure by acid is one of the characteristics of cyclohepta[*b*][1,4]benzoxazine **11** and its derivatives.[6] In paticular, *N*-methyl derivative **25** is readily saponified to 2-(*N*-methyl-*o*-hydroxyanilino)-tropone **27** (even with water at room temperature), by the attack of hydroxide ion at C-5a. Although *S*-analogue **12** is stable to warm alkali, its *N*-methyl

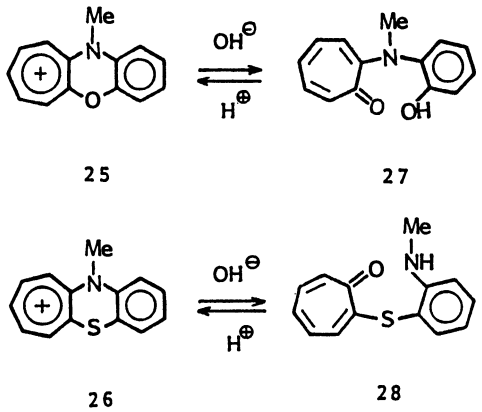

cation **26** is saponified with cold alkali to give 2-[*o*-(methylamino)phenylthio]tropone **28** by an attack of the hydroxide ion at C-10a.[8]

On the contrary, 5-methyl-5*H*-cyclohepta[*b*]quinoxaline **21a** is quite stable to warm alkali, whereas its *N*,*N*′-dimethyl cation **23a** give a colorless conjugate base by dilute alkali, but is restored to **23a** upon acidification. When a methanolic solution of **23a** containing 5 equiv of sodium hydroxide was allowed to stand overnight at room temperature, various products were formed (accompanied by autoxidation), from which a 6.5% yield of 5,10-dihydro-5,10-dimethyl-2-phenazinecarbaldehyde (**30**)[12] and 11% of benzamide **29** were isolated. Possible pathways for the formation of these compounds are shown in Scheme 4. It is considered that in path (i), intermediate a_1, produced by the attack of a hydroxide anion at C-5 of **23**, gives **29** via norcaradiene a_2 as illustrated in the scheme, whereas in path (ii) intermediate b_1, produced by the attack of a hydroxide anion at C-7, aromatizes to **30** via b_2 by autoxidation. In concentrated methanolic alkali, however, **23** rearranges to benzamide **29** in 89% yield.

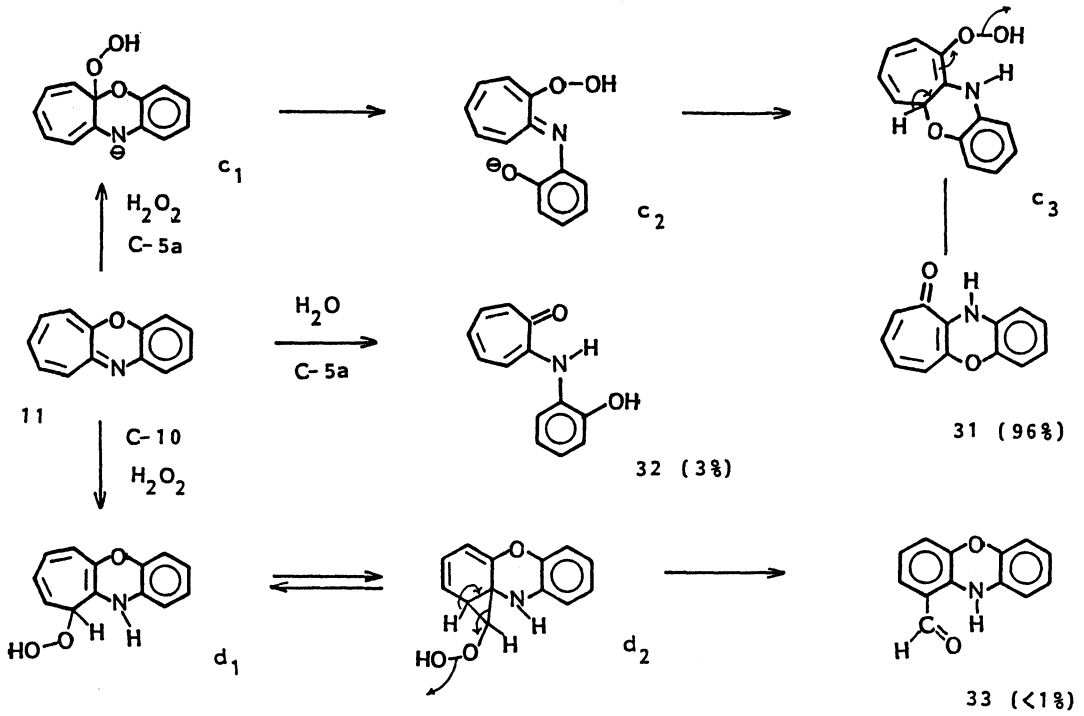

Scheme 5.

We then examined the reaction of **10a** (or **9a**) with hydrogen peroxide for a comparison with the behavior of the H_2O_2 to *O*- and *S*-analogues (**11**,[6] **12**[7,8]). Our previous findings may be summerized as follows: (1) Treatment of *O*-analogue **11** with H_2O_2 in MeOH gave almost exclusively (96%) cyclohepta[*b*][1,4]benzoxazin-10(11*H*)-one (**31**) and 2—3% of the hydrolyzed product **32**, along with a small proportion (<1%) of 1-formyl-10*H*-phenoxazine (**33**); for the reaction pathways, see Scheme 5. (2) The *S*-analogue **12** reacted[8] with H_2O_2 in MeOH slightly more slowly than **11**, producing many kinds of rearranged products, 10*H*-phenothiazine (**34**), its 1- and 3-formyl derivatives (**35**, **36**).

On the other hand, oxidation of **10a** with H_2O_2 in acetic acid gave mainly the dehydro dimer **16a** mentioned above and a small quantity of **E**, **F**, and 6*H*-cyclohepta[*b*]quinoxalin-6-one (**37**).[13] Compound **21a** is stable under basic conditions and also to H_2O_2 in MeOH at room temperature; upon heating at 60 °C, however, it was gradually oxidized to a complex mixture of products. One of them was separated as a reddish oil, which was identified spectroscopically as 10-methyl-2(10*H*)-phenazinone (**39**).[14] It was considered that **39** was formed by the oxidation of 5,10-dihydro-5-methylphenazine (**38**), derived from an oxidative rearrangement of **21a**, because phenothiazines usually form quinone derivatives upon radical oxidation.[15]

It is interesting to note that cyclohepta[*b*][1,4]benzoxazine (**11**), its *S*-analogue **12**, and *N*-analogues **10**, **21** have considerable different chemical properties. These compounds can be regarded as π-excessive heteroaromatics[16] fused with benzene and cycloheptatriene rings. Therefore, the diversity of these reactivities could be explained in terms of the electronegativity and porarizability of the hetero atoms as well as the nature of the attaching reagents. However, detailed studies (including theoretical calculations) on the π-electron system of cyclohepta[*b*]quinoxalines and those *O*- and *S*-analogues in relation to their chemical properties are currently in progress, and the results will be reported in a future paper.[17]

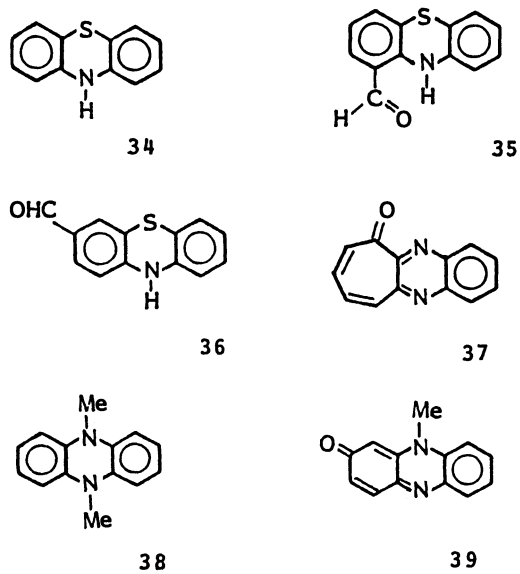

Experimental

Melting points were determined with a Yanagimoto MP-

3S apparatus and are uncorrected. The IR spectra were taken on a Shimadzu IR-400 or IR-450, and the UV spectra were recorded with a Shimadzu UV-202 or a Hitachi 557 spectrometer. The NMR spectra were recorded with JEOL JNM-PS100 (100-MHz) and GX270 (270-MHz) spectrometers using TMS as the internal standard. The mass spectra were taken on Shimadzu LKB9000 and JEOL JMS-01SG mass spectrometers. The HPLC was carried out on Hitachi gel #3011 with MeOH–hexane (9 : 1) as the solvent. The UV spectra in acid and alkali were taken after adding a drop of 3 M HCl or 3 M NaOH (1 M=1 mol dm^{-3}) to the sample solution. TLC analyses were carried out with Merck Kieselgel 60F-254 and Aluminium oxide F-254 plates.

Reaction of 2-Methoxytropone (4b) with *o*-Phenylenediamine (2a). A solution of **4b** (250 mg, 1.84 mmol) and **2a** (240 mg, 2.22 mmol) in EtOH (5 cm^3) was heated in a sealed tube for 6 h at 80 °C and then the solution was set aside at room temperature, depositing crystals after several hours. The precipitates were filtered off, giving **13a** (238 mg, 61%, combined with second crop). Compound **10a** (37 mg, 10%) and unreacted **4b** (56 mg, 22%) were isolated by preparative HPLC.

Heating of an ethanolic solution of **13a** in a sealed tube at 120 °C for 6 h gave a quantitative yield of **10a**.

2-(*o*-Aminophenylamino)tropone (13a): Yellow needles (from EtOH), mp 183—183.5 °C; UV (MeOH) λ_{max} 235, 338, and 401 nm (log ε 4.45, 4.00, and 4.10), (MeOH+HCl) 236, 280, 289, 333, 345, 439, 464, and 490 nm (log ε 4.22, 4.41, 4.52, 3.95, 3.92, 3.92, 4.04, and 3.90); IR (KBr) 3460, 3320 (NH_2), 3240 (NH), and 1620 cm^{-1} (C=O); ^{1}H NMR ($CDCl_3$) δ=3.75 (2H, br, NH_2), 6.64 (1H, dd, J=10.3 and 1.0 Hz, H-7), 6.75—7.46 (9H, m, ar-H), and 8.33 (1H, br, NH); MS, m/z 212 (M^+).

Anal. ($C_{13}H_{12}N_2O$) C, H, N.

***6H*-Cyclohepta[*b*]quinoxaline (10a):** Pale yellow needles (from $CHCl_3$); mp 68—69 °C; UV (MeOH) λ_{max} 235, 243, and 342 nm (log ε 4.21, 4.21, and 3.94), (MeOH+HCl) 238, 280, 289, 333, 345, 449, 464, and 491 nm (log ε 4.21, 4.34, 4.42, 3.92, 3.90, 3.79, 3.91, and 3.79), (MeOH+NaOH) 231, 247, 270, 349, and 392 nm (log ε 4.27, 4.26, 4.17, 3.94, and 3.48); ^{1}H NMR (CD_3 CN) δ=3.59 (2H, d, J=5.8 Hz, CH_2), 6.08 (1H, dt, J=10.3 and 5.8 Hz, H-7), 6.28 (1H, dd, J=10.3 and 5.3 Hz, H-8), 6.80 (1H, dd, J=11.7 and 5.3 Hz, H-9), 7.71 (2H, m, H-2,3), 7.28 (1H, d, J=11.7 Hz, H-10) and 8.05 (2H, m, H-1,4); MS, m/z 194 (M^+).

Anal. ($C_{13}H_{10}N_2$) C, H, N.

Reaction of 5-Isopropyl-2-methoxytropone (4d) with 2a. Reaction of **4d** (200 mg, 1.12 mmol) with **2a** (145 mg, 1.34 mmol) as described above gave **13b** (153 mg, 54%), **10b** (18 mg, 7%) and unreacted **4d** (54 mg, 27%).

Heating of **13b** (100 mg, 0.39 mmol) as described for **13a** (see above) gave **10b** (73 mg, 79%) and unreacted **13b** (27 mg, 27%).

2-(*o*-Aminoanilino)-5-isopropyltropone (13b): Yellow needles (from EtOH); mp 155—156 °C; UV (MeOH) λ_{max} 236, 341, and 405 nm (MeOH+HCl) 236, 283, 291, 334, 347, 448, 471, and 500 nm; ^{1}H NMR ($CDCl_3$) δ=1.20 (6H, d, J=6.8 Hz, $2CH_3$), 2.79 (1H, sept, J=6.8 Hz, CH), 3.77 (2H, br, NH_2), 6.57 (1H, d, J=10.3 Hz, H-7), 6.78—7.28 (7H, m, ar-H), and 8.14 (1H, br, NH); MS, m/z 254 (M^+).

Anal. ($C_{16}H_{18}N_2O$) C, H, N.

8-Isopropyl-6*H*-cyclohepta[*b*]quinoxaline (10b): Pale yellow oil; UV (MeOH) λ_{max} 213, 247, and 340 nm (MeOH+HCl) 215, 249, 292, 340, and 468 nm ; ^{1}H NMR ($CDCl_3$) δ=1.05 (6H, d, J=6.8 Hz, $2CH_3$), 2.48 (1H, sept, J=6.8 Hz, CH), 3.51 (2H, d, J=6.3 Hz, CH_2), 5.81 (1H, t, J=6.3 Hz, H-7), 7.72 (1H, d, J=12.2 Hz, H-9), 7.71 (2H, m, H-2,3), 7.80 (1H, d, J=12.2 Hz, H-10), and 8.03 (2H, m, H-1,4); MS, m/z 236 (M^+).

Anal. ($C_{16}H_{16}N_2$) C, H, N.

***5H*-Cyclohepta[*b*]quinoxalinium Salts (9a).** A solution of **10a** (100 mg, 0.52 mmol) in EtOH (2 cm^3) was treated with various acids (1 : 2); the mixture was set aside at room temperature, depositing crystals. The precipitates were filtered off, giving **9a** (BF_4^- salt, 121 mg, 85%) as dark green needles. BF_4^- salt: mp 227.2—229 °C; UV (MeOH) λ_{max} 236, 279sh, 289, 331, 445, 449sh, 464, and 481sh (log ε 4.16, 4.37, 4.46, 3.89, 3.84, 3.96, 4.00, and 3.94), (MeOH+NaOH) 231, 246, 347, and 391 (log ε 4.24, 4.22, 3.85, and 3.31); ^{1}H NMR (CD_3CN) δ=5.68 (2H, d, J=11.2 Hz, H-6,10), 6.04 (1H, t, J=9.5 Hz, H-8), 6.14 (2H, m, H-1,4), 6.52 (2H, m, H-2,3), 6.62 (2H, dd, J=11.2 and 9.5 Hz, H-7,9), and 7.95 (2H, br, NH).

Anal. ($C_{13}H_{11}N_2BF_4$) C, H, N.

ClO_4^- salt: mp 227—228.5 °C. CF_3COO^- salt: mp 198—199 °C. Br^- salt: mp 300 °C. Cl^- salt: mp 190—190.5 °C.

8-Isopropyl-5*H*-cyclohepta[*b*]quinoxalinium Salts (9b). Treatment of **10b** (50 mg, 0.21 mmol) with acid (as described above) gave **9b** (BF_4^- salt, 57 mg, 83%) as dark green needles. BF_4^- salt: mp 237—238 °C; UV (MeOH) λ_{max} 236, 283, 291, 338, 347, 446, 470, and 500 nm (log ε 4.18, 4.35, 4.48, 3.91, 3.83, 3.96, 4.04, and 3.87), (MeOH+NaOH) 245 and 341 nm (log ε 4.29 and 3.85); ^{1}H NMR (CD_3CN) δ=1.10 (6H, d, J=6.8 Hz, $2CH_3$), 2.39 (1H, m, J=6.8 Hz, CH), 5.71 (2H, d, J=11.5 Hz, H-6,10), 6.10 (2H, m, H-1,4), 6.48 (2H, m, H-2,3), 6.64 (2H, J=11.5 Hz, H-7,9), and 7.75 (2H, br, NH).

Found: C, 58.97; H, 5.51; N, 8.43%. Calcd for $C_{16}H_{17}N_2BF_4$: C, 59.29; H, 5.29; N, 8.64%.

ClO_4^- salt: mp 289—290 °C.

6,6′-Bi-6*H*-cyclohepta[*b*]quinoxaline (16a): Aqueous $NaHCO_3$ was slowly added to a suspension of **9a** (BF_4^- salt, 100 mg, 0.35 mmol) in EtOH (1 cm^3); the mixture was allowed to stand overnight exposed to air. The precipitates were filtered off and extracted with $CHCl_3$. The extracts were combined with the precipitates and purified by preparative HPLC, giving **16a** (57 mg, 84%, RT 32 min) as colorless plates: mp 193.5—194.5 °C (from $CHCl_3$); UV (MeOH) λ_{max} 215, 233, and 338 nm; ^{1}H NMR (270 MHz in $CDCl_3$) δ=4.59 (2H, br, H-6,6′), 6.20 (2H, d, J=10.2 Hz, H-7,7′), 6.43 (2H, dd, J=10.2 and 5.1 Hz, H-8,8′), 7.02 (1H, dd, J=11.7 and 5.1 Hz, H-9,9′), 7.40 (2H, t, J=8.1 Hz, H-3,3′ or 2,2′), 7.49 (2H, d, J=8.1 Hz, H-4,4′ or 1,1′), 7.53 (2H, t, J=8.1 Hz, H-2,2′ or 3,3′), 7.54 (2H, d, J=11.7 Hz, H-10,10′), and 7.96 (2H, d, J=8.1 Hz, H-1,1′ or 4,4′); MS, m/z 386 (M^+, 7), 294 (58), 193 (100), and 192 (30).

Anal. ($C_{26}H_{18}N_4$) C, H, N.

6,6′-Bicycloheptiden[*b*]quinoxaline (19): Heating of **16a** of 220 °C in vacuo in a sealed tube gave **10a** and **19** (observed by HPLC). **19**: reddish brown needles, mp 300 °C decomp.; MS m/z 384 (M^+, 100), 193 (6), and 191 (23); UV (Hexane-MeOH) λ_{max} 217, 249, 349, and 404 nm.

8,8′-Diisopropyl-6,6′-bi-6*H*-cyclohepta[*b*]quinoxaline (16b). Treatment of **9b** (BF_4^- salt, 50 mg, 0.15 mmol) with alkali (as described above) gave **16b** (27 mg, 74%) as pale yellow needles: mp 134—135 °C; UV (MeOH) λ_{max} 220, 244, and 336 nm; ^{1}H NMR ($CDCl_3$) δ=1.08 (6H, d, J=6.8 Hz, $2CH_3$), 1.13 (6H, d, J=6.8 Hz, $2CH_3$), 2.59 (2H, m, J=6.8 Hz, CH), 4.50 (2H, br, H-6,6′), 5.88 (2H, br, H-7,7′), 7.00 (2H, d,

J=11.7 Hz, H-9,9'), 7.39—7.61 (8H), and 7.91—8.01 (2H); MS, m/z 470 (M^+).

Anal. ($C_{32}H_{30}N_4$) C, H, N.

5-Methyl-5*H*-cyclohepta[*b*]quinoxaline (21a). A solution of **4b** (224 mg, 1.65 mmol) and *N*-methyl-*o*-phenylenediamine (**20a**) (251 mg, 2.06 mmol) in EtOH (2 cm^3) was heated in a sealed tube for 24 h at 120 °C. After removing the solvent, the residue was taken in a small amount of $CHCl_3$ and chromatographed on silica-gel thin-layer plates with acetonitrile as the eluant, giving **21a** (237 mg, 69%) as dark green needles along with unreacted **4b** (16 mg, 7%) : mp 68 °C; UV (MeOH) λ_{max} 229, 274, 324, 429, 458, 525, 568, 630, and 696 nm (log ε 4.09, 4.22, 3.87, 3.98, 3.75, 2.62, 2.61, 2.45, and 2.15), (MeOH+HCl) 237, 288, 334, 430, 451, 485, 565, 616, 670, and 752 nm (log ε 4.17, 4.33, 3.91, 3.79, 3.91, 3.76, 3.01, 2.91, 2.83, and 2.34); ^{1}H NMR (270 MHz in CD_3CN) δ=2.67 (3H, s, CH_3), 4.47 (1H, d, J=9.7 Hz, H-6), 5.22 (1H, dd, J=10.8 and 7.6 Hz, H-8), 5.40 (1H, J=12.3 Hz, H-10), 5.79 (1H, ddd, J=12.3, 7.6, and 1.5 Hz, H-9), 5.84 (1H, ddd, J=10.8, 9.7, and 1.5 Hz, H-7), 6.24 (1H, dd, J=8 and 1.5 Hz, H-4), 6.48 (1H, dd, J=8 and 1.5 Hz, H-6), 6.52 (1H, td, J=8 and 1.5 Hz, H-2), and 6.68 (1H, td, J=8 and 1.5 Hz, H-3), (250 MHz in CF_3COOD) δ=3.02 (3H, s, CH_3), 5.95 (1H, d, J=11 Hz, H-10), 6.08 (1H, d, J=11 Hz, H-10), 6.35 (1H, t, J=9 Hz, H-8), 6.37 (1H, dd, J=7.5 and 1.5 Hz, H-4), 6.51 (1H, dd, J=8 and 1.5 Hz, H-1), 6.78 (1H, td, J=8, 7.5 and 1.5 Hz, H-3), 6.88 (1H, ddd, J=11, 9 and 1.5 Hz, H-9), 6.88 (1H, td, J=8 and 1.5 Hz, H-2) and 7.01 (1H, ddd, J=11, 9, and 1.5 Hz, H-7); MS, m/z 208 (M^+).

Anal. ($C_{14}H_{12}N_2$) C, H, N.

8-Isopropyl-5-methyl-5*H*-cyclohepta[*b*]quinoxaline (21b). The reaction of **4c** and **20a** was conducted in a manner similar to that described above for **21a**, giving **21b** in 51% yield: Dark green oil; mp 200 °C (picrate); UV (MeOH) λ_{max} 228, 260, 282, 324, 432, 525, 568, 628, and 686 nm (log ε 4.19, 4.18, 4.27, 3.29, 3.99, 2.88, 2.81, 2.62, and 2.30), (MeOH+HCl) 237, 299, 332, 428, 446, 488, 564, 616, 672, and 760 nm (log ε 4.24, 4.60, 3.97, 3.88, 4.00, 3.83, 3.01, 2.99, 2.84, and 2.23); ^{1}H NMR (100 MHz in $CDCl_3$) δ=0.98 (6H, d, J=6.6 Hz, $2CH_3$), 2.09 (1H, sept, J=6.6 Hz, CH), 2.70 (3H, s, N-CH_3), 4.41 (1H, d, J=9.8 Hz, H-6), 5.47 (1H, d, J=12.5 Hz, H-9), 5.74 (1H, d, J=9.8 Hz, H-7), 6.01 (1H, d, J=12.5 Hz, H-10), 6.12 (1H, d, J=7.3 Hz, H-4), 6.61 (3H, m, H-1,2,3), (CF_3COOD) δ=1.15 (6H, d, J=7.1 Hz, $2CH_3$), 2.51 (1H, sept, J=7.1 Hz, CH), 2.98 (3H, s, N-CH_3), 5.93 (1H, d, J=12 Hz, H-6), 6.07 (1H, d, J=12 Hz, H-10), 6.30 (1H, d, J=7 Hz, H-4), 6.41 (1H, d, J=7 Hz, H-1), 6.70 (2H, m, H-2,3), 6.88 (1H, d, J= 12 Hz, H-9 or 7) and 6.98 (1H, d, J=12 Hz, H-7 or 9); MS, m/z 250 (M^+).

Anal. ($C_{17}H_{18}N_2$) C, H, N.

5,11-Dimethyl-5*H*-cyclohepta[*b*]quinoxalinium Salts (23). (a) Concd HCl (100 mg) was added to a solution of **4a** (300 mg, 2.14 mmol) and *N,N'*-dimethyl-*o*-phenylenediamine **20b** (436 mg, 3.21 mmol) in EtOH (2 cm^3); the mixture was heated in a sealed tube for 20 h at 120 °C. After cooling, the precipitates were collected, giving **23** (481 mg, 87% with the second crop). (b) The reaction of **4b** (120 mg, 0.88 mmol) with **20b** (180 mg, 1.32 mmol) and 42% HBF_4 as above gave the BF_4^- salt (106 mg, 39%). Cl^- salt: Dark green needles; mp 230 °C (from EtOH); UV (MeOH) λ_{max} 238, 287, 328, 440, 580, 620, and 630 nm. (log ε 4.18, 4.23, 3.84, 3.81, 3.07, 3.05, and 2.56); ^{1}H NMR (270 MHz in CD_3CN) δ=3.10 (6H, s, $2CH_3$), 6.25 (2H, d, J=11 Hz, H-6, 10), 6.57 (1H, t, J=9.5 Hz, H-8), 6.71 (2H, m, H-1, 4), 6.95 (2H, m, H-2, 3), and 7.24 (2H, dd, J=11.3 and 9.5 Hz, H-7,9).

Anal. ($C_{15}H_{16}N_2Cl$) C, H, N.

BF_4^- salt: Dark green needles; mp 223 °C

Reaction of 23 with NaOH. (a) Aqueous NaOH (1 g/3 cm^3 of H_2O) was added to a green solution of **23** (150 mg, 0.58 mmol) in MeOH (150 cm^3); the solution turned to colorless. After removing the solvent, the residue was extracted with $CHCl_3$. The combined extracts were concentrated and chromatographed on a silica-gel column with 10 : 1 benzene-MeOH as the eluant, giving **29** (124 mg, 89%). (b) Aqueous NaOH (80 mg/ H_2O, 0.5 cm^3) was added to a solution of **23** (100 mg, 0.39 mmol) in MeOH (100 cm^3) and the solution was set aside overnight at room temperature; it slowly became reddish brown. After removing the solvent, the residue was chromatographed on silica-gel thin-layer plates with 10 : 1 benzene-MeOH as the eluant, giving **30** (5 mg, 6.5%) besides **29** (11%) and many products.

***N*-Methyl-*N*-[*o*-(methylamino)phenyl]benzamide (29):** Colorless needles (from MeOH), mp 140 °C; MS, m/z 240 (M^+); UV (MeOH) λ_{max} 238 and 301 nm (log ε 4.19 and 3.57), (MeOH+HCl) 233, 271, and 278 nm (log ε 4.15, 4.08, and 4.14); IR (KBr) 3360 (NH) and 1630 cm^{-1} (CO); ^{1}H NMR (270 MHz in $CDCl_3$) δ=2.92 (3H, d, J=5.5 Hz, CH_3), 3.29 (3H, s, CH_3), 4.19 (1H, q, J=5.5 Hz, NH), 6.46 (1H, t, J=7.7 Hz), 6.61 (1H, d, J=8.2 Hz), 6.71 (1H, d, J=7.7 Hz), 7.12 (3H, m), 7.20 (1H, d, J=7.1 Hz) and 7.29 (2H, dd, J=7.7 and 7.1 Hz); MS, m/z 240 (M^+, 41), 163 (12), 135 (31), 120 (28), 119 (78), 106 (9), 105 (42), 91 (9), and 77 (100).

Anal. ($C_{15}H_{16}N_2O$) C, H, N.

5,10-Dihydro-5,10-dimethyl-2-phenazinecarbaldehyde (30): Reddish orange crystals; mp 83 °C (lit,[12] red plates, mp 185 °F); UV (MeOH) λ_{max} 237, 288, 351, and 432 nm (log ε 4.38, 4.37, 3.65, and 3.37), (MeOH+HCl) 241, 260, 290, 348, and 442 nm (log ε 4.36, 4.16, 4.25, 3.68, and 3.69); ^{1}H NMR (270 MHz in C_6D_6) δ=2.28 (3H, s, CH_3), 2.30 (3H, s, CH_3), 5.82 (1H, d, J=7.7 Hz, H-4), 5.99 (2H, m, H-6,9), 6.64 (2H, m, H-7,8), 6.81 (1H, d, J=1.7 Hz, H-1), and 6.89 (1H, dd, J=7.7 and 1.7 Hz, H-3); MS, m/z 238 (M^+, 77), 238 (86), 195 (100), and 180 (48).

Found: m/z 238.1113. Calcd for $C_{15}H_{14}N_2O$: M, 238.1105.

5,11-Dihydro-8,11-dimethyl-6*H*-cyclohepta[*b*]quinoxaline-5,6-sultone (24b). A solution of **21a** (100 mg, 0.96 mmol) and methyl fluorosulfate (200 mg, 1.75 mmol) in dichloromethane (0.5 cm^3) was shaken in a sealed flask for 40 h at room temperature. After removing the solvent and excess sulfate in vacuo, the residue was diluted with aqueous $NaHCO_3$ and then extracted with $CHCl_3$. The extracts were combined and concentrated in vacuo. The residue was chromatographed on silica-gel thin-layer plates with 10 : 1 benzene-MeOH as the eluant, giving **24** (178 mg, 61%) as green needles: mp 127—128.5 °C (from $CHCl_3$); UV (MeOH) λ_{max} 268, 276, 328, 443, 464, 616, 676, and 680 nm (log ε 4.43, 4.38, 4.09, 4.27, 4.22, 3.20, 3.08, 2.72) (MeOH+NaOH) 230, 250, 280, and 354 nm. (MeOH+HCl) 240, 284, 334, 432, 460, 490, 564, 622, and 684 nm (log ε 4.31, 4.45, 4.21, 4.04, 4.29, 4.30, 3.07, 3.01, 2.80), (hexane) 265, 322, and 434 nm; IR (KBr) 1160, 1340 cm^{-1} (-SO_2-); ^{1}H NMR (270 MHz in C_6D_6) δ=1.63 (3H, s, CH_3), 3.29 (3H, s, N-CH_3), 3.33 (1H, d, J=10.2 Hz, H-6), 5.49 (1H, d, J=12.8 Hz, H-10), 5.61 (1H, dt, J=9.5 and 3.3 Hz, H-1), 5.98 (1H, dd, J=12.8 and 2.2 Hz, H-9), 6.44 (1H, dd, J=10.2 and 2.2 Hz, H-7), 6.44 (2H, m, H-2,3), and 6.88 (1H, dt, J=9.5 and 3.3 Hz, H-4), (270 MHz in CD_3CN) δ=2.86 (3H, s, CH_3), 3.74 (3H, s, N-CH_3), 4.47 (1H, d, J=11.0

Hz, H-6), 5.38 (1H, d, J=13.2 Hz, H-10), 5.90 (1H, dd, J=13.2 and 2.2 Hz, H-9), 6.51 (1H, dd, J=11.0 and 2.2 Hz, H-7), 6.54 (1H, d, J=6.6 Hz, H-1), 6.69 (1H, dd, J=6.5 and 1.5 Hz, H-4), 6.74 (1H, td, J=6.5 and 1.5 Hz, H-3), 6.86 (1H, td, J=6.5 and 1.5 Hz, H-2), (270 MHz in CD_3CN+CF_3COOD) δ=2.99 (3H, s, CH_3), 3.81 (3H, s, CH_3), 5.69 (1H, d, J=11.7 Hz, H-10), 5.83 (1H, d, J=11.7 Hz, H-6), 6.56 (1H, dd, J=7.5 and 1.5 Hz, H-4), 6.71 (1H, dd, J=7.5 and 1.5 Hz, H-1), 6.87 (1H, td, J=7.5 and 1.5 Hz, H-2), 6.95 (1H, td, J=7.5 and 1.5 Hz, H-3), 7.05 (1H, dd, J=11.7 and 2.2 Hz, H-9) and 7.20 (1H, dd, J= 11.7 and 2.2 Hz, H-7); MS, m/z 302 (M^+, 100), 287 (13), 223 (13), 208 (14), 207 (38), 206 (11), 205 (12), 193 (13), 192 (23), 191 (17), and 182 (31).

Found: m/z 302.0679. Calcd for $C_{15}H_{14}N_2O_3S$: M, 302.0724.

Oxidation of 10a with H_2O_2: To a solution of **10a** (20 mg) in acetic acid (2 cm^3) was added 28% H_2O_2 (100 mg), and the mixture was set aside for 24 h at room temperature. Each product was separated and identified by means of HPLC, giving **16a** (80%), **E** and **F** (7%), and **37**[13] (5%). The yields were based on the peak areas.

Oxidation of 21a with H_2O_2: Compound **21a** (50 mg) was treated with 28% H_2O_2 (0.1 cm^3) in methanol (0.5 cm^3) at 60 °C for 70 h. Many product spots were seen on TLC, and **39** was separated (10% yield) by using preparative TLC with benzene-MeOH (10 : 1) as eluant.

10-Methyl-2(10*H*)-phenazinone (39):[14] Red solid; UV (MeOH) λ_{max} 229, 276sh, 284, 355, 512, and 550sh nm (log ε 4.69, 4.57, 4.60, 3.86, 3.83, and 3.70); ^{1}H NMR (270 MHz in $CDCl_3$) δ=7.02 (1H, s, H-1), 7.35 (1H, d, J=9 Hz, H-3), 7.64 (1H, t, J=8 Hz, H-6), 7.80 (1H, d, J=8 Hz, H-8), 7.85 (1H, d, J=9 Hz, H-4), 7.89 (1H, t, J=8 Hz, H-7), 8.19 (1H, d, J=8 Hz, H-6); MS, m/z 210 (M^+, 74), 182 (100), and 167 (29).

Found: m/z 210.0803. Calcd for $C_{13}H_{10}N_2O$: M, 210.0793.

We wish to thank Drs. Masafumi Yasunami and Kazuko Takahashi (Tohoku Univ.) and Professor Hiroshi Yamamoto (Okayama Univ.) for their helpful advice, and Mr. Nobuyuki Yoshida (Tokyo Reserch Laboratories, Kao Corp.) for his help in the early stages of this work.

References

1) Presented at the 43rd National Meeting of the Chemical Society of Japan, Tokyo, April 1981, Abstr., No. 1H41; at the 47th Meeting, Tokyo, April 1983, Abstr., No. 4F34; at the 50th Meeting, Tokyo, April 1985, Abstr., No. 1T25.

2) T. Nozoe, *Pure Appl. Chem.*, **54**, 975 (1982); T. Nozoe, *Chemistry* (Chinese Chem. Soc. Taiwan), **41**, A43 (1983).

3) T. Nozoe, M. Sato, and T. Matsuda, *Sci. Rep. Tohoku Univ.*, First Series, **37**, 407 (1953).

4) T. Nozoe, T. Kitahara, K. Takase, and M. Sasaki, *Proc. Jpn. Acad.*, **32**, 349 (1956). Compound **6a** was also formed from the reaction of 1,2-cycloheptanedione and **2a**, and **7a** was obtained by the reduction of **6a**.

5) T. Fukunaga, presented at the 23rd IUPAC Congress, Boston, 1971, Abstr., p. 103; also private communication.

6) T. Nozoe, H. Okai, and T. Someya, *Bull. Chem. Soc. Jpn.*, **51**, 2185 (1978); T. Nozoe and T. Someya, *ibid.*, **51**, 3316 (1978); T. Nozoe, T. Someya, and H. Okai, *ibid.*, **56**, 2756 (1983).

7) T. Nozoe, T. Asao, and K. Takahashi, *Bull. Chem. Soc. Jpn.*, **34**, 146 (1961); **39**, 1980 (1966)

8) K. Shindo, S. Ishikawa, and T. Nozoe, *Bull. Chem. Soc. Jpn.*, **58**, 165 (1985)

9) Presented at the 50th National Meeting of the Chemical Society of Japan, Tokyo, April 1985, Abstr., No. 1T26.

10) A little later, Mukai et al also obtained the same compound (as iodide salt) by methylation of **21a** with methyl iodide: Y. Yamashita, K. Hagiya, Y. Nishizawa, and T. Mukai, presented at the 50th National Meeting of the Chemical Society of Japan, Tokyo, April 1985, Abstr., No. 3T35; at the 18th Japanese Symposium on the Chemistry of Nonbenzenoid Aromatic Compounds, Toyama, Abstr., p. 107 (1985). See also Y. Yamashita, K. Hagiya, G. Saito, and T. Mukai, *Bull. Chem. Soc. Jpn.*, **61**, 271 (1988).

11) W. Brasen, H. Holmquist, and R. Benson, *J. Am. Chem. Soc.*, **83**, 3125 (1961).

12) M. G. Khristiansen, A. Ya. Il'cheenko, Yu. S. Rozum, *Dopov. Akad. Nauk Ukr. RSR, Ser. B*, **32**, 829 (1970).

13) M. Hirama, A. Kawamata, and S. Itô, *Chem. Lett.*, **1979**, 855.

14) F. Kehrmann and F. Cherpillod, *Helv. Chim. Acta*, **7**, 973 (1924).

15) A. R. Katritzky and C. W. Rees, "Comprehensive Heterocyclic Chemistry," ed by M. Sainsbury, Pergamon Press, Oxford (1984), Vol. 3, p. 1010.

16) A. Albert, "Heterocyclic Chemistry," Athlone Press London, 1968.

17) K. Shindo, K. Kurihara, S. Ishikawa, and T. Nozoe, to be published.

An Efficient Route to Both Enantiomers of *N*-(*p*-Tolylsulfonyl)-benzenesulfonimidamide and Their Use for Asymmetric Allylic Amination of Olefins

Susumu TSUSHIMA,§ Yasuhiro YAMADA,§ Tetsuo ONAMI,*,† Koichiro OSHIMA,††,§ Michael O. CHANEY,†††
Noel D. JONES,††† and John K. SWARTZENDRUBER†††
Department of Chemistry, Stanford University, Stanford, CA 94305, U.S.A.
†Department of Chemistry, Fukushima Medical College, Hikarigaoka, Fukushima-shi 960-12
††Department of Chemistry, Massachusetts Institute of Technology, Cambridge, MA 02139, U.S.A.
†††Lilly Research Laboratories, A Division of Eli Lilly and Company, Lilly Corporate Center, Indianapolis, IN 46285, U.S.A.
(Received October 17, 1988)

The chiral compounds (*R*)- and (*S*)-*N*-(*p*-tolylsulfonyl)benzenesulfonimidamide have been prepared efficiently from *N*-(*p*-tolylsulfonyl)benzenesulfonimidoyl chloride and both enantiomers were transformed into chiral selenium diimide reagents, (*S*)- and (*R*)-*N*,*N*′-bis[*N*-(*p*-tolylsulfonyl)benzenesulfonimidoyl]selenium diimide, respectively, for the asymmetric allylic amination of olefins. Asymmetric allylic amination of methylenecyclohexane with the *S*-configured selenium diimide reagent afforded allylic amide, (1*S*)-*N*-[(*R*)-*N*-(*p*-tolylsulfonyl)benzenesulfonimidoyl]-2-methylenecyclohexylamine as a major diastereomer (42% diastereomeric excess). Similarly, cyclohexene, 1-heptene, and cyclooctene gave chiral allylic amides with 34%, 32%, and 20% diastereomeric excess, respectively. It is apparent that the *S*-configured diimido selenium reagent gives *S*-configured allylic amides, and that the *R*-configured reagent affords *R*-configured allylic amides as the major diastereomers in all of the cases investigated.

Great progress has been made in the area of asymmetric oxygenations of prochiral olefins since the finding of the enantioselective epoxidation of allylic alcohols by Sharpless and Katsuki in 1980.[1] However, the aza analogues of direct asymmetric oxygenations of olefins have not been studied extensively, and only chiral aziridination of the special olefins such as α-methylene-γ-butyrolactone is reported[2] to date as a direct asymmetric nitrogenation of prochiral olefins, although an indirect but excellent method for the synthesis of chiral primary amines through 2-alkyl-1,3,2-dioxaborinanes is developed by Brown et al.[3]

In 1976, we reported a method for the direct allylic amination of olefins and acetylenes by selenium diimide compounds.[4] The probable mechanism for the allylic amination is the aza analogue of the well-established mechanism for the allylic oxygenation of olefins by selenium dioxide.[5] If the substituent on the nitrogen atom in the selenium diimide reagent were chiral, some asymmetric induction would be anticipated in the allylic amination. This report describes the application of this concept to achieve asymmetric allylic amination of olefins. It must be admitted at the outset that this approach to asymmetric allylic amination by means of the chiral substituent on the nitrogen introduced is not likely to be of much practical value, for it involves the stoichiometric use of a resolved chiral reagent. However, the area of asymmetric amination is new enough that the factors which enable one to achieve good enantioselectivities are poorly understood, and there are only a few literatures[6,7] to refer to about it. In this circumstance it seems defensible, even desirable, to engage in studies which involve the stoichiometric use of a chiral agent which is not a commercially available natural product. Of course, the real future for a practical asymmetric allylic amination process lies in the development of highly effective chiral catalysts.

Jones and Cram have reported the synthesis of the chiral *N*-(menthyloxycarbonyl)-*p*-toluenesulfonimidamide (**1**).[8] The amide **1** was prepared following their procedure and transformed into its sodiochloramine derivative **2**, which was found to be effective in the selenium mediated allylic amination of methylenecyclohexane, as shown in Scheme 1. Although the allylic amination product **3** was shown to have a diastereomeric purity of about 48%,[9] it was very difficult to obtain more than a few hundred milligrams of the optically pure amide **1** due to the difficulty of its isolation from the diastereomeric mixture. However, this preliminary result encouraged us to devise a more practical route to other chiral alkylbenzenesulfonimidamides.

Results and Discussion

After several false starts, the exceedingly efficient sequence shown in Scheme 2 for the preparation of chiral *N*-(*p*-tolylsulfonyl)benzenesulfonimidamide [(*R*)-**8** and (*S*)-**8**] was developed. The racemic sulfonimidoyl chloride **6** is readily available from diphenyl disulfide (**4**) by sequential application of two literature procedures.[10] The nitrogen was introduced into sulfonimidamide **7** in the form of (*S*)-α-methylbenzylamine. At this point we had the good fortune to expe-

§ Present address: S. T.: Chemistry Laboratories, Central Research Division, Takeda Chemical Industries, Ltd., Juso-hommachi, Yodogawa, Osaka 532; Y. Y.: Department of Fermentation Technology, Faculty of Engineering, Osaka University, Yamadaoka, Suita-shi 565; and K. O.: Department of Industrial Chemistry, Faculty of Engineering, Kyoto University, Sakyo-ku, Kyoto 606.

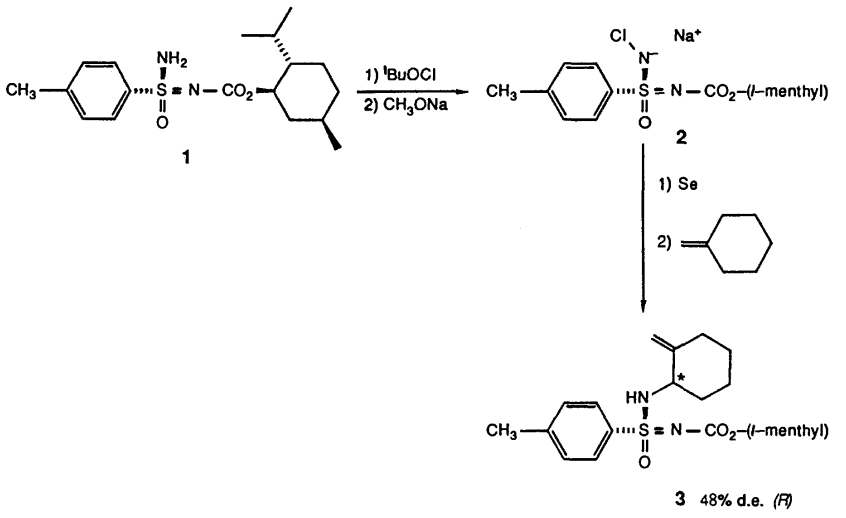

Scheme 1.

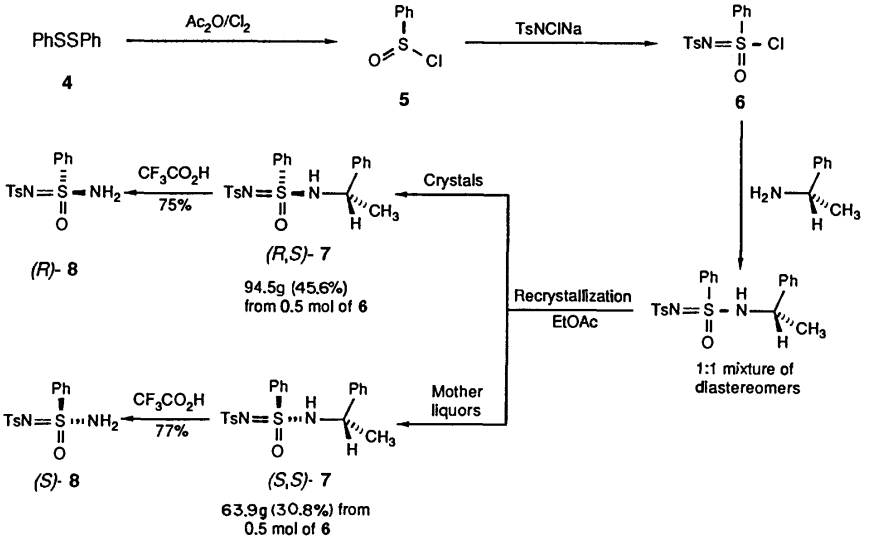

Scheme 2.

rience a completely painless resolution. One of the diastereomeric sulfonimidamides [(*R*,*S*)-**7**] is almost completely insoluble in ethyl acetate. Thus, a single recrystallization from ethyl acetate led to its isolation in 45.6% yield. The other diastereomer (*S*,*S*)-**7** was isolated in 30.8% yield by concentrating the mother liquor and adding diethyl ether to induce its crystallization. Therefore, the total yield of the two diastereomers was 76.4% from the sulfonimidoyl chloride **6**, and it will be noted in Scheme 2 that large amounts of (*R*,*S*)-**7** and (*S*,*S*)-**7** were easily obtained by carrying out a 0.5 mole scale reaction. A single-crystal X-ray analysis of (*S*,*S*)-**7** allowed assignment of the absolute stereochemistry at the chiral sulfur center; it is *S* as shown in Fig. 1.

Numerous unsuccessful attempts were made to cleave the α-methylbenzyl moiety from (*R*,*S*)-**7** and (*S*,*S*)-**7** by hydrogenolysis. Finally, a literature

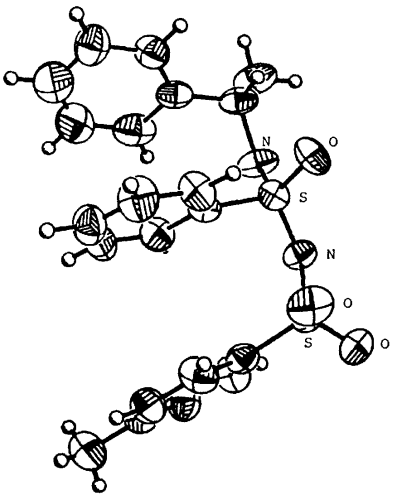

Fig. 1. The perspective drawing of the (*S*,*S*)-**7** molecule.

method[11] involving solvolysis in trifluoroacetic acid was found to be very effective. A priori one might have expected these acidic conditions to either racemize or hydrolyze the desired chiral sulfonimidoyl amides (*R*)-**8** and (*S*)-**8**, but no such difficulties were encountered. We, therefore, now had a good route to the chiral benzenesulfonimidamides (*R*)-**8** and (*S*)-**8**.[12] Sulfonimidamide (*R*)-**8** is readily converted to the corresponding chloramine salt (*S*)-**9**, as shown in Scheme 3. The salt (*S*)-**9** is stable for months at room temperature. The salt (*S*)-**9** is slightly soluble in dry dichloromethane, and when exposed to selenium metal in this solvent it reacts to afford an uncharacterized substance which behaves as if it were the selenium(IV) diimide species (*S*)-**10**.[13] The putative diimide reagent (*S*)-**10** is effective for the allylic amination of olefins.

The probable mechanism for the allylic amination process is that shown in Scheme 4, and it is simply the aza analogue of the rather well-established mechanism for the allylic oxygenation of olefins by selenium dioxide.[5] The key events bearing on the question of chirality transfer from the selenium reagent to the allylic

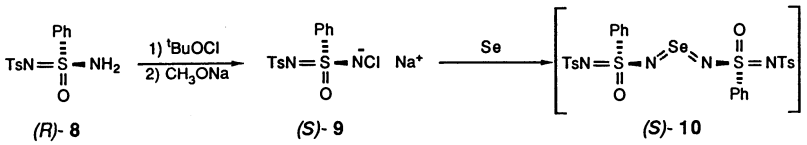

Scheme 3.

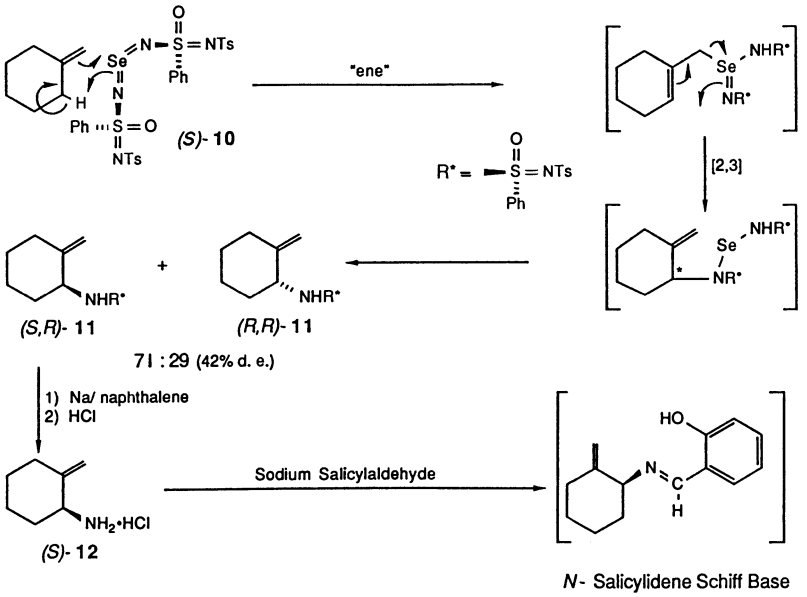

Scheme 4.

Table 1. Asymmetric Inductions

Entry	Olefin	Configuration of R*N=Se=NR* a)	Product	Ratio of diastereomers	Diastereomeric excess	Yield
1	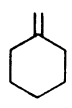	*S*	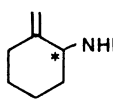	29 : 71	42% (*S*)	51%
2	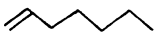	*R*	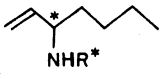	34 : 66	32% (*R*)	25%
3		*R*	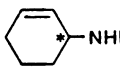	33:67	34% (*R*)	29%
4		*R*	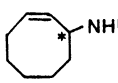	4.0 : 6.0	20% (*R*)	30%

a) R*= -S*(=O)(=NTs)-Ph.

amination product are the ene step and the [2,3]sigmatropic step. For an olefin which bears a terminal double bond such as methylenecyclohexane or 1-heptene (Entry 2, Table 1), the ene step would induce a chiral center at the selenium, but leads to an intermediate which has no chirality in the olefinic part of the structure. In this case, therefore, the asymmetric selection could take place in the [2,3]sigmatropic step.[7] For example, the diimide reagent (*S*)-**10** (*S* configuration at sulfur) derived from the optically active sulfonimidamide (*R*)-**8**, reacted with methylenecyclohexane at 0 °C to give the expected allylic amide **11** as the mixture of diastereomers in the ratio of 29 : 71 (42% diastereomeric excess). The ratio was not changed even when the reaction was performed at various temperatures between −40 °C and 25 °C. The diastereomers were distinguished clearly by their ^{1}H NMR spectra and were separated by column chromatography on silica gel to give (*S*,*R*)-**11** as the major isomer and (*R*,*R*)-**11** as the minor isomer. The circular dichroism of the *N*-salicylidene Schiff base of the allylic amine (*S*)-**12**, which was derived from (*S*,*R*)-**11** by naphthalene-sodium reduction,[14] showed positive Cotton effects at 253 and 317nm. Therefore, the newly induced chiral center at carbon in the major diastereomer was assigned the *S*-configuration[15] following the salicylideneamino chirality rule.[16]

An acyclic olefin such as 1-heptene was aminated with the selenium diimide reagent (*R*)-**10** which contains *R*-configured sulfurs, and a somewhat lower diastereomeric excess (32%) was observed for the allylic amination product **13** (Scheme 5).[17] The absolute configuration of the newly induced chiral center in **13** was correlated to the corresponding chiral center in an authentic sample of *N*-(*N*-trifluoroacetyl-L-prolyl)-L-norleucine methyl ester [(2*S*)-**15**] which was derived from commercially available L-norleucine as shown in Scheme 5. The GC retention time of the major diastereomer of **15** which was derived from the diastereomeric mixture **13** was the same as that of (2*S*)-**15** from L-norleucine. Therefore the induced chiral center in the major diastereomer of **13** was proved to be *S*-configured.

For the majority of olefins which do not bear a terminal double bond (e.g. Entries 3 and 4, Table 1), the ene product possesses chirality in the olefinic part of the structure, and in this case the chirality of the final product is determined only by the asymmetric induction in the ene step. An example is shown in Scheme 6

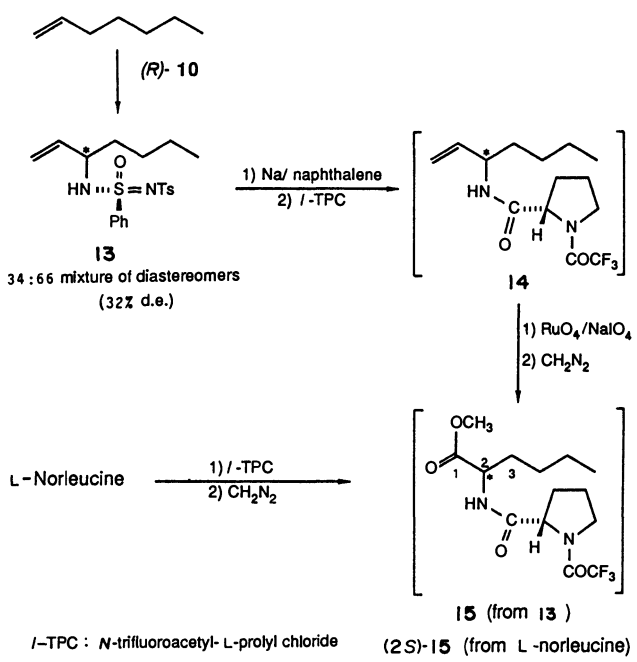

Scheme 5.

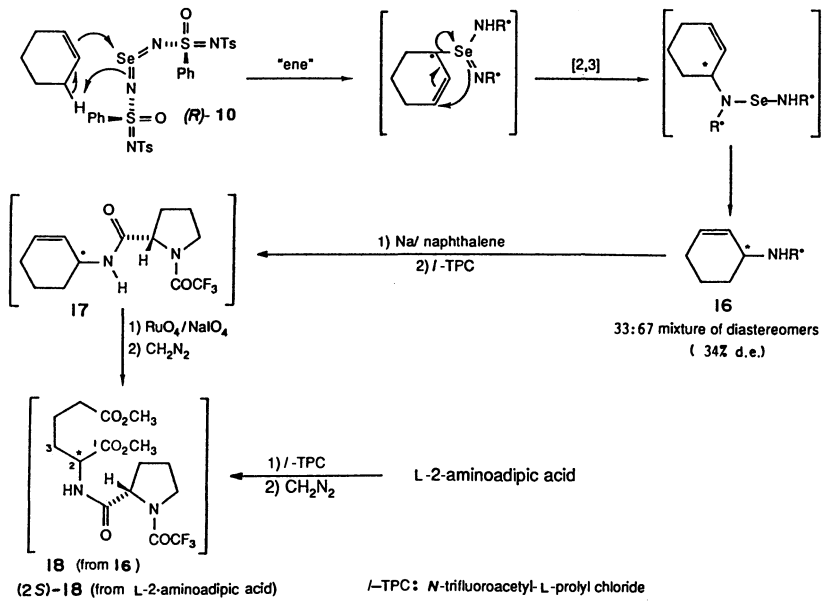

Scheme 6.

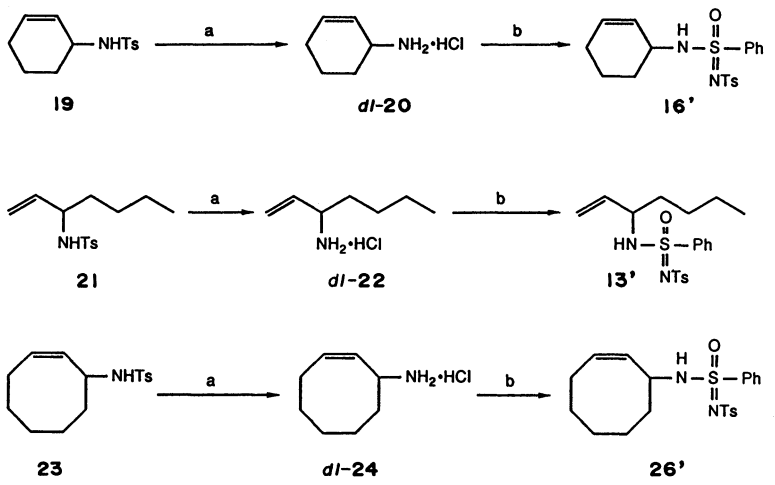

a: 1) Na/naphthalene, 2) HCl. b: PhSO(=NTs)Cl.

Scheme 7. Preparation of authentic samples.

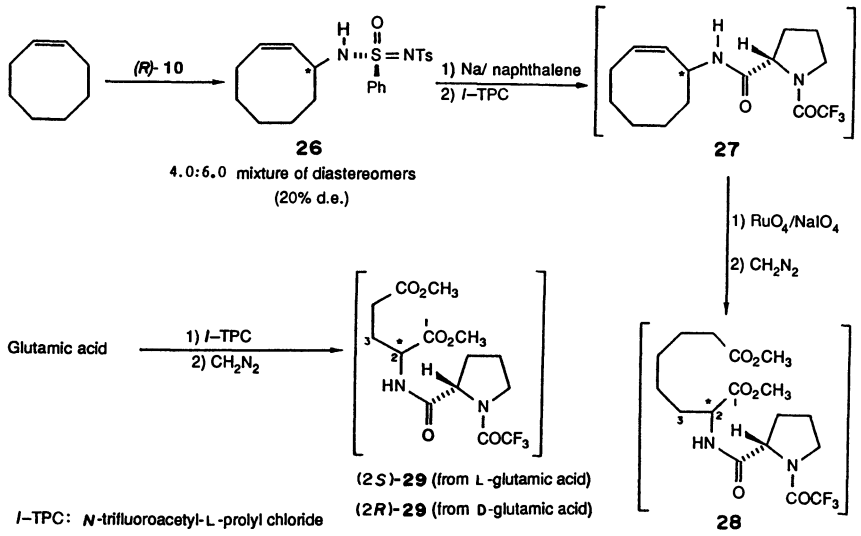

Scheme 8.

for cyclohexene as the olefin. When the aminating reagent (*R*)-**10** was used, two diastereomers (**16**) were produced in the ratio of 33 : 67 (34% diastereomeric excess). As they are not separable by column chromatography on silica gel, the structure was confirmed by comparison of the diastereomeric mixture with an authentic sample of diastereomeric mixture **16'** which was derived from racemic allylic amine *dl*-**20** as shown in Scheme 7. In order to determine the absolute configuration of the newly induced chiral center in the major diastereomer of **16**, the diastereomeric mixture (**16**) was converted to methyl *N*-(*N*-trifluoroacetyl-L-prolyl)-2-aminoadipate (**18**) as shown in Scheme 6. As the GC retention time of the major diastereomer of **18** was the same as that of an authentic sample of methyl *N*-(*N*-trifluoroacetyl-L-prolyl)-L-2-aminoadipate [(2*S*)-**18**], which was derived from L-2-aminoadipic acid, the induced chiral center in the major diastereomer of **16** must be *S*-configured.

A medium-sized cyclic olefin such as cyclooctene afforded two diastereomers (**26**) upon the asymmetric allylic amination with the diimido selenium reagent (*R*)-**10** (Scheme 8). However, the asymmetric induction (20% diastereomeric excess) was somewhat lower than for the other olefins already described. As shown in Scheme 8, the diastereomeric mixture **26** was converted to **28** in order to assign the absolute configuration of the induced chiral center in the major diastereomer of the allylic amide. The GC analysis of **28** showed two peaks on PEG, and the major diastereomer eluted before the minor one. While diastereomers with *S*-configuration at C-2, such as (2*S*)-**18** (Scheme 6), (2*S*)-**15** (Scheme 5), and (2*S*)-**29** (Scheme 8) have in all cases longer retention times than the corresponding diastereomers with *R*-configuration at C-2 on the same GC column as shown in Table 2.[18] Therefore, as the major diastereomer of **28** has a shorter retention time than the minor one, the *R*-configuration was assigned

Table 2. GC Retention Times of *N*-(*N*-Trifluoroacetyl-L-prolyl) Derivatives of Amino Acid Methyl Ester

Amino acid	D-Enantiomer	L-Enantiomer	Column temp, flow rate[a)]
Norleucine	7.80 min	10.50 min	170 °C, 24 mL min^{-1}
Glutamic acid	18.20 min	22.20 min	180 °C, 45 mL min^{-1}
2-Aminoadipic acid	15.17 min	17.40 min	200 °C, 24 mL min^{-1}

a) 1m 1% PEG-20M-P.

to C-2 in the major diastereomer of **28**, and accordingly the induced chiral center in the major diastereomer of **26** was assigned the same *R*-configuration.

It seems noteworthy that the *R*-configured selenium reagent (*R*)-**10** gives the *R*-configured allylic amides in all four cases examined (Table 1). As can also be seen in Table 1 the asymmetric inductions we have observed are in the unimpressive 20—42% range. We had hoped for better inductions as chiral transfer is known to be excellent for [2,3]sigmatropic processes.[19] There are at present far too many unknown factors to support any speculation about the reasons for the modest inductions we have observed. However, since the relative bulk of the substituents around the chiral sulfurs in the imido selenium reagent could play an important part in determining the geometry of the transition states, the asymmetric inductions might be improved by exploring structural variations in the chiral sulfonimidamide **8** (Scheme 2). Fortunately, the synthetic route to the chiral sulfonimidamides (*R*)-**8** and (*S*)-**8** is straight-forward and should lend itself to the introduction of structural modifications.

Experimental

Melting points were determined on a capillary tube melting point apparatus and are uncorrected. Optical rotations were measured using a Perkin-Elmer 241 polarimeter. Infrared (IR) spectra were recorded on a Jasco A-100 grating infrared spectrometer and proton nuclear magnetic resonance (^{1}H NMR) spectra were recorded on a Jeol FX-90Q spectrometer (90 MHz). Tetramethylsilane (TMS) was used as an internal standard; however, when the solvent was D_2O, the standard was sodium 3-(trimethylsilyl)propionate-d_4 (TSP-d_4); chemical shifts are denoted in ppm downfield from TMS or TSP-d_4 at δ=0. Elemental analyses were performed by Stanford university or Takeda Chemical Industries Ltd., Chemistry Laboratories. Gas chromatographic (GC) analyses were performed on a Hitachi 163 gas chromatograph with a flame ionization detector using glass columns (3 mm i.d.) and nitrogen carrier gas. All the column packings used were purchased from Gasukuro Kogyo Inc. Analytical high-performance liquid chromatography (HPLC) was carried out on a Jasco BIP-1 high-performance liquid chromatograph equipped with a UV detector (adjusted to 260 nm). The CD spectrum was recorded on a Jasco J-20 spectropolarimeter at Takeda Chemical Industries Ltd., Chemistry Laboratories. Analytical thin-layer chromatography was performed on precoated silica-gel glass plates (0.25 mm, Kieselgel 60, F-254, E. Merck) and siica gel (Wakogel C-300, Wako Pure Chemical Industries Ltd.) was used for column chromatography.

(*R*)-*N*-[(*S*)-α-Methylbenzyl]-*N*′-(*p*-tolylsulfonyl)benzenesulfonimidamide [(*R*,*S*)-7] and (*S*)-*N*-[(*S*)-α-Methybenzyl]-*N*′-(*p*-tolylsulfonyl)benzenesulfonimidamide [(*S*,*S*)-7]. To an ice-cooled solution of 165 g (0.5 mol) of *N*-(*p*-tolylsulfonyl)benzenesulfonimidoyl chloride (prepared according to the published procedure[10]) in 1 L of dichloromethane was added a mixture of 66.5 g (0.55 mol) of (*S*)-(−)-α-methylbenzylamine (Aldrich) and 50.4 g (0.6 mol) of sodium hydrogencarbonate in 550 ml of water, and the mixture was stirred at room temperature overnight. After the separation of the organic layer, it was washed with 10% HCl, and water, successively, and concentrated in vacuo to afford crude crystals. Recrystallization from 1.5 L of ethyl acetate gave 94.5 g (45.6%) of (*R*,*S*)-**7** as needles (mp 166.5—168.0 °C), which was diastereomerically pure by ^{1}H NMR. An analytical sample was obtained by recrystallization from ethyl acetate: mp 167.5—168.5 °C; $[\alpha]_D^{23}$ −60.3° (*c* 1.02, acetone); IR (KBr) 3240, 1600, 1450, 1430, 1306, 1265, 1150, 1092, 1055, and 952 cm^{-1}; ^{1}H NMR ($CDCl_3$) δ=1.33 (3H, d, *J*=6.9 Hz, methyl), 2.37 (3H, s, aryl methyl), 4.50 (1H, q, *J*=6.9 Hz, CH-N), 7.0—8.0 (15H, NH and aromatic). Found: C, 60.84; H, 5.32; N, 6.77%. Calcd for $C_{21}H_{22}N_2O_3S_2$: C, 60.85; H, 5.35; N, 6.76%.

The mother liquor was concentrated and 1.2 L of diethyl ether was added to the residue to give 69.8 g of the other diastereomer (*S*,*S*)-**7** as prisms (mp 89.5—91.5 °C, contains approximately 1% of (*R*,*S*)-**7** judging from its ^{1}H NMR spectrum). Concentration of the mother liquor afforded a second crop of 17.2 g of crude crystals, which were dissolved in 75 mL of hot ethyl acetate and 3.29 g of crystals (mp 164—166.5 °C) were precipitated on cooling to room temperature. [These precipitated crystals were further recrystallized from 50 mL of ethyl acetate to give 2.9 g of diastereomerically pure (*R*,*S*)-**7**, mp 167.5—168.5 °C. Therefore, the total yield of (*R*,*S*)-**7** is 97.4 g (47%).] After separating the crystals, the mother liquor was concentrated and 200 mL of diethyl ether was added to the residue to give 13.1 g of (*S*,*S*)-**7** (mp 89.5—91.5 °C, contains approximately 2% of (*R*,*S*)-**7** judging from its ^{1}H NMR spectrum). The combined (*S*,*S*)-**7** (82.9 g) was dissolved in 100 mL of hot ethanol, and addition of hexane (100 mL) afforded 63.9 g (30.8%) of diastereomerically pure (*S*,*S*)-**7**: mp 91.5—92.5 °C; $[\alpha]_D^{23}$ −70.6° (*c* 1.08, acetone); IR (KBr) 3240, 1600, 1450, 1290, 1260, 1150, 1092, 1062, and 967 cm^{-1}; ^{1}H NMR ($CDCl_3$) δ=1.54 (3H, d, *J*=6.9 Hz, methyl), 2.37 (3H, s, aryl methyl), 4.48 (1H, d of q, *J*=6.9 and 6.9 Hz, CH-N), 6.71 (1H, d, *J*=6.9 Hz, NH), 6.9—8.0 (14H, aromatic). Found: C, 60.55; H, 5.47; N, 6.57%. Calcd for $C_{21}H_{22}N_2O_3S_2$: C, 60.85; H, 5.35; N, 6.76%.

X-Ray Diffraction Studies on (*S*)-*N*-[(*S*)-α-Methylbenzyl]-*N*′-(*p*-tolylsulfonyl)benzenesulfonimidamide [(*S*,*S*)]-7].

Compound (*S,S*)-**7** exists as colorless prisms in the space group $P2_12_12_1$, with four molecules in a unit cell having the dimensions: a =11.500±0.003; b=8.254±0.002; c=21.384± 0.005 Å. The calculated density is 1.356 g cm^{-3}. A total of 1626 reflections were measured on an automated four-circle diffractometer, using monochromatic copper radiation. A partial solution was found using the direct method routines of the SHELXTL program library, with the remaining peaks being located through successive difference E maps. The solution was refined by the least squares method to R=0.0755, with anisotropic temperature factors for all atoms except hydrogen. Hydrogen atoms were included with isotropic temperature factors at calculated positions. Supplementary materials (unit cell atomic coordinates, bond lengths, bond angles, anisotropic temperature factors, hydrogen atom coordinates, and nonbonded distances) are deposited as Document No. 8864 at the Office of the Editor of the Bulletin of the Chemical Society of Japan.

(*R*)-*N*-(*p*-Tolylsulfonyl)benzenesulfonimidamide [(*R*)-8] and (*S*)-*N*-(*p*-Tolylsulfonyl)benzenesulfonimidamide [(*S*)-8]. To 40 mL of trifluoroacetic acid was added 16.56 g (40 mmol) of (*R,S*)-**7**. After stirring for 40 h at 35 °C, trifluoroacetic acid was removed in vacuo to give crude crystals. Recrystallization of the crystals from 600 mL of ethyl acetate afforded 10.63 g (86%) of (*R*)-**8** ([α]$_D^{23}$ +97.8°), which was further recrystallized from the same solvent to give 9.3 g (75%) of pure (*R*)-**8**, mp 178.5—179.5 °C,[20] [α]$_D^{23}$ +103° (*c* 1.03, acetone). Further recrystallization of this material did not change the rotation: IR (KBr) 3220 (sh), 3170, 3060, 1590, 1558, 1448, 1388, 1290, 1259, 1135, 1042, 930, 800, and 750 cm^{-1}; ^{1}H NMR ($CDCl_3$/DMSO-d_6, ca. 1 : 1) δ=2.36 (3H, s, aryl methyl), 4.39 (2H, broad s, NH), and 7.0—8.0 (9H, aromatic). Found: C, 50.47; H, 4.48; N, 8.93%. Calcd for $C_{13}H_{14}N_2O_3S_2$: C, 50.31; H, 4.55; N, 9.02%.

The other enantiomer (*S*)-**8** (6.3 g, 77%) was obtained from 12.52 g (30 mmol) of (*S,S*)-**7** following the same procedure: mp 178.5—179.5 °C, [α]$_D^{23}$ −103° (*c* 1.03, acetone). The ^{1}H NMR and IR spectra were identical to those of (*R*)-**8**.

Sodium Salt of (*R*)-*N*-Chloro-*N'*-(*p*-tolylsulfonyl)benzenesulfonimidamide [(*R*)-9] and Sodium Salt of (*S*)-*N*-Chloro-*N'*-(*p*-tolylsulfonyl)benzenesulfonimidamide [(*S*)-9]. To an ice-cooled, stirred suspension of 14.23 g (46 mmol) of (*S*)-**8** in 115 mL of methanol was added dropwise 5.21 mL (4.99 g, 46 mmol) of *t*-butyl hypochlorite (Tokyo Kasei Kogyo Co., Ltd.) under a nitrogen atmosphere. After stirring for 15 min, 2.53 g (47 mmol) of sodium methoxide was added while still stirring under ice-bath cooling. The solution was concentrated on a rotary evaporator at 30 °C to a volume of approximately 30 mL, and addition of 300 mL of diethyl ether to the concentrated solution induced crystallization. After standing overnight at room temperature, the crystals were separated and washed with diethyl ether under nitrogen to avoid contact with moisture (if this procedure is done without nitrogen, some of the crystals melt presumably due to the absorption of moisture), and dried at 80 °C in vacuo (ca. 1 mmHg; 1 mmHg≈133.322 Pa) for 1 h, to give 15.62 g (93%) of (*R*)-**9**. Titration of this material with 0.1 M (1 M=1 mol dm^{-3}) sodium thiosulfate showed a purity of 96%, and this anhydrous (*R*)-**9** was stable for months at room temperature if protected from the atmosphere in a well-sealed bottle. An analytical sample of these crystals was obtained by recrystallization from isopropyl alcohol, which afforded fine needles: mp 175.5—176.5 °C (decomp). Found: C, 42.32; H, 3.19; N, 7.58%. Calcd for $C_{13}H_{12}ClN_2NaO_3S_2$: C, 42.57; H, 3.30; N, 7.64%.

The other enantiomer (*S*)-**9** was prepared from (*R*)-**8** in the same manner.

Preparation of Diimido Selenium Reagents (*S*)-10 and (*R*)-10. To a stirred suspension of 3.67 g (10 mmol) of the chloramide salt (*S*)-**9** (dried at 80 °C in vacuo for 1 h) in 20 mL of dry dichloromethane (methanol-free dichloromethane was passed through a column of neutral aluminum oxide, activity grade I, Woelm, and stored over 3A Molecular Sieves) was added 474 mg (6 mmol) of selenium powder (dried at 80 °C in vacuo for 1 h) under a nitrogen atmosphere. The resulting mixture was stirred vigorously at room temperature and almost all the solids in the solution disappeared within 30 min, only a small amount of the excess selenium powder remained. After stirring for an additional 3 h, the reaction mixture was used as reagent (*S*)-**10** for the amination of olefins.

Reagent (*R*)-**10** was similarly prepared from the chloramide salt (*R*)-**9**.

Allylic Amination of Methylenecyclohexane with the Diimido Selenium Reagent (*S*)-10. To reagent (*S*)-**10**, which was prepared from 3.67 g (10 mmol) of chloramide salt (*S*)-**9** and 6 mmol of selenium powder according to the method described above, was added dropwise 768 mg (8 mmol) of methylenecyclohexane at 0 °C (an ice bath) while stirring under a nitrogen atmosphere. After stirring for 24 h in the refrigerator (0 °C), the reaction mixture was allowed to warm to room temperature (15 min), and stirring was continued for 1 h. the reaction mixture was then diluted with 200 mL of 1 : 1 ethyl acetate/diethyl ether and 50 mL of an alkaline aqueous solution consisting of 2 parts 1 M NaOH and 1 part saturated NaCl solution. After stirring for 30 min, the red mixture was filtered through Celite 545 and the organic layer of the filtrate was washed again with 50 mL of the above mentioned alkaline brine solution (2×50 mL), dried (Na_2SO_4) and concentrated to give an oil. The crude product was chromatographed on 60 g of silica gel (dichloromethane/ethyl acetate, 95 : 5 as eluent) to give 1.66 g (51% based on the olefin) of a crystalline diastereomeric mixture of (*S,R*)-**11** and (*R,R*)-**11**, which showed two spots by TLC analysis [hexane/ethyl acetate, 3:2, R_f 0.464 (major) and R_f 0.536 (minor)]. GC analysis (1m 1% PEG-HT on 60/80 mesh Uniport HP, 270 °C, flow rate: 38 mL min^{-1}) of the crystalline diastereomeric mixture showed two peaks at 10.03 min and 12.50 min in a ratio of 29 : 71, respectively. The ratio matched that obtained by comparison of the integrated vinyl proton resonances for each of the diastereomers in the ^{1}H NMR spectrum.

A part of the diastereomeric mixture (0.1 g) was chromatographed on 20 g of silica gel (elution with 10—20% ethyl acetate/hexane) to yield two fractions. Eluting first was the minor diastereomer (*R,R*)-**11**, which was recrystallized from ethyl acetate/hexane to give 21 mg of pure crystals: mp 92—93 °C; [α]$_D^{23}$ + 25.4° (*c* 1.00, acetone); IR (KBr) 3196, 1651, 1599, 1450, 1311, 1255, 1154, 1124, 1090, and 1069 cm^{-1}; ^{1}H NMR ($CDCl_3$) δ=1.1—2.3 (8H, m, methylene), 2.39 (3H, s, aryl methyl), 3.76 (1H, m, CH-N), 4.57 (2H, s, vinyl), 6.40 (1H, d, J=8 Hz, NH), 7.0—8.1 (9H, m, aromatic). Found: C, 59.34; H, 5.91; N, 7.04%. Calcd for $C_{20}H_{24}N_2O_3S_2$: C, 59.38; H, 5.98; N, 6.92%.

Eluting second was the major diastereomer (*S,R*)-**11**, which was recrystallized from ethyl acetate/hexane to afford

39 mg of pure crystals: mp 132—133 °C; $[\alpha]_D^{23}$ +6.9° (*c* 1.01, acetone); IR (KBr) 3246, 1648, 1599, 1450, 1313, 1303, 1252, 1156, 1119, and 1080 cm^{-1}; ^1H NMR ($CDCl_3$) δ=1.1—2.3 (8H, m, methylene), 2.39 (3H, s, aryl methyl), 3.76 (1H, m, CH-N), 4.80 (1H, s, vinyl), 5.04 (1H, s, vinyl), 6.22 (1H, d, *J*=8.0 Hz, NH), 7.0—8.1 (9H, m, aromatic). Found: C, 59.38; H, 5.84; N, 7.05%. Calcd for $C_{20}H_{24}N_2O_3S_2$: C, 59.38; H, 5.98; N, 6.92%.

Determination of the Absolute Configuration of (*S,R*)-11. To a stirred solution of naphthalene-sodium reagent[14] [prepared by stirring a mixture of 11 mg (0.49 mmol) of sodium metal and 66 mg (0.51 mmol) of naphthalene in 1 mL of freshly distilled dry 1,2-dimethoxyethane for 2 h at room temperature under nitrogen] was added 20 mg (0.049 mmol) of (*S,R*)-**11** under nitrogen at room temperature, and stirring was continued for 2 h. After addition of chilled water (3 mL) to the reaction mixture cooled in an ice bath, 1 M HCl was added until the solution became acidic (pH<1), and the resulting mixture was washed twice with 10 mL of diethyl ether. The aqueous layer was separated, made strongly basic (pH>11) with aqueous 30% NaOH and extracted with chloroform (3×5 mL). After drying the combined extracts with sodium sulfate, 0.05 mL of concd HCl was added and the resulting mixture was evaporated to dryness in vacuo to give 4.2 mg of crude crystals, which was recrystallized from 1-propanol/hexane to afford 1.3 mg of (*S*)-**12**. The ^1H NMR spectrum was identical with that of *dl*-2-methylenecyclohexylamine hydrochloride (*dl*-**12**), which was prepared as described below.

For observation of the circular dichroism, the *N*-salicylidene derivative of (*S*)-**12** was prepared in situ according to Smith's procedure.[21] Sodium salicylaldehyde[22] (1.26 mg, 8.74 μmol) and 1.14 mg (7.72 μmol) of (*S*)-**12** were weighed into a 5-mL volumetric flask on a microgram balance. Methanol (3 mL) was added and the mixture was warmed for 15 min with steam, cooled, and made up to 5 mL. This solution was diluted (1 : 10) for observation of the CD maxima: CD (*c* 0.0033, MeOH, 25 °C) $[\theta]_{317}^{peak}$ +7800, $[\theta]_{253}^{peak}$ +16000.[23]

Allylic Amination of Methylenecyclohexane at Various Temperatures. Four test tubes (10 cm, 13 mm i.d.) containing 0.25 mmol of diimido selenium reagent (*R*)-**10** in 2 ml of dichloromethane were kept at −40 °C (Dry Ice-aqueous ethanol bath), −20 °C (Dry Ice-carbon tetrachloride bath), −5 °C (ice-salt bath), and 25 °C, respectively. After an addition of 60 μL (0.5 mmol) of methylenecyclohexane to each of the tubes under nitrogen, they were stirred magnetically for 1 week maintaining their initial temperatures in freezers (−40, −20, or −5 °C) or in the room (25 °C). One drop of water was added to each tube to destroy the reagent and the resulting mixtures were then diluted with 4 mL of diethyl ether and 1 mL of an alkaline aqueous solution consisting of 2 parts 1 M NaOH and 1 part saturated NaCl solution. After stirring for 30 min at room temperature, the reaction mixtures were filtered through Celite 545 and the organic layers of the filtrates were concentrated to give oils. Each crude product was analyzed by GC (1 m 1% PEG-HT on 60/80 mesh Uniport HP, 270 °C, flow rate: 38 mL min^{-1}), and the diastereomeric ratios were determined as 29 : 71 (42% diastereomeric excess) in four cases.

Allylic Amination of Cyclohexene with Diimido Selenium Reagent (*R*)-10. Cyclohexene (493 mg, 6 mmol) was aminated with reagent (*R*)-**10** according to the method and conditions described for allylic amination of methylenecyclohexane with reagent (*S*)-**10**. The crude product (oil) was chromatographed on 60 g of silica gel using 50—60% dichloromethane/hexane to give 686 mg (29%) of a diastereomeric mixture (**16**) as crystals in a ratio of 33:67 (34% diastereomeric excess); mp 160—166 °C; IR (KBr) 3245, 1647, 1599, 1452, 1311, 1303, 1154, 1117, 1090, 1060, and 1050 cm^{-1}. The NMR spectrum was identical with an authentic sample of a 73 : 27 diastereomeric mixture of **16'** (vide infra) with the exception of differing peak intensities in the olefinic proton region. HPLC (4 mm i.d. 250 mm LiChrosorb Si 60, 5 μm, 55 : 1 hexane/isopropyl alcohol, 1 mL min^{-1}) retention times of the major (t_r=17.20 min) and minor (t_r=16.00 min) diastereomers in the mixture were identical with those of the authentic sample of **16'**. The above diastereomeric ratio (33 : 67) was determined by GC analysis of *N*-trifluoroacetyl-L-prolyl derivative **17**, which was derived by reductive cleavage of the diastereomeric mixture **16** and subsequent acylation with *N*-trifluoroacetyl-L-prolyl chloride as shown in Scheme 6 (see the following general method for the determination of diastereomeric ratios).

General Method for the Determination of Diastereomeric Ratios. As diastereomeric mixture **16** was not well-resolved either by analytical GC or by analysis of its NMR spectrum, *N*-trifluoroactyl-L-prolyl chloride was used to derivatize[24] the amine enantiomers which were derived by reductive cleavage of the diastereomeric mixture **16**. Separation of the newly derived diastereomeric mixture **17** was achieved by GC. This method was also applied to diastereomeric mixtures **13** and **26**.

To a 0.01 mmol diastereomeric mixture of asymmetric amination product was added 0.4 mL (0.2 mmol) of naphthalene-sodium reagent[14] at room temperature [the reagent was prepared by stirring a mixture of 115 mg (5 mmol) of sodium metal and 673 mg (5.25 mmol) of naphthalene in 10 mL of freshly distilled dry 1,2-dimethoxyethane for 2 h under a nitrogen atmosphere, and 0.4 mL of the resulting deep green solution was used. The rest was stored at 0 °C in the refrigerator for the next use]. After stirring for 1 h, 1 mL of water was added to the ice-chilled (ca. 0 °C) reaction mixture to quench the reaction and the mixture was acidified with an addition of 3 drops of 6 M HCl to pH<1. The resulting solution was washed with diethyl ether (2×1 mL), made strongly basic (pH>11) with 30% aqueous NaOH (ca. 4 drops), saturated with NaCl, and extracted with diethyl ether (2 mL), and the extract was dried (Na_2SO_4). To the ethereal solution was added 0.1 mL (0.01 mmol) of *N*-trifluoroactyl-L-prolyl chloride solution (Regis, 0.1 M in chloroform, contains 6.2% D-isomer), and the resulting mixture was stirred for 30 min. Fifteen minutes after addition of 1 drop of triethylamine and 1 drop of water, the organic layer was separated, dried (Na_2SO_4), and evaporated. A diastereomeric ratio of the diastereomers in the resulting product was analyzed by GC.

Determination of Absolute Configuration of the Major Diastereomer of 16. To the mixture of 8 mg (0.05 mmol) of L-2-aminoadipic acid (Calbiochem) and 5.5 mg of magnesium oxide (heavy) in 0.2 mL of water was added 0.5 mL (0.05 mmol) of *N*-trifluoroacetyl-L-prolyl chloride solution (Regis, 0.1 M in chloroform, contains 6.2% D-isomer) at 0 °C (ice bath), and the mixture was stirred for 2 h at 0 °C, and then for 4 h at room temperature. After dilution with 2 mL of ethyl acetate, the solid material (MgO) was filtered off

through Celite 545 (water wash, 0.5 mL). To the filtrate was added 6 M HCl until the aqueous layer became acidic (pH<1) with stirring. The organic layer was separated, dried (Na_2SO_4), and treated with excess diazomethane (diethyl ether solution). After stirring for 5 min, the excess diazomethane and solvents were removed in vacuo to afford 9 mg of an oil. Analysis by GC (1 m 1% PEG-20M-P on 80/100 mesh Uniport HP, 200 °C, flow rate: 24 mL min^{-1}) afforded single peak[25] (t_r=17.40 min) due to (2*S*)-**18** (*S*-configuration at the asterisk in Scheme 6). The reaction was repeated with *dl*-2-aminoadipic acid and GC analysis of the product showed a 1.0:1.0 ratio of (2*R*)-**18** (t_r=15.17 min) to (2*S*)-**18** (t_r=17.40 min).

To 1.2 mL of the naphthalene-sodium reagent (see above) was added 12 mg (0.03 mmol) of the diastereomeric mixture **16** (33:67) under a nitrogen atmosphere. After stirring for 1 h, the reaction mixture was cooled to 0 °C (ice bath), quenched by addition of 2 mL of ice-water, and acidified to pH<1 with concd HCl (ca. 3 drops). The resulting mixture was washed with diethyl ether (3×1 mL) to remove naphthalene and other nonbasic substances. The separated aqueous layer was made strongly basic (pH>11) with 30% aqueous NaOH (ca. 6 drops), saturated with NaCl, and extracted into diethyl ether (3×2 mL). The ethereal solution (dried with Na_2SO_4) was treated with 0.3 mL (0.03 mmol) of *N*-trifluoroacetyl-L-prolyl chloride (Regis, 0.1 M in chloroform, contains 6.2% D-isomer) and allowed to stand for 1 h. After addition of 1 drop of triethylamine and 3 drops of water, the reaction mixture was stirred for 30 min, and successively washed with 1 mL of 1 M HCl, 1 mL of 1 M NaOH, and brine (2×2 mL), dried (Na_2SO_4), and concentrated to give amide **17** as an oil. The oil was dissolved in 1 mL of ethyl acetate. To this solution was added RuO_4/$NaIO_4$ reagent [a mixture of 52 mg (0.24 mmol) of $NaIO_4$, 0.3 mg (0.0018 mmol) of $RuO_2 \cdot 2H_2O$, 0.5 mL of CCl_4, and 1 mL of water was stirred until all the $RuO_2 \cdot 2H_2O$ dissolved (ca. 2 min) and the resulting mixture was used as the reagent] to cleave the carbon-carbon double bond and the mixture was stirred vigorously for 3 h. Then isopropyl alcohol (3 drops) was added and the reaction mixture was stirred for 30 min. After acidification of the aqueous layer with 3 M sulfuric acid to pH<1, the organic layer was extracted with 3 mL of ethyl acetate, and dried ($MgSO_4$). The ethyl acetate solution was treated with excess diazomethane (diethyl ether solution). After standing for 5 min, the excess diazomethane and solvent were removed in vacuo to afford 8 mg of a crude oil. Analysis by GC (1 m 1% PEG-20M-P, the same conditions as above) showed a 67:33 ratio of (2*R*)-**18** (t_r=15.17 min) to (2*S*)-**18** (t_r=17.40 min), thus establishing the *R*-configuration at the carbon bearing the nitrogen in the major diastereomer of the amination product **16**.

Allylic Amination of 1-Heptene with Diimido Selenium Reagent (*R*)-10. 1-Heptene (471 mg, 4.8 mmol) was aminated with reagent (*R*)-**10** according to the method and conditions described for the allylic amination of methylenecyclohexane with diimido selenium reagent (*S*)-**10**. The crude product (oil) was chromatographed on 70 g of silica gel using 5—10% EtOAc/hexane to give 488 mg (25%) of the diastereomeric mixture **13** in a ratio of 34:66 (32% diastereomeric excess) as an oil: IR (neat) 3228, 2962, 2938, 2864, 1601, 1451, 1318, 1303, 1290, 1263, 1155, 1114, 1095, 1020, and 929 cm^{-1}. The NMR spectrum was identical with an authentic sample of a 1.0:1.0 diastereomeric mixture of **13′** (vide infra) except for intensities of the peaks in the olefinic proton region. HPLC (4.6 mm i.d. 150 mm Finepak SIL C_{18} S; 3:7 H_2O/MeOH, 1 mL min^{-1}) retention times of the major (t_r=8.35 min) and minor (t_r=9.23 min) diastereomers in the mixture were identical with those of the authentic sample of **13′**. The above diastereomeric ratio (34:66) was determined by GC analysis of the *N*-trifluoroacetyl-L-prolyl derivative **14**, which was derived by reductive cleavage of the diastereomeric mixture **13** and subsequent acylation with *N*-trifluoroacetyl-L-prolyl chloride as shown in Scheme 5 (see general method for the determination of diastereomeric ratios).

Determination of the Absolute Configuration of the Major Diastereomer of 13. L-Norleucine (L-2-aminohexanoic acid, 6 mg) was acylated with *N*-trifluoroacetyl-L-prolyl chloride and the resulting amide was then methylated with diazomethane (Scheme 5) according to the method and conditions described for the determination of absolute configuration of the major diastereomer of **16**. GC analysis (2 m 3% Silicone OV-17 on 80/100 mesh Uniport HP, 180 °C, flow rate: 50 mL min^{-1}) of the crude product revealed a single peak[25] (t_r=39.60 min) attributed to (2*S*)-**15**. The reaction was repeated with *dl*-norleucine and GC analysis of the product showed a 1.0:1.0 ratio of (2*R*)-**15** (t_r=34.60 min) to (2*S*)-**15** (t_r=39.60 min).

The diastereomeric mixture **13** (34:66, 12 mg) was converted to amido ester **15** according to the method and conditions described for the conversion of diastereomeric mixture **16** to amido ester **18**. GC analysis (2 m 3% Silicone OV-17 on 80/100 mesh Uniport HP, 180 °C, flow rate: 50 mL min^{-1}) of the crude product showed a 66:34 ratio of (2*R*)-**15** (t_r=34.60 min) to (2*S*)-**15** (t_r=39.60 min), thus providing the *R*-configuration at the carbon bearing the nitrogen in the major diastereomer of **13**.

Allylic Amination of Cyclooctene with Diimido Selenium Reagent (*R*)-10. Cyclooctene (330 mg, 3 mmol) was aminated with reagent (*R*)-**10** according to the method and conditions described for allylic amination of methylenecyclohexane with reagent (*S*)-**10**. The crude product (oil) was chromatographed on 40 g of silica gel using 5—10% EtOAc/hexane to give 379 mg (30%) of the diastereomeric mixture **26** in a ratio of 4.0:6.0 (20% diastereomeric excess) as crystals: mp 117—127 °C; IR (KBr) 3205, 2920, 2850, 1650, 1599, 1447, 1326, 1302, 1217, 1150, 1113, 1088, 1052, and 1023 cm^{-1}. The NMR spectrum was identical with an authentic sample of a 62:38 diastereomeric mixture of **26′** (vide infra) with the exception of differing peak intensities in the olefinic proton region and the shape of proton signal due to the NH. The NH proton signal appeared at 6.10 ppm as a broad singlet. HPLC (4.6 mm i.d. 150 mm Finepak SIL C_{18} S; 3:7 H_2O/MeOH, 1 mL min^{-1}) retention times of the major (t_r=7.95 min) and minor (t_r=8.41 min) diastereomers in the mixture were identical with those of the authentic sample of **26′**. The above diastereomeric ratio (4.0:6.0) was determined by GC analysis of *N*-trifluoroacetyl-L-prolyl derivative **27**, which was obtained by reductive cleavage of the diastereomeric mixture **26** and subsequent acylation with *N*-trifluoroacetyl-L-prolyl chloride as shown in Scheme 8 (see general method for the determination of diastereomeric ratio).

GC Studies for the Determination of Absolute Configuration of the Major Diastereomer of 26. The diastereomeric mixture **26** (4.0:6.0, 13 mg) was converted to amido ester **28** (Scheme 8) according to the method and conditions de-

scribed for the conversion of diastereomeric mixture **16** to amido ester **18**. GC analysis (1 m 1% PEG-20M-P on 80/100 mesh Uniport HP, 195 °C, flow rate: 45 mL min^{-1}) of the product showed a 4.0:6.0 ratio of the minor (t_r=23.02 min) to the major diastereomer (t_r=28.17 min).

L-Glutamic acid (7 mg) was acylated with *N*-trifluoroacetyl-L-prolyl chloride and the resulting amide was then methylated with diazomethane according to the method and conditions described for the determination of absolute configuration of the major diastereomer of **16**. GC analysis (the same column as above, 180 °C, flow rate: 45 mL min^{-1}) of the product afforded a single peak[25] (t_r=22.20 min) assigned to (2*S*)-**29**. The reaction was repeated with *dl*-glutamic acid and GC analysis of the product showed a 1.0:1.0 ratio of (2*R*)-**29** (t_r=18.20 min) to (2*S*)-**29** (t_r= 22.20 min).

A 1:1 diastereomeric mixture of (2*R*)-**15** and (2*S*)-**15** were analyzed by GC using the same column as above (170 °C, flow rate: 24 mL min^{-1}). Retention times of (2*R*)-**15** and (2*S*)-**15** were 7.80 and 10.50 min, respectively.

***dl*-2-Cyclohexenylamine Hydrochloride (*dl*-20).** To naphthalene-sodium reagent[14] [prepared by stirring the mixture of 276 mg (12 mmol) of sodium metal, 1.62 g (12.6 mmol) of naphthalene and 24 mL of freshly distilled dry 1,2-dimethoxyethane for 2 h under nitrogen] was added 503 mg (2 mmol) of *dl*-*N*-*p*-tolylsulfonyl-2-cyclohexenylamine (**19**).[4] After stirring for 1 h, the reaction was quenched by addition of ice-water (10 mL), acidified with 1 M HCl to pH<1, and the resulting solution was washed with diethyl ether (3×35 mL) to eliminate naphthalene and other nonbasic substances. The aqueous layer was then made strongly basic (pH>11) with 30% NaOH, saturated with NaCl, and extracted with chloroform three times (30, 10, and 10 mL). The combined chloroform extracts were dried by passing through a cone of anhydrous sodium sulfate. After addition of 0.5 mL of concd HCl, the mixture was concentrated and the crystalline residue was washed succesively with 1 mL of hexane and 1 mL of benzene to give 187 mg (70%) of *dl*-**20** as off-white crystals. An analytical sample was obtained by recrystallization from 1-propanol/hexane to afford white crystals, mp 159.5—160.5 °C; IR (KBr) 2910, 2714, 2604, 2516, 2042, 1653, 1600, 1502, 1450, 1400, 729, and 670 cm^{-1}; ^{1}H NMR (D_2O) δ=1.4—2.3 (6H, methylene), 3.87 (1H, m, CH-N), 4.78 (3H, s, $NH_2 \cdot HCl$), 5.62 (1H, m, C=CH-C-N), 6.10 (1H, m, CH=C-C-N). Found: C, 54.01; H, 8.79; N, 10.40%. Calcd for $C_6H_{12}ClN$: C, 53.93; H, 9.05; N, 10.48%.

***N*-(2-Cyclohexenyl)-*N'*-(*p*-tolylsulfonyl)benzenesulfonimidamide (16').** To the stirred mixture of 134 mg (1 mmol) of *dl*-2-cyclohexenylamine hydrochloride (*dl*-**20**), 1 g of ice, 2 mL of dichloromethane, and 330 mg (1 mmol) of *N*-(*p*-tolylsulfonyl)benzenesulfonimidoyl chloride (**6**)[10] was added 1 mL of 17% aqueous sodium hydrogencarbonate solution under ice-bath cooling. The reaction mixture was allowed to warm to room temperature (ca. 1 h) and stirred for an additional 24 h. The reaction mixture was twice extracted with ethyl acetate (10 mL, 5 mL), and the combined extracts were dried (Na_2SO_4). Evaporation of the solvent gave crude product which was then passed through a short plug of silica gel (3 g) using 1:1 EtOAc/hexane as eluent. Polar impurities were thus removed and evaporation of the solvent gave crystals, which were further recrystallized from EtOH/hexane to give 169 mg (43%) of optically inactive diastereomeric mixture **16'** (73:27[26]): mp 147—153 °C; HPLC (4 mm i.d. 250 mm LiChrosorb Si 60, 5 μm, 55:1 hexane/isopropyl alcohol, 1 mL min^{-1}) t_r=17.20 min (major), t_r=16.00 min (minor); IR (KBr) 3245, 1647, 1599, 1452, 1311, 1303, 1154, 1117, 1090, 1060, and 1050 cm^{-1}; ^{1}H NMR ($CDCl_3$) δ=1.2—2.1 (6H, methylene), 2.40 (3H, s, aryl methyl), 3.85 (1H, m, CH-N), 5.45—6.20 (3H, m, two vinyl protons and NH), and 7.10—8.10 (9H, aromatic). Found: C, 58.34; H, 5.86; N, 7.17%. Calcd for $C_{19}H_{22}N_2O_3S_2$: C, 58.44; H, 5.68; N, 7.17%.

***dl*-*N*-*p*-Tolylsulfonyl-2-cyclooctenylamine (23).** A mixture of 729 mg (10.5 mmol) of dry selenium powder (dried in vacuo at 80 °C for 1 h) and 4.55 g (10 mmol) of anhydrous Chloramine-T (commercially available Chloramine-T was dehydrated in vacuo at 80 °C for 1 h) in 35 mL of dry dichloromethane (methanol-free dichloromethane was passed through activated alumina, Woelm neutral alumina activity I and stored over 3A Molecular Sieves) was vigorously stirred (magnetically) for 14 h at room temperature under a nitrogen atmosphere (a white or white-gray slurry was usually produced after stirring for 2 to 4 h). Several minutes after addition of 1.56 mL (1.32 g, 12 mmol) of cyclooctene to the stirred slurry at room temperature, a gentle exothermic reaction was observed and the stirring was continued overnight (for about 14 h). The solvent was then removed in vacuo, and the residue was dissolved in a mixture of 150 mL 1:1 ethyl acetate/diethyl ether and 90 mL of an alkaline aqueous solution consisting of 2 parts 1 M NaOH and 1 part saturated NaCl solution. After stirring for 30 min, the entire reaction mixture was filtered through Celite 545 and the organic layer of the filtrate was washed again with the above mentioned alkaline brine solution (2×50 mL), dried (Na_2SO_4), and concentrated to give crude crystals. The crystals were dissolved in 20 mL of acetone. The acetone solution was refluxed for 2 min with 30 mg of activated charcoal and the mixture was passed through a two layered column (13 mm i.d.) consisting of 1.3 g of Celite 545 (lower layer) and 100 mg of activated charcoal (upper layer). More acetone (30 mL) was used to ensure elution of **23** and the combined eluates were concentrated to give white crystals, which were recrystallized from carbon tetrachloride/hexane (ca. 10 mL:15 mL) to give 2.66 g (84%) of **23**: mp 125.0—125.5 °C; IR (KBr) 3230, 2910, 2845, 1595, 1437, 1300, 1144, 1087, and 1060 cm^{-1}; ^{1}H NMR ($CDCl_3$) δ=1.0—2.2 (10H, methylene), 2.41 (3H, s, aryl methyl), 4.19 (1H, m, CH-N), 4.92 (1H, d, J=6.81 Hz, NH), 5.14 (1H, d of d, J=7.69 and 10.55 Hz, C=CH-C-N), 5.54 (1H, d of t, J=10.55 and 5.54 Hz, CH=C-C-N), 7.1—7.9 (4H, aromatic). Found: C, 64.44; H, 7.66; N, 5.02%. Calcd for $C_{15}H_{21}NO_2S$: C, 64.48; H, 7.58; N, 5.01%.

***dl*-2-Cyclooctenylamine Hydrochloride (*dl*-24).** *dl*-2-Cyclooctenylamine hydrochloride (*dl*-**24**) was prepared from 1 g (3.58 mmol) of **23** according to the method and conditions described for the preparation of *dl*-2-cyclohexenylamine hydrochloride (*dl*-**20**), and the crude crystalline hydrochloride was recrystallized from isopropyl alcohol/hexane to give 407 mg (70%) of *dl*-**24**: mp 268—269 °C (sealed tube under nitrogen); IR (KBr) 2926, 2652, 2576, 2040, 1655, 1609, 1586, 1519, 1457, 1410, 758, and 716 cm^{-1}; ^{1}H NMR (D_2O) δ=1.2—2.4 (10H, methylene), 4.26 (1H, m, CH-N), 4.80 (3H, s, $NH_2 \cdot HCl$), 5.47 (1H, d of d, J=7.91 and 10.54 Hz, C=CH-C-N), 5.96 (1H, m, CH=C-C-N). Found: C, 59.54; H, 10.20; N, 8.62%. Calcd for $C_8H_{16}ClN$: C, 59.43; H; 9.97; N, 8.66%.

***N*-(2-Cyclooctenyl)-*N'*-(*p*-tolylsulfonyl)benzenesulfonimidamide (26').** Compound **26'** was prepared from 162 mg (1 mmol) of *dl*-**24** according to the method and conditions

described for the preparation of *N*-(2-cyclohexenyl)-*N'*-(*p*-tolylsulfonyl)benzenesulfonimidamide (**16'**), and recrystallization from ethanol/hexane gave 307 mg (73%) of diastereomeric mixture **26'** (62:38[26]): mp 123—134 °C; HPLC (4.6 mm i.d. 150 mm Finepak SIL C_{18} S; 3:7 H_2O/MeOH, 1 mL min^{-1}) t_r=7.95 min (major), t_r=8.41 min (minor); IR (KBr) 3205, 2920, 2850, 1650, 1599, 1447, 1326, 1302, 1217, 1150, 1113, 1088, 1052, and 1023 cm^{-1}; ^1H NMR ($CDCl_3$) δ=1.0—2.2 (10H, methylene), 2.39 (3H, s, aryl methyl), 4.14 (1H, m, CH-N), 4.8—5.8 (2H, m, CH=CH), 5.98 (0.62H, d, J=6.8 Hz, NH in the major diastereomer), 6.20 (0.38H, d, J=7.3 Hz, NH in the minor diastereomer), 7.1—8.0 (9H, aromatic). Found: C, 60.12; H, 6.23; N, 6.49%. Calcd for $C_{21}H_{26}N_2O_3S_2$: C, 60.26; H, 6.26; N, 6.69%.

***dl*-*N*-*p*-Tolylsulfonyl-1-butyl-2-propenylamine (21).** *dl*-*N*-*p*-Tolylsulfonyl-1-butyl-2-propenylamine (**21**) was prepared by allylic amination of 1-heptene (1.18 g, 12 mmol) according to the method and conditions described for the preparation of *dl*-*N*-*p*-tolylsulfonyl-2-cyclooctenylamine (**23**). The crude product (oil) was chromatographed on 80 g of silica gel using 50—75% benzene/hexane to give 2.08 g (65%) of **21** as an oil. An analytical sample was obtained by Kugelrohr distillation of a portion of this oil (180 °C, 13 Pa): IR (neat) 3280, 2970, 2940, 2860, 1648, 1600, 1500, 1432, 1330, 1163, 1098, 923, and 817 cm^{-1}; ^1H NMR ($CDCl_3$) δ=0.80 (3H, diffuse t, J=5.9 Hz, methyl), 1.0—1.7 (6H, methylene), 2.41 (3H, s, aryl methyl), 3.72 (1H, m, CH-N), 4.8—5.1 (2H, three peaks, CH=C), 5.18 (1H, d, J=7.0 Hz, NH), 5.55 (1H, m, C=CH-N), 7.1—7.9 (4H, aromatic). Found: C, 62.80; H, 8.13; N, 5.14%. Calcd for $C_{14}H_{21}NO_2S$: C, 62.98; H, 7.92; N, 5.24%.

***dl*-1-Butyl-2-propenylamine Hydrochloride (*dl*-22).** *dl*-1-Butyl-2-propenylamine hydrochloride (*dl*-**22**) was prepared from 1 g (3.74 mmol) of **21** according to the method and conditions described for the preparation of *dl*-2-cyclohexenylamine hydrochloride (*dl*-**20**). the crude crystalline hydrochloride was recrystallized from isopropyl alcohol/hexane to give 243 mg (43%) of *dl*-**22**: mp 118—119 °C; IR (KBr) 2928, 2666, 2548, 2060, 1617, 1504, 1439, 1000, and 960 cm^{-1}; ^1H NMR (D_2O) δ=0.887 (3H, t, J=5.93 Hz, methyl), 1.1—1.9 (6H, methylene), 3.78 (1H, d of t, J=6.81 and 6.81 Hz, CH-N), 4.79 (3H, s, aryl methyl), 5.2—5.5 (2H, m, CH=C), 5.6—6.1 (1H, m, C=CH-C-N). Found: C, 56.30; H, 11.06; N, 9.22%. Calcd for $C_7H_{16}ClN$: C, 56.18; H, 10.78; N, 9.36%.

***N*-(1-Butyl-2-propenyl)-*N'*-(*p*-tolylsulfonyl)benzenesulfonimidamide (13').** *N*-(1-Butyl-2-propenyl)-*N'*-(*p*-tolylsulfonyl)benzenesulfonimidamide (**13'**) was prepared from 150 mg (1 mmol) of *dl*-**22** according to the method and conditions described for the preparation of *N*-(2-cyclohexenyl)-*N'*-(*p*-tolylsulfonyl)benzenesulfonimidamide (**16'**). The crude product (oil) was purified by preparative TLC (silica-gel plates, 1:2 EtOAc/hexane) to give 124 mg (30%) of diastereomeric mixture **13'** (1.0:1.0) as an oil: HPLC (4 mm i.d. 150 mm Finepak SIL C_{18} S; 3:7 H_2O/MeOH, 1 ml min^{-1}) t_r=8.35 min (major), t_r=9.23 min (minor); IR (neat) 3228, 2962, 2938, 2864, 1601, 1451, 1318, 1303, 1290, 1263, 1155, 1114, 1095, 1020, and 929 cm^{-1}; ^1H NMR ($CDCl_3$) δ=0.6—1.8 (9H, methyl and methylene), 2.38 (3H, s, aryl methyl), 3.65 (1H, m, CH-N), 4.6—6.0 (3H, m, vinyl), 6.30 (1H, broad s, NH), 7.0—8.1 (9H, aromatic); Anal. by high resolution MS (Hitachi M-80A mass spectrometer): Found: m/z 406.1372. Calcd for $C_{20}H_{26}N_2O_3S_2$: M, 406.1362.

***dl*-2-Methylenecyclohexylamine Hydrochloride (*dl*-12).** *dl*-2-Methylenecyclohexylamine hydrochloride (*dl*-**12**) was prepared from 500 mg (1.88 mmol) of *dl*-*N*-(*p*-tolylsulfonyl)-2-methylenecyclohexylamine (**25**)[4] according to the method and conditions described for the preparation of *dl*-2-cyclohexenylamine hydrochloride (*dl*-**20**). The crude crystalline hydrochloride was recrystallized from isopropyl alcohol/hexane to give 154 mg (55%) of *dl*-**12**: mp 218—220 °C; IR (KBr) 2936, 2056, 1659, 1595, 1513, 1452, 1399, and 910 cm^{-1}; ^1H NMR (D_2O) δ=1.2—2.6 (8H, methylene), 3.75 (1H, m, CH-N), 4.72 (1H, s, vinyl), 4.79 (3H, s, $NH_2 \cdot HCl$), 5.01 (1H, s, vinyl). Found: C, 56.57; H, 9.52; N, 9.37%. Calcd for $C_7H_{14}ClN$: C, 56.94; H, 9.56; N, 9.49%.

The authors wish to express their heartfelt gratitude to Professor K. Barry Sharpless of M. I. T. for his guidance in this work. This research was partially supported by grants to K. B. Sharpless from the United States National Science Foundation (CHE77-14628) and the United States National Institutes of Health (GM24551).

References

1) T. Katsuki and K. B. Sharpless, *J. Am. Chem. Soc.*, **102**, 5974 (1980).

2) R. S. Atkinson, J. Fawcett, D. R. Russell, and G. Tughan, *J. Chem. Soc., Chem. Commun.*, **1986**, 832; R. S. Atkinson and G. Tughan, *ibid.*, **1986**, 834.

3) H. C. Brown, K-W. Kim, T. E. Cole, and B. Singaram, *J. Am. Chem. Soc.*, **108**, 6761 (1986).

4) K. B. Sharpless, T. Hori (Tetsuo Onami), L. K. Truesdale, and C. O. Dietrich, *J. Am. Chem. Soc.*, **98**, 269 (1976).

5) K. B. Sharpless and R. F. Lauer, *J. Am. Chem. Soc.*, **94**, 7154 (1972); D. Arigoni, A. Vasella, K. B. Sharpless, and H. P. Jensen, *ibid.*, **95**, 7917 (1973); L. M. Stephenson and D. R. Speth, *J. Org. Chem.*, **44**, 4683 (1979).

6) The ene reaction mechanisms have been extensively studied on the sulfur analogues of selenium diimide aminating reagents: H. Münsterer, G. Kresze, V. Lamm, and A. Gieren, *J. Org. Chem.*, **48**, 2833 (1983).

7) An investigation to get optically active allylic amines from achiral allylic phenyl selenides has been reported: R. G. Shea, J. N. Fitzner, J. E. Fankhauser, A. Spaltenstein, P. A. Carpino, R. M. Peevey, D. V. Pratt, B. J. Tenge, and P. B. Hopkins, *J. Org. Chem.*, **51**, 5243 (1986).

8) M. R. Jones and D. J. Cram, *J. Am. Chem. Soc.*, **96**, 2183 (1974).

9) K. Oshima, T. Onami, and K. B. Sharpless, unpublished results.

10) I. B. Douglass and R. V. Norton, *J. Org. Chem.*, **33**, 2104 (1968); E. S. Levchenko, N. Ya. Derkach, and A. V. Kirsanov, *Zh. Obshch. Khim.*, **30**, 1971 (1960).

11) B. Loev, M. A. Haas, and F. Dowalo, *Chem. Ind. (London)*, **20**, 973 (1968).

12) Both α-methylbenzylamine enantiomers are available at almost equal cost. This means that the enantiomer of the insoluble (*R,S*)-**7** could be prepared with equal convenience [using (*R*)-(+)-α-methylbenzylamine for the reaction **6**→**7**], and the resulting less soluble enantiomer of (*S,R*)-**7** would afford (*S*)-**8** on solvolysis.

13) Some selenium diimides (e.g. phenylsulfonylselenium diimide) are isolated: N. Ya. Derkach and G. G. Barashenkov,

Zh. Org. Khim., **12**, 2484 (1976); N. Ya. Derkach, G. G. Barashenkov, and E. S. Levchenko, *ibid.*, **18**, 70 (1982).

14) S. Ji, L. B. Gortler, A. Waring, A. Battisti, S. Bank, W. D. Closson, and P. Wriede, *J. Am. Chem. Soc.*, **89**, 5311 (1967).

15) Examination of a Dreiding model of the *N*-salicylidene Schiff base indicates a preferred conformation such that the hydrogen atom at the chiral center is eclipsed with the carbon-nitrogen double bond. For this conformation, if positive Cotton effects are observed near 316 and 251 nm, the chirality of the relevant transition moments is positive, and the *S*-configuration is assigned to the chiral center in the *N*-salicylidene Schiff base. See Ref. 16.

16) B. Ringdahl, H. E. Smith, and F.-M. Chen, *J. Org. Chem.*, **42**, 4184 (1977); H. E. Smith, *Chem. Rev.*, **83**, 359 (1983).

17) Hopkins et al. studied the synthesis of optically active allylic amines from achiral allylic phenyl selenides by oxidative rearrangement in conjunction with chiral amides, and observed the asymmetric induction ranging from 17% to 37%. See Ref. 7.

18) Iwase and Murai studied gas chromatographic separation of 13 neutral or acidic amino acids, and showed that L-amino acids had longer retention times than their D-enantiomers when converted to *N*-(*N*-trifluoroacetyl-L-prolyl) amino acid methyl esters on all the stational phases (22) investigated: H. Iwase and A. Murai, *Chem. Pharm. Bull.*, **22**, 8 (1974). For similar studies, see: B. Halpern and J. W. Westley, *Tetrahedron Lett.*, **1966**, 2283; B. Halpern and J. W. Westley, *Biochem. Biophys. Res. Commun.*, **19**, 361 (1965).

19) P. Bickert, F. W. Carson, J. Jacobus, E. G. Miller, and K. Mislow, *J. Am. Chem. Soc.*, **90**, 4868 (1968); M. Moriwaki, S. Sawada, and Y. Inouye, *Chem. Commun.*, **1970**, 419; M. Moriwaki, Y. Yamamoto, J. Oda, and Y. Inouye, *J. Org. Chem.*, **41**, 300 (1976); B. M. Trost and R. F. Hammen, *J. Am. Chem. Soc.*, **95**, 963 (1973).

20) Melting point of the racemate; 167—169 °C. See; E. S. Levchenko, N. Ya. Derkach, and A. V. Kirsanov, *Zh. Obshch. Khim.*, **32**, 1208 (1962).

21) H. E. Smith, E. P. Burrows, M. J. Marks, R. D. Lynch, F.-M. Chen, *J. Am. Chem. Soc.*, **99**, 707 (1977).

22) To 1.47 g (12 mmol) of salicylaldehyde in 3 mL of absolute MeOH was added 1.93 g (10 mmol) of 28% NaOMe in MeOH while cooling in an ice bath under nitrogen. The precipitated crystals were separated, and washed successively with absolute EtOH and dry benzene under nitrogen, and dried in vacuo to give 1.14 g (79%) of yellow crystals, which did not melt even at 280 °C.

23) Concentration (c) and molecular ellipticity [θ] were calculated for the in situ formed derivative on the basis of complete formation of the Schiff base.

24) T. Nambara and J. Goto, *Bunseki Kagaku*, **23**, 704 (1974).

25) As *N*-trifluoroacetyl-L-prolyl chloride contains 6.2% of the D-enantiomer, a small peak (ca. 6%) due to the other diastereomer containing the D-enantiomer appears on the GC trace.

26) The ratio of two diastereomers (each diastereomer is a 1 : 1 mixture of *d*- and *l*-enantiomers) was changed by recrystallization owing to the different solubilities in the solvent.

 © 1989 The Chemical Society of Japan Bull. Chem. Soc. Jpn., 62, 1179—1187 (1989)

Stereochemical Control in Microbial Reduction. 9. Diastereoselective Reduction of 2-Alkyl-3-oxobutanoate with Bakers' Yeast

Kaoru NAKAMURA,* Takehiko MIYAI,† Ashish NAGAR,†,†† Shinzaburo OKA,† and Atsuyoshi OHNO†
Department of Chemistry, Shiga University of Medical Science, Seta, Ohtsu 520—21
†Institute for Chemical Research, Kyoto University, Uji, Kyoto 611
(Received October 24, 1988)

Bakers' yeast reduces esters of 2-alkyl-3-oxobutanoic acid ($CH_3COCHRCO_2R'$; R=methyl, ethyl, propyl, propargyl, and allyl) into the corresponding (*S*)-hydroxy esters with exclusive stereoselectivity, while the configuration at the 2-position of the hydroxy esters is either *S* (anti) or *R* (syn) depending on the structure of the alkoxyl group in the carboalkoxyl moiety of the ester. Oftenly, the stereoselectivity with respect to the 2-position is not satisfactory. In general, the reduction of *t*-butyl esters exerts predominancy in the products, whereas that of 1,1-dimethylpropyl esters exerts the syn predominancy. A marked difference between these two esters in diastereoselectivity is discussed from the view point of plausible conformations of the esters.

Esters of 2-alkyl-3-hydroxybutanoic acids are important chiral building blocks for syntheses of antibiotics and other natural products. There are three major methods in the literatures to prepare the esters with high diastereo- and enantioselectivities. First of all is the aldol condensation of chiral enolates with aldehydes,[1,2] and the second method is α-alkylation of a dianion from a chiral 3-hydroxybutanoate.[3] The latter method is restricted to synthesize the hydroxy ester of anti conformation. These two methods are chemical transformations and require an optically active starting material(s) in order to obtain an optically active product. The third and biological method involves the reduction of achiral 2-alkyl-3-oxobutanoate by means of certain microbes.[4,5] The biological method has some advantages over the chemical methods in that two chiral centers are introduced into the product in one step starting from an achiral compound, and that some microbes such as bakers' yeast (BY) are quite cheap and easily obtainable. However, on the other hand, diastereoselectivity of microbial reduction is not always satisfactory and sometimes both syn and anti products are produced in nearly equal amounts, which means that dehydrogenases

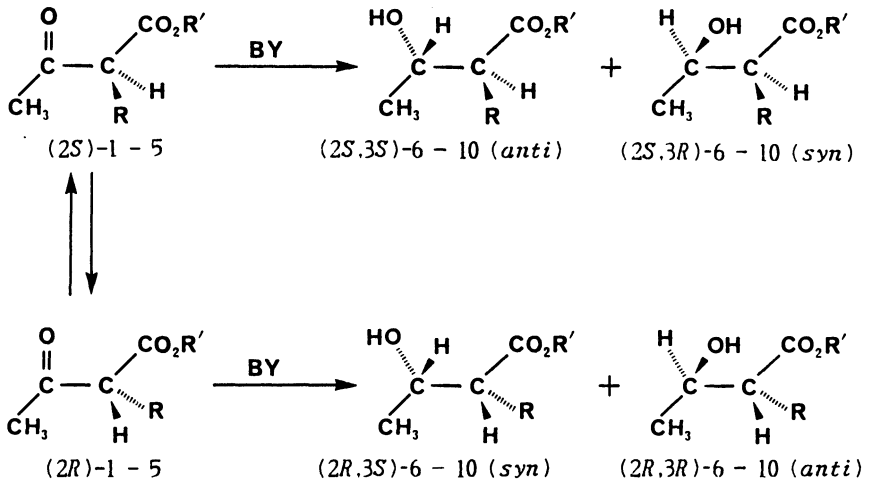

1, **6**; R = CH_3-
2, **7**; R = C_2H_5-
3, **8**; R = *n*-C_3H_7-
4, **9**; R = $HC{\equiv}CCH_2$-
5, **10**; R = $H_2C{=}CHCH_2$-

a; R′ = CH_3-
b; R′ = C_2H_5-
c; R′ = *n*-C_4H_9-
d; R′ = *n*-C_6H_{13}-
e; R′ = *n*-C_8H_{17}-
f; R′ = Me_2CH-
g; R′ = Me_2CHCH_2-
h; R′ = Me_3C-
i; R′ = Me_2EtC-
j; R′ = Me_3CCH_2-

k; R′ = *cyclo*-C_5H_9-
l; R′ = *cyclo*-C_6H_{11}-
m; R′ = *cyclo*-$C_6H_{11}CH_2$-
n; R′ = $PhCH_2$-
o; R′ = $H_2C{=}CHCH_2$-
p; R′ = $MeO(CH_2)_2$-
q; R′ = $EtO(CH_2)_2$-
r; R′ = *n*-$BuO(CH_2)_2$-
s; R′ = $MeS(CH_2)_2$-
t; R′ = $Cl(CH_2)_2$-

Scheme 1.

†† Present address: Chemistry Section, D. V. Project, ONGC, Jorhat, Assam, India.

present in the microbe and responsible for the reduction cannot recognize the configuration at the α (or 2)-position of racemic α-substituted β-keto esters (alkyl 3-oxocarboxylates).

It is known that the stereochemistry of the reduction of β-keto esters by BY affords the corresponding (*S*)-hydroxy esters with moderate to high enantioselectivities,[6] and the substitution by an alkyl group at the α-position of the ester increases the selectivity.[7,8] Therefore, if an α-substituted β-keto ester has a structure which exerts a large difference in rate of reduction between its 2*S*- and 2*R*-enantiomeric isomers, one can expect to obtain the product with a high diastereomeric excess (d.e.). There remains another problem, i.e., if the rate of isomerization between the 2*S*- and 2*R*-isomers is not fast enough compared to the rate of reduction, the chemical yield of the product cannot exceed 50% even though the recognition between 2*S*- and 2*R*-isomers with an enzyme is excellent. On the other hand, if racemization at the α-position takes place much faster than the reduction, the starting material remains racemic whole through the reaction period and the product is expected to be highly diastereoselective after 100% completion of the reaction.

We would like to report in this paper that the diastereoselectivity of the reduction of an α-substituted β-keto ester with BY can be controlled by the change in the structure of alkoxyl group: the presence and absence of a methylene group next to the alkoxyl oxygen play a crucial role in determining the syn/anti selectivity, therefore the d.e., of the reduction.

Results

Various esters of 2-methyl- (**1**), 2-ethyl- (**2**), 2-propyl- (**3**), 2-propargyl- (**4**), and 2-allyl-3-oxobutanoates (**5**) were prepared from the corresponding unsubstituted esters by alkylation and subjected to the reducion with BY. The diastereoselectivities of the reduction (syn/anti ratio in the product) were monitored on GLC. The authentic samples for the anti isomers were prepared by the reaction of the dianion of 3-hydroxybutanoates with the corresponding alkyl halides.[3]

The rate of deuterium incorporation at the 2-position of ethyl 2-methyl-3-oxobutanoate (**1b**) in neutral deuterium oxide was measured on a ^{1}H NMR spectrometer. The signal from the methine proton of **1b** (δ_{TMS}: 3.8) was compared with that from the methylene protons in the ethyl group (δ_{TMS}: 4.3). The intensity of the former signal decreased gradually with a half-life of about 1.5 hours, which is at least an order of magnitude faster than the rate of reduction. On the other hand, practically no incorporation of deuterium was observed with 2-methyl-3-hydroxybutanoate (**6b**) under the same reaction conditions.

Results from the reduction of various esters are summarized in Table 1.[9] The diastereomeric composition of 2,2-dimethylpropyl 2-methyl-3-hydroxybutanoate (**6j**) obtained by the reduction with BY was measured in detail, after it was converted into **6a**, and found the ratio of 2*R*, 3*S* : 2*S*, 3*S* : 2*R*, 3*R* : 2*S*, 3*R* to be 96 : 4 : $<$1 : $<$1. Thus, it was confirmed that the contamination of the (3*R*)-isomers is negligible, if any.

Discussion

Since H-D exchange and racemization at the α-position of a β-keto ester pass through the same intermediate (enolate), there remains no doubt that fast incorporation of deuterium in **1b** under neutral conditions reveals that the starting material stays in a racemic mixture with respect to the enantiomorphism at the α-position whole through the reduction by BY, where there are many acid and base catalysts to promote the enolization. That is, all starting materials subjected to the present reduction can, at least theoretically, be converted into the product of desired configuration (kinetic resolution), provided the difference in rate of reduction for two enantiomers is large enough.

Elongation of alkyl chain in alkoxyl group of the β-keto ester did not show remarkable difference in the diastereoselectivity of the reduction for all α-substituents so far studied. This is in contrast to the reduction of β-keto esters unsubstituted at the α-position.[10] In addition, substitution of a methylene group in the alkyl chain by either a heteroatom such as oxygen or sulfur or an aromatic group did not affect the selectivity in recognizable extent as can be seen in Table 1. Thus, the change in the polarity (or hydrophobicity) of the alkoxyl group seems to exert very little effect, if any, on the selectivity. Another interesting trend seen in Table 1 is that α-allyl substituent tends to afford the anti product, whereas others prefer to yield the syn product. The latter trend is the strongest with the α-methyl substituent, the shortest alkyl group. Since the propargyl group belongs to the syn-preferential substituent, it is clear that the anti-orientation with the allyl group is not due to the presence of a π-bonding in this substituent.

A remarkable change in the diastereoselectivity can be seen in anti preference with 2-allyl-3-oxobutanoates (**10**) when the alkoxyl oxygen is bound directly to a tert-carbon such as in *t*-butyl (**10h**) and 1,1-dimethylpropyl (**10i**) esters. The same structure also shifts the selectivity toward the anti direction in 2-methyl-3-hydroxybutanoates (**6**), and the syn/anti ratio becomes the worst in **6h**. Instead, the insertion of a methylene group between the alkoxyl oxygen and a bulky alkyl substituent such as in 2,2-dimethylpropyl (**j**) or cyclohexylmethyl (m) esters shifts the selectivity to syn direction. Consequently, the syn/anti ratio in **6** is improved by the alkoxyl group of this kind, but the value for **10** with these alkoxyl groups becomes worse.

It is interesting to note that one methylene group in the alkoxyl moiety affects the stereochemistry of the reduction. It should be emphasized that the reduction

Table 1. Syn/Anti Ratio in the β-Hydroxy Esters Obtained by the Reduction of α-Substituted β-Keto Esters by Bakers' Yeast[a)]

Compd.	R′ in ester	R in ester				
		Me **6**	Et **7**	*n*-Pr **8**	$HC{\equiv}CCH_2$- **9**	$H_2C{=}CHCH_2$- **10**
a	CH_3-	81/19 (11)	62/38 (70)	72/28 (80)	57/43 (39)	27/73 (25)
b	C_2H_5-	87/13 (59)	74/26 (80)	74/26 (70)	68/32 (80)	35/65 (59)
c	*n*-C_4H_9-	88/12 (67)	50/50 (60)	49/51 (40)	69/31 (97)	36/64 (24)
d	*n*-C_6H_{13}-	94/6 (76)	74/26 (50)	—	—	48/52 (22)
e	*n*-C_8H_{17}-	92/8 (63)	76/24 (84)	b)	—	b)
f	Me_2CH-	—	—	65/35 (70)	66/34 (86)	31/69 (27)
g	Me_2CHCH_2-	93/7 (87)	60/40 (75)	—	70/30 (82)	51/49 (43)
h	Me_3C-	72/28 (85)	21/79 (55)	25/75 (76)	17/83 (68)	6/94 (36)
i	Me_2EtC-	69/31 (19)	21/79 (4)	23/77 (5)	22/78 (48)	3/97 (9)
j	Me_3CCH_2-	96/4 (57)	69/31 (70)	80/20 (68)	77/23 (76)	56/44 (66)
k	*cyclo*-C_5H_9-	81/19 (82)	—	—	—	52/48 (63)
l	*cyclo*-C_6H_{11}-	90/10 (81)	—	—	—	25/75 (25)
m	*cyclo*-$C_6H_{11}CH_2$-	94/6 (83)	—	—	—	—
n	$PhCH_2$-	82/18 (79)	—	50/50 (70)	—	16/84 (54)
o	$H_2C{=}CHCH_2$-	—	53/47 (65)	68/32 (65)	61/39 (84)	25/75 (49)
p	$MeO(CH_2)_2$-	87/13 (75)	53/47 (80)	63/37 (80)	62/38 (—)	30/70 (37)
q	$EtO(CH_2)_2$-	87/13 (80)	58/42 (73)	57/43 (63)	—	35/65 (60)
r	*n*-$BuO(CH_2)_2$-	87/13 (90)	66/34 (82)	81/19 (80)	50/50 (—)	24/76 (56)
s	$MeS(CH_2)_2$	89/11 (84)	—	—	—	34/66 (78)
t	$Cl(CH_2)_2$	85/15 (60)	—	—	—	—

a) Numbers in parentheses are chemical yields. b) No reaction.

with BY is catalyzed by a variety of catalysts, dehydrogenases, and reductases, in this microbe, and we cannot nominate any one of enzymes as the sole candidate for the catalyst. Zhou and his co-workers reported that there are at least three dehydrogenases in BY to reduce 4-chloro-3-oxobutanoates.[11)] Furuichi and his co-workers found that benzyl 2-methyl-3-oxobutanoate is reduced by a pure enzyme into the corresponding β-hydroxy ester with the syn/anti ratio of 8/1, whereas the reduction of the same ester with a yeast affords the syn/anti ratio to be 2/1[12)] suggesting the contribution of plural enzymes in yeast. Nevertheless, the sum of individual diastereoselectivities of all enzymes involved in the reduction can be attributed to the diastereoselectivity of an "imaginary" enzyme.[13)]

Inspection of molecular structures of the esters with the aid of CPK-models seems to suggest a simple rule; *a principle of the smallest volume*. Figures 1a and 1b show molecular models for (2*R*,3*S*)-**6j** (syn) and (2*S*,3*S*)-**6j** (anti), respectively, where a bulky substituent is represented by an iodine atom. Suppose that the carboxylate oxygen assumes the syn-conformation with respect to the carbonyl oxygen to be reduced and the "hydride" from NAD(P)H attacks the carbonyl group from the front side to give the (3*S*)-hydroxy ester as seen in Fig. 1. Also suppose that the molecule is folded in the pocket of the "imaginary" enzyme so that the alkoxyl oxygen in the ester can assume the syn-conformation in the molecular plane. From Fig. 1, it is recognized that the alkoxyl oxygen in the *syn*-**6j** can assume the full syn-conformation in the molecular plane without being suffered from any strain, whereas

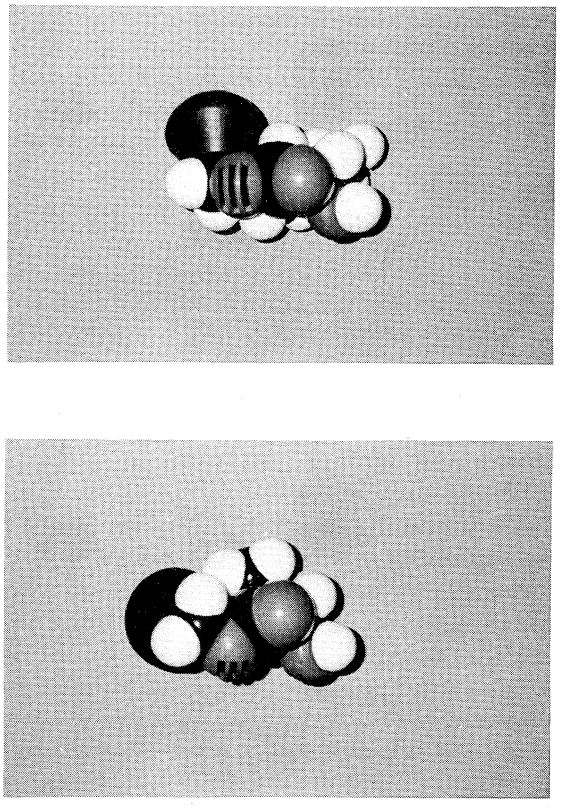

Fig. 1. CPK-models for (a) 2*R*,3*S* (*syn*)- and (b) 2*S*,3*S* (*anti*)-alkyl 2-methyl-3-hydroxybutanoates. The bulky substituent in the alkoxyl group is represented by an iodine model.

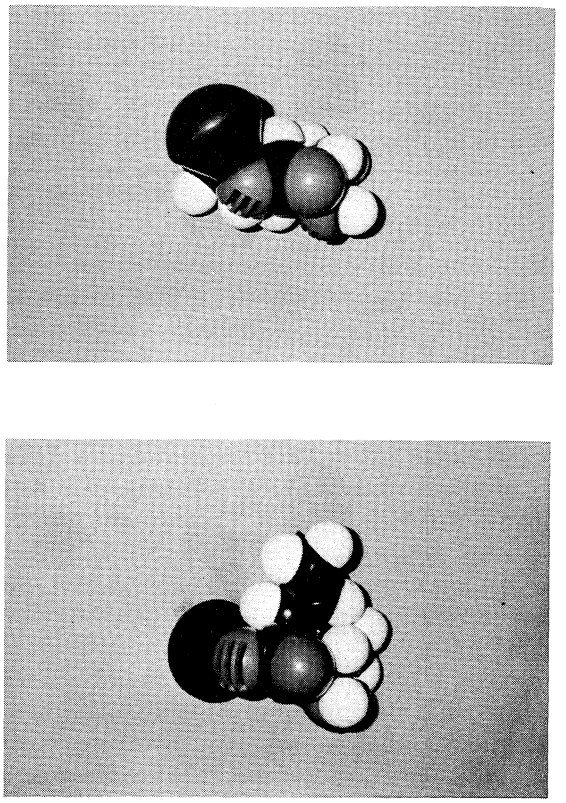

Fig. 2. CPK-models for (a) 2*R*,3*S* (*syn*)- and (b) 2*S*,3*S* (*anti*)-alkyl- 2-allyl-3-hydroxybutanoates. The bulky substituent in the alkoxyl group is represented by an iodine model.

the oxygen in the *anti*-**6j** has to be twisted from the plane to be in the syn-conformation.

Contrary, the alkoxyl oxygen can assume the full syn-conformation in (2*S*,3*S*)-**10h** (anti), as shown in Fig. 2 in which a bulky substituent is again represented by an iodine, but it is largely twisted from the planarity in (2*R*, 3*S*)-**10h** (syn). Thus, the reduction affords satisfactory diastereoselectivity only when the structure of an ester is such that in which the alkoxyl oxygen can assume *a planar syn-conformation* in the product β-hydroxy ester. In other words, the pocket of the "imaginary" enzyme does not have enough room and elasticity to accept a bulky molecule, and the stereoselectivity appears large either in syn or anti direction when the fundamental skeleton of β-keto ester can assume the smallest volume. The presence or absence of a methylene group adjacent to the alkoxyl oxygen is crucial to make the syn or anti conformation more stable than the other, respectively. Since the substituent at the 2-position of **7**, **8**, or **9** is larger than that in **6**, the steric bulk of the alkoxyl group becomes more important in these esters, and the syn/anti predominancy is reversed in **7h**, **8h**, and **9h**. The conformational effect is more important than the hydrophobicity of the alkoxyl group to determine the selectivity. Similar trend in the steric bulk of the alkoxyl group was also observed in the reduction of 2-methyl-3-oxopropanoates.[14] It should be emphasized again that the argument has been done for a pocket of imaginary enzyme composed of a pack of many real enzymes.

In order to confirm the proposed principle, and to prove its versatility, we have to accumulate further results from various esters. However, we believe that the principle at the present stage can suggest the structure of substituents we should try in order to obtain the β-hydroxy ester of certain configuration at least as a working hypothesis.

Experimental

Instruments. ^{1}H NMR spectra were recorded on a Varian VXR-200 spectometer in $CDCl_3$ with tetramethylsilane (TMS) as an interal reference or in D_2O with sodium 3-(trimethylsilyl)-1-propanesulfonate-1,1,2,2-d_4 (DSS) as an internal reference. Gas chromatography was recorded on a Yanaco G-1800 and a G-2800 gas chromatographs. Optical rotations were measured with a Perkin-Elmer 241 polarimeter.

Materials. Organic reagents were purchased from Nacalai Tesque Co., Tokyo Kasei Co., and Aldrich Chemical Co. unless otherwise indicated. Solvents and commercially available starting materials were generally used without additional purification unless otherwise indicated. Pyridine and benzene were refluxed on calcium hydride for 1 day and distilled before the use. Satisfactory results were obtained from elemental analyses of all of the products.

Rate of Enolization. Into 0.5 ml of D_2O containing DSS in an NMR sample tube, 20 mg of ethyl 2-methyl-3-oxobutanoate (**1b**) was added and the solution was immediately subjected to ^1H NMR spectroscopy. The intensity of signal from the methine proton (δ_{DSS}: 3.8) was compared with that from the methylene proton in the ethyl group (δ_{DSS}: 4.3). Initially, the ratio of the intensities of both signals was 1/2, but it decreased to 1/4 after 1.5 h, revealing that the rate of enolization takes place much faster than the reduction.

Preparation of Alkyl 2-Alkyl-3-oxobutanoate. In general, into 200 ml of a benzene solution containing 0.1 mol of an alkyl 3-oxobutanoate and 0.1 mol of 1,8-diazabicyclo[5.4.0]-undec-7-ene (DBU) was added 0.1 mol of an appropriate alkyl iodide in 100 ml of benzene. The resulted mixture was stirred for 3 h at room temperature and filtered. The filtrate was washed with water, dried over anhydrous sodium sulfate, and concentrated under reduced pressure. The residue was distilled to give an alkyl 2-alkyl-3-oxobutanoate. For 1,1-dimethylpropyl esters, the residue was subjected to a column chromatography on silica gel using hexane-ether (100:3) as an eluent. 2-Methyl-3-oxobutanoates, except for **1a**, **1b**, **1h**, and **1i**, were prepared by transesterification with the corresponding ethyl ester (**1b**) according to the literature procedure.[14] Chemical yields (%), boiling points (°C/mmHg[15]), and ^1H NMR spectral data (δ_{TMS} in $CDCl_3$) of the esters are summalized below in this order.

1a: 59; 68 (16); 1.34 (3H, d, J=7.2 Hz), 2.23 (3H, s), 3.51 (1H, q, J=7.2 Hz), and 3.73 (3H, s). **1c**: 66; 110 (15); 0.92 (3H, t, J=7.2 Hz), 1.33 (3H, d, J=7.2 Hz), 1.31—1.73 (4H, m), 2.23 (3H, s), 3.49 (1H, q, J=7.2 Hz), and 4.13 (2H, t, J=6.8 Hz). **1d**: 81; 84 (1.5); 0.88 (3H, t, J=6.5 Hz), 1.18—1.72 (8H, m), 1.33 (3H, d, J=7.2 Hz), 2.23 (3H, s), 3.49 (1H, q, J=7.2 Hz), and 4.12 (2H, t, J=6.6 Hz). **1e**: 91; 78 (0.4); 0.87 (3H, t, J=6.5 Hz), 1.15—1.72 (12H, m), 1.33 (3H, d, J=7.0 Hz), 2.23 (3H, s), 3.49 (1H, q, J=7.2 Hz), and 4.12 (2H, t, 6.7 Hz). **1g**: 59; 96—98 (16); 0.92 (6H, d, J=6.8 Hz), 1.34 (3H, d, J=7.2 Hz), 1.94 (1H, m), 2.24 (3H, s), 3.52 (1H, q, J=7.2 Hz), and 3.91 (2H, dd, J=6.8 Hz, 1.3 Hz). **1h**: 60; 90 (21); 1.27 (3H, d, J=7.2 Hz), 1.44 (9H, s), 2.21 (3H, s), and 3.38 (1H, q, J=7.2 Hz). **1i**: 14; —; 0.86 (3H, t, J=7.5 Hz), 1.28 (3H, d, J=7.0 Hz), 1.42 (6H, s), 1.76 (2H, q, J=7.5 Hz), 2.22 (3H, s), and 3.40 (1H, q, J=7.0 Hz). **1j**: 45; 108 (20); 0.93 (9H, s), 1.35 (3H, d, J=7.2 Hz), 2.25 (3H, s), 3.53 (1H, q, J=7.2 Hz), and 3.82 (2H, d, J=2.2 Hz). **1k**: 76; 125 (19); 1.31 (3H, d, J=7.1 Hz], 1.49—1.97 (8H, m), 2.21 (3H, s), 3.44 (1H, q, J=7.1 Hz), and 5.17—5.25 (1H, m). **1l**: 68; 141 (21); 1.21—1.89 (10H, m), 1.32 (3H, d, J=7.2 Hz), 2.22 (3H, s), 3.46 (1H, q, J=7.2 Hz), and 4.73—4.87 (1H, m). **1m**: 72; 91 (0.5); 0.75—1.8 (11H, m), 1.33 (3H, d, J=7.2 Hz), 2.23 (3H, s), 3.50 (1H, q, J=7.2 Hz), and 3.93 (2H, d, J=6.2 Hz). **1n**: 71; 111 (1); 1.35 (3H, d, J=7.2 Hz), 2.18 (3H, s), 3.54 (1H, q, J=7.2 Hz), 5.17 (2H, s), and 7.34 (5H, s). **1p**: 55; 119 (21); 1.32 (3H, d, J=7.2 Hz), 2.22 (3H, s), 3.34 (3H, s), 3.52 (1H, q, J=7.2 Hz), 3.57 (2H, m), and 4.27 (2H, m). **1q**: 26; 130 (20); 1.19 (3H, t, J=7.0 Hz), 1.34 (3H, d, J=7.2 Hz), 2.24 (3H, s), 3.51 (2H, q, J=7.0 Hz), 3.62 (2H, t, J=4.8 Hz), 4.19 (1H, q, J=7.2 Hz), and 4.26—4.31 (2H, m). **1r**: 77; 153 (24); 0.90 (3H, t, J=7.2 Hz), 1.24—1.63 (4H, m), 1.34 (3H, d, J=7.2 Hz), 2.24 (3H, s), 3.44 (2H, t, J=6.5 Hz), 3.53 (1H, q, J=7.2 Hz), 3.61 (2H, t, J=4.8 Hz), and 4.25—4.31 (2H, m). **1s**: 55; 150 (20); 1.35 (3H, d, J=6.8 Hz), 2.13 (3H, s), 2.25 (3H, s), 2.72 (2H, t, J=6.8 Hz), 3.52 (1H, q, J=7.2 Hz), and 4.30 (2H, t, J=6.8 Hz). **1t**: 50; 128 (19); 1.37 (3H, d, J=7.1 Hz), 2.27 (3H, s), 3.56 (1H, q, J=7.1 Hz), 3.70 (2H, t, J=5.6 Hz), and 4.36—4.42 (2H, m). **2a**: 74; 78 (17); 0.90 (3H, t, J=7.5 Hz), 1.86 (2H, m), 2.20 (3H, s), 3.33 (1H, t, J=7.5 Hz), and 3.72 (3H, s). **2b**: 50; 85 (17); 0.90 (3H, t, J=7.4 Hz), 1.24 (3H, t, J=7.2 Hz), 1.85 (2H, m), 2.19 (3H, s), 3.30 (1H, t, J=7.4 Hz), and 4.16 (2H, q, J=7.2 Hz). **2c**: 67; 109 (17); 0.89 (6H, t, J=7.4 Hz), 1.22—1.43 (2H, m), 1.51—1.66 (2H, m), 1.75—1.90 (2H, m), 2.18 (3H, s), 3.29 (1H, t, J=7.4 Hz), and 4.09 (2H, t, J=6.6 Hz). **2d**: 40; 135 (17); 0.86 (3H, t, J=6.6 Hz), 0.91 (3H, t, J=7.5 Hz), 1.15—1.40 (6H, m), 1.53—1.69 (2H, m), 1.79 —1.93 (2H, m), 2.20 (3H, s), 3.31 (1H, t, J=7.4 Hz), and 4.11 (2H, t, J=6.7 Hz). **2e**: 79; 150 (17); 0.87 (3H, t, J=7.2 Hz), 0.92 (3H, t, J=7.4 Hz), 1.12—1.40 (10H, m), 1.53—1.71 (2H, m), 1.79—1.98 (2H, m), 2.21 (3H, s), 3.32 (1H, t, J=7.4 Hz), and 4.12 (2H, t, J=6.7 Hz). **2g**: 41; 104 (17); 0.90 (6H, d, J=6.8 Hz), 0.90 (3H, t, J=7.4 Hz), 1.86 (3H, m), 2.20 (3H, s), 3.33 (1H, t, J=7.4 Hz), and 3.89 (2H, d, J=6.6 Hz). **2h**: 38; 86 (17); 0.89 (3H, t, J=7.4 Hz), 1.44 (9H, s), 1.80 (2H, m), 2.22 (3H, s), and 3.20 (1H, t, J=7.2 Hz). **2i**: 13; —; 0.87 (3H, t, J=7.4 Hz), 0.91 (3H, t, J=7.5 Hz), 1.42 (6H, s), 1.76 (2H, q, J=7.5 Hz), 1.82 (2H, m), 2.20 (3H, s), and 3.23 (1H, t, J=7.4 Hz). **2j**: 93; 106 (17); 0.92 (9H, s), 0.92 (3H, t , J=7.4 Hz), 1.88 (2H, m), 2.22 (3H, s), 3.36 (1H, t, J=7.4 Hz), and 3.81 (2H, s). **2o**: 42; 100 (17); 0.91 (3H, t, J=7.4 Hz), 1.87 (2H, m), 2.20 (3H, s), 3.35 (1H, t, J=7.4 Hz), 4.58—4.63 (2H, m), 5.19—5.36 (2H, m), and 5.78—5.99 (1H, m). **2p**: 42; 124 (17); 0.89 (3H, t, J=7.5 Hz), 1.85 (2H, m), 2.19 (3H, s), 3.32 (3H, s), 3.35 (1H, t, J=7.5 Hz), 3.52—3.58 (2H, m), and 4.23—4.28 (2H, m). **2q**: 70; 88 (3); 0.92 (3H, t, J=7.5 Hz), 1.17 (3H, t, J=7.0 Hz), 1.87 (2H, m), 2.21 (3H, s), 3.36 (1H, t, J=7.5 Hz), 3.49 (2H, q, J=7.0 Hz), 3.58—3.64 (2H, m), and 4.25—4.80 (2H, m). **2r**: 74 108 (3); 0.90 (3H, t, J=7.3 Hz), 0.93 (3H, t, J=7.4 Hz), 1.24—1.62 (4H, m), 1.88 (2H, m), 2.23 (3H, s), 3.32—3.48 (3H, m), 3.59—3.64 (2H, m), and 4.26—4.31 (2H, m). **3a**: 66; 51 (1); 0.89 (3H, t, J=7.2 Hz), 1.28 (2H, m), 1.18—1.87 (2H, m), 2.19 (3H, s), 3.41 (1H, t, J=7.4 Hz), and 3.70 (3H, s). **3b**: 48; 90 (17); 0.91 (3H, t, J=7.2 Hz), 1.25 (3H, t, J=7.2 Hz), 1.21—1.39 (2H, m), 1.74—1.87 (2H, m), 2.20 (3H, s), 3.39 (1H, t, J=7.3 Hz), and 4.17 (2H, q, J=7.2 Ha). **3c**: 62; 67 (1); 0.90 (6H, t, J=7.2 Hz), 1.20—1.87 (8H, m), 2.19 (3H, s), 3.39 (1H, t, J=7.5 Hz), and 4.11 (2H, t, J=6.6 Hz). **3e**: 74; 105 (1); 0.85 (3H, t, J=6.6 Hz), 0.90 (3H, t, J=7.5 Hz), 1.13—1.40 (12H, m), 1.51—1.70 (2H, m), 1.72—1.88 (2H, m), 2.19 (3H, s), 3.49 (1H, t, J=7.4 Hz), and 4.09 (2H, t, J=6.6 Hz). **3f**: 54; 70 (1); 0.90 (3H, t, J=7.2 Hz), 1.22 (6H, d, J=6.2 Hz), 1.30 (2H, m), 1.72—1.86 (2H, m), 2.20 (3H, s), 3.35 (1H, t, J=7.5 Hz), and 5.04 (1H, m). **3h**: 60; 55 (1.5); 0.90 (3H, t, J=7.2 Hz), 1.19—1.38 (2H, m), 1.43 (9H, s), 1.69—1.82 (2H, m), 2.18 (3H, s), and 3.28 (1H, t, J=7.6 Hz). **3i**: 7; —; 0.87 (3H, t, J=7.5 Hz), 0.91 (3H, t, J=7.3 Hz), 1.18—1.48 (2H, m), 1.42 (6H, s), 1.71—1.83 (2H, m), 1.76 (2H, q, J=7.3 Hz), 2.20 (3H, s), and 3.32 (1H, t, J=7.5 Hz). **3j**: 62; 113 (17); 0.86—1.00 (3H, m), 0.92 (9H, s), 1.31 (2H, m), 1.77—1.89 (2H, m), 2.22 (3H, s), 3.44 (1H, t, J=7.4 Hz), and 3.80 (2H, s). **3n**: 59 135 (1); 0.90 (3H, t, J=7.2 Hz), 1.29 (2H, m), 1.78—1.90 (2H, m), 2.16 (3H, s), 3.46 (1H, t, J=6.4 Hz), 5.16 (2H, s), and 7.34 (5H, s). **3o**: 51; 61 (1); 0.92 (3H, t, J=7.1 Hz), 1.31 (2H, m), 1.84 (2H, m), 2.22 (3H, s), 3.44 (1H, t, J=7.2 Hz), 4.59—4.64 (2H, m), 5.21—5.37 (2H, m), and 5.80—6.01 (1H, m). **3p**: 62; 84 (1); 0.88 (3H, t, J=7.2 Hz), 1.28 (2H, m), 1.89 (2H, m), 2.19 (3H, s), 3.32 (3H, s), 3.43 (1H, t, J=7.5 Hz), 3.53—3.57 (2H, m), and 4.22—4.27 (2H, m). **3q**: 66; 90 (2); 0.91 (3H, t, J=7.4 Hz), 1.18 (3H, t, J=7.0 Hz), 1.14—1.41 (2H, m), 1.73—1.89 (2H, m), 2.22 (3H, s), 3.44 (1H, t, J=7.4 Hz), 3.49 (2H, q, J=7.0 Hz), 3.57—3.66 (2H, m), and 4.25—4.30 (2H, m). **3r**: 60; 133

(5); 0.87 (3H, t, J=7.1 Hz), 0.89 (3H, t, J=7.2 Hz), 1.20—1.62 (6H, m), 1.70—1.90 (2H, m), 2.20 (3H, s), 3.37—3.45 (3H, m), 3.56—3.61 (2H, m), and 4.25 (2H, m). **4a**: 37; 111 (19); 1.99 (1H, t, J=2.7 Hz), 2.30 (3H, s), 2.72 (2H, m), 3.71 (1H, t, J=7.5 Hz), and 3.76 (3H, s). **4b**: 19; 116 (20); 1.28 (3H, t, J=7.1 Hz), 1.99 (1H, t, J=2.6 Hz), 2.30 (3H, s), 2.71 (2H, dd, J=2.6 Hz, 7.2 Hz), 3.68 (1H, t, J=7.4 Hz), and 4.22 (2H, q, J=7.1 Hz). **4c**: 21; 136 (17); 0.92 (3H, t, J=7.2 Hz), 1.29—1.47 (2H, m), 1.56—1.70 (2H, m), 1.98 (1H, t, J=2.7 Hz), 2.30 (3H, s), 2.71 (2H, m), 3.69 (1H, t, J=7.5 Hz), and 4.16 (2H, t, J=6.6 Hz). **4f**: 25; 112 (17); 1.25 (3H, d, J=6.4 Hz), 1.26 (3H, d, J=6.4 Hz), 1.98 (1H, t, J=2.6 Hz), 2.28 (3H, s), 2.69 (2H, m), 3.64 (1H, t, J=7.5 Hz), and 5.07 (1H, m). **4g**: 33; 124 (15); 0.93 (6H, d, J=6.8 Hz), 1.95 (1H, m), 1.98 (1H, t, 2.6 Hz), 2.31 (3H, s), 2.72 (2H, m), 3.71 (1H, t, J=7.5 Hz), and 3.94 (2H, d, J=6.6 Hz). **4h**: 20; 102 (17); 1.46 (9H, s), 1.97 (1H, t, J=2.7 Hz), 2.28 (3H, s), 2.65 (2H, m), and 3.58 (1H, t, J=7.5 Hz). **4i**: 19;—; 0.87 (3H, t, J=7.4 Hz), 1.43 (6H, s), 1.77 (2H, q, J=7.4 Hz), 1.97 (1H, t, J=2.7 Hz), 2.28 (3H, s), 2.65 (2H, m), and 3.60 (1H, t, J=7.5 Hz). **4j**: 25; 131 (18); 0.93 (9H, s), 1.98 (1H, t, J=2.6 Hz), 2.31 (3H, s), 2.71 (2H, m), 3.73 (1H, t, J=7.5 Hz), and 3.84 (2H, s). **4o**: 30; 130 (18); 1.99 (1H, t, J=2.6 Hz), 2.31 (3H, s), 2.72 (2H, m), 3.73 (1H, t, J=7.5 Hz), 4.65 (2H, m), 5.22—5.38 (2H, m), and 5.80—5.99 (1H, m). **4p**: 35; 144 (21); 1.98 (1H, t, J=2.6 Hz), 2.30 (3H, s), 2.71 (2H, m), 3.35 (3H, s), 3.58 (2H, t, J=4.7 Hz), 3.73 (1H, t, J=7.4 Hz), and 4.29 (2H, t, J=4.7 Hz). **4r**: 21; 105 (0.8) 0.90 (3H, t, J=7.3 Hz), 1.35—1.62 (4H, m), 1.99 (1H, t, J=2.7 Hz), 2.26 (3H, s), 2.71 (2H, m), 3.38—3.48 (3H, m), 3.58—3.64 (2H, m), and 4.23—4.32 (2H, m). **5a**: 3; 95 (20); 2.21 (3H, s), 2.58 (2H, t, J=7.2 Hz), 3.52 (1H, t, J=7.2 Hz), 3.71 (3H, s), 4.93—5.18 (2H, m), and 5.51—5.93 (1H, m). **5b**: 41; 100 (20); 1.26 (3H, t, J=6.7 Hz), 2.21 (3H, s), 2.58 (2H, t, J=6.7 Hz), 3.51 (1H, t, J=6.7 Hz), 4.18 (2H, q, J=6.7 Hz), 4.95—5.19 (2H, m), and 5.53—5.97 (1H, m). **5c**: 30; 123 (15); 0.94 (3H, t, J=7.2 Hz), 1.28—1.49 (2H, m), 1.56—1.69 (2H, m), 2.24 (3H, s), 2.60 (2H, t, J=7.1 Hz), 3.53 (1H, t, J=7.5 Hz), 4.15 (2H, t, J=6.6 Hz), 5.02—5.16 (2H, m), and 5.65—5.86 (1H, m). **5d**: 21; 143 (15); 0.89 (3H, m), 1.29 (6H, m), 1.56—1.68 (3H, m), 2.24 (3H, s), 2.60 (2H, m), 3.53 (1H, t, J=7.5 Hz), 4.13 (2H, t, J=6.7 Hz), 5.01—5.15 (2H, m), and 5.65—5.85 (1H, m). **5e**: 45; 100 (0.7); 0.86 (3H, t, J=6.8 Hz), 1.14—1.40 (10H, m), 1.57—1.68 (2H, m), 2.21 (3H, s), 2.57 (2H, m), 3.50 (1H, t, J=7.5 Hz), 4.11 (2H, t, J=6.7 Hz), 4.91—5.13 (2H, m), and 5.62—5.83 (1H, m). **5f**: 81; 106 (20); 1.24 (6H, d, J=6.2 Hz), 2.22 (3H, s), 2.57 (2H, m), 3.47 (1H, t, J=7.4 Hz), 4.99—5.14 (3H, m), and 5.62—5.84 (1H, m). **5g**: 28; 119 (16); 0.93 (6H, d, J=6.8 Hz), 1.75—2.08 (1H, m), 2.25 (3H, s), 2.61 (2H, t, J=6.3 Hz), 3.55 (1H, t, J=7.3 Hz), 3.92 (2H, d, J=6.9 Hz, 4.99—5.18 (2H, m), and 5.56—5.97 (1H, m). **5h**: 11; 105 (16); 1.44 (9H, s), 2.21 (3H, s), 2.53 (2H, t, J=7.4 Hz), 3.40 (1H, t, J=7.4 Hz), 4.93—5.17 (2H, m), and 5.52—5.93 (1H, m). **5i**: —; —; 0.86 (3H, t, J=7.5 Hz), 1.42 (6H, s), 1.75 (2H, q, J=7.5 Hz), 2.22 (3H, s), 2.54 (2H, m), 3.42 (1H, t, J=7.5 Hz), 4.98—5.14 (2H, m), and 5.62—5.82 (1H, m). **5j**: 81; 70 (3); 0.94 (9H, s), 2.25 (3H, s), 2.61 (2H, m), 3.56 (1H, t, J=7.5 Hz), 3.82 (2H, s), 4.99—5.15 (2H, m), and 5.65—5.84 (1H, m). **5k**: 83; 145 (20); 1.51—1.95 (8H, m), 2.19 (3H, s), 2.54 (2H, m), 3.45 (1H, t, J=7.4 Hz), 4.97—5.22 (3H, m), and 5.61—5.82 (1H, m). **5l**: 62; 152 (21); 1.15—1.92 (10H, m), 2.21 (3H, s), 2.57 (2H, m), 3.47 (1H, t, J=7.4 Hz), 4.72—4.88 (1H, m), 4.98—5.13 (2H, m), and 5.62—5.82 (1H, m). **5n**: 75; 142 (2); 2.18 (3H, s), 2.60 (2H, m), 3.56 (1H, t, J=7.4 Hz), 4.98—5.12 (2H, m), 5.16 (2H, s), 5.61—5.82 (1H, m), and 7.34 (5H, s). **5o**: 89; 113 (20); 2.22 (3H, s), 2.58 (2H, m), 3.54 (1H, t, J=7.4 Hz), 4.58—4.62 (2H, m), 5.00—5.36 (4H, m), and 5.61—5.99 (2H, m). **5p**: 78; 140 (20); 2.23 (3H, s), 2.58 (2H, m), 3.35 (3H, s), 3.44—3.60 (3H, m), 4.25—4.30 (2H, m), 5.00—5.13 (2H, m), and 5.62—5.82 (1H, m). **5q**: 81; 96 (3); 1.18 (3H, t, J=7.0 Hz), 2.23 (3H, s), 2.58 (2H, m), 3.44—3.65 (5H, m), 4.24—4.31 (2H, m), 4.99—5.15 (2H, m), and 5.62—5.83 (1H, m). **5r**: 74; 132 (2) 0.89 (3H, t, J=7.1 Hz), 1.25—1.75 (4H, m), 2.23 (3H, s), 2.58 (2H, m), 3.38—3.63 (5H, m), 4.24—4.30 (2H, m), 4.99—5.13 (2H, m), and 5.65—5.84 (1H, m). **5s**: 62; 117 (1); 2.11 (3H, s), 2.27 (3H, s), 2.57 (2H, m), 2.67 (2H, m), 3.52 (1H, t, J=7.4 Hz), 4.27 (2H, m), 4.98—5.13 (2H, m), and 5.61—5.82 (1H, m).

Preparation of Racemic Esters of 3-Hydroxy-2-alkylbutanoate. Sodium borohydride (9.5 mg, 0.25 mmol) was added to a stirred and cooled solution composed of 1 mmol of alkyl 2-alkyl-3-oxobutanoate and 10 ml of tetrahydrofuran (THF) in an ice bath. The resulted solution was stirred at room temperature for 1 h and the THF was removed under reduced pressure, then the residual solution was acidified with dilute aqueous hydrochloric acid. The organic portion was extracted with ether (30 ml), and the ether layer was washed with water, aqueous sodium hydrogencarbonate, and water (10 ml each), respectively. The ethereal solution was dried over anhydrous sodium sulfate, and the solvent was evaporated under reduced pressure. Esters of 3-hydroxy-2-alkylbutanoate were obtained by distillation of the residue with a Kugelrohr apparatus. Chemical yields (%), boiling points (°C/mmHg[15]), and ^{1}H NMR spectral data (δ from TMS in $CDCl_3$) of the esters are summarized below in this order.

6a: 46; 75 (17); 1.17 (syn: s), 1.21 (anti: a) (3H, d, J=6.4 Hz), 1.22 (3H, d, J=6.4 Hz), 2.40—2.67 (2H, m), 3.70 (3H, s), and 4.01—4.28 (1H, m). **6b**: 42; 75 (17); 1.17 (s), 1.21 (a) (3H, d, J=6.3 Hz), 1.17 (3H, d, J=7.0 Hz), 1.26 (3H, t, J=7.2 Hz), 2.35—2.55 (1H, m), 2.59—2.72 (1H, b), 3.79—4.12 (1H, m), and 4.16 (2H, q, J=7.2 Hz). **6c**: 63; (17); 0.92 (3H, t, J=7.2 Hz), 1.16—1.22 (3H, m), 1.17 (3H, d, J=7.2 Hz), 1.28—1.46 (2H, m), 1.55—1.69 (2H, m), 2.36—2.53 (1H, m), 2.59—2.72 (1H, b), 3.79—4.22 (1H, m), and 4.10 (2H, t, J=6.6 Hz). **6d**: 92; 80 (2); 0.88 (3H, t, J=6.6 Hz), 1.16 (s), 1.20 (a) (3H, d, J=6.4 Hz), 1.17 (3H, d, J=6.8 Hz), 1.20—1.40 (6H, m), 1.56—1.68 (2H, m), 2.35—2.56 (1H, m), 2.63 (1H, b), 3.79—4.22 (1H, m), and 4.09 (2H, t, J=6.8 Hz). **6e**: 80; 100 (1.5); 0.87 (3H, t, J=6.5 Hz), 1.15—1.22 (6H, m), 1.15—1.40 (10H, m), 1.57—1.70 (2H, m), 2.37—2.56 (1H, m), 2.55—2.75 (1H, b), 3.81—4.22 (1H, m), and 4.09 (2H, t, J=6.6 Ha). **6g**: 66; 80 (18); 0.96 (6H, d, J=6.8 Hz), 1.17 (s), 1.21 (a) (3H, d, J=6.6 Hz), 1.19 (3H, d, J=7.2 Hz), 1.80 (1H, b), 1.84—2.04 (1H, m), 2.38—2.58 (1H, m), 3.89 (2H, d, J=6.6 Hz), and 3.77—4.21 (1H, m). **6h**: 84; 100 (16); 1.11—1.21 (6H, m), 1.45 (9H, s), 2.25—2.45 (2H, m), 3.75—4.06 (1H, m). **6i**: 68; 100 (20); 0.88 (3H, t, J=7.5 Hz), 1.12—1.21 (6H, m), 1.42 (6H, s), 1.77 (2H, q, J=7.5 Hz), 2.25—2.47 (2H, m), and 3.96—4.21 (1H, m). **6j**: 37; 130 (18); 0.94 (9H. s), 1.18 (s), 1.22 (a) (3H, d, J=6.4 Hz), 1.20 (3H, d, J=7.2 Hz), 2.40—2.60 (1H, m), 2.56—2.77 (1H, b), 3.81 (2H, s), and 3.83—4.12 (1H, m). **6k**: 75; 145 (19); 1.15 (3H, d, J=7.2 Hz), 1.16 (s), 1.20 (a) (3H, d, J=6.1 Hz), 1.50—1.98 (8H, m), 2.26—2.51 (1H, m), 2.55—2.85 (1H, b), 3.78—4.10 (1H, m), and 5.14—5.24 (1H, m). **6l**: 87; 160 (21); 1.15—1.22 (6H, m), 1.25—1.89 (11H, m), 2.34—2.53 (1H, m), 3.79—4.10 (1H, m), and 4.72—4.85 (1H, m). **6m**: 88; 175 (21); 1.17 (s), 1.21 (a) (3H, d, J=6.3 Hz), 1.18 (3H, d, J=7.2 Hz), 0.88—1.79 (11H,

m), 2.37—2.57 (1H, m), 2.44—2.85 (1H, b), 3.91 (s), 3.92 (a) (2H, d, J=6.1 Hz), and 3.81—4.12 (1H, m). **6n**: 73; 180 (19); 1.14—1.22 (6H, m), 2.43—2.64 (2H, m), 3.86—4.16 (1H, m), 5.14 (2H, s), and 7.35 (5H, s). **6p**: 44; 130 (22); 1.16 (s), 1.20 (a) (3H, d, J=6.4 Hz), 1.17 (3H, d, J=7.0 Hz), 2.17 (1H, b), 2.41—2.62 (1H, m), 3.37 (3H, s), 3.58 (2H, t, J=4.5Hz), 3.80—4.14 (1H, m), and 4.14—4.38 (2H, m). **6q**: 64; 120 (20); 1.15—1.23 (9H, m), 2.00 (1H, b), 2.47—2.64 (1H, m), 3.52 (2H, q, J=7.0 Hz), 3.63 (2H, t, J=4.8 Hz), 3.79—4.15 (1H, m), and 4.15—4.40 (2H, m). **6r**: 91; 170 (20); 0.90 (3H, t, J=7.1 Hz), 1.16 (s), 1.21 (a) (3H, d, J=6.4 Hz), 1.17 (3H, d, J=7.4 Hz), 1.29—1.62 (5H, m), 2.40—2.62 (1H, m), 3.45 (2H, t, J=6.5 Hz), 3.61 (2H, t, J=4.7 Hz), 3.79—4.13 (1H, m), and 4.14—4.38 (2H, m). **6s**: 79; 165 (18); 1.16—1.23 (6H, m), 2.14 (3H, s), 2.42—2.66 (2H, m), 2.74 (2H, t, J=6.6 Hz), 3.83—4.18 (1H, m), and 4.19—4.40 (2H, m). **6t**: 58; 125 (18); 1.17—1.24 (6H, m), 2.37—2.63 (2H, m), 3.70 (2H, t, J=5.5 Hz), and 4.34—4.39 (2H, m). **7a**: 35; 90 (17); 0.88 (a), 0.89 (s) (3H, t, J=7.5 Hz), 1.15 (s), 1.18 (a) (3H, d, J=6.4 Hz), 1.55—1.73 (2H, m), 2.24—2.38 (1H, m), 2.55—2.67 (1H, b), 3.67 (s), 3.68 (a) (3H, s), and 3.72—4.00 (1H, m). **7b**: 48; 70 (17); 0.90 (a), 0.91 (s) (3H, t, J=7.4 Hz), 1.17 (s), 1.20 (a) (3H, d, J=6.3 Hz), 1.26 (3H, t, J=7.2 Hz), 1.59—1.75 (2H, m), 2.22—2.63 (2H, m), 3.74—4.00 (1H, m), and 4.16 (s), 4.17 (a) (2H, q, J=7.2 Hz). **7c**: 53; 90 (17); 0.92 (6H, t, J=7.4 Hz), 1.17 (s), 1.21(a) (3H, d, J=6.4 Hz), 1.28—1.46 (2H, m), 1.54—1.76 (4H, m), 2.23—2.59 (2H, m), 3.74—4.01 (1H, m), and 4.10 (s), 4.12 (a) (2H, t, J=6.4 Hz). **7d**: 52; 110 (17); 0.87 (3H, t, J=6.6 Hz), 0.91 (a), 0.92 (s) (3H, t, J=7.4 Hz), 1.17 (s), 1.20 (a) (3H, d, J=6.2 Hz), 1.14—1.37 (6H, m), 1.56—1.73 (4H, m), 2.24—2.61 (2H, m), 3.75—4.26 (1H, m), and 4.09 (s), 4.11 (a) (2H, t, J=6.6 Hz). **7e**: 51; 150 (17); 0.86 (3H, t, J=6.8 Hz), 0.90 (a), 0.92 (s) (3H, t, J=7.4 Hz), 1.16 (s), 1.20 (a) (3H, d, J= 6.2 Hz), 1.15—1.41 (10H, m), 1.52—1.78 (4H, m), 2.20—2.63 (2H, m), 3.75—4.24 (1H, m), and 4.08 (s), 4.10 (a) (2H, t, J=6.6 Hz). **7g**: 57; 95 (17); 0.93 (6H, d, J=6.8 Hz), 0.88—0.96 (3H, t), 1.18 (s), 1.21 (a) (3H, d, J=6.1 Hz), 1.59—1.71 (2H, m), 1.82—2.03 (1H, m), 2.26—2.60 (2H, m), 3.88 (s), 3.90 (a) (2H, d, J=6.6 Hz), and 3.77—4.25 (1H, m). **7h**: 38; 70 (17); 0.92 (a), (s) (3H, t, J=7.4 Hz), 1.16 (s), 1.20 (a) (3H, d, J=6.4 Hz), 1.44 (9H, s), 1.54—1.73 (2H, m), 2.12—2.54 (2H, m), and 3.77—4.72 (1H, m). **7i**: 99; 110 (20); 0.89 (3H, t, J=7.5 Hz), 0.93 (3H, t, J=7.5 Hz), 1.18 (s), 1.21 (a) (3H, d, J=6.2 Hz), 1.53—1.72 (2H, m), 1.77 (2H, q, J=7.5 Hz), 2.13—2.26 (2H, m), and 3.79—4.00 (1H, m). **7j**: 62; 100 (17); 0.92 (s), 0.93 (a) (9H, s), 0.88—0.96 (3H, t), 1.17 (s), 1.20 (a) (3H, d, J=6.2 Hz), 1.60—1.73 (2H, m), 2.21—2.63 (2H, m), and 3.78 (s), 3.79 (a) (2H, s). **7o**: 31; 85 (17); 0.92 (a), 0.93 (s) (3H, t, J=7.5 Hz), 1.18 (s), 1.21 (a) (3H, d, J=6.4 Hz), 1.60—1.77 (2H, m), 2.28—2.72 (2H, m), 3.76—4.02 (1H, m), 4.59—4.62 (2H, m), 5.21—5.37 (2H, m), and 5.81—6.01 (1H, m). **7p**: 48; 90 (17); 0.92 (a), 0.93 (s) (3H, t, J=7.4 Hz), 1.17 (s), 1.21 (a) (3H, d, J=6.6 Hz), 1.58—1.74 (2H, m), 2.32—2.76 (2H, m), 3.36 (3H, s), 3.58 (2H, t, J=4.8 Hz), 3.71—4.03 (1H, m), and 4.18—4.40 (2H, m). **7q**: 58; 125 (21); 0.93 (a), 0.94 (s) (3H, t, J=7.4 Hz), 1.19 (3H, t, J=7.0 Hz), 1.18 (s), 1.22 (a) (3H, d, J= 6.2 Hz), 1.57—1.80 (2H, m), 2.27—2.77 (2H, m), 3.52 (2H, q, J=7.0 Hz), 3.63 (2H, t, J=5.2 Hz), 3.75—4.02 (1H, m), and 4.18—4.41 (2H, m). **7r**: 75; 120 (17); 0.89 (3H, t, J=7.1 Hz), 0.92 (a), 0.93 (s) (3H, t, J=7.4 Hz), 1.17 (s), 1.21 (a) (3H, d, J=6.4 Hz), 1.24—1.75 (6H, m), 2.27—2.77 (2H, m), 3.44 (2H, t, J=6.4 Hz), 3.61 (2H, t, J=4.8 Hz), 3.64—4.02 (1H, m), and 4.17—4.40 (2H, m). **8a**: 45; 100 (17); 0.90 (3H, t, J=7.2 Hz), 1.17 (s), 1.20 (a) (3H, d, J=6.4 Hz), 1.15—1.40 (2H, m), 1.45—1.75 (2H, m), 2.32—2.54 (2H, m), 3.69 (3H, s), and 3.78—4.06 (1H, m). **8b**: 48; 90 (18); 0.91 (3H, t, J=7.1 Hz), 1.18 (s), 1.21 (a) (3H, d, J=6.4 Hz), 1.26 (3H, t, J=7.2 Hz), 1.15—1.40 (2H, m), 1.43—1.77 (2H, m), 2.33—2.46 (2H, m), 3.78—4.06 (1H, m), and 4.16 (2H, q, J=7.2 Hz). **8c**: 60; 130 (21); 0.90 (3H, t, J=7.0 Hz), 0.92 (3H, t, J=7.2 Hz), 1.17 (s), 1.20 (a) (3H, d, J=6.2 Hz), 1.15—1.76 (8H, m), 2.31—2.62 (2H, m), 3.83—4.02 (1H, m), and 4.06—4.14 (2H, m). **8e**: 48; 110 (17); 0.86 (3H, t, J=7.0 Hz), 0.90 (3H, t, J=7.2 Hz), 1.15—1.34 (15H, m), 1.54—1.67 (4H, m), 2.25—2.60 (2H, m), and 3.80—4.13 (3H, m). **8f**: 66; 90 (17); 0.89 (3H, t, J=7.2 Hz), 1.22 (6H, d, J=6.4 Hz), 1.09—1.76 (7H, m), 2.26—2.42 (1H, m), 2.55—2.69 (1H, b), 3.78—4.00 (1H, m), and 4.93—5.14 (1H, m). **8h**: 60; 100 (17); 0.89 (3H, t, J=7.2 Hz), 1.15 (s), 1.18 (a) (3H, d, J=6.5 Hz), 1.44 (9H, s), 1.15—1.76 (4H, m), 2.19—2.36 (1H, m), 2.60—2.77 (1H, b), 3.73—3.96 (1H, m). **8i**: 80; 120 (20); 0.89 (3H, t, J=7.5 Hz), 0.92 (3H, t, J=7.4 Hz), 1.18 (s), 1.21 (a) (3H, d, J=6.6 Hz), 1.24—1.69 (4H, m), 1.43 (6 H, s), 1.77 (2H, q, J=7.4 Hz), 2.22—2.35 (1H, m), 2.45—2.74 (1H, b), and 3.76—4.00 (1H, m). **8j**: 50; 110 (21); 0.90 (3H, t, J=7.8 Hz), 0.93 (9H, s), 1.17 (s), 1.20 (a) (3H, d, J=6.0 Hz), 1.15—1.74 (4H, m), 2.35—2.49 (1H, m), 2.49—2.64 (1H, b), 3.77 (a), 3.79 (s) (2H, s), and 3.65—4.00 (1H, m). **8n**: 45; 140 (17); 0.85—0.94 (3H, m), 1.14—1.34 (5H, m), 1.45—1.90 (2H, m), 2.39—2.52 (2H, m), 3.85—4.28 (1H, m), 5.14 (a), 5.15 (s) (2H, s), and 7.35 (5H, s). **8o**: 55; 100 (17); 0.90 (3H, t, J=7.2 Hz), 1.18 (s), 1.21 (a) (3H, d, J=6.2 Hz), 1.20—1.81 (4H, m), 2.36—2.51 (2H, m), 3.82—4.02 (1H, m), 4.58—4.62 (2H, m), 5.20—5.37 (2H, m), and 5.81—6.03 (1H, m). **8p**: 40; 100 (17); 0.89 (3H, t, J=7.3 Hz), 1.16 (s), 1.20 (a) (3H, d, J=6.2 Hz), 1.12—1.79 (4H, m), 2.35—2.52 (1H, m), 2.57— 2.76 (1H, b), 3.35 (3H, s), 3.55—3.60 (2H, m), 3.80—3.98 (1H, m), and 4.15—4.39 (2H, m). **8q**: 50; 105 (17); 0.89 (3H, t, J=7.2 Hz), 1.76 (3H, t, J=7.0 Hz), 1.20 (s), 1.22 (a) (3H, d, J=6.2 Hz), 1.15—1.77 (4H, m), 2.33—2.52 (1H, m), 2.62—2.71 (1H, b), 3.46 (2H, q, J=7.0 Hz), 3.58—3.63 (2H, m), 3.81—4.00 (1H, m), and 4.16—4.40 (2 H, m). **8r**: 58; 140 (17); 0.88 (6H, t, J=7.2 Hz), 1.15 (s), 1.19 (a) (3H, d, J=6.4 Hz), 1.22—1.77 (8H, m), 2.32—2.51 (1H, m), 2.60—2.80 (1H, b), 3.43 (2H, t, J=6.5 Hz), 3.57—3.62 (2H, m), 3.77—4.00 (1H, m), and 4.14—4.38 (2H, m). **9a**: 83; 115 (18); 1.20—1.30 (3H, m), 1.97—2.02 (1H, m), 2.34—2.97 (4H, m), 3.74 (s and a) (3H, s), and 3.81—4.17 (1H, m). **9b**: 66; 120 (19); 1.21—1.32 (6H, m), 1.18—2.01 (1H, m), 2.16—2.88 (4H, m), 3.78—4.27 (1H, m), and 4.20 (s), 4.21 (a) (2H, q, J=7.4 Hz). **9c**: 87; 130 (15); 0.92 (3H, t, J=7.2 Hz), 1.22 (s), 1.25 (a) (3H, d, J=6.2 Hz), 1.25—1.70 (4H, m), 1.98—2.04 (1H, m), 2.27—2.98 (4H, m), and 3.78—4.23 (3H, m). **9f**: 73; 115 (18); 1.20—1.30 (3H, m), 1.25 (6H, d, J=6.2 Hz), 1.97—2.03 (1H, m), 2.34—2.94 (4H, m), 3.76—4.21 (1H, m), and 5.02—5.20 (1H, m). **9g**: 77; 120 (15); 0.94 (6H, d, J=6.6 Hz), 1.22 (s), 1.26 (a) (3H, d, 6.4 Hz), 1.82—2.03 (2H, m), 2.27—2.96 (4H, m) 3.81—4.11 (3H, m). **9h**: 71; 115 (28); 1.21 (s), 1.25 (a) (3H, d, J=6.6 Hz), 1.47 (9H, s), 1.98—2.02 (1H, m), 2.34—2.83 (4H, m), and 3.81—4.16 (1H, m). **9i**: 79; 120 (15); 0.90 (3H, t, J=7.4 Hz), 1.22 (s), 1.25 (a) (3H, d, J=6.1 Hz), 1.45 (6H, s), 1.60 (1H, b), 1.79 (2H, q, J=7.4 Hz), 1.98—2.01 (1H, m), 2.44—2.58 (3H, m), and 3.96—4.14 (1H, m). **9j**: 69; 135 (18); 0.95 (9H, s), 1.23 (s), 1.26 (a) (3 H, d, J=5.6 Hz), 1.98—2.01 (1H, m), 2.18—2.94 (4H, m), and 3.76—4.18 (3H, m). **9o**: 76; 120 (20); 1.23 (s), 1.26 (a) (3H, d, J=6.2 Hz), 1.65 (1H, b), 2.00 (1H, m), 2.49—2.74 (3H, m), 4.06—4.22 (1H, m), 4.62—4.66 (2H, m), 5.21—5.40 (2H, m), and 5.82—6.01 (1H, m). **9p**: 54; 130 (20); 1.22 (s), 1.26 (a) (3H, d, J=6.4 Hz), 1.73 (1H, b), 1.98—2.04

(1H, m), 2.25—2.78 (3H, m), 3.37 (3H, s), 3.60 (2H, m), 3.77—4.22 (1H, m), and 4.22—4.42 (2H, m). **9r**: 72; 130 (17); 0.90 (3H, t, J=7.2 Hz), 1.21 (3H, d, J=6.6 Hz), 1.28—1.61 (4H, m), 1.97—2.01 (1H, m), 2.38—2.80 (3H, m), 3.05 (1H, b), 3.45 (2H, t, J=6.5 Hz), 3.59—3.65 (2H, m), and 4.03—4.42 (3H, m). **10a**: 33; 95 (21); 1.21 (s), 1.24 (a) (3H, d, J=3.4 Hz), 2.32—2.58 (4H, m), 3.71 (3H, s), 3.88—4.08 (1H, m), 5.01—5.14 (2H, m), and 5.70—5.85 (1H, m). **10b**: 53; 100 (20); 1.21—1.29 (6H, m), 2.37—2.67 (4H, m), 3.90—4.04 (1H, m), 4.18 (2H, q, J=6.7 Hz), 5.00—5.14 (2H, m), and 5.71—5.85 (1H, m). **10c**: 64; 125 (15); 0.94 (3H, t, J=7.2 Hz), 1.21 (s), 1.24 (a) (3H, d, J=6.3 Hz), 1.30—1.43 (2H, m), 1.54—1.69 (2H, m), 2.03—2.34 (1H, m), 2.36—2.68 (3H, m), 3.63—4.16 (3H, m), 4.99—5.14 (2H, m), and 5.65—5.90 (1H, m). **10d**: 44; 130 (21); 0.89 (3H, m), 1.21 (s), 1.24 (a) (3H, d, J=6.2 Hz) 1.28—1.42 (6H, m), 1.51—1.72 (2H, m), 2.37—2.67 (4H, m), 3.87—4.18 (3H, m), 4.99—5.16 (2H, m), and 5.65—5.94 (1H, m). **10e**: 86; 145 (21); 0.87 (3H, m), 1.20 (s), 1.23 (a) (3H, d, J=6.2 Hz), 1.24—1.38 (10H, m), 1.53—1.70 (2H, m), 2.28—2.62 (4H, m), 3.89—4.17 (3H, m), 4.99—5.16 (2H, m), and 5.66—5.90 (1H, m). **10f**: 50; 111 (21); 1.21 (6H, d, J=6.4 Hz), 1.21 (s), 1.23 (a) (3H, d, J=6.4 Hz), 2.34—2.59 (3H, m), 2.70 (1H, b), 3.82—4.00 (1H, m), 4.96—5.13 (3H, m), and 5.62—5.88 (1H, m). **10g**: 34; 140 (17); 0.94 (s), 0.95 (a) (6H, d, J=6.8 Hz), 1.22 (s), 1.25 (a) (3H, d, J=6.3 Hz), 1.89—2.00 (1H, m), 2.37—2.65 (4H, m), 3.85—4.06 (3H, m), 5.01—5.13 (2H, m), and 5.71—5.85 (1H, m). **10h**: 40; 100 (21); 1.21(s), 1.24 (a) (3H, d, J=6.8 Hz), 1.46 (s), 1.47 (a) (9H, s), 2.25—2.47 (4H, m), 3.85—4.01 (1H, m), 5.01—5.13 (2H, m), and 5.72—5.86 (1H, m). **10i**: 90; 120 (20); 0.88 (3H, t, J=7.4 Hz), 1.20 (s), 1.23 (a) (3H, d, J=6.0 Hz), 1.42 (6H, s), 1.75 (2H, q, J=7.4 Hz), 2.29—2.46 (3H, m), 2.42—2.83 (1H, b), 3.78—4.04 (1H, m), 4.97—5.14 (2H, m), and 5.65—5.89 (1H, m). **10j**: 30; 105 (17); 0.94 (9H, s), 1.21 (s), 1.23 (a) (3H, d, J=5.9 Hz), 1.65 (1H, b), 2.25—2.61 (3H, m), 3.78 (s), 3.79 (a) (2H, s), 3.87—4.08 (1H, m), 4.99—5.13 (2H, m), and 5.65—5.89 (1H, m). **10k**: 52; 160 (21); 1.19 (s), 1.22 (a) (3H, d, J=6.4 Hz), 1.52—1.92 (9H, m), 2.35—2.47 (3H, m), 3.86—4.03 (1H, m), 4.98—5.23 (3H, m), and 5.67—5.88 (1H, m). **10l**: 56; 180 (21); 1.19 (s), 1.22 (a), (3H, d, J=6.4 Hz), 1.20—1.86 (11H, m), 2.35—2.61 (3H, m), 3.82—4.06 (1H, m), 4.73—4.88 (1H, m), 4.98—5.12 (2H, m), and 5.64—5.89 (1H, m). **10n**: 57; 145 (2); 1.12 (s), 1.18 (a) (3H, d, J=6.2 Hz), 1.58—1.71 (1H, b), 2.32—2.63 (3H, m), 3.87—4.09 (1H, m), 4.96—5.11 (2H, m), 5.13 (s), 5.15 (a) (2H, s), 5.62—5.88 (1H, m), and 7.35 (5H, s). **10o**: 56; 125 (17); 1.21 (s), 1.22 (a) (3H, d, J=5.8 Hz), 2.25—2.62 (4H, m), 3.86—4.09 (1H, m), 4.57—4.62 (2H, m), 4.99—5.36 (4H, m), and 5.64—6.00 (2H, m). **10p**: 17; 150 (21); 1.20 (s), 1.23 (a) (3H, d, J=6.4 Hz), 2.30—2.74 (4H, m), 3.37 (3H, s), 3.55—3.61 (2H, m), 3.87—4.08 (1H, m), 4.16—4.38 (2H, m), 4.98—5.13 (2H, m), and 5.49—5.89 (1H, m). **10q**: 60; 135 (17); 1.19 (3H, t, J=7.0 Hz), 1.18(s), 1.23 (a) (3H, d, J=6.4 Hz), 2.35—2.63 (4H, m), 3.47 (2H, q, J=7.0 Hz), 3.57—3.65 (2H, m), 3.86—4.04 (1H, m), 4.13—4.38 (2H, m), 4.96—5.13 (2H, m), and 5.68—5.89 (1H, m). **10r**: 68; 140 (21); 0.89 (3H, t, J=7.2 Hz), 1.19 (s), 1.23 (a) (3H, d, J= 6.4 Hz), 1.28—1.40 (2H, m), 1.47—1.58 (2H, m), 1.61—1.79 (1H, b), 2.22—2.64 (3H, m), 3.44 (2H, t, J=6.5 Hz), 3.56—3.63 (2H, m), 3.82—4.07 (1H, m), 4.14—4.37 (2H, m), 4.97—5.13 (2H, m), and 5.63—5.89 (1H, m). **10s**: 55; 125 (17); 1.19 (s), 1.22 (a) (3H, d, J=6.4 Hz), 2.12 (3H, s), 1.61—1.86 (1H, b), 2.38—2.61 (3H, m), 2.64—2.74 (2H, m), 3.87—4.08 (1H, m), 4.21—4.35 (2H, m), 4.98—5.14 (2H, m), and 5.62—5.88 (1H, m).

Reduction of Alkyl-3-oxobutanoates with Bakers' Yeast. One mmol of an alkyl 2-alkyl-3-oxobutanoate was added to a suspension of 20 g of bakers' yeast in 25 ml of water and the mixture was stirred at room temperature for 2 days. Then Hyflo-Super-Cell (10 G) was added to the mixture and the resulted suspension was filtered. The organic portion was concentrated under reduced pressure and the residue was subjected to column chromatography on silica gel with an eluent of hexane-ethyl acetate (9 : 1) mixture to give the corresponding hydroxy ester. The diastereomeric ratios and chemical yields are listed in Table 1.

Determination of Syn/Anti Ratio. The syn/anti ratio in the product was determined on GLC (PEG. 1.5 m) with column temperatures: **6a**, 80 °C; **6b**, 90 °C; **6c**, 110 °C; **6d**, 120 °C; **6e**, 150 °C; **6g**, 110 °C; **6h**, 80 °C; **6i**, 120 °C; **6j**, 100 °C; **6k**, 120 °C; **6l**, 130 °C; **6m**, 150 °C; **6n**, 160 °C; **6p**; 130 °C; **6q**, 130 °C; **6r**, 130 °C; **6s**, 130 °C; **6t**, 130 °C.

Determination of Diastereomeric Composition. The reduced product **6j** was converted into the corresponding methyl ester and the ^{1}H NMR spectrum of its MTPA ester[16] was compared with those of the authentic samples prepared by methylation of racemic and (*S*)-methyl 3-hydroxybutanoates.[3]

The authors wish to thank for financial support by a Grant-in-Aid from the Ministry of Education, Science and Culture under the Grant No. 62216011.

References

1) S. Masamune, W. Choy, F. A. J. Kerdesky, and B. Imperiali, *J. Am. Chem. Soc.*, **103**, 1566 (1981).

2) P. A. Barlett, *Tetrahedron*, **36**, 3 (1980).

3) G. Fráter, U. Muller, and W. Günther, *Tetrahedron*, **40**, 1269 (1984).

4) H. Akita, A. Furuichi, H. Koshiji, K. Horikoshi, and T. Oishi, *Chem. Pharm. Bull.*, **31**, 4376 (1983).

5) K. Nakamura, T. Miyai, K. Nozaki, K. Ushio, S. Oka, and A. Ohno, *Tetrahedron Lett.*, **27**, 3155 (1986).

6) B. S. Deol, D. D. Ridley, and G. W. Simpson, *Aust. J. Chem.*, **29**, 2459 (1976).

7) T. Fujisawa, T. Itoh, and T. Sato, *Tetrahedron Lett.*, **25**, 5083 (1984).

8) H. Akita, H. Matsukura, and T. Oishi, *Tetrahedron Lett.*, **27**, 5397 (1986).

9) The diastereomeric composition of the product seems to depend on the activity of bakers' yeast employed for the reduction. For example, the ratio preliminary reported for **6e** was 95/5,[5] which turned out to be 92/8 in the present report. In the preliminary experiment which was run 2 years ago, the yeast employed was less active than that employed presently and unable to reduce the substrate completely unless glucose was added at each 6 h. The yeast in the present work reduced **6e** within 1 day without adding extra glucose.

10) M. Hirama, M. Shimizu, and M. Iwashita, *J. Chem. Soc., Chem. Commun.*, **1983**, 559.

11) B. N. Zhou, A. S. Gopalan, F. van Middlesworth, W. R. Shieh, and C. J. Sih, *J. Am. Chem. Soc.*, **105**, 3958 (1983).

12) A. Furuichi, H. Akita, H. Matsukura, T. Oishi, and K. Horikoshi, *Agric. Biol. Chem.*, **51**, 293 (1987).

13) Kinetic parameters for a reaction composed of multi-

steps are treated as those for an "imaginary" single-step process. Contrary, a real system which is in resonance is expressed by a sum of "imaginary" canonical forms. Thus, to have an image for a nonexistent subject is a common procedure in chemistry.

14) K. Nakamura, T. Miyai, K. Ushio, S. Oka, and A. Ohno, *Bull. Chem. Soc. Jpn.*, **61**, 2089 (1988).

15) All Boiling points are uncorrected. $t/°C=T/K-273.15$. $p/mmHg=P/13.5951\times980.665\times10^{-2}Pa=P/133.322Pa$.

16) J. A. Dale, D. L. Dull, and H. S. Mosher, *J. Org. Chem.*, **34**, 2543 (1969).

Synthesis and Properties of the Tridecafulvene Derivatives. The Substituent Effect at the 14-Position on the Tropicity of Thirteen-Membered Fulvene System

Juro OJIMA,* Masayuki MASUMOTO, Jyunji KATSUYAMA, Keiko KITAMURA, and Masahiko IYODA†,*
Department of Chemistry, Faculty of Science, Toyama University, Gofuku, Toyama 930
†Department of Chemistry, Faculty of Science, Osaka University, Toyonaka, Osaka 560
(Received October 26, 1988)

Dimethylbisdehydrotridecafulvene derivatives bearing various substituents at the exocyclic bond have been synthesized and the inductive effect of substituents upon the tropicity of the thirteen-membered ring is discussed on the basis of the spectral data.

The cyclic cross-conjugated π-electron systems, fulvalene (**1**) and fulvene (**2**), containing small- and medium-rings have been extensively studied.[1] However, there is little study on those containing a monocyclic large-membered ring. It is expected that an examination of the ring current effect of the large-membered ring system can be made more readily than those of the small- and medium-ring ones, since the former has both the olefinic inner and outer protons, as compared with that the latter has only the olefinic outer protons.[2]

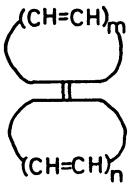

1

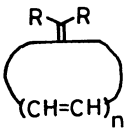

2

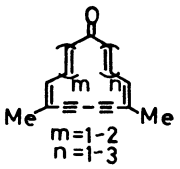

3

Recently, we have investigated the cross-conjugated π-electron systems **4**—**9** as well as their 15-, 17-, and 19-membered counterparts,[3] which were derived from the bisdehydroannulenones (**3**).[4] Among these compounds, the diphenyl (**4**)[3a] and the dichloro derivative (**5**)[3b] proved to be atropic, reflecting little cross-conjugation of π-electrons, or of little contribution from dipolar structures (**4a**) and (**5a**), respectively, in the ground state. In contrast, the dinitrile derivative (**6**)[3c] exhibited the ring current effect (paratropicity), owing to polarization of an exocyclic bond. These results and relatively easy preparation of **6** directed us to prepare the various derivatives of tridecafulvene in order to study the inductive effect of substituents upon the tropicity of the thirteen-membered ring.

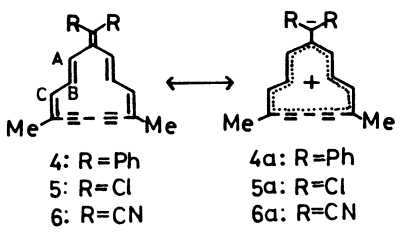

4: R=Ph
5: R=Cl
6: R=CN

4a: R=Ph
5a: R=Cl
6a: R=CN

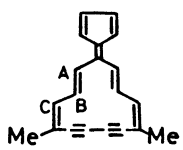

7

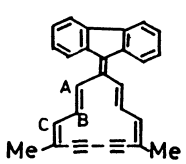

8

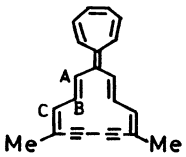

9

Results and Discussion

Synthesis. Reduction of **6** with a little excess of diisobutylaluminum hydride (DIBAH)[5] gave only the nitrile aldehyde derivative **11** in 53% yield, along with recovery of a small amount of **6**. A further reduction of **11** with the same reagent resulted in formation of the hydroxy aldehyde derivative **12** (9%) and the hydroxy nitrile derivative **13** (12%), but the diformyl derivative was not obtained in these reductions. Compound **13** was also obtained from **11** by reduction with $NaBH_4$ (75%). Treatment of **13** with phosphorus tribromide gave the bromomethyl nitrile derivative **14** (84%), which was led to the methyl ether derivative **15** (15%) by reaction with NaOMe. The reaction of **11** with MnO_2-NaCN-MeOH, according to the procedure of Corey et al.,[6] afforded the methyl ester derivative (**16**) (42%). Similarly, the reaction of **11** with MnO_2-NaCN-NH_3[7] afforded the amide derivative (**17**) (17%). Oxidation of **11** with Jone's reagent[8] resulted in formation of the annulenone (**10**), arising from the attack of the pinch bond of **11**.

^{1}H NMR and Electronic Spectra. The chemical shifts of the olefinic protons, labeled in the formulas, of the compounds **11**—**17** as well as the closely related compounds **4**—**10**[3a-e,4a] are listed in Table 1. The chemical shift differences between the inner (H^B, $H^{B'}$) and the outer (H^A, $H^{A'}$, H^C, $H^{C'}$) protons, $\Delta\delta=H^i-H^o$ (H^i=inner protons; H^o=outer protons), which would be an experimental measure of the magnitude of ring current of these compounds, are also given in Table 1.

Considering the chemical shift differences ($\Delta\delta$), the following decreasing order of the tropicity of the 13-membered ring of these compounds may be established: **6** (CN, CN)>**10** (annulenone)>**16** (CN,

Table 1. ^{1}H NMR Data of Compounds **4**—**17** (δ Values, $CDCl_3$, 90 or 200 MHz)

Compd	A	A′	B	B′	C	C′	$\Delta\delta(H^i-H^0)$
4	6.27		7.05		6.68		0.57
5	6.51		7.45		6.65		0.87
6	6.34		9.78		6.29		3.46
7	6.81		8.19		6.62		1.47
8	6.93		7.97		6.73		1.14
9	6.49		6.63		6.79		−0.01
10	6.10		9.39		6.29		3.19
11	6.59	6.88	9.38	8.48	6.49	6.32	2.36
12	6.66		7.90	6.72	6.65	6.44	0.71
13	6.49	6.31	8.27	8.09	6.51	6.44	1.75
14	6.46	6.29	8.54	8.35	6.46	6.44	2.03
15	6.61	6.32	8.31	8.13	6.54	6.43	1.74
16	6.45	7.11	9.41		6.35[a]	6.32[a]	2.85
17	6.42	7.16	9.23	9.19	6.38[b]	6.34[b]	2.63

a, b) Assignments may be reversed in each group.

Table 2. Electronic Absorption Maxima of Fulvenes **11**—**17**[a]

11	a	254 (13500), 266 (12800), 306 (20500), 376 (17300)
	b	251 (0.640), 262 (0.591), 304 (1.000), 375 (0.828)
12	a	257 (11900), 302 (19000), 362 (11100)
	b	255 (0.582), 300 (1.000), 358 (0.539)
13	a	254sh (15200), 268sh (19900), 291 (28400), 351 (15400)
	b	250sh (0.490), 265sh (0.675), 289 (1.000), 347 (0.510)
14	a	254 (14900), 268 (16900), 297 (25000), 362 (17900)
	b	252 (0.554), 266 (0.646), 294 (1.000), 356 (0.667)
15	a	252sh (14700), 266sh (19800), 292 (29100), 349 (15500)
	b	250sh (0.473), 264sh (0.659), 289 (1.000), 345 (0.518)
16	a	247 (14400), 262 (14000), 295 (21800), 366 (19400)
	b	247 (0.645), 262 (0.601), 296 (1.000), 366 (0.873)
17	a	253sh (12600), 266sh (15000), 294 (20300), 361 (14900)
	b	251 (0.581), 265sh (0.678), 293 (1.000), 357 (0.725)

a) a. in THF: λ_{max} (nm) (ε_{max}/1 $mol^{-1}cm^{-1}$); b. in acetonitrile: λ_{max} (nm) (relative extinction coefficients)

CO_2Me)>**17** (CN, $CONH_2$)>**11** (CN, CHO)>**14** (CN, CH_2Br)>**13** (CN, CH_2OH)>**15** (CN, CH_2OMe)>**7** (pentafulvalene)>**8** (dibenzopentafulvalene) >**5** (Cl, Cl)≃**12** (CHO, CH_2OH)≃**4** (Ph, Ph)>**9** (heptafulvalene). Since both the inner H^B and $H^{B'}$ protons suffer a rather large local anisotropy of the diacetylene bond in these compounds,[9] the tropicity of **12** as well as **4** and **5** is quite small, i.e., **4**, **5** (as mentioned above), and **12** are atropic. This result also supports the interpretation that the heptafulvalene (**9**) ($\Delta\delta$: −0.01) is diatropic, as reported previously.[3e] All other tridecafulvene derivatives including the fulvalenes **7** and **8** are paratropic and show the contribution of the dipolar structure such as **6a**.

Among the compounds in which one substituent is nitrile group, the paratropicity decreases in the following order of another substituent: CN (**6**)>COOMe (**16**)>$CONH_2$ (**17**)>CHO (**11**)>CH_2Br (**14**)>CH_2OH (**13**)>CH_2OMe (**15**). This is roughly in accord with a decreasing order of the inductive, electron-withdrawing effect of their substituents, except that of the CHO group.

Since the chemical shifts of H^A, H^B, H^C, and $H^{C'}$ protons are similar in compounds **11** , **16**, and **17**, the deviation of **11** from the order of the electron-withdrawing effect is ascribed to the rather large difference of the chemical shifts of $H^{A'}$ and $H^{B'}$ protons between **11** and **16** (and **17**). Although the higher field shift of $H^{B'}$ proton of **11** as compared with those of **16** and **17**, could not be explained, the higher field shift of $H^{A'}$ proton of **11** might be attributed to a local anisotropic effect of the formyl group at 14-position.

The electronic absorption maxima of compounds **11**—**17**, determined in both tetrahydrofuran (THF) and acetonitrile, are listed in Table 2. It is evident from Table 2 that all the maxima of compounds **11**—**17** show a small hypsochromic shift or do not show any shift on changing the solvent from less polar (THF) to polar (acetonitrile). This solvent effect also supports the interpretation that the polarization, depicted in structure (**6a**), from the large rings to the exocyclic moiety occurs in these systems **11** and **13**—**17**,

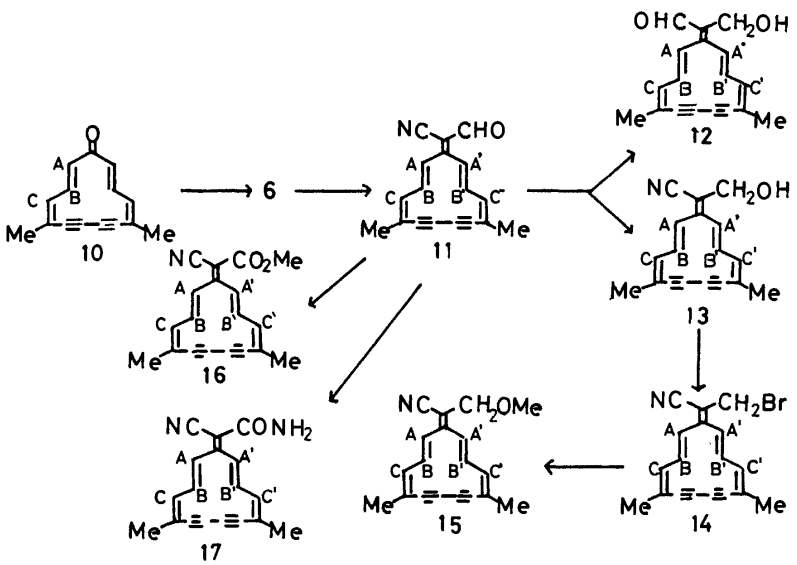

as revealed by ^{1}H NMR spectral data.

In conclusion, it was found that the paratropicity of the tridecafulvene system decreases with the decreasing electron-withdrawing order of the inductive effect of substituents at 14-position.

Experimental

Melting points were determined on a hot-stage apparatus and are uncorrected. IR spectra were measured on a Hitachi 260—50 spectrophotometer as KBr disk; only significant maxima are reported. Electronic spectra were determined on a Hitachi 220A spectrophotometer (sh=shoulder). ^{1}H NMR spectra were measured on a JEOL FX-90Q (90 MHz) and refer to solutions in $CDCl_3$, in δ-values with TMS as an internal standard. The coupling constants (J) are given in Hz. Assignments were assisted by decoupling experiments where necessary. Mass spectra were determined with a JMS D-200 spectrometer at 75 eV using a direct inlet system. Silica gel (Merck) and alumina (Merck, activity II—III) were used for column chromatography and preparative thin-layer chromatography was carried out on 20×20 cm plate (Merck, 0.5 mm thick). Dichloromethane was distilled over calcium hydride before use. Reactions were followed by TLC aluminum sheets precoated with Merck silica gel F_{254}. Organic extracts were dried over anhydrous sodium sulfate prior to solvent removal.

14,14-Dicyano-5,10-dimethyl-6,8-bisdehydrotridecafulvene (6). This compound was prepared with a slight modification of the reported method.[3c] To a stirred solution of dimethylbisdehydro[13]annulenone (**10**)[4a] (500 mg, 2.40 mmol) and malononitrile (286 mg, 4.33 mmol) in dry dichloromethane (27 ml) was added dropwise a solution of titanium tetrachloride (1.1 ml, 10 mmol) in dry dichloromethane (17 ml) during 50 min under ice-bath. Then a solution of pyridine (2.3 ml) in dry dichloromethane (17 ml) was added dropwise during 40 min to the ice-cooled mixture. After stirring for 1 h at room temperature, a solution of titanium tetrachloride (1.1 ml) in dry dichloromethane (17 ml) was added to the ice-cooled mixture. Then a solution of malononitrile (286 mg) in dry dichloromethane (27 ml) was added dropwise during 90 min, and a solution of pyridine (2.3 ml) in dry dichloromethane (17 ml) was added dropwise during 30 min. The mixture was stirred for 1 h at room temperature. Then 7% hydrochloric acid (17 ml) was added and the mixture was stirred for a further 10 min. Then the mixture was separated and the aqueous layer was extracted with dichloromethane. The combined organic layer was washed with aqueous sodium hydrogencarbonate solution and brine, successively, and dried. The residue after solvent removal was chromatographed on silica gel (4.1×10.5 cm). The fractions eluted with 35% benzene in hexane afforded fulvene **6** (356 mg, 58%).

14-Cyano-14-formyl-5,10-dimethyl-6,8-bisdehydrotridecafulvene (11). To a stirred solution of fulvene **6** (150 mg, 0.59 mmol) in dry toluene (105 ml) was added a solution of diisobutylaluminum hydride (1.8 ml, 1.77 mmol) in toluene by a syringe under argon during 10 min at −7 °C, and the solution was stirred for 50 min at the same temperature. Then 5% sulfuric acid (30 ml) was added and the mixture was extracted with benzene. The combined extracts were washed with aqueous sodium hydrogencarbonate solution and brine, successively, and dried. The residual red liquid was chromatographed on silica gel (3.8×10.0 cm). The early fractions eluted with 30—50% benzene in hexane gave the recovered **6** (18 mg). The later fractions eluted with 80% benzene in hexane afforded fulvene **11** (83 mg, 53%). It formed dark brown needles, mp 195—197 °C (decomp), from hexane-benzene; MS m/z 259 (M^+, 50%) and 214 (100); mol wt 259.2; IR 2225, 2160 (C≡N), 2100 (C≡C), 1665 (CHO), 1610 (C=C), and 980 cm^{-1} (trans C=C); UV Table 2; ^{1}H NMR δ=9.89 (s, 1H, CHO), 9.38 (dd, J=16, 10 Hz, 1H, H^B), 8.48 (dd, J=16, 8 Hz, 1H, $H^{B'}$), 6.88 (d, J=16 Hz, 1H, $H^{A'}$), 6.59 (d, J=16 Hz, 1H, H^A), 6.49 (d, J=10 Hz, 1H, H^C), 6.32 (d, J=8 Hz, 1H, $H^{C'}$), 1.82 (s, 3H, Me), and 1.81 (s, 3H, Me).

Found: C, 83.60; H, 5.15; N, 5.41%. Calcd for $C_{18}H_{13}NO$: C, 83.37; H, 5.05; N, 5.40%.

14-Formyl-14-hydroxymethyl-5,10-dimethyl-6,8-bisdehydrotridecafulvene (12) and 14-Cyano-14-hydroxymethyl-5,10-dimethyl-6,8-bisdehydrotridecafulvene (13). To a stirred solution of fulvene **11** (112 mg, 0.43 mmol) in dry toluene (130 ml) was added a solution of diisobutylaluminum hydride (1.0 ml, 0.99 mmol) in toluene by a syringe at −7 °C. After stirring for 1 h at −7 °C, the mixture was poured into 5% sulfuric acid and extracted with benzene. The combined extracts were worked up as for the isolation of **11**. The residue after solvent removal was chromatographed on silica gel (3.4×8.5 cm). The early fractions eluted with 40% benzene in hexane gave recovered **11** (5 mg). The later fractions eluted with 40—70% benzene in dichloromethane gave a mixture of **12** and **13** as a liquid. The liquid was purified by preparative plate chromatography (dichloromethane-acetone (7 : 3) as eluent). The fast moving, first band gave fulvene **13** (14 mg, 12%). It formed red needles, mp 151—152 °C, from hexane-benzene: MS m/z 261 (M^+, 58%) and 189 (100); mol wt 261.7; IR 3400 (OH), 2200, 2160 (C≡N), 2100 (C≡C), and 970 cm^{-1} (trans C=C); UV Table 2; ^{1}H NMR δ=8.27 (dd, J=16.5, 10 Hz, 1H, H^B), 8.09 (dd, J=16.5, 9 Hz, 1H, $H^{B'}$), 6.51 (d, J=10 Hz, 1H, H^C), 6.49 (d, J=16.5 Hz, 1H, H^A), 6.44 (d, J=9 Hz, 1H, $H^{C'}$), 6.31 (d, J=16 Hz, 1H, $H^{A'}$), 4.46 (d, J=5 Hz, 2H, -CH_2-), 1.95 (broad t, J=5 Hz, 1H, -OH, exchangeable with D_2O), 1.83 (s, 3H, Me), and 1.84 (s, 3H, Me).

Found: C, 82.40; H, 5.85; N, 5.29%. Calcd for $C_{18}H_{15}NO$: C, 82.73; H, 5.79; N, 5.36%.

The fast moving, second band gave fulvene **12** (10 mg, 9.0%). It formed red needles, mp 138—139 °C, from hexane-benzene: IR 3400 (OH), 2170 (C≡N), 2100 (C≡C), 1660 (CHO), and 975 cm^{-1} (trans C=C); UV Table 2; ^{1}H NMR δ=10.12 (s, 1H, CHO), 7.90 (dd, J=16, 10 Hz, 1H, H^B), 6.72 (dd, J=16, 7 Hz, 1H, $H^{B'}$), 6.66 (d, J=16 Hz, 2H, H^A and $H^{A'}$), 6.65 (d, J=10 Hz, 1H, H^C), 6.44 (d, J=7 Hz, 1H, $H^{C'}$), 4.52 (s, 2H, -CH_2-), 2.45 (broad s, 1H, -OH, exchangeable with D_2O), 1.87 (s, 3H, Me), and 1.89 (s, 3H, Me).

HRMS: Found: m/z 264.1088. Calcd for $C_{18}H_{16}O_2$: M, 264.1148.

Preparation of 13 from 11 by Reduction with $NaBH_4$. To a stirred solution of fulvene **11** (158 mg, 0.61 mmol) in dry ethanol (170 ml) was added sodium borohydride (26.5 mg, 0.72 mmol) in one portion, and the mixture was stirred for 3 h at room temperature. After cooling under ice-bath, water (30 ml), and then 2 M hydrochloric acid (27 ml) were added, and the mixture was extracted with benzene. After usual work up, the residual liquid was chromatographed on silica gel (3.2×8.3 cm). The fractions eluted with dichloromethane gave fulvene **13** (120 mg, 75%).

14-Bromomethyl-14-cyano-5,10-dimethyl-6,8-bisdehydrotridecafulvene (14). To a stirred solution of fulvene **13** (142 mg, 0.54 mmol) in dry dichloromethane (21 ml) was added dropwise a solution of phosphorus tribromide (214 mg, 0.79 mmol) in dry dichloromethane (11 ml) during 40 min at −6 °C under argon, and the mixture was stirred overnight at room temperature. After refluxing for a further 3 h, the mixture was poured into water and extracted with dichloromethane. The extracts were washed with aqueous sodium hydrogencarbonate solution and brine, successively, and dried. The residual red liquid after solvent removal was passed through a short column of silica gel (3.2×4.6 cm). The fractions eluted with benzene gave fulvene **14** (148 mg, 84%). It formed dark red needles, mp 159—161 °C, from hexane-benzene: MS *m/z* 325 (M^+, 10%), 323 (M+, 10%), and 228 (100); mol wt 323.2; IR 2210, 2175 (C≡N), 2100 (C≡C), 1620, 1600 (C=C), and 980 cm^{-1} (trans C=C); UV Table 2; ^1H NMR δ=8.54 (dd, J=16, 9.5 Hz, 1H, H^B), 8.35 (dd, J=16, 9 Hz, 1H, $H^{B'}$), 6.46 (d, J=16 Hz, 1H, H^A), 6.46 (d, J=9.5 Hz, 1H, H^C), 6.44 (d, J=9 Hz, 1H. $H^{C'}$), 6.29 (d, J=16 Hz, 1H, $H^{A'}$), 4.23 (s, 2H, $-CH_2-$), and 1.81 (s, 6H, Me).

Found: C, 66.43; H, 4.32; N, 4.20%. Calcd for $C_{18}H_{14}BrN$: C, 66.68, H, 4.35; N, 4.32%.

14-Cyano-14-methoxymethyl-5,10-dimethyl-6,8-bisdehydrotridecafulvene (15). A solution of sodium methoxide, prepared from sodium (45 mg, 1.96 mg atm) and dry methanol (200 ml), was added dropwise during 12 h to a stirred solution of fulvene **14** (148 mg, 0.456 mmol) in dry benzene (60 ml) at room temperature and the solution was stirred for 2 h at the same temperature. The precipitates formed were filtered and washed with hexane. The filtrate was poured into water, and the aqueous layer was extracted with benzene. The combined organic layer was washed with brine, and dried. The residue after solvent removal was chromatographed on alumina (3.2×9.4 cm). The fractions eluted with 10—25% benzene in hexane afforded fulvene **15** (19 mg, 15%). It formed orange cubes, mp 95—96 °C, from hexane: MS *m/z* 275 (M^+, 38%) and 228 (100); mol wt 275.3; IR 2200, 2170 (C≡N), 2100 (C≡C), and 970 cm^{-1} (trans C=C); UV Table 2; ^1H NMR δ=8.31 (dd, J=15, 10 Hz, 1H, H^B), 8.13 (dd, J=15, 10 Hz, 1H, $H^{B'}$), 6.61 (d, J=15 Hz, 1H, H^A), 6.54 (d, J=10 Hz, 1H, H^C), 6.43 (d, J=10 Hz, 1H, $H^{C'}$), 6.32 (d, J=15 Hz, 1H, $H^{A'}$), 4.22 (s, 2H, $-OCH_2-$), 3.40 (s, 3H, OMe), 1.83 (s, 3H, Me), and 1.82 (s, 3H, Me).

Found: C, 82.64; H, 6.29; N, 5.06%. Calcd for $C_{19}H_{17}NO$: C, 82.88; H, 6.22; N, 5.09%.

14-Cyano-14-methoxycarbonyl-5,10-dimethyl-6,8-bisdehydrotridecafulvene (16). Manganese dioxide (350 mg), sodium cyanide (75 mg), and acetic acid (27 ml) were added in one portion, respectively, to a stirred solution of fulvene **11** (70 mg, 0.27 mmol) in dry methanol (160 ml), and the mixture was refluxed for 3 h. Then a further quantity of manganese dioxide (210 mg) was added and stirring was continued overnight at room temperature. Then a further quantity of manganese dioxide (350 mg), sodium cyanide (37 mg), acetic acid (10 ml) were added and the mixture was refluxed for further 5 h. After cooling, inorganic materials were filtered and washed with dichloromethane. Then the filtrate was poured into water, and the aqueous layer was extracted with dichloromethane. The combined organic layer was washed with aqueous sodium hydrogencarbonate solution and brine, successively, and dried. The residue after solvent removal was chromatographed on silica gel (3.6×6.0 cm). The fractions eluted with 30—40% benzene in hexane afforded fulvene **16** (33 mg, 42%). It formed dark red needles, mp 147—148 °C, from ether-methanol: MS *m/z* 289 (M^+, 63%) and 214 (100); mol wt 289.3; IR 2200, 2150 (C≡N), 2100 (C≡C), 1710 (CO_2-), and 960 cm^{-1} (trans C=C); UV Table 2; ^1H NMR δ=9.41 (dd, J=16, 10 Hz, 2 H, H^B and $H^{B'}$), 7.11 (d, J=16 Hz, 1H, $H^{A'}$), 6.45 (d, J=16 Hz, H^A), 6.35 (d, J=10 Hz, 1H, H^C or $H^{C'}$), 6.32 (d, J=9 Hz, 1H, H^C or $H^{C'}$), 3.82 (s, 3H, $-CO_2Me$). and 1.74 (s, 6H, Me).

Found: C, 78.58; H, 5.27; N, 4.75%. Calcd for $C_{19}H_{15}NO_2$: C, 78.87; H, 5.23; N, 4.84%.

14-Carbamoyl-14-cyano-5,10-dimethyl-6,8-bisdehydrotridecafulvene (17). To isopropyl alcohol (30 ml) saturated with ammonia at −3 °C, was added powdered sodium cyanide (180 mg, 3.65 mmol) in one portion. After 10 min, fulvene **11** (120 mg, 0.463 mmol) was added in one portion, then manganese dioxide (1.10 g) was added in two equal portions 10 min apart. After stirring for 5 h at −3 °C, the mixture was diluted with dichloromethane (30 ml) and was filtered to remove inorganic materials. The filtrate was poured into water, and the aqueous layer was extracted with dichloromethane. The combined organic layer was washed with aqueous sodium hydrogencarbonate solution and brine, successively, and dried. The residue after solvent removal was chromatographed on alumina (3.2×6.8 cm). The fractions eluted with hexane-dichloromethane (1 : 9) afforded fulvene **17** (22 mg, 17%). It formed brown needles, mp 198 °C (dec), from hexane-benzene: MS *m/z* 274 (M^+, 54%) and 214 (100); mol wt 274.3; IR 3350, 3170 ($-NH_2$), 2200, 2100 (C≡N), 2100 (C≡C), 1660 (C=O), 1600 (C=C), and 980 cm^{-1} (trans C=C); UV Table 2; ^1H NMR δ=9.23 (dd, J=16, 10 Hz, 1H, H^B), 9.19 (dd, J=15.5, 9 Hz, 1H, $H^{B'}$), 7.16 (d, J=16.5 Hz, 1H, $H^{A'}$), 6.42 (d, J=16 Hz, 1H, H^A), 6.38 (d, J=9 Hz, 1H, H^C or $H^{C'}$), 6.34 (d, J=10.5 Hz, 1H, H^C or $H^{C'}$), 6.11 (broad s, 1H, $-NH_2$), 5.61 (broad s, 1H, NH_2), 1.76 (s, 3H, Me), and 1.74 (s, 3H, Me).

Found: C, 78.92; H, 5.48; N, 9.54%. Calcd for $C_{18}H_{14}N_2O$: C, 78.81; H, 5.14; N, 10.21%.

Oxidation of Fulvene 11. A chromium trioxide solution (0.4 ml), prepared from chromium trioxide (13.3 g), sulfuric acid (11.5 ml), and water (50 ml), was added to a stirred solution of fulvene **11** (70 mg, 0.27 mmol) in acetone (50 ml) at room temperature. After stirring for 1 h at the same temperature, a further quantity of the chromium trioxide solution (0.5 ml) was added, and stirring was continued for a further 4 h. Then the mixture was poured into water and extracted with dichloromethane. The extracts were washed with brine, and dried. The residue after solvent removal was chromatographed on silica gel (3.8×3.5 cm). The fractions eluted with 10% dichloromethane in benzene gave annulenone **10** (12 mg, 16%).

This work was partly supported by a Grant-in-Aid (No. 61470023) for Scientific Research from the Ministry of Education, Science and Culture.

References

1) For reviews, see E. D. Bergmann, *Chem. Rev.*, **68**, 41 (1968); F. Pietra, *ibid.*, **73**, 203 (1973); G. Becker in Houben-Weyl, "Methoden der Organischen Chemie," Georg Thieme Verlag, Stuttgart (1985), Vol. V, IIc, p. 697.

2) J. Ojima, *Yuki Gosei Kagaku Kyokai Shi*, **46**, 244

(1988).

3) a) S. Kuroda, J. Ojima, K. Kitatani, M. Kirita, and T. Nakada, *J. Chem. Soc., Perkin Trans. 1*, **1983**, 2987; b) J. Ojima, K. Itagawa, S. Hamai, T. Nakada, and S. Kuroda, *ibid.*, **1983**, 2997; c) J. Ojima, S. Ishizaka, Y. Shiraiwa, E. Ejiri, T. Kato, S. Kuroda, and H. Takeda, *ibid.*, **1987**, 1505; d) J. Ojima, K. Itagawa, and T. Nakada, *Bull. Chem. Soc. Jpn.*, **59**, 1723 (1986); e) T. Asao, N. Morita, J. Ojima, M. Fujiyoshi, K. Wada, and S. Hamai, *ibid.*, **59**, 1713 (1986).

4) a) T. M. Cresp, J. Ojima, and F. Sondheimer, *J. Org. Chem.*, **42**, 2130 (1977); b) J. Ojima, Y. Shiroishi, K. Wada, and F. Sondheimer, *ibid.*, **42**, 2130 (1977).

5) E. Winterfeld, *Synthesis*, **1975**, 617.

6) E. J. Corey, N. W. Gilman, and B. E. Ganem, *J. Am. Chem. Soc.*, **90**, 5616 (1968).

7) N. W. Gilman, *J. Chem. Soc., Chem. Commun.*, **1971**, 733.

8) K. Bowden, I. M. Heilbron, E. R. H. Jones, and B. C. L. Weedon, *J. Chem. Soc.*, **1946**, 39.

9) J. Ojima, E. Ejiri, T. Kato, M. Nakamura, S. Kuroda, S. Hirooka, and M. Shibutani, *J. Chem. Soc., Perkin Trans. 1*, **1987**, 831.

 © 1989 The Chemical Society of Japan Bull. Chem. Soc. Jpn., 62, 1193—1197 (1989)

Sequential Reactions of Michael Addition and Peterson Condensation of 1-Silylvinyl Ketones with Grignard Reagents: Study of Stereoselectivity

Junji TANAKA, Hiroshi KOBAYASHI, Shuji KANEMASA,* and Otohiko TSUGE*
Institute of Advanced Material Study, and Department of Molecular Science and Technology, Interdisciplinary Graduate School of Engineering Sciences, Kyushu University, Kasugakoen, Kasuga 816
(Received October 26, 1988)

1-Silylvinyl ketones undergo smooth Michael addition with Grignard reagents generating magnesium enolates which are then trapped with benzaldehyde to give *E*- and *Z*-isomers of enones after Peterson condensation. (*E*)-Olefins become major products under a thermodynamic control when the condensation with benzaldehyde is carried out at room temperature in diethyl ether, while *Z*-isomers are more favored as kinetically controlled products at −78 °C in THF. Reaction mechanism is briefly discussed.

Nucleophilic addition of organocopper reagents to α,β-unsaturated carbonyl compounds and subsequent trapping of the intermediate enolates with a variety of electrophiles are now synthetically useful.[1] Applications of this sequence to α,β-unsaturated ketones followed by enolate-trapping with aldehydes lead to β-hydroxy ketones.

Michael addition of organometallics to 3-silyl-3-buten-2-ones[2,3] would offer a convenient and direct route to silyl-substituted metal enolates with a variety of counter cations. Hopefully the intermediate enolates may be utilized, in the same flask, to the Peterson condensation with carbonyl compounds leading to highly substituted enones.

In a previous communication,[4] we have reported the Michael addition-Peterson condensation sequence of methyl 2-(trimethylsilyl)acrylate with organomagnesium and -lithium compounds. As an extension of this program we have investigated the Michael addition-Peterson condensation sequence of 1-silylvinyl ketones with Grignard reagents. The details are presented here.

Results and Discussion

The Michael addition and Peterson condensation sequence of 3-trimethylsilyl-3-buten-2-one (**1**) was simply carried out by the initial treatment of **1** with a Grignard reagent followed by the reaction with benzaldehyde after completion of the Michael addition. No copper catalyst was needed in the Michael addition. For example, methylmagnesium iodide was added to a solution of **1** in diethyl ether at −15 °C, benzaldehyde was introduced after 1 h, and the reaction was continued at the same temperature for additional 1 h. The mixture was quenched with aqueous ammonium chloride to give a 6.7:1 mixture (by GLC) of *E*- and *Z*-isomers of 3-ethyl-4-phenyl-3-buten-2-one (**2a**) in 45% yield based on **1** (Scheme 1 and Entry 1 in Table 1). Both isomers could be separated from each other by column chromatography on silica gel.

Formation of (*E*)-olefins was again preferred in the

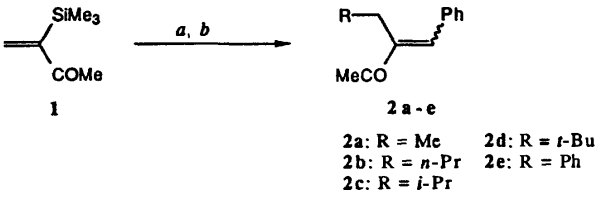

1 **2a-e**

2a: R = Me **2d**: R = *t*-Bu
2b: R = *n*-Pr **2e**: R = Ph
2c: R = *i*-Pr

a: RMgX in diethyl ether or THF *b*: PhCHO

Scheme 1.

reactions of **1** with propyl-, isopropyl-, and phenylmagnesium bromides under the equal conditions, **2b** (*E*:*Z*=5.2:1, Entry 3), **2c** (5:1, Entry 6), and **2e** (6.5:1, Entry 21) being produced. However, *Z*-isomer was predominantly produced (*E*:Z=1:4.7, Entry 20) in the reaction of **1** with *t*-butylmagnesium chloride, which was carried out in tetrahydrofuran (THF).[5] This unusual selectivity will be discussed below.

Stereostructures of (*E*)-**2** and (*Z*)-**2** were based on the chemical shifts of the olefin proton and the acetyl methyl protons. One typical example is shown as follows in the case of **2b**. (*E*)-**2b**: δ=2.44 (MeCO) and 7.46 (4-H). (*Z*)-**2b**: 2.05 (MeCO) and 6.64 (4-H).

The reaction of **1** with isopropylmagnesium bromide and benzaldehyde was performed under a variety of conditions to know factors by which the *E*/*Z* selectivity is influenced. The *E*/*Z* ratios were determined by gas-liquid chromatography (GLC) using (*E*)-4-phenyl-3-buten-2-one as an internal reference.

The *E*/*Z* ratio was found to be dependent upon the reaction temperature as shown in Entries 5—8. Since (*E*)-**2c** was relatively more favored at a higher temperature (Entry 8, *E*:*Z*=5.4:1), (*E*)-**2c** must be a thermodynamically controlled product, and hence (*Z*)-**2c** is a kinetically controlled one. This indicates that either the Michael addition step or the Peterson condensation step is reversible.

Figure 1 shows a possible reaction course for the formation of both isomers of olefin **2c**. The Michael addition between **1** and isopropylmagnesium bromide forms (*E*)- **C** and/or (*Z*)-enolate(s) **D**. As the carbonyl

Table 1. The Michael-Peterson Sequence of 3-Trimethylsilyl-3-buten-2-one (**1**)

Entry	RMgX[a]	Solvent	Additive	Michael addition		Peterson condensation		Product	Yield/%[b]	$E:Z$[c]
				Temp/°C	Time/h	Temp/°C	Time/h			
1	MeMgI	Et_2O		−15	1	−15	1	**2a**	45	6.7:1
2	MeMgI	Et_2O		rt	1	rt	1	**2a**	59	*E* only
3	*n*-PrMgBr	Et_2O		−15	1	−15	1	**2b**	61	5.8:1
4	*n*-PrMgBr	Et_2O		rt	1	rt	1	**2b**	67	5.7:1
5	*i*-PrMgBr	Et_2O		−78	1	−78	1	**2c**	59	1.6:1[d]
6	*i*-PrMgBr	Et_2O		−15	1	−15	1	**2c**	48	5:1[d]
7	*i*-PrMgBr	Et_2O		0	1	0	1	**2c**	55	5.1:1[d]
8	*i*-PrMgBr	Et_2O		rt	2	rt	1	**2c**	45	5.4:1[d]
9	*i*-PrMgBr	Et_2O		−78 °C 1 h then rt 1 h		rt	1	**2c**	73	6.8:1[d]
10	*i*-PrMgBr	Et_2O		rt 1 h then −78 °C 1 h		−78	1	**2c**	57	2.2:1[d]
11	*i*-PrMgBr	Et_2O		rt	1	−78[e]	1	**2c**	77	6.8:1[d]
12	*i*-PrMgBr	THF		−78	1.5	−78	1	**2c**	64	1:1.9[d]
13	*i*-PrMgBr	THF		−15	1	−15	1	**2c**	60	1:2.6[d]
14	*i*-PrMgBr	Et_2O	THF[f]	−15	1	−15	1	**2c**	59	1:2[d]
15	*i*-PrMgBr	Et_2O	HMPA[g,h]	−15	1	−15	1	**2c**	51	1.1:1[d]
16	*i*-PrMgBr	Et_2O	HMPA[g,i]	−15	1	−15	1	**2c**	52	1.1:1[d]
17	*i*-PrMgBr	Et_2O	$SnCl_4$[g,h]	−78	1	−78	1	**2c**	51	1.6:1[d]
18	*i*-PrMgBr	Et_2O	$SnCl_4$[g,j]	−78	1	−78	1	**2c**	53	1.8:1[d]
19	*t*-BuMgCl	THF		−78	1	−78	1	**2d**	47	1:5.8
20	*t*-BuMgCl	THF		−15	1	−15	1	**2d**	40	1:4.7
21	PhMgBr	Et_2O		−15	1	−15	1	**2e**	63	6.5:1

a) 1.2 Equivalnt of a Grignard reagent was employed. b) Yield of isolated products based on **1**. c) Ratio of isolated isomers. d) Detemined by GLC. e) Cooled to −78 °C immediately after benzaldehyde was added. f) THF:Et_2O=1:3 v/v. g) Additive was added 0.5 h after the Michael addition was started. h) A catalytic amount. i) HMPA:Et_2O=1:2 v/v. j) 1 Equivalent was used.

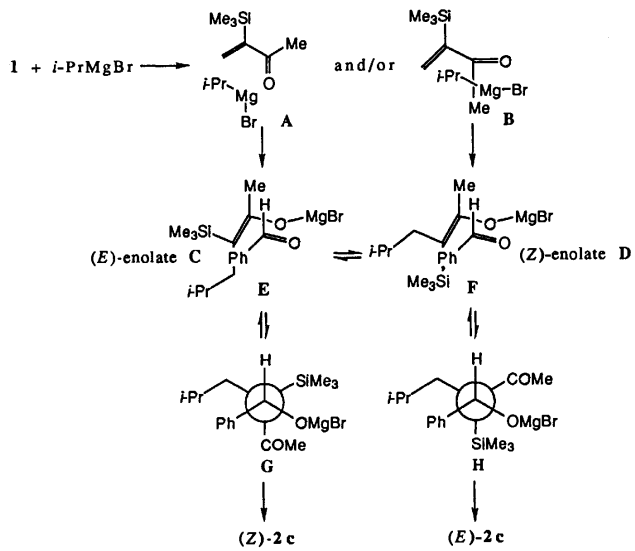

Fig. 1. Stereochemical course of the Michael-Peterson sequence between enone **1** and isopropylmagnesium bromide.

addition of magnesium enolates should be chelation-controlled,[6] the chair transition state **E** involving (*E*)-enolate **C** forms adduct alkoxide **G**; similarly its diastereomeric alkoxide **H** is formed from **F**. Cis-elimination is the far major path in the alkoxide-mediated Peterson condensation.[7] Therefore, (*Z*)-**2c** and (*E*)-**2c** are produced from **G** and **H**, respectively.

A high isomer ratio ($E:Z$=6.8:1, Entry 9) was obtained when the Michael adduct formed at −78 °C was warmed at room temperature for 1 h and the reaction with benzaldehyde was followed at the same temperature, while the stereoselectivity was poor ($E:Z$=2.2:1, Entry 10) when the adduct formed at room temperature was cooled to −78 °C and reacted with benzaldehyde.

It is concluded, on the ground of these results, that the stereostructures of product **2c** do not reflect those of magnesium enolate intermediates **C** and **D**,[8] and that the step of carbonyl addition is reversible. Thus, the thermodynamically controlled olefin, (*E*)-**2c**, was produced as a major product from the mixture of adduct alkoxides **G** and **H** which were equilibrating via **E** and **F**. The thermodynamic preference of (*E*)-**2c** might be due to the higher stabilization of (*Z*)-enolate **D** than **C** by an attractive interaction between the silyl and the alkoxide moieties.

Unlike in diethyl ether, (*Z*)-**2c** was produced as a major isomer in the reaction of **1** with isopropylmagnesium bromide and benzaldehyde in THF where the $E:Z$ ratio was not very much affected by the reaction temperature (Entries 12 and 13). A similar result was observed when THF (25 vol%) was added as an additive in the reaction performed in diethyl ether (Entry 14).

The aforementioned reaction of **1** with *t*-butylmagnesium chloride and benzaldehyde (Entry 20) in THF became a little more selective in favor of (*Z*)-**2c** when carried out at −78 °C ($E:Z$=1:5.8, Entry 19).

Thus the reaction in THF is kinetically controlled. As shown in Fig. 1, the Grignard reagent adds to enone **1** leading to (*E*)-enolate **C** as a kinetic adduct which

Table 2. The Michael-Peterson Sequence of 4,4-Dimethyl-2-trimethylsilyl-1-penten-3-one (**3**)

Entry	RMgX	Solvent	Michael addition		Peterson condensation		Product	Yield/%[a]	$E:Z$[b]
			Temp/°C	Time/h	Temp/°C	Time/h			
1	MeMgI	Et_2O	−78	1	−78 °C 1 h then	0 °C 30 min	Recovered **3**		
2	MeMgI	Et_2O	rt	1	rt	1	**4a**	80	1 : 1
3	*i*-PrMgBr	Et_2O	rt	1	rt	1	**4b**	84	1 : 1.5
4	*t*-BuMgCl	THF	−15	1	−15 °C 1 h then	0 °C 30 min	Recovered **3**		
5	*t*-BuMgCl	THF	rt	1	rt	1	**4c**	85	1 : 3.7

a) Yield of isolated products based on **3**. b) Determined by GLC.

gradually isomerizes into (*Z*)-enolate **D**. This isomerization presumably took place also in the reactions carried out in diethyl ether. As soon as the chelation-controlled addition of **C** to benzaldehyde forms the adduct alkoxide **G**, the elimination of silanol takes place quickly to give (*Z*)-**2c**. The elimination reaction is accelerated in THF because THF has a greater solvation ability than diethyl ether and therefore the oxygen-magnesium bond is much more polarized in this solvent.

Addition of hexamethylphosphoric triamide (HMPA) or tin(IV) chloride, either with a catalytic or a comparable amount, lowered the $E:Z$ ratio (Entries 15 to 18). These additives presumably broke down the chelation in the transition state of carbonyl addition.

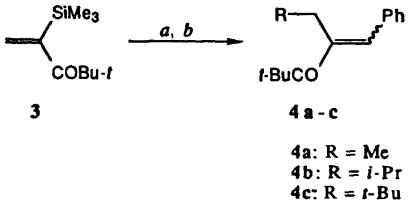

3 **4a-c**

4a: R = Me
4b: R = *i*-Pr
4c: R = *t*-Bu

a: RMgX in diethyl ether at rt
b: PhCHO at rt

Scheme 2.

The vinylsilane with a bulky acyl substituent, 4,4-dimethyl-2-trimethylsilyl-1-penten-3-one (**3**), was employed to the Michael-Peterson sequence. No Michael addition of **3** proceeded with methylmagnesium iodide at −78 °C, and *t*-butylmagnesium chloride as a bulky Grignard reagent could not react even at −15 °C. The starting enone **3** was recovered in both cases (Entries 1 and 4 in Table 2). Therefore, all the sequences were carried out at room temperature.

Both reactions of **3** with methylmagnesium iodide (Entry 2) and isopropylmagnesium bromide (Entry 3) in diethyl ether gave almost 1 : 1 mixtures of the *E*- and *Z*-isomers of olefins **4**. The $E:Z$ selectivity was poor also in the reaction of **3** with *t*-butylmagnesium chloride in THF (Entry 5, $E:Z$=1 : 3.7).

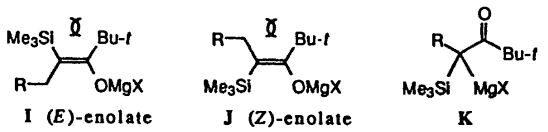

Two sterically congested magnesium enolates, **I** and **J**, which are expected to form in the Michael additions of **3** with Grignard reagents, seem too unstable to be involved as reacting intermediates. Even if they exist, their thermodynamic stability can not be sufficiently high so as to fully contribute to such an equilibrium as Fig. 1 shows. Therefore the adduct anions formed in the Michael additions of **3** should have reacted with benzaldehyde in a way different from the case of **1**. Probably they were involved in the carbonyl condensations, at least partly, in the form of β-oxo Grignard reagents **K**. This would be the major reason why the $E:Z$ selectivity was so decreased both in the reactions in diethyl ether and THF.

Experimental

General. Melting points were determined on a Yanagimoto melting point apparatus and are uncorrected. IR spectra were taken with a JASCO IRA-1 or a JASCO A-702 spectrometer. ^{1}H NMR spectra were recorded on a Hitachi R-40 (90 MHz), a JEOL FX-100 (100 MHz), or a JEOL GSX-270 instrument (270 MHz), and ^{13}C NMR on a JEOL FX-100 (25.05 MHz) or a JEOL GSX-270 spectrometer (67.94 MHz). Chemical shifts are expressed in parts per million downfield from tetramethylsilane as an internal standard. Mass spectra as well as high-resolution mass spectra were measured with a JEOL-01SG-2 spectrometer at 70 eV of ionization energy. Elemental analyses were performed on a Hitachi 026 CHN analyzer. For preparative column chromatography, Wakogel C-200, C-300 (Wako), and Silicagel 60 (Merck) were employed. Flash chromatography was carried out on an EYELA EF-10 apparatus using a column (20×180 mm) packed with Silicagel 60 (Merck, size: 0.04—0.063 mm). Gas liquid chromatography (GLC) was accomplished on a Yanaco G-2800 gas chromatograph (Yanagimoto) with an ionization flame detector using a glass column (SE-30, 3×2000 mm) or a glass capillary column (Silicone GE, SE-30, 0.25×50000 mm). Micro vacuum distillation was carried out on a Sibata GTO-250R Kugelrohr distilling apparatus. Solvents were evaporated with a Tokyo Rikakikai rotary evaporator type-V at about 50 °C unless otherwise stated.

Material. 3-Trimethylsilyl-3-buten-2-one (**1**) was prepared according to the reported method using 1-(trimethylsilyl)vinylmagnesium bromide.[2]

General Procedure for the Michael Addition and Peterson Condensation Sequence of 1-Silylvinyl Ketone 1. As a typical procedure, the reaction of **1** with methylmagnesium iodide and benzaldehyde is described. To a solution of freshly

prepared methylmagnesium iodide (1.2 mmol) in diethyl ether (3 ml) was added **1** (0.142 g, 1 mmol in diethyl ether (1 ml)) at −15 °C under dry nitrogen. After stirring for 1 h at this temperature, benzaldehyde (0.127 g, 1.2 mmol in diethyl ether (1 ml)) was added. The mixture was stirred at −15 °C for 1 h and then at 0 °C for 0.5 h. Saturated aqueous ammonium chloride was added and the organic products were collected in diethyl ether (30 ml×2). The combined extracts were dried over magnesium sulfate and evaporated in vacuo. The residue was chromatographed over silica gel by using hexane-ethyl acetate (30 : 1 v/v) to give (*Z*)-**2a** (0.01 g, 6%) and then (*E*)-**2a** (0.067 g, 39%).

In all other cases, the *E*- and *Z*-isomers were separated by silica-gel chromatography with hexane-ethyl acetate (30:1 v/v). The results are summarized in Table 1.

3-Ethyl-4-phenyl-3-buten-2-one (2a): (*E*)-**2a**: Colorless oil; IR (neat) 1662, 1490, 1380, 1345, 1228, 1115, 1020, 755, and 690 cm^{-1}; ^1H NMR ($CDCl_3$) δ=1.11 (3H, t, J=7.0 Hz, Et), 2.45 (3H, s, MeCO), 2.53 (2H, q, J=7.0 Hz, Et), 7.40 (5H, br s, Ph), and 7.47 (1H, s, 4-H); ^{13}C NMR ($CDCl_3$) δ=13.78, 19.63 (each Et), 26.09 (MeCO), 128.22, 128.58, 129.23, 135.81 (each Ph), 139.35 (4-C), 144.11 (3-C), and 200.08 (MeCO); MS m/z (rel intensity, %) 174 (M^+, base peak), 173 (62), 159 (56), 131 (72), 129 (19), 116 (23), 115 (28), 91 (55), 73 (50), and 43 (68). HRMS Found: m/z 174.1033. Calcd for $C_{12}H_{14}O$: M, 174.1044. (*Z*)-**2a**: Pale yellow liquid; IR (neat) 1655, 1430, 1380, 1340, 1220, 1115, 1020, 755, and 690 cm^{-1}; ^1H NMR ($CDCl_3$) δ=1.15 (3H, t, J=7.0 Hz, Et), 2.05 (3H, s, MeCO), 2.3—2.6 (2H, m, Et), 6.66 (1H, s, 4-H), and 7.1—7.5 (5H, m, Ph); MS m/z (rel intensity, %) 174 (M^+, base peak), 173 (66), 159 (74), 131 (93), 129 (25), 128 (18), 116 (31), 115 (49), 102 (24), 91 (85), 77 (36), 51 (25), and 43 (97). HRMS Found: m/z 174.1044. Calcd for $C_{12}H_{14}O$: M, 174.1044.

3-Butyl-4-phenyl-3-buten-2-one (2b): (*E*)-**2b**: Colorless liquid; IR (neat) 1660, 1375, 1350, 1240, 1215, 740, and 690 cm^{-1}; ^1H NMR ($CDCl_3$) δ=0.90 (3H, t, *n*-Bu), 1.3—1.5 (4H, m, *n*-Bu), 2.44 (3H, s, MeCO), 2.50 (2H, t, J=7.0 Hz, *n*-Bu), 7.3—7.4 (5H, m, Ph), and 7.46 (1H, s, 4-H); ^{13}C NMR ($CDCl_3$) δ=13.85, 22.98, 26.16, 31.35 (each *n*-Bu), 31.35 (MeCO), 128.53, 129.24, 135.89, (each Ph), 139.38 (4-C), 143.12 (3-C), and 200.27 (MeCO); MS m/z (rel intensity, %) 202 (M^+, 31), 201 (15), 159 (22), 129 (30), 117 (47), 116 (17), 115 (49), 91 (36), 77 (16), and 43 (base peak). HRMS Found: m/z 202.1350. Calcd for $C_{14}H_{18}O$: M, 202.1357. (*Z*)-**2b**: Colorless oil; IR (neat) 1680, 1485, 1345, 1190, 1115, 750, and 690 cm^{-1}; ^1H NMR ($CDCl_3$) δ=0.7—1.1 (3H, m, *n*-Bu), 1.1—1.6 (4H, m, *n*-Bu), 2.04 (3H, s, MeCO), 2.2—2.5 (2H, m, *n*-Bu), 6.64 (1H, s, 4-H), and 7.1—7.6 (5H, m, Ph); ^{13}C NMR ($CDCl_3$) δ=13.88, 22.38, 30.40 (each *n*-Bu), 30.87 (MeCO), 35.20 (*n*-Bu), 127.83, 128.38, 128.46, 130.16 (each Ph), 136.52 (4-C), 145.01 (3-C), and 208.00 (MeCO); MS m/z (rel intensity,%) 202 (M^+, 4), 129 (20), 128 (15), 117 (47), 116 (16), 115 (60), 91 (35), 77 (16), and 43 (base peak). HRMS Found: m/z 202.1361. Calcd for $C_{14}H_{18}O$: M, 202.1357.

3-(2-Methylpropyl)-4-phenyl-3-buten-2-one (2c): (*E*)-**2c**: Colorless oil; IR (neat) 1670, 1470, 1380, 1350, 1225, 1130, 750, and 700 cm^{-1}; ^1H NMR ($CDCl_3$) δ=0.82 (6H, d, J=6.6 Hz, *i*-Bu), 1.6—1.8 (1H, m, *i*-Bu), 2.45 (3H, s, MeCO), 2.48 (2H, d, J=7.3 Hz, *i*-Bu), 7.3—7.4 (4H, m, Ph), and 7.50 (1H, s, 4-H); ^{13}C NMR ($CDCl_3$) δ=22.59, 26.34 (each *i*-Bu), 28.06 (MeCO), 34.47 (*i*-Bu), 128.35, 128.52, 129.25, 136.06 (each Ph), 139.78 (4-C), 142.70 (3-C), and 200.80 (MeCO); MS m/z (rel intensity, %) 202 (M^+, 7), 128 (10), 116 (12), 115 (52), 91 (12), and 43 (base peak). HRMS Found: m/z 202.1350. Calcd for $C_{14}H_{18}O$: M, 202.1357. (*Z*)-**2c**: Colorless oil; IR (neat) 1685, 1460, 1365, 1350, 1200, 1120, 755, and 695 cm^{-1}; ^1H NMR ($CDCl_3$) δ=0.79 (6H, d, J=6.6 Hz, *i*-Bu), 1.6—1.7 (1H, m, *i*-Bu), 1.86 (3H, s, MeCO), 2.10 (2H, dd, J=7.3 and 1.1 Hz, *i*-Bu), 6.49 (1H, s, 4-H), and 7.0—7.2 (5H, m, Ph); ^{13}C NMR ($CDCl_3$) δ=22.62 (*i*-Bu), 27.30 (MeCO), 31.08, 45.39 (each *i*-Bu), 128.17, 128.67, 128.73 (each Ph), 132.01 (4-C), 136.75 (Ph), 144.27 (3-C), and 208.02 (MeCO); MS m/z (rel intensity, %) 202 (M^+, 24), 159 (17), 117 (21), 116 (19), 115 (35), 91 (16), and 43 (base peak). HRMS Found: m/z 202.1354. Calcd for $C_{14}H_{18}O$: M, 202.1357.

3-(2,2-Dimethylpropyl)-4-phenyl-3-buten-2-one (2d): (*E*)-**2d**: Colorless oil; IR (neat) 1675, 1470, 1360, 1235, 1200, 1160, 755, and 695 cm^{-1}; ^1H NMR ($CDCl_3$) δ=0.69 (9H, s, *t*-Bu), 2.45 (3H, s, MeCO), 2.66 (2H, s, *t*-BuCH_2), 7.2—7.5 (5H, m, Ph), and 7.50 (1H, s, 4-H); ^{13}C NMR ($CDCl_3$) δ=29.86 (*t*-Bu), 33.23 (MeCO), 36.76 (*t*-Bu), 49.08 (*t*-BuCH_2), 128.45, 128.48, 129.00, 136.76 (each Ph), 139.61 (4-C), 142.43 (3-C), and 201.51 (MeCO); MS m/z (rel intensity, %) 216 (M+, 10), 160 (34), 159 (24), 145 (29), 117 (21), 116 (30), 115 (36), 56 (59), and 42 (base peak). HRMS Found: m/z 216.1510. Calcd for $C_{15}H_{20}O$: M, 216.1513. (*Z*)-**2d**: Pale yellow oil; IR (neat) 1675, 1470, 1360, 1200, 1155, 760, and 695 cm^{-1}; ^1H NMR ($CDCl_3$) δ=0.94 (9H, s, *t*-Bu), 2.00 (3H, s, MeCO), 2.39 (2H, s, *t*-BuCH_2), 6.74 (1H, br s, 4-H), and 7.2—7.4 (5H, m, Ph); ^{13}C NMR ($CDCl_3$) δ=29.60 (*t*-Bu), 30.60 (MeCO), 32.17 (*t*-Bu), 49.07 (*t*-BuCH_2), 127.99, 128.43, 128.47 (each Ph), 135.11 (4-C), 136.70 (Ph), 143.15 (3-C), and 207.19 (MeCO); MS m/z (rel intensity, %) 216 (M^+, 27), 201 (16), 160 (base peak), 159 (48), 145 (42), 117 (30), 116 (78), 115 (30), and 56 (87). HRMS Found: m/z 216.1512. Calcd for $C_{15}H_{20}O$: M, 216.1513.

3-Benzyl-4-phenyl-3-buten-2-one (2e): (*E*)-**2e**: Colorless needles; mp 68—70 °C; IR (KBr) 1665, 1495, 1450, 1350, 1255, 1215, 970, 750, and 695 cm^{-1}; ^1H NMR ($CDCl_3$) δ=2.43 (3H, s, MeCO), 3.94 (2H, s, PhCH_2), 7.1—7.4 (10H, m, Ph), and 7.74 (1H, s, 4-H); ^{13}C NMR ($CDCl_3$) δ=26.29 (PhCH_2), 32.21 (MeCO), 126.04, 127.96, 128.55, 128.64, 128.94, 129.24, 135.36, 139.49 (each Ph), 139.87 (4-C), 141.22 (3-C), and 199.29 (MeCO); MS m/z (rel intensity, %) 236 (M^+, 35), 192 (25), 133 (20), 121 (69), 115 (62), 105 (43), 94 (27), 91 (49), 77 (28), 75 (24), 73 (40), 65 (35), and 43 (base peak). HRMS Found: m/z 236.1197. Calcd for $C_{17}H_{16}O$: M, 236.1200. (*Z*)-**2e**: Pale yellow oil; IR (neat) 1680, 1495, 1445, 1350, 1245, 1200, 830, 755, and 700 cm^{-1}; ^1H NMR ($CDCl_3$) δ=1.95 (3H, s, MeCO), 3.81 (2H, d, J=1.4 Hz, PhCH_2), 6.80 (1H, br s, 4-H), and 7.2—7.6 (10H, m, Ph); MS m/z (rel intensity, %) 236 (M^+, base peak), 235 (30), 221 (20), 193 (47), 192 (41), 178 (23), 115 (69), 91 (46), and 43 (36). HRMS Found: m/z 236.1196. Calcd for $C_{17}H_{16}O$: M, 236.1200.

4,4-Dimethyl-2-trimethylsilyl-1-penten-3-one (3): This compound was prepared by an application of the synthetic method of **1**.[2] From 1-bromo-1-(trimethylsilyl)ethene (5.0 g, 28 mmol), magnesium metal (0.83 g), and 2,2-dimethylpropanal (2.4 g, 28 mmol), enone **3** was obtained in 32% yield: Pale yellow liquid; bp 97—99 °C/4790 Pa (bulb-to-bulb); IR (neat) 2970, 1670, 1480, 1365, 1250, 1180, 1050, 1000, 940, 850, 760, and 695 cm^{-1}; ^1H NMR ($CDCl_3$) δ=0.15 (9H, s, Me_3Si), 1.19 (9H, s, *t*-Bu), 5.67, and 5.84 (each 1H, d, J=2.2 Hz, $=CH_2$); ^{13}C NMR ($CDCl_3$) δ=−1.02 (Me_3Si), 27.39, 44.06 (each *t*-Bu), 126.62 ($=CH_2$), 155.66 (2-C), and 215.57 (CO); MS m/z (rel intensity, %) 184 (M^+, 6), 127 (37), 73 (72), 57 (49), 45 (21), and 43 (base peak).

General Procedure for the Michael Addition and Peterson Condensation Sequence of 1-Silylvinyl Ketone 3. As a typical procedure, the reaction of **3** with methylmagnesium iodide and benzaldehyde is described. To a solution of freshly prepared methylmagnesium iodide (1.2 mmol) in diethyl ether (3 ml) was added **3** (0.168 g, 0.91 mmol in diethyl ether (1 ml)) at −15 °C under dry nitrogen. After stirring for 1 h at this temperature, benzaldehyde (0.127 g, 1.2 mmol in diethyl ether (1 ml)) was added. The mixture was stirred at −15 °C for 1 h. Saturated aqueous ammonium chloride was added and the organic products were collected in diethyl ether (30 ml × 2). The combined extracts were dried over magnesium sulfate and evaporated in vacuo. The residue was chromatographed over silica gel by using hexane-ethyl acetate (50 : 1 v/v) to give an inseparable mixture of *E*- and *Z*-isomers of **4a** (0.158 g, 80%, *E* : *Z*=1 : 1 (GLC)).

All results obtained in other cases are listed in Table 2.

2-Ethyl-4,4-dimethyl-1-phenyl-1-penten-3-one (4a): Obtained as an inseparable 1 : 1 mixture of *E*- and *Z*-isomers (GLC). Colorless oil; IR (neat) 1680, 1475, 1460, 1390, 1360, 1170, 1080, 1065, 930, 750, and 695 cm^{-1}; ^1H NMR ($CDCl_3$) *E*-isomer: δ=1.32 (9H, s, *t*-Bu), 1.17 (3H, t, J=7.7 Hz, Et), 2.54 (2H, dq, J=7.7 and 1.8 Hz, Et), 6.82 (1H, s, 1-H), and 7.2—7.4 (10H, m, Ph). *Z*-isomer: δ=0.99 (9H, s, *t*-Bu), 1.03 (3H, t, J=7.7 Hz, Et), 2.34 (2H, dq, J=7.7 and 1.8 Hz, Et), 6.35 (1H, s, 1-H), and 7.2—7.4 (10H, m, Ph); ^{13}C NMR ($CDCl_3$) δ=12.54, 13.43 (each Et), 22,52, 29,21 (each Et), 27.44, 28,29 (each *t*-Bu), 44.19, 44.25 (each *t*-Bu), 127.30, 127.57, 128.32, 128.38, 128.85, 129.72, 130.65, (each Ph), 136.04, 137.23, (each 1-C), 145.34, 144.39 (each 2-C), 212.65, and 218.50 (each CO); MS *m*/*z* (rel intensity, %) 216 (M^+, 9), 159 (base peak), 131 (90), 129 (26), 116 (37), 115 (58), 91 (87), 57 (37), and 41 (43). HRMS Found: *m*/*z* 216.1515. Calcd for $C_{15}H_{20}O$: M, 216.1513.

4,4-Dimethyl-2-(2-methylpropyl)-1-phenyl-1-penten-3-one (4b): Obtained as an inseparable 1 : 1.3 mixture of *E*- and *Z*-isomers (GLC). Colorless oil; IR (neat) 1685, 1480, 1465, 1370, 1095, 985, 755, and 700 cm^{-1}; ^1H NMR ($CDCl_3$) *E*-isomer: δ=0.84 (6H, d, J=6.6 Hz, *i*-Bu), 1.33 (9H, s, *t*-Bu), 2.43 (2H, dd, J=7.3 and 1.1 Hz, *i*-Bu), 6.89 (1H, br s, 1-H), and 7.2—7.4 (10H, m, Ph). *Z*-isomer: δ=0.97 (6H, d, J=6.6 Hz, *i*-Bu), 1.00 (9H, s, *t*-Bu), 2.17 (2H, dd, J=7.3 and 1.1 Hz, *i*-Bu), 6.32 (1H, br s, 1-H), and 7.2—7.4 (10H, m, Ph); ^{13}C NMR ($CDCl_3$) *E*-isomer: δ=22.61, 27.92 (each *i*-Bu), 28.55 (*t*-Bu), 37.68 (*i*-Bu), 44.15 (*t*-Bu), 143.11 (2-C), and 212.84 (CO). *Z*-isomer: δ=22.35, 26.80 (each *i*-Bu), 27.47, 44.28 (each *t*-Bu), 46.12 (*i*-Bu), 142.80 (2-C), and 217.65 (CO). Other signals are overlapped: δ=127.08, 127.32, 127.44, 128.30, 128.38, 128.91, 132.18, 136.22, 137.09; MS *m*/*z* (rel intensity, %) 244 (M^+, 3), 115 (32), 57 (98), 43 (38), and 41 (base peak). HRMS Found: *m*/*z* 244.1823. Calcd for $C_{17}H_{24}O$: M, 244.1826.

4,4-Dimethyl-2-(2,2-dimethylpropyl)-1-phenyl-1-penten-3-one (4c): Obtained as a 1 : 3.7 mixture of *E*- and *Z*-isomers (GLC) from which each isomer was roughly separated by column chromatography on silica gel with hexane-ethyl acetate (50 : 1 v/v). (*E*)-**4c**: Colorless oil; ^1H NMR ($CDCl_3$) δ=0.76, 1.38 (each 9H, s, *t*-Bu), 2.60 (2H, s, *t*-$BuCH_2$), 7.07 (1H, s, 1-H), and 7.2—7.4 (5H, m, Ph); ^{13}C NMR ($CDCl_3$) δ=29.45 (*t*-Bu), 29.69, 32.67, 40.03 (each *t*-$BuCH_2$), 44.06 (*t*-Bu), 127.35, 128.35, 128.81, (each Ph), 134.29 (1-C), 136.70 (Ph), 141.88 (2-C), and 212.69 (CO); MS *m*/*z* (rel intensity, %) 258 (M^+, 7), 201 (base peak), 145 (30), 115 (29), 57 (68), and 40 (40). HRMS Found: *m*/*z* 258.1968. Calcd for $C_{18}H_{26}O$: M, 258.1982. (*Z*)-**4c**: Colorless solid; mp 47—49 °C; IR (KBr) 1670, 1450, 1350, 1220, 1110, 980, 745, and 690 cm^{-1}; ^1H NMR ($CDCl_3$) δ=0.99, 1.00 (each 9H, s, *t*-Bu), 2.21 (2H, d, J=1.1 Hz, *t*-$BuCH_2$), 6.36 (1H, br s, 1-H), and 7.2—7.3 (5H, m, Ph); ^{13}C NMR ($CDCl_3$) δ=27.76 (*t*-Bu), 29.92, 32.89 (each *t*-$BuCH_2$), 44.22 (*t*-Bu), 49.66 (*t*-$BuCH_2$), 127.31, 128.17, 128.65 (each Ph), 129.93 (1-C), 136.84 (Ph), 141.67 (2-C), and 216.88 (CO); MS *m*/*z* (rel intensity, %) 258 (M^+, 6), 201 (base peak), 145 (24), 115 (25), 57 (60), and 40 (35). HRMS Found: *m*/*z* 258.1988. Calcd for $C_{18}H_{26}O$: M, 258.1982.

References

1) As a review: R. J. K. Taylor, *Synthesis*, **1985**, 364.

2) G. Stork and B. Ganem, *J. Am. Chem. Soc.*, **95**, 6152 (1973); R. K. Boeckman, Jr., *ibid.*, **95**, 6867 (1973).

3) R. Boeckman, Jr., *J. Am. Chem. Soc.*, **96**, 6179 (1974); G. Stork and J. Singh, *ibid.*, **96**, 6181 (1974); G. Quinkert, U. Schwartz, H. Stark, W. -D. Weber, H. Baier, F. Adam, and G. Durner, *Angew. Chem.*, **92**, 1062 (1980); A. P. S. Narula and D. I. Schuster, *Tetrahedron Lett.*, **22**, 3707 (1981).

4) O. Tsuge, S. Kanemasa, and Y. Ninomiya, *Chem. Lett.*, **1984**, 1993.

5) A solution of *t*-butylmagnesium chloride in THF was employed as it is commercially available.

6) H. E. Zimmerman and M. D. Traxler, *J. Am. Chem. Soc.*, **79**, 1920 (1957); F. Naf and R. Decorzant, *Helv. Chim. Acta*, **57**, 1317 (1974); P. Fellmann and J.-Emile Dubois, *Tetrahedron*, **34**, 1349 (1978); Y. Tamaru, T. Harada, S. Nishi, M. Mizutani, T. Hioki, and Z. Yoshida, *J. Am. Chem. Soc.*, **102**, 7808 (1980).

7) D. J. Ager, *Synthesis*, **1984**, 384; W. P. Weber, "Silicon Reagents for Organic Synthesis," Springer-Verlag, Berlin, Heidelberg, New York (1983), p. 58; E. W. Colvin, "Silicon in Organic Synthesis," Butterworths, London, Boston, Sydney, Wellington, Durbarr, Toronto (1981), p. 141.

8) All attempts to trap the enolates **C** and **D** with trimethylsilyl chloride were unsuccessful. As to the enolate trapping: E. J. Corey and A. W. Gross, *Tetrahedron Lett.*, **25**, 495 (1984).

Diene-Transmissive Hetero Diels-Alder Reactions of 3-Oxo-1,4-pentadiene Equivalents Leading to Functionalized 2-Chromanones

Eiji WADA,* Shuji KANEMASA,* and Otohiko TSUGE
Institute of Advanced Material Study, and Department of Molecular Science and Technology, Interdisciplinary Graduate School of Engineering Sciences, Kyushu University, Kasugakoen, Kasuga 816
(Received October 26, 1988)

Through hetero Diels-Alder reaction with a vinyl ether and Horner-Emmons olefination, diethyl 2-oxo-3-butenylphosphonate leads to 2-ethoxy-6-(1-alkenyl)-3,4-dihydro-2*H*-pyrans which are further transformed into 2-chromanones via regioselective Diels-Alder reactions with activated acetylenes followed by hydrolysis and oxidation.

Diene-transmissive Diels-Alder reactions of cross-conjugated trienes offer a direct and stereoselective synthetic route to highly functionalized hydronaphthalene skeletons.[1] The cross type of reactions with activated trienes[2] as well as the reaction sequences with some cross-conjugated triene equivalents[3] has been also developed.

In the preceding article we have opened a new synthetic route of diethyl 2-oxo-3-alkenylphosphonates which can be successfully applied to regioselective Diels-Alder reactions with vinyl ethers to give 4-substituted 2-alkoxy-6-[(diethoxyphosphinyl)methyl]-3,4-dihydro-2*H*-pyrans.[4] As these pyrans have an allylphosphonate functionality, they should be transformed into 1,3-dienes by a Horner-Emmons olefinations.[5] Diels-Alder reactions of the resulting 6-(1-alkenyl)-3,4-dihydro-2*H*-pyrans with acetylenes would become a convenient route to highly functionalized chroman derivatives after dehydrogenation. The present article describes details of the research performed along these lines.

Results and Discussion

The Diels-Alder reaction between diethyl 2-oxo-3-butenylphosphonate (**1**) and ethoxyethene regioselectively leads to 2-ethoxy-6-[(diethoxyphosphinyl)methyl]-3,4-dihydro-2*H*-pyran (**2**) in 83% yield.[4] As Horner-Emmons olefinations of **2** as an allylphosphonate are expected to produce 1,3-dienes,[5] the reaction of **2** with benzaldehyde was examined under various conditions. Deprotonation of **2** readily took place with butyllithium in tetrahydrofuran (THF) and the resulting anion reacted with bezaldehyde at room temperature to give the expected diene **3a** (Scheme 1). Under these conditions, however, the yield of **3a** was poor (34%) and some starting phosphonate **2** was recovered unchanged (37%), indicating the participation of a competitive retro carbonyl addition which has been often observed when the phosphonate anions are not so highly stabilized.[6]

It was found that the elimination reaction was accelerated by hexamethylphosphoric triamide (HMPA),

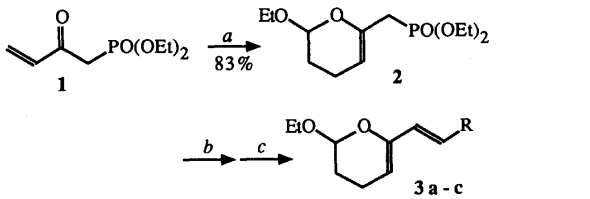

3a: R = Ph 66%
3b: R = *p*-MeOC$_6$H$_4$ 63%
3c: R = *n*-Pr 54% (recovered **2**: 28%)

a CH_2=CHOEt
b *n*-BuLi in THF-HMPA (5:1 v/v)
c RCHO

Scheme 1.

but still a temperature higher than 5 °C was needed to complete the elimination. After some efforts, the reaction was optimized as follows: The anion of **2** was generated with butyllithium (1.2 equiv) in THF containing HMPA (THF : HMPA=5 : 1 v/v) at −78 °C and benzaldehyde (1.2 equiv) was added. The reaction temperature was gradually raised to 10 °C and the reaction was continued for 6 h. Thus (*E*)-1,3-diene **3a** was obtained as the sole product in 66% yield.

Similar condensations with *p*-methoxybenzaldehyde and butanal produced (*E*)-6-(1-alkenyl)-2-ethoxy-3,4-dihydro-2*H*-pyrans **3b**, **c** in 63 and 54% yields, respectively (Scheme 1).

Three activated acetylene dienophiles such as dimethyl acetylenedicarboxylate (DMAD), methyl propynoate (MPR), and 3-butyn-2-one (BYO) were employed in the Diels-Alder reactions with these dienes **3a—c**. The Diels-Alder reactions were carried out in benzene in a sealed tube at 90—115 °C, and a catalytic amount of hydroquinone or 2,5-di(*t*-butyl)hydroquinone was used as an inhibitor for the homolytic polymerization of **3**.

Since the starting 1,3-dienes **3a—c** are 2-alkoxy-substituted *E*-isomers, the cycloadducts **4a—h** must be regiochemically pure and accordingly consist of only two isomers of cycloadducts, 2,4a-cis and 2,4a-trans isomers, on the basis of the high regio control by an

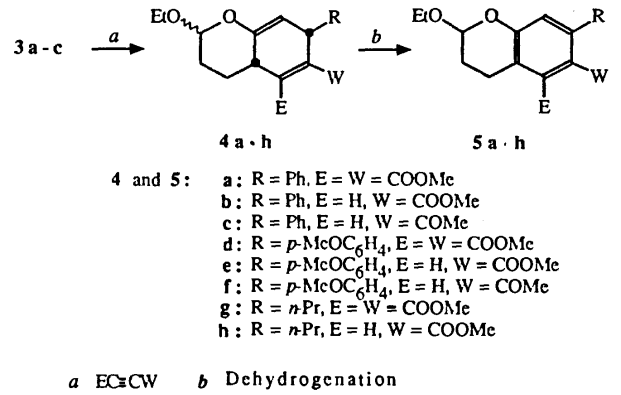

Scheme 2.

oxygen substituent and the stereochemical integrity of Diels-Alder cycloadditions (Scheme 2 and Table 1). Thus the Diels-Alder reactions of 1-aryl-substituted dienes **3a, b** with MPR and BYO afforded a clean mixture of two stereoisomers of regioselective cycloadducts **4a, b**. Only in the reaction of **3c** bearing a 1-alkyl substituent with MPR a trace of regioisomer **5h** (R=*n*-Pr, E=COOMe, W=H) was produced. In one case where the Diels-Alder reaction was carried out at such a high temperature as 155 °C for 60 h, spontaneous dehydrogenation of the cycloadduct **4b** took place.

Assignment of each stereoisomer of Diels-Alder cycloadducts **4** as well as determination of the isomer ratio was not thought so important in this particular sequence directed to 2-chromanones that characterization was made only for limited cases. The stereostructures of 2,4a-cis and 2,4a-trans isomers were determined on the basis of ^{1}H NMR spectra. As for two stereoisomers of **4b**, the major isomer with lower ethoxy methyl protons (δ=1.22) was assigned to be 2,4a-trans and the minor one with higher protons (1.05) 2,4a-cis. The major isomer should have an axial 2-H, and this was confirmed by the coupling constant $J_{2\text{-}3}$ (8.8 and 2.6 Hz).[7,8] An abnormally large 1,4-long-

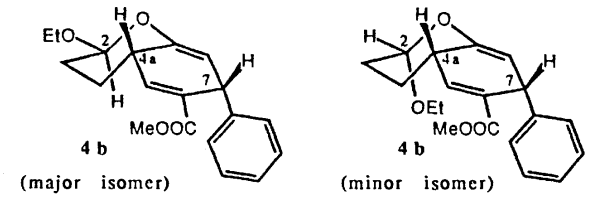

$J_{2\text{-}3}$ = 8.8 and 2.6 Hz
$J_{4a\text{-}7}$ = 8.1 Hz

range coupling constant was observed between 4a-H and 7-H of the major isomer of **4b** ($J_{4a\text{-}7}$=8.1 Hz). This large coupling is anticipated for the 4a,7-cis structure with two methine hydrogen in a pseudo-axial configuration.[9]

As shown in Table 1, 2,4a-trans isomers were a little more favored than 2,4a-cis isomers, indicating the preference of the sterically less hindered approach of an acetylene dienophile to **3** from the face opposite to the axial 2-ethoxy substituent.[10]

The 1,4-cyclohexadiene rings of the Diels-Alder cycloadducts **4a—h** were readily aromatized by treatment with 2,3-dichloro-5,6-dicyano-1,4-benzoquinone (DDQ) or tetrachloro-1,4-benzoquinone (*p*-chloranil) under reflux in benzene or toluene, respectively, to give 2-ethoxychromans **5a—h** (Scheme 2 and Table 1). As DDQ is stronger dehydrogenating reagent than chloranil, a less amount of DDQ and a lower reaction temperature were enough to complete the dehydrogenation. Existence of an acetyl moiety in **4** resulted in

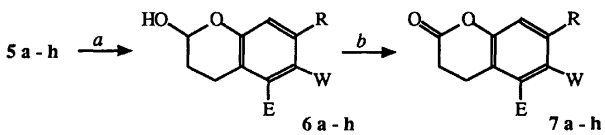

(*Suffixes* **a-h** *designated in Scheme 2*)

a 4M-HCl in THF
b PCC (3 equiv) in CH_2Cl_2

Scheme 3.

Table 1. Diels-Alder Reactions of 6-(1-Alkenyl)-2-ethoxy-3,4-dihydro-2*H*-pyrans **3a—c** Followed by Dehydrogenation Leading to 2-Ethoxychromans **5a—h**

Diene	Dienophile[a]	Diels-Alder reaction[b]		Product			Dehydrogenation[c]	Product	
		Temp/°C	Time/h	4	Yield/%[d]	Isomer ratio[e]		5	Yield/%[d,f]
3a	DMAD	115	24	**4a**	70	g)	A or B	**5a**	90 (80)
3a	MPR	115	60	**4b**	87	8:3[h]	A or B	**5b**	90 (73)
3a	BYO	90	48	**4c**	69	9:5	A or B	**5c**	50 (50)
3b	DMAD	115	20	**4d**	75	3:1	B	**5d**	(80)
3b	MPR	115	60	**4e**	88	2:1	A or B	**5e**	70 (74)
3b	BYO	90	48	**4f**	79	1:1	A or B	**5f**	36 (57)
3c	DMAD	105	84	**4g**	66	g)	A	**5g**	85
3c	MPR	105	84	**4h**	72	g)	A	**5h**	80[i]

a) DMAD: dimethyl acetylenedicarboxylate. MPR: methyl propynoate. BYO: 3-butyn-2-one. b) Carried out in a sealed tube in the presece of a catalytic amount of hydroquinone or 2,5-di(*t*-butyl)hydroquinone. c) A: DDQ (2 equiv), reflux in benzene, 24 h. B: *p*-chloranil (5 equiv), reflux in toluene, 48 h. d) Yield of isolated products. e) Ratio of 2,4a-trans : 2,4a-cis isomers (^{1}H NMR). f) Yield in parenthesis from procedure B. g) No ^{1}H NMR taken. h) Contaminated by a trace of **5b** (**4b** : **5b**=12 : 1 mol/mol). i) Contaminated by a trace of *m*-isomer (**5h** : R=*n*-Pr, E=COOMe, W=H).

the low-yield formation of **5c** and **5f**; *p*-chloranil gave better yields of **5e, f** than DDQ in dehydrogenations of *p*-methoxyphenyl-substituted cycloadducts **4e, f**.

The coupling constants between 2-H and 3-Hs of **5a—h** are relatively small ($J_{2\text{-}3}$=2.6 to 2.9 Hz). This indicates that the benzo-fused 2-ethoxy-3,4-dihydro-2*H*-pyran ring exclusively takes one conformation, in a chloroform solution, with the 2-ethoxy substituent axial.

The acetal moiety of 2-ethoxychromans **5a—h** was readily hydrolyzed with 4 M hydrochloric acid (1 M=1 mol dm^{-3}) in THF at room temperature; the products **6a—e** excellently produced were characterized as not 3-(*o*-hydroxyaryl)propanals but as 2-chromanols (Scheme 3) on the basis of the absence of formyl proton in ^{1}H NMR spectra. However, they were smoothly oxidized into 2-chromanones **7a—e** with pyridinium chlorochromate (PCC) in good yields. In most cases, both steps of hydrolysis and oxidation of **5** were performed in a single procedure without trouble. Total yields of 2-chromanones **7** were as good as 68 to 78% based on **5a—h**, not depending upon the isolation procedure of **6** (Table 2).

In conclusion, a new entry to the synthesis of 2-chromanones has been presented here. The method starts with diethyl 2-oxo-3-butenylphosphonate (**1**) through the Diels-Alder reaction with a vinyl ether, the Horner-Emmons olefination, the Diels-Alder reaction with acetylenes, and the PCC oxidation. Through the above sequence of reactions, the phosphonate **1** can be regarded as a synthetic equivalent of 1,4-pentadien-3-ones, a hetero cross-conjugated triene. 7-Substituted 2-chromanones bearing functional groups at 5- and 6-positions were synthesized in this article, and further introduction of several substituents or functional groups would be possible at the 4- and 8-positions of 2-chromanones by a simple extension of the present method.

Table 2. Transformation of 2-Ethoxychromans **5a—h** into 2-Chromanones **7a—h** by a Sequence of Hydrolysis and Pyridinium Chlorochromate Oxidation

2-Ethoxychromans	2-Chromanols[a]		2-Chromanones[b]	
	6	Yield/%[c]	**7**	Yield/%[d]
5a	**6a**	90	**7a**	83 (75)
5b	**6b**	90	**7b**	81 (73)
5c	**6c**	90	**7c**	80 (72)
5d	**6d**	92	**7d**	85 (78)
5d	**6d**	e)	**7d**	(74)
5e	**6e**	90	**7e**	84 (76)
5f	**6f**	e)	**7f**	(68)
5g	**6g**	e)	**7g**	(70)
5h	**6h**	e)	**7h**	(69)

a) Obtained by hydrolysis of **5** with 4M-HCl in THF at room temperature for 15 h. b)Obtained by oxidation of **6** with PCC (3 equiv) in dichloromethane at room temperature for 24 h. c) Yield of isolated product based on **5**. d) Yield of isolated product based on **6**. Yield based on **5** in parenthesis e) Crude **6** was used in the subsequent transformation without isolation.

Experimental

General. Melting points were determined on a Yanagimoto melting point apparatus and are uncorrected. IR spectra were taken with a JASCO IRA-1 or a JASCO A-720 spectrometer. ^{1}H NMR spectra were recorded on a Hitachi R-40 (90 MHz), a JEOL FX-100 (100 MHz), or a JEOL GSX-270 instrument (270 MHz), and ^{13}C NMR on a JEOL FX-100 (25.05 MHz) or a JEOL GSX-270 spectrometer (67.94 MHz). Chemical shifts are expressed in parts per million downfield from tetramethylsilane as an internal standard. Mass spectra as well as high-resolution mass spectra were measured with a JEOL-01SG-2 spectrometer at 70 eV of ionization energy. Elemental analyses were performed on a Hitachi 026 CHN analyzer. For preparative column chromatography, Wakogel C-200, C-300 (Wako), and Silicagel 60 (Merck) were employed. Flash chromatography was carried out on an EYELA EF-10 apparatus using a column (20×180 mm) packed with Silicagel 60 (Merck, size: 0.04—0.063 mm). Gas liquid chromatography (GLC) was accomplished on a Yanaco G-2800 gas chromatograph (Yanagimoto) with an ionization flame detector using a glass column (SE-30, 3×2000 mm) or a glass capillary column (Silicone GE, SE-30, 0.25×50000 mm). Micro vacuum distillation was carried out on a Sibata GTO-250R Kugelrohr distilling apparatus. Solvents were evaporated with a Tokyo Rikakikai rotary evaporator type-V at about 50 °C unless otherwise stated.

Material. Compound **2**[4] was prepared according to the previously reported method.

General Procedure for the Horner-Emmons Olefination of 2-Ethoxy-6-[(diethoxyphosphinyl)methyl]-3,4-dihydro-2*H*-pyran (2) Leading to 6-(1-Alkenyl)-3,4-dihydro-2*H*-pyrans 3a—c. As a typical example the preparation of **3a** is described as follows: To a solution of **2** (1.7 g, 6.11 mmol) and HMPA (5 ml) in dry THF (25 ml) was added butyllithium (15% in hexane, 4.57 ml, 7.33 mmol) at −78 °C under nitrogen. After 1 h at the same temperature, benzaldehyde (0.777 g, 7.33 mmol) was added and stirring was continued at 10 °C for 6 h. The mixture was poured into saturated aqueous ammonium chloride and extracted with diethyl ether (25 ml×2). The combined extracts were dried over anhydrous magnesium sulfate and evaporated in vacuo. The residue was chromatographed over silica gel by using hexane-diethyl ether (96 : 4 v/v) as an eluent to give **3a** (0.93 g, 66%).

(*E*)-2-Ethoxy-6-(2-phenylethenyl)-3,4-dihydro-2*H*-pyran (3a): Colorless liquid; IR (neat) 1640, 1610, 1490, 1445, 1120, 1030, 955, 750, and 690 cm^{-1}; ^{1}H NMR ($CDCl_3$) δ=1.24 (3H, t, J=7.0 Hz, EtO), 1.8—1.9 (2H, m, 3-H), 2.0—2.2, 2.3—2.5 (each 1H, m, 4-H), 3.66, 3.93 (each 1H, dq, J_{gem}=9.9 and J=7.0 Hz, EtO), 5.00 (1H, t, $J_{5\text{-}4}$=4.4 Hz, 5-H), 5.18 (1H, t, $J_{2\text{-}3}$=3.3 Hz, 2-H), 6.44 (1H, d, J=15.8 Hz, 6-CH=), 6.83 (1H, d, J=15.8 Hz, =CHPh), and 7.2—7.5 (5H, m, Ph); ^{13}C NMR ($CDCl_3$) δ=15.25 (EtO), 17.80 (4-C), 26.54 (3-C), 63.81 (EtO), 97.19 (2-C), 104.47 (5-C), 124.33, 125.94, 126.46, 127.28, 128.55, 137.23, 147.77 (6-C); MS *m/z* (rel intensity, %) 230 (M^+, 30), 131 (67), 129 (37), 128 (46), 115 (46), 105 (36), 103 (71), 102 (25), 91 (37), 76 (base peak), 55 (24), and 51 (44). HRMS Found: *m/z* 230.1332. Calcd for $C_{15}H_{18}O_2$: M, 230.1306.

(*E*)-2-Ethoxy-6-[2-(*p*-(methoxyphenyl)ethenyl]-3,4-dihydro-2*H*-pyran (3b): Pure **3b** was obtained in 63% yield by silica-gel column chromatography of the curde product by using hexane-diethyl ether (7 : 1 v/v) as an eluent: Colorless solid (hexane); mp 62—64 °C; IR (KBr) 1640, 1595, 1500, 1440, 1245, 1175, 1110, 1040, 970, and 820 cm^{-1}; ^1H NMR ($CDCl_3$) δ=1.25, (3H, t, J=7.0 Hz, EtO), 1.8—2.0 (2H, m, 3-H), 2.11, 2.33 (each 1H, m, 4-H), 3.67, 3.94 (each 1H, dq, J_{gem}=9.9 and J=7.0 Hz, EtO), 3.80 (3H, s, *p*-MeO), 4.95 (1H, t, $J_{5\text{-}4}$=4.4 Hz, 5-H), 5.17 (1H, t, $J_{2\text{-}3}$=3.3 Hz, 2-H), 6.32 (1H, d, J=16.1 Hz, 6-CH=), 6.77 (1H, d, J=16.1 Hz, =CHPh), 6.85 (2H, dt, J=8.8 and 1.9 Hz, Ar), and 7.34 (2H, dt, J=8.8 and 1.9 Hz, Ar); ^{13}C NMR ($CDCl_3$) δ=15.25 (EtO), 17.83 (4-C), 26.64 (3-C), 55.26 (*p*-MeO), 63.79 (EtO), 97.23 (2-C), 103.35 (5-C), 114.05, 122.36, 125.51, 127.66, 130.06, 147.94 (6-C), and 159.10 (Ar); MS m/z (rel intensity, %) 260 (M^+, 74), 178 (25), 161 (48), 136 (64), 135 (base peak), 92 (21), and 77 (33). Found: C, 74.01; H, 7.79%. Calcd for $C_{16}H_{20}O_3$: C, 73.82; H, 7.74%.

(*E*)-2-Ethoxy-6-(1-pentenyl)-3,4-dihydro-2*H*-pyran (3c): Pure **3c** was obtained in 54% yield by silica-gel column chromatography of the crude product by using hexane-diethyl ether (9 : 1 v/v) as an eluent: Pale yellow liquid; IR (neat) 1660, 1625, 1440, 1370, 1120, 1035, 955, and 920 cm^{-1}; ^1H NMR ($CDCl_3$) δ=0.86 (3H, t, J=7.3 Hz, *n*-Pr), 1.10 (3H, t, J=7.0 Hz, EtO), 1.37 (2H, sex, J=7.3 Hz, *n*-Pr), 1.6—1.9 (3H, m, 3- and 4-H), 2.03 (2H, q, J=7.3 Hz, *n*-Pr), 2.30 (1H, m, 4-H), 3.43, 3.88 (each 1H, J_{gem}=9.5 and J=7.0 Hz, EtO), 4.72 (1H, dd, $J_{5\text{-}4}$=5.2 and 3.6 Hz, 5-H), 4.98 (1H, dd, $J_{2\text{-}3}$=3.3 and 2.7 Hz, 2-H), 5.84 (1H, br d, J=15.4 Hz, 6-CH=), and 6.24 (1H, br dt, J=15.4 and 7.3 Hz, =CHPr-*n*); ^{13}C NMR ($CDCl_3$) δ=13.87 (*n*-Pr), 15.45 (EtO), 17.68 (4-C), 22.94 (*n*-Pr), 26.98 (3-C), 34.82 (*n*-Pr), 63.70 (EtO), 97.35 (2-C), 101.12 (5-C), 126.89, 128.23, 148.17 (6-C); MS m/z (rel intensity, %) 196 (M^+, 78), 153 (39), 151 (21), 150 (41), 121 (20), 109 (20), 107 (23), 97 (34), 86 (45), 79 (31), and 73 (base peak). HRMS Found: m/z 196.1470. Calcd for $C_{12}H_{20}O_2$: M, 196.1462.

General Procedure for the Diels-Alder Reaction and Dehydrogenation of 6-(1-Alkenyl)-2-ethoxy-3,4-dihydro-2*H*-pyrans 3a—c Leading to 2-Ethoxychromans 5a—h. As a typical example the reaction of **3a** with methyl propynoate is described as follows: A solution of **3a** (0.105 g, 0.46 mmol), methyl propynoate (0.084 g, 1 mmol), and a catalytic amount of hydroquinone in dry benzene (2 ml) was charged in a sealed tube and heated at 115 °C for 60 h. The benzene was evaporated in vacuo and the residue was chromatographed over silica gel with hexane-diethyl ether (6 : 1 to 4 : 1 v/v) to give **4b** which was contaminated by a trace of **5b** (**4b** : **5b**=12 : 1 mol/mol by ^1H NMR).

The product **4b** consisted of two stereoisomers (2,4a-trans : 2,4a-cis=8 : 3 by ^1H NMR) from which 2,4a-*trans*-**4b** was separated by crystallization. 2,4a-*trans*-**4b**: Colorless prisms (diethyl ether-hexane); mp 131—132 °C; IR (KBr) 1710, 1690, 1430, 1250, 1130, 1040, 960, 830, 740, and 700 cm^{-1}; ^1H NMR ($CDCl_3$) δ=1.22 (3H, t, J=7.0 Hz, EtO), 1.56 (1H, dq, J_{gem}=$J_{4\text{-}3}$=$J_{4\text{-}4a}$=12.4 and $J_{4\text{-}3}$=8.8 Hz, 4(ax)-H), 1.83 (1H, dddd, J_{gem}=13.6, $J_{3\text{-}4}$=12.4, 4.8, and $J_{3\text{-}2}$=8.8 Hz, 3(ax)-H), 2.03 (1H, m, 3(eq)-H), 2.21 (1H, m, 4(ax)-H), 3.01 (1H, m, 4a-H), 3.53, 3.94 (each 1H, dq, J_{gem}=9.9 and J=7.0 Hz, EtO), 3.56 (3H, s, COOMe), 4.46 (1H, ddd, $J_{7\text{-}4a}$=8.1, $J_{7\text{-}8}$=3.7, and $J_{7\text{-}5}$=1.5 Hz, 7-H), 4.58 (1H, dd, $J_{2\text{-}3}$=8.8 and 2.6 Hz, 2-H), 5.20 (1H, dd, $J_{8\text{-}7}$=3.7 and $J_{8\text{-}4a}$=1.5 Hz, 8-H), 6.85 (1H, dd, $J_{5\text{-}4a}$=3.7 and $J_{5\text{-}7}$=1.5 Hz, 5-H), and 7.2—7.4 (5H, m, Ph); ^{13}C NMR ($CDCl_3$) δ=15.21 (EtO), 28.45 (4-C), 31.16 (3-C), 34.86 (4a-C), 42.68 (7-C), 51.52 (COOMe), 64.58 (EtO), 103.14 (2-C), 109.15 (8-C), 126.46, 128.04, 128.42 (each Ph), 131.10 (6-C), 138.15 (5-C), 143.93 (Ph), 148.61 (8a-C), and 166.73 (COOMe); MS m/z (rel intensity, %) 314 (M^+, 3), 165 (15), 153 (24), 152 (26), 141 (20), 115 (37), 85 (27), and 77 (28). Found: C, 72.40; H, 7.11%. Calcd for $C_{19}H_{22}O_4$: C, 72.59; H, 7.05%.

A solution of **4b** (0.47 g, 1.495 mmol) and DDQ (0.679 g, 2.99 mmol) in dry benzene (25 ml) was heated under reflux for 20 h. The solid precipitated was removed off by filtration through Celite 545 and the filtrate was again filtered through alumina by using ethyl acetate as an eluent. The eluate was evaporated in vacuo and the residue was chromatographed over silica gel with hexane-diethyl ether (5 : 1 v/v) to give **5b** (0.418 g, 90%).

In other cases, Diels-Alder cycloadducts **4a** and **4c—h** were not characterized, but the cis/trans ratio was determined by ^1H NMR spectrum of the unpurified mixture. The ratio between the 3,4a-trans and 3,4a-cis isomers was determined on the basis of the relative integration of the 2-ethoxy methyl protons (in parenthesis): **4b**: 8 : 3 (δ=1.22 and 1.05); **4c**: 9 : 5 (1.20 and 1.08); **4d**: 3 : 1 (1.23 and 1.05); **4e**: 2 : 1 (1.22 and 1.08); **4f**: 1 : 1 (1.20 and 1.11). The reaction conditions and results are summarized in Table 1.

Dimethyl 2-Ethoxy-7-phenylchroman-5,6-dicarboxylate (5a): Colorless viscous oil; IR (neat) 1725, 1600, 1560, 1320, 1270, 1040, 960, 880, and 700 cm^{-1}; ^1H NMR ($CDCl_3$) δ=1.20 (3H, t, J=7.0 Hz, EtO), 1.91, 2.08 (each 1H, m, 3-H), 2.74 (1H, ddd, J_{gem}=17.3, $J_{4\text{-}3}$=5.5, and 3.3 Hz, 4(eq)-H), 3.03 (1H, ddd, J_{gem}=17.3, $J_{4\text{-}3}$=11.4, and 5.9 Hz, 4(ax)-H), 3.53 (3H, s, 6-COOMe), 3.62, 3.86 (each 1H, dq, J_{gem}=9.9 and 7.0 Hz, EtO), 3.87 (3H, s, 5-COOMe), 5.28 (1H, t, $J_{2\text{-}3}$=2.9 Hz, 2-H), 6.92 (1H, s, 8-H), and 7.2—7.5 (5H, m, Ph); ^{13}C NMR ($CDCl_3$) δ=14.97 (q, EtO), 18.25 (t, 4-C), 25.85 (t, 3-C), 51.83, 52.29 (each q, COOMe), 63.98 (t, EtO), 96.87 (d, 2-C), 120.28 (s), 120.28 (d), 127.41 (d), 128.00 (d), 133.50 (s), 140.05 (s), 140.99 (s), 153.62 (s), 168.01, and 168.48 (each s, COOMe); MS m/z (rel intensity, %) 370 (M^+, 26), 338 (base peak), 281 (25), 279 (27), 249 (24), 185 (21), 165 (24), and 154 (21). HRMS Found: m/z 370.1418. Calcd for $C_{21}H_{22}O_6$: M, 370.1415.

Methyl 2-Ethoxy-7-phenylchroman-6-carboxylate (5b): Colorless prisms (hexane); mp 46—48 °C; IR (KBr) 1700, 1610, 1550, 1480, 1440, 1290, 1155, 960, and 880 cm^{-1}; ^1H NMR ($CDCl_3$) δ=1.19 (3H, t, J=7.0 Hz, EtO), 1.95, 2.08 (each 1H, m, 3-H), 2.68 (1H, br ddd, J_{gem}=16.8, $J_{4\text{-}3}$=6.0, and 3.6 Hz, 4(eq)-H), 3.20 (1H, br ddd, J_{gem}=16.8, $J_{4\text{-}3}$=12.1, and 6.2 Hz, 4(ax)-H), 3.56 (3H, s, COOMe), 3.64, 3.88 (each 1H, dq, J_{gem}=9.5 and J=7.0 Hz, EtO), 5.29 (1H, t, $J_{2\text{-}3}$=2.6 Hz, 2-H), 6.80 (1H, s, 8-H), 7.2—7.5 (5H, m, Ph), and 7.65 (1H, s, 5-H); ^{13}C NMR ($CDCl_3$) δ=15.03 (EtO), 20.00 (4-C), 26.32 (3-C), 51.48 (COOMe), 63.88 (EtO), 97.28 (2-C), 119.22, 121.50, 122.44, 126.94, 127.71, 128.23, 131.86, 141.39, 142.92, 154.79 (each Ph and Ar), and 168.31 (COOMe); MS m/z (rel intensity, %) 312 (M^+, 28), 266 (23), 74 (30), 59 (66), 57 (28), 45 (51), 43 (51), and 31 (base peak). Found: C, 73.30; H, 6.54%. Calcd for $C_{19}H_{20}O_4$: C, 73.06; H, 6.45%.

6-Acetyl-2-ethoxy-7-phenylchroman (5c): Colorless prisms (hexane); mp 51—53 °C; IR (KBr) 1675, 1600, 1545, 1475, 1275, 1145, 1100, 1045, 955, and 875 cm^{-1}; ^1H NMR ($CDCl_3$) δ=1.20 (3H, t, J=7.0 Hz, EtO), 1.96 (1H, m, one of 3-H), 1.96 (3H, s, MeCO), 2.09 (1H, m, the other of 3-H), 2.70 (1H, ddd, J_{gem}=16.2, $J_{4\text{-}3}$=6.0, and 3.6 Hz, 4(eq)-H), 3.03 (1H,

ddd, J_{gem}=16.2, J_{4-3}=12.6, and 5.4 Hz, 4(ax)-H), 3.66, 3.90 (each 1H, dq, J_{gem}=9.5 and J=7.0 Hz, EtO), 5.30 (1H, t, J_{2-3}=2.9 Hz, 2-H), 6.82 (1H, s, 8-H), and 7.2—7.5 (6H, 5-H and Ph); ^{13}C NMR ($CDCl_3$) δ=15.10 (EtO), 20.09 (4-C), 26.42 (3-C), 30.27 (MeCO), 63.96 (EtO), 97.28 (2-C), 118.67, 121.77, 127.70, 128.51, 128.76, 130.23, 133.16, 140.97, 141.15, 154.47 (each Ph and Ar), and 203.10 (MeCO); MS m/z (rel intensity, %) 296 (M^+, 41), 281 (57), 235 (31), 209 (21), 165 (28), 153 (27), 152 (38), and 43 (base peak). Found: C, 77.19; H, 6.85%. Calcd for $C_{19}H_{20}O_4$: C, 77.00; H, 6.80%.

Dimethyl 2-Ethoxy-7-(*p*-methoxyphenyl)chroman-5,6-dicarboxylate (5d): Colorless prisms (hexane); mp 94—95 °C; IR (KBr) 1725, 1600, 1430, 1320, 1265, 1230, 1020, 955, and 830 cm^{-1}; ^{1}H NMR ($CDCl_3$) δ=1.18 (3H, t, J=7.3 Hz, OEt), 1.92, 2.07 (each 1H, m, 3-H), 2.73 (1H, ddd, J_{gem}=17.3, J_{4-3}=5.5, and 3.3 Hz, 4(eq)-H), 3.03 (1H, ddd, J_{gem}=17.3, J_{4-3}=11.4, and 5.9 Hz, 4(ax)-H), 3.58 (3H, s, 6-COOMe), 3.63, 3.83 (each 1H, dq, J_{gem}=9.5 and J=7.3 Hz, OEt), 3.81 (3H, s, 5-COOMe), 3.87 (3H, s, *p*-MeO), 5.27 (1H, t, J_{2-3}=2.6 Hz, 2-H), 6.90 (1H, s, 8-H), 6.90 (2H, dt, J=8.8 and 2.2 Hz, Ar), and 7.22 (2H, dt, J=8.8 and 2.2 Hz, Ar); ^{13}C NMR ($CDCl_3$) δ=15.08 (EtO), 18.39 (4-C), 26.02 (3-C), 52.08, 52.44 (each COOMe), 55.23 (*p*-MeO), 64.00 (EtO), 96.97 (2-C), 113.69, 120.11, 120.38, 124.03, 129.24, 132.47, 133.42, 140.64, 153.65, 159.19 (each Ar), 168.19, and 168.86 (each COOMe); MS m/z (rel intensity, %) 400 (M^+, 32), 368 (43), 58 (35), and 43 (base peak). Found: C, 66.11; H, 6.02%. Calcd for $C_{22}H_{24}O_7$: C, 65.99; H, 6.04%.

Methyl 2-Ethoxy-7-(*p*-methoxyphenyl)chroman-6-carboxylate (5e): Colorless viscous oil; IR (neat) 1725, 1610, 1490, 1280, 1240, 1160, 960, 880, 830, and 730 cm^{-1}; ^{1}H NMR ($CDCl_3$) δ=1.19 (3H, t, J=7.0 Hz, EtO), 1.95, 2.08 (each 1H, m, 3-H), 2.68 (1H, ddd, J_{gem}=16.8, J_{4-3}=6.0, and 3.6 Hz, 4(eq)-H), 3.02 (1H, ddd, J_{gem}=16.8, J_{4-3}=12.1, and 6.2 Hz, 4(ax)-H), 3.63 (3H, s, COOMe), 3.65, 3.88 (each 1H, dq, J_{gem}=9.9 and J=7.0 Hz, EtO), 3.83 (3H, s, *p*-MeO), 5.29 (1H, t, J_{2-3}=2.9 Hz, 2-H), 6.87 (1H, s, 8-H), 6.91 (2H, dt, J=8.8 and 2.2 Hz, Ar), 7.21 (2H, dt, J=8.8 and 2.2 Hz, Ar), and 7.62 (1H, s, 5-H); ^{13}C NMR ($CDCl_3$) δ=15.10 (EtO), 20.04 (4-C), 26.41 (3-C), 51.65 (COOMe), 55.22 (*p*-MeO), 63.96 (EtO), 97.35 (2-C), 113.33, 119.28, 121.22, 122.50, 129.44, 131.89, 133.76, 142.53, 154.77, 158.83 (each Ar), and 168.65 (COOMe); MS m/z (rel intensity, %) 342 (M^+, 14), 248 (27), 246 (21), 58 (26), 44 (37), and 43 (base peak). HRMS Found: m/z 342.1459. Calcd for $C_{20}H_{22}O_5$: M, 342.1466.

6-Acetyl-2-ethoxy-7-(*p*-methoxyphenyl)chroman (5f): Colorless prisms (hexane); mp 99—101 °C; IR (KBr) 1675, 1600, 1570, 1270, 1230, 1145, 1100, 1045, 870, and 825 cm^{-1}; ^{1}H NMR ($CDCl_3$) δ=1.20 (3H, t, J=7.0 Hz, EtO), 1.97 (3H, s, MeCO), 1.97, 2.07 (each 1H, m, 3-H), 2.68 (1H, ddd, J_{gem}=16.1, J_{4-3}=5.9, and 3.5 Hz, 4(eq)-H), 3.02 (1H, ddd, J_{gem}=16.1, J_{4-3}=12.1, and 6.2 Hz, 4(ax)-H), 3.65, 3.90 (each 1H, dq, J_{gem}=9.5 Hz, and J=7.0 Hz, EtO), 3.84 (3H, s, *p*-MeO), 5.30 (1H, t, J_{2-3}=2.9 Hz, 2-H), 6.80 (1H, s, 8-H), 6.94 (2H, dt, J=8.8 and 2.2 Hz, Ar), 7.24 (2H, dt, J=8.8 and 2.2 Hz, Ar), and 7.36 (1H, s, 5-H); ^{13}C NMR ($CDCl_3$) δ=15.12 (EtO), 20.06 (4-C), 26.44 (3-C), 30.32 (MeCO), 55.29 (*p*-MeO), 63.96 (EtO), 97.33 (2-C), 114.01, 118.50, 121.44, 129.87, 130.13, 133.26, 133.29, 140.73, 154.41, 159.43 (each Ar), and 203.52 (MeCO); MS m/z (rel intensity, %) 326 (M^+, base peak), 311 (58), 265 (21), 247 (27), 246 (38), 245 (23), 231 (46), 221 (42), 217 (22), 123 (27), 109 (20), 108 (69), 57 (38), and 56 (20). Found: C, 73.83; H, 6.94%. Calcd for $C_{20}H_{22}O_4$: C, 73.60; H, 6.79%.

Dimethyl 2-Ethoxy-7-propylchroman-5,6-dicarboxylate (5g): Colorless liquid; IR (neat) 1725, 1605, 1570, 1440, 1300, 1140, and 1060 cm^{-1}; ^{1}H NMR ($CDCl_3$) δ=0.93 (3H, t, J=7.3 Hz, EtO), 1.18 (3H, t, J=7.0 Hz, *n*-Pr), 1.59 (2H, sex, J=7.3 Hz, *n*-Pr), 1.89, 2.04 (each 1H, m, 3-H), 2.6—2.8 (3H, m, *n*-Pr and 4(eq)-H), 2.95 (1H, ddd, J_{gem}=16.9, J_{4-3}=11.7, and 6.2 Hz, 4(ax)-H), 3.63, 3.81 (each 1H, dq, J_{gem}=9.9 and J=7.0 Hz, EtO), 3.82, 3.86 (each 3H, s, COOMe), 5.24 (1H, t, J_{2-3}=2.9 Hz, 2-H), and 6.78 (1H, s, 8-H); ^{13}C NMR ($CDCl_3$) δ=14.00 (*n*-Pr), 15.09 (EtO), 18.36 (4-C), 24.46 (*n*-Pr), 26.09 (3-C), 35.64 (*n*-Pr), 52.12, 52.31 (each COOMe), 63.99 (EtO), 96.99 (2-C), 119.12, 120.18, 123.54, 133.66, 141.91, 155.93 (each Ar), 168.37 (COOMe), and 168.53 (COOMe); MS m/z (rel intensity, %) 336 (M^+, 28), 304 (base peak), 289 (40), 275 (21), 245 (18), 215 (12), 163 (14), and 43 (12). HRMS Found: m/z 336.1574. Calcd for $C_{18}H_{24}O_6$: M, 336.1571.

Methyl 2-Ethoxy-7-propylchroman-6-carboxylate (5h): This compound is contaminated by a trace of regioisomer **5h** (R=*n*-Pr, E=COOMe, W=H). Colorless viscous oil; IR (neat) 1715, 1610, 1560, 1430, 1270, 1135, 1055, 970, and 870 cm^{-1}; ^{1}H NMR ($CDCl_3$) δ=0.97 (3H, t, J=7.3 Hz, *n*-Pr), 1.19 (3H, t, J=7.0 Hz, EtO), 1.60 (2H, sex, J=7.3 Hz, *n*-Pr), 1.92, 2.04 (each 1H, m, 3-H), 2.62 (1H, ddd, J_{gem}=16.2, J_{4-3}=5.5, and 4.1 Hz, 4(eq)-H), 2.8—3.0 (3H, m, 4(ax)-H and *n*-Pr), 3.64, 3.88 (each 1H, dq, J_{gem}=9.5 and J=7.0 Hz, EtO), 3.84 (3H, s, COOMe), 5.26 (1H, t, J_{2-3}=2.9 Hz, 2-H), 6.69 (1H, s, 8-H), and 7.68 (1H, s, 6-H); ^{13}C NMR ($CDCl_3$) δ=14.77 (*n*-Pr), 15.12 (EtO), 20.03 (4-C), 24.69 (*n*-Pr), 26.54 (3-C), 36.40 (*n*-Pr), 51.52 (COOMe), 63.94 (EtO), 97.41 (2-C), 118.99, 119.90, 121.39, 132.64, 145.03, 155.33 (each Ar), and 167.68 (COOMe); MS m/z (rel intensity, %) 278 (M^+, base peak), 247 (22), 233 (29), 232 (52), and 231 (24). HRMS Found: m/z 278.1520. Calcd for $C_{16}H_{22}O_4$: 278.1517.

General Procedure for the Hydrolysis and Oxidation of 2-Ethoxychromans 5a—h Leading to 2-Chromanones 7a—h. As a typical example the sequence of hydrolysis and PCC-oxidation of **5a** is described as follows: A solution of **5a** (0.53 g, 1.43 mmol) in THF (50 ml) containing 4M hydrochloric acid (25 ml) was stirred at room temperature for 15 h. The THF was evaporated in vacuo and the residual solution was extracted with dichloromethane (25 ml×2). The combined extracts were dried over magnesium sulfate and evaporated in vacuo. The residue was chromatographed over silica gel with hexane-ethyl acetate (1 : 1 v/v) to give **6a** (0.44 g, 90%).

6a: ^{1}H NMR ($CDCl_3$) δ=1.8—2.1 (2H, m, 3-H), 2.77 (1H, dt, J_{gem}=16.9 Hz, and J_{4-3}=5.5 Hz, 4(eq)-H), 3.01 (1H, ddd, J_{gem}=16.9, J_{4-3}=10.2, and 6.9 Hz, 4(ax)-H), 3.52 (3H, s, 6-COOMe), 3.86 (3H, s, 5-COOMe), 3.93 (1H, d, J=2.7 Hz, OH), 5.57 (1H, q, J_{2-3}=J_{2-OH}=2.7 Hz, 2-H), 6.85 (1H, s, 8-H), and 7.2—7.4 (5H, m, Ph); ^{13}C NMR ($CDCl_3$) δ=18.32 (3-C), 26.52 (4-C), 52.12, 52.57 (each COOMe), 92.14 (2-C), 119.89, 120.41, 124.03, 127.54, 128.06, 128.19, 133.49, 140.02, 141.22, 153.73 (each Ar), 168.25, and 168.81 (each COOMe).

A mixture of this compound **6a** (0.065 g, 0.19 mmol) and PCC (0.123 g, 0.57 mmol) in dichloromethane (3 ml) was stirred at room temperature for 24 h. Diethyl ether (10 ml) was added and the ether layer was decanted. This procedure was repeated three times. The combined ether extracts were filtered through a short column packed with silica gel and the silica gel was washed with ethyl acetate. The ether and the ethyl acetate were combined and evaporated in vacuo.

The residue was again chromatographed over silica gel with hexane–diethyl ether (4 : 1 v/v) to give **7a** (0.054 g, 83%).

The eluents used for the final column chromatography are as follows: **7b**: hexane–diethyl ether (4:1 v/v); **7c**, **7d**, **7f**: hexane–ethyl acetate (1 : 1 v/v); **7e**, **7h**: hexane–ethyl acetate (3 : 1 v/v); **7g**: hexane–ethyl acetate (3 : 2 v/v). The results are summarized in Table 2.

Dimethyl 2-Oxo-7-phenylchroman-5,6-dicarboxylate (7a): Colorless needles (dichloromethane–hexane); mp 205—207 °C; IR (KBr) 1780, 1730, 1715, 1600, 1430, 1330, 1275, 1220, 1180, and 1150 cm^{-1}; ^1H NMR ($CDCl_3$) δ=2.81 (2H, dd, $J_{3\text{-}4}$=7.7 and 5.9 Hz, 3-H), 3.17 (2H, dd, $J_{4\text{-}3}$=7.7 and 5.9 Hz, 4-H), 3.58 (3H, s, 6-COOMe), 3.90 (3H, s, 5-COOMe), 7.17 (1H, s, 8-H), and 7.2—7.5 (5H, m, Ph); ^{13}C NMR ($CDCl_3$) δ=21.57 (3-C), 28.41 (4-C), 52.38, 52.85 (each COOMe), 120.53, 121.22, 128.03, 128.17, 128.49, 128.59, 131.82, 138.81, 141.87, 152.94 (each Ph and Ar), 166.88, 167.08, and 168.10 (each COOMe and 2-C); MS *m/z* (rel intensity, %) 340 (M^+, 8), 339 (27), 309 (44), 308 (78), 281 (40), 280 (base peak), 265 (25), 249 (80), 222 (21), 221 (27), 194 (53), 166 (24), 165 (75), 153 (25), 152 (42), 151 (22), and 139 (34). Found: C, 66.80; H, 4.60%. Calcd for $C_{19}H_{16}O_6$: C, 67.05; H, 4.75%.

Methyl 2-Oxo-7-phenylchroman-6-carboxylate (7b): Colorless prisms (diethyl ether–hexane); mp 144—145 °C; IR (KBr) 1755, 1725, 1270, 1230, 1130, 1080, and 900 cm^{-1}; ^1H NMR ($CDCl_3$) δ=2.84 (2H, dd, $J_{3\text{-}4}$=7.6 and 5.5 Hz, 3-H), 3.08 (2H, dd, $J_{4\text{-}3}$=7.6 and 5.5 Hz, 4-H), 3.62 (3H, s, COOMe), 7.04 (1H, s, 8-H), 7.2—7.5 (5H, m, Ph), and 7.73 (1H, s, 5-H); ^{13}C NMR ($CDCl_3$) δ=23.33 (3-C), 29.00 (4-C), 51.99 (COOMe), 119.10, 121.45, 126.71, 127.64, 128.13, 130.22, 140.20, 143.68, 153.73 (each Ph and Ar), 167.57 (2-C), and 168.03 (COOMe); MS *m/z* (rel intensity,%) 282 (M^+, base peak), 251 (85), 223 (61), 181 (27), 166 (21), 165 (63), 153 (43), 152 (85), 151 (25), 139 (36), 127 (21), 115 (22), and 77 (21). Found: C, 72.05; H, 4.86%. Calcd for $C_{17}H_{14}O_4$: C, 72.33; H, 5.00%.

6-Acetyl-2-oxo-7-phenylchroman (7c): Colorless prisms (diethyl ether–hexane); mp 134—135 °C; IR (KBr) 1755, 1675, 1610, 1470, 1350, 1275, 1135, 900, 770, and 695 cm^{-1}; ^1H NMR ($CDCl_3$) δ=1.96 (3H, s, MeCO), 2.85 (2H, dd, $J_{3\text{-}4}$=8.4 and 5.9 Hz, 3-H), 3.09 (2H, dd, $J_{4\text{-}3}$=8.4 and 5.9 Hz, 4-H), 7.06 (1H, s, 8-H), 7.3—7.4 (2H, m, Ph), and 7.4—7.5 (4H, m, 5-H and Ph); ^{13}C NMR ($CDCl_3$) δ=23.35 (3-C), 29.03 (4-C), 30.34 (MeCO), 118.47, 121.77, 128.40, 128.69, 128.87, 136.96, 139.62, 141.64, 153.36 (each Ph and Ar), 167.63 (2-C), and 203.28 (MeCO); MS *m/z* (rel intensity, %) 266 (M^+, 41), 251 (base peak), 223 (22), 209 (28), 165 (52), 153 (45), 152 (50), 139 (22), and 63 (25). Found: C, 76.77; H, 5.20%. Calcd for $C_{17}H_{14}O_3$: C, 76.67; H 5.30%.

Dimethyl 7-(*p*-Methoxyphenyl)-2-oxochroman-5,6-dicarboxylate (7d): Colorless needles (diethyl ether–hexane); mp 164—165 °C; IR (KBr) 1775, 1725, 1710, 1600, 1435, 1335, 1280, 1225, 1185, and 1150 cm^{-1}; ^1H NMR ($CDCl_3$) δ=2.80 (2H, dd, $J_{3\text{-}4}$=7.7 and 7.0 Hz, 3-H), 3.14 (2H, dd, $J_{4\text{-}3}$=7.7 and 7.0 Hz, 4-H), 3.62 (3H, s, 6-COOMe), 3.83 (3H, s, 5-COOMe), 3.89 (3H, s, *p*-MeO), 6.92 (2H, br d, J=8.4 Hz, Ar), 7.14 (1H, s, 8-H), and 7.22 (2H, dt, J=8.4 and 1.8 Hz, Ar); ^{13}C NMR ($CDCl_3$) δ=21.59 (3-C), 28.47 (4-C), 52.44, 52.86 (each COOMe), 55.30 (*p*-MeO), 113.99, 120.53, 120.83, 128.56, 129.27, 131.11, 131.66, 141.48, 152.90, 159.65 (each Ar), 166.91, 167.17, and 168.32 (each COOMe and 2-C); MS *m/z* (rel intensity, %) 370 (M^+, base peak), 339 (46), 338 (70), 311 (25), 310 (98), 279 (59), 224 (33), 152 (31), and 139 (27). Found: C, 64.98; H, 4.87%. Calcd for $C_{20}H_{18}O_7$: C, 64.86; H, 4.90%.

Methyl 7-(*p*-Methoxyphenyl)-2-oxochroman-6-carboxylate (7e): Colorless prisms (cyclohexane); mp 85—87 °C; IR (KBr) 1775, 1720, 1615, 1490, 1250, 1130, and 840 cm^{-1}; ^1H NMR ($CDCl_3$) δ=2.83 (2H, dd, $J_{3\text{-}4}$=8.1 and 5.8 Hz, 3-H), 3.05 (2H, dd, $J_{4\text{-}3}$=8.1 and 5.8 Hz, 4-H), 3.65 (3H, s, COOMe), 3.84 (3H, s, *p*-MeO), 6.93 (2H, dd, J=8.8 and 2.2 Hz, Ar), 7.02 (1H, s, 8-H), 7.20 (2H, dd, J = 8.8 and 2.2 Hz, Ar), and 7.69 (1H, s, 5-H); ^{13}C NMR ($CDCl_3$) δ=23.28 (3-C), 29.01 (4-C), 52.05 (COOMe), 55.26 (*p*-MeO), 113.63, 119.02, 121.05, 126.65, 129.37, 130.15, 132.44, 143.22, 153.67, 159.27 (each Ar), 167.64 (2-C), and 168.26 (COOMe); MS *m/z* (rel intensity, %) 312 (M^+, base peak), 281 (24), 239 (10), and 152 (9). Found: C, 69.03; H, 5.13%. Calcd for $C_{18}H_{16}O_5$: C, 69.22; H, 5.16%.

6-Acetyl-7-(*p*-methoxyphenyl)-2-oxochroman (7f): Colorless prisms (diethyl ether–hexane); mp 118—120 °C; IR (KBr) 1760, 1670, 1605, 1480, 1270, 1250, 1130, 900, and 830 cm^{-1}; ^1H NMR ($CDCl_3$) δ=1.97 (3H, s, MeCO), 2.84 (2H, dd, $J_{3\text{-}4}$= 7.7 and 5.5 Hz, 3-H), 3.07 (2H, dd, $J_{4\text{-}3}$=7.7 and 5.5 Hz, 4-H), 3.86 (3H, s, *p*-MeO), 6.92 (2H, dt, J=8.8 and 2.2 Hz, Ar), 7.04 (1H, s, 8-H), 7.23 (2H, dt, J=8.8 and 2.2 Hz, Ar), and 7.42 (1H, s, 5-H); ^{13}C NMR ($CDCl_3$) δ=23.31 (3-C), 29.06 (4-C), 30.32 (MeCO), 55.35 (*p*-MeO), 114.34, 118.28, 121.35, 128.30, 129.87, 131.85, 136.96, 141.25, 153.38, 159.91 (each Ar), 167.73 (2-C), and 203.68 (MeCO); MS *m/z* (rel intensity, %) 296 (M^+, base peak), 295 (20), 281 (76), 239 (32), and 55 (25). Found: C, 72.81; H, 5.47%. Calcd for $C_{18}H_{16}O_4$: C, 72.96; H, 5.44%.

Dimethyl 2-Oxo-7-propylchroman-5,6-dicarboxylate (7g): Colorless prisms (hexane); mp 81—83 °C; IR (KBr) 1770, 1720, 1580, 1440, 1310, 1200, 1140, 990, and 790 cm^{-1}; ^1H NMR ($CDCl_3$) δ = 0.94 (3H, t, J = 7.3 Hz, *n*-Pr), 1.61 (2H, sex, J = 7.3 Hz, *n*-Pr), 2.69 (2H, t, J = 7.3 Hz, *n*-Pr), 2.76 (2H, dd, $J_{3\text{-}4}$=7.7 and 5.5 Hz, 3-H), 3.10 (2H, dd, $J_{4\text{-}3}$=7.7 and 5.5 Hz, 4-H), 3.87, 3.88 (each 3H, s, COOMe), and 7.03 (1H, s, 8-H); ^{13}C NMR ($CDCl_3$) δ = 13.85 (*n*-Pr), 21.51 (3-C), 24.26 (*n*-Pr), 28.51 (4-C), 35.36 (*n*-Pr), 52.50, 52.72 (each COOMe), 120.03, 120.33, 128.38, 131.73, 142.62, 153.13 (each Ar), 167.17, 167.35, and 167.93 (each 2-C and COOMe); MS *m/z* (rel intensity,%) 306 (M+, 5), 279 (25), 274 (31), 217 (43), 201 (21), 167 (27), 149 (55), and 40 (base peak). Found: C, 62.53; H, 5.99%. Calcd for $C_{16}H_{18}O_6$: C, 62.74; H, 5.92%.

Methyl 2-Oxo-7-propylchroman-6-carboxylate (7h): Colorless prisms (hexane); mp 50—51 °C; IR (KBr) 1775, 1700, 1610, 1430, 1400, 1260, 1110, and 895 cm^{-1}; ^1H NMR ($CDCl_3$) δ=0.97 (3H, t, J=7.3 Hz, *n*-Pr), 1.61 (2H, sex, J=7.3 Hz, *n*-Pr), 2.80 (2H, dd, $J_{3\text{-}4}$=7.7 and 5.5 Hz, 3-H), 2.92 (2H, dd, J=7.3 Hz, *n*-Pr), 3.01 (2H, dd, $J_{4\text{-}3}$=7.7 and 5.5 Hz, 4-H), 3.89 (3H, s, COOMe), 6.92 (1H, s, 8-H), and 7.77 (1H, s, 5-H); ^{13}C NMR ($CDCl_3$) δ=14.05 (*n*-Pr), 23.23 (3-C), 24.59 (*n*-Pr), 29.14 (4-C), 36.15 (*n*-Pr), 51.96 (COOMe), 118.99, 119.79, 125.43, 130.97, 146.03, 154.19 (each Ar), 167.84 (2-C), and 168.36 (COOMe); MS *m/z* (rel intensity, %) 248 (M^+, 40), 217 (base peak), 201 (48), 91 (24), 57 (66), 56 (32), and 43 (27). Found: C, 67.96; H, 6.57%. Calcd for $C_{14}H_{16}O_4$: C, 67.73; H, 6.50%.

References

1) O. Tsuge, E. Wada, and S. Kanemasa, *Chem. Lett.*, **1983**, 279. As a review: O. Tsuge, S. Kanemasa, E. Wada, and H. Sakoh, *Yuki Gosei Kagaku Kyokai Shi*, **44**, 756 (1986).

2) O. Tsuge, S. Kanemasa, H. Sakoh, and E. Wada,

Chem. Lett., **1984**, 277; *Bull. Chem. Soc. Jpn.*, **57**, 3234 (1984).

3) S. Kanemasa, H. Sakoh, and E. Wada, *Bull. Chem. Soc. Jpn.*, **58**, 3312 (1985) and *ibid.*, **59**, 1869 (1986); O. Tsuge, E. Wada, and S. Kanemasa, *Chem. Lett.*, **1984**, 469 and 709.

4) E. Wada, S. Kanemasa, and O. Tsuge, *Bull. Chem. Soc. Jpn.*, **62**, 860 (1989).

5) E. J. Corey and B. W. Erickson, *J. Org. Chem.*, **39**, 821 (1974); G. Lavielle and G. Sturtz, *Bull. Soc. Chim. Fr.*, **1970**, 1369; G. Lavielle, *Comp. Rend. C*, **270**, 86 (1970).

6) E. J. Corey and G. T. Kwiatowski, *J. Am. Chem. Soc.*, **88**, 5652 (1966); O. Tsuge, S. Kanemasa, and H. Suga, *Bull. Chem. Soc. Jpn.*, **61**, 2133 (1988).

7) The pyran ring of 2,4a-*trans*-**4b** exists in a stable chair confornation where 2-EtO group is forced to take an equatorial position. Thus, a general rule of the stereoelectronic preference of axial alkoxy group does not accord in this case.

8) R. A. John, V. Schmid, and H. Wyler, *Helv. Chim. Acta*, **70**, 600 (1987); A. J. Duggan and S. S. Hall, *J. Org. Chem.*, **40**, 2234 (1975).

9) L. J. Durham, J. Studebaker, and M. J. Perkins, *J. Chem. Soc., Chem. Commun.*, **1965**, 456; J. L. Marshall and T. K. Folsom, *J. Org. Chem.*, **36**, 2011 (1971).

10) Two small coupling constants of $J_{2\text{-}3}$ (3.3 Hz) show the stable conformation of **3a** with an axial 2-ethoxyl moiety. A similar coupling pattern was observed on compound **2** (Ref. 4).

 © 1989 The Chemical Society of Japan Bull. Chem. Soc. Jpn., 62, 1205—1210 (1989)

Magnesium Ion Assisted Highly Regio- and Chemoselective Reduction of 5*H*-Pyrrolo[3,4-*b*]pyridine-5,7(6*H*)-diones with Sodium Borohydride. A Convenient Synthesis of 6,7-Dihydro-7-hydroxy-5*H*-pyrrolo[3,4-*b*]pyridin-5-ones

Takehiko GOTO,* Michio KONNO, Minoru SAITO, and Ryu SATO
Department of Resource Chemistry, Faculty of Engineering, University of Iwate, Ueda, Morioka 020
(Received October 31, 1988)

6-Substituted and unsubstituted 6,7-dihydro-7-hydroxy-5*H*-pyrrolo[3,4-*b*]pyridin-5-ones were predominantly obtained in excellent yield by the reduction of the corresponding 5,7-diones with sodium borohydride in the presence of Mg ion at 0 °C. The highly regioselective production of the 7-hydroxy lactam in preference to the 5-hydroxy isomer was reasonably interpreted in terms of a chelate complex formation between the dione and Mg ion. The regioisomeric assignment was achieved by the transformation of the 7-hydroxy lactam to 2-(hydroxymethyl)-3-pyridinecarboxamides which could be converted to the known azaphthalide, furo[3,4-*b*]-pyridin-5(7*H*)-one. Furthermore, the high chemoselectivity was found to be retained below 0 °C to give the partial reduction product, hydroxy lactam, exclusively.

The partial reduction of 6-substituted 5*H*-pyrrolo-[3,4-*b*]pyridine-5,7(6*H*)-diones (quinolinimides **1**) with sodium borohydride ($NaBH_4$) has been known to produce 6-substituted 6,7-dihydro-7-hydroxy-5*H*-pyrrolo-[3,4-*b*]pyridin-5-ones (**2**) along with the corresponding 5-hydroxy-7-oxo isomers (**3**).[1—3] Recent attention has been directed to these hydroxy lactams as precursors to pharmacologically active compounds[1,2] or to aza analogs of fused heterocyclic systems.[3] The partial $NaBH_4$-reduction of cyclic imides, which involve alicyclics[4] and aromatics,[5] to the corresponding hydroxy lactams has been well investigated. However, in the case of the unsymmetrical imide **1**, the study on the control of the regioselectivity as well as the chemoselectivity of the reduction is scanty. We previously reported[6] that the chemoselectivity of the $NaBH_4$-reduction of *N*-unsubstituted quinolinimide (**1a**) could be thermally controlled; the partial reduction to the corresponding hydroxy lactams **2a** and **3a** was effected at −20 °C. In contrast, the regioselectivity of the reduction was unsatisfactory (**2a** : **3a**=3 : 1). Therefore, we turned our attention to improving the regioselectivity and expanding the scope of this method to the synthesis of *N*-substituted hydroxy lactams. Eventually, we found that the addition of Mg ion lead to the highly regioselective $NaBH_4$-reduction of *N*-substituted and *N*-unsubstituted quinolinimides (**1a—g**) to the corresponding hydroxy lactams **2a—g**. In this paper, we wish to describe the detail of this selective reduction.

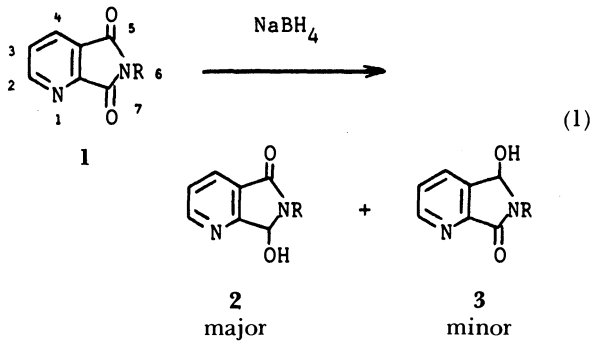

(1)

1

2 major + **3** minor

a: R = H **e**: R = CH_2Ph
b: R = Me **f**: R = Ph
c: R = Et **g**: R = *p*-MePh
d: R = *i*-Pr

Results and Discussion

First of all, the $NaBH_4$-reduction of *N*-unsubstituted quinolinimide (**1a**) to the hydroxy lactam **2a** and **3a** was examined under the various reaction conditions as shown in Table 1. A mixed solvent (MeOH-$CHCl_3$ (1 : 1 (v/v)) was principally employed for the reduction because of the relatively high solubility of the substrate **1a**. Although the reduction also proceeded in MeOH uneventfully, the degree of regioselectivity was diminished (Runs 1 and 2). We could not find any merit at a lowered temperature (−40 °C, Run 3), while at an elevated temperature (0 °C), the over-reduction took place to give 3-(hydroxymethyl)-2-pyridinecarboxamide (**5a**) as a by-product (Run 4). In our further efforts to find the reaction conditions for high degree of regioselectivity, we reasoned that the formation of a chelate complex, in which the 1-nitrogen atom and the oxygen atom of 7-carbonyl group of imide **1** coordinate to

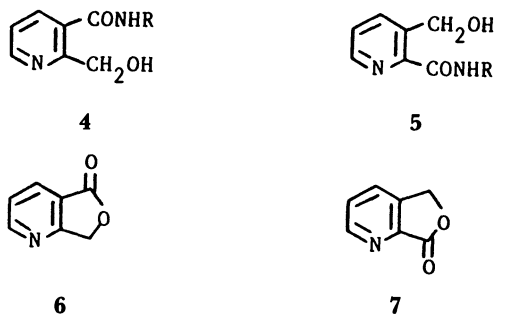

4 **5**

6 **7**

Chart 1. Over-reduction products.

Table 1. Partial $NaBH_4$-Reduction of *N*-Unsubstituted Quinolinimide (**1a**)[a]

Run	Solvent	React. temp/°C	$Mg(ClO_4)_2$ /mmol	Yield of **2a**+**3a**/%	Regioisomer ratio (**2a**:**3a**)[b]
1	MeOH-$CHCl_3$[c]	−20	None	93[d]	76:24
2	MeOH	−20	None	89[d]	66:34
3	MeOH-$CHCl_3$[c]	−40	None	77[d]	75:25
4	MeOH-$CHCl_3$[c]	0	None	69[d,f]	72:28
5	MeOH-$CHCl_3$[c]	−20	2	97[e]	>99: 1
6	MeOH-$CHCl_3$[c]	0	2	95[e]	>99: 1
7	MeOH-$CHCl_3$[c]	r.t.	2	70[e,g]	>99: 1

a) **1a**, 1 mmol; $NaBH_4$, 1.5 mmol; solvent, 10 ml; reaction time, 30 min. b) Determined by ^1H NMR integration. c) MeOH:$CHCl_3$=1:1(v/v). d) Isolated by column chromatography. e) Isolated by continuous extraction with $CHCl_3$ for 4 d. f) **5a** was obtained as a by-product in 17% yield. g) **6** was obtained as a by-product in 21% yield.

Table 2. Partial $NaBH_4$-Reduction of *N*-Methylquinolinimide (**1b**)

Run[a]	Solvent	React. temp/°C	Metal salt (mmol)	Yield of **2b**+**3b**/%[e]	Regioisomer ratio (**2b**:**3b**)[b]
1[f]	MeOH-$CHCl_3$[c]	0	None	99	67:33
2	MeOH-$CHCl_3$[c]	0	$Mg(ClO_4)_2$(0.5)	93	87:13
3	MeOH-$CHCl_3$[c]	0	$Mg(ClO_4)_2$(1)	95	90:10
4	MeOH-$CHCl_3$[c]	0	$Mg(ClO_4)_2$(2)	99	94: 6
5	MeOH-$CHCl_3$[c]	0	$Mg(ClO_4)_2$(3)	93	95: 5
6	MeOH-$CHCl_3$[c]	−20	$Mg(ClO_4)_2$(2)	99	94: 6
7	MeOH-$CHCl_3$[c]	−40	$Mg(ClO_4)_2$(2)	96	94: 6
8[g]	MeOH-$CHCl_3$[c]	0	$Mg(ClO_4)_2$(20)	99	96: 4
9	EtOH	0	$Mg(ClO_4)_2$(2)	96	90:10
10	MeCN	0	$Mg(ClO_4)_2$(2)	93	90:10
11[f]	MeOH-$CHCl_3$[c]	0	$LiClO_4$(2)	88	74:26
12	MeOH-$CHCl_3$[c]	0	$AgClO_4$(2)	34	74:26
13	MeOH-$CHCl_3$[c]	0	$Zn(ClO_4)_2$(2)	4	—[d]
14	EtOH	0	$Zn(ClO_4)_2$(2)	4	—[d]
15	MeCN	0	$Zn(ClO_4)_2$(2)	13	—[d]

a) **1b**, 1 mmol; $NaBH_4$, 2 mmol; solvent, 10 ml; reaction time, 15 min. b) Determined by ^1H NMR integration. c) MeOH:$CHCl_3$=1:1 (v/v). d) Not observed. e) Isolated by continuous extraction with $CHCl_3$ for 1 d. f) Reaction time, 30 min. g) 10-fold scale.

a metal ion, should activate the 7-carbonyl group in preference to the 5-carbonyl group for the reduction. Indeed, when magnesium perchlorate was added into the reduction system, ^1H NMR of the product indicated the predominant formation of 7-hydroxy lactam **2a**. Unfortunately, the hydroxy lactam **2a** could not be separated from the magnesium salt by usual methods because **2a** was less soluble in normal organic solvents such as chloroform. When a polar solvent such as methanol was employed as an eluent for column chromatography, a mixture of the hydroxy lactam and the magnesium salt was obtained. The similar problem also occurred in the case of using magnesium chloride instead of the perchlorate. This trouble could be avoided by "continuous extraction." Thus, the worked-up reaction mixture was continuously extracted with refluxing chloroform for 4 d to give the hydroxy lactam **2a** in an excellent yield (Run 5). Surprisingly, in the presence of Mg salt, the chemoselectivity was completely retained at 0 °C (Run 6). Even at r.t., the hydroxy lactam was obtained in 70% yield along with a minor over-reduction product (Run 7). It deserves emphasis that this result is a striking contrast to the reduction in the absence of Mg ion at r.t., in which the over-reduction products, 2-(hydroxymethyl)-3-pyridinecarboxamide (**4a**) and its regioisomer **5a** was produced exclusively.[6] In a word, Mg ion controlled not only the regioselectivity but also the chemoselectivity.

Encouraged by the success of this selective reduction, we turned to the synthesis of *N*-substituted hydroxy lactams. In order to obtain the best reaction conditions, *N*-methylquinolinimide (**1b**) was reduced under the various reaction conditions as shown in Table 2. The Mg ion was apparently effective for the highly regioselective reduction (Runs 1—4), and the degree of regioselectivity came to a maximum when two equivalents of Mg ion was used (Runs 4 and 5). On the other hand, lowered temperatures (−20 and −40 °C) did not influence the regioselectivity (Runs 6 and 7). This highly regioselective and chemoselective reduction could be also carried out in a synthetic scale (Run 8). The major regioisomer **2b** was readily available in the pure form by the recrystallization of the crude product obtained by the continuous extraction.

Although the minor product **3b** could not be isolated in the pure form, the formation of **3b** was confirmed by the conversion of **3b** to the over-reduction product, 3-(hydroxymethyl)-2-pyridinecarboxamide (**5b**). It should be noted that the present reduction was also successful in EtOH (Run 9) and MeCN (Run 10), since it has been reported that the partial reduction of cyclic imide required MeOH as a solvent[7] or an addition of acid in EtOH.[8] The univalent Li and Ag ions have no essential effect for the regioselectivity (Runs 11 and 12). This fact suggests the formation of a divalent metal ion chelate complex at the initial stage of the reaction (vide infra). Although an alternative divalent ion, Zn^{2+}, was expected the desirable effect as well as Mg^{2+}, the continuous extraction of the reaction mixture gave only low yield of the hydroxy lactam without any other products and recovered substrate (Run 13). Furthermore, we observed a similar unsuccessful result with $Zn(BH_4)_2$. The reasons for the unusual low yields in the presence of Zn ion as well as Ag ion (Run 12) are uncertain. It is likely that in the methanol-involved solvent, Zn or Ag ion accelerates the formation of hemiacetal or acetal of the imide, which inhibits the $NaBH_4$-reduction.[9] But, this possibility is ruled out because (i) we could not observe any products such as acetal before addition of $NaBH_4$ into the solution of the substrate and the metal salt, and (ii) similarly low yield was obtained with dry acetonitrile (Run 15). Hence, it is supposed that another pathway lead to a product which could not be obtained by the continuous extraction.

According to Speckamp and co-workers,[10] the present reduction will proceed through the pathways depicted in Scheme 1. As aforementioned, in the presence of Mg ion, a chelate complex **8** might be formed, and then 7-carbonyl group would be more strongly activated for the attack of a hydride ion in comparison with 5-carbonyl group. As the result, oxide anion **9** will be produced regioselectively. The formation of such a magnesium ion chelate on a pyrrolo[3,4-*b*]-pyridine[3] or furo[3,4-*b*]pyridine[11] ring has been suggested in the case of regioselective addition reactions of magnesium Grignard reagents. However, as far as we know, the present reaction is the first example of Mg ion assisted regioselective reduction on the pyrrolo-[3,4-*b*]pyridine ring. If the oxide anion **9** undergoes ring-cleavage to formyl amide **10**, the over-reduction will readily occur to afford the hydroxymethyl amide **4**. It is easily envisioned, however, that in the presence Mg ion, the oxide anion would be stabilized by the chelation, and the ring-cleavage might become an unfavorable pathway. Ultimately, direct protonation of **9** would afford the hydroxy lactam **2**. Thus, Mg ion precludes the over-reduction to improve the chemoselectivity as mentioned above. In the case of the reduction of *N*-methylquinolinimide (**1b**), the high chemoselectivity was retained at 0 °C even in the absence of Mg ion (Run 1, Table 2). This is not surprising when one considers that the methyl group is an electron-donating group, and the ring-cleavage of *N*-methylated **9** to **10** will be more unfavorable in comparison with *N*-unsubstituted one.

Since we have been able to optimize the reaction conditions, we applied this selective reduction to several *N*-alkylated and *N*-arylated quinolinimides (**1c—g**) in a synthetic scale to demonstrate the general synthetic utility of this method. As listed in Table 3, the

Table 3. Partial $NaBH_4$-Reduction of *N*-Substituted Quinolinimides (**1c—g**)[a]

Imide	*N*-Substituent	Yield of **2**+**3**/%	Regioisomer ratio (**2**:**3**)[b]
1c	Et	95[c]	96:4
1d	*i*-Pr	97[c]	98:2
1e	$PhCH_2$	96[d]	92:8
1f	Ph	92[d]	93:7
1g	*p*-MePh	96[d]	92:8

a) **1**, 10 mmol; $NaBH_4$ 20 mmol; $Mg(ClO_4)_2$, 20 mmol; solvent, MeOH-$CHCl_3$ (1:1 v/v 100 ml); reaction temperature, 0 °C; reaction time, 15 min. b) Determined by ^1H NMR integration. c) Isolated by continuous extraction for 1 d. d) Isolated by continuous extraction for 2 d.

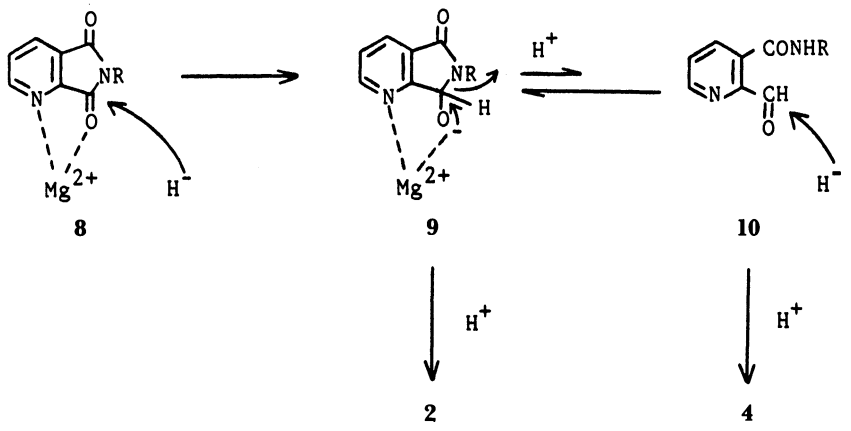

Scheme 1.

reduction was smoothly effected in the presence of Mg ion to produce the corresponding hydroxy lactams **2c—g** in excellent yields with high degree of regioselectivity and chemoselectivity. Consequently, the present method is potentially fruitful for the synthesis of the 7-hydroxy lactam **2** because of excellent yield, high selectivity, simple manipulation, and easy availability of the substrate and reducing reagent.

Finally, we studied the assignment of the regioisomeric structure of **2b—g**. Although Hitchings and Vernon described the regioisomeric assignment of such a hydroxy lactam by ^{1}H NMR,[3] the directly definitive evidence has not been obtained. In our previous study,[6] the regioisomeric assignment of hydroxy lactams **2a** and **3a** has been clearly attained by transformation of **2a** and **3a** to the corresponding (hydroxymethyl)pyridinecarboxamides **4a** and **5a**, which could be converted to the known azaphthalides **6** and its regioisomer **7**, respectively. Because the (hydroxymethyl)pyridinecarboxamides **4** and **5** are key compounds to determine the regioisomeric structures, our initial attention was focused on the preparation of the over-reduction products, *N*-substituted (hydroxymethyl)pyridinecarboxamides **4b—g** and **5b—g** from the corresponding quinolinimide **1b—g** followed by the conversion to **6** and **7**, respectively. When *N*-methylquinolinimide (**1b**) was treated with $NaBH_4$ in MeOH-$CHCl_3$ at r.t. according to previous report,[6] the desired products **4b** and **5b** were produced in very low yield. After examining reaction conditions, the best result was obtained in EtOH at 50 °C for 1.5 h. These conditions could be applied with equal success to other *N*-substituted quinolinimides **1c—g** as shown in Table 4. Table 4 also exhibits that the hydrolysis and cyclization of the (hydroxymethyl)pyridinecarboxamide **4b—g** and **5b—g** smoothly proceeded in hot acidic methanol to give the known azaphthalides **6** and **7**, respectively. Consequently, we could assign the regioisomeric structures of **4** and **5**. Eventually, we carried out the reduction of aforementioned hydroxy lactams **2b—g** with $NaBH_4$ to confirm their regioisomeric structure. As listed in Table 5, the 2-(hydroxymethyl)-3-pyridinecarboxamides (**4b—g**) were obtained in moderate to good yields. From the synthetic point of view, it is noteworthy that the sequential combination of the two steps (**1**→**2**→**4**) amounts to a regioselective synthesis of *N*-substituted 2-(hydroxymethyl)-3-pyridinecarboxamides (**4**), which can be recognized as a precursor to nicotinamide derivatives bearing side chain on 2-position.

In summary, the present partial $NaBH_4$-reduction of quinolinimide **1** in the presence of Mg ion proceeded with high degree of regioselectivity and chemoselectivity. This procedure provides an attractive synthetic route to the 7-hydroxy lactam **2** as a useful synthetic precursor to biologically active compounds, whose isomeric structure can be clearly established by the conversion to the known azaphthalide **6** via (hydroxymethyl)pyridinecarboxamide **4**.

Table 4. Reduction[a] of *N*-Substituted Quinolinimides (**1b**—g) with $NaBH_4$ to **4b**—g and **5b**—g, and Transformation[b] of **4b**—g and **5b**—g to **6** and **7**

Imide	*N*-Substituent	Isolated yield/%			
		4	**5**	**6**	**7**
1b	Me	44	31	64	69
1c	Et	47	31	62	74
1d	*i*-Pr	43	31	70	72
1e	$PhCH_2$	41	31	71	67
1f	Ph	35	30	53	66
1g	*p*-MePh	32	31	64	71

a) **1**, 10 mmol; $NaBH_4$ 20 mmol; solvent, EtOH (100 ml); reaction temperature, 50 °C; reaction time, 1.5 h. b) 2 or 3, 1 mmol; reaction temperature 80 °C; reaction time, 2 d.

Table 5. Reduction of Hydroxy Lactams **2b**—g with $NaBH_4$ to **4b**—g[a]

Lactam	*N*-Substituent	Isolated yield of **4**/%
2b	Me	71
2c	Et	73
2d	*i*-Pr	67
2e	$PhCH_2$	58
2f	Ph	51
2g	*p*-MePh	48

a) **2**, 1 mol; $NaBH_4$, 2 mmol; solvent, EtOH (10 ml); reaction temperature, 50 °C; reaction time, 1 h.

Experimental

Measurements. Melting points were uncorrected. ^{1}H NMR spectra at 90 MHz were recorded with Hitachi R-22. IR spectra were recorded with Hitachi 295 and 260-50. Mass spectra were recorded with Hitachi RMU-6M and M-2000. Elemental analyses were determined with Yanagimoto MT-3.

Materials. Magnesium, zinc, and lithium perchlorate were dried over phosphorus pentachloride for 1 d under reduced pressure at 100 °C. Acetonitrile was dried over calcium hydride and distilled before use.

6-Substituted and Unsubstituted 5*H*-Pyrrolo[3,4-*b*]pyridine-5,7(6*H*)-dione (1a—g) were prepared according to a procedure in the literature.[12]

Partial $NaBH_4$-Reduction of 1. A representative procedure is described with **1a**: Into a solution of **1a** (0.148 g, 1 mmol) and $Mg(ClO_4)_2$ (0.446 g, 2 mmol) in MeOH-$CHCl_3$ (10 ml (1:1 v/v)) cooled at 0 °C under argon was added $NaBH_4$-powder (0.057 g, 1.5 mmol) with stirring. After 30 min, the reaction mixture was acidified with aqueous HCl approximately to pH 2. The resulting mixture was stirred for 10 min and basified with aqueous NaOH approximately to pH 11. After being warmed up to room temperature, the mixture was concentrated in vacuo until the evaporation of water began. This aqueous residue was continuously extracted with refluxing $CHCl_3$ for 4 d. The extract was concentrated in vacuo to give a colorless solid of **2a** (0.146 g, 97%).[6]

1b—g were reduced to **2b**—g with a similar procedure.

2b: Mp 146—147 °C (from MeCN); ^{1}H NMR ($CDCl_3$) δ= 3.14 (3H, s, CH_3), 5.84 (1H, s, H-7), 6.87 (1H, s, OH), 7.37 (1H, dd, J=8 and 5 Hz, H-3), 8.02 (1H, dd, J=8 and 3 Hz, H-4), and 8.57 (1H, dd, J=5 and 3 Hz, H-2); IR (KBr) 1710 (C=O) and 3070 (OH) cm^{-1}; MS (70 eV) m/z 164 (M^+); Found: C, 58.64; H, 4.90; N, 16.99%. Calcd for $C_8H_8N_2O_2$: C, 58.53; H, 4.91; N, 17.06%.

2c: Mp 153—154 °C (from MeCN); ^{1}H NMR ($CDCl_3$) δ= 1.30 (3H, t, J=8 Hz, CH_3), 3.3—4.0 (2H, m, CH_2), 5.99 (1H, s, H-7), 6.95 (1H, s, OH), 7.41 (1H, dd, J=8 and 5 Hz, H-3), 8.06 (1H, dd, J=8 and 2 Hz, H-4), and 8.60 (1H, dd, J=5 and 2 Hz, H-2); IR (KBr) 1670 (C=O) and 3150 (OH) cm^{-1}; MS (70 eV) m/z 178 (M^+); Found: C, 60.67; H, 5.65; N, 15.77%. Calcd for $C_9H_{10}N_2O_2$: C, 60.67; H, 5.66; N, 15.72%.

2d: Mp 169—170 °C (from MeCN); ^{1}H NMR ($CDCl_3$) δ= 1.50 (6H, d, J=7 Hz, CH_3×2), 4.46 (1H, quint, J=7 Hz , CH), 6.10 (1H, d, J=8 Hz, H-7), 6.75 (1H, d, J=8 Hz, OH), 7.42 (1H, dd, J=8 and 5 Hz, H-3), 8.06 (1H, dd, J=8 and 2 Hz, H-4), and 8.62 (1H, dd, J=5 and 2 Hz, H-2); IR (KBr) 1660 (C=O) and 3150 (OH) cm^{-1}; MS (70 eV) m/z 192 (M^+); Found: C, 62.45; H, 6.31; N, 14.78%. Calcd for $C_{10}H_{12}N_2O_2$: C, 62.49; H, 6.29; N, 14.57%.

2e: Mp 192—193 °C (from EtOH); ^{1}H NMR (DMSO-d_6) δ=4.41 and 4.96 (2H, d+d, J_{gem}=16 Hz, $PhCH_2$), 5.65 (1H, d, J=9 Hz, H-7), 6.93 (1H, d, J=9 Hz, OH), 7.2—7.4 (5H, m, arom), 7.50 (1H, dd, J=8 and 5 Hz, H-3), 8.10 (1H, dd, J=8 and 2 Hz, H-4), and 8.77 (1H, dd, J=5 and 2 Hz, H-2); IR (KBr) 1650 (C=O) and 3170 (OH) cm^{-1}; MS (70 eV) m/z 240 (M^+); Found: C, 70.07; H, 4.97; N, 11.73%. Calcd for $C_{14}H_{12}N_2O_2$: C, 69.99; H, 5.03; N, 11.66%.

2f: Mp 209—210 °C (from MeOH); ^{1}H NMR (DMSO-d_6) δ=6.44 (1H, d, J=10 Hz, H-7), 7.00 (1H, d, J=10 Hz, OH), 7.1—7.9 (6H, m, arom+H-3), 8.14 (1H, dd, J=8 and 2 Hz, H-4), and 8.83 (1H, dd, J=5 and 2 Hz, H-2); IR (KBr) 1700 (C=O) and 3150 (OH) cm^{-1}; MS (70 eV) m/z 226 (M^+); Found: C, 69.24; H, 4.40; N, 12.52%. Calcd for $C_{13}H_{10}N_2O_2$: C, 69.02; H, 4.46; N, 12.38%.

2g: Mp 216—218 °C (from MeOH); ^{1}H NMR (DMSO-d_6) δ=2.30 (3H, s, CH_3), 6.40 (1H, d, J=10 Hz, H-7), 6.99 (1H, d, J=10 Hz, OH), 7.22 (2H, d, J=9 Hz, arom), 7.58 (1H, dd, J=8 and 5 Hz, H-3), 7.66 (2H, d, J=9 Hz, arom), 8.13 (1H, dd, J=8 and 2 Hz, H-4), and 8.82 (1H, dd, J=5 and 2 Hz, H-2); IR (KBr) 1710 (C=O) and 3100 (OH) cm^{-1}; MS (70 eV) m/z 240 (M^+); Found: C, 70.15; H, 5.09; N, 11.55%. Calcd for $C_{14}H_{12}N_2O_2$: C, 69.99; H, 5.03; N, 11.66%.

***N*-Substituted 2-(Hydroxymethyl)-3-pyridinecarboxamides (4b—g) and 3-(Hydroxymethyl)-2-pyridinecarboxamides (5b—g) by the Reduction of 1b—g with $NaBH_4$.** As a general procedure, into a solution of **1** (10 mmol) in EtOH (100 ml) was added $NaBH_4$-powder (20 mmol) at room temperature. After 15 min, the solution was heated at 50 °C for 1.5 h. The reaction mixture was cooled to room temperature and acidified with aqueous HCl approximately to pH 2. The resulting mixture was stirred for 5 min and basified with aqueous NaOH approximately to pH 9. The evaporation of the solvent in vacuo gave a solid which was extracted with hot ethanol (30 ml×4). The combined extracts were concentrated in vacuo to give the mixture of **4** and **5**. When the crude product was chromatographed (silica gel, MeOH-$CHCl_3$ (1 : 10 v/v)), **5** was obtained from the first fraction. The second fraction gave **4**.

4b: Mp 88—89 °C (from MeCN); ^{1}H NMR ($CDCl_3$) δ= 2.94 (3H, d, J=5 Hz, CH_3), 4.78 (2H, d, J=5 Hz, CH_2O), 5.39 (1H, t, J=5 Hz, OH), 7.23 (1H, dd, J=9 and 5 Hz, H-5), 7.60 (1H, br s, NH), 7.89 (1H, dd, J=9 and 2 Hz, H-4), and 8.50 (1H, dd, J=5 and 2 Hz, H-6); IR (KBr) 1630 (C=O) and 3250 (NH and OH) cm^{-1} ; MS (70 eV) m/z 166 (M^+); Found: C, 57.96; H, 6.06; N, 16.89%. Calcd. for $C_8H_{10}N_2O_2$: C, 57.82; H, 6.07, N, 16.86%.

5b: Mp 58—59 °C (from Et_2O); ^{1}H NMR ($CDCl_3$) δ=3.00 (3H, d, J=5 Hz, CH_3), 4.81 (2H, d, J=8 Hz, CH_2O), 5.29 (1H, t, J=8 Hz, OH), 7.34 (1H, dd, J=9 and 5 Hz, H-5), 7.75 (1H, dd, J=9 and 2 Hz, H-4), and 8.45 (2H, dd+br s, J=5 and 2 Hz, H-6 and NH); IR (KBr) 1650 (C=O) and 3230 (NH and OH) cm^{-1}; MS (70 eV) m/z 166 (M^+); Found: C, 57.91; H, 6.07; N, 16.79%. Calcd for $C_8H_{10}H_2O_2$: C, 57.82; H, 6.07, N, 16.86%.

4c: Mp 76—77 °C (from AcOEt); ^{1}H NMR ($CDCl_3$) δ= 1.23 (3H, t, J=7 Hz, CH_3), 3.3—3.6 (2H, m, CH_2), 4.81 (2H, s, CH_2O), 5.25 (1H, br s, OH), 7.24 (2H, dd+br s, J=8 and 5 Hz, H-5 and NH), 7.88 (1H, dd, 8 and 2 Hz, H-4), and 8.50 (1H, dd, J=5 and 2 Hz, H-6); IR (KBr) 1640 (C=O) and 3280 (NH and OH) cm^{-1}; MS (70 eV) m/z 180 (M^+); Found: C, 59.99; H, 6.73; N, 15.53%. Calcd for $C_9H_{12}N_2O_2$: C, 59.99; H, 6.71; N, 15.55%.

5c: Mp 32—34 °C (from Et_2O); ^{1}H NMR ($CDCl_3$) δ=1.28 (3H, t, J=8 Hz, CH_3), 3.4—3.7 (2H, m, CH_2), 4.82 (2H, d, J=8 Hz, CH_2O), 5.32 (1H, t, J=8 Hz, OH), 7.36 (1H, dd, J=8 and 5 Hz, H-5), 7.73 (1H, dd, J=8 and 2 Hz, H-4), and 8.46 (2H, dd+br s, J=5 and 2 Hz, H-6 and NH); IR (KBr) 1660 (C=O) and 3340 (NH and OH) cm^{-1}; MS (70 eV) m/z 180 (M^+); Found: C, 57.90; H, 6.70; N, 15.48%. Calcd for $C_9H_{12}N_2O_2$: C, 59.99; H, 6.71; N, 15.55%.

4d: Mp 86—87 °C (from AcOEt);^{1}H NMR ($CDCl_3$) δ=1.24 (6H, d, J=7 Hz, CH_3×2), 4.0—4.4 (1H, m, CH), 4.74 (2H, d, J=6 Hz, CH_2O), 5.41 (1H, t, J=6 Hz, OH), 7.17 (1H, dd, J=9 and 5 Hz, H-5), 7.35 (1H, br s, NH), 7.83 (1H, dd, J=9 and 2 Hz, H-4), and 8.43 (1H, dd, J=5 and 2 Hz, H-6); IR (KBr) 1650 (C=O) and 3370 (NH and OH) cm^{-1}; MS (70 eV) m/z 194 (M^+); Found: C, 61.92; H, 7.36; N, 14.57%. Calcd for $C_{10}H_{14}N_2O_2$: C, 61.84; H, 7.26; N, 14.42%.

5d: Mp 40—41 °C (from Et_2O-hexane); ^{1}H NMR ($CDCl_3$) δ=1.29 (6H, d, J=7 Hz, CH_3×2), 4.1—4.4 (1H, m, CH), 4.81 (2H, d, J=8 Hz, CH_2O), 5.35 (1H, t, J=8 Hz, OH), 7.37 (1H, dd, J=9 and 5 Hz, H-5), 7.73 (1H, dd, J=9 and 2 Hz, H-4), 8.17 (1H, br s, NH), and 8.46 (1H, dd, J=5 and 2 Hz, H-6); IR (KBr) 1640 (C=O), 3420 and 3280 (NH and OH) cm^{-1}; MS (70 eV) m/z 194 (M^+); Found: C, 61.92; H, 7.33; N, 14.47%. Calcd for $C_{10}H_{14}N_2O_2$: C, 61.84; H, 7.26; N, 14.42%.

4e: Mp 79—80 °C (from AcOEt); ^{1}H NMR ($CDCl_3$) δ= 4.52 (2H, d, J=7 Hz, CH_2Ph), 4.74 (1H, s, CH_2O), 5.15 (1H, br s, OH), 7.1—7.3 (6H, m, arom+H-5), 7.82 (2H, dd+br s, J=9 and 2 Hz, H-4 and NH), and 8.42 (1H, dd, J=5 and 2 Hz, H-6); IR (KBr) 1660 (C=O) and 3250 (NH and OH) cm^{-1}; MS (70 eV) m/z 242 (M^+); Found: C, 69.46; H, 5.81; N, 11.53%. Calcd for $C_{14}H_{14}N_2O_2$: C, 69.41; H, 5.82, N, 11.56%.

5e: Mp 65—66 °C (from Et_2O); ^{1}H NMR ($CDCl_3$) δ=4.63 (2H, d, J=6 Hz, CH_2Ph), 4.83 (2H, d, J=8 Hz, CH_2O), 5.19 (1H, t, J=8 Hz, OH), 7.2—7.4 (6H, m, arom+H-5), 7.73 (1H, dd, J=8 and 3 Hz, H-4), 8.42 (1H, dd, J=5 and 3 Hz, H-6) and 8.66 (1H, br s, NH); IR (KBr) 1650 (C=O), 3340 and 3430(NH and OH) cm^{-1}; MS (70 eV) m/z 242 (M^+); Found: C, 69.38; H, 5.81; N, 11.52%. Calcd for $C_{14}H_{14}N_2O_2$: C, 69.41; H, 5.82; N, 11.56%.

4f: Mp 118—120 °C (from AcOEt); ^{1}H NMR ($CDCl_3$) δ= 4.86 (2H, s, CH_2O), 5.39 (1H, br s, OH), 7.0—7.7 (7H, m, H-5+arom+NH), 8.04 (1H, dd, J=8 and 2 Hz, H-4), and 8.48

(1H, dd, J=6 and 2 Hz, H-6); IR (KBr) 1660 (C=O) and 3280 (NH and OH) cm^{-1}; MS (70 eV) m/z 228 (M^+); Found: C, 68.40; H, 5.28; N, 12.20%. Calcd for $C_{13}H_{12}N_2O_2$: C, 68.41; H, 5.30, N, 12.27%.

5f: Mp 108—109 °C (from AcOEt); ^1H NMR ($CDCl_3$) δ= 4.90 (3H, s, CH_2O+OH), 7.1—7.8 (7H, m, H-5,+arom+NH), 7.82 (1H, dd, J=9 and 2 Hz, H-4), and 8.53 (1H, dd, J=9 and 2 Hz, H-6); IR (KBr) 1680 (C=O), 3320 and 3500 (NH and OH) cm^{-1}; MS (70 eV) m/z 228 (M^+); Found: C, 68.30; H, 5.25; N, 12.27%. Calcd for $C_{13}H_{12}N_2O_2$: C, 68.41; H, 5.30, N, 12.27%.

4g: Mp 155—156 °C (from AcOEt); ^1H NMR (DMSO-d_6) δ=2.27 (3H, s, CH_3), 4.75 (2H, d, J=6 Hz, CH_2O), 5.30 (1H, t, J=6 Hz, OH), 7.15 (2H, d, J=8 Hz, arom), 7.42 (1H, dd, J=8 and 5 Hz, H-5), 7.61 (3H, d, J=8 Hz, arom+NH), 7.96 (1H, dd, J=8 and 2 Hz, H-4), and 8.60 (1H, dd, J=5 and 2 Hz, H-6); IR (KBr) 1650 (C=O) and 3280 (NH and OH) cm^{-1}; MS (70 eV) m/z 242 (M^+); Found: C, 69.54; H, 5.78; N, 11.50%. Calcd for $C_{14}H_{14}N_2O_2$: C, 69.41; H, 5.82; N, 11.56%.

5g: Mp 117—118 °C (from AcOEt). ^1H NMR (DMSO-d_6) δ=2.27 (3H, s, CH_3), 4.97 (2H, d, J=6 Hz, CH_2O), 5.34 (1H, t, J=6 Hz, OH), 7.12 (2H, d, J=8 Hz, arom), 7.59 (1H, dd, J=8 and 5 Hz, H-5), 7.70 (3H, d, J=8 Hz, arom+NH), 8.17 (1H, dd, J=8 and 3 Hz, H-4), and 8.53 (1H, dd, J=5 and 3 Hz, H-6); IR (KBr) 1670 (C=O) and 3320 (NH and OH) cm^{-1}; MS eV) m/z 242 (M^+); Found: C, 69.28; H, 5.78;N, 11.61%. Calcd for $C_{14}H_{14}N_2O_2$: C, 69.41; H, 5.82, N, 11.56%.

Starting with **2b**—g, a similar procedure gave **4b**—g, respectively.

Furo[3,4-*b*]pyridin-5(7*H*)-one(6) and Furo[3,4-*b*]pyridin-7(5*H*)-one(7). As a general procedure, a solution of **4** or **5** (1 mmol) in MeOH (5 ml) added HCl (1 mol dm^{-3}, 5 ml) was heated at 80 °C for 2 d. The reaction mixture was neutralized with aqueous NaOH and concentrated in vacuo. After the residue was extracted with $CHCl_3$ (10 ml×5), the combined extracts were washed with water, dried over Na_2SO_4, and concentrated in vacuo to afford spectroscopically pure **6** or **7**.[13]

The present work was partially supported by a Grant-in-Aid for Scientific Research No. 63740271 from the Ministry of Educstion, Science and Culture.

References

1) C. Cotrel, C. Crisan, C, Jeanmart, and M. N. Messer, Ger. Offen., 2423650 (1974) [*Chem. Abstr.*, **82**, 112103k (1975)]; C. Cotrel, C. Crisan, C, Jeanmart, and M. N. Messer, Fr. Demande, 2263752 (1975) [*Chem. Abstr.*, **84**, 121901n (1976)]; C. Cotrel, C. Crisan, C. Jeanmart, and A. Leger, Ger. Offen., 2615067 (1976) [*Chem. Abstr.*, **86**, 43743n (1977)].

2) G. Goto and Y. Saji, *Jpn. Kokai Tokkyo Koho*, JP 61130290 (1986) [*Chem. Abstr.*, **106**, 33014t (1987)].

3) G. J. Hitchings and J. M. Vernon, *J. Chem. Soc., Chem. Commun.*, **1988**, 623.

4) Reviews: W. N. Speckamp, *Recl. Trav. Chim. Pays-Bas*, **100**, 345 (1981); W. N. Speckamp and H. Hiemstra, *Tetrahedron*, **41**, 4367 (1985).

5) Z. Horii, C. Iwata, and Y. Tamura, *J. Org. Chem.*, **26**, 2273 (1961); F. C. Uhle, *ibid.*, **26**, 2998 (1961); R. T. Major and R. J. Hedrick, *ibid.*, **30**, 1270 (1965); Y. Kondo and B. Witkop, *ibid.*, **33**, 206 (1968); Y. Maki, K. Kikuchi, H. Sugiyama, and S. Seto, *Chem. Ind.*, **1976**, 322; T. Watanabe, F. Hamaguchi, and S. Ohki, *Chem. Pharm. Bull.*, **26**, 530 (1978).

6) T. Goto, M. Saito, and R. Sato, *Bull. Chem. Soc. Jpn.*, **60**, 4178 (1987).

7) D. A. Burnett, J.-K. Choi, D. J. Hart, and Y.-M. Tsai, *J. Am. Chem. Soc.*, **106**, 8201 (1984); A. R. Chamberlin, H. D. Nguyen, and J. Y. L. Chung, *J. Org. Chem.*, **49**, 1682 (1984).

8) J. C. Hubert, W. Steege, W. N. Speckamp, and H. O. Huisman, *Synth. Commun.*, **1**, 103 (1971).

9) A. J. Showler and P. A. Darley, *Chem. Rev.*, **67**, 427 (1967).

10) J. C. Hubert, J. B. P. A. Wijnberg, and W. N. Speckamp, *Tetrahedron*, **31**, 1437 (1975).

11) P. Canonne and M. Belley, *Can. J. Chem.*, **65**, 1885 (1987).

12) H. von Dobeneck and B. Hansen, *Chem. Ber.*, **105**, 3611 (1972).

13) W. R. Ashcroft, M. G. Beal, and J. A. Joule, *J. Chem. Soc., Perkin Trans. 1*, **1981**, 3012, and references cited therein.

Monosubstituted Tetramethoxynaphthalenes[1)]

Yasuhiro TANOUE, Akira TERADA,* Kazuhiko TORISU, and Hiroshige TANIGUCHI
Department of Chemistry, Kyushu Institute of Technology, Tobata, Kitakyushu, Fukuoka 804
(Received November 7, 1988)

As new intermediates for the syntheses of monosubstituted naphthazarins and anthracyclines, several tetramethoxynaphthalenes having a substituent such as CH_3, COOH, CN, Br, OAc, OH, and OMe groups were prepared from 1,4,5,8-tetramethoxynaphthalene and 2-formyl-1,4,5,8-tetramethoxynaphthalene.

We have already reported that 1,4,5,8-tetramethoxynaphthalene (**1**) could be converted to 2-formyl-1,4,5,8-tetramethoxynaphthalene (**2**) in almost quantitative yield; from this, (±)shikonin was first prepared.[2)] Generally, tetramethoxynaphthalens could be easily demethylated by our methods to give the corresponding naphthazarin compounds[3)] (Scheme 1). The tetramethoxynaphthalene **1** was used as an intermediate in the synthesis of nogalamycin,[4)] which belonged to anthracycline series antibiotics.

These results suggest to us the possibility that these monosubstituted tetramethoxynaphthalenes will become new intermediates for naphthoquinones and anthracyclines. Here, we consider the syntheses of monosubstituted tetramethoxynaphthalenes having CH_3, COOH, CN, Br, OAc, OH, or OMe as the substituent.

Results and Discussion

Reduction of the aldehyde **2** with $LiAlH_4$ gave 2-hydroxymethyl-1,4,5,8-tetramethoxynaphthalene (**3**),[3)] followed by hydrogenolysis in the presence of palladium carbon, 2-methyl-1,4,5,8-tetramethoxynaphthalene (**4**) resulted in 58% yield.

Although the oxidation of **2** with potassium permanganate gave a negative result, tetrabutylammonium permanganate[5)] was tried and our proposed 1,4,5,8-tetramethoxy-2-naphthoic acid (**5**) was obtained in 87% yield.

With chlorosulfonyl isocyanate[6)] in dichloromethane the tetramethoxynaphthalene **1** gave an *N*-chlorosulfonyl amide intermediate; subsequent treatment with DMF afforded 2-cyano-1,4,5,8-tetramethoxynaphthalene (**6**) in 71% yield (Scheme 3).

With an equimolar amount of bromine in chloroform, **1** gave 2-bromo-1,4,5,8-tetramethoxynaphthalene (**7**) (44% yield) and 2,6-dibromo-1,4,5,8-tetramethoxynaphthalene (**8**) (17%) at the same time. However, two molar equiv. of bromine wholly afforded the dibromide (**8**); the product yield was 87%. Since the structure of this dibromide was either 2,6-dibromide (**8**) or 2,7-

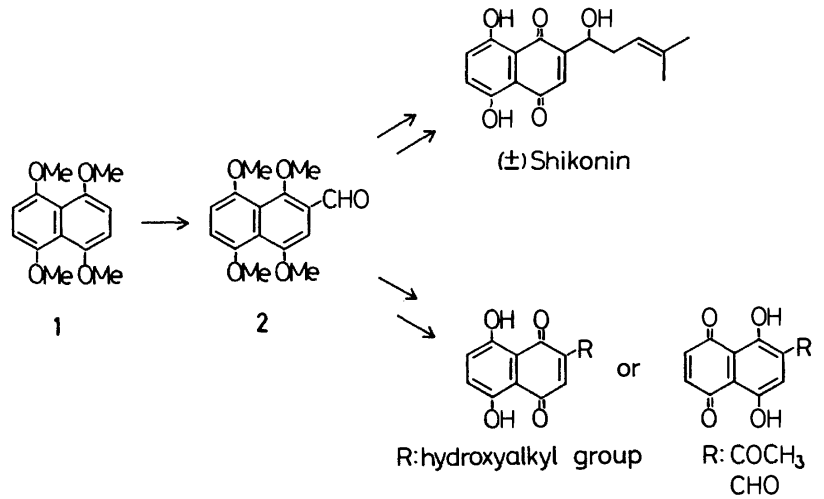

Scheme 1.

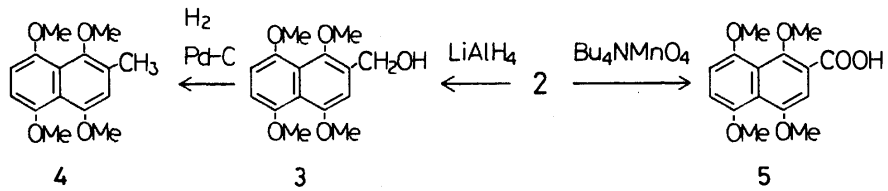

Scheme 2.

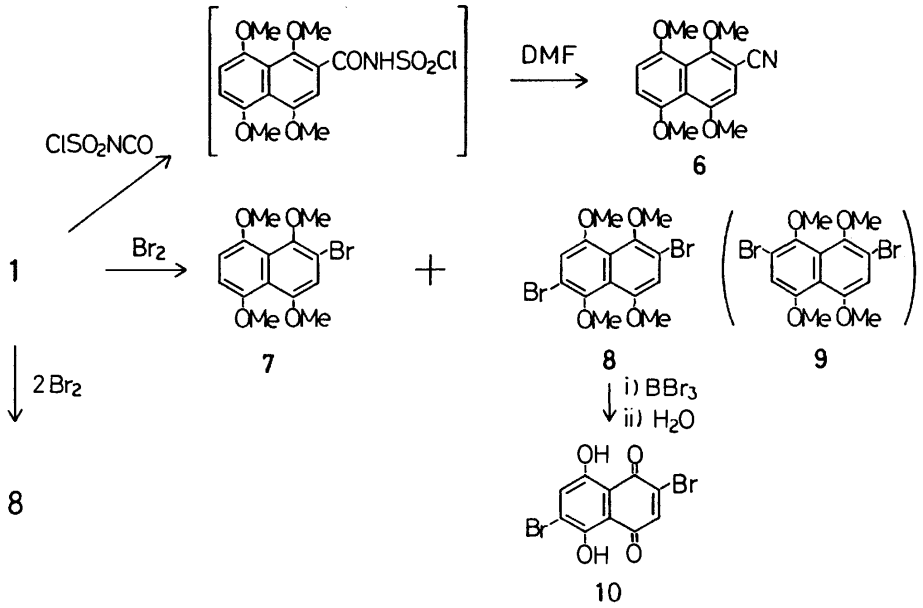

Scheme 3.

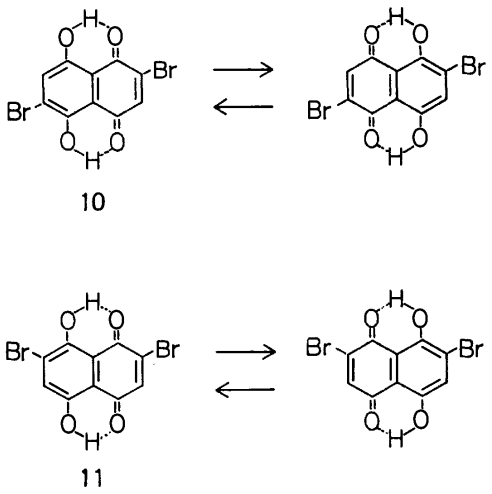

Chart 1.

dibromide (**9**), shown in Scheme 3, the dibromide was changed into a dibromonaphthazarin and identified as follows. Both the naphthazarin dibromides, **10** and **11** in Chart 1, are tautomers of each other. The dibromonaphthazarin which we obtained showed a sharp single peak in the ^{1}H NMR at δ 12.56 due to two equivalent hydroxyl groups. Since the naphthazarin was, therefore, **10**, the above dibromide was proved to be **8**. If the naphthazarin product was another **11**, its hydroxyl signal in ^{1}H NMR had to be separated into two peaks as like A in Chart 2.[7]

The treatment of **1** with lead tetraacetate in benzene gave 2-acetoxy-1,4,5,8-tetramethoxynaphthalene (**12**) (40% yield) and 5,8-dimethoxy-1,4-naphthoquinone (**13**) (46%). The structure of **13** was identical with that of the authentic sample[3] already obtained in our laboratory by the oxidative demethylation of **1** with cerium(IV) ammonium nitrate.

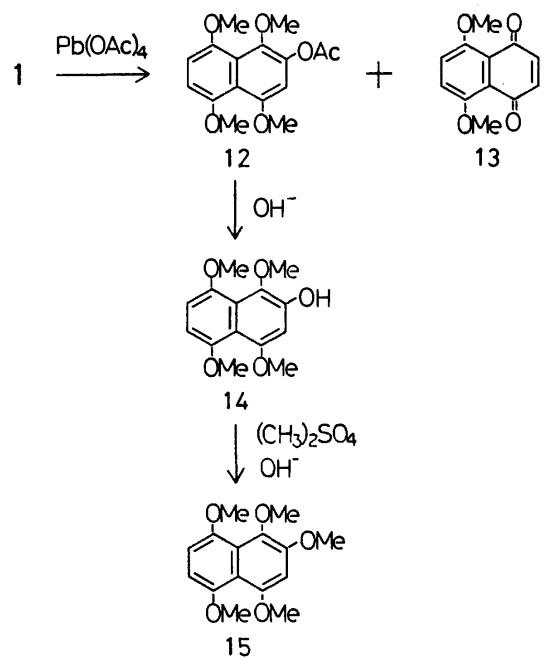

Scheme 4.

Alkali hydrolysis of **12** gave 1,4,5,8-tetramethoxy-2-naphthol (**14**) in 91% yield, and methylation with dimethyl sulfate afforded 1,2,4,5,8-pentamethoxynaphthalene (**15**) (Scheme 4).

Experimental

Melting points were determined with a Yanagimoto micromelting point apparatus and were uncorrected. ^{1}H and ^{13}C NMR spectra were taken on a JEOL JNM-60 in $CDCl_3$ using Me_4Si and $CDCl_3$ as internal standards, respectively. Mass spectra and IR spectra were obtained with a JEOL DX-300 spectrometer, and a Hitachi 260-30 spectrometer, respectively. Column chromatography was carried

out on silica gel (Wakogel C-200) or alumina (Sumitomo, KCG-30) eluting with chloroform.

2-Methyl-1,4,5,8-tetramethoxynaphthalene (4). A mixture of 2-hydroxymethyl-1,4,5,8-tetramethoxynaphthalene (**3**)[3] (189 mg, 0.68 mmol) and palladium carbon (200 mg, Pd content 5%) in tetrahydrofuran (5 ml) and ethanol (30 ml) was stirred at 60 °C for 8 h under 50 kg cm^{-2} of hydrogen in an autoclave. After filtration and washing the residue with chloroform, evaporation of the combined filtrate gave a solid which was purified by alumina chromatography to give a sample of **4** (102 mg, 58%). Recrystallization from hexane gave an analytical sample, mp 95.5—96.5 °C. IR (KBr) 1600, 1355, 1260, and 1070 cm^{-1}; ^{1}H NMR δ=2.41 (s, 3H, CH_3), 3.73, 3.89 (each s, 3H, OCH_3), 3.92 (s, 6H, 2×OCH_3), 6.7 (s, 1H, ArH), and 6.78 (s, 2H, 2×ArH); MS, *m/z* 262 (M^+), 247 (M^+-CH_3), 204. Calcd for $C_{15}H_{18}O_4$: C, 68.69; H, 6.92%. Found: C, 68.30; H, 6.58%.

1,4,5,8-Tetramethoxy-2-naphthoic Acid (5). Tetrabutylammonium permanganate[5] (360 mg, 1 mmol) was added to a solution of 2-formyl-1,4,5,8-tetramethoxynaphthalene[2] (**2**) (138 mg, 0.5 mmol) in pyridine (3 ml) and stirred at room temperature for 20 h under a nitrogen atmosphere. The reaction mixture was poured into dil. hydrochloric acid (100 ml) containing sodium hydrogensulfite and extracted with chloroform. The chloroform solution was washed with dil. hydrochloric acid (100 ml ×2), brine (100 ml) and dried over anhydrous sodium sulfate, and concentrated. The crude product was chromatographed on silica gel to give 127 mg (87%) of **5**. Recrystallization from hexane-ethanol (5:1) gave an analytical sample, mp 131—132 °C. IR (KBr) 3100—2500 (broad, OH), 1695, 1670 (each C=O), 1610, 1585, 1265 (C-O), and 1070 cm^{-1}; ^{1}H NMR δ=3.91, 3.94, 3.98, 3.99 (each s, 3H, OCH_3), 6.99 (s, 2H, 2×ArH), 7.46 (s, 1H, ArH), and 11.23 (broad, 1H, COOH); ^{13}C NMR δ=56.70, 56.87, 57.90, 64.41 (each OCH_3), 106.36 (C-3), 108.94 (C-7), 111.85 (C-6), 118.37, 121.17, 123.28, 150.49 (C-5), 150.83 (C-4), 151.46 (C-8), 153.92 (C-1), and 165.81 (COOH); MS, *m/z* 292 (M^+), 277, 259, 247. Calcd for $C_{15}H_{16}O_6$: C, 61.64; H, 5.52%. Found: C, 61.36; H, 5.45%.

2-Cyano-1,4,5,8-tetramethoxynaphthalene (6). A solution of chlorosulfonyl isocyanate (700 mg, 4.4 mmol) in dichloromethane (2 ml) was added to a solution of 1,4,5,8-tetramethoxynaphthalene(**1**)[2] (992 mg, 4 mmol) in dichloromethane (28 ml) and stirred at room temperature for 2 h. *N,N*-Dimethylformamide (800 mg) was added and stirred at room temperature for 3.5 h. The reaction mixture was poured into ice water and extracted with dichloromethane (100 ml×3). The dichloromethane solution was washed with brine (100 ml) and dried over anhydrous sodium sulfate, and concentrated. The residue was purified by silica-gel chromatography to give 778 mg (71%) of **6**. Recrystallization from hexane gave an analytical sample, mp 127—128 °C. IR (KBr) 2225 (CN), 1605, 1390, 1370, 1270, 1080, and 1050 cm^{-1}; ^{1}H NMR δ=3.89, 3.94 (each s, 3H, OCH_3), 3.95 (s, 6H, 2×OCH_3), 6.82 (s, 1H, ArH), and 6.97 (s, 2H, 2×ArH); ^{13}C NMR δ=57.04, 57.15, 58.01, 63.56 (each OCH_3), 104.02 (C-2), 106.71 (C-3), 109.28 (C-7), 112.19 (C-6), 117.11, 122.34, 122.71, 150.72 (C-5), 151.35 (C-8), 153.69 (C-4), 155.46 (C-1); MS, *m/z* 273 (M^+), 258, 243, 215. Calcd for $C_{15}H_{15}O_4N$: C, 65.93; H, 5.53; N, 5.13%. Found: C, 65.85; H, 5.61; N, 5.07%.

2-Bromo-1,4,5,8-tetramethoxynaphthalene (7) and 2,6-Dibromo-1,4,5,8-tetramethoxynaphthalene (8). A solution of bromine (323 mg, 2.02 mmol) in chloroform (5 ml) was added dropwise to a solution of 1,4,5,8-tetramethoxynaphthalene (500 mg, 2.02 mmol) in chloroform (20 ml) at room temperature. The solution was stirred for 2 h, poured into water, and extracted with chloroform. The chloroform solution was washed with aqueous sodium hydrogensulfite, sodium hydrogencarbonate and brine and dried over anhydrous sodium sulfate, and concentrated. The residue was chromatographed on silica gel to give 291 mg (44%) of **7**, 140 mg (17%) of **8** and 14 mg (3%) of the starting material **1**.

7: mp 104—105 °C (from hexane); IR(KBr) 1605, 1580, 1380, 1365, 1310, 1260, 1070, and 1040 cm^{-1}; ^{1}H NMR δ=3.82, 3.88 (each s, 3H, OCH_3), 3.92 (each s, 6H, 2×OCH_3), 6.86 (s, 2H, 2×ArH), and 7.00 (each s, 1H, ArH); MS, *m/z* 328 (M^++2, 99%), 326 (M^+, 100), 313, 311, 232, 217, 204. Calcd for $C_{14}H_{15}O_4Br$: C, 51.40; H, 4.62%. Found: C, 51.27; H, 4.55%.

8: mp 215—216 °C (from methanol); IR (KBr) 1570, 1355, 1310, 1240, 1070, 1030, and 795 cm^{-1}; ^{1}H NMR δ=3.80 (s, 6H, 2×OCH_3), 3.95 (s, 6H, 2×OCH_3), 7.04 (s, 2H, 2×ArH); MS, *m/z* 408 (M^++4, 51%), 406 (M^++2, 100), 404 (M^+, 50), 391, 312, and 310. Calcd for $C_{14}H_{14}O_4Br_2$: C, 41.41; H, 3.47%. Found: C, 41.00; H, 3.46%.

2,6-Dibromo-5,8-dihydroxy-1,4-naphthoquinone (10). To a solution of the tetramethoxydibromide **8** (200 mg, 0.49 mmol) in dichloromethane (15 ml) was added dropwise boron tribromide (500 mg, 1.96 mmol) in dichloromethane (5 ml) at −70 °C. After stirring at −70 °C for 4 h, the solution was allowed to warm to room temperature and to stand overnight. It was then decomposed with dil. hydrochloric acid (100 ml) and extracted with dichloromethane (100 ml×3). The dichloromethane solution was worked up as usual and gave a crude product which was chromatographed on a silica-gel column to give 156 mg (91%) of **10**. Recrystallization from ethanol gave an analytical sample, mp 258—261 °C (decomp). IR (KBr) 1610 (C=O), 1580, 1560, 1420, 1400, 1260, 1180, and 995 cm^{-1}; ^{1}H NMR δ=7.61 (s, 2H, 2×ArH) and 12.56 (s, 2H, 2×OH); MS, *m/z* 350 (M^++4, 51%), 348 (M^++2, 100), 346 (M^+, 52), 304, 302, 269, and 267. Calcd for $C_{10}H_4O_4Br_2$: C, 34.52; H, 1.16%. Found: C, 34.40; H, 1.28%.

2-Acetoxy-1,4,5,8-tetramethoxynaphthalene (12) and 5,8-Dimethoxy-1,4-naphthoquinone (13). Lead tetraacetate (244 mg, 0.55 mmol) was added to a solution of the tetramethoxynaphthalene **1** (124 mg, 0.5 mmol) in benzene (20 ml) and stirred at 60 °C for 1 h. It was then decomposed by the addition of water and extracted with dichloromethane. The usual work-up and chromatography on silica gel gave 62 mg (40%) of **12** and 60 mg (46%) of **13**.

12: mp 85—85.5 °C (from hexane); IR (KBr) 1760 (C=O), 1600, 1365, 1265, 1205, 1090, 1065, 1025, and 990 cm^{-1}; ^{1}H NMR δ=2.37 (s, 3H, $COCH_3$), 3.78, 3.88 (each s, 3H, OCH_3), 3.91 (s, 6H, 2×OCH_3), 6.64 (s, 1H, ArH), and 6.82 (s, 2H, 2×ArH). Calcd for $C_{16}H_{18}O_6$: C, 62.74; H, 5.92%. Found: C, 62.73; H, 5.89%.

13: mp 157—159 °C (lit,[3] mp 160—161 °C). This did not depress the melting point of an authentic sample of **13** on admixture.

1,4,5,8-Tetramethoxy-2-naphthol (14). Aqueous sodium hydroxide (1 M, 6 ml; 1 M=1 mol dm^{-3}) was added to a solution of the ester **12** (343 mg, 1.12 mmol) in methanol (8 ml) under a nitrogen atmosphere and stirred at room temperature for 3 h. The solution was acidified by the addition of 1 M hydrochloric acid (100 ml) and extracted with chloroform. The chloroform solution was concentrated to

give 269 mg (91%) of **14**, mp 149—152 °C. This was unstable and decomposed during usual recrystallization or column chromatography. IR (KBr) 3400 (sharp OH), 1600, 1375, 1260, 1070 cm^{-1}; ^1H NMR δ=3.81, 3.88 (each s, 3H, OCH_3), 3.92 (s, 6H, 2×OCH_3), 5.20 (broad, 1H, OH), 6.69 (s, 2H, 2×ArH), 6.74 (s, 1H, ArH); MS, *m/z* 264 (M^+), 249, 221, 203, and 104. HRMS, Calcd for $C_{14}H_{16}O_5$: M, 264.0997. Found: *m/z* 264.0989.

1,2,4,5,8-Pentamethoxynaphthalene (15). Under a nitrogen atmosphere aqueous sodium hydroxide (1 M, 4 ml) was added to a solution of the naphthol **14** (223 mg, 0.84 mmol) in methanol (20 ml) at room temperature. To this solution was altenately added dropwise dimethyl sulfate (1.2 g, 8.4 mmol) and aqueous sodium hydroxide (1 M, 4 ml) at room temperature. After stirring at 50 °C for 2 h, the solution was concentrated until 10 ml and then extracted with chloroform, dried, and concentrated. The residue was chromatographed on silica-gel column to give 141 mg (60%) of **15**. Recrystallization from hexane afforded an analytical sample, mp 104—105 °C. IR (KBr) 1600, 1390, 1370, 1355, 1265, 1070, 1045, and 805 cm^{-1}; ^1H NMR δ=3.82 (s, 3H, OCH_3), 3.90 (s, 6H, 2×OCH_3), 3.94 (s, 3H, OCH_3), 3.99 (s, 3H, OCH_3), 6.64 (s, 1H, ArH), 6.74 (s, 2H, 2×ArH); MS, *m/z* 274 (M^+), 264, 263, 249, 231, and 124. Calcd for $C_{15}H_{18}O_5$: C, 64.74; H, 6.52%. Found: C, 64.26; H, 6.74%.

References

1) Paper VIII, on Synthesis of Naphthoquinone Derivatives. Paper VII, Y. Tanoue and A. Terada, *Bull. Chem. Soc. Jpn.*, **61**, 2039 (1988).

2) A. Terada, Y. Tanoue, A. Hatada, and H. Sakamoto, *J. Chem. Soc., Chem. Commun.*, **1983**, 987; *Bull. Chem. Soc. Jpn.*, **60**, 205 (1987).

3) Y. Tanoue and A. Terada, *Bull. Chem. Soc. Jpn.*, **61**, 2039 (1988).

4) M. Kawasaki, F. Matsuda, and S. Terashima, *Tetrahedron Lett.*, **27**, 2145 (1986).

5) T. Sala and M. V. Sargent, *J. Chem. Soc., Chem. Commun.*, **1978**, 253.

6) The reaction mechanism of aromatic compounds with chlorosulfonyl isocynate was shown in the following paper. G. Lohaus, *Chem. Ber.*, **100**, 2719 (1967).

7) R. E. Moore and P. J. Scheuer, *J. Org. Chem.* **31**, 3272 (1966). For example, in ^1H NMR of 2,7-dimethoxynaphthazarin (**A**), two hydroxyl signals were observed at δ 12.70 and 13.12 (Chart 2).

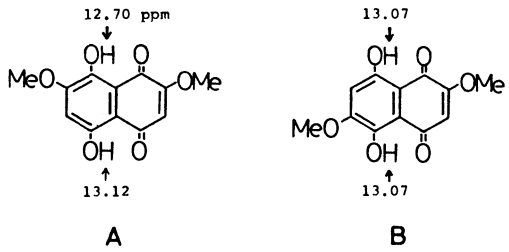

Chart 2.

 © 1989 The Chemical Society of Japan Bull. Chem. Soc. Jpn., 62, 1215—1225 (1989)

Nonacidic and Highly Chemoselective Protection of the Carbonyl Function. 3-Methylbenzothiazolines as a Base- and Acid-Resistant Protected Form for the Carbonyl Groups

Hidenori CHIKASHITA,* Shun-ichiro KOMAZAWA, Nishiki ISHIMOTO, Koji INOUE, and Kazuyoshi ITOH

Department of Applied Chemistry, Faculty of Engineering, Kansai University, Suita, Osaka 564

(Received November 21, 1988)

A simple and useful new type of protection method for carbonyl groups by conversion into 3-methylbenzothiazoline derivatives with *o*-(methylamino)benzenethiol was described. With this method, 3-methylbenzothiazolines were conveniently obtained in excellent yields from various aldehydes and ketones. This method allows efficient protection and deprotection under mild and neutral conditions and affords protection of the carbonyl group against both basic and acidic conditions. The difference in reactivity between different carbonyl groups was successfully utilized for the chemoselective benzothiazolination of the formyl group of 4-oxopentanal and also for the chemoselective conversion of 4-androstene-3,17-dione and progesteron into the corresponding benzothiazolines with the nonconjugated keto groups remaining intact. 2-Substituted benzothiazolines derived from aldehydes were efficiently converted into 2,2-disubstituted benzothiazolines via alkylation, with a variety of Grignard or organolithium reagents, of 2-substituted 3-methylbenzothiazolium salts which were readily obtained by the treatment of the former thiazolines with trityl perchlorate in acetonitrile. These salts were also obtained in good yields from aldehydes in one-pot syntheses by the treatment with *o*-(methylamino)benzenethiol in acetonitrile followed by addition of trityl perchlorate. 3-Methylbenzothiazolium iodide was found to be also effective as a formyl cation equivalent and the reactions with Grignard or organolithium reagents produced the corresponding 2-substituted benzothiazolines in good yields. With this reaction, 2-deuterio-3-methylbenzothiazolium iodide was effectively applied as a deuterated formyl cation equivalent for the synthesis of aldehyde-*d*.

The protection of carbonyl groups as acetals is now widely and frequently used as an important synthetic operation during the course of various synthetic projects. Acetalization of carbonyl compounds is generally performed in the presence of various acidic catalysts and the protected form is known to be very stable under various basic conditions while it can be easily deprotected by treating with acid.[1] However, this simplicity is disadvantageous at the same time because acetalized compounds can not be treated with acid except for removing the protection and in addition, acid-sensitive molecules can not be protected and deprotected as acetals. Furthermore, a convenient and at the same time highly chemoselective acetalization method capable of discrimination between aldehydes and ketones has not yet been achieved in spite of its great importance and necessity.[2] On the other hand, thioacetalization is an important and widely used protecting method for carbonyl compounds as well as acetalization. However, this method is also not exempted from some of these disadvantages.

In this paper, we report a new type of convenient and highly chemoselective protection of carbonyl compounds by conversion into 3-methylbenzothiazoline derivatives with *o*-(methylamino)benzenethiol (MABT). This method allows efficient protection and deprotection under mild and neutral conditions and affords protection of carbonyl groups against both basic and acidic conditions. We will also show that the benzothiazoline ring system is very useful as a functional protective group via 3-methylbenzothiazolium salts (**5** and **6**) as an acyl and a formyl cation equivalent (Scheme 1).

Benzothiazolination of Aldehydes and Ketones with MABT. In order to establish optimum conditions, the rates of benzothiazolination for pentanal (**1a**) and 2-pentanone (**2a**) with one equiv of MABT in various solvents at reflux temperatures were followed by GLC. The results are presented in Figs. 1 and 2. Regarding the benzothiazolination of aldehyde **1a**, the reaction proceeded using a protic or an aprotic solvent in excellent yields (>88%) during the 6 h reaction time and the rates did not vary significantly based on type of solvent (Fig. 1). However, ethanol was apparently the most effective and the reaction proceeded almost quantitatively during the 6 h reaction time even in 98% ethanol. On the other hand, the reaction of ketone **2a** with MABT occurred more slowly as compared to **1a** and did not proceed in hexane at all. Although the reaction rates varied considerably based on type of solvent, the rate in alcohols or acetonitrile was sufficiently rapid to be synthetically useful for the protection of ketones (Fig. 2). The different reactivity of **1a** and **2a** is advantageous from a synthetic viewpoint since it enables the selective protection of aldehydes in the presence of ketones. It is noteworthy and very attractive that these reactions were performed under neutral conditions without any additives by a very simple operation which does not require even the removal of the water formed during the reaction.

By this simple method, benzothiazolinations of several aldehydes were successfully performed with the

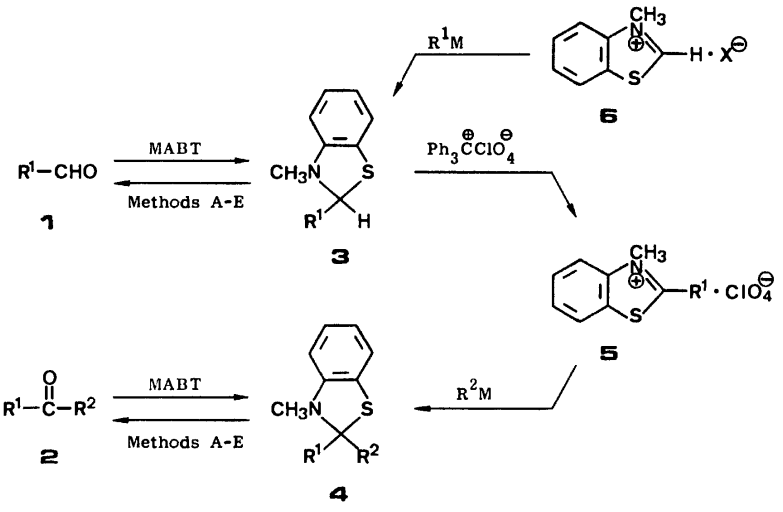

Scheme 1.

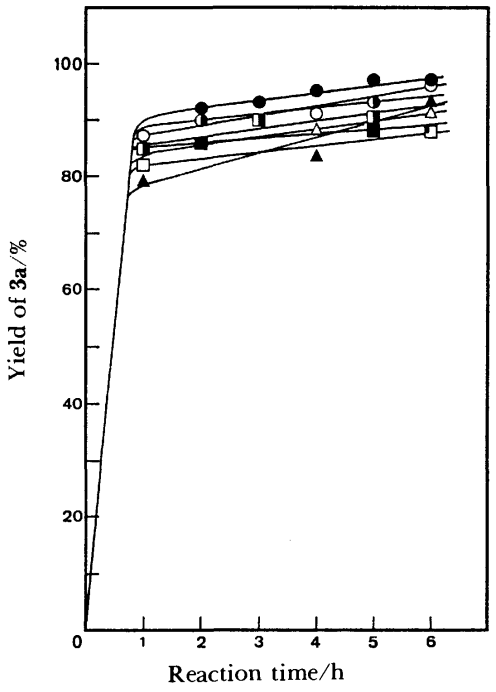

Fig. 1. Benzothiazolination of pentanal (**1a**) with one equiv of MABT in various solvents at reflux temperatures: ethanol (●), 98% ethanol (○), methanol (◑), acetonitrile (▲), THF (△), dichloromethane (■), benzene (□), and hexane (◧).

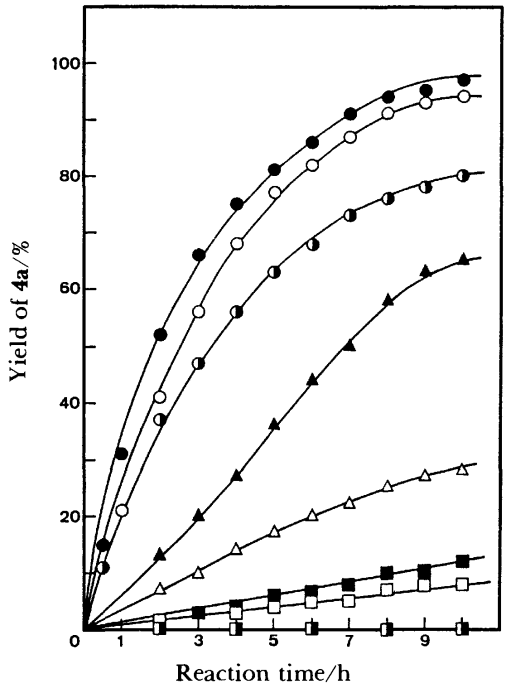

Fig. 2. Benzothiazolination of 2-pentanone (**2a**) with one equiv of MABT in various solvents at reflux temperatures. Symbols are identical with those used in Fig. 1.

results summarized in Table 1. As is seen in Table 1, aliphatic as well as aromatic aldehydes **1a—k** were all cleanly converted to the corresponding 2-substituted benzothiazolines **3a—k** with MABT in ethanol. Unexpectedly, the benzothiazolination of conjugated enal (**1l**) proceeded very slowly under the present conditions to afford **3l** in low yield. Benzothiazolination with MABT in ethanol was also examined with several ketones and the results are listed in Table 2. The linear ketones **2a—e** except for highly hindered ketone, 2,4-dimethyl-3-pentanone (**2f**) which almost did not react, were all cleanly converted to the corresponding 2,2-disubstituted benzothiazolines **4a—e** in almost quantitative yields. In the case of linear conjugated enones **2i** and **2j**, the reaction proceeded very slowly and much of the substrate was recovered unchanged. It is noteworthy that the benzothiazolination of the cyclic ketone **2g** and cyclic enone **2h** proceeded much more rapidly than the linear ketones and enones to afford **4g** and **4h** in quantitative and good yields, respectively. Thus, the order of relative reactivity of ketones in the present benzothiazolination was as

Table 1. Preparation and Hydrolysis of 2-Substituted Benzothiazolines **3**

R^1	Aldehyde	Benzothiazoline	Benzothiazolination[a]		Hydrolysis[b]
			Time/h	Yield/%[c]	Yield/%[d]
n-C_4H_9-	**1a**	**3a**	6	87	—
n-C_9H_{19}-	**1b**	**3b**	24	82	86
n-$C_4H_9(C_2H_5)CH$-	**1c**	**3c**	24	84	83
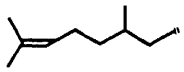	**1d**	**3d**	24	85	93
i-C_3H_7-	**1e**	**3e**	6	91	—
t-C_4H_9-	**1f**	**3f**	24	89	—
C_6H_5-	**1g**	**3g**	6	80	95
p-ClC_6H_4-	**1h**	**3h**	6	86	—
p-$CH_3OC_6H_4$-	**1i**	**3i**	6	82	—
	1j	**3j**	6	85	96
	1k	**3k**	6	90	94
(Z)-C_6H_5CH=CH-	**1l**	**3l**	24	28	84

a) Aldehyde (5 mmol) was reacted with MABT (5 mmol) in ethanol (5 ml) at reflux temperature. b) Hydrolysis was carried out under the conditions of Method A (see Table 3). c) Yield of pure product after short column chromatography or recrystallization. d) Yield of crude, nearly pure product.

Table 2. Preparation and Hydrolysis of 2,2-Disubstituted Benzothiazolines **4**

R^1	R^2	Ketone	Benzothiazoline	Benzothiazolination[a]		Hydrolysis[b]
				Time/h	Yield/%[c]	Yield/%[d]
n-C_3H_7-	CH_3-	**2a**	**4a**	10	88	—
n-C_3H_7-	n-C_3H_7-	**2b**	**4b**	10	90	—
n-C_5H_{11}-	n-C_5H_{11}-	**2c**	**4c**	24	90	94
i-C_3H_7-	CH_3-	**2d**	**4d**	24	91	—
C_6H_5-	CH_3-	**2e**	**4e**	10	89	90
i-C_3H_7-	i-C_3H_7-	**2f**	**4f**	24	Trace	—
-$(CH_2)_5$-		**2g**	**4g**	4	97	92
-CH=$CH(CH_2)_3$-		**2h**	**4h**	24	69	92
(E)-C_6H_5CH=CH-	CH_3-	**2i**	**4i**	24	32	90
(E)-C_6H_5CH=CH-	C_6H_5-	**2j**	**4j**	24	21	98

a) Ketone (5 mmol) was reacted with MABT (5 mmol) in ethanol (5 ml) at reflux temperature. b) Hydrolysis was carried out under the conditions of Method A (see Table 3). c) Yield of pure product after short column chromatography or recrystallization. d) Yield of crude, nearly pure product.

follows: cyclohexanone > linear ketones > 1-cyclohexen-1-one > linear conjugated enones > 2,4-dimethyl-3-pentanone.

Selective Benzothiazolination of Carbonyl Groups in the Presence of a Different Carbonyl Group. In order to examine the selectivity of the present benzothiazolination with MABT, experiments with compounds having two different carbonyl groups were performed (Scheme 2). As seen in the successful conversion of the keto carboxylic acid **7** and the keto ester **8** into the corresponding benzothiazolines **12** and **13** (94 and 92% yields, respectively) with one equiv of MABT in ethanol at reflux temperature, the benzothiazolination of keto groups can be easily performed in the presence of carboxylic acid or similar ester functional group. The benzothiazolination by the same method also exhibited splendid selectivity towards the formyl group. For example, the reaction of keto aldehyde **9** gave **14** as the sole product in 99% yield. The striking chemoselectivity of the present method was also emphasized by the fact that perfect selectivity could be realized in the benzothiazolination of steroid ketones **10** and **11** to **15** and **16** in dichloromethane and ethanol, respectively, with one equiv of MABT at reflux temperatures. After completion of the reactions, the products **15** and **16** were obtained in 93 and 97% yields, respectively and neither starting materials nor any by-products derived from the benzothiazolination at the nonconjugated keto carbonyl group was observed. These excellent chemoselectivities are in sharp contrast to acetalization or thioacetalization of the same steroid ketones.[3]

Hydrolysis and Stabilities of Benzothiazolines. Hydrolysis of benzothiazolines to the parent carbonyl

compounds was examined using two test substances **3g** and **4e**. As shown in Table 3, the hydrolysis could be effectively accomplished under neutral conditions in four ways (Methods A—D) using $AgNO_3$, $HgCl_2$, NBS, and Chloramine T to afford benzaldehyde (**1g**) and acetophenone (**2e**) in excellent yields, although the hydrolysis of **4e** by Method D gave exceptionally low yield of **2e**. Using another method, methylation with $MeOSO_2F$ followed by hydrolysis under mildly basic conditions was also effective to afford the products **1g** and **2e** in excellent yields. Notable in the case of Method A is the fact that such mild conditions did not affect the epimerizable center[4] or the α-hydroxyl group.[5] In addition, the mild nature of Method A is also illustrated in the conversion of 2-(β-hydroxyalkyl)-benzothiazolines **17** and **18** to the corresponding β-hydroxy ketones **19** and **20** (88 and 94% yields, respectively) without any evidence of dehydration (Scheme 3). Further results for the deprotection of benzothiazolines using Method A are given in Tables 1 and 2. All the tested benzothiazolines derived from aldehydes and ketones were cleanly cleaved with no difficulties and produced the corresponding carbonyl compounds in nearly quantitative yields.

Stabilities of the benzothiazolines were checked using **3g** and **4b** as samples. As shown in Table 4, both of these compounds survived the severe conditions

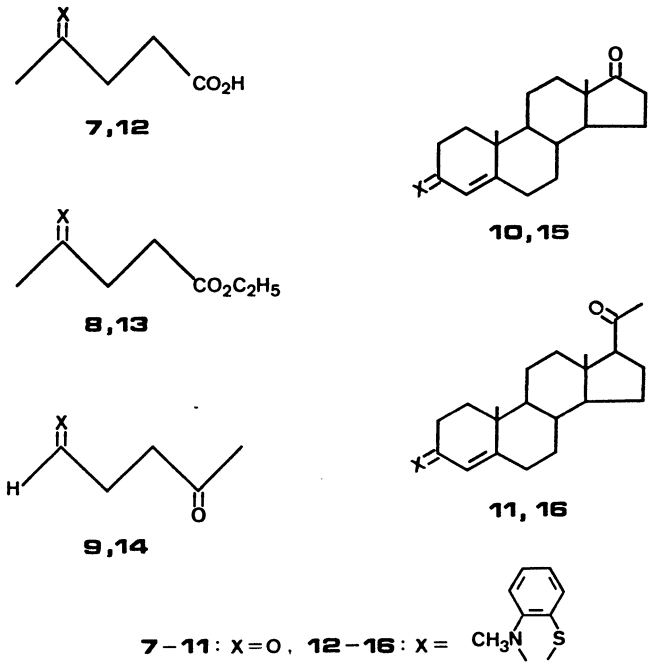

Scheme 2.

Table 4. Stabilities of Benzothiazolines

Reaction conditions	Recovery/%[a]	
	3g	4b
$LiAlH_4$/THF/r.t./24 h	94	97
$NaBH_4$/CH_3OH/reflux/24 h	98	94
20% H_2SO_4/70 °C/7 h	99	95
1M KOH/CH_3OH/reflux/7 h	97	93
Al_2O_3/CH_3OH/reflux/24 h	93	97
CF_3COOH/r.t./24 h	95	98
H_2(1 atom)/5% Pd-C/EtOH/r.t./18 h	94	94

a) Yields of the isolated benzothiazolines.

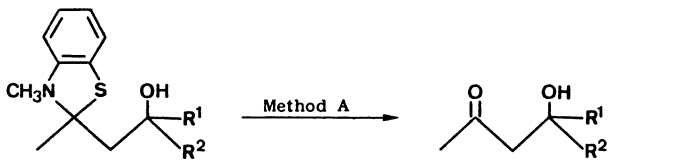

17: $R^1=H, R^2=n\text{-}C_9H_{19}$
18: $R^1=R^2=CH_3$
19: $R^1=H, R^2=n\text{-}C_9H_{19}$
20: $R^1=R^2=CH_3$

Scheme 3.

Table 3. Methods for Hydrolysis of Benzothiazolines into Aldehydes or Ketones

Method[a]	Reagent	Solvent	Isolated yield/%	
			1g	2e
A	$AgNO_3$	aq. CH_3CN	95	90
B	$HgCl_2$	aq. CH_3CN	93	94
C	NBS	H_2O	91	86
D	Chloramine T	C_2H_5OH	85	21
E	CH_3OSO_2F/K_2CO_3	CH_2Cl_2/aq. THF	92	96

a) Method A: benzothiazoline (4 mmol), $AgNO_3$ (12 mmol), CH_3CN-phosphate buffer (pH 7, 0.05 M)-H_2O (15 : 3 : 5 v/v), r.t. for 40 min (for the aldehyde) or r.t. to 40 °C for 100 min (for the ketone), $(C_2H_5)_3N$ (4 mmol). Method B: benzothiazoline (4 mmol), $HgCl_2$ (6 mmol), CH_3CN-H_2O (4 : 1 v/v), reflux temp, 4 h. Method C: benzothiazoline (4 mmol), NBS (8 mmol), H_2O, r.t., 10 min. Method D: benzothiazoline (4 mmol), Chloramine T (4.8 mmol), C_2H_5OH, r.t., 1 h (for the aldehyde) or 24 h (for the ketone). Method E: benzothiazoline (4 mmol), CH_3OSO_2F (4.8 mmol), CH_2Cl_2, r.t., 18 h (for the aldehyde) or 24 h (for the ketones), and then 5% aq. K_2CO_3-THF (4 : 5 v/v), r.t., 4 h.

commonly required for removal of other protecting groups. The resistability to both basic and acidic conditions is especially attractive and increases the importance of the present protection method.

Conversion of 2-Substituted Benzothiazolines 3 into 2,2-Disubstituted One 4 via Benzothiazolium Salts 5 as Acyl Cation Equivalents. During the course of a study about the reactivity of 2-substituted benzothiazolines **3**, we have found that 3-methylbenzothiazolium perchlorates **5** are readily prepared in excellent yields by the reaction of **3** with trityl perchlorate in acetonitrile with the results summarized in Table 5. As shown in Table 5, these easily handled and stable carbocations were also conveniently obtained in good yields from aldehydes by the one-pot reaction with MABT in acetonitrile followed by the addition of trityl perchlorate. In order to demonstrate the possibility of using these salts as an acyl cation equivalent, we have studied the reaction of **5** with a variety of Grignard or organolithium reagents. The results are summarized in Table 6. The conversion of **5** into 2,2-disubstituted benzothiazolines **4** was most conveniently achieved by the addition of 1.2 equiv of Grignard or organolithium reagent to the suspension of **5** in THF or ether at −78 °C. These reactions generally proceeded quite cleanly and nearly pure products were obtained in excellent yields after a simple workup procedure. Thus, by these methods not only alkyl including tertiary but also aryl, allyl, and alkynyl groups were substituted for the hydrogen at the C-2 position of **3**. The ready availability of benzothiazolium salts **5** from aldehydes and facile convertibility of them into 2,2-

Table 5. Conversion of 2-Substituted Benzothiazolines **3** into Benzothiazolium Salts **5**

Substrate	Benzothiazolium salt	Method[a]	Yield/%[b]
3a	**5a** (R^1=C_4H_9)	A	91
3a	**5a**	B	83
3c	**5b** (R^1=$C_4H_9(C_2H_5)CH$)	A	96
3c	**5b**	B	76
3e	**5c** (R^1=*i*-C_3H_7)	A	94
3e	**5c**	B	79
3g	**5d** (R^1=C_6H_5)	A	95
3g	**5d**	B	72
3h	**5e** (R^1=*p*-ClC_6H_4)	A	96
3h	**5e**	B	71
3i	**5f** (R^1=*p*-$CH_3OC_6H_4$)	A	98
3i	**5f**	B	65
3k	**5g** (R^1=)	A	93
3k	**5g**	B	70

a) Method A: Benzothiazoline (5 mmol) was reacted with trityl perchlorate (5 mmol) in acetonitrile at room temperature. Method B (one-pot reaction): Aldehyde (5 mmol) was reacted with MATP (5 mmol) in refluxing acetonitrile followed by the addition of trityl perchlorate (10 mmol). b)Yield of crude, nearly pure product (in Method A). Yield of pure product after recrystallization (in Method B).

Table 6. Alkylation of 2-Substituted Benzothiazolium Salts **5** into 2,2-Disubstituted Benzothiazolines **4**[a]

Substrate	R^2M	Product	Solvent	Yield/%[b]
5a	*n*-C_4H_9Li	**4k**	THF	93
5a	*n*-$C_7H_{15}C{\equiv}CLi$	**4l**	THF	92
5a	$C_6H_5C{\equiv}CLi$	**4m**	THF	95
5a	*n*-C_4H_9MgBr	**4k**	THF	92
5a	*t*-C_4H_9MgCl	**4n**	THF	59
5a	C_6H_5MgBr	**4o**	Ether	42[c]
5b	*n*-C_4H_9MgBr	**4p**	THF	87[d]
5c	*n*-C_4H_9MgBr	**4q**	THF	77[d]
5d	*n*-C_4H_9MgBr	**4o**	THF	93[c]
5d	C_6H_5MgBr	**4r**	THF	75[c]
5d	$C_6H_5CH_2MgCl$	**4s**	Ether	88[c]
5f	*n*-C_4H_9Li	**4t**	THF	90
5g	*n*-C_4H_9MgBr	**4u**	THF	99[d]

a) Benzothiazolium salt (4 mmol) was reacted with alkylating reagent (4.8 mmol) at −78 °C (30 min) to room temperature (1 h). b) Yield of crude, nearly pure product unless otherwise noted. c) Yield of pure product after recrystallization. d) Yield of pure product after short column chromatography.

Table 7. Alkylation of Benzothiazolium Salts **6** into 2-Substituted Benzothiazolines **3**[a]

Salt	X	R^2M	Solvent	Product	Yield/%[b,c]
6a	I	*n*-C_4H_9MgBr	THF	**3a**	61[d](70)
6b	SO_3F	*n*-C_4H_9Li	THF	**3a**	(62)[e]
6c	SO_4CH_3	*n*-C_4H_9MgBr	THF	**3a**	(40)
6d	BF_4	*n*-C_4H_9MgBr	THF	**3a**	(32)
6a	I	$(n\text{-}C_4H_9)_2CuMgBr$	THF	**3a**	(64)
6a	I	$CH_2{=}CHCH_2MgBr$	Ether	**3m**	92
6a	I	$CH_3CH{=}CHCH_2MgCl$	THF	**3n**	98[f]
6a	I	$C_6H_5C{\equiv}CLi$	THF	**3o**	90
6a	I	C_6H_5MgBr	THF	**3g**	98
6a	I	*p*-$CH_3OC_6H_4MgBr$	THF	**3i**	95

a) Benzothiazolium salt **6** (4 mmol) was reacted with alkylating reagent (4.8 mmol) at −78 °C (30 min) to room temperature (1 h). b) Yield of isolated, nearly pure product. c) Values in parentheses indicate yields determined by GLC. d) Yield of pure product after short column chromatography. e) Benzothiazolium salt **6** was reacted with the alkylating reagent (4.8 mmol) at −78 °C (30 min) to room temperature (24 h). f) 2-(2-Butenyl)-3-methylbenzothiazoline was selectively obtained.

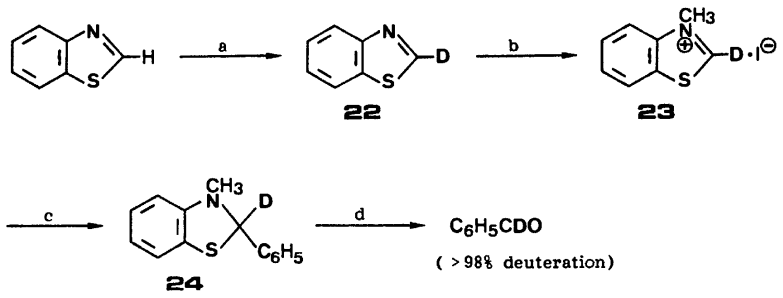

(a) n-BuLi, THF, -78°C, (2) D_2O; (b) CH_3I, DMF, reflux;
(c) C_6H_5MgBr, THF, -78°C-r.t.; (d) Method A (see Table 3).

Scheme 4.

disubstituted benzothiazolines **4** illustrate the synthetic usefulness of the benzothiazoline ring system as a functional protected form for carbonyl groups.

Preparation of 2-Substituted Benzothiazolines 3 by the Reaction of Grignard or Organolithium Reagents with 3-Methylbenzothiazolium Salt 6. 1,3-Dithienium tetrafluoroborate,[6] 2-chloro-1,3-dithiane,[7] and heteroaromatic cations such as 1,3-benzodithiolylium salts[8] are well-known as promising candidates for heterocyclic formyl cation equivalents. However, the reaction of former two compounds with either Grignard or organolithium reagents does not produce or produces with difficulty the corresponding 1,3-dithianes.[7,9] As another synthetic advantage of the benzothiazoline ring system, we have found that Grignard and organolithium reagents react with 3-methylbenzothiazolium salts **6** to give the expected adducts **3** in good yields (Table 7). The reactions were conveniently achieved by a procedure similar to the alkylation of the salts **5**. When **6** was reacted with butylmagnesium bromide or butyllithium, 2-butyl-3-methylbenzothiazoline (**3a**) was most effectively obtained in 70% yield in the case of the reaction using the iodide **6a**. Butylmagnesium cupurate was also used to alkylate **6a** but the yield of **3a** was not improved. The uppermost limit of yields in these reactions is probably due to formation of the ylide **21**

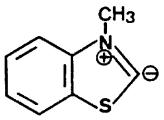

21

derived from proton abstraction from the salt **6** by organometallic reagents. On the other hand, the reaction of **6a** with aryl, allyl, or alkynyl Grignard reagent went to completion yielding the corresponding 2-substituted benzothiazolines in near quantitative yields. Thus, it appears that the reaction of 3-methylbenzothiazolium iodide (**6a**) as a formyl cation equivalent with Grignard or organolithium reagents is a useful way to produce 2-substituted benzothiazolines **3**.

With the aim of evaluating the synthetic potential of **6a**, we present a useful method for the preparation of aldehydes-*d* according to Scheme 4. 2-Deuterated 3-methylbenzothiazolium iodide (**23**) was conveniently prepared in high yield by methylation of benzothiazole-2-*d* (**22**) with iodomethane, which was readily prepared by the lithiation of commercially available benzothiazole with butyllithium followed by quenching with D_2O.[5] The reaction of **23** with phenylmagnesium bromide and subsequent hydrolysis by method A gave benzaldehyde-*d* in excellent yield with almost complete deuterium incorporation. The easy accessibility of **22**, the high yields of the products and the excellent deuterium incorporation offers promise for a new method of synthesizing aldehydes-*d* from Grignard reagents via carbon-carbon bond formation with the deuterated formyl cation equivalent **23**. The deuterated heteroaromatic cation, 2-deuterio-1,3-benzodithiolylium salt, has already been reported as a deuterated formyl cation equivalent for the synthesis of aldehydes-*d* by Degani et al.[10] However, compared with their original method or the improved one,[11] the present method is advantageous because of its high simplicity.

Conclusion

Benzothiazolination with MABT is a very effective, convenient, and mild (no acidic catalyst is required) method for the protection of aldehydes and ketones. The mildness of benzothiazolination and effective convertibility of benzothiazolines into parent carbonyl compounds under neutral and very mild conditions are suitable for the synthetic operation of acid-sensitive multifunctional molecules. High chemoselectivity of benzothiazolination makes the present method more attractive and should be useful for selective protection of carbonyl groups in the presence of a

different carbonyl group. In addition, the resistability of benzothiazolines to both basic and acidic conditions allows one to use the protected form under these conditions. Furthermore, the functionality of the benzothiazoline ring system via benzothiazolium salts as an acyl or formyl cation equivalent increases the value of benzothiazolines in use as a protected form for carbonyl compounds.

Experimental

Melting points were recorded on a Yanagimoto micro melting-point apparatus and are uncorrected. ^{1}H NMR spectra were measured with a JEOL PMX-60 spectrometer at 60 MHz using tetramethylsilane as an internal reference. IR spectra were recorded on a JASCO A-202 spectrophotometer. Mass spectra were obtained on a JMS-QH100 GC-Mass spectrometer. The yields by quantitative GLC were measured on a Shimadzu Gas Chromatograph GC-6AM equipped with a hydrogen flame ionization detector using glass columns (1.5 m) packed with 2% Silicone OV-7 on Uniport HP (60—80 mesh), by the internal standard method using dodecane as an internal standard. Silica gel (Wakogel C-300) was used for short column chromatography.

Materials. Solvents were purified and dried according to standard procedures. MABT was prepared by the reductive ring opening reaction of commercially available benzothiazole with $LiAlH_4$ according to a slightly modified method of Huning et al.[12] Phosphate buffer (0.05 M, pH 7; 1 M=1 mol dm^{-3}) was prepared by dilution of the 0.1 M solution (0.4 M Na_2HPO_4+0.4 M KH_2PO_4) which was commercially available. Trityl perchlorate was prepared by the method of Dauben et al.[13] Carbonyl compounds and the other reagents were obtained as high-grade commercial products.

Benzothiazolination of Aldehydes and Ketones; General Procedure. MABT (0.70 g, 5 mmol) was added to a solution of aldehyde or ketone (5 mmol) in ethanol (5 ml) and the mixture was refluxed for an appropriate reaction time (monitored with TLC; see Tables 1 and 2). The solvent was removed under reduced pressure to give crude product. Purification of the crude oily products (**3a—f**, **31**, **4a—d**, **4g—j**) and crystalline products (**3g—k**, **4e**) was carried out by short column chromatography or recrystallization from ethanol, respectively, to afford pure samples. Product yields are summarized in Tables 1 and 2.

3a: colorless oil; IR (neat) 2940, 1660, 1580, 1670, 1380, 1280, 1120, 1060, and 740 cm^{-1}; ^{1}H NMR ($CDCl_3$) δ=0.88 (t, 3H), 1.08—2.08 (m, 6H), 2.67 (s, 3H), 4.78 (dd, 1H), and 6.00—7.00 (m, 4H). Calcd for $C_{12}H_{17}NS$: C, 69.51; H, 8.26; N, 6.76%. Found: C, 69.40; H, 8.55; N, 6.28%.

3b: pale yellow oil; IR (neat) 2900, 2850, 1660, 1580, 1480, 1380, 1300, 1110, 1020, and 740 cm^{-1}; ^{1}H NMR ($CDCl_3$) δ=0.87 (t, 3H), 1.03—2.07 (br, 16H), 2.70 (s, 3H), 4.80 (t, 1H), and 6.00—6.90 (m, 4H). Calcd for $C_{17}H_{27}NS$: C, 73.59; H, 9.81; N, 5.05%. Found: C, 73.74; H, 9.92; N, 5.35%.

3c: pale yellow oil; IR (neat) 2940, 1660, 1580, 1480, 1380, 1300, 1110, 1020, 730, and 700 cm^{-1}; ^{1}H NMR ($CDCl_3$) δ= 0.50—2.17 (m, 15H), 2.70 (s, 3H), 5.12 (d, 1H), and 6.03—7.27 (m, 4H). Calcd for $C_{15}H_{23}NS$: C, 72.23; H, 9.29; N, 5.62%. Found: C, 72.90; H, 8.91; N, 5.81%.

3d: colorless oil; IR (neat) 2900, 1660, 1580, 1480, 1380, 1300, 1110, 1010, and 740 cm^{-1}; ^{1}H NMR ($CDCl_3$) δ=0.67—2.17 (m, 16H), 2.67 (s, 3H), 4.87 (m, 2H), and 6.00—6.90 (m, 4H). Calcd for $C_{17}H_{25}NS$: C, 74.13; H, 9.15; N, 5.08%. Found: C, 73.94; H, 9.22; N, 5.13%.

3e: pale yellow oil; IR (neat) 2950, 1660, 1580, 1480, 1380, 1340, 1300, 1220, 1110, 1020, 1000, and 730 cm^{-1}; ^{1}H NMR ($CDCl_3$) δ=1.00 (d, 6H), 2.00 (m, 1H), 2.68 (s, 3H), 5.10 (d, 1H), and 5.84—6.84 (m, 4H). Calcd for $C_{11}H_{15}NS$: C, 68.35; H, 7.82; N, 7.25%. Found: C, 68.33; H, 7.74; N, 7.07%.

3f: colorless oil; IR (neat) 2950, 1570, 1470, 1380, 1350, 1290, 1200, 1120, 1100, 1020, 980, 880, and 740 cm^{-1}; ^{1}H NMR ($CDCl_3$) δ=0.90 (s, 9H), 2.90 (s, 3H), 4.42 (s, 1H), and 6.17—6.90 (m, 4H). Calcd for $C_{12}H_{17}NS$: C, 69.51; H, 8.26; N, 6.76%. Found: C, 69.33; H, 8.32; N, 6.58%.

3g: colorless needles; mp 113 °C; IR (KBr) 1580, 1480, 1450, 1340, 1300, 1190, 1110, 1020, 740, and 700 cm^{-1}; ^{1}H NMR ($CDCl_3$) δ=2.70 (s, 3H), 5.80 (s, 1H), and 6.10—7.50 (m, 4H). Calcd for $C_{14}H_{13}NS$: C, 73.97; H, 5.76; N, 6.16%. Found: C, 73.66; H, 5.73; N, 5.90%.

3h: colorless needles; mp 78—78.5 °C; IR (KBr) 1570, 1460, 1400, 1320, 1300, 1260, 1180, 1100, 1080, 1010, 860, 830, 780, and 740 cm^{-1}; ^{1}H NMR ($CDCl_3$) δ=2.47 (s, 3H), 5.75 (s, 1H), and 6.07—7.40 (m, 8H). Calcd for $C_{14}H_{12}NSCl$: C, 64.24; H, 4.62; N, 5.35%. Found: C, 64.11; H, 4.53; N, 5.22%.

3i: colorless needles; mp 106—106.5 °C; IR (KBr) 1600, 1570, 1510, 1460, 1330, 1280, 1250, 1160, 1100, 1030, 860, 830, 790, and 750 cm^{-1}; ^{1}H NMR ($CDCl_3$) δ=2.52 (s, 3H), 3.70 (s, 3H), 5.80 (s, 1H), and 6.33—7.50 (m, 8H). Calcd for $C_{15}H_{15}NOS$: C, 70.01; H, 5.87; N, 5.44%. Found: C, 69.94; H, 5.92; N, 5.29%.

3j: colorless needles; mp 43—43.5 °C; IR (KBr) 2900, 2850, 1580, 1480, 1370, 1300, 1110, 1020, 880, 740, and 710 cm^{-1}; ^{1}H NMR ($CDCl_3$) δ=0.85—2.33 (m, 11H), 3.17 (s, 3H), 4.45 (d, 1H), and 6.84—7.50 (m, 4H). Calcd for $C_{14}H_{19}NS$: C, 72.05; H, 8.21; N, 6.00%. Found: C, 71.48; H, 8.09; N, 5.82%.

3k: colorless needles; mp 89—89.5 °C; IR (KBr) 2900, 1580, 1490, 1430, 1380, 1310, 1220, 1120, 1020, 740, and 670 cm^{-1}; ^{1}H NMR ($CDCl_3$) δ=1.17—2.50 (m, 7H), 2.77 (s, 3H), 5.02 (d, 1H), 5.53 (m, 2H), and 6.00—7.00 (m, 4H). Calcd for $C_{14}H_{17}NS$: C, 72.68; H, 7.41; N, 6.05%. Found: C, 72.36; H, 7.38; N, 5.85%.

3l: colorless oil; IR (neat) 1640, 1570, 1470, 1420, 1340, 1300, 1120, 1040, 1020, 960, 740, and 700 cm^{-1}; ^{1}H NMR ($CDCl_3$) δ=2.67 (s, 3H), 5.43 (dd, 1H), and 6.00—7.33 (m, 11H). This compound is slightly unstable in air.

4a: colorless oil; IR (neat) 2950, 1580, 1480, 1360, 1300, 1120, 1050, 1020, 740, and 720 cm^{-1}; ^{1}H NMR (CCl_4) δ=0.92 (t, 3H), 1.13—2.07 (m, 4H), 1.52 (s, 3H), 2.60 (s, 3H), and 5.87—6.90 (m, 4H). Calcd for $C_{12}H_{17}NS$: C, 69.51; H, 8.26; N, 6.76%. Found: C, 69.41; H, 8.18; N, 6.63%.

4b: colorless oil; IR (neat) 2950, 1580, 1480, 1360, 1300, 1210, 1120, 1050, 1020, and 740 cm^{-1}; ^{1}H NMR ($CDCl_3$) δ=0.67—2.00 (m, 14H), 2.60 (s, 3H), and 5.73—6.83 (m, 4H). Calcd for $C_{14}H_{21}NS$: C, 71.44; H, 8.99; N, 5.95%. Found: C, 71.26; H, 8.89; N, 5.91%.

4c: colorless oil; IR (neat) 2900, 1580, 1480, 1360, 1300, 1220, 1120, 1050, 1020, 900, and 730 cm^{-1}; ^{1}H NMR (CCl_4) δ=0.50—2.00 (m, 22H), 2.53 (s, 3H), and 5.73—6.77 (m, 4H). Calcd for $C_{18}H_{29}NS$: C, 74.17; H, 10.03; N, 4.81%. Found: C, 73.99; H, 10.10; N, 4.81%.

4d: pale yellow oil; IR (neat) 1950, 1580, 1480, 1370, 1300, 1220, 1120, 1020, and 740 cm^{-1}; ^{1}H NMR ($CDCl_3$) δ=0.94 (d, 6H), 1.55 (s, 3H), 2.03 (m, 1H), 2.58 (s, 3H), and 5.83—6.83

(m, 4H). Calcd for $C_{12}H_{17}NS$: C, 69.51; H, 8.26; N, 6.76%. Found: C, 69.14; H, 8.11; N, 6.66%.

4e: colorless needles; mp 62—63 °C; IR (KBr) 2900, 1580, 1470, 1440, 1370, 1300, 1110, 1040, 1020, 900, 740, and 700 cm^{-1}; ^1H NMR ($CDCl_3$) δ=1.97 (s, 3H), 2.55 (s, 3H), and 6.10—7.67 (m, 9H). Calcd for $C_{15}H_{15}NS$: C, 74.65; H, 6.26; N, 5.80%. Found: C, 74.38; H, 6.29; N, 5.61%.

4g: pale yellow needles; mp 34—34.5 °C; IR (neat) 2900, 1680, 1470, 1360, 1300, 1200, 1100, 1040, 1020, and 740 cm^{-1}; ^1H NMR ($CDCl_3$) δ=1.00—2.23 (m, 10H), 2.67 (s, 3H), and 6.00—7.00 (m, 4H). Calcd for $C_{13}H_{17}NS$: C, 71.18; H, 7.81; N, 6.39%. Found: C, 71.26; H, 7.88; N, 6.27%.

4h: colorless oil; IR (neat) 2900, 1580, 1500, 1480, 1420, 1300, 1210, 1160, 1120, 1030, 960, 740, and 680 cm^{-1}; ^1H NMR ($CDCl_3$) δ=1.00—2.13 (m, 6H), 2.60 and 2.73 (each s, 3H), and 6.00—7.33 (m, 6H). Calcd for $C_{13}H_{15}NS$: C, 71.85; H, 6.96; N, 6.44%. Found: C, 71.48; H, 6.88; N, 6.80%.

4i: colorless oil; IR (neat) 2950, 1580, 1470, 1420, 1350, 1300, 1120, 1050, 1020, 960, 740, and 700 cm^{-1}; ^1H NMR ($CDCl_3$) δ=1.73 (s, 3H), 2.58 (s, 3H), and 6.00—7.37 (m, 11H). This compound is slightly unstable in air.

4j: colorless oil; IR (neat) 1580, 1470, 1420, 1360, 1300, 1220, 1120, 1050, 1020, 990, 740, and 700 cm^{-1}; ^1H NMR ($CDCl_3$) δ=2.67 (s, 3H) and 6.13—7.87 (m, 16H). Calcd for $C_{22}H_{19}NS$: C, 80.20; H, 5.81; N, 4.25%. Found: C, 80.36; H, 5.72; N, 4.14%.

Benzothiazolination of Keto Carboxylic Acid 7, Keto Ester 8, and Keto Aldehyde 9. Benzothiazolination of these compounds **7—9** was carried out on a 5 mmol scale for 24 h according to standard procedure. Purification of the crude products which did not contain any by-product or regioisomer (monitored by TLC and ^1H NMR) by recrystallization from ethanol or short column chromatography afforded pure products (**12—14**).

12 (1.12 g, 94%): colorless needles; mp 82.5—83.5 °C; IR (KBr) 2900, 1700, 1580, 1480, 1420, 1350, 1300, 1220, 1160, 1110, 1020, and 740 cm^{-1}; ^1H NMR ($CDCl_3$) δ=1.57 (s, 3H), 2.00—2.50 (m, 4H), 2.62 (s, 3H), 5.97—7.00 (m, 4H), and 11.00 (br, 1H). Calcd for $C_{12}H_{15}NO_2S$: C, 60.73; H, 6.37; N, 5.90%. Found: C, 60.30; H, 6.26; N, 5.75%.

13 (1.22 g, 92%): colorless oil; IR (neat) 2950, 1720, 1580, 1480, 1360, 1300, 1180, 1120, 1020, amd 740 cm^{-1}; ^1H NMR (CCl_4) δ=1.17 (t, 3H), 1.57 (s, 3H), 1.67—2.57 (m, 4H), 2.63 (s, 3H), 3.95 (q, 2H), and 5.90—6.83 (m, 4H). Calcd for $C_{14}H_{19}NO_2S$: C, 63.36; H, 7.22; N, 5.28%. Found: C, 63.18; H, 7.27; N, 5.31%.

14 (1.23 g, 99%): pale yellow oil; IR (neat) 2900, 1720, 1660, 1580, 1480, 1360, 1300, 1120, 1020, 910, and 740 cm^{-1}; ^1H NMR ($CDCl_3$) δ=0.50—1.83 (m, 11H), 2.70 (s, 3H), 4.76 (br, 1H), and 6.17—7.27 (m, 4H). Calcd for $C_{14}H_{19}NOS$: C, 67.43; H, 7.68; N, 5.62%. Found: C, 67.26; H, 7.29; N, 5.63%.

Benzothiazolination of Steroid Ketones 10 and 11. MABT (0.14 g, 1 mmol) was added to a solution of 4-androstene-3,17-dione (**10**) (0.29 g, 1 mmol) in dichloromethane (1 ml) and the mixture was refluxed for 48 h. After removal of the solvent under reduced pressure, the residual crystalline product which did not contain the other isomers (monitored by TLC, ^1H NMR and IR) was recrystallized from methanol to afford pure **15** as colorless plates (0.38 g, 93%): mp 191—192 °C; IR (KBr) 2950, 2900, 1740, 1590, 1480, 1450, 1400, 1300, 1210, 1120, 1030, 860, and 740 cm^{-1}; ^1H NMR ($CDCl_3$) δ=0.87 (s, 3H), 1.05 (s, 3H), 1.10—2.45 (m, 19H), 2.62 (s, 3H), 5.47 (bs, 1H), and 6.00—7.00 (m, 4H). Calcd for $C_{26}H_{33}NOS$: C, 76.61; H, 8.16; N, 3.44%. Found: C, 76.98; H, 8.04; N, 3.15%.

Benzothiazolination of progesterone (**11**) was carried out on a 1 mmol scale for 24 h according to standard procedure. Recrystallization of crude product which did not contain the other isomers (monitored by TLC, ^1H NMR, and IR) from ethanol afforded pure **16** as colorless needles (0.42 g, 97%): mp 203—204 °C; IR (KBr) 2950, 2870, 1710, 1580, 1480, 1450, 1360, 1310, 1110, 1030, and 740 cm^{-1}; ^1H NMR ($CDCl_3$) δ=0.63 (s, 3H), 1.03 (s, 3H), 1.13—2.03 (m, 20H), 2.07 (s, 3H), 2.63 (s, 3H), 5.47 (bs, 1H), and 6.03—7.00 (m, 4H). Calcd for $C_{28}H_{37}NOS$: C, 77.19; H, 8.56; N, 3.21%. Found: C, 76.98; H, 8.58; N, 3.09%.

Benzothiazolination of β-Hydroxy Ketones 19 and 20. Benzothiazolination of **19** and **20** was carried out on a 5 mmol scale for 72 h according to standard procedure. Purification of the crude products by short column chromatography afforded pure **17** and **18**.

17 (0.81 g, 48%): pale yellow oil; IR (neat) 3400, 2900, 2850, 1580, 1470, 1360, 1290, 1160, 1120, 1040, 1020, and 730 cm^{-1}; ^1H NMR ($CDCl_3$) δ=0.67—1.83 (m, 24H), 2.60 and 2.65 (ds, 3H), 2.97 (br, 1H), 4.00 (br, 1H), and 5.98—6.93 (m, 4H). Calcd for $C_{20}H_{33}NOS$: C, 71.59; H, 9.91; N, 4.17%. Found: C, 71.83; H, 9.69; N, 4.35%.

18 (0.29 g, 24%): colorless needles after recrystallization from ethanol; mp 83.5—84 °C; IR (KBr) 3350, 2950, 1580, 1470, 1370, 1330, 1300, 1260, 1170, 1100, 940, 790, and 740 cm^{-1}; ^1H NMR ($CDCl_3$) δ=1.33 (s, 6H), 1.57 (s, 3H), 2.12 (d, 2H), 2.69 (s, 3H), 3.10 (br, 1H), and 6.17—7.14 (m, 4H). Calcd for $C_{13}H_{19}NOS$: C, 65.78; H, 8.07; N, 5.90%. Found: C, 65.49; H, 8.02; N, 5.80%.

Hydrolysis of 3-Methylbenzothiazolines. Method A (General). Silver nitrate (1.02 g, 6 mmol) dissolved in water (10 ml) was added to a stirred solution of benzothiazoline **3** (4 mmol) in acetonitrile (60 ml) and 0.05 M phosphate buffer (pH 7) (12 ml). After 15 min at room temperature, additional silver nitrate (1.02 g, 6 mmol) dissolved in water (10 ml) was added. After another 20 min at room temperature, triethylamine (0.6 ml, 6 mmol) was added to neutralize the released acid (HNO_3) and stirring was continued for 5 min. Saturated aq. NaCl solution was added to the reaction mixture and filtered through Celite. The filtrate was extracted with ether and the extract was filtered through silica gel (Wakogel C-300). Removal of the solvent afforded almost pure aldehyde **1** that was free of MABT. Benzothiazoline **4** was similarly hydrolized, except that stirring was continued for 1 h at 45 °C after the addition of triethylamine, to afford almost pure ketone **2** that was free of MABT. Product yields are summarized in Tables 1 and 2. The compounds **17** and **18** were hydrolyzed by the similar method to benzothiazoline **4** to give the corresponding β-hydroxy ketones **19** (88%) and **20** (94%).

Method B. Mercury(II) chloride (1.63 g, 6 mmol) was added to a solution of benzothiazoline **3g** or **4e** (4 mmol) in 4:1 (v/v) acetonitrile-water (25 ml). The mixture was refluxed for 4 h and then cooled. After filtration to remove the precipitate, the aqueous solution was extracted with dichloromethane. The extract was dried with $MgSO_4$ and concentrated under reduced pressure to afford almost pure aldehyde **1g** (0.39 g, 93%) or ketone **2e** (0.45 g, 94%) as a colorless oil.

Method C. *N*-Bromosuccinimide (1.42 g, 8 mmol) was added to a suspension of benzothiazoline **3g** or **4e** (4 mmol)

in water (40 ml) and the mixture was stirred at room temperature for 10 min. After filtration, the filtrate was extracted with dichloromethane and the extract was dried with $MgSO_4$. Removal of the solvent under reduced pressure afforded almost pure aldehyde **1g** (0.39 g, 93%) or ketone **2e** (0.41 g, 86%).

Method D. Chloramine T (1.35 g, 4.8 mmol) was added to a solution of benzothiazoline **3g** (4 mmol) in ethanol (40 ml) and the mixture was stirred at room temperature for 1 h. After concentration of the mixture under reduced pressure, the residue was diluted with dichloromethane and washed thoroughly with water. The dichloromethane solution was dried with $MgSO_4$ and concentrated to give almost pure aldehyde **1g** (0.36 g, 85%). Benzothiazoline **4e** (0.97 g, 4 mmol) was similarly treated with Chloramine T (1.35 g, 4.8 mmol) for 24 h to give almost pure ketone **2e** (0.10 g, 21%).

Method E. Methyl fluorosulfate (0.55 g, 4.8 mmol) was added to a stirred solution of benzothiazoline **3g** or **4e** (4 mmol) in dichloromethane (16 ml) and stirring was continued at room temperature until no starting material remained (monitored with TLC; 18 h for **3g**, 24 h for **4e**). The excess reagent was quenched with ether (4 ml) for 30 min and the solvent was removed under reduced pressure. The residue was taken up in a mixture of 5% aq. K_2CO_3 solution (8 ml) and THF (10 ml) and the mixture was stirred at room temperature for 4 h. The solution was extracted with ether and the extract was washed with 5% aq. HCl, 5% aq. $NaHCO_3$, and saturated aq. NaCl solutions. It was then dried with $MgSO_4$. Concentration of the organic layer under reduced pressure afforded almost pure aldehyde **1g** (0.39 g, 92%) or ketone **2e** (0.46 g, 96%).

Identification of the carbonyl products obtained in these hydrolysis experiments was performed by spectroscopic (NMR, IR, and MS) methods. These spectral data were in satisfactory agreement with those of the corresponding authentic samples.

Preparation of 3-Methylbenzothiazolium Perchlorates 5; General Procedure. (A) From 3-Methylbenzothiazolines 3: Trityl perchlorate (3.43 g, 10 mmol) was added to a stirred solution of benzothiazoline **3** (10 mmol) in dry acetonitrile (10 ml). The mixture was warmed to 50—60 °C and continuously stirred for 30 min after the mixture became a complete solution. After cooling for 30 min at 0 °C, ether was added to completely precipitate product. The separated precipitate was collected by filtration and washed with dry ether to give crude product which was sufficiently pure to use directly in the next alkylation step. Recrystallization of crude products from methanol afforded pure salts as colorless needles. Product yields are summarized in Table 5.

(B) From Aldehyde 1 (One-Pot Reaction): MABT (1.39 g, 10 mmol) was added to a solution of aldehyde (10 mmol) in acetonitrile (10 ml) and the mixture was refluxed until the starting aldehyde disappeared (monitored with TLC; similar reaction times when compared to the benzothiazolination in ethanol were required). After cooling to room temperature, trityl perchlorate (6.86 g, 20 mmol) was added with stirring and warmed to 50—60 °C. The mixture was stirred for 10 min at the same temperature after the mixture became a complete solution and then stirred for 30 min at 0 °C. Ether was added to precipitate product completely and separated precipitate was collected by filtration and then washed with ether. The crude salt was decolorized in methanol with active charcoal and recrystallized from methanol to give pure **5** as colorless needles. Product yields are summarized in Table 5.

5a: mp 163.5—164.5 °C (decomp); IR (KBr) 2950, 1580, 1520, 1460, 1440, 1340, 1200, 1090, 760, and 620 cm^{-1}; ^1H NMR (DMSO-d_6) δ=0.97 (t, 3H), 1.17—2.17 (m, 4H), 3.43 (t, 2H), 4.13 (s, 3H), 7.67 (m, 2H), and 8.17 (m, 2H). Calcd for $C_{12}H_{16}NO_4SCl$: C, 47.14; H, 5.27; N, 4.58%. Found: C, 46.83; H, 5.11; N, 4.41%.

5b: mp 84.5—85 °C (decomp); IR (KBr) 2950, 1520, 1460, 1380, 1340, 1200, 1080, 760, and 620 cm^{-1}; ^1H NMR (DMSO-d_6) δ=0.67—2.17 (m, 14H), 3.87 (m, 1H), 4.33 (m, 3H), 7.83 (m, 2H), and 7.97 (m, 2H). Calcd for $C_{15}H_{22}NO_4SCl$: C, 51.79; H, 6.37; N, 4.03%. Found: C, 51.85; H, 6.31; N, 3.77%.

5c: mp 138.5—139 °C (decomp); IR (KBr) 2950, 1580, 1520, 1460, 1340, 1220, 1080, 820, 760, 720, and 620 cm^{-1}; ^1H NMR (DMSO-d_6) δ=1.48 (d, 6H), 3.83 (m, 1H), 4.17 (s, 3H), 7.67 (m, 2H), and 8.17 (m, 2H). Calcd for $C_{11}H_{14}NO_4SCl$: C, 45.29; H, 4.84; N, 4.80%. Found: C, 45.09; H, 4.73; N, 4.78%.

5d: mp 213—214 °C (decomp); IR (KBr) 1580, 1540, 1450, 1340, 1250, 1090, 760, 700, and 620 cm^{-1}; ^1H NMR (DMSO-d_6) δ=4.17 (s, 3H), 7.03 (m, 2H), 7.73 (m, 5H), and 8.27 (m, 2H). Calcd for $C_{14}H_{12}NO_4SCl$: C, 51.62; H, 3.71; N, 4.30%. Found: C, 51.43; H, 3.63; N, 4.06%.

5e: mp 216—217 °C (decomp); IR (KBr) 1590, 1480, 1470, 1400, 1240, 1090, 840, 700, and 620 cm^{-1}; ^1H NMR (DMSO-d_6) δ=4.20 (s, 3H), 7.75 (m, 6H), and 8.27 (m, 2H). Calcd for $C_{14}H_{11}NO_4SCl_2$: C, 46.68; H, 3.08; N, 3.89%. Found: C, 46.30; H, 3.42; N, 3.86%.

5f: mp 195—196 °C (decomp); IR (KBr) 1600, 1500, 1460, 1400, 1340, 1310, 1260, 1180, 1080, 830, 770, and 620 cm^{-1}; ^1H NMR (DMSO-d_6) δ=3.88 (s, 3H), 4.20 (s, 3H), 7.18 (m, 2H), 7.77 (m, 4H), and 8.23 (m, 2H). Calcd for $C_{15}H_{14}NO_5SCl$: C, 50.64; H, 3.97; N, 3.94%. Found: C, 50.83; H, 3.89; N, 3.68%.

5g: mp 173—174 °C (decomp); IR (KBr) 2950, 1580, 1520, 1450, 1300, 1200, 1080, 760, 700, and 620 cm^{-1}; ^1H NMR (DMSO-d_6) δ=2.00—2.83 (m, 6H), 3.83 (m, 1H), 4.27 (s, 3H), 5.77 (m, 2H), 7.72 (m, 2H), and 8.22 (m, 2H). Calcd for $C_{14}H_{16}NO_4SCl$: C, 50.99; H, 4.89; N, 4.25%. Found: C, 50.86; H, 4.76; N, 3.78%.

Alkylation of Benzothiazolium Salts 5 with Grignard or Organolithium Reagents; General Procedure. A solution of Grignard reagents (prepared from 20% excess of the corresponding bromide or chloride) in dry THF or ether (20 ml) was added dropwise to a stirred and cooled suspension at −78 °C of benzothiazolium salt **5** (4 mmol) in THF or ether (40 ml). The mixture was stirred for 30 min at −78 °C and allowed to warm to room temperature. After being stirred for 1 h at room temperature, the mixture was quenched by the addition of saturated aq. NH_4Cl solution. The aqueous mixture was extracted with ether and the extract was dried with $MgSO_4$. Concentration of the solution under reduced pressure to afford the crude products **4k**, **4n—s**, and **4u**. A 20% excess of butyllithium in hexane or a solution of nonynyllithium or phenylethynyllithium in THF (prepared by lithiation of 20% excess of 1,1-dibromo-1-nonene[14] or phenylacetylene with butyllithium) was similarly used in place of the Grignard reagents, giving **4k—m** and **4t**. Purification was carried out by short column chromatography for compounds **4p**, **4q**, and **4u** and by recrystallization from ethanol for compounds **4o**, **4r**, and **4s**. The other products were almost pure (monitored with TLC) without purification.

Product yields are summarized in Table 6.

4k: pale yellow oil; IR (neat) 2900, 1580, 1480, 1360, 1300, 1260, 1120, 1050, 1020, and 740 cm^{-1}; ^1H NMR ($CDCl_3$) δ=0.67—2.00 (m, 18H), 2.73 (s, 3H), and 5.83—6.97 (m, 4H). Calcd for $C_{16}H_{25}NS$: C, 72.95; H, 9.56; N, 5.32%. Found: C, 73.22; H, 9.77; N, 5.10%.

4l: pale yellow oil; IR (neat) 2900, 2850, 2200, 1580, 1470, 1340, 1290, 1120, 1020, and 740 cm^{-1}; ^1H NMR ($CDCl_3$) δ=0.53—2.30 (m, 24H), 2.93 (s, 3H), and 6.38—7.05 (m, 4H). Calcd for $C_{21}H_{31}NS$: C, 76.54; H, 9.48; N, 4.25%. Found: C, 76.71; H, 9.77; N, 4.11%.

4m: pale yellow oil; IR (neat) 2950, 2850, 2200, 1580, 1470, 1350, 1300, 1260, 1120, 1070, 1020, 740, and 700 cm^{-1}; ^1H NMR ($CDCl_3$) δ=0.57—2.33 (m, 9H), 2.75 (s, 3H), and 6.05—7.47 (m, 9H). Calcd for $C_{20}H_{21}NS$: C, 78.13; H, 6.88; N, 4.56%. Found: C, 78.17; H, 6.73; N, 4.04%.

4n: pale yellow oil; IR (neat) 2950, 1580, 1480, 1380, 1360, 1300, 1200, 1120, 1050, 1020, and 730 cm^{-1}; ^1H NMR ($CDCl_3$) δ=0.67—2.00 (m, 18H), 2.73 (s, 3H), and 5.83—6.97 (m, 4H). Calcd for $C_{16}H_{25}NS$: C, 72.95; H, 9.56; N, 5.32%. Found: C, 72.59; H, 9.58; N, 5.45%.

4o: colorless needles; mp 70.5—71 °C; IR (neat) 2900, 1580, 1480, 1440, 1360, 1300, 1220, 1100, 1040, 1020, 730, and 700 cm^{-1}; ^1H NMR ($CDCl_3$) δ=0.67—1.67 (m, 9H), 2.58 (s, 3H), and 6.40—7.60 (m, 9H). Calcd for $C_{18}H_{21}NS$: C, 76.28; H, 7.47; N, 4.94%. Found: C, 76.11; H, 7.49; N, 4.74%.

4p: colorless oil; IR (neat) 2950, 1620, 1580, 1480, 1370, 1300, 1220, 1120, 1020, and 730 cm^{-1}; ^1H NMR ($CDCl_3$) δ=0.67—2.00 (m, 24H), 2.60 (s, 3H), and 5.67—6.83 (m, 4H). Calcd for $C_{19}H_{31}NS$: C, 72.95; H, 9.57; N, 5.32%. Found: C, 73.14; H, 9.91; N, 4.81%.

4q: colorless oil; IR (neat) 2950, 1580, 1480, 1360, 1300, 1220, 1120, 1020, and 730 cm^{-1}; ^1H NMR (CCl_4) δ=0.50—2.13 (m, 16H), 2.57 (s, 3H), and 5.67—6.77 (m, 4H). Calcd for $C_{15}H_{23}NS$: C, 72.23; H, 9.29; N, 5.62%. Found: C, 72.37; H, 9.59; N, 5.37%.

4r: colorless needles; mp 140—140.5 °C; IR (KBr) 1570, 1480, 1440, 1340, 1300, 1220, 1150, 1100, 1120, 980, 890, 730, and 700 cm^{-1}; ^1H NMR ($CDCl_3$) δ=2.55 (s, 3H) and 6.33—7.50 (m, 14H). Calcd for $C_{20}H_{17}NS$: C, 79.17; H, 5.65; N, 4.62%. Found: C, 79.66; H, 5.42; N, 4.35%.

4s: colorless needles; mp 98.5—99 °C; IR (KBr) 3100, 2950, 1580, 1480, 1440, 1370, 1300, 1220, 1180, 1120, 1050, 1020, 770, 740, and 700 cm^{-1}; ^1H NMR ($CDCl_3$) δ=2.62 (s, 3H), 3.53 (s, 2H), and 6.07—7.67 (m, 14H). Calcd for $C_{21}H_{19}NS$: C, 79.46; H, 6.03; N, 4.41%. Found: C, 78.84; H, 6.04; N, 4.16%.

4t: pale yellow oil; IR (neat) 2950, 1580, 1500, 1420, 1320, 1160, 1040, and 740 cm^{-1}; ^1H NMR ($CDCl_3$) δ=0.67—1.83 (m, 9H), 2.53 (s, 3H), 3.68 (s, 3H), and 6.37—7.50 (m, 8H). Calcd for $C_{19}H_{23}NOS$: C, 72.80; H, 7.40; N, 4.47%. Found: C, 72.66; H, 7.62; N, 4.82%.

4u: colorless oil; IR (neat) 2900, 1650, 1580, 1460, 1360, 1300, 1220, 1120, 1020, 960, 920, and 730 cm^{-1}; ^1H NMR (CCl_4) δ=0.67—2.23 (m, 16H), 2.64 (s, 3H), 5.47 (m, 2H), and 5.73—6.83 (m, 4H). Calcd for $C_{18}H_{25}NS$: C, 75.21; H, 8.77; N, 4.87%. Found: C, 75.69; H, 9.08; N, 4.61%.

3-Methylbenzothiazolium Iodide (6a). A solution of benzothiazole (1.1 g, 8 mmol) in DMF (3 ml) and iodomethane (3 ml, 48 mmol) was refluxed for 2 h. The mixture was diluted with ether and cooled in an ice bath to completely precipitate the product. The pale yellow needles obtained were collected by filtration and washed thoroughly with ether. Recrystallization of the crude product from methanol afforded pure **6a** as colorless needles (2.1 g, 95%): mp 217 °C (decomp); IR (KBr) 3000, 1580, 1520, 1450, 1400, 1370, 1110, 1030, 880, 750, and 695 cm^{-1}; ^1H NMR (DMSO-d_6) δ=4.33 (s, 3H), 7.75 (m, 2H), 8.28 (m, 2H), and 10.38 (s, 1H). Calcd for C_8H_8NSI: C, 34.67; H, 2.91; N, 5.05%. Found: C, 34.48; H, 2.83; N, 4.86%.

3-Methylbenzothiazolium Fluorosulfate (6b). Methyl fluorosulfate (3.42 g, 30 mmol) was added to a solution of benzothiazole (1.35 g, 10 mmol) in dichloromethane (10 ml) and the mixture was refluxed for 24 h. After cooling to room temperature and a similar workup as in the preparation of **6a**, recrystallization of crude product from methanol afforded pure **6b** (2.24 g, 90%): mp 107—108 °C (decomp); IR (KBr) 3450, 3050, 1720, 1620, 1580, 1520, 1440, 1400, 1280, 1080, 900, 880, 820, 760, and 580 cm^{-1}; ^1H NMR (DMSO-d_6) δ=4.35 (s, 3H), 7.72 (m, 2H), 8.27 (m, 2H), and 10.38 (s, 1H). Calcd for $C_8H_8NO_3S_2F$: C, 38.55; H, 3.23; N, 5.62%. Found: C, 38.46; H, 3.18; N, 5.61%.

3-Methylbenzothiazolium Methyl Sulfate (6c). Benzothiazole (1.35 g, 10 mmol) was methylated for 72 h with dimethyl sulfate (3.78 g, 30 mmol) in dichloromethane (10 ml) by the same procedure for **6b**. Recrystallization of crude product from methanol afforded pure **6c** (0.42 g, 16%): mp 122—124 °C (decomp); IR (KBr) 3450, 3050, 1610, 1580, 1520, 1440, 1400, 1280, 1250, 1210, 1060, 1020, 900, 760, 720, and 570 cm^{-1}; ^1H NMR (DMSO-d_6) δ=3.32 (s, 3H), 4.33 (s, 3H), 7.72 (m, 2H), 8.25 (m, 2H), and 10.33 (s, 1H). Calcd for $C_9H_{11}NO_4S_2$: C, 41.37; H, 4.24; N, 5.36%. Found: C, 40.92; H, 4.10; N, 5.26%.

3-Methylbenzothiazolium Tetrafluoroborate (6d). Trimethyloxonium tetrafluoroborate (1.63 g, 10 mmol) was added in portions to a solution of benzothiazole (1.35 g, 10 mmol) in dichloromethane (10 ml). After the reaction mixture was refluxed for 20 min, the solvent was removed by evaporation under reduced pressure. The residual sirup was crystallized from acetone-dichloromethane-ether to give the crude product as colorless needles. Recrystallization from acetone-dichloromethane afforded pure **6d** as colorless needles (2.26 g, 95%): mp 118.5—119.5 °C (decomp); IR (KBr) 3050, 1580, 1520, 1440, 1400, 1370, 1320, 1280, 1080, 900, 760, 720, 570, and 520 cm^{-1}; ^1H NMR (DMSO-d_6) δ=4.37 (s, 3H), 7.73 (m, 2H), 8.23 (m, 2H), and 10.33 (s, 1H). Calcd for $C_8H_8NSBF_4$: C, 40.54; H, 3.40; N, 5.91%. Found: C, 40.42; H, 3.19; N, 5.88%.

Alkylation of 3-Methylbenzothiazolium Salts 6. Benzothiazolium salts **6a—d** (4 mmol) were allowed to react with 1.2 equiv of organometallic reagent according to standard procedure for the alkylation of the salt **5**, giving **3a**, **3g**, **3i**, and **3m—o**. In the case of **3a** obtained in the reaction of **6a** with butylmagnesium bromide, purification by short column chromatography was carried out to give pure **3a** as pale yellow oil. The other products were almost pure (monitored with TLC) without purification. Product yields are summarized in Table 7.

3m: pale yellow oil; IR (neat) 3050, 2900, 2850, 1640, 1580, 1480, 1370, 1330, 1300, 1120, 1020, 920, and 740 cm^{-1}; ^1H NMR (CCl_4) δ=2.50 (t, 2H), 2.68 (s, 3H), 4.67—5.17 (m, 3H), 5.50 (m, 1H), and 5.87—6.83 (m, 4H). Calcd for $C_{11}H_{13}NS$: C, 69.06; H, 6.85; N, 7.32%. Found: C, 69.29; H, 6.83; N, 7.38%.

3n: pale yellow oil; IR (neat) 3050, 2800, 1950, 1680, 1580, 1480, 1370, 1330, 1290, 1120, 1020, 1000, 920, and 740 cm^{-1};

^{1}H NMR ($CDCl_3$) δ=1.05 (d, 3H), 2.74 (s, 3H), 5.06 (m, 3H), and 6.21—7.25 (m, 4H). This compound is slightly unstable in air.

3o: pale yellow oil; IR (neat) 2200, 1670, 1580, 1470, 1420, 1350, 1320, 1280, 1100, 1020, 740, and 690 cm^{-1}; ^{1}H NMR ($CDCl_3$) δ=3.13 (s, 3H), 6.00—7.50 (m, 9H), and 7.93 (s, 1H). This compound is slightly unstable in air.

Benzothiazole-2-*d* (22). A stirred solution of benzothiazole (6.0 g, 45 mmol) in dry THF (90 ml) under nitrogen was cooled to −78 °C and 20% excess of butyllithium in hexane (1.6 M solution) was added dropwise. 2-Lithiobenzothiazole was immediately formed. This orange-colored anion solution was quickly quenched at −78 °C with D_2O (4.5 ml) after the addition of butyllithium. The mixture was allowed to warm to room temperature and diluted with water. The aqueous mixture was extracted with ether. The ether extract was dried with $MgSO_4$. Removal of the solvent under reduced pressure afforded almost pure **22** as a pale yellow oil (5.85 g, 95%; >98% deuteration by ^{1}H NMR): bp 73 °C/2 mmHg (1 mmHg≈133.322 Pa); ^{1}H NMR (CCl_4) δ=6.50—7.50 (m, 4H).

2-Deuterio-3-methylbenzothiazolium Iodide (23). Benzothiazole-2-*d* (**22**) (4.1 g, 30 mmol) was methylated with iodomethane (11.2 ml, 180 mmol) in DMF (16.8 ml) according to the procedure for the preparation of **6a**. Recrystallization of crude product from methanol afforded pure **23** as colorless needles (7.8 g, 94%): mp 217 °C (decomp); ^{1}H NMR (DMSO-d_6) δ=4.33 (s, 3H), 7.75 (m, 2H), and 8.23 (m, 2H).

3-Methyl-2-phenylbenzothiazoline-2-*d* (24). Benzothiazolium salt **23** (7.23 g, 26 mmol) was alkylated with phenylmagnesium bromide (1.2 eq) in THF according to standard procedure described previously. Recrystallization of the crude product as pale yellow needles from ethanol afforded pure **24** as colorless needles (4.7 g, 80%; >98% deuteration by ^{1}H NMR): mp 113 °C; ^{1}H NMR ($CDCl_3$) δ=2.58 (s, 3H) and 6.17—7.67 (m, 9H).

Benzaldehyde-2-*d*. Benzothiazoline **24** (4.6 g, 20 mmol) was hydrolyzed by Method A to afford almost pure benzaldehyde-*d* as a colorless oil (1.99 g, 94%; >98% deuteration by ^{1}H NMR): bp 72.5 °C/20 mmHg; ^{1}H NMR (CCl_4) δ=7.30—7.87 (m, 5H).

References

1) J. F. W. McOmie, "Protective Groups in Organic Chemistry," Plenum Press, London (1973); T. W. Green, "Protective Groups in Organic Synthesis," Wiley, New York(1981).

2) Recently convenient and chemoselective acetalization and thioacetalization methods using alumina or silica gel have been reported: Y. Kamitori, M. Hojo, R. Masuda, and T. Yoshida, *Tetrahedron Lett.*, **26**, 4767 (1985); Y. Kamitori, M. Hojo, R. Masuda, T. Kimura, and T. Yoshida, *J. Org. Chem.*, **51**, 1427 (1986).

3) J. W. Ralls and B. Riegel, *J. Am. Chem. Soc.*, **76**, 4479 (1954); J. R. Williams and G. M. Sarkisian, *Synthesis*, **1974**, 32; D. A. Evans, L. K. Truesdale, K. G. Grimm, and S. L. Nesbitt, *J. Am. Chem. Soc.*, **99**, 5009 (1977).

4) Pure *cis*-2-acetonylcyclohexanecarbaldehyde have been obtained from the corresponding pure *cis*-benzothiazoline derivative with no trace of the corresponding and more stable *trans*-aldehyde: E. J. Corey and D. L. Boger, *Tetrahedron Lett.*, **1978**, 9.

5) The cleavage of 2-(α-hydroxyalkyl)benzothiazolines with Method A causes no dehydration to produce the corresponding α-hydroxy carbonyl compounds in good yields: H. Chikashita and K. Itoh, *Heterocycles*, **23**, 295 (1985); H. Chikashita, M. Ishibaba, K. Ori, and K. Itoh, *Bull. Chem. Soc. Jpn.*, **61**, 3637 (1988).

6) E. J. Corey and S. W. Walinsky, *J. Am. Chem. Soc.*, **94**, 8932 (1972).

7) B. T. Grobel, A. Wijsman, and A. Van der Gen, *J. Org. Chem.*, **44**, 1847 (1979).

8) I. Degani and R. Fochi, *J. Chem. Soc., Perkin Trans. 1*, **1976**, 1886.

9) G. Picotin and P. Miginiac, *J. Org. Chem.*, **50**, 1299 (1985).

10) I. Degani, R. Fochi, and V. Regondi, *Tetrahedron Lett.*, **22**, 1821 (1981).

11) J. Nakayama, *Bull. Chem. Soc. Jpn.*, **55**, 2289 (1982).

12) V. S. Huning, D. Scheutzow, H. Schlaf, and H. Quast, *Justus Liebigs Ann. Chem.*, **765**, 113 (1972).

13) J. Dauben, Jr., L. R. Honnen, and K. M. Harmon, *J. Org. Chem.*, **25**, 1442 (1960).

14) E. J. Corey and P. L. Fuchs, *Tetrahedron Lett.*, **1972**, 3769.

Vanadium Oxides (V_2O_x) Catalysts for Dry-Type and Simultaneous Removal of Sulfur Oxides and Nitrogen Oxides with Ammonia at Low Temperature

Shigeaki KASAOKA,* Eiji SASAOKA, and Hideto IWASAKI
Faculty of Engineering, Okayama University, Okayama 700
(Received August 11, 1988)

In order to develop highly functional catalysts for a dry-type, simultaneous removal of sulfur oxides (SO_x) and nitrogen oxides (NO_x) the catalytic activities of V_2O_x/TiO_2, V_2O_x/TiO_2/AC(activated carbon) and V_2O_x/AC ($4<x<5$) were studied using a fixed bed flow reactor. In this process SO_2 is catalytically oxidized to SO_3 and then fixed on the catalyst as ammonium sulfates by reactions with H_2O and NH_3; NO_x are reduced to N_2 with NH_3 over the same catalyst at low temperature (ca. 130 °C). The sulfates deposited on the catalyst must be periodically removed for regeneration in order to realize repeated use of the catalyst. V_2O_x/TiO_2 was found to be a suitable catalyst for the simultaneous removal and to have an acceptable tolerance for reiterative regeneration. Also, water washing of the used catalyst after a NH_3 pretreatment was found to be preferable for regeneration. The sulfates deposited on the catalyst could be recovered as $(NH_4)_2SO_4$ by this type regeneration. The deposited sulfates were amorphous and could be regarded as being a mixture of NH_4HSO_4 and $(NH_4)_2SO_4$. These sulfates reacted with NO_x to produce N_2.

SO_x and NO_x in the flue gases emitted from stationary sources have been removed by two consecutive processes. NO_x in flue gas are catalytically reduced to N_2 with NH_3 by a dry process at around 350 °C; SO_x are absorbed by a wet process at around 50 °C. These processes are well established, though complicated and not very energy saving-type processes. Furthermore, in wet-type desulfurization, waste water must be cleaned. For both simplification and energy saving, it is desirable to estabish a low-temperature, dry-type process for the removal of SO_x and NO_x.

The authors have already reported a dry-type, simultaneous removing process, in which CuO containing metal oxides (TiO_2, SiO_2, etc.) are used as the catalyst and sorbent. In this case SO_2 is oxidized to SO_3, and then fixed as $CuSO_4$ ($SO_3 \rightarrow CuO$). NO_x are catalytically reduced to N_2 with NH_3 over the $CuSO_4$ formed. This dry-type process gives a high completion rate for the simultaneous removal of SO_x and NO_x at around 350 °C. Furthermore, it was found that CuO containing multi-component metal oxides has sufficient tolerance for reiterative regeneration from $CuSO_4$ to CuO.[1-3]

A new dry-type, simultaneous process using active carbon or coke was proposed[4,5] and studied regarding practical applications.[6-9] In this process SO_2 is oxidized to SO_3 over the catalyst and then fixed on the catalyst:

$$SO_2 + (1/2)O_2 + H_2O = H_2SO_4, \quad (1)$$

and

$$H_2SO_4 + NH_3 = NH_4HSO_4. \quad (2)$$

NO is reduced to N_2 with NH_3 over the same catalyst:

$$NO + (1/4)O_2 + NH_3 = N_2 + (3/2)H_2O. \quad (3)$$

The catalysts are claimed to be highly active for simultaneous removal, even when a lot of the sulfate is fixed on the catalyst surface. Furthermore, the catalyst which lost its activity at last has to be regenerated, because of the deposition of sulfate. That is, the sulfate has to be removed from the used catalyst without loss and deactivation of the catalyst.

The regeneration of the used catalyst can be achieved according to the reactions:

$$H_2SO_4 + (1/2)C = SO_2 + H_2O + (1/2)CO_2, \quad (4)$$

and

$$NH_4HSO_4 + (1/2)C = NH_3 + H_2O + SO_2 + (1/2)CO_2. \quad (5)$$

Therefore, loss of the carbon catalysts during regeneration is unavoidable.

In the present study, vanadium oxides catalysts were studied to develop a dry-type, simultameous removal process; reiterative regeneration by a wet-type method was also studied in order to establish a regeneration method in which the used catalyst could be regenerated without loss and deactivation. Vanadium oxides catalysts have been used as a commercial denitrification catalyst, and are highly active even at low temperature if the preparation is adequate.[10] The sulfation of SO_x with H_2O and NH_3 over the vanadium oxides catalysts were also studied.[11-14] The object of this work is to clarify the performance and the possibility of any practical applications of vanadium oxides catalysts.

Experimental

Materials. Gases (NO, SO_2, NH_3, O_2, N_2, and He) from commercial cylinders were used. NH_3 and H_2O were supplied as aqueous ammonia. All chemicals used for the preparation of catalysts were reagent grade. Before use, AC(activated carbon) was washed with hot water (ca. 100 °C), dried at 110 °C for 25 h and then calcined at 900 °C for 1 h in a stream of N_2.

Catalysts. The support TiO_2(anatase) was prepared by the precipitation method. A 10 wt% $TiCl_4$ aqueous solution was poured instantly into a 7 wt% NH_3 aqueous solution under intensive mixing at room temperature. The precipi-

tate was washed with repeated decantation, filtered, dried at 110 °C for 25 h, calcined at 400 °C for 3 h in the stream of air, crushed, and then sieved to average diameter of 1.0 mm (surface area: 90 $m^2 g^{-1}$, bulk density: 0.83 g cm^{-3}). The AC as a support was crushed and sieved to an average diameter of 1.0 mm (surface area: 1460 m^2 g^{-1}, bulk density: 0.42 g cm^{-3}). TiO_2/AC was prepared by a chemical vapor deposition method. That is, the AC was packed in a glass tube reactor and dried at 150 °C for 1 h in a N_2 stream, cooled down to room temperature, exposed to $TiCl_4$ vapor using a mixed gas of 1% $TiCl_4$ and N_2(100 $cm^3N\,min^{-1}$) for 3 h, and then exposed to a mixed gas of 40% NH_3, 2% H_2O and N_2 (180 $cm^3N\,min^{-1}$) for 3 h. After this procedure, the sample was washed with water, dried at 110 °C for 25 h and calcined at 400 °C for 3 h in a N_2 stream (surface area: 1040 $m^2 g^{-1}$, bulk density: 0.53 g cm^{-3}). The TiO_2 content in the TiO_2/AC was ca. 21 wt%.

Catalysts, V_2O_x/TiO_2, V_2O_x/AC, and V_2O_x/TiO_2/AC, were prepared by an impregnation method. The supports were impregnated in aqueous ammonia of NH_4VO_3 at room temperature for 25 h, dried in a rotary evaporator under evacuation at 40 °C, and then dried at 110 °C for 25 h. The amount of NH_4VO_3 loaded on the support was ca. 5 wt% as V_2O_5. The NH_4VO_3 loaded on the support was changed to an active state V_2O_x ($4<x<5$)[10] by a pretreatment with a mixed gas of 250 ppm NO, 250 ppm NH_3, 5% O_2 and N_2(500 $cm^3N\,min^{-1}$) at 200 °C for 3 h.

Reaction Procedure. The simultaneous removal of SO_x and NO_x was carried out in a fixed bed flow reactor under an atmospheric pressure, in the temperature range 130 to 150 °C (mainly 130 °C). Two glass tube reactors were used. The one (inner dia.: 12 mm) was used for 3 ml of catalyst (SV: 1.0×10^4 h^{-1}) and the another (inner dia.: 20 mm) was used for 12 ml (SV: 2.5×10^{-3} h^{-1}) or 18 ml (1.7×10^3 h^{-1}) of catalyst. Inlet gases were a mixture of 250 ppm SO_2, 250 ppm NO, (0—750) ppm NH_3, 5% O_2, 10% H_2O and N_2, and were fed with the total flow rate of 500 $cm^3N\,min^{-1}$. The concentrations of SO_x and NO_x in inlet and outlet gas were measured by the method of Arsenazo III (JIS K0103) and a chemiluminescence-type NO_x meter (YANACO ECL300), respectively. The concentration of NH_3 was measured by the conventional absorption-titration method.[15] Confirmation of the reduction of NO_x to N_2 with NH_3 was carried out using helium instead of N_2 as a balanced gas. The concentration of N_2 was measured by a gas chromatograph using a column packed with Molecular Sieves 5A (zeolite).

The reactivity of NH_4HSO_4 with NH_3 and the thermal stability of NH_4HSO_4, $(NH_4)_3H(SO_4)_2$ and $(NH_4)_2SO_4$ were measured with a flow-type auto-recording micro-thermobalance. Identifications of the sulfates were carried out by X-ray diffraction (XRD) analysis. The pore volume of the catalyst was measured using a mercury porosimeter (Erba MOD-220).

Results and Discussion

Simultaneous Removal of SO_x and NO_x with V_2O_x/AC, V_2O_x/TiO_2, and V_2O_x/TiO_2/AC. Results on the simultaneous removal of SO_x and NO_x over V_2O_x/AC and V_2O_x/TiO_2 are shown in Fig. 1. A comparison of the catalytic activities of the two catalysts led to the conclusion that V_2O_x/AC is more suitable for SO_x removal than V_2O_x/TiO_2, and that V_2O_x/TiO_2 is more suitable for NO_x removal than V_2O_x/AC.

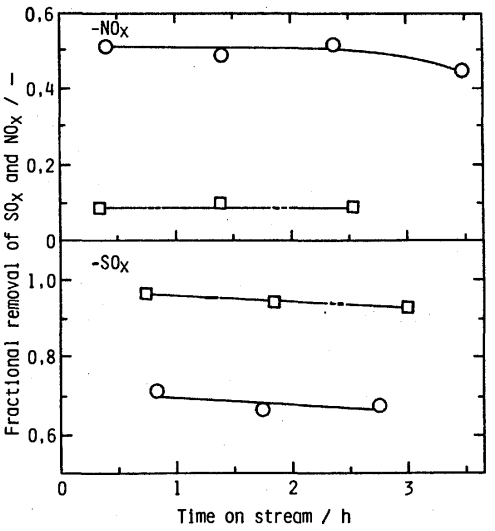

Fig. 1. Simultaneous removal of SO_x and NO_x with V_2O_x/TiO_2 and V_2O_x/AC. Catalysts: virgin, 3.0 ml, reaction conditions: 250 ppm SO_2-250 ppm NO-500 ppm NH_3-5% O_2-10% H_2O-N_2(500 $cm^3N\cdot min^{-1}$, 1.0×10^4 h^{-1}), 403.2 K.
○: V_2O_x/TiO_2, □: V_2O_x/AC.

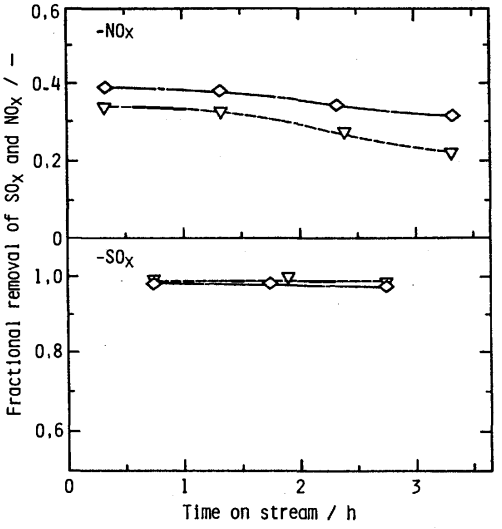

Fig. 2. Simultaneous removal of SO_x and NO_x with V_2O_x/TiO_2/AC and mixture of equi-volume of V_2O_x/TiO_2 and V_2O_x/AC. Catalysts: virgin, 3.0 ml, reaction conditions: 250 ppm SO_2-250 ppm NO-500 ppm NH_3-5% O_2-10% H_2O-N_2(500 $cm^3N\cdot min^{-1}$, 1.0×10^4 h^{-1}) 403.2 K.
▽: V_2O_x/TiO_2/AC, ◇: V_2O_x/TiO_2+V_2O_x/AC.

For the utilization of the characteristics of V_2O_x/AC and V_2O_x/TiO_2, the combination of the two catalysts was studied. That is, the activity of V_2O_x/TiO_2/AC was measured and compared with that of a mixture of the equi-volume of V_2O_x/AC and V_2O_x/TiO_2. These results are shown in Fig. 2. The order of catalytic activities was as follows:

For NO_x removal: $V_2O_x/TiO_2 > (V_2O_x/AC + V_2O_x/TiO_2) > V_2O_x/TiO_2/AC \gg V_2O_x/AC$

For SO_x removal: $V_2O_x/TiO_2/AC$, $(V_2O_x/AC+V_2O_x/TiO_2)$, $V_2O_x/AC>V_2O_x/TiO_2$

Unfortunately, the expected effect with the combination was not found. From the above results, it was found that V_2O_x/TiO_2 is most suitable among the three catalysts for the simultaneous removal of SO_x and NO_x (especially, for the concentration of $NO_x>$ that of SO_x).

Confirmation of the Fixation of SO_x on the Catalyst and the Reduction of NO_x to N_2. The fixation of SO_x on the catalyst was confirmed by the following procedure. The used catalysts (V_2O_x/AC and V_2O_x/TiO_2 used for 3.5 h (Fig. 1)) were washed with water at room temperature, and the amount of ammonium sulfates in the filtrate was measured by Arsenazo III method. The ratios of the amount recovered by the above method to the amount of SO_x removal were from 0.9 to 1.0.

For the comfirmation that NO_x are reduced to N_2 with NH_3, helium was used instead of N_2 as a balance gas. As the results, it was found that almost all of SO_x and NO_x were removed.

Effects of Reaction Temperature and Concentration of NH_3 on the Simultaneous Removal of SO_x and NO_x. The effect of the reaction temperature on the removal of SO_x and NO_x with V_2O_x/TiO_2 is shown in Fig. 3. With the temperature rise, the activity for NO_x removal increased and that for SO_x removal decreased. Although the reason for the decrease of SO_x removal is unknown, it may be possible that the sulfate (such as NH_4HSO_4 (mp 147 °C)) melted and plugged the pores of the catalyst. This plugging probably disturbed the removal of SO_x more than that of NO_x.

The effect of the inlet concentration of NH_3 on the removal of SO_x and NO_x with V_2O_x/TiO_2 is shown in Fig. 4. The fractional removal of NO_x increased with increasing NH_3 concentration, and then reached a constant value above the stoichiometric concentration of NH_3 (calculated from Eq. 3). This means that the dependency of the reduction rate of NO on the concentration of NH_3 is zero order. This result is consistent with the previous results reported.[1,16,17] On the other hand, the fractional removal of SO_x increased with increasing NH_3 concentration. This suggests that NH_3 plays an important role in SO_x removal, and that the rate-determining step of SO_x removal is not the oxidation of SO_2 to SO_3 with O_2.

Stabilities of V_2O_x/TiO_2 and V_2O_x/AC for Regeneration. The experiments on the regeneration of the used catalyst were tried by wet-type methods. In the early stage, the used catalysts were washed with water at room temperature without any pretreatment. In this method part of the V_2O_x on the supports was slightly dissolved with the water. This was due to the acidity of the solution. Therefore, to prevent leaching of V_2O_x from the catalysts, the used catalysts were treated with NH_3 (0.5% NH_3-5% O_2-N_2, 450 cm^3N min^{-1}, 130→100 °C, 0.5 h); that is, the sulfates deposited on the catalyst were neutralized with NH_3. After this treatment, the ammonium salts formed on the catalysts were extracted with water. the ammonium salts taken out from the aqueous solution by drying were identified as $(NH_4)_2SO_4$ by XRD analysis.

The stabilities of V_2O_x/TiO_2 and V_2O_x/AC for reiterative regeneration by the improved regeneration

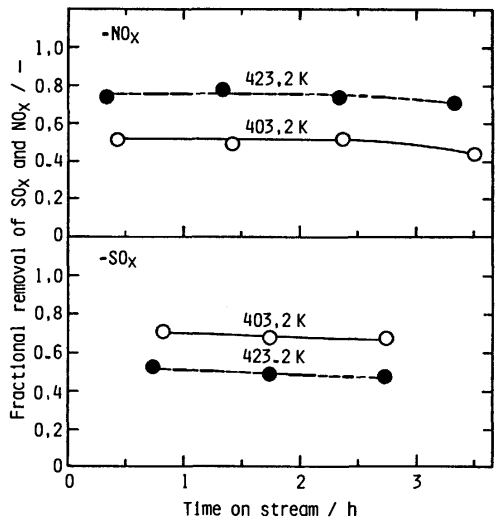

Fig. 3. Effect of reaction temperature on simultaneous removal of SO_x and NO_x with V_2O_x/TiO_2. Catalyst: virgin, 3.0 ml, reaction conditions: 250 ppm SO_2-250 ppm NO-500 ppm NH_3-5% O_2-10% H_2O-N_2 (500 $cm^3N \cdot min^{-1}$, 1.0×10^4 h^{-1}).

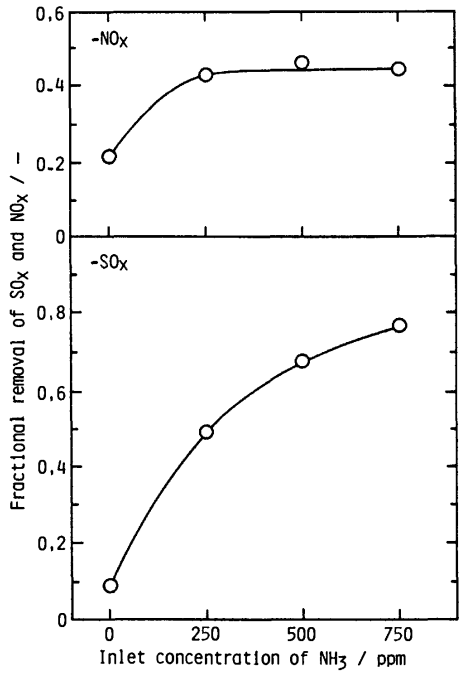

Fig. 4. Effect of inlet concentration of NH_3 on simultaneous removal of SO_x and NO_x with V_2O_x/TiO_2. Catalyst: virgin, 3.0 ml, reaction conditions: 250 ppm SO_2-250 ppm NO-0—750 ppm NH_3-5% O_2-10% H_2O-N_2 (500 cm^3 $N \cdot min^{-1}$, 1.0×10^4 h^{-1}), 403.2 K.

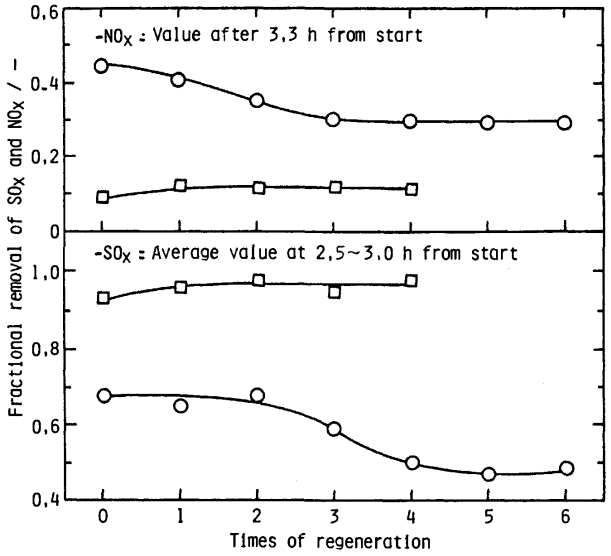

Fig. 5. Regeneration stability of V_2O_x/TiO_2 and V_2O_x/AC for simultaneous removal of SO_x and NO_x catalysts: 3.0 ml, reaction conditions: 250 ppm SO_2-250 ppm NO-500 ppm NH_3-5% O_2-10% H_2O-N_2 (500 $cm^3N \cdot min^{-1}$, 1.0×10^4 h^{-1}), 403.2 K.
○: V_2O_x/TiO_2, □: V_2O_x/AC.

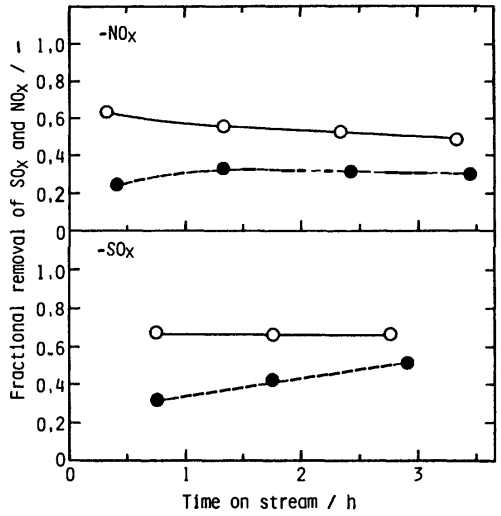

Fig. 6. Comparison of catalytic activity of V_2O_x/TiO_2* and V_2O_5/TiO_2* for simultaneous removal of SO_x and NO_x. TiO_2*: calcined at 550 °C for 3 h in air stream, catalysts: virgin, 3.0 ml, reaction conditions; 250 ppm SO_2-250 ppm NO-500 ppm NH_3-5% O_2-10% H_2O-N_2 (500 cm^3 $N \cdot min^{-1}$, 1.0×10^4 h^{-1}), 403.2 K.
○: V_2O_x/TiO_2*, ●: V_2O_5/TiO_2*.

method are shown in Fig. 5. V_2O_x/AC was found to have good stability, but the activity of V_2O_x/TiO_2 decreased up to the fifth regeneration, and then sustained adequate activity. One of the reasons for the deactivation of V_2O_x/TiO_2 up to fifth regeneration run might be a decrease of the specific surface area; however, the difference of the surface area of the virgin catalyst and that of the seventh regenerated catalyst was small (94→87 m^2g^{-1}). Another reason might be the change of V_2O_x to another vanadium oxide, such as V_2O_5. Therefore, the activities of V_2O_x/TiO_2 and V_2O_5/TiO_2 were compared. TiO_2, which were calcined at 550 °C for 3 h, were used (surface area: 72 m^2g^{-1}, bulk density: 1.1 gcm^{-3}). V_2O_5/TiO_2 was prepared from TiO_2 supported NH_4VO_3 by calcining at 550 °C for 3 h in a stream of air. The activity of V_2O_x/TiO_2 for the simultaneous removal was higher than that of V_2O_5/TiO_2, as shown in Fig. 6. It was indicated that the change of V_2O_x to V_2O_5 might be one of the causes of the deactivation.

Identification of the Sulfates Deposited on the Catalyst. As described previously, SO_x were fixed on a catalyst, though the kinds of sulfates were unknown. Therefore, the identification of deposited sulfates was carried out by XRD analysis; however, no clear X-ray diffraction pattern was found. This indicated that the sulfates were amorphous.

Because of the difficulty of a direct identification of the sulfates by XRD analysis, an indirect identification was tried by the following method. The used catalyst was washed with water; then, the filtrate was dried in a rotary evaporator under evacuation at 40 °C. The sulfates from the filtrate were dried at 110 °C for 25 h, and were then analyzed by XRD. As a result, $(NH_4)_3H(SO_4)_2$(equi-gram-mole mixture of NH_4HSO_4) and $(NH_4)_2SO_4$),[17] and $(NH_4)_2SO_4$ were identified. Since these sulfates might be produced via NH_4HSO_4, the possibility of conversion from NH_4HSO_4 to another sulfate was studied. That is, the reactivity of NH_4HSO_4 with NH_3 under the coexistence of water vapor was studied at 130 °C using a thermobalance. The conversions of the NH_4HSO_4 to $(NH_4)_3H(SO_4)_2$ and $(NH_4)_2SO_4$ were confirmed by thermal gravimetrical and XRD analysis. Furthermore, it was confirmed by a gravimetrical method that the decompositions of NH_4HSO_4, $(NH_4)_3H(SO_4)_2$ and $(NH_4)_2SO_4$ are not detectable by a temperature-programmed method (2 °C min^{-1}) in the temperature range 130 to 150 °C.

From the above results, it was suggested that the sulfates could be regarded as a mixture of NH_4HSO_4 and $(NH_4)_2SO_4$, and that the side reaction of NH_4HSO_4 with NH_3 proceeds according to the following equation:

$$NH_4HSO_4 + NH_3 = (NH_4)_2SO_4. \quad (6)$$

It was also suggested that $(NH_4)_2SO_4$ is the final product from SO_x on the catalyst, if it does not react with SO_x and NO_x.

Reactivities of the Sulfates Deposited on the Catalyst. Shikada et al.[18] already reported that NH_4HSO_4 in a molten salt of $NH_4HSO_4/NaHSO_4$ reacted with NO under the coexistence of V_2O_5. Therefore, the reactivities of the sulfates deposited on the catalyst with NO_x were measured by the following procedure.

For the complete removal of NH_3 remaining on V_2O_x/TiO_2 after the activation step of $NH_4VO_3 \rightarrow V_2O_x$, the sample V_2O_x/TiO_2 was further treated with a mixed gas (250 ppm NO-5% O_2-N_2) at 200 °C. This treatment was stopped when the outlet concentration of NO_x became equal to the concentration in the inlet gas. The treated catalyst was crushed under 100 mesh, mechanically mixed with NH_4HSO_4 or $(NH_4)_2SO_4$ using a mortar, pelletized, crushed, again, and then sieved to an average dieameter of 1.0 mm. The content of the sulfate was ca. 10 wt%. Figure 7 shows the reactivity of the NH_4HSO_4 or $(NH_4)_2SO_4$ loaded on V_2O_x/TiO_2 with NO_x. It was obviously found that $(NH_4)_2SO_4$ and NH_4HSO_4 reacted with NO_x. Furthermore, the reduction of NO_x to N_2 with the sulfates was confirmed by using helium as a balanced gas, and the gas chromatograph, as follows:

$$NO + (1/4)O_2 + NH_4HSO_4 = N_2 + (3/2)H_2O + H_2SO_4, \quad (7)$$

and

$$NO + (1/4)O_2 + (NH_4)_2SO_4 = N_2 + (3/2)H_2O + NH_4HSO_4. \quad (8)$$

On the other hand, small amount of SO_x were removed; the fracional removal of SO_x was almost the same as the value measured without the coexistence of NH_3 (Fig. 4).

The active site of the cataltst for the reactions of Eqs. 7 and 8 will finally be covered by the deposited sulfates. Therefore, any NH_4HSO_4 formed will be converted to $(NH_4)_2SO_4$ with NH_3.

Evaluation of V_2O_x/TiO_2 as a Catalyst for the Simultaneous Removal of SO_x and NO_x. For practical applications, the life of a catalyst and the reaction conditions demanding an almost complete removal of both SO_x and NO_x are important. From these view points, the fractional conversions of SO_x and NO_x were measured for 30 h. The results under the conditions that the inlet concentration of NH_3 was set to be equal to the stoichiometric value in Eqs. 2 and 3 (NO: 250 ppm, SO_2: 250 ppm, $NH_3/(SO_2+NO)$ mole ratio: 1.0) are shown in Fig. 8. At a higher space velocity (1.0×10^4 h^{-1}), both of the conversions of SO_x gradually decreased with the time on stream. From a comparison of the fractional removal of SO_x and NO_x, the SO_x removal proceeded predominantly under this conditions. Since the reason for the decline of the fractional removal of both SO_x and NO_x was considered to be the deposition of the sulfates, the surface area and pore volume of a virgin catalyst and that of a used catalyst were measurd. In this case, NH_4HSO_4 in the used catalyst absorbed water vapor and melt if the catalyst was exposed to the atmosphere at room temperature. Therefore, before the measurements of the surface area and the pore volume, the used catalyst was treated with NH_3, and NH_4HSO_4 was converted to $(NH_4)_2SO_4$ by the same procedure as that of the NH_3 treatment in the regemeration. The surface area of the catalyst decreased ca. 40% after the use (94→54 m^2 g^{-1}) and the pore volume of the catalyst also fell down ca.30% after the use (pore diameter>6 nm : 0.26→0.17 cm^3 g^{-1}). From these results it was confirmed that the reason of the declines of the fractional removal of SO_x and NO_x was the deposition of the sulfates.[11-13] At lower space velocity (2.5×10^3 h^{-1}), NO_x were almost completely removed up to 6 h from the start, but the fractional removal of SO_x fell down gradually up to 12 h. The effect of the space velocity (SV) on the removal of SO_x is not justified, because the conversion of SO_x at the lower SV should be considerably larger than that of the

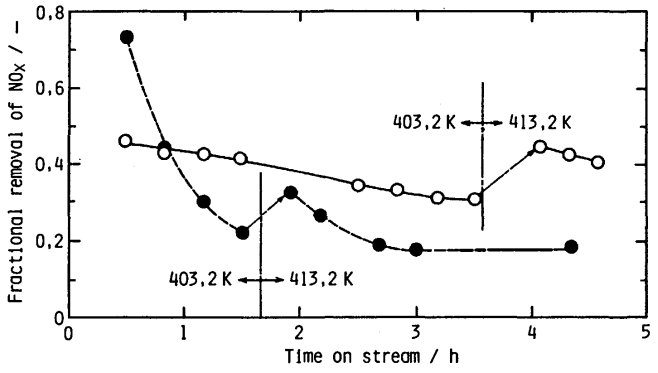

Fig. 7. Reactivity of NH_4HSO_4 and $(NH_4)_2SO_4$ loaded on V_2O_x/TiO_2 with NO_x. 10 wt% $NH_4HSO_4/(V_2O_x/TiO_2)$, 10 wt% $(NH_4)_2SO_4/(V_2O_x/TiO_2)$: Virgin, 3.0 ml, reaction conditions: 250 ppm SO_2-250 ppm NO-5% O_2-10% H_2O-N_2 (500 cm^3 N·min^{-1}, 1.0×10^4 h^{-1}).
○: $(NH_4)_2SO_4/(V_2O_x/TiO_2)$, ●: $NH_4HSO_4/(V_2O_x/TiO_2)$.

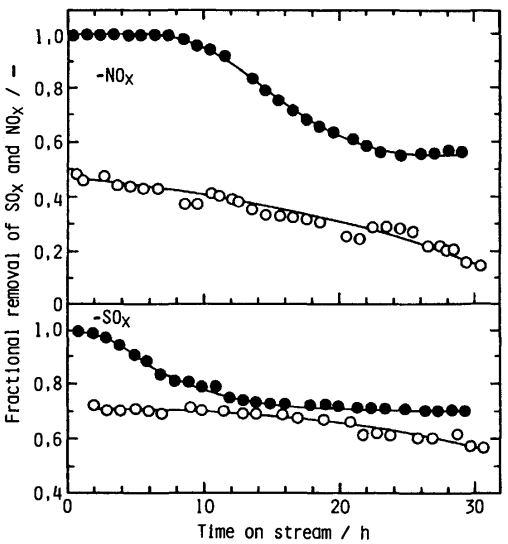

Fig. 8. Effect of space velocity on simultaneous removal of SO_x and NO_x with V_2O_x/TiO_2 in long run. Catalyst: virgin, 3.0, 12.0 ml, reaction conditions: 250 ppm SO_2-250 ppm NO-500 ppm NH_3-5% O_2-10% H_2O-N_2(500 cm^3 N·min^{-1}), 403.2 K.
○: 3.0 ml, 1.0×10^4 h^{-1}, ●: 12.0 ml, 2.5×10^3 h^{-1}.

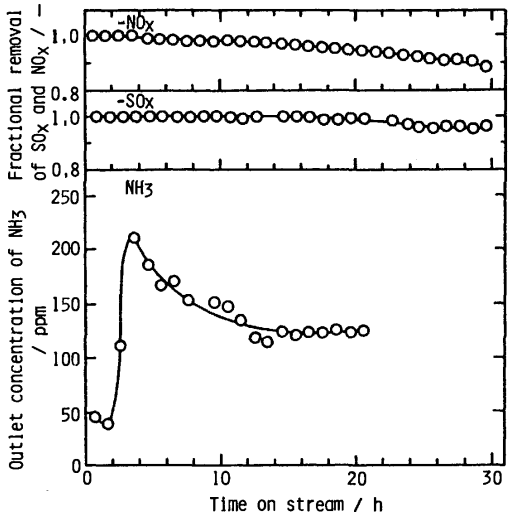

Fig. 9. Complete simultaneous removal of SO_x and NO_x with V_2O_x/TiO_2. Catalyst: virgin, 12.0 ml, reaction conditions: 250 ppm SO_2-250 ppm NO-750 ppm NH_3-5% O_2-10% H_2O-N_2(500 cm^3 N·min^{-1}, 2.5×10^3 h^{-1}), 403.2 K.

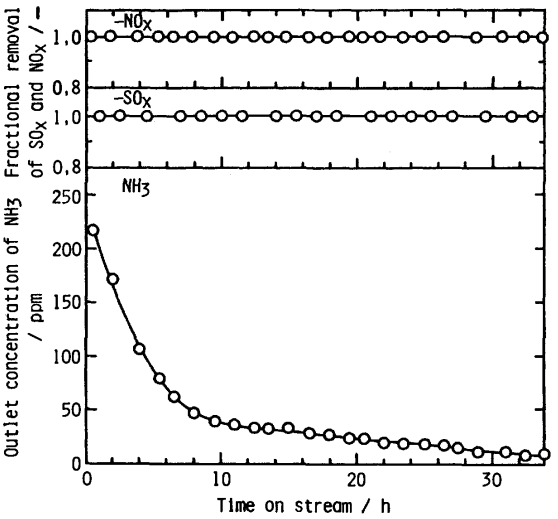

Fig. 10. Complete simultaneous removal of SO_x and NO_x with V_2O_x/TiO_2. Catalyst: virgin, 18.0 ml, reaction conditions: 100 ppm SO_2-250 ppm NO-400 ppm NH_3-5% O_2-10% H_2O-N_2(500 cm^3 N·min^{-1}, 1.7×10^3 h^{-1}), 403.2 K.

higher SV. Furthermore, the NO_x removal proceeded predominantly in the early time at the lower SV, being inconsistent with the results obtained at the higher space velocity. It was suggested that these results were due to the insufficiency of the amount of NH_3 supplied. In these experiments, the amount of NH_3 used was just sufficient to form NH_4HSO_4 and to reduce NO_x to N_2; however, $(NH_4)_2SO_4$ was produced in addition to NH_4HSO_4. This formation of $(NH_4)_2SO_4$ caused the insufficiency of the amount of NH_3 for the complete removal of SO_x and NO_x.

Based on the above results, in a following experiment, NH_3 was used in stoichiometric amount (750 ppm NH_3 for 250 ppm SO_2 and 250 ppm NO) according to Eqs. 2 to 6. That is, this amount of NH_3 is just sufficient to form $(NH_4)_2SO_4$ and to reduce NO_x to N_2. SO_x were almost completely removed from start up to 20 h, and the fractional removal of NO_x was kept above 90% for 20 h, as shown in Fig. 9. However, in this case, a considerable amount of NH_3 was detected in the reactor outlet. Furthermore, during the early hours the concentration of NH_3 changed abnormally. It may be considered that the adsorption of NH_3 onto the catalyst occurred, and also that the contributions of the reactions of Eqs. 2 to 6 to the consumption of NH_3 depended on the time on stream. Using the data at the quasi-steady state in Fig. 9 (from 14 to 20 h), the consumption mole ratio of NH_3 to (SO_x +NO_x) was obtained as ca. 1.25. This means that the sulfates produced seem to be a mixture of equi-gram-mole of NH_4HSO_4 and $(NH_4)_2SO_4$. Although, the simultaneous complete removal of SO_x and NO_x was possible under a sufficient amount of NH_3, the practical application of the catalyst claims the almost complete removal of SO_x and NO_x without any leakage of NH_3. Therefore, in the next experiment the inlet mole ratio of NH_3 to (SO_x+NO_x) was decreased from 1.5 to 1.25, and the space velosity was lowered to 1.7×10^3 h^{-1}. In this case, from the start up to 20 h, NO_x were almost completely removed, and SO_x were almost completely removed after 12 h. From these results and the dependency of the removal of SO_x on the concentration of NH_3, it was suggested that the removal rate of SO_x is lower under a smaller amount of NH_3 and, hence, the amount of the catalyst was not sufficient for a complete removal of SO_x.

From the results shown in Fig. 4, it was also suggested that the removal rate of SO_x could be kept higher under a higher mole ratio of NH_3 to SO_x. This claim for the removal of SO_x was satisfied by the application of a catalyst to the NO_x-rich flue gas(concentration of NO_x>that of SO_x). In the next experiment, SO_2, NO, and NH_3 were set to be 100, 250, and 400 ppm, respectively. The almost complete simultaneous removal of SO_x and NO_x without leakage of NH_3 was achieved, except during the early hours, as shown in Fig. 10.

The above-mentioned results might suggest that a just sufficient amount of NH_3 to form a mixture of equi-gram-mole of NH_4HSO_4 and $(NH_4)_2SO_4$, and to reduce NO_x to N_2, had to be used for the complete removal of SO_x and NO_x without leakage of NH_3. However, from previous fundamental studies, it was concluded that the most stable form of the sulfate was $(NH_4)_2SO_4$, and that the mole ratio of NH_4HSO_4 to $(NH_4)_2SO_4$ depended on the time on stream and/or the concentration of NH_3. In any case, it was experimentally clarified that the simultaneous complete removal of SO_x and NO_x in a NO_x-rich gas without leakage of NH_3 was possible.

Conclusion

V_2O_x/TiO_2 was found to be a suitable catalyst for the simultaneous removal of SO_x and NO_x in NO_x-rich flue gas by reactions with NH_3, even at low temperature, such as 130 °C.

V_2O_x/AC was suitable only for the removal of SO_x, and the activity for the removal of SO_x was better than that of the V_2O_x/TiO_2. The water washing of the used catalyst after treatment with NH_3 was found to be a preferable regeneration method for the prevention of the V_2O_x leaching. By this method the SO_x fixed on the catalysts could be recovered as $(NH_4)_2SO_4$. It was found that sulfates deposited on the catalysts are amorphous and can be regarded as being a mixture of NH_4HSO_4 and $(NH_4)_2SO_4$. It was also found that these sulfates reacted with NO_x and did not react with SO_x.

Although, the amount of NH_3 for the complete removal of SO_x and NO_x without leakage of NH_3 for a given flue gas could not be theoretically predicted, it was experimentally confirmed that for the NO_x-rich flue gas, SO_x and NO_x could be completely removed without the leakage of NH_3. For the SO_x-rich flue gas, the use of (V_2O_x/AC+V_2O_x/TiO_2) or V_2O_x/TiO_2 /AC may be suitable. Furthermore, we already found another type catalyst containing Cr_2O_3 for SO_x-rich flue gas.[19] Details of the characteristics of this catalyst will be reported later.

The present work was partially supported by a Grant-in-Aid for Scientific Research No. 61035044 from the ministry of Education, Science and Culture.

References

1) S. Kasaoka, E. Sasaoka, M. Funahara, and S. Nakashima, *Nenryo Kyokaishi*, **61**, 126 (1982).
2) S. Kasaoka, E. Sasaoka, and S. Nakashima, *Nenryo Kyokaishi*, **63**, 53 (1984).
3) S. Kasaoka, E. Sasaoka, and H. Nagano, *Nenryo Kyokaishi*, **65**, 273 (1986).
4) H. Juntgen, *Carbon*, **15**, 273 (1977).
5) K. Knoblauch, E. Richer, and H. Juntgen, *Fuel*, **60**, 832 (1981).
6) I. Mochida, M. Ogaki, H. Fujitsu, Y. Komatsubara, and S. Ida, *Fuel*, **62**, 868 (1983).
7) Y. Komatsubara, S. Ida, H. Fujitsu, and I. Mochida, *Fuel*, **63**, 1738 (1984).
8) I. Mochida, M. Kogaki, H. Fujitsu, Y. Komatsubara, and S. Ida, *Nippon Kagaku Kaishi*, **1985**, 680.
9) I. Mochida, T. Mizoshiri, H. Fujitsu, Y. Komatsubara, and S. Ida, *Nippon Kagaku Kaishi*, **1985**, 1685.
10) S. Kasaoka and E. Sasaoka, *Kankyo Gijyutu*, **8**, 676 (1979).
11) K. Fujimoto, T. Shikada, T. Kunugi, and H. Tominaga, *Nenryo Kyoukaishi*, **56**, 666 (1977).
12) T. Shikada, K. Fujimoto, T. Kunugi, and H. Tominaga, *Nenryo Kyoukaishi*, **57**, 991 (1978).
13) T. Shikada, K. Fujimoto, T. Kunugi, and H. Tominaga, *Ind. Eng. Prod. Res. Dev.*, **20**, 91 (1981).
14) S. Morikawa, K. Takahashi, H. Yoshida, O. Harasaki, and S. Kurita, *Nenryo Kyokaishi*, **61**, 1024 (1982).
15) S. Kasaoka and E. Sasaoka, *Nippon Kagaku Kaishi*, **9**, 1619 (1975).
16) M. Inomata, A. Miyamoto, and Y. Murakami, *J. Catal.*, **62**, 140 (1980).
17) R. Kiyoura and K. Urano, *Ind. Eng. Chem. Process Des. Develop.*, **9**, 489 (1970).
18) T. Shikada, T. Oba, K. Fujimoto, and H. Tominaga, "Proceedings 8th International Congress on Catalysis, Berlin, 1984," Verlag Chemie, Weiheim (1984), Vol. 3, p. 637.
19) S. Kasaoka, E. Sasaoka, and H. Iwasaki, the 58th Meeting of Catalysis Society of Japan, A, 290 (1986).

A Study of Dielectric Solvent Effect on Silicon-29 NMR Chemical Shifts of Some Chlorosilanes

Toshio TAKAYAMA,* Isao ANDO,† and Tetsuo ASAKURA††
Department of Applied Chemistry, Faculty of Technology, Kanagawa University, Rokkakubashi, Kanagawa-ku, Yokohama 221
†Department of Polymer Chemistry, Tokyo Institute of Technology, Ookayama, Meguro-ku, Tokyo 152
††Department of Biopolymer Engineering, Faculty of Technology, Tokyo University of Agriculture and Technology, Nakamachi 2-chome, Koganei, Tokyo 184
(Received October 8, 1988)

The dielectric solvent effect on the ^{29}Si NMR chemical shifts of some chlorosilanes is calculated by means of the finite perturbation theory within the CNDO/2 framework using the solvaton theory which is employed to estimate specific solute-solvent bonded interactions as a function of the dielectric constant of the medium. The calculated variations are reasonably compared with the gross trend of the observed solvent effects of ^{29}Si chemical shifts. Further, the origin of the dielectric solvent effect is discussed.

Chemical shift in NMR is known to be solvent dependent. ^{13}C NMR chemical shifts in various solvents have been observed and have been well-interpreted theoretically by means of the "solvaton"-MO theory.[1] The polar effects of aprotic solvents on nuclear shielding may be accounted for by means of an imaginary particle called the "solvaton" model.[2-4] This has been successfully employed in the calculation of solvent effects on ^{13}C chemical shifts in a number of molecules.[5-7] According to our best knowledge, there is little systematic calculation by sophisticated methods of solvent effect on ^{29}Si chemical shift considered here.

Therefore, the above approach can be extended to ^{29}Si chemical shifts of some organic compounds containing silicon atom.[8] The purpose of this work is to measure the ^{29}Si NMR chemical shifts of chlorosilanes in various kinds of solvents over a wide range of dielectric constants. Further, we aim to study theoretically dielectric solvent effects on ^{29}Si chemical shifts of chlorosilanes by the finite perturbation theory (FPT)[6] within the CNDO/2 framework.[9] For this, the solvaton model has been employed to study the effect of solvation on the screening of this nucleus in aprotic solvents. It is anticipated that its model may provide a substantial insight into the effects of solute-solvent interactions on the experimentally observed chemical shifts.

Theoretical

For convenience, we describe briefly the "solvaton" theory. In this theory it is assumed that (1) a number of charges (the "solvaton") are induced in the solvent when a solute is infinitely diluted with an aprotic solvent of dielectric constant, ε; and (2) one solvaton is associated with each atomic center of the solute molecule and its charge is equal in magnitude but opposite in sign; and (3) there are no interactions between them. From these assumptions it follows that the strength of the interaction between the solute and the "solvaton" depends on the polar nature of the solvent. The Hamiltonian, H, of the specified molecular system with M electrons and N nuclei consists of the inherent term, H_{inh}, and the solvent interaction term, H_{solv}, and is given as (in atomic units)

$$H = H_{\mathrm{inh}} + H_{\mathrm{solv}}, \tag{1}$$

where

$$H_{\mathrm{inh}} = \sum_{i=1}^{M}\left[-\frac{1}{2}\nabla_i^2 - \sum_{n=1}^{N}\frac{Z_n}{r_{ni}}\right] + \frac{1}{2}\sum_{i}^{M}\sum_{j}^{M}\frac{1}{r_{ij}} + \frac{1}{2}\sum_{k}^{N}\sum_{l}^{N}\frac{Z_k Z_l}{r_{kl}}, \tag{2}$$

$$H_{\mathrm{solv}} = \frac{(\varepsilon-1)}{2\varepsilon}\left[\sum_{i}^{M}\sum_{s}^{N}\frac{Q_s}{r_{si}} - \sum_{k}^{N}\sum_{s}^{N}\frac{Q_s Z_k}{r_{sk}}\right], \tag{3}$$

in which Q_s is the induced "solvaton" charge, r_{si} and r_{sk} are the "solvaton"-electron and "solvaton"-nucleus distances respectively, and Z_i is the nuclear charge. The first term in Eq. 3 is the interaction energy of the electrons and the induced solvent charges while the last term represents the interaction energy between the induced solvent charges (solvaton) and the nuclear core charges. The function of the solvent dielectric constant, $(\varepsilon-1)/2\varepsilon$ determines the degree of solvent-solute interaction. In these calculations, if the AO's and "solvaton" are associated with the same atomic center as the "solvaton"-electron distance r_{si}, the van der Waals radius of the particular atom type is used and if the AO's and "solvaton" are associated with different atomic centers, the "solvaton" is assumed to be centered on the atomic center associated with S and then r_{si} is evaluated. The solvent interaction was incorporated into the FPT-CNDO/2 method proposed by Pople et al.[9,10] As the effective van der Waals radius of silicon atom, 2.00 Å is used.[11] The detail of the calculation is described elsewhere.[1,4]

In this calculation, values used for bond lengths were 2.01, 1.87, 1.48, and 1.09 Å for the Si-Cl, Si-C,

Si-H, and C-H, respectively, and all the ∠C-Si-Cl, ∠Cl-Si-Cl, ∠H-Si-Cl, and ∠Si-C-H bond angles were set at 109.47°.[12] All calculations were carried out by means of a FACOM VP-30 computer at the Computer Center of Kanagawa University, a HITAC M-280H computer of the Tokyo Institute of Technology, and a HITAC S810 computer at the Institute for Molecular Science, Okazaki.

Experimental

All of chlorosilanes, $(CH_3)_3SiCl$, $(CH_3)_2SiCl_2$, $(CH_3)SiCl_3$, $(CH_3)_2HSiCl$, $(CH_3)HSiCl_2$, $HSiCl_3$, and $SiCl_4$ were commercially available spectral-grade products. Solvents used were dried under usual precautions and distilled under an atmosphere of nitrogen: Hexane (ε=1.9), carbon tetrachloride (ε=2.23), chloroform (ε=4.6), tetrahydrofuran (ε=7.39), and acetone (ε=20.7), where the value of the dielectric constant at 20 °C is indicated in parenthesis.[13]

The ^{29}Si NMR spectra were measured by means of a JEOL FX90Q spectrometer operating at 17.75 MHz equipped with a Fourier transform accessory. The measurements were made using the 20% (v/v) solutions of the above-mentioned solvents for chlorosilanes at the probe temperature of 22.4 °C in a 10 mm o.d. NMR tube, and deuterated benzene and tetramethylsilane sealed off in a 5 mm o.d. capillary were used as ^2D lock and an external reference. The observed free-induction decay after a 45° pulse width of 7.0 μs was sampled in 8192 data points and the pulse recycle time was 20 s. The ^{29}Si chemical shift was corrected for bulk magnetic susceptibility.[14] The bulk magnetic susceptibility for a solution, X_{soln}, is given as

$$X_{soln} = \sum_i^n \phi_i X_i, \quad (4)$$

where ϕ_i and X_i are the volume fraction and the bulk magnetic susceptibity of the i-th component molecule in solution, respectively.

Results and Discussion

Observed dielectric solvent effect of NMR chemical shift: The observed ^{29}Si chemical shifts of chlorosilanes in various solvents are plotted as a function of $(\varepsilon-1)/2\varepsilon$ in Fig. 1.

The factor $(\varepsilon-1)/2\varepsilon$ was chosen as abscissa because the chemical shielding is found to be proportional to $(\varepsilon-1)/2\varepsilon$ as described previously.[1] $(CH_3)_2SiCl_2$, $(CH_3)_3SiCl$, $(CH_3)SiCl_3$, $(CH_3)_2HSiCl$, $(CH_3)HSiCl_2$, and $HSiCl_3$ chlorosilanes show linearly downfield shift with increasing $(\varepsilon-1)/2\varepsilon$, but the chemical shift of $SiCl_4$ is almost independent of ε. This indicates that ^{29}Si chemical shift is linearly proportional to $(\varepsilon-1)/2\varepsilon$ as well as in the case of ^{13}C chemical shift. The observed ^{29}Si shifts for chlorosilanes can be fitted approximately by

$$\delta = A\left(\frac{\varepsilon-1}{2\varepsilon}\right) + B. \quad (5)$$

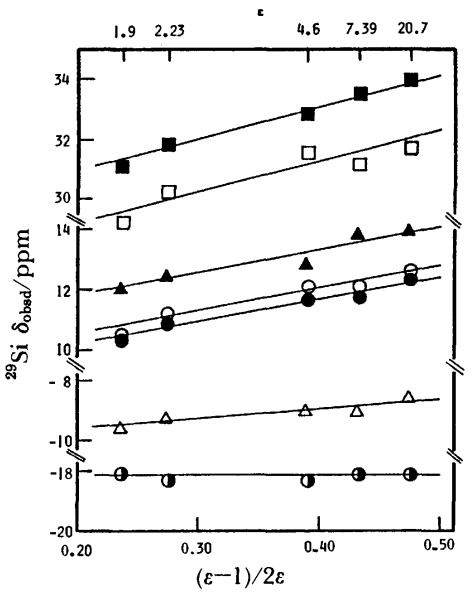

Fig. 1. Dependence on dielectric constant e of the observed ^{29}Si NMR chemical shifts δ in chlorosilanes. The positive sign means downfield shift. The sysmbols used refer to the following compounds: $(CH_3)_2SiCl_2$ (■),$(CH_3)_3SiCl$ (□), $(CH_3)SiCl_3$ (▲), $(CH_3)_2HSiCl$ (○),$(CH_3)HSiCl_2$ (●), $HSiCl_3$ (△), $SiCl_4$ (◑). The straight line was obtained by the linear least-squares fitting.

Table 1. The Variation of the Observed ^{29}Si Chemiccal Shift in Chlorosilanes as in Going from ε=1.9 to 20.7

Compound	Parameter/ppm[b]			
	$\Delta\delta_{obsd}$/ppm[a]	A_{obsd}	B_{obsd}	r[c]
$(CH_3)_3SiCl$	2.3	9.8	27.2	0.93
$(CH_3)_2SiCl_2$	2.8	11.8	28.3	0.99
$(CH_3)SiCl_3$	1.9	7.7	10.2	0.96
$(CH_3)_2HSiCl$	1.9	8.0	8.8	0.97
$(CH_3)HSiCl_2$	1.8	7.8	8.6	0.99
$HSiCl_3$	0.8	3.4	−10.4	0.91
$SiCl_4$	ca. 0	ca. 0	−18.2	0.2

a) $\Delta\delta_{obsd}=\delta_{obsd}(\varepsilon=20.7)-\delta_{obsd}(\varepsilon=1.9)$. A valus of δ_{obsd} corresponds to the linear least-squares fitting. The positive sign means downfild shift. b) The parameters are given by $\delta_{obsd}=A((\varepsilon-1)/2\varepsilon)+B$. c) Correlation coefficient.

The observed data fall approximately on a straight line plot of δ against $(\varepsilon-1)/2\varepsilon$. The magnitude of A provides a measure of the solvent effect on δ, whereas B is the value of δ in an isolated molecule. The parameters A and B can be obtained from the linear least-squares fitting. The variation of the observed ^{29}Si chemical shift ($\Delta\delta_{obsd}$) and the estimated values of parameters A_{obsd} and B_{obsd} for chlorosilanes in going from ε=1.9 to 20.7 are summarized in Table 1.

As seen from Table 1, the ^{29}Si chemical shifts of these compounds give an excellent correlation coefficient except for $SiCl_4$. The value of A_{obsd} for ^{29}Si nucleus is positive except for $SiCl_4$. This means that

the trend of the solvent effect is downfield shift. The observed chemical shift values cover a range from 0 ppm to 2.8 ppm with respect to hexane (ε=1.9).

Calculated dielectric solvent effect: Let us discuss the ^{29}Si chemical shift in chlorosilanes calculated as a function of ε by the CNDO/2 MO method using the "solvaton" theory. The results of the calculation of electron density (d), screening constants (σ^d, σ^P, and $\sigma^T(=\sigma^d+\sigma^P)$), chemical shift difference ($\Delta\sigma_{calcd}$), and correlation parameter (A_{calcd}) as a function of dielectric constant, are presented in Table 2.

Note that the calculated chemical shift (σ) is a nuclear shielding constant and so the negative sign means deshielding. On the other hand, the negative sign of the observed chemical shift (δ) means shielding. Therefore, the relative difference in the calculated chemical shift should be compared with the observed chemical shift. As seen from Table 2, the diamagnetic term, σ^d, moves slightly up-field in going from ε=1.0 to 20.7 for all compounds. This variation is consider-

Table 2. Dependences of the Calculated ^{29}Si Chemical Shifts and Correlation Parameters of Chlorosilanes and Electron Density on the Silicon Atom upon Dielectric Constant

	ε[a]	d	^{29}Si chemical shift/ppm				Parameter/ppm
			σ^d	σ^P	σ^T[b]	$\Delta\sigma_{calcd}$[c]	A_{calcd}[d]
$(CH_3)_3SiCl$	1.0	3.5475	68.01	−368.72	−300.70	−2.00	
	1.9	3.5733	68.36	−371.06	−302.70	0.0	
	2.23	3.5771	68.42	−371.40	−302.99	0.29	7.03
	4.6	3.5881	68.57	−372.37	−303.81	1.11	
	7.39	3.5919	68.62	−372.71	−304.09	1.39	
	20.7	3.5958	68.67	−373.05	−304.38	1.68	
$(CH_3)_2SiCl_2$	1.0	3.5519	68.07	−375.76	−307.69	−1.76	
	1.9	3.5822	68.49	−377.93	−309.45	0.0	
	2.23	3.5867	68.55	−378.22	−309.67	0.22	5.56
	4.6	3.5995	68.72	−379.05	−310.33	0.88	
	7.39	3.6038	68.78	−379.33	−310.55	1.10	
	20.7	3.6082	68.84	−379.62	−310.78	1.33	
$(CH_3)SiCl_3$	1.0	3.5556	68.12	−382.64	−314.51	−1.55	
	1.9	3.5917	68.61	−384.68	−316.06	0.0	
	2.23	3.5970	68.69	−384.95	−316.27	0.21	4.73
	4.6	3.6120	68.89	−385.71	−316.82	0.76	
	7.39	3.6170	68.96	−385.96	−317.00	0.94	
	20.7	3.6222	69.02	−386.22	−317.19	1.13	
$(CH_3)_2HSiCl$	1.0	3.5539	68.10	−364.73	−296.63	−2.47	
	1.9	3.5767	68.41	−367.52	−299.10	0.0	
	2.23	3.5803	68.46	−367.92	−299.46	0.36	8.95
	4.6	3.5904	68.60	−369.11	−300.51	1.41	
	7.39	3.5938	68.64	−369.51	−300.87	1.77	
	20.7	3.5974	68.69	−369.93	−301.24	2.14	
$(CH_3)HSiCl_2$	1.0	3.5496	68.04	−369.29	−301.25	−2.17	
	1.9	3.5786	68.44	−371.86	−303.42	0.0	
	2.23	3.5830	68.50	−372.25	−303.76	0.34	7.70
	4.6	3.5955	68.67	−373.31	−304.65	1.23	
	7.39	3.5998	68.72	−373.67	−304.95	1.53	
	20.7	3.6042	68.78	−374.04	−305.26	1.84	
$HSiCl_3$	1.0	3.5453	67.98	−374.67	−306.69	−2.21	
	1.9	3.5823	68.49	−377.39	−308.90	0.0	
	2.23	3.5878	68.56	−377.77	−309.21	0.31	7.03
	4.6	3.6034	68.77	−378.80	−310.03	1.13	
	7.39	3.6086	68.84	−379.15	−310.30	1.40	
	20.7	3.6141	68.92	−379.50	−310.58	1.68	
$SiCl_4$	1.0	3.5573	68.15	−390.78	−322.64	−1.47	
	1.9	3.6009	68.74	−392.85	−324.11	0.0	
	2.23	3.6073	68.82	−393.09	−324.27	0.16	3.77
	4.6	3.6251	69.06	−393.79	−324.72	0.61	
	7.39	3.6310	69.14	−394.01	−324.87	0.76	
	20.7	3.6371	69.22	−394.23	−325.01	0.90	

a) Dielectric constants are employed (20 °C): Isolated molecule (ε=1.0), hexane (ε=1.9), carbon tetrachloride (ε=2.23), chloroform (ε=4.6), tetrahydrofuran (ε=7.39), and acetone (ε=20.7). b) $\sigma^T=\sigma^d+\sigma^P$. c) Calculated chemical shifts converted to the hexane scale. The positive sign means downfield shift. d) The parameter is given by $\sigma^T=A((\varepsilon-1)/2\varepsilon)+B$.

ably small. On the other hand, the paramagnetic term, σ^P, moves linearly downfield in going from ε=1.0 to 20.7. This means that the solvent effect of the ^{29}Si chemical shift is predominantly governed by the variation of the paramagnetic term.

It would be interesting to compare these calculated value with some observed data. The same relationship (Eq. 5) as the case of the observed data is also found in the calculated data. This agreement implies that there are no specific interactions between chlorosilanes and solvent molecules. This table has two features for the calculated solvent-induced shifts. First, we discuss the solvent-induced ^{29}Si chemical shift variations of $(CH_3)_3SiCl$, $(CH_3)_2SiCl_2$, $(CH_3)SiCl_3$, and $SiCl_4$ series. The magnitude of the calculated solvent-induced shift becomes larger in the order of $SiCl_4$ (A_{calcd}=3.77)< $(CH_3)SiCl_3$ (A_{calcd}=4.73)<$(CH_3)_2SiCl_2$ (A_{calcd}=5.56)< $(CH_3)_3SiCl$ (A_{calcd}=7.03) as ε increases from 1.9 to 20.7. This means that as the number of substituted chlorine atoms is decreased, the value of parameter A_{calcd} is increased. The calculated results reproduce qualitatively the observed trend except for $(CH_3)_2SiCl_2$. Especially, for $SiCl_4$ the calculated chemical shift variation shows the smallest value compared with all the other compounds in going from ε=1.9 to 20.7. This result agrees qualitatively with the trend of the observed one. Therefore, it can be said that this is inactive in various solvent. The above results can be understood from the observed facts that the magnitude of dipole moment μ for these compounds[15] becomes in the order of $SiCl_4$ ($\mu\simeq$0)<$(CH_3)SiCl_3$ (μ=1.87)<$(CH_3)_2SiCl_2$ (μ=1.89)< $(CH_3)_3SiCl$ (μ=2.09) and therefore the magnitude of reaction field becomes in the same order. This means that the reaction field plays an important role in the solvent effect of ^{29}Si chemical shifts. Next, we discuss the solvent-induced ^{29}Si chemical shift variation of $(CH_3)_2HSiCl$, $(CH_3)HSiCl_2$, $HSiCl_3$, and $SiCl_4$ series. The magnitude of parameter A_{obsd} for them become larger in the order of $SiCl_4$<$HSiCl_3$<$(CH_3)HSiCl_2$ <$(CH_3)_2HSiCl$. The calculated results (A_{calcd}) reproduce this result. The calculated results[16] of their dipole moment show that the value of the dipole moment is increased in the order of $SiCl_4$ (μ=0)< $HSiCl_3$ (μ=1.0)<$(CH_3)HSiCl_2$ (μ=1.7)<$(CH_3)_2HSiCl$ (μ=1.8) as the number of substituted chlorine atoms is increased (the experimental data are unknown). Therefore, the above results can be explained reasonably by the same reason as the case of the first compound series.

Finally, we will consider the relationship between the ^{29}Si chemical shift and electron density as a function of the dielectric constant of the medium. In the previous work,[8] it is shown that the ^{29}Si chemical shifts move roughly downfield as an increase of the electron density on the silicon atom. The direction of such a shift is opposite to general consideration[14] that the increase of electron density leads to upfield shift. As seen from Table 2, the electron density on the silicon atom in the molecules considered here increase with an increase of ε. According to general consideration, this leads to upfield shift with an increase in ε. However, this is in disagreement with the observed results. Thus, it is apparent that such arguments must be done by the direct calculation of the ^{29}Si chemical shift as above mentioned.

From the above results, it can be concluded that the general trend found in this work would suggest the potential applicability of the FPT-CNDO/2 calculation with the "solvaton" model in interpreting solvent effects in aprotic polar media which influence ^{29}Si chemical shift.

References

1) I. Ando and G. A. Webb, *Org. Magn. Reson.*, **15**, 111 (1981).
2) G. Klopman, *Chem. Phys. Lett.*, **1**, 200 (1967).
3) G. Klopman, *J. Am. Chem. Soc.*, **90**, 223 (1968).
4) H. A. Germer, Jr., *Theoret. Chim. Acta*, **34**, 145 (1974).
5) I. Ando, A. Nishioka, and M. Kondo, *J. Magn. Reson.*, **21**, 429 (1976).
6) I. Ando, Y. Kato, M. Kondo, and A. Nishioka, *Makromol. Chem.*, **178**, 803 (1977).
7) M. Jallali-Heravi and G. A. Webb, *Org. Magn. Reson.*, **13**, 114 (1980).
8) T. Takayama and I. Ando, *Bull. Chem. Soc. Jpn.*, **60**, 3125 (1987).
9) M. Kondo, I. Ando, R. Chujo, and A. Nishioka, *J. Magn. Reson.*, **24**, 315 (1976).
10) J. A. Pople and G. A. Segal, *J. Chem. Phys.*, **44**, 3289 (1966).
11) L. Pauling, "The Nature of the Chemical Bond," 3rd ed., Cornell University Press, Ithaca (1960), pp. 260.
12) "Tables of Interatomic Distances and Configuration in Molecules and Ions," ed by L. E. Sutton, Chemical Society, London (1958), Spec. Publ., No. 11.
13) J. A. Dean, "Lange's Handbook of Chemistry," McGraw-Hill, New York (1973), Section 10.
14) J. W. Emsley, J. Feeney, and L. H. Sutcliffe, "High Resolution Nuclear Magnetic Resonance Spectroscopy," Pergamon Press, Oxford (1965), Vol. 1.
15) A. L. Mcclellan, "Tables of Experimental Dipole Moments," W. H. Freeman and Company, San Francisco (1963).
16) For calculation from available bond moments, see: A. P. Altshuller and L. Rosenblum, *J. Am. Chem. Soc.*, **77**, 272 (1955).

Inhibiting Effects of Ethanethiol, Dimethyl Sulfide, and Dimethyl Disulfide on the Corrosion of Stainless Steel (405) in Sulfuric Acid

Jalal Mohammed SALEH*,† and Yousif Kadim AL-HAIDARI
Department of Chemistry, College of Science, University of Baghdad, Baghdad, Jadiriya, Republic of Iraq
(Received February 19, 1988)

The corrosion behavior of stainless steel (405) specimen in 5 M H_2SO_4 solution has been investigated potentiostatically at four temperatures in the range 303—323 K. The inhibiting effects of ethanethiol (EtSH), dimethyl sulfide (Me_2S), and dimethyl disulfide (Me_2S_2) have thereafter been tested for four inhibitor concentrations of 0.5, 1, 5, and 10 mmol dm^{-3}. The sulfur compound addition to the H_2SO_4 solution caused a shift, mainly in the cathodic direction, of the corrosion potential, the electrode potential at low current densities as well as of the linear section of the cathodic Tafel line. The protection efficiency of each sulfur compound was determined at various temperatures and inhibitor concentrations. The sulfur compound acted as a corrosion inhibitor in the H_2SO_4 solution through adsorption on the stainless steel surface. The kinetic results, operating through a compensation effect, could well account for the variation of the inhibiting capacities of the various sulfur compounds. The results indicated that inhibition process involved the shift of the stainless steel corrosion to those surface sites which are associated with progressively higher energy of activation. EtSH was the most efficient of the three sulfur compounds for inhibiting the corrosion of the stainless steel in H_2SO_4 solution.

There have been a number of corrosion and corrosion inhibition investigations on various types of stainless steel in the acid media.[1-7] The majority of the previous literature was devoted to the effect of the type of stainless steel on the polarization behavior of this alloy in the corrosion medium, as well as to the ability of organic compounds in general to inhibit the steel corrosion.[8-10]

Organic sulfur compounds have widely been used as inhibitors for the corrosion of various iron alloys.[11-15] The literature in this respect discusses some effects of such inhibitors which could result in the corrosion inhibition, and these involved:

(i) altering the nature of the corrosion product;

(ii) changing the type and the extent of adsorption of the inhibitor on the electrode surface, and;

(iii) rearranging the corrosion current and potential.

There are several other aspects of the corrosion inhibition which are still lacking. Among such aspects are the thermodynamics of the feasibility of inhibition and the kinetics of the corrosion in the presence and absence of the inhibitor in the corrosion medium, and these need careful attention and thorough investigation.

The present research involves the potentiostatic study of the corrosion of a stainless steel specimen (type 405) in 5 M H_2SO_4 (1 M=1 mol dm^{-3}) at four temperatures in the range 303—323 K. The protection efficiencies of three sulfur compounds have been studied at the four experimental temperatures using four concentrations of the inhibitor over the range 0.5 to 10 mmol dm^{-3}. An attempt was made to predict the thermodynamic feasibility of inhibition from the coverages of the stainless steel surface by the adsorbed inhibitor. The effect of the inhibitor on the kinetics of the stainless steel corrosion was also attempted from the rates of corrosion under various experimental conditions.

Experimental

The stainless steel (405) specimen had the following composition as revealed by emission spectroscopic analysis:

element :	Cr	Al	C	Mn	Si	P	S
Wt% :	11.5	0.1	0.08	1.0	1.0	0.04	0.03

Cylinderical working electrodes were made of 8.5 mm thickness and 12.7 mm diameter. The surface of each electrode was carefully polished and then degreased and washed as described earlier.[16] A tight fitting Teflon sleeve was fitted over one end of the stainless steel electrode to expose an apparent surface area of about 1.0 cm^2 of the stainless steel. The surface preparation procedure was shown to give reproducible polarization curves, with an error in corrosion current density of less than 0.1%. The surface area of the electrode was determined by measuring all dimensions to the nearest 0.01 mm and subtracting the area under the Teflon gasket. A two-dimensional measuring microscope (Pye 6147 M) was used for area measurements.

The experimental cell which had a working compartment capacity of 750 cm^3 contained the stainless steel electrode and two platinum auxiliary electrodes and a saturated calomel electrode connected through a Luggin capillary bridge. The cell compartment was provided with a stirror and arrangements for bubbling gases through the cell solution. Before each experiment, the solution was deaerated by bubbling highly pure nitrogen gas for 2 h. The cell solution was prepared from triply distilled water and Analar grade H_2SO_4. Ethanethiol (EtSH), dimethyl sulfide (Me_2S), and dimethyl disulfide (Me_2S_2) were purum grades, obtained from Fluka, with a purity exceeding 99.5%.

The potential-current curves were plotted[16] using 'corrosoript' obtained from Tacussel electronique, which was composed of a potentiostat, an electronic millivoltmeter and

† Saddam University for Engineering and Science, College of Science, Baghdad, Jadiriya, P.O. Box 47077, Iraq.

a chart recorder. The potentiostat had an output voltage of ±10 V, output current of ±500 mA and a response time of 2—3 μs. The recorder enabled the working electrode current to be recorded in either linear or logarithmic coordinates.

Both the cathodic and anodic current-potential curves were obtained with decreasing and increasing polarization and this was repeated several times. The potential scan began initially 1 h after the specimen immersion in the acid solution, beginning at about −1.5 V and proceeded through to 1.0 V versus a saturated calomel electrode. A potentiodynamic potential sweep rate of 15 mV min^{-1} was used recording the current continuously with the change of potential.

Corrosion current densities (i_{corr}) and corrosion potentials (E_{corr}) were calculated from the polarization curves. The linear logarithmic sections of the cathodic and anodic Tafel lines were extrapolated to the point of intersection from which both i_{corr} and E_{corr} were determined.

Results and Discussion

Corrosion Potential (E_{corr}). Table 1 shows the variation of E_{corr} for the stainless steel specimen in 5 M H_2SO_4 solution with temperature and inhibitor concentration. Values of E_{corr} for the stainless steel in the acid solution in the absence of the inhibitor shifted to less negative values with increasing temperature from 303 to 323 K. E_{corr} generally shifted to more negative values with increasing inhibitor concentration in the case of Me_2S and Me_2S_2 at all the experimental temperatures. A similar behavior was observed with EtSH over the concentration range 0.5—1.0 mmol dm^{-3} at 313 and 323 K; at 303 and 308 K the shift of E_{corr} with increasing EtSH concentration was towards less negative values. A similar trend was detected with ethanethiol at 313 and 323 K over the concentration variation from 5 to 10 mmol dm^{-3}.

Tafel Slope. The influence of the inhibitor concentration on the current-potential polarization curve for the stainless steel in the H_2SO_4 solution may be summarized as:

1. The electrode potential at low current densities shifted considerably relative to the values in the absence of the inhibitor. The shift was generally towards more cathodic direction except in the case of EtSH at 303 and 308 K for all inhibitor concentrations and at 313 and 323 K for 5—10 mmol dm^{-3} where the shift was in the anodic direction (Table 1).
2. The linear part of the cathodic Tafel lines shifted parallel with respect to the original line in the absence of the inhibitor. The shift was generally in the cathodic direction (Fig. 1).
3. The Tafel lines generally maintained their linearity and slope at all inhibitor concentrations and temperatures.

The first two effects (1 and 2) indicate that all the three sulfur compounds had significant effects on the hydrogen evolution reaction. The transfer coefficient (β) which was calculated from the Tafel slope had values close to 0.5 (Table 2) in agreement with the generally accepted values of this parameter.[17,18] This suggests that sulfur compound adsorption in the double layer does not change the mechanism of hydrogen evolution reaction despite its effect on the rate. This probably indicates that the sulfur compounds which have been used as inhibitors in the present work act through adsorption on the stainless steel surface.[10,19,20]

Table 1. Potentials (V) and Currents (A cm^{-2}) for the Corrosion (E_{corr}, i_{corr}) of Stainless Steel in 5 M H_2SO_4 at Different Inhibitor Concentrations (C) and Temperatures (T)

T	C	EtSH		Me_2S		Me_2S_2	
K	mmol dm^{-3}	$-E_{corr}$	i_{corr}	$-E_{corr}$	i_{corr}	$-E_{corr}$	i_{corr}
303	0.0	0.413	5.35×10^{-3}	0.413	5.35×10^{-3}	0.413	5.35×10^{-3}
	0.5	0.402	2.70×10^{-3}	0.430	4.10×10^{-3}	0.425	3.20×10^{-3}
	1.0	0.390	1.55×10^{-4}	0.454	2.98×10^{-3}	0.434	1.18×10^{-3}
	5.0	0.370	6.26×10^{-5}	0.448	2.00×10^{-3}	0.447	9.54×10^{-4}
	10.0	0.366	3.15×10^{-5}	0.442	6.08×10^{-4}	0.445	5.93×10^{-4}
308	0.0	0.410	8.50×10^{-3}	0.410	8.50×10^{-3}	0.410	8.50×10^{-3}
	0.5	0.407	3.50×10^{-3}	0.422	7.50×10^{-3}	0.416	6.00×10^{-3}
	1.0	0.402	6.50×10^{-4}	0.439	6.00×10^{-3}	0.436	4.20×10^{-3}
	5.0	0.390	1.70×10^{-4}	0.444	3.40×10^{-3}	0.442	3.00×10^{-3}
	10.0	0.372	5.00×10^{-5}	0.450	1.40×10^{-3}	0.446	1.40×10^{-3}
313	0.0	0.407	1.14×10^{-2}	0.407	1.14×10^{-2}	0.407	1.14×10^{-2}
	0.5	0.414	9.20×10^{-3}	0.415	1.10×10^{-2}	0.421	9.00×10^{-3}
	1.0	0.428	6.80×10^{-3}	0.427	1.04×10^{-2}	0.430	7.50×10^{-3}
	5.0	0.400	7.00×10^{-4}	0.447	5.16×10^{-3}	0.443	5.15×10^{-3}
	10.0	0.382	5.70×10^{-5}	0.418	2.37×10^{-3}	0.448	2.37×10^{-3}
323	0.0	0.400	2.95×10^{-2}	0.400	2.95×10^{-2}	0.400	2.95×10^{-2}
	0.5	0.419	2.65×10^{-2}	0.416	2.70×10^{-2}	0.439	2.30×10^{-2}
	1.0	0.438	2.30×10^{-2}	0.428	2.55×10^{-2}	0.460	1.58×10^{-3}
	5.0	0.420	1.75×10^{-2}	0.438	1.65×10^{-2}	0.464	8.60×10^{-3}
	10.0	0.392	6.69×10^{-4}	0.450	7.75×10^{-3}	0.466	8.15×10^{-3}

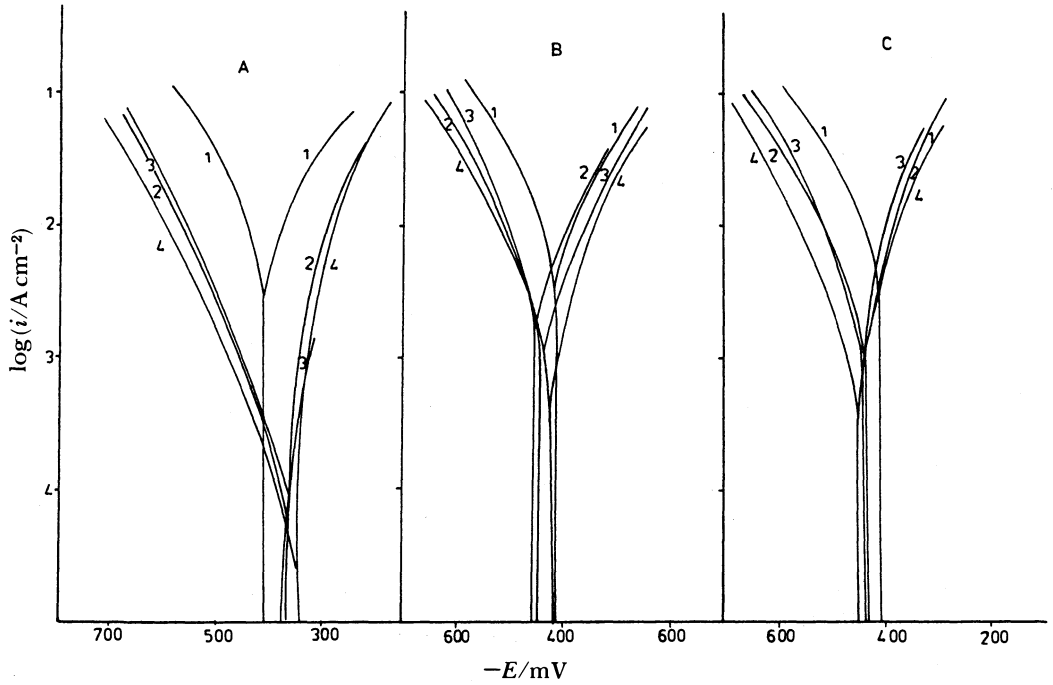

Fig. 1. Effect of the inhibitor on the cathodic and anodic polarization curves for the stainless steel (405) in 5 M H_2SO_4 at 303 K. Numbers 1, 2, 3, and 4 refer respectively to the inhibitor concentrations of zero, 1, 5, and 10 mmol dm^{-3}. A, EtSH; B, Me_2S; C, Me_2S_2.

Table 2. Effect of Inhibitor Concentration and Temperature on the Surface Coverage (θ), Tafel Slop (β) and Polarization Resistance (R_p) for the Stainless Steel Specimen in 5 M H_2SO_4

T	C	EtSH			Me_2S			Me_2S_2		
K	mmol dm^{-3}	θ	β	R_p[a)]	θ	β	R_p[a)]	θ	β	R_p[a)]
303	0.0	—	0.44	1.68	—	0.44	1.68	—	0.44	1.68
	0.5	0.74	0.45	37.4	0.15	0.45	2.20	0.36	0.43	5.7
	1.0	0.80	0.47	98.9	0.23	0.46	3.27	0.50	0.42	10.2
	5.0	0.82	0.47	163.4	0.51	0.37	3.74	0.73	0.42	8.4
	10.0	0.91	0.46	440.9	0.62	0.43	17.60	0.76	0.49	13.4
313	0.0	—	0.37	1.5	—	0.37	1.53	—	0.37	1.53
	0.5	0.38	0.39	2.3	0.11	0.36	1.40	0.21	0.42	1.55
	1.0	0.47	0.40	2.9	0.17	0.36	1.81	0.30	0.50	1.67
	5.0	0.87	0.41	56.1	0.45	0.40	2.82	0.60	0.49	4.35
	10.0	0.92	0.42	180.4	0.58	0.46	14.5	0.68	0.51	7.35
323	0.0	—	0.63	0.43	—	0.63	0.43	—	0.63	0.43
	0.5	0.16	0.60	0.60	0.11	0.60	0.44	0.10	0.51	0.95
	1.0	0.29	0.58	0.62	0.13	0.61	0.46	0.18	0.45	1.24
	5.0	0.54	0.56	1.01	0.40	0.58	0.86	0.48	0.45	2.02
	10.0	0.62	0.59	22.52	0.55	0.40	2.16	0.62	0.47	1.91

a) R_p is expressed in cm^{-2}.

Polarization Resistance. The polarization resistance (R_p) may be taken as a measure of the efficiency of the sulfur compounds to operate as corrosion inhibitors for the stainless steel in the H_2SO_4 solution, where

$$R_p = d(E-E_{corr})/di \quad (1)$$

where E and E_{corr} are in V, i in A cm^{-2}, and R_p in Ω cm^{-2}. For small polarization, values of $(E-E_{corr})$ are proportional to the current density i. Such a relationship was found in the present work to exist for the low cathodic polarization region where $(E-E_{corr})<20$ mV. This is an indication for the fact that some stage in the discharge of hydrogen ions at the electrode should be the rate-determining process. Figure 2 shows the relationship between such small $(E-E_{corr})$ values and the corresponding values of i, for the polarization in the absence and the presence of the inhibitors. Values of R_p have been derived from the slopes of various plots in Fig. 2 and these are presented in Table 2.

Protection Efficiency. The protection efficiency (P) of the sulfur compounds, operating as inhibitors, could be calculated from equation:[15,16,21]

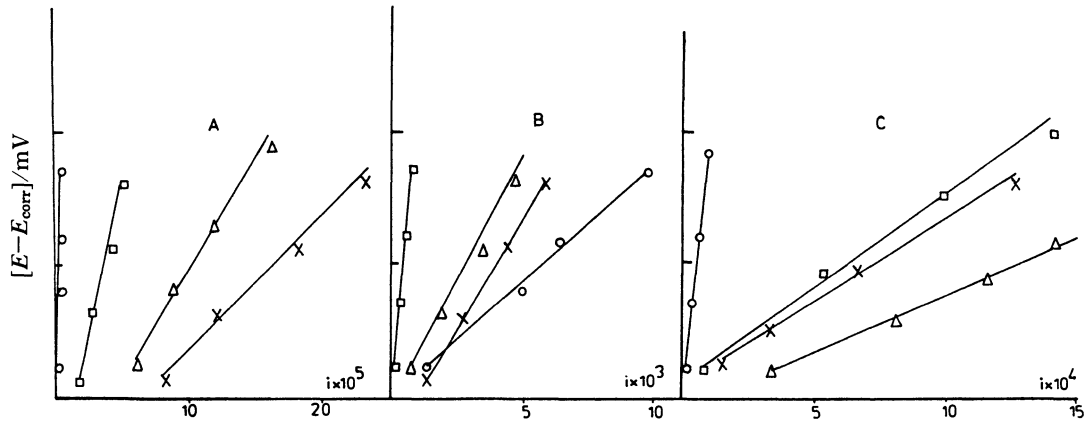

Fig. 2. Values of $(E-E_{corr})$ plotted against the current density (i) for low cathodic polarization of the stainless steel (405) in 5 M H_2SO_4 at 303 K. Symbols ○, ×, △, and □ refer respectively to inhibitor concentrations of zero, 1, 5, and 10 mmol dm^{-3}. Other symbols (A, B, and C) as in Fig. 1.

Table 3. Effect of Inhibitor Concentration (C) at Three Temperatures on the Values of the Protection Efficiency (P) of the Various Inhibitors in the 5 M H_2SO_4 Solution of the Stainless Steel Specimen

C / mmol dm^{-3}	P								
	303 K			313 K			323 K		
	EtSH	Me_2S	Me_2S_2	EtSH	Me_2S	Me_2S_2	EtSH	Me_2S	Me_2S_2
0.5	54.7	23.4	40.2	19.3	4.5	19.0	10.2	8.5	21.1
1.0	97.1	44.3	77.9	40.6	8.0	34.1	22.0	13.6	46.4
5.0	98.8	62.6	82.2	99.3	40.6	54.7	40.7	44.1	70.8
10.0	99.4	88.7	88.9	99.5	79.2	79.1	97.3	73.7	72.4

$$P=100[1-(i_c)_2/(i_c)_1] \quad (2)$$

where $(i_c)_1$ and $(i_c)_2$ are respectively the corrosion current densities (i_{corr}) for the stainless steel in the absence and the presence of the sulfur compound in the acid solution at the same temperatures; $(i_c)_1$ and $(i_c)_2$ are assumed to be proportional respectively to the corrosion rates under similar experimental conditions in the absence and the presence of the inhibitor in the corrosion medium.[22] Values of P that have been calculated, for the three sulfur compounds, from the data of Table 1 are indicated in Table 3.

Values of P generally increased at all the experimental temperatures with increasing concentration of the inhibitor (Table 3). The highest protection efficiency (P_h) of the sulfur compounds was attained at 303 K, as well as at 313 K in the case of EtSH, and corresponded to inhibitor concentration of 10 mmol dm^{-3}. P_h values of the three sulfur compounds could be arranged in the order: EtSH>Me_2S_2>Me_2S. Values of P at 303 K remained relatively high for EtSH even at 1 mmol dm^{-3} and the values of P for this inhibitor at this temperature showed the least dependence on the inhibitor concentration. The least dependencies on the inhibitor concentration were observed with EtSH and Me_2S at 313 and 323 K. At 10 mmol dm^{-3} of either Me_2S and Me_2S_2 in the acid solution, P became higher at 313 K than the values at 323 K in contrast to the behavior at 1 and 5 mmol dm^{-3}. Values of P decreased only slightly in the case of EtSH at 10 mmol dm^{-3}, while the decrease of P for this inhibitor was sharp and substantial at 1 and 5 mmol dm^{-3} beginning at 303 K in the former case and at 313 K at the latter inhibitor concentration. The decrease of P with temperature for Me_2S and Me_2S_2 was gradual at 10 mmol dm^{-3}, but the decrease at the other inhibitor concentrations was rather sharp over the range 303—313 K increasing thereafter on raising the temperature to 323 K (Table 3).

Inhibitor Adsorption. The coverage (θ) of the stainless steel surface by the adsorbed inhibitor was estimated from the current densities at constant potential in the presence (i_2) and absence (i_1) of the inhibitor in the acid solution using the equation:[15,23]

$$\theta=1-(i_2)/(i_1) \quad (3)$$

Table 2 gives the calculated values of θ for the various inhibitors at different experimental temperatures and inhibitor concentrations. At any experimental temperature, θ increased with increasing inhibitor concentration. On the other hand, values of θ, at a given inhibitor concentration, decreased with the rise of the temperature from 303 to 323 K.

The manner in which the values of θ for each inhibitor varied at a constant temperature with the concentration (C) of the inhibitor conformed to Langmuir

adsorption isotherm which may be put as:

$$\frac{C}{\theta} = \frac{1}{b} + C \quad (4)$$

A plot of C/θ values against the corresponding values of C was found to be linear with respect to each inhibitor as seen in Fig. 3. The values of b for each sulfur compound could be estimated from the reciprocal of the intercept of the appropriate plot in Fig. 3. Table 4 gives values of b for the various sulfur compounds which have been utilized as inhibitors for the corrosion of the stainless steel in the H_2SO_4 solution.

The parameter b in Eq. 4 may be defined as:[24,26]

$$b = a \exp(-\Delta H_a/RT) \quad (5)$$

where ΔH_a is the heat of inhibitor adsorption on the stainless steel surface and a is a constant.[24] A plot of $\log b$ versus $1/T$ for each sulfur compound should result in a straight line if a and ΔH_a remained constant over the experimental temperature range as was found with the present results indicated in Fig. 4. Values of ΔH_a for the temperature range 303—323 K have been derived for the various inhibitors from the slopes of the plots in Fig. 4 and these have been listed in Table 4. Values of ΔH_a are shown (Table 4) to be all negative reflecting the exothermic behavior of the inhibitor adsorption on the stainless steel surface. The magnitude of ΔH_a is less negative in the case of Me_2S as compared with the remaining two sulfur compounds. This is an indication for the stronger inhibitor adsorption in the case of EtSH and Me_2S_2 as compared with that of Me_2S. This result well agrees with that presented in Table 3 for the variation of the protection efficiency of the inhibitors with concentration; values of P are shown in Table 3 to be generally higher for EtSH and Me_2S_2 at all inhibitor concentrations than of Me_2S.

The parameter b, given in Eq. 4 represents the equilibrium constant for the adsorption/desorption processes of the inhibitor on the stainless steel surface and could be expressed as;[24]

$$b = \exp(-\Delta G_a/RT) = \exp(\Delta S_a/R)\exp(-\Delta H_a/RT) \quad (6)$$

where ΔG_a, ΔS_a, and ΔH_a are respectively the changes in the free energy, entropy, and enthalpy of the inhibitor adsorption on the stainless steel surface. Values of

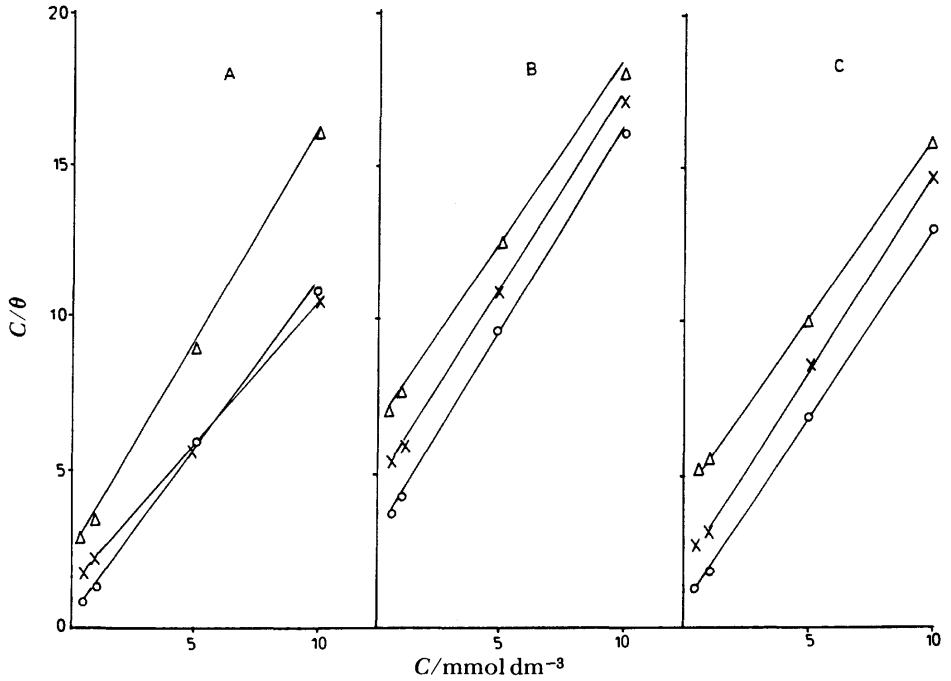

Fig. 3. Langmuir adsorption isotherms plotted as C/θ versus C for the three inhibitors at 303 (○), 313 (×), and 323 K(△).

Table 4. Values of b, ΔG_a (kJ mol^{-1}), ΔH_a (kJ mol^{-1}), and ΔS_a (J K^{-1} mol^{-1}) for the Adsorption of the Inhibitors on the Stainless Steel Specimen at Three Temperatures, in the Range 303—323 K

T	EtSH				Me_2S				Me_2S_2			
K	b	$-\Delta H_a$	$-\Delta G_a$	$-\Delta S_a$	b	$-\Delta H_a$	$-\Delta G_a$	$-\Delta S_a$	b	$-\Delta H_a$	$-\Delta G_a$	$-\Delta S_a$
303	2857		20	184	328		14.6	153	1432		18.3	185
313	1053	76.9	18	184	213	31.7	14.0	146	491	74.3	16.0	186
323	433		16	184	151		13.5	140	231		14.7	185

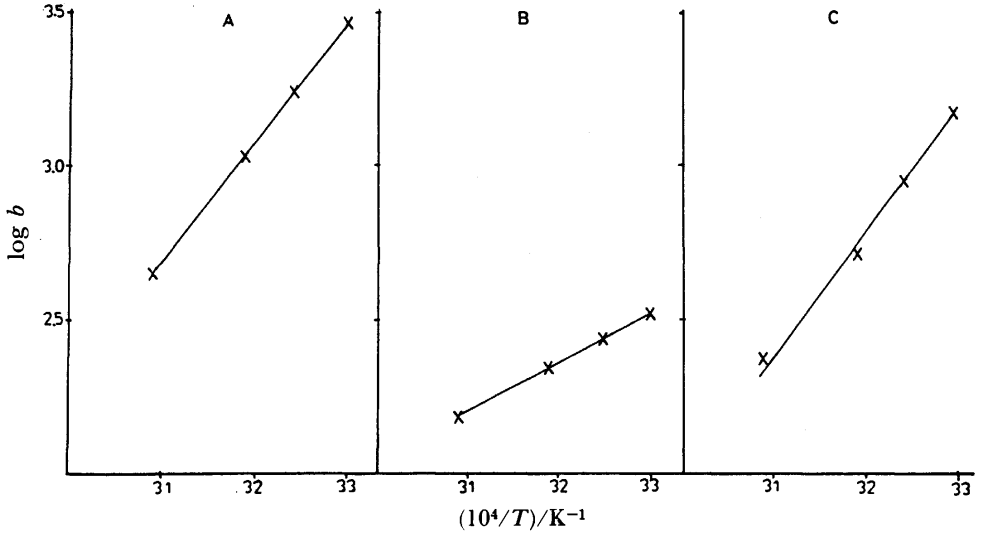

Fig. 4. Values of $\log b$ plotted versus $1/T$ for the three inhibitors in the stainless steel/sulfuric acid system.

ΔH_a have previously been derived from the plots of Fig. 4 which have been presented in Table 4. Using values of b and ΔH_a from Table 4 at each of the four experimental temperatures in the range 303—323 K, it was possible to deduce the corresponding values of ΔG_a and ΔS_a and these have been inserted in Table 4. Values of ΔG_a indicate inhibition of the stainless steel corrosion in the H_2SO_2 solution by the sulfur compounds became less favorable as the temperature increased from 303 to 323 K. This conclusion generally agrees with the results of Table 3 where the values of P were higher at 303 K than at the higher temperatures. The overall changes in ΔG_a and ΔS_a over the temperature range 303—323 K are shown in Table 4 to be almost the same for both EtSH and Me_2S_2 and the values are more negative than for Me_2S. The less negative values of ΔS_a for Me_2S than for EtSH and Me_2S_2 should reflect a far less decrease in the degrees of freedom subsequent to adsorption on the electrode surface in the case of the former inhibitor than of the latter two sulfur compounds. This suggests a weaker adsorbed species as a consequence of Me_2S adsorption on the stainless steel than those resulting throughout adsorption of EtSH or Me_2S_2.

Kinetics of Corrosion. The rate (r) of the stainless steel corrosion in the H_2SO_4 solution increased generally with the rise of the temperature from 303 to 323 K, and the behavior followed Arrhenius equation:

$$r = A \exp(-E/RT) \quad (7)$$

where A and E are respectively the preexponential factor and the energy of activation. Due to the linearity of the Tafel slope segment of the current-potential polarization curve, the value of r in Eq. 7 was taken to be directly proportional to the corrosion current density (i_{corr}) through such relation as:[21]

$$r = 0.13(\theta/d)i_{corr} \quad (8)$$

where θ is the equivalent weight of the metal and d its density. Using the appropriate conversion factor, the values of i_{corr} at each temperature could be converted into rate (i) in units of 'atom cm^{-2} s^{-1}'. Figure 5 shows Arrhenius plots for the blank (absence of inhibitor) and various inhibitor concentrations; values of E and A have been derived from the slopes and intercepts of the plots respectively. Table 5 gives the resulting values of E and $\log A$ for the corrosion of the stainless steel specimen in the acid solution. Both $\log A$ and E increased smoothly with increasing inhibitor concentration.

A linear relationship was found to exist between the experimental values of $\log A$ and the corresponding values of E which could be expressed as:[27]

$$\log A = mE + l \quad (9)$$

where m and l are respectively the slope and the intercept of the plot in Fig. 6. Such a relationship is termed a 'compensation effect' which is frequently found to describe the kinetics of catalytic and a number of tarnishing reactions on metals.[28-31] Equation 9 shows that simultaneous increases or decreases in E and $\log A$ for a particular system tend to compensate from the standpoint of the reaction rate. A number of interpretations have been offered for the phenomenon of the compensation effect in surface reactions,[32-35] among which the effect could be ascribed to the presence of energetically heterogeneous reaction sites on the metal surface; and the corrosion reaction should therefore occur first on surface sites with low energy of activation and spreading thereafter to those sites where E values are progressively higher.

The activation energy (E) of the stainless steel corrosion in the H_2SO_4 solution in the absence of the inhibitor was 69.5 kJ mol^{-1}; the corrosion should thus be confined to surface sites with such energy of activa-

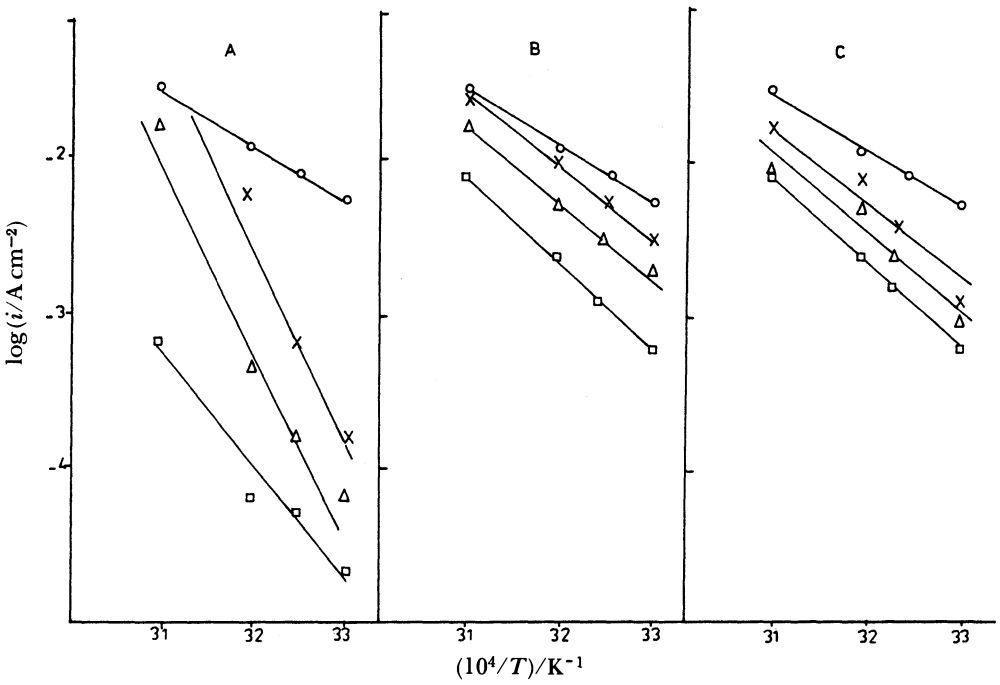

Fig. 5. Arrhenius plots, relating log i_{corr} to $1/T$, for the corrosion of the stainless steel (405) in 5 M H_2SO_4 in the absence and the presence of the inhibitors in the acid. Symbols as in Fig. 2.

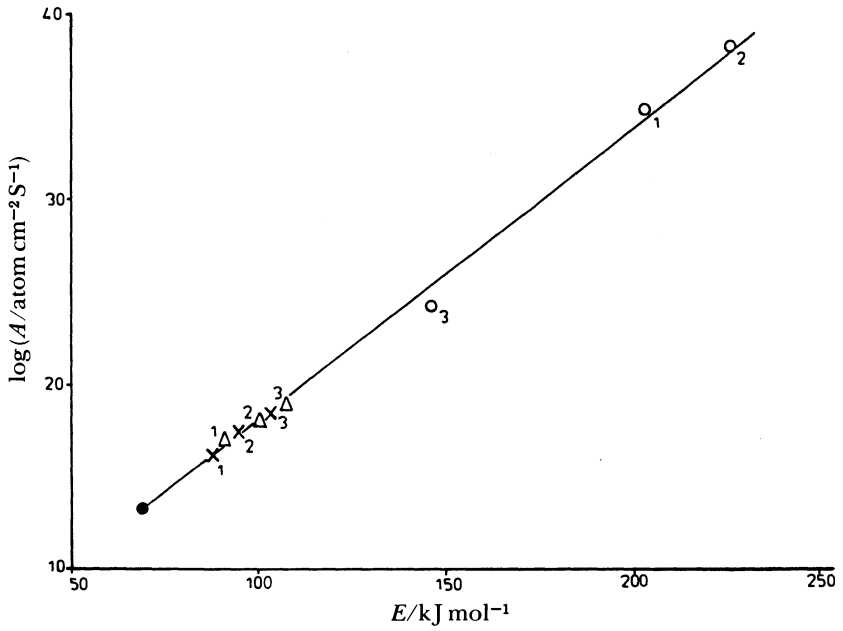

Fig. 6. Variation of the activation energy (E) with the preexponential factor ($\log A$) for the corrosion of the stainless steel (405) in 5 M H_2SO_4. EtSH, O; Me_2S, △; Me_2S_2, ×. Numbers 1, 2, and 3 refer respectively to inhibitor concentrations of 1, 5, and 10 mmol dm^{-3}. ●, corresponds to the value in the absence of the inhibitor.

tion. The presence of the sulfur compound in the acid solution accordingly shifts the corrosion reaction to those sites where E values are greater. The corrosion reaction will further be pushed to surface sites which are characterized with progressively higher values of E as the concentration of the inhibitor in the acid solution became greater.

The results of Fig. 6 and Table 5 reveal the following:

1. For all inhibitor concentrations in the acid, the variation of E values for the three sulfur compounds, followed the sequence:

Table 5. Activation Energies (E) and Preexponential Factors (A/atom cm^{-2} s^{-1}) for the Corrosion of the Stainless Steel Specimen in 5 M H_2SO_4 at Four Inhibitor Concentrations (C)

Inhibitor	C / mmol dm^{-3}	log A	E / kJ mol^{-1}
EtSH	0.0	11.6	69.5
	0.5	32.2	186.5
	1.0	34.7	204.7
	5.0	38.0	227.2
	10.0	24.1	147.0
Me_2S	0.0	11.6	69.5
	0.5	14.8	78.0
	1.0	16.1	87.7
	5.0	16.8	93.6
	10.0	18.2	103.8
Me_2S_2	0.0	11.6	69.5
	0.5	15.4	86.5
	1.0	16.8	91.9
	5.0	17.8	100.5
	10.0	18.7	106.8

$$EtSH > Me_2S_2 > Me_2S$$

This reflects the greatest tendency of the stainless steel for corrosion in the acid solution containing Me_2S as compared with the behavior of the specimen in the presence of EtSH under similar inhibitor concentration and temperature. This conclusion agrees with the protection efficiency results which have been presented in Table 3. The results are also in line with the variation of the ΔG_a values (Table 4) which have been obtained for the inhibitor adsorption on the stainless steel electrode.

2. The dependence of the E and log A values on the inhibitor concentration is seen in Fig. 6 to be far more smaller in the case of Me_2S and Me_2S_2 as compared with that of EtSH.

Molecular Structure Consideration. The tendencies of the sulfur compounds to adsorb on, and hence protect, the stainless steel surface are shown from the kinetic results to decrease from EtSH, through Me_2S_2, to Me_2S. A qualitative explanation of this sequence may be found from the consideration of the electronic structures of these compounds. Each of EtSH and Me_2S has one lone pair of electrons on sulfur while there are two such pairs in Me_2S_2. The lone pairs of electrons on the sulfur atoms are delocalized and hence produce delocalization or resonance energy which stabilizes the sulfur compound.[36] Thus the larger the number of delocalized electrons, the more stable is the charge density on the 'anchoring' atoms (in this case the sulfur) and hence the larger is the strength of adsorption on the metal surface. Comparing Me_2S_2 with Me_2S, one would expect stronger adsorption of the former, and therefore greater inhibition, than of the latter. Furthermore, both Me_2S_2 and Me_2S do not contain hydrogen atoms linked to sulfur as in the case of EtSH. This should produce an additional adsorption tendency for this compound (EtSH) on the electrode surface as compared with the remaining two sulfur compounds.

The organic sulfur compounds which have been dealt with in the present work are classified as toxic substances and can inhibit the catalytic activity of metal surfaces due to the presence of lone pairs of electrons on the sulfur atoms.[37] The poisoning effect results from the formation of strong dative bonds between the toxic molecules and the surface atoms. It has been established that the poisoning effect among a series of alkyl sulfides and disulfides increased by lengthening the chain in these compounds.[38] These facts showed that Me_2S_2 was more toxic than Me_2S and that EtSH behavior was comparable with that of Me_2S_2. This conclusion well agrees with the calculated values of ΔH_a (Table 4) as the heat of adsorption is known to be a good measure of the strength of adsorption on a surface.

References

1) T. Ishikawa and G. Okamoto, 1st Intr. Congr. Metal Corrosion, 10—15 April, 1961, Butterworths, London (1961), p. 444.

2) I. G. Mugulescu and O. Radevici, 1st Intr. Congr. Metal Corrosion, 10—15 April, 1961, Butterworths, London (1961), p. 302.

3) W. O. Binder, J. Thomson, and C. R. Bishop, *Proc. Am. Soc. Test. Mater.*, **56**, 903 (1956).

4) M. A. Streicher, *Corrosion*, **14**, 19 (1958).

5) D. Warren, *Corrosion*, **16**, 101 (1960).

6) V. A. Suprunov and M. Kh. Fried, *Khim-Tekhnol. Inst.*, **12**, 180 (1970) (Russ.).

7) J. E. Truman, "Corrosion; Metal/Environment," ed by L. L. Shreir, Newness, Butterworths, Boston, Mass. (1976), Vol. 1, p. 352.

8) M. B. Lawson, *Corrosion*, **36**, 493 (1980).

9) B. Danmelly, T. C. Downie, and R. Grzeskowiak, *Corros. Sci.*, **14**, 597 (1974).

10) H. Brandt, M. Fischer, and K. Schwabe, *Corros. Sci.*, **10**, 631 (1970).

11) G. Trabanelli, F. Zucchi, G. Gullini, and V. Carassiti, *Werkst. Korros.*, **20**, 1012 (1969).

12) K. Schwabe, G. Reinhard, M. Fischer, and K. Schaarschmidt, *Werkst. Korros.*, **22**, 302 (1971).

13) P. Markov, C. Roumian, and S. Chorbadziev, *Corros. Sci.*, **18**, 103 (1978).

14) N. Subramanyan, K. Ramakrishnaiah, S. V. Iyer, and V. Kapali, *Corros. Sci.*, **18**, 1083 (1978).

15) B. G. Ateya, B. E. Anadouli, and F. M. A. El-Nizamy, *Bull. Chem. Soc. Jpn.*, **54**, 3157 (1981).

16) L. A. Al-Shamma, J. M. Saleh, and N. A. Hikmat, *Corros. Sci.*, **27**, 221 (1987).

17) B. E. Conway, "Electrochemical Data," Elsevier, New York (1952), p. 347.

18) N. Tanaka and R. Tamamushi, *Electrochim. Acta*, **9**, 953 (1964).

19) T. P. Hoar and R. D. Holliday, *J. Appl. Chem.*, **3**, 502 (1953).

20) H. Kassche, "Die Korrosion der Metalle," Springer-

Verlag, Berlin (1966), p. 159.
21) W. J. Larans, F. R. G. Karlaruhe, and F. Mansfeld, Proc. 8th. Inter. Congr. Metal Corrosion, Dechema, West Germany, 6—11, September (1981).
22) G. Trabanelli and V. Carassiti, "Advances in Corrosion Science and Technology," Plenum Press, New York (1950), Vol. 1, p. 147.
23) I. A. Amer and S. A. Darwish, *Corros. Sci.*, **7**, 579 (1967).
24) G. C. Bond, "Catalysis by Metals," Academic Press, New York (1962), pp. 70—71, 126.
25) H. E. Ries, Jr., "Catalysis," ed by P. H. Emmett, Reinhol Publishing Corp. (1954), pp. 6—8.
26) G. Schay, *Acta Chim. Acad. Sci. Hung.*, **3**, 511 (1953).
27) G. C. Bond, "Catalysis by Metals," Academic Press, New York (1962), p. 140.
28) S. A. Isa and J. M. Saleh, *J. Phys. Chem.*, **76**, 2560 (1972).
29) Y. M. Dadiza and J. M. Saleh, *J. Chem. Soc., Faraday Trans. 1*, **68**, 269 (1972).
30) Y. K. Al-Haidari, J. M. Saleh, and M. H. Matloob, *J. Phys. Chem.*, **89**, 3286 (1985).
31) Y. K. Al-Haidari and J. M. Saleh, *J. Chem. Soc., Faraday Trans. 1*, **84**, 3027, 3043 (1988).
32) F. H. Constable, *Proc. R. Soc. London, Ser. A*, **108**, 355 (1952).
33) E. Cremer and G. M. Schwab, *Z. Phys. Chem. (Leipzig), A*, **144**, 243 (1929).
34) E. Cremer, "Advances in Catalysis," Academic Press, New York (1955), Vol. 7, p. 75.
35) C. Kemball, *Proc. R. Soc. London, Ser. A*, **217**, 276 (1953).
36) E. B. Maxted, "Advances in Catalysis," Academic Press, New York (1951), Vol. 3, p. 129.
37) R. H. Griffith and J. D. F. Mrash, "Contact Catalysis," Oxford University Press (1957), pp. 193—207.

Viscosity *B*-Coefficients of Tetraalkylammonium Bromides in 2-Methoxyethanol at 25 °C

Debasis DASGUPTA, Susanta DAS, and Dilip K. HAZRA*
Department of Chemistry, North Bengal University, Darjeeling 734430, India
(Received April 18, 1988)

The relative viscosities of solutions of tetraalkylammonium bromides, R_4NBr, ($R=C_2H_5$ to C_7H_{15}) have been measured in 2-methoxyethanol (ME) at 25 °C. The data have been analyzed in the form of associated electrolytes and the *B*-coefficients have been evaluated. The ionic *B*-values have been determined using the "reference electrolytes" viz. Bu_4NBBu_4 and Bu_4NBPh_4. The results have been discussed on the basis of Einstein's equation and in terms of a transition state treatment.

The potentiality of 2-methoxyethanol (ME) as a solvent for use in nonaqueous batteries and its application in synthesis[1] and electrochemical[2] studies have been widely stressed. These necessitate the study of the transport properties of various ions in this 'quasi-aprotic' medium[3] both conductometrically and viscometrically. The viscometric method is known to give valuable information regarding ion-solvent interactions which are the controlling forces in dilute solutions where ion-ion interactions are absent.[4] The variations of the solvational properties are reflected in the viscosity *B*-coefficients of ions. Although a number of extensive viscometric studies[5,6] have been made in various solvents with different electrolytes, but literature provides no information regarding the viscometric studies of tetraalkylammonium halides in 2-methoxyethanol. This led us to undertake the title investigation and the results are reported in this article.

Experimental

2-Methoxyethanol (G.R.E. Merck) was distilled twice in an all-glass distillation set before use. The properties at 25 °C obtained for the purified sample were 0.96002 g cm^{-3} for the density and 1.5414 cP (1 P=0.1 Pa s) for the viscosity (η_0) and these values are in good agreement with the literature values.[7]

Tetraalkylammonium bromides were of Fluka's purum or puriss grade and purified in the manner as given in the literature[8] and also described by us earlier.[9] The salts were purified by recrystallization and the higher homologues were recrystallized twice to ensure highest purity. The recrystallized salts were dried in vacuum at elevated temperatures for 12 h.

Tetrabutylammonium tetraphenylborate (Bu_4NBPh_4) was prepared by mixing equimolar quantities of $NaBPh_4$ and Bu_4NBr as described in the literature.[10] Tetrabutylammonium tetrabutylborate (Bu_4NBBu_4) (Alfa product) was purified as suggested by Lawrence et al.[11]

The concentration of the salts was generally varied from 0.009 M to 0.05 M (1M=1 mol dm^{-3}) which was prepared by weight dilution of the stock solution (ca. 0.1 M). The conversion of the molality into molarity was done using the density values. The kinetic viscosities were measured at the desired temperature (accuracy ±0.01 °C) using a suspended Ubbelohde-type viscometer. The densities were measured using an Ostwald-Sprengal type pycknometer. The details of the experimental procedure employed have been described previously.[9] The accuracies of the density and viscosity measurements were $\pm 3\times10^{-5}$ g cm^{-3} and 0.01% respectively. The electrical conductivities were measured with a Pye-Unicam conductivity meter (PW 9509) within an accuracy of ±0.1%.

The dielectric constant of ME (ε=16.93) was taken from the literature.[12]

Results and Discussion

The relative viscosities of the electrolytes in solution are generally analyzed by the well-known Jones-Dole equation,[13]

$$(\eta/\eta_0-1)/\sqrt{c}=A+B\sqrt{c}, \quad (1)$$

where η and η_0 are the viscosities of the solution and the solvent respectively and c is the molar concentration.

As these electrolytes have been found to be strongly associated in this solvent from conductivity measurements,[14] so the viscosity data have been analyzed by Eq. 2 as recently done by Feakins et al.[15] instead of Eq. 1,

$$\eta_r=1+A\sqrt{\alpha c}+B_i(\alpha c)+B_p(1-\alpha)c, \quad (2)$$

where, A, B_i, B_p are the characteristic constants and α is the degree of dissociation of the ion pair. The values of ion-pair dissociation constants for the electrolytes were calculated from the conductivity data[14] using the set of equations as described in the literature.[15]

Equation 2 was rearranged to give

$$(\eta_r - 1 - A\sqrt{\alpha c})/\alpha c = B_i + B_p\left(\frac{1-\alpha}{\alpha}\right). \quad (3)$$

The $(\eta_r-1-A\sqrt{\alpha c})/\alpha c$, concentration c, density ρ, and $(1-\alpha)/\alpha$ values of the solutions of different electrolytes at 25 °C are reported in Table 1.

The A-values were calculated theoretically from the physical properties of the solvent and the limiting ionic equivalent conductances[14] using the Falkenhagen and Vernon equation,[16]

$$A_{Theo} = \frac{0.2577\,\Lambda^\circ}{\eta_0(\varepsilon T)^{1/2}\lambda_+^\circ\lambda_-^\circ}\left[1-0.6863\left(\frac{\lambda_+^\circ-\lambda_-^\circ}{\Lambda^\circ}\right)^2\right] \quad (4)$$

Table 1. Density (ρ), Concentration (c), Relative Viscosity (η_r), $(1-\alpha)/\alpha$ and $(\eta_r-1-A\sqrt{\alpha c}\,)/\alpha c$ of Tetraalkylammonium Bromides and the Two Reference Electrolytes viz. Bu_4NBBu_4 and Bu_4NBPh_4 in 2-Methoxyethanol at 25 °C

Salt	$(\eta_r-1-A\sqrt{\alpha c}\,)/\alpha c$	η_r	c / mol dm^{-3}	$(1-\alpha)/\alpha$	ρ / g cm^{-3}
Tetraethylammonium bromide	0.700	1.005	0.00963	0.970	0.96064
	1.299	1.012	0.02417	2.209	0.96158
	1.478	1.014	0.02904	2.581	0.96188
	1.667	1.019	0.03883	2.971	0.96250
	1.816	1.024	0.04867	3.281	0.96312
Tetrapropylammonium bromide	0.801	1.007	0.00963	0.498	0.96057
	1.010	1.014	0.01933	0.721	0.96112
	1.100	1.018	0.02419	0.811	0.96139
	1.180	1.022	0.02908	0.891	0.96167
	1.301	1.029	0.03890	1.028	0.96221
	1.421	1.037	0.04878	1.149	0.96275
Tetrabutylammonium bromide	1.350	1.009	0.00964	0.776	0.96042
	1.651	1.019	0.01934	1.029	0.96082
	1.900	1.024	0.02422	1.235	0.96102
	2.350	1.030	0.02912	1.614	0.96121
	2.475	1.049	0.04889	1.720	0.96208
Tetrapentylammonium bromide	1.347	1.010	0.00964	0.750	0.96038
	1.660	1.019	0.01936	1.071	0.96075
	1.781	1.023	0.02425	1.197	0.96093
	1.880	1.028	0.02916	1.308	0.96111
	2.082	1.037	0.03905	1.500	0.96146
	2.281	1.046	0.04902	1.672	0.96182
Tetrahexylammonium bromide	1.600	1.013	0.00964	0.551	0.96026
	2.001	1.025	0.01937	0.802	0.96049
	2.175	1.032	0.02428	0.900	0.96061
	2.325	1.039	0.02920	0.992	0.96073
	2.575	1.052	0.03912	1.152	0.96095
	2.850	1.066	0.04913	1.321	0.96118
Tetraheptylammonium bromide	2.001	1.006	0.00965	0.624	0.96023
	2.505	1.028	0.01939	1.050	0.96043
	2.550	1.040	0.02925	1.107	0.96064
	2.775	1.053	0.03920	1.278	0.96084
	2.950	1.066	0.04926	1.426	0.96104
Tetrabutylammonium tetrabutylborate	1.350	1.013	0.00964	0.368	0.95939
	1.700	1.026	0.01986	0.543	0.95878
	1.851	1.033	0.02425	0.616	0.95847
	1.950	1.039	0.02917	0.679	0.95816
	2.200	1.067	0.03906	0.793	0.95757
	2.400	1.069	0.04903	0.890	0.95696
Tetrabutylammonium tetraphenylborate	1.661	1.002	0.00964	0.993	0.96024
	2.027	1.034	0.01979	1.540	0.96045
	2.441	1.041	0.02418	1.742	0.96075
	2.628	1.047	0.02951	1.923	0.96087
	2.803	1.077	0.04922	2.096	0.96095

The A-coefficient values thus obtained have been recorded in Table 2. These A-values have been used for analysis of the data.

The plots of $(\eta_r-1-A\sqrt{\alpha c})/\alpha c$ against $(1-\alpha)/\alpha$ were linear in all cases. The intercept at $(1-\alpha)/\alpha=0$ were taken as the required value of B_i. The B-coefficients (B_i-values) reported in Table 2 for the electrolytes were obtained using the least square method.

Viscosity data have also been analyzed on the basis of the transition state treatment of the relative viscosity of electrolytic solutions as suggested by Feakins et al.[17]

The B-coefficient is expressed by

$$B = \frac{\bar{V}_1^\circ - \bar{V}_2^\circ}{1000} + \frac{\bar{V}_1^\circ}{1000}\left(\frac{\Delta\mu_2^{\circ\neq} - \Delta\mu_1^{\circ\neq}}{RT}\right), \quad (5)$$

where $\bar{V}_1^\circ$ and $\bar{V}_2^\circ$ are the partial molar volumes of the solvent and the solute respectively. $\Delta\mu_2^{\circ\neq}$, the contribution per mole of solute to the free energy of activation for viscous flow of the solution, has been determined from the above relationship. $\Delta\mu_1^{\circ\neq}$, the free energy of activation per mole of the pure solvent, is given by

Table 2. A-Coefficients (Theoretical), B-Coefficients and $\Delta\mu_2^{\circ\neq}$ Values for the Electrolytes in 2-Methoxyethanol at 25 °C

Salt	A	B-Coefficient	$\Delta\mu_2^{\circ\neq}$
	$dm^{3/2}\,mol^{-1/2}$	$dm^3\,mol^{-1}$	$kJ\,mol^{-1}$
Et_4NBr	0.0215	0.231	23.69
Pr_4NBr	0.0244	0.327	28.76
Bu_4NBr	0.0260	0.425	34.09
$(C_5H_{11})_4NBr$	0.0281	0.607	41.76
$(C_6H_{13})_4NBr$	0.0308	0.703	47.01
$(C_7H_{15})_4NBr$	0.0345	1.258	66.26
Bu_4NBBu_4	0.0326	0.609	48.41
Bu_4NBPh_4	0.0201	0.678	50.36

The maximum uncertainty of the B-coefficient is ±0.005. Errors in $\Delta\mu_2^{\circ\neq}$ values are generally ±0.1 or less.

$$\Delta\mu_1^{\circ\neq} = \Delta G_1^{\circ\neq} = RT \ln\left(\frac{\eta_0 \bar{V}_1^{\circ}}{hN}\right), \tag{6}$$

and the value for 2-methoxyethanol at 25°C is 14.18 kJ mol^{-1}. The activation parameters for viscous flow for the electrolytes are given in Table 2.

The viscosity B-coefficients (Table 2) are larger and positive and increase as we go from Et_4NBr to $(C_7H_{15})_4NBr$. This is a common feature in most nonaqueous solvents.[18] The B-coefficients for tetraalkylammonium halides in almost in all dipolar aprotic solvents show a weak temperature dependence[18] whereas those in ME show a strong temperature dependence as observed in water.[18] This may be due to the 'quasi-aprotic' nature of ME. The changes in the $\Delta\mu_2^{\circ\neq}$ follows the same pattern as the B-values.

In order to distinguish the effect each single has in 2-methoxyethanol, the ionic B-values were calculated using Bu_4NBBu_4[18-21] and Bu_4NBPh_4[14,22,23] as reference electrolytes by

$$B_{Bu_4N^+} = B_{Bu_4B^-} = \frac{1}{2} B_{Bu_4NBBu_4} \tag{7}$$

and

$$\frac{B_{Ph_4B^-}}{B_{Bu_4N^+}} = \frac{r^3_{Ph_4B^-}}{r^3_{Bu_4N^+}} = \left(\frac{5.35}{5.00}\right)^3. \tag{8}$$

The average B_{ion}-values of tetraalkylammonium ions are recorded in Table 3. The ionic $\Delta\mu_2^{\circ\neq}$ values have also been recorded in Table 3.

The ionic B-coefficients for the tetraalkylammonium ions have been found to increase continuously from Et_4N^+ to $(C_7H_{15})_4N^+$ in ME. An analysis of B-coefficients can be made on the basis of Einstein's equation,[24]

$$B_{\pm} = 2.5 \times \frac{4}{3}\pi \frac{R_{\pm}^3 N}{1000}, \tag{9}$$

where $R_{\pm}$ is the radius of the ion assumed as a rigid sphere moving in a continuum and 2.5 is the shape factor for a sphere. The number (n_s) of solvent molecules bound to the ion in the primary sphere of solvation can be calculated by combining the Jones-Dole equation with Einstein's[25]

$$B_{\pm} = \frac{2.5}{1000}(V_i + n_s v_s), \tag{10}$$

where V_i represents the bare ion molar volume and is related to the crystallographic radius r_c of the ion, v_s is the solvent molar volume. The values of $R_{\pm}$ and n_s are shown in Table 4. The values may be compared with the corrected Stokes' radii obtained from conductance studies. For cations R_+ values are much less than r_c values, showing that these ions are scarcely solvated in this medium. On the other hand the comparatively high n_s as well as R value for Br^- ion indicate this ion's capacity for interactions in the solvent as already found in other aprotic solvents.[6]

From Table 3 we find that the change in ionic $\Delta\mu_2^{\circ\neq}$ values is much more in case of larger ions than the smaller ones. If the solvent offers no appreciate structure resistance to the coordination of the solvent molecules in the ground state, steric inhibition will now limit the coordination of ions and this will effect the smaller ion more than the larger. With a bond breaking mechanism the effects on $\Delta\mu_2^{\circ\neq}$ will be complex, but the relief of steric hindrance in the transition state would be one factor tending to decrease $\Delta\mu_2^{\circ\neq}$ for the smaller relative to the larger ions. Moreover, $\Delta\mu_2^{\circ\neq}$ for all the ions is positive, thus, the formation of the transition state is less favorable by these ions. $\Delta\mu_2^{\circ\neq}$ for

Table 3. $B_{\pm}$-Coefficients and Ionic $\Delta\mu_2^{\circ\neq}$ Values in 2-Methoxyethanol at 25 °C

Ion	$B_{\pm}$-Coefficient/$dm^3\,mol^{-1}$		$\Delta\mu_2^{\circ\neq}$/$kJ\,mol^{-1}$
	a)	b)	
Et_4N^+	0.112	0.111	13.81
Pr_4N^+	0.207	0.206	18.88
Bu_4N^+	0.305	0.304	24.21
$(C_5H_{11})_4N^+$	0.488	0.487	31.88
$(C_6H_{13})_4N^+$	0.583	0.583	37.13
$(C_7H_{15})_4N^+$	1.138	1.138	56.38
Br^-	0.119	—	9.88
BPh_4^-	—	0.373	27.72

a) Calculations based on Bu_4NBBu_4. b) Calculations based on Bu_4NBPh_4.

Table 4. Ionic Radii ($R_{\pm}$) and Solvation Number (n_s) of Ions in 2-Methoxyethanol at 25 °C

Ion	r_c[a]	$R_{\pm}$[b]	r_s[c]	n_s
Et_4N^+	4.00	2.61	2.48	−1.47
Pr_4N^+	4.52	3.20	3.22	−1.89
Bu_4N^+	4.94	3.64	3.69	−2.29
$(C_5H_{11})_4N^+$	5.29	4.26	4.35	−2.24
$(C_6H_{13})_4N^+$	5.60	4.52	5.37	−2.64
$(C_7H_{15})_4N^+$	5.88	5.65	5.89	−0.725
Br^-	1.95	2.67	2.38	0.369
BPh_4^-	4.20	3.89	4.02	−0.473

a) R. A. Robinson and R. H. Stokes, "Electrolyte Solutions," 2nd ed, Butlerworths, London (1959). b) From viscometric data. c) From Ref. 14.

the Br^- ion is lower than the cations and this suggests that cations interact with ME more strongly than the anion.

One of the authors (D.D) thanks the CSIR, New Delhi, for the award of a Junior Research Fellowship.

References

1) J. F. Garst, "Solute-Solvent Interactions," ed by J. F. Coetzee and C. D. Ritchie, Marcel Dekker, New York (1969), Chap. 8.
2) A. G. Schwartz and J. B. Barkar, *Talanta*, **22**, 773 (1975).
3) F. Franks and D. J. G. Ives, *Q. Rev. Chem. Soc.*, **20**, 1 (1966).
4) B. S. Krumgalz, *J. Chem. Soc., Faraday Trans. 1*, **76**, 1275 (1980).
5) M. D. Archer and R. P. H. Gasser, *Trans. Faraday Soc.*, **62**, 345 (1966).
6) N. P. Yao and D. N. Bennion, *J. Phys. Chem.*, **75**, 1727 (1971).
7) J. A. Riddick and W. B. Bunger, "Organic Solvents," 3rd ed, "Techniques of Chemistry, Vol. II," ed by A. Weissburger, Wiley, New York (1970).
8) D. F. Evans, C. Zawoyski, and R. L. Kay, *J. Phys. Chem.*, **69**, 387 (1965).
9) S. Das, D. K. Hazra, and S. C. Lahiri, *Z. Phys. Chem. (Frankfurt/Main)*, **138**, 185 (1983).
10) M. Castagnolo, A. Sacco, and A. D. Giglio, *J. Chem. Soc., Faraday Trans. 1*, **80**, 2669 (1984).
11) K. G. Lawrence and A. Sacco, *J. Chem. Soc., Faraday Trans. 1*, **79**, 615 (1983).
12) H. Sadek, Th. F. Tadros, and A. A. El-Harakany, *Electrochim. Acta*, **16**, 339 (1971).
13) G. Jones and M. Dole, *J. Am. Chem. Soc.*, **51**, 2950 (1929).
14) D. Dasgupta, S. Das, and D. K. Hazra, *J. Chem. Soc., Faraday Trans. 1*, **84**, 1057 (1988).
15) J. Crudden, G. M. Delaney, D. Feakins, P. J. O'Reilly, W. E. Waghorne, and K. G. Lawrence, *J. Chem. Soc., Faraday Trans. 1*, **82**, 2195 (1986).
16) H. Falkenhagen and E. L. Vernon, *Phys. Z.*, **33**, 140 (1932).
17) D. Feakins, D. J. Fremantle, and K. G. Lawrence, *J. Chem. Soc., Faraday Trans. 1*, **70**, 795 (1974).
18) A. N. Sharma and D. S. Gill, *J. Chem. Soc., Faraday Trans. 1*, **78**, 475 (1982) and references therein.
19) B. S. Krumgalz, *J. Phys. Chem.*, **83**, 763 (1979).
20) A. Sacco, M. D. Monica, A. D. Giglio, and K. G. Lawrence, *J. Chem. Soc., Faraday Trans. 1*, **79**, 2631 (1983).
21) K. G. Lawrence, T. M. Bicknell, A. Sacco, and A. Dell'Atti, *J. Chem. Soc., Faraday Trans. 1*, **81**, 1133 (1985).
22) D. S. Gill and M. B. Sekhri, *J. Chem. Soc., Faraday Trans. 1*, **78**, 119 (1982).
23) D. F. Tuan and R. M. Fuoss, *J. Phys. Chem.*, **67**, 1343 (1963).
24) A. Einstein, *Ann. Phys.*, **19**, 289 (1906).
25) D. Feakins and K. G. Lawrence, *J. Chem. Soc. A*, **1966**, 212.

A New Method for the Calculation of the Sextet Polynomial of Unbranched Catacondensed Benzenoid Hydrocarbons

Ivan GUTMAN*,† and Sven J. CYVIN
Division of Physical Chemistry, The University of Trondheim, N-7034 Trondheim-NTH, Norway
(Received May 28, 1988)

A method for the calculation of the sextet polynomial of unbranched catacondensed benzenoid molecules is proposed. It requires the multiplication of a small number of 2×2 matrices and is therefore very simple.

The concept of the sextet polynomial was introduced by Hosoya and Yamaguchi[1] in 1975 and was thereafter subject of numerous investigations.[2-19] The theory based on the sextet polynomial and its various chemical applications can be found in the reviews[20,21] and books.[22,23]

The sextet polynomial is defined via the resonant sextet numbers $r(B, k)$. Let B be a benzenoid system. Then $r(B, k)$ is the number of distinct Clar-type formulas for B, in which exactly k hexagons contain a resonant sextet, $k=1,2,\cdots,s$. Here s is the maximal number of aromatic sextets which can be inserted in a Clar-type formula for B, i.e. $r(B, s)\neq 0$, $r(B, s+1)=0$. By definition, $r(B, 0)=1$.

Then the sextet polynomial of B is

$$\sigma(B, x)=\sum_{k=0}^{s} r(B, k)\, x^k. \qquad (1)$$

If B is an unbranched catacondensed benzenoid system, then an acyclic graph G=G(B) can be constructed,[4] such that for all values of k,

$$r(B, k)=m(G, k) \qquad (2)$$

where $m(G, k)$ is the number of k-matchings of the graph G. When Eq. 2 is substituted back into Eq. 1 we obtain

$$\sigma(B, x)=\sum_{k=0}^{s} m(G, k)\, x^k. \qquad (3)$$

The right-hand side of Eq. 3 is exactly the so-called "Z-counting polynomial" (of the graph G), introduced in 1971 by Hosoya.[24] Therefore in the case of unbranched catacondensed benzenoids, the calculation of the sextet polynomial reduces to the finding of the Z-counting polynomial of the associated graph.

The graph G has the following structure. Suppose that the unbranched catacondensed molecule considered possesses n hexagons of type A (i.e. n kinks). The number of hexagons of type L between the i-th and the $(i+1)$-th A hexagon is t_i, $i=1, 2,\cdots, n-1$. Further, t_0 is the number of L hexagons lying between the terminal (T) hexagon and the first A hexagon.

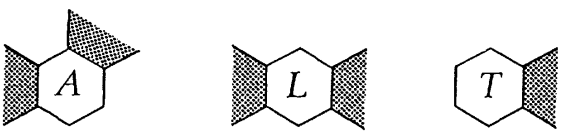

† Permanent address: Faculty of Science, University of Kragujevac, P. O. Box 60, YU-34000 Kragujevac, Yugoslavia.

Similarly, t_n counts the L hexagons between the n-th A hexagon and the other terminal hexagon. With these conventions, the LA-sequence[4] of a general unbranched catacondensed benzenoid system has the form

$$TL^{t_0}AL^{t_1}AL^{t_2}A\cdots L^{t_{n-1}}AL^{t_n}T \qquad (4)$$

where LL, LLL, LLLL etc. is abbreviated by L^2, L^3, L^4 etc. Note that t_i may be equal to zero, which simply means that the i-th and the $(i+1)$-th hexagon of the type A are first neighbors.

For example, the below unbranched benzenoid system B_0 has $n=4$ kinks and its LA-sequence is TL^3A-$LAAL^2AT$; hence $t_0=3$, $t_1=1$, $t_2=0$, $t_3=2$, and $t_4=0$.

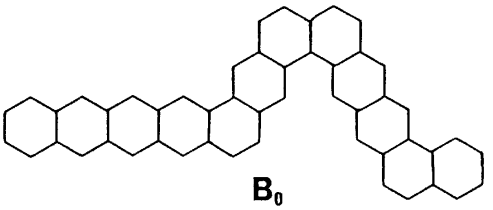

Now, the graph G in Eqs. 2 and 3 is of the form:[4]

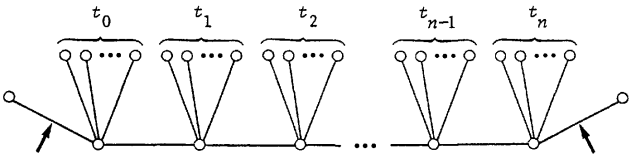

$G = G(t_0, t_1, t_2, \ldots, t_{n-1}, t_n)$

The graphs of the above type are called caterpillars[15,21] or sometimes[19,21] Gutman trees.

One should observe that the caterpillar G has n horizontal edges, each corresponding to a hexagon of type A. This explains why the branching points of G are numbered from 0 to n (and not from 1 to n as, at the first glance, may look more appropriate). Anyway, it should not be forgotten that the main object of the present paper are benzenoid hydrocarbons whereas their LA-sequences and the associated Gutman trees are auxiliary mathematical constructions needed only to deduce our expression for the sextet polynomial.

The caterpillar corresponding to B_0 is $G(B_0)$:

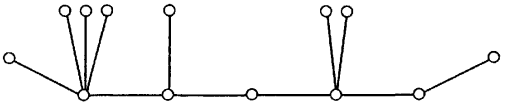

$G(B_0)$

As already mentioned, the Z-counting polynomial of $G(t_0, t_1, t_2 \cdots, t_{n-1}, t_n)$ coincides with the sextet polynomial of an unbranched catacondensed hydrocarbon whose LA-sequence is given by Eq. 4.

The properties of the matching numbers $m(G, k)$, the Z-counting polynomial $Q(G, x)$ and the closely related matching polynomial have been studied in detail.[25] In the present paper we need only two simple relations[24] for $Q(G, x)$.

(i) Let G be an arbitrary graph, e its arbitrary edge, and let e connect the vertices u and v. Then

$$Q(G, x) = Q(G\text{-e}, x) + xQ(G\text{-u-v}, x). \tag{5}$$

(ii) Let G be a graph composed of two components G_1 and G_2. Then

$$Q(G, x) = Q(G_1, x) \cdot Q(G_2, x). \tag{6}$$

The Main Result. The sextet polynomial of an unbranched catacondensed benzenoid system whose LA-sequence is given by Eq. 4 is equal to $U_{11}+U_{12}+U_{21}+U_{22}$ where

$$\begin{pmatrix} U_{11} & U_{12} \\ U_{21} & U_{22} \end{pmatrix} = M_0 M_1 M_2 \cdots M_{n-1} M_n \begin{pmatrix} 1 & 0 \\ 0 & x \end{pmatrix} \tag{7}$$

and

$$M_i = \begin{pmatrix} 1 + t_i x & 1 \\ x & 0 \end{pmatrix}.$$

For the previous example,

$$\begin{pmatrix} U_{11} & U_{12} \\ U_{21} & U_{22} \end{pmatrix} = \begin{pmatrix} 1+3x & 1 \\ x & 0 \end{pmatrix}\begin{pmatrix} 1+x & 1 \\ x & 0 \end{pmatrix}\begin{pmatrix} 1 & 1 \\ x & 0 \end{pmatrix}$$
$$\begin{pmatrix} 1+2x & 1 \\ x & 0 \end{pmatrix}\begin{pmatrix} 1 & 1 \\ x & 0 \end{pmatrix}\begin{pmatrix} 1 & 0 \\ 0 & x \end{pmatrix}$$

which after simple matrix multiplication gives

$$\begin{pmatrix} U_{11} & U_{12} \\ U_{21} & U_{22} \end{pmatrix} = \begin{pmatrix} 1+10x+29x^2+21x^3 & x+9x^2+23x^3+15x^4 \\ x+6x^2+7x^3 & x^2+5x^3+5x^4 \end{pmatrix}$$

yielding the sextet polynomial of B_0:

$$\begin{aligned} \sigma(B_0, x) &= (1+10x+29x^2+21x^3)+(x+9x^2+23x^3+15x^4) \\ &\quad +(x+6x^2+7x^3)+(x^2+5x^3+5x^4) \\ &= 1+12x+45x^2+56x^3+20x^4. \end{aligned}$$

Two special cases of Eq. 7 are worth mentioning. If on the left-hand side from the first kink there are no L-type hexagons (i.e. $t_0=0$), then

$$\begin{pmatrix} U_{11} & U_{12} \\ U_{21} & U_{22} \end{pmatrix} = \begin{pmatrix} 1 & 1 \\ x & 0 \end{pmatrix} M_1 M_2 \cdots M_n \begin{pmatrix} 1 & x \\ 0 & x \end{pmatrix}.$$

If on the right-hand side from the last kink there are no hexagons of the type L (i.e. $t_n=0$), then

$$\begin{pmatrix} U_{11} & U_{12} \\ U_{21} & U_{22} \end{pmatrix} = M_0 M_1 \cdots M_{n-1} \begin{pmatrix} 1 & x \\ x & 0 \end{pmatrix}.$$

Verification of Equation 7. We first apply Eqs. 5 and 6 to the two edges of $G(t_0, t_1, t_2, \cdots, t_{n-1}, t_n)$ which on the previous diagram are indicated by arrows. Bearing in mind that for the graph E_p with p vertices but without edges $Q(E_p)\equiv 1$, we straightforwardly obtain:

$$\begin{aligned} &Q[G(t_0, t_1, t_2, \cdots, t_{n-1}, t_n), x] \\ &\quad = Q[F(t_0, t_1, t_2, \cdots, t_{n-1}, t_n), x] \\ &\quad + xQ[F(t_0, t_1, t_2, \cdots, t_{n-1}), x] \\ &\quad + xQ[F(t_1, t_2, \cdots, t_{n-1}, t_n), x] \\ &\quad + x^2 Q[F(t_1, t_2, \cdots, t_{n-1}), x] \end{aligned} \tag{8a}$$

where the caterpillar F is defined as follows:

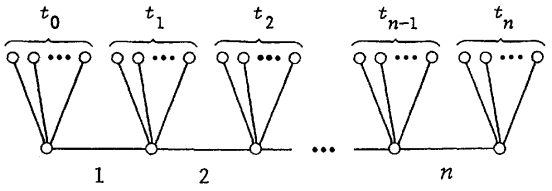

$F(t_0, t_1, t_2, \ldots, t_{n-1}, t_n)$

It is expedient to use the shorthand notation

$$Q[F(t_0, t_1, t_2, \cdots, t_{n-1}, t_n), x] \equiv (0, n).$$

Then Eq. 8a is simplified as

$$\begin{aligned} &Q[G(t_0, t_1, t_2, \cdots, t_{n-1}, t_n), x] \\ &\quad = (0, n) + x \cdot (0, n-1) + x \cdot (1, n) + x^2 \cdot (1, n-1). \end{aligned} \tag{8b}$$

Another way to deduce the identity Eq. 8 is to apply the inclusion and exclusion principle to the Q polynomial. Let a and b denote the edges of G indicated by arrows. Then the first term on the right-hand side of either Eq. 8a or 8b corresponds to the subgraph of G from which both a and b are excluded. The second term in Eqs. 8a and 8b corresponds to the subgraph of G in which a is included, but b is excluded; the third term corresponds to the subgraph from which a is excluded, but b is included. Finally, the last term in Eqs. 8a and 8b corresponds to the subgraph to which both a and b are included. The authors are indebted to the referee for pointing out this observation.

Applying Eqs. 5 and 6 to the i-th horizontal edge of $F(t_0, t_1, t_2, \cdots, t_{n-1}, t_n)$ we arrive at

$$(0, n) = (0, i)(i+1, n) + x \cdot (0, i-1)(i+2, n)$$

and in a fully analogous manner:

$$\begin{aligned} (0, n-1) &= (0, i)(i+1, n-1) + x \cdot (0, i-1)(i+2, n-1) \\ (1, n) &= (1, i)(i+1, n) + x \cdot (1, i-1)(i+2, n) \\ (1, n-1) &= (1, i)(i+1, n-1) + x \cdot (1, i-1)(i+2, n-1). \end{aligned}$$

These four equations can be written in a matrix form as

$$\begin{pmatrix} (0, n) & (0, n-1) \\ x \cdot (1, n) & x \cdot (1, n-1) \end{pmatrix} =$$
$$\begin{pmatrix} (0, i) & (0, i-1) \\ x \cdot (1, i) & x \cdot (1, i-1) \end{pmatrix} \begin{pmatrix} (i+1, n) & (i+1, n-1) \\ x \cdot (i+2, n) & x \cdot (i+2, n-1) \end{pmatrix}. \tag{9}$$

The above relations hold for $2 \leq i \leq n-3$. They can eas-

ily be extended to apply for all values of i, $i=0, 1, \cdots, n-1$ if one sets $(j,j-1)\equiv 1$ and $(j+1,j-1)\equiv 0$. One should recall that $(j,j)=1+t_j x$.

Setting $i=n-1$ in Eq. 9 we obtain

$$\begin{pmatrix} (0,n) & (0,n-1) \\ x\cdot(1,n) & x\cdot(1,n-1) \end{pmatrix} = \begin{pmatrix} (0,n-1) & (0,n-2) \\ x\cdot(1,n-1) & x\cdot(1,n-2) \end{pmatrix} \begin{pmatrix} 1+t_n x & 1 \\ x & 0 \end{pmatrix}$$

i.e.

$$\begin{pmatrix} (0,n) & (0,n-1) \\ x\cdot(1,n) & x\cdot(1,n-1) \end{pmatrix} = \begin{pmatrix} (0,n-1) & (0,n-2) \\ x\cdot(1,n-1) & x\cdot(1,n-2) \end{pmatrix} M_n$$

from which is immediately seen that

$$\begin{pmatrix} (0,n) & (0,n-1) \\ x\cdot(1,n) & x\cdot(1,n-1) \end{pmatrix} = M_0 M_1 M_2 \cdots M_{n-1} M_n \ .$$

Equation 7 follows now from the fact that

$$\begin{pmatrix} U_{11} & U_{12} \\ U_{21} & U_{22} \end{pmatrix} = \begin{pmatrix} (0,n) & (0,n-1) \\ x\cdot(1,n) & x\cdot(1,n-1) \end{pmatrix} \begin{pmatrix} 1 & 0 \\ 0 & x \end{pmatrix} .$$

Discussion

Another form in which we can express our main result is

$$\sigma(\mathrm{B}, x) = \begin{pmatrix} 1 \\ 1 \end{pmatrix}^T M_0 M_1 \cdots M_n \begin{pmatrix} 1 \\ x \end{pmatrix} . \qquad (10)$$

For $x=1$ the sextet polynomial reproduces the number of Kekulé structures.[1,3] Therefore Eq. 10 provides an expression for the Kekulé structure count of unbranched catacondensed benzenoid systems, viz.

$$K\{\mathrm{B}\} = \begin{pmatrix} 1 \\ 1 \end{pmatrix}^T L_0 L_1 \cdots L_n \begin{pmatrix} 1 \\ 1 \end{pmatrix} \qquad (11)$$

where

$$L_i = \begin{pmatrix} t_i & +1 & 1 \\ & 1 & 0 \end{pmatrix} .$$

Formulas of this type, but not Eq. 11, are previously known.[26]

We wish to point at a property of the matrix elements U_{ij}, Eq. 7, whose meaning and possible significance are not understood. We have seen that $U_{11}+U_{12}+U_{21}+U_{22}$ is the sextet polynomial. In addition,

$$U_{11}U_{22} - U_{12}U_{21} = (-1)^n x^{n+1}. \qquad (12)$$

The above relation is obtained if one calculates the determinants of the left- and right-hand sides of Eq. 7, taking into account that $\det M_i = -x$. The special case of Eq. 12 for $x=1$ was observed previously.[27]

One of the authors (I. G.) thanks the Royal Norwegian Council for Scientific and Industrial Research for financial support.

References

1) H. Hosoya and T. Yamaguchi, *Tetrahedron Lett.*, **1975**, 4659.
2) J. Aihara, *Bull. Chem. Soc. Jpn.*, **50**, 2010 (1977).
3) I. Gutman, H. Hosoya, T. Yamaguchi, A. Motoyama, and N. Kuboi, *Bull. Soc. Chim. Beograd*, **42**, 503 (1977).
4) I. Gutman, *Theor. Chim. Acta*, **45**, 309 (1977).
5) I. Gutman, *Bull. Chem. Soc. Jpn.*, **51**, 2729 (1978).
6) I. Gutman, *Z. Naturforsch., A*, **33**, 840 (1978).
7) N. Ohkami, A. Motoyama, T. Yamaguchi, H. Hosoya, and I. Gutman, *Tetrahedron*, **37**, 1113 (1981).
8) I. Gutman, *Match*, **11**, 127 (1981).
9) I. Gutman, *Z. Naturforsch., A*, **37**, 69 (1982).
10) N. Ohkami and H. Hosoya, *Theor. Chim. Acta*, **64**, 153 (1983).
11) S. El-Basil, *Bull. Chem. Soc. Jpn.*, **56**, 3152 (1983).
12) I. Gutman and S. El-Basil, *Chem. Phys. Lett.*, **94**, 188 (1983).
13) I. Gutman and S. El-Basil, *Z. Naturforsch., A*, **39**, 276 (1984).
14) I. Gutman and S. El-Basil, *J. Serb. Chem. Soc.*, **50**, 25 (1985).
15) I. Gutman and S. El-Basil, *Z. Naturforsch., A*, **40**, 923 (1985).
16) F. J. Zhang and R. S. Chen, *Match*, **19**, 179 (1986).
17) W. C. He and W. J. He, *Theor. Chim. Acta*, **70**, 43 (1986).
18) S. El-Basil, *Theor. Chim. Acta*, **70**, 53 (1986).
19) S. El-Basil, *J. Chem. Soc., Faraday Trans. 2*, **82**, 299 (1986).
20) I. Gutman, *Bull. Soc. Chim. Beograd*, **47**, 453 (1982).
21) S. El-Basil, *J. Math. Chem.*, **1**, 153 (1987).
22) N. Trinajstić, "Chemical Graph Theory," CRC Press, Boca Raton (1983), Vol. II, pp. 44—46.
23) I. Gutman and S. J. Cyvin, "Introduction to the Theory of Benzenoid Hydrocarbons," Springer-Verlag, Berlin (1988).
24) H. Hosoya, *Bull. Chem. Soc. Jpn.*, **44**, 2332 (1971).
25) D. Cvetković, M. Doob, I. Gutman, and A. Torgašev, "Recent Results in the Theory of Graph Spectra," North-Holland, Amsterdam (1988), Chaps. 4 and 5.
26) D. Cvetković and I. Gutman, *Croat. Chem. Acta*, **46**, 15 (1974).
27) S. J. Cyvin, *Chem. Phys. Lett.*, **147**, 384 (1988).

 © 1989 The Chemical Society of Japan Bull. Chem. Soc. Jpn., 62, 1253—1257 (1989)

Conductometric Determination of Thermodynamics Dissociation Constants of Benzoic and Nitrobenzoic Acid in Methanol-Water Mixtures at 298 K

M. S. K. Niazi
Department of Chemistry, Quaid-I-Azam University, Islamabad, Pakistan
(Received July 4, 1988)

The thermodynamic dissociation constants and the limiting molar conductivities of 2-, 3-, 4-nitrobenzoic and benzoic acids have been determined in water-methanol mixtures at 298 K. The experimental data are analyzed with the Lee and Wheaton conductance equation incorporating modifications. The derived results are compared with the ones in literature, pertaining to analogous media. The findings are interpreted in terms of solute-solvent interactions, intramolecular hydrogen bonding, resonance and inductive effect and the substituent position. The study showed that the dissociation order decreases as 2-nitrobenzoic acid> 3-nitrobenzoic acid≈ 4-nitro benzoic acid> benzoic acid.

Protonation/deprotonation equilibria leading to the study of acid-base equilibria have been under investigation in pure and mixed solvents since many years. The ionization constant of an acid is largely influenced mostly by the structure of the acid but also by the nature of the solvent.[1-4] Potentiometric and spectrophotometric techniques are quite popular for obtaining dissociation constants of acids and bases.[5-7] However, the ionization of acids in methanol-water (MeOH-H_2O) mixtures varies with solvent composition in a manner which is still not completely understood.[8,9] In contranst to potentiometry, the conductimetry provides a simple and accurate method for the determination of dissociation constants of acids without any primary and secondary buffer solutions required for calibration of the platinum electrode.[10-12]

In this paper the conductance behavior of 2-, 3-, 4-nitrobenzoic acids along with benzoic acid (as a model compound) in MeOH-H_2O mixtures at 298 K is examined. The pK_a values (thermodynamic dissociation constants) are derived from conductance data using the Lee and Wheaton conductance equation (in series form) incorporating modifications.[13,14] Finished results are compared with those by other workers pertaining to the same and similar acids in analogous media.

Experimental

Benzoic and nitrobenzoic acids used in the present work were Merck products of ultrahigh purity. They were crystallized twice from ethanol-water mixtures, dried under vacuum over P_2O_5 and stored in a desiccator.

Methanol (Analar BDH) was distilled over sulfanilic acid and the middle fraction was collected for use. The deionized conductivity water (triply distilled) was used as an aqueous medium and for preparation of MeOH-H_2O mixtures (w/w composition). The purity of solvents was checked from their physical parameters such as density, viscosity, and dielectric constant at 298 K.

The conductance measurements were made in the same way as described elsewhere.[15,16] An Orion Research conductivity meter model 101, was used for the purpose. Two platinized platinum electrodes (cell constants: 0.857 and 1.151 cm^{-1}) were used. The temperature of water baths was controlled at 25±0.01 °C. No appreciable variations in conductance were observed in changing frequency range from 80 Hz to 3 kHz. Duplicate measurements for each mixture were made, the results varied within±0.1% only.

Viscosities, densities, and dielectric constants of various mixtures were measured in the same way as described earlier,[17] which have been found in good agreement with the values cited in literature.[18]

Results

Physical properties of MeOH-H_2O mixtures are listed in Table 1. The corresponding values of the molar conductances are given in Table 2 for all the four acids in solvent mixtures of different composition listed therein. The experimental data were analyzed with the Lee and Wheaton conductance equation in its series form.[13,14] The selection of the equation was tentative since it was based on a model warranting the study of the dissociation process and short range interactions closely. The limiting molar conductance (Λ_0) and association constant (K_A) for the process $[H^+ + A^- \overset{K_A}{\rightleftarrows} H^+A^-]$ were deduced from the equations:

$$\Lambda = \gamma[\Lambda_0(1+\Delta X/X)-\Delta\Lambda_{el}] \quad (1)$$

$$K_A = (1-\gamma)/\gamma^2 f^2 c \quad (2)$$

$$-\ln f = bk/2(1+kR),\ b = e^2/DKT \quad (3)$$

for Λ_0 and K_A values which minimize

$$\sigma_\Lambda = \sum_i [\Lambda_i(\text{cal})-\Lambda_i(\text{obs})]^2/n-2 \quad (4)$$

Table 1. Physical Properties of MeOH-H_2O Mixtures at 298 K

% MeOH (w/w)	ρ / g·cm^{-3}	η / cP[a]	D
0	0.9971	0.890	78.65
10	0.9806	1.153	74.23
30	0.9437	1.581	63.93
50	0.9129	1.545	55.17
70	0.8481	1.215	37.88

ρ=density; η=viscosity; D=dielectric constant.
a) 1 cP=10^{-3} Pa s.

The symbols have their usual significance. The study revealed that in the case of carboxylic acids no minimum is observed in a R-σ_A (%) plot. The value of distance parameter R was set equal to $2b$ as suggested by Fuoss.[22] The derived conductance parameters are given in Table 3.

From the K_A values, the respective pK_a (i.e. dissociation constant) values were calculated using the relationship:

$$pK_a = -\log K_d = -\log (1/K_A) \quad (5)$$

Values of pK_a for benzoic and nitrobenzoic acids at 298 K are presented in Table 4. The solvent effect of MeOH on the dissociation of these acids is shown in Fig. 2, where the difference between pK_a^s (the value of pK_a in the fixed solvent-mixture) and pK_a^w (the value of pK_a in water) is plotted as a function x, the mole fraction of MeOH in methanol-water mixtures. The

Table 2. Molar Conductances of Solutions of Acids in MeOH–H_2O Mixtures at 298 K

Wt. % MeOH	0	10	30	50	70
10^4C	Λ	Λ	Λ	Λ	Λ
mol·dm^{-3}	S·cm^2·mol^{-1}	S·cm^2·mol^{-1}	S·cm^2·mol^{-1}	S·cm^2·mol^{-1}	S·cm^2·mol^{-1}
		Benzoic acid			
1.961	168.13	82.42	42.39	21.36	9.55
5.660	111.05	52.42	26.28	12.91	5.75
9.091	90.71	42.41	21.08	10.27	4.56
12.281	79.55	37.00	18.29	8.88	3.94
12.254	72.21	33.46	16.51	7.98	3.54
18.033	67.01	31.20	15.24	7.36	3.27
20.635	63.04	29.08	14.29	6.89	3.06
23.077	59.91	27.59	13.56	6.53	2.90
25.373	57.39	26.40	12.94	6.23	2.77
27.536	55.30	25.39	12.44	5.98	2.65
		2-Nitrobenzoic acid			
1.961	390.87	268.37	176.45	92.27	46.92
5.660	374.92	251.64	153.99	69.65	30.31
9.091	362.57	239.50	140.53	59.67	24.64
12.281	352.57	230.11	131.24	53.68	21.54
15.254	344.21	222.55	124.32	49.57	19.52
18.033	337.13	216.30	118.91	46.54	18.09
20.635	330.99	211.02	114.53	44.20	17.01
23.077	325.63	206.48	110.89	42.30	16.15
25.373	320.89	202.54	107.81	40.75	15.46
27.536	316.67	199.03	105.03	39.86	14.88
		3-Nitrobenzoic acid			
1.961	292.95	207.85	114.65	50.81	25.88
5.660	220.80	155.55	79.61	33.82	16.13
9.091	188.95	132.75	66.22	27.73	12.71
12.281	169.82	119.15	58.60	24.36	10.93
15.254	156.71	109.84	53.54	22.15	9.87
10.033	147.05	103.01	49.88	20.57	9.15
20.635	139.54	97.71	47.09	19.37	8.53
23.077	133.53	93.46	44.87	18.42	8.10
25.373	128.56	89.96	43.05	17.65	7.72
27.536	124.34	86.99	41.52	16.99	7.43

Wt. % MeOH	0	10		30	
10^4C	Λ	10^4C	Λ	10^4C	Λ
mol·dm^{-3}	S·cm^2·mol^{-1}	mol·dm^{-3}	S·cm^2·mol^{-1}	mol·dm^{-3}	S·cm^2·mol^{-1}
		4-Nitrobenzoic acid			
1.48	296.75	1.481	249.87	1.081	166.57
3.871	233.25	3.871	197.06	2.927	124.46
5.714	212.89	5.714	174.95	4.444	107.61
7.179	191.39	7.179	162.27	5.714	98.12
8.377	181.40	8.373	153.87	6.772	91.89
9.362	174.33	9.362	148.04	7.719	87.44
10.196	169.01	9.795	145.67	8.525	84.10
10.566	166.82	10.196	143.36	8.888	82.73
10.909	164.87	10.568	140.82	9.231	81.50

Table 2. (Continued)

50		70	
10^4C	Λ	10^4C	Λ
mol·dm^{-3}	S·cm^2·mol^{-1}	mol·dm^{-3}	S·cm^2·mol^{-1}
1.481	73.89	1.961	26.47
3.871	51.24	5.660	16.23
5.714	45.48	9.091	12.96
7.179	39.58	12.281	11.19
8.373	37.07	15.259	10.06
9.362	25.31	18.033	9.29
10.196	33.02	20.635	8.72
10.566	33.49	21.675	8.48
10.909	33.03	23.077	8.26

Table 3. Conductance Parameters of Acids in MeOH-H_2O Mixtures at 298 K

% MeOH w/w	Λ_0	σ	K_A
	S·cm^2·mol^{-1}	%	dm^3·mol^{-1}
	Benzoic acid		
0	393.08	0.084	16635
10	262.16	0.028	20700
30	197.77	0.031	87625
50	190.94	0.011	366481
70	105.44	0.008	1574078
	2-Nitrobenzoic acid		
0	402.08	0.032	125
10	280.43	0.051	214
30	196.24	0.057	620
50	128.83	0.017	2830
70	133.55	0.035	27432
	3-Nitrobenzoic acid		
0	408.73	0.012	2834
10	295.17	0.008	3091
30	206.97	0.013	7534
50	144.67	0.003	14708
70	161.49	0.031	170260
	4-Nitrobenzoic acid		
0	376.54	0.049	2785
10	336.95	0.008	3712
30	251.82	0.010	7235
50	169.44	0.040	20123
70	173.82	0.021	189459

Table 4. pK_a Values and Difference of Standard Molar Gibbs Energy of Transfer $\Delta_{tr}G^\circ_m$ at 298 K of Acids for Water to Methanol-Water

% MeOH (w/w) Acid	0	10	30	50	70
	pK_a values				
Benzoic	4.22	4.31	4.94	5.56	6.20
2-Nitrobenzoic	2.10	2.33	2.79	3.45	4.44
3-Nitrobenzoic	3.45	3.49	3.88	4.17	5.23
4-Nitrobenzoic	3.45	3.50	3.86	4.30	5.27
	$\Delta_{tr}G^\circ_m$/kJ·mol^{-1}				
Benzoic		0.51	2.97	7.65	11.30
2-Nitrobenzoic		1.31	3.94	7.70	13.35
3-Nitrobenzoic		0.23	2.45	4.11	10.16
4-Nitrobenzoic		0.29	2.34	4.85	10.39

observed changes of pK_a^s and standard molar Gibbs free energy of transfer $\Delta_{tr}G^\circ_m$ were calculated from:

$$\Delta_{tr}G^\circ_m = -RT \ln 10\Delta pK_a = 5.707\,[pK_a^s - pK_a^w]\ \text{kJ·mol}^{-1} \quad (6)$$

and are presented in Table 4.

Discussion

The pK_a values of benzoic and 2-, 3-, and 4-nitrobenzoic acids in aqueous medium are in good agreement with those quoted in literature, mainly derived by potentiometric and some other methods.[23] The dissociation study of benzoic and the nitrobenzoic acid in alcohol-water mixtures is available in literature.[1,19–21] The present pK_a values for benzoic acid (in some MeOH-H_2O mixtures) are in good agreement with previous study in Fig. 1. In this figure, the derived results are compared with those by Lahiri et al.[19] for 4-nitrobenzoic acid in MeOH-H_2O mixtures. As is obvious, their pK_a values in 8—60 wt% MeOH-H_2O mixtures are higher than our derived values. This could be attributed to their so called corrections in pH values of acidic solutions in binary solvent mixtures. Also, procedural digression from the normal potentiometric method for determination of pK_a values of carboxylic acids in mixed solvent systems could also be another cause for this effect.[1,4] On similar ground, the present results do not agree with those derived by Dash et al.[21] who undertook potentiometric calibration with reference to aqueous phase. Therefore, a direct comparison with their results could be oversimplification of actual situation.

The solvent effect on the dissociation of these acids is shown in Fig. 2. The plots of pK_a vs. mole fraction x of methanolic contents in MeOH-H_2O mixtures are not linear. A similar behavior of these acids in pK_a vs. $(1/D_s - 1/D_w)$ plots, may also be observed, where D_s and D_w are dielectric constants of mixtures and water, respectively. If only electrostatic interactions among the ions would have been operational these plots should have been linear, detailed by Born.[24] The present investigation thus suggest that in case of nitrobenzoic acids a nonelectrostatic part of the standard free

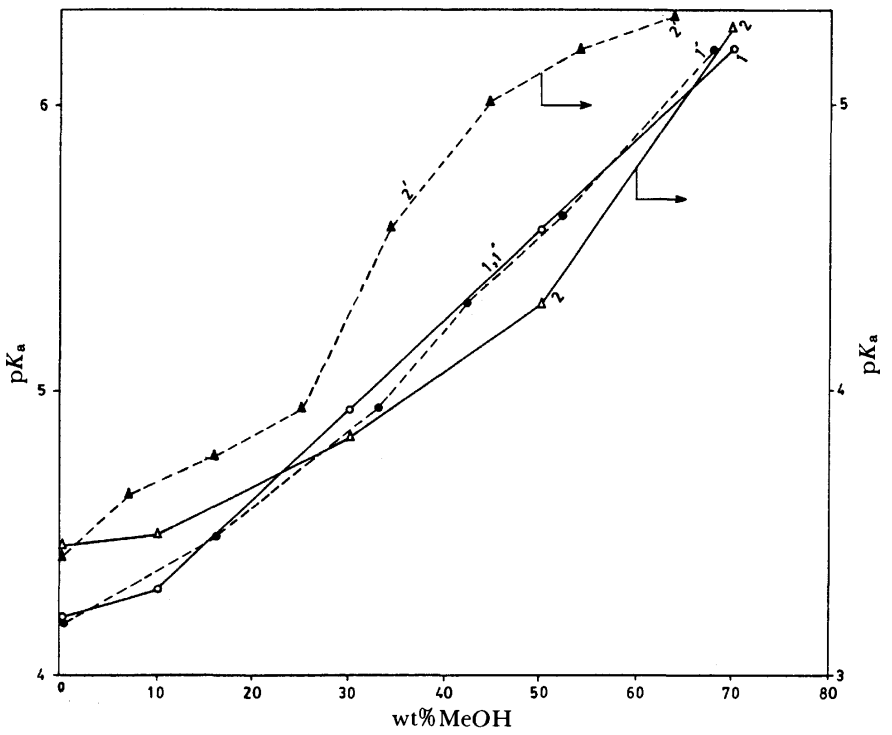

Fig. 1. Dependence of pK_a values of benzoic (○,●) and 4-nitrobenzoic acids (△,▲) on composition of MeOH-H_2O mixtures at 298 K: 1, 2 present work; 1′, 2′ taken from Refs. 26 and 19.

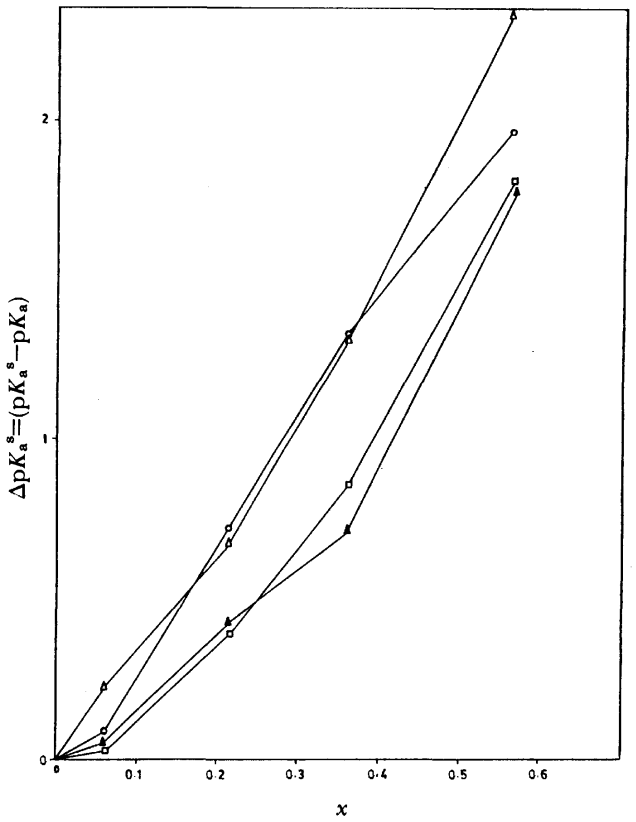

Fig. 2. Effect of changes of solvent composition on the pK_a values of benzoic (○); 2-nitrobenzoic (△); 3-nitrobenzoic (▲); and 4-nitrobenzoic (□) acids in $x\{CH_3OH+(1-x)\ H_2O\}$ at 298 K.

energy of transfer from aqueous to aqueous-methanol mixtures is playing a dominant role. It means that these are specific chemical interactions going on between ions of these acids and the solvent.

The dissociation order in respect of the acids studied in MeOH-H_2O mixtures turns out to be; 2-nitrobenzoic acid > 3-nitrobenzoic acid ≃ 4-nitrobenzoic acid > benzoic acid. This observed difference of acidities among the same isomers of nitrobenzoic acid could be explained on basis of intramolecular hydrogen bonding, inductive and resonance effects of the substituent and its respective position on the benzene ring with respect to carboxyl group.[25]

The normalized Walden products ($\Lambda_0\eta/\Lambda_{0w}\eta_w$) against percentage of methanol in MeOH-H_2O system, decreases as the solvent mixture is enriched in methanol. The changes in the Walden product are not only due to viscosity or dielectric constant variations but also to an altering proton transfer mechanism.[7]

The assistances rendered by the following persons are acknowledged gratefully: M. Zafar Iqbal Khan for conductance measurements, Mahmood Hussain for preparation of typescript, and Dr. M. Jaffar for correcting the manuscript.

References

1) M. S. K. Niazi and J. Mollin, *Bull. Chem. Soc. Jpn.*, **60**, 2605 (1987).

2) L. E. Strong, L. C. Brummel, and P. Lindower, *J.*

Solution Chem., **16**, 105 (1987).
3) J. Mollin, Z. Pavelek, J. Navratilova, and A. Recmanova, *Collect. Czech. Chem. Commun.*, **50**, 2670 (1985).
4) Z. Pawlák, *J. Chem. Thermodyn.*, **19**, 443 (1987).
5) S. Glab, E. Skrzydlewska, and A. Hulanicki, *Talanta*, **34**, 411 (1987).
6) S. K. Chakravorty, S. K. Sarkar, and S. C. Lahiri, *Thermochim. Acta*, **114**, 245 (1987).
7) G. Poulias, N. Papadopoulos, and D. Jannakoudakis, *Electrochim. Acta*, **30**, 431 (1985).
8) G. Parsons and C. H. Rochester, *J. Chem. Soc., Faraday Trans. 1*, **71**, 1058 (1975); **68**, 523 (1972).
9) J. Juillard, *Bull. Soc. Chim. Fr.*, **1968**, 1894.
10) L. E. Strong, T. Kinney, and P. Fischer, *J. Solution Chem.*, **8**, 329 (1979).
11) A. Pal and S. C. Lahiri, *Z. Phys. Chem. (Leipzig)*, **268**, 378 (1987).
12) G. Poulias, N Papadopoulous, and D. Jannakoudakis, *Talanta*, **33**, 461 (1986).
13) W. H. Lee and R. J. Wheaton, *J. Chem. Soc., Faraday Trans. 2*, **74**, 743, 1456 (1978).
14) A. D. Pethybridge and S. S. Taba, *J. Chem. Soc., Faraday Trans. 1*, **76**, 368 (1980).
15) M. S. K. Niazi, *Bull. Chem. Soc. Jpn.*, **61**, 2165 (1988).
16) M. S. K. Niazi, O. Fischer, and E. Fischerova, *J. Solution Chem.*, **15**, 957 (1986).
17) O. Fischer, M. S. K. Niazi, and E. Fischerova, *Electrochim. Acta*, **27**, 791 (1982).
18) G. Akerlof and O. A. Short, *J. Am. Chem. Soc.*, **58**, 1241 (1936).
19) B. P. Dey, S. C. Dutta, and S. C. Lahiri, *Indian J. Chem.*, **25A**, 1105 (1986).
20) A. K. Mandal and S. C. Lahiri, *J. Prakt. Chem.*, **319**, 377 (1977).
21) U. N. Dash, B. B. Das, U. K. Biswal, T. Panda, and M. K. Mishra, *J. Electrochem. Soc. India*, **36**, 173 (1987).
22) R. M. Fuoss, *J. Phys. Chem.*, **82**, 2427 (1978).
23) G. K. W. Vogel and K. Andrussow, "Dissociation Constants of Organic Acids in Aqueous Solution," Butterworth, London (1961).
24) M. Born, *Z. Phys.*, **1**, 45 (1920).
25) E. J. King, "Acid Base Equilibria," Pergamon Press, Oxford (1965).
26) A. Van Veen, A. J Hoefnagel, and B. M. Wepster, *Rec. Trav. Chem.*, **90**, 289 (1971).

Nonequilibrium Thermodynamic Studies on Membrane Phenomena. Transport of Electrolytic Solutions through Progesterone Plug Membrane

M. L. SRIVASTAVA and Bali RAM*,†
Department of Chemistry, University of Gorakhpur, Gorakhpur 273009, India
†Department of Chemistry, College of Basic Sciences & Humanities, G. B. Pant Univ. of Agric. & Technology, Pantnagar 263145, Nainital, India
(Received August 4, 1988)

Studies on hydrodynamic and electroosmotic permeation of water and aqueous solutions of NaCl, KCl, and $MgCl_2$ across progesterone plug membrane have been carried out to characterize the electrical nature of progesterone interfaces. Electrophoretic mobilities of progesterone particles dispersed in these aqueous solutions have also been measured. Experiments were confined to the range where linear flux/force relationships hold. Membrane parameters have been evaluated with the data obtained and the membrane/solution electrical interface has been explained using electrical double layer model and theory of nonequilibrium thermodynamics. Zeta potentials have been evaluated from electroosmotic and electrophoretic flux data and their dependence on concentration examined.

A variety of transport phenomena is known to take place when a membrane system is subjected to various driving forces such as gradients of electric potential, concentration, and hydrostatic pressure. The phenomenon of mass transmission through natural membranes is very complex[1] having immense physiological and medicinal applications.[2] In view of the complexities of these membranes considerable interest has developed in the study of transport behavior through model membranes.[3] It has been found that these model membranes possess certain dimensional, electrical permeability, and excitability characteristics that closely resemble the behavior of natural membranes.[4] Recently we have made extensive studies on the application of nonequilibrium thermodynamics to the transport phenomenon across testosterone plug membrane[5-7] (model membrane).

This paper is concerned with the study of the transport properties of an isothermal system consisting of a progesterone plug membrane, water, and aqueous solutions of NaCl, KCl, and $MgCl_2$ in the concentration range of 10^{-4} to 10^{-3} mol l^{-1} on the basis of nonequilibrium thermodynamics. Such studies with respect to progesterone interfaces in various types of electrolytic solutions are expected to throw light on various facets of its functions.[8] For this purpose measurements on hydrodynamic permeability, electroosmosis and electrophoresis have been carried out on progesterone/aqueous electrolyte systems and the data so obtained have been analysed in the light of nonequilibrium thermodynamic theories with a view to ascertaining the form of transport equation and evaluating the phenomenological coefficients.

Experimental

(a) Materials: Progesterone obtained from Sigma Chemical Company (Saint Louis, USA) was used as such to prepare the membrane plug. Analytical grade NaCl, KCl, and $MgCl_2$ obtained from BDH, India were used to prepare their aqueous solutions in distilled water (specific conductance of the order 10^{-6} S). Various solutions of $MgCl_2$ were prepared from its stock solution standardized by EDTA titration.

(b) Experimental Cell/Membrane-Plug Assembly and Silver-Silver Chloride Electrodes: A known amount of progesterone powder was mixed with a small amount of araldite which was then cast in the form of a plug, in a Pyrex glass cell having a constriction in the middle by mechanical compression as described elsewhere.[9] The thickness of the membrane was 5.02 mm and the area of the surface was nearly 3.24×10^{-4} m^2. Reversible silver-silver chloride electrodes were prepared by anodic deposition of chloride ions on a silver disc attached with a silver rod, from 0.1 M NaCl solution (1 M=1 mol dm^{-3}) at 0.4 mA cm^{-2}. It was found that anodically formed chloride layer on silver was very thin.

(c) Measurement of Electroosmotic Permeabilities: The experimental cell was filled with the permeants under investigation and left for 24 h for equilibration. The cell was subsequently filled with degassed fresh permeant to ensure that the concentration of experimental solution remained the same as compounded before equilibration. An electronically operated power supply (HIL, India) was used to apply potential gradients upto 50 V employing Ag-AgCl electrodes. The electrodes were adjusted to cover the maximum surface area of the plug from both the sides.

The volumetric flux was measured by following the rate of displacement of solution/air meniscus in a horizontally placed graduated capillary tube of cross sectional area 1.484×10^{-6} m^2. The electroosmotic flux was found to take place from negative to positive electrode.

The hydrodynamic permeability was measured with the same cell as used for electroosmosis. A constant hydrostatic pressure difference was maintained across the membrane by a constant pressure head device and the volume flow was calculated from the movement of solution/air meniscus in the horizontally placed graduated capillary attached to the cell. The difference of the pressure on the two surfaces of the membrane was measured to $\pm$ 0.001 cm with a cathetometer.

It was observed that the flow of solution takes place in the measuring capillary even when pressure difference and potential difference on both sides of the plug membrane is zero. This residual flow arises due to capillary active forces operating at the solution/air interface in the measuring capillary tube. The data given in these measurements have

been corrected for this residual flow.

(d) Conductance of Membrane Equilibrated with Permeants: Conductance of membrane equilibrated with various solutions were measured with a conductivity bridge (Toshniwal, India) at 50 Hz. Conductances of the permeants were measured before and after electroosmosis with the same apparatus.

(e) Measurement of Electrophoretic Velocities: The electrophoretic velocities of progesterone particles dispersed in the aqueous solutions were measured by the method described elsewhere.[10] Corrections were made for the downward movement due to the action of gravitational forces. Movement of the boundary was from anode to cathode. Measurements of electroosmotic permeability and electrophoretic velocities for a particular system were repeated several times. The deviation from the average value was always less than 5% showing that the measurements are fairly reproducible.

All the measurements were carried out in an air thermostat maintained at 25±0.5 °C.

Results and Discussion

According to nonequilibrium thermodynamics, the isothermal volume flux J_v and the electric current I, through a permeant-equilibrated membrane under the simultaneous action of a hydrodynamic pressure difference ΔP and an electric potential difference $\Delta\Phi$, are given by[11,12]

$$J_v = L_{11}\left(\frac{\Delta P}{T}\right) + L_{12}\left(\frac{\Delta\Phi}{T}\right) \quad (1)$$

$$I = L_{21}\left(\frac{\Delta P}{T}\right) + L_{22}\left(\frac{\Delta\Phi}{T}\right) \quad (2)$$

The parameters L_{ij} (i, j=1, 2) are called phenomenological coefficients. We restrict ourselves to the examination of the applicability of Eq. 1 only. This equation predicts a linear relationship between $(J_v)_{\Delta\Phi=0}$ and ΔP with the slope yielding the value of hydrodynamic transport coefficient L_{11}/T. A linear relationship was also observed between the electroosmotic volume flux $(J_v)_{\Delta P=0}$ and $\Delta\Phi$, whose slope yielded the value of L_{12}/T. L_{22}/T, the conductance of membrane equilibrated with permeant was directly noted by conductivity bridge.

Further the classical theory[13] of electrical double layer reveals that for a plug membrane consisting of an array of n parallel capillaries and equivalent pore radius r, the transport coefficients are given by:

$$\frac{L_{11}}{T} = \frac{n\pi r^4}{8\eta l} \quad (3)$$

$$\frac{L_{12}}{T} = \frac{n\varepsilon r^2}{4\eta l}\cdot\zeta_{e.o.} \quad (4)$$

$$\frac{L_{22}}{T} = \frac{n\pi r^2}{l}\cdot\kappa \quad (5)$$

where η is the coefficient of viscosity of the permeating solutions, l is the average length of membrane capillaries, $\zeta_{e.o.}$ is the zeta potential causing electroosmosis and κ is the specific conductance of the permeant. Values of these transport coefficients are recorded in Table 1.

The electroosmotic flow was found to occur towards positive electrode. This behavior may be explained on the basis of the electrical double layer formed at the membrane permeant interface. The oxygen atom of >C=O groups at C-3 and C-20 and electron density around the olefinic bond is collectively responsible for generating overall negative charge at the progesterone molecules present in the membrane matrix. The cations and anions present in the solution are hydrated and move with the same linear velocity as respective ions.[14] Water dipoles present in the permeating solution get preferentially adsorbed at the negatively charged matrix oriented with their positive ends towards the membrane surface and form the inner Helmholtz plane (IHP). The hydrated cations are attracted towards the negative part of water dipoles forming outer Helmholtz plane (OHP). The diffusely dispersed part of the electrical double layer (Fig. 1) has an excess of hydrated chloride ions with the result that electroosmotic transport would occur towards the anode in accordance with our observation.

Electrophoresis. Electrophoretic migration of progesterone particles dispersed in these electrolytic solutions occur towards the cathode. The following linear relationship holds between the electrophoretic velocity $(V_e)_{g=0}$ and applied potential difference $\Delta\Phi$ as found earlier.[5]

$$(V_e)_{g=0} = \frac{L_{12}^*}{T}\cdot\Delta\Phi \quad (6)$$

Table 1. Phenomenological Coefficients for Progesterone/Aqueous Electrolyte Solution Systems

$C\times10^4$	$\frac{L_{11}}{T}\times10^{13}$			$\frac{L_{12}}{T}\times10^{12}$			$\frac{L_{22}}{T}\times10^{6}$			$\frac{L_{12}^*}{T}\times10^{8}$		
mol l^{-1}	$m^5 S^{-1} N^{-1}$			$m^3 S^{-1} V^{-1}$			S			$mS^{-1} V^{-1}$		
	NaCl	KCl	$MgCl_2$	NaCl	KCl	$MgCl_2$	NaCl	KCl	$MgCl_2$	NaCl	KCl	$MgCl_2$
0.0	8.01	8.10	8.04	2.90	2.92	2.92	0.20	0.20	0.19	17.8	17.7	17.8
1.0	8.20	8.42	8.35	3.12	3.30	3.04	0.24	0.31	0.29	19.4	19.9	18.8
2.0	8.52	8.80	8.72	3.30	3.52	3.20	0.41	0.54	0.58	20.0	20.6	18.9
4.0	9.31	9.64	9.25	3.54	3.91	3.35	0.86	1.06	1.14	21.2	21.4	19.6
6.0	11.02	9.60	21.80	3.92	4.40	3.48	1.35	1.74	9.94	21.8	21.9	21.0
10.0	11.88	13.80	10.10	4.38	5.42	3.80	2.42	3.23	2.95	24.8	22.7	22.3

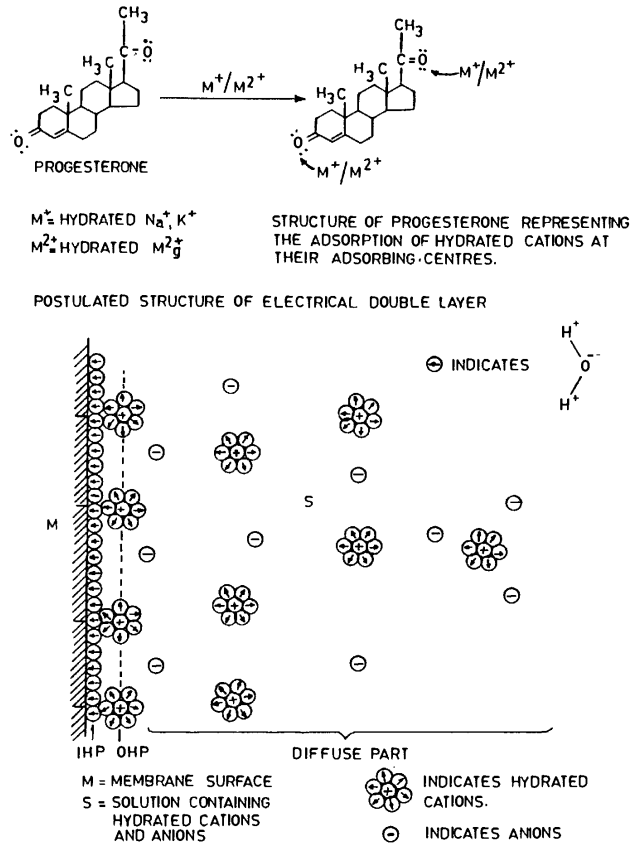

Fig. 1.

where

$$\frac{L_{12}^*}{T} = \frac{\varepsilon \zeta_{e.p.}}{4\pi\eta l'} \tag{7}$$

L_{12}^*/T is the electrophoretic transport coefficient, ε and η are the dielectric constant and viscosity of the solution, respectively. $\zeta_{e.p.}$ is the zeta potential and l' is the distance between the two electrodes of the electrophoretic cell.

The values of L_{12}^*/T obtained from the slope of linear plots of $(V_e)_{g=0}$ vs. $\Delta\Phi$ are recorded in Table 1.

The preferential adsorption of hydrated cations at the surface of progesterone particles cause it to have net positive charge. This facilitates the electrophoretic migration towards cathode.

Membrane Parameters/Characterization of Membrane Structure. The extent of flow and nature of flow through a membrane is determined to a great extent by the characteristics of membrane itself. Hence, certain important parameters which provide an insight into the structural details viz., (i) average pore radii and average number of pores, (ii) zeta potential have been determined using fluid permeation measurements e.g., electroosmosis and hydrodynamic permeation, conductance of the membrane equilibrated with permeants. The average pore radii r and average number of pores n, have been evaluated using the equations[5]

$$r = \left[\frac{8\eta\kappa L_{11}/T}{L_{22}/T}\right]^{1/2} \tag{8}$$

and

$$n = \frac{\frac{L_{22}}{T} \times l}{\pi r^2 \kappa} . \tag{9}$$

The values of these parameters are recorded in Table 2.

Evaluation of Zeta-Potentials: Electrokinetic phenomena are only directly related to the nature of the mobile part of the electric double layer and may, therefore, only be interpreted in terms of potential (zeta) or the charge density at the surface of shear. No direct information is given about the charge density at the surface of the membrane. Zeta potentials have been calculated using the following equations[5]

$$\zeta_{e.o.} = \frac{4\pi\eta\kappa}{\varepsilon\left(\frac{L_{22}}{T}\right)} \times \left(\frac{L_{12}}{T}\right)_{e.o.} \times 9 \times 10^4 \text{ V} \tag{10}$$

and

$$\zeta_{e.p.} = \frac{4\pi\eta l'}{\varepsilon} \times \frac{L_{12}^*}{T} \times 9 \times 10^4 \text{ V} \tag{11}$$

where $\zeta_{e.o.}$ and $\zeta_{e.p.}$ are the zeta potentials calculated using electroosmotic and electrophoretic transport coefficients respectively. There are instances where the above relationships are not applicable due to complicating effects arising on account of double layer polarization.[15]

It is evident from Table 2 that the zeta potentials calculated from electroosmotic and electrophoretic data are not comparable, which observation is consistent with our earlier findings.[5,7]

The discrepancy in the two values of zeta potentials

Table 2. Membrane Parameters for Progesterone/Aqueous Electrolyte Systems[a]

$C\times10^4$	$r\times10^6$			$n\times10^3$			$\zeta_{e.o.}\times10^3$			$\zeta_{e.p.}\times10^3$		
mol l^{-1}	m						V			V		
	NaCl	KCl	$MgCl_2$	NaCl	KCl	$MgCl_2$	NaCl	KCl	$MgCl_2$	NaCl	KCl	$MgCl_2$
1.0	6.66	6.65	6.68	4.80	5.46	5.27	31.7	32.1	29.5	43.3	44.3	41.5
2.0	6.70	6.64	6.65	6.09	4.66	5.71	32.2	32.9	30.1	44.5	45.9	42.4
4.0	6.82	6.71	6.77	5.46	6.03	5.82	32.5	33.7	30.6	45.7	47.5	43.1
6.0	6.72	6.81	6.81	6.22	6.48	6.06	32.7	34.2	31.0	46.3	48.4	43.5
10.0	6.97	6.01	6.72	6.49	6.11	6.84	33.0	34.8	31.4	47.2	49.7	44.0

a) Average pore radii r, average no. of pores n, and zeta potentials $\zeta_{e.o.}$ and $\zeta_{e.p.}$.

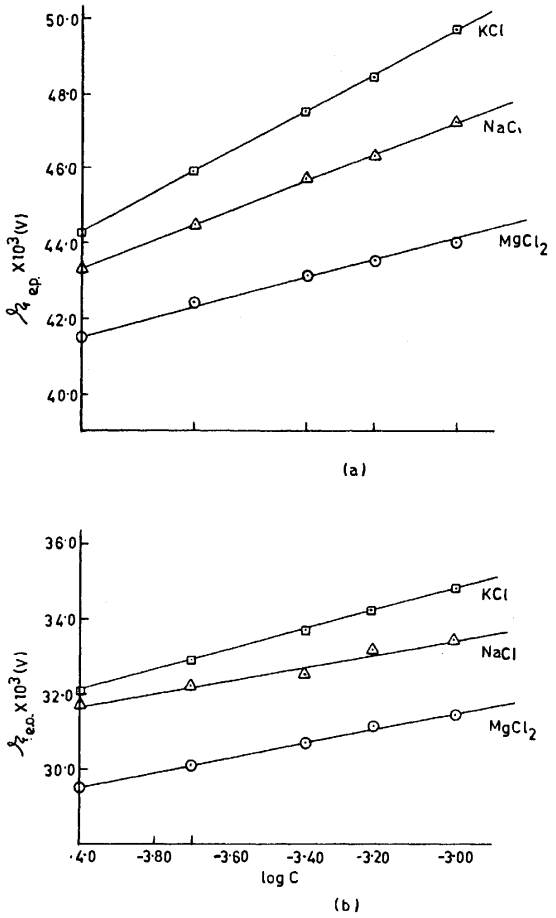

Fig. 2. Dependence of zeta potential (ζ) on log$C$ for progesterone/aq electrolyte solution systems (concn 10^{-3} mol l^{-1}).

is attributable to: i) change in the electrokinetic behavior owing to the decrease in particle size for electrophoretic measurements, ii) change in the hydrodynamic environment in the two cases, and iii) variation of the dielectric constant ε and the viscosity η in the double layer. It is not possible to calculate these quantities directly within the double layer. Therefore, no definite conclusion could be drawn.[16]

Zeta potentials vary nonlinearly with concentration of solutions while its dependence with log C is found to be linear (Fig. 2) and the following equation[5] holds good.

$$\zeta = A + B \log C \quad (20)$$

where A is taken as approximately constant for conditions under which the charge on the membrane surface does not change sign and B is another constant. The existence of positive zeta potentials may be attributed to the firm attachment of cations at the surface of capillary channels of the membrane.

The authors would like to express their thanks to late Prof. S. C. Tripathi, Head, Chemistry Department, Gorakhpur University, Gorakhpur, for providing laboratory facilities. Financial support by CSIR, New Delhi, to one of us (Bali Ram) is thankfully acknowledged.

References

1) W. D. Stein, "The Movement of Molecules Across Cell Membranes," Academic Press, New York (1967), p. 9.
2) S. T. Hwang and K. Kammermeyer, "Membranes in Separations," Wiley, N. Y. (1975), Vol. VII.
3) H. T. Tien, "Bilayer Lipid Membranes," Dekker, N. Y. (1974), p. 9.
4) Ref. 3, p. 4.
5) M. L. Srivastava and B. Ram, *J. Membrane Sci.*, **19**, 137 (1984).
6) M. L. Srivastava and B. Ram, *Carbohydr. Res.*, **132**, 209 (1984).
7) M. L. Srivastava and B. Ram, *J. Non-Equilib. Thermodyn.*, **10**, 57 (1985).
8) B. K. Chakrabarti, H. N. Ghosh, and S. N. Sahana, "Modern Human Physiology," Mahendra Nath Paul, Calcutta-9 (1972), pp. 1101—1105.
9) A. F. Hadermann, P. F. Walters, and J. W. Woo, *J. Phys. Chem.*, **78**, 65 (1974).
10) M. L. Srivastava and B. Ram, *Bull. Chem. Soc. Jpn.*, **61**, 2175 (1988).
11) S. R. de Groot, "Thermodynamics of Irrversible Processes," North Holland, Amesterdam (1961), p. 186.
12) A. Katchalsky and P. F. Curran, "Non-Equilibrium Thermodynamics in Biophysics." Harvard University Press, Cambridge, Mass. (1964).
13) J. Th. G. Overbeek, "Article in Colloid Science," ed by H. R. Kruyt, Amesterdam, Elsevier, N. Y. (1952), Vol. 1, p. 198.
14) K. S. Spiegler, *Trans. Faraday Soc.*, **54**, 1408 (1958).
15) S. S. Dukhin, "Surface and Colloid Science," ed by E. Matjevic, Wiley, New York (1974), Vol. 7, pp. 36, 37.
16) Ref. 15, pp. 181—184.

Molecular and Electronic Structures of Thieno[3,4-*b*]thiophene-2-carboxylic Acid and Acetic Thieno[3,4-*b*]thiophene-2-carboxylic Anhydride. An AM1, MNDO, and CNDO/S Study

Giuseppe BUEMI
Dipartimento di Scienze Chimiche, Università di Catania, Viale A. Doria 6-95125 Catania, Italy
(Received August 8, 1988)

AM1 and MNDO methods have been used for optimizing the molecular geometry of all the possible conformations of thieno[3,4-*b*]thiophene-2-carboxylic acid (**1**), of its methyl ester (**2**) and of acetic thieno[3,4-*b*]thiophene-2-carboxylic anhydride (**3**). Both methods give comparable results for the thieno[3,4-*b*]thiophene framework but rather different bond angles for the substituent group of **3**. In any case, an equilibrium between two (**1**,**2**) or more (**3**) conformations is conceivable. Although the most stable conformations are predicted to be planar, the rotation of the substituent group implies only low energy increase (rotation barriers are calculated to be about 2 kcal mol^{-1}) which allows wide oscillations. The $\pi \rightarrow \pi^*$ electronic transitions do not differ appreciably from those of the parent thieno[3,4-*b*]thiophene molecule and are better accounted for by the conformations having remarkable rotation around the C_7-C_9 bond.

Thieno[3,4-*b*]thiophene-2-carboxylic acid (**1**), its methyl ester (**2**) and acetic thieno[3,4-*b*]thiophene-2-carboxylic anhydride (**3**) are stable derivatives[1] of the unstable thieno[3,4-*b*]thiophene. The geometry and electronic structure of this latter bicyclic compound have been previously studied at MNDO and CNDO/S level.[2] In spite of the increasing of the π system dimension, the UV absorption bands of the parent compound are still present—only slightly affected by substitution—also in the spectra of **1**—**3**, together with a new band of moderate intensity lying on the long wavelengths side (about 340 nm).[1] This band is certainly peculiar of the substituent group and probably involves oxygen(s) lone pairs.

Aim of the present study is the investigation of the electronic structures of the title compounds in order to evidence what changes occur in the electronic transitions as well as in the involved frontier MO's, with respect to those of the thieno[3,4-*b*]thiophene, consequently to the substitution of an H atom with a carboxyl or more extensive group. Moreover, we propose to investigate the role played by the molecular geometry on the electronic spectra.

Since different possible accomodations of the atoms constituting the lateral chain are conceivable, and, therefore, quite a lot of conformations can be originated, a preventive conformational analysis study has been accomplished in order to determine the relative stabilities of these conformations to select the most probable conformers.

Calculation

The geometry optimization, including all the independently variable parameters needed for geometry definition, was carried out by means of AM1 method[3] since it is claimed to evaluate the "core-core" repulsion energy better than other semiempirical methods. Further optimization at MNDO level[4] was carried out too, in order to get geometries of **1**—**3** homogeneous with those previously obtained for the parent thieno[3,4-*b*]thiophene, and, on the same time, to evidence what differences, if any, characterize the molecular structures coming from the two different methods.

All the possible conformations arising from the different possible geometrical arrangements of -COOH, -$COOCH_3$, or -$COOCOCH_3$ groups of **1**—**3** were taken into account in the present study. In a first step full planarity was imposed to the molecules, then the obtained minimum energy structures were again optimized allowing free rotation to the substituent groups in order to check if loss of planarity leads to energy gain. Since MNDO is often not able to give correct geometries when rotation is considered,[5] because of its tendency to underestimation of rotation barrier energies, only AM1 was used in exploring nonplanar conformations. Calculations were performed on a Vax-11-750 computer by using the AMPAC program (in which MINDO/3, MNDO, and AM1 options are included) furnished by Q.C.P.E.[6]

The electronic transitions were evaluated by means of CINDO/SHIFT/UV program[†7] which allows (if wanted) inclusion of 3d atomic orbitals of S atoms. 80 monoexcited configurations were taken into account in the CI procedure. The importance of doubly excited configurations was also tested by means of the CNDUV99 program.[8]

Results and Discussion

Molecular Conformations. The most stable conformers of **1**—**3** are shown in Fig. 1. The relative stabilities resulting from our calculations are given in Table 1, where also the theoretical dipole moments are reported.

† CNDO-SHIFT-UV program furnished by Q. C. P. E was properly modified by us to run on VAX computers and to allow calculations of the excited state dipole moments. At present a version of the same program running on IBM-PC is available too.[7b]

Table 1. Stability Order (Energies in kcal mol^{-1}) and Dipole Moments (in Debyes) of the Various Conformers

	ΔE		μ	
	MNDO	AM1	MNDO	AM1
1-A	0.367	0.0	3.21	3.37
1-ARP	9.736	5.562	5.49	5.66
1-B	0.0	0.483	2.07	2.38
1-BRP	7.874	4.828	4.76	4.95
Rotation barrier 1-A → 1-B=2.040 kcal mol^{-1}				
2-A	0.381	0.0	3.25	3.16
2-ARP[a)]	9.736	9.055	5.40	5.69
2-RNP	—	5.920	—	5.23
2-B	0.0	0.405	1.78	1.74
2-BRP[a)]	7.874	7.762	4.34	4.52
Rotation barrier 2-A → 2-B=1.803 kcal mol^{-1}				
3-A1	0.754	0.436	5.84	5.87
3-A2	3.355	0.0	2.06	2.51
3-A2RP[a)]	21.975	20.698	7.41	7.76
3-B1	0.0	0.353	4.40	4.18
3-B2	3.550	0.817	3.27	3.86
3B2RP[a)]	18.861	16.991	7.01	7.25
Rotation barrier 3-A2 → 3-B2=2.41 kcal mol^{-1}				

a) Pseudo minimum. P=Planar, NP=Nonplanar.

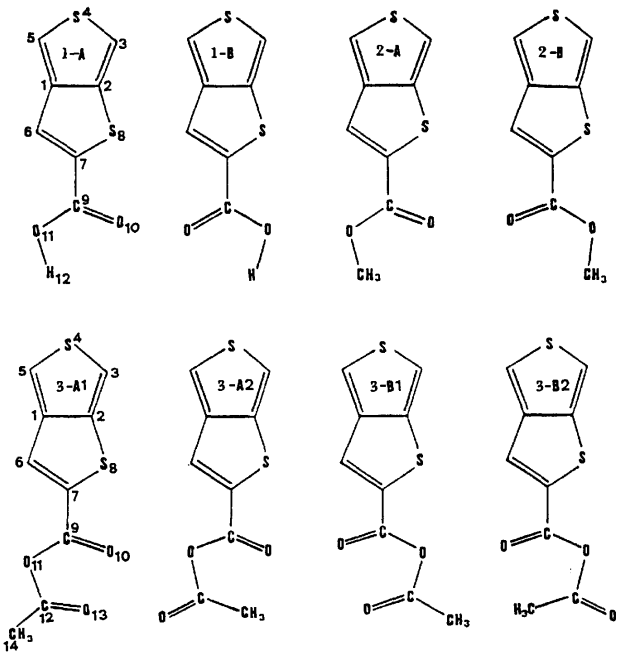

Fig. 1. Numbering system and molecular structure of the most stable conformations of **1**—**3**.

Additionally to the conformations of Fig. 1, we took into account also the less probable structures in which the H, CH_3, or $COCH_3$ groups are oriented towards the bicyclic framework, i.e. having $\omega_{10\text{-}9\text{-}11\text{-}12}=180°$. They will be indicated as **1**-AR, **2**-BR, **2**-AR, and so on. **1**-AR and **1**-BR minimum energy geometries retain their planarity after optimization but are less stable than **1**-A and **1**-B by 5.56 and 4.83 kcal mol^{-1}, respectively. The corresponding planar conformations of **2** and **3**

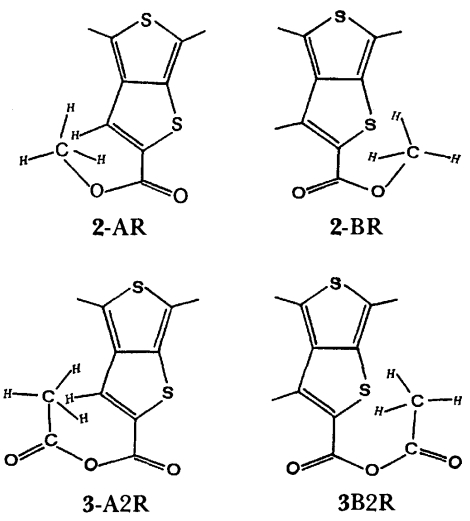

Fig. 2. Pseudo minima found when S_8 or the H bonded to C_6 bisects the bond angle of the methyl out-of-plane H atoms.

(**2**-ARP, **2**-BRP, **3**-A2RP, and **3**-B2RP) reach pseudo minima when the two out of plane H atoms of the CH_3 group are arranged as shown in Fig. 2. In such a situation, owing to the interaction with the H atom bonded to C_6 or with the S_8 electronic cloud, any rotation of the methyl group causes energy increasing which prevents the displacement towards the most stable structures **2**-A, **2**-B, **3**-A2, and **3**-B2 (a similar pseudo minimum was previously noticed in studying the molecular structures of methoxy derivatives of heptalenediones.[9)] Since **2**-ARP, **2**-BRP, **3**-A2RP, and **3**-B2RP forms are by far less stable than **2**-A, **2**-B, **3**-A2, and **3**-B2, no detail about their geometrical parameters is reported here. When the above cited pseudo minima were avoided a different behavior of **2** and **3** was found. In particular, both **2**-AR and **2**-BR converge towards a nonplanar single minimum energy structure (indicated as **2**-RNP in Table 1) in which the CH_3 group is still oriented towards the thieno[3,4-*b*]thiophene framework but has the whole $COOCH_3$ group rotated by about 80° around the C_7-C_9 bond.

Differently from **3**-A2R and **3**-B2R, the conformers **3**-A1R and **3**-B1R show no minimum and after optimization, come back to **3**-A1 and **3**-B1 respectively. **3**-A2 and **3**-B2 are all planar conformations whilst **3**-A1 and **3**-B1 are not, because of repulsion between O_{10} and O_{13} which causes rotation of about 20° around to the C_9-O_{11} and O_{11}-C_{12} bond; however, the energy difference between the planar and nonplanar structures is very low: ≃0.3 kcal mol^{-1}. These results lead to the conclusion that the $OCOCH_3$ group in **3** can widely oscillate. Although null or negligible rotation around the C_7-C_9 bond is predicted for the most probable conformations of **1**—**3** the calculated torsion barriers are not excessively high and the related potential well is rather flattened (in **1** and **2** a rotation of 45° of the substituent group implies an energy increase lower

Table 2. Optimized Molecular Geometry of Thieno[3,4-*b*]thiophene Framework of **1**-A Conformer

	AM1	MNDO	MNDO[a]		AM1[b]	MNDO	MNDO[a]
r_{1-2}	1.468	1.475	1.478	δ_{5-1-2}	111.8	111.2	110.8
r_{2-3}	1.362	1.370	1.364	δ_{1-2-3}	112.2	111.8	112.6
r_{3-4}	1.680	1.682	1.690	δ_{2-3-4}	109.9	110.7	110.4
r_{4-5}	1.673	1.677	1.689	δ_{3-4-5}	95.9	95.3	94.9
r_{5-1}	1.367	1.376	1.371	δ_{4-5-1}	110.2	110.9	111.3
r_{1-6}	1.442	1.456	1.457	δ_{6-1-2}	110.7	110.4	110.3
r_{6-7}	1.366	1.376	1.365	δ_{1-6-7}	111.7	111.5	111.1
r_{7-8}	1.712	1.711	1.702	δ_{6-7-8}	113.4	113.3	114.6
r_{2-8}	1.677	1.674	1.687	δ_{7-8-2}	93.4	94.1	93.3
r_{C-H}	1.090	1.081	1.082	δ_{8-2-1}	110.8	110.7	110.7

a) Isolated molecule. The geometry of this framework does not change significantly in the other conformers. b) $\delta_{H-C_3-C_2}$=129.5; $\delta_{H-C_5-C_4}$=128.9; $\delta_{H-C_6-C_4}$=123.3.

Table 3. Optimized Geometries of the Substituent Groups in the Studied Molecules

	1-A		**1**-B		**2**-A		**2**-B	
	AM1	MNDO	AM1	MNDO	AM1	MNDO	AM1	MNDO
r_{7-9}	1.453	1.482	1.454	1.481	1.456	1.484	1.457	1.484
r_{9-10}	1.235	1.232	1.238	1.233	1.233	1.229	1.236	1.230
r_{9-11}	1.369	1.360	1.365	1.358	1.374	1.363	1.370	1.360
r_{11-12}	0.972	0.949	0.972	0.950	1.430	1.407	1.431	1.407
$r_{CH(methyl)}$	—	—	—	—	1.117	1.108[a]	1.117	1.108[a]
δ_{6-7-9}	125.6	127.9	122.9	124.9	125.9	128.2	122.7	124.8
δ_{7-9-10}	129.9	126.4	127.4	126.0	129.4	126.1	126.9	125.6
δ_{7-9-11}	114.0	115.3	116.4	115.5	112.9	114.0	115.1	114.3
$\delta_{9-11-12}$	109.0	115.2	108.9	115.3	116.1	125.2	116.1	125.2
$\delta_{HCH(methyl)}$	—	—	—	—	107.8	110.3	107.8	110.3
	3-A1		**3**-A2		**3**-B1		**3**-B2	
	AM1	MNDO	AM1	MNDO	AM1	MNDO	AM1	MNDO
r_{7-9}	1.455	1.485	1.455	1.482	1.457	1.484	1.457	1.483
r_{9-10}	1.226	1.223	1.230	1.226	1.228	1.224	1.233	1.227
r_{9-11}	1.390	1.374	1.378	1.366	1.384	1.371	1.372	1.364
r_{11-12}	1.387	1.374	1.393	1.379	1.388	1.374	1.396	1.380
$r_{CH(methyl)}$	1.117	1.108[a]	1.118	1.108[a]	1.117	1.108[a]	1.118	1.108[a]
r_{12-13}	1.224	1.221	1.229	1.226	1.223	1.222	1.228	1.225
r_{12-14}	1.488	1.525	1.482	1.523	1.488	1.525	1.482	1.523
δ_{6-7-9}	126.0	128.4	125.7	128.2	122.6	124.6	122.4	124.5
δ_{7-9-10}	130.1	126.4	129.3	126.5	127.5	126.1	126.7	126.0
δ_{7-9-11}	112.3	113.3	111.7	113.4	114.5	113.4	114.1	113.7
$\delta_{9-11-12}$	121.5	131.5	124.4	133.9	121.7	131.8	124.2	133.6
$\delta_{HCH(methyl)}$	109.5	110.6	109.8	110.8	109.5	110.6	109.8	110.8
$\delta_{11-12-13}$	118.5	120.8	109.6	111.5	118.7	120.7	109.6	111.5
$\delta_{11-12-14}$	111.6	112.3	122.4	123.8	111.4	112.3	122.4	123.9
$\omega_{10-9-7-8}$	1.5	—	0.2	—	−178.6	—	180.0	—
$\omega_{12-11-9-7}$	−156.5	—	179.9	—	157.0	—	180.0	—
$\omega_{13-12-11-9}$	21.4	—	178.7	—	−19.2	—	180.0	—

a) This bond length was not optimized at MNDO level. MNDO geometries refer to all planar conformations (see text).

than 1 kcal mol^{-1}) so that wide oscillations around this bond are also possible. Let we now analyze more carefully the details of AM1 and MNDO geometries of the bicyclic framework and of the substituent groups, reported in Tables 2 and 3, respectively.

A first remark to point out is that, independently of the adopted method, the geometry of the thieno[3,4-*b*]-thiophene framework is practically the same calculated for the parent compound and it does not change significantly on changing the attached group. As it can be seen by comparing the geometrical data of **1**-A, reported in Table 2, the ring bond lengths differ by about 0.01 Å and bond angles by about one degree on passing from AM1 to MNDO or from the substituted to the unsubstituted molecule. These findings are noticed in compounds **2** and **3** too. More important

differences between AM1 and MNDO geometries occur in the -COOR and, mainly, in the $-COOCOCH_3$ framework (see Table 3). In particular, the C_7-C_9 bond length, in all the examined compounds, and the C_{12}-C_{14} bond length in **3** are predicted by AM1 about 0.03 Å shorter than the MNDO ones, whilst $r_{O\text{-}CH_3}$ in **2**-A and **2**-B is calculated by AM1 about 0.02 Å longer than that calculated by MNDO.

In all conformers of A type $\delta_{6\text{-}7\text{-}9}$ is 3—4 degrees larger than in the conformers of B type: being $\delta_{6\text{-}7\text{-}9}$ value practically constant, the substituent group is bent towards the right more than it is in B type conformers. This could be due, at least partially, to a lower repulsion between S_8 and oxygen with respect to that between C_6-H and oxygen owing to a greater interatomic distance in the former case, deriving from the large C_7-S_8 bond length in comparison with C_6=C_7 double bond length. Moreover the MNDO values concerning $\delta_{9\text{-}11\text{-}12}$ are, in general, from six to ten degrees larger than AM1 ones. These large angle differences are to be ascribed to the overestimation of "core-core" repulsion by MNDO with respect to AM1 method. As a consequence, the two methods lead to different final stability order, at least for the most probable conformations. So MNDO predicts structures **1**-B, **2**-B, and **3**-B1 to be the most stable ones, in contrast with AM1, which indicates **1**-A, **2**-A, and **3**-A2 as the most stable conformers. Indeed, apart from the question about which of them is the most stable, the ΔE between structures **1**-A and **1**-B and between **2**-A and **2**-B, both at MNDO and AM1 level, is less than 0.5 kcal mol^{-1}, whilst the ΔE among **3**-A2, **3**-B1, **3**-A1, and **3**-B2, at AM1 level, are less than, or, at the most, equal to 1 kcal mol^{-1}. On this ground an equilibrium between these structures is conceivable.

At present, at best of our knowledge, no experimental support is available in favor of one or another conformation. Unfortunately, the calculated electronic spectra of the above conformers are not sufficiently different from each other. However we note that the calculated dipole moments of the cited conformations are rather unlike one another, therefore an important contribution to the problem could be achieved from their measurement.

Electronic Spectra. As previously pointed out for thieno[3,4-*b*]thiophene,[2] the contribution of 3d orbitals of sulfur atoms to the orbitals involved in the low energy electronic transitions is very low.

The molecular orbitals involved in the electronic transitions responsible of the UV absorption maxima of **1**—**3** are chiefly the two highest occupied (π_1 and π_2) and the two lowest vacant (π_1* and π_2*) together with the *n* ones. In **1** and **2** the n orbital is mainly localized on O_{10}, whilst in **3** we have two n orbitals whose highest coefficients are located mainly on O_{10} and O_{13}, respectively.

Figure 3 shows the coefficient distribution of π_1, π_2, π_1*, and π_2* of **1** and **3** (the coefficient distribution of the frontier MO's of **2** is not reported because it is practically coincident with that of the MO's of **1**). In the same figure also the corresponding MO's of the thieno[3,4-*b*]thiophene are reported for comparison. It appears clearly that the coefficient distribution on the bicyclic framework is practically equal in the parent and in the derivative compounds, although non-negligible coefficients are found also on O_{10} (π_1 and π_2) and on the C_9=O_{10} fragment (π_1* and π_2*). Owing to the fact that these MO's in **3** do not span appreciably the extreme $COCH_3$ framework (which is the most rotated with respect to the molecular plane), the electronic transitions calculated by adopting the minimum energy conformations (nonplanar) or the planar ones, are practically coincident (differences are limited to 1 or 2 nm). Similarly, no appreciable difference exists between the calculated transitions of A and B type structures.

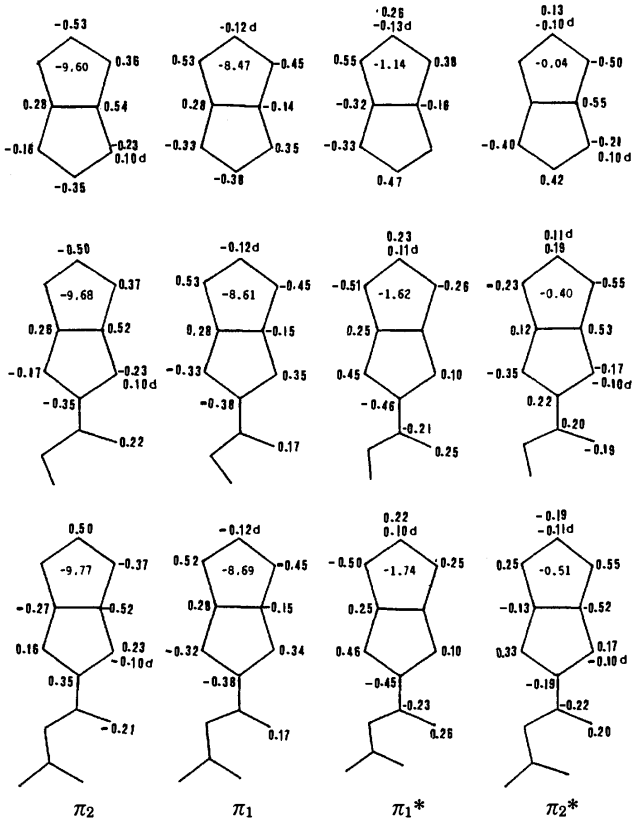

Fig. 3. Coefficient distribution of the two highest occupied (HOMO and NHOMO) and the two lowest unoccupied (LUMO and NLUMO) MO's of thieno[3,4-*b*]thiophene and its derivatives **1** and **3**. The figures inside the rings are the orbital energies (in eV). The n-type orbitals were calculated at −11.32 eV in **1**-A, at −11.23 eV in **2**-A, and at −11.06 and −11.68 eV in **3**-A2.

The charge densities on the atoms of the bicyclic framework mantain the same order noted in the parent compound,[2] so that also in **1**—**3** the C atoms in α position with respect to S are once again the most negatively charged.

Table 4. Electronic Transitions (eV) of **1—3** in Their Minimum Energy Conformation (Geometries from AM1 method).

E	λ	f	Pol.[a]	Nature	Exp.[b] λ	Exp.[b] E	Exp.[b] log ε
			Thieno[3,4-*b*]thiophene[c]				
4.43(4.53)	280	0.32(0.35)	27(31)	$\pi_1 \rightarrow \pi_1^*$	297	4.18	3.73
					276	4.50	3.56
4.65(4.82)	266	0.02(0.02)	102(74)	$\pi_1 \rightarrow \pi_2^*$; $\pi_2 \rightarrow \pi_1^*$	266	4.66	3.56
					257	4.82	3.53
5.39(5.41)	230	0.51(0.49)	97(99)	$\pi_1 \rightarrow \pi_2^*$; $\pi_2 \rightarrow \pi_1^*$	235	5.27	4.23
5.54(5.71)	224	0	—				
5.98(6.06)	207	0.05(0.09)	49(73)	$\pi_1 \rightarrow \pi_3^*$; $\pi_2 \rightarrow \pi_2^*$			
			Thieno[3,4-*b*]thiophene-2-carboxylic acid[c] (**1**-A)				
3.60(3.58)	344	0	—	$n \rightarrow \pi^*$	336	3.69	3.64
4.18(4.22)	296	0.35(0.38)	39(43)	$\pi_1 \rightarrow \pi_1^*$	292	4.24	4.18
					283	4.38	4.20
4.59(4.75)	270	0.23(0.29)	107(74)	$\pi_2 \rightarrow \pi_1^*$; $\pi_1 \rightarrow \pi_2^*$	260	4.77	4.07
					255_{sh}	4.86	4.06
5.07(5.12)	244	0.52(0.42)	104(70)	$\pi_1 \rightarrow \pi_2^*$; $\pi_2 \rightarrow \pi_1^*$	232	5.34	3.74
5.46(5.60)	227	0	—	$\sigma,n \rightarrow \pi^*$			
5.76(5.85)	215	0.02(0.09)	86(81)	$\pi_1 \rightarrow \pi_3^*$; $\pi_2 \rightarrow \pi_2^*$	226	5.50	3.73
5.98(6.09)	207	0.04(0.10)	94(101)	$\pi_3 \rightarrow \pi_1^*$; $\pi_2 \rightarrow \pi_2^*$			
			Thieno[3,4-*b*]thiophene-2-carboxylic ester[d] (**2**-A)				
3.58(4.01)	346	$10^{-5}(10^{-4})$	—	$n \rightarrow \pi^*$	340	3.65	3.62
4.20(4.46)	295	0.35(0.35)	141	$\pi_1 \rightarrow \pi_1^*$	293	4.23	4.23
					284	4.36	4.22
4.59(4.64)	270	0.22(0.04)	73	$\pi_2 \rightarrow \pi_1^*$; $\pi_1 \rightarrow \pi_2^*$	262	4.74	4.02
					256_{sh}	4.84	4.00
5.07(5.33)	244	0.53(0.57)	104	$\pi_1 \rightarrow \pi_2^*$; $\pi_2 \rightarrow \pi_1^*$	234	5.31	3.66
5.51(5.50)	225	0	—	$\sigma,n \rightarrow \pi^*$			
5.77(5.92)	215	0.02(0.03)	83	$\pi_1 \rightarrow \pi_3^*$; $\pi_2 \rightarrow \pi_2^*$			
5.99(5.98)	207	0.10(0)	92	$\pi_3 \rightarrow \pi_1^*$; $\pi_2 \rightarrow \pi_2^*$			
			Acetic thieno[3,4-*b*]thiophene-2-carboxylic anhydride (**3**-A2)				
3.74	332	0	—	$n \rightarrow \pi^*$	343	361	3.58
4.03	308	10^{-3}	—	$n \rightarrow \pi^*$			
4.18	297	0.35	140	$\pi_1 \rightarrow \pi_1^*$	292	4.24	4.22
					284_{sh}	4.36	4.14
4.60	270	0.24	107	$\pi_2 \rightarrow \pi_1^*$; $\pi_1 \rightarrow \pi_2^*$	260	4.78	3.98
5.06	245	0.52	114	$\pi_1 \rightarrow \pi_2^*$; $\pi_2 \rightarrow \pi_1^*$	238_{sh}	5.21	3.69
5.55	224	0	—	$\sigma,n \rightarrow \pi^*$			
5.75	215	0.02	86	$\pi_2 \rightarrow \pi_2^*$; $\pi_1 \rightarrow \pi_4^*$			
5.98	207	0.20	75	$\pi_3 \rightarrow \pi_1^*$; $\pi_2 \rightarrow \pi_2^*$			

a) Angle between the transition moment vector and the short molecular axis. b) Ref. 1 (95% ethanol). c) Values in parentheses are those obtained without d orbitals inclusion. d) Values in parentheses refer to the conformation rotated by 90° around C_7-C_9.

The CNDO/S results obtained for the most stable conformers (AM1 geometries) are collected in Table 4, together with those of thieno[3,4-*b*]thiophene, for which the optimized geometry coming from AM1 method was adopted too. Here also the literature experimental absorption maxima are reported. These latter were recorded in 95% EtOH solution. According to Skancke[10] the vapor phase values of thieno[3,4-*b*]-thiophene would be roughly 0.08 eV higher than the solution ones. A similar correction could be accepted also for **1—3**.

By comparing the experimental absorption maxima of thieno[3,4-*b*]thiophene and those of **1—3** we observe two noteworthy features: i) The maxima centered at 297 and 266 nm in the spectrum of the parent compound shift by 4—5 nm towards the blue after substitution; ii) the two maxima recorded at 276 and 257 nm in the thieno[3,4-*b*]thiophene spectrum, where they are equidistant from the band at 266 nm, show to be differently affected by substitution: The former shifts towards the red and is found in the range of 280 nm, the latter remains unchanged in **1—2** and is absent in **3**.

Theory predicts that the lowest energy transition of **1** and **2** and the lowest two transitions of **3** are $n \rightarrow \pi^*$ in nature: they are responsible of the absorption band observed in the range of 3.6 eV.

Owing to the slight changes noted in the frontier orbitals of the title molecules, also the lowest energy $\pi \rightarrow \pi^*$ transitions undergo negligible changes with

Table. 5. Electronic Transitions (eV) of the Title Compounds after Inclusion of Doubly Excited Configurations

E	λ	*f*	log ε	%DEC[a)]	*E*	λ	*f*	log ε	%DEC[a)]
Thieno[3,4-*b*]thiophene							**1**		
4.43	280	0.02	2.96	18	4.09	303	0.11	3.78	7
4.63	268	0.16	3.94	4	4.54	273	0.12	3.81	10
5.18	239	0.02	3.13	37	4.83*	256	0	—	—
5.70	218	0.27	4.16	9	5.04	246	0.17	3.96	18
6.37	195	10^{-3}	1.84	8	5.46	227	0.17	3.96	25
					6.00	207	$7\cdot10^{-3}$	2.55	6
		2					**3**		
4.08	304	0.10	3.74	8	4.08	304	0.15	3.91	5
4.54	273	0.13	3.85	11	4.59	270	0.08	3.63	12
4.83*	257	0	—	—	5.01*	248	0	—	—
5.05	246	0.16	3.95	18	5.03	247	0.24	4.12	11
5.44	228	0.21	4.06	22	5.19*	239	10^{-4}	0.91	—
6.02	206	0.01	2.70	—	5.48	226	0.10	3.72	30
					5.98	207	$6\cdot10^{-3}$	2.52	6

a) Total percentage of doubly excited configurations. Values marked with * refer to n→π^* transitions.

respect to those of the parent compound. So the band at 4.2 eV is mainly due to the $\pi_1\rightarrow\pi_1^*$, HOMO→LUMO transition, whilst the two bands recorded at 4.7 and 5.3 eV originate from HOMO→NLUMO and NHOMO→LUMO transitions. The oscillator strength of the transition calculated at 4.6 eV is strongly enhanced by substitution but it becomes gradually weaker as the substituent goes away from planarity.

The two experimental maxima centered at 284 nm and at about 255 nm, corresponding to the maxima at 276 and 257 nm of thieno[3,4-*b*]thiophene, are not supported by calculations: this occurred also in the parent compound, where they lie in a wavelengths range affected by a vibrational progression and were assigned to vibrational modes. Although in **1—3** they are no more equidistant from the band recorded at 266 nm, we think they originate once again from molecular vibrations.

The two lowest virtual orbitals of **1—3** are stabilized by substitution more than the two highest occupied ones, so that the calculated $\pi\rightarrow\pi^*$ transitions involving them are calculated 10—15 nm shifted towards the red with respect to those of thieno[3,4-*b*]thiophene. This result, seems contrasting with the weak blue shift appearing in the experimental findings, even if it is in line with the red shift observed on passing from the spectrum of benzene to that of the benzoic acid.[11] However, the eletronic transition energies of **1—3** shift towards the blue when remarkable rotation around C_7-C_9 is considered (see values in parentheses for **2** in Table 4). This behavior, together with the fact that the rotation barrier of the carboxyl group (calculated by the same method[2]) in the benzoic acid is $\simeq$1 kcal mol^{-1} higher than in **1**, suggest that contributions from conformers highly rotated around C_7-C_9 are important in the electronic structure description of the title compounds.

Calculations carried out by using CNDUV/99 program,[8] in order to test the importance of doubly excited configurations, are reported in Table 5. Apart from an overestimation of the n→π^* transition(s) (a peculiarity of this program), also these last results support the above assignments and conclusions as regards the $\pi\rightarrow\pi^*$ transitions. Double excitations are present in percentages comparable with those noticed in the parent molecule and the highest total value was found for the transitions lying at $\simeq$5—5.4 eV.

Conclusion

The results of the present study indicate that the most stable conformations of **1—3** have the substituent group coplanar to the bicyclic framework. The low energy difference between the most stable conformers (two in **1**, **2**, four in **3**) suggests the possibility of an equilibrium among them; moreover the rather flattened potential well when rotation around C_7-C_9 is considered allows a wide out of plane oscillation of the substituent group.

The frontier molecular orbitals of **1—3** show a coefficient distribution similar to that observed for thieno[3,4-*b*]thiophene with a weak extension on C_9 and O_{10}. The absorption band on the long wavelengths side originates from n→π^* transitions. The two maxima lying in the range of 280 and 250 nm are probably to be assigned to vibrational modes. The slight blue shift (4—5 nm) shown by the lowest energy bands on passing from the parent compound to its derivatives can be accounted for if a remarkably contribution from the conformers with high rotation around the C_7-C_9 bond is assumed.

Financial support from the Italian Ministero della Pubblica Istruzione, Roma, is acknowledged.

References

1) H. Wynberg and D. J. Zwanenburg, *Tetrahedron Lett.*, **1967**, 761.

2) G.Buemi, *J. Chim. Phys.*, **84**, 1147 (1987).

3) M. J. S. Dewar, E. G. Zoebisch, E. F. Healy, and J. J. P. Stewart, *J. Am. Chem. Soc.*, **107**, 3902 (1985).

4) M. J. S. Dewar and W. Thiel, *J. Am. Chem. Soc.*, **99**, 4899 and 4907 (1977).

5) G. Buemi, F. Zuccarello, and A. Raudino, *J. Mol. Struct. Theochem.*, **164**, 379 (1988).

6) Dewar Research Group and J. J. Stewart; AMPAC: Austin Model 1 Package; *Q.C.P.E. Bulletin*, Vol. 6 (1986), program nr.506.

7) a) M. Rajzmann and P. Francois; CINDO/SHIFT/UV: Shielding Tensors and Electronic Transitions Including Singly Excited Configurations; *Q.C.P.E. Bulletin*, Newsletter 67 (1979), program nr. 382.

b) Program QCMPO29, *Q.C.P.E. Bulletin*, **7** (1987).

8) H. Baumann; CNDUV99: Computation of Electronic Transitions, SCF-CNDO-CI Method, Including Singly and Doubly Excited Configurations; *Q.C.P.E. Bulletin*, Newsletter 59 (1977), program nr. 333.

9) G. Buemi and F. Zuccarello, *Gazz. Chim. Ital.*, **117**, 169 (1987).

10) A. Skancke and P. N. Skancke, *Acta Chem. Scand.*, **24**, 23 (1970).

11) C. N. R. Rao, "Ultraviolet and Visible Spectroscopy," Butterworths, London (1961).

 © 1989 The Chemical Society of Japan Bull. Chem. Soc. Jpn., 62, 1269—1274 (1989)

The Effect of Cadmium Ions on the Polarographic Reduction of Poly[(*p*-methylbenzyl)viologen] Dibromide in Water

Bhim Bali PRASAD
Analytical Division, Chemistry Department, Faculty of Science, Banaras Hindu University, Varanasi-221 005, India
(Received February 25, 1988)

The d.c. polarographic reduction of a redox polyelectrolyte, poly[(*p*-methylbenzyl)viologen] dibromide, in the presence of cadmium sulfate salt demonstrated two well-defined, irreversible diffusion-controlled cathodic waves corresponding to the reduction of protonated form as well as the cadmium complex of the polyelectrolyte in aqueous buffers (pH 2.00—6.00). No wave was observed due to the reduction of the unprotonated form of the polymer in the present instance, however, another ill-defined wave of irreversible nature was emerged at relatively higher negative potential presumably because of the catalytic evolution of hydrogen, at the dropping mercury electrode. An attempt has been made to correlate these results in terms of cadmium ion interaction with the polyelectrolyte during the course of electrode processes.

A comprehensive study on the polarography of the redox polymers, viz., poly[(*p*-methylbenzyl)viologen] dibromides (*o*, *m*, *p*-$PMVBr_2$) has recently been made to understand their reduction mode as well as electron-transfer mechanism involved.[1] The present paper deals with the effect of cadmium ions on the polarographic reduction of poly[(*p*-methylbenzyl)viologen] dibromide (*p*-$PMVBr_2$) in the aqueous solutions of pH 2.00—6.00 range.

Polyelectrolytes have been found to demonstrate a significant impact over their conformational alterations with the addition of simple salts.[2] As a consequence of such salt-induced conformational transition, i.e., the coiling or contraction of cationic polyelectrolyte in interaction with the anions of the added salt in dilute solution and sometimes the possibility of a chemical reaction of polyelectrolyte with the added salt, the reduction behavior of these systems would likely to differ than those of the salt-free polymeric materials. As is evident from the structural formulation of *p*-$PMVBr_2$ [represented by the structure **1**], one of the two nitrogens of the terminal bipyridine is not quaternized and may therefore serve as the proton acceptor allowing the system to exhibit an equilibrium between its protonated and unprotonated form as *p*-$PMVBr_2 + H^+ \rightleftarrows$ *p*-$PMVBr_2H^+$. However, in the presence of Cd^{2+} ions, this uncharged nitrogen of the compound would act as a potential site for the complexation as well. It seems to be feasible that both the protonation and complexation may occur simultaneously and/or compete with each other on the time scale involved for the electroreduction. Thus, a different type of electrode process as compared to that of the polymer alone could be expected, in the presence of cadmium sulfate in this investigation.

Experimental

Materials. Demineralized water, distilled twice from a Pyrex glass still, with specific conductivity ranging between 1×10^{-6} to 2.5×10^{-6} $S\,cm^{-1}$ was used in the preparation of solutions.

The preparation and characterization of the polymer *p*-$PMVBr_2$ (MW=11000) was followed according to the earlier recipes.[1c,3] All other chemicals were of analytical grade.

Methods. All the polarograms were recorded in the usual manner[1c] at room temperature (ca. 25 °C) with the help of Leeds Northrup Type E Electrochemograph using a dropping mercury electrode (DME) and a saturated calomel electrode (SCE) as working and reference electrodes, respectively. First, a known volume (15 ml) of the supporting electrolyte was introduced into the cell and purged with nitrogen gas, and the residual current was obtained. Then, desired amounts of solid depolarizer(s) were added to the solution in the cell; after each addition, the nitrogen gas was allowed to pass through the mixture until the solid completely dissolved and then the final polarogram was run under the blanket of this gas.

The DME used had following characteristics in the open circuit: m=1.90 mg s^{-1} and t=4.3 s (h_{Hg}=35 cm; 0.1 M aqueous KCl, M=mol dm^{-3}). The supporting electrolytes used were a KCl-HCl mixture (pH= 2.00) and citrate buffers (pH=4.40 and 6.00); the ionic strength was maintained at 0.1 M with the addition of requisite amounts of KCl. In each case of these buffers, polarograms were run in two ways: (i) keeping the concentration of *p*-$PMVBr_2$ in the buffer fixed and recording the current-voltage curves with subsequent addition of different known amount of cadmium sulfate, (ii) varying the concentration of polymer by introducing the weighed amount of *p*-$PMVBr_2$ into the buffer containing fixed concentration of cadmium ions.

It must be mentioned that any investigation in an alkaline medium may arise some complications of dequaternization[4] or ylide formation[5] in the system. Therefore all investiga-

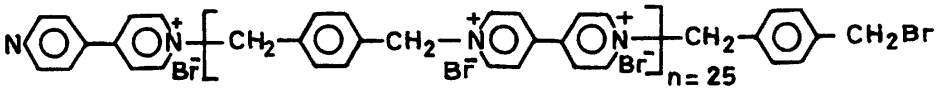

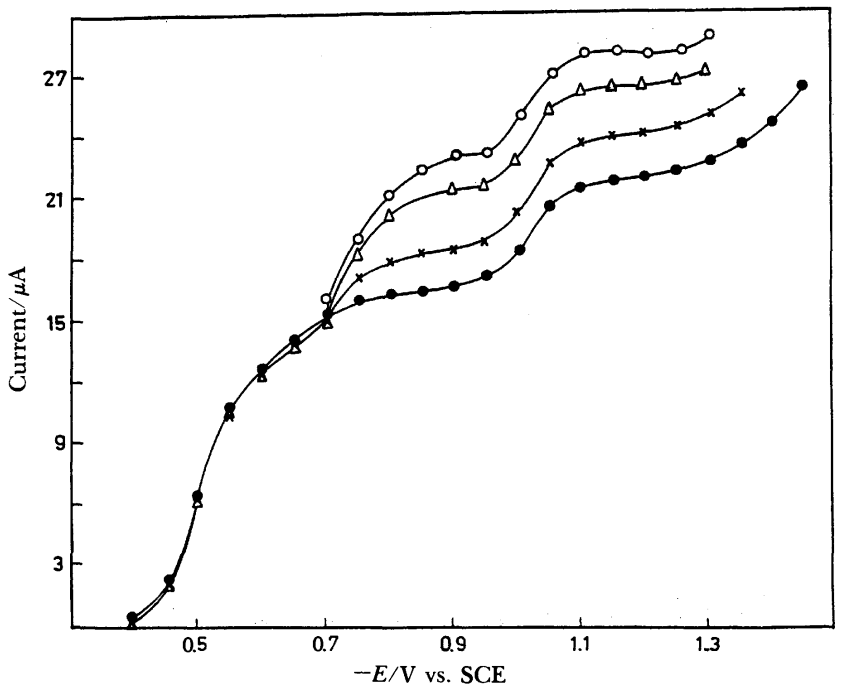

Fig. 1. Polarograms for aqueous solutions of poly[*p*-methylbenzyl)viologen] dibromide at 25 °C in the presence of various concentration of Cd^{2+} ions (in mg cm^{-3}): 0.215 (×); 0.420 (△); 0.640 (○) ([$PMVBr_2$]=4.65 mg cm^{-3} (●), pH=2.00, h_{Hg}=35 cm).

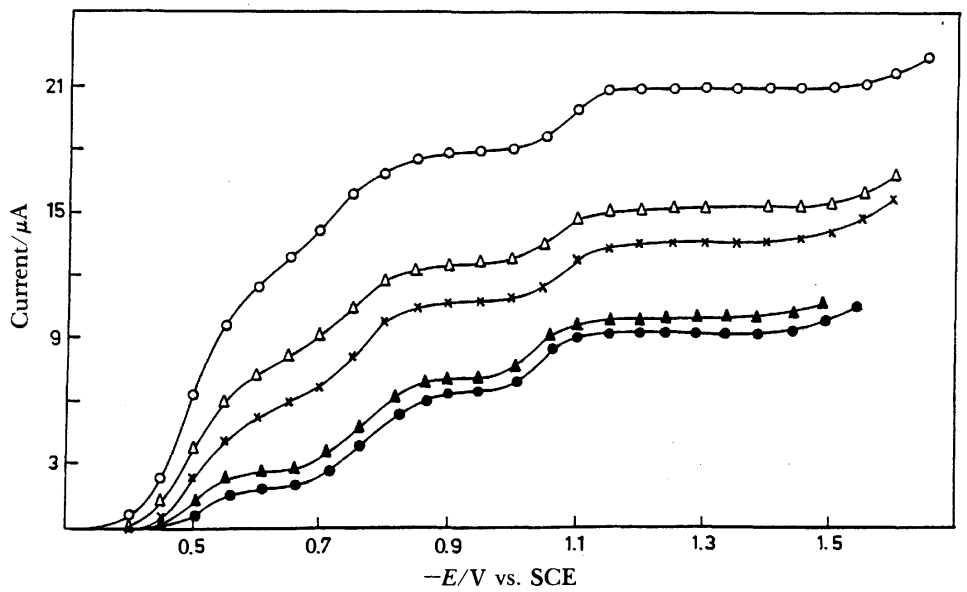

Fig. 2. Polarograms for aqueous solution of poly[(*p*-methylbenzyl)viologen] dibromide having varying concentrations (in mg cm^{-3}) of 0.410 (●), 0.800 (▲), 1.812 (×), 2.340 (△), and 3.962 (○) at 25 °C. ([Cd^{2+}]=0.40 mg cm^{-3} (fixed), pH=2.00, h_{Hg}=35 cm).

tions made in this case had to be confined to only acidic buffers.

The currents and potentials used in the final calculations have been corrected for the residual currents as well as the *iR* drops involved.

Results and Discussion

The representative polarograms of (i) *p*-$PMVBr_2$ with varying amount of Cd^{2+} ions and (ii) Cd^{2+} solution with increasing concentration of *p*-$PMVBr_2$ in a KCl-HCl mixture (pH=2.00) are illustrated in Figs. 1 and 2, respectively. All results obtained with different buffers from analysis of both kinds of polarograms are summarized in Tables 1 and 2.

As is evident from Fig. 1 , two irreversible waves ($E_{1/2}$(I)=−0.520 V and $E_{1/2}$ (II)=−1.00 V vs. SCE) were

Table 1. Summary of Results of Polarographic Measurements on Aqueous Solutions of Poly[(*p*-methylbenzyl)viologen] Dibromide (4.65 mg cm^{-3}) in the Presence of Varying Concentration of Cadmium Sulfate at ca. 25 °C (h_{Hg}=35 cm)

pH[a]	[$CdSO_4$]/mg cm^{-3}	Limiting current, $i_l/\mu A$		
		Wave I[b]	Wave II[b]	Wave III[b]
2.00	0	16.50	6.00	—
(KCl-HCl)		(−0.510)	(−1.00)	
	0.215	16.20	2.70	5.10
		(−0.515)	(−0.770)	(−1.02)
	0.420	16.15	5.40	5.00
	0.640	16.20	6.95	4.95
4.40	0	14.20	10.10	—
(citrate buffer)	0.225	13.94	3.80	4.35
		(0.510)	(−0.775)	(−1.20)
	0.418	14.00	6.10	4.50
	0.635	14.45	6.78	4.50
6.00	0	12.10	13.30	—
(citrate buffer)	0.200	12.45	3.75	2.15
		(−0.510)	(−0.770)	(−1.50)
	0.425	12.65	6.00	2.20
	0.645	12.40	6.95	2.28

a) Ionic strength adjusted to 0.1 M by adding calculated amount of KCl. b) Values in parentheses denote half-wave potentials ($E_{1/2}$) in V vs. SCE.

Table 2. Results of Polarographic Studies on Solutions of Varying Concentrations of Poly[(*p*-methylbenzyl)viologen] Dibromide (*p*-$PMVBr_2$) Contsining Fixed Amount of Cadmium Sulfate (0.40 mg cm^{-3}) in Water at ca. 25 °C

pH[a]	[*p*-$PMVBr_2$]×10^2	h_{Hg}/cm	Limiting current, $i_l/\mu A$		
	mg cm^{-3}		Wave I[b]	Wave II[b]	Wave III[b]
2.00	0	35	—	15.00	—
(KCl-HCl)				(−0.700)	
	41.0	35	2.10	4.60	2.68
			(−0.515)	(−0.790)	(−1.30)
	80.0	35	2.80	4.50	2.79
			(−0.505)	(−0.775)	(−1.25)
	181.2	35	6.00	4.50	2.70
			(−0.510)	(−0.770)	(−1.08)
	234.0	35	7.80	4.80	2.60
			(−0.500)	(−0.750)	(−1.07)
	396.2	35	13.20	4.80	2.85
			(−0.510)	(−0.740)	(−1.08)
		50	15.84	5.52	3.60
		65	17.20	6.20	4.50
4.40	0	35	—	15.10	—
(citrate buffer)	37.5	35	1.50	4.70	2.48
	85.0	35	2.60	4.65	2.45
	179.4	35	5.40	4.65	2.50
	236.5	35	6.27	4.90	2.45
	401.5	35	12.95	5.00	2.60
			(−0.510)	(−0.760)	(−1.35)
6.60	0	35	—	14.95	—
(citrate buffer)	35.0	35	0.75	4.90	1.55
	90.0	35	1.80	5.00	1.50
	180.0	35	3.40	4.70	1.55
	241.3	35	4.98	4.85	1.60
	403.3	35	10.95	5.10	1.65
			(−0.510)	(−0.760)	(−1.50)

a) Ionic strength maintained at 0.1 M by adding calculated amount of KCl. b)Values in parentheses denote half-wave potentials ($E_{1/2}$) in V vs. SCE.

obtained for pure *p*-$PMVBr_2$ (concentration: 4.65 mg cm^{-3}; pH=2.00). The cathodic currents for these waves (which are also obtained with other buffers studied; Table 1) have been previously correlated in terms of a protonation equilibrium *p*-$PMVBr_2+H^+ \rightleftarrows$ *p*-$PMVBr_2H^+$.[1c] Keeping in view of the gross effect of pH variation on the wave height which decreases for first wave and increases for the second one with decreasing acidity of the medium, both waves have been attributed to the reduction of protonated and unprotonated form of the polymer, respectively. However, more interesting results are obtained in the presence of $CdSO_4$ which still demonstrated two well-defined waves with their pH-independent half-wave potentials approximately at −0.51 V and −0.75 V vs. SCE, and a third ill-defined wave emerging beyond −1.00 V depending upon the pH of the solution (Table 1). Similar results are also observed with the solution having fixed amounts of Cd^{2+} ions and varying concentration of *p*-$PMVBr_2$ (Fig. 2). In this case, the wave height for wave I increases while the limiting currents of waves II and III are practically constant at a certain pH with the successive increment in the polymer concentration (Table 2). It may be noted that the variation of Cd^{2+} ions concentration only affects the height of second wave which is found to be increasing; others remaining constant as before for a certain solution (Table 1). All three waves are, however, found to be increasing with the height of the mercury pressure.

The appearance of the first wave of the polymer in the presence of cadmium ions seems to be similar in every respect with the wave obtained for the reduction of the protonated form of *p*-$PMVBr_2$ alone.[1c] The wave II, whose wave height remains uneffected by the pH variation, may be assigned to a cadmium-$PMVBr_2$ complex. The negative shift in half-wave potential as compared to that of free Cd^{2+} ions and moreover the gradual decrease in $E_{1/2}$ values of wave II with the increase of *p*-$PMVBr_2$ concentration conforms the existance of a pH-independent complexation process in the solution (Table 2). It is of interest to note that the acidity of the medium is not effective at all in controlling the limiting current for wave II (Tables 1 and 2) since even smallest amount of unprotonated polymer ($PMVBr_2$) at any pH, is found to be sufficient enough to cause complete complexation with Cd^{2+} ions taken in the present instance. The increasing trend of the height of the wave II with the increase of Cd^{2+} ions concentration (Table 1) may reflect the spontaneous complexation process with high molecular weight unprotonated compound ($PMVBr_2$) obtained after the protonation equilibrium. However, a constant limiting current of wave II, irrespective of the variation of polymer concentration (Table 2), interestingly indicates the limiting magnitude of complexation between Cd^{2+} (fixed) and minimum concentration of unprotonated polymeric species available, at any pH.

The rates of electron-transfer processes and hence the limiting currents for the reduction of *p*-$PMVBr_2H^+$ (wave I) and Cd^{2+}-$PMVBr_2$ complex (wave II) are diffusion-controlled as slopes for the plots of $\log i_l$ vs. $\log h_{Hg}$ (Table 2; pH=2.00; [$PMVBr_2$]=3.962 mg cm^{-3}) are found to be close to 0.5 for both waves. However, a slope value of 0.8 in the case of wave III indicates that the electroreduction is not governed by a diffusion process. Further, on substitution of $E_{1/4}$ and $E_{3/4}$ values of waves I and II (Fig. 1, [Cd^{2+}]=0.215 mg cm^{-3}, pH=2.00) in the following relationships of an irreversible (Eq. 1) and a reversible wave (Eq. 2) at 25 °C

$$E_{3/4}-E_{1/4}=-0.0517/\alpha n \quad (1)$$

$$E_{3/4}-E_{1/4}=-0.0564/n \quad (2)$$

the fractional values of αn and n obtained for first and second waves [wave I (αn=0.47, n=0.51); wave II (αn=0.35, n=0.37)] reveal the irreversible nature of the reduction in either case. Moreover, the negative shift in half-wave potentials with the increase of ionic strength (>0.1 M) of the supporting electrolyte in the respective buffer is typically suggestive of the irreversibility of all the three waves appeared in the present case.[6a]

It is interesting to emphasis that wave I is still noticeable even at higher pH (in the presence of Cd^{2+} ions) whose wave height decreases with the pH of the solution conforming the reduction of *p*-$PMVBr_2H^+$ and therefore, one may conclude that the prospect of a protonation equilibrium is not at all hampered by the addition of Cd^{2+} ions. It appears that as and when protonation equilibrium exhibits in the solution, the Cd^{2+} ions subsequently start complexing to a maximum extent as discussed earlier with the unprotonated species (*p*-$PMVBr_2$) of the compound available, irrespective of the pH of the medium concerned. The complete omission of waves owing to the reductions of free unprotonated polymer and Cd^{2+} ions, surplus if any, in the solution after complexation is quite surprising and seems to reflect the nonavailability of the these species in the vicinity of the electrode for the reduction as such. One may speculate the existance of a somesort of interaction or binding between metal ion and ligand (not complexation) which probably restricts the process of reduction of these species individually on the time scale involved. Although D(complex)<D(Cd^{2+}), the relatively large decrease in the magnitude of free cadmium current (Table 2) when complexed with the polymeric material, might also corroborate the fact that all Cd^{2+} ions are not consumed in complexation with the unprotonated polymer; however some of these ions would presumably behave like electroinactive substance as a consequence of their possible interactions with *p*-$PMVBr_2$ and/or the cationic radical species[1c] obtained after the first reduction.

The nature of third wave is rather more interesting. The height of this wave, which is irreversible in

nature, remains practically constant irrespective of the amount of *p*-$PMVBr_2$ added in the solution. The half-wave potentials realised in the case of *p*-$PMVBr_2$ (without Cd^{2+} ions) are pH-independent[1c] whereas the same for wave III, in the present instance, shifts towards more negative potential with the increase of pH of the solution. Furthermore, the height of this wave in the presence of cadmium salt decreases with the pH in contrast to the wave obtained for the polymer alone which increases with increase of the pH of the medium concerned. As is apparent from the above experimental facts, the wave III in the present study, thus, might be considered due to the reduction of some different species other than unprotonated *p*-$PMVBr_2$. Further, this wave does not appear in shape as a polarographic maximum; however, an attempt to suppress the wave by the use of several maximum suppressors (e.g., gelatine, Triton X-100, soap etc.) was failed. On the basis of these observations, the wave III could reasonably be assigned to only a catalytic hydrogen current, appearing in the shape of a wave, before the normal evolution of hydrogen.[6b] It should be mentioned in this connection that Brdička[7] has discovered somewhat similar kind of catalysis and polarographic behavior during an investigation of proteins in the presence of cobalt salts. The interpretation of catalytic wave in the present investigation might be correlated with the first reduction of *p*-$PMVBr_2$. The catalytic effect corresponds to the first reduction product i.e., a cation radical *p*-$PMVBr_2H^{\ddagger}$; from which, under the influence of cadmium, hydrogen is irreversibly reduced at the DME with decreased overvoltage.[8] Thus, the following overall scheme for wave III can be tentatively suggested.

$$p\text{-}PMVBr_2H^{\ddagger} + Cd^{2+} + e^- \rightarrow (p\text{-}PMVBr_2Cd^{2+})^- + 1/2\ H_2$$

The interaction of *p*-$PMVBr_2H^{\ddagger}$ with cadmium ions must be considered as further conditions necessary for the formation of a catalytic wave[7] in the present case. As no catalytic wave was observed in the absence of Cd^{2+} ions in the case of the reduction of *p*-$PMVBr_2$ compound alone[1c] in the similar concentration ranges (cf., Table 2), it seemed reasonable to consider some sort of intercoulombic bond between *p*-$PMVBr_2H^{\ddagger}$ and Cd^{2+} ion on the electrode surface which essentially facilitates the reduction of hydrogen with decreased overvoltage. The cation radical protons consumed in the electrode process are replaced by a reaction with proton of the medium. Normally, the height of the catalytic wave should increase with the concentration of *p*-$PMVBr_2$ (and hence *p*-$PMVBr_2H^{\ddagger}$) and Cd^{2+} ions[8] but it was found to be practically unaltered at a certain pH. This supports the fact that the surface of mercury electrode becomes fully covered, mainly at higher negative potential under the force of electrostatic attraction, by the adsorption of even small amount of high-molecular-weight catalytically-active cationic reduction product [a cation radical *p*-$PMVBr_2H^{\ddagger}$ under the interaction of Cd^{2+} ions in the present instance] which eventually limits the height of the catalytic wave to a constant magnitude.[9] The anticipated decrease in current of this wave at lower acidities is quite interesting which reflects somewhat implicit behavior in context to the adsorption phenomenon as proposed above. However, the remarkable decrease in the catalytic wave height at pH=6.00 might be attributed to the scavenging of the electrode by the hydroxide ions of the medium.[1b] It should be further noted that the possibility of partial adsorption of cationic cluster of *p*-$PMVBr_2H^{\ddagger}$ and Cd^{2+} ion [i.e., *p*-$PMVBr_2H^{\ddagger}$-Cd^{2+}] even in the lower potential range of wave II cannot be fully ignored. This eventually appears to impede the reduction current of wave II to some extent, supporting as one of the possible reasons for the drastic decrease in the magnitude of free cadmium current after complexation (Table 2).

The catalytic wave height was observed to be decreasing with the increase of ionic strength (>0.1 M) by addition of KCl.[8,9] This probably suggests the significant desorption of catalytic active cluster of cation radical reduction product with Cd^{2+} ions [*p*-$PMVBr_2H^{\ddagger}$-Cd^{2+}] from the surface of the mercury electrode by the large amount of KCl added in the solution. The process of adsorption of "cationic cluster" at higher negative potential under the electrostatic influences might be apparently mitigated by the large excess of KCl present in the solution. Furthermore, a higher concentration of KCl may also induce curling or the contraction[2] of the polyelectrolyte envelop around the electrode surface which, in turn, may cause desorption phenomenon. It should be pointed out in this connection that the cadmium salt or supporting electrolyte present in the solution might have also similar impact over the conformation of the polymeric film but not showed up effectively at the DME. On the other hand, the *p*-$PMVBr_2H^{\ddagger}$-Cd^{2+} interaction appears to be instigating the catalytic reduction of hydrogen at ionic strength <0.1 M in the present study.

Acknowledgement is made to the Head of the Chemistry Department for providing necessary facilities for this research.

References

1) a) B. B. Prasad, *J. Macromol. Sci. Chem.*, **A22**, 1 (1985); b) B. B. Prasad, *ibid.*, **A21**, 1493 (1984); c) L. M. Mukherjee and B. B. Prasad, *ibid.*, **A16**, 1263 (1981).

2) R. M. Fuoss and U. P. Strauss, *J. Polym. Sci.*, **3**, 246, 602 (1948); A. Tager, "Physical Chemistry of Polymers," 2nd ed., Mir Publishers, Moscow (1978), p. 461

3) A. Factor and G. E. Heinsohn, *J. Polym. Sci., Part B*, **9**, 289 (1971).

4) C. L. Bird and A. T. Kuhn, *Chem. Soc. Rev.*, **10**, 49 (1981).

5) "Pyridine and its Derivatives," ed by E. Klingsberg, Part II, Interscience, New York (1960), pp. 43, 57.

6) a) L. Meites, "Polarographic Techniques", 2nd ed., Wiley-Interscience, New York (1965), p. 291.
b) B. B. Prasad, *Electrochim. Acta*, **30**, 597 (1985).
7) R. Brdička, *Collect. Czech. Chem. Commun.*, **5**, 112, 148, 238 (1933).
8) J. Heyrovský and J. Kůta, "Principles of Polarography," Czech. Acad. Sci. Prague (1965), pp. 234, 419, 421—424.
9) S. G. Mairanovskii, L. D. Klyukina, and A. N. Frumkin, *Dokl. Akad. Nauk SSSR*, **141**, 147 (1961).

 © 1989 The Chemical Society of Japan Bull. Chem. Soc. Jpn., 62, 1275—1278 (1989)

Polarography of Metal Hydroxamates. Individual and Simultaneous Determination of Tungsten and Molybdenum Using Benzo- and Cinnamohydroxamic Acids

Sabooj Kumar BHOWAL* and Mita BHATTACHARYYA
Department of Chemistry, Jadavpur University, Calcutta 700032, India
(Received May 16, 1988)

Methods for the determination of traces of tungsten have been developed by directly subjecting the organic extracts of its benzo- and cinnamohydroxamic acid complexes to d. c. and derivative pulse polarography. Well defined waves and peaks are obtained in a ternary solvent mixture containing the extract, methanolic lithium chloride and aqueous phase. The methods are highly selective and allow determination of the metal in the ppm range. A procedure has also been developed for the simultaneous determination of tungsten and molybdenum using their benzohydroxamates. Effects of acids and solvents on the system have been studied and the probable mechanism of reduction of the complexes has also been discussed.

Studies on the extraction-polarography of metal hydroxamates directly in the organic phase have led to the development of excellent methods for the determination of traces of molybdenum.[1-3] In this article is reported similar investigations carried out to develop methods of analysis of traces of tungsten and simultaneous determination of tungsten and molybdenum. Investigations carried out with the benzohydroxamic acid (BHA) and cinnamohydroxamic acid (CHA) complexes of tungsten reveal that the complexes after extraction into a mixture of chloroform and isobutyl alcohol or chloroform can directly be subjected to d.c. and derivative pulse polarography (D.P.P.) in a mixture of solvents containing the extract, methanolic lithium chloride and water in a definite ratio. The systems yield well defined waves or peaks which have been utilized for the determination of trace quantities of tungsten. Solvent extraction separation and direct submission of the extract to polarography have resulted in the development of highly selective and quick determination methods which are superior to those known up to date. Furthermore a quick and sensitive method for the simultaneous determination of molybdenum and tungsten, two closely related metals, have also been worked out utilizing the benzohydroxamic complexes of the elements. Highly reproducible results have been obtained with synthetic mixtures of the metals. The probable mechanism of reduction of the complexes have been discussed.

Experimental

Apparatus. A Tacussel PRG 5 Pulse polarograph was used as reported earlier.[1-3] The capillary characteristics were as follows in the different solvent extracts at the mercury height of 45 cm.

Chloroform-isobutyl alcohol extract
m=0.376 mg s^{-1} t=9.78 s.
Chloroform extract
m=0.371 mg s^{-1} t=9.90 s.

All d.c. and D.P.P. were recorded with a controlled drop time of 1 and 3 s respectively, 4 mV s^{-1} recorder speed and 50 mV pulse amplitude.

Reagents and Solutions. Standard tungsten solution was prepared from $Na_2WO_4 \cdot 2H_2O$ (analar grade) and standardized as the oxine complex.[4] Standard molybdenum solution was prepared as described earlier.[1-3]

Benzohydroxamic acid (BHA) and cinnamohydroxamic acid (CHA) were prepared as mentioned earlier.[1,3] 1.0% (w/v) ethanolic solution of BHA and 0.2% (w/v) ethanolic solution of CHA were used for the investigations.

Lithium chloride (analar, Riedel) was used as the supporting electrolyte. Methanol (G.R.S. Merck) was distilled before use. All other metal salts, solvents, acids, and chemicals used were of analytical reagent grade. Twice distilled water was used in all the studies.

Results and Discussion

Procedure for Determination of Tungsten and Simultaneous Determination of Molybdenum and Tungsten with BHA. An aliquot of standard tungsten solution or a mixture of standard molybdenum and tungsten solutions were taken in a 50 ml separatory funnel and diluted to 10 ml with water. After addition of 3 ml of BHA the acidity was adjusted to 1.5 mol dm^{-3} with 6 mol dm^{-3} hydrochloric acid and the mixture was shaken with 3 ml of 1 : 1 chloroform and isobutyl alcohol for one minute. The organic layer was drained into a 50 ml flask and aqueous layer was washed with 3 ml of the same solvent mixture. The washing was mixed with the main extract. To the combined extract was added 7 ml 1% methanolic lithium chloride, 12 ml 0.5 mol dm^{-3} perchloric acid solution and the mixture was made up to volume with methanol. Direct current and D.P.P. were recorded from −500 to −950 mV after deaeration with nitrogen for ten minutes.

Procedure for Determination of Tungsten with Cinnamohydroxamic Acid. A standard aliquot of tungsten solution taken in a 50 ml separatory funnel was diluted to 10 ml with water. The solution was treated with 5 ml of CHA solution. After adjusting acidity to 1.5 mol dm^{-3} with 6 mol dm^{-3} hydrochloric acid the mixture was extracted with 4 ml of chloroform and the organic layer was taken in a 50 ml flask. The

aqueous layer was washed with 2 ml chloroform and the washing was taken with the main extract. The organic layer was made up to volume with 7 ml 1% methanolic lithium chloride, 12 ml 4 mol dm^{-3} perchloric acid and methanol. Direct current and D.P.P. were recorded from −300 to −800 mV after deaeration with nitrogen for ten minutes.

Extraction and Polarographic Behavior of W-BHA and W-CHA Complexes. The colorless complex of tungsten with BHA is found to be sparingly soluble in common extracting solvents like chloroform, benzene, methyl isobutyl ketone, and 3-methyl-1-butanol. However, the complex can be easily extracted into a 1 : 1 mixture of chloroform and isobutyl alcohol from 1.0 to 6.0 mol dm^{-3} hydrochloric acid solutions. The extract when mixed with methanolic lithium chloride and an aqueous phase containing 0.5 mol dm^{-3} perchloric acid in the ratio 3:16:6 furnishes excellent polarograms with d.c. and D.P.P. techniques. The pulse polarogram yields a sharp peak at −800 mV and d.c. polarogram shows a single wave with $E_{1/2}$ value at −780 mV (Fig. 1). Inspite of the fact that tungsten benzohydroxamate produces a single reduction wave like molybdenum,[1] the nature of reduction happens to be quite different. The value of the slope obtained from the log plot of the d.c. wave (50.8 mV) is nearly compatible with a one electron reduction step which is not totally reversible. The transfer coefficient, α, 1.16, being close to unity points towards a quasireversible reduction. The peak half width (123 mV) of the D.P.P. at 50 mV amplitude is, however, indicative of a reversible one electron process. Thus it may be concluded that the d.c. wave and pulse peak indicate the reduction of W(VI) to W(V) species. Like molybdenum, reduction of tungstate ion in aqueous medium observed by other workers[5] show two reduction waves W(VI) to W(V) and W(V) to W(III) where the first wave appears at a potential of zero volt. So in the present case the reduction of tungsten appears to happen in the complexed form as the $E_{1/2}$ of the first wave is shifted to negative direction and that of second one cannot be obtained due to the same reason. The linear relationship of current with square root of mercury height indicates that the reduction is diffusion controlled.

The W-CHA complex is freely soluble in chloroform due to presence of a conjugation in the reagent molecule. The complex is completely extracted into the said solvent from 0.5 to 2.5 mol dm^{-3} hydrochloric acid solution. The organic phase can be mixed with aqueous phase and methanol in the ratio 3 : 6 : 16 to give a homogeneous phase whose D.P.P. produce a sharp peak at −620 mV. $E_{1/2}$ of the d.c. polarogram lies at −625 mV (Fig. 2). The average slope (50.2 mV) obtained from the log plot of the d.c. wave and transfer coefficient, 1.17 suggest the reduction to be a one electron quasireversible one. The peak half width 115 mV is also indicative of the same. That the wave appears due to reduction of complex rather than the uncomplexed oxo ion, WO_2^{2+}, is evidenced by the fact that free tungstate ion under the same conditions does not show any wave or peak. The linear relationship of current with square root of mercury height indicates the reduction is diffusion controlled.

We have previously reported[1] the determination of traces of molybdenum after extraction of its benzohydroxamate in chloroform and subjecting the extract to polarography in a solvent mixture containing chloroform, methanol, and an aqueous phase in a definite ratio. It has now been observed that molybdenum benzohydroxamate can be extracted into a chloroform isobutyl alcohol mixture like that of the tungsten complex. The extract when subjected to polarography in the same solvent mixture as used in the case of tungsten, furnishes well defined peak in D.P.P. with an E_p of −330 mV. Simultaneous determination of

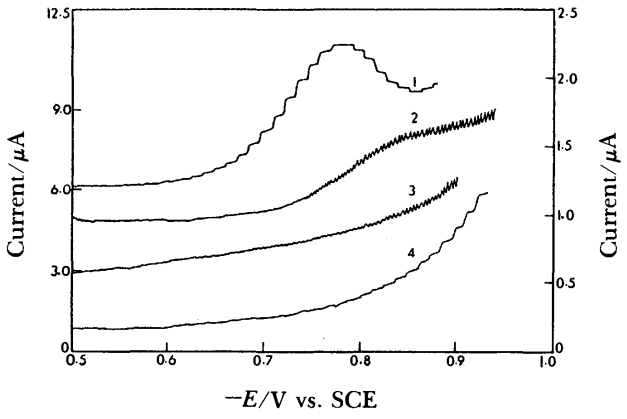

Fig. 1. Polarograms of W-benzohydroxamic acid complex; concentration of W=8×10^{-5} mol dm^{-3}; Curve 1-pulse polarogram; Curve 2-d.c. polarogram; Curve 3-d.c. polarogram of reagent blank; Curve 4-pulse polarogram of reagent blank; Curves 3 and 4 right hand side scale.

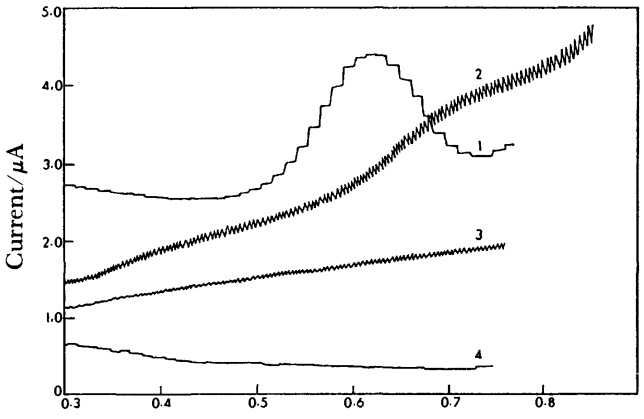

Fig. 2. Polarograms of W-cinnamohydroxamic acid complex; concentration of W=8×10^{-5} mol dm^{-3}; Curve 1-pulse polarogram; Curve 2-d.c. polarogram; Curve 3-d.c. polarogram of reagent blank; Curve 4-pulse polarogram of reagent blank.

Table 1. Simultaneous Determination of Molybdenum and Tungsten in a Mixture

Ratio W : Mo	Concn of metals taken	Current	Concn of metals found
	mol dm^{-3}	μA	mol dm^{-3}
1 : 1	2.0×10^{-5} W	0.82	1.84×10^{-5} W
	2.0×10^{-5} Mo	0.46	2.30×10^{-5} Mo
1 : 3	2.0×10^{-5} W	0.84	1.90×10^{-5} W
	6.0×10^{-5} Mo	1.20	6.0×10^{-5} Mo
3 : 1	3.0×10^{-5} W	1.28	2.90×10^{-5} W
	1.0×10^{-5} Mo	0.26	1.10×10^{-5} Mo
1 : 5	2.0×10^{-5} W	0.82	1.84×10^{-5} W
	1.0×10^{-4} Mo	2.0	1.01×10^{-4} Mo
5 : 1	5.0×10^{-5} W	2.10	4.80×10^{-5} W
	1.0×10^{-5} Mo	0.24	1.09×10^{-5} Mo

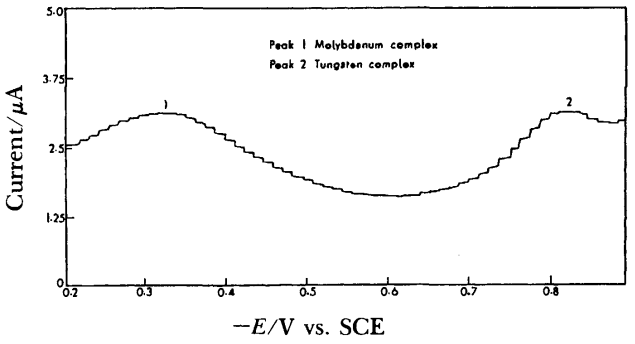

Fig. 3. Pulse polarogram of mixture of molybdenum and tungsten-benzohydroxamic acid complexes. Concentration of Mo=4×10^{-5} mol dm^{-3}; concentration of W=2×10^{-5} mol dm^{-3}.

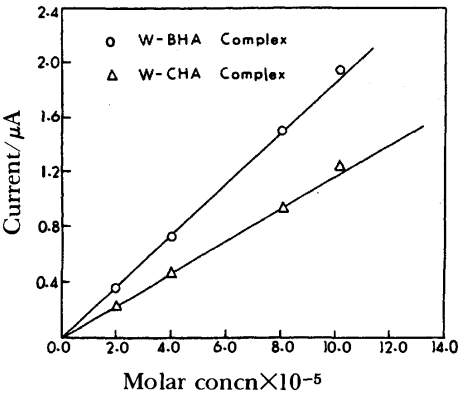

Fig. 4. Current-concentration relationship of benzo- and cinnamohydroxamates of W. (d.c. polarography).

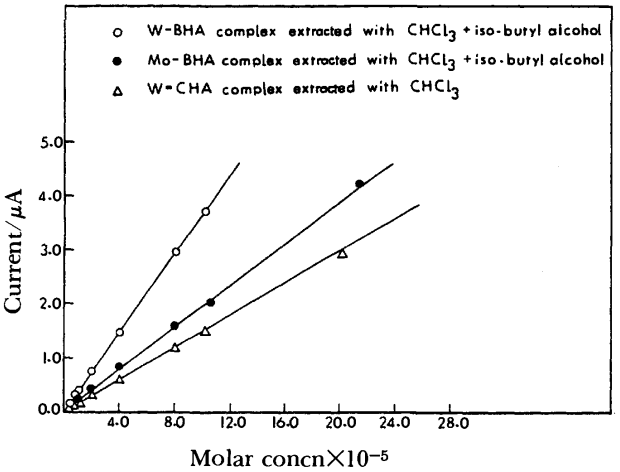

Fig. 5. Current-concentration relationship of benzo- and cinnamohydroxamates of W and Mo (D.P.P.).

trace quantities of the said metals has become possible in a ratio of 1 : 5 and vice versa (Fig. 3). The results are given in Table 1. Attempts have been made to develop a method for the simultaneous determination of molybdenum and tungsten after extraction of their cinnamohydroxamates in chloroform. But the method could not be worked out as the peaks of the two metals happened to be overlapping with each other.

Extracting Solvents, Supporting Electrolyte, Composition of Solvent Mixture and Current-Concentration Relationship. Chloroform-isobutyl alcohol mixture in a ratio of 1 : 1 was found to be the best extractant for the W-BHA complex. A homogeneous solution was obtained by mixing 6 ml of the extract, 7 ml 1% methanolic lithium chloride, 12 ml of aqueous phase and 25 ml of methanol in a total volume of 50 ml. Acids like HCl, H_2SO_4, CH_3COOH, H_3PO_4, and also NH_3 in the aqueous phase did not furnish well defined waves or peaks. Most well defined and reproducible polarograms were produced only when the aqueous phase contained 0.25 to 1.0 mol dm^{-3} $HClO_4$. For the tungsten-CHA complex chloroform alone was found to be the best extractant. A mixture of the chloroform extract, methanolic lithium chloride, and aqueous phase containing 3 mol dm^{-3} to 5 mol dm^{-3} $HClO_4$ in the ratio 3 : 16 : 6 produced the best polarogram in this case. Acids such as HCl, H_2SO_4, H_3PO_4, CH_3COOH were not found suitable as an aqueous phase. Methanolic solution of LiCl was used as the supporting electrolyte in all the cases. For both W-BHA and W-CHA complexes the diffusion current is found to vary linearly with concentration of the metal and the said ranges applicable for d.c. and D.P.P. techniques are shown in Figs. 4 and 5.

Effect of Diverse Ions. The effects of diverse ions and complexing agents are given in Table 2. It is observed W-CHA system can tolerate larger concentration of metals like iron(III) and cerium(IV) and complexing agents like ascorbic acid, tartaric acid, oxalic acid, and fluoride. This behavior may be attributed to the greater stability of the W-CHA complex in comparison to W-BHA complex. However, benzo and cinnamohydroxamates of tungsten cannot be extracted in presence of metals like copper(II), cobalt(II), manganese(II), chromium(III), cadmium(II), mercury(II), titanium(IV), tin(IV). Molybdenum(VI) is found to interfere with determination of tungsten with CHA.

Table 2. Tolerance Limits of Diverse Ions and Complexing Agents
Concentration of W=2.0×10^{-5} mol dm^{-3}

Metal ion or complexing agent	Tolerance ratio of the metal ion or complexing agent to complexes of W with		Remarks
	BHA	CHA	
Fe(III)	10	70	Extracted in presence of ascorbic acid
Pb(II)	100	100	Extracted from 1.5 mol dm^{-3} perchloric acid solution
Ni(II)		2	
Re(VII)	100	100	
Ce(IV)	10	100	Extracted in presence of ascorbic acid
V(V)	10	100	Extracted in presence of ascorbic acid
Zr(IV)	10	50	Extracted in presence of fluoride
U(VI)	50	50	
Mo(VI)	5		
Ascorbic acid	20	500	
Tartaric acid	200	500	
Citric acid	500	500	
Oxalic acid	40	70	
Fluoride	40	100	
EDTA	500	500	

Statistical Errors in the Determination of Tungsten. The relative standard deviation values for the pulse polarographic determination of tungsten with benzo- and cinnamohydroxamic acids have been calculated from a set of ten determinations in each case. The said values are ±6.37% for the W-BHA and ±2.78% for W-CHA complexes.

The authors express their thanks to the authorities of Alexander Von Humboldt-Stiftung, West Germany for the donation of the Pulse Polarograph. One of the authors (M.B.) likes to thank the U.G.C., India, for the award of a research fellowship.

References

1) S. K. Bhowal and Mita Bhattacharyya, *Fresenius' Z. Anal. Chem.*, **310**, 124 (1982).
2) S. K. Bhowal and Mita Bhattacharyya, *Indian J. Chem.*, **23A**, 736 (1984).
3) S. K. Bhowal and Mita Bhattacharyya, *Talanta*, in press.
4) A. I. Vogel, "A Text Book of Quantitative Inorganic Analysis," E.L.B.S and Longman (1973), p. 567.
5) J. J. Lingane and L. A. Small, *J. Am. Chem. Soc.*, **71**, 973 (1949).

 © 1989 The Chemical Society of Japan Bull. Chem. Soc. Jpn., 62, 1279—1280 (1989)

Preparation and Crystal Structure of Diaquabis-(1,8-naphthyridine 1-oxide)cobalt(II) Nitrate

Zhu YIN, Gan XINMIN, Tang NING, and Tan MINYU*
Department of Chemistry, Lanzhou University, Lanzhou, P. R. China
(Received May 21, 1988)

The complex $[Co(napyo)_2(H_2O)_2](NO_3)_2$ was formed by the reaction of cobalt(II) nitrate with 1,8-naphthyridine 1-oxide (napyo) in methanol medium. The complex crystallizes in the monoclinic system, space group $P2_1/n$ with Z=2. Lattice parameters are: a=7.165(2), b=11.797(2), c=11.830(3) Å, β=95.14(3)°, V=995.9(4) Å^3, D_c=1.705 g cm^{-3}, D_o=1.714 g cm^{-3}, λ(Mo $K\alpha$)=0.71069 Å, μ=9.26 cm^{-1}, F(000)=522. The final R=0.036 for 1433 unique observed reflections. Co^{2+} ion is coordinated by two nitrogen atoms and four oxygen atoms to form a distorted octahedron.

Many complexes of aromatic amine *N*-oxide with metal ions have been synthesized and characterized in recent twenty years.[1] However any complexes of 1,8-naphthyridine 1-oxide (napyo), which belongs to the kind of aromatic amine *N*-oxide, with transition metal ions have never been reported. In order to investigate the coordinating power of napyo with transition metal ions we recently synthesized a series of complexes of napyo with 3d metal ions. The present paper reports on the synthesis and crystal and molecular structure of the title compound.

Experimental

Preparation of $[Co(napyo)_2(H_2O)_2](NO_3)_2$. 0.1 mmol $Co(NO_3)_2 \cdot 6H_2O$ and 0.2 mmol napyo[2] were dissolved in 40 ml methanol. Then the solution was placed in a desiccator with $CaCl_2$ at room temperature. After about two weeks pink needle-like crystals of the title compound were obtained. Calcd for $C_{16}H_{16}CoN_6O_{10}$: C, 37.59; H, 3.15; N, 16.44; Co, 11.53%. Found: C, 37.70; H, 3.21; N, 16.13; Co, 11.79%).

Crystal Structure Determination of $[Co(napyo)_2(H_2O)_2](NO_3)_2$. Crystal Data: $C_{16}H_{16}CoN_6O_{10}$, M=511.27, monoclinic, space group $P2_1/n$, a=7.165(2), b=11.797(2), c=11.830(3) Å, β=95.14(3)°, V=995.9 Å^3, Z=2, D_c=1.705 g cm^{-3}, D_o (flotation in CCl_4/CH_2I_2)=1.714 g cm^{-3}, λ(Mo $K\alpha$)=0.71069 Å, μ=9.26 cm^{-1}, F(000)=522.

A crystal of approximate dimension 0.2×0.2×0.3 mm was selected for the data collection on an Enraf-Nonius CAD4 diffractometer with graphite-monochromated Mo $K\alpha$ radiation, $\omega/2\theta$ scan. 25 reflections were used for measuring lattice parameters. 1928 independent reflections were collected in the range of $2° \leqslant 2\theta \leqslant 50°$. 1433 reflections with $I > 3\sigma(I)$ were used in the structure determination and refinement. The intensity data were corrected for LP effect and empirical absorption. The structure was solved by the direct method and Fourier techniques, refined by full-matrix least-squares with anisotropic temperature parameters for all non-hydrogen atoms and isotropic thermal parameters for H atoms. Atomic scattering factors were taken from Ref. 3. All calculations were done by using computer programs from the Enraf-Nonius SDP package.[4] Final R=0.036, R_w=0.038.

Results and Discussion

The final atomic coordinates and equivalent isotropic temperature factors are given in Table 1,[5] selected bond lengths and bond angles in Tables 2 and 3. The equations of the least-squares planes concerned, deviations of atoms and dihedral angles between these planes are given in Table 4. The structure of complex cation $[Co(napyo)_2(H_2O)_2]^{2+}$ and the packing of the molecules in the unit cell are presented in Figs. 1 and 2, respectively. The crystal of the complex consists of discrete $[Co(napyo)_2(H_2O)_2]^{2+}$ cations and nitrate group anions. All the atoms in both napyo rings are fairly coplanar, as shown in Table 4. It can be seen from Fig. 1 that the cobalt atom locates at the inversion center of the complex cation and is bonded to two oxygen atoms and two nitrogen atoms of two different napyo ligands and two oxygen atoms of two water molecules. The six coordinating bonds are nearly equal in length (2.037—2.096 Å) but the three coordinating planes (Table 4) are not strictly vertical with each other. So the coordinated configuration of Co atom is a distorted octahedron.

Table 1. Final Atomic Coordinates and Equivalent Isotropic Temperature Factors

Atom	x/a	y/b	z/c	B_{eq}/Å^{2} a)
Co	0.0000	0.0000	0.0000	2.59(1)
O(1)	0.2120(4)	0.0498(2)	−0.0925(2)	3.73(5)
O(2)	0.1640(4)	0.0439(2)	0.1478(2)	4.36(6)
O(21)	−0.6090(4)	0.2315(2)	−0.8790(2)	4.42(6)
O(22)	−0.5608(5)	0.4070(3)	−0.8414(3)	6.42(8)
O(23)	−0.8117(4)	0.3313(3)	−0.8034(3)	7.49(8)
N(1)	0.2083(4)	0.1586(2)	−0.1170(2)	3.02(6)
N(2)	−0.0668(4)	0.1711(2)	−0.0293(2)	2.98(6)
N(21)	−0.6605(4)	0.3234(3)	−0.8417(2)	3.21(6)
C(1)	0.3434(5)	0.2052(4)	−0.1717(3)	4.04(8)
C(2)	0.3381(6)	0.3183(4)	−0.1995(3)	5.3(1)
C(3)	0.2000(6)	0.3844(3)	−0.1734(3)	4.83(9)
C(4)	0.0548(5)	0.3395(3)	−0.1151(3)	3.30(7)
C(5)	0.0614(5)	0.2250(3)	−0.0859(3)	2.63(6)
C(6)	−0.1026(6)	0.3997(3)	−0.0832(4)	4.62(9)
C(7)	−0.2320(6)	0.3443(4)	−0.0258(4)	4.47(9)
C(8)	−0.2073(5)	0.2302(3)	−0.0004(3)	3.54(8)

a) The equivalent isotropic temperature factors were computed using the following expression: $B_{eq}=4/3 \cdot (B_{11}a^2+B_{22}b^2+B_{33}c^2+B_{12}ab\cos\gamma+B_{13}ac\cos\beta+B_{23}bc \cdot \cos\alpha)$.

Table 2. Bond Lengths l/Å

Co-O(1)	2.037(3)	N(2)-C(5)	1.350(6)
Co-O(2)	2.083(3)	N(2)-C(8)	1.295(5)
Co-N(2)	2.096(3)	C(1)-C(2)	1.374(6)
O(1)-N(1)	1.316(4)	C(2)-C(3)	1.318(6)
O(21)-N(21)	1.239(4)	C(3)-C(4)	1.402(6)
O(22)-N(21)	1.218(4)	C(4)-C(5)	1.394(5)
O(23)-N(21)	1.215(4)	C(4)-C(6)	1.413(6)
N(1)-C(1)	1.330(5)	C(6)-C(7)	1.364(6)
N(1)-C(5)	1.388(4)	C(7)-C(8)	1.352(5)

Table 3. Bond Angles θ/°

O(1)-Co-O(2)	89.3(1)	C(3)-C(4)-C(6)	125.9(3)
O(1)-Co-N(2)	101.3(1)	C(5)-C(4)-C(6)	115.5(3)
O(2)-Co-N(2)	89.9(1)	N(1)-C(5)-C(4)	119.4(3)
O(1)-Co-O(1′)	180.0(0)	N(2)-C(5)-C(4)	124.2(3)
O(2)-Co-O(2′)	180.0(0)	N(2)-C(5)-N(1)	116.4(4)
N(2)-Co-N(2′)	180.0(0)	C(4)-C(6)-C(7)	119.2(4)
O(1)-N(1)-C(1)	120.5(3)	C(6)-C(7)-C(8)	120.3(3)
O(1)-N(1)-C(5)	119.6(3)	C(7)-C(8)-N(2)	123.4(4)
C(1)-N(1)-C(5)	119.9(3)	C(8)-N(2)-C(5)	117.4(3)
N(1)-C(1)-C(2)	120.8(4)	O(21)-N(21)-O(22)	121.1(3)
C(1)-C(2)-C(3)	121.6(4)	O(21)-N(21)-O(23)	120.3(3)
C(2)-C(3)-C(4)	119.8(4)	O(22)-N(21)-O(23)	118.6(3)
C(3)-C(4)-C(5)	118.6(3)		

Table 4. Least-Squares Planes,[a] the Deviations of Atoms (l/Å)[b] and Dihedral Angles between the Planes (θ/°)

Plane (1) [C(1), C(2), C(3),C(4), C(5), C(6), C(7), C(8), N(1), N(2)]
$-0.4376X-0.2277Y-0.8699Z-0.0468=0$
C(1), 0.006; C(2), −0.010; C(3), −0.009; C(4), −0.004; C(5), −0.003; C(6), 0.015; C(7), 0.009; C(8), −0.012; N(1), 0.019; N(2), −0.011

Plane (2) [C(1′), C(2′), C(3′), C(4′), C(5′), C(6′), C(7′), C(8′), N(1′), N(2′)]
$-0.4376X-0.2277Y-0.8699Z+0.0468=0$
C(1′), −0.006; C(2′), 0.010; C(3′), 0.009; (4′), 0.004; C(5′), 0.003; C(6′), −0.015; C(7′), −0.009; C(8′), 0.012; N(1′), −0.019; N(2′), 0.011

Plane (3) [Co, O(1), O(2), O(1′), O(2′)]
$-0.3742X+0.9257Y-0.0563Z=0$

Plane (4) [Co, O(1), N(2), O(1′), N(2′)]
$-0.4774X-0.2497Y-0.8425Z=0$

Plane (5) [Co, O(2), N(2), O(2′), N(2′)]
$0.8460X+0.0979Y-0.5241Z=0$

Plane No.	Plane No.	Dihedral Angle
(1)	(2)	0.0
(1)	(3)	89.9
(1)	(4)	3.0
(1)	(5)	86.4
(2)	(3)	89.9
(2)	(4)	3.0
(2)	(5)	86.4
(3)	(4)	90.3
(3)	(5)	101.3
(4)	(5)	89.2

a) X, Y, and Z in the equations of the planes are orthogonalized coordinates. b) Deviations of the atoms in Planes (3), (4), and (5) are 0.000.

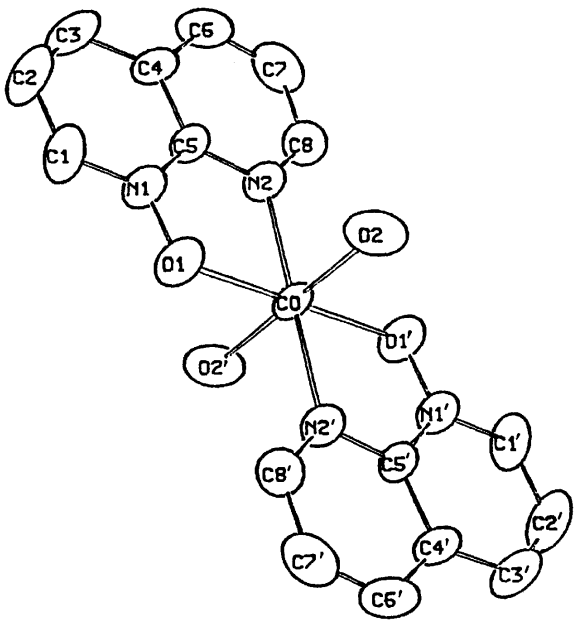

Fig. 1. The structure of the complex cation $[Co(napyo)_2(H_2O)_2]^{2+}$.

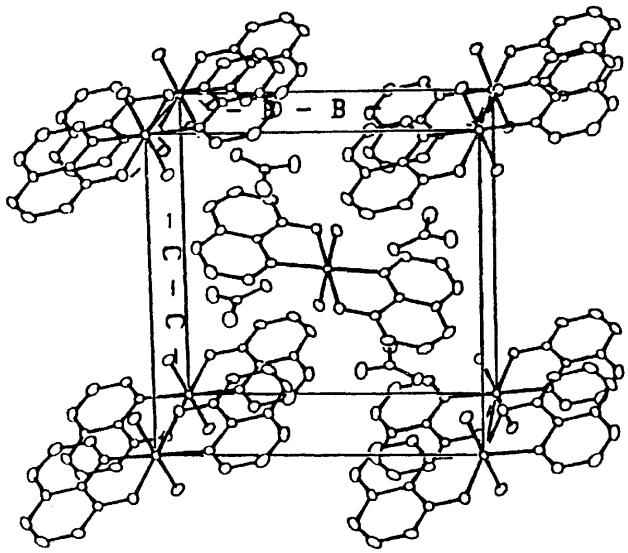

Fig. 2. The packing of the molecules in the unit cell.

References

1) N. M. Karayannis, A. N. Spaca, D. E. Chasan, and L. L. Pytlewski, *Coord. Chem. Rev.*, **20**, 37 (1976).

2) Y. Kobayashi, I. Kumadaki, H. Sato, Y. Sekine, and T. Hara, *Chem. Pharm. Bull.*, **22**, 2097 (1974).

3) "International Tables for X-Ray Crystallography," Kynoch Press, Birmingham, U.K. (1974), Vol. IV.

4) "Enraf-Nonius SDP Package," B. A. Frenz & Associates, Inc., College Station, Texas 77840; Enraf-Nonius, Delft, Holland.

5) Atomic parameters for H atoms, anisotropic thermal parameters for non-H atoms and F_o-F_c tables are deposited as Document No. 8846 at the Office of the Editor of the Bulletin of the Chemical Society of Japan.

 © 1989 The Chemical Society of Japan Bull. Chem. Soc. Jpn., 62, 1281—1286 (1989)

Carbohydrate Complexes with Lead(II) Ion. Interaction of Pb(II) with β-D-Glucurono-6,3-lactone, D-Glucono-1,5-lactone, and Their Acid Anions and the Effects of Metal Ion Binding on the Sugar Hydrolysis

Heidar-Ali TAJMIR-RIAHI
Department of Chemistry, University of Laval, Quebec, G1K 7P4 Canada
(Received April 27, 1988)

The interaction of Pb(II) ion with β-D-glucurono-6,3-lactone, D-glucuronic acid, D-glucono-1,5-lactone, and their acid anions has been investigated in aqueous solution and solid compounds of the type Pb(D-glucurono-6,3-lactone)$(NO_3)_2$, Pb(D-glucuronic acid)$(NO_3)_2$, Pb(II)-D-glucuronate, Pb(D-glucono-1,5-lactone)$(NO_3)_2$, and Pb(II)-D-gluconate have been isolated. These compounds are characterized by means of FT-IR, ^1H and ^{13}C NMR spectroscopy and molar conductivity measurements. Among these Pb-sugar complexes, the crystal structure of the Pb(II)-D-gluconate is known through X-ray diffraction measurements, in which the lead(II) ion is hexa-coordinated, binding to four D-gluconate anions via a carboxylato oxygen and an α-hydroxyl group of the two anions (chelation) and to a carboxylato oxygen atom of the other two sugar anions (unidentately). Spectroscopic evidence suggested that in the Pb-lactone or Pb-acid adducts, the metal ion could be bonded to a lactone or acid molecule through one of the carbonyl oxygen atom and other sugar donor group as well as to two bridging nitrato groups. In the Pb(II)-D-glucuronate, the metal ion could be bonded to four sugar moieties (similar to that of the Pb(II)-D-gluconate) via a carboxylato oxygen atom and other sugar donor group of the two anions and to a carboxylato oxygen atom of the other two acid anions, resulting into a hexa-coordinated lead(II) ion. The β-anomer sugar configuration is predominant in the free D-glucurono-6,3-lactone, D-glucuronic acid, D-glucuronate anion and in these Pb-sugar complexes.

The highly toxic effect of lead on the environmental pollution have been known for some years,[1] and correlations between lead poisoning[2,3] and its carcinogenic action in animals have been established.[4] It has been also demonstrated that the injected lead in rats accumulates in the cell nuclei.[5] In recent years, the stabilizing or destabilizing effects of the Pb(II) ion interaction on the double-helix structure of DNA have been investigated and the mode of Pb-DNA binding has been the subject of several studies.[6-8] Sugar is a part of nucleic acids and lead-sugar interaction could have biological importance. On the other hand, D-glucurono-6,3-lactone and D-glucono-1,5-lactone show biological properties and are readily hydrolyzed to D-glucuronic and D-gluconic acid in aqueous solution (Scheme 1).

In our recent report, it was shown how the silver nitrate complexes with the free β-D-glucurono-6,3-lactone, D-glucuronic acid, and D-glucono-1,5-lactone in aqueous solutions, while the silver acetate facilitates the lactone hydrolysis and the acid ionization.[9-11] Similarly, the alkaline earth metal ions (Mg^{2+} and Ca^{2+}) coordinate with D-glucuronate anion in aqueous solutions, whereas in ethanolic solution, the binding of these metal ions to the free lactone is preferred.[12] In this work, we describe the Pb(II) ion interaction with β-D-glucurono-6,3-lactone, D-glucuronic acid, and D-glucono-1,5-lactone, in aqueous solution and the isolation and characterization of the complexes formed, using FT-IR, ^1H and ^{13}C NMR spectroscopy and molar conductivity measurements, that have not been reported so far. Furthermore, the effects of metal ion binding on the sugar hydrolysis have been discussed here.

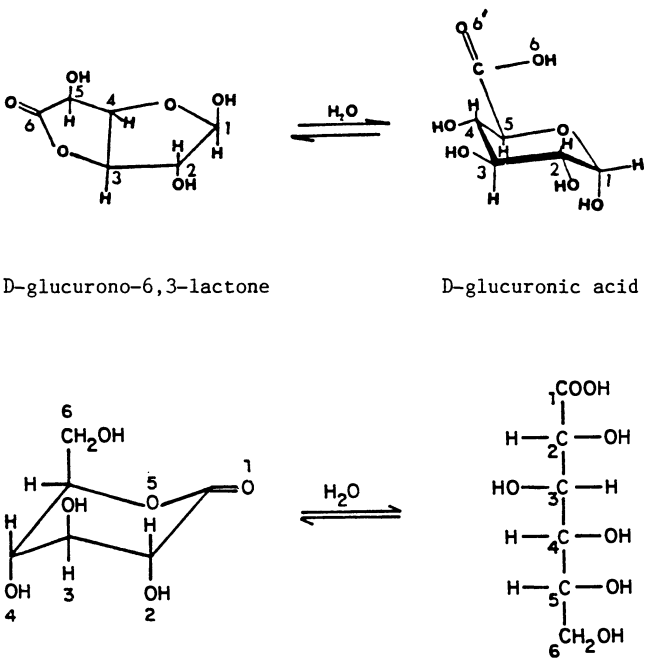

D-glucurono-6,3-lactone D-glucuronic acid

D-glucono-1,5-lactone D-gluconic acid

Scheme 1.

Experimental

Materials and Methods. β-D-Glucurono-6,3-lactone, D-glucuronic acid, and D-glucono-1,5-lactone were purchased from Aldrich Chemical Co., and were used as supplied. Other chemicals were reagent grade and were used without further purification.

Synthesis of Pb-Sugar Adducts. The Pb-lactone adducts

Table 1. Analytical Data for Pb-Sugar Complexes

Compound	Calcd(Found)		
	%Pb	%C	%H
Pb(D-glucurono-6,3-lactone)$(NO_3)_2$	40.93	14.25	1.58
	(39.90	13.95	1.70)
Pb(D-glucuronic acid)$(NO_3)_2$	39.43	13.17	1.91
	(38.80	13.55	1.75)
Pb(D-glucuronate)$_2$	34.90	24.44	3.05
	(33.55	23.80	2.90)
Pb(D-glucono-1,5-lactone)$(NO_3)_2$	40.66	14.15	1.97
	(39.70	13.85	2.10)
Pb(D-gluconate)$_2$	34.46	24.20	3.69
	(33.80	23.50	3.85)

were prepared by the addition of $Pb(NO_3)_2$, 1 mmol in H_2O (20 ml) to a solution of the free lactone 1 mmol in H_2O (10 ml). The solution mixtures were left at room temperature for a period of 48 h under slow evaporation and then ethanol-acetone (50/50) was used to bring down the white precipitate (avoid heating the solution, due to rapid lactone hydrolysis and acid ionization). This was filtered off and washed with acetone several times and dried over $CaCl_2$. The Pb-acid adducts were also prepared in a similar fashion, using D-glucuronic acid instead of the lactone and using ethanolic solution to bring down the metal-acid precipitate. The analytical results given in Table 1, showed the composition of the type Pb(D-glucurono-6,3-lactone)$(NO_3)_2$, Pb(D-glucuronic acid)$(NO_3)_2$, and Pb(D-glucono-1,5-lactone)-$(NO_3)_2$. The Pb-lactone adducts are very hygroscopic and should be kept in a desiccator over $CaCl_2$.

Synthesis of Pb-Sugar Salts. The Pb-sugar salts were prepared by the addition of the equimolar amount of the $PbCO_3$ and the lactone or acid in H_2O (50 ml) and the mixtures were heated up till all the lead carbonate was dissolved. After cooling down the solution to room temperature, ethanol was used to precipitate the white Pb-sugar salt. This was filtered off and washed with ethanol several times and dried over $CaCl_2$. The analytical data given in Table 1, showed the composition of Pb(D-gluconate)$_2$ and Pb(D-glucuronate)$_2$. The Pb-sugar salts synthesized here, are very soluble in water, but they are not soluble in common organic solvents.

Physical Measurements. The infrared spectra have been recorded on a NICOLET 5DXB Fourier Transform infrared instrument with DTGS detector. The spectra were taken as KBr pellets with a resolution of 2—4 cm^{-1}. The ^1H NMR spectra were recorded with a Varian XL-200 instrument in D_2O solution containing DSS as reference. The ^{13}C NMR spectra have been recorded on a Bruker WH-80 instrument in D_2O solution containing dioxane as reference. Conductance measurements were carried out at room temperature in aqueous solution (10^{-3} mol dm^{-3}) with a conductivity meter type CDM2e (Radiometer, Copenhagen).

Results and Discussion

FT-IR Spectra. The infrared spectra of the free D-glucurono-6,3-lactone, D-glucuronic acid, and D-glucono-1,5-lactone and their lead complexes have been recorded in the region of 4000—500 cm^{-1} and a comparison has been made with those of the structurally identified D-glucuronate-CaBr·$3H_2O$,[13] Mn(II)-D-gluconate·$2H_2O$[14] and the corresponding Ag-sugar compounds[9-11] and the results of the spectral analysis will be discussed below.

Sugar OH Stretching Vibrations and Lead(II) Binding. The assignments of the infrared vibrational frequencies of the free D-glucurono-6,3-lactone, D-glucuronic acid, and D-glucono-1,5-lactone were reported earlier.[9-12] The free lactone and acid OH stretching vibrations appeared as several strong and broad absorption bands in the region of 3500—3200 cm^{-1} of their spectra[9-12] and exhibited considerable intensity changes and shifting towards lower frequencies, on sugar metalation or acid ionization. The observed spectral changes in this region, are related to the participation of sugar OH group in lead-sugar binding. Similar trends were observed in the IR spectra of the structurally known D-glucuronate-CaBr·$3H_2O$ and Mn(II)-D-gluconate·$2H_2O$, where sugar bindings were found to be via sugar OH groups as well as the carboxylate anion.[13-15]

Lactone Carbonyl Stretching Vibrations and Lead(II) Ion Binding. Drastic spectral changes were observed for each sugar carbonyl stretching vibration, upon lead ion interaction, which will be dealt with separately.

D-Glucurono-6,3-lactone. The carbonyl stretching vibration of the free D-glucurono-6,3-lactone was observed as a strong band at 1758 cm^{-1} and exhibited shifting and splitting at 1760 and 1757 cm^{-1}, in the spectrum of the Pb(D-glucurono-6,3-lactone)$(NO_3)_2$ adduct (Fig. 1). The shifting and splitting of the lactone C=O stretching vibration are related to the direct metal-carbonyl binding. Similar spectral changes were observed for the carbonyl stretching vibration, in the IR spectra of the $AgNO_3$, $AgClO_4$, and alkaline earth metal halide (Mg^{2+} and Ca^{2+}) adducts with D-glucurono-6,3-lactone molecule, where metal sugar binding was concluded to be through the carbonyl oxygen atom.[11,12] The carbonyl stretching vibration of the free D-glucuronic acid was observed at 1709 cm^{-1} and showed shifting and splitting at 1758 and 1730 cm^{-1}, in the spectrum of the Pb(D-glucuronic acid)$(NO_3)_2$ adduct (Fig. 1). The observed changes for the carbonyl group are due to the participation of the acid C=O group in metal ligand bonding, in the Pb(D-glucuronic acid)$(NO_3)_2$ compound. Similar trends were observed in the spectrum of the Ag(D-glucuronic acid)(NO_3) adduct, where metal-acid binding was suggested to be through the acid carbonyl oxygen atom.[11] It should be noted that, one of the components of the C=O stretching vibration at 1758 cm^{-1} in the spectrum of the Pb-acid adduct bears similarity to that of the free lactone (1758 cm^{-1}) or to that of the lactone at 1757 cm^{-1}, in the Pb-lactone adduct (Fig. 1). This can lead to the question of the purity of the Pb-acid compound that might be contaminated with the free lactone or Pb-lactone adduct (since the reaction has been carried out in aqueous solution, where acid $\rightleftarrows$ lactone conver-

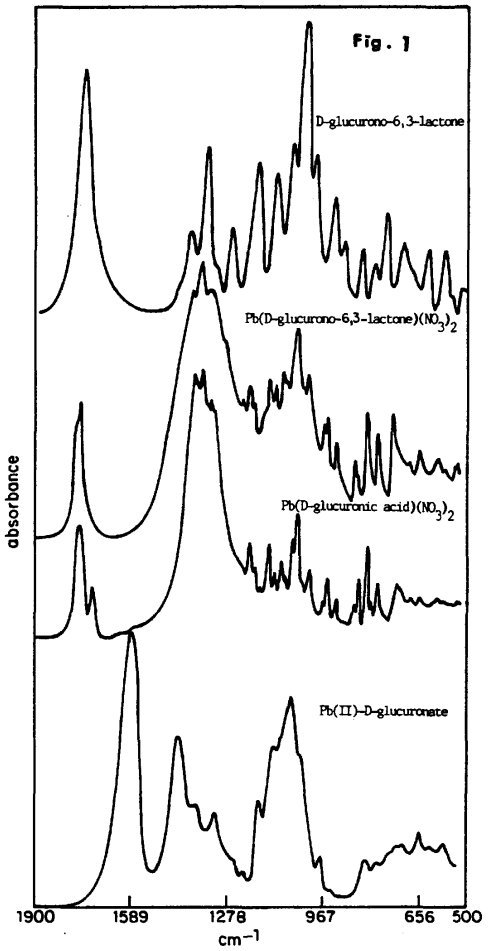

Fig. 1. The FT-IR spectra of D-glucurono-6,3-lactone and its lead(II) complexes in the region of 1900—500 cm^{-1}.

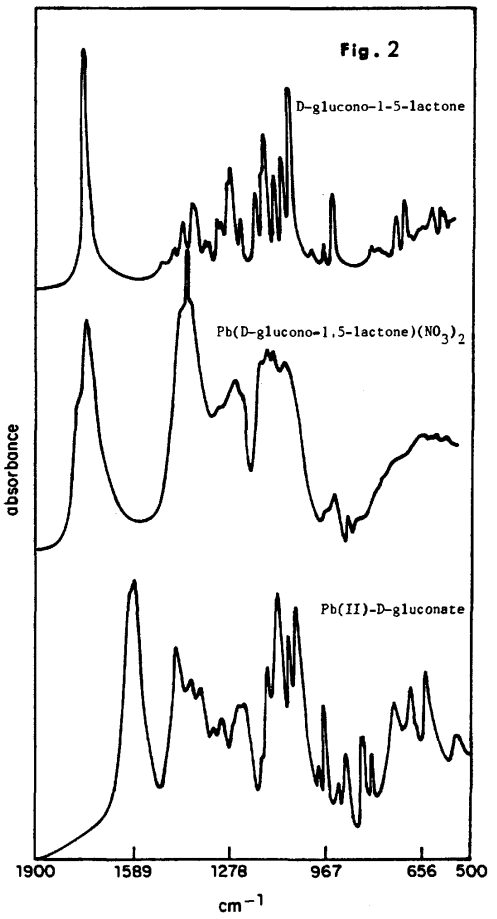

Fig. 2. The FT-IR spectra of D-glucono-1,5-lactone and its lead(II) complexes in the region of 1900—500 cm^{-1}.

sion is readily occurred). Since the separation between the two components of the C=O groups in the Pb-acid ($\Delta\bar{\nu}$=28 cm^{-1}) and Pb-lactone adducts ($\Delta\bar{\nu}$=3 cm^{-1}) are different, therefore, the spectral changes observed for the carbonyl groups are related to two different metal-sugar complexes. On the other hand, even an absorption band is present at about 1758 cm^{-1}, both in the free lactone and the Pb-acid adduct, the one at 1758 cm^{-1} in the free lactone has lost most of its intensity in the spectrum of the Pb-acid adduct (Fig. 1) and this is indicative of the complexed C=O group and it is not related to the free lactone (present in the lead-acid compound). However, the purity of these Pb-sugar adducts are also confirmed from their ^{13}C NMR spectra (see next pages). On comparing the IR spectra of the Pb-sugar adducts with that of the Pb(II)-D-glucuronate (Fig. 1), one can see that the carbonyl stretching vibration of the free acid at 1709 cm^{-1}, shifted towards lower frequencies and split into two components at 1583 and 1420 cm^{-1}, in the spectrum of the lead-D-glucuronate. These two absorption bands are related to the antisymmetric and symmetric OCO^- stretching vibrations.[11,12] The observed spectral changes for the carboxylate group, in the spectrum of the lead-D-glucuronate are due to the ionization and the participation of the sugar OCO^- group in metal-ligand bonding.

D-Glucono-1,5-lactone. The C=O stretching vibration of the free D-glucono-1,5-lactone was observed as a strong band at 1728 cm^{-1} and exhibited shifting and splitting at 1775 and 1741 cm^{-1}, in the spectrum of the Pb(D-glucono-1,5-lactone)$(NO_3)_2$ adduct (Fig. 2). The shifting and splitting of the carbonyl stretching vibration is indicative of the Pb-sugar binding through the lactone carbonyl oxygen atom. Similar changes were observed for the C=O group in the Ag(D-glucono-1,5-lactone) NO_3 adduct, where the silver sugar binding was suggested to be through carbonyl oxygen atom.[9] On the other hand, in the IR spectrum of the Pb(II)-D-gluconate, the carbonyl stretching vibration showed splitting and shifting towards lower frequency (Fig. 2). The two broad and strong bands at 1586 and 1430 cm^{-1} in the spectrum of the lead-gluconate are attributed to the antisymmetric and symmetric OCO^- stretching vibrations.[9] It should be noted that, in the crystal structure of the Pb(II)-D-gluconate,[16] the Pb(II) ion was bonded to four D-gluconate residues through a carboxylato oxygen atom and an OH group (in α-

position) of the two sugar anions (chelation) and to a carboxylato oxygen atom of the other two sugar anions (unidentately). It is worth mentioning that, no Pb-sugar containing bonded D-gluconic acid can be isolated, due to the partial acid ionization and salt formation and this is evident, by the presence of a strong band at about 1600 cm^{-1}, which is related to the antisymmetric sugar OCO^- stretching vibration.[9]

Other sugar absorption bands in the region of 1350—900 cm^{-1} related to the strongly coupled OH, CO, and CH modes,[17,18] exhibited drastic changes, upon Pb(II) interaction (Figs. 1 and 2). The shifting and intensity changes observed in this region for the OH bending and C-O stretching vibrations are related to the participation of the sugar OH and CO groups in metal sugar bindings.

Nitrato Group Vibrational Frequencies and Binding Modes. The strong and broad absorption band at about 1400 cm^{-1} related to the ν_3 of the ionic nitrate in D_{3h} symmetry,[19] exhibited shifting and splitting in the spectra of the Pb(D-glucurono-6,3-lactone)$(NO_3)_2$, Pb(D-glucuronic acid)$(NO_3)_2$, and Pb(D-glucono-1,5-lactone)$(NO_3)_2$ adducts (Figs. 1 and 2). The splitting of the NO_3^- band at 1380 cm^{-1} is indicative of the presence of the nitrato group in lower symmetry and the possible Pb-NO_3 coordination. Similar changes were observed for the nitrato group vibration in the IR spectra of the Ag(D-glucurono-6,3-lactone)NO_3, Ag(D-glucuronic acid)NO_3, and Ag(D-glucono-1,5-lactone)-$NO_3 \cdot H_2O$ adducts,[9-12] where the possibility of the bridging NO_3^- group (sugar-Ag-NO_3-Ag-sugar) and the ionic NO_3^- was proposed. Thus a similar nitrate binding modes (bridging and ionic) could be suggested, in these Pb-sugar adducts. This is also consistent with the molar conductivities observed for the free $Pb(NO_3)_2$ and its sugar adducts, which indicated the presence of both bonded and ionic NO_3^- groups, in aqueous solutions. Other nitrate absorption bands in the region of 1300—7000 cm^{-1} were masked by the strong sugar vibrations (Figs. 1 and 2).

Solution Spectra. In D_2O solution, the IR spectra of the free lactones, acids, and their lead(II) complexes in the region of 1900—1400 cm^{-1}, showed marked similarities with those of the corresponding solid compounds. The C=O stretching vibrations of the free lactones at about 1750 cm^{-1} (D-glucurono-6,3-lactone), 1700 cm^{-1} (D-glucuronic acid), and 1720 cm^{-1} (D-glucono-1,5-lactone) showed splitting and shifting towards higher frequencies, in the spectra of the $Pb(NO_3)_2$-sugar adducts. These changes are consistent with the Pb(II) ion binding to the carbonyl oxygen atoms of the free lactone and acid. On the other hand, in the spectra of the Pb(II)-D-glucuronate and Pb(II)-D-gluconate, the carboxyl stretching vibrations showed splitting and shifting towards lower frequencies, which are characteristic of the acid ionization and salt formation. The observed spectral changes in aqueous solution also indicate the participation of the sugar C=O group in the Pb-lactone and Pb-acid complexation, while in the Pb-sugar salts the OCO^- is mainly involved in metal-sugar bindings.

^{13}C and ^1H NMR Spectra. The ^{13}C NMR spectra of D-glucurono-6,3-lactone, D-glucuronic acid, D-glucono-1,5-lactone, and D-gluconic acid have been reported.[20,21] In this work, in D_2O solution, the ^{13}C NMR chemical shifts (δ/ppm) were observed for D-glucono-1,5-lactone, 175.20 (C-1), 82.24 (C-2), 75.70 (C-3), 72.00 (C-4), 67.95 (C-5), 60.80 (C-6), for the Pb(D-glucono-1,5-lactone)$(NO_3)_2$, 177.50 (C-1), 83.20 (C-2), 73.70 (C-3), 72.20 (C-4), 67.90 (C-5), 60.88 (C-6), for D-gluconic acid, 176.40 (C-1), 73.25 (C-2), 72.30 (C-3), 71.95 (C-4), 71.50 (C-5), 63.50 (C-6), for Pb(II)-D-gluconate, 180.50 (C-1), 75.40 (C-2), 72.99 (C-3), 71.99 (C-4), 71.77 (C-5), 63.40 (C-6), for β-D-glucurono-6,3-lactone, 103.60 (C-1), 74.90 (C-2), 85.60 (C-3), 78.55 (C-4), 70.50 (C-5), 177.50 (C-6), for Pb(D-glucurono-6,3-lactone)$(NO_3)_2$, 103.7 (C-1), 74.95 (C-2), 85.60 (C-3), 78.60 (C-4), 71.20 (C-5), 178.50 (C-6), for β-D-glucuronic acid, 96.90 (C-1), 74.65 (C-2), 76.35 (C-3), 72.45 (C-4), 75.40 (C-5), 173.40 (C-6), for Pb(D-glucuronic acid)$(NO_3)_2$, 96.80 (C-1), 74.70 (C-2), 76.40 (C-3), 73.20 (C-4), 75.50 (C-5), 174.50 (C-6), and for Pb(II)-D-glucuronate, 96.85 (C-1), 74.80 (C-2), 76.40 (C-3), 72.90 (C-4), 73.60 (C-5), and 177.40 (C-6). As it is evident, D-glucono-1,5-lactone and D-gluconate anion bind the Pb(II) ion via O-1, and O-2 (due to the downfield shifts of the C-1 and C-2 chemical shifts for both lactone and acid) and this is consistent with the structural analysis of the Pb(II)-D-gluconate, which showed Pb(II) ion binding through O-1 (carboxylato) and O-2 oxygen atoms.[16] Similarly, the major downfield shifts for the C-6 and C-5 chemical shifts of the β-D-glucurono-6,3-lactone, C-6 and C-4 of the β-D-glucuronic acid would indicate the Pb(II) binding via a carbonyl oxygen atom in concert with O(5)-H (lactone) or O(4)-H (acid) (chelation). Similar binding of the D-glucuronate anion was observed in the crystal structure of D-glucuronate-$CaBr \cdot 3H_2O$, with one of the sugar anion being bonded to Ca(II) ion via a OCO^- oxygen and O(4)-H group.[13]

The ^1H NMR spectra of the free D-glucurono-6,3-lactone and D-glucuronic acid in D_2O solution showed both α- and β-anomer forms with the α-H chemical shift at δ 5.56, and β-H at δ 5.45 for the free lactone and α-H at δ 5.58 and β-H at δ 5.28 for the free acid, with the β-anomer domination for both lactone and acid. In the spectra of the Pb(D-glucurono-6,3-lactone)$(NO_3)_2$ and Pb(D-glucuronic acid)$(NO_3)_2$ and Pb(II)-D-glucuronate, the β-anomer was found. It has been suggested[22] that the binding modes of the α- and β-anomers of D-glucuronic acid are different and in order one can have a better understanding of the binding modes of D-glucuronate or D-gluconate anion, a comparison between the coordination chemistry of the two acids has been made here.

Coordination Chemistry of D-Glucuronic Acid. Among all the metal D-glucuronats compounds

formed, the crystal structures of potassium-D-glucuronate·$2H_2O$,[23] and D-glucuronate-CaBr·$3H_2O$[13] are known through X-ray diffraction measurements. In the potassium salt, the potassium ion is surrounded by the sugar O-1, O-3, O-6, O-6′, and two H_2O molecule, with sugar anion having β-anomer configuration.[23] In the D-glucuronate-CaBr·$3H_2O$, the calcium ion is bonded to three sugar anions, through O-6, O-5 of the first, O-6′, O-4 of the second, and O-1, O-2 of the third sugar anion as well as to two H_2O molecule, with sugar having α-anomer form.[13] As it is evident, the α-anomer complexes via both carboxylate oxygen atoms and in concert with ring O-5 or O(4)-H group (chelation). Recently, on the basis of the ^{13}C NMR spectroscopy,[24] and other techniques,[25] it has been shown how copper and molybdenum ions bind to D-glucuronate anion, in aqueous solution and the solid state. In the presence of the Cu(II) ion of different concentrations and at variable pH's, the binding modes of D-glucuronic acid have been monitored[24] and the flexibility of this sugar moiety towards metal ion coordination has been shown. The main binding sites are the carboxylate oxygen atom (unidentately) or chelation in concert with other sugar OH groups,[25] while molybdenum binding was suggested to be through sugar hydroxyl groups as well as the carboxylate anion.[25] Therefore, the binding of the Pb(II) ion could be through a carboxylate oxygen atom and O-4 (chelation)(in both acid and anion), while lactone binding is possibly through carbonyl O-6 and O(5)-H group.

Coordination Chemistry of D-Gluconic Acid. The crystal structures of the sodium-D-gluconate,[26] potassium-D-gluconate,[27] potassium-D-gluconate·H_2O,[28] ammonium-D-gluconate,[29] manganese-D-gluconate·$2H_2O$,[14] and lead-D-gluconate[16] are known through X-ray diffraction analysis. The Na^+ ion binds to six oxygen atoms belonging to six different D-gluconate anions with the participation of the OCO^- group and other sugar OH groups (except O-3).[26] The K^+ ion in the potassium-D-gluconate is bonded to both carboxylate and OH group oxygen atoms,[27] whereas the potassium-D-gluconate·H_2O contains two different types of crystals, in which one of the potassium ion is bonded to the sugar OH groups and not the carboxylate group,[30] while in the other crystal potassium ion binding is through both sugar OH and OCO^- groups as well as H_2O molecule.[28] In the ammonium-D-gluconate, the NH_4^+ has a strong hydrogen bonding network with all the sugar OH groups, which stabilizes the crystal structure.[29] In the manganese(II)-D-gluconate·$2H_2O$, the Mn(II) ion is coordinated to two sugar anions through a carboxylate oxygen atom and an OH group of each anion as well as to two H_2O, forming hexa-coordinated metal ion.[14] In the Pb(II)-D-gluconate, the Pb(II) ion is bonded to four sugar anions via a carboxylate oxygen atom and O(2)-H group of the two anions and to a OCO- oxygen atom of the other two anions, resulting into a hexa-coordinate Pb(II) ion.[16] Therefore, it seems that the main binding of the D-gluconate anion is through carboxylato oxygen atoms and O(2)-H hydroxyl group (in α-position), forming a five-membered ring with metal cations. This is also true for the Pb(II) ion binding here, which is through a carboxylato oxygen atom and O(2)-H group of each D-gluconate anion, while in the Pb-lactone adduct, the binding could be through the C=O oxygen atom and the O(2)-H hydroxyl group.

Conclusion

On the basis of the spectroscopic (FT-IR, ^1H and ^{13}C NMR) and structural properties of the D-glucurono-6,3-lactone, D-glucuronic acid, and D-glucono-1,5-lactone and their Pb(II) complexes, the following points can be emphasized:

(a) In the Pb(D-glucurono-6,3-lactone)$(NO_3)_2$ adduct, the Pb(II) ion could be coordinated to a lactone molecule via C(6)=O and O(5)-H oxygen atoms as well as to two nitrato groups, while in the Pb(D-glucuronic acid)$(NO_3)_2$, the lead ion is bonded to an acid molecule, through carbonyl O(6′) and O(4)-H as well as to two nitrato groups. In the Pb(II)-D-glucuronate, the metal ion is bonded to carboxylato group (one or both oxygen atom) or a carboxylato oxygen atom and O(4)-H group (chelation) of the two acid anions and to a OCO^- oxygen atom of the other two sugar anions, forming a hexa-coordinated Pb(II) ion (similar to that of the Pb(II)-D-gluconate salt).

(b) In the Pb(D-glucono-1,5-lactone)$(NO_3)_2$, the metal ion would be bonded to a lactone molecule via C(1)=O and O(2)-H oxygen atoms as well as to two nitrato groups. In the Pb(II)-D-gluconate, the lead ion is hexa-coordinated, binding to four sugar anions through a carboxylato oxygen atom and an O(2)-H group of the two anions and to a OCO^- oxygen atom of the other two D-gluconate anions, which is known through X-ray structural determination.[16]

(c) The β-anomer sugar configuration is predominant in the free D-glucurono-6,3-lactone, D-glucuronic acid, and their lead sugar complexes.

References

1) K. R. Mahaffey, *Fed. Proc.*, **42**, 1730 (1983).
2) J. A. Valcinkas, R. Lilis, and M. Petrococci, *Am. J. Ind. Med.*, **2**, 261 (1981).
3) J. A. Valcinkas and R. Lilis, *Int. Arch. Occup. Health*, **51**, 1 (1982).
4) M. R. Moore and P. A. Meredith, *Arch. Toxicol.*, **42**, 87 (1979).
5) E. Sabbioni and E. Mafarante, *Chem.-Biol. Interact.*, **15**, 1 (1976); J. G. Poundt, R. Wright, and R. L. Kodelt, *Toxicol. Appl. Pharmacol.*, **66**, 88 (1982).
6) G. L. Eichhorn, *Nature(London)*, **194**, 474 (1962).
7) K. Gasiorowski, J. Swiatek, and H. Kozbowski, *Inorg. Chim. Acta*, **106**, L1 (1983).

8) H. A. Tajmir-Riahi, M. Langlais, and R. Savoie, *Nucleic Acids Res.*, **16**, 751 (1988).
9) H. A. Tajmir-Riahi, *J. Inorg. Biochem.*, **27**, 205 (1986).
10) H. A. Tajmir-Riahi, *Inorg. Chim. Acta*, **125**, 43 (1986).
11) H. A. Tajmir-Riahi, *Inorg. Chim. Acta*, **136**, 93 (1987).
12) H. A. Tajmir-Riahi, *Carbohydr. Res.*, **172**, 327 (1988).
13) L. Delucas, C. E. Bugg, A. Terzis, and R. Rivest, *Carbohydr. Res.*, **41**, 9 (1975).
14) T. Lis, *Acta Crystallogr., Sect. B*, **35**, 1690 (1979); H. A. Tajmir-Riahi, *Can. J. Chem.*, in press.
15) H. A. Tajmir-Riahi, *Carbohydr. Res.*, **122**, 241 (1983); *J. Inorg. Biochem.*, **24**, 127 (1985).
16) T. Lis, *Acta Crystallogr., Sect. C*, **40**, 374 (1984).
17) M. Hineno, *Carbohydr. Res.*, **56**, 219 (1977).
18) J. J. Cael, J. L. Koenig, and J. Blackwell, *Carbohydr. Res.*, **32**, 79 (1974).
19) J. I. Bullock, *J. Inorg. Nucl. Chem.*, **29**, 2257 (1967).
20) P. E. Pfeffer, K. M. Valentine, and F. W. Parish, *J. Am. Chem. Soc.*, **101**, 1265 (1979).
21) K. Bock and C. Pedersen, *Adv. Carbohydr. Chem. Biochem.*, **41**, 27 (1983).
22) K. Izumi, *Agric. Biol. Chem.*, **44**, 1623 (1980).
23) G. E. Gurr, *Acta Crystallogr.*, **16**, 690 (1963).
24) I. B. Cook, R. J. Magee, R. Payne, and T. Bela, *Aust. J. Chem.*, **39**, 1307 (1986).
25) S. Stojkovski, R. J. Magee, and J. Liesegang, *Aust. J. Chem.*, **39**, 1205 (1986).
26) T. Lis, *Acta Crystallogr, Sect. C*, **40**, 376 (1984)
27) C. D. Littleton, *Acta Crystallogr.*, **6**, 775 (1953).
28) N. C. Panagiotopoulos, G. A. Jeffrey, S. J. LaPlace, and W. C. Hamilton, *Acta Crystallogr., Sect. B*, **30**, 1421 (1974).
29) T. Lis, *Acta Crystallogr., Sect. B*, **37**, 1957 (1981).
30) G. A. Jeffrey and E. J. Fasiska, *Carbohydr. Res.*, **21**, 187 (1972).

 © 1989 The Chemical Society of Japan Bull. Chem. Soc. Jpn., 62, 1287—1291 (1989)

Photocycloadditions of Cyclodienes to Hexafluorobenzene

Boris ŠKET, Nataša ZUPANČIČ, and Marko ZUPAN*
Department of Chemistry and "Jožef Stefan" Institute, E. Kardelj University of Ljubljana, Ljubljana, Yugoslavia
(Received May 18, 1988)

The stereochemistry of photocycloaddition reactions of various cyclodienes to hexafluorobenzene in cyclohexane solution depends on the structure of the cyclodiene and [2+2]cycloadducts are mainly observed. Photoreaction of 1,5-cyclooctadiene with hexafluorobenzene gives nearly equal amounts of syn and anti [2+2]adducts, which are further transformed to tetracyclic systems, contrary to this, the stereochemistry observed by reactions with 1,4-cyclohexadiene depends on the molar ratio of cyclodiene-hexafluorobenzene and 30—54% of syn addition is observed, the syn adduct, however, being further transformed to 2,3,4,5,6,7-hexafluoropentacyclo-[6.4.0.0^{2,7}.0^{3,11}.0^{6,10}]dodec-4-ene. Syn selectivity of [2+2]cycloaddition was enhanced when bicyclic dienes were used and it is interesting that in the case of norbornadiene and benzonorbornadiene only exo attack was observed, and no anti attack occurred in the case of benzonorbornene. The quantum yields of [2+2]photocycloaddition reactions depend on the structure of the cyclodiene and the concentrations of hexafluorobenzene and cyclodiene. The quantum yields for norbornadiene and 1,4-cyclohexadiene are nearly the same, while it is two times higher in a photoreaction with 1,5-cyclooctadiene, when equal amounts of hexafluorobenzene and 1,5-cyclooctadiene were irradiated in cyclohexane at λ=253.7 nm.

Aromatic molecules undergo various photochemical transformations, depending on their structure, the reagents and the reaction conditions which initiated wide ranging investigations in the last twenty years.[1] Photocycloaddition reactions of benzene derivatives with alkenes and dienes resulted in 1,2-, 1,3-, or 1,4-cycloaddition products, the course of the reaction depending on the substituent on the phenyl ring and on the structure of the olefin and diene. The advantage of fluorine as a substituent in investigations of phototransformations of organic molecules have been shown in several studies.[2] We have already demonstrated that hexafluorobenzene readily reacted with various cycloalkenes when irradiation was carried out in cyclohexane solution, however, the structure of the olefin played the major role in the stereochemistry of [2+2]cycloaddition reactions: cyclopentene gave predominantly anti products[3] while with indene stereospecific syn addition was observed.[4] We now report investigations of the effect of the structure of the cyclodienes on photocycloaddition reactions to hexafluorobenzene.

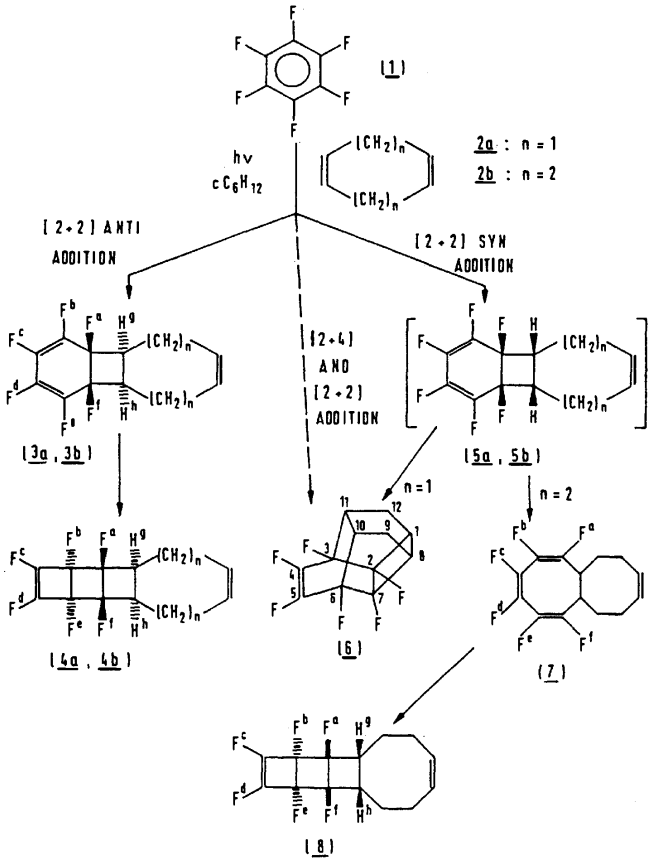

Scheme 1.

Results and Discussion

Cyclohexane solution of 1,4-cyclohexadiene (1 mmol) and hexafluorobenzene (2 mmol) was irradiated for 1 h at λ=253.7 nm, the solvent evaporated and the crude reaction mixture analyzed by ^{19}F NMR spectroscopy and nine signals, corresponding to three different products in the following relative yields: 61% (**3a**), 16% (**4a**), and 23% (**6**) (Scheme 1), were observed.

Products were separated by preparative TLC and VPC and the structures of the products determined on the basis of their NMR, MS, and X-ray data. The major product **3a** shows in its ^{19}F NMR the following signals at δ=−169.5, −171.75, and −198.0, while ^{1}H NMR spectrum confirms the presence of olefinic protons, CH_2 group and a signal at δ=3 with a coupling constant $^{3}J_{FH}$=7.5 Hz. Mass spectrum confirms the presence of 1:1-adduct, while irradiation of the pure product **3a** gave exclusively product **4a**, which shows the following three signals in its ^{19}F NMR spectrum at δ=−129.0, −190.5, and −204.25, and in its ^{1}H NMR spectrum olefinic protons at δ=5.9, methylenic protons at δ=2.3 and a signal at δ=3.08 with $^{3}J_{FH}$=7.5 Hz. The third product formed (**6**) shows a

quite different ^{19}F NMR spectrum with a signal at $\delta=-167.25$ (corresponding to fluorine atoms on olefinic carbon atom), and two signals at a much higher field: $\delta=-216.75$ and -217.5, corresponding to fluorine atoms bonded to saturated carbon atoms. ^{1}H NMR spectrum also shows only signals at higher fields: $\delta=3.2$ (2H), 2.64 (2H), and 1.8 (4H). However, mass spectrum (m/z 266 (M^+, 24%)) confirms the formation of 1 : 1 adduct, whose structure was finally proven by X-ray analysis.[5] 2,3,4,5,6,7-hexafluoropentacyclo-[6.4.0.$0^{2,7}$.$0^{3,11}$.$0^{6,10}$]dodec-4-ene (**6**) could be formed either by the primary [2+2] syn addition, followed by intramolecular [2+4] or by primary [2+4] addition, followed by [2+2] addition; we were unable to detect the presence of primary formed [2+2] or [2+4] adducts and so the origin of the product **6** formation remains open. However, further studies of the stereochemistry of [2+2]cycloaddition reaction with 1,5-cyclooctadiene (**2b**) where four products were formed (Scheme 1) diminished the possibility of the formation of product **6** via primary [2+4]cycloaddition. The irradiation of cyclohexane solution of 1,5-cyclooctadiene (**2b**) and hexafluorobenzene gave the crude reaction mixture containing four products (**3b**, 41%; **4b**, 9%; **7**, 41%; and **8**, 9%) which were partly separated by preparative TLC. The mixture containing **3b** and **7** was further irradiated for forty hours and the formation of two isomeric tetracyclic products **4b** and **8** was established. On the basis of the spectroscopic data we have found that the formation of the four products corresponds to the exclusively [2+2]cycloaddition process (syn attack 50%). In Scheme 1, the course of photocycloaddition reactions with 1,4-cyclohexadiene and 1,5-cyclooctadiene is presented.

Further, we have studied the stereochemistry of photocycloaddition reactions with norbornadiene (**9a**) and benzonorbornene (**9c**), where there are four possible [2+2] attacks: exo-syn, exo-anti, endo-syn, and endo-anti. As in the case of norbornene (**9b**),[6] only exo-attack was observed with **9a** and **9c**, while the amount of anti attack was diminished from 20% observed with norbornadiene to the exclusive exo-syn attack, occurring in the case of benzonorbornene. The course of cycloaddition reactions is presented in Scheme 2.

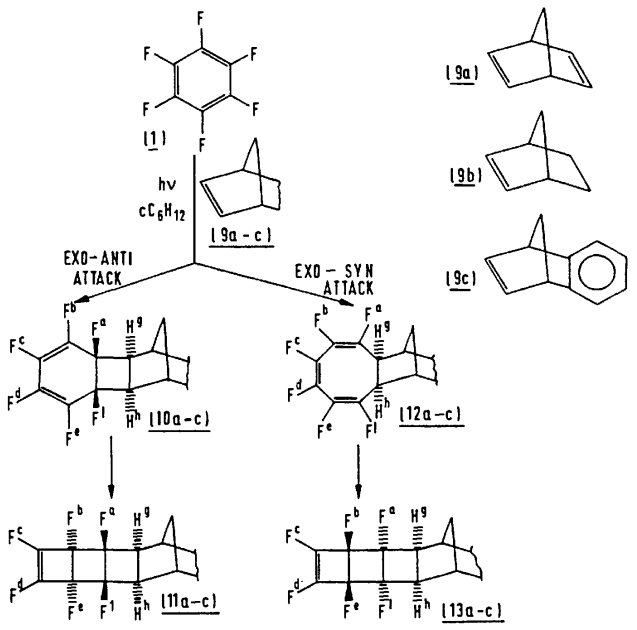

Scheme 2.

Table 1. The Effect of Cyclodiene or Cycloalkene Ring Size on the Stereochemistry of the [2+2]-Photocycloaddition[a] to Hexafluorobenzene

Cyclodiene or ycloalkene	exo-syn		exo-anti
	12	**13**	**11**
9a	47	33	20
9b	57	38	5
9c	72	28	—

a) The relative yields were determined by ^{19}F NMR spectroscopy; concentration of C_6F_6 0.111 mol l^{-1}; concentration of cyclodienes or cycloalkenes 0.055 mol l^{-1}; solvent cyclohexane; 35 °C, λ 253.7 nm.

Table 2. ^{19}F NMR Spectroscopic Data for Photoadducts[a]

	Product	δ_F/ppm		
		$F^{c,d}$	$F^{b,e}$	$F^{a,f}$
2a	**4a**	−129	−204.25	−190.5
2b	**4b**	−125.5	−195	−190
	7	−158.5	−155.2	−165.5
	8	−126	−195	−161.25
9a	**11a**	−123.75	−194.23	−180.8
	12a	−161.25	−159	−168
	13a	−125.25	−180	−164.25
9b	**11b**	−123	−193.5	−177.4
	12b	−159.75	−156	−163.5
	13b	−124.5	−179.25	−158.25
9c	**12c**	−158.3	−156.75	−165
	13c	−124.9	−180	−163

The starting cycloalkenes or cyclodienes were as follows: **2a;** 1,4-cyclohexadiene, **2b;** 1,5-cyclooctadiene, **9a;** norbornadiene, **9b;** norbornene, **9c;** benzonorbornene.

a) All signals correspond to 2F.

The structures of the products were determined on the basis of their mass spectra, NMR spectra, and X-ray data. Selected NMR data for photoadducts are presented in Table 2, the exact determination of the stereochemistry of the products was, however, enabled by the fact that the structures of **11a**[7] and **13b**[8] were confirmed by X-ray analysis.

In Scheme 3 various thermal and photochemical transformations of [2+2]adducts formed by irradiation of norbornadiene and hexafluorobenzene are presented. Product **12a** is converted stereospecifically to the pentacyclic system **13a** under photochemical conditions, while heating **12a** to 150 °C resulted in the primary formed anti adduct **10a**, which was further transformed under photochemical conditions to the pentacyclic system **11a**. Heating of the pentacyclic

Table 3. The Effect of Cyclodiene or Cycloalkene and Hexafluorobenzene Concentration on Quantum Yield of Photocycloaddition[a)]

Cyclodiene or cycloalkene	Concentration[b)]		ϕ/mol Einstein^{-1}			% syn addition	R[c)]
	A	B	ϕ_{syn}	ϕ_{anti}	$\phi_{[2+2]}$		
2a	0.1	0.5	0.049	0.041	0.09	54	1.32
	0.1	0.1	0.030	0.038	0.068	44	1.00
	0.5	0.1	0.043	0.067	0.11	39	1.62
2b	0.1	0.5	0.08	0.07	0.15	53	1.10
	0.1	0.1	0.071	0.065	0.136	52	1.00
	0.5	0.1	0.115	0.105	0.22	52	1.62
9a	0.1	0.4	0.042	0.006	0.048	88	0.70
	0.1	0.1	0.061	0.008	0.069	88	1.00
	0.5	0.1	0.090	0.011	0.101	89	1.46
9b	0.1	0.1	0.051	0.003	0.054	95	1.00

a) Solvent cyclohexane; λ 253.7 nm; T 30 °C; light intensity 2.4×10^{15} photons ml^{-1}s^{-1}. b) Concentration A: C_6F_6 concentration (mol l^{-1}). Concentration B: cyclodiene or cycloalkene concentration (mol l^{-1}). c) R; ratio of [2+2]photocycloaddition quantum yield at the given concentration to [2+2]photocycloaddition quantum yield at concentration of both C_6F_6 and cyclodiene or cycloalkene 0.1 mol l^{-1}.

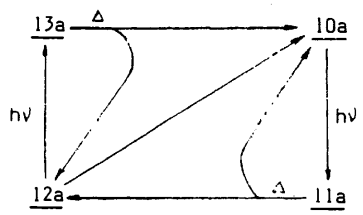

Scheme 3.

products **11a** and **13a** at 150 °C gave mixtures of **10a** and **12a** .

Photocycloaddition reactions of hexafluorobenzene and norbornadiene at λ=350 nm as well as in the presence of benzophenone as sensitizer did not occur, while photoreaction was completely quenched by 1,3-pentadiene and resulted in a complex mixture of the 1,3-pentadiene-hexafluorobenzene adducts.

The effect of the cyclodiene structure on the quantum yield of photocycloaddition reactions to hexafluorobenzene in cyclohexane solutions is presented in Table 3.

It is evident that the photoreactions of norbornadiene and 1,4-cyclohexadiene with hexafluorobenzene are 30% more efficient than the photoreaction of norbornene, while as much as a 1.5-fold increase of efficiency was observed in the case of [2+2]cycloaddition with 1,5-cyclooctadiene. The effect of the molar ratio of cyclodiene and hexafluorobenzene on photocycloaddition and on the efficiency of syn and anti addition is also presented in Table 1. Variations in the amount of reactants did not play significant role on the efficiency of syn/anti addition in the case of norbornadiene and 88% of syn addition was observed, the increase of the amount of cyclodiene diminished the quantum yield, while an increased amount of hexafluorobenzene increased the quantum yield for 46%. A similar absence of the effect of the reactant concentration on stereochemistry was also observed by 1,5-cyclooctadiene, where only 52% syn addition was observed, however, a variation of the reactant concentration increased the quantum yield, i.e., 10% by changing concentration of cyclodiene from 0.1 to 0.5 mol l^{-1}, and 62% by increasing the hexafluorobenzene concentration from 0.1 to 0.5 mol l^{-1}. The change of the concentration of the reactants influenced in the case of 1,4-cyclohexadiene photoreaction both the stereospecificity and the efficiency of the [2+2]cycloaddition. Irradiation of equal amounts of the reactants hexafluorobenzene and 1,4-cyclohexadiene resulted in 44% of syn attack, an increase of cyclodiene concentration increased the syn addition to 54% and the quantum yield for 32%, while an increase in hexafluorobenzene concentration decreased the syn attack to 39% but increased the efficiency of the photoprocess by 62%.

Experimental

Preparative experiments were carried out with a Rayonet Model RPR 100 with RPR 253.7 nm lamps. IR spectra were recorded using a Perkin Elmer 727B spectrometer and ^{1}H and ^{19}F NMR spectra by JEOL JNM-PS-100 spectrometer from $CDCl_3$ or CCl_4 solutions with $(CH_3)_4Si$, or CCl_3F as internal reference. Mass spectra and high resolution measurements were taken on a CEC 21-110 spectrometer. TLC was carried out on Merck PSC Fertigplatten F 254, and GLC on Varian Aerograph, Model 1800.

Materials: Hexafluorobenzene, 1,4-cyclohexadiene, 1,5-cyclooctadiene, norbornadiene, were commercially available and distilled before use, while benzonorbornene was synthesized. Cyclohexane was purified and distilled before use. It had been demonstrated in a separate experiment that the presence of oxygen had no significant effect on product distribution and quantum yields and thus no special attention was paid to air exclusion.

Photocycloaddition Reactions of Hexafluorobenzene with Cyclodienes. 1 mmol of cyclodiene and 2 mmol of hexafluorobenzene were dissolved in 18 ml of cyclohexane, the solution irradiated for various times (1—60 h) at λ=253.7 nm, the solvent evaporated in vacuo, the crude reaction mixture

analyzed by ^{19}F NMR and the products separated by preparative TLC or GLC.

Reaction with 1,4-Cyclohexadiene (2a). After 1 h irradiation, the reaction mixture was separated by preparative TLC (SiO_2, petroleum ether), and 23% of oily product **3a**, 7% of white crystalline product **4a**, mp=56—58 °C, and 10% of white crystalline product **6**, mp=137—139 °C, was obtained.

Spectroscopic Data for 3a: NMR δ_F −169.5 (m, 2F), −171.75 (broad s, 2F), −198 (m, 2F), δ_H 2.2 (m, 4H), 3.0 (m, 2H), 5.8 (m, 2H), $^3J_{FH}$=7.5 Hz; MS: Calcd for $C_{12}H_8F_6$: M, 266.0931. Found: *m/z* 266.0930; *m/z* 266 (M^+, 5%), 212 (20), 186 (30), 169 (20), 133 (35), 109 (25), 93 (20), 80 (80), 79 (95), 54 (55), 51 (60), 39 (100), 30 (40).

Spectroscopic Data for Product 4a: NMR (numbering of fluorine atoms is evident from Scheme 1): $\delta_{F^{c,d}}$ −129.0 (d, 2F), $\delta_{F^{b,e}}$ −204.25 (m, 2F), $\delta_{F^{a,f}}$ −190.5 (m, 2F, $^3J_{FH}$=7.5 Hz); δ_H 2.3 (m, 4H), 3.08 (m, 2H), 5.9 (m, 2H); MS: Calcd for $C_{12}H_8F_6$: M, 266.05301. Found: *m/z* 266.05272; *m/z* 266 (M+, 4%), 169 (31), 133 (43), 109 (37), 80 (100), 79 (98), 77 (43), 54 (63), 39 (64).

Spectroscopic Data for Product 6: NMR δ_F −167.25 (m, 2F), −216.75 (m, 2F), −217.5 (m, 2F); δ_H 1.88 (m, 4H), 2.64 (dm, 2H), 3.2 (m, 2H); MS: Calcd for $C_{12}H_8F_6$: M, 266.0530. Found: *m/z* 266.0530; *m/z* 266 (M^+, 24%), 164 (30), 134 (31), 133 (100), 115 (40), 80 (36), 79 (76).

Reaction with 1,5-Cyclooctadiene (2b). After 1 h irradiation, the reaction mixture was separated by preparative TLC (SiO_2, petroleum ether), and 36% of mixture of **3b** and **7** and 9% of mixture of **4b** and **8** was isolated. All attempts to separate the products were unsuccessful, however, when 80 mg of mixture of **3b** and **7** was dissolved in 5 ml of cyclohexane and irradiated at λ=253.7 nm for 40 h the formation of isomeric tetracyclic products **4b** and **8** was established.

NMR Data for Product 3b: δ_F −150.75 (m, 2F), −157.0 (broad s, 2F), −204 (m, 2F).

NMR Data for Product 7 (numbering of fluorine atoms is evident from Scheme 1): $\delta_{F^{c,d}}$ −158.5 (m, 2F), $\delta_{F^{b,e}}$ −155.2 (m, 2F), $\delta_{F^{a,f}}$ −165.5 (broad s, 2F), mass spectrum of mixture of **3b** and **7**: Calcd for $C_{14}H_{12}F_6$: M, 294.0844. Found: *m/z* 294.0841.

NMR Data for Product 4b (numbering of fluorine atoms is evident from Scheme 1): $\delta_{F^{c,d}}$ −125.5 (m, 2F), $\delta_{F^{b,e}}$ −195.0 (m, 2F), $\delta_{F^{a,f}}$ −190.0 (m, 2F).

NMR Data for Product 8 (numbering of fluorine atoms is evident from Scheme 1): $\delta_{F^{c,d}}$ −126 (m, 2F), $\delta_{F^{b,e}}$ −195 (m, 2F), $\delta_{F^{a,f}}$ −161.25 (m, 2F); MS of mixture of **4b** and **8**: Calcd for $C_{14}H_{12}F_6$: M, 294.0844. Found: *m/z* 294.0844.

Reaction with Norbornadiene (9a). After 3 h irradiation the reaction mixture was separated by preparative TLC (SiO_2, petroleum ether) and 2% of white crystalline product **10a**, mp=83—85 °C, and 9% of white crystalline product **12a**, mp=85—87 °C was isolated.

Spectroscopic Data for Product 10a: NMR δ_F −162.3 (m, 2F), −163.9 (broad s, 2F), −188.62 (m, 2F); δ_H 6.12 (broad s, 2H), 3.36 (broad s, 2H), 2.34 (m, 2H), 1.35 (m, 2H), $^3J_{FH}$=7.5 Hz; MS: Calcd for $C_{13}H_8F_6$: M, 278.0530. Found: *m/z* 278.0535; *m/z* 278 (M^+, 6%), 232 (43), 186 (71), 117 (50), 92 (83), 91 (100).

Spectroscopic Data for Product 12a: NMR (numbering of fluorine atoms is evident from Scheme 2): $\delta_{F^{c,d}}$ −161.25 (broad s, 2F), $\delta_{F^{b,e}}$ −159.0 (m, 2F), $\delta_{F^{a,f}}$ −168.0 (m, 2F); δ_H 6.2 (broad s, 2H), 3.09 (broad s, 2H), 2.7 (m, 2H), 1.5 (m, 2H), $^3J_{FH}$=26 Hz, $^3J_{F^bF^a}$=13 Hz; MS: Calcd for $C_{13}H_8F_6$: M, 278.0530. Found: *m/z* 278.0518; *m/z* 278 (M^+, 9%), 232 (16), 97 (22), 92 (32), 91 (40), 66 (100).

After 60 h irradiation, the reaction mixture was separated by preparative TLC, and 27% of solid **12a** and 29% of mixture of **11a** and **13a** was isolated. Isomeric pentacyclic products **11a** and **13a** were separated by preparative VPC (FFAP 30%, Chrom A AW, T=120 °C) and 7% of white crystalline product **11a**, mp=92—94 °C, and 50% of white crystalline product **13a**, mp =98—100 °C, was isolated.

Spectroscopic Data for Product 11a: NMR (numbering of fluorine atoms is evident from Scheme 2): $\delta_{F^{c,d}}$ −123.75 (d, 2F), $\delta_{F^{b,e}}$ −194.25 (dd, 2F), $\delta_{F^{a,f}}$ −180.75 (dd, 2F); δ_H 6.33 (s, 2H), 3.24 (s, 2H), 2.55 (d, 2H), 1.74 (broad s, 2H), $^3J_{FH}$=7.5 Hz, $^3J_{F^cF^a}$=15 Hz, $^3J_{F^cF^b}$=9 Hz; MS: Calcd for $C_{13}H_8F_6$: M, 278.0530. Found: *m/z* 278.0550; *m/z* 278 (M^+, 10%), 237 (19), 232 (7), 109 (21), 93 (24), 92 (14), 91 (42), 79 (43), 67 (44), 66 (100).

Spectroscopic Data for Product 13a (numbering of fluorine atoms is evident from Scheme 2): $\delta_{F^{c,d}}$ −125.25 (broad s, 2F), $\delta_{F^{b,e}}$ −180 (d, 2F), $\delta_{F^{a,f}}$ −164.25 (d, 2F); δ_H 6.24 (d, 2H), 3.18 (s, 2H), 2.7 (d, 2H), 1.53 (broad s, 2H), $^3J_{FH}$=24 Hz, $^3J_{F^bF^a}$=15 Hz, $^3J_{F^cF^b}$=4.5 Hz; MS: Calcd for $C_{13}H_8F_6$: M, 278.0530. Found: *m/z* 278.0545; *m/z* 278 (M^+, 6%), 237 (5), 232 (18), 97 (20), 92 (25), 91 (44), 79 (20), 67 (14), 66 (100).

0.5 mmol of product **12a** dissolved in 9 ml of cyclohexane, was irradiated at λ=253.7 nm for 60 h, the solvent evaporated in vacuo and the crude reaction mixture, containing only pentacyclic product **13a**, was isolated. 0.5 mmol of product **10a**, dissolved in 9 ml of cyclohexane, was irradiated at λ=253.7 nm for 60 h, the solvent evaporated in vacuo and the reaction mixture, containing only pentacyclic product **11a**, was isolated.

0.5 mmol of pentacyclic product **13a** was heated for 5 min at 150 °C in a sealed glass tube. The crude reaction mixture contained 65% of **10a** and 35% of **12a**. Similar heating of 0.5 mmol of isomeric pentacyclic product **11a** gave a mixture, containing 67% of **10a** and 33% of **12a**.

0.5 mmol of product **12a** was heated for 5 min in a sealed glass tube. The crude reaction mixture contained 30% of the starting material and 70% of **10a**.

After 60 h irradiation of mixture of hexafluorobenzene and norbornadiene at λ=350 nm no products were formed.

Reaction of Benzonorbornene (9c). After 60 h irradiation the reaction mixture was separated by preparative TLC (SiO_2, petroleum ether), 15% of white crystalline product **13c**, mp=132—134 °C and 37% of white crystalline product **12c**, mp=141—143 °C, was isolated.

Spectroscopic Data for Product 12c: NMR (numbering of fluorine atoms is evident from Scheme 2): $\delta_{F^{c,d}}$ −158.3 (broad s, 2F), $\delta_{F^{b,e}}$ −165.75 (d, 2F), $\delta_{F^{a,f}}$ −165 (dd, 2F); δ_H 7.2 (m, 4H), 3.6 (s, 2H), 2.85 (m, 2H), 1.89 (m, 2H), $^3J_{F^bF^a}$=15 Hz, $^3J_{FH}$=25 Hz; MS: *m/z* 328 (M^+, 13%), 282 (19), 186 (57), 181 (20), 147 (40), 143 (27), 142 (100), 141 (81), 129 (68), 128 (25), 116 (77), 115 (76); Calcd for $C_{17}H_{12}F_6$: C, 61.8; H, 3.6%. Found: C, 61.2; H, 3.4%.

Spectroscopic Data for Product 13c: NMR (numbering of fluorine atoms is evident from Scheme 2): $\delta_{F^{c,d}}$ −124.9 (broad s, 2F), $\delta_{F^{b,e}}$ −180 (d, 2F), $\delta_{F^{a,f}}$ −163 (dd, 2F); δ_H 7.2 (m, 4H), 3.66 (s, 2H), 2.85 (d, 2H), 1.89 (m, 2H), $^3J_{F^bF^a}$=15 Hz, $^3J_{FH}$=24 Hz; MS: *m/z* 328 (M^+, 7%), 142 (13), 141 (16), 129 (23), 128 (16), 117 (45), 116 (100), 115 (64); Calcd for $C_{17}H_{12}F_6$: C, 61.8; H, 3.6%. Found: C, 61.8; H, 3.4%.

Determination of Quantum Yields. Quantum yields

were measured by using a trioxalatoferrate(III) actinometer and in each experiment the amount of transmitted light was measured. Quartz cuvettes (12 ml) were filled with 10 ml of a cyclohexane solution of hexafluorobenzene and cyclodiene and thermostated by external cooling and the temperature of the solution measured. The light source was an RPR 253.7 nm lamp without filters. In a separate experiment with filters only 2—3% difference was found. The products were analyzed using ^{19}F NMR spectroscopy with $CF_3C_6H_5$ or octafluoronaphthalene as the internal standard, which was added after solvent evaporation. Irradiation times were chosen so that conversion of hexafluorobenzene did not exceed 5—7% of its initial amount. Each quantum yield determination was repeated at least three times and the average data are presented in Table 3, together with the data on concentrations of reagents, light intensity, and temperatures.

References

1) D. Bryce-Smith, "Photochemistry," Vols. 1—14, The Chemical Society, Burlington House, London (1970—1983); D. Bryce-Smith and A. Gilbert, *Tetrahedron*, **32**, 1309 (1976); **33**, 2459 (1977); G. Kaupp, *Angew. Chem.*, **92**, 245 (1980); T. Wagner-Jauregg, *Synthesis*, **1980**, 165; **1980**, 769; J. Cornelise and E. Havings, *Chem. Rev.*, **75**, 353 (1975).

2) M. Zupan and B. Šket, *Isr. J. Chem.*, **17**, 92 (1978).

3) B. Šket and M. Zupan, *J. Chem. Soc., Chem. Commun.*, **1977**, 365.

4) B. Šket and M. Zupan, *J. Chem. Soc., Chem. Commun.*, **1976**, 1053.

5) L. Golič and I. Leban, *Acta Crystallogr., Sect. B.*, **36**, 1520 (1980).

6) B. Šket, N. Zupančič, and M. Zupan, *J. Chem. Soc., Perkin Trans. 1*, **1987**, 981.

7) L. Golič and I. Leban, *Cryst. Struct. Commun.*, **9**, 739 (1980).

8) L. Golič and I. Leban, *Cryst. Struct. Commun.*, **7**, 53 (1978).

Electronic Spectra of 9,10-Phenanthrenediamine: Effects of Solvents and Acid Concentrations

R. MANOHARAN and Sneh K. DOGRA*
Department of Chemistry, Indian Institute of Technology, Kanpur-208 016, India
(Received June 20, 1988)

Dual fluorescence is observed from 9,10-phenanthrenediamine (PDA) in defferent solvents. Normal Stokes shifted fluorescence band is a structured one with vibrational frequency of ca. 750 cm^{-1} and is polarized along the longer axis (^1L_b state). Large Stokes shifted fluorescence is a broad band and is polarized along the shorter axis of phenanthrene (^1L_b state). Fluorescence intensities of both the bands decrease with the increase of polarity and hydrogen-bond formation tendency of the solvents, but the preferential decrease in the fluorescence intensity of latter band system is more than that of the former band system under the above environments. Equilibrium for the prototropic reaction of monocation-free base is not established in the S_1 state within the lifetimes of the conjugate acid-base pair. Proton-induced fluorescence quenching constant for monocation is found to be 2×10^7 $dm^3 mol^{-1} s^{-1}$ and this low value, as compared to that for neutral aromatic amines, is because of the presence of positive charge on the monocation.

In the cata-condensed aromatic hydrocarbons, generally three electronic absorption bands are very prominent.[1,2] The long wavelength band (also known as α or ^1L_b band) is a long axis polarized weak band. Next band of high energy [polar(p) or ^1L_a band] is short axis polarized and is stronger than the α band. The third one is either a mixture of short axis and long axis polarized transitions (^1B_a or ^1B_b) or a single band i.e. β (^1B_b) and it is the most intense band. p-band is more easily susceptible to any change in the geometry of the molecule or to the presence of basic substituent along the short axis. For example α- and p-bands are well separated in benzene but are mixed in case of anthracene. In 1-naphthoic acid,[3] the long wavelength absorption band is of ^1L_a character whereas in naphthalene it is ^1L_b, which is of the lowest singlet energy.

As said earlier, the p-band is more polar and easily succeptible to the changes in the molecule or environments than the α-band. The presence of basic substituent at position-1 of linearly condensed systems will affect the p-band very much because roughly speaking the transition moment vector coincides with dipole moment vector. On the other hand the presence of basic substituent at 2-position affects both the α- and p-bands because dipole moment vector is lying in between the long axis and the short axis. Due to this, the dipole moment vector will have finite value along the short and the long axes of the molecule. However, the long axis polarized band will be affected more than the short axis polarized.

Because of the presence of benzo group along the angular direction, phenanthrene molecule belongs to C_{2v} symmetry point group. Due to this, unlike anthracene, α- and p-bands are well-separated and α-band possesses a nice vibrational structure, with vibrational frequency of 705 cm^{-1}. As can be seen from the structure of the phenanthrene molecule, the presence of basic groups at positions 9 and 10 will affect the p-band more than the α-band. The present study on

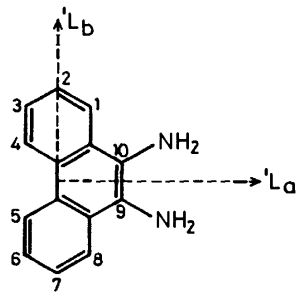

Scheme 1.

9,10-phenanthrenediamine (PDA) is in continuation of our earlier studies on the molecules containing similar two functional groups[4-6] to find out (i) how the amino groups affect the various band systems of phenanthrene and (ii) how the various prototropic species formed by the protonation or deprotonation of the amino groups will affect the α- and the p-bands. The conclusions are based on the absorption and fluorescence spectra recorded in different solvents and at various proton concentrations. The pK_a values for the different prototropic reactions have been determined in s_0 and s_1 states and are discussed. Lastly, this study was undertaken because the molecule, 9-phenanthrenamine is studied thoroughly.[7-9]

Experimental

9,10-Phenanthrenediamine (PDA) was obtained from Aldrich Chemical Company and was recrystallized from benzene. Finally, PDA was purified by vacuum sublimation and was stored under nitrogen atmosphere. The purity was checked by noting its sharp melting point, absorption spectrum and getting the similar fluorescence band maxima when excited at different wavelengths. Being very sensitive to air and light, the compound and the stock solutions were kept in amber-colored bottles and in oxygen free nitrogen atmosphere. Spectrograde methanol (BDH), trifluoroacetic acid (TFA, Fluka), analytical grade sulfuric acid, sodium hydroxide, and orthophosphoric acid were used without

further purifiction. Whereas cyclohexane, ether, and acetonitrile were further purified according to the procedure suggested in the literature.[10] Triply distilled water was used for aqueous solutions. pH of the solutions in the range of 3—10 was adjusted by adding appropriate quantities of sodium hydroxide and orthophosphoric acid, since the small quantities or phosphate buffers do not quench the fluorescence of the species and do not alter the pK_a of the prototropic reactions.[11] Hammett's acidity scale[12] for the solutions with pH<1 (prepared by the mixture of H_2SO_4 and water) and Yagil's basicity scale[13] for the solutions with pH>13 (prepared by the mixture of NaOH and water) were used.

The abosrption spectra were recorded on Shimadzu 190UV spectrophotometer, equipped with 135U recorder. The fluorescence measurements were carried out on a recording spectrofluorimeter fabricated in our laboratory of which details are available elsewhere.[14] Both the monochromators were calibrated from time to time with low-pressure mercury lamp. The band width used for excitation purposes is 8 nm. The concentration of the solution was kept at 5×10^{-5} M (1 M=1 moldm^{-3}), containing not more than 5% (v/v) methanol. For titration purposes, the solutions were prepared just before taking the measurements and the solutions were excited using the isosbestic wavelengths. The excitation wavelength used in determining the equilibrium constants for dication-monocation, monocation-free base and free base-monoanion equilibria in S_1 state were 300, 370, and 350 nm. The fluorescence quantum yields were determined from the solutions whose absorbances were less than 0.1. The fluorescence spectra were corrected[15] and quantum yields were calculated using quinine sulfate in 0.05 M H_2SO_4 as a standard.[16] The wavelength used for excitation was 385 nm. The pH of the solutions in the range of 1—13 were measured with Toshniwal's pH meter model CL 44A.

Results

The absorption spectra of PDA in different solvents and at different proton concentrations are depicted in Figs. 1 and 2 respectively. The relevant data are compiled in Table 1. Data of Table 1 clearly indicate that the absorption spectra of PDA can be divided into three band systems above 250 nm. One around 400 nm, the second around 330 nm and the third around 270 nm. The 400 nm band is broad and less structured as compared to the long wavelength band of phenanthrene,[1] whereas the structure is observed in the 274 nm band system and unlike other band systems, the structure of this band is retained in polar as well as hydrogen-bonding solvents. The vibrational frequency observed in the long wavelength band in cyclohexene is nearly equal to 730±30 cm^{-1}. A small red shift is noticed in the long wavelength absorption band in going from cyclohexane to acetonitrile, whereas a blue shift is observed in 400 and 330 nm bands in methanol and water.

With the decrease of pH (ca. 2), the 400 nm band system develops into a very nice vibrational structured absorption band which is red-shifted as compared to neutral one, whereas the other band systems follow a small blue shft. The absorption band systems at 303

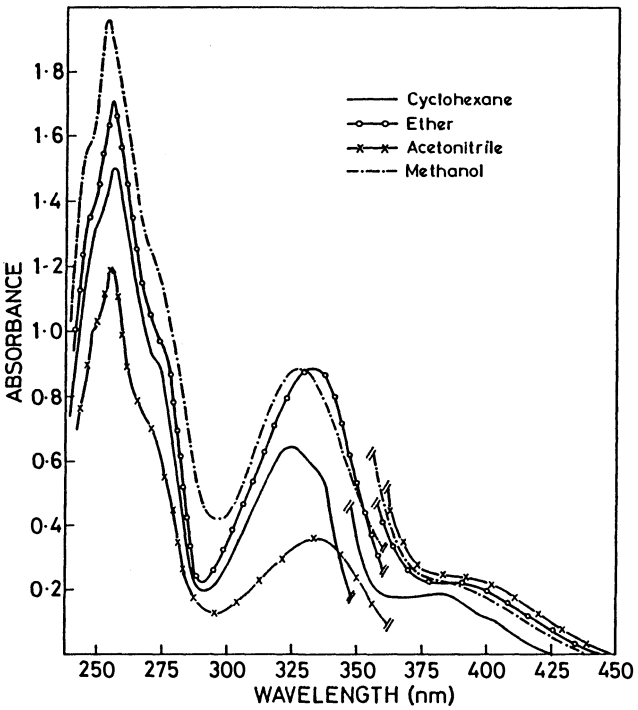

Fig. 1. Absorption spectra of PDA in different solvents at 298 K, concn=7×10^{-5}M.

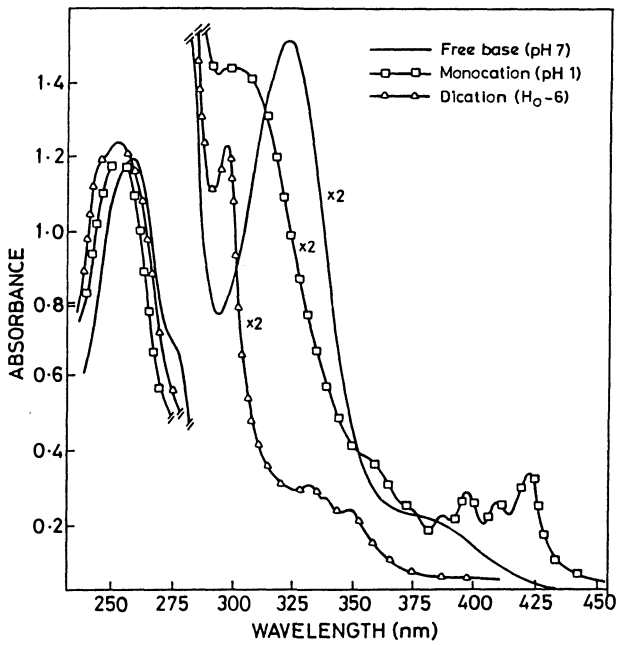

Fig. 2. Absorption spectra of the various prototropic species of PDA at 298 K.

and 252 nm resemble with that of 9-phenanthrenamine.[7] The vibrational frequency observed in the long wavelength band is 740±20 cm^{-1}. This spectrum is assigned to the monocation of PDA formed by the protonation of one of the amino groups. With further increase of proton concentration, all the band systems are blue-shifted and exactly agree with the band systems of phenanthrene,[1] both in the band maxima

Table 1. Absorption and Fluorescence Maxima (nm), $\log \varepsilon_{max}$ and ϕ_f of 9,10-Phenanthrenediamine in Different Solvents and at Various Proton Concentrations

Solvent/ species	λ_{max}(abs) ($\log \varepsilon_{max}$)			λ_{max}(flu) (ϕ_f)	
Cyclohexane	408	333	274	422, 438	—
	384	324	260	(0.07)	
			253		
Ether	395	333	277(4.23)	431	
	(3.15)	(4.05)	270(4.20)	418	492(0.04)
			259(4.32)	405	485[a]
Acetonitrile	400	332	274(4.27)	434	
	(3.10)	(4.05)	270(4.36)	420	511(0.02)
			258(4.53)	408	490[a]
Methanol	388	328	275(4.16)	430	
	(2.9)	(3.91)	270(4.22)	416	522(0.01)
			256(4.30)	406	475[a]
Water pH 7	383	323	275(4.21)		—
(Free base)	(3.13)	(3.96)	260(4.45)	—	448[a]
Monocation	421	303	252		430(0.02)
pH 1	408	(3.35)	(4.36)	—	400, 425[a]
	396				410[b]
	385				405[c]
	374				
	360				
Dication	348	299	252	—	390
H_0-6	(3.15)	(3.56)	(4.25)		368(0.31)
	337	288	246		354
	(3.22)	(3.53)	(4.19)		343, 359, 380, 390[a]
	332	278			
	(3.26)	(3.67)			
		265			
		(3.91)			
Monoanion	395	330	248	—	410
(H_-16)		304	227		

a) 77 K. b) Cyclohexane+0.5% (v/v) trifluoroacetic acid. c) 0.75 M H_2SO_4 in methanol.

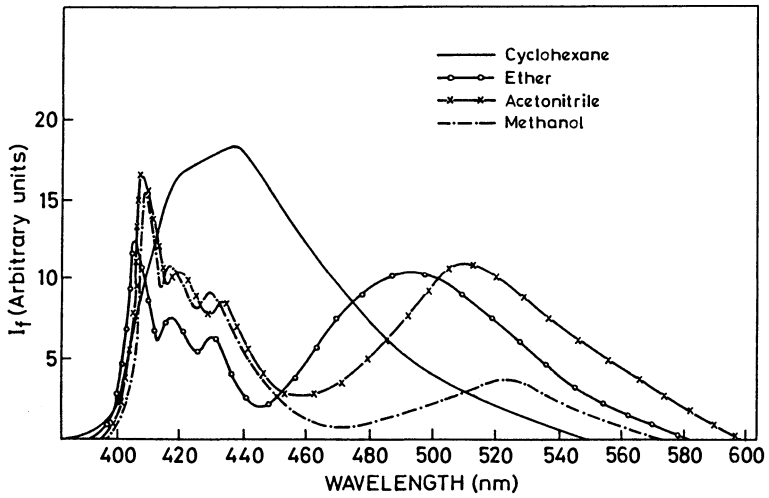

Fig. 3. Fluorescence spectra of PDA in different solvents at 298 K, concn=3×10^{-5}M.

and the vibrational frequencies observed in α- and p-bands. This species is thus assigned to dication formed by the protonation of both the amino groups. In the basic region above pH 14, a red shift is observed in the absorption spectrum, indicating the formation of monoanion. This equilibium is not complete, even at H_- 16, the highest basic solution used.

The fluorescence spectra of PDA in different solvents and at various proton concentrations are depicted in Figs. 3 and 4 respectively. The relevant

data are compiled in Table 1. In cyclohexane, only one normal stokes shifted fluorescence band (422 nm) is observed, whereas in other solvents, both the normal Stokes shifted and large Stokes shifted fluorescence (495 nm) bands are noticed. The normal Stokes shifted fluorescence band is nicely structured in all the solvents, with the vibrational frequency of ca. 720±20 cm^{-1}, whereas a large stokes shifted fluorescence emission is a broad band. With the increase in solvent polarity and proton donor capacity of the solvets, the fluorescence band maximum of large Stokes shifted band gets red-shifted, whereas that of normal Stokes shifted band remains unaffected. The fluorescence intensities of both the bands decrease under the above environments, but the relative decrease in the fluorescence intensity of the large Stokes shifted band is more than that of the normal Stokes shifted one. In water as solvent, PDA is nonfluorescent.

The prototropic species formed in the excited singlet state are the same as formed in the ground state. That is a blue-shifted fluorescence band (430 nm) is ovserved at pH 1 and this resembles with that of 9-phenanthrenamine in water as a solvent[9] and thus can be assigned to the monocation. At H_0-6 a large blue shifted structured fluorescence band is observed, agreeing nicely with that of phenanthrene.[17] The species formed thus a dication, obtained by protonating both the amino groups. No other fluorescence bands are observed even on increasing the proton concentration to H_0-10. Free base is nonfluorescent in the pH range of 6—14. Only at H_- 15, a fluorescence band (ca. 410 nm) appears and it reaches maximum intensity at H_- 16.5. This band system agrees with the fluorescence band maximum observed in case of 9-phenanthrenamine[9] at H_- 15. This can be assigned to monoanion.

The pK_a values of the various prototropic reactions are determined spectrophotometrically and are listed in Table 2. The pK_a for the monocation-free base equilibrium is much lower than that observed for similar reactions of other aromatic amines,[18] but agrees with the pK_a value obtained in case of 2,3-naphthaleneamine.[6] Similar is the case for dication-monocation equilibrium. The smaller pK_a value is because of the steric hindrance offerred by the two adjacent amino groups. The ground state pK_a value for the free base-monoanion equilibrium cannot be determined because the formtion of monoanion is not complete even at H_- 16.5, the highly basic solution used. The excited singlet state pK_a values are determined with the fluorimetric titrations (Fig. 5) and the values so obtained are listed in Table 2. Förster cycle method[19] cannot be used for the monocation-free base equilibrium as free base molecule is nonfluorescent in water at 298 K and the absorption spectrum of cation gets some complex structure (see later). Fluo-

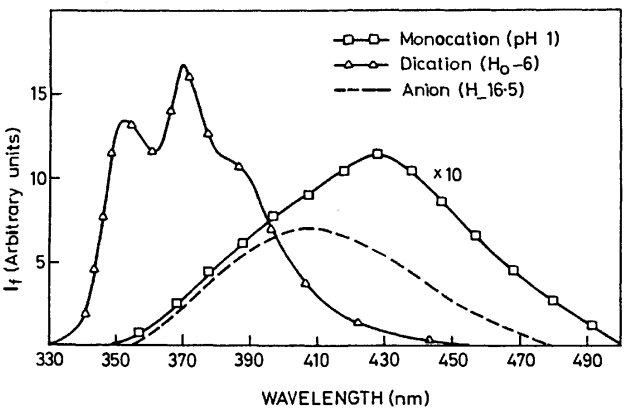

Fig. 4. Fluorescence spectra of the different prototropic species of PDA at 298 K.

Table 2. pK_a Values of Various Prototropic Reactions in S_0 and S_1 States

Equilibrium	pK_a	pK_a^{*} a)		
		abs	flu	Ft
Dication ⇄ Monocation	0.25	−10.2	−4.7	−4.2
Monocation ⇄ Free base	3.5	8.4		3.3
Monoanion ⇄ Dianion	>16	—	—	14.5

a) pK_a^{*} values using Förster cycle method and absorption and fluorescence data. Ft=Fluorimetric titration.

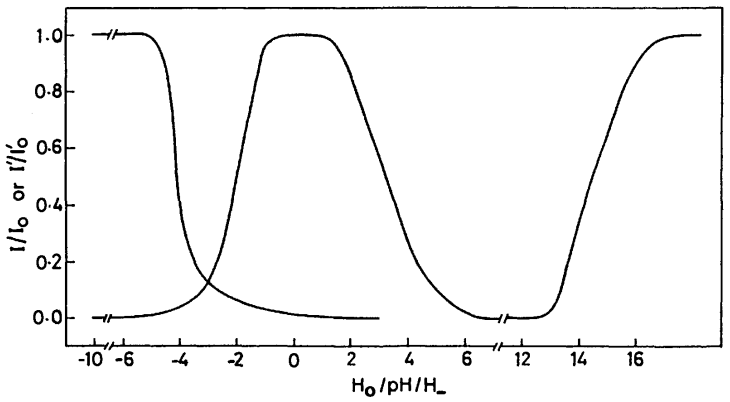

Fig. 5. Plot of relative fluorescence intensities of various prototropic species versus H_0/pH/H_-.

rescence data at 77 K and Förster cycle method do indicate that the ammonium ion becomes stronger acid in S_1 state. On the other hand, fluorimetric titrations have yielded the ground state pK_a for the monocation-free base equilibrium. This indicates that the prototropic equilibrium is not attained in the S_1 state during the short lifetimes of the conjugate acid-base species. Similar results have been observed in some other systems,[4-6,20] although it is anomalous. Similar to the normal behavior of aromatic amines, no correspondence is observed between the decrease in fluorescence intensity of monocation and the increase in the fluorescence intensity of the dication. The pK_a^* values for this reaction has been determined using fluorimetric titrations but from the formation curve of the dication only (Fig. 5) and is listed in Table 2.

As described earlier no correspondence is observed between the decrease and increase in the fluorescence intensity of the monocation and dication of PDA respectively. This has been attributed to the proton-induced fluorescence quenching of monocation.[21-29] This is because there was no quenching effect due to the counterion SO_4^{2-} under the experimental conditions. Applying the similar model as suggested by Shizuka et al.[27] and under conditions that proton concentration is small and thus rate for the backward protonation reaction is small as compared to its lifetime, the final equation reduces to a simple Stern-Volmer equation i.e.

$$I_0/I = 1 + k_q\tau[H^+]$$

where I and I_0 are fluorescence intensities in the presence and absence of quencher, k_q is the proton-induced fluorescence quenching rate constant and τ is the lifetime of the monocation. I_0/I vs. $[H^+]$ has been plotted in Fig. 6 and the slope obtained is 0.02 $dm^3 mol^{-1}$. The natural lifetime τ_{FM} is calculated using Strickler and Berg[30] equation and τ by using $\tau=\tau_{FM}\phi_f$ equation. The value of τ obtained is 1.1 ns and that of k_q is 2×10^7 $dm^3 mol^{-1} s^{-1}$. This value is quite small as compared to that observed for the similar reactions of other aromatic amines.

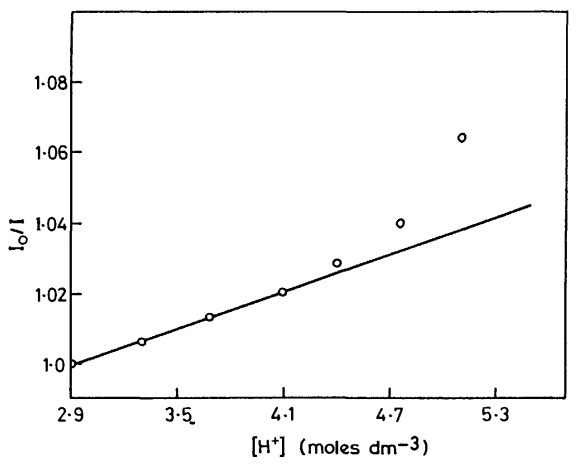

Fig. 6. Stern-Volmer plot for proton-induced fluorescence quenching of the monocation of PDA.

Discussion

Phenanthrene molecule has three band systems, one near 340 nm, highly structured with vibrational frequency 705 cm^{-1} (α-band), the other at 290, moderately structured with vibrational frequency 1320 cm^{-1} (p-band) and the third around 250 nm (β-band). Tsutsumi et al.[31] have clearly indicated with the help of semi-empirical SCF-MO-CI method that the charge migration from the amino group to the phenanthrene ring in the ^1L_a (p-band) occurs much more than in the other states in case of 9-phenanthrenamine. Thus based on these results the two amino groups in phenanthrene will perturb the above transitions but the effect will be more on the p-band than on the α- and β-bands. This is clear from the Scheme 1 shown earlier. Though the perturbation due to the presence of amino groups is more on the p-band, it is believed that the long wavelength band in PAD and its prototropic species is still the α-band. This is based on the following results:

(i) Molecular extinction coefficient of the long wavelength band (1.26×10^3 $dm^3 mol^{-1} cm^{-1}$) is less than that of second band (1.1×10^4 $dm^3 mol^{-1} cm^{-1}$). The former is more close to that of phenanthrene (0.4×10^3 dm^3 $mol^{-1} cm^{-1}$). The increase in the ε_{max} of this band of PDA is due to the interaction of amino groups with the phenanthrene moiety.

(ii) The difference between the two band maxima in phenanthrene is ca. 56 nm. Though the two band systems may get mixed up in PDA but it is highly improbable that the p-band will be of lower energy than that of α-band. It is also clear from the absorption spectrum (Fig. 1) that ca. 400 nm band appears as shoulder to the 333 nm band system.

(iii) Lastly the vibrational frequency observed in the long wavelength band (730 ± 30 cm^{-1}) resembles with that noticed in the absorption spectrum of phenanthrene (705 cm^{-1}).

The loss in the vibrational structure of α- and p-bands is because of the interation of lone pairs of the amino groups with the aromatic ring, which is commonly observed. Further, the loss of vibrational structure with the increase in the polarity and hydrogen-bond-forming tendency of the solvents is due to the interaction of the solvents with PDA. The data of Table 1 indicate that the molecule is acting as a proton acceptor in the ground state.

The blue shift observed in the p- and β-bands of the absorption spectra of PDA with the increase of proton concentration is consistent with the protonation of one of the amino groups, leading to the formation of monocation and protonation of both the amino groups, to the formation of dication. The band maximum in the former resembles with that of 9-

phenanthrenamine[9] and that of latter resembles with phenanthrene molecule.[1] But the behavior of α-band system is different from that of the other two. The absorption band maximum is slightly red-shifted and the band system has very nice structure, with vibrational frequency of 720±20 cm^{-1}. This structure is similar to the α-band system of phenanthrene molecule. The similar behavior is also observed in the α-band of PDA in cyclohexane when different amounts of TFA is added. Though the formation of monocation of PDA is confirmed but it is difficult to explain the appearance of a red-shifted structured absorption spectrum.

From the data of Table 1, we assign the normal Stokes shifted fluorescence band to the transition from ^1L_b. This is because the vibrational frequency observed in the short wavelength emission (ca. 750 cm^{-1}) spectrum agrees with that noticed in the absorption spectrum, indicating that the mirror image symmetry is observed between the long wavelength band of absorption and the short wavelength of fluorescence spectrum. This proves that the excited electronic state involved in the long wavelength absorption band and the short wavelength fluorescence band is the same i.e. ^1L_b. More evidences will be given later on. We assign the long wavelength fluorescence band to ^1L_a transition. This assignment is further based on the following evidences:

(i) The excitation spectra were recorded in two different solvents (ether and acetonitrile) at both the fluorescence band maxima and are shown in Fig. 7. The excitation spectrum recorded at long wavelength band does possess a small peak at 400 nm but the vibrational structure present in the absorption band is absent and the most intense band is around 350 nm, agreeing with the ^1L_a transition of absorption spectrum. On the other hand the excitation spectrum recorded at short wavelength fluorescence band possesses the vibrational structure, with the similar vibrational frequency as noticed in the long wavelength absorption spectrum. This spectrum does not contain the band around 350 nm, arising out of ^1L_a transition. The mixing of the small absorbance due to 400 nm band in the excitation spectra recorded at 500 nm is due to the mixing of these two bands in the absorption spectrum of PDA. (ii) ^1L_a electronic excited state is generally more polar than the ^1L_b electronic state. The presence of electron donating groups in the proper direction makes it further more polar. It has been shown by Tsutsumi et al.[31] that the charge migration from amino group to phenanthrene ring, in case of 9-phenanthrenamine, is much larger in the ^1L_a state than others. Due to this ^1L_a state is stabilized much more as compared to that of ^1L_b in more polar solvents and thus it appears at lower energy than the ^1L_b state. This is further manifested from the effect of solvents on the fluorescence spectrum of PDA, recorded in different solvents. The fluorescence band maximum at 400 nm is hardly affected by the polarity or proton-donor capacity of the solvents, whereas a large red shift is noticed in 500 nm band under the similar environments. (iii) Although the fluorescence intensities of both the fluorescence bands decrease in going from ether to water (molecule is nonfluorescent in water), the ratio of I_{500}/I_{400} decreases very rapidly in the above environments. This could be due to the fact that ^1L_a state is more polar and will have more interactions with the polar and proton donor or aceptor solvents. This will increase the rates of radiationless processes of the polar state. (iv) The more polar nature of ^1L_a state is further confirmed from the results of the fluorescence spectra of PDA recorded in cyclohexane containing TFA. The cyclohexane solution containing TFA upto 2×10^{-2} % (v/v) does produce a blue shift in the ^1L_a band system of absorption spectrum but ^1L_b band system becomes more structured, similar to the results observed in the absorption spectrum of PDA in aqueous solution containing H_2SO_4. But the fluorescence spectrum contains both the band systems and the red shift in the large Stokes shifted fluorescence band

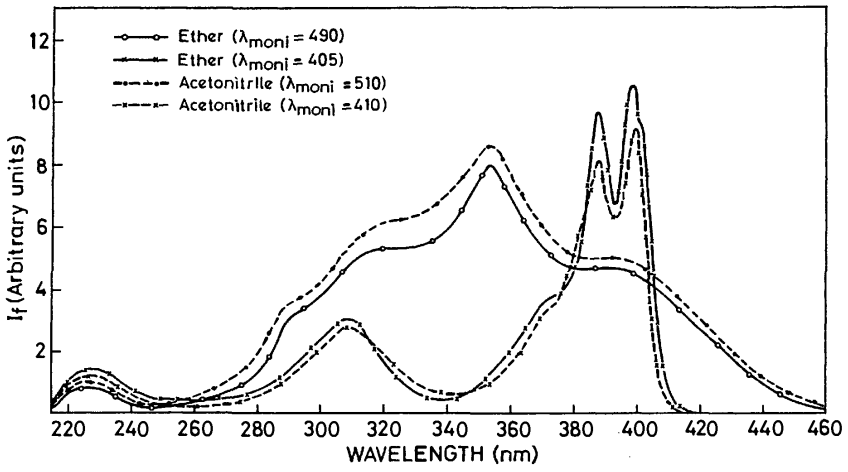

Fig. 7. Excitation spectra (uncorrected) of PDA recorded at 510 and 400 nm.

Table 3. Absorption and Fluorescence Band Maxima of PAD in Cyclohexane + Different Amount of Trifluoroacetic Acid (TFA)

% TFA (v/v)	λ_{max}(ab) nm			λ_{max}(fluo) nm	
Cyclohexane+0.00	408	333	274	438	—
	384	324	268	422	
			253		
0.001	408		287	442	
	396	309	277	430	494
	385			416	
	375			410	
	365				
	348				
0.002	408		288	442	
	396	312	277	430	502
	385			416	
	375			410	
	—				
	341				
0.02	408		286	430	502
	396	320		416	
	385	300		400	
	375				
	350				
	341				
0.2	357			Nonfluorescent	
	340	325			
		312			
1.0				410	

increases with the increase in the TFA concentration upto 2×10^{-2} % (Table 3). This is because TFA makes the cyclohexane polar and stabilizes the ^1L_a electronic state more than the ^1L_b one. This is further manifested from the fact that fluorescence intensities of both the emission bands decrease with increase of TFA in cyclohexane and PDA is nonfluorescent in cyclohexane containing 0.2% (v/v) TFA. (v) Last possibility that the long wavelength fluorescence belongs to the excimer is ruled out on the ground that the ratio of I_{500}/I_{400} does not change with the increase in the concentration of PDA by thousand fold.

The fluorescence spectra of the various prototropic species of PDA are consistent with the behavior of aromatic amines. The 430 nm fluorescence band of monocation, formed by protonating one of the amino group is originating from the ^1L_a electronic state, because this band maximum, similar to large Stokes shifted fluorescence band of PDA, is solvent dependent i.e. band maximum is red-shifted with the increase in the polarity of the solvent. Further monocation of PDA is similar to 9-phenanthrenamine, where it has been shown that ^1L_a is the lowest excited singlet state.[8] Finally, the structured fluorescence spectrum at H_0-6 is assigned to dication, formed by protonating both the amino groups, as this spectrum resembles with that of phenanthrene. In general, the fluorescence intensity of neutral aromatic amine is quenched by pH 14, without observing fluorescence from the monoanion, formed by the deprotonation of amino group, with few exceptions.[32] In our case, the additional problem is that the free base is also nonfluorescent in pH range 6—14, so it cannot be said with certainity that monoanion is formed in the excited state, but from the results of literature, the formation of this species can be speculated in the excited state. Based on our earlier results on 9-phenanthrenamine,[9] the 410 nm band can be assigned to a dianion formed by the deprotonation of either $-NH^-$ or $-NH_2$ group. This was further based on the similar results observed for 1- and 2-naphthylamine.[33] The results of Choudhury and Chatopadhyay,[34] on 2-naphthylamine and *N,N*-dimethyl-2-naphthylamine have clearly shown that the fluorescence band ovserved at *H*- 15 is due to the species formed by the deprotonation of ring hydrogen rather than from $-NH^-$, as *N,N*-dimethyl-2-naphthylamine has no dissociable proton. Based on these results and the similarity of the fluorescence band observed in PDA, with that of 9-phenanthrenamine it is possible that this species is similar to that formed in case of 2-naphthylamine. Fluorimetric titration curve has indicated that pK_a^* value for the equilibrium between the monoanion and the latter species (may also be monoanion) is 14.5, which actually agrees with the results of 9-phenanthrenamine.[9]

Results of fluorimetric titrations indicate that the prototropic equilibrium between monocation and free base pair is not established in the excited state during the lifetimes of the conjugate acid-base pair. This result is anomalous but similar behavior has been shown by the aromatic systems containing two amino groups,[4-6] 6-indazolamine,[35] and 4-(9-anthryl)-*N,N*-dimethylaniline.[20] This can be attributed to the short lifetimes of the two species. The pK_a^* value for the dication-monocation equilibrium has indicated that the ammonium ion becomes stronger acid on excitation.

Lastly, the small value of k_q observed for the proton-induced fluorescence quenching as compared to that for normal aromatic amines, is due to the presence of positive charge on the monocation.

Conclusion

Following conclusions can be drawn from the above study. (i) Dual fluorescence is observed in all the solvents. Abnormal Stokes shifted fluorescence arises from more polar and short axis polarized state, whereas the normal Stokes shifted, structured fluorescence is assigned to the less polar, long axis polarized state. (ii) The equilibrium between the monocation-free base species is not attained in the S_1 state and is due to the short lifetimes of the conjugate acid-base pair. (iii) Proton-induced fluorescence quenching for the monocation is observed and k_q value is found to be 2×10^7 $dm^3\,mol^{-1}\,s^{-1}$. The small value is due to the presence of positive charge on the monocation.

The authors are thankful to the Department of Science and Technology for the financial support to the project entitled, "Proton Transfer Reactions in the Excited States."

References

1) H. H. Jaffe and M. Orchin, "Theory and Applications of Ultraviolet Spectroscopy," John Wiley, New York (1962), Chap. 13.
2) N. Mataga and T. Kubota, "Molecular Interactions and Electronic Spectra," Marcel Dekker, New York (1970).
3) P. J. Kovi and S. G. Schulman, *Anal. Chim. Acta*, **63**, 39 (1973).
4) R. Manoharan and S. K. Dogra, *Can. J. Chem.*, **65**, 2013 (1987).
5) R. Manoharan and S. K. Dogra, *Bull. Chem. Soc. Jpn.*, **60**, 4409 (1987).
6) R. Manoharan and S. K. Dogra, *J. Phys. Chem.*, in press.
7) K. Tsutsumi, K. Aoki, H. Shizuka, and T. Morita, *Bull. Chem. Soc. Jpn.*, **44**, 3245 (1971).
8) K. Tsutsumi, S. Sekiguchi, and H. Shizuka, *J. Chem. Soc., Faraday Trans. 1*, **78**, 1087 (1982).
9) M. Swaminathan and S. K. Dogra, *Can. J. Chem.*, **61**, 1064 (1983).
10) J. A. Riddick and W. B. Bunger, "Organic Solvents," Wiley Interscience, New York (1970), pp. 632, 695, 801.
11) A. K. Mishra, M. Swaminathan, and S. K. Dogra, *J. Photochem.*, **26**, 49 (1984).
12) M. J. Jorgenson and R. D. Hartter, *J. Am. Chem. Soc.*, **85**, 878 (1963).
13) G. Yagil, *J. Phys. Chem.*, **71**, 1034 (1967).
14) M. Swaminathan and S. K. Dogra, *Indian J. Chem.*, **22A**, 853 (1983).
15) C. A. Parker, "Photoluminescence of Solutions with Applications to Photochemistry and Analytical Chemistry," Elsevier, Amsterdam (1968), p. 261.
16) G. G. Guilbault, "Practical Fluorescence, Theory Methods and Techniques," Marcel and Dekker, New York (1973), p. 149.
17) J. W. Longworth, R. O. Rahn, and R. G. Schulman, *J. Chem. Phys.*, **45**, 2930 (1964).
18) J. F. Ireland and P. A. H. Wyatt, *Adv. Phys. Org. Chem.*, **12**, 159 (1976).
19) Th. Förster, *Z. Elektrochem.*, **54**, 50 (1950).
20) H. Shizuka, T. Ogiwara, and E. Kimura, *J. Phys. Chem.*, **89**, 4302 (1985).
21) K. Tsutsumi and H. Shizuka, *Chem. Phys. Lett.*, **52**, 485 (1977).
22) H. Shizuka and K. Tsutsumi, *J. Photochem.*, **9**, 334 (1978).
23) H. Shizuka, K. Tsutsumi, H. Takeuchi, and I. Tanaka, *Chem. Phys. Lett.*, **62**, 408 (1979).
24) H. Shizuka, K. Tsutsumi, H. Takeuchi, and I. Tanaka, *Chem. Phys.*, **59**, 183 (1981).
25) H. Shizuka and S. Tobita, *J. Am. Chem. Soc.*, **104**, 6919 (1982).
26) H. Shizuka, M. Nakamura, and T. Morita, *J. Phys. Chem.*, **84**, 989 (1980).
27) K. Tsutsumi, S. Sekiguchi, and H. Shizuka, *J. Chem. Soc., Faraday Trans. 1*, **78**, 1087 (1982).
28) A. K. Mishra and S. K. Dogra, *J. Photochem.*, **23**, 163 (1983).
29) R. V. Subbarao, M. Krishnamurthy, and S. K. Dogra, *Indian J. Chem.*, **25A**, 517 (1986).
30) S. J. Strickler and R. A. Berg, *J. Phys. Chem.*, **37**, 814 (1962).
31) K. Tsutsumi, A. Aoki, H. Shizuka, and T. Morita, *Bull. Chem. Soc. Jpn.*, **44**, 3245 (1971).
32) Th. Förster, *Z. Elektrochem.*, **54**, 531 (1950).
33) A. K. Mishra, M. Swaminathan, and S. K. Dogra, *J. Photochem.*, **28**, 87 (1985).
34) M. Choudhury and N. Chatopadhyay, *J. Photochem. Photobiol., A: Chem.*, **41**, 337 (1988).
35) A. K. Mishra and S. K. Dogra, *Indian J. Chem.*, **24A**, 285 (1985).

Kinetics of Electron Transfer from Cyclic Ketones to Ni(IV) Periodate Complex in Aqueous Alkaline Medium

Jaffar Ali KHAN, U. CHANDRAIAH, B. Kishore KUMAR, and Sushama KANDLIKAR*
Department of Chemistry, Nizam College, Hyderabad-500 001, India
(Received June 27, 1988)

The kinetics of electron transfer from cyclic ketones (represented by (S)) to Ni(IV) periodate complexes has been studied in aqueous alkaline medium. The kinetics exhibit a pseudo-first-order disappearance of Ni(IV) periodate complexes when the [substrate] is present in excess. The pseudo-first-order rate constants, k_{obs}, were linearly dependent on [S] and the order in [S] were found to be unity. The rate of the reaction increased with the increase in [OH^-], however the rates were retarded with the increase in [periodate]. Salt and solvent effect studies indicate that the reaction is of ion-dipole type. A suitable mechanism involving slow adduct formation between enol and oxidant, and its decomposition in a fast step have been suggested. A rate law consistent with the proposed mechanism has also been derived. The products of oxidation were identified as corresponding decarboxylic acids.

The metal complexes containing nickel in the trivalent[1,2] and tetravalent[3-6] states have recently received considerable attention and significant progress has been made in understanding Ni(III) species. A few reports are also available on the preparation and characterization of Ni(IV) oxime complexes and their reactions with different organic and inorganic substrates.

In the kinetic studies of electron transfer reactions from ascorbate ion[5] and tris(1,10-phenanthroline)-cobalt(II),[6] it is reported that electron transfer at above pH 5 takes place by a two seperate one-electron reductive steps. In some cases electron transfer, such as from ascorbic acid[7] and hexacyanoferrate(II)[8] to tris (dimethylglyoximato)nickelate(IV), is assumed to proceed through a kinetically indistinguishable Ni(III) species. Kinetic studies on oxidation of organic compounds by dihydroxydiperiodatonickelate(IV) were reported earlier from our laboratory.[9-11] However, the present investigation is intended to study the mode of electron transfer from cyclic ketones to Ni(IV) periodate complexes and to suggest a suitable mechanism.

Material and Methods

All the solutions were prepared afresh in twice distilled water. Cyclic ketones viz. cyclopentanone, cyclohexanone, cycloheptanone, and cyclooctanone were of Fluka (puriss) and were used as such. The other chemicals such as KOH, KIO_4, $NaClO_4$, *t*-butyl alcohol were of BDH AnalaR grade.

Preparation of Oxidant. The nickel(IV) periodate complex, $KNiIO_6 \cdot 1/2\,H_2O$, was prepared by the method suggested by Ray[12] and standardized as given earlier.[9]

Kinetic Measurements. The kinetics of the reaction between the diperiodatonickelate(IV) ion and the substrate was followed in the temperature range 293—313 K by monitoring the disappearance of Ni(IV) at 410 nm employing a UV-vis double beam spectrophotometer model 140.02 (Shimadzu Corporation, Japan). A mixture containing requisite quantities of aqueous solution of cyclic ketone and potassium hydroxide and the solution of the Ni(IV) periodate complex were thermally equilibrated at desired temperature (±0.1 °C) separately for about 30 min and the known volume of aqueous solution of the Ni(IV) periodate complex was transferred to alkaline substrate solution. The supporting electrolyte for maintaining ionic strength was sodium perchlorate.

Pseudo-first-order rate constants, k_{obs}, were calculated from linear least square fit from Eq. 1, which was found to be valid well over three half-lives of disappearance of the Ni(IV) periodate complex

$$-\ln (A_t - A_\infty / A_0 - A_\infty) = k_{obs} t \quad (1)$$

where A_t, A_0, and A_∞, respectively, represent the absorbances at time *t*, before commencement of the reaction and at infinite time. Ni(II) periodate, a product of reduction of Ni(IV) periodate, was found to have negligible absorbance at 410 nm.

Results

Products of oxidation of cyclic ketones by the diperiodatonickelate(IV) ion were identified as corresponding dicarboxylic acids as determined by their characteristic tests.[13]

The stoichiometric experiments were conducted at different [OH^-] range viz. 5.0×10^{-2} mol dm^{-3} to 10.0×10^{-2} mol dm^{-3}, [Ni(IV)]=2.0×10^{-4} mol dm^{-3} and $[S]_0=1.0\times10^{-5}$ mol dm^{-3}. Unreacted Ni(IV) was estimated spectrophotometrically at the end of the reaction. It was found that three moles of Ni(IV) reacted with one mole of cyclic ketone. The stoichiometric equation is

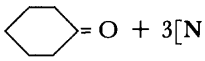

$$= O + 3[Ni(OH)_2(H_3IO_6)_2]^{2-} \longrightarrow$$

$$HOOC(CH_2)_4COOH + 3Ni(II) + 6H_3IO_6^{2-} + 3H_2O \quad (2)$$

The kinetic results can be summarized as follows:

i) The rate of the reaction increased linearly with the increase in $[S]_0$. Under the conditions $[S]_0 \gg$ [Ni(IV)] the plot of $\log[(abs)_0/(abs)_t]$ versus time was linear passing through origin, showing first-order dependence on [Ni(IV)]. From the slope of such plots the pseudo-first-order rate constants, k_{obs}, were evalu-

ated (Table 1). The plot of log k_{obs} versus log $[S]_0$ was linear and from the slope of such plots the order in [S] was found to be unity for all the cyclic ketones.

ii) The reactions were conducted at different $[OH^-]$. The rate of the reaction, at fixed $[S]_0$, [Ni(IV)], and [periodate] increased with the increase in $[OH^-]$ (Table 2).

iii) At fixed [Ni(IV)], [ketone], and $[OH^-]$ increase in [periodate] decreased the rate of the reaction. For example, under the conditions $[Ni(IV)]=1.0\times10^{-4}$ mol dm^{-3}, $[S]_0=5.0\times10^{-2}$ mol dm^{-3}, $[OH^-]=1.0\times10^{-2}$ mol dm^{-3}, increase in [periodate] from 1.0×10^{-5} mol dm^{-3} to 1.0×10^{-4} mol dm^{-3} decreased the $10^4\times k_{obs}$ values from 5.76 s^{-1} to 3.19 s^{-1} at 298 K.

iv) Effect of changing dielectric constant of the medium by using aqueous *t*-butyl alcohol as a solvent had negligible effect on the rate of the reaction. For example, under identical conditions as above and at $[periodate]=5.0\times10^{-5}$ mol dm^{-3} decreased negligibly the $10^4\times k_{obs}$ values from 4.35 s^{-1} to 4.16 s^{-1} at 298 K when the percentage of *t*-butyl alcohol was increased from 0—60% (v/v).

v) The rate of the reaction, at fixed $[S]_0$, $[OH^-]$, [Ni(IV)], and [periodate], was not altered by added sodium perchlorate.

vi) The reactions were carried out at different temperatures in the range of 293—313 K. Activation energy of the reaction and other thermodynamic parameters were evaluated (Table 3).

vii) The addition of acrylamide to deaerated reaction mixture did not alter the reaction rates nor there was any polymerization showing the absence of free radicals in the reaction.

viii) The observed order of the oxidation rate was found to be decreased in the order, cyclohexanone > cyclooctanone > cyclopentanone > cycloheptanone. Probably this may be due to enolic content of the above cyclic ketones decreasing in the same order.[14]

Table 1. Effect of [substrate] on the Rate of the Reaction

$10^2\times[S]$ / mol dm^{-3}	$10^4\times k_{obs}$ / s^{-1}
2.00	1.28
4.00	2.57
5.00	3.19
6.00	3.85
8.00	5.05
10.0	6.44

[Ni(IV)])=1.0×10^{-4} mol dm^{-3}, $[OH^-]=1.0\times10^{-2}$ mol dm^{-3}, [periodate]=1.0×10^{-4} mol dm^{-3}, T=298 K.

Table 2. Effect of $[OH^-]$ on the Rate of the Reaction

$10^2\times[OH^-]$ / mol dm^{-3}	$10^4\times k_{obs}$ / s^{-1}
0.500	2.27
1.00	3.19
2.00	4.63
5.00	6.08
8.00	7.93
10.0	8.51

[Ni(IV)]=1.0×10^{-4} mol dm^{-3}, [S]=5.0×10^{-2} mol dm^{-3}, [periodate]=1.0×10^{-4} mol dm^{-3}, T=298 K.

Discussion

Mukherjee et al.[15] reported the structre of the water-soluble Ni(IV) periodate complex as $[Ni(OH)_2(HIO)_6)_2]^{6-}$. The electronic spectrum of the water-soluble Ni(IV) periodate complex was reported to have a hump at 410 nm assignable to charge transfer from metal t_{2g} to ligand orbital and a strong band at 210 nm, due to IO_6 octahedron. The electronic spectrum of the complex prepared by us also showed similar spectral characteristics. However, in aqueous alkaline medium and in the pH range employed, the periodate cannot exist as HIO_6^{4-}.

Crouthamel and co-workers[16,17] suggested the following equilibria at different pH ranges

$$H_5IO_6 \overset{K_1}{\rightleftharpoons} H_4IO_6^- + H^+ \quad (3)$$

$$H_4IO_6^- \overset{K_2}{\rightleftharpoons} H_3IO_6^{2-} + H^+ \quad (4)$$

$$H_3IO_6^{2-} \overset{K_3}{\rightleftharpoons} H_2IO_6^{3-} + H^+ \quad (5)$$

The dissociation constants K_1, K_2, and K_3 at 298 K are 2.3×10^{-2}, 4.35×10^{-9}, and 1.05×10^{-15} respectively. Among the above species periodic acid, H_5IO_6 exist in acidic media and $H_4IO_6^-$ near pH 7. Hence in the pH range employed in the present study, the main species can be $H_3IO_6^{2-}$ and $H_2IO_6^{3-}$. The existence of $H_2IO_6^{3-}$ looks improbable owing to very low value of K_3 and

Table 3. Activation Parameters for the Oxidation of Cyclic Ketones with Diperiodatonickelate(IV) Ion in Aqueous Alkaline Medium

Substrate	$10^3\times k''$ / dm^3 mol^{-1} s^{-1}					E_a	$\Delta H^{\#}$	$\Delta G^{\#}$	$-\Delta S^{\#}$
	293 K	298 K	303 K	308 K	313 K	kJ mol^{-1}	kJ mol^{-1}	kJ mol^{-1}	J mol^{-1} K^{-1}
Cyclopentanone	3.47	5.64	9.01	14.2	21.9	70.3	67.8	85.8	60.3
Cyclohexanone	8.00	12.6	19.6	30.0	45.3	66.1	63.6	83.8	67.8
Cycloheptanone	1.29	2.13	3.47	5.57	8.77	73.1	70.1	88.2	59.0
Cyclooctanone	3.96	6.40	10.2	15.9	24.7	69.9	67.4	85.5	60.8

[NI(IV)]=1.0×10^{-4} mol dm^{-3}, [S]=5.0×10^{-2} mol dm^{-3}, $[OH^-]=1.0\times10^{-2}$ mol dm^{-3}, [periodate]=1.0×10^{-4} mol dm^{-3}.

periodate exists in the dimerized form $I_2O_9^{4-}$ only when it is present in higher concentrations. Hence the soluble complex may be represented by the formula $[Ni(OH)_2(H_3IO_6)_2]^{2-}$.

The $[OH^-]$ depenednce of oxidation of cyclic ketones by the Ni(IV) periodate complex indicates the equilibrium between deprotonated reactive species **2** and deprotonated unreactive species **1**:

$$[Ni(OH)_2(H_3IO_6)_2]^{2-} + OH^- \rightleftharpoons [Ni(OH)_2(H_2IO_6)(H_3IO_6)]^{3-} + H_2O \quad (6)$$

The dependence of the rate of oxidation on the periodate complex indicates a dissociative equilibrium in which Ni(IV) moiety loses a periodate ligand from its coordination sphere forming the monoperiodatonickelate (IV) ion (**3**):

$$[Ni(OH)_2(H_2IO_6)(H_3IO_6)]^{3-} \rightleftharpoons [Ni(OH)_2(H_2IO_6)]^- + H_3IO_6^{2-} \quad (7)$$

The formation of species **3** directly from **1** is also possible:

$$[Ni(OH)_2(H_3IO_6)_2]^{2-} + OH^- \rightleftharpoons [Ni(OH)_2(H_2IO_6)]^- + H_3IO_6^{2-} + H_2O \quad (8)$$

A sequence of Eqs. 6 and 7 is preferred as the loss of the periodate ion occurs preferentially from a species having higher negetive charges. Hence deprotonated species **3** is assumed to be an active oxidant species. Such protonated and deprotonated forms in the inner sphere also exist for tris(dimethylglyoximato)nickelate(IV) complex[4] and the periodato and tellurato complexes of copper and the peptide complexes of silver in their trivalent states.[18-20] The assumption that **3** is the reactive species of oxidant is also in conformity with the earlier findings.[21] In the oxidation of the thiocyanate ion by the dihydroxydiperiodatonickelate(IV) complex the charge on the reactive species of oxidant was found to be unit negetive from the observed salt effect.

Oxidation of ketones may proceed by any one of the following stages:

(a) If the rate of oxidation>rate of enolization, the oxidation process can be represented as

$$\text{Ketone} + \text{Oxidant} \longrightarrow \text{Products} \quad (9)$$

with first-order dependence in oxidant.

(b) If the rate of enolization>rate of oxidation and the order in oxidant is unity, the oxidation can be represented as

$$\text{Ketone} + OH^- \rightleftharpoons \text{Enol} \quad (10)$$

$$\text{Enol} + \text{Oxidant} \xrightarrow[\text{slow}]{} \text{Products} \quad (11)$$

(c) If the rate of enolization > rate of oxidation and the order in oxidant is zero, the oxidation can be represented as

$$\text{Ketone} + OH^- \overset{\text{slow}}{\rightleftharpoons} \text{Enol} \quad (12)$$

$$\text{Enol} + \text{Oxidant} \xrightarrow[\text{fast}]{} \text{Products} \quad (13)$$

In the present study, the order in [oxidant] was found to be unity as the log (absorbance) versus time plot was perfectly straight line (correlation coefficient, r=0.9992) and the rate of oxidation of cyclic ketones was found to be in the order of ca. 10^{-8}. The rates of enolization of all cyclic ketones determined by iodination method were found to be in the order of ca. 10^{-6} to ca. 10^{-5} which are very much higher than the rate of oxidation of cyclic ketones with the diperiodatonickelate(IV) ion. Hence, it may be concluded that enol may be reacting with oxidant. One of the possibilities of an electron transfer may be due to the reaction between species **3** and enol giving an unstable adduct which decomposes subsequently to given an intermediate and Ni(II) in the fast step. The intermediate may react with two moles of Ni(IV) to give the final products. The other posibility of the electron transfer may be by two seperate one-electron reductive steps, the first step of which produces Ni(III) and enol free radical (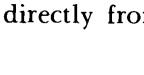) which induces polymerization of acrylamide. However, no polymerization was observed by adding acrylamide to deaerated reaction mixture, showing the absence of one-electron reductive step. Hence in the absence of polymerization one could envisage that the adduct of 3-enol is formed in the slow step which dissociates with the electron transfer in the fast step.

A plausible mechanism, based on the above discussions for the electron transfer is shown in Scheme 1.

Though an adduct formation is envisaged no evidence could be given for its formation as it must be unstable and because of its low concentration it is difficult to detect it kinetically. A plot of $1/k_{obs}$ versus $1/[S]_0$ was linear yielding a straight line passing almost through origin. The observed stoichiometry

$$[DPN]^{a)} + OH^- \overset{K_1}{\rightleftharpoons} [Ni(OH)_2(H_2IO_6)(H_3IO_6)]^{3-} + H_2O \quad (14)$$

$$[Ni(OH)_2(H_2IO_6)(H_3IO_6)]^{3-} \overset{K_2}{\rightleftharpoons} [Ni(OH)_2(H_2IO_6)]^- + H_3IO_6^{2-} \quad (15)$$

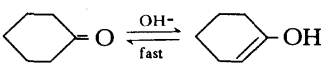

(16)

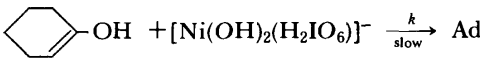

(17)

$$\text{Adduct} \xrightarrow[\text{fast}]{} \text{Intermediate} + \text{Ni(II)} \quad (18)$$

$$\text{Intermediate} + 2[Ni(OH)_2(H_2IO_6)]^- \xrightarrow[\text{fast}]{} \text{Products} + 2\text{Ni(II)} \quad (19)$$

Scheme 1. a) Diperiodatonickelate(IV) ion, $[(Ni(OH)_2(H_3IO_6)_2]^{2-}$ is represented as [DPN] for simplicity.

i.e., 1 cyclic ketone: 3Ni(IV), salt and solvent effects also reinforce the above mechanism.

The rate of oxidation could be written as

$$\text{rate}=k[\text{enol}][\mathbf{3}]. \quad (20)$$

As enol is consumed in product formation more and more ketone is converted into enol form. As [ketone] is far excess to [oxidant], [ketone] can be taken as equal to [enol]. The concentration of **3** can be calculated by taking into consideration the two equilibria, Eqs. 14 and 15, in terms of $[\text{DPN}]_{\text{total}}$.

$$[\text{DPN}]_t=[\mathbf{1}]+[\mathbf{2}]+[\mathbf{3}] \quad (21)$$

As the disappearance of [DPN] is monitored, the rate of the reaction, Eq. 20 can be written as

$$\text{rate} = -\frac{d[\text{DPN}]}{dt} = \frac{kK_1K_2[\text{DPN}]_t[\text{ketone}][\text{OH}^-]}{K_1K_2[\text{OH}^-]+\{K_1[\text{OH}^-]+1\}[\text{H}_3\text{IO}_6^{2-}]}$$

$$\equiv k_{\text{obs}}[\text{DPN}]_t \quad (22)$$

The above equation envisages a linear plot for $1/k_{\text{obs}}$ versus $1/[\text{OH}^-]$. In fact such a plot was obtained giving further support to the derived rate law. The above rate law also explains all experimental observations, such a first order in [DPN] and [ketone], fractional order in $[\text{OH}^-]$ and inverse fractional order in [periodate].

The equilibrium constants, K_1 and K_2 in Eqs. 14 and 15, were calculated kinetically from a kinetic study of oxidation of benzyl alcohol with diperiodatonickelate(IV) ion.[22] The K_2 values were found to be 4.59×10^{-4}, 3.78×10^{-4}, and 3.39×10^{-4} at 300, 305, and 310 K respectively and K_1 values were found to be 33.1, 43.6, and 52.1 at 300, 305, and 310 K respectively. The K_1 and K_2 values were used to calculate k of the rate law and from this it follows that the concentration of **3** (monoperiodatonickelate(IV) ion, $[\text{Ni(OH)}_2(\text{H}_2\text{IO}_6)]^-$) is around 10^{-7} mol dm^{-3}. Even if whole of the concentration of **3** is undergoing adduct formation with enol, the concentration of adduct of **3**-enol at any given time will not be more than 10^{-7} mol dm^{-3}. This may be the reason for non-detectability of adduct of **3**-enol.

The bimolecular rate constants, k'' obtained by dividing k_{obs} with [S], along with activation parameters are listed in Table 3. An examination of the data shows that the reactions are enthalpy controlled as the reaction with lowest enthalpy ($\Delta H^{\#}$) has highest rate. This is also confirmed from the fact that the plot of $\Delta H^{\#}$ versus $\Delta S^{\#}$ was found to be linear with isokinetic temperature, β=693 K (correlation coefficient, r= 0.9985) which is much higher than experimental temperature range (293—313 K). The consistency in $\Delta G^{\#}$ values indicates the similar mechanism to be operative in the present study.

The authors express their thanks to Professors T. Navneeth Rao and B. Sethuram for ecouragement and useful discussions. One of the authors (JAK) is thankful to Principal, Nizal College, for providing laboratory facilities, and another author (UC) is thankful to CSIR, New Delhi for the award of senior research fellowship.

References

1) R. I. Haines and A. McAuley, *Coord. Chem. Rev.*, **39**, 77 (1981).
2) K. Nag and A. Chakravarthy, *Coord. Chem. Rev.*, **33**, 87 (1980).
3) D. H. Macartney and A. McAuley, *Inorg. Chem.*, **22**, 2062 (1983).
4) S. Acharya, G. Neogi, R. K. Panda, and D. Ramaswamy, *Int. J. Chem. Kinet.*, **14**, 1253 (1982).
5) A. G. Lappin, M. C. M. Laranjeira, and L. Youdi Owei, *J. Chem. Soc., Dalton Trans.*, **1981**, 721.
6) A. G. Lappin and M. C. M. Laranjeira, *J. Chem. Soc., Dalton Trans.*, **1982**, 1861.
7) R. Sahu, G. Neogi, S. Acharya, and R. K. Panda, *Int. J. Chem. Kinet.*, **15**, 945 (1983).
8) S. Acharya, G. Neogi, R. K. Panda, and D. Ramaswamy, *J. Chem. Soc., Dalton Trans.*, **1984**, 1471.
9) U. Chandraiah, Jaffar Ali Khan, C. P. Murthy, and Sushama Kandlikar, *Indian J. Chem.*, **26A**, 481 (1987).
10) U. Chandraiah, C. P. Murthy, and Sushama Kandlikar, *Indian J. Chem.*, in press.
11) U. Chandraiah, C. P. Murthy, and Sushama Kandlikar, *Indian J. Chem.*, in press.
12) P. Ray, *Inorg. Synth.*, Vol. V, 201 (1957).
13) F. Feigl, "Spot Tests in Organic Analysis," Elsevier, New York (1966), p. 213.
14) M. Prasad Rao, B. Sethuram, and T. Navneeth Rao, *Indian J. Chem.*, **19A**, 582 (1980).
15) H. G. Mukherjee, Bhansidhar Mandal, and Shyamali De, *Indian J. Chem.*, **23A**, 426 (1984).
16) C. E. Crouthamel, H. V. Meek, D. S. Martin, and C. V. Banks, *J. Am. Chem. Soc.*, **71**, 3031 (1949).
17) C. E. Crouthamel, H. V. Meek, and D. V. Martin, *J. Am. Chem. Soc.*, **73**, 82 (1951).
18) G. I. Rozovskii, A. Yu Prokopchik, and R. P. Yankanskas, *Kinet. Katal.*, **12**, 82 (1971).
19) G. I. Rozovskii, A. K. Misyavichyus, and A. Yu Prokopchik, *Kinet. Katal.*, **16**, 402 (1975).
20) J. Kirschenbaum Louis and J. D. Rush, *J. Am. Chem. Soc.*, **106**, 1003 (1984).
21) U. Chandraiah, Ph. D. Thesis (1987), Osmania University, Hyderabad, India.
22) Jaffar Ali Khan, U. Chandraiah, B. Kishore Kumar, and Sushama Kandlikar, *Indian J. Chem.*, to be submitted.

An Investigation into the Mechanism of Acid-Catalyzed Hydrolysis of *N*-Benzylbenzohydroxamic Acid†

Kallol K. GHOSH* and Shiv G. TANDON
Department of Chemistry, Ravishankar University, Raipur 492 010, India
(Received July 27, 1988)

The catalytic effects of hydrochloric, perchloric, and sulfuric acids on the hydrolysis of *N*-benzylbenzohydroxamic acid (BBHA) have been examined in 10% (v/v) dioxane-water at 55 °C. Plots of the pseudo-first-order rate constants k_ψ against $[H^+]$ show maxima which arise from extensive protonation of the substrate. Analyses of the kinetic data by Bunnett and Bunnett-Olsen criteria, solvent deuterium isotope effects, salt effects and entropies of activation are consistent with a bimolecular mechanism.

As a part of a broad program on the hydrolysis reaction of hydroxamic acids in concentrated mineral acids,[1-6] we have presently undertaken the study of the acid catalyzed hydrolysis of *N*-benzylbenzohydroxamic acid (BBHA). No kinetic study of the hydrolysis of BBHA have previously been reported. BBHA has been found to be a highly selective reagent for the spectrophotometric determination of vanadium(V).[7] However, due to hydrolysis of hydroxamic acids into the parent carboxylic acids and hydroxylamines in concentrated mineral acids severe problems are faced in achieving the desired objectives. Hence, reaction mechanisms and hydrolytic stabilities have been investigated.

In investigating the mechanism we have examined our kinetic data in 10% (v/v) dioxane-water medium, with reference to four different diagnostic criteria; the effect of mineral acid and of added salt, the solvent isotope effect, and the effect of temperature.

Experimental

BBHA was provided by Prof. Usha Tandon of this laboratory and characterized by mp, elemental analysis, UV, IR, NMR, and mass spectral data. The acids used were of analytical reagent quality. Their concentrations were determined by titration with standard alkali. Sodium perchlorate was a recrystallized commercial sample. It was dehydrated at 150 °C. Anhydrous sodium chloride was dried similarly. Dioxane (BDH, AR) was used after purification. Deuterium oxide, D_2O (isotopic purity>99.8%), DCl (isotopic purity> 95%), and D_2SO_4 (isotopic purity>95%) were procured from BARC, Bombay. Iron(III)-chloride solution used in colorimetric procedure was prepared by the standard method.

Kinetic measurements were made by use of the spectrophotometric method reported previously[1] using a SPEKOL set at 520 nm.

Results

Rate Profiles. The observed pseudo-first-order rate constants for the catalytic effect of hydrochloric, perchloric and sulfuric acids are given in Table 1. In order to emphasise the difference in the catalytic efficiencies of the different acids and to illustrate that the rate acidity profiles go through maxima, these data have been plotted in Fig. 1. In sulfuric and hydrochloric acid the dependance of BBHA is characterized by an initial rate increase with the acid concentration, passing through a maximum, followed by a rate decrease with further increasing acid concentration. In the case of perchloric acid, the same trend is observed with a maximum except that the final increase occurs at higher acid concentration. We have previously observed,[1] and commented on, similar maxima in the hydrolysis of *N*-phenylbenzohydroxamic acid (PBHA). Such maxima are attributed to two opposing effects of increasing the acid concentration. On the one hand increased acidity raises the concentration of the reactive conjugate acid form of the substrate, but at the same time reduces the available water needed to complete the hydrolysis. The rate maxima that we observe are superficially similar to those found in acid hydro-

Table 1. Observed Pseudo-First-Order Rate Constants for Hydrolysis of *N*-Benzylbenzohydroxamic Acid (BBHA) (Temp=50 °C, Solvent: Dioxane 10% (v/v))

Acid	$k_\psi \cdot 10^3/\mathrm{min}^{-1}$		
M	HCl	H_2SO_4	$HClO_4$
0.72	—	2.71	—
1.16	4.23	—	2.52
1.45	5.06	5.08	4.36
2.02	—	7.00	—
2.32	8.29	—	6.74
2.90	10.5	10.1	8.05
3.50	11.9	12.0	8.80
4.00	13.6	14.2	9.30
4.50	15.4	14.8	8.97
5.00	—	14.2	8.19
5.22	17.1	—	—
5.80	18.5	—	6.23
6.00	—	12.0	—
6.50	19.0	8.67	4.24
7.00	18.5	7.44	—
7.50	17.6	—	1.81
8.00	16.3	3.56	1.06
8.50	14.6	—	1.00
9.00	13.1	1.24	0.257
9.50	11.1	—	—
10.0	—	0.597	—
10.1	—	—	0.745
10.4	9.06	—	—

† Presented in part at the 7th IUPAC Conference on Physical Organic Chemistry, Auckland, New Zealand, August 1984.

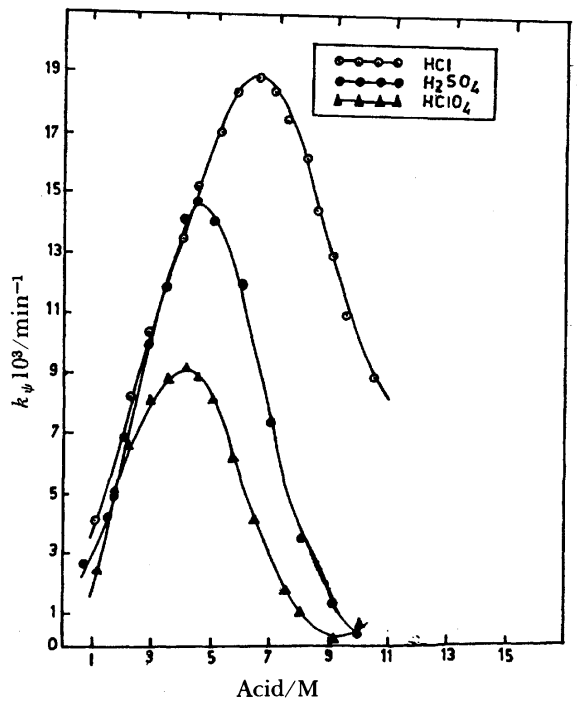

Fig. 1. Rate acidity profiles of pseudo-first-order rate constants for the hydrolysis of BBHA at 55 °C.

lyses of esters,[8] amides,[9] lactams,[10] and hydrazines.[11]

At acid concentrations in the range 0.72 to 4.5 M the catalytic effect (1M=1 mol dm^{-3}) of acids decreases in the order $HCl \approx H_2SO_4 > HClO_4$. At acid concentration above 5.0 M, the catalytic effectiveness of the acids decreases in the sequence $HCl > H_2SO_4 > HClO_4$. Bunton[12] and his co-workers have suggested that such an order is associated with an A-2 mechanism. They attributed this behavior in part to a propensity of perchlorate ion, a large ion of low charge density, to associate preferentially with carbenium ions, actual or partially formed in a transition state. They also consider that transition states with little or no carbenium ion character but with good sites for hydrogen bonding with the medium will be favored in mineral acids having anions of higher charge density (e.g., HSO_4^- or Cl^-). Studies at higher molarities are not possible because of the strong oxidizing and dehydrating properties of H_2SO_4.

The rate of hydrolysis of BBHA is fast as compared to PBHA[1] upto particular acidity region (0.72 to 7.0 M H_2SO_4 and 1.16 to 6.5 M $HClO_4$). It may be due to electron donating nature of $-CH_2$ group attached between C_6H_5 and the nitrogen of the functional group. This may facilitate the protonation of substrate.

Treatment of Rate Data. For all the sets of data in Table 1, we have correlated the data in terms of the acidity function H_0[13] and H_A,[14] activity of water a_{H_2O} and total concentration of hydrogen ion $[H^+]$.

One of the difficulties in the present study in using criteria which utilize acidity function (H_0 and H_A) or activity of water (a_{H_2O}) values is the difference between the temperature and medium at which the hydrolysis of BBHA was studied (55 °C and 10% (v/v) dioxane) and that for which the vast majority of such data is available (25 °C and aqueous medium), and the lack of precise information on the protonation behavior of BBHA. Very few detailed studies of the variation of acidity function with temperature and medium have been reported. We have therefore in the present study used acidity function and water activity at 25 °C for all the acids used. Bunnett and Olsen[15] adopted a similar approach in a study of the acid-catalyzed hydrolysis of *o*-tolunitrile at 133 °C.

The results of Bunnett and Bunnett-Olsen analysis are summarized in Table 3. Most of the correlations

Table 3. Kinetic Solvent Isotope Effect at 55 °C

Solvent	Catalyst	$k_\psi \cdot 10^3$ / min^{-1}	k_D/k_H
H_2O	1.45 M HCl	5.06	2.1
D_2O	1.45 M DCl	11.0	
H_2O	2.90 M HCl	10.5	1.58
D_2O	2.90 M DCl	16.6	
H_2O	5.80 M HCl	18.5	1.37
D_2O	5.80 M DCl	25.4	
H_2O	10.4 M HCl	9.06	1.16
D_2O	10.4 M DCl	10.6	
H_2O	0.72 M H_2SO_4	2.71	1.62
D_2O	0.72 M D_2SO_4	4.40	
H_2O	4.0 M H_2SO_4	14.2	1.52
D_2O	4.0 M D_2SO_4	21.6	
H_2O	5.0 M H_2SO_4	14.2	1.19
D_2O	5.0 M D_2SO_4	17.0	
H_2O	8.50 M H_2SO_4	1.90	0.63
D_2O	8.50 M D_2SO_4	1.20	

Table 2. Analysis of Rate Data[a] for the Hydrolysis of BBHA at 55 °C by Use of Bunnett and Bunnett-Olsen Lfer

Acid	Bunnett			Bunnett-Olsen lfer ϕ	
	w		w^*		
	H_0	H_A		H_0	H_A
HCl	5.6 (1.45—9.00)	4.4 (2.32—10.4)	1.7 (4.5—10.4)	1.26 (2.9—10.4)	1.14 (1.16—8.12)
H_2SO_4	4.2 (2.02—9.00)	3.9 (2.02—10.0)	0.93 (2.02—6.0)	1.08 (0.72—6.0)	1.24 (2.02—6.00)
$HClO_4$	6.4 (1.16—8.00)	4.1 (2.9—9.00)	1.12 (1.16—8.00)	1.32 (1.45—6.00)	1.56 (1.45—6.00)

a) The acid concentration range in which the parameters are calculated is inserted in the parentheses.

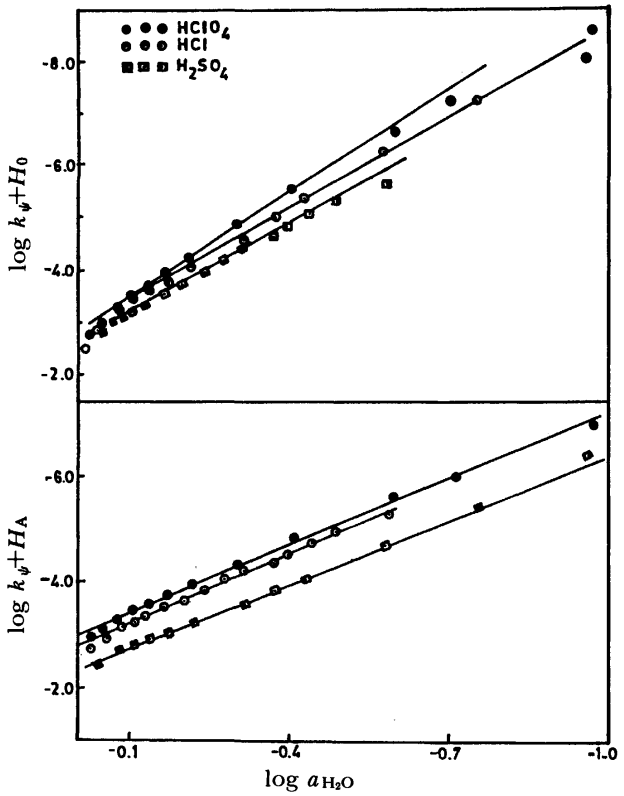

Fig. 2. Bunnett 'w' plots for the hydrolysis of BBHA at 55°C.

are good rather than superb, because of scatter of experimental points. Bunnett[16] plots for the hydrolysis of BBHA (using H_0 and H_A values) are shown in Fig. 2. A good linear correlation is obtained with slopes (w values) in the range 3.9 to 6.4 for all three acids used. Such values of 'w' fall into the range normally associated with water acting as a proton-transfer agent. Plots of ($\log k_\psi - \log [H^+]$) versus $\log a_{H_2O}$ gave Bunnett 'w^*' values of 1.70, 0.92, and 1.12 for hydrochloric, sulfuric, and perchloric acids respectively. Such values are consistent with the mechanistic classification indicated by the Bunnett 'w' values.

Treatment of the data according to Bunnett-Olsen,[17] which does not involve any water-activity data, gave linear plots with slope values ϕ (Table 2). The Bunnett-Olsen plots were far less satisfactory and showed a scattering of points at higher acidities, which could only be resolved into straight lines by omitting certain points and considering limited acid concentration ranges. The 'ϕ' values implies that water plays some additional role in the rate-determining step besides behaving as a nucleophile.

Solvent Isotope Effect. The values obtained for the deuterium kinetic solvent effect, k_D/k_H, for the hydrolysis of BBHA are shown in Table 3. The values for hydrolysis in various concentrations of hydrochloric acid lie in the range 2.1—1.16 which is consistent with specific hydrogen ion catalysis.[18] The values in sulfuric acid are all greater than unity and lie in the range 1.62 to 1.19 approaching less than unity at high concentrations of acid. Thus, the magnitude of the solvent isotope effect at a given acid strength reflects the relative importance of the protonation and the hydrolytic N-acyl bond cleavage steps at that acid strength. These values are also consistent with a reaction involving a preequilibrium at lower acidities followed by a rate-determining nucleophilic attack of D_2O or H_2O.

Salt Effects. Table 4 shows the effect of added sodium chloride and perchlorate on the rate of hydrolysis of BBHA. It is seen that both salts assist the rate of hydrolysis, chlorides doing so more than perchlorates. Bunton et al.[12] have shown that the salt effect of anions of low charge density such as ClO_4^- is slightly negative in A-2 acid-catalyzed ester hydrolysis and anions of high charge density such as Cl^- hinder only slightly or assist the hydrolysis. Thus the data in Table 4 suggest that the substrate is undergoing reaction by an A-2 pathway.

Activation Parameters. The various activation parameters are given in Table 5. The entropy (ΔS^*) and enthalpy (ΔH^*) of activation were calculated from the equation $k=(kT/h)\exp(\Delta S^*/R)\exp(-\Delta H^*/RT)$ by a least-square procedure. These values are fairly typical for A-2 reactions.[19]

Mechanism. On the basis of the above results the plausible mechanism (Scheme 1) appears to involve a rapid protonation equilibrium of BBHA followed by a slow reaction of water with the protonated form, leading to the transition complex and subsequent hydrolysis resulting in the fission of N-acyl bond giving benzoic acid and N-benzylhydroxylamine as the products. At the present time there is no direct evidence as to

Table 4. Salt Effects on the Hydrolysis of BBHA in $HClO_4$ at 55°C

$HClO_4$	Added salt	$k_\psi \cdot 10^3/min^{-1}$		
M	M	Nil	Added NaCl	Added $NaClO_4$
1.45	1.00	4.36	5.47	4.51
1.45	2.00	4.36	5.50	4.45
1.45	3.00	4.36	5.86	4.52
2.90	1.00	8.05	8.92	8.20

Table 5. Activation Parameters for Hydrolysis of BBHA

Acid	ΔE	$\Delta H^{\neq}$	$\Delta S^{\neq}$
	kJ mol^{-1}	kJ mol^{-1}	J K^{-1}mol^{-1}
1.45 M H_2SO_4	75.4(45—55)	72.7	−93.8
2.9 M H_2SO_4	74.4(45—65)	71.6	−91.3
6.0 M H_2SO_4	73.7(45—65)	71.0	−91.7
8.0 M H_2SO_4	78.5(45—65)	76.2	−87.3
2.9 M $HClO_4$	78.4(45—55)	76.2	−78.9
2.9 M HCl	77.4(45—65)	74.6	−81.7
6.5 M HCl	77.6(45—65)	74.8	−75.9
9.0 M HCl	78.8(45—65)	76.1	−75.4

Temperature range is indicated in the parentheses.

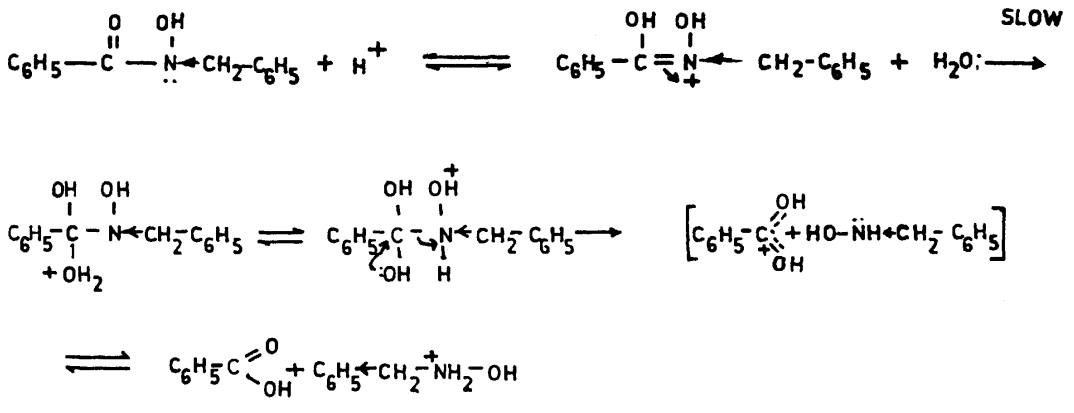

Scheme 1.

whether initial protonation of hydroxamic acid occurs on nitrogen or on oxygen. Protonation studies[20] on *N*-methylhydroxamic acid in concentrated sulfuric acid reveal the presence of both the species. Below 60% (w/w) H_2SO_4 *N*-protonation is preferred and above 60% (w/w) *O*-protonation. Recently, Novak et al.[21] have suggested that for the acid-catalyzed hydrolysis of *N*-hydroxyacetanilides, the protonation of the carbonyl oxygen is favored over the hydroxyl oxygen by ca. 7 orders of magnitude.

One of the authors (KKG) is grateful to CSIR, New Delhi for financial support. We are grateful to Dr. Robin A. Cox, Dr. A. Bagno, and Prof. G. Modena for stimulating correspondence.

References

1) K. K. Ghosh and S. G. Tandon, *Indian J. Chem.*, **23A**, 1004 (1984).

2) K. K. Ghosh and S. G. Tandon, *Bull. Soc. Chim. Belg.*, **91**, 5 (1981).

3) K. K. Ghosh and S. G. Tandon, Proceed. 7th IUPAC Conf. on Phys. Org. Chem., Auckland, New Zealand, August (1984).

4) K. K. Ghosh and S. G. Tandon, Proceed. 8th IUPAC Conf. on Phys. Org. Chem., Tokyo, Japan (1986).

5) K. K. Ghosh, Proceed, 9th IUPAC Conf. on Phys. Org. Chem., Regensburg (F. R. Germany), p. 217, No. p. 82 (1988).

6) C. S. Rao and S. G. Tandon, *Indian J. Chem.*, **14A**, 765 (1976).

7) R. R. Nanewar, Ph. D. Thesis, Ravishankar University, Raipur (1978).

8) K. Yates, *Acc. Chem. Res.*, **4**, 136 (1971); J. T. Edward and S. C. Wong, *J. Am. Chem. Soc.*, **99**, 7224 (1977).

9) C. R. Smith and K. Yates, *J. Am. Chem. Soc.*, **93**, 6578 (1971); R. A. Cox and K. Yates, *Can. J. Chem.*, **59**, 2853 (1981).

10) P. Wan, T. A. Modro, and K. Yates, *Can. J. Chem.*, **58**, 2423 (1980).

11) M. Mashima, F. Ikeda, T. Doi, and S. Nishikawa, *Bull. Chem. Soc. Jpn.*, **54**, 3659 (1981).

12) C. A. Bunton, J. H. Crabtree, and L. Robinson, *J. Am. Chem. Soc.*, **90**, 1258 (1968).

13) L. Zucker and L. P. Hammett, *J. Am. Chem. Soc.*, **61**, 2791 (1939); L. P. Hammett, "Physical Organic Chemistry," McGraw-Hill, New York (1940), pp. 267—277; C. H. Rochester, "Acidity Function," Academic Press, London (1970).

14) K. Yates, J. B. Stevens, and A. R. Katritzky, *Can. J. Chem.*, **42**, 1957 (1964); J. L. Jensen and A. I. Thibeault, *J. Org. Chem.*, **42**, 2168 (1977); S. Geribaldi, A. G. Luciano, P. C. Maria, and M. Azzaro, *J. Chim. Phys. Phys.-Chim. Biol.*, **79**, 103 (1982); M. Liler, "Reaction Mechanisms in Sulfuric Acid," Academic Press, New York (1971), p. 41.

15) J. F. Bunnett and F. P. Olsen, *J. Org. Chem.*, **39**, 1156 (1974).

16) J. F. Bunnett, *J. Am. Chem. Soc.*, **83**, 4956, 4968, 4973, 4978 (1961).

17) J. F. Bunnett and F. P. Olsen, *Can. J. Chem.*, **44**, 1899, 1917 (1966).

18) C. A. Bunton and V. J. Shiner, Jr., *J. Am. Chem. Soc.*, **83**, 3207 (1961).

19) L. L. Schaleger and F. A. Long, "Advances in Physical Organic Chemistry," ed. by V. Gold, Academic Press, London (1963), Vol. 1, p. 24.

20) A. M. Lobo, S. Prabhakar, M. T. C. Fonseca, and A. M. B. Rodriguez, *Tetrahedron Lett.*, **1977**, 3167.

21) M. Novak, G. A. Bonham, L. K. Mohler, and K. M. Peet, *J. Org. Chem.*, **53**, 3903 (1988).

A Time-Resolved CIDEP Study of the Laser Photoreduction of Pyruvic Acid by Lactic Acid

Marjory T. CRAW, M. Catherine DEPEW, Frank J. ADRIAN,† and Jeffrey K. S. WAN*
Department of Chemistry, Queen's University, Kingston, Ontario, K7L 3N6 Canada
(Received July 29, 1988)

In addition to the well-known initial phototriplet polarization, unusual Chemically Induced Dynamic Electron Polarization (CIDEP) behavior in solutions of neat pyruvic acid/lactic acid has been attributed to ST_ Radical Pair Mechanism (RPM) polarization in combination with absorptive initial Triplet Mechamism (TM) polarization and ST_0 RPM polarization. Significant ST_ RPM contributions to such carbon centered radicals with small hyperfine splittings have rarely been observer in solution at room temperature.

Pyruvic acid has been utilized quite extensively in this laboratory in studies of free radical reactions with compounds of biological interest including vitamin C, vitamin E, and several quinones.[1-3] The first demonstration of enhanced absorptive triplet mechanism polarization was evidenced in the photoreduction of pyruvic acid;[1] subsequently photolysis of pyruvic acid in glassy ethanol matrices was utilized to demonstrate the concept of spin conservation in energy transfer processes in randomly oriented matrices.[4]

While the pyruvic acid system was an earlier model in our studies to establish the simultaneous contributions of both the initial Triplet Mechanism and the additional ST_0 Radical Pair mechamism in both CIDEP and CIDNP[1] phenomena, the possible operation of the ST- radical pair polarization had eluded our attention until our recent understanding of this mechanism in a more general, but separate chemical system.[5] (The designations ST- and ST_0 refer to polarizations that arise from the interaction or mixing of the singlet and T- or T_0 triplet energy sublevels of the radical pair during the period of separation of the members of the radical pair in which the energies of the two sublevels are nearly degenerate.) In this report, we show the unusual polarization patterns in a series of photoreduction studies of neat pyruvic acid by lactic acid. The complex CIDEP behavior of these systems is due to the substantial and simultaneous contributions of ST- RPM polarization in addition to the expected ST_0 contributions. The significant ST- contribution in the present pyruvic/lactic acid system is mainly due to the very strong molecular interaction between the pair leading to a very high molecular viscosity.

Experimental

Pyruvic acid, lactic acid, and hexafluoro-2-propanol were obtained from Aldrich. Solution viscosities were measured at 25 °C using a falling ball viscosimeter. The CIDEP experiments were conducted using a modified Varian E3 spectrometer without field modulation, as described previously.[6] The solutions were irradiated in situ with a Lambda Physik EMG101-MSC XeCl excimer laser at 308 nm. The path length of the cell used was 0.8 mm in order to reduce any inner filter effects for light absorption.

† Permanent address: Milton S. Eisenhower Research Center, Applied Physics Laboratory, the Johns Hopkins University, Laurel, Maryland 20707, U. S. A.

Results and Discussion

Photolysis of pyruvic acid/lactic acid solutions results in the initial formation of a pair of identical ketyl radicals as shown below.

$$CH_3COCOOH + CH_3CHOHCOOH \longrightarrow 2\,CH_3\dot{C}OHCOOH$$

The time-resolved CIDEP spectrum of a 1:1 v/v mixture of pyruvic acid (PA), and lactic acid (LA) in 50% ethanol is shown in Fig. 1a. There is very good agreement between the experimental spectrum and a spectrum simulated for 40% TM and 60% ST_0 polariza-

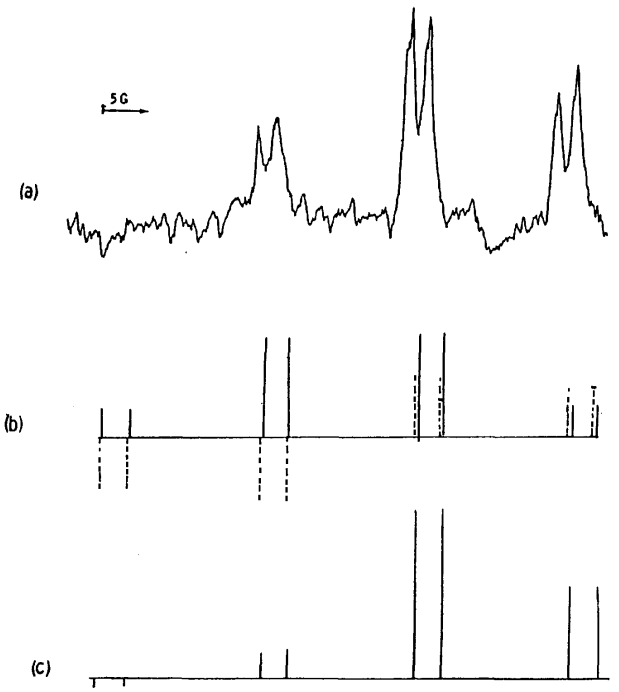

Fig. 1. (a) Time-resolved magnetic resonance spectrum of pyruvate radicals formed following photolysis of a 1:1 v/v PA/LA mixture in 50% ethanol. (b) Expected intensity distribution and phase of TM (——) polarization and ST_0 (----) (right shifted for observation). (c) Simulated CIDEP spectrum for 40% TM and 60% ST_0 radical pair mechanism polarization.

tion (Fig. 1b and 1c).

However, when neat solutions of PA and LA are mixed the resulting solution appears to have a substantially increased viscosity and the relative intensity distribution and phase of the hyperfine lines in the CIDEP spectrum of the ketyl radical changes rather dramatically. Figure 2a—c represents typical spectra observed for neat PA/LA mixtures as a function of relative concentrations of each component, measured at 3 μs after the laser flash. These spectra show that as the pyruvic acid concentration increases the LF/HF ratio also becomes larger and more negative, thus suggesting some additional contribution from ST– mixing.

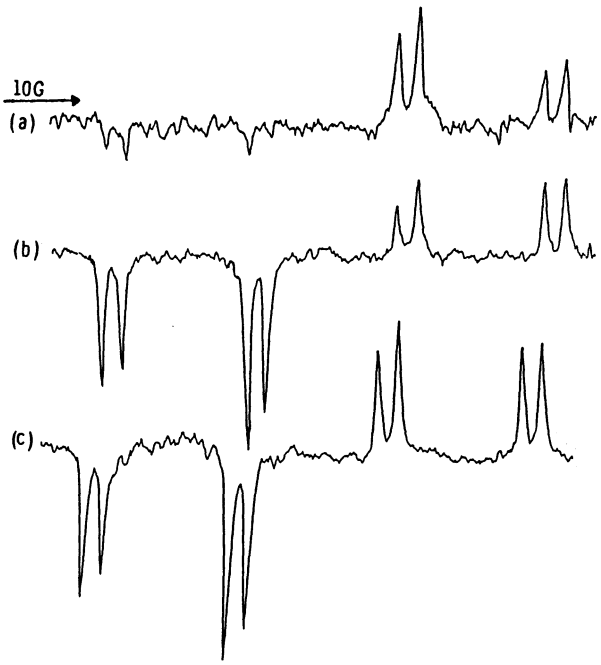

Fig. 2. The time-resolved (3 μs) CIDEP spectra recorded at 25 °C for: (a) 1 : 2 v/v mixture of pyruvic acid/lactic acid, (b) 1 : 1 v/v mixture of pyruvic acid/lactic acid, (c) 2 : 1 v/v mixture of pyruvic acid/lactic acid.

While several examples of a rather large hyperfine induced ST– contributions to polarization spectra have been published,[5,8] the development of "viscosity" induced ST– polarization has not been well-characterized. The CIDEP spectra of 1 : 1 v/v PA/LA at varying temperatures as shown in Fig. 3a—c clearly exhibit a dramatic temperature effect. At 25 °C the relative ratios of the LF/HF lines indicate the presence of an ST– contribution to the observed polarization spectrum. On lowering the temperature the relative intensity of the high field lines diminishes until at −15 °C the phase of these hyperfine lines changes entirely to emission. These observations are consistent with an increase in the ST– contribution to the CIDEP spectrum as the molecular viscosity of the system increases.

Additional insight into the effects of viscosity on this system was obtained by examining the effects of a variety of solvents with a wide range of viscosities from glycerol/water mixtures to nonviscous solvents such as ethanol, hexafluoro-2-propanol, benzene, and formic acid. In neat 1 : 1 v/v mixtures of PA/LA and in solutions containing 50% ethanol or glycerol/water mixtures the viscosity of each solution was measured at 30 °C, ranging from 13 cP (1P=0.1 Pa s) for a solution of 50% ethanol/PA/LA to 73 cP for neat PA/LA system, to 580 cP for a 1 : 1 mixture of PA/LA and glycerol. The time-resolved CIDEP spectra observed

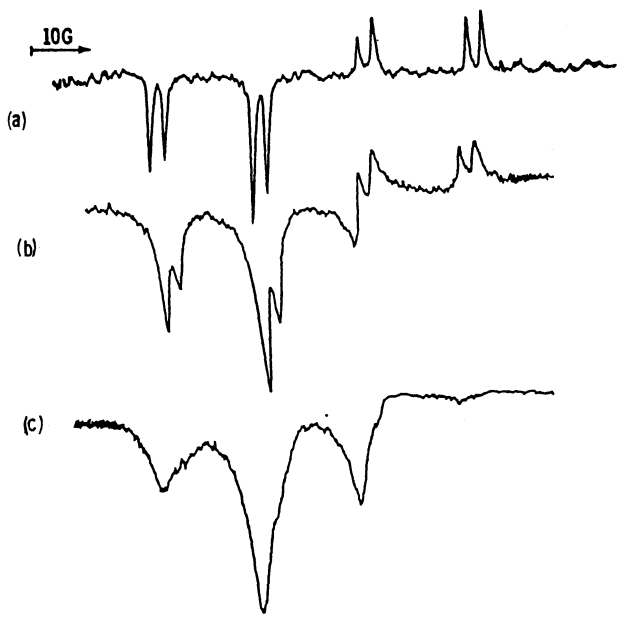

Fig. 3. The CIDEP spectra for a 1 : 1 v/v mixture of pyruvic acid/lactic acid at (a) 25 °C, (b) −2 °C, (c) −15 °C.

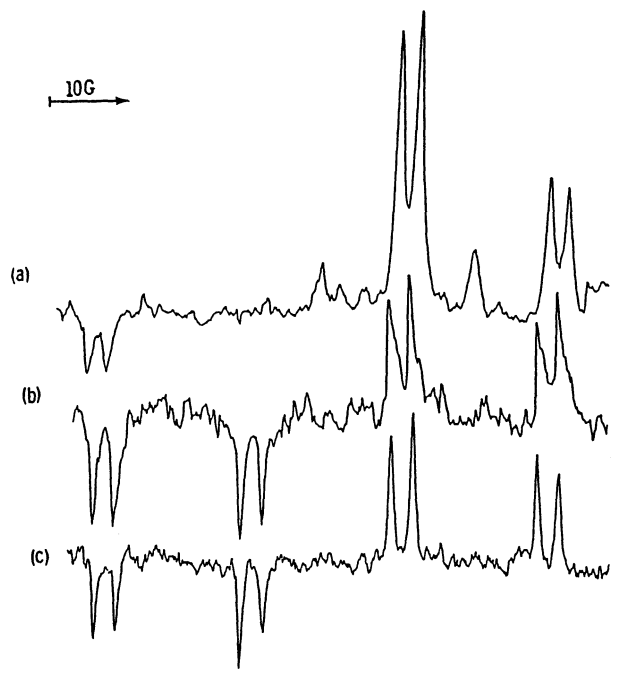

Fig. 4. The time-resolved (3 μs) CIDEP spectra for 1 : 1 PA/LA in 50%. (a) Glycerol, (b) hexafluoroisopropanol, (c) benzene.

for pyruvate radicals under various solvent conditions are shown in Fig. 2a—c. There is no apparent direct correlation between solvent viscosity and the development of ST- polarization for pyruvate radicals, since the most viscous solvent-glycerol-resulted in less ST- contribution than benzene or hexafluoro-2-propanol, or neat PA/LA itself (Fig. 3a).

Pyruvic acid molecules under certain circumstances may dimerize or trimerize, presumably through their carboxyl moieties.[9] This unique property of pyruvic acid may lead to a strong interaction between it and its reduced form, lactic acid. Such a strong molecular interaction may occur both in the ground state and in the radical pair state. Thus ST- mixing may be enhanced when the residence time of an initially formed radical pair in the level crossing region is increased according to[11]

$$\rho_{ST-} = (\pi A^2/4g\,\mu_B{}^H)\,(r_c/2\lambda D) \quad (1)$$

where A is the difference in hyperfine frequencies of the pair and D is the diffusion coefficient. We have used the Smoluchowski equation and the previously published rate constants for the disproportionation of pyruvate radicals in various solvents[7] to calculate D as a function of viscosity,

$$K = 4\pi\sigma\rho DN/1000 \quad (2)$$

where $K=1/2$ the termination rate constant, σ the spin statistical factor for free radical reaction, N is Avogadro's number and ρ the distance of closest approach estimated to be in the region of 6 Å.

The data are presented in Table 1; the assumptions made here suggest that D for pyruvate radicals in $2-4\times10^{-6}$ M pyruvic acid (1 M=1 mol dm^{-3}) in ethanol (viscosity 1.2 cP) is aproximately 10E−5 cm^{2}s^{-1}, not unreasonable for organic radicals in solution.[12] As the viscosity is increased the diffusion of the radicals in a pair would be expected to be very restricted leading to a significant contribution of ST- polarization. While a qualitative analysis suggests that the ST- mechanism becomes more important as the viscosity is increased in a particular solvent, several of the experimentally observed spectra indicate that viscosity arguments alone cannot account for the magnitude of the ST- polarization contributions in defferent solvents. Clearly in solvents such as glycerol and glycerol/water systems the CIDEP spectrum shows contributions from ST_0, TM, and ST- polarizations. However, while the development of ST- polarization for C centered radicals has been observed previously at low temperature[13] and in systems where the solvent viscosity was high,[14] in both cases the ratio of ST-/ST_0 polarization was relatively small.

Table 1. Estimated Diffusion Coefficients for Pyruvate Radicals as a Function of Solvent Viscosity[7]

Solvent	D	Viscosity
	cm^{2}s^{-1}	cP
Ethanol	1.5×10^{-5}	1.2
2-Propanol	7.05×10^{-6}	2.3
1-Butanol	4.23×10^{-6}	3.9
2-Methyl-1-propanol	4.75×10^{-6}	3.9
Benzyl alcohol	4.4×10^{-6}	4.1

As mentioned above pyruvic acid is known to form a polymeric structure, dimer or trimer, in nonpolar solvents.[15] This dimer presumably arises via a hydrogen bonding type of interaction similar to that previously reported for acetic acid.[9] Therefore, it is not surprising that solvent interactions that affect this hydrogen bonding should result in changes in the observed time-resolved spectra. Pyruvic acid has a pK_a of 2.39, while that for lactic acid is 3.83,[16] therefore when ethanol, pK_a=10, is added to a PA/LA acid, it is possible that the concentrations of the protonated forms of the acids are reduced which may limit the extent of such a hydrogen bonding interaction. Comparing the spectra for PA/LA in 50% ethanol with those observed for PA/LA in 50% formic acid and for PA/LA/50% $(CF_3)_2COH$ in which the viscosities of the solutions are similar, a much larger contribution from ST- polarization is found in both of the latter cases. Both $(CF_3)_2CHOH$ have pK_a values in the region of 4—6,[16] therefore in these systems the hydrogen bonding interaction may still be significant, as a result of the acidity of the solvent. This may be further substantiated by the PA/ethyl lactate experiments in which the apparent ST- contribution decreases markedly when the acid functionality of LA is esterified.

When glycerol is used as solvent, the viscosity of the system increases but pK_a for glycerol is $\simeq$14.[16] Therefore the contribution of ST- polarization predicted on the basis of viscosity comparisons may be somewhat lower than expected since in this solvent system the extent of hydrogen bonding and thus the degree of "internal" restricted diffusion may itself be reduced as a result of deprotonation of the acid functionalities. Furthermore, the observed substantial ST- polarization in benzene solutions are consistent with the reduced deffusion expected as a result of the known preference of PA to exist in a polymeric structure in this nonpolar solvent.[15] Also the observed increase in the relative contribution of ST- mixing with increasing concentrations of pyruvic acid is consistent with an increase in the extent of association of pyruvic acid molecules as the concentration relative to LA is increased.

Obviously the complexity of both the physicochemical interactions between the reagants and the solvents in this system and the presence of three contributing polarization mechanisms does not render

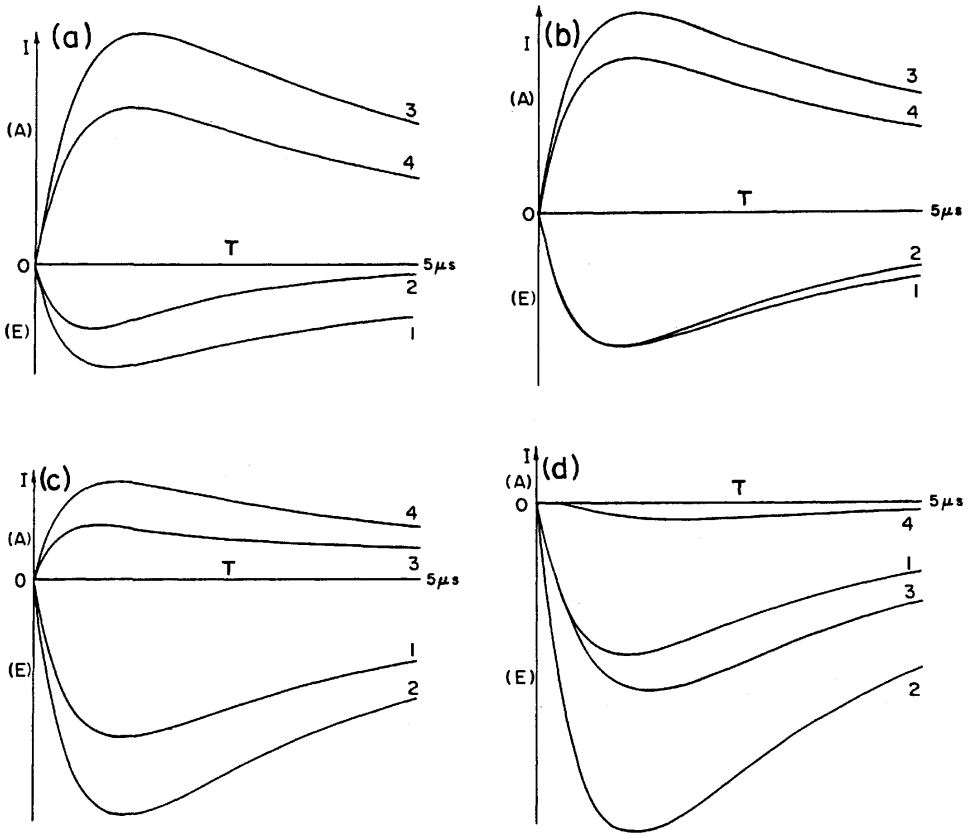

Fig. 5. The calculated line intensities and phases for RPM polarization of pyruvate ketyl radical at various values of D.
(a) $D=10^{-5}$ cm^2s^{-1}, $\rho_{ST_0}=0.033$, $\rho_{ST-}=10^{-4}$, (b) $D=10^{-6}$ cm^2s^{-1}, $\rho_{ST_0}=0.063$, $\rho_{ST-}=10^{-3}$, (c) $D=10^{-7}$ cm^2s^{-1}, $\rho_{ST_0}=0.103$, $\rho_{ST-}=0.01$, (d) $D=10^{-8}$ cm^2s^{-1}, $\rho_{ST_0}=0.151$, $\rho_{ST-}=0.1$.

quantitative examination possible. However an analysis of the variation of the relative hyperfine line intensities and phases with decreasing deffusion between the members of the radical pair which contributes differing relative ST_0 and ST- components to the expected polarization shows some interesting results. Computer simulation of the effects of decreasing D from 10^{-5} to 10^{-8} cm^2s^{-1} is shown in Fig. 5. The relative probabilities of ST_0 to ST- mixing (ρ_{SY_0}/ρ_{ST-}) vary from 330 to 1.5 on going from Fig. 5a to 5d. It is interesting to note the close correlation of line intensity changes with decreasing D value expected in several of the experimental situations; for example, in 50% ethanol the time-resolved spectrum (Fig. 1a) is consistent with the pattern predicted in 5a (with an additional absorptive contribution due to the TM), while in 1 : 2 PA/LA (Fig. 2a) the pattern is quite similar to that shown in 5b. The line intensity changes exhibited in Fig. 3a—c as a result of decreased diffusion due to lowering of the temperature are in good agreement with the changes predicted in Fig. 5c and d.

Finally it is interesting to note the biological role of pyruvic acid and the environment that these molecules exist in in vivo, which can also be studied by CIDEP. We hope to extend this study to other systems in which the possibility of molecular interactions influencing the development of CIDEP may be of importance.

References

1) K. Y. Choo and J. K. S. Wan, *J. Am. Chem. Soc.*, **97**, 7127 (1975).
2) M. C. Depew, B. B. Adeleke, and J. K. S. Wan, *Can. J. Chem.*, **59**, 2708 (1981).
3) J. K. S. Wan, *J. Photochem.*, **17**, 517 (1981).
4) D. Weir and J. K. S. Wan, *J. Am. Chem. Soc.*, **106**, 427 (1984); K. Obi and T. Imamura, *Rev. Chem. Intermed.*, **7**, 225 (1986).
5) T. J. Burkey, J. Lusztyk, K. U. Ingold, J. K. S. Wan, and F. J. Adrian, *J. Phys. Chem.*, **89**, 4268 (1985).
6) J. W. DeBoer, T. Y. C. Chan Chung, and J. K. S. Wan, *Can. J. Chem.*, **59**, 2708 (1981); E. Kam, M. T. Craw, M. C. Depew, and J. K. S. Wan, *J. Mag. Reson.*, **67**, 556 (1986).
7) P. B. Ayscough and R. C. Sealy, *J. Chem. Soc., Perkin Trans. 2*, **1973**, 543.
8) K. Akiyama, private communication.
9) R. W. Taft and M. J. Kamlet, *J. Chem. Soc., Perkin Trans. 2*, **1979**, 1723.
10) S. Yamauchi, K. Tominaga, and N. Hirota, *J. Phys. Chem.*, **90**, 236 (1986).
11) F. J. Adrian and L. Monchick, *J. Chem. Phys.*, **71**, 2600 (1979).

12) T. J. Burkey, D. Griller, D. A. Lindsey, and J. C. Scaiano, *J. Am. Chem. Soc.*, **106**, 1983 (1984).
13) C. D. Buckley and K. A. McLauchlan, *Chem. Phys. Lett.*, **137**, 86 (1987).
14) A. D. Trifunac, D. J. Nelson, and C. Mottley, *J. Magn. Res.*, **30**, 263 (1978).
15) P. A. Leermakers and G. F. Vesley, *J. Am. Chem. Soc.*, **85**, 3776 (1963).
16) R. Stewart, "The Proton: Applications to Organic Chemistry," Academic Press, Inc., New York (1984), Vol. 46, Chap. 2; P. Ballinger and F. A. Long, *J. Am. Chem. Soc.*, **82**, 795 (1960); "Ionization Constants of Organic Acids in Aqueous Solutions–IUPAC–," Pergammon Press, IUPAC (1979), Vol. 23, pp. 41, 45.
17) C. D. Buckley, D. A. Hunter, P. J. Hore, and K. A. MacLauchlan, *Chem. Phys. Lett.*, **135**, 307 (1987).

 © 1989 The Chemical Society of Japan Bull. Chem. Soc. Jpn., 62, 1313—1315 (1989)

Direct Determination of the Intermolecular Potential for Krypton

Ali BOUSHEHRI* and Jalil Moghadasi ABSARDI
Department of Chemistry, Shiraz University, Shiraz, Iran
(Received September 16, 1988)

In recent years a procedure has been developed for determining potential energy functions directly from measurements of gaseous transport properties, without assuming any particular functional form for the interaction potential. Previous applications of this procedure have required that the potential well depth be known independently. It is shown that this requirement is not necessary, and that the entire potential can be directly obtained with reasonable accuracy from the accurate viscosity data presently avilable. The interaction potential discussed is that for the inert gases.

Many attempts have been made to obtain the forces between molecules, as they are important in determining the physical and chemical properties of matter. Without direct ways of measuring the interaction potential energy function, it has become customary to postulate a parameterized functional form and adjust the parameters for best agreement between the calculated and experimental results. A method for accurately determining the potential energy function for the inert gases by fitting a number of measured quantities has been developed.[1] Here, we reexamine the problem of determining the potential energy function directly from measurements of a single property.

Our method for determining the neutral-neutral interaction potential is based on the method developed by Smith and others[2-6] and recently tested by Boushehri[7,8] in connection with the Extended Law of Corresponding State.[9] Previous applications of this inversion procedure required independent knowledge of the well depth ε. In this work the method used by Boushehri et al.,[10] to determine ε from viscosity data is adapted, so that the value of ε can be obtained from gas viscosities measurements alone. Here we use a unified formulation of viscosity, the ratio η/η_0 of the viscosity η to its value η_0 in the limit of zero temperature. This ratio first rises with increasing temperature to a maximum and then decreases, and the heigth of this maximum can be used to determine the well depth, and a method for its determination using the rate of iteration is described.

Recently a knowledge of the vibrational energy levels has been used to obtain the width of the potential energy well as a function of its depth, and that may be used to determine the shape of the internuclear potential energy function.[11] Lee and his co-workers have been able to obtain potential-energy functions for the inert gases from high-resolution measurements of the differential cross sections.[12] It is unlikely, other than for the simplest molecules, that an accurate potential can be developed from spectroscopic and high-resolution scattering cross section measurements. The method discussed in this paper is an attempt to estimate this quantity purely from viscosity data, which would be considered extremely valuable for substanes where other sources of data are unavailable.

The Kinetic Theory

Our starting point is the well-known equation[13] for the viscosity of an atomic gas

$$\eta = \frac{26.9654(MT)^{1/2} f_\eta^{(3)}}{r_m^2 \Omega^{(2,2)^*}(T^*)} \tag{1}$$

where $T^*=KT/\varepsilon$ and where η is measured in micropoise. The function $f_\eta^{(3)}$, which is nearly unity, and the quantity $\Omega^{(2,2)^*}(T^*)$ are functionals of the potential energy function. It is convenient to write viscosity in a different form. To do this we note that at low temperatures the interactions are dominated by an r^{-6} attractive term. Since $V \simeq C_6\, r^{-6}$, $\Omega^{(2,2)^*}$ takes on the form.[14]

$$\Omega^{(2,2)^*} \rightarrow 1.1943\,(C_6/K_B T)^{1/3}/r_m^2 \tag{2}$$

we can then introduce the viscosity limit η_0 defined by[15]

$$\eta_0 = 22.3903\,(MT)^{1/2}/(C_6/K_B T)^{1/2} \tag{3}$$

and rewrite Eq. 1 as

$$\eta/\eta_0 = 0.85167\, C_6^{1/3}\, \eta/M^{1/2}T^{5/6} \tag{4}$$

where η is in micropoise and C_6 is in atomic units.

We are now in a position to consider Eq. 4 as a unified formulation of the viscosity for all gases. The estimate of well depth is obtained conveniently from the observation of the maximum η/η_0 only.

Inversion Procedure

The experimental collision integral may be used to define the intermolecular potential energy function from which they arise, $V(r)$. A separation distance r_0, for a given temperature, may be defined such that

$$\overline{\Omega}^{(2,2)} = \pi r_0^2 \tag{5}$$

where r_0 represents the collision diameter for hard-sphere molecules which would have the same viscosity as the real molecule and where $\overline{\Omega}^{(2,2)}/\pi r_m^2 = \Omega^{(2,2)^*}$. The potential $V(r_0)$ is given by the relation.

$$V(r_0) = G\, K_B T \tag{6}$$

where G is a temperature dependent function that may be calculated using a model system whose intermolec-

ular potential energy function is known. This process may be repeated to refine the $G(T^*)$ values and hence to obtain an improved $V(r)$ that precisely represent the intermolecular potential energy function. Thus knowing the well depth, the values of viscosity as a function of T can be converted to the potential V as a function of r_0.

In order to obtain a collision integral $\Omega(2,2)$, three successive numerical integrations are needed. Estimation of the triple integral is made by employment of Gatland version of the Computer Program developed by O'Hara and Smith.[16]

To establish the value of the well depth, one may carry out a search procedure. That is, at each stage in the iteration process the values η/η_0 are back calculated from the improved $V(r)$ using an assumed well depth. Several iteration may be used until agreement with the previous iteration is achieved. For findig $V(r)$ directly from measurement of viscosity, one may estimate an initial value of the well depth ε. This estimate value of well depth is obtained conveniently from the observation of the maximum η/η_0, if the maximum η/η_0 is too large, the estimated ε needs to be increased and vice versa, so that a different value of ε is chosen, and the process repeated until agreement with experiment is reached.

In summary, values of collision integral $\Omega(2,2)$ must be obtained from Eq. 1 using highly accurate data. Three interation may be used, if agreement with the previous iteration is not achieved, then a different value of ε is chosen and the process repeated until agreement with experiment is reached. An inital value

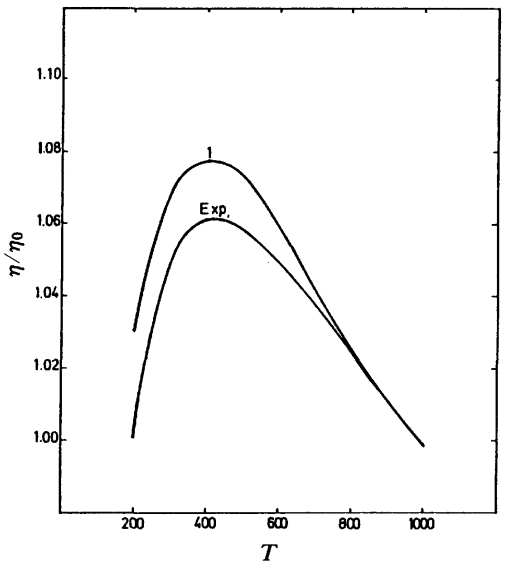

Fig. 1. The ratio η/η_0 as a function of T. Values of η/η_0 in the range $140<T<200$ and $1000<T<2000$ have been omitted for the sake of clarity. The lower curve (Exp.) represents the smoothed viscosity data (Ref. 19). The other curve 1 assuming a well depth $\varepsilon/k=184$. The results in 2nd iteration are nearly identical with those obtained in the first iteration, and are therefore not shown separately.

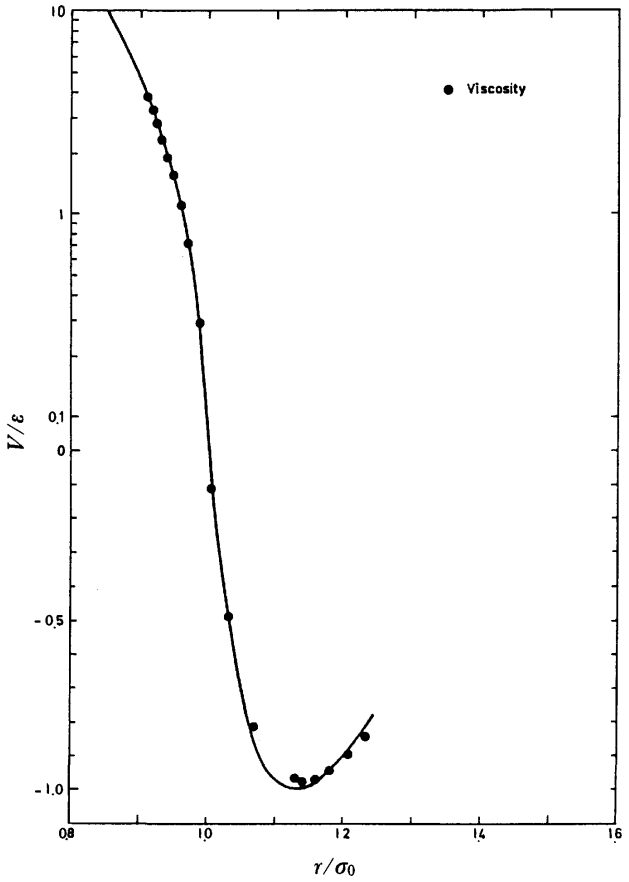

Fig. 2. Reduced pair potential obtained by direct inversion based on the smoothed viscosity data compiled by Smith for krypton (●), $\varepsilon/k=184$ K. Also shown for comparison is a typical curve obtained primarily from thermal scattering data (Kr-Kr, Ref. 18), $\varepsilon/k=198$ K. Note that the scale changes from linear to logrithm at $V/\varepsilon=0.1$.

for the well depth $\varepsilon/k=184$ K is used. The inversion function from Ref. 17 used for an initial estimate of $G(T^*)$. Following the inversion procedure, we obtain calculated values (η/η_0, T) shown as curve 1 in Fig. 1 and compared with the "Smoothed" data shown as Exp. The difference between maximum values, η/η_0 of the two curves is about 1.5%. The (η/η_0, T) values in second iteration are virtually indistinguishable from curve 1 in Fig. 1 and hence is not shown. Thus three steps may be followed in the inversion scheme:

1) Two iteration may be performed to find $V(r)$ for a given ε and a given set of highly accurate data.

2) If the calculated and experimental (η/η_0, T) does not agree within some limit then estimated ε needs to be increased for large value of η/η_0 and vice versa.

3) Return to step 1 and continue until the correct value of ε is obtained.

These three steps should provide a useful technique for the determination of ε values for substances where other source of data are unavailable.

It is of interest to note that the potential obtained for Krypton when plotted in reduced form, using σ and ε/k

determined in this work, is in good agreement with Lee Potential[18] (see Fig. 2).

Conclusion

The present work indicates an application of the concept in Ref. 10 to the smoothed viscosity data. Other than the simplest molecules, it is unlikely to obtain accurate well depth from spectroscopic measurements. The availability of highly accurate viscosity data over a reasonable range of temperature opens up the possibility of obtaining the well depth ε from measure of this single property without the use of additional experimental information or assumption of any mathematical form for the interaction energy function. This method would be considered extremely valuable for substances where other sources of data are unavailable.

We are thankful to Shiraz University Research Council for the support of this work through Grant No. 58-AS-276-256.

References

1) E. B. Smith, *Physica*, **73**, 211 (1974).
2) D. W. Gough, G. C. Maitland, and E. B. Smith, *Mol. Phys.*, **24**, 151 (1972).
3) D. W. Gough, E. B. Smith, and G. C. Maitland, *Mol. Phys.*, **25**, 1433 (1973).
4) P. Clancy and M. Rigby, *Mol. Phys.*, **29**, 1035 (1975).
5) P. Clancy, D. W. Gough, G. Matthews, E. B. Smith, and G. C. Maitland, *Mol. Phys.*, **30**, 1397 (1975).
6) L. A. Viehland, M. M. Harrington, and E. A. Mason, *Chem. Phys.*, **17**, 433 (1976).
7) A. Boushehri, L. A. Viehland, and E. A. Mason, *Physica*, **91A**, 424 (1978).
8) A. Boushehri, *Physica*, **97A**, 206 (1979).
9) J. Kestin, S. T. Ro, and W. A. Wakeham, *Physica (Utrecht)*, **58**, 165 (1972).
10) A. Boushehri, L. A. Viehland, and E. A. Mason, *Chem. Phys.*, **28**, 313 (1978).
11) G. C. Maitland and E. B. Smith, *Mol. Phys.*, **22**, 861 (1971).
12) P. E. Siska, J. M. Parson, T. P. Schafew, and Y. T. Lee, *J. Chem. Phys.*, **55**, 5762 (1971).
13) J. O. Hirschfelder, C. F. Curtiss, and R. B. Bird, "Molecular Theory of Gases and Liquids," Wiley, New York (1964), Chap. 8.
14) L. D. Higgins and F. J. Smith, *Mol. Phys.*, **14**, 399 (1968).
15) E. A. Mason, *J. Chem. Phys.*, **22**, 169 (1954).
16) H. O'Hara and F. J. Smith, *J. Comput. Phys.*, **5**, 328 (1970); *Comput. Phys. Commun.*, **2**, 47 (1971).
17) P. Clancy, D. W. Gough, G. P. Matthews, E. B. Smith, and G. C. Maitland, *Mol. Phys.*, **30**, 1397 (1975).
18) J. M. Farra, T. P. Schafer, and Y. T. Lee, in, Transport Phenomena-1973, J. Kestin, ed., AIP Conf. Proc. **11**, 279 (1973).
19) G. C. Maitland and E. B. Smith, *J. Chem. Eng. Data*, **17**, 150 (1972).

4-(2-Quinolylazo)phenol as a Spectrophotometric Reagent for Palladium(II), Osmium(VIII), and Gold(III)

Ishwar SINGH,* Pratap Singh KADYAN, B. S. GARG,† and Sudarsan BARUA†,††
Department of Chemistry, M. D. University, Rohtak 124001, India
†Department of Chemistry, University of Delhi, Delhi 110007, India
(Received May 26, 1988)

Reaction behavior of 4-(2-quinolylazo)phenol (*p*-QAP) is established with three noble metals, i.e. palladium(II), osmium(VIII), and gold(III), under various conditions. Palladium(II) forms a 1:1 greenish violet complex at pH 8—10 (absorption maximum at 580 nm), while osmium(VIII) forms a 1:1 violet compex at pH 8—9.5 (absorption maximum at 550 nm) with the ethanolic solution of *p*-QAP. Color reaction with gold(III) with ethanolic solution of *p*-QAP is instantaneous, but fades away with time. However, a 4:4:2 mixture of water, ethanol, and cyclohexanol stabilizes this color for 45 min. Thus a 1:1 red gold(III) complex formed at pH 8—9.5 absorbs maximum at 550 nm. The Sandell's sensitivities (ng cm^{-2}) of the color reactions are 2.7, 3.9, and 9.8 with palladium(II), osmium(VIII), and gold(III) respectively. Other physicochemical characteristics of the complexes are established. A number of foreign ions tested for their interferences and use of masking agents wherever necessaty it tabulated. Synthetic solutions identical in composition to some palladium(II) and gold(III) alloys are estimated to ascertain the suitability of the reagent.

4-(2-Quinolylazo)phenol (*p*-QAP) was used as an analytical reagent for copper in blood serum[1] and in milk;[2] and for silver[3] and the silver-(*p*-QAP) complex for the indirect determination of iodide.[3] This reagent showed further good analytical potentialities against the micro determination of some other noble metals. Whereas, a very limited number of heterocyclic azo dyes find their uses for the determination of noble metals,[4-19] comparatively this reagent has been found a potential reagent for palladium(II), osmiun(VIII), and gold(III).

Experimental

Apparatus. A Unicam SP 600 spectrophotometer with matched 10-mm glass cells was used for recording the spectra. A Beckman Expandomatic SS-2 pH meter was used for the pH adjustments.

Reagents. *p*-QAP Solution. *p*-QAP was synthesized[1,3] as described earlier, and used as a 1×10^{-3} mol·cm^{-3} solution prepared by dissolving 0.249 g in 1 dm^3 of ethanol. The dark red solid (*p*-QAP) synthesized was quite stable for several months however, *p*-QAP solution more than a week old were discarded, as the older soutions gave slightly less absorbances with metal ions in comparison to freshly prepared solutions.

Palladium(II) Solution. A stock solution of palladium(II) was prepared by dissolving appropriate amount of palladium chloride (Johnson and Mathey, U.K.) in 2 mol·cm^{-3} hydrochloric acid. The solution was standardized gravimetrically with dimethylglyoxime.[20]

Osmium(VIII) Solution. A 1-g ampoule of osmium tetraoxide (Johnson and Mathey, U.K.) was broken beneath the surface of about 100 ml of normal sodium hydroxide solution, contained in a glass-stoppered flask, as described by Ayres and Wells.[21] The orange-red solution was washed into a one litre volumetric flask and made upto volume with doubly distilled water. The solution was standardized iodometrically by the method of Klobbie.[22]

Gold(III) Solution. A stock solution of gold(III) was prepared by dissolving appropriate amount of gold(III) chloride (Johnson and Mathey, U.K.) in doubly distilled water. The solution was 1 mol·dm^{-3} with respect to hydrochloric acid. The solution was standardized iodometrically.[23]

All other reagents were of analytical grade and doubly distilled water was used throughout.

Determination of Palladium(II). To a suitable volume of sample containing 4.7—25.7 μg of palladium(II) add 2 ml of 1×10^{-3} mol·dm^{-3} *p*-QAP solution followed by 1 ml of borate/HCl buffer. Dilute to 10 ml with water and ethanol keeping 50% (v/v) ethanol concentration. Heat on a boiling water bath for 5 min, cool and add ethanol to compensate the loss of volume on heating. Measure the absorbance at 580 nm against a corresponding reagent blank prepared under identical conditions.

Determination of Osmium(VIII). To a suitable volume of sample containing 7.9—32.4 μg of osmium(VIII) add 1 ml of 1 mol·dm^{-3} sodium acetate solution and 2 ml of 1×10^{-3} mol·dm^{-3} *p*-QAP. Raise the volume to 10 ml keeping 50% (v/v) ethanol concentration. Measure the absorbance at 550 nm against a reagent blank and deduce the amount of osmium(VIII) present from the calibration curve.

Determination of Gold(III). To a suitable volume of sample containing 17.4—58.9 μg of gold(III) add 3 ml of 1×10^{-3} mol·dm^{-3} *p*-QAP solution. Add 2 ml of cyclohexanol and 1 ml of aqueous solution 0.05 mol·dm^{-3} $Na_2B_4O_7$. Dilute to 10 ml with water and ethanol, adjusting water, ethanol and cyclohexanol in the ratio 4:4:2(v/v) in the final solution. Measure the absorbance of the solution at 550 nm against a corresponding reagent blank.

Results and Discussion

Among platinum metals, palladium is the easiest to determine and a number of organic reagents are known. Heterocyclic azo dyes are an important class of sensitive reagents for palladium. But very few are known for other noble metals. 4-(2-Quinolylazo)-phenol forms a greenish violet complex with palladium at higher pH's. Full colour development takes place when the mixture is heated on a boiling water bath for about 5 min. Under the appropriate condi-

†† Presently with Cotton College, Gauhati (Assam) India.

Table 1. Physicochemical Characteristics of the Metal-*p*-QAP Complexes

Characteristic	Pd(II)-*p*-QAP comlex	Os(VIII)-*p*-QAP complex	Au(III)-*p*-QAP complex
λ_{max}/nm	580	550	550
pH range	8.0—10.0	8.0—9.5	8.0—9.5
Reagent required for full complexation (mol)	4	4	5
Beer's law range (ppm)	0.0—2.75	0.0—3.80	0.0—6.30
Optimum concentration range (ppm)	0.47—2.57	0.79—3.24	1.74—5.89
Sandell's sensitivity ($\mu g \cdot cm^{-2}$)	0.0027	0.0039	0.0098
Molar absorptivity (ε) ($l \cdot mol^{-1} \cdot cm^{-1}$)	3.98×10^4	4.9×10^4	2.0×10^4
Composition(M : L) by job's method	1 : 1	1 : 1	1 : 1

tions found for palladium(II), complexes of zinc, cadmium, mercury, cobalt, and gold decompose and therefore can be tolerated in varying amounts. Platinum metals, except osmium, do not form complexes and thus 50-fold of each are tolerated. A fair amount of EDTA does not interfere and has been used to mask many common metals. On the other hand, *p*-QAP forms violet complex with osmium(VIII) in alkaline medium and no warming is required for the color development. However formation of this complex can be obviated by nitrite and thus palladium can be determined selectively. However palladium(II) interferes in the determination of osmium(VIII).

Preliminary investigations on the colour reaction of gold(III) with ethanolic solution of *p*-QAP showed instantaneous red colour formation at higher pH's. The color, however, fades away with time. To stabilise the colour developed different solvents, singly of their mixtures have been tried and found that a mixture of water, ethanol and cyclohexanol in the ratio 4 : 4 : 2 can be used conveniently since the complex has maximum absorbance and is quite stable for 45 min. The effect of different solvents on the stability of gold(III)-*p*-QAP complex with time has been shown in Fig. 1.

Physicochemical Characteristics. In Fig. 2 are the spectra recorded for the complexes of *p*-QAP with the three metals. The optimum conditions and other physicochemical constants established for the complexes have been given in Table 1.

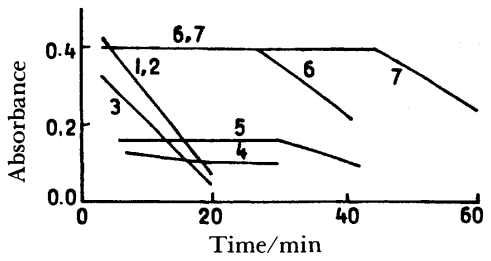

Fig. 1. Effect of different solvents on the stability of Au(III)-(*p*-QAP) complex with time (curves 1 and 2, 50% ethanol and 50% dioxane; 3, 50% DMF; 4, DMF : BuOH : water=5 : 2 : 3; 5, DMF : *c*-$C_6H_{11}OH$: BuOH : water=5 : 1 : 1 : 3; 6, ethanol : *c*-$C_6H_{11}OH$: water=5 : 1 : 4 and 7, ethanol : *c*-$C_6H_{11}OH$: water=4 : 2 : 4).

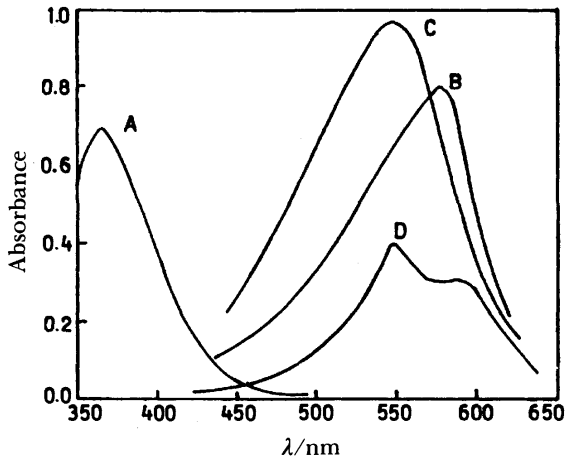

Fig. 2. Absorption spectra of *p*-QAP and its metal complexes at pH 8.0(A) 2.5×10^{-5} mol dm^{-3} *p*-QAP in 50% ethanol (v/v), (B) 2×10^{-5} mol dm^{-3} Pd(II)+1×10^{-4} mol dm^{-3} *p*-QAP[in 50% ethanol (v/v)], (C) 2×10^{-5} mol dm^{-3} Os(VIII)+1×10^{-4} mol dm^{-3} *p*-QAP[in 50% ethanol (v/v)], (D) 2×10^{-5}mol dm^{-3} Au(III)+1×10^{-4} mol dm^{-3} *p*-QAP(in ethanol: water : cyclohexanol=4 : 4 : 2).

Comparison of Sensitivities of the Methods. However many classes of organic spectrophotometric reagents, like oximes, nitroso compounds, hydrazones, reagents containing sulfur as ligand atom, are known for palladium, a number of heterocyclic azo dyes have also been suggested as sensitive reagents for this metal. Sensitivity index[8] 'ϕ' (defined as number of micrograms of an element, present as the absorbing species, in a column of solution of 1 cm^2 cross section giving an absorbance of 0.001 at a specified wavelength) of some important heterocyclic azo dyes are: 1-(2-pyridylazo)-2-naphthol[9] (0.0075 at 678 nm), 4-(2-pyridylazo)resorcinol[10] (0.0057 at 440 nm and 0.012 at 630 nm), 4-(2-thiazolylazo)resorcinol[11] (0.013 at 650 nm), 5-(ethylamino)-2-(2-pyridylazo)-*p*-cresol[12] (0.0039 at 520 nm), 3-(2-thiazolylazo)-2,6-diaminopyridine[13] (0.0077 at 665 nm) and 4-(2-thiazolylazo)-1,3-benzenediamine[14] (0.002 at 585 nm). The present method has the sensitivity index of 0.0027 μg Pd(II)/cm^2 at 580 nm.

A very few heterocyclic azo dyes are known as reagents for gold and osmium. 4-(2-Thiazolylazo)-resorcinol[19] forms a red colored complex with gold-

Table 2. Tolerance Limits of the Foreign Ions in the Determination of the Metal Ions

Foreign ion	For 2.13 $\mu g\,ml^{-1}$ of Pd(II)		For 1.90 $\mu g\,ml^{-1}$ of Os(VIII)		For 3.98 $\mu g\,ml^{-1}$ of Au(III)	
	Toleranse limits /$\mu g\,ml^{-1}$	Masking agent	Tolerance limits /$\mu g\,ml^{-1}$	Masking agent	Tolerance limits /$\mu g\,ml^{-1}$	Masking agent
Fluoride	1000	—	1000	—	500	—
Chloride	1000	—	1000	—	1000	—
Bromide	1000	—	1000	—	1000	—
Iodide	80	—	15	—	Interfere	—
Nitrate	1000	—	1000	—	1000	—
Nitrite	200	—	Interfere	—	400	—
Phosphate	200	—	100	—	80	—
Sulfate	1000	—	80	—	1000	—
Sulfite	200	—	1000	—	Interfere	—
Sulfide	Interfere	—	Interfere	—	Interfere	—
Borate	1000	—	1000	—	1000	—
Cyanide	Interfere	—	—	—	Interfere	—
Thiocyanate	Interfere	—	Interfere	—	Interfere	—
Thiosulfate	Interfere	—	Interfere	—	Interfere	—
Thiourea	Interfere	—	Interfere	—	Interfere	—
Thiosemicarbazide	5	—	Interfere	—	Interfere	—
Oxalate	80	—	Interfere	—	60	—
Citrate	80	—	60	—	50	—
Tartrate	20	—	60	—	50	—
EDTA	150	—	150	—	300	—
Zinc(II)[a]	20	—	20	—	20	—
Cadmium(II)[a]	20	—	20	—	7	—
Mercury(II)	5	—	20	—	5	—
Copper(II)	12	Masked by EDTA	12	Masked by EDTA	50	Masked by EDTA
Silver(I)[c]	10	Masked by Cl^-	6	Masked by Cl^-	20	Masked by Cl^-
Gold(III)	15[b]	—	15	Masked by SO_3^{2-}	—	—
Tin(II)	5	—	5	—	Interfere	—
Lead(II)	20	—	20	—	50[c]	—
Iron(II)	5	Masked by EDTA	5	Masked by EDTA	7	Masked by EDTA
Iron(III)[c]	20	—	20	—	40	—
Cobalt(II)	10	Masked by EDTA	10	Masked by EDTA	10	Masked by EDTA
Nickel(II)	15	Masked by EDTA	15	Masked by EDTA	50	Masked by EDTA
Uranyl(II)	20	—	20	—	50	—
Palladium(II)	—	—	Interfere	—	Interfere	—
Osmium(VIII)	10	Masked by NO_2^-	—	—	20	Masked by NO_2^-

a) Metal-(*p*-QAP) complexes unstable. b) Gold-(*p*-QAP) complex in 50% ethanol medium decompose fastly on warming. c) Precipitate centrifuged.

Table 3. Determination of Palladium in Synthetic Solutions Corresponding to Some of Its Alloys[36]

Alloy	Amount of Pd(II) taken (ppm)	Amount of foreign ions taken (ppm)	Amount of Pd(II) found (ppm)	Percentage error
Palladium-copper alloy of vicker hardness 145 (composition-40% Cu, 60% Pd)	(i) 2.0	1.33 Cu(II)	2.01	+0.50
	(ii) 2.0	1.33 Cu(II)	2.01	+0.50
	(iii) 2.0	1.33 Cu(II)	2.02	+1.00
Palladium-silver alloy (composition-40% Ag, 60% Pd)	(i) 2.0	1.33 Ag(I)	2.00	0.00
	(ii) 2.0	1.33 Ag(I)	1.99	−0.50
	(iii) 2.0	1.33 Ag(I)	2.00	0.00
Palladium-gold alloy of vicker hardness 85 (composition-50% Au, 50% Pd)	(i) 2.0	2.0 Au(III)	2.00	0.00
	(ii) 2.0	2.0 Au(III)	2.01	+0.50
	(iii) 2.0	2.0 Au(III)	2.00	0.00

(III) in xylene and 1-butanol mixture (4 : 1) and has the sensitivity index 0.013 μg Au(III)/cm^2 at 520 nm. The sensitivity index of some other organic reagents known for gold could be enlisted as dithizone[24] (0.007 at 420 nm), methylviolet[25] (0.0017 at 600 nm), chromopyrazole I[26] (0.003 at 580 nm), di-2-pyridyl ketone oxime[27] (0.0098 at 459 nm), furil-α-dioxime[28] (0.0062 at 550 nm), and rhodamine B[29] (0.002 at 565 nm). For

Table 4. Determination of Gold in Synthetic Solutions Corresponding to Some of Its Alloys[36]

Alloy	Amount of Au(III) taken (ppm)	Amount of foreign ions taken (ppm)	Amount of Au(III) found (ppm)	Percentage error
Purple gold	(i) 4.0	1.0 Al(III)	3.98	−0.50
(composition-79% Au, 21% Al)	(ii) 4.0	1.0 Al(III)	3.95	−1.25
	(iii) 4.0	1.0 Al(III)	4.00	0.00
Gold 16 carat	(i) 4.0	0.5 Cu(II)+1.5 Ag(I)	4.05	+1.25
(compositon-67% Au, 8—27% Cu, 6.6—26% Ag)	(ii) 4.0	1.0 Cu(II)+1.0 Ag(I)	3.99	−0.25
	(iii) 4.0	1.5 Cu(II)+0.5 Ag(I)	4.07	+1.75
Gray gold	(i) 4.0	0.66 Fe(II)	4.01	+0.25
(composition-86% Au, 5.7—17% Fe, 0—8.6% Ag)	(ii) 4.0	0.4 Fe(II)+0.26 Ag(I)	4.03	+0.75
	(iii) 4.0	0.33 Fe(II)+0.33 Ag(I)	4.0	0.00
White gold	(i) 4.0	0.4 Ni(II)+0.4 Zn(II)	4.02	+0.50
(composition-75—85% Au, 8—10% Ni, 2—9% Zn)	(ii) 4.0	0.4 Ni(II)+0.3 Zn(II)	3.95	−1.25
	(iii) 4.0	0.5 Ni(II)+0.3 Zn(II)	3.96	−1.00

osmium, very less reagents are known. Diphenylcarbazide[30] forms a blue-green complex, absorbing maximum at 560 nm (ϕ, 0.00127). A simple thiourea method[5,6] is popular but is insensitive. Some other known methods have the following sensitivity indices: acenaphthoquinone monoxine[31] (0.0323 at 430 nm), 1-naphthylamine-4,6,8-trisulfonic acid[32] (0.0063 at 573 nm), *o*-aminophenol-*p*-sulfonic acid[33] (0.01 at 440 nm), 3-nitroso-2,6-pyridinediol[34] (0.0079 at 550 nm), and 2-amino-3-pyridinol[35] (0.038 at 600 nm and 0.024 at 540 nm). The sensitivity indices for the present methods are 0.0098 at 550 nm for gold(III) and 0.0039 at 550 nm for osmium(VIII).

Effect of Foreign Ions on the Determination of Palladium(II), Osmium(VIII), and Gold(III). In the determination of the three metal ions [Pd(II)=2.13 $\mu g\,ml^{-1}$, Os(VIII)=1.90 $\mu g\,ml^{-1}$ and Au(III)=3.98 $\mu g\,ml^{-1}$] calcium, magnesium, barium, strontium, aluminium, gallium, indium, antimony(III), manganese(II), lanthanoids upto 100-fold excess and vanadium(V), molybdenum(VI), platinum(IV), rhodium(III), iridium(IV), ruthenium(III) upto 25-fold excess do not interfere. The tolerance limits of other ions which do not cause a deviation of more than ±2% in the absorbance in the determination of the metals are given in Table 2.

Determination of Palladium(II) and Gold(III) in Synthetic Solution of Their Alloys. To ascertain the suitability of the reagent for the determination of palladium(II) and gold(III) in alloys, estimation has been carried out, adopting the appropriate conditions, in synthetic solutions identical in composition to some of their alloys.[36] The results obtained are recorded in Tables 3 and 4 and the percentage recovery obtained suggest that the methods are fairly successful.

References

1) S. Barua, Y. S. Varma, B. S. Garg, R. P. Singh, and I. Singh, *Analyst*, **106**, 799 (1981).

2) S. Barua, B. S. Garg, R. P. Singh, and I. Singh, *J. Ind. Chem. Soc.*, **60**, 64 (1983).

3) S. Barua, B. S. Garg, R. P. Singh, and I. Singh, *Analyst*, **105**, 996 (1980).

4) F. E. Beamish, *Talanta*, **12**, 743 (1965).

5) F. E. Beamish and J. C. Van Loon, "Recent Advances in the Analytical chemistry of the Noble Metals," Pergamon Press, London (1972).

6) F. D. Snell, "Photometric and fluorometric Methods of Analysis," Metals, Part 2, John Wiley, New York (1978).

7) H. A. Flaschka and A. J. Barnard, Jr., "Chelates in Analytical Chemistry," Marcel Dekker, Inc., New York (1972), Vol. 4.

8) E. B. Sandell and H. Onishi, "Photometric Determination of Traces of Metals," John Wiley, New York (1978), Vol. 3, Part I.

9) A. I. Busev and L. V. Kiseleva, *Vestnik Mosk. Univ. Ser. Mat'. Mekh. Astron., Fiz. Khim.*, **13**, 179 (1958); *Chem. Abstr.*, **53**, 11105f (1959).

10) A. I. Busev and V. M. Ivanov, *Zh. Anal. Khim.*, **19**, 232 (1964).

11) H. K. Lin, K. Chen, and Y. F. Chen, *Hua Hsueh Tung Pao*, **1966**, 365; *Chem. Abstr.*, **66**, 25818y (1967).

12) S. I. Gusev and V. A. Vinkova, *Zh. Anal. Khim.*, **22**, 376 (1967).

13) M. F. Garcia, D. V. Gonzalez, and C. R. Tallo, *Microchem. J.*, **27**, 194 (1982); *Chem. Abstr.*, **97**, 48806x (1982).

14) M. F. Garcia, D. V. Gonzalez, and C. R. Tallo, *Analusis*, **9**, 353 (1981); *Chem. Abstr.*, **95**, 214494z (1981).

15) O. Coufalova, G. Rudzitis, G. Mezaraup, and L. Cermakova, *Microchem. J.*, **32**, 24 (1985); *Chem. Abstr.*, **103**, 226549t (1985).

16) P. Suthivaiyakit and A. Kettrup, *Fresenius Z. Anal. Chem.*, **320**, 769 (1985); *Chem. Abstr.*, **103**, 47481t (1985).

17) Y. Gong, H. Zhou, and Z. Gao, *Fenxi Hauxue*, **14**, 291 (1986); *Chem. Abstr.*, **105**, 107523m (1986).

18) M. Siroki and M. Koren, *Mikrochim. Acta*, **1**, 75 (1983); *Chem. Abstr.*, **98**, 118734u (1983).

19) B. Subrahmanyam and M. C. Eshwar, *Anal. Chim. Acta*, **82**, 435 (1976).

20) A. I. Vogel, "A Text Book of Quantitative Inorganic Analysis," 3rd ed, Longman, London (1975).

21) G. H. Ayres and W. N. Wells, *Anal. Chem.*, **22**, 317 (1950).
22) D. A. Klobbie, *J. Chem. Soc.*, **76ii**, 184 (1899).
23) "Treatise on Analytical Chemistry," ed by I. M. Kolthoff and P. J. Elving, Interscience, New York (1966), Part II, Vol. 4, p. 92.
24) Z. Marczenko and M. Krasiejko, *Chem. Anal. (Warsaw)*, **17**, 1201 (1972).
25) L. Ducret and H. Maurel, *Anal. Chim. Acta*, **21**, 74 (1959).
26) N. N. Gorbunova, A. I. Busev, and V. M. Ivanov, *Zh. Anal. Khim.*, **25**, 461, 1471 (1970).
27) W. J. Holland and Z. Bozic, *Anal. Chem.*, **39**, 109 (1967).
28) P. S. Patil and V. M. Shinde, *Mikrochim. Acta*, **1971**, 151; **1977**, 331.
29) H. Onishi, *Mikrochim. Acta*, **1959**, 9.
30) G. Goldstein, D. L. Manning, O. Menis, and J. A. Dean, *Talanta*, **7**, 296, 301, 307 (1961).
31) S. K. Sindhwani and R. P. Singh, *Microchem. J.*, **18**, 627 (1973).
32) E. L. Steele and J. H. Yoe, *Anal. Chem.*, **29**, 1622 (1957).
33) A. K. Mujumdar and J. G. S. Gupta, *Anal. Chim. Acta*, **22**, 306 (1960).
34) C. W. McDonald and R. Carter, Jr., *Anal. Chem.*, **41**, 1478 (1969).
35) Y. L. Mehta, B. S. Garg, and R. P. Singh, *Talanta*, **23**, 53 (1976).
36) "Comprehensive Inorganic chemistry," ed by J. C. Bailer, H. J. Emeleus, R. Nyholm, and A. F. Trotman-Dicknson, Pergamon, Oxford (1973), Vol. 3, pp. 134, 1179.

 © 1989 The Chemical Society of Japan Bull. Chem. Soc. Jpn., 62, 1321—1324 (1989)

Natural 2,6-Dialkyl-3-piperidinols. 9. Total Synthesis of (±)-Prosafrinine and ^{13}C NMR Studies of Some Analogous Compounds

Michel PATERNE,* Robert DHAL, and Eric BROWN
Laboratoire de Synthèse Organique (U. A. n° 482), Faculté des Sciences,
Route de Laval, BP 535, F-72017 Le Mans, France
(Received June 25, 1988)

1,7-Dibromoheptane was used to alkylate both ketoesters **2** and **4** successively. Hydrolysis and decarboxylation of the resulting intermediate afforded the ethylenic diketone (**6**). Ozonolysis of the double bond of **6** gave the diketonic aldehyde (**8**). Alkaline condensation of nitroethane on the aldehydic carbonyl of the latter, followed by hydrogenation using a Pd-Pt catalyst, afforded 3-*r*-hydroxy-6-*c*-(10-oxododecyl)-2-*c*-methylpiperidine [(±)-prosafrinine] (**1a**) and (±)-3-epiprosafrinine (**1b**). The structures of **1a**, **1b**, and some analogues were confirmed by ^{13}C NMR studies.

The alkaloid prosafrinine (**1a**) was isolated from the leaves of *Prosopis africana*, and its structure was established in 1972.[1] Prosafrinine (**1a**) is a 2,6-dialkyl-3-piperidinol in which the three substituents are cis. We describe here a racemic total synthesis of the alkaloid (**1a**) following a general reaction scheme previously developed in our laboratory for the synthesis of 2,6-dialkyl-3-piperidinols.[2] We have confirmed or established the relative stereochemistry of prosafrinine (**1a**) and some related compounds, more particularly by ^{13}C NMR studies, and by comparison with the data published in a recent paper.[3]

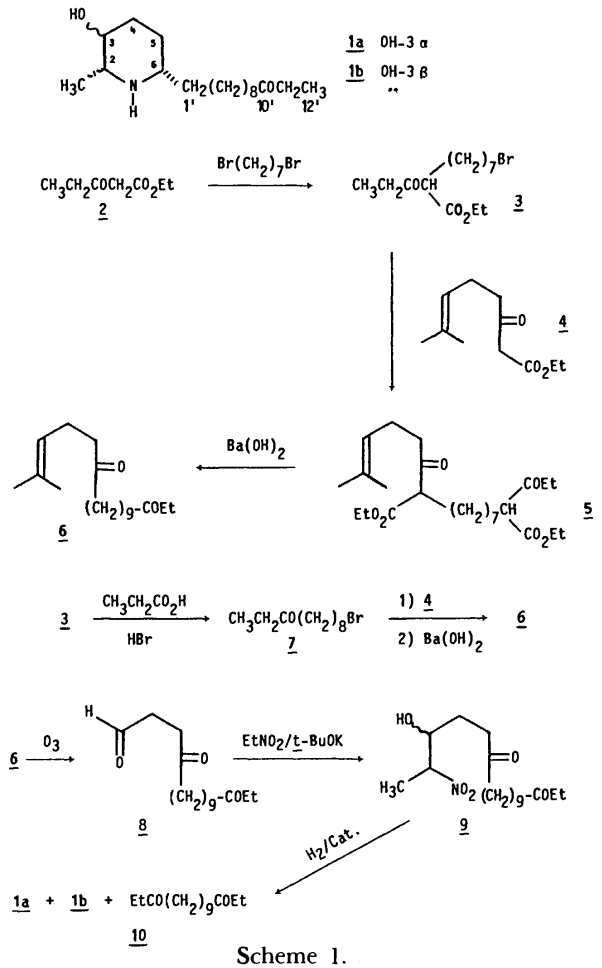

Scheme 1.

γ,δ-Unsaturated ketones are key-intermediates in our synthetic scheme for 2,6-dialkyl-3-piperidinols. In the present case, we needed to prepare 17-methyl-16-octadecene-3,13-dione (**6**), which contains the carbon atoms at the positions 3 to 6 of the final piperidine ring, as well as the twelve carbon substituent at the position 6 of the same ring. Thus, ethyl 3-oxopentanoate (**2**), prepared from Meldrum's acid,[4] was alkylated with 1,7-dibromoheptane and afforded the monobromo intermediate (**3**) (Scheme 1). Alkylation of the β-keto ester **4**[5] with the bromide **3** gave the diketonic diester **5**, which was next hydrolyzed and decarboxylated in refluxing aqueous barium hydroxide, thus leading to the ethylenic diketone **6** in about 40% yields of purified product, with regards to the starting 1,7-dibromoheptane. Another route to the ethylenic diketone **6** consisted in the decarboxylation of the intermediate **3**, in order to obtain 11-bromo-3-undecanone (**7**) following a known analogous method.[6] Next, the alkylation of the β-keto ester **4** with the bromide **7**, followed by hydrolysis and decarboxylation, afforded the ethylenic diketone **6**. However, this route was found less satisfactory than the former one, which was less toilsome and gave higher yields of **6**.

Ozonolysis of the double bond of **6** in dichloromethane (in the presence of pyridine) at low temperature, followed by reduction of the intermediate ozonide with zinc in acetic acid, afforded the dioxo aldehyde **8** in about 80% yields of purified product. Selective condensation of nitroethane with the aldehydic carbonyl of **8** using potassium *t*-butoxide in a THF/ethanol mixture, gave the β-nitro alcohol **9** as a crystalline mixture of both erythro and threo diastereomers, and in about 80% yields of recrystallized product. The hydrogenation of the mixture of diastereomers **9** was next carried out in ethanol under a pressure of 3 bar, using a mixed catalyst composed of palladium (8%) and platinum (2%) deposited on charcoal. Thin-layer chromatography of the crude reaction product revealed the presence of compounds of high R_f values, together with the piperidinols **1a** and **1b** whose R_f's are very different. By column chromatography on silica

gel, we isolated 3,13-pentadecanedione (**10**) (30%) as well as a mixture of the 3-piperidinols **1a** and **1b** (40—50% yields). The dione **10** probably resulted from a palladium-catalyzed decarbonylation of the γ-keto aldehyde **8** liberated by retrocondensation of the β-nitro alcohols **9**. The above mixture of epimers **1a** and **1b** was easily separated by high-pressure liquid chromatography on an inversed-phase column and using aqueous methanol for the elution. This afforded (±)-prosafrinine (**1a**), mp 69—72 °C and (±)-3-epiprosafrinine (**1b**), mp 76—80 °C, whose structures were confirmed as indicated below.

In principle, four racemic diastereomers could be formed by reduction-cyclization of the mixture of the epimeric β-nitro alcohols **9** (Scheme 2). According to former studies from our laboratory,[7] the catalytic hydrogenation of compounds such as **9** generally yields 2,6-dialkyl-3-piperidinols of types **a** and **b** in which the groups at the positions 2 and 6 are *cis*-diequatorial. In the case of the epimer **a**, the axial hydroxyl can be intramolecularly bound with the lone pair of electrons on the nitrogen atom by hydrogen bonding, which is not possible in the case of the epimer **b** where the hydroxyl is equatorial. Until quite recently, both structures **a** and **b** could be identified essentially by two spectroscopic methods. The infrared spectrum of a dilute carbon tetrachloride solution shows, for the hydroxyl at the position 3, two absorption bands (free and associated OH) for **a** and a single band (free OH) for **b**.[8] On the other hand, the ^{1}H NMR signal of the equatorial carbinolic proton of **a** shows up as a peak whose half-height width is about 6 Hz, whereas the axial carbinolic proton of **b** gives a much flatter peak having a half-height width of about 20 Hz.[9]

Additional information was gained from the examination of the 300 MHz ^{1}H NMR spectra of the isomers **1a** and **1b**. In the case of prosafrinine (**1a**), the H-3 proton shows up as a peak at δ 3.71 whose half-height width is about 5 Hz. This poorly resolved signal having the coupling constants $J_{3\text{-}2,\,4ax,\,4eq}<2$ Hz is characteristic of an equatorial proton, and its selective irradiation allowed the signals at δ 2.99 and 2.76 to be assigned to the H-2 and H-6 protons respectively.

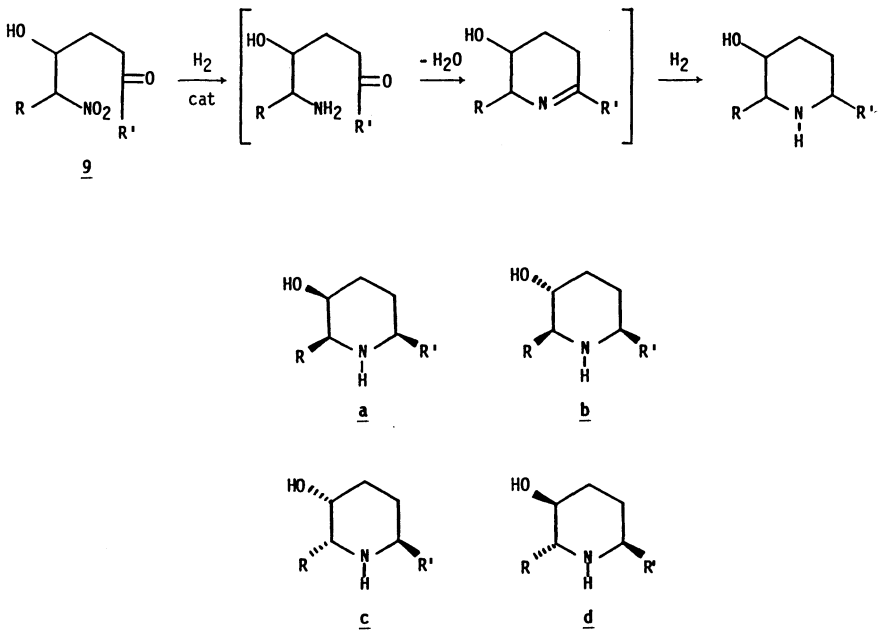

Scheme 2.

Table 1. Characteristic ^{13}C NMR Data of Various 2,6-Dialkyl-3-piperidinols

		δ/ppm			
		C-2	C-3	C-6	C-7
a	**11a** R′=-CH_3	55.80	67.52	52.67	18.48
	12a R′=-$(CH_2)_{12}$-CO-CH_3 (±)-spectaline	57.24	67.90	55.81	18.61
	1a R′=-$(CH_2)_9$-CO-Et (±)-prosafrinine	57.27	67.59	55.92	18.16
b	**11b** R′=-CH_3	58.50	73.61	51.87	18.85
	1b R′=-$(CH_2)_9$-CO-Et (±)-3-epiprosafrinine	58.74	73.72	56.62	19.16

In the case of the epimer (**1b**), the H-3 proton shows up at δ 3.17 as a multiplet whose high coupling constants J_{3-2}=8.8 Hz and J_{3-4}=10.4 Hz are characteristic of trans-diaxal couplings. The selective irradiation of H-3 allowed the signals at δ 2.49, 2.04, and 1.32 to be assigned to the H-2, H-4eq, and H-4ax protons respectively, and made it possible the complete attribution of all the remaining protons of the piperidine ring. However, the H-6 proton at δ 2.52 could not be analyzed because of the overlap with the H-2 signal. The signals and chemical shifts we observed for **1a** and **1b** are in agreement with those reported for (−)-deoxocassine and 3-epideoxocassine, respectively.[3]

The information provided by the infrared and ^1H NMR spectra were confirmed and completed by the study of ^{13}C NMR spectra (see Table 1).

In the case of prosafrinine (**1a**), it can be seen that the C-3 carbon atom, which bears an axial hydroxyl, gives a signal at δ 67.59 whereas in the 3-epimer (**1b**) the same carbon atom (bearing an equatorial hydroxyl) gives a signal at δ 73.72 which corresponds to a difference $\Delta\delta$ =6.13 ppm. This difference has almost the same value in the case of the 2,6-dimethyl-3-piperidinols (**11a** and **11b**) ($\Delta\delta$ =6.09 ppm).[7] It can also be noticed that the C-7 carbon atom of the methyl groups (at the position 2 of the ring) has δ values ranging from 18.16 to 19.16 and which are therefore very close, in all the cases where this methyl group and the substituent at position 6 are cis-diequatorial. These various data confirm the all-cis structure of the epimers of type a.[10]

Experimental

The IR spectra were recorded with a Nicolet 5DX spectrophotometer. The NMR spectra were recorded with Varian EM 390 and Bruker 300 spectrometers for the proton, and Varian FT 80 or Jeol FX 90 Q spectrometers for ^{13}C. NMR spectra were run with samples in $CDCl_3$ solutions. TMS was the internal standard. Chemical shifts are expressed in ppm values (δ scale). Elemental analyses were carried out by the "Centre de Microanalyse du CNRS" (Lyon). Melting points were taken with a Reichert microscope. Thin layer chromatographies (TLC) were carried out using precoated silica gel plates. Preparative column chromatographies were carried out under pressure (1—3 bar) using Merck silica gel (Kieselgel 60). The following abbreviations are used: RP, reduced pressure; RT, room temperature; THF, tetrahydrofuran.

11-Bromo-4-ethoxycarbonyl-3-undecanone (3). To a solution of sodium ethoxide (2.42 g of sodium in 300 ml of anhydrous ethanol) cooled to 0 °C, ethyl 3-oxopentanoate (**2**; 14.4 g) was added dropwise, followed by NaI (100 mg). 1,7-Dibromoheptane (25.8 g) was then added and the mixture was refluxed under stirring for 24 h. The ethanol was removed under RP, the residue was acidified with 0.5 M H_2SO_4 (1 M=1 mol dm^{-3}) and was extracted with ether. The ethereal phase was washed with water until neutral, dried ($MgSO_4$) and evapored under RP. The crude compound (**3**; 29.2 g) was thus obtained in 91% yield, having bp 155—165 °C/0.1 mmHg (1 mmHg≈133.322 Pa). It was used without further purification in the next step; ^1H NMR δ=1.06 (6H, mult., $C\underline{H}_3$-CH_2), 1.33 (12H, -CH_2-), 2.56 (2H, -CH_2-CO), 3.30 (3H, -CH< and -CH_2Br), 4.26 (2H, q, CH_2-O-CO-); IR (film) 1743, 1713, 1186, 1028 cm^{-1}.

4,12-Bis(ethoxycarbonyl)-17-methyl-16-octadecene-3,13-dione (5). To a solution of sodium ethoxide (2.1 g of sodium in 100 ml of anhydrous ethanol) cooled to 0 °C, ethyl 7-methyl-3-oxo-6-octenoate (**4**; 18.01 g)[2] was added, followed by NaI (200 mg). After stirring for 30 min, a solution of crude 11-bromo-4-ethoxycarbonyl-3-undecanone (**3**; 29.2 g) in anhydrous ethanol (150 ml) was added dropwise, and the mixture was refluxed under stirring for 24 h. The ethanol was removed under RP, the residue was acidified with 0.5 M H_2SO_4 and was extracted with ether. The ether phase was washed with water until neutral, dried ($MgSO_4$) and evaporated under RP. The crude compound (**5**; 39.1 g) was thus obtained in 98% yield. It was used without purification in the next step; ^1H NMR δ=1.65 (6H, d, $(CH_3)_2$ C=C), 2.33 (4H, -CH_2-CO-), 3.46 (2H, tertiary CH), 4.20 (4H, q, -CH_2-OCO-), 5.05 (1H, ethylenic proton); IR (film) 1737, 1717, 1180, 1034 cm^{-1}.

17-Methyl-16-octadecene-3,13-dione (6). Crude 4,12-bis-(ethoxycarbonyl)-17-methyl-16-octadecene-3,13-dione (**5**; 39.4 g) was treated with barium hydroxide octahydrate (70 g) in water (1200 ml). After refluxing for 16 h under vigorous stirring, the mixture was cooled down, then acidified with HCl and stirred until complete dissolution of the barium salts. The mixture was then extracted with ether, the organic phase was washed with water, and was dried ($MgSO_4$) and evaporated under RP. The residue was crystallized from pentane, thus giving the purified diketone (**6**; 12.2 g) in 46% yield and as white crystals, mp 71—72 °C (pentane); ^1H NMR δ=1.05 (3H, t, $C\underline{H}_3$-CH_2-), 1.25 (14H, methylenes), 1.65 (6H, d, $(CH_3)_2$C=C-), 2.45 (10H, -CH_2-CO- and $C\underline{H}_2$-CH=C-), 5.0 (1H, ethylenic proton); IR (film) 1716 cm^{-1}; HRMS Found: 294.481; Calcd for $C_{19}H_{34}O_2$: 294.530.

11-Brom-3-undecanone (7). Crude 11-bromo-4-ethoxycarbonyl 3-undecanone (**3**; 14 g) in a mixture of propionic acid (35 ml) and 48% aqueous hydrobromic acid (50 ml) was refluxed for 2.5 h. After cooling, the mixture was added to ice and extracted with toluene. The organic phase was washed with water, dried ($MgSO_4$) and evapored under RP. Crystallization of the residue from pentane afforded the bromide (**7**; 6.5 g) in 60% yield and as white crystals, mp 17—18 °C (pentane); **7** is unstable and should be kept in the refrigerator; ^1H NMR δ=1.0 (3H, t, CH_3-), 1.33 (12H, -CH_2-), 2.30 (4H, -CH_2-CO-), 3.40 (2H, t, -CH_2-Br); IR (film) 1716, 1110, 731 cm^{-1}.

4,14-Dioxohexadecanal (8). Ozone was bubbled through a solution of 17-methyl-16-octadecene-3,13-dione (**6**; 2 g) in dichloromethane (500 ml) at −70 °C until persistence of a blue colour in the ozonolysis reactor. After purging for 5 min, the solution was added to zinc powder (3.4 g), followed by a slow addition of acetic acid (6.8 g) and the resulting mixture was magnetically stirred at RT for 3 h, at which time the peroxide test was found to be negative. The solids were filterd through celite and the filtrate was washed with water. The solution was dried ($MgSO_4$) and evapored under RP and the crystalline residue was chromatographed over silica gel. Elution with 95:5 CH_2Cl_2/ether afforded the dioxo aldehyde (**8**; 1.46 g) in 80% yield, mp 67—69 °C (ether/pentane); ^1H NMR δ=1.03 (2H, t, $C\underline{H}_3$-CH_2), 1.26 (14H, CH_2), 2.43 (8H, CH_2CO), 2.69 (4H, s HCO-$C\underline{H}_2C\underline{H}_2$CO-),

9.95 (1H, s, CHO); ^{13}C NMR δ=211.59 (C-14), 208.67 (C-4), 200.27 (C-1), 42.75 (C-5), 42.40 (C-13), 37.54 (C-2), 35.85 (C-15), 34.70 (C-3), 29.29 (C-7 to C-11), 23.94 (C-6 and C-12), 7.87 (C-16); IR (film) 1712, 1420, 823 cm^{-1}; HRMS Found: 268.2033; Calcd for $C_{16}H_{28}O_3$: 268.2038; Found: C, 71.25; H, 10.29; O, 17.84%. Calcd for $C_{16}H_{28}O_3$: C, 71.60; H, 10.51; O, 17.88%.

16-Hydroxy-17-nitro-3, 13-octadecanedione (9). (Erythro and Threo Isomers). To a solution of potassium *t*-butoxide (0.446 g) in anhydrous ethanol (1 ml) and anhydrous THF (10 ml), a solution of nitroethane (0.343 g) in anhydrous THF (20 ml) was added dropwise. Then a solution of 4,14-dioxohexadecanal (**8**; 0,97 g) in anhydrous THF (20 ml) was added dropwise and the reaction mixture was stirred at RT for 14 h. The potassium salt was destroyed by addition of acetic acid (0.24 g) in THF (5 ml), followed by water (1 ml). The solids were removed by filtration and the solution was dried ($MgSO_4$) and evapored under RP at RT, thus leaving a white crystalline product in quantitative yield. Recrystallization of the latter from ether afforded the mixture of isomers **9** (1 g) in 80% yield, mp 75—76 °C (ether); ^{1}H NMR δ=1.04 (3H, t, C$\underline{H}_3$-CH_2), 1.27 (14H, broad peak, -CH_2-), 1.56 (3H, d, C$\underline{H}_3$-CH-), 2.26 to 2.83 (8H, -CH_2-CO-), 3.0 (1H, -OH), 4.1 (1H, m, -C$\underline{H}$OH), 4.6 (1H, CH-NO_2); IR (film) 3849, 1709, 1559, 1116, 972, 822 cm^{-1}; Found: C, 62.67; H, 9.84; O, 23.35; N, 4.14%. Calcd for $C_{18}H_{33}NO_5$: C, 62.94; H, 9,68; O, 23.29; N, 4.07%.

Hydrogenation of β-Nitro Alcohols (9). (±)-Prosafrnine (1a) and (±)-3-Epiprosafrinine (1b). The hydrogenation was carried out in a Parr apparatus. 16-Hydroxy-17-nitro-3,13-octadecanedione (**9**; 0.73 g) in 95% ethanol (80 ml), and in the presence of a mixed palladium (8%)-platinum (2%) on charcoal catalyst, was hydrogenated under 3 bars at 30 °C for 14 h. After filtration of the catalyst through Celite and evaporation of the solvent under RP, a crude product (0.63 g) was obtained, and whose IR spectrum did not contain a nitro band. TLC over silica gel using 30:9:1 AcOMe/MeOH/15 M aqueous NH_3 as eluent revealed the presence of compounds of high R_f values and two distinct spots at R_f 0.72 and 0.41 corresponding to **1a** and **1b** respectively. The product was chromatographed on a column of silica gel (Merck, 230—400 mesh) using CH_2Cl_2/EtOH/15 M aqueous NH_3 (100:10:1) as eluent, to give a mixture (0.23 g) of (±)-prosafrinine (**1a**) and (±)-3-epiprosafrinine (**1b**) after elimination of less polar head fractions; HRMS of the mixture $[M-C_2H_5]^+$: Found: 268.2287; Calcd: 268.2276; among the head fractions, 3,13-pentadecanedione (**10**) was isolated as a white crystalline solid, mp 78—80 °C (ether), which was characterized as follows; ^{1}H NMR δ=1.06 (6H, t, C$\underline{H}_3$-CH_2), 1.27 (10H, broad peak, -CH_2-), 1.60 (4H, -CH_2CH_2CO-), 2.40 (8H, m, -CH_2-CO-): ^{13}C NMR δ=211.35 (C-3 and C-13), 42.38 (C-4 and C-12), 35.82 (C-2 and C-14), 29.43 and 29.33 (C-6 to C-10), 23.97 (C-5 and C-11), 7.84 (C-1 and C-15): IR (film) 1708, 1701, 1420, 1104, 823 cm^{-1}; HRMS Found: 240.2112; Calcd: 240.2089.

The separation of the mixture of epimers **1a** and **1b** was carried out by high-pressure liquid chromatography on an inversed-phase column (Bondapack Waters C_{18}, 7.8 mm×30 cm, 2 ml min^{-1}) and using MeOH/H_2O (90:10) for the elution. Thus, starting from a solution of the mixture of **1a** and **1b** (250 mg in 1 ml of 90:10 MeOH/H_2O), each 100 µl injection afforded (±)-3-epiprosafrinine (**1b**; 12 mg) and (±)-prosafrinine (**1a**; 9 mg). (±)-3-Epi-prosafrinine (**1b**): mp 76—80 °C (acetone/pentane); ^{1}H NMR (300 MHz) δ=1.05 (3H, t, $J_{12'-11'}$=7.4 Hz, CH_3-12'), 1.18 (1H, m, $J_{5ax-4eq}$=3.6 Hz, $J_{5ax-6ax}\approx$11.5 Hz, $J_{ab}\approx J_{5ax-4ax}$=13.1 Hz, H-5ax), 1.21 (3H, d, J_{7-2}=6.2 Hz, CH_3-7), 1.28 (14H, s, CH_2-1' to 7'), 1.32 (1H, m, $J_{4ax-5eq}$=3.8 Hz, J_{4ax-3}=10.5 Hz, $J_{AB}\approx J_{4ax-5ax}$=13.4 Hz, H-4ax), 1.56 (1H, m, CH_2-8'), 1.75 (1H, dq, $J_{5eq-4eq,\ 4ax,\ 6}\approx$3.0 Hz, J_{AB}=12.5 Hz, H-5eq), 1.81 (2H, large s, OH and NH), 2.04 (1H, dq, $J_{4eq-3,\ 5eq,\ 5ax}\approx$3.5 Hz, J_{AB}=12.0 Hz, H-4eq), 2.39 (2H, t, $J_{9'-8'}$=7.4 Hz, CH_2-9'), 2.42 (2H, q, $J_{11'-12'}$=7.4 Hz, CH_2-11'), 2.49 (1H, m, H-2), 2.52 (1H, m, H-6), 3.17 (1H, ddd, J_{3-4eq}=4.4 Hz, J_{3-2}=8.8 Hz, J_{3-4ax}=10.4 Hz, H-3); ^{13}C NMR δ=212.13 (C-10'), 73.72 (C-3), 58.74 (C-2), 56.62 (C-6), 42.54 (C-9'), 36.64 (C-1'), 35.96 (C-11'), 34.28 (C-4), 31.79 (C-5), 29.85, 29.59, 29.51, 29.37 (C-3' to C-7'), 26.34 (C-2'), 24.07 (C-8'), 19.16 (C-7), 8.01 (C-12'); IR (film) 3261, 3120, 1713, 1113, 1044 cm^{-1}. (±)-Prosafrinine (**1a**): mp 69—72 °C (acetone/pentane); ^{1}H NMR (300 MHz) δ=1.05 (3H, t, $J_{12'-11'}$=7.3 Hz, CH_3-12'), 1.26 (18H, s, CH2-1' to 7'), 1.32 (3H, d, J_{7-2}=6.5 Hz, CH_3-7), 1.56 (m, CH_2-8'), 1.45 to 1.8 (m, H-4ax and CH_2-5), 1.99 (1H, m, H-4eq), 2.39 (2H, t, $J_{9'-8'}$=7.4 Hz, H-9'), 2.42 (2H, q, $J_{11'-12'}$=7.3 Hz, H-11'), 2.76 (1H, m, H-6), 2.99 (1H, q, J_{2-7}=6.3 Hz, H-2), 3.71 (1H, s, H-3), in agreement with the literature;[1,3] ^{13}C NMR δ=211.83 (C-10'), 67.59 (C-3), 57.27 (C-2), 55.92 (C-6), 42.35 (C-9'), 36.34 (C-1'), 35.79 (C-11'), 31.84 (C-4), 29.64, 29.45, 29.32, and 29.11 (C-3' to C-7'), 25.69 (C-5), 25.39 (C-2'), 23.90 (C-8'), 18.16 (C-7), 7.71 (C-12'); IR (film) 3302, 1713, 1107, 1000, 913, 863 cm^{-1}; IR (in dilute CCl_4 solution) 3640 (free OH), 3540 (bound OH) cm^{-1}, $\varepsilon_{ass}/\varepsilon_{free}$: 2.

References

1) Q. Khuong-Huu, G. Ratle, X. Monseur, and R. Goutarel, *Bull. Soc. Chim. Belg.*, **81**, 443 (1972).

2) M. Paterne and E. Brown, *J. Chem. Res. (S)*, **1985**, 278.

3) K. Kurihara, T. Sugimoto, Y. Saitoh, Y. Igarashi, H. Hirota, Y. Moriyama, T. Tsuyuki, T. Takahashi, and Q. Khuong-Huu, *Bull. Chem. Soc. Jpn.*, **58**, 3337 (1985).

4) Y. Oikawa, K. Sugano, and O. Yonemitsu, *J. Org. Chem.*, **43**, 2087 (1978).

5) M. S. Schechter, N. Green, and F. B. Laforgue, *J. Am. Chem. Soc.*, **71**, 3165 (1949).

6) T. Sato, R. Nishida, Y. Kuwahara, H. Fukami, and S. Ishii, *Agric. Biol. Chem.*, **40**, 391 (1976).

7) E. Brown and R. Dhal, *Bull. Soc. Chim. Fr.*, **1972**, 4292; E. Brown, R. Dhal, and P. F. Casals, *Tetrahedron*, **28**, 5607 (1972).

8) M. Tichy and J. Sicher, *Tetrahedron Lett.*, **1962**, 511.

9) R. E. Lyle, D. H. McMahon, W. E. Krueger, and C. K. Spicer, *J. Org. Chem.*, **31**, 4164 (1966).

10) Q. Khuong-Huu, X. Monseur, M. J. Gasic, P. M. Wovkulich, and E. Wenkert, *J. Chem. Soc. Pak.*, **4**, 267 (1982).

 © 1989 The Chemical Society of Japan Bull. Chem. Soc. Jpn., 62, 1325—1327 (1989)

Epoxidation of Alkenes Catalyzed by Iron(III) Schiff Base Chelates. A Monooxygenase Model

Mathew JACOB, Pabitra Krishna BHATTACHARYA,* Pralhad A. GANESHPURE,†
Sheo SATISH,† and Swaminathan SIVARAM†
Department of Chemistry, Faculty of Science, M. S. University of Baroda, Vadodara 390002, India
†Research Centre, Indian Petrochemicals Corporation Limited, Vadodara 391346, India
(Received October 3, 1988)

Iron(III) Schiff base chelates $[Fe_2(PA_2ppd)_2Cl_4]Cl_2$ (**1**), $[Fe_2(PA_2mpd)_2Cl_4]Cl_2$ (**2**), and $[Fe(PA_2opd)Cl_2]Cl$ (**3**), were synthesized, where (PA_2ppd), (PA_2mpd), and (PA_2opd) are the Schiff bases derived from 2-pyridinecarbaldehyde (PA), and *p*-phenylenediamine (ppd), *m*-phenylenediamine (mpd), and *o*-phenylenediamine (opd) respectively. The complexes **1**, **2**, and **3** catalyzed the epoxidation of alkenes with iodosylbenzene as an oxidant providing a chemical model for cytochrome P-450. The binuclear complexes (**1**, **2**) were superior to the mononuclear complex (**3**) as the catalyst for epoxidation of norbornene. Addition of pyridine bases increased the rates, and yields of epoxidation.

The selective addition of oxygen to a hydrocarbon provides a direct means of increasing its commercial potential. But there are only a few preparatively or industrially useful liquid-phase catalytic oxidation processes which do not compromise on the selectivity. In contarst, nature has evolved monooxygenase enzymatic systems, such as cytochrome P-450 which catalyzes oxygenation reactions with utmost selectivity. Hemin forms part of the composition of cytochrome P-450 which are responsible for detoxification of living organisms by hydroxylation of saturated hydrocarbons and epoxidation of alkenes employing molecular oxygen, in their cells.[1]

In the last few years, several chemical models of monooxygenases have been studied. In such systems a metalloporphyrin catalyzes the transfer of an oxygen atom to an alkene, either from a single oxygen donor (e.g. PhIO, $KHSO_5$, NaOCl) or from the combination of molecular oxygen and a reductant (e.g. ascorbic acid, $NaBH_4$).[2-11] Recently, metal complexes other than metalloporphyrins have also been used for catalytic epoxidation of alkenes with iodosylbenzene or alkyl hydroperoxide as an oxygen source.[12-14] However, the systems using iron complexes are limited to porphyrin ligands only.

In the present communication, we report studies on Fe(III) Schiff base chelates as catalysts for epoxidation of alkenes.

Experimental

The elemental analyses were carried out on a Coleman carbon, hydrogen analyzer. The IR spectra were recorded on Shimadzu IR-408 and UV-VIS spectra on Shimadzu UV-240 spectrophotometer. The thermal analyses were performed on Shimadzu DT-30 thermal analyzer. Magnetic moments were determined by Guoy method at room temperature. The conductivity measurements were carried out on Toshniwal conductivity bridge. Gas chromatography analysis were performed on Shimadzu GC 7AG.

Syntheses of Binuclear Complexes. To a solution of 2-pyridinecarbaldehyde (2 mmol), in dry ethanol (50 ml) was added a solution of *p*-phenylenediamine or *m*-phenylenediamine (1 mmol) in dry ethanol (70 ml) and the mixture stirred for 15 min. The Schiff base, thus formed, was added dropwise to a solution of anhydrous $FeCl_3$ (1 mmol) in dry ethanol (100 ml). The mixture was stirred at room temperature for 0.5 h and refluxed on a water bath for 5 h. After cooling to room temperature, the complex was filtered, washed thoroughly with ethanol and dried under vacuum at 100 °C.

Synthesis of Mononuclear Complex. To a solution of 2-pyridinecarbaldehyde (2 mmol) in dry ethanol (20 ml) was added a solution of *o*-phenylenediamine (1 mmol) in dry ethanol (35 ml) and the mixture stirred for 15 min. The mixture was warmed slowly to 45 °C and allowed to cool to room temperature. The Schiff base formed was then added dropwise to a solution of anhydrous $FeCl_3$ in dry ethanol (70 ml) and the mixture refluxed for 5 h. It was then cooled to room temperature, filtered and the filtrate was concentrated to one third. To the above solution was added excess of ether and the precipitated complex was filtered, washed first with ethanol and finally with ether, and dried under vacuum at 100 °C.

Epoxidation of Alkenes. All reactions were carried out in a Schlenk tube under nitrogen atmosphere. To a solution of catalyst (0.012 mmol) in acetonitrile (6 ml) and water (1 ml) were added alkene (2.5 mmol), an appropriate quantity of anisole as an internal standard, and iodosylbenzene (0.5 mmol). The mixture was stirred at ambient temperature for 5.5 h. Aliquots (1 μl) were withdrawn and analyzed by gas chromatography (GC column (3 M), Carbowax 20M, 15% on Chromosorb W, carrier gas nitrogen, flow 30 ml min^{-1}, detector FID, injector temp 240 °C).

Results

The metal complex $[Fe_2(PA_2ppd)_2Cl_4]Cl_2$, $[Fe_2(PA_2mpd)_2Cl_4]Cl_2$, and $[Fe(PA_2opd)Cl_2]Cl$, were characterized by elemental (C, H, N, and metal), spectral (IR and UV-VIS) and thermal analyses, and by conductivity and magnetic moment measurements. The elemental analyses and the magnetic moment data are presented in Table 1. Molecular conductivity was measured in water, methanol, and in a mixture of acetonitrile-water (6 : 1). However, molar conductance of **1** in methanol could not be measured because of its poor solubility. Molar conductance data have been

Table 1. Analytical and Magnetic Moment Data for the Metal Complexes

Complex	C%		H%		N%		M%		μ_{eff}
	Calcd	Found	Calcd	Found	Calcd	Found	Calcd	Found	(B.M.)
$[Fe_2(PA_2ppd)_2Cl_4]Cl_2$	48.18	49.30	3.12	3.08	12.49	12.27	12.46	12.9	5.13
$[Fe_2(PA_2mpd)_2Cl_4]Cl_2$	48.18	49.01	3.12	3.42	12.49	12.49	12.46	12.19	4.2
$[Fe(PA_2opd)Cl_2]Cl$	48.18	48.7	3.12	3.56	12.49	12.86	12.46	12.36	4.6

Table 2. Molar Conductance of the Metal Complexes

Complex	Solvent	Molar conductance $\Omega^{-1}cm^2mol^{-1}$
1	H_2O	576
	CH_3OH	—[a]
	CH_3CN-H_2O(6:1)	341
2	H_2O	598
	CH_3OH	205
	CH_3CN-H_2O(6:1)	279
3	H_2O	344
	CH_3OH	144
	CH_3CN-H_2O(6:1)	133

a) Poor solubility.

Table 3. Epoxidation of Norbornene with Iodosylbenzene Catalyzed by Metal Complexes (**1**—**3**)

Metal complex	Yield[a] of norbornene oxide (%)
1	6
2	8
3	2

a) Yields based on iodosylbenzene charged.

presented in Table 2. All the three complexes are soluble in water, but sparingly soluble in acetonitrile, dichloromethane and benzene. However, they are soluble in the acetonitrile-water (6:1) solvent mixture, which was used as a reaction medium for the epoxidation reactions.

The effectiveness of the complexes (**1**—**3**) as catalysts for epoxidation were compared using norbornene as the substrate and iodosylbenzene as an oxidant. The addition of iodosylbenzene to a system containing catalytic amounts of the complex and norbornene in an acetonitrile-water solvent mixture leads to complete reaction within 4 h. The results are given in Table 3. Control experiments showed that norbornene gave extremely low quantity of epoxide in the absence of catalyst. The credibility of anisole as an internal standard was checked by carrying out an oxidation reaction using anisole as the substrate. Anisole did not react under these conditions.

From the catalytic epoxidation of norbornene using the three catalysts, **2** was selected as the catalyst of choice. Oxidation capability of this complex was then screened against various alkenes. The results are presented in Table 4. Effect of various base additives, such as pyridine, 4-picoline, and imidazole has been studied. These results are shown in Fig. 1.

Table 4. Epoxidation of Various Alkenes Catalyzed by $[Fe_2(PA_2mpd)_2Cl_4]Cl_2$

Alkene	Yield[a] of epoxide %
Norbornene	8
Styrene	3
Cyclohexene	4[b]
cis-Cyclooctene	7
trans-4-Octene	2

a) Based on iodosylbenzene charged. b) 2-Cyclohexen-1-ol (7%) and 2-cyclohexen-1-one (22%) were also formed.

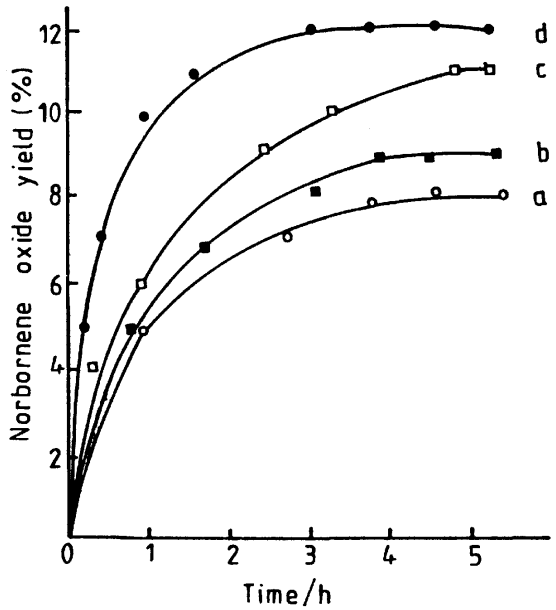

Fig. 1. Influence of base addition (3 mol equivalent) on epoxidation of norbornene catalyzed by $[Fe_2(PA_2mpd)_2Cl_4]Cl_2$. Conditions as given in experimental. a, without base; b, with imidazole; c, with pyridine and d, with 4-picoline.

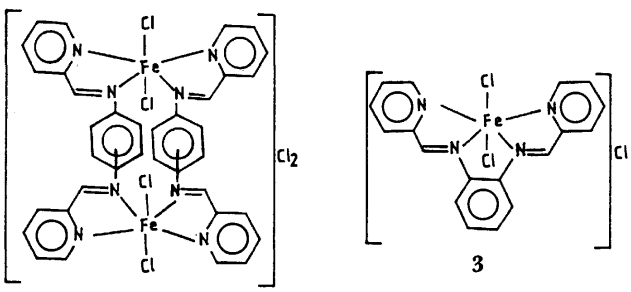

1, Bridge=*p*-phenylenediamine
2, Bridge=*m*-phenylenediamine

3

Fig. 2. Structures of the metal complexes.

Discussion

The analytical data presents the formula as $C_{36}H_{28}N_8Cl_6Fe_2$ for binuclear complexes and $C_{18}H_{14}N_4Cl_3Fe$ for the mononuclear complex. The structures of the complexes are shown in Fig. 2. Molecular conductivity measurements in water and in methanol show that four chloride ions in the binuclear complexes are inside, and two chlorides are outside the coordination sphere, whereas in the mononuclear complex one chloride is present outside and two inside the coordination sphere. Thermogravimetric analyses from ambient temperature to 800 °C rules out the possibility of any associated water molecules. The magnetic susceptibility measurements at room temperature show that the complexes (**1—3**) are high-spin paramagnetic compounds (4.2—5.13 BM). Infrared spectra of the complexes showed bands at 1615 cm^{-1} corresponding to the coordinated azomethine C=N-stretching, and at 1330 cm^{-1} corresponding to the coordinated C=N-stretching of the pyridyl ring.

Catalytic oxygenation of olefins is taken as evidence for the formation of the highly reactive oxoiron species. In iron porphyrin systems, this species have been identified as the Fe(IV) porphyrin π-radical complex $[FeO(P\cdot)]^+$. However, with one apparent exception no such oxoiron species has been isolated, but several have been spectroscopically detected in situ.[15]

In the present study, where iron Schiff base complexes are involved, the reaction probably proceeds through an oxoiron intermediate as in the porphyrin systems (Scheme 1). But electronic spectra of the complexes (**1—3**) in acetonitrile-water mixture (6 : 1) in the presence of iodosylbenzene did not show any new band for the transient oxoiron species. This may be due to the charge-transfer band masking the dd transition bands. However, it may be suggested that the catalytic reaction occurs via an oxoiron species as shown below (Scheme 1):

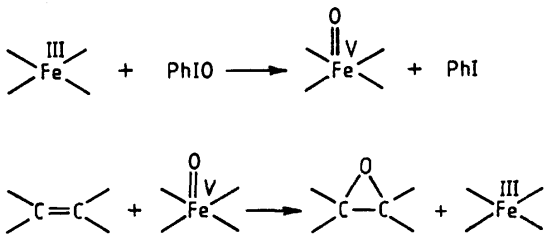

Scheme 1.

All the three catalysts were screened against norbornene to compare their oxidation capabilities. From the yields of norbornene oxide formed (Table 3), it is clear that both the binuclear complexes (**1**, **2**) are superior to the mononuclear complex (**3**). Out of the two binuclear complexes, the one with *m*-phenylenediamine Schiff base (**2**), is a better catalyst than the one with *p*-phenylenediamine Schiff base (**1**).

The formation of the oxo-bridged binuclear species Fe^{IV}-O-Fe^{IV} may be the reason for the termination of the catalytic activity. In case of binuclear complexes the formation of oxo-bridged species appear to be less probable than the mononuclear complex because of its bigger molecular size. However, the reasons for the superiority of the binuclear complex having *m*-phenylenediamine Schiff base over the one with *p*-pheneylenediamine Schiff base is not clear at present.

Addition of bases are known to increase the rates of the reaction dramatically without affecting much the overall yields.[16] However, in the present study of the epoxidation of norbornene, addition of various bases such as imidazole, pyridine, and 4-picoline, not only enhanced the rates but showed marked increase in the yields of epoxide. Addition of 4-picoline gave higher yield of epoxide, as compared to that with pyridine. In contrast to this, imidazole was comparatively less effective (Fig. 1).

Conclusion

The metal Schiff base complexes described here catalyze the epoxidation of olefins providing a good chemical model for monooxygenases. Their easy preparation from readily available materials as compared to that of metalloporphyrins makes them attractive catalyst for monooxygenase model studies.

References

1) J. E. Lyons, *Hydrocarbon Processing*, **1980**, 107.
2) N. S. Enikolopyan, K. A. Bogdanova, and K. A. Askarov, *Russ. Chem. Rev.*, **52**, 13 (1983).
3) D. Mansuy, M. Fontecave, and J. F. Bartoli, *J. Chem. Soc., Chem. Commun.*, **1983**, 253.
4) M. Perree-Fauvet and A. Gaudemer, *J. Chem. Soc., Chem. Commun.* **1981**, 874.
5) J. T. Groves, T. E. Nemo, and R. S. Myers, *J. Am. Chem. Soc.*, **101**, 1032 (1979).
6) E. Guilmet and B. Meunier, *Tetrahedron Lett.*, **21**, 4449 (1980).
7) A. Gold, W. Ivey, and M. Bowen, *J. Chem. Soc., Chem. Commun.*, **1981**, 293.
8) R. E. White, S. G. Sligar, and M. J. Coon, *J. Biol. Chem.*, **225**, 11108 (1980).
9) I. Tabushi and N. Koga, *J. Am. Chem. Soc.*, **101**, 6456 (1979).
10) E. Guilmet and B. Meunier, *Tetrahedron Lett.*, **23**, 2449 (1982).
11) S. Oae, Y. Watanabe, and K. Fujimori, *Tetrahedron Lett.*, **23**, 1189 (1982).
12) C. Floriani and G. Fachinetti, *J. Chem. Soc., Chem. Commun.*, **1973**, 17.
13) K. Srinivasan and J. K. Kochi, *Inorg. Chem.*, **24**, 4671 (1985).
14) E. G. Samsel, K. Srinivasan, and J. K. Kochi, *J. Am. Chem. Soc.*, **107**, 7606 (1985).
15) R. H. Holm, *Chem. Rev.*, **87**, 1401 (1987).
16) K. Srinivasan, S. Perrier, and J. K. Kochi, *J. Mol. Catal.*, **36**, 297 (1986).

Crystal and Molecular Structure of the Dicobalt(III) Complex Containing Bridging Di-μ-hydroxo Ligands, $[(gly)(en)Co(\mu\text{-}OH)_2Co(gly)(en)]^{2+}$

Kensaku HAMADA, Etsuko OHTA, Takaji FUJIWARA,* and Tomoharu AMA†
Department of Chemistry, Faculty of Science, Shimane University, Nisikawatsu, Matsue 690
†Department of Chemistry, Faculty of Science, Kochi University, Akebono-cho, Kochi 780
(Received August 11, 1988)

Synopsis. The molecular and crystal structure of the title compound has been determined by the X-ray method. The cation structure consists of well-separated dimeric pairs of the octahedrally coordinated cobalt(III) atom linked by two μ-hydroxo bridges. There are two intramolecular N-H···O hydrogen bonds bridging the two chromophores.

There have been many reports on the preparation and characterization of dicobalt(III) complexes containing two bridging hydroxo ligands.[1] The complexes of this type are fundamental in the study of the polynuclear complexes, and a comparative study of the geometrical isomers of the $(\mu\text{-}OH)_2$ complexes is important in clarifying the factor stabilizing the polynuclear structure. Recently, three isomers of the $[(gly)(en)Co(\mu\text{-}OH)_2Co(gly)(en)]^{2+}$ complex ion were synthesized by one of the present authors.[2] However, there are so many possible isomers (theoretically 20 isomers) in the complex ion that it is necessary to confirm the structure of the synthesized isomers by the X-ray method.

Experimental

$[(en)(gly)Co(\mu\text{-}OH)_2Co(en)(gly)]\cdot 2ClO_4$ was prepared by the method reported previously[2] and then recrystallized from a water-ethanol solution. A wine-red crystal with approximate dimensions of 0.30×0.18×0.15 mm^3 was used for the X-ray measurement. The unit-cell parameters and reflection intensities were measured on a Rigaku AFC-4 automatic four-circle diffractometer with graphite-momochromated Mo $K\alpha$ radiation (λ=0.71073 Å). Independent reflections with the range of $2\theta<55°$ were collected by the 2θ-ω scan technique. The scan width, scan rate, and background counting time at both ends of scan were $\Delta\omega=(1.2+0.35\tan\theta)°$, $4°(2\theta)min^{-1}$, and 4 s respectively. Three standard reflections were measured after every 100 reflections; they showed no decay during the intensity measurement. The Lorentz and polarization effects were corrected, but no corrections for absorption and extinction were applied. 2116 independent reflections with $F_o>3\sigma(F_o)$ were used for the structure analysis. The structure was solved by the direct method (MULTAN 78)[3] and refined by the block-diagonal least-squares procedure (HBLS-V),[4] with anisotropic thermal parameters for nonhydrogen atoms. The function minimized was $\sum w(|F_o|-|F_c|)^2$, where a unit weight was applied throughout the refinement. All the hydrogen atoms were found in the difference Fourier map and included in the refinements with isotropic thermal parameters. The final R-value was 0.051 (R_w=0.056). The final atomic parameters are listed in Table 1.[5] The atomic-scattering factors were taken from International Tables for X-ray Crystallography.[7] The computations were carried out on an IBM-3081 computer at the Information Processing Center of Shimane University.

Crystal data: $C_8H_{26}N_6O_6Co_2\ 2ClO_4\ 2H_2O$, $F.W.$=655.11, Monoclinic, $P2_1/n$, a=15.982(2), b=11.732(2), c=6.086(1) Å, β=94.51(1)°, Z=2, D_x=1.912 Mg m^{-3}, D_m=1.913(3) Mg m^{-3}, μ=1.84 mm^{-1}, $F(0\ 0\ 0)$=672.

Table 1. Final Atomic Coordinates (×10^5 for Co and Cl, ×10^4 for C, N, and O), with Estimated Standard Deviations in Parentheses, and Their Equivalent Isotropic Thermal Parameters

Atom	x	y	z	B_{eq}/Å^2 [6]
Co	−1818(4)	11767(5)	4148(9)	1.4
Cl	12628(8)	56596(11)	53719(25)	2.9
C(1)	−1806(3)	1602(5)	1612(8)	2.2
C(2)	−1311(3)	1045(4)	3564(8)	2.0
C(3)	1002(3)	2335(5)	−1870(8)	2.5
C(4)	822(4)	3144(4)	−39(9)	2.8
N(1)	−1222(2)	2041(3)	23(6)	1.9
N(2)	230(2)	1637(3)	−2327(6)	1.8
N(3)	484(2)	2440(3)	1730(6)	1.9
O(1)	−542(2)	801(3)	3279(5)	1.9
O(2)	−1639(2)	817(4)	5275(6)	3.1
O(3)	−747(2)	−142(3)	−786(5)	1.6
O(4)	2141(3)	5914(5)	5492(10)	5.7
O(5)	1111(4)	4554(4)	4559(10)	5.6
O(6)	977(4)	5710(6)	7568(11)	4.1
O(7)	826(4)	6506(6)	4172(15)	9.8
O(w)	2147(3)	1500(4)	3706(7)	4.0

Table 2. Bond Lengths and Angles, with Estimated Standard Deviations in Parentheses

(a) Bond lengths (Å)

Co-O(1)	1.929(3)	Co-O(3)	1.908(3)	Co-O[a]	1.917(3)
Co-N(1)	1.946(4)	Co-N(2)	1.919(4)	Co-N(3)	1.958(4)
N(1)-C(1)	1.488(7)	C(1)-C(2)	1.522(7)	C(2)-O(1)	1.287(6)
C(2)-O(2)	1.231(6)	N(2)-C(3)	1.489(7)	C(3)-C(4)	1.509(8)
C(4)-N(3)	1.491(7)	Cl-O(4)	1.431(6)	Cl-O(5)	1.403(6)
Cl-O(6)	1.447(7)	Cl-O(7)	1.388(10)		

(b) Bond angles (°)

O(1)-Co-O(3)	89.7(1)	O(1)-Co-N(1)	85.2(2)
O(1)-Co-N(2)	175.7(2)	O(1)-Co-N(3)	89.7(2)
O(3)-Co-N(1)	90.1(2)	O(3)-Co-N(2)	94.6(2)
O(3)-Co-N(2)	174.8(2)	N(1)-Co-N(2)	95.5(2)
N(1)-Co-N(3)	95.0(2)	N(2)-Co-N(3)	86.0(2)
O(3)-Co-O(3)[a]	82.6(1)	Co-O(3)-Co[a]	97.4(2)
Co-O(1)-C(2)	115.3(3)	Co-N(1)-C(1)	108.3(3)
Co-N(2)-C(3)	109.2(3)	Co-N(3)-C(4)	109.9(4)
N(1)-C(1)-C(2)	110.0(5)	C(1)-C(2)-O(1)	115.7(5)
C(1)-C(2)-O(2)	121.6(5)	O(1)-C(2)-O(2)	122.7(5)
N(2)-C(3)-C(4)	106.3(3)	C(3)-C(4)-N(3)	106.6(3)
O(4)-Cl-O(5)	110.7(4)	O(4)-Cl-O(6)	108.9(4)
O(4)-Cl-O(7)	109.2(5)	O(5)-Cl-O(6)	107.8(4)
O(5)-Cl-O(7)	114.2(5)	O(6)-Cl-O(7)	105.9(5)

a) $-x, -y, -z$.

Results and Discussion

The crystal structure consists of well-separated dimeric cations, perchlorate ions, and H_2O molecules. The bond distances and angles of the complex are listed in Table 2. A perspective view of the complex cation is shown in Fig. 1. The complex cation has an inversion center at the middle of the dimer. The coordination of Co(III) is roughly octahedral, and the bridging unit, Co-O-Co-O, is strictly planar. The Co-Co and O-O separations in the bridging unit are 2.874 (1) and 2.524 (4) Å respectively. The two independent bridging Co-O bond lengths are essentially the same (1.917 (3) and 1.908 (3) Å). The Co-O-Co and O-Co-O angles are 97.4 (2)° and 82.6 (1)° respectively. The geometry of the Co-O-Co-O bridging unit is similar to that of the Cr-O-Cr-O unit found in $[Cr(gly)_2(OH)_2]$[9] and $[Cr(L\text{-}Pro)_2(OH)_2]$.[10] There are two intramolecular hydrogen bonds formed between the N(2)-H ethylenediamine ligating to one of the two cobalt atoms and the O(1) of glycinate coordinated to the other cobalt atom, whose N(2)···O(1) length is 2.968(5) Å. The hydrogen bonds significantly contribute to stabilizing the dinuclear structure. The ethylenediamine-chelate ring adopts a gauche conformation, where C(3) and C(4) are 0.482(8) and −0.203(8) Å, from the plane of the three remaining atoms (Co, N(2), and N(3)). On the other hand, the glycinate-chelate ring adopts an envelope conformation, where C(1) and C(2) are 0.491(7) and 0.252(7) Å, from the plane of the remaining atoms (Co, N(1), and O(1)). As shown in Fig. 2, the O(2) and N(3) form intermolecular hydrogen bonds with the water molecules, and the lengths of O(2)···O(w) ($-x$, $-y$, $1-z$) and N(3)···O(w) (x, y, z) are 2.918(6) and 3.037(6) Å respectively. The N(2) forms an intermolecular hydrogen bond with the O(7) of the perchlorate ion, and

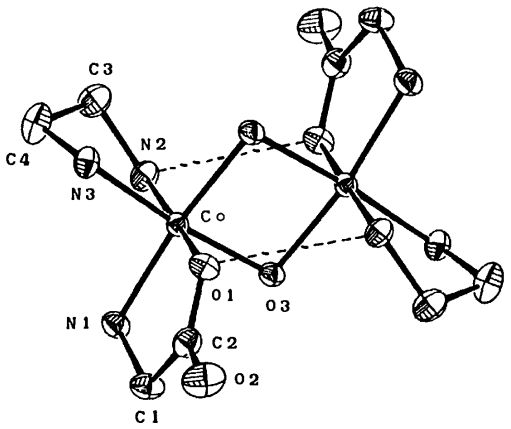

Fig. 1. A perspective view of the $[(gly)(en)Co(\mu\text{-}OH)_2Co(gly)(en)]^{+2}$ drawn by a ORTEP.[8] Thermal ellipsoids are drawn at the 50% probability. Hydrogen bonds are indicated by broken lines.

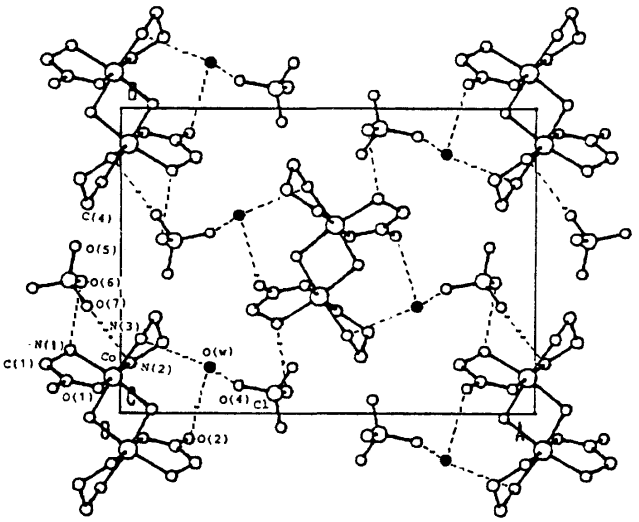

Fig. 2. A crystal structure of the complex along c-axis. Water molecules are drawn in solid circles. Hydrogen bonds are indicated by broken lines.

the length of N(2)···O(7) ($-x$, $1-y$, $-z$) is 2.925(10) Å. The N(1) also forms a hydrogen bond with the O(6), whose N(1)···O(6) ($-x$, $1-y$, $1-z$) length is 3.029(8) Å. The water molecule also forms an intermolecular hydrogen bond with O(4) of the perchlorate ion, O(w)···O(4) ($1/2-x$, $-1/2+y$, $1/2-z$) being 2.958(8) Å.

The authors wish to express their thanks to Professor Yukiteru Katsube of the Crystallographic Research Center, Institute for Protein Research, Osaka University, for the use of the diffractometer.

References

1) T. Ama, H. Kawaguchi, and T. Yasui, *Bull. Chem. Soc. Jpn.*, **60**, 1183 (1987).
2) T. Ama, A. Mukai, K. Miyauchi, H. Kawaguchi, and T. Yasui, *Mem. Fac. Sci. Kochi Univ., Ser. C*, **7**, 1 (1986).
3) P. Main, S. E. Hull, L. Lessinger, G. Germain, J.-P. Declercq, and M. M. Woolfson, MULTAN 78 "A System Computer Program for the Automatic Solution of Crystal Structures from X-ray Diffraction Data," Univs. of York, England, and Louvain, Belgium, 1978.
4) T. Ashida, HBLS V, "The Universal Crystallographic Computing System-Osaka," The Computation Center, Osaka University, 1979.
5) Tables of the observed and calculated structure factors, the anisotropic thermal parameters for nonhydrogen atoms, and the atomic parameters for hydrogen atoms are deposited at the Chemical Society of Japan as Document No. 8862.
6) W. C. Hamilton, *Acta Crystallogr.*, **12**, 609 (1959).
7) "International Tables for X-ray Crystallography," Kynoch Press, Birmingham, England (1974), Vol. IV, p. 71.
8) C. K. Jonson, ORTEP II, Report ORNL-5138, Oak Ridge National Laboratory, Tennessee, 1976.
9) J. T. Veal, W. Hatfield, D. Y. Jeter, J. C. Hempel, and D. J. Hodgson, *Inorg. Chem.*, **12**, 342 (1973).
10) H. Oki and H. Yoneda, *Inorg. Chem.*, **20**, 3875 (1981).

Intrinsic Reaction Coordinates for the Dissociation and the Isomerization Reactions of Formaldehyde

Seikichi CHO
Department of Chemistry, Faculty of Education, Gunma University, Aramakicho 4-2, Maebashi, Gunma 371
(Received September 9, 1988)

Synopsis. Static and dynamic intrinsic reaction coordinates are defined by using the eigenvectors of the force constant matrix, and the simultaneous eigenvectors of the relative kinetic energy and the force constant matrix, respectively. The theory was applied to the dissociation and the isomerization reactions of the formaldehyde molecule. It is shown that the intrinsic reaction coordinate of the dissociation reaction of formaldehyde left from the normal coordinate of the equilibrium formaldehyde with the second lowest wavenumber, the rocking mode of vibration, while that of the isomerization reaction departed from the scissoring mode having the third lowest wavenumber.

The transition state is usually defined as a stationary point, that is, all the first-order differentials are vanishing, and the force constant matrix has only one negative eigenvalue.[1] A unit vector along the direction of the eigenvector with a negative eigenvalue is called the transition vector by McIver and Stanton.[2] Fukui[3] defined the intrinsic reaction coordinate (IRC) as a curve passing through the initial and the transition points and orthogonal to the energy equipotential contour surface. He also proved that at a stationary point, the IRC merges with one of the eigenvectors of the force constant matrix. From these considerations we might infer that the IRC is alternatively defined as a curve along one of the eigenvectors of the force constant matrix with a negative or a small positive eigenvalue, and all the first order differentials along the eigenvectors other than the IRC are null. This statement can also be applicable to the normal coordinate space,[4] where the eigenvectors of the force constant matrix should be replaced by the simultaneous eigenvectors of the relative kinetic energy and the force constant matrix.[5]

The IRC's in ordinary space and in the normal coordinate space may differ, since the transformation matrix is not unitary, nor orthogonal. The former is *'static'* as it lies on an adiabatic potential surface, while the latter is *'dynamic'* as the normal coordinates are the solutions of the classical equations of motion, despite of vibration or 'infinitely slow' motion.[5] However, actual calculations showed that the two IRC's are unexpectedly simillar to each other. This is partially because at each stage corrections were made so that the first order differentials along eigenvectors other than the IRC were zero. To follow the 'dynamic' IRC has some merit; it gives the vibrational mode of the initial state from which the reaction departs, and also the change of vibration wavenumbers during the course of the reaction.

The IRC's of the formaldehyde molecule were treated by normal coordinate analysis using the STO-3G potential surface. Although the potential surface of the formaldehyde molecule has been extensively investigated with the more extended basis sets,[6] we apted to choose the minimal basis set as a consideration of cost and quality.

Now we briefly review the procedure to determine the IRC. At first a normal coordinate analysis is applied to a transition state and the resulting normal coordinates are normalized, as the normal coordinates are usually not normalized. Choosing the transition vector as the IRC vector, we proceed downwards along the IRC at a constant stepwidth. At the next point we repeat the normal coordinate analysis and again normalize the resulting normal coordinates. From these normalized normal coordinates we choose a new IRC vector by calculating the overlaps between these and the IRC vector at the previous point. If necessary, the correction is made so that the first-order differentials along the normal coordinates other than the IRC vector are zero.[5] Thus the steepest-descent requirement of IRC[7] is automatically satisfied. These procedures are repeated until an equilibrium point is attained, where the first-order differential along the IRC vector is zero.

The program was implemented into HONDO76[8] and the calculations were carried out on the HITAC M-240H computer located at Gunma University.

The vibrational wavenumbers of the equilibrium state calculated on the STO-3G potential surface were in the correct order, although the calculated values were generally larger than the observed ones. The numbering of the normal coordinates is in an increasing order of wavenumber, and that of the eigenvectors of the force constant matrix is also in an increasing order of the magnitude of the eigenvalues. The Q_1

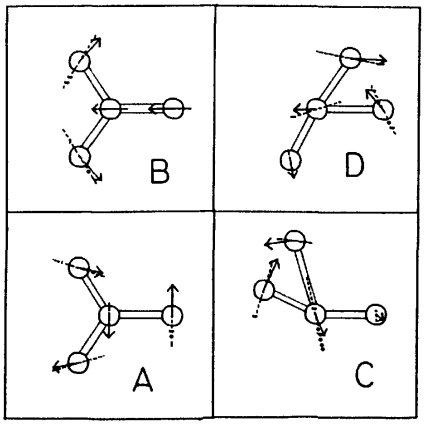

Fig. 1. Normalized normal coordinates and the nearest valleys on the formaldehyde STO-3G potential surface. (A) Q_2 and V_1; (B) Q_3 and V_2 at the equilibrium state; (C) Q_1 and V_1 at the dissociation transition state; (D) Q_1 and V_1 at the isomerization transition state (C_s symmetry).

normal coordinate is an out-of-plane wagging vibration and corresponds to the third eigenvector (V_3) of the force constant matrix, the third 'valley' of the potential energy surface. Q_1 is thus omitted from a candidate of IRC of the dissociation or the isomerization reaction. Q_2 and Q_3 might be chosen as IRC vectors, and are graphically shown in Fig. 1 with the nearest valleys. At this time it is difficult to decide, which normal coordinate, Q_2 or Q_3, lead to the dissociation reaction or the isomerization reaction of the formaldehyde molecule. The dissociation reaction IRC should pass the dissociation transition state,[9] and the isomerization IRC should go through the isomerization transition state.[9]

The transition vectors of the dissociation and the isomerization transition states are also shown in Fig. 1. (Actually using the geometry shown in Fig. 1-D, the formaldehyde molecule on the STO-3G potential surface has two imaginary wavenumbers and may be said to be on a '*hilltop*'. The lowest wavenumber vibration has C_s symmetry while the second one is in an out-of-plane mode. The more elaborate calculations[6] mentioned above gave C_s symmetry for the isomerization transition state of formaldehyde, so we ignored the second imaginary wavenumber vibration and adopted the C_s symmetry transition state.) The mode of the transition vector at the isomerization transition state (Fig. 1,D) is closely related to Q_3 of the equilibrium state (Fig. 1,B), while the correspondence between that of the dissociation transition state (Fig. 1,A) and Q_2 of the equilibrium state (Fig. 1,C) is not clear.

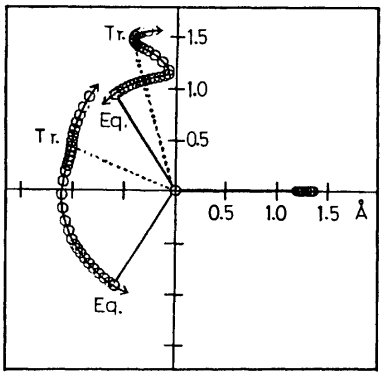

Fig. 2. Dissociation IRC of the formaldehyde on the STO-3G potential surface. The carbon atom is fixed at the origin and the oxygen atom is floating on the abscissa.

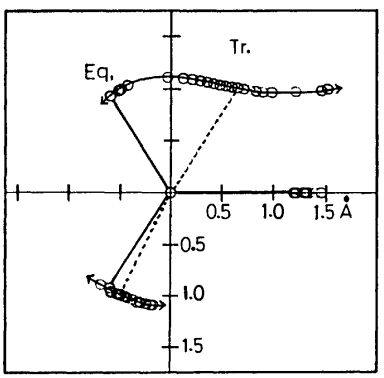

Fig. 3. Isomerization IRC of the formaldehyde on the STO-3G potential surface.

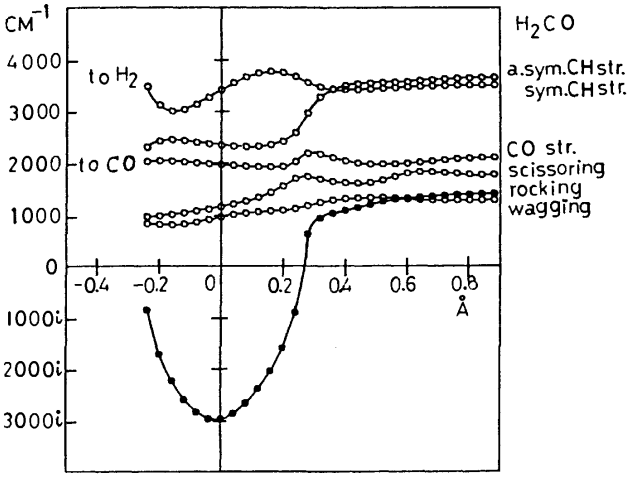

Fig. 4. Variations of vibrational wavenumbers in the course of the dissociation IRC of formaldehyde, calculated on the STO-3G potential surface.

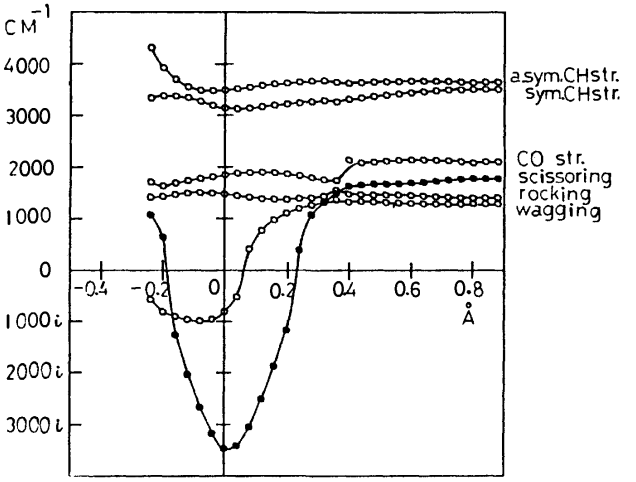

Fig. 5. Variations of vibrational wavenumbers in the course of the isomerization IRC of formaldehyde, calculated on the STO-3G potential surface.

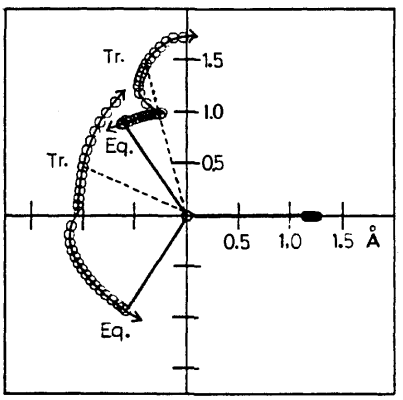

Fig. 6. '*Static*' IRC of the dissociation reaction of formaldehyde, calculated on the STO-3G potential surface.

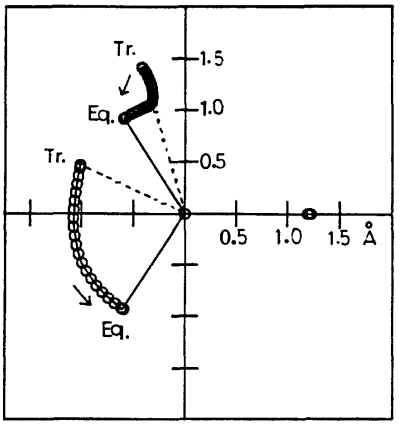

Fig. 7. *'Steepest descent'* IRC of the dissociation reaction of formaldehyde, calculated on the STO-3G potential surface, using the program GAMESS.[10]

The IRC's of the dissociation and the isomerization reactions of the formaldehyde molecule are shown in Figs. 2 and 3. The variations of the wavenumbers during the course of the IRC's are also shown in Figs. 4 and 5. From these figures it can be easily seen that the dissociation IRC and the isomerization IRC tend to the Q_2 (rocking) and the Q_3 (scissoring) mode of the equilibrium formaldehyde molecule, respectively. Finding these, we can follow the IRC's upwards to each transition state by leaving from Q_2 and Q_3, respectively.

The *'static'*, and the *'steepest descent'* IRC's calculated by GAMESS,[10] of the dissociation reaction of formaldehyde are shown in Figs. 6 and 7 for the comparison. Figure 6 resembles to the results by Cerjan and Miller[9] obtained on the adiabatic potential surface. On the other hand, the *'steepest descent'* IRC cannot reverse the direction, the uphill side from the equilibrium to the transition state.

In conclusion, the dissocation IRC of formaldehyde reaches the Q_2 normal coordinate (the rocking mode) at the equilibrium state, and the isomerization IRC leads to the Q_3 normal coordinate (the scissoring mode), respectlvely. The rocking and scissoring vibrations may be said to be 'key vibrations' of the dissociation and the isomerization reactions of equillbrium formaldehyde, in a sense recently described by Fuke et al.[11]

References

1) J. N. Murrel and K. J. Laidler, *Trans. Faraday Soc.*, **64**, 371 (1968).
2) J. W. McIver and R. E. Stanton, *J. Am. Chem. Soc.*, **94**, 8618 (1972).
3) K. Fukui, *J. Phys. Chem.*, **74**, 4161 (1970).
4) E. B. Wilson, Jr., *J. Chem. Phys.*, **7**, 1047 (1938); **9**, 76 (1941).
5) S. Cho, *Bull. Chem. Soc. Jpn.*, **58**, 3405 (1985); **60**, 1534 (1987).
6) J. D. Goddard and H. F. Schaefer, III, *J. Chem. Phys.*, **70**, 5117 (1979); J. D. Goddard, Y. Yamaguchi, and H. F. Schaefer, *ibid.*, **75**, 3459 (1981); L. B. Hardling, H. B. Schlegel, R. Krishnan, and J. A. Pople, *J. Phys. Chem.*, **84**, 3394 (1980).
7) K. Ishida, K. Morokuma, and A. Komornicki, *J. Chem. Phys.*, **66**, 2153 (1977).
8) M. Dupui, J. Rys, and H. King, HONDO76, QCPE No. 338. The present author would express sincere thanks to Prof. H. Ichikawa, Hoshi College of Pharmacy, for permitting to use the program.
9) C. J. Cerjan and W. H. Miller, *J. Chem. Phys.*, **75**, 2800 (1981); J. D. Goddard and F. Schaefer, *ibid.*, **70**, 5117 (1979).
10) M. Dupuis, D. Spangler, and J. J. Wendoloski, GAMESS, NRCC Software Catalog, Vol. 1, program QGO1 (1980).
11) K. Fuke, T. Yabe, N. Chiba, T. Kohida, and K. Kaja, *J. Phys. Chem.*, **90**, 2309 (1986).

The Amidation of Carboxylic Acid with Amine over Hydrous Zirconium(IV) Oxide

Kyoko TAKAHASHI, Makoto SHIBAGAKI,* Hideyuki KUNO, Hiroshi KAWAKAMI, and Hajime MATSUSHITA
Life Science Research Laboratory, Japan Tobacco, INC., 6-2 Umegaoka, Midori-ku, Yokohama, Kanagawa 227
(Received November 5, 1988)

Synopsis. The reaction of a carboxylic acid or an ester with an amine to give the corresponding amide was carried out efficiently over hydrous zirconium(IV) oxide, whether in the vapor phase or in the liquid phase.

Hydrous zirconium(IV) oxide is a colorless, translucent, amorphous, and hard solid. It is insoluble in organic solvents and stable at room temperature in air. In previous papers,[1-3] we reported that the reduction of aldehydes and ketones with 2-propanol proceeded efficiently over hydrous zirconium(IV) oxide. During our studies to clarify the scope and the limitations of the reaction and to characterize the hydrous zirconium(IV) oxide, it was found that the oxide could also catalyze the amidation of carboxylic acid with amine. A homogeneous catalyst such as phosphoric acid or alkoxide[4] of titanium or zirconium was ordinarily used in the amidation, but the isolation of the products involves tedious work-up procedures. On the other hand, alumina,[5-7] silica gel,[8,9] and silica-alumina have also been reported as heterogeneous catalysts of the amidation, and they had such advantages as the easy isolation of products. In order to compare the catalytic activity, amidations were carried out using hydrous zirconium(IV) oxide and other catalysts.

Experimental

Materials. The hydrous zirconium(IV) oxide was prepared in the manner reported earlier.[1-3] Commercial reagents were used for the amidation without further purification.

Vapor-Phase Reaction Procedure. The catalytic amidation was carried out in a glass-flow reactor (6.5 mm or 7.0 mm in diameter) with a fixed-bed catalyst: flow rate of nitrogen gas=30—60 $cm^3 min^{-1}$, catalyst=2.0 g, reaction temperature=150—200 °C. A mixture of carboxylic acid or ester, amine or aqueous ammonia (28%), and dodecane or tridecane as an internal standard was fed, by means of a microfeeder, into the reactor (5 $cm^3 h^{-1}$). In the case of the reaction with ammonia gas, a benzene solution of carboxylic acid or ester was fed an excess amount of ammonia gas. The products were then analyzed by means of gas chromatography (a capillary column; PEG 20M 30 m).

Liquid-Phase Reaction Procedure. In a 25 cm^3 round-bottomed flask equipped with a reflux condenser were placed the catalyst (2.0 g), a carboxylic acid or ester, an amine, and a hydrocarbon as an internal standard. The contents were heated under a gentle reflux. In the reaction with ammonia, excess ammonia was supplied to the reaction solution of benzene before heating. In some reactions, xylene or toluene was added to the solution in order to raise the reaction temperature. The reaction mixture was col-

Table 1. Vapor-Phase Amidations over Hydrous Zirconium(IV) Oxide[a]

Entry	Reactant		Conditions[b]	Temp/°C	Yield/%
1	CH_3COOH	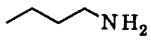	A	200	100
2	$CH_3COOC_2H_5$	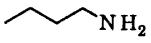	B	200	100
3	$CH_3COOC_2H_5$	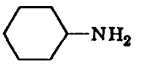	B	200	100
4	$CH_3COOC_2H_5$	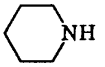	B	200	96
5	CH_3COOH	NH_3	C	150	97
6	C_2H_5COOH	NH_3	C	150	88
7	CH_3COOH	NH_3	C	100	—
8	CH_3COOH	NH_3	C	200	Tr[c]
9	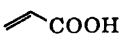	NH_3	C	150	—[d]
10	C_2H_5COOH	aq. NH_3	D	150	33
11	C_2H_5COOH	aq. NH_3	D	200	53
12	CH_3COOH	aq. NH_3	E	200	58
13	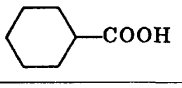	aq. NH_3	E	200	57

a) Catalyst: 2.0g, N_2: 30—60 $cm^3 min^{-1}$, sample feed: 5 $cm^3 h^{-1}$. b) Conditions A: CH_3COOH: n-$C_4H_9NH_2$=1:5; Conditions B: $CH_3COOC_2H_5$:amine=10:1; Conditions C: acid: 0.20 mol dm^{-3} in benzne; Conditions D: acid: 0.20 mol dm^{-3} in aq NH_3 (28%); Conditions E: acid: 0.10 mol dm^{-3} in aq NH_3 (28%). c) Acetonitrile was mainly produced. d) Polymerization.

Table 2. Liquid-Phase Amidations with Hydrous Zirconium(IV) Oxide[a)]

Entry	Reactant (mmol)				Yield/%
1	CH_3COOH	(10)		(50)	100
2[b)]	CH_3COOH	(10)	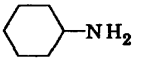	(15)	60
3[c)]	CH_3COOH	(10)	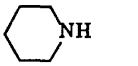	(15)	75
4	$CH_3COOC_2H_5$	(50)		(5)	79
5	$CH_3COOC_2H_5$	(50)	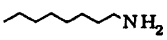	(5)	10
6	$C_2H_5COOC_2H_5$	(50)	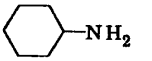	(5)	80
7	$CH_3COOC_2H_5$	(50)	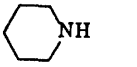	(5)	60
8[b)]	C_2H_5COOH	(10)	NH_3[d)]		31
9[c)]	C_2H_5COOH	(10)	NH_3[d)]		27
10[c)]	C_2H_5COOH	(10)	NH_3[d)]		51[e)]
11[c)]	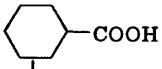	(10)	NH_3[d)]		34[e)]
12[c)]		(10)	NH_3[d)]		44[e)]
13[b)]	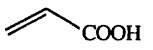	(10)	NH_3[d)]		—[f)]

a) Catalyst: 2.0 g, reflux for 5 h. b) Toluene: 8 cm^3. c) Xylene: 8 cm^3. d) NH_3 was saturated in the solvent. e) NH_3 was added during the reaction. f) Polymerization.

lected after 5 hours' reflux, and the products were analyzed by means of gas chromatography. The products was identified by a comparison of their retention times with those of authentic samples.

Results and Discusion

Vapor-Phase Reaction. The results of the vapor-phase amidation of some carboxylic acids or esters with amine, ammonia, and aqueous ammonia over hydrous zirconium(IV) oxide are listed in Table 1. The amidation of acetic acid or ethyl acetate with amine gave a corresponding amide in high yields at 200 °C (Entries 1—4). The amidation of acetic acid with ammonia at 150 °C gave acetamide in a high yield (Entry 5). At 100 °C, the amidation did not proceed (Entry 7). At 200 °C, acetonitrile was mainly obtained by the subsequent dehydration of the product (Entry 8). These results suggest that the selectivity of the reaction is strongly affected by the reaction temperature. The reaction of acrylic acid with ammonia caused undesirable polymerization (Entry 9). The amidation of carboxylic acid with aqueous ammonia at 200 °C gave the corresponding amides (Entries 10—13), though in lower yields.

Liquid-Phase Reaction. The results of the liquid-phase amidation of carboxylic acid or ester with amine or ammonia over hydrous zirconium(IV) oxide are shown in Table 2. The hydrous zirconium(IV) oxide also catalyzed the amidation of carboxylic acid with ammonia in the liquid phase. Since ammonia gas was liberated under the reflux conditions, an additional supply of ammonia during the reaction could improve the yield, as is shown in the case of the amidation of propionic acid (Entry 10).

Table 3. Catalytic Activities of Several Catalysts

Catalyst	Yield/%	
	A	B
Hydrous zirconium(IV) oxide	100	100
Hydrous titanum(IV) oxide	92	63
Hydrous tin(IV) oxide	90	3
Hydrous cerium(IV) oxide	—	39
Hydrous aluminum(III) oxide	14	1
Hydrous iron(III) oxide	29	8
Hydrous niobium(V) oxide	75	24
Silica gel	87	2
Zeolite, A-4	25	8
Al_2O_3	1	2
ZrO_2	1	2
Al_2O_3-SiO_2	91	2

Catalyst: 2.0 g. A Vapor-phase: 200 °C, N_2; 60 cm^3 min^{-1}, CH_3COOH: n-$C_4H_9NH_2$=1:5, sample feed; 5 cm^3h^{-1}. B Liquid-phase: reflux 5 h, CH_3COOH; 10 mmol, n-$C_4H_9NH_2$; 50 mmol.

Comparison of Catalytic Activity among Several Catalysts. The liquid-phase and vapor-phase amidations of acetic acid with butylamine were carried out by using different heterogeneous catalysts. The results are shown in Table 3. In the case of vapor-phase amidation, hydrous zirconium(IV) oxide, hydrous titanium(IV) oxide, hydrous tin(IV) oxide, silica gel, and silica-alumina worked efficiently. However, only hydrous zirconium(IV) oxide acted as an efficient catalyst for the liquid-phase amidation. It was concluded that the hydrous zirconium(IV) oxide is the most active catalyst in these types of amidations.

References

1) M. Shibagaki, K. Takahashi, and H. Matsushita, *Bull. Chem. Soc. Jpn.*, **61**, 3283 (1988).
2) H. Matsushita, S. Ishiguro, H. Ichinose, A. Izumi, and S. Mizusaki, *Chem. Lett.*, **1985**, 731.
3) H. Matsushita and S. Ishiguro, *Agric. Biol. Chem.*, **49**, 3071 (1985).
4) Achim Werdehausen, Herbert Weisse, and Hartwig Schuette (Henkel und Cie. G. m. b. H.), Ger. Offen. 2026832 (1971); *Chem. Abstr.*, **76**, 45768s (1972).
5) A. S. Basov, Sh. A. Zelenaya, and T. I. Pantelei, *Maslo-Zhir. Prom.*, **32**, 14 (1966); *Chem. Abstr.*, **64**, 14431e (1966).
6) Sh. A. Zelenaya, A. S. Basov, and G. M. Shubina, *Maslo-Zhir. Prom.*, **35**, 23 (1969); *Chem. Abstr.*, **72**, 54692g (1970).
7) Artur Blade-font, *Tetrahedron Lett.*, **21**, 2443 (1980).
8) M. Takahisa, M. Osugi, and K. Takeuchi, *Jpn. Kokai Tokkyo Koho* JP **82** 38754 (1982).
9) T. Ota, Jpn. Patent **69** 10249 (1969).

Voltammetric Characterization of α- and β-Dodecamolybdophosphates in Aqueous Organic Solutions

Sadayuki HIMENO,* Toshiyuki OSAKAI, and Atsuyoshi SAITO
Department of Chemistry, College of Liberal Arts, Kobe University, Nada-ku, Kobe 657
(Received April 28, 1988)

Synopsis. The electrochemical properties of α- and β-dodecamolybdophosphates were characterized at the glassy carbon (GC) electrode. It was found that the β-isomer was only stable in neat organic solvents. When molybdophosphate was prepared in aqueous organic solutions, a mixture of α- and β-isomers formed.

It has been known that heteropolymolybdates known as Keggin anions exist in α- and β-modifications.[1,2] According to Halasz and Pungor,[3] the β-modification converts spontaneously into the α-modification for silico- and germanomolybdic acids while α-arsenomolybdic acid changes into the β-modification.

As for phosphomolybdic acid, the increase of the absorbance by the presence of water-miscible organic solvents has been accounted for in terms of the formation of the β-form.[4] It has been assumed that both α- and β-forms are stable and no isomerization occurs. Recently Hori and Fujinaga have obtained spectrophotometric evidence that the irreversible change of β-molybdophosphate into the α-form occurs in aqueous organic solvents.[5] However, the solution chemistry of the β-form is still obscure.

Electrochemical measurements have proved to be suitable for distinguishing clearly between both forms of molybdophosphate. The purpose of the present study is to characterize both isomers in aqueous organic solutions.

Experimental

The electrochemical measurements were made with a PAR (Princeton Applied Research) Model 174-A polarographic analyzer and a computer-controlled voltammetry system.[6] The voltammograms were recorded on a Riken Denshi Model D-8CP X-Y recorder. Working electrodes were GC rods of 3 mm diameter (GC-30S, Tokai Carbon) which were mounted in a Teflon tube by means of silicone rubber tubing. A saturated calomel electrode (SCE) was used as a reference and a platinum wire as a counter electrode.

Ultraviolet(UV)-visible spectra were obtained with a Hitachi Model 220-A spectrophotometer equipped with a constant temperature housing for the cell. Electrochemical and spectrophotometric measurements were carried out at 25±0.1 °C.

β-$[(n\text{-}C_4H_9)_4N]_3PMo_{12}O_{40}$ was prepared by the method of Rocchiccioli-Deltcheff et al.[7] Phosphomolybdic acid, $H_3PMo_{12}O_{40}\,xH_2O$ was purchased from E. Merck. This acid is referred to as the stable α-compound. The anhydrous acid obtained by heating at 150 °C was used. For the sake of brevity, Keggin anions, $XMo_{12}O_{40}^{m-}$ will be designated as XMo_{12} in the following, where X=P, Si, Ge, and As. All other reagents were of analytical grade and were used as received.

Results and Discussion

Electrochemistry of α- and β-PMo_{12}. Figure 1(a) shows a cyclic voltammogram of 1.60×10^{-4} M (M= mol dm^{-3}) α-PMo_{12} in 80% (v/v) CH_3CN containing 0.1 M HCl. Reduction waves were observed with peak potentials (E_p's) of +0.25, +0.14, −0.10, and −0.29 V. The anodic peaks occurred at +0.27, +0.16, −0.08, and −0.25 V in the reverse scan.[8-11]

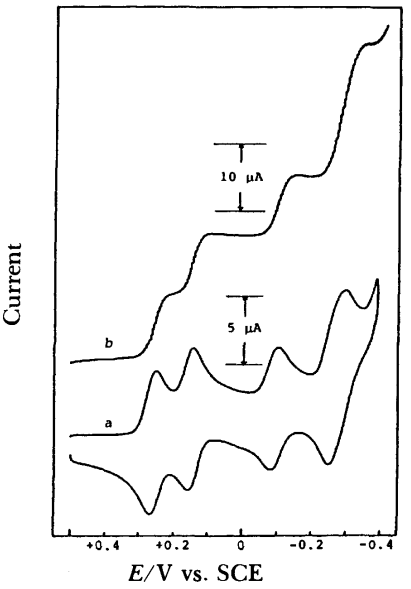

Fig. 1. A cyclic voltammogram (a) and a normal pulse polarogram (b) of 1.60×10^{-4} M α-PMo_{12} in 80% (v/v) CH_3CN containing 0.1 M HCl. Scan rate, (a) 100 mV s^{-1}; (b) 10 mV s^{-1}.

For the reduction of $SiMo_{12}$, $GeMo_{12}$, and $AsMo_{12}$, the polarographic half-wave potentials ($E_{1/2}$'s) of the β-isomers are more positive than those of the corresponding α-isomers.[2] According to Fruchart and Souchay,[12] a four-electron reduction species of β-PMo_{12} showed two oxidation waves with $E_{1/2}$'s of +0.55 and +0.37 V and a reduction wave with an $E_{1/2}$ of −0.07 V in 1 M $HClO_4$, while the oxidized form of α-PMo_{12} showed four reduction waves with $E_{1/2}$'s of +0.36, +0.22, −0.01, and −0.15 V vs. SCE in 1 M $HClO_4$ containing 50% dioxane at a rotating platinum electrode. On the basis of their findings, it has been assumed that β-PMo_{12} is electroreduced at more positive potentials than α-PMo_{12}. However, there have been no previous studies on the voltammetric behavior of the oxidized form of β-PMo_{12}.

Figure 2(a) shows a typical cyclic voltammogram of 1.68×10^{-4} M β-PMo_{12} in 80% (v/v) CH_3CN containing 0.1 M HCl. The peak potentials for the cathodic waves are: +0.35, +0.25, −0.15, and −0.34 V while those for the anodic waves are: +0.38, +0.28, −0.12, and −0.27 V. Each wave is diffusion-controlled. Coulometric analysis showed that the first three waves corresponded to a

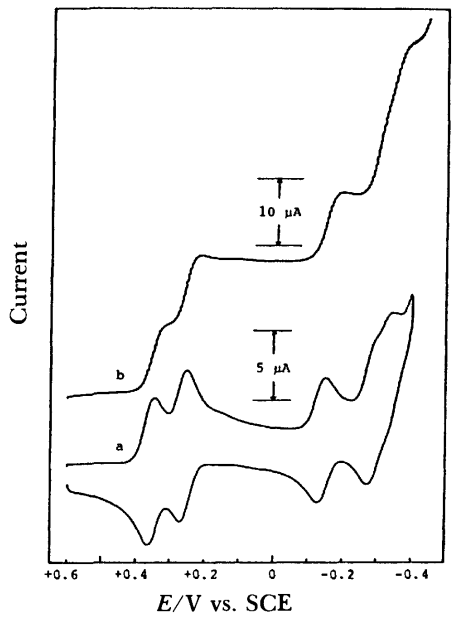

Fig. 2. A cyclic voltammogram (a) and a mormal pulse polarogram (b) of 1.68×10^{-4} M β-PMo_{12} in 80% (v/v) CH_3CN containing 0.1 M HCl. Scan rate, (a) 100 $mV\,s^{-1}$; (b) 10 $mV\,s^{-1}$.

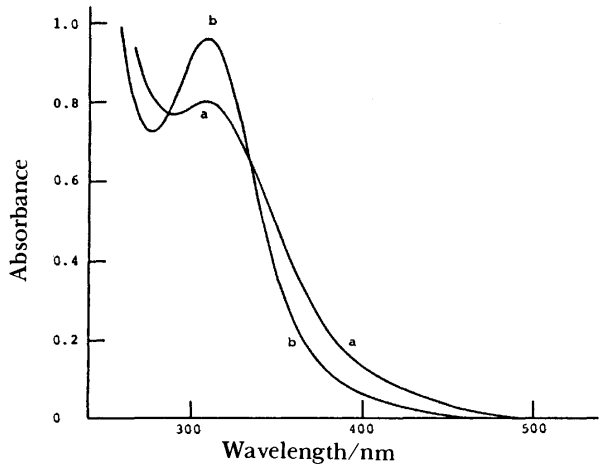

Fig. 3. UV-visible spectra of 4.2×10^{-5} M α- and β-PMo_{12}. (a) β-PMo_{12} in neat CH_3CN; (b) α-PMo_{12} in 70% (v/v) CH_3CN. Path length, 1 cm.

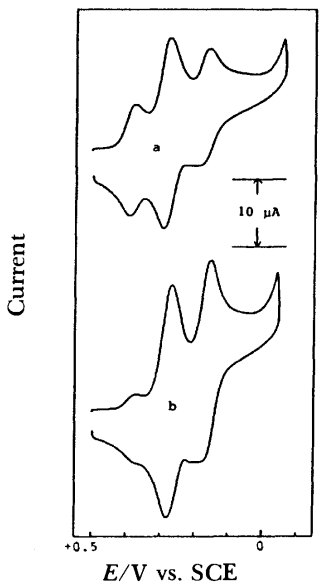

Fig. 4. Cyclic voltammograms of the 10.0 mM Mo(VI)/0.5 M HCl/40% (v/v) CH_3CN/0.5 mM phosphate system. (a) Immediately after the addition of phosphate; (b) 60 min after the addition of phosphate. Scan rate, 100 $mV\,s^{-1}$.

two-electron reduction and the fourth to a four-electron reduction. Curve (a) was obtained immediately after the addition of β-PMo_{12} in the solution. When the solution was allowed to stand, a reduction wave with an E_p of +0.14 V appeared. From a comparison with curve (a) of Fig. 1 it follows that β-PMo_{12} changes gradually into the α-form. It should be noted that the E_p for the 1st wave of α-PMo_{12} is identical with that for the 2nd wave of β-PMo_{12}. Curves (b) in Figs. 1 and 2 show the corresponding normal pulse polarograms of α- and β-PMo_{12} in 80% (v/v) CH_3CN containing 0.1 M HCl. Both polarograms resemble in shape and their limiting current ratios are 1 : 1 : 1 : 2, fitting the 2 : 2 : 2 : 4 electron ratios.

Formation of α- and β-PMo_{12} in Aqueous Organic Solutions. The yellow color of PMo_{12} is enhanced by the presence of water-miscible organic solvents such as acetonitrile and acetone. Since the color enhancement has been used for the spectrophotometric determination of the orthophosphate ion, it seems important to clarify the properties of α- and β-PMo_{12} in aqueous organic solutions. Figure 3(a) shows a UV-visible spectrum of 4.2×10^{-5} M β-PMo_{12} in neat CH_3CN. The spectrum was unchanged under these conditions. In 70% (v/v) CH_3CN solutions, on the other hand, the yellow color faded with time. Simultaneously, the gradual change of the spectrum was observed. Curve (b) is the spectrum of α-PMo_{12} obtained after standing for 3 h; as discussed below, the complete transformation of β-PMo_{12} to α-PMo_{12} was confirmed by the voltammetric measurements. The oxidized form of each isomer shows a common absorption maximum at 308 nm. The molar absorption coefficients of α- and β-PMo_{12} at 420 nm are calculated as 990 and 2120 $cm^{-1}M^{-1}$, respectively. Since UV-visible spectra of α- and β-forms are very similar, it is difficult to identify individual anions when both anions coexist in solution. As shown in Figs. 1 and 2, on the other hand, α- and β-PMo_{12} showed their characteristic reduction waves.

Therefore voltammetric measurements were made to elucidate the formation and conversion reactions of α-and β-PMo_{12} in aqueous organic solutions. Similar experiments were carried out with coulopotentiography.[13] An aliquot of 0.1 M phosphate solution was added to a 20 ml solution consisting of 10 mM Mo(VI)/0.5 M HCl/40% (v/v) CH_3CN, and the cyclic voltammogram was taken immediately after the addition of phosphate. As shown in Fig. 4(a), three reduction waves appeared with E_p's of +0.37, +0.27, and +0.15 V until the final current rise due to the reduction

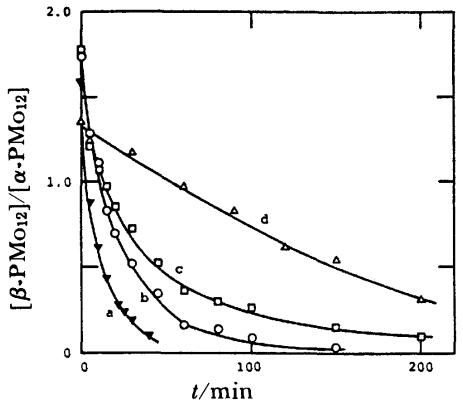

Fig. 5. Dependence of the ratio of [β-PMo_{12}] to [α-PMo_{12}] on time for 50 mM Mo(VI)/0.5 M HCl/0.5 mM phosphate systems containing 40% (v/v) organic solvents; (a) ethanol, (b) acetonitrile, (c) 1,4-dioxane, (d) acetone.

of Mo(VI). The 1st and 2nd waves correspond to the reduction of β-PMo_{12}, and the 2nd and 3rd waves to the reduction of α-PMo_{12}. When the solution was allowed to stand, as shown in curve (b) of Fig. 4, the 1st wave decreased with a simultaneous increase of the 3rd wave, which indicates the spontaneous conversion of β-PMo_{12} to α-PMo_{12}.

Normal pulse polarographic measurements were carried out in order to study the kinetics of the transformation of β-PMo_{12} to α-PMo_{12} in aqueous organic solutions. Figure 5 shows the change of the ratio of [β-PMo_{12}] to [α-PMo_{12}] with time for 50 mM Mo(VI)/0.5 M HCl/0.5 mM phosphate systems containing 40% (v/v) ethanol, acetonitrile, 1,4-dioxane, and acetone. The ratio of [β-PMo_{12}] to [α-PMo_{12}] in solution was determined by measuring the limiting currents of the 1st and 2nd waves.[9] It was found that the transformation rate was the slowest in the acetone-containing solution. Kinetic analysis for the curves showed that the conversion reaction was of the first-order, and the rate constants were calculated as 7.6×10^{-4}, 3.3×10^{-4}, 1.9×10^{-4}, and 0.6×10^{-4} s^{-1} in solutions containing ethanol, acetonitrile, 1,4-dioxane, and acetone, respectively. As the concentrations of organic solvents were increased, the transformation rates became slower. However, the ratio of [β-PMo_{12}] to [α-PMo_{12}] did not exceed 2 in solutions containing the organic solvents examined here. It should be emphasized that a mixture of α- and β-PMo_{12} is always obtained in aqueous organic solvents.

References

1) J. D. H. Strickland, *J. Am. Chem. Soc.*, **74**, 868 (1952).
2) M. T. Pope, "Heteropoly and Isopoly Oxometalates," Springer-Verlag, Berlin (1983).
3) A. Halasz and E. Pungor, *Talanta*, **18**, 569 (1971).
4) R. A. Chalmers and A. G. Sinclair, *Anal. Chim. Acta*, **33**, 384 (1965); **34**, 412 (1966).
5) T. Hori and T. Fujinaga, *Bull. Chem. Soc. Jpn.*, **58**, 1380 (1985).
6) T. Osakai, T. Nuno, T. Kakutani, and M. Senda, *Rev. Polarogr. (Kyoto)*, **33**, 73 (1987).
7) C. Rocchiccioli-Deltcheff, M. Fournier, R. Franck, and R. Thouvenot, *Inorg. Chem.*, **22**, 207 (1983).
8) E. Itabashi, *Bull. Chem. Soc. Jpn.*, **60**, 1333 (1987).
9) J. P. Launay, R. Massart, and P. Souchay, *J. Less-Common Metals*, **36**, 139 (1974).
10) G. A. Tsigdinos and C. J. Hallada, *J. Less-Common Metals*, **36**, 79 (1974).
11) K. Unoura and N. Tanaka, *Inorg. Chem.*, **22**, 2963 (1983).
12) J. M. Fruchart and P. Souchay, *C. R. Acad. Sci. Ser. C*, **266**, 1571 (1968).
13) T. Hori and T. Fujinaga, *Chem. Lett.*, **1983**, 687; *Talanta*, **30**, 925 (1983).

Kinetics of the Thermal Intramolecular Redox Reaction of Pentaamminenitrosylcobalt(III) Chloride in the Solid State

Kikuo MIYOKAWA,*,† Hakaru MASUDA, and Hisanobu WAKITA
Department of Chemistry, Faculty of Science, Fukuoka University, Fukuoka 814-01
(Received August 17, 1988)

Synopsis. The kinetics of the thermal intramolecular redox reaction between NO^- and Co(III) in $[Co(NH_3)_5NO]Cl_2$ has been studied by means of thermogravimetric and thermomagnetic analyses. The reaction is found to follow the first-order equation, with $\Delta H^*=129\pm6$ kJ mol^{-1} and $\Delta S^*=14\pm16$ J mol^{-1} K^{-1}. These results are compared with the kinetics of other nitrosylcobalt(III) and hexaamminecobalt(III) complexes.

It is well-known that the thermal decomposition of cobalt(III) complexes is often accompanied by an intramolecular redox reaction between the Co(III) ion and the ligand.[1] However, the kinetics of the reaction which characterizes the thermal property of Co(III) complexes has not been studied well[2—4] because the complicated decomposition reaction of the ligand oxidized by the Co(III) ion makes it difficult to examine the kinetics by means of a usual technique like thermogravimetry.

Pentaamminenitrosylcobalt(III) chloride has a "bent" NO group and has been depicted formally as having the bonding unit[5] Co(III)-NO^-. This complex decomposes around 350 K to evolve nitrogen monoxide and ammonia, yielding the amminecobalt(II) complex as the solid product.[6] As the decomposition temperature is fairly low for a cobalt(III) complex it seems of interest to compare its kinetic properties with those of other cobalt(III) complexes. Since the diamagnetic nitrosyl complex yields a paramagnetic, high-spin cobalt(II) complex, the kinetics of the intramolecular redox reaction can be effectively followed by measuring the change in the magnetic susceptibility of the sample. We wish to report here the kinetics of the intramolecular redox reactions of $[Co(NH_3)_5NO]Cl_2$ as examined by means of thermomagnetic analysis,[7] which has previously been successfully applied to the kinetic study of low spin $\rightleftarrows$ high spin transformation of bis(*N*-substituted-salicylideneaminato)nickel(II) in the solid state.[8]

Experimental

$[Co(NH_3)_5NO]Cl_2$ was prepared according to the published procedure;[9] it was identified by means of elemental analyses and magnetic-susceptibility measurements. The thermomagnetic analysis was carried out using a thermomagnetic analysis instrument constructed by assembling a Faraday-type magnetobalance, an infrared-lamp furnace, and a temperature-controller.[8,10] The isothermal thermomagnetic curves (hereafter abbreviated as ITM curves) were obtained by plotting the change in the sample weight induced when the magnetic field was applied to the sample against the time, while the sample was kept under isothermal conditions; the sample was usually heated to the desired temperature at a heating rate of 200 K min^{-1}. The strength of the applied magnetic field was regulated to an appropriate constant value of around 0.85 T. The isothermal weight-loss curves (hereafter abbreviated as IWL curves) were recorded on the same instrument when no magnetic field was applied to the sample.

Results and Discussion

The thermogravimetric (heating rate=1 K min^{-1}) and pyrolysis gas-chromatographic analyses have indicated that the thermal decomposition of $[Co(NH_3)_5NO]Cl_2$ proceeds through three stages:[6]

$$[Co(NH_3)_5NO]Cl_2 \xrightarrow{353-413\ K} Co(NH_3)_2Cl_2 + 3NH_3 + NO$$

$$Co(NH_3)_2Cl_2 \xrightarrow{413-427\ K} Co(NH_3)Cl_2 + NH_3$$

$$Co(NH_3)Cl_2 \xrightarrow{>427\ K} CoCl_2 + NH_3$$

As the redox reaction occurs in the first stage of decomposition, the kinetic analysis was carried out in the temperature range of 363—377 K.

The apparent increase in the sample weight at the time t induced by applying the magnetic field, ΔW_t, is given by Eq. 1:

$$\Delta W_t = H_c(\chi_r W_{r,t} + \chi_p W_{p,t}) \quad (1)$$

where χ_r and $W_{r,t}$ denote, respectively, the gram magnetic susceptibility and the weight of $[Co(NH_3)_5NO]Cl_2$ in the sample at the time t; χ_p and $W_{p,t}$ are corresponding values for $Co(NH_3)Cl_2$. The H_c is a constant value determined by the apparatus and the strength of the applied magentic field. The weight change when the reaction has been completed, ΔW_f, is expressed by:

$$\Delta W_f = H_c \chi_p W_{p,f} \quad (2)$$

where $W_{p,f}$ is the final weight of the product. Then the ratio of ΔW_t to ΔW_f is given by:

$$\Delta W_t/\Delta W_f = \chi_r/\chi_p(W_{r,t}/W_{p,f}) + W_{p,t}/W_{p,f} \quad (3)$$

In the present experiments, χ_r/χ_p was virtually zero ($<1\times10^{-3}$), so that the first term on the right-hand side of Eq. 3 can be neglected, and the fraction of $[Co(NH_3)_5NO]Cl_2$-reduced α_{ITM}, which is defined as $W_{p,t}/W_{p,f}$, becomes equal to $\Delta W_t/\Delta W_f$:

$$\alpha_{ITM} = \Delta W_t/\Delta W_f$$

From the IWL curves α_{IWL} is calculated as:

$$\alpha_{IWL} = (W_t - W_i)/(W_i - W_f)$$

where W_i and W_f represent the initial and final weights of the sample respectively and W_t, the weight

† Present address: Laboratory of Chemistry, Hitotsubashi University, Kunitachi, Tokyo 186.

Table 1. Kinetic Data of Intramolecular Redox Reactions of $[Co(NH_3)_5NO]Cl_2$ and Related Complexes

Complex	T/K	$k/10^{-4}\,s^{-1}$	$\Delta H^{\ddagger}_{300}$ / kJ mol^{-1}	$\Delta S^{\ddagger}_{300}$ / J K^{-1} mol^{-1}	$-\log(k_{300}/s^{-1})$
$[Co(NH_3)_5NO]Cl_2$[a]	362.6	1.37±0.01 (1.50±0.02)	127±8 (131±9)	9±21 (18±25)	7.72
	367.4	2.33±0.04 (2.26±0.04)			
	371.5	4.27±0.07 (4.27±0.05)			
	377.2	7.16±0.19 (7.70±0.20)			
CoL^4NO[b]			120—124	−(52—67)	10.2—10.5
$[Co(NH_3)_6]Cl_3$[c]			153±5	−9±3	13.1
$[Co(NH_3)_6]I_3$[c]			113±17	−57±45	8.62

a) Kinetic data from isothermal weight-loss curves are given in parentheses. b) Ref. 3. c) Ref. 4.

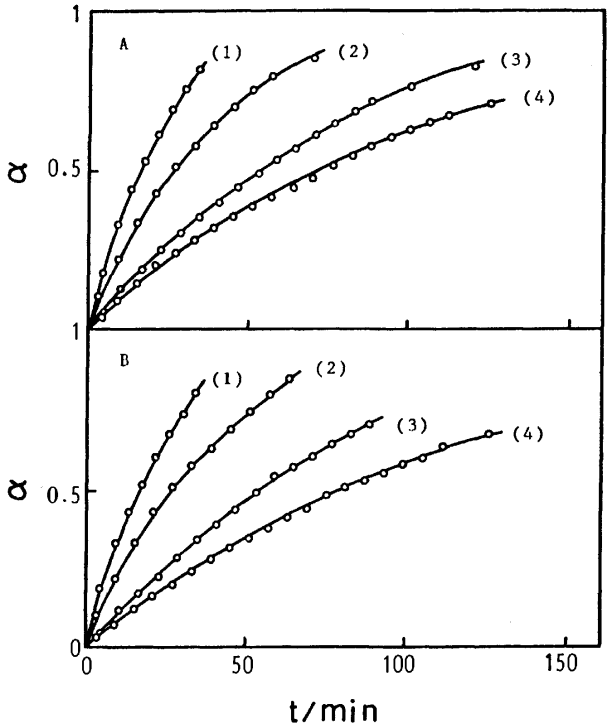

Fig. 1. α vs. t curves calculated from (A) ITM and (B) IWL curves. (1) 362.6 K, (2) 367.4 K, (3) 371.5 K, (4) 377.2 K.

of sample at the time t.

Figure 1 shows α_{ITM} and α_{IWL} versus the t curves thus calculated from the ITM and IWL data. From these curves, it was found that the reactions fit the first-order equation:

$$-\ln(1-\alpha)=kt \quad (k\text{: rate constant})$$

in the range of α=0.05—0.60, with no distinct induction period. The rate constants, k, and its standard deviation, as estimated from the residue of the least-square line for each run, are given in Table 1. The temperature dependence of the rate constants conforms to the Arrehenius rate law; the activation energy (E_a) and the preexponential factor (A) are calculated by the least-square analysis. Then they are converted to the activation enthalpy $\Delta H^{\ddagger}$ and entropy $\Delta S^{\ddagger}$ at 300 K, assuming that the Eyring equation is valid for the solid state reaction:

$$\Delta H^{\ddagger}=E_a-RT$$
$$\Delta S^{\ddagger}=R(\ln A+h/kT-1)$$

Furthermore the assumptive rate constant at 300 K, k_{300}, was evaluated from E_a and A in order to compare quantitatively the reactivities of the complexes. They are listed in Table 1. As Table 1 shows, the rate constants obtained from the ITM and IWL curves agree with each other within the limits of experimental error, indicating no intermediary formation of any cobalt(II) species other than $Co(NH_3)_2Cl_2$ in the first stage of the decomposition reaction.

Although it is practically impossible to draw up a general rule applicable to the kinetics of the redox reaction of Co(III) complexes from the limited number of data now available, some aspects can be pointed out by comparing the present results with the kinetics of other Co(III) complexes thus far reported. The nitrosylcobalt(III) complexes of the CoL^4NO** type dissociate nitrogen monoxide on heating to yield its parent complexes. As Co(salen)NO** and Co(bzacen)NO** have a bent nitrosyl group[11,12] like $[Co(NH_3)_5NO]Cl_2$, the dissociation reaction is considered to be accompanied by an intramolecular redox reaction between the Co(III) ion and the NO^- group. It has been reported that the reaction follows the first-order equation and that the activation paramerters and k_{300} values are nearly invariable, regardless of the nature of the L^4 ligand.[3] As Table 1 shows, in spite of the large difference in the reactivity between $[Co(NH_3)_5NO]Cl_2$ and CoL^4NO (i.e., their k_{300} values differ by more than two orders of magnitude), there is almost no difference in their activation enthalpies. This is somewhat surprising because the reactivity of a compound is usually considered to be determined by the magnitude of its activation enthalpy. As these complexes have nothing in common in their molecular and crystal structures

**L^4 represents the tetradentate Schiff base dianion; N,N'-ethylenebis(1-phenyl-3-oxobutylideneaminate) dianion (bzacen), N,N'-ethylenebis(salicylideneaminate) dianion (salen), and its 5-nitro, 5-chloro, and 5-methyl derivatives.

other than the Co(III)-NO^- moiety, these findings seem to suggest that the enthalpies of activation of these complexes are mainly determined by the energetic feature of the electron-transfer process from the NO^- group to the Co(III) ion and that the reactivity of these complexes is dominated by the activation entropy. In fact, the difference in the ΔS^* values of these complexes exceeds 60 $J\,K^{-1}\,mol^{-1}$.

It is also of interest to compare the activation parameters of $[Co(NH_3)_5NO]Cl_2$ with those of hexaamminecobalt(III) halides, which have the same CoN_6 coordination structure as the nitrosyl complex. Hexaamminecobalt(III) halides undergo a thermal redox reaction between the ligands and the Co(III) ion; the stoichiometry[13] and relatively reliable kinetic parameters have been reported[4] for $[Co(NH_3)_6]Cl_3$ and $[Co(NH_3)_6]I_3$. The cobalt(III) ion of the former complex has been considered to be reduced by the NH_2^- produced by the thermally induced autoionization of the NH_3 ligand,[6] and that of the latter complex, by the iodide anion. As Table 1 shows, whereas the reactivities of these complexes increase in the order of: $[Co(NH_3)_6]Cl_3 < [Co(NH_3)_6]I_3 < [Co(NH_3)_5NO]Cl_2$ the activation enthalpies increase in the order of: $[Co(NH_3)_6]I_3 < [Co(NH_3)_5NO]Cl_2 < [Co(NH_3)_6]Cl_3$. These facts indicate that the activation enthalpy does not solely determine the reactivities of these cobalt(III) complexes, as in the case of the nitrosyl complexes. The order of the activation enthalpy is explainable in terms of the reducing power of the NH_2^-, NO^-, and I^- anions. The standard electrode potential (SEP) of the NO/NO^- couple (0.712 eV) is higher than $SEP(I_2/I^-) = 0.536$ eV.[14] Presently $SEP(NH_2/NH_2^-)$ is not known; however, since those potentials of the $N_2H_5^+/NH_4^+$ (1.275 eV) and NH_3OH/NH_4^+ (1.35 eV) couples with the same change in the oxidation number of nitrogen in the reduction of the amide ion are around 1.3 eV,[14] $SEP(NH_2/NH_2^-)$ may not differ largely from 1.3 eV, which is considerably higher than the SEP's of nitrogen monoxide and iodine. Therefore, as far as the cobalt(III) complexes so far studied are concerned, it can be said that the activation enthalpy of the redox reaction of cobalt(III) complexes is determined mainly by the reducing power of the reductant and that the activation entropy plays an important role in determining the thermal stability of these complexes. It has been reported that, in the thermal redox reactions of Co(salen)(β-diketonato) compleses, the activation entropy dominates the reactivity of these complexes.

References

1) S. Kinoshita, K. Miyokawa, H. Wakita, and I. Masuda, *Bull. Chem. Soc. Jpn.*, **57**, 381 (1984) and the references cited therein.

2) W. W. Wendlandt and J. P. Smith, *J. Inorg. Nucl. Chem.*, **25**, 843 (1963).

3) H. Masuda, K. Miyokawa, and I. Masuda, *Thermochim. Acta*, **84**, 337 (1985).

4) N. Tanaka and K. Nagase, *Bull. Chem. Soc. Jpn.*, **40**, 546 (1964).

5) C. P. Pratt, B. A. Coyle, and J. A. Ibers, *J. Chem. Soc. A*, **1971**, 2146.

6) K. Miyokawa, H. Masuda, and I. Masuda, *Bull. Chem. Soc. Jpn.*, **53**, 3573 (1980).

7) W. W. Wendlandt, "Thermal Methods of Analysis," 2nd ed, John Wiley and Sons, New York (1974), p 459.

8) K. Miyokawa, H. Hirashima, and I. Masuda, *Bull. Chem. Soc. Jpn.*, **54**, 3361 (1981).

9) O. Bostrup, *Inorg. Synth.*, **8**, 191 (1966).

10) K. Miyokawa and I. Masuda, *Fukuoka Univ. Science Reports*, **10**, 83 (1980).

11) K. J. Haller and J. H. Enemark, *Acta Crystallogr., Sect. B*, **34**, 102 (1978).

12) R. Wiest and R. Weiss, *J. Organomet. Chem.*, **30**, C33 (1971).

13) W. W. Wendlandt, *J. Inorg. Nucl. Chem.*, **25**, 545 (1963).

14) "Kagaku Binran Kisohen II," The Chemical Society of Japan, Maruzen, Tokyo (1975).

A Glassy Carbon Electrode Modified with *N*-(2-Hydroxybenzyl)chitosan for Voltammetric Determinations of Cu^{2+} and Pb^{2+}

Yoshiaki KURAUCHI, Eiichi TSURUMORI, and Kazuya OHGA*
Department of Environmental Chemistry and Engineering, Faculty of Engineering,
Oita University, Dannoharu, Oita 870-11
(Received November 24, 1988)

Synopsis. A glassy carbon electrode was chemically modified with *N*-(2-hydroxybenzyl)chitosan which could act as an agent to preconcentrate Cu^{2+} and Pb^{2+}. The modified electrode was stable for 30 d and its calibration curves for the voltammetric determination of these ions are linear in the concentration range of $(1—10)\times10^{-7}$ mol dm^{-3}. The usage limitation of this electrode has also been discussed.

High metal-chelating ability is one of the most attractive functions of chitosan which is obtained by deacetylation of chitin, a naturally occurring polysaccharide.[1] The chelating ability arises primarily from the amino group of the 2-amino-2-deoxy-D-glucose (glucosamine) unit and is enhanced by chemical modification of the amino group. For example, the capacity of *N*-(2-hydroxybenzyl)chitosan (HBC) to adsorb Cu^{2+} is 47 times as much as that of chitosan itself.[2]

Recently much attention has been drawn to the voltammetric determination of metal ions using electrodes modified with preconcentrating agents or media. The agents frequently used to preconcentrate transition metal ions are chelating compounds, including 2,9-dimethyl-1,10-phenanthroline[3] and cross-linked polystyrene with bis(carboxymethyl)amino groups.[4] Chitosan and its derivatives with high chelating abilities are therefore anticipated to act as efficient agents for transition metal ions. In this research, we prepared a glassy carbon (GC) electrode modified with HBC and examined its applicability to the determination of trace amounts of Cu^{2+} and Pb^{2+}.

Experimental

Reagents. Chitosan (100% deacetylation) was kindly donated by Katokichi Co., Kagawa, Japan. Commercial salicylaldehyde and dicyclohexylcarbodiimide (DCC) were distilled under reduced pressure just before use. Water was purified by reverse osmosis (Millipore Milli RO15) and deionization. All other chemicals were of reagent grade or better and used without further purification.

Modification of a GC Electrode. *N*-Salicylidenechitosan was formed from chitosan and salicylaldehyde[5] and reduced with $NaBH_3CN$ to give a HBC gel.[2] The molar quantity of salicylaldehyde used was half that of the glucosamine unit. A GC electrode (Tokai Carbon GC-30S, 6 mm diameter) covered with a Teflon tube was polished with alumina (FUJIMI FM-No. 4, 0.5 μm) and then oxidized with H_2SO_4 according to the procedure reported by Wingard and Gurecka.[6] After being washed with water and dried at 120 °C for 2 h, the oxidized surface was coated with 20 mm^3 of 2% aqueous acetic acid–methanol (7:3) containing 0.08 mg of HBC and was dried again at room temperature for 5 h and further at 120 °C for 12 h. The dried electrode having a thin HBC film was immersed in 20 cm^3 of DMF–acetonitrile (1 : 1) containing 2 g of DCC for 5 h at room temperature. The HBC-modified electrode (HME) thus obtained was washed successively with DMF, 2% aqueous acetic acid, and water and was stored in 0.05 M (1 M=1 mol dm^{-3}) aqueous KNO_3.

Cyclic Voltammetry. After being soaked in 0.05 M aqueous KNO_3 containing a metal ion to be analyzed for a prescribed period, the HME was rinsed briefly with water and then subjected to a cyclic voltammetry in 0.05 M KNO_3 which had previously been deaerated with N_2 and thermostated at (25.0±0.5) °C. The cyclic voltammetry was carried out with a Hokuto Denko HB 104 function generator, a Hokuto Denko HA 301 potentiostat, and a Yokogawa 3086 X-Y recorder. The HME was used as a working electrode, and reference and counter electrodes were Ag/AgCl and Pt, respectively.

Results and Discussion

The IR spectrum of HBC showed no absorption band at 1640 cm^{-1} which is assigned to the C=N stretching vibration of *N*-salicylidenechitosan, while the band assigned to the aromatic C-H bending vibration (760 cm^{-1}) still remained. These suggest that the reduction reaction took place sufficiently. The presence of the remaining amino groups was confirmed by observation of a band at 1600 cm^{-1}. The treatment with DCC during the modification of the GC electrode with HBC was carried out with the intention of forming amide bonds from the amino groups and the carboxylato groups on the oxidized electrode surface (Fig. 1), and resulted in formation of a thin HBC film adhering firmly to the electrode surface.

Figure 2 shows typical cyclic voltammograms

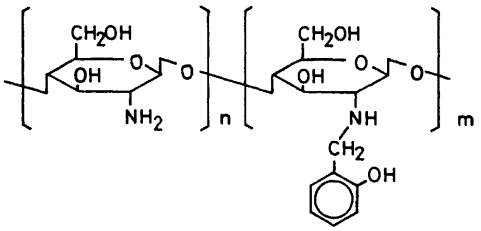

HBC

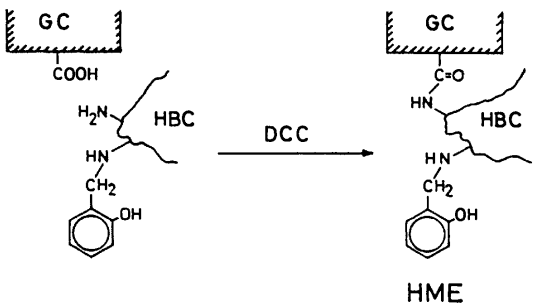

HME

Fig. 1. Modification of a GC electrode with HBC.

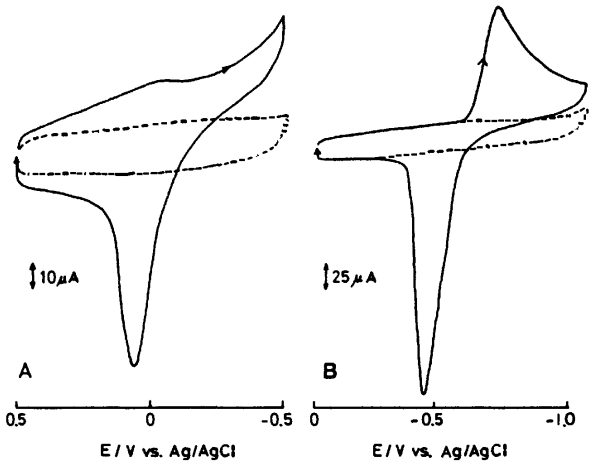

Fig. 2. Cyclic voltammetric *I-E* curves after soaking in 1.0×10^{-5} M Cu^{2+} (A) and 1.0×10^{-5} M Pb^{2+} (B) solutions: scan rate, 100 mVs^{-1}; soaking time, 60 min; electrolyte, 0.05 M KNO_3. Dashed lines represent the curves before soaking.

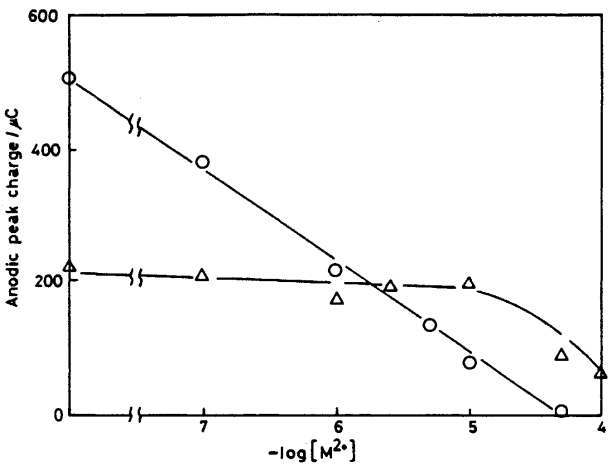

Fig. 3. Anodic-peak-charge changes for 1.0×10^{-5} M Pb^{2+} by the addition of Cu^{2+} (○) and for 1.0×10^{-5} M Cu^{2+} by the addition of Pb^{2+} (△). The left edge of the abscissa implies the absence of the coexisting divalent cation. Other conditions are as in Fig. 2.

obtained with the modified electrode HME which was soaked in 1.0×10^{-5} M Cu^{2+} and Pb^{2+} solutions for 60 min. Large anodic waves were observed at +0.04 V for Cu^{2+} and −0.45 V for Pb^{2+}. The anodic peak charge of Pb^{2+} (273 μC) calculated from the peak area is about twice as large as that of Cu^{2+} (132 μC). At lower metal-ion concentrations, 10^{-7} M, the uptake was slower and hence a longer soaking time was required to obtain such well-defined anodic peaks. The accumulated Cu^{2+} and Pb^{2+} were completely removed by dipping in 0.1 M EDTA for 10 min.

The anodic peak charge of the 1.0×10^{-5} M Pb^{2+} sample was reproducible to ±4% for 10 accumulation/measurement/renewal cycles. The ability of the HME to accumulate Cu^{2+} or Pb^{2+} lowered only slightly with repeated runs. The peak charge of 1.0×10^{-5} M Pb^{2+} was 90% of its initial value even after the cycle was repeated about 100 times for 30 d. In addition, the calibration curves of peak charge vs. concentration for Cu^{2+} and Pb^{2+} were both linear in the concentration range of $(1-10)\times10^{-7}$ M (soaking time, 120 min; correlation coefficient, 0.990 for Cu^{2+} and 0.999 for Pb^{2+}). These results suggest that the HME is available for the voltammetric determination of trace amounts of Cu^{2+} and Pb^{2+}.

On the other hand, when no DCC treatment was applied, the HBC film peeled off after three cycles and the accumulation ability disappeared nearly completely. Further, when chitosan itself was used in place of HBC, the electrode obtained showed a Pb^{2+} peak charge only one fifth of that of the HME, though having a stable film.

In the case of the other metal ions, Cd^{2+}, UO_2^{2+}, Co^{2+}, and Ni^{2+}, no redox waves were observed when the HME was soaked for 60 min in a 1.0×10^{-5} M solution of each metal ion. The selectivity of the HME toward Cu^{2+} agrees with the fact that HBC has a high ability to adsorb Cu^{2+},[2] though the reason why the peak charge of Pb^{2+} is larger than that of Cu^{2+} is not yet clear.

As shown in Fig. 3, the anodic peak charge of Pb^{2+} ($[Pb^{2+}]=1.0\times10^{-5}$) was reduced enormously by the presence of Cu^{2+} and to nearly zero when the Cu^{2+} concentration increased up to 5×10^{-5} M. The peak charge of Cu^{2+}, in contrast, was not so much affected by the addition of Pb^{2+} of concentrations below 1×10^{-5} M ($<[Pb^{2+}]/[Cu^{2+}]=1$). Such a more significant reduction of the Pb^{2+} peak charge may be explained in terms of the weaker coordination ability of hydroxyl and amino groups to Pb^{2+} than to Cu^{2+}.[7] Thus, in the Pb^{2+} determination, it is necessary to previously remove other metal cations which can strongly form complexes with HBC, if present.

References

1) R. A. A. Muzzarelli and O. Tubertini, *Talanta*, **16**, 1571 (1969).
2) L. D. Hall and M. Yalpani, *Carbohydr. Res.*, **83**, C5 (1980).
3) S. V. Prabhu and R. P. Baldwin, *Anal. Chem.*, **59**, 1074 (1987).
4) N. Egashira, M. Kudo, and F. Hori, *Chem. Lett.*, **1986**, 1045.
5) S. Hirano, N. Matsuda, O. Miura, and H. Iwaki, *Carbohydr. Res.*, **71**, 339 (1979).
6) L. B. Wingard, Jr. and J. L. Gurecka, Jr., *J. Mol. Catal.*, **9**, 209 (1980).
7) D. Hopgood and D. L. Leussing, *J. Am. Chem. Soc.*, **91**, 3740 (1969).

The Photochemistry of Steroidal 6-Membered Cyclic α-Nitro Enones[1)]

Hiroshi SUGINOME* and Yoshitaka KUROKAWA
Organic Synthesis Division, Department of Chemical Process Engineering, Faculty of Engineering, Hokkaido University, Sapporo 060
(Received September 7, 1988)

Synopsis. The products of the photolysis of two steroidal cyclic α-nitro enones, newly synthesized, were compared with those of the cyclic α-nitro ketones and cyclic enones. Direct irradiation of 2α-nitrocholest-4-en-3-one in protic solvents resulted in an unexpected α-cleavage of the carbonyl group and gave 3-alkoxy-2-nitro-2,3-secocholest-4-en-3-one while irradiation of 4α-nitro-5α-cholest-1-en-3-one gave the parent cholest-1-en-3-one which arose from the removal of the nitro group.

In a previous paper,[2)] we have reported the results of the photolysis of several 6-membered cyclic α-nitro ketones in ethanol.

We have found that two versions of the products, the corresponding α-diketones and α-diketone monooximes, can be obtained when 6-membered cyclic α-nitro ketones which exist exclusively or predominantly in their enol forms in protic solvents, are irradiated in ethanol. We have also found that the corresponding α-diketone monooximes are products which do not accompany any corresponding α-diketones when the 6-membered cyclic α-nitro ketones, which exist in their keto forms, are irradiated in ethanol.

In this paper, we wish to report the results of a further investigation in this area: the photolysis of two steroidal cyclic α-nitro enones, 2α-nitrocholest-4-en-3-one (**2**) and 4α-nitro-5α-cholest-1-en-3-one (**6**). The study was carried out to help us to understand more fully the behavior of the excited nitro group in protic solvents.

Preparation of α-Nitro Enones 2 and 6. The two steroidal α-nitro enones **2** and **6** chosen for the present investigation were prepared in a standard manner by nitration of the corresponding steroidal α,β-unsaturated ketones **1** and **5** with an alkyl nitrate and a base.[3-5)] The IR spectra of α-nitro enones **2** and **6** exhibited strong bands assignable to the α,β-unsaturated carbonyl and nonconjugated nitro groups. These α-nitro enones therefore exist almost exclusively as their keto form in the Nujol. An ^{1}H NMR spectra of both α-nitro enones also indicated that these α-nitro enones in $CHCl_3$ exist in their keto form.

The UV spectrum of α-nitro enone **2**, on the other hand, exhibited an absorption maximum with a medium intensity at 375 nm (ε; 1620), besides an intense absorption maximum at 244 nm (ε; 13200). The former is attributable to the presence of a small portion of α-nitro enone **2** in its enol form. The UV spectrum of α-nitro ketone **6** in ethanol exhibited a weak absorption maximum at 335 nm attributable to the $\pi \rightarrow \pi^*$ transition of the nitro group of the corresponding enol form[2)] besides a strong absorption maximum at 231 nm due to the $\pi \rightarrow \pi^*$ transition.

It has been reported that in the mass spectra of Δ^4- and Δ^1-androstan-3-ones, the base peaks occur at *m/z* 124 and 122 respectively. Both base peaks arise from a cleavage across ring B as indicated in the formulae **A** and **B**.[6)] On the basis of deuterium labelling studies

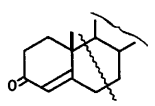

A *m/z* 124

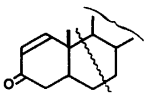

B *m/z* 122

Shapiro and Djerassi have suggested that the mechanism for the production of the base peak at *m/z* 124 involves the migration of hydrogen atoms from C-8 and C-11 of the steroid to the ring A fragment while the formation of the base peak at *m/z* 122 involves the reciprocal migration of hydrogen to the ring **A** fragment. It should be noted that in contrast to the simple enones studied by Shapiro and Djerassi, the mass spectra of both α-nitro enones **2** and **6** exhibited a base peak at *m/z* 121. Both ions seem to be formed as a result of the loss of NO_2 and a cleavage across the ring **B** as indicated in the formulae C and D.

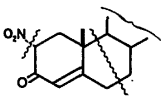

C *m/z* 121

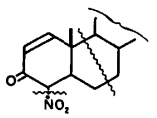

D *m/z* 121

Photochemistry of α-Nitro Enones 2 and 6. Photolysis of α-nitro enone **2** in ethanol with a 450-W high-pressure Hg arc through a Pyrex filter for 6 h gave a product mixture from which a product **3** (25%) was isolated by means of preparative TLC as the only indentifiable product (Scheme 1). The high-resolution mass spectrometry indicated that the photoproduct **3** had the molecular formula $C_{29}H_{49}NO_4$. The UV and IR spectra indicated that the new product was an α,β-unsaturated ester carrying a nitro group (see Experimental). The analysis of ^{1}H NMR spectrum of **3** with the aide of a double resonance study indicated that the structure of product **3** was 3-ethoxy-2-nitro-

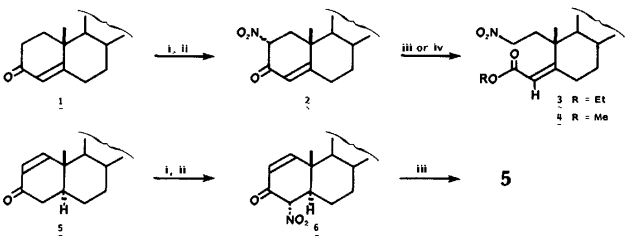

i) $CH_3CH_2CH_2ONO_2$-$(CH_3)_3COK$ ii) CH_3COOH iii) EtOH-*hν* iv) MeOH-*hν*

Scheme 1.

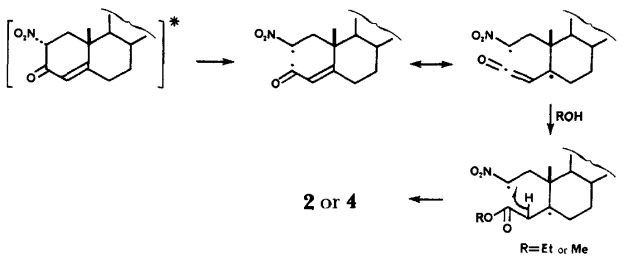

Scheme 2.

2,3-secocholest-4-en-3-one (**3**) (See Experimental). The ^{13}C NMR spectrum exhibited five signals at δ 167.0, 165.5, 112.0, 71.5, and 59.6 in the downfield. On the basis of the results revealed by the INEPT technique and by considering the known structure-shift correlations, these signals were assigned respectively to the C=O of the ethoxycarbonyl, the trigonal α-carbon of the α,β-unsaturated ester, the trigonal β-carbon of the α,β-unsaturated ester, the methylene carbon carrying a nitro group, and the methylene carbon of the ethoxycarbonyl group of **3**.

The photolysis of **2** was also undertaken by using methanol as the solvent to give 3-methoxy-2-nitro-2,3-secocholest-4-en-3-one **4** in a 30% yield.

Photolysis of α-nitro enone **6** in ethanol under conditions similar to those described above gave the parent ketone **5** (37%) as the only identifiable product.

Although the photochemistry of nitro compounds has been extensively investigated,[7] the photochemistry of cyclic α-nitro enones has never been reported. The foregoing experiments have shown that the photoreaction of an α,β-unsaturated carbonyl group preceded the photoreaction of the nitro group in 2α-nitrocholest-4-en-3-one (**2**), while the photoreaction of nitro group preceded that of α,β-unsaturated carbonyl group in 4α-nitrocholest-1-en-3-one **6**. The probable pathway which led to the secosteroid **3** is outlined in Scheme 2.

Although the photoreactions of enones[8] have been extensively investigated only a few examples of the photochemical α-fission of α,β-unsaturated carbonyl group have so far been reported.[9] The general process of α,β-unsaturated ketones in hydrogen-donating solvents such as ethanol appears to be a photoreduction.[10] Thus, irradiation of testosterone acetate in ethanol has been reported to give a mixture of products from which only the corresponding saturated ketone have been isolated.[10] It is well-known that the irradiation of steroidal 4-en-3-ones in *t*-butyl alcohol leads to fascinating photorearrangements.[8,10,12,13]

The present α-cleavage of excited steroid-4-en-3-one therefore, is apparently due to the presence of the 2α-nitro group which directs the α-cleavage over other photochemical processes common to the excited α,β-unsaturated carbonyl group.

Experimental

For instruments and general procedure see Ref. 2.

Preparation of 2α-Nitrocholest-4-en-3-one (2). To THF (14 ml) containing potassium *t*-butoxide (0.5 g), cholest-4-en-3-one (1 g, 2.6 mmol) dissolved in THF (22 ml) was added over the course of 30 min at −30 °C. To this solution, propyl nitrate (0.6 g) in THF (5 ml) was added and the solution was stirred for 45 min during which period the temperature of the solution was raised to 0 °C. The solution was neutralized with glacial acetic acid. The solution was then poured into iced water (200 ml) and the aq solution was extracted twice with dichloromethane. The combined organic layers were dried over Na_2SO_4 and worked up in the usual way to give an oily product (1.173 g). This crude product was recrystallized from ethanol to yield yellow crystals (0.637 g, 57%), mp 140—142 °C. (Found: C, 75.44; H, 9.98; N, 3.28%. Calcd for $C_{27}H_{43}NO_3$: C, 75.48; H, 10.09; N, 3.26%): IR (Nujol) 1695 (C=O), 1605 (C=C), and 1544 cm^{-1} (NO_2); ^1H NMR (270 MHz) δ=0.71 (3H, s, 18-H), 1.3 (3H, s, 19-H), 2.06 (1H, dt, J=12.82, 3.3 and 3.3 Hz, 6α-H), 5.31 (1H, dd, J=13.19 and 5.86 Hz, 2β-H), 5.84 (1H, s, 4-H); MS *m/z* (rel intensity) 429 (M^+, 17) 413 [$(M-O)^+$, 12.4], 397 (14), 383 [$(M-NO_2)^+$, 27.5], 316 (20.3), 261 (16.7), 147 (36.7), 135 (40.3), 121 (100), 109 (27.1), 95 (42.3), 81 (33.7), 69 (35.5), 57 (44.2), and 43 (47.2); UV (C_2H_5OH) λ_{max} 375 nm (ε: 1620) and 2.44 (ε: 13240).

Preparation of 4α-Nitro-5α-cholest-1-en-3-one (6). To THF (28 ml) containing potassium *t*-butoxide (1 g), 5α-cholest-1-en-3-one (2 g, 5.21 mmol) dissolved in THF (44 ml) was added over the courses of 30 min at −30 °C. To this solution, propyl nitrate (1.2 g) in THF (10 ml) was added and the solution was stirred for 45 min during which time the temperature of the solution was raised to 0 °C. The solution was neutralized with glacial acetic acid until the pH of the solution became ca. 3. The solution was then poured into water (300 ml) and the aq solution was extracted with dichloromethane. The organic layers were combined and the solution was dried over Na_2SO_4 and worked up in the usual way to give an oily product (2.381 g). The crude product was subjected to column chromatrography (silica gel, 40 g). Elution with benzene gave a crude α-nitro ketone **5** (1.080 g, 48.3%) which was recrystallized from methanol. Mp 149—151 °C. (Found: C, 75.52; H, 9.97; N, 3.14%. Calcd for $C_{27}H_{43}NO_3$; C, 75.48; H, 10.09; N, 3.26%); IR (Nujol) 1694 (C=O), 1616 (C=C), and 1542 cm^{-1} (NO_2); ^1H NMR (270 MHz) δ=0.70 (3H, s, 18-H), 1.12 (3H, s, 19-H), 5.12 (1H, d, J=13.56 Hz, 4β-H), 6.01 (1H, d, J=10.25 Hz, 2-H), and 7.31 (1H, d, J=10.25 Hz, 1-H); MS *m/z* (rel intensity), 429 (M^+, 20.4%), 383 [$(M-NO_2)^+$, 26.7], 229 (31), 173 (15.4), 147 (43.4), 121 (100), 109 (24.5), 95 (35.4), 81 (30), 69 (33.4), 55 (42.2), and 43 (42.9); UV (EtOH) λ_{max} 335 nm (ε: 60).

Photolysis of 2α-Nitrocholest-4-en-3-one (2). The nitro ketone **2** (400 mg, 0.93 mmol) in ethanol (400 ml) was flushed with nitrogen and irradiated for 6 h with a Hanovia 450-W high-pressure Hg arc through a Pyrex filter in an atmosphere of dry nitrogen. The solvent was then removed to give an oily product (455 mg). The product was subjected to preparative TLC with benzene to give product **3** (122 mg, 25.2%). (Found: *m/z* 475.3623; Calcd for $C_{29}H_{49}NO_4$: M, 475.3659); IR (Nujol) 1710 (COOEt), 1626 (C=C), 1548 (NO_2), 1191, 1183, and 1161 cm^{-1} (C-O-C); ^1H NMR (270 MHz) δ=0.70 (3H, s, 18-H), 1.14 (3H, s, 19-H), 1.29 (3H, t, J=7.14 Hz, CH_3-CH_2O), 3.38 (1H, dt, J=14.29, 3.3 and 3.3 Hz, 6α-H), 4.15 (2H, q, J=7.14, CH_3CH_2-O), 4.33 (1H, ddd, J=12.8, 12,8 and 6.2 Hz, 2-H), 4.49 (1H, ddd, J=12.8, 12.8 and 4.8 Hz, 2-H), and 5.67 (1H, s, 4-H); MS *m/z* (rel intensity) 475 (M^+, 3.4), 458 (27.7), 440 (11.2), 430 [$(M-OEt)^+$, 15.8], 402 [$(M-COOEt)^+$, 68.9], 372 (100), 147 (20.8), 133 (22.0), 121 (23.6), 107 (31.6), 95 (20.0), 82 (47.1), 69 (47.7), 55 (65.7), and 43 (74.6). UV(ethanol) λ_{max} 212 nm (ε; 13850).

The photoreaction of **2** (400 mg) in methanol (400 mg) for 8 h under the above conditions gave a product. The product was subjected to preparative TLC (3 : 1 dichloromethane-hexane) to yield a methoxy analogue **4** (180 mg, 47%, based on the converted nitro ketone) and the starting nitro ketone (41

mg). (Found: *m/z* 461.3457: Calcd for $C_{28}H_{47}NO_4$: M, 461.3505); IR (Nujol) 1710 (COOEt), 1630 (C=C), and 1577 cm^{-1} (NO_2); ^1H NMR (270 MHz) δ=0.70 (3H, s, 18-H), 1.14 (3H, s, 19-H), 3.70 (3H, s, OMe), 3.84 (1H, td, J=14.3 and 3.7 Hz, 6α-H), 4.33 (1H, ddd, J=12.8, 11.0 and 6.2 Hz, 2-H), 4.48 (1H, ddd, J=12.8, 11.4 and 4.8 Hz, 2-H), and 5.69 (1H, s, 4-H): ^{13}C NMR δ=56.1 (OMe), 71.5 (CH_2NO_2), 11.6 (the α-carbon of the α,β-unsaturated ester), 165.9 (the β-carbon of the α,β-unsaturated ester), and 167.3 (the C=O of the methoxycarbonyl); MS *m/z* (rel intensity) 461 (M^+, 9.2), 444 (38.9), 430 [$(M-OMe)^+$, 13.3], 426 (15.3), 402 [$(M-COOMe)^+$, 53.6], 386 (33.8), and 372 (100).

Photolysis of 4α-Nitro-5α-cholest-1-en-3-one (6). α-Nitro ketone **6** (300 mg, 0.7 mmol) in ethanol (350 ml) was flushed with nitrogen and irradiated for 3 h with a EIKOSHA 500-W high-pressure mercury arc through a Pyrex filter under an atmosphere of a nitrogen. The removal of the solvent left an oily residue (326 mg) which was subjected to preparative TLC with dichloromethane to yield two fractions. The most mobile fraction (26 mg, 8.7%) was starting nitro ketone. The next mobile fraction (91 mg, 36.8%) was 5α-cholest-1-en-3-one, **4** which was purified by recrystallization from methanol (55 mg), mp 149—151 °C.

References

1) Photoinduced Molecular Transformations. Part 101. Previous paper in this series. H. Suginome, C. F. Liu, S. Seko, K. Kobayashi, and A. Furusaki, *J. Org. Chem.*, **53**, 5952 (1988).

2) H. Suginome and Y. Kurokawa, *Bull. Chem. Soc. Jpn.*, **61**, 4005 (1988).

3) H. Feuer and P. M. Pivawer, *J. Org. Chem.*, **31**, 3152 (1966); H. Feuer, J. W. Shepherd, and S. Savides, *J. Am. Chem. Soc.*, **78**, (1956).

4) R. E. Schaub, W. Fulmor, and M. J. Weiss, *Tetrahedron*, **20**, 373 (1964).

5) For reviews, see a) N. Kornblum, *Org. React.*, **12**, 101 (1962); b) R. H. Fischer and H. M. Weitz, *Synthesis*, **1980**, 216.

6) R. H. Shapiro and C. Djerassi, *J. Am. Chem. Soc.*, **86**, 2825 (1964).

7) For reviews, see a) H. A. Morrision, "The Chemistry of Functional Groups" general ed by S. Patai; The Chemistry of the Nitro and Nitroso Groups, part 1," ed by H. Feuer, Interscience Publ., New York, (1969), pp. 165—213. b) Y. L. Chow, "The Chemistry of Functional Groups" general ed by S. Patai; The Chemistry of Amino, Nitroso, Nitro Compounds and their Derivatives," ed by S. Patai, Wiley, New York (1982), pp. 181—290.

8) For reviews on photochemistry of enones and dienones, see a) N. J. Turro, "Technique of Organic Chemistry, Vol. 14, Energy Transfer and Organic Photochemistry," ed by A. Weissberger, Interscience Publ. New York (1969) p. 232. b) K. Schaffner in "Advances in Photochemistry, Vol. 4," ed by W. A. Noyes, G. S. Hammond, and J. N. Pitts, Jr., Interscience Publ., New York (1966), p. 81. c) P. J. Kropp, "Organic Photochemistry, Vol. 1," ed by O. L. Chapman, Marcel Dekker, New York (1967), p. 1.

9) W. C. Agosta and A. B. Smith, *J. Am. Chem. Soc.*, **93**, 5513 (1971); T. H. Koch and R. J. Sluski, *Tetrahedron Lett.*, **1970**, 2391.

10) B. Nann, D. Gravel, R. Schorta, H. Wehri, K. Schaffner, and O. Jeger, *Helv. Chim. Acta*, **46**, 2473 (1963).

11) I. A. Williams and P. Bladon, *Tetrahedron Lett.*, **1964**, 257.

12) O. L. Chapman, T. A. Rettig, A. A. Griswold, A. I. Dutton, and P. Fitton, *Tetrahedron Lett.*, **1963**, 2049. W. W. Kwie, B. A. Shoulder, and P. D. Gardner, *J. Am. Chem. Soc.*, **84**, 2268 (1962); B. A. Shoulder, W. W. Kwie, W. Klyne, and P. D. Gardner, *Tetrahedron*, **21**, 2973 (1965); G. Marsh, D. R. Kearns, and K. Schaffner, *Helv. Chim. Acta*, **51**, 1890 (1968).

13) D. Bellus, D. R. Kearns, and K. Schaffner, *Helv. Chim. Acta*, **52**, 971 (1969).

Nontemplate Synthesis of Macrocyclic Tetraimine Schiff Bases Incorporating Dithienylmethane Units[1)]

Tyo SONE,* Yoshihiro OHBA, and Ryuji WATANABE
Department of Applied Chemistry, Faculty of Engineering, Yamagata University, Yonezawa 992
(Received October 11, 1988)

Synopsis. Novel 26- and 28-membered macrocyclic tetraimine Schiff bases incorporating four thiophene units as ring constituents were synthesized by a nontemplate method starting from bis(5-formyl-2-thienyl)methane derivatives and aliphatic diamines under high-dilution conditions.

Recently, much attention has been given to the synthesis and characterization of macrocyclic tetraimine Schiff bases and their metal complexes.[2)] In addition to ligands, macrocyclic Schiff bases are potential precursors[3)] of the cyclic tetramines, which are also ligands,[4)] and potential inclusion hosts[5)] for organic molecules. Although several macrocyclic Schiff bases incorporating a heteroaromatic unit as a ring constituent have been reported,[6)] most of them have been derived from 2,6-pyridinedicarbonyl compounds and isolated as metal complexes. In spite of growing interest as mixed donor macrocyclic ligands, macrocyclic Schiff bases incorporating a heteroaromatic unit other than a pyridine nucleus have received less attention. Regarding the thiophene family, for example, it is limited to those[7-9)] derived from 2,5-thiophenedicarbaldehyde, all of which contain two thiophene units as a ring constituent. We investigated the synthesis of a novel-type macrocyclic Schiff bases (**3** and **4**)[5)] which contain four thiophene units, namely two di-2-thienylmethane units substituted at the methylene bridges. The results are reported.

Macrocyclic Schiff bases have generally been synthesized by the condensation of dicarbonyl compounds with diamines by employing a metal template procedure. However, it is rather difficult to isolate metal-free Schiff bases from the metal complex, because of the instability of the macrocycles under demetalation conditions. Only a few examples[3,5,7,9)] for the nontemplate synthesis of macrocyclic Schiff bases have been reported, including those prepared by the [2+2] condensation of 2,5-thiophenedicarbaldehyde with α,ω-alkanediamines[7,9)] under reflux in ethanol.

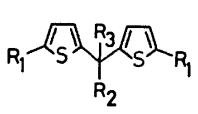

1, 2

1a: R_1=H, R_2=R_3=-CH_3
1b: R_1=H, R_2=-CH_3, R_3=-C_2H_5
1c: R_1=H, R_2=-CH_3, R_3=-i-C_3H_7
2a: R_1=-CHO, R_2=R_3=H
2b: R_1=-CHO, R_2=R_3=-CH_3
2c: R_1=-CHO, R_2=-CH_3, R_3=-C_2H_5
2d: R_1=-CHO, R_2=-CH_3, R_3=-i-C_3H_7

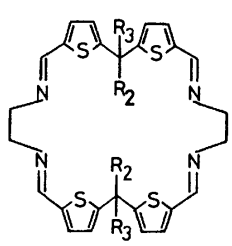

3

3a: R_2=R_3=H
3b: R_2=R_3=-CH_3
3c: R_2=-CH_3, R_3=-C_2H_5
3d: R_2=-CH_3, R_3=-i-C_3H_7

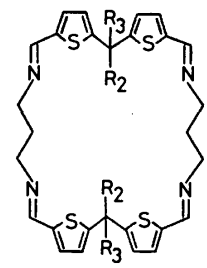

4

4: R_2=R_3=-CH_3

The 26-membered macrocycles, **3a—d**, which contain four thiophene units, could also be synthesized in high yields in the absence of a template metal by using a high-dilution procedure. Thus, when equimolar amounts of bis(5-formyl-2-thienyl)methane derivatives, **2a—d**, and 1,2-ethanediamine were allowed to react in a highly diluted $CHCl_3$ solution at room temperature, the expected **3a—d** were obtained in 70—86% yields. The 28-membered macrocycle (**4**) was obtained similarly by the condensation of **2a** and 1,3-propanediamine, but in rather low yield (18%). The condensation of **2b** with 1,4-butanediamine or 1,6-hexanediamine for the synthesis of 30- or 34 membered macrocycles gave no macrocyclic imines, but only polymeric materials. These results indicate that 1,2-ethanediamine is the most suitable building block for the construction of the macrocyclic tetraimine Schiff bases derived from bis(5-formyl-2-thienyl)methane derivatives, **2a—d**. The reason why **2** efficiently undergoes the [2+2] condensation with 1,2-ethanediamine, but not with its higher homologs, is not clear at present. The contribution of the facile precipitation of the products in the reaction media as well as the conformation of the starting dicarbonyl compounds were suggested to be the result of efficient [2+2] condensation of 2,5-pyrrole- or 2,5-thiophenedicarbaldehyde with 2-hydroxy-1,3-propanediamine.[9)] However, this is not the case regarding the condensation of **2** with 1,2-ethanediamine; products **3** and **4** are soluble in the reaction media, $CHCl_3$, and are derived from the same dicarbonyl compound, **2**. There must be a favoured mutual positioning between the two end groups of the noncyclic intermediates in the final stage of the ring closure between **2** and 1,2-ethanediamine.

The structures of **3a—d** and **4** were determined by elemental analysis as well as spectral data (MS, IR, ^1H and ^{13}C NMR). The IR spectra display an absorption band in the 1620—1630 cm^{-1} region (C=N stretching band). The ^1H NMR spectra show singlets at δ 8.15—8.18, while ^{13}C NMR singlets at ca. 156 ppm are ascribable to the four equivalent imine protons and imine

carbons, respectively. Any signals due to aldehyde and primary amine were not detected in the IR and NMR spectra.

All of the macrocyclic Schiff bases oblained are, contrary to our expectation, only slightly soluble in most solvents, except $CHCl_3$. Variatons of the alkyl group at the methylene bridges and of amine produced little effect on solubility. This makes it difficult to utilize **3** (or **4**) as inclusion hosts or a precursor for the macrocyclic polyamines.

Experimental

All melting points are uncorrected. The ^1H and ^{13}C NMR spectra were obtained on a Hitachi R-90H (90.0 MHz) and Hitachi R-90H (22.6 MHz) spectrometer, using TMS as an internal reference. The IR and Mass spectra were recorded on Hitachi EPI-S2 and UMU-5MG spectrometers. 2,2-Di(2-thienyl)propane (**1a**) and 2,2-bis(5-formyl-2-thienyl)propane (**2b**) were obtained according to methods described in the literature.[10]

Synthesis of 2,2-Di(2-thienyl)butane (1b). The procedure is a modification of the method used for the synthesis of **1a**.[10] 2-Butanone (48.3 g, 0.67 mol) was added to a mixture of thiophene (84 g, 1 mol) and 72% aqueous H_2SO_4 (126 g) over a period of 30 min at room temperature; the mixture was then stirred at 70—75 °C for 4 h. The cooled mixture was extracted with $CHCl_3$ (300 ml×2) and washed with water and dried over Na_2SO_4. After removing the solvent, the residue was distilled under reduced pressure to give **1b** (41.8 g, 38%). Colorless oil, bp 108—115 °C/3 Torr (1 Torr=133.322 Pa). IR ($CHCl_3$) 2980, 2950, 850, and 825 cm^{-1}; ^1H NMR ($CDCl_3$) δ=0.90 (3H, t, J=7.2 Hz), 1.78 (3H, s), 2.23 (2H, q, J=7.2 Hz), 6.82 (2H, d, J=2.4 Hz), 6.85 (2H, d, J=4.2 Hz), and 7.08 (2H, d,d, J=4.2, 2.4 Hz); MS m/z 222 (M^+, 28%). Anal. ($C_{12}H_{14}S_2$) C, H.

Synthesis of 2,2-Di(2-thienyl)-3-methylbutane (1c). By a similar procedure used for the preparation of **1b**, **1c** was obtained in 19% yield. Yellow oil, bp 137—145 °C/5 Torr. IR ($CHCl_3$) 2970, 2860, and 840 cm^{-1}; ^1H NMR ($CDCl_3$) δ=0.90 (6H, d, J=5.4 Hz), 1.75 (3H, s), 2.40—2.80 (1H, m), and 6.80—7.20 (3H, m); MS m/z 236 (M^+, 11%). Anal. ($C_{13}H_{16}S_2$) C, H.

Synthesis of Bis(5-formyl-2-thienyl)methane (2a). This compound was not obtained in satisfactory yield by the reported procedure.[11] Another route described below was used. A solution of bis(5-bromo-2-thienyl)methane[12] (6.3 g, 19 mmol) in dry ether (40 ml) was added over a period of 10 min to 15% buthyllithium-hexane solution (19 g) in dry diethyl ether (30 ml) at −40 °C—−50 °C under N_2 atmosphere. Then, *N,N*-dimethylformamide (DMF) (2.8 g, 38 mmol) in dry diethyl ether (20 ml) was added over a period of 5 min; the mixture stirred for 1 h at room temperature. After this solution was added to crushed ice (100 g) the ether layer was washed successively by a 5% HCl aqueous solution, a saturated $NaHCO_3$ solution, and a saturated NaCl solution and then dried over Na_2SO_4. After removing the solvent, the crude product was crystallized with ethanol to give **2a** (1.9 g, 42%). Colorless prisms, mp 95 °C (lit.[11] 95 °C). IR (KBr) 1645 cm^{-1} (CHO); ^1H NMR ($CDCl_3$) δ=4.43 (2H, s), 7.00 (2H, d, J=3.6 Hz), 7.62 (2H, d, J=3.6 Hz), and 9.83 (2H, s, CHO); MS m/z 236 (M^+, 100%).

Synthesis of 2,2-Bis(5-formyl-2-thienyl)butane (2c). To a mixture of **1b** (22.2 g, 0.1 mol) and DMF (9.2 g, 0.13 mol), $POCl_3$ (19.2 g, 0.13 mol) was added under cooling in a water bath with stirring. The mixture was stirred at 80—90 °C for 1 h and then cooled to room temperature. DMF (9.2 g, 0.13 mol) and $POCl_3$ (19.2 g, 0.13 mol) were added to this mixture. After heating at 80 °C for 2 h, the reaction mixture was poured into crushed ice (100 g), neutralized with sodium acetate, and then extracted with $CHCl_3$ (250 ml×2). The $CHCl_3$ layer was washed with water (200 ml×2) and dried over Na_2SO_4. The solvent was removed and the residue was chromatographed on silica gel (Wako C-200, hexane/ethyl acetate=1/1) to give the crude product, which was recrystallized from ethanol gave **2c** (12.2 g, 48%). Yellow powder, mp 63—63.5 °C. IR (KBr) 2975, 2950, 2850, 1655, and 810 cm^{-1}; ^1H NMR ($CDCl_3$) δ=0.90 (3H, t, J=6.9 Hz), 1.80 (3H, s), 2.24 (2H, q, J=6.9 Hz), 6.91 (2H, d, J=3.6 Hz), 7.53 (2H, d, J=3.6 Hz), and 9.74 (2H, s, CHO); MS m/z 278 (M^+, 14%). Anal. ($C_{14}H_{14}S_2$) C, H.

Synthesis of 2,2-Bis(5-formyl-2-thienyl)-3-methylbutane (2d). Diformyl compound **2d** was obtained in 55% yield by a similar procedure to that used for the synthesis of **2c**. Pale-yellow powder, mp 88—89.5 °C. IR (KBr) 1660 and 1650 cm^{-1} (CHO); ^1H NMR ($CDCl_3$) δ=0.94 (6H, d, J=6.0 Hz), 1.80 (3H, s), 2.47—2.90 (1H, m), 7.07 (2H, d, J=3.6 Hz), 7.59 (2H, d, J=3.6 Hz), and 9.78 (2H, s, CHO); MS m/z 292 (M^+, 12%). Anal. ($C_{15}H_{16}O_2S_2$) C, H.

Synthesis of 31,32,33,34-Tetrathia-3,6,18,21-tetraazapentacyclo[26.2.1.1^{8,11}.1^{13,16}.1^{23,26}]tetratriaconta-1(30),2,6,8,10,13,15,17,21,23,25,28-dodecaene (3a). A solution of **2a** (0.25 g, 1.0 mmol) in $CHCl_3$ (20 ml) and a solution of 1,2-ethanediamine (0.06 g, 1.0 mmol) in $CHCl_3$ (20 ml) were added simultaneously to the $CHCl_3$ (20 ml) over a period of 1.5 h with stirring at room temperature. After stirring for 30 min, the reaction mixture was filtered in order to remove any insoluble precipitate; the filtrate was then dried over Na_2SO_4 and concentrated. The yellow powder, thus obtained, was washed with ethanol (20 ml×2) giving **3a** (2.2 g, 83%). Colorless powder, mp 158—165 °C (decomp). IR (KBr) 2820, 1620, and 840 cm^{-1}; ^1H NMR ($CDCl_3$) δ=3.83 (8H, s), 4.20 (4H, s), 6.73 (4H, d, J=3.6 Hz), 7.03 (4H, d, J=3.6 Hz), and 8.15 (4H, s); MS m/z 520 (M^+, 10%). Anal. ($C_{26}H_{24}N_4S_4$) C, H.

Synthesis of 12,12,27,27-Tetramethyl-31,32,33,34-tetrathia-3,6,18,21-tetraazapentacyclo[26.2.1.1^{8,11}.1^{13,16}.1^{23,26}]tetratriaconta-1(30),2,6,8,10,13,15,17,21,23,25,28-dodecaene (3b). (Typical procedure) The solution of 2,2-bis(5-formyl-2-thienyl)propane (2.6 g, 10 mmol) in $CHCl_3$ (50 ml) and 1,2-ethanediamine (0.6 g, 10 mmol) in $CHCl_3$ (100 ml) were added simultaneously to 50 ml of $CHCl_3$ over a period of 15 h with stirring at room temperature; the mixture was stirred for an additional 30 h. After usual work-up, the crude product was obtained as yellow powder, which was recrystallized with $CHCl_3$-hexane to give **3b** (2.4 g, 84%). Pale-yellow powder, mp 233—236 °C (decomp). IR (KBr) 2970, 2930, 2830, 1630, and 800 cm^{-1}; ^1H NMR ($CDCl_3$) δ=1.80 (12H, s), 3.79 (8H, s), 6.74 (4H, d, J=3.6 Hz), 6.99 (4H, d, J=3.6 Hz), and 8.18 (4H, s); ^{13}C NMR ($CDCl_3$) δ=32.41, 40.92, 61.07, 123.61, 130.04, 155.83, and 158.09; MS m/z 576 (M^+, 26%). Anal. ($C_{30}H_{32}N_4S_4$) C, H, N.

The cyclic tetraimines, **3c**, **3d**, and **4a**, were synthesized in a similar manner.

12,27-Diethyl-12,27-dimethyl-31,32,33,34-tetrathia-3,6,18,21-tetraazapentacyclo[26.2.1.1^{8,11}.1^{13,16}.1^{23,26}]tetratriaconta-1(30),2,6,8,10,13,15,17,21,23,25,28-dodecaene (3c). Yield 86%. Pale yellow powder, mp 197—200 °C. IR (KBr) 2970, 2930, 2830, 1630, and 790 cm^{-1}. ^1H NMR ($CDCl_3$) δ=0.90 (6H, t, J=7.2 Hz), 1.78 (6H, s), 2.22 (4H, q, J=7.2 Hz), 3.80 (8H, s), 6.75 (4H, d, J=3.6 Hz), 7.00 (4H, d, J=3.6 Hz), and 8.15 (4H, s); ^{13}C NMR ($CDCl_3$) δ=9.71, 27.96, 37.11, 44.70, 61.04, 124.06, 129.98, 140.28, 155.86, and 157.33; MS m/z 604 (M^+, 28%). Anal. ($C_{32}H_{36}N_4S_4$) C, H, N.

12,27-Diisopropyl-12,27-dimethyl-31,32,33,34-tetrathia-3,6,18,21-tetraazapentacyclo[26.2.1.1^{8,11}.1^{13,16}.1^{23,26}]tetratriaconta-1(30),2,6,8,10,13,15,17,21,23,25,28-dodecaene (3d). Yield 70%. Pale yellow powder, mp 188—191 °C. IR (KBr) 2980, 2840,

and 1630 cm^{-1}. ^1H NMR ($CDCl_3$) δ=0.90 (12H, d, J=6.2 Hz), 1.70 (6H, s), 2.30—2.50 (2H, m), 3.79 (8H, s), 6.87 (4H, d, J=3.6 Hz), 7.03 (4H, d, J=3.6 Hz), and 8.17 (4H, s); ^{13}C NMR ($CDCl_3$) δ=18.42, 22.17, 39.18, 48.11, 61.07, 124.09, 130.01, 139.95, 155.93, and 157.08; MS m/z 632 (M^+, 5%). Anal. ($C_{34}H_{40}N_4S_4$) C, H, N.

13,13,29,29-Tetramethyl-33,34,35,36-tetrathia-3,7,19,23-tetraazapentacyclo[28.2.1.$1^{9,12}$.$1^{14,17}$.$1^{25,28}$]hexatriaconta-1(32), 2,7,9,11,14,16,18,23,25,27,30-dodecaene (4). Yield 14%. Colorless powder, mp 270—275 °C. IR (KBr) 2975, 2840, and 1630 cm^{-1}; ^1H NMR ($CDCl_3$) δ=1.40—2.40 (16H, m), 3.53 (8H, t, J=7.2 Hz), 6.76 (4H, d, J=3.6 Hz), 7.00 (4H, d, J=3.6 Hz), and 8.20 (4H, s); ^{13}C NMR ($CDCl_3$) δ=31.74, 32.38, 40.89, 58.60, 123.54, 129.64, 140.56, 154.46, and 157.94; MS m/z 604 (M^+, 1%). Anal. ($C_{32}H_{36}N_4S_4$) C, H, N.

The authors with to thank Mr. Takayuki Ebisawa and Yasuo Nagai for their assistance with some experiments and Mr. Kazuaki Sato for elemental analyses.

References

1) Presented at the Tohoku District Meeting of the Chemical Society of Japan, Iwaki, October 1987.

2) For example, M. G. B. Drew, P. C. Yates, J. Trorha-Grismshaw, A. Lavery, K. P. Mckillop, and S. M. Nelson, *J. Chem. Soc., Dalton Trans.*, **1988**, 347; D. E. Fenton, S. J. Kitchen, C. M. Spencer, S. Tamburini, and A. Vigato, *ibid.*, **1988**, 685; J. Nelson, B. P. Murphy, M. G. B. Drew, P. C. Yates, and S. M. Nelson, *ibid.*, **1988**, 1001; D. Luneau. J.-M. Savariault, P. Cassoux, and J.-P. Tuchagues, *ibid.*, **1988**, 1225; M. J. Cook, A. J. Dunn, A. A. Gold, A. J. Thomson, and M. F. Daniel, *ibid.*, **1988**, 1583; H-R. Chang, S. K. Larsen, P. D. W. Boyd, C. G. Pierpont, and D. N. Hendrickson, *J. Am. Chem. Soc.*, **110**, 4565 (1988), and references cited therein.

3) N. W. Alcock, R. G. Kingston, P. Moore, and C. Pierpoint, *J. Chem. Soc., Dalton Trans.*, **1984**, 1937.

4) Certain macrocyclic polyamines have been recognized as good hosts: For example, K. Odashima and K. Koga, "Cyclophanes," ed by P. M. Kheen and S. M. Rosenfeld, Academic Press, New York (1983), pp. 629—678.

5) While our work was in progress, a publication appeared on the synthesis of a similar type of macrocyclic Schiff base by starting from bis(4-formylphenyl)methane and its inclusion property. J. Jazwinski, L-M. Lehn, R. Meric, J-P. Vigneron, M. Cesario, J. Guilhem, and C. Pascard, *Tetrahedron Lett.*, **28**, 3489 (1987).

6) D. E. Fenton, *Pure Appl. Chem.*, **58**, 1437 (1986) and the references cited therein.

7) N. A. Bailey, M. M. Eddy, D. E. Fenton, G. Jones, S. Moss, and A. Mukhopadhyay, *J. Chem. Soc., Chem. Commun.*, **1981**, 628; N. A. Bailey, M. M. Eddy, D. E. Fenton, S. Moss, A. Mukhopadhyay, and G. Jones, *J. Chem. Soc., Dalton Trans.*, **1984**, 2281.

8) M. G. B. Drew, P. C. Yates. J. Trocha-Grimshaw, K. P. Mckillop, and S. M. Nelson, *J. Chem. Soc., Chem. Commun.*, **1985**, 262.

9) D. E. Fenton and R. Moody, *J. Chem. Soc., Dalton Trans.*, **1987**, 219.

10) M. Sy and M. Maillet, *Bull. Soc. Chim. Fr.*, **1965**, 1495.

11) M. Ahmed and O. Meth-Cohn, *J. Chem. Soc. C*, **1971**, 2104.

12) Y. L. Gol'dfarb and M. L. Kirmalova, *Zh. Obshch. Khim.*, **26**, 3409 (1956).

Halogenation Using Quaternary Ammonium Polyhalides. XVII.[1] Iodination of Acetanilide Derivatives with Benzyltrimethylammonium Dichloroiodate and Zinc Chloride

Shoji KAJIGAESHI,* Takaaki KAKINAMI,† Fumiko WATANABE,† and Tsuyoshi OKAMOTO†
Department of Industrial Chemistry, Faculty of Engineering, Yamaguchi University, Tokiwadai, Ube 755
†Department of Industrial Chemistry, Ube Technical College, Tokiwadai, Ube 755
(Received October 24, 1988)

Synopsis. The reaction of acetanilide derivatives with benzyltrimethylammonium dichloroiodate in acetic acid in the presence of $ZnCl_2$ at room temperature or at 70 °C gave iodo-substituted acetanilide derivatives in good yields.

The nuclear iodo-substituted acetanilide derivatives (**2**) have usually been prepared by the *N*-acetylation of iodo-substituted anilines. As an iodinating agent for acetanilide derivatives (**1**) iodine monochloride (ICl) has considerably been used in place of molecular iodine.[2] However, experimental data concerning the direct iodination of **1** have not been appreciably revealed in the literature.

Recent work in this series has shown that benzyltrimethylammonium dichloroiodate (BTMA ICl_2) is an excellent iodinating agent to phenols,[3] aromatic amines,[4] aromatic ethers,[5] and arenes.[6] In this paper we wish to report on the iodination of **1** by the use of BTMA ICl_2 in the presence of $ZnCl_2$.

Results and Discussion

The reaction of **1** with a calculated amount of BTMA ICl_2 and $ZnCl_2$ in acetic acid at room temperature or at 70 °C gave **2** in good yields. The results are summarized in Table 1, and ^1H NMR data and analyt-

Table 1. Iodination of Acetanilide Derivatives by Use of BTMA $ICl_2/ZnCl_2$ in Acetic Acid

Substrate **1**	Molar ratio BTMA ICl_2/**1**	Reaction conditions Time/h	Temp/°C	Product **2**	Yield[a] %	Mp/°C Found[b]	Mp/°C Reported
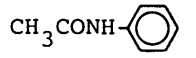 (**1a**)	1.1	2	rt	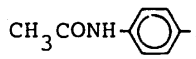 (**2a**)	77	186—187	184[2]
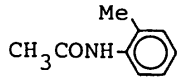 (**1b**)	1.1	4	rt	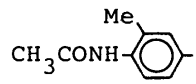 (**2b**)	86	172—173	170.5[7]
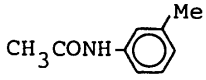 (**1c**)	1.1	0.5	rt	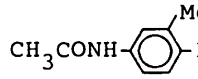 (**2c**)	97	145—146	147—148[8]
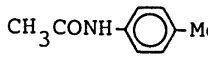 (**1d**)	1.1	24	70	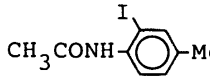 (**2d**)	76	124—126	133[9]
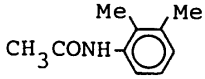 (**1e**)	1.1	2	rt	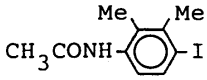 (**2e**)	88	166—167	—
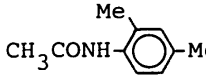 (**1f**)	1.1	18	rt	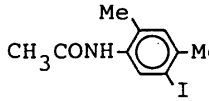 (**2f**)	73	168—169	—
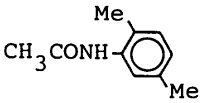 (**1g**)	1.1	1	rt	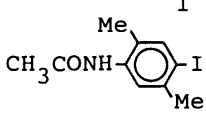 (**2g**)	91	212—214	—
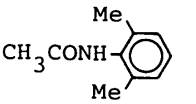 (**1h**)	1.1	24	70	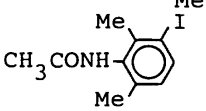 (**2h**)	93	190—192	—
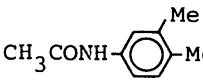 (**1i**)	1.1	5	rt	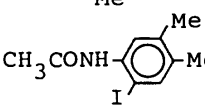 (**2i**)	60	166—167.5	—
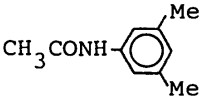 (**1j**)	1.0	1	rt	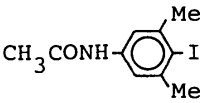 (**2j-1**)	80	171—172	—
1j	2.1	16	70	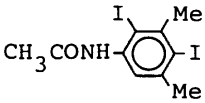 (**2j-2**)	89	194—195.5	—

Table 1. (Continued)

Substrate 1	Molar ratio BTMA ICl_2/1	Reaction conditions Time/h	Temp/°C	Product 2	Yield[a] %	Mp/°C Found[b]	Mp/°C Reported
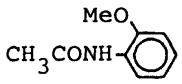 (**1k**)	1.0	2	rt	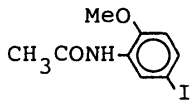 (**2k-1**)	67	147—148	—
1k	2.1	21	70	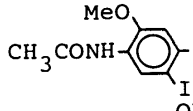 (**2k-2**)	95	136—137.5	—
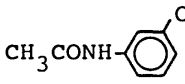 (**1l**)	2.1	1	rt	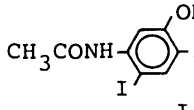 (**2l**)	86	210—211	—
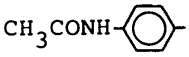 (**1m**)	1.1	48	rt	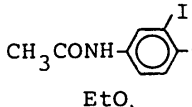 (**2m**)	90	149—151	—
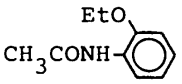 (**1n**)	1.0	3	rt	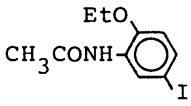 (**2n-1**)	82	156—158	—
1n	2.1	21	70	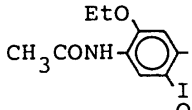 (**2n-2**)	88	176—177	—
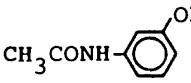 (**1o**)	2.1	1	rt	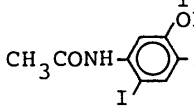 (**2o**)	95	210—211.5	—
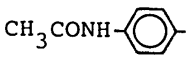 (**1p**)	1.1	48	rt	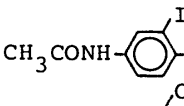 (**2p**)	95	140—141	—
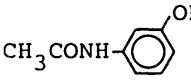 (**1q**)	2.1	3	rt	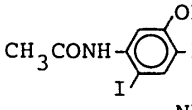 (**2q**)	96	223.5—225	—
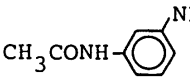 (**1r**)	2.1	2	rt	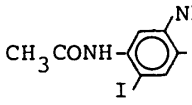 (**2r**)	84	186—187	172—174[10]

a) Yield of isolated product. b) All new compounds prepared were recrystallized from ethanol-water (1 : 3).

Table 2. ^1H NMR Data and Analytical Data of **2**

Product	^1H NMR ($CDCl_3$/TMS) δ, J/Hz			Found(%) and (Calcd(%))		
	CH_3CONH,	Alkyl or Alkoxyl	Aromatic protons	C	H	N
2e	2.02 (s)	2.15 (s, 2-CH_3)	6.87 (d, J=4, 6-H)	41.42	3.92	4.67
	9.28 (br.s)	2.38 (s, 3-CH_3)	7.53 (d, J=4, 5-H)	(41.54	4.18	4.84)
2f	2.05 (s)	2.12 (s, 2-CH_3)	7.00 (s, 6-H)	41.52	3.92	4.62
	9.03 (br.s)	2.30 (s, 4-CH_3)	7.77 (s, 3-H)	(41.54	4.18	4.84)
2g	2.07 (s)	2.15 (s, 2-CH_3)	7.40 (s, 6-H)	41.52	3.95	4.59
	9.15 (br.s)	2.32 (s, 5-CH_3)	7.60 (s, 3-H)	(41.54	4.18	4.84)
2h	2.07 (s)	2.13 (s, 6-CH_3)	6.77 (d, J=4, 5-H)	41.33	4.11	4.81
	9.23 (br.s)	2.30 (s, 2-CH_3)	7.45 (d, J=4, 4-H)	(41.54	4.18	4.84)
2i	2.07 (s)	2.18 (s, 3 and 4-CH_3)	7.17 (s, 2-H)	41.37	4.39	4.62
	8.93 (br.s)		7.48 (s, 5-H)	(41.54	4.18	4.84)
2j-1	2.08 (s)	2.42 (s, 3 and 5-CH_3)	7.38 (s, 2 and 6-H)	41.51	4.10	4.80
	9.57 (br.s)			(41.54	4.18	4.84)
2j-2	2.07 (s)	2.40 (s, 5-CH_3)	7.20 (s, 6-H)	28.97	2.57	3.35
	9.23 (br.s)	2.87 (s, 3-CH_3)		(28.94	2.67	3.38)
2k-1	2.13 (s)	3.83 (s, OCH_3)	6.73 (d, J=4, 3-H)	37.02	3.34	4.79
	8.90 (br.s)		7.27 (dd, J=4 and 2, 4-H)	(37.14	3.46	4.81)
			8.33 (d, J=2, 6-H)			
2k-2	2.12 (s)	3.82 (s, OCH_3)	7.28 (s, 6-H)	26.09	2.18	3.54
	8.70 (br.s)		8.57 (s, 3-H)	(25.92	2.18	3.36)

Table 2. (Continued)

Product	^{1}H NMR ($CDCl_3$/TMS) δ, J/Hz			Found(%) and (Calcd(%))		
	CH_3CONH,	Alkyl or Alkoxyl	Aromatic protons	C	H	N
2l	2.12 (s)	3.80 (s, OCH_3)	7.24 (s, 2-H)	25.83	2.00	3.28
	8.93 (br.s)		8.03 (s, 5-H)	(25.92	2.18	3.36)
2m	2.03(s)	3.77 (s, OCH_3)	6.78 (d, J=4, 5-H)	36.95	3.28	4.78
	9.67 (br.s)		7.47 (dd, J=4 and 2, 6-H)	(27.14	3.46	4.81)
			8.02 (d, J=2, 2-H)			
2n-1	2.12 (s)	1.40 (t, J=7, $OCH_2\underline{CH_3}$)	6.70 (d, J=4, 3-H)	39.23	3.86	4.57
	8.72 (br.s)	4.07 (q, J=7, $OC\underline{H_2}CH_3$)	7.25 (dd, J=4 and 2, 4-H)	(39.36	3.97	4.59)
			8.33 (d, J=2, 6-H)			
2n-2	2.08 (s)	1.37 (t, J=7, $OCH_2\underline{CH_3}$)	7.31 (s, 6-H)	27.90	2.50	3.15
	8.82 (br.s)	4.03 (q, J=7, $OC\underline{H_2}CH_3$)	8.44 (s, 3—H)	(27.87	2.57	3.25)
2o	2.05 (s)	1.35 (t, J=4, $OCH_2\underline{CH_3}$)	7.10 (s, 2-H)	27.82	2.31	3.23
	9.22 (br.s)	4.02 (q, J=4, $OC\underline{H_2}CH_3$)	8.03 (s, 5-H)	(27.87	2.57	3.25)
2p	2.03 (s)	1.37 (t, J=7, $OCH_2\underline{CH_3}$)	6.75 (d, J=4, 5-H)	39.38	3.84	4.55
	9.67 (br.s)	4.00 (q, J=7, $OC\underline{H_2}CH_3$)	7.45 (dd, J=4 and 2, 6-H)	(39.36	3.97	4.59
			8.00 (d, J=2, 2-H)			
2q	2.07 (s)	3.33 (br.s, OH)	7.13 (s, 2-H)	23.84	1.53	3.40
	8.97 (br.s)		7.92 (s, 5-H)	(23.85	1.75	3.48)

ical data of the new **2** are shown in Table 2.

Although BTMA ICl_2 is slightly soluble in acetic acid at room temperature, the addition of $ZnCl_2$ makes this reagent soluble in acetic acid, and the iodination reaction of **1** smoothly proceeds under mild conditions. In this case an equimolar amount of $ZnCl_2$ is required for BTMA ICl_2. Therefore, we assumed the existence of a complex, formed from BTMA ICl_2 with equimolar $ZnCl_2$, as the active species.[6]

We believe that the procedure for the iodination of **1** using BTMA $ICl_2/ZnCl_2$ is an efficient method owing to its ease, mildness of conditions, and good product yields.

As a limitation of this iodinating method, the less reactive **1** such as nitro-, chloro-, and bromoacetanilides gave no product. The reactions of 3-methoxy- (**1l**), 3-ethoxy-(**1o**), 3-hydroxy- (**1q**), and 3-aminoacetanilide (**1r**) with 1-equiv of BTMA $ICl_2/ZnCl_2$ were so vigorous that mixtures of mono, and diiodinated products were obtained, respectively.

Experimental

4-Iodoacetanilide (2a); Typical Procedure: To a solution of acetanilide (**1a**) (0.50 g, 3.70 mmol) in acetic acid (20 ml) was added BTMA ICl_2 (1.42 g, 4.08 mmol) and $ZnCl_2$ (0.7 g, 5.14 mmol). The mixture was stirred for 2 h at room temperature. The yellow color of the solution gradually changed to light brown. The solvent was distilled and a 5% aq solution of $NaHSO_3$ (10 ml) was added to the obtained residue. A 5% aq solution of $NaHCO_3$ was added to the mixture to neutralize; then, the solution was extracted with dichloromethane (40 ml×4). The dichloromethane layer was dried over $MgSO_4$, and passed through a short alumina column. The elute (dichloromethane solution) was concentrated in vacuo to give **2a** as colorless crystals; 0.75 g (77%); mp 186—187 °C (lit,[2] mp 184 °C).

References

1) Part XVI. S. Kajigaeshi, T. Kakinami, M. Shimizu, M. Takahashi, S. Fujisaki, and T. Okamoto, *Tech. Rep. Yamaguchi Univ.*, **4**, 139 (1988).

2) F. D. Chattaway and A. B. Constable, *J. Chem. Soc.*, **105**, 124 (1914).

3) S. Kajigaeshi, T. Kakinami, H. Yamasaki, S. Fujisaki, M. Kondo, and T. Okamoto, *Chem. Lett.*, **1987**, 2109.

4) S. Kajigaeshi, T. Kakinami, H. Yamasaki, S. Fujisaki, and T. Okamoto, *Bull. Chem. Soc. Jpn.*, **61**, 600 (1988).

5) S. Kajigaeshi, T. Kakinami, M. Moriwaki, M. Watanabe, S. Fujisaki, and T. Okamoto, *Chem. Lett.*, **1988**, 795.

6) S. Kajigaeshi, T. Kakinami, M. Moriwaki, T. Tanaka, S. Fujisaki, and T. Okamoto, *Bull. Chem. Soc. Jpn.*, **62**, 439 (1989).

7) H. L. Wheeler and L. M. Liddle, *J. Am. Chem. Soc.*, **42**, 498 (1909).

8) H. Burton and J. Kenner, *J. Chem. Soc.*, **121**, 675 (1922).

9) H. L. Wheeler and L. M. Liddle, *Am. Chem. J.*, **42**, 441 (1909).

10) B. H. Nicolet and J. R. Sampey, *J. Am. Chem. Soc.*, **49**, 1796 (1927).

A Facile and Practical Synthesis of 1-Aryl-3,3,3-trifluoropropynes

Tamejiro HIYAMA,* Ken-ichi SATO, and Makoto FUJITA
Sagami Chemical Research Center, 4-4-1 Nishiohnuma, Sagamihara, Kanagawa 229
(Received October 26, 1988)

Synopsis. A facile and practical method for the synthesis of $ArC{\equiv}CCF_3$ is described which involves (1) conversion of aldehydes ArCHO into $ArCH{=}CClCF_3$ with 1,1,1-trichloro-2,2,2-trifluoroethane, zinc powder, and acetic anhydride in one-pot and (2) dehydrochlorination with sodium *t*-butoxide or sodium amide/*t*-butyl alcohol.

In view of rapidly growing role of organofluorine compounds particularly in material and pharmaceutical science, synthesis of organofluorine compounds is becoming more and more important.[1] Introduction of fluorine and polyfluoroalkyl groups to organic molecule at the late stage of the synthesis often encounters technical and economical problems.[2,3] Use of fluorine-containing building blocks[2] is the alternative approach to the synthesis of organofluorine compounds. Of various trifluoromethyl-substituted building blocks, 1-aryl-3,3,3-trifluoropropynes, which were studied previously with structural interest,[4] have recently been attracting much attention from polymer chemists,[5] organometallic chemists,[6] and synthetic chemists[7] as well as pharmaceutical scientists.[8] Synthetic methods of this type of acetylenes reported so far are classified into four categories: (1) Bromination of trifluoromethylethenes followed by double dehydrobromination,[9] (2) thermal decomposition of triphenylphosphonium trifluoroacetylmethylylides,[8] (3) palladium-mediated coupling reaction of 3,3,3-trifluoropropyne with iodoarenes,[5] and (4) trifluoromethylation of stannylacetylenes.[10] The method (1) is chronologically the first one but suffers restricted application, since we failed to apply the procedure to an acetylene of higher boiling points, e.g. 1-(1-naphthyl)-3,3,3-trifluoropropyne. The second one is suitable only for laboratory-scale synthesis. The third method apparently have practical advantage, but trifluoropropyne should be generated in situ from a relatively expensive precursor.[11] The last one is of no practical use. We report herein a readily accessible two-step entry for the synthesis of 1-aryl-3,3,3-trifluoropropynes.

$$\mathrm{RCHO} + \mathrm{CCl_3CF_3} \longrightarrow \underset{\mathbf{1}}{\mathrm{RCH{=}CClCF_3}} \longrightarrow \underset{\mathbf{2}}{\mathrm{RC{\equiv}CCF_3}}$$

Results and Discussion

Aldehydes RCHO are readily transformed to olefins $RCH{=}CClCF_3$ (**1**) by the one-pot reaction which employs 1,1,1-trichloro-2,2,2-trifluoroethane, zinc powder, and acetic anhydride.[12] Dehydrochlorination of the olefins should give rise to the desired acetylenes $RC{\equiv}CCF_3$ (**2**). We studied various bases to effect the β-elimination. Tertiary amines and lithium amides were totally ineffective. Potassium *t*-butoxide gave fair amount of the acetylenes. Changing the counter ion to sodium or employing a reagent derived from sodium amide and *t*-butyl alcohol was found to be highly effective. Various olefins of $RCH{=}CClCF_3$ were treated with the sodium amide/*t*-butyl alcohol system. Although the olefins which have R = aliphatic or alicylic were either recovered unchanged or decomposed, those having aryl groups gave excellent yields of acetylenes. Results are listed in Table 1.

Table 1. Dehydrochlorination of **1**

Run	Olefin	Product	Yield/%[a]
1	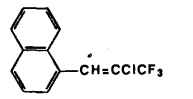	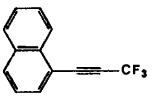	90[b]
2	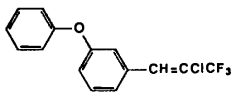	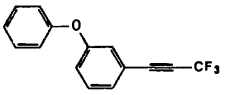	91[c]
3	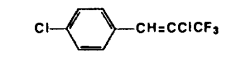	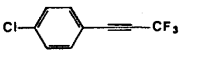	51[d]
4	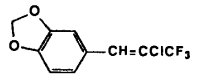	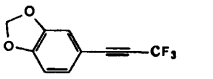	77[c]
5	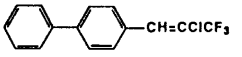	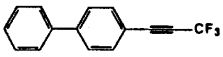	81[c] 95[f]
6	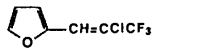		60[g]

a) Isolated yields after distillation unless otherwise stated. b) The reaction was carried out in 0.78 mmol scale. c) The reaction was carried out in 2 mmol scale. d) The reaction was carried out in 0.46 mmol scale. e) The reaction was carried out in 1 mmol scale. f) The reaction was carried out in 0.01 mol scale. g) Estimated by ^{19}F NMR with 1,3,5-trichloro-2,4,6-trifluorobenzene as an internal standard. This reaction was carried out in 2 mmol scale.

In addition to 3,3,3-trifluoropropynyl-substituted carbocyclic aromatics (Runs 1—5), a furan derivative (Run 6) is now accessible. Our strategy is based on two-carbon elongation of ArCHO by using inexpensive reagents and thus find wide practical application.

Experimental

Boiling points were measured by use of Büchi Kugelrohor or Glass Tube Oven (Shibata) and are given in °C/Torr(1 Torr=133.322 Pa). ^1H NMR spectra (tetramethylsilane as an internal standard) were obtained with a Hitachi R-90H or Varian EM-390 spectrometer and ^{19}F NMR spectra (trichlorofluoromethane as an internal standard) with a Hitachi R-20B spectrometer. IR data were recorded with a JASCO A-202 spectrometer. MS spectra (70 eV) were recorded with a Hitachi RMU-6MC machine. Sodium amide was purchased

from Yoneyama Chem. Ind. and used directly. Benzene and *t*-butyl alcohol were freshly distilled before use over benzophenone ketyl and calcium hydride respectively. The chlorotrifluoromethyl substituted olefins **1** were prepared through a modified procedure of our previous publication.[12]

2-Chloro-3,3,3-trifluoro-1-(1-naphthyl)propene. To a *N,N*-dimethylformamide (DMF) (20 ml) solution of 1-naphthalenecarbaldehyde (3.12 g, 20.0 mmol) were added 1,1,1-trichloro-2,2,2-trifluoroethane (2.84 ml, 24.0 mmol) and zinc powder (1.44 g, 22.0 mmol), and the mixture was stirred at room temperature for 1 h and at 50 °C for 24 h before treatment with acetic anhydride (3 ml) and zinc powder (2.62 g, 40 mmol). The resulting mixture was stirred at 50 °C for 2 h, poured to 10% hydrochloric acid (100 ml) and extracted with diethyl ether (100 ml×3 times). The ethereal extract was washed with sat sodium hydorgencarbonate (50 ml) aq solution and then with sat sodium chloride aq solution (50 ml×twice) and dried over magnesium sulfate. Filtration and concentration followed by distillation in vacuo gave the desired olefin (3.2 g, 62% yield) as a colorless oil. Bp 89 °C (bath temp)/0.3 Torr; ^{1}H NMR ($CDCl_3$) δ=7.3—7.6 (m, 3H), 7.7—7.9 (m, 4.5H); ^{19}F NMR ($CDCl_3$-$CFCl_3$) δ=69.0 (s) for (*Z*)-isomer, 62.2 (s) for (*E*)-isomer, intensity ratio (*Z*):(*E*)=7:1. IR (neat) 3060, 1640, 1285, 1260, 180, 1160, 1140, 960, 800, 770 cm^{-1}; MS *m/z* (rel intensity) 256 (48, M$^+$), 221 (100), 201 (74), 152 (79). Found: C, 60.93; H, 3.34%. Calcd for $C_{13}H_8ClF_3$: C, 60.84; H, 3.14%.

2-Chloro-3,3,3-trifluoro-1-(2-furyl)propene. To furfural (1.66 ml, 20.0 mmol) dissolved in DMF (20 ml) were added 1,1,1-trichloro-2,2,2-trifluoroethane (2.85 ml, 24 mmol) and zinc powder (1.44 g, 22 mmol), and the resulting mixture was stirred at 50 °C for 4 h. Acetic anhydride (3.0 ml, 27 mmol) and zinc powder (2.62 g, 40 mmol) were added to the mixture at 0 °C, and the whole was stirred at 50 °C for 1 h and then at 50 °C for 18 h. After workup as above, the ether solvent was stripped off by atmospheric distillation through 10 cm-Vigreux column. Final distillation afforded the title olefin (2.12 g, 54% yield) as a colorless oil. Bp 60 °C (bath temp)/20 Torr. ^{1}H NMR ($CDCl_3$) δ=6.55 (dd, 1H), 7.13 (dd, 1H), 7.22 (s, 1H) for the (*Z*)-isomer, 6.47 (dd, 1H), 6.69 (d, 1H), 6.94 (s, 1H), 6.49 (d, 1H) for the (*E*)-isomer, (*Z*):(*E*)=6:1. ^{19}F NMR ($CDCl_3$-$CFCl_3$) δ=69.0 (s) for (*Z*)-isomer, 63.0 for (*E*)-isomer; IR (neat) 3160, 3070, 2950, 1650, 1480, 1290, 1180, 1140, 1020, 970, 880, 742 cm^{-1}; MS *m/z* (rel intensity) 196 (100, M$^+$), 167 (27), 133 (31), 113 (17), 99 (16), 83 (10), 63 (20). Found: C, 42.77; H, 1.84%. Calcd for $C_7H_4ClF_3O$: C, 42.78; H, 2.05%.

1-(1-Naphthyl)-3,3,3-trifluoropropyne. A Typical Procedure for Dehydrochlorination of 1. A benzene (1 ml) solution of 2-chloro-1-(1-naphthyl)-3,3,3-trifluoropropene (0.20 g, 0.78 mmol) and *t*-butyl alcohol (0.5 ml) was added to sodium amide (0.22 g, 5.2 mmol) suspended in benzene (2 ml), and the mixture was heated to reflux for 5 h. The reaction mixture was poured to 10% hydrochloric acid (10 ml) and extracted with ether (20 ml×3). The combined ethereal extract was washed with aq sodium hydrogencarbonate solution (20 ml×2) and dried over magnesium sulfate. Filtration, concentration under reduced pressure followed by preparative TLC (silica gel, hexane) afforded 1-(1-naphthyl)-3,3,3-trifluoropropyne (0.156 g, 90% yield) and the recovered starting material (3%). The acetylene showed bp 95 °C (bath temp)/0.7 Torr; ^{1}H NMR ($CDCl_3$) δ=7.20—7.90 (m, 6H), 8.10—8.20 (m, 1H); ^{19}F NMR ($CDCl_3$-$CFCl_3$) δ=49.5 (s); IR (neat) 3800, 2250, 1400, 1315, 1260, 1205, 1140, 800, 770 cm^{-1}; MS *m/z* (rel intensity) 220 (100, M$^+$), 201 (48), 170 (28), 150 (10), 85 (14). Found: C, 70.85; H, 3.31%. Calcd for $C_{13}H_7F_3$: C, 70.91; H, 3.20%.

1-(1-Naphthyl)-3,3,3-trifluoropropye. An Alternative Procedure with Sodium *t*-Butoxide. Sodium *t*-butoxide was prepared by heating a mixture of sodium amide (0.29 g, 74 mmol), benzene (2 ml), and *t*-butyl alcohol (0.7 ml) at reflux temperature for 1 h. 2-Chloro-1-(1-naphthyl)-3,3,3-trifluoropropene (0.26 g, 1.0 mmol) dissolved in benzene (1 ml) was added, and the mixture was heated to reflux for 5 h. Workup as above followed by purification by TLC gave the desired acetylene (161 mg, 73% yield) and the starting material (9%).

Other acetylenes in Table 1 were prepared by the typical procedure and showed following physical properties.

1-(3-Phenoxyphenyl)-3,3,3-trifluoropropyne: Bp 140 °C (bath temp)/1.5 Torr; ^{1}H NMR ($CDCl_3$): δ=6.93—7.40 (m); ^{13}C NMR ($CDCl_3$): δ=75.9 (q, $J_{C\text{-}CF_3}$=52.6 Hz), 85.9 (sextet, *J*=6.4 Hz), 114.8 (q, J_{CF_3}=256.9 Hz), 119.5 (d), 119.8 (d), 121.3 (d), 127.2 (d), 121.8 (d), 124.2 (d), 127.0 (d), 130.0 (d), 130.1 (d), 156.1 (s), 157.7 (s); ^{19}F NMR ($CDCl_3$-$CFCl_3$) δ=50.3 (s); IR (KBr) 3100, 3050, 2260, 1580, 1490, 1325, 1203, 1140, 695, 685 cm^{-1}; MS *m/z* (rel intensity) 262 (100, M$^+$), 165 (42), 94 (5), 77 (56), 51 (39). Found: C, 68.76; H, 3.36%. Calcd for $C_{15}H_8F_3O$: C, 68.97; H, 3.09%.

1-(4-Chlorophenyl)-3,3,3-trifluoropropyne: Bp 60 °C (bath temp)/5 Torr (lit[8] 64 °C/44 Torr); ^{1}H NMR ($CDCl_3$) δ=7.32 (d, 2H), 7.48 (d, 2H); ^{19}F NMR ($CDCl_3$-$CFCl_3$) δ=50.3 (s); IR (neat) 2940, 2870, 2260, 1598, 1495, 1325, 1310, 1130—1180, 1105, 1085, 1015, 870, 830, 750, 530 cm^{-1}; MS *m/z* (rel intensity) 204 (100, M$^+$), 185 (32), 169 (64), 154 (16), 99 (11), 74 (11), 50 (11).

1-(3,4-Methylenedioxyphenyl)-3,3,3-trifluoropropyne: Bp 95 °C (bath temp)/5 Torr; ^{1}H NMR ($CDCl_3$): δ=6.00 (s, 2H), 6.75 (d, 1H), 6.90 (α, 1H), 7.70 (dd, 1H); ^{13}C NMR ($CDCl_3$): δ=74.4 (q, $J_{C\text{-}CF_3}$=52.3 Hz), 86.8 (sextet, $J_{C\text{-}CF_3}$=6.0 Hz), 101.8 (t), 108.8 (d), 111.5 (s), 111.9 (d), 115.0 (q, J_{CF_3}=256.4 Hz), 128.0 (d), 147.7 (s), 150.1 (s); ^{19}F NMR ($CDCl_3$-$CFCl_3$) δ=49.5 (s); IR (neat) 2920, 2250, 1500, 1440, 1315, 1240, 1180, 1140, 1100, 1040, 930, 860, 810, 610, 540 cm^{-1}; MS *m/z* (rel intensity) 214 (100, M$^+$), 195 (14), 156 (12), 106 (9), 87 (27). Found: C, 56.05; H, 2.56%. Calcd for $C_{10}H_5F_3O_2$: C, 56.09; H, 2.35%.

1-(2-Furyl)-3,3,3-trifluoropropyne: Boiling point of this compound could not be measured as it distilled with low-boiling solvents. Its analytical sample was obtained by preparative GLC. ^{1}H NMR ($CDCl_3$) δ=6.47 (dd, 1H), 6.92 (d, 1H), 7.53 (d, 1H); ^{13}C NMR ($CDCl_3$) δ=80.3 (q, $J_{C\text{-}CF_3}$=53.3 Hz), 111.4 (d), 114.9 (q, J_{CF_3}=257.5 Hz), 120.1 (d), 128.4 (s), 133.4 (q, *J*=1.9 Hz), 146.1 (d); ^{19}F NMR ($CDCl_3$-$CFCl_3$) δ=51.0 (s); IR (neat) 3150, 2260, 2240, 1300, 1220, 1190, 1150, 1010 cm^{-1}; MS *m/z* (rel intensity) 160 (100, M$^+$), 141 (25), 131 (29), 106 (14), 81 (39), 78 (29), 63 (65). Found: C, 52.30; H, 1.82%. Calcd for $C_7H_3F_3O$: C, 52.52; H, 1.89%.

1-(4-Phenylphenyl)-3,3,3-trifluoropropyne. A Procedure for Gram-Order Synthesis. Sodium amide (2.73 g, 0.07 mol) was added to a benzene (50 ml) solution of 2-chloro-1-(4-phenylphenyl)-3,3,3-trifluoropropene (2.82 g, 0.01 mol) under an argon atmosphere. To the resulting mixture was added *t*-butyl alcohol (6.64 ml, 0.07 mol) at room temperature. The mixture immediately turned to thick under slightly exothermal evolution of ammonia. Benzene (30 ml) was added to facilitate stirring, and the whole was stirred for 2 h before treatment with 10% hydrochloric acid (100 ml). The organic layer was separated, and the aqueous layer was extracted with ether (50 ml×2). The combined organic layer was washed with sat sodium hydrogencarbonate aq solution (50 ml×2) and dried over sodium sulfate. Concentration followed by column chromatography (silica gel, hexane) afforded the title acetylene (2.34 g, 95% yield) as colorless solid. Mp 87 °C; ^{1}H NMR ($CDCl_3$): δ=7.30—7.60 (m); ^{13}C NMR ($CDCl_3$): δ=76.3 (q, $J_{C\text{-}CF_3}$=52.9 Hz), 86.6 (m), 114.0 (q, J_{CF_3}=256.6 Hz), 117.2 (m), 127.1 (d), 127.2 (d), 128.3 (d), 129.0 (d), 132.9(d), 139.6 (s), 143.7 (s); ^{19}F NMR ($CDCl_3$-$CFCl_3$) δ=49.9 (s); IR (KBr) 3100, 3050, 2270, 2200, 1530, 1490, 1410, 1330, 1220, 1170, 1120—1140, 875, 848, 767, 720, 690 cm^{-1}; MS *m/z* (rel intensity) 246 (100, M$^+$), 227 (10), 196 (5),

176 (7), 123 (5). Found: C, 72.90; H, 3.59%. Calcd for $C_{15}H_9F_3$: C, 73.17; H, 3.68%.

This work was partially supported by a Grant-in-Aid for Special Research on Organic Resources (No. 62101001) from the Ministry of Education, Science and Cultrure.

References

1) M. Hudlkicky, "Chemistry of Organic Fluorine Compounds," Ellis Horwood (1976); N. Ishikawa and Y. Kobayashi, "Fluorine Compounds—Chemistry and Application," Kodansha (1979); N. Ishikawa, *Yuki Gosei Kagaku Kyokai Shi*, **42**, 770 (1984).

2) T. Fuchikami, *Yuki Gosei Kagaku Kyokai Shi*, **42**, 775 (1984); Y. Takeuchi, *ibid.*, **46**, 145 (1988).

3) S. T. Purrington, B. S. Kagen, and T. B. Patrick, *Chem. Rev.*, **86**, 997 (1986); A. Haas and M. Lieb, *Chimia*, **39**, 134 (1985); M. R. C. Gerstenberger and A. Haas, *Angew. Chem., Int. Ed. Engl.*, **20**, 647 (1981); S. Silngh, D. D. DesMarteau, S. S. Zuberi, M. Witz, and H.-N. Huang, *J. Am. Chem. Soc.*, **109**, 7194 (1987); T. Umemoto, K Kawada, and K. Tomita, *Tetrahedron Lett.*, **27**, 4465 (1986) and references cited therein.

4) W. R. Cullen, D. C. Frost, and W. R. Leeder, *J. Fluorine Chem.*, **1**, 227 (1971/72); A. E. Lutskii, E. M. Obukhova, L. M. Yagupol'skii, Y. A. Fialkov, and A. G. Panteleimonov, *Russ. J. Phys. Chem.*, **42**, 986 (1968).

5) J. E. Bunch and C. L. Bumgaradner, *J. Fluorine Chem.*, **36**, 313 (1987).

6) R. Fields, R. N. Haszeldine, and A. F. Hubbard, *J. Chem. Soc. C*, **1971**, 3838; H. C. Clark, P. L. Fiess, and C. S. Wong, *Can. J. Chem.*, **55**, 177 (1977); T. G. Attig, H. C. Clark, and C. S. Wong, *ibid.*, **55**, 189 (1977); H. C. Clark and C. R. Milne, *J. Organomet. Chem.*, **161**, 51 (1978); H. C. Clark, G. Ferguson, A. B. Goel, E. G. Janzen, H. Ruegger, P. Y. Siew, and C. S. Wong, *J. Am. Chem. Soc.*, **108**, 6961 (1986).

7) C. L. Bumgardner, J. E. Bunch, and M.-H. Whangbo, *Tetrahedron Lett.*, **27**, 1883 (1986).

8) Y. Kobayashi, T. Yamashita, K. Takahashi, H. Kuroda, and I. Kumadaki, *Tetrahedron Lett.*, **23**, 343 (1982); *Chem. Pharm. Bull.*, **32**, 4402 (1984).

9) L. M. Yagupol'skii and Y. A. Fialkov, *Zh. Obshche. Khim.*, **30**, 1291 (1960); Y. A. Fialkov and L. M. Yagupol'skii, *ibid.*, **36**, 739 (1966).

10) S. A. Klyuchinskii, V. S. Zavgorodnii, V. B. Lebedev, and A. A. Petrov, *Zh. Obshch. Kim.*, **56**, 1663 (1986); *J. Gen. Chem. USSR*, **56**, 1474 (1987).

11) K. Okuhara and K. Kodaira, *Jpn. Kokai Tokkyo Koho*, 87-56496.

12) M. Fujta and T. Hiyama, *Bull. Chem. Soc. Jpn.*, **60**, 4377 (1987); M. Fujita, K. Kondo, and T. Hiyama, *ibid.*, **60**, 4385 (1987) and references cited therein.

A Synthesis of (+)-Cyclaradine, Carbocyclic Analogue of 9-β-D-Arabinofuranosyladenine

Kin-ichi TADANO,* Hiroshi KIMURA, and Seiichiro OGAWA
Department of Applied Chemistry, Faculty of Science and Technology, Keio University, Hiyoshi, Kohoku-ku, Yokohama 223
(Received November 16, 1988)

Synopsis. The title compound, a promising antiviral carbocyclic nucleoside analogue, was synthesized enantiospecifically. The present synthesis involves a coupling reaction of 5-amino-4,6-dichloropyrimidine and (1*R*,2*R*,3*R*,4*R*)-2,3-dihydroxy-4-(hydroxymethyl)cyclopentanamine which was in turn prepared from D-xylose.

Aristeromycin[1] and neplanocin A[2] known as antimicrobial and antitumor agents are representatives of carbocyclic analogue of nucleosides. Sugar moieties of nucleosides are replaced by (hydroxymethyl)cyclopentanepolyol or (hydroxymethyl)-1-cyclopentenepolyol in their structures. The synthesis and biological evaluation of the carbocyclic analogues of nucleosides are current concerns from a pharmacological viewpoint.[3] In 1977, Vince and Daluge reported a synthesis of racemic carbocyclic analogue of arabinosyladenine.[4] This synthetic carbocyclic analogue (**1**) of nucleoside, simply called cyclaradine, arouses much attention owing to its remarkable cytotoxicity against P-388 mouse lymphoid leukemia cells ($LD_{50}=1\times10^{-5}$ M†). Compound **1** was completely resistant to deamination by adenosine deaminase under the conditions in which the antiviral nucleoside 9-β-D-arabinosyladenine was completely deaminated.[4] Furthermore, the racemic **1** inhibits the replication of herpes simplex virus types 1 and 2.[5] This inhibition effect may regard **1** as a candidate for antiherpes agent. We describe herein an enantiospecific synthesis of (+)-cyclaradine (**1**).

Recently, we have reported the synthesis of (3*S*,4*S*)-3-(benzyloxy)-1-[[(*t*-butyldiphenylsilyl)oxy]methyl]-4-hydroxy-1-cyclopentene (**3**) from D-xylose.[6] Our synthesis of **1** commenced with **3**. Mesylation of **3** gave **4** in 96% yield. The mesyloxy group in **4** was displaced by azido group with inversion of configuration at C-4 by treatment with NaN_3 in hot DMF in 81% yield. The silyl protecting group in the resultant azide **5** was then removed with tetrabutylammonium fluoride to give **6** quantitatively. Hydroboration of **6** with borane-THF complex in THF at 0 °C and successive treatment of the product with H_2O_2 in an alkaline solution followed by acetylation provided **7** as a sole product in 79% yield. This highly stereoselective hydroboration with the preferential attack of borane from the less hindered α-side was similar to our previous result obtained by employing the structurally resembling model.[6] Treatment of **7** with H_2S in aqueous pyridine followed by acetylation gave **8** in 98% yield. Debenzylation of **8** according to the Hanessian's procedure[7] followed by acetylation provided the fully acetylated derivative (**9**) of (1*R*,2*R*,3*R*,4*R*)-2,3-dihydroxy-4-(hydroxymethyl)cyclopentanamine (**2**) in 93% yield. Hydrolysis of **9** with aqueous HCl gave **2** in 81% yield after purification by passage through Amberlite CG-120 column.

Coupling of **2** and 5-amino-4,6-dichloropyrimidine (**10**)[8] in boiling 1-butanol in the presence of triethylamine gave a carbocyclic analogue of pyrimidine nucleoside **11**. Cyclization of **11** to a purine derivative **12** was achieved by treatment with triethyl orthoformate in the presence of *p*-toluenesulfonic acid at 60 °C under reduced pressure. Finally, desired **1** was obtained by heating a solution of **12** in saturated methanolic ammonia at 60 °C in an autoclave. The conversion of **2** into **1** was achieved in an overall yield

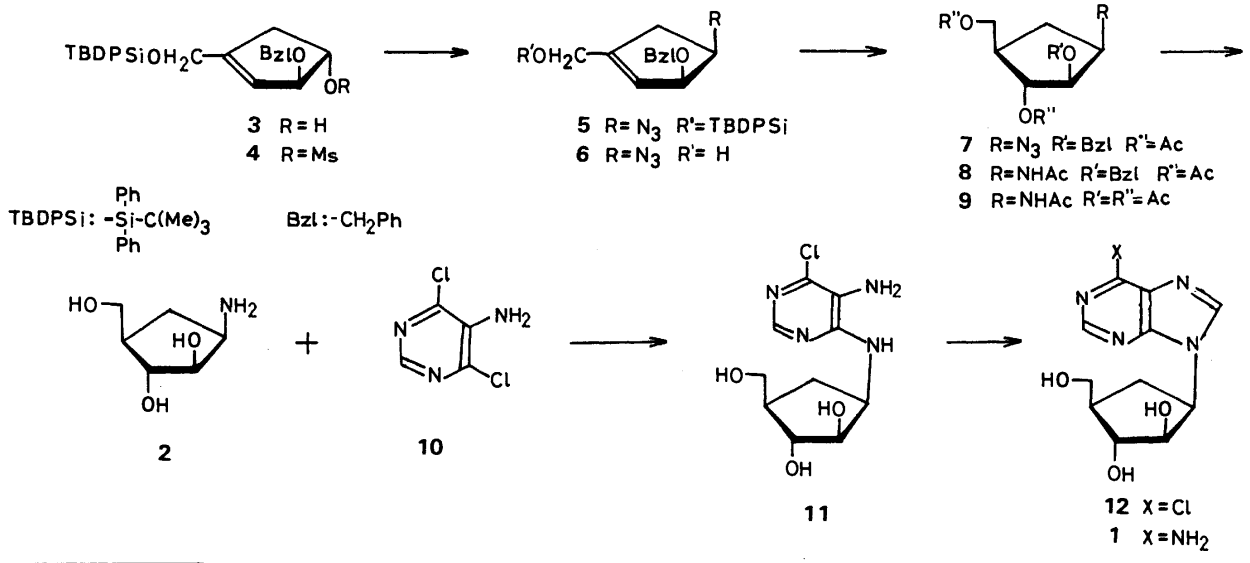

† 1 M=1 mol dm^{-3}.

of approximately 50% (compounds **11** and **12** were not purified to obtain analytical samples). The synthetic **1** was fully characterized by spectral means.

The IC_{50} of the synthetic **1** for P-388 mouse lymphoid leukemia cells (in vitro) was 4.25 μg ml^{-1}.

Experimental

General procedure was described in the previous paper.[6]

(3*S*,4*S*)-3-(Benzyloxy)-4-[(methylsulfonyl)oxy]-1-[[(*t*-butyldiphenylsilyl)oxy]methyl]-1-cyclopentene (4). A solution of **3** (1.01 g, 2.2 mmol) and methanesulfonyl chloride (0.51 ml, 6.6 mmol) in pyridine (10 ml) was stirred at room temperature for 1 h. The reaction mixture was diluted with CH_2Cl_2 (200 ml) and washed with water (100 ml). The aqueous layer was extracted with CH_2Cl_2 (200 ml×3). The combined organic phases were dried (Na_2SO_4) and concentrated in vacuo. The residue was chromatographed on silica gel (AcOEt/hexane 1 : 10) to give **4** (1.13 g, 96%) as a colorless oil: TLC R_f 0.60 (AcOEt/hexane 1 : 3); $[\alpha]_D^{25}$+38.7° (*c* 0.86, $CHCl_3$); IR ν_{max}^{neat} 3090, 2875, 1670, 1185 cm^{-1}; ^{1}H NMR (90 MHz, $CDCl_3$) δ=1.05 (9H, s, Me_3CSi), 2.0—2.2 (2H, m, H-5,5′), 2.94 (3H, s, $MeSO_2O$), 4.16 (2H, br s, $CH_2OTBDPSi$), 4.59 (2H, s, $OC\underline{H}_2C_6H_5$), 4.5—4.8 (1H, m, H-3), 5.13 (1H, dt, *J*=5 and 9 Hz, H-4), 5.69 (1H, br s, H-2), 7.2—8.0 (15H, m, 3×C_6H_5). Found: C, 67.43; H, 6.76%. Calcd for $C_{30}H_{36}O_5SSi$: C, 67.13; H, 6.76%.

(3*S*,4*R*)-4-Azido-3-(benzyloxy)-1-[[(*t*-butyldiphenylsilyl)oxy]methyl]-1-cyclopentene (5). A mixture of **4** (1.12 g, 2.1 mmol) and sodium azide (814 mg, 12.5 mmol) in DMF (60 ml) was heated at 130 °C with stirring for 7 h. The mixture was diluted with AcOEt (400 ml) and washed with water (100 ml×3). The combined aqueous phases were extracted with CH_2Cl_2 (200 ml×3). The combined organic phases were dried (Na_2SO_4) and concentrated in vacuo. The residue was chromatographed on silica gel (AcOEt/hexane 1 : 100) to give **5** (822 mg, 81%) as a colorless oil [42.5 mg (4%) of **4** was recovered]: TLC R_f 0.88 (AcOEt/hexane 1 : 10); $[\alpha]_D^{25}$+37.4° (*c* 0.71, $CHCl_3$); IR ν_{max}^{neat} 3075, 2860, 2100, 1590, 1430 cm^{-1}, ^{1}H NMR (90 MHz, $CDCl_3$) δ=1.03 (9H, s, Me_3CSi), 2.49, 2.56 (each 1H, each br s, H-5,5′), 3.85 (1H, dd, *J*=6 and 12 Hz, H-4), 4.22 (2H, br s, $CH_2OTBDPSi$), 4.4—4.7 (1H, m, H-3), 4.65 (2H, d, *J*=4.5 Hz, $OC\underline{H}_2C_6H_5$), 5.82 (1H, br s, H-2), 7.3—7.9 (15H, m, 3×C_6H_5). Found: C, 72.02; H, 6.81; N, 8.61%. Calcd for $C_{29}H_{33}N_3O_2Si$: C, 72.02; H, 6.88; N, 8.69%.

(3*S*,4*R*)-4-Azido-3-(benzyloxy)-1-cyclopentene-1-methanol (6). A solution of **5** (797 mg, 1.65 mmol) in THF (20 ml) was stirred in the presence of tetrabutylammonium fluoride (1 M in THF, 2.5 ml, 2.5 mmol) at room temperature for 30 min. The solution was concentrated in vacuo. The residue was chromatographed on silica gel (AcOEt/hexane 1 : 7) to give **6** (401 mg, 99%) as a colorless oil: TLC R_f 0.57 (AcOEt/hexane 1 : 1); $[\alpha]_D^{29}$+43.4° (*c* 0.67, $CHCl_3$); IR ν_{max}^{neat} 3610, 2100, 1420 cm^{-1}. ^{1}H NMR (90 MHz, $CDCl_3$) δ=2.37 (1H, br s, OH), 2.51, 2.57 (each 1H, each br s, H-5,5′), 3.87 (1H, dd, *J*=6 and 12 Hz, H-4), 4.13 (2H, br s, $C\underline{H}_2OH$), 4.49 (1H, br s, H-3), 4.55, 4.74 (each 1H, each d, *J*=12 Hz, $OC\underline{H}_2C_6H_5$), 5.75 (1H, m, H-2), 7.37 (5H, s, $OCH_2C_6\underline{H}_5$).

(1*R*,2*R*,3*R*,4*R*)-2-Acetoxy-1-(acetoxymethyl)-4-azido-3-(benzyloxy)cyclopentane (7). To a solution of **6** (400 mg, 1.6 mmol) in THF (30 ml) was added BH_3-THF (1 M in THF, 13.0 ml, 13.0 mmol) at 0 °C under an argon atmosphere. The mixture was stirred at 0 °C for 2 h, and to it were added water (15 ml), 3 M aqueous NaOH (18 ml), and 35% aqueous H_2O_2 (20 ml) successively. The mixture was then stirred at room temperature for 4 h. To it was added saturated aqueous $NaSO_3$ (20 ml). This was extracted with CH_2Cl_2 (300 ml×4) and AcOEt (300 ml×2). The combined organic phases were dried (Na_2SO_4) and concentrated in vacuo. The residue was acetylated with acetic anhydride (3 ml) in pyridine (3 ml) for 2 h. The mixture was concentrated in vacuo. The residue was chromatographed on silica gel (AcOEt/hexane 1 : 14) to give **7** (446 mg, 79%) as a colorless oil: TLC R_f 0.60 (AcOEt/hexane 1 : 3); $[\alpha]_D^{29}$−12.8° (*c* 0.80, $CHCl_3$); IR ν_{max}^{neat} 3020, 2110, 1730, 1450, 1360 cm^{-1}; ^{1}H NMR (90 MHz, $CDCl_3$) δ=1.5—2.5 (3H, m, H-1,5,5′), 2.02 (6H, s, 2×OAc), 3.5—3.9 (2H, m, H-3,4), 4.09 (2H, dd, *J*=4.5 and 6 Hz, CH_2OAc), 4.68 (2H, s, $OC\underline{H}_2C_6H_5$), 4.99 (1H, t, *J*=4.5 Hz, H-2), 7.32 (5H, s, $OCH_2C_6\underline{H}_5$). Found: C, 58.47; H, 5.99; N, 11.81%. Calcd for $C_{17}H_{21}N_3O_5$: C, 58.78; H, 6.09; N, 12.10%.

(1*R*,2*R*,3*R*,4*R*)-1-Acetamido-3-acetoxy-4-(acetoxymethyl)-2-(benzyloxy)cyclopentane (8). To a solution of **7** (440 mg, 1.3 mmol) in a mixture of water and pyridine (1 : 4, 50 ml) was bubbled H_2S at room temperature for 2 h. This solution was stirred more 24 h, and then concentrated in vacuo. The residue was acetylated with acetic anhydride (4 ml) in pyridine (4 ml) for 1 h. The mixture was concentrated in vacuo. The residue was chromatographed on silica gel ($PhCH_3$, then AcOEt/hexane 1 : 1) to give **8** (452 mg, 98%) as a colorless oil: TLC R_f 0.56 (EtOH/$PhCH_3$ 1 : 5); $[\alpha]_D^{26}$+41.5° (*c* 1.42, $CHCl_3$); IR ν_{max}^{neat} 3300, 2925, 1730, 1650, 1535, 1360, 1230 cm^{-1}; ^{1}H NMR (90 MHz, $CDCl_3$) δ=1.4-2.5 (3H, m, H-4, 5, 5′), 1.93 (3H, s, $NCOCH_3$), 2.04, 2.06 (each 3H, each s, 2×$OCOCH_3$), 3.71 (1H, d, *J*=5 Hz, H-2), 4.1—4.5 (3H, m, H-1, CH_2OAc), 4.51, 4.81 (each d, each 1H, *J*=12 Hz, $OC\underline{H}_2C_6H_5$), 4.99 (1H, dd, *J*=1 and 3.5 Hz, H-2), 5.90 (1H, d, *J*=8 Hz, NH), 7.3—7.4 (5H, m, $OCH_2C_6\underline{H}_5$); high-resolution mass spectrum, Calcd for $C_{19}H_{25}NO_6$: M, 363.1680, Found: *m/z* 363.1680.

(1*R*,2*R*,3*R*,4*R*)-1-Acetamido-2,3-diacetoxy-4-(acetoxymethyl)cyclopentane (9). A solution of **8** (443 mg, 1.2 mmol) in a mixture of cyclohexene (10ml) and EtOH (6 ml) in the presence of 20% $Pd(OH)_2$ on charcoal (600 mg) was refluxed for 2 h. The catalyst was removed through a Celite pad, and the filtrate was concentrated in vacuo. The residue was acetylated with acetic anhydride (4 ml) in pyridine (4 ml) for 2 h. The reaction mixture was concentrated in vacuo. The residue was chromatographed on silica gel (EtOH/$PhCH_3$ 1 : 20) to give **9** (356 mg, 93%) as colorless needles, mp 125.5—126.5 °C: TLC R_f 0.36 (EtOH/$PhCH_3$ 1 : 5); $[\alpha]_D^{31}$+28.8° (*c* 0.86, $CHCl_3$); IR ν_{max}^{neat} 3300, 1745, 1660, 1545, 1440, 1375 cm^{-1}; ^{1}H NMR (400 MHz, $CDCl_3$) δ=1.40—1.48 (1H, m, H-5), 1.99 (3H, s, $NCOCH_3$), 2.07, 2.13 (6H, 3H, each s, 3×$OCOCH_3$), 2.25—2.40 (2H, m, H-4, 5′), 4.07—4.19 (2H, m, CH_2OAc), 4.55—4.63 (1H, m, H-1), 4.92 (1H, dd, *J*=2.4 and 4.9 Hz, H-3), 5.08 (1H, dd, *J*=2.4 and 5.4 Hz, H-2), 5.62 (1H, d, *J*=8.8 Hz, NH); high-resolution mass spectrum, Calcd for $C_{14}H_{22}NO_7$: M+H, 316.1394. Found: *m/z* 316.1387. Found: C, 53.14; H, 6.49; N, 4.47%. Calcd for $C_{14}H_{21}NO_7$: C, 53.33; H, 6.71; N, 4.44%.

(1*R*,2*R*,3*R*,4*R*)-2,3-Dihydroxy-4-(hydroxymethyl)cyclopentanamine (2). A solution of **9** (32 mg, 0.1 mmol) in 2 M aqueous HCl (2 ml) was heated at 70 °C for 2 h, and then concentrated in vacuo. The residue was dissolved in water (2 ml) and the aqueous solution was neutralized by addition of Amberlite IRA-400 (OH^-). The resin was removed, and the filtrate was concentrated in vacuo. The residue in a small amount of water was applied on a column of Amberlite CG-120 (H^+). The column was eluted with 0.1 M aqueous NH_4OH to give **2** (12 mg, 81%) as a colorless oil: TLC R_f 0.43 (MeOH/water 1 : 2); $[\alpha]_D^{22}$−125.8° (*c* 0.56, H_2O); ^{1}H NMR (90 MHz, CD_3OD) δ=1.1—2.4 (4H, m, H-1, 4, 5, 5′), 3.50, 3.56 (2H, each s, $C\underline{H}_2OH$), 3.4—4.0 (2H, m, H-2, 3); ^{13}C NMR (100 MHz, $CD_3\underline{O}D$) δ=33.69, 47.24, 53.55, 64.79, 79.74, 79.86; high-resolution mass spectrum, Calcd for $C_6H_{13}NO_3$: M, 147.0894. Found: *m/z* 147.0886.

9-[(1*R*,2*R*,3*R*,4*R*)-2,3-Dihydroxy-4-(hydroxymethyl)cyclopentyl]adenine, (+)-Cyclaradine (1). Compound **9** (216 mg) was hydrolyzed as described above. After neutralization of the reaction solution with Amberlite IRA-400, the filtrate was concentrated to give **2** (141 mg) which was used without further purification. A mixture of **2** and 5-amino-4,6-dichloropyrimidine (674 mg, 4.1 mmol) in 1-butanol (45 ml) was refluxed for 22 h in the presence of triethylamine (0.96 ml, 6.9 mmol). The reaction mixture was then concentrated in vacuo. The residue was dissolved in water (100 ml), and this was washed with $CHCl_3$ (20 ml×5). The combined organic phases were extracted with water (100 ml×2). The combined aqueous phases were concentrated, and the residual yellow crystals were dissolved in water (3 ml), then this aqueous solution was heated with active carbon. This was filtered, and the filtrate was concentrated in vacuo. The resultant white solids were chromatographed on silica gel (EtOH/$PhCH_3$ 1 : 9) to give 5-amino-4-chloro-6-[[(1*R*,2*R*,3*R*,4*R*)-2,3-dihydroxy-4-(hydroxymethyl)cyclopentyl]amino-pyrimidine (**11**) (140 mg) as white powders: IR ν_{max}^{KBr} 3340, 2920, 1570, 1410 cm^{-1}; ^1H NMR (90 MHz, CD_3OD) δ=1.3—2.6 (3H, m, H-4, 5, 5′ of the cyclopentane ring), 3.59, 3.65 (each 1H, each s, $C\underline{H}_2OH$), 3.7—3.9, 3.9—4.1 (each 1H, each m, H-2, 3 of the cyclopentane ring), 7.74 (1H, s, H-2 of the pyrimidine ring).

A solution of **11** (115 mg) in a mixture of DMF (12 ml) and triethyl orthoformate (0.7 ml) was heated at 60 °C under 13 mmHg[††] in the presence of *p*-TsOH (80 mg). After 1 h, *p*-TsOH (10 mg) was added and the mixture was heated for total 2 h. The reaction mixture was neutralized with Amberlite IRA 400 (OH^-), and the resin was removed. The filtrate was concentrated in vacuo. The residue in a small amount of water was applied on a column of Amberlite CG-120 (H^+). The column was eluted with water to give 6-chloro-9-[(1*R*,2*R*,3*R*,4*R*)-2,3-dihydroxy-4-(hydroxymethyl)cyclopentyl]-purine (**12**) (89 mg) as white powders: IR ν_{max}^{KBr} 3380, 2920, 1595,1560, 1490 cm^{-1}; ^1H NMR (90 MHz, CD_3OD) δ=1.9—2.6 (3H, m, H-4, 5, 5′ of the cyclopentane ring), 3.65, 3.70 (each 1H, each s, $C\underline{H}_2OH$), 3.88 (1H, t, J=3 Hz, H-2 or 3 of the cyclopentane ring), 4.01 (1H, dd, J=3 and 6 Hz, H-3 or 2 of the cyclopentane ring), 5.0—5.3 (1H, m, H-1 of the cyclopentane ring), 8.49, 8.53 (each 1H, each s, H-2 and 8 of purine ring).

A solution of **12** (40 mg) in saturated methanolic ammonia (20 ml) was heated at 60 °C in an autoclave for 15 h. The reaction solution was concentrated in vacuo, and the residue was purified by repeated PTLC (EtOH/$PhCH_3$ 1 : 1, four times development) to give **1** (39 mg) as white powders, mp 235—245 °C (decomp): TLC R_f 0.15 (EtOH/$PhCH_3$ 1 : 1); $[\alpha]_D^{22}$+48° (*c* 1.50, MeOH): IR ν_{max}^{KBr} 3300, 2920, 2840, 1630, 1250 cm^{-1}; ^1H NMR (400 MHz, CD_3OD) δ=2.13—2.21, 2.40—2.47 (2H, 1H, each m, H-4, 5, 5′ of the cyclopentane ring), 3.71—3.81 (2H, m, $C\underline{H}_2OH$), 3.97 (1H, dd, J=2.7 and 4.2 Hz, H-2 or 3 of the cyclopentane ring), 4.10 (1H, dd, J=2.7 and 5.2 Hz, H-3 or 2 of the cyclopentane ring), 5.08—5.14 (1H, m, H-1 of the cyclopentane ring), 8.19, 8.28 (each 1H, each s, H-2 and 8 of adenine ring); ^{13}C NMR (100 MHz, CD_3OD) δ=31.51, 47.52, 56.83, 64.58, 78.22, 80.02, 119.70, 142.54, 151.01, 153.45, 157.13; high-resolution mass spectrum, Calcd for $C_{11}H_{16}N_5O_3$: M+H, 266.1251, Found: *m/z* 266.1251.

We are grateful to Sumitomo Pharmaceuticals Co., Ltd. for performing the biological test. Our thanks are also due to Mr. Hisao Arita of our university for carring out elemental analyses.

[††] 1 mmHg=133.322 Pa.

References

1) Isolation: a) T. Kusaka, H. Yamamoto, M. Shibata, M. Muroi, T. Kishi, and K. Mizuno, *J. Antibiot.*, **21**, 255 (1968); b) T. Kishi, M. Muroi, T. Kusaka, M. Nishikawa, K. Kamiya, and K. Mizuno, *Chem. Pham. Bull.*, **20**, 940 (1972). Total synthesis: c) Y. F. Shealy and J. D. Clayton, *J. Am. Chem. Soc.*, **88**, 3885 (1966); d) M. Arita, K. Adachi, Y. Ito, H. Sawai, and M. Ohno, *ibid.*, **105**, 4049, (1983); e) A. K. Saksena, *Tetrahedron Lett.*, **21**, 133 (1980); f) G. V. B. Madhavan and J. C. Martin, *J. Org. Chem.*, **51**, 1287 (1986).

2) Isolation: a) S. Yaginuma, N. Muto, M. Tsujino, Y. Sudate, M. Hayashi, and M. Otani, *J. Antibiot.*, **34**, 359 (1981); b) M. Hayashi S. Yaginuma, H. Yoshioka, and K. Nakatsu, *ibid.*, **34**, 675 (1981). Total synthesis: c) M. Jung, G. Offenbacher, and J. Retey, *Helv. Chim. Acta*, **66**, 1915 (1983); d) M.-I. Lim and V. E. Marquez, *Teretrahedron Lett.*, **24**, 4051 and 5559 (1983). See also Ref. 1d.

3) A leading review for this area: V. E. Marquez and M.-I. Lim, *Med. Res. Rev.*, **6**, 1 (1986).

4) S. Daluge and R. Vince, *J. Med. Chem.*, **20**, 612 (1977).

5) R. Vince, S. Daluge, H. Lee, W. M. Shannon, G. Arnett, T. W. Schafer, T. L. Nagabhushan, P. Reichert, and H. Tsai, *Science*, **221**, 1405 (1983); W. M. Shannon, L. Westbrock, G. Arnett, S, Daluge, H. Lee, and R. Vince, *Antimicrob. Agents Chemother.*, **24**, 538 (1983).

6) K. Tadano, H. Kimura, M. Hoshino, S. Ogawa, and T. Suami, *Bull. Chem. Soc. Jpn.*, **60**, 3673 (1987).

7) S. Hanessian, T. J. Liak, and B. Vanasse, *Synthesis*, **1981**, 396.

8) Commercially available from Aldrich Chemical Co., Inc. For related coupling reactions: A. B. Cheikh, L. E. Craine, S. G. Recher, and J. Zemlicka, *J. Org. Chem.*, **53**, 929 (1988), and also see Refs. 1d, 1f, and 2d.

Sodium Telluride-Mediated Sulfenylation of α-Halo Carbonyl Compounds with Diphenyl Disulfide

Seetharamaiyer PADMANABHAN, Takuji OGAWA, and Hitomi SUZUKI*
Department of Chemistry, Faculty of Science, Ehime University, Bunkyo-cho, Mastuyama 790
(Received November 19, 1988)

Synopsis. Under mild aprotic conditions α-halo carbonyl compounds react with diphenyl disulfide in the presence of sodium telluride to give the corresponding α-phenylthio derivatives in good to moderate yields. The reaction appears to proceed involving the sulfur-sulfur bond cleavage of diphenyl disulfide by sodium telluride.

Introduction of a phenylthio unit adjacent to a carbonyl function is an important step for achieving facile structural modifications.[1] Generally the sulfenylated compounds are synthesized by reacting metal enolates with organic disulfides[2,3] or thiosulfonates,[4] by the action of sulfenyl chloride on α-diazo ketones,[5] enamines,[6] 1,3,2-dioxaphospholes,[7] and silyl enol ethers,[8] and also from α-halo carbonyl compounds and thiolate ion,[9] thallium(I) benzenethiolate,[10] or α-thio iminium salts.[11] Other methods include the sulfenylation of active methylene carbon with sulfenamides,[12] thermal decomposition of β-keto sulfonium salts,[13] and controlled oxidation of β-hydroxy sulfides.[14] Sulfenylation accompanied by dealkoxycarbonylation of β-keto esters affords α-thio ketones.[15] Sophisticated approaches using [bis(phenylthio)methyl]lithium[16] and α,β-epoxy sulfoxides[17] were also reported.

As part of our continuing efforts to explore the synthetic utility of sodium telluride, we now wish to report a method for preparing monothio carbonyl compounds from α-halo carbonyl compounds and diphenyl disulfide.

$$\underset{\mathbf{1}}{RCOCH_2X} + Ph_2S_2 \xrightarrow[DMF,\ -40\,^\circ C]{Na_2Te} \underset{\mathbf{2}}{RCOCH_2SPh} \quad (1)$$

When a solution of α-halo carbonyl compounds (**1**) in *N*,*N*-dimethylformamide (DMF) was added to a mixture of sodium telluride and diphenyl disulfide (excess) in DMF at −40 °C, the monosulfenylated compound (**2**) was obtained in fairly good yields (Table 1). Bissulfenylated compounds and dehalogenation products were also isolated in a few cases. Formation of significant amount of dehalogenated compound from bromodibenzoylmethane could be probably due to the desulfenylation of the monosulfenylated compound initially formed by the thiolate ion. Such desulfenation by thiolate ions has been reported earlier.[18]

The monosulfenylated product **2** arises from the reaction between the thiolate, generated in situ from diphenyl disulfide and sodium telluride, and α-halo carbonyl compound **1**. This was concluded by changing the mode of addition: Addition of phenacyl bromide to sodium telluride at −40 °C generated the enolate anion, which was allowed to react with the added diphenyl disulfide. This resulted in the isolation of bissulfenylated product (**2e**) in addition to acetophenone. Simultaneous formation of these two products can be best explained by assuming the rapid proton removal from the initially formed monosulfenylated compound (**2a**) by the enolate anion present in large excess. Isolation of bissulfenylated products from lithium enolates has been observed earlier.[2] Addition of diphenyl disulfide to sodium telluride at −40 °C resulted in the immediate separation of free tellurium and subsequent addition of ethyl iodide led to the isolation of ethyl phenyl sulfide in 45% isolated yield. Thus the overall reaction (1) can be depicted as follows:

$$PhSSPh + Te^{2-} \longrightarrow 2\,PhS^- + Te$$
$$RCOCH_2X + PhS^- \longrightarrow RCOCH_2SPh + X^-$$

From the reaction of phenacyl bromide with dimethyl disulfide, however, bissulfenylated product and acetophenone were the only major products isolated. This result is very much similar to the one obtained by the addition of diphenyl disulfide to the enolate anion. This indicates that the reaction between phenacyl bromide and dimethyl disulfide may proceed through the nucleophilic attack of the enolate anion on the sulfur atom without any involvement of the reductive cleavage of S-S bond by telluride anion. Trost and co-workers[2] observed that simple ketone enolates are not sufficiently reactive toward dimethyl disulfide. Confirmation of the proposed non-cleavage of S-S bond was provided by an attempted reaction between dimethyl disulfide and benzyl chloride. Formation of benzyl methyl sulfide could not be observed under our conditions from the ^{1}H NMR analysis of the reaction mixture.[19]

It has been reported that the bissulfenylated products can be converted to monosulfenylated compounds with sodium ethanethiolate in the presence of excess base.[20] Any doubt regarding the formation of monosulfenylated compounds by such a possible reduction by sodium telluride in the present study was eliminated by a separate experiment. Reaction of bis(phenylthio)acetophenone with excess of sodium telluride under similar reaction conditions resulted only in the recovery of the starting material in 62% isolated yield and no formation of monosulfenylated product was observed from the ^{1}H NMR of the reaction mixture.

Efforts to effect the selenylation under similar conditions using diphenyl diselenide led to the dehalogenated compounds in most of the cases. Only in the case of ω-bromo-ω-phenylsulfonylacetophenone monoselenylated product was obtained in an acceptable yield.

This paper reports a synthesis of α-phenylthio carbonyl compounds without actually handling the evil-

Table 1. α-Phenylthio and α,α-Bis(phenylthio) Carbonyl Compounds Obtained

Compound			Mp (Bp)	Yield[b]	IR	^{1}H NMR ($CDCl_3$/TMS)
			°C (°C/mm Hg[a])	%	cm^{-1}	δ (ppm)
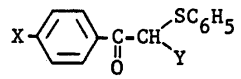						
	X	Y				
2a:	H	H	49—50 (lit,[22] 53—54)	61	1665, 1590, 1570, 1440, 1270, 1010, 800, 750, 740, 690	4.19 (s, 2H), 7.1—8.0 (m, 10H)
2b:	Br	H	59—60	57 (24)	1680, 1580, 1480, 1395, 1190, 995, 740	4.13 (s, 2H), 7.1—7.4 (m, 5H), 7.48 (d, 2H; J=7.8 Hz), 7.71 (d, 2H; J=7.8 Hz)
2c:[c]	H	$SO_2C_6H_5$	131—134	87	1680, 1440, 1320, 1310, 1275, 1140, 1080, 750, 680	5.73 (s, 1H), 7.2—8.0 (m, 15H)
2d:	H	COC_6H_5	89—91 (lit,[12] 93—94)	38[d]	1690, 1680, 1595, 1580, 1450, 1285, 1250-1260, 1200, 760, 740, 690	5.95 (s, 1H), 6.9—8.0 (m, 15H)
2e:	H	SC_6H_5	94—99 (lit,[22] 99—100	33	1670, 1580, 1470, 1450, 1265, 1180, 1150, 995, 810, 755, 695	5.67 (s, 1H) 7.1—8.1 (m, 15H)
2f:[c]	Br	SC_6H_5	68—69	24	—[f]	5.56 (s, 1H), 7.0—7.8 (m, 14H)
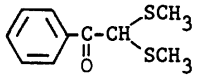 **2g:**[g]			57—62	30	1650, 1585, 1440, 1310, 1280, 1190, 1170, 1000, 720, 700, 680	2.09 (s, 6H) 5.26 (s, 1H) 7.2—7.6 (m, 3H) 7.8—8.1 (m, 2H)
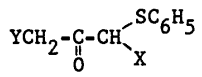						
2h:	H	CH_3	115—120/2 (lit,[7] 78—80/0.003)	85	1710, 1480, 1440, 1360, 1030, 750, 690	1.28 (d, 3H) 2.16 (s, 3H) 3.69 (q, 1H) 7.1—7.6 (m, 5H)
2i:	$COOC_2H_5$	H	135—140/3 (lit,[23] 140/1)	74	1730, 1660, 1580, 1485, 1440, 1370, 1320, 1250, 1185, 1090, 1025, 745, 690	1.18 (t, 3H; J=7 Hz) 3.52 (s, 2H) 3.74 (s, 2H) 4.07 (q, 2H: J=7 Hz) 7.23 (s, 5H)
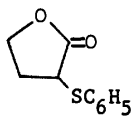 **2j:**			145—150/3 (lit,[10] 140—145/1.3)	85 (10)	1760, 1475, 1435, 1370, 1200, 1150, 1020, 740, 685	2.0—2.8 (m, 2H) 3.73 (d, 1H; J=6 Hz) 3.88 (d, 1H: J=5.4 Hz) 4.19 (t, 2H; J=6.6 Hz) 7.2—7.6 (m, 5H)

a) Bulb-to-bulb distillation (1 mmHg=133.322 Pa). b) Isolated yields based on α-halo carbonyl compounds are not optimised. The values in parentheses refer to the yields of bissulfenylated products. c) Found: C, 64.99; H, 4.49%. Calcd for $C_{20}H_{16}O_3S_2$: C, 65.22; H, 4.35%. d) Dehalogenated product was obtained in 57% yield. e) Found: C, 57.58; H, 3.76%. Calcd for $C_{20}H_{15}BrOS_2$: C, 57.83; H, 3.64%. f) Not determined. g) Found: C, 56.29; H, 5.66%. Calcd for $C_{10}H_{12}OS_2$: C, 56.60; H, 5.66%.

smelling thiol under mild aprotic conditions in fairly good yields and also discloses one more new property of sodium telluride to cleave the S-S bond in aromatic disulfide, but not in aliphatic one. To the best of our knowledge this is the first report employing both α-halo carbonyl compounds and an organic disulfide in a "one pot" way for preparing the α-phenylthio carbonyl compounds.

Experimental

All melting and boiling points were uncorrected. IR spectra were measured as KBr pellets or as neat films between NaCl plates by using a Hitachi 260-10 spectrophotometer

and only prominent peaks between 2000 and 650 cm^{-1} are indicated. ^1H NMR spectra were determined on a Hitachi R-600 spectrometer using chloroform-*d* as solvent and TMS as internal standard. Mass spectra were obtained on a Hitachi M-80B spectrometer using 70 eV.

General Procedure for Sulfenylation: To a suspension of sodium telluride (2.0 mmol; prepared from tellurium and sodium hydride[21]) in DMF was added at −40 °C under nitrogen diphenyl disulfide (4.0 mmol) in DMF (5 ml), followed by the addition of α-halo carbonyl compound (2.0 mmol) in the same solvent (3 ml). The dark reaction mixture was kept with stirring at −40 °C for 2 h and then at room temperature for 1 h. The reaction was quenched with saturated aqueous ammonium chloride solution (10 ml) and the mixture was extracted with benzene. The extract was filtered through a thin bed of Celite, washed with 0.5 M (1 M=1 $mol dm^{-3}$) sulfuric acid and water, and dried over sodium sulfate. The solvent was removed and the crude product was purified by column chromatography on silica gel using hexane as eluent to give the unchanged diphenyl disulfide. Further elution with a mixture of hexane and dichloromethane afforded the sulfenylated compound. Different sulfenylated products prepared and their physical characteristics are given in Table 1.

ω,ω-Bis(phenylthio)acetophenone (2e): To sodium telluride (2.0 mmol) in DMF was added at −40 °C phenacyl bromide (2.0 mmol) in the same solvent (3 ml). The reaction mixture turned black immediately with the separation of free tellurium. After 5 min, diphenyl disulfide (4.0 mmol) in DMF (5 ml) was added. Following the general procedure given above, the bissulfenylated product was isolated in 33% yield. Mp 94—99 °C.

ω,ω-Bis(methylthio)acetophenone (2g) was obtained similarly using dimethyl disulfide instead of diphenyl disulfide. Yield, 30%. Mp 57—62 °C.

ω-Phenylseleno-ω-phenylsulfonylacetophenone: To a mixture of sodium telluride (1.0 mmol) and diphenyl diselenide (2.0 mmol) was added at −40 °C under nitrogen a solution of ω-bromo-ω-phenylsulfonylacetophenone (1.0 mmol) in DMF (2 ml). The reaction mixture was stirred at this temperature for 2 h and then at room temperature for 1 h. After the usual work up the monoselenylated product was isolated in 29% yield in addition to ω-phenylsulfonylacetophenone in 57% yield. The seleno compound was crystallized from ethanol as colorless crystals mp 157—159 °C. MS: *m/z* (rel intensity) 416 (M, 4.4), 275 (21), 167 (23), and 105 (100); IR (KBr): 1690, 1445, 1330, 1315, 1280, 1145, 1085, 745, and 685 cm^{-1}. ^1H NMR ($CDCl_3$): δ=5.71 (s, 1H) and 7.1—8.0 (m, 15H). Found: C, 57.67; H, 3.98%. Calcd for $C_{20}H_{16}O_3SSe$: C, 57.83; H, 3.86%.

We thank the Ministry of Education, Science and Culture for a Scholarship (to S. P.).

References

1) B. M. Trost, *Chem. Rev.*, **78**, 363 (1978); *Acc. Chem. Res.*, **11**, 453 (1978).

2) B. M. Trost and T. N. Salzmann, *J. Am. Chem. Soc.*, **95**, 6840 (1973); B. M. Trost, T. N. Salzmann, and K. Hiroi, *ibid.*, **98**, 4887 (1976).

3) D. Seebach and M. Teschner, *Tetrahedron Lett.*, **1973**, 5113; S. Kurozumi, T. Toru, and T. Tanaka, *ibid.*, **1976**, 4091; P. A. Zoretic and P. Soja, *J. Org. Chem.*, **41**, 3587 (1976); P. G. Gassman, D. P. Gilbert, and S. M. Cole, *ibid.*, **42**, 3233 (1977); K. Hiroi, Y. Matsuda, and S. Sato, *Synthesis*, **1979**, 621; P. Groenewegen, H. Kallenberg, and A. van der Gen, *Tetrahedron Lett.*, **1979**, 2817.

4) B. M. Trost and G. S. Massiot, *J. Am. Chem. Soc.*, **99**, 4405 (1977).

5) F. Weygand and H. J. Bestmann, *Z. Naturforsch., B*, **10**, 296 (1955).

6) M. E. Kuehne, *J. Org. Chem.*, **28**, 2124 (1963).

7) D. N. Harpp and P. Mathiaparanam, *J. Org. Chem.*, **36**, 2540 (1971).

8) S. Murai, Y. Kuroki, K. Hasegawa, and S. Tsutsumi, *J. Chem. Soc.*, **1972**, 946.

9) C. K. Bradsher, F. C. Brown, and R. J. Grantham, *J. Am. Chem. Soc.*, **76**, 114 (1954). Recently phase-transfer catalyst has been employed for preparing α-thio ketones from α-halo ketones and thiolate anions: M. Lissel, *J. Chem. Res. (S)*, **1982**, 286.

10) M. R. Detty and G. P. Wood, *J. Org. Chem.*, **45**, 80 (1980).

11) H. Singh and M. S. Batra, *Indian J. Chem., Sect. B*, **26**, 1111 (1987).

12) T. Kumamoto, S. Kobayashi, and T. Mukaiyama, *Bull. Chem. Soc. Jpn.*, **45**, 866 (1972).

13) A. J. H. Labuschagne, J. S. Malherbe, C. J. Meyer, and D. F. Schneider, *Tetrahedron Lett.*, **1976**, 3571.

14) G. H. Posner and M. J. Chapdelaine, *Tetrahedron Lett.*, **1977**, 3227.

15) M. Asaoka, K. Miyake, and H. Takei, *Bull. Chem. Soc. Jpn.*, **51**, 3008 (1978).

16) I. Kuwajima and Y. Kurata, *Chem. Lett.*, **1972**, 291.

17) T. Satoh, Y. Kaneko, T. Kumagawa, T. Izawa, K. Sakata, and H. Yamakawa, *Chem. Lett.*, **1984**, 1957.

18) M. Oki. W. Funakoshi, and A. Nakamura, *Bull. Chem. Soc. Jpn.*, **44**, 828 (1971); V. S. Karavan, D. A. Simonov, and T. I. Temnikova, *Zh. Org. Khim.*, **18**, 1767 (1982).

19) The sulfur-sulfur bond in dimethyl disulfide is reported to be three times stronger than that in diphenyl disulfide; E. N. Gur'yanova, *Quart. Reports. Sulfur Chem.*, **5**, 113 (1970); *Chem. Abstr.*, **73**, 109114y (1970).

20) J. S. Grossert and P. K. Dubey, *J. Chem. Soc., Chem. Commun.*, **1982**, 1183.

21) H. Suzuki, H. Manabe, T. Kawaguchi, and M. Inouye, *Bull. Chem. Soc. Jpn.*, **60**, 771 (1987).

22) W. J. Kenney, J. A. Walsh, and D. A. Davenport, *J. Am. Chem. Soc.*, **83**, 4019 (1961).

23) C. B. Troostwijk and R .M. Kellogg, *J. Chem. Soc., Chem. Commun.*, **1977**, 932.

Photochemical Decarbonylation of (α-Arylacyl)triphenylgermane

Syun-ichi KIYOOKA,* Tsutomu SHIBUYA, Fuminori SHIOTA, and Ryoji FUJIYAMA
Department of Chemistry, Kochi University, Akebono-cho, Kochi 780
(Received September 12, 1988)

Synopsis. (α-Arylacyl)triphenylgermanes were prepared from the corresponding esters with triphenylgermyllithium at room temperature in good yields. Photochemical decarbonylation of (α-arylacyl)triphenylgermanes took place under UV irradiation to quantitatively give (α-arylalkyl)-triphenylgermanes without by-products.

Organogermaniums are gradually attracting the attention of synthetic organic chemists because of their inherent properties, which are different from organosilicons and organotins.[1] Acylgermanes, among them, are expectantly situated to be relatively unique reagents by considering the acylsilane chemistry.[2] We recently wrote a preliminary report regarding the preparation of acylgermanes from the corresponding esters with triphenylgermyllithium,[3] the process is easier than the other routes.[4]

Upon studying the utility of acylgermanes to organic synthesis, we became aware of the instability of acylgermanes dissolved in solvents toward sunlight. Although the photochemistry of acylsilanes has been well-investigated,[5] little is known concerning that of acylgermanes. The germyl radical via a Norrish type-I cleavage has been observed in the laser photolysis (266 nm) of acylgermanes.[6] When (α-arylacyl)triphenylgermanes were irradiated, decarbonylation was found to take place. We therefore report here the synthesis of (α-arylacyl)triphenylgermanes and the subsequent photochemical decarbonylation to give (α-arylalkyl)-triphenylgermanes.

Results and Discussion

The reaction of *N*,*N*-dimethylpivalamide with triethylgermyllithium, from bis(triethylgermyl)mercury and metallic lithium, in hexane at 20 °C has been reported to give pivaloyltriethylgermane in 30% yield with a by-product of 1,1-bis(triethylgermyl)-2,2-dimethyl-1-propanol (24%).[1c] We examined the reaction of esters with triphenylgermyllithium, which is known to have sufficient nucleophilicity.[7] Triphenylgermyllithium can be produced by the addition of equimolar quantities of butyllithium into a tetrahydrofuran (THF) solution of triphenylgermane.[8] To a flesly produced THF solution of triphenylgermyllithium were added equimolar quantities of esters at ambient temperature. After stirring for 5—10 min, the reaction mixture was quenched with a saturated aqueous ammonium chloride solution to give acylgermanes in satisfactory yields (60—80%). The yield was independent of the bulkyness of R (methyl, ethyl, and *t*-butyl groups).

$$RCOOR' + Ph_3GeLi \rightleftharpoons RCOGePh_3 + LiOR'$$

However, small amounts of triphenylgermane were always recovered without any other by-products. Thus, the reaction is not prone to proceed quantitatively. The incompleteness of the reaction can presumably be attributed to an equilibrium attainted under the basic conditions; but here, by the use of 10% excess of esters, the yield was not improved. Further, the reaction of esters having α-active hydrogen (e.g., (+)-methyl (*S*)-2-phenylpropionate) gave almost racemic acylgermanes under such conditions. The results of a synthesis of (α-arylacyl)triphenylgermanes are presented in Table 1.

The acyl carbon-germanium bond of acyltriphenylgermanes was found to be smoothly fissioned with light with a wavelength >300 nm. Actually, benzoyltriphenylgermane and propionyltriphenylgermane in THF was rapidly degradated in a Pyrex flask upon irradiation by a sunlamp (1 h) or a high-pressure mercury lamp (20 min). Though the reaction is apparently complex (many spots on their thin-layer chroma-

Table 1. Synthesis of Benzylic Acylgermanes from the Corresponding Esters

Compd	Yield[a] %	Mp °C	IR (C=O) cm^{-1}	^1H NMR δ/ppm (*J*/Hz)	Found (Calcd)/% C	H
1a	70	81—83	1655	4.05(s, 2H), 7.18—7.70 (m, 20H)	73.88 (73.82)	5.25 (5.24)
1b	74	74—76	1660	2.23(s, 3H), 3.86(s, 2H), 6.81—6.73(m, 4H), 7.30(m, 15H)	74.42 (74.20)	5.51 (5.53)
1c	66	136—138	2220,[b] 1675	3.95(s, 2H), 7.40(m, 19H)	72.43 (72.38)	4.69 (4.72)
1d	71	115—117	1660	1.33(d, *J*=7, 1H), 4.30 (q, *J*=7, 1H), 7.13—7.70 (m, 20H)	74.18 (74.20)	5.55 (5.53)
1e	65	133—139	1665	4.36(ABq, *J*=11 and 23, 2H), 4.85(s, 1H), 6.80—7.75(m, 25H)	75.00 (74.90)	5.30 (5.33)

a) Isolated yield. b) Absorption of C≡N group.

Table 2. Synthesis of Benzyltriphenylgermanes by Photochemical Decarbonylation

Compd	Yield[a] %	Mp °C	^{1}H NMR δ/ppm (J/Hz)	Found (Calcd)/% C	H
2a	95	84—87[b]	2.96(s, 2H), 7.12(m, 20H)	76.09 (76.01)	5.64 (5.61)
2b	97	78—80	2.17(s, 3H), 2.87(s, 2H), 6.75(m, 4H), 7.22(m, 15H)	76.46 (76.34)	5.86 (5.91)
2c	88	135	2.95(s, 2H), 7.26(m, 19H)	74.27 (74.35)	5.02 (5.04)
2d	92	119—120	1.60(d, J=7.5,3H), 3.26 (q, J=7.5, 1H), 6.8—7.15 (m, 5H), 7.31(br s, 15H)	76.44 (76.34)	5.96 (5.91)
2e	90	125—127	4.49(ABq, J=12 and 31, 2H), 5.15(s, 1H), 6.90—7.60 (m, 25H)	76.70 (76.69)	5.59 (5.63)

a) Isolated yield. b) 86.5 °C in the literature; H. Gilman and C. W. Gerow, *J. Am. Chem. Soc.*, **77**, 5509 (1955).

tography after irradiation), the corresponding carboxylic acids were obtainted by a treatment of crude materials with 10% hydrochloric acid in low yields with hexaphenyldigermane.

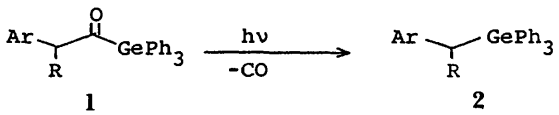

1 **2**

	Ar	R
a	Ph	H
b	p-$CH_3C_6H_4$	H
c	p-CNC_6H_4	H
d	Ph	CH_3
e	Ph	$PhCH_2O$

In contrast, α-arylacylgermanes upon irradiation resulted in a different mode of fission. The stability of benzyl radical is well-known in various kinds of photochemistry[9] and the photochemical fission of germanium-carbon bonds with shorter wavelengths has been observed regarding the benzyl radical,[10] as well as that of silicon-carbon bonds via a benzyl radical-silyl radical pair in a primary photochemical process.[11] When a THF solution containing α-arylacylgermanes in a Pyrex flask filled with argon was irradiated at ambient temperature with a 400-W high-pressure mercury lamp for 30 min, the reaction quantitatively gave α-arylalkylgermanes. (α-Arylacyl)triphenylgermanes absorbed light in their n→π* excited states,[12] and might have fissured to give an acyl radical-germyl radical pair; then, decarbonylation might have taken place at the acyl radical, because of the inherent stability of the α-arylalkyl radical. The photoreaction of α-arylacylgermanes in the presence of olefin (e.g., methyl acrylate) did not give any addition products; thus, the recombination between the resulting α-arylalkyl and triphenylgermyl radicals might have been an intramolecular process in a solvent cage.

Experimental

Unless otherwise noted, materials were obtained from commercial suppliers and used without further purification. Tetrahydrofuran (THF) was distilled from sodium/bezophenone immediately prior to use. All melting points were uncorrected. IR spectra were determined with a JASCO A-302 infrared spectrophotometer. UV spectra were measured with a JASCO UNIDEC 670 spectrophotometer. ^{1}H NMR spectra were obtained with a Hitachi R-90H spectrometer. Chemical shifts are expressed in ppm downfield from internal tetramethylsilane. Merck silica gel 60 (230—400 mesh) was used for flash column chromatography and Merck aluminium sheets (silica gel 60) was used for thin layer chromatography. Ethyl 2-benzyloxyphenylacetate was prepared by the treatment of ethyl 2-hydroxyphenylacetate with benzyl bromide/sodium hydride in *N,N*-dimethylformamide.

General Procedure for the Reaction of Esters with Triphenylgermyllithium. Preparation of (Phenylacetyl)triphenylgermane (1a): To a solution of triphenylgermane (304.6 mg, 1 mmol) in THF (10 cm^3) was added butyllithium (15% solution in hexane, 0.62 cm^3, 1 mmol) at 0—−5 °C. The solution was stirred at room temperature for 1 h. Methyl phenylacetate (150.2 mg, 1 mmol) was added via syring to the solution. After stirring for 10 min, the reaction mixture was quenched with a saturated aqueous ammonium chloride solution and the organic layer was extracted with diethyl ether. The ethereal layer was dried over magnesium sulfate. After evaporation of the solvent, a crude solid was obtained and then purified by flash column chromatography (9 g of silica gel with 3% ethyl acetate in hexane) to give (phenylacetyl)triphenylgermane **1a** (296 mg) in 70% yield.

General Procedure for the Photochemical Decarbonylation of (α-Arylacyl)triphenylgermanes. Preparation of Benzyltriphenylgermane (2a): The solution of **1a** (84.6 mg, 0.2 mmol) in THF (10 cm^3) was irradiated with a 400-W high-pressure mercury lamp with stirring under argon for 30 min. The solvent was removed with a rotary evaporator to give a solid which was purified by flash column chromatography (6 g of silica gel with hexane) to give benzyltriphenylgermane (75 mg) in 95% yield.

References

1) a) A. G. Brook and S. A. Fieldhouse, *J. Organomet. Chem.*, **10**, 235 (1967); b) W. Kitching, H. A. Olszowy, and K. Harvey, *J. Org. Chem.*, **47**, 1893 (1982); c) D. A. Bravo-Zhivotovskii, S. D. Pigarev, I. D. Kalikhman, O. A. Vyazankina, and N. S. Vyazankin, *J. Organomet. Chem.*, **248**, 51 (1983); d) H. Oda, Y. Morizawa, K. Oshima, and H. Nozaki, *Tetrahedron Lett.*, **25**, 3217 (1984); e) S. Inoue and Y. Sato, *Organometallics*, **6**, 2568 (1987); f) S. Kiyooka

and M. Nakata, *Chem. Lett.*, **1988**, 721.

2) a) E. W. Colvin, "Silicon in Organic Synthesis," Butterworths, London (1981); b) W. P. Weber, "Silicon Reagents for Organic Synthesis," Springer-Verlag, New York (1983).

3) a) S. Kiyooka and A. Miyauchi, *Chem. Lett.*, **1985**, 1829; b) S. Kiyooka, F. Shiota, and T, Shibuya, *ibid.*, **1987**, 495; Acylgermanes did not appreciably hydrolyze in 10% HCl and 10% NaOH aqueous solutions and were relatively inert toward lithium diisopropylamide and Lewis acids.

4) a) A. G. Brook, J. M. Duff, P. F. Jones, and N. R. Davis, *J. Am. Chem. Soc.*, **89**, 431 (1967); b) G. J. D. Peddle, *J. Organomet. Chem.*, **14**, 139 (1968).

5) a) N. A. Porter and P. M. Iloff, *J. Am. Chem. Soc.*, **96**, 6200 (1974); b) M. E. Scheller, G. Iwasaki, and B. Frei, *Helv. Chim. Acta*, **69**, 1378 (1986).

6) K. Mochida, K. Ichikawa, S. Okui, Y. Sakaguchi, and H. Hayashi, *Chem. Lett.*, **1985**, 1433; Hexaphenyldigermane was isolated after the photolysis of benzoyltriphenylgermane. However no informations were given about acyl moiety.

7) H. Gilman and C. W. Gerow, *J. Am. Chem. Soc.*, **77**, 4675 (1955).

8) H. Gilman and C. W. Gerow, *J. Am. Chem. Soc.*, **78**, 5435 (1956); The other preparative methods of triphenylgermyllithium using metallic lithium with hexaphenyldigermane, tetraphenylgermane, or chlorotriphenylgermane, were not so adequate for the following synthetic reactions because of the remaining excess lithium.

9) a) A. G. Harrison and F. P. Lossing, *J. Am. Chem. Soc.*, **82**, 1052 (1960); b) R. S. Givens and W. F. Oettle, *ibid.*, **93**, 3301 (1971); c) M. B. Zimmt, C. Doubleday, and N. J. Turro, *ibid.*, **108**, 3618 (1986).

10) a) M. Kobayashi, M. Yoshida, and M. Kobayashi, *Bull. Chem. Soc. Jpn.*, **59**, 3169 (1986); b) K. Mizuno, M. Yasueda, and Y. Otzuji, *Chem. Lett.*, **1988**, 229.

11) M. Kira, H. Yoshida, and H. Sakurai, *J. Am. Chem. Soc.*, **107**, 7767 (1985).

12) The UV spectra of compounds **1a—1c** were measured in 99% ethanol; **1a**: λ_{max}363 (ε 185), **1b**: λ_{max} 365 (ε 208), **1c**: λ_{max} 360 (ε 313) and λ_{max} 374 nm (ε 293).

Stereospecific Preparation of Chiral 1,5-Diketone by One-Methylene Incorporated Dimerization Reaction of *d*-Camphor Enolate and Reduction of the 1,5-Diketone

Syun-ichi KIYOOKA,* Tsuneo YAMASHITA, Akihisa YAMAMOTO, and Ryoji FUJIYAMA
Department of Chemistry, Kochi University, Akebono-cho, Kochi 780
(Received September 19, 1988)

Synopsis. The reaction of *d*-camphor with *N*,*N*-dimethylformamide (DMF) in the presence of potassium hydride stereoselectively gave bis[(1*R*,3*S*,4*R*)-2-oxo-3-bornyl]methane (**1**). This new condensation reaction is proposed to proceed by an attack of the *d*-camphor enolate to DMF and a subsequent reduction. Three chiral diols were obtained from the reduction of **1**.

New-type chiral auxiliaries can be expected to facilitate new developments and some improvements of asymmetric reactions. Such auxiliaries are worth consideration, provided they can be readily prepared from natural compounds by simple procedures. Since *d*-camphor is a cheap chiral pool, a number of effective chiral auxiliaries has been produced by its structural modification and then used for some potential asymmetric reactions.[1)]

We found a new reaction under way to prepare new chiral auxiliaries from *d*-camphor.[2)] In the reaction of *d*-camphor with equimolar quantities of sodium/benzyl chloride in DMF solvent at ambient temperature, the expected α-benzylated compound was obtained in very low yield. By applying conditions of more elevated temperature (50—80 °C) and/or potassium hydride[3)] in order to increase the yield of the α-alkylated product, an unknown compound (mp 198.5—199.5 °C) (**1**) having a similar IR spectrum to that of starting *d*-camphor was mainly obtained. The reaction without alkyl halide under the same conditions also gave only the compound **1** in high yield.

The structure of **1** was determined to be bis-[(1*R*,3*S*,4*R*)-2-oxo-3-bornyl]methane by analyzing the physical data (as described below). The formura $C_{21}H_{32}O_2$ of **1**, derived from its elemental analysis and MS (M^+ 316), corresponded to that of a compound to be made up of two camphors and one methylene. A characteristic structure suited for **1** could be deduced to have high symmetry from eleven different peaks of carbon resonance, in which each camphor binds with a methylene at the carbonyl α-position (C-3).

The stereochemistry at C-3, while that at C-3′ is treated in the same manner from the symmetry, was ascertained to be endo on the basis of the following NMR studies. a) The observed γ effect on the ^{13}C chemical shift at C-5 suggests that the methylene bridge situates in endo direction; the ^{13}C chemical shift at C-5 of **1** was observed 6.9 ppm upfield than that at C-5 of *d*-camphor, as observed in *endo*-3-methyl-2-norbornanone system.[4)] b) In addition, in the ^1H NMR spectra such a rigid camphor system permits the application of the Karplus equation[5)] to compound **1** with confidence. If the methylene bridge of **1** is endo at C-3, the dihedral angle between H-3 and H-4 is close to about 40°. From 2D cosy and 2DJ experiments with the 200 MHz NMR, the coupling constant between H-3 and H-4 was determined to be 5.0 Hz which supports to be the endo configuration. Further, the long-range coupling (1.5 Hz) between H-3 and H-5β was observed in **1** by virtue of the "W" configuration[6)] of these protons.

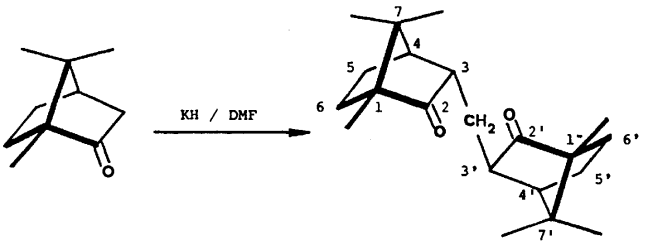

1

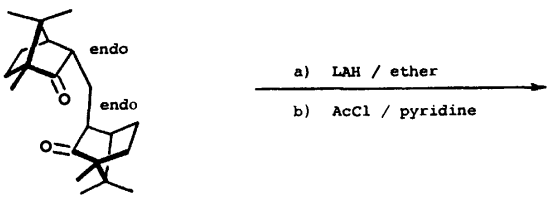

1

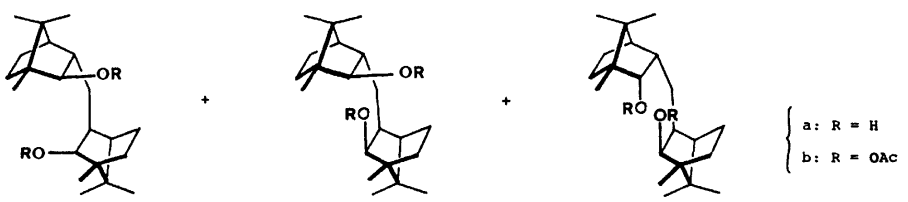

2a, b (exo, exo) **3a, b** (exo, endo) **4a, b** (endo, endo)

Consequently, in the one-methylene incorporated dimerization reaction of *d*-camphor enolate, thermodynamically more stable endo, endo-isomer turned out to be predominantly produced under the applied conditions, in which steric repulsions are minimized between the methyl groups at C-7 and C-7′ and the bridged methylene reductively incorporated from the formyl group of DMF used as a solvent.[2] This chiral diketone **1** expected to find utility for various asymmetric reactions.

As several chiral diols have been used as chiral modificators of lithium aluminum hydride (LAH),[7] we also tried the reduction of the chiral 1,5-diketone **1** in order to obtain new chiral diols. The reduction of **1** with LAH in diethyl ether easily gave a mixture of diols **2a—4a**.

The stereochemistry of **2a—4a** was determined on the basis of the coupling constants between H-2 and H-3 and/or H-2′ and H-3′ in the diols and diacetates. Compound **2a** with a coupling constant of 4.0 Hz is exo,exo-isomer and compound **3a** with two different coupling constants (4.0 and 9.5 Hz) is exo,endo-isomer, while the compound **4a** with J=9.9 Hz corresponds to endo,endo-isomer. Furthermore, the peak numbers in the ^{13}C NMR spectra of **2a** and **4a** suggested that both are symmetrical structures.

Diols, **2a** (47%) and **3a** (40%), are major and diol **4a** (6%) is minor in the reduction of **1** with LAH (ether, room temperature). The selectivity in the reduction of **1** with diisobutylaluminum hydride (THF, −78 °C) is not so different from that with LAH. On the other hand, the reduction of **1** with lithium tri-*s*-butylhydroborate (THF, −78 °C) gave only diol **2a** in a low yield.

Experimental

Unless otherwise noted, materials were obtained from commercial suppliers and used without further purification. Tetrahydrofuran (THF) was distilled from sodium/benzophenone, diethyl ether (ether) was distilled from lithium aluinum hydride (LAH), and *N*,*N*-dimethylformamide (DMF) was distilled from K_2CO_3 immediately prior to use. All the melting points were uncorrected. IR spectra were determined with a JASCO A-302 infrared spectrophotometer. Optical rotations were observed with a Union Giken PM-101 polarimeter. ^{1}H NMR and ^{13}C NMR spectra were determined with Hitachi R-90H and R-250H NMR spectrometers. 2D cosy and 2DJ experiments were performed with a Varian XL-200E NMR spectrometer. Mass spectra were measured on a Hitachi RMU-6L instrument at 70 eV. Merck silica gel 60 (230—400 mesh) was used for flash column chromatography.

Synthesis of Bis[(1*R*,3*S*,4*R*)-2-oxo-3-bornyl]methane (1). Potassium hydride (200 mg, 5 mmol) dispersed in mineral oil (35 wt%) was washed several times with petroleum ether. Onto the hydride was added DMF (10 cm^3) under argon atmospher. The solution was stirred at room temperature until the evolution of gas ceased. To the resulting mixture was added dropwise a solution of (1*R*)-(+)-camphor (609 mg, 4 mmol) in THF (3 cm^3). Then the reaction mixture was stirred at 50 °C for 3 h and quenched with 5% HCl at 0 °C. After extraction with ether, the ethereal solution was washed with brine and dried over $MgSO_4$. Filtration and removal of the solvent gave a residue, which was purified by flash

Table 1. Diols Prepared from **1** and Their Diacetates

Compd	Mp / °C	$[\alpha]_D^{20}$/° (c 1.0, $CHCl_3$)	IR/cm^{-1} (Nujol)	^{1}H NMR δ/ppm (J/Hz) ($CDCl_3$)	^{13}C NMR δ/ppm ($CDCl_3$)	Anal.[a] (C, H)
2a	202—206	−15.4	3320 (OH)	0.85 (s, 6H); 0.87 (s, 6H); 1.09 (s, 6H); 1.30—1.60 (m, 12H); 2.04—2.32 (m, 2H); 2.91 (s, 2H); 3.21 (d, 2H, J=4.0)	11.8; 20.1; 20.8; 21.1; 31.7; 34.9; 47.3; 47.9; 49.7; 50.0; 84.6	$C_{21}H_{36}O_2$
3a	184—186	+31.9	3400 (OH)	0.84 (s, 12H); 0.90 (s, 6H); 1.45 (s, 2H); 1.03—2.25 (m, 14H); 3.08 (d, 1H, J=4.0); 3.91 (d, 1H, J=9.5)	11.8; 14.4; 18.8; 19.9; 20.4; 20.5; 21.2; 26.0; 27.0; 34.8; 37.6; 46.4; 47.0; 47.8; 48.1; 48.5; 49.8; 50.6; 77.1; 87.0	$C_{21}H_{36}O_2$
4a	209—212	+26.1	3350 (OH)	0.83 (s, 6H); 0.89 (s, 12H); 1.26—2.13 (m, 16H); 3.90 (d, 2H, J=9.9)	14.1; 18.0; 20.1; 20.3; 22.0; 25.8; 36.9; 46.1; 47.7; 50.1; 76.9	$C_{21}H_{36}O_2$
2b	128—129	−25.8	1735 (OAc)	0.75 (s, 6H); 0.84 (s, 6H); 0.99 (s, 6H); 1.34—1.58 (m, 14H); 4.32 (d, 2H, J=3.7)	11.5; 19.3; 19.9; 20.4; 21.2; 31.6; 34.0; 44.6; 47.8; 48.1; 49.7; 86.6; 170.2	$C_{25}H_{40}O_4$
3b	Oil	+27.8	1730 (OAc) (Neat)	0.75 (s, 6H); 0.84 (s, 3H); 0.90 (s, 3H); 0.93 (s, 3H); 0.99 (s, 3H); 1.34—1.58 (m, 14H); 2.03 (s, 3H); 2.13 (s, 3H); 4.29 (d, 1H, J=3.7); 4.98 (d, 1H, J=9.9)	11.5; 13.9; 18.5; 19.4; 19.9; 20.5; 21.1; 21.2; 25.8; 26.8; 34.0; 36.1; 44.2; 46.5; 47.6; 47.7; 49.5; 78.8; 86.6; 170.4; 171.2	$C_{25}H_{40}O_4$
4b	109—112	+81.2	1735 (OAc)	0.76 (s, 6H); 0.89 (s, 6H); 0.93 (s, 6H); 1.13—1.55 (m, 14H); 2.06 (s, 6H); 4.97 (d, 2H, J=10.1)	14.0; 18.6; 20.0; 20.6; 21.0; 27.0; 35.8; 46.6; 47.5; 49.5; 79.3; 171.1	$C_{25}H_{40}O_4$

a) Microanalyses for all compounds were satisfactorily done in ±0.3% of calculated values.

column chromatography to give diketone **1** (537 mg) in 85% yield: mp 198.5—199.5 °C; $[\alpha]_D^{18}$+82° (*c* 1.07, $CHCl_3$); IR (neat) 1740 cm^{-1}; ^1H NMR ($CDCl_3$) δ=0.88 (s, 3H×2), 0.89 (s, 3H×2), 1.00 (s, 3H×2), 1.25—1.38 (m, 1H×2), 1.52—1.77 (m, 4H×2), 1.69 (t, *J*=7.0 Hz, 2H), 2.03 (t, *J*=5.0 Hz, 1H×2), 2.39 (tdd, *J*=7.0, 5.0, and 1.5 Hz, 1H×2); ^{13}C NMR ($CDCl_3$) δ=9.5 (q), 19.3 (q), 19.5 (q), 20.1 (t), 24.7 (t), 31.1 (t), 45.8 (s), 46.0 (d), 47.5 (s), 58.7 (s), 220.8 (s); MS (70 eV) 316 (M^+ 19.4), 301 (2.8), 288 (base), 273 (8.9), 260 (2.7), 255 (2.4), 245 (2.0), 165 (6.2), 152 (43.7), 137 (13.6), 124 (24.5), 109 (20.0); Calcd for $C_{21}H_{32}O_2$: C, 79.70; H, 10.19%. Found: C, 79.82; H, 10.62%.

Synthesis of Diols (2a, 3a, and 4a) by the Reduction of Diketone 1 with LAH. To a suspension of excess LAH (3.0 g, 79 mmol) in ether (300 cm^3) was added dropwise a solution of **1** (13.6 g, 43 mmol) in ether (50 cm^3) at room temperature under argon atmosphere. The solution was refluxed for 1 h and then quenched with ethyl acetate (10 cm^3) at 0 °C. After the addition of water (80 cm^3), the ethereal layer was separated and washed with 10% HCl (20 cm^3), 10% Na_2CO_3 (10 cm^3), and brine (20 cm^3). The organic layer was dried over $MgSO_4$. Evaporation of the solvent gave a mixture of diols; bis[(1*R*,2*R*,3*S*,4*R*)-2-hydroxy-3-bornyl]methane **2a**, [(1*R*,2*R*,-3*S*,4*R*)-2-hydroxy-3-bornyl][(1*R*,2*S*,3*R*,4*R*)-2-hydroxy-3-bornyl]methane **3a**, and bis[(1*R*,2*S*,3*S*,4*R*)-2-hydroxy-3-bornyl]methane **4a**, (12.8 g) in 93% yield. The mixture showed R_f values of 0.5, 0.2, and 0.15, corresponding to **2a**, **3a**, and **4a**, respectively, on its thin-layer chromatography using Merck silica gel 60 on an aluminium sheet with ethyl acetate/hexane (1 : 5). Each diol was isolated by flash column chromatography with ethyl acetate/hexane (1 : 10). Their physical data, along with that of their diacetates, are listed in Table 1.

References

1) W. Oppolzer, *Angew. Chem., Int. Ed. Engl.*, **23**, 876 (1984); R. W. Hoffmann and H. J. Zeiss, *ibid.*, **19**, 218 (1980); A. A. Bothner, *J. Am. Chem. Soc.*, **73**, 846 (1951); A. Nakamura, A. Konishi, Y. Tatsuno, and S. Otsuka, *ibid.*, **100**, 3443 (1978); R. L. Halterman and K. P. C. Vollhardt, *Organometallics*, **7**, 883 (1988).

2) Preriminary report: S. Kiyooka, T. Yamashita, J. Tashiro, K. Takano, and Y. Uchio, *Tetrahedron Lett.*, **27**, 5629 (1986).

3) C. A. Brown, *J. Org. Chem.*, **39**, 3913 (1974).

4) J. B. Grutzner, M. Jantelat, J. B. Dence, P. A. Smith, and J. D. Roberts, *J. Am. Chem. Soc.*, **92**, 7107 (1970).

5) M. Karplus, *J. Chem. Phys.*, **30**, 11 (1959); N. L. McClure, G.-Y. Dai, and H. S. Mosher, *J. Org. Chem.*, **53**, 2617 (1988).

6) J. Meinwald and A. Lewis, *J. Am. Chem. Soc.*, **83**, 2769 (1961).

7) J. D. Morrison, "Asymmetric synthesis," Academic press, New York (1983), Vol. 2.

A 3-Methylene-1,2-dioxetane as a Possible Chemiluminescent Intermediate in Singlet Oxygenation of Allene

Takeshi AKASAKA, Koichiro FUKUOKA, and Wataru ANDO*
Department of Chemistry, University of Tsukuba, Tsukuba, Ibaraki 305
(Received November 1, 1988)

Synopsis. Photosensitized oxygenation of bis(adamantylidene)methane and vinylideneadamantane at −78 °C afforded adamantanone and the former also emitted light when warmed up to room temperature in the presence of a fluorescer. A 3-methylene-1,2-dioxetane as a possible chemiluminescent intermediate is proposed.

The chemistry of 1,2-dioxetanes (**1**) has been extensively studied and utilized for the synthetic and mechanistic exploration of chemienergized electronic excitation in connection with chemiluminescence and bioluminescence systems.[1-3] The thermal stability of 1,2-dioxetanes is affected by a substituent on the dioxetane ring.[4] Work on the synthesis and characterization of dioxetanones[1,2] (**2**) and dioxetanimines[5] (**3**) through the singlet oxygenation of ketenes and ketene imines has recently been reported. Greibrokk[6] and Gollnick et al.[7] reported that the photosensitized oxygenation of allenes yields the corresponding ketones and CO_2, in which singlet oxygen ($^1O_2$) cycloaddition is considered to give the bi(dioxetane) and methylene-1,2-dioxetane (**4**). Recently, Sander and Patyk reported the matrix isolation of a ter(dioxetane) at 10 K in photooxidation of 2,5-dimethyl-2,3,4-hexatriene, in which a methylene-substituted dioxetane intermediate is proposed.[8] As a part of our continuing research for new chemiluminescence systems,[9] we report here our results on the photosensitized oxygenation of bis(adamantylidene)methane[10] (**5a**) and vinylideneadamantane[11] (**5b**) and the chemiluminescence of the product (**4a**) in the presence of a fluorescer.

1 **2** **3** **4**

Results and Discussion

Photosensitized oxygenation of **5a** in dichloromethane at 15 °C with Methylene Blue (MB) as sensitizer led to formation of adamantanone in 87% yield as an isolable product accompanied by polymeric products.[12] Very similar results were obtained with allene **5b** (adamantanone; 56% yield). **5** is stable under the reaction conditions in the absence of the sensitizer and light, and 1,4-diazabicyclo[2.2.2]octane, a $^1O_2$ quencher,[13] inhibits the reaction. Moreover addition of triphenylmethane as free radical scavenger[14] and *p*-dimetoxybenzene as an electron-transfer quencher[15] left the photooxygenation unaffected. These results reveal that $^1O_2$ is an actual oxidizing species.

When the reaction of **5a** was carried out at −78 °C with polymer-bound Rose Bengal[16] as sensitizer and then warmed up to room temperature, no direct chemiluminescence could be observed with the naked eye. However, the irradiated solution emitted a strong pale-blue light in the presence of 9,10-diphenylanthracene (DPA) as a fluorescer. The experimental and spectroscopic results suggest that the dioxetane intermediate might be formed during the oxidation. One plausible rationale for these observations is that the oxidation seems to involve [2+2]cycloaddition to yield 3-methylene-1,2-dioxetane **4**. Subsequent decomposition of these dioxetanes may produce adamantanone and the corresponding ketenes **6** as shown in Scheme 1 (with light emission in the presence of a fluorescer in the case of **5a**). To test these possibilities of the formation of ketenes, the following experiments were done. In order to trap the ketene intermediate, the photooxygenations were carried out in the presence of alcohols which were demonstrated ketene acceptors.[17] The formation of the corresponding ester was observed together with that of adamantanone (Scheme 2).[18] Ketene **6a** may react with $^1O_2$ to afford the correspond-

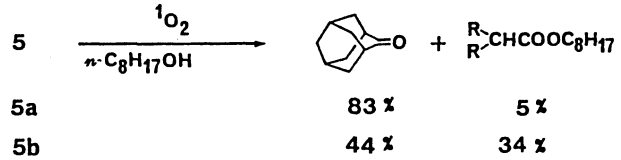

Scheme 2.

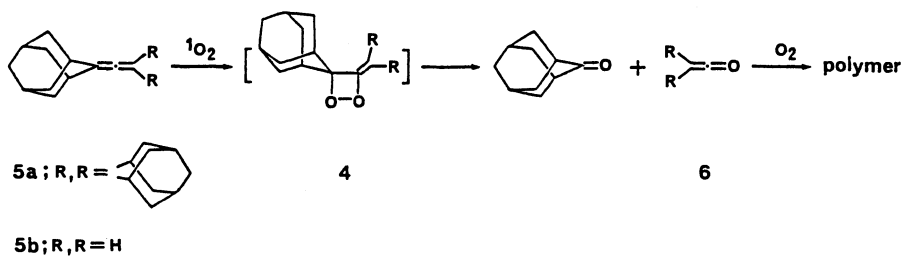

Scheme 1.

ing dioxetanone followed by decomposition to give adamantanone and CO_2.[19] This possibility may be ruled out by the following fact that the adamantanone formation was unaffected in the presence of 1-octanol. Since the reaction enthalpy (ΔH)[20] for the conversion **4a** → adamantanone + **6a** was estimated to be ca. 100 kcal mol^{-1}, both singlet (E_S=85 kcal mol^{-1} for acetone, 84 kcal mol^{-1} for adamantanone) and triplet (E_T=78 kcal mol^{-1} for acetone, 87 kcal mol^{-1} for ketene **5b**[25]) excited states of adamantanone and ketene **5a** are energetically accessible from the transition state. The relative intensities of chemiluminescence from the thermolysis of 3-methylene-1,2-dioxetane **4a** were approximately 1, 1, 3, and 22 for no additive, perylene, 9,10-dibromoanthracene and DPA as fluorescers, respectively (see Experimental) (Fig. 1). This result indicates that the role of CIEEL (chemically initiated electron-exchange luminescence) path in the light production from dioxetane **4a** is unimportant,[3,5a] similar to the case of the dioxetanimine[5] and 2-azaspiro[cyclopropane-1,3′-[1,2]dioxetane][9a] and in contrast to that of the dioxetanone.[3] This difference is presumably due to the general property of carbonyl compounds which can undergo one-electron reduction more easily than olefins. Direct ^{13}C NMR observation of **4a** was unsuccessful because of low solubility of **5a** in NMR solvent at low temperature.

It thus appears that singlet oxygen is able to undergo [2+2]cycloaddition with electron-rich allenes[26] to give methylene-substituted dioxetanes which decompose with light emission in the presence of a fluorescer.

Experimental

The light source was two 500-W tungsten-halogen lamps. Irradiations were carried out in Pyrex tubes in a water bath while oxygen passed through them.

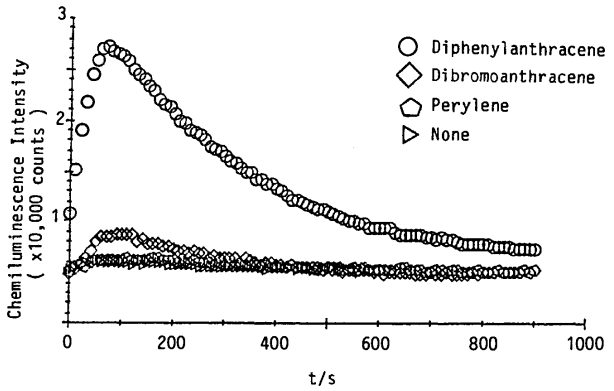

Fig. 1. Chemiluminescence from decomposition of dioxetane **4a**.

Materials. MB (Kanto Chemical) was used as received. Polymer-bound Rose Bengal (Ⓟ-RB) was prepared by the procedure given in the literature,[16] and this was also true of allene **5b**.[11] Oxidation potential (E_{ox} vs. SCE) of **5b** is +1.95 V.

Synthesis of Allene 5a. Triene **7**[27] (4.3 mmol) was treated with potassium peroxomonosulfate (8.8 mmol) by the modified method of Edwards et al.[28] in dichloromethane (70 mL), acetone (17 mL), buffered water (pH 7.5, phosphate buffer, 65 mL) and 18-crown-6 (0.75 mmol), and kept at 10 °C. During the addition of potassium peroxomonosulfate the pH was monitored with a pH-stat and kept at 7.5 by addition of 0.5 M (1 M=1 mol dm^{-3}) NaOH solution. The mixture was stirred at 10 °C. After consumption of **7** monitored by GLC, photolysis of the reaction mixture containing **8** (C=O; 1790 cm^{-1}) with a 400-W high-pressure mercury arc lamp was carried out.[29] (Scheme 3) The mixture was dried over $MgSO_4$ and then removed in vacuo. The residue was chromatographed on silica gel using hexane as an eluent. **5a** was isolated in 60% yield. **5a**: mp 245—247 °C (lit,[10] 224—226 °C); IR (KBr) 1960 cm^{-1} (C=C=C); ^1H NMR ($CDCl_3$) δ=1.67—2.08 (24H, m), 2.26—2.51 (4H, m); ^{13}C NMR ($CDCl_3$) δ=28.4 (d), 36.2 (d), 39.3 (t), 108.5 (s), 184.0 (s); MS (20 eV) m/z 280 (M^+). Anal. ($C_{21}H_{28}$) C,H. E_{ox}=+1.51 V vs. SCE.

Photosensitized Oxygenation of Allene 5. In a typical experiment, **5a** (0.11 mmol) was dissolved in dichloromethane with MB as sensitizer, and this solution was photooxygenated for 7.5 h at 15 °C. After separation by preparative gel permeation chromatography (Japan Analytical Industry Co.), adamantanone was obtained in 87% yield accompanied by polymeric products.

Photosensitized Oxygenation of Allene 5 in the Presence of Alcohol. A typical experiment was as follows: **5a** (0.1 mmol) was dissolved in 4 mL of dichloromethane containing 1 mL of 1-octanol with MB as sensitizer and the resulting solution was photooxygenated. Formation of adamantanone (83%) and 2-adamantanecarboxylic acid octyl ester (5%) was confirmed by comparison of their retention times on GLC (4 mm×1.5 m, 2% OV-1 on Uniport HP) with those of the authentic samples and GC-Mass analysis.

Chemiluminescence Analysis. Chemiluminescence was detected through a quartz window by a photomultiplier (Hamamatsu TV Ind., Model R878) with a chemiluminescence analyzer Model OX-70 (Tohoku Denshi Co.). For quantitative chemiluminescence measurement, a sample solution of **4a** was prepared by photooxygenation of **5a** in dichloromethane using Ⓟ-RB as sensitizer, followed by filtration at −78 °C. To the solution of **4a** thus prepared was added an equal volume of the stock solution of each fluorescer in dichloromethane, and the chemiluminescence was measured at −26 °C.

We thank Drs. Fujio Mizukami and Shu-ichi Niwa, National Chemical Laboratory for Industry, for the chemiluminescent measurements. This work was supported by a Grant-in-Aid for Scientific Research on Priority Areas (No. 62607003) from the Ministry of Education, Science and Culture.

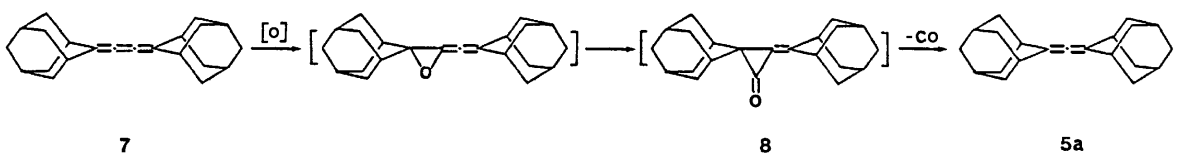

7 8 5a

Scheme 3.

References

1) W. Adam and K. Zinner, "Chemical and Biological Generation of Excited States," ed by W. Adam and G. Cilento, Academic, New York (1982), pp. 153—190; A. I. Baumstark, "Singlet O_2," ed by A. A. Frimer, CRC, Boca Raton (1985), pp. 1—36,

2) O. Shimomura, "Chemical and Biological Generation of Excited States," ed by W. Adam and G. Cilento, Academic, New York (1982), pp. 249—277.

3) S. P. Schmidt and G. B. Schuster, *J. Am. Chem. Soc.*, **100**, 1966 (1978).

4) W. Adam and W. J. Paader, *J. Am. Chem. Soc.*, **107**, 410 (1985) and references cited therein.

5) a) Y. Ito, T. Matsuura, and H. Kondo, *J. Am. Chem. Soc.*, **101**, 7105 (1979); b) W. Adam, O. De Lucchi, H. Quast, R. Rectenwald, and F. Yany, *Angew. Chem., Int. Ed. Engl.*, **18**, 788 (1979); c) Y. Ito, H. Yokoya, K. Kyono, S. Yamamura, Y. Yamada, and T. Matsuura, *J. Chem. Soc., Chem. Commun.*, **1980**, 898.

6) T. Greibrokk, *Tetrahedron Lett.*, **1973**, 1663.

7) K. Gollnick and A. Schnatterer, *Tetrahedron Lett.*, **26**, 5029 (1985).

8) W. Sander and A. Patyk, *Angew. Chem., Int. Ed. Engl.*, **26**, 475 (1987).

9) a) T. Akasaka, Y. Nomura, and W. Ando, *J. Org. Chem.*, **53**, 1670 (1988); b) T. Akasaka, R. Sato, and W. Ando, *J. Am. Chem. Soc.*, **107**, 5539 (1985); c) T. Akasaka, R. Sato, Y. Miyama, and W. Ando, *Tetrahedron Lett.*, **26**, 843 (1985); d) W. Ando and Y. Kabe, *J. Chem. Soc., Chem. Commun.*, **1984**, 741.

10) J. Strating, A. H. Alberts, and H. Wynberg, *J. Chem. Soc., Chem. Commun.*, **1970**, 818.

11) T. Sasaki, S. Eguchi, and Y. Hirako, *Tetrahedron Lett.*, **1976**, 541.

12) It is known that polymerization of dimethylketene as well as reaction with $^1O_2$ or $^3O_2$ affords resinous products: W. Adam and H. C. Steinmetzer, *Angew. Chem., Int. Ed. Engl.*, **11**, 540 (1972): H. Staudinger, K. Dyckerhoff, H. W. Klever, K. Ruzicka, *Ber. Dtsch. Chem. Ges.*, **58**, 1079 (1925).

13) C. S. Foote, E. R. Peterson, and K.-W. Lee, *J. Am. Chem. Soc.*, **94**, 1032 (1972).

14) G. A. Russell, *J. Am. Chem. Soc.*, **78**, 1047 (1956).

15) J. Eriksen and C. S. Foote, *J. Am. Chem. Soc.*, **102**, 6083 (1980).

16) A. P. Schaap, A. L. Thayer, E. L. Blossey, and D. C. Neckers, *J. Am. Chem. Soc.*, **97**, 3741 (1975).

17) P. Blake, "The Chemistry of Ketenes, Allenes, and Related Compounds," ed by S. Patai, Wiley, New York (1980), Chap. 9, pp. 310—362.

18) Any product which come from trapping of **4** with alcohol was not obtained.

19) N. J. Turro, Y. Ito, M.-F. Chow, W. Adam, O. Rodriguez, and F. Yany, *J. Am. Chem. Soc.*, **99**, 5836 (1977); W. Adam, A. Alzerreca, J.-C. Liu, and F. Yany, *ibid.*, **99**, 5768 (1977).

20) The reaction enthalpy, ΔH, was estimated by Benson's method[21] as ca. 100 kcal mol^{-1}. This is based on the assumption that the strain energies for the 1,2-dioxetane ring and the spiro carbon are 26[22] and 5 kcal mol^{-1},[23] respectively; $\Delta H = -(152^{22)} \times 2) - 58.6^{24)} - (70^{24)} \times 2) - 34.9^{24)} + 26 + 5 = -101.5$ kcal mol^{-1}.

21) S. W. Benson, F. R. Cruickshank, D. M. Golden, G. R. Haugen, H. E. O'Neal, A. S. Rodgers, R. Sham, and R. Walsh, *Chem. Rev.*, **69**, 279 (1969).

22) A. Greenberg and J. F. Liebman, "Strained Organic Molecules," Academic, New York (1978).

23) Y. Hata, "Chemistry of Highly Strained Molecules," Kagakudojin, Kyoto (1972), pp. 59—80.

24) L. F. Fieser and M. Fieser, "Basic Organic Chemistry," Heath, Boston(1972).

25) J. V. M. Jungen and A. Beauchamp, *Chem. Phys. Lett.*, **40**, 500 (1976).

26) (2+2) Cycloaddition and ene-reactions of allenes with enophiles such as dimethyl acetylenedicarboxylate and diethyl azodiformate have been reported: C. B. Lee, J. J. Newman, and D. R. J. Taylor, *J. Chem. Soc., Perkin Trans. 1*, **1978**, 1161.

27) G. Karich and J. C. Jochims, *Chem. Ber.*, **110**, 2680 (1977).

28) J. O. Edwards, R. H. Pater, R. Curci, and F. DiFuria, *Photochem. Photobiol.*, **30**, 63 (1979); R. Curci, M. Fiorentino, L. Troishi, J. O. Edwards, and R. H. Pater, *J. Org. Chem.*, **45**, 4758 (1980); A. R. Gallopo and J. O. Edwards, *J. Org. Chem.*, **46**, 1684 (1981).

29) W. Ando, H. Hayakawa, and N. Tokitoh, *Tetrahedron Lett.*, **27**, 6357 (1986).

A ^{13}C NMR Relaxation Study of Octyltrimethylammonium Salts in D_2O

Yuhei UZU,* Yasushi SAITO, and Masatoki YOKOI
Department of Chemistry, Faculty of Science, Shinshu University, Asahi, Matsumoto 390
(Received October 3, 1988)

Synopsis. The concentration dependence of the ^{13}C spin-lattice relaxation times (T_1) of the alkyl carbons in octyltrimethylammonium salts was analyzed by means of applying the phase separation model. At higher concentration, the $1/T_1$ value deviates from a linear plot and depends on the magnetic field strength. The molecular motions in monomer and micellar states are discussed, along with the overall motions of the molecule and its internal motion.

Micelles formed by surfactants in aqueous media have been the subject of numerous studies involving various techniques. Especially, in studying micellar solutions on the molecular level, NMR spectroscopy has proved to be one of the most useful experimental techniques. Recently, the internal structure and dynamics of micelles have been examined by a ^{13}C NMR study,[1-3] since the spin-lattice relaxation times (T_1) for individual carbons of the molecules provide quantitative information concerning the rotational mobility of the corresponding C-H vector. Further, a significant observation in ^{13}C T_1 measurements at different magnetic fields is that the relaxation times are dependent on the magnetic field strength at higher surfactant concentrations.[4,5]

In the present work, we systematically examined the ^{13}C-T_1 behavior of octyltrimethylammonium salts in D_2O. For these surfactants, the critical micelle concentrations (cmc) are rather high (ca. 0.3 M; 1 M=1 mol dm^{-3}). Therefore, it is feasible to obtain structural information concerning the motions of the alkyl chain segments in surfactant both in monomer and micellar states.

Experimental

Octyltrimethylammonium bromide (C_8TAB) and octyltrimethylammonium chloride (C_8TAC) were used as the surfactants in this study. The preparative procedures for the surfactants have been described elsewhere.[6] As a check of the purity of the surfactants, cmc determinations were performed by means of a surface tension method; the cmc's agreed closely with those values from the literature.[7]

^{13}C NMR spectra and T_1 values were obtained with complete proton decoupling at 22.5 MHz (2.10 T) on a JEOL-FX90QNMR spectrometer. T_1 measurements were also made at 62.9 MHz (5.87 T) using a Brucker-AC250 NMR spectrometer to examine the magnetic field dependence. The deuterium signal from solvent D_2O was used as a lock signal. T_1 values were obtained by the inversion recovery method, using a 180°-τ-90° pulse sequence. The experimental temperature was controlled by a controller unit. It's reliability was monitored by the alternative insertion of a thermister into the sample position. All T_1 measurements were performed at 36 °C.

Results and Discussion

The representative ^{13}C NMR spectrum in a C_8TAB solution at 36 °C is shown in Fig. 1. With C_8TAB, almost all carbons appear as a resolved resonance. For surfactants containing longer alkyl chains, the differences in chemical shifts of the methylene carbons near the center of the chain are insufficient to obtain a complete resolution of the spectrum, as shown in C-4 and C-5 in the figure: hence, an averaged value of T_1 values of these carbons was given. Similar spectral behavior has been observed for C_8TAC. The assignments for the surfactants studied have been given previously.[2,8]

It is assumed that the ^{13}C spin-lattice relaxation of protonated carbon in large and intermediate sized molecules like an aggregated surfactant system is in general dominated by three kinds of contributions from: (1)the overall motion of micelles, (2)the overall motions of surfactant molecules in a micellar and a bulk phases, and (3)the chain segmentary motion (internal motion) of the hydrocarbon chain in a molecule. Of three, the overall motion of micelle is slow compared with the other two motions and hence it can be neglected.[9]

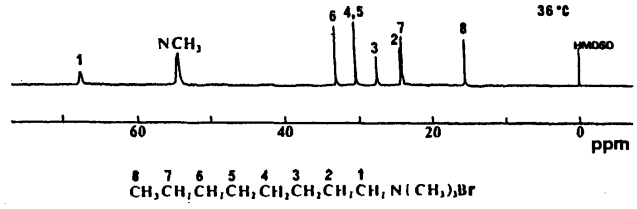

Fig. 1. ^{13}C NMR specturm of C_8TAB in D_2O at 36 °C. Hexamethyldisiloxane (HMDSO) was used as an external reference.

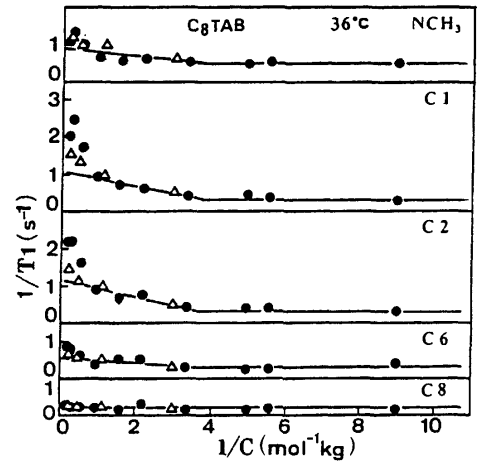

Fig. 2. Plots of $1/T_1$ of carbons for C_8TAB at two different magnetic field strengths against the inverse of surfactant concentration: (△) corresponds to 5.87 T and (●) to 2.10 T. The carbons are numbered as in Fig. 1.

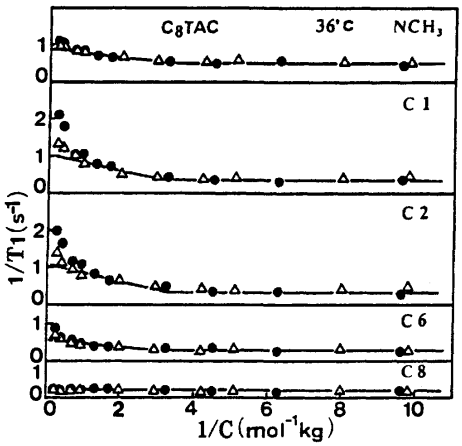

Fig. 3. Plots $1/T_1$ of carbons for C_8TAC at two different magnetic field strengths against the inverse of surfactant concentration: (△) corresponds to 5.87 T and (●) to 2.10 T. The carbons are numbered as in Fig. 2.

The observed relaxation rates, $1/T_1$, for alkyl carbons in the C_8TAB and C_8TAC at two different magnetic field strengths are plotted in Figs. 2 and 3, as functions of the inverse of surfactant concentrations (C). It can be seen that relaxation times are almost constant at low concentrations (high values of $1/C$); however, at high concentrations, there is an increase in the relaxation rate for all carbon atoms, except C-8 of the terminal methyl group. The increase in the $1/T_1$ value indicates an increased restriction on the mobility of the entire chain. Similar ^{13}C-T_1 behavior has been observed for aqueous micellar solutions of sodium hexanoate.[10] The changes in $1/T_1$ are due to the formation of micelles. The obtained cmc values are nearly equal to those by the surface tension method: C_8TAB 0.27 mol kg^{-1}, C_8TAC 0.32 mol kg^{-1}. It can be seen that the cmc of C_8TAB is lower than that of the corresponding chloride. As for T_1 values of individual alkyl carbons in the surfactants, there was no striking difference between C_8TAB and C_8TAC, indicating that both of these micelles are of nearly the same size and shape. Considered together with previously published results,[6] these micelles tend to remain nearly spherical up to high concentrations (above the cmc). In the limited range of concentration above the cmc (ca. 0.3—1.0 mol kg^{-1}), an approximately linear relationship exists between $1/T_1$ and $1/C$. We can also see that there is little difference between both T_1 values at 2.10 T and at 5.87 T in this concentraion range, as well as below cmc. Following the phase separation model, the observed relaxation rate $(1/T_1)_{obsd.}$ is assumed to be a weighted average of the relaxation rates in the micelles and monomers. Then, T_1 in this concentraion range is given by[10,11]

$$\left(\frac{1}{T_1}\right)_{obsd.} = \frac{cmc}{C}\left(\frac{1}{T_1}\right)_{mon.} + \frac{C-cmc}{C}\left(\frac{1}{T_1}\right)_{mic.}.$$

This equation suggests that a plot of the $(1/T_1)_{obsd.}$ against the inverse of the concentration should give two straight lines intersecting at the cmc, as shown in the Figs. 2 and 3. The $1/T_1$ values for all carbons in monomer and micellar states can, therefore, be obtained from the intercepts at cmc and at $1/C=0$, respectively. Thus, the relaxation times obtained for C_8TAB are summarized in Table 1, together with the correlation time (τ_c). In the monomer state, variation of the relaxation along the hydrocarbon chain within a molecule was not large, as compared with those in the micellar state. Precisely, there seems to be a slight increase in the segmentary mobility as one moves away from the polar head. As indicated by the higher T_1 values all along the chain, the overall reorientation motion is faster with a slight degree of segmentary motions along the chain in a molecule, suggesting that the relaxation behavior below cmc is mainly governed by the overall motion of the octyltrimethylammonium ion. From Fig. 2 and Table 1, a marked increase in the $1/T_1$ value above cmc is found along the alkyl chain from C-8 toward C-1 next to the N-methyl head groups. This behavior may be attributed to a severe immobilization at the polar head, because surfactant molecules interact strongly with neighboring molecules, counterions and water molecules at the micellar surface. Accordingly, the overall motion of the molecule becomes more and more restricted, implying that the internal motions become more important for the relaxation behavior. On the other hand, the $1/T_1$ value of N-methyl carbon is rather small, as shown in Table 1. Probably, such N-methyl groups are expected to extend outward from the micellar surface into the solvent. Consequently, they would possess a larger degree of motional freedom than that of the carbons next to the polar group. As for the C-8 carbon, it has a prominent segmentary mobility, irrespective of the surfactant concentration. The micellar interior is likely to have properties that approach those of a liquid-like environment, as already stated by others.[1,12,13] In Figs. 2 and 3 it is remarkable that at the highest concentration range, $1/T_1$ values tend to deviate from the linear plots and the degree of deviation is relatively larger at 2.10 T than that at 5.87 T, suggesting a magnetic field strength dependence for the relaxation behavior. Especially, a marked field dependence is found for the first three methylene car-

Table 1. ^{13}C Spin-Lattice Relaxation Times (T_1) and Correlation Times (τ_c) for the Alkyl Carbons of C_8TAB Solution at 2.10 T

Carbon atom	Micelles		Monomers at cmc	
	T_1/s	τ_c/ps[a]	T_1/s	τ_c/ps[a]
N-CH_3	0.99	16	2.0	7.8
C-1	0.73	32	2.6	8.6
C-2	0.78	30	2.4	9.8
C-3	0.87	27	2.4	9.8
C-4,5	1.3	19	2.7	8.6
C-6	1.6	15	3.3	7.0
C-7	2.2	10	3.6	6.5
C-8	4.4	3.6	4.4	3.6

a) Calculated from $1/T_1=N\hbar^2\gamma_C^2\gamma_H^2 r_{CH}^{-6}\tau_C$, where γ_C and γ_H: gyromagnetic ratios of ^{13}C and ^{1}H, N: number of directly bonded hydrogen, r_{CH}: C-H distance. $\hbar$: Plank's constant.

bons next to the polar head group. For this field dependence, Wennerström et al.[4] have proposed from ^{13}C T_1 measurements on sodium octanoate that the slow micellar motion contributes to the relaxation, particularly for carbons near the polar head. In addition, the deviation from linearity may suggest that some structural change affecting the relaxation occurs in the micelles. From the results presented above, T_1 is found to be magnetic field independent at low concentrations, so that the relaxation is determined by a correlation time τ_c on the order of 10^{-11} to 10^{-12} s based upon the rotational motion of isotropic reorienting molecule, where extreme narrowing condition is fulfilled. At higher concentrations with field dependence, such a surfactant system is expected to have slow motions on the order of 10^{-8} to 10^{-9} s (or longer), such as the rotation of micelle as a single entity and surfactant lateral diffusion along the micelle surface.[14] Further analysis using a two-step model[4,14] from the multifield relaxation data would be necessary to obtain detailed information on both chain dynamics and orientation.

We express our sincere thanks to Prof. Ryozo Irie, Faculty of Agriculture, Shinshu University, for the NMR measurement at 5.87 T.

References

1) E. Williams, B. Sears, A. Allerhand, and E. H. Cordes, *J. Am. Chem. Soc.*, **95**, 4871 (1973).
2) G. C. Levy, R. A. Komoroski, and J. A. Halstead, *J. Am. Chem. Soc.*, **96**, 5456 (1974).
3) H. Maeda, S. Ozeki, S. Ikeda, H. Okabayashi, and K. Matsushita, *J. Colloid Interface Sci.*, **76**, 532 (1980).
4) H. Wennerström, B. Lindman, O. Söderman, T. Drakenberg, and J. Rosenholm, *J. Am. Chem. Soc.*, **101**, 6860 (1979).
5) H. Walderhaug, O. Söderman, and P. Stilbs, *J. Phys. Chem.*, **88**, 1655 (1984).
6) Y. Uzu, J. Nakagawa, and M. Yokoi, *Bull. Chem. Soc. Jpn.*, **59**, 2891 (1986).
7) P. Mukerjee and K. J. Mysels, "Critical Micelle Concentration of Aqueous Surfactant Systems," Nat. Stand. Ref. Data Series, Nat. Bur. Stand. (U. S) Feb., 1961.
8) J. Ulmius, B. Lindman, G. Lindblom, and T. Drakenberg, *J. Colloid Interface Sci.*, **65**, 88 (1978).
9) K. Tsuji and F. Tokiwa, *Yukagaku*, **27**, 2 (1978).
10) U. Henriksson and L. Ödberg, *Kolloid Z. Z. Polym.*, **254**, 35 (1976).
11) T. Nakagawa and F. Tokiwa, "Surface and Colloid Science," Vol. 9, ed. by E. Matijevic, John Wiley & Sons, New York (1976), p. 69.
12) A. S. Waggoner, O. H. Griffith, and C. R. Christensen, *Proc. Natl. Acad. Sci. U. S. A.*, **57**, 1198 (1967).
13) K. Shinoda, T. Nakagawa, B. Tamamushi, and T. Isemura, "Colloidal Surfactants," Academic, New York (1963), Chap. 1.
14) B. Lindman, O. Söderman, and H. Wennerström, "Surfactant Solutions," ed. by R. Zana, Dekker, New York (1987), Vol. 22, Chap. 6.

Effects of Some Variables on the Point of Zero Charge of TiO_2-ZrO_2 Double Oxides

Basudeb KARMAKAR and Dibyendu GANGULI*
Central Glass & Ceramic Research Institute, Calcutta 700032, India
(Received July 4, 1988)

Synopsis. Effects of variables such as acid/base reaction temperature, presence of impurities, method of oxide powder preparation, and calcination temperature on the point of zero charge (p.z.c) were investigated for TiO_2-ZrO_2 (79.41—20.59, wt.%) mixed oxides. The visually determined p.z.c. values were also compared with those arrived at by a computational method to obtain an estimate of the error of determination.

Interfacial charge-transfer reactions play a key role in many chemical process industries[1,2] like ceramic, paint, and catalyst industries. The potentiometric investigations of Bolt,[3] and Parks and de Bruyn[4] confirmed that H^+ and OH^- are the potential or charge determining ions for oxides in aqueous medium. They extended the potentiometric titration data to estimate the surface-charge densities as a function of pH and at the same time to detemine the p.z.c. The p.z.c. is determined from the intersecting point of the surface charge density vs. pH curves with the zero surface charge density line. Difficulties arise in determining the exact location of the point of intersection when different ionic concentrations of the supporting inert electrolyte are considered. The p.z.c. values have been found to depend on several factors such as acid/base reaction temperature,[5] impurities,[6] calcination temperature[7] etc.

The present communication intends to show the effects of (i) acid/base reaction temperature, (ii) cationic and anionic impurities, (iii) methods of preparation, and (iv) calcination temperature on the p.z.c. of a TiO_2-ZrO_2 (79.41—20.59, wt.%) double oxide. The visually determined p.z.c. values have also been compared with those arrived at by a computational method to obtain an estimate of the error of determination.

Experimental

Preparation of Double Oxide Powders. Powder samples (Table 1) of TiO_2-ZrO_2 (79.41—20.59, wt%) were prepared in the following way. Sample TZ-1 was prepared by the thermal decomposition of mixed hydroxides which were coprecipitated from a mixture of aqueous $TiCl_4$ (Riedel-de-Haën) and $ZrO(NO_3)_2$ (BDH) solution with aqueous ammonia solution (BDH). Powders having the particle size range of 74—175 μm (obtained by sieving) were used. Sample TZ-2 was prepared from a mixed alkoxide of $Ti(OPr^i)_4$ (Fluka) and $Zr(OPr^n)_4$ (Fluka) by hydrolyzing with doubly distilled deionized water. The average agglomerated particle size was 3.1 μm. This powder sample was impregnated with aqueous H_2SO_4 (Sample TZ-2A, SO_4^{2-} content 0.40 mmol g^{-1}) and NaOH (Sample TZ-2B, Na^+ content 0.04 mmol g^{-1}) solution to observe the effects of impurities on the p.z.c. Sample TZ-3 was prepared from high purity TiO_2 (rutile, National Lead Co.) and $Zr(OPr^n)_4$ (Fluka) by hydrolyzing the latter with water. The average agglomerated particle size of the double oxide was 9.1 μm. Sample TZ-4 was prepared from $Ti(OPr^i)_4$ (Fluka) and pure ZrO_2 (monoclinic, Riedel-de-Haën) by hydrolyzing the former with water. The average agglomerated particle size was 4.0 μm. All the samples were calcined at 500 °C for 3 h in static air unless otherwise mentioned.

Method of Study. A potentiometric titration method described previously by Kita et al.,[8] and Karmakar and Ganguli[9] was used. Briefly, aqueous solutions (200 ml) of 0.004 mol dm^{-3} HNO_3+KNO_3 (10^{-1}, 10^{-2}, and 10^{-3} mol dm^{-3}) were carefully poured into beakers containing accurately weighed 1.000 g of the sample powder, and the suspension equilibrated overnight; potentiometric titration against 0.1 mol dm^{-3} KOH aqueous solution was carried out with the suspension at 40±0.5 °C (some experiments were carried out at 30, 50, and 60±0.5 °C) under a nitrogen stream to avoid CO_2 contamination from air.

The surface-charge density as a function of pH was estimated from the difference between the titration curves obtained without and with the sample. The p.z.c. values were determined from the common point of intersection of the surface-charge density vs. pH curves for 10^{-3}, 10^{-2}, and 10^{-1} mol dm^{-3} KNO_3.

Results and Discussion

The p.z.c.'s of several TiO_2-ZrO_2 (79.41—20.59, wt%) powders were determined following the above described method by varying different parameters and the results have been listed in Table 1. Effects of specific variables are described below in brief.

Effect of Acid/Base Reaction Temperature. The observed p.z.c. values of the Sample TZ-2 indicated decrease with increase in acid/base reaction temperature (in the range of 30 to 60 °C). Such decrease in p.z.c. was apparently caused by the decrease in the relative affinity of the charge-determining ions (i.e. H^+ and OH^-) for the oxide surface with increasing temperature.[5]

The standard thermodynamic functions (ΔH^*=the standard differential heats of transfer of H^+ and OH^- from the bulk solution to the interfacial region, and ΔS^*=the difference in standard ionic entropy of hydration of H^+ and OH^- at p.z.c.) have been calculated (ΔH^*=−92.30 kJ mol^{-1} and ΔS^*=−343.88 J deg^{-1} mol^{-1}) from the slope and intercept of the linear plot of ($1/2$ pK_w−$pH_{p.z.c.}$) vs. $1/T$ (Fig. 1) following the equation proposed by Berube and de Bruyn.[5] Here ΔH^* is negative, ΔS^* is also negative and numerically $T\Delta S^*$ (of the Gibbs-Helmholtz equation) is greater than ΔH^* which make ΔG^* positive. The temperature dependent ΔG^* values, therefore, suggest that the transferring reactions of H^+ and OH^- from the bulk solution to the interfacial region were not a spontaneous process. The negative ΔH^* value also suggests that the deprotonation process of the surface MOH_2^+ and MOH groups was exothermic.

Effect of Impurity. Samples TZ-2A and TZ-2B con-

Table 1. Computed and Visually Determined $pH_{p.z.c}$ Data for Different TiO_2-ZrO_2 (79.41—20.59, wt%) Double Oxides

Sample[a] (For details, see under "Experimental")	Crystal phase	Acid/base reaction temperature °C	Minimum standard deviation considering all the three surface charge density vs. pH curves at the computed $pH_{p.z.c.}/\mu C\,g^{-1}$	Computed $pH_{p.z.c.}$ m	Visually determined $pH_{p.z.c.}$ p	$(p-m)$ pH unit
TZ-1	Anatase	40	9.30	6.88	6.95	0.07
TZ-1[b]	Rutile, $ZrTiO_4$	40	0.84	10.03	10.10	0.07
TZ-2	Anatase	30	11.15	5.76	5.90	0.14
TZ-2	Anatase	40	9.62	5.49	5.45	−0.04
TZ-2	Anatase	50	10.42	5.20	5.15	−0.05
TZ-2	Anatase	60	7.83	4.85	4.75	−0.10
TZ-2[b]	Rutile, $ZrTiO_4$	40	3.97	6.09	6.25	0.16
TZ-2A	Anatase	40	10.62	2.33	2.45	0.12
TZ-2B	Anatase	40	11.02	5.63	5.75	0.12
TZ-3	Rutile	40	5.52	4.54	4.45	−0.09
TZ-4	Anatase, Monoclinic ZrO_2	40	6.09	6.03	6.30	0.27

a) Calcined at 500°C for 3 h unless otherwise stated. b) Calcined at 1000 °C for 3 h.

tained intentionally introduced SO_4^{2-} and Na^+ as typical anionic and cationic impurities respectively. The p.z.c. values of the above samples (Table 1) clearly indicated that on impregnation with (i) SO_4^{2-}, the p.z.c. shifted to the lower pH value, and with (ii), Na^+, the p.z.c. shifted to the higher pH value. Several researchers[6,10] also reported similar trends on single oxides. The SO_4^{2-} apparently greatly increased the amount of surface Brønsted acid sites (any Lewis acid that might form would be transformed to the Brønsted type in an aqueous medium) of the sample TZ-2A, thereby causing a shift of p.z.c. towards the lower pH value. On the other hand, the Na^+ increased the surface basic sites of the Sample TZ-2B due to the neutralization of the acid sites by NaOH, thereby causing a shift of p.z.c. towards higher pH value.

Effect of Methods of Preparation. On comparison of the p.z.c. values among the Samples TZ-1, TZ-2 (40 °C), TZ-3, and TZ-4, it was observed that the p.z.c. depended on the method of preparation and varied in the pH range of 4.45—6.95. The p.z.c. of the anatase containing Samples TZ-1, TZ-2 (40 °C), and TZ-4 remained in a higher pH range than that of the rutile-containing Sample TZ-3. Here the degree of intermixing of the reacting constituents, product homogeneity and the sources of starting materials of samples TZ-3 and TZ-4 were completely different from each other, due to the difference in their methods of preparation (see "Experimental"). Further, the Samples TZ-3 and TZ-4 were obviously less homogeneous than the Samples TZ-1 and TZ-2 (40 °C).

Again, both the Samples TZ-1 and TZ-2 (40 °C) contained the anatase crystal phase, although they were prepared from inorganic salts and metal alkoxides respectively. The excellent chemical homogeneity in mixed oxide systems prepared via mixed alkoxides is well-known.[11] Samples prepared via inorganic salt solutions, though much more homogeneous than those prepared via solid-solid reactions, are less so

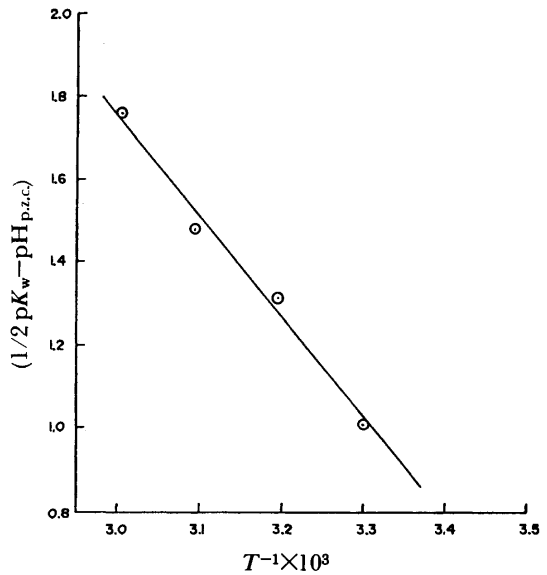

Fig. 1 Plot of $(1/2\,pK_w - pH_{p.z.c.})$ vs. T^{-1} (reciprocal of temperature in Kelvin) for Sample TZ-2.

than alkoxide-derived ones. They are also less pure because of the presence of dissolved ionic impurities etc. Thus, the differences in the origin of starting materials and mode of preparation are amply reflected in the p.z.c. values.

Effect of Calcination Temperature. The p.z.c. values of TZ-1 and TZ-2 (Table 1) indicated that the p.z.c. of TiO_2-ZrO_2 double oxides shifted to higher pH on calcination at 1000 °C. Important factors responsible for changing p.z.c. with calcination temperature are, e.g. change in crystal structure,[7] change in the nature of atomic arrangements (i.e. amorphous to crystalline, or separate components to compound formation), dehydration and dehydroxylation etc. In the present case the formation of $ZrTiO_4$ in addition to anatase-rutile conversion should be considered as a

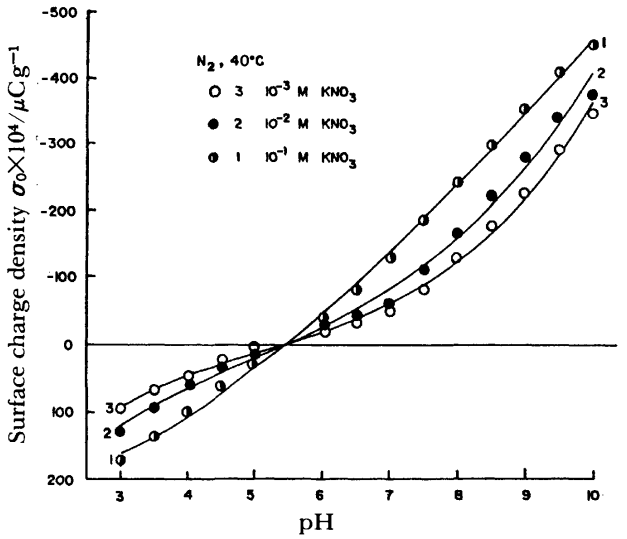

Fig. 2. Experimental and computed surface-charge density as a function of pH for Sample TZ-2 (40 °C). Solid lines are calculated by fitting cubic equations at the minimum standard deviation considering all the three curves; the experimental data points (circles) are shown for comparison.

determining factor.

It is evident from the above discussion that p.z.c. values can be sensitive to various preparative and experimental parameters. However, all such comparisons must ensure a minimum of relative errors in the experimental measurements. To check on this in the present case, where p.z.c. values were determined from the visually estimated cut points of three titration curves at different electrolyte concentrations, cubic equations for the titration curves were set up. The process is described below.

Cubic Equations for Surface-Charge Density vs. pH Curves and Determination of p.z.c. A careful examination of the nature of the experimental surface-charge density vs. pH curve (Fig. 2) showed that this curve having a single inflection point should correspond to cubic (third degree) polynomials.[12,13] For this reason, cubic regression analyses were performed on the experimental points of surface-charge density vs. pH curves and p.z.c. values were determined. The cubic equation (y=surface charge density, x=pH) could be written as:

$$y = A_0 + A_1 x + A_2 x^2 + A_3 x^3 \cdots \quad (1)$$

The values of A_0, A_1, A_2, and A_3, (dependent on both the concentration of supporting electrolyte and the nature of oxide powder considered) were obtained by using a computer program in the following way. Following the theory of p.z.c. two conditions were applied:

(i) At p.z.c., according to the equation[8,14]

$$\sigma_0 = F(\Gamma_{H^+} - \Gamma_{OH^-}),$$

where F is the Faraday constant (C/equiv. wt.), Γ_{H^+} and Γ_{OH^-} are the net adsorption densities of H^+ and OH^- respectively, y=0 and x must have a real and positive value.

(ii) All the three curves (of 10^{-3}, 10^{-2}, and 10^{-1} mol dm^{-3} KNO_3) should pass through the point having coordinates of y=0, x=single fixed value mentioned in (i).

Standard deviations were computed for all the three curves of σ_0 vs. pH in each set of data, considering a large number of points on the line y=0 to be their possible points of intersection. Mean standard deviations were then computed for all such points. The point corresponding to the minimum standard deviation was selected as the point of intersection of the three curves, i.e. the p.z.c. The eleven sets of experimental data on TiO_2-ZrO_2 powders were processed following the above-mentioned procedure and the results have been listed in Table 1. The curves of Sample TZ-2 (40 °C) indicating the difference between the experimental (circles) and the computed (solid lines) points of σ_0 at the corresponding pH values, have been shown in Fig. 2 as an example.

The above diagram indicates the goodness of fit of cubic equations with the experimental points. The differences between the visually determined and the computed p.z.c.'s for the eleven sets of experimental data were found to vary in the range of −0.10 to +0.27 pH unit. These differences arose possibly due to the fact that for visually determined p.z.c., weightage was given to only some experimental points near the p.z.c., whereas for computed p.z.c., uniform importance was given also to the points very much away from the p.z.c. The above differences of p.z.c.'s were, however, not too large in the present case and remained within the errors of measurement.

The authors are thankful to Dr. S. Kumar, Director of the Institute, for his permission to publish this note. Thanks are also due to Dr. R. K. Das, Computer Cell of the Institute for his kind help in the programming.

References

1) A. Bleier, *J. Mater. Educ.*, **7**, 429 (1985).
2) H. K. Bowen, *Mater. Sci. Eng.*, **44**, 1 (1980).
3) G. H. Bolt, *J. Phys. Chem.*, **61**, 1166 (1957).
4) G. A. Parks and P. L. de Bruyn, *J. Phys. Chem.*, **66**, 967 (1962).
5) Y. G. Berube and P. L. de Bruyn, *J. Colloid Interface Sci.*, **27**, 305 (1968).
6) K. Jiratova, *Appl. Catal.*, **1**, 165 (1981).
7) H. Watanabe and J. Seto, *Bull. Chem. Soc. Jpn.*, **59**, 2683 (1986).
8) H. Kita, N. Henmi, K. Shimazu, H. Hattori, and K. Tanabe, *J. Chem. Soc., Faraday Trans. 1*, **77**, 2451 (1981).
9) B. Karmakar and D. Ganguli, *Trans. Ind. Ceram. Soc.*, **46**, 53 (1987).
10) G. A. Parks, *Chem. Rev.*, **65**, 177 (1965).
11) S. Sakka, *Trans. Ind. Ceram. Soc.*, **46**, 1 (1987).
12) C. H. Goulden, "Methods of Statistical Analysis," 2nd Ed., Asia Publishing House, New Delhi (1959), p. 173.
13) B. Ostle, "Statistics in Research," The Iowa State College Press, Ames, Iowa (1958), p. 138.
14) M. R. Houchin and L. J. Warren, *J. Colloid Interface Sci.*, **100**, 278 (1984).

A Lattice Gas Model for Neopentane

Masato SHINMI and Dale A. HUCKABY*
Department of Chemistry, Texas Christian University, Fort Worth, Texas 76129, U.S.A.
(Received August 16, 1988)

Synopsis. A lattice gas model for neopentane on a bcc lattice was considered. The equation of state and critical point were calculated using a Guggenheim-McGlashan approximation. The liquid phase in the model exhibits the same type of short-range orientational ordering proposed by Nishikawa to exist in liquid neopentane.

Nishikawa recently carried out structure simulation studies for liquid neopentane[1] and reported that the X-ray diffraction intensities from the liquid observed by Narten[2] were reproduced well by a local body centered cubic (bcc) lattice structure model.[1] In this bcc cluster model, the central carbon atoms of the neopentane molecules occupy the sites of a bcc lattice, the molecules are all in the same orientation, and the four carbon-carbon bonds of each molecule point toward the central carbon atoms of neighboring molecules. This local orientational ordering was proposed to occur over a wide range of temperatures.[1] Nishikawa and Murata[3] previously used this bcc cluster model to accurately reproduce the X-ray diffraction intensities from liquid carbon tetrachloride. The X-ray diffraction intensities from liquid 1,1,1-trichloroethane have also been accurately reproduced using the bcc cluster model.[4]

Using a five force center Lennard-Jones potential, Mountain and Brown[5] carried out a molecular dynamics study of neopentane. Their results were consistent with radial distribution functions derived from Narten's diffraction data,[2] and their study indicated that long-range angular correlations in liquid neopentane are weak.[5]

The bcc cluster model[1,3] for short-range orientational ordering has the same local structure as does the long-range orientational ordering proved to exist in a lattice gas of tetrahedral molecules on a bcc lattice.[6,7] We[8] have previously fitted a Guggenheim-McGlashan approximation[9,10] of this lattice gas model to the properties of carbon tetrachloride at the critical point. The lattice gas has properties which are consistent with several aspects of the bcc cluster model[3,11] and provides a fairly good model for carbon tetrachloride.[8]

In the present work we use this bcc lattice gas of tetrahedral molecules as a model for neopentane. A lattice site in the model can be either vacant or occupied by a molecule in either of the two orientations in which the carbon-carbon bonds of the molecule point toward neighboring lattice sites. One such orientation is illustrated in Fig. 1. If two molecules occupy neighboring lattice sites, they repel with a steric bond-bond repulsion $\gamma>0$ if each points a bond toward the other, they attract with an energy $\varepsilon\leq 0$ if exactly one points a bond toward the other, and they attract with an energy $\delta\leq 0$ if neither points a bond toward the other.

An extension of the Peierls argument[12,13] has been used to prove that if $2\varepsilon<\gamma+\delta$, then at sufficiently low temperature and sufficiently high chemical potential an orientationally ordered phase exists in the lattice gas model in which most of the sites are occupied by molecules in a single orientation.[8] Within the Guggenheim-McGlashan approximation, this orientationally ordered structure was found to exist locally in the liquid phase of the lattice gas over a wide range of temperatures.[8]

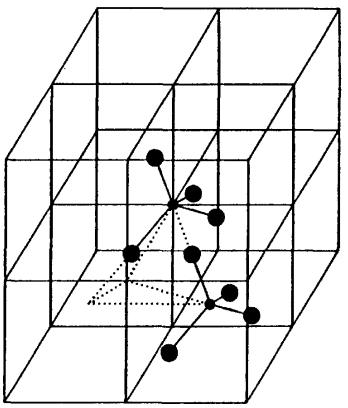

Fig. 1. One of two possible orientations of a neopentane molecule in the bcc lattice gas is shown. A tetrahedron is illustrated which is used in the Guggenheim-McGlashan approximation.

We shall now use a Guggenheim-McGlashan approximation of this bcc lattice gas[8] to model the properties of the liquid and vapor phases of neopentane. The approximation considers the interactions within the various molecular configurations possible on a cluster of sites and then approximates the interactions between various clusters on the lattice.

The following outline of the Guggenheim-McGlashan approximation is described in more detail in Ref. 8. The bcc lattice is composed of tetrahedra, one of which is illustrated in Fig. 1. We consider the set τ consisting of all translates of a single tetrahedron. Each lattice site is covered by a vertex from each of four tetrahedra in τ, and each first neighbor lattice bond is covered by an edge from exactly one tetrahedron in τ.

The set of possible molecular configurations about a tetrahedron in τ is illustrated in Fig. 2 of Ref. 8. For a configuration of type i, the energy ε_i, the number of molecules n_i, and the number of such configurations ω_i are listed in Table II of Ref. 8.

For a lattice of N sites containing M molecules, we let ψ_i be the probability that a given unit tetrahedron in τ has a molecular configuration i. The energy per lattice site is given as

$$E=\sum_i \varepsilon_i\omega_i\psi_i.$$

The entropy per lattice site is given in the

Guggenheim-McGlashan approximation as

$$S=N^{-1}k\ln\Omega_0-k\sum_i\omega_i\psi_i\ln\psi_i.$$

Here there are N tetrahedra in τ, and Ω_0 in a constant which is determined by calculating S at extremely high temperatures.

At equilibrium the Helmholtz free energy, $A=E-TS$, is minimized at constant T, M, and N under the restrictions

$$\sum_i\omega_i\psi_i=1$$

$$\sum_i n_i\omega_i\psi_i=\rho,$$

where $\rho=M/N$ is the number density of occupied sites. The order parameter ρ is sufficient to locate the liquid phase-vapor phase equilibrium and the associated critical point.

The Lagrange multiplier technique then gives expressions for the chemical potential μ, the pressure P, and the density ρ as functions of a parameter r.[8] These equations can be solved to obtain the phase diagram for the model. An iterative technique we developed[8] was used to locate the critical point in the model. For plotting purposes we define the reduced variables $P'=Pv_0/|\varepsilon|$, $T'=kT/|\varepsilon|$, $\gamma'=\gamma/|\varepsilon|$, and $\delta'=\delta/|\varepsilon|$. Here v_0 is the volume per lattice site.

Since steric repulsions are very strong between the methyl groups on neighboring molecules in the bcc cluster model for neopentane,[1] we consider here only the case of infinite bond-bond repulsion, $\gamma'\to\infty$, in the bcc lattice gas model. Using the experimental critical values[14] P_c=31.545 atm, T_c=433.75 K, and $\bar{V}_c$=311 cm^3 mol^{-1} for neopentane, the parameters δ', v_0, and ε in the lattice gas model can be fitted to experiment at the critical point.

The critical compressibility factor $Z_c=P_c'/(\rho_cT_c')$ for the lattice gas is plotted against δ' in Fig. 4 of Ref. 8. Since $Z_c=P_c\bar{V}_c/(RT_c)$, this quantity can be readily fitted to experiment. The best fit occurs at $\delta'=-0.78$.

For the case $\gamma'\to\infty$ and $\delta=0.78\ \varepsilon$, steric bond-bond repulsions are certainly central in producing the orientational ordering, for the two orientations of a pair of neighboring molecules which are attractive have nearly the same energy. The effect of steric repulsion on this ordering can be readily seen within the Guggenheim-McGlashan approximation, for packing considerations (see Fig. 2 of Ref. 8) even in a tetrahedral arrangement of four sites preclude all four sites from being occupied such that an attraction δ occurs in the tetrahedron without the simultaneous occurrence of a steric repulsion γ.

The critical parameters for the lattice gas model with $\gamma'\to\infty$ and $\delta'=-0.78$ were computed to be P_c'=0.08922, T_c'=0.8558, and ρ_c=0.3784. The volume per lattice site, v_0, was then fixed at the critical point using the equation $v_0=\rho_c\bar{V}_c/N_0$, where $\bar{V}_c$ is the experimental critical molar volume and N_0 is Avogadro's number. This gives a value $v_0=1.954\times10^{-22}$ cm^3, and a resulting first neighbor central carbon-central carbon separation of r_{cc}=6.33 Å. This compared quite well with the separations r_{cc}=6.14 Å at −17 °C to r_{cc}=6.90 Å at 150 °C which were used in the bcc cluster model[1] to accurately simulate the experimental X-ray diffraction intensities of the liquid at different temperatures under high pressure.[2]

The energy ε was fitted to experiment using the equation $|\varepsilon|=kT_c/T_c'$, where T_c is the experimental critical temperature. This yields $N_0|\varepsilon|$=4.21 kJ mol^{-1}. In order to compare the fitted value of $|\varepsilon|$ with experiment, we assume the liquid at the normal boiling point is ordered in the bcc local lattice structure. Then $N_0|\varepsilon|\approx\Delta\bar{E}_v/4=(\Delta\bar{H}_v-P\Delta\bar{V}_v)/4$. The experimental values[14] $\Delta\bar{H}_v$=22.64 kJ mol^{-1} and $\Delta\bar{V}_v$=21893.4 cm^3 mol^{-1} at the normal boiling point (T_b=282.628 K and P=1 atm) yields $N_0|\varepsilon|$=5.11 kJ mol^{-1}, which agrees fairly well with the fitted value.

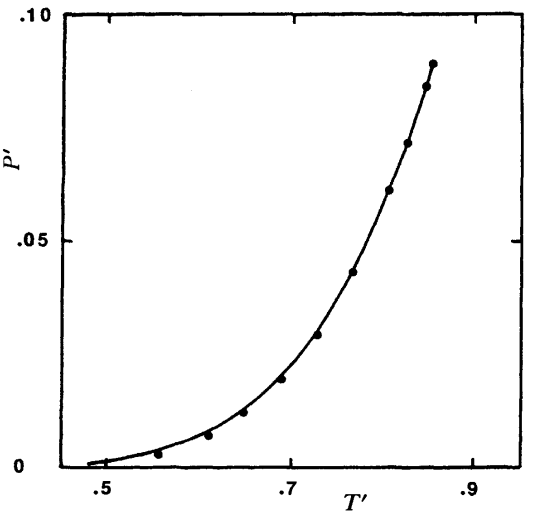

Fig. 2. The liquid-vapor coexistence curve in the (P', T') plane is plotted for the lattice gas case in which $\gamma'\to\infty$ and $\delta'=-0.78$. Several experimental points[14] are illustrated as dots in the figure.

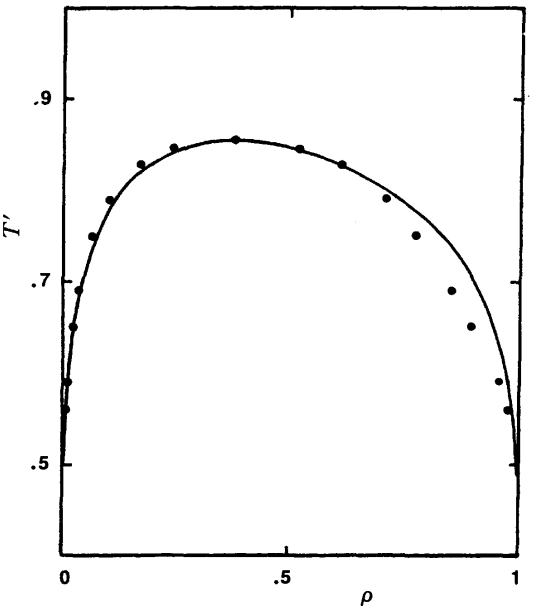

Fig. 3 The liquid-vapor coexistence curve in the (T', ρ) plane is plotted for the lattice gas case in which $\gamma'\to\infty$ and $\delta'=-0.78$. Several experimental points[14] are illustrated as dots in the figure.

The liquid-vapor coexistence curves in the (P', T') plane and in the (T', ρ) plane are plotted in Figs. 2 and 3, respectively, for the lattice gas case in which $\gamma' \to \infty$ and $\delta' = -0.78$. Using the equations $P' = Pv_0/|\varepsilon|$, $T' = kT/|\varepsilon|$, and $\rho = v_0 N_0/V$, several experimental points[14] (P, T) and (T, V) on the liquid-vapor coexistence curve were converted to (P', T') and (T', ρ) values and illustrated in Figs. 2 and 3, respectively.

In conclusion, the lattice gas model studied here is consistent with many aspects of Nishikawa's local bcc lattice structure model and seems to provide a fairly good model for neopentane.

This research was supported by the Robert A. Welch Foundation, grant P-446.

References

1) K. Nishikawa, *Bull. Chem. Soc. Jpn.*, **59**, 2920 (1986).
2) A. H. Narten, *J. Chem. Phys.*, **70**, 299 (1979).
3) K. Nishikawa and Y. Murata, *Bull. Chem. Soc. Jpn.*, **52**, 293 (1979).
4) K. Nishikawa and T. Iijima, *Bull. Chem. Soc. Jpn.*, **61**, 217 (1988).
5) R. D. Mountain and A. C. Brown, *J. Chem. Phys.*, **82**, 4236 (1985).
6) D. A. Huckaby, *J. Stat. Phys.*, **17**, 371 (1977).
7) D. A. Huckaby, A. M. Dougherty, and A. Pękalski, *Phys. Rev. A*, **26**, 3528 (1982).
8) M. Shinmi and D. A. Huckaby, *J. Chem. Phys.*, **84**, 951 (1986).
9) E. A. Guggenheim and M. C. McGlashan, *Proc. R. Soc. London*, **206**, 335 (1951).
10) G. M. Bell and D. A. Lavis, *J. Phys. A*, **3**, 568 (1970).
11) K. Nishikawa and T. Iijima, *Bull. Chem. Soc. Jpn.*, **58**, 1215, 1220 (1985).
12) R. Peierls, *Proc. Cambridge Philos. Soc.*, **32**, 477 (1936).
13) O. J. Heilmann, *Commun. Math. Phys.*, **36**, 91 (1974).
14) T. R. Das, C. O. Reed, Jr., and P. T. Eubank, *J. Chem. Eng. Data*, **22**, 16 (1977).

Molecular Complexes of Cyclophanes. XV. Charge-Transfer Complexes of Sterically Hindered[2.2]metapara- and [2.2]paracyclophanes with π-Acceptors

Aboul-fetouh E. MOURAD*, Alaa El-Din A. HASSAN, and Jörg DANNHEIM†
Chemistry Department, Faculty of Science, El-Minia University, El-Minia, Egypt
†Institut für Organische Chemie, Technische Universität Braunschweig, Hagenring 30, D-3300 Braunschweig, Federal Republic of Germany
(Received April 18, 1988)

Synopsis. The charge-transfer (CT) complexes of some sterically hindered [2.2]metapara- and [2.2]paracyclophanes as π-donors with 2,3-dichloro-5,6-dicyano-*p*-benzoquinone (DDQ) and tetracyanoethylene (TCNE) as π-acceptors have been investigated by electronic as well as infrared spectroscopy. Electronic, steric, and transannular effects governing the formation and stability of the CT complexes studied are discussed.

The transannular electronic interactions in the [2.2]paracyclophanes were the subject of several spectroscopic investigations in the last decades.[1-9] These studies dealt mainly with the question of how the electronic effects of substituents in one ring are transferred to the second ring of the [2.2]paracyclophane molecule.

This paper dealt with the visible and infrared spectra of intermolecular complexes of di-*t*-butyl[2.2]-metaparacyclophanes (**1—3**), diisopropyl[2.2]paracyclophanes (**4,5**), 4-*t*-butyl[2.2]paracyclophane (**6**) as well as 4-trimethylsilyl[2.2]paracyclophane (**7**) and both acceptors DDQ and TCNE. A new absorption band due to neither donor **1—7** nor acceptor was observed in the visible region for the CT complexes studied. In two cases two new absorption bands were observed (Table 1). These two absorption bands may be explained as due to electron transition from two highest occupied π-molecular orbitals of an electron donor to the lowest vacant π-molecular orbital of an electron acceptor.

It has been reported that the λ_{max} values for the CT complexes were used as a measure of the π-base strengths of the donors used.[2] Comparison of the λ_{max} values for the CT complexes of the donors **1—5** with both DDQ and TCNE demonstrates that the π-base strengths of the donors follow the order: 4>5>1>2>3. Also, [2.2]paracyclophanes (**4** and **5**) are more basic

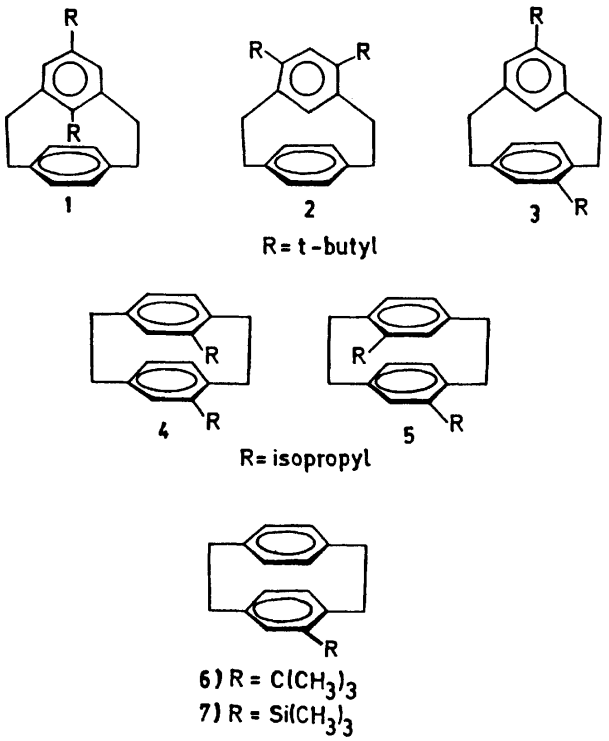

Table 1. CT Spectral Data for Complexes between Donors **1—7** and DDQ, TCNE in Dichloromethane at 20 °C

Donor	Acceptor	λ_{max}	ε	*K*	IP
		nm	$l\,mol^{-1}cm^{-1}$	$l\,mol^{-1}$	eV
1	DDQ	632	109	121.45	8.17
2	DDQ	597	100	93.71	8.31
3	DDQ	562	117	72.24	8.46
4	DDQ	659	98	137.56	8.07
5	DDQ	650	118	129.43	8.10
6	DDQ	597	144	95.26	8.31
7	DDQ	587	196	91.44	8.35
1	TCNE	563, 425	49	78.08	8.14, 9.09
2	TCNE	537, 425	69	65.27	8.28, 9.09
3	TCNE	499	86	52.56	8.52
4	TCNE	580	95	86.12	8.05
5	TCNE	575	108	81.03	8.08
6	TCNE	541	115	70.52	8.26
7	TCNE	532	136	67.36	8.31

than [2.2]metaparacyclophanes (**1—3**). In order to explain this trend of basicity two factors must be discussed; electronic and steric. In the metaparacyclophanes (**1—3**) the transannular electronic interactions are absent, since the two aromatic nuclei are perpendicular to each other,[10] and thus the unsubstituted part of compound **1** and **2** may be formally considered as *p*-xylene. The higher values of the λ_{max}'s of the CT complexes of donors **1—3** with TCNE in Table 1 relative to *p*-xylene-TCNE complex (λ_{max}=460 nm[11]) indicated that the substituted ring in **1** and **2** mainly formed complexes with the acceptors. Accordingly, the electronic effects of the *t*-butyl groups are prevailing over steric ones. The presence of two *t*-butyl groups in the *p*-position in **1** and in the *m*-position in **2** is responsible for the greater steric hindrance and consequently lower π-basicity of **2** relative to **1**.[1]

As reported in Table 1, the CT complexes of **4** with DDQ and TCNE absorb at 659 and 580 nm respectively. The CT complexes of its analogue 4,13-di-*t*-butyl[2.2]paracyclophane (**4**, R=*t*-butyl) with the same acceptors absorb at 663 and 595 nm respectively.[12] These results reveal that the *t*-butyl-substituted cyclophane is more basic than the isopropyl-substituted one. In other words, the electron-releasing character is stronger than the steric one. Accordingly if we compare the basicity of di-*t*-butyl-substituted [2.2]metaparacyclophanes (**1—3**) with that of diisopropyl-substituted [2.2]paracyclophanes (**4** and **5**) the former basicity is expected to be larger than that of the latter. Contrary to the expectation the latter was larger than the former as shown in Table 1. This behevior arises undoubtly from transannular electronic interactions within paracyclophanes **4** and **5**.

The existence of steric hindrance in a donor-acceptor system tends to inhibit the interections between the electron-poor π-orbitals of acceptor with the electron-rich π-orbitals of donor, and hence the basic character of donor will be decreased with increasing the steric hindrance, i.e., the absorption of its CT complexes will be shifted to shorter wavelengths. Consequently, on the basis of steric requirements, the CT complexes of **4** with DDQ and TCNE should absorb at shorter wavelengths than those of **5**, since the two isopropyl groups in **4** are pseudo-geminally oriented, and hence more sterically hindered than in the pseudo-ortho case (**5**) On the contrary, the donor **4** exerts higher basic character than **5** as reported in Table 1 for the values of λ_{max}. This may be explained as due to the difference in exiton splitting of the electronic states of the two donor molecules.

The association constants for complex formaation indicate a marked sensitivity to substituent effects and follow the same sequence as the corresponding λ_{max} values. A linear correlation between the association constants and the position of the λ_{max} of the long wavelength CT band has been observed for the two series of complexes.

It is worthwhile to point out that the low *K* values of the CT complexes of 4-trimethylsilyl[2.2]paracyclophane (**7**) with DDQ and TCNE and the absorption at relatively shorter wavelengths than the CT complexes of 4-*t*-butyl[2.2]paracyclophane (**6**) with the same acceptors are in agreement with the low electronegativity of the silicon atom with respect to the carbon one.

It has been reported that for a series of CT complexes the relationship between *K* and ε values is generally linear,[13] and when the electron donor is sterically hindered the ε values will be reduced.[11] The CT complexes in the present work reveal no regular relationship between *K* and ε values. This behavior is believed to be due to the steric hindrance in the donor molecules, which decreases in the following order:

2>1>3 and **4>5>6**.

The empirical relation derived by Aloisi and Pignataro[14] were used to determine the ionization potentials (IP) of the free donors (**1—7**) and their values are given in Table 1; they are another measure of the relative π-basicities of these electron donors. The high IP values in case of the DDQ-complexes is due to the high electron affinity of DDQ with respect to TCNE.[15]

The infrared spectra of some CT complexes as well as their free components are summarized in Table 2. The data reveals that in case of the CT complexes with

Table 2. IR Spectra (KBr) of Some Free Donors and Acceptors and Their CT Complexes (cm^{-1})

Complex	Free acceptor	Compl. acceptor	Free donor	Compl. donor
2-DDQ	2225(CN)	Very weak	1353, 1240,	1360, 1250
	1670(CO)	1690, 1660	925(CMe_3)	930
	1555(C=C)	1550	790, 720(ArH)	800, 728
	1175(C-Cl)	1160		
2-TCNE	2260, 2220(CN)	2240, 2200	1100(CMe_3)	1105
	1085, 960, 920	1077, 950, 910	880, 790, 728	885, 800, 732
	(C-CN)		(ArH)	
5-DDQ	2225(CN)	Very weak	2850(aliph. CH)	2857
	1670(CO)	1685, 1660	1370, 1350	1378, 1360
	1175, 800(C-Cl)	1170, 793	($CHMe_2$)	
			882, 840(ArH)	890, 845
5-TCNE	2260, 2220(CN)	2245, 2208	2850(aliph. CH)	2855
	1110, 1085, 960	1105, 1080, 952	1370, 1350	1375, 1356
	(C-CN)		($CHMe_2$)	
			840, 720(ArH)	845, 727

DDQ the C=O at 1670 cm^{-1} splits into two bands, whereas that of the C≡N group is weaken. In case of the TCNE-complexes, the two bands characteristic of the C≡N groups show a red shift. Comparison of the infrared spectra of the CT complexes with those of the free components reveals an apparent shift of the bands of the acceptor to lower wavenumbers. However those of the donor are shifted to higher values indicating a decrease in the electron density in the donor part of the CT complex. This behavior is characteristic of π-π^* transitions.[16]

In conclusion, the spectroscopic studies of this type of donor-acceptor interactions revealed the important role played by both electronic effects of the electron-releasing groups and the transannular electronic interactions of the π-electron clouds of the two aromatic rings with one another in [2.2]paracyclophane relative to the eteric factors.

Experimental

Reagents. The electron donors **1—7** were prepared according to the procedure described in Ref 17. Tetracyanoethylene and 2,3-dichloro-5,6-dicyano-*p*-benzoquinone (Janssen Chimica) were used without further purification. Dichloromethane (Merck) was dried over phosphorus pentaoxide and distilled as described in Organicum.[18]

Physical Measurements. Association constants (K) and molar extinction coefficients (ε) of the CT complexes studied have been determined by utilizing the Rose-Drago equation:[19,20]

$$K^{-1} = \frac{C_D C_A(\varepsilon - \varepsilon_A)}{d - d_A} - C_D - C_A + \frac{d - d_A}{\varepsilon - \varepsilon_A},$$

where C_D and C_A are the initial concentrations of donor and acceptor respectively, ε_A is the molar absorbance of the acceptor, d_A is the absorbance at the initial concentration of the acceptor, and d corresponds to the total absorbance at any given wavelength for a cell of 1.0 cm path length.

The visible spectra were scanned on a Beckman UV 5230 recording spectrophotometer in stoppered silica cells (1.0 cm). All scans covered the range from 350 to 800 nm. The infrared spectra were recorded on a Perkin-Elmer 157 G spectometer.

A. M. is grateful to the Alexander von Humboldt Foundation for the award of a fellwoship for 1986—1987 and to Prof. H. Hopf for providing working facilities at Braunschweig. J. D. thanks the Volkswagenwerk Foundation for financial support.

References

1) D. J. Cram and R. H. Bauer, *J. Am. Chem. Soc.*, **81**, 5971 (1959).
2) L. A. Singer and D. J. Cram, *J. Am. Chem. Soc.*, **85**, 1080 (1963).
3) D. J. Cram and D. I Wilkinson, *J. Am. Chem. Soc.*, **82**, 5721 (1960).
4) A. E. Mourad, A. M. Nour-el-Din, and M. R. Mahmoud, *Spectrochim. Acta, Part A*, **38**, 993 (1982).
5) A. E. Mourad and A. M. Nour-el-Din, *Spectrochim. Acta, Part A*, **39**, 533 (1983).
6) A. E. Mourad and A. M. Nour-el-Din, *Gazz. Chim. Ital.*, **113**, 213 (1983).
7) A. E. Mourad, F. W. Raulfs, and H. Hopf, *Monatsh. Chem.*, **116**, 701 (1985).
8) A. E. Mourad, E. H. Eltamany, and H. Hopf, *Z. Phys. Chem. (Leipzig)*, **267**, 507, 937 (1986).
9) A. E. Mourad, A. M. Nour-el-Din, and H. A. Abdel-Nabi, *Gazz. Chim. Ital.*, **116**, 381 (1986).
10) H. J. Lindner, *Tetrahedron*, **32**, 753 (1976).
11) R. E. Merrifield and W. D. Phillips, *J. Am. Chem. Soc.*, **80**, 2778 (1958).
12) A. E. Mourad and J. Dannheim, unpublished.
13) R. S. Mulliken, *J. Am. Chem. Soc.*, **74**, 811 (1952); *J. Phys. Chem.*, **56**, 801 (1952).
14) G. G. Aloisi and S. Pignataro, *J. Chem. Soc., Faraday Trans. 1*, **69**, 534 (1972).
15) R. Foster, "Organic Charge Transfer Complexes," Academic Press, London (1969).
16) R. M. Issa, M. Gaber, A. L. El-Ansary, and H E. Rizk, *Bull. Soc. Chim. Fr.*, **1985**, 173.
17) J. Dannheim, "Diplomarbeit," TU Braunschweig (1986).
18) Organicum, "Practical Handbook of Organic Chemistry," 1st ed., Pergamon Press, Oxford (1973).
19) N. J. Rose and R. S. Drago, *J. Am. Chem. Soc.*, **81**, 6138 (1959).
20) B. K. Seal, A. K. Mukherjee, and D. C. Mukherjee, *Bull. Chem. Soc. Jpn.*, **52**, 2088 (1979).

Reduction of Halonitrobenzenes with Disodium Ditelluride in *N,N*-Dimethylformamide

Ralph A. ZINGARO* and Chris HERRERA
Department of Chemistry, Texas A & M University, College Station, Texas 77843, U.S.A.
(Received June 6, 1988)

Synopsis. The reaction of disodium ditelluride in *N,N*-dimethylformamide with *o*-halonitrobenzenes results in displacement of the halide, reduction of the nitro group and a ring closure reaction which yields phenazines.

Recently, we reported on the unusual stabilities of bis(benzenetellurenyl) selenides when a carbonyl group is located ortho to the tellurium atom.[1,2] This stability was attributed to a strong Te··· O=C interaction as reflected in a relatively short Te··· O distance (2.658 Å). As an extension of this observation it was decided to synthesize bis(*o*-nitrophenyl) ditelluride and determine its crystal structure. It would be of interest to determine the geometry of the Te-O-C-C-N-O sequence and the Te··· O bond length in order to learn whether the Te··· O interaction represents a more general phenomenon. Because bis(*o*-nitrophenyl) diselenide has been prepared by the reaction between *o*-chloronitrobenzene and sodium diselenide,[3a] the synthesis of the ditelluride by the aromatic nucleophilic displacement reaction of sodium ditelluride on *o*-chloronitrobenzene in *N,N*-dimethylformamide was attempted. However, the only products isolated were phenazine and, in very low yield, bis(dimethylcarbamoyl) ditelluride. The latter compound was first obtained by Suzuki and Inouye[3b] and its crystal structure was determined by us.[4] In this same study, the latter investigators reported that aromatic nitro compounds are reduced to azo compounds by sodium telluride in DMF. These workers investigated the reaction between several substituted nitrobenzenes and sodium ditelluride in DMF. Among these were some *m*- and *p*-chloro derivatives. Both were found to yield the azo compounds without nucleophilic displacement of the halide. It is interesting to note in the work reported herein, that in the reaction between *o*-halonitrobenzenes and sodium ditelluride in DMF there occurs an aromatic nucleophilic displacement of the halide together with deoxygenation of the nitro group and ring closure to the phenazine.

Before proceeding to a presentation and discussion of other experimental observations, we wish to report that nitrobenzene, nitrosobenzene, and azoxybenzene all underwent reaction with Na_2Te_2 in DMF to yield the same product, viz., azobenzene. This confirms the observation of Suzuki et al.[5]

Phenazine was unequivocally identified by its mp, 175 °C, elemental analysis, and ^{13}CNMR spectrum: δ 130.2 ($C_{1,4}$), 129.5 ($C_{2,3}$), and 143.3 (C_{11}). The yields of phenazine were generally of the order of 25—35%. Phenazine was readily identified (GC/MS, comparison with retention time and m./c. of known standard) as the major product formed in the reaction between sodium ditelluride in DMF with *o*-chloro, *o*-bromo, *o*-iodonitrobenzene.

When 4-chloro-3-nitroanisole was used as the substrate the major product was 3,7-dimethoxyphenazine. Similarly, 4-chloro-3-nitro-1-(trifluoromethyl)benzene, as observed from GC/MS data, gave 3,7-bis(trifluoromethyl)phenazine as the major product [(major mass peak at 316)].

Of unusual interest is the evidence for the formation of biphenylenes **1** and carbazoles **2**. The formation of

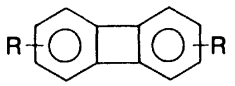

1
R=-H, -CF_3, -OCH_3

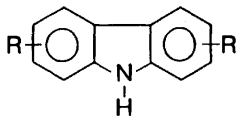

2
R=-H, -CF_3, -OCH_3

biphenylene as one of the products was confirmed in the case of the reaction between *o*-chloronitrobenzene and sodium ditelluride in DMF. The residue remaining after removal of the solids (including phenazine) was subjected to GC/MS. A strong molecular ion at 152 was observed. The experiment was repeated, first using an authentic sample of biphenylene to establish retention time, peak shape, and location, and second with the addition of a small amount of biphenylene to the reaction residue. The retention times and peak shapes and locations were completely superimposable.

Strong molecular ion peaks were observed for the indicated molecular ions **1** and **2** when *o*-bromo-, *o*-iodonitrobenzene, 4-chloro-3-nitroanisole, or 4-chloro-3-nitro-1-(trifluoromethyl)benzene were used as substrates in the reaction with Na_2Te_2. However, the identification of the peaks was not corroborated in these cases by comparison with authentic samples.

The results of other experiments performed for the purpose of elucidating the nature of the reaction are summarized below.

a. The reaction between 4-chloro-3-nitroaniline and Na_2Te_2 in DMF gave 2,2′-dinitro-4,4′-diaminobiphenyl as the main product. No reduction of the nitro groups was observed.

b. No evidence of formation of phenazine was noted in the reaction between 2-chloroaniline and Na_2Te_2 in DMF.

c. Equimolar quantities of *o*-chloronitrobenzene and 4-chloro-3-nitroanisole were allowed to undergo reaction with Na_2Te_2 in DMF. The major product, as determined from GC/MS studies was methoxyphenazine, but both phenazine and dimethoxyphenazine were also formed. These results are not quantitative because authentic samples of the methoxyphenazines were not used. However, they clearly suggest the occurrence of a bimolecular condensation.

d. Solutions containing Na_2Te_2 and *o*-chloronitro-

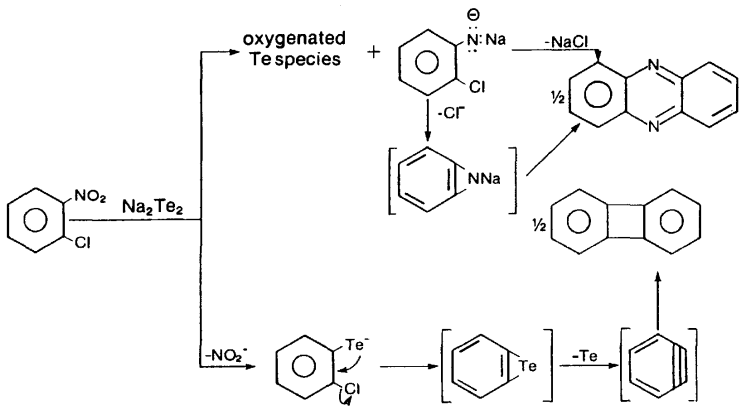

Scheme 1.

benzene in DMF were measured, during the course of the reaction, for paramagnetic susceptibility. No evidence of paramagnetism was observed. This, however, does not rule out the possibility for the formation of free radical species since the measurement is not sufficiently sensitive.

e. The grey residue formed from the reaction between Na_2Te_2 and *o*-chloronitrobenzene was separated under oxygen-free conditions and was found to contain 16.5% oxygen (by fast neutron activation analysis). This gives evidence for the deoxygenation of the nitro group, but does not establish the actual chemical form of the oxygen-containing species.

The observed reactions are exceedingly complex. They are difficult to study mechanistically because of the formation and persistence of the tellurium-rich solid phase. While experimental evidence for a detailed mechanism is lacking, product formation does suggest some reasonable possibilities.

The observation of Suzuki and co-workers on the reduction of aromatic nitro compounds to diazo derivatives by Na_2Te in DMF has already been referred to.[5] This group of investigators has also observed the displacement of the nitro group by NaHTe in ethanol.[5,6] In the present study the ditelluride ion is involved in halide displacement and reduction and elimination of the aromatic nitro group ortho to a halogen. The anionic tellurium species presumably function as deoxygenating agents and, as previously indicated,[5,6] are able to displace the nitro groups. An additional example of the displacement of a nitro group by a nucleophile has been reported by Loudon[7] who observed the conversion of 3,4-dinitro-1-chlorobenzene to 3-phenylthio-4-nitro-1-chlorobenzene by treatment with thiophenol.

In the mechanisms proposed in Scheme 1, the formation of diphenylenes is strongly indicative of a benzyne intermediate. One likely possibility, not shown in the scheme, involves the initial nucleophilic displacement of chloride by Te_2^{2-}. Deoxygenation can then be accomplished either by the ring substituted tellurium or by unreacted ditelluride in the reaction medium.

Experimental

Melting points were determined in capillary tubes on a Büchi-SMP 20 melting point apparatus and are uncorrected. Gas chromatographic/mass spectroscopic (GC/MS) measurements were performed on the Hewlett-Packard model 5995C instrument. Nuclear magnetic resonance spectroscopic measurements were performed on the Varian XL-200 instrument. *N,N*-Dimethylformamide (DMF), was stirred with KOH and distilled from BaO (bp 152 °C). Powdered tellurium (99.9% purity) was obtained as a gift from the Selenium-Tellurium, Assn., Inc. Organic reagents were purchased from the Aldrich Chemical Co. and were used as received.

Preparation of Disodium Ditelluride. All reactions were carried out under an atmosphere of nitrogen or argon. Reactions were carried out in the dark or under a red light. The procedure followed was that described by Sandman et al.[8] Powdered tellurium (15.24 g, 0.19 mol) was placed in a three-necked flask (300 ml) containing 100 ml of dried DMF. A thermometer was inserted through one of the necks, another was sealed with a rubber septum, and to the other was attached a reflux condenser. Metallic sodium (2.73 g, 0.119 mol) in 100 ml of DMF was added and the mixture was heated slowly, with continuous magnetic stirring, until it reached a temperature of 110 °C. The reaction can be quite violent at the mp of sodium (ca. 97 °C) and slow, gradual heating is desirable. The mixture was stirred for 1 h at 110 °C and then allowed to cool to 55 °C. The solution is deep purple in color.

Reaction of Aromatic Nitro Compounds with Excess Na_2Te_2. The reactions were carried out using a three-to four-fold excess of Na_2Te_2. A solution of the reagent in 100 ml of DMF was added to the Na_2Te_2 in DMF through the rubber septrum and the mixture was stirred for 23 h at 50 °C. The solution was then filtered under nitrogen and the precipitate was washed with 80 ml of hot DMF. The filtrate was evaporated under reduced pressure. The solid or heavy viscous liquid that remained was then taken up in an appropriate solvent, usually benzene, and allowed to crystallize in the cold. Isolated crystalline solids were recrystallized from appropriate solvents until reproducible mp's were obtained. In those cases where the residual oils were formed, solutions in appropriate solvents, usually benzene, were taken for GC/MS measurements. Details of a specific experiment are given in the next paragraph.

A solution of disodium ditelluride was prepared according to the method previously described from 15.30 g, 0.119 mol of powdered tellurium and 2.78 g, 0.121 mol of sodium in 200 ml of DMF under an atmosphere of nitrogen. The solution was cooled to 60 °C and to it was added with magnetic stirring, through the attached rubber septum, a solution containing 5.15 g, 0.0275 mol of 4-chloro-3-nitroanisole. The temperature jumped to 98 °C upon the addition of the ani-

sole. The mixture was stirred for 20 h at 35 °C. The mixture was filtered, under nitrogen, and the filtrate was evaporated under reduced pressure with heating (external hot water bath) to a viscous dark syrup. This was refluxed with 200 ml dry benzene containing decolorizing charcoal, filtered and again taken to a viscous syrup under reduced pressure. Storage in a refrigerator overnight showed the presence of a crystalline solid. This was recrystallized from ethanol/chloroform in the presence of decolorizing charcoal which was removed by filtration. The final product, green crystals of 3,7-dimethoxyphenazine were obtained in yields of 24, 30, and 37% on three different runs (based on recrystallized material). The recrystallized solid melted at 251—253 °C: A low resolution mass spectral peak corresponding to the molecular ion was observed at 240.17; for $C_{14}H_{12}N_2O_2$. Calcd (Found): C, 69.99 (70.07); H, 5.03 (5.11); N, 11.65% (11.65%); the ^{13}C NMR spectrum showed resonances at δ 55.8 assigned to $-OCH_3$ at δ 160.2 assigned to quaternary ring carbons attached to methoxy groups (C_3 and C_7) and at δ 143.4 and 140.4 (quaternary carbons attached to ring nitrogen atoms). Resonances at δ 129.9 and 125.9 are assigned to ring carbons $C_{2,6}$ and $C_{4,8}$ and at δ 104.9 to ring carbons $C_{1,5}$, but this group of assignments cannot be made unequivocally.

The financial assistance of the Robert A. Welch Foundation in support of this work is gratefully acknowledged.

References

1) N. L. M. Dereu, R. A. Zingaro, E. A. Meyers, and M. Renson, *Organometallics*, **1**, 111 (1982).
2) E. A. Meyers, N. L. M. Dereu, and R. A. Zingaro, *Cryst. Struct. Commun.*, **10**, 1353 (1981).
3) a) M. T. Bogert and A. Stull, *J. Am. Chem. Soc.*, **49**, 2011 (1927); b) H. Suzuki and M. Inouye, *Chem. Lett.*, **1985**, 1671.
4) R. A. Zingaro, C. Herrera, and E. A. Meyers, *J. Organomet. Chem.*, **306**, C36 (1986).
5) H. Suzuki, H. Manabe, T. Kawaguchi, and M. Inouye, *Bull. Chem. Soc. Jpn.*, **60**, 771 (1987).
6) A. Osuka, H. Shimizu, and H. Suzuki, *Chem. Lett.*, **1983**, 1373.
7) J. D. Loudon, *J. Chem. Soc.*, **1939**, 902.
8) D. J. Sandman, J. C. Stark, and B. M. Foxman, *Organometallics*, **1**, 739 (1982).

Structural Features and Biological Studies of Dioxomolybdenum(VI) Complexes of Thiosemicarbazones

Neeta KANOONGO, Ranvir SINGH, and Jagdish Prasad TANDON*
Department of Chemistry, University of Rajasthan, Jaipur 302004, India
(Received August 22, 1988)

Synopsis. Synthesis, characterization, and spectral features of six-coordinated dioxomolybdenum(VI) complexes of the type, $[MoO_2(tscz)_2]$ (where Htscz represents the thiosemicarbazone moiety) are reported. These have been characterized by elemental analysis, conductance measurements, molecular weight determinations, and magnetic studies. Based on IR, ^1H NMR, ^{13}C NMR, and electronic spectral studies, an octahedral geometry with *cis*-MoO_2 structure has been proposed. The antibacterial and fungicidal activities of two representative ligands and their dioxomolybdenum complexes have also been evaluated and discussed.

Molybdenum exhibits a large number of stable and accessible oxidation states as well as varying coordination numbers from four to eight.[1] A large number of important chemical reactions catalyzed by molybdenum compounds, e.g. industrial process such as hydrodesulfurization[2] and olefin epoxidation[3] are carried out in presence of molybdenum catalyst. Nature has also incorporated molybdenum into a number of important[4] redox enzymes.

In view of industrial and biological importance of molybdenum complexes,[5,6] it was considered of interest to synthesize some molybdenum(VI) complexes of bidentate Schiff bases and study their structural features as well as biological activity. The ligands used are biologically active thiosemicarbazones and the results of these investigations are being presented in this paper.

Experimental

All the chemicals of analytical grade were used and the solvents were dried by the standard methods. Thiosemicarbazones[7] and $MoO_2(acac)_2$[8] were prepared according to the literature methods and analyzed before use. The ligands derived from 2-furancarbaldehyde, 2-pyridinecarbaldehyde, 2-thiophenecarbaldehyde, 3-indolecarbaldehyde, cinnamaldehyde 2-propanone, 1-phenylethanone and 4-methyl-2-pentanone are abbrevied as $Htscz_1$, $Htscz_2$, $Htscz_3$, $Htscz_4$, $Htscz_5$, $Htscz_6$, $Htscz_7$ and $Htscz_8$, respectively.

Synthesis of $[MoO_2(tscz)_2]$. To a calculated amount (1 mol) of $MoO_2(acac)_2$ in dry MeOH (ca. 40 cm^3) the requisite amount (2 mol) of thiosemicarbazone was added. The resulting mixture was refluxed for 4 h. After the completion of the reaction the solvent was removed and the residue dried in vacuo for 3 h. The analytical data (C, H, N, S, and Mo) of the complexes are within the limit of experimental errors. Molybdenum was determined gravimetrically as bis(8-quinolinalato) dioxomolybdenum(VI). Other methods of analyses and physical measurements are same as reported earlier.[7]

Results and Discussion

The reactions between $MoO_2(acac)_2$ and monobasic bidentate, thiosemicarbazones were carried out in 1 : 2 molar ratio in methanol. The replacement of acetylacetonato group by the ligands resulted in the formation of the products of the type $[MoO_2(acac)_2]$. The resulting derivatives were recrystallized by adding solvent ether to the methanolic solution of the complexes and their purity was further checked by TLC on silica gel G using anhydrous methanol as the solvent. These are soluble in methanol, DMSO, and DMF.

The low values of molar conductance in DMF (10—14 $ohm^{-1}\,cm^2\,mol^{-1}$) show these complexes to be non-electrolytes and the molecular weight determinations by the Rast camphor method correspond to the formula weight indicating their monomeric nature. All the derivatives are diamagnetic as expected for $4d^0$ configuration for Mo(VI) species.

The IR spectra of thiosemicarbazones[7] show a strong band at ca. 3280 cm^{-1} due to ν_{NH} vibrations and which disappears in the metal complexes suggesting its deprotonation on complexation with the metal ion. In the IR spectra of ligands in solution, bands due to ν(C=S) and ν_{NH}, which are observed in the IR spectra in KBr optics do not appear. This may be attributed to the existence of two tautomeric forms, viz, an thioamide form in the solid state and iminothiol form in solution.[9] On complex formation, these bands disappear indicating the coordination of the ligand through the thiolic sulfur. A strong band in the ligands in the region, 1610—1620 cm^{-1} due to the azomethine (>C=N) group shifted to the lower frequency region in the molybdenum complexes.[10]

In the spectra of the complexes, two bands in the regions, 900—920 and 890—900 cm^{-1} can be ascribed to ν_{sym}(O=Mo=O) and ν_{asym}(O=Mo=O) vibrations[11] respectively. The presence of these bands is indicative of *cis*-MoO_2 structure as the *trans*-MoO_2 structure would show only one ν_{asym}(O=Mo=O) band in this region. Further, medium to weak intensity bands in the regions, 450—430 and 370—300 cm^{-1} which do not appear in the ligands, may be attributed to νMo-N and νMo-S, respectively.[12,13]

The electronic spectrum of $Htscz_1$ shows one band of weak intensity at 245 nm and a broad band at 340 nm attributable to π-π^* (double bond) and n-π^* (azomethine) electronic transitions, respectively. In $[MoO_2(tscz_1)_2]$ the first band remains almost unchanged whereas, the second band shows a blue shift due to the donation of nitrogen lone pair of the azomethine group to molybdenum atom. The spectrum of complex also exhibits a strong band at 380—450 nm due to the ligand to metal charge transfer transitions between the lowest empty molybdenum d orbital and the highest occupied ligand molecular orbital as reported earlier.[1]

The proton magnetic resonance spectra of $Htscz_1$

Table 1. ^{1}H NMR Data (δ/ppm) of Ligands and Dioxomolybdenum(VI) Complexes

S. No.	Compound	-NH	Aromatic	Azomethine	$-NH_2$
1	$Htscz_1$[a)]	11.40bs	6.60—7.68m	8.00s	2.40bs
2	$[MoO_2(tscz_1)_2]$[a)]	—	7.35—8.16m	8.20s	2.66bs
3	$Htscz_2$	11.08bs	6.32—6.80m	8.40s	2.55bs
4	$[MoO_2(tscz_2)_2]$	—	7.00—7.72m	8.50s	2.60bs
5	$Htscz_4$	11.78bs	6.00—7.60m	8.32s	2.40bs
6	$[MoO_2(tscz_4)_2]$	—	7.46—8.00m	8.48s	2.80bs

s=singlet, bs=broad singlet, and m=complex multiplets.
a) ^{13}C NMR data: Ligand; C_1 (179.48), C_2 (150.79), C_3 (134.77), C_4 (114.75), C_5 (146.14), C_6 (199.9).
Complex; C_1 (176.77), C_2 (148.49), C_3 (131.78), C_4 (111.87), C_5 (144.00), C_6 (188.69).

Table 2. Fungicidal Data of Ligands and Their Dioxomolybdenum Complexes

Compound	Average percentage inhibition after 96 h					
	Aspergillus Flaves		Aspergillus niger		Alternaria alternata	
	50 ppm	75 ppm	50 ppm	75 ppm	50 ppm	75 ppm
$Htscz_1$	40	48	32	45	65	70
$[MoO_2(tscz_1)_2]$	52	61	38	50	68	75
$Htscz_3$	44	55	37	47	70	79
$[MoO_2(tscz_3)_2]$	60	67	48	59	77	85

(**1**), $Htscz_2$ (**3**), $Htscz_4$ (**5**), and their corresponding dioxomolybdenum complexes **2**, **4**, and **6** respectively have been recorded in DMSO-d_6 using TMS as the internal standard. The chemical shifts value (δ/ppm) of the different protons have been recorded in Table 1. The broad signals due to NH protons at δ 11.40 (**1**), δ 11.08 (**3**), and δ 11.78 (**5**) in the ligands disappear in the case of molybdenum complexes showing ligation of molybdenum to nitrogen as well as sulfur atoms. The azomethine proton signals (-C(H)=N) appearing at δ 8.00 (**1**), δ 8.40 (**3**), and δ 8.32 (**5**) in the ligands undergo deshielding and appear at δ 8.20 (**2**), δ 8.50 (**4**), and δ 8.48 respectively in the molybdenum complexes indicating the coordination of the azomethine nitrogen to the molybdenum atom. The positions and assignment of other protons are recorded in Table 1.

^{13}C NMR spectra of $Htscz_1$ and its molybdenum complex have also been recorded in Table 1 (foot note). The shifts of the carbons attached to the donor S and N atoms further substantiate the bonding pattern discussed earlier.

Thus on the basis of above evidences the following cis-octahedral structure can be proposed for the molybdenum(VI) complexes with $Htscz_1$ as the ligand:

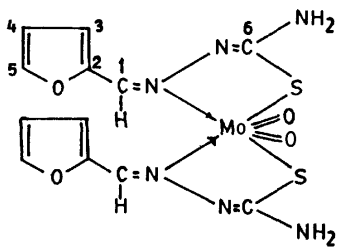

The antibacterial activity of $Htscz_1$ and $Htscz_3$ and their dioxomolybdenum complexes has been evaluated in vitro against *E. Coli, S. aureus, Eutrobactor aerogenus, Citrobactor, P. Pyocyancus,* and *S. Citrus* at 1000 ppm concentration using the inhibition zone technique.[14] A 5 mm diameter sterilized filter paper disc impregnated with the compound was placed on agar plate seeded with the test organism. The plates were incubated for 24 h at 37 °C. The zone of inhibition of bacterial growth around the disc was observed. The screening data show moderate activity against *E. Coli, S. aureus, Eutrobactor aerogenus,* while all the compounds are highly active against *P. Pyocyancus* and *S. citrus.* The above ligands and complexes were also screened for their fungicidal activity by determining the percentage inhibition of colonial growth in comparison to the growth in control. From the data recorded in Table 2, it is evident that the compounds are capable of inhibiting the fungal growth to a considerable extent both at high and low dilutions.

One of us (N.K.) is thankful to the U.G.C. New Delhi, India for financial assistance.

References

1) E. I. Stiefel, *Prog. Inorg. Chem.*, **22**, 1 (1977).
2) B. C. Gates, J. R. Katzer, and G. C. Aschuit "Chemistry of Catalytic Process," McGraw Hill, New York (1979), p. 390.
3) M. L. H. Green, Proc. 3rd Int. Conf. on the Chemistry and Uses of Molybdenum Climax, Molybdenum Co., Ann. Arbor MI, p. 34 (1979).
4) R. C. Bray, *Enzyme*, **12**, 299 (1975).
5) T. D. Tullius, D. M. Kurtz, Jr., S. D. Conradson, and K. O. Hodgson, *J. Am. Chem. Soc.*, **101**, 2776 (1969).
6) S. P. Cramer, H. B. Gray, and K. V. Rajagopalan, *J. Am. Chem. Soc.*, **101**, 2772 (1979).
7) N. Kanoongo, R. V. Singh, and J. P. Tandon, *Transition Met. Chem.*, **12**, 271 (1987).
8) G. J.-J. Chen, W. J. McDonald, and W. E. Newton, *Inorg. Chem.*, **15**, 2612 (1976).
9) S. P. Mital, R. V. Singh, and J. P. Tandon, *Synth. React.*

Inorg. Met.-Org. Chem., **11**, 547 (1981).
10) R. H. Holm, G. W. Everett, Jr., and A. Chakravorty, *Prog. Inorg. Chem.*, **7**, 83 (1966).
11) P. W. Moore and M. L. Larsen, *Inorg. Chem.*, **6**, 998 (1967).
12) K. Nakamoto, "The Infrared Spectra of Inorganic and Coordination Compounds," Wiley Eastern, New Delhi (1967).
13) S. K. Sengupta and S. Kumar, *Indian J. Chem.*, **22A**, 257 (1983).
14) R. S. Verma and S. A. Imam, *Indian J. Microbiol.*, **13**, 45 (1973).

A Simple Iterative Approach to the Synthesis of *cis-cisoid-cis*-Tricyclo[6.3.0.0^{2,6}]undecane Carbon Skeleton

Padma S. VANKAR and Srinivasan CHANDRASEKARAN*
Department of Chemistry, Indian Institute of Technology, Kanpur 208016, India
(Received September 5, 1988)

Synopsis. In an iterative synthesis utilizing only four reagents, cyclopentanone has been converted into *cis-cisoid-cis*-tricyclo[6.3.0.0^{2,6}]undecane carbon skeleton in high yield.

There is much current interest in the synthesis of linearly fused tricyclopentanoids (triquinanes) which is mainly due to their wide occurance in nature with promising biological properties and their likely role as building blocks for the synthesis of the $C_{20}H_{20}$ regular (pentagonal) polycycle, dodecahedrane.[1] As a result, several novel approaches to this ring system have been developed in recent years.[2] In the course of our studies on oxidative transformations with hexadecyltrimethylammonium permanganate (CTAP)[3] we developed a general two step methodology for the synthesis of γ-lactones **2** from ketones **1** (Scheme 1) in very good yield.[4]

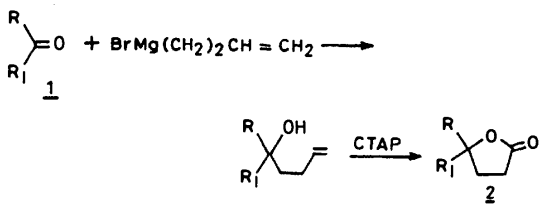

Scheme 1.

Herein, we report an efficient application of this oxidative cyclization strategy in an iterative approach to set up the *cis-cisoid-cis*-tricyclo[6.3.0.0^{2,6}]undecane carbon skeleton. It is anticipated that easy accessibility to **3** and its derivatives would open new possibilities for further synthetic exploitation.

Reaction of cyclopentanone with Grignard reagent derived from 4-bromo-1-butene[5] gave the alcohol **4**[6] (62%) which was then subjected to oxidative cyclization with hexadecyltrimethylammonium permanganate (CTAP) to yield the spirolactone **5**[4] (71%). Treatment of the lactone **5** with phosphorus pentaoxide in methanesulfonic acid[8] for 2 h at 50 °C led to the bicyclic enone **6**[8] (98%). Hydrogenation of **6** in ethyl acetate containing palladium on carbon produced the saturated cis-bicyclic ketone **7**[9] (99%).

To continue the synthesis the bicyclic ketone **7** was subjected to the same sequence of reactions. Thus, reaction with the Grignard reagent produced the adduct **8** (64%). Oxidative cyclization with CTAP afforded the spirolactone **9** (60%). On action of phosphorus pentaoxide in methanesulfonic acid the lactone **9** yielded the tricyclic enone **10** (92%). Catalytic hydrogenation of **10** with palladium on carbon resulted in the cis addition of hydrogen to the less hindered face of the olefin[10] to give the product **3** (95%) (Scheme 2).

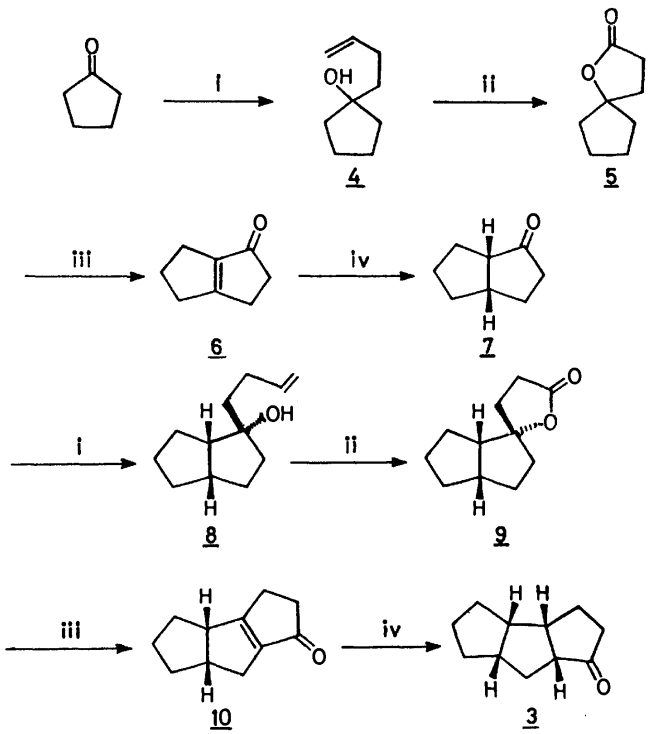

Scheme 2. Reagents:
i, $BrMgCH_2CH_2CH{=}CH_2$; ii, CTAP, CH_2Cl_2; iii, P_2O_5-$MeSO_3H$; iv, Pd/C, H_2

Experimental

The NMR spectra were taken on a Varian EM-390 spectrometer and Brucker WP-80 spectrometer. IR spectra were measured using a Perkin Elmer 1320 spectrometer and mass spectra were obtained from a VG micromass 7070F mass spectrometer.

Oxidative Cyclization of 4 with CTAP. To a solution of **4**[6] (1.4 g, 10 mmol) in chloroform (30 ml) was added a solution of CTAP (8.08 g, 20 mmol) in chloroform (25 ml) at room temperature (28 °C) and the mixture was stirred for 6 h. Solvent was evaporated under reduced pressure and ether (200 ml) was added to the residue which was filtered through a pad of Celite. The filter cake was washed thoroughly with ether and the combined filtrate was evaporated. The residue was purfied by flash chromatography on silica gel (elution with 4:1 ether-petroleum ether) to get the spirolactone **5**[4] (0.980 g, 71%) as a colorless oil. IR(CCl_4) 1780 cm^{-1}; ^1H NMR ($CDCl_3$) δ=1.5—2.35 (m, 10H) and 2.4—2.7 (m, 2H); MS *m/z* 140 (M^+).

Reaction of 5 with Methanesulfonic Acid-Phosphorous Pentaoxide. A solution of **5** (0.700 g, 5 mmol) in freshly distilled methanesulfonic acid (50 g) containing phsophorus pentaoxide (5 g) was stirred under nitrogen at 50 °C for 2 h. The mixture was cooled in an ice bath and water (150 ml) was carefully added. It was then extracted with ether (3×100

ml). The combined ether extract was washed with 10% potassium carbonate solution and water and then dried over anhydrous magnesium sulfate. After evaporation of solvent the product was purified by flash chromatography on silica gel (elution with 1:10 ether-petroleum ether) to afford **6**[8] (0.600 g, 98%) as a colorless oil. IR(CCl_4) 1645, 1710 cm^{-1}; ^1H NMR($CDCl_3$) δ=1.8—2.0 (m, 2H) and 2.3—2.7 (m, 8H): MS *m/z* 122 (M^+).

Catalytic Hydrogenation of 6. To a solution of **6** (0.610 g, 5 mmol) in ethyl acetate (20 ml) was added 5% palladium on charcoal (0.100 g) and treated with hydrogen at 40 psi for 1 h. The catalyst was filtered and the solvent was evaporated to yield the bicyclic ketone **7**[9] (0.605 g, 99%) as an oil. IR(CCl_4) 1735 cm^{-1}; ^1H NMR($CDCl_3$) δ=1.4—2.0 (m, 9H), 2.2—2.4 (m, 2H), and 2.5—2.7 (m, 1H); MS *m/z* 124 (M^+).

Grignard Reaction of 7 with 4-Bromo-1-butene. Grignard reagent derived from 4-bromo-1-butene[5] (1.35 g, 10 mmol) and magnesium powder (0.288 g, 12 mmol) in dry THF (25 ml) was treated with **7** (1.240 g, 10 mmol) in dry THF (10 ml) at 0 °C for 1 h. The product was purified by flash chromatography on silica gel (elution with 1:2 ether-petroleum ether) to yield the alcohol **8** (1.152 g, 64%) as a coloress oil. IR(CCl_4) 3480, 3080, 1640 cm^{-1}; ^1H NMR ($CDCl_3$) δ=1.2—2.0 (m, 15H), 2.1—2.3 (m, 2H), 4.8—5.1 (m, 2H), and 5.5—5.9 (m, 1H); MS *m/z* 180 (M^+). Found: *m/z* 180.1510. Calcd for $C_{12}H_{20}O$: M, 180.1515.

Oxidative Cyclization of 8 with CTAP. To a solution of **8** (0.360 g, 2 mmol) in dichloromethane (8 ml) was added CTAP (1.62 g, 4 mmol) in dichloromethane (10 ml) and the mixture was stirred at room temperature for 4 h. The product after purification by flash chromatography on silica gel (elution with 1:2 ether-petroleum ether) yielded the spiro lactone **9** (0.216 g, 60%) as an oil. IR(neat) 1770 cm^{-1}; ^1H NMR ($CDCl_3$) δ=1.3—1.8 (m, 14H) and 2.2—2.5 (t, 2H); MS *m/z* 180 (M^+).

Reaction of 9 with Methanesulfonic Acid-Phosphorus Pentaoxide. A solution of **9** (0.360 g, 2 mmol) in freshly distilled methanesulfonic acid (30 g) was added to phsophorus pentaoxide (3 g) and the mixture was heated under nitrogen at 50 °C for 2 h. The product was worked up as described in the synthesis of **6**. The tricyclic enone **10** (0.300 g, 92%) was isolated as an oil after chromatographic purification. IR(neat) 1700, 1640 cm^{-1}; ^1H NMR ($CDCl_3$) δ=1.3—1.8 (m, 7H) and 2.1—2.6 (m, 7H); MS *m/z* 162 (M^+). Found: *m/z* 162.1041. Calcd for $C_{11}H_{14}O$: M, 162.1045.

Catalytic Hydrogenation of 10. A solution of **10** (0.162 g, 1 mmol) in ethyl acetate (5 ml) was added to 5% Pd-C and treated with hydrogen at 40 psi for 2 h. The ctalyst was filtered and the solvent was removed to give the tricyclic ketone **3** (0.155 g, 95%) as an oil homogeneous to TLC. IR(neat) 1725 cm^{-1}; ^1H NMR ($CDCl_3$) δ=1.2—2.0 (m, 13H) and 2.2—2.6 (m, 3H); MS *m/z* 164 (M^+). Found: *m/z* 164.1198. Calcd for $C_{11}H_{16}$: M, 164.1201.

The authors are thankful to DST, New Delhi for financial support.

References

1) G. Mehta, *J. Sci. Ind. Res. (India)*, **37**, 256 (1978): L. A. Paquette, *Topics in Current Chemistry*, **79**, 43 (1979); P. E. Eaton, *Tetrahedron*, **35**, 2189 (1979).

2) L. A. Paquette, *Topics in Current Chemistry*, **119**, 1 (1984); L. A. Paquette, Y. Miyahara, and C. W. Doecke, *J. Am. Chem. Soc.*, **108**, 1716 (1986).

3) V. Bhushan, R. Rathore, and S. Chandrasekaran, *Synthesis*, **1984**, 431.

4) R. Rathore, P. S. Vankar, and S. Chandrasekaran, *Tetrahedron Lett.*, **27**, 4079 (1986).

5) G. A. Kraus and L. Langrebe, *Synthesis*, **1984**, 885.

6) G. E. Gream, A. K. Serelis and T. I. Stoneman, *Aust. J. Chem.*, **27**, 1711 (1974).

7) P. E. Eaton and R. H. Mueller, *J. Am. Chem. Soc.*, **94**, 1015 (1972).

8) S. Dev and C. Rai, *J. Ind. Chem. Soc.*, **34**, 266 (1957); F. Cooke, R. Moerck, J. Schwindeman, and P. Magnus, *J. Org. Chem.*, **45**, 1046 (1980); A. C. Cope and W. Schmitz, *J. Am. Chem. Soc.*, **72**, 3056 (1950); H. Jones and H. T. Taylor, *J. Chem. Soc.*, **1959**, 4017; G. Mehta and K. S. Rao, *Tetrahedron Lett.*, **25**, 1839 (1984).

9) B. M. Trost and M. J. Bogdanowicz, *J. Am. Chem. Soc.*, **95**, 5311 (1973); A. C. Cope, M. Brown, and H. E. Petree, *ibid.*, **80**, 2852 (1958); Y. Fujikura, N. Takaishi, and Y. Inamato, *Tetrahedron*, **37**, 4465 (1981).

10) P. E. Eaton, R. S. Sidhu, G. E. Langford, D. A. Cullison, and C. L. Pietruszewski, *Tetrahedron*, **37**, 4479 (1981).

Optical Resolution of C3 Cyclotriveratrylenes and D3 Cryptophanes by Liquid Chromatography on Chiral Stationary Phase Chiralpak-OT(+)

André TAMBUTÉ, Josette CANCEILL,† and André COLLET*,††
Direction des Recherches et Etudes Techniques, Centre d'Etudes du Bouchet, B. P. 3, 91710 Vert-Petit, France
†Chimie des Interactions Moléculaires, Collège de France, 11 Place Marcelin-Berthelot, 75231 Paris cedex 05, France
††Ecole Normale Supérieure de Lyon, 46 Allée d'Italie, 69007 Lyon, France
(Received October 6, 1988)

Synopsis. A series of C3 cyclotriveratrylenes and D3 cryptophanes have been resolved by HPLC on Chiralpak-OT (+), allowing the first direct enantiomeric excess assessments for these substances. These results confirm the usefulness of this chiral stationary phase for the resolution of aromatic compounds and extend its scope of application to new classes of highly symmetrical molecules.

Since the first reports on the synthesis of optically active C3 cyclotriveratrylenes (CTV's **1**)[1] in 1978 and D3 cryptophanes (**2**)[2] in 1981, a number of molecules of this kind have been described and have found applications in several fields,[3] including spectroscopy (exciton optical activity),[4-6] liquid crystals,[7] and host-guest chemistry.[8-10] Although a cryptophane was used as a *chiral host shift reagent* for the determination of the enantiomeric composition of a weakly rotating sample of CHFClBr,[11] paradoxically, simple means of establishing the enantiomeric excess (ee) of the resolved CTV's and cryptophanes themselves did not exist so far.

We report herein that the commercially available chiral stationary phase (CSP) Chiralpak-OT(+) is effective for analytical optical resolution of certain C3 CTV's and D3 cryptophanes by HPLC. This CSP can also be used for the structural assignment of D3 (**2**, *dl*) vs. C3h (**3**, *meso*) cryptophane isomers.

1a-f

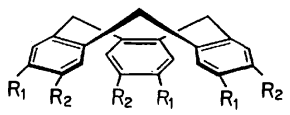

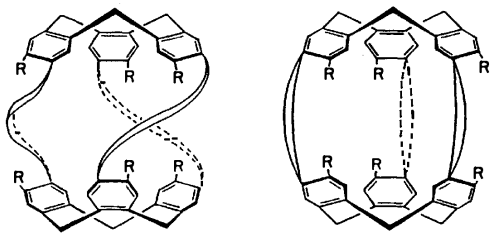

R = OCH_3

(-)-**2a-e** **3b-e**

Results and Discussion

The use of poly(triphenylmethyl methacrylate), an optically active polymer with a stable helical conformation, was introduced in 1979 by Okamoto et al.[12] This polymer either finely ground or coated on silica gel has since been used for analytical resolution of a wide range of racemates under reversed phase conditions, using a polar eluent such as methanol.[13] Such CSP's and especially Chirapak-OT(+) have proven particularly efficient with regard to two main categories of substances.

Table 1. Optical Resolution of C3 Cyclotriveratrylenes **1a—f**[a]

Compd.	First eluted isomer			k'_2[b]	α	T	estd.
	R_1	R_2	confg.			°C	R_s[c]
1a	H	OCH_3	M(+)	25.5	2.29	15	>3
				26.9	2.35	5	
1b	OC_2H_5	OCH_3	P(−)	13.9	1.41	15	≈1
				14.4	1.48	5	
1c	(*O*-allyl	OCH_3)[d]		16.6	1.37	15	≈1.25
				17.2	1.43	5	
1d	$OC_3H_7^i$	OCH_3	P(+)	14.8	1.43	15	≈1.1
				15.4	1.50	5	
1e	$OCOCH_3$	OCH_3	P(+)	12.5	1.38	15	≈1.15
				12.9	1.43	5	
1f	Br	OCH_3	P(−)	16.3	1.48	15	≈1.3
				16.2	1.50	5	

a) Column: Chiralpak-OT(+), 250×4.6 mm i.d.; methanol, 0.5 ml min^{-1}; all solutes were injected in chloroform solution; detection was effected by recording the UV absorption at 230 nm. b) Capacity factor of the slowest eluted enanitiomer; $k'_2=(t_2/t_0)-1$, where t_2 is the retention time of the slowest enantiomer and t_0 that of a nonretained solute. c) The resolution factor R_s is estimated from the depth of valley between the peaks;[14] base line separation corresponds to $R_s>1.3$. d) The enantiomers of this compounds are hitherto unknown.

The first one gathers weakly polar compounds such as oxiranes, halogenated hydrocarbons, some phosphorus insecticides, metal complexes ($M(acac)_3$), as well as more polar compounds such as alcohols and esters. The second category encompasses a variety of molecules (mostly aromatic) that belong to the C2 symmetry point group, such as binaphthol and related atropisomers, spiro (bis) indanones, etc.[13]

In our hands, Chiralpak-OT(+) proved suitable for the resolution of the C3 CTV's **1a—f**. Cyclotriveratrylenes **1b—f**, bearing two different substituents of comparable size on each benzene ring, showed separation factors α ca. 1.4—1.5 (Table 1); **1a** which bears a single substituents on each ring (OCH_3), and hence is "more chiral," was even better separated ($\alpha \approx 2.3$). A slight selectivity increase was obtained by lowering the temperature to 5 °C, as is generally observed. The resolution factor R_s was low (1 to 1.3) for **1b—f**, and good for **1a** (>3). Baseline separations were obtained for **1a** and **1f**, and were almost obtained for the other compounds (see Fig. 1).

Optically active samples of **1a, b, d—f**, which in earlier works[4] had been considered, on the basis of indirect arguments, to have>90% ee, were analyzed by this method. In all cases none or trace amounts of the others enantiomer was detected, thus confirming that the reported maximum rotation data are correct.[4] These experiments also allowed us to establish the order of elution of the two enantiomers in all cases but **1c** (not available in optically active form). For the "disubstituted" series **1b, d—f**, the P isomer, in which R_1 is bulkier than R_2 (see the stereoformula) was eluted first; the "monosubstituted compound **1a** (R_1=H) showed an inverse behavior. Further comments or interpretation of these results would be premature, as the helicity of C3 CTV's is not easy to define and to compare with that of the C2 binaphthyles and analogous compounds discussed by Okamoto.[13]

D3 Cryptophanes **2a—d** were also resolved on this CSP with good selectivities (Table 2). As expected, the achiral C3h isomers **3b—d** each showed a single peak, and this method can therefore be useful to distinguish between *racemic* and *meso* cryptophanes. The elution orders were determined by using the previously described optically active samples of **2a,b,d**.[6] The helicity

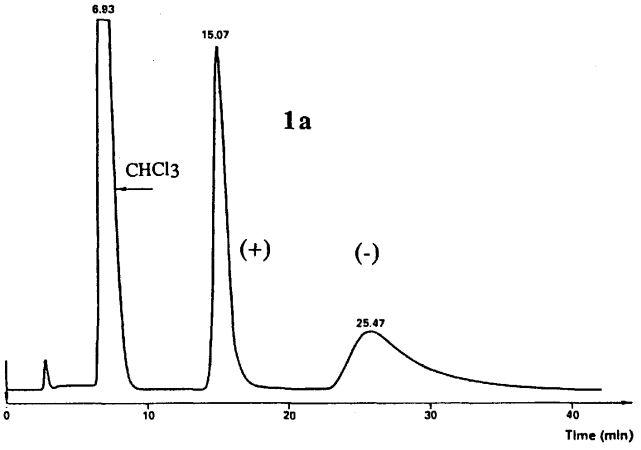

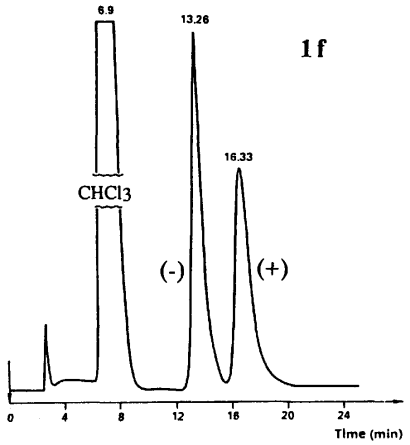

Fig. 1. Chromatographic resolution of (±)-**1a** and (±)-**1f** at 15 °C (conditions indicated in Table 1).

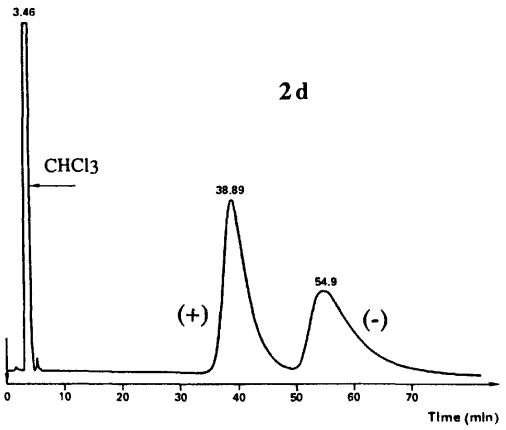

Fig. 2. Chromatographic resolution of(±)-**2d** (conditions indicated in Table 2).

Table 2. Analysis of D3 and C3h Cryptophanes on Chiralpak-OT(+)[a]

Compd.	Symmetry	Bridges	Retn. times/min	k'_2	α
2a	D3	$O(CH_2)_2O$	22.1(+) 30.0(−)	7.58	1.43
2b	D3	$O(CH_2)_3O$	27.4(+) 37.6(−)	9.75	1.42
3b	C3h	$O(CH_2)_3O$	36.0	9.52	
2c	D3	$O(CH_2)_4O$	30.3(?)[b] 75.3(?)	21.1	2.67
3c	C3h	$O(CH_2)_4O$	27.5	6.86	
2d	D3	$OCH_2 \setminus\setminus CH_2O$	38.9(+) 54.9(−)	14.7	1.45
3d	C3h	$OCH_2 \setminus\setminus CH_2O$	31.5	8.0	

a) Same conditions as indicated in Table 1 except flow rate: 1.0 ml min^{-1}; temperature 15 °C.
b) Enantiomers not available.

of the more retained (−) isomers is that of a right-handed screw, when the molecule is viewed along its C3 axis. Typical chromatograms are shown in Fig. 2.

These results raise interesting questions on the mechanisms of the chiral discrimination between a helical polymer and molecules of high symmetry,[15] and suggest that preparative optical resolution of these substances could be carried out on suitable chiral stationary phases.

References

1) A. Collet and J. Jacques, *Tetrahedron Lett.*, **1978**, 1265.
2) J. Gabard and A. Collet, *J. Chem. Soc., Chem. Commun.*, **1981**, 1137.
3) A. Collet, *Tetrahedron*, **43**, 5725 (1987).
4) J. Canceill, A. Collet, J. Gabard, G. Gottarelli, and G. P. Spada, *J. Am. Chem. Soc.*, **107**, 1299 (1985).
5) J. Canceill and A. Collet, *Nouv. J. Chim.*, **10**, 17 (1986).
6) J. Canceill, A. Collet, G. Gottarelli, and P. Palmieri, *J. Am. Chem. Soc.*, **109**, 6454 (1987).
7) J. Malthête and A. Collet, *J. Am. Chem. Soc.*, **109**, 7544 (1987).
8) J. Canceill, L. Lacombe, and A. Collet, *J. Am. Chem. Soc.*, **108**, 4230, (1986).
9) J. Canceill, L. Lacombe, and A. Collet, *J. Chem. Soc., Chem. Commun.*, **1987**, 219.
10) J. Canceill, L. Lacombe, and A. Collet, *C. r. Acad. Sci. Paris Sér. II*, **304**, 815 (1987).
11) J. Canceill, L. Lacombe, and A. Collet, *J. Am. Chem. Soc.*, **107**, 6993 (1985).
12) Y. Okamoto, K. Suzuki, K. Otha, K. Hatada, and H. Yuki, *J. Am. Chem. Soc.*, **101**, 4763 (1979).
13) Y. Okamoto and K. Hatada, *J. Liq. Chromatogr.*, **9**, 369 (1986) and references therein.
14) L. R. Snyder, *J. Chromatogr. Sci.*, **10**, 200 (1972).
15) For a recent relevant discussion, see: O. Wennerström, R. Isaksson, and H. Wennerström, Abstracts of the Ist International Symposium on Separation of Chiral Molecules, Société Française de Chimie, Paris, 1988.

Electrochemical Studies of Poly(mercaptohydroquinone) and Poly(mercapto-*p*-benzoquinone) Films Prepared by Electropolymerization. III. Basic Behavior and Properties in Aqueous Solutions

Gorou ARAI,* Shigehiko SHIMAMURA, Yasunobu OHTOMO, and Iwao YASUMORI
Department of Applied Chemistry, Faculty of Engineering, Kanagawa University, Kanagawa-ku, Yokohama 221
(Received August 4, 1988)

Electrochemical behavior and properties of poly(mercaptohydroquinone)/poly(mercapto-*p*-benzoquinone) (SQ) films prepared on glassy carbon electrodes (GCE) by anodic polymerization of mercaptohydroquinone were examined in detail by cyclic voltammetry. Almost all hydroquinone and/or *p*-benzoquinone moieties in SQ films of less than ca. 100 monolayers are electroactive in acidic and neutral buffer solutions. The formal redox potential (as estimated from anodic and cathodic peak potentials) vs. solution pH plot, the slope of which is −60 mV/pH, suggests that the overall electrode reaction of SQ films is an H^+/e (1:1) reaction. As to the voltammetric behavior of SQ films, the peak current decreased and the peak potential separaxtion (ΔE_p) increased appreciably in unbuffered solutions as compared with those in buffered solutions. The difference of these voltammetric behaviors in unbuffered and buffered solutions increased with increasing pH. Moreover, the peak current increased and ΔE_p decreased with rising solution temperature. These noticeable behaviors observed on SQ films are discussed in connection with the charge-transport mechanism within SQ films. SQ films on GCE showed good durability over a wide potential range from the hydrogen evolution potential to +1.0 V vs. SCE.

Much attention has recently been drawn to the preparation and properties of thin films of polymeric materials covalently bonded to or coated on glassy carbon electrodes (GCE). Especially electroconductive polymers having hydroquinone/quinone moieties are of particular interest as electrocatalysts because they can act as selective chemical oxidants[1,2] and reductants.[3] However, for all electroactive polymers on GCEs having quinone and/or hydroquinone functionalities so far reported, as far as we know, only a few monolayers are electroactive unless small mediator molecules are present that can penetrate the polymer matrix and carr electrons between redox sites.[4]

In a series of our recent papers,[5-8] we have reported of (i) a preparation method of poly(mercaptohydroquinone/mercapto-*p*-benzoquinone)(SQ) films on GCE and on Pt electrode, (ii) applications of SQ film-coated electrodes to various metal sensors and an electrochromic display, and (iii) the electrocatalytic oxidation of NADH to NAD^+. In the present paper, we will report on basic electrochemical behavior and properties of SQ films on a GCE with particular reference to the following points: (i) the redox response behavior of SQ films of ca. 4 to ca. 100 monolayers in thickness, (ii) the influence of solution pH and solution temperature on the charge-transport process within SQ films, and (iii) the applied potential range in which stable voltammetric response is obtained for SQ films on a GCE.

Experimental

Materials and Preparation of SQ Films. Mercaptohydroquinone was synthesized and purified according to the method described in our previous paper.[5] The chemicals used for the synthesis of mercaptohydroquinone were of reagent grade. The other inorganic reagents and ethanol used for rinsing SQ films were of reagent grade and used without further purification. Deionized water was used for the preparation of solutions, final washing of electrode surface, and rinsing SQ films. The substrate electrode used was a GCE 3 mm in diameter. SQ films on the GCE were prepared by anodic polymerization of mercaptohydroquinone at a constant potential of +0.5 V vs. a saturated calomel electrode (SCE) in a Britton-Robinson buffer solution (pH 5.0) containing 20 vol% ethanol, as previously described.[5] The surface concentration (Γ^x, where the superscript x stands for x nmol cm^{-2}) of the electroactive sites, i.e., the hydroquinone and/or *p*-benzoquinone moieties, in SQ films was controlled by the amount of charges passed during the electrochemical polymerization and estimated by measuring the area of cyclic voltammograms for the oxidation-reduction reaction of SQ films themselves, obtained at a scan rate of 2 mV s^{-1} in the Britton-Robinson buffer solution.

Apparatus and Procedure. The apparatus used for the preparation of SQ films on the GCE was the same as that used in our previous work.[5] Voltammetric measurements were carried out with a standard three-electrode system consisting of an SQ film-coated GCE working electrode, a Pt plate counter electrode, and an SCE reference electrode having an agar salt bridge of saturated KCl. Cyclic voltammetry was performed by using a potentiostat/galvanostat (Model HA-304, Hokuto Denko Co.). Purified nitrogen gas was bubbled for 30 min to remove dissolved oxygen. Unless otherwise noted, all measurements were run under nitrogen atmosphere at room temperature. All potential values cited in this paper are those referred to the SCE.

Results and Discussion

Cyclic Voltammetric Behavior. Figure 1 shows a typical cyclic voltammogram representing the electrochemical response of an SQ film-coated GCE in the Britton-Robinson buffer solution (pH 6.5) at a scan

rate of 50 mV s^{-1}. The SQ film examined has $\Gamma^{10.2}$ corresponding to ca. 17 monolayers based on a close-packed monolayer of ca. 0.6 nmol cm^{-2} for 4-methyl-1,2-benzenediol lying flat on a perfectly flat carbon surface.[2] The voltammetric response remained qualitatively unchanged even after a potential scan cycling of several hours in acidic and neutral buffered aqueous solutions and is similar to that obtained for the ordinary electrode reaction of a solution-phase redox species at an uncoated electrode, that is, the voltammogram has diffusional tails and its shape is unsymmetric as shown in Fig. 1. Cyclic voltammetric behavior at various scan rates in a Britton-Robinson buffer solution of pH 6.0 was examined for SQ film-coated GCEs loaded with three different amounts of Γs, viz., $\Gamma^{2.17}$(=ca. 3.6 monolayers), $\Gamma^{10.2}$, and $\Gamma^{56.0}$(=ca. 93.3 monolayers). The results are summarized in Table 1. For all the three SQ films examined, linear relationships exist between the anodic and cathodic peak currents (i_p^a and i_p^c) and the square root of scan rate ($\sqrt{v}$) on the time scale of 100 mV s^{-1}. At scan rates lower than 50 mV s^{-1}, the anodic and cathodic peak currents are proportional to the Γ values, and the peak separation (ΔE_p) is almost constant irrespective of the film thickness. Thus the amount of the charges consumed in the oxidation-reduction reaction of SQ films are almost proportional to the Γ value. On the other hand, at scan rates higher than 50 mV s^{-1}, the anodic and cathodic peaks were observed to be broader and ΔE_p was increased with increasing scan rate and/or Γ value. These results show that almost all hydroquinone and/or *p*-benzoquinone moieties in SQ films are electroactive even at the scan rate of 50 mV s^{-1} although the charge transport in SQ film was rather slow, and suggest that the electron transfer between the substrate electrode (GCE) and the innermost sublayer of SQ film may be faster than the charge transport within SQ film which may be controlled by electron hopping and/or proton transfer between adjacent electroactive sites, ion migration, polymer motions, or combinations of these actions. From the fact that the SQ film of ca. 100 monolayers may be electroactive on the time scale of 50 mV s^{-1}, SQ film-coated GCEs are superior to other poly(hydroquinone) film-coated electrodes[1-3] in respect of the charge transport within polymer layers.

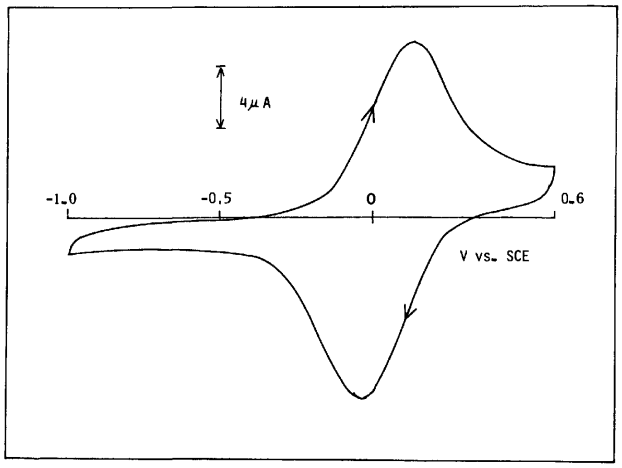

Fig. 1. A typical cyclic voltammogram of SQ film-coated GCE in a Britton-Robinson buffer solution (pH 6.5) at a scan rate of 50 mV s^{-1}. The surface concentration of hydroquinone and/or quinone moieties in SQ film was 10.2 nmol cm^{-2} ($\Gamma^{10.2}$). The arrow indicates the direction of potential scan.

Response in Buffered and/or Unbuffered Solutions. In order to clarify the charge-transport process within SQ film, the pH dependence of cyclic voltammograms of SQ film-coated GCEs was examined over the pH region 2—8 using Britton-Robinson buffer solution. The anodic and cathodic peak potentials (E_p^a and E_p^c) shifted to the negative potential side with increasing pH. E_p^a, E_p^c, and the formal redox potential ($E^{0'}$) which is estimated as the average of E_p^a and E_p^c values, are shown in Fig. 2. Over the pH region 2—8, the slope of the $E^{0'}$ vs. pH plot is about −60 mV/pH. This result suggests that the overall electrode reaction of SQ film is the H^+/e (1:1) reaction in the examined pH region on the time scale examined. On the basis of the fact that SQ film is a hydroquinone/*p*-benzoquinone redox polymer and that the slope of the $E^{0'}$ vs. pH plot is ca. −60 mV/pH in the pH range below 8, and with the assumption that the negative logarithm of the first dissociation constant (pK_1) of the hydroquinone moiety in SQ film is from 9 to 10 based on the pK_1

Table 1. Change in Peak Current and Peak Separation of Cyclic Voltammograms of SQ Film-Coated GCEs of Various Values with Scan Rates of Potential Sweeping in a Britton-Robinson Buffer Solution (pH 6.0). Γ Values Were Controlled by the Electrolysis Time of Mercaptohydroquinone

	$\Gamma^{2.17}$			$\Gamma^{10.2}$			$\Gamma^{56.0}$		
Scan rate	i_p^a	i_p^c	ΔE_p	i_p^a	i_p^c	ΔE_p	i_p^a	i_p^c	ΔE_p
mV s^{-1}	μA	μA	mV	μA	μA	mV	μA	μA	mV
10	0.63	0.64	120	2.9	3.0	120	16.0	16.3	130
20	1.20	1.22	130	5.5	5.7	130	28.5	27.5	140
50	2.55	2.70	160	11.5	12.0	170	54.0	56.5	210
100	4.40	4.95	180	18.0	20.5	200	80.0	86.5	270
200	7.60	9.00	210	31.5	34.5	245	134.5	154.0	350

value of hydroquinone (pK_1=9.9), the overall reduction-oxidation reaction of SQ film in aqueous solutions of pH 2 to 8 may be written as

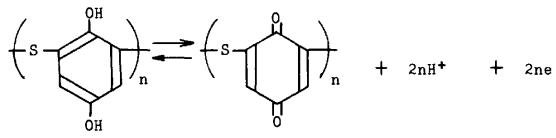

The other pH effects in the buffered solutions on the cyclic voltammograms for SQ film-coated GCEs are summarized in Table 2. The anodic and cathodic peak currents decreased slightly and ΔE_p decreased with increasing pH below 4, while in the pH region higher than 5, both the peak currents increased and ΔE_p decreased with increasing pH. At pH higher than 8, the cyclic voltammograms for SQ films were largely distorted in shape and the integrated current was decreased with increasing pH as shown in Fig. 3, where cyclic voltammograms are illustrated just after 10 cycles since the distortion in shape became more complicated as the potential scan was cycled. Even though the SQ film-coated electrode was transferred to acidic or neutral solution after successive potential sweepings in alkaline solution, the observed distortion remained unchanged. These results show that the distortion in wave shape resulted from some chemical or structural change of SQ film itself because in alkaline aqueous solution *p*-benzoquinone is susceptible to addition of OH^- ion.[9] Turning to the pH dependence of cyclic voltammograms, very similar behavior is seen to an anthraquinone polymer film reported by Degrand[10] with respect to the pH dependence of i_p^a, i_p^c, and i_p^a/i_p^c. To date, a similar pH dependence of redox behavior has also been reported with other types of conductive polymers.[11-13] In order to further detail the pH dependence of the charge transport within SQ films, the cyclic voltammetric

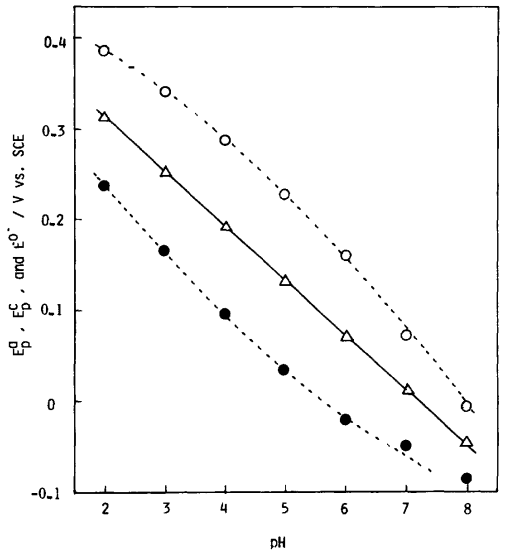

Fig. 2. pH-dependences of the anodic and cathodic peak potentials (E_p^a and E_p^c) and the formal redox potential ($E^{0'}$) of the cyclic voltammograms of SQ film-coated GCE using Britton-Robinson buffer solutions. Other experimental conditions are the same as in Fig. 1. O: E_p^a, ●: E_p^c, Δ: $E^{0'}$.

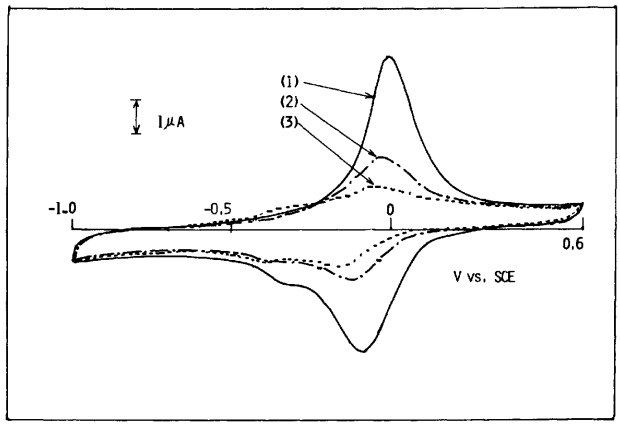

Fig. 3. Wave distortion observed on the cyclic voltammograms for SQ film-coated GCE's of $\Gamma^{13.0}$ just after 10 cycles in alkaline buffer solutions. Scan rate: 50 mV s^{-1}. (1) pH 8.5, (2) pH 9.0, (3) pH 9.5.

Table 2. pH Dependence of the Peak Current and Peak Separation of SQ Film-Coated GCEs Obtained at a Scan Rate of 50 mV s^{-1} in Britton-Robinson Buffer Solutions

pH	i_p^a	i_p^c	i_p^a/i_p^c	ΔE_p	$\Gamma^{a)}$
	μA	μA		mV	nmol cm^{-2}
2	15.8	18.3	0.86	150	13.4
3	15.5	16.5	0.94	160	13.0
4	14.2	15.0	0.95	190	13.2
5	14.0	14.5	0.97	190	12.5
6	14.3	14.7	0.97	180	12.6
6.5	14.3	15.5	0.99	160	12.9
7	14.6	13.5	1.08	120	12.4
7.5	17.3	15.0	1.15	100	12.6
8	17.5	14.8	1.18	90	12.4

a) All the SQ films examined were prepared on GCEs by a constant-potential electrolysis for 30 min at the same conditions as described in Experimental section.

behavior of SQ film-coated GCEs was examined in unbuffered aqueous solutions since the pH change within SQ films resulting from the oxidation-reduction reaction of SQ films in unbuffered solutions may be more rapid and larger than in buffered solutions. It is, therefore, expected that the charge transport within SQ films will be affected remarkably by this rapid and large pH change. Figure 4 shows cyclic voltammograms for an SQ film-coated GCE having $\Gamma^{13.1}$ (ca. 22.0 monolayers) in unbuffered solutions of various pH values. The wave shapes in the unbuffered solutions differed considerably from those in the buffered solutions. The difference in the wave shapes increased with increasing pH, that is, in the unbuffered solutions the peak current dramatically decreased and ΔE_p remarkably increased with increasing pH, whereas in the buffered solution of pH 5.0 the peak current slightly decreased and ΔE_p slightly increased (see Fig. 2) and at pH 7 two anodic and two cathodic peaks were obscurely observed on the examined time scale. Such voltammetric behavior observed in the unbuffered solutions may be explained as follows: Consider the electro-oxidation process of SQ film (reduced form). The electro-oxidation of one hydroquinone moiety gives one *p*-benzoquinone moiety and two protons over the pH range examined. The numbers of the hydroquinone moieties in the SQ film used were almost equal because the same electrode ($\Gamma^{13.1}$) was used in the examined three cases. The increments of the protons resulting from the electro-oxidation of all the hydroquinone moieties in the SQ film may, therefore, be equal in the three cases. Hence the pH change in the SQ film induced by the electro-oxidation of the film may increase in the order of pH 7>pH 5>pH 3. The pH change in the SQ film results in variation of the redox potential of hydroquinone/*p*-benzoquinone couple in the film. It is clear on the basis of the Nernst equation that the redox potential of hydroquinone/*p*-benzoquinone moieties in SQ films become more negative with increasing pH and more positive with decreasing pH in SQ films. In the case of the oxidation process of SQ films, the decrease in pH within inner layers of SQ films (in the immediate neighborhood of the GCE) may retard the further oxidation of hydroquinone moieties in their outer layers. On the other hand, in the case of the reduction process of SQ films the increase in pH within inner layers may also retard the further reduction of *p*-benzoquinone moieties in outer layers. Judging from their pH dependence described above and their reduction-oxidation behavior in unbuffered solutions, it may safely be said that the propagation of the redox reaction between adjacent hydroquinone/*p*-benzoquinone moieties participates predominantly in the charge-transport process within SQ films on the time scale examined.

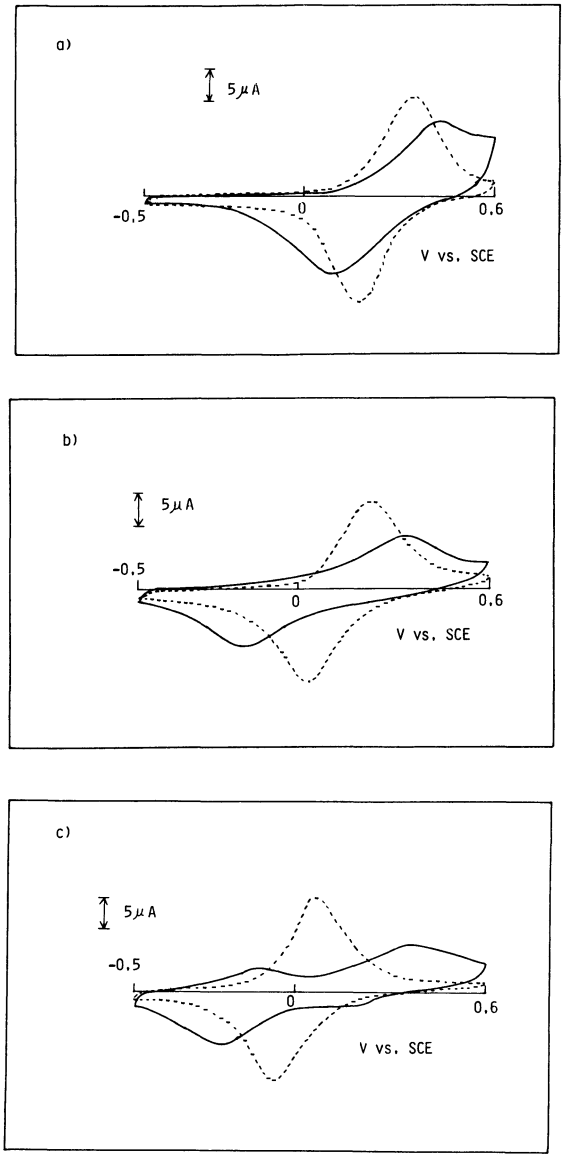

Fig. 4. Comparison between the cyclic voltammograms of SQ film-coated GCE of $\Gamma^{13.1}$ in buffer solutions and those in no buffer solutions. Full lines were obtained in 0.1 mol cm^{-3} KCl solution adjusted to each pH value by addition of an appropriate quantity of dilute HCl or NaOH while broken lines were obtained in Britton-Robinson buffer solutions. Scan rate: 50 mV s^{-1}. a) pH 3.0, b) pH 5.0, c) pH 7.0.

Influence of Temperature. Cyclic voltammetric measurements on the SQ film-coated GCE having $\Gamma^{13.0}$ were carried out over the solution temperatures from 1 to 50 °C. The peak currents increased and ΔE_p decreased with rising temperature, as shown in Fig. 5. The temperature dependence observed is completely reproducible and suggests that the rate of the charge transport through SQ films may be facilitated by rising the temperature. It seems to be a reason for the temperature dependence of the charge transport within SQ films that the rise in temperature makes the segmental polymeric chains in SQ films more mobile

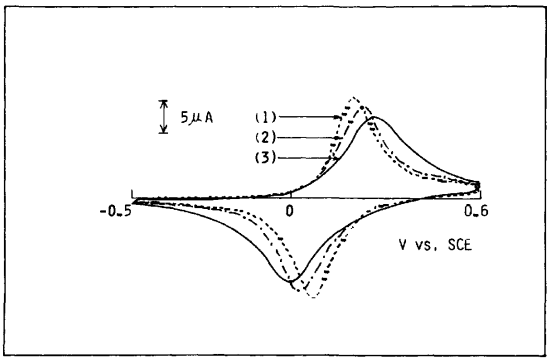

Fig. 5. Temperature-dependence of the cyclic voltammogram of SQ film-coated GCE of $\Gamma^{13.0}$ in the Britton-Robinson buffer solution (pH 5.0). Scan rate: 50 mV s^{-1}. (1) 50 °C, (2)20 °C, (3) 1 °C.

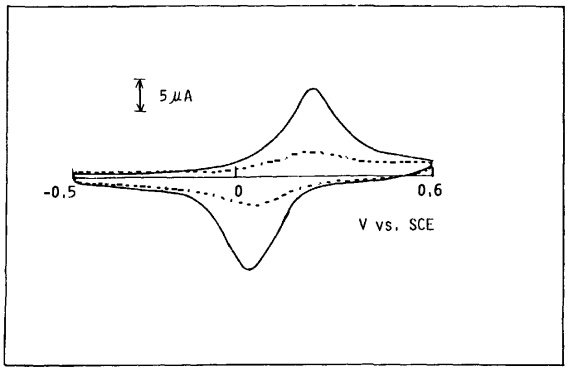

Fig. 7. Change in the cyclic voltammogram of SQ film-coated GCE of $\Gamma^{12.6}$ before and after holding the electrode potential at +1.2 V. Scan rate: 50 mV s^{-1}. ——: 0 min, ---------: 30 min.

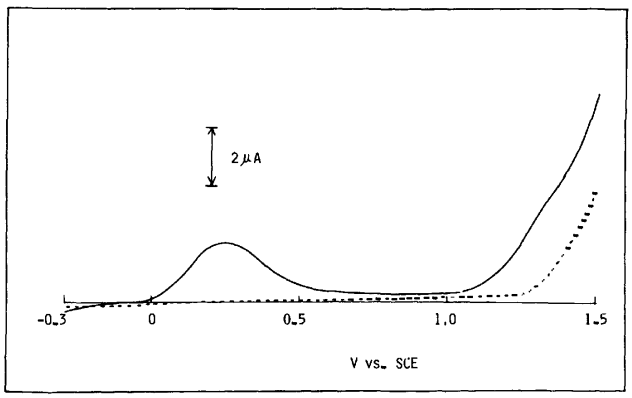

Fig. 6. Current-potential curves of an SQ film-coated GCE and of an uncoated GCE in the Britton-Robinson buffer solution of pH 5.0. Full line was obtained with the SQ film-coated GCE and broken line was obtained with the uncoated GCE. Scan rate: 5 mV s^{-1}.

and that thereby the counter electroactive sites, hydroquinone, and *p*-benzoquinone may be brought more closely together. In addition, the rate of the redox reaction, or the proton migration and electron hopping, between adjacent electroactive sites will also be increased with rising temperature. Thus these two effects are considered to be responsible for the temperature dependence of the charge-transfer rate within SQ films. A similar phenomenon has been reported with a polymerized vinylferrocene.[14]

Stability to Applied Potential. The stability of SQ films on GCE to applied potential was examined over a wide potential range using a weakly acidic Britton-Robinson buffer solution in which SQ films were very stable as described above. Figure 6 shows anodic voltammograms for an SQ film-coated GCE and an uncoated GCE in the Britton-Robinson buffer solution of pH 5.0. The anodic wave in the potential range of +0.2 to +0.4 V observed on the SQ-coated GCE corresponds to the oxidation reaction of hydroquinone moieties to *p*-benzoquinone ones in the SQ film. At more positive potentials than +1.1 V, appreciable increase in anodic current is observed for the SQ-coated GCE, as compared with the uncoated GCE. This increase in anodic current may probably be caused either by some further oxidation of the oxidized SQ film itself or by an unexpected oxidation of some species in the buffer solution. In order to study this increase in anodic current in more ditail, anodic response for the SQ film was examined after the potential of the SQ-coated GCE had been held for 30 min in the Britton-Robinson buffer solution of pH 5.0 at +1.2 V where the increase in anodic current of the SQ film was observed. As shown in Fig. 7, peak currents significantly decreased while peak potentials remained almost unchanged. A similar decrease in peak current was observed in a potential scanning at 50 mV s^{-1} from −0.5 to +1.2 V in the same buffer solution. The cyclic voltammetric wave caused by the reduction-oxidation reaction of the SQ film got smaller as the potential cycling was repeated and almost disappeared after ca. 100 cycles. These results strongly suggest that the increase in anodic current of the SQ film-coated GCE above +1.1 V may result from some further oxidation of the oxidized SQ film itself, followed by an electrochemical inactivation of the film. At present, the mechanism of the further oxidation reaction is obscure. On the other hand, SQ films on GCE were observed to be very stable for the negative shift up to the potential of hydrogen evolution which depends on the solution pH. Judging from the fact that SQ films, even though of ca. 100 layers in thickness, are stable and conductive over a wide potential range in acidic and neutral aqueous solutions, the SQ film-coated GCE may be used as an excellent dehydrogenating and/or hydrogenating agent because the potential of electroactive sites can be controlled exactly to a desired potential with a potentiostat. We will report elsewhere of the electroreduction of quinones and the electrooxidation

of hydroquinones with SQ film-coated GCEs.

References

1) C. Degrand and L. L. Miller, *J. Am. Chem. Soc.*, **102**, 5728 (1980).
2) M. Fukui, A. Kitani, C. Degrand, and L. L. Miller, *J. Am. Chem. Soc.*, **104**, 28 (1982).
3) M. C. Pham and J. E. Dubois, *J. Electroanal. Chem. Interfacial Electrochem.*, **199**, 153 (1986).
4) C. Degrand, L. Roullier, L. L. Miller, and B. Zinger, *J. Electroanal. Chem. Interfacial Electrochem.*, **178**, 101 (1984).
5) G. Arai and M. Furui, *Nippon Kagaku Kaishi*, **1984**, 673.
6) G. Arai, T. Ishii, S. Yamamoto, and I. Yasumori, *Bull. Chem. Soc. Jpn.*, **61**, 7871 (1988).
7) G. Arai, K. Enomoto, and I. Yasumori, *Chem. Lett.*, **1988**, 733.
8) G. Arai, M. Matsushita, and I. Yasumori, *Nippon Kagaku Kaishi*, **1985**, 894.
9) M. Eigen and P. Matthies, *Chem. Ber.*, **94**, 3309 (1961).
10) C. Degrand and L. L. Miller, *J. Electroanal. Chem. Interfacial Electrochem.*, **117**, 267 (1981).
11) A. F. Diaz and J. A. Logan, *J. Electroanal. Chem. Interfacial Electrochem.*, **111**, 111 (1980).
12) A. Kitani, J. Izumi, J. Yano, Y. Hiromoto, and K. Sasaki, *Bull. Chem. Soc. Jpn.*, **57**, 2254 (1984).
13) N. Oyama, T. Osaka, K. Chiba, and K. Takahashi, *Bull. Chem. Soc. Jpn.*, **61**, 1095 (1988).
14) P. Daum, J. Lenhard, D. Rolison, and R. Murray, *J. Am. Chem. Soc.*, **102**, 4649 (1980).

Two-Bond Deuterium Isotope Effects on ^{13}C Chemical Shifts of Phenols

Yasuki NAKASHIMA, Akihiro YOSHINO, and Kensuke TAKAHASHI*
Department of Applied Chemistry, Nagoya Institute of Technology, Gokiso-cho, Showa-ku, Nagoya 466
(Received September 14, 1988)

Two-bond deuterium isotope effects on ^{13}C chemical shifts of 28 substituted phenols are reported and explained in terms of the additivity of substituent parameters which are correlated with the SCS of ^{13}C NMR.

Deuterium isotope effects on ^{13}C chemical shifts are useful parameters for spectral assignments, kinetic studies, and biomechanic studies.[1] The cause of the effect is still unclear, especially regarding further remote effects over one-bond.[2-5] If the magnitudes of the shifts are correlated with any molecular parameters, their applications would be extended in further use. Among such isotope effects, the long-range effects, however, have rarely been reported for aromatic compounds.[6,7] Therefore, more data must be accumulated.

In this study, 28 substituted phenols were selected for the purpose of studying two-bond isotope effects on ^{13}C NMR shifts. One of the reasons for our selection was for an easy preparation of deuterium-labeled compounds. From the sixty nine data points obtained, substituent isotope shifts (hereafter abbreviated as SIS) for seven substituents were quantitatively determined. The SIS's are correlated linearly with the SCS's of the aromatic carbons. Then, the two-bond isotope shifts ($^2\Delta$) can be evaluated from the knowledge of the SCS's. They can also be correlated with the electron densities of the sites under study.

Experimental

Deuterium-labeled compounds were prepared with acid- or base-catalyzed proton-deuteron exchange-reactions of substituted phenols.[8] The starting materials used were commercially available and were used without further purification. Reaction vessels were hand-made Pyrex ampoules. About 0.01 mol of a starting material and a small amount of catalyst (0.1 wt%) dissolved in 1 g of D_2O were sealed into the ampoule, and kept at 80 °C in the thermostatted air oven. After the reaction had reached an extent of about 5—50 D%, the sample was cooled by immersing it in water; the contents were then separated into aqueous and oily (or solid) phases. The latter phase was used for an NMR measurement. Protium-deuterium exchange reactions occurred at 2, 4, and 6-positions and not at 1, 3, and 5-positions of the substituted phenols when they were examined with NMR spectroscopy. The hydroxyl hydrogen of phenol exchanges with that of water and cannot be separately observed on the NMR time scale. Then, the labeled substituent such as OD, ND_2, or NHD did not have any effect on the ^{13}C chemical shifts, as described by Newmark and Hill.[9] Other substituents did not suffer any exchange. Therefore, one- and three-bond isotope effects were observed at the C_2, C_4, and C_6 atoms on the ^{13}C spectra. However, the carbon signals were broadened by the quadrupole effect of deuteron. Thus, accurate values of their isotope effects could not be determined. However, two- and four-bond isotope effects were observed at the C_1, C_3, and C_5 signals. In their spectra two-bond carbon-deuteron couplings are negligibly small and seem to have no effect on their line-widths. An example of the measurement is given in Fig. 1. For the purpose of observing the isotope effect, the extent of the reaction was devised to be nearly 50%. If this is so, the labeled and unlabeled phenols are suitably mixed for their NMR measurements, as shown in Fig. 1. Therefore, the $^2\Delta$ values can be evaluated by using the data obtained from the labeled and unlabeled phenols in a solution contained in the same NMR tube. This might be helpful for decreasing the experimental error of the measurement, which was evaluated to be within 5 ppb. Six C_1 or C_3 signals were observed in Fig. 1. The assignments of the six signals were carried out according to changes in their heights with time. At the starting time of the proton-deuteron exchange reaction only the most downfield signal was observed. When the reaction proceeded with time, five upfield signals appeared in the spectra with gradually increasing heights. Then, the substituent effect of deuteron is an upfield shift. It was also assumed that in polydeuterated compounds deuterons exert their effects additively. If this is so, the six

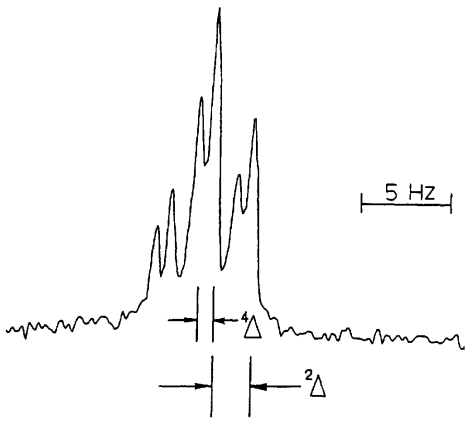

Fig. 1. ^{13}C NMR signals of C_1 or C_3 atoms of the products obtained from the proton-deuteron exchange reaction of 1,3-benzenediol in a 0.14 wt% NaOH-D_2O solution. The signals were averaged for 64 scans. The six signals are assigned as coming from (a) 2,4,6-trideuterated, (b) 2,4- or 2,6-dideuterated, (c) 2,4-, 4,6-, or 2,6-dideuterated, (d) 2- or 6-deuterated, (e) 4-deuterated, and (f) undeuterated 1,3-benzenediols from the right-hand to the left-hand side.

signals can be assigned straightforwardly. The six signals are divided into three groups with a splitting of $^2\Delta$. The three groups can be assigned as those in which the two adjacent sites of the C_1 of the sample have two H's, one H and one D, and two D's. Each of the three groups shows a further small splitting of $^4\Delta$. The six signals were then assigned to be signals coming from (a) 2,4,6-trideuterated, (b) 2,4- or 2,6-dideuterated, (c) 2,4-, 4,6-, or 2,6-dideuterated, (d) 2- or 4-deuterated, (e) 4-deuterated, and (f) undeuterated 1,3-benzenediols from the right-hand (upfield) to the left-hand side (downfield). The value of $^2\Delta$ can be evaluated from the difference of two signals, for example a and c, or c and e. Four-bond isotope effects were accidentally observed in the sample shown in Fig. 1. However, they were generally not determined because of their small magnitudes.

NMR spectra were measured with a Varian XL-200 FT-NMR spectrometer at 50.3 MHz and at about 22 °C. The concentration of the NMR sample solution was neat for the liquid sample and ca. 50 wt%, mostly in dioxane or any other solvent for the solid sample. The ^{13}C NMR spectra were measured by using a gated decoupling technique with no NOE pulse sequence. Data acquisition was carried out under the following conditions: a 45° flip angle of pulse, 24—128 transients, 32000 data points, a delay time of 40 s, and a spectral width of 2600—3500 Hz. Linear regression calculations of the experimental data were carried out on an NEC PC9801VX personal computer in our laboratory using a BASIC program. Details of acid- or base-catalyzed proton-deuteron exchange reactions will be published elsewhere.

Results and Discussion

Sixty-nine two-bond isotope effects of 28 phenols were determined. They are in a range from 32 to 112 ppb (Table 1). All of the observed two-bond isotope effects were toward the high filed. Therefore, the values given in Table 1 should be negative in the conventional manner. However, the signs are neglected in the table. As can be seen in Table 1, the values of $^2\Delta$ of the C_1's are always smaller than those of the C_5's. The values of the C_3's are intermediate between those of the C_1's and C_5's, except for several cases. The $^2\Delta$'s are then correlated with the ^{13}C chemical shifts, which are cited from several articles,[10-13] as shown in Fig. 2. $^2\Delta$ in ppb can be expressed as follows:

$$^2\Delta(\text{ppb}) = -2.06\delta_c(\text{ppm}) + 365. \quad (1)$$

The $^2\Delta$ are roughly related to the ^{13}C chemical shifts. Therefore, their correlation with kinds of substituents might be considered. Then, the contributions of the various substituents to the two-bond isotope shifts were determined by linear regression analyses using

$$^2\Delta = B_0 + n_i a + n_o b + n_m c, \quad (2)$$

where B_0 is the two-bond isotope shift of the unsubstituted benzene (cited as 111 ppb[7]). Three parameters (a, b, and c) are the contributions from ipso, ortho, and meta positioned substituents, respectively. n_i, n_o, or n_m is a weight factor for each substituent parameter. An example of a calculation

Table 1. Two-Bond Deuterium Isotope Effects on ^{13}C Chemical Shifts of Substituted Phenols in ppb[a]

No.	Substituent	Solvent	C-1	C-3	C-5
1	None	Neat	44	107	107
2	2-Me	Neat	39	105	112
3	3-Me	Neat	47	84	107
4	4-Me	Neat	43	96	96
5	2,3-Me_2	1,4-Dioxane	42	84	111
6	2,4-Me_2	Neat	43	—	105
7	2,5-Me_2	1,4-Dioxane	38	111	86
8	2,6-Me_2	1,4-Dioxane	—	111	111
9	3,4-Me_2	1,4-Dioxane	46	76	101
10	3,5-Me_2	1,4-Dioxane	45	86	86
11	2-OMe	Neat	39	105	109
12	3-OMe	Neat	48	46	107
13	4-OMe	Neat	51	92	92
14	2,3-$(OMe)_2$	Neat	47	42	110
15	2-Cl	Neat	38	99	108
16	3-Cl	Neat	46	88	106
17	4-Cl	Neat	45	91	91
18	2,3-Cl_2	1,4-Dioxane	40	83	106
19	3,4-Cl_2	1,4-Dioxane	48	76	b)
20	3,5-Cl_2	Neat	50	86	86
21	2-*t*-Bu	$CDCl_3$	32	108	108
22	3-*t*-Bu	Neat	40	66	100
23	4-*t*-Bu	Neat	44	101	101
24	3-OH	0.14 wt% NaOH-D_2O	47	47	107
25	2-NO_2	D_2O	b)	110	102
26	3-NO_2	CH_3OH	54	61	97
27	4-NO_2	CH_3OH	b)	98	98
28	3-NH_2	0.10wt% HCl-D_2O	43	63	104

a) Errors are estimated to be within 5 ppb. b) Not available.

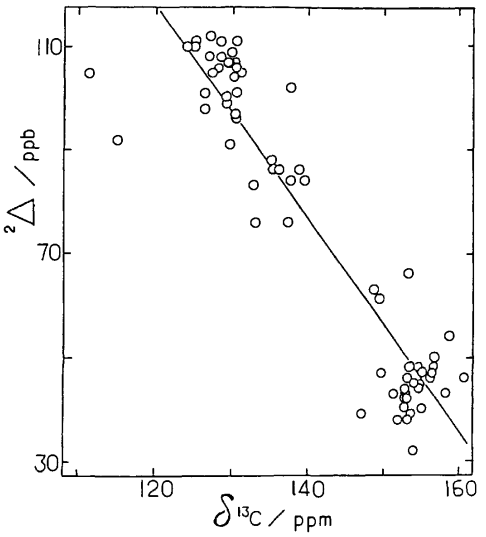

Fig. 2. Correlation between $^2\Delta$ (ordinate in ppb) and δ_c (abscissa in ppm) for substituted phenols with r=0.932 and the standard deviation of 10.4 ppb.

Table 2. Statistical Parameters for Eq. 2[a]

Parameter	Substituent						
	OH	OMe	*t*-Bu	Me	Cl	NO_2	NH_2
a	−64.8	−60.3	−41.5	−22.7 (−26.4)[b]	−19.7	−46.5	−44.5
b	−3.0[c]	−6.5	−6.8	−4.1 (−5.5)	−9.5	−3.5	d)
c	−3.5	2.8	−6.9	0.3 (0)	0.8	−1.4	−3.4

a) RMS error=4.4 ppb. Linear correlation coefficient between experimental and calculated data=0.991. Standard deviation=3.8 ppb. b) The value in parentheses is cited from Ref. 7. c) See text. d) Not available.

using Eq. 2 with three substituent parameters and three weight factors can be illustrated as follows. An example is 1,3-benzenediol (**24**). Its C_1 is affected by a directly bonded substituent and a meta-positioned one. Its C_5 is affected by two meta-positioned substituents. Therefore, its calculated $^2\Delta$ can be expressed as follows:

$$\text{1,3-position: } n_i = 1,\ n_o = 0, \text{ and } n_m = 1;$$
$$^2\Delta = B_0 + a + c;$$
$$\text{5-position : } n_i = 0,\ n_o = 0,\ n_m = 2;$$
$$^2\Delta = B_0 + 2c.$$

The experimentally observed values given in Table 1 are used to evaluate these parameters for each substituent by using linear regression analyses. The parameters obtained for seven kinds of substituents are given in Table 2. These parameters (*a*, *b*, and *c*) are called Substituent Isotope Shift (SIS). The observed two-bond isotope shifts can be calculated with Eq. 2 by using these SIS values with an RMS error of 4.4 ppb and a correlation coefficient of 0.991. So far, a similar analysis has been reported only for one substituent of the CH_3 group by Berger et al.[7] They explained that two-bond isotope shifts for CH_3 can be obtained by two parameters, *a* and *b*, which are consistent with our values given in Table 2. Although the value is rather small, one additional parameter of *c* is included in our analysis.

Correlation between SIS and SCS for ^{13}C NMR. The parameters of SIS decrease in magnitude from *a*, *b*, to *c*. All values of *a* and *b* are large and negative. However, *c* is rather small and either positive or negative. This means that $^2\Delta$ becomes small when any substituent is introduced in the aromatic ring. The magnitudes of *a* are in an order OH>OMe>NO_2>NH_2>*t*-Bu>Me>Cl. This order is parallel to that of the SCS values of the ^{13}C NMR. The SIS values of seven substituents are plotted in Fig. 3, correlated with the SCS values of ^{13}C NMR.[14] As can be seen in Fig. 3, the points are linearly correlated, except for those of the ortho-positions, which are shown by black-filled circles. The correlation coefficient gives a rise from 0.924 to 0.980 when the points of the ortho-positions

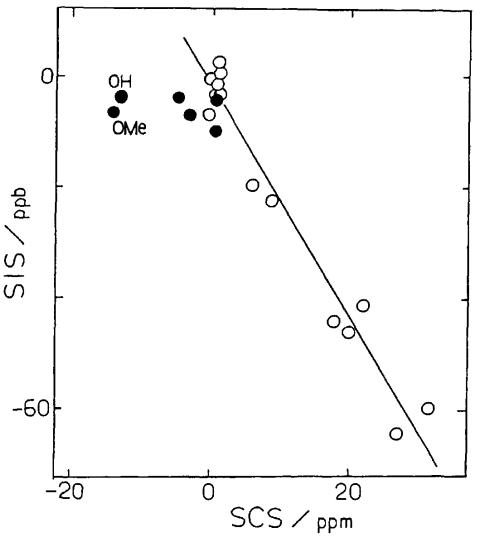

Fig. 3. Correlation between the SIS and SCS values of the ^{13}C NMR determined for substituted phenols. A correlated straight line is expreseed as SIS(ppb)= −2.11 SCS(ppm)−1.30 with r=0.980 and the standard deviation of 5.0 ppb when the black-filled points are excluded.

are excluded. Therefore, both the SIS's and the SCS's are linearly correlated with each other at the ipso and meta positions. This fact means that the factors controlling the SIS's are partly the same as those of the SCS's. Especially the deviation of the black-filled circles are downward from the correlated straight line. The magnitudes of their deviations are in the order OMe>NO_2>*t*-Bu>Cl>Me. Therefore, the deviation seems to be affected by a steric effect of bulky substituents, such as OMe, NO_2, and *t*-Bu groups. The ^{13}C chemical shifts sometime suffer a steric compression effect from bulky substituents.[15,16] The isotope effect, on the contrary, is said not to suffer such a contribution.[7] The deviations of the black-filled circles are thus explained by such steric effects which are effective for SCS but ineffective for SIS. This idea is supported by the fact that the observed deviation of the OMe, NO_2, or *t*-Bu group is given at the negative side of the SCS from a straight line, as can be seen in Fig. 3. Among those black-filled points, however, the

deviation of OMe is much larger than others. Therefore, it must be necessary to consider other effects. In order to clarify this point we made an examination in order to obtain the value of b for OH. The $^2\Delta$ of m-deuterophenol is 108 ppb.[17] From this value b equals to -3.0 ppb (plotted in Fig. 3). The deviation of OH is similar to that of OMe. Therefore, the origin of the deviation must be explained by other effects, such as the lone pair of the oxygen atom.

Presently, the origins of the isotope shifts are considered to be entirely or partly due to the vibration.[18] However, for deuteromethyl-substituted aromatic compounds two explanations have been presented, in which the hyperconjugational part is reversed in sign to the vibrational one.[2,3,7,19] But in cases where the deuterium atom is directly bonded to the aromatic ring, the hyperconjugational effect is not considered.[20] Furthermore, as shown in Figs. 2 and 3, and Eq. 1, the isotope shifts studied here have been correlated to the chemical shifts of the corresponding carbons. A similar discussion was also presented by Arrowsmith and Kresge.[21] These examples suggest the electron densities of the carbon atoms under study can become the origin of the isotope shifts.

Conclusion

Two-bond isotope shifts for the substituted phenols are represented additively by three parameters assigned to each substituent. This additivity can also be applied to polysubstituted benzenes. Further, the SIS values were correlated with the SCS values of the substituents of ^{13}C NMR. This would be a key for considering the origins of the isotope effect.

References

1) a) P. E. Hansen, *Ann. Repts. NMR Spectr.*, **15**, 105 (1983); b) D. A. Forsyth, "Isotopes in Organic Chemistry," ed. by E. Buncel and C. C. Lee, Elsevier, New York (1984), Vol. **6**, Chap. 1.

2) L. Ernst, H. Hopf, and D. Wullbrandt, *J. Am. Chem. Soc.*, **105**, 4469 (1983).

3) J. R. Wesener and H. Günther, *Tetrahedron Lett.*, **23**, 2845 (1982).

4) R. Aydin and H. Günther, *J. Am. Chem. Soc.*, **103**, 1301 (1981).

5) K. L. Servis and R. L. Domenick, *J. Am. Chem. Soc.*, **108**, 2211 (1986).

6) R. A. Bell, C. L. Chan, and B. G. Sayer, *J. Chem. Soc., Chem. Commun.*, **1972**, 67.

7) S. Berger and W. K. Diehl, *Magn. Reson. Chem.*, **24**, 1073 (1986).

8) A. Murry, III and D. L. Williams, "Organic Syntheses with Isotopes," Interscience Publishers, Inc., New York (1958), Part 1, p. 1652.

9) R. A. Newmark and J. R. Hill, *Org. Magn. Reson.*, **13**, 40 (1980).

10) D. A. Netzel, *Org. Magn. Reson.*, **11**, 58 (1978).

11) M. Ilczyzyn, Z. Lstsjka, and H. Ratajczak, *Org. Magn. Reson.*, **13**, 132 (1980).

12) W. B. Smith and T. W. Proulx, *Org. Magn. Reson.*, **8**, 205 (1976).

13) L. F. Johnson and W. C. Jankowski, "Carbon-13 NMR Spectra," John Wiley & Sons, New York (1972), p. 385.

14) D. A. Ewing, *Org. Magn. Reson.*, **12**, 499 (1979).

15) D. M. Grant and B. V. Cheney, *J. Am. Chem. Soc.*, **89**, 5315 (1967).

16) J. B. Grutzner, M. Jautelat, J. B. Dence, R. A. Smith, and J. D. Roberts, *J. Am. Chem. Soc.*, **92**, 7107 (1970).

17) m-Deuterophenol was prepared from m-chlorophenol by using a method described by M. Tashiro et al. (*J. Org. Chem.*, **43**, 196 (1978)).

18) A. Bernheim, *Progr. Nucl. Magn. Reson. Spectr.*, **3**, 63 (1967).

19) S. Berger, B. W. K. Diehl, and H. Künzer, *Chem. Ber.*, **120**, 1059 (1987).

20) S. Berger and H. Künzer, *Tetrahedron*, **39**, 1327 (1983).

21) C. H. Arrowsmith and A. J. Kresge, *J. Am. Chem. Soc.*, **108**, 7918 (1986).

Continuous Electrochemiluminescence of [Ru(2,2′-bipyridine)$_3$]$^{2+}$ in Solution

Ryuji IGARASHI, Yoshio NOSAKA,* Nobuyuki FUJII, and Hajime MIYAMA
Department of Chemistry, Nagaoka University of Technology,[1] Nagaoka 940-21
(Received September 28, 1988)

Electrochemiluminescence (ECL) of tris(2,2′-bipyridine)ruthenium(2+) ([Ru(bpy)$_3$]$^{2+}$) was observed in a propylene carbonate–dimethylacetamide–water mixed solvent by applying direct current (dc) voltage to a cell which consists of a sheet cathode of metals such as Al and Pt and a wire anode of Pt. The intensity of the dc ECL increased with the water concentration (up to 30 vol%) and the applied voltage. Besides water, oxygen was found to be necessary for observing the dc ECL. A plausible mechanism is the formation of [Ru(bpy)$_3$]$^{2+*}$ from the reaction of [Ru(bpy)$_3$]$^{+}$ and HO_2, those species are both produced at the cathode. This mechanism was supported by a separate experiment in which the chemiluminescence was observed by the reactions with a reducing agent.

The continuous electrochemiluminescence (ECL) of tris(2,2′-bipyridine)ruthenium(2+) ([Ru(bpy)$_3$]$^{2+}$) in acetonitrile solution with a small amount of water was observed recently by the authors.[2] Some unique characteristics of the dc-ECL observation were (i) a quick response to the direct current (dc) application, (ii) the restriction to Al for cathode materials when the applied voltage was 10 V, and (iii) a special arrangement for the electrodes in which the area of the anode was much smaller than that of the cathode. On the application of ac voltage to the same cell, these characteristics did not appear, although the ECL intensity was significantly large. Accordingly the reaction mechanism of the dc ECL should be different from the conventional ac ECL in which a diffusion process is involved. Although the emitting species was considered to be [Ru(bpy)$_3$]$^{2+*}$, its formation mechanism was not clarified in the previous study, where a two-electrode cell was used in connection with its application to ECL devices.[2] In the present study, however, a three-electrode cell was also used to explain the unique characteristics of the dc-ECL. For comparison with the previous study, the cathode potential in the two-electrode cell was measured against the concentration of the supporting electrolyte and by changing the cathode materials. A mechanism of the dc ECL will be proposed based on the influence of oxygen on the emission intensity and the observation of chemical luminescence by using a reducing agent.

Experimental

Materials. Tris(2,2′-bipyridine)ruthenium(2+) complex ([Ru(bpy)$_3$]$Cl_2 \cdot 6H_2O$), obtained from Aldrich Chemical Co., was purified by recrystallizing three times from distilled water followed by drying in vacuum. Propylene carbonate (PC, extra pure reagent) and *N*,*N*-dimethylacetamide (DMA, guaranteed reagent) obtained from Nakarai Chemicals, Ltd. were dried with molecular sieve followed by vacuum distillation. A mixture of PC, DMA, and H_2O was used as a solvent, unless otherwise stated. Tetrabutylammonium perchlorate (TBAP, polarographic grade of Nakarai Chemicals) was used without further purification. Aluminum sheet (0.08 mm in thickness) obtained from Tokai Kinzoku Co., Ltd., was used as received. A copper sheet (0.3-mm thick), a titanium sheet (0.05 mm thick), and a molybdenum sheet (0.1-mm thick) from the Japan Lamp Industrial Co., Ltd., and a Pt sheet (0.023-mm thick), from Itimura Metal Co., Ltd., were rinsed with a 1.2-M HCl solution (1 M=1 mol dm^{-3}) and subsequently with distilled water before use.

Method. The two-electrode cell consists of a metal sheet of 8-mm width and 2-cm effective height and a wire of Pt of 0.5-mm diameter and 1-cm effective length. The sheet was used as a working electrode (WE) while the wire was used as a counter electrode (CE). The three-electrode cell consists of an Al or a Pt sheet WE, a Pt wire CE, and an Ag/Ag$^+$ reference electrode (RE) which are placed in a H-shaped glass vessel having a sintered-glass filter separator. The WE and CE were the electrodes as used in the two-electrode cell, respectively. The ECL intensity was measured for a 0.2-mM [Ru(bpy)$_3$]$^{2+}$ solution under controlled polarization with a potentiostat (Toho Technical Research, Type 2090). The potential was usually supplied by a function generator (Leader, LFG-1300). The ECL light after passing through a grating monochromator (Ritsu, MC-25N) was detected by a photomultiplier (Hamamatsu Photonics, R928). The experimental setup for the two-electrode cell was similar to that in the previous report.[2]

Effective potentials of the metal sheet WE against the Ag/Ag$^+$ RE were measured by using the Pt wire CE, which were the same as for the two-electrode cell. Cyclic voltammograms were measured by using a square Pt WE (0.5 cm×0.5 cm), and a Pt coil CE, and the Ag/Ag$^+$ RE in the H-shaped vessel.

The measurement of chemiluminescence of [Ru(bpy)$_3$]$^{2+}$ was performed by adding 1 M HCl to the mixture of PC, DMA, and H_2O containing 1-mM [Ru(bpy)$_3$]$^{2+}$ and a piece of Mg ribbon.

Results

In our previous study on the dc ECL,[2] acetonitrile was used as a solvent. Since acetonitrile is a volatile and virulent substance, propylene carbonate (PC) was used as a solvent in the present study. In order to observe the dc ECL, a small amount of water had been required in the previous study. Since water is poorly soluble in the PC solution, DMA was added to the mixture to increasing the water solubility. DMA is

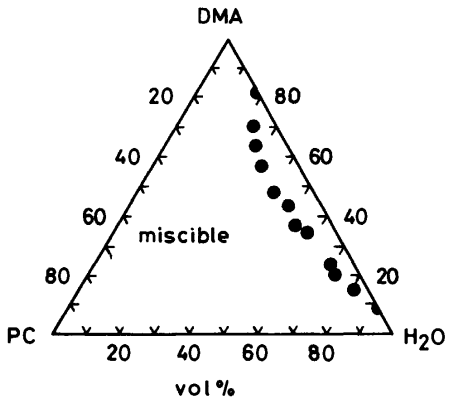

Fig. 1. Limits of miscibility in the ternary system of PC, DMA, and H_2O.

also an aprotic nonvolatile substance used commonly as a solvent. Figure 1 shows the limit of miscibility for the three-component system consisting of PC, DMA, and H_2O. On this basis a DMA concentration of 20 vol% was chosen for this study. The three compositions are completely miscible at this concentration.

The dc-ECL intensity was measured by changing the water concentration. When the water was absent from the solution no emission was observed. The intensity of the emission increased with the water concentration which became saturated at 30 vol%. Therefore, in the following experiments, the contents of the mixed solvent were fixed to be 50 vol% of PC, 30 vol% of H_2O, and 20 vol% of DMA. The dc ECL was observed without delay (less than 0.2 s) and continued for several hours similarly to the case of the acetonitrile-H_2O solution.[2] However, the emission intensity is higher and more stable than that observed in the previous study,[2] although no quantitative comparison was performed.

Redox potentials of $[Ru(bpy)_3]^{2+}$ in the mixture were examined to investigate the mechanism of the dc ECL. The cyclicvoltammetric behavior at the Pt electrode was measured for the PC-DMA-H_2O solution containing 1-mM $[Ru(bpy)_3]^{2+}$ and a supporting electrolyte of 0.1 M TBAP. The potential for each peak obtained from the voltammogram is given in Table 1. These electrode reactions are one-electron reversible processes, because the potential differences between the reduction and oxidation peaks, $E_{pa}-E_{pc}$, were approximately equal to 59 mV.[3] This observation indicates that the mixed solvent does not participate in the electrode reaction over the potential range. For the following discussion, note that $[Ru(bpy)_3]^{2+}$ was reduced to $[Ru(bpy)_3]^{+}$ at −1.52 V vs. Ag/Ag^+ in this solvent.

The emission intensity was measured under the controlled potential using the three-electrode cell. Figure 2 shows the relationship between the dc-ECL intensity

Table 1. Peak Potentials at Cathodic (E_{pc}) and Anodic (E_{pa}) Sweeps of the Cyclic Voltammogram for $Ru(bpy)_3Cl_2$ in PC-DMA-H_2O Mixed Solvent[a]

Oxidation state	I	II	III	IV
E_{pc}	0.96	−1.52	−1.70	−1.91
E_{pa}	1.02	−1.47	−1.64	−1.85

a) In V vs. Ag/Ag^+ reference electrode. Sweep rate; 200 mV s^{-1}.

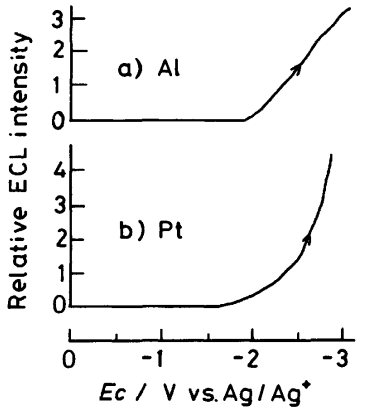

Fig. 2. ECL intensity-potential (E_c) curves at (a) Al and (b) Pt sheet cathodes in PC-DMA-H_2O solution containing 0.2-mM $[Ru(bpy)_3]^{2+}$ and 0.1-M TBAP.

and the electrode potential of the Al and Pt sheet cathodes in the PC-DMA-H_2O solution containing 0.2-mM $[Ru(bpy)_3]^{2+}$ and 0.1-M TBAP. For the Al electrode, emission was observed at −1.9 V vs. Ag/Ag^+ and the intensity increased with the potential. For the Pt sheet cathode, the dc ECL was observed above −1.6 V vs. Ag/Ag^+. This onset potential roughly agrees with the reduction potential for $[Ru(bpy)_3]^{2+}$ mentioned above.

In the experiments using the two-electrode cell with 10-V application, the dc ECL was not observed at the Pt cathode similarly to the case in the previous study. Therefore, the actual potential of the cathode in the two-electrode cell against RE was measured. Table 2 shows the observed potential for various metal sheets to Ag/Ag^+ RE when −10 V was applied against the Pt-wire electrode. The values of the redox potential of the metals and whether the dc-ECL was observed or not are also shown in the table. The dc ECL was observed at the Al and Ti sheet cathodes whose actual potentials were lower than the reduction potential of $[Ru(bpy)_3]^{2+}$. At the Mo, Cu, and Pt sheet cathodes the dc ECL was not observed because the potential was not high enough to reduce the ruthenium complex. The cathode potential appears to correlate with the standard electrode potential.

The actual potential at the Al and Pt sheet cathodes was measured by adding various amount of TBAP as shown in Fig. 3. For both electrodes, the negative

Table 2. Cathode Potential (E_c) and the Standard Electrode Potential (E_s) with dc-ECL[a]

Sheet cathode	E_c V vs. Ag/Ag$^+$	E_s V vs. NHE	dc-ECL emission
Aluminum	−2.00	−1.66[b]	○
Titanium	−1.74	−1.63[b]	○
Molybdenum	−1.31	−0.2[c]	×
Copper	−1.18	0.34[b]	×
Platinum	−0.93	1.12[b]	×

a) Applied voltage is 10 V without TBAP. E_c=cathode potential, E_s=standard electrode potential. b) "CRC Handbook of Chemistry and Physics" 66th ed, ed by R. C. Weast, CRC Press, D151-D155 (1985). c) "Electrochemical Data," D. Dobos, Elsevier Scientific Publishing Company, (1975), p. 255.

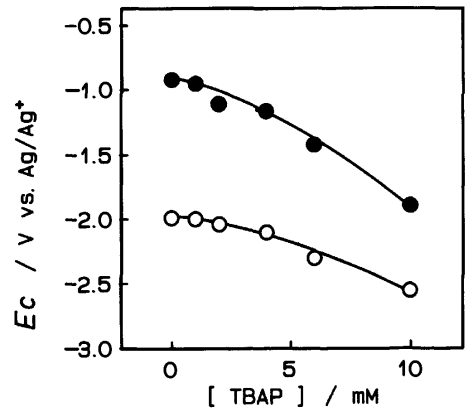

Fig. 3. Observed potentials (E_c) at the Pt (●) and Al (○) cathodes for various concentration of TBAP. At the cathode, −10 V was applied against the Pt wire. PC-DMA-H_2 solution containing 0.2-mM $[Ru(bpy)_3]^{2+}$ was used.

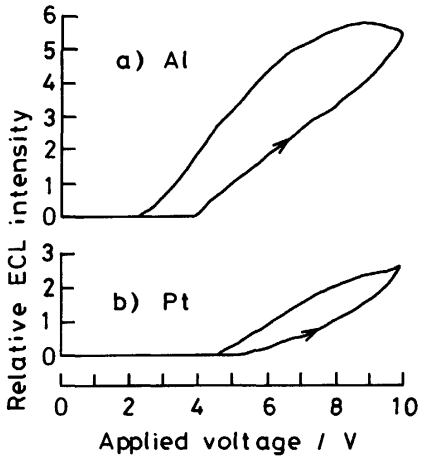

Fig. 4. ECL intensity-applied voltage curves at (a) Al and (b) Pt sheet cathodes in PC-DMA-H_2O solution containing 0.2-mM $[Ru(bpy)_3]^{2+}$ and 0.1-M TBAP.

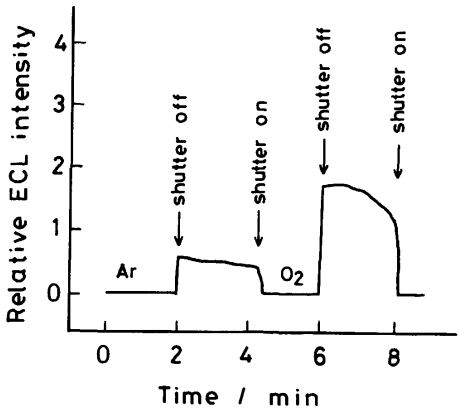

Fig. 5. Effect of oxygen on ECL intensity at Al sheet cathode in PC-DMA-H_2O solution containing 0.2-mM $[Ru(bpy)_3]^{2+}$. Both O_2 and Ar gases were purged alternatively when the shutter for the photomultiplier was on.

potential increased with the TBAP concentration. In the presence of 10-mM TBAP, the cathode potential at the Pt sheet became more negative than −1.52 V which is the reduction potential of $[Ru(bpy)_3]^{2+}$. Consequently, in the presence of TBAP, the dc ECL may be observed for the Pt cathode in the two-electrode cell at a lower applied voltage. Figure 4 shows the dc-ECL intensity in the presence of 0.1-M TBAP as a function of the applied voltage at the Al and Pt sheet cathodes. As mentioned previously, in the absence of a supporting electrolyte, no emission was observed at applied voltages ranging from 0 to 10 V at the Pt cathode. However, when TBAP was added in the solution, emission was observed at the Pt cathode as shown in Fig. 4. The thresholds of the applied voltage for the emission at the Al and Pt cathodes were 3.8 V and 5.5 V, respectively. The threshold voltage for emission at the Al sheet cathode was smaller than that at the Pt sheet cathode. This originates from the fact that the potential of the Al sheet cathode was more negative than the Pt cathode at the same applied voltage as shown in Fig. 3. Thus the influence of the cathode materials on the dc ECL in the two-electrode cell is explained by the cathode potential instead of the participation to the emission mechanism as a chemical reactant.

As mentioned above, H_2O is necessary for the dc-ECL. Besides H_2O, atmospheric oxygen is considered to contribute to the mechanism of the dc ECL. The dc ECL was next measured by alternating the conditions between those in the presence of oxygen by bubbling oxygen gas and in the absence of oxygen by bubbling argon gas through the solution. As shown in Fig. 5, the ECL intensity was weakened without oxygen and recovered on adding oxygen. These results suggest that oxygen participates in the emission mechanism of the dc ECL.

The emission occurs only at the cathode surface, indicating that some reduction process accounts for

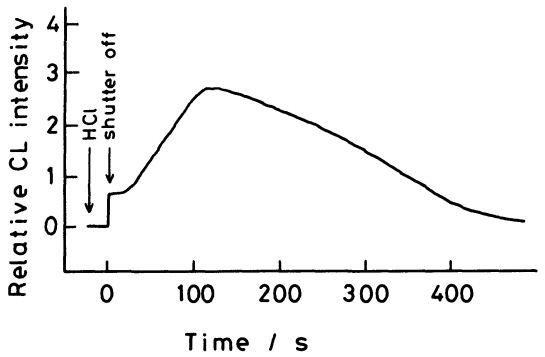

Fig. 6. Emission profile of chemiluminescence (CL) obtained by adding 1-M HCl to the 1-mM $[Ru(bpy)_3]^{2+}$ solution containing a piece of Mg ribbon.

the dc ECL. The chemiluminescence was next measured in order to confirm that the emission is caused by a reduction process. Figure 6 shows the chemiluminescence obtained by adding 1-M HCl to a 1-mM $[Ru(bpy)_3]^{2+}$ solution containing a piece of Mg ribbon. This result suggests that the mechanism of the dc ECL involves a process similar to the chemiluminescence.

Discussion

Although the separation between the anode and the cathode is as large as 8 mm, the dc ECL was observed without delay on the dc application. This phenomenon suggests that the electrochemical reaction proceeds through the short diffusion length at only one electrode. Bard et al. demonstrated that the ECL phenomenon occurred at only one electrode when a sacrificial reagent such as oxalate[4] and peroxodisulfate[5] was employed. In the case of peroxodisulfate, for example, a strong oxidant, $SO_4^{\cdot-}$, was produced by the reduction of $S_2O_8^{2-}$ at the cathode. Then $[Ru(bpy)_3]^{2+*}$ was formed by oxidizing $[Ru(bpy)_3]^{+}$ with $SO_4^{\cdot-}$.[5] In the present study, oxygen and water are essential to the appearance of the dc ECL. Therefore, O_2 and H_2O may be replaced to the peroxodisulfate in the ECL mechanism. For example, Reaction 1 may take place at the cathode.

$$O_2 + e^- \longrightarrow O_2^- \quad (1)$$

At the low pH the super oxide ion becomes the $HO_2^{\cdot}$ radical.

$$O_2^- + H^+ \rightleftharpoons HO_2^{\cdot} \quad pK\ 4.8^{6} \quad (2)$$

The reduction potential of Eq. 1 is −0.32 V vs. NHE.[7] The observation of the $HO_2^{\cdot}$ radical with a UV spectrophotometer failed because of the low estimated concentration and the overlapping of the solvent at the maximum of $HO_2^{\cdot}$ (225 nm).[8] However, the formation of $HO_2^{\cdot}$ by the reduction of water has been reported already.[8] Since the product $HO_2^{\cdot}$ radical is a strong oxidant, it may act in the same role as the $SO_4^{\cdot-}$ radical. Then, $[Ru(bpy)_3]^{2+*}$ was produced via electron transfer from $[Ru(bpy)_3]^{+}$ to $HO_2^{\cdot}$ as expressed by Eq. 3.

$$[Ru(bpy)_3]^{+} + HO_2^{\cdot} + H^+ \longrightarrow [Ru(bpy)_3]^{2+*} + H_2O_2 \quad (3)$$

Here, the redox potencials of $HO_2^{\cdot}+H^+/H_2O_2$ and $[Ru(bpy)_3]^{2+}$ in aqueous solution are +1.495 V[9] and −1.28 V[10,11] vs. NHE, respectively. The difference of the potentials, 1.495−(−1.28), is 2.775 V. This value is larger than the excitation energy for $[Ru(bpy)_3]^{2+}$ of 2.7 eV which corresponds to the absorption maximum of 455 nm. Therefore, $[Ru(bpy)_3]^{2+*}$ is probably produced by the Reaction 3.

At the anode the oxidation of $[Ru(bpy)_3]^{2+}$ and water may occur. One of the products is likely to be oxygen. This oxygen may be used for the reduction at the cathode. Thus the ECL continued for hours.

The contribution of $HO_2^{\cdot}$ in the dc-ECL mechanism was supported by the experiment with a reducing reagent. As shown in Fig. 6 the chemiluminescence was observed when a $[Ru(bpy)_3]^{2+}$ aqueous solution was reduced with the Mg metal in the presence of O_2. In this case the reaction scheme is considered as follows;

$$1/2Mg + [Ru(bpy)_3]^{2+} \longrightarrow 1/2Mg^{2+} + [Ru(bpy)_3]^{+} \quad (4)$$

$$1/2Mg + H^+ + O_2 \longrightarrow 1/2Mg^{2+} + HO_2^{\cdot} \quad (5)$$

Here, the two reactions are highly exothermic as calculated to be ΔG=−105.2 and −372.9 kJ mol^{-1} for Eqs. 4 and 5, respectively. The products of these reactions may produce $[Ru(bpy)_3]^{2+*}$ as shown by Eq. 3, followed by light emission.

The discussion next turns to the third feature of the dc ECL at which the area of the anode is smaller than that of the cathode. In the two-electrode cell, the applied voltage V is represented by

$$V = E_a(i) + (-E_c(i)) + Vr(I) \quad (6)$$

Here, $E_a(i)$ and $E_c(i)$ are the anode and cathode potentials with the current density i, and $Vr(I)$ is the ohmic drop associated with the solution resistance and the current I through the cell. When the area of the cathode is considerably larger than that of the anode, the current density of the cathode is very small and $E_c(i)$ is close to the standard electrode potential of the electrode substance. This explains the fact that the cathode potential correlates with the redox potential of the electrode materials as shown in Table 2. Further-

more, by adding TBAP to the solution, the resistance of the solution decreases and consequently $Vr(I)$ decreases. Thus the cathode potential increases with the TBAP concentration at a constant applied potential as shown in Fig. 3.

In the present study, the current through the cell is limited by the substance transport at a wire CE having a small surface area. Then, at the larger sheet WE the current density is low although the potential is high enough for oxygen and $[Ru(bpy)_3]^{2+}$ to be reduced. This situation may be necessary to produce both $[Ru(bpy)_3]^{+}$ and $HO_2^{\cdot}$ at the cathode. In order to prevent the further reduction of $HO_2^{\cdot}$ and $[Ru(bpy)_3]^{+}$, the species produced must quickly diffuse from the cathode surface to the solution. This may also be achieved by the small current density at the cathode.

Conclusion

The most plausible mechanism of the dc ECL in the two-electrode cell is the formation of $[Ru(bpy)_3]^{2+*}$ by the reaction between $[Ru(bpy)_3]^{+}$ and $HO_2^{\cdot}$ both of which are produced at the cathode. The potential of the sheet cathode in the two-electrode cell is affected by the standard potential of the electrode material and the concentration of the supporting electrolyte. This observation is used to reveal the emission mechanism and to solve the questions in the previous report.

We are grateful to Professor A. J. Bard for very useful discussions on the dc-ECL mechanism and to Dr. Masao Kaneko for valuable discussions. This work was supported by Nippon Seiki Co., Ltd.

References

1) Former name is the Technological University of Nagaoka.
2) R. Igarashi, Y. Nosaka, H. Miyama, M. Kaneko, and M. Yokoyama, *J. Electrochem. Soc.*, **135**, 2987 (1988).
3) N. E. Tokel and A. J. Bard, *J. Am. Chem. Soc.*, **94**, 2862 (1972).
4) I. Rubinstein and A. J. Bard, *J. Am. Chem. Soc.*, **103**, 512 (1981).
5) H. S. White and A. J. Bard, *J. Am. Chem. Soc.*, **104**, 6891 (1982).
6) D. Meisel and G. Gzapski, *J. Phys. Chem.*, **79**, 1503 (1975).
7) P. George, "Oxidases and Related Redox Systems," ed by T. E. King, H. S. Mason, and M. Morison, Wiley, New York (1965), p. 3.
8) J. Divisek and B. Kastening, *J. Electroanal. Chem.*, **65**, 603 (1975).
9) "CRC Handbook of Chemistry and Physics" 66th ed, ed by R. C. Weast (1985).
10) N. Sutin and C. Creutz, *Adv. Chem. Ser.*, **168**, 1 (1978).
11) F. Bolletta, M. Ciano, V. Balzani, and N. Serpone, *Inorg. Chim. Acta*, **62**, 207 (1982).

 © 1989 The Chemical Society of Japan Bull. Chem. Soc. Jpn., 62, 1410—1414 (1989) [Vol. 62, No. 5

Theoretical Investigation of the Interaction Potential of Helium Trimer

Akira ICHIHARA* and Reikichi ITOH
Department of Chemistry, Faculty of Science and Engineering, Waseda University,
3-4-1 Ohkubo Shinjuku-ku, Tokyo 160
(Received September 28, 1988)

Using the help of an ab initio calculation along with a configuration interaction treatment, the interaction potential of a He trimer has been calculated. The basis set superposition error in the He trimer system could be avoided using a reference calculation approximated by a simple formula.

There have been several reports in which the interaction potential between He atoms was calculated by the use of an ab initio MO method. It is known that the He dimer system has a repulsive ground state, with only a van der Waals minimum. We have recently calculated the interaction potential of the He dimer through the configuration interaction (CI) method.[1] For a weakly bonded system the basis set superposition error (BSSE)[2-7] in the He dimer energies could not be neglected and reference calculations had to be performed in order to correct this error. In this paper we will report on the results of CI calculations for the interaction potential of the He trimer. The CI calculations contain all single and double excitations from the SCF ground state (SD CI). A simple formula is proposed for estimating the BSSE for three-body interaction energies. The formulation was performed using a procedure described by Price and Stone.[5]

The Function Counterpoise Method for Three-Body Interactions. In principle the interaction energy (ΔE) of three closed-shell systems (atoms or molecules: A, B, and C) with energies E^A, E^B, and E^C can be written

$$\Delta E^{ABC} = E^{ABC} - E^A - E^B - E^C, \tag{1}$$

where E^{ABC} is the energy of supersystem ABC at some nuclear geometry. However, this expression takes no account of the BSSE. The BSSE arises from the incompleteness of the basis set, and each of the interactuing systems can make partial use of the basis sets centered on the other systems in order to improve its own property. It leads to a nonphysical energy lowering in the supersystem. Boys and Bernardi proposed the function counterpoise (CP) method for correcting the BSSE in two-body interaction energies.[2] This is often denoted as a "full" CP method.[2-7] A generalization of the full CP method to many-body interactions was attempted by Wells and Wilson.[8-10]

In the CP method, the interaction energy for a three-body system can be calculated using the difference between E^{ABC} and an appropriate reference energy, E_{ref};

$$\Delta E^{ABC} = E^{ABC} - E_{ref}. \tag{2}$$

The reference energy, E_{ref}, may be defined as

$$E_{ref} = E^{AG}{}_{BC} + E^{BG}{}_{CA} + E^{CG}{}_{AB}, \tag{3}$$

where $E^{iG}{}_{jk}$ represents the energy for system i with "ghost" orbitals of systems j and k. The term "ghost" represents a nucleus with a nuclear charge of zero and without any electrons. In practice, system i should be calculated with the full basis set of the supersystem. Wells and Wilson called this the "site-site" CP method.[8-10] This method is valid only for both E^{ABC} and E_{ref} calculations which are size consistent.

In the present investigation, however, calculations of the interaction potential were performed using the SD CI treatment; Eq. 3 was not directly used. We therefore propose an approximate formula for calculating the true reference energy. This approach is used to describe the correct reference state by the product $\psi^A\psi^B\psi^C$ of correlated wavefunctions, using ghost orbitals, for three closed shell systems. Then, since each wavefunction (ψ^A, ψ^B, and ψ^C) includes all single and double excitations from the SCF ground state, for size consistency, an elimination of the effect of triple and higher excitations is performed. The formulation is carried out using a procedure proposed by Price and Stone for two-body interactions[5] and the full CP technique.

Development of the Formula. The normalised wavefunction for a closed shell system A, including all single and double excitations, may be written

$$\psi^A = a_0\psi_0^A + a_1\psi_1^A + a_2\psi_2^A, \tag{4}$$

with

$$a_0^2 + a_1^2 + a_2^2 = 1, \tag{5}$$

where ψ_0^A is the normalised SCF function, ψ_i^A is the part of the normalised wavefunctions containing i-fold excitations, and the a_i's the corresponding coefficients.

The wavefunctions for closed shell systems B and C can be written similarly; these three wavefunctions are orthogonal to each other.

Then, the product wavefunction for the three separated systems with ghost orbitals is

$$\begin{aligned}\psi^A\psi^B\psi^C &= (a_0\psi_0^A + a_1\psi_1^A + a_2\psi_2^A)(b_0\psi_0^B + b_1\psi_1^B + b_2\psi_2^B)\\ &\quad (c_0\psi_0^C + c_1\psi_1^C + c_2\psi_2^C)\\ &= a_0b_0c_0\psi_0^A\psi_0^B\psi_0^C + a_1b_0c_0\psi_1^A\psi_0^B\psi_0^C\\ &\quad + \text{--------} + a_2b_2c_2\psi_2^A\psi_2^B\psi_2^C.\end{aligned} \tag{6}$$

In order to obtain our estimated wavefunction for the correct reference calculation, we discard the terms which represent the triple and higher excitations, and obtain

$$\begin{aligned}\psi^{ABC} = Z^{-1}(&a_0b_0c_0\psi_0^A\psi_0^B\psi_0^C + a_1b_0c_0\psi_1^A\psi_0^B\psi_0^C + a_0b_1c_0\psi_0^A\psi_1^B\psi_0^C \\ &+ a_0b_0c_1\psi_0^A\psi_0^B\psi_1^C + a_1b_1c_0\psi_1^A\psi_1^B\psi_0^C + a_1b_0c_1\psi_1^A\psi_0^B\psi_1^C \\ &+ a_0b_1c_1\psi_0^A\psi_1^B\psi_1^C + a_2b_0c_0\psi_2^A\psi_0^B\psi_0^C + a_0b_2c_0\psi_0^A\psi_2^B\psi_0^C \\ &+ a_0b_0c_2\psi_0^A\psi_0^B\psi_2^C),\end{aligned} \tag{7}$$

where z^{-1} is the renormalisation factor.

This product is a CI expansion which includes all single and double excitations from the SCF ground state $\psi_0^A\psi_0^B\psi_0^C$, though the coefficients in Eq. 7 are not variationally optimised. However, as has been noted in the previous calculations for the He-He by Dacre[4] and for the H_2-H_2 by Price and Stone,[5] the product wavefunction with the coefficients of separated systems might be a reasonable approximation to the variational function. We therefore expect that ψ^{ABC} will be a reliable estimation for the variational function.

Normalising Eq. 7, we obtain

$$\begin{aligned}Z^2 = {} & a_0^2b_0^2c_0^2 + a_1^2b_0^2c_0^2 + a_0^2b_1^2c_0^2 + a_0^2b_0^2c_1^2 + a_1^2b_1^2c_0^2 \\ & + a_1^2b_0^2c_1^2 + a_0^2b_1^2c_1^2 + a_2^2b_0^2c_0^2 + a_0^2b_2^2c_0^2 + a_0^2b_0^2c_2^2.\end{aligned} \tag{8}$$

Using the fact that terms like $a_1^2b_1^2c_0^2$ are small (because of Brillouin's theorem), Eq. 8 can be approximated as

$$Z^2 = a_0^2b_0^2 + b_0^2c_0^2 + c_0^2a_0^2 - 2a_0^2b_0^2c_0^2. \tag{9}$$

Rearranging Eqs. 6 and 7, we obtain

$$\psi^A\psi^B\psi^C = Z\psi^{ABC} + (\text{triple and higher excitation terms}), \tag{10}$$

which is used to obtain the energy relationship

$$\begin{aligned}&\langle\psi^A\psi^B\psi^C|H_A + H_B + H_C|\psi^A\psi^B\psi^C\rangle \\ &= Z^2\langle\psi^{ABC}|H_A + H_B + H_C|\psi^{ABC}\rangle \\ &+ a_0^2(b_1^2c_2^2 + b_2^2c_1^2 + b_2^2c_2^2)\langle\psi_0^A|H_A|\psi_0^A\rangle \\ &+ a_1^2(b_1^2c_1^2 + b_0^2c_2^2 + b_2^2c_0^2 + b_1^2c_2^2 \\ &+ b_2^2c_1^2 + b_2^2c_2^2)\langle\psi_1^A|H_A|\psi_1^A\rangle \\ &+ a_2^2(b_0^2c_1^2 + b_1^2c_0^2 + b_1^2c_1^2 + b_0^2c_2^2 + b_2^2c_0^2 \\ &+ b_1^2c_2^2 + b_2^2c_1^2 + b_2^2c_2^2)\langle\psi_2^A|H_A|\psi_2^A\rangle \\ &+ 2a_2a_0(b_0^2c_1^2 + b_1^2c_0^2 + b_1^2c_1^2 + b_0^2c_2^2 + b_2^2c_0^2 \\ &+ b_1^2c_2^2 + b_2^2c_1^2 + b_2^2c_2^2)\langle\psi_2^A|H_A|\psi_0^A\rangle \\ &+ 2a_2a_1(b_0^2c_1^2 + b_1^2c_0^2 + b_1^2c_1^2 + b_0^2c_2^2 + b_2^2c_0^2 \\ &+ b_1^2c_2^2 + b_2^2c_1^2 + b_2^2c_2^2)\langle\psi_2^A|H_A|\psi_1^A\rangle \\ &+ b_0^2(c_1^2a_2^2 + c_2^2a_1^2 + c_2^2a_2^2)\langle\psi_0^B|H_B|\psi_0^B\rangle \\ &+ b_1^2(c_1^2a_1^2 + c_0^2a_2^2 + c_2^2a_0^2 + c_1^2a_2^2 \\ &+ c_2^2a_1^2 + c_2^2a_2^2)\langle\psi_1^B|H_B|\psi_1^B\rangle \\ &+ b_2^2(c_0^2a_1^2 + c_1^2a_0^2 + c_1^2a_1^2 + c_0^2a_2^2 + c_2^2a_0^2 \\ &+ c_1^2a_2^2 + c_2^2a_1^2 + c_2^2a_2^2)\langle\psi_2^B|H_B|\psi_2^B\rangle \\ &+ 2b_2b_0(c_0^2a_1^2 + c_1^2a_0^2 + c_1^2a_1^2 + c_0^2a_2^2 + c_2^2a_0^2 \\ &+ c_1^2a_2^2 + c_2^2a_1^2 + c_2^2a_2^2)\langle\psi_2^B|H_B|\psi_0^B\rangle \\ &+ 2b_2b_1(c_0^2a_1^2 + c_1^2a_0^2 + c_1^2a_1^2 + c_0^2a_2^2 + c_2^2a_0^2 \\ &+ c_1^2a_2^2 + c_2^2a_1^2 + c_2^2a_2^2)\langle\psi_2^B|H_B|\psi_1^B\rangle \\ &+ c_0^2(a_1^2b_2^2 + a_2^2b_1^2 + a_2^2b_2^2)\langle\psi_0^C|H_C|\psi_0^C\rangle \\ &+ c_1^2(a_1^2b_1^2 + a_0^2b_2^2 + a_2^2b_0^2 + a_1^2b_2^2 \\ &+ a_2^2b_1^2 + a_2^2b_2^2)\langle\psi_1^C|H_C|\psi_1^C\rangle \\ &+ c_2^2(a_0^2b_1^2 + a_1^2b_0^2 + a_1^2b_1^2 + a_0^2b_2^2 + a_2^2b_0^2 \\ &+ a_1^2b_2^2 + a_2^2b_1^2 + a_2^2b_2^2)\langle\psi_2^C|H_C|\psi_2^C\rangle \\ &+ 2c_2c_0(a_0^2b_1^2 + a_1^2b_0^2 + a_1^2b_1^2 + a_0^2b_2^2 + a_2^2b_0^2 \\ &+ a_1^2b_2^2 + a_2^2b_1^2 + a_2^2b_2^2)\langle\psi_2^C|H_C|\psi_0^C\rangle \\ &+ 2c_2c_1(a_0^2b_1^2 + a_1^2b_0^2 + a_1^2b_1^2 + a_0^2b_2^2 + a_2^2b_0^2 \\ &+ a_1^2b_2^2 + a_2^2b_1^2 + a_2^2b_2^2)\langle\psi_2^C|H_C|\psi_1^C\rangle\end{aligned} \tag{11}$$

where H_i is the Hamiltonian for system i.

On the other hand, the SCF energy (E_{SCF}) and the total SCF CI energy (E_T) of the individual system A can be written as

$$E_{SCF}^A = \langle\psi_0^A|H_A|\psi_0^A\rangle, \tag{12}$$

$$\begin{aligned}E_T^A = {} & \langle\psi^A|H_A|\psi^A\rangle = a_0^2E_{SCF}^A \\ & + 2a_2a_0\langle\psi_2^A|H_A|\psi_0^A\rangle + a_1^2\langle\psi_1^A|H_A|\psi_1^A\rangle \\ & + 2a_2a_1\langle\psi_2^A|H_A|\psi_1^A\rangle + a_2^2\langle\psi_2^A|H_A|\psi_2^A\rangle,\end{aligned} \tag{13}$$

and similarly for systems B and C.

Then, taking into account the relationships

$$\begin{aligned}&a_0^2b_1^2 + a_1^2b_0^2 + a_0^2b_2^2 + a_2^2b_0^2 \\ &\quad = a_0^2(1 - b_0^2) + b_0^2(1 - a_0^2)\end{aligned} \tag{14}$$

and

$$a_1^2b_1^2 + a_1^2b_2^2 + a_2^2b_1^2 + a_2^2b_2^2 = (1 - a_0^2)(1 - b_0^2), \tag{15}$$

and ignoring terms like $a_1^2b_1^2c_0^2\langle\psi_1^A|H_A|\psi_1^A\rangle$, the reference energy can be approximated as

$$\begin{aligned}E_{ref} = {} & \langle\psi^{ABC}|H_A + H_B + H_C|\psi^{ABC}\rangle \\ = {} & [\{b_0^2c_0^2E_T^A + a_0^2(b_0^2 + c_0^2 - 2b_0^2c_0^2)E_{SCF}^A\} \\ & + \{c_0^2a_0^2E_T^B + b_0^2(c_0^2 + a_0^2 - 2c_0^2a_0^2)E_{SCF}^B\} \\ & + \{a_0^2b_0^2E_T^C + c_0^2(a_0^2 + b_0^2 - 2a_0^2b_0^2)E_{SCF}^C\}] \\ & \times (a_0^2b_0^2 + b_0^2c_0^2 + c_0^2a_0^2 - 2a_0^2b_0^2c_0^2)^{-1}.\end{aligned} \tag{16}$$

The error made in this approximation depends on the values of a_1, b_1, and c_1, as well as a_2, b_2, and c_2. Moreover, changes in these coefficients depend only on the position of the ghost orbitals. As noted by Dacre[4] and by Price and Stone,[5] however, these coefficients vary slightly between different relative positions of the interacting systems. Therefore, we also expect the

error in Eq. 16 to be nearly constant.

On the other hand, if three systems are to be infinitely separated, both the interaction energy and the BSSE must be zero. In this case the reference energy becomes equal to the total energy of super-system (E^{ABC}). Thus, we can estimate the error in Eq. 16 as a constant ε. A final formula is given by adding the constant ε:

$$E_{ref} = [\{b_0^2c_0^2E_T^A + a_0^2(b_0^2 + c_0^2 - 2b_0^2c_0^2)E_{SCF}^A\} + \{c_0^2a_0^2E_T^B + b_0^2(c_0^2 + a_0^2 - 2c_0^2a_0^2)E_{SCF}^B\} + \{a_0^2b_0^2E_T^C + c_0^2(a_0^2 + b_0^2 - 2a_0^2b_0^2)E_{SCF}^C\}] \times (a_0^2b_0^2 + b_0^2c_0^2 + c_0^2a_0^2 - 2a_0^2b_0^2c_0^2)^{-1} + \varepsilon. \quad (17)$$

The reference energy can be calculated using the SCF, total (SD CI) energies, and the corresponding SCF ground state coefficients of separated systems with the ghost orbitals.

For reference, let E_{SCF}^C and E_T^C be zero and c_0 one. We then obtain E_{ref} for two-body interactions:

$$E_{ref} = [b_0^2E_T^A + a_0^2E_T^B + a_0^2(1 - b_0^2)E_{SCF}^A + b_0^2(1 - a_0^2)E_{SCF}^B] \times (a_0^2 + b_0^2 - a_0^2b_0^2)^{-1} + \varepsilon, \quad (18)$$

which is equivalent to the formula proposed by Price and Stone.[5]

Results and Discussion

In all ab initio calculations, a Gaussian-type basis set [4slpld][1] for the He atom was employed. This [4slpld] set could give an improved description for the interaction potential of the He dimer by the use of the SD CI treatment and the CP method of Price and Stone.[1]

The MO calculations were performed by using the Gaussian 82 program provided by J.A. Pople et al. and the graphical unitary group approach (GUGA) program of our group.

Tables 1 and 2 indicate the interaction potentials ($E_{int}^{He_3}$) of the He trimer for two different spatial configurations: (i) an equilateral triangle and (ii) a linear configuration. The BSSE was estimated by $E_{ref}(R) - E_{SD\,CI}^{He_3}(\infty)$. R in Tables 1 and 2 designates the internuclear distance between nearest-neighbour He atoms. For a triangular configuration, Eq. 17 can be simplified to

$$E_{ref} = 3[E_T + 2(1 - a_0^2)E_{SCF}]/(3 - 2a_0^2) + \varepsilon, \quad (19)$$

where E_{SCF}, E_T, and a_0 represent the SCF, total (SD CI) energy, and the SCF ground state coefficient of the He atom with ghost orbitals. For a linear configuration, Eq. 17 can also be simplified to

$$E_{ref} = [b_0^2E_T^A + 2a_0^2E_T^B + 2a_0^2(1 - b_0^2)E_{SCF}^A + 2(a_0^2 + b_0^2 - 2a_0^2b_0^2)E_{SCF}^B]/(2a_0^2 + b_0^2 - 2a_0^2b_0^2) + \varepsilon, \quad (20)$$

where suffix A represents a He atom fixed at the

Table 1. The He Trimer Interaction Potential ($E_{int}^{He_3}$) for the Triangular Configuration

R/Bohr[a]	E^{He_3}/a.u.[b]		E_{ref}		$E_{int}^{He_3}$/K	$E_{int}^{He_3}$[e]/K
	SCF	correlation	E_{ref}[c]/a.u.	$E_{ref}(R) - E^{He_3}(\infty)$/K[d]		
5.0	−8.5846669	−0.0608697	−8.6455975	−1149.0	19.2	5.5
5.3	−8.5848581	−0.0600871	−8.6448892	−925.4	−17.7	−7.0
5.6	−8.5849514	−0.0594304	−8.6442898	−736.1	−29.0	−10.6
6.0	−8.5850058	−0.0587151	−8.6436302	−527.8	−28.7	−10.1
7.0	−8.5850359	−0.0575822	−8.6425718	−193.6	−14.6	−5.1
8.0	−8.5850384	−0.0571179	−8.6421364	−56.1	−6.3	−2.2
10.0	−8.5850386	−0.0569353	−8.6419697	−3.4	−1.3	−0.4
15.0	−8.5850386	−0.0569202	−8.6419588	0.0	0.0	0.0

a) R is the internuclear distance between He atoms. 1 Bohr=0.529177×10^{-10} m. b) 1 a.u.=4.359814×10^{-18} J. c) ε in E_{ref} is −3.43 K. d) 1 K=1.380662×10^{-23} J. e) See Ref. 1.

Table 2. The He Trimer Interaction Potential ($E_{int}^{He_3}$) for the Linear Configuration

R/Bohr[a]	E^{He_3}/a.u.[b]		E_{ref}		$E_{int}^{He_3}$/K
	SCF	correlation	E_{ref}[c]/a.u.	$E_{ref}(R) - E^{He_3}(\infty)$/K[d]	
5.0	−8.5847862	−0.0600077	−8.6448236	−904.7	9.4
5.3	−8.5849166	−0.0593530	−8.6442227	−714.9	−14.8
5.6	−8.5849799	−0.0588114	−8.6437230	−557.1	−21.6
6.0	−8.5850166	−0.0582370	−8.6431889	−388.5	−20.4
7.0	−8.5850368	−0.0573815	−8.6423863	−135.0	−10.1
8.0	−8.5850384	−0.0570546	−8.6420794	−38.1	−4.3
10.0	−8.5850386	−0.0569302	−8.6419661	−2.3	−0.9
15.0	−8.5850386	−0.0569201	−8.6419587	0.0	0.0

a) R is the internuclear distance between nearest-neighbor He atoms. 1 Bohr=0.529177×10^{-10} m. b) 1 a.u.= 4.359814×10^{-18} J. c) ε in E_{ref} is −3.40 K. d) 1 K=1.380662×10^{-23} J.

midpoint of the linear system, and a_0 is the corresponding SCF ground state coefficient. Similarly, suffix B represents the He atom at each side and b_0 the corresponding coefficient.

It can be seen from Tables 1 and 2 that the SCF energy of the He trimer system contributes to the repulsion between He atoms and that the correlation contributes to the attraction. A He dimer interaction potential ($E_{\text{int}}^{\text{He}_2}$) is also indicated in Table 1. In the dimer calculation the same [4slpld] basis set was employed and the BSSE was avoided using the reference calculation of Price and Stone. For the triangular configuration, the interaction energies were found to be about three-times larger than those of dimer calculations. On the other hand, the interaction energies in the linear configuration were almost twice the corresponding dimer energies. This difference is due to the fact that there are only two He-He nearest-neighbor interactions in the linear configuration, as opposed to three in the triangular configuration. It is appearant that the interaction potentials of the He trimer can be mainly described by the sum of two-body interactions.

Then, in order to investigate the accuracy of the interaction potentials, we calculated the three-body components of these potentials. The Three-body component could be calculated using $E_{\text{int}}^{\text{He}_3}(R)-3E_{\text{int}}^{\text{He}_2}(R)$ for the triangular configuration, and $E_{\text{int}}^{\text{He}_3}(R)-2E_{\text{int}}^{\text{He}_2}(R)-E_{\text{int}}^{\text{He}_2}(2R)$ for the linear configuration. The results are indicated in Table 3.

As can be seen from Table 3, the three-body component in the triangular configuration is positive for the whole range of calculated R. A many-body perturbation calculation of Wells and Wilson indicates a three-body component of -0.43 μa.u. (-0.14 K) at R=5.6 Bohr.[9] In their calculation, an even-tempered Gaussian basis set [8s4p2d1f] was employed and the site-site CP method was applied. Our calculated value (2.7 K at R=5.6 Bohr) is significantly larger than the many-body perturbation calculation and of opposite sign. This discrepancy is considered to be mainly due to our small [4slpld] basis set used in the interaction calculation. In fact, this [4slpld] set was optimised just to describe the interaction of the He dimer system. Therefore, the contribution of the three-body component was not included sufficiently in the trimer calculations. Thus, the $E_{\text{SD CI}}^{\text{He}_3}$ was smaller than expected.

On the other hand, the three-body component of the interaction potential for the linear configuration is much less than that for the triangular configuration. For the linear configuration, Wells and Wilson obtained a value of 0.00 μa.u. (0.0 K) at R=5.6 Bohr.[9] Since two He atoms of both sides are far separated, the three-body effect is expected to be quite small. Then, the defect of the basis set may become trivial. From Table 3 we assume that the error in the interaction potential is less than ±0.1 K; the three-body component was estimated to be -0.1—-0.3 K at R=5.6 Bohr. This result is comparable with the calculation of Wells and Wilson.

Finally, we discuss the error made in the reference calculation. It may be pointed out that the error appears in Eq. 17 in two ways. First, we consider that the error made in the approximation is almost constant and substituted it for ε, though the error is not exactly constant. Secondly, Eq. 17 overestimates the BSSE in the trimer system.[6,7] However, a serious error in the reference calculaton is not expected from the interaction calculation of the linear system. Thus, the error in Eq. 17 can be considered to be small.

Conclusion

It has been shown that a reliable interaction potential of the He trimer for the linear configuration can be obtained by the use of the SD CI treatment and a reference calculation approximated by a simple formula. This result indicates that our reference calculation for deriving the interaction potential of the three-body system from the SD CI calculation can be used in general. On the other hand, the interaction potential for the triangular configuration is less reliable compared with the linear configuration. It seems that the difference between these potentials is mainly due to the defect of the basis set employed here.

Table 3. The Three-Body Component of the Interaction Potentials

R/Bohr[a]	Equilateral triangle	Linear
	$E_{\text{int}}^{\text{He}_3}(R)-3E_{\text{int}}^{\text{He}_2}(R)$/K[b]	$E_{\text{int}}^{\text{He}_3}(R)-2E_{\text{int}}^{\text{He}_2}(R)-E_{\text{int}}^{\text{He}_2}(2R)$/K
5.0	2.8	−2.0
5.3	3.2	−0.6
5.6	2.7	−0.2
6.0	1.7	−0.1
7.0	0.6	0.1
8.0	0.2	0.0
10.0	0.0	0.0

a) R is the internuclear distance between nearest-neighbor He atoms. 1 Bohr=0.529177×10^{-10} m. b) 1 K=1.380662×10^{-23} J.

We would like to thank Kazuhide Mori for his interest and encouragement. We also would like to thank Kohtoku Sasagane for making his program code avaiable to us. The calculations presented here were performed on the HITAC M680H system of the Computer Center of the Institute for Molecular Science (IMS).

References

1) A. Ichihara, K. Sasagane, T. Izaki, T. Miyazaki, and R. Itoh, *Bull. Chem. Soc. Jpn.*, **61**, 1014 (1988).
2) S. F. Boys and F. Bernardi, *Mol. Phys.*, **19**, 553 (1970).
3) N. S. Ostlund and D.L. Merrifield, *Chem. Phys. Lett.*, **39**, 612 (1976).
4) P. D. Dacre, *Mol. Phys.*, **37**, 1529 (1979).
5) S. L. Price and A.J. Stone, *Chem. Phys. Lett.*, **65**, 127 (1979).
6) J. R. Collins and G. A. Gallup, *Chem. Phys. Lett.*, **123**, 56 (1986).
7) J. H. van Lenthe, J. G. C. M. van Duijneveldt-van de Rijdt, and F. B. van Duijneveldt, "Weakly Bonded Systems," in "Advances in Chemical Physics Volume LXIX, Ab Initio Methods in Quantum Chemistry, Part II," ed by K. P. Lawley, John Wiley and Sons, Chichester (1987), pp. 521—566.
8) B. H. Wells and S. Wilson, *Chem. Phys. Lett.*, **101**, 429 (1983).
9) B. H. Wells and S. Wilson, *Mol. Phys.*, **55**, 199 (1985).
10) B. H. Wells and S. Wilson, *Mol. Phys.*, **57**, 421 (1986).

 © 1989 The Chemical Society of Japan Bull. Chem. Soc. Jpn., 62, 1415—1420 (1989)

Detection of Photoinduced Intramolecular Electron Transfer in 4-(1-Pyrenyl)butyl 9-Anthracenecarboxylate by Transient Absorption and Resonance CARS Spectra

Toshio KAMISUKI, Naotoshi AKAMATSU, Yukio ADACHI, Chiaki HIROSE,*
Noritaka YAMAMOTO,† Keiichi TAKUMA,† and Michiko IWAMURA†
Research Laboratory of Resources Utilization, Tokyo Institute of Technology,
Nagatsuta, Midori-ku, Yokohama 227
†Department of Chemistry, Faculty of Science, Toho University,
2-2-1 Miyama, Funabashi, Chiba 274
(Received October 19, 1988)

Transient absorption and resonance CARS spectra of title molecule have been observed in acetonitrile solution to show the presence of cationic pyrenyl group and anionic 9-anthryl group (or 9-anthracenecarbonyloxy group). The 337 nm UV pulse was used for the excitation. The result was combined with the linear dependence of the signals on the intensity of UV pulse to prove that the ionic radicals were produced by the intramolecular electron transfer from the locally excited pyrenyl group to the 9-anthryl group (or 9-anthracenecarbonyloxy group).

As reviewed by De Schryver et al.[1] the intramolecular exciplex formation on electron transfer, which occurs in molecules having two chromophores separated by unconjugated spacer group, have been investigated with such interests as to study the kinetics and mechanisms of intermolecular interactions under the control of separation and mutual orientation of interacting moieties,[2-6] to design and control photochemical reactions,[7,8] or to probe the structure of macromolecules.[9,10] Molecules consisting of identical halves with arylic chromophores such as 1,2-di(9- and 1-anthryl)ethane[11] or 1,3-di(1-pyrenyl)propane[4] and those in which arylic rings and *N,N*-dimethylamino group, functioning as electron acceptor and donor, respectively, are separated by alkyl chains,[2,5] have been studied extensively. The use of alkyl chains as spacer group sometimes poses problem in defining the separation and orientation of the two chromophore groups bacause of low barrier of internal rotation around the carbon–carbon single bonds of alkyl chain, and the investigation of cyclophanes[12,13] or bridged molecules[3] were made to avert this problem by rigidly fixing the chromophores. Vanderauwera et al. carried out an experiment[2] in which alkyl ester groups with various chain length were used to separate dimethylamino group and 9-anthryl group. Aromatic esters are characterized by the C–O single bond where the alkyl group and carbonyl oxygen are in cis conformation and the carbonyl, *O*-alkyl bond, and aryl rings are coplanar. Combining this with the flexibility of alkyl chain, Vanderauwera et al. adjusted the separation between the chromophores by the length of alkyl chain in their investigation of the kinetics of intramolecular exciplex formation and electron transfer in the series of ω-(dimethylamino)alkyl esters of 2-anthracenecarboxylic acid.

Recently, however, the present authors (M. I. and K. T.) have unveiled several unexpected features in the photochemical behavior of 1-pyrenylmethyl 9-anthracenecarboxylate;[4] broad emission band was observed for the solution (10^{-5} M; 1 M=1 mol dm^{-3}) in polar solvent (acetonitrile) when either the pyrenyl (at 313 nm) or the anthracene (at 365 nm) moieties were excited by UV pulse, the intensity of the excitation with respect to that of fluorescence by locally excited species increased monotonically from 200 K to 293 K, and the broad emission of the solution in nonpolar isooctane was asymmetric and double-peaked.

In this paper we describe about the combined use of transient resonant CARS and transient absorption spectroscopy to the characterization of one-photonically produced ionic radical group.

It should be mentioned that the analysis of fluorescence and exciplex emission spectra has been the principal tool for the investigation of the intramolecular exciplex formation and electron transfer, and even in those papers that reported on the transient absorption spectrum of ionic species the possibility that the ionic species can also be produced from the two-photon processes was overlooked, thus the experimental verification of the one-photonical production of ionic species has been lacking.

Transient absorption and the transient resonance Raman spectra have been used for the study of photoinduced species. The resonance Raman effect is particularly useful because we get information of the molecular vibrations in the electronic state. The CARS (coherent anti-Stokes Raman spectroscopy) is a nonlinear Raman spectroscopy having its exclusive advantage for the observation of luminous samples because conventional resonance Raman spectroscopy is not operative in such samples. The vibrational spectrum of the various transient species produced in photoexcited pyrene has been studied by this method.[15,16]

Present study of transient absorption and transient resonance CARS spectra was undertaken to get solid evidence for the occurrence of intramolecular electron

transfer and to investigate the direction and degree of the transfer that takes place between the two chromophores in the UV excited 4-(1-pyrenyl)butyl 9-anthracenecarboxylate (**1**) that is abbreviated as P4A hereafter.

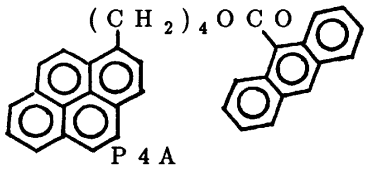

P 4 A

The absorption spectrum of P4A as well as those of other 1-pyrenylalkyl 9-anthracenecarboxylates studied so far exhibits the feature that is the 1 : 1 superposition of the spectra of 1-pyrenylmethanol and 9-anthracenecarboxylic acid, with just slight shifts by a few nm in peak positions, indicating the absence of any specific interaction between the chromophores in the ground state.[14]

Experimental

The preparation of purified sample has been described elsewhere.[14] The purified P4A was dissolved in acetonitrile (spectrograde) to make the sample solution of 10^{-3} M concentration.

The output beam of an N_2 laser (Molectron UV-24) with output power of 9 mJ/pulse and duration time of 10 ns was used both to excite the sample and to pump the dye lasers. No time delay was imposed between the UV and dye laser pulses. The confirmation that the observed signals originated from the transient species of P4A and not from the decomposition products was made by examining the absorption spectrum taken after the experiment. The transient absorption spectrum was obtained by alternately blocking the UV pulse that excited P4A and comparing the intensity of the transmitted dye laser with and without the irradiation by the UV pulse. The two laser beams were adjusted so that the transient absorption was maximal. The intensity I of the transmitted dye laser beam with the UV beam irradiating the cell was divided by the intensity I_0 that is the value recorded without the irradiation at various wavelengths of the dye laser. The derived values of $\log(I_0/I)$ for the deaerated solution are plotted against wavenumber in Fig. 1a for the region where the spectrum of pyrene cation radical is expected. Figure 1c shows the result of the observation in the region where the absorption by anthracene anion radical is expected. Partly owing to the lower sensitivity of the used photomultiplier and the lower intensity of the dye laser output in the longer wavelength region, the observation in the region failed to give distinct absorption peak although the presence of transient absorption was evident from the attenuation of the laser beam on the excitation by UV light.

The procedure for the transient resonance CARS experiment has been described in our previous paper.[15] Briefly, two dye lasers pumped by the N_2 laser were used when ω_1 beam (pump beam) was set resonant with the transient absorption while ω_2 beam (probe beam) was scanned over the range where the difference $\omega_1-\omega_2$ varied from 1000 to 1700 cm^{-1}.

The dependence of both the transient absorption and the resonance CARS signals on the power of excitation UV beam was measured by attenuating the UV beam. The sets of filters with 76% transmission per sheet at 337.1 nm were used.

Results and Discussion

Transient Absorption Spectrum. The transient absorption spectra observed on the photoexcitation of pyrene have been reported by several authors. Post et al. reported the observation of absorption peaks at 19500 cm^{-1} and 21200 cm^{-1} that they assigned to $S_n \leftarrow S_1$ and $S_m \leftarrow S_1$ bands, respectively.[17] The $T_n \leftarrow T_1$ absorption band at 24000 cm^{-1} was reported by the same authors and by Grellmann[18] who also reported on the absorption spectra of anion and cation radicals of pyrene at 20400 cm^{-1} and 22500 cm^{-1}, respectively. Siomos and Christophorou verified that the ion radicals are produced by two-photon ionization and gave the value of 38700 cm^{-1} as the threshold energy of the process.[19] Typical results of our observations of the transient species of pyrene are reproduced in Fig. 1b.

We find from the comparison of Figs. 1a and 1b that the transient absorption spectrum of P4A exhibits close resemblance with that of pyrene in methanol. Considering that the fluorescence lifetime of the S_1 state of pyrene is longer than 100 ns and that the related molecule P1A was found to give the emission with the quantum yield of about 1% and the emission lifetime of less than 1 ns,[14] it is expected under the present experimental condition that the sample contained such transients as the species in which the pyrenyl group was locally excited to the S_1 state, the species where the pyrenyl group was in the lowest triplet state T_1 and the ones that had undergone the intramolecular electron transfer with or without the formation of exciplexes. We thus associate the peaks at 23800 cm^{-1} and 20000 cm^{-1} in Fig. 1a with the pyrenyl-localized $T_n \leftarrow T_1$ and $S_m \leftarrow S_1$ absorption bands, respectively, and the peak at 21500 cm^{-1} is assigned as the overlap of pyrenyl-localized $S_n \leftarrow S_1$ band and the absorption band of cationic pyrenyl group. The presence of cationic pyrenyl group was confirmed by the CARS experiment as described below. The formation of the T_1 species of P4A was verified by the observation of the resonance (ω_1=23750 cm^{-1}) CARS signal at 1365 cm^{-1} that corresponds to the intense Raman band of pyrene in the T_1 state. We note that the $T_n \leftarrow T_1$ absorption of P4A shows up in both the deaerated and air-saturated solutions while the band of pyrene is observed only in the air-saturated solution. The reason for the appearance of the $T_n \leftarrow T_1$ band of pyrene in only air-saturated solutions

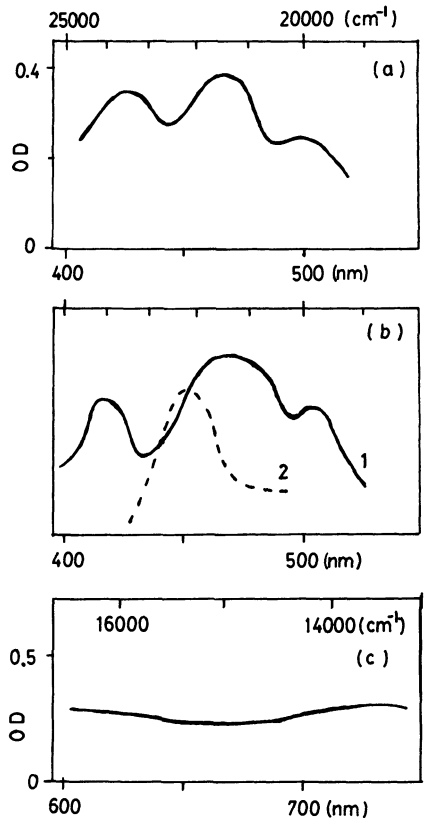

Fig. 1. Transient absorption spectra of the photoproduced transient species of P4A and pyrene. (a): the spectrum from 400 to 550 nm of the deaerated solution of P4A in acetonitrile (10^{-3} M concentration) under the irradiation of UV pulse at 337.1 nm, (b): the spectra from 400 to 550 nm of the UV produced transient species of molecular pyrene and curve 1 is the spectrum observed in air-saturated methanol solution in which the S_1 and T_1 species of pyrene are present and curve 2 is the spectrum of pyrene cation radicals that were produced in the aqueous micellar solution of hexadecyltrimethylammonium bromide, and (c): the spectrum observed from 600 to 740 nm region for the same system as described in (a). The UV pulse at 337.1 nm having the pulse duration time of 10 ns and the repetition rate of 10 pps was used throughout.

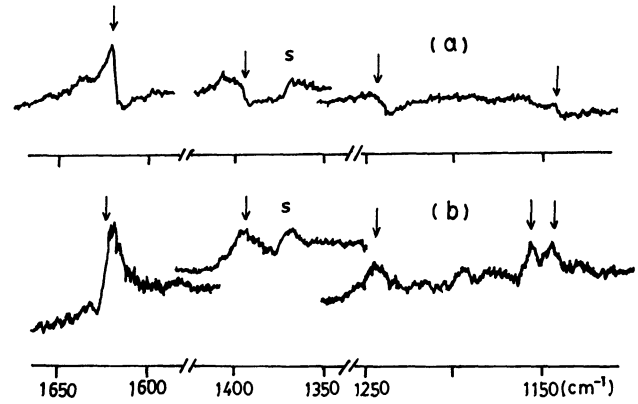

Fig. 2. Transient resonance CARS spectra of P4A in deaerated acetonitrile solution (10^{-3} M concentration) observed when the solution was irradiated by 337.1 nm pulse under the conditions (a): ω_1= 21000 cm^{-1} and (b): 21800 cm^{-1}. Arrow and s denote the Raman bands of the transient species and the solvent molecule, respectively.

is attributed as owing to the dissolved oxygen working as the effective promoter of intersystem crossing. The present observation suggests that the production pathway of the T_1 state from the S_1 state, both localized to the pyrenyl group, of P4A is different from that of pyrene.

Anthracene anion radical has been known to have the peak of the absorption band at 13700 cm^{-1} (730 nm).[20] Actually, the question whether the ionic moiety of the present transient is either the 9-anthryl group, 9-anthracenecarbonyl group, or 9-anthracenecarbonyloxy group remains to be solved and we expect that absorption peak may be shifted outside the present observation for latter two groups. In any event, it is likely that the obvious absorption giving the change of 0.3 in the optical density under the optical pass length of 1 mm in the region.of 730 nm in P4A (see Fig. 1c) originates from one of the above-mentioned species.

Transient Resonance CARS Spectrum. The resonance CARS spectrum of P4A was observed by setting the ω_1 beam resonant with the transient absorption band at 21500 cm^{-1}. Figures 2a and 2b show the results for the settings of ω_1=21800 cm^{-1} and ω_1=21000 cm^{-1}, respectively. From Figs. 2a and 2b one notes that the Raman band at 1622 cm^{-1} shows dispersion dips on mutually opposite side of the peak. The feature shows that one-photon electronic resonance effect is at work on the totally symmetric vibrations and that of the absorption band is the 0–0 band origin located near 21500 cm^{-1}. The wavenumbers of the observed six Raman bands that showed up only when the UV light was incident are listed in the first column of Table 1. The reported values of pyrene in various states are also listed in the following columns. The present result is close to the reported values of the Raman shifts for the cation radical of pyrene that has been produced by UV-irradiation of pyrene in such systems as acetonitrile, methanol, cationic micelle, and pyrene–dicyanobenzene in acetonitrile solutions.[15] It should be noted that the Raman frequencies of the present study were obtained under electronically resonant condition and thus the participation of the pyrenyl group in the ground state can be disregarded.

The behavior of the CARS signals by the change of the intensity of UV light was examined to prove that the signals were associated with the cationic pyrenyl group and not with either the free pyrenyl cation radicals that could have resulted from two-photonic ionization or the photofragmented pyrenyl radicals.

Table 1. Observed Raman Shifts of Photo-excited P4A and Various Species Pyrene (cm^{-1})

P4A*, CARS (acetonitrile solution)[a]	S_0, Raman (solid)[b]	S_1, CARS (pentane-d_{12} solution)[c]	T_1, CARS (heptane solution)[c]	Anion, Raman (THF solution)[c]	Cation, CARS (CTAB[d] aqueous micellar solution)[c]
	1642 s (b_{1g})				
		1633 vw (a_g?)			
1622	1627 vs (a_g)				1627 m (a_g)
			1595 s (a_g)	1604 s (a_g)	
	1584 s (a_g)				
		1565 m (b_{1g})			
	1549 w (b_{1g})				
		1500 m (a_g)			
		1445 s (a_g)			
1396	1405 vs (a_g)	1433 s (b_{1g})			1410 s (a_g)
			1365 vs (a_g)	1364 m (a_g)	
	1371 m (b_{1g})		1345 m (a_g)		
	1359 vw (a_g, b_{1g})	1329 s (a_g)	1340 m (a_g)		
		1315 vw (b_{1g})			
1240	1236 vs (a_g)	1246 s (a_g)			1245 m (a_g)
	1206 vw (b_{1g})			1225 m (a_g)	
	1174 vw (b_{1g})		1188 w (a_g)		
1155	1142 s (a_g)			1123 m (a_g)	1138 m (a_g)
1142		1113 w (b_{1g})	1110 m (a_g)		
	1107 vw (b_{1g})	1107 vw (a_g?)			
	1066 s (a_g)				
		1032 w (a_g)			

a) Originating from transient species of P4A, present study. b) S. J. Cyvin, B. N. Cyvin, J. Brunvoll, J. C. Whitmer, K. Klaeboe, and J. E. Gustavsen, *Z. Natureforsch.*, **34a**, 876 (1979). Symmetry species of the vibrational mode based on D_{2h} symmetry are shown in parentheses. c) Ref. 15. Symmetry species of the vibrational mode based on D_{2h} symmetry are shown in parentheses. d) Hexadecyltrimethylammonium bromide.

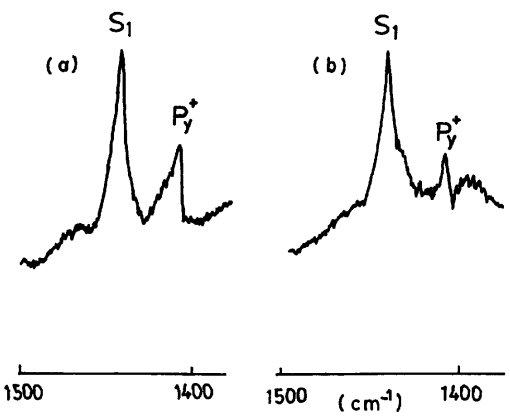

Fig. 3. The effect of UV power on the transient CARS signal of photoproduced species of pyrene under ω_1=21800 cm^{-1}; (a) without attenuation and (b) under attenuation by about 50% of UV power. The methanol solution (10^{-3} M) of pyrene were used for the measurement and the signals from the one-photon excited S_1 species and that from the two-photon ionized pyrene cation radical (marked by S_1 and P_y^+, respectively) are seen to exhibit distinctly different dependence on the intensity of UV pulse.

Figure 3 shows the population change in the pyrene/methanol system as observed on the resonance CARS signals of the pyrene cation radical and the S_1 state species. The frequency of ω_1 was set at 21800 cm^{-1}. The signal at 1445 cm^{-1} originates from the S_1 state of pyrene produced by one-photon excitation and the signal at 1410 cm^{-1} is from the pyrene cation radical that is produced by two-photon ionization. Figure 3 shows that the relative intensity of the two CARS signals changed by the intensity of UV excitation and the change evidently resulted from the difference in the population processes of the two species; the production of S_1 species by one-photon processes vs. the two-photon process to produce the cation radical. Figure 4 shows the decrease of CARS signal of cationic pyrenyl group in P4A at 1396 cm^{-1} (marked by arrow) and that of solvent acetonitrile (marked by s) when the UV power (at 337.1 nm) was attenuated by 0%(a), 58%(b), and 100%(c). Figures 4d—4g are the results of computer simulation. Of three components of CARS susceptibility, the Raman nonresonant background term and the term that is resonant to the Raman band of solvent molecule stay constant of the intensity of UV radiation and their relative magnitude was determined by simulating the feature of Fig. 4c to give the curve shown in Fig. 4f. The term causing the 1396 cm^{-1} band is proportional to the population of photoproducts and its relative magnitude with respect to other terms was determined for the condition that gives the trace in Fig. 4a and the trace shown in Fig. 4d was derived from the simulation. The attenuation of UV power causes the

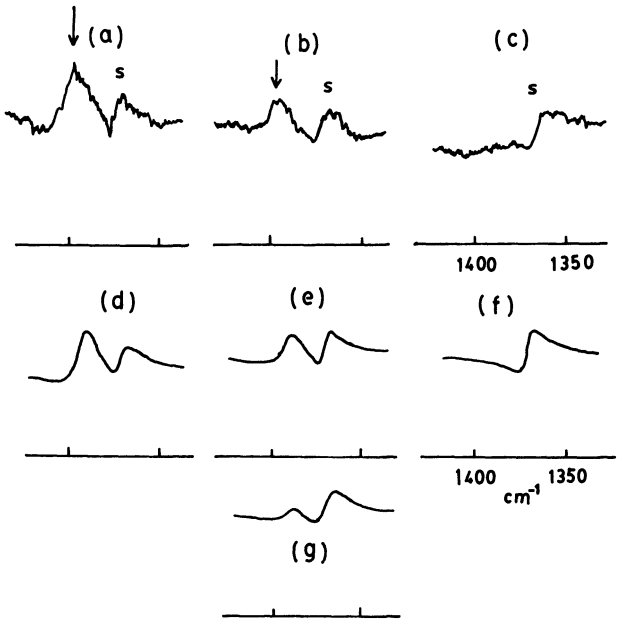

Fig. 4. The UV-power-dependent variation of the observed and simulated features of the CARS spectrum in the region where the resonance CARS signal of photoexcited P4A (marked by arrows) and the CARS signal of solvent acetonitrile are observed. The signals observed under the attenuation of UV power by 0%, 58%, and 100% are shown in (a), (b), and (c), respectively, while the simulation was made by using the traces in (a) and (c) as references giving the reference curves of (d) and (f), respectively, and the theoretical curves of (e) and (g) were obtained for the cases when the population of the transient species changes linearly (e) and quadratically (g), with intensity of UV pulse.

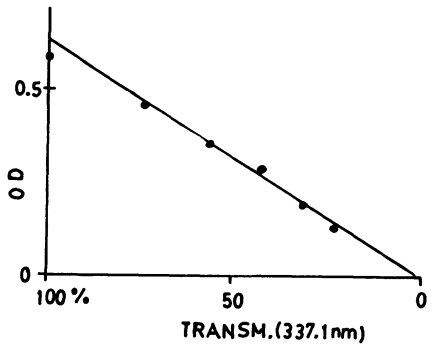

Fig. 5. Plot of the change in the intensity of transient absorption at 21800 cm^{-1} by the intensity of UV irradiation. Linear increase of the absorption with increasing UV power is derived from the plot.

population of the photoproduced species to decrease leading to the change in the spectral profiles. Figures 4e and 4g are the results of the simulations for the linear and quadratic dependencies, respectively, of the population on UV power, and we note that Fig. 4e is the better reproduction of the observed feature of Fig. 4b.

The frequency (21800 cm^{-1}) of the ω_1 beam is inside the absorption band of transient cationic species and the intensity of the ω_1 beam changed by the intensity of UV beam. The intensity of the ω_1 beam at the point through the sample is plotted in Fig. 5 against the UV power used for the photoexcitation where the intensity of ω_1 beam is expressed in the unit of optical density of the sample. The linear production of the cationic pyrenyl radicals with respect to the intensity of UV beam as verified above is in clear contrast with the two-photonic production of the pyrene cation radicals.

The overall feature of the transient absorption spectrum of P4A in the acetonitrile solution resembles that of UV-irradiated pyrene in methanol where the signals from both the cation radical and the S_1 state of pyrene have been observed. The resonance CARS signals of only the cationic pyrenyl group were, however, observed in the present sample, suggesting the different processes of the production of cationic species in the two systems.

The present result points to the conclusion that the cationic species in P4A resulted by the internal conversion and successive intramolecular relaxation from one-photonically excited Franck–Condon state of pyrenyl group. We have also mentioned from the observation of weak yet distinct transient absorption around 730 nm region that either the anthryl group or the anthracenecarbonyloxy group in P4A acquired anionic nature following the photoexcitation of pyrenyl group. Hence the present observation is a direct indication that the pyrenyl group becomes cationic through the intramolecular electron transfer of nearly unit charge from the locally excited 1-pyrenyl group to the 9-anthryl group (or 9-anthracenecarbonyloxy group). Although the attempt to observe the transient CARS signal of negatively charged anthryl group failed owing to small electronic resonance effect and the technical difficulty in obtaining enough power of the dye lasers in the near infrared region, the present picture of intramolecular transfer of an electron from pyrenyl to anthryl group (or anthracenecarbonyloxy group) fits the model that was presented in Ref. 14, that is, through-bond electron transfer takes place before the Coulombic attraction between the two oppositely charged moieties enables the rotation around the C–O bond to let the s-trans conformation of P4A in ground state change into s-cis conformation that is necessary for the formation of stable intramolecular exciplex with two chromophores sitting in face-to-face conformation. The Coulombic attraction is needed to overcome the potential barrier of about 50 kJ mol^{-1} lying expectedly between the two conformations.

In conclusion, the occurrence of intramolecular electron transfer from the locally excited 1-pyrenyl

group to the 9-anthryl group (or 9-anthracenecarbonyloxy group) in the acetonitrile solution of P4A has been confirmed from the observation of transient absorption and resonance CARS spectra. Further work is under way to solve the remaining questions such as if the species under study was identical with the species for which the broad exciplex-like emission band was observed and if the two chromophores are of elongated end-to-end conformation or of sandwitch type. The undertaken experiments on related molecules and of time-resolved spectroscopy are expected to provide further informations on the chemical and physicochemical characteristics of bichromophoric carbohydrates.

References

1) F. C. De Schryver, P. Collart, J. Vandendriessche, R. Goedeweeck, A. M. Swinnen, and M. Van der Auweraer, *Acc. Chem. Res.*, **20**, 159 (1987).

2) P. Vanderauwera, F. C. De Schryver, A. Weller, M. A. Winnik, and K. A. Zachariasse, *J. Phys. Chem.*, **88**, 2964 (1984).

3) H. Oevering, M. N. Paddon-Row, M. Heppener, A. M. Oliver, E. Cotsaris, J. W. Verhoeven, and N. S. Hush, *J. Am. Chem. Soc.*, **109**, 3258 (1987) and references cited therein.

4) K. A. Zachariasse, R. Busse, B. Duveneck, and W. Kuhnle, *J. Photochem.*, **28**, 237 (1985).

5) A. M. Swinnen, M. Van der Auweraer, F. C. De Schryver, K. Nakatani, T. Okada, and N. Mataga, *J. Am. Chem. Soc.*, **109**, 321 (1987) and references cited therein.

6) T. Ebata, Y. Suzuki, N. Mikami, T. Miyashi, and M. Ito, *Chem. Phys. Lett.*, **110**, 597 (1984).

7) H. Sakuragi, K. Tokumaru, H. Itoh, K. Terakawa, K. Kikuchi, R. A. Caldwell, and C.-C. Hsu, *J. Am. Chem. Soc.*, **104**, 6796 (1982).

8) A. Castellan, J. M. Lacoste, and H. Bouas-Laurent, *J. Chem. Soc., Perkin Trans. 2*, **1979**, 411.

9) H. Takagi, H. Horie, and I. Mita, *Macromolecules*, **16**, 1395 (1983) and references cited therein.

10) J. Vandendriessche, M. Van der Auweaer, and F. C. De Schryver, *Bull. Soc. Chim. Belg.*, **94**, 991 (1985).

11) T. Hayashi, T. Suzuki, N. Mataga, Y. Sakata, and S. Misumi, *J. Phys. Chem.*, **81**, 420 (1977).

12) T. Hayashi, N. Mataga, T. Umemoto, Y. Sakata, and S. Misumi, *J. Phys. Chem.*, **81**, 424 (1977).

13) H. Masuhara, N. Mataga, M. Yoshida, H. Tatemitsu, Y. Sakata, and S. Misumi, *J. Phys. Chem.*, **81**, 879 (1977).

14) M. Iwamura, K. Takuma, N. Koga, and H. Iwamura, *Chem. Lett.*, **1988**, 1249.

15) S. Maeda, T. Kamisuki, H. Kataoka, and Y. Adachi, *Appl. Spectrosc. Rev.*, **21**, 211 (1985).

16) T. Kamisuki, I. Moriyama, R. Igarashi, Y. Adachi, and S. Maeda, *J. Chem. Phys.*, **73**, 3500 (1980).

17) M. F. M. Post, J. Langelaar, and J. D. W. Van Voorst, *Chem. Phys. Lett.*, **10**, 468 (1971).

18) K. H. Grellmann and A. R. Watkins, *J. Am. Chem. Soc.*, **95**, 983 (1973); W. I. Aalbersberg, G. J. Hoijtink, E. L. Mackor, and W. P. Weijland, *J. Chem. Soc.*, **1959**, 3049.

19) K. Siomos and L. G. Christophorou, *Chem. Phys. Lett.*, **72**, 43 (1980).

20) T. Shida and S. Iwata, *J. Am. Chem. Soc.*, **95**, 3473 (1973).

Studies of Liquid Water by Computer Simulations. VI. Transport Properties of Carravetta-Clementi Water

Yosuke KATAOKA
Department of Chemistry, Faculty of Science, Kyoto University, Kyoto 606
(Received October 24, 1988)

The micro canonical molecular dynamics simulations of liquid water were performed at different temperatures and densities in order to investigate the anomalies of the transport coefficients. The nonempirical Carravetta-Clementi potential was used for the system with 216 molecules in a cubic cell. The order of magnitude of the nonempirically calculated self-diffusion coefficient, shear viscosity, bulk viscosity, and thermal conductivity were in agreement with experimental results. These transport properties were recognized as anomalous as in real liquid water. The temperature-dependence of these quantities was in agreement with the observed values under pressure of 50 MPa. The effects of compression on these transport coefficients were reproduced qualitatively. The obtained bulk viscosity was larger than the shear viscosity at low temperatures in accordance with experiments. The contribution of rotational motion to thermal conductivity seems to be responsible for the anomalous temperature-dependence of thermal conductivity. Several decay constants of the time correlation functions were obtained. The frequency spectra of the correlation functions were discussed. No marked molecule number dependence was observed in the calculated transport coefficients of Matsuoka-Clementi-Yoshimine water.

We have carried out the molecular dynamics (MD) simulation to study the effect of density and temperature on the transport properties of liquid water. This problem was examined in the fourth paper[1] of this series by a simplified 2-dimensional water-like model.[2,3] Although most of the transport properties were reproduced qualitatively, the maximum of thermal conductivity as a function of temperature was not verified.[1]

In the preceding paper[4] we showed that the anomalous thermodynamic properties observed experimentally are nonempirically reproduced on a semi-quantitative level with Carravetta-Clementi (CC) potential.[5] Our study on the liquid-vapor interface of CC water gave reasonable thermodynamic properties.[6] For these reasons we will report in the present paper on MD simulations with CC potential to examine the transport properties of liquid water.

The most interesting characteristics of the transport properties of liquid water are summarized as follows:[7] The initial application of pressure decreases the viscosity and increases the self-diffusion coefficient below about 300 K. The thermal conductivity of liquid water has a maximum as a function of temperature under a constant pressure. Although the density dependence of the self-diffusion coefficient was already studied by MD,[8-14] it seems that the viscosity and the thermal conductivity of liquid water have been studied only at normal conditions (at room temperature and volume, $V=18\ \mathrm{cm^3\ mol^{-1}}$).[13] Therefore, we are going to perform MD simulations at different temperatures and densities. Transport coefficients were calculated by the standard Kubo formula.[15-17]

The dynamical properties of liquid water were studied by Matsuoka-Clementi-Yoshimine (MCY) potential[18] at several state points by Impey et al.[9] They showed that the main features of spectroscopic and transport properties of real water are interpreted by their MD simulations, although some spectra are not reproduced. The collective dynamics in MCY and three body water was studied by Wojcik and Clementi.[13] The calculated shear viscosity is well compared with the experimental value at room temperature and normal density. For this reason, MCY potential is one of the most promising models in the study of transport properties of liquid water. We will further survey the fluid state over a wide range of temperature and density. For such purpose, CC potential is more convenient than MCY model, because the equation of state of CC water has been given by us.[4]

In the fourth paper of this series,[1] we used the constant temperature-pressure MD,[19,20] because this method is more convenient to obtain temperature dependence or pressure dependence of the system. We found, however, that the bulk viscosity obtained by the constant pressure MD is wrong.[1] The value of the shear viscosity calculated by constant temperature-pressure MD seemed to scatter more than that by the micro canonical MD.[1] For this reason the micro canonical MD method is used in this paper.

The molecule number dependence of the transport coefficients was examined with MCY water.[18] The transport coefficients of the systems with 216 and 1000 molecules were compared with the Wojcik and Clementi's result on a 512-molecule system.[13]

The contribution of rotational motion to thermal conductivity is calculated in order to examine the origin of the anomalous temperature dependence. The decaying and oscillatory characters of the time correlation functions related to the transport coefficients are analyzed and compared with those of simple liquids.[21-29]

Molecular Dynamics Calculations

The molecular dynamics method is essentially the same as the previous one.[4] The program MDMPOL coded by Smith and Fincham[30] is used as the basis of the present program. The program calculates the time evolution of the system using a leapfrog algorithm for the center of mass motion and a leapfrog-quaternion algorithm for the angular motion. The electrostatic forces and energy were calculated by the Ewald method. The short range terms were cut off at half of the MD cell width for the 216-molecule system. When the system has 1000 molecules, the cutoff distance is the same as that of the 216-molecule system of the same number density. The cpu time was 0.23 and 1.3 s/step for 216- and 1000-molecule systems respectively by FACOM VP-400E vector processor at Kyoto University Data Processing Center, which includes the calculations of stress tensor components and heat currents.

The time step in this work was 0.5 fs. The root mean square fluctuation of the total energy was less than 0.02% in the case of 40000-step run. The initial data at each state were those of the aged state obtained by the previous calculations.[4] The 18000-, 24000-, or 40000-step runs were repeated several times, from which the molecular dynamics statistical averages were obtained.

The self-diffusion coefficient D was calculated from the mean square displacement $<\Delta r^2>$ and the velocity auto-correlation function given below:[31]

$$D = \lim_{t\to\infty} \frac{<\Delta r^2>}{6t} \tag{1}$$

and

$$D = \frac{1}{3}\int_0^\infty <\boldsymbol{v}(t)\cdot\boldsymbol{v}(0)>\mathrm{d}t. \tag{2}$$

The shear viscosity η_S and the bulk viscosity η_B were calculated by the standard Kubo type formula:[15–17]

$$\eta_s = \frac{1}{\kappa_B TV}\int_0^\infty <J^{xy}(t)J^{xy}(0)>\mathrm{d}t, \tag{3}$$

$$\eta_B = \frac{1}{9\kappa_B TV}\sum_{\substack{\alpha=x\\ \beta=x}}^{z}\int_0^\infty <[J^{\alpha\alpha}(t) - <J^{\alpha\alpha}>]\cdot[J^{\beta\beta}(0) - <J^{\beta\beta}>]>\mathrm{d}t, \tag{4}$$

$$J^{\alpha\beta} = M\sum_{i=1}^{N} v_{i\alpha}v_{i\beta} + \sum_{i=1}^{N} r_{i\alpha}f_{i\beta}, \tag{5}$$

where M is the mass of the molecule, v_i the velocity of the i-th molecule, r_i means the position of the i-th molecule, and f_i is the force that the i-th molecule feels. The suffix α means the α-component of the vector. The Boltzmann constant, temperature, volume, and number of molecules in the basic cell are written as κ_B, T, V, and N, respectively.

The thermal conductivity λ was calculated by the correlation function of the heat current $\boldsymbol{S}(t)$:[15–17]

$$\lambda = \frac{1}{3\kappa_B T^2 V}\int_0^\infty <\boldsymbol{S}(t)\cdot\boldsymbol{S}(0)>\mathrm{d}t \tag{6}$$

and

$$\boldsymbol{S}(t) = \frac{\mathrm{d}}{\mathrm{d}t}\sum_{i=1}^{N} H_i\boldsymbol{r}_i, \tag{7}$$

where H_i is the contribution of the i-th molecule to the total Hamiltonian of the system $\mathscr{H}$:

$$\mathscr{H} = \sum_{i=1}^{N} H_i$$

and

$$H_i = K_{\mathrm{TRANS}}(i) + K_{\mathrm{ROT}}(i) + \frac{1}{2}\sum_{j=1}^{N} U_{ij}, \tag{8}$$

where $K(i)$ is the kinetic energy and U_{ij} is the molecular interaction energy between molecule i and j.

The representative range of the time integration of the correlation function is $0 \leqq t \leqq 1$ ps. The averages of at least 14000 values were taken for the initial time. An example of convergence characteristics is shown in Fig. 1 for shear viscosity. It is seen that the cumulative average is stable although the partial average scatters.

Molecule Number Dependence

As the first step, we are going to see whether 216 molecules are enough for the calculation of transport coefficients. For this purpose, the coefficients of the 216-, 512-, and 1000-molecule system are compared with each other. Wojcik and Clementi[13] gave the results on the 512-molecule system with MCY potential[18] at normal conditions. The systems with 216 and 1000 MCY molecules are compared with their results

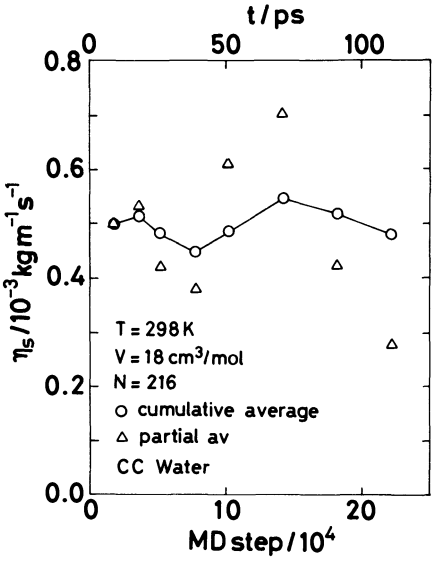

Fig. 1. Convergence characteristics of the shear viscosity.

Table 1. Molecule Number Dependence of the Properties of MCY Water, N=512 case is given by Wojcik and Clementi[13]

	MCY water			CC water	obs
N	1000	512	216	216	obs
T/K	300±2	296	295±1	298±1	298
V cm^3 mol^{-1}	18	18.018	18	18	18.050
P/MPa	829±7	843	832±12	248±8	20
U/kJ mol^{-1}	−28.23±0.06	−28.3	−28.46±0.05	−31.5±0.05	−33.9
G_K	1.6		1.5	1.9	4.1
D/10^{-9} m^2 s^{-1}	2.9 ±0.1		2.4 ±0.3	3.9±0.3	2.85
η_s/10^{-3} kg ms^{-1}	0.4 ±0.2	0.6	0.6 ±0.1	0.5±0.1	0.9
η_B/10^{-3} kg ms^{-1}	0.8 ±0.2	0.8	1.1 ±0.4	0.9±0.4	1.2
l/W mK^{-1}	1.6 ±0.3	1.35	1.3 ±0.3	1.1±0.3	0.59

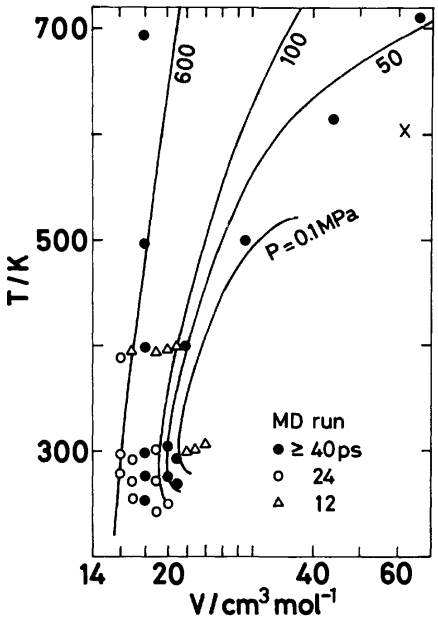

Fig. 2. Map of simulated state points. The G-type equation of sate[4] is drawn by solid lines. The symbol cross means the critical point in the G-type equation of state.

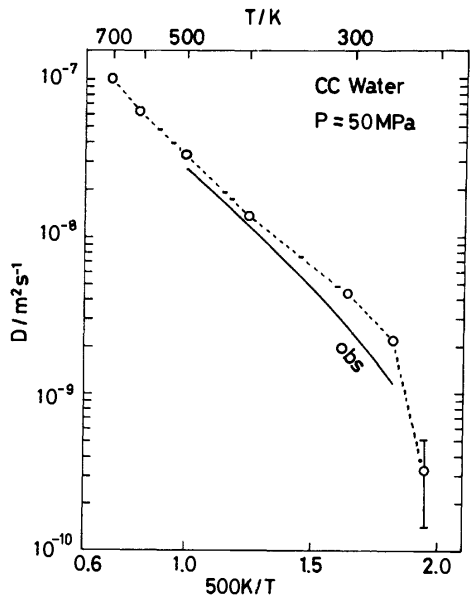

Fig. 3. The self-diffusion coefficient D is plotted against 500 K/T, where pressure P is about 50 MPa. The experimental results at P=50 MPa are shown by the solid line.[35-39]

in Table 1. No marked molecule number dependence is seen in this table. Hence, the basic cell with 216 molecules has been employed hereafter because of simplicity.

Table 1 also includes the coefficients of CC water. They are not so different from those of MCY water. As we have obtained the equation of state (EOS)[4] for CC model, we use CC potential[5] hereafter.

The values of Kirkwood orientational correlation factor G_K are also given, although they are preliminary; it is known that very long MD run is needed to evaluate this quantity.[32-34] These are obtained as follows:

$$G_K = <(\sum_{i=1}^{N} \mu_i)^2>/N, \quad (9)$$

where μ_i is the unit vector along the dipole direction of molecule i. The obtained values of G_K for MCY and CC water were small compared with the experimental values.[32] A similar result on MCY water was given by Neumann.[32]

Temperature and Volume Dependence

In this section, the calculated transport coefficients are compared with the experimental results. We carried out many MD simulations of the 216-molecule system with CC potential[5] in order to examine the temperature and density dependence of the transport coefficients as shown in Fig. 2. Some state points correspond to the states with pressure P of about 50 MPa. The others were selected around the normal density (V=18 cm^3 mol^{-1}).

The calculated self-diffusion coefficient D is plotted against the inverse of temperature T in Fig. 3 by circles where pressure P is about 50 MPa. The experimental results at P=50 MPa are shown by the solid line.[35-39] The calculated D is in agreement with the observed one with respect to the temperature dependence. The

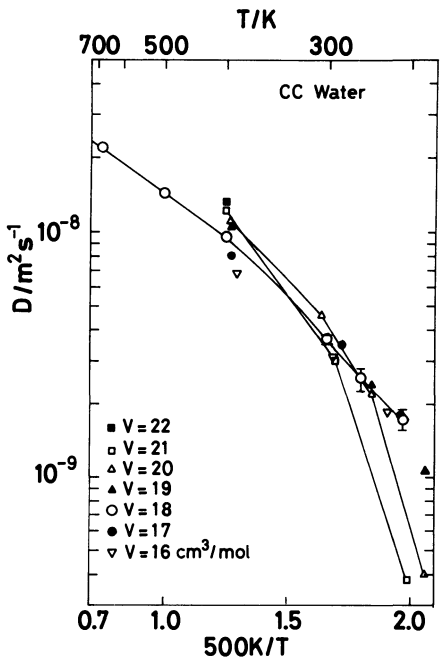

Fig. 4. The self-diffusion coefficient D is plotted against 500 K/T at several volumes.

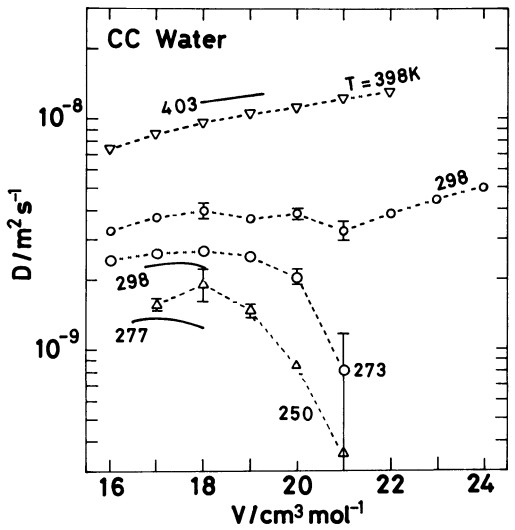

Fig. 5. The self-diffusion coefficient D is plotted against volume V at several temperatures. The experimental results are shown by the solid lines.[35-39]

calculations were repeated at different densities as seen in Fig. 4, where the setting temperatures were 260, 273, 298, 398, 500, and 700 K. As each average temperature was different from set temperature, the self-diffusion coefficients were obtained by interpolation as a function of temperature at each volume. The volume dependence of D obtained is shown in Fig. 5. The anomaly of the self-diffusion coefficient is semi-quantitatively reproduced as shown in Fig. 5. At lower temperatures, D has a maximum around volume V of

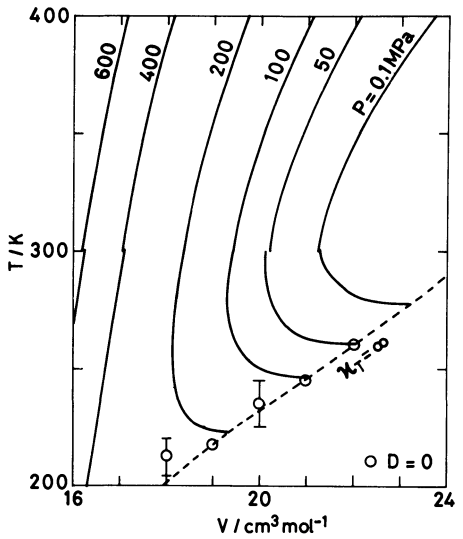

Fig. 6. The equation of state in the T-V plane. Above 300K the G-type EOS is used and below 300K the L-type EOS is shown.[4] The stability limit of the liquid phase is drawn by the dashed line.[4] The temperature where D is equal to zero at each volume is shown by circle.

18 $cm^3 mol^{-1}$ at a given temperature. Because the volume of the low density ice with CC potential is 11% larger than the observed one,[4] the volume with the maximum D at a given temperature varies correspondingly.

In this paper, the nonempirical calculation of the transport coefficients is intended; scaling of volume or adjusting have never been tried. The pressure effect on the self-diffusion coefficient of liquid water has been examined by a simple water-like model[1] and also by TIP4P model.[11]

When temperature is decreased, the self-diffusion coefficient D tends to approach to zero at a finite temperature under constant pressure as seen experimentally.[40] This temperature was discussed with the anomaly of the thermodynamic and transport properties of supercooled liquid water.[40-42] In the previous paper this temperature was assigned to the stability limit of liquid phase.[4]

Now we are going to see the relation between the stability limit of the liquid phase and the temperature of zero diffusion coefficient in this calculation.[43] We can get the temperature of zero D in the condition of fixed density as shown in Fig. 4. We used linear extrapolation for the D vs. T plot. The result is shown in Fig. 6. The circle means the temperature where D is equal to zero and the dotted line is the stability limit of the liquid phase obtained by the L-type equation of state.[4] We see that the zero D points are almost on the stability limit within the error bar. This means that the present calculations on the self-diffusion coefficient are consistent with the static properties obtained before.[4]

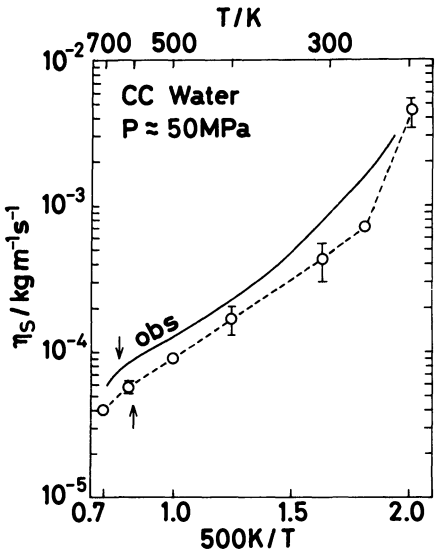

Fig. 7. The shear viscosity η_s is plotted against 500 K/T, where pressure is about 50 MPa. The experimental results at P=50 MPa are shown by the solid line.[44-50] An arrow indicates the critical temperature.

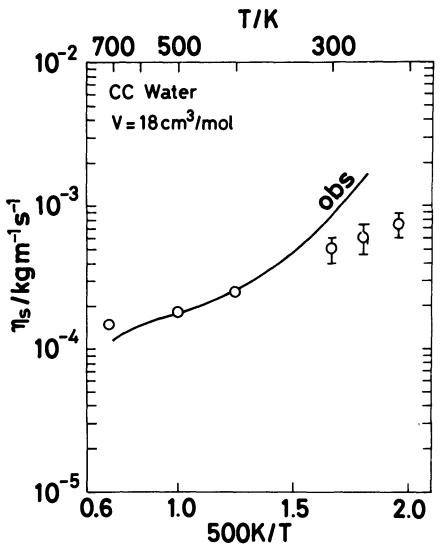

Fig. 8. The shear viscosity η_s is plotted against 500 K/T, where volume is 18 cm^3 mol^{-1}. The experimental results at V=18 cm^3 mol^{-1} are shown by the solid line.[44-50]

The shear viscosity η_s is plotted against the inverse of temperature in Fig. 7, where pressure P is about 50 MPa, and in Fig. 8 with the condition of the normal density (V=18 cm^3 mol^{-1}). The experimental results at P of 50 MPa are shown by solid line.[40-50] As regards the temperature dependence in Fig. 7, the obtained shear viscosity is in agreement with the observed one. Under the condition of normal density (Fig. 8), the calculated shear viscosity is a little smaller than the experimental results below room temperature. This can be understood qualitatively by the facts that the

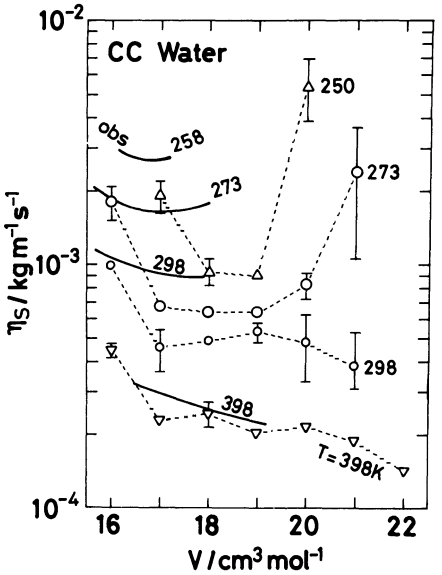

Fig. 9. The shear viscosity η_s is plotted against volume at several temperatures. The experimental reults are shown by the solid lines.[44-50]

shear viscosity of real liquid water at low temperatures has a minimum around P of 2×10^2 MPa as a function of pressure[7] and that the pressure is 2×10^2 MPa at room temperature by the present model.[4]

The volume dependence of η_s at several temperatures is shown in Fig. 9. This was obtained by interpolation as in the case of D. We see that the calculated shear viscosity has a peculiar volume dependence at low temperatures as observed in real water.[40-50] This property is shown much more clearly by the present simulation than in real water because our calculation includes the supercooled and/or minus pressure region. At a given temperature below room temperature, the volume of minimum viscosity is 18.5±0.5 cm^3 mol^{-1}, which is different a little from the observed one (around 17 cm^3 mol^{-1}). This comes from the reason that the length of hydrogen bond of the CC potential is larger than the observed one (see Table IV of Ref. 4).

The bulk viscosity η_B at normal density is plotted against the inverse of temperature in Fig. 10. The order of magnitude of the calculated values around room temperature is in agreement with the observed one.[51-53] As the bulk viscosity η_B is usually discussed by the ratio η_B/η_s, this quantity is plotted as a function of temperature in Fig. 11, where pressure is about 50 MPa for the calculation and the experimental results were obtained under normal pressure. Because of the large fluctuation of the virial term, the bulk viscosity at low temperatures was difficult to calculate in our case. The ratio η_B/η_s was larger than 1 below 500 K in accordance with the observed results.[51-53] The present calculation predicts that this quantity is less than 1 at higher temperatures, around or above the

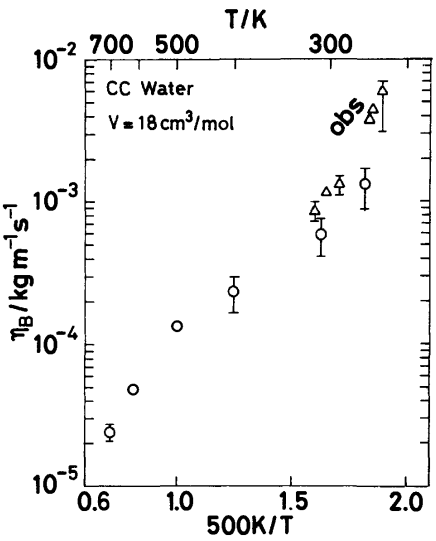

Fig. 10. The bulk viscosity η_B is plotted against 500 K/T, where volume is 18 cm^3 mol^{-1}. The experimental results are shown by the triangles.[51-53]

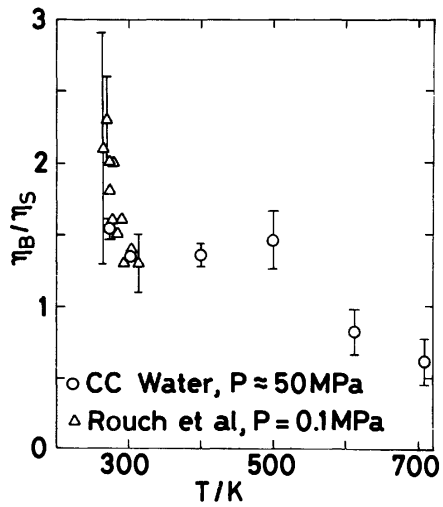

Fig. 11. The ratio η_B/η_s is plotted against temperature, where pressure is about 50 MPa for the calculation. The triangles show the experimental results[51-53] under normal pressure.

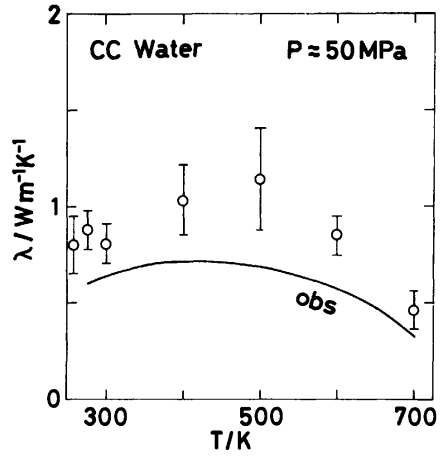

Fig. 12. The thermal conductivity λ is plotted against temperature, where pressure P is about 50 MPa. The experimental results at P=50 MPa are shown by the solid line.[50,54,55]

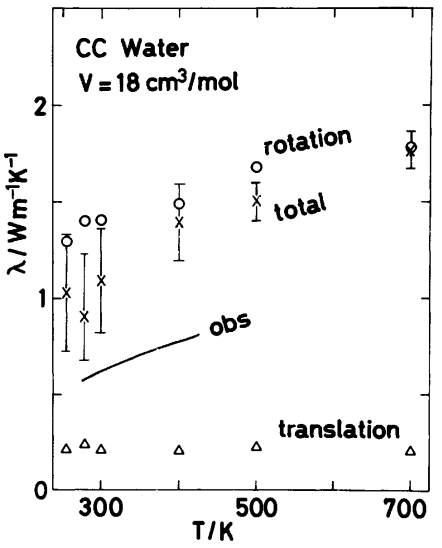

Fig. 13. The thermal conductivity λ is plotted against temperature, where volume is 18 cm^3 mol^{-1}. The cross means the total conductivity. The contribution from rotation and translation are plotted by circle and triangle respectively. The experimental results at V=18 cm^3 mol^{-1} are shown by the solid line.[50]

critical temperature (603 K for CC water).

The calculated thermal conductivity λ is shown as a function of temperature by open circle in Fig. 12, where pressure is about 50 MPa. We see that the present result is in agreement with the observed one at P of 50 MPa shown by the solid curve.[50,54,55] The thermal conductivity decreases as temperature increases above 500 K, because the density decreases abruptly around the critical temperature. So the essential point of anomaly in the thermal conductivity of liquid water is its increasing property with temperature at constant density. For this reason the thermal conductivity is plotted against temperature under the condition of normal density (V=18 cm^3 mol^{-1}) in Fig. 13. The cross indicates the calculated thermal conductivity at normal density, which is to be compared with the observed result shown by the solid curve at the same density.[50] The order of magnitude and the temperature dependence of the present values are in agreement with experiments.

In order to see the origin of this anomaly, partitioning of the thermal conductivity is tried as follows. The heat current $S(t)$ was divided into three parts, which are tentatively called translational, rotational, and molecular Hamiltonian part;

$$S(t) = S_{TRANS}(t) + S_{ROT}(t) + S_{MH}(t), \qquad (10)$$

$$S_{\mathrm{TRANS}}(t) = \sum_{i=1}^{N}\{\frac{\mathrm{d}K_{\mathrm{TRANS}}(i)}{\mathrm{d}t} + \frac{1}{2}\sum_{i=1}^{N}(\frac{\partial U_{ij}}{\partial x_j}\frac{\mathrm{d}x_j}{\mathrm{d}t} + \frac{\partial U_{ij}}{\partial y_j}\frac{\mathrm{d}y_j}{\mathrm{d}t} + \frac{\partial U_{ij}}{\partial z_j}\frac{\mathrm{d}z_j}{\mathrm{d}t})\}r_i, \quad (11)$$

$$S_{\mathrm{ROT}}(t) = \sum_{i=1}^{N}\{\frac{\mathrm{d}K_{\mathrm{ROT}}(i)}{\mathrm{d}t} + \frac{1}{2}\sum_{i=1}^{N}(\frac{\partial U_{ij}}{\partial \omega_{1j}}\frac{\mathrm{d}\omega_{1j}}{\mathrm{d}t} + \frac{\partial U_{ij}}{\partial \omega_{2j}}\frac{\mathrm{d}\omega_{2j}}{\mathrm{d}t} + \frac{\partial U_{ij}}{\partial \omega_{3j}}\frac{\mathrm{d}\omega_{3j}}{\mathrm{d}t})\}r_i, \quad (12)$$

and

$$S_{\mathrm{MH}}(t) = \sum_{i=1}^{N} H_i \frac{\mathrm{d}r_i}{\mathrm{d}t} \quad (13)$$

where ω is the Euler angle. The total heat current was calculated by means of numerical differentiation as Eq. 7. The first and third terms of Eq. 10 were obtained at each MD step by Eqs. 11 and 13,[17] and the second term was indirectly calculated from other terms.

It was found that the contribution from molecular Hamiltonian part is negligible. The contributions from $S_{\mathrm{TRANS}}(t)$ and $S_{\mathrm{ROT}}(t)$ are shown as a function of temperature at normal density in Fig. 13. Although the contribution from the cross term of $S_{\mathrm{TRANS}}(t)$ and $S_{\mathrm{ROT}}(t)$ is not shown, we can estimate it graphically from the rest in Fig. 13. The main part is the contribution from the rotational one shown by circles. This part increases as temperature increases. On the other hand, the contribution from the translation part $S_{\mathrm{TRANS}}(t)$ is almost constant as a function of temperature and the magnitude is much less than that of the rotational one. The strong anisotropic interaction seems to be responsible to the rotational part.

Here we are going to understand the temperature dependence of the thermal conductivity in terms of the time correlation functions. For this purpose, we define the time correlation function as follows:

$$f_\lambda(t) = \langle S(t)\cdot S(0)\rangle. \quad (14)$$

The time correlation functions (translational and rotational parts) are shown in Figs. 14 and 15, respectively. The normal temperature case and the high temperature one are compared at normal density. As temperature increases, the correlation function of the rotational part changes more than that of the translational one at normal density as seen in Figs. 14 and 15.

For quantitative discussion on the temperature dependence, the time integral of the normalized correlation function is shown in Table 2. It is found that the time integral changes only a little with temperature under the condition of normal density (V=18 cm^3 mol^{-1}). However, not only the time integral but also the normalization constant $\langle S(0)^2\rangle$

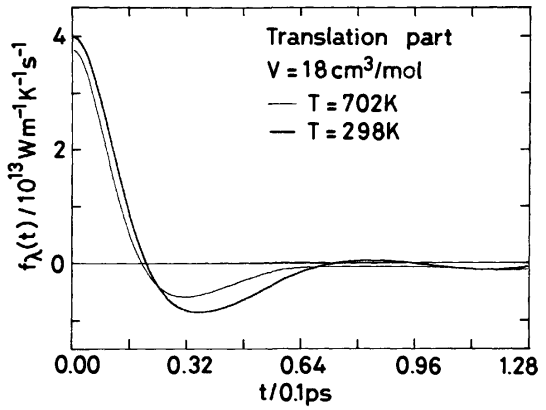

Fig. 14. The time correlation function related to the thermal conductivity, translational part.

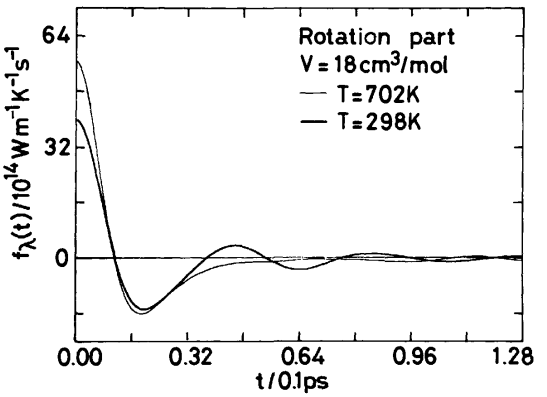

Fig. 15. The time correlation function related to the thermal conductivity, rotational part.

depends on temperature. These are summarized in Table 2 (cf. Eq. 6). From this table, it is seen that the increase of the factor $\langle S(0)^2\rangle/T^2$ of the rotational part as a function of temperature is the main cause for the anomaly in the temperature dependence of the thermal conductivity of liquid water. The excitation of rotational motion is responsible to the increase of this factor.

In this paragraph we will try to compare liquid water with a simple liquid by the correlation function related to thermal conductivity. The heat current autocorrelation function in Lennard-Jones liquid does not have any clear oscillatory character.[27] On the other hand, the translational part of the correlation function of liquid water oscillates clearly as shown in Fig. 14. The Fourier transform has a maximum around 70 ps^{-1} although the figure is not shown. The above difference between simple liquid and liquid water comes from rotational motion and anisotropic interaction. The anisotropic potential energy has high frequency component because of the rotational motion in liquid water. This effect will be discussed in the next section.

Table 2. Rotational and Translational Parts of Thermal Conductivity, V=18 cm^3 mol^{-1}

			T/K	
			298	702
Rotational	$\int_0^\infty \frac{<S(t)\cdot S(0)>}{<S(0)^2>} dt$	10^{-15} s	0.36	0.32
	$\frac{<S(0)^2>}{3\kappa_B T^2 V}$	10^{15} W mK^{-1} s^{-1}	3.9	5.6
	λ_{ROT}	W mK^{-1}	1.4	1.8
Translational	$\int_0^\infty \frac{<S(t)\cdot S(0)>}{<S(0)^2>} dt$	10^{-15} s	5.0	5.5
	$\frac{<S(0)^2>}{3\kappa_B T^2 V}$	10^{13} W mK^{-1} s^{-1}	4.0	3.7
	λ_{TRANS}	W mK^{-1}	0.20	0.20

Time Correlation Functions

As the CC model[5] is not so different from MCY potential,[18] the kinetic properties of CC water are similar to those of MCY water.[9] Qualitatively these properties are not so different from those of BNS water.[8] The frequency spectrum of the velocity autocorrelation function has peaks at 8 and 30 ps^{-1}. The frequency spectra of angular velocity autocorrelations have peaks at 76, 120, and 100 ps^{-1} for α=1, 2, and 3 components in the Rahman and Stillinger's notation.[8]

The normalized correlation function related to shear viscosity is drawn in Fig. 16 at normal conditions (at room temperature and V of 18 cm^3 mol^{-1}). Its Fourier transform is compared with that at a higher temperature (T=702 K) in Fig. 17. We see two characteristic frequencies 40 and 160 ps^{-1} in Fig. 17 at room temperature. At high temperature (T=702 K), these peaks shift to lower frequencies. The oscillation of the time correlation function related to shear viscosity is not intrinsic in Lennard-Jones liquid.[26] However oscillation is clear in liquid water. Since there is strong anisotropic interaction in liquid water, the rotation-translation coupling can cause such an oscillatory behavior as discussed below in the paragraph on the thermal conductivity.

The bulk viscosity was obtained by the time integration of time correlation functions as shown in Fig. 18. In this case, an exponential decay is clear in short term. It is also possible to analyze the second part as another exponential decay as shown by the dotted line. The Fourier transform is given in Fig. 19, where the abscissa is in logarithmic scale. The zero-frequency is the main component at room temperature and a peak is seen around 6 ps^{-1} at T of 702 K in Fig. 19.

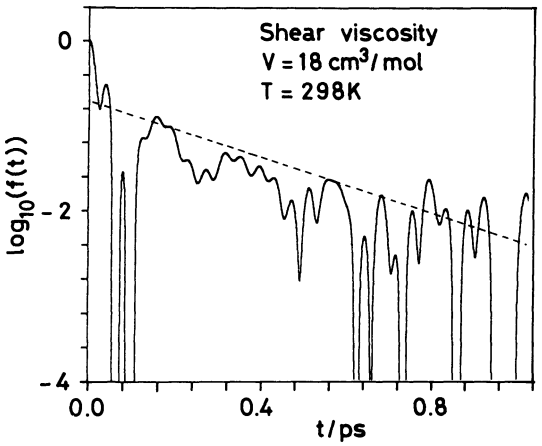

Fig. 16. The normalized time correlation function related to the shear viscosity. A decay character of the envelope is analyzed as shown by the dotted line.

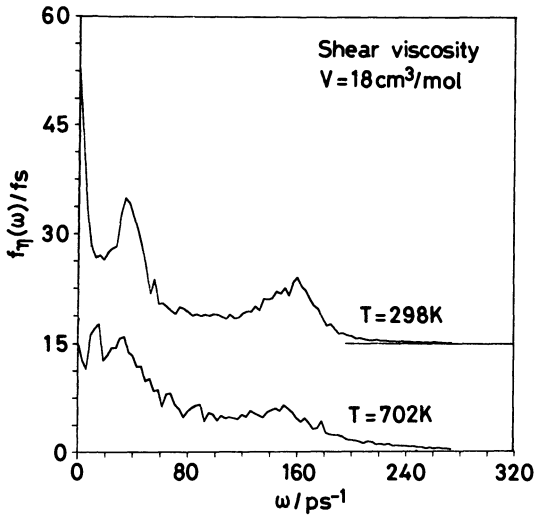

Fig. 17. The Fourier spectrum of the normalized time correlation function related to the shear viscosity.

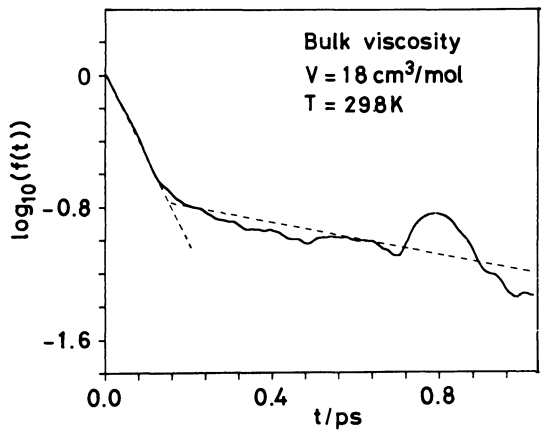

Fig. 18. The normalized time correlation function related to the bulk viscosity.

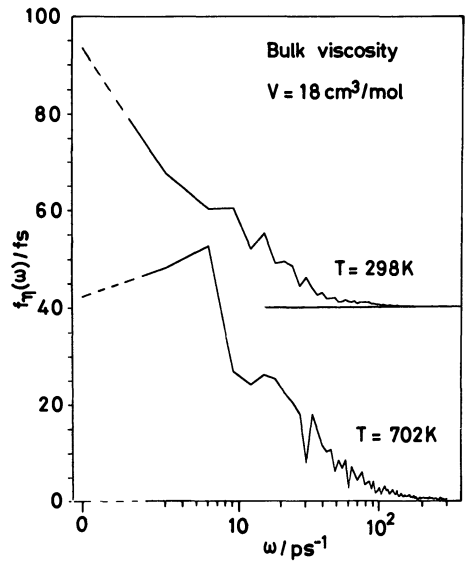

Fig. 19. The Fourier spectrum of the normalized time correlation function related to the bulk viscosity.

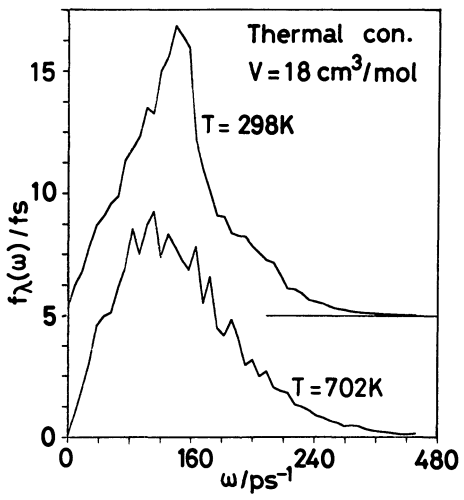

Fig. 20. The Fourier spectrum of the normalized time correlation function related to the thermal conductivity.

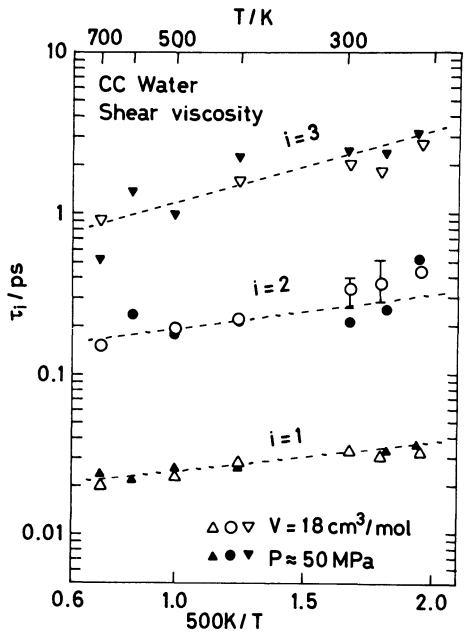

Fig. 21. The decay constant τ_i in Eq. 15, shear viscosity.

The decay character of the time correlation function related to bulk viscosity shown in Fig. 18 is qualitatively similar to that of Lennard-Jones liquid[28] in contrast with the case of shear viscosity.

Because the rotational part is main, the time correlation function related to thermal conductivity is not so different from that given in Fig. 15. The Fourier transform of the total correlation function related to thermal conductivity is plotted in Fig. 20. An oscillatory character is very clear. It is interesting to see that the characteristic frequency at about 140 ps^{-1} in thermal conductivity is close to the frequency seen in shear viscosity. The translational motion coupled with rotational one may have this frequency.

The long tails of the normalized time correlation functions are analyzed by the time averaged correlation functions which are averaged over a period of 0.144 ps, because the time correlation function oscillates with high frequency. The decay character of the time averaged correlation function was obtained by its envelope at long term. The short term was, however, analyzed by the original time correlation function. The following function was assumed (see Fig. 18):

$$f(t) = C_1 \exp(-t/\tau_1)\ t<0.1\ \mathrm{ps}(\eta_S),\ t<0.2\ \mathrm{ps}(\eta_B),$$

$$f(t) = C_2 \exp(-t/\tau_2)\ 0.1\ \mathrm{ps}<t<0.5\ \mathrm{ps}(\eta_S),\ 0.2\ \mathrm{ps}<t(\eta_B),$$

and

$$f(t) = C_3 \exp(-t/\tau_3)\ 0.5\ \mathrm{ps}<t<4\ \mathrm{ps}(\eta_S). \quad (15)$$

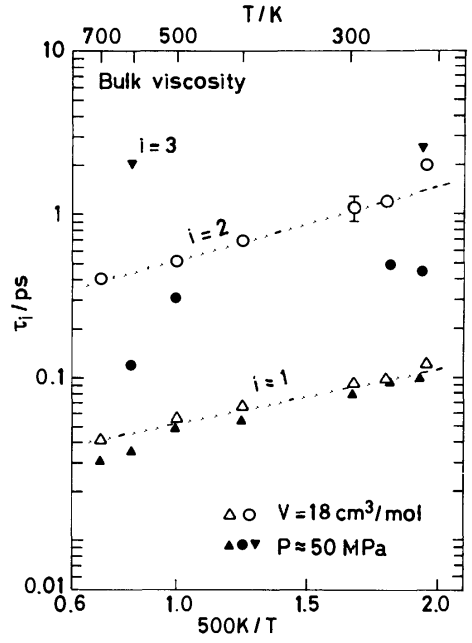

Fig. 22. The decay constant τ_i in Eq. 15, bulk viscosity.

The results on the decay constants τ_i are summarized in Figs. 21 and 22 for shear and bulk viscosity. It was difficult to perform such analysis on the time correlation function related to thermal conductivity, because of too high frequency components. These figures show that there are several decay constants and that the order of magnitude of them are 0.01, 0.1, and 1 ps. Wide distribution of decay constants means that there are so many time constants in the molecular motion in liquid water.

It is shown in this paper that anomalous behavior of the transport coefficients of liquid water can be reproduced nonempirically on a qualitative level. Some microscopic characteristics were revealed by the time correlation function related to the transport coefficients. The dynamical structure of liquid water will be studied in the next step.

The author would like to thank Prof. Nobuhiro Go and Mr. Mitsuhiro Matsumoto for valuable discussions. He also thanks Dr. D. Fincham, Queen Mary College, and Dr. W. Smith, Science and Research Council, Daresbury Laboratory, UK for their program MDMPOL as the basis of the present program. This work has been supported in part by a Grant-in-Aid for Scientific Research (Nos. 62103012, 62124039, and 63430023) from the Ministry of Education, Science and Culture. The author thanks the Computer Center of the Institute for Molecular Science for the use of HITAC M-680H and S-820/80 computers. The computation was also done by FACOM VP-400E and M-780 computers at Kyoto University Data Processing Center.

References

1) Y. Kataoka, *Bull. Chem. Soc. Jpn.*, **59**, 1425 (1986).
2) K. Okazaki, S. Nosé, Y. Kataoka, and T. Yamamoto, *J. Chem. Phys.*, **75**, 5864 (1981).
3) Y. Kataoka, *Bull. Chem. Soc. Jpn.*, **57**, 1522 (1984).
4) Y. Kataoka, *J. Chem. Phys.*, **87**, 589 (1987).
5) V. Carravetta and E. Clementi, *J. Chem. Phys.*, **81**, 2646 (1984).
6) M. Matsumoto and Y. Kataoka, *J. Chem. Phys.*, **88**, 3233 (1988).
7) G. S. Kell, "Water, a Comprehensive Treatise," ed by F. Franks, Plenum, New York (1972), Vol. 1, p. 363.
8) A. Rahman and F. H. Stillinger, *J. Chem. Phys.*, **55**, 3336 (1971). F. H. Stillinger and A. Rahman, *J. Chem. Phys.*, **61**, 4973 (1974).
9) R. W. Impey, P. A. Madden, and I. R. McDonald, *Mol. Phys.*, **46**, 513 (1982).
10) G. Jancso, P. Bopp, and K. Heinzinger, *Chem. Phys.*, **85**, 377 (1984).
11) M. R. Reddy and M. Berkowitz, *J. Chem. Phys.*, **87**, 6682 (1987).
12) M. W. Evans, G. C. Lie, and E. Clementi, *J. Chem. Phys.*, **88**, 5157 (1988).
13) M. Wojcik and E. Clementi, *J. Chem. Phys.*, **85**, 6085 (1986).
14) As for more comprehensive references on MD of liquid water, see the review articles cited in Ref. 4 and the references cited in Ref. 4. See also: A. C. Belch and S. A. Rice, *J. Chem. Phys.*, **86**, 5676 (1987). M. W. Evans, G. C. Lie, and E. Clementi, *J. Chem. Phys.*, **87**, 6040 (1987). H. Tanaka and I. Ohmine, *J. Chem. Phys.*, **87**, 6128 (1987).
15) R. Zwanzig, *Ann. Rev. Phys. Chem.*, **16**, 67 (1965).
16) D. J. Evans and W. B. Streett, *Mol. Phys.*, **36**, 161 (1978).
17) R. Kubo, "Water and Steam, Their Properties and Current Industrial Applications", Proc. 9th Intern. Conf. on Prop. of Steam, held at München, 1979, Pergamon (1980), p. 303.
18) O. Matsuoka, E. Clementi, and M. Yoshimine, *J. Chem. Phys.*, **64**, 1351 (1976).
19) S. Nosé, *Mol. Phys.*, **52**, 255 (1984); S. Nosé, *J. Chem. Phys.*, **81**, 511 (1984).
20) H. C. Andersen, *J. Chem. Phys.*, **72**, 2384 (1980).
21) D. Levesque, L. Verlet, and J. Kürkijarvi, *Phys. Rev. A*, **7**, 1690 (1973).
22) W. T. Ashurst and W. G. Hoover, *Phys. Rev.*, **11**, 658 (1975).
23) J. Vermesse and D. Levesque, *Phys. Rev.*, **19**, 1801 (1979).
24) D. M. Heyes, *J. Chem. Soc., Faraday Trans. 2*, **79**, 1741 (1983).
25) D. Fincham and D. M. Heyes, *Chem. Phys.*, **78**, 425 (1983).
26) M. Schoen and C. Hoheisel, *Mol. Phys.*, **56**, 653 (1985).
27) R. Vogelsang, C. Hoheisel, and G. Ciccotti, *J. Chem. Phys.*, **86**, 6371 (1987).
28) C. Hoheisel, *J. Chem. Phys.*, **86**, 2328 (1987). C. Hoheisel, R. Vogelsang, and M. Schoen, *J. Chem. Phys.*, **87**, 7195 (1987).
29) D. Levesque and L. Verlet, *Mol. Phys.*, **61**, 143 (1987).

30) W. Smith and D. Fincham, CCP5 Newsletter, an informal letter freely available from Science & Research Council, Daresbury Laboratory, Warrington WA4, 4AD, England.
31) J. Kushick and B. J. Berne, "Statistical Mechanics, Part B: Time-Dependent Processes," ed by B. J. Berne, Plenum, New York (1967), p. 41.
32) M. Neumann, *J. Chem. Phys.*, **82**, 5663 (1985).
33) M. Neumann, *J. Chem. Phys.*, **85**, 1567 (1986).
34) J. Anderson, J. J. Ullo, and S. Yip, *J. Chem. Phys.*, **87**, 1726 (1987).
35) L. A. Woolf, *J. Chem. Soc., Faraday Trans. 1*, **71**, 784 (1975).
36) L. A. Woolf, *J. Chem. Soc., Faraday Trans. 1*, **72**, 1267 (1976).
37) D. J. Wilbur, T. DeFries, and J. Jonas, *J. Chem. Phys.*, **65**, 1783 (1976).
38) K. Krynicki, C. D. Green, and D. W. Sawyer, *Faraday Discuss. Chem. Soc.*, **66**, 199 (1978).
39) K. R. Harris and L. A. Woolf, *J. Chem. Soc., Faraday Trans. 1*, **76**, 377 (1980).
40) R. J. Speedy and C. A. Angell, *J. Chem. Phys.*, **65**, 851 (1976).
41) C. A. Angell, "Water, a Comprehensive Treatise," ed by F. Franks, Plenum, New York (1981), Vol. 7, p. 1.
42) R. J. Speedy, *J. Phys. Chem.*, **86**, 982 (1982).
43) R. J. Speedy showed that the self-diffusion coefficient of the stretched model water tends to zero at low temperatures, "Abstracts of Lectures and Posters of Eighth International Symposium on Solute-Solute-Solvent Interactions," (1987), ed by J. Barthel and G. Schmeer, p. 29.
44) P. W. Brigeman, *Proc. Am. Acad. Arts Sci.*, **61**, 57 (1926).
45) K. E. Bett and J. B. Cappi, *Nature (London)*, **207**, 620 (1965).
46) E. M. Stanley and R. C. Batten, *J. Phys. Chem.*, **73**, 1187 (1969) and the references cited herein.
47) J. Kestin, H. E. Khalifa, H. Sookiazian, and W. A. Wakeham, *Ber. Bunsenges. Phys. Chem.*, **82**, 180 (1978).
48) T. DeFries and J. Jonas, *J. Chem. Phys.*, **66**, 896 (1977).
49) T. DeFries and J. Jonas, *J. Chem. Phys.*, **66**, 5393 (1977).
50) J. Kestin, J. V. Sengers, B. Kamgar-Parsi, and J. M. H. Levelt Sengers, *J. Phys. Chem. Ref. Data*, **13**, 175 (1984).
51) J. Rouch, C. C. Lai, and S.-H. Chen, *J. Chem. Phys.*, **65**, 4016 (1976).
52) J. Rouch and C. C. Lai and S.-H. Chen, *J. Chem. Phys.*, **66**, 5031 (1977).
53) J. Teixeira and J. Leblond, *J. de Phys.*, **39**, L83 (1978).
54) E. McLaughlin, *Chem. Eng.*, **64**, 389 (1964).
55) J. Yata, T. Minamiyama, T. Kim, and H. Murai, "Water and Steam, Their Properties and Current Industrial Applications," Proc. 9th Intern. Conf. on Prop. of Steam, held at München, 1979, Pergamon (1980), p. 431.

Electrical and Magnetic Properties of (BEDT-TTF)$_4$Ni(CN)$_4$ Complex

Masashi TANAKA,* Hideo TAKEUCHI, Mitsuru SANO, Toshiaki ENOKI,†
Kazuya SUZUKI,† and Kenichi IMAEDA††
Department of Chemistry, College of General Education, Nagoya University, Chikusa-ku, Nagoya 464-01
†Department of Chemistry, Faculty of Science, Institute of Tokyo Technology, Megro-ku, Tokyo 152
††Institute for Molecular Science, Myodaiji, Okazaki 444
(Received October 31, 1988)

The electrical conductivity and the ESR spectra of the single crystal of (BEDT-TTF)$_4$Ni(CN)$_4$ complex were measured. This crystal exhibits a metal-insulator transition at 160 K. The ESR signals show the presence of the [Ni^{III}(CN)$_4$]$^-$ anion in addition to the BEDT-TTF cation radical. The spin concentration of Ni(III) ion was estimated to be 0.01 of the total Ni ions from the temperature dependence of the spin susceptibility of these components. The X-ray photoelectron spectra were also taken.

The discovery of superconductivity in β-(BEDT-TTF)$_2$I$_3$ at T_c=1.3 K under ambient pressure[1-3] has promoted the preparation of radical salts of BEDT-TTF (bis(ethylenedithio)tetrathiafulvalene) with the linear triatomic anion such as I_2Br^-[4] and AuI_2^-.[5] After that, the studies of many complexes including the metal salts as the counter anion were made and the stable organic superconductor, (BEDT-TTF)$_2$Cu(NCS)$_2$, exhibiting complete superconductivity around 10 K at ambient pressure was discovered.[6] Such charge transfer complexes between BEDT-TTF and metal salts are interesting on magnetic properties in addition to electrical properties, because the metal ion can have the incompletely occupied electron shell. From this point of view, we investigated the magnetic and electronic properties of (BEDT-TTF)$_2$CuCl$_2$[7] and obtained the result that the Cu atoms in (BEDT-TTF)-CuCl$_2$ are in a mixed-valence state consisting of mono and bivalent cations. In the present paper, we report the complex of (BEDT-TTF)$_4$Ni(CN)$_4$.

Experimental

Black plate-like crystals were grown by the electrochemical crystallization of BEDT-TTF in 1,1,2-trichloroethane by using $K_2Ni(CN)_4$ as a supporting electrolyte. The electrical conductivity of the single crystal was measured by the four probe method using gold paste as a contact. The ESR spectra were taken by a Varian E112 at X-band with a continuous helium flow cryostat and a rectangular microwave cavity. The crystal was rotated around the a axis and was measured over a temparature range of 4—300 K. The X-ray photoelectron spectra were recorded on a VG ESCALAB MkII. Mg $K\alpha$ radiation (1253.6 eV) was used as the X-ray excitation source and the measurements were carried out at 10^{-7} Torr (1 Torr≈133.322 Pa) or below.

Results and Discussion

Figure 1 shows the temperature dependence of electrical conductivity of the single crystal. The room temperature conductivity was about 20 S cm^{-1}. The crystal was metallic between 230 and 300 K and became

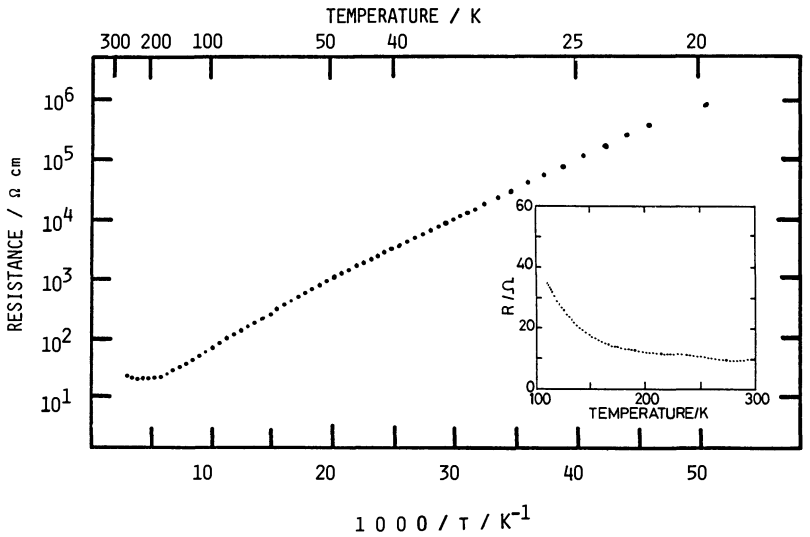

Fig. 1. Temperature dependence of the a axis electrical conductivity of the single crystal of (BEDT-TTF)$_4$Ni(CN)$_4$.

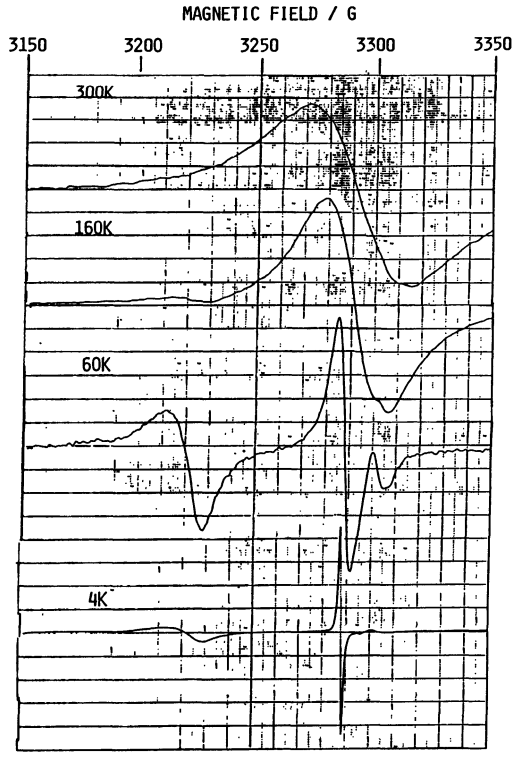

Fig. 2. ESR spectra of (BEDT-TTF)$_4$Ni(CN)$_4$ for the field direction giving the maximum g value around the a axis.

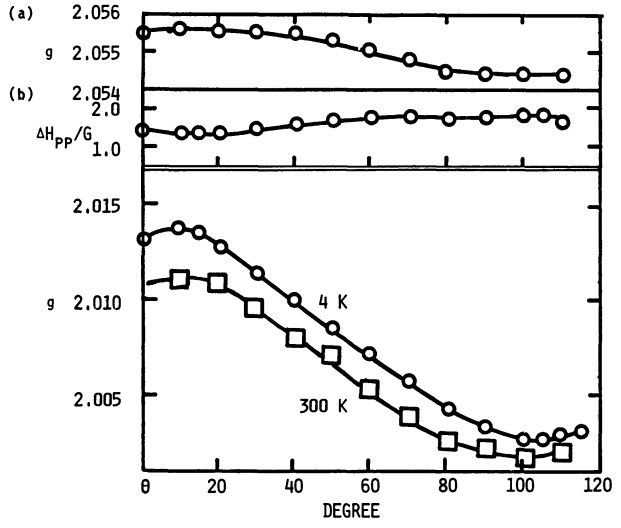

Fig. 3. Angular dependence of the g value around the a axis. The field is perpendicular to the ac plane at 0 degree. (a) Weak band at 4 K (—○—○—). (b) Strong band at 4 K (—○—○—) and 300 K (—□—□—).

semi-conductive with the energy gap of 100 K below 160 K after the temperature dependence of the conductivity was not observed between 160 and 230 K. This kind of resistance behavior may be explained by the phase transition of the crystal between 160 and 230 K.

The ESR spectra of the single crystal of (BEDT-TTF)$_4$Ni(CN)$_4$ are shown in Fig. 2. The angular

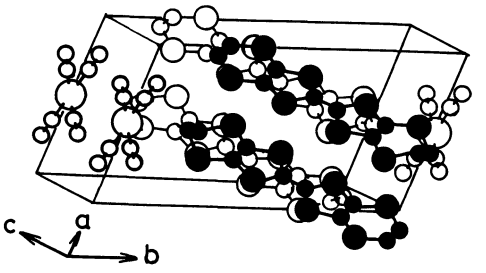

Fig. 4. Crystal structure of (BEDT-TTF)$_4$Ni(CN)$_4$.[8]

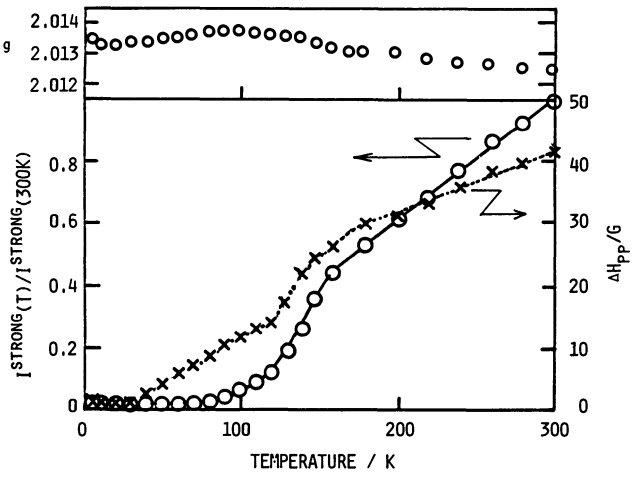

Fig. 5. Temperature dependence of the g value, the linewidth and the absorption intensity of the ESR spectra of the strong band for the field giving the maximum g value.

dependence of the g value and linewidth for the strong and weak bands at 4 and 300 K is shown in Fig. 3. The g value exhibits the maximum for the field applied nearly perpendicular to the ac plane. As is shown in Fig. 4, the molecular plane of BEDT-TTF is almost normal to the ac plane and the Ni(CN)$_4$ anion is located in the ac plane.[8] Accordingly the direction of the maximum g value is in accordance with the direction normal to the Ni(CN)$_4$ anion plane or parallel to the long axis of BEDT-TTF molecule.

The ESR spectrum at 4 K consists of the strong band at g=2.013 (3300 G; 1G=10^{-4} T), the weak band at g=2.056 (3220 G) and the satellite band at g=2.004 (3305 G). The strong band is assigned to the unpaired π-electron of the BEDT-TTF cation radical.[7] The weak band can be assigned to the d electron of [Ni^{III}(CN)$_4$]$^-$ in a square planar arrangement.[9]

Figure 5 shows the temperature dependence of the g value, the linewidth ΔH_{pp} and the absorption intensity of the ESR spectra of the strong band for (BEDT-TTF)$_4$Ni(CN)$_4$. The magnetic susceptibility $\chi^{strong}(T)$ at temperature T is given by the absorption intensity of the ESR signal,

$$\chi^{strong}(T) = C\{I^{strong}(T)/I^{strong}(300\ \mathrm{K})\}. \quad (1)$$

The coefficient C may be estimated with the observed static magnetic susceptibility at room temperature of 9×10^{-4} emu mol^{-1}. This value was corrected by considering the diamagnetic effect of the constitution atoms. The magnetic susceptibility and the linewidth of the strong band decrease almost linearly with decreasing temperature between 300 and 160 K and exponentially below 160 K. The activated behavior below 160 K corresponds to that of the electrical conductivity and means the occurence of the metal-semiconductor transition. If the susceptibility at room temperature may be described by the Pauli paramagnetism of the tight binding model, the calculated susceptibility is given the simple equation,[10]

$$\chi = \frac{N_0\mu_B^2}{\pi t \sin(\rho\pi/2)}, \tag{2}$$

where N_0 is Avogadro's number, μ_B is the Bohr magneton and t is the transfer integral. The degree of the charge transfer (ρ=1/2) per BEDT-TTF molecule and the observed susceptibility of 9×10^{-4} emu mol^{-1} gives t=0.016 eV.

The temperature dependence of the absorption intensity of the weak band can be depicted by the Curie law as shown in Fig. 6. The magnetic susceptibility of $[Ni(III)(CN)_4]^-$ ion is given by the next equation,

$$\chi^{weak}(T) = n_{Ni}\frac{N_0 g_{Ni}^2\mu_B^2}{3kT}s(s+1) \tag{3}$$

$$= C\{I^{weak}(T)/I^{strong}(300\text{ K})\}. \tag{4}$$

Then, the number of spins per $[Ni(CN)_4]^-$ anion is estimated to be n_{Ni}=0.01.

Figure 7 shows the X-ray photoelectron spectra (ESCA) of $(BEDT\text{-}TTF)_4Ni(CN)_4$ complex and $K_2Ni(CN)_4$. The Ni 2p3/2 and Ni 2p1/2 peaks were observed in both components and no difference of the

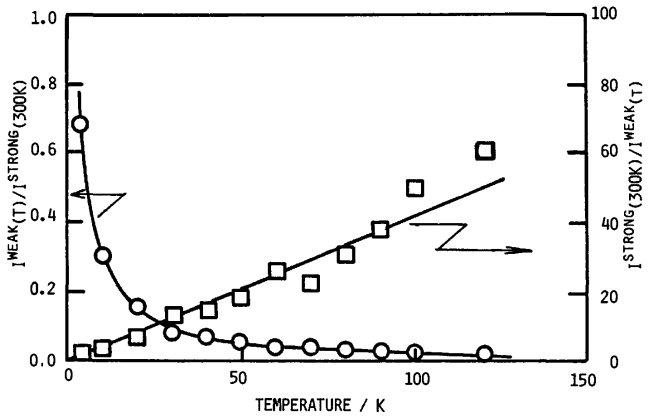

Fig. 6. Temperature dependence of the absorption intensity of the ESR spectra of the weak band.

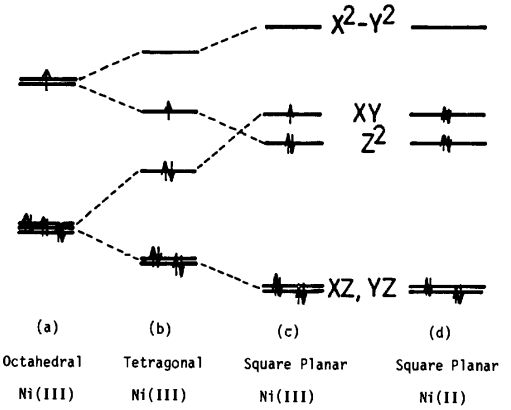

Fig. 8. Energy level diagram for Ni(III) and Ni(II) ions. The z axis is normal to the $Ni(CN)_4$ plane.

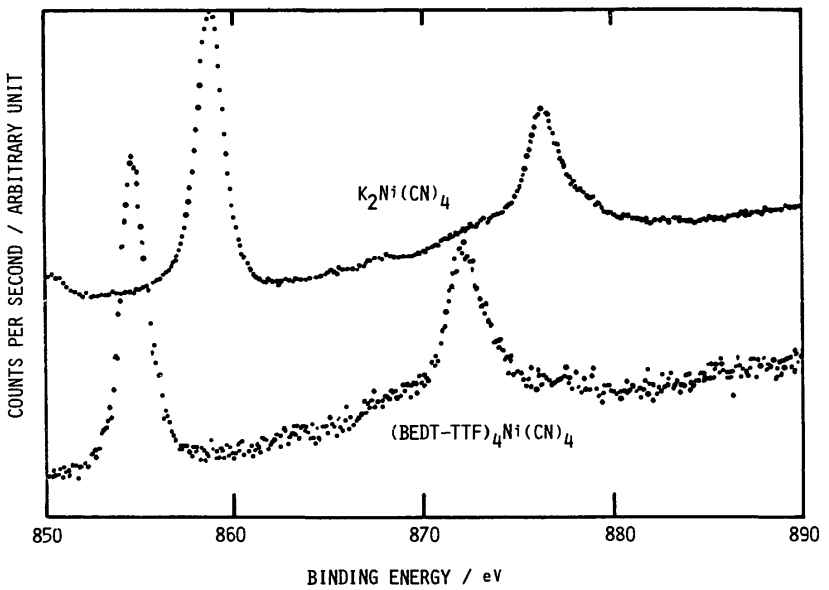

Fig. 7. X-Ray photoelectron spectra (ESCA) of $(BEDT\text{-}TTF)_4Ni(CN)_4$.

line shape and the intensity ratio is found between them. That is, most parts of the Ni atoms in (BEDT-TTF)$_4$Ni(CN)$_4$ complex are in the bivalence state and the low spin d^8 configuration of Ni(II) ion forms the closed shell in the square-planar arrangement as is shown in Fig. 8, while a few Ni(III) complexs prepared by the electrochemical oxidation have the unpaired electron in the d_{xy} orbital. Such mixed valence state of the metal ion in the BEDT-TTF complex was observed for the Cu ion in (BEDT-TTF)$_2$CuCl$_2$.[7] These ESR spectra consist of both signals of BEDT-TTF cation and metal ion. This fact shows the possibility of the coexist of the free carrier in the conducting BEDT-TTF band and the paramagnetic electron in the metal ion.

The above-mentioned results about the magnetic and electrical measurements show that the electrical conductivity of (BEDT-TTF)$_4$Ni(CN)$_4$ complex is metallic at room temperature and the metal-insulator transition occurs at 160 K by the dimerization of the BEDT-TTF molecules.

The authors would like to thank Dr. Tetsuo Asaji of Nagoya university for the measurement of the static magnetic susceptibility.

References

1) E. B. Yagubskii, I. F. Schegolev, V. N. Laukhin, P. A. Kononovich, M. V. Kartsovnik, A. V. Zvarykina, and L. L. Buravov, *Sov. Phys. JETP Lett.*, **39**, 12 (1984).

2) J. M. Williams, T. J. Emge, H. H. Wang, M. A. Beno, P. T. Copps, L. N. Hall, K. D. Carlson, and G. W. Crabtree, *Inorg. Chem.*, **23**, 2558 (1984).

3) H. Schwenk, C. P. Heidmann, F. Gross, E. Hess, K. Andres, D. Schweitzer, and H. J. Keller, *Phys. Rev. B*, **31**, 3138 (1985).

4) T. J. Emge, H. H. Wang, M. A. Beno, P. C. W. Leung, M. A. Firestone, H. C. Jenkins, J. D. Cook, K. D. Carlson, J. M. Williams, E. L. Venturini, L. J. Azedo, and J. E. Schirber, *Inorg. Chem.*, **24**, 1736 (1985).

5) H. H. Wang, M. A. Beno, U. Geiser, M. A. Firestone, K. S. Webb, L. Nunez, G. W. Crabtree, K. D. Carlson, J. M. Williams, L. J. Azevedo, J. F. Kwak, and J. E. Schirber, *Inorg. Chem.*, **24**, 2465 (1985).

6) H. Urayama, H. Yamochi, G. Saito, K. Nozawa, T. Sugano, M. Kinoshita, S. Sato, K. Oshima, A. Kawamoto, and J. Tanaka, *Chem. Lett.*, **1988**, 558.

7) M. Tanaka, A. Kawamoto, J. Tanaka, M. Sano, T. Enoki, and H. Inokuchi, *Bull. Chem. Soc. Jpn.*, **60**, 2531 (1987).

8) A. Kawamoto, M. Tanaka, and J. Tanaka, *Chem. Lett.*, to be submitted.

9) A. G. Lappin, C. K. Murray, and D. W. Margerum, *Inorg. Chem.*, **17**, 1630 (1978).

10) J. B. Torrance, Y. Tomkiewicz, and B. D. Silverman, *Phys. Rev. B*, **15**, 4738 (1977).

The Crystal and Molecular Structures of Two 1:2 Complexes of 1,4-Diazabicyclo[2.2.2]octane (DABCO) with 1-(*o*-Chlorophenyl)-1-phenyl-2-propyn-1-ol (CPPOH), and Those of Two 1:2 Complexes of *N,N'*-Dimethylpiperazine (DMP) with CPPOH

Masanori YASUI, Tetsuro YABUKI, Masaaki TAKAMA, Shigeharu HARADA, Nobutami KASAI,* Koichi TANAKA,† and Fumio TODA*,†
Department of Applied Chemistry, Faculty of Engineering, Osaka University, Suita, Osaka 565
†Department of Industrial Chemistry, Faculty of Engineering, Ehime University, Matsuyama 790
(Received April 22, 1988)

X-Ray crystal structure analysis of the title four complexes showed that crystals consist of CPPOH···achiral diamine···CPPOH units. In the first two crystals a DABCO molecule is bound by two (−)-CPPOH molecules (**1**) or by (+)- and (−)-CPPOH (**2**) to form 1:2 complex by strong intermolecular O-H···N hydrogen bonds [O-H···N=2.707(3) and 2.755(3) (**1**) and 2.704(4) and 2.747(4) Å (**2**)]. The latter two crystals are respectively formed by (+)-CPPOH···DMP···(−)-CPPOH complex (**3**) [O-H···N=2.771(3) Å] and (−)-CPPOH···DMP···(−)-CPPOH complex (**4**) [O-H···N=2.768(5) and 2.730(6) Å].

In a series of studies on the novel optical resolution of tertiary acetylenic alcohols by complexation with naturally chiral alkaloids,[1-3] Toda and Tanaka found that the partially resolved enantiomers, obtained after the separation of the 1:1 complex of optically pure enantiomers with alkaloid, can easily be purified by complexation with simple achiral diamines such as DABCO, *N,N'*-dialkylpiperazine, *N,N,N',N'*-tetramethylethylenediamine, or pyrazine to give the optically pure alcohols.[4] Among the complexation reactions mentioned above, achiral DABCO forms 1:2 complex selectively with two (−)-CPPOH molecules to give **1** crystal, and in result optically pure (+)-CPPOH remains in solution. On the other hand, achiral DMP easily forms 1:2 complex (**3**) with (+)- and (−)-CPPOH molecules. However, under appropriate but severe conditions, DABCO and DMP were found to form the other 1:2 complex crystals of (+)-CPPOH···DABCO···(−)-CPPOH (**2**) and (−)-CPPOH···DMP···(−)-CPPOH (**4**), respectively. In order to obtain a clue to clarify the fact that leads the selective 1:2 complex formation of achiral DABCO with two chiral (−)-CPPOH molecules, the crystal and molecular structures of **1** has been determined by means of X-ray diffraction. As a reference, the structure of **2**, which is not formed under ordinary condition, has also been determined. The crystal and molecular structures of 1:2 complexes of DMP with two CPPOH molecules, (+)-CPPOH··· DMP···(−)-CPPOH (**3**) and (−)-CPPOH···DMP···(−)-CPPOH (**4**, obtained under severe condition), which have been already reported briefly,[5] are compared with those of **1** and **2**.

Experimental

Crystal Data. $C_6H_{12}N_2$,2($C_{15}H_{11}OCl$), *F.W.* 597.6; **1**, monoclinic, space group $P2_1$, a=15.785(2), b=11.511(1), c=8.878(1) Å, β=102.89(1)°, V=1565.6(3) Å^3, D_c=1.262 g cm^{-3} for Z=2. **2**, monoclinic, space group $C2/c$, a=49.319(13), b=9.237(1), c=14.343(1) Å, β=105.96(1)°, V=6281.8(19) Å^3, D_c=1.264 g cm^{-3} for Z=8. $C_6H_{14}N_2$,2($C_{15}H_{11}OCl$), *F.W.* 599.6; **3**, triclinic, space group $P\bar{1}$, a=10.752(4), b=9.057(4),

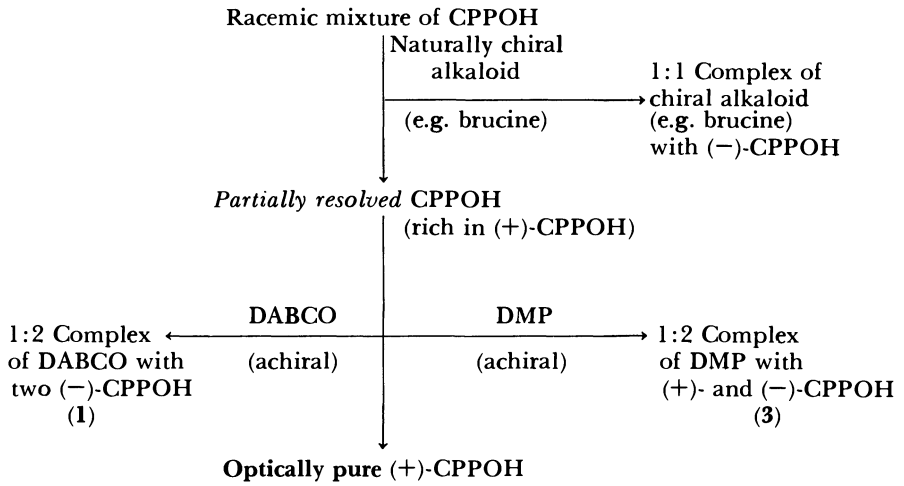

c=8.350(5) Å, α=100.28(4), β=81.87(3), γ=102.38(2)°, V=777.0(7) Å^3, D_c=1.282 g cm^{-3} for Z=1. **4**, monoclinic, space group $P2_1$, a=17.511(2), b=7.606(1), c=13.311(2) Å^3, β=111.55(1)°, V=1648.9(5) Å^3, D_c=1.208 g cm^{-3} for Z=2.

The crystals used has approximate dimensions of 0.4×0.3×0.2 mm (**1**) and 0.5×0.3×0.2 mm (**2**). X-Ray diffraction data were collected on a Rigaku four-circle diffractometer by the θ-2θ scan technique ($2\theta_{max}$=120°). For **1** and **4**, hkl and $h\bar{k}l$ reflections were measured in order to determine the absolute configuration of (−)-CPPOH molecule. Nickel-filtered Cu $K\alpha$ radiation was used (λ=1.5418 Å). The θ-scan rate was 4° min^{-1} and the scan width $\Delta\theta$=(1.2+0.15 tan θ)°. Backgrounds were counted for 4 s at both ends of a scan. Three standard reflections measured after every 100 reflections to monitor the stability and orientation of the crystal showed no significant decay throughout the experiment. Of the 2461 and 4663 independent reflections measured, 2393 and 3834 reflections were observed for **1** and **2**, respectively ($|F_o|>2\sigma(F_o)$, where σ is the standard deviation obtained by the counting statistics of reflections). Usual Lorentz and polarization corrections were applied but absorption effect was ignored [μ(Cu $K\alpha$)=21.4 cm^{-1} for both **1** and **2**]. X-Ray experiments on **3** and **4** crystals have been already descrived in the previous letter.[5]

Bijvoet pair reflections were used for the determination of absolute configuration of (−)-CPPOH molecule in **1** and **4**. These pair reflections were also included in the Hamilton's R value test,[6] but intensities of each pair reflections were averaged for the ordinary use of the structure determination.

Structure Solution and Refinement

The structure of **1** was solved by the heavy atom method and that of **2** by the direct method (*MULTAN* 78).[7] Both structures were refined anisotropically by the block-diagonal least-squares procedure (*HBLS*

Table 1. Final Atomic Coordinates and Equivalent Isotropic Temperature Factors[9] for Non-Hydrogen Atoms with Estimated Standard Deviations in Parentheses

Atom	x	y	z	B_{eq}/Å^2
(**1**) 1:2 Complex of DABCO with two (−)-CPPOH				
C(1A)	−0.0422(2)	0.3264(3)	0.2884(4)	3.7
C(2A)	−0.0115(2)	0.4396(3)	0.3612(4)	4.3
C(3A)	0.0176(3)	0.5260(3)	0.4258(5)	5.4
C(4A)	−0.0378(2)	0.3316(3)	0.1163(3)	3.6
C(5A)	−0.0860(2)	0.4087(3)	0.0108(4)	4.4
C(6A)	−0.0775(3)	0.4149(4)	−0.1425(4)	5.4
C(7A)	−0.0198(3)	0.3416(4)	−0.1921(4)	6.2
C(8A)	0.0256(3)	0.2598(4)	−0.0916(5)	5.8
C(9A)	0.0179(2)	0.2555(3)	0.0616(4)	4.9
C(10A)	−0.1322(2)	0.2925(3)	0.3087(4)	3.9
C(11A)	−0.1717(3)	0.3488(3)	0.4126(4)	5.0
C(12A)	−0.2517(3)	0.3086(4)	0.4382(5)	6.5
C(13A)	−0.2904(3)	0.2129(4)	0.3583(5)	6.6
C(14A)	−0.2505(3)	0.1555(4)	0.2536(5)	6.1
C(15A)	−0.1726(3)	0.1962(3)	0.2301(4)	4.9
O(1A)	0.0139(1)	0.2375(2)	0.3665(3)	4.5
Cl(1A)	−0.16303(6)	0.50005(9)	0.06128(11)	5.7
C(1B)	0.5403(2)	0.0482(3)	0.7575(4)	3.8
C(2B)	0.5102(2)	−0.0398(3)	0.6350(4)	4.2
C(3B)	0.4851(3)	−0.1084(4)	0.5361(4)	5.4
C(4B)	0.6410(2)	0.0442(3)	0.8022(4)	4.0
C(5B)	0.6882(2)	−0.0508(3)	0.8717(4)	4.4
C(6B)	0.7778(2)	−0.0557(4)	0.9117(5)	5.5
C(7B)	0.8232(3)	0.0388(4)	0.8755(5)	6.6
C(8B)	0.7806(3)	0.1352(4)	0.8062(5)	6.8
C(9B)	0.6884(2)	0.1375(4)	0.7700(5)	5.5
C(10B)	0.4993(2)	0.0288(3)	0.8950(4)	3.9
C(11B)	0.4367(2)	−0.0559(3)	0.8960(4)	4.7
C(12B)	0.3981(3)	−0.0688(4)	1.0209(5)	6.1
C(13B)	0.4224(3)	0.0010(5)	1.1478(5)	6.7
C(14B)	0.4855(3)	0.0874(5)	1.1496(5)	6.8
C(15B)	0.5237(2)	0.1003(4)	1.0242(4)	5.1
O(1B)	0.5183(2)	0.1615(2)	0.6958(3)	4.8
Cl(1B)	0.63560(6)	−0.17730(9)	0.91309(10)	5.6
C(16)	0.2275(3)	0.1955(4)	0.3869(4)	5.6
C(17)	0.1901(3)	0.1965(4)	0.6351(5)	5.4
C(18)	0.2349(3)	0.3713(3)	0.5319(5)	5.6
C(19)	0.3244(3)	0.1778(4)	0.4592(4)	5.4
C(20)	0.2848(2)	0.1563(3)	0.7031(4)	4.8
C(21)	0.3286(2)	0.3427(4)	0.6255(5)	5.3
N(1)	0.1859(2)	0.2624(3)	0.4916(3)	4.4
N(2)	0.3438(2)	0.2160(3)	0.6206(3)	4.3

Table 1. (Continued)

Atom	x	y	z	B_{eq}/Å^2
(2) 1:2 Complex of DABCO with (+)- and (−)-CPPOH				
C(1A)	0.67481(8)	0.1509(4)	0.3187(3)	3.1
C(2A)	0.64823(9)	0.1834(4)	0.2424(3)	3.9
C(3A)	0.6263(1)	0.2081(5)	0.1862(4)	5.7
C(4A)	0.69572(8)	0.0684(4)	0.2763(3)	2.9
C(5A)	0.70428(9)	0.1127(4)	0.1962(3)	3.6
C(6A)	0.7242(1)	0.0362(5)	0.1632(3)	4.8
C(7A)	0.7356(1)	−0.0894(5)	0.2106(4)	5.6
C(8A)	0.7276(1)	−0.1365(5)	0.2895(3)	5.0
C(9A)	0.70761(9)	−0.0600(4)	0.3220(3)	3.7
C(10A)	0.68873(8)	0.2895(4)	0.3678(3)	2.9
C(11A)	0.6806(1)	0.4262(4)	0.3323(3)	4.1
C(12A)	0.6942(1)	0.5493(5)	0.3804(4)	5.2
C(13A)	0.7153(1)	0.5349(5)	0.4648(3)	4.8
C(14A)	0.7234(1)	0.3988(5)	0.5025(3)	4.8
C(15A)	0.70979(9)	0.2754(4)	0.4543(3)	3.9
O(1A)	0.66819(6)	0.0590(3)	0.3877(2)	3.7
Cl(1A)	0.69161(3)	0.27027(13)	0.13346(8)	5.3
C(1B)	0.57488(8)	0.3400(4)	0.7882(3)	3.1
C(2B)	0.60295(9)	0.3033(4)	0.8549(3)	3.8
C(3B)	0.6256(1)	0.2753(5)	0.9052(4)	5.3
C(4B)	0.55802(8)	0.4310(4)	0.8417(3)	3.4
C(5B)	0.55105(9)	0.3855(4)	0.9243(3)	3.8
C(6B)	0.5362(1)	0.4718(6)	0.9721(3)	5.2
C(7B)	0.5273(1)	0.6073(6)	0.9356(4)	5.7
C(8B)	0.5334(1)	0.6566(5)	0.8520(4)	5.4
C(9B)	0.5487(1)	0.5687(4)	0.8062(3)	4.1
C(10B)	0.55831(9)	0.2042(4)	0.7439(3)	3.2
C(11B)	0.5713(1)	0.0690(4)	0.7506(3)	4.0
C(12B)	0.5559(1)	−0.0504(5)	0.7040(3)	5.0
C(13B)	0.5281(1)	−0.0324(5)	0.6518(4)	5.9
C(14B)	0.5154(1)	0.1022(6)	0.6432(4)	6.7
C(15B)	0.5305(1)	0.2213(5)	0.6898(3)	5.5
O(1B)	0.57934(7)	0.4268(3)	0.7122(2)	3.9
Cl(1B)	0.56110(3)	0.21371(12)	0.97352(7)	4.9
C(16)	0.6344(1)	0.3549(5)	0.4812(4)	5.2
C(17)	0.6112(1)	0.1306(6)	0.4745(4)	6.0
C(18)	0.6544(1)	0.1667(6)	0.5935(3)	5.9
C(19)	0.6170(1)	0.4099(5)	0.5513(4)	5.3
C(20)	0.5955(1)	0.1768(6)	0.5487(4)	6.2
C(21)	0.6391(1)	0.2291(5)	0.6653(3)	5.1
N(1)	0.63876(8)	0.1283(3)	0.4941(2)	3.6
N(2)	0.61191(8)	0.2913(3)	0.6109(2)	3.6
(3) 1:2 Complex of DMP with (+)- and (−)-CPPOH				
C(1)	0.2600(2)	0.7065(3)	0.3562(3)	3.2
C(2)	0.3320(3)	0.8505(3)	0.3028(3)	3.5
C(3)	0.3817(3)	0.9687(4)	0.2598(4)	4.7
C(4)	0.3255(3)	0.5726(3)	0.2719(3)	3.3
C(5)	0.4526(3)	0.5689(3)	0.2857(3)	3.8
C(6)	0.5101(3)	0.4484(3)	0.2052(4)	4.5
C(7)	0.4422(3)	0.3301(3)	0.1065(4)	4.6
C(8)	0.3163(3)	0.3294(4)	0.0932(4)	5.0
C(9)	0.2584(3)	0.4491(3)	0.1754(3)	4.1
C(10)	0.2429(2)	0.7153(3)	0.5425(3)	3.2
C(11)	0.3041(3)	0.8378(3)	0.6470(3)	3.8
C(12)	0.2817(3)	0.8416(4)	0.8156(4)	4.6
C(13)	0.1986(3)	0.7222(4)	0.8807(4)	5.1
C(14)	0.1372(3)	0.6014(4)	0.7780(4)	4.9
C(15)	0.1589(3)	0.5966(3)	0.6092(4)	4.1
O(1)	0.1358(1)	0.6757(2)	0.2999(2)	3.7
Cl(1)	0.54804(6)	0.71576(9)	0.40454(9)	4.9
C(16)	−0.1079(3)	0.8840(4)	0.4830(5)	6.5
C(17)	0.0534(3)	1.0619(4)	0.3582(4)	6.0

Table 1. (Continued)

Atom	x	y	z	B_{eq}/Å^2
C(18)	−0.0703(5)	0.8445(6)	0.1927(6)	10.7
N(1)	−0.0081(3)	0.9026(3)	0.3456(3)	5.7
(**4**) 1:2 Complex of DMP with two (−)-CPPOH				
C(1A)	−0.0131(3)	0.2562(6)	0.1959(4)	3.7
C(2A)	0.0111(3)	0.1285(6)	0.1295(4)	3.9
C(3A)	0.0271(4)	0.0323(7)	0.0707(4)	5.1
C(4A)	0.0588(3)	0.3825(6)	0.2496(4)	3.5
C(5A)	0.1339(3)	0.3294(6)	0.3248(4)	4.0
C(6A)	0.1975(3)	0.4472(7)	0.3734(4)	4.7
C(7A)	0.1868(3)	0.6225(8)	0.3449(5)	5.2
C(8A)	0.1140(3)	0.6768(7)	0.2694(5)	5.1
C(9A)	0.0503(3)	0.5605(6)	0.2224(4)	4.5
C(10A)	−0.0403(3)	0.1675(7)	0.2799(4)	4.2
C(11A)	−0.0494(3)	−0.0129(7)	0.2845(4)	5.0
C(12A)	−0.0766(4)	−0.0896(11)	0.3582(6)	7.5
C(13A)	−0.0952(4)	0.0127(12)	0.4295(5)	8.4
C(14A)	−0.0871(4)	0.1955(13)	0.4276(5)	8.0
C(15A)	−0.0599(4)	0.2734(9)	0.3520(4)	5.7
O(1A)	−0.0793(2)	0.3589(5)	0.1254(3)	4.2
Cl(1A)	0.15269(8)	0.11505(19)	0.36437(11)	5.6
C(1B)	−0.4886(3)	−0.1713(7)	−0.1988(4)	4.2
C(2B)	−0.5023(3)	−0.3130(8)	−0.1322(4)	4.8
C(3B)	−0.5118(4)	−0.4201(9)	−0.0732(5)	6.3
C(4B)	−0.5679(3)	−0.0658(7)	−0.2509(4)	4.1
C(5B)	−0.6392(3)	−0.1332(7)	−0.3248(4)	4.6
C(6B)	−0.7101(4)	−0.0360(9)	−0.3701(5)	5.9
C(7B)	−0.7108(4)	0.1359(11)	−0.3389(6)	7.5
C(8B)	−0.6415(5)	0.2090(9)	−0.2643(6)	7.1
C(9B)	−0.5713(4)	0.1090(8)	−0.2214(5)	5.8
C(10B)	−0.4564(3)	−0.2407(7)	−0.2828(4)	4.6
C(11B)	−0.4306(4)	−0.4152(10)	−0.2840(5)	6.7
C(12B)	−0.3999(5)	−0.4688(12)	−0.3590(7)	8.9
C(13B)	−0.3935(4)	−0.3574(15)	−0.4333(6)	9.5
C(14B)	−0.4189(4)	−0.1872(14)	−0.4360(5)	8.9
C(15B)	−0.4499(4)	−0.1239(11)	−0.3587(5)	6.7
O(1B)	−0.4301(2)	−0.0539(6)	−0.1280(3)	5.7
Cl(1B)	−0.64471(9)	−0.3500(3)	−0.36675(12)	6.5
C(16)	−0.2557(4)	0.0582(8)	0.0970(4)	5.3
C(17)	−0.2745(4)	0.2349(8)	−0.0564(5)	5.9
C(18)	−0.2685(4)	0.3733(10)	0.1093(6)	7.7
C(19)	−0.2267(4)	−0.0883(9)	0.0471(5)	5.9
C(20)	−0.2450(4)	0.0892(9)	−0.1057(5)	5.7
C(21)	−0.2327(5)	−0.2258(11)	−0.1202(6)	8.1
N(1)	−0.2375(3)	0.2277(6)	0.0608(4)	4.8
N(2)	−0.2640(3)	−0.0817(6)	−0.0707(4)	4.8

V).[8] The function minimized was $\sum w\Delta F^2$. The hydrogen atoms which could be located on the difference Fourier maps were refined with isotropic temperature factors. The final R indices are 0.045 (R_w=0.038) and 0.063 (R_w=0.092) for **1** and **2**, respectively. The weighting schemes used at the final stage of the refinement were $w=(\sigma^2+a|F_o|+b|F_o|^2)^{-1}$, where a=−0.65941 and 0.12269 and b=0.03381 and 0.00105 for **1** and **2**, respectively.

The structures of **3** and **4** have been determined in a similar manner as mentioned above.[5] R=0.060 (R_w=0.074) (**3**) and R=0.077 (R_w=0.083) (**4**).

The absolute configuration of the (−)-CPPOH molecule has been determined by examining the magnitude of structure factors of Bijvoet pair reflections of the **1** and **4** crystals, and the chirality of the asymmetric C(1) atom of the (−)-CPPOH in both complexes was found as R. Hamilton's R value test for the **1** and **4** is consistent with this result.

Final atomic parameters of **1**, **2**, **3**, and **4** are given in Table 1.†† Atomic scattering factors used were taken from those of International Tables for X-Ray Crystallography, Vol. IV.[10] Computations were done on an ACOS S850 computer at the Crystallographic Research Center, Institute for Protein Research, Osaka University.

†† Tables of anisotropic thermal parameters and those of observed and calculated structure factors of **1**, **2**, **3**, and **4** are kept at the Chemical Society of Japan, Document No. 8871.

Results and Discussion

Crystal Structures. The packings of molecules in **1** and **2** crystals[11] are depicted in Fig. 1, which are compared with those of **3** and **4**. The remarkable feature of the structure is that all these crystals consist of discrete 1:2 host-guest complexes of CPPOH···achiral diamine···CPPOH consolidated by O-H···N hydrogen bonds. Each DABCO molecule is bound to two (−)-CPPOH in **1** and bound to (+)- and (−)-CPPOH molecules in **2** by strong hydrogen bondings [O-H···N=2.707(3) and 2.755(3) Å (**1**) and 2.704(4) and 2.747(4) Å (**2**) (Fig. 2, (a) and (b))]. This 1:2 complex formation seems to be similar to that of achiral DMP with (+)- and (−)-CPPOH (**3**) and two (−)-CPPOH molecules (**4**) (Fig. 2, (c) and (d)). The geometry about the hydrogen bondings in **1** and **2** complexes are compared with those in **3** and **4** in Table 2. In **1** and **2**, the H(1) atom of CPPOH locates at the direction of lone pair electrons of the N atom which occupies the apex of the pyramid made by one N and three C atoms at one end of DABCO. The O(1), H(1), and N atoms of each of the hydrogen bonds lie approximately on a line. In **3** and **4**, the H(1) atom of CPPOH is approximately at the direction of lone pair electrons of one of the N atoms of DMP. The O(1), H(1), and N atoms of each of the hydrogen bonds are not on a line in **3** [O-H(1)···N=161(3)°].

In **1** crystal very close inter-complex atomic contacts are observed. The closest distance, 3.160(5) Å was found between the hydroxyl oxygen atom of one complex, O(1A)(x, y, z) and the acetylenic carbon atom of the adjacent complex, C(3A)($-x$, $-0.5+y$, $1-z$). The second closest contact, 3.290(5) Å was observed between the chlorine atom of the *o*-chlorophenyl group of one complex, Cl (1B)(x, y, z) and the carbon atom of the phenyl group of the other complex, C(14B)($1-x$, $-0.5+y$, $2-z$)]. On the other hand, no close contact shorter than 3.465(5) Å [Cl(1A)(x, y, z)···C(13A)(x, $1-y$, $-0.5+z$)] was observed in **2**. In addition to this, most of the close inter-complex contact distances involved with hydrogen atoms in **1** are shorter than those in **2**. These facts suggest that the stronger inter-complex interaction leads the selective crystallization of (−)-CPPOH···DABCO···(−)-CPPOH (**1**), which makes the optical resolution of (−)-CPPOH enantiomers from the partially resolved CPPOH.

In **3** and **4** crystals, however, no short inter-complex contact distances are found between non-hydrogen atoms. Instead, intercomplex atomic contacts involved with hydrogen atoms in **3** are mostly shorter than those in **4**, and the **3** crystal has the denser structure (D_c=1.282 g cm^{-3}) than **4** (D_c=1.208 g cm^{-3}).

Molecular Structures. Selected bond distances and bond angles in **1**, **2**, **3**, and **4** are listed in Table 3.

1-(*o*-Chlorophenyl)-1-phenyl-2-propyn-1-ol(CPPOH). The C(2)-C(3) acetylenic bonds have distances of 1.187(5) and 1.180(5) Å (**1**) and 1.179(6) and 1.181(6) Å (**2**), which are slightly shorter than the standard C-C triple bond distance, 1.204(2) Å. The C(1)-C(2)-C(3) angles are smaller than 180° [175.5(4) and 178.8(4)° (**1**) and 175.9(4) and 177.6(4)° (**2**)].

Two benzene rings of *o*-Cl-Ph and Ph groups are planar, which make angles of 88.6(1) and 89.1(1)° in **1** and 80.4(1) and 89.1(1)° in **2**. The corresponding angles in **3** and **4** are 82(1)° and 87.7(1) and 85.8(1)°, respectively. Among the bond angles around the C(5) atom, the C(4)–C(5)-Cl(1) angle is approximately equal to the C(4)-C(5)-C(6), which are larger than the C(6)–C(5)–Cl(1) throughout the complexes **1** to **4** (Table 2).

The (−)-1-(*o*-bromophenyl)-1-phenyl-2-propyn-1-ol molecule in its 1:1 complex with brucine and also that with (−)-sparteine[3] have similar structure as (−)-CPPOH in the present complexes of **1** and **2**.

1,4-Diazabicyclo[2.2.2]octane (DABCO). The DABCO molecule completely lost its original $\bar{6}m2$ symmetry by the formation of 1:2 complex with CPPOH. However, in the 1:2 complex with *p*-cresol, it was observed that the molecular symmetry of DABCO decreased down to 2. All the thermal ellipsoids of carbon atoms of DABCO are much larger than those of the other carbon atoms, and they also show remarkable elonga-

Table 2. Hydrogen Bondings in the 1:2 Complexes of DABCO and DMP with CPPOH. Estimated Standard Deviations in Parentheses

	1	2	3	4
Distance [l/Å]				
O(1)·····N	2.707(3)	2.704(4)	2.771(3)	2.768(5)
	2.755(3)	2.747(4)		2.730(6)
O(1)-H(1)	1.05(4)	1.07(6)	1.05(3)	1.00(6)
	1.06(4)	1.03(5)		1.01(8)
H(1)·····N	1.66(4)	1.63(6)	1.76(4)	1.77(6)
	1.70(4)	1.71(5)		1.72(8)
Angle [ϕ/°]				
O(1)-H(1)·····N	177(4)	178(5)	161(3)	175(5)
	176(4)	179(4)		173(7)

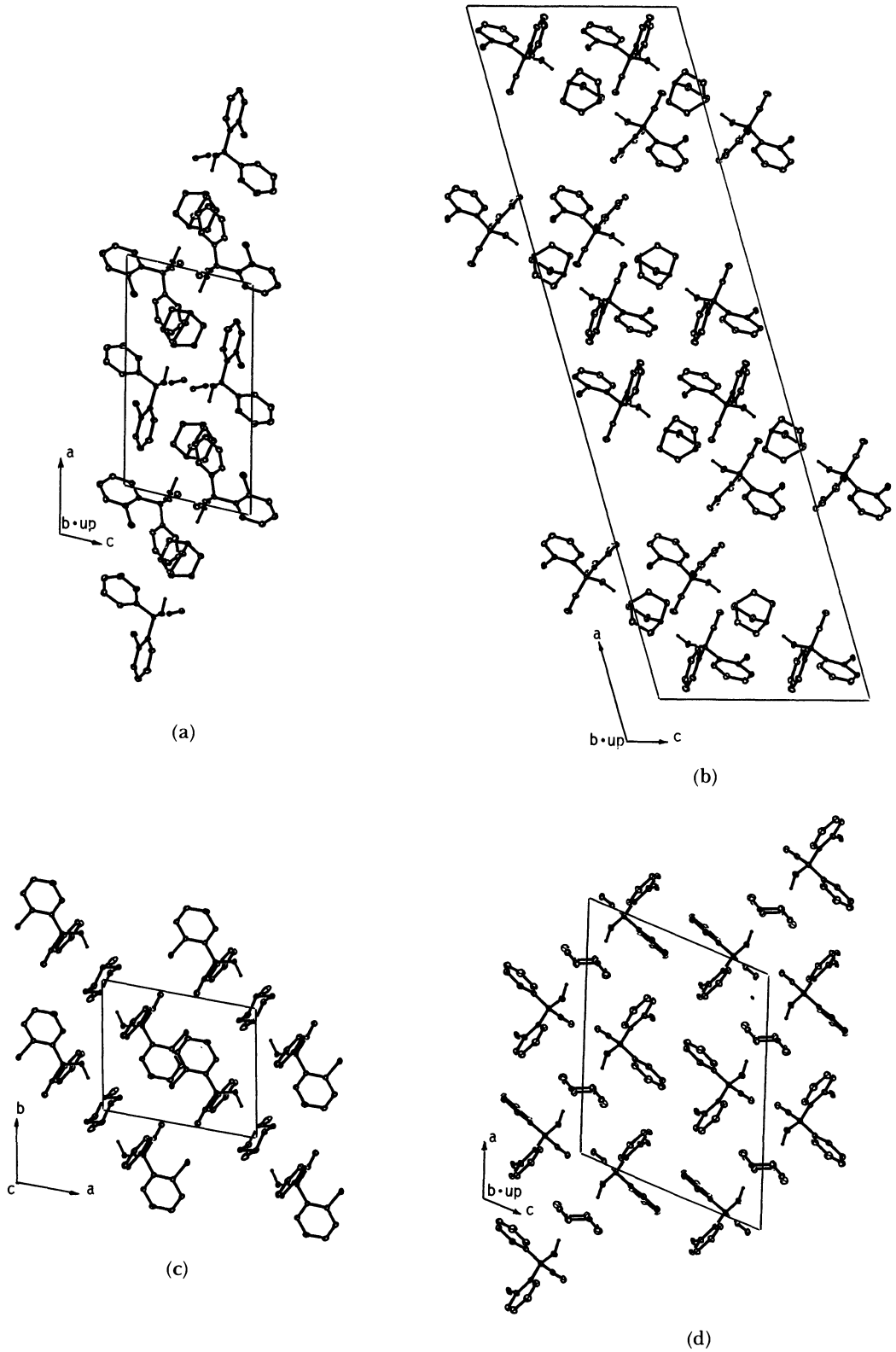

Fig. 1. Packing of 1:2 complex molecules[11] in the **1**(a) and **2**(b) crystals are compared with that of **3**(c) and **4**(d). Non-hydrogen atoms are drawn as thermal elliposids with 10% probability level, and hydrogen atoms only engaged in hydrogen bondings are shown as spheres with B=1.0 Å^2.

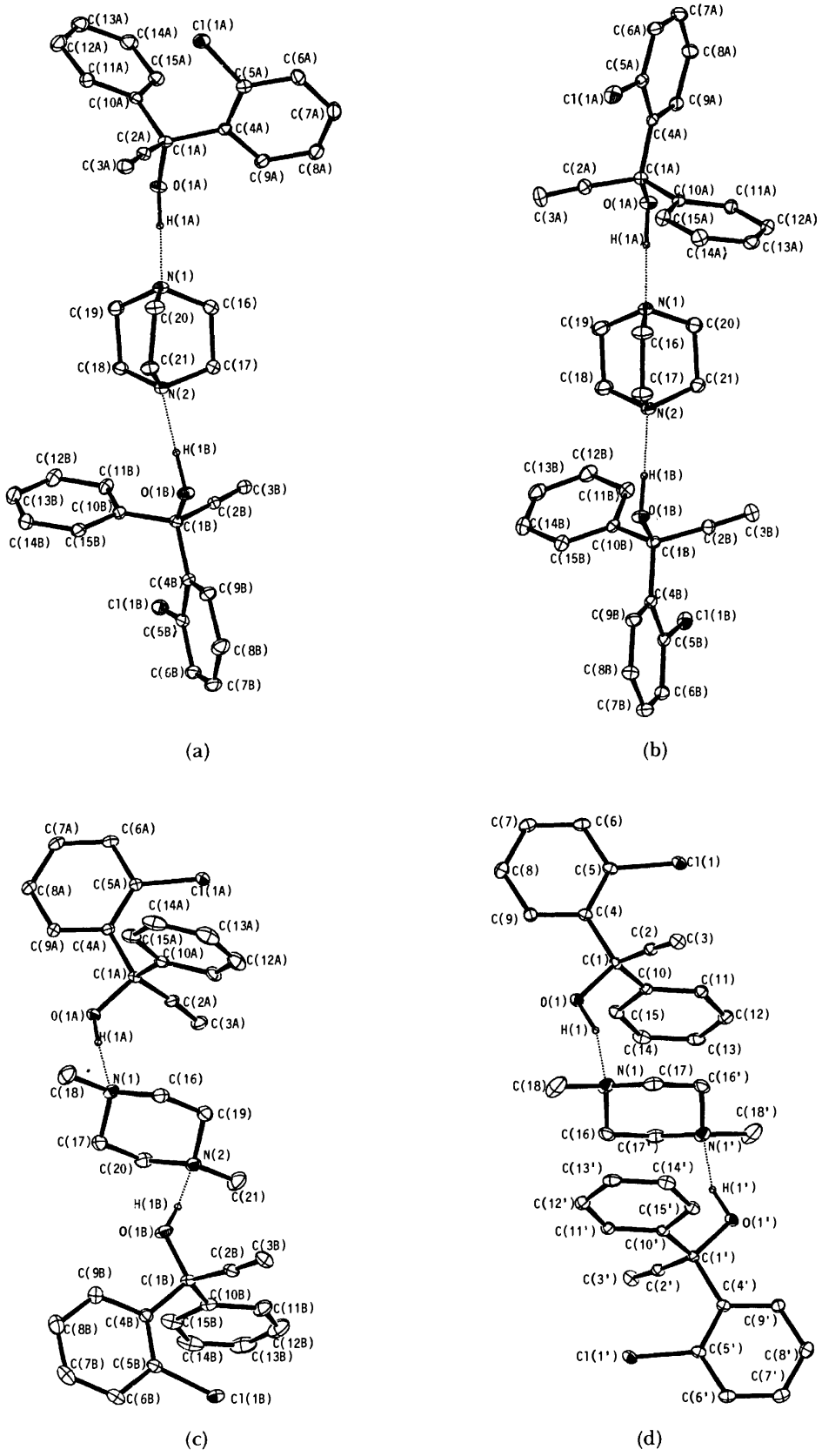

Fig. 2. A perspective view[11] of **1**(a) and **2**(b) complexes with the numbering scheme of atoms compared with that of **3**(c) and **4**(d). Non-hydrogen atoms are drawn as thermal ellipsoids with 10% probability level, and hydrogen atoms only engaged in hydrogen bonding are shown as spheres with B=1.0 Å^2.

Table 3. Selected Bond Distances and Bond Angles in the 1:2 Complex of DABCO with Two (−)-CPPOH (**1**) and that with (+)- and (−)-CPPOH (**2**) Compared with Those in the 1:2 Complex of *N,N'*-Dimethylpiperazine with (+)- and (−)-CPPOH (**3**) and That with Two (−)-CPPOH (**4**). Estimated Standard Deviations in Parentheses

	1	**2**	**3**	**4**
Bond distances [*l*/Å]	1-(*o*-Chlorophenyl)-1-phenyl-2-propyn-1-ol (CPPOH)			
C(1)-O(1)	1.425(4)	1.409(4)	1.434(3)	1.427(5)
	1.426(4)	1.417(5)		1.424(7)
C(1)-C(2)	1.485(4)	1.489(5)	1.475(3)	1.476(6)
	1.482(4)	1.490(5)		1.469(7)
C(1)-C(4)	1.543(4)	1.536(5)	1.544(3)	1.536(6)
	1.549(4)	1.529(5)		1.532(7)
C(1)-C(10)	1.521(4)	1.530(4)	1.529(3)	1.525(6)
	1.518(4)	1.536(5)		1.520(7)
C(2)-C(3)	1.187(5)	1.179(6)	1.182(4)	1.177(7)
	1.180(5)	1.181(6)		1.185(9)
C(4)-C(5)	1.385(4)	1.390(4)	1.395(3)	1.388(6)
	1.385(4)	1.387(5)		1.373(7)
C(4)-C(9)	1.402(4)	1.403(5)	1.384(3)	1.395(6)
	1.374(5)	1.400(5)		1.393(8)
C(5)-C(6)	1.397(5)	1.393(5)	1.392(4)	1.390(7)
	1.378(5)	1.384(6)		1.379(9)
C(5)-Cl(1)	1.737(3)	1.735(4)	1.743(3)	1.708(5)
	1.753(3)	1.753(4)		1.732(6)
C(6)-C(7)	1.381(6)	1.384(6)	1.371(4)	1.380(8)
	1.377(6)	1.380(7)		1.374(10)
C(7)-C(8)	1.380(6)	1.368(6)	1.373(4)	1.365(8)
	1.369(6)	1.390(7)		1.373(11)
C(8)-C(9)	1.391(5)	1.392(5)	1.392(4)	1.381(7)
	1.417(6)	1.389(7)		1.379(9)
C(10)-C(11)	1.382(4)	1.379(5)	1.389(3)	1.385(7)
	1.386(5)	1.395(5)		1.405(9)
C(10)-C(15)	1.385(4)	1.388(5)	1.392(4)	1.389(8)
	1.392(5)	1.385(6)		1.380(9)
C(11)-C(12)	1.409(6)	1.401(6)	1.389(4)	1.369(9)
	1.385(5)	1.401(6)		1.359(11)
C(12)-C(13)	1.375(6)	1.368(6)	1.386(4)	1.356(12)
	1.365(6)	1.378(7)		1.338(14)
C(13)-C(14)	1.398(6)	1.384(6)	1.372(4)	1.399(13)
	1.404(7)	1.383(7)		1.365(15)
C(14)-C(15)	1.373(5)	1.405(5)	1.390(4)	1.394(11)
	1.385(6)	1.393(7)		1.413(13)
	1,4-Diazabicyclo[2.2.2]octane (DABCO)		*N,N'*-Dimethylpiperazine (DMP)	
C(16)-N(1)	1.467(5)	1.466(6)	1.463(5)	1.452(7)
C(17)-N(1)	1.469(4)	1.452(6)	1.445(4)	1.453(8)
C(18)-N(1)	1.473(5)	1.451(6)	1.485(6)	1.482(9)
C(19)-N(2)	1.462(5)	1.454(6)		1.461(8)
C(20)-N(2)	1.474(4)	1.474(6)		1.459(8)
C(21)-N(2)	1.479(5)	1.470(5)		1.484(9)
C(16)-C(19)	1.533(6)	1.567(7)	1.481(5)[a]	1.480(9)
C(17)-C(20)	1.550(5)	1.540(7)		1.475(9)
C(18)-C(21)	1.560(5)	1.546(7)		
Bond angles [ϕ/°]	1-(*o*-Chlorophenyl)-1-phenyl-2-propyn-1-ol (CPPOH)			
C(2)-C(1)-C(4)	108.2(3)	111.1(3)	109.9(2)	108.9(4)
	108.0(3)	109.9(3)		109.6(5)
C(2)-C(1)-C(10)	113.3(3)	111.3(3)	112.6(2)	112.5(4)
	111.3(3)	112.0(3)		112.1(5)
C(2)-C(1)-O(1)	108.1(3)	108.1(3)	107.8(2)	108.0(4)
	109.4(3)	108.1(3)		107.3(5)
C(4)-C(1)-C(10)	112.0(3)	109.4(3)	111.4(2)	111.0(4)
	112.7(3)	110.8(3)		111.6(5)
C(4)-C(1)-O(1)	110.4(3)	106.8(3)	106.4(2)	107.1(4)
	105.8(3)	107.2(3)		106.5(4)

Table 3. (Continued)

	1	2	3	4
C(10)-C(1)-O(1)	104.7(3)	110.0(3)	108.4(2)	109.1(4)
	109.4(3)	108.8(3)		109.5(5)
C(1)-C(2)-C(3)	175.5(4)	175.9(5)	175.4(3)	175.6(5)
	178.8(4)	177.6(4)		175.9(6)
C(1)-C(4)-C(5)	123.6(3)	124.8(3)	123.1(3)	123.5(4)
	123.8(3)	124.0(3)		124.2(5)
C(1)-C(4)-C(9)	119.2(3)	118.3(3)	120.1(3)	119.6(4)
	119.8(4)	119.1(3)		119.8(5)
C(5)-C(4)-C(9)	117.2(3)	116.9(3)	116.8(3)	116.9(4)
	116.3(3)	116.9(4)		116.0(5)
C(4)-C(5)-C(6)	122.1(4)	122.2(3)	121.9(3)	122.2(5)
	124.4(4)	122.5(4)		123.2(6)
C(4)-C(5)-Cl(1)	121.5(3)	121.9(3)	121.7(2)	121.6(4)
	120.9(3)	120.6(3)		121.0(4)
C(6)-C(5)-Cl(1)	116.4(3)	115.9(3)	116.4(2)	116.2(4)
	114.7(3)	116.8(4)		115.8(5)
C(5)-C(6)-C(7)	119.4(4)	119.2(4)	119.9(3)	119.3(5)
	117.7(4)	119.3(5)		119.0(6)
C(6)-C(7)-C(8)	119.6(4)	120.1(5)	119.4(3)	119.4(5)
	120.9(4)	120.2(5)		120.0(7)
C(7)-C(8)-C(9)	120.6(4)	120.5(4)	120.6(3)	121.4(5)
	119.5(5)	119.4(4)		119.6(7)
C(4)-C(9)-C(8)	120.9(4)	121.0(4)	121.4(3)	120.8(5)
	121.1(4)	121.7(4)		122.2(6)
C(1)-C(10)-C(11)	122.0(3)	123.2(3)	123.1(3)	122.9(5)
	122.6(3)	121.4(3)		122.9(5)
C(1)-C(10)-C(15)	118.8(3)	117.6(3)	117.9(3)	118.3(5)
	118.9(3)	118.1(4)		117.9(5)
C(11)-C(10)-C(15)	119.0(3)	119.1(4)	119.0(3)	118.8(5)
	118.5(3)	120.3(4)		119.2(6)
C(10)-C(11)-C(12)	120.4(4)	120.7(4)	120.5(3)	122.0(6)
	121.3(4)	119.6(4)		120.5(7)
C(11)-C(12)-C(13)	119.3(4)	120.1(4)	120.1(3)	119.5(7)
	120.2(4)	119.5(5)		121.1(8)
C(12)-C(13)-C(14)	120.4(5)	120.2(5)	119.7(3)	120.4(8)
	119.5(5)	121.1(5)		120.3(10)
C(13)-C(14)-C(15)	119.4(4)	119.8(4)	120.6(3)	120.0(8)
	120.1(5)	119.7(5)		120.9(10)
C(10)-C(15)-C(14)	121.5(4)	120.2(4)	120.1(3)	119.3(7)
	120.4(4)	119.8(5)		118.1(8)
C(1)-O(1)-H(1)	123(3)	112(4)	109(2)	121(4)
	114(3)	112(3)		122(4)
	DABCO		DMP	
N(1)-C(16)-C(19)[b]	110.5(3)	108.8(4)	111.0(3)	111.4(5)
N(1)-C(17)-C(20)[c]	110.1(3)	111.7(4)	110.9(3)	111.0(5)
N(1)-C(18)-C(21)	109.5(3)	110.7(4)		
N(2)-C(19)-C(16)	109.9(4)	110.2(4)		111.4(5)
N(2)-C(20)-C(17)	109.2(3)	108.6(4)		111.7(5)
N(2)-C(21)-C(18)	109.4(3)	109.5(4)		
C(16)-N(1)-C(17)	109.7(3)	107.7(4)	108.7(3)	108.9(5)
C(16)-N(1)-C(18)	108.3(3)	110.1(4)	107.4(3)	111.0(5)
C(17)-N(1)-C(18)	108.0(3)	108.7(4)	113.2(3)	110.5(5)
C(19)-N(2)-C(20)	109.2(3)	109.9(4)		108.0(5)
C(19)-N(2)-C(21)	109.0(3)	109.1(4)		111.0(5)
C(20)-N(2)-C(21)	108.6(3)	108.1(4)		106.5(5)

a) C(16)-C(17′) in **3**. b) N(1)-C(16)-C(17′) in **3**. c) N(1)-C(17)-C(16′) in **3**.

tion along the direction perpendicular to the N(1)···N(2) axis of DABCO molecule. This suggests an existence of hindered rotation of the molecule along the N(1)···N(2) axis, similar to that in the 1:2 complex of DABCO with *p*-cresol.[12] The C-N bond distances are equal in each molecule [av. 1.469 Å(**1**) and av. 1.461 Å(**2**)] and also equal to that observed in uncomplexed DABCO by the neutron diffraction study [1.470(7) Å][13] within the range of errors. The C-C distances [av. 1.548 Å (**1**) and av. 1.554 Å (**2**)] are

larger than those in DABCO crystal [1.513(5) Å]. The C-N-C and N-C-C bond angles of **1** and **2** showed no significant difference respectively from the corresponding angles of DABCO in the crystal[108.4(2) and 110.5(4)°].

***N,N'*-Dimethylpiperazine (DMP).** The DMP molecule in **3** takes a chair form, the center of which lies on a crystallographic center of symmetry. In **4**, the DMP molecule is also in a chair form but not centrosymmetric structure.

Part of the cost of the present study was defrayed by the Grant-in-Aid by the Ministry of Education, Science and Culture, for which the authors thanks are due.

References

1) F. Toda, K. Tanaka, and H. Ueda, *Tetrahedron Lett.*, **22**, 4669 (1981).

2) F. Toda, K. Tanaka, H. Ueda, and T. Oshima, *J. Chem. Soc., Chem. Commun.*, **1983**, 1513.

3) F. Toda, K. Tanaka, H. Ueda, and T. Oshima, *Israel J. Chem.*, **25**, 338 (1985).

4) F. Toda and K. Tanaka, *Chem. Lett.*, **1986**, 1905.

5) T. Yabuki, M. Yasui, H. Tezuka, S. Harada, N. Kasai, K. Tanaka, and F. Toda, *Chem. Lett.*, **1988**, 749.

6) W. C. Hamilton, *Acta Crystallogr.*, **18**, 502 (1965).

7) P. Main, S. E. Hull, L. Lessinger, G. Germain, J. P. Decrelercq, and M. M. Woolfson, *MULTAN* 78, "A System Computer Programs for the Automatic Solution of Crystal Structure from X-Ray Diffraction Data," Univs. of York, England, and Louvain, Belgium, 1978.

8) T. Ashida, *HBLS* V, "The Universal Crystallographic Computing System-Osaka," The Computation Center, Osaka Univ., 1979.

9) W. C. Hamilton, *Acta Crystallogr.*, **12**, 609 (1959).

10) "International Tables for X-Ray Crystallography," Kynoch Press, Birmingham, England, Vol. IV (1974), p. 71.

11) C. K. Johnson, *ORTEP* II, Report ORNL-5138, Oak Ridge National Laboratory, Tennessee (1976).

12) M. Takama, M. Yasui, S. Harada, N. Kasai, K. Tanaka, and F. Toda, *Bull. Chem. Soc. Jpn.*, **61**, 567 (1988).

13) J. K. Nimmo and B. W. Lucas, *Acta Crystallogr., Sect. B*, **32**, 348 (1976).

Adsorption of 2-(Octylsulfinyl)ethanol at Ethanol-Water Mixture/Air Interface

Hidemi IYOTA* and Kinsi MOTOMURA†
Kagoshima Women's Jr. College, Murasakibaru, Kagoshima 890
†Department of Chemistry, Faculty of Science, Kyushu University 33, Fukuoka 812
(Received November 11, 1988)

The surface tension of the solution of 2-(Octylsulfinyl)ethanol (OSE) in ethanol-water mixture was measured as a function of molality of OSE at constant composition of ethanol at 298.15 K under atmospheric pressure. The slope of surface tension vs. molality curve decreased with increasing composition. Two break points were observed on the curve: the break point at a low molality was attributed to the phase transition of the adsorbed film of OSE and the one at a high molality to the micelle formation of OSE. The surface excess numbers of moles per unit area of OSE and ethanol and their ratio were evaluated by applying the thermodynamic equations developed previously to the experimental results. It was clarified that the adsorbed film of OSE expels ethanol molecules from the surface region at a small composition of ethanol. The ratio of the excess number of molecules of ethanol per micelle particle to that of OSE was found to be similar to the corresponding ratio of the surface excess number of moles at the critical micelle concentration. This fact led us to the conclusion that the OSE molecules in the micelle behave similarly to those in the adsorbed film even in the mixed solvent.

The adsorption of surface active substances at various oil/water interfaces has been studied thermodynamically and the significant influence of solvent has been revealed in the previous papers.[1,2] Furthermore, the thermodynamic treatment has been extended so as to be applicable to the adsorption of surfactant from mixed solvent.[3] It is now necessary to examine the effect of the composition of mixed solvent on the interfacial behavior of surfactant molecules. Such examinations were rarely conducted by investigators.[4-6] The present purpose is that the surface tension of the solution of 2-(octylsulfinyl)ethanol in ethanol-water mixture is measured as a function of the concentration of OSE and the composition of the mixture and analyzed thermodynamically.

Experimental

2-(Octylsulfinyl)ethanol was synthesized and purified by the method described in the previous paper.[7] Its purity was checked by gas-liquid chromatography; no minimum was observed on the surface tension vs. concentration curve around the critical micelle concentration. Ethanol (Nakarai Chemicals Ltd., specially prepared reagent for spectroscopy) was dried by the refluxion over calcium oxide and then distilled. Water was triply distilled, the second and third steps being carried out from dilute alkaline permanganate solution.

Surface tension was measured by the drop volume technique[8] at 298.15 K under atmospheric pressure. The error inherent in the surface tension measurement was less than 0.02 mN m^{-1} throughout this experiment. Temperature was regulated to a precision of 0.01 K by the use of thermister controller.

The surface tension γ of the solution of 2-(octylsulfinyl)-ethanol (OSE) in ethanol-water mixture was measured as a function of molality of OSE, m, at a given mole fraction of ethanol, X, in the mixed solvent at 298.15 K under atmospheric pressure.

Results

Figures 1a and 1b show the γ vs. m curves at constant X. The γ value decreases steeply with increasing m and remains almost constant at concentrations above the critical micelle concentration (cmc) when X is smaller than about 0.05. Further, another break point is seen at a very small m value on γ vs. m curve, which is designated by the arrow on the curve in Fig. 1b. The m value at the break point and the cmc value increase as X increases. At larger mole fractions of ethanol, however, the slope of the γ vs. m curve

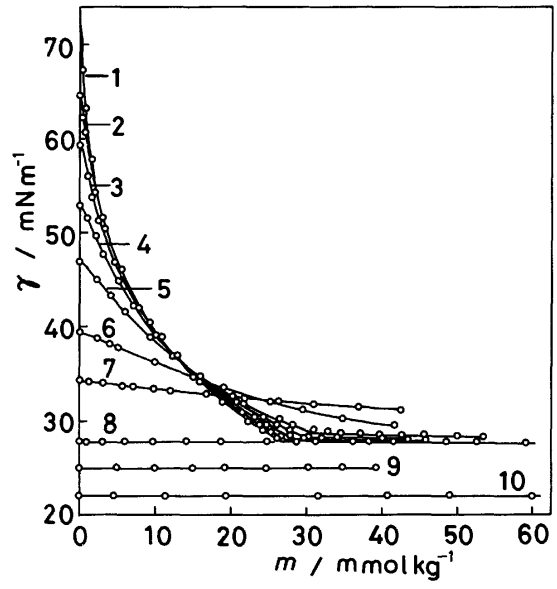

Fig. 1a. Surface tension vs. molality of OSE curves at constant mole fraction of ethanol at 298.15 K under atmospheric pressure: (1) X=0, (2) 0.0060, (3) 0.0130, (4) 0.0258, (5) 0.0439, (6) 0.0798, (7) 0.1253, (8) 0.2903, (9) 0.5694, (10) 1.

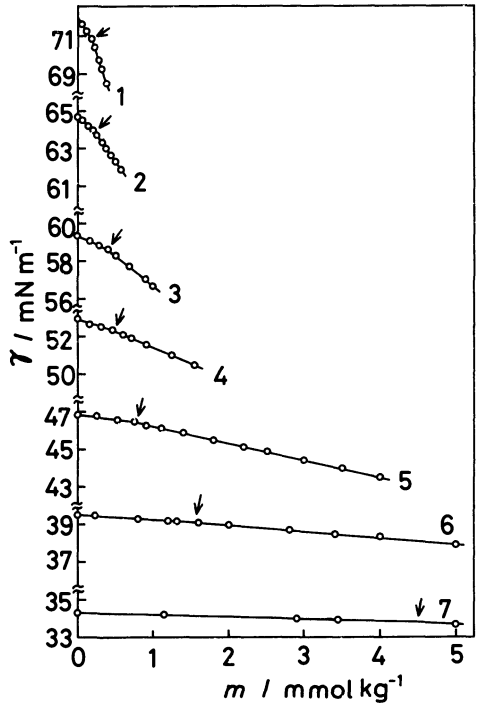

Fig. 1b. Surface tension vs. molality of OSE curves at constant mole fraction of ethanol at 298.15 K under atmospheric pressure: (1) X=0, (2) 0.0060, (3) 0.0130, (4) 0.0258, (5) 0.0439, (6) 0.0798, (7) 0.1253.

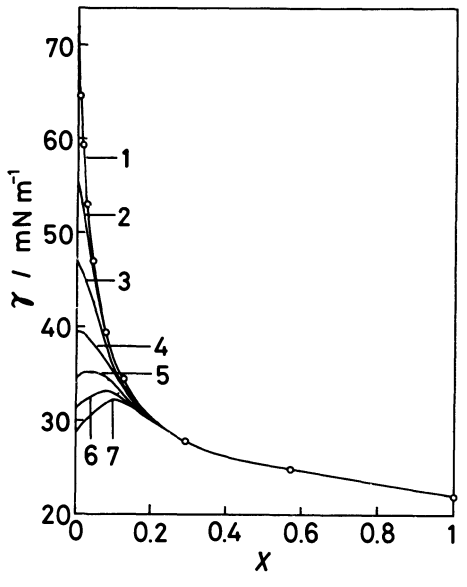

Fig. 2. Surface tension vs. mole fraction of ethanol curves at constant molality of OSE at 298.15 K under atmospheric pressure: (1) m=0 mmol kg^{-1}, (2) 2, (3) 5, (4) 10, (5) 15, (6) 20, (7) 25.

becomes gentle. It should be noticed that the γ value does not vary with m at compositions above X=ca. 0.3.

In order to examine the variation of surface tension with the composition of mixed solvent, the values of γ taken from Fig. 1a at constant m are plotted against X in Fig. 2. The γ value decreases monotonously with increasing X at low concentrations of OSE. At high concentrations of OSE, the γ vs. X curve has a distinct maximum at small X. However, all the curves approach each other above at X=ca. 0.3.

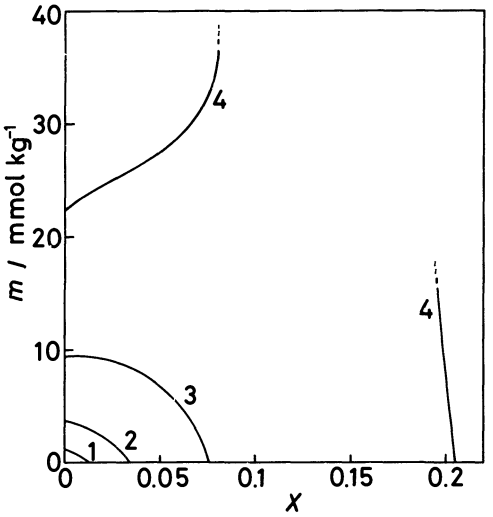

Fig. 3. Molality of OSE vs. mole fraction of ethanol curves at constant surface tension at 298.15 K under atmospheric pressure: (1) γ=60 m N m^{-1}, (2) 50, (3) 40, (4) 30.

In Fig. 3 shown is how the molality m changes with the composition X at constant surface tension. The value of m decreases with an increase in X at large γ, while the m vs. X curve has a maximum at small γ.

Discussion

Since the system under consideration consists of 2-(octylsulfinyl)ethanol, ethanol, water, and air, the information regarding the surface of the system is provided by applying the thermodynamic equations derived in the previous paper[3] to the above experimental results. Employing the molality of OSE m and the mole fraction of ethanol X as the independent variables at constant temperature T and pressure p, the fundamental equation is written in the form

$$d\gamma = -RT[(1-X)X]^{-1}[1+(\partial nf/\partial \ln X)_{T,p,m}]\Gamma_1^H dX - RTm^{-1}\Gamma_2^H dm, \quad (1)$$

where OSE is assumed to behave ideally at any X value and f is the activity coefficient of ethanol in the mixture. The interfacial density of ethanol Γ_1^H and that of OSE Γ_2^H are defined with respect to the dividing planes which satisfy the condition that the interfacial density of air Γ_a^H and the sum of those of ethanol and water $\Gamma_1^H+\Gamma_w^H$ are zero simultaneously. Now, the following equations derived from Eq. 1 enable us to evaluate the thermodynamic quantities $\Gamma_1^H(=-\Gamma_w^H)$, Γ_2^H, and Γ_1^H/Γ_2^H from the experimental

results:

$$-(\partial\gamma/\partial m)_{T,p,X} = RTm^{-1}\Gamma_2^{H}, \quad (2)$$

$$-(\partial\gamma/\partial X)_{T,p,m} = RT[(1-X)X]^{-1}[1+(\partial\ln f/\partial\ln X)_{T,p,m}]\Gamma_1^{H} \quad (3)$$

and

$$-(\partial m/\partial X)_{T,p,\gamma} = m[(1-X)X]^{-1}[1+(\partial\ln f/\partial\ln X)_{T,p,m}]\Gamma_1^{H}/\Gamma_2^{H}. \quad (4)$$

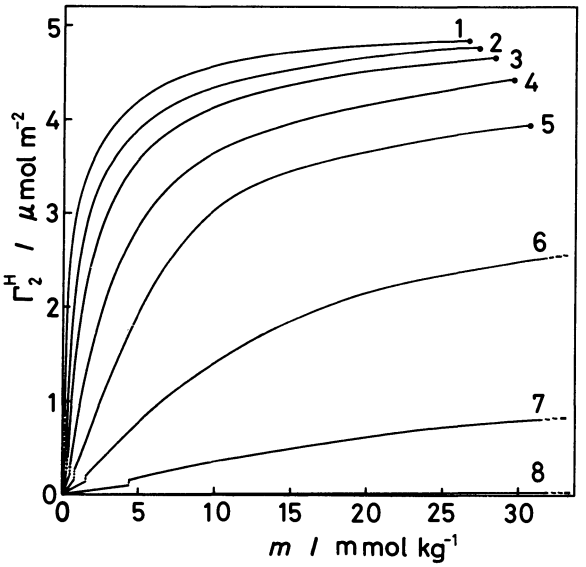

Fig. 4a. Interfacial density of OSE vs. molality of OSE curves at constant mole fraction of ethanol at 298.15 K under atmospheric pressure: (1) X=0, (2) 0.0060, (3) 0.0130, (4) 0.0258, (5) 0.0439, (6) 0.0798, (7) 0.1253, (8) 0.2903.

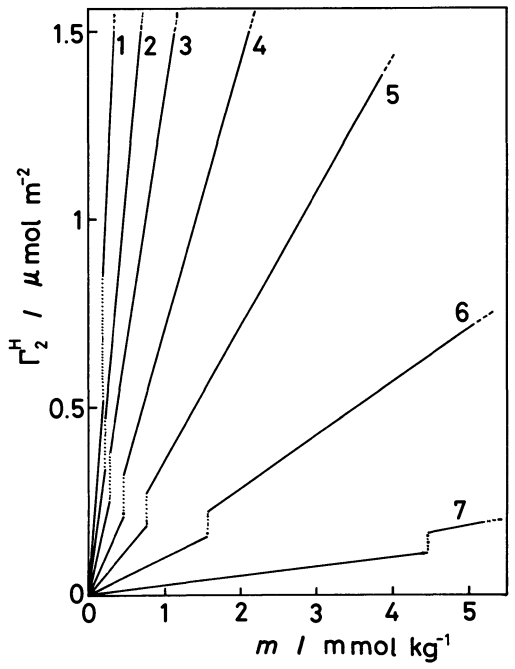

Fig. 4b. Interfacial density of OSE vs. molality of OSE curves at constant mole fraction of ethanol at 298.15 K under atmospheric pressure: (1) X=0, (2) 0.0060, (3) 0.0130, (4) 0.0258, (5) 0.0439, (6) 0.0798, (7) 0.1253.

First, the numerical values of Γ_2^H were estimated by applying Eq. 2 to the curves in Figs. 1a and 1b and plotted against m at constant X in Figs. 4a and 4b. It is seen from Fig. 4a that the Γ_2^H value increases steeply with m and then approaches that of saturation adsorption at the cmc indicated by the closed circle when X is small. With increasing X, the Γ_2^H value decreases and becomes zero at a composition above X=ca. 0.3. Therefore, it can be said that the enhancement of ethanol in the mixed solvent diminishes the adsorption of OSE. Now, let us focus our attention on the variation of Γ_2^H with m in the dilute concentration region depicted in Fig. 4b. The Γ_2^H value changes discontinuously at the concentration where the γ vs. m curve breaks. This discontinuous change in the Γ_2^H vs. m curve is attributed to the phase transition of the adsorbed film between a gaseous and an expanded state which has been observed in the previous papers.[8-10] It is also seen that the concentration at which the phase transition takes place increases with increasing X and eventually vanishes at a

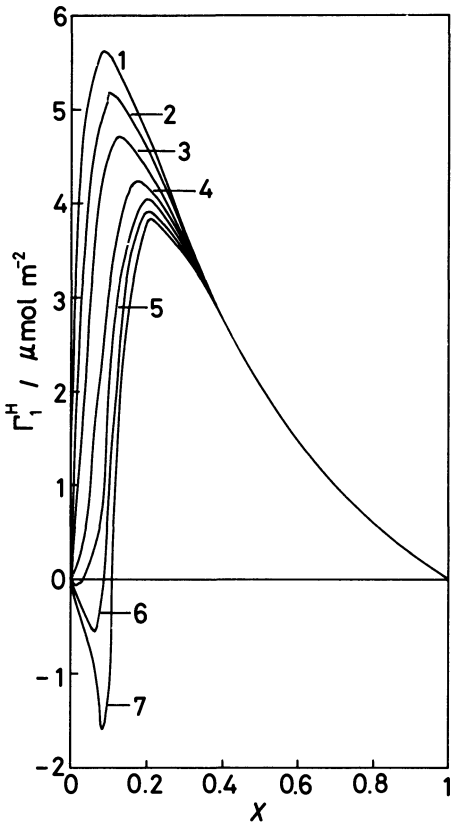

Fig. 5. Interfacial density of ethanol vs. mole fraction of ethanol curves at constant molality of OSE at 298.15 K under atmospheric pressure: (1) m= 0 mmol kg^{-1}, (2) 2, (3) 5, (4) 10, (5) 15, (6) 20, (7) 25.

composition above X=ca. 0.3. This fact is reconciled with the view that the enhancement of ethanol diminishes the adsorption of OSE.

Next, the value of Γ_1^H was evaluated by applying Eq. 3 to the γ vs. X curve drawn in Fig. 2 and using the activity coefficient of ethanol.[11] The Γ_1^H vs. X plot at constant m is shown in Fig. 5. The value of Γ_1^H at m=0 is positive over the whole range of composition and has a maximum. With increasing m, the value decreases considerably and becomes negative at a small X value, though it remains unchanged at a high X value. Taking into account that the maximum value of Γ_1^H is comparable with the value of the saturated adsorption of normal aliphatic alcohol,[12] we may say that ethanol molecules pack closely in the adsorbed film. However, the dependence of Γ_1^H on m suggests that the formation of OSE film expels ethanol molecules from the surface region. On the other hand, we notice that the surface activity of OSE becomes extinct in an ethanol-rich solution. Therefore, it seems to be useful to examine the relation of the adsorption of OSE to that of ethanol. This can be achieved by evaluating the ratio Γ_1^H/Γ_2^H.

The numerical values of Γ_1^H/Γ_2^H were evaluated by making use of Eq. 4 and the m vs. X curves in Fig. 3; they are plotted against X at fixed γ in Fig. 6, where r^H denotes Γ_1^H/Γ_2^H. The values at γ=60, 50, and 40 mN m^{-1} are seen to increase greatly with increasing X. On the other hand, the value at γ=30 mN m^{-1} first decreases and then increases steeply. These findings indicate that the competitive adsorption of OSE and ethanol molecules takes place at the surface.

Now it is useful to examine the adsorption of OSE from its micellar solution in the ethanol-water mixture. The behavior of micelles can be described by the excess thermodynamic quantities with reference to the spherical dividing surface around the micelle chosen so that the sum of the excess number of water molecules per micelle particle N_w^M and that of ethanol molecules N_1^M is equal to zero. The analogue of the Gibbs-Duhem equation for the micelle particle is written as[13]

$$N_w^M d\mu_w + N_1^M d\mu_1 + N_2^M d\mu_2 = 0, \quad (5)$$

where N_2^M is the excess number of OSE molecules per micelle particle and μ_i the chemical potential of component i. Adopting T, p, X, and m as the independent variables and assuming that OSE behaves ideally in the solution, Eq. 5 is rewritten in the following form at constant T and p

$$[(1-X)X]^{-1}[1+(\partial \ln f/\partial \ln X)_{T,p,m}]N_1^M dX + m^{-1}N_2^M dm = 0. \quad (6)$$

Combination of Eqs. 1 and 6 yields the relation representing the variation of surface tension of the micellar solution with X:

$$-d\gamma = RT[(1-X)X]^{-1}[1+(\partial \ln f/\partial \ln X)_{T,p,m}]\Gamma_2^H(r^H - r^M)dX, \quad (7)$$

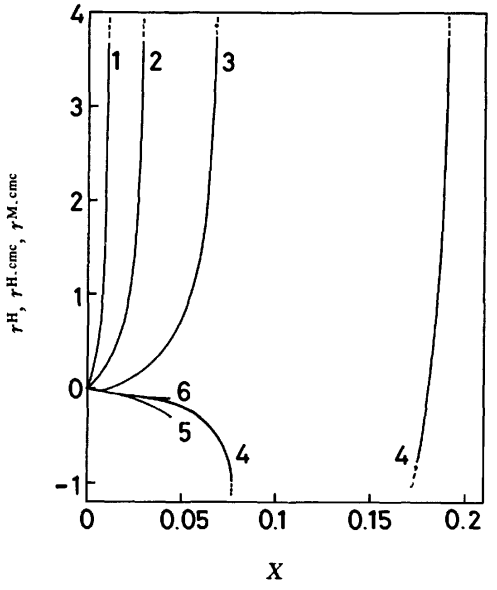

Fig. 6. Ratios r^H, $r^{H,cmc}$, and $r^{M,cmc}$ vs. mole fraction of ethanol curves at constant surface tension at 298.15 K under atmospheric pressure: (1) γ=60 mN m^{-1}, (2) 50, (3) 40, (4) 30, (5) $r^{H,cmc}$ vs. X, (6) $r^{M,cmc}$ vs. X.

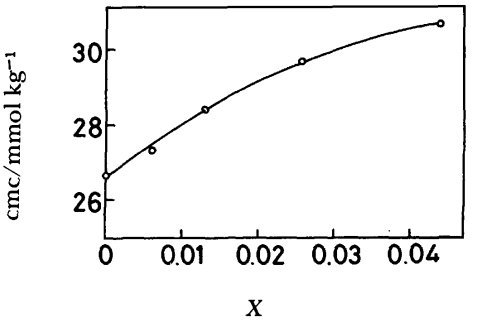

Fig. 7a. Critical micelle concentration vs. mole fraction of ethanol curve at 298.15 K under atmospheric pressure.

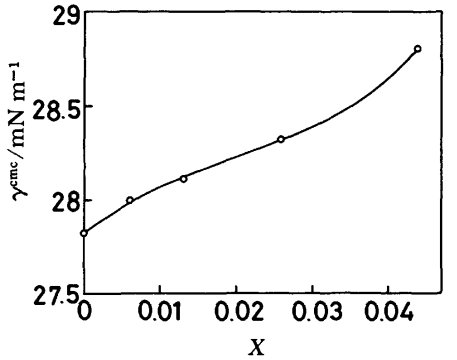

Fig. 7b. Surface tension at critical micelle concentration vs. mole fraction of ethanol at 298.15 K under atmospheric pressure.

where r^{M} expresses N_1^M/N_2^M. Since $\gamma \cong \gamma^{cmc}$ and $m \cong$cmc in the vicinity of the cmc, the following equations are obtained from Eqs. 6 and 7:

$$-(\partial \mathrm{cmc}/\partial X)_{T,p} = (\mathrm{cmc})[(1-X)X]^{-1}[1+(\partial \ln f/\partial \ln X)_{T,p,m}] \times r^{M,cmc} \quad (8)$$

and

$$-(\partial \gamma^{cmc}/\partial X)_{T,p} = RT[(1-X)X]^{-1}[1+(\partial \ln f/\partial \ln X)_{T,p,m}] \times \Gamma_2^{H,cmc}(r^{H,cmc} - r^{M,cmc}), \quad (9)$$

where the superscript cmc indicates that the values of the thermodynamic quantities are those at the cmc. Therefore, we can evaluate the values of $r^{H,cmc}$ and $r^{M,cmc}$ by applying Eqs. 8 and 9 to the experimental results.

The values of cmc and γ^{cmc} obtained from the γ vs. m curves in Fig. 1a are plotted against X at constant T and p in Figs. 7a and 7b. The cmc vs. X curve is qualitatively consistent with those observed by some other work.[4-6,14-17] The numerical values of $r^{H,cmc}$ and $r^{M,cmc}$ estimated are drawn as a function of X at 298.15 K under atmospheric pressure in Fig. 6. Comparing these curves with the r^{H} vs. X curves, the values of $r^{H,cmc}$ and $r^{M,cmc}$ may be said to be not so different from each other. Therefore, we can conclude that the behavior of OSE molecules in the micelle is similar to that in the adsorbed film. Moreover, the negative values of $r^{H,cmc}$ and $r^{M,cmc}$ indicate that ethanol molecules are expelled from the adsorbed film and the micelle particle of OSE.

Further information about the interaction between OSE and ethanol molecules in the adsorbed film and the micelle will be provided by a thermodynamic treatment which regards the present system as an aqueous solution of surfactant mixture.

References

1) T. Ikenaga, N. Matubayasi, M. Aratono, K. Motomura, and R. Matuura, *Bull. Chem. Soc. Jpn.*, **53**, 653 (1980).
2) H. Iyota, M. Aratono, M. Yamanaka, K. Motomura, and R. Matuura, *Bull. Chem. Soc. Jpn.*, **56**, 2402 (1983).
3) K. Motomura, H. Iyota, N. Ikeda, and M. Aratono, *J. Colloid Interface Sci.*, **126**, 26 (1988).
4) L. Cantu, M. Corti, V. Degiorgio, H. Hoffmann, and W. Ulbricht, *J. Colloid Interface Sci.*, **116**, 384 (1987).
5) L. G. Ionescu, T. Tokuhiro, and B. J. Czerniawski, *Bull. Chem. Soc. Jpn.*, **52**, 922 (1979).
6) M. Koshinuma, *Bull. Chem. Soc. Jpn.*, **52**, 1790 (1979).
7) K. Motomura, S. Iwanaga, S. Uryu, H. Matsukiyo, M. Yamanaka, and R. Matuura, *Colloids and Surfaces*, **9**, 19 (1984).
8) K. Motomura, S. Iwanaga, Y. Hayami, S. Uryu, and R. Matuura, *J. Colloid Interface Sci.*, **80**, 32 (1981).
9) S. Uryu, M. Aratono, M. Yamanaka, K. Motomura, and R. Matuura, *Bull. Chem. Soc. Jpn.*, **56**, 3219 (1983).
10) M. Aratono, S. Uryu, Y. Hayami, K. Motomura, and R. Matuura, *J. Colloid Interface Sci.*, **98**, 33 (1984).
11) H. J. E. Dobson, *J. Chem. Soc.*, **1925**, 2866.
12) R. Defay, I. Prigogine, and A. Bellemans, (translated by D. H. Everett), "Surface Tension and Adsorption," Longmans, London (1966), p. 94.
13) K. Motomura, S. Iwanaga, M. Yamanaka, M. Aratono, and R. Matuura, *J. Colloid Interface Sci.*, **86**, 151 (1982).
14) P. Becher, *J. Colloid Sci.*, **20**, 728 (1965).
15) A. Goto, M. Takemoto, and F. Endo, *Bull. Chem. Soc. Jpn.*, **58**, 247 (1985).
16) D. Oakenfull, *J. Colloid Interface Sci.*, **88**, 562 (1982).
17) R. Zana, S. Yiv, C. Strazielle, and P. Lianos, *J. Colloid Interface Sci.*, **80**, 208 (1981).

Host-Guest Complexation of Mono[6-(1-pyridinio)-6-deoxy]-α-cyclodextrin with Several Inorganic Anions

Yoshihisa MATSUI,* Masahiko FUJIE, and Kaori HANAOKA
Faculty of Agriculture, Shimane University, Nishikawatsu, Matsue 690
(Received November 16, 1988)

Mono[6-(1-pyridinio)-6-deoxy]-α-cyclodextrin (**1**) formed 1:1 charge-transfer complexes with such inorganic anions as I^-, SCN^-, and Br^- in an aqueous solution to afford characteristic UV absorption bands. The binding constant (K_a) for a I^- complex with **1** was ca. 45 times as large as that with a nonmacrocyclic analog of **1**, ca. 10 times that with native α-cyclodextrin, and 4.4 times that with a β-cyclodextrin analog. The I^- ion was bound to a dipyridinio analog of **1** more strongly than to **1** by a factor of 10. The K_a values decreased with an increase in the ionic strength of the medium. The complexation was competitively inhibited by ClO_4^-. Hydrophobic, van der Waals, electrostatic, and charge-transfer interactions were supposed to take part in the complexation co-operatively.

Cyclodextrin (CD) forms host-guest complexes with a variety of molecules or ions in aqueous solutions. Several intermolecular interactions have been proposed as being responsible for the complexation:[1—4] Hydrophobic interactions, van der Waals interactions including dipole-dipole interactions and London dispersion forces, hydrogen-bonding, interactions due to the relief of high-energy water from the CD cavity upon guest complexation, and interactions due to the relief of conformational strain in a CD-water complex upon guest inclusion. Recently, the modification or functionalization of CD has attracted much attention to enhancing the binding force and/or the selectivity of a host. For example, a CD derivative in which the OH groups of CD are displaced by the apolar OCH_3 groups forms a host-guest complex with an apolar guest more stable than the native CD does.[5] In this case, the modification enhances hydrophobic and van der Waals interactions between a host and a guest. The replacement of the OH group(s) of CD with positively or negatively charged group(s) results in an increase in the affinity of the host for the oppositely charged guests.[6—9] Electrostatic interactions between the host and guests are responsible for the binding.

In the course of an investigation of charged CD,[8—10] we recently found that a positively charged CD, mono[6-(1-pyridinio)-6-deoxy]-α-CD (**1**), forms stable 1:1 charge-transfer (CT) complexes with such inorganic anions as I^- and SCN^- to give characteristic absorption bands in the UV spectra. It has been known that the 1-alkylpyridinium ions form CT complexes with a few inorganic anions.[11—13] However, the interactions between them are very weak in an aqueous solution.[12] In contrast, the binding constant (K_a) for a complex of I^- with **1** is considerably larger than that for a complex of I^- with either the native α-CD or the 1-alkylpyridinium ion. This finding seems interesting in view of the development of host compounds to which inorganic anions are bound strongly and/or selectively. Only a few host compounds with such ability have hitherto been reported.[14—17] The present article deals with the binding properties of **1** and related compounds in aqueous solutions, together with the effects of environmental factors, such as the ionic strength (I_c) and polarity of the medium, on the complexation of **1** with the I^- and SCN^- ions.

Experimental

Materials. The α- and β-CD's were kindly supplied by the Nihon Shokuhin Kako Co., Ltd., and were dried overnight in vacuo at 110 °C. Reagent-grade pyridine and dimethyl sulfoxide (DMSO) were dried over calcium hydride and distilled in the presence of fresh calcium hydride before use. The hydrogencarbonate salts of **1** and A,D-bis[6-(1-pyridinio)-6-deoxy]-α-CD (**2**) were prepared by refluxing solutions of the corresponding C(6)-*O*-sulfonylated α-CD's in dry pyridine, followed by the column chromatography of the products on a CM-cellulose column with the elution of aqueous ammonium hydrogencarbonate solutions.[10] The hydrogencarbonate salts of mono[6-(1-pyridinio)-6-deoxy]-β-CD (**3**)[9] and methyl 6-(1-pyridinio)-6-deoxy-α-D-glucopyranoside (**4**)[10] were also prepared in a similar manner. Reagent-grade methanol was used after distillation. The inorganic salts, such as KI, KSCN, KBr, KCl, $KClO_4$, K_2SO_4, and NH_4HCO_3, were reagent grade and were used without further purification. The ionic strengths of aqueous solutions were adjusted, if necessary, using K_2SO_4 or KCl. The deuterium oxide (Merck, 99.75%) and sodium 2,2-dimethyl-2-silapentane-5-sulfonate (DSS) were available for ^1H NMR use.

Apparatus. The absorption spectra were measured with a Hitachi Model 220 spectrophotometer. The quartz cells (1.0 cm) were maintained at a constant temperature (25 °C) by means of a jacket through which water was circulated from a constant-temperature bath. The ^1H NMR spectra were recorded using a JEOL Model JNM-GX270 FT NMR spectrometer (270 MHz).

Results

Formation of CT Complexes of 1—4 with I^-. Aqueous solutions of 0.4—0.8 mmol dm^{-3} **1**—**3** (pH 8.1—8.5[18]) or 5 mmol dm^{-3} **4** (pH 8.8[18]) exhibited virtually nothing of either UV or visible absorption in the region of wavelengths longer than 280 nm. When KI was added to the solutions, characteristic absorp-

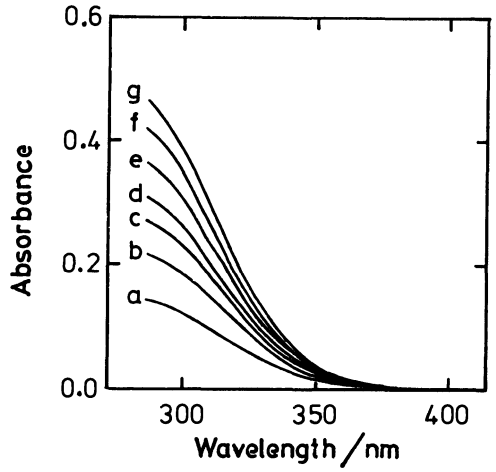

Fig. 1. Absorption spectra of 0.80 mmol dm^{-3} **3** in aqueous solutions containing various amounts of KI at 25 °C. [KI]/mmol dm^{-3}: (a) 10, (b) 20, (c) 29, (d) 39, (e) 57, (f) 83, and (g) 115.

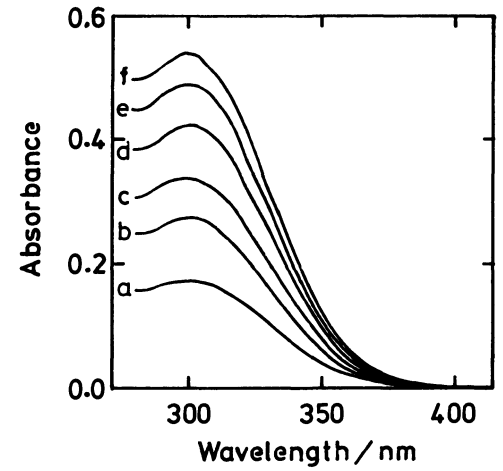

Fig. 2. Absorption spectra of 0.80 mmol dm^{-3} **1** in aqueous solutions containing various amounts of KI at 25 °C. [KI]/mmol dm^{-3}: (a) 2.5, (b) 4.9, (c) 7.1, (d) 11.3, (e) 17.0, and (f) 23.5.

tion bands appeared in the wavelength region from 280 to 350 nm. In a **3**–KI system (Fig. 1), the absorbance gradually increased with a decrease in the wavelength. No absorption maximum was observed in this wavelength region, similarly to the case of a CT complex of the 1-methylpyridinium ion (**5**) with I$^-$.[11] On the other hand, a **1**–KI system (Fig. 2) gave an apparent absorption maximum (λ_{max}) at 300 nm, indicating that a CT complex between **1** and I$^-$ is more stable than one between **3** and I$^-$.[13] The addition of KI to an aqueous solution of the dipyridinium derivative **2** also resulted in the appearance of a CT absorption band (λ_{max}=297 nm) very similar to that for a **1**–KI system. A CT band observed for an aqueous mixture of a nonmacrocyclic analog **4** with KI resembled that for a **3**–KI system.

The binding constants, K_a, for CT complexes of **1**—

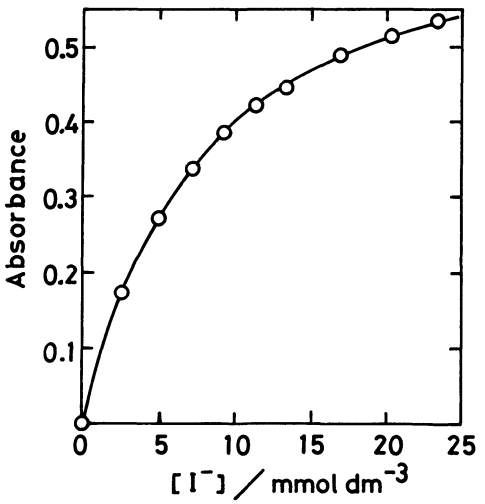

Fig. 3. Changes in absorbance at λ=300 nm of an aqueous **1** solution with increasing [I$^-$] at 25 °C. The solid line was obtained by the curve-fitting analysis upon an assumption of 1:1 complexation between **1** and I$^-$.

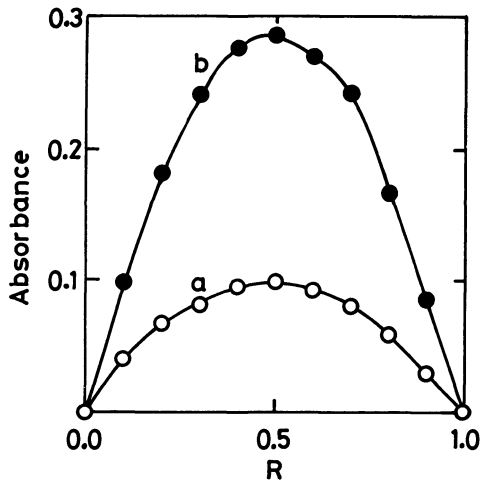

Fig. 4. Plots of absorbance at 300 nm against the ratio R=[host]/([host]+[guest]) for a **1**–KI system (a) at [host]+[guest]=2.0 mmol dm^{-3} and a **2**–KI system (b) at [host]+[guest]=1.0 mmol dm^{-3}.

4 with I$^-$ were determined by the curve-fitting analysis, by means of a microcomputer, of the changes in the absorbance at a given wavelength with the KI concentration, upon an assumption of a 1:1 complexation. The curves thus calculated were well fitted to the observed data (Fig. 3), indicating that the assumption of a 1:1 complexation is valid. The 1:1 stoichiometry was also confirmed by the continuous-variation method for complexes of **1** and **2** with I$^-$. Figure 4 shows the plots of the absorbance at 300 nm against the R=[host]/([host]+[guest]) ratio. The plots for both **1**–I$^-$ and **2**–I$^-$ systems gave maximum absorbances at R=0.5, indicating the 1:1 complexation. No indication of 1:2 complexation was

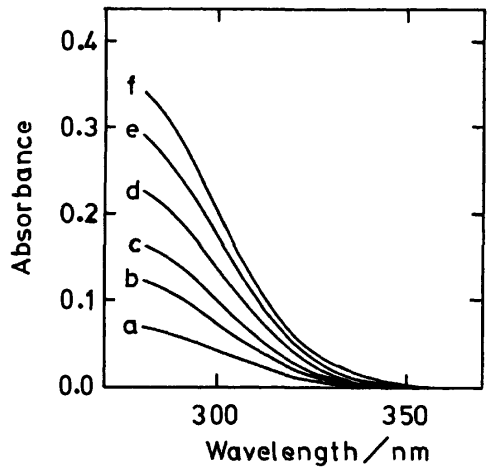

Fig. 5. Absorption spectra of 0.80 mmol dm^{-3} **1** in aqueous solutions containing various amounts of KSCN at 25 °C. [KSCN]/mmol dm^{-3}: (a) 0.6, (b) 1.2, (c) 1.8, (d) 3.0, (e) 4.8, and (f) 7.2.

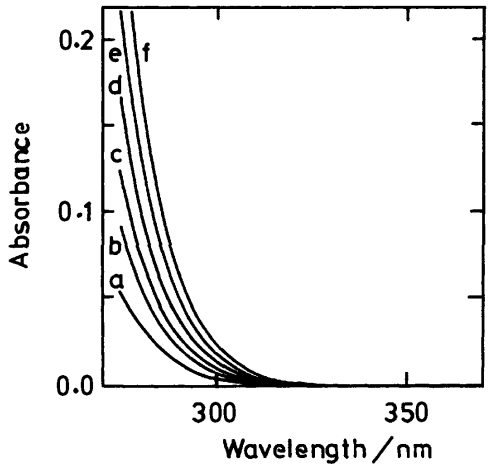

Fig. 6. Absorption spectra of 0.50 mmol dm^{-3} **1** in aqueous solutions containing various amounts of KBr at 25 °C. [KBr]/mmol dm^{-3}: (a) 14, (b) 28, (c) 41, (d) 63, (e) 103, and (f) 173.

recognized, even for a dipyridinio derivative **2**. The K_a values thus determined are shown in Table 1. The K_a value (3.0 mol^{-1} dm^3) for a nonmacrocyclic compound **4** was close to that (2.3 mol^{-1} dm^3) for **5**.[12] Interestingly, the K_a value (136 mol^{-1} dm^3) for **1** was remarkably larger than those for **4** and native α-CD by factors of about 45 and 10 respectively. It is evident that the hydrophobic cavity of **1** contributes to the stabilization of a CT complex of **1** with I$^-$. The K_a value (31 mol^{-1} dm^3) for a β-CD analog **3** was significantly smaller than that for **1**, though it was larger than those for **4** and native β-CD. Since the cavity size of **3** is larger than that of **1**, the van der Waals interactions between **3** and I$^-$ may be weaker than that between **1** and I$^-$. The K_a value (1320 mol^{-1} dm^3) for a dipyridinio derivative **2** was about 10 times as large as that for the monopyridinio derivative **1**. It is also noteworthy that the molar absorption coefficient (ε) for a **2**–I$^-$ CT complex was about twice that for a **1**-I$^-$ complex. The two pyridinio groups in **2** may participate cooperatively in the stabilization of a CT complex with I$^-$.

Formation of CT Complexes of 1 and 2 with Inorganic Anions Other than I$^-$. According to Kosower and Klinedinst,[11] 1-alkylpyridinium ions form CT complexes not only with I$^-$, but also with SCN$^-$ and Br$^-$. Hence, the complexation of **1** and **2** with inorganic anions other than I$^-$ was examined by means of absorption spectrophotometry. The addition of KSCN or KBr to an aqueous solution of **1** resulted in the appearance of UV absorption in the wavelength region from 280 to 350 nm; such absorption is characteristic of a CT complex (Figs. 5 and 6). An aqueous mixture of **2** with KSCN or KBr also gave a similar CT band. The spectral data were analyzed by the curve-fitting method described in the preceding paragraph. The results indicated that **1** and **2** form 1 : 1 complexes with SCN$^-$ and Br$^-$. The K_a values thus determined are summarized in Table 1. The K_a values for the **1**– and **2**–SCN$^-$ systems were, respectively, about 12 and 80 times as large as that for a native α-CD-SCN$^-$ system. The K_a values for the **1**– and **2**–Br$^-$ systems were also larger than that for a native α-CD–Br$^-$ system by factors of ca. 10 and 42 respectively. No CT absorption band was observed for aqueous mixtures of **1** and **2** with such inorganic salts as KCl, $KClO_4$, and K_2SO_4. Kosower and Klinedinst[11] also reported that the ClO_4^- ion forms no CT complex with **5**.

Effect of the Ionic Strength on the Binding Constants for CT Complexes of 1—3 with I$^-$ and SCN$^-$. Kosower and Burbach[12] suggested that the K_a value for a CT complex of **5** with I$^-$ is sensitive to the ionic strength, I_c, of the medium. Hence, the effect of I_c on the K_a values was examined for CT complexes of **1** and **2** with I$^-$ and SCN$^-$. The I_c of the medium was adjusted by K_2SO_4. It is known that the sulfate ion forms no inclusion complex with α- and β-CD.[19–22] The K_a values were spectrophotometrically determined at I_c=1.0; they are summarized in Table 2. An increase in I_c caused a marked decrease in K_a values for the systems examined. Thus, the K_a values for the **1**–I$^-$ and **1**–SCN$^-$ systems at I_c=1.0 were 0.54—0.58 times those determined at I_c<0.024. The effect of I_c on K_a was more remarkable in divalent **2** systems than in monovalent **1** systems. In the **2**-I$^-$ and **2**–SCN$^-$ systems, the K_a values were only 0.25—0.28 times those at I_c<0.007. The addition of K_2SO_4 causes a decrease in the ionic activities of the host and guest ions, thus weakening the complexation between them. Thus, it is evident that electrostatic interactions are also responsible for the complexation of **1** and **2** with I$^-$ and SCN$^-$ and that the contribution of the electrostatic interactions to the complexation is larger in divalent **2**

Table 1. Binding Constants, K_a, for CT Complexes of **1** and the Related Compounds with a Few Inorganic Anions in an Aqueous Solution at 25 °C

Anion	Host	K_a / mol^{-1} dm^3	$\varepsilon \times 10^{-3}$ [a] / mol^{-1} dm^3 cm^{-1}	I_c / mol dm^{-3}
I^-	**1**	136 ± 2	0.88	<0.024[b]
	2	1320 ±20	1.86	<0.004[b]
	3	31 ± 2	0.60	<0.095[b]
	4	3.0 ± 0.1	0.45	<0.15[b]
	5[c]	2.3 ± 0.3	0.34[d]	0.01
	α-CD[e]	13.2		0.02
	β-CD[e]	3.9		0.02
SCN^-	**1**	286 ± 7	0.39	<0.008[b]
	2	1850 ±20	0.77	<0.006[b]
	3	14 ± 1	0.33	1.00
	α-CD[e]	22.8		0.02
	β-CD[e]	4.5		0.02
Br^-	**1**	8.4 ± 0.2	0.57[f]	<0.18[b]
	2	36 ± 1	0.16	<0.32[b]
	α-CD[g]	0.87± 0.02		0.50

a) Molar absorption coefficients at λ=300 nm, unless otherwise noted. b) The I_c was not kept constant. c) The 1-methylpyridinium ion; Ref. 12. d) λ=308 nm. e) Ref. 21. f) λ=280 nm. g) Ref. 25.

Table 2. The K_a/mol^{-1} dm^3 Values for Complexes of **1**—**3** with Inorganic Anions at 25 °C and I_c=1.0 as Adjusted by the Use of K_2SO_4 and KCl

Guest	Host	K_2SO_4	Ratio[a]	KCl	Ratio[a]
I^-	**1**	79 ± 1	0.58	45 ±1	0.33
	2	364 ± 7	0.28		
	3	10.2± 0.3	0.33	5.5±0.2	0.18
SCN^-	**1**	155 ± 5	0.54	83 ±2	0.29
	2	470 ±10	0.25		
	3	14 ± 1			

a) The ratio of K_a at I_c=1.0 to K_a in Table 1.

systems than in monovalent **1** systems.

Table 2 also includes the K_a values for CT complexes of **1** and **3** with I^- and SCN^- at I_c=1.0, as adjusted by the use of KCl. It is known that Cl^- forms inclusion complexes with α-CD, though the K_a value is very small.[19,23,24] The K_a values at I_c=1.0 (KCl) were always smaller than those at I_c=1.0 (K_2SO_4) by a factor of ca. 0.55. It is reasonable to consider that Cl^- retards the complexation of **1** or **3** with I^- or SCN^- not only electrostatically but also by competitive binding to the host cavity. The competitive binding of an inorganic anion to the host cavity was distinctly demonstrated by an examination of the effect of $KClO_4$ on the complexation of **1** with I^-. The perchlorate ion is known to form a relatively stable inclusion complex with α-CD.[22-26] The addition of $KClO_4$ to an aqueous solution of 0.792 mmol dm^{-3} **1** containing 19.8 mmol dm^{-3} KI caused an apparent decrease in the absorbance in the wavelength region from 280 to 350 nm due to a CT complex (Fig. 7). The I_c value of the medium was maintained at 1.0 by the use of K_2SO_4. Since the I_c of the medium was kept constant, the retarding effect of $KClO_4$ on the complexation of **1** with I^- is attributable to the competitive binding of ClO_4^- to the host cavity. In other words, the inclusion of I^- within the host

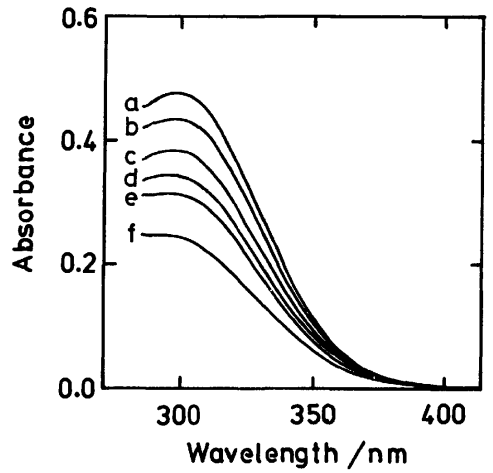

Fig. 7. Absorption spectra of a CT complex of **1** with I^- in aqueous solutions containing various amounts of $KClO_4$ at I_c=1.00 (K_2SO_4) and 25 °C. [**1**]=0.792 mmol dm^{-3}, and [KI]=19.8 mmol dm^{-3}. [$KClO_4$]/ mmol dm^{-3}: (a) 0.0, (b) 2.5, (c) 6.4, (d) 10.4, (e) 13.8, and (f) 27.8.

cavity is essential for the formation of a stable CT complex of **1** with I^-. The K_a value for a **1**-ClO_4^- system was determined to be 110 mol^{-1} dm^3 by the analysis of the inhibitory effect of ClO_4^- on the

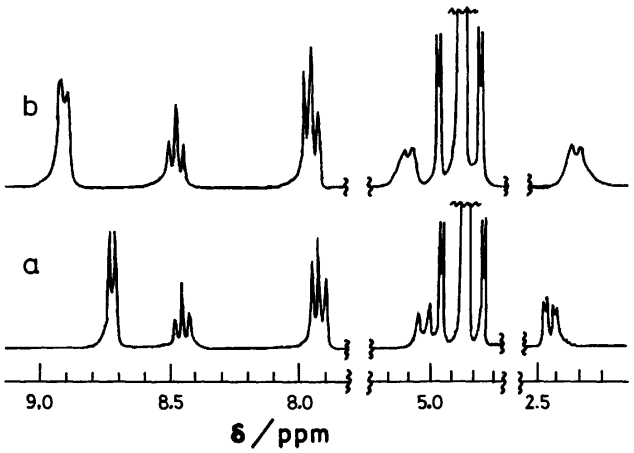

Fig. 8. Partial ^{1}H NMR spectra (270 MHz, D_2O, ref. DSS, 30 °C) of 20 mmol dm^{-3} **1** in the absence (a) and in the presence (b) of 92 mmol dm^{-3} KI.

complexation of **1** with I^-.[27] The K_a value is 3.7 times as large as that for a native α-CD-ClO_4^- system (K_a=30.6 mol^{-1} dm^3).[22]

^{1}H NMR Spectrometry of a CT Complex of 1 with I^-. The complexation of **1** with I^- was also examined by means of ^{1}H NMR spectrometry. Figure 8-a illustrates parts of the ^{1}H NMR spectrum of **1** in the absence of KI. The ortho-, meta-, and para-protons of the pyridinio group of **1** gave a doublet at δ=8.72 (2H, J=5.9 Hz), a triplet at δ=7.92 (2H, J=7.1 Hz), and a triplet at δ=8.45 (1H, J=8.1 Hz) respectively. An apparently doublet signal at δ=5.04 (1H, J=13.2 Hz) was assigned to one of the diastereotopic geminal C(6)-H's involved in the substituted glucopyranose ring [GP(A)], and a doublet-doublet signal at δ=2.43 (1H, J=3.3, 12.1 Hz), to one of geminal C(6)-H's involved in the unsubstituted glucopyranose ring [GP(B)] adjacent to GP(A).[10] The doublets at δ=4.76—4.96 (6H, J=ca. 3.2 Hz) were due to the anomeric C(1)-H's. Figure 8-b shows parts of the ^{1}H NMR spectrum of **1** in the presence of KI. The addition of KI caused a marked lower-field shift of the doublet signal due to the ortho-H's of the pyridinio group from δ=8.72 to 8.93. Furthermore, the doublet signal was significantly broadened by the addition of KI. In contrast to the signal of the ortho-H's, the triplet signals due to the meta- and para-H's of the pyridinio group showed only slight lower-field shifts and virtually no broadening of the signals upon the addition of KI. On the other hand, the apparent doublet signal and the dd-signal, due to the C(6)-H's of GP(A) and GP(B) respectively, showed a significant lower- or higher-field shift and signal broadening, whereas virtually no change was observed for the doublet signals due to the C(1)-H's. These facts indicate that the complexed I^- ion is located in the vicinity of the ortho- and C(6)-H's of **1**. The protons other than those described above gave ^{1}H NMR signals at δ=2.7—4.7; those signals were too complex to be completely assigned at the present stage of investigation. However, we also found that the complexation of **1** with I^- causes some changes in the pattern of the signals in this region.

Table 3. Effects of Organic Solvents on the λ_{max} and K_a Values of a CT Complex of **1** with I^- at 25 °C

Solvent	λ_{max}/nm	K_a/mol^{-1} dm^3
H_2O only	300	136 ±2
25% (v/v) MeOH	303	68.1±0.3
50% (v/v) MeOH	303	39.9±0.4
80% (v/v) MeOH	308	33.0±0.2
10% (v/v) DMSO	306	165 ±4
20% (v/v) DMSO	308	141 ±2
30% (v/v) DMSO	310	90.7±2.2
40% (v/v) DMSO	312	61.1±0.3
50% (v/v) DMSO	314	34.7±0.9
60% (v/v) DMSO	317	20.9±0.6
70% (v/v) DMSO	320	9.5±0.2
80% (v/v) DMSO	321	6.9±0.6

The Effect of Organic Solvents on the Complexation of 1 with I^-. Kosower showed that the CT absorption bands of 1-alkylpyridinium iodides are very sensitive to the polarity of the medium.[13] In the present work, we examined the effect of such organic solvents as methanol and DMSO on the CT absorption band and the K_a value of a **1**-I^- system (Table 3). The absorption maximum of the CT complex shifted to the direction of longer wavelengths. The effect was larger in DMSO than in methanol. These results are in agreement with those observed for 1-alkyl-4-(methoxycarbonyl)pyridinium iodides by Kosower.[13] The K_a value of a CT complex of **1** with I^- increased slightly with an increase in the DMSO concentration from 0 to 10% (v/v). A further increase in the DMSO concentration resulted in a significant decrease in the K_a value. The K_a value also decreased with the addition of methanol. DMSO and methanol are less polar than water. A decrease in the polarity of the medium with an increase in the concentration of the organic solvents is favorable for both electrostatic and CT interactions between **1** and I^-. However, it is unfavorable for hydrophobic interactions between them. Moreover, both DMSO and methanol are included within the α-CD cavity,[27,28] so they competitively inhibit the complexation of **1** with I^-. These unfavorable effects of the organic solvents may surpass the favorable effects in the systems examined, except for the cases of 10 and 20% DMSO.

Discussion

Judging from the results described in the preceding section, it seems that at least four kinds of intermolecular interactions are responsible for the complexation

of **1** with I^-: (1) Hydrophobic interactions, (2) van der Waals interactions, (3) electrostatic interactions, and (4) CT interactions. The host, **1**, forms relatively stable complexes with I^-, SCN^-, and ClO_4^-, which are known to be chaotropic or lipophilic anions.[29] On the other hand, **1** binds very weakly, if at all, to SO_4^{2-} and Cl^-, which are known to be antichaotropic or hydrophilic.[29] This fact indicates that hydrophobic interactions are involved in the complexation. The binding constant (K_a) for a I^- complex with **1** was ca. 45 times that with a nonmacrocyclic analog **4** and ca. 4.4 times that with a β-CD analog **3**. This suggests that the macrocyclic cavity of α-CD is essential for the formation of a stable complex of **1** with I^-. The I^- ion may be in close van der Waals contact with the α-CD cavity. The β-CD cavity in **3** may be too large to be in close contact with I^-. The host **1** is positively charged, and the guest, negatively charged. Thus, electrostatic interactions must also take part in the complexation. In fact, the K_a value for a **1**–I^- system decreases significantly with an increase in the I_c value of the medium. CT interactions may also contribute to the stabilization of the complex. This postulate is supported by the following observations. A mixture of **1** with I^-, SCN^-, or Br^- affords an distinct absorption band characteristic of a CT complex. The I^- and SCN^- ions are bound to **1** more strongly than to the native α-CD by factors of 6—7 at I_c=1.0. On the other hand, the K_a value for a **1**–ClO_4^- system at I_c=1.0 is only 3.7 times that for a native α-CD–ClO_4^- system. The ClO_4^- ion forms no CT complex with **1**. In conclusion, the four kinds of intermolecular interactions described above may take part cooperatively in the complexation of **1** with such inorganic anions as I^-, SCN^-, and Br^-.

Kosower and Burbach[12] suggested that, in a complex of **5** with I^-, the I^- ion is located over the center of the pyridine ring, although it is undeniable that the complexed I^- ion is located near the nitrogen of the pyridinio group. In the present **1**–I^- system, we found that ^1H NMR signals due to the ortho-H's of the pyridinio group and C(6)–H's of GP(A) and GP(B) are significantly influenced by the complexation, whereas only small changes, if any, in the signals are observable for the meta- and para-H's of the pyridinio group and the C(1)–H's of the GP's. This suggests that the complexed I^- ion is located in the vicinity of the nitrogen of the pyridinio group. The nitrogen is positively charged, so that the location of the complexed I^- ion near the nitrogen is advantageous for electrostatic interactions.

We have showed that I^- forms more stable complexes with the C(6)-mono- and C(6)-dipyridinio derivatives, **1** and **2**, than with the native α-CD by factors of ca. 10 and 100 respectively at I_c<0.024. This finding directed our attention to the development of a host compound to which inorganic anions are bound strongly and/or selectively. Very recently, we have found that the I^- is bound to the C(6)-tri- and C(6)-hexapyridinio derivatives of α-CD more strongly than to the native α-CD by factors of ca. 10^3 and 10^5 respectively at I_c<0.01. Thus, the effect of the number of the pyridinio groups on the stability is extremely large. The C(6)-di- and C(6)-tripyridinio derivatives of α-CD involve three and four regioisomers respectively. The effects of the positions of the pyridinio groups on the stability may also be interesting. The experimental results on these subjects will be presented elsewhere in detail.

It is anticipated that electrostatic and CT interactions between **1** and I^- will be strengthened by lowering the polarity of the medium. However, the addition of an organic solvent to the medium caused virtually no such favorable effect on the complexation as had been anticipated; this was because of the competitive binding of the organic molecule to the host cavity. It may be advantageous, for strengthening the electrostatic and CT interactions, to make the microenvironment around the pyridinio group less polar. In fact, we recently found that I^- is bound to the peracetylated derivative of **1** more strongly than to **1** by a factor of ca. 4 at I_c<0.024. Further details will be reported elsewhere.

References

1) D. W. Griffith and M. L. Bender, *Adv. Catal.*, **23**, 209 (1973).
2) W. Saenger, *Angew. Chem., Int. Ed. Engl.*, **19**, 344 (1980).
3) I. Tabushi, *Acc. Chem. Res.*, **15**, 66 (1982).
4) Y. Matsui, T. Nishioka, and T. Fujita, *Topics Current Chem.*, **128**, 61 (1985).
5) B. Casu, M. Reggiani, and G. R. Sanderson, *Carbohydr. Res.*, **76**, 59 (1979).
6) I. Tabushi, N. Shimizu, T. Sugimoto, M. Shiozuka, and K. Yamamura, *J. Am. Chem. Soc.*, **99**, 7100 (1977).
7) J. Boger and J. R. Knowles, *J. Am. Chem. Soc.*, **101**, 7631 (1979).
8) Y. Matsui and A. Okimoto, *Bull. Chem. Soc. Jpn.*, **51**, 3030 (1978).
9) Y. Matsui, K. Ogawa, S. Mikami, M. Yoshimoto, and K. Mochida, *Bull. Chem. Soc. Jpn.*, **60**, 1219 (1987).
10) Y. Matsui, M. Fujie, and H. Sakate, *Bull. Chem. Soc. Jpn.*, **61**, 3409 (1988).
11) E. M. Kosower and P. E. Klinedinst, Jr., *J. Am. Chem. Soc.*, **78**, 3493 (1956).
12) E. M. Kosower and J. C. Burbach, *J. Am. Chem. Soc.*, **78**, 5838 (1956).
13) E. M. Kosower, *J. Am. Chem. Soc.*, **80**, 3253 (1958).
14) E. Graf and J.-L. Lehn, *J. Am. Chem. Soc.*, **98**, 6403 (1976).
15) I. Tabushi, Y. Kimura, and K. Yamamura, *J. Am. Chem. Soc.*, **100**, 1304 (1978).
16) J. Cullinane, R. I. Gelb, T. N. Margulis, and L. J. Zompa, *J. Am. Chem. Soc.*, **104**, 3048 (1982).
17) E. Kimura, M. Komada, and T. Yatsunami, *J. Am.*

Chem. Soc., **104**, 3182 (1982).
18) All the aqueous solutions were unbuffered and slightly basic due to the hydrogencarbonate salts of the hosts. The concentration of the OH^- ion was too low to affect the association of the hosts with the guest anion.
19) K. Mochida, A. Kagita, Y. Matsui, and Y. Date, *Bull. Chem. Soc. Jpn.*, **46**, 3703 (1973).
20) A. Buvari and L. Barcza, *Inorg. Chim. Acta*, **33**, L179 (1979).
21) J. P. Diard, E. Saint-Aman, and D. Serve, *J. Electroanal. Chem. Interfacial Electrochem.*, **189**, 113 (1985).
22) H. Hoeiland, L. H. Hald, and O. J. Kvammen, *J. Soln. Chem.*, **10**, 775 (1981).
23) R. P. Rohrbach, L. J. Rodriguez, E. M. Eyring, and J. F. Wojcik, *J. Phys. Chem.*, **81**, 944 (1977).
24) I. Sanemasa, M. Fujiki, and T. Deguchi, *Bull. Chem. Soc. Jpn.*, **61**, 2663 (1988).
25) F. Cramer, W. Saenger, and H.-Ch. Spatz, *J. Am. Chem. Soc.*, **89**, 14 (1967).
26) R. I. Gelb, L. M. Schwartz, M. Radeos, and D. A. Laufer, *J. Phys. Chem.*, **87**, 3349 (1983).
27) Y. Matsui and K. Mochida, *Bull. Chem. Soc. Jpn.*, **52**, 2808 (1979).
28) R. I. Gelb, L. M. Schwartz, M. Radeos, R. B. Edmonds, and D. A. Laufer, *J. Am. Chem. Soc.*, **104**, 6283 (1982).
29) W. P. Jencks, "Catalysis in Chemistry and Enzymology," McGraw-Hill, New York (1969), p. 358.

 © 1989 The Chemical Society of Japan Bull. Chem. Soc. Jpn., 62, 1458—1462 (1989) [Vol. 62, No. 5

Light-Induced Generation of Charge Carriers in Porphyrin Solids Doped with Electron-Accepting and Donating Molecules

Yutaka HARIMA,* Kazuyo YAMAMOTO, Kazuhiko TAKEDA, and Kazuo YAMASHITA
Department of Material and Life Sciences, Faculty of Integrated Arts and Sciences, Hiroshima University, Naka-ku, Hiroshima 730
(Received November 24, 1988)

Fluorescence and photocurrent generation efficiencies of thin films of 5,10,15,20-tetraphenylporphyrin (TPP) and its zinc complex (ZnTPP) doped with electron-accepting and -donating molecules were investigated to get an insight into a charge-carrier generation in organic solid films upon irradiation. Photogeneration of charge carriers in I_2-doped ZnTPP solids was found to consist mainly of a direct ionization process via an excited singlet state of ZnTPP while that in TPP solids was consistent with an exciplex formation model. From a practical view point, the doping of acceptor molecules into p-type porphyrin solids was effective to improve photovoltaic efficiencies of Al/porphyrin/Au sandwich-type cells.

The effect of electron acceptors or donors upon the conductivity and photoconductivity of molecular solids is well-known. As early as in 1960, Calvin et al. examined electrical properties of phthalocyanine (Pc) films on addition of *o*-chloranil and found the increase in the dark conductivity and photoconductivity by orders of magnitude.[1,2] Based on the ESR measurement, they ascribed the striking enhancement of the currents to an electron transfer from Pc to the acceptor molecule in the dark, which produces holes in the Pc layer and *o*-chloranil anion radicals. More recently, Loutfy and Menzel have investigated a correlation between fluorescence and charge-carrier photogeneration efficiencies of an X-type Pc film doped with 2,4,7-trinitrofluorenone (TNF).[3] In consequence, they have found that with an increase in TNF concentration the carrier generation efficiency increases while the fluorescence is quenched. Their finding is explained by the singlet exciton diffusion to the surface of the X-Pc at the dopant site, followed by the exciplex formation and its subsequent dissociation into charge carriers. In other words, the former authors have postulated a dominant role of the ground-state complex for the doping effect, which is equivalent to the band model of doped semiconductors,[4] as opposed to the exciplex formation proposed by the latter.

The electronic processes in molecular solids are complicated and their interpretation occasionally requires molecular level considerations.[5-8] However, a close examination of the doping effect on the organic semiconductors could be a clue to understand the electronic processes such as a charge-carrier generation upon irradiation, the process being essential in photosynthesis and in solar energy conversion.

In this report, we describe the effects of doping with electron acceptors and donors on the fluorescence intensity of porphyrin films as well as on the performance of photovoltaic cells based on these porphyrins. The reasons of using porphyrins as host molecules are four-fold: 1) Electronic processes in nondoped porphyrin films have been the subject of recent investigations.[9,10] Especially, the choice of the two porphyrins, i.e. 5,10,15,20-tetraphenylporphyrin (TPP) and its zinc derivative (ZnTPP), is due to the large differences in exciton diffusion length[9,10] and in oxidation potential[11] between these porphyrins. 2) Different from phthalocyanines most investigated, porphyrins are soluble in some organic solvents to allow a preparation of organic thin films by use of a spinner coating method. This enables us to distribute guest molecules into the porphyrin layers uniformly. In most of previous studies[2,3,12] a surface doping in place of our bulk doping is employed. 3) Fluorescence from porphyrin solids is intense and gives us the information on the fate of excited states. 4) Aggregates of porphyrin molecules, organic oxidizing agents (quinones, coenzyme Q, etc.) and reducing agents (carotenoids) occur together in photosynthetic materials, and their interaction may be of importance in the primary quantum conversion process.

Experimental

TPP and its metal complex (ZnTPP) were purchased from Strem Chemicals Inc. ZnTPP was purified according to the literature method to remove a trace of chlorin.[13] Thin films of TPP and ZnTPP are known to exhibit a p-type semiconducting behavior. Iodine (I_2) was of reagent grade from Katayama Chemicals and used without further purification. Tetracyanoquinodimethane (TCNQ) from Tokyo Kasei Co. was recrystallized twice from ethyl acetate. *o*-Chloranil (Chl) and phenothiazine (Pz) from Tokyo Kasei Co. were purified by recrystallization from acetone and toluene, respectively. I_2, TCNQ, and Chl are well-known to be electron acceptors while Pz is an electron donor. Dichloromethane was redistilled after desiccation with calcium hydride. Sandwich-type photovoltaic cells of Al/(porphyrin+dopant)/Au were fabricated by first evaporating aluminum directly onto a precleaned glass substrate at 10^{-4} Pa by use of a Tokuda CFS-8EP vacuum deposition apparatus. The transmittance of the aluminum film was 20—50%. Porphyrin films doped with acceptors and donors were prepared using a Kyowa-Riken K359SW spinner as follows: a given amount of dopant molecules was dissolved into a 8 mM (1 M=1 mol dm^{-3}) TPP or ZnTPP solution of dichloromethane, and then one drop of the solution of

porphyrin plus dopant was put onto the aluminum-coated glass slide spinning at the rate of 4600 rpm. Absorbance of the films prepared in this manner was 0.8—1.0 at the Soret band of the porphyrin films irrespective of the amount of dopant molecules involved. Only uniformly prepared samples were used for further vacuum-deposition of gold on the porphyrin films to make an ohmic contact. Measurements of spectral responses of the short-circuit (s.c.) photocurrents were performed with the aid of a microcomputer, where photocurrents were normalized in such a way that the intensity of monochromatic light incident on the interface between the dye film and Al was at 10 μW cm^{-2}. The light source consisted of a 300 W tungsten halogen lamp and a JASCO CT-10S monochromator. Open-circuit photovoltages (V_{oc}) of photovoltaic cells were measured by a Takeda Riken TR8651 electrometer. Samples for fluorescence measurements were prepared by the spinner coating onto Pyrex glass substrates. Measurements of fluorescence from spun films of porphyrins were made by use of a Hitachi MPF-4 fluorescence spectrophotometer. In most experiments, the angle of the exciting light to the normal of the sample side of the glass slides was adjusted within 65±5° to give a maximum fluorescence intensity, and the luminescence was detected at the right angle to the exciting beam. All measurements were carried out at room temperature.

Results

Figure 1 depicts spectral responses of s.c. photocurrents for a) Al/TPP/Au and b) Al/ZnTPP/Au photovoltaic cells with and without doping of electron accepting I_2 and TCNQ molecules. In all cases, illumination is carried out from the Al/p-type porphyrin interface which provides an effective site for the light-induced generation of charge carriers. Photocurrents (i_p) flow from Au to Al through the external circuit. It is seen that the addition of I_2 or TCNQ enhances the photocurrents greatly over the entire spectral range investigated. In addition, the spectral responses of photocurrents for the doped samples coincide well in shape with the absorption and action spectra of the corresponding pure porphyrin films, suggesting that no spectral sensitization by the dopants takes place. The photocurrent quantum yield (η), defined as the number of electrons produced per photon incident on the dye film, at the Soret band changes from 1.4% for pure TPP to 6.3% for I_2-doped TPP and from 2.9% for pure ZnTPP to 11% for I_2-doped ZnTPP. In addition to this, no appreciable decay of i_p with a lapse of time indicates that the doping is an important technique to improve efficiencies of solar cells based on organic materials.

Figure 2a shows changes of s.c. photocurrents at the Soret band for the Al/TPP/Au photovoltaic cells when I_2, Chl, TCNQ, or Pz are doped into the TPP solids at various mole fractions, where η_0 in ordinate denotes the η value in the absence of dopant. Figure 2b depicts similar plots for the Al/ZnTPP/Au photovoltaic cells with I_2 or TCNQ as a dopant. With I_2 being doped, the photocurrents for the both cells start to increase at the I_2 mole fraction as high as 0.1, whereas the TCNQ doping is effective at its mole fraction as low as 0.01. In the TCNQ case, the photocurrents for TPP as well as ZnTPP level off at a 0.2 mole fraction and decrease with TCNQ mole fractions beyond this value. The photocurrent reduction when TCNQ is doped heavily might be ascribed to a steric effect which prevents an intermolecular interaction between porphyrin molecules. As is seen in Fig. 2a, the doping of Chl into the TPP film was the most effective and enhanced the photocurrent by almost one order of magnitude. On the other hand, the photocurrent is slightly reduced by the addition of electron-donating Pz molecules into the TPP film.

Figure 3 summarizes the results of fluorescence measurements, where F and F_0 correspond to intensities of fluorescence from porphyrin solids with and

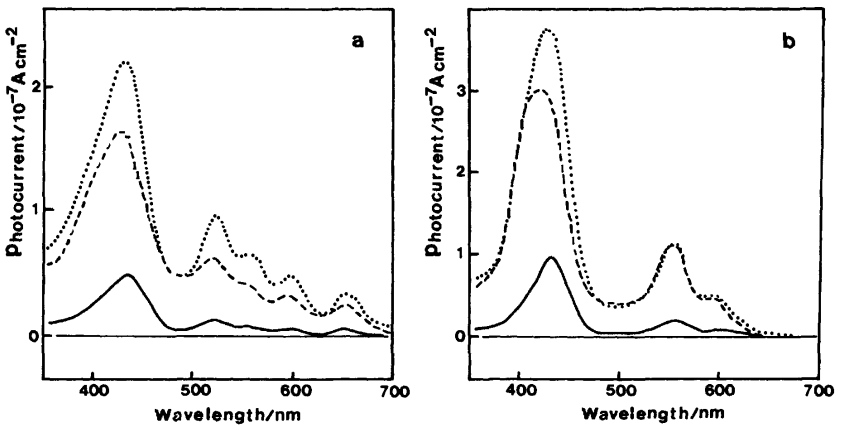

Fig. 1. Spectral responses of s.c. photocurrents for a) Al/TPP/Au and b) Al/ZnTPP/Au photovoltaic cells, where porphyrin solids are nondoped (solid line) and doped with I_2 (dotted line) and TCNQ (broken line).

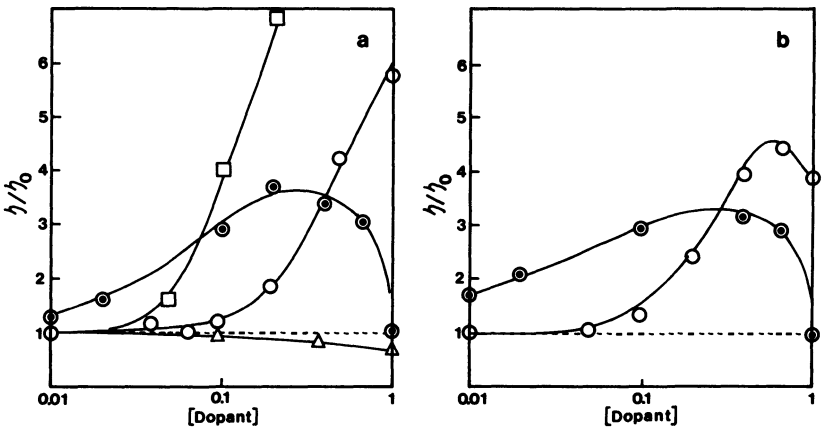

Fig. 2. Effect of doping on photocurrent quantum yield (η) for a) Al/TPP/Au and b) Al/ZnTPP/Au photovoltaic cells, where photocurrents are measured at the respective Soret bands of TPP and ZnTPP solids. Abscissas in Figs. 2 and 3 denote a mole fraction of the respective dopants: (○) I_2; (◉) TCNQ; (□) Chl and (△) Pz.

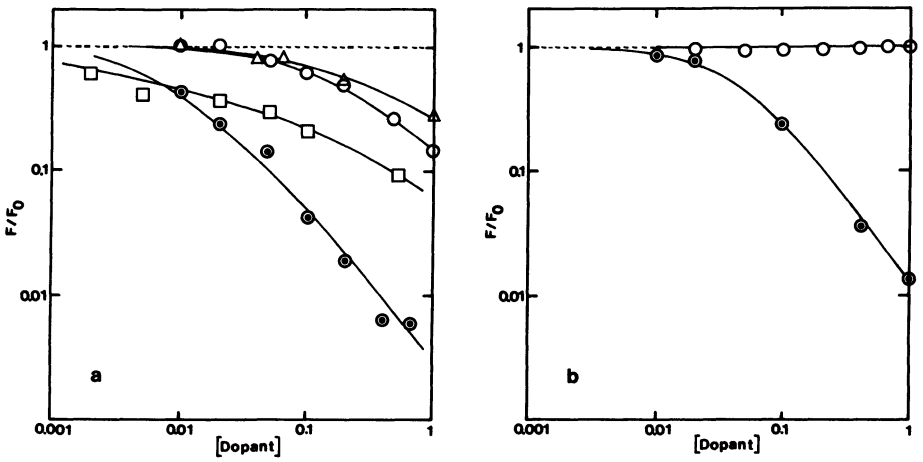

Fig. 3. Effect of doping on fluorescence intensity (F) of TPP and ZnTPP films, where excitation is made at 430 nm in both cases and emission is detected at 655 nm for TPP and 605 nm for ZnTPP. Each symbol has the same meaning as that of Fig. 2.

without doping, respectively. The excitation is made at the respective Soret bands of TPP and ZnTPP films, and the emission is detected at 655 nm for TPP and 605 nm for ZnTPP. It is seen from this figure first that TCNQ is the most effective in quenching ability among dopants used in the present study and second that fluorescence of TPP is quenched by TCNQ or I_2 more strongly than that of ZnTPP is. The second feature of the fluorescence quenching may be associated with the exciton diffusion length being greater for TPP than ZnTPP,[9] if the quenching ability of either of the dopants is similar between the two porphyrins. It should be noticed in Fig. 3 that fluorescence from the ZnTPP films is not quenched at all by I_2 ranging in mole fraction up to unity although the photocurrents are enhanced by the factor of 4 at the highest I_2 mole fraction. In contrast to this, fluorescence of the TPP films is quenched by Pz with an electron donating character although the photocurrents for the Pz-doped porphyrin films are almost constant irrespective of the amount of Pz doped. When the data in Fig. 3 were replotted as a reciprocal of a fluorescence intensity against a dopant mole fraction, all the plots yielded straight lines in the ranges of mole fractions up to 0.2—0.5 depending on the sort of the dopant. This finding indicates that the present bulk-doping technique using the spinner is successful to attain a uniform distribution of dopants in the solid films at low doping levels, at least.

Figure 4 displays the effect of I_2-doping on relative

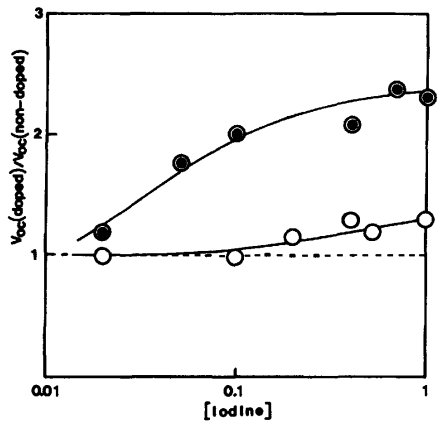

Fig. 4. Effect of I_2-doping on relative photovoltages of (○) Al/TPP/Au and (◉) Al/ZnTPP/Au photovoltaic cells.

open-circuit photovoltages of a) Al/TPP/Au and b) Al/ZnTPP/Au cells, where V_{oc}'s for the doped samples are divided by V_{oc} for the nondoped sample. V_{oc} for TPP stays almost constant irrespective of concentrations of I_2 doped, while that for ZnTPP increases with increasing I_2 concentration.

Discussion

According to the exciplex formation model,[3] deactivation routes for singlet excitons (S_1) consist of the following two competitive reactions:

$$S_1 \longrightarrow S_0 + h\nu(\text{fluorescence}) \quad (1)$$

$$S_1 + Q \longrightarrow (S.Q)^* \quad (2)$$

where Q is the quencher or the electron acceptor in the present case, S_0 the ground state of an organic dye molecule and $(S.Q)^*$ denotes the exciplex. The exciplex is assumed to dissociate into free charge carriers with a probability of $\phi(E)$ or into S_0 and Q as follows:

$$(S.Q)^* \xrightarrow{\phi(E)} e^- + h^+ \quad (3)$$

$$(S.Q)^* \xrightarrow{1-\phi(E)} S_0 + Q \quad (4)$$

Obviouly, this mechanism predicts the increase in charge carrier photogeneration efficiency on addition of Q concomitant with a decrease in fluorescence, in accord with the observations for the I_2-, TCNQ-, and Chl-doped TPP films. The same effects of doping can be expected also by assuming a dissociation of the exciton due to a local electric field caused by the charge-transfer complex between S_0 and Q in the dark. However, neither of these mechanisms explains the increase in photocurrents of the Al/ZnTPP/Au cell on addition of I_2, accompanied by no quenching of fluorescence. Concurrent changes in efficiencies of fluorescence and charge-carrier generation are essential in both models because a charge-carrier generation and a fluorescence quenching follow the reaction of S_1 with Q or with the CT complex comprising S_0 and Q.

One possible way to account for the results with ZnTPP is to assume, in place of the above impurity-dependent route, a direct charge-carrier generation from the S_1 state and/or the excited state of ZnTPP together with the band model description of the ZnTPP solid. In a preceding paper,[10] we have estimated diffusion lengths of excitons as 3±2 nm for ZnTPP and 15±10 nm for TPP on the basis of the analysis of the optical filtering effect observed for the Al/porphyrin/Au photovoltaic cells. In view of the fact that our estimate of the exciton diffusion length involves a contribution from the direct ionization process as well, the short exciton diffusion length found for the ZnTPP solid suggests that the direct charge-carrier generation may prevail in the ZnTPP solid in support of the above assumption. On the other hand, the ZnTPP molecule is known to be more easily oxidized than the TPP molecule.[11] This suggests that the valence band edge of the ZnTPP solid locates above that of TPP. Therefore, the postulated relative positions of energy levels denote that the acceptor doping should be more effective in ZnTPP than in TPP or that the acceptor molecule is likely to produce a ground-state complex, as suggested by Calvin et al.,[2] with the ZnTPP molecule more easily than with TPP. The ground-state complex formation leading to a production of the majority carrier (hole) in the ZnTPP solid in the dark induces a shift of the Fermi level of the molecular solid toward the valence band. The lowering of the Fermi level of the p-type solid leads to the increase of a built-in potential in the ZnTPP bulk close to Al, consistent with the increase in V_{oc} with increasing I_2 concentrations as shown in Fig. 4. Furthermore, the increase in the built-in potential can be responsible for the improvement in the photocurrent quantum yield since the enhanced electrostatic field in the depletion layer reduces a recombination probability of electron-hole pairs produced by the direct ionization process. It is quite evident that this model, in place of the exciplex formation model, does not necessarily require a parallelism between the fluorescence quenching and the improvement in the photocurrent quantum yield.

A spectroscopic attempt to detect the ground-state complex between ZnTPP and I_2 was performed by measuring absorption and fluorescence spectra of pure ZnTPP films and ZnTPP films doped with I_2 at various concentrations. However, no change at all was found in both spectra, suggesting that the equilibrium concentration of the ground-state complex is very low in comparison with that of the dopant added unless it has an absorption and a fluorescence spectra essentially indistinguishable from those of ZnTPP itself. The low concentration is not in conflict with the

observed changes in V_{oc} and i_p on addition of I_2 because even a small amount of the ground-state complex, if its concentration being higher than the hole concentration of the pure ZnTPP film, can be sufficient to alter electrical properties of the ZnTPP solids greatly.

For the TCNQ-doped ZnTPP solids, one can expect a similar carrier generation mechanism with the above one. In this case, however, fluorescence was quenched highly on addition of TCNQ. The result shows clearly an involvement of deactivation routes of S_1 such as expressed by Eqs. 1 and 2 besides, probably, the direct carrier generation path, which is predominant in the illuminated I_2-doped ZnTPP film.

Finally, the fluorescence quenching and no change of i_p observed with the Pz-doped TPP film are understandable by assuming the exciplex model with a small $\phi(E)$ value.

In conclusion, the present study shows that the mechanism of photogeneration of charge carriers depends on the combination of a dopant and an organic solid. Measurements of fluorescence and charge-carrier generation efficiency for the TPP solids doped with Chl, I_2, TCNQ, or Pz were consistent with those expected from the exciplex formation model. On the other hand, the mechanism of charge-carrier generation upon irradiation for the I_2-doped ZnTPP was explained based on the band model for the doped semiconductors together with the assumption of the direct photoionization process, in which the photocurrent increase was ascribed to a reduction in recombination rate of electron-hole pairs in the depletion layer. In the case of TCNQ-doped ZnTPP, both direct and indirect processes appeared to prevail.

References

1) G. Tollin, D. R. Kearns, and M. Calvin, *J. Chem. Phys.*, **32**, 1013 (1960).
2) D. R. Kearns, G. Tollin, and M. Calvin, *J. Chem. Phys.*, **32**, 1020 (1960).
3) R. O. Loutfy and E. R. Menzel, *J. Am. Chem. Soc.*, **102**, 4967 (1980).
4) H. Meier, "Monographs in Modern Chemistry," ed by H. F. Ebel, Verlag Chemie, Weinheim (1974), Vol. 2, p. 375.
5) H. Hoegl, *J. Phys. Chem.*, **69**, 755 (1965).
6) R. F. Chaiken and D. R. Kearns, *J. Chem. Phys.*, **45**, 3966 (1966).
7) D. F. Barbe and C. R. Westgate, *J. Chem. Phys.*, **52**, 4046 (1970).
8) J. Noolandi and K. M. Hong, *J. Chem. Phys.*, **70**, 3230 (1979).
9) K. Tanimura, T. Kawai, and T. Sakata, *J. Phys. Chem.*, **84**, 751 (1980).
10) K. Yamashita, Y. Harima, and H. Iwashima, *J. Phys. Chem.*, **91**, 3055 (1987).
11) R. H. Felton, "The Porphyrins," ed by D. Dorphin, Academic Press, New York (1978), Vol. V, p. 53.
12) P. Leempoel, F-R. Fan, and A. J. Bard, *J. Phys. Chem.*, **87**, 2948 (1983).
13) J.-H. Fuhrhop and K. M. Smith, "Porphyrins and Metalloporphyrins," ed by K. M. Smith, Elsevier, New York (1975), p. 770.

 © 1989 The Chemical Society of Japan Bull. Chem. Soc. Jpn., 62, 1463—1467 (1989)

The Model Compounds and the Conformational Analysis of Poly(thiomethylene)

Taira MIYASAKA* and Takaichi YOSHIDA
Department of Dental Materials Science, School of Dentistry at Tokyo, The Nippon Dental University, 1-9-20, Fujimi, Chiyoda-ku, Tokyo 102
(Received November 29, 1988)

The conformational energies of model compounds of poly(thiomethylene), $CH_3(SCH_2)_nSCH_3$, (n=1—6) were calculated by the molecular-mechanics method. Based on these conformational energy differences, the configuration-dependent properties of poly(thiomethylene) were estimated under the rotational isomeric-state approximations. The first-order interaction energy of the $C\diagdown S\diagup C\diagdown S$ bond, obtained from the energy differences among the conformers of $CH_3(SCH_2)_3SCH_3$, is coincident with that estimated from the same bond sequence for poly(1,3-dithiocane). Based on this coincidence, the monomeric sequential length of the model compound, which is representative of poly(thiomethylene), was decided. The propriety of the method of coupling the molecular-mechanics with the statistical-mechanics was also demonstrated.

Because of the structural similarity between poly(oxyalkylenes) and poly(thioalkylenes), the anomalous preference of the gauche states to the trans, i.e. the "gauche effect," which had been found in poly(oxyalkylenes),[1] is expected also to be present in poly(thioalkylenes). Based on the success of the estimation of the "gauche effect" and that of the proper approximation for rotational states of poly(oxyalkylenes),[2-4] poly(thiotrimethylene) was studied by the molecular-mechanics method in a previous report.[5] This polymer has the simplest chemical structure among the analogous poly(thioalkylenes), whose configuration-dependent properties had previously been observed experimentally. In that earlier paper,[5] the dipole-moment ratio and its temperature coefficient, observed experimentally, were reproduced with satisfactory success under the isomeric-state approximation of the molecular-mechanics method. It was shown that the "gauche effect" caused by sulfur atoms is significantly different from that of poly(oxyalkylenes); in the case of poly(thiotrimethylene), a longer-range steric interaction plays an important role. It was also shown that the molecular mechanics is effective in the analysis of the anomeric gauche effect of poly(thiotrimethylene).

Poly(thiomethylene) is the simplest member of the poly(thioalkylenes) and possesses the characteristic $C\diagdown S\diagup C\diagdown S$ sequence. Therefore, it can be expected to exhibit the even more characteristic "sulfur gauche effect." Recently, a vibrational analysis of poly(thiomethylene) was done[6] based on the group-coordinate force-field method, which clarified that the dominant conformational state of the skeletal bonds in the crystal, liquid, and gaseous states is gauche, although the energy difference between possible conformers had not yet been estimated accurately.

In this paper, the molecular conformation and the related properties of poly(thiomethylene) are studied by the method of statistical mechanics coupled with the molecular mechanics, since the configuration-dependent properties have not been observed experimentally because of the low solubility of poly(thiomethylene) in any solvents and its high melting point. Several model compounds possessing various chain lengths are investigated in an attempt to estimate the rotational isomeric-state approximations of the polymer. The most suitable chain length for the model compound of poly(thiomethylene) should satisfy the following conditions: it gives all the statistical and geometrical parameters required in the statistical-mechanics calculations for poly(thiomethylene), and it gives a first-order interaction ($C\diagdown S\diagup C\diagdown S$) parameter of the same magnitude as that which has experimentally estimated for poly(1,3-dithiocane). Using the parameters thus obtained, the configuration-dependent properties of poly(thiomethylene) are calculated.

Theoretical

Molecular-Mechanics Method. The molecular-mechanics method, also called the force-field method, has become one of the most popular methods in the field of computer chemistry. In this calculation, a molecule is treated as a system of particles held to one another with classical mechanical interatomic forces. The steric energy of the molecule is obtained as a function of the bond-stretching, bending, torsional, van der Waals, and electrostatic interactions; then, the optimum conformation is searched for.

Although many force fields have been suggested, Allinger's force-field[7] can be used for a wide range of problems in organic chemistry because its parameters for hydrocarbons and some hetero atoms are made carefully. An old type of this type of force field, i.e., MMI,[7] has been successfully used in a series of our studies of the conformational analysis of poly(oxyalkylenes); a newer version, i.e., MM2[8] has also been used in our previous reports on a similar analysis of poly(thiotrimethylene). In the present calculation, we used the new version of MM2,[9] which can run on a microcomputer.

In order to ascertain the optimal length of model compounds used as representative poly(thiomethylenes), the following compounds including one to six $-SCH_2-$ units with terminal methyl and methylthio groups were selected for study; 2,4-dithiapentane [**2T**] $CH_3-SCH_2-SCH_3$, 2,4,6-trithiaheptane [**4T**] $CH_3-(SCH_2)_2-SCH_3$, 2,4,6,8-tetrathianonane [**6T**] $CH_3-(SCH_2)_3-SCH_3$, 2,4,6,8,10-pentathiaundecane [**8T**] $CH_3-(SCH_2)_4-SCH_3$, 2,4,6,8,10,12-hexathiatridecane [**10T**] $CH_3-(SCH_2)_5-SCH_3$, and 2,4,6,8,10,12,14-heptathiapentadecane [**12T**] $CH_3-(SCH_2)_6-SCH_3$. Here ***n*T** in square brackets denotes the number of skeletal bonds whose internal rotations experience the butane interaction between CH_2 groups and S atoms; these abbreviations will be used hereafter instead of the full names of the model compounds. The all-trans conformer, the conformers including one gauche state, and those including two consecutive gauche bonds with the same or opposite signs are calculated by means of the molecular-mechanics.

Results and Discussion

Model Compounds of Poly(thiomethylene). The results of molecular-mechanics calculations on the six above-mentioned kinds of model compounds of poly(thiomethylene) are listed in Table 1, where the energy differences between the conformers including one or two consecutive gauche states and the corresponding all-trans conformer are also shown.

In the case of the simplest model compound, **2T**, the GG conformer has the lowest energy, the TG conformer is next, and the TT has the highest. In the vibrational analysis of this model compound, more than two conformers were found in the liquid or gaseous states.[6] These results can be compared with those for the corresponding model compounds of poly(oxymethylene),[2] i.e. 2,4-dioxapentane, in which the energy differences of the TG, GG, and G$\bar{\text{G}}$ conformers from TT are −10.84, −18.45, and −3.18 kJ mol^{-1} respectively. Comparing these values with the values of **2T** shows that the energy of TG, i.e., −4.01 kJ mol^{-1}, is much higher than that of 2,4-

Table 1. The Energy Differences between the All-Trans State and Other Conformers (in kJ mol^{-1})

2,4-Dithiapentane	E/kJ mol^{-1}	2,4,6-Trithiaheptane	E/kJ mol^{-1}	2,4,6,8-Tetrathianonane	E/kJ mol^{-1}	2,4,6,8,10-Pentathiaundecane	E/kJ mol^{-1}
TT	0.0	TTTT	0.0	TTTTTT	0.0	TTTTTTTT	0.0
TG	−4.012	TTTG	−4.289	TTTTTG	−4.376	TTTTTTTG	−4.427
GG	−8.209	TTGT	−5.142	TTTTGT	−5.540	TTTTTTGT	−5.745
G$\bar{\text{G}}$	−1.950	TTGG	−9.703	TTTGTT	−5.590	TTTTTGTT	−5.728
		TGGT	−10.196	TTTTGG	−10.188	TTTTGTTT	−6.138
		TTG$\bar{\text{G}}$	−7.895	TTTGGT	−11.088	TTTTTTGG	−10.414
		TG$\bar{\text{G}}$T	−9.644	TTGGTT	−11.531	TTTTTGGT	−11.431
				TTTTG$\bar{\text{G}}$	−2.481	TTTTGGTT	−12.184
				TTTG$\bar{\text{G}}$T	−4.531	TTTGGTTT	−12.226
				TTG$\bar{\text{G}}$TT	−9.309	TTTTTTG$\bar{\text{G}}$	−2.435
						TTTTTG$\bar{\text{G}}$T	−4.682
						TTTTG$\bar{\text{G}}$TT	−5.280
						TTTG$\bar{\text{G}}$TTT	−4.757

2,4,6,8,10,12-Hexathiatridecane	E/kJ mol^{-1}	2,4,6,8,10,12,14-Heptathiapentadecane	E/kJ mol^{-1}
TTTTTTTTTT	0.0	TTTTTTTTTTTT	0.0
TTTTTTTTTG	−4.464	TTTTTTTTTTTG	−4.523
TTTTTTTTGT	−5.879	TTTTTTTTTTGT	−6.017
TTTTTTTGTT	−5.879	TTTTTTTTTGTT	−6.033
TTTTTTGTTT	−6.443	TTTTTTTTGTTT	−6.724
TTTTTGTTTT	−6.217	TTTTTTTGTTTT	−6.561
TTTTTTTTGG	−10.535	TTTTTTGTTTTT	−6.657
TTTTTTTGGT	−11.652	TTTTTTTTTTGG	−10.640
TTTTTTGGTT	−12.552	TTTTTTTTTGGT	−11.862
TTTTTGGTTT	−12.740	TTTTTTTTGGTT	−12.887
TTTTGGTTTT	−12.912	TTTTTTTGGTTT	−13.175
TTTTTTTTG$\bar{\text{G}}$	−2.377	TTTTTTGGTTTT	−13.489
TTTTTTTG$\bar{\text{G}}$T	−4.837	TTTTTGGTTTTT	−13.422
TTTTTTG$\bar{\text{G}}$TT	−6.092	TTTTTTTTTTG$\bar{\text{G}}$	−2.330
TTTTTG$\bar{\text{G}}$TTT	−4.887	TTTTTTTTTG$\bar{\text{G}}$T	−5.000
TTTTG$\bar{\text{G}}$TTTT	−11.301	TTTTTTTTG$\bar{\text{G}}$TT	−6.276
		TTTTTTTG$\bar{\text{G}}$TTT	−4.619
		TTTTTTG$\bar{\text{G}}$TTTT	−14.322
		TTTTTG$\bar{\text{G}}$TTTTT	−4.920

dioxapentane. The energies of the two consecutive gauche states of 2,4-dioxapentane (E_{GG} and $E_{G\bar{G}}$) are larger than twice the energy difference in the conformer including one gauche state ($2E_{TG}$), while the energy of E_{GG} of **2T** is smaller than $2E_{TG}$. Such a difference may be caused by the difference in the skeletal-bond length: the long C-S bond and the short C-O bond. The energy differences between the conformers of **2T** are mainly caused by the difference in the torsional and electrostatic interactions. These interactions also play an important role in the energy difference among the conformers of 2,4-dioxapentane. However, the energy difference between **2T** and 2,4-dioxapentane may also be caused by the electrostatic interactions: the electrostatic attraction in 2,4-dioxapentane is much larger than that in **2T**. This model compound, **2T**, is too short in length to give all the statistical-weight parameters required in the statistical-mechanics calculations for poly(thiomethylene). The smallest model compound giving the five required statistical-weight parameters is **4T**.

The conformers of **4T** including the two consecutive gauche bonds with the same sign are the lowest in energy, those including one gauche bond are the next lower, and the all-trans conformer is the highest. In the case of the corresponding model compounds of poly(oxymethylene),[2] i.e., 2,4,6-trioxaheptane, the order of the conformers in terms of energetic stability are the same as in **4T**, although the energy of the conformer including one gauche is lower by a factor of about 2.7 than that of the corresponding conformer of **4T**. The energy difference among the conformers is mainly caused by the torsional and electrostatic interactions. Especially the electrostatic interaction plays an important role in the steric-energy difference between **4T** and 2,4,6-trioxaheptane. The vibrational and normal-coordinate analysis of poly(thiomethylene) and its model compounds[10] made it clear that the lone-pair electrons on the sulfur atoms in the trans form are all located in the same direction and that the repulsion force between the lone-pairs becomes large (rabbit-ear effect), resulting in the stability of the gauche state.[10] This stability of the gauche state is consistent with the calculated results for the model compounds in this study.

Based on the calculated results for the various conformers from **2T** to **12T**, it was clarified that the conformation energy is smaller for the compound which includes the gauche bond in the inner position of the skeletal chain. This is always true for the conformers with a gauche state located within the fourth position from the terminal point, except for the sequence of TTTTTTGT and TTTTTGTT of **8T**. On the contrary, the conformers of **10T** and **12T**, which include a gauche bond at a position more inward than the fourth from the terminal point, show larger energies than those of the conformers which include a gauche bond at the fourth position. It seems that, when the length of the chain becomes long, the gauche state of the central position experiences a severe steric interaction because of the large substituent groups being brought close to each other. Therefore, the **10T** and **12T** molecules seem too long to be adopted as suitable model compounds of poly(thiomethylene). For the conformers including two consecutive gauche bonds of the same sign, the energy becomes lower as the two gauche bonds are positioned at the inner part of the chain, except for the cases of the TTTTTTGGTTTT and TTTTTGGTTTTT of **12T**.

Statistical-Mechanics Calculation of Configuration-Dependent Properties. A parameter of the first-order interaction and the four parameters of the second-order interactions are required to make statistical-mechanics calculations of configuration-dependent properties of poly(thiomethylene). The statistical-weight parameter of the first-order interaction for a gauche in the 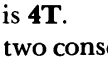 bond sequence is denoted by σ. The parameters of the second-order interaction in the sequence are denoted by ϕ and ω for the two consecutive gauche bonds with the same and with opposite signs respectively. The second-order interaction parameters of the two other consecutive gauches in the sequence are defined by ϕ' and ω' for the GG($\bar{G}\bar{G}$) and G$\bar{G}$($\bar{G}$G) respectively. These parameters are obtained from the above-mentioned results of the molecular-mechanics calculation of the conformers of each model compound. The first-order interaction energy E_σ is calculated as the averaged value of the conformational-energy differences between the conformers including one gauche state and the all-trans conformer. The second-order interaction energy is obtained as the energy increment upon the introduction of one additional gauche state into the corresponding conformation with one gauche bond; for example, $E_{\phi'}=E_{TTGG}-E_{TTGT}-E_{TTTG}$. These energy values are averaged over all the model compounds. The energies of the first- and second-order interactions thus obtained are plotted for the number of skeletal bonds of model compounds in Fig. 1. The first-order interaction energy E_σ decreases with the increase in the chain length: -4.02 kJ mol^{-1} in **2T** and -6.11 kJ mol^{-1} in **12T**. In contrast, E_ϕ and $E_{\phi'}$ are held at almost the same level; E_ϕ is nearly zero, and $E_{\phi'}$ is between -0.17 and -0.33 kJ mol^{-1}. The second-order interaction energies for the two consecutive oppositely signed gauche sequences, i.e., E_ω and $E_{\omega'}$, vary significantly. The E_ω increases with an increase in the chain length, while the $E_{\omega'}$ tends to decrease slightly with some vibration. The conformations of poly(thiomethylene) are estimated from these energy parameters. The gauche state occurs most frequently because of a large negative value of E_σ. The

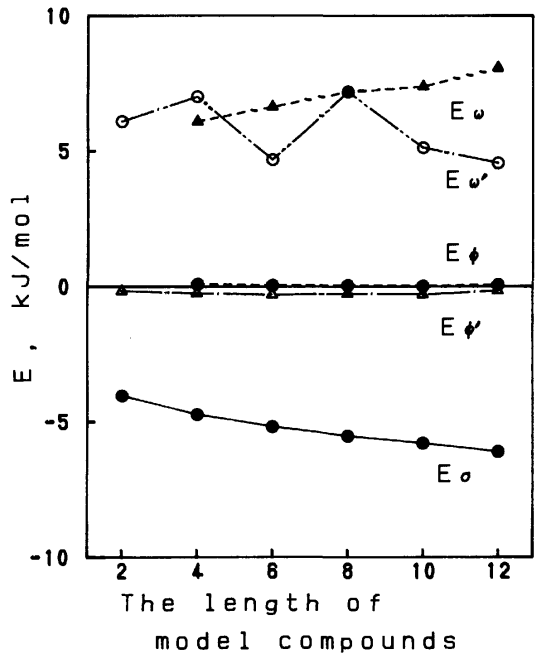

Fig. 1. The variation of statistical-weight parameters plotted against the chain length of model compounds of poly(thiomethylene).

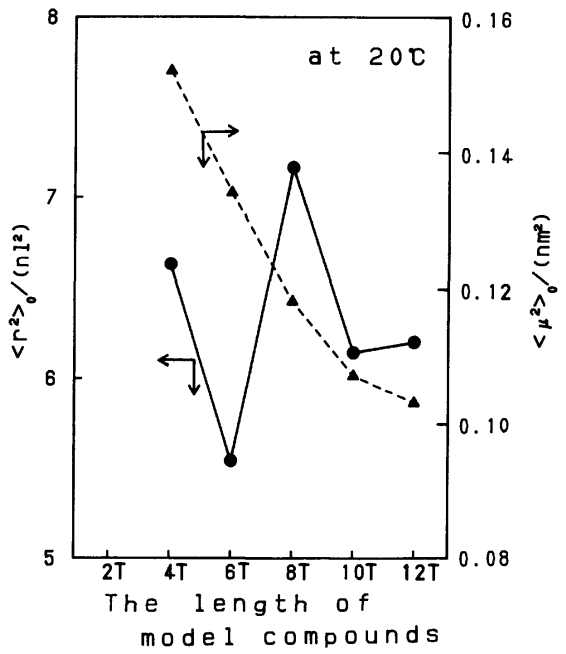

Fig. 2. The dependence of the characteristic ratio and the dipole-moment ratio of poly(thiomethylene) on the chain length of model compounds. Filled circles represent the characteristic ratios and filled triangles represent the dipole-moment ratios.

conformers containing two consecutive gauche states with the same sign in the $^{C}_{S}\!\!\diagup\!\!\diagdown^{C}_{S}\!\!\diagup\!\!\diagdown^{C}$ bond sequence occur more frequently than those in $^{S}_{C}\!\!\diagup\!\!\diagdown^{S}_{C}\!\!\diagup\!\!\diagdown^{S}$ because the value $E_{\phi'}$ is negative and smaller than $E_{\phi}(\simeq 0)$. The $E_{\omega'}$ value is apparently smaller than E_{ω} in **6T**, **10T**, and **12T**; therefore, the conformers containing two consecutive gauche states with the opposite signs in the $^{C}_{S}\!\!\diagup\!\!\diagdown^{C}_{S}\!\!\diagup\!\!\diagdown^{C}$ bond sequence occur more frequently than those in $^{S}_{C}\!\!\diagup\!\!\diagdown^{S}_{C}\!\!\diagup\!\!\diagdown^{S}$. Such an estimation can be compared with the experimental results of poly(thiomethylene) and its model compounds. The crystal structure of this polymer had been investigated,[11] and the molecular form in the solid state has been confirmed to be the [G] form. However, this X-ray study was carried out in the solid state, and so the results could not be directly compared with the present results, for in this study the conformation of poly(thiomethylene) in a liquid (dilute solution) or an isolated molecule has been investigated. A recent study of the vibrational analysis of poly(thiomethylene) and its model compounds[10] pointed out that many forms coexist in a liquid or gaseous state: for example, GG, TT, TG in **2T**. Their results correspond well with those obtained in this study.

The geometrical parameters necessary for the statistical-mechanics calculations were also obtained from the results of the molecular-mechanics calculations on each model compound. All the geometrical parameters for the conformers of each model compound were then averaged, taking the weight of their energy differences and occurrence into account. The Boltzmann-averaged geometric parameters thus obtained were found to be scarcely influenced at all by the chain length of the model compounds; $\angle$CSC=80.6°—81.2°, $\angle$SCS=64.2°—66.4°, $\phi^{T}_{C\text{-}C}$=−0.8°—0.7°, $\phi^{G}_{C\text{-}C}$=109.3°—112.5°, $l_{C\text{-}S}$=1.819 Å, and $m_{C\text{-}S}$=1.20 D, where ϕ^{T}, ϕ^{G}, and m are the torsional angles of the trans and gauche states, and the bond dipole-moment, respectively.

The configuration-dependent properties of poly(thiomethylene) that is, the characteristic ratio, the dipole-moment ratio, and their temperature coefficients were calculated as functions of the chain length of the model compound by using these statistical-mechanics parameters; the results are shown in Figs. 2 and 3. Although the characteristic ratios $\langle r^2\rangle_0/(nl^2)$ ($\langle r^2\rangle_0$: an unperturbed dimension, n: the number of skeletal bonds, l: the length of the bond) show some variation (from 5.5 to 7.2) for **6T** and **8T**, those of **4T**, **10T**, and **12T** are all at almost the same level (6.1—6.3). The dipole-moment ratio $\langle\mu^2\rangle_0/(nm^2)$ decreases from 0.17 to 0.10 with the increase in the chain length, although the decrement rate becomes small. As is shown in Fig. 3, the temperature coefficient of the dipole-moment ratio $d\log_e\langle\mu^2\rangle_0/dT$ is positive and increases with the increase in the chain length. The temperature coefficients of the characteristic ratio $d\log_e\langle r^2\rangle_0/dT$ are all negative and show a rapid decrease from -3.2×10^{-3} K^{-1} at **4T**

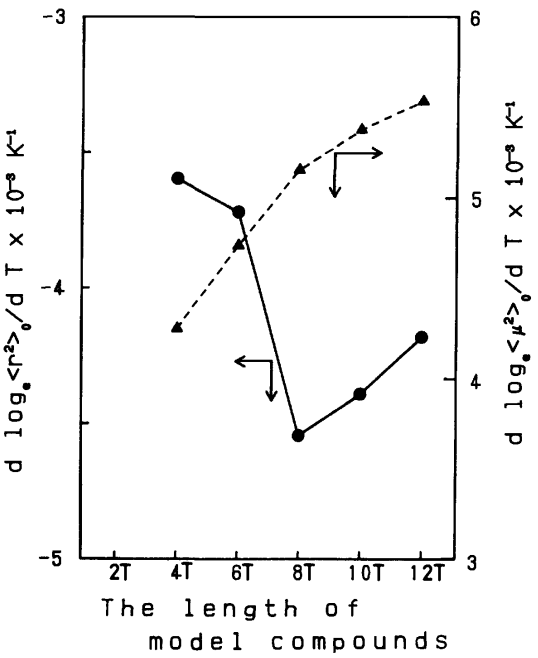

Fig. 3. The dependence of the temperature coefficients of the configuration-dependent properties of poly(thiomethylene) on the chain length of model compounds. Filled circles represent the temperature coefficients of characteristic ratios and filled triangles represent those of dipole-moment ratios.

to $-4.5\times10^{-3}K^{-1}$ at **8T**, after which they slightly increase to -4.2×10^{-3} K^{-1} for **12T**. The reliability of these forecast values depends upon the reliability of the statistical-mechanics parameters obtained from the molecular-mechanics calculations on the model compounds. No experimentally obtained value of the configuration-dependent properties of poly(thiomethylene) has yet been reported. The configurational study of poly(1,3-dithiocane)[12] is the only experimental report available for comparison with the calculated values of poly(thiomethylene). The experimental values of the dipole-moment ratio and its temperature coefficient of poly(1,3-dithiocane) were reproduced by using the value of $E_\sigma=-5.02$ kJ mol^{-1}. This value of the first-order interaction energy is very close to those obtained from the model compounds of poly(thiomethylene); $E_\sigma=-4.73$ kJ mol^{-1} for **4T**, and -5.19 kJ mol^{-1} for **6T**. This fact suggests the reliability of the results obtained by the molecular-mechanics calculations on these model compounds of poly(thiomethylene). Our previous report[5] on poly(thiotrimethylene) showed that the approximate model compound of this polymer contains two or three repeating units with proper terminal groups. According to this conclusion, the appropriate model compounds of poly(thiomethylene) may be either **6T** or **8T**. The present calculation also supports this result, because: (1) the E_σ value of the model compound is of the same magnitude as that of poly(1,3-dithiocane), and (2) the gauche states in the central position of the long model compounds (above the **10T**) experience a severe steric interaction. When the **6T** is adopted as the model compound of poly(thiomethylene), the configuration-dependent properties are calculated as follows; $\langle r^2\rangle_0/(nl^2)=5.54$, $\langle\mu^2\rangle_0/(nm^2)=0.13$, d log$_e$ $\langle r^2\rangle_0$/d $T=-3.72\times10^{-3}$ K^{-1} and d log$_e\langle\mu^2\rangle_0$/d $T=4.73\times10^{-3}$ K^{-1}.

In an earlier report on poly(1,3-dithiocane),[12] the energy of the first-order interaction for the $\overset{C}{\diagdown}\!\!\underset{S}{\diagup}\overset{C}{\diagdown}\!\!\underset{S}{\diagup}$ bond sequence was estimated as $E_\sigma=-1.42$ kJ mol^{-1} on the basis of the calculation of the model compound, but the experimental data of the dipole-moment ratio and its temperature coefficient could not be reproduced well by this energy value. The E_σ was, therefore, modified so as to fit the experimentally obtained configuration-dependent properties; then $E_\sigma=-5.02$ kJ mol^{-1} was obtained, as has been reported above. This energy variation of E_σ, 3.60 kJ mol^{-1}, was named the "extra stabilization energy" and assumed to be the first evidence for a large attractive sulfur gauche effect in poly(sulfides).[12] In the present study, this energy difference between the trans and gauche states was estimated to be 5.19 kJ mol^{-1} for the **6T** molecule by the molecular-mechanics method.

The present authors wish to thank Prof. Dr. Yoshio Imamura of the Science University of Tokyo for his valuable advice and guidance. They also wish to thank a referee for his helpful suggestions and observations and for his critical reading of the manuscript.

References

1) P. J. Flory and J. E. Mark, *Makromol. Chem.*, **75**, 11 (1964).
2) T. Miyasaka, Y. Kinai, and Y. Imamura, *Makromol. Chem.*, **182**, 353 (1981).
3) T. Miyasaka, T. Yoshida, and Y. Imamura, *Makromol. Chem.*, **184**, 1285 (1983).
4) T. Miyasaka, T. Yoshida, and Y. Imamura, *Makromol. Chem.*, **187**, 1515 (1986).
5) T. Miyasaka and T. Yoshida, *Bull. Chem. Soc. Jpn.*, **61**, 4231 (1988).
6) M. Ohsaku, Y. Shiro, and H. Murata, *Bull. Chem. Soc. Jpn.*, **45**, 113 (1972); H. Matsuura and H. Murata, *Bull. Chem. Soc. Jpn.*, **55**, 2853 (1982).
7) N. L. Allinger and D. Y. Chung, *J. Am. Chem. Soc.*, **98**, 6798 (1976).
8) N. L. Allinger, *J. Am. Chem. Soc.*, **99**, 8127 (1977).
9) This revised program was provided to us by Prof. Dr. Eiji Osawa of Hokkaido University.
10) M. Ohsaku, *Bull. Chem. Soc. Jpn.*, **47**, 965 (1974).
11) G. Carazzolo and G. Valle, *Makromol. Chem.*, **90**, 66 (1966).
12) W. J. Welsh, *Makromol. Chem.*, **183**, 2565 (1982).

Solvent Extraction of Various Metal Picrates with Benzo-18-crown-6 into $CHCl_3$

Yasuyuki TAKEDA* and Minoru NISHIDA
Department of Chemistry, Faculty of Science, Chiba University,
Yayoi-cho, Chiba 260
(Received December 16, 1988)

Overall extraction equilibrium constants (K_{ex}) of various metal picrates (MA_m) with benzo-18-crown-6 (B18C6) and distribution constant ($K_{D,L}$) of B18C6 were determined at 25 °C between water and chloroform. The K_{ex} values were analyzed by constituent equilibria, e.g., $K_{D,L}$, formation constant in water and ion-pair extraction constant ($K_{ex,ip}$) with a picrate anion of the B18C6–metal ion complex. K_{ex} orders for univalent and bivalent metal ions are $Tl^+>K^+>Rb^+>Ag^+>Cs^+>Na^+$ and $Pb^{2+}\gg Sr^{2+}>Ca^{2+}$, respectively. Extraction selectivities of B18C6 for the alkali and alkaline earth metal ions are consistent with the size-fit concept; namely, the more closely a cation fits into a crown ether cavity, the more extractable the complex is. For a given B18C6–M^{m+} system, $K_{ex,ip}$ value is much larger than values of the other constituent equilibria. Thus, the magnitude of K_{ex} value is determined largely by that of $K_{ex,ip}$ value. $K_{ex,ip}$ value of B18C6 for univalent and bivalent metal ions increases in the order $Na^+<Ag^+<Cs^+<K^+<Rb^+<Tl^+$ and $Sr^{2+}<Ca^{2+}<Pb^{2+}$, respectively. Factors governing the magnitude of the $K_{ex,ip}$ value were discussed in detail.

Overall extraction equilibrium constant of a crown ether with a metal picrate consists of several constituent equilibria. In a series of our solvent-extraction studies regarding crown ethers,[1] the overall extraction equilibrium constants of metal picrates with crown ethers and some constituent equilibria have been measured, and the overall extraction equilibrium constants have been analyzed by the constituent equilibria in order to clarify factors governing selectivities and extractabilities of crown ethers for metal ions, and, moreover, obtain information on solute–solvent interactions of the crown ether complexes.

In this study, the overall extraction equilibrium constants of various metal picrates with benzo-18-crown-6 (B18C6) between water and chloroform were determined at 25 °C and analyzed by constituent equilibria. The role of B18C6 in the metal ion-extraction process was discussed.

Experimental

Materials. Benzo-18-crown-6 was prepared according to Pedersen.[2] The product was recrystallized four times from heptane and, prior to use, dried at 40 °C in a vacuum oven. Its purity was checked by melting point, elemental analysis, and NMR. Chloroform, picric acid, NaOH, KOH, $AgNO_3$, $TlNO_3$, $Ca(NO_3)_2$, $Sr(NO_3)_2$, and $Pb(NO_3)_2$ were analytical grade reagents. Rubidium and caesium hydroxides were reagent-grade. Chloroform was washed three times with distilled water. The other reagents were used without further purification.

The experimental procedures were almost the same as those described in previous papers.[3,4] Extractions were conducted at 25±0.2 °C. Concentrations of B18C6, metal salts, and picric acid were 1×10^{-5}—7×10^{-3} M (1 M=1 mol dm^{-3}), 1×10^{-3}—5×10^{-2} M, and (1—5)$\times10^{-3}$ M, respectively. For hydroxide and nitrate systems, the extractions were performed at pH 11.2—12.1 and pH 2.4—3.1, respectively. For the Ba system, turbidity was always found in the interface between chloroform and water under all experimental conditions.

The Distribution Coefficient of B18C6. A 10 ml portion of a chloroform solution of B18C6 and an equal volume of distilled water were placed in a stoppered glass tube (volume 30 ml) and shaken in a thermostated water bath for 2 h at 25±0.2 °C. The concentration range of B18C6 was from 0.1 M to 0.2 M. After centrifugation, the B18C6 concentration of the aqueous phase was spectrophotometrically determined at 273 nm ($\varepsilon=2.49_5\times10^3$ cm^{-1} M^{-1}). The distribution coefficient value of B18C6 is 371±4, which is the average of twenty measurements.

Results

In an equilibrium between a chloroform solution of a crown ether (L) and an aqueous solution of a metal ion (M^{m+}) and a picrate ion (A^-), the equilibrium constants are defined as

$$K_{ex} = [MLA_m]_o[H^+]^m/[M^{m+}][L]_o[HA]_o^m, \quad (1)$$
$$K_{D,L} = [L]_o/[L], \quad (2)$$
$$K_{ex}(HA) = [HA]_o/[H^+][A^-], \quad (3)$$
$$K_{ML} = [ML^{m+}]/[M^{m+}][L], \quad (4)$$
$$K_{ex,ip} = [MLA_m]_o/[ML^{m+}][A^-]^m, \quad (5)$$

where the subscript "o" and the lack of subscript denote the organic and the aqueous phase, respectively. The overall extraction equilibrium constant (K_{ex}) can be written as

$$K_{ex} = K_{ML}K_{ex,ip}K_{D,L}^{-1}K_{ex}(HA)^{-m}. \quad (6)$$

The distribution ratio of the metal is represented by

$$D = [MLA_m]_o/([M^{m+}] + [ML^{m+}]). \quad (7)$$

In the case of $[M^{m+}]\gg[ML^{m+}]$, Eq. 7 is transformed into

$$D = K_{ex}K_{ex}(HA)^m[L]_o[A^-]^m. \quad (8)$$

For the univalent metal ion system, $\log(D/[A^-])$ vs. $\log[L]_o$ plot in Fig. 1 shows a straight line with a slope

of 1 in every case. This indicates that B18C6 forms a 1:1 complex with the univalent metal ion. For the bivalent metal ion system, $\log(D/[A^-]^2)$ vs. $\log[L]_o$ plot in Fig. 2 always shows a line with a slope of 1. This indicates that B18C6 forms a 1:1 complex with the bivalent metal ion.

From the mass balances, $[L]_o$, $[M^{m+}]$, and $[HA]_o$ are given by

$$[L]_o = ([L]_t - [MLA_m]_o)/(\alpha + \beta[M^{m+}]), \quad (9)$$

$$[M^{m+}] = ([M]_t - [MLA_m]_o)/(1 + \beta[L]_o), \quad (10)$$

$$[HA]_o = ([HA]_t - m[MLA_m]_o)/\{1 + ([H^+]^{-1} + K_{HA})K_{ex}(HA)^{-1}\}, \quad (11)$$

where the subscript "t" denotes the total concentration, $\alpha = 1 + K_{D,L}^{-1}$, and $\beta = K_{ML}K_{D,L}^{-1}$. The K_{ex} value was determined by using the $[L]_o$ value of Eq. 9, the $[M^{m+}]$ value of Eq. 10, and the $[HA]_o$ value of Eq. 11. The value of $K_{ex}(HA)$ was spectrophotometrically determined as 87.1±0.4 using the association constant ($K_{HA}=1.9_5$ at 25 °C[5]) of picric acid in water, $K_{HA}=[HA]/[H^+][A^-]$. Equilibrium constants are summarized in Table 1.

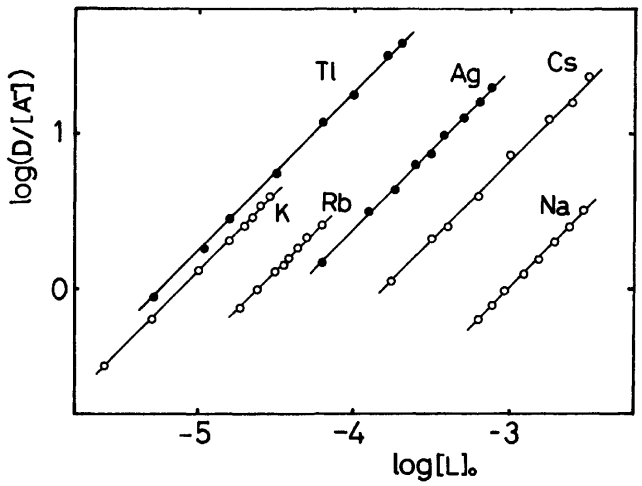

Fig. 1. Plots of $\log(D/[A^-])$ vs. $\log[L]_o$ for B18C6-univalent metal picrate systems at 25 °C.

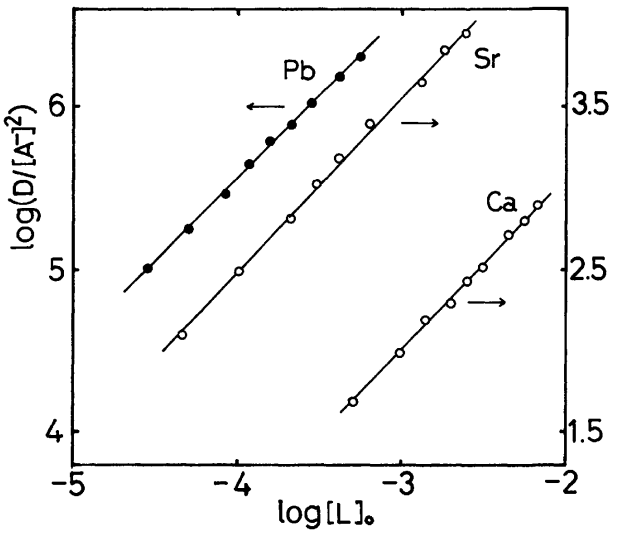

Fig. 2. Plots of $\log(D/[A^-]^2)$ vs. $\log[L]_o$ for B18C6-bivalent metal picrate systems at 25 °C.

Table 1. Summary of Equilibrium Constants at 25 °C

Crown ether	$\log K_{D,L}$	Cation	Ionic radius (Å)[a]	$\log K_{ex}$	$\log K_{ML}$	$\log K_{ex,ip}$
B18C6	2.569±0.005	Na^+	1.02	1.08±0.02	1.38[6]	4.21
		K^+	1.38	3.17±0.02	1.744[6]	5.94
		Rb^+	1.49	2.67±0.01	1.15[6]	6.03
		Cs^+	1.70	1.90±0.02	0.88[6]	5.53
		Ag^+	1.15	2.46±0.02	1.83[6]	5.14
		Tl^+	1.50	3.29±0.05	1.68[6]	6.12
		Ca^{2+}	1.00	1.16±0.03	0.48[7]	7.13
		Sr^{2+}	1.13	2.74±0.03	2.41[6]	6.78
		Pb^{2+}	1.19	5.30±0.01	3.19[6]	8.56
18C6	0.78[6]	Na^+		1.53[8]	0.80[10]	3.46
		K^+		4.13[8]	2.03[10,11]	4.83
		Rb^+		3.71[8]	1.56[10]	4.88
		Cs^+		2.68[8]	0.99[10]	4.42
		Sr^{2+}		5.55[9]	2.72[10]	7.50
DB18C6	3.91[2]	Na^+		0.1_6[13]	1.1_6[16]	4.84
		K^+		2.6_6[13]	1.6_7[16]	6.83
		Rb^+		2.2_6[13]	1.0_8[16]	7.02
		Cs^+		1.2_6[13]	0.8_3[16]	6.27
		Ag^+		1.3_6[12]	1.4_1[16]	5.79
		Tl^+		2.7_6[14]	1.5_0[16]	7.10
		Sr^{2+}		1.0_2[15]	1.0_0[16]	7.80
		Pb^{2+}		2.7_2[15]	1.8_8[16]	8.62

a) R. D. Shannon and C. T. Prewitt, *Acta Crystallogr., Sect. B*, **25**, 925 (1969).

Discussion

The contribution of an ether oxygen atom to log $K_{D,L}$ (Π_O) and that of a methylene group to extraction constants of ion pairs (Π_{CH_2}) at 25 °C for the $CHCl_3$/water system are −0.79[8] and 0.47,[17] respectively. The contribution of a benzo group to log $K_{D,L}$ ($\Pi_{C_6H_4}$) can be calculated to be 2.61 from the log $K_{D,L}$ value of B18C6 by using the values of Π_O and Π_{CH_2} ($\Pi_{C_6H_4}$=2.57−{0.47×10+(−0.79×6)}). Values of $\Pi_{C_6H_4}$ are 2.5_9 for benzo-15-crown-5 (B15C5) and 2.4_4 for dibenzo-18-crown-6 (DB18C6).[8] They are nearly equal. The $\Pi_{C_6H_4}$ value is 2.5_4 on the average. From these empirical parameters, the log $K_{D,L}$ value of B18C6 at 25 °C between $CHCl_3$ and H_2O can be estimated to be 2.5_0. This is consistent with the experimental log $K_{D,L}$ value of B18C6 (2.569± 0.005). The same is true for the cases of B15C5 (2.3_5(calcd), 2.4(exptl)[18]) and DB18C6 (4.1_0(calcd), 3.9 (exptl)[13]).

From Table 1, the order of log K_{ex} of B18C6 for the univalent metal ions is $Tl^+ > K^+ > Rb^+ > Ag^+ > Cs^+ > Na^+$. The extraction selectivity of B18C6 for the alkali metal ions is in accord with the size-fit concept; namely, the more closely a cation fits into a crown ether cavity, the more extractable the crown ether-cation complex is (cavity radius of 18-crown-6 (18C6)=1.38 Å (CPK model)[19]). Although log K_{ML} values of Ag^+ and Tl^+ are the largest and the third greatest of all the univalent metal ions, B18C6 shows the third lowest and the highest extractability for Ag^+ and Tl^+, respectively; this is attributed completely to the second smallest and the largest log $K_{ex,ip}$ values of Ag^+ and Tl^+, respectively. log K_{ex} value sequences of B18C6 for the alkali metal ions are consistent with log K_{ML} value sequences except for Na^+ and log $K_{ex,ip}$ value sequences except for K^+. Although log K_{ML} value of Na^+ and log $K_{ex,ip}$ value of K^+ are the second largest of all the alkali metal ions, extractabilities of B18C6 for Na^+ and K^+ are the lowest and the highest, respectively; this is ascribed to the smallest log $K_{ex,ip}$ value of Na^+ and the greatest log K_{ML} value of K^+, respectively.

For the bivalent metal ions, the log K_{ex} value of B18C6 decreases in the order, $Pb^{2+} \gg Sr^{2+} > Ca^{2+}$ (Table 1). The highest extractability of B18C6 for Pb^{2+} of all the metal ions in this study depends on both the greatest log K_{ML} and log $K_{ex,ip}$ value.

For a given B18C6-M^{m+} system, log $K_{ex,ip}$ value is much larger than log K_{ML}, log $K_{D,L}$, and $m$log K_{ex}(HA) value. Thus, the magnitude of log K_{ex} value is determined largely by that of log $K_{ex,ip}$ value. The same is true for the cases of 18C6 and DB18C6 (Table 1). The K_{ex} value of a given metal ion among 18C6, B18C6, and DB18C6 increases with a decrease in the size of the crown ether; the same tendency is observed for the K_{ML} value of a metal ion among the crown ethers except for the case of a Na^+-18C6 complex; but, the reverse is true for the $K_{ex,ip}$ value except for the cases of Sr^{2+}-B18C6 and 18C6 complexes. Since the $K_{D,L}^{-1}$-value sequence is in the order DB18C6<B18C6<18C6, the K_{ex}-value sequence of a metal ion among the crown ethers depends on both the $K_{D,L}^{-1}$- and K_{ML}-value sequence (Eq. 6).

It can be seen from Table 1 that log $K_{ex,ip}$ value of B18C6 varies with a cation of the same charge trapped in the cavity. The same is true for 18C6 and DB18C6. For alkali metal ions, log $K_{ex,ip}$ value of B18C6 increases in the order, $Na^+ < Cs^+ < K^+ < Rb^+$ (Table 1). The same trend is observed for the cases of 18C6 and DB18C6. This shows that, generally, a crown ether–metal ion complex, where the metal ion has a suitable size for the cavity, is more extractable as an ion pair with a picrate ion. From the structure of the crown ether complex with the univalent metal ion held in the cavity, anion- and solvent-contact are possible in respective directions perpendicular to the plane of the ring. It thus appears that strength of interaction between the central univalent metal ion and water molecules is one of the most important factors in determining the magnitude of $K_{ex,ip}$ value of the univalent metal ion. Consequently, the lowest $K_{ex,ip}$ value of Na^+ among all the alkali metal ions listed in Table 1 is probably attributed to the strongest interaction of Na^+ with water molecules. Gibbs free energies of hydration ($\Delta G_h°$/kJ mol^{-1}) of K^+, Rb^+, and Cs^+ are −338, −320, and −297, respectively.[20] The interaction of Cs^+ with water is weaker than those of K^+ and Rb^+. The interaction with water of Cs^+ held in the crown ether cavity is expected to be weaker than those of K^+ and Rb^+. Association constant of Cs^+ with a picrate ion in water is larger than those of K^+ and Rb^+.[21] Association constant with a picrate ion of Cs^+ held in the crown ether cavity is expected to be greater than those of K^+ and Rb^+. However, $K_{ex,ip}$ value of a Cs^+-crown ether complex is smaller than those of the corresponding K^+- and Rb^+-crown ether complex. Judging from the structure of a crown ether-univalent metal ion complex. this may be attributable to negligible effect of water on association of the K^+- and Rb^+-crown ether complex with a picrate ion and/or very weak interactions with water of the K^+- and Rb^+-complex. The above discussion is supported by the following data. When L=18C6, B18C6, and DB18C6, differences in the numbers of water molecules coextracted into nitrobenzene among ML^+ complexes (M=K, Rb, Cs) are small, whereas those among uncomplexed K^+, Rb^+, and Cs^+ are relatively large.[22]

Ionic radii of Rb^+ and Tl^+ are nearly identical (Table 1); $-\Delta G_h^\circ$ value of Tl^+ (343 kJ mol^{-1})[20] is slightly greater than that of Rb^+; $K_{ex,ip}$ values of RbL^+ and TlL^+ complexes (L=B18C6 and DB18C6) are approximately equal. This indicates that strength of interaction with a picrate ion of the RbL^+ complex is nearly equal to that of the corresponding TlL^+ complex. The sizes of Na^+ and Ag^+ are smaller than those of B18C6- and DB18C6-

cavity; $-\Delta G_h^\circ$ of Ag^+ (479.1 kJ mol^{-1})[20] is greater than that of Na^+ (411.3 kJ mol^{-1});[20] but, in each case of B18C6 and DB18C6, $K_{ex,ip}$ value of Ag^+ is larger than that of Na^+. Since specific interaction between Ag^+ and $CHCl_3$ is considered to be impossible, the higher $K_{ex,ip}$ value of Ag^+ may be caused by stronger association with a picrate ion and weaker interaction with water of the Ag^+ complex compared with the case of the corresponding Na^+ complex.

From the structure of a crown ether-bivalent metal ion complex, two picrate anion-contacts are possible in respective directions perpendicular to the plane of the ring. Sizes of Sr^{2+} and Pb^{2+} are almost the same; they are smaller than the B18C6- and DB18C6-cavity; $-\Delta G_h^\circ$ value of Sr^{2+} (1447 kJ mol^{-1})[20] is nearly equal to that of Pb^{2+} (1497 kJ mol^{-1}).[20] However, in each case of B18C6 and DB18C6, $K_{ex,ip}$ value of Pb^{2+} is larger than that of Sr^{2+}. This may be ascribed to stronger interaction with two picrate anions of the Pb^{2+} complex compared with the corresponding Sr^{2+} complex.

$K_{ex,ip}$ value of a univalent metal ion increases with an increase in the size of crown ether (18C8<B18C6< DB18C6) (Table 1). However, it does not always hold for the bivalent metal ions. For a univalent metal ion, the difference in $\log K_{ex,ip}$ values between 18C6 and B18C6 is 0.75—1.15, which is approximately constant; that between B18C6 and DB18C6 is 0.6_3—0.9_9, which is approximately constant; they are roughly equal. This indicates that an increment of $\log K_{ex,ip}$ value per a benzo group is about 0.9 (on the average).

$K_{ex,ip}=K_{MLA}K_{D,MLA}$, where $K_{MLA}=[MLA]/[ML^+][A^-]$ and $K_{D,MLA}=[MLA]_o/[MLA]$. Since $K_{D,MLA}$ is a distribution constant of a neutral complex MLA between water and $CHCl_3$, an increment of $\log K_{D,MLA}$ per a benzo group is estimated to be about 2.5 on the basis of $\Pi_{C_6H_6}$ value (2.5_4). From an increment of $\log K_{ex,ip}$ per a benzo group (ca. 0.9), a decrement of $\log K_{MLA}$ per a benzo group is calculated to be 1.6. This indicates that the larger the size of a crown ether-univalent metal ion complex is, the smaller the $\log K_{MLA}$ value is. It is interesting from a structural point of view that the two-dimensional increase in the size of the crown ether-univalent metal ion complex causes the constant decrease in the $\log K_{MLA}$ value.

Since MLA_2 is a neutral complex, it seems reasonable to assume that the K_{D,MLA_2} value increases with an increase in the size of the crown ether (18C6<B18C6< DB18C6), where $K_{D,MLA_2}=[MLA_2]_o/[MLA_2]$. Consequently, the $K_{ex,ip}$-value sequences of a bivalent metal ion among the crown ethers may be determined chiefly by the K_{MLA_2}-value sequences, where $K_{MLA_2}=[MLA_2]/[ML^{2+}][A^-]^2$.

References

1) Y. Takeda, "The Solvent Extraction of Metal Ions by Crown Compounds, Host Guest Complex Chemistry III," Springer-Verlag, Topics in Current Chemistry, Vol. 121, Heidelberg (1984), Chap. 1.

2) C. J. Pedersen, *J. Am. Chem. Soc.*, **89**, 7017 (1967).

3) Y. Takeda and H. Kato, *Bull. Chem. Soc. Jpn.*, **52**, 1027 (1979).

4) Y. Takeda and H. Goto, *Bull. Chem. Soc. Jpn.*, **52**, 1920 (1979).

5) "Dissociation Constants of Organic Acids in Aqueous Solution," ed by G. Kortün, W. Vogel, and K. Andrussov, Butterworths, London (1961).

6) Y. Takeda, R. Kohno, Y. Kudo, and N. Fukada, *Bull. Chem. Soc. Jpn.*, **62**, 999 (1989).

7) Estimated value from K_{ML} values of 18C6 (3.0^{23}) and DB18C6 ($<1^{16}$) complexes in H_2O.

8) Y. Takeda and A. Tanaka, *Bull. Chem. Soc. Jpn.*, **59**, 733 (1986).

9) Y. Takeda et al., unpublished datum.

10) R. M. Izatt, R. E. Terry, B. L. Haymore, L. D. Hansen, N. K. Dalley, A. G. Avondet, and J. J. Christensen, *J. Am. Chem. Soc.*, **98**, 7620 (1976).

11) Y. Takeda and O. Arima, *Bull. Chem. Soc. Jpn.*, **58**, 3403 (1985).

12) Y. Hasegawa, N. Iizima, and T. Sekine, *J. Inorg. Nucl. Chem.*, **43**, 633 (1981).

13) Y. Hasegawa, H. Wakabayashi, M. Sakuma, and T. Sekine, *Bull. Chem. Soc. Jpn.*, **54**, 2427 (1981).

14) T. Sekine, H. Wakabayashi, and Y. Hasegawa, *Bull. Chem. Soc. Jpn.*, **51**, 645 (1978).

15) T. Sekine, K. Shioda, and Y. Hasegawa, *J. Inorg. Nucl. Chem.*, **41**, 571 (1979).

16) E. Shchori, N. Nae, and J. Jagur-Grodzinski, *J. Chem. Soc., Dalton Trans.*, **1975**, 2381.

17) H. Matsunaga and T. Yotsuyanagi, *Nippon Kagaku Kaishi*, **1982**, 785.

18) Y. Hasegawa, T. Nakano, Y. Odori, and Y. Ishikawa, *Bull. Chem. Soc. Jpn.*, **57**, 8 (1984).

19) "Progress in Macrocyclic Chemistry," ed by R. M. Izatt and J. J. Christensen, John Wiley and Sons, New York (1981), Vol. 2.

20) H. L. Friedman and C. V. Krishnan, "Water," ed by F. Franks, Plenum, New York (1973), Vol. 3, p. 55.

21) M. Yamane, T. Iwachido, and K. Tōei, *Bull. Chem. Soc. Jpn.*, **44**, 745 (1971).

22) T. Iwachido, M. Minami, M. Kimura, A. Sadakane, M. Kawasaki, and K. Tōei, *Bull. Chem. Soc. Jpn.*, **53**, 703 (1980).

23) H. Høiland, J. A. Ringseth, and T. S. Brun, *J. Solution Chem.*, **8**, 779 (1979).

 © 1989 The Chemical Society of Japan Bull. Chem. Soc. Jpn., 62, 1472—1476 (1989) [Vol. 62, No. 5

Preferential Solvation of Ni(II) and Mg(II) Ions in Water-Acetonitrile Mixtures. Enthalpies of Transfer and the Electronic Spectra

Kiyoshi MIYAJI,* Kiyokazu NOZAWA,† and Kenichi MORINAGA
Department of Chemistry, Faculty of Science, Saitama University, Urawa, Saitama 338
(Received May 10, 1988)

The enthalpies of transfer (ΔH_t°) from water to water-acetonitrile (W-AN) mixtures for Ni^{2+} and Mg^{2+} ions were estimated using the enthalpies of dilution of the concentrated aqueous electrolyte solutions into water and mixtures, and the enthalpies of solution of water in the mixtures. The ΔH_t° values for these ions decreased with an increase in the mole fraction of AN (x_{AN}) in the range of x_{AN}<ca. 0.9, however, they increased rapidly in the range x_{AN}>ca. 0.9. The values of ΔH_t° for the Ni^{2+} ion were more negative than those for the Mg^{2+} ion throughout the x_{AN} regions, especially in the extremely AN-rich region and in pure AN. The average number of coordinated water molecules, N, for the $[Ni(AN)_{6-N}(W)_N]^{2+}$ ion in the mixtures (x_{AN}=0.2, 0.6, and 0.9), as estimated from the electronic absorption spectra, was always greater than that calculated on the basis of the bulk-solvent composition, indicating that the Ni^{2+} ion was preferentially solvated by water. These results, including the conductance data, were discussed in terms of the principle of hard and soft acid and base.

The preferential solvation of an ion in a mixed solvent has been one of the most fundamentally important problems in solution chemistry, and some phenomena have been applied in chemical technology.[1,2] Although various types of ion-solvent interactions have been noted to contribute to the ionic solvation in pure solvents,[3] in mixed solvents the concept of hard and soft acid (cation) and base (solvent) (i.e., the HSAB principle) is considered to be one of the most important factors. We have studied previously the preferential solvation behavior of ions in water-acetonitrile (W-AN) mixtures by means of the conductance[4,5] and the enthalpies of transfer (ΔH_t°). The majority of papers on ionic solvation so far have been concerned with monovalent ion. A difference in limiting ionic conductances was observed between the Ni^{2+} and Mg^{2+} ions in the mixtures, while they have equal conductance values in both water and acetonitrile.[5] Since the Ni^{2+} and Mg^{2+} ions have similar ionic radii, the electrostatic contributions to the overall ion-solvent interaction for the free ions can be regarded as similar. Therefore, the difference in the solvation property of the Ni^{2+} and Mg^{2+} ions should reflect the difference in the covalency of ion-solvent bonding. The nickel ion is expected to have a stronger affinity for acetonitrile than the Mg^{2+} ion, since the former ion is less hard than the latter. The ΔH_t° method was found to be a powerful tool in studying the preferential solvation of ions in the mixtures,[6,7] so the ΔH_t° values for the Ni^{2+} and Mg^{2+} ions from water to water-acetonitrile mixtures were estimated in this study.

It is not easy to measure directly the enthalpies of solution for highly hygroscopic salts of divalent cations. In such cases, the enthalpic measurements of dilution of a concentrated aqueous electrolyte solution into water and a mixed solvent, as proposed by Valera et al., are very attractive.[9] We have applied this method to estimate the enthalpies of transfer for nickel and magnesium perchlorates from water to the mixtures. The electronic absorption spectra have also been measured for nickel perchlorate solutions.

Experimental

Materials. Hexakis(acetonitrile)nickel perchlorate, $[Ni(CH_3CN)_6](ClO_4)_2$, was prepared from the hexaaqua salt and purified by the method described in the literature.[10] Commercially available magnesium perchlorate, $Mg(ClO_4)_2$ ("Anhydron"), was used without further purification. For the measurement of the enthalpies of solution it was dried in vacuo at 250 °C just before its use. The anhydrous salt was weighed in a glove bag filled with dried nitrogen gas. The other reagents and solvents were purified as described previously.[7,11] The alkali and acid solutions were prepared and standardized by the usual method. The concentrations of aqueous perchlorate solutions were determined by the EDTA titration method.

Enthalpic Measurements. The enthalpies of solution and dilution were measured by a heat-exchange type calorimeter.[12] Liquid samples were introduced continuously into the mixtures via a peristatic pump (LKB 2132) after having been passed through a Teflon heat exchanger at 25±0.02 °C. Aliquots of a solution (0.1—0.5±0.001 ml) were added to ca. 40 ml of the solvent in the reaction vessel. The enthalpies of dilution were determined in series by measuring the enthalpy changes accompanying the successive addition of the concentrated solution in the reaction vessel.

The calorimeter was calibrated by the measurements of the enthalpies of neutralization for NaOH and HCl solutions[12] and also the enthalpies of dilution for aqueous KNO_3 solution.

Spectral Measurements. The electronic absorption spectra were measured with a Hitachi 340 spectrophotometer.

Results and Discussion

Principle of Measurements. The enthalpy change, ΔH_R^C(mixt), when a small aliquot of a concentrated

† Present address: The Institute for Solid State Physics, The University of Tokyo, Roppongi, Minato-ku, Tokyo 106.

aqueous electrolyte solution is added to a large amount of a mixed solvent can be regarded as involving the enthalpy of dilution for electrolytes to a definite concentration and the enthalpy of solution of the water contained in the original electrolyte solution with the mixed solvent. The latter enthalpy of solution of water in a mixed solvent, ΔH_W^C(mixt), can be measured directly by the use of the present titration calorimeter. The enthalpy of dilution for an electrolyte, ΔH_D^C(mixt) ($=\Delta H_R^C$(mixt)$-\Delta H_W^C$(mixt)), changes with the electrolyte concentration according to the following equation:

$$\Delta H_D^C(\text{mixt}) = \Delta H_D^\circ(\text{mixt}) + (2/3)A_H C^{1/2} + BC, \quad (1)$$

where A_H is the Debye-Hückel coefficient (1.48 kJ mol$^{-1/2}$ for a 1:1 electrolyte aqueous solution and 5.12$_9$ kJ mol$^{-3/2}$ dm$^{-3/2}$ for a 2:1 electrolyte aqueous solution)[13] and where B is the experimental parameter.

Defining the enthalpy of solution for preparing a concentrated aqueous electrolyte solution as ΔH_S^C(W),[9] the standard enthalpy of solution for electrolytes in an aqueous solution, ΔH_S°(W), and in a mixed solvent, ΔH_S°(mixt), can be expressed as follows:

$$\Delta H_S^\circ(\text{W}) = \Delta H_S^C(\text{W}) + \Delta H_D^\circ(\text{W}) \quad (2)$$

$$\Delta H_S^\circ(\text{mixt}) = \Delta H_S^C(\text{W}) + \Delta H_D^\circ(\text{mixt}). \quad (3)$$

The enthalpy of transfer for an electrolyte from water to a mixed solvent, ΔH_t°, can be then obtained as:

$$\Delta H_t^\circ = \Delta H_D^\circ(\text{mixt}) - \Delta H_D^\circ(\text{W}). \quad (4)$$

Relative Partial Molar Enthalpies for Water in Water-Acetonitrile Mixtures. The enthalpy of solution of water in the mixtures, ΔH_W^C(mixt), was found to vary linearly with the concentration of water added. An extrapolation of the experimental ΔH_W^C (mixt) values to zero concentration of water will give the relative partial molar enthalpies of water ($\bar{L}_W$) in the mixtures. The values thus obtained are shown in Table 1, together with those values estimated by the method of graphical intercepts[14] on the basis of excess enthalpy data.[15] The values estimated in this experiment are derived from directly measurable quantities and are, therefore, more accurate than those in the literature.[15]

Table 1. Relative Partial Molar Enthalpies of Water in Water-Acetonitrile Mixtures, $\bar{L}_W$/kJ mol^{-1}

x_{AN}	$\bar{L}_W$	
	This Exper.	Lit.[a]
0	0	0
0.1	−0.154±0.002	−0.15±0.14
0.2	−0.049±0.003	−0.04±0.07
0.4	0.276±0.006	0.30±0.05
0.6	0.864±0.001	0.79±0.01
0.8	2.51 ±0.05	2.5 ±0.1
0.9	4.41 ±0.06	4.5 ±0.1

a) From Ref. 15.

As may be seen in Table 1, $\bar{L}_W$ decreases with the addition of a small amount of AN, passes through a minimum at the mole fraction of AN(x_{AN}) (ca. 0.1), and then increases with an increase in x_{AN}. Beyond x_{AN} ca. 0.2, the $\bar{L}_W$ values become positive, increase almost linearly until x_{AN} reaches ca. 0.65. With a further increase in x_{AN}, the $\bar{L}_W$ values increase more rapidly. The x_{AN} dependence of $\bar{L}_W$ appears to reflect the change in the solvent structure of these mixtures: a water-rich region, an intermediate region, and an acetonitrile-rich region.[7]

Enthalpies of Transfer for Nickel and Magnesium Perchlorates. The enthalpies of dilution, ΔH_D^C(mixt), change with the electrolyte concentration in the final electrolyte concentration range from 5×10^{-3} to 0.09 mol dm^{-3}. Examples of the plots for obtaining the ΔH_D°(mixt) values are shown in Fig. 1. The ΔH_D°(mixt) values were obtained using the A_H values for water. There were no significant differences between the ΔH_D°(mixt) values calculated using A_H value for water and those calculated using the A_H value for AN. The enthalpies of transfer obtained on the basis of Eq. 4 for nickel and magnesium perchlorates are given in Table 2. As may be seen in Table 2, the change in the initial concentration of an electrolyte aqueous solution does not seem to cause any significant error in the estimation of the ΔH_t° values.

The enthalpy of transfer for $Mg(ClO_4)_2$ from water to AN was obtained from the direct measurements of the enthalpies of solution. The enthalpy of solution in water is found to be −157.$_3$±2 kJ mol^{-1} in good agreement with the literature value of −156.6$_1$ kJ mol^{-1}.[16] The enthalpy of solution in AN was difficult to measure because of its high hygroscopicity, but the most careful repeated measurements (more than ten times) gave the enthalpy of solution of −185.$_5$±5 kJ mol^{-1}. The enthalpy of transfer for $Mg(ClO_4)_2$ from water to AN was taken as −28±5 kJ mol^{-1}. The

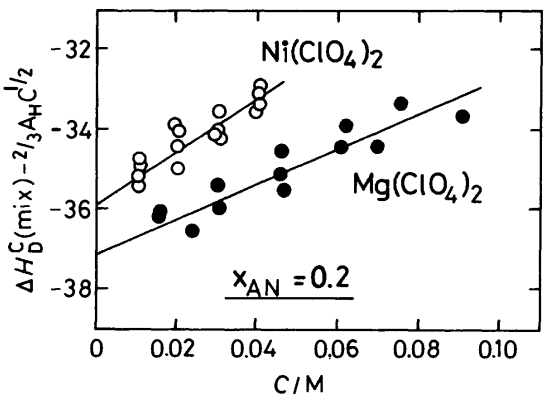

Fig. 1. Plots based on Eq. 1 for the enthalpies of dilution in the mixtures.

Table 2. Enthalpies of Dilution at Infinite Dilution in Water and Water-Acetonitrile Mixtures, ΔH_D°, and Enthalpies of Transfer for Electrolytes, ΔH_t°/kJ mol^{-1}

x_{AN}	$Ni(ClO_4)_2$		$Mg(ClO_4)_2$	
	$-\Delta H_D^\circ$	$-\Delta H_t^\circ$	$-\Delta H_D^\circ$	$-\Delta H_t^\circ$
0	4.3[a]	0	10.4	0
0	3.5	0	5.8[b]	0
0.1	16.2	12.7±0.6	20.8	10.4±0.2
0.2	34.6	31.1±0.5	36.8	26.4±0.3
0.4	54.5[a]	50.2±1.0[a]	55.7	45.3±0.3
0.4	54.3	50.8±0.9		
0.6	72.4	68.9±1.1	75.1	64.7±1.3
0.8	90.8	87.3±0.7	93.9	83.5±0.5
0.9	93.6	95.1±0.2	101.9	91.5±0.6
0.9			100.4[b]	94.6±0.2[b]

a) The initial concentration of nickel perchlorate solutions is 2.08$_8$ mol dm^{-3} unless otherwise noted in which case it is 2.11$_5$ mol dm^{-3}. b) The initial concentration of magnesium perchlorate solutions is 2.09$_6$ mol dm^{-3} unless otherwise noted in which case it is 3.10$_4$ mol dm^{-3}.

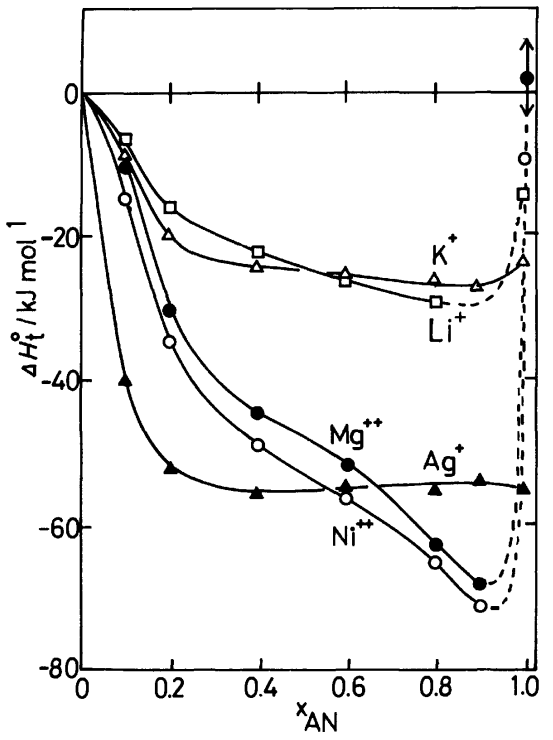

Fig. 2. Plots of the ionic enthalpies of transfer (ΔH_t°) vs. the mole fraction of acetonitrile (x_{AN}). Data for M^+ ions were cited from Ref. 6.

enthalpy of transfer for $Ni(ClO_4)_2$ from water to AN was cited from the literature.[17]

The ionic enthalpies of transfer were calculated by using the reported values of the ClO_4^- ion estimated on the basis of the TATB assumption $\{\Delta H_t^\circ(Ph_4As^+) = \Delta H_t^\circ(Ph_4B^-)\}$.[6] The estimated ΔH_t° values for the Ni^{2+} and Mg^{2+} ions are plotted as a function of x_{AN} in Fig. 2. For convenience of comparison, the x_{AN} dependences of ΔH_t° for the Li^+, K^+, and Ag^+ ions are also shown in Fig. 2.[6] It has been established by several kinds of measurements that the Ag^+ ion is preferentially solvated by AN in this mixed solvent system.[8] The ΔH_t° values for the Ag^+ ion decrease very rapidly in the water-rich region, but change only slightly in the other regions. The ΔH_t° values for the K^+ ion, similar in ionic size to the Ag^+ ion, decrease much less rapidly in the water-rich region, and its x_{AN} dependence profile in the other regions is nearly the reverse of that of the Ag^+ ion. The values of ΔH_t° for the Li^+ ion decrease a little more slowly than that for the K^+ ion in the water-rich region, continue to decrease less slowly in the intermediate region, and increase rapidly in the AN-rich region. Such an x_{AN} dependence profile of the Li^+ ion is characteristic of the most preferentially hydrated monovalent cation.

Previously, the present authors have discussed semiquantitatively the solvation enthalpies for halide ions in the W-rich and intermediate regions based on a modified hydration model, and noted that the exothermic shift of the ΔH_t° values in the intermediate region may be attributed to the reduction in the cavity formation energy.[7] Therefore, the exothermic shift of ΔH_t° values for cations in the range of x_{AN} may also be attributed to the change in the solvent structure of the mixtures, although it is difficult to discuss the solvation enthalpies for cations quantitatively. However, the difference in ΔH_t° values at an x_{AN} value between Ni^{2+} and Mg^{2+} ions may not be influenced by the solvent structure, since these ions have similar ionic radii.

As shown in Fig. 2, when a small amount of water is added to a pure AN solution, the ΔH_t° values for the Ni^{2+} and Mg^{2+} ions decrease markedly. And the ΔH_t° values for both ions are almost twice as negative as those for the Li^+ ion in the range of x_{AN}<ca. 0.9. Therefore, the x_{AN} dependence of the ΔH_t° values suggests that both Ni^{2+} and Mg^{2+} ions are totally preferentially hydrated in water-acetonitrile mixtures. The same conclusion can be drawn from the electronic spectral measurements of a nickel perchlorate solution to be described below. However, the more negative ΔH_t° values for the Ni^{2+} ion than for the Mg^{2+} ion indicate that the Ni^{2+} ion has a stronger affinity for AN than the Mg^{2+} ion over the whole x_{AN} region. The nickel and Mg^{2+} ions have quite different electronic configurations in spite of the similar ionic sizes. The magnesium ion is a hard divalent cation, while the Ni^{2+} ion is situated on the borderline between hard and soft divalent cations.[18] The σ value, which is used as a parameter of the softness for metal ions, is largest for the Ni^{2+} ion among the borderline cations.[19] Furthermore, as has been pointed out by Munatake, Kitagawa, and Myajima, the covalent bonding in the metal ion-CH_3CN bonds is enhanced in this order;

$Mg^{2+}<Ni^{2+}<Ag^{+}$. Therefore, the stronger solvation of the Ni^{2+} ion in AN can be ascribed to its acid property being less hard than the Mg^{2+} ion. In view of the HSAB principle it is very reasonable, that the much more rapid increase in ΔH_t° values is observed for the Mg^{2+} ion in the extremely AN-rich region.

Electronic Absorption Spectra of Nickel Perchlorate Solutions in Water-Acetonitrile Mixtures. The electronic absorption spectra have been measured in order to obtain more information concerning the average number of water molecules in the solvation cosphere of the Ni^{2+} ion in these solvent mixtures. Figure 3 shows the variation in the electronic absorption maxima, λ_{max}, as a function of the $Ni(ClO_4)_2$ concentration at x_{AN}=0.2, 0.6, and 0.9; Fig. 3-a corresponds to those with shorter wavelength λ_{max} values, and Fig. 3-b, to those with longer wavelength λ_{max} values. In aqueous solutions, the absorption maxima λ_{max} are 395 and 656 nm, while in AN solutions they are 365 and 580 nm. It has been confirmed that there is a linear relationship between the number of water molecules coordinated in the $[Ni(NH_3)_{6-N}(H_2O)_N]^{2+}$ ion and the wavenumber ν.[11] Since a similar relationship is expected to hold in the case of the $[Ni(CH_3CN)_{6-N}(H_2O)_N]^{2+}$ ion, the number of water molecules coordinated in the aquaacetonitrile nickel complex ion can be estimated from the absorption spectral data. The values estimated at the electrolyte concentrations of 0.005, 0.05, and 0.32 M (1 M=1 mol dm^{-3}) are 5.0, 5.1, and 5.5 (x_{AN}=0.2); 4.9, 5.3, and 4.4 (x_{AN}=0.6), and 3.2, 3.2, and 2.0 (x_{AN}=0.9), respectively. The number of water molecules in the actual solvation sphere is always greater than that calculated on the basis of the bulk solvent composition, therefore, water is clearly enriched preferentially in the cosphere of the nickel ion. The λ_{max} value in the W-rich region (x_{AN}=0.2) approaches that observed as in an aqueous solution as the electrolyte concentration increases. In contrast with this, in the AN-rich region (x_{AN}=0.9), the λ_{max} value approaches that observed as in the AN solution. In the intermediate region (x_{AN}=0.6), the increase in electrolyte concentration causes the shift of λ_{max} to the longer wavelength side, as in the W-rich region when electrolyte concentration is small. On the contrary, a further increase in the electrolyte concentration beyond a certain limit causes a shift of the λ_{max} value to the shorter wavelength side, as in the AN-rich region. Such dependence of the λ_{max} value on the electrolyte concentration in the mixtures may be attributed to the ion-pair formation of nickel species, since it is difficult to explain the such behavior in terms only of the variation in the equilibrium concentration of the $[Ni(CH_3CN)_{6-N}(H_2O)_N]^{2+}$ species.

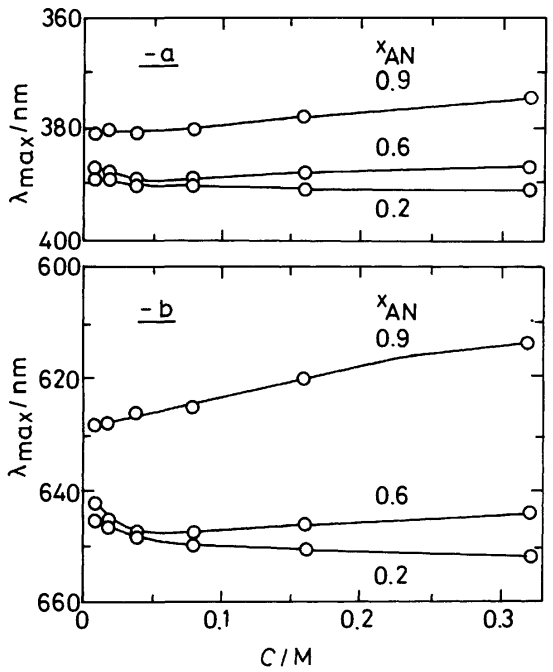

Fig. 3. Dependences of the electronic absorption maxima (λ_{max}) for Ni^{2+} ion on the electrolyte concentration in the mixtures; -a: maximum at shorter wavelength, -b: maximum at longer wavelength.

Relationship between Enthalpies of Transfer and Conductance for Nickel and Magnesium Perchlorates. Finally, the difference in the conductance behavior of nickel and magnesium perchlorates in the mixtures will be discussed in connection with the ΔH_t° values described above. It has been reported that the Ni^{2+} and Mg^{2+} ions were differentiated only in the x_{AN} range from 0 to 0.4, that is, the limiting ionic conductances (λ_0^+) for the Ni^{2+} ion were smaller than those for the Mg^{2+} ion in this range.[5] In this range, the ΔH_t° values for the Ni^{2+} ion are found to be more negative than those for the Mg^{2+} ion. This indicates that the Ni^{2+} ion has a stronger affinity for acetonitrile than does the Mg^{2+} ion. The smaller limiting ionic conductance for the Ni^{2+} ion may be related to the larger ionic species resulting from the displacement of the water molecule by a larger acetonitrile molecule in its solvation cosphere. Spectral measurements show that the Ni^{2+} ion becomes increasingly hydrated with an increase in the concentration in this range. Consequently, the hydration state of the Ni^{2+} ion can be expected to be similar to that of the Mg^{2+} ion at a certain concentration. In fact, nearly equal molar conductances are observed for 10 mmol dm^{-3} solutions of $Ni(ClO_4)_2$ and $Mg(ClO_4)_2$.[5]

The enthalpies of transfer from pure acetonitrile to mixtures (x_{AN}=0.9) clearly indicate that the Mg^{2+} ion is more strongly hydrated than the Ni^{2+} ion. In the extremely AN-rich region ($x_{AN}\geqq 0.95$), the limiting ionic conductances are found to be nearly equal for the Ni^{2+} and Mg^{2+} ions. However, the molar conductance for $Mg(ClO_4)_2$ is much smaller than that for $Ni(ClO_4)_2$ at 10 mmol dm^{-3}. From spectral measurements at x_{AN}=0.9, acetonitrile appears to be increasingly enriched in the cosphere of the Ni^{2+} ion with an increase in

the electrolyte concentration. A similar concentration dependence may not necessarily be expected for the Mg^{2+} ion in view of its stronger affinity for water. The notable decrease in molar conductance for $Mg(ClO_4)_2$ in the extremely AN-rich region may be due to the easier formation of the solvent (water)-separated ion-pair, as is suggested by the ^{35}Cl NMR measurements for the 1.0 mol dm^{-3} AN solution containing a small amount of water.[21]

References

1) H. Schneider, "Solute-Solvent Interactions," ed by J. F. Coetzee and C. D. Richie, Vol. 2, Chap. 11, Marcel Dekker, N. Y. (1976).

2) A. K. Covington and K. E. Newman, *Pure Appl. Chem.*, **51**, 2041 (1979).

3) A. J. Parker, *Electrochim. Acta*, **21**, 671 (1976).

4) K. Morinaga and K. Miyaji, *Denki Kagaku*, **50**, 736 (1982).

5) K. Miyaji and K. Morinaga, *Denki Kagaku*, **51**, 115 (1983).

6) K. Miyaji and K. Morinaga, *Bull. Chem. Soc. Jpn.*, **56**, 1861 (1983).

7) K. Miyaji and K. Morinaga, *Bull. Chem. Soc. Jpn.*, **59**, 1695 (1986).

8) H. Strehlow and H. -N. Koepp, *Z. Elektrochem.*, **62**, 373 (1958); H. Schneider and H. Strehlow, *Z. Phys. Chem. N. F.*, **49**, 44 (1966).

9) E. D. Valera, D. Feakins, and W. E. Waghorne, *J. Chem. Soc., Faraday Trans. 1*, **76**, 560 (1980); Y. Pointud, J-P. Morel, and J. Juillard, *J. Phys. Chem.*, **80**, 2381 (1976).

10) A. E. Wickenden and R. A. Krause, *Inorg. Chem.*, **4**, 404 (1965).

11) K. Morinaga and K. Miyaji, *Nippon Kagaku Kaishi*, **1977**, 1478.

12) M. Nakanishi and S. Fujieda, *Anal. Chem.*, **44**, 404 (1972).

13) H. S. Harned and B. B. Owen, "The Physical Chemistry of Electrolytic Solutions," Reinhold, N. Y. (1950).

14) J. S. Rowlinson and F. L. Swinton, "Liquids and Liquid Mixtures," Butterworths, London (1982).

15) K. W. Marcom and R. W. Smith, *J. Chem. Thermodyn.*, **1**, 503 (1969).

16) "Kagaku Binran Kiso-hen 11," Maruzen, Tokyo (1984), p. 277.

17) W. Libus, M. Mecik, and H. Strzelecki, *J. Soln. Chem.*, **9**, 723 (1980).

18) F. Basolo and R. G. Pearson, "Mechanisms of Inorganic Reactions," 2nd ed., John Wiley & Sons, Inc., N. Y. (1967).

19) S. Yamada and M. Tanaka, *J. Inorg. Nucl. Chem.*, **37**, 587 (1975).

20) M. Munakata, S. Kitagawa, and M. Miyajima, *Inorg. Chem.*, **24**, 1638 (1985).

21) H. A. Berman, H. J. C. Yehand, and T. R. Stengle, *J. Phys. Chem.*, **79**, 2551 (1975).

Thermal Stability of Substituted Pyridine Adducts of Bis(acetylacetonato)-oxovanadium(IV) in Solid State

Yasuhiko SHIBUTANI* and Koichiro SHINRA†
Department of Applied Chemistry, Osaka Institute of Technology,
Omiya, Asahi-ku, Osaka 535
(Received August 22, 1988)

The kinetic of the elimination reaction of axial ligand B in [VO(acac)$_2$B] complexes (Hacac=acetylacetone; B=pyridine, its derivatives, and ammonia) was studied in solid state by the Coats-Redfern method. The frequency factor and activation energy were determined, from which the activation free energy (ΔG^*) was calculated. The ΔG^* values varied with the nature of pyridine derivatives in the range of 99—109 kJ mol^{-1}. The insight into ΔG^* values suggests that the kinetic stability of vanadium-substituted pyridine bond is influenced by both the basicity (pK_a) and heat of sublimation ($\Delta H_{(sub)}$) of the axial ligand. Furthermore, the E' values which appear to reflect coordination ability of base B were determined by reflectance spectra of the complexes. The E' value was found to increase linearly with the increase in pK_a and $\Delta H_{(sub)}$ of the axial ligand.

The stability and reactivity of metal complexes have generally been discussed on the basis of kinetic and thermodynamic data of substitution reactions in solution. Since the reactant and product are naturally solvated with medium molecules, the kinetic and thermodynamic data have to be corrected for interaction between reactants and solvent. On the other hand, the thermal reaction in solid state will directly provide information concerning not only the strength of metal–ligand bond,[1] but also the formation of intermediate products.[2] We studied previously the thermal aniline elimination reaction of [Co(Hbhpn)A$_2$]X$_2$[3] and [Ni(acac)$_2$A$_2$][4] complexes, where H$_2$bhpn: *N,N'*-bis(2-hydroxyimino-1-methylpropylidene)-1,3-propanediamine, A: aniline or its derivatives, X: Cl^-, Br^-, or I^- ion, and Hacac: acetylacetone. The results revealed that the kinetic stability of metal-substituted aniline bond for these complexes mainly depends on the pK_a and the heat of sublimation of aniline and its derivatives; a linear correlation between the experimental ΔG^* of the elimination reaction and pK_a values of the aniline derivatives was observed except the complexes with *p*-chloroaniline and *p*-bromoaniline having larger heat of sublimation than other aniline derivatives.

In the present work, thermal analysis has been carried out on the thermal elimination reaction of a series of adduct complexes, mono(substituted pyridine)bis(acetylacetonato)oxovanadium(IV) shown in Fig. 1-[I], (abbreviated as [VO(acac)$_2$B], B=pyridine, its derivatives,[5] and ammonia) to elucidate the influence of heat of sublimation of axial ligand on thermal stability of these complexes. In the thermal analysis of [VO(acac)$_2$B] complexes, it was confirmed that these complexes endothermically dissociate the axial ligand to give green [VO(acac)$_2$] complex shown in Fig. 1-[II]. The activation free energy of the elimination reaction will be briefly discussed in connection with the nature of vanadium-substituted pyridine bond.

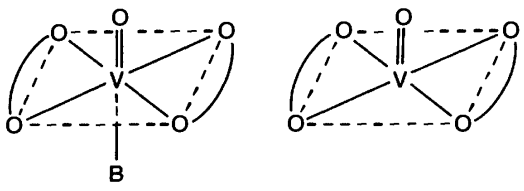

[I] [VO(acac)$_2$B] [II] [VO(acac)$_2$]

Fig. 1. [VO(acac)$_2$B][I] and [VO(acac)$_2$][II].

† Present address: Okamachiminami, Toyonaka-shi 560.

Experimental

Materials. The parent complex [VO(acac)$_2$] was prepared as described in the literature.[6] Its pyridine adducts, [VO(acac)$_2$B], were prepared as described in the literature,[7] except those with 4-CN-py and 3-CN-py. Because 4-CN-py and 3-CN-py are slightly soluble in ether, they were first dissolved in a minimum quantity of water and then added to [VO(acac)$_2$] in ether. The mixture was refluxed for about 1 h and solid residue was filtered off as the complex desired. The ammonia adduct, [VO(acac)$_2$(NH$_3$)], was prepared by the method of Claunch et al.[8] These adducts were identified by elemental analyses and IR spectroscopy.

Analytical Data for [VO(acac)$_2$B]. Found: C, 52.37; H, 5.45; N, 4.14; V, 14.38%. Calcd for [VO(acac)$_2$(py)]: C, 52.33; H, 5.57; N, 4.07; V, 14.80%. Found: C, 52.38; H, 5.74; N, 3.90; V, 13.90%. Calcd for [VO(acac)$_2$(4-CH$_3$-py)]; C, 53.68; H, 5.92; N, 3.91; V, 14.22%. Found: C, 54.58; H, 6.14; N, 3.92; V, 13.33%. Calcd for [VO(acac)$_2$(4-C$_2$H$_5$-py)]: C, 54.84; H, 6.24; N, 3.76; V, 13.68%. Found: C, 48.92; H, 4.76; N, 6.93; V, 13.50%. Calcd for [VO(acac)$_2$(4-CN-py)]: C, 52.04; H, 4.92; N, 7.59; V, 13.79%. Found: C, 49.53; H, 4.78; N, 7.03; V, 13.60%. Calcd for [VO(acac)$_2$(3-CN-py)]: C, 52.04; H, 4.92; N, 7.59; V, 13.79%. Found: C, 40.96; H, 4.09; N, 3.20; V, 11.95%. Calcd for [VO(acac)$_2$(3-Br-py)]: C, 42.58; H, 4.29; N, 3.31; V, 12.04%. Found: C, 41.68; H, 5.96; N, 4.88; V, 17.83%. Calcd for [VO(acac)$_2$(NH$_3$)]: C, 42.57; H, 6.07; N, 4.96; V, 18.04%.

Measurements. The TG and DSC curves were recorded in a flowing nitrogen atmosphere of 100 cm^3 min^{-1} at a heating rate of 10 °C min^{-1} on a Rigaku Denki 8002 thermal analyzer. α-Al$_2$O$_3$ was used as reference material. The heat of the elimination reaction was determined by measuring the DSC peak area. The instrument was calibrated against the heat of

transition of potassium nitrate and silver nitrate. The kinetic analysis under nonisothermal conditions was carried out on the TG curves recorded at a heating rate of 1 °C min^{-1} for 8—9 mg of sample. The particle size of samples for the measurements was under 100 mesh.

Reflectance spectra of the complexes in the visible region were recorded on a Hitachi Model 340 spectrophotometer equipped with a R-10A integrating sphere, using MgO as the reference substance.

Results and Discussion

Thermal Analysis. The TG and DSC curves for [VO(acac)$_2$B] complexes are shown in Figs. 2-(a) and 2-(b). The DSC data are summarized in Table 1.

As shown in Fig. 2-(a), in the case of [VO(acac)$_2$(py)] complex, the weight-loss (21.3%) on the TG curve in the temperature range of 83—142 °C, can be attributed to the elimination of one mole of pyridine (22.9%). An endothermic phenomenon was observed on the DSC curve corresponding to this weight decrease. For other complexes, the decrease in weight and endothermic phenomenon corresponding to the ligand elimination were similarly observed in the range of 90—170 °C; the weight loss was 25.8% (Calcd 26.0%) for [VO(acac)$_2$(4-CH$_3$-py)], 29.0%(28.8%) for [VO(acac)$_2$(4-C$_2$H$_5$-py)], 26.6%(28.2%) for [VO(acac)$_2$(4-CN-py)], 27.1%(28.2%) for [VO(acac)$_2$(3-CN-py)], 36.5%(37.3%) for [VO(acac)$_2$-(3-Br-py)], and 5.8%(6.0%) for [VO(acac)$_2$(NH$_3$)].

The infrared spectra of the decomposition products were measured at appropriate steps of the reaction process appearing in the TG and DSC curves. As mentioned above, [VO(acac)$_2$(py)] loses one mole of pyridine at about 142 °C. The IR spectrum of [VO-(acac)$_2$(py)] at 142 °C does not give the bands of pyridine ring[9,10] at 1444, 1218, and 711 cm^{-1} at room temperature. However, substantial change in the bands at 1523, 1371, and 934 cm^{-1} due to the coordinated acetylacetonate[10] were not observed, and the spectrum of this decomposition product was found to be the same as that of [VO(acac)$_2$]. Analyses of the infrared spectra of thermal decomposition products suggested that the thermal decomposition of complexes was elimination of pyridine derivatives from [VO(acac)$_2$B] as expressed below:

$$[VO(acac)_2B] \xrightarrow[endo.]{} [VO(acac)_2] + B\uparrow.$$

As seen in Table 1, the enthalpy changes (ΔH) for [VO(acac)$_2$(py)] and [VO(acac)$_2$(4-CH$_3$-py)] were 69.4 and 81.4 kJ mol^{-1}, respectively, which are comparable

Table 1. DSC Data of [VO(acac)$_2$B] Complexes

Base	pK_a	$\Delta H_{(sub)}$[a] / kJ mol^{-1}	(K)[b]	ΔH[c] / kJ mol^{-1}
py	5.25	47.8	404	69.4
4-CH$_3$-py	6.02	56.9	421	81.4
4-C$_2$H$_5$-py	6.17	54.0**	425	73.2
4-CN-py	1.90	75.6*	399	65.5
3-CN-py	2.28	79.0*	391	68.2
3-Br-py	2.84	59.4*	402	74.7
NH$_3$	9.26	29.0	370	51.3

a) $\Delta H_{(sub)}$[a], enthalpy of sublimation for pyridine derivatives. *, $\Delta H_{(sub)}$ values determined by DSC measurement; **, enthalpy of vaporization. b) DSC maximum peak temperature. c) ΔH, heat of reaction.

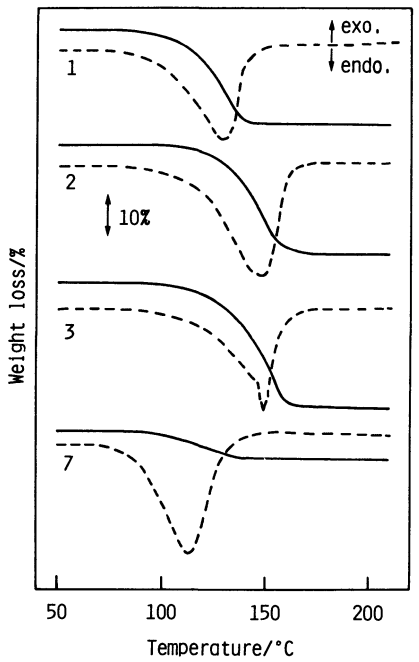

Fig. 2a. TG (—) and DSC (----) curves of [VO-(acac)$_2$B] complexes; heating rate 10 °C min^{-1}. B= 1: py, 2: 4-CH$_3$-py, 3: 4-C$_2$H$_5$-py, 7: NH$_3$.

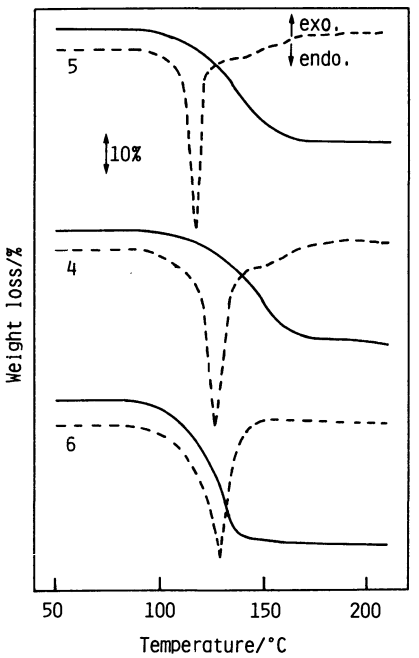

Fig. 2b. TG (—) and DSC (----) curves of [VO-(acac)$_2$B] complexes; heating rate 10 °C min^{-1}. B= 4: 4-CN-py, 5: 3-CN-py, 6: 3-Br-py.

to those of the thermal elimination of [VO(dbm)2(py)] (71.5 kJ mol^{-1}) and [VO(dbm)2(4-CH3-py)] (93.5 kJ mol^{-1}), where dbm is dibenzoylmethane.[11]

Kinetic Stability. The thermal stability of complexes has often been discussed in terms of the initiation temperature of decomposition reaction or the DSC maximum peak temperature. Since the temperature observed on the thermoanalytical curves is affected by the experimental conditions and the reaction mechanism, the thermal stability concerning the bond strength of metal-ligand linkage should be discussed by using a kinetic parameter rather than the initiation temperature.

Hence the kinetic analysis was carried out in order to ascertain the kinetic feature of [VO(acac)2B] complexes. The rate plot under nonisothermal conditions was obtained by use of the following Eq. 1 proposed by Coats and Redfern:[12]

$$\left.\begin{array}{l}\text{(when } n=1)\ \log\left\{\dfrac{-\log(1-\alpha)}{2.303T^2}\right\}\\ \text{(when } n\neq 1)\ \log\left\{\dfrac{1-(1-\alpha)^{1-n}}{T^2(1-n)}\right\}\end{array}\right\} = \log\frac{AR}{\phi E_a}\left(1-\frac{2RT}{E_a}\right)-\frac{E_a}{2.303RT}, \quad (1)$$

where E_a is activation energy; A, frequency factor; α, molar fraction of complex decomposed; T, absolute temperature; R, gas constant; ϕ, heating rate; and n, order of reaction. The plot of $\log\{-\log(1-\alpha)/(2.303T^2)\}$ against $1/T$ when $n=1$ gives a straight line, as shown in Fig. 3. The E_a and A values were calculated from the slopes and intercepts of these straight lines, respectively. The activation enthalpy ΔH^* was calculated from $\Delta H^*=E_a-RT$, while the activation entropy ΔS^* was obtained from $\Delta S^*=R[\ln(Ah/kT)-1]$, where k is the Boltzman constant, and h, the Planck constant, assuming the transmission coefficient to be 1. In addition, in order to disclose the contribution of the entropic term to the reaction, the activation free energy ΔG^* was calculated by the relation, $\Delta G^*=\Delta H^*-T\Delta S^*$. The kinetic characteristics are tabulated in Table 2.

Since the thermal reaction of [VO(acac)2B] complexes belongs to the elimination reaction of base B, the kinetic stability of the vanadium-base bond was expected to vary with the basicity of the bases. However, as seen in Table 2, in spite of pK_a values of the bases varying in wide range of 1.90—9.26, the activation free energy ΔG^* change in narrow range of 99—109 kJ mol^{-1}. On the other hand, when pyridine or its derivative forms a complex with a transition metal, the bonding consists of σ and π interactions between metal and substituted pyridine. It has been reported that in the thermal decomposition of [Ag(B)2NO3][13] and [Co(salen)(B)][14] (salen=*N*,*N*′-ethylenebis(salicylideneaminato)dianion), the complex with 4-CN-py has unusually large E_a value in comparison with those of py, 3-CH3-py, and 3-CN-py complexes. The large E_a value observed in 4-CN-py complex has been interpreted by taking into account a significant contribution of metal-base π-back-bonding to the bond stability. In the present complexes, [VO(acac)2(4-CN-py)] was also expected to be more stable than [VO(acac)2(3-CN-py)], [VO(acac)2(3-Br-py)], and [VO(acac)2(py)]. However, no remarkable difference in ΔG^* values among these complexes was observed.

These facts suggest that the thermal stability of

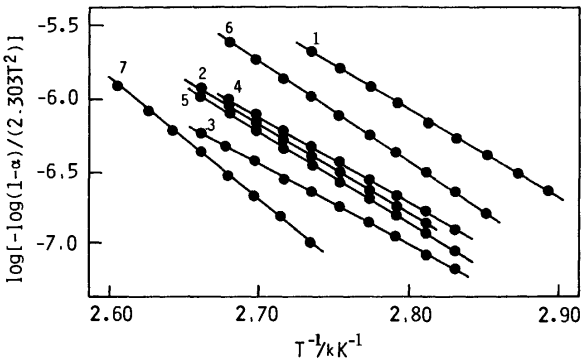

Fig. 3. Plots by the Coats-Redfern method for pyridine elimination of [VO(acac)2B] complexes. B= 1: py, 2: 4-CH3-py, 3: 4-C2H5-py, 4: 4-CN-py, 5: 3-CN-py, 6: 3-Br-py, 7: NH3.

Table 2. Kinetic Data of Pyridine Derivatives for the Elimination Reactions of [VO(acac)2B] Complexes

Base	E_a / kJ mol^{-1}	log(A/s^{-1})	ΔH^*(400 K) / kJ mol^{-1}	ΔS^*(400 K) / J K^{-1} mol^{-1}	ΔG^*(400 K) / kJ mol^{-1}
py	123±9	16.1±1.2	120±9	52±12	99±2
4-CH3-py	123±10	15.3±1.4	119±10	37±15	105±2
4-C2H5-py	103±9	12.3±1.2	100±9	−20±10	108±0.2
4-CN-py	113±4	13.9±0.6	110±4	11±6	105±0.2
3-CN-py	119±0.6	14.9±0.1	116±0.3	29±0.4	104±0.4
3-Br-py	126±7	16.2±1.1	123±7	54±7	101±0.7
NH3	157±1	19.2±0.5	153±1	110±2	109±0.5

E_a, activation energy; A, frequency factor; ΔH^*, activation enthalpy; ΔS^*, activation entropy; ΔG^*, activation free energy.

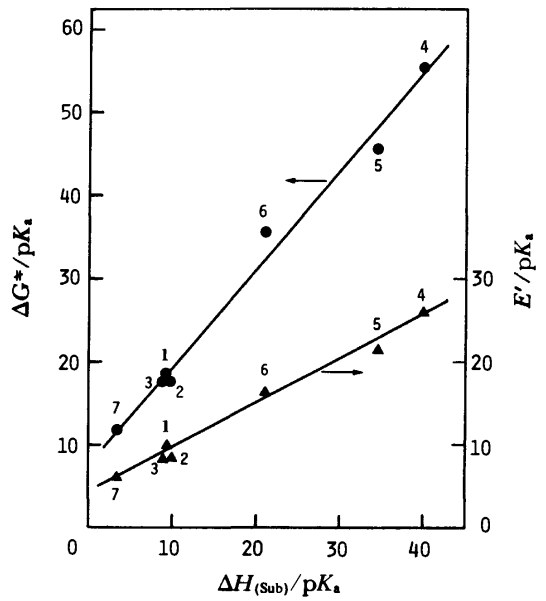

Fig. 4. Plots (—●—●—) of $\Delta G^*/pK_a$ against $\Delta H_{(sub)}/pK_a$, plots (—▲—▲—) of E'/pK_a against $\Delta H_{(sub)}/pK_a$. B=1: py, 2: 4-CH_3-py, 3: 4-C_2H_5-py, 4: 4-CN-py, 5: 3-CN-py, 6: 3-Br-py, 7: NH_3.

complexes is affected by various interactions, including the metal–base σ-bond, π-bond, and steric interaction.

As mentioned before, our previous studies[3,4] for the thermal reactions of $[Ni(acac)_2A_2]$ and $[Co(Hbhpn)A_2]X_2$ complexes revealed that the thermal stability of these complexes is influenced by the heat of sublimation of base A itself as well as basicity of the base. As for $[VO(acac)_2B]$, it is assumed that the thermal stability may be influenced by the thermal properties such as the heat of fusion and vaporization in the following equation:

$$\Delta G^* = \alpha pK_a + \beta \Delta H_{(sub)}, \quad (2)$$

where α and β are constants determined by the reaction system, and $\Delta H_{(sub)}$ is the heat of sublimation (sum of heat of fusion and vaporization). Dividing both sides of Eq. 2 by pK_a yields Eq. 2′:

$$\Delta G^*/pK_a = \alpha + \beta \Delta H_{(sub)}/pK_a, \quad (2')$$

If the above assumption is adequate, a straight line with slope β will be obtained. As shown in Fig. 4, the plot between $\Delta G^*/pK_a$ and $\Delta H_{(sub)}/pK_a$ indicates that $\Delta G^*/pK_a$ and $\Delta H_{(sub)}/pK_a$ bear a linear correlation. This result suggests that the thermal stability of $[VO(acac)_2B]$ complexes investigated here depends mainly on the basicity and the heat of sublimation of base B.

Reflectance Spectra. The reflectance spectral data for $[VO(acac)_2B]$ are summarized in Table 3. The lowest energy band can be assigned to $^2E \leftarrow {}^2B_2$ transition and the second band to $^2B_1 \leftarrow {}^2B_2$ transition (10 Dq). Selbin et al.[15] reported that a parameter D_{12}, the difference in positions between the first and the second

Table 3. Reflectance Spectral Data of $[VO(acac)_2B]$ Complexes in Solid State

Base	Band 1	Band 2	D_{12}	E'
	cm^{-1}	cm^{-1}	cm^{-1}	kJ mol^{-1}
py	12890	17300	4410	52.7
py[15]	(13000)	(17390)	(4390)	
4-CH_3-py	13000	17240	4240	50.7
4-C_2H_5-py	12990	17180	4190	50.1
4-CN-py	12950	17060	4110	49.1
3-CN-py	13120	17180	4150	49.6
3-Br-py	13370	17270	3900	46.6
NH_3	12630	17180	4550	55.4

E', Calculated from D_{12} values.

band maxima, is more sensitive than 10 Dq in the coordination ability of ligands. Then, the D_{12} values for these complexes were determined and converted to energy E'(kJ mol^{-1}) as shown in the 5th column of Table 3.

The tendency in E' value for each complex is similar to that for ΔG^* value as described above. In other words, no dependence of E' on basicity of the bases was observable. Therefore, in this case, Eq. 2″ was assumed:

$$E'/pK_a = \alpha' + \beta' \Delta H_{(sub)}/pK_a, \quad (2'')$$

where α' and β' are constants. As seen in Fig. 4, a linear correlation was observed between E'/pK_a and $\Delta H_{(sub)}/pK_a$. These results support the assumption that the stability in connection with the strength of metal-ligand bond is affected by the electron donating power and the heat of sublimation of base B.

Variations in the values of ΔG^* and E' with different ligand can be attributed to changes in the strength of metal–ligand σ-bond, the magnitude of metal-ligand π-bond, and the steric interaction. The basicity of ligand will relate to the strength of σ-bond. However, it is difficult to evaluate the degree of the character of π-bond and steric interaction. Although the heat of fusion and vaporization of ligand does not necessarily reflect the character of π-bond and steric interaction, both the characters may have correlation to the thermal property through hydrogen bond and van der Waals force. Therefore, the thermal properties such as heat of fusion and vaporization were used for explaining the difference in ΔG^* and E' values. Thus, the thermal stability of $[VO(acac)_2B]$ complexes seems to depend mainly on the pK_a and $\Delta H_{(sub)}$ of base B. A similar observation has been reported for dehydration-anation reaction of $[Cu(en)_2(H_2O)_2]X_2$[16] (en=ethylenediamine, X=Cl^-, Br^- ion) and $CoCl_2 \cdot nH_2O$ (n=1—6)[17] to discuss the influence of intermolecular hydrogen bonds on the activation energy and the enthalpy change of dehydration reaction.

References

1) G. Beech and C. T. Mortimer, *J. Chem. Soc. A*, **1967**,

1115; J. C. Van Dam, G. Hakvoort, and J. Reedijk, *J. Therm. Anal.*, **20**, 3 (1981); K. Boguslawska and A. Cygański, *J. Therm. Anal.*, **24**, 15 (1982).

2) J. G. Murgulescu, E. Segal, and D. Fătu, *J. Inorg. Nucl. Chem.*, **27**, 2677 (1965); P. Pfeiffer and Fr. Tappermann, *Z. Anorg. Allg. Chem.*, **214**, 273 (1933); W. W. Wendlandt and C. H. Stembridge, *J. Inorg. Nucl. Chem.*, **27**, 575 (1965).

3) Y. Shibutani and K. Shinra, *Nippon Kagaku Kaishi*, **1988**, 143.

4) Y. Shibutani, H. Tachikawa, and K. Shinra, *Nippon Kagaku Kaishi*, **1988**, 1816.

5) The following abbreviations are used: py, pyridine; 4-CH_3-py, 4-methylpyridine; 4-C_2H_5-py, 4-ethylpyridine, 4-CN-py, 4-cyanopyridine; 3-CN-py, 3-cyanopyridine, 3-Br-py, 3-bromopyridine.

6) R. A. Rowe and M. M. Jones, *Inorg. Synth.*, **5**, 115 (1957).

7) M. M. Jones, *J. Am. Chem. Soc.*, **76**, 5995 (1954).

8) R. T. Claunch, T. W. Martine, and N. M. Jones, *J. Am. Chem. Soc.*, **83**, 1073 (1961).

9) H. Horiguchi, "Sekigai Kyukozusetsu Soran," Sankyo Shuppan, Tokyo (1979), Chap. 7.

10) K. Nakamoto, Y. Morimoto, and A. E. Martell, *J. Am. Chem. Soc.*, **83**, 4533 (1961).

11) R. Lozano, J. Martiney, A. Martiney, and A. D. Lōpey, *Polyhedron*, **2**, 977 (1983).

12) A. W. Coats and J. P. Redfern, *Nature* (*London*), **201**, 68 (1964).

13) A. Akhavein and J. E. House, Jr., *J. Inorg. Nucl. Chem.*, **32**, 1479 (1970).

14) K. Miyokawa, M. Takumi, S. Kinoshita, and I. Masuda, *Thermochim. Acta*, **95**, 227 (1985).

15) J. Selbin and T. R. Ortolano, *J. Inorg. Nucl Chem.*, **26**, 37 (1964).

16) H. Langfelderová, V. Karia, M. Lirkešová, and J. Gažo, *J. Therm. Anal.*, **26**, 95 (1983).

17) W. K. Grindstaff and N. Fogel, *J. Chem. Soc., Dalton Trans.*, **1972**, 1476.

The Spectrophotometric Determination of Phosphate Following the Collection of Ion Pair of Molybdophosphate with Bis[2-(5-chloro-2-pyridylazo)-5-diethylaminophenolato]cobalt(III) on an Organic Solvent-Soluble Membrane Filter

Mitsuhiko TAGA* and Masahiko KAN
Department of Chemistry, Faculty of Science, Hokkaido University, Sapporo 060
(Received September 1, 1988)

A rapid and sensitive method of determining phosphate was described. The ion pair of molybdophosphate with bis[2-(5-chloro-2-pyridylazo)-5-diethylaminophenolato]cobalt(III) (Co-5-Cl-PADAP) formed in 0.075 mol dm^{-3} sulfuric acid, 0.225 mmol dm^{-3} ammonium molybdate, and 25 μmol dm^{-3} Co-5-Cl-PADAP was collected on an organic solvent-soluble membrane filter made of cellulose nitrate. The membrane filter with the ion pair was then dissolved into *N,N*-dimethylformamide, and the absorbance of the solution was measured for the determination of phosphate. The calibration curve was linear up to 0.4 μg as phosphorus, with the correlation coefficient of 0.999, and the apparent molar absorption coefficient of phosphate was 2.9×10^5 dm^3 mol^{-1} cm^{-1}. The relative standard deviation was 1.7% for 0.4 μg of phosphorus. Although dodecyl sulfate existing in an amount ten times that of phosphorus caused a positive error, no ions commonly existing in natural waters interfere with the determination of phosphate. The proposed method was applied to the determination of μg dm^{-3} levels of phosphate-phosphorus in natural waters, and satisfactory results were obtained.

Since the determination of traces of phosphate in environmental samples is important for environmental chemistry and geochemistry, the development of a sensitive and rapid method of determining phosphate has been promoted. In addition to conventional heteropoly blue methods, many more sensitive methods have been reported, such as spectrophotometry using Malachite Green[1,2] and differential-pulse anodic voltammetry.[3]

For the determination of traces of phosphate in natural waters, an extraction procedure using a separating funnel is required in most determination methods. For the rapid and sensitive determination of phosphate and silicate, the collection of the ion pair of molybdophosphate or molybdosilicate with a cationic surfactant on an organic solvent-soluble membrane filter has been reported.[4-6] These methods are superior to the extraction method using a separating funnel because there is no use of toxic and combustible solvents and the operation is easy. However, greater sensitivity is required for the determination of traces of phosphate in natural waters.

For the highly sensitive determination of phosphate with membrane-filter collection, the use of Malachite Green as the ion pair reagent has been reported.[7] Although this method had a high sensitivity, the interferences caused by silicon and iron(III) were so serious that pretreatment was required for the determination of phosphate in natural waters.

In their previous studies, the present authors have developed highly sensitive methods of determining phosphate by means of indirect atomic absorption spectrophotometry using the copper(II)-1,10-phenanthroline complex[8] and have also developed flotation-spectrophotometry[9] and indirect atomic absorption spectrophotometry[10] using bis[2-(5-chloro-2-pyridylazo)-5-diethylaminophenolato]cobalt(III) chloride (Co-5-Cl-PADAP), which has previously been used for the extraction-spectrophotometric determination of anionic surfactants.[11,12]

In the present paper, the present authors have developed a highly sensitive and rapid method of determining phosphate. In the acidic solution, phosphate forms molybdophosphate with molybdate. The ion pair of the molybdophosphate anion with the Co-5-Cl-PADAP cation is formed and collected on the organic solvent-soluble membrane filter made of cellulose nitrate. The membrane filter with the ion pair is dissolved into *N,N*-dimethylformamide (DMF). The absorbance of the solution is proportional to the concentration of phosphate. By using this procedure, traces of phosphate in natural waters can easily be determined.

Experimental

Reagents. A standard solution of phosphate was prepared by dissolving potassium dihydrogenphosphate (special grade, Wako Pure Chemical Industries, Ltd.) in water. The Co-5-Cl-PADAP was purchased from Dojindo Laboratories and used as an aqueous solution without any further purification.

Apparatus. A Hitachi Model 124 double-beam spectrophotometer was used for measuring the absorbance. The absorption spectra were constructed with a Hitachi Model U-3200 recording spectrophotometer.

Procedure. A sample is placed in a 20-cm^3 beaker, and 1-cm^3 portions of 0.75 mol dm^{-3} sulfuric acid, 2.25 mmol dm^{-3} ammonium molybdate, and 0.25 mmol dm^{-3} Co-5-Cl-PADAP are added, after which the total volume is made up to 10 cm^3 with water. The solution is filtered through a 3.0-μm-pore sized membrane filter made of cellulose nitrate 25 mm in diameter (Toyo Roshi Kaisha, Ltd.). After washing with two portions of 10 cm^3 of water, the membrane

filter with the ion pair is transferred into a 10-cm³ beaker. By the addition of 5.0 cm³ of DMF, both the ion pair and the membrane filter are dissolved. The absorbance of the solution is measured at the absorption maximum wavelength of 560 nm against water with a 1-cm measuring cell.

Results and Discussion

Absorption Spectra. The absorption spectra of the ion pair of molybdophosphate with Co-5-Cl-PADAP and a reagent blank are shown in Fig. 1. The maximum absorbance is observed at the wavelength of 560 nm.

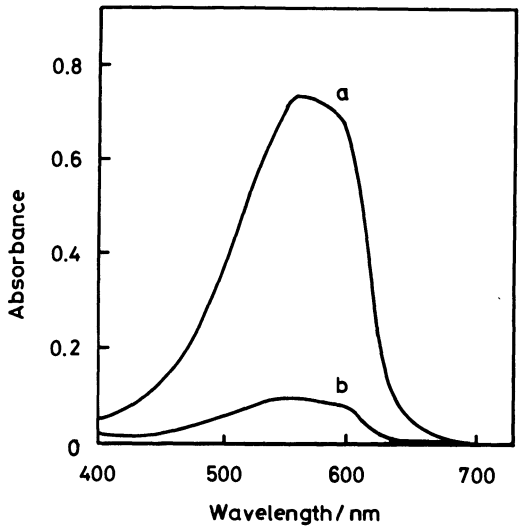

Fig. 1. Absorption spectra of ion pair of Co-5-Cl-PADAP with molybdophosphate and reagent blank. a: 0.4 μg phosphorus against reagent blank, b: reagent blank against water. [H_2SO_4]: 0.075 mol dm^{-3}, [$(NH_4)_6Mo_7O_{24}$]: 0.225 mmol dm^{-3}, [Co-5-Cl-PADAP]: 25 μmol dm^{-3}.

Selection of Acid. For adjusting the concentration of acid, sulfuric acid and hydrochloric acid can be used because of the small absorbance of the blank. The use of nitric acid or perchloric acid leads to a large absorbance of the blank due to the formation of the ion pair of nitrate or perchlorate with Co-5-Cl-PADAP. In the proposed method, sulfuric acid is used because the preservation and pretreatment needed for the determination of total phosphorus in natural waters often require the use of sulfuric acid.[13,14]

Effect of Concentration of Sulfuric Acid. Figure 2 shows the effect of the concentration of sulfuric acid on the absorbance of the ion pair and the reagent blank. The absorbance of the reagent blank was small above the concentrations of 0.05 mol dm^{-3}. The maximum absorbance of the ion pair was obtained in the concentration range from 0.05 to 0.1 mol dm^{-3}. The reason for the large absorbance of the reagent blank in the concentrations below 0.05 mol dm^{-3} was the formation and collection of the ion pair of Co-5-Cl-PADAP with molybdate. No molybdophosphate was formed in the concentration range above 0.2 mol dm^{-3}. The concentration of 0.075 mol dm^{-3} was chosen as the concentration of sulfuric acid.

Effect of Concentration of Ammonium Molybdate. The effect of the concentration of ammonium molybdate is shown in Fig. 3. The maximum and constant absorbance of the ion pair was obtained in the concentration range above 0.15 mmol dm^{-3}. As the concentration of ammonium molybdate, 0.225 mmol dm^{-3} was chosen.

Effect of Concentration of Co-5-Cl-PADAP. Figure 4 shows the effect of the concentration of Co-5-Cl-PADAP on the absorbance. The maximum and constant absorbance of the ion pair was obtained

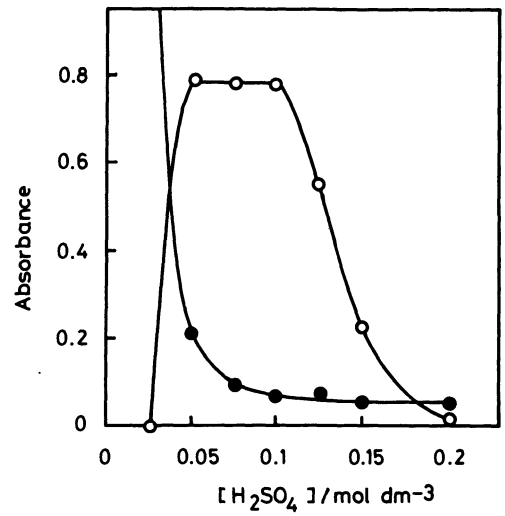

Fig. 2. Effect of concentration of sulfuric acid on absorbance. [$(NH_4)_6Mo_7O_{24}$]: 0.225 mmol dm^{-3}, [Co-5-Cl-PADAP]: 25 μmol dm^{-3}. ○: 0.4 μg phosphorus against reagent blank, ●: reagent blank against water.

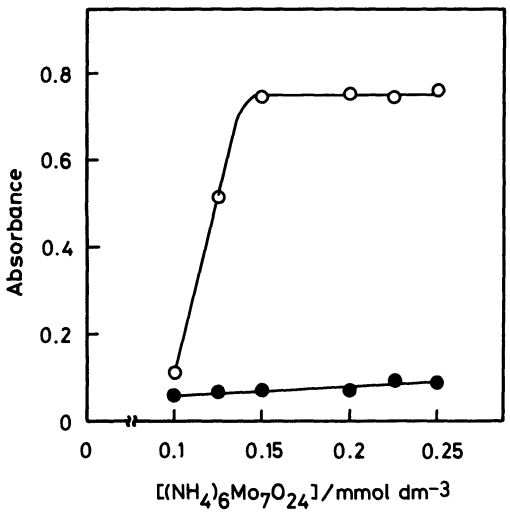

Fig. 3. Effect of concentration of ammonium molybdate on absorbance. [H_2SO_4]: 0.075 mol dm^{-3}, [Co-5-Cl-PADAP]: 25 μmol dm^{-3}. ○: 0.4 μg phosphorus against reagent blank, ●: reagent blank against water.

Table 1. Effects of Diverse Ions on the Determination of Phosphate[a)]

Ion	Added as	Amount/μg	Relative error/%
As(V)	Na_2HAsO_4	0.4	+42
As(III)	As_2O_3	40	0
DS[b)]	Na salt	4.0	+5
		40	+29
Si(IV)	Na_2SiO_3	400	+8
Fe(III)	$FeCl_3$	400	−2
ClO_4^-	$KClO_4$	400	+8
SCN^-	KSCN	400	+7
$S_2O_3^{2-}$	$Na_2S_2O_3$	400	+1

a) Phosphorus taken; 0.4 μg. b) Dodecyl sulfate.

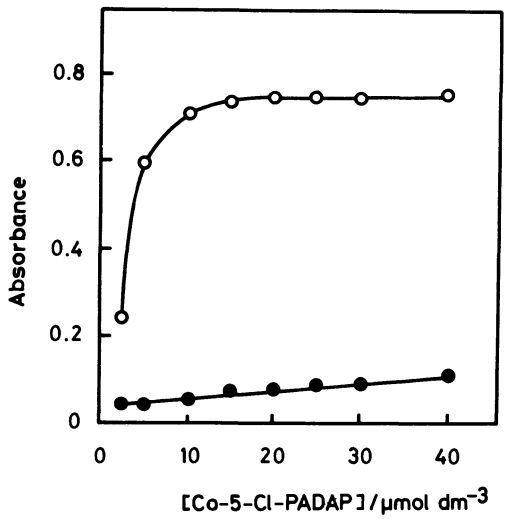

Fig. 4. Effect of concentration of Co-5-Cl-PADAP on absorbance. [H_2SO_4]: 0.075 mol dm^{-3}, [$(NH_4)_6Mo_7O_{24}$]: 0.225 mmol dm^{-3}. ○: 0.4 μg phosphorus against reagent blank, ●: reagent blank against water.

above the concentrations of 15 μmol dm^{-3}, while the absorbance of the reagent blank increased with the increase in the concentration of Co-5-Cl-PADAP. This increase in the absorbance of the reagent blank was explained by the formation and collection of the ion pair of molybdate with Co-5-Cl-PADAP. A concentration of 25 μmol dm^{-3} was chosen as the concentration of Co-5-Cl-PADAP.

Selection of Membrane Filter. The membrane filter collecting the ion pair of Co-5-Cl-PADAP with molybdophosphate must be dissolved into such organic solvents as DMF. Membrane filters made of cellulose nitrate, cellulose acetate, and a mixture of cellulose acetate and cellulose nitrate can be dissolved in DMF; a cellulose nitrate filter was used.

Effect of Pore Size of Membrane Filter. The effect of the pore size of the membrane filter on the absorbance was also studied. The constant absorbance of the ion pair was obtained in the pore-size range from 1.0 μm to 5.0 μm. The absorbance of the blank was also constant in this region. With the decrease in the pore size to less than 1.0 μm, the absorbance of the blank increased and the absorbance of the ion pair decreased. These results are similar to those reported in the collection of the ion pair of Malachite Green with molybdophosphate on a membrane filter.[7)]

As the pore size of the membrane filter, 3.0 μm was used because of the constant absorbance of the ion pair and the facility of the filtration.

Other Conditions. The effect of the standing time on the absorbance was examined for the reaction after the addition of Co-5-Cl-PADAP. From 30 s to 5 min, the constant absorbance was obtained for both the ion pair and the reagent blank.

Two portions of 10 cm^3 of water were sufficient for washing the membrane filter with the ion pair.

As the solvent dissolving the membrane filter with the ion pair, DMF was used. Dimethyl sulfoxide and Methyl Cellosolve could also be used. Although 5.0 cm^3 of DMF was used for dissolving the membrane filter with the ion pair, 2.0 cm^3 was sufficient for a complete dissolution.

Calibration Curve, Sensitivity, and Precision. The calibration curve of phosphate was linear up to 0.4 μg of phosphorus, with a correlation coefficient of 0.999. The apparent molar absorption coefficient of phosphate was 2.9×10^5 dm^3 mol^{-1} cm^{-1}. The relative standard deviation was 1.7% for 0.4 μg of phosphorus.

Effect of Diverse Ions. The effect of diverse ions on the determination of phosphate is shown in Table 1. Arsenic(V) showed a serious positive error when it coexisted in the same amount as phosphorus. This is due to the formation and collection of the ion pair of molybdoarsenate with Co-5-Cl-PADAP. For the elimination of the error caused by arsenic(V), the reduction of arsenic(V) to arsenic(III) with thiosulfate[15)] can be used. In the proposed method, arsenic(III) and thiosulfate showed no interference with the determination of phosphate.

Dodecyl sulfate, an anionic surfactant, exhibited a positive error of 5% when coexisting in an amount ten times that of phosphorus.

Although silicon showed a little positive error when coexisting in a 1000-fold amount, no serious problem arise in the determination of phosphate in natural waters.

Table 2. Determination of Phosphate-Phosphorus in Natural Waters[a]

Sample	Phosphorus content[b]/μg l^{-1}	
	Proposed method	Other method[c]
River water	3.6±0.3	4±1
Ground water	19.4±0.3	18±1

a) Sample taken; 5.0 cm^3. b) Mean±standard deviation (n=3). c) Flotation-spectrophotometry using Co-5-Cl-PADAP previously proposed by the present authors.[9]

Table 3. Spike and Recovery Test for Phosphate-Phosphorus in River Water[a]

Phosphorus/μg		Recovery/%
Added	Found	
0.000	0.035	—
0.050	0.089	108
0.100	0.130	95
0.150	0.193	105

a) Sample taken; 5.0 cm^3.

Iron(III) showed no interference with the proposed method. In the method using Malachite Green proposed by Matsubara et al.,[7] the presence of iron(III) in an amount equal to that of phosphorus caused an increase in the absorbance. Therefore, the pretreatment of samples with cation-exchange resin was required to remove iron(III). The proposed method is superior in the points of little interference caused by silicon and no interference by iron(III).

No ions commonly existing in natural waters, such as sodium, potassium, magnesium, calcium, chloride, and sulfate, interfere with the determination of phosphate. Organic substances, such as tartrate, citrate, ascorbate, and ethylenediaminetetraacetate, also showed no interference.

Determination of Phosphate in Natural Waters. The proposed method was applied to the determination of phosphate-phosphorus in natural waters. The samples were filtered with a 0.45 μm pore sized membrane filter and analyzed immediately or stored in a freezer until determination.[13] The results are shown in Table 2, in comparison with those of flotation-spectrophotometry using Co-5-Cl-PADAP previously proposed by present authors.[9] A satisfactory agreement was obtained between the two methods.

The spike and recovery test was examined for phosphate-phosphorus in another river water sample. The result, shown in Table 3, was satisfactory.

Enrichment of the Ion Pair on the Membrane Filter. Although the proposed method has a high sensitivity for the determination of traces of phosphate in natural waters, the enrichment of the ion pair on a membrane filter leads to an even more sensitive determination method.

To a 100-cm^3 portion of a sample, 1-cm^3 portions each of 7.5 mol dm^{-3} sulfuric acid, 22.5 mmol dm^{-3} ammonium molybdate, and 2.5 mmol dm^{-3} Co-5-Cl-PADAP were added. After filtration, the membrane filter with the ion pair was washed with three 30 cm^3 portions of water.

The calibration curve of phosphate was also linear up to 0.4 μg of phosphorus, with a correlation coefficient of 0.998. The molar absorption coefficient had the same value as that obtained by using 7 cm^3 of the sample. The absorbance of the reagent blank was 0.25, while that of 1 μg dm^{-3} of phosphrus was 0.19 against the reagent blank. The determination of 0.1 μg dm^{-3} levels of phosphorus can be made by using 100 cm^3 of the sample.

References

1) T. Nasu and M. Kan, *Analyst*, **113**, 1683 (1988).
2) S. Motomizu, T. Wakimoto, and K. Tôei, *Talanta*, **31**, 235 (1984).
3) K. Matsunaga, I. Kudo, M. Yanada, and K. Hasebe, *Anal. Chim. Acta*, **185**, 355 (1986).
4) S. Taguchi, E. Ito-oka, and K. Goto, *Bunseki Kagaku*, **33**, 453 (1984).
5) S. Taguchi, E. Ito-oka, K. Masuyama, I. Kasahara, and K. Goto, *Talanta*, **32**, 391 (1985).
6) I. Kasahara, R. Terai, Y. Murai, N. Hata, S. Taguchi, and K. Goto, *Anal. Chem.*, **59**, 787 (1987).
7) C. Matsubara, Y. Yamamoto, and K. Takamura, *Analyst*, **112**, 1257 (1987).
8) M. Taga, H. Yoshida, and M. Kan, *Bunseki Kagaku*, **36**, 18 (1987).
9) M. Taga and M. Kan, *Anal. Sci.*, **4**, 181 (1988).
10) M. Taga and M. Kan, *Talanta*, in press.
11) S. Taguchi, I. Kasahara, Y. Fukushima, and K. Goto, *Talanta*, **28**, 616 (1981).
12) S. Taguchi, T. Tonoshima, I. Kasahara, and K. Goto, *Kogyo Yosui*, No. 278, 23 (1981).
13) Y. Nasu, N. Yogo, and H. Tachibana, "Mizuno Bunseki (Water Analysis)," 3rd ed, ed by the Japan Society for Analytical Chemistry (Hokkaido), Kagakudojin, Kyoto (1981), pp. 408—413.
14) "Testing Methods for Industrial Wastewater, Japanese Industrial Standard K 0102," Japanese Industrial Standards Committee, Japanese Standards Association, Tokyo (1986), p. 4.
15) S. Motomizu, T. Wakimoto, and K. Tôei, *Bunseki Kagaku*, **31**, 717 (1982).

Complexation of Lanthanoid(III) with Substituted Benzoic or Phenylacetic Acids and Extraction of These Acids

Yuko HASEGAWA,* Yoko MORITA, Masako HASE, and Mayumi NAGATA
Department of Chemistry, Science University of Tokyo,
Kagurazaka, Shinjuku-ku, Tokyo 162
(Received September 8, 1988)

The stability constants of lathanoid(III) complexes with several benzoic and phenylacetic acids substituted with -OH, $-OCH_3$, or $-NH_2$ groups as well as the dissociation constants of these acids have been determined potentiometrically in 0.1 mol dm^{-3} sodium perchlorate solution at 25 °C. The distribution constants of these acids between the perchlorate media and chloroform and the dimerization constants in chloroform were also determined. The distribution constants of ortho-substituted benzoic acids seem to be larger than those of α-substituted phenylacetic acids with the same substituent. There is a trend that the higher the pK_a, the larger the dimerization constant. The order of pK_a is : *o*-aminobenzoic>*o*-methoxybenzoic>β-hydroxy-β-phenylpropanoic>α-hydroxyphenylacetic(mandelic)>α-methoxyphenylacetic>*o*-hydroxybenzoic acid and the sequence of the stability constants of their complexes for a given lanthanoid is also in a same order except for the mandelate. Mandelic acid forms more stable complexes with the heavier lanthanoid(III) while others are similar to each other regardless of the lanthanoid.

Most α-hydroxy carboxylic acids have been used as eluents in the mutual separation of lanthanoid(III) by ion-exchange method, because these form more stable complexes with the heavier lanthanoid(III). It has also been reported that most carboxylic acids, such as benzoic acid[1] and benzilic acid (α-hydroxydiphenylacetic acid[2]), form adducts with tris(β-diketonato)-lanthanoid(III) in organic solvents.

However, it is not always clear what properties of the acids are effective to form stable complexes with lanthanoid(III) in organic and in aqueous solutions. In order to get some information about this point, the effect of the characteristics of acids such as the acid strength, the structure, and the nature of the functional group on the liquid–liquid distribution and the dimerization constants has been examined, using several benzoic and phenylacetic acids substituted with -OH, $-OCH_3$, or $-NH_2$ group at the 2-position of the parent acids. Furthermore, the stability constants of these complexes with lanthanoid(III) have been determined potentiometrically.

Experimental

Reagents. All reagents used were of analytical grade. Mandelic acid (α-hydroxyphenylacetic acid) and tropic acid (β-hydroxy-β-phenylpropanoic acid) were obtained from Nacalai Tesque, Inc., salicylic acid (*o*-hydroxybenzoic acid) and anthranilic acid (*o*-aminobenzoic acid) from Kanto Chemicals, *o*-anisic acid (*o*-methoxybenzoic acid) from Tokyo Kasei Co., and α-methoxyphenylacetic acid from Aldrich Chemical Co. Lanthanoid oxides(III) were obtained from the following companies: Aldrich Chemicals (lanthanum), Mitsuwa Chemicals (neodymium, europium, thulium), Shin-Etsu Chemical Co. (praseodymium, samarium, and lutetium), and American Potash & Chemical Corporation (others). The purity of each oxide was 99.99%. Sodium perchlorate was prepared from sodium carbonate and perchloric acid; it was recrystallized twice from water. Chloroform was washed three times with deionized water. The other reagents were employed without further purification.

Procedures. All the procedures were carried out in a thermostated room at 25 °C. The total anion concentration was adjusted to 0.1 M (1 M=1 mol dm^{-3}) with sodium perchlorate. The solution containing 0.010 M $HClO_4$+0.09 M $NaClO_4$ solution was employed as the standard of $-\log[H^+]=2.00$ (hereafter $-\log[H^+]$ is abbreviated as pC_H).

i) Dissociation, Distribution, and Dimerization Constants of the Carboxylic Acids.

Dissociation Constants of Carboxylic Acids. A certain volume (about 50 cm^3) of a buffered carboxylic acid solution ($[A^-]/[HA]=1$), in other words, the acid solution in which a half of the acid was neutralized with sodium hydroxide, was titrated with perchloric acid potentiometrically. The total acid concentration was about 0.02 M. The other dissociation constant of anthranilic acid owing to the amino group associated with proton, K_a' ($=[H^+][HA]/[H_2A^+]$), was similarly determined by titrating the acid solution, in which perchloric acid equivalent to a half concentration of the total anthranilic acid had been added, with sodium hydroxide solution. The titrations were repeated several times. In all cases, the repetitive runs agreed satisfactorily.

Distribution and Dimerization Constants of the Acids. A portion of chloroform solution containing one of the acids at various concentrations and an equal volume of 0.1 M sodium perchlorate solution adjusted to a certain pC_H were placed in a stoppered glass tube and the two phases were agitated vigorously. After then, the mixtures were centrifuged. The pC_H in the aqueous solution was measured. The acid concentrations in the aqueous phases were determined by measuring the absorbance at a certain wavelength, near the wavelength giving the maximum absorbance, e.g., for salicylic acid, at 301.7 nm where the molar absorptivity was 3.53×10^3, and for mandelic acid at 260 nm (the absorptivity was 1.64×10^2). The concentration in the organic phases was also determined by measuring the absorbance directly except for anthranilic acid. The molar absorptivity was 4.10×10^3 at 309 nm for salicylic acid, and 1.85×10^2 for mandelic acid at 260 nm. The concentration of anthranilic acid in chloroform was determined from the absorbance after back-extraction into sodium hydroxide

solution. The molar absorptivity of anthranilic acid at the wavelength was constant at $pC_H>7$. However, at lower pC_H, the absorptivity decreased.

The distribution ratio is defined as,

$$D = [HA]_{org,total}/[HA]_{aq,total}$$

hereafter, the organic phase is denoted by the subscript "o" and the aqueous phase has no subscript. The distribution ratio of the monocarboxylic acid can generally be represented as follows:

$$D = \frac{[HA]_o + 2[(HA)_2]_o}{[HA] + [A^-]} = \frac{K_d(1 + 2K_dK_{dim}[HA])}{1 + K_a/[H^+]} \quad (1)$$

where K_d is the distribution constant of the acid ($K_d=[HA]_o/[HA]$) and K_{dim} is the dimerization constant ($K_{dim}=[(HA)_2]_o/[HA]_o^2$).

The distribution ratio was also measured at various pC_H for each acid at 1.0×10^{-3} M.

ii) Stability Constants of the Complexes. The metal(III) solutions were prepared by dissolving the respective weighed oxide in perchloric acid. The lanthanoid(III) concentration was determined by titration with EDTA using Xylenol Orange as the indicator at about $pC_H=5$. The pC_H in the metal(III) solution was adjusted, just prior to use to a similar pC_H in the buffered ligand acid solution in order to avoid the change in the pC_H due to the acid-base neutralization. The stability constants of the lanthanoid(III) complexes were determined by titrating the metal(III) solutions with the half-neutralized carboxylate solution potentiometrically. The potentiometric titration data were analyzed using the following equation based on the Bjerrum formation function.

$$\frac{\bar{n}}{1-\bar{n}} \cdot \frac{1}{[A^-]} = \beta_1 + \beta_2 \frac{2-\bar{n}}{1-\bar{n}} [A^-] \quad (2)$$

where $\bar{n}$ is the average number of ligands combined with the metal ion. More detailed data treatment is reported elsewhere.[3]

Results and Discussion

i) Dissociation, Distribution, and Dimerization Constants of the Carboxylic Acids. The pK_a values obtained by potentiometric titration are listed in Table 1. Since the pK_a of the parent acids, i.e., benzoic and phenylacetic acids, is almost 4,[6,7b] the introduction of these functional groups decreases the values of pK_a except for $-NH_2$. The values of the dissociation constant obtained in the present work agree with the several results reported earlier.[7] The pK_a of salicylic acid reported in the literature scatters. However, a value which agrees with the present result, (2.70±0.02 in 0.10 M ionic medium), has also been reported.[8]

Figure 1-a shows the log–log plots of the distribution ratio of salicylic and anthranilic acids against the undissociated acid concentration in the aqueous phase. Since the distribution ratio depends on the pC_H as given in Eq. 1, the pC_H at equilibrium was measured and $\log D(1+K_a/[H^+])$ for salicylic acid and $\log D(1+K_a/[H^+]+[H^+]/K_a')$ for anthranilic acid instead of $\log D$ are plotted against log[HA]. The undissociated acid concentration was calculated from the total acid concentration in the aqueous phases (A_T) and the K_a, according to $[HA]=A_T/(1+K_a/[H^+])$ while that of anthranilic acid was calculated according to $[HA]=A_T/(1+K_a/[H^+]+[H^+]/K_a')$. The data were analyzed by a curve-fitting method using a normalized curve, $Y=\log(1+v)$ where $v=2K_d\times K_{dim}[HA]$ (see Eq. 1). Consequently, K_d and K_{dim} were obtained. Since the distribution ratio could not be determined over a wide range of [HA] for the other acids (due to the restriction of solubilities), the relation in Eq. 1 was plotted in antilog units (an example is shown in Fig. 1-b) and from the intercept and the slope of the straight lines obtained, the constants were determined. All the constants obtained are listed in Table 1. The solid curves in Fig. 1 were calculated using the constants obtained. The curves fit well to the data.

Table 1. Equilibrium Constants of Acids
Aqueous Solution : 0.1 M $NaClO_4$
Organic Solvent : $CHCl_3$

Acid	pK_a	$\log K_d$	$\log K_{dim}$
Salicylic (*o*-Hydroxybenzoic)	2.72	0.48	1.64
Anisic (*o*-Methoxybenzoic)	3.92	1.58	—
Anthranilic (*o*-Aminobenzoic)	4.68 (2.15)[a]	−0.20	2.15
Mandelic (α-Hydroxyphenylacetic)	3.18	−1.47[4]	1.50[4]
α-Methoxyphenylacetic	2.97	0.40	1.10
Tropic (β-Hydroxy-β-phenylpropanoic)	3.90	−1.09	1.54
Benzoic	4.01[6]	0.44[5]	2.22[5]

a) In the parentheses $K_a'=[HA][H^+]/[H_2A^+]$.

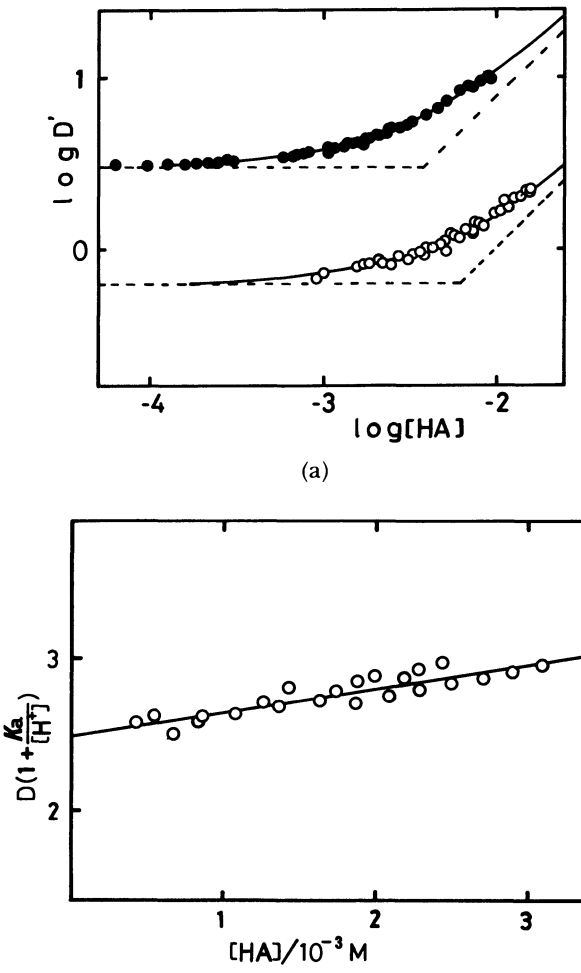

Fig. 1. Typical examples of extraction curves as a function of undissociated acid concentration in aqueous phases. a) Log-log plot of distribution ratio of salicylic and anthranilic acids as a function of [HA]. The $-\log[H^+]$ is around 2.0 for salicylic acid (●) and 3.4 for anthranilic acid (○). $\log D' = \log D(1+K_a/[H^+])$ for salicylic acid and $\log D' = \log D(1+K_a/[H^+]+[H^+]/K_a')$. The dotted lines are $Y = \log K_d$ and $Y = \log[HA] + \log 2K_d^2K_{dim}$. b) Distribution ratio of α-methoxyphenylacetic acid against [HA]. The solid line is $Y = 2.49 + 1.57\times10^2[HA]$. The correlation coefficient is 0.89₄. The $-\log[H^+]$ is around 2.0.

In order to ascertain the validity of Eq. 1 and of applying pK_a, which was determined in 0.1 M sodium perchlorate media without saturation with chloroform, to the analysis of the solvent extraction data, the distribution ratio was measured at various pC_H at a constant acid concentration. Figure 2 shows the plots of the distribution ratio of salicylic, anthranilic, and mandelic acids against pC_H using a total acid concentration of 10^{-3} M. The solid curves are calculated from Eq. 1 using all the constants in Table 1. The curves fit well to the data. The data obtained by similar experiments with other acids fitted well to

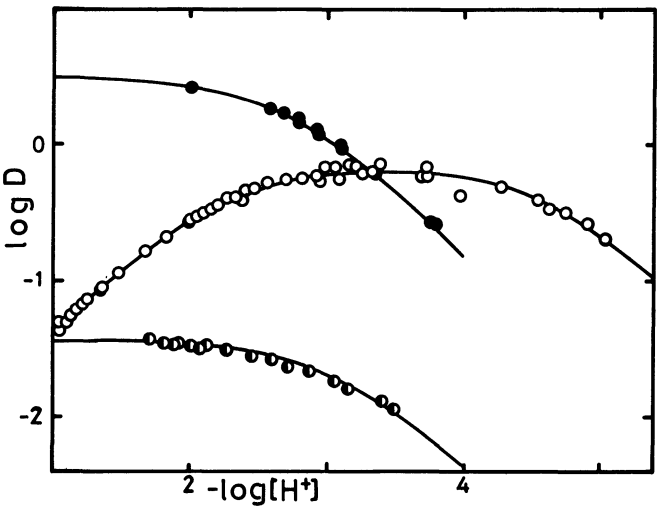

Fig. 2. Distribution ratio of salicylic, anthranilic, or mandelic acid as a function of $-\log[H^+]$. Total acid concentration: 1.0×10^{-3} M. Aqueous phase: 0.1 M $NaClO_4$, organic phase: $CHCl_3$. Salicylic (●), anthranilic (○), and mandelic (◐) acids.

the values calculated from the constants obtained. The fact that all the constants, including pK_a, explain the data well would suggest that the constants obtained in an aqueous solution without saturation with organic solvents can be applied to solvent extraction data.

As seen from Table 1, it is not easy to find definite correlation among pK_a, K_d, and/or K_{dim}. The distribution constants of the substituted benzoic acids seem to be larger than those of the phenylacetic acids substituted with the same functional group. There is a trend that the higher the pK_a, the larger K_{dim}, at least in the family of phenylacetic acid. The trend would be explained as: the acid anion capable of attracting hydrogen ion strongly, i.e., the oxygen atom in carboxyl group to be the stronger Lewis base, may also attract a hydrogen atom in other acid molecules to form a hydrogen bond. This result suggests that a carboxylic acid having higher pK_a may form more stable adducts with lanthanoid(III) chelates such as tris(β-diketonato)lanthanoid(III) in organic phases. The high pK_a and small K_{dim} of *o*-anisic acid may be caused by the methoxyl group at the ortho position. This could form an inner complex with the hydrogen atom in the carboxyl group. Consequently, the dissociation is depressed and the distribution constant is large, due to less hydration. Furthermore it would not easily associate with other *o*-anisic acid, i.e., low K_{dim}. We can not explain the low pK_a, and high distribution and dimerization constants of salicylic acid, most presumably, owing to inner complexation in salicylate ion.

ii) Complexation of Lanthanoid(III) with These Acids. Table 2 gives typical examples of the potentiometric titration data. Using these data, $\bar{n}/((1-\bar{n})[A^-])$ and $(2-\bar{n})[A^-]/(1-\bar{n})$ were calculated (see Eq. 2),

Table 2. Potentiometric Titration Data in 0.10 M ($NaClO_4$) at 25 °C

(1) Terbium(III) anthranilate

Volume of titrant/cm³	−log [H⁺]	[A⁻]ᵃ⁾/10⁻⁴ M	$\bar{n}$
3.0	4.25_6	2.15	0.04_1
4.0	4.24_8	2.80	0.05_3
5.0	4.24_3	3.42	0.06_6
6.0	4.24_3	4.06	0.07_8
7.0	4.24_3	4.68	0.09_0
8.0	4.24_4	5.29	0.10_2
9.0	4.24_8	5.92	0.11_3
10.0	4.24_9	6.51	0.12_5
11.0	4.25_3	7.11	0.13_6
12.0	4.25_6	7.70	0.14_7
13.0	4.26_0	8.29	0.15_8

in the cup; initial volume=50.0 cm³
initial $-\log[H^+]=4.80_7$
initial terbium(III) concentration=1.02×10^{-2} M
in the buret; titrant concentration=2.08×10^{-2} M

(2) Dysprosium(III) mandelate

Volume of titrant/cm³	−log [H⁺]	[A⁻]ᵃ⁾/10⁻⁴ M	$\bar{n}$
6.0	2.75_5	3.51	0.32_1
7.0	2.73_8	4.21	0.36_2
8.0	2.72_3	4.85	0.40_3
9.0	2.71_3	5.54	0.44_1
10.0	2.70_4	6.21	0.47_9
11.0	2.69_7	6.88	0.51_5
12.0	2.69_4	7.60	0.55_0
13.0	2.68_9	8.23	0.58_6
14.0	2.68_9	8.99	0.61_7
15.0	2.68_7	9.67	0.65_0

in the cup; initial volume=50.0 cm³
initial $-\log[H^+]=3.19_4$
initial dysprosium(III) concentration=1.03×10^{-2} M
in the buret; titrant concentration=3.96×10^{-2} M

a) Free carboxylate ion concentration at equilibrium.

and the former was plotted against the latter. Straight lines having positive slopes were obtained. The first and second stability constants were determined from the intercept and the slope, respectively. The constants so obtained are listed in Table 3 together with the error limits based on the agreement in repetitive titrations. In these experiments, owing primarily to two reasons, high $\bar{n}$ could not be obtained, that is, i) lanthanoid(III) does not form stable complexes with these ligands except for mandelate ions, and ii) since the solubility of the acids employed in water is not high, the free carboxylate anion concentration at equilibrium was not over 2×10^{-3} M. Consequently, the second stability constants have rather big errors.

It would appear from the values in Table 3 that the order of the stability constants for a given lanthanoid(III) is in the following sequence: mandelates≫anthranilates>*o*-anisates≃tropates≃α-methoxyphenylacetates≃benzoates>salicylates. This sequence may be due to the differene of pK_a of the ligand acids. Actually, it has been reported[6] that the correlation

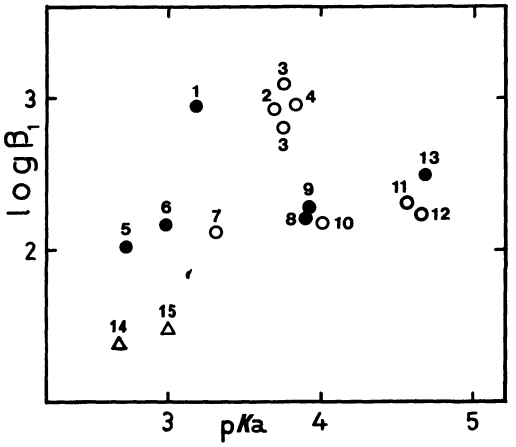

Fig. 3. Correlation between the first stability constants (log β_1) of Eu^{III} complexes and the dissociation constants of the ligand acids (pK_a). 1. Mandelate, 2. hydroxyacetate, 3. α-hydroxymethylpropanoate, 4. α-hydroxypropanoate, 5. salicylate, 6. α-methoxyphenylacetate, 7. methoxyacetate, 8. β-hydroxy-β-phenylpropanoate, 9. *o*-methoxybenzoate, 10. benzoate, 11. acetate, 12. propanoate, 13. anthranilate, 14. chloroacetate, 15. iodoacetate, solid circles: present work, open circles: taken from Refs. 6 and 7, triangles: taken from Ref. 9.

between log β_1 and pK_a is linear, when the interaction between lanthanoid ion and a ligand is ionic and there is no variation in the steric effects. Figure 3 shows the correlation between the first stability constants of europium(III) complexes (log β_1) and pK_a of the ligand acid together with that reported for several monocarboxylates in the literature. The constants are classified into two different groups. The α-hydroxy carboxylic acids which may form five-membered chelates belong to the upper group, and other carboxylic acids belong to the lower group. Although α-methoxyphenylacetic acid may form a five-membered ring, it does not belong to the upper group. Similarly, methoxyacetic acid[10] also does not belong to the upper group. In the lower group, the order of the stability constants in magnitude seems to be correlated with the difference of pK_a. Furthermore, as seen in Table 1, only mandelic acid forms more stable complexes with the heavier lanthanoid(III), and the stability constants (log β_1) of the series of lanthanoid(III) complexes with other carboxylic acids employed in the present work are similar to each other.

In a word, the presence of the OH group at the α-position of carboxylates seems to be very effective to form a more stable complex with the heavier lanthanoid(III). However, β-position of carboxylates, *o*-position of benzoic acid or other functional group such as methoxyl group are not effective. Further accumulation of data would be necessary in order to know the reason why α-hydroxy carboxylic acids form more stable complexes with the heavier lanthanoid.

Table 3. Stability Constants of Lanthanoid(III) Complexes with Substituted Benzoic and Phenylacetic Acids in 0.1 M $NaClO_4$ at 25°C

	Mandelate		Salicylate	
a) -OH substitution	$\log(\beta_1\pm\delta)$[a]	$\log(\beta_2\pm\delta)$	$\log(\beta_1\pm\delta)$	$\log(\beta_2\pm\delta)$
La	2.55±0.06	4.14±0.08	1.80±0.06	3.55±0.23
Pr	2.76±0.01	4.65±0.08	1.88±0.02	3.70±0.33
Nd	2.83±0.03	4.77±0.12	1.90±0.04	3.56±0.09
Sm	2.90±0.09	4.75±0.08	2.06±0.03	3.82±0.21
Eu	2.95±0.01	5.07±0.13	2.02±0.05	3.84±0.03
Gd	2.88±0.03	5.01±0.15	1.89±0.06	3.78±0.03
Tb	3.01±0.03	5.25±0.05	1.95±0.02	3.86±0.02
Dy	3.03±0.04	5.29±0.08	1.71±0.03	3.76±0.04
Ho	3.05±0.06	5.35±0.09	1.83±0.08	3.79±0.23
Er	3.15±0.07	5.41±0.05	1.78±0.05	3.59±0.17
Tm	3.20±0.07	5.56±0.06	1.75±0.07	3.67±0.08
Yb	3.29±0.01	5.76±0.02	1.78±0.07	3.45±0.06
Lu	3.25±0.03	5.83±0.04	1.65±0.04	3.75±0.05
	α-Methoxyphenylacetate		*o*-Anisate	
b) $-OCH_3$ substitution	$\log(\beta_1\pm\delta)$	$\log(\beta_2\pm\delta)$	$\log(\beta_1\pm\delta)$	$\log(\beta_2\pm\delta)$
La	2.09±0.00	3.84±0.12	2.07±0.00	4.05±0.05
Pr	2.16±0.06	3.57±0.23	2.20±0.01	4.17±0.04
Nd	2.16±0.02	3.83±0.06	2.26±0.01	4.20±0.08
Sm	2.24±0.02	3.64±0.10	2.31±0.03	4.22±0.14
Eu	2.17±0.02	4.12±0.22	2.28±0.02	4.26±0.02
Gd	2.14±0.01	3.59±0.17	2.19±0.01	3.99±0.17
Tb	2.19±0.04	3.97±0.20	2.15±0.01	4.12±0.06
Dy	2.19±0.03	3.82±0.11	2.11±0.02	4.08±0.10
Ho	2.19±0.11	3.85±0.26	2.07±0.02	4.06±0.05
Er	2.19±0.02	3.61±0.07	2.06±0.01	3.95±0.03
Tm	2.14±0.03	3.86±0.15	2.05±0.03	4.11±0.08
Yb	2.23±0.05	4.10±0.12	2.06±0.07	3.90±0.17
Lu	2.31±0.05	3.97±0.01	2.10±0.03	4.09±0.14
	Tropate		Anthranilate	
c) Miscellaneous	$\log(\beta_1\pm\delta)$	$\log(\beta_2\pm\delta)$	$\log(\beta_1\pm\delta)$	$\log(\beta_2\pm\delta)$
La	2.02±0.07	3.90±0.08	1.96±0.04	4.08±0.08
Pr	2.14±0.01	4.00±0.09	2.33±0.03	4.39±0.04
Nd	2.23±0.05	4.11±0.04	2.44±0.02	4.26±0.17
Sm	2.24±0.06	4.11±0.18	2.44±0.02	4.78±0.05
Eu	2.21±0.01	4.02±0.02	2.49±0.02	4.78±0.05
Gd	2.17±0.02	4.12±0.08	2.36±0.03	4.51±0.17
Tb	2.07±0.02	4.00±0.07	2.28±0.01	4.40±0.10
Dy	2.10±0.01	3.92±0.03	2.27±0.04	4.39±0.10
Ho	2.05±0.02	4.02±0.09	2.17±0.04	4.22±0.12
Er	1.99±0.03	3.93±0.02	2.16±0.04	4.21±0.12
Tm	2.02±0.10	3.78±0.2	2.22±0.01	4.39±0.06
Yb	2.05±0.02	3.98±0.19	2.24±0.00	4.40±0.06
Lu	2.09±0.05	3.97±0.20	2.22±0.03	4.53±0.11

a) δ denotes error limits based on the agreement in repetitive titrations.

The larger stability constants and the monotonical increase of $\log \beta_1$ against the atomic number could be caused by the match of the bond angle of the hydroxyl group and the carboxyl group to the smaller sized lanthanoid(III). In α-methoxy carboxylates, the one carbon and the three hydrogen atoms in the methoxyl group could interfere with taking up an appropriate bond angle to accept lanthanoid(III).

As seen from Fig. 3, the stability constant of the salicylate seems to be a little larger than estimated from the correlation between pK_a and $\log \beta_1$ of monocarboxylates. This may be due to the formation of stable chelates between the salicylic acid and lanthanoid(III),[11] or due to a proper character of salicylate ion.

The above results may suggest that: 1) there is a trend that the acid of higher pK_a has a larger dimerization constant. When the ligand acids are not

α-hydroxy carboxylic acids, log β_1 increases in proportion to pK_a. Accordingly, pK_a will be one of the important parameters for the complexation in the organic phases as well as in the aqueous solutions. 2) The behavior of salicylic acid in aqueous and/or in organic solvents including complexation with lanthanoid(III) is different from that of other carboxylic acids. 3) Only carboxylic acids having a hydroxyl group at the α-position are effective to form the more stable complexes with the heavier lanthanoid(III). Other functional groups, and hydroxyl group at the β-position or the *o*-position are not effective.

The authors are grateful to Misses Satoko Usui, and Tomomi Ishizawa, and Messers Masami Ajihara, Masato Ohshita and Alim Abdurahman for their experimental aid. This research was partially supported by the Grant-in-Aid for Scientific Research No. 61540429 from the Ministry of Education, Science and Culture.

References

1) Y. Hasegawa, T. Nakano, and G. R. Choppin, *Solv. Extr. and Ion Exchange*, **1**, 745 (1983).

2) Y. Hasegawa, H. Tanaka, A. Kobashi, and T. Tominaga, *Solv. Extr. and Ion Exchange*, **6**, 293 (1988).

3) K. Suzuki, T. Hattori, and K. Yamasaki, *J. Inorg. Nucl. Chem.*, **30**, 161 (1968).

4) Y. Hasegawa, et al. unpublished data.

5) Y. Hasegawa, T. Unno, and G. R. Choppin, *J. Inorg. Nucl. Chem.*, **43**, 2154 (1981).

6) G. R. Choppin, P. A. Bertrand, Y. Hasegawa, and E. N. Rizkalla, *Inorg. Chem.*, **21**, 3722 (1982).

7) a) "Stability Constants of Metal-Ion Complexes," spec. pub. No. 17, compiled by L. G. Sillen and A. E. Martell, The Chemical Society (London) (1964), b) *ibid.*, Supplement No. 1, c) *ibid.*, Part B No. 22, compiled by D. D. Perrin, Pergamon Press, Oxford (1979).

8) G. E. Mont and A. E. Martell, *J. Am. Chem. Soc.* **88**, 1387 (1966).

9) A. E. Martell and R. M. Smith, "Critical Stability Constants," Plenum, New York (1977), Vol. 3.

10) J. E. Powell, R. S. Kolat, and G. S. Paul, *Inorg. Chem.*, **3**, 518 (1964).

11) G. R. Choppin, Q. Liu, and C. Niu, *Lanthanide and Actinide Res.*, **1**, 285 (1986).

Dispersion Behavior of Solutes in an Ideal Laminar Flow with Small-Bore Glass Tubes†

Takashi KORENAGA,* Fenghua SHEN, Hirofumi YOSHIDA, and Teruo TAKAHASHI
Department of Applied Chemistry, Faculty of Engineering, Okayama University, Tsushima, Okayama 700
(Received September 14, 1988)

The dispersion behavior of solute molecules injected as a sample plug into an ideal laminar capillary flow was experimentally analyzed by means of microscopic and microphotometric methods. The flow pattern in small-bore glass tubes was directly observed by the microscopic method using a camera. The peak responses obtained for the colored solutes by means of the microphotometric method consist of double-humped peak features which resulted from both laminar flow convection and the molecular diffusion of solute molecules at the parabolic interface between the sample plug and the carrier fluid. The influences of the diffusion coefficient of the solute, the flow rate, the tube length, the tube diameter, etc. were mainly investigated in order to guide the design and optimization of the flow systems of capillary liquid chromatography (CLC), capillary electrophoresis (CEP), flow-injection analysis (FIA), etc. The experimental results obtained here are in good agreement with the theoretical results obtained by the numerical solution for the diffusion-convection equation.

Many open-tubular glass capillary columns have been utilized in the fields of analytical separation chemistry, such as in gas or liquid chromatography, since 1956.[1] Their main advantage is in the use of long glass capillary columns in order to obtain a high resolution, but it is difficult to operate and provide instrumentation for the apparatus. Therefore, an understanding of the dispersion behavior of the solute molecules in the sample plug flowing with the carrier stream through a small-bore glass tube or the characterization of the response peak feature is important in designing flow systems with or for capillary liquid chromatography (CLC), capillary electrophoresis (CEP), flow-injection analysis (FIA), electrokinetic chromatography (EKC), field-flow fractionation (FFF), membrane-separation analysis (MSA), etc. In CLC, for example, the band broadening is just an important parameter to obtain a higher sensitivity and resolution, and it is mainly controlled by the eddy diffusion from unions, joints, and connectors,[2] the molecular diffusion in both mobile and stationary phases, and the interactions between stationary and mobile phases.[3]

For the dispersion phenomena in straight open tubes, several theoretical approaches have been studied in order to overcome the above-mentioned problems,[4-8] but few experimental studies have been carried out. Recently, though, Atwood and Golay[9] theoretically and experimentally reported the dispersion behavior of peak features using short, straight tubes in LC systems. In their experiments, however, a usual chromatographic apparatus was used, and it was difficult to obtain an ideal laminar flow because of the turbulence resulting from the sample injection, unions, joints, connectors, or the detector flow cell. Since the theoretical analyses were based on the assumption that the capillary flow was completely laminar, a model apparatus which achieves an ideal laminar flow should be used for the experimental research.

The present authors[10] previously analyzed the transport phenomena and dispersion behavior of a small quantity of a sample solution injected as a plug into a carrier fluid flowing through open-tubular small-bore tubes and built a simple simulation without considering the molecular diffusivities of the solutes in the sample-solution plug.

The present paper will mainly describe some experimental results on sample-dispersion behavior obtained for open tubular and small-bore glass capillary tubes with a circular cross-section using some diffusive solutes or a nondiffusive one in the injected sample plug. Using an ideally-composed model experimental apparatus with the microcomputer developed here, we investigated the fundamental dispersion behavior and transport phenomena of the solute dissoved in the sample solution plug in order to compare them quantitatively with the theoretical results obtained by the numerical solution for Taylor's diffusion-convection equation.[4]

Experimental

Apparatus. A schematic description of the experimental apparatus used for taking photographs continuously is given in Fig. 1. It is simply constructed of a Furue (Tokyo, Japan) model JP-V-W microfeeder-type syringe pump, an Olympus (Tokyo, Japan) model BH-2 microscope (equipped with an Olympus model OM-2N camera with a motor-drive unit and a shutter control unit), and various kinds (various diameters and lengths) of small-bore (capillary: less than 1 mm i.d.) glass tubes.

In order to investigate the dispersion behavior, the residence-time distribution of solutes injected as a plug were measured by means of a hand-made microphotometric detection system, as is shown in Fig. 2. The detector is mainly constructed of a Sugiura (Tokyo, Japan) model SL-

† This paper was partly presented at the 7th International Symposium on Capillary Chromatography, held in May, 1986, at Gifu, Japan.

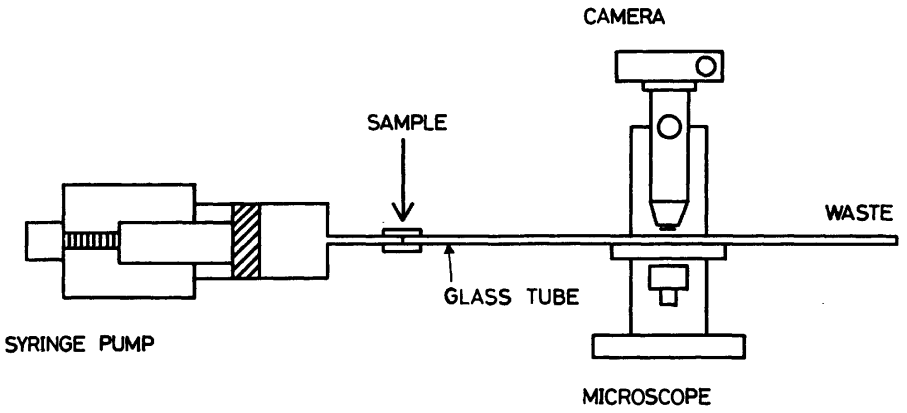

Fig. 1. Experimental apparatus with a microscope as a detector.

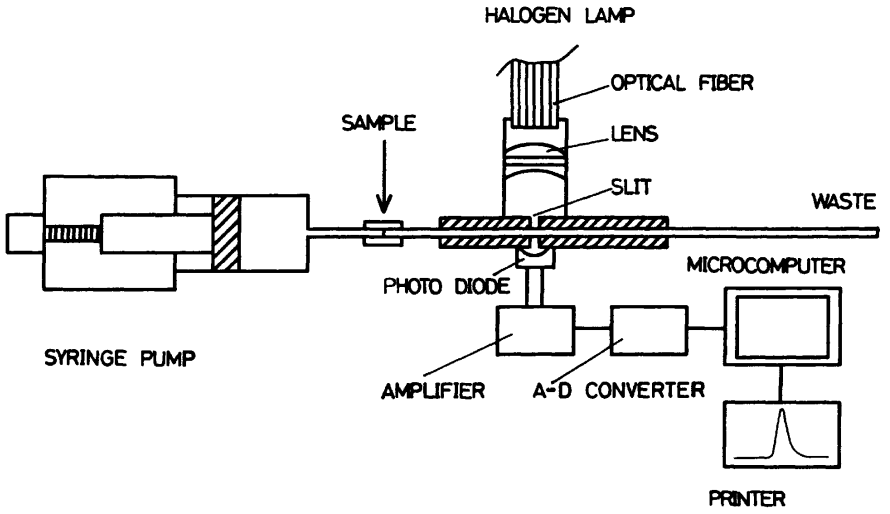

Fig. 2. Model experimental apparatus with a hand-made microphotometric detection system.

FI-150T cold light source using a halogen lamp and an optical fiber, a Hamamatsu Photonics model S-1033-01 photodiode, an Analog Devices model 757N logarithmic amplifier, and a data-recording and -processing system using a Sharp model MZ-80C microcomputer.

Reagents. Colored aqueous sample solutions of potassium permanganate, Methylene Blue dye (MB; Colour Index 52015), and commercially available blue ink containing submicron pigment particles were used in the present experiments. The potassium permanganate solution was prepared by dissolving analytical-reagent-grade potassium permanganate in distilled water. The dye solution was directly prepared by dissolving analytical-reagent-grade MB dye (Wako Pure Chemicals, Japan) in distilled water. The ink solution was prepared from a commercial submicron pigment ink (Sakura Color Products, Japan) by removing relatively large particles using a centrifugal separation technique. The molecular diffusion coefficient of potassium permanganate in water at a concentration of 2.5×10^{-3} mol l^{-1} is 1.2×10^{-3} $mm^2 s^{-1}$,[4] and that of MB in water is 3.0×10^{-4} $mm^2 s^{-1}$.[10] The ink consists of colored submicron pigment particles, and its molecular diffusion coefficient is assumed to be about 10^{-5} $mm^2 s^{-1}$, so that the dispersion in water occurs mainly by means of the laminar-flow convection. Distilled water and glycerol/water (1+1) mixture were used as the carrier fluids in this work.

Procedure. A small portion of the sample solution, dissolved in the respective carrier fluid, was injected precisely by the use of a micro syringe into a stopped-flow carrier fluid, and the syringe pump was then immediately started. By this open-column sample-injection method, the dead volumes, abrupt changes in the internal diameter, and disturbances of the flow can be reduced to a minimum. The injected sample volume was less than 10 μl, and the injected sample length was less than 12 mm in the 1.0 mm-i.d. glass capillary column.

In the photographic experiments, a motor-drive camera was started as soon as the sample zone entered in the view of the microscope. Many photographs were taken at every 0.25 s. In the case of microphotometric detection, the BASIC program for data recording was started when the pump started. The signals obtained from the photodiode were transmitted to the microcomputer after the conversion of the analog signals to digital ones. The data stored on floppy

disk were then treated and printed out to a dotted printer or a X-Y plotter to observe the response-peak features.

Results

Theory on Laminar-Flow Model of Sample Plug in Small-Bore Tube. In small-bore capillary tubes, the flow pattern of the nondiffusive sample plug can theoretically be described as a laminar-flow profile. The diameters of the capillary tubes used in this research are below 1 mm, and the average flow rates are below 110 mm s^{-1}, so the Reynolds number is smaller than 110, much smaller than the critical Reynolds number of the laminar flow (2000—2300) in a round pipe.

The velocity profile of the laminar flow may be described as follows:

$$u_r = 2u(1 - r^2/R^2) \quad (1)$$

where u_r denotes the flow rate at the tube radius r of the capillary and where u and R denote the average flow rate and the tube radius respectively. Equation 1 shows that the laminar-flow velocity profile has a parabolic dispersion of the injected sample plug and that the velocity profile possesses a large possibility of the molecular diffusion of the solute molecules caused by the concentration gradient. Equation 1 shows that the smaller the tube radius, the steeper the parabolic profile (velocity gradient) in capillary columns.

Assuming that the solute molecule used in a sample solution is nondiffusive, the following equation is obtained:

$$d_s = 2ut \quad (2)$$

where d_s and t denote the traveling distance of the sample zone head (front) and time respectively.

The apparent sample arrival time at the detection point $t_{a'}$, that is, the time required for the sample-zone front to reach the detector, can be calculated for the nondiffusive solute molecules by means of Eq. 3:

$$t_{a'} = d_s/(2u) \quad (3)$$

where the d_s nearly equals the tube length of the capillary column (L), since short joint tubes are necessary in column connections.

For diffusive solute molecules, the baseline-to-baseline time Δt_b, which is the band-width in time, was investigated as a means of measuring the dispersion behavior in the response-peak profile. Vanderslice et al.[8] solved Taylor's convection-diffusion equation by the finite differential method and obtained Eq. 4 for the calculation of Δt_b:

$$\Delta\tau_b = 1.93X^{0.64} \quad (4)$$

where $\Delta\tau_b$ and X denote the dimensionless baseline-to-baseline time and the dimensionless traveling distance respectively, as defined by Eqs. 5 and 6:

$$\Delta\tau_b = D\Delta t_b/R^2 \quad (5)$$
$$X = DL/(2R^2u) \quad (6)$$

where D denotes the molecular diffusion coefficient of the solute in the injected sample plug.

Evaluation of the Apparatus by Eye Measurement of Sample-Dispersion Behavior. The traveling distances (d_{MB}) of the colored-sample-zone front as a function

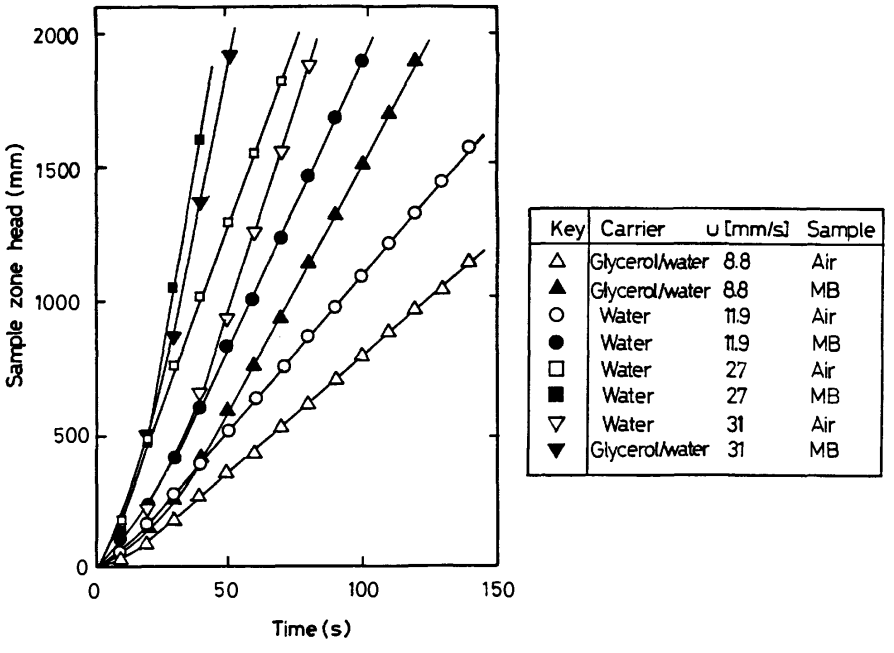

Fig. 3. Relationship between traveling distance of sample zone head and time.

of the time were measured with the eye for the solute molecules of MB dye (Fig. 3). The traveling distances of the air-segment front (d_{air}), which was injected instead of the colored-sample-solution plugs containing solute molecules, were also represented as typical examples for the comparison of the dispersion behavior. When the air segment is injected, the flow rate of the air segment just equals the average flow rate (u) of the carrier fluid according to Eq. 2. In the case of the plots for the air segment, the slopes of the curves equal u except for each transition period. The laminar capillary-flow model of the MB solute in the injected sample plug is shown in Fig. 4(a). The traveling distances of the front interface of the MB solute were smaller than that calculated by Eq. 2. This might be because the MB molecule diffuses to the radial direction at the interface of the sample plug. The component substance (i.e., the MB solute) at the front interface of the sample plug naturally diffuses to the low-velocity-gradient region in the laminar capillary flow near the tube wall. Of course, the MB molecule at the back interface of the sample plug zone conversely diffuses to the high-velocity-gradient region in the center of the tube. Thus, the sample-dispersion length between the sample-zone front in the tube center and at the back in the tube wall decreases, so that the peak broadening on response-peak profiles can be minimized, as is shown in Fig. 4(b). This phenomenon can easily be understood by comparing the results obtained by using the same MB dye as a solute molecule in water and a glutinous glycerol/water (1+1) (G/W) solution as a carrier fluid, and those obtained by using the MB dye and nondiffusive submicron ink in a water carrier. When the G/W carrier was used, the measured d_{MB} value was about twice as large as the d_{air} one, because the apparent molecular diffusivity of the MB dye molecule in the G/W solution is negligibly small, probably less than 10^{-5} mm^2 s^{-1}. The relationship between the measured d_{MB} and d_{air} values is studied in this work. The ordinate represents the slopes of the d_{MB} values in Fig. 3; the abscissa represents those of the d_{air} values. The results obtained by using glass tubes with an inner diameter between 0.5 mm and 1 mm i.d. show that a narrower glass column has a larger velocity gradient and that the profile of the colored sample plug loses its sharpness as a result of the molecular diffusivities of the solute molecules into a water carrier larger than 10^{-4} mm^2 s^{-1}. The model apparatus is, therefore, useful for fundamental and experimental studies of the dispersion behavior of an injected sample plug containing solute molecules as tracers in a flowing carrier stream in small-bore glass tubes.

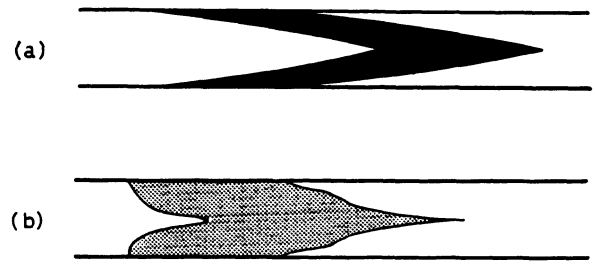

Fig. 4. Models of the flowing sample plug zones in laminar capillary flow. (a) Nondiffusive solute, (b) diffusive solute.

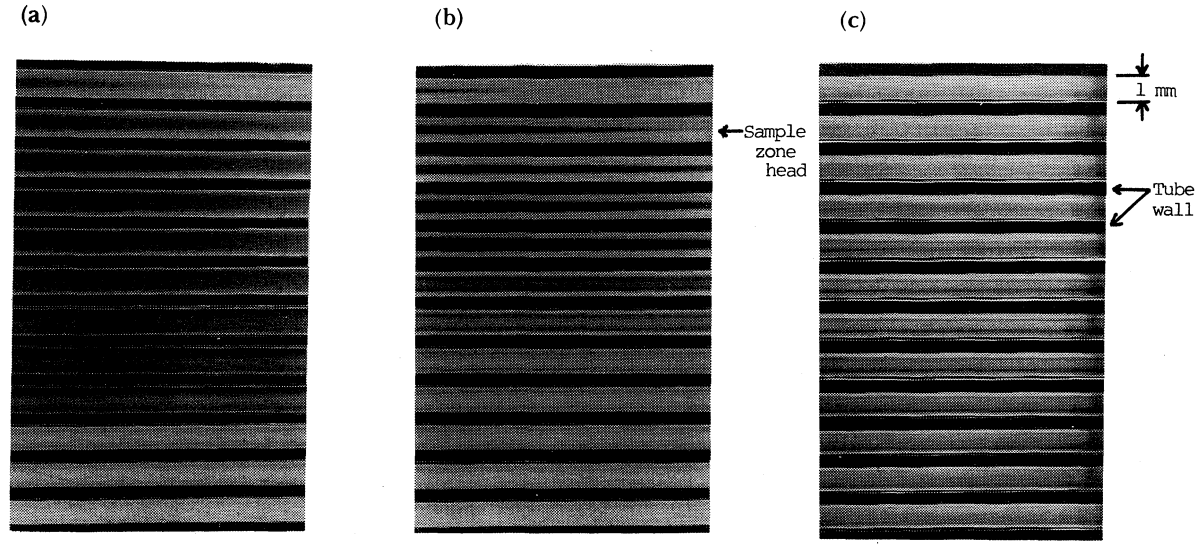

Fig. 5. Photographs continuously obtained with a microscope for the mobile sample plug zones. Ten-μl of 1 mM MB dye or submicron particle ink solutions were injected by the open-column method into a water carrier. A glass tubing (1 mm i.d. and 200 mm detection distance) was used as a capillary column. (a) MB dye; flow velocity: 11.9 mm s^{-1}, (b) MB dye; flow velocity: 110 mm s^{-1}, and (c) submicron ink; flow velocity: 21 mm s^{-1}.

Flow Pattern Analysis by Means of a Photographic Method with a Microscope. A typical flow pattern, obtained by the present photographic method with a microscope, is shown in Fig. 5, where the mobile colored sample zone travels through the capillary tube. According to the procedure, a motor-drive camera starts and many photographs are continuously taken, using a 100-feet roll film, as soon as the injected sample zone front enters the view of the microscope. The photographs show that the injected-sample zone flows with the laminar-flowing carrier fluid and rapidly broadens along with the flow-velocity profile in the axial direction. The flowing sample zone contains a sharply-pointed, needle-like top and has two parabolic interfaces (front and back) lying between the sample plug and the carrier fluid. According to the parabolic-velocity distribution in the laminar flow, represented by Eq. 1, the flow pattern of the sample zone becomes sharper with the increase in the flow rate of the carrier fluid, as is shown in Figs. 5(a) and 5(b). This result is due to the difference in the diffusion time.

Many photographs were taken for the MB-dye samples under various operating conditions by changing the flow rate and the tube length. All the photographs show the same results as those presented above; that is, the sample zone became sharper and spread wider in the axial direction with an increase in the flow rate and/or the tube length. The mixing of the sample component (i.e., the solute) with the carrier component depends on the convection (i.e., the laminar flow profile), and their molecular diffusivities occurred at the porabolic interfaces (front and back). By comparing Figs. 5(a) and (b), it is also found that the interfaces become more distinct because of the smaller extension of the molecular diffusion when the flow rate becomes faster, viz., when the mean residence time ($t_m=L/u$) decreases. Furthermore, when the nondiffusive ink sample was injected, the front and back interfaces were much more distinct than the diffusive ones because the molecular diffusion of the component substances was one of the most important parameters in controlling peak dispersion (cf. the photographs in Fig. 5(c)).

Peak-Dispersion Observation by Means of a Micro-Photometric-Detection System. In stead of the qualitative photographic method, the hand-made micro-photometric-detection system developed here was used to evaluate quantitatively the axial dispersion, that is, the sample-zone broadening as the response-peak profile. In order to optimize the operating conditions in several analytical instrumentation methodologies using small-bore tubes as reactors, the physical properties of the injected-sample plug and the carrier solutions are the most important parameters for the design of the flowing systems. The effects of the molecular diffusivities of the solutes were first studied; the peak features are shown in Fig. 6. For a large molecular diffusivity (i.e., the potassium permanganate solute), the second peak is more apparent than the first one, the width of the peak feature being much narrower and the dispersion in the axial direction being reduced because of the molecular diffusion of the solute in the radial direction in the water carrier. When the ink sample, which contains colored submicron particles and has much less molecular diffusivity than the potassium permanganate and MB-dye samples, is injected as the sample plug, the double-peak features cannot be obtained as expected for a molecule having a molecular-diffusion coefficient of less than 10^{-5} mm^2 s^{-1} by means of the computer simulation.[10]

The response-peak features under various operating conditions are very interesting, as is shown in Fig. 7. Nine figures are summarized at different flow rates and different tube lengths in the present apparatus with a horizontally placed capillary tube (Fig. 2). Almost all of these response peaks show the clear double-humped peak features expected from computer simulation using the numerical-analysis method.[8] This means that the experimental apparatus used in this study is quite satisfactory for studying the dispersion behavior of the solutes in a laminar capillary flow, since many theoretical analyses were carried out on the basis of the assumption that the flow was really laminar.[4-8] From these figures, the sharper part (the first peak) is seem to

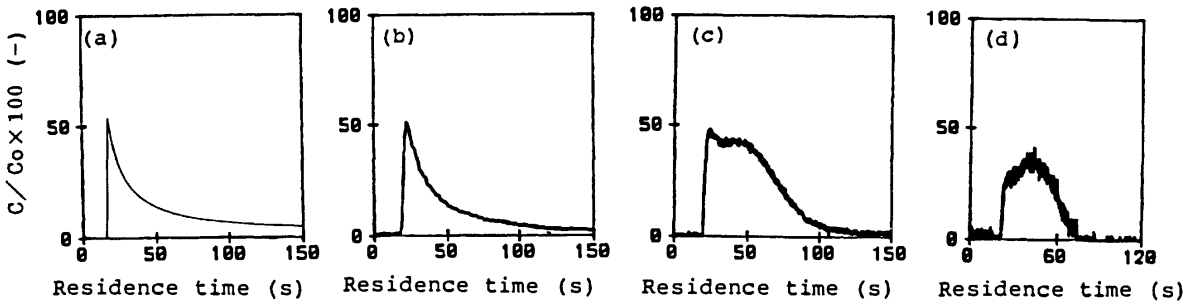

Fig. 6. Difference of peak features for different molecular diffusion coefficient samples. (a) Simulation results for nondiffusive solute, (b) submicron particle ink, (c) MB dye, and (d) potassium permanganate. Each 10 μl of the sample solutions was injected into distilled water flowing in a 1 mm i.d. and 400 mm length glass tubing as a capillary column.

result from convection by the parabolic-velocity profiles, while the other part (the second peak) is caused by the molecular diffusion of the solute injected as the plug of the sample solution.

It may be found in Fig. 7 that the second diffusion peak becomes more apparent when the flow rate is relatively slow and that the peak height becomes lower and the peak width increases with a longer traveling distance (i.e., tube length). When the column reactor becomes longer in various analytical instruments, the sample zone is dispersed along with a longer laminar-flow velocity profile in the axial direction; the large concentration distribution of the solute in the sample solution causes the lower peak-height response. It can also be found that the response-peak feature becomes nearly a Gaussian distribution for a long retention time (e.g., for a long traveling distance and/or a slow flow rate).

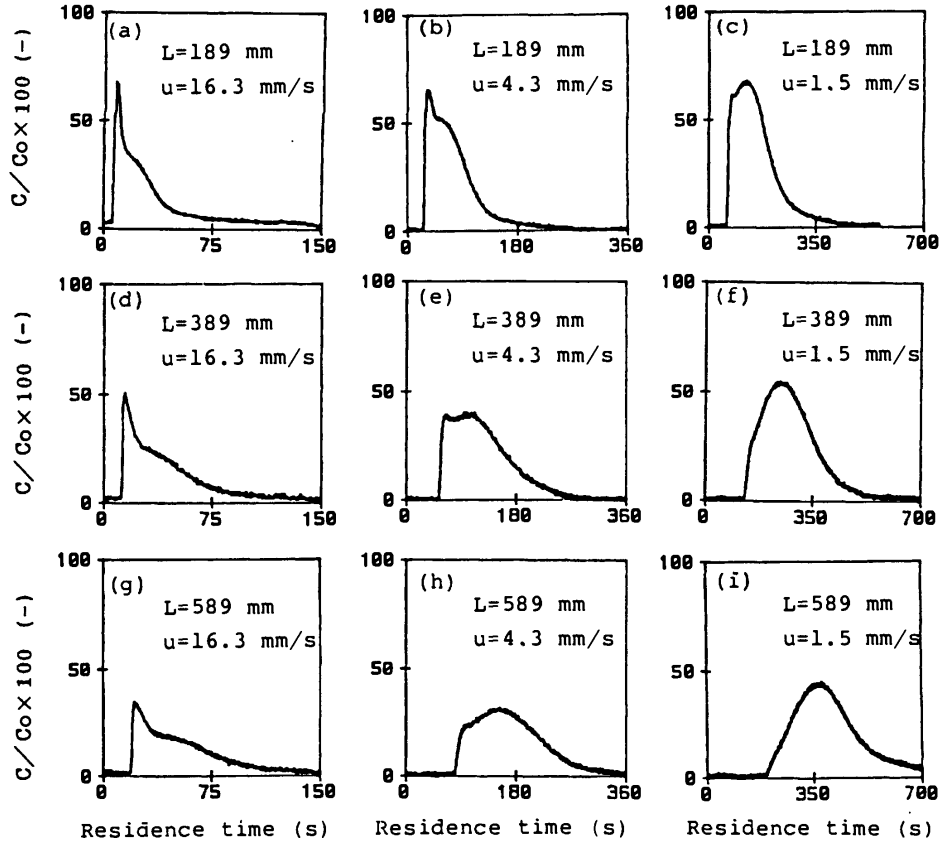

Fig. 7. Peak features obtained for MB dye sample solutions by the microphotometric detection system. Capillary column: 1 mm i.d. glass tubing. Carrier fluid: distilled water. u denotes the average velocity, c and c_0 denote the respective and original concentrations of the MB dye sample respectively.

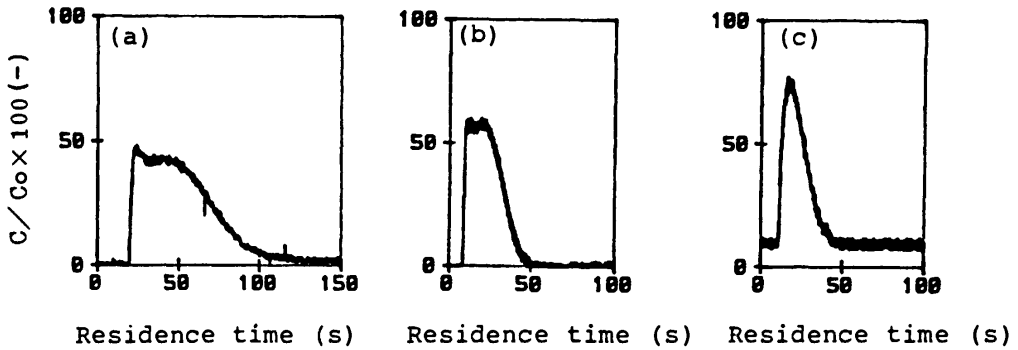

Fig. 8. Peak features obtained by changing capillary conditions. MB dye sample and a 400 mm length glass tubing were used. (a) 1 mm i.d. straight capillary column, (b) 0.6 mm i.d. straight capillary column, and (c) 0.6 mm i.d. coiled capillary column (one loop, 100 mm in loop diameter) were used.

Figs. 8(a) and (b) directly illustrate the qualitative results for the column-radius effect on the peak features. It is found that the narrower capillary tube is effective in obtaining a higher and narrower peak. When the inner diameter of the capillary column decreases, the velocity profile becomes more adrupt between the wall and the center of the capillary tube, according to Eq. 1. Thus, the sample broadening in the axial direction is strongly reduced by the molecular diffusion in the radial direction.

Peak broadening, caused by the sample dispersion in the capillary columns, may generally be far more reduced in the coiled capillary tubes than in straight tubes in consequence of the coiling effect induced by the secondary flow phenomenon,[12] for the secondary flow effectively enhances mixing and mass transfer in the radial direction. Coiled capillary tubes are, therefore, examined in this work. As is also shown in Figs. 8(b) and 8(c), on the basis of Tijssen's theoretical work on FIA[12] it has been concluded that peak broadening can be far more reduced by coiling tubes than in straight tubes in consequence of the coiling effect induced by the secondary flow phenomenon. Because the secondary flow enhances mixing and mass transfer in the radial direction, reduces the dispersion in the axial direction, its peak feature consequently becomes nearly a Gaussian distribution, as is suggested by Fig. 8(c). It is, therefore, recommended that the column of CLC also be coiled into a helical configuration in order to reduce the peak broadening and to obtain a high sensitivity and resolution.

Traveling Distance and Sample Arrival Time. As has been noted in the former section, the traveling distance of the sample-zone head (d_{head}) is smaller than that calculated because of molecular diffusion. A similar phenomenon of the shortening effect can also be seen by comparing the sample traveling time measured (t_a) with the one calculated (Fig. 9). Figure 9 shows the relationship between the measured t_a value and the tube length. Each broken line is a theoretical line based on Eq. 3. All the t_a values measured seem to be larger than the theoretical values since the sample-zone head has lost its sharpness by molecular diffusion at the front of the interfaces, as is suggested in Fig. 4(b). Hence, it requires a longer arrival time for the sample-plug-zone head to reach the detector view.

Effect of Flow Rate. The variations in the peak height as a function of the flow rate are shown in Fig. 10 for different lengths of tubes. As the peak consists of double-humped peak features, the peak-height data presented here are the heights of the higher among the first- and second-peak features. The flow rate at which the peak height reaches a minimum just corresponds to the double-humped peaks with the same two peak heights, that is, a critical flow rate (CFR). At just this point, both diffusion and convection are found significant. Below this critical point on the flow rate, the second peak is higher than the first one because of sufficient molecular diffusions; thereafter, its height decreases with the increases in the flow rate, as has been discussed before. Over the point of CFR, however, the first convection peak is higher than the secondary one, because it is mainly controlled by convection. The first peak, unlike the secondary peak, represents the concentration distribution of the component substance (i.e., the solute) in the sample-plug head. The first peak height seldom varies with the flow rate, as is shown in Fig. 10, when the flow rate becomes faster. These results, therefore, show that the CFR point can be used as a judging point for the flow rate on the dispersion behavior of the response-peak features by molecular diffusion. Below the point of CFR, the peak features are controlled predominantly by the diffusion in order to make higher the peak

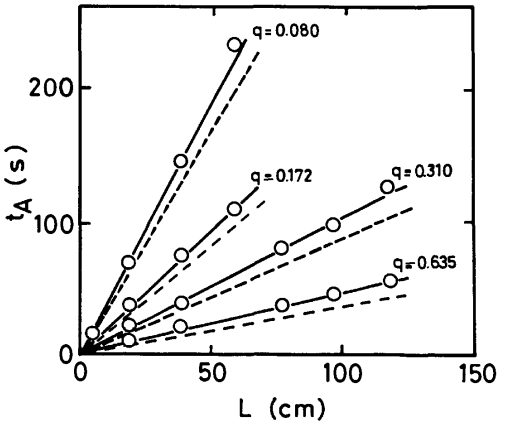

Fig. 9. Relationship between traveling time of sample zone head and the length. Each 10 µl of MB dye sample solution was injected into distilled water flowing in a 1 mm i.d. glass capillary column. q denotes the volume flow rate, and dotted lines show the calculated values against each q values.

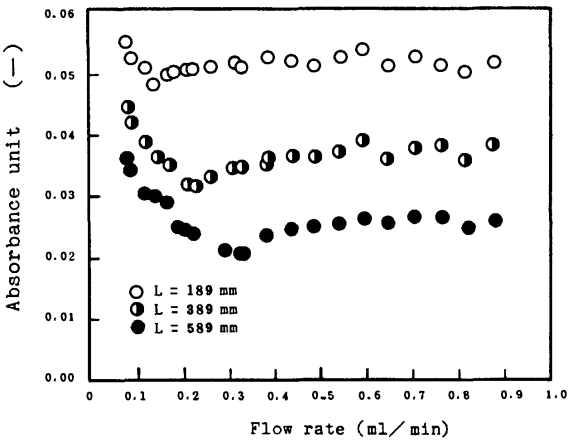

Fig. 10. Peak height value in absorbance unit vs. volume flow rate for three different tube lengths. Each 10 µl of MB dye sample solution was injected in distilled water flowing in a 1 mm glass tubing as a capillary column.

height with the Gaussian distribution and to minimize the dispersion of the flowing-sample plug, as is shown in Fig. 10, although such slower flow-rate regions have seldom been studied.

Discussion

The dispersion of the injected-sample plug in capillary-column reactors was experimentally investigated by means of direct observation, microscopic photographs, and photometric-detection methods newly developed. The baseline-to-baseline times are measured in those response peaks obtained by the microphotometric detection system. According to Eq. 4,[10] the dimensionless baseline-to-baseline time values are then compared with the dimensionless traveling-distance values (Fig. 11). It is concluded that they have a good agreement with the various experimental results obtained with the present model apparatus. This means that an ideal laminar capillary flow can be attained by the use of the model experimental apparatus described above. A great advantage of the present work is, therefore, that an ideal laminar flow can be attained by the model experimental apparatus. It is essential to use such a model apparatus for fundamental and/or experimental approaches since several theoretical analyses of this problem have been carried out on the assumption of a complete laminar capillary flow. In usual LC systems, however, disagreements between experimental and theoretical results are often found, as was pointed out first by Atwood and Golay.[9] They attributed the disturbance to the laminar flow resulting from the unions. Since the parts and components used in the LC, CGC, and CLC systems, such as a high-pressure double-reciprocating micropump, a loop-injection valve, or a detector with flow-throu h cells, cannot suppress the dead volume, abrupt changes in the internal diameter of the flowing stream, the turbulence of the flow, or the occurrence of large time constants in detectors and recorders, etc., it is not desirable to use these components for the model experiments under just a laminar flow. Before starting the work, we elaborated the apparatus in order to obtain as ideal a lamilar flow as is possible. In the present experiment, a syringe pump was used to obtain a steady and smooth pumping. In order to reduce the disturbance of the laminar flow, a stopped-flow injection technique for sample injection and a hand-made microphotometric detection system were adopted. The light source and the light accepter as the detector were mounted on the small-bore glass tube wall without any disturbance to the flowing stream. As has been described above, the results presented here show a primary success in the development of an ideally-composed model experimental apparatus for undertaking sample-dispersion-behavior analysis in capillary tubes. Although the results presented in this paper support only fundamental and qualitative conclusions, they are very important to attempts to improve, design, and optimize the FIA, CLC, and other LC families.

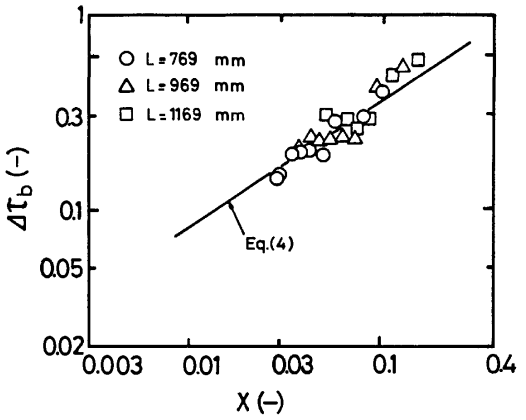

Fig. 11. Comparison of experimental results and numerical-analysis equation between dimensionless baseline-to-baseline time ($\Delta\tau_b$) and dimensionless traveling distance (X).[8]

Since the disturbance to the laminar flow by the apparatus itself has been eliminated in this work, the influences on sample dispersion by a variety of parameters, such as tube length, diameter, flow rate, and molecular-diffusion coefficient, can be clearly found, as has been discussed above. For example, Fig. 10 shows the influence of the flow rates on the peak height. For three tube lengths, below a flow rate of about 0.1 ml min^{-1}, the peak height depends closely on the flow rate, while above that flow rate the peak height tends to be constant. Therefore, if one wants to obtain a high sensitivity by adjusting the flow rate, the operation should be conducted at flow rates below 0.1 ml min^{-1}.

This research was funded in part by the Grants-in-Aid for Scientific Reasearch from the Japanese Ministry of Education, Science and Culture, and also by the Shorai Foundation for Science and Technology.

References

1) M. J. E. Golay, "Gas Chromatography, 1957" (Lansing Symposium), ed by V. J. Coates, H. J. Noebels, and I. S. Fagerson, Academic Press, New York (1958), p. 1.

2) T. Korenaga, Doctoral Dissertation, Kyoto University (1985).

3) L. C. Truesdell, Jr., and R. J. Adler, *Am. Inst. Chem. Eng. J.*, **16**, 1010 (1970).

4) G. Taylor, *Proc. R. Soc. London, Ser. A*, **219**, 186 (1953).

5) R. Aris, *Proc. R. Soc. London, Ser. A*, **252**, 538 (1959).

6) V. Ananthakrishnan, W. N. Gill, and A. J. Barduhn, *AIChE J.*, **11**, 1063 (1965).

7) H. Bate, S. Rowlands, J. A. Sirs, and H. W. Thomas, *Brit. J. Appl. Phys. (J. Phys. D.)*, **2**, 1147 (1969).

8) J. T. Vanderslice, K. K. Stewart, A. G. Rosenfeld, and D. J. Higgs, *Talanta*, **28**, 11 (1981).

9) J. G. Atwood and M. J. E. Golay, *J. Chromatogr.*, **218**, 97 (1981).
10) T. Korenaga, H. Yoshida, Y. Yokota, S. Kaseno, and T. Takahashi, *J. Flow Injection Anal.*, **3**, 91 (1986).
11) "Bussei Josu," ed by The Society of Chemical Engineers, Japan, Maruzen, Tokyo (1968), Vol. 6, p. 246.
12) R. Tijssen, *Anal. Chim. Acta*, **114**, 71 (1980).

The Determination of a Small Amount of a Biological Constituent by the Use of Chemiluminescence. XV. A Zeolite Column-Chemiluminescence Detection System for the Separation and the Determination of a Protein Mixture

Tadashi HARA,* Kazuhiko TSUKAGOSHI, and Yuichiro KURITA
Department of Chemical Engineering, Faculty of Engineering, Doshisha University, Karasuma Imadegawa, Kamigyo-ku, Kyoto 602
(Received September 27, 1988)

To make use of zeolite as the packing material for the separation of proteins by means of adsorption chromatography, the adsorption behavior of protein onto the Na-X type of zeolite (Molecular Sieve 13X) in an aqueous solution or onto a column (3 mm i.d.×50 mm) packed with the same zeolite as above was examined using a ultraviolet absorption detector and model proteins, such as human-serum albumin and human-serum γ-globulin. The following results were obtained: 1) Human-serum γ-globulin was much more adsorbed onto the zeolite than was human-serum albumin and 2) in general, more protein was adsorbed in an acidic solution than in an alkaline solution. Moreover, a chemiluminescence detector using a 1,10-phenanthroline-hydrogen peroxide-copper(II) system, which has been developed by the present authors, was modified to improve its sensitivity for the determination of protein. Both the carrier solution and the eluting solution which were used in combination with a zeolite column with a chemiluminescence detector were optimized so as to give a smooth baseline on a recorder. A microbore zeolite column (1 mm i.d.×250 mm)-chemiluminescence detection system suitable for the separation and the determination of a small amount of a protein mixture was established on the basis of these experimental results. Since human-serum albumin passed through a microbore zeolite column, while human-serum γ-globulin was retained on the column, when a model sample containing human-serum albumin and human-serum γ-globulin was injected into the column, human-serum albumin was first determined, followed by the determination of human-serum γ-globulin after its desorption. Both human-serum albumin and human-serum γ-globulin in the concentration range of 2×10^{-5}—5×10^{-3} g dm^{-3} could be determined economically and conveniently, with a detection limit of about 1 ng (injected sample volume: 50 mm^3; S/N=2). The present method was, therefore, applicable to the separation and the determination of albumin and globulin in a serum sample.

It has been desired to develop a new method for the determination of a trace amount of a protein, such as a tumor marker in serum. The present authors have already reported a flow-injection analysis (FIA) method for the determination of a small amount of a protein, in which method a chemiluminescence (CL) detector using the CL reaction of a 5-amino-2,3-dihydro-1,4-phthalazinedione (luminol)-hydrogen peroxide (H_2O_2)-copper(II) (Cu(II)) system or a 1,10-phenanthroline (phen)-H_2O_2-Cu(II) system is used.[1,2] The determination of a protein was based on the measurement of the decreasing catalytic activity of Cu(II) for the CL reaction in the presence of the protein. These methods were about 10^2—10^6 times as sensitive as the conventional methods,[3-7] such as colorimetry and fluorometry.

Immunoaffinity chromatography and metal-chelate-affinity chromatography, in which conventional affinity columns were combined with the CL detector for the separation of protein, have also previously been established by the present authors for the analysis of a model sample containing albumin and globulin.[8,9] These affinity columns were confirmed to have some excellent characteristics for the separation of proteins, but they were, in general, expensive, difficult to operate, and time-consuming, and they required a complicated operation for their pretreatment and regeneration. Furthermore, some serious problems, such as an abnormally large blank value and a lowering of the sensitivity for the detection of protein, appeared since protein was eluted from the column with an acidic solution, and so the resulting acidic eluate was subjected to the measurement of the CL intensity in an alkaline solution.

In addition to the packing materials used in the above affinity columns, there are several commercially available ones. However, these packing materials are ordinarily difficult to handle and expensive because most of them necessitate a specific regand or functional group. On the other hand, some metal-oxide beads, such as silica and alumina, have been used as the packing material for the separation column of a protein[10,11] because of their ease of handling and their inexpensiveness. Since zeolite is a crystalline aluminosilicate and is stable enough in an alkaline solution, unlike silica, it seems a possible packing material which is inexpensive, easy to handle, and durable enough for use in an alkaline solution. And zeolite shows a cation-exchange phenomenon and has a specific and definite diameter of its cavity. Moreover, zeolite has often been utilized as a packing material for gas chromatography, but only rarely for liquid chromatography,[12] and its adsorption behavior against protein has not yet been examined. The present authors were, therefore, interested in the application of zeolite to protein-separation.

On the basis of the results obtained in the preliminary experiment, the present paper with deal with zeolite as a packing material for the separation of proteins by adsorption chromatography. First, the adsorption behavior of protein onto the Na-X type of zeolite will be examined using a ultraviolet absorption (UV) detector. Moreover, a CL detector using a phen-H_2O_2-Cu(II) system will be modified to improve the sensitivity for the determination of protein. Then, both the carrier solution and the eluting solution used in the combination of a zeolite column with a CL detector will be optimised. A microbore zeolite column-CL detection system suitable for the separation and the determination of a small amount of a protein mixture will be established on the basis of these experimental results.

Experimental

All of the reagents used were of a commercially available special grade. Deionized water was distilled for use. A sodium dihydrogenphosphate (NaH_2PO_4)-disodium hydrogenphosphate (Na_2HPO_4) buffer solution (pH 5.8—8.3) and a sodium hydroxide (NaOH)-sodium chloride (NaCl) buffer solution (pH 12.0—13.0) were mainly used. HSA (Chemical Dynamics Co.) and HγG (SIGMA), which comprise most of the serum protein and the determination of which is regarded as significant in a clinical laboratory, were used as the model proteins. Control serum (Q-PAK-Chemistry Control Serum I, Human) from Hyland Diagnostics was also used. A Molecular Sieve 13X (Nishio Kogyo, Ltd.) (chemical formula; $Na_{86}[(AlO_2)_{86}(SiO_2)_{106}]\cdot 276H_2O$; particle size 100—120 mesh; and cavity diameter 10 Å) was used as the Na-X type of zeolite. Cation-exchanged zeolites, such as Mg-, Ca-, and Zn-X types of zeolites, were prepared from the Molecular Sieve 13X in accordance with the procedure described in the literature.[13-15]

The zeolite was packed in an ordinary (3 mm i.d. ×50 mm) or a microbore column (1 mm i.d. ×250 mm) which has been manufactured by the present authors using a Teflon tube (2 mm o.d. ×1 mm i.d.) and a Teflon line-filter (Nishio Kogyo, Ltd.) (Fig. 1).

The adsorption behavior of protein onto the zeolite in an aqueous solution was examined by means of the depletion method (indirect-determination method)[16,17] (Scheme 1) using a UV detector (measured at 280 nm). The adsorption behavior of protein onto a zeolite column (3 mm i.d. ×50 mm) was also examined by means of the determination of the protein in an eluate by means of a UV detector (measured at 280 nm) connected to a column.

A schematic flow diagram of a zeolite column-CL detection system is shown in Fig. 2. A CL detector using a phen-H_2O_2-Cu(II) system was used, in which the concentrations of phen, H_2O_2, and Cu(II) in the individual solutions were the same as in a previous paper.[2] A carrier solution (d) and an eluting solution (e) were fed is at the flow rate of 1.0 ml min^{-1} by means of a pump (Pharmacia Fine Chemicals, High-precision Pump, P-500) (j). A 50-mm^3 portion of the sample solution was injected into the carrier solution line through a sampling loop (m) and a six-way cock (l), and then passed through a zeolite column (o).

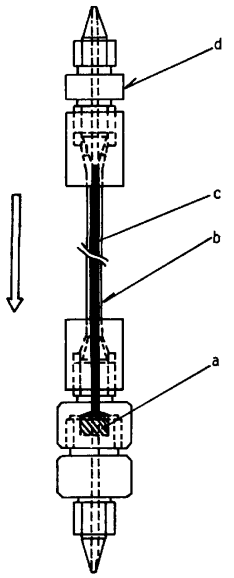

Fig. 1. Setup of a microbore column. a) 10 μm Teflon filter, b) 2 mm o.d.×1 mm i.d. Teflon tube, c) zeolite, and d) joint (0.6 mm i.d.).

(Zeolite + Protein soln)
↓
Degassing
↓
Shaking
(3 h, 4 °C)
↓
Centrifugation
(20 min, 10000 rpm)
↓
Diluting the supernatant with
a buffer soln
↓
Detection using a UV detector

Scheme 1. Outline of a depletion method.

Globulin was adsorbed selectively onto the zeolite column, but albumin was not adsorbed. Then the eluting solution was fed into the column by operating a four-way cock (k) to elute the globulin. The protein in the eluate was detected by the CL detector.

The CL intensity of the solution containing no protein was recorded as a baseline on a recorder, while the CL intensity of the solution containing protein was recorded as a negative peak because the catalytic activity of Cu(II) decreased due to the formation of a complex compound between Cu(II) and the protein. The amount of protein was

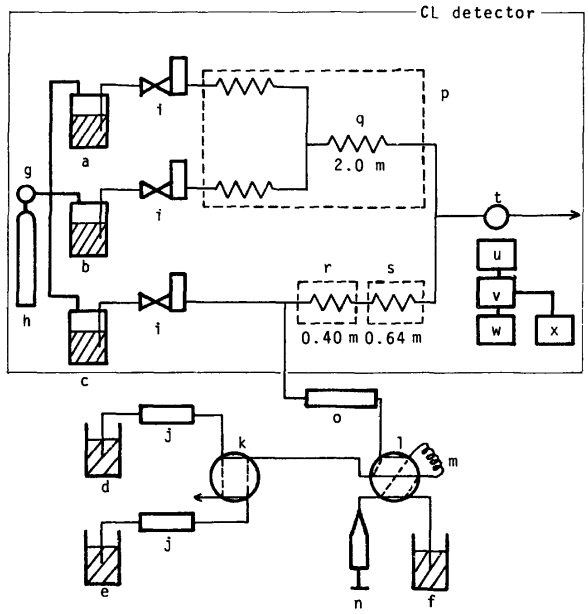

Fig. 2. Schematic flow diagram of the zeolite column-CL detection system. a) Phen soln, b) H_2O_2 soln, c) Cu(II) catalyst soln, d) carrier soln, e) eluting soln, f) sample soln, g) regulator, h) N_2 cylinder, i) flowmeter equipped with a needle valve, j) pump, k) four-way cock, l) six-way cock, m) sampling loop, n) syringe, o) microbore zeolite column, p) thermostat, q) mixing coil, r) reaction tube, s) cooling tube, t) flow cell, u) photomultiplier, v) amplifier, x) recorder, and w) integrator.

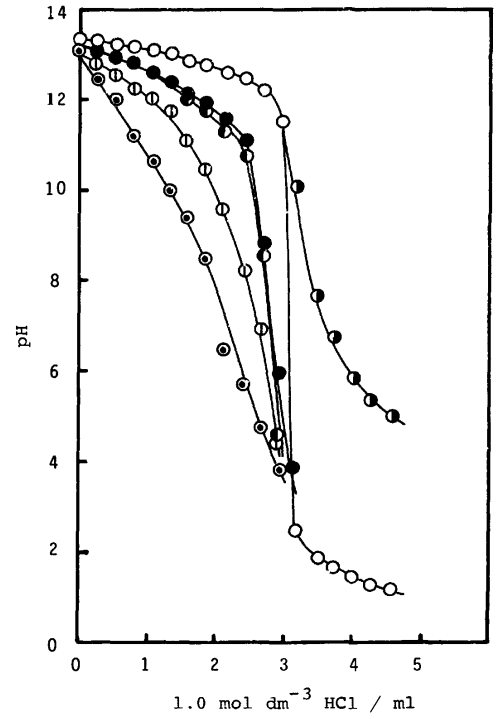

Fig. 3. Titration curves. ○: Zeolite-free, ●: commercially available zeolite (A), ◑: zeolite treated with an alkaline solution (B), ◐: zeolite treated with a neutral solution (C), ⓓ: zeolite treated with an acidic solution (D), and ⊙: proton-type of zeolite (E). Condition: 0.1 mol dm^{-3} NaOH solution (30 ml) containing 0.20 g zeolite was titrated with 1.0 mol dm^{-3} HCl solution.

estimated from the peak area.

Results and Discussion

Preliminary Experiment. To make use of zeolite as a packing material for each mode of chromatography, such as chromatofocusing, metal-chelate-affinity, molecular exclusion, and adsorption chromatographies, preliminary experiments were carried out.

The pH buffering action, which is indispensable for a material used as packing in chromatofocusing,[18,19] was examined by titrating a sodium hydroxide solution containing a definite amount of zeolite with a standard hydrochloric acid solution. The following Na-X-type zeolites were used: A) Commercially available zeolite (untreated zeolite); B) zeolite treated with an alkaline solution (1.32×10^{-1} mol dm^{-3} NaOH-5.00×10^{-2} mol dm^{-3} NaCl; pH 13.0); C) zeolite treated with a neutral solution (3.90×10^{-2} mol dm^{-3} NaH_2PO_4-6.10×10^{-2} mol dm^{-3} Na_2HPO_4; pH 7.0); D) zeolite treated with an acidic solution (7.35×10^{-2} mol dm^{-3} NaH_2PO_4-2.65×10^{-2} mol dm^{-3} Na_2HPO_4; pH 6.4), and E) a proton-type zeolite prepared from the Na-X type of zeolite.[20] As can be seen from Fig. 3, zeolite B, with less proton, showed a buffer capacity in an acidic region, whereas zeolite A≃C, D, and E showed a buffer capacity in an alkaline region, in that order.

In the mode of metal-chelate-affinity chromatography, different affinities of proteins against cation-exchanged zeolite are utilized for the separation of proteins. The amounts of cation on each Mg-, Ca-, and Zn-X-type zeolite, as estimated by chelatometric titration, were 1.0, 1.3, and 1.2 mequiv g^{-1} respectively. Each cation on the cation-exchanged zeolite was held in the cavity of the zeolite crystal; no cation was found in a solution, even after standing for 3 h in a phosphate buffer solution (pH 7.0). Then, the amount of protein adsorbed onto the cation-exchanged zeolite was determined by means of a depletion method after 3 hours' shaking with the phosphate buffer solution (pH 7.0) (Table 1). As is shown in Table 1, the amounts of HSA adsorbed onto the four types of zeolites were almost definite, whereas the amount of HγG adsorbed onto the Zn-X type zeolite was about 6% larger than the amounts of HγG adsorbed onto the other types of zeolites.

Since zeolite, having a definite diameter of its cavity, is quite different from the packing material, which has a pore-size distribution for molecular exclusion chromatography, the molecular-sieve effect on peptide and protein of a column packed with the Na-X type of zeolite was examined. The retention times obtained in

Table 1. Amount of Protein Adsorbed onto Each Cation-Exchanged Zeolite

Zeolite	Relative peak area	
	HSA	HγG
None	1.00	1.00
Molecular sieve 13X (Na-X type)	0.95	0.14
Mg-X type	0.96	0.17
Ca-X type	0.96	0.16
Zn-X type	0.95	0.10

a) Conditions: Zeolite, 1.5 g; soln volume, 3.0 ml; protein concn, 1.0×10^{-1} g dm^{-3}; shaking time, 3 h, and pH 7.0 (Na_2HPO_4-NaH_2PO_2).

Table 2. Retention Times for Polypeptides and Proteins

Sample	Retention time/s
Glycylglycine	321
Glycylglycylglycine	276
Glycylglycylglycylglycine	252
HSA	245
HγG	244

Conditions: Column, 3 mm i.d.×50 mm; polypeptide concn, 1.0×10^{-3} mol dm^{-3}; protein concn, 1.0×10^{-1} g dm^{-3}; injection volume, 50 mm^3; flow rate, 0.1 ml min^{-1}, and measurement wavelength, 220 nm.

the zeolite column for several kinds of polypeptides, HSA, and HγG are shown (Table 2). Here, a phosphate buffer solution containing 1.0 mol dm^{-3} of NaCl was used as the carrier solution because several kinds of polypeptides, HSA, and HγG were not adsorbed onto the zeolite column in a 1.0 mol dm^{-3} NaCl solution. No difference was observed between the retention times of HSA and HγG, but some differences were observed between the retention times of protein and polypeptides or among the retention times of polypeptides. These differences seemed to be based on the molecular-sieve effect, since the retention time decreased with an increase in the molecular weight of the polypeptides and proteins.

To investigate if zeolite could be used as a packing material for adsorption chromatography, much like silica beads,[10] the effect of the pH on the amount of protein adsorbed onto the Na-X type of zeolite in an aqueous solution was examined by means of a depletion method. The experiment was carried out in a solution of pH 5.8—8.3, in which the crystal structure of zeolite was stable and the protein was not denatured. The following results were obtained: 1) much more HγG was adsorbed onto the zeolite than HSA, and 2) more protein was adsorbed in an acidic solution than in an alkaline solution.

On the basis of the results thus obtained, a column packed with the Na-X type of zeolite was used in the present paper for the separation of proteins by means

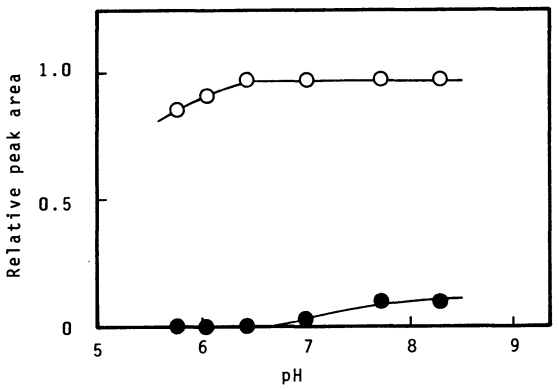

Fig. 4. Adsorption of protein onto column packed with zeolite. ○: HSA and ●: HγG. Conditions: Column size 3 mm i.d.×50 mm, protein concn 1.0×10^{-1} g dm^{-3}, injection volume 50 mm^3, and flow rate 0.1 ml min^{-1}.

of adsorption chromatography. The application of a zeolite column to the other chromatography will be described later.

Adsorption Behavior of Protein onto Zeolite. The adsorption behavior of protein onto the Na-X type of zeolite was further examined.

The adsorption equilibrium of protein on the zeolite in an aqueous solution was attained in about 1 h; thereafter, the amount of adsorbed protein did not change, even an standing for 5 h. In the present study, the amount of protein adsorbed at equilibrium was determined after 3 hours' standing.

It was found that the adsorption behavior of protein onto the zeolite in an aqueous solution was shown by Langmuir's adsorption isotherm.[16,17] The amount of HSA or HγG adsorbed onto the zeolite was constant above protein concentrations of about 4 g dm^{-3} or 6 g dm^{-3} respectively.

The effect of the pH on the amount of protein adsorbed onto the zeolite column was also shown (Fig. 4). Here, a series of experiments were carried out at an individual, definite pH value as follows: A 50-mm^3 protein solution was placed in the column, and then the corresponding buffer solution was fed, followed by the measurement of the protein eluted from the column by means of a UV detector connected to the column. The relative peak area in Fig. 4 was referred to as the ratio of the peak area of the protein passing through the column to the peak area of the protein obtained without passing through the column. The results obtained using the zeolite column showed a trend similar to that obtained in a preliminary experiment using the zeolite in an aqueous solution.

The adsorption of protein onto a silica bead is known to be attributable to the negative charge due to a hydroxyl group on its surface in an aqueous solution. Since the adsorption of protein onto the zeolite was thought to be similar, Results 1) and 2)

described in the preliminary experiment were explained as follows: 1) was explained by considering that globulin, having a much more positive charge than albumin, showed a larger affinity than albumin against the negative charge due to a hydroxyl group on the zeolite surface, while 2) was explained by considering that protein, as an amphoteric electrolyte, had a much more positive charge in an acidic solution than in an alkaline solution.

As is shown in Fig. 4, HγG was completely adsorbed onto the zeolite column from the phosphate buffer solution (pH 6.4), while HSA was not adsorbed from the same buffer solution. The effect of the coexisting substance on the adsorption of HγG onto the zeolite column was examined by the use of the phosphate buffer solution (about pH 6.4) containing: 1) NaCl as a moderator of the ionic strength, 2) urea as a denaturing agent, 3) glycine as a competitive inhibitor, and 4) ethylene glycol or 1,4-dioxane as a representative of a polar-to-nonpolar solvent (Table 3). The amount of HγG adsorbed onto the zeolite column tended to decrease with the use of all these solutions except the glycine solution. Neither HSA nor HγG was adsorbed onto the column at all by the use of a phosphate buffer solution (pH 6.4) containing 1.0 mol dm^{-3} of NaCl.

On the basis of these results, albumin and globulin in a control serum were separated and determined using a zeolite column-UV detection system. A control serum sample diluted 100 times (50 mm^3) was placed in the zeolite column, after which a phosphate buffer solution (pH 6.4) was fed in. Here, globulin was adsorbed onto the column, while albumin passed through the column. The globulin on the column was eluted by a phosphate buffer solution (pH 6.4) containing 1.0 mol dm^{-3} of NaCl. As can be seen from Fig. 5, the practical peak for globulin is given by II′, which corresponds to the difference between the true peak II for globulin and the negative peak II″ for the interference fringe appearing in the mixing area of two kinds of solutions. The recovery of 50 mm^3 of the 1.0×10^{-1} g dm^{-3} HγG solution was 80% by the present method.

Table 3. Effects of the Coexisting Substance on Adsorption of Protein onto Zeolite Column

Solution	Relative peak area	
	HSA	HγG
Phosphate buffer soln (pH 6.4)	0.97	0.00
Phosphate buffer soln (pH 8.3)	0.97	0.10
Phosphate buffer soln -1.0 mol dm^{-3} sodium chloride (pH 6.4)	0.96	0.97
Phosphate buffer soln -1.0 mol dm^{-3} Urea (pH 6.4)	0.97	0.07
Phosphate buffer soln -1.0 mol dm^{-3} glycine (pH 6.4)	0.96	0.00
Phosphate buffer soln (pH 6.4) -ethylene glycol (9:1)	0.97	0.15
Phosphate buffer soln (pH 6.4) -1,4-dioxane (9:1)	0.97	0.10

Conditions: Column, 3 mm i.d.×50 mm; protein concn, 1.0×10^{-1} g dm^{-3}; injection volume, 50 mm^3, and flow rate, 0.1 ml min^{-1}.

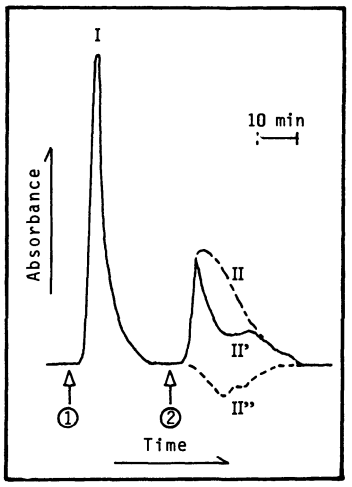

Fig. 5. Chromatogram of control serum using a zeolite column-UV detection system. ①: Sample was injected, ②: eluent was fed. I: Peak for albumin, II: true peak for globulin, II′: practical peak for globulin, and II″: negative peak for interference fringe.

Improvement of the Sensitivity of a CL Detector and Optimization of a Carrier Solution and an Eluting Solution. In the previous papers,[1,2] the reaction between Cu(II) and protein in the CL detector was done at pH 10.2 using a borate buffer solution. On the other hand, the biuret reaction for the determination of protein based on the formation of a complex compound between Cu(II) and protein is generally carried out in a solution above pH 12. This suggests that the effect of the pH on the reaction between Cu(II) and protein should be reinvestigated in order to improve the sensitivity of a CL detector.

Then, the pH (pH ①) of the solution being passed through a reaction tube (r in Fig. 2), the pH (pH ②) of the solution being passed through a flow cell (t in Fig. 2), the CL intensity of a base-line (CL_{BL}), and the percentage of the decrease in the rate of CL intensity (CL_{DR}) ($|$(the lowering of the CL intensity in the presence of protein)/(CL_{BL})$|\times100$) were measured using various pH values of phen, the Cu(II) catalyst, and the carrier solutions. Based on the results obtained, the relationship between pH ① and CL_{DR}, as well as that between pH ② and CL_{BL}, were established (cf. Figs. 6 and 7). From Figs. 6 and 7, the optimum values may be supposed to be about pH 13 for pH ① and about pH 10.5 for pH ②.

In order to separate and determine a small amount

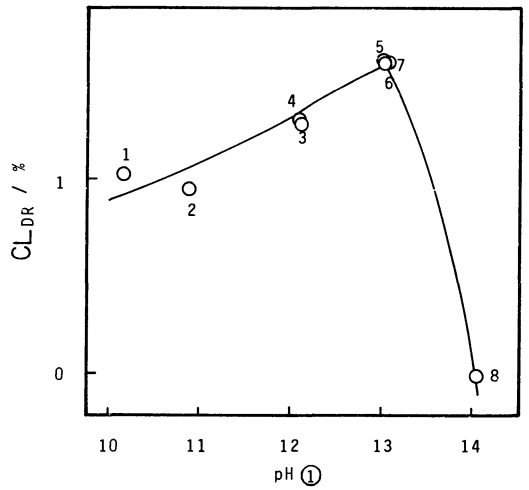

Fig. 6. Relationship between pH ① and CL_{DR}.

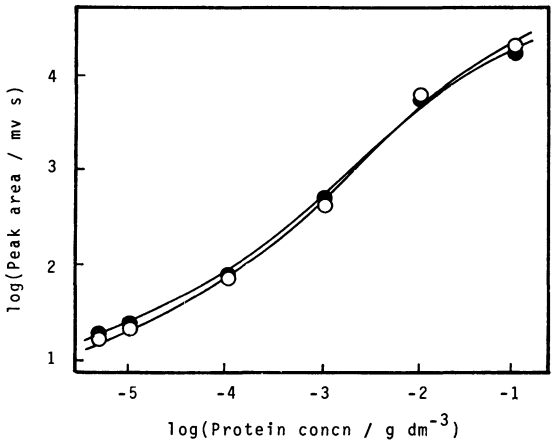

Fig. 8. Calibration curves of proteins using a FIA method. O: HSA and ●: HγG.

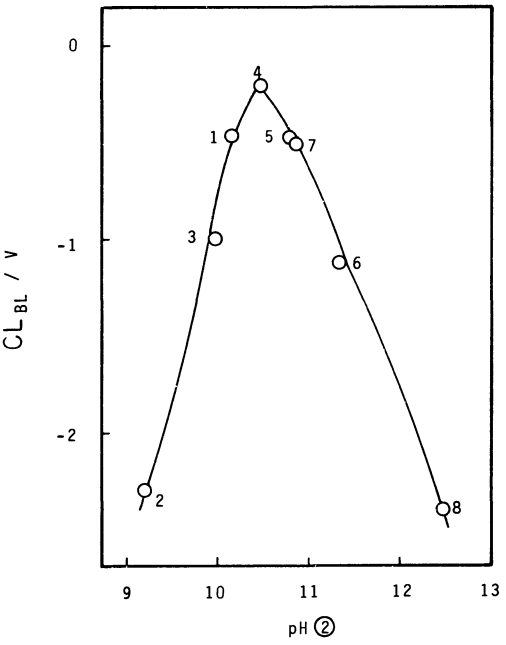

Fig. 7. Relationship between pH ② and CL_{BL}.

of a protein mixture using a zeolite column-CL detection system, the following conditions are required: 1) pH ① and pH ② were satisfied with the optimum pH values, as above, and 2) the change in CL_{BL} with the change in from a carrier solution to an eluting solution was negligible. The buffer capacities of the Cu(II) catalyst, carrier, and eluting solutions, which significantly influenced the pH ①, pH ②, and the change in CL_{BL}, were changed, and then the change in CL_{BL} was measured. Here, the phosphate buffer solutions (pH 6.4—6.5) were used as carrier solutions because these buffer solutions gave the most favorable results for the separation of HSA and HγG on the zeolite column. The NaOH-NaCl buffer solutions (pH 12.0—13.0) were also used as eluting solutions, because all the proteins adsorbed onto the zeolite column were expected to be eluted. As a result, the conditions using a Cu(II) catalyst solution (3.96×10^{-1} mol dm^{-3} NaOH-1.50×10^{-1} mol dm^{-3} NaCl; pH 13.2), a carrier solution (7.35×10^{-3} mol dm^{-3} NaH_2PO_4-2.65×10^{-3} mol dm^{-3} Na_2HPO_4; pH 6.5), and an eluting solution (1.32×10^{-2} mol dm^{-3} NaOH-5.00×10^{-3} mol dm^{-3} NaCl; pH 12.0) were recommended for the following experiments, because the change in CL_{BL} with the change from a carrier solution to an eluting solution was negligibly small and because the pH ① and pH ② were near to the optimum values of about 13 and about 10.5 under these conditions.

The calibration curves for HSA and HγG under the above conditions were obtained by means of an FIA method without using a zeolite column (Fig. 8). Both proteins could be determined in the concentration range of 5×10^{-6}—1×10^{-1} g dm^{-3}, with the detection limit of 250 pg (injected sample volume 50 mm^3, S/N=2). The present FIA method was about 4 times as sensitive as the previous method,[2] in which up to 250 pg of protein could be detected only by the use of the amplifying effect of an amino acid. Though several FIA methods for the determination of protein have recently been reported,[21-24] the present FIA method is much superior to these FIA mehods in termes of the detection limit and the concentration range.

Development of a Zeolite Column-CL Detection System. A zeolite column-CL detection system was investigated in an attempt to develop a method for the separation and determination of a small amount of a protein mixture. To minimize the dilution of a sample solution in a columm, a microbore column was used in the present study. An ordinary zeolite column (3 mm i.d.×50 mm) or a microbore zeolite column (1 mm i.d.×250 mm), both packed with the Na-X type of zeolite, was combined with the CL

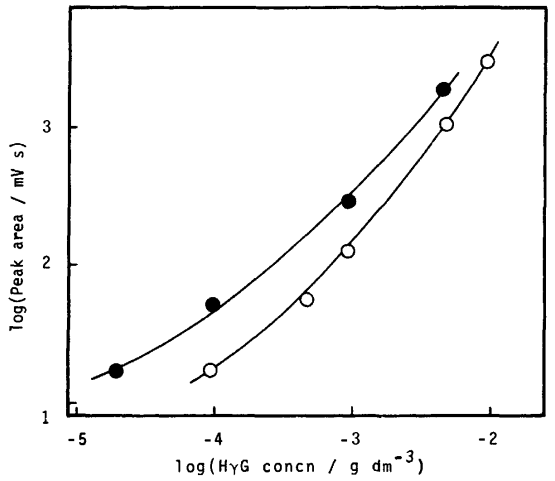

Fig. 9. Comparison of HγG calibration curves obtained on a microbore and an ordinary columns. ○: Ordinary column (3 mm i.d.×50 mm) and ●: microbore column (1 mm i.d.×250 mm).

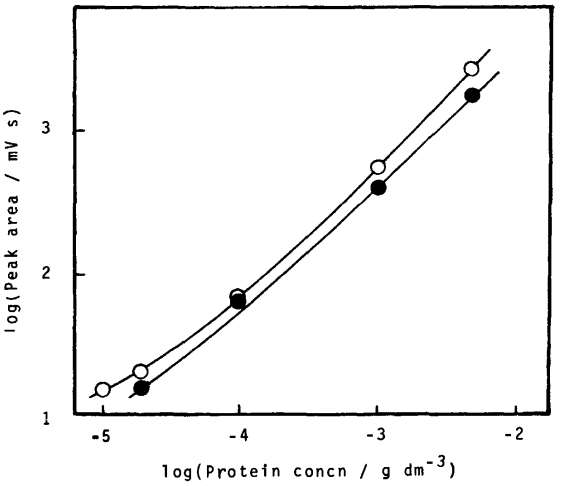

Fig. 10. Calibration curves of proteins using a microbore zeolite column-CL detection system. ○: HSA and ●: HγG.

detector; they were then used under the conditions specified above. 50-mm^3 HγG sample solutions in various concentrations were injected and adsorbed on the column, followed by elution and the measurement of the HγG. The calibration curves of HγG eluted from an ordinary zeolite column and a microbore zeolite column are shown in Fig. 9. As can be seen from Fig. 9, HγG could be determined by the use of a microbore column less well than by the use of an ordinary column.

It was first confirmed that 5.0×10^{-3} g dm^{-3} HSA was not adsorbed onto the microbore zeolite column, while the same concentration of HγG was completely adsorbed by the carrier solution. The model sample containing HSA and HγG was separated on the microbore zeolite column, and then the HSA passing through the column was first determined, followed by the determination of the HγG after its desorption. According to the present method using the microbore zeolite column, both HSA and HγG in the concentration range of 2×10^{-5}—5×10^{-3} g dm^{-3} could be determined with a detection limit of about 1 ng (injected sample volume, 50 mm^3; S/N=2) (Fig. 10). Here, the recovery of 1.0×10^{-3} g dm^{-3} of HγG was 84%, the coefficients of the variation of HSA and HγG were 5.4% and 8.3% (1.0×10^{-3} g dm^{-3} protein; n=5), and the time necessary for an analysis was about 16 min, including adsorption, elution, and regeneration. The present method may, therefore, be characterized as follows: 1) High sensitivity and a wide dynamic range for the determination of protein; 2) a consecutive operation for the separation and the determination of protein by means of high-performance liquid chromatography, and 3) the advantage of a zeolite column, that is, its inexpensiveness, ease of operation, and convenience for pretreatment and regeneration.

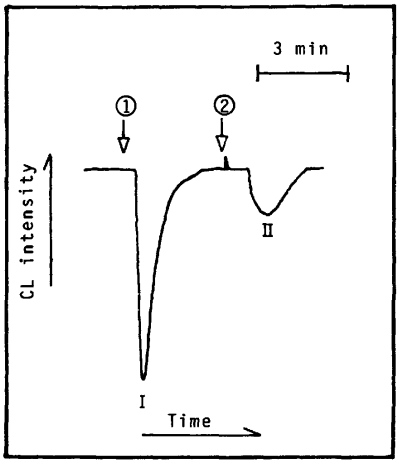

Fig. 11. Chromatogram of control serum using a microbore zeolite column-CL detection system. ①: Sample was injected, ②: eluent was fed, I: peak for albumin, and II: peak for globulin.

The immunoaffinity chromatography and metal-chelate-affinity chromatography using the CL detector previously developed by the present authors could determine up to 15 ng of HSA or 5 ng of bovine serum γ-globulin.[8,9] However, the present method could determine up to 1 ng of HγG. The high sensitivity of the present method may be supposed to be due to: 1) Improvement in the sensitivity in the CL detector, 2) utilization of a microbore column, and 3) the combination of the zeolite column with the CL detector using an alkaline-eluting method. The separation and the determination of several kinds of proteins using a pH-gradient method or a step-by-step eluting method are now in progress.

Finally, the present method was applied to a control serum sample. A control serum sample was diluted 10^4 times, and then an aliquot (50 mm^3) of it was analyzed

by the present method (Fig. 11). As is shown in Fig. 11, there were two peaks, I and II; Peak I corresponded to albumin, and Peak II, to globulin.

The authors wish to thank Mr. Masakatsu Imaki (Horiba, Ltd.) for providing the apparatus necessary for the present study.

The present study was supported by a Grant-in-Aid for General Scientific Research from the Ministry of Education, Science and Culture.

References

1) T. Hara, M. Toriyama, and K. Tsukagoshi, *Bull. Chem. Soc. Jpn.*, **57**, 1551 (1984).
2) T. Hara, T. Ebuchi, A. Arai, and M. Imaki, *Bull. Chem. Soc. Jpn.*, **59**, 1833 (1986).
3) K. Sano, "Bunseki-library 3 Rinsho Kagaku Bunseki II," ed by the Japan Society for Analytical Chemistry, Tokyo Kagaku Dojin, Tokyo (1979).
4) K. Sugawara and M. Soejima, "Seibutsu Kagaku Jikken-ho 7 Tanpakushitsu No Teiryo-ho," Japan Scientific Societies Press, Tokyo (1981).
5) Y. Izumi, H. Nakagawa, and T. Miwatani, "Seibutsu Kagaku Jikken No Tebiki Tanpakushitsu No Bunri·Bunseki-ho," Kagaku Dojin, Kyoto (1985).
6) J. A. Johnson and J. A. Lott, *Chin. Chem.*, **24**, 1931 (1978).
7) T. Kinoshita, F. Iinuma, K. Atsumi, and A. Tsuji, *Anal. Biochem.*, **77**, 471 (1977).
8) T. Hara, K. Tsukagoshi, A. Arai, and T. Iharada, *Bull. Chem. Soc. Jpn.*, **61**, 301 (1988).
9) T. Hara, K. Tsukagoshi, and T. Yoshida, *Bull. Chem. Soc. Jpn.*, **61**, 2779 (1988).
10) T. Mizutani and A. Mizutani, *J. Chromatogr.*, **120**, 206 (1976).
11) C. J. C. M. Laurent, H. A. H. Billiet, and L. Degalan, *J. Chromatogr.*, **287**, 45 (1984).
12) M. Arai, H. Fukuda, and H. Morikawa, The Meeting of the Society of Fermentation Technology of Japan, Abstr. No. 550, 202 (1986).
13) H. S. Sherry, *J. Phys. Chem.*, **70**, 1158 (1966).
14) J. L. White, A. N. Jelli, J. M. Andre, and J. J. Fripiat, *Trans. Faraday Soc.*, **63**, 461 (1967).
15) H. A. Szymanski, D. N. Stamiers, and G. R. Lynch, *J. Opt. Soc. Am.*, **50**, 1323 (1960).
16) E. I. Hitchcock, *J. Gen. Physiol.*, **8**, 6 (1925).
17) Y. K. Hanson, K. Chuang, W. F. King, and R. Mason, *J. Lab. Clin. Med.*, **92**, 483 (1978).
18) L. A. AE. Sluyterman and O. Elgersma, *J. Chromatogr.*, **150**, 17 (1978).
19) L. A. AE. Sluyterman and J. Wijdenes, *J. Chromatogr.*, **150**, 31 (1978).
20) J. B. Uytterhoeven, L. G. Christner, and W. K. Hall, *J. Phys. Chem.*, **69**, 2117 (1965).
21) T. Shuto, M. Koga, I. Tanaka, T. Akiyama, and H. Igisu, *Bunseki Kagaku*, **36**, 256 (1987).
22) C. J. Yaun and C. O. Huber, *Anal. Chem.*, **57**, 180 (1985).
23) L. C. Davis and G. A. Radke, *Anal. Biochem.*, **161**, 152 (1987).
24) R. A. Salerno, C. Odell, N. Cyanovich, B. P. Bubnis, W. Morges, and A. Gray, *Anal. Biochem.*, **151**, 309 (1985).

Dynamic NMR as a Nondestructive Method for the Determination of Rates of Dissociation. XVI. Mechanism of Sulfur Inversion in Platinum(II)-Thioether Complexes Revisited[1)]

Shinji TOYOTA, Yasuhisa YAMADA, Masami KANEYOSHI, and Michinori ŌKI*,†
Department of Chemistry, Faculty of Science, The University of Tokyo, Bunkyo-ku, Tokyo 113
(Received October 24, 1988)

The mechanism of sulfur inversion in some platinum(II)-thioether complexes was reinvestigated with the use of the dynamic NMR technique. Activation parameters for the sulfur inversion in [(isopropylthio)acetato-*O*,*S*]bis(triphenylphosphine)platinum(II) perchlorate in $CDCl_3$ were obtained by taking advantage of the line shape changes in its ^1H NMR spectra at various temperatures as follows: ΔH^* 18.0±0.4 kcal mol^{-1}, ΔS^* 4.0±1.4 cal mol^{-1} K^{-1}. The kinetic parameters varied little, though the rates of inversion were determined in other solvents. The entropy of activation and the solvent effects together with the presence of coupling between the phosphine-^{31}P and the methine-^1H throughout the temperature range of investigation evidence the sulfur inversion without breaking the Pt–S bond. The sulfur inversion in dichlorobis(dialkyl sulfide)platinum(II) in nonpolar solvents was also concluded to take place without bond breakage.

While it is well known that the sulfur inversion in organic sulfonium ions is slow to make it possible to isolate enantiomers at room temperature,[2)] if they are properly substituted, that in coordination compounds is much faster to make it amenable to dynamic NMR study and consequently isolation of isomers due to the sulfur inversion impossible at room temperature. The typical examples among the coordination compounds are *cis*-dichlorobis(dialkyl sulfide)platinum(II) (**1**) and *trans*-dichlorobis(3,3-dimethylthietane)platinum(II) (**2**).

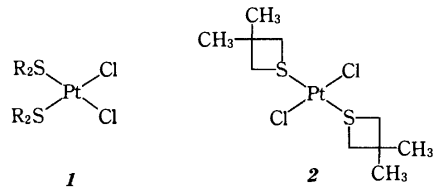

1 *2*

Dynamic NMR spectral study on the inversion of the thioether ligands in compound **1** was carried out and it was concluded that the inversion did not involve the scission of the Pt–S bond by observing the coupling between ^{195}Pt and ^1H nuclei even at temperatures where coalescence of diastereotopic proton signals took place.[3,4)] However, close examination of the published figure discloses that the peaks attributed to the coupling are rather broad. In addition, it might be possible to argue that, since the compounds in question possess a pair of dialkyl sulfide ligands, one of the sulfur-ligands may be bonded to the platinum during the process of sulfur-detachment, thus the coupling being observed always.

We have shown in our previous works that, if the process involves bond-breakage in compounds of which ground state is ionic, the entropy of activation must be large positive, whereas it is large negative, if the compound in question is of covalence in its ground state.[5)] Using this generalization, we have shown that sulfur compounds are no exceptions. The entropy of activation for sulfur inversion in a thioether-borane and another complex was shown to be large negative, because the mechanism involves bond-dissociation,[1)] suggesting that the thioether complex possesses ionic nature at its ground state. By contrast, sulfonium salts, in which bond-dissociation was not likely, showed nearly zero entropy of activation by both classical[6)] and dynamic NMR method.[7)]

Actually, the dynamic NMR study of compounds **1** and **2** has been carried out. However, the method used for compound **1** was the line-width method which is known to tend to give erroneous entropy of activation.[8)] The total line shape analysis was carried out for compound **2**.[9)] However, due to the simplicity of the line shapes of the diastereotopic gem-dimethyl group,[10)] the reliability of the entropy of activation can be questioned.

Based on these experiences, we felt it would be appropriate to apply the total line shape analysis with the use of probes which would give complex signals[10)] for diagnosis of the mechanism of sulfur inversion in platinum-thioether complexes. This paper is to report the results of such investigation.

Results and Discussion

Platinum(II) Complexes with One Thioether Ligand. Clearly, a compound which has only one thioether ligand is desirable to avoid the complexity. A recent publication described the preparation of compound **3**, of which thioether ligand showed the dynamics in its NMR spectra, though the free energies of activation only have been reported.[11)]

† Present address: Department of Chemistry, Faculty of Science, Okayama University of Science, Ridaicho, Okayama 700.

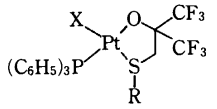

3

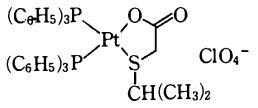

4

We decided to use this type of compounds for our investigation and prepared compound **4** by treating *cis*-dichlorobis(triphenylphosphine)platinum(II) with potassium (isopropylthio)acetate followed by silver perchlorate. We have selected this compound because the isopropyl probe for the exchange of their magnetic sites on inversion should not show coupling with platinum to make it much easier to carry out the line shape simulation and the isopropyl-methyls give complex enough signals to assure the reliability of the data thus obtained.

Although similarly prepared chloro[(isopropylthio)-acetato-*O,S*](triphenylphosphine)platinum(II) did show the change in the line shapes on heating at above 100 °C, decomposition set in at the same time. Compound **4** by contrast showed the desired line shape change without decomposition, thanks to the trans influence.[12] The process may be written as in the following scheme.

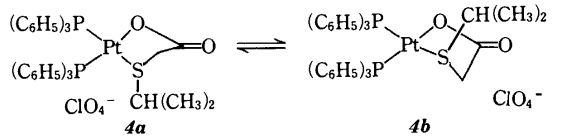

4a 4b

Kinetic parameters obtained by simulation of the line shapes are shown in Table 1. The feature of the kinetic parameters is the near zero entropy of activation. From our experience in the past, the results support the idea that the sulfur inversion in the platinum complex takes place without bond dissociation, namely the simple inversion of sulfur. Further support for the mechanisms proposed is obtained from the following observations.

One is the coupling between the isopropyl-methine proton and one of the phosphorus atoms in the ligands. This coupling was observed at room temperature and was persistent at 90 °C where the coalescence of the signals due to the isopropyl-methyl group took place.

The other piece of evidence is the solvent effects. The activation parameters obtained with **4** in various solvents are listed in Table 1. The data clearly show that the activation parameters are not dependent on the solvent used and entropy of activation is always close to zero. If the mechanism of the sulfur-inversion involved the S-Pt bond scission, the inversion would have been fast in the solvents of which affinity toward platinum was high.

Platinum(II) Complexes with Two Thioether Ligands. Coming back to the problem of the platinum complexes that contain two molecules of sulfur ligands, we were interested in knowing whether these compounds as well demonstrate the near zero entropy of activation for sulfur inversion. We selected *cis*- and *trans*-dichlorobis(diisobutyl sulfide)platinum(II) (**5** and **6** respectively) for our investigation. These compounds were prepared by the known method from potassium tetrachloroplatinate(II) and diisobutyl sulfide. Their cis- and trans-isomers were assigned by the behavior in chromatography as well as the coupling constants between the platinum and the α-proton of the isobutyl group: the cis compound gives a larger coupling constant than the trans.[13]

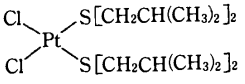

5

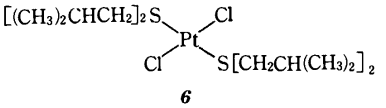

6

The kinetic parameters obtained by total line shape analysis of these compounds are shown in Table 2, in which rate constants rather than free energies of activation are shown to demonstrate small differences in the rates. The results clearly show that the inversion of the thioether ligands in the trans isomer is more facile than in the cis, again due to the trans influence. The entropy of activation is not very far from zero.

The results can be interpreted on the basis of sulfur inversion without bond dissociation and that the complexity in the sulfur-inversion due to the presence of two thioether ligands can be ruled out. The existence of coupling between ^{195}Pt and ^{1}H at the α-position of the thioether ligand at temperatures higher than the coalescence point of the isopropyl-methyl

Table 1. Kinetic Parameters for Sulfur Inversion in Compound **4** in Various Solvents[a]

Solvent	$\Delta H^{\ddagger}$/kcal mol^{-1}	$\Delta S^{\ddagger}$/kcal mol^{-1} K^{-1}	$\Delta G^{\ddagger}_{298}$/kcal mol^{-1}
$CDCl_3$	18.0±0.4	4.0±1.4	16.8
$(CD_3)_2CO$	18.5±0.7	4.8±2.0	17.1
CD_3NO_2	17.8±0.3	3.6±1.0	16.7
$(CD_3)_2SO$	17.9±0.4	2.6±1.3	17.1

a) 1 cal=4.184 J.

Table 2. Kinetic Parameters for Sulfur Inversion in Compounds **5** (Cis) and **6** (Trans) in Various Solvents

Form	Solvent	$\Delta H^{\ddagger}$/kcal mol^{-1}	$\Delta S^{\ddagger}$/cal mol^{-1} K^{-1}	k_{298}/s^{-1}
Cis	C_7D_8[a]	15.1±0.3	−2.6±0.8	15.1
	$CDCl_3$	17.2±0.5	4.7±1.4	17.3
	$(CD_3)_2CO$	17.6±0.6	7.5±1.8	33.6
	CD_3OD	16.6±0.4	3.6±1.3	26.3
Trans	C_7D_8[a]	12.6±0.3	−2.0±1.1	11.5×10^3
	CD_2Cl_2	11.7±0.3	−6.1±1.0	7.9×10^3

a) Toluene-d_8.

proton signals was confirmed.

Factors Affecting Sulfur-Inversion. Interesting is the fact that the solvent effect on the rates of sulfur-inversion in **5** is significant. The rates of inversion is larger in more polar solvents than in the less polar. We postulate that in these compounds solvent-assisted inversion of sulfur is involved to some extent. The difference between **4** and **5** may be attributed to the trans influence: if the Pt-S bond is weakened, the solvent assistance becomes more important.

The results provide a hint in considering the cause of the fast or slow inversion of sulfur. It was suggested in the literature[4] that the stabilization of the transition state for inversion due to the pπ-dπ interaction would be the cause for more facile inversion in the platinum complexes than in the sulfonium ions. It may be argued that the sulfur inversion in the platinum complexes is easier than in organic sulfonium compounds because the pyramidality[14] of the sulfur which is connected to the platinum and two alkyl ligands is smaller in the ground state than the sulfonium ions because of the pπ-dπ interaction. However, if it were the case, the thioethers that are bonded by a short bond should invert more rapidly than that connected by a long bond. Thus we agree with the old postulate as the explanation of the easier sulfur inversion in the platinum complexes.

The relatively slow inversion of the thioether ligand in compound **4**, despite the fact that the strong trans effect of the phosphine ligand[4] should reduce the barrier, deserves mention here. We believe this is due to the ring puckering of the ligand. The facts that the chemical shift difference between the two protons of the α-methylene group in the acetate ligand is as large as ca. 1 ppm and that only one of these protons shows couplings with ^{195}Pt and ^{31}P support that the five-membered ring made by the ligand and the platinum is fairly puckered. Probably the planar transition state for inversion in this compound is accordingly of high energy.

Experimental

***cis*-[(Isopropylthio)acetato-*O,S*]bis(triphenylphosphine)-platinum(II) Perchlorate (4).** (Isopropylthio)acetic acid[16] (34 mg or 0.25 mmol) was added to 19 mg (0.34 mmol) of potassium hydroxide in 20 mL of ethanol. To this solution was added 0.20 g (0.25 mmol) of *cis*-dichlorobis(triphenylphosphine)platinum(II)[17] in 10 mL of dichloromethane and the whole was stirred for 2.5 h at room temperature. The precipitate was removed by filtration and 60 mg (0.29 mmol) of silver perchlorate was added to the filtrate. The resulting silver chloride was immediately removed by filtration and the filtrate was stirred for 20 h. The solvent was evaporated and the residue was extracted with dichloromethane and the extract was washed with water. After evaporation of the solvent, the residue was recrystallized from ethanol to afford 0.12 g (49%) of the desired compound which contained 1/2 molecule of ethanol, mp 155—160 °C (decomp). Found: C, 51.72; H, 4.34%. Calcd for $C_{41}H_{39}ClO_6P_2PtS\cdot0.5C_2H_6O$: C, 51.45; H, 4.41%. ^{1}H NMR ($CDCl_3$, −20 °C) δ=0.98 (3H, d, J=6.8 Hz), 1.55 (3H, d, J=6.8 Hz), 2.74(1H, double septet, J=6.8 and 1.6 Hz), 3.36 (1H, dd, J=17.1 and 3.2 Hz), 4.26 (1H, d, J=17.1 Hz), 7.3—7.7 (30H, m).

***cis*- and *trans*-Dichlorobis(diisobutyl sulfide)platinum(II) (5 and 6).** To a solution of 0.88 g (2.1 mmol) of potassium tetrachloroplatinate(II) in 40 mL of water was added 0.31 g (2.1 mmol) of diisobutyl sulfide[18] in 6 ml of ethanol. The mixture was stirred for ca. 90 h at room temperature and an oily product was separated by decantation. The product was submitted to chromatography on silica gel with a 1:1 hexane-dichloromethane eluent. The trans form was eluted first and then came the cis form. The separated products were recrystallized from ethanol.

Cis-form, yellowish green crystals, mp 130 °C, was obtained in 21% yield. Found: C, 34.13; H, 6.57; Cl, 12.82; S, 11.79%. Calcd for $C_{16}H_{36}Cl_2PtS_2$: C, 34.41; H, 6.50; Cl, 12.69; S, 11.48%. ^{1}H NMR ($CDCl_3$, −20 °C) δ=1.00 (3H, d, J=6.6 Hz), 1.05 (3H, d, J=6.6 Hz), 2.20 (1H, app septet J=ca. 6.5 Hz), 2.43 (1H, dd, J=11.9 and 8.5 Hz), 3.19 (1H, dd, J=11.9 and 5.7 Hz).

Trans-form, yellow crystals, mp 106 °C, was obtained in 16% yield. Found: C, 34.12; H, 6.55; Cl, 12.85; S, 11.46%. Calcd for $C_{16}H_{36}Cl_2PtS_2$: C, 34.41; H, 6.50; Cl, 12.69; S, 11.48%. ^{1}H NMR (toluene-d_8, −18 °C) δ=0.94 (6H, d, J=6.4 Hz), 1.82 (1H, br s), 2.27 (1H, app septet, J=ca. 6.3 Hz), 3.08 (1H, br s).

Dynamic NMR Spectroscopy. The spectra were obtained with a JEOL GX270 spectrometer. The temperature was calibrated with a thermocouple. The sample was dissolved in appropriate solvents to make up a ca. 50 mmol L^{-1} solution. The simulation of the line shapes was performed with the use of DNMR3 program[19] by assuming the site exchange process of $A_3B_3X\rightleftarrows B_3A_3X$ which was approximated as $ABX\rightleftarrows BAX$.

Table 4. Rate Constants of Sulfur Inversion in Compounds **4**, **5**, and **6** in Various Solvents

Compound	Solvent	k/s^{-1} (temperature/°C)
4	$CDCl_3$	7.4 (33.9), 10.5 (37.9), 16.0 (41.9), 34.0 (49.9), 54 (55.4), 82 (60.4)
4	$(CD_3)_2CO$	7.4 (38.0), 11.2 (42.0), 16.5 (45.9), 22.0 (49.4), 28.5 (52.1), 38 (55.2)
4	CD_3NO_2	11.1 (37.9), 16.9 (41.9), 24.8 (46.0), 36.8 (50.0), 58 (55.4), 88 (60.4), 196 (70.4), 410 (80.4)
4	$(CD_3)_2SO$	7.6 (40.0), 12.0 (44.9), 19.2 (50.0), 32.5 (55.4), 51 (60.5), 112 (70.4), 235 (80.4), 460 (90.3)
5	C_7D_8[a]	6.1 (14.8), 8.2 (17.8), 10.6 (20.9), 13.9 (23.9), 18.0 (26.8), 23.4 (29.8)
5	$CDCl_3$	6.2 (14.8), 8.0 (17.3), 10.4 (19.8), 13.5 (22.4), 16.4 (25.2), 22.6 (27.9)
5	$(CD_3)_2CO$	3.8 (4.8), 5.1 (7.4), 6.5 (9.8), 8.5 (12.3), 11.1 (14.8), 15.2 (17.3)
5	CD_3OD	3.9 (6.9), 5.0 (8.8), 6.3 (10.9), 7.6 (12.9), 9.6 (15.1), 11.5 (16.9)
6	C_7D_8[a]	3.8 (−35.8), 4.5 (−34.4), 5.6 (−32.8), 6.5 (−31.4), 7.6 (−30.0), 11.5 (−26.,3)
6	CD_2Cl_2	3.7 (−36.9), 4.4 (−35.3), 5.4 (−33.1), 6.6 (−31.2), 8.4 (−29.1), 10.7 (−26.9)

a) Toluene-d_8.

Table 3. Relationships between the Chemical Shift Differences of the Diastereotopic Protons and Temperature

Compound	Solvent	$\Delta\nu/s^{-1}=At/°C+B$	
		A	B
4	$CDCl_3$	−0.3512	145.55
4	$(CD_3)_2CO$	−0.2946	125.65
4	CD_3NO_2	−0.3153	136.34
4	$(CD_3)_2SO$	−0.2626	109.98
5	C_7D_8[a]	0.0274	13.52
5	$CDCl_3$	0.0351	12.69
5	$(CD_3)_2CO$	0.0009	5.36
5	CD_3OD	0.0347	9.38
6	C_7D_8[a]	0.150	3.63
6	CD_2Cl_2	0.0102	5.43

a) Toluene-d_8.

The coupling constants and the chemical shift differences at various temperatures were estimated by the tendency observed from the several points in the slow exchange limit. The coupling constants were constant throughout the temperature range to let us assume they were the same at temperatures where the line shapes changed. The chemical shift differences drifted when the temperature was changed and were correlated linearly with temperature. The relationships are given in Table 3. These lines were extrapolated to the temperature where the line shape change was observed. T_2 was estimated from the line width due to the protons which were not involved in the exchange and varied from 0.08 to 0.17 s for compound **4** and 0.14—0.24 s for compounds **5** and **6** according to the conditions of the measurement. The T_2 was adjusted, when necessary, to make the fit of the calculated line shapes better than the fixed value. The rate constants of site exchange thus obtained are compiled in Table 4.

This work was supported by a Grant-in-Aid (62124039) for Fundamental Scientific Research of the Ministry of Education, Science and Culture.

References

1) For Part XV of the series, see M. Ōki and Y. Yamada, *Bull. Chem. Soc. Jpn.*, **61**, 1191 (1988).
2) M. Mikolajczyk and J. Drabowicz, *Top. Stereochem.*, **13**, 333 (1982).
3) P. Haake and P. C. Turley, *J. Am. Chem. Soc.*, **89**, 4611 (1965).
4) P. C. Turley and P. Haake, *J. Am. Chem. Soc.*, **89**, 4617 (1965).
5) T. Morita and M. Ōki, *Bull. Chem. Soc. Jpn.*, **59**, 3603 (1986) and papers cited therein.
6) R. Scartazzini and K. Mislow, *Tetrahedron Lett.*, **1967**, 2719: M. Ōki, Y. Yamada, and S. Murata, *Bull. Chem. Soc. Jpn.*, **61**, 707 (1988).
7) M. Ōki and Y. Yamada, *Bull. Chem. Soc. Jpn.*, **61**, 1181 (1988).
8) M. Ōki, "Applications of Dynamic NMR Spectroscopy to Organic Chemistry," VCH Publishers, Deerfield Beach (1985), pp. 22—30.
9) E. W. Abel, M. Booth, and K. G. Orrell, *J. Chem. Soc., Dalton Trans.*, **1974**, 1994.
10) M. Nakamura, H. Kihara, N. Nakamura, and M. Ōki, *Org. Magn. Reson.*, **12**, 702 (1979): G. Binsch and H. Kessler, *Angew. Chem., Int. Ed. Engl.*, **19**, 411 (1980).
11) R. T. Boere and C. J. Willis, *Can. J. Chem.*, **64**, 492 (1986).
12) A. Pidcock, R. E. Richards, and L. M. Venanzi, *J. Chem. Soc. A*, **1966**, 1707: T. G. Appleton, H. C. Clark, and L. E. Manzer, *Coord. Chem. Rev.*, **10**, 335 (1973).
13) S. M. Grim, R. L. Keiter, and W. McFarlane, *Inorg. Chem.*, **6**, 1133 (1967).
14) J. D. Dunitz, "X-Ray Analysis and the Structure of Organic Molecules," Cornell University Press, Ithaca (1979), pp. 366—384.
15) R. Gosling and M. L. Tobe, *Inorg. Chem.*, **22**, 1235 (1983). See also Ref. 12.
16) L. D. Petit and C. Sherrington, *J. Chem. Soc. A*, **1968**, 3078.
17) J. C. Bailar, Jr., and H. Itatani, *Inorg. Chem.*, **4**, 1618 (1965).
18) D. T. McAllan, T. V. Cullum, R. A. Dean, and F. A. Fidler, *J. Am. Chem. Soc.*, **73**, 3627 (1951).
19) G. Binsch, *Top. Stereochem.*, **3**, 97 (1968).

EXAFS and XANES Spectra of Cobalt(III) EDTA Complexes in Solids and Solutions

Hideto SAKANE,* Iwao WATANABE, and Shigero IKEDA†
Department of Chemistry, Faculty of Science, Osaka University, Toyonaka, Osaka 560
†Institute of Science and Technology, Ryukoku University, Fushimi, Kyoto 612
(Received November 17, 1988)

The Co K-edge XANES (X-ray Absorption Near-Edge Structure) of $[Co(edta)]^-$ ($edta^{4-}$=ethylenediamine-*N*,*N*,*N*′,*N*′-tetraacetate) complex in crystal varies with the kind of counter cations and it also varies with the kind of solvents when it is dissolved. The amplitude of the oscillation in its EXAFS (Extended X-ray Absorption Fine Structure), or the peak height in its Fourier transform, also varies as much as threefold depending on the kind of counter cations or solvents. The most plausible cause for the variations is the difference in the thermal disorder of the bonds which is enhanced by the formation of hydrogen bonding between carboxylato groups in the complex and the water molecules in crystal or the solvent molecules in solution.

The structures of metal–edta complexes are not necessarily the same. They are known to take various coordination structures.[1] The structures can also vary with the environments, i.e. in crystals[2] or in solutions.[3,4] The EXAFS and XANES techniques appear to be suitable for the structural studies of such complexes since these spectroscopic techniques extract the information regarding the local structure around the central metal irrespective of the environments. The complex treated in this work is $[Co(edta)]^-$ which is considered to be so stable that no structural change in its inner sphere would occur against the variation of the environments. In spite of the expected rigidity of the complex, it was found that its EXAFS and XANES spectra are highly sensitive to the environments. This paper reports the X-ray absorption spectra of the complex in various environments and the possible effects of hydrogen bonding on the Debye–Waller factors or the EXAFS oscillation amplitudes.

Experimental

Samples. Li[Co(III)(edta)]·$3H_2O$ and Na[Co(III)(edta)]·$4H_2O$ were prepared according to the literatures.[5,6] Rb[Co(III)(edta)]·$2H_2O$ was synthesized in the following way; Rb_2CO_3 was added to a warm slurry solution containing RbCl, $(CH_3COO)_2Co·4H_2O$, and H_4edta until the pH of the solution became 4. The $[Co(II)(edta)]^{2-}$ ion was oxidized by adding 3% H_2O_2 aqueous solution. After filtration, this solution was concentrated and cooled, and ethanol was added to crystallize Rb[Co(edta)]·$2H_2O$. NH_4[Co(III)(edta)]·$2H_2O$ was synthesized using a similar method from $Co(NO_3)_2·6H_2O$, H_4edta, and NH_4OH. All the solid samples were recrystallized twice or more from water and ethanol. Elemental analysis: Found for Li[Co(edta)]·$3H_2O$: C, 29.32; H, 4.55; N, 6.85%. Na[Co(edta)]·$4H_2O$: C, 26.56; H, 4.26; N, 6.19%. Rb[Co(edta)]·$2H_2O$: C, 24.21; H, 3.49; N, 5.65%. NH_4[Co(edta)]·$2H_2O$: C, 29.63; H, 5.06; N, 10.41%.

Aqueous solutions of 0.1 mol·dm^{-3} $[Co(edta)]^-$ were prepared from the above Na salt. HNO_3 or NaOH were used to adjust their pH to 3.0, 5.0, 7.0, and 9.0. The solutions of pH 7.0 and 9.0 turned to be pH 6.9 and 8.1, respectively, after the X-ray absorption measurements. DMF (*N*,*N*-dimethylformamide) solution was prepared from K[Co(edta)]·$2H_2O$ which was synthesized by the conventional method.[6] Excess of 18-crown-6 ether was added to raise the solubility of the complex. KBr disks of solid samples were prepared for the measurements of infrared absorption spectra.

Measurements and Calculations. Co K-edge X-ray absorption spectra were obtained at BL-7C of the Photon Factory in the National Laboratory for High Energy Physics using a Si(111) double crystal monochromator. Powder samples of ca. 0.5 mm thick were held between two sheets of adhesive tape. Solution samples were placed in polyethylene pouches. Fourier transform calculations of EXAFS were performed by using the phase shift and scattering amplitude parameters tabulated by Teo and Lee.[7] Transformations were performed over the k range of 2.9—16.75 Å^{-1}. In order to reduce ripple peaks in Fourier transforms, Hamming window function was used.

Results and Discussion

Figure 1 shows XANES spectra and Fourier transforms of EXAFS for aqueous solutions. Both spectra show no dependence on pH. Their Raman scattering and UV-Visible absorption spectra were also measured and showed no dependence on pH. According to Higginson et al.,[4] the form of Co(III)–EDTA is either [Co(Hedta)(H_2O)], [Co(edta)(H_2O)]$^-$, $[Co(edta)]^-$, or $[Co(edta)(OH)]^{2-}$ depending on pH of the solution. In the pH range of 3.0 to 8.1, most of the complex has been known to form $[Co(edta)]^-$. The present results indicate that the structure of $[Co(edta)]^-$ in aqueous solutions is very stable over this pH range.

Figure 2 shows Co K-edge XANES spectra for (a) aqueous solution, (b) Na[Co(edta)]·$4H_2O$, (c) NH_4[Co(edta)]·$2H_2O$, (d) Rb[Co(edta)]·$2H_2O$, (e) Li[Co(edta)]·$3H_2O$, and (f) DMF solution. They can be classified into three groups; (A) aqueous solution and Na salt, (B) NH_4 and Rb salts, and (C) Li salt and DMF solution. The spectra for group A have the lowest threshold energies and the lowest peak heights at around 7740 eV. In contrast, group C has the highest

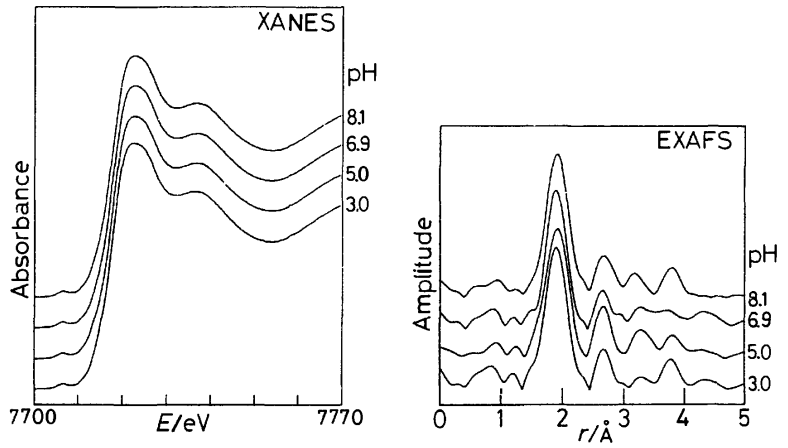

Fig. 1. Co K-edge XANES spectra and Fourier transforms of EXAFS for $[Co(edta)]^-$ in different pH aqueous solutions.

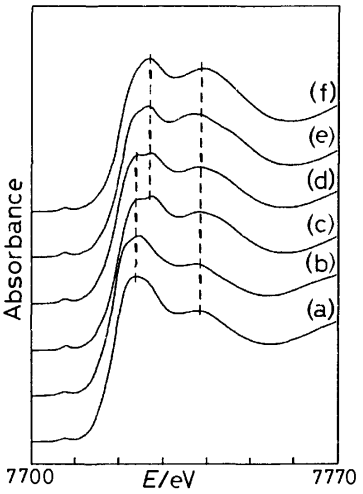

Fig. 2. Co K-edge XANES spectra for (a) aqueous solution, (b) $Na[Co(edta)]\cdot 4H_2O$, (c) $NH_4[Co(edta)]\cdot 2H_2O$, (d) $Rb[Co(edta)]\cdot 2H_2O$, (e) $Li[Co(edta)]\cdot 3H_2O$, and (f) DMF solution.

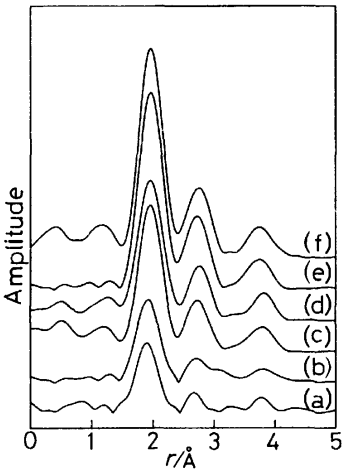

Fig. 3. Fourier transforms of Co K-edge EXAFS for (a) aqueous solution, (b) $Na[Co(edta)]\cdot 4H_2O$, (c) $NH_4[Co(edta)]\cdot 2H_2O$, (d) $Rb[Co(edta)]\cdot 2H_2O$, (e) $Li[Co(edta)]\cdot 3H_2O$, and (f) DMF solution.

threshold energies and the highest peak heights at 7740 eV. Group B is intermediate between A and C. The highest peaks, so called white line, in A or C are composed of a single peak possibly accompanying a shoulder, while those of B are composed of double peaks and the position of its higher energy component agrees with the position of the peak in C.

There are two possibilities which may contribute to the differences in the XANES spectra of three groups. One is the photoelectron scattering by the counter cations or solvent molecules. The other is the indirect effects of the cations or the solvents on the electronic and/or structural conditions of the complex anion, $[Co(edta)]^-$. There is a reason to reject the former possibility, i.e. although the N in NH_3 and Rb are quite different photoelectron scatterers in respect to the amplitude and phase shift (the distances of Co-N and Co-Rb are similar 5.68 and 5.81 Å, respectively[5]), the XANES spectra of the samples having these atoms as counter cations are almost the same. In addition to this, there seems to be no systematic correlation between the XANES spectrum and the kind of counter cation. Therefore, it is almost impossible to consider that the variety of XANES spectra is caused by the direct photoelectron scattering by the counter cation.

Fourier transforms of EXAFS for $[Co(edta)]^-$ in various environments are shown in Fig. 3. One easily finds three peaks in each of the Fourier transforms. By referring to the crystallographic data for NH_4 salt,[5] these peaks are assigned to the bond distances between Co and the scatterers as follows; the most intense peaks at around 1.9 Å correspond to four oxygens (O_1 in Fig. 4) and two nitrogens, the second peaks at around 2.7 Å to ten carbons, and the third peaks at around 3.8 Å to

Table 1. Peak Positions and Their Heights in Fourier Transforms of Co K-edge EXAFS for $[Co(edta)]^-$ Complexes

Sample	Peak position/Å			Peak height[a]		
	1st	2nd	3rd	1st	2nd	3rd
(a) Average of aqueous solution	1.92	2.69	—	0.5	0.4	—
(b) $Na[Co(edta)]\cdot 4H_2O$	1.92	2.75	3.80	0.5	0.5	0.5
(c) $NH_4[Co(edta)]\cdot 2H_2O$	1.96	2.76	3.79	1.0	1.0	1.0
(d) $Rb[Co(edta)]\cdot 2H_2O$	1.95	2.76	3.83	1.0	1.1	1.1
(e) $Li[Co(edta)]\cdot 3H_2O$	1.97	2.75	3.77	1.4	1.4	1.1
(f) DMF solution	1.97	2.78	3.75	1.5	1.3	1.2
$NH_4[Co(edta)]\cdot 2H_2O$	1.91[b]	2.73[b]	3.85[b]	—	—	—
$[Co(sarmp)(NH_3)_3][Co(edta)]\cdot H_2O$	1.92[c]	2.74[c]	3.89[c]	—	—	—

a) Relative intensity. b) and c) The average of the distances of corresponding bonds for $[Co(edta)]^-$ from crystallographic data of Refs. 5 and 9, respectively. $sarmp^{2-}$=sarcosinate-*N*-propionate.

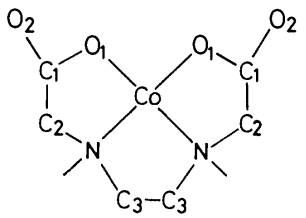

Fig. 4. Numbering on some atoms in $[Co(edta)]^-$ complex.

four oxygens (O_2) not coordinating to Co. In spite of its long distance, the third peaks due to O_2 appear with an unusual intensity, particularly for the samples of groups B and C. Binsted et al.[8] studied EXAFS of cobalt carbonyls such as $[Co(CO)_4]^-$ and found that the linear configuration of Co-C-O atoms enhances the peak corresponding to Co-O bond because of the multiple scattering effect. In the present case, it is plausible that the intensity of the third peak results from the same multiple scattering effect because the angles of $Co\text{-}C_1\text{-}O_2$ are known to be about 160° and those of $Co\text{-}O_2\text{-}C_1$ about 14° from the crystallographic data for NH_4 salt.[5]

Table 1 lists the peak positions in each Fourier transform and the mean distances of corresponding bonds taken from the crystallographic data.[5,9] The third peaks are not clear for some samples of aqueous solutions.

There are large differences in the amplitude of EXAFS oscillation. The ratio of the heights of the first peaks in Fourier transforms is roughly 1:2:3 between groups A, B, and C, respectively. Since the coordination numbers of Co in all the samples are known to be constantly six,[10] the large differences in peak heights must be resulted from the differences in the root-mean-square displacement of Debye-Waller factor. The Debye-Waller factor of a peak originates from two contributions, static bond length distribution and dynamic or thermal disorder. In order to examine the contribution of static distribution, some simulation calculations were performed. The simulated EXAFS spectra were obtained by using a constant value of Debye-Waller factor to each kind of bonds and distributed bond lengths limited within reasonable ranges. However, the spectra could not give such large differences in peak heights in Fourier transforms as shown in experimental spectra. Therefore there must be some large differences in thermal disorder among the samples of group A, B, and C.

One of the origins for the large differences in thermal disorder may be the presence of hydrogen bonding which donates electrons from carboxylato group to water molecule. A water molecule can approach to O_2 and even to O_1 to form hydrogen bonding. This effect appears in other experimental phenomena, e.g. UV absorption spectra[11] and ^{13}C NMR spectra.[12] The presence of such hydrogen bonding has also been known in the $[Co(edta)]^-$ crystals[9] and in an analogous complex, $[Co(III)(trdta)]^-$ ($trdta^{4-}$=trimethylenediamine-*N*,*N*,*N*′,*N*′-tetraacetate) crystal.[13] $NH_4[Co(edta)]\cdot 2H_2O$ crystal must have such hydrogen bonding, since some distances between O in water molecule and O_2 or O_1 are less than 3.0 Å. More hydrogen bonding may exist in Na salt than in NH_4 salt, because the volume of an unit cell of Na salt is larger only about 10% than that of NH_4 salt and the number of waters of crystallization are twice as much. The fact that the spectrum for DMF solution sample is most intense should be due to the absence of the hydrogen bonding.

It is quite interesting to note that the weaker the peak in the Fourier transform, the shorter the bond length read from the first peak position. This may be due to the fact that the Debye-Waller factors for Co-O bonds of longer lengths increase more than the shorter ones upon the hydrogen bonding formation. (cf. the bond lengths are 1.870, 1.896, 1.913, 1.922 Å for Co-O and 1.921 and 1.925 Å for Co-N in NH_4 salt.[5])

The authors thank Drs. Tadashi Matsushita and Masaharu Nomura of the National Laboratory for High Energy Physics (KEK) for their help with X-ray absorption measurements.

References

1) S. Harada, Y. Funaki, and T. Yasunaga, *J. Am. Chem. Soc.*, **102**, 136 (1980); S. Kaizaki and H. Mizu-uchi, *Inorg. Chem.*, **25**, 2732 (1986); W. C. E. Higginson and B. Samuel, *J. Chem. Soc. A*, **1970**, 1579; J. Oakes and E. G. Smith, *J. Chem. Soc., Faraday Trans. 1*, **79**, 543 (1983); S. Richards, B. Pedersen, J. V. Silverton, and J. L. Hoard, *Inorg. Chem.*, **3**, 27 (1964).

2) C. H. L. Kennard, *Inorg. Chim. Acta*, **1**, 347 (1967); M. D. Lind and J. L. Hoard, *Inorg. Chem.*, **3**, 34 (1964); M. J. Hamor, T. A. Hamor, and J. L. Hoard, *ibid.*, **3**, 34 (1964); X. Solans, M. Font Altaba, and J. Garcia-Oricain, *Acta Crystallogr., Sect. C*, **40**, 635 (1984); N. V. Novozhilova, T. N. Polynova, and M. A. Porai-Koshits, *Zh. Struct. Khim.*, **16**, 865 (1975).

3) W. D. Wheeler and J. I. Legg, *Inorg. Chem.*, **23**, 3798 (1984); K. Kanamori and K. Kawai, *ibid.*, **25**, 3711 (1986).

4) I. A. W. Shimi and W. C. E. Higginson, *J. Chem. Soc.*, **1958**, 260; R. Dyke and W. C. E. Higginson, *ibid.*, **1960**, 1998.

5) H. A. Weakliem and J. L. Hoard, *J. Am. Chem. Soc.*, **81**, 549 (1959).

6) F. P. Dwyer, E. C. Gyarfas, and D. P. Mellor, *J. Phys. Chem.*, **59**, 296 (1955); S. Kirschner and E. C. Gyarfas, *Inorg. Synth.*, Vol. V, 186.

7) B. K. Teo and P. A. Lee, *J. Am. Chem. Soc.*, **101**, 2815 (1979).

8) N. Binsted, S. L. Cook, J. Evans, R. J. Price, and G. N. Greaves, *J. Phys. (Paris), Colloq.*, **47**, C8-589 (1986); N. Binsted, S. L. Cook, J. Evans, G. N. Greaves, and R. J. Price, *J. Am. Chem. Soc.*, **109**, 3669 (1987).

9) K. Okamoto, T. Tsukihara, J. Hidaka, and Y. Shimura, *Bull. Chem. Soc. Jpn.*, **51**, 3534 (1978).

10) Y. Kushi, K. Morimasa, and H. Yoneda, 49th National Meeting of the Chemical Society of Japan, Tokyo, April 1984, Abstr., No. 1N31; Y. Kushi, K. Morimasa, and H. Yoneda, to be published.

11) T. Taura, *Chem. Lett.*, **1984**, 2011.

12) T. Taura, *Inorg. Chem.*, **27**, 2845 (1988).

13) R. Nagao, F. Marumo, and Y. Saito, *Acta Crystallogr., Sect. B*, **28**, 1852 (1972).

Preparation and Characterization of Cobalt(III) Complexes Containing (2-Aminoethyl)dimethylarsine (edma). Resolution and Racemization of *fac*-[Co(edma)$_3$]$^{3+}$

Kazuhiro NEMOTO, Masakazu KITA, Masaaki KOJIMA, and Junnosuke FUJITA*
Department of Chemistry, Faculty of Science, Nagoya University,
Chikusa-ku, Nagoya 464-01
(Received December 1, 1988)

(2-Aminoethyl)dimethylarsine (edma) and its cobalt(III) complexes, *trans*(*X*,*X*),*cis*(*As*,*As*)-[CoX$_2$(edma)$_2$]$^+$ (X=Cl, Br, and I), *trans*(*As*,*As*)- and *trans*(*As*,*N*)-[Co(acac)(edma)$_2$]$^{2+}$ (acac=acetylacetonate ion), *trans*(*As*,*N*)-[Co(CO$_3$)(edma)$_2$]$^+$, [Co(acac)$_2$(edma)]$^+$, and *fac*-[Co(edma)$_3$]$^{3+}$ were prepared and characterized. From a comparison of the first d-d absorption bands of analogous diamine and (2-aminoethyl)dimethylphosphine (edmp) complexes, the spectrochemical series of Group 5B elements was found to be P>As>N. The *fac*-[Co(edma)$_3$]$^{3+}$ complex was resolved and the absolute configuration of the $(+)_{490}^{CD}$-isomer was assigned to *Λ* on the basis of the CD spectrum. Racemization of *fac*-[Co(edma)$_3$]$^{3+}$ was studied in aqueous solutions in the pH and temperature ranges of 7.88—9.32 and 35.0—50.0 °C, respectively. The racemization obeyed a rate law of the form, $R=k$[OH$^-$][complex]. The activation enthalpy and entropy values were found to be $\Delta H^*=132\pm4$ kJ mol^{-1} and $\Delta S^*=171\pm11$ J K^{-1} mol^{-1}, respectively.

In previous papers, we reported the preparation of a number of cobalt(III) complexes containing (2-aminoethyl)dimethylphosphine (edmp)[1,2] and its derivatives.[3-5] To our knowledge, however, no cobalt(III) complex with the arsine analog is known. An (aminoalkyl)arsine is an intermediate ligand between a diamine and a diarsine and its complexes will be useful in studying properties of cobalt(III)–arsine complexes, for which several studies have been reported.[6,7] This paper deals with the preparation and characterization of (2-aminoethyl)dimethylarsine (edma) and its several cobalt(III) complexes, including the resolution and absolute configuration of *fac*-[Co(edma)$_3$]$^{3+}$, and its racemization occured in aqueous solution catalyzed by OH$^-$.

Experimental

The arsine ligand was handled under an atmosphere of nitrogen until it formed air-stable cobalt(III) complexes. Tetrahydrofuran was dried with sodium and deoxygenated by distillation in a stream of nitrogen. Other solvents used for the preparation of complexes were deoxygenated by bubbling nitrogen for 20 min immediately before use. Absorption, circular dichroism, and ^{1}H NMR spectra were recorded on JASCO 610B and Hitachi U-3400 spectrophotometers, a JASCO J-40CS spectropolarimeter, and a Hitachi R-90HS spectrometer, respectively.

(2-Aminoethyl)dimethylarsine (edma). A tetrahydrofuran solution of sodium dimethylarsine was prepared by a modified method of Phillips and Vis.[8] To a mixture of tetrahydrofuran (60 cm^3) and metallic sodium (15.4 g, 0.67 mol) in a 300 cm^3 three-necked round bottom flask was added dropwise a tetrahydrofuran solution (80 cm^3) of iododimethylarsine[9] (46.4 g, 0.20 mol) over a period of 90 min with stirring at 0 °C. After a while the mixture was refluxed for 30 min and then cooled to room temperature. The resulting greenish brown solution was filtered to remove precipitated sodium iodide and unreacted sodium. To the filtrate was added aziridine[10] (10.8 g, 0.25 mol), and the solution was stirred at 35 °C for 60 h, the color of the solution becoming pale gradually. Water (40 cm^3) was added dropwise to the solution, and tetrahydrofuran was removed under reduced pressure. The residue was shaken with diethyl ether to extract edma. The extract was evaporated under reduced pressure to give oily, pale yellow edma. Yield: 15.3 g (51% based on AsI(CH$_3$)$_2$). The ligand could not be purifed by distillation because of its decomposition under usual distilling conditions, but done via the nickel(II) complex. The yellow nickel(II) complex (presumably [Ni(edma)$_2$](ClO$_4$)$_2$) was precipitated immediately by the addition of crude edma (15.3 g) to a methanol solution (100 cm^3) of Ni(ClO$_4$)$_2$·6H$_2$O (18.7 g), filtered, washed with methanol and diethyl ether, and air dried. Yield: 14.1 g. The complex is stable in air but tends to be explosive by mechanical or thermal shock. Thus the elemental analysis was not carried out. The free ligand can be obtained from the complex by treating with KCN in water and by extracting with diethyl ether. ^{1}H NMR edma (=(CH$_3$)$_2$AsCH$_2$CH$_2$NH$_2$)(CDCl$_3$, TMS): δ=0.88 (s, 6H, As(CH$_3$)$_2$), 1.53 (t, 2H, AsCH$_2$), 1.83 (s, 2H, NH$_2$), 2.76 (t, 2H, NCH$_2$). The nickel(II) complex (CD$_3$NO$_2$, TMS): δ=1.67 (s, 6H, As(CH$_3$)$_2$), 2.18 (t, 2H, AsCH$_2$), 2.97 (m, 2H, NCH$_2$), 3.56 (br, 2H, NH$_2$).

***trans*(*Cl*,*Cl*)-[CoCl$_2$(edma)$_2$]ClO$_4$.** To an ethanol solution (50 cm^3) of CoCl$_2$·6H$_2$O (5.0 g, 21.0 mmol) was added crude edma (5.0 g, 33.5 mmol) in ethanol (50 cm^3). A pale blue precipitate was observed. Into this mixture air was bubbled for 1 h, then water (1 cm^3) and concd HCl (1 cm^3) were added, and ethanol was removed under reduced pressure. To the resulting green solution was added NaClO$_4$·H$_2$O (10 g) in water (5 cm^3), and the complex was extracted with dichloromethane. The extract was evaporated to dryness, giving green needle crystals, which were filtered and recrystallized from hot methanol. Yield: 2.20 g. Found: C, 17.83; H, 4.62; N, 5.04%. Calcd for C$_8$H$_{24}$N$_2$As$_2$Cl$_3$O$_4$Co: C, 18.21; H, 4.59; N, 5.31%. ^{1}H NMR (CD$_2$Cl$_2$, TMS): δ=1.54 (s, 12H, As(CH$_3$)$_2$), 2.45 (t, 4H, AsCH$_2$), 3.24 (br, 4H, NCH$_2$), 4.80 (br, 4H, NH$_2$).

***trans*(*Br*,*Br*)-[CoBr$_2$(edma)$_2$]ClO$_4$.** A hot methanol solution (10 cm^3) of *trans*(*Cl*, *Cl*)-[CoCl$_2$(edma)$_2$]ClO$_4$ (1.46 g, 2.77 mmol) was mixed with a hot aqueous solution (10 cm^3) of Na$_2$CO$_3$ (0.32 g, 3.0 mmol), and the mixture was warmed at 60 °C for 15 min to give a red solution. Methanol was

removed under reduced pressure, and the solution was passed through a column of QAE-Sephadex (ClO_4^--form) to remove chloride ions. The eluate was concentrated to ca. 2 cm^3 under reduced pressure. On addition of concd HBr (2 cm^3) the concentrate yielded green crystals, which were filtered, washed with methanol and diethyl ether. Recrystallization was carried out from hot methanol. Yield: 1.64 g. Found: C, 15.86; H, 3.40; N, 4.71%. Calcd for $C_8H_{24}N_2As_2Br_2ClO_4Co$: C, 15.59; H, 3.92; N, 4.71%. ^1H NMR (CD_2Cl_2, TMS): δ=1.70 (s, 12H, $As(CH_3)_2$), 2.50 (t, 4H, $AsCH_2$), 3.36 (m, 4H, NCH_2), 5.05 (br, 4H, NH_2).

***trans*(*I*,*I*)-[CoI_2(edma)$_2$]ClO_4.** This complex was obtained as brown crystals by a method similar to that for the above dibromo complex using KI and 60% $HClO_4$ instead of concd HBr. Yield: 76%. Found: C, 14.03; H, 3.40; N, 4.18%. Calcd for $C_8H_{24}N_2As_2ClI_2O_4Co$: C, 13.53; H, 3.41; N, 3.94%. ^1H NMR (CD_2Cl_2, TMS): δ=1.96 (s, 12H, $As(CH_3)_2$), 2.54 (t, 4H, $AsCH_2$), 3.42 (m, 4H, NCH_2), 4.98 (br, 4H, NH_2).

***trans*(*As*,*N*)-[Co(CO_3)(edma)$_2$]$B(C_6H_5)_4$.** A red solution prepared from *trans*(*Cl*,*Cl*)-[$CoCl_2$(edma)$_2$]ClO_4 (1.46 g, 1.77 mmol) and Na_2CO_3 (0.32 g, 3.0 mmol) by the method for *trans*(*Br*, *Br*)-[$CoBr_2$(edma)$_2$]$^+$ was diluted with water (1 dm^3), and the solution was applied on a column (ϕ 3.0×50 cm) of SP-Sephadex C-25. By elution with 0.05 mol dm^{-3} Na_2SO_4 only one red band developed. The eluate was concentrated to a small volume under reduced pressure, and filtered. On addition of $NaB(C_6H_5)_4$ in water the concentrate yielded a red precipitate, which was filtered, washed with water and methanol, and air dried. The complex with other anions such as Cl^- or ClO_4^- was very soluble and could not be isolated. Found: C, 53.80; H, 6.19; N, 3.86%. Calcd for $C_{33}H_{44}N_2As_2BO_3Co$: C, 53.83; H, 6.02; N, 3.80%. ^1H NMR (DMSO-d_6, TMS): δ=1.34, 1.44, 1.55, 1.66 (s, $As(CH_3)_2$).

***trans*(*As*,*As*)- and *trans*(*As*,*N*)-[Co(acac)(edma)$_2$]$(ClO_4)_2$ (acac=acetylacetonate ion).** A mixture of *trans*(*Cl*, *Cl*)-[$CoCl_2$(edma)$_2$]ClO_4 (300 mg, 0.57 mmol) and Li(acac) (61 mg, 0.57 mmol) in a mixture of water and methanol (2:1, 20 cm^3) was warmed at 60 °C for 3 h. The resulting red solution was diluted with water (500 cm^3) and applied on a column (ϕ 2.0×150 cm) of SP-sephadex C-25. The adsorbed product was eluted with 0.1 mol dm^{-3} Na_2SO_4, giving a faster-moving violet band ([Co(acac)$_2$(edma)]$^+$) and then two red bands. The separation between the latter two bands was small. The eluate containing each red band was collected, diluted 10 times with water, applied again on a small column of SP-Sephadex C-25, and the adsorbed complex was eluted with 1 mol dm^{-3} $NaClO_4$. The eluate containing the first red band was evaporated to a small volume under reduced pressure, and the complex was extracted with dichloromethane. The extract was concentrated to a small volume under reduced pressure. Dark red crystals of *trans*(*As*, *As*)-[Co(acac)(edma)$_2$]$(ClO_4)_2$ were precipitated by slow addition of diethyl ether to the concentrate, filtered, washed with diethyl ether, and air dried. Yield: 29 mg (8%). Found: C, 23.47; H, 4.71; N, 4.12%. Calcd for $C_{13}H_{31}N_2As_2Cl_2O_{10}Co$: C, 23.84; H, 4.77; N, 4.28%. ^1H NMR (CD_3OD, TMS): δ=1.66, 1.91, 2.02 (s, $As(CH_3)_2$ and CCH_3), 5.61 (s, CH), 2.1—2.7 (m, CH_2).

The eluate containing the second red band was concentrated under reduced pressure, yielding red crystals of *trans*-(*As*,*N*)-[Co(acac)(edma)$_2$]$(ClO_4)_2$, which were filtered, washed with a small amount of cold water, and recrystallized from methanol and diethyl ether. Yield: 42 mg (11%). Found: C, 23.85; H, 4.70; N, 4.66%. Calcd for $C_{13}H_{31}N_2As_2Cl_2O_{10}Co$: C, 23.84; H, 4.77; N, 4.28%. ^1H NMR (CD_3OD, TMS): δ=1.58, 1.61, 1.70, 1.88, 1.92, 2.28 (s, $As(CH_3)_2$ and CCH_3), 5.70 (s, CH).

[Co(acac)$_2$(edma)]ClO_4. The free ligand was extracted with diethyl ether from a mixture of [Ni(edma)$_2$]$(ClO_4)_2$ (780 mg, 1.4 mmol) and KCN (560 mg, 8.4 mmol) in water (3 cm^3), and ether was removed under reduced pressure. To this were added a methanol solution (60 cm^3) of [Co(acac)$_3$] (1.0 g, 2.8 mmol) and active charcoal (ca. 0.3 g). The mixture was stirred at room temperature for 13 h, and active charcoal was filtered off. The filtrate was diluted 10 times with water and applied on a column (ϕ 3.0×20 cm) of SP-Sephadex C-25. The column was washed with water to remove unreacted [Co(acac)$_3$], and then the violet adsorbed product was eluted with 0.05 mol dm^{-3} NaCl, a trace of a pink product remaining on the column. The eluate was evaporated under reduced pressure to ca. 5 cm^3. On addition of a few drops of a saturated aqueous solution of $NaClO_4$ the concentrate yielded violet crystals, which were filtered, washed with a small amount of cold water, and recrystallized from methanol and diethyl ether. Yield: 0.91 g (67%). Found: C, 33.36; H, 2.66; N, 5.15%. Calcd for $C_{14}H_{26}NAsClO_8Co$: C, 33.25; H, 2.77; N, 5.18%. ^1H NMR (D_2O, TSP): δ=1.46, 1.71, 1.99, 2.02, 2.06, 2.33 (s, $As(CH_3)_2$ and CCH_3), 5.69, 5.77 (s, CH).

The complex was also yielded as a by-product in the preparation of [Co(acac)(edma)$_2$]$^{2+}$ from *trans*(*Cl*,*Cl*)-[$CoCl_2$-(edma)$_2$]$^+$ and Li(acac) (1:1) (vide ante).

***fac*-[Co(edma)$_3$]$Br_3\cdot 3H_2O$.** To edma, which was obtained from [Ni(edma)$_2$]$(ClO_4)_2$ (560 mg, 1 mmol) and KCN (400 mg, 6 mmol) by the above method, were added $Na_3[Co(CO_3)_3]\cdot 3H_2O$[11] (210 mg, 0.58 mmol) and water (3 cm^3), and the mixture was stirred at 40 °C for 30 min. To the resulting orange solution was added excess $NaClO_4$ (ca. 1 g) dissolved in a minimum amount of water. After 2 h a yellow precipitate ([Co(edma)$_3$]$(ClO_4)_3$) was filtered, and dissolved in water. The solution was applied on a column (ϕ 3.0×90 cm) of SP-Sephadex C-25, and the adsorbed product was eluted with 0.5 mol dm^{-3} KBr, giving a single yellow band. Yellow-brown crystals which were precipitated by concentrating the eluate under reduced pressure were filtered, washed with ethanol, and recrystallized from water. Yield: 230 mg (43%). Found: C, 18.10; H, 5.83; N, 5.20%. Calcd for $C_{12}H_{42}N_3As_3Br_3O_3Co$: C, 18.02; H, 5.29; N, 5.25%. ^1H NMR (D_2O, TSP): δ=1.87, 1.97(s, $As(CH_3)_2$).

Resolution of *fac*-[Co(edma)$_3$]$^{3+}$. Complete resolution of *fac*-[Co(edma)$_3$]$^{3+}$ was achieved by a column-chromatographic method similar to that for [Co(en)$_3$]$^{3+}$ (en=NH_2-$CH_2CH_2NH_2$).[12] An aqueous solution of *fac*-[Co(edma)$_3$]-$Br_3\cdot 3H_2O$ (ca. 100 mg) was applied on a column (ϕ 3.0×90 cm) of SP-Sephadex C-25, and the adsorbed complex was eluted with 0.1 mol dm^{-3} $Na_2[Sb_2\{(+)\text{-tartrate}\}_2]$. Two yellow bands were eluted in good separation. Each eluate was diluted 10 times with water and applied on a small column of SP-Sephadex C-25. The column was washed thoroughly with water, and the adsorbed complex was eluted with 1 mol dm^{-3} KBr. Yellow-brown crystals of optically active *fac*-[Co(edma)$_3$]$Br_3\cdot 3H_2O$ were obtained from the eluate by the same procedure as that for the racemate. The $(+)_{490}^{CD}$-*A* isomer was obtained from the faster-moving band. Found: C, 17.94; H, 4.88; N, 5.30%. Calcd for $C_{12}H_{42}N_3As_3$-Br_3O_3Co=[Co(edma)$_3$]$Br_3\cdot 3H_2O$: C, 18.02; H, 5.29; N, 5.25%.

Kinetic Measurements. Optically active *fac*-$[Co(edma)_3]^{3+}$ (ca. 1.10 mmol dm^{-3}) was racemized in sodium 5,5-diethylbarbiturate ($NaC_8H_{11}N_2O_3$)-HCl buffer solution (pH: 7.88—9.32) with ionic strength of 1.0 (LiCl) in the temperature range of 35.0—50.0 °C. Portions of the solution were withdrawn at intervals, and the decreases in CD strength were recorded in the region of 390—540 nm. In each kinetic run, the plot of ln ($\Delta\varepsilon_t$(492 nm)) vs. time gave a straight line for at least three half-lives, where $\Delta\varepsilon_t$(492 nm) denotes the CD strength at time t and at 492 nm. No change in absorption spectrum was observed during the racemization.

Attempts to examine the racemization of *fac*-$[Co(edmp)_3]^{3+}$ [1] were unsuccessful. The complex was stable to racemization in neutral or acidic solution and decomposed in basic solution to give a blue-white precipitate.

Results and Discussion

Preparation and Characterization of the Complexes. The edma ligand was prepared by a method similar to that for the phosphorus analog, (2-aminoethyl)-dimethylphosphine (edmp)[1] from sodium dimethylarsenide and aziridine in a yield of ca. 50%. 2-Chloroethylamine hydrochloride can be used instead of aziridine but the yield was a little poorer. The ligand could not be purified by vacuum distillation because it decomposed at ca. 40 °C. The purification was carried out via $[Ni(edma)_2](ClO_4)_2$ which easily liberated edma by the addition of excess KCN in water. The yellow $[Ni(edma)_2](ClO_4)_2$ complex in CD_3NO_2 shows sharp signals in the ^1H NMR spectrum and is assumed to be a diamagnetic planar complex. The complex tends to be explosive by mechanical or thermal shock, while the perchlorates of Co(III)-edma complexes prepared in this study are rather stable and burn by heating without exploding.

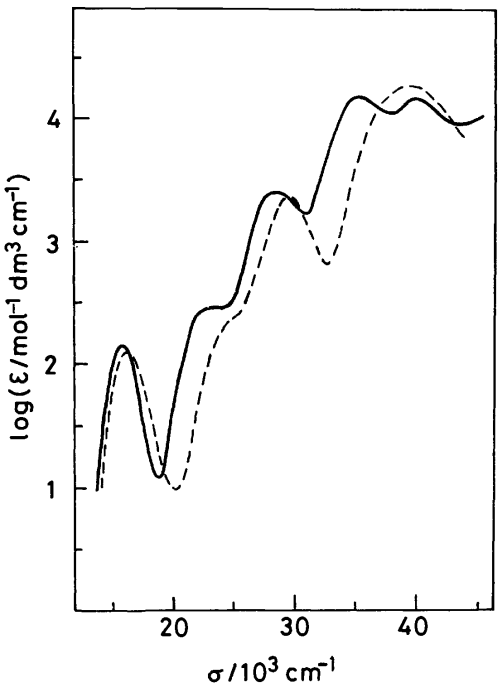

Fig. 1. Absorption spectra of *trans(Cl,Cl),cis(As,As)*-$[CoCl_2(edma)_2]^+$ (——) and *trans(Cl,Cl),cis(P,P)*-$[CoCl_2(edmp)_2]^+$ (----) in methanol.

Only one isomer of $[CoCl_2(edma)_2]^+$ was formed by oxidizing a mixture of $CoCl_2 \cdot 6H_2O$ and edma in ethanol with air, although five geometrical isomers are possible for this type of complex. The reaction of $[Co(CO_3)(edma)_2]^+$ with hydrochloric acid yielded the same isomer. The complex is green in color and shows a medium intensity band at 15800 cm^{-1} in the absorption spectrum. The band is characteristic of a *trans(Cl,Cl)* configuration, and can be assigned to the split component (Ia) of the first d-d band ($^1T_{1g} \leftarrow {}^1A_{1g}$ (O_h)) (Fig. 1). The broad band around 22500 cm^{-1} can be assigned to the other split component (Ib) overlapping with the second d-d band ($^1T_{2g} \leftarrow {}^1A_{1g}(O_h)$). This spectral pattern is very similar to that of *trans(Cl, Cl), cis(P, P)*-$[CoCl_2(edmp)_2]^+$ [3] shown in Fig. 1. Thus the complex can be assingned to the *trans(Cl, Cl), cis(As, As)* isomer, although no clear evidence for the *cis(As, As)* configuration could be obtained from the absorption and ^1H NMR spectra. Table 1 lists the data of absorption spectra.

Figure 2 shows absorption spectra of $[CoX_2(edma)_2]^+$ (X=Br, I), which were prepared from $[Co(CO_3)(edma)_2]^+$ and HX, together with the spectrum of dichloro complex. The lowest energy bands around 15000 cm^{-1} of the dibromo and diiodo complexes are similar in pattern to that of the dichloro complex, and their energies decrease in the order Cl>Br>I in accordance with the spectrochemical series. Thus these dihalogeno complexes can be assigned to the same *trans(X, X), cis(As, As)* isomer.

No *cis(X, X)* isomer was obtained by the reaction of

Table 1. Absorption Spectral Data of Mixed Ligand Complexes

Complex	$\sigma_{max}/10^3$ cm^{-1} ($\log(\varepsilon/cm^{-1}\,mol^{-1}\,dm^3)$)
trans(Cl,Cl)-$[CoCl_2(edma)_2]^{+a)}$	15.8 (2.16), 22.5 (sh, 2.49), 28.4 (3.40), 35.2 (4.17), 39.7 (4.14)
trans(Br,Br)-$[CoBr_2(edma)_2]^{+a)}$	15.0 (2.23), 27.9 (sh, 3.34), 25.5 (3.27), 34.8 (4.36), 42.7 (4.09)
trans(I,I)-$[CoI_2(edma)_2]^{+a)}$	14.1 (2.23), 21.5 (3.69), 29.9 (4.12), 37.8 (4.10)
$[Co(acac)_2(edma)]^{+b)}$	19.0 (2.50), 29.9 (sh, 3.80), 35.7 (sh, 4.23), 39.0 (4.37), 45.0 (4.30)
trans(As,As)-$[Co(acac)(edma)_2]^{2+b)}$	19.2 (3.19), 25.4 (sh 3.80), 28.1 (3.90), 33.0 (4.24), 39.0 (4.10), 45.5 (4.23)
trans(As,N)-$[Co(acac)(edma)_2]^{2+b)}$	20.4 (2.71), 26.3 (sh, 2.80), 29.9 (sh, 3.56), 35.0 (sh, 4.30), 37.8 (4.49), 42.7 (4.13), 46.6 (4.10)
trans(As,N)-$[Co(CO_3)(edma)_2]^{+c)}$	19.7 (2.57), 25.6 (sh, 2.43), 36.2 (4.19)

Solvent, a): CH_3OH, b): H_2O, c): CH_3CN.

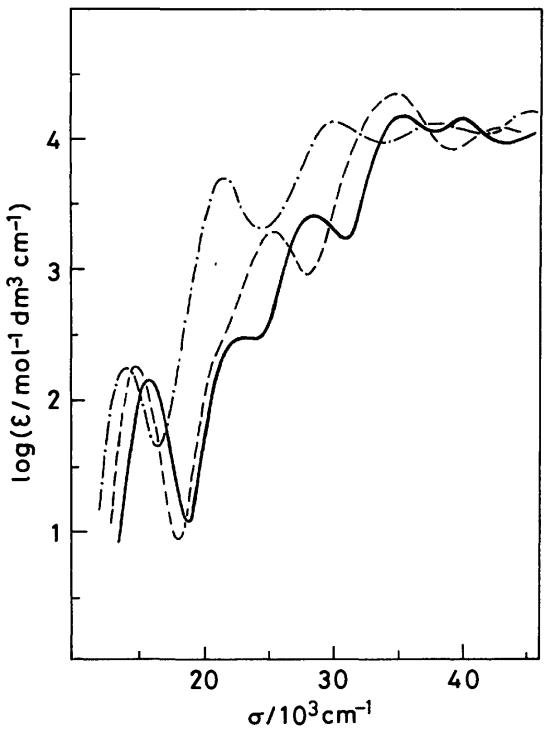

Fig. 2. Absorption spectra of *trans*(*X*,*X*),*cis*(*As*,*As*)-$[CoX_2(edma)_2]^+$ in methanol, X=Cl (——), X=Br (----), and X=I (-·-·-).

$[Co(CO_3)(edma)_2]^+$ with HX under cooling (0 °C). The *cis*(*X*,*X*) isomers of edmp and related (aminoalkyl) phosphine complexes are not known either, while *cis*(*X*,*X*)-$[CoX_2\{(CH_3)_2E(CH_2)_nE(CH_3)_2\}_2]^+$ (n=2, 3. X=Cl, Br. E=P,[13] As[6]) can be prepared from the carbonato complexes by similar procedures. A red aqueous solution of $[Co(CO_3)(edma)_2]^+$ changed to violet and then green fairly rapidly on addition of HX at 0 °C, and gave a green precipitate of the trans dihalogeno complex. The rapid color change from violet to green indicates rapid cis to trans isomerization of the dihalogeno complex.

The $[Co(CO_3)(edma)_2]^+$ complex yielded only one of three possible geometrical isomers, *trans*(*As*, *As*) (C_2 symmetry), *trans*(*As*, *N*) (C_1 symmetry) and *trans*(*N*, *N*) (C_2 symmetry), by the reaction of $[CoCl_2(edma)_2]^+$ with Na_2CO_3. The complex exhibits four kinds of methyl signal in the ^1H NMR spectrum and is clearly assigned to the *trans*(*As*, *N*) isomer from symmetry argument. For the corresponding acac complex, two isomers were obtained by a similar reaction with Li(acac). The isomers are red and dark red in color. The red isomer shows six kinds of methyl signal in the ^1H NMR spectrum and is assigned unequivocally to the *trans*(*As*, *N*) isomer. On the other hand, the dark red isomer gives three kinds of methyl signal, but the structure can not be assigned from the spectrum, since both *trans*(*As*, *As*) and *trans*(*N*, *N*) isomers have a C_2 axis. An analogous phosphine complex, [Co(acac)-$\{(C_6H_5)_2PCH_2CH_2NH_2\}_2]^{2+}$ also yields two isomers.[4]

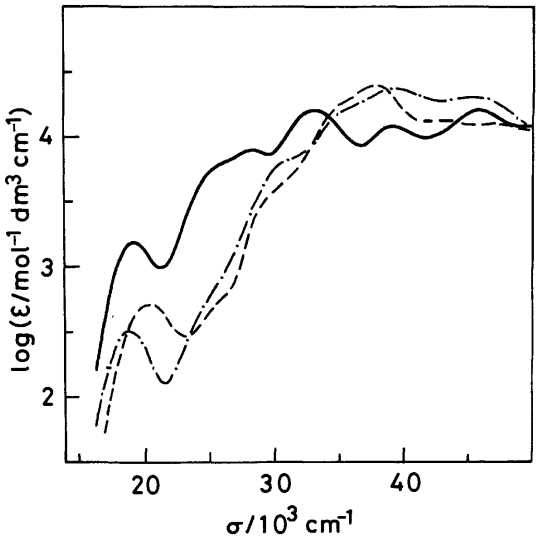

Fig. 3. Absorption spectra of $[Co(acac)_2(edma)]^+$ (-·-·-), *trans*(*As*,*As*)-$[Co(acac)(edma)_2]^{2+}$ (——), and *trans*(*As*,*N*)-$[Co(acac)(edma)_2]^{2+}$ (----) in water.

They were assigned to the *trans*(*P*, *P*) and *trans*(*P*, *N*) isomers on the basis of the coupling constant values between proton or carbon and phosphorus in ^1H and ^{13}C NMR spectra. The isomers of the phosphine complex exhibit absorption spectra quite different from each other; the *trans*(*P*, *P*) isomer shows the first d-d band of strong intensity and a remarkable red shift of charge transfer bands as compared with the corresponding bands of the *trans*(*P*, *N*) isomer. A similar spectral difference is seen between the two isomers of $[Co(acac)(edma)_2]^{2+}$ (Fig. 3). Thus the dark red isomer can be assigned to the *trans*(*As*, *As*) one.

Molecular models indicate that the steric crowding caused by the bulky dimethylarsino group in the three isomers of $[Co(acac)(edma)_2]^{2+}$ increases in the order *trans*(*As*, *As*)<*trans*(*As*, *N*)<*trans*(*N*, *N*). The reason for the *trans*(*N*, *N*) isomer being not formed will be attributable to the most crowded structure. For other two isomers, the more crowded *trans*(*As*,*N*) isomer was formed in a larger amount than the less crowded *trans*(*As*, *As*) isomer. The formation ratio of the dark red *trans*(*As*, *As*) isomer to the red *trans*(*As*, *N*) one was found to be 1:2 by column chromatography of the reaction products. The smaller abundance (less stability) of the less crowded *trans*(*As*, *As*) isomer may be attributable to the trans effect of the arsine donor group. For $[Co(acac)\{(C_6H_5)_2PCH_2CH_2NH_2\}_2]^{2+}$, the formation ratio of the *trans*(*P*, *P*) isomer to the *trans*(*P*, *N*) one is reported to be 1:4.[4] The same reason may be given for the selective formation of more crowded *trans*(*Cl*,*Cl*), *cis*(*As*,*As*)-$[CoCl_2(edma)_2]^+$ than its *trans*-(*Cl*,*Cl*), *trans*(*As*,*As*) isomer.

The violet $[Co(acac)_2(edma)]^+$ complex was obtained by the reaction of $[Co(acac)_3]$ with edma in the presence of active charcoal or as a by-product in the synthesis of $[Co(acac)(edma)_2]^{2+}$. The absorption

spectrum is compared with those of $[Co(acac)(edma)_2]^{2+}$ in Fig. 3.

The reaction of $Na_3[Co(CO_3)_3]$ with edma yielded only one isomer of $[Co(edma)_3]^{3+}$. The isomer showed two kinds of sharp methyl signal in the ^1H NMR spectrum and was assigned to the *fac*-isomer. The phosphorus analog, $[Co(edmp)_3]^{3+}$ also forms only the *fac*-isomer. The selective formation of the *fac*-isomer in these complexes may also be attributable to the trans effect of the arsine or phosphine donor group. The complex was easily resolved on an SP-Sephadex column by elution with an aqueous solution of $Na_2[Sb_2\{(+)\text{-tartrate}\}_2]$. The optically active complex is stable in acidic water but racemizes in basic water (vide infra).

Figure 4 compares the absorption spectrum of *fac*-$[Co(edma)_3]^{3+}$ with those of *fac*-$[Co(edmp)_3]^{3+}$ and

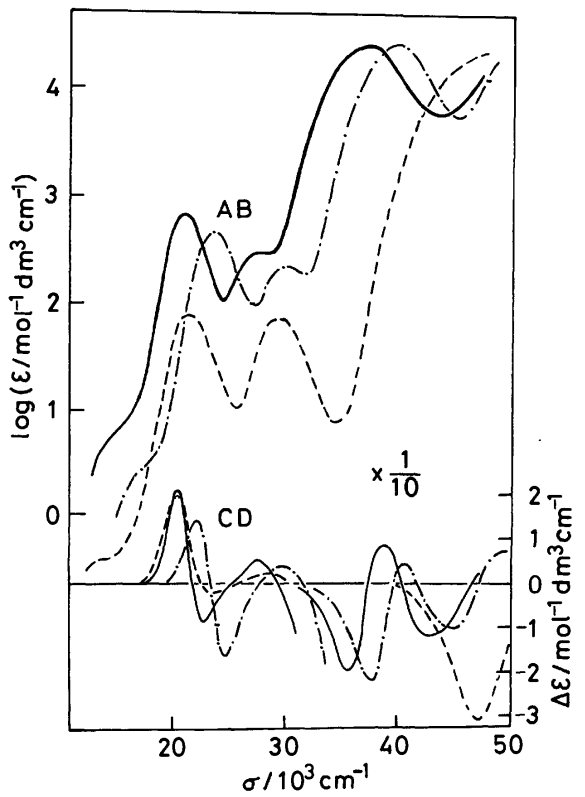

Fig. 4. Absorption and CD spectra of *Λ*-*fac*-$[Co(edma)_3]^{3+}$ (——), *Λ*-*fac*-$[Co(edmp)_3]^{3+}$ (-·-·-), and *Λ*-$[Co(en)_3]^{3+}$ (----) in water.

$[Co(en)_3]^{3+}$, and the data are listed in Table 2. The first absorption band of *fac*-$[Co(edma)_3]^{3+}$ is observed at 21300 cm^{-1}. The energy is almost the same as that of $[Co(en)_3]^{3+}$ (21400 cm^{-1})[14] and much lower than that of *fac*-$[Co(edmp)_3]^{3+}$ (23700 cm^{-1}).[1] The tris-type complex of $(CH_3)_2NCH_2CH_2NH_2$ (Me_2-en) corresponding to edma and edmp is not known. Attempts to prepare $[Co(Me_2\text{-en})_3]^{3+}$ were unsuccessful and bis-diamine complexes such as $[Co(H_2O)_2(Me_2\text{-en})_2]^{3+}$ were yielded even in the presence of a large excess of Me_2-en. However, it is known that cobalt(III) complexes containing Me_2-en exhibit the first d-d band at fairly lower energy than that of the corresponding en complex.[15] For example, the bands of $[Co(acac)_2(Me_2\text{-en})]^+$ and $[Co(acac)_2(en)]^+$ are at 17800 and 18450 cm^{-1}, respectively.[16] Thus it is concluded that the spectrochemical series for the three ligands with donors of the grounp 5B elements is edmp(P)>edma(As)>Me_2-en(N). Besides the first d-d band, *fac*-$[Co(edma)_3]^{3+}$ shows a weak, broad triplet d-d band around 14600 cm^{-1}, the second d-d band at 28000 cm^{-1} and the As to Co(III) charge-transfer band at 37700 cm^{-1}. All these bands are shifted to lower energy by ca. 2000 cm^{-1} than the corresponding bands of *fac*-$[Co(edmp)_3]^{3+}$, but both spectral patterns are very similar. The energy difference between the first and second d-d bands of *fac*-$[Co(edma)_3]^{3+}$ is 6700 cm^{-1}. The value is similar to that of *fac*-$[Co(edmp)_3]^{3+}$ (6500 cm^{-1}) but much smaller than that of $[Co(en)_3]^{3+}$(8100 cm^{-1}). Thus the interelectronic repulsion of the cobalt(III) ion is largely reduced in the edma and edmp complexes. Such large reduction has been reported for other phosphine[1] and arsine complexes[6] of cobalt(III).

Figure 4 shows the CD spectrum of $(+)^{CD}_{490}$-*fac*-$[Co(edma)_3]^{3+}$ togehter with those of *Λ*-*fac*-$[Co(edmp)_3]^{3+}$ [1] and *Λ*-$[Co(en)_3]^{3+}$.[14,17] The $(+)^{CD}_{490}$-$[Co(edma)_3]^{3+}$ isomer gives a similar CD pattern in the first d-d band region to those of other two complexes and can be assigned to the same *Λ* isomer. These isomers are all eluted faster than their antipodes on SP-Sephadex column chromatography by elution with $Na_2[Sb_2\{(+)\text{-tartrate}\}_2]$. In previous papers,[1,18] we reported that the small negative CD component in the first d-d band region of *Λ*-$[Co(en)_3]^{3+}$ is enhanced by replacing en by edmp or $(CH_3)_2PCH_2CH_2P(CH_3)_2$. The strength of the negative CD component of the edma complex is intermedi-

Table 2. Absorption and CD Spectral Data of Tris(chelate)cobalt(III) Complexes in Water

Complex	Absorption $\sigma_{max}/10^3$ cm^{-1} ($\log(\varepsilon/cm^{-1}\ mol^{-1}\ dm^3)$)	CD $\sigma_{ext}/10^3$ cm^{-1} ($\log(\Delta\varepsilon/cm^{-1}\ mol^{-1}\ dm^3)$)
Λ-*fac*-$[Co(edma)_3]^{3+}$	14.6 (sh, 0.67), 21.3 (2.82), 28.0 (2.50), 37.7 (4.43)	20.4 (+2.06), 22.7 (−0.87), 27.6 (+0.55), 35.8 (−19.2), 38.9 (+8.76), 42.7 (−11.7)
Λ-*fac*-$[Co(edmp)_3]^{3+}$ [a]	16.7 (sh, 0.43), 23.7 (2.68), 30.2 (2.36), 39.9 (4.42)	22.3 (+1.54), 24.8 (−1.57), 30.0 (+0.49), 37.9 (−20.6), 41.0 (+4.74), 45.5 (−9.33)
Λ-$[Co(en)_3]^{3+}$ [b]	21.4 (1.97), 29.5 (1.93), 47.1 (4.36)	20.3 (+1.89), 23.4 (−0.16), 28.5 (+0.25), 47.4 (−31)

a) From Ref. 1. b) From Ref. 14.

ate between those of the edmp and en complexes. In the ultraviolet region, both edma and edmp complexes exhibit a negative and a positive CD band from the lower to higher energy side corresponding to each charge-transfer band between the arsine (37700 cm^{-1}), the phosphine (39900 cm^{-1}) or the amine donor group (ca. 50000 cm^{-1}) and the cobalt(III) ion. These CD patterns are also known to be characteristic of *Λ*-[Co(diamine)$_3$]-type complex.[14,19]

Racemization of *fac*-[Co(edma)$_3$]$^{3+}$. Racemization of *fac*-[Co(edma)$_3$]$^{3+}$ was studied in aqueous solutions in the pH and temperature ranges of 7.88—9.32 and 35.0—50.0 °C, respectively. Figure 5 shows a representative CD spectral change of *Λ*-[Co(edma)$_3$]$^{3+}$ in a sodium 5,5-diethylbarbiturate ($NaC_8H_{11}N_2O_3$)-HCl buffer solution (pH: 8.36) at 40 °C in a period of 4225 min. In each kinetic run the plot of $\ln(\Delta\varepsilon_t(492\ nm))$ vs. time at a constant pH gave a straight line for at least three half-lives. Thus the rate of racemization at a constant pH can be expressed as $-d[complex]/dt = k_{obsd}$ [complex], where k_{obsd} is the pseudo-first-order rate constant for racemization at a constant pH. The $k_{obsd}/[OH^-]$ ($=k$) values are constant at a given temperature, indicating that the reaction is first order in $[OH^-]$. The values of k_{obsd} and k are listed in Table 3, where the variation of ionic product of water $k_W=[H^+][OH^-]$ with a change in temperature[20] was taken into consideration. From the temperature dependence of k values, the activation enthalpy and entropy were obtained as 132±4 kJ mol^{-1} and 171±11 J K^{-1} mol^{-1}, respectively. No detectable change in absorption spectrum was observed during the racemization.

The mechanism for racemization of *fac*-[Co(edma)$_3$]$^{3+}$ is not clear at present. The fact that the racemization is catalyzed by OH^- indicates that the first step of the racemization is deprotonation of the amine hydrogen(s). For the present complex a dissociative mechanism involving the rupture of the Co-As bond will be ruled out, since the absorption spectrum of the complex remained unchanged during the racemization; if the arsine part of edma were released from the cobalt(III) ion the ligand would be oxidized by atmospheric oxygen to cause the decomposition of the complex.

The values of activation parameters for racemization

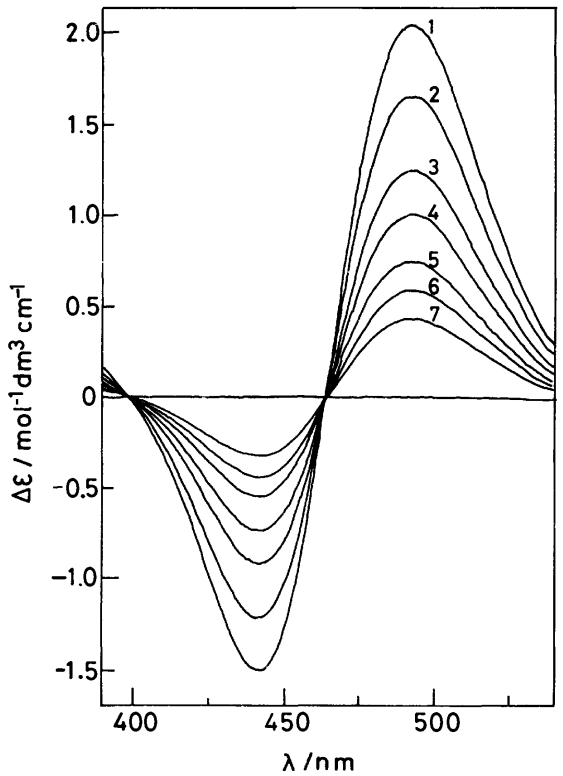

Fig. 5. Change in CD spectrum of *Λ*-*fac*-[Co(edma)$_3$]$^{3+}$ in water at pH 8.36 and 40.0 °C. Spectra 1—7 were measured after 0, 585, 1360, 1960, 2755, 3385, 4225 min, respectively.

Table 3. Racemization Rates of *fac*-[Co(edma)$_3$]$^{3+}$

t / °C	pH	k_{obsd} / 10^{-6} s^{-1}	k / mol^{-1} dm^3 s^{-1}	k (av.) / mol^{-1} dm^3 s^{-1}
50.0	8.39	26.7	1.98	
	8.19	17.3	2.04	2.16 ±0.19
	8.06	13.8	2.20	
	7.88	10.0	2.41	
45.0	8.83	26.3	0.968	
	8.70	19.3	0.958	0.973±0.017
	8.48	12.1	0.997	
	8.32	8.12	0.967	
40.0	8.89	10.6	0.468	
	8.75	7.60	0.463	0.481±0.018
	8.52	4.76	0.493	
	8.39	3.58	0.499	
35.0	9.32	8.10	0.186	
	9.12	3.73	0.171	0.181±0.007
	8.87	2.77	0.179	
	8.68	1.90	0.186	

of *fac*-$[Co(edma)_3]^{3+}$ are similar to those ($\Delta H^{\ddagger}=132\pm6$ kJ mol^{-1}, $\Delta S^{\ddagger}=204\pm18$ J K^{-1} mol^{-1}) reported for racemization of $[Co(stn)]^{3+}$ (stn=$CH_3C(CH_2NHCH_2CH_2CH_2NH_2)_3$), which is also catalyzed by OH^-.[21] For this racemization, a twist intramolecular mechanism via a trigonal twist about the threefold axis of the deprotonated intermediate was proposed. A similar twist mechanism may be assumed for the racemization of *fac*-$[Co(edma)_3]^{3+}$, although it is unknown whether the rupture of the Co-N bond is involved or not.

The *fac*-$[Co(edmp)_3]^{3+}$ complex was stable to racemization in acidic water, but decomposed in basic water to give a blue-white precipitate which was supposed to be cobalt(III) species. The decomposition rate observed by a decrease in intensity of the first d-d band was nearly the same as the diminishing rate of the CD strength. The decomposition of the complex is supposed to take place in preference to the racemization. On the other hand, it is known that $[Co(en)_3]^{3+}$ in water does not racemize and does in the presence of excess en[22] or active charcoal.[23] Such different properties in racemization of three typical complexes, $[Co(en)_3]^{3+}$, *fac*-$[Co(edmp)_3]^{3+}$, and *fac*-$[Co(edma)_3]^{3+}$ will provide useful information in elucidating bonding character between cobalt(III) and 5B group donor atoms.

The present work was supported by a Grant-in-Aid for Scientific Research No. 61430013 from the Ministry of Education, Science and Culture.

References

1) I. Kinoshita, K. Kashiwabara, J. Fujita, K. Matsumoto, and S. Ooi, *Bull. Chem. Soc. Jpn.*, **54**, 2683 (1981).

2) a) T. Ohishi, K. Kashiwabara, H. Ito, T. Ito, and J. Fujita, *Bull. Chem. Soc. Jpn.*, **56**, 1551 (1983). b) T. Ohishi, K. Kashiwabara, and J. Fujita, *ibid.*, **56**, 1553 (1983). c) T. Ohishi, S. Ohba, K. Kashiwabara, Y. Saito and J. Fujita, *ibid.*, **57**, 877 (1984).

3) I. Kinoshita, Y. Yokota, K. Matsumoto, S. Ooi, K. Kashiwabara, and J. Fujita, *Bull. Chem. Soc. Jpn.*, **56**, 1067 (1983).

4) M. Atoh, I. Kinoshita, K. Kashiwabara, and J. Fujita, *Bull. Chem. Soc. Jpn.*, **55**, 3179 (1982).

5) a) K. Kashiwabara, I. Kinoshita, T. Ito, and J. Fujita, *Bull. Chem. Soc. Jpn.*, **54**, 725 (1981). b) M. Atoh, K. Kashiwabara, H. Ito, T. Ito, and J. Fujita, *ibid.*, **57**, 3139 (1984). c) M. Takata, K. Kashiwabara, H. Ito, T. Ito, and J. Fujita, *ibid.*, **58**, 2247 (1985).

6) K. Iwata, M. Kojima, and J. Fujita, *Bull. Chem. Soc. Jpn.*, **58**, 3003 (1985).

7) a) R. S. Nyholm, *J. Chem. Soc.*, **1950**, 2071. b) F. H. Burstall and R. S. Nyholm, *ibid.*, **1952**, 3570. c) T. M. Dunn, R. S. Nyholm, and S. Yamada, *ibid.*, **1962**, 1564. d) R. G. Pearson, *J. Am. Chem. Soc.*, **85**, 3553 (1963); *J. Chem. Educ.*, **45**, 581 (1968). e) B. K. W. Baylis and J. C. Bailar, Jr., *Inorg. Chem.*, **9**, 641 (1970). f) P. K. Bernstein, G. A. Rodley, R. Marsh, and H. B. Gray, *ibid.*, **11**, 3040 (1972). g) B. Bosnich, W. G. Jackson, and W. McLaren, *ibid.*, **13**, 1133 (1974). h) R. D. Feltham, H. G. Metzger, and W. Silverthorn, *ibid.*, **7**, 2003 (1968). i) H. C. Jewiss, W. Levason, and M. Webster, *ibid.*, **25**, 1997 (1986).

8) J. R. Phillips and J. H. Vis, *Can. J. Chem.*, **45**, 676 (1967).

9) G. J. Burrows and E. E. Turner, *J. Chem. Soc.*, **1920**, 1373.

10) V. P. Wystrach and F. C. Schaefer, *J. Am. Chem. Soc.*, **78**, 1263 (1956).

11) H. F. Bauer and W. C. Drinkard, *J. Am. Chem. Soc.*, **82**, 5031 (1960).

12) Y. Yoshikawa and K. Yamasaki, *Inorg. Nucl. Chem. Lett.*, **6**, 523 (1970).

13) T. Ohishi, K. Kashiwabara, and J. Fujita, *Bull. Chem. Soc. Jpn.*, **60**, 575 (1987).

14) M. Kojima, H. Yamada, H. Ogino, and J. Fujita, *Bull. Chem. Soc. Jpn.*, **50**, 2325 (1977).

15) K. Akamatsu and Y. Shimura, *Bull. Chem. Soc. Jpn.*, **51**, 2586 (1978).

16) Y. Ouyang, M. Kojima, and J. Fujita, *Bull. Chem. Soc. Jpn.*, **57**, 3574 (1984).

17) Y. Saito, K. Nakatsu, M. Shiro, and H. Kuroya, *Acta Crystallogr.*, **8**, 729 (1955); *Bull. Chem. Soc. Jpn.*, **30**, 795 (1957).

18) T. Ohishi, K. Kashiwabara, and J. Fujita, *Bull. Chem. Soc. Jpn.*, **56**, 3441 (1983).

19) a) K. Ogino, K. Murano, and J. Fujita, *Inorg. Nucl. Chem. Lett.*, **4**, 351 (1968); A. J. MaCaffery, S. F. Mason, B. J. Norman, and A. M. Sargeson, *J. Chem. Soc. A*, **1968**, 1304; S. F. Mason and R. H. Seal, *Mol. Phys.*, **31**, 755 (1976).

20) H. S. Harned and R. A. Robinson, *Trans. Faraday Soc.*, **36**, 973 (1940).

21) U. Sakaguchi, K. Tomioka, T. Kashihara, and H. Yoneda, *Inorg. Chem.*, **24**, 463 (1985).

22) B. Douglas, *J. Am. Chem. Soc.*, **76**, 1020 (1954).

23) W. G. Gehman and W. C. Fernelius, *J. Inorg. Nucl. Chem.*, **9**, 71 (1959).

A New Method for the Preparation of α-Methylene-γ-butyrolactones Using 3-Ethoxycarbonyl-3-(phenylsulfonyl)cyclobutanone

Tooru FUJIWARA, Koichi MORITA, and Takeshi TAKEDA*
Department of Industrial Chemistry, Faculty of Technology, Tokyo University of Agriculture and Technology, Koganei, Tokyo 184
(Received July 6, 1988)

The reaction of 3-ethoxycarbonyl-3-(phenylsulfonyl)cyclobutanone with Grignard reagent or aryllithium gave 1-(alkyl or aryl)-3-ethoxycarbonyl-3-(phenylsulfonyl)cyclobutanol which was treated with potassium hydride, reduced with $LiBH_4$ in the presence of $ZnCl_2$, and treated with *p*-TsOH or aluminum triisopropoxide successively to give α-methylene-γ-butyrolactone in good yield.

In recent years, much attention has been paid on the synthesis of the compounds possessing α-methylene-γ-butyrolactone moiety because of their wide range of biological activity and various methods have been developed for the construction of such a structural unit.[1]

Previously, we showed that β-methylene ketones were obtained by the base-promoted ring-opening reaction of 1,3-dialkyl-3-(phenylsulfonyl)cyclobutanols.[2] Based on the results of above study, we investigated a new synthetic route to α-methylene-γ-butyrolactone (**9**) using 3-ethoxycarbonyl-3-(phenylsulfonyl)cyclobutanone (**5**) as a starting material as shown in the following scheme. The cyclobutanone (**5**) was synthesized from 3-(phenylthio)-3-(trimethylsilyl)cyclobutanol (**1**) which was easily prepared by the reaction of epichlorhydrin with α,α-bis(trimethylsilyl)phenylthiomethyllithium.[3] The cyclobutane (**1**) was oxidized with potassium peroxymonosulfate (oxone) to give the corresponding sulfone (**2**). Hydrolysis of the trimethylsilyl group and trimethylsilylation of the hydroxy group gave **3**. The trimethylsilyl ether (**3**) was treated with lithium diisopropylamide and ethyl chloroformate successively to give the hydroxy ester (**4**) which was then oxidized with dimethyl sulfoxide-acetic anhydride[4] to afford the cyclobutanone (**5**).

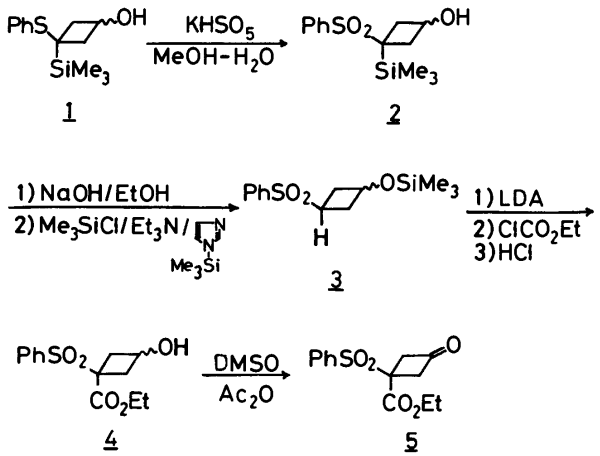

Scheme 1.

3-Ethoxycarbonyl-1-phenyl-3-(phenylsulfonyl)cyclobutanol (**6c**) was obtained in good yield by the reaction of the cyclobutanone (**5**) with phenylmagnesium bromide in THF at 0 °C. Then **6c** was treated with 4 equimolar amounts of KH in THF in the presence of HMPA to give γ-oxo-α-methylene ester (**7c**) along with a trace amount of the isomeric α,β-unsaturated ester. The selective reduction of **7c** was performed with $LiBH_4$ in ether at 0 °C in the presence of a catalytic amount of $ZnCl_2$ and a mixture of γ-hydroxy-α-methylene ester (**8c**) and α-methylene-γ-phenyl-γ-butyrolactone (**9c**) was obtained. The treatment of the mixture with *p*-TsOH in toluene at room temperature gave **9c** in good yield.

In a similar manner, several α-methylene-γ-butyrolactones (**9**) were synthesized using Grignard and aryllithium reagents and the results were summarized in Table 1. Since the treatment of **8d** and **8e** with *p*-TsOH gave complex mixtures, the lactonization of these compounds was carried out with an equimolar amount of aluminum triisopropoxide in refluxing THF.

The most coventional methods for the preparation of γ-substituted α-methylene-γ-butyrolactone (**9**) consist of the reaction of aldehyde with various carbanions which have an ester function or its equivalent. It is noted that the γ-substituent of **9** is introduced using carbanion species, which is the distinctive feature of the present method.

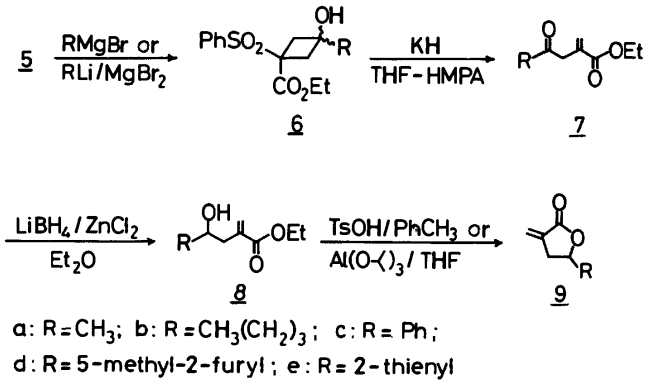

Scheme 2.

Table 1. Preparation of α-Methylene-γ-butyrolactones (**9**)

	R	Products (yield/%)		
		6	**7**	**9**
a	CH_3	62	67	65
b	$CH_3(CH_2)_3$	51	71	85
c	Ph	81	85	83
d	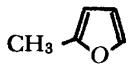	84	78	83
e		70	73	74

Experimental

Preparation of 3-(Phenylsulfonyl)-3-(trimethylsilyl)cyclobutanol (2). To a MeOH (4 ml) solution of 3-(phenylthio)-3-(trimethylsilyl)cyclobutanol (**1**)[3] (252 mg, 1 mmol) was added an aqueous solution (4 ml) of 49.5% $KHSO_5$ (922 mg, 3 mmol) under cooling with ice. After stirring for 1.5 h at room temperature, the reaction mixture was diluted with water. The organic material was extracted with CH_2Cl_2. The extract was dried over Na_2SO_4 and condensed under reduced pressure. The residue was chromatographed on silica gel (AcOEt–hexane) and 3-(phenylsulfonyl)-3-(trimethylsilyl)cyclobutanol (**2**) (265 mg) was isolated in 93% yield.

2: mp 113—115 °C (hexane–benzene); IR (KBr) 3500, 2990, 2940, 1453, 1300, 1256, 1141, 1120, 1090, 850, and 748 cm^{-1}; ^1H NMR ($CDCl_3$) δ=0.02 and 0.19 (2s, 9H), 1.98—3.11 (m, 5H), 3.34—4.25 (m, 1H), and 7.21—8.02 (m, 5H). Found: C, 54.99; H, 7.14; S, 11.24%. Calcd for $C_{13}H_{20}O_3SSi$: C, 54.89; H, 7.09; S, 11.27%.

Preparation of 1-(Phenylsulfonyl)-3-(trimethylsiloxy)cyclobutane (3). To a EtOH (200 ml) solution of the cyclobutanol (**2**) (14.22 g, 50 mmol) was added pellet NaOH (1.0 g, 25 mmol). After stirring for 1 h at room temperature, the reaction mixture was diluted with water and neutralized with 1 M hydrochloric acid (1 M=1 mol dm^{-3}). The organic material was extracted with AcOEt and the extract was dried over Na_2SO_4. The extract was condensed under reduced pressure to give crude 3-(phenylsulfonyl)cyclobutanol. A THF (80 ml) solution of the crude cyclobutanol was slowly added to a mixture of triethylamine (7.7 ml, 55 mmol), chlorotrimethylsilane (7.0 ml, 55 mmol), and *N*-(trimethylsilyl)imidazole (0.29 ml, 2 mmol) in THF (50 ml) under cooling with ice. The reaction mixture was stirred overnight at room temperature. The reaction was quenched by addition of saturated aqueous solution of $NaHCO_3$ and the organic material was extracted with AcOEt. The extract was dried (Na_2SO_4) and condensed in vacuo. The residue was purified by column chromatography on silica gel (AcOEt–hexane) to give 1-(phenylsulfonyl)-3-(trimethylsiloxy)cyclobutane (**3**) (12.84 g) in 90% yield.

3: oil; IR (neat) 3080, 2970, 1453, 1312, 1256, 1155, 1132, 1094, 993, 907, 850, 736, and 698 cm^{-1}; ^1H NMR ($CDCl_3$) δ=0.08 (s, 9H), 2.00—4.81 (m, 6H), and 7.33—7.98 (m, 5H). Found: C, 54.72; H, 7.10; S, 11.23%. Calcd for $C_{13}H_{20}O_3SSi$: C, 54.89; H, 7.09; S, 11.27%.

Preparation of 3-Ethoxycarbonyl-3-(phenylsulfonyl)cyclobutanol (4). To a THF (45 ml) solution of lithium diisopropylamide prepared from diisopropylamine (4.912 g, 48.5 mmol) and butyllithium (46.3 mmol) was slowly added a THF (60 ml) solution of the (trimethylsiloxy)cyclobutane (**3**) (12.55 g, 44.1 mmol) under cooling with ice. After stirring for 40 min, the reaction mixture was cooled to −78 °C. A THF solution (20 ml) of ethyl chloroformate (4.6 ml, 48.6 mmol) was added to the reaction mixture and stirred for 2 h at the same temperature. Then 2 M hydrochloric acid (50 ml) was added under cooling with ice and the mixture was stirred for 15 min. The organic material was extracted with AcOEt and the extract was dried over Na_2SO_4. After evaporation of the solvent, the residue was chromatographed on silica gel (AcOEt–hexane) to give 3-ethoxycarbonyl-3-(phenylsulfonyl)cyclobutanol (**4**) (10.96 g) in 87% yield.

4: viscous oil; IR (neat) 3510, 3060, 2960, 1727, 1450, 1308, 1290, 1151, 1085, 860, 730, and 695 cm^{-1}; ^1H NMR ($CDCl_3$) δ=1.11 (t, J=7 Hz, 3H), 2.33—3.40 (m, 4H), 3.40—3.82 (m, 1H), 4.03 (q, J=7 Hz, 2H), 4.25 —4.85 (m, 1H), and 7.30—8.07 (m, 5H). MS (FAB) m/z 285 (M^++H).

Preparation of 3-Ethoxycarbonyl-3-(phenylsulfonyl)cyclobutanone (5). To a dimethyl sulfoxide (31 ml) solution of the cyclobutanol (**4**) (2.92 g, 10.3 mmol) was added acetic anhydride (20.5 ml) and the mixture was stirred for 17 h at room temperature. Then it was diluted with a phosphate buffer solution (pH 7) under cooling with ice to form brownish precipitate. The precipitate was collected and dried in vacuo. The crude material was recrystallized from hexane–benzene to give pure 3-ethoxycarbonyl-3-(phenylsulfonyl)cyclobutanone (**5**) (1.91 g) in 68% yield.

5: mp 134—135 °C (hexane–benzene); IR (KBr) 3080, 2990, 2950, 1801, 1730, 1452, 1380, 1314, 1288, 1152, 1089, 765, 734, and 700 cm^{-1}; ^1H NMR ($CDCl_3$) δ=1.20 (t, J=7 Hz, 3H), 3.10—4.25 (m, 4H), 4.16 (q, J=7 Hz, 2H), and 7.27—8.00 (m, 5H). Found: C, 55.34; H, 4.98; S, 11.35%. Calcd for $C_{13}H_{14}O_5S$: C, 55.31; H, 5.00; S, 11.35%.

Reaction of 3-Ethoxycarbonyl-3-(phenylsulfonyl)cyclobutanone (5) with Phenylmagnesium Bromide. To a THF (0.5 ml) solution of phenylmagnesium bromide (0.55 mmol) was slowly added a THF (2 ml) solution of 3-ethoxycarbonyl-3-(phenylsulfonyl)cyclobutanone (**5**) (141 mg, 0.5 mmol) under cooling with ice. After stirring for 10 min at the same temperature, the reaction was quenched by addition of saturated aqueous solution of NH_4Cl and the organic material was extracted with AcOEt. The extract was dried over Na_2SO_4 and condensed under reduced pressure. The residual crude crystal was purified by recrystallization from hexane–benzene and 3-ethoxycarbonyl-1-phenyl-3-(phenylsulfonyl)cyclobutanol (**6c**) (146 mg) was obtained in 81% yield.

6c: mp 141—142 °C (hexane–benzene); IR (KBr) 3480, 3050, 3020, 2980, 1714, 1445, 1368, 1301, 1140, 1086, 1021, 916, 870, 853, 702, and 669 cm^{-1}; ^1H NMR ($CDCl_3$) δ=0.98 and 1.10 (2t, J=7 and 6 Hz, 3H), 2.56—3.60 (m, 5H), 3.91 and 4.06 (2q, J=7 and 6 Hz, 2H), and 6.93—7.90 (m, 10H). Found: C, 63.31; H, 5.55; S, 8.88%. Calcd for $C_{19}H_{20}O_5S$: C, 63.31; H, 5.59; S, 8.90%.

By a similar manner, the cyclobutanol (**6a**) was obtained. The cyclobutanols (**6b**, **6d**, and **6e**) were prepared by the reaction of **5** with butyllithium, 5-methyl-2-furyllithium,

and 2-thienyllithium in the presence of an equimolar amount of $MgBr_2$, respectively. These compounds were isolated by TLC (AcOEt-hexane).

All the cyclobutanols (**6**) were obtained as a mixture of diastereomers and the ratio of isomers of these compounds was not determined.

3-Ethoxycarbonyl-1-methyl-3-(phenylsulfonyl)cyclobutanol (6a): viscous oil; IR (neat) 3500, 3060, 2970, 1724, 1447, 1308, 1290, 1174, 1140, 1085, 955, 725, and 690 cm^{-1}; ^1H NMR ($CDCl_3$) δ=1.10 (t, J=7 Hz, 3H), 1.29 (s, 3H), 2.42—3.28 (m, 4H) 3.28—3.80 (br s, 1H), 4.06 (q, J=7 Hz, 2H), and 7.28—7.95 (m, 5H). MS (FAB) m/z 299 (M^++H). **1-Butyl-3-ethoxycarbonyl-3-(phenylsulfonyl)cyclobutanol (6b):** viscous oil; IR (neat) 3500, 3060, 2950, 2870, 1723, 1446, 1307, 1141, 1085, 1024, 932, 850, 724, and 692 cm^{-1}; ^1H NMR ($CDCl_3$) δ=1.09 (t, J=7 Hz, 3H), 0.62—1.93 (m, 9H), 2.23—3.20 (m, 4H), 3.33—3.73 (br s, 1H), 4.03 (q, J=7 Hz, 2H), and 7.27—7.93 (m, 5H). MS (FD) m/z 341 (M^++H). **3-Ethoxycarbonyl-1-(5-methyl-2-furyl)-3-(phenylsulfonyl)cyclobutanol (6d):** mp 95—96 °C (hexane-benzene); IR (KBr) 3500, 3080, 3070, 2980, 2960, 1710, 1447, 1310, 1145, 1086, 1024, 955, 858, 802, 766, 727, and 696 cm^{-1}; ^1H NMR ($CDCl_3$) δ=1.04 (t, J=7 Hz, 3H), 2.21 (s, 3H), 3.20 (s, 4H), 3.44 (br s, 1H), 3.96 (q, J=7 Hz, 2H), 5.73—5.90 (m, 1H), 6.08 (d, J=3 Hz, 1H), and 7.30—7.98 (m, 5H). Found: C, 59.34; H, 5.52; S, 8.77%. Calcd for $C_{18}H_{20}O_6S$: C, 59.33; H, 5.53; S, 8.80%. **3-Ethoxycarbonyl-3-(phenylsulfonyl)-1-(2-thienyl)-cyclobutanol (6e):** mp 110—111 °C (hexane-benzene): IR (KBr) 3490, 3070, 2990, 1720, 1290, 1156, 1141, 1086, 729, and 703 cm^{-1}; ^1H NMR ($CDCl_3$) δ=1.00 (t, J=7 Hz, 3H), 3.27 (br s, 4H), 3.91 (q, J=7 Hz, 2H), 3.67—4.23 (m, 1H), 6.68—6.93 (m, 2H), 7.02—7.23 (m, 1H), and 7.37—7.92 (m, 5H). Found: C, 55.82; H, 4.95; S, 17.30%. Calcd for $C_{17}H_{18}O_5S_2$: C, 55.72; H. 4.95; S, 17.50%.

Preparation of Ethyl 2-Methylene-4-oxo-4-phenylbutyrate (7c). To a suspension of KH (144 mg, 3.6 mmol) in THF (4 ml)-HMPA (3 ml) was added a THF (6 ml) solution of 3-ethoxycarbonyl-1-phenyl-3-(phenylsulfonyl)cyclobutanol (**6c**) (325 mg, 0.9 mmol) at −23 °C. After being stirred for 50 min at the same temperature, the reaction was quenched by addition of a phosphate buffer solution (pH 7). The organic material was extracted with ether and the extract was dried (Na_2SO_4). After removal of the solvent, the residue was chromatographed on silica gel (AcOEt-hexane) and **7c** (168 mg) was isolated in 85% yield. **7c:** viscous oil; IR (neat) 3060, 2980, 1708, 1686, 1632, 1321, 1303, 1199, 1146, 1026, 952, 758, and 690 cm^{-1}; ^1H NMR (CCl_4) δ=1.23 (t, J=7 Hz, 3H), 3.82 (s, 2H), 4.06 (q, J=7 Hz, 2H), 5.49 (br s, 1H), 6.17 (br s, 1H), 7.13—7.53 (m, 3H), and 7.58—7.97 (m, 2H). Found: C, 71.22; H, 6.47%. Calcd for $C_{13}H_{14}O_3$: C, 71.54; H, 6.47%.

In the same procedure, α-methylene-γ-oxo esters (**7a**, **7b**, **7d**, and **7e**) were synthesized. **Ethyl 2-methylene-4-oxovalerate (7a):** viscous oil; IR (neat) 2980, 2950, 2920, 1715, 1635, 1335, 1308, 1205, 1148, 1028, and 950 cm^{-1}; ^1H NMR (CCl_4) δ=1.26 (t, J=7 Hz, 3H), 2.09 (s, 3H), 3.25 (br s, 2H), 4.13 (q, J=7 Hz, 2H), 5.51 (br s, 1H), and 6.18 (br s, 1H). MS m/z 156 (M^+). **Ethyl 2-methylene-4-oxooctanoate (7b):** viscous oil; IR (neat) 2960, 2940, 2880, 1740, 1720, 1633, 1333, 1305, 1190, 1151, 1030, and 954 cm^{-1}; ^1H NMR (CCl_4) δ=1.27 (t, J=7 Hz, 3H), 0.65—1.80 (m, 7H), 2.37 (br t, J=6 Hz, 2H), 3.21 (br s, 2H), 4.08 (q, J=7 Hz, 2H), 5.45 (br s, 1H), and 6.11 (br s, 1H). Found: C, 66.25; H, 9.22%. Calcd for $C_{11}H_{18}O_3$: C, 66.64; H, 9.15%. **Ethyl 2-Methylene-4-(5-methyl-2-furyl)-4-oxobutyrate (7d):** viscous oil; IR (neat) 3110, 2980, 1720, 1707, 1671, 1637, 1515, 1317, 1202, 1147, 1062, 1030, 956, and 804 cm^{-1}; ^1H NMR (CCl_4) δ=1.21 (t, J=7 Hz, 3H), 2.33 (s, 3H), 3.64 (s, 2H), 4.09 (q, J=7 Hz, 2H), 5.54 (br s, 1H), 6.03 (br d, J=3 Hz, 1H), 6.18 (br s, 1H), and 6.93 (d, J=3 Hz, 1H). MS (FAB) m/z 223 (M^++H). **Ethyl 2-methylene-4-oxo-4-(2-thienyl)butyrate (7e):** viscous oil; IR (neat) 3090, 2970, 1720, 1706, 1658, 1519, 1411, 1313, 1200, 1147, 1024, 951, 855, 818, and 728 cm^{-1}; ^1H NMR (CCl_4) δ=1.20 (t, J=7 Hz, 3H), 3.80 (s, 2H), 4.08 (q, J=7 Hz, 2H), 5.59 (br s, 1H), 6.21 (br s, 1H), 6.97 (dd, J=5 and 4 Hz, 1H), 7.50 (dd, J=5 and 1 Hz, 1H), and 7.62 (dd, J=4 and 1 Hz, 1H). MS (FAB) m/z 225 (M^++H).

Preparation of 4,5-Dihydro-3-methylene-5-phenyl-2(3*H*)-furanone (9c). The ethereal solution (1.8 ml) of $LiBH_4$ (1.1 mmol) was added to a suspension of $ZnCl_2$ (41 mg, 0.3 mmol) in ether (2 ml) under cooling with ice. An ether (2 ml) solution of **7c** (218 mg, 1 mmol) was slowly added to a resulting white suspension and the reaction mixture was stirred for 15 min under cooling with ice. The reaction was quenched by addition of 2 M hydrochloric acid and the organic material was extracted with ether. The extract was washed with water and dried over Na_2SO_4. After evaporation of the solvent, the residue was dissolved in toluene (4 ml) and p-toluenesulfonic acid (75 mg, 0.44 mmol) was added at room temperature. After being stirred for 2 h, the reaction mixture was diluted with ether (10 ml) and the organic layer was washed with water and brine, dried (Na_2SO_4), and condensed under reduced pressure. The residue was chromatographed on silica gel (AcOEt-hexane) and **9c** (138 mg) was obtained in 83% yield.

9c: mp 50—51 °C (lit,[18] 48—49.5 °C); IR (neat) 3020, 2960, 1760, 1704, 1664, 1320, 1276, 1130, 1026, 816, 758, and 701 cm^{-1}; ^1H NMR ($CDCl_3$) δ=2.76 (ddt, J=17, 7, and 2.5 Hz, 1H), 3.39 (ddt, J=17, 8, and 2.5 Hz, 1H), 5.46 (dd, J=7 and 8 Hz, 1H), 5.63 (t, J=2.5 Hz, 1H), 6.25 (t, J=2.5 Hz, 1H), and 7.32 (s, 5H).

In a similar manner, α-methylene-γ-butyrolactones (**9a** and **9b**) were synthesized. **9d** and **9e** were prepared by the treatment of the crude reduction product (**8**) with an equimolar amount of aluminum triisopropoxide in refluxing THF (10 ml per 1 mmol of **8**) for 2 h.

4,5-Dihydro-3-methylene-5-methyl-2(3*H*)-furanone (9a): oil; IR (neat) 2980, 2930, 1760, 1665, 1440, 1400, 1340. 1280, 1261, 1116, 1042, 957, and 818 cm^{-1}; ^1H NMR (CCl_4) δ=1.42 (d, J=6 Hz, 3H), 2.47 (ddt, J=17, 6, and 3 Hz, 1H), 3.10 (ddt, J=17, 7, and 3 Hz, 1H), 4.58 (d quint, J=7 and 6 Hz, 1H), 5.55 (t, J=3 Hz, 1H), and 6.04 (t, J=3 Hz, 1H). Found: C, 63.98; H, 7.37%. Calcd for $C_6H_8O_2$: C, 64.27; H, 7.19%. **5-Butyl-4,5-dihydro-3-methylene-2(3*H*)-furanone (9b):** oil; IR (neat) 2960, 2930, 2870, 1760, 1665, 1399, 1350, 1280, 1118, 1007, 933, and 818 cm^{-1}; ^1H NMR (CCl_4) δ=0.60—1.92 (m, 9H), 2.47 (ddt, J=17, 6, and 2.5 Hz, 1H), 3.04 (ddt, J=17, 7, and 2.5 Hz, 1H), 4.01—4.63 (m, 1H), 5.48 (t, J=2.5 Hz, 1H), and 6.00 (t, J=2.5 Hz, 1H). Found: C, 69.55; H, 9.29%. Calcd for $C_9H_{14}O_2$: C, 70.10; H, 9.15%. **3,5-Dihydro-5-(5-methyl-2-furyl)-3-methylene-2(3*H*)-furanone (9d):** viscous oil; IR (neat) 3120, 3100, 2920, 1760, 1663, 1512, 1438, 1398, 1317, 1280, 1259, 1128, 1030, 966, 906, and 801 cm^{-1}; ^1H NMR (CCl_4) δ=2.17 (s, 3H), 3.01 (dt, J=7 and 2.5 Hz, 2H), 5.18 (t,

J=7 Hz, 1H), 5.45 (t, J=2.5 Hz, 1H), 5.75 (br s, 1H), 5.99 (t, J=2.5 Hz, 1H), and 6.03 (d, J=3 Hz, 1H). Found: C, 66.95; H, 5.73%. Calcd for $C_{10}H_{10}O_3$: C, 67.40; H, 5.66%. MS (FD) m/z 178 (M^+). **3,5-Dihydro-3-methylene-5-(2-thienyl)-2(3*H*)-furanone (9e):** viscous oil; IR (neat) 3100, 2970, 2930, 1759, 1664, 1435, 1277, 1251, 1125, 1020, 854, 815, and 710 cm^{-1}; ^1H NMR (CCl_4) δ=2.48—3.60 (m, 2H), 5.33—5.73 (m, 2H), 6.03 (t, J=3 Hz, 1H), and 6.67—7.28 (m, 3H). Found: C, 59.76; H, 4.60; S, 17.52%. Calcd for $C_9H_8O_2S$: C, 59.98; H, 4.47; S, 17.79%.

References

1) For general reviews: P. A. Grieco, *Synthesis,* **1975**, 67; H. M. R. Hoffmann and J. Rabe, *Angew. Chem.,* **97**, 96 (1985). Recent reports for the synthesis of α-methylene-γ-butyrolactones: a) H. Saimoto, K. Nishio, H. Yamamoto, M. Shinoda, T. Hiyama, and H. Nozaki, *Bull. Chem. Soc. Jpn.,* **56**, 3093 (1983) and references cited therein; b) A. P. Kozikowski and A. K. Ghosh, *Tetrahedron Lett.,* **24**, 2623 (1983); c) T. Mandai, K. Mori, K. Hasegawa, M. Kawada, and J. Otera, *ibid.,* **25**, 5225 (1984); d) W. R. Jackson, P. Perlmutter, and A. J. Smallridge, *J. Chem. Soc., Chem. Commun.,* **1985**, 1509; e) Y. Okuda, S. Nakatsukasa, K. Oshima, and H. Nozaki, *Chem. Lett.,* **1985**, 481; f) S. E. Drew and R. F. A. Hoole, *Synth. Commun.,* **15**, 1067 (1985); g) K. Tanaka, H. Yoda, Y. Isobe, and A. Kaji, *Tetrahedron Lett.,* **26**, 1337 (1985); h) D. Bravo, G. Resnati, and F. Viani, *ibid.,* **26**, 2913 (1985); i) H. Mattes and C. Benezra, *ibid.,* **26**, 5697 (1985); j) W. E. Fristad, J. R. Peterson, and A. B. Ernst, *J. Org. Chem.,* **50**, 3143 (1985); k) K. Tanaka, H. Yoda, Y. Isobe, and A. Kaji, *ibid.,* **51**, 1856 (1986); l) J. Nokami, T. Tamaoka, H. Ogawa, and S. Wakabayashi, *Chem. Lett.,* **1986**, 541; m) K. Uneyama, K. Ueda, and S. Torii, *ibid.,* **1986**, 1201; n) T. Fujisawa, K. Umezu, M. Suzuki, and T. Sato, *ibid.,* **1986**, 1675; o) J. E. Baldwin, R. M. Adlington, and J. B. Sweeney, *Tetrahedron Lett.,* **27**, 5423 (1986); p) K. Boch, I. M. Castilla, I. Lundt, and C. Pedersen, *Acta. Chem. Scand., Ser. B,* B41, 13 (1987); q) J. Tsuji, M. Nisar, and I. Minami, *Chem. Lett.,* **1987**, 23; r) H. Mattes, K. Hamada, C. Benezra, *J. Med. Chem.,* **30**, 1948 (1987); s) Y. Tsuji, T. Kondo, and Y. Watanabe, *J. Mol. Catal.,* **40**, 295 (1987)., t) G. P. Boldrini, L. Lodi, E. Tagliavini, C. Tarasco, C. Trombini, and A. Umani-Ronchi, *J. Org. Chem.,* **52**, 5447 (1987); u) A. Srikrishna, *J. Chem. Soc., Chem. Commun.,* **1987**, 587.

2) T. Takeda, K. Ando, and T. Fujiwara, *Chem. Lett.,* **1983**, 1285.

3) T. Takeda, S. Naito, K. Ando, and T. Fujiwara, *Bull. Chem. Soc. Jpn.,* **56**, 967 (1983).

4) J. D. Albright and L. Goldman, *J. Am. Chem. Soc.,* **89**, 2416 (1967).

Optical Resolution of 2′-Methoxy-1,1′-binaphthyl-2-carboxylic Acid, and Application to Chiral Derivatizing Agent for HPLC Separation of Enantiomeric Alcohols and Amines

Sotaro MIYANO,* Shin-ichi OKADA, Hiroki HOTTA, Masayuki TAKEDA, Chizuko KABUTO,† and Harukichi HASHIMOTO
Department of Biochemistry and Engineering, Faculty of Engineering, Tohoku University, Aramaki-Aoba, Sendai 980
†Department of Chemistry, Faculty of Science, Tohoku University, Aramaki-Aoba, Sendai 980
(Received July 18, 1988)

Racemic 2′-methoxy-1,1′-binaphthyl-2-carboxylic acid was separated on a multi-gram scale into its antipodes via silica-gel column chromatography followed by alkaline hydrolysis of the diastereomeric esters prepared from (*R*)-1-phenylethanol or (−)-menthol. The molecular structure of (−)-menthyl (a*S*)-2′-methoxy-1,1′-binaphthyl-2-carboxylate was determined by single-crystal X-ray analysis. The (a*S*)-acid was converted to crystalline acid chloride, which was conveniently utilized as efficient chiral derivatizing agent for differentiation of enantiomeric alcohols and amines by high-performance liquid chromatography on silica gel. The elution behavior of a pair of diastereomeric esters or amides was explained by the steric interactions between the solutes and the silica-gel stationary phase on the basis of the X-ray analysis.

During the last two decades, a number of chiral derivatizing agents have been developed for discrimination of enantiomers.[1,2] Almost all of these possess C-centrochirality to exert stereo-differentiating ability, among which, Mosher's α-methoxy-α-trifluoromethylphenylacetic acid (MTPA) has been most widely used.[3]

It has been well-recognized recently that axially dissymmetric biaryls are efficient chiral auxiliaries in a variety of asymmetric reactions,[4] and then, these biaryls should also be good candidates for chiral derivatizing agents. Only a few reports, however, have appeared dealing with atropisomeric biaryls as such.[5,6] This seems mainly because of the difficulties accompanying the preparation of prerequisite chiral biaryl components. For example, the synthesis of optically active 2′-methyl-1,1′-binaphthyl-2-carbonyl cyanide (**1′**), the first chiral derivatizing agent with axially chiral binaphthyl unit reported in 1982 by Goto et al., required lengthy and subtle manipulations via 1,1′-binaphthyl-2,2′-dicarboxylic acid.[5]

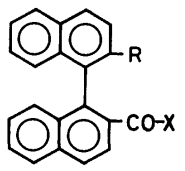

1 ; R = CH_3, X = OH
1′; R = CH_3, X = CN
2 ; R = OCH_3, X = OH
2′; R = OCH_3, X = Cl

We previously reported a practical method for the synthesis of 1,1′-binaphthyl-2-carboxylic acids.[7] As part of a program in our laboratory directed toward the use of these acids for elaboration of efficient chiral recognizing elements,[8] we wish to report herein a multi-gram scale optical resolution of 2′-methoxy-1,1′-binaphthyl-2-carboxylic acid (**2**) and its application to chiral derivatizing agent for differentiation of enantiomeric alcohols and amines by high-performance liquid chromatography (HPLC).

Results and Discussion

Optical Resolution of 2. Wilson and Cram reported the preparation of optically pure (a*S*)-**2**[9] by repeated crystallization of quinidine salt of rather pure (a*S*)-**2** (81%ee) which had been obtained by a chiral version of the oxazoline-assisted nucleophilic displacement on alkoxyarenes (the Meyers reaction).[10] We repeated the resolution procedure starting from racemic **2**, but realized that it was very sensitive to the experimental conditions, thus making difficult to obtain reproducible results. Furthermore, preferential precipitation of the racemate caused frequent decrease of the optical rotations of partially active samples of **2** during manipulations.[10]

We noticed, however, that many of the pairs of diastereomeric esters prepared from (±)-**2** and chiral alcohols gave two distinct spots on silica-gel TLC. This implies the possibility of optical resolution of **2** via chromatographic separation of the diastereomeric esters followed by hydrolytic removal of the chiral alcohol residue. Our expectation was realized by the fact that a multi-gram sample of diastereomeric esters prepared from (±)-**2** and (*R*)-1-phenylethanol was readily separated into (*R*)-1-phenylethyl (a*S*)-2′-methoxy-1,1′-binaphthyl-2-carboxylate ((a*S*,*R*)-**3a**) and the (a*R*,*R*)-counterpart by a silica-gel column chromatography. Upon alkaline hydrolysis, each of the diastereomers afforded the corresponding optically pure **2** as judged by HPLC on Pirkle column as *N*-butylamide. Practically, inexpensive (−)-menthol was ad-

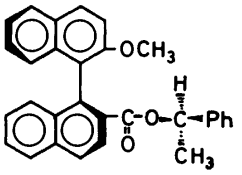

(aS,R)-3a

vantageously replaced for enantiomeric 1-phenylethanol; although hydrolysis of the diastereomeric esters (**3b**) required longer heating at reflux in aqueous ethanol in the presence of potassium hydroxide, no trace of racemization was observed.

Utilization of Axially Chiral 2 as Chiral Derivatizing Agent. Treatment of (aS)-**2** with thionyl chloride and recrystallization from hexane gave the acid chloride (aS)-**2′** as pale yellow prisms. Several partially active alcohols or amines of known enantiomeric composition were acylated with a small excess of (aS)-**2′** in benzene-pyridine (or triethylamine) in the presence of a catalytic amount of 4-dimethylaminopyridine (DMAP) to give the corresponding diastereomeric pairs of esters or amides. These pairs were subjected to HPLC analysis, and Tables 1 and 2 list the results of separation of alcohols and amines, respectively. Although reversed-phase HPLC on a ODS column eluting with aqueous ethanol or acetonitrile gave not so good separation, normal-phase HPLC on a spherical silica-gel column

Table 1. HPLC Separation of Diastereomeric Esters Derived from (aS)-**2**[a]

HO-R	k'[b] (aS,R)	k'[b] (aS,S)	α[c]	R_s[d]
HO-CH(Me)-Ph	5.85	8.39	1.43	7.40
	8.91[e]	9.65	1.08	0.95
	9.98[f]	9.98	1.00	0
Menthol	2.24	2.91	1.30	4.44
	14.44[e]	14.44	1.00	0
	18.30[f]	19.30	1.05	0.72
Borneol	3.50	4.48	1.28	4.35
HO-CH(Me)-Et	4.60	5.54	1.21	3.83
HO-CH(Me)-CHMe$_2$	3.82	5.16	1.35	6.05
HO-CH(Me)-C$_6$H$_{13}$	2.74	3.99	1.46	6.41
α-Tetralol	4.58	5.61	1.22	4.10

a) Operating conditions: column, silica gel; eluent, 2.5% AcOEt/hexane, 1 ml min^{-1}. b) Capacity factor = (retention volume of diastereomer − void volume of column)/(void volume of column). c) Separation factor = $k'_{(aS,S)}/k'_{(aS,R)}$. d) Resolution factor = 2X (distance between the peaks of two diastereomers)/(sum of bandwidth of the two peaks). e) ODS column; MeOH/H$_2$O (80/20), 1 ml min^{-1}. f) ODS column; MeCN/H$_2$O (80/20), 1 ml min^{-1}.

Table 2. HPLC Separation of Diastereomeric Amides Derived from (aS)-**2**[a]

H$_2$N-R	k' (aS,R)	k' (aS,S)	α	R_s
H$_2$N-CH(Me)-Ph	6.17	10.24	1.66	7.56
H$_2$N-CH(Me)-(1-Naphthyl)	4.09	6.76	1.65	4.30
H$_2$N-CH(Me)-(2-Naphthyl)	8.05	13.97	1.74	9.02
H$_2$N-CH(Me)-Et	10.84	13.53	1.25	3.40
H$_2$N-CH(Me)-C$_5$H$_{11}$	8.94	14.68	1.64	8.73
H$_2$N-CH(Me)-C$_6$H$_{13}$	4.63	7.58	1.64	5.30
Bornylamine	8.77	12.53	1.45	6.30
Isobornylamine	10.18	14.38	1.41	5.48
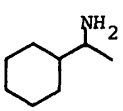	13.06	19.53	1.50	6.97
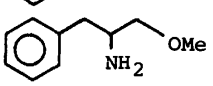	18.61	36.61	1.97	12.27

a) Operating conditions: column, silica gel; eluent, 1% *i*-PrOH/hexane, 2 ml min^{-1}.

cleanly differentiated two diastereomeric esters with base-line separation (Table 1). It should be noted that among a given diastereomeric pair of esters or amides of α-chiral alcohols or amines, the (a*S*,*R*)-isomer eluted faster than the (a*S*,*S*)-counterpart (vide infra).

Kinetic resolution is a potential problem in using a chiral derivatizing agent, but it was shown that acylation of racemic 1-phenylethanol or 1-phenylethylamine by (a*S*)-**2′** under standard conditions gave essentially 1:1 mixture of (a*S*,*R*)- and (a*S*,*S*)-isomer within the limits of ^{1}H NMR detection at 60 MHz.[11] Furthermore, it was also shown that the diastereomeric composition of a mixture of diastereomeric esters prepared from a sample of partially active 1-phenylethanol was identical to the enantiomeric composition of the starting alcohol as determined by HPLC analysis (see Experimental). These facts indicate that axially chiral **2** is useful as a chiral derivatizing agent for HPLC determination of absolute configuration and enantiomeric purity of α-chiral alcohols and amines.

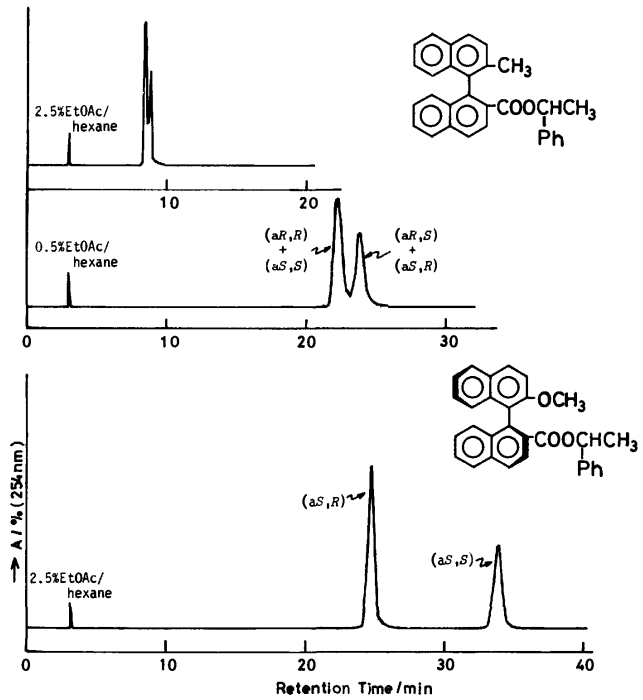

Fig. 1. HPLC resolution of diastereomeric 1-phenylethanol esters of **1** and **2**.

Effects of the Presence of 2′-Methoxyl Group. Figure 1 shows HPLC chromatograms of diastereomeric 1-phenylethanol esters of **1** and **2**. It should be noted that replacement of 2′-methoxyl for 2′-methyl functionality significantly increases both of the retention volumes and the separation factor α.

X-Ray Structure of (−)-Menthyl Ester of (a*S*)-2. Wilson and Cram assigned the absolute configuration of (−)-**2** to a*S* by correlating it to (a*S*)-(−)-1,1′-bi-2-naphthol.[10] Their assignment is now unambiguously confirmed here on the basis of the fact that the configuration of the (−)-menthyl carbon, C_4 in **3b** is *R*: Recrystallization of (−)-menthyl ester of (a*S*)-**2** ((a*S*,*R*)-**3b**) from hexane gave cubic crystals proper for X-ray diffraction. The ORTEP drawings in Fig. 2 show the complete connectivity established by the crystal structure analysis. It was shown that there are two independent molecules in the unit cell (**3b-1** and **3b-2**).

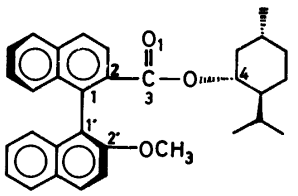

(a*S*,*R*)-**3b**

These two molecules have no significant differences in the bond lengths and angles, but take slightly different conformations around the single bond linking the two naphthalene rings as shown in the ORTEP drawings; the dihedral angle (θ, C_2-C_1-$C_{1'}$-$C_{2'}$) is 89.0° in **3b-1** (see Fig. 3), while that is 97.8° in **3b-2**. At the same time, the torsion angles of the carbonyl groups are also slightly different; the dihedral angles (φ, C_1-C_2-C_3-O_1) are 1.1° and 10.5° for **3b-1** and **3b-2**, respectively.

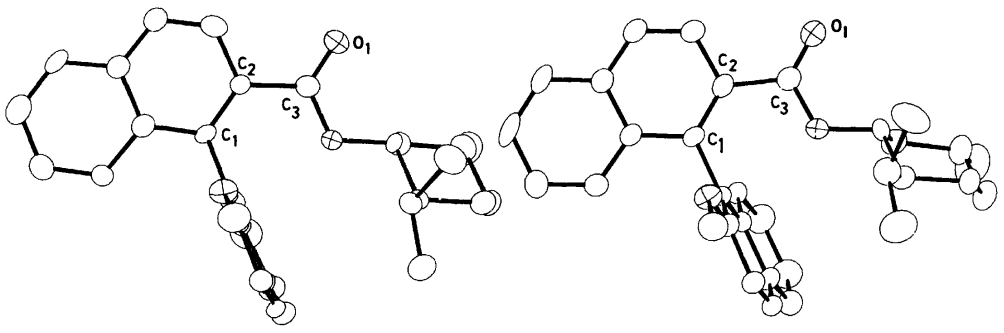

3b-1 **3b-2**

Fig. 2. ORTEP drawings of (a*S*,*R*)-**3b**.

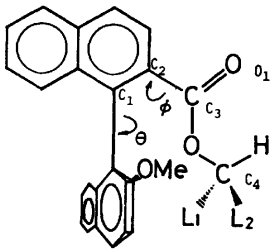

Fig. 3. Schematic view of crystal structure of alcohol (CL_1L_2H–OH) ester of (a*S*)-**2**.

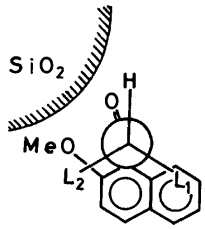

Fig. 4. Schematic view of the interaction of alcohol (CL_1L_2H–OH) ester of (a*S*)-**2** with silica-gel stationary phase.

Thus, the molecule **3b-1** has an almost orthogonal conformation concerning the naphthalene rings with almost coplanar carboxyl group with one of the naphthalene rings, while the molecule **3b-2** has a slightly deviated conformation from that of **3b-1**. These deviations seem to be due to subtle differences in the packing effect into the crystalline state.

Mechanistic Aspects of the Differentiation of Enantiomeric Alcohols and Amines by Axially Chiral 2. The most characteristic features of (a*S*,*R*)-**3b** based on the X-ray analysis are approximated as follows; 1) the dihedral angle confined by the two naphthalene rings is almost orthogonal, 2) CO–O–C_4–H atoms are nearly on the same plane that contains the naphthalene ring connecting the carboxyl function at the C_2-position, and 3), thus the plane roughly bisects the two other ligands (L_1 and L_2) attached at the C_4-carbon. These stereochemical features can be simplified as schematically shown in Fig. 3.

It is said that adsorptions of the solutes to the stationary phase mainly control the chromatographic behavior of the solutes on a normal-phase silica-gel HPLC. In this context, interactions of the diastereomeric esters or amides of **2** with the silica-gel surface by virtue of the carbonyl oxygen and/or methoxyl oxygen may play critical role.

On the assumption that prevailing conformations of these diastereomers in HPLC conditions are deducible from those of the X-ray structure of the (a*S*,*R*)-**3b**,[12] Fig. 4 shows a schematic model for the interaction of the solute with silica-gel surface based on the structure depicted in Fig. 3. It may be said that, among a given diastereomeric pair, the (a*S*,*S*)-isomer should be adsorbed more strongly than the (a*S*,*R*)-counterpart, because in the former the ligand L_2, which is arrayed toward the adsorbent, is smaller than L_1, while in the latter, the relationship of the steric bulk of the two ligands is reversed.

As mentioned above, the idea of utilizing axially chiral biaryl derivatives as chiral derivatizing agent for enantiomeric compounds was first reported by Goto et al.[5] Their 2'-methyl-1,1'-binaphthyl-2-carbonyl moiety was highly efficient for HPLC differenciation of several alcohols which contained oxycarbonyl function. At our hand, however, the moiety did not show so much discrimination, as compared with **2**, for simple alcohols such as 1-phenylethanol (Fig. 1). This is another support for the above reasoning that HPLC behavior of the diastereomeric esters and amides of **2** is largely determined by the coordination to silica-gel surface by the carbonyl oxygen as well as the methoxyl oxygen.

In conclusion, we have shown here that axially chiral **2**, which is readily obtainable in a multi-gram scale,[13] serves as an efficient chiral derivatizing agent for differentiation of enantiomeric alcohols and amines by HPLC.

Experimental

Instruments. HPLC measurements were carried out on a JASCO TRIROTAR-III and/or a Shimadzu LC-5A, with UV detection at 254 nm. Stainless-steel columns (0.46 cm i.d. ×25 cm) were packed with Hitachi Gel 3056 for the silica-gel column and JASCO FINPAK C_{18} for the ODS column, respectively, using conventional slurry techniques. IR and UV spectra were measured on a Shimadzu IR-430 grating spectrophotometer and a Shimadzu UV 160 spectrophotometer, respectively. ^{1}H NMR spectra were recorded on a JEOL JNM-FX60 instrument in benzene-d_6 using tetramethylsilane as an internal standard. Optical rotations were recorded on a Union PM-101 automatic digital polarimeter in a 1-cm cell at 23—25 °C. Melting points were measured on a Yamato MP-21 and uncorrected.

Materials. Racemic binaphthylcarboxylic acids **1** and **2** were prepared as described in previous paper.[7] Samples of partially active alcohols and amines (20—70%ee) were prepared by adding commercial enantiomers to the corresponding racemates unless otherwise noted. (*S*)-(+)-2-Octanamine was the sample obtained in this laboratory.[14] Solvents were purified as usual. Wako Gel C-200 was dried by heating at 120 °C for several hours before use for silica-gel column chromatography. Analytical, and preparative TLC were performed using Merck Kieselgel 60 F_{254}, and Merck Kieselgel 60 G, respectively. Water-sensitive reactions were routinely carried out in a nitrogen atmosphere.

Optical Resolution of 2 via (*R*)-1-Phenylethanol Ester. Racemic **2** (5.0 g, 15.2 mmol) was boiled in 30 ml of freshly distilled thionyl chloride for 5 h. After volatiles were evaporated in vacuo, residual thionyl chloride was removed by addition and evaporation of small portions of benzene (×3) to give (±)-**2'** as a brown solid. The acid chloride was dissolved in 70 ml of benzene. This was added dropwise to a

solution of (*R*)-1-phenylethanol (2.3 g, 18.9 mmol) and 4-dimethylaminopyridine (1 g) in benzene (80 ml) and pyridine (5 ml). The mixture was stirred overnight at ambient temperature, and then heated at ca. 70 °C for 3 h. The cool mixture was diluted with benzene, washed (2 M[††] HCl, 1 M Na_2CO_3, and water), and dried over $MgSO_4$ in the presence of activated charcoal. After filtration and evaporation of volatiles in vacuo, the organic residue was subjected to chromatography using a 7 cm i.d. ×30 cm silica-gel column with benzene as the eluent. Fractions containing two components were combined together and chromatographed again, finally affording the following diastereomerically pure samples beside 0.65 g of a mixture of **3a**:

(a*S*,*R*)-**3a**: 2.75 g (42% based on (±)-**2**); IR (KBr) 3060, 1705, 1272, and 765 cm^{-1}; UV (MeOH) 232.4 (λ_{max}) (ε 10.3×10^4) and ε 1.05×10^4 at 254 nm; ^1H NMR δ=0.68 (3H, d, J=6.45 Hz, C-CH_3), 3.15 (3H, s, O-CH_3), 5.79 (1H, q, J=6.45 Hz, -CH-), and 6.7—8.5 (17H, m, Ar-H). The sense of axial chirality was confirmed by the optical rotaion of **2** obtained by hydrolysis (vide infra).

(a*R*,*R*)-**3a**: 2.40 g (36%); IR (KBr) 3060, 1710, 1272, and 763 cm^{-1}; UV (MeOH) 232.4 (λ_{max}) (ε 9.35×10^4) and ε 1.02×10^4 at 254 nm; ^1H NMR δ=0.86 (3H, d, J=6.45 Hz, C-CH_3), 3.20 (3H, s, O-CH_3), 5.85 (1H, q, J=6.45 Hz, -CH-), and 6.4—8.5 (17H, m, Ar-H).

A sample of (a*S*,*R*)-**3a** (2.0 g, 4.62 mmol) was boiled in a solution of KOH (10 g) in ethanol (100 ml) and water (5 ml) for 3 h. Solvents were evaporated in vacuo, and the residue was dissolved in water. After extracted with ether, the aqueous layer was made acidic with concd HCl, and extracted with ether. Combined ether extracts were treated as usual to give (a*S*)-**2**, 1.50 g (99% yield); IR (KBr) 1690 cm^{-1}; $[\alpha]_D$ −25.5° (*c* 2.60, THF) (lit,[10] $[\alpha]_D$ −25.98° (*c* 1.22, THF)). A sample of (a*S*)-**2** (ca. 20 mg) was treated with excess butylamine in the presence of dicyclohexylcarbodiimide to give the *N*-butylamide,[8] which was confirmed to be more than 99.5%ee by HPLC on a Pirkle column.

Similar treatment of 2.30 g of (a*R*,*R*)-**3b** gave 1.71 g of (a*R*)-**2** which was confirmed enantiomerically pure by HPLC as above; $[\alpha]_D$ +25.4° (*c* 2.66, THF).

Synthesis and Separation of (−)-Menthyl Ester Diastereomers of (±)-2. (−)-Menthol (12.8 g, 82.1 mmol) was treated with (±)-**2′** (prepared from 9.15 g (27.8 mmol) of **2**) in the presence of DMAP (1 g) in benzene (100 ml) and pyridine (5 ml) as above. After as much menthol as possible was removed by sublimation under vacuum, remaining organic material was chromatographed twice on silica-gel column eluting with toluene to give 3.79 g of diastereomerically pure (a*S*,*R*)-**3b** (29% yield based on (±)-**2**)), 4.10 g of (a*R*,*R*)-**3b** (32%), and 2.64 g of a mixture of the diastereomers.

(a*S*,*R*)-**3b**: mp 145—146 °C (hexane); ^1H NMR δ=3.28 (3H, s, OCH_3); $[\alpha]_D$ −142° (*c* 2.11, $CHCl_3$).

(a*R*,*R*)-**3b**: mp 126—129 °C (hexane); ^1H NMR δ=3.24 (3H, s, OCH_3); $[\alpha]_D$ −55.4 °C (*c* 2.75, $CHCl_3$).

Both diastereomers of **3b** were heated at reflux with KOH in aqueous ethanol for 8—10 h to give optically pure acids as judged by HPLC as above.

Preparation of (a*S*)-2′. In a typical run, (a*S*)-**2** (1.09 g, 3.32 mmol) was treated with thionyl chloride as above, dissolved in hot hexane, filtered hot from activated charcoal, and allowed to stand to give (a*S*)-**2′** as prisms, 0.98 g (85% yield), mp 139—142 °C, IR (KBr) 1770 cm^{-1}.

Preparation of Diastereomeric Esters and Amides of (a*S*)-2. General procedure for the preparation of HPLC samples of diastereomers is as follows: To a stirred mixture of partially active alcohol or amine (0.3—0.4 mmol) and DMAP (0.1 g) in benzene (5 ml) and pyridine (1 ml) was added dropwise a solution of 1.2—1.5 equiv of (a*S*)-**2′** in benzene (10 ml). The mixture was stirred overnight, and then heated at 60—70 °C (amines) or at gentle reflux (alcohols) for 2—3 h. To the cool mixture was added 0.1 ml of 3-(dimethylamino)propylamine. It was diluted with ether, washed successively with 2 M HCl, 1 M Na_2CO_3, and water, and dried over $MgSO_4$. After volatiles were evaporated in vacuo, the mixture of diastereomeric esters or amides were recovered by TLC, care being taken not to cause fractionation of either of the diastereomers.

In case of (−)-borneol (*endo*-(1*S*)-1,7,7-trimethylbicyclo-[2.2.1]heptan-2-ol), (−)-menthol ((1*R*, 2*S*, 5*R*)-2-isopropyl-5-methylcyclohexanol), (+)-bornylamine (*endo*-(1*R*)-1,7,7-trimethylbicyclo[2.2.1]heptan-2-amine), and (+)-isobornylamine (*exo*-(1*R*)-1,7,7-trimethylbicyclo[2.2.1]heptan-2-amine), excess of optically pure enantiomers was allowed to react with partially active (−)-**2′** of known enantiomeric composition (ca. 50%ee). For the sake of simplicity, diastereomers of these alcohols and amines were also presented in Tables 1 and 2 as if they were those prepared from (a*S*)-**2′** and partially active enantiomers.

^1H NMR Study of the Diastereomeric Ester or Amide Mixture of (±)-1-Phenylethanol or (±)-1-Phenylethylamine. (±)-1-Phenylethanol (50 mg, 0.41 mmol) was acylated with (a*S*)-**2′** (0.21 g, 0.61 mmol) as above. The diastereomeric ester mixture **3a**, which was obtained in 81% yield (0.144 g) after preparative TLC, was subjected to ^1H NMR measurement. The methoxyl protons of (a*S*,*R*)-**3a** which appeared at δ 3.15 shifted to δ 4.84 on addition of 1 equiv amount of lanthanoide shift reagent Eu(fod)$_3$ to the diastereomeric **3a**, while those of (a*S*,*S*)-**3a** which appeared at δ 3.19 shifted to δ 4.42. The ratio of peak areas of those lanthanoide-shifted methoxyl signals was 50.3:49.7, which should be regarded to indicate that the diastereomeric composition was practically 1:1 whithin the error limits of the integration of NMR peak areas at 60 MHz (vide infra).

Similar treatment of (±)-1-phenylethylamine with (a*S*)-**2′** gave the amide mixture in 93% yield. Addition of 1 equiv amount of Eu(fod)$_3$ caused shift of the methoxyl protons of (a*S*,*R*)-amide from δ 3.04 to δ 5.47, while those of (a*S*,*S*)-isomer from δ 3.12 to δ 5.19, with base-line separation of the two peaks. The ratio of areas of those two peaks measured to be 49.8:50.2.

HPLC Estimation of the Diastereomeric Composition of Partially Active 1-Phenylethanol Esters of (a*S*)-2. A sample of partially active 1-phenylethanol enriched in (*R*)-isomer was prepared to be 50%ee by addition of the racemate to the (*R*)-enantiomer. Aliquot of the sample was converted to the 3,5-dinitrophenylcarbamates. HPLC analysis of the carbamates on a chiral column developed in our laboratory[15] demonstrated that the mixture should be 49.9%ee.

The remainder of the partially active alcohol was converted to the diastereomeric esters by treatment with (a*S*)-**2′**. HPLC analysis of the mixture on silica-gel column showed the peaks of (a*S*,*R*)- and (a*S*,*S*)-**3a** in the ratio of

[††] 1 M=1 mol dm^{-3}.

3.07:1 in the order of increasing retention time. The peak ratio was corrected for molar response indicating that the diastereomeric composition of the sample should be 49.7% de (diastereomeric excess), on the basis that the ratio of the peak areas of the aforementioned diastereomeric (a*S*,*R*)- and (a*S*,*S*)-**3a** from racemic 1-phenylethanol was 1.03:1 (see footnote a in Table 1 for the HPLC operating conditions).

Crystal Structure Determination of (a*S*,*R*)-3b. A prism-like crystal of (a*S*,*R*)-**3b** with the dimensions of 0.2×0.2×0.3 mm was used for the data collection on a Rigaku-Denki automated four-circle diffractometer (Rigaku AFC-5R), equipped with a rotating anode (40 kV, 200 mA) using Mo $K\alpha$ radiation (λ=0.71029 Å). Crystal data are as follows: M.F.=$C_{32}H_{34}O_3$, M.W.=466.59, orthorhombic space group $P2_12_12_1$, a=16.852(3), b=22.307(4), c=14.047(2) Å, V=5280.5(9) Å^3, Z=8, D_{calcd}=1.17 g cm^{-3}, μ(Mo $K\alpha$)=0.688 cm^{-1}. A total of 6027 reflections within 2θ=52° were measured using 2θ-θ scan mode and 3567 reflections with $|F_o|>3\sigma|F_o|$ were used for the structure determination. The structure was solved by the direct method and refined by the block-diagonal least-squares method to give an R factor of 0.09 including all hydrogen atoms which were calculated and verified by the difference Fourier synthesis.

Tables of atomic coordinates, temperature factors, bond lengths, bond angles, and the F_o—F_c list are kept at the Chemical Society of Japan (Document No. 8867).

We are grateful to the Asahi Glass Foundation for Industrial Technology and a Grant-in-Aid for Scientific Research (No. 62101001) from the Ministry of Education, Science and Culture for financial support of this work. We also thank Mr. Takatsugu Suzuki for experimental help and Professor Shozo Yamaguchi and Ms. Fujiko Yasuhara of our university for helpful discussions.

References

1) S. Yamaguchi, *Asymm. Synth.*, **1**, 125 (1983).

2) Recent examples: K. Saigo, K. Sekimoto, N. Yonezawa, F. Ishii, and M. Hasegawa, *Bull. Chem. Soc. Jpn.*, **58**, 1006 (1985); D. Terunuma, M. Kato, M. Kamei, H. Uchida, S. Ueno, and H. Nohira, *ibid.*, **59**, 3581 (1986); R. E. Doolittle and R. R. Heath, *J. Org. Chem.*, **49**, 5041 (1984); B. M. Trost, J. L. Belletire, S. Godleski, P. G. McDougal, and J. M. Balkovec, *ibid.*, **51**, 2370 (1986).

3) J. A. Dale and H. S. Mosher, *J. Am. Chem. Soc.*, **95**, 512 (1973).

4) S. Miyano and H. Hashimoto, *Yuki Gosei Kagaku Kyokai Shi*, **44**, 713 (1986).

5) J. Goto, N. Goto, and T. Nambara, *Chem. Pharm. Bull.*, **30**, 4597 (1982).

6) A. Aigner, F. Vögtle, S. Franken, and H. Puff, *Chem. Ber.*, **118**, 3643 (1985).

7) S. Miyano, S. Okada, T. Suzuki, S. Handa, and H. Hashimoto, *Bull. Chem. Soc. Jpn.*, **59**, 2044 (1986).

8) Cf., J. Yamashita, T. Numakura, H. Kita, T. Suzuki, S. Ôi, S. Miyano, H. Hashimoto, and N. Takai, *J. Chromatogr.*, **403**, 275 (1987).

9) The descriptor (a*S*) or (a*R*) refers to axial chirality.

10) J. M. Wilson and D. J. Cram, *J. Org. Chem.*, **49**, 4930 (1984).

11) Deatails of discrimination of diastereomeric esters and amides of (a*S*)-**2** by ^{1}H NMR will be reported elsewhere.

12) The assumption indicates that the ligand L_1 in Fig. 3 should magnetically be more shielded than L_2 by the relevant naphthalene ring, which was just the like in case of diastereomeric **3a**s (see Experimental).

13) Merits and demerits of optical resolution via covalent diastereomers: J. Jacques, A. Collet, and S. H. Wilen, "Enantiomers, Racemates and Resolutions," John Wiley and Sons., Inc., New York, NY (1981).

14) Y. Inoue, M. Taguchi, and H. Hashimoto, *Synthesis*, **1986**, 332.

15) S. Ôi, M. Shijo, J. Yamashita, and S. Miyano, *Chem. Lett.*, **1988**, 1545.

 © 1989 The Chemical Society of Japan Bull. Chem. Soc. Jpn., 62, 1534—1538 (1989) [Vol. 62, No. 5

Novel Synthesis of Carbamate Ester from Carbon Dioxide, Amines, and Alkyl Halides

Yasuhiko YOSHIDA,* Shigeru ISHII, Masayo WATANABE, and Tadataka YAMASHITA
Department of Applied Chemistry, Faculty of Engineering, Toyo University,
Kujirai, Kawagoe, Saitama 350
(Received September 6, 1988)

A novel synthesis of carbamate ester using carbon dioxide as a direct material is reported in this article. The direct reaction of carbon dioxide, aliphatic amines, and alkyl halides was found to give the corresponding alkyl carbamate esters in good yields. Reactions using secondary alkyl bromides gave carbamate esters in higher yields than those using primary or tertiary alkyl bromides. The carbamate ester yields increased with the addition of *N*,*N*-dimethylformamide to the reaction system of carbon dioxide, amines and, alkyl halides. This reaction is considered to proceed by an S_N2 displacement reaction of the alkyl halide by the carbamate anion formed from the reaction of carbon dioxide and the amine.

The chemical utilization of carbon dioxide as a raw material in the synthetic chemical industry has so far been limited, because the reactivity of carbon dioxide is considered to be one of the lowest of all carbon compounds. However, carbon dioxide is well-known, to easily react with nucleophilic reagents, such as Grignard reagent or organometallic compounds.[1] Similarly, amine attacks carbon dioxide to form carbamic acid:

$$R_2NH + CO_2 \rightarrow R_2NCOOH \quad (1)$$

Carbamic acid, itself, however, has not been isolated and has been known only as a reaction intermediate in the hydrolysis reaction of carbamate ester or in the hydration reaction of isocyanate.[2] Thus, carbamic acid is very unstable by easy decomposition to carbon dioxide and amine; its esters, however, are stable compounds.

Carbamate esters[3] have so far been prepared by the reactions of amines with alkyl chloroformate, and alcohols with carbamoyl chloride or isocyanate, which were made from phosgene as a starting material. The starting materials for the preparation of carbamate esters, such as phosgene, isocyanate, carbamoyl chloride, and chloroformate, are highly toxic and inconvenient to use for the syntheses of carbamate esters.

The syntheses of carbamate esters by reactions using carbon dioxide as a direct starting component have been reported in recent years.[4-11] Also, we have previously reported that carbon dioxide and aliphatic amine reacted with epoxide to give 2-hydroxyalkyl carbamate in high yields,[12,13] with vinyl ether to give 1-alkoxyalkyl carbamate selectively,[14] and with ortho ester to give the corresponding alkyl carbamate in high yields.[15] In the course of further studies we found that the reaction of carbon dioxide and amines with alkyl halides formed the corresponding carbamate esters (Eq. 2).[16]

$$R_2NH + CO_2 + R'X \rightarrow R_2NCOOR' + [R_2NH_2]^+X^- + [R_2R'NH]^+X^- \quad (2)$$

The structures and reactivities of alkyl halides and amines are considered to be of importance for reactions with carbon dioxide, since the amine reacts directly with the alkyl halide to form an ammonium halide salt. In this paper, we describe the details of reactions of carbon dioxide with amines and alkyl halides to yield carbamate esters.

Results and Discussion

Carbon dioxide reacted with secondary aliphatic amines and alkyl halides to give the corresponding alkyl carbamates with two kinds of ammonium halide salts, depending on the reactivities and structures of the amine and alkyl halide and the reaction conditions (Eqs. 2—4):

$$R_2NH + CO_2 + R'\text{-}X \rightarrow R_2NCOOR' + [R_2NH_2]^+X^- \quad (3)$$
$$R_2NH + R'\text{-}X \rightarrow [R_2R'NH]^+X^- \quad (4)$$

One of the ammonium halide salts is a secondary ammonium salt which is formed by a reaction of the amine and hydrogen halide released as by-products of carbamate ester formation. The other is a tertiary ammonium salt which is obtained by a direct reaction of the amine and alkyl halide.

Reactions of carbon dioxide, diethylamine (Et_2NH) and various isomeric butyl halides were investigated in detail concerning the reaction conditions for the synthesis of the carbamate ester. Table 1 shows the carbamate ester yield and the total recovered amount of ammonium salt under various reaction conditions. Butyl chloride hardly gave the carbamate ester at 60 °C, but carbamate ester was obtained in 18% yield at 100 °C and increased slightly at higher temperature (Runs 1—3).

The yield of carbamate ester was nearly constant for longer reaction times, but the formation of tertiary ammonium salt, which was obtained by the direct reaction of diethylamine and butyl chloride, increased (Runs 2 and 4). In the case of butyl bromide, the carbamate ester was obtained in 8% yield at 40 °C, though the amount of secondary ammonium salt,

Table 1. The Reaction of Diethylamine, CO_2, and Various Butyl Halides[a]

Run	*n*-Bu-X	Temp	Time	Yield of products	
				Carbamate	Ammonium salt
		°C	day	%[b]	g[c]
1	*n*-Bu-Cl	60	1	0.9	0
2	*n*-Bu-Cl	100	1	18	4.7
3	*n*-Bu-Cl	120	1	22	7.4
4	*n*-Bu-Cl	100	2	25	6.3
5	*n*-Bu-Cl	120	2	22	6.2
6	*n*-Bu-Br	40	1	8	1.5
7	*n*-Bu-Br	60	1	21	9.8
8	*n*-Bu-Br	70	1	21	12.6
9	*n*-Bu-Br	80	1	22	14.4
10	*n*-Bu-Br	100	1	20	14.1
11	*n*-Bu-Br	120	1	17	14.4
12	*n*-Bu-Br	70	2	31	14.4
13	*n*-Bu-Br	70	4	31	14.5
14	*n*-Bu-I	20	1	12	0
15	*n*-Bu-I	40	1	20	9.0
16	*n*-Bu-I	60	1	14	17.3
17	*n*-Bu-I	70	1	13	15.8
18	*n*-Bu-I	100	1	10	15.4
19	*n*-Bu-I	120	1	8	18.1
20	*n*-Bu-I	40	2	20	10.3

a) Et_2NH: 0.2 mol, R-X: 0.1 mol, CO_2: 40 atm. b) The corresponding alkyl diethylcarbamate. Yield based on R-X by GLC analysis. c) Recovered amount of ammonium salt.

Table 2. The Reaction of Diethylamine, CO_2, and Various Alkyl Bromides[a]

Run	Bu-X	Temp	Time	Yield of products	
				Carbamate	Ammonium salt
		°C	day	%[b]	g[c]
1	*s*-Bu-Br	60	1	17	1.6
2	*s*-Bu-Br	70	1	30	4.0
3	*s*-Bu-Br	100	1	56	10.7
4	*s*-Bu-Br	120	1	54	12.0
5	*s*-Bu-Br	70	2	48	7.3
6	*s*-Bu-Br	100	2	62	12.7
7	*t*-Bu-Br	60	1	14	6.7
8	*t*-Bu-Br	70	1	19	11.6
9	*t*-Bu-Br	100	1	18	17.6
10	*t*-Bu-Br	120	1	12	13.1
11	*t*-Bu-Br	70	2	24	13.0
12	*n*-Bu-Br	70	2	31	14.4

a) Et_2NH: 0.2 mol, R-X: 0.1 mol, CO_2: 40 atm. b) The corresponding alkyl diethylcarbamate. Yield based on R-X by GLC analysis. c) Recovered amount of ammonium salt.

which corresponded to the amount of ammonium salt obtained as the by-product of the carbamate ester synthesis, was also obtained (Run 6). The carbamate ester yield was 20—22% from 60 to 100 °C (Runs 7—10). Also, the amount of tertiary ammonium salt, obtained by a direct reaction of the amine and alkyl halide, increased with increasing the reaction temperature (Runs 6—11). Under reaction conditions greater than 80 °C, about 50% of the butyl bromide directly reacted with the amine to give the tertiary ammonium salt (Eq. 4). At 70 °C for 2 days, carbamate ester was obtained in 31% yield; then, the ester yield was almost constant (Runs 12 and 13). Butyl iodide gave the carbamate ester in 20% yield at 40 °C; however, a direct reaction of amine and alkyl halide was preferred to a carbamate ester synthesis at higher temperatures (Runs 14—20).

In conclusion, various butyl halides such as the chloride, bromide, and iodide reacted with carbon dioxide and diethylamine to yield butyl diethylcarbamate in 25, 31, and 20%, respectively, under each best reaction condition (Runs 4, 12, and 15). Since the reactivity of butyl chloride to nucleophilic reagents is low, a higher reaction temperature was required for the carbamate ester synthesis. In the case of butyl iodide, the reaction was accompanied by the formation of a considerable amount of tertiary ammonium iodide salt, which was obtained from a direct reaction of

Table 3. Reaction of CO_2, Various Amines, and Alkyl Halides[a]

Run	Amine	Alkyl halide	Product	
			Carbamate	Yield/%[b]
1	Et_2NH	CH_3CH_2-Br	Et_2NCOO-CH_2CH_3	22
2		CH_3CH_2-Br		3.5
3		CH_3CH_2-Br		0
4	Et_2NH	$CH_3CH_2CH_2$-Br	Et_2NCOO-$CH_2CH_2CH_3$	32
5		$CH_3CH_2CH_2$-Br		0.5
6	$((CH_3)_2CH)_2NH$	$CH_3(CH_2)_3$-Br	$((CH_3)_2CH)_2NCOO$-$(CH_2)_3CH_3$	11
7	Et_2NH	$PhCH_2$-Cl	Et_2NCOO-CH_2Ph	7
8	Et_2NH	$(CH_3)_2CH$-Br	Et_2NCOO-$CH(CH_3)_2$	53
9		$(CH_3)_2CH$-Br		37
10	Et_2NH	$(CH_3)_2CHCH_2$-Br	Et_2NCOO-$CH_2CH(CH_3)_2$	29
11	Et_2NH	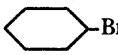	Et_2NCOO-	3
12[c]	$CH_3CH_2CH_2NH_2$	CH_2Br_2	$(CH_3CH_2CH_2NHCOO)_2CH_2$	1[d]
13	Ph_2NH	$CH_3CH_2CH_2$-Br	—	0
14	$Ph(CH_3)NH$	$CH_3CH_2CH_2$-Br	—	0
15	$PhNH_2$	$CH_3(CH_2)_3$-Br	—	0

a) Amine; 0.25 mol, alkyl halide; 0.1 mol, CO_2; 40 atm, time; 48 h, temp; 70°C. b) The carbamate ester yields based on alkyl halide were determined by GLC. c) $CH_3CH_2CH_2NH_2$: 0.4 mol, CH_2Br_2: 0.1 mol. d) The isolated yield.

diethylamine and butyl iodide. The reaction of butyl bromide, carbon dioxide and diethylamine gave the carbamate ester in the highest yield of all butyl halides.

The steric effect of the alkyl group in the reaction of carbon dioxide, diethylamine, and various isomeric butyl bromides was studied (Table 2). The carbamate ester yields obtained using a secondary alkyl bromide were compared with those using primary and tertiary alkyl bromides. In the case of using *s*-butyl bromide, the formation of the carbamate ester was preferred to the formation of ammonium salt (the direct reaction of amine and alkyl bromide), and occurred in higher yields (Run 6). Since the reactivities of primary alkyl bromides, such as butyl and isobutyl bromides, with an amine are higher than that of *s*-butyl bromide, the direct reaction with the amine was preferred to the carbamate ester synthesis (Table 2: Runs 5 and 12, and Table 3: Run 10). Owing to the steric hindrance of the tertiary alkyl group, the reactivity of the *t*-butyl bromide to the nucleophilic reagents was low (Runs 7—11).

The effect of the molar ratio of diethylamine to butyl bromide, [Et_2NH]/[*n*-BuBr], on carbamate ester yield, was examined in detail, as shown in Fig. 1. The carbamate ester yield increased with an increase in the molar ratio, [Et_2NH]/[*n*-BuBr]. The ester yield was approximately constant when the value of [Et_2NH]/[*n*-BuBr] was over 2.

The results of the reaction of carbon dioxide, various amines, and various alkyl halides are summarized in Table 3. While aliphatic amines gave the corresponding carbamate esters (Runs 1, 2, and 4—12), no aromatic amines gave the carbamate esters at all (Runs 13—15). Also, the aliphatic substituent groups of the amine exerted an influence on the synthesis of the carbamate ester by the reaction of carbon dioxide, amine, and alkyl halide (Runs 1, 2 and 3: 4 and 5: 8 and 9).

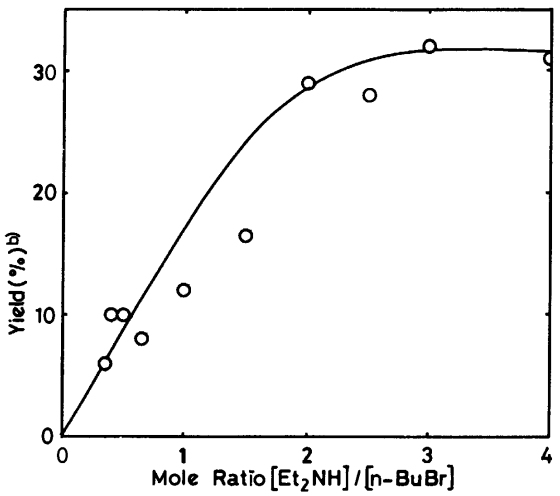

Fig. 1. Effect of [Et_2NH]/[*n*-BuBr] mole ratio on the reaction of Et_2NH, *n*-BuBr, and CO_2.[a]
a) Time: 24 h, temp: 70°C. b) Yield of Et_2NCOO-*n*-Bu based on *n*-BuBr.

As the carbon number in the alkyl bromides increased, the yield of the carbamate ester increased. The reaction of carbon dioxide and diethylamine with ethyl, propyl, or butyl bromide, gave the corresponding carbamate ester in 22, 32, or 42%,[16] respectively (Runs 1 and 4). The carbamate ester yields by a reaction using secondary alkyl bromides are higher than those

using primary alkyl bromides (Runs 4 and 8: 5 and 9). Cyclohexyl bromide gave the corresponding carbamate ester in 3% yield, because of the steric effect of the cyclohexane ring (Run 11). Methylene dibromide reacted with carbon dioxide and propylamine to give methylene bis(propylcarbamate) (Run 12). This product can not be obtained by other synthetic methods, since it is the ester of methanediol and propylcarbamic acid, which are both unstable and not isolable.

It was considered that the polarity of the reaction system influenced the reaction rate, since the synthetic reaction of carbamate ester from aliphatic amines, alkyl halides, and carbon dioxide is a nucleophilic substitution. The addition of DMF (*N,N*-dimethylformamide) into the reaction mixture resulted in an increase in the carbamate ester yield at the lower temperatures. By the addition of 5 mol% DMF for diethylamine, the carbamate ester yield increased from 8 to 11% at 40 °C, and from 22 to 32% at 80 °C. However, the addition of DMF did not exert any influence on the carbamate ester yield at 120 °C. The carbamate ester yields gradually decreased with an increase in the DMF concentration at any temperature, because the addition of DMF resulted in a dilution of the reaction system. No additive effects of other solvents such as dimethyl sulfoxide, acetonitrile, alcohols, tertiary amine, and ether were observed in the synthetic reaction of carbamate ester at any reaction temperature using any additive amount.

The reaction is considered to proceed as follows. Carbon dioxide reversibly reacts with the aliphatic amine to form carbamic acid (Eq. 1). Carbamic acid dissociates to a carbamate anion and a proton (Eq. 5). Then, the carbamate anion attacks the alkyl halide to produce the carbamate ester (Eq. 6). This reaction is considered to be an S_N2 displacement reaction, because the yield of the carbamate ester obtained using cyclohexyl bromide is considerably lower than that using acyclic alkyl bromides.[17] Also, any reactions of carbon dioxide, amines, and alkyl halides give the corresponding carbamate esters without the formation of other isomeric alkyl carbamate esters:

$$R_2NCOOH \rightarrow R_2NCOO^- + H^+ \quad (5)$$

$$R_2NCOO^- + R'\text{-}X \rightarrow R_2NCOOR' + X^- \quad (6)$$

In conclusion, the reaction of amine, carbon dioxide, and alkyl halide to form the carbamate ester accompanied the direct reaction of amine and alkyl halide to yield ammonium salt. In this reaction the secondary alkyl bromides gave the corresponding carbamate ester in high yields. This reaction mechanism is an S_N2 displacement reaction in which the carbamate anion, formed from carbon dioxide and amine, attacks alkyl halide.

Experimental

Materials. Various commercially available amines and alkyl halides were purified by refluxing and distilling over calcium hydride and stored under a nitrogen atmosphere. Commercial available high-purity carbon dioxide gas was introduced directly into an autoclave from a gas cylinder without further purification.

Measurements. IR spectra were recorded on a Hitachi 260-50 apparatus, and NMR spectra were recorded on a Hitachi R-24 spectrometer operating at 60 MHz and JEOL FX90Q at 90 MHz, using hexamethyldisiloxane (HMDS) as the internal standard. GC-MS spectra were measured by a Shimadzu QP-1000 spectrometer, and gas-liquid chromatogram (GLC) were recorded on a Shimadzu GC-4C apparatus with a thermal conductivity detector.

Preparations of Carbamate Ester. A typical example for the synthesis of 1-methylpropyl diethylcarbamate (*s*-butyl diethylcarbamate) is as follows.

A 100 cm^3 stainless-steel autoclave was swept free of air by displacement with nitrogen. Into the autoclave was added a mixture of diethylamine (18.3 g, 0.25 mol) and *s*-butyl bromide (13.7 g, 0.10 mol). Carbon dioxide gas was then introduced directly from the gas cylinder until the pressure reached 40 atm (4.1×10^6 Pa). After the autoclave was allowed to stand in an oil bath controlled at 70 °C for 48 h, the excess carbon dioxide gas was released and the contents of the reaction mixture were filtered to remove any ammonium bromide salts. The filtrate was subjected to fractional distillation under reduced pressure to isolate the product, *s*-butyl diethylcarbamate, bp 67.0—67.3 °C/6 mmHg† (7.5 g, 43%).

Preparations of other carbamate esters were carried out using a similar procedure.

Identification of the Products. Butyl Diethylcarbamate: bp 111.2—111.4 °C/30 mmHg (lit,[18] 60 °C/0.05 mmHg); IR (neat) 1705 cm^{-1} (ester C=O); ^1H NMR($CDCl_3$) δ=0.8—1.8 (13H, m, ($CH_3CH_2)_2N$ and $CH_3CH_2CH_2CH_2$-O), 3.30 (4H,q,($CH_3CH_2)_2N$), and 4.06 (2H, t, $CH_3CH_2CH_2CH_2$-O); MS(70 eV) *m/z* 173(M^+); Calcd for $C_9H_{19}NO_2$: M, 173.

2-Methylpropyl Diethylcarbamate (Isobutyl Diethylcarbamate): bp 73.0—73.8 °C/5.0 mmHg; IR (neat) 1700 cm^{-1} (ester C=O); ^1H NMR($CDCl_3$) δ=0.6—1.3 (12H, m, ($CH_3CH_2)_2N$ and $(CH_3)_2CHCH_2$-O), 1.8 (1H, m, $(CH_3)_2CHCH_2$-O), 3.17 (4H, q, ($CH_3CH_2)_2N$), and 3.70 (2H, d, $(CH_3)_2CHCH_2$-O); Found: C, 62.21; H, 11.00; N, 8.13%; M^+, 173. Calcd for $C_9H_{19}NO_2$: C, 62.39; H, 11.05; N, 8.09%; M, 173.

1-Methylpropyl Diethylcarbamate (*s*-Butyl Diethylcarbamate): bp 67.0—67.3 °C/6.0 mmHg; IR (neat) 1695 cm^{-1} (ester C=O); ^1H NMR($CDCl_3$) δ=0.6—1.9 (14H, m, ($CH_3CH_2)_2N$ and $CH_3CH_2CH(CH_3)$-O), 3.17 (4H, q, ($CH_3CH_2)_2N$), and 4.63 (1H, m, $CH_3CH_2CH(CH_3)$-O); Found: C, 62.41; H, 11.07; N, 8.09%; M^+, 173. Calcd for $C_9H_{19}NO_2$: C, 62.39; H, 11.05; N, 8.09%; M, 173.

1,1-Dimethylethyl Diethylcarbamate (*t*-Butyl Diethylcarbamate): bp 28.4 °C/3.0 mmHg; IR (neat) 1690 cm^{-1} (ester C=O); ^1H NMR($CDCl_3$) δ=0.74 (6H, t, ($CH_3CH_2)_2N$), 1.07 (9H, s, $(CH_3)_3C$-O), and 2.87 (4H, q, ($CH_3CH_2)_2N$); Found: C, 62.32; H, 11.05; N, 8.08%; M^+, 173. Calcd for $C_9H_{19}NO_2$: C, 62.39; H, 11.05; N, 8.09%; M, 173.

† 1 mmHg≈133.322 Pa.

Ethyl Diethylcarbamate: bp 60.8—61.2 °C/13 mmHg (lit,[19] bp 62—63 °C/14 mmHg); IR (neat) 1700 cm^{-1} (ester C=O); ^1H NMR($CDCl_3$) δ=1.1 (9H, m, (CH_3CH_2)$_2$N and CH_3CH_2-O), 3.24 (4H, q, (CH_3CH_2)$_2$N), and 4.12 (2H, t, CH_3CH_2-O).

***N*-Ethoxycarbonylpiperidine:** bp 57.7—58.0 °C/1.5 mmHg (lit,[20] bp 55—56 °C/0.9 mmHg); IR (neat) 1705 cm^{-1} (ester C=O); ^1H NMR($CDCl_3$) δ=0.97 (3H, t, CH_3CH_2-O), 1.3 (6H, m, -(CH_2)$_3$-), 3.20 (4H, m, -CH_2NCH_2-), and 3.75 (2H, q, CH_3CH_2-O).

Propyl Diethylcarbamate: bp 58.6—59.0 °C/4.9 mmHg; IR (neat) 1700 cm^{-1} (ester C=O); ^1H NMR($CDCl_3$) δ=0.7—1.4 (9H, m, (CH_3CH_2)$_2$N and $CH_3CH_2CH_2$-O), 1.6 (2H, m, $CH_3CH_2CH_2$-O), 3.27 (4H, q, (CH_3CH_2)$_2$N), and 3.98 (2H, t, $CH_3CH_2CH_2$-O); Found: C, 60.16; H, 10.81; N, 8.57%; M$^+$, 159. Calcd for $C_8H_{17}NO_2$: C, 60.34; H, 10.76; N, 8.79%; M, 159.

***N*-(Propyloxycarbonyl)piperidine:** bp 86.0—86.5 °C/4.4 mmHg; IR (neat) 1695 cm^{-1} (ester C=O); ^1H NMR($CDCl_3$) δ=0.87 (3H, t, $CH_3CH_2CH_2$-O), 1.1—1.9 (8H, m, CH_3CH_2-CH_2-O and -(CH_2)$_3$-), 3.27 (4H, m, -CH_2NCH_2-), and 3.94 (2H, t, $CH_3CH_2CH_2$-O); Found: C, 63.13; H, 10.11; N, 8.09%; M$^+$, 171. Calcd for $C_9H_{17}NO_2$: C, 63.12; H, 10.00; N, 8.17%; M, 171.

Butyl Bis(1-methylethyl)carbamate: bp 55.9—56.9 °C/2.0 mmHg; IR (neat) 1695 cm^{-1} (ester C=O); ^1H NMR ($CDCl_3$) δ=0.6—1.8 (13H, m, ((CH_3)$_2$CH)$_2$N and CH_3CH_2-CH_2CH_2-O), 3.8 (2H, m, ((CH_3)$_2$CH)$_2$N), and 4.00 (2H, t, $CH_3CH_2CH_2CH_2$-O); Found: C, 65.63; H, 11.55; N, 6.96%; M$^+$, 201. Calcd for $C_{11}H_{23}NO_2$: C, 65.63; H, 11.51; N, 6.95%; M, 201.

Benzyl Diethylcarbamate: bp 93.0—94.0 °C/2.0 mmHg; IR (neat) 1700 cm^{-1} (ester C=O); ^1H NMR($CDCl_3$) δ=0.9 (6H, t, (CH_3CH_2)$_2$N), 3.07 (4H, q, (CH_3CH_2)$_2$N), 5.00 (2H, s, $C_6H_5CH_2$-O), and 7.13 (5H, s, $C_6H_5CH_2$-O); Found: C, 69.66; H, 8.35; N, 6.71%; M$^+$, 207. Calcd for $C_{12}H_{17}NO_2$: C, 69.54; H, 8.26; N, 6.76%; M, 207.

1-Methylethyl Diethylcarbamate: bp 44.8—45.4 °C/3.6 mmHg; IR (neat) 1700 cm^{-1} (ester C=O); ^1H NMR($CDCl_3$) δ=0.6-1.5 (12H, m, (CH_3CH_2)$_2$N and (CH_3)$_2$CH-O), 3.13 (4H, q, (CH_3CH_2)$_2$N), and 4.73 (1H, m, (CH_3)$_2$CH-O); Found: C, 60.06; H, 10.75; N, 8.39%; M$^+$, 159. Calcd for $C_8H_{17}NO_2$: C, 60.34; H, 10.76; N, 8.79%; M, 159.

***N*-(1-Methylethoxycarbonyl)piperidine:** bp 61.2—61.4 °C/1.4 mmHg; IR (neat) 1695 cm^{-1} (ester C=O); ^1H NMR ($CDCl_3$) δ=0.8—1.8 (12H, m, (CH_3)$_2$CH-O and -(CH_2)$_3$-), 3.27 (4H, m, -CH_2NCH_2-), and 4.76 (1H, m, (CH_3)$_2$CH-O); Found: C, 63.14; H, 9.98; N, 8.15%; M$^+$, 171. Calcd for $C_9H_{17}NO_2$: C, 63.12; H, 10.00; N, 8.17%; M, 171.

Cyclohexyl Diethylcarbamate: bp 83.1—83.7 °C/1.0 mmHg; IR (neat) 1710 cm^{-1} (ester C=O); ^1H NMR($CDCl_3$) δ=0.6—2.0 (16H, m, (CH_3CH_2)$_2$N and -(CH_2)$_5$-), 3.14 (4H, q, (CH_3CH_2)$_2$N), and 4.50 (1H, m, CH-O); Found: C, 66.23; H, 10.80; N, 7.03%; M$^+$, 199. Calcd for $C_{11}H_{21}NO_2$: C, 66.29; H, 10.62; N, 7.03%; M, 199.

Methylene Bis(propylcarbamate): mp 80.0—81.0 °C; IR (KBr pellet) 1695 cm^{-1} (ester C=O); ^1H NMR ($CDCl_3$) δ=0.85 (6H, m, ($CH_3CH_2CH_2NHCOO$)$_2$), 1.50 (4H, m, (CH_3CH_2-CH_2NHCOO)$_2$), 3.10 (4H, m, ($CH_3CH_2CH_2NHCOO$)$_2$), 5.40 (2H, s, ($CH_3CH_2CH_2NHCOO$)$_2$), and 5.6 (2H, s, O-CH_2-O); Found: C, 49.75; H, 8.52; N, 12.71%. Cacld for $C_9H_{18}N_2O_4$: C, 49.53; H, 8.31; N, 12.84%.

References

1) S. Inoue and N. Yamazaki, "Organic and Bio-organic Chemistry of Carbon Dioxide," Kodansha Ltd., (1981).
2) H. A. Rawi and A. Williams, *J. Am. Chem. Soc.*, **99**, 2671 (1977).
3) P. Adams and F. A. Baron, *Chem. Rev.*, **65**, 567 (1965).
4) T. Toda, *Chem. Lett.*, **1977**, 957.
5) T. Asano, N. Saito, S. Ito, K. Hatakeda, and T. Toda, *Chem. Lett.*, **1978**, 311.
6) T. Toda, *Nippon Kagaku Kaishi*, **1982**, 282.
7) N. Saito, K. Hatakeda, S. Ito, T. Asano, and T. Toda, *Bull. Chem. Soc. Jpn.*, **59**, 1629 (1986).
8) K. Soga, S. Hosoda, and S. Ikeda, *Nippon Kagaku Kaishi*, **1978**, 246.
9) K. Soga, S. Hosoda, H. Nakamura, and S. Ikeda, *J. Chem. Soc., Chem. Commun.*, **1976**, 617.
10) Y. Sasaki and P. H. Dixneuf, *J. Chem. Soc., Chem. Commun.*, **1986**, 79.
11) Y. Sasaki and P. H. Dixneuf, *J. Org. Chem.*, **52**, 314 (1987).
12) Y. Yoshida and S. Inoue, *Chem. Lett.*, **1978**, 139.
13) Y. Yoshida and S. Inoue, *J. Chem. Soc., Perkin Trans. 1*, **1979**, 3146.
14) Y. Yoshida and S. Inoue, *Chem. Lett.*, **1977**, 1375.
15) S. Ishii, H. Nakayama, Y. Yoshida, and T. Yamashita, *Bull. Chem. Soc. Jpn.*, in press.
16) Y. Yoshida, S. Ishii, and T. Yamashita, *Chem. Lett.*, **1984**, 1571.
17) M. S. Newman, "Steric Effect in Organic Chemistry," John Wiley and Sons, Inc., (1956), p. 126.
18) V. G. Parra, F. Sanchez, and T. Torres, *Synthesis*, **1985**, 282.
19) O. Schmit, *Chem. Ber.*, **36**, 2477 (1954).
20) W. Ried, H. Hillenbrand, and G. Oertel, *Justus Liebigs Ann. Chem.*, **590**, 123 (1954).

Novel Electron Acceptors Bearing a Heteroquinonoid System. I. Synthesis and Conductive Complexes of 5,5′-Bis(dicyanomethylene)-5,5′-dihydro-$\Delta^{2,2'}$-bithiophene and Related Compounds

Koji YUI, Yoshio ASO, Tetsuo OTSUBO, and Fumio OGURA*
Department of Applied Chemistry, Faculty of Engineering, Hiroshima University, Saijo, Higashi-Hiroshima 724
(Received September 12, 1988)

Novel electron acceptors bearing a heteroquinonoid system, 5,5′-bis(dicyanomethylene)-5,5′-dihydro-$\Delta^{2,2'}$-bithiophene, its 3,3′-dichloro, 3,3′-dibromo, and 3,3′,4,4′-tetrabromo derivatives, and 5,5″-bis(dicyanomethylene)-5,5″-dihydro-$\Delta^{2,2':5',2''}$-terthiophene were synthesized by the action of tetracyanoethylene oxide or by Pd(0)-catalyzed substitution reactions with sodium dicyanomethanide on the corresponding α,α'-dihalogeno-heteroaromatics. They showed very small on-site Coulomb repulsion as expected, and afforded several highly conductive molecular complexes with electron donors such as hexamethylenetetratellurafulvalene.

A very large amount of recent work in terms of structural organic chemistry and of material science has been directed toward the design and synthesis of new electron acceptor molecules which can be a potential component of organic electrical conductors. In particular, an excellent acceptor, 7,7,8,8-tetracyano-*p*-quinodimethane (TCNQ), giving many conductive charge-transfer complexes, has been widely modified to improve its physical properties up to date.[1] In this current, extension of quinonoid conjugation of TCNQ has been examined to develop new acceptors with smaller on-site Coulomb repulsion in dianion state.[2] Though 13,13,14,14-tetracyanodiphenoquinodimethane (TCNDQ) had attracted considerable interest as one of such candidates, it turned out to be a nonpersistent molecule in neutral state owing to steric repulsion between the biphenylic ortho hydrogens.[3] This was followed by stable isolation of an ethano-bridged derivative of TCNDQ (**1**).[2a] On the other hand, 2,5-bis(dicyanomethylene)-2,5-dihydrothiophene (**2**) has been known as a heteroquinonoid isologue of TCNQ, which was casually synthesized by Gronowitz and Uppström.[4] Though the introduced sulfur atom is expected to act advantageously on the formation of its molecular complexes, **2** has stirred little attention because of its inferior electron-accepting ability and insulating molecular complex formation.[5] Much more extension of quinonoid conjugation in **2** might improve its ability as a component of conductive complex regarding effective diminution of on-site

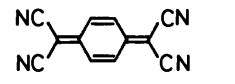
TCNQ

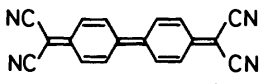
TCNDQ

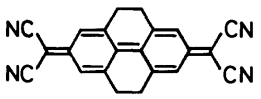
1

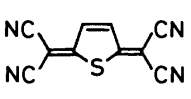
2

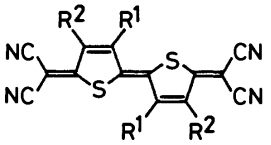
3a : $R^1 = R^2 = H$
3b : $R^1 = Cl$, $R^2 = H$
3c : $R^1 = Br$, $R^2 = H$
3d : $R^1 = R^2 = Br$

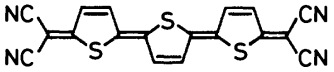
4

Coulomb repulsion and enlargement of band width. The most expected compounds are 5,5′-bis(dicyanomethylene)-5,5′-dihydro-$\Delta^{2,2'}$-bithiophene (**3a**) and 5,5″-bis(dicyanomethylene)-5,5″-dihydro-$\Delta^{2,2':5',2''}$-terthiophene (**4**). Supposedly, the trans geometry is more preferable for **3a**, because the biphenylic hydrogen repulsion must be advantageously avoided. On the other hand, **4** is a moreover extended homologue of **2**, in which some advanced character involving much smaller on-site Coulomb repulsion and large polarizability is expected.[6] Now we would like to report the syntheses and properties of **3a**, its derivatives with halogeno-substituents (**3b—d**), and **4**. As expected, these acceptors showed very small on-site Coulomb repulsion in their dianion state, and afforded semi- to highly conductive molecular complexes with various electron donors.

Results and Discussion

Synthesis. Gronowitz and Uppström reported that 2,5-dibromothiophene reacted with tetracyanoethylene oxide (TCNEO) in refluxing 1,2-dibromoethane to afford **2** and carbonyldicyanide.[4] At the same time, 2,3,5-tri- and 2,3,4,5-tetrabromothiophenes were formed as minor by-products because the reaction stoichiometrically generated bromine. We have found a similar reaction to be applicable toward bi- and terthiophene systems. 5,5′-Dibromo-2,2′-bithiophene (**5a**)[7] was treated with 0.75 equivalent of TCNEO in

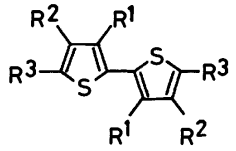

5a : $R^1 = R^2 = H$, $R^3 = Br$
5b : $R^1 = R^3 = Cl$, $R^2 = H$
5c : $R^1 = Br$, $R^2 = R^3 = H$
5d : $R^1 = R^3 = Br$, $R^2 = H$
5e : $R^1 = R^2 = R^3 = Br$

refluxing 1,2-dibromoethane for 8 h to afford **3a** in 42% yield on TCNEO. 3,3′,5,5′-Tetrachloro-2,2′-bithiophene (**5b**) was prepared from one-step treatment of thiophene with sulfuryl chloride and iron powder according to the procedure of Sone et al.[8] In a similar reaction of **5b** and TCNEO, the resulting 3,3′-dichloro-5,5′-bis(dicyanomethylene)-5,5′-dihydro-$\Delta^{2,2'}$-bithiophene (**3b**) was contaminated by further chlorinated one which was caused by chlorine stoichiometrically generated in the reaction, and was difficult to sufficiently purify. This reaction needed to be carried out in the presence of excessive copper(I) chloride as a reducing agent in refluxing 1,3-dibromopropane to obtain pure **3b** in a reasonable yield of 30%. 3,3′,5,5′-Tetrabromo-2,2′-bithiophene (**5d**) was prepared by bromination of 3,3′-dibromo-2,2′-bithiophene (**5c**)[9] (81% yield) or **5a** (90% yield) with NBS in refluxing chloroform–acetic acid (1:1 v/v). When **5d** was treated with an excess of TCNEO in refluxing 1,3-dibromopropane, 3,3′-dibromo-5,5′-bis(dicyanomethylene)-5,5′-dihydro-$\Delta^{2,2'}$-bithiophene (**3c**) was obtained in 27% yield. Treatment of **5a** with an excess of bromine in refluxing carbon disulfide afforded 3,3′,4,4′,5,5′-hexabromo-2,2′-bithiophene (**5e**) in 95% yield. A similar treatment of **5e** with TCNEO gave 3,3′,4,4′-tetrabromo-5,5′-bis(dicyanomethylene)-5,5′-dihydro-$\Delta^{2,2'}$-bithiophene (**3d**) in only 1.5% yield, whereas addition of an excess of copper(I) bromide fairly improved the yield up to 12%.

In the presence of palladium(0) catalyst, a cross coupling reaction[10] between 2,5-dibromothiophene and tributyl(2-thienyl)tin (**7**), which was prepared in 89% yield from 2-thienyllithium and chlorotributyltin, afforded 2,2′:5′,2″-terthiophene (**6a**) in 59% yield as shown in Scheme 1. This procedure is a practical alternative to the reported methods to obtain **6a**.[11,12] The NBS treatment of **6a** in chloroform–acetic acid (1:1 v/v) afforded 5,5″-dibromo-2,2′:5′,2″-terthiophene (**6b**) in 94% yield. The subsequent reaction of **6b** with 0.75 equiv of TCNEO in 1,2-dibromoethane at reflux gave 5,5″-bis(dicyanomethylene)-5,5″-dihydro-$\Delta^{2,2':5',2''}$-terthiophene (**4**) in 11% yield on TCNEO.

Sodium dicyanomethanide prepared in situ from malononitrile and sodium hydride was allowed to react with **5a** and **6b** in refluxing 1,2-dimethoxyethane containing a catalytic amount of tetrakis(triphenylphosphine)palladium(0),[13] followed by oxidation with bromine water, to successfully synthesize **3a** and **4** in 68% and 73% yield, respectively. Scheme 2 illustrates the conversion of **5a** into **3a**.

Nickel(0)-catalyzed coupling reaction[14] of 5-bromo-2,2′-bithiophene (**5f**)[15] gave 2,2′:5′,2″:5″,2‴-quaterthiophene (**8a**) in 87% yield, and its subsequent reaction with NBS afforded 5,5‴-dibromo derivative (**8b**) in 87% yield as shown in Scheme 3. Both TCNEO and malononitrile treatments, however, failed in synthesizing 5,5‴-bis(dicyanomethylene)-5,5‴-dihydro-

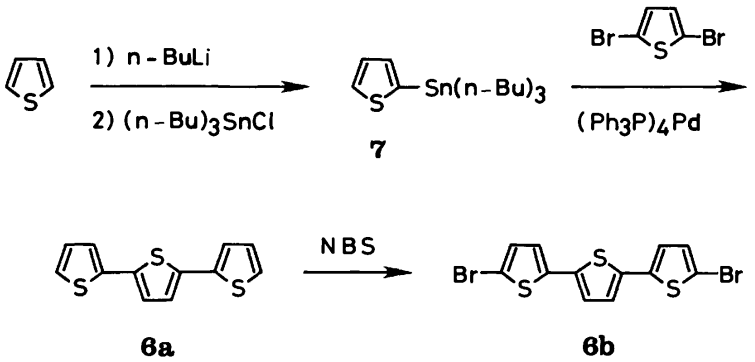

Scheme 1.

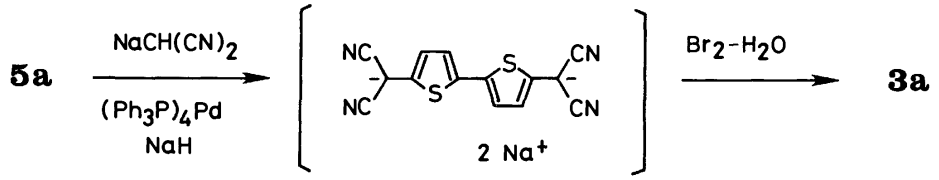

Scheme 2.

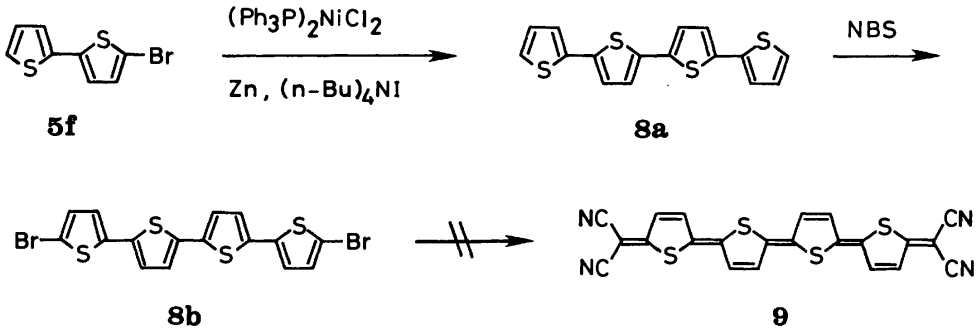

Scheme 3.

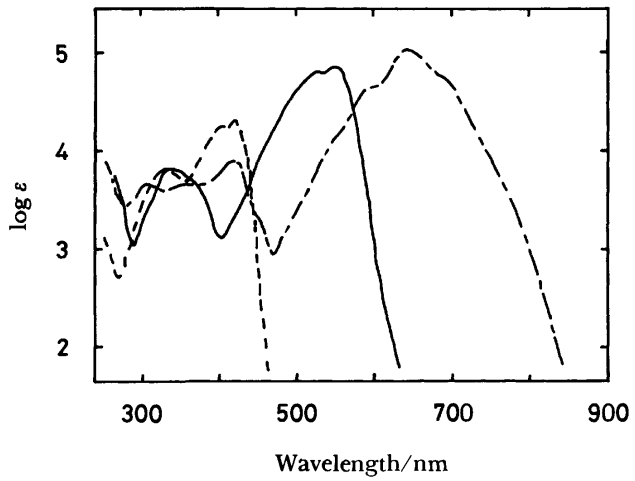

Fig. 1. Electronic spectra of **2** (-------), **3a** (——), and **4** (— — —) in dichloromethane.

$\Delta^{2,2':5',2'':5'',2'''}$-quaterthiophene (**9**).

Structure. The electronic spectra of **2**, **3a**, and **4** are shown in Fig. 1. These spectra strikingly resemble each other in shape, and their absorption maxima in the visible region are bathochromically shifted largely with extending their conjugation systems (**2**: $\lambda_{max}(\varepsilon)$ 330(6400), 400(18000), 421(20300); **3a**: 343(7000), 525 (65700), 550(73100); **4**: 304(4710), 358(4530), 415(7640), 643(106000) nm), suggesting nearly planar quinonoid structures in these molecules. Although TCNDQ is too unstable to isolate as mentioned before,[3] **3a—d** and **4** are extremely stable compounds whose decomposition points are not observed below 300 °C. These facts are attributable to trans geometry of these molecules, being capable of avoiding steric repulsion between hydrogen or halogen atoms at 3,3'-position.

Table 1 shows electrical conductivities of these acceptors (**3a—d** and **4**) on a compressed pellet together with those of **2** and TCNQ. It is very interesting that **3a—d** and **4** are all highly conductive for a pellet sample of a neutral organic compound in contrast to much lower conductivities of **2** and TCNQ, and reminicent of the most conductive, neutral organic compound, tetrakis(methyltelluro)tetrathiafulvalene.[16] This is realized as an increase of the intermolecular interactions due to extension of their heteroquinonoid conjugation.

Table 1. Conductivities of Acceptors

Acceptor	Conductivity[a]/S cm^{-1}
2	$<10^{-11}$
3a	1.2×10^{-6}
3b	4.9×10^{-7}
3c	2.7×10^{-6}
3d	6.9×10^{-5}
4	1.7×10^{-6}
TCNQ	8.1×10^{-10}

a) Measured on compressed pellets with a two-probe method at RT.

Table 2. Half-Wave Reduction Potentials[a]

Acceptor	$E^1_{1/2}$	$E^2_{1/2}$	ΔE/V
2	0.07	−0.54	0.61
3a	−0.03	−0.26	0.23
3b	0.18	−0.06	0.24
3c	0.20	0.03	0.17
3d	0.28	0.13	0.15
4	−0.03	−0.03	0
TCNQ	0.25	−0.47	0.72

a) Cyclic voltammetry was carried out at RT in dichloromethane containing 0.1 mol dm^{-3} tetrabutylammonium perchlorate using Ag/AgCl as a reference electrode and platinum as a working electrode at a scan rate of 100 mV s^{-1}.

Redox Property. The redox behavior of acceptors **3a—d** and **4** was determined by cyclic voltammetry in dichloromethane. Table 2 summarizes their half-wave reduction potentials together with those of **2** and TCNQ. All **3a—d** show two pairs of reversible redox waves. The first half-wave potential ($E^1_{1/2}$) of **3a** is lower than that of **2**, indicating a smaller electron affinity of **3a**. However, since its second one ($E^2_{1/2}$) is higher, the difference (ΔE) between $E^1_{1/2}$ and $E^2_{1/2}$ becomes smaller. This unambiguously demonstrates much more diminution of on-site Coulomb repulsion in the dianion state of **3a**. Acceptor **4** shows almost the same $E^1_{1/2}$ value as **3a** does. It is remarkable that its

second wave coalesces into its first one as if its on-site Coulomb repulsion were minimized.

The electron-withdrawing halogen substituents of **3b** and **3c** can actually increase the weak electron-accepting ability of parent **3a**, resulting in the $E^1_{1/2}$ values comparable to that of TCNQ. The additional 5,5′-dibromo substituents of **3d**, however, do not so much raise its $E^1_{1/2}$ as its 3,3′-dibromo substituents. Compounds **3b—d** also show very small ΔE values. Both large electron affinity and quite small on-site Coulomb repulsion thus allow **3b—d** to behave as superior electron acceptors.

Molecular Complex. These acceptors did form molecular complexes with electron donors such as tetrathiafulvalene (TTF), tetrathiotetracene (TTT), hexamethylenetetrathiafulvalene (HMTTF), tetramethylphenylenediamine (TMPDA), tetraphenylbipyranylidene (TPBP), hexamethylenetetratellurafulvalene (HMTTeF), 5,6-dihydroacenaphtho[5,6-*cd*]-1,2-ditellurole (ADTe), and bis(ethylenedithio)tetrathiafulvalene (BEDT-TTF). Table 3 summarizes physical properties of the isolated complexes.

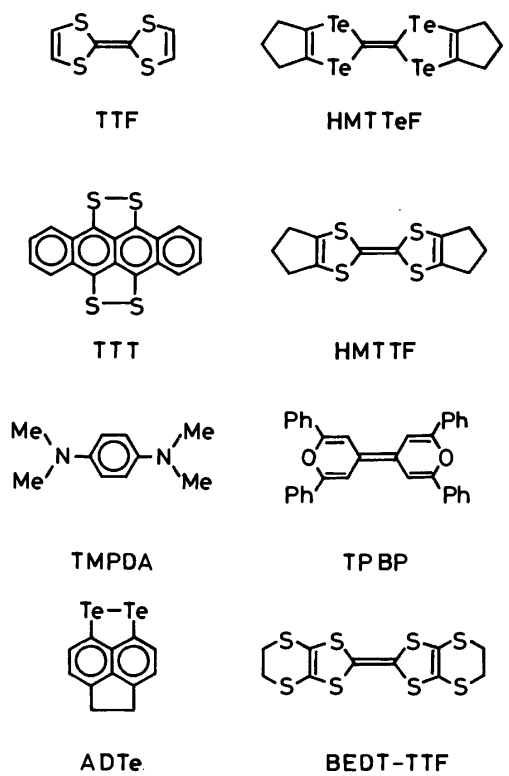

Acceptor **2** gave no crystalline complexes with typical donors such as TTT, TMPDA, HMTTF, ADTe, and BEDT-TTF because of its weak accepting ability. It, however, formed nearly insulating 1:1 complexes with TTF and HMTTeF. The TTF and HMTTeF complexes carry no charge transfer, as indicated by no shift in wavenumber of the nitrile stretching vibration absorption (ν_{CN}) in the IR spectra on complexation.[17] On the other hand, **2** formed a highly conductive 1:1 complex with a stronger donor TPBP. A considerable lower wavenumber shift of ν_{CN} (2184 cm^{-1}) of the complex than that (2222 cm^{-1}) of neutral **2** clearly indicates the existence of certain charge transfer, which might be related to its high conductivity.

Acceptor **3a** gave 1:1 complexes with TTF and TTT. These complexes are little ionic on the basis of ν_{CN} nearly comparable to that (2220 cm^{-1}) of **3a** but semiconductive. Acceptor **4** complexed TTF, TTT, TPBP, and HMTTeF. The stoichiometry of these complexes except TTT complex is rich in acceptor. Their ν_{CN} values, referring to that (2213 cm^{-1}) of **4**, indicate no charge transfer in the TTF and HMTTeF complexes and some charge transfer in the TTT and TPBP complexes. Their conductivities are, however, close to metallic, regardless of degree of the charge transfers. Comparison of three TTF complexes of **2**, **3a**, and **4**, though they are all nonionic, demonstrates a marked increase in conductivity in order of the extensive acceptor. These results strongly support that the diminished on-site Coulomb repulsion of the extensive conjugated acceptor makes a significant contribution to the formation of conductive molecular complexes.

Acceptors **3b—d**, further endowed by stronger electron-accepting abilities, could form complexes with all the given donors. However, complexation of **3b** with ADTe and of **3d** with BEDT-TTF failed. Most of complexes obtained were very highly conductive. In particular, marvelously high conductivity of 170 S cm^{-1} was observed for **3b**·HMTTeF in a compressed pellet state.

Conclusion

The accepting ability of 2,5-bis(dicyanomethylene)-2,5-dihydrothiophene (**2**) was successfully improved by

Table 3. Molecular Complexes of **2**, **3a—d**, and **4**

Complex[a]	Appearance	Found (Calcd)[b]/%			ν_{CN}[c]/cm^{-1}	dp[d]/°C	Conductivity[e] /S cm^{-1}
		C	H	N			
2·TTF[f]	Golden yellow needles	46.12; (46.36;	1.41; 1.46;	13.22 13.52)	2221	168	6.8×10^{-9}[g]
2·TPBP	Dark brown powder	78.29; (78.32;	3.83; 3.88;	7.57 8.30)	2184	193	4.9×10^{-1}

Table 3. (Continued)

Complex[a]	Appearance	Found (Calcd)[b]/%			ν_{CN}[c]/cm^{-1}	dp[d]/°C	Conductivity[e] /S cm^{-1}
		C	H	N			
2·HMTTeF	Dark brown powder	30.14; (30.14;	1.77; 1.61;	5.54 6.39)	2221	200	5.5×10^{-9}[g]
3a·TTF[f]	Brown powder	48.15; (48.37;	1.62; 1.62;	11.37 11.28)	2217	195	2.2×10^{-4}
3a·TTT	Deep blue fine needles	58.79; (59.60;	1.65; 1.88;	8.93 8.69)	2219	>300	3.0×10^{-4}
3b·TTF[f]	Deep brown powder	42.45; (42.48;	1.07; 1.07;	9.88 9.91)	2197	228	19
3b·TTT	Green needles	53.72; (53.85;	1.41; 1.41;	7.55 7.85)	2190	>300	4.6
(**3b**)$_2$·TMPDA	Black fine cryst	51.93; (51.47;	2.16; 2.27;	14.92 15.80)	2192	>300	7.3×10^{-1}
3b·TPBP	Deep green fine cryst	69.67; (69.82;	3.04; 3.17;	6.50 6.78)	2193	>300	8.3×10^{-5}[g]
3b·HMTTF	Black fine needles	48.58; (48.37;	1.92; 2.19;	8.68 8.68)	2199	>300	6.3
3b·HMTTeF	Dark brown powder	30.12; (30.38;	1.30; 1.37;	5.23 5.45)	2180	236	170
(**3b**)$_2$·BEDT -TTF	Deep green needles	41.80; (41.23;	1.10; 1.09;	10.14 10.12)	2218	274	2.3×10^{-7}[g]
3c·TTF[f]	Green fine needles	36.70; (36.70;	0.92; 0.92;	8.56 8.56)	2203	235	15
3c·TTT	Green fine needles	47.86; (47.87;	1.26; 1.26;	6.78 6.98)	2203	>300	13
3c·TMPDA[f]	Dark green fine needles	46.22; (46.92;	2.83; 2.95;	13.15 13.65)	2198	220	2.9×10^{-2}
3c·TPBP	Green powder	62.66; (63.03;	2.73; 2.87;	5.39 6.13)	2196	>300	4.5×10^{-1}
3c·HMTTF	Dark blue prisms	42.46; (42.51;	1.91; 1.92;	7.50 7.63)	2194	220	22
3c·(HMTTeF)$_2$	Dark green powder	25.75; (25.59;	1.62; 1.47;	3.12 3.14)	2169	270	57
3c·ADTe	Dark green powder	36.41; (36.42;	1.10; 1.18;	6.24 6.53)	2193	250	6.3×10^{-1}
3c·BEDT -TTF	Dark green powder	34.65; (34.53;	1.50; 1.21;	6.61) 6.71)	2218	265	2.2×10^{-7}[g]
3d·TTF	Deep green fine needles	29.87; (29.57;	0.47; 0.50;	6.90 6.90)	2200	202	31
3d·TTT	Deep green fine needles	40.17; (40.02;	0.77; 0.84;	5.75 5.83)	2193	>300	18
(**3d**)$_3$·(TMPDA)$_2$	Green powder	34.35; (34.60;	1.22; 1.50;	9.32 10.41)	2192	161	7.1×10^{-1}
3d·TPBP	Deep green powder	54.17; (53.76;	2.18; 2.26;	4.84 5.22)	2195	294	11
3d·HMTTF	Dark brown powder	35.16; (34.99;	1.29 1.36;	6.11 6.28)	2200	>300	39
3d·HMTTeF	Black powder	24.24; (24.54;	0.97; 0.95;	3.30 4.40)	2182[i]	225	29
3d·ADTe	Black powder	30.73; (30.76;	0.83; 0.79;	4.78 5.52)	2195	278	6.6×10^{-1}
(**4**)$_5$·TTF[h]	Black powder	55.53; (56.26;	1.65; 1.84;	13.49 11.74)	2215	>300	3.3×10^{-3}
4·TTT	Black powder	58.58; (59.48;	1.88; 1.94;	7.20 7.71)	2204	>300	7.2×10^{-1}
(**4**)$_5$·(TPBP)$_2$	Black powder	67.10; (67.84;	2.97; 2.81;	8.32 10.01)	2209	286	3.7×10^{-1}
(**4**)$_2$·HMTTeF	Dark brown powder	39.97; (40.73;	2.32; 1.71;	6.72 7.92)	2215	214	1.1

a) Obtained from chlorobenzene unless otherwise described. b) Calculated as stoichiometry indicated for the complex. c) Measured with a KBr disk method unless otherwise mentioned. d) Decomposition point. e) Measured on compressed pellets at RT with a four-probe method unless otherwise described. f) Obtained from acetonitrile. g) Measured on compressed pellets with a two-probe method at RT. h) Obtained from benzonitrile. i) Measured with a Nujol mull method.

introduction of both extensive heteroquinonoid conjugation and electron-withdrawing substituents. For compounds **3a** and **4** the extensive conjugation was very effective for diminution of on-site Coulomb repulsion, which is a requisite for designing conductive molecular complexes. In addition, it was proved that compounds **3b—d** possessing both small on-site Coulomb repulsion and large electron affinity are reliable electron acceptors for forming a variety of very high conductive molecular complexes.

Experimental

General. Melting points are uncorrected. All solvents are of reagent grade. Elemental analyses were measured by Mr. Hideaki Iwatani, Microanalytical Laboratory in Department of Applied Chemistry, Faculty of Engineering, Hiroshima University. Electron donors used to prepare the molecular complexes, TTF,[18] TTT,[19] HMTTF,[20] TPBP,[21] BEDT-TTF,[22] and ADTe[23] were obtained according to the published procedures except commercially available TMPDA and HMTTeF. NMR spectra were recorded on a JEOL PMX-60 spectrometer (60 MHz) using tetramethylsilane as an internal standard. IR spectra were taken on a Hitachi 260-30 or Perkin-Elmer 1600 FTIR spectrophotometer with a nujol mull or a KBr disk method. MS spectra were measured on a Shimadzu GC-MS QP-1000A Mass spectrometer at 70 eV using a direct insertion technique. Electronic absorption spectra were recorded on a Shimadzu UV-160 spectrophotometer. Cyclic voltammetry was carried out on a Hokuto Denko HA-301 potentiostat and a Hokuto Denko HB-104 function generator.

5,5′-Bis(dicyanomethylene)-5,5′-dihydro-$\Delta^{2,2'}$-bithiophene (3a). A) Using TCNEO. A mixture of **5a** (324 mg, 1.00 mmol) and TCNEO (216 mg, 1.50 mmol) in dry 1,2-dibromoethane (15 cm^3) was heated under reflux for 8 h, and the solution was diluted with carbon tetrachloride (60 cm^3) at 0 °C. The resulting precipitate was collected by filtration and purified by column chromatography on silica-gel with dichloromethane, followed by recrystallization from acetonitrile, giving **3a** as deep violet fine needles (92 mg, 42% yield on TCNEO): mp>300 °C; IR (KBr) 2220 (CN), 1525, 1500 (C=C) cm^{-1}; MS *m/z* 292 (M^+, 100%); Anal. ($C_{14}H_4N_4S_2$) C, H, N.

B) Using Sodium Dicyanomethanide. Malononitrile (156 mg, 2.40 mmol) was added to an ice-cooled suspension of sodium hydride (192 mg, 60% oily, 4.80 mmol) in 1,2-dimethoxyethane (8 cm^3) under nitrogen atmosphere, and the mixture was stirred at RT for 20 min. To this solution were added **5a** (324 mg, 1.00 mmol) and tetrakis(triphenylphosphine)palladium(0) (156 mg, 0.100 mmol), and the mixture was heated under reflux for 4 h. The reaction mixture was treated with saturated bromine water (30 cm^3) at 0 °C and diluted with cold water (50 cm^3). The resulting precipitate was collected by filtration on Hyflo Super-Cel, Soxhlet-extracted with dichloromethane, concentrated in vacuo, and recrystallized from chlorobenzene to give **3a** (199 mg, 68%).

3,3′-Dichloro-5,5′-bis(dicyanomethylene)-5,5′-dihydro-$\Delta^{2,2'}$-bithiophene (3b). A mixture of **5b** (2.43 g, 8.00 mmol), TCNEO (11.5 g, 80.0 mmol), and copper(I) chloride (5.54 g, 56.0 mmol) in dry 1,3-dibromopropane (130 cm^3) was heated under reflux for 6 h. The solution was twice column-chromatographed on silica gel with dichloromethane, followed by recrystallization from acetonitrile to give **3b** as deep violet fine crystals (880 mg, 30%): mp>300 °C; IR (KBr) 2217 (CN), 1503 (C=C) cm^{-1}; MS *m/z* 360 (M^+, 100%); Anal. ($C_{14}Cl_2H_2N_4S_2$) C, H, N.

3,3′,5,5′-Tetrabromo-2,2′-bithiophene (5d). A) From 3,3′-Dibromo-2,2′-bithiophene (5c). A mixture of **5c** (1.30 g, 4.00 mmol) and NBS (1.50 g, 8.43 mmol) in chloroform–acetic acid (8 cm^3, 1:1 v/v) was heated under reflux for 5 h. The resulting solution was poured into water and extracted with chloroform. The organic layer was washed with 5% sodium hydrogencarbonate aqueous solution and water, and dried on anhydrous magnesium sulfate. After concentration in vacuo, the residual solid was recrystallized from chloroform–hexane to give **5d** as colorless prisms (1.57 g, 81%): mp 138.5—140.5 °C (lit,[24] 139—140 °C); ^1H NMR ($CDCl_3$) δ= 6.97 (s).

B) From 5a. NBS (392 mg, 2.20 mmol) was added to a solution of **5a** (324 mg, 1.00 mmol) in chloroform–acetic acid (9 cm^3, 1:1 v/v), and the mixture was heated under gentle reflux for 3 d. The solution was poured into water, and extracted with chloroform. The organic layer was worked up in the same way as described in Method A to give **5d** (436 mg, 90%).

3,3′-Dibromo-5,5′-bis(dicyanomethylene)-5,5′-dihydro-$\Delta^{2,2'}$-bithiophene (3c). A mixture of **5d** (120 mg, 0.25 mmol) and TCNEO (288 mg, 2.00 mmol) in dry 1,3-dibromopropane (3 cm^3) was heated under reflux for 2 h. The mixture was twice column-chromatographed on silica gel with dichloromethane, followed by recrystallization from acetonitrile to give **3c** as deep violet fine needles (31 mg, 27%): mp>300 °C; IR (KBr) 2224 (CN), 1510, 1495 (C=C) cm^{-1}; MS *m/z* 450 (M^+, 100%); Anal. ($C_{14}Br_2H_2N_4S_2$) C, H, N.

3,3′,4,4′,5,5′-Hexabromo-2,2′-bithiophene (5e). A mixture of **5a** (648 mg, 2.00 mmol), carbon disulfide (25 cm^3), and bromine (3.3 cm^3, 64 mmol) was heated under gentle reflux for 26 h. To this mixture was carefully added a saturated sodium hydrogensulfite aqueous solution (50 cm^3), and the mixture was vigorously stirred for several min. The resulting precipitate was collected by filtration, washed with water and methanol, and dried in vacuo. The organic layer of the filtrate was washed with 5% sodium hydrogencarbonate aqueous solution and water, and dried on anhydrous magnesium sulfate. After concentration in vacuo, the residual solid was combined with the above collected precipitate and recrystallized from chlorobenzene to give **5e** as colorless needles (1.21 g, 95%): mp 262—264 °C (lit,[25] 257—258 °C).

3,3′,4,4′-Tetrabromo-5,5′-bis(dicyanomethylene)-5,5′-dihydro-$\Delta^{2,2'}$-bithiophene (3d). A mixture of **5e** (128 mg, 0.200 mmol), TCNEO (576 mg, 4.00 mmol), and copper(I) bromide (201 mg, 1.40 mmol) in dry 1,3-dibromopropane (5 cm^3) was heated under reflux for 6 h. The solution was column-chromatographed on silica gel with chloroform, followed by recrystallization from chloroform to give **3d** as deep violet fine needles (15 mg, 12%): mp>300 °C; IR (KBr) 2217 (CN), 1500 (C=C) cm^{-1}; MS *m/z* 608 (M^+, 100%); Anal. ($C_{14}Br_4N_4S_2$) C, H, N.

Tributyl(2-thienyl)tin (7). Butyllithium (94 cm^3, 0.15 mol, 1.6 mol dm^{-3} hexane solution) was added to a solution

of thiophene (12.6 g, 0.150 mol) in THF (120 cm³) at 0 °C under nitrogen atmosphere, and the mixture was stirred at 50 °C for 30 min. To this solution was added chlorotributyltin (51.3 g, 0.150 mol, 95% purity) at 0 °C. The resulting suspension was stirred overnight at RT, concentrated, and filtered. The filtrate was distilled in vacuo to give **7** as colorless liquid (50.1 g, 89%): bp 118—125 °C/0.22 mmHg (lit,[26] 150 °C/1 mmHg; 1 mmHg≈133.322 Pa); ^{1}H NMR (CCl_4) δ=0.5—2.3 (m, 27H), 6.9—7.3 (m, 2H), 7.3—7.6 (m, 1H).

2,2′:5′,2″-Terthiophene (6a). A solution of **7** (48.5 g, 130 mmol), 2,5-dibromothiophene (14.5 g, 60.0 mmol), and tetrakis(triphenylphosphine)palladium(0) (3.47 g, 3.00 mmol) in toluene (200 cm³) was heated at reflux for 18 h under nitrogen atmosphere. The reaction mixture was concentrated in vacuo and chromatographed on silica gel with hexane, followed by recrystallization from hexane to give **6a** as pale yellow plates (8.77 g, 59%): mp 89—91 °C (lit,[27] 94—95 °C); ^{1}H NMR ($CDCl_3$) δ=6.9—7.2 (m); Anal. ($C_{12}H_8S_3$) C, H.

5,5″-Dibromo-2,2′:5′,2″-terthiophene (6b). NBS (11.9 g, 66.7 mmol) was portionwise added to a solution of **6a** (8.28 g, 33.3 mmol) in chloroform-acetic acid (1:1 v/v) at RT. The resulting suspension was suirred for an additional hour and then at 50—60 °C for 30 min. Precipitated solid was collected by filtration. The filtrate was successively washed with water, 5% sodium hydrogencarbonate aqueous solution, and again water, and dried on anhydrous magnesium sulfate. After concentration in vacuo, the residual solid was combined with the above precipitate and recrystallized from hexane-chloroform to give **6b** as yellow needles (12.7 g, 94%): mp 158—158.5 °C (lit,[28] 160—161 °C); ^{1}H NMR (CS_2) δ=6.86 (s, 2H), 6.84 (d, J=3.7 Hz, 2H), 6.78 (d, J=3.7 Hz, 2H).

5,5″-Bis(dicyanomethylene)-5,5″-dihydro-$\Delta^{2,2':5',2''}$-terthiophene (4). A) Using TCNEO. A mixture of **6b** (406 mg, 1.00 mmol) and TCNEO (216 mg, 1.50 mmol) in dry 1,2-dibromoethane (16 cm³) was heated under reflux for 2 h. The solution was twice column-chromatographed on silica gel with dichloromethane to give **4** (32 mg, 11% yield on TCNEO): deep green powder from chlorobenzene, mp> 300 °C; IR (KBr) 2213 (CN), 1480 (C=C) cm^{-1}; Found: m/z 374.0294. Calcd for $C_{18}H_6N_4S_3$: M, 373.9755.

B) Using Sodium Dicyanomethanide. Under a nitrogen stream, malononitrile (312 mg, 4.80 mmol) was added to an ice-cooled suspension of sodium hydride (384 mg, 9.60 mmol, 60% oily) in 1,2-dimethoxyethane (24 cm³), and the mixture was stirred at RT for 20 min. To this suspension were added **6b** (812 mg, 2.00 mmol) and tetrakis(triphenylphosphine)palladium(0) (312 mg, 0.200 mmol). The mixture was heated under reflux for 4 h, and treated with saturated bromine water (40 cm³). After dilution with cold water (20 cm³), the resulting precipitate was collected by filtration on Hyflo Super-Cel, and Soxhlet-extracted with dichloromethane, followed by recrystallization from chlorobenzene to give **4** (546 mg, 73%).

2,2′:5′,2″:5″,2‴-Quaterthiophene (8a). A mixture of zinc powder (785 mg, 12.0 mmol), bis(triphenylphosphine)nickel(II) chloride (393 mg, 0.600 mmol), and tetrabutylammonium iodide (2.22 g, 6.00 mmol) in THF (15 cm³) was stirred at RT under nitrogen atmosphere for 30 min. To the resulting reddish brown solution was added a solution of **5f** in THF (5 cm³), and the solution was stirred at 50 °C for 2 h. After addition of water, precipitated solid was collected by filtration, and column-chromatographed on silica gel with carbon disulfide, followed by recrystallization from chloroform to give **8a** as yellow leaflets (867 mg, 87%): mp 216.5—218 °C (lit,[12] 211—212 °C).

5,5‴-Dibromo-2,2′:5′,2″:5″,2‴-quaterthiophene (8b). NBS (911 mg, 5.12 mmol) was added to a solution of **8a** in carbon disulfide-chloroform-acetic acid (270 cm³, 2:5:2 v/v), and the mixture was heated under gentle reflux for an hour. After cooling to 0 °C, the resulting precipitate was collected by filtration, washed with methanol, and dried. The filtrate was successively washed with water, 5% sodium hydroxide aqueous solution, and water, and dried over anhydrous magnesium sulfate. After concentration in vacuo, the residual solid was combined with the above precipitate, and recrystallized from chlorobenzene to give **8b** as orange leaflets (1.09 g, 87%): mp 260—263 °C (lit,[24] 248 °C).

Preparation of Molecular Complexes. All molecular complexes described in this report were prepared by mixing the two hot saturated solutions of donor and acceptor in chlorobenzene, acetonitrile, or benzonitrile. The resulting complexes precipitated out immediately or on cooling appropriately, which were collected by filtration and dried in vacuo.

This work was partially supported by Grants-in-Aid for Scientific Research Nos. 62550635 and 63604576 from the Ministry of Education, Science and Culture.

References

1) For excellent articles on organic metals composed of TCNQ and its derivatives: R. C. Wheland and E. L. Martin, *J. Org. Chem.*, **40**, 3101 (1975); R. C. Wheland and J. L. Gillson, *J. Am. Chem. Soc.*, **98**, 3916 (1976); M. Narita and C. U. Pittman, Jr., *Synthesis*, **1976**, 489; J. B. Torrance, *Acc. Chem. Res.*, **12**, 79 (1979); M. R. Bryce and L. C. Murphy, *Nature (London)*, **309**, 119 (1984) and literatures cited therein.

2) a) E. Ahalon-Shalom, J. Y. Becker, and I. Agranat, *Nouv. J. Chim.*, **3**, 643 (1979); M. Maxfield, D. O. Cowan, A. N. Bloch, and T. O. Poehler, *ibid.*, **3**, 647. b) M. Maxfield, S. M. Willi, D. O. Cowan, A. N. Bloch, and T. O. Poehler, *J. Chem. Soc., Chem. Commun.*, **1980**, 947; N. Acton, D. Hou, J. Schwarz, and T. J. Katz, *J. Org. Chem.*, **47**, 1011 (1982); M. Maxfield, A. N. Bloch, and D. O. Cowan, *J. Org. Chem.*, **50**, 1789 (1985).

3) W. R. Hertler, U. S. Patent, 1964, No. 3153658 (*Chem. Abstr.*, **62**, 4145 (1965)); D. J. Sandman and A. F. Garito, *J. Org. Chem.*, **39**, 1165 (1974); M. Morinaga, T. Nogami, and H. Mikawa, *Bull. Chem. Soc. Jpn.*, **52**, 3739 (1979).

4) S. Gronowitz and B. Uppström, *Acta Chem. Scand., Ser. B*, **28**, 981 (1974).

5) M. L. Kaplan, R. C. Haddon, F. B. Bramwell, F. Wudl, J. H. Marshall, D. O. Cowan, and S. Gronowitz, *J. Phys. Chem.*, **84**, 427 (1980).

6) K. Yui, Y. Aso, T. Otsubo, and F. Ogura, *J. Chem. Soc., Chem. Commun.*, **1987**, 1816.

7) R. M. Kellog, A. P. Shaap, and H. Wynberg, *J. Org. Chem.*, **34**, 343 (1969).

8) T. Sone, K. Sakai, and K. Kuroda, *Bull. Chem. Soc. Jpn.*, **43**, 1411 (1970).

9) S. Gronowitz, *Acta Chem. Scand.*, **15**, 1393 (1961).

10) A. Donboni, A. R. Mastellari, A. Medici, E. Negrini, and P. Pedrini, *Synthesis*, **1986**, 757.
11) B. J. R. Philogene, J. T. Arnason, C. W. Berg, F. Duval, D. Champagne, R. G. Taylor, L. C. Leitch, and P. Moland, *J. Econ. Entomol.*, **78**, 121 (1985); A. Carpita, R. Rossi, and C. A. Veracini, *Tetrahedron*, **41**, 1919 (1985); J. Nakayama, M. Shimomura, M. Iwamoto, and M. Hoshino, *Heterocycles*, **23**, 1907 (1985) and references cited therein.
12) J. Kagan and S. K. Arora, *Tetrahedron Lett.*, **24**, 4043 (1983).
13) M. Uno, K. Seto, and S. Takahashi, *J. Chem. Soc., Chem. Commun.*, **1984**, 932; M. Uno, K. Seto, M. Sasuda, W. Ueda, and S. Takahashi, *Tetrahedron Lett.*, **26**, 1553 (1985).
14) M. Iyoda, K. Sato, and M. Oda, *Tetrahedron Lett.*, **26**, 3829 (1985).
15) R. F. Curtis and G. T. Phillips, *J. Chem. Soc.*, **1965**, 5134.
16) K. Imaeda, T. Enoki, Z. Shi, P. Wu, N. Okada, H. Yamochi, G. Saito, and H. Inokuchi, *Bull. Chem. Soc. Jpn.*, **60**, 3163 (1987).
17) J. S. Chappell, A. N. Bloch, W. A. Bryden, M. Maxfield, T. O. Poehler, and D. O. Cowan, *J. Am. Chem. Soc.*, **103**, 2442 (1981).
18) L. R. Melby, H. D. Hartzler, and W. A. Sheppard, *J. Org. Chem.*, **39**, 2456 (1974).
19) E. P. Goodings, D. A. Mitchard, and G. Owen, *J. Chem. Soc., Perkin Trans. 1*, **1972**, 1310.
20) H. K. Spencer and M. P. Cava, *J. Org. Chem.*, **41**, 730 (1976).
21) G. A. Reynolds, C. H. Chen, and J. A. Van Allan, *J. Org. Chem.*, **44**, 4456 (1979).
22) E. M. Engler, V. Y. Lee, R. R. Schumaker, S. S. P. Parkin, R. L. Greene, and J. C. Scott, *Mol. Cryst. Liq. Cryst.*, **107**, 19 (1984).
23) Y. Aso, K. Yui, T. Miyoshi, T. Otsubo, F. Ogura, and J. Tanaka, *Bull. Chem. Soc. Jpn.*, **61**, 2013 (1988).
24) W. Steinkopf, H. Pertersdorff, and R. Gording, *Justus Liebigs Ann. Chem.*, **527**, 272 (1937).
25) W. Steinkopff, *Justus Liebigs Ann. Chem.*, **543**, 128 (1940).
26) S. Gopinathan, C. Gopinathan, and J. Gupta, *Indian J. Chem.*, **12**, 623 (1974).
27) W. Steinkopff, R. Leitsmann, and K. H. Hofmann, *Justus Liebigs Ann. Chem.*, **546**, 180 (1941).
28) J. W. Sease and L. Zechmeister, *J. Am. Chem. Soc.*, **69**, 270 (1947).

Novel Electron Acceptors Bearing a Heteroquinonoid System. II. Synthesis and Conductive Complexes of 2,5-Bis(dicyanomethylene)-2,5-dihydrothieno-[3,2-*b*]thiophene, 2,6-Bis(dicyanomethylene)-2,6-dihydrodithieno[3,2-*b*:2′,3′-*d*]thiophene, and Their Derivatives

Koji YUI, Hideki ISHIDA, Yoshio ASO, Tetsuo OTSUBO, Fumio OGURA,*
Atsushi KAWAMOTO,† and Jiro TANAKA†
Department of Applied Chemistry, Faculty of Engineering, Hiroshima University, Saijo, Higashi-Hiroshima 724
†Department of Chemistry, Faculty of Science, Nagoya University, Chikusa-ku, Nagoya 464
(Received November 19, 1988)

Novel heteroquinonoid compounds as potential electron acceptors, 2,5-bis(dicyanomethylene)-2,5-dihydrothieno[3,2-*b*]thiophene (**4a**), 3,6-dibromo derivative, 2,6-bis(dicyanomethylene)-2,6-dihydrodithieno[3,2-*b*:2′,3′-*d*]thiophene, 3,5-dibromo derivative, and 4,4-dioxide were synthesized by the action of tetracyanoethylene oxide or by a Pd(0)-catalyzed substitution reaction with sodium dicyanomethanide on the corresponding α,α′-dihalo-substituted fused thiophenes. They show effectively diminished on-site Coulomb repulsion owing to the extensive conjugation, and most of their molecular complexes with various electron donors exhibit very high electrical conductivities up to metallic region. In addition, X-ray crystallographic analysis of the complex of **4a** with bis(ethylenedithio)tetrathiafulvalene has elucidated that sulfur atoms embedded in **4a** molecule are capable of inducing a significant intermolecular interaction, forming a sheet-like network structure.

Intermolecular interactions of heteroatoms often play an important role on molecular assemblies. In particular, interstack contacts of chalcogen atoms in the cation radical salts of two organic electron donors, tetramethyltetraselenafulvalene and bis(ethylenedithio)-tetrathiafulvalene (BEDT-TTF), served to suppress typical Peierls-type insulating transitions, leading to the discovery of first organic superconductors.[1] On the other hand, similar multi-dimensionality based on chalcogen atoms has been designed for electron acceptors. Yamashita's and Kobayashi's groups have independently examined the condensation effect of heterocyclic rings on an excellent electron acceptor, 7,7,8,8-tetracyano-*p*-quinodimethane (TCNQ).[2] Our previous work has developed novel electron acceptors (**1**, its derivatives, and **2**) as extensively conjugated

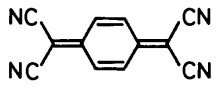

TCNQ

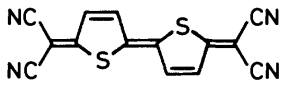

1

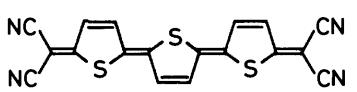

2

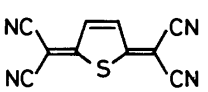

3

homologues of 2,5-bis(dicyanomethylene)-2,5-dihydrothiophene (**3**).[3] These acceptors have advantages of inducing not only increasing intermolecular interactions due to the sulfur atoms embedded in the quinonoid system but also very small on-site Coulomb repulsion due to the extensive conjugation, accordingly forming highly conductive molecular complexes.

Our present aim is to study condensed homologues of **3** as another potential acceptors. 2,5-Bis(dicyanomethylene)-2,5-dihydrothieno[3,2-*b*]thiophene (**4a**) is

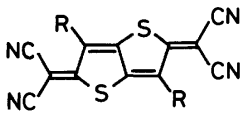

4a : R = H
4b : R = Br

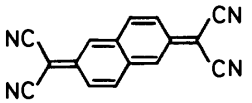

TNAP

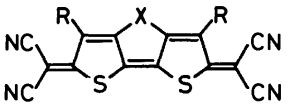

5a : X = S, R = H
5b : X = S, R = Br
5c : X = $-S(O_2)-$, R = H
5d : X = $-S(O)-$, R = H

the first molecule of the series and isoelectronic with 11,11,12,12-tetracyano-2,6-naphthoquinodimethane (TNAP), which has better accepting properties, that is, smaller on-site Coulomb repulsion, larger electron affinity, and higher polarizability than TCNQ.[4] A benzenoid compound corresponding to 2,6-bis(dicyanomethylene)-2,6-dihydrodithieno[3,2-*b*:2′,3′-*d*]thiophene (**5a**) is hitherto unknown. Now we wish to report the syntheses of **4a** and **5a** and their conductive molecular complexes as well as those of **4b** and **5b—c**.[5] In addition, the crystal structure of **4a**·BEDT-TTF complex is described, in which the sulfur atoms embedded in the quinonoid conjugation system are capable of inducing a significant intermolecular interaction.[6]

Results and Discussion

Synthesis. *Gronowitz reaction* which refers to a conversion of 2,5-dihalogenothiophene into **3** by a pyrolytic reaction with tetracyanoethylene oxide (TCNEO)[7] was successfully applicable toward bi- and terthiophene systems to synthesize the corresponding heteroquinonoid compounds **1** and **2**.[5] We found that a similar procedure was equally well-applicable toward fused thieno- and dithienothiophene systems. 2,5-Dibromothieno[3,2-*b*]thiophene (**6a**) was treated with an excess of TCNEO at 167 °C of refluxing 1,3-dibromopropane for 2 h to afford **4a** in 36% yield. When accomplished at 131 °C of refluxing 1,2-dibromoethane as done in the synthesis of **1**, **2**, and **3**, the reaction proceeded very slowly and resulted in a lower yield (23%) of **4a**. On the other hand, Gronowitz reaction of 2,6-dibromodithieno[3,2-*b*:2′,3′-*d*]thiophene (**7a**) in refluxing 1,2-dibromoethane for 1.5 h simply produced a 39% yield of **5a**.

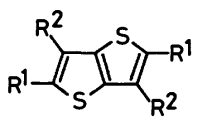

6a : $R^1 = Br$, $R^2 = H$
6b : $R^1 = R^2 = Br$
6c : $R^1 = R^2 = H$

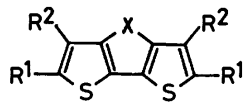

7a : $X = S$, $R^1 = Br$, $R^2 = H$
7b : $X = S$, $R^1 = R^2 = Br$
7c : $X = -S^{O_2}-$, $R^1 = Br$, $R^2 = H$
7d : $X = -S^{O}-$, $R^1 = Br$, $R^2 = H$

2,3,5,6-Tetrabromothieno[3,2-*b*]thiophene (**6b**) and 2,3,6,7-tetrabromodithieno[3,2-*b*:2′,3′-*d*]thiophene (**7b**) were prepared in 87% and 94% yields by the treatment of thieno[3,2-*b*]thiophene (**6c**) and **7a**, respectively with a large excess of bromine in refluxing carbon disulfide. These tetrabromides **6b** and **7b** were allowed to react with TCNEO in refluxing 1,3-dibromopropane containing an excess of copper(I) bromide to afford 3,6-dibromo-2,5-bis(dicyanomethylene)-2,5-dihydrothieno[3,2-*b*]thiophene (**4b**) in 40% yield and 3,5-dibromo-2,6-bis(dicyanomethylene)-2,6-dihydrodithieno-[3,2-*b*:2′,3′-*d*]thiophene (**5b**) in 27% yield, respectively.

Oxidation of **7a** with 2 equiv of *m*-chloroperbenzoic acid (MCPBA) in refluxing dichloromethane gave 2,6-dibromodithieno[3,2-*b*:2′,3′-*d*]thiophene 4,4-dioxide (**7c**) in 46% yield. The subsequent Gronowitz reaction of this sulfone **7c** in refluxing 1,3-dibromopropane afforded 2,6-bis(dicyanomethylene)-2,6-dihydrodithieno-[3,2-*b*:2′,3′-*d*]thiophene 4,4-dioxide (**5c**) in 34% yield. When **7a** was oxidized with 1.2 equivalent of MCPBA at 0 °C, 2,6-dibromodithieno[3,2-*b*:2′,3′-*d*]thiophene 4-oxide (**7d**) was obtained as a major product in 46% yield together with **7c** (25%). In contrast to the above sulfone, TCNEO treatment of sulfoxide **7d** did not afford the corresponding heteroquinonoid acceptor **5d** but **5a** in 26% yield. The mechanism of this deoxygenation remains unclarified yet.

An alternative reaction used to synthesize **1** and **2** is nucleophilic substitution reaction of the precursory dibromides by sodium dicyanomethanide in refluxing 1,2-dimethoxyethane containing a catalytic amount of tetrakis(triphenylphosphine)palladium(0), followed by oxidation with bromine water. Scheme 1 shows a similar sequence of preparing **5a** in overall yield of 78%, whereas this procedure failed to synthesize **4a**, **5c**, and **5d**.

Redox Property. The redox behavior of acceptors **4a**, **b** and **5a—c** was determined by cyclic voltammetry in dichloromethane. Table 1 summarizes their half-wave reduction potentials together with those of **3** and TCNQ. All of these acceptors show two pairs of reversible redox waves. The first half-wave potentials ($E^1_{1/2}$) of **4a** and **5a** are comparable to that of **3**, indicating that the extension of heteroquinonoid skelton *in a condensed manner* is not capable of improving the electron accepting ability of **3**. As shown in Fig. 1, the longest wavelength maxima in the electronic absorption spectra of **3**, **4a**, and **5a** are bathochromically shifted largely with extending the conjugation system (**3**: $\lambda_{max}(\varepsilon)$ 330 (6400), 400 (18000), and 421 (20300); **4a**: 444 (66400) and 470 (71000); **5a**: 263

Table 1. Half-Wave Reduction Potentials[a]

Acceptor	$E^1_{1/2}$	$E^2_{1/2}$	ΔE/V
4a	0.06	−0.36	0.42
4b	0.25	−0.13	0.38
5a	0.05	−0.23	0.28
5b	0.16	−0.11	0.27
5c	0.28	−0.05	0.33
3	0.07	−0.54	0.61
TCNQ	0.25	−0.47	0.72

a) Cyclic voltammetry was carried out at RT in dichloromethane containing 0.1 mol dm^{-3} tetrabutylammonium perchlorate using Ag/AgCl as a reference electrode and platinum as a working electrode at a scan rate of 100 mV s^{-1}.

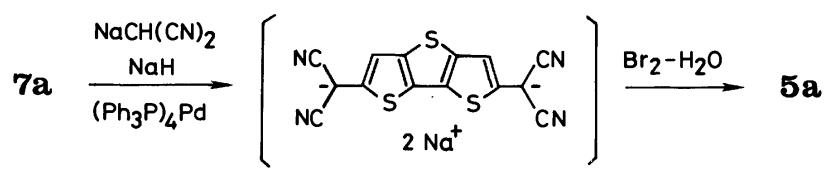

Scheme 1.

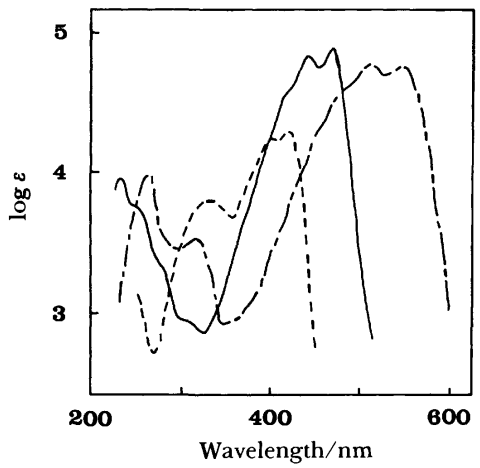

Fig. 1. Electronic spectra of **3** (-----), **4a**, (——), and **5a** (----) in dichloromethane.

Table 2. Conductivities of Acceptors

Acceptor	Conductivity[a]/S cm^{-1}
4a	6.7×10^{-9}
4b	1.1×10^{-7}
5a	5.6×10^{-7}
5b	2.8×10^{-7}
5c	5.5×10^{-8}
3	$<10^{-11}$
TCNQ	8.1×10^{-10}

a) Measured on compressed pellets with a two-probe method at RT.

almost insulating behavior of **3**, being probably due to an increasing intermolecular contacts of the present extensive systems.

Charge-Transfer Salts. These acceptors did form a variety of molecular complexes with known electron donors such as tetrathiafulvalene (TTF), 5,6:11,12-bis(dithio)naphthacene (so-called tetrathiotetracene, TTT), bis(trimethylene)tetrathiafulvalene (HMTTF), *N,N,N′,N′*-tetramethylphenylenediamine (TMPDA), tetraphenylbipyranylidene (TPBP), bis(trimethylene)-tetratellurafulvalene (HMTTeF), 5,6-dihydroacenaphtho[5,6-*cd*]-1,2-ditellurole (ADTe), and BEDT-TTF. They are mostly of 1:1 stoichiometry, but some are of 2:1 rich in either donor or acceptor and include a solvent used for complexation. Table 3 summarizes the physical properties of these isolated complexes.

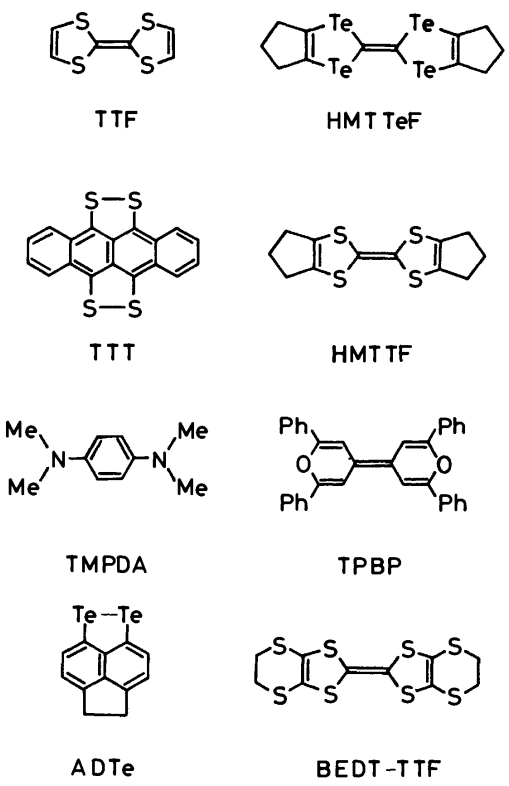

Acceptors **1**, **2**, and **3** formed CT complexes only with strong electron donors such as TTF, TTT, HMTTeF, and TPBP, and the conductivities of the resulting complexes increased with the extensive conjugation of the acceptor.[5,8] On the other hand, **4a**, having the almost same accepting ability as **1**—**3**, formed complexes with all the other donors except ADTe. In this regard, **3a** of a condensed conjugated type is superior to acceptors **1** and **2** of a linear conjugated type. Moreover, most of the complexes showed very high electrical conductivities as measured on a compressed pellet at room temperature. In particular, the HMTTeF complex recorded the highest value of 140 S cm^{-1}. The BEDT-TTF and TTT complexes, however, exhibited exceptionally low

(9270), 315 (3000), 511 (60300), and 549 (59800) nm). These facts imply that such an extension does not lower the π-LUMO level of the heteroquinonoid acceptors but raises π-HOMO level, so that the energy gap between their HOMO and LUMO decreases in the order of the extensive acceptors. The differences (ΔE) between $E^1_{1/2}$ and $E^2_{1/2}$ values decrease as the quinonoid conjugation extend. This demonstrates that such an extension certainly cotributes to diminution of on-site Coulomb repulsion in dianion state. This effect, however, is not so conspicuous as that of the extension *in a linear manner* seen in molecule **1**, in which ΔE value is down to 0.23 V.[5]

Two bromo substituents on **4b** and **5b** fairly enhance the electron-accepting power. The dibromide **4b**, as a result, is as strong an acceptor as TCNQ. The ΔE values of **4b** and **5b** are also diminished.

The accepting ability of **5a** is markedly strengthened by the conversion into the dioxide **5c** whose $E^1_{1/2}$ value is higher than that of TCNQ. The ΔE value of **5c**, however, becomes a little larger than that of **5a**, indicating that the sulfonation is not available for diminution of on-site Coulomb repulsion.

Table 2 shows electrical conductivities on pellet samples of neutral organic compounds. All new acceptors are relatively conductive in contrast to

Table 3. Charge-Transfer Salts Composed of **4a**, **b**, and **5a—c**

Complex or salt[a]	Appearance	Found (Calcd)[b]/%			ν_{CN}[c]/cm^{-1}	dp[d]/°C	Conductivity[e] /S cm^{-1}
		C	H	N			
4a·TTF[f]	Black fine needles	46.33; (45.94;	1.39; 1.28;	11.90 11.90)	2199	157	13
4a·TTT	Green powder	57.37; (58.23;	1.51; 1.63;	8.11 9.05)	2216	228	1.9×10^{-7}[g]
(**4a**)$_2$·TMPDA[f]	Black powder	57.56; (58.60;	2.69; 2.89;	19.15 20.10)	2196	165	5.0×10^{-3}[g]
4a·HMTTF	Black fine needles	52.10; (52.34;	2.32; 2.56;	9.39 10.17)	2201	>300	4.7
(**4a**)$_2$·TPBP·CB	Deep violet fine needles	69.17; (69.40;	2.72; 3.00;	10.03 10.12)	2195	>300	2.7
4a·HMTTeF	Black fine needles	30.88; (30.90;	1.51; 1.51;	5.68 6.01)	2200	>300	140
4a·BEDT-TTF	Black leaflets	40.30; (40.59;	1.26; 1.55;	7.89 8.61)	2223	254	6.9×10^{-10}[g]
4b·TTF	Black needles	34.35; (34.40;	0.59; 0.64;	8.88 8.92)	2195	175	11
4b·(TTT)$_2$	Dark green fine needles	51.14; (51.06;	1.19; 1.43;	4.66 4.96)	2194	>300	3.1
4b·TMPDA	Dark blue fine cryst	44.62; (44.91;	2.50; 2.74;	13.21 14.28)	2193	157	2.0×10^{-1}
4b·HMTTF·(CB)$_{0.5}$	Black needles	42.67; (42.40;	1.89; 1.91;	7.42 7.33)	2192	160	7.5
4b·(HMTTeF)$_2$	Greenish brown fine cryst	25.47; (24.60;	1.83; 1.38;	3.22 3.19)	2192	222	170
4b·ADTe	Deep blue powder	34.60; (34.67;	0.93; 0.97;	6.12 6.74)	2200	298	3.7
4b·BEDT-TTF	Dark green fine needles	32.60; (32.67;	1.72; 1.00;	6.66 6.93)	2220	241	7.0×10^{-8}[g]
5a·TTF[f]	Deep green powder	45.65; (45.61;	1.33; 1.15;	10.45 10.64)	2198	184	2.3
5a·(TTT)$_2$	Black powder	56.95; (58.45;	1.45; 1.77;	5.75 5.45)	2172[i]	256	3.0
(**5a**)$_2$·TPBP	Dark green powder	66.42; (67.25;	2.61; 2.55;	9.47 10.12)	2202	>300	6.2×10^{-1}
5a·HMTTeF	Dark brown powder	31.43; (31.58;	1.47; 1.43;	5.38 5.66)	2200	277	20
5b·TTF	Greenish brown powder	36.01; (35.09;	0.68; 0.59;	8.01 8.18)	2205	245	23
5b·TTT	Dark green powder	46.13; (46.16;	0.97; 0.97;	6.60 6.73)	2194	>300	5.8
(**5b**)$_2$·HMTTF	Deep green powder	38.05; (38.60;	1.30; 0.97;	9.30 9.00)	2205	242	2.3
(**5b**)$_2$·TMPDA	Deep green fine needles	40.59; (40.59;	1.43; 1.43;	12.00 12.46)	2197	213	2.4
(**5b**)$_2$·TPBP	Dark green powder	53.19; (52.26;	1.79; 1.70;	7.10 7.86)	2190	>300	4.9
5b·HMTTeF	Black powder	27.38; (27.23;	0.91; 1.05;	4.60 4.89)	2192	244	14
5b·(ADTe)$_2$	Dark brown powder	34.88; (35.25;	1.42; 1.25;	5.03 4.33)	2192	238	2.3×10^{-1}
5c·TTF	Brown fine needles	43.61; (43.00;	1.76; 1.08;	10.20 10.02)	2192	262	1.2×10^{-2}
5c·(TTT)$_2$	Deep violet powder	55.65; (56.69;	1.48; 1.71;	5.22 5.29)	2193	285	2.1
5c·TPBP	Golden brown powder	70.24; (70.40;	3.41; 3.20;	6.25 6.84)	2192	295	7.7×10^{-6}[g]
5c·(HMTTeF)$_2$	Violet powder	27.63; (27.04;	2.00; 1.55;	2.99 3.32)	2192	210	7.7
4a·$Na_{0.7}$[f]	Black needles	51.39; (51.04;	0.70; 0.71;	19.32 19.84)	2204	>300	3.1×10^{-3}
4a·$K_{0.6}$[f]	Black powder	50.07; (49.74;	2.10; 0.70;	18.78 19.34)	2195	255	1.9

Table 3. (Continued)

Complex or salt[a]	Appearance	Found (Calcd)[b]/% C	H	N	ν_{CN}[c]/cm^{-1}	dp[d]/°C	Conductivity[e] /S cm^{-1}
(**4a**)$_3$·(n-Bu)$_4$N[f]	Black powder	59.82; (59.98;	3.80; 4.07;	16.48 17.49)	2170	279	6.3×10^{-4}
5a·Na[f,j]	Dark violet powder	44.13;	0.76;	14.27	2180	>300	5.3×10^{-1}
(**5a**)$_5$·(n-Bu)$_4$N[f]	Dark violet powder	54.71; (55.70;	2.88; 2.50;	14.14 15.86)	2183	273	1.9×10^{-1}
5c·Na[f]	Dark green powder	43.78; (44.56;	1.27; 0.53;	14.04 14.85)	2200	>300	1.1×10^{-4}[g]
5c·K[f]	Dark blue powder	42.77; (42.74;	0.67; 0.51;	14.21 14.24)	2192	>300	2.0×10^{-5}[g]

a) Obtained from chlorobenzene, which is abbreviated as CB when contained in the complex, unless otherwise described. b) Calculated as stoichiometry indicated for the complex. c) Measured with a KBr disk method unless otherwise mentioned. d) Decomposition point. e) Measured on compressed pellets at RT with a four-probe method unless otherwise described. f) Obtained from acetonitrile. g) Measured on compressed pellets with a two-probe method at RT. h) Obtained from benzonitrile. i) Measured with a Nujol mull method. j) Composition was not estimated by an elemental analysis of C, H, and N.

conductivities. The case of the BEDT-TTF complex is probably because of lack of charge transfer due to the weak electron-donating ability of BEDT-TTF, as indicated by no shift of the CN frequency of the complex relative to neutral **4a** (2223 cm^{-1}).[9] The case of the TTT complex may be ascribed to the formation of a Mot insulator due to the poor fit of a strong donor TTT to **4a**. Acceptor **4b** complexed all the given donors except TPBP. The resulting complexes, except the BEDT-TTF complex, had also very high conductivities including a marverously high value 170 S cm^{-1} of the HMTTeF complex for a pellet sample. It may be furthermore noted as a result of the elevated electron affinity of **4b** that the TTT, TMPDA,and BEDT-TTF complexes are considerably more conductive than the corresponding ones of **4a**. A similar but somewhat different situation is the case for more fused heteroquinonoid system **5**. Acceptor **5a** thus formed complexes with only four strong donors, TTF, TTT, TPBP, and HMTTeF, and its dibromo derivative **5b** with all the given donors. The latter complexes are generally more conductive than the former ones. On the other hand, sulfone acceptor **5c**, though the strongest of the present acceptors, complexed only just the same strong donors as did **5a**. In addition, the conductivities of **5c** complexes are not so high as those of the corresponding **5b** complexes. The sterical bulkiness of the sulfone moiety is realized to interfere crystallization with a conductive molecular arrangement on complexation.

Acceptors **4a**, **5a**, and **5c** were reduced with sodium iodide, potassium iodide, and tetrabutylammonium iodide to form the corresponding anion radical salts. The physical properties of these salts are also summarized in Table 3. Some of these salts are found to have mixed valences in the acceptor because of nonstoichiometric composition, and accordingly they show higher conductivities than the other salts with 1:1 composition.

Table 4. Fractional Atomic Coordinates and Equivalent Temperature Factors (Å^2)

	x(×10^4)	y(×10^4)	z(×10^4)	B_{eq}[a]
S1	646 (2)	590 (1)	2413 (2)	3.7 (1)
C2	870 (7)	1594 (4)	5146 (7)	2.6 (2)
C3	487 (8)	1287 (4)	6068 (8)	3.0 (2)
C4	−2 (8)	259 (4)	5936 (7)	2.8 (2)
C5	1398 (8)	2559 (4)	3690 (8)	2.8 (2)
C6	1684 (8)	2765 (4)	1747 (9)	3.5 (2)
N7	1869 (8)	2899 (4)	173 (8)	4.8 (2)
C8	1663 (8)	3407 (4)	5067 (8)	3.2 (2)
N9	1897 (8)	4108 (4)	6123 (7)	4.4 (2)
S10	4502 (2)	9118 (1)	2599 (2)	3.6 (1)
C11	4715 (7)	9518 (4)	157 (8)	2.8 (2)
S12	4184 (2)	8546 (1)	−1755 (2)	3.4 (1)
C13	3568 (7)	7579 (4)	−242 (8)	2.9 (2)
C14	3718 (8)	7841 (4)	1675 (8)	3.0 (2)
S15	3271 (3)	7086 (1)	3577 (2)	4.4 (1)
C16	2253 (11)	5875 (4)	2230 (10)	5.1 (2)
C17	3304 (10)	5652 (4)	639 (9)	4.2 (2)
S18	2842 (2)	6375 (1)	−1484 (2)	3.6 (1)

a) $B_{eq}=(4/3)\sum_{ij}\beta_{ij}(a_i\cdot a_j)$.

Molecular and Crystal Structure of 4a·BEDT-TTF Complex. An X-ray crystallographic analysis was undertaken to elucidate the function of the embedded sulfur atoms in the crystal structures of the present complexes. Most of the complexes, however, appeared as fine crystals or powders. Only the molecular complex of **4a** with BEDT-TTF gave a good single crystal being suitable for the analysis. The crystal is triclinic with space group $P\bar{1}$, the unit cell contains one donor and one acceptor, and each component is present on the crystallographic inversion center. Table 4 summarizes the final atomic parameters.

Figure 2 illustrates the molecular geometries of both components. Acceptor **4a** takes a planar conformation; the largest deviation from the least squares plane is 0.057 Å for the sulfur atoms. On the other hand, the

structure of the BEDT-TTF molecule closely resembles those found in various cation radical salts of BEDT-TTF;[10] the TTF moiety keeps a planar conformation within 0.03 Å deviation and the terminal ethylene groups appreciably deviate from the optimal plane. The bond lengths of the TTF skelton can be used to estimate roughly the degree of charge transfer, ρ.[11] Table 5 shows a comparison of the present complex with neutral BEDT-TTF molecule[12] as a standard of $\rho=0$ and a cation radical salt α-(BEDT-TTF)$_2$PF$_6$[11] with $\rho=0.5$. The central C=C bond length (a) of the complex is between those of the neutral species and the salt, but the other C=C bond length (d) and C-S bond length (b and c) are quite identical to the corresponding ones of the neutral species. This indicates the degree of charge transfer in the present complex to be almost nil, as already judged from the examination of the nitrile stretching frequency.

Figure 3 shows the crystal structure viewed along the c axis (the transverse projection of the molecules) and along the orthogonal axis (the longitudinal projection of the molecules). The segregate stacking columns of both components are observed along the a axis, which is nearly perpendicular to the molecular planes, but the interplanar distances are as long as the unit length

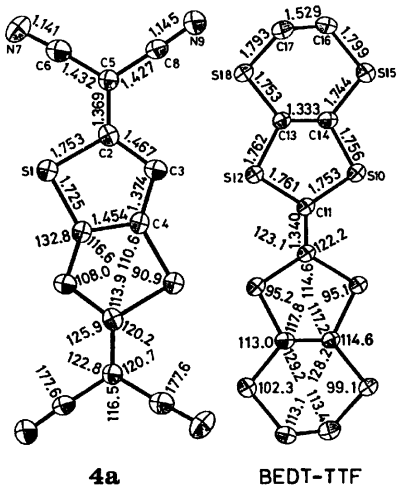

Fig. 2. Bond lengths and bond angles of **4a** and BEDT-TTF in this complex. Estimated standard deviations are 0.005—0.011 Å and 0.3—0.6° for lengths and angles, respectively.

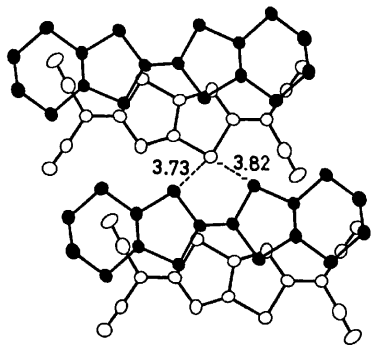

Fig. 4. The mode of the molecular overlap. The view direction is perpendicular to the molecular plane.

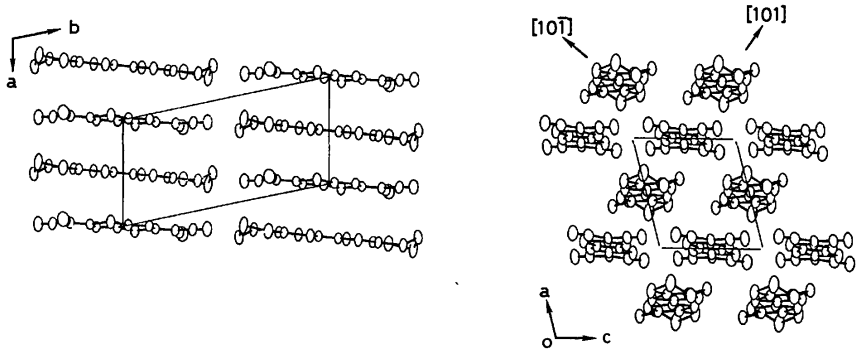

Fig. 3. Crystal structures viewed (a) along c axis and (b) approximately along the long axis of the molecule.

Table 5. A Comparison of the Mean Bond Lengths (Å) of BEDT-TTF

Compound	ρ	a	b	c	d
BEDT-TTF[12]	0	1.319	1.753	1.755	1.328
α-(BEDT-TTF)$_2$PF$_6$[11]	0.5	1.365(4)	1.740(2)	1.750(2)	1.345(3)
Present complex	ca. 0	1.340(9)	1.757(6)	1.759(5)	1.333(8)

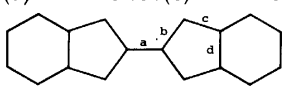

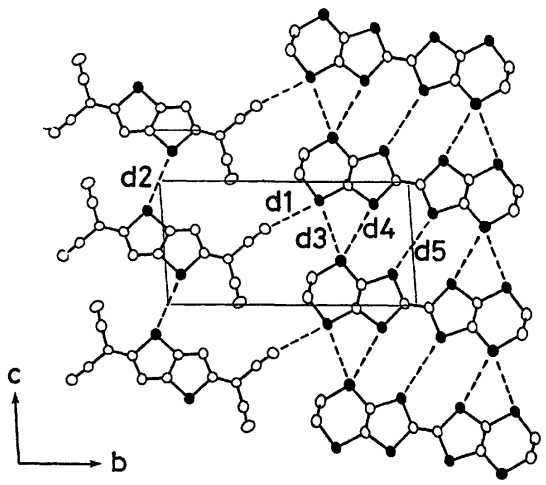

Fig. 5. Sheet-like net works in the $(2\bar{1}0)$ plane. Some of short contacts: d1=3.33, d2=3.48, d3=3.64, d4=3.59, and d5=3.98 Å.

(7.205 Å) of the a axis. On the other hand, an alternate stacking arrangement is observed with a little face-to-face overlap along [101] or [10$\bar{1}$] direction, as illustrated in Fig. 4.

The intermolecular S···S contact distances (3.73 and 3.82 Å) between the alternately stacked components are slightly longer than the sum of van der Waals radius (3.70 Å). On the other hand, several short intermolecular contacts exist in $(2\bar{1}0)$ plane, as shown in Fig. 5. The two components are separately arranged side by side along the transverse direction and alternately along the longitudinal direction, constituting a sheet-like network. In accordance with the structural features of various BEDT-TTF salts[10,11] and neutral BEDT-TTF,[12] the sulfur atoms of the ethylenedithio moiety in BEDT-TTF component play an important role on this side-by-side arrangement, that is, they strongly interact with the same kind of atom (3.64 Å) and the sulfur atoms (3.59 Å) of the 1,3-dithiole ring of the neighboring BEDT-TTF. In addition, they interact with the nitrogen atom of the acceptor with van der Waals contact (3.33 Å). On the other hand, there is no van der Waals contact between the sulfur atoms of the 1,3-dithiole rings (3.98 Å). Figure 5 also demonstrates that there exists a strong S···S interaction between the acceptors (3.48 Å). This indicates that the sulfur atoms embedded in the quinonoid conjugation system are capable of inducing multi-dimensionality in molecular complexes.

Conclusion

Novel compounds **4a**, **b** and **5a—c** of a fused conjugated type have been found to be superior electron acceptors with very small on-site Coulomb repulsion. They formed a variety of molecular complexes with π-electron donors, most of which exhibited high conductivities up to metallic bound. In particular, the HMTTeF complexes of **4a** and **4b** recorded 140 and 170 S cm^{-1}, respectively, marverously high for a pellet measurement at room temperature. The X-ray crystallographic analysis of **4a**·BEDT-TTF complex has elucidated that sulfur atoms embedded in the quinonoid conjugation contribute to intermolecular interactions in the crystal structure. Thus the present fused heteroquinonoid compounds are promising electron acceptors to design multi-dimensional organic metals directed towards a superconductor.

Experimental

General. Melting points are uncorrected. All solvents are of reagent grade. Electron donors used to prepare the molecular complexes, TTF,[13] TTT,[14] HMTTF,[15] TPBP,[16] BEDT-TTF,[17] and ADTe[18] were obtained according to the published procedures except commercially available TMPDA and HMTTeF. NMR spectra were recorded on a JEOL PMX-60 spectrometer (60 MHz) using tetramethylsilane as an internal standard. IR spectra were taken on a Hitachi 260-30 or a Perkin-Elmer 1600 FTIR spectrophotometer with a Nujol mull or a KBr disk method. MS spectra were measured on a Shimadzu GC-MS QP-1000A Mass spectrometer at 70 eV using a direct insertion technique. Electronic absorption spectra were recorded on a Shimadzu UV-160 spectrophotometer. Cyclic voltammetry was carried out on a Hokuto Denko HA-301 potentiostat and a Hokuto Denko HB-104 function generator.

2,5-Bis(dicyanomethylene)-2,5-dihydrothieno[3,2-*b*]thiophene (4a). A mixture of **6a**[19] (838 mg, 2.81 mmol), TCNEO (1.61 g, 11.2 mmol), and dry 1,3-dibromopropane (21 cm^3) was heated under reflux for 2 h. The resulting solution was twice column-chromatographed on silica gel with dichloromethane, followed by recrystallization from acetonitrile to give **4a** (268 mg, 36%) as reddish brown needles: mp>300 °C; IR (KBr) 2223 (CN) and 1508 (C=C) cm^{-1}; MS *m/z* 266 (M^+, 100%); Anal. ($C_{12}H_2N_4S_2$) C, H, N.

2,3,5,6-Tetrabromothieno[3,2-*b*]thiophene (6b). A solution of bromine (2.4 cm^3, 49 mmol) in carbon disulfide (3 cm^3) was dropwise added to a solution of **6c** (200 mg, 1.43 mmol) in carbon disulfide (5 cm^3), and the mixture was heated under gentle reflux for 23 h. To the resulting suspension was carefully added a saturated sodium hydrogensulfite aqueous solution. The precipitated solid was collected by filtration, washed with water and ethanol, and dried in vacuo. The organic layer of the filtrate was washed with brine, 5% sodium hydrogencarbonate aqueous solution, and again brine, and dried over anhydrous magnesium sulfate. After concentration in vacuo, the residual solid was combined with the above precipitate, and recrystallized from benzene to give **6b** (567 mg, 87%) as colorless needles: mp 237—238.5 °C (in a sealed tube); Anal. ($C_6Br_4S_2$) C.

3,6-Dibromo-2,5-bis(dicyanomethylene)-2,5-dihydrothieno-[3,2-*b*]thiophene (4b). A mixture of **6b** (1.60 g, 3.50 mmol), TCNEO (5.04 g, 35.0 mmol), copper(I) bromide (3.51 g, 24.5 mmol), and dry 1,3-dibromopropane (70 cm^3) was heated under reflux for 4 h. The mixture was column-chromatographed on silica gel with dichloromethane, followed by recrystallization from chlorobenzene to give **4b** (627 mg, 40%) as purple micro prisms: mp>300 °C; IR (KBr) 2224 (CN) and 1508 (C=C) cm^{-1}; MS *m/z* 422 (M^+−2, 53%), 424 (M^+, 100%),

and 426 (M^++2, 56%); Anal. ($C_{12}Br_2N_4S_2$) C, N.

2,6-Bis(dicyanomethylene)-2,6-dihydrodithieno[3,2-*b*:2′,3′-*d*]thiophene (5a). A) Using TCNEO. A mixture of **7a** (354 mg, 1.00 mmol),[20] TCNEO (576 mg, 4.00 mmol), and dry 1,2-dibromoethane (16 cm³) was heated under reflux for 1.5 h. The mixture was column-chromatographed on silica gel with dichloromethane, followed by recrystallization from acetonitrile to give **5a** (125 mg, 39%) as deep violet fine crystals: mp>300 °C; IR (KBr) 2219 (CN) and 1496 (C=C) cm^{-1}; MS *m/z* 322 (M^+, 100%); Anal. ($C_{14}H_2N_4S_3$) C, H, N.

B) Using Sodium Dicyanomethanide. Malononitrile (79 mg, 1.2 mmol) was added to an ice-cooled suspension of sodium hydride (96 mg, 2.4 mmol, 60% oily) in absolute 1,2-dimethoxyethane (4 cm³) under nitrogen stream, and the mixture was stirred at RT for 20 min. To this solution was added **7a** (142 mg, 0.40 mmol) and tetrakis(triphenylphosphine)palladium(0) (46 mg, 0.04 mmol), and the mixture was heated under reflux for 2 h. The resulting solution was treated with saturated bromine water (15 cm³) at 0 °C, and filtered on Hyflo Super-cel. The collected solid was extracted with boiling chlorobenzene, and recrystallized from chlorobenzene to give **5a** (101 mg, 78%).

2,3,6,7-Tetrabromodithieno[3,2-*b*:2′,3′-*d*]thiophene (7b). Bromine (2.1 cm³, 41.2 mmol) was added to a solution of **7a** (1.91 g, 5.39 mmol) in carbon disulfide (40 cm³), and the solution was heated at gentle reflux for 24 h. The solution was carefully treated with 10% sodium hydrogensulfite aqueous solution, and diluted with hexane. The resulting precipitate was collected by filtration, washed thoroughly with water and methanol, dried in vacuo, and recrystallized from chlorobenzene to give **7b** (2.59 g, 94%) as off-white leaflets: mp>300 °C; Anal. ($C_8Br_4S_3$) C.

3,5-Dibromo-2,6-bis(dicyanomethylene)-2,6-dihydrodithieno-[3,2-*b*:2′,3′-*d*]thiophene (5b). A mixture of **7b** (2.10 g, 4.10 mmol), TCNEO (5.91 g, 41.0 mmol), copper(I) bromide (4.12 g, 28.7 mmol), and dry 1,3-dibromopropane (120 cm³) was heated under reflux for 1.2 h. The reaction mixture was column-chromatographed on silica gel with dichloromethane, and recrystallized from chlorobenzene to give **5b** (530 mg, 27%) as deep green prisms: mp>300 °C; IR (KBr) 2221 (CN) and 1490 (C=C) cm^{-1}; MS *m/z* 478 (M^+−2, 50%), 480 (M^+, 100%), and 482 (M^++2, 62%); Anal. ($C_{14}Br_2N_4S_3$) C, N.

2,6-Dibromodithieno[3,2-*b*:2′,3′-*d*]thiophene 4,4-Dioxide (7c). MCPBA (216 mg, 1.00 mmol, 80% purity) was added to a solution of **7a** (177 mg, 0.500 mmol) in dichloromethane (15 cm³), and the mixture was heated under gentle reflux for 2 d. The reaction mixture was poured into a concentrated sodium hydrogensulfite aqueous solution, and extracted with dichloromethane. The organic layer was washed with 5% sodium hydrogencarbonate aqueous solution and water, and dried over anhydrous magnesium sulfate. After concentration in vacuo, the residue was purified by column chromatography on silica gel with dichloromethane to give **7c** (90 mg, 47%): yellow prisms from chloroform; mp 248 °C (decomp); IR (KBr) 1348, 1303, 1282, 1154, 1132 (SO_2) cm^{-1}; ^1H NMR ($CDCl_3$) δ=7.21 (s); Anal. ($C_8H_2Br_2O_2S_3$) C, H.

2,6-Bis(dicyanomethylene)-2,6-dihydrodithieno[3,2-*b*:2′,3′-*d*]thiophene 4,4-Dioxide (5c). A mixture of **7c** (1.47 g, 3.81 mmol), TCNEO (5.49 g, 38.1 mmol), and dry 1,3-dibromopropane (50 cm³) was heated under reflux for 5 h. The reaction mixture was twice column-chromatographed on silica gel with dichloromethane–acetone (96:4 v/v), and recrystallized from acetonitrile to give **5c** (462 mg, 34%) as deep violet prisms: mp>300 °C; IR (KBr) 2222 (CN) and 1510 (C=C), 1343, 1323, 1172 (SO_2) cm^{-1}; MS *m/z* 354 (M^+, 100%); Anal. ($C_{14}H_2N_4O_2S_3$) C, H, N.

2,6-Dibromodithieno[3,2-*b*:2′,3′-*d*]thiophene 4-Oxide (7d). MCPBA (517 mg, 2.40 mmol, 80% purity) was added to a solution of **7a** (708 mg, 2.00 mmol) in chloroform (26 cm³) at 0 °C. The mixture was stirred at 0 °C for 9 h and at RT for 4 h, poured into 10% sodium hydrogensulfite aqueous solution, and extracted with chloroform. The organic layer was washed with 5% sodium hydrogencarbonate aqueous solution and water, and dried over anhydrous magnesium sulfate. After concentration in vacuo, the residue was column-chromatographed on silica gel with chloroform to give **7c** (190 mg, 25%) and **7d** (340 mg, 46%): yellow crystals from hexane–chloroform; mp 172.5—174 °C; IR (KBr) 1052 (SO) cm^{-1}; ^1H NMR ($CDCl_3$) δ=7.34 (s); Anal. ($C_8H_2Br_2OS_3$) C, H.

Reaction of 7d with TCNEO. A mixture of **7d** (143 mg, 0.386 mmol), TCNEO (556 mg, 3.86 mmol), and dry 1,3-dibromopropane (7 cm³) was heated under reflux for 2 h. The reaction mixture was worked up according to the procedure of Method A described in the synthesis of **5a**, and the yield was 26%.

Preparation of Molecular Complexes and Anion Radical Salts. All molecular complexes described in this report were each prepared by mixing saturated solutions of donor and acceptor in hot chlorobenzene, acetonitrile, or benzonitrile. All anion radical salts were obtained by the reaction of the acceptors with the corresponding metal iodide or tetrabutylammonium iodide in hot acetonitrile or benzonitrile. The complexes or salts precipitated out immediately or on cooling appropriately, and were collected by filtration and dried in vacuo.

Crystal Structure Analysis of 3a·BEDT-TTF. The intensities of X-ray diffractions were collected with a Rigaku automated diffractometer using Cu $K\alpha$ radiation monochromatized with a graphite plate. We obtained 1969 independent diffractions within 2θ=126° which had intensities larger than the statistical counting error, and used all of them for analysis. The dimension of the measured crystal was 0.50×0.40×0.01 mm³. The crystal belonged to the triclinic system with the space group, $P\bar{1}$, crystal data being a=7.205(1), b=13.654(1), c=6.898(2) Å, α=91.76(1), β=103.85-(2), γ=101.32(1)°, Z=1, and V=643.9(2) Å³, D_{obs}=1.626, and D_{calcd}=1.679 g cm^{-3}. The structure was solved by the direct method combined with the Monte-Carlo method[21] for the selection of the initial set of phase. It was refined by the full-matrix least squares method after applying the absorption corrections.[22] Atomic scattering factors were taken from International Tables for X-ray Crystallography.[23] Anisotropic temperature factors were used for the refinement, and hydrogen atoms were not included in the refinement. The final R value was 0.073. Computations were carried out partly at the Information Processing Center of Hiroshima University and mainly at the Computation Center of Nagoya University using the library program of CRYSTAN system. Tables of structure factors and anisotropic thermal parameters are deposited as Document No. 8869 at the Office of the Editor of Bull. Chem. Soc. Jpn.

This work was partially supported by Grants-in-Aid for Scientific research Nos. 62550635 and 63604576 from the Ministry of Education, Science and Culture. The authors wish to thank Mr. Hideaki Iwatani, Hiroshima University, for elemental analysis.

References

1) For a review, see: J. M. Williams, M. A. Beno, H. H. Wang, P. C. W. Leung, T. J. Emge, U. Geiser, and K. D. Carlson, *Acc. Chem. Res.*, **18**, 261 (1985).

2) Y. Yamashita, T. Suzuki, T. Mukai, and G. Saito, *J. Chem. Soc., Chem. Commun.*, **1985**, 1044; K. Kobayashi and C. L. Gajurel, *ibid.*, **1986**, 1779.

3) K. Yui, Y. Aso, T. Otsubo, and F. Ogura, *J. Chem. Soc., Chem. Commun.*, **1987**, 1816.

4) J. Diekmann, W. R. Hertler, and R. E. Benson, *J. Org. Chem.*, **28**, 2719 (1963); D. J. Sandman and A. F. Garito, *ibid.*, **39**, 1165 (1974).

5) A preliminary result was published in the following paper: K. Yui, H. Ishida, Y. Aso, T. Otsubo, and F. Ogura, *Chem. Lett.*, **1987**, 2339.

6) A preliminary report has appeared in the following paper: Y. Aso, K. Yui, H. Ishida, T. Otsubo, F. Ogura, A. Kawamoto, and J. Tanaka, *Chem. Lett.*, **1988**, 1069.

7) S. Gronowitz and B. Uppström, *Acta Chem. Scand., Ser. B*, **28**, 981 (1974).

8) M. L. Kaplan, R. C. Haddon, F. B. Bramwell, F. Wudl, J. H. Marshall, D. O. Cowan, and S. Gronowitz, *J. Phys. Chem.*, **84**, 427 (1980).

9) J. S. Chappell, A. N. Bloch, W. A. Bryden, M. Maxfield, T. O. Poehler, and D. O. Cowan, *J. Am. Chem. Soc.*, **103**, 2442 (1981).

10) R. Kato, H. Kobayashi, A. Kobayashi, and Y. Sasaki, *Chem. Lett.*, **1984**, 1693; R. Kato, A. Kobayashi, Y. Sasaki, and H. Kobayashi, *ibid.*, **1984**, 993; K. Bender, I. Henning, D. Schweizer, K. Dietz, H. Endres, and H. J. Keller, *Mol. Cryst. Liq. Cryst.*, **108**, 359 (1984); H. Kobayashi, R. Kato, A. Kobayashi, G. Saito, M. Tokumoto, H. Anzai, and T. Ishiguro, *Chem. Lett.*, **1986**, 93.

11) H. Kobayashi, A. Kobayashi, Y. Sasaki, G. Saito, and H. Inokuchi, *Chem. Lett.*, **1984**, 183.

12) H. Kobayashi, A. Kobayashi, Y. Sasaki, G. Saito, and H. Inokuchi, *Bull. Chem. Soc. Jpn.*, **59**, 301 (1986).

13) L. R. Melby, H. D. Hartzler, and W. A. Sheppard, *J. Org. Chem.*, **39**, 2456 (1974).

14) E. P. Goodings, D. A. Mitchard, and G. Owen, *J. Chem. Soc., Perkin Trans. 1*, **1972**, 1310.

15) H. K. Spencer, M. P. Cava, F. Yamagishi, and A. F. Garito, *J. Org. Chem.*, **41**, 730 (1976).

16) G. A. Reynolds, C. H. Chen, and J. A. Van Allan, *J. Org. Chem.*, **44**, 4456 (1979).

17) E. M. Engler, V. Y. Lee, R. R. Schumaker, S. S. P. Parkin, R. L. Greene, and J. C. Scott, *Mol. Cryst. Liq. Cryst.*, **107**, 19 (1984).

18) Y. Aso, K. Yui, T. Miyoshi, T. Otsubo, F. Ogura, and J. Tanaka, *Bull. Chem. Soc. Jpn.*, **61**, 2013 (1988).

19) A. Bugge, *Acta Chem. Scand.*, **23**, 2704 (1969).

20) G. F. Pedulli, M. Tiecco, M. Guerra, G. Martelli, and P. Zanirato, *J. Chem. Soc., Perkin Trans. 2*, **1978**, 212.

21) A. Furusaki, *Acta Crystallogr., Sect. A*, **35**, 220 (1979).

22) C. Katayama, N. Sakabe, and K. Sakabe, *Acta Crystallogr., Sect. A*, **28**, S207 (1972).

23) "International Tables for X-ray Crystallography," Kynoch Press, Birmingham, England (1974), Vol. IV.

Topochemical Photopolymerization and Photo-Copolymerization of the Crystals of Unsymmetrically Substituted Diolefin Compounds Having Pyrimidine Ring

Masaki HASEGAWA,* Yasuhiro ENDO, Masato AOYAMA, and Kazuhiko SAIGO
Department of Synthetic Chemistry, Faculty of Engineering, The University of Tokyo, Hongo, Bunkyo-ku, Tokyo 113
(Received September 27, 1988)

Several new diolefin compounds, methyl and ethyl 4-[2-(4-pyrimidyl)ethenyl]cinnamates (**1a** and **1b**), and methyl, ethyl, and propyl α-cyano-4-[2-(4-pyrimidyl)ethenyl]cinnamates (**1c**, **1d**, and **1e**) were synthesized, and their photoreactivity in the crystalline state was investigated. The crystals of **1c**, **1d**, and **1e** gave amorphous oligomers having cyclobutane skeletons (average degree of polymerization was approximately 10) through the [2+2] photocycloaddition. The dimers (**2c**, **2d**, and **2e**) were formed in high yields by the exclusive photoexcitation of the monomers. The dimers were isolated by column chromatography. The cyclobutane structure of **2c** and **2d** was β-type homo adduct whereas that of **2e** was β-type hetero adduct. As only one type of adduct was detected for each crystal, photodimerization was interpreted as being of a crystal lattice controlled process. The conversions of these reactions were not as high as that of the reaction in α-type of 2,5-distyrylpyrazine (DSP). The lower conversion was interpreted as being due to alternative reacting sites which inevitably result from the β-type molecular packing and to the drastic displacement of molecules which causes the distortion of crystal lattice. The mixed crystals (**1f**) of **1d** and **1e** (molar ratio 1.3/1), of which the X-ray diffraction pattern is similar to that of **1e**, photopolymerized to give amorphous cooligomers (average degree of polymerization was approximately 5). The reaction went through an intermediate similar to dimer **2e**.

In previous studies we have demonstrated that the topochemical reactivity of various types of diolefin compounds and the configuration of their photoproducts were accurately predictable from the molecular arrangements of these crystals.[1]

Although the correlation between chemical and crystal structures of organic compounds is very sophisticated, it is obvious that the interaction between electron-donating and -accepting groups in the molecule contributes greatly to determining their crystal structure. From recent results of studies on the photochemical behavior of several unsymmetrically substituted diolefinic crystals, we have revealed that pyridyl, cyano and carbonyl groups were the electron-accepting groups which are potent in affording the photoreactive α-type crystal packing.[2] In a preceeding report, we have reported that the unsymmetrically substituted diolefin monomer crystals which have a pyrazine ring produce extremely high molecular weight of crystalline linear polymers.[3]

As the pyrimidine ring is also expected to induce much stronger donor–acceptor interactions with benzene rings, in our present work, we synthesized several new diolefin compounds having pyrimidine rings, as is represented in Scheme 1, and investigated the photochemical behaviors of these crystals. Furthermore, we attempted to prepare several mixed crystals, and investigated these crystals from the point of view of topochemical photo-copolymerization.

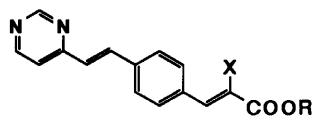

comp.	X	R
1a	H	Me
1b	H	Et
1c	CN	Me
1d	CN	Et
1e	CN	n-Pr

Scheme 1.

Results and Discussion

The photoreactivity of **1a,b** (alkyl 4-[2-(4-pyrimidyl)ethenyl]cinnamates) and **1c—e** (alkyl α-cyano-4-[2-(4-pyrimidyl)ethenyl]cinnamates) in crystalline state was checked by methods 1 and 2 (see Experimental section).

From the results, it was found that three monomer crystals, **1c—e**, were highly photoreactive and gave the products through [2+2] cycloaddition. On the other hand, the crystal of **1a** was photostable and that of **1b** gave intractable cross-linked photoproducts.

Following the photoreaction of **1c—e**, IR spectra of the products showed the decrease in the absorptions due to olefin bonds and the shift to higher wavenumbers of the absorptions of the carbonyl and cyano groups. ^{1}H NMR spectra of the photoproducts also showed the disappearance of olefin protons in the monomer and the appearance of cyclobutane protons. These spectral evidences indicate that the photoreaction is a [2+2] photocyclopolymerization.

The photoproducts after 24 h irradiation were amorphous white-brown powders. From gel permeation chromatogram (GPC) (eluent: *N,N*-demethylformamide), the photoproducts were found to consist of the dimer (**2**) and the oligomers (**3**) of which the average degree of polymerization was about 10.

In order to clarify the structure of the products, isolation of dimers was attempted.

For the purpose of depressing the photoexcitation of the terminal olefins in the oligomers which reduces the polymerization, the crystalline **1c—e** were irradiated through an optical filter which cuts off the shorter

wavelengths.

The irradiation using L38 filter (cut off <350 nm) for **1c** and **1e**, and using L40 filter (cut off <380 nm) for **1d**, respectively, resulted in the accumulation of a great amount (≈90%) of the dimers.

The photoproducts from **1c** and **1d** consisted mostly (≈90%) of the dimer retaining crystallinity whereas the products from **1e** were amorphous. The dimers (**2c—e**) were isolated from the photoproducts and purified by flash column chromatography.

^{1}H NMR and mass analyses revealed that **2c** and **2d** had head-to-head homo adduct type cyclobutane structures, in which two 2-(4-pyrimidyl)ethenyl groups are neighboring, and that **2e** had head-to-head hetero adduct type, in which 2-(4-pyrimidyl)ethenyl and α-cyanocinnamate groups are neighboring to each other, as shown in Scheme 2.

Since only a single structure of the dimers was detected, it was concluded that the photoreaction of **1c—e** crystals proceeded, at least at the photocyclodimerization stage, under the strict control of the monomer crystal lattice.

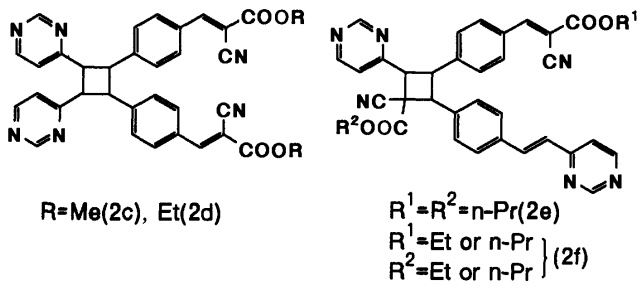

Scheme 2.

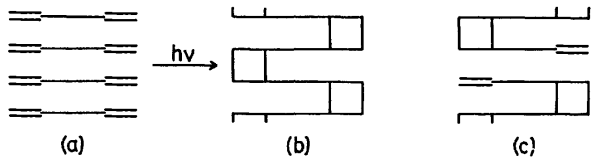

Fig. 1. Schematic illustration of the photopolymerization of (a) β-type crystals of diolefin compounds into (b) zigzag polymers and (c) termination resulting from alternative reactivity of the monomer.

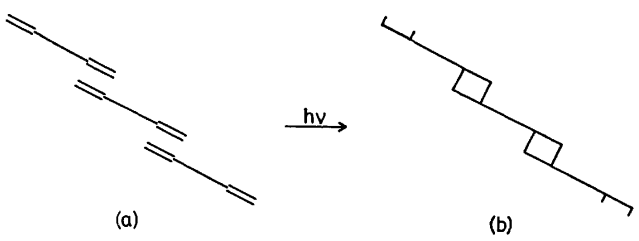

Fig. 2. Schematic illustration of photopolymerization of (a) α-type crystal of diolefin compounds into (b) a linear polymer.

The remarkable change of the dimer skeleton from **1d** to **1e** should doubtlessly correspond to the change of relative orientation of reacting olefins. IR, DSC (differential scanning calorimetry), and PAS (photoacoustic spectra) analyses of the **1d** and **1e** crystals, however, revealed no evident difference between these two crystal structures.

The structures of **2c—e** suggest that the crystals of **1c—e** consist of β-type packing monomers (Fig. 1a), and that the final oligomers are of a zigzag type (Fig. 1b).

In the case of α-type crystals two reacting olefin groups are related with a center of symmetry as is illustrated in the crystals of α-DSP. Therefore, one olefin can react only with one olefin of the neighboring molecule, and the center of gravity of the reacting monomer scarcely moves. These topochemical conditions make possible the α-type crystals to produce linear crystalline polymers of high molecular weight (Fig. 2). On the other hand, such a high crystalline polymer with a high conversion (almost quantitative) has not resulted from the photoreaction of β-type diolefin crystals, not only in the present results but in some of our previous works.[3,4]

The low degree of polymerization with an incomplete conversion (≈85%) and the lack of crystallinity of the photoproducts from β-type crystals can be explained by the following two reasons.

The first reason is that if we assume all olefins are in the same topochemical environment there are four possible reactive sites of the [2+2] photodimerization for each photoexcited molecule in a typical β-type packing crystal. This may cause the termination of further chain growth of the polymer by some probabilities as schemed in Fig. 1c. The second is that with the formation of cyclobutane a large displacement of the reacting molecules may occur to result in serious distortion of crystal lattice. Such a large displacement may make the reacting crystal to be amorphous at latter stages of the photoreaction. In contrast to β-type crystals, the extremely clean-cut photoreaction of the α-type crystals has been interpreted in terms of "seesaw" mechanism,[5] in which the reacting monomer rotates around its center of gravity, that scarcely moves.

In view of the molecular arrangements, the β-type packing is not explicable by electrostatic interactions which seem to be effective in α-type packing. The π-π orbital interaction of facing pyrimidine and benzene rings and/or N–N interaction may contribute to the formation of β-type packings.

It is of great interest to extend the study of a topochemical [2+2] photopolymerization into that of the photocopolymerization. Although there have been a few preliminary reports on the formation of mixed diolefin crystals,[6,7] none of them described [2+2] topochemical copolymerization. In our present work

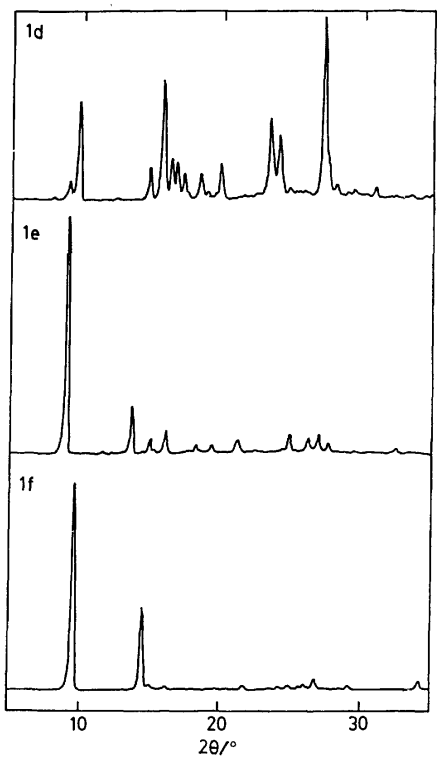

Fig. 3. X-Ray diffraction patterns of the crystals of **1d** (upper), **1e** (middle), and **1f** (lower).

after several attempts a well-defined mixed crystal consisting of two derivatives **1d** and **1e** was successfuly prepared, as was expected from their similar chemical structures. However, no other mixed crystals were obtained from any other combination of the monomers.

A mixed crystal of **1d** and **1e** (molar ratio 1.3:1, **1f**) was obtained by recrystallization from a 1-propanol solution containing an equimolar amount of the two monomers. **1f** had a melting point (160.0—165.0 °C) which is intermediate between those of **1d** (mp 184.0—185.0 °C) and **1e** (mp 149.5—151.0 °C), and showed almost the same X-ray diffraction pattern as that of **1e**, suggesting nearly the same crystal structure (Fig. 3).

The photoirradiation of **1f** for 24 h with a 100 W high-pressure mercury lamp gave amorphous co-oligomers, which had an average polymerization degree of about 5. Structure of the dimer isolated (**2f**) was proved to be head-to-head hetero adduct by mass analysis (Scheme 2), which is the same as that of **2e**, as was expected from the X-ray diffraction pattern of **1f**.

These results indicate that **1d** is included in the crystal lattice of **1e** as isomorphous and that the mixed crystal behaved analogously to **1e**, to afford the head-to-head hetero zigzag type co-oligomers on photoirradiation.

In spite of the electrostatic interaction between electron donating groups of the molecule (benzene ring) and one of the accepting groups (pyrimidine ring, carbonyl, and cyano groups in present crystals), the π-π orbital interaction of facing benzene and pyrimidine rings and/or N-N interaction is considered to contribute to the formation of the β-type stacking.

Experimental

Measurements. Infrared spectra were recorded on a JASCO IR-810 spectrophotometer. ^{1}H NMR spectra were recorded on a JEOL PMX-60SI spectrophotometer or a JEOL GX-400 spectrometer. X-Ray diffraction pattern was recorded on a Rigaku Rotaflex RU-200 spectrometer (λ=1.54184 Å). Melting points were determined by a Laboratory Devices MEL-TEMP and are uncorrected. Gel permeation chromatography (GPC) of the photoproducts was performed at 40 °C on a Shodex (GPC AD 800/P+AD 805/S+AD 803/S+AD 802/S) column (DMF solution).

Preparation of Monomers. 4-[2-(4-Pyrimidyl)ethenyl]-benzaldehyde. Terephthalaldehyde (9.2 g, 69 mmol) was dissolved in a mixed solvent of acetic anhydride (24 ml) and acetic acid (16 ml) at 70 °C. 4-Methylpyrimidine (5.0 g) was added to the solution and refluxed for 4 h. After cooling to room temperature, 50 ml of benzene was added and extracted with 100 ml of 1 mol l^{-1} hydrochloric acid three times, followed by neutralization by 2 mol l^{-1} sodium hydroxide. The precipitates were collected by filtration and dried under reduced pressure. The solid mass was purified by flash column chromatography (Wako gel C-300, eluent: dichloromethane:methanol=99.5:0.5 (v/v)), followed by recrystallization from benzene-hexane. 3.6 g of 4-[2-(4-Pyrimidyl)-ethenyl]benzaldehyde was obtained. Yield 33%; mp 162.0—163.5 (benzene-hexane); IR (KBr) 2850, 1700, 1600, 1390, 1310, 1210, 970, 800 cm^{-1}; ^{1}H NMR ($CDCl_3$) δ=10.04 (1H, s, formyl), 9.21 (1H, d, J=1.5 Hz, pyrimidyl), 8.74 (1H, d, J=5.2 Hz, pyrimidyl), 7.96 (1H, d, J=15.6 Hz, olefin), 7.93 (2H, d, J=8.2 Hz, phenylene), 7.76 (2H, d, J=8.2 Hz, phenylene), 7.35 (1H, dd, J=1.5 and 5.2 Hz, pyrimidyl), 7.19 (1H, d, J=15.6 Hz); UV (99.5% CH_2Cl_2): 325 (ε=35000). Found: C, 74.12; H, 4.79; N, 13.31%. Calcd for $C_{13}H_{10}N_2O$: C, 74.27; H, 4.79; N, 13.32%.

4-[2-(4-Pyrimidyl)ethenyl]cinnamic Acid. To a solution of 4-[2-(4-pyrimidyl)ethenyl]benzaldehyde (1.00 g, 4.8 mmol) in 25 ml of pyridine were added malonic acid (1.98 g, 19.0 mmol) and piperidine (0.1 ml), and the solution was stirred for 13 h at 90 °C. After cooling to room temperature, 50 ml of 2 mol l^{-1} hydrochloric acid was added. The precipitates were collected and dried under reduced pressure, and recrystallized from *N,N*-dimethylformamide. 4-[2-(4-Pyrimidyl)ethenyl]cinnamic acid (0.63 g) was obtained as the complex with DMF. The final crystals, containing about 10% molar ratio of DMF, were supplied to the following esterification procedure.

Alkyl 4-[2-(4-Pyrimidyl)ethenyl]cinnamates (1a and 1b). To a suspension of the complex of 4-[2-(4-pyrimidyl)-ethenyl]cinnamic acid with DMF (0.180 g) in methanol (40 ml) was added concentrated sulfuric acid (1.0 ml), and the mixture was refluxed for 3 h to give a homogeneous solution. After cooling to room temperature, the solution was filtered to remove unreacted acid, and the filtrate was neutralized by 1 mol l^{-1} aqueous sodium hydroxide and extracted with dichloromethane. After evaporation of the

solvent, the residue was recrystallized from methanol. 0.091 g of **1a** was obtained. Mp 159.0—160.5 °C (methanol); IR (KBr) 1710, 1580, 1310, 990 cm^{-1}; ^1H NMR ($CDCl_3$) δ=9.19 (1H, d, J=1.5 Hz, pyrimidyl), 8.70 (1H, d, J=5.5 Hz, pyrimidyl), 7.89 (1H, d, J=15.9 Hz, olefin), 7.70 (1H, d, J=16.2 Hz, olefin), 7.62 (2H, d, J=8.2 Hz, phenylene), 7.56 (2H, d, J=8.2 Hz, phenylene), 7.32 (1H, dd, J=1.5 and 5.5 Hz, pyrimidyl), 7.10 (1H, d, J=15.9 Hz, olefin), 6.48 (1H, d, J=16.2 Hz, olefin), 3.82 (3H, s, methyl); UV (99.5% CH_2Cl_2) 343 (ε=46700). Found: C, 71.88; H, 5.24; N, 10.52%. Calcd for $C_{16}H_{14}N_2O_2$: C, 72.15; H, 5.31; N, 10.52%.

In a similar manner, 0.150 g of the same complex was esterified with ethanol to give 0.064 g of **1b**. Mp 106.0—108.0 °C (ethanol); IR (KBr) 1720, 1640 ,1210, 980 cm^{-1}; ^1H NMR ($CDCl_3$) δ=9.18 (1H, d, J=1.2 Hz, pyrimidyl), 8.70 (1H, d, J=5.2 Hz, pyrimidyl), 7.89 (1H, d, J=16.2 Hz, olefin), 7.68 (1H, d, J=15.9 Hz, olefin), 7.62 (2H, d, J=8.5 Hz, phenylene), 7.56 (2H, d, J=8.5 Hz, phenylene), 7.32 (1H, dd, J=1.2 and 5.2 Hz, pyrimidyl), 7.10 (1H, d, J=16.2 Hz, olefin), 6.48 (1H, d, J=15.9 Hz, olefin), 4.28 (2H, q, J=7.0 Hz, methylene), 1.35 (3H, t, J=7.0 Hz, methyl); UV (99.5% CH_2Cl_2) 343 (ε=34400). Found: C, 72.54; H, 5.77; N, 10.04%. Calcd for $C_{17}H_{16}N_2O_2$: C, 72.83; H, 5.76; N, 9.99%.

Alkyl α-Cyano-4-[2-(4-pyrimidyl)ethenyl]cinnamates) (1c, 1d, and 1e). To a solution of 4-[2-(4-pyrimidyl)ethenyl]-benzaldehyde (1.99 g, 9.4 mmol) in 200 ml of methanol were addedmethyl cyanoacetate (1.21 g, 12.2 mmol) and piperidine (0.1 ml), and the mixture was refluxed for 7 h. The yellow precipitates appeared during the reaction. After cooling, the precipitates were collected by filtration, and recrystallized from methanol to give 1.23 g of **1c**. Yield 72%; mp 223.0—225.0 °C; IR (KBr) 2210, 1740, 1600, 1290, 990 cm^{-1}; ^1H NMR ($CDCl_3$) δ=9.21 (1H, d, J=1.5 Hz, pyrimidyl), 8.74 (1H, d, J=5.5 Hz, pyrimidyl), 8.26 (1H, s, olefin), 8.05 (2H, d, J=15.9 Hz, phenylene), 7.93 (1H, d, J=15.9 Hz, olefin), 7.72 (2H, d, J=8.6 Hz, phenylene), 7.36 (1H, dd, J=1.5 and 5.5 Hz, pyrimidyl), 7.19 (1H, d, J=15.9 Hz, olefin), 3.95 (3H, s, methyl); UV (99.5% CH_2Cl_2) 360 (ε=65900). Found: C, 70.24; H, 4.46; N, 14.33%. Calcd for $C_{17}H_{13}N_3O_2$: C, 70.10; H, 4.47; N, 14.43%.

Similar condensations of 4-[2-(4-pyrimidyl)ethenyl]benzaldehyde with ethyl and propyl cyanoacetate gave **1d** and **1e** in 83% and 71% yield, respectively.

1d. Mp 184.0—185.0 °C (ethanol); IR (KBr) 2220, 1710, 1590, 1270, 970 cm^{-1}; ^1H NMR ($CDCl_3$) δ=9.21 (1H, d, J=1.2 Hz, pyrimidyl), 8.74 (1H, d, J=5.2 Hz), 8.24 (1H, s, olefin), 8.05 (2H, d, J=8.5 Hz, phenylene), 7.93 (1H, d, J=16.0 Hz, olefin), 7.72 (2H, d, J=8.5 Hz, phenylene), 7.36 (1H, dd, J=1.2 and 5.2 Hz, pyrimidyl), 7.19 (1H, d, J=16.0 Hz, olefin), 4.40 (2H, q, J=7.3 Hz, methylene), 1.41 (3H, t, J=7.3 Hz, methyl); UV (99.5% CH_2Cl_2) 359 (ε=43200). Found: C, 70.55; H, 4.84; N, 13.75%. Calcd for $C_{18}H_{15}N_3O_2$: C, 70.82; H, 4.92; N, 13.77%.

1e. Mp 149.5—151.0 °C (1-propanol); IR (KBr) 2230, 1730, 1600, 1280, 980 cm^{-1}; ^1H NMR ($CDCl_3$) δ=9.21 (1H, d, J=1.2 Hz, pyrimidyl), 8.74 (1H, d, J=5.2 Hz, pyrimidyl), 8.24 (1H, s, olefin), 8.05 (2H, d, J=8.6 Hz, phenylene), 7.93 (1H, d, J=16.2 Hz, olefin), 7.72 (2H, d, J=8.6 Hz, phenylene), 7.35 (1H, dd, J=1.2 and 5.2 Hz, pyrimidyl), 7.19 (1H, d, J=16.2 Hz, olefin), 4.30 (2H, t, J=6.7 Hz, methylene), 1.81 (2H, m, methylene), 1.00 (3H, t, J=1.2 Hz, methyl); UV (99.5% CH_2Cl_2) 360 (ε=69800). Found: C, 71.41; H, 5.47; N, 12.89%. Calcd for $C_{19}H_{17}N_3O_2$: C, 71.47; H, 5.33; N, 13.17%.

Mixed Crystal (1f). Recrystallization of an equimolar mixture of **1d** (300 mg, 0.98 mmol) and **1e** (313 mg, 0.98 mmol) from 180 ml of propanol gave 350 mg of 1.3:1 mixed crystal (**1f**). The ratio was determined by 400 MHz ^1H NMR. Mp 160.0—165.0 °C (1-propanol).

Isolation of Dimers. The crystals of **1c—f** were photoirradiated by method 3. The dimers **2c, d** (1,2-bis[4-[2-cyano-2-(alkoxycarbonyl)ethenyl]phenyl]-3,4-di(4-pyrimidyl)cyclobutane) and **2e,f** (alkyl 1-cyano-3-[4-[2-cyano-2-(alkoxycarbonyl)-ethenyl]phenyl]-2-[4-[2-(4-pyrimidyl)ethenyl]phenyl]-4-(4-pyrimidyl)-1-cyclobutanecarboxylate) were isolated from the products by flash column chromatography (eluent: dichloromethane with 1—5% methanol). IR, ^1H NMR, and mass spectra analyses of **2c—f** were performed without further purification.

2c. IR (KBr) 2220, 1740, 1600, 1580, 1470, 1440, 1390, 1270, 1215, 1190, 1090, 840 cm^{-1}; ^1H NMR ($CDCl_3$) δ=9.01 (2H, d, J=1.2 Hz, pyrimidyl), 8.52 (2H, d, J=5.2 Hz, pyrimidyl), 8.14 (2H, s, olefin), 7.83 (4H, d, J=8.4 Hz, phenylene), 7.26 (4H, d, J=8.4 Hz, phenylene), 7.14 (2H, dd, J=5.2 and 1.2 Hz, pyrimidyl), 4.99 (2H, m, cyclobutane), 4.63 (2H, m, cyclobutane), 3.90 (6H, s, methyl); MS m/z 582 (M^+), 398, 290 ($M^+/2-1$), 276, 258, 230.

2d. IR (KBr) 2230, 1730, 1600, 1580, 1550, 1470, 1390, 1270, 1220, 1195, 1090, 1020, 840 cm^{-1}; ^1H NMR ($CDCl_3$) δ=9.01 (2H, d, J=1.1 Hz, pyrimidyl), 8.52 (2H, d, J=5.2 Hz, pyrimidyl), 8.12 (2H, s, olefin), 7.83 (4H, d, J=8.4 Hz, phenylene), 7.24 (4H, d, J=8.4 Hz, phenylene), 7.12 (2H, dd, J=5.2 and 1.1 Hz, pyrimidyl), 4.97 (2H, m, cyclobutane), 4.61 (2H, m, cyclobutane), 4.36 (4H, q, J=7.0 Hz, methylene), 1.38 (6H, t, J=7.0 Hz, methyl); MS m/z 610 (M^+), 426, 304 ($M^+/2-1$), 276, 232.

2e. IR (KBr) 2220, 1730, 1580, 1460, 1390, 1270, 1210, 1190 cm^{-1}; ^1H NMR ($CDCl_3$) δ=9.25 (1H, d, J=1.2 Hz, pyrimidyl), 9.15 (1H, d, J=1.0 Hz, pyrimidyl), 8.80 (1H, d, J=5.2 Hz, pyrimidyl), 8.67 (1H, d, J=5.2 Hz, pyrimidyl), 8.11 (1H, s, olefin), 7,82 (2H, d, J=8.2 Hz, phenylene), 7.78 (1H, d, J=15.9 Hz, olefin), 7.47 (2H, d, J=8.2 Hz, phenylene), 7.41 (1H, dd, J=5.2 and 1.2 Hz, pyrimidyl), 7.28 (1H, dd, J=5.2 and 1.0 Hz, pyrimidyl), 7.20 (2H, d, J=8.2 Hz, phenylene), 7.06 (2H, d, J=8.2 Hz, phenylene), 6.99 (1H, d, J=15.9 Hz, olefin), 5.19 (1H, t, J=11.3 and 10.4 Hz, cyclobutane), 4.93 (1H, d, J=11.3 Hz, cyclobutane), 4.72 (1H, d, J=10.4 Hz, cyclobutane), 4.24 (2H, t, J=6.6 Hz, methylene), 3.99 (2H, m, methylene), 1.75 (2H, m, methylene), 1.48 (2H, m, methylene), 0.99 (3H, t, J=7.5 Hz, methyl), 0.84 (3H, t, J=7.5 Hz, methyl); MS m/z 638 (M^+), 551, 463, 421, 318 ($M^+/2-1$), 276, 232.

2f. IR (KBr) 2220, 1725, 1600, 1580, 1470, 1390, 1270, 1210, 1190, 1090, 840 cm^{-1}; ^1H NMR ($CDCl_3$) δ=9.25 (1H, d, J=1.2 Hz, pyrimidyl), 9.14 (1H, s, pyrimidyl), 8.80 (1H, m, pyrimidyl), 8.66 (1H, d, J=5.2 Hz, pyrimidyl), 8.11 (1H, s, olefin), 7.82 (2H, d, J=8.2 Hz, phenylene), 7.78 (1H, d, J=16.0 Hz, olefin), 7.47 (2H, d, J=8.2 Hz, phenylene), 7.41 (1H, m, pyrimidyl), 7.28 (1H, m, pyrimidyl), 7.20 (2H, d, J=8.2 Hz, phenylene), 7.06 (2H, d, J=8.2 Hz, phenylene), 6.99 (1H, d, J=16.0 Hz, olefin), 5.19 (1H, m, cyclobutane), 4.94 (1H, d, J=11.3 Hz, cyclobutane), 4.72 (1H, d, J=10.4 Hz, cyclobutane), 4.37—3.89 (4.5H, m, methylene), 1.82—0.82 (number of H is unknown for impurities, m, methylene and methyl); MS m/z 638 (M^+, R^1=Pr, R^2=Pr), 624 (M^+, R^1=Et,

R^2=Pr or R^1=Pr, R^2=Et), 610 (M^+, R^1=Et, R^2=Et), 531, 421, 407, 396, 318 ($M^+/2-1$, R=Pr), 304 ($M^+/2-1$, R=Et), 276, 260, 232.

Photoreaction. Photoreaction was carried out as follows. Method 1) KBr pellets containing a small amount of monomer crystals were irradiated with a 500 W super high-pressure mercury lamp under nitrogen atomosphere. Method 2) Finely powdered crystals of **1c—f** (200—500 mg) were dispersed in 300 ml of water containing a few drops of surfactant (NIKKOL TL-10FF), and irradiated with a 100 W high-pressure mercury lamp (Eikosha EHBWF-100) through a uranium glass filter with rigorous stirring under nitrogen atomosphere. Method 3) Finely powdered crystals of **1c—f** (100—200 mg) were dispersed in 90 ml of water containing a few drops of surfactant (NIKKOL TL-10FF) and irradiated with a 500 W super high-pressure mercury lamp (Ushio USH-500D) through a L38 filter (cut off <350 nm) for **1c**, **1e**, and **1f**, or a L40 filter (cut off <380 nm) for **1d** with stirring under nitrogen atomosphere.

We gratefully thank Prof. Tsuguo Sawada and Dr. Norio Teramae, Faculty of Engineering, the University of Tokyo, for the measurement of photoacoustic spectra.

References

1) M. Hasegawa, *Chem. Rev.*, **83**, 507 (1983); *Pure Appl. Chem.*, **58**, 1179 (1986).

2) M. Hasegawa, S. Kato, K. Saigo, S. R. Wilson, C. L. Stern, and I. C. Paul, *J. Photochem. Photobiol.*, **A41**, 385 (1988); M. Hasegawa, H. Harashina, S. Kato, and K. Saigo, *Macromolecules*, **19**, 1276 (1986).

3) M. Hasegawa, M. Aoyama, Y. Maekawa, and Y. Ohhashi, *Macromolecules*, in press.

4) M. Hasegawa, K. Saigo, T. Mori, H. Uno, M. Nohara, and H. Nakanishi, *J. Am. Chem. Soc.*, **107**, 2788 (1985).

5) H. Nakanishi, M. Hasegawa, and Y. Sasada, *J. Polym. Sci. A-2*, **10**, 1537 (1972).

6) H. Nakanishi, W. Jones, and G. M. Parkinson, *Acta Crystallogr., Sect. B*, **35**, 3103 (1979).

7) L. Addadi, van J. Mil, and M. Lahav, *J. Am. Chem. Soc.*, **104**, 3422 (1982).

Reduction of N_3^- by $[Mo_2Fe_6S_8(SPh)_9]^{3-}$ Modified Glassy Carbon Electrode—Model Study of Nitrogenase

Koji TANAKA,* Susumu KUWABATA, Satoshi DENNO, and Toshio TANAKA
Department of Applied Chemistry, Faculty of Engineering, Osaka University,
Yamada-oka, Suita, Osaka 565
(Received October 6, 1988)

The reduction of N_3^- by a $(Bu_4N)_3[Mo_2Fe_6S_8(SPh)_9]$ modified glassy carbon electrode has been conducted in a pH region 5 to 12 in water. In neutral and acidic conditions, N_3^- undergoes two-and six-electron reductions to afford not only N_2 and NH_3 but also N_2H_4, and the total amounts of N_2 and N_2H_4 produced were essentially consistent with that of NH_3. On the other hand, no N_2H_4 formation was observed in the pH region higher than 10, where an equal amount of N_2 and NH_3 was formed. The rate of N_2H_4 formation was linearly proportional to a concentration of N_3H, which exists as an equilibrium mixture with N_3^- in the aqueous phase, while that of N_2 evolution was controlled by the concentration of free N_3^- in H_2O. These observations indicate that N_2H_4 and N_2 result from the coordination of N_3H and N_3^- to the molybdenum-iron sulfur cluster, respectively.

Nitrogenase is composed of iron proteins and molybdenum-iron proteins and reduces not only N_2 but also various unsaturated small molecules such as C_2H_2, N_3^-, RCN, RNC, and N_2O.[1] Among those nitrogenase substrates, N_3^- is the only anionic substrate which is reduced with inequivalent numbers of electrons and protons. In the initial study on the reduction of N_3^- by crude nitrogenase in the presence of MgATP, N_3^- was reduced with two electrons to give an equal amount of N_2 and NH_3.[2] Later, Hardy et al. have reported that the reduction of N_3^- afforded one N_2 molecule and two NH_3 molecules at low concentration of N_3^-, and the excess NH_3 has been attributed to result from the further reduction of the N_2 formed.[3] Furthermore, the formation of N_2H_4 in addition to N_2 and NH_3 was observed in the reduction of N_3^- by purified nitrogenase.[4] It has been argued whether N_3^- or N_3H is the actual substrate of nitrogenase[2-5] since both species exist as an equilibrium mixture around pH 7. Furthermore, N_3^- has been shown to disturb the electron flow in enzymatic reaction by inhibiting the rate of MgATP hydrolysis by nitrogenase.[3,6] Despite these difficulties, N_3H has been suggested to be a potent substrate for the formation of N_2H_4 based on the reduction of N_3^- conducted in a restricted pH range 6.5—7.3.[7]

It has been demonstrated that various nitrogenase substrates such as C_2H_2,[8] CH_3CN,[9] CH_3NC,[9] and N_2O[10] are reduced by the reduced species of $[Fe_4S_4(SPh)_4]^{2-}$ and $[Mo_2Fe_6S_8(SPh)_9]^{3-}$. One of the principal advantage of those model studies is that the reduction of nitrogenase substrates can be conducted in wide pH range, where proteins are readily denatured. The reduction of N_3^- by a model study, therefore, may give a clue to elucidate whether N_3^- or N_3H is the actual substrate of nitrogenase. The construction of a system which can not only rapidly but also continuously transport electrons to a catalyst having ability of multi-electron reduction of N_3^- is required in order to simulate the enzymatic reaction since N_3^- undergoes two-, six-, and eight-electron reductions by nitrogenase.[3,4] This paper describes the reduction of N_3^- on a $(Bu_4N)_3[Mo_2Fe_6S_8(SPh)_9]$ modified glassy carbon electrode in H_2O.

Experimental

Commercially available guaranteed reagent grade of NaN_3, H_3PO_4, and NaOH were used without further purification. Water insoluble and soluble MoFeS clusters, $(Bu_4N)_3[Mo_2Fe_6S_8(SPh)_9]$[11] ($(Bu_4N)_3$[Mo-Fe]) and $(Et_4N)_3[Mo_2Fe_6S_8(SCH_2CH_2OH)_9]$,[12] and $(Et_4N)N_3$[13] were prepared according to the literature. Solvents used for electrochemical measurements were purified by distillation over appropriate desiccants; DMF from CaH_2 under reduced pressure and CH_3CN from P_2O_5, and stored under N_2 atmosphere. Immediately before the electrochemical reduction of N_3^-, those solvents were bubbled with He at least for 1 h to remove nitrogen dissolved in the solvents. A $(Bu_4N)_3$[Mo-Fe] modified glassy carbon electrode was prepared by dropping a CH_3CN solution of $(Bu_4N)_3$[Mo-Fe] (1.0 mmol dm^{-3}) on a glassy carbon plates with areas 3.0 and 1.0 cm^2 (Tokai Carbon Co., Ltd., SC-2), and dried under N_2 atmosphere. The details of the cluster modified glassy carbon electrode was described in previous papers.[10,14]

Physical Measurements. Electronic absorption spectra were measured with a Union SM-401 spectrophotometer. Spectroelectrochemical experiments were carried out by the use of an optically transparent thin layer electrode.[15] Cyclic voltammetry was carried out by using a potentiostat (Hokuto Denko HA-301), a function generator (Hokuto Denko HB-107A), and an X-Y recorder (Yokogawa Electric Inc., 3077).

Reduction of N_3^- by the [Mo-Fe]/GC Electrode. The reduction of N_3^- by the [Mo-Fe]/GC electrode in water were carried out under the controlled potential electrolysis conditions using an electrolysis cell consisting of three components; a working, a counter, and an SCE reference electrode compartments.[8] A cation exchange membrane (Nafion film) was used as a separator between the working electrode and the counter electrode compartments. After passing He through the electrolysis cell for 1 h to remove air, an aqueous buffer solution (H_3PO_4–NaOH) of NaN_3 was introduced into the working electrode compartment by syringe techniques. Then, the electrolysis cell was placed in a thermostat at 30 °C and the reduction of N_3^- was started by

applying a fixed potential to the [Mo-Fe]/GC electrode with a potentiostat. The charge consumed in the course of reduction was measured with a Hokuto Denko HF-201 coulometer. Analyses of H_2 and N_2 evolved in the reduction were conducted on a Shimadzu GC-3BT gas chromatograph with a 2.0 m column filled with Molecular Sieves 13X and on a Shimadzu GC-7A gas chromatograph with Porapack Q, respectively. Ammonia and N_2H_4 formed in solutions were determined by Shimadzu GC-6A gas chromatograph with Chromosorb 103 and by colorimetric titration,[16] respectively.

Results and Discussion

Interaction of $[Mo\text{-}Fe]^{3-}$ with N_3^-. The electronic absorption spectrum of $(n\text{-}Bu_4N)_3[Mo\text{-}Fe]$ in DMF shows two absorption bands at 360 and 460 nm (a broken line in Fig. 1), which did not change at all by addition of $(Et_4N)N_3$ to the solution. The electrochemical reduction of $[Mo\text{-}Fe]^{3-}$ to $[Mo\text{-}Fe]^{4-}$ at -1.10 V vs. SCE[17] in DMF resulted in a decrease of the absorptivity at the 460 nm band (a dotted broken line in Fig. 1), while the electrochemical reduction of the cluster conducted in the presence of $(Et_4N)N_3$ under otherwise the same conditions leads to an appearance a new band at 306 nm (a solid line of Fig. 1). The 306 nm band can be assigned to PhS^-[14,18] dissociated from $[Mo\text{-}Fe]^{4-}$, and the intensity of this band corresponds to one molecule of PhS^- per one molecule of the cluster. On the other hand, this band gradually disappeared by reoxidation of $[Mo\text{-}Fe]^{4-}$ at -0.60 V vs. SCE, and the final spectrum became almost same as that of original $[Mo\text{-}Fe]^{3-}$ in DMF. These results indicate that the oxidized cluster $[Mo\text{-}Fe]^{3-}$ has no interaction with N_3^-, while a PhS^- ligand of $[Mo\text{-}Fe]^{4-}$ is substituted by N_3^- to afford the 1:1 adduct. Such a substitution reaction may take place on the Fe atom of $[Mo\text{-}Fe]^{4-}$ rather than the Mo atom, since a terminal RS^- is subject to a substitution reaction, while the bridging RS^- ligands of the cluster are inert for substitutions.[19]

Cyclic Voltammograms of the [Mo-Fe]/GC Electrode. The cyclic voltammogram of the [Mo-Fe]/GC electrode in H_2O (pH 8) shows a cathodic wave around -1.25 V vs. SCE, followed by an irreversible cathodic current due to H_2 evolution catalyzed by the reduced species of the cluster, and an anodic wave around at -0.75 V in the reverse scan (a dotted line in Fig. 2). Although the charge consumed in the cathodic process cannot be determined exactly due to the following irreversible cathodic current, that of the anodic one is just two electrons per a cluster modified on the glassy carbon plate. Thus, all the clusters modified on a glassy carbon plate undergo simultaneous two-electron reduction in water. The $[Mo\text{-}Fe]^{3-/5-}$ redox cycle stably works on the glassy carbon plate since the cyclic voltammogram was essentially unchanged by successive potential scan at least for 2 h.[14] The cathodic current density at more negative potentials than -1.1 V fairly increases by addition of NaN_3 (0.2 mol dm^{-3}) to the aqueous buffer solution at the same pH value (a solid line of Fig. 2). The threshold potential of the cathodic current in the presence of NaN_3 is essentially consistent with the reduction wave from $[Mo\text{-}Fe]^{3-}$ to $[Mo\text{-}Fe]^{5-}$ in the absence of NaN_3, suggesting that the reduced forms of the cluster can effectively reduce N_3^- in water. The current density at more negative potentials than -1.1 V increases with decreasing the pH value (dotted broken and broken lines in Fig. 2).

Reduction of N_3^- by the [Mo-Fe]/GC Electrode. As expected from the cyclic voltammograms of the

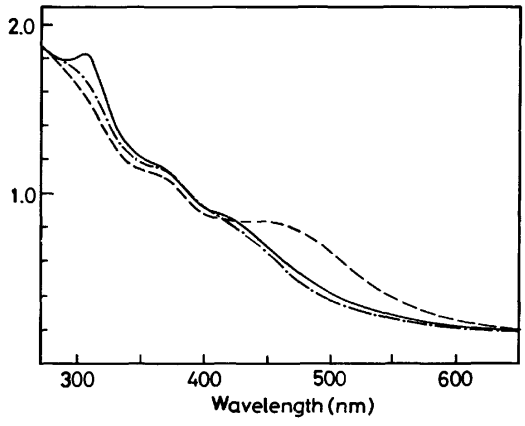

Fig. 1. Electronic absorption spectra of $(Bu_4N)_3[Mo_2Fe_6S_8(SPh)_9]$ (4.0×10^{-4} mol dm^{-3}) (-----) and the reduced species produced at -1.10 V vs. SCE in the absence (—·—) and the presence (-----) of $(Bu_4N)N_3$ (5.0×10^{-2} mol dm^{-3}) in DMF.

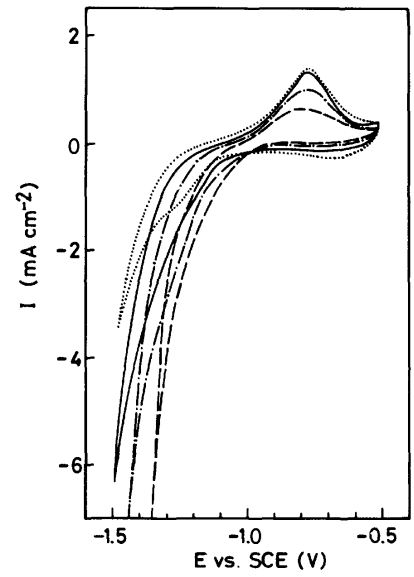

Fig. 2. Cyclic voltammograms of the [Mo-Fe]/GC electrode in H_2O (pH 8.0) in the absence (·····) and the presence of NaN_3 (0.2 mol dm^{-3}) in H_2O at pH 8.0 (——), 7.0 (—·—), and 6.0 (----) : dE/dt= 100 mV s^{-1}.

[Mo-Fe]/GC in the presence of NaN_3 at various pH, the reduction of N_3^- by the [Mo-Fe]/GC electrode at pH 6.0 is much faster than that at pH 12.0 under the controlled potential electrolysis at −1.25 V vs. SCE (Fig. 3). In addition, the reduction products are also altered by the change of pH; N_3^- is reduced to not only N_2 and NH_3 but also N_2H_4 at pH 6.0 (Fig. 3b), while only N_2 and NH_3 are formed in the same reduction at pH 12.0 (Fig. 3a). Thus, in acidic solutions both two- and six-electron reductions of N_3^- (Eqs. 1, 2) take place, and two-electron reduction of N_3^- (Eq. 1) occurs predominantly in

$$N_3^- + 3H^+ + 2e^- \longrightarrow N_2 + NH_3 \quad (1)$$

$$N_3^- + 7H^+ + 6e^- \longrightarrow N_2H_4 + NH_3 \quad (2)$$

alkaline solutions. In order to elucidate such a pH dependency of the N_3^- reduction, reduction of N_3^- was conducted under various reaction conditions, and the results are summarized in Table 1.

The formation of N_2H_4 (Eq. 2) was observed in the pH less than 10 (Entries 1—7 in Table 1). The sum of the amounts of N_2 and N_2H_4 formed in that pH region is essentially consistent with the amount of NH_3, suggesting that N_2H_4 is not the precursor of NH_3. In fact, N_2H_4 was not reduced by the [Mo-Fe]/GC electrode in H_2O under the present experimental conditions. Thus, the [Mo-Fe]/GC electrode can catalyze two- (Eq. 1) and six-electron (Eq. 2) reductions of N_3^- but has no ability to catalyze the eight-electron reduction of N_3^- (Eq. 3). The amounts of not only the

$$N_3^- + 9H^+ + 8e^- \longrightarrow 3NH_3 \quad (3)$$

reduction products of N_3^- but also H_2 increase with decreasing the pH value of the aqueous phase. It should, however, be noticed that the amount of H_2 evolved are controlled by the potential of the [Mo-Fe]/GC electrode under a constant pH, while the amounts of N_2, NH_3, and N_2H_4 are not largely dependent on the electrode potential (Entries 2—4 in Table 1). The result indicates that H_2 evolution is controlled principally by the electron transfer from the GC plate to the cluster, and that the rate of the N_3^- reduction is governed mainly by the chemical reaction. Thus, the cluster modified on the glassy carbon plate effectively functions as a catal st for the reduction of N_3^-. Holm et al. have reported that the reduced species of the present molybdenum-iron sulfur cluster has an

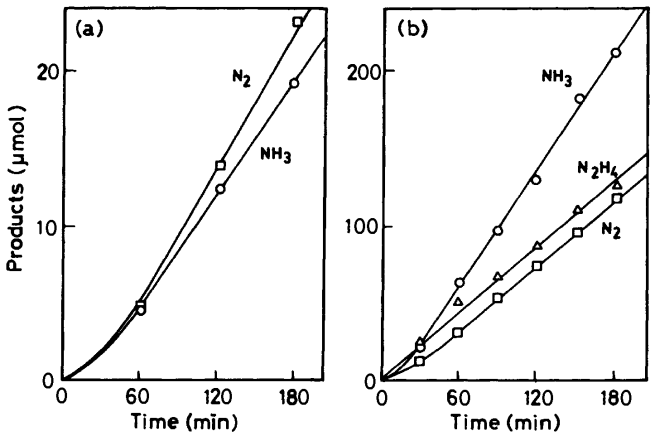

Fig. 3. Reduction of NaN_3 catalyzed by the [Mo-Fe]/GC under the controlled potential electrolysis at −1.25 V vs. SCE in H_2O at pH 12.0 (a) and 6.0 (b). The concentrations of NaN_3 are 0.5 mol dm^{-3} (a) and 0.05 mol dm^{-3} (b).

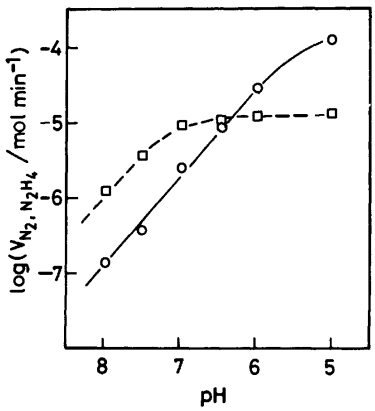

Fig. 4. Rates of the N_2H_4 (○) and N_2 (□) formation against pH of the electrolyte solutions in the reduction of NaN_3 (0.05 mol dm^{-3}) by the [Mo-Fe]/GC electrode at −1.25 V vs. SCE.

Table 1. The Reduction of N_3^- Catalyzed by the [Mo-Fe]/GC Electrode in H_2O for 150 min

Entry	NaN_3	pH	E	Products[a]			
	mmol dm^{-3}		V vs. SCE	NH_3	N_2	N_2H_4	H_2
1	50	5	−1.25	254	96	165	453
2	50	6	−1.10	179	92	89	16
3	50	6	−1.25	183	86	103	234
4	50	6	−1.40	188	89	95	1235
5	25	7	−1.25	49	23	28	77
6	50	7	−1.25	83	45	34	58
7	50	8	−1.25	3.6	3.2	0.3	51
8	50	10	−1.25	2.8	2.5	0	18.2
9	50	12	−1.25	1.3	1.3	0	1.1

a) μmol.

ability to reduce protons and metal-hydride species has been proposed as the precursor for the H_2 evolution.[20] The difference of the rate determining steps in the reductions of protons and N_3^- by the [Mo-Fe]/GC electrode suggests that the reaction mechanisms of those two reactions are different from each other. The reduction of N_3^- may, therefore, be initiated by the coordination of N_3^- to the molybdenum-iron sulfur cluster modified on the GC plate since N_3^- is not reduced at all by a glassy carbon electrode at −1.25 V vs. SCE in H_2O.

As described above, the rates of N_2 and N_2H_4 formation[21] increased with decreasing pH values. The former, however, reaches a constant value below around 7 (a broken line in Fig. 4), and the latter also show the saturation behavior around 5 (a solid line in Fig. 4). Such a distinct difference in the formation rates between N_2H_4 and N_2 toward the pH change suggests that the reductions of Eqs. 1 and 2 take place independently. It is well-known that N_3^- exists as an equilibrium mixture with N_3H in H_2O, and the pK_a of N_3H is 4.6 at 30 °C (Eq. 4).[22] The presence of the turning point in the plot of $\log V(N_2H_4)$ vs. pH ($V(N_2H_4)$: the rate of N_2H_4 formation) around pH 5 may, therefore, be associated with the pK_a. The concentrations of N_3H and N_3^- are expressed by Eqs. 5 and 6, where $[N_3^-]_0$ is the initial concentration of NaN_3. Equations 5 and 6 also can be converted into Eqs. 7 and 8 in terms of pK_a and pH in place of

$$N_3H \rightleftharpoons N_3^- + H^+ \quad (4)$$

$$[N_3H] = [N_3^-]_0[H^+]/(K_a + [H^+]) \quad (5)$$

$$[N_3^-] = K_a[N_3^-]_0/(K_a + [H]^+) \quad (6)$$

$$[N_3H] = [N_3^-]_0/(10^{(pH-pK_a)} + 1) \quad (7)$$

$$[N_3^-] = 10^{(pH-pK_a)}[N_3^-]_0/(10^{(pH-pK_a)} + 1) \quad (8)$$

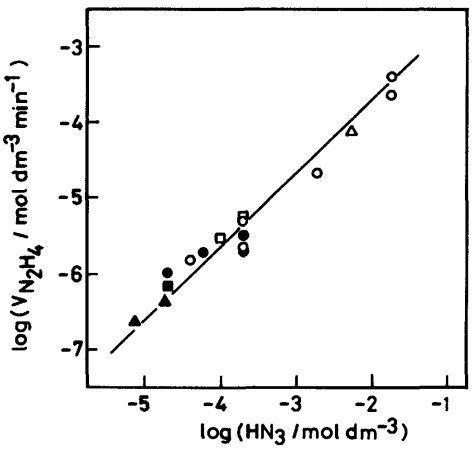

Fig. 5. Relationship between the rate of N_2H_2 formation and the N_3H concentration in the reduction of NaN_3 by the [Mo-Fe]/GC electrode at pH 6.0 (○), 6.5 (△), 7.0 (□), 8.0 (■), and 10.0 (▲).

K_a and $[H^+]$, respectively. Although any linear relationship was not observed between $\log V(N_2H_4)$ and $\log[N_3^-]$ calculated from Eq. 8, a plot of $\log V(N_2H_4)$ vs. $\log[N_3H]$ obtained from Eq. 7 gives a straight line, as shown in Fig. 5. A linear dependence of $V(N_2H_4)$ upon the N_3H concentration in the aqueous phase suggests that N_3H is the actual substrate for the formation of N_2H_4. This conclusion may be supported by the fact that N_2H_4 is not produced above pH 10, where N_3H essentially does not exist as an equilibrium mixture of N_3^-. Equation 9 rather than Eq. 2 may,

$$N_3H + 6H^+ + 6e^- \longrightarrow N_2H_4 + NH_3 \quad (9)$$

therefore, be appropriate for the formation of N_2H_4 in the present study.

The saturation behavior of $\log V(N_2)$ around 7 (Fig. 4) also may be explained by a protonation equilibrium of the reaction intermediate. The reduction of N_3H formed in the aqueous phase may be initiated by the coordination of N_3H to the cluster on the [Mo-Fe]/GC, followed by the electron transfer to the N_3H from the cluster. It should be noticed that N_3^- also can coordinate to the reduced cluster but the rate of the electron transfer to the N_3^- from the cluster may be fairly slower than that to the N_3H ligated on the cluster since N_3^- is apparently much more basic than N_3H. Accordingly, smooth electron transfer from the cluster to the N_3^- coordinated may take place when the N_3^- undergoes a reversible protonation, as expressed by Eq. 10,

$$[[Mo\text{-}Fe]\text{-}N_3^-]_{sur} + H^+ \rightleftharpoons [[Mo\text{-}Fe]\text{-}HN_3]_{sur} \quad (10)$$

where $[[Mo\text{-}Fe]\text{-}N_3^-]_{sur}$ and $[[Mo\text{-}Fe]\text{-}HN_3]_{sur}$ are the cluster-N_3^- adduct and its protonated species, respectively, on the [Mo-Fe]/GC. The protonated cluster-N_3^- adduct ($[[Mo\text{-}Fe]\text{-}HN_3]_{sur}$) formed by the protonation (Eq. 10) is not necessarily the same species as the reaction intermediate involved in the reduction of N_3H affording N_2H_4 and NH_3 (Eq. 9) (vide infra). The proton dissociation constant pK_a' of $[[Mo\text{-}Fe]\text{-}HN_3]_{sur}$ (Eq. 10) may be fairly different from the pK_a of free HN_3 (Eq. 4; pK_a=4.6). As similar to Eq. 5, the surface concentration of $[[Mo\text{-}Fe]\text{-}HN_3]_{sur}$ of Eq. 10 can be expressed by Eq. 11,

$$[[Mo\text{-}Fe]\text{-}HN_3]_{sur} = [[Mo\text{-}Fe]\text{-}N_3^-]_0[H^+]/(K_a' + [H^+]) \quad (11)$$

where $[[Mo\text{-}Fe]\text{-}N_3^-]_0$ is the total surface concentration of the cluster-N_3^- adduct ($[[Mo\text{-}Fe]\text{-}N_3^-]_{sur}$) and its protonated species ($[[Mo\text{-}Fe]\text{-}HN_3]_{sur}$). As discussed in a previous section, the formation of H_2, N_2, and N_2H_4 takes place independently on the [Mo-Fe]/GC. To avoid an extreme difficulty in the determination of each surface concentrations of the active species in those reductions, the surface concentration of [[Mo-

Fe]-N_3^-]$_0$ is assumed to be proportional to the bulk concentration of N_3^- calculated from Eq. 8. The surface concentration of the cluster-N_3^- adduct ([[Mo-Fe]-N_3^-]$_{sur}$ and its protonated species ([[Mo-Fe]-HN_3]$_{sur}$), therefore, can be expressed in terms of [N_3^-], K_a', and [H+] (Eqs. 12, 13). On the basis of the fact

$$[[Mo\text{-}Fe]\text{-}N_3^-]_{sur} \propto K_a'[N_3^-]/(K_a' + [H']) \quad (12)$$

$$[[Mo\text{-}Fe]\text{-}HN_3]_{sur} \propto [N_3^-][H^+]/(K_a' + [H^+]) \quad (13)$$

that $V(N_2)$ is saturated around pH 7, a simulation fitting was conducted in the plots of log $V(N_2)$ vs. log[[Mo-Fe]-N_3^-]$_{sur}$ and log[[Mo-Fe]-HN_3]$_{sur}$ by changing K_a' value around 10^{-7}. The best result was obtained at K_a' is $10^{-6.8}$ in the plot of log $V(N_2)$ vs. log[[Mo-Fe]-HN_3]$_{sur}$, where the rate of N_2 formation in the reduction of N_3^- under various conditions shows a linear dependence on the calculated value $[N_3^-][H^+]/(K_a'+[H^+])$, as shown in Fig. 6, suggesting that [[Mo-Fe]-HN_3]$_{sur}$ selectively affords N_2 and NH_3 (Eq. 1). The large pK_a' value (6.8) of [[Mo-Fe]-HN_3]$_{sur}$ compared with the pK_a value (4.6) of N_3H in water can be explained by an increase in the electron density of N_3^- moiety upon the coordination to the cluster. Such an enhancement of the basicity of N_3^- may be caused by electron transfer through the terminal nitrogen atom bonded to the cluster, since N_3^- usually coordinates to metal complexes with a terminal nitrogen.[23] The initial protonation of N_3^- ligated on the cluster may, therefore, take place on the nitrogen atom bonded to the cluster to produce [Mo-Fe]-HN-N=N (**1**) rather than [Mo-Fe]-N=N=NH (**2**). The structure of **1** seems to explain reasonably the dissociation of the terminal N_2 moiety upon further protonation coupled with electron transfer from the cluster to HN-N=N moiety. In accordance with this, protonation of M-N_3^- complexes (M=Ru,[24] Co,[25]

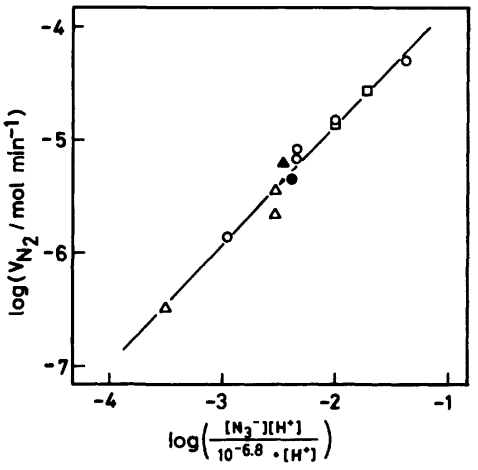

Fig. 6. Relationship between the rate of N_2 formation and log ($[N_3^-][H^+]/(10^{-6.8}+[H^+])$) in the reduction of NaN_3 by the [Mo-Fe]/GC electrode at pH 6.0 (○), 6.5 (△), 7.0 (□), and 10.0 (▲).

$$\bar{N}=\overset{+}{N}=\bar{N} + H^+ \rightleftharpoons \bar{N}=\overset{+}{N}=NH$$

Scheme 1.

Ir[26]) also occurs at the nitrogen atom bonded to the metal, followed by the dissociation of terminal N_2.

The protonation of N_3^- in a solution has been shown to occur at one of a terminal nitrogen atom of N_3^-[27] (Scheme 1). The linear dependence of the rate of N_2H_4 formation upon the concentration of N_3H in the aqueous phase (Eq. 4) indicates the appropriateness of Eq. 9. In contrast to the protonation of [Mo-Fe]-$\bar{N}=\overset{+}{N}=\bar{N}$ affording [Mo- Fe]-HN-$\bar{N}=\overset{+}{N}=\bar{N}$ (**1**), N_3H may bind to the cluster with the nonprotonated terminal nitrogen atom affording [Mo-Fe]-$\bar{N}=\overset{+}{N}=NH$ (**2**) rather than **1**. The intramolecular electron transfer from the cluster to the N_3H moiety of **2** may cause also the increase of the basicity of the nitrogen atom bonded to the cluster, resulting in further protonation to form [Mo-Fe]-NH-N=NH (**3**). The following electron transfer coupled with protonation of **3** may lead the dissociation of N_2H_4. It should be noticed that such the six-electron reduction of N_3^- (Eq. 2) hardly took place under the controlled potential electrolysis of an aqueous solution (pH 7.0, 12 cm^3) containing $(Et_4N)_3[Mo_2Fe_6S_8(SCH_2CH_2OH)_9]$ (0.37 mmol dm^{-3}) and NaN_3 (0.37 mol dm^{-3}) at −1.25 V vs. SCE, where the two-electron reduction of N_3^- (Eq. 1) predominantly occurred with concomitant H_2 evolution. The mole ratios of N_2 and H_2 to NH_2NH_2 formed in this homogeneous system were 25 and 194, respectively, and the turnover number for the formation of N_2H_4 was as low as 0.385/h based on the amount of the cluster. On the other hand, the [Mo-Fe]/GC catalyzes the six-electron reduction of N_3^- affording N_2H_4 with the turnover number 235/h under the same electrolysis potential at pH 7 (Entry 6 in Table 1). Despite that both $[Mo_2Fe_6S_8(SPh)_9]^{3-}$ and $[Mo_2Fe_6S_8(SCH_2CH_2OH)_9]^{3-}$ similarly undergo two successive one-electron reduction at more positive potentials than −1.25 V in solutions, the outstanding ability of the former modified glassy carbon electrode for the six-electron reduction of N_3^- may be explained by the view that the cluster of the [Mo-Fe]/GC exists as the reduced form even after two-electron reduction of N_3^- due to fast and continuous electron transport to $[Mo_2Fe_6S_8(SPh)_9]^{3-}$ from the glassy carbon plate. This assumption is supported by the fact that the cyclic voltammogram of the [Mo-Fe]/GC clearly exhibits the anodic wave of the cluster even in the presence of N_3^- (Fig. 2). Thus, the system which is provided with rapid and continuous electron transport to a redox catalyst may be one of the essential factor to catalyze a multi-electron reduction involving unstable reaction intermediates.

The reduction of N_3^- by nitrogenase affords also N_2, NH_3, and N_2H_4 around pH 7, and the amount of NH_3 has been shown to be larger than the total amount of

N_2 and N_2H_4. This has been ascribed to further six-electron reduction of N_2 formed in the two-electron reduction of N_3^-. The [Mo-Fe]/GC electrode has no ability of catalyzing the eight-electron reduction of N_3^- though the [Mo-Fe]/GC reasonably explains the difference in the two- and six-electron reduction of N_3^- in a wide pH range.

References

1) H. Dalton and L. E. Mortenson, *Bacteriol. Rev.*, **1972**, 231. L. E. Mortenson and R. N. F. Thorneley, *Ann. Rev. Biochem.*, **48**, 387 (1979).

2) R. Schollhorn and R. H. Burris, *Proc. Natl. Acad. Sci. U.S.A.*, **57**, 1317 (1967).

3) R. W. F. Hardy and E. Knight, Jr., *Biochim. Biophys. Acta*, **139**, 69 (1967).

4) M. J. Dilworth and R. N. F. Thorneley, *Biochem. J.*, **193**, 971 (1981).

5) J. -G. Li, B. K. Burgess, and J. L. Corbin, *Biochemistry*, **21**, 4393 (1982). T. E. Hermann and P. W. Wilson, *J. Bacteriol.*, **126**, 743 (1976).

6) T. Lijones, *Biochim. Biophys. Acta*, **321**, 103 (1973).

7) J. F. Rubinson, B. K. Burgess, J. L. Corbin, and M. J. Dilworth, *Biochemistry*, **24**, 273 (1985).

8) R. S. McMillan, J. Renaud, J. G. Reynolds, and R. H. Holm, *J. Inorg. Biochem.*, **11**, 213 (1979). K. Tanaka, M. Honjo, and T. Tanaka, *ibid.*, **22**, 187 (1984).

9) K. Tanaka, Y. Imasaka, M. Tanaka, M. Honjo, and T. Tanaka, *J. Am. Chem. Soc.*, **104**, 4258 (1982).

10) S. Kuwabata, S. Uezumi, K. Tanaka, and T. Tanaka, *Inorg. Chem.*, **25**, 3018 (1986).

11) G. Christou, C. D. Garner, and R. M. Miller, *J. Chem. Soc., Dalton Trans.*, **1980**, 2363.

12) G. Christou, C. D. Garner, F. E. Mabbs, and M. G. B. Drew, *J. Chem. Soc., Chem. Commun.*, **1979**, 91.

13) R. E. Palermo, R. Singh, J. K. Bashkin, and R. H. Holm., *J. Am. Chem. Soc.*, **106**, 2600 (1984).

14) D. Lexa, J. M. Savent, and J. Zickler, *J. Am. Chem. Soc.*, **99**, 2786 (1977).

15) S. Kuwabata, K. Tanaka, and T. Tanaka, *Inorg. Chem.*, **25**, 1691 (1986).

16) G. W. Watt and J. Chrips, *Anal. Chem.*, **24**, 2066 (1952).

17) G. Christou, P. K. Mascharak, W. H. Armstrong, G. Papaefthymiou, R. B. Frankel, and R. H. Holm, *J. Am. Chem. Soc.*, **104**, 2820 (1982).

18) K. Tanaka, M. Moriya, S. Uezumi, and T. Tanaka, *Inorg. Chem.*, **27**, 137 (1988).

19) R. E. Palermo, P. P. Power, and R. H. Holm, *Inorg. Chem.*, **21**, 173 (1982).

20) T. Yamamura, G. Christou, and R. H. Holm, *Inorg. Chem.*, **22**, 939 (1983).

21) An induction period was observed for the formation of N_2 and N_2H_4 in the reduction of N_3^- by the [Mo-Fe]/GC electrode in H_2O. So the rates of the N_2 and N_2H_4 formation were obtained after 30 min, where both products linearly were produced with time (Fig. 3).

22) J. H. Boughton and R. N. Keller, *J. Inorg. Nucl. Chem.*, **28**, 2851 (1966).

23) Z. Dori and R. F. Ziolo, *Chem. Rev.*, **73**, 247 (1973).

24) L. A. P. Kane-Maguire, P. S. Sheridon, F. Basolo, and R. G. Person, *J. Am. Chem. Soc.*, **92**, 5685 (1970).

25) F. Monacelli, G. Mattogno, D. Gattegno, and M. Matese, *Inorg. Chem.*, **9**, 686 (1970).

26) B. C. Lome, J. W. McDonald, F. Basolo, and R. G. Person, *J. Am. Chem. Soc.*, **94**, 3786 (1972).

27) A. Mertens, K. Lammertsma, M. Arvanaghi, and G. A. Olah, *J. Am. Chem. Soc.*, **105**, 5657 (1983).

Synthetic Photochemistry. XLIX.[1] Synthesis and Photoisomerization of 2-Acetyl-2-azatricyclo[6.2.2.0^{1,5}]dodeca-4,6,9,11-tetraen-3-one. An MO Explanation of the Cycloaddition of Cyclohepta[*b*]pyrrol-2(1*H*)-ones

Guan Rong TIAN,† Akira MORI, Hitoshi TAKESHITA,* Miwako HIGASHI,†† and Hiroyuki YAMAGUCHI††
Institute of Advanced Material Study, 86, Kyushu University, Kasuga-koen, Kasuga, Fukuoka 816
††College of Technology, Ibaraki University, 4-12-1, Nakanarusawa, Hitachi 316
(Received October 17, 1988)

Thermal cycloaddition reactions of 2,3-bis(methoxycarbonyl)-7-oxabicycloheptadiene with cyclohepta[*b*]-pyrrol-2(1*H*)-ones gave the [4+2]adducts and products derived from the [8+2]adducts. Among [4+2]adducts, a new adduct was isolated. Cyclohepta[*b*]pyrrol-2(1*H*)-ones, having a substituent at the C-3 position exclusively, gave [4+2]adducts. The photolysis of 2-azatricyclo[6.2.2.0^{1,5}]dodeca-4,6,9,11-tetraen-3-one afforded substituted 9-methylenebarbaralane, 5-methylenetricyclo[4.3.0.0^{2,9}]nonadiene, and 1-methylenedihydroindene derivatives.

Currently, we have been interested in the thermal cycloaddition-cycloreversion process of 2,3-bis(methoxycarbonyl)-7-oxabicyclo[2.2.1]heptadiene, an acetylene equivalent, with tropones,[2] cyclohepta[*b*]furan-2(2*H*)-ones,[3] and anthracenes.[4] Since this procedure is useful to construct various cage compounds, we have now investigated the reaction with cyclohepta-[*b*]pyrrol-2(1*H*)-ones (**1**) to obtain 2-azatricyclo-[6.2.2.0^{1,5}]dodeca-4,6,9,11-tetraen-3-ones. Although Abe and Takehiro recently showed that the thermal cycloaddition between **1** and dimethyl butynedioate (DMBD) gave the products via a [8+2]cycloaddition,[5] we have now found that the reactions of **1** and 2,3-bis(methoxycarbonyl)-7-oxabicyclo[2.2.1]heptadiene (**2**) under 3000 bar afforded [4+2] and [8+2]adducts. In addition, the photorearrangement of 2-azatricyclo-[6.2.2.0^{1,5}]dodeca-4,6,9,11-tetraen-3-one furnished similar products as in the oxa analogues, 2-oxatricyclo-[6.2.2.0^{1,5}]dodeca-4,6,9,11-tetraen-3-ones.

Results and Discussion

Cycloaddition Reaction of 1 and 2. When a chlorobenzene solution of 1-acetylcyclohepta[*b*]pyrrol-2(1*H*)-one (**1a**) and **2** was heated at 120 °C under 3000 bar, four products (**3a**, and **4**—**6**) were formed and isolated via silica-gel chromatography in 12, 4, 8, and 6% yields, respectively (Scheme 1). Products **3a** and **4** were 1:1-cycloadducts, respectively; the ^{1}H NMR spectrum of product **3a** revealed five methine protons with coupling constants ($J_{1,2}$=$J_{2,3}$=$J_{6,7}$=0—1.1 Hz), which are very similar to those of endo [4+2]adducts formed by the addition of cyclohepta[*b*]furan-2(2*H*)-ones and **2**.[3] On the other hand, the structure of **4** was deduced to be another endo [4+2]adduct; the ^{1}H NMR spectrum showed the presence of four olefinic and six methine protons with coupling constants ($J_{1,2}$=$J_{2,3}$=

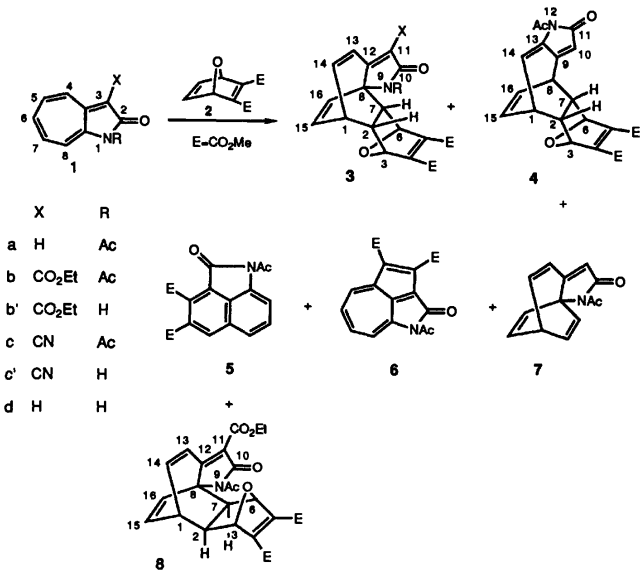

Scheme 1.

Table 1. Product Distribution of **1** and **2**

	Conditions[a]	Products (Yield/%)
1a	3000, 120, 20, CB,[b]	**3a** (12), **4** (4), **5** (8), **6** (6),
	1, 130, 20, CB	**5** (16), **7** (13)
1b	3000, 120, 20, anhydrous dioxane	**3b** (26), **8** (6.5)
	3000, 115, 20, dioxane	**3b'** (45)
1c	3000, 120, 20, anhydrous dioxane	**3c** (20), **3c'** (24)
1d	3000, 120, 20, anhydrous dioxane	No reaction[c]

a) Pressure/bar, temperature/°C, time/h, and solvent. b) Chlorobenzene. c) The reaction of **1d** and DMBD in refluxing acetonitrile gave five products derived from a [8+2]adduct.[5]

† On leave from Yanbian University, Yanji, Jilin, People's Republic of China.

$J_{6,7}=J_{7,8}=0$—1.1 Hz). Additionally, H-14 appeared at δ 7.69 (dd, J=9.5, 1.8 Hz). This signal at the low-field could be explained in terms an α-position to the *N*-acetyl group. These observations were consistent to the structure of **4**. The connectivities of the hydrogens of **3** and **4** were further confirmed by the ^{1}H COSY spectra. Product **5** was the naphthalene derivative, being identical with an authentic sample.[6] Product **6** was assigned as 1-acetyl-3,4-bis(methoxycarbonyl)pyrrolo[4,3,2-*cd*]azulen-2(1*H*)-one by comparing the spectral data with related compounds.[5] The product distributions of **1** and **2** are summarized in Table 1.

When the reaction between **1a** and **2** was performed at 130 °C in a sealed tube, a new product **7** was obtained in 13% yield together with **5** (16%). Since this new product **7** was also formed together with 3,4-bis(methoxycarbonyl)furan from **3a** by heating at 135 °C and its NMR spectrum indicated to have a symmetry element in a molecule, **7** was assigned to be 2-acetyl-2-azatricyclo[6.2.2.0^{1,5}]dodeca-4,6,9,11-tetraen-3-one.

The reaction of 1-acetyl-3-ethoxycarbonylcyclohepta-[*b*]pyrrol-2(1*H*)-one (**1b**) and **2** in anhydrous dioxane gave a 1:1-adduct (**3b**) and another 1:1-adduct (**8**) together with a deacetylated derivative (**1b'**)[7] of **1b**. Also, in a moistened medium a deacetylated 1:1-adduct (**3b'**) was isolated instead of **3b**. The structure of **3b** was elucidated to be an endo [4+2]adduct by a direct comparison with the spectral data of **3a**; in the ^{1}H NMR spectrum, **3b** showed signals at δ 6.95—7.15, which were ascribable to H-13 and H-14, being lower than the corresponding signals of **3a**. This low-field shift indicated an intact ethoxycarbonyl group at C-11. The exo [4+2]adduct structure for **8** was deduced from the coupling constant (5.9 Hz) between H-1 and H-2 in the ^{1}H NMR spectrum.

The reaction between 1-acetyl-3-cyanocyclohepta-[*b*]pyrrol-2(1*H*)-one (**1c**) and **2** in anhydrous dioxane under 3000 bar afforded two products (**3c** and **3c'**) and a deacetyl derivative (**1c'**)[8] of **1c**. The latter adduct **3c'** was a deacetylated derivative of **3c**.

Photorearrangement of 7. The irradiation of **7** with a high-pressure mercury lamp (1 kW) gave three products (**9**—**11**). The structures of these products were similar to those obtained from the photolysis of 2-oxatricyclo[6.2.2.0^{1,5}]dodeca-4,6,9,11-tetraen-3-one derivatives (**12**).[9] Interestingly, a dihydroindenone (**11**) was isolated as a proto-photoisomer from **7** in this case; a similar photolysis of **12** gave an aromatized indan derivative (**13**).

Reaction Modes of 1 and 2. There was observed nearly equal amounts of two types of products in the cycloaddition reaction between **1** and **2**, as shown in Table 1. The product distributions were not similar to those of the reactions of **1** and DMBD in a refluxing acetonitrile.[5] For example, the reaction of cyclohepta-[*b*]pyrrol-2(1*H*)-one (**1d**) and DMBD gave two ene

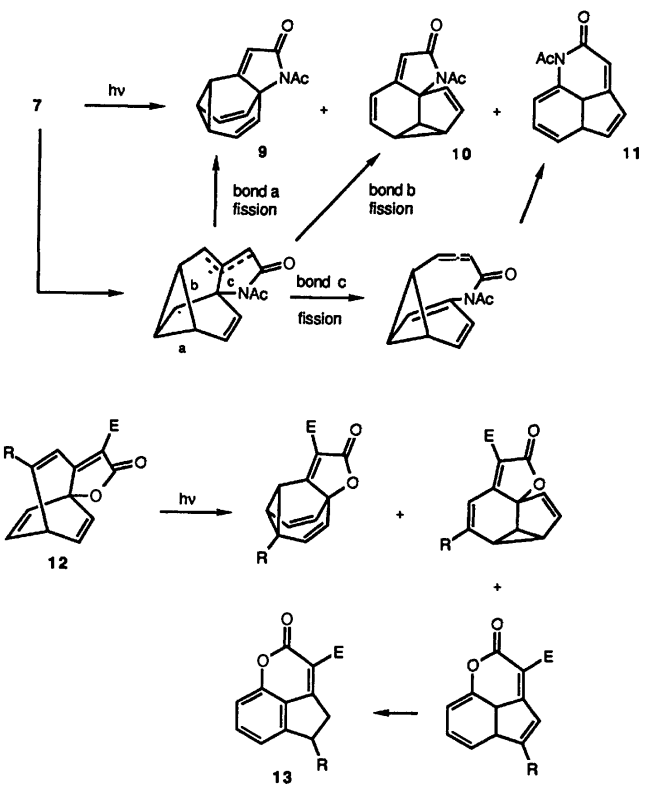

Scheme 2.

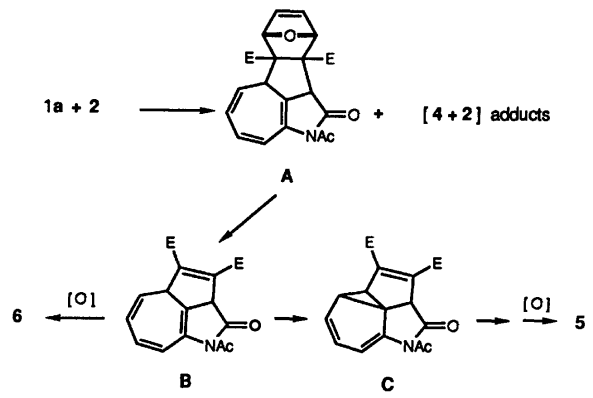

Scheme 3.

products in 51% and the deacetyl derivative of **5** in 35% together with a deacetyl derivative of **6** in 5% yields. The reaction of **1d** and **2** did not proceed even at 120 °C under 3000 bar, and the product distributions in the reactions of **1d** with DMBD and **1a** and **2** were completely different. Therefore, products **5** and **6** were formed via a 1:1-adduct (**A**) of **1a** and **2** and not formed from **1a** and DMBD, although DMBD could be available by a cycloreversion of **2** under the reaction conditions. An elimination of furan from **A** and a subsequent autooxidation, via **B**, should yield **6**. A valence bond isomerization of the cycloheptatriene function in **B** followed by a dehydrogenation should afford **5**. Thus, the [8+2]addition occurred exclusively

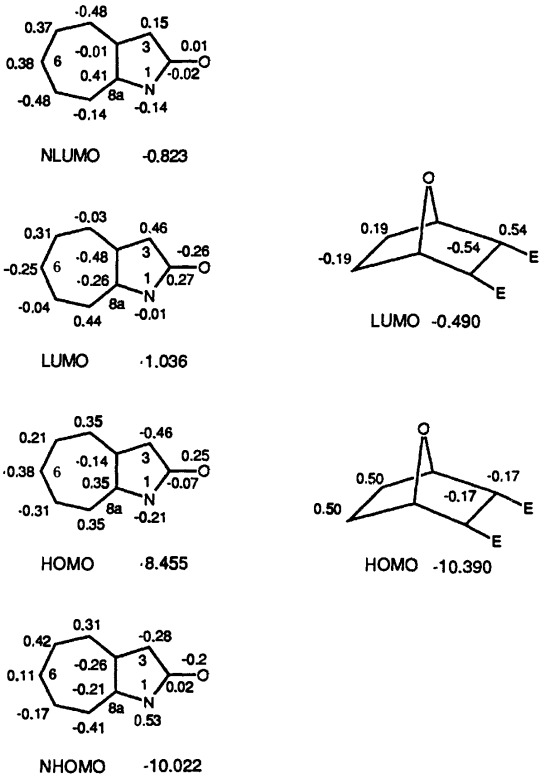

Fig. 1. Coefficients and energy levels of selected molecular orbitals of **1a** and **2**.

at positions of C-3 and C-4 in **1**. So far, no product reacted at C-3 and C-8a of **1** has been isolated, although the coefficient of C-4 in HOMO of **1a** was identical with that of C-8a from the MNDO calculation. An acetyl group might prevent an approach to the C-8a position of **2**. The reaction site of **2** in the [8+2]addition could be reasonably explained by the interaction of HOMO(**1a**) and LUMO(**2**), which favored a reaction to occur at the double bond with methoxycarbonyl groups.

Among [4+2]adducts identified, a new type of an adduct, **4**, should be worthy of note. This type of the product has never been isolated from reactions between cyclohepta[*b*]furan-2(2*H*)-ones and **2**.[3] Therefore, the formation of **4** might be explained in terms of the steric effect of an acetyl group on the nitrogen atom, which prevents an approach of **2** to the C-8a position of **1a**. The interactions of both LUMO(**1a**)-HOMO(**2**) and the NLUMO(**1a**)-HOMO(**2**) favored a [4+2]addition at a double bond having no substituents of **2**.[10]

Experimental

Elemental analyses were performed by Miss S. Hirashima, of Institute of Advanced Material Study, Kyushu University. NMR spectra were measured by a JEOL GSX 270 H Model spectrometer in a $CDCl_3$ solution (unless otherwise specified); chemical shifts are expressed in δ unit. Apparent coupling constants were obtained from the first-order analyses. Mass spectra were measured with a JEOL OlSG-2 spectrometer. IR spectra were taken as KBr disks or as a liquid film inserted between NaCl plates using a Jasco IR-A 102 spectrometer. UV spectra were measured by a Hitachi U-3200 spectrophotometer.

Cycloaddition of 1a and 2. a) A chlorobenzene solution (3 cm^3) of **1a** (191 mg) and **2** (293 mg) was heated at 120 °C for 20 h under 3000 bar. The solvent was removed under reduced pressure and the residue was chromatographed on a silica-gel column to give 45 mg (12%) of **3a**, 15 mg (4%) of **4**, 26.6 mg (8%) of **5**, 20 mg (6%) of **6**, and recovered **1a** (12.4 mg) and **2** (20 mg).

3a: colorless crystals, mp 202—203 °C; ^{1}H NMR δ=2.26 (1H, dd, J=8.1, 1.1 Hz), 2.56 (1H, d, J=8.1 Hz), 2.67 (3H, s), 3.43 (1H, dd, J=8.4, 8.1 Hz), 3.77 (3H, s), 3.81 (3H, s), 4.93 (1H, d, J=1.1 Hz), 5.69 (1H, d, J=1.1 Hz), 5.72 (1H, s), 6.21 (1H, d, J=10.3 Hz), 6.25 (1H, t, J=8.1 Hz), 6.30 (1H, dt, J=8.1, 1.1 Hz), and 6.72 (1H, dd, J=10.3, 8.4 Hz); ^{13}C NMR δ=26.6, 38.8, 46.2, 51.4, 52.4 (2C), 71.8, 83.7, 85.8, 117.3, 122.3, 128.8, 129.5, 144.5, 144.7, 146.4, 160.3, 162.7, 162.9, 170.8, and 171.6; IR 3010, 2890, 1740, 1705, 1640, and 1610 cm^{-1}; UV (MeOH) 245.6 (ε 9600) and 282.8 nm (7300).

Found: C, 63.67; H, 4.84; N, 3.54%. Calcd for $C_{21}H_{19}NO_7$: C, 63.46; H, 4.82; N, 3.52%.

4: colorless crystals, mp 202 °C; ^{1}H NMR δ=2.39 (1H, d, J=8.1 Hz), 2.55 (3H, s), 2.70 (1H, d, J=8.1 Hz), 3.52 (1H, dd, J=9.5, 8.1 Hz), 3.81 (6H, s), 3.89 (1H, d, J=7.0 Hz), 4.93 (1H, s), 5.06 (1H, s), 5.87 (1H, d, J=1.8 Hz), 6.14 (1H, dd, J=8.4, 7.0 Hz), 6.45 (1H, dd, J=8.4, 8.1 Hz), and 7.69 (1H, dd, J=9.5, 1.8 Hz); ^{13}C NMR δ=26.6, 37.8, 41.0, 44.4, 47.9, 52.4 (2C), 86.0, 86.2, 115.5, 127.2, 127.4, 136.6, 138.0, 144.7, 145.7, 154.4, 162.7 (2C), 168.4, and 171.1; IR 2890, 1710, 1630, 1595, and 1430 cm^{-1}; UV (MeOH) 246.4 (ε 11700), 285.4 (9100), and 421.4 nm (500).

Found: C, 63.55; H, 4.83; N, 3.47%. Calcd for $C_{21}H_{19}NO_7$: C, 63.46; H, 4.82; N, 3.52%.

5: yellow prisms, mp 172—173 °C (lit,[5] mp 174—176 °C).

6: reddish crystals, mp 183—185 °C; ^{1}H NMR δ=2.82 (3H, s), 3.97 (3H, s), 4.07 (3H, s), 7.91 (1H, dd, J=10.3, 9.5 Hz), 8.26 (1H, t, J=10.3 Hz), 9.06 (1H, d, J=10.3 Hz), and 9.36 (1H, d, J=9.5 Hz); ^{13}C NMR δ=26.5, 52.1, 53.0, 113.7, 120.9, 122.1, 131.4, 137.3, 137.5, 139.2, 142.7, 143.1, 147.2, 161.0, 164.1, 165.3, and 172.4; IR 2880, 1740, 1695, and 1595 cm^{-1}; UV (MeOH) 232.4 (ε 21600), 257.6 (42300), 283.2 (26300), and 367.4 nm (9500).

Found: C, 62.32; H, 3.98; N, 4.05%. Calcd for $C_{17}H_{13}NO_6$: C, 62.39; H, 4.00; N, 4.28%.

b) A chlorobenzene solution (1 cm^3) of **1a** (130 mg) and **2** (350 mg) was heated at 130 °C for 20 h in a sealed tube under a nitrogen atmosphere. After removing the solvent, the residue was chromatographed on a silica-gel column to give 35.8 mg (16%) of **5**, 18 mg (13%) of **7**, and recovered **1a** (52.2 mg) and **2** (106 mg).

7: colorless crystals, mp 136—138 °C; ^{1}H NMR δ=2.63 (3H, s), 3.90 (1H, dtm, J=8.1, 7.7 Hz), 5.73 (1H, s), 5.90 (1H, d, J=10.3 Hz), 6.28 (2H, dd, J=7.7, 1.5 Hz), 6.54 (2H, t, J=7.7 Hz), and 6.57 (1H, dd, J=10.3, 8.1 Hz); ^{13}C NMR δ=25.2, 39.5, 70.5, 118.0, 119.6, 131.5 (2C), 133.1 (2C), 140.2, 153.2, 169.7, and 170.3; IR 2905, 1730, 1620, and 1380 cm^{-1}; UV (MeOH) 260.6 nm (ε 9300).

Found: C, 73.28; H, 5.22; N, 6.58%. Calcd for $C_{13}H_{11}NO_2$: C, 73.23; H, 5.20; N, 6.57%.

Cycloaddition of 1b and 2. a) An anhydrous dioxane solution (2.5 cm^3) of **1b** (54 mg) and **2** (100 mg) was heated at 120 °C under 3000 bar for 20 h. Silica-gel chromatography of the residue gave 16 mg (26%) of **3b**, 4 mg (6.5%) of **8**, and recovered **2** (50 mg) and **1b'** (16 mg).

3b: colorless crystals, mp 125—126 °C; ^1H NMR δ=1.38 (3H, t, J=7.3 Hz), 2.27 (1H, d, J=7.7 Hz), 2.59 (1H, dd, J=7.7, 1.1 Hz), 2.71 (3H, s), 3.53 (1H, m), 3.78 (3H, s), 3.81 (3H, s), 4.37 (2H, q, J=7.3 Hz), 4.94 (1H, d, J=1.1 Hz), 5.64 (1H, d, J=1.1 Hz), 6.3 (2H, m), and 6.95—7.15 (2H, m); ^{13}C NMR δ=14.2, 27.0, 39.5, 46.4, 51.7, 52.5 (2C), 61.6, 70.6, 83.8, 85.7, 117.3, 121.2, 128.8, 130.4, 144.5, 146.8, 149.7, 161.8, 162.4, 162.7, 162.8, 166.8, and 171.8; IR 3000, 1740, 1640, 1610, and 1580 cm^{-1}; UV (MeOH) 248.2 (ε 11100) and 296.4 nm (11700).

Found: C, 61.48; H, 4.96; N, 3.05%. Calcd for $C_{24}H_{23}NO_9$: C, 61.40; H, 4.94; N, 2.98%.

8: colorless crystals, mp 172—173 °C; ^1H NMR δ=1.39 (3H, t, J=7.3 Hz), 2.65 (1H, dd, J=8.8, 5.9 Hz), 2.69 (3H, s), 3.7 (1H, m), 3.73 (1H, d, J=8.8 Hz), 3.75 (3H, s), 3.81 (3H, s), 4.37 (2H, q, J=7.3 Hz), 4.61 (1H, s), 4.89 (1H, d, J=1.1 Hz), 6.18 (1H, d, J=8.4 Hz), 6.42 (1H, dd, J=8.4, 7.3 Hz), 6.69 (1H, dd, J=10.6, 8.4 Hz), and 7.31 (1H, d, J=10.6 Hz); ^{13}C NMR δ=14.3, 26.2, 38.1, 42.8, 48.5, 52.4, 52.5, 61.5, 70.4, 79.9, 83.8, 118.6, 125.9 (2C), 133.2, 134.4, 143.9, 145.6, 161.5, 161.7, 161.8, 162.6, 166.4, and 170.4; IR 3000, 2950, and 1720 cm^{-1}; UV (MeOH) 243.8 (ε 10000) and 299.4 nm (10300).

Found: C, 61.19; H, 4.94; N, 2.99%. Calcd for $C_{24}H_{23}NO_9$: C, 61.40; H, 4.94; N, 2.98%.

1b': mp 185—188 °C (lit,[7] mp 189—190 °C).

b) A dioxane solution (2 cm^3) of **1b** (80 mg) and **2** (240 mg) was heated at 115 °C for 20 h under 3000 bar. Silica-gel chromatography of the mixture gave 35 mg (45%) of **3b'**, 26 mg of **1b'**, and recovered **2** (125 mg).

3b': colorless crystals, mp 197—198 °C; ^1H NMR δ=1.34 (3H, t, J=7.0 Hz), 2.27 (1H, d, J=8.1 Hz), 2.50 (1H, d, J=8.1 Hz), 3.52 (1H, dd, J=8.4, 7.7 Hz), 3.72 (3H, s), 3.81 (3H, s), 4.33 (2H, q, J=7.0 Hz), 4.95 (1H, s), 5.45 (1H, s), 6.00 (1H, d, J=8.8 Hz), 6.29 (1H, dd, J=8.8, 7.7 Hz), 6.78 (1H, dd, J=10.6, 8.4 Hz), 7.06 (1H, d, J=10.6 Hz), and 8.63 (1H, br s); ^{13}C NMR δ=14.2, 39.5, 43.5, 49.8, 52.4, 52.5, 61.1, 65.8, 84.3, 85.5, 118.4, 121.9, 130.6, 132.0, 145.0, 145.4 (2C), 162.1, 162.3, 162.5, 162.6, and 169.9; IR 3400, 3200, 3100, 1740, 1640, and 1570 cm^{-1}; UV (MeOH) 248.6 (ε 10150) and 285.8 nm (11400).

Found: C, 61.46; H, 4.78; N, 3.26%. Calcd for $C_{22}H_{21}NO_8$: C, 61.82; H, 4.95; N, 3.28%.

Cycloaddition of 1c and 2. An anhydrous dioxane solution (1 cm^3) of **1c** (50 mg) and **2** (120 mg) was heated at 120 °C under 3000 bar for 20 h. Silica-gel chromatography of the mixture gave 4 mg (20%) of **3c**, 4.5 mg (24%) of **3c'**, and **1c'** (30 mg).

3c: colorless crystals, mp 198 °C (decomp); ^1H NMR δ=2.28 (1H, d, J=8.1 Hz), 2.59 (1H, dd, J=8.1, 1.1 Hz), 2.70 (3H, s), 3.6 (1H, m), 3.79 (3H, s), 3.81, (3H, s), 4.95 (1H, d, J=1.4 Hz), 5.64 (1H, s), 6.32 (2H, m), 6.53 (1H, d, J=10.3 Hz), and 7.14 (1H, dd, J=10.3, 8.8 Hz); ^{13}C NMR δ=26.7, 39.9, 46.6 (2C), 51.9, 52.6, 72.2, 83.7, 85.8, 102.6, 110.6, 120.7, 127.9, 130.8, 144.3, 146.7, 152.2, 162.4, 162.6, 165.4, 166.9, and 171.3; IR 2975, 2240, 1720, and 1620 cm^{-1}; UV (MeOH) 243.8 (ε 5700) and 300.8 nm (6300).

Found: m/z 380.1015 ($M^+ - CH_3CO$). Calcd for $C_{20}H_{15}N_2O_6$: 380.1008.

3c': colorless crystals, mp 201—203 °C; ^1H NMR δ=2.27 (1H, d, J=8.1 Hz), 2.55 (1H, d, J=8.1 Hz), 3.60 (1H, t, J=8.8 Hz), 3.79 (3H, s), 3.83 (3H, s), 4.95 (1H, d, J=1.5 Hz), 5.26 (1H, s), 5.99 (1H, d, J=8.8 Hz), 6.33 (1H, t, J=8.8 Hz), 6.55 (1H, d, J=10.6 Hz), 6.93 (1H, dd, J=10.6, 8.8 Hz), and 7.76 (1H, br s); ^{13}C NMR (DMSO-d_6) δ=42.8, 49.2, 52.2, 52.3, 67.0, 78.9, 82.8, 84.8, 101.5, 112.4, 119.8, 129.4, 132.5, 143.1, 146.6, 149.3, 161.9, 162.6, 166.4, and 166.6; IR 3400, 2975, 2240, 1710, 1640, and 1620 cm^{-1}; UV (MeOH) 285.4 (ε 13000) and 423.4 nm (1300).

Found: C, 62.14; H, 4.05; N, 7.03%. Calcd for $C_{20}H_{16}N_2O_6 \cdot 1/3H_2O$: C, 62.18; H, 4.31; N, 7.25%.

1c': mp>280 °C (lit,[8] mp 305 °C (decomp)).

Cycloaddition of 1d and 2. A chlorobenzene solution (1 cm^3) of **1d** (72 mg) and **2** (138 mg) was heated at 120 °C under 3000 bar for 20 h. Silica-gel chromatography of the mixture gave only **1d**.

Cycloreversion of 3a. A xylene solution (1 cm^3) of **3a** (55 mg) was heated at 140 °C for 20 h in a sealed tube. The mixture was chromatographed on a silica-gel column to give 12 mg (56%) of **7**, 11 mg (60%) of 3,4-bis(methoxycarbonyl)-furan, and recovered **3a** (15 mg).

Photolysis of 7. A $CHCl_3$ solution (1 cm^3) of **7** (30 mg) was irradiated by a high-pressure mercury lamp (1 kW) for 3 h. The mixture was chromatographed on a silica-gel column to give 4.7 mg (19%) of **9**, 4.5 mg (18%) of **10**, and 3.8 mg (15%) of **11**.

9: colorless crystals, mp 130 °C; ^1H NMR δ=2.58 (3H, s), 2.77 (2H, m), 3.13 (1H, t, J=7.0 Hz), 5.65—5.75 (2H, m), 5.71 (1H, s), and 6.37 (2H, d, J=8.8 Hz); ^{13}C NMR δ=21.6, 25.3, 30.3 (2C), 67.2, 112.8, 119.2 (2C), 129.3 (2C), 162.9, 169.7, and 169.9; IR 3000, 1720, and 1650 cm^{-1}; UV (MeOH) 222.2 (ε 15900) and 268.4 nm (3850).

Found: C, 72.88; H, 5.10; N, 6.43%. Calcd for $C_{13}H_{11}NO_2$: C, 73.23; H, 5.20; N, 6.57%.

10: colorless crystals, mp 129—131 °C; ^1H NMR δ=2.10 (1H, td, J=7.7, 4.8 Hz), 2.55 (3H, s), 2.76 (1H, dd, J=7.7, 6.2 Hz), 2.95 (1H, ddd, J=7.7, 6.2, 2.2 Hz), 5.18 (1H, d, J=5.1 Hz), 5.69 (1H, s), 5.96 (1H, dd, J=5.1, 2.2 Hz), 6.12 (1H, dd, J=9.9, 4.8 Hz), and 6.59 (1H, d, J=9.9 Hz); ^{13}C NMR δ=25.5, 26.6, 37.0, 42.0, 74.2, 114.7, 122.4, 131.9, 133.4, 134.0, 161.4, 169.7, and 170.2; IR 3000, 1720, and 1625 cm^{-1}; UV (MeOH) 238.0 (ε 9800) and 302.6 nm (5900).

Found: C, 73.28; H, 4.94; N, 6.58%. Calcd for $C_{13}H_{11}NO_2$: C, 73.23; H, 5.20; N, 6.57%.

11: colorless crystals, mp 123 °C; ^1H NMR δ=2.64 (3H, s), 3.56 (1H, dm, J=12.1 Hz), 4.0—4.2 (1H, m), 5.51 (1H, dd, J=9.5, 4.0 Hz), 5.71 (1H, dd, J=2.9, 2.6 Hz), 5.79 (1H, dd, J=6.2, 1.8 Hz), 5.88 (1H, ddd, J=9.5, 6.2, 2.6 Hz), 6.61 (1H, dd, J=5.5, 2.6 Hz), and 6.77 (1H, dd, J=5.5, 2.9 Hz); ^{13}C NMR δ=28.0, 40.3, 46.2, 110.2, 114.8, 121.9, 122.5, 129.8, 132.7, 152.1, 166.1, 167.8, and 172.3; IR 3010 and 1695 cm^{-1}; UV (MeOH) 265.8 nm (ε 19100).

Found: C, 73.05; H, 5.07; N, 6.49%. Calcd for $C_{13}H_{11}NO_2$: C, 73.23; H, 5.20; N, 6.57%.

References

1) Part. XLVIII. N. Kato, S. Ohbuchi, and H. Takeshita, *Kyushu Daigaku Kino Bussitsu Kagaku Kenkyusho Hokoku*, **2**, 241 (1988).

2) G. R. Tian, S. Sugiyama, A. Mori, and H. Takeshita, *Chem. Lett.*, **1987**, 1557; *idem, Bull. Chem. Soc. Jpn.*, **61**, 2393 (1988).

3) G. R. Tian, S. Sugiyama, A. Mori, H. Takeshita, M. Higashi, and H. Yamaguchi, *Chem. Lett.*, **1988**, 941.

4) G. R. Tian, S. Sugiyama, A. Mori, and H. Takeshita, *Kyushu Daigaku Kino Bussitsu Kagaku Kenkyusho Hokoku*, **2**, 95 (1988); *idem, Kyushu Daigaku Sogo Rikogaku Kenkyuka Hokoku*, **10**, 171 (1988).

5) N. Abe and T. Takehiro, *Bull. Chem. Soc. Jpn.*, **61**, 1225 (1988).

6) A. Mori, G. R. Tian, H. Takeshita, T. Takehiro, and N. Abe, *Bull. Chem. Soc. Jpn.*, **62**, 1663 (1989).

7) T. Nozoe, S. Seto, S. Matsumura, and T. Terasawa, *Chem. Ind. (London)*, **1954**, 1356.

8) T. Nozoe, S. Seto, and S. Nozoe, *Proc. Jpn. Acad.*, **32**, 472 (1956).

9) G. R. Tian, S. Sugiyama, A. Mori, and H. Takeshita, *Bull. Chem. Soc. Jpn.*, **61**, 4397 (1988).

10) G. R. Tian, S. Sugiyama, A. Mori, H. Takeshita, M. Higashi, and H. Yamaguchi, *Bull. Chem. Soc. Jpn.*, **62**, 1136 (1989).

Oxetane Derivatives and Their Polymers for Designing Functional Polymers Containing a Soft, Somewhat Polar Polyether Network as a Polymer Support

Masatoshi MOTOI,* Shinsuke NAGAHARA, Mitsuru YOKOYAMA, Eiichi SAITO, Osamu NISHIMURA, Shigeyoshi KANOH, and Hiroshi SUDA
Department of Chemistry and Chemical Engineering, Faculty of Technology, Kanazawa University, Kodatsuno, Kanazawa-shi 920
(Received October 25, 1988)

Several oxetane derivatives having functional groups, such as ester, ketone, ether, acetal, and azo, at the end of 2-oxapolymethylene spacers which were linked to the C-3 carbon of an oxetane ring were readily prepared by a substitution reaction of the corresponding bromide of the oxetane. These oxetanes were polymerized by cationic ring-opening polymerization to give their polymers with molecular weights ranging from 16000 to 1000, depending on the structure of the functional group of the monomer used. When using bisoxetanes as a cross-linking agent in the above polymerization, insoluble resins containing soft, somewhat polar polyether networks as a polymer support were obtained. Some chemical reactions of the pendant functional groups were also examined for the oxetane derivatives and their polymers.

Since the mid-1960s, synthesis of functional polymers has been increasingly recognized to be one of the most interesting subjects in polymer chemistry. So far, a variety of monomers and their polymers have been prepared in order to design polymers which realize respective functionalities desired in using those polymers under applied conditions.[1-3] However, there have been few studies on the use of polyethers as materials for producing the functional polymers, particularly as polymer supports. In the course of our investigations of cationic ring-opening polymerization of oxetanes, we hoped to utilize oxetane derivatives for preparing various functional polymers which possess functional groups in the pendant groups of a soft, somewhat polar, polyether network. Accordingly, we have prepared oxetanes **3a** and **3b**, which have a bromine atom at the end of 2-oxapolymethylene spacers, as well as bisoxetanes **4a** and **4b**, which were used successfully as a cross-linking agent capable of forming polyether networks by cationic ring-opening copolymerizations with **3a** and **3b**.[4]

In the ordinary way of obtaining oxetanes with functional substituents, chlorine atoms of 3,3-bis(chloromethyl)oxetane were replaced with acetoxyl, alkoxyl, cyano, and azido groups.[5-8] Substitution reactions on the chloromethyl groups of poly[3,3-bis(chloromethyl)oxetane] were also examined to form ester, ether, thioether, and cyano groups at the side chain end of the uncross-linked polyoxetane.[9] In this article, we report the preparation and chemical reactions of oxetane derivatives and their polymers which will be used conveniently for designing various functional polyethers.

Results and Discussion

Oxetane Derivatives. Bromine atoms in oxetanes **3a** and **3b**, which were readily obtained by a reaction between **1** and **2** in the presence of tetrabutylammonium bromide (TBAB) as a phase-transfer catalyst (PTC), were replaced with several nucleophiles to give the corresponding functional groups at the C-3 position of an oxetane ring in fairly good yields. Results of the substitution reactions are summarized in Scheme 2 and Table 1.

The ^{1}H NMR spectrum of **5b** is exemplified in Fig.

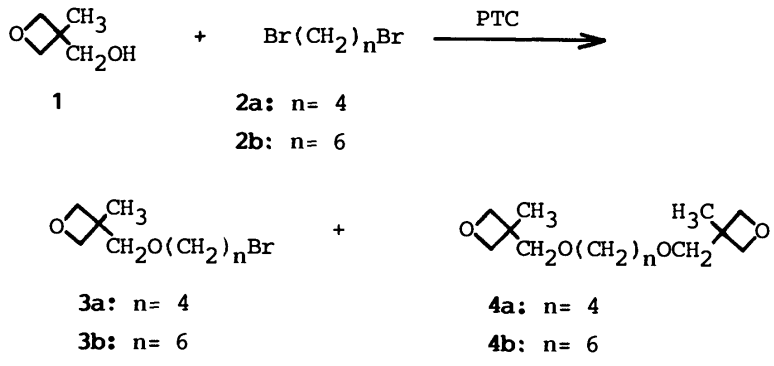

Scheme 1.

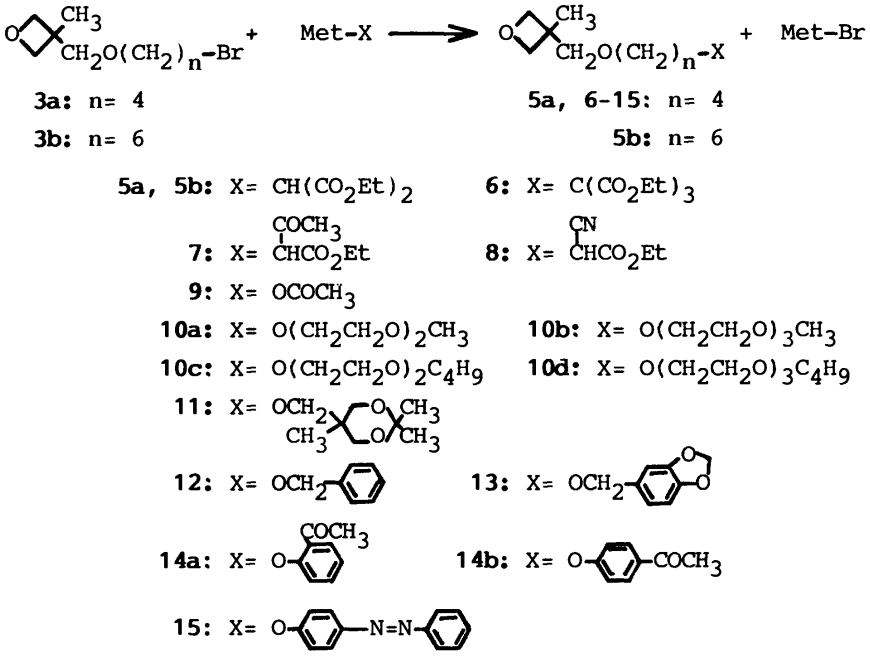

Scheme 2.

Table 1. Preparation of Oxetane Derivatives by Substitution Reaction of **3a** with Nucleophilic Reagents

Nucleophilic reagent	Conditions	Product	
	Base or PTC/solvent/temp	No.	Yield/%
$CH_2(CO_2Et)_2$	NaOEt/EtOH/reflux	**5a**	88
$CH_2(CO_2Et)_2$	NaOEt/EtOH/reflux[a)]	**5b**	75
$NaC(CO_2Et)_3$	TBAB/PhMe/reflux	**6**	74
$AcCH_2CO_2Et$	NaOEt/EtOH/reflux	**7**	54
$NCCH_2CO_2Et$	NaOEt/EtOH/reflux	**8**	52
KOAc	TBAB/PhH/reflux	**9**	84
$HO(CH_2CH_2O)_2Me$	TBAB/hexane-50%NaOH/rt[b)]	**10a**	69
$HO(CH_2CH_2O)_3Me$	TBAB/hexane-50%NaOH/rt	**10b**	68
$HO(CH_2CH_2O)_2Bu$	TBAB/hexane-50%NaOH/rt	**10c**	59
$HO(CH_2CH_2O)_3Bu$	TBAB/hexane-50%NaOH/rt	**10d**	67
HTMDO[c)]	TBAB/hexane-50%NaOH/reflux	**11**	58
$HOCH_2Ph$	TBAB/hexane-50%NaOH/rt	**12**	73
MDOBA[d)]	TBAB/hexane-50%NaOH/rt	**13**	72
(*o*)-HOArAc	TBAB/PhH-50%NaOH/reflux	**14a**	81
(*p*)-HOArAc	TBAB/PhH-50%NaOH/reflux	**14b**	88
(*p*)-HOArN=NPh	TBAB/PhMe-50%NaOH/70°C	**15**	41

a) **3b** was used in place of **3a**. b) Room temperature. c) HTMDO refers to 5-hydroxymethyl-2,2,5-trimethyl-1,3-dioxane. d) MDOBA refers to 3,4-methylenedioxybenzyl alcohol.

1(A) to demonstrate the characteristic signals of these oxetane derivatives. Generally, methylene protons (H_a) of an oxetane ring show an AB quartet around δ 4.5—5.3, and methylene protons (H_b) adjacent to the oxetane ring and methyl protons (H_g) on the oxetane ring exhibit their singlets at about δ 3.5 and 1.3, respectively. Furthermore, in the IR spectra of oxetane derivatives, cyclic and acyclic ethers possess absorption bands due to a C-O-C stretching vibration, respectively, at 980 and 830, and 1100 cm^{-1}, as described in our previous report.[4)]

In *C*-alkylation reactions of malonic and acetoacetic esters with the bromide of **3a** or **3b**, their oxetane rings were not susceptible to the attack of carbanions, derived from the esters with sodium ethoxide as a base, while it is known that an oxirane ring is attacked by such carbanions to give a γ-lactone ring.[10,11)] *C*-Alkylation products of triethyl methane-1,1,1-tricarboxylate have been obtained by Newkome and coworkers by a reaction between alkyl bromide and triethyl sodiomethane-1,1,1-tricarboxylate in a benzene/*N*,*N*-dimethylformamide (DMF) mixture (1 : 1).[12)]

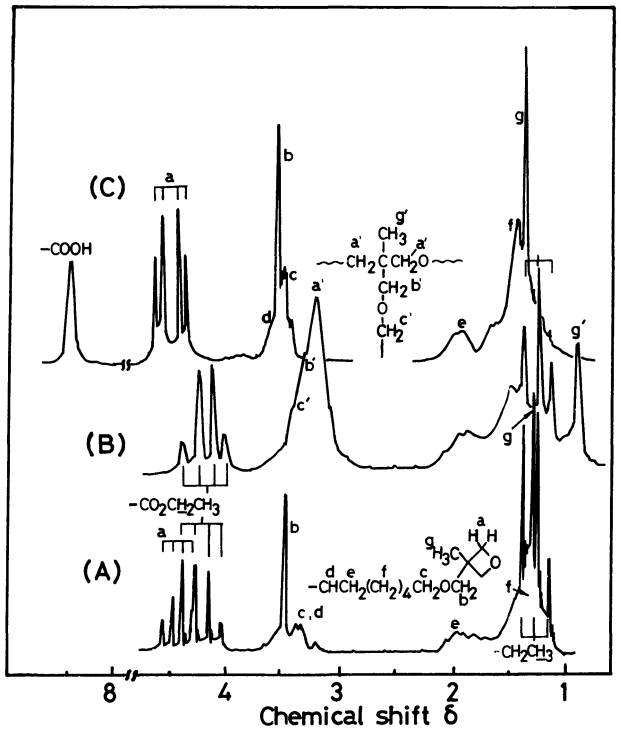

Fig. 1. ^{1}H NMR spectra of (A) **5b**, (B) poly (**5a**), and (C) **16b** (hydrolysis product from **5b**).

However, we have found that the *C*-alkylation product **6** was more readily prepared in an isolated yield of 74% by a phase-transfer catalytic equimolar reaction between the sodium salt of the triester and the bromide **3a** using TBAB as a PTC in toluene at 100 °C.

In connection with the further conversion of diesters **5** and **7** into other oxetane derivatives, some of their chemical reactions were examined. 1,1-Dicarboxylic esters in **5** were converted into the corresponding dicarboxylic acid of **16**, but not to a monocarboxylic acid, on hydrolysis of **5** with an aqueous sodium hydroxide (NaOH) solution in methanol at reflux temperature. As shown obviously from the ^{1}H NMR spectrum of **16b** in Fig. 1(C), a signal due to a carboxyl proton at δ 8.58 and an AB quartet due to methylene protons of the oxetane ring at δ 4.3—4.7 appear in an integral intensity ratio of 2:4, indicating that a decarboxylation reaction of **5** is difficult to achieve under the hydrolysis conditions applied. However, heating keto ester **7** in 1.0 mol dm^{-3} NaOH at 90 °C gave the corresponding ketone **17** via a decarboxylation of the sodium carboxylate formed from **7**. The ^{1}H NMR spectrum of **17** showed a distinct singlet due to an acetyl group and an AB quartet due to methylene protons of the oxetane ring, respectively, at δ 2.12 and 4.4—4.7, but did not show any signals due to the ester group or to a carboxyl proton.

As reported by Shih and Tirrell, polyoxiranes carrying ω-hydroxyalkyl pendant chains were prepared by methanolysis of the corresponding ω-acetoxyl and -benzoyloxyl groups of the pendants. The benzoate was derived from the chloride of a 3-chloropropyl pendant group by a phase-transfer catalytic reaction using tetrabutylammonium benzoate as a PTC in DMF.[13] These resulting polyoxiranes are considered to be new hydrophilic polyether elastomers. Concerning this preparation method for elastic polyhydroxyl polyethers, we have also found a facile method for preparing the elastic polyoxetane networks carrying a terminal hydroxyl group in the side chain; a bromine atom of **3a** was converted into a hydroxyl group of **18** by a phase-transfer catalytic reaction using potassium acetate in refluxing benzene in the presence of TBAB and by subsequent hydrolysis of the resultant acetate **9** with a 2.5 mol dm^{-3} aqueous NaOH solution in methanol under reflux. Alcohol **18** was soluble in water, although both the bromide **3a** and the acetate **9** were insoluble in water. The hydroxyl group of **18** can be further changed to esters of other carboxylic acids by reactions of **18** with acid chlorides in the presence of pyridine; thus, the cinnamate **19** was obtained in a 77% yield when using cinnamoyl chloride as an acid chloride. Additionally, acetates with aromatic residues **20a** and **20b** were readily obtained by reduction of the corresponding acetophenone derivatives **14a** and **14b**

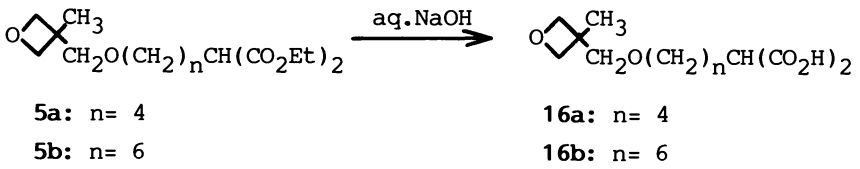

Scheme 3.

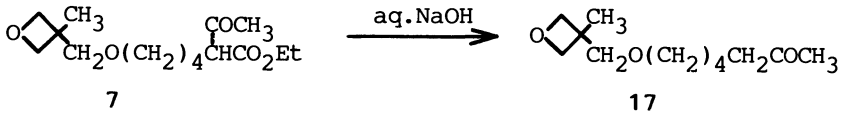

Scheme 4.

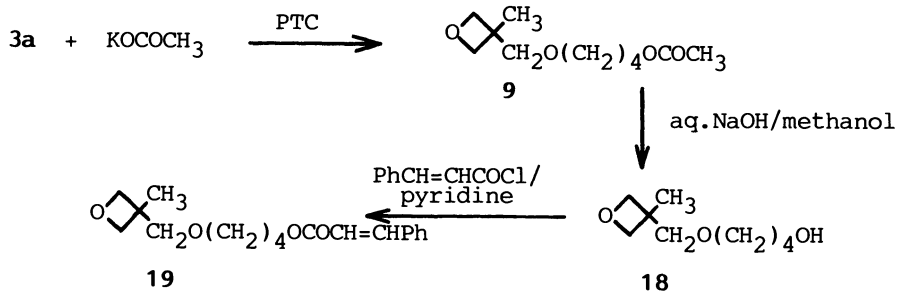

Scheme 5.

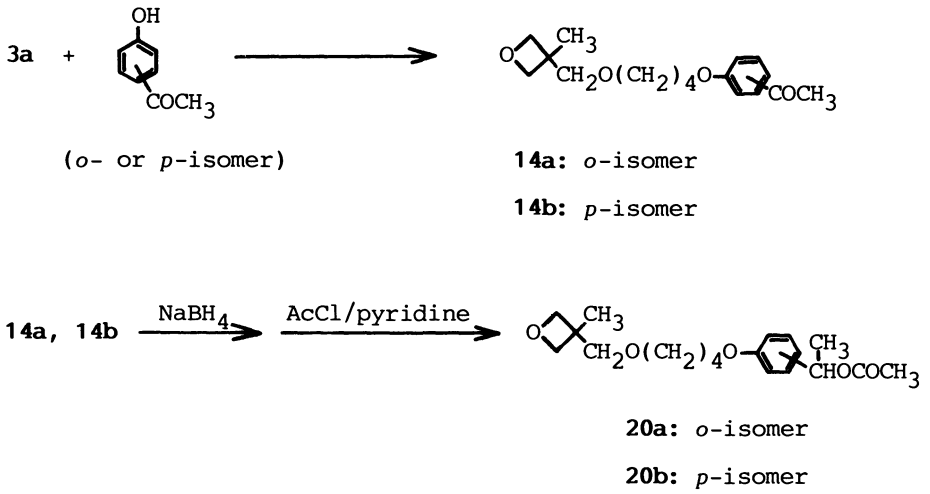

Scheme 6.

with $NaBH_4$ in ethanol, followed by *O*-acylation of the resultant secondary alcohols with acetyl chloride. In the preparation of such esters as **19**, **20a**, and **20b** via the *O*-acylation of the pendant alcohol moiety with acyl chlorides, pyridine should be employed as a base in order to avoid a ring-opening reaction of the oxetane ring by the used acyl chloride. When pyridine was not added to the above reaction mixture, the required ester was not obtained, since none of the IR bands (980 and 830 cm^{-1}) and of ^1H NMR signals (δ 4.3—4.7) assignable to the oxetane ring were indicated in the spectra of the product.

Phase-transfer catalysis of **3a** with hydroxyl compounds having such functional groups as cyclic acetal, ketone, and azo also afforded desirable products in the presence of TBAB in 50% NaOH and either of hexane or benzene. In the preparation of these products, use of an equimolar amount of the hydroxyl compound to **3a** was enough to realize fairly good yields of products. By the Williamson synthesis, sodium salts of alkoxides and phenoxides have been prepared using sodium metal, sodium hydride, or potassium carbonate as a base in dry alcoholic (which give their alkoxide anions with the base too) or aprotic polar solvents such as DMF, in order to obtain ether products by a reaction of the sodium salts with halides. The present method using a small amount of TBAB in 50% NaOH as a base and commercially available hexane or benzene as the solvent is more facile and less expensive. In particular it can be applied conveniently when the sodium salts are insoluble or hardly soluble in the reaction medium used in the Williamson synthesis. An example is described for the synthesis of **3a** and **4a** by a phase-transfer catalytic reaction between **1** and **2a**.[4]

Preparation of Polyoxetanes. Those oxetanes carrying a functional group at the C-3 position of an oxetane ring can be used as a monomer of the cationic ring-opening polymerization in dichloromethane (DCM) at 0 °C with a boron trifluoride (BF_3)–THF (tetrahydrofuran) complex as an initiator. A 20-h polymerization of those oxetanes gave viscous liquid polymers, which were soluble in such common organic solvents as DCM, chloroform, benzene, acetone, ether, DMF, and THF. Uncross-linked polymers with the comb-like oligo(oxyethylene) side chains were soluble in methanol but not in water, although all the corresponding monomers were appreciably soluble in water because of the hydrophilicity of their oligo(oxyethylene) groups. When the bisoxetane **4a** was used as a comonomer in the above polymerizations of the oxetane derivatives, elastic gel polymers insoluble in the ordinary solvents were produced.

Table 2. Cationic Ring-Opening Polymerization of Oxetane Derivatives in CH_2Cl_2 at 0 °C for 20 h[a]

Monomer (Mole ratio)	Polymer[b]			
	Name	Yield/%	$10^{-3}\overline{M}_n$	Wavenumber[c]/cm^{-1}
5a	Poly (**5a**)	92	12.0	1750, 1250, 1030 (ester); 1100 (acyclic ether)
5a+**4a** (85/15)	**R-1**	89	Gel	
5b+**4a** (70/30)	**R-2**	89	Gel	
6	Poly (**6**)	91	5.9	1760, 1740, 1260, 1040 (ester) 1100 (acyclic ether)
7	Poly (**7**)	85	1.1	1740, 1250, 1070 (ester); 1720 (C=O); 1620 (C=C); 1100
8	—	0	—	—
9	Poly (**9**)	52[d]	16.4	1740, 1250, 1040 (ester); 1100
9+**4a** (91/9)	**R-3**	89	Gel	
19	Poly (**19**)	100	12.0	1715, 1170 (ester); 1640 (C=C) 765 (phenyl)
20a	Poly (**20a**)	66	n.d[e]	1740, 1240, 1060 (ester); 1100; 755 (ortho)
20b	Poly (**20b**)	96	n.d.	1740, 1240, 1060; 1100; 830 (para)
17	Poly (**17**)	53[f]	1.0	1720 (C=O); 1100 (acyclic ether)
17+**4a** (76/24)	**R-4**	57	Gel	
14a	Poly (**14a**)	90	1.3	1675 (C=O); 1240 (aromatic ether); 1120; 760 (ortho)
14a+**4a** (59/41)	**R-5**	75	Gel	
14b	Poly (**14b**)	90	1.5	1680; 1255; 1110; 835 (para)
14b+**4a** (90/10)	**R-6**	78	Gel	
10a	Poly (**10a**)	87	n.d	1110 (acyclic ether)
10b	Poly (**10b**)	78	n.d	
10c	Poly (**10c**)	83	n.d	
10d	Poly (**10d**)	72	n.d	
11+**4a** (72/28)	**R-7**	87	Gel	1110; 985, 830 (acetal)
12	Poly (**12**)	94	2.2	1100; 735, 700 (phenyl)
15	Poly (**15**)	33[g]	3.7	1255; 1110; 840 (para); 690 (phenyl)

a) Initiator, BF_3·THF (0.5 mol% to monomer); initial monomer concentration, 1.0—3.5 mol dm^{-3}. b) For a methanol-insoluble fraction. c) IR bands characteristic of functional groups are presented. d) For the rest, 39% yield of polymer with $\overline{M}_n$ of 2000 was obtained as a methanol-soluble fraction. e) Not determined. f) 37% of lower-molecular-weight polymer was obtained as a methanol-soluble fraction. g) In a methanol-soluble fraction, a considerable amount of unreacted monomer was present.

Existence of an ester group at the end of a 2-oxapolymethylene spacer did not prevent the oxetane monomer from expanding into its polymer with a considerably high molecular weight. It has been found by Corey and Raju that some esters of **1** are converted into the 2,6,7-trioxabicyclo[2.2.2]octane structure, but not the polyoxetane structure, via the zwitterion intermediate **21** which was derived from the (3-methyl-3-oxetanyl)methyl ester of a carboxylic acid in the presence of a 25 mol% of BF_3 etherate.[14] We also confirmed that (3-methyl-3-oxetanyl)methyl acetate could not give its polymer in the presence of a 0.5 mol% of BF_3·THF. However, **9** can be converted into its polymer, poly(**9**), but not an 11-membered heterocyclic intermediate **23**, via formation of a cyclic oxonium ion **24**, which is highly susceptible to a nucleophilic attack of **9**, by BF_3 besides a trace of moisture present in a reaction mixture.[15] Difficulty in forming the intermediate **23** may be ascribed to requiring a higher ring-strain energy for the formation of **23** than that of a stable six-membered ring in **21**, following the theory of ring-strain energies of cycloalkanes.[16]

Ester groups of poly(**9**), poly(**19**), and their **4a**-cross-linked analogues were hydrolyzed with 1.0 mol dm^{-3} NaOH in methanol at reflux temperature within reaction periods of 1 to 5 h, depending on the structure of the polymer used. The resultant uncross-linked polyols were soluble in methanol, but not in water. A **4a**-cross-linked polymer of **11** was also used to obtain a polyoxetane resin carrying a 1,3-glycol moiety at the spacer end; a cyclic acetal of **11** was refluxed in acetone containing 3.0 mol dm^{-3} aqueous HCl to give the 1,3-glycol moiety. The presence of this 1,3-glycol in the product is confirmed by its IR spectrum indicating absorption bands of the primary alcohol at 3400 and 1040 cm^{-1} as well as disappearance of bands due to the cyclic acetal at 1085 and 830 cm^{-1} (Fig. 2C). On the other hand, these acetal ring bands appear in the IR spectra of the copolymer **R-7** and monomer **11**, although IR bands due to the acetal and oxetane rings in **11** overlap each other at 830 cm^{-1} (Figs. 2A and 2B).

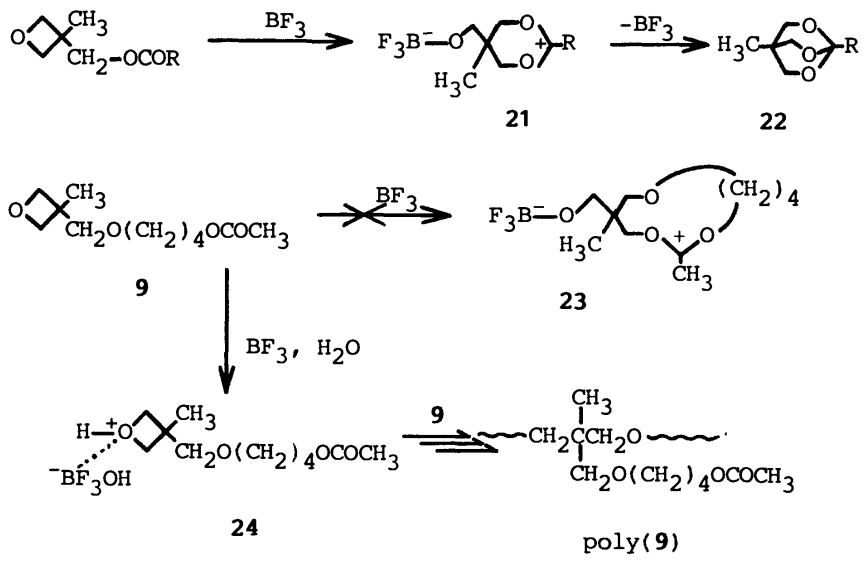

Scheme 7.

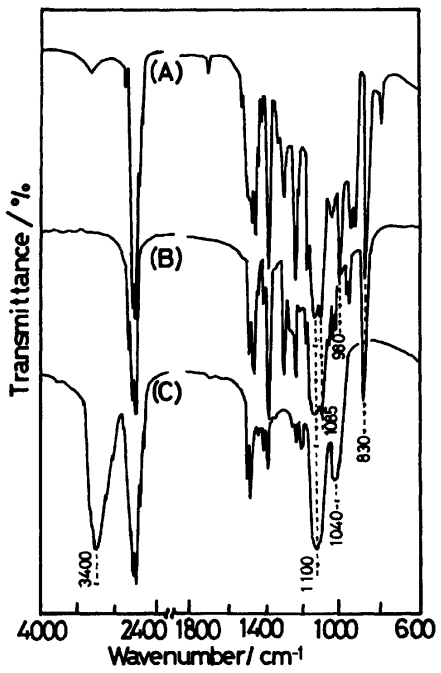

Fig. 2. IR spectra of (A) monomer **11**, (B) **4a**-cross-linked polymer of **11**, and (C) product polymer obtained by hydrolysis of the pendant cyclic acetal.

Polyoxetanes with terminal aliphatic and aromatic ketones in the side chain were prepared by cationic ring-opening polymerizations of **7**, **17**, **14a**, and **14b**, although they had low molecular weights of about 1000. In each of these polymerizations, the polymerization solution changed from colorless to orange or wine red during polymerization. This color disappeared on adding methanol to the solution after a reaction time of 20 h. Residual monomer was not detected by gas chromatography (GC) analysis of the polymerization mixture. These facts suggest that some other undesired side reaction than a termination reaction produced such low-molecular-weight polymers. On the other hand, **20a** and **20b** having an acetoxyl group in their side chains were polymerized under the same polymerization conditions as those applied for the polymerization of **14a** and **14b**, and gave colorless gel polymers, which were insoluble in the usual solvents, in spite of using no cross-linking agents such as **4a** and **4b** in this polymerization. The insolubility of those polymers may be interpreted as due to a high molecular weight, highly crystallized structure, or a cross-linked structure formed by an unexpected side reaction. The acetyl group of poly(**14a**) and poly(**14b**), which showed a strong IR band at 1680 cm^{-1}, were completely reduced with $NaBH_4$ to the corresponding secondary alcohol, a broad band of which appeared around 3400 cm^{-1}. IR spectra of the $NaBH_4$-reduced polymers were identified, respectively, with IR spectra of the polymers obtained by hydrolysis of poly(**20a**) and poly(**20b**) with 2.0 mol dm^{-3} NaOH in methanol. Presumably, the acetyl carbonyl group seems to be involved in the occurrence of a side reaction during the polymerization. A mechanism for this side reaction has not yet been clarified. The investigation of cationic ring-opening polymerization of **14a**, **14b**, **20a**, and **20b** is in progress in our laboratory. Oxetane **8** with a pendant cyano group did not give the corresponding polymer, presumably due to the existence of the cyano group which is considered to be a Lewis base capable of coordinating with a BF_3 initiator, resulting in lack of a reaction step initiated by BF_3.

Concerning the hydrolysis of the malonic ester group of **5**, a hydrolysis of the corresponding diester of a cross-linked polymer was also examined by warming

it in 1.0 mol dm^{-3} aqueous NaOH and methanol. One gram of the resultant polymer, which showed no IR bands due to the ester group, was neutralized with 7.3 mmol of NaOH, indicating that the hydrolyzed polymer had a pendant dibasic acid group. The calculated amount of the carboxyl group is 6.5 mmol per 1.0 g of the dry polymer containing a 15 mol% of **4a** as a cross-linking agent. If the polymer has a monobasic acid pendant group by decarboxylation of the dibasic acid formed intermediately upon the hydrolysis, the amount of carboxyl group is calculated to be 3.7 mmol per 1.0 g of the resultant polymer. Therefore, it is also confirmed that the decarboxylation reaction does not take place under reaction conditions applied for the hydrolysis of the malonic ester at the spacer end of the polyoxetane resin. Oxetane **16b** with a pendant carboxyl group polymerized on leaving **16b** in a test tube at room temperature for at least 3 months, as confirmed by the IR spectrum lacking absorption bands due to an oxetane ring.

The preceding information about the chemical reactions of the oxetane derivatives and their polymers will be of assistance in guiding work on the design of functional polymers that are composed of a soft, somewhat polar polyether network with qualities different from those of a hard, less polar polystyrene support widely used in functional polymer synthesis.

Experimental

Materials. Oxetanes **3a** and **3b**, and bisoxetanes **4a** and **4b** were obtained according to the method described by us previously.[4]

Diethyl 7-(3-Methyl-3-oxetanyl)-6-oxaheptane-1,1-dicarboxylate (5a) and Diethyl 9-(3-Methyl-3-oxetanyl)-8-oxanonane-1,1-dicarboxylate (5b): Diethyl sodiomalonate was formed from diethyl malonate (26 mmol) and sodium metal (21 mmol) in dry ethanol (200 ml) and, subsequently, allowed to react with **3a** or **3b** (17 mmol) under reflux for 2 h. After removing ethanol from the reaction mixture by evaporation, the residue was neutralized with acetic acid and shaken both with ether and water. The organic layer was separated from the aqueous layer, dried over Na_2SO_4, and distilled to give **5a** (88%) or **5b** (75%).

5a: bp 140—142 °C (79 Pa); IR (neat) 1750, 1735, 1240, 1155, and 1025 (ester), 1115 (acyclic ether), and 980 and 835 cm^{-1} (cyclic ether); ^1H NMR ($CDCl_3$) δ=1.25 (6H, t, J=7.0 Hz, CH_2CH_3), 1.28 (3H, s, CH_3 on the oxetane ring), 1.6—2.2 [6H, m, $CH_2OCH_2(CH_2)_3CH$], 3.28—3.70 [total 5H: s (δ=3.46), CH_2 adjacent to the oxetane ring; m, $CH_2OCH_2(CH_2)_3CH$], 4.18 (4H, q, J=7.0 Hz, CH_2CH_3), and 4.31 and 4.47 (each 2H, AB quartet, J=6.0 Hz, CH_2 of the oxetane ring).

Found: C, 60.65; H, 9.03%. Calcd for $C_{16}H_{28}O_6$: C, 60.73; H, 8.94%.

5b: bp 173—175 °C (53 Pa); IR (neat) 1755, 1735, 1240, and 1025 (ester), 1115 (acyclic ether), and 980 and 835 cm^{-1} (cyclic ether); ^1H NMR ($CDCl_3$) δ=1.00—2.13 [total 19H: t (δ=1.26), J=7.0 Hz, CH_2CH_3; s (δ=1.31), CH_3 on the oxetane ring; m, $CH_2OCH_2(CH_2)_5CH$], 3.25—3.65 [total 5H: s (δ=3.48), CH_2 adjacent to the oxetane ring; m, $CH_2OCH_2(CH_2)_5CH$], 4.23 (4H, q, J=7.0 Hz, CH_2CH_3), and 4.35 and 4.49 (each 2H, AB quartet, J=5.0 Hz, CH_2 of the oxetane ring).

Found: C, 62.48; H, 9.57%. Calcd for $C_{18}H_{32}O_6$: C, 62.75; H, 9.38%.

9-(3-Methyl-3-oxetanyl)-8-oxanonane-1,1-dicarboxylic Acid (16b): **5b** was allowed to react with 1.0 mol dm^{-3} NaOH (twofold equivalence to the ester) in 50% aqueous methanol at reflux temperature for 5 h. After the reaction mixture has been concentrated by means of an evaporator, the residue was acidified to pH 5 with aqueous HCl, saturated with Na_2SO_4, and extracted three times with ether. The combined extracts were evaporated to obtain an oily hydrolysis product **16b** in a 72% yield: IR (neat) 3400 and 1720 (COOH), 1110 (acyclic ether), and 980 and 830 (cyclic ether) cm^{-1}; ^1H NMR ($CDCl_3$) δ=1.10—1.74 [total 11H: s (δ=1.31), CH_3; m, $CH_2OCH_2(CH_2)_4CH_2CH$], 1.74—2.10 [2H, m, $CH_2CH(COOH)_2$], 3.20—3.60 [total 5H: s (δ=3.46), CH_2 adjacent to the oxetane ring; m, $CH_2OCH_2(CH_2)_4CH_2CH$], 4.41 and 4.59 (each 2H, AB quartet, J=5.9 Hz, CH_2 of the oxetane ring), and 8.58 (2H, bs, COOH).

Triethyl 7-(3-Methyl-3-oxetanyl)-6-oxaheptane-1,1,1-tricarboxylate (6): Prepared in a 74% yield by a phase-transfer catalytic reaction between triethyl sodiomethane-1,1,1-tricarboxylate[17] (21 mmol) and **3a** (21 mmol) in the presence of TBAB (1.1 mmol) in toluene (50 ml) at 100 °C for 7 h: bp 156 °C (10 Pa); IR (neat) 1760, 1749, 1260, and 1040 (ester), 1110 (acyclic ether), and 980 and 830 cm^{-1} (cyclic ether); ^1H NMR ($CDCl_3$) δ=1.29 (9H, t, J=6.6 Hz, CH_2CH_3), 1.31 (3H, s, CH_3 on the oxetane ring), 1.46—1.95 [4H, m, $CH_2OCH_2(CH_2)_2CH_2C$], 1.95—2.39 [2H, m, $CH_2OCH_2(CH_2)_2CH_2C$], 3.37—3.70 [total 4H: m, $CH_2OCH_2(CH_2)_2CH_2C$; s (δ=3.50), CH_2 adjacent to the oxetane ring], 4.29 (6H, q, J=6.6 Hz, CH_2CH_3), and 4.35 and 4.53 (each 2H, AB quartet, J=5.8 Hz, CH_2 of the oxetane ring).

Found: C, 58.57; H, 8.34%. Calcd for $C_{19}H_{32}O_8$: C, 58.74; H, 8.32%.

Ethyl 8-(3-Methyl-3-oxetanyl)-2-acetyl-7-oxaoctanoate (7) and 9-(3-Methyl-3-oxetanyl)-8-oxa-2-nonanone (17): **7** was prepared from ethyl acetoacetate (50 mmol), bromide **3a** (42 mmol), and sodium metal (50 mmol) in dry ethanol. Working up the reaction mxture and distilling the resultant organic layer gave **7** with a purity of 98% by GC analysis: bp 116—124 °C (57 Pa); IR (neat) 1740, 1240—1150, and 1060—1020 (ester), 1710 (C=O), 1620 (C=C of an enol form), 1120 (acyclic ether), and 980 and 830 cm^{-1} (cyclic ether); ^1H NMR ($CDCl_3$) δ=1.0—2.0 [total 12H: t (δ=1.27), J=7.0 Hz, CH_2CH_3; s (δ=1.30), CH_3 on the oxetane ring; m, $CH_2OCH_2(CH_2)_3CH$], 2.21 (3H, s, $COCH_3$), 3.28—3.70 [total 5H: s (δ=3.47), CH_2 adjacent to the oxetane ring; m, $CH_2OCH_2(CH_2)_3CH$], 4.21 (2H, q, J=7.0 Hz, CH_2CH_3), and 4.31 and 4.39 (each 2H, AB quartet, J=5.0 Hz, CH_2 of the oxetane ring).

Oxo ester **7** (42 mmol) was stirred in 1.0 mol dm^{-3} NaOH (84 mmol) at 50 °C for 3 h until an oily layer of **7** disappeared completely. The alkaline solution was heated at 90 °C for 4 h. The resulting organic layer was extracted with ether, separated from the aqueous layer, dried over Na_2SO_4, and distilled to give pure **17** in a 53% yield based on **3a**: bp 110—115 °C (107 Pa); IR (neat) 1710 (C=O), 1120 (acyclic ether), and 980 and 835 cm^{-1} (cyclic ether); ^1H NMR ($CDCl_3$)

δ=1.21—1.96 [total 9H: s (δ=1.29), CH_3 on the oxetane ring; m, $CH_2OCH_2(CH_2)_3CH_2$], 2.12 (3H, s, $COCH_3$), 2.24—2.63 (2H, m, CH_2Ac), 3.31—3.64 [total 4H: s (δ=3.46), CH_2 adjacent to the oxetane ring; m, $CH_2OCH_2(CH_2)_3CH_2$], and 4.32 and 4.47 (each 2H, AB quartet, J=5.6 Hz, CH_2 of the oxetane ring).

6-(3-Methyl-3-oxetanyl)-5-oxahexyl Acetate (9) and 3-(6-Hydroxy-2-oxahexyl)-3-methyloxetane (18): **3a** (84.3 mmol) was heated with powdered potassium acetate (0.28 mol) in benzene (50 ml) in the presence of TBAB (4.3 mmol) under reflux for 6 h with efficiently stirring. The organic layer was washed with water and dried over Na_2SO_4. After removing the solvent from the reaction mixture, fractional distillation of the residue gave slightly impure **9** in about 84% yield: bp 107 °C (116 Pa); IR (neat) 1745, 1245, and 1040 (ester), 1110 (acyclic ether), and 980 and 830 cm^{-1} (cyclic ether); ^1H NMR ($CDCl_3$) δ=1.33 (3H, s, CH_3), 1.48—1.90 [4H, m, $OCH_2(CH_2)_2CH_2OAc$], 2.05 (3H, s, $COCH_3$), 3.35—3.78 [total 6H: m, $CH_2OCH_2(CH_2)_2CH_2OAc$; s (δ=3.49), CH_2 adjacent to the oxetane ring], 4.13 (2H, t, J=5.6 Hz, CH_2OAc), and 4.37 and 4.53 (each 2H, AB quartet, J=6.0 Hz, CH_2 of the oxetane ring).

The acetate **9** was refluxed with 2.5 mol dm^{-3} NaOH in methanol for 2 h. The methanol was evaporated and the residue shaken with hexane. The alkaline aqueous layer was separated from the organic layer, saturated with sodium chloride, and shaken with ether to extract an alcoholic product. The ethereal layer was concentrated and distilled to give **18** in a 73% yield based on **3a**: bp 98—99 °C (93 Pa); IR (neat) 3400 and 1065 (alcohol), 1120 (acyclic ether), and 980 and 835 cm^{-1} (cyclic ether); ^1H NMR ($CDCl_3$) δ=1.31 (3H, s, CH_3), 1.43—1.90 [4H, m, $OCH_2(CH_2)_2CH_2OH$], 3.12—3.86 [total 7H: m, $CH_2OCH_2(CH_2)_2CH_2OH$; s (δ=3.50), CH_2 adjacent to the oxetane ring], and 4.35 and 4.51 (each 2H, AB quartet, CH_2 of the oxetane ring).

Found: C, 61.89; H, 10.64%. Calcd for $C_9H_{18}O_2$: C, 62.02; H, 10.43%.

6-(3-Methyl-3-oxetanyl)-5-oxahexyl Cinnamate (19): The alcohol **18** (32 mmol) was esterified with cinnamoyl chloride (33 mmol) and pyridine (3 ml) in DCM (30 ml) at −10 to 0 °C for 5 h. The desired product **19** was isolated in a 77% yield by distillation: bp 172—174 °C (12 Pa); IR (neat) 1580, 1500, 1450, and 770 (phenyl), 1715, 1315, and 1175 (ester), 1640 (C=C), 1120 (acyclic ether), and 980 and 835 cm^{-1} (cyclic ether); ^1H NMR ($CDCl_3$) δ=1.34 (3H, s, CH_3), 1.57—2.07 [4H, m, $CH_2OCH_2(CH_2)_2$], 3.36—3.73 [total 4H: s (δ=3.50), CH_2 adjacent to the oxetane ring; m, $CH_2OCH_2(CH_2)_2$], 4.41—4.69 [total 6H: m, CH_2OCO; AB quartet (δ=4.39 and 4.55), J=6.9 Hz, CH_2 of the oxetane ring], 6.49 (1H, d, J=16.0 Hz, CH=CHPh), and 7.34—7.69 [total 6H: m, ArH; d (δ=7.27), J=16.0 Hz, CH=CHPh].

3-(2,7,10,13-Tetraoxatetradecyl)- (10a), 3-(2,7,10,13,16-Pentaoxaheptadecyl)- (10b), 3-(2,7,10,13-Tetraoxaheptadecyl)- (10c), and 3-(2,7,10,13,16-Pentaoxaicosyl)-3-methyloxetanes (10d): Each of these compounds was prepared by the phase-transfer catalytic reaction of **3a** (41 mmol) with an appropriate di- or triethylene glycol monoalkyl ether (21 mmol) in hexane (20 ml) and 50% NaOH (28 g) for 5 h under reflux in the presence of TBAB (1.1 mmol). The reaction mixture was diluted with water (70 ml), saturated with Na_2SO_4, and extracted continuously with ether for 30 h. The ether extract was distilled to give **10a** (69%), **10b** (59%), **10c** (68%), or **10d** (67%). These compounds had characteristic IR bands at 1110 (acyclic ether) and 980 and 835 cm^{-1} (cyclic ether).

10a: bp 116—119 °C (20 Pa); ^1H NMR ($CDCl_3$) δ=1.30 (3H, s, CH_3 on oxetane ring), 1.50—1.85 [4H, m, $CH_2OCH_2(CH_2)_2CH_2$], 3.31—3.89 [total 17H: s (δ=3.38), OCH_3; s (δ=3.48), CH_2 adjacent to the oxetane ring; s (δ=3.62), $(CH_2CH_2O)_2$; m, $CH_2OCH_2(CH_2)_2CH_2$], and 4.32 and 4.50 (each 2H, AB quartet, J=6.0 Hz, CH_2 of the oxetane ring).

10b: bp 144—145 °C (49 Pa); ^1H NMR ($CDCl_3$) δ=1.30 (3H, s, CH_3 on the oxetane ring), 1.40—1.84 [4H, m, $CH_2OCH_2(CH_2)_2CH_2O$], 3.30—3.80 [total 21H: s, (δ=3.37), OCH_3; s (δ=3.47), CH_2 adjacent to the oxetane ring; s (δ=3.60), $OCH_2CH_2OCH_2CH_2OCH_2CH_2O$; s ($\delta$=3.66), $OCH_2CH_2OCH_2CH_2OCH_2CH_2O$; m, $CH_2OCH_2(CH_2)_2CH_2O$], and 4.32 and 4.48 (each 2H, AB quartet, J=6.0 Hz, CH_2 of the oxetane ring).

Found: C, 60.02; H, 10.27%. Calcd for $C_{16}H_{32}O_6$: C, 59.96; H, 10.09%.

10c: bp 120—132 °C (45 Pa); ^1H NMR ($CDCl_3$) δ=0.71—1.06 (3H, m, CH_3 of butyl), 1.22—1.81 [total 11H: s (δ=1.24), CH_3 on the oxetane ring; m, $CH_2OCH_2(CH_2)_2CH_2O$ and $OCH_2(CH_2)_2CH_3$], 3.29—3.78 [total 16H: s (δ=3.46), CH_2 adjacent to the oxetane ring; s (δ=3.60), $O(CH_2CH_2O)_2$; m, $CH_2OCH_2(CH_2)_2CH_2O$ and $OCH_2(CH_2)_2CH_3$], and 4.31 and 4.49 (each 2H, AB quartet, J=6.0 Hz, CH_2 of the oxetane ring).

10d: bp 142—157 °C (51 Pa); ^1H NMR ($CDCl_3$) δ=0.76—1.12 (3H, m, CH_3 of butyl), 1.24—1.94 [total 11H: s (δ=1.31), CH_3 on the oxetane ring; m, $CH_2OCH_2(CH_2)_2CH_2O$ and $OCH_2(CH_2)_2CH_3$], 3.32—3.48 [total 20H: s (δ=1.47), CH_2 adjacent to the oxetane ring; s (δ=1.61), $OCH_2CH_2OCH_2CH_2OCH_2CH_2O$; s ($\delta$=1.66), $OCH_2CH_2OCH_2CH_2OCH_2CH_2O$; m, $OCH_2(CH_2)_2CH_2O$ and $OCH_2(CH_2)_2CH_3$], and 4.33 and 4.49 (each 2H, AB quartet, J=6.0 Hz, CH_2 of the oxetane ring).

3-[8-(2,2,5-Trimethyl-1,3-dioxan-5-yl)-2,7-dioxaoctyl]-3-methyloxetane (11): **11** was prepared by a phase-transfer catalytic reaction using **3a** (21 mmol) and 5-hydroxymethyl-2,2,5-trimethyl-1,3-dioxane (21 mmol) in hexane (30 ml) and 50% NaOH (28 g) in the presence of TBAB (1.1 mmol) at reflux temperature for 12 h. The ordinary work-up gave pure **11** in a 58% yield: bp 126.0—126.5 °C (69 Pa); IR (neat) 1110 (acyclic ether), 980 and 830 (cyclic ether), and 1085 and 830 cm^{-1} (cyclic acetal); ^1H NMR ($CDCl_3$) δ=0.87 (3H, s, nongeminal CH_3 on the acetal ring), 1.31 (3H, s, CH_3 on the oxetane ring), 1.39 and 1.42 (each 3H, each s, geminal CH_3), 1.50—1.74 [4H, m, $CH_2OCH_2(CH_2)_2CH_2OCH_2$], 3.32—3.80 [total 12H: s (δ=3.39), CH_2 adjacent to the acetal ring; s (δ=3.47), CH_2 adjacent to the oxetane ring; m (δ=3.32—3.52), $CH_2OCH_2(CH_2)_2CH_2OCH_2$; AB quartet ($\delta$=3.53 and 3.70), J=11.0 Hz, CH_2 of the acetal ring], and 4.43 and 4.50 (each 2H, AB quartet, J=5.6 Hz, CH_2 of the oxetane ring).

3-[8-Phenyl-2,7-dioxaoctyl]-3-methyloxetane (12): A phase-transfer catalytic reaction of **3a** (42 mmol) with benzyl alcohol (38 mmol) gave **12** in a 72% yield in the presence of TBAB (1.9 mmol) in hexane (40 ml) and 50% NaOH (50 g): bp 144.0—144.5 °C (67 Pa); IR (neat) 1605, 1590, 1500, 740, and 700 (monosubstituted benzene), 1110 (acyclic ether), and 980 and 835 cm^{-1} (cyclic ether); ^1H NMR ($CDCl_3$) δ=1.28 (3H, s, CH_3), 1.47—1.97 [4H, m, $OCH_2CH_2(CH_2)_2CH_2O$], 3.29—3.71 [total 6H: m, $OCH_2(CH_2)_2CH_2O$; s (δ=3.43), CH_2 adjacent to the oxetane ring], 4.23—4.65 [total 6H: s

(δ=4.49), CH_2Ph; AB quartet (δ=4.31 and 4.49), J=5.5 Hz, CH_2 of the oxetane ring], and 7.3—7.5 (5H, m, ArH).

Found: C, 72.73; H, 9.39%. Calcd for $C_{16}H_{24}O_3$: C, 72.68; H, 9.17%.

3-[8-(3,4-Methylenedioxyphenyl)-2,7-dioxaoctyl]-3-methyloxetane (13): In the same way as above, **13** was prepared from **3a** and piperonyl alcohol in a 72% yield: bp 152—160 °C (7.3 Pa); IR (neat) 1110 (acyclic ether), 980 and 830 (cyclic ether), 1040 and 930 (cyclic acetal), and 1610, 1505, 1495, and 810 cm^{-1} (1,2,4-trisubstituted benzene); ^1H NMR ($CDCl_3$) δ=1.29 (3H, s, CH_3), 1.56—1.76 [4H, m, CH_2OCH_2-(CH_2)$_2CH_2$], 3.36—3.56 [total 6H: s (δ=3.47), CH_2 adjacent to the oxetane ring; m, $CH_2OCH_2(CH_2)_2CH_2OCH_2Ar$], 4.39 (2H, s, CH_2Ar), 4.33 and 4.49 (each 2H, AB quartet, J=5.8 Hz, CH_2 of the oxetane ring), 5.93 (2H, s, CH_2 of acetal), and 6.72—6.87 (3H, m, ArH).

Found: C, 66.10; H, 8.08%. Calcd for $C_{17}H_{24}O_5$: C, 66.20; H, 7.86%.

3-[7-(2- and 4-Acetylphenyl)-2,7-dioxaheptyl]-3-methyloxetanes (14a and 14b): These products were prepared by the phase-transfer catalytic reaction of *o*- or *p*-hydroxyacetophenone (37 mmol) with **3a** (37 mmol) in benzene (50 ml) and 50% NaOH (49 g) at 80 °C for 6—8 h in the presence of TBAB (1.8 mmol). The ordinary work-up of the reaction mixture gave **14a** (81%) or **14b** (88%).

14a: bp 172 °C (19 Pa); IR (neat) 1600, 1580, 1490, and 760 (1,2-disubstituted benzene), 1675 (acetyl C=O), 1240 (aromatic ether), 1115 (acyclic ether), and 980 and 830 cm^{-1} (cyclic ether); ^1H NMR ($CDCl_3$) δ=1.29 (3H, s, CH_3 on the oxetane ring), 1.52—2.20 [4H, m, $CH_2OCH_2(CH_2)_2CH_2O$], 2.62 (3H, s, $COCH_3$), 3.37—3.70 [total 4H: s (δ=3.47), CH_2 adjacent to the oxetane ring; m, $CH_2OCH_2(CH_2)_2CH_2OAr$], 4.08 (2H, bt, CH_2OAr), 4.32 and 4.50 (each 2H, AB quartet, CH_2 of the oxetane ring), and 6.8—7.9 (4H, m, ArH).

Found: C, 69.66; H, 8.29%. Calcd for $C_{17}H_{24}O_4$: C, 69.82; H, 8.29%.

14b: bp 154—156 °C (8Pa); IR (neat) 1600, 1575, 1515, and 835 (1,4-disubstituted benzene), 1680 (acetyl C=O), 1255 (aromatic ether), 1115 (acyclic ether), and 980 and 830 cm^{-1} (cyclic ether); ^1H NMR ($CDCl_3$) δ=1.12 (3H, s, CH_3 on the oxetane ring), 1.40—1.97 [4H, m, $CH_2OCH_2(CH_2)_2CH_2O$], 2.34 (3H, s, $COCH_3$), 3.25—3.52 [total 4H: s (δ=3.30), CH_2 adjacent to the oxetane ring; m, $CH_2OCH_2(CH_2)_2CH_2OAr$], 3.88 (2H, bt, CH_2OAr), 4.15 and 4.33 (each 2H, AB quartet, CH_2 of the oxetane ring), and 6.6—7.9 (4H, AB quartet-like, ArH).

Found: C, 69.65; H, 8.46%. Calcd for $C_{17}H_{24}O_4$: C, 69.82; H, 8.29%.

3-[7-[2- and 4-(1-Acetoxyethyl)phenyl]-2,7-dioxaheptyl]-3-methyloxetanes (20a and 20b): **14a** or **14b** (17 mmol) was stirred with $NaBH_4$ (17 mmol) in ethanol (80 ml) at 60 °C for 2 h. The ethanol was evaporated, and the residue shaken with both water and ether. The organic layer was separated from the aqueous layer and dried over Na_2SO_4. The crude product, which was obtained by removing the solvent from the organic layer, was allowed to react with acetyl chloride (17 mmol) in DCM (50 ml) containing pyridine (3 ml) at 20—25 °C for 9 h. The reaction mixture was poured into ice and extracted with DCM. The organic layer was washed with water and dried over Na_2SO_4. Removal of the solvent followed by distillation of the residue gave **20a** (90%) or **20b** (83%).

20a: bp 151 °C (23 Pa); IR (neat) 1740, 1250, and 1060 (ester), 1605, 1590, 1500, 1475, 755 (1,2-disubstituted benzene), 1240 (aromatic ether), 1120 (acyclic ether), and 980 and 835 cm^{-1} (cyclic ether); ^1H NMR ($CDCl_3$) δ=1.21 (3H, s, CH_3 on the oxetane ring), 1.50 [3H, s, J=6.6 Hz, CH_3CH-(OAc)Ar], 1.64—2.05 [4H, m, $CH_2OCH_2(CH_2)_2CH_2O$], 2.07 (3H, s, $OCOCH_3$), 3.34—3.70 [total 4H: s (δ=3.49), CH_2 adjacent to the oxetane ring; t-like, $CH_2OCH_2(CH_2)_2CH_2$-OAr], 3.87—4.19 (3H, t-like, CH_2OAr), 4.33 and 4.51 (each 2H, AB quartet, J=6.0 Hz, CH_2 of the oxetane ring), 6.30 (1H, q, J=6.6 Hz, CHAr), and 6.2—7.5 (4H, m, ArH).

20b: bp 174—175 °C (41 Pa); IR (neat) 1744, 1245, and 1060 (ester), 1620, 1590, 1520, and 835 (1,4-disubstituted benzene), 1240 (aromatic ether), 1120 (acyclic ether), and 980 and 835 cm^{-1} (cyclic ether); ^1H NMR ($CDCl_3$) δ=1.29 (3H, s, CH_3 on the oxetane ring), 1.39 [3H, d, J=7.0 Hz, CH_3CH-(OAc)Ar], 1.63—1.93 [4H, m, $CH_2OCH_2(CH_2)_2CH_2O$], 2.04 (3H, s, $OCOCH_3$), 3.41—3.69 [total 4H: s (δ=3.51), CH_2 adjacent to the oxetane ring; t-like, $CH_2OCH_2(CH_2)_2CH_2$-OAr], 3.88—4.18 (2H, t-like, CH_2OAr), 4.35 and 4.53 (each 2H, AB quartet, J=5.0 Hz, CH_2 of the oxetane ring), 5.87 (1H, q, J=7.0 Hz, CHAr), and 6.8—7.5 (4H, AB quartet-like, ArH).

4-[[6-(3-Methyl-3-oxetanyl)-5-oxahexyl]oxy]azobenzene (15): **15** was prepared by a phase-transfer catalytic reaction using **3a** (21 mmol) and 4-hydroxyazobenzene (21 mmol) in toluene (30 ml) and 50% NaOH (30 g) in the presence of TBAB (1.1 mmol) at reflux temperature. After working up the reaction mixture in the ordinary way, recrystallization of the crude product from ethanol-DCM gave a yellow-colored **15** in a 41% yield: mp 57—59 °C; IR (KBr) 1615, 1580, 1475, 840, and 685 (mono- and disubstituted benzenes), 1260 (aromatic ether), 1110 (acyclic ether), and 980 and 840 cm^{-1} (cyclic ether); ^1H NMR ($CDCl_3$) δ=1.31 (3H, s, CH_3), 1.36—2.00 [4H, m, $CH_2OCH_2(CH_2)_2CH_2$], 3.40—3.60 [total 4H: s (δ=3.48), CH_2 adjacent to the oxetane ring; t-like, CH_2OCH_2-$(CH_2)_2CH_2OAr$], 3.92—4.14 (2H, t-like, CH_2OAr), 4.35 and 4.52 (each 2H, AB quartet, J=5.9 Hz, CH_2 of the oxetane ring), and 6.8—8.0 (9H, m, ArH).

Preparation of Polymers: Polymers of oxetane derivatives were prepared by their cationic ring-opening polymerization in DCM with BF_3·THF as an initiator, according to the method we previously reported.[4]

Polymer Reactions. Hydrolysis of Malonic Ester Groups of Cross-Linked Resins: The ester groups were hydrolyzed by warming the resins with an excess amount of 1.0 mol dm^{-3} NaOH in methanol under reflux. The reaction mixture was concentrated by means of an evaporator and acidified to pH 5 with aqueous HCl. The resinous product was filtered and washed with water and then with methanol. After drying the resin, its weight was measured (yield, 94%). After immersing the resin in 0.05 mol dm^{-3} NaOH for 24 h, an aliquot of the alkaline supernatant was withdrawn to determine acid equivalent of the carboxyl group of the resin by back titration with 0.05 mol dm^{-3} HCl; 1 g of the dry resin was neutralized with 7.28 mmol of NaOH.

Hydrolysis of Polymers Carrying Acetate and Cinnamate Groups in the Side Chain: These polymers were stirred with an excess amount of 2.5 mol dm^{-3} NaOH in methanol under reflux for 1—5 h. After removing the methanol by evaporation, the residue was extracted with ether or benzene in the case of the hydrolysis of uncross-linked polymers.

When using cross-linked polymers, the resultant polymers were filtered and washed successively with water and methanol. Hydrolyzed polymers were obtained in 85—95% yields. IR spectra of these product polymers indicated a strong band due to the hydroxyl group around 3400 cm^{-1}, but did not show bands due to ester and carboxylate groups.

Hydrolysis of a Cyclic Acetal of Resin R-7: A **4a**-cross-linked polymer, **R-7**, was stirred in acetone containing 10% of its volume of 3.0 mol dm^{-3} aqueous HCl for 8 h under reflux. The acetone was removed by evaporation. A polymerized product was collected by filtration and washed successively with water and methanol. After being dried at 70 °C for 7 h in vacuo, the polymer was weighed (yield, 95%).

Measurement. GC analysis of the products was performed in a Shimadzu GC-8A apparatus: glass column (3.2ϕ×1 m) packed with Silicone High Vacuum Grease (30%)/Celite (80—100 mesh); carrier gas, He (66 cm^3 min^{-1}); temp, 200 °C. The IR spectra were recorded on a JASCO A-202 spectrometer and ^1H NMR on a 60 (Hitach R-24B) or 100 MHz instrument (JEOL FX-100S) using $CDCl_3$ as a solvent and TMS as an internal standard at 25 °C. Molecular weight measurements were made by VPO in a Corona molecular weight apparatus (model 117).

References

1) A. Akelah and D. C. Sherrington, *Chem. Rev.*, **81**, 557 (1981).

2) A. Akelah, *Synthesis*, **1981**, 413.

3) M. Kinoshita, *Kaigai Kobunshi Kenkyu*, **22**, 201 (1978).

4) M. Motoi, H. Suda, K. Shimamura, S. Nagahara, M. Takei, and S. Kanoh, *Bull. Chem. Soc. Jpn.*, **61**, 1653 (1988).

5) A. C. Farthing, *J. Chem. Soc.*, **1955**, 3648.

6) K. Hardenstine, C. J. Murphy, R. B. Jones, L. H. Sperling, and G. E. Manser, *J. Appl. Polym. Soc.*, **30**, 205 (1985).

7) M. B. Frankel and E. R. Wilsov, U.S. Patent 383421 (1983); *Chem. Abstr.*, **98**, 160570 (1983).

8) K. Hiratani, K. Taguchi, H. Sugihara, and T. Okada, *Chem. Lett.*, **1986**, 197.

9) Y. Minoura, K. Shiina, and K. Yoshikawa, *J. Polym. Soc.*, **A-1**, 5, 3843 (1967).

10) R. R. Russell and C. A. Vanderwerf, *J. Am. Chem. Soc.*, **69**, 11 (1947).

11) S. A. Glickman and A. C. Cope, *J. Am. Chem. Soc.*, **67**, 1012 (1945).

12) G. R. Newkome, G. R. Buker, M. J. Saunders, P. S. Russo, V. K. Gupta, Z. Yao, J. E. Miller, and K. Bouillion, *J. Chem. Soc., Chem. Commun.*, **1986**, 752.

13) J. S. Shih and D. A. Tirrell, *J. Polym. Soc., Polym. Chem. Ed.*, **22**, 781 (1983).

14) E. J. Corey and N. Raju, *Tetrahedron Lett.*, **24**, 5571 (1983).

15) J. B. Rose, *J. Chem. Soc.*, **1956**, 546.

16) E. L. Elil, N. L. Allinger, S. J. Angyal, and G. A. Morrison, "Conformational Analysis," John Wiley & Sons, N.Y. (1965), Chap. 4.

17) H. C. Padgett, I. G. Csendes, and H. Rapoport, *J. Org. Chem.*, **44**, 3492 (1979).

Dinuclear Complexes of Tetrathia[10]metallocenophanes with Silver(I) Ion: Slightly Distorted Square-Pyramidal Coordination of Ag(I) Ion

Sadatoshi AKABORI,* Sadao SATO,*,† Masaru SATO,†† and Yoshinori TAKANOHASHI
Department of Chemistry, Faculty of Science, Toho University, Funabashi, Chiba 274
†Analytical and Metabolic Research Laboratories, Sankyo Co., Ltd., Hiromachi, Shinagawa-ku, Tokyo 140
††Chemical Analysis Center, Saitama University, Urawa, Saitama 334
(Received November 1, 1988)

Tetrathia[10](1,1′)ferrocenophane reacts with silver(I) perchlorate and/or trifluoromethamesulfonate to form dimeric 1:1 complexes (**2c** and **2d**) in 73 and 60% yields, respectively. The corresponding complexes (**2a** and **2b**) of tetrathia[10](1,1′)ruthenocenophane were also obtained in 45 and 33% yields, respectively. The crystal structure of complex **2c** was determined by the X-ray method. The crystal data: monoclinic, space group $P2_1/a$, a=19.227(3), b=10.619(3), c=9.739(2) Å, β=91.71(2)°, U=1987.8 Å^3, D_c=2.02 g cm^{-3}, Z=4, μ(Mo $K\alpha$)=23 cm^{-1}, R=0.075. In complex **2c** the inner coordination sphere of the silver is completed by a sulfur atom of another ligand bonded axially to produce a five-coordinate silver ion with an overall slightly distorted square-pyramidal geometry. The temperature dependence of the ^{1}H NMR spectra of **2** was also examined. The rate between the silver free ligand **1a** and complex **2b** at room temperature was very first by the ^{1}H NMR scale.

Transition metal complexes with thioether ligands are of much current interest from the viewpoint of coordination chemistry and biological aspects. Such complexes have been extensively reviewed recently.[1] Of particular interest in coordination chemistry are the metal complexes of macrocyclic polythiaethers. For example, the polythiacrown ether ligands, such as 1,4,7-trithiacyclononane and 1,4,7,10,13,16-hexathiacyclooctadecane, often impose novel electronic properties on transition metal ions.[2,3] It is well-known that the complexes of silver(I) exhibit a preference for linear two coordination and occasionally, tetrahedral four coordination. Higher numbers of coordination can be forced by polydentate macrocyclic ligands, though such complexes generally show irregular geometries and ambiguous coordination numbers due to a poor fit between the metal ion and ligand.[4-13] For example, six and four coordination of Ag(I) are typical examples. However, to the best of the author's knowlege, no mention has been made in the literature about the fivehold coordination of thiaethers on Ag(I) ion. We have previously reported on the preparation of polythia[n]ruthenocenophanes,[14] -ferrocenophanes,[15] and 1,n-dioxathia[n]ruthenocenophanes,[16] which exhibited considerably enhanced Ag(I) cation binding compared with the corresponding ring membered crown ethers. We report here the preparation and the first novel structure of tetrathiaferrocenocrown ether complex of silver(I).

Silver(I) perchlorate or silver(I) trifluoromethanesulfonate (0.1 mmol) in acetonitrile (5 ml) was slowly added to a gently refluxing acetonitrile solution (10 ml) containing tetrathia[10]metallocenophane (**1**, 0.1 mmol). The resulting crystals were collected by filtration and washed with a small amount of acetonitrile to give 1:1 complexes (**2**) in 33—73% yields.

X-Ray Analyses. Recrystallization of **2c** from hot acetonitrile afforded brown crystals suitable for X-ray diffaction studies. The conformation of the complex (**2c**) is illustrated in Fig. 1, which also shows the atom

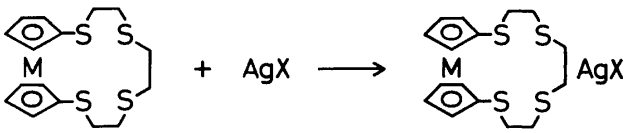

1a: M=Ru
1b: M=Fe

2a: M=Ru, X=ClO_4
2b: M=Ru, X=CF_3SO_3
2c: M=Fe, X=ClO_4
2d: M=Fe, X=CF_3SO_3

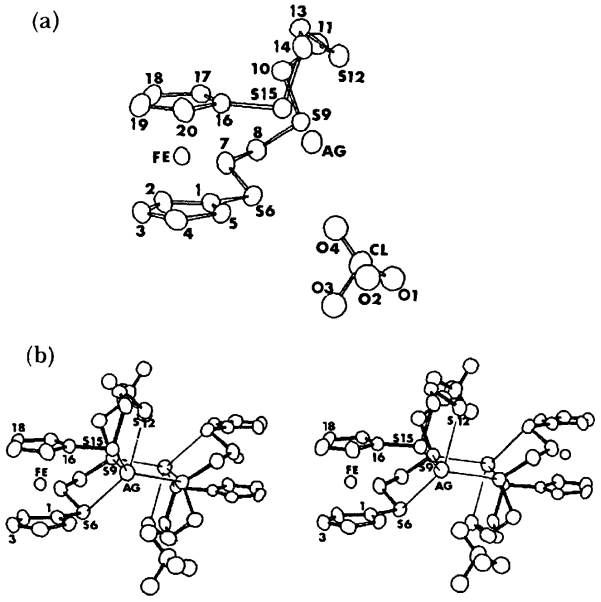

Fig. 1. ORTEP drowing of **2c**. (a) Molecular conformation and atomic labelling. (b) Stereoscopic drowing of the molecule.

labels used. The positional parameters for nonhydrogen atoms are listed in Table 1. Also, the bond lengths, bond angles and torsion angles are listed in Table 2.

As shown in Fig 1, **1b** forms a 1:1 complex with silver perchlorate which is dimeric in relation to the center of symmetry; two silver atoms are sandwiched between the two ferrocenophanes to yield a five-coordinated complex, in which each silver atom is coordinated with four sulfur atoms (S(6), S(9), S(12), and S(15)) of the organic ligand moiety and one sulfur atom (hereafter denoted as S(9')) of another ligand. The deviations of the four sulfur atoms from their mean plane are between +0.14 and −0.11 Å, and such that the configuration of these four atoms is a very flattened tetrahedron. The Ag atom is 0.87 Å out of the plane. The inner coordination sphere of the silver atom is completed by the S(9') atom bonded at the apex to produce a five-coordinate silver atom with overall square-pyramidal geometry. However, the line Ag···S(9') is displaced from the normal square-pyramidal geometry, the angle S(9')-Ag-X ranging from 77.3(4) to 133.4(4)°. The perchlorate ion does not appear to be coordinated to the silver ion, and the shortest interatomic distance between the Ag and O atoms is 3.035(18) Å. Silver-sulfur distances range from 2.629(4) to 2.883(4) Å. Although bond lengths of Ag-S(6)(2.668(4) Å), Ag-S(15)(2.629(4) Å) and Ag-S(9')(2.474(4) Å) are in same range as those observed in bis(1,4,7-trithiacyclononane)silver(I) trifluoromethanesulfonate (which contains a six-coordinate silver atom)[17] and in 1,3,5-trithiane silver(I) perchlorate (which contains both four- and five-coordinate silver),[18] the bond lengths of Ag-S(9)(2.883(4) Å) and Ag-S(12)(2.805(4) Å) are comparable with that in μ-(1,3,5-trithiane-S^1,S^3)-bis[bis(1,3,5-trithiane)silver(I)] bis-[hexafluoroarsenate(V)]-sulfur dioxide (in which contains five-coordinate silver).[6] The Cp rings take an eclipsed conformation, in which the dihedral angle between them is 3.9(6)° and the torsion angle C(1)-Cp1-Cp2-C(16) (Cp1 and Cp2 being the centroids of the Cp rings) is 57.7(15)°. These results agree well with those in the platinum complex of 1,4,7,10-tetrathia[10](1,1')ruthenocenophane.[19] The distances between the iron atom and the carbon atoms of the Cp rings range from 2.002(12) to 2.056(14) Å. The perpendicular distances from the iron atom to the least square planes of the two Cp rings, 1.631 and 1.636 Å, respectively, are both slightly shorter than those found in the NaSCN complex[20] of pentaoxa[12](1,1')ferrocenophane but agree well with those of some bridged ferrocenophanes. The intramolecular atomic distances between the Fe and Ag(I) atoms is 4.101(2) Å. This value is much longer than the sum of the covalent radii of the Fe and Ag(I) atoms[21] and indicates no direct metal–metal interaction between the coordinated Ag(I) atom and the iron atom of the ferrocene nucleus in the complex **2c**.

Table 1. Fractional Atomic Coordinates (×10⁴) and Thermal Parameters (Å²), with Estimated Standard Deviations in Parentheses

Atom	x	y	z	B_{eq}[22]
Ag	4331(1)	4927(1)	6790(1)	2.55
Fe	2358(1)	5742(2)	8010(2)	3.01
Cl	4100(2)	1018(3)	7722(4)	2.89
C(1)	2497(6)	4519(12)	6443(12)	3.43
C(2)	1834(6)	5123(13)	6285(13)	2.81
C(3)	1467(6)	4826(12)	7500(13)	2.81
C(4)	1878(7)	4075(13)	8347(14)	2.98
C(5)	2545(6)	3871(12)	7713(13)	3.15
S(6)	3183(2)	4462(3)	5268(3)	3.09
C(7)	3060(6)	5936(13)	4327(12)	3.41
C(8)	3672(7)	6152(13)	3373(13)	3.68
S(9)	4512(2)	6223(3)	4225(4)	3.76
C(10)	4555(7)	7770(13)	5014(14)	3.07
C(11)	5210(7)	7898(13)	5866(14)	3.30
S(12)	5295(2)	6856(4)	7346(4)	2.78
C(13)	4803(6)	7695(12)	8630(13)	2.21
C(14)	4601(7)	6805(13)	9798(13)	2.63
S(15)	3967(2)	5572(3)	9274(3)	3.36
C(16)	3194(6)	6436(11)	9024(11)	3.24
C(17)	3026(6)	7225(11)	7914(12)	2.84
C(18)	2334(7)	7677(12)	8066(14)	3.37
C(19)	2092(7)	7162(13)	9313(13)	1.93
C(20)	2615(6)	6401(13)	9897(12)	3.90
O(1)	452(1)	36(2)	683(2)	10.8(0.4)
O(2)	402(1)	49(2)	900(2)	11.6(0.5)
O(3)	348(1)	33(2)	754(2)	15.6(0.6)
O(4)	401(1)	223(2)	759(2)	12.0(0.5)

^{1}H NMR Spectra. The 400 MHz ^{1}H NMR spectra of **1b** in acetonitrile-d_3 showed a pair of triplets corresponding to the α- and β-ring protons of the ferrocene nucleus at δ 4.29 (t, J=1.8 Hz, 4H) and 4.27 (t, J=1.8 Hz, 4H), in addition to a singlet at δ 3.05 (s, 4H, -SCH_2CH_2S-) and two triplets at δ 3.15 (t, J=7.0 Hz, 4H, -SCH_2-) and 2.85 (t, J=7.0 Hz, 4H, -SCH_2-). The ^{1}H NMR spectra of **2c** in acetonitrile-d_3 showed a pair of triplets due to the α- and β-protons of Cp-rings at δ 4.43 (t, J=1.8 Hz, 4H) and 4.36 (t, J=1.8 Hz, 4H) together with two broad singlets at δ 3.12 (8H) and 3.06 (4H) due to the methylene protons, although these peaks shifted downfield to about 0.12—0.29 ppm. This result suggests that the counter ion (ClO_4^-) of the complex **2c** is completely separated from the silver(I) ion and the Fe atom of the ferrocene nuclues, and that the anions are surrounded by the acetonitrile-d_3 in solution. Furthermore, the change in the methylene protons' absorption pattern upon complexing (compared with the corresponding silver free ligand) can be explained by the coordination of the sulfur atoms to the silver atom described below. That is, the methylene protons at 7-, 8-, 13-, and 14-, and 10- and 11-positions become equivalent to each other upon complexing. The ^{1}H NMR spectra of **2a** in acetonitrile-d_3 showed also a pair of triplets corresponding to the α- and β-ring protons of the

Table 2. Bond Lengths (Å), and Bond and Torsion Angles (°)

1	2	3	4	1-2	1-2-3	1-2-3-4
Tetrathia-crown moiety						
S(6)	C(1)	C(2)	C(3)	1.775(13)	128.2(10)	177.0(6)
S(6)	C(1)	C(5)	C(4)		121.2(9)	176.6(8)
C(2)	C(1)	S(6)	C(7)			29.2(13)
C(5)	C(1)	S(6)	C(7)			−154.0(11)
C(1)	S(6)	C(7)	C(8)		102.1(6)	172.3(8)
S(6)	C(7)	C(8)	S(9)	1.825(14)	110.0(9)	−58.8(13)
C(7)	C(8)	S(9)	C(10)	1.538(19)	114.9(10)	−76.4(11)
C(8)	S(9)	C(10)	C(11)	1.795(14)	105.2(6)	174.9(8)
S(9)	C(10)	C(11)	S(12)	1.814(14)	110.1(10)	−64.4(13)
C(10)	C(11)	S(12)	C(13)	1.49(2)	116.0(10)	−82.6(11)
C(11)	S(12)	C(13)	C(14)	1.821(15)	102.1(6)	161.3(8)
S(12)	C(13)	C(14)	S(15)	1.823(14)	110.8(9)	−67.3(12)
C(13)	C(14)	S(15)	C(16)	1.538(19)	114.2(9)	−71.6(11)
C(14)	S(15)	C(16)	C(17)	1.850(14)	102.5(6)	74.9(12)
C(14)	S(15)	C(16)	C(20)			−108.3(11)
S(15)	C(16)	C(17)	C(18)	1.757(12)	126.5(9)	176.3(7)
S(15)	C(16)	C(20)	C(19)		125.3(9)	−176.9(5)
Cyclopentadienyl ring						
C(1)	C(2)	C(3)	C(4)	1.431(18)	105.6(11)	−0.6(16)
C(2)	C(3)	C(4)	C(5)	1.431(19)	109.5(12)	1.1(16)
C(3)	C(4)	C(5)	C(1)	1.379(19)	109.2(12)	−1.1(15)
C(4)	C(5)	C(1)	C(2)	1.457(19)	105.2(11)	0.7(15)
C(5)	C(1)	C(2)	C(3)	1.411(18)	110.5(11)	−0.1(15)
C(16)	C(17)	C(18)	C(19)	1.398(17)	108.5(11)	1.2(15)
C(17)	C(18)	C(19)	C(20)	1.425(19)	106.8(12)	−1.0(16)
C(18)	C(19)	C(20)	C(16)	1.423(19)	108.7(12)	0.4(16)
C(19)	C(20)	C(16)	C(17)	1.397(19)	108.0(11)	0.4(15)
C(20)	C(16)	C(17)	C(18)	1.422(18)	108.1(11)	−1.0(15)
Ag coordination						
S(6)	Ag	S(9)		2.668(4)	74.1(1)	
S(9)	Ag	S(12)		2.853(4)	73.9(1)	
S(12)	Ag	S(15)		2.805(4)	80.0(1)	
S(15)	Ag	S(9)*		2.629(4)	133.4(1)	
S(9)*	Ag			2.747(4)		*: 1−x, 1−y, 1−z
O(4)	Ag			3.035(18)		
Fe	Ag			4.101(2)		
Cl	Ag			4.275(4)		
Ag*	Ag			4.393(2)		

ruthenocene nucleus at δ 4.84 (J=1.7 Hz, 4H) and 4.76 (t, J=1.7 Hz, 4H), in addition to a broad singlet at δ 3.03 (bs, 4H) and a multiplet at δ 3.05—3.14 (m, 8H). The peak due to the methylene protons at the 7-, 8-, 13-, and 14-positions of the ruthenocenophane complex **2a** is broadened and appears as a multiplet, although the chemical shift value is very similar to that of the ferrocenophane complex **2c**. Furthermore, the methylene protons at the 10- and 11-positions of **2a** and **2c** also showed nearly the same chemical shift values. These results suggest that **2a** in solution forms a 1:1 complex similar to that of **2c**, but the methylene protons at 7- and 8- (and/or 13- and 14-) positions become nonequivalent environments due to the long distance between the two Cp-rings of the ruthenocene nucleus in **2a** compared with that of the ferrocene nucleus in **2c**. A similar relationship is observed between **2b** and **2d**.

In order to investigate the stability of the silver complex, the VT NMR technique was used. According to the rise in temperature the spectral pattern and chemical shift of **2b** in DMSO-d_6 changed. At 65 °C a sharp singlet due to the methylene protons at the 7-, 8-, 13-, and 14-positions became a broad singlet and then the broad singlet separated completely to two multiplet peaks at 90 °C. Furthermore the methylene protons at the 7-, 8-, 13-, and 14-positions became a pair of A_2B_2 triplets at δ 3.11 (J=6.6 Hz) and 2.94 (J=6.6 Hz), and the peaks of the Cp ring protons shifted up-field and showed a pair of AA'BB' triplets at δ 4.82 and 4.68 at 170 °C. The spectrum of **2b** at 170 °C is very similar to that found in the silver-free ligand **1a** at room temperature. These results suggest that the dissociation of **2b** to (**1a**+$AgCF_3SO_3$) began at 65 °C and finished completely at about 170 °C. In order to calculate the formation energy of **2b** from **1a**

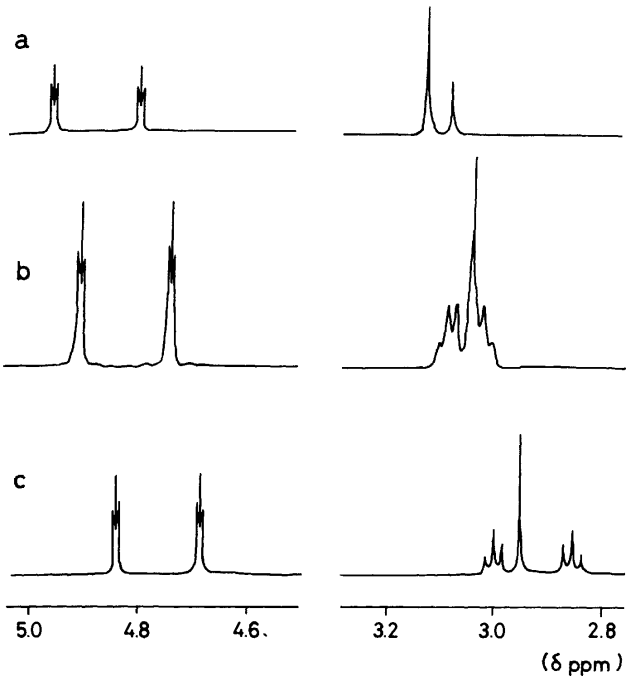

Fig. 2. ^{1}H NMR spectra (in DMSO-d_6) of (a) **2b**, (b) an equimolar mixture of **1a**+**2b**, and (c) **1a**.

and $AgCF_3SO_3$, a VT NMR measurement of the 1:1 mixture of **1a** and **2b** was carried out. First, the 1:1 mixture of the complex **2b** and silver free ligand **1a** in DMSO-d_6 was measured at room temperature. The spectrum showed a pair of AA'BB' triplets corresponding to the α- and β-ring protons at δ 4.91 (J=1.8 Hz) and 4.74 (J=1.8 Hz), a singlet due to the methylene protons at the 10- and 11-positions, together with a broad pair of triplets due to the methylene protons at the 7-, 8-, 13-, and 14-positions. However the spectrum did not show any peaks due to the methylene protons at the 7-, 8-, 13-, and 14-positions of **1a** and **2a** at room temperature. These results showed that there is a relatively fast equilibrium by ^{1}H NMR scale between the following equations. Then, low-temperature measurements of the mixture in various solvents were attempted. Unfortunately, though, they failed because of the low solubility of the samples at low temperatures.

Experimental

The melting points are uncorrected. The IR spectra were measured on a JASCO IRA-2 Diffraction Grating Infrared Spectrometer. The ^{1}H NMR spectra were obtained on a JEOL GX400 spectrometer with TMS as the internal standard. Elemental analyses of **2b** and **2d** were not carried out because of the explosive property of these complexes at high temperature.

Materials. 1,4,7,10-Tetrathia[10]ruthenocenophane[19] and 1,4,7,10-tetrathia[10]ferrocenophane[23] were prepared according to a method discussed in the previous papers. Silver(I) perchlorate and trifluoromethanesulfonate (triflate) were commercially available. The solvents used were reagents grade and/or purified by distillation.

(1,4,7,10-Tetrathia[10]ruthenocenophane)silver(I) Perchlorate (2a). To a solution of **1a** (11.0 mg, 2.5×10^{-2} mmol) in acetonitrile (2 cm^3) was added a solution of silver(I) perchlorate (5.2 mg, 2.5×10^{-2} mmol) in acetonitrile (1 cm^3). After the solution was refluxed for 3 min, it was diluted with diethyl ether (1 cm^3). The solution was kept overnight in a refrigerator. The resulting crystals were collected by filtration and washed with small amounts of acetonitrile to give **2a** in 45% yield as white needles. Mp 170 °C (decomp). ^{1}H NMR (in CD_3CN) δ=4.84 (t, J=1.7 Hz, 4H), 4.76 (t, J=1.7 Hz, 4H), 3.14—3.05 (m, 8H), and 3.04—3.01 (m, 4H). IR (KBr) 3090, 2910, 1410, 1090, 1050, 820, 618, and 490 cm^{-1}.

(1,4,7,10-Tetrathia[10]ruthenocenophane)silver(I) Triflate (2b). Complex **2b** was prepared using the same method as described above. Yield 33%. Mp 190 °C (decomp). Found: C, 29.59; H, 2.90%. Calcd for $C_{17}H_{20}AgF_3O_3RuS_5$: C, 29.23; H, 2.89%. ^{1}H NMR (in CD_3CN) δ=4.84 (t, J=1.7 Hz, 4H), 4.76 (t, J=1.7 Hz, 4H), 3.14—3.05 (m, 8H), and 3.03 (s, 4H). IR (KBr) 3100, 2910, 1410, 1280, 1110, 810, 625, and 570 cm^{-1}.

(1,4,7,10-Tetrathia[10]ferrocenophane)silver(I) Perchlorate and Triflate (2c and 2d). Complexes **2c** and **2d** were prepared using a method described in a previous paper.[15]

2c was identified by a comparison with melting point and the spectral data of an authentic sample.

2d. Yield 60%. Mp 195 °C (decomp). Found: C, 31.16; H, 3.06%. Calcd for $C_{17}H_{20}AgF_3FeO_3S_5$; C, 31.25; H, 3.06%. ^{1}H NMR (in CD_3CN) δ=4.43 (t, J=1.8 Hz, 4H), 4.36 (t, J=1.8 Hz, 4H), 3.12 (s, 8H), and 3.06 (s, 4H). IR (KBr) 3090, 2910, 1410, 1275, 1250, 1023, 622, and 510 cm^{-1}.

X-Ray Crystallography of 2c. Lattice constants were determined by a least-squares fit of angular settings of 2θ reflections within the range $15<2\theta<25°$. Intensity data were obtained on a Rigaku AFC-5R apparatus equipped with graphite monochromated Mo $K\alpha$ radiation and using the ω-2θ scan technique ($2\theta\leq50°$). During data collection three standards (measured g before every 200 reflections) showed no significant variation. Of 3510 independent reflections measured, only 3122 were considered as being observed on the basis of the criterion $F_o>2\sigma(F_o)$. All intensities were corrected for Lorentz and polarization effects, but not for absorption. Crystal data: $C_{16}H_{20}S_4FeAgClO_4$, Mw=603.8, crystal size 0.5×0.5×0.15 mm, monoclinic, space group $P2_1/a$, a=19.227(3), b=10.619(3), c=9.739(2) Å, β=91.71(2)°, U=1987.8 Å^3, Z=4, D_c=2.02 g cm^{-3}, μ(Mo $K\alpha$)=23 cm^{-1}, T=

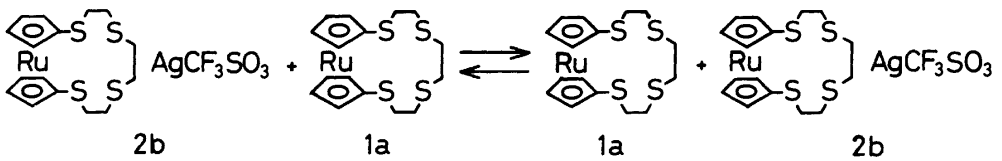

297 K. The structure was solved by heavy-atom methods, and refined by block-diagonal least-squares methods. The positions of the hydrogen atoms were estimated from standard geometry. The final refinements with anisotropic temperature factors for the nonhydrogen atoms and isotropic temperature factors for the hydrogen atoms lowered the R value to 0.075 (R_w=0.086, $w=1/\sigma^2(F_o)$). The goodness of fit was 5.6. The excursions in the final difference Fourier synthesis were within ± 0.7 e Å^{-3}.

The complete F_o-F_c data are deposited as Document No. 8868 at the office of the editor of Bull. Chem. Soc. Jpn.

References

1) S. G. Murray and F. R. Hartley, *Chem. Rev.*, **81**, 365 (1981).

2) J. R. Hartman and S. R. Cooper, *J. Am. Chem. Soc.*, **108**, 1202 (1986).

3) J. R. Hartman, E. J. Hinsta, and S. R. Cooper, *J. Am. Chem. Soc.*, **108**, 1208 (1986); *J. Chem. Soc., Chem. Commun.*, **1984**, 386.

4) R. Louis, D. Pelissard, and R. Weiss, *Acta Crystallogr., Sect. B*, **32**, 1480 (1976).

5) M. G. B. Drew, D. A. Rice, and S. bin Sitong, *Acta Crystallogr., Sect. C*, **40**, 2014 (1984).

6) H. W. Roesky, H. Hofmann, P. G. Jones, W. Pinkert, and G. M. Sheldick, *J. Chem. Soc., Dalton Trans.*, **1983**, 1215.

7) T. Ito, H. Ito, and K. Toriumi, *Chem. Lett.*, **1981**, 1101.

8) B. Noren and A. Okarsson, *Acta Chem. Scand. Ser. A*, **38**, 479 (1984).

9) H. W. Roesky, E. Peymann, J. Schimkowiak, M. Noltmeyer, W. Pinkert, and G. M. Sheldrick, *J. Chem. Soc., Chem. Commun.*, **1983**, 981.

10) P. G. Jones, T. Gries, H. Grutzmacher, H. W. Roesky, J. Schimkowiak, and G. M. Sheldrick, *Angew. Chem., Int. Ed. Engl.*, **23**, 376 (1984).

11) G. Ferguson, R. McCrindle, and M. Paruez, *Acta Crystallogr., Sect. C*, **1984**, 354.

12) A. L. Spek, E. A. Klop, and C. Brevard, *Inorg. Chem.*, **24**, 1367 (1985).

13) P. G. Duarte, J. Sola, J. Vives, and X. Solans, *J. Chem. Soc., Chem. Commun.*, **1987**, 1641.

14) S. Akabori, Y. Habata, H. Munegumi, and M. Sato, *Chem. Lett.*, **1984**, 1991; S. Akabori, H. Munegumi, Y. Habata, S. Sato, K. Kawazoe, C. Tamura, and M. Sato, *Bull. Chem. Soc. Jpn.*, **58**, 2185 (1985).

15) M. Sato, S. Tanaka, S. Akabori, and Y. Habata, *Bull. Chem. Soc. Jpn.*, **59**, 1515 (1986).

16) S. Akabori, Y. Habata, H. Munegumi, and M. Sato, *Chem. Lett.*, **1985**, 1063; Y. Habata, S. Akabori, and M. Sato, *Bull. Chem. Soc. Jpn.*, **58**, 3540 (1985).

17) J. Clarkson, R. Yagbasan, P. J. Blower, S. C. Rawle, and S. R. Cooper, *J. Chem. Soc., Chem. Commun.*, **1987**, 950.

18) R. S. Ashworth, C. K. Prout, A. Domenicano, and A. Vaciago, *J. Chem. Soc. A*, **1986**, 93.

19) S. Akabori, S. Sato, T. Tokuda, Y. Habata, K. Kawazoe, C. Tamura, and M. Sato, *Bull. Chem. Soc. Jpn.*, **59**, 3189 (1986).

20) S. Akabori, Y. Habata, and M. Sato, *Bull. Chem. Soc. Jpn.*, **57**, 68 (1984).

21) L. Pauling, "Nature of the Chemical Bond," 3rd ed., Cornell University Press, Ithaca, New York (1960).

22) W. C. Hamilton, *Acta Crystallogr.*, **12**, 609 (1959).

23) M. Sato, S. Tanaka, S. Ebine, and S. Akabori, *Bull. Chem. Soc. Jpn.*, **57**, 1929 (1984).

Phosphonylation of Biomolecules with Inorganic Diphosphonate. III.[1] Formation of an H-phosphonate Analogue of Adenosine 5′-Triphosphate by Phosphonylation of Adenosine 5′-Diphosphate

Yoshinobu BABA,* Tomoko SUMIYAMA,† Mitsutomo TSUHAKO,† and Norimasa YOZA††
Chemical Laboratory, Faculty of Education, Oita University, Dannoharu, Oita 870-11
†Kobe Women's College of Pharmacy, Kitamachi, Motoyama, Higashinada-ku, Kobe 658
††Department of Chemistry, Faculty of Science, Kyushu University,
Hakozaki, Higashi-ku, Fukuoka 812
(Received November 9, 1988)

Phosphonylation of adenosine 5′-diphosphate (ADP) with inorganic diphosphonate was investigated by use of ^{31}P NMR spectroscopy and the coupled system of high-performance liquid chromatography and flow injection analysis. ADP was phosphonylated by inorganic diphosphonate to form an H-phosphonate analogue of adenosine 5′-triphosphate (ATP) in aqueous solutions. The yield of the H-phosphonate analogue of ATP varied strongly depending on reaction conditions: pH and initial concentration of inorganic diphosphonate. The maximum yield of the H-phosphonate analogue of ATP was 56% under the following conditions: initial concentration of inorganic diphosphonate and ADP were 1.8 and 0.1 mol dm^{-3}, respectively; 50 °C; pH 5; 90 min. In basic solutions, 2′ or 3′-hydroxyl group on ADP was predominantly phosphonylated.

More recently much interest has been focused on an H-phosphonate approach for the development of new and efficient methods of synthesizing DNA and RNA,[2-4] nucleoside-phospolipid conjugates,[5a] and internucleotide phosphate analogues[5b] which are widely used as metabolic regulators.[6] The increasing significance of H-phosphonate approach has also stimulated further research in organic synthesis. The application of H-phosphonate approach, however, has been limited to the syntheses of monophosphate analogues, such as nucleoside 3′-H-phosphonate.

One of our current projects is the synthesis of H-phosphonates involving a P-O–P linkage as analogues of nucleoside polyphosphates, the analogues which become new important probes for the mechanistic studies on enzymatic reactions. We have recently reported that the phosphonylation of nucleoside 5′-monophosphate such as adenosine 5′-monophosphate (AMP) using a new phosphonylating agent, inorganic diphosphonate (P^{III}-O-P^{III}), gave an H-phosphonate analogue of nucleoside 5′-diphosphate such as adenosine 5′-diphosphate (ADP) in aqueous solutions according to Eq. 1.[1,7,8]

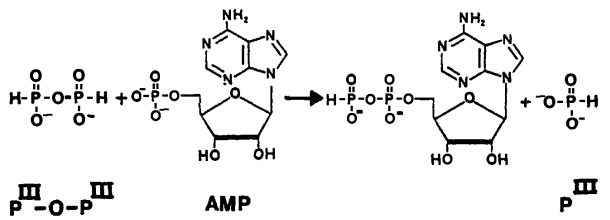

(1)

This method using P^{III}–O-P^{III} is extended in the present paper to phosphonylation of ADP to obtain an H-phosphonate analogue of adenosine 5′-triphosphate (ATP).

Experimental

Chemicals. Unless otherwise stated, guaranteed reagents from Wako (Osaka, Japan) were used without further purification. Disodium adenosine 5′-diphosphate dihydrate was purchased from Oriental Yeast (Tokyo, Japan).

Disodium inorganic diphosphonate, $Na_2P_2H_2O_5$, was prepared according to the previous paper.[1] The purity of disodium diphosphonate thus obtained was checked by HPLC[9-11] to be 98% (as P).

Phosphonylation of ADP with Diphosphonate. Initial concentration of diphosphonate varied from 0.5 to 1.8 mol dm^{-3}, keeping the initial concentration of ADP at 0.1 mol dm^{-3} constant. The pH of aqueous reaction mixture was ca. 5. If necessary, the reaction mixture was adjusted to the prescribed pH value (10, 8, 7, 6, or 4) with a sodium hydroxide or hydrochloric acid solution. The reaction mixtures with and without pH adjustment were allowed to react at 50, 60, and 70 °C. The pH change during the reactions was not controlled strictly.

HPLC Measurement. Two HPLC systems were used in the present study: 1) an HPLC system with UV-detector for determination of ADP and products; 2) an HPLC system coupled with a flow injection analysis (FIA) designed for the sensitive detection of phosphate and phosphonate groups.[1,9-13]

A TRI ROTAR VI system (Jasco, Tokyo, Japan) was used as an HPLC system with UV-detector. An aliquot (0.1 ml) of reaction mixture was injected onto a separation column (250×4.6 mm I.D.). Two kinds of anion-exchange columns were used: 1) an MCI column (MCI Gel CDR-10, 7 μm, Mitsubishi Chemical Industry, Tokyo, Japan) in Fig. 1; 2) a TSK column (TSKgel SAX, 10 μm, TOSOH, Tokyo, Japan) in Figs. 2 and 3. Flow rate was 1.0 ml min^{-1} and column temperature was kept at 40 °C. Separated ADP and products were detected at 260 nm by use of UV spectrophotometer (UVIDEC-340, Jasco, Tokyo, Japan). Eluent for the MCI column was composed of 0.4 mol dm^{-3} ammonium sulfate, 0.2 mol dm^{-3} potassium dihydrogenphosphate, 0.2 mol dm^{-3} dipotassium hydrogenphosphate, and 4% (V/V) acetonitrile

(pH 6.6). Eluent for the TSK column was composed of 0.3 mol dm^{-3} potassium chloride and 0.1% (W/V) tetrasodium ethylenediaminetetraacetate (pH 10).

To detect ADP, diphosphonate, phosphonate, and products simultaneously, an FIU-300 FIA system (Jasco, Tokyo, Japan) was coupled with the TRI-ROTAR VI HPLC system. The separation was performed on the TSK column. Flow rate, column temperature, and eluent were the same as described above. Phosphate and phosphonate groups on separated reactants and products were monitored by the on-line coupled FIA system.[1,9-13] A molybdenum(V)-molybdenum(VI) reagent[12] was used as a chromogenic agent. To oxidize phosphonate to detectable phosphate, sodium hydrogensulfite was introduced into the FIA system.[9-11]

^{31}P NMR Measurement. Pulse FT ^{31}P NMR spectra were recorded at room temperature by use of Varian XL-VXR300 (121 MHz) and Varian XL-200 (81.0 MHz). Orthophosphoric acid (85%) was used as an external standard.

Results and Discussion

Characterization of Phosphonylated Products by HPLC. A chromatographic peak (A) in Fig. 1 for a phosphonylated product appeared after 5 min incubation of ADP (0.1 mol dm^{-3}) with P^{III}-O-P^{III} (1.8 mol dm^{-3}) at 70 °C and pH 5 in an aqueous solution. Area of the peak (A) increased gradually to a maximum value, 55%, after 15 min incubation and then decreased slowly. The retention time for (A) was 16.4 min measured by the HPLC system with UV-detector using the MCI column. No peaks for other phosphonylated products were observed by the HPLC measurements. A small peak for adenosine 5′-monophosphate (AMP) which would be formed by hydrolysis of ADP was also recorded.

The peak (A) for the phosphonylated product involves both phosphate and phosphonate groups as shown in Fig. 2b, because the solid line represents the sum of the absorbances (830 nm) due to phosphate and phosphonate groups and the dotted line represents the absorbance (830 nm) due to phosphate group measured by the HPLC system coupled with the FIA using the TSK column. The peak (A) (Fig. 2a) measured by use of the HPLC system with UV-detector using the TSK column was also observed at the same retention time as that of the peak (A) in Fig. 2b. The retention time (35.4 min) for (A) measured by use of the TSK column (Fig. 2) was longer than that for (A) measured by use of the MCI column (Fig. 1).

Three chromatographic peaks (Fig. 3) for two main

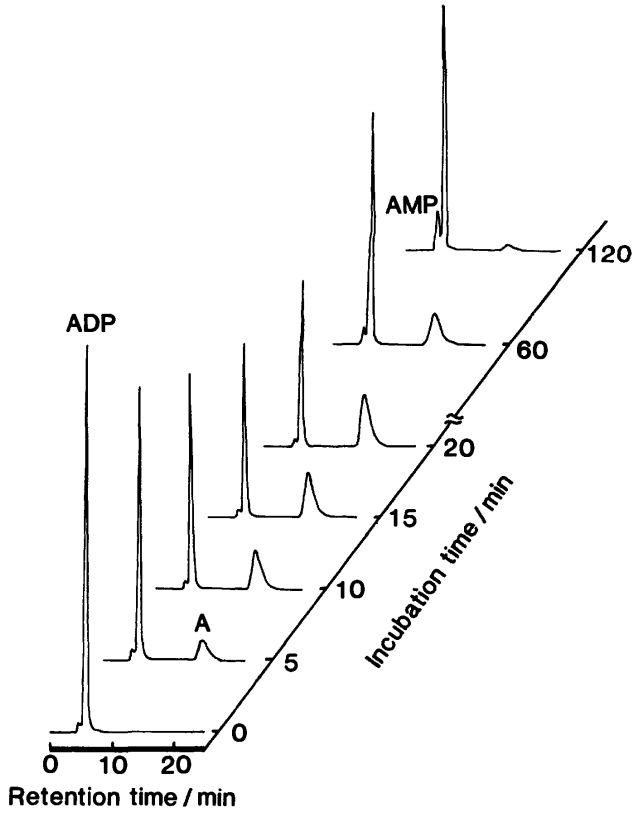

Fig. 1. Kinetic HPLC profile for phosphonylation of ADP (0.1 mol dm^{-3}) with inorganic diphosphonate (1.8 mol dm^{-3}) at 70 °C and pH 5. Column: the MCI anion-exchange column. Eluent: 0.4 mol dm^{-3} $(NH_4)_2SO_4$, 0.2 mol dm^{-3} KH_2PO_4, 0.2 mol dm^{-3} K_2HPO_4, and 4% CH_3CN (pH 6.6). Wavelength: 260 nm.

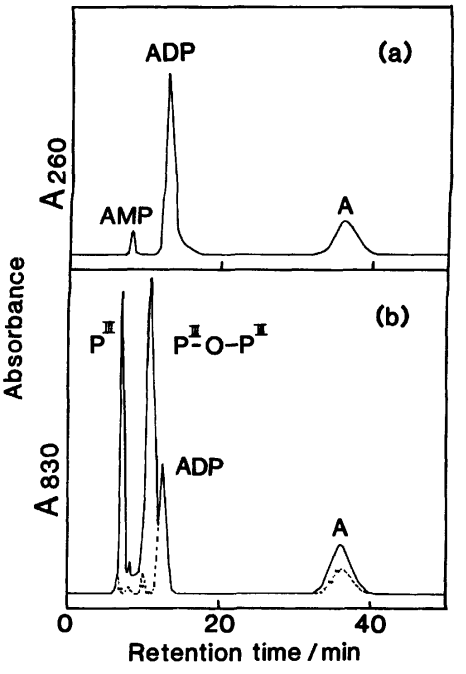

Fig. 2. HPLC profiles for ADP (0.1 mol dm^{-3}) phosphonylated by inorganic diphosphonate (1.0 mol dm^{-3}) at pH 5 and 70 °C for 50 min. Column: the TSK anion-exchange column. Eluent: 0.3 mol dm^{-3} KCl and 0.1% EDTA 4Na (pH 10). Wavelength: 260 nm(a) and 830 nm(b). The solid line in (b) indicates the sum of the absorbances due to both phosphate and phosphonate groups and the dotted line indicates the absorbance due to only a phosphate group.

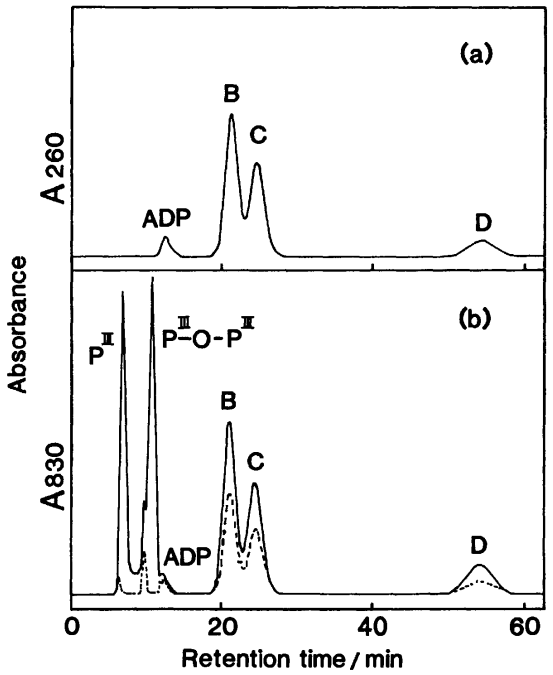

Fig. 3. HPLC profiles for ADP (0.1 mol dm^{-3}) phosphonylated by inorganic diphosphonate (1.0 mol dm^{-3}) at pH 10 and room temperature for 30 min. Other conditions are the same as in Fig. 2.

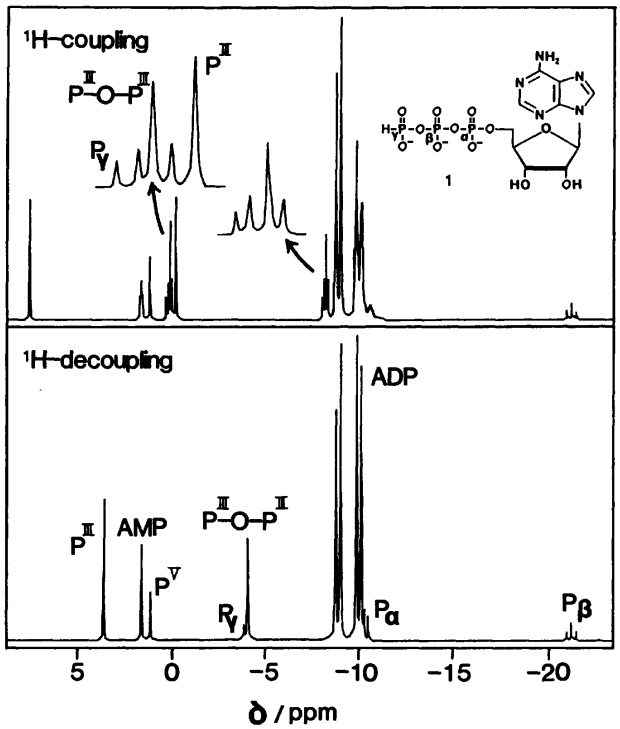

Fig. 4. ^{31}P NMR spectra for ADP (0.5 mol dm^{-3}) phosphonylated by inorganic diphosphonate (0.1 mol dm^{-3}) at pH 5 and 70 °C for 90 min.

products (B and C) and a by-product (D) were observed for the reaction mixture incubated at pH 10 by use of the same HPLC systems in Fig. 2. Although these peaks also involve phosphate and phosphonate groups as shown in Fig. 3b, retention times of these peaks are different from that of peak (A). This shows that in an alkaline solution different products are formed.

Structure of Phosphonylated Products by ^{31}P NMR. To establish the structure of phosphonylated products, ^{31}P NMR spectra were recorded. Figure 4 shows ^{31}P NMR spectra for the reaction mixture of ADP (0.5 mol dm^{-3}) and P^{III}-O-P^{III} (0.1 mol dm^{-3}) incubated at pH 5 and 70 °C for 90 min.

A proton-decoupled spectrum (Fig. 4) represents two unknown doublets (−4.1 and −10.4 ppm) and an unknown triplet (−21.2 ppm) in addition to the signals assigned to phosphonate (P^{III}; 3.5 ppm), AMP (1.5 ppm), orthophosphate (P^{V}; 1.0 ppm), P^{III}-O-P^{III} (−4.2 ppm), and ADP (two doublets at −9.0 and −10.0 ppm) on the basis of the chemical shifts for the authentic samples. These unknown peaks are the signals for the phosphonylated product observed by the HPLC measurement in Figs. 1 and 2. AMP and P^{V} would be formed by hydrolysis of ADP in the course of reaction.

The triplet at −21.2 ppm is the most important signal to characterize the chemical structure of the phosphonylated product, because the triplet at around −20 ppm is caused by the middle-group phosphorus on triphosphate species such as ATP[14,15] and inorganic triphosphate.[16,17] In addition, coupling constant (19.0 Hz) of the triplet is approximately equal to that (19.3 Hz) of ATP.[15] We concluded that, as shown in Fig. 4, product **1** similar in structure to ATP (H-phosphonate analogue of ATP) was fromed by phosphonylation of ADP with P^{III}-O-P^{III} at pH 5. The triplet is assigned to middle phosphorus atom (P_β of **1**). Other unknown doublets at −4.1 and −10.4 ppm would be signals for P_γ and P_α atom of **1**. A signal of the doublet at −4.1 ppm overlapped with that of P^{III}-O-P^{III}.

The doublet at −10.4 ppm is further split into a double-triplet in a proton-coupled spectrum (Fig. 4). The double-triplet is assigned to P_α atom of **1**, because the double-triplet shows a splitting of 4.5 Hz, the value of which is similar to the three-bond coupling constant ($^3J_{PH}$) for P_α atom on ATP split by the 5′-hydrogens of the ribose moiety.[16]

Further splitting of the doublet at −4.1 ppm into a double-doublet is shown in a proton-coupled spectrum. The double-doublet is assigned to P_γ atom of **1** for phosphonyl group transferred from P^{III}-O-P^{III} to ADP, because the double-doublet shows the splitting of 669.1 Hz for the hydrogen atom attached directly to a phosphorus atom.[1,18]

The ^{31}P NMR spectra (Fig. 5) for the reaction mixture adjusted to pH 10 differ from those observed at pH 5. A proton-decoupled spectrum shows four singlets and three doublets. The singlets at 6.3 and

−1.8 ppm are assigned to P^{III} and P^{III}–O–P^{III}, respectively. Two unknown singlets (E and F) and three unknown doublets are the signals for the main phosphonylated products observed in Fig. 3.

In a proton-coupled spectrum, both singlets (E and F) are split into double-doublets. These double-doublets are assigned to the signals for compounds **2** and **3** (Fig. 5) producing the phosphonylation of 2′- or 3′-hydroxyl group, because each double-doublet shows one-bond coupling constant ($^1J_{PH}$=650 Hz) and three-bond coupling constant ($^3J_{PH}$=10 Hz).[1] Doublet at −7.1 ppm is then assigned to P_α of these compounds and two doublets at −2.4 ppm are assigned to P_β of these compounds. ^{31}P NMR spectrum of a by-product could not be observed, owing to a low yield.

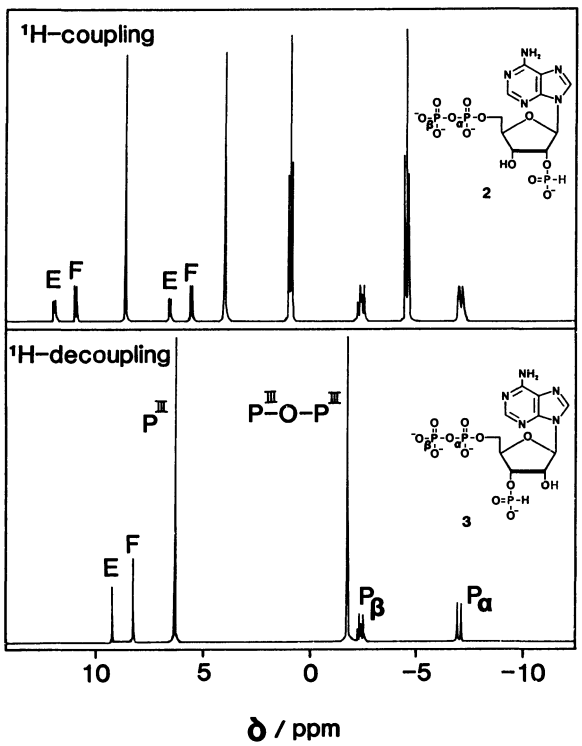

Fig. 5. ^{31}P NMR spectra for ADP (0.1 mol dm^{-3}) phosphonylated by inorganic diphosphonate (0.5 mol dm^{-3}) at pH 10 and room temperature for 20 min.

Effect of pH on the Phosphonylation of ADP. The product **1** was predominantly formed at pH 5 as shown in Figs. 1 and 6. The amount of the product **1** increased gradually with time at pH 5 as shown in Fig. 6. The yield of **1** reached a maximum (about 40%) at 120 min, and then slowly decreased.

In the reaction at pH 10, very little amount of **1** was formed, so that the datum for **1** was omitted in Fig. 7. The amount of both products **2** and **3** showed a gradual increase with time, reaching a maximum (about 74%) after 60 min. The maximum amount remained constant at least after 100 min incubation. The unknown by-product was formed in the amount of ca. 20% after 240 min.

Table 1 which lists the yields of products **1**, **2**, and **3** in the pH 4 to 10 region shows that the yield of product **1** at pH 6 is higher than those at any other pH's. To get product **1** selectively without impurities of **2** and **3**, however, ADP should react in more acidic solu-

Table 1. Yields[a] of Phosphonylated Products in the pH Region from **4** to **10**

pH	Yield/%		Time/min
	1	**2**+**3**	
4	27	0	80
5	40	0	120
6	45	7	100
7	37	11	100
8	21	30	40
10	0	74	60

a) Reaction conditions: initial concentrations of ADP and P^{III}–O–P^{III} were 0.1 mol dm^{-3} and 1.0 mol dm^{-3}; 60 °C.

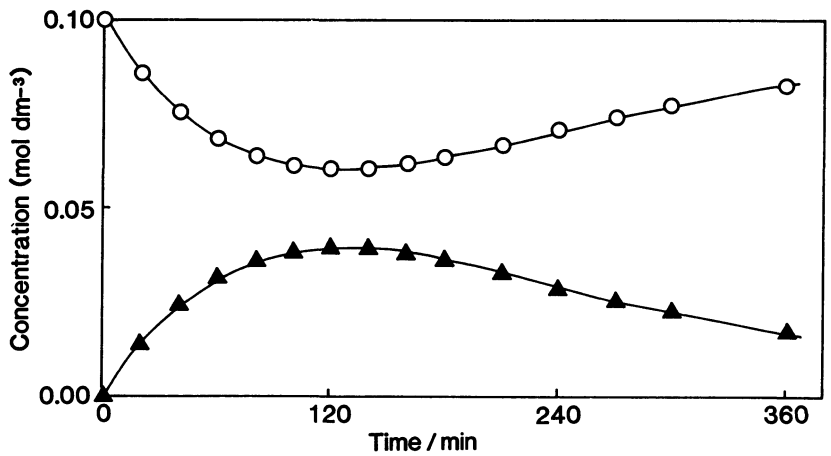

Fig. 6. Time dependence of the reaction components of phosphonylation for ADP (0.1 mol dm^{-3}) with inorganic diphosphonate (1.0 mol dm^{-3}) at pH 5 and 60 °C. Plots of the observed molar concentrations of ADP (○) and product **1** (▲) vs. time.

tions, because small amount of **2** and **3** was formed at pH 6.

Products **2** and **3** were formed in alkaline solutions more favorably than in acidic solutions. For example, the yield of **2** and **3** at pH 6 was only 7%, while the yield reached a maximum value of 74% at pH 10. The results show that the hydroxyl group at 2′- or 3′-position becomes reactive by dissociation of a proton in a basic solution, because such hydroxyl groups have very large protonation constant more than 12 in log scale.[19] Phosphonylation of hydroxyl groups will be described in more detail in a subsequent paper of this series.

It is interesting that the yields of these products strongly depend on pH of reaction solution. The pH dependence can be explained as follows: the degradation of products is in competition with the formation of products. In acidic and neutral solutions, diphosphate group on ADP reacts with P^{III}-O-P^{III} to form product **1**, which is relatively stable as shown in Fig. 6. The hydroxyl groups at 2′- and 3′-positions are protonated in acidic and neutral solutions, so that the hydroxyl groups do not react with P^{III}-O-P^{III}. On the other hand, in basic solution product **1** is very unstable and undergoes rapid hydrolysis to ADP and phosphonate in spite of the formation of **1** from ADP and P^{III}-O-P^{III}. A hydroxyl group is deprotonated in a basic solution, consequently, a deprotonated hydroxyl group reacts with P^{III}-O-P^{III} to form products **2** and **3**, which are very stable even in a basic solution as shown in Fig. 7. To provide further support for the proposed reaction pathway, we carried out an additional ^{31}P NMR experiment by addition of sodium hydroxide solution to the reaction mixture shown in Fig. 4. As a result, the NMR signals for **1** disappeared rapidly and the signals for **2** and **3** appeared.

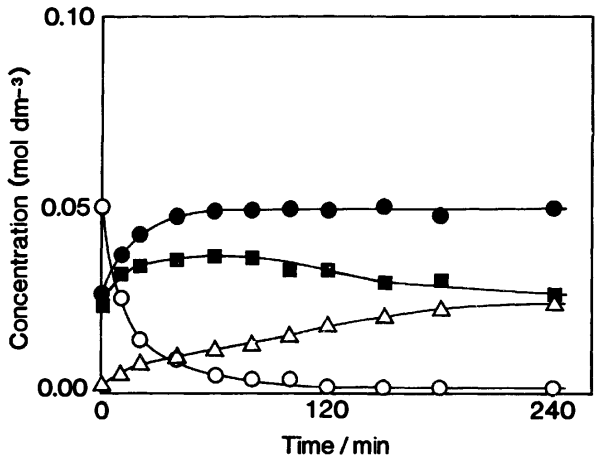

Fig. 7. Time dependence of the reaction components of phosphonylation for ADP (0.1 mol dm^{-3}) with inorganic diphosphonate (1.0 mol dm^{-3}) at pH 10 and 50 °C. Plots of the observed molar concentrations of ADP (○) and product **2** and **3** (●, ■), and unknown product (△) vs. time.

Effects of Initial Concentrations of Diphosphonate and Temperature on Yield of Product 1. As shown in Fig. 8, phosphonylation of ADP gave H-phosphonate analogue of ATP (**1**) at pH 5 selectively, while 2′- or 3′-hydroxyl group was phosphonylated at pH 10. The yields of **1** were measured at pH 5 varying initial concentration of P^{III}-O-P^{III} and temperature to find the optimal conditions for phosphonylation of ADP.

Yield of **1** (Table 2) increased with increasing initial concentration of P^{III}-O-P^{III}: from 28% (0.5 mol dm^{-3}) to 54—56% (1.8 mol dm^{-3}). Yield was found to be maximum at initial concentration of 1.8 mol dm^{-3} in the temperature range studied here. The solution of P^{III}-O-P^{III} is saturated at 1.8 mol dm^{-3}. No improvements of the yields were observed with an increase in temperature, in spite of an decrease in time required to

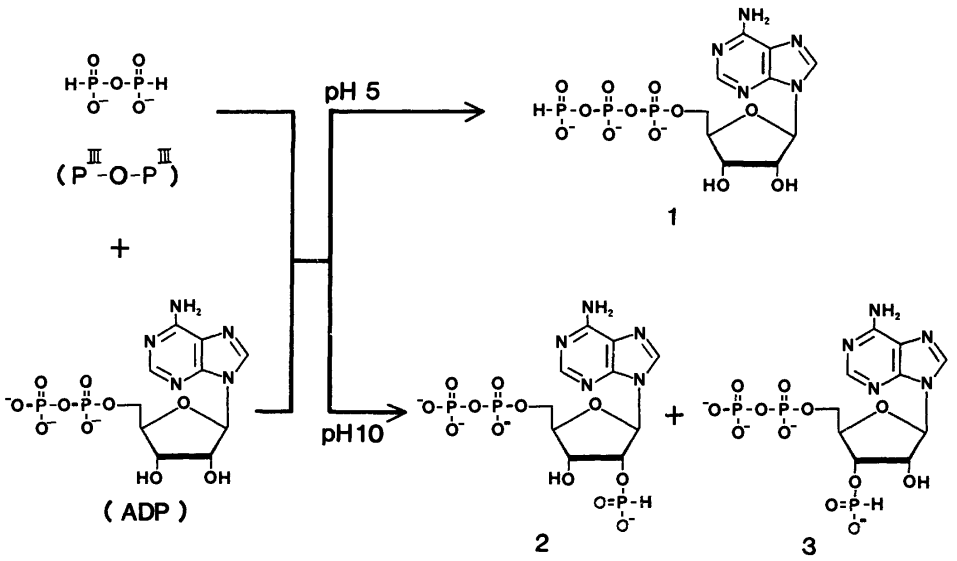

Fig. 8. Reaction scheme for phosphonylation of ADP with P^{III}-O-P^{III} at pH's 5 and 10.

Table 2. Phosphonylation of ADP with Diphosphonate at pH 5

Reaction conditions				Yield of 1/%
Molarity/mol dm^{-3}		Temp/°C	Time/min	
P^{III}-O-P^{III}	ADP			
0.5	0.1	40	1680	28
		50	420	28
		60	240	28
		70	140	28
1.0	0.1	40	420	42
		50	200	41
		60	120	40
		70	50	41
1.5	0.1	40	330	51
		50	120	51
		60	60	50
		70	30	48
1.8	0.1	40	210	55
		50	90	56
		60	30	54
		70	15	55

reach a maximum amount. The optimal conditions for phosphonylation of ADP with P^{III}-O-P^{III} were found to be initial concentration of P^{III}-O-P^{III} 1.8 mol dm^{-3}, pH 5, and 50 °C.

The overall tendencies of the results are similar to those obtained in the phosphonylation of AMP,[1] except that the yield of **1** is smaller than that of H-phosphonate analogue of ADP (ca. 70%).[1] The difference in yield between ATP analogue and ADP ananlogue is attributalbe to the different negative charges on nucleophiles, ADP and AMP, because more negatively charged ADP is repulsed and slowed down to higher degree in attacking dianionic P^{III}-O-P^{III}.

We appreciate Professor Tsujiaki Hata and Dr. Mitsuo Sekine at Tokyo Institute of Technology for their helpful discussions on the synthesis of H-phosphonates and sending us many valuable reprints. We are indebted to Professor Jacek Stawinski at University of Stockholm, Dr. Brian Froehler at Genentech, Inc., and Associate Professor Hiroshi Takaku at Chiba Institute of Technology, for sending us many valuable reprints. The authors wish to express their thanks to Dr. Makiko Sugiura of Kobe Women's College of Pharmacy for her help in measuring ^{31}P NMR spectra.

References

1) Part II of this series. Y. Yamamoto, Y. Baba, M. Mizokuchi, M. Onoe, T. Sumiyama, M. Tsuhako, N. Yoza, and S. Ohashi, *Bull. Chem. Soc. Jpn.*, **61**, 3217 (1988).

2) a) P. J. Garegg, T. Regberg, J. Stawinski, and R. Strömberg, *Chem. Scr.*, **25**, 280 (1985); **26**, 59 (1986); b) P. J. Garegg, I. Lindh, T. Regberg, J. Stawinski, and R. Strömberg, *Tetrahedron Lett.*, **27**, 4051, 4055 (1986).

3) a) B. C. Froehler and M. D. Matteucci, *Tetrahedron Lett.*, **27**, 469 (1986); b) B. C. Froehler, P. G. Ng, and M. D. Matteucci, *Nucleic Acids Res.*, **14**, 5399 (1986).

4) a) J. E. Marugg, M. Tromp, E. Kuyl-Yeheskiely, G. A. van der Marel, and J. H. van Boom, *Tetrahedron Lett.*, **27**, 2661 (1986); b) T. Tanaka, S. Tamatsukuri, and M. Ikehara, *Nucleic Acids Res.*, **15**, 7235 (1987); c) A. Andrus, J. W. Efcavitch, L. J. McBride, and B. Giusti, *Tetrahedron Lett.*, **29**, 861 (1988); d) M. Sekine, S. Narui, and T. Hata, *ibid.*, **29**, 1037 (1988); e) H. Takaku, S. Yamakage, O. Sakatsume, and M. Ohtsuki, *Chem. Lett.*, **1988**, 1675.

5) a) I. Lindh and J. Stawinski, Nucleic Acids Res. Symp. Ser., No. 18, 189 (1987); b) B. C. Froehler, *Tetrahedron Lett.*, **27**, 5575 (1986).

6) R. Engel, *Chem. Rev.*, **77**, 349 (1977).

7) Y. Baba, M. Tsuhako, Y. Yamamoto, N. Yoza, and S. Ohashi, Nucleic Acids Res. Symp. Ser., No. 17, 69 (1986).

8) Y. Baba, M. Onoe, T. Sumiyama, M. Tsuhako, N. Yoza, and S. Ohashi, *Chem. Lett.*, **1987**, 1389.

9) H. Hirai, N. Yoza, and S. Ohashi, *J. Chromatogr.*, **206**, 501 (1981).

10) Y. Baba, N. Yoza, and S. Ohashi, *J. Chromatogr.*, **295**, 153 (1984).

11) Y. Baba, N. Yoza, and S. Ohashi, *J. Chromatogr.*, **318**, 319 (1985).

12) Y. Baba, N. Yoza, and S. Ohashi, *J. Chromatogr.*, **348**, 27 (1985).

13) Y. Baba, Y. Yamamoto, N. Yoza, and S. Ohashi, *Bunseki Kagaku*, **34**, 692 (1985).

14) H. J. Vogel, "Phosphorus-31 NMR Principles and Applications," ed by D. G. Gorenstein, Academic Press, New York (1984), Chap. 4, p. 114.

15) M. Cohn and T. R. Hughes, Jr., *J. Biol. Chem.*, **235**, 3250 (1960).

16) M. M. Crutchfield, C. H. Dungan, and J. R. Van Wazer, "^{31}P Nuclear Magnetic Resonance," in "Topics in Phosphorus Chemistry," ed by M. Grayson and E. F. Griffith, Wiley Interscience, New York (1967), Vol. 5, Chap. 1, pp. 12, 13.

17) T. Glonek, A. J. R. Costello, T. C. Myers, and J. R. Van Wazer, *J. Phys. Chem.*, **79**, 1214 (1975).

18) D. G. Gorenstein, "Phosphorus-31 NMR Principles and Applications," ed by D. G. Gorenstein, Academic Press, New York (1984), Chap. 2, p. 39.

19) R. M. Izatt, J. J. Christensen, and J. H. Rytting, *Chem. Rev.*, **71**, 439 (1971).

A Spectroscopic Characterization of Metal Ion-Complexed NADH Models and Their Kinetic Behavior in Nitrosobenzene Reduction

Seizo TAMAGAKI, Yoshitaka SIMOJO, Takasi MIMURA, and Waichiro TAGAKI*
Department of Applied Chemistry, Faculty of Engineering, Osaka City University, Sugimoto 3-3-138, Sumiyoshi-ku, Osaka 558
(Received November 14, 1988)

The structures of metal ion complexes of a series of NADH models were spectrophotometrically investigated. The electronic spectra were sensitive to variation of both the 1,4-dihydropyridines and the metals; particularly, 1-benzyl-3,5-bis(1-pyrrolidylcarbonyl)-1,4-dihydropyridine (BPDH) was recognized to produce two types of complexes with zinc and lead perchlorates, whereas 1-benzyl-1,4-dihydronicotinamides (BNAH) complexed metal ion only at the amide oxygen. In order to elucidate these structures, the effect of changing perchlorate ion concentrations was examined. In addition, reduction of nitrosobenzene in the presence of bivalent metal cations was kinetically investigated.

The coordination between zinc and NADH plays an important role in alcohol dehydrogenase enzymes.[1] Thus, the role of metal ion is fundamental to our better understanding of NADH coenzymes. Then, there do exist a number of reports on NADH models. Ohno and other workers have demonstrated that metal ion coordination to NADH models such as BNAH and its optical active analogs exhibits a significant influence on rate acceleration[2a] and stereodifferentiation[2b] in carbonyl reductions. However, the systematic spectroscopic study on metal ion complexation has received less attention thus far.[3] This study provides a spectroscopic analysis of zinc and lead complexes with NADH models, the results of which are discussed in this paper and also presents experimental data on the reduction of nitrosobenzenes by these complexes, since interest in a fundamental understanding of the relationship between the structure and the reactivity of NADH models continues to be an area of considerable experimental effort.

1,4-Dihydronicotinamides themselves have a disadvantage for their applications as coenzyme models owing to their relative instability toward electrophilic reagents. In order to overcome this drawback, we have recently synthesized symmetrically substituted 1,4-dihydropyridines and have used them for studies under acidic conditions. In this study we have employed such NADH models as a proper choice.

Experimental

Materials. 1-Benzyl-3,5-bis(pyrrolidylcarbonyl)-1,4-dihydropyridine (BPDH, **1**) and its 1-(substituted benzyl) derivatives was prepared according to the method described in the previous paper.[4] Special grade metal perchlorates as the hydrates from Kishida Chemicals Co. were used without further purification. Tetrabutylammonium perchlorate of special grade was purchased from Tokyo Kasei Kogyo Co. and dried in vacuo at 50 °C for one day. *p*-Substituted nitrosobenzenes were prepared according to the literature method.[5] Acetonitrile was distilled from P_4O_{10}.

Kinetic Procedure. The kinetic data were determined at 25 °C in acetonitrile under anaerobic conditions, as described in our previous paper.[6] UV-visible spectra and absorbance-time measurements were recorded on a Hitachi model-220 spectrophotometer equipped with constant temperature cell holders. The progress of the reaction was monitored by the disappearance of the absorbance at, for example, 355 nm due to **1**. Generally, the initial concentrations of **1** and nitrosobenzene were 0.1 mM and 1.0 mM, respectively, throughout this work (M=mol dm^{-3}).

Results and Discussion

Spectral Changes of Dihydropyridine-Zinc(II) Complexes. The spectral changes in acetonitrile as solvent were monitored by UV-visible spectrometry in an appropriate region 300—400 nm. In Table 1 are summarized the spectroscopic data for a series of substituted 1-benzyl-1,4-dihydronicotinamides in the presence and absence of a 100-fold molar excess of zinc perchlorate. All these compounds have a strong absorption band somewhere ranging from 300 nm to 400 nm, depending on the metal ion and the substituents. It has been proposed that these absorption could be

Table 1. Electronic Absorption Bands for NADH Model Compounds in the Presence and Absence of Zinc Perchlorate in Acetonitrile[a]

Model compound[b]	R, R′	λ/nm without $Zn(ClO_4)_2$	λ/nm with $Zn(ClO_4)_2$
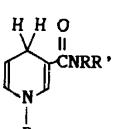	H, H	345	360
	H, Et	340	355
	$(CH_2)_5$	333	345
	Et, Et	330	338
	i-Pr, *i*-Pr	325	—
	$(CH_2)_4$	345	350
	H, Et	372	380
	Et, Et	355	368
	$(CH_2)_5$	340	370
	$(CH_2)_4$	355	320

a) $[Zn(ClO_4)_2]/[NADH\ Model]=100$. b) Bz: $CH_2C_6H_5$.

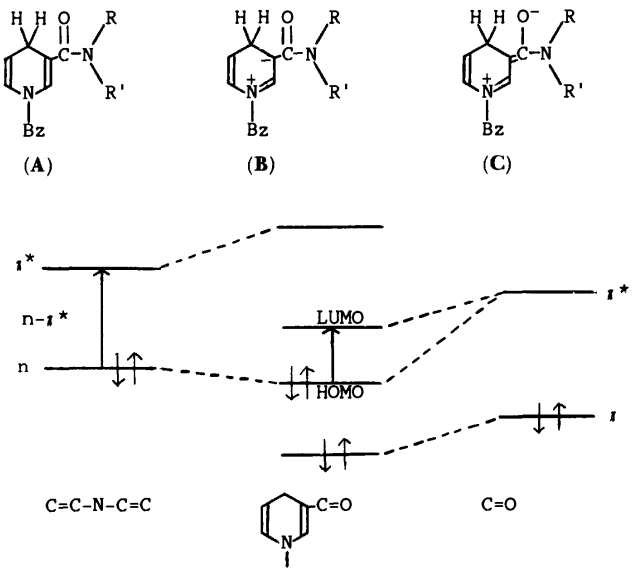

Fig. 1. Construction of the orbitals of 1,4-dihydronicotinamide. Only the major interactions are illustrated.

ascribed to the n-π^* transition.[7]

There are a few limiting resonance structures (**A**, **B**, and **C**) for 1,4-dihydronicotinamide in which the lone pair of electrons on N-1 is delocalized into the ring and conjugates further with the π-system of the carbonyl group. The delocalization will be maximized when the carbonyl group lies in the plane of the ring. Therefore, the twist of the bulky amide group out of the dihydropyridine ring destabilizes the LUMO more than destabilizes the HOMO, resulting in a blue shift of the electronic absorption band (Fig. 1). Indeed, the λ_{max} values shift toward a shorter wavelength in going from R,R'=H,H (345 nm) to R,R'=H,Et (340 nm) and to R,R'=Et,Et (330 nm). Obviously, the steric repulsions diminish π-conjugation. Nevertheless, despite its bulkiness, R,R'=$(CH_2)_4$ substitution affords an electronic absorption band at an exceptionally rather longer wavelength.

Upon complexation with zinc ion, the dihydronicotinamides undergo spectral shifts toward long wavelengths without exception. The extent of the spectral shift for a less bulky amide is twice as large as that for a more bulky amide. This is because the relative extent of delocalization in nonplanar dihydropyridine molecules is originally small. Thus, two isopropyl groups in an amide may extremely destabilize the metal complex and actually the λ_{max} could not be defined.

A similar situation is continued in 3,5-disubstituted 1,4-dihydropyridines; bulky carbamoyl groups may destabilize the dihydropyridines and causes a blue shift irrespective of with and without the metal ion. In Table 1 are collected observed λ_{max} values in the presence or absence of a 100-fold excess of zinc perchlorate. The most remarkable feature is the unusual behavior of the dihydropyridine having R,R'=$(CH_2)_4$, which shows a greater red shift and exceptional stability inspite of the bulkiness of the carbamoyl substituent. The exact reason for this behavior is not understood at present. This anomaly, however, may be understood if we accept the view that the hydrogens α to the nitrogen in a rigidly planar pyrrolidine ring fit well between the ring methylenes of the dihydropyridine without significant steric interference, making possible a nearly planar molecule with almost maximum conjugation.[7] Owing to this stability, only the dihydropyridines bearing 1-pyrrolidinylcarbonyl groups were used for further investigations.

The absorption peak of BPDH in acetonitrile was only at 355 nm (ε: 6070) in the absence of zinc perchlorate. An addition of a large excess of zinc perchlorate to that solution resulted in the displacement of the absorption maximum to 320 nm accompanied by a poor shoulder at a slightly longer wavelength than the original, i.e., at around 365 nm, which lies within the envelope of bands with λ_{max} 355 nm and 320 nm. In a previous paper,[6] the blue shift toward 320 nm (343 nm for $Mg(ClO_4)_2$) was attributed to complexation of the metal ion on the dihydropyridine nitrogen.[8] In contrast, the bathochromic shift toward 365 nm would be that generally expected for the complexation with the amide oxygen. The existence of the corresponding complex is not strictly recognized by the spectrum of the 1-benzyl or 1-(*p*-chlorobenzyl) derivative (Figs. 4 and 2a). However, the band of the 1-(*p*-methyl- or *p*-methoxybenzyl)-1,4-dihydropyridine derivative (**e'**) explicitly distinguishes itself as an independent band with a slightly smaller extinction coefficient in the presence of a 100-fold excess of zinc perchlorate relative to BDPH (Fig. 2b). The absorption belonging to the same category was also found with less Lewis acidic zinc nitrate (361, 5680) as well as perchlorates of manganese (λ_{max} 355 nm, ε 5590 M^{-1} cm^{-1}), cobalt (359, 5870), nickel (356, 5640), where no largely blue-shifted bands could be seen (Fig. 3).

With the 1-benzyl or 1-(*p*-chlorobenzyl) derivative, the stronger absorption at 320 nm than at around 365 nm suggests that the complexation with the dihydropyridine nitrogen (**d'**) is dominant, while with the 1-(*p*-methylbenzyl) derivative, the amide oxygen is a major coordination site (**e'**).

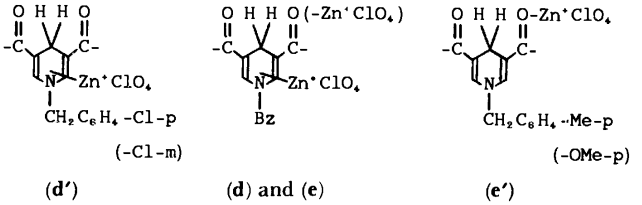

These observations can be well-explained as follows: an electron-accepting group increases the contribution

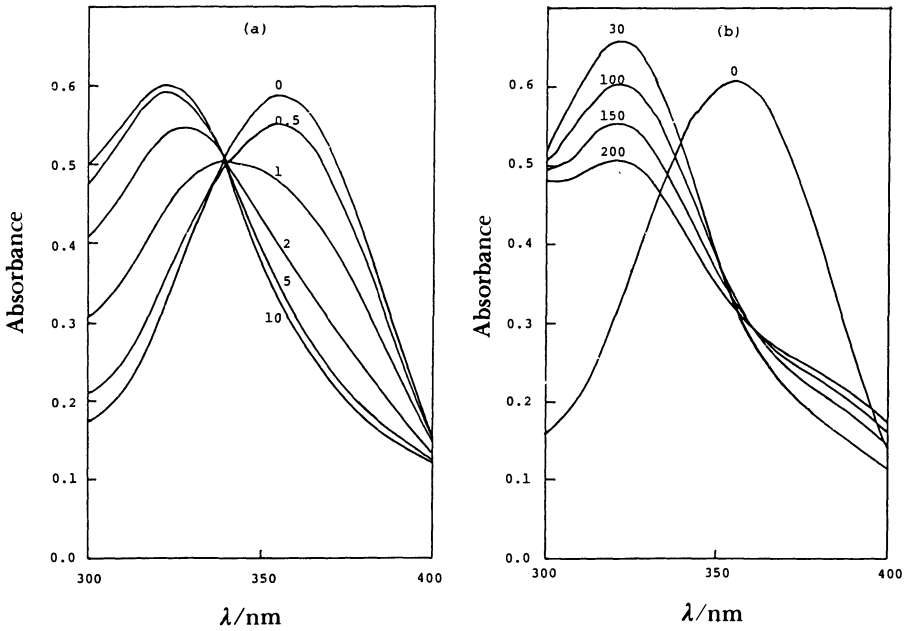

Fig. 2. Spectral changes of 1-(substituted benzyl)dihydropyridines (BPDH) in the presence of various amounts of zinc perchlorate in CH_3CN. [dihydropyridine]=0.1 mM. The numbers indicate the ratio [$Zn(ClO_4)_2$]/[dihydropyridine]. a) *p*-Cl, b) *p*-Me.

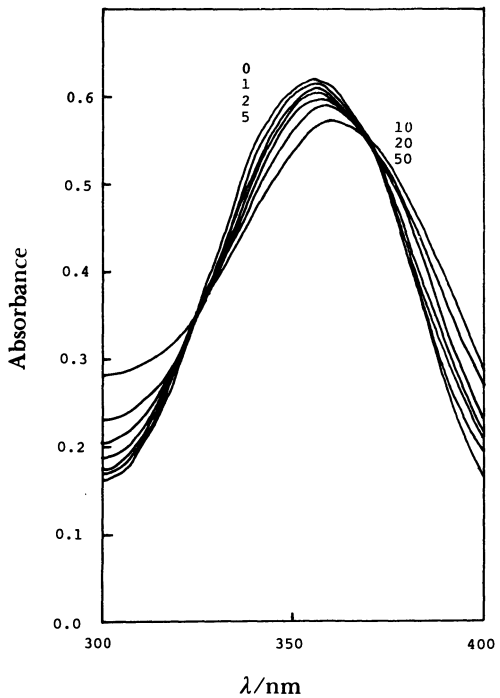

Fig. 3. Spectral changes of BPDH in the presence of $Zn(NO_3)_2$. The numbers indicate the ratio [$Zn(NO_3)_2$]/[BPDH].

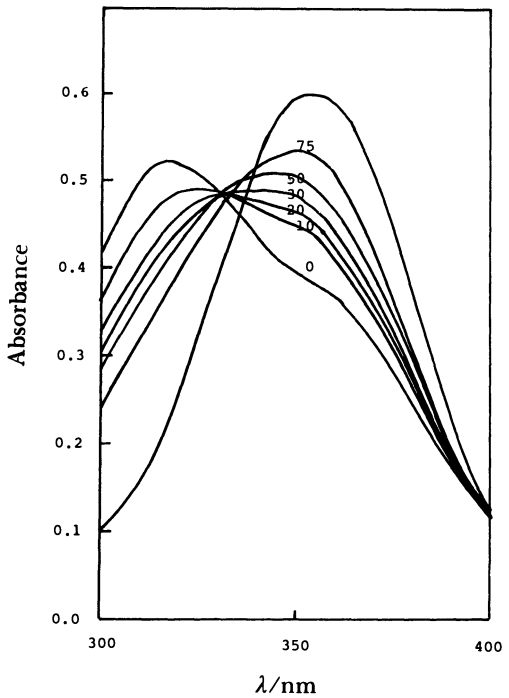

Fig. 4. Spectral changes of the BPDH-zinc ion complexes induced by addition of TBAP. [BPDH]= 0.1 mM; [$Zn(ClO_4)$]=3 mM. The numbers indicate the ratio [TBAP]/[$Zn(ClO_4)_2$].

of the resonance form **A** (shown in Fig. 1) and then the geometry around the ring nitrogen becomes more pyramidal to be suitable for accomodation of a metal cation, whereas an electron-donating group increases the contribution of the resonance form **C**, which makes the carbonyl oxygen more Lewis basic than the ring nitrogen.

Figure 4 illustrates the spectral changes as a function of the concentration of tetrabutylammonium perchlorate (TBAP); as the 320 nm band diminishes, the original 355 nm band develops. These observations can only be consistent with the conclusion that the absorption at 320 and 365 nm should be ascribed to cationic complexes of zinc monoperchlorate with the dihydropyridine nitrogen and the amide oxygen, respectively, and these positively charged complexes would be readily decomposed by addition of perchlorate anion. In the meantime, these complexes are completely hydrolyzed by water in excess to regenerate the original BPDH. Thus, the following are the overall equilibria established for the complexation between zinc and BPDH in solution:

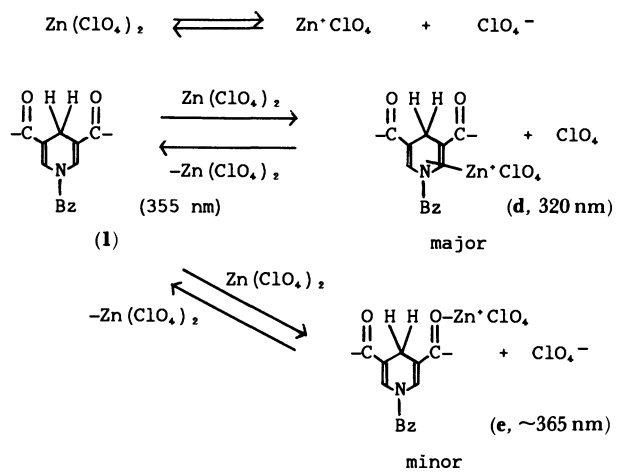

Scheme 1.

Meanwhile, the 1-methyl derivative (MPDH, **2**) behaves in spectroscopically a similar manner to the 1-benzyl derivative. In a series of the spectral changes an excellent isosbestic point can be seen at 342 nm on the original MPDH curve and no complex characterized by a red shift is produced in detectable concentration. Thus, metal coordination onto the dihydropyridine moiety rather than onto the amide carbonyl is dominating, since the ability of the 1-methyldihydropyridine moiety for coordination is superior to that of the 1-benzyldihydropyridine moiety owing to the less sterically hindering nature of the methyl vs. benzyl group rather than the electronic origin.

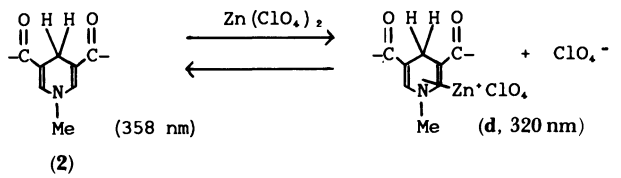

On the other hand, an absorption maximum of a typical NADH model, 1-benzyl-1,4-dihydronicotinamide (BNAH, **3**, λ_{max} 345 nm), was previously reported to shift toward a longer wavelength on complexation;[6] for example, 357 and 358 nm with magnesium and zinc perchlorates, respectively. It should be emphasized, however, that no spectral change was observed even by addition of a large excess (100-fold relative to BNAH) of TBAP probably because of the strong ability of the metal complexation of BNAH relative to the association of Zn^+ClO_4 with ClO_4^-.[6] Incidentally, the complexing ability (K_m) of BNAH has been estimated to be one order of magnitude greater than that of BPDH.[3,6]

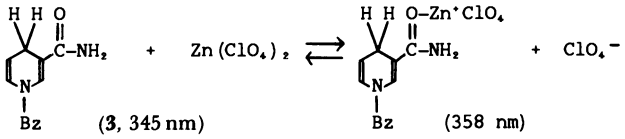

Spectral Changes of Dihydropyridine-Lead(II) Complexes. Inspection of the spectra in Fig. 5a and 5b is quite instructive. Upon addition of lead perchlorate to a BPDH solution, two positively charged complexes may be inferred to be produced; a definite absorption band appears at 325 nm in the range of lead perchlorate concentrations 0—1 mM, which corresponds to a 1:1 complex of the dihydropyridine nitrogen and Pb^+ClO_4 (**g**). Further addition of the metal perchlorate gives, at the sacriface of the 325 nm band, another band at around 385 nm due probably to the complex between the dihydropyridine nitrogen and lead perchlorate (**h**). In order to verify this assignment, the effect of addition of TBAP on spectral changes was examined. The results are displayed in Fig. 6; as the band at 325 nm diminished, the corresponding broad band newly developed at around 385 nm and there was observed a single definite isosbestic point between these bands over the wide range of changing perchlorate concentrations. It is of particular interest to point out that the isosbestic point is not on the original BPDH curve, indicating that, in contrast to zinc complexes, the positively charged lead complexes do not furnish the free BPDH, even if large excesses of perchlorate anions are added to the solution. Instead, the proportion of the uncharged complex **h** is increased with increasing concentrations of TABP; namely, in the presence of excess TABP only the complex **h** can exist in a relatively stable form. This result allows the conclusion that bonding of BPDH to Pb^{2+} may be much stronger than that to Zn^{2+} because of the smaller hydration enthalpy and/or the larger ionic radii of Pb^{2+} than Zn^{2+} to be capable of accomodating two bulky perchlorate anions. Therefore, we may say that the ring nitrogen can be complexed not by lead perchlorate but by a lead monoperchlorate cation probably for its steric requirements.

In contrast to the characteristic feature of zinc com-

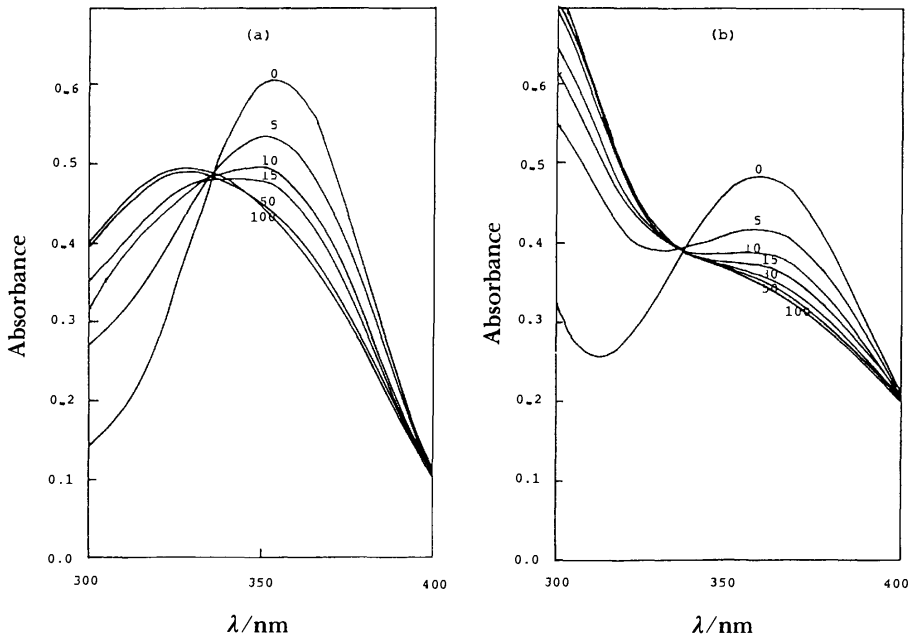

Fig. 5. Spectral changes of BPDH in the presence of various amounts of lead perchlorate: (a) 0—1.0 mM; (b) 3.0—20.0 mM. The numbers indicate the ratio $[Pb(ClO_4)_2]/[BPDH]$.

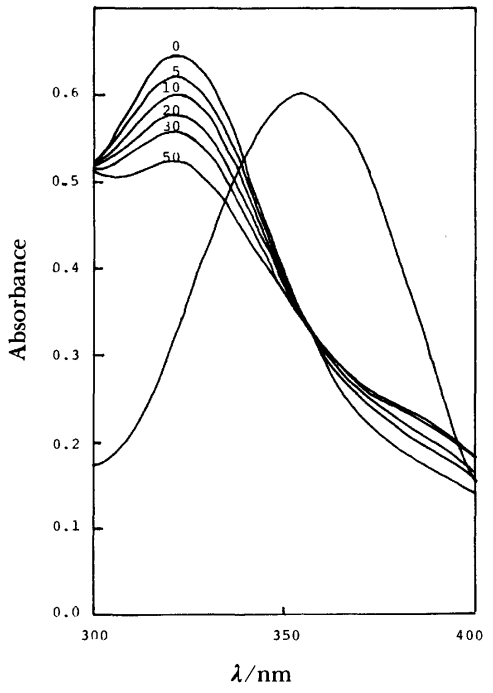

Fig. 6. Spectral changes of BPDH induced by addition of various amounts of TBAP in the presence of lead perchlorate. [BPDH]=0.1 mM; $[Pb(ClO_4)_2]$=3.0 mM. The numbers indicate the ratio $[TBAP]/[Pb(ClO_4)_2]$.

plexation, definite evidence for the presence of a complex **f** bearing a red-shifted band was not obtained. Even in any case examined here, the presence of a complex between the metal ion and the dihydropyridine with a stoichiometry of 1:2 or more was not evidenced under the present conditions, although such a higher metal complex of a dihydropyridine has been precedented with 3,5-diethoxy-2,6-dimethyl-1,4-dihydropyridine as was reported by Pandit.[9] From the above results, the complexation events can be summarized as in Scheme 2:

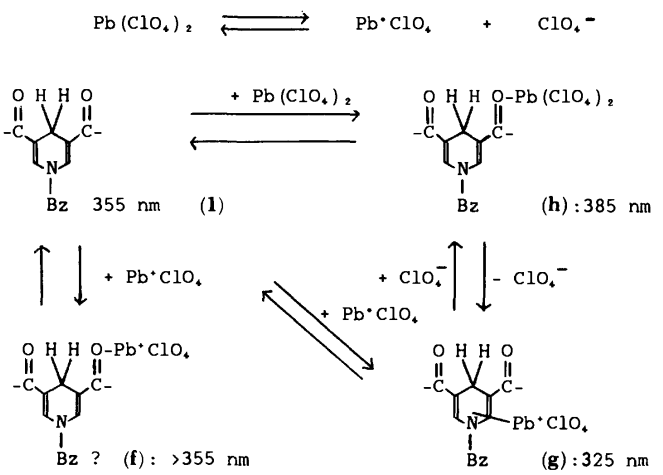

Scheme 2.

We shall discuss in the next section that the kinetic and spectroscopic features are closely interrelated.

Effect of Metal Cations on the Rate of Reduction. In the previous paper, we reported that bivalent metal ions catalyze the nitrosobenzene reduction with BPDH according to a Michaelis-Menthen type saturation kinetics and a linear relationship was found between

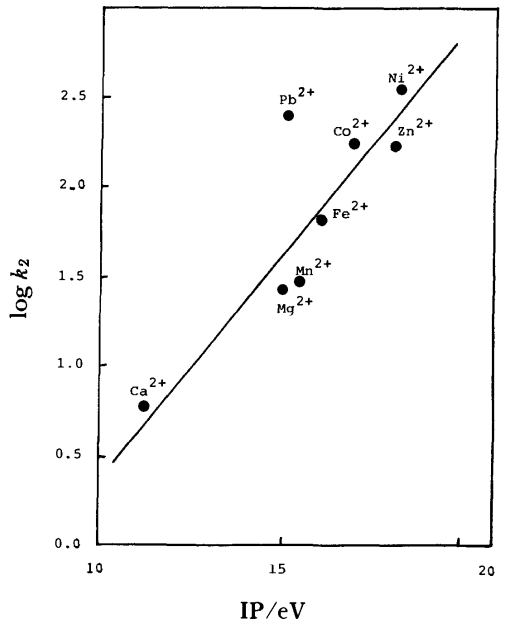

Fig. 7. Plot of log k_2 vs. ionization potential of the metal ion for the reduction of nitrosobenzene with BPDH in the presence of bivalent metal ions in CH_3CN under nitrogen at 25 °C. [metal perchlorates]=3.0 mM; [nitrosobenzene]=1.0 mM.

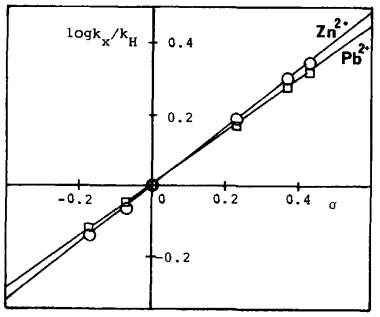

Fig. 8. Hammett plots for reduction of substituted nitrosobenzenes with BPDH in the presence of zinc and lead perchlorates in CH_3CN under nitrogen. [metal perchlorates]=3.0 mM; [nitrosobenzenes]=1.0 mM.

log k_2 and the ionization potentials of metal ions with a positive slope.[6]

We have found here that the rate with lead perchlorate as catalyst is somewhat higher than the rate with zinc perchlorate and lead ion is one order of magnitude active than metal ions such as Mn^{2+} and Mg^{2+} having a similar ionization potential (Fig. 7). As for zinc and lead perchlorates, the effect of the substituents (X) in nitrosobenzenes was studied, the metal ion concentration being kept constant at 30×10^{-4} M. When σ parameters are used, the Hammett plots exhibit straight lines (ρ: 0.81 and 0.75 for zinc and lead salts, respectively). The similarlity in magnitude of the Hammett ρ values is indicative of both reductions as occurring by way of the same mechanism (Fig. 8).

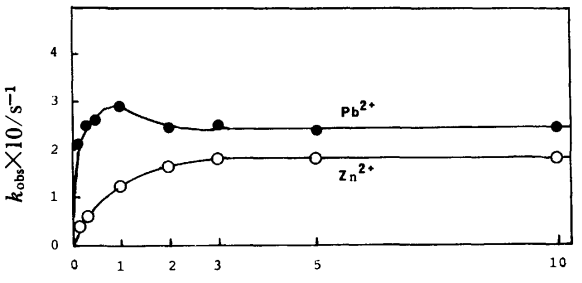

Fig. 9. Reduction of nitrosobenzene in the presence of changing amounts of bivalent metal perchlorates in CH_3CN at 25 °C under nitrogen. [BPDH]= 0.1 mM; [nitrosobenzene]=1.0 mM.

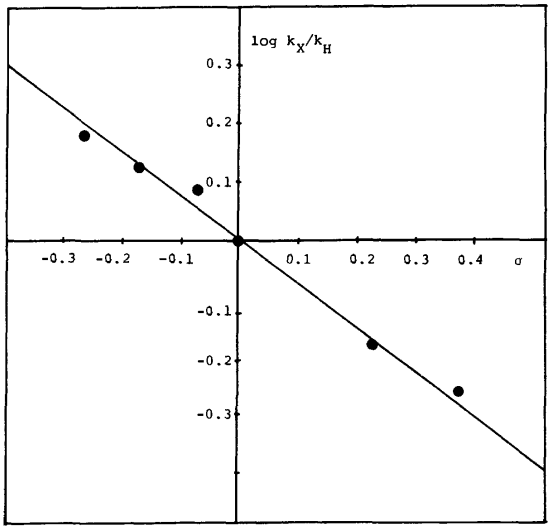

Fig. 10. Hammett plot for metal ion-catalyzed reduction of nitrosobenzene with 1-(substituted benzyl) BPDH in CH_3CN under nitrogen. [metal perchlorates]=5.0 mM. The reaction conditions are the same as described in Fig. 9, unless noted otherwise.

In Fig. 9 are depicted the plots of k_{obs} versus the concentrations of $Pb(ClO_4)_2$ and $Zn(ClO_4)_2$ for comparison. The clear saturation curve for zinc perchlorate might be explained by either or both of the following assumptions; the 320 and 360 nm zinc complexes (**d** and **e** types) are kinetically almost equivalent, or these complexes exist in the same ratio throughout changing concentrations of zinc perchlorate. In order to test the former assumption, an experiment was done, in which the reduction of nitrosobenzene with 1-(substituted benzyl)dihydropyridines was studied. The plotting of the logarithm of the observed rate constant against the Hammett σ constant affords a linear correlation within the experimental error (Fig. 10), which would presents a piece of evidence that, despite the overall differences in structure between complexes **d** and **e**, their kinetic behavior is inherently identical. Thus, we may safely say that zinc ion in any complex is displaced to the same position most suitable for the

Table 2. K_m and k_2 Values for Metal Ion-Catalyzed Nitrosobenzene Reduction

Metal ion	Ionization potential/eV	Ionic radius/Å	K_m/M^{-1}	$10^{-3}k_2/M^{-1}s^{-1}$
Zn^{2+} [a]	17.96	0.74	1870	1.80
Zn^{2+} [b]			1350	0.75
Pb^{2+} [a]	15.03	1.24	18400	2.44

a) Counter anion: ClO_4^-. b) Counter anion: NO_3^-.

transition state of reduction, as illustrated below:[5]

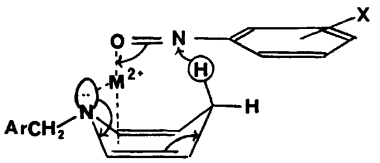

Unlike zinc perchlorate giving a usual saturation plot, lead perchlorate exhibits a significant feature in the rate-concentration plot; the maximum rate is observed at around 1 mM, suggesting that at least two kinetically important species are present in solution; namely, at its lower concentrations (<1 mM) added $Pb(ClO_4)_2$ would almost completely dissociate into Pb^+ClO_4 and ClO_4^- and the BPDH·Pb^+ClO_4 complex (**g**) thus formed could be the major species active for reduction, while at concentrations above 1 mM the BPDH·$Pb(ClO_4)_2$ complex (**h**) might also participate in the reaction. It is natural to conclude that the reaction with the former complex is faster than is the reaction with the latter and then the maximum rate has been observed. The contribution of the not identified complex **f** toward the overall rate, if any, is negligible, because of its only minor existence. Thus, the overall reaction proceeds by two competitive pathways involving totally different transition state, as illustrated below;

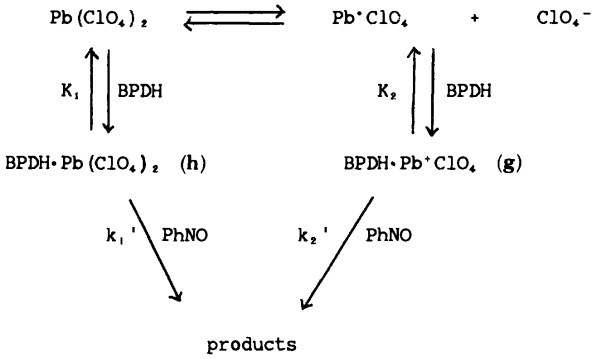

Scheme 3.

In Table 2 are compared the K_m and k_2 values calculated by assuming a Michaelis-Menthen equation, in which K_m is an association constant between BPDH and metal ion and k_2 is a second-order rate constant for the reaction of BPDH·metal complex and the substrate ArNO.[6] In the case of lead perchlorate, the data

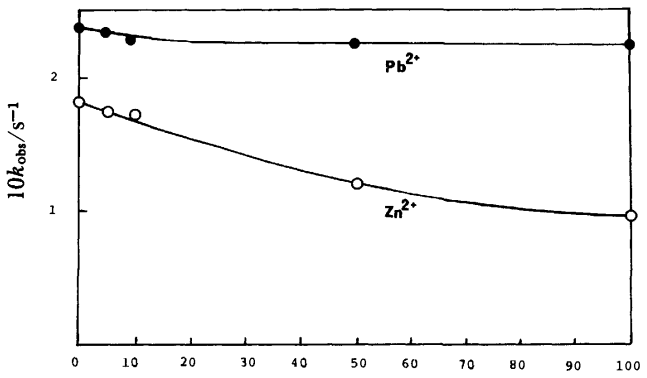

Fig. 11. Effect of addition of altering amounts of TBAP on rate of metal ion-catalyzed reduction of nitrosobenzene with BPDH in CH_3CN under nitrogen. [metal perchlorates]=3.0 mM.

points at lower metal ion concentrations (<1 mM) were only used for the calculation of K_m and k_2 values. The table shows that the apparent association

$$DH + M^{2+} \overset{K_m}{\rightleftharpoons} [DH\cdot M^{2+}] \xrightarrow{k_2[ArNO]} D^+ + PhNHO^- + M^{2+}$$

constant (K_m) for zinc complexes is tenfold smaller than that for lead complexes. This implies that the zinc complexes are relatively quite unstable as compared with the corresponding lead complexes. In order to verify this statement further, the effect of TBAP on the rate was also examined and the results thus obtained are depicted in Fig. 11; as for zinc perchlorate, the rate decreases steadly with increasing concentrations of added TBAP, indicating again all of the zinc complexes being unstable toward addition of perchlorate anions. On the other hand, as for the lead complexes, only a little rate depression resulted. This is in line with the conclusion which would be expected from the spectroscopic analysis and suggests that the uncharged BPDH·$Pb(ClO_4)_2$ (**h**) complex is slightly less reactive than the cationic BPDH·Pb^+ClO_4 complex (**g**).

References

1) C.-I. Brändén, H. Jörnvall, H. Eklund, and B. Furugren, "Alcohol Dehydrogenases" in "The Enzymes," ed. by P. D. Boyer, Academic Press, New York (1975), Vol. II; A. Frerst, "Enzyme Structure and Mechanism," 2nd ed., W. H. Freeman and Co., New York (1985), pp. 390—404; E.

Cedergren-Zeppezauer, J-P. Samama, and H. Eklund, *Biochemistry*, **21**, 4895 (1982).

2) a) D. J. Creighton and D. S. Sigman, *J. Am. Chem. Soc.*, **98**, 4619 (1976); J. B. Steeven and U. K. Pandit, *Tetrahedron*, **39**, 1395 (1983). b) Y. Ohnishi, M. Kagami, and A. Ohno, *J. Am. Chem. Soc.*, **97**, 4766 (1975); Y. Ohnishi, T. Numakunai, T. Kimura, and A. Ohno, *Tetrahedron Lett.*, **1976**, 2699; A. Ohno, M. Ikeguchi, T. Kimura, and S. Oka, *J. Chem. Soc., Chem. Commun.*, **1978**, 328; J. G. de Vries and R. M. Kellogg, *J. Am. Chem. Soc.*, **101**, 2759 (1979); A. Ohno and S. Ushida, "Lecture Notes in Bio-organic Chemistry," No. 1, Springer Verlag, Heiderberg (1986).

3) D. J. Creighton and D. S. Sigman, *J. Am. Chem. Soc.*, **93**, 6314 (1971); D. C. Dittmer, A. Lombardo, F. H. Batzold, and C. S. Greene, *J. Org. Chem.*, **41**, 2976 (1976); A. Ohno, T. Kimura, H. Yamamoto, S. G. Kim, S. Oka, and Y. Ohnishi, *Bull. Chem. Soc. Jpn.*, **50**, 2385 (1977); S. Fukuzumi, Y. Kondo, and T. Tanaka, *Chem. Lett.*, **1983**, 485.

4) H. Awano, T. Hirabayashi, and W. Tagaki, *Tetrahedron Lett.*, **25**, 2005 (1984); H. Awano and W. Tagaki, *Bull. Chem. Soc. Jpn.*, **59**, 3117 (1986).

5) E. V. Brown and W. H. Kipp, *J. Org. Chem.*, **36**, 170 (1971); R. E. Lutz and M. R. Lytton, *ibid.*, **2**, 68 (1937); R. A. Abramovitch, S. R. Challand, and E. F. V. Scriven, *ibid.*, **37**, 2705 (1972); K. Tabei and A. Nagakura, *Bull. Chem. Soc. Jpn.*, **38**, 965 (1965).

6) H. Awano, K. Takemoto, H. Ohya, M. Tomio, S. Tamagaki, and W. Tagaki, *Bull. Chem. Soc. Jpn.*, **60**, 1887 (1987).

7) E. M. Evleth, *J. Am. Chem. Soc.*, **89**, 6445 (1967); A. Ohno, T. Kimura, H. Yamamoto, S. G. Kim, S. Oka, and Y. Ohnishi, *Bull. Chem. Soc. Jpn.*, **50**, 1535 (1977); G. R. Hays, R. Huis, B. Coleman, D. Clague, J. W. Verhoeven, and F. Rob, *J. Am. Chem. Soc.*, **103**, 5140 (1981); A. Glasfeld, P. Zbinden, M. Dobler, S. A. Benner, and J. D. Dunitz, *J. Am. Chem. Soc.*, **110**, 5152 (1988).

8) F. C. Paul, H. Arora, and S. I. Chadha, *Inorg. Nucl. Chem. Lett.*, **6**, 469 (1970); M. Hughes and R. H. Prince, *Chem. Ind. (London)*, **1975**, 648. S. Shinkai, Y. Kusano, T. Ide, T. Sone, and O. Manabe, *Bull. Chem. Soc. Jpn.*, **51**, 3544 (1978).

9) R. A. Gase, G. Boxhoorn, and U. K. Pandit, *Tetrahedron Lett.*, **1976**, 2889.

Synthesis of 2-Alkyl-Substituted 1,3-Diketones via the 1,4-Addition of the Grignard Reagents to α,β-Unsaturated Imidates

Seiichi Inoue, Osamu Suzuki, and Kikumasa Sato*
Department of Applied Chemistry, Faculty of Engineering, Yokohama National University, Tokiwadai, Hodogaya-ku Yokohama 240
(Received November 17, 1988)

4-Propyl-3,5-nonanedione was selectively formed by the reaction of methyl *N*-phenylacrylimidate with ethylmagnesium bromide in 80% yield. Similar diketones were obtained from methyl *N*-phenylcrotonimidate and *N*-phenylcinnamimidate with the Grignard reagents. The coupling of *N*-magnesio α-methoxy enamine and ketenimine, both of which are formed through the initial 1,4-addition of the Grignard reagent to α,β-unsaturated imidate, is the most plausible pathway for the formation of the diketones.

There is presently an interest in imidates (imino ethers) and related compounds from both synthetic and mechanistic points of view.[1] When imidates were treated with acyl halides, imidates gave amides. This reaction has been very important for amide side chain syntheses of β-lactam antibiotics.[2] On the other hand, Meyers et al. reported that the reaction of 2-alkenyldihydro-1,3-oxazines, cyclic version of α,β-unsaturated imidates, with organolithium or the Grignard reagents gave aldehydes or ketones via ketenimines as the key intermediates.[3] It has been reported by Adams and Reifschneider[4] that methyl *N*-phenylsulfonyl-3,3-diphenylpropionimidate is formed by the reaction of methyl *N*-phenylsulfonylcinnamimidate with phenylmagnesium bromide. In this case, however, elimination of methoxymagnesium bromide from the initial 1,4-addition product has not been observed. In this instance we became interested in whether acyclic α,β-unsaturated imidates may afford nucleophilic species upon reaction with organometallic compounds or afford electrophilic species such as ketenimines through further elimination of metal alkoxide. Now we found that the acrylimidates selectively undergo initial 1,4-addition of the Grignard reagents to finally produce 2-alkyl-1,3-diimines as a result of selective coupling between the two intermediates, magnesio enamines and ketenimines.[5] In this paper we wish to report the results in detail and discuss the pathway of the reaction.

Results and Discussion

A series of α,β-unsaturated imidates (**1**) was prepared by the reaction of the corresponding amides and trimethyloxonium tetrafluoroborate according to the literature.[6]

Treatment of methyl *N*-phenylacrylimidate (**1a**) with one equiv. of ethylmagnesium bromide in ether at 0 °C, followed by work-up with dilute hydrochloric acid, afforded 4-propylnonane-3,5-dione (**3a**) as a colorless liquid in 10% yield.

It was then found out that the yield of dione **3a** increased with increase of the amount of ethylmagnesium bromide and the maximum yield (80% yield) was obtained with 6 equiv. of the Grignard reagent (Fig. 1). Ethyl *N*-phenylacrylimidate gave the same diketone (**3a**). Similar treatment of **1a** with 6 equiv. of 2-phenylethylmagnesium and phenylmagnesium bromide also afforded 1,3-diketones **3b** and **3c**, respectively (Table 1, Eq. 1). It was thought that these diketones came out from two moles of **1a** and three moles of the Grignard reagents.

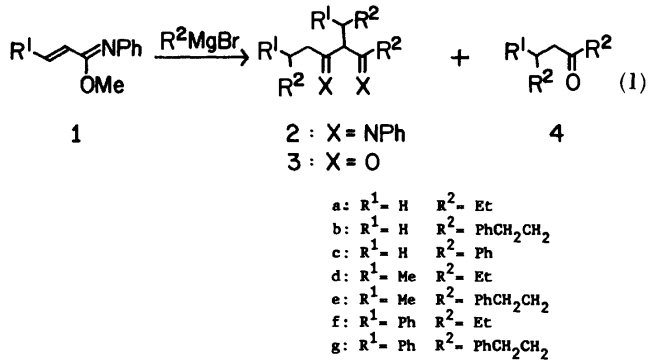

Reaction of crotonimidate (**1b**) and cinnamimidate (**1c**) with the alkyl Grignard reagents afforded 1,3-diimines **2** as stable liquids along with minor amounts of monoketones **4**. The diimines (**2**) could be hydrolyzed with 1 M HCl (1 M=1 mol dm^{-3}) at room tem-

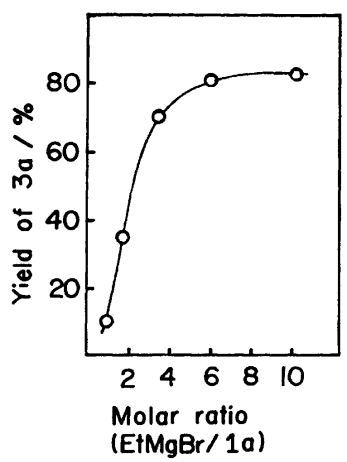

Fig. 1. Effect of the amount of the Grignard reagent.

Table 1. Diimines and Diketones from **1**[a]

1	R^1	R^2	Reaction conditions		Yield/%[b]		
			Temp	Time/h	2	3	4
1a	H	Et	0 °C	7	—	80	—
1a	H	$PhCH_2CH_2$	0 °C	5	—	64	—
1a	H	Ph	0 °C	8	—	74	—
1b	Me	Et	0 °C	4.5	75	80[c]	18
1b	Me	$PhCH_2CH_2$	r.t.	7.5	69	72[c]	21
1c	Ph	Et	0 °C	4	72	85[c]	13
1c	Ph	$PhCH_2CH_2$	r.t.	7.5	26	75[c]	44

a) Reactions were carried out in ether with 6 equiv. of the Grignard reagents. b) Isolated yield. c) The yield of **3** formed by hydrolysis of **2**.

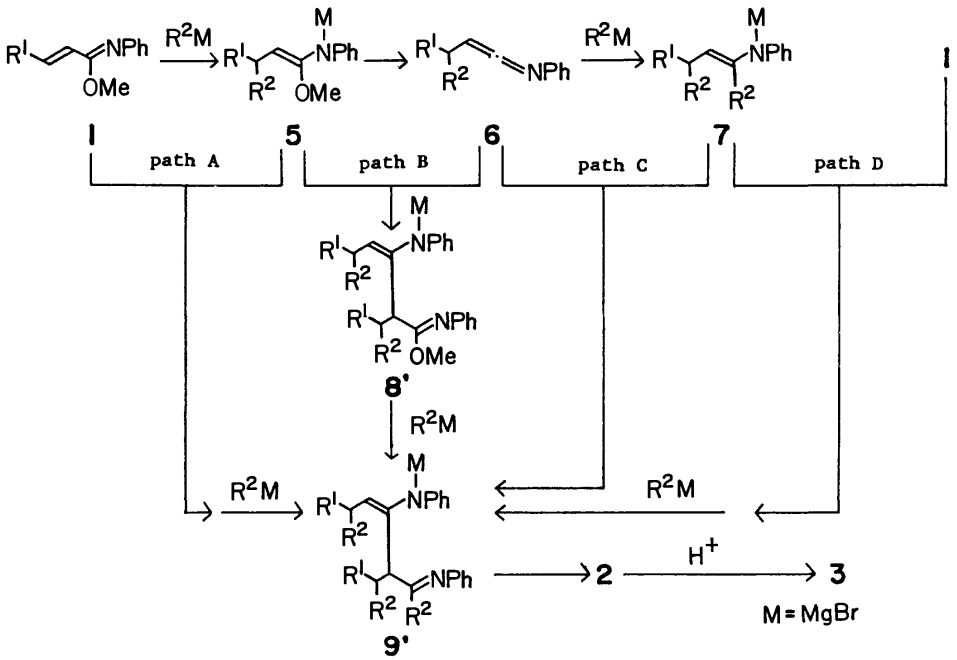

Scheme 1.

perature for 1—4 days to give 1,3-diketones **3** (Table 1). These results clearly suggest that the reaction of **1a** with the Grignard reagents leads to diimines **2** which are susceptible to hydrolysis during the work-up.

In contract with acryl or β-monosubstituted acrylimidates, α-substituted and β,β-disubstituted imidates, e.g., methacrylimidate, (*E*)-2-methyl-2-butenimidate, and 3-methyl-2-butenimidate gave only monoketones (**4**) upon reaction with alkyl and aryl Grignard reagents.

Several interpretations can be afforded as to the mechanism of formation of diketone **3** (Scheme 1). At first, we tried to detect a presumable key intermediate **6**. But ketenimine **6** was not isolated even by the use of limited quantities of the Grignard reagent or by carring out the reaction at low temperature. When 6 equiv. of *t*-butylmagnesium chloride was used to intercept the reaction at an intermediary stage by preventing further reactions by steric hindrance, β-imino imidate **8a** was obtained in 60% yield (Eq. 2). Moreover, treatment of **1a** with 6 equiv. of ethylmagnesium bromide in tetrahydrofuran (THF), followed by work-up with dilute hydrochloric acid gave 2-valerylpentanoate (**8b**) in 36% yield along with diketone **3a** (29% yield) (Eq. 3). The above results of the formation of β-imino or β-keto esters strongly suggest the presence of **8'** as intermediates in the reaction.

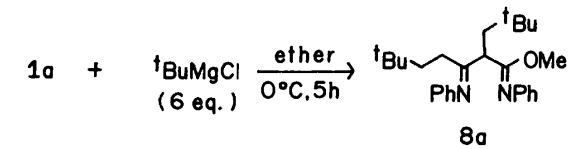

(2)

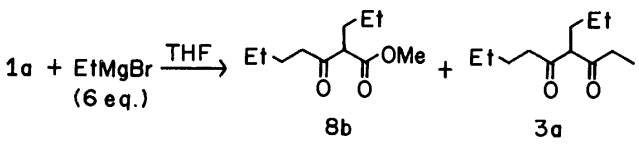

(3)

When a mixture of **1a** and 1-phenylimino-1-propene (**6a**), prepared by the reaction of *N*-phenylpropionimidoyl chloride with triethylamine,[7] was treated with 10 equiv. of ethylmagnesium bromide, 4-propyl-3,5-heptanedione (**10a**) was formed in 15% yield as well as **3a** in 43% yield (Eq. 4).

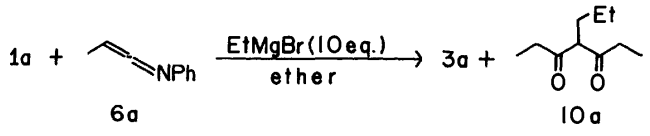

(4)

The formation of diketone **10a** suggests that the coupling reaction of *N*-magnesio α-methoxy enamine (**5**) with ketenimine (**6**) is probable (path B). Furthermore, the addition of **1c** to an ethereal solution of the *N*-magnesio enamine, which was in situ prepared from *N*-(1-methylhexylidene)aniline and ethylmagnesium bromide, at 0 °C resulted only in recovering the starting imidate (**1c**) and the imine. These results are not favorable to paths C and D.

In order to test whether the coupling of unsaturated imidate **1** and *N*-magnesio α-methoxy enamine **5** (path A) was possible, the reaction of **1a** with ethylmagnesium bromide was carried out in the presence of methyl *N*-phenylpropionimidate (**5a**). If the coupling reaction between **1** and **5** is possible, *N*-magnesio α-methoxy enamine (**5**) should also react with **5a** to give diketone **10a** and methyl 2-propyl-3-oxopentanoate (**11**) as well as diketone **3a**. The reaction of an equimolar mixture of **1a** and **5a** with 6 molar equiv. of ethylmagnesium bromide in ether at 0 °C for 3 h turned out to give **3a** in 77% yield as a sole product and **5a** was recovered quantitatively (Eq. 5).

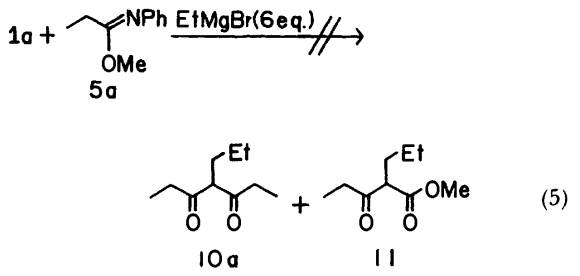

(5)

Although the methoxyl group in **5a** was not replaced by the ethyl group upon reaction with ethylmagnesium bromide as shown above, this fact does not deny the path from **8′** to **9′**. A facile replacement of the methoxy group with the Grignard reagent in imidates of the type of **8′** was demonstrated as follows. β-Imino imidate **8c**, the precursor of **8b**, was prepared by the reaction of **1a** and 6 equiv. of ethylmagnesium bromide in THF at 0 °C (vide supra) followed by work-up with aqueous ammonium chloride. When this β-imino imidate **8c** was treated with methylmagnesium iodide in ether at 0 °C, diimine **10b** was formed immediately and, after work-up with dilute hydrochloric acid, diketone **10c** was isolated in 31% yield (Eq. 6). This facilitated alkylation of imidates at the imino nitrogen can be explained by the chelating effect of the imino nitrogen at the β-position toward alkylmagnesium species.

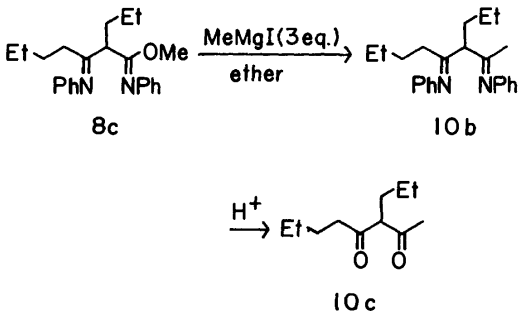

(6)

Finally, the possibility of the initial 1,2-addition, instead of the 1,4-addition discussed so far, of the Grignard reagent to imidate **1** can be deniable by the fact that the reaction of magnesio enamine **7** and **1** did not occur.

By the fact mentioned above, the most plausible pathway seems to involve the initial conjugate addition of the Grignard reagent to imidates affording very reactive *N*-magnesio α-methoxy enamine **5**, which leads to unstable, electrophilic ketenimine **6** upon β-elimination of metal methoxide. The ketenimine (**6**) is selectively alkylated by the strongly nucleophilic species **5** to yield **8′** which are then alkylated at the imidate carbon by the Grignard reagent to give diimine precursor (**9′**). When α-methylated and β,β-dimethylated unsaturated imidates were used, ketenimines **6** could not react with **5** by the steric hindrance, then **6** are attacked by the Grignard reagent to give **7**.

When organolithium reagent was used instead of the Grignard reagents, ketenimine (**6**) was exclusively trapped by the organolithium reagent instead of **5** to give monoketone (**4**).

The most unusual feature of the reaction of α,β-unsaturated imidates with the Grignard reagents is the facile formation of 2-branched 1,3-diketones by the selective coupling of **5** and **6**.

Experimental

General. Boiling points and melting points are uncorrected. IR spectra were measured on a Hitachi 260-10 spectrometer. ^{1}H NMR spectra were obtained with a JEOL JNM-C-60M or a JEOL FT-90-Q with tetramethylsilane as an internal standard. Column chromatography was normally effected with Wakogel C-200 (Wako Pure Chemical Industries). GLC analyses were performed on a Shimadzu GC-7A chromatograph using a column packed with Silicone OV-17 (3 mm×3 m). Trimethyloxonium tetrafluoroborate[9] and α,β-unsaturated imidate[6] were prepared according to the literature. The structure of the known compounds were

established on the basis of their spectroscopic properties and from descriptions in the literature.

Reaction of Methyl *N*-Phenylacrylimidate (1a) with Grignard Reagents. To a stirred ether solution of the Grignard reagent (18.6 mmol), **1a** (0.50 g, 3.1 mmol) was added at 0 °C and stirred for 5—8 h at 0 °C. Then the solution was poured into 1 M HCl at 0 °C and stirred for 1 h. The resulting mixture was extracted with ether and the organic layer was washed with $NaHCO_3$ aq. then brine and dried over $MgSO_4$. After filtration, the solvent was removed and the residue was purified by column chromatography (silica gel-hexane/chloroform) to give diketone.

4-Propyl-3,5-nonanedione (3a): bp 129—130 °C/11 mmHg (1 mmHg=133.322 Pa.); IR (neat) 2970, 1730, and 1700 cm^{-1}; ^1H NMR ($CDCl_3$) δ=0.91 (6H, m), 1.04 (3H, t, J=7 Hz), 1.27 (4H, m), 1.53 (2H, m), 1.82 (2H, m), 2.46 (2H, t, J=7 Hz), 2.49 (2H, q, J=7 Hz), and 3.67 (1H, t, J=7 Hz); MS m/z 198 (M^+).

Found: C, 72.70; H, 11.43%. Calcd for $C_{12}H_{22}O_2$: C, 72.68; H, 11.18%.

1,9-Diphenyl-4-(3-phenylpropyl)-3,5-nonanedione (3b): IR (neat) 3060, 2860, 1725, 1695, 750, and 700 cm^{-1}; ^1H NMR (CCl_4) δ=1.50 (8H, m), 2.60 (10H, m), 3.42 (1H, t, J=7 Hz), and 7.12 (15H, s).

Found: C, 84.51; H, 8.13%. Calcd for $C_{30}H_{34}O_2$: C, 84.46; H, 8.03%.

1,5-Diphenyl-2-benzyl-1,3-pentanedione (3c): mp 66—67 °C (MeOH); IR (KBr) 1710, 1680, 740, and 700 cm^{-1}; ^1H NMR ($CDCl_3$) δ=2.79 (4H, bs), 3.30 (2H, d, J=7 Hz), 4.79 (1H, t, J=7 Hz), 7.23 (10H, s), and 7.70 (5H, m); MS m/z 342 (M^+).

Found: C, 83.96; H, 6.46%. Calcd for $C_{24}H_{22}O_2$: C, 84.18; H, 6.48%.

Reaction of Methyl *N*-Phenylcrotonimidate (1b), Methyl *N*-Phenylcinnamimidate (1c) with Alkyl Grignard Reagents. To a stirred ether solution of Grignard reagent (18.6 mmol), imidate (3.1 mmol) was added at 0 °C. After further stirring at 0 °C or r.t., the resulting mixture was poured into aqueous ammonium chloride then extracted with ether and dried over $MgSO_4$. After filtration, the solvent was removed and distilled with Glass Tube Oven to give monoketone. The resulting residue was purified by column chromatography (silica gel-hexane/chloroform) to give diimine. To a solution of diimine (1 mmol) in ether (10 ml), 1 M HCl (40 ml) was added and stirred for 1—4 days. The resulting mixture was extracted with ether and washed with brine, dried over $MgSO_4$. After filtration, the solvent was removed and the residue was purified by column chromatograpy (silica gel-hexane/chloroform) to give diketone. The following compounds were prepared.

5-Methyl-3-heptanone (4d): bp 152—154 °C (lit,[10] 153—155 °C).

***N,N'*-Diphenyl-7-methyl-4-(1-methylpropyl)-3,5-nonanediimine (2d):** IR (neat) 2960, 1640, 1595, 755, and 700 cm^{-1}; ^1H NMR ($CDCl_3$) δ=1.00 (15H, m), 2.20 (10H, m), 3.73 (1H, d, J=7 Hz), and 6.87 (10H, m).

Found: C, 82.71; H, 9.64; N, 7.60%. Calcd for $C_{26}H_{36}N_2$: C, 82.93; H, 9.64; N, 7.44%.

7-Methyl-4-(1-methylpropyl)-3,5-nonanedione (3d): bp 133—134 °C/17 mmHg; IR (neat) 2960, 1720, and 1695 cm^{-1}; ^1H NMR (CCl_4) δ=0.89 (19H, m), 2.10 (8H, m), and 3.34 (1H, d, J=7 Hz); MS m/z 226 (M^+).

Found: C, 74.50; H, 11.57%. Calcd for $C_{14}H_{26}O_2$: C, 74.29; H, 11.58%.

5-Methyl-1,7-diphenyl-3-heptanone (4e): bp 174—175 °C/0.30 mmHg; IR (neat) 3030, 2930, 1715, 750, and 700 cm^{-1}; ^1H NMR (CCl_4) δ=1.10 (3H, d, J=7 Hz), 2.10 (10H, m), 3.37 (1H, m), and 7.12 (10H, s).

Found: C, 85.65; H, 8.61%. Calcd for $C_{20}H_{24}O$: C, 85.67; H, 8.63%.

***N,N'*-Diphenyl-7-methyl-4-(1-methyl-3-phenylpropyl)-1,9-diphenyl-3,5-nonanediimine (2e):** IR (neat) 3030, 2930, 1640, 1595, 750, and 700 cm^{-1}; ^1H NMR (CCl_4) δ=0.97 (6H, m), 2.10 (16H, m), 3.50 (1H, d, J=7 Hz), and 6.89 (25H, m).

Found: C, 87.66; H, 8.25; N, 4.33%. Calcd for $C_{44}H_{48}N_2$: C, 87.37; H, 8.00; N, 4.63%.

7-Methyl-4-(1-methyl-3-phenylpropyl)-1,9-diphenyl-3,5-nonanedione (3e): IR (neat) 3030, 2930, 1690, 750, and 700 cm^{-1}; ^1H NMR (CCl_4) δ=0.80 (3H, d, J=7 Hz), 0.83 (3H, d, J=7 Hz), 2.00 (16H, m), 3.32 (1H, d, J=7 Hz), and 7.05 (15H, s).

Found: C, 84.75; H, 8.35%. Calcd for $C_{32}H_{38}O_2$: C, 84.45; H, 8.42%.

5-Phenyl-3-heptanone (4f): bp 120—125 °C/2.5 mmHg (lit,[11] 255 °C).

***N,N'*-Diphenyl-4-(1-phenylpropyl)-7-phenyl-3,5-nonanediimine (2f):** IR (neat) 3030, 2930, 1640, 1595, 750, and 700 cm^{-1}; ^1H NMR (CCl_4) δ=1.54 (19H, m), 3.48 (1H, d, J=7 Hz), and 6.90 (20H, m).

Found: C, 86.62; H, 8.00; N, 5.20%. Calcd for $C_{36}H_{40}N_2$: C, 86.35; H, 8.05; N, 5.59%.

4-(1-Phenylpropyl)-7-phenyl-3,5-nonanedione (3f): IR (neat) 3040, 2970, 1720, 1700, 760, and 705 cm^{-1}; ^1H NMR (CCl_4) δ=0.68 (9H, m), 1.67 (8H, m), 3.17 (2H, m), 3.93 (1H, d, J=7 Hz), and 7.15 (10H, s); MS m/z 350 (M^+).

Found: C, 82.51; H, 8.74%. Calcd for $C_{24}H_{30}O_2$: C, 82.24; H, 8.63%.

1,5,7-Triphenyl-3-heptanone (4g): bp 194—196 °C/0.19 mmHg; IR (neat) 3030, 2915, 1715, 750, and 700 cm^{-1}; ^1H NMR (CCl_4) δ=2.10 (11H, m), 7.12 (15H, s).

Found: C, 87.97; H, 7.37%. Calcd for $C_{25}H_{26}O$: C, 87.68; H, 7.65%.

***N,N'*-Diphenyl-1,7,9-triphenyl-4-(1,3-diphenylpropyl)-3,5-nonanediimine (2g):** IR (neat) 3030, 2930, 1640, 750, and 700 cm^{-1}; ^1H NMR (CCl_4) δ=2.08 (16H, m), 3.50 (1H, d, J=7 Hz), and 6.89 (35H, m).

Found: C, 89.26; H, 6.91; N, 3.54%. Calcd for $C_{54}H_{52}N_2$: C, 88.97; H, 7.19; N, 3.84%.

1,7,9-Triphenyl-4-(1,3-diphenylpropyl)-3,5-nonanedione (3g): IR (neat) 3040, 2970, 1720, 1700, 760, and 705 cm^{-1}; ^1H NMR (CCl_4) δ=1.60 (6H, m), 1.76 (10H, m), 3.95 (1H, d, J=7 Hz), and 7.15 (25H, s).

Found: C, 87.41; H, 7.35%. Calcd for $C_{42}H_{42}O_2$: C, 87.16; H, 7.31%.

Reaction of 1a with *t*-Butylmagnesium Chloride. To a stirred ether solution of *t*-butylmagnesium chloride (31 mmol), ether solution of **1a** (0.50 g, 3.1 mmol) was added at 0 °C and stirred at r.t. for 5 h. After usual work-up, the residue was purified by column chromatography (alumina-dichloromethane) to give methyl *N*-phenyl-2-(2,2-dimethylpropyl)-6,6-dimethyl-3-phenyliminoheptanimidate (**8a**) (0.38 g, 60%); bp 165—170 °C/0.80 mmHg; IR (neat) 3030, 2960, 1660, 1245, 750, and 700 cm^{-1}; ^1H NMR (CCl_4) δ=0.77 (18H, m), 1.90 (6H, m), 3.67 (1H, t, J=7 Hz), 3.80 (3H, s), and 6.95 (10H, m); MS m/z 406 (M^+). Found: C, 79.74; H, 9.71; N,

6.58%. Calcd for $C_{27}H_{38}N_2O$: C, 79.76; H, 9.42; N, 6.89%.

Reaction of 1a with Ethylmagnesium Bromide in THF. According to the general procedure, 0.50 g (3.1 mmol) of **1a** and ethylmagnesium bromide (31 mmol) were treated in THF. After usual work-up, the residue was purified by column chromatography (silica gel-hexane/ethyl acetate) to give **3a** (111 mg, 36%), methyl 2-valerylpentanoate (**8b**) (89 mg, 29%); bp 130—135 °C/20 mmHg; IR (neat) 2960, 1740, and 1235 cm^{-1}; ^1H NMR (CCl_4) δ=0.95 (6H, m), 1.83 (10H, m), 3.29 (1H, t, J=7 Hz), and 3.67 (3H, s); MS m/z 200 (M^+).

Reaction of 1a and *N*-(1-Propenylidene)aniline (6a) with Ethylmagnesium Bromide. According to the general procedure, **1a** 0.50 g (3.1 mmol) and **6a** 0.40 g (3.1 mmol) were treated with 31 mmol of ethylmagnesium bromide in ether at 0 °C. After usual work-up, the residue was purified by column chromatography (silica gel-hexane/chloroform) to give **3a** (132 mg, 43%), 4-propyl-3,5-heptanedione (**10a**) (40 mg, 15%); IR (neat) 2950, 1720, 1695, and 1460 cm^{-1}; ^1H NMR (CCl_4) δ=0.90 (3H, t, J=7 Hz), 0.99 (6H, t, J=7 Hz), 1.45 (4H, m), 2.38 (4H, q, J=7 Hz), and 3.49 (1H, t, J=7 Hz); MS m/z 170 (M^+).

Reaction of Methyl *N*-Phenyl-3-(phenylimino)-2-propylheptanimidate (8c) with Methylmagnesium Iodide. 1a (0.50 g, 3.1 mmol) and 10 equiv. of ethylmagnesium bromide were treated in THF at 0 °C, then poured into aqueous ammonium chloride, and extracted with ether, the organic layer was dried ($MgSO_4$) and concentrated. The crude mixture was dissolved in ether (5 ml), added to methylmagnesium iodide in ether at 0 °C and stirred for 5 min then poured into 1 N HCl, stirred for 1 h. After usual work-up and distillation (125—130 °C/10 mmHg) to give a mixture of **3a** and 3-propyl-2,4-octanedione (**10c**); MS m/z 184 (M^+), which was separated by GLC.

References

1) R. Roger and D. G. Neilson, *Chem. Rev.*, **61**, 179 (1961); D. G. Neilson, "The Chemistry of Amidines and Imidates," ed by S. Patai, Wiley, New York (1975), pp. 385—489; J. P. Lokensgard, J. W. Fisher, and W. J. Bartz, *J. Org. Chem.*, **50**, 5609 (1985); A. Bongini, G. Cardillo, M. Orena, S. Sandri, and C. Tomasini, *ibid.*, **51**, 4905 (1986).

2) A. Koda, K. Takanobu, I. Isaka, T. Kashiwagi, K. Takahashi, S. Kawahara, and M. Murakami, *J. Pharm. Soc, Jpn.*, **92**, 459 (1972); T. Saito, K. Nishihata, and S. Fukatsu, *J. Chem. Soc., Perkin Trans. 1*, **1981**, 1085.

3) A. I. Meyers, E. M. Smith, and M. S. Ao., *J. Org. Chem.*, **38**, 2129 (1973); A. I. Meyers, A. C. Kovelesky, and A. F. Jurjevich, *ibid.*, **38**, 2136 (1973).

4) R. Adams and W. Reifschneider, *J. Am. Chem. Soc.*, **78**, 3825 (1956).

5) S. Inoue, O. Suzuki, and K. Sato, *J. Chem. Soc., Chem. Commun.*, **1985**, 1773.

6) K. Sato, O. Miyamoto, S. Inoue, and T. Ota, *Synthesis*, **1982**, 137.

7) C. L. Stevens and J. C. French, *J. Am. Chem. Soc.*, **76**, 4398 (1954).

8) R. E. Dessy, *J. Am. Chem. Soc.*, **83**, 3530 (1961).

9) T. J. Curphey, *Org. Synth.*, **51**, 142 (1971).

10) S. G. Powell and C. H. Secoy, *J. Am. Chem. Soc.*, **53**, 767 (1931).

11) E. P. Kohler, *Am. Chem. J.*, **38**, 511 (1907).

Kinetic Study for Reactions of Nitrate Radical (NO_3·) with Alcohols in Solutions

Osamu Ito,* Seiji Akiho, and Masashi Iino
Chemical Research Institute of Nonaqueous Solutions, Tohoku University, Katahira, Sendai 980
(Received November 18, 1988)

The rate constants for the reaction of nitrate radical (NO_3·) with alcohols have been determined by flash photolysis method in aqueous and nonaqueous solutions. The reactivity of NO_3· in acetonitrile was higher than that in aqueous solution, suggesting that hydrogen bonds between solvent and NO_3· or alcohols decrease the reaction rate. From the deuterium-isotope effect, the main reaction path was confirmed to be hydrogen atom abstraction from the carbon atom bonded with the OH group. For 2-methyl-2-propanol, the hydrogen atom abstraction from the OH group was presumed. These reaction paths were confirmed, since the reaction rate constants decreased with an increase in the corresponding bond-dissociation energies. From strong dependency of the rate constants upon the ionization energies of alcohols, the polar transition states of the reactions were suggested.

By photolysis of $(NH_4)_2[Ce(NO_3)_6]$ in the presence of alcohols, the intermediate radicals produced by the loss of the hydrogen atom from alcohols were observed by the low temperature ESR measurements and spin trapping technique.[1-3] As the initial step, it has been presumed that the electron transfer from alcohols to cerium(IV) ion occurs producing the radical cations of alcohols (Reaction 1), which undergo deprotonation forming the neutral radicals of alcohols (Reaction 2).[1-3]

$$R'R''CHOH + Ce^{4+} \xrightarrow{h\nu} R'R''CHOH^{+\cdot} + Ce^{3+} \quad (1)$$

$$R'R''CHOH^{+\cdot} \longrightarrow R'R''C{\cdot}OH + H^{+} \quad (2)$$

On the other hand, it was also reported by flash photolysis method that the nitrate radical (NO_3·) was efficiently produced from $(NH_4)_2[Ce(NO_3)_6]$ in aqueous solution[4,5] and in nonaqueous solution.[6,7] For a few alcohols, the rate constants for the reaction with NO_3· in aqueous solution were determined by using the flash photolysis[8] and pulse radiolysis method.[9] The high reactivities of NO_3· with alcohols suggest that different reactions from Reactions 1 and 2 are responsible to the photooxidation of alcohols by $(NH_4)_2[Ce(NO_3)_6]$.

Since NO_3· also plays an important role in air pollution, many kinetic studies in gas phase have been reported.[10,11] By comparing the rate constants in gas phase with the corresponding ones in solutions, considerable differences attributable to the medium effect were found for the reactions with aldehydes in our previous paper.[12] In this study, we report the rate constants for the reactions of NO_3· with various alcohols in acetonitrile and in aqueous solution by using flash photolysis technique. In order to reveal the reaction paths, the deuterium-isotope effects on the reaction rates were investigated. The correlation of the observed rate constants with bond-dissociation energies also afforded information about the reaction mechanisms. The polar nature of the transition state for the reaction was also revealed.

Experimental

$K_2[Ce(NO_3)_6]$, which was used as a radical source, was prepared from the ammonium salt by the action of KOH. Alcohols were purified by distillation before use. Commercially available deuterium derivatives (Merck Co. INC.) were used as received; deuterium degrees for both CH_3OD and CD_3OD are >99%. Distilled acetonitrile (over P_2O_5 under N_2) and distilled water were used as solvents.

The xenon flash photolysis apparatus was of a standard design with two xenon flash-lamps (Xenon Corp. N-815C);[13,14] the half-duration was ca. 10 μs and input energy was ca. 100 J. By using the light filters, $K_2[Ce(NO_3)_6]$ was flash-photodecomposed with the light between 310 and 450 nm. The temperature of the reaction was controlled by dipping the flash cell (1 dm of optical lenght and 0.1 dm of diameter) in a cooled methanol bath or water bath. For the measurements of Arrhenius parameters, temperature was varied from −40 to 20 °C. Within this temperature range, spontaneous reaction between the radical source and alcohols was not observed in the dark. Above 50 °C, bleaching of yellow color of the radical source was observed on the addition of benzene-methanol (benzyl alcohol) as reported in the literature.[15]

Results and Discussion

Figure 1 shows a transient absorption spectrum appeared by the flash photolysis of $K_2[Ce(NO_3)_6]$ in acetonitrile. The absorption bands with vibronic structure (peak at 635 nm) are attributed to the absorption bands of NO_3· in acetonitrile, indicating that photodissociation Reaction 3 occurs efficiently even in acetonitrile.[6-9]

$$K_2[Ce^{IV}(NO_3)_6] \underset{k_b}{\overset{h\nu}{\rightleftharpoons}} NO_3{\cdot} + K_2[Ce^{III}(NO_3)_5] \quad (3)$$

Insert of Fig. 1 shows the first-order plots for the decay of NO_3· in the presence of alcohols. In the absence of alcohol, the decay of NO_3· was attributed to the back process of Reaction 3. The half-life of NO_3· in the absence of alcohols was ca. 1000 μs which is long enough to follow decay kinetics of NO_3· by our flash photolysis apparatus with half-duration of flash lamp

of 10 μs even in the presence of excess of alcohols. In the presence of alcohol, a sufficiently linear line was obtained for each concentration. The slope yields pseudeo first-order rate constant ($k_{first\text{-}order}$). The decay rate increases with the concentration of additive. Since the concentration of NO_3· produced by each flash exposure was evaluated less than ca. 1×10^{-6} mol dm^{-3} by assuming the extinction coefficient to be ca. 1000 dm^3 mol^{-1} cm^{-1} at 635 nm in acetonitrile,[3,4,16] the addition of alcohols higher than ca. 1×10^{-5} mol dm^{-3} is enough to establish pseudo first-order kinetics.

Figure 2 shows the pseudo first-order plots for various alcohols. The linear lines are obtained; from the slopes the second-order rate constants, which are referred to as k_{obs}, are evaluated. The k_{obs} values at 20 °C obtained in acetonitrile and 6 M HNO_3 (1 M=1 mol dm^{-3}) aqueous solution are summarized in Tables 1 and 2, respectively. In Table 2, the reported rate constants in aqueous solutions are also listed. Agreement between the rate constants in this study and those of pulse radiolysis method by Neta and Huie[9] is better than that with flash photolysis method by Dogliotti and Hayon.[8] With the change of acidity of aqueous solution from 6 M HNO_3 to 2 M HNO_3, appreciable change was not observed. The k_{obs} values in acetonitrile are ca. 10 times larger than the rate constants for hydrogen atom abstraction of $(CH_3)_3CO$·

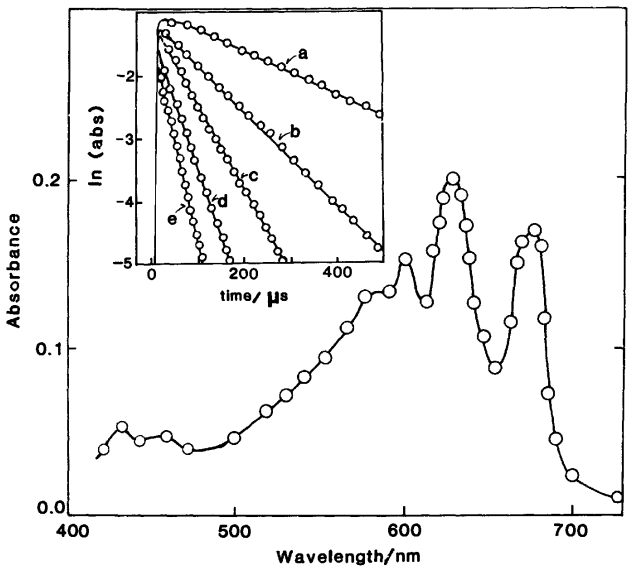

Fig. 1. Transient absorption spectrum observed by flash photolysis of $K_2[Ce(NO_3)_6]$ (10^{-3} mol dm^{-3}). Absorbance at 10 μs after each flash exposure is plotted. Insert: First-order plots for decay of absorbance at 635 nm in acetonitrile (at 20 °C) in the presence of 2-propanol; (a) 0, (b) 0.6, (c) 1.3, (d) 1.9, and (e) 2.5 mmol dm^{-3}.

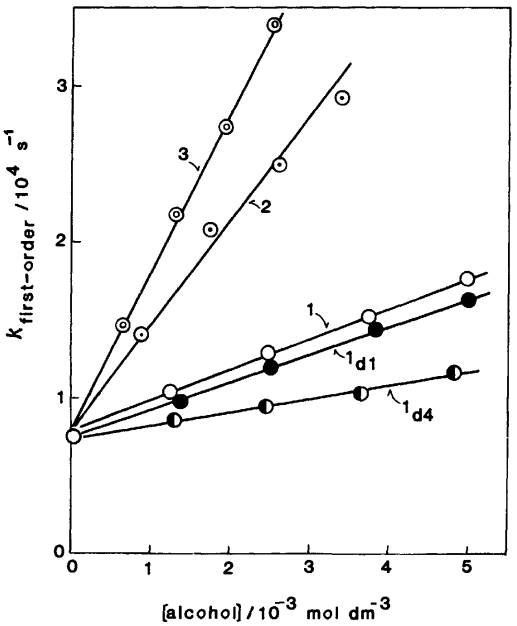

Fig. 2. Pseudo first-order plots for some alcohols in acetonitrile at 20 °C; numbers in figure are referred to as Tables.

Table 1. Rate Constants (at 20 °C) and Arrhenius Parameters for Reactions of NO_3· with Various Alcohols in Acetonitrile;[a] Bond Dissociation Energy (BDE)[b] and Ionization Energy (IE)[c]

	Alcohol	10^{-6} k_{obs}	10^{-6} k_H	log A_H	E_a	BDE	IE
		mol^{-1} dm^3 s^{-1}	mol^{-1} dm^3 s^{-1}		kJ mol^{-1}	kJ mol^{-1}	eV
1	CH_3OH	2.1	0.70	8.00	11	395	10.85
1_{d1}	CH_3OD	1.9	0.63	7.85	11		
1_{d4}	CD_3OD	0.61	0.20	7.75	14		
2	CH_3CH_2OH	6.7	3.4	8.08	9	390	10.50
3	$(CH_3)_2CHOH$	14	14	8.51	7	382	10.15
4	$(CH_3)_3COH$[d]	0.23	0.23			441	10.24
			0.03			386	
5	CH_2OHCH_2OH	6.6	1.7	8.20	10		10.55
6	$C_6H_5CH_2OH$	310	160	8.8	<3	348	9.53
7	CH_2=$CHCH_2OH$[e]	260	130	8.7	<3	343	9.63
			260	8.9			

a) Each rate constant contains an estimation error of ±5%; activation energy contains an estimation error of ±1 kJ mol^{-1}. b) Ref. 26. c) Ref. 23. d) Arrhenius parameters were not evaluated because of small $k_{first\text{-}order}$; upper row is for O-H and lower row is for C-H. e) Upper row is for hydrogen-atom abstraction and lower row is for addition reaction.

Table 2. Rate Constants for Reactions of $NO_3^{\cdot}$ with Various Alcohols in Aqueous Solution (6 M HNO_3 at 20 °C)

	Alcohol	$10^{-6}\,k_{obs}$	$10^{-6}\,k_H$
		$mol^{-1}\,dm^3\,s^{-1}$	$mol^{-1}\,dm^3\,s^{-1}$
1	CH_3OH[a]	0.31 (0.2,[c] 1.0[d])	0.10
$\mathbf{1}_{d1}$	CH_3OD	0.30	0.10
$\mathbf{1}_{d4}$	CD_3OD	0.15	0.05
2	CH_3CH_2OH	1.2 (1.4,[c] 3.9[d])	0.60
3	$(CH_3)_2CHOH$[b]	2.7 (2.4,[c] 3.6[d])	2.7
4	$(CH_3)_3COH$	0.047	0.047
			0.005
5	CH_2OHCH_2OH	0.76	0.19
6	$C_6H_5CH_2OH$	450	280
7	$CH_2{=}CHCH_2OH$	210	210
		230 (2M HNO_3)	230

a) E_a=19±2 kJ mol^{-1}; log A_H=8.4±0.2. b) E_a=11±2 kJ mol^{-1}; log A_H=8.6±0.2. c) Pulse radiolysis data (Ref. 9). d) Flash photolysis data (Ref. 8).

from alcohols in organic solvent determined with laser flash photolysis.[17]

In Fig. 2, it is noticeable that the slope of CH_3OD is practically equal to that of CH_3OH (rate constant is referred to as k^H), whereas that of CD_3OD (k^D) is considerably small. This difference (k^H/k^D=3.4) is clearly larger than estimation errors (±5%) which were contained in our method. Although this deuterium-isotope effect is larger than that expected from the primary deuterium-isotope effect (k^H/k^D=1.63), further large ratios were reported for the hydrogen-atom abstraction reaction by various radicals.[18] Especially, the reported ratio (3.2)[17] for the reaction of $(CH_3)_3CO^{\cdot}$ with 2-propanol is in good agreement with our value. These observations clearly indicate that the reaction path of $NO_3^{\cdot}$ with alcohols with hydrogen atoms at the carbon atom with the OH group is direct hydrogen (deuterium) atom abstraction as shown in Reaction 4.

$$R'R''CHOH + NO_3^{\cdot} \longrightarrow R'R''C^{\cdot}OH + HNO_3 \quad (4)$$

Since the oxygen-centered radicals are known to be highly reactive to hydrogen atom abstraction,[19,20] the observed large rate constants of $NO_3^{\cdot}$ suggest that $NO_3^{\cdot}$ can be shown in canonical structures **I** and **II**, in which an unpaired electron localizes on one oxygen atom.

$$\underset{\mathbf{I}}{{}^{\cdot}O\text{-}N^{+}(O^{-})=O} \longleftrightarrow \underset{\mathbf{II}}{{}^{\cdot}O\text{-}N^{+}(=O)\text{-}O^{-}}$$

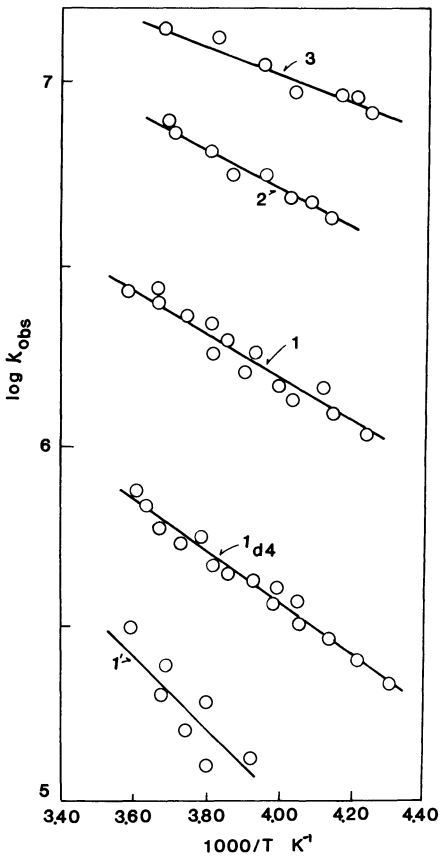

Fig. 3. Arrhenius plots for some alcohols. Numbers are referred to as Tables; **1'** is for methanol in aqueous solution.

In Tables 1 and 2, the rate constants per an active hydrogen (k_H and k_D) are also added by assuming that hydrogen atoms at the α-carbon are predominantly abstracted by $NO_3^{\cdot}$. In the case of 2-methyl-2-propanol (*t*-butyl alcohol), two possible reaction paths (i.e., hydrogen atom abstraction from O–H and from C–H) must be taken into consideration. For 2-propen-1-ol (allyl alcohol), addition reaction mode must be considered besides the hydrogen atom abstraction from allyl position. In each Table, the k_H values increase in the order of $CH_3OH < CH_3CH_2OH < (CH_3)_2CHOH <$ benzenemethanol (benzyl alcohol); this order is in good agreement with the reported tendency for other oxygen-centered radicals such as $(CH_3)_3CO^{\cdot}$ and $OH^{\cdot}$.[17-20]

Figure 3 shows the Arrhenius plots for the rate con-

stants for some alcohols between −40 and 20 °C. Fairly good linear lines are obtained for various alcohols. In the case of methanol in acetonitrile, the rate constant at 20 °C is about three times larger than that at −40 °C. In Table 1, the activation energies (E_a) and frequency factors per an active hydrogen atom ($\log A_H$) obtained in acetonitrile are summarized. By the variation of ±1 kJ mol^{-1} in E_a, the A value varies ±30%; thus, they are shown in the form of $\log A$. The E_a values for aliphatic alcohols seem to be smaller than the reported values for the carbon-centered radicals.[19] In the reported activation energies, we can find a tendency that the activation energies for the hydrogen-atom abstraction reactions by the oxygen-centered radicals are smaller than those by other radicals.[19] For example, the reported E_a value of 22.2 kJ mol^{-1} for $(CH_3)_3CO$·-methanol is comparable with our value for NO_3· by taking smaller rate constant for $(CH_3)_3CO$· (1.3×10^5 mol^{-1} dm^3 s^{-1}) into consideration.[21]

In Table 1, the E_a values decrease with an increase in the k_H values, showing linear free energy relationship.[19] With the increase in the k_H values, the $\log A_H$ values seem to increase. The reactivity at ambient temperature is determined by the combination of both E_a and A.

In Fig. 4, the rate constants in acetonitrile are plotted against the rate constants in aqueous solution. In the range of k_H smaller than 10^8 mol^{-1} dm^3 s^{-1}, the rate constants in acetonitrile are larger than the corresponding rate constants in aqueous solution by a factor of ca. 10. This difference may be attributed to the interaction between the attacking radical and acidic aqueous solvent via hydrogen bond. From the canonical structures of NO_3· (**I** and **II**), the electron-deficient oxygen radical center may interact with oxygen atom of H_2O. Such interaction may interfere the approach of alcohols to NO_3·. In addition, the hydrogen bonds between alcohols and H_2O also tend to decrease the reaction rates.

For benzyl alcohol, the rate constants in both solvents approach to the same value. Interchange of the reaction modes from hydrogen atom abstraction was not expected, since the rate constant of benzyl alcohol is similar to that of toluene, in which benzylic hydrogen atom is abstracted.[7,22] Taking the high ionization energy of benzyl alcohol into consideration,[23] electron-transfer reaction is not probable. Addition of NO_3· to the benzene ring is not probable, because the reactivity for addition to the phenyl ring is low.[12] Thus, the approach of the rate constants in the both solvents suggests the reactivity-selectivity principle;[24] for fast reactions, selectivity is reduced. Indeed, the rate constants are only ca. 1/10 of the diffusion controlled limits in the both solvents.[25] In the case of allyl alcohol, although the addition reaction of NO_3· to the double bond must be taken into consideration, the similar behavior was found.

In Fig. 5, the rate constants ($\log k_{obs}$ and $\log k_H$) in acetonitrile are plotted against the bond-dissociation energies between C-H at the α-position; for *t*-butyl alcohol, the plot for O-H is also shown. A general tendency was found, showing that the reactivities of alcohols increase with a decrease in the bond-dissociation energies.[26] Since the reactivities of alcohols are correlated linearly with the bond-dissociation energy at C_α-H, the reaction mode was confirmed to be Reaction 4. For *t*-butyl alcohol, the rate constant plotted against the bond-dissociation energy for O-H is found near the extrapolated line for $\log k_{obs}$ and for $\log k_H$. The reported ESR spectra support the hydrogen-atom

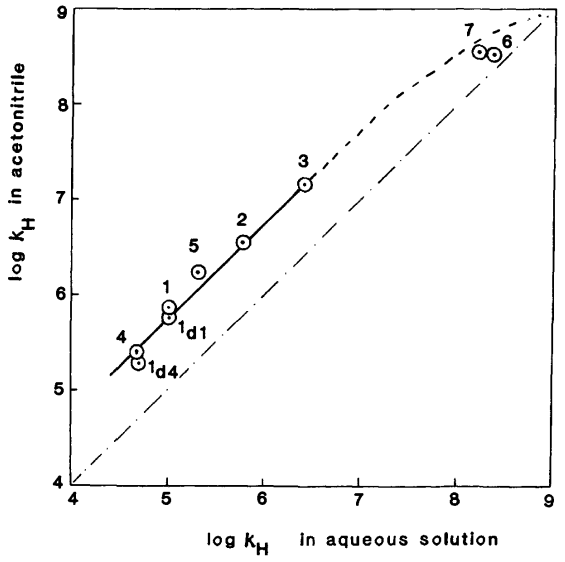

Fig. 4. Correlation between $\log k_H$ in acetonitrile and $\log k_H$ in 6 M HNO_3 at 20 °C.

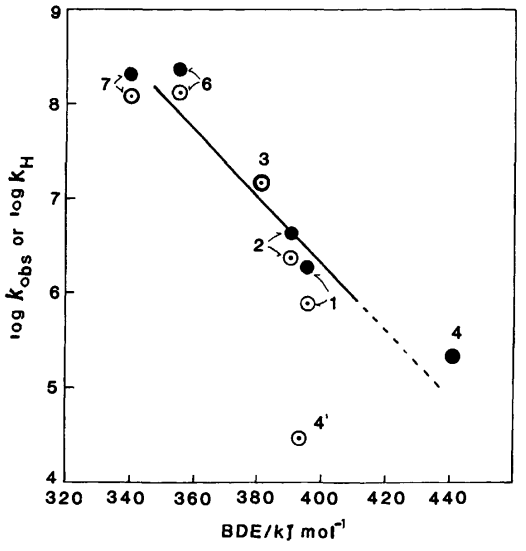

Fig. 5. $\log k_{obs}$ (●) or $\log k_H$ (⊙) at 20 °C in acetonitrile vs. bond-dissociation energy (BDE); **4** is for BDE(O-H) and **4'** for BDE(C-H).

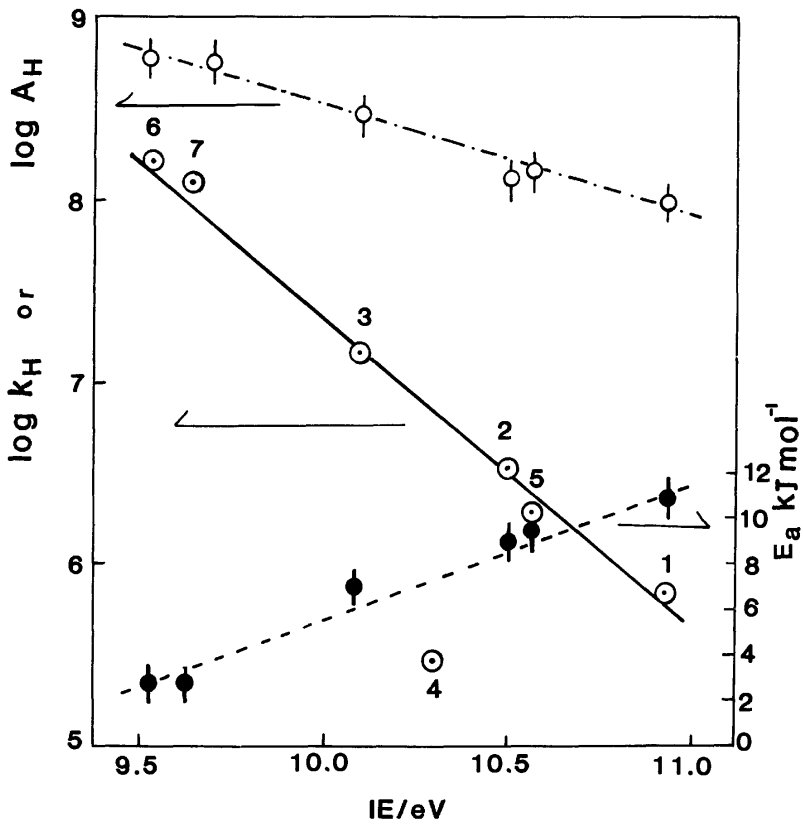

Fig. 6. $\log k_H$ (⊙), $\log A_H$ (○), and E_a (●) at 20 °C in acetonitrile vs. ionization energy (IE).

abstraction reaction from the OH group [Reaction 5].[1-3]

$$R_3COH + NO_3^{\cdot} \longrightarrow R_3CO^{\cdot} + HNO_3 \qquad (5)$$

In the case of allyl alcohol, since the rate constant is found near the line, the hydrogen-atom abstraction reaction from allylic position was suggested.

Figure 6 shows the plot of $\log k_H$, $\log A_H$, and E_a, against the ionization energies of alcohols.[23] Fairly good linear relationship is found for $\log k_H$ of alcohols except *t*-butyl alcohol. There seems to be a general tendency that the reactivity increases with a decrease in the ionization energy. This suggests a high electrophilicity of $NO_3^{\cdot}$, which is in good agreement with the reported high electron affinity (3.5 eV).[27] Furthermore, it is indicated that there are contributions of the polar resonance structures to the transition state; charge transfer from alcohols to $NO_3^{\cdot}$ occurs in the transition state as shown by **III** and **IV**.[18] By the contribution of these polar resonance structures, it is expected that the activation energy is decreased; indeed, a decrease in E_a with a decrease in the ionization energy was seen in Fig. 6.

$$[R'R''\overset{\cdot}{C}\cdot H\cdot O\text{-}NO_2] \longleftrightarrow [R'R''\overset{+}{C}H{:}O^{-}\text{-}NO_2]$$
$$\quad\;\; | \qquad\qquad\qquad\quad |$$
$$\quad OH \qquad\qquad\qquad OH$$
$$\quad \textbf{III} \qquad\qquad\qquad \textbf{IV}$$

The $\log A_H$ values are also influenced by the ionization energies of alcohols, suggesting that polar effect also presents in the orientation factor.[12]

The slightly lower reactivity of 1,2-ethanediol than that of ethanol is attributed to its higher ionization energy. Downward deviation of k_H of *t*-butyl alcohol suggests a different reaction mode having less polar transition state. The hydrogen atom of the OH group in *t*-butyl alcohol is more electron-deficient than that of C-H; thus, Reaction 5 proceeds via less polar transition state.

Although the point for allyl alcohol in Fig. 6 is on a line for the hydrogen-atom abstraction [Reaction 4], one can not exclude a possibility of addition reaction path, because the rate constant for vinyl acetate (2.5×10^8 mol^{-1} dm^3 s^{-1} at 5 °C in acetonitrile),[28] which is a nonconjugate vinyl monomer similar to allyl alcohol, is close to that of allyl alcohol.

We are thankful to the Grant-in-Aid (No. 63550676) for Scientific Research from the Ministry of Education, Science and Culture.

References

1) D. Greatorex and T. J. Kemp, *Trans. Faraday Soc.*, **67**, 56 (1971).

2) D. Greatorex, R. J. Hill, T. J. Kemp, and T. J. Stone, *Trans. Faraday Soc.*, **70**, 216 (1974).

3) D. Rehorex, *Acta. Chim. Acad. Sci. Hung.*, **101**, 395 (1979).
4) T. W. Martin, R. E. Rummel, and R. C. Cross, *J. Am. Chem. Soc.*, **86**, 2595 (1964).
5) R. W. Glass and T. W. Martin, *J. Am. Chem. Soc.*, **92**, 5084 (1970).
6) O. Ito, "The 8th IUPAC Conference on Physical. Organic Chemistry," Tokyo (1986), p. 218.
7) E. Baciocchi, T. G. Giacco, S. M. Murgia, and G. V. Sebastiani, *J. Chem. Soc., Chem. Commun.*, **1987**, 1246.
8) L. Dogliotti and E. Hayon, *J. Phys. Chem.*, **71**, 3802 (1967).
9) P. Neta and R. E. Huie, *J. Phys. Chem.*, **90**, 4645 (1986).
10) R. Atkinson, C. N. Plum, A. M. Weiner, and J. N. Pitts, Jr., *J. Phys. Chem.*, **88**, 2361 (1984).
11) C. A. Cantrell, W. R. Stockwell, L. G. Anderson, K. L. Busarow, D. Perner, A. Schmeltekopf, J. Calvert, and H. S. Johnston, *J. Phys. Chem.*, **89**, 139 (1985).
12) O. Ito, S. Akiho, and M. Iino, *J. Phys. Chem.*, in press.
13) G. Porter and M. A. West, "Techniques of Chemistry," ed. by A. Weissberger, Wiley, New York (1974), Vol. VI, p. 367.
14) O. Ito, *J. Am. Chem. Soc.*, **105**, 850 (1983).
15) W. S. Trahanovsky and N. S. Fox, *J. Am. Chem. Soc.*, **96**, 7968 (1974).
16) S. P. Sander, *J. Phys. Chem.*, **90**, 4135 (1986).
17) H. Paul, R. D. Small, and J. C. Scaiano, *J. Am. Chem. Soc.*, **100**, 4520 (1978).
18) G. A. Russell, "Free Radicals," ed. by J. K. Kochi, Wiley, New York (1973), Vol. I, p. 275.
19) J. A. Kerr, "Comprehensive Chemical Kinetics," ed. by C. H. Bamford and C. F. H. Tipper, Elsevier, Amsterdam (1976), Vol. 18, p. 39.
20) R. Atkinson, *Chem. Rev.*, **85**, 69 (1985).
21) S. K. Wong, *J. Am. Chem. Soc.*, **101**, 1235 (1979).
22) E. Baciocchi, T. D. Giacco, C. Rol, and G. V. Sebastiani, *Tetrahedron Lett.*, **26**, 541 (1985).
23) M. Bachiri, G. Mouvier, P. Carlier, and J. E. Dubois, *J. Chim. Phys. Phys.-Chim. Biol.*, **77**, 899 (1980).
24) G. S. Hammond, *J. Am. Chem. Soc.*, **77**, 334 (1955).
25) O. Ito and M. Matsuda, *Can. J. Chem.*, **56**, 1080 (1978).
26) D. F. McMillen and D. M. Golden, *Ann. Rev. Phys. Chem.*, **33**, 493 (1982).
27) J. P. Lowe, *J. Am. Chem. Soc.*, **99**, 5557 (1977).
28) O. Ito, unpublished data.

Syntheses and Properties of Quinonoid Mesoionic Compounds

Shuki ARAKI,* Naomitsu AOYAMA, and Yasuo BUTSUGAN
Department of Applied Chemistry, Nagoya Institute of Technology,
Gokiso-cho, Showa-ku, Nagoya 466
(Received November 21, 1988)

Quinonoid mesoionic compounds having a 2,3-diphenyltetrazolium ring were synthesized and characterized spectroscopically. Compounds possessing an inserted benzene ring were found that a dipolar (5-tetrazolylio)-phenolate structure contributes importantly to the ground state of the mesoions. On the contrary, a mesoion having an inserted anthracene ring is a less polar compound, anthraquinone methide structures being dominant in its ground state electronic structure.

Mesoionic compounds of the general formula **1**, where a—f are suitably substituted carbons or heteroatoms, are an interesting family of heterocycles because of their unique structure, reaction behavior, and pharmaceutical activity; and numerous works have been focused on the chemistry of these novel electronic systems.[1] Quinonoid mesoionic compounds **2**, derived from **1** by insertion of a benzene ring into the exocyclic e–f bond of **1**, are one of unique modifications of mesoions, and their properties are intriguting in connection with those of the original mesoions **1**. Recently, we reported[2] the preparation of (2,3-diphenyl-5-tetrazolylio)phenolates (**3a**—c) as the first representatives of such quinonoid mesoions. Now, we describe here the synthesis and physicochemical properties of the further examples of the related quinonoid mesoions possessing a tetrazolium ring, together with a full account of the study on **3a**—c.

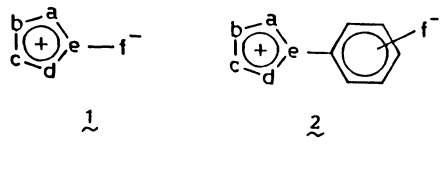

1 **2**

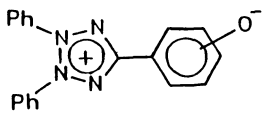

3

Synthesis. The synthetic pathway of the tetrazoliums **3a**—c is illustrated in Scheme 1. Phenylhydrazones of anisaldehydes (*o*, *m*, and *p*) were reacted with benzenediazonium chloride to give formazanes **5a**—c. Oxidation of **5a**—c with chromium(VI) oxide[3] or *N*-bromosccinimide[4] (NBS) afforded tetrazolium salts **6a**—c. The salts **6a**—c were isolated as tetra-

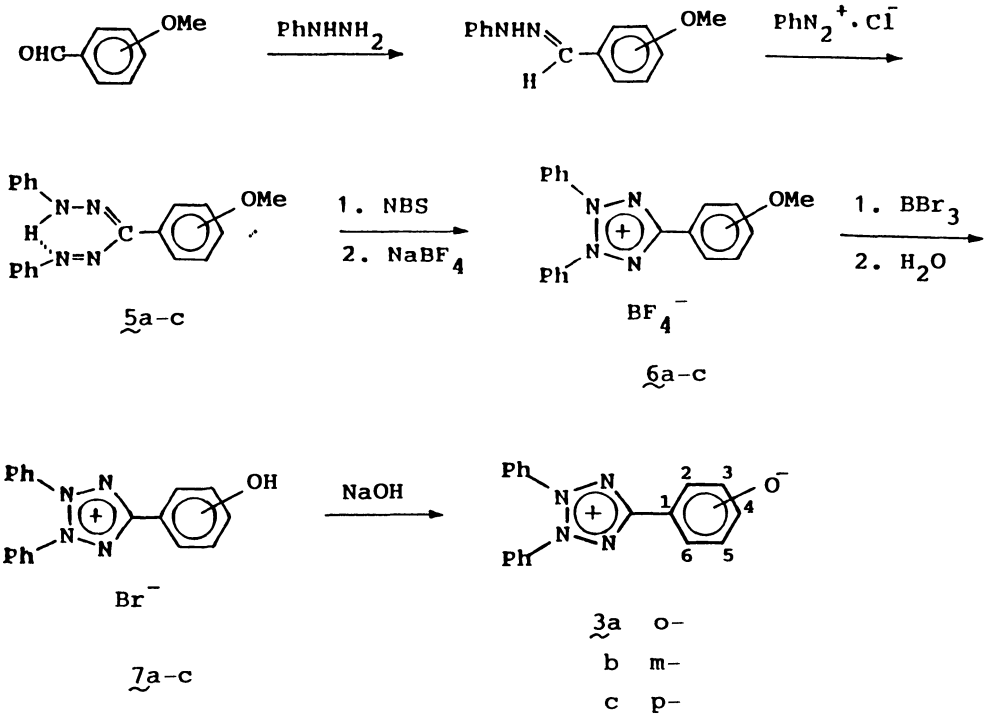

Scheme 1.

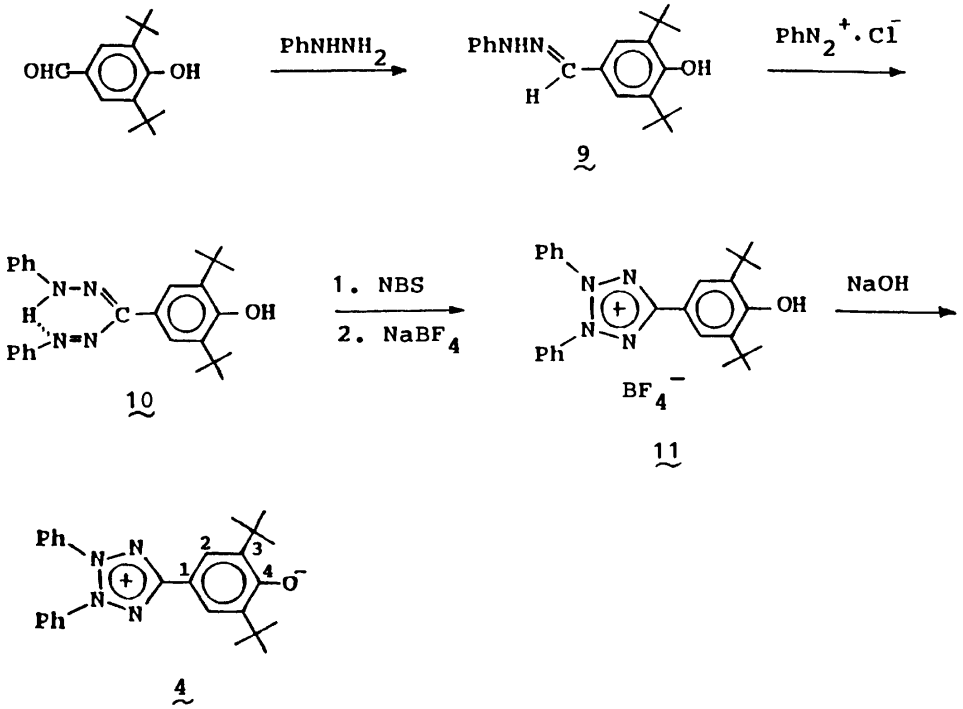

Scheme 2.

fluoroborates after an anion exchange with sodium tetrafluoroborate. Demethylation with boron tribromide furnished phenols **7a—c** in good yields. Deprotonation with a base followed by column chromatography on Sephadex 20 afforded quinonoid mesoions **3a—c** as hydrated crystals.

2,6-Di-*t*-butyl derivative **4** was synthesized by a similar synthetic scheme (Scheme 2) starting with 3,5-di-*t*-butyl-4-hydroxybenzaldehyde. In this synthesis, the protection of the hydroxyl group was unnessesary. The phenolate **4** was isolated as stable pale blue crystals.

Quinonoid mesoion **16** having three phenolate rings was synthesized according to Scheme 3. The dianion **16** is hygroscopic orange-red crystals. Upon the treatment of **16** with bromine, hexabrominated salt **17** was obtained. Deprotonation of **17** gave the conjugate anion **18** as brownish red crystals.

Quinonoid mesoionic compound **23** having an inserted anthracene ring instead of a benzene ring is of particular interest from the viewpoint of the comparison of the effects of the inserted aromatic ring (benzene vs. anthracene ring) upon the electronic structure of the quinonoid mesoions. The compound **23** was synthesized as shown in Scheme 4 and isolated as greenish brown crystals. It is worth noting here that compound **22** was isolated as the anthrol form rather than the anthrone form, despite the equilibrium between 9-anthrol and anthrone which lies to anthrone.[5] All the quinonoid mesoions **3a—c**, **4**, **16**, **18**, and **23** gave back to the corresponding conjugate acids

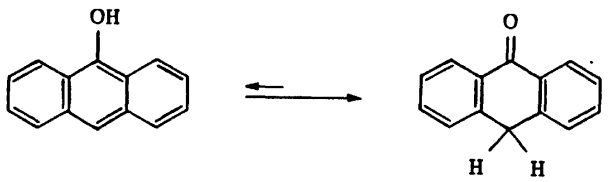

reversively by an acid treatment.

Properties of Quinonoid Mesoions 3a—c. The conjugate acids **7a—c** are stable pale yellow crystals. Their pK_a values measured by a UV method are 7.75 (for **7a**), 8.65 (**7b**), and 8.08 (**7c**), which are smaller by 1.3—2.2 than of phenol itself (pK_a=9.96) owing to the substitution of the strongly electron-withdrawing tetrazolium ring. Treatment of the salts **7a—c** with a base such as aqueous sodium hydroxide and 1,8-diazabicyclo[5.4.0]undec-7-ene (DBU) in dimethyl sulfoxide (DMSO) gave quinonoid mesoions **3a—c**.

Electronic Spectra: The quinonoid mesoions **3a—c** are brown (**3a**) to purple crystals (**3b**, **c**) and soluble in polar solvents such as water, methanol, and DMSO but practically insoluble in nonpolar solvents such as benzene, carbon tetrachloride, and hexane. The mesoions **3a—c** showed lowest excitation absorptions at 496—513 nm in the electronic spectra (see Experimental). These bands showed a distinctive negative solvatochromism: by decreasing a solvent polarity, large bathochromic shifts were observed. For example, by changing the solvent from water to less polar chloroform, the absorption maximum of **3c** was shifted by $\Delta\lambda$=152 nm. As shown in Fig. 1, linear

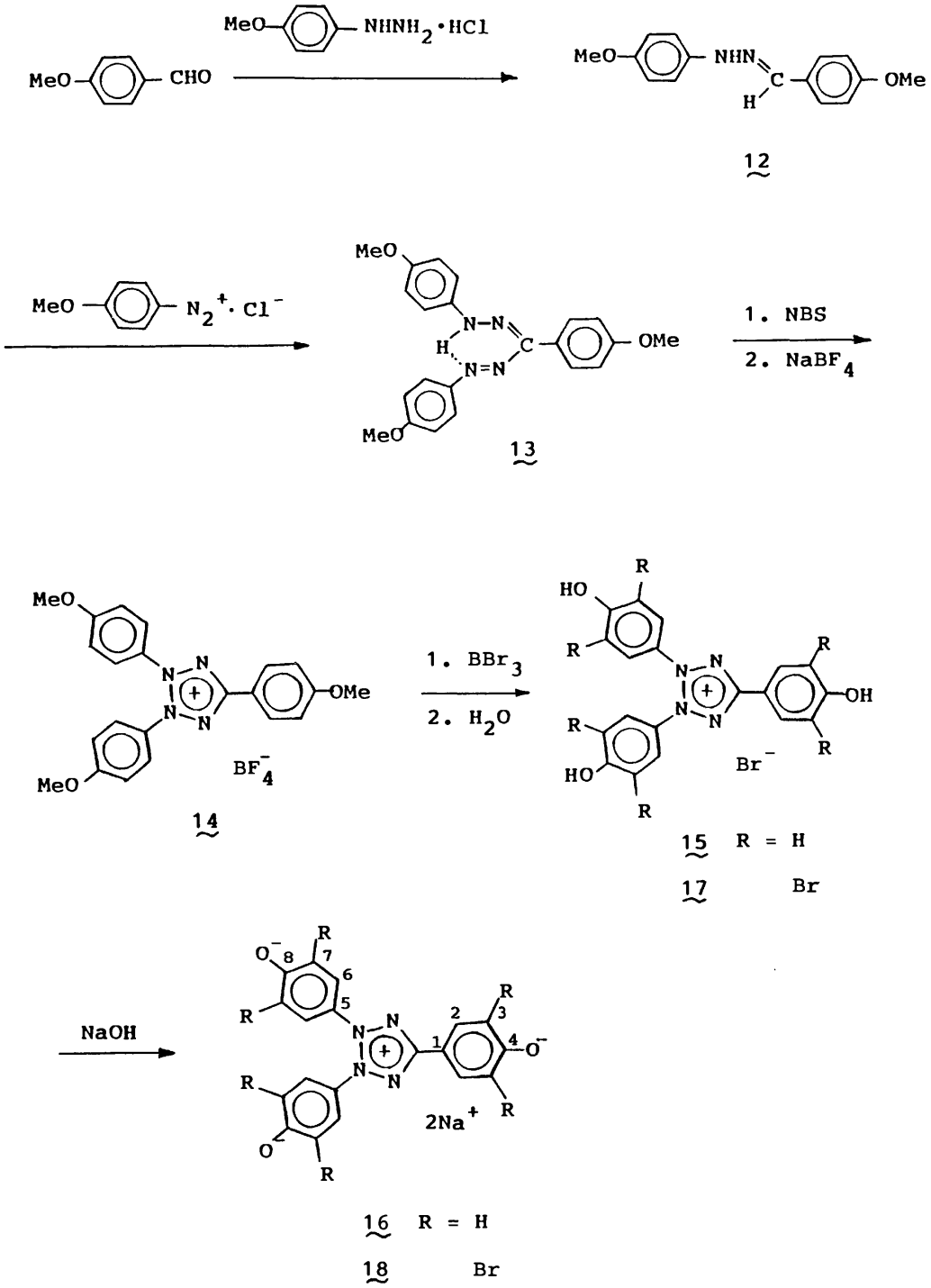

Scheme 3.

relation was observed between the wavenumber ($\tilde{\nu}$) of the longest-wavelength absorption and solvent polarity (E_T parameter[6]). The observed large solvent effect indicates that **3a—c** are polar compounds, mesoionic dipolar character contributing importantly to their ground state structures.[7]

^{1}H and ^{13}C NMR Spectra: The ^{1}H NMR parameters of the compounds **3a—c** are listed in Table 1 together with those of the corresponding conjugate acids **7a—c**. By deprotonation, the chemical shifts of the phenol ring protons of **7a—c** were shifted to higher field. For example, the AA'BB' pattern of the *p*-isomer **7c** at δ 7.08 and 8.15 (J=9 Hz) was shifted to 6.29 and 7.74 (J=9 Hz). On the other hand, the chemical shifts of the phenyl protons of **3a—c** and **7a—c** are almost coincident. This means the negative charge of the

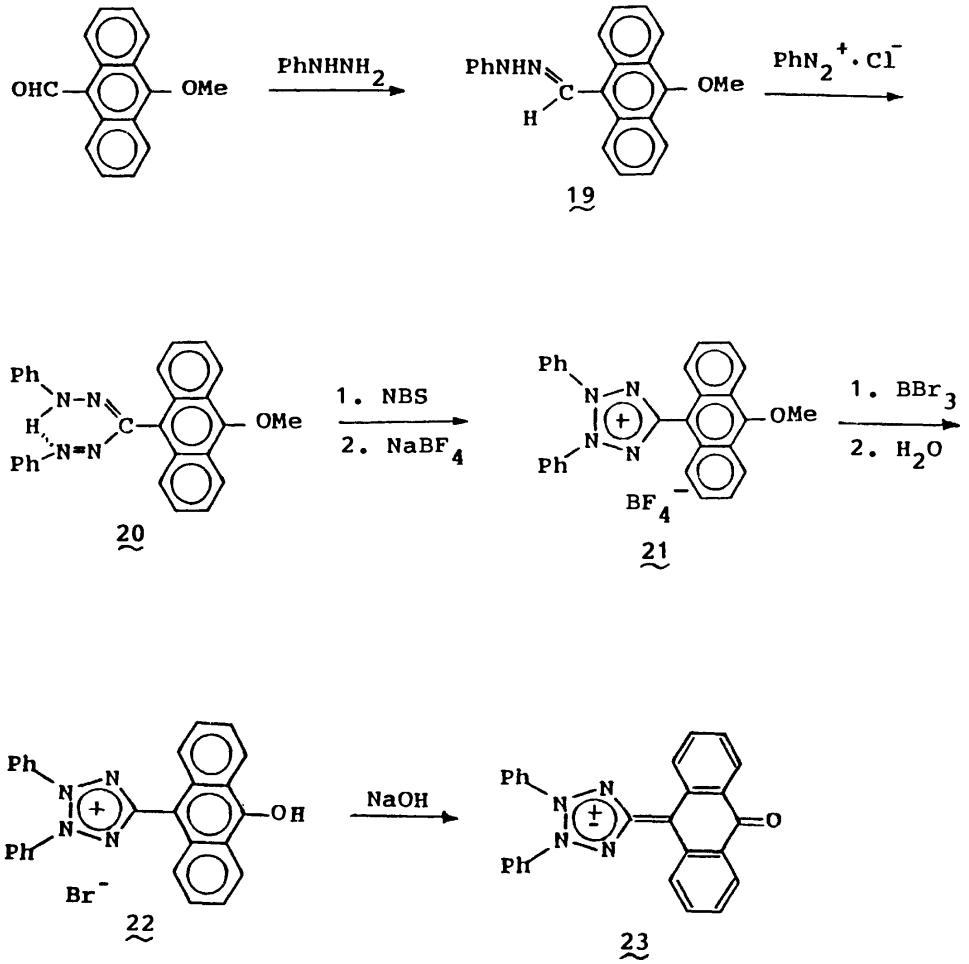

Scheme 4.

Table 1. ^{1}H NMR Data of **7a**—c and **3a**—c[a)]

Compd	δ
7a	7.00—8.10 (m, 14H, Ph and H-3—H-6), 10.95 (s, 1H, OH)
7b	7.10—8.00 (m, 14H, Ph, H-2, and H-4—H-6), 10.30 (s, 1H, OH)
7c	7.08 (d, *J*=9 Hz, 2H, H-3 and H-5), 7.65—7.85 (m, 10H, Ph), 8.15 (d, *J*=9 Hz, 2H, H-2 and H-6), 11.00 (s, 1H, OH)
3a	6.24 (t, *J*=8 Hz, 1H, H-5), 6.57 (d, *J*=8 Hz, 1H, H-3), 7.09 (d, *J*=8 Hz, 1H, H-4), 7.64—7.84(m, 7H, H-6 and Ph), 7.91 (d, *J*=7 Hz, 4H, Ph)
3b	6.64 (d, *J*=8 Hz, 1H, H-4), 7.01 (d, *J*=8 Hz, 1H, H-6), 7.17 (m, 2H, H-2 and H-5), 7.68—7.82 (m, 6H, Ph), 7.89 (d, *J*=7 Hz, 4H, Ph)
3c	6.29 (d, *J*=9 Hz, 2H, H-3 and H-5), 7.63—7.81 (m, 6H, Ph), 7.74 (d, *J*=9 Hz, 2H, H-2 and H-6), 7.87 (d, *J*=7 Hz, 4H, Ph)

a) Measured in DMSO-d_6.

Table 2. ^{13}C NMR Data of **7a**—c and **3a**—c[a)]

Compd	C-1	C-2	C-3	C-4	C-5	C-6	C+	Phenyl			
								ipso	ortho	meta	para
7a	109.8	157.1	117.4	130.2[b)]	120.1	134.6[b)]	163.1	133.2	126.6	130.4	134.1
7b	124.0	117.9[c)]	158.5	113.4[c)]	131.4	120.6	164.1	133.0	126.5	130.2	134.0
7c	113.5	129.4	117.0	162.2	117.0	129.4	164.5	133.1	126.5	130.4	134.0
3a	107.1	170.6	123.0	129.4[d)]	108.6	133.2[d)]	166.8	133.5	126.6	130.0	133.4
3b	124.0	123.0[e)]	170.3	115.9[e)]	130.3	107.5	166.4	133.1	126.4	130.2	133.8
3c	99.7	128.9	120.4	176.4	120.4	128.9	166.6	133.3	126.5	130.2	133.5

a) Measured in DMSO-d_6. b—e) These values may be interchanged.

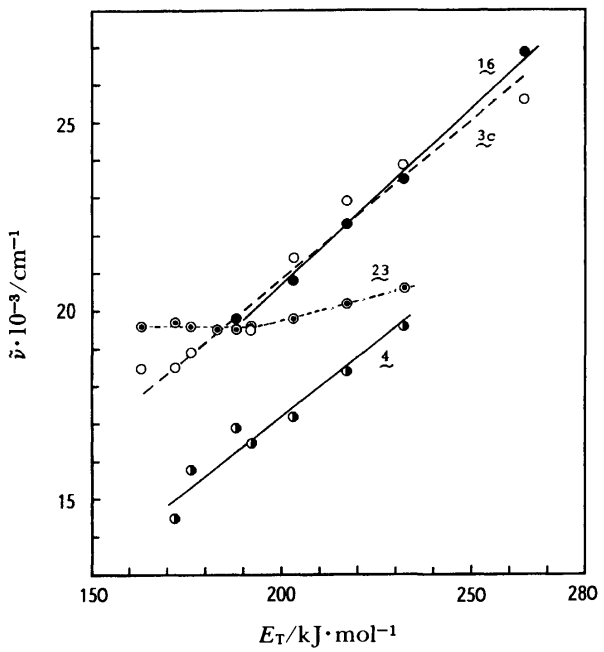

Fig. 1. Solvent dependence of the longest wavelength absorptions of 3c (○), 4 (◑), 16 (●), and 23 (⊙).

mesoions 3a—c is locarized in the phenolate ring. By comparison of the ^{13}C chemical shifts (Table 2) of 3a—c and 7a—c, it is evident that the oxygen-bearing carbons were shifted to lower field (by 11.8—14.2 ppm) by deprotonation. This corresponds well to the chemical shift difference (12.7 ppm) between the corresponding carbons of phenol (δ 155.6) and phenolate anion (δ 168.3). In contrast, the tetrazolium ring carbon and phenyl carbons were very little affected on going from 7a—c to 3a—c. These magnetic properties indicate that the mesoions 3a—c can be regarded as phenolate anions substituted by a 2,3-diphenyltetrazolium ring.

Mass Spectra: The electron-impact mass spectra of the three quinonoid mesoions 3a—c were essentially identical; no molecular ion peaks were observed but a characteristic fragment ion appeared at m/z 286. This peaks is considered due to mesoionic fulvalene **24** arising from the elimination of carbon monoxide from the quinonoid mesoions 3a—c. The fulvalene **24** is an isomer of the 1,3-diphenyl derivative **25** which was recently prepared and fully characterized.[8] Attempts to synthesize **24** by flash vacuum thermolysis of 3a—c are now in progress.

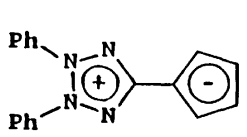

24

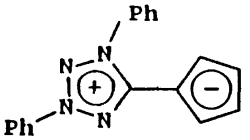

25

Adducts with Hydrobromic Acid: When an excess of DBU was added into a suspension of phenol **7c** in dichloromethane, the mixture turned to reddish purple and **7c** went into solution. After a few minutes, orange crystals of **8c** were precipitated. They were filtered and purified by recrystallization. Elemental analysis of the compound **8c** revealed that **8c** is the 2:1 adduct of mesoion 3c and hydrobromic acid. Similar adducts **8a, b** were obtained in the same manner. The electronic spectra of **8a—c** were the sum of the absorptions of both mesoions 3a—c and phenols 7a—c. Moreover, the ^1H and ^{13}C NMR chemical shifts (Table 3) of **8a—c** are average of those of 3a—c and 7a—c, indicating that **8a—c** exist as the rapid equiliblium between 3a—c and 7a—c in the solution.

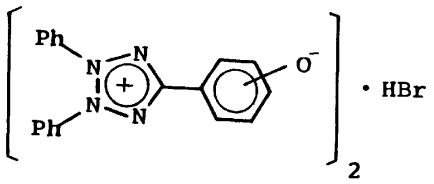

8a o-
b m-
c p-

Properties of Quinonoid Mesoions 4 and 16. The quinonoid mesoion **4** having two *t*-butyl groups at the ortho positions of the oxygen atom revealed similar spectroscopic properties to the parent compound **3c**. The lowest excitation band in the electronic spectrum showed large bathochromic shift on going from polar to less polar solvent (Fig. 1). The phenol ring protons of **11** at 8.00 ppm shifted to 7.64 by deprotonation, indicating high electron density of the phenolate ring of **4**. The phenolate ring carbons of **4** resonate at higher field than those of the phenol **11** (Table 4),

Table 3. ^{13}C NMR Data of **8a—c**[a]

Compd	C-1	C-2	C-3	C-4	C-5	C-6	C+	Phenyl			
								ipso	ortho	meta	para
8a	111.1	168.6	122.0	129.5[b]	109.0	133.3[b]	166.0	133.5	126.6	130.1	133.4
8b	123.4	122.6[c]	165.6	114.9[c]	130.7	112.2	165.2	133.0	126.6	130.2	133.9
8c	106.7	129.1	118.6	170.3	118.6	129.1	165.6	133.2	126.5	130.2	133.8

a) Measured in DMSO-d_6. b, c) These values may be interchanged.

Table 4. ^{13}C NMR Data of **4** and **11**[a)]

Compd	*t*-Bu		C-1	C-2	C-3	C-4	C+	Phenyl			
	Me	-C-						ipso	ortho	meta	para
11	30.0	34.7	117.0	124.0	140.4	159.6	162.7	133.0	126.5	130.3	134.0
4	29.8	34.8	95.9	123.0	138.1	175.4	168.2	133.4	126.4	130.1	133.4

a) Measured in DMSO-d_6.

except for the oxygen-bearing carbon whose chemical shift is δ 175.4, 15.8 ppm downfield than that of **11**. In contrast to **3a—c**, the mass spectrum of **4** exhibits the intense molecular ion peak at *m/z* 426 and the daughter ion corresponding to M^+-CO was not observed at all. This is because fulvalene **26**, which is expected to be formed by the loss of carbon monoxide from **4**, is energetically unfavorable owing to the presence of the two adjacent *t*-butyl groups.

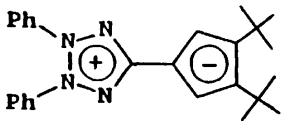

26

The triphenolate **16** prepared by the base treatment of the triphenol **15** was isolated as a disodium salt. It showed similar solvatochromism and magnetic properties to the quinonoid mesoions **3a—c** and **4**, as shown in Fig. 1. The three negative charges are located in the three phenolate rings, and this compound is rationalized as a tetrazolium cation having three phenolate rings in the 2, 3, and 5 positions. Attempts to oxidize **16** to its anion radical or other oxidized species with various oxidants (potassium hexacyanoferrate(III), silver(I) oxide, lead tetracetate, etc.) were unsuccessful. Only with bromine, hexabrominated compound **17** was isolated. The conjugate anion **18** of the acid **17** is an another example of quinonoid mesoions.

Properties of Anthracene-Inserted Mesoion 23. The compound **23** having an inserted anthracene ring shows marked differences in its electronic structure from those of the benzene-ring-inserted mesoions **3a—c, 4, 16**, and **18**. The longest wavelength absorption of **23** in its visible spectrum exhibits very smaller solvent effect than **3c, 4**, and **16** do as shown in Fig. 1. The carbonyl carbon of **23** resonates at δ 185.9, more than 17 ppm downfield than that of phenolate anion (δ 168.3). The chemical shift of the tetrazolium ring carbon is δ 175.7 and this value is also shifted downfield by 7.5—13.4 ppm compared with those of **3a—c, 4, 16**, and **18**. These spectroscopic properties clearly indicate that the compound **23** has a different type of electronic structures from the mesoions with an inserted benzene ring; the dipolar 10-(5-tetrazolylio)-anthrolate structure **27** is not important but the mesoionic betain **28** and/or bis(phenylazo)methylene structure **29** make(s) a significant contribution to the ground state of the compound **23**. This large difference in the ground state electronic structure between the benzene-inserted mesoions **3a—c, 4, 16**, and **18** and the anthracene-inserted mesoion **23** can be explained in terms of little stabilization of **27** compared to **28** or **29**, whereas **30** has a larger aromatic resonance energy compared to **31** or **32**.

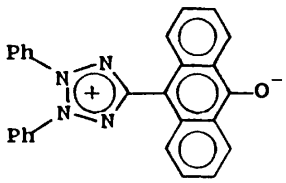

27

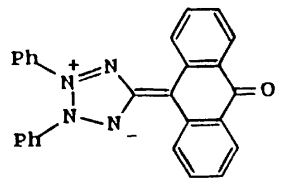

28

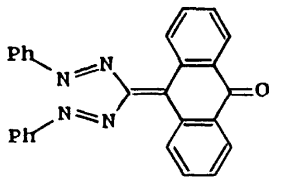

29

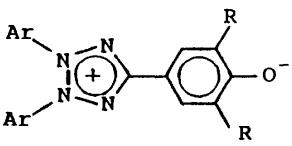

30

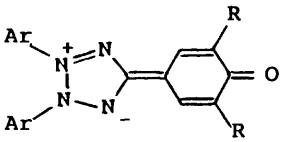

31

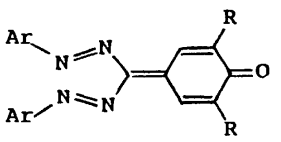

32

Experimental

General. Melting points were determined with a hot-stage apparatus and uncorrected. IR spectra were taken for KBr discs with a JASCO A-102 instrument. Electronic spectra were measured on a Hitachi 124 spectrophotometer. Mass spectra were recorded with a Hitachi M-52 instrument at 20 eV using a direct inlet system. ^1H NMR spectra were run with Hitachi R-24A (60 MHz) and Varian XL-200 (200 MHz) spectrometers. ^{13}C NMR spectra were recorded with a Varian XL-200 (50.3 MHz) spectrometer. Elemental

analysis were performed at Elemental Analysis Center in Kyoto University.

1,5-Diphenyl-3-(*o*-methoxyphenyl)formazane (5a). *o*-Anisaldehyde phenylhydrazone (9.09 g, 40.2 mmol) in pyridine (60 cm³) was slowly added below 5 °C to a solution of benzenediazonium chloride prepared from aniline (3.7 cm³, 40.8 mmol) and sodium nitrite (2.82 g, 40.9 mmol) in a mixture of acetic acid (5 cm³) and concd hydrochloric acid (15 cm³). After stirring for 2 h, the mixture was poured into water (300 cm³). The precipitate was filtered, washed with warm water and a small amount of ethanol and then dried giving formazane **5a** (10.2 g, 77%), a reddish orange powder. The corresponding *m*- (**5b**) and *p*-isomers (**5c**) were synthesized in the same manner in 55 and 89% yields, respectively.

5a: Mp 147—149 °C; IR: 3250, 3050, 2850, 1602, 1564, 1508, 1490, 1460, 1438, 1410, 1290, 1168, 1136, 1090, 1070, 1044, 1020, 760, 750, 690 cm⁻¹; MS: *m/z* 330 (M^+).

1,5-Diphenyl-3-(*m*-methoxyphenyl)formazane (5b): Mp 126 °C; IR: 3050, 2950, 2850, 1598, 1580, 1514, 1488, 1452, 1432, 1356, 1318, 1242, 1220, 1078, 1060, 1038, 920, 884, 860, 770, 750, 690, 684 cm⁻¹; MS: *m/z* 330 (M^+).

1,5-Diphenyl-3-(*p*-methoxyphenyl)formazane (5c): Mp 155 °C (lit,[8] mp 156—158 °C); IR: 3050, 2950, 2850, 1610, 1600, 1520, 1500, 1456, 1360, 1318, 1300, 1252, 1230, 1180, 1080, 1048, 1030, 1010, 844, 822, 776, 760, 740, 690, 660 cm⁻¹; MS: *m/z* 330 (M^+).

2,3-Diphenyl-5-(*o*-methoxyphenyl)tetrazolium Tetrafluoroborate (6a). A mixture of formazane **5a** (2.20 g, 6.7 mmol) and chromium(VI) oxide (2.16 g, 21.6 mmol) in acetic acid (50 cm³) and 5—6 drops of water was refluxed for 15 min. When the mixture turned to green, it was cooled and poured into water (200 cm³). The yellow precipitate deposited was collected by filtration. The precipitate was dissolved in dichloromethane and shaked with aqueous sodium tetrafluoroborate. The dichloromethane layer was separated and dried over anhydrous sodium sulfate. After evaporation, the residue was recrystallized from dichloromethane–ether giving **6a** (723 mg, 26%), a pale yellow powder. Oxidation with NBS (vide infra) gave a much better yield (79%).

6a: Mp 200 °C; IR: 3090, 2950, 2850, 1610, 1586, 1520, 1490, 1440, 1280, 1260, 1164, 1140—1000, 776, 760, 690 cm⁻¹; ¹H NMR (DMSO-d_6): δ=4.00 (s, 3H, OMe), 7.20—8.20 (m, 14H, Ph); Found: C, 57.70; H, 4.08; N, 13.18%. Calcd for $C_{20}H_{17}BF_4N_4O$: C, 57.72; H, 4.12; N, 13.46%.

2,3-Diphenyl-5-(*m*-methoxyphenyl)tetrazolium Tetrafluoroborate (6b). Into a solution of formazane **5b** (1.70 g, 5.2 mmol) in ethyl acetate (16 cm³) was added a solution of NBS (1.86 g, 10.5 mmol) in ethyl acetate (12 cm³) at 50 °C and the mixture was stirred at 50 °C for 2 h. After evaporation, the residue was dissolved in dichloromethane and shaked with aqueous sodium tetrafluoroborate. The dichloromethane layer was separated and dried (Na_2SO_4). After evaporation, the residue was recrystallized from dichloromethane–ether giving **6b** (0.77 g, 36%), pale yellow needles. The *p*-isomer **6c** was similarly prepared as pale yellow crystals.

6b: Mp 201 °C; IR: 3090, 2970, 2850, 1620, 1588, 1534, 1490, 1440, 1286, 1250, 1230, 1170, 1126, 1110—1000, 880, 856, 800, 776, 770, 750, 690 cm⁻¹; ¹H NMR (DMSO-d_6): δ=3.90 (s, 3H, OMe), 7.30—7.95 (m, 14H, Ph); Found: C, 57.95; H, 3.99; N, 13.41%. Calcd for $C_{20}H_{17}BF_4N_4O$: C, 57.72; H, 4.12; N, 13.46%.

6c: Mp 230 °C; IR: 3100, 2980, 2850, 1612, 1490, 1468, 1440, 1310, 1280, 1266, 1180, 1162, 1130—1030, 1000, 930, 856, 770, 750, 688 cm⁻¹; ¹H NMR (DMSO-d_6): δ=3.90 (s, 3H, OMe), 7.25 (d, J=9.0 Hz, 2H, Ar), 7.65—7.75 (m, 10H, Ph), 8.20 (d, J=9.0 Hz, 2H, Ar); Found: C, 57.96; H, 4.03; N, 13.38%. Calcd for $C_{20}H_{17}BF_4N_4O$: C, 57.72; H, 4.12; N, 13.46%.

2,3-Diphenyl-5-(*o*-hydroxyphenyl)tetrazolium Bromide (7a). To a solution of tetrazolium salt **6a** (1.49 g, 3.58 mmol) in dichloromethane (10 cm³) was added boron tribromide (0.60 cm³, 6.3 mmol) at −78 °C under argon. The reddish brown mixture was gradually warmed to room temperature and poured into water. The precipitate was filtered, dried, and recrystallized from ethanol giving pale yellow needles of **7a** as the 1:1 complex with ethanol (1.19 g, 84%). Phenols **7b** and **7c** were similarly synthesized and obtained as pale yellow crystals.

7a: Mp 259 °C (decomp); IR: 3600—3300, 3050, 1616, 1600, 1522, 1484, 1456, 1410, 1370, 1294, 1260, 1162, 1110, 1070, 1068, 1022, 1000, 938, 880, 840, 778, 760, 690 cm⁻¹; UV (MeCN): λ_{max} (log ε) 216 nm (4.42), 248 (4.28), 300 (4.01); Found: C, 57.24; H, 4.70; N, 12.82%. Calcd for $C_{19}H_{15}BrN_4O \cdot C_2H_5OH$: C, 57.15; H, 4.80; N, 12.70%.

7b: Mp 258 °C (decomp); IR: 3550—3350, 3150, 1620, 1590, 1530, 1486, 1440, 1346, 1290, 1216, 1160, 1126, 1076, 1042, 1000, 920, 888, 870, 794, 766, 740, 682 cm⁻¹; UV (MeCN): λ_{max} (log ε) 218 nm (4.56), 252 (4.37), 297 (3.96); Found: C, 57.71; H, 3.71; N, 14.19%. Calcd for $C_{19}H_{15}BrN_4O$: C, 57.74; H, 3.82; N, 14.17%.

7c: Mp 280 °C (decomp); IR: 3550—3350, 3100—2950, 1610, 1588, 1486, 1460, 1448, 1278, 1224, 1170, 1160, 1000, 856, 770, 750, 690, 680 cm⁻¹; UV (MeCN): λ_{max} (log ε) 213 nm (4.21), 271 (4.40); Found: C, 57.79; H, 3.63; N, 14.01%. Calcd for $C_{19}H_{15}BrN_4O$: C, 57.74; H, 3.82; N, 14.17%.

2-(2,3-Diphenyl-5-tetrazolylio)phenolate (3a). Phenol **7a** (246 mg, 0.62 mmol) was dissolved in an aqueous sodium hydroxide solution (1 M, 1.5 cm³; 1 M=1 mol dm⁻³) at room temperature. Water was removed under reduced pressure and the residue was purified by column chromatography on Sephadex LH-20 using dichloromethane as an eluent. Mesoion **3a** was obtained as a brown powder (186 mg, 95%). By the same method, **3b** and **3c** were isolated in 84 and 68% yields, respectively, purple crystals.

3a: Mp 140 °C (decomp); IR: 3060, 1602, 1504, 1478, 1434, 1318, 1240, 1152, 1000, 846, 760, 686 cm⁻¹; UV (MeCN): λ_{max} (log ε) 220 nm (4.18), 258 (sh, 4.00), 381 (4.03), 496 (2.59); solvent dependence of the longest wavelength band: 398 nm (sh) (H_2O), 412 (MeOH), 425 (EtOH), 460 (*i*-PrOH), 491 (DMSO), 499 (Me_2C=O), 496 (CH_2Cl_2), 525 ($CHCl_3$); MS: *m/z* (rel intensity) 286 (M−CO, 15), 238 (23), 211 (50), 169 (14), 167 (14), 119 (14), 91 (100); Found: C, 70.44; H, 4.37; N, 17.18%. Calcd for $C_{19}H_{14}N_4O \cdot 0.5H_2O$: C, 70.57; H, 4.68; N, 17.33%.

3b: Mp 141 °C (decomp); IR: 3060, 1588, 1570, 1504, 1486, 1460, 1316, 1282, 1160, 1000, 982, 892, 764, 746, 688 cm⁻¹; UV (MeCN): λ_{max} (log ε) 250 nm (4.42), 320 (sh, 3.64), 535 (2.61); solvent dependence of the longest wavelength band: 396 nm (sh) (H_2O), 428 (MeOH), 443 (EtOH), 484 (*i*-PrOH), 536 (DMSO), 477 (Me_2C=O), 537 (CH_2Cl_2), 538 ($CHCl_3$); MS: *m/z* (rel intensity) 286 (M−CO, 19), 211 (92), 91 (100); Found: C, 68.12; H, 4.57; N, 16.17%. Calcd for $C_{19}H_{14}N_4O \cdot H_2O$: C, 68.66; H, 4.85; N, 16.86%.

3c: Mp 154 °C (decomp); IR: 3060, 1590, 1442, 1336, 1162, 1000, 980, 844, 762, 690 cm^{-1}; UV (MeCN): λ_{max} (log ε) 213 nm (4.06), 228 (3.97), 300 (sh, 4.05), 347 (4.54), 513 (2.68); solvent dependence of the longest wavelength band: 390 nm (H_2O), 419 (MeOH), 437 (EtOH), 467 (*i*-PrOH), 512 (DMSO), 530 (Me_2C=O), 542 (CH_2Cl_2), 542 ($CHCl_3$); MS: *m/z* (rel intensity) 286 (M−CO, 47), 211 (60), 169 (17), 167 (17), 91 (100); Found: C, 65.14; H, 4.91; N, 16.14%. Calcd for $C_{19}H_{14}N_4O \cdot 2H_2O$: C, 65.13; H, 5.13; N, 15.99%.

Adducts 8a—c of Mesoions 3a—c and Hydrobromic Acid. The following preparation of **8c** represents the general procedure. Phenol **7c** (143 mg, 0.36 mmol) was suspended in dichloromethane (15 cm^3) and DBU (0.1 cm^3, 0.67 mmol) was added at room temperature. Phenol **7c** went into solution and the mixture turned to reddish purple. After a few minutes, orange crystals deposited which were filtered off and dried giving **8c** (113 mg, 89%).

8c: Mp 179 °C (decomp); IR: 1610, 1486, 1460, 1174, 1000, 842, 770, 750, 692, 682 cm^{-1}; ^1H NMR (DMSO-d_6): δ=6.72 (d, 2H, *J*=9 Hz, H-3), 7.57—7.80 (m, 10H, Ph), 7.91 (d, 2H, *J*=9 Hz, H-2); Found: C, 63.55; H, 4.27; N, 16.26; Br, 11.29%. Calcd for $C_{38}H_{29}BrN_8O_2$: C, 64.37; H, 4.09; N, 15.80; Br, 11.28%.

Adducts **8a** and **8b** were similarly synthesized in almost quantitative yields.

8a: Mp 143 °C (decomp); IR: 1642, 1608, 1584, 1440, 1370, 1322, 1296, 1160, 1104, 1000, 836, 768, 752, 686 cm^{-1}. ^1H NMR (DMSO-d_6): δ=6.38—6.50 (m, 1H, Ar), 6.69—6.74 (m, 1H, Ar), 7.14—7.24 (m, 1H, Ar), 7.66—8.00 (m, 11H, Ar and Ph).

8b: Mp 180 °C (decomp); IR: 1500, 1490, 1422, 1260, 1160, 1074, 1016, 1000, 992, 894, 880, 870, 790, 762, 740, 680 cm^{-1}; ^1H NMR (DMSO-d_6): δ=6.93—7.02 (m, 1H, Ar), 7.36—7.40 (m, 2H, Ar), 7.52 (s, 1H, Ar), 7.70—7.97 (m, 10H, Ph).

1,5-Diphenyl-3-(3,5-di-*t*-butyl-4-hydroxyphenyl)formazane (10). This compound was synthesized in 94% yield as a dark purple powder by a similar synthetic method to **5a—c** from 3,5-di-*t*-butyl-4-hydroxybenzaldehyde phenylhydrazone (**9**). Mp 122 °C; IR: 3650—3370, 2960, 2910, 2870, 1600, 1510, 1500, 1438, 1360, 1314, 1254, 1236, 1150, 1118, 1080, 1068, 996, 920, 898, 884, 796, 770, 744, 698 cm^{-1}; ^1H NMR ($CDCl_3$): δ=1.44 (s, 18H, *t*-Bu), 5.25 (s, 1H, OH), 7.02—7.71 (m, 10H, Ph), 7.90 (s, 2H, Ar), 8.58 (s, 1H, NH).

2,3-Diphenyl-5-(3,5-di-*t*-butyl-4-hydroxyphenyl)tetrazolium Tetrafluoroborate (11). Formazane **10** was oxidized with NBS as described above and tetrafluoroborate **11** was obtained in 28% yield, colorless crystals, after an anion exchange with sodium tetrafluoroborate. Mp 246 °C (decomp). IR: 3630—3330, 3080, 2960, 1604, 1516, 1488, 1410, 1120—1030, 762, 690 cm^{-1}; ^1H NMR (DMSO-d_6): δ=1.46 (s, 18H, *t*-Bu), 5.73 (s, 1H, OH), 7.65—7.84 (m, 6H, Ph), 7.89—7.96 (m, 4H, Ph), 8.00 (s, 2H, Ar); UV (MeCN): λ_{max} (log ε) 217 nm (4.56), 272 (4.46); Found: C, 62.34; H, 6.11; N, 10.89%. Calcd for $C_{27}H_{31}BF_4N_4O \cdot 0.25H_2O$: C, 62.50; H, 6.12; N, 10.80%.

2,6-Di-*t*-butyl-4-(2,3-diphenyl-5-tetrazolylio)phenolate (4). Into a solution of **11** (630 mg, 1.23 mmol) in methanol (5 cm^3) was added aqueous sodium hydroxide (1 M, 2 cm^3). The mixture turned to purple and a precipitate deposited. Water was evaporated under reduced pressure and the residue was chromatographed on Sephadex LH-20 (dichloromethane–acetone) giving **4** quantitatively, pale blue crystals. Mp 209 °C; IR: 3060, 2950, 2910, 1586, 1478, 1440, 1350, 1334, 992, 900, 808, 760, 684 cm^{-1}; ^1H NMR (DMSO-d_6): δ=1.38 (s, 18H, *t*-Bu), 7.64 (s, 2H, Ar), 7.64—7.78 (m, 6H, Ph), 7.82—7.88 (m, 4H, Ph); UV (MeCN): λ_{max} (log ε) 249 nm (sh, 3.97), 282 (4.08), 373 (4.48), 605 (2.50); solvent dependence of the longest wavelength band: 510 nm (MeOH), 543 (EtOH), 583 (*i*-PrOH), 591 (DMSO), 631 (Me_2C=O), 690 (CH_2Cl_2); MS: *m/z* (rel intensity) 426 (M^+, 100), 411 (77), 384 (73), 342 (47), 322 (67), 105 (40), 77 (40). Found: C, 75.04; H, 7.11; N, 12.83%. Calcd for $C_{27}H_{30}N_4O \cdot 0.25H_2O$: C, 75.24; H, 7.12; N, 12.99%.

1,3,5-Tris(*p*-methoxyphenyl)formazane (13). This compound was prepared in 81% yield from *p*-anisaldehyde *p*-methoxyphenylhydrazone[9] (**12**) (7.05 g, 27.5 mmol) and *p*-methoxybenzenediazonium chloride (35.1 mmol) in a similar manner as **5a—c**. Mp 136—138 °C (lit,[9] mp 140 °C); IR: 3020, 2950, 2850, 1600, 1580, 1510, 1460, 1440, 1422, 1306, 1256, 1230, 1182, 1166, 1142, 1102, 1022, 836, 824, 796, 740, 702 cm^{-1}; ^1H NMR (DMSO-d_6): δ=3.75 (s, 9H, OMe), 6.80 (d, 4H, *J*=9 Hz, Ar), 6.84 (d, 2H, *J*=9 Hz, Ar), 7.55 (d, 4H, *J*=9 Hz, Ar), 7.68 (d, 2H, *J*=9 Hz, Ar), 14.35 (s, 1H, NH); MS: 390 (M^+).

2,3,5-Tris(*p*-methoxyphenyl)tetrazolium Tetrafluoroborate (14). This salt was obtained by the oxidation of **13** (1.98 g, 5.07 mmol) with NBS (3.60 g, 20.2 mmol) in 65% yield. Mp 176 °C; IR: 3100, 2970, 2850, 1616, 1600, 1588, 1510, 1460, 1438, 1310, 1260, 1178, 1160, 1130—1020, 990, 840, 750, 660 cm^{-1}; ^1H NMR (DMSO-d_6): δ=3.82 (s, 6H, 2 OMe), 3.86 (s, 3H, OMe), 7.16 (d, 4H, *J*=9 Hz, H-7), 7.23 (d, 2H, *J*=9 Hz, H-3), 7.72 (d, 4H, *J*=9 Hz, H-6), 8.20 (d, 2H, *J*=9 Hz, H-2); ^{13}C NMR (DMSO-d_6): δ=55.7 (OMe), 56.1 (2 OMe), 115.2 (C-1), 115.4 (C-7), 115.6 (C-3), 125.4 (C-5), 128.1 (C-6), 129.1 (C-2), 162.8 (C-8), 163.1 (C-4), 163.7 (C^+); Found: C, 55.71; H, 4.33; N, 11.79%. Calcd for $C_{22}H_{21}BF_4N_4O_3$: C, 55.49; H, 4.44; N, 11.76%.

2,3,5-Tris(*p*-hydroxyphenyl)tetrazolium Bromide (15). The compound **14** (1.28 g, 2.69 mmol) was demethylated by the action of boron tribromide (0.85 cm^3, 8.95 mmol) in the same manner as **7a—c** giving yellow needles of **15** in 94% yield. Mp 279 °C (decomp); IR: 3450—3050, 1616, 1594, 1512, 1462, 1452, 1350, 1290, 1260, 1220, 1172, 1160, 1104, 1028, 1000, 840, 748, 710, 684 cm^{-1}; ^1H NMR (DMSO-d_6); δ=6.98 (d, 4H, *J*=9 Hz, H-7), 7.07 (d, 2H, *J*=9 Hz, H-3), 7.62 (d, 4H, *J*=9 Hz, H-6), 8.10 (d, 2H, *J*=9 Hz, H-2), 10.58 (s, 1H, OH); ^{13}C NMR (DMSO-d_6): δ=113.9 (C-1), 116.4 (C-7), 116.9 (C-3), 124.1 (C-5), 128.2 (C-6), 129.2 (C-2), 161.7 (C-8), 161.9 (C-4), 163.8 (C^+); UV (MeCN): λ_{max} (log ε) 217 nm (4.52), 262 (4.45), 272 (sh, 4.42), 308 (sh, 4.07), 352 (sh, 3.80); Found: C, 53.16; H, 3.43; N, 12.88%. Calcd for $C_{19}H_{15}BrN_4O_3$: C, 53.42; H, 3.54; N, 13.11%.

Disodium 4,4′,4″-(Tetrazole-2,3,5-triylio)tris[phenolate] (16). Bromide **15** (160 mg, 0.38 mmol) was dissolved in a sodium hydroxide solution (1 M, 2 cm^3) at room temperature. Water was pumped off and the residue was recrystallized twice from methanol–ether giving reddish orange crystals of **16** quantitatively. Mp 190 °C (decomp); IR: 1580, 1496, 1446, 1332, 1320, 1164, 1140, 842 cm^{-1}; ^1H NMR (DMSO-d_6): δ=6.36 (d, 4H, *J*=9 Hz, H-7), 6.69 (d, 2H, *J*=9 Hz, H-3), 7.23 (d, 4H, *J*=9 Hz, H-6), 7.82 (d, 2H, *J*=9 Hz, H-2); ^{13}C NMR (D_2O): δ=111.7 (C-1), 121.7 (C-5), 121.9 (C-7), 122.7 (C-3), 129.2 (C-6), 131.9 (C-2), 173.3 (C-4), 174.3 (C-8), 167.2

(C^+); UV (MeOH): λ_{max} (log ε) 260 nm (4.29), 274 (sh, 4.24), 320 (sh, 3.93), 425 (3.79); solvent dependence of the longest wavelength band: 372, 413 nm (sh) (H_2O), 425 (MeOH), 448 (EtOH), 480 (*i*-PrOH), 506 (DMSO); Found: C, 48.51; H, 4.62; N, 11.49%. Calcd for $C_{19}H_{12}N_4Na_2O_3 \cdot 4.5H_2O$: C, 48.41; H, 4.49; N, 11.89%.

2,3,5-Tris(3,5-dibromo-4-hydroxyphenyl)tetrazolium Bromide (17). 2,3,5-Tris(*p*-hydroxyphenyl)tetrazolium bromide (**15**) (222 mg, 0.52 mmol) was dissolved in aqueous sodium hydroxide (1 M, 20 cm^3) and bromine (0.16 cm^3, 3.2 mmol) was added at room temperature. The reaction mixture was stirred at room temperature for 3 h. The mixture was acidified with hydrochloric acid (2 M) and the resulting solid was filtered. Recrystallization from methanol–ether gave a yellow powder of **17** (403 mg, 86%). Mp ca. 200 °C; IR: 3630—3310, 3090, 1600, 1560, 1470, 1436, 1312, 1240, 1170—1000, 880, 750, 736 cm^{-1}; ^1H NMR (DMSO-d_6): δ=4.80 (s, 3H, OH), 8.12 (s, 4H, H-6), 8.33 (s, 2H, H-2); ^{13}C NMR (DMSO-d_6): δ=111.7 (C-7), 113.0 (C-3), 116.3 (C-1), 124.0 (C-5), 130.3 (C-6), 131.3 (C-2), 155.6 (C-4), 156.6 (C-8), 161.8 (C^+); UV (MeCN): λ_{max} (log ε) 218 nm (4.46), 266 (4.08), 315 (3.78), 520 (3.62); Found: C, 25.38; H, 0.97; N, 5.85%. Calcd for $C_{19}H_9Br_7N_4O_3$: C, 25.34; H, 1.01; N, 6.22%.

Disodium 4,4′,4″-(Tetrazole-2,3,5-triylio)tris[2,6-dibromophenolate] (18). The acid **17** (400 mg, 0.44 mmol) was dissolved in methanol (2 cm^3) and an aqueous solution of sodium hydroxide (1 M, 1.5 cm^3) was added. Water was pumped off and the residue was purified by recrystallization from methanol–ether and then column chromatography on Sephadex LH-20 giving brownish red plates of **18** (333 mg, 88%). Mp 235 °C (decomp); IR: 1578, 1560, 1410—1320, 1358, 1168, 1140, 880, 758, 742, 730 cm^{-1}; ^1H NMR (DMSO-d_6): δ=7.41 (s, 4H, H-6), 7.76 (s, 2H, H-2); ^{13}C NMR (DMSO-d_6): δ=102.1 (C-1), 112.1 (C-3), 113.1 (C-7), 115.4 (C-5), 128.1 (C-6), 129.5 (C-2), 162.3 (C^+), 162.5 (C-4), 164.2 (C-8); UV (MeOH) λ_{max} (log ε) 217 nm (4.77), 314 (4.55), 399 (4.17), 448 (sh, 4.02); Found: C, 25.67; H, 1.46; N, 6.14%. Calcd for $C_{19}H_6Br_6N_4Na_2O_3 \cdot 2H_2O$: C, 25.36; H, 1.12; N, 6.23%.

1,5-Diphenyl-3-(10-methoxy-9-anthryl)formazane (20). From 10-methoxy-9-anthraldehyde phenylhydrazone (**19**) (1.05 g, 3.20 mmol) and benzenediazonium chloride (3.2 mmol), **20** was obtained as an orange powder (1.32 g, 96%). Mp 174—175 °C (decomp); IR: 1600, 1562, 1558, 1500, 1438, 1360, 1286, 1260, 1216, 1200, 1160, 1092, 982, 962, 780, 750, 726, 700, 680 cm^{-1}; ^1H NMR ($CDCl_3$): δ=4.24 (s, 3H, OMe), 7.12—7.56 (m, 12H, Ar), 7.63—7.76 (m, 4H, Ar), 8.40—8.48 (m, 2H, Ar).

2,3-Diphenyl-5-(10-methoxy-9-anthryl)tetrazolium Tetrafluoroborate (21). Formazane **20** (680 mg, 1.58 mmol) was oxidized with NBS (1.12 g, 6.29 mmol) as the same manner to **5a**—c. The crude product was purified by column chromatography on silica gel with dichloromethane–acetone (1:1) as the eluent. Pure **21** was obtained as pale yellow crystals. Mp 150—153 °C; IR: 1664, 1600, 1488, 1458, 1324, 1266, 1122, 1100—1020, 760, 720, 704, 682 cm^{-1}; ^1H NMR (DMSO-d_6): δ=4.06 (s, 3H, OMe), 7.24—7.94 (m, 14H, Ar), 8.06—8.44 (m, 4H, Ar); ^{13}C NMR (DMSO-d_6): δ=64.2 (OMe), 111.7 (=C–), 122.8 (=C–), 123.8 (=CH–), 125.2 (=CH–), 126.4 (=CH–), 126.4 (ortho), 128.9 (=CH–), 130.6 (meta), 132.0 (=C–), 133.3 (ipso), 134.3 (para), 158.2 (C–O), 163.9 (C^+).

2,3-Diphenyl-5-(10-hydroxy-9-anthryl)tetrazolium Bromide (22). The compound **21** (335 mg, 0.65 mmol) was demethylated with boron tribomide (0.20 cm^3, 2.1 mmol) as the cases of **6a**—c yielding **22** (239 mg, 74%), orange powder. Mp 215 °C (decomp); IR: 3600—3350, 1558, 1500, 1486, 1422, 1348, 1312, 1176, 1162, 1140, 998, 924, 770, 686 cm^{-1}; ^1H NMR (DMSO-d_6): δ=7.61—7.95 (m, 10H, Ar), 8.03—8.09 (m, 4H, Ar), 8.49 (d, 2H, J=9 Hz, Ar), 8.70 (d, 2H, J=9 Hz, Ar), 11.56 (s, 1H, OH); ^{13}C NMR (DMSO-d_6): δ=103.8 (=C–), 119.4 (=C–), 123.3 (=CH–), 124.5 (=CH–), 124.6 (=CH–), 126.4 (ortho), 128.7 (=CH–), 130.4 (meta), 132.0 (=C–), 133.3 (ipso), 134.1 (para), 154.5 (C–O), 163.2 (C^+); UV (MeCN): λ_{max} (log ε) 214 nm (4.40), 259 (4.69), 275 (sh, 4.18), 386 (sh, 3.60), 400 (3.63): Found: C, 64.14; H, 3.95; N, 10.97%. Calcd for $C_{27}H_{19}BrN_4O \cdot 0.5H_2O$: C, 64.29; H, 4.00; N, 11.11%.

Synthesis of 23 by the Deprotonation of 22. Into a solution of **22** (60 mg, 0.12 mmol) in methanol (10 cm^3) was added an aqueous solution of NaOH (1 M, 0.5 cm^3) at room temperature. The solvent was removed under reduced pressure and the residue was chromatographed on Sephadex LH-20. Recrystallization from acetonitrile–ether gave pure **23** as greenish brown crystals in a quantitative yield. Mp 125 °C (decomp); IR: 3060, 1602, 1558, 1480, 1440, 1424, 1334, 1260, 1180, 1120, 1030, 1016, 996, 772, 768, 732, 690, 674 cm^{-1}; ^1H NMR (DMSO-d_6): δ=7.01—7.13 (m, 2H, Ar), 7.37—7.49 (m, 2H, Ar), 7.53—7.85 (m, 6H, Ph), 7.93—8.01 (m, 4H, Ph), 8.44—8.60 (m, 4H, Ar); ^{13}C NMR (DMSO-d_6): δ=118.4 (=C–), 118.4 (=CH–), 122.0 (=C–), 123.9 (=CH–), 126.5 (ortho), 126.7 (=CH–), 128.6 (=CH–), 130.4 (meta), 133.4 (para), 133.5 (ipso), 135.6 (=C–), 175.7 (C^+), 185.9 (C=O); UV (MeCN): λ_{max} (log ε) 257 nm (4.67), 275 (4.82), 343 (sh, 4.27), 366 (4.37), 425 (sh, 3.75), 450 (3.98), 478 (4.19), 509 (4.19); solvent dependence of the longest wavelength band; 486 nm (sh) (MeOH), 495 (EtOH), 504 (*i*-PrOH), 513 (DMSO), 510 (Me_2C=O), 508 (CH_2Cl_2), 509 ($CHCl_3$), 513 (DMF); MS: *m/z* (rel intensity) 414 (M^+, 45), 413 (100), 325 (41), 324 (59), 308 (34), 237 (32), 232 (54), 93 (59), 92 (43), 77 (64); Found: C, 72.33; H, 5.30%. Calcd for $C_{27}H_{18}N_4O \cdot 2H_2O$: C, 71.99; H, 4.92%.

References

1) W. D. Ollis and C. A. Ramsden, *Adv. Heterocycl. Chem.*, **19**, 1 (1976); C. G. Newton and C. A. Ramsden, *Tetrahedron*, **38**, 2965 (1982).

2) S. Araki, N. Aoyama, and Y. Butsugan, *Tetrahedron Lett.*, **28**, 4289 (1987).

3) J. N. Ashley, B. M. Davis, A. W. Nineham, and R. Slack, *J. Chem. Soc.*, **1953**, 3881.

4) W. Ried and D. Schendzielorz, *Justus Liebigs Ann. Chem.*, **682**, 156 (1965).

5) Y. Bansho and K. Nukada, *Bull. Chem. Soc. Jpn.*, **33**, 579 (1960).

6) C. Reichardt, *Angew. Chem.*, **77**, 30 (1965).

7) N. S. Bayliss and E. G. McRae, *J. Phys. Chem.*, **58**, 1002 (1954); E. M. Kosower, *J. Am. Chem. Soc.*, **80**, 3253 (1958).

8) S. Araki and Y. Butsugan, *J. Chem. Soc., Chem. Commun.*, **1983**, 789; *Tetrahedron Lett.*, **25**, 441 (1984); *J. Chem. Soc., Perkin Trans. 1*, **1984**, 2545.

9) D. Jerchel and H. Fischer, *Justus Liebigs Ann. Chem.*, **590**, 216 (1954).

Aryliminodimagnesium Reagents. XVI.[1] Formation of *o*-Hydroxyazoarenes by Condensation with *o*-Hydroxynitroarenes. Favorable Role of *o*-Hydroxyl Group in the Reaction

Masao Ōkubo,* Takanori Nakashima, and Haruko Shiku
Department of Chemistry, Faculty of Science and Engineering, Saga University, Honjō-machi, Saga 840
(Received November 24, 1988)

Hydroxy(HO)-azoxy- and -azoarenes were formed by condensation of $ArN(MgBr)_2$ with *o*-, *m*-, and *p*-HO-nitrobenzenes; nuclear substitution took place as a minor or a major pathway. *o*-HO-azobenzene was obtained in sufficiently high yield. Relative yields of the products varied according to the position of HO group and reaction conditions. The yield variation was explained by the effects of relative efficiency of single electron transfer, σ-complexation, and cooperation of reagent molecules.

o-Hydroxyazoarenes are useful chelating reagents,[2] and have usually been prepared by diazotization of appropriate phenols and naphthols.[3] This paper concerns exploration of an alternative procedure for preparing hydroxyazoarenes by condensation of N-Mg reagent, aryliminodimagnesium ($ArN(MgBr)_2$ derived from aniline, IDMg), with some hydroxy(HO)-substituted nitroarenes (Scheme 1).

Grignard-type reagent has seldom been applied to HO-substituted substrate, although an example of conversion of 2-HO-5-Me-nitrobenzene (**1a**) into *o*-HO-azoxy- and -azobenzenes by use of *p*-MeC_6H_4-IDMg was reported.[4] A large molar excess of IDMg was used, because at least one mol of the reagent is consumed by exchange with HO-proton. Nevertheless, according to the general pathway,[5] *o*-HO-azoxy product (**2a**) is formed and deoxygenated by molar excess of reagent to give *o*-HO-azo product (**3a**). The alternative procedure using HO-substituted IDMg was impossible.[4]

In order to establish the grounds for synthetic application of IDMg reaction, the effect of HO group on the product distribution was examined using isomeric HO-nitrobenzenes and some related substrates. Condensation and nuclear substitution took place, and the product yields depended greatly on the position of HO group, electron-accepting and -donating abilities (EAA and EDA) of reactants (due to involvement of single electron transfer (SET)), and reaction conditions. Reasons for the variations in types and relative yields of products will be discussed.

Results and Discussion

The distribution of major and minor products in IDMg reaction of **1a** was compared with that of the products from two positional isomers, 3-HO-4-Me- and 4-HO-2-Me-nitrobenzenes (**1b** and **1c**). The position of HO group of **1a**, **1b**, and **1c** to nitro groups is ortho, meta, and para, respectively. By typical treatments of **1a** with a small (1.9 or 2.0) and a large (8.0) molar excess of *p*-RC_6H_4-IDMg (R=Me, MeO, Cl) at 55 °C for 3 h, the HO-azoxy and HO-azo products (**2** and **3**), symmetrical azoarene (**4** formed via oxidative coupling of IDMg[5]), and nuclear substitution products (**5—10**) were obtained. The yields of products including those obtained from some related substrates (**1d—1h**) are given in Table 1 (Runs 1—18).

The results of Runs 1—6 using *p*-Me reagent and **1a—1c** were complicated, but reveal three noticeable features unexpected from the reported product distributions in IDMg reactions with ordinary nitroarenes.[5-9] First, nuclear substitution products were formed from **1a** and **1b** and not from **1c** (Run 1, 3, and 5). Second, independent of molar amount of reagent used, combined yield of **2** and **3** from **1a** (Runs 1 and 2) was

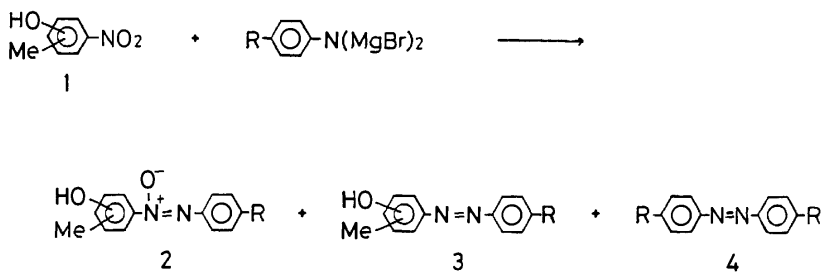

Scheme 1.

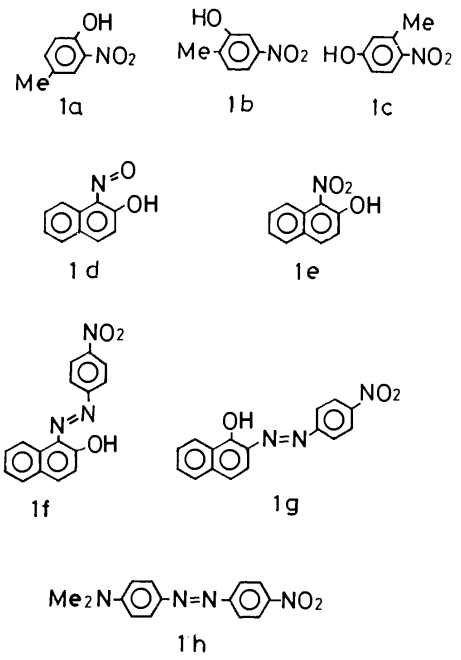

higher than that from **1b** and **1c** (Runs 3—6). Third, also independent of molar amount of IDMg, yield of **3a** was higher than that of **2a** (Runs 1 and 2). Reasons for the unexpected features, however, were explained on the basis of governing factors generally reported for reactions with C-Mg (Grignard) and N-Mg reagents; the relative SET efficiency as a major factor,[6] and σ-complexation[6] and cooperation of reagent molecules[7,8] as minor factors. Discussion will be described in the following sections.

Product Distribution and SET Efficiency. The "first feature" concerns relative SET efficiency estimated by the combination of EAA and EDA.[6] If the redox potentials of substrates cited in Table 1 are compared with the relative yields of **2** plus **3** with reference to those of substitution products (depending on molar amount of IDMg, vide infra), formation of **2** and **3** is favored with strong EAA's (small negative potentials of **1a**, **1b**, **1d**, and 1-nitro-2-naphthol (**1e**)) and not with weak EAA (large negative potential of **1c**). Strong EAA is explained by participation of *o*-quinonoid structure of **1a**, **1d**, and **1e** (Fig. 1). The similar substitution on aromatic ring having low π-electron density is observed in IDMg reactions of quinones without electron-repelling MeO group.[6,9] In contrast to **1c** having *p*-HO group, fairly strong EAA of **1b** due to the lack of electron-repelling resonance of *m*-HO group causes intramolecular successive substitution leading to novel phenazine-type products (**7** and **8**, see Experimental).

The product distribution in the reaction with **1a** is also affected by relative EDA of IDMg (MeO>Me>Cl,[6]

Table 1. Product Distribution in the Reaction of Hydroxynitroarenes with *p*-RC_6H_4-IDMg

Run No.	Substrate (Redn. Pot) (/V)	IDMg R	IDMg molar equiv.	Yield/%[a] 2	3	4	5	6	7	8	9	10	Recovery/%
1	**1a** (−1.080)	Me	1.9	14	33	6	27	—	—	—	—	—	0
2	**1a**	Me	8.0	7	57	19	0	—	—	—	—	—	0
3	**1b** (−1.308)	Me	1.9	13	18	1	—	0	12	0	—	—	37
4	**1b**	Me	8.0	35	7	12	—	0	0	0	—	—	0
5	**1c** (−1.634)	Me	1.9	0	6	2	—	—	—	—	—	—	30
6	**1c**	Me	8.0	3	22	19	—	—	—	—	—	—	0
7	**1a**	MeO	2.0	4	15	3	4	—	—	—	—	—	12
8	**1a**	MeO	8.0	3	43	0	0	—	—	—	—	—	0.6
9	**1a**	Cl	2.0	20	4	2	3	—	—	—	—	—	43
10	**1a**	Cl	8.0	43	17	11	0	—	—	—	—	—	0
11[b]	**1b**	Me	2.0	5	10	0	—	2	20	19	—	—	23
12[c]	**1b**	Me	1.0	0	0	2	—	0	0	0	—	—	93
13	**1d** (−0.898)	Me	3.0	—	5	0.7	—	—	—	—	59[d]	—	20
14	**1e** (−1.068)	Me	3.0	13	13	4	—	—	—	—	13[d]	—	18
15	**1e**	Me	8.0	2	16	13	—	—	—	—	19[d]	—	0
16	**1f** (−0.823)	Me	3.0	34	41	7	—	—	—	—	—	17[e]	0
17	**1g** (−0.870)	Me	3.0	36	44	7	—	—	—	—	—	11[e]	0
18	**1h** (−1.081)	Me	2.0	55	18	9	—	—	—	—	—	—	0

a) Yield based on the amount of substrate used. b) IDMg was added in reverse manner for 100 min and the mixture was heated at 55 °C for 3 h. c) IDMg was added in normal manner and the mixture was heated at 55 °C for 1 h. d) Nuclear substitution and replacement product was obtained as a mixture of tautomer (see Experimental). Product formed via replacement of hydroxynaphthylazo group (see text).

Runs 7—10). In comparison with the results of Runs 1 and 2, strong EDA of *p*-MeO reagent causes rapid deoxygenation leading to higher yield of **3** than **2** but to low overall yield due to self-decomposition of substrate via vigorous SET.[6] Weak EDA of *p*-Cl reagent leads sluggishly to fairly high combined yield of **2** and **3** (the yield of **2** was higher than that of **3**) and leaves a part of **1a** unreacted.

The effects of addition manner and molar ratio are remarkable. By comparison of the results of Runs 3 and 11, "normal addition" of *p*-Me reagent to solution of **1b** favors condensation slightly over substitution compared with "reverse addition." Further comparison of the results of Runs 1 and 2 (using **1a**) reveals that "normal addition" of substrate to large molar excess of IDMg favors condensation. The advantage of these conditions for the condensation with nitro group, due to "cooperation of reagent molecules essential for the pathway," was previously shown by the reaction of *p*-MeC_6H_4-IDMg with *o*-MeO- and *o*-halo-nitrobenzenes[7] and by that of IDMg having long-chain *p*-alkoxyl substituent.[8] An equimolar amount of *p*-Me reagent added even in "normal manner" to **1b** leads to almost complete recovery (Run 12); this indicates that HO-proton of substrate is precedently exchanged with reagent (vide infra) and the derived

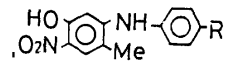

5 (R=Me, MeO, Cl)

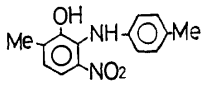

6

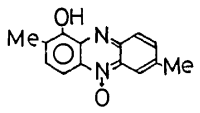

7

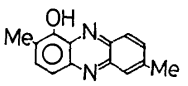

8

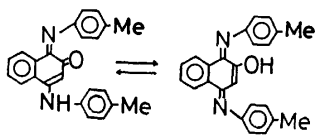

9

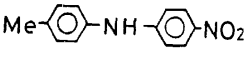

10

5a^R from **1a**; **6**, **7**, and **8** from **1b**;
9 (tautomer) from **1d** and **1e**; **10** from **1f** and **1g**.

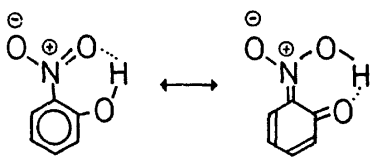

ortho-Quinonoid Structure

Fig. 1. Quinonoid structure of *o*-hydroxynitrobenzene.

-OMgBr and -NHMgBr species form a stable complex which is incapable of SET.

Special Role of *o*-Hydroxyl Group. The "second feature" concerns good overall yeilds of four products from **1a** (**2**—**5**, over 80% yield, Runs 1 and 2) and a small amount of unidentified materials compared to the results of Runs 3—6. Though the clean reaction involving effective condensation of **1a** compared to **1b** and **1c** is appropriate for synthetic use of *o*-hydroxy-substituted nitroarenes, the cleanliness seems to contradict with **1a**'s strong EAA causing usually remarkable substitution or decomposition with much rapid SET.[6] The contradiction arises from special role of *o*-HO group, which is converted into "OMgBr acting as a center of IDMg aggregate in the proximity of nitro group" to facilitate the cooperation of IDMg molecules for condensation.[7,8] The aggregation of Grignard molecules in the presence of alkoxymagnesium species was reported.[10] The conversion of *o*-OH into OMgBr prior to SET is established by Run 12 (vide supra), and by the recovery (over 85%) of **1a** from an equimolar mixture with EtMgBr (having stronger EDA than IDMg[6]), which was added at −70 °C in 1 h. The mixture was gradually warmed up to room temperature, stirred at 55 °C for 1 h, and quenched with aqueous NH_4Cl.

It is likely that in the case of **1b** or **1c**, IDMg molecules are gathered by *m*- or *p*-OMgBr group apart from nitro group; condensation is thus retarded and strong EAA of **1b** will cause substitution. The *p*-HO and weak EAA of **1c** are unfavorable for both the pathways, and consequently result in self-decomposition even with mild SET. The steric repulsion caused by *o*-Me group of **1c** may be negligible (see poor combined product yield and recovery in Runs 5 and 6),[7] because the comparable result was obtained by the reverse addition of 8.0 mol of *p*-Me reagent to noncrowded 4-HO-nitrobenzene though the yields of **2**, **3**, and **4** were slightly improved by the normal addition.

Azoxyarene Precursor. Concerning the "third feature," the higher yield of **3a** than **2a** in spite of consumption of one of the two mol of IDMg used in Run 1 is noted. This fact seems to contradict to the usual tendency of yield variation,[5] i.e., the use of small molar excess of IDMg in the reaction with ordinary nitroarenes leads to a lower yield of **3** than **2**.[5] In order to examine the reason for the contradiction, two attempts were carried out: the one to test facile deoxygenation of **2a**, and the other to test facile condensation of *o*-HO-nitrosoarene[5] expected as an intermediate from deoxygenation of **1a**.

Both the two attempts were unsuccessful. First, treatment of pure **2a** (reduction peak potential: −1.438 V) at 55 °C with 5.0 mol of *p*-MeO reagent for 3 h,[5] caused sluggish deoxygenation leading to **3a** in 15% yield and 75% recovery of **2a**. Another attempt was

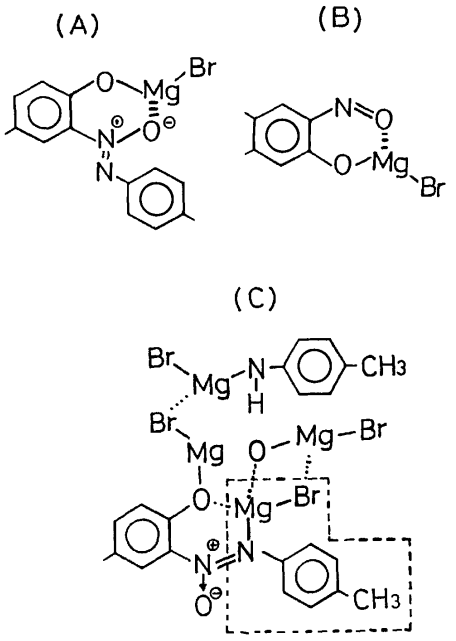

Fig. 2. Depiction of chelates formed in the IDMg reaction. (A): Formed from isolated **2a**. (B): Formed from **1d**. (C): Precursor of **2a** formed from **1a**. A fragment of IDMg is enclosed by broken line.

the treatment of 1-nitroso-2-naphthol (**1d**, reduction peak potential: 0.898 V) with 3.0 mol of *p*-Me reagent at 55 °C (Run 13, **1d** was used instead of nitrosophenol which is difficult to handle because of its high volatility). Yield of the expected 1-arylazo-2-naphthol was 5%, and a nuclear substitution product (cf. Run 14) was obtained in 59% yield. Poor results of the attempts (irrespective of the potential) using isolated **2a** and nitrosonaphthol are ascribed to the formation of Mg chelates (Fig. 2A, 2B): The azoxy and nitroso oxygen atoms incorporated in the chelates may be weakly reactive or almost inert toward IDMg.

As shown by the alternative chelate depicted in Fig. 2C, the "precursor of **2a** formed in the reaction mixture" must involve the ArN moiety of IDMg (enclosed by broken line). As discussed in the preceding section, the precursor 2C must be flanked further by an aggregate of N-Mg species around the OMgBr group. The azoxy oxygen of 2C, not incorporated in the chelate, will be easily attacked by IDMg aggregate and removed.

Reactions of Related Nitroarenes. The results obtained by use of some related nitroarenes (Runs 14—18) were explained similarly as the above discussion. The low overall yield from **1e** by use of both small and large molar excesses of *p*-Me reagent (Runs 14 and 15) is due to decomposition via SET caused by strong EAA. The nitro group of **1e** is sterically hindered by peri-hydrogen, and, at the expense of condensation products (**2e** and **3e**), gives tautomeric compound via substitution-replacement (**9**, the same as that obtained in Run 13, see Experimental). Two noncrowded hydroxy-substituted azonitroarenes (1-(4-NO_2-phenyl-azo)-2-naphthol and its 2,1-isomer (**1f** and **1g**)) condensed effectively with *p*-Me reagent (3.0 mol, Runs 16 and 17) giving azoxy-azo (**2f** and **2g**, 34—36%) and bis-azo (**3f** and **3g**, 41—44%) products. The slightly higher yield of **3** than **2** is ascribed to azo-OMgBr chelation (Fig. 3). The chelation will enhance the positive charge on azoxy nitrogen to facilitate the removal of oxygen,[5] and will also be responsible for the novel replacement of hydroxynaphthylazo groups leading to 4-Me-4′-NO_2-diphenylamine (**10**, 11—17%).

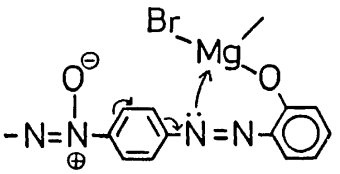

Fig. 3. Illustration of chelation effect on the deoxygenation and replacement in the reaction of **1f** and **1g**.

By comparison, 4-Me_2N-4′-nitroazobenzene (**1h** having no HO group) was treated with 2.0 mol of *p*-Me reagent (Run 18). In spite of strong EAA of **1h**, comparable to **1a** in isolated state, a moderate reaction took place leading to a good combined yield of azoxy-azo (**2h**, 55%) and bis-azo (**3h**, 18%) products. Lack of HO group may be at least partly responsible for the higher yield of **2h** than **3h**. The reaction must be moderated by stabilization of IDMg due to coordination of dimethylamino nitrogen to Mg atom, because the oxidation peak potential of *p*-Me reagent in the presence of equimolar amount of *N,N*-dimethylaniline is larger by ca. 200 mV than the potential in the absence.[5] A similar example of IDMg stabilization by interaction with a remote substituent of nitroarene was reported.[11]

Conclusion

The complicated results of IDMg reactions with HO-substituted nitroarenes were explained on the basis of governing factors and effects of various types of coordination[5-11] originating from strong affinity of Mg with O, Br, and N atoms of substrates. The moderate reactivity of IDMg[6] is responsible for observation of the coordination factors. Though the precise mechanism of condensation still remains to be studied, the grounds for synthetic use of *o*-HO-nitroarenes seem to be established.

Experimental

Procedures and Products. The nitrophenols and nitro- and nitrosonaphthols were commercially available. The isomeric (nitrophenylazo)naphthols were prepared from 1- and 2-naphthols by diazotization using 4-nitroaniline. The preparation of IDMg was previously described,[4] and most of its reactions were carried out under typical conditions at 55 °C for 3 h.

After quenching the reaction mixture with saturated

Table 2. Melting Points and ^1H NMR Data of Products

Product No.	Mp θ_m/°C	^1H NMR data/δ
2a^{Me}	109—109.5	11.94 (1H, s), 7.80—6.99 (7H, m), 2.42 (3H, s), 2.36 (3H, s)
2b^{Me}	163.5	8.12—7.21 (8H, m), 2.43 (3H, s), 2.33 (3H, s)
2c^{Me}	—[a]	8.12—6.82 (8H, m), 2.60 (3H, s), 2.34 (3H, s)
2a^{MeO}	95	11.91 (1H, s), 8.22—6.97 (7H, m), 3.81 (3H, s), 2.34 (3H, s)
2a^{Cl}	136—137	11.71 (1H, s), 8.09—7.00 (7H, m), 2.36 (3H, s)
2e	—[a]	10.91 (1H, s), 8.55—7.20 (10H, m), 2.39 (3H, s)
2f	244.5—245	16.30 (1H, s), 8.51 (1H, d), 8.43 and 7.77 (4H, ABq. J=8.8 Hz), 8.18 (1H, s), 8.15 (1H, s), 7.74—7.29 (6H, m), 6.79 (1H, d), 2.34 (3H, s)
2g	221—221.5	16.10 (1H, s), 8.42 (1H, s), 8.39 (1H, s), 8.15 (1H, d), 7.56—6.99 (9H, m), 7.69 (1H, s), 7.66 (1H, s), 2.43 (3H, s)
2h	198—199	8.41 and 6.77 (4H, ABq, J=9.3 Hz), 8.17 and 7.30 (4H, ABq, J=8.4 Hz), 7.96—7.90 (4H, m), 3.12 (6H, s), 2.43 (3H, s)
3f	222—222.5	16.41 (1H, s), 8.55 (1H, d), 8.06—7.32 (1sH, m), 6.82 (1H, d), 2.45 (3H, s)
3g	245—246	16.26 (1H, s), 8.43 (1H, d), 8.04—7.51 (11H, m), 7.34—6.87 (2H, m), 2.45 (3H, s)
5^{Me}	153 (sublimed)	11.18 (1H, s), 7.87 (1H, s), 7.23 and 7.13 (4H, ABq, J=8.3 Hz), 6.46 (1H, s), 6.06 (1H, s), 2.38 (3H, s), 2.24 (3H, s)
5^{MeO}	—[a]	11.20 (1H, s), 7.86 (1H, s), 7.15 and 6.97 (4H, ABq, J=2.4 Hz), 6.30 (1H, s), 6.01 (1H, s), 3.85 (3H, s), 2.24 (3H, s)
5^{Cl}	—[a]	7.87 (1H, s), 7.39 and 7.18 (4H, ABq, J=8.8 Hz), 6.50 (1H, s), 6.03 (1H, s), 2.25 (3H, s)
6	Oil	7.58—6.56 (5H, m), 5.78 (1H, s), 2.28 (3H, s), 2.19 (3H, s)
7	167 (sublimed)	8.42 (1H, s), 8.23 (1H, s), 8.03—7.49 (4H, m), 2.62 (3H, s), 2.47 (3H, s)
8	185 (sublimed)	8.22 (1H, s), 8.09—7.60 (5H, m), 2.63 (3H, s), 2.52 (3H, s)
9[b]	178	12.84 (1H, s), 8.90 (1H, d), 7.80—7.12 (13H, m), 2.36 (3H, s), 2.31 (3H, s)
10	138—139	8.11 and 6.85 (4H, ABq, J=2.2 Hz), 7.26—7.09 (4H, m), 6.27 (1H, broad s), 2.36 (3H, s)

a) Melting point was undetermined, because the product was not purified. b) One of the tautomers: the signal at δ 12.84 is assigned to HO-proton.

aqueous NH_4Cl, the products were separated by column and thin-layer chromatography on silica gel (Wako Gel C-200 and C-300). The elemental analyses of products gave satisfactory results. The melting points (uncorrected) and ^1H NMR data of **2a—2h**, **3f** and **3g**, **5**[R], and **6—10** are given in Table 2. The data for **3a—3e** and **4** are known.

The phenazine-type products (**7** and **8**) formed from **1b** (Runs 3 and 4) arise from substitution at 2-position (cf. **6**) followed by intramolecular attack of a nitrogen radical (derived from nitro group) at the *o*-position of anilino moiety, the precise mechanism being ambiguous. The two tautomeric products (**9**) formed from nitroso- and nitronaphthols (Runs 13—15) arise from substitution at 4-position followed by replacement of nitroso or nitro group; the physical data for the stable one having HO group is given in Table 2. The structure of **9** was confirmed by hydrolysis with aqueous hydrochloric acid to convert into 2-HO-1,4-naphthoquinone and 4-Me-aniline.

Reduction (redox) potentials of substrates were measured by the reported method[9] using bis(biphenyl)chromium(I) tetraphenylborate (BCTB) as an internal reference.

The gift of BCTB samples by Professor Gerhard Gritzner, University of Linz, is gratefully acknowledged. The authors thank Mr. Kōji Matsuo for measuring redox potentials of substrates and the recovery experiment using **1a** and EtMgBr. They are grateful to the Advanced Instrumentation Center for Chemical Analyses, Ehime University, for elemental analyses. A part of this work was financially supported by Grants-in-Aid for Scientific Research (Nos. 60470024 and 63540405) from the Ministry of Education, Science and Culture.

References

1) Part XIV: See Ref. 7.

2) For example, G. Schetty, *Helv. Chim. Acta*, **52**, 1016 (1969); G. Schetty and E. Steiner, *ibid.*, **55**, 1509 (1972), and literatures cited therein.

3) H. Zollinger, "Color Chemistry," Verlagsgesellschaft, Weinheim (1987).

4) M. Ōkubo, M. Tokisada, and T. Gondo, *Nippon Kagaku Kaishi*, **1985**, 303.

5) M. Ōkubo, T. Takahashi, and K. Koga, *Bull. Chem. Soc. Jpn.*, **56**, 199 (1983); M. Ōkubo and K. Koga, *ibid.*, **56**, 203 (1983).

6) M. Ōkubo, T. Tsutsumi, and K. Matsuo, *Bull. Chem. Soc. Jpn.*, **60**, 2085 (1987); M. Ōkubo, T. Tsutsumi, A. Ichimura, and T. Kitagawa, *ibid.*, **57**, 2679 (1984).

7) M. Ōkubo, Y. Inatomi, N. Taniguchi, and K. Imamura, *Bull. Chem. Soc. Jpn.*, **61**, 3581 (1988).

8) M. Ōkubo, K. Matsuo, and A. Yamauchi, *Bull. Chem. Soc. Jpn.*, **62**, 915 (1989), and literatures cited therin.

9) M. Ōkubo and K. Matsuo, unpublished results.

10) A. D. Vreugdenhil and C. Blomberg, *Recl. Trav. Chim. Pays-Bas*, **84**, 38 (1965); H. O. House, R. A. Latham, and G. M. Whitesides, *J. Org. Chem.*, **32**, 3481 (1967); M. Ōkubo, *Bull. Chem. Soc. Jpn.*, **58**, 3108 (1985).

11) M. Ōkubo, K. Asao, and H. Hyakutake, *Bull. Chem. Soc. Jpn.*, **60**, 3781 (1987).

Strongly Deformed TCNQ Derivatives: Syntheses and Properties of 7,12-Bis(dicyanomethylene)-7,12-dihydrobenz[*a*]-anthracene (BDCNBA) Derivatives

Kazuhiro MARUYAMA,* Hiroshi IMAHORI, Katsuhiko NAKAGAWA,† and Nobuo TANAKA††
Department of Chemistry, Faculy of Science, Kyoto University, Kyoto 606
†Department of Industrial Chemistry, Niihama National College of Technology, Niihama 792
††Department of Life Science, Faculty of Science, Tokyo Institute of Technology, Yokohama 227
(Received November 26, 1988)

In spite of large steric repulsion between aromatic quinone moiety and dicyanomethylene moiety the title compounds (BDCNBA) were synthesized by $TiCl_4$-catalyzed reactions of the corresponding aromatic quinones and malononitrile. BDCNBA showed electronic spectra indicating the intramolecular charge-transfer interaction and redox properties similar to 11,11,12,12-tetracyano-9,10-anthraquinodimethane (TCNAQ) derivatives. BDCNBA showed a low electrical conductivity ($\approx 10^{-7}\ \Omega^{-1}\ cm^{-1}$). Strongly deformed structure of BDCNBA was established by X-ray crystallographic analysis.

Recently much attentions have been centered to organic metals.[1] Organic metals are generally composed of donors and acceptors, but acceptors investigated so far have been limited mostly to tetracyanoquinodimethane (TCNQ) analogues, while a variety of donors have been examined. 11,11,12,12-Tetracyano-9,10-anthraquinodimethane (TCNAQ) deviates deform from flat molecular plane of the corresponding anthraquinone, having butterfly form, because of steric repulsion between peri-hydrogen of aromatic moiety and dicyanomethylene group.[2] Nevertheless they make complex with aromatic donors in many cases.[3] It is important to elucidate the relationship between steric factor in organic metals and complex formation between donors and acceptors or electrical conductivity for designing excellent organic metals. We synthesized polyaromatic TCNQ compounds to investigate the effect of aromaticity and steric repulsion between dicyanomethylene moiety and aromatic moiety by introducing a benzene ring to TCNAQ framework. Now we wish to report here syntheses and properties of 7,12-bis(dicyanomethylene)-7,12-dihydrobenz[*a*]anthracene derivatives.

Table 1. $TiCl_4$-Catalyzed Reaction between Quinone **1** and Malononitrile

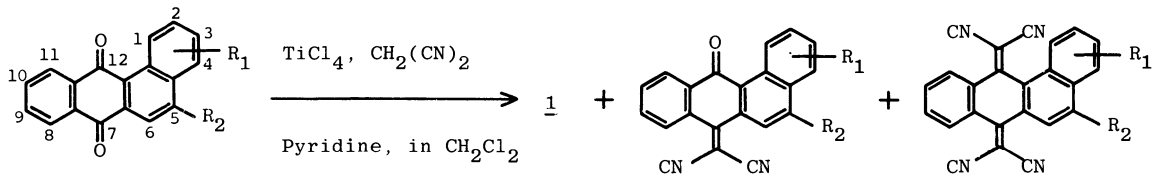

Run		Quinone **1**	Quinone conversion/%	Yields of products/% **2**		**3**	
1	**1a**:	R_1=2-F, R_2=H	100	**2a**:	0	**3a**:	70
2	**1b**:	R_1=2-Cl, R_2=H	100	**2b**:	0	**3b**:	64
3	**1c**:	R_1=2-H, R_2=H	100	**2c**:	0	**3c**:	88
4	**1d**:	R_1=2-Me, R_2=H	100	**2d**:	0	**3d**:	64
5	**1e**:	R_1=2-OMe, R_2=H	100	**2e**:	0	**3e**:	70
6	**1f**:	R_1=3-OMe, R_2=H	100	**2f**:	0	**3f**:	48
7	**1g**:	R_1=4-OMe, R_2=H	100	**2g**:	0	**3g**:	70
8	**1h**:	R_1=2-F, R_2=4-FC_6H_4	100	**2h**:	53	**3h**:	40
9	**1i**:	R_1=2-Cl, R_2=4-ClC_6H_4	63	**2i**:	8	**3i**:	22
10	**1j**:	R_1=2-H, R_2=C_6H_5	100	**2j**:	80	**3j**:	18
11	**1k**:	R_1=2-Me, R_2=4-MeC_6H_4	96	**2k**:	74	**3k**:	21
12	**1l**:	R_1=2-OMe, R_2=4-$OMeC_6H_4$	97	**2l**:	63	**3l**:	30
13	**4**:	5,12-naphthacenequinone	100	**5**:	0	**6**:	60

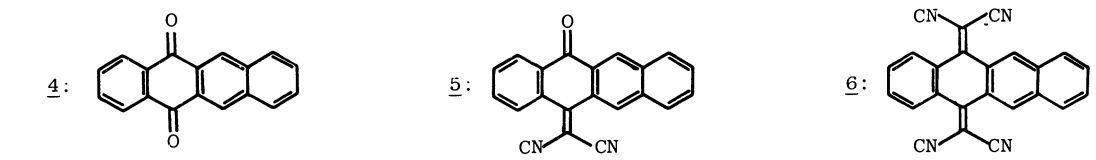

Results and Discussion

Synthesis of BDCNBA. 7,12-Bis(dicyanomethylene)-7,12-dihydrobenz[*a*]anthracenes (BDCNBA) **3** were synthesized from the corresponding benz[*a*]anthracene-7,12-diones **1** according to the Aumüller[4] and Ong[5] method. The results are summarized in Table 1. In spite of large steric repulsion between dicyanomethylene groups and aromatic moieties, especially naphthalene moiety, BDCNBA **3a—g** were produced in high yields compared to the case of TCNAQ,[3-6] while 7-(dicyanomethylene)benz[*a*]anthracen-12(7*H*)-ones (DCNBA) **2a—g** were not obtained. 5,12-Bis-(dicyanomethylene)-5,12-dihydronaphthacene **6** which is less crowded than **3c** was also obtained in similar yield. In Runs 8—12, BDCNBA **3h—l** were obtained in low yields, whereas DCNBA **2h—l** were obtained majorly. The respective structures of compounds **2**, **3** were assigned by the spectroscopic data as well as X-ray analyses of **2j** and **3c**. A proton at C-1 of **2** showed characteristic shift in the ^{1}H NMR spectrum ($\delta \approx 9$—10) similar to that in the corresponding quinone **1** due to the additional deshielding of carbonyl group, while no similar downfield shift of C-1 proton in the ^{1}H NMR spectrum of the corresponding BDCNBA **3** was observed (see Experimental section). This indicates that the position of dicyanomethylene group in **2** probably is at less crowded C-7 site. The structure was unambiguously determined by X-ray analysis of **2j**. It is known that only 1,3-dimethyl-10-(dicyanomethylene)anthrone was formed exclusively when 1,3-dimethylanthraquinone was subjected to the same reaction,[5] while 1,5-dichloro-9,10-bis(dicyanomethylene)-9,10-dihydroanthracene was obtained in a low yield (19%) when the corresponding anthraquinone was used.[4] In our case it is amazing that BDCNBA **3** was produced in a high yield in spite of supposedly larger steric repulsion between aromatic moieties and dicyanomethylene groups compared to other cases.

UV-Visible Absorption Spectrum. The UV-visible absorption spectrum of BDCNBA **3c** in dichloromethane shows bands at 231 (log ε=4.29), 285 (4.19), 337 (4.46), and 431 (3.46) nm. Thus, the lowest energy electronic transition (λ_{max}=431 nm) is red-shifted by ca. 80, 30, 30 nm, compared to those of TCNAQ,[7] 9,9,10,10-tetracyano-1,4-naphthoquinodimethane (TCNNQ),[7] tetracyanoquinodimethane (TCNQ), respectively (Table 2). In addition, the longest wavelength band (λ_{max}) of TCNAQ is blue-shifted by ca. 70 nm compared with that of anthraquinone, while that of **3c** is red-shifted by ca. 100 nm compared with that of **1c** (Table 2). It is well-known that the central ring in TCNAQ is bent into a boat form and the two benzene rings are noncoplanar to avoid the severe steric interactions between the cyano groups and the peri-hydrogens.[2] Since the structure of **3c** deforms more severely than that of TCNAQ as discussed later, the observed large red shift (λ_{max}) in the longest wavelength band is unusual. These data suggest that the large red shift of the longest wavelength bands is not ascribed to the larger delocalization of the π system, but to the intramolecular charge-transfer (CT) interaction[8] between dicyanomethylene groups and aromatic moieties. The peak values (λ_{max}^{CT}) in the longest wavelength region were more blue-shifted for **3a—g** and **3h—l**, as electron-withdrawing substituent groups were introduced into the naphthalene moiety (Table 3). As the polarity of solvent increased,[9] blue shifts of the λ_{max}^{CT} were observed in the UV spectra of **3c** and **3j** (Table 4). Since the corresponding CT band

Table 3. Longest Wavelength Band (λ_{max}^{CT}) of **2** and **3** in CH_2Cl_2

3	λ_{max}^{CT}/nm	3	λ_{max}^{CT}/nm	2	λ_{max}^{CT}/nm
3a	424	**3h**	449	**2h**	422
3b	426	**3i**	458	**2i**	425
3c	431	**3j**	458	**2j**	427
3d	444	**3k**	478	**2k**	450
3e	474	**3l**	502	**2l**	477
3f	462				
3g	480				
6	424				

Table 4. Solvent Effects for CT Band

Solvent	*Z* value[a]	λ_{max}^{CT}/nm[b] 3c	3j	2j
C_6H_6	54	433	459	432
CH_2Cl_2	64.2	431	458	427
CH_3CN	71.3	418	441	420
CH_3OH	83.6	416	438	—[c]

a) Kosower's solvent parameter.[9] b) Measured at 1.0×10^{-4} mol dm^{-3}. c) For low solubility of **2j** in methanol.

Table 2. UV-Visible Spectra of TCNQ Derivatives in CH_2Cl_2

Compound	λ_{max} (log ε)/nm
TCNQ	235 (3.57), 380 (4.42), 401 (4.63)
TCNNQ	290 (3.89), 388 (4.53), 404 (4.50)[a]
9,10-Anthraquinone	253 (4.73), 264 (4.33), 274 (4.26), 326 (3.76), 414 (1.90)
TCNAQ	283 (4.48), 305 (4.22), 347 (4.43)[a]
1c	242 (4.41), 249 (4.35), 284 (4.55), 336 (3.65)
3c	231 (4.29), 285 (4.19), 337 (4.46), 431 (3.46)

a) From Ref. 7.

was also observed in **6**, these effects are not due to the deformation derived from larger steric interaction compared to TCNAQ, but due to the easier electron-releasing character from naphthalene moiety to dicyanomethylene group caused by replacement of benzene ring to naphthalene one. Indeed, similar substituent (Table 3) and solvent effects (Table 4) in **2h—l** were observed. That is, the values of λ_{max}^{CT} were blue-shifted as electron-withdrawing substituent groups were introduced in the naphthalene moiety. The similar inclination was observed as the polarity of solvent increased. Thus, these longest bands are due to the intramolecular CT interaction.

Electrochemical Studies. Table 5 shows the results of cyclic voltammogram of TCNQ derivatives in acetonitrile, taken at room temperature using with tetraethylammonium perchlorate as the supporting electrolyte. For BDCNBA only one reversible redox wave, which corresponds to two electron reduction observed in the case of TCNAQ,[2-4,7] was observed in the range from 0 to −2.0 V and the value of $E_{1/2}^{red}$ is much lower than that in TCNQ, but is a little lower than that in TCNAQ. These facts suggest that extension of aromatic system contributes only slightly to the reduction potential, but decrease of the aromaticity due to big steric repulsion between dicyanomethylene groups and aromatic moieties has a greater effect. From the value of $E_{1/2}^{red}(1)-E_{1/2}^{red}(2)$ (+0.016) obtained by Myers and Shain's method,[10] we can estimate the value of semiquinone formation constant K_{sem} as the following;

$$\log K_{sem} = \log([BDCNBA^{-}]^2/[BDCNBA][BDCNBA^{2-}]) = (E_{1/2}^{red}(1) - E_{1/2}^{red}(2))/0.058$$

The small log K_{sem} (+0.28) value of **3c** relative to that of TCNQ, but nearly equal to that of TCNAQ indicates that anion radical $\mathbf{3c}^{-}$ is unstable. It has been concluded from the ESR and the ENDOR studies of TCNQ derivatives that the negative charges in the dianions tend to localize on the two dicyanomethylene groups.[11] This inclination is enhanced in $TCNAQ^{2-}$ because of the steric repulsion between peri-hydrogen and dicyanomethylene group.[6,7] Since C7—C13 and C12—C16 bonds (see Fig. 2) turn to be single in the dianion of **3c**, steric repulsion between dicyanomethylene groups and aromatic moieties including peri-hydrogen atoms in $\mathbf{3c}^{2-}$ would be readily released by twisting the two negatively charged dicyanomethylene groups out of the aromatic plane rather than by bending the central benzene ring (consisting of C6a, C7, C7a, C11a, C12, C12a) in the benz[*a*]anthracene moiety. Thus, disproportionation between dianion $\mathbf{3c}^{2-}$ and **3c** easily would occur because of the steric interaction.[12]

Table 5. Reduction Potentials[a] and Semiquinone Formation Constants of TCNQ Derivatives

Compound	$E_{1/2}^{red}$ (1)	$E_{1/2}^{red}$ (2)	log K_{sem}[e]
TCNQ[b]	+0.18	−0.36	9.31
TCNAQ[c]	−0.37		−0.03
BDCNBA[d]	−0.44		+0.28

a) V vs. SCE, 0.1 mol dm^{-3} Et_4NClO_4 in CH_3CN, platinum electrode. b) From Ref. 6. c) From Ref. 3. d) This work. e) From Ref. 10.

Electrical Conductivity. Mukai et al. reported that TCNAQ forms CT complex with many aromatic donors and steric factor is important to form complexation.[3,6] On the contrary, 2,3,5,6-tetramethyl-7,7,8,8-tetracyanoquinodimethane (TMTCNQ), which has strong deformation of the TCNQ skeleton into a boat-conformation,[13] formed no complex with tetrathiafulvalene (TTF), tetramethyltetrathiafulvalene (TMTTF), tetramethyltetraselenafulvalene (TMTSF).[14] In our case, no complex was formed between **3c** and a variety of electron donors, like as naphthalene, pyrene, anthracene, TMTTF, although they showed charge-transfer bands in dichloromethane solution similar to the cases observed between TCNAQ and aromatic donors (Table 6 and Experimental section), indicating that the larger steric hindrance between donor and

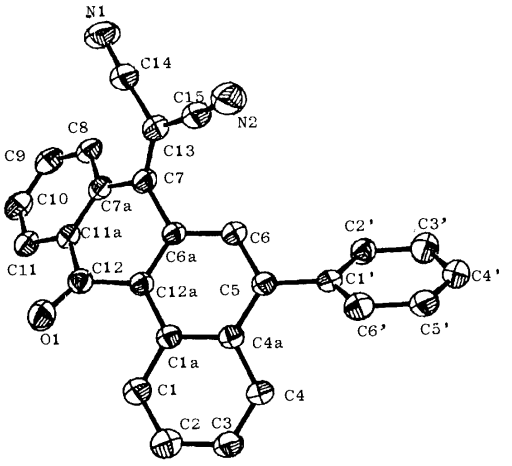

Fig. 1. ORTEP view of **2j**.

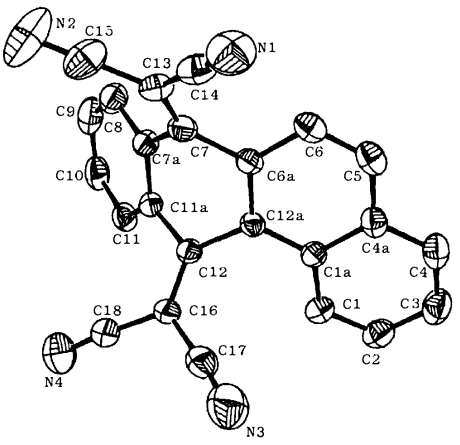

Fig. 2. ORTEP view of **3c**.

acceptor interrupts the complex formation.

It is well-known that partial charge transfer from donor to acceptor is important for high quality of organic metals.[1] Thus, **3c** itself has possibility of showing high electrical conductivity, since **3c** has intramolecular CT character. Against our expectation, **3c** showed low electrical conductivity (1×10^{-7} Ω^{-1} cm^{-1}) at room temperature. These results suggest that large steric deformation reduces intermolecular interaction and results in low electrical conductivity.

X-Ray Structures of DCNBA 2j and BDCNBA 3c. The structures of DCNBA and BDCNBA frameworks were definitely confirmed by X-ray diffraction analyses of **2j** and **3c** (Figs. 1 and 2). The atomic positional and equivalent isotropic thermal parameters are listed in Table 7. Bond distances and angles of **2j** and **3c** are listed in Tables 8 and 9, respectively.

Table 6. Charge-Transfer Absorption Maxima of BDCNBA **3c** and Aromatic Donors[a] (λ_{max}/nm in CH_2Cl_2)

Naphthalene	Pyrene	Anthracene	TMTTF
485	502	518	632

a) BDCNBA: 2.5×10^{-3} mol dm^{-3}, donors: 5.0×10^{-2} mol dm^{-3}.

Bond lengths and angles of TCNQ unit (consisting of C6a, C7, C7a, C11a, C12, C12a) in **3c** are almost the same as those in TCNAQ. However, deformation of the structure of **3c** is larger than that of TCNAQ. The dihedral angle between planes A (consisting of C8, C9, C10, C11, C11a, C7a) and B (consisting of C1, C2, C3, C4, C4a, C5, C6, C6a, C12a, C1a) is 49.5° for **3c**, while that of TCNAQ is 35.4° (see Fig. 2 and Table 10). The dihedral angle between planes A and B in **2j** is 33.3°, and that in 10-dicyanomethyleneanthrone is 28°.[15] These facts indicate that introduction of naphthalene unit into TCNAQ causes the larger deformation of the structure because of the steric repulsion between naphthalene moiety and dicyanomethylene group. Comparison of bond distances of naphthalene moiety for benz[*a*]anthracene-7,12-dione vs. **3c** or **2j** reveals us degree of the deformation for naphthalene moiety, for example, 142.0 pm for **3c**, 144.4 pm for **2j** vs. 147.2 pm for 8-methylbenz[*a*]anthracene-7,12-dione (MBAD) (C1a-C12a); 134.8 pm for **3c**, 138.5 pm for **2j** vs. 139.3 pm for MBAD (C5-C6).[16] Thus, bond lengths of naphthalene moiety in **3c** and **2j** (C1-C1a, C1a-C12a, C6a-C12a, C6–C6a, C5-C6, C4a-C5, C4-C4a) are different from those in MBAD due to effect of the butterfly form. On the other hand, bond lengths of

Table 7. Atomic Positional and Equivalent Isotropic Thermal Parameters for **2j** and **3c**

2j					**3c**				
Atom	*x*	*y*	*z*	B_{eq}/B_{iso}[a]	Atom	*x*	*y*	*z*	B_{eq}/B_{iso}[a]
O1	0.3136(2)	0.6576(2)	0.1908(3)	4.2	N1	0.6169(4)	0.7284(2)	0.8259(5)	5.1
N1	−0.1948(3)	0.7725(3)	0.0408(5)	5.4	N2	0.7082(5)	0.9748(3)	0.5380(5)	7.3
N2	0.0910(3)	1.1228(3)	0.3780(5)	5.4	N3	−0.2323(4)	0.7063(2)	0.4057(5)	4.9
C1	0.5652(3)	0.8909(3)	0.2914(4)	3.2	N4	−0.1311(4)	0.9332(2)	0.0911(6)	5.9
C2	0.6957(3)	0.9657(3)	0.3538(4)	3.7	C1	−0.1759(4)	0.5558(2)	0.1029(4)	3.0
C3	0.7596(3)	1.1056(3)	0.3796(4)	3.6	C2	−0.2764(4)	0.4676(2)	0.0778(5)	3.6
C4	0.6909(3)	1.1692(3)	0.3473(4)	3.3	C3	−0.2137(4)	0.3937(2)	0.1634(5)	3.8
C5	0.4811(3)	1.1635(3)	0.2566(4)	2.8	C4	−0.0489(4)	0.4090(2)	0.2680(5)	3.4
C6	0.3503(3)	1.0867(3)	0.1888(4)	3.0	C5	0.2334(4)	0.5143(2)	0.3984(5)	3.1
C7	0.1457(3)	0.8653(3)	0.0800(4)	3.0	C6	0.3400(4)	0.5986(2)	0.4194(4)	3.0
C8	0.0046(3)	0.6681(3)	−0.1817(4)	3.5	C7	0.3916(3)	0.7673(2)	0.3497(4)	2.6
C9	−0.0277(3)	0.5384(4)	−0.2867(4)	4.0	C8	0.4494(4)	0.8588(2)	0.0827(5)	3.3
C10	0.0381(3)	0.4697(3)	−0.2559(4)	3.9	C9	0.3868(4)	0.8914(2)	−0.0983(5)	3.7
C11	0.1379(3)	0.5298(3)	−0.1187(4)	3.5	C10	0.2179(5)	0.8812(2)	−0.1898(5)	3.8
C12	0.2835(3)	0.7271(3)	0.1284(4)	3.0	C11	0.1083(4)	0.8374(2)	−0.1019(5)	3.2
C13	0.0556(3)	0.9085(3)	0.1360(4)	3.4	C12	0.0614(3)	0.7492(2)	0.1736(4)	2.4
C14	−0.0835(3)	0.8290(3)	0.0790(4)	3.8	C13	0.5278(4)	0.8079(2)	0.5103(5)	3.2
C15	0.0829(3)	1.0307(3)	0.2716(5)	3.9	C14	0.5767(4)	0.7623(2)	0.6858(5)	3.6
C1a	0.4904(3)	0.9531(3)	0.2550(4)	2.7	C15	0.6290(4)	0.9010(3)	0.5222(5)	4.4
C4a	0.5540(3)	1.0968(3)	0.2884(4)	2.7	C16	−0.0576(3)	0.7812(2)	0.2040(4)	2.7
C6a	0.2869(3)	0.9451(3)	0.1508(4)	2.8	C17	−0.1548(4)	0.7364(2)	0.3156(5)	3.3
C7a	0.1058(3)	0.7301(3)	−0.0439(4)	3.0	C18	−0.0936(4)	0.8672(2)	0.1394(5)	3.5
C11a	0.1733(3)	0.6607(3)	−0.0148(4)	2.9	C1a	−0.0037(3)	0.5750(2)	0.2179(4)	2.4
C12a	0.3546(3)	0.8773(3)	0.1809(4)	2.7	C4a	0.0606(4)	0.4988(2)	0.2979(4)	2.8
C1′	0.5416(3)	1.3125(3)	0.2955(4)	2.8	C6a	0.2800(3)	0.6754(2)	0.3430(4)	2.5
C2′	0.6128(3)	1.3988(3)	0.4569(4)	3.2	C7a	0.3403(4)	0.8129(2)	0.1692(4)	2.6
C3′	0.6686(3)	1.5384(3)	0.4932(4)	3.6	C11a	0.1683(3)	0.8021(2)	0.0754(4)	2.5
C4′	0.6532(3)	1.5936(3)	0.3680(5)	4.1	C12a	0.1097(3)	0.6641(2)	0.2486(4)	2.3
C5′	0.5809(3)	1.5094(3)	0.2076(5)	4.3					
C6′	0.5238(3)	1.3683(3)	0.1723(4)	3.3					

a) $B_{eq}=\frac{4}{3}(B_{11}a^2+B_{22}b^2+B_{33}c^2+B_{12}ab\cos\gamma+B_{13}ac\cos\beta+B_{23}bc\cos\alpha))$.

Table 8. Bond Distances for **2j** and **3c**

From	To	Distance/pm	ESD	From	To	Distance/pm	ESD
			2j				
O1	C12	122.9	0.4	N1	C14	114.8	0.5
N2	C15	114.0	0.5	C1	C2	137.1	0.5
C1	C1a	142.5	0.5	C2	C3	140.8	0.5
C3	C4	136.8	0.5	C4	C4a	142.7	0.5
C5	C6	138.5	0.5	C5	C4a	143.7	0.5
C5	C1′	148.9	0.5	C6	C6a	141.3	0.5
C7	C13	136.2	0.5	C7	C6a	148.9	0.5
C7	C7a	147.7	0.5	C8	C9	139.0	0.6
C8	C7a	140.4	0.5	C9	C10	138.9	0.6
C10	C11	139.2	0.5	C11	C11a	139.2	0.5
C12	C11a	149.3	0.5	C12	C12a	149.3	0.5
C13	C14	144.8	0.5	C13	C15	143.9	0.5
C1a	C4a	143.8	0.5	C1a	C12a	144.4	0.5
C6a	C12a	139.4	0.5	C7a	C11a	140.6	0.5
C1′	C2′	140.2	0.5	C1′	C6′	140.2	0.5
C2′	C3′	139.5	0.5	C3′	C4′	140.0	0.5
C4′	C5′	139.4	0.6	C5′	C6′	141.1	0.5
			3c				
N1	C14	113.3	0.5	N2	C15	113.3	0.6
N3	C17	113.6	0.5	N4	C18	113.4	0.6
C1	C2	136.8	0.5	C1	C1a	142.4	0.5
C2	C3	140.9	0.5	C3	C4	136.0	0.6
C4	C4a	141.5	0.5	C5	C6	134.8	0.5
C5	C4a	141.5	0.5	C6	C6a	141.9	0.4
C7	C13	136.4	0.5	C7	C6a	147.3	0.4
C7	C7a	147.5	0.4	C8	C9	139.3	0.5
C8	C7a	139.0	0.5	C9	C10	138.8	0.6
C10	C11	139.1	0.5	C11	C11a	138.7	0.5
C12	C16	134.4	0.4	C12	C11a	147.5	0.4
C12	C12a	148.8	0.4	C13	C14	144.3	0.5
C13	C15	144.3	0.5	C16	C17	144.7	0.5
C16	C18	144.1	0.5	C1a	C4a	143.5	0.5
C1a	C12a	142.0	0.4	C6a	C12a	139.8	0.4
C7a	C11a	141.2	0.4				

C1-C2, C2-C3, and C3-C4 in **3c** and **2j** are similar to those in MBAD due to the less effect of the butterfly form. The larger values of dihedral angle between planes A and C (consisting of C6a, C7a, C11a, C12a) (25.2°) or planes B and C (24.4°) compared to that of TCNNQ (15.3°),[17] TCNAQ (16.6°, 18.9°),[2] tetracyanobianthraquinodimethane (TBAQ) (23.6°, 26.1°),[18] and **2j** (15.1°, 18.3°) show that planes A and B in **3c** are more folded out of the central ring plane C than those in TCNQ derivatives. Planes D (consisting of C6a, C7, C7a, C13) and F (consisting of C16, C12, C11a, C12a) are tilted more sharply from the central ring plane C by 34.4°, 41.0°, respectively than those of TCNNQ (16.7°, 21.6°), TCNAQ (30.1°, 30.7°), TBAQ (29.8°, 35.4°), and **2j** (33.1°). Dihedral angle between planes D and E (consisting of C7, C13, C14, C15, N1, N2) (3.6°) or planes F and G (consisting of C12, C16, C17, C18, N3, N4) (3.9°) is small, thus, planes D and E (or planes F and G) are almost coplanar. Yamaguchi et al.[18] reported that TBAQ, which is the most strongly deformed of all TCNQ derivatives, was synthesized from bianthron and malononitrile, while tetracyanodiphenoquinodimethane could not be synthesized. Comparison of the corresponding dihedral angles of TBAQ and BDCNBA **3c** reveals that BDCNBA is more strongly deformed than TBAQ.

In conclusion, BDCNBA and TCNAQ are very similar except that BDCNBA shows intramolecular CT character. BDCNBA has the most strongly deformed structure of all TCNQ derivatives due to the steric interaction between benzene rings and dicyanomethylene groups.

Experimental

General Procedures. All melting points were determined with a Yanagimoto micro melting point apparatus and uncorrected. Mass spectra were taken on a JEOL JMS-DX 300 mass spectrometer. The electronic spectra were obtained by Shimadzu UV-200 spectrometer. ^{1}H NMR spectra were taken by using a JEOL-JNM-PS-100 spectrometer or a JEOL JNM-GX-400 spectrometer and chemical shifts were recorded in parts per million (ppm) on the δ scale from tetramethylsilane as an internal standard. IR spectra were obtained by using a JASCO IRA-1 spectrometer on KBr

Table 9. Bond Angles for **2j** and **3c**

	Angle/degree	ESD		Angle/degree	ESD		Angle/degree	ESD
				2j				
C2-C1-C1a	120.89	0.33	C1-C2-C3	120.68	0.35	C2-C3-C4	120.18	0.35
C3-C4-C4a	121.36	0.33	C6-C5-C4a	118.95	0.30	C6-C5-C1′	119.03	0.30
C4a′-C5-C1′	122.02	0.29	C5-C6-C6a	121.72	0.31	C13-C7-C6a	122.39	0.31
C13-C7-C7a	121.14	0.31	C6a-C7-C7a	116.24	0.29	C9-C8-C7a	119.25	0.35
C8-C9-C10	120.84	0.37	C9-C10-C11	120.40	0.36	C10-C11-C11a	119.39	0.33
O1-C12-C11a	119.74	0.30	O1-C12-C12a	124.23	0.31	C11a-C12-C12a	115.97	0.28
C7-C13-C14	123.67	0.33	C7-C13-C15	125.07	0.33	C14-C13-C15	110.94	0.32
N1-C14-C13	175.62	0.42	N2-C15-C13	172.99	0.42	C1-C1a-C4a	118.55	0.30
C1-C1a-C12a	122.67	0.30	C4a-C1a-C12a	118.75	0.29	C4-C4a-C5	121.57	0.30
C4-C4a-C1a	118.24	0.30	C5-C4a-C1a	120.15	0.29	C6-C6a-C7	120.55	0.30
C6-C6a-C12a	120.79	0.30	C7-C6a-C12a	118.65	0.29	C7-C7a-C8	124.20	0.31
C7-C7a-C11a	116.12	0.30	C8-C7a-C11a	119.65	0.32	C11-C11a-C12	119.45	0.30
C11-C11a-C7a	120.44	0.31	C12-C11a-C7a	120.12	0.30	C12-C12a-C1a	122.54	0.29
C12-C12a-C6a	117.85	0.29	C1a-C12a-C6a	119.57	0.30	C5-C1′-C2′	120.96	0.30
C5-C1′-C6′	120.01	0.30	C2′-C1′-C6′	118.99	0.31	C1′-C2′-C3′	120.75	0.33
C2′-C3′-C4′	119.99	0.35	C3′-C4′-C5′	120.11	0.36	C4′-C5′-C6′	119.64	0.35
C1′-C6′-C5′	120.48	0.33						
				3c				
C2-C1-C1a	120.26	0.31	C1-C2-C3	121.46	0.34	C2-C3-C4	119.78	0.36
C3-C4-C4a	121.01	0.35	C6-C5-C4a	121.93	0.33	C5-C6-C6a	120.14	0.31
C13-C7-C6a	123.07	0.29	C13-C7-C7a	122.91	0.29	C6a-C7-C7a	114.00	0.26
C9-C8-C7a	119.36	0.33	C8-C9-C10	120.84	0.36	C9-C10-C11	120.12	0.37
C10-C11-C11a	119.68	0.33	C16-C12-C11a	121.74	0.28	C16-C12-C12a	124.85	0.28
C11a-C12-C12a	113.18	0.25	C7-C13-C14	122.27	0.31	C7-C13-C15	122.92	0.32
C14-C13-C15	114.74	0.31	N1-C14-C13	178.50	0.40	N2-C15-C13	177.49	0.45
C12-C16-C17	123.71	0.30	C12-C16-C18	123.12	0.31	C17-C16-C18	113.04	0.30
N3-C17-C16	175.90	0.39	N4-C18-C16	175.52	0.44	C1-C1a-C4a	118.00	0.28
C1-C1a-C12a	123.93	0.30	C4a-C1a-C12a	117.96	0.28	C4-C4a-C5	121.32	0.32
C4-C4a-C1a	119.39	0.31	C5-C4a-C1a	119.24	0.30	C6-C6a-C7	122.39	0.28
C6-C6a-C12a	119.89	0.28	C7-C6a-C12a	117.64	0.27	C7-C7a-C8	123.71	0.29
C7-C7a-C11a	116.38	0.27	C8-C7a-C11a	119.74	0.29	C11-C11a-C12	123.71	0.29
C11-C11a-C7a	120.22	0.29	C12-C11a-C7a	116.03	0.27	C12-C12a-C1a	124.00	0.27
C12-C12a-C6a	115.15	0.26	C1a-C12a-C6a	120.72	0.27			

Table 10. Dihedral Angles for **2j** and **3c**

Plane A	C8, C9, C10, C11, C11a, C7a
Plane B	C1, C2, C3, C4, C4a, C5, C6, C6a, C12a, C1a
Plane C	C6a, C7a, C11a, C12a
Plane D	C6a, C7, C7a, C13
Plane E	C7, C13, C14, C15, N1, N2
Plane F	C11a, C12a, C12, C16
Plane G	C12, C16, C17, C18, N3, N4

		Angle between the planes I and II/degree	
I	II	**2j**	**3c**
A	B	33.3(1)	49.5(1)
A	C	15.1(1)	25.2(1)
B	C	18.3(1)	24.4(1)
C	D	33.1(2)	34.4(2)
C	E		36.7(2)
C	F		41.0(2)
C	G		44.6(1)

pellets. Elemental analyses were performed at the Micro Analytical Center of Kyoto University. Cyclic voltammetry was performed with a PAR Model 174. The working electrode was platinum wire. A Ag/Ag^+ (0.1 M; 1 M=1 mol dm^{-3}) electrode was used as a reference and 0.1 M tetraethylammonium perchlorate as supporting electrolyte. The reduction potential was measured in a nitrogen-purged acetonitrile solution and the value measured was corrected to that relative to SCE (+0.24 V). The impedance measurements (pellet) were made in the frequency range 10 Hz—1 MHz using a gain-phase meter YHP 4276A LCZ METER at room temperature. All the solvents were used after distillation.

Starting Material. Quinone **1c** was purchased from Aldrich, Inc. and used without further purification. Quinones **1a—b, d—g** were prepared from naphthoquinone and the corresponding styrenes.[19] Quinone **4** was prepared according to the reported method.[20] Quinones **1h—l** were prepared by photochemical reactions of 2,3-dichloro-1,4-naphthoquinone with corresponding 1,1-diphenylethylenes.[21] Anthraquinone was purchased from Nacalai tesque Co. and used after recrystallization. TCNQ was prepared according to the reported method.[22]

Preparation of 2 and 3 (or 6). **2** and **3** (or **6**) were prepared according to Ong and Aumüller method. To a well-stirred mixture of 1 mmol of quinone **1** (or **4**) and 10 mmol of malononitrile in 20 ml of dichloromethane at an ice-bath temperature were added dropwise 10 ml of 1 mol dm^{-3} $TiCl_4$ solution and 20 mmol of pyridine. After end of addition, ice bath was removed to continue reaction at room temperature for overnight. The reaction mixture was treated with 50 ml of 10% aqueous HCl solution with vigorous stirring. Organic layer was separated and washed with brine and

dried. Purification of the products was accomplished by column chromatography developing hexane-benzene (2:1) and subsequently benzene. First bands contains **1** (or **6**), second one contains **2**, and third one contains **3**. The products were assigned from the following spectroscopic data.

7-Dicyanomethylene-2-fluoro-5-(4-fluorophenyl)benz[*a*]anthracen-12(7*H*)-one (2h): Red crystals from hexane-chloroform; mp>300 °C. MS; *m/z* 418 (M^+). Found: C, 77.57; H, 2.74; F, 8.91; N, 6.47%. Calcd for $C_{27}H_{12}F_2N_2O$: C, 77.51; H, 2.89; F, 9.08; N, 6.70%. IR (KBr); 2230 (C≡N), 1660 (C=O) cm^{-1}. ^1H NMR ($CDCl_3$) δ=7.2—8.5 (11H, m), 9.56 (1H, dd, *J*=11, 3 Hz). UV (CH_2Cl_2) λ_{max}: 234 (log ε=4.36), 257 (4.25), 315 (4.48), 377 (3.92), 422 (3.41) nm.

2-Chloro-5-(4-chlorophenyl)-7-(dicyanomethylene)benz[*a*]anthracen-12(7*H*)-one (2i): Orange crystals from hexane-chloroform; mp>300 °C. MS; *m/z* 450, 452, 454 (M^+). Found: C, 71.89; H, 2.61; Cl, 15.62; N, 6.17%. Calcd for $C_{27}H_{12}Cl_2N_2O$: C, 71.86; H, 2.68; Cl, 15.71; N, 6.21%. IR (KBr); 2210 (C≡N), 1650 (C=O) cm^{-1}. ^1H NMR ($CDCl_3$) δ=7.4—8.7 (11H, m), 9.88 (1H, d, *J*=3 Hz). UV (CH_2Cl_2) λ_{max}: 236 (4.56), 259 (4.38), 316 (4.56), 379 (4.01), 425 (3.50) nm.

7-Dicyanomethylene-5-phenylbenz[*a*]anthracen-12(7*H*)-one (2j): Orange crystals from hexane-chloroform; mp> 300 °C. MS; *m/z* 382 (M^+). Found: C, 85.08; H, 3.50; N, 7.31%. Calcd for $C_{27}H_{14}N_2O$: C, 84.80; H, 3.69; N, 7.33%. IR (KBr); 2200 (C≡N), 1650 (C=O) cm^{-1}. ^1H NMR ($CDCl_3$) δ=7.4—8.7 (13H, m), 9.77 (1H, d, *J*=10 Hz). UV (CH_2Cl_2) λ_{max}: 234 (4.46), 257 (4.27), 317 (4.61), 380 (3.98), 427 (3.49) nm.

7-Dicyanomethylene-2-methyl-5-(4-methylphenyl)benz[*a*]anthracen-12(7*H*)-one (2k): Orange needles from hexane-chloroform; mp>300 °C. MS; *m/z* 410 (M^+). Found: C, 84.85; H, 4.26; N, 7.00%. Calcd for $C_{29}H_{18}N_2O$: C, 84.86; H, 4.42; N, 6.82%. IR (KBr); 2230 (C≡N), 1650 (C=O) cm^{-1}. ^1H NMR ($CDCl_3$) δ=2.50 (3H, s), 2.68 (3H, s), 7.3—8.6 (11H, m), 9.58 (1H, s). UV (CH_2Cl_2) λ_{max}: 235 (4.51), 265 (4.33), 325 (4.58), 383 (3.96), 450 (3.46) nm.

7-Dicyanomethylene-2-methoxy-5-(4-methoxyphenyl)-benz[*a*]anthracen-12(7*H*)-one (2l): Red crystals from hexane-chloroform; mp>300 °C. MS; *m/z* 442 (M^+). Found: C, 78.79; H, 4.18; N, 6.14%. Calcd for $C_{29}H_{18}N_2O_3$: C, 78.72; H, 4.10; N, 6.33%. IR (KBr); 2220 (C≡N), 1640 (C=O) cm^{-1}. ^1H NMR ($CDCl_3$) δ=3.94 (3H, s), 4.12 (3H, s), 7.1—8.5 (11H, m), 9.32 (1H, d, *J*=3 Hz). UV (CH_2Cl_2) λ_{max}: 235 (4.63), 265 (4.45), 332 (4.58), 395 (3.97), 477 (3.61) nm.

7,12-Bis(dicyanomethylene)-2-fluoro-7,12-dihydrobenz[*a*]anthracene (3a): Orange cubics from acetonitrile; mp> 300 °C. MS; *m/z* 372 (M^+). Found: C, 77.51; H, 2.17; F, 5.16; N, 15.15%. Calcd for $C_{24}H_9FN_4$: C, 77.42; H, 2.44; F, 5.10; N, 15.05%. IR (KBr); 2240 (C≡N) cm^{-1}. ^1H NMR ($CDCl_3$) δ=7.54 (1H, m), 7.7—7.8 (3H, m), 8.04 (1H, m), 8.1—8.3 (4H, m). UV (CH_2Cl_2) λ_{max}: 232 (4.30), 285 (4.23), 334 (4.40), 424 (3.42) nm.

2-Chloro-7,12-bis(dicyanomethylene)-7,12-dihydrobenz[*a*]anthracene (3b): Orange cubics from acetonitrile; mp> 300 °C. High-resolution mass spectrum. Found: *m/z* 388.0521. Calcd for $C_{24}H_9N_4{}^{35}Cl$: M, 388.0515. Found: *m/z* 390.0483. Calcd for $C_{24}H_9N_4{}^{37}Cl$: M, 390.0486. IR (KBr); 2240 (C≡N) cm^{-1}. ^1H NMR ($CDCl_3$) δ=7.6—7.8 (3H, m), 7.97 (1H, d, *J*=8.9 Hz), 8.07 (1H, s), 8.17 (1H, d, *J*=8.5 Hz), 8.2—8.3 (3H, m). UV (CH_2Cl_2) λ_{max}: 232 (4.66), 286 (4.37), 336 (4.54), 426 (3.52) nm.

7,12-Bis(dicyanomethylene)-7,12-dihydrobenz[*a*]anthracene (3c): Orange plates from acetonitrile; mp>300 °C. MS; *m/z* 354 (M^+). Found: C, 81.29; H, 2.61; N, 15.76%. Calcd for $C_{24}H_{10}N_4$: C, 81.35; H, 2.84; N, 15.81%. IR (KBr); 2240 (C≡N) cm^{-1}. ^1H NMR ($CDCl_3$) δ=7.7—7.9 (4H, m), 8.02 (1H, d, *J*=8.2 Hz), 8.11 (1H, d, *J*=8.1 Hz), 8.1—8.3 (4H, m). UV (CH_2Cl_2) λ_{max}: 231 (4.29), 285 (4.19), 337 (4.46), 431 (3.46) nm.

7,12-Bis(dicyanomethylene)-2-methyl-7,12-dihydrobenz[*a*]anthracene (3d): Red cubics from acetonitrile; mp>300 °C. MS; *m/z* 368 (M^+). Found: C, 81.32; H, 3.04; N, 15.51%. Calcd for $C_{24}H_{12}N_4$: C, 81.51; H, 3.28; N, 15.21%. IR (KBr); 2230 (C≡N) cm^{-1}. ^1H NMR ($CDCl_3$) δ=2.67 (3H, s), 7.57 (1H, d, *J*=8.2 Hz), 7.6—7.8 (2H, m), 7.83 (1H, s), 7.90 (1H, d, *J*=8.3 Hz), 8.12 (1H, d, *J*=8.2 Hz), 8.19 (1H, d, *J*=8.5 Hz), 8.2—8.3 (2H, m). UV (CH_2Cl_2) λ_{max}: 232 (4.42), 286 (4.28), 345 (4.48), 444 (3.43) nm.

7,12-Bis(dicyanomethylene)-2-methoxy-7,12-dihydrobenz[*a*]anthracene (3e): Red crystals from acetonitrile; mp>300 °C. High-resolution mass spectrum. Found: *m/z* 384.1008. Calcd for $C_{25}H_{12}N_4O$: M, 384.1010. IR (KBr); 2230 (C≡N) cm^{-1}. ^1H NMR ($CDCl_3$) δ=4.08 (3H, s), 7.23 (1H, d, *J*=2.1 Hz), 7.39 (1H, dd, *J*=8.8, 2.1 Hz), 7.7—7.8 (2H, m), 7.90 (1H, d, *J*=9.2 Hz), 8.0—8.2 (2H, m), 8.2—8.3 (2H, m). UV (CH_2Cl_2) λ_{max}: 234 (4.56), 289 (4.39), 349 (4.39), 474 (3.41) nm.

7,12-Bis(dicyanomethylene)-3-methoxy-7,12-dihydrobenz-[*a*]anthracene (3f): Orange needles from acetonitrile; mp> 300 °C. MS; *m/z* 384 (M^+). Found: C, 78.27; H, 2.94; N, 14.42%. Calcd for $C_{25}H_{12}N_4O$: C, 78.12; H, 3.15; N, 14.58%. IR (KBr); 2230 (C≡N) cm^{-1}. ^1H NMR ($CDCl_3$) δ=3.99 (3H, s), 7.25 (1H, m), 7.44 (1H, dd, *J*=9.4, 2.4 Hz), 7.7—7.8 (2H, m), 7.98 (1H, d, *J*=9.4 Hz), 8.02 (1H, d, *J*=8.5 Hz), 8.1—8.3 (3H, m). UV (CH_2Cl_2) λ_{max}: 234 (4.54), 294 (4.28), 349 (4.56), 462 (3.76) nm.

7,12-Bis(dicyanomethylene)-4-methoxy-7,12-dihydrobenz-[*a*]anthracene (3g): Orange needles from acetonitrile; mp> 300 °C. MS; *m/z* 384 (M^+). Found: C, 78.40; H, 2.92; N, 14.51%. Calcd for $C_{25}H_{12}N_4O$: C, 78.12; H, 3.15; N, 14.58%. IR (KBr); 2230 (C≡N) cm^{-1}. ^1H NMR ($CDCl_3$) δ=4.06 (3H, s), 7.04 (1H, d, *J*=7.6 Hz), 7.63 (1H, d, *J*=8.8 Hz), 7.7—7.8 (3H, m), 8.2—8.3 (3H, m), 8.66 (1H, d, *J*=9.2 Hz). UV (CH_2Cl_2) λ_{max}: 233 (4.40), 286 (4.34), 346 (4.46), 480 (3.31) nm.

7,12-Bis(dicyanomethylene)-2-fluoro-5-(4-fluorophenyl)-7,12-dihydrobenz[*a*]anthracene (3h): Orange crystals from hexane-chloroform; mp>300 °C. High-resolution mass spectrum. Found: *m/z* 466.1029. Cacld for $C_{30}H_{12}F_2N_4$: M, 466.1029. IR (KBr); 2240 (C≡N) cm^{-1}. ^1H NMR ($CDCl_3$) δ=7.3—8.6 (12H, m). UV (CH_2Cl_2) λ_{max}: 234 (4.51), 287 (4.35), 343 (4.49), 449 (3.64) nm.

2-Chloro-5-(4-chlorophenyl)-7,12-bis(dicyanomethylene)-7,12-dihydrobenz[*a*]anthracene (3i): Orange crystals from hexane-chloroform; mp>300 °C. MS; *m/z* 498, 500, 502 (M^+). Found: C, 71.96; H, 2.30; Cl, 14.43; N, 11.14%. Calcd for $C_{30}H_{12}Cl_2N_4$: C, 72.16; H, 2.42; Cl, 14.20; N, 11.22%. IR (KBr); 2250 (C≡N) cm^{-1}. ^1H NMR ($CDCl_3$) δ=7.4—8.7 (12H, m). UV (CH_2Cl_2) λ_{max}: 234 (4.59), 288 (4.33), 343 (4.48), 458 (3.59) nm.

7,12-Bis(dicyanomethylene)-5-phenyl-7,12-dihydrobenz[*a*]anthracene (3j): Red crystals from hexane-chloroform; mp>300 °C. MS; *m/z* 430 (M^+). Found: C, 83.67; H, 3.15; N,

12.79%. Calcd for $C_{30}H_{14}N_4$: C, 83.71; H, 3.28; N, 13.02%. IR (KBr); 2240 (C≡N) cm^{-1}. ^1H NMR ($CDCl_3$) δ=7.6—8.7 (14H, m). UV (CH_2Cl_2) λ_{max}: 233 (4.56), 288 (4.40), 345 (4.61), 458 (3.70) nm.

7,12-Bis(dicyanomethylene)-2-methyl-5-(4-methylphenyl)-7,12-dihydrobenz[*a*]anthracene (3k): Orange crystals from hexane–chloroform; mp>300 °C. MS; *m/z* 458 (M^+). Found: C, 84.02; H, 3.83; N, 11.96%. Calcd for $C_{32}H_{18}N_4$: C, 83.82; H, 3.96; N, 12.22%. IR (KBr); 2230 (C≡N) cm^{-1}. ^1H NMR ($CDCl_3$) δ=2.50 (3H, s), 2.71 (3H, s), 7.2—8.8 (12H, m). UV (CH_2Cl_2) λ_{max}: 236 (4.60), 290 (4.47), 354 (4.59), 478 (3.70) nm.

7,12-Bis(dicyanomethylene)-2-methoxy-5-(4-methoxyphenyl)-7,12-dihydrobenz[*a*]anthracene (3l): Purple crystals from hexane–chloroform; mp>300 °C. MS; *m/z* 490 (M^+). Found: C, 78.09; H, 3.43; N, 11.42%. Calcd for $C_{32}H_{18}N_4O_2$: C, 78.36; H, 3.70; N, 11.42%. IR (KBr); 2220 (C≡N) cm^{-1}. ^1H NMR ($CDCl_3$) δ=3.92 (3H, s), 4.11 (3H, s), 7.0—8.5 (12H, m). UV (CH_2Cl_2) λ_{max}: 238 (4.61), 287 (4.45), 358 (4.45), 502 (3.68) nm.

5,12-Bis(dicyanomethylene)-5,12-dihydronaphthacene (6): Yellow needles from hexane–chloroform; mp>300 °C. MS; *m/z* 354 (M^+). Found: C, 81.10; H, 2.66; N, 15.64%. Calcd for $C_{25}H_{12}N_4$: C, 81.35; H, 2.84; N, 15.81%. IR (KBr); 2240 (C≡N) cm^{-1}. ^1H NMR ($CDCl_3$) δ=7.76 (4H, m), 8.05 (2H, m), 8.27 (2H, m), 8.72 (2H, s). UV (CH_2Cl_2) λ_{max}: 233 (4.39), 260 (4.51), 306 (4.51), 424 (3.96) nm.

Molecular Complexes of 3c. Naphthalene, pyrene, anthracene was purchased from Nacalai tesque Co. and used after recrystallization. TMTTF was prepared according to the reported method.[23] **3c** and an excess amounts of a donor were dissolved in dichloromethane, and ethanol was added to precipitate a complex and prevent the precipitate of excess donor. The mixture was concentrated by distillation, and then cooled, but complex did not precipitate. However, a dichloromethane solution containing **3c** (0.0025 mol dm^{-3}) and donors (0.05 mol dm^{-3}) showed a CT band, which was obtained by substracting the "background" absorption of samples (absorption of **3c** and donors). Intensity of these CT bands increased as donors were added into the mixture.

X-Ray Structure Analyses. The X-ray structure analyses were made with a Rigaku Denki AFC-4 automatic four-circle diffractometer [Ni-filtered Cu $K\alpha$ radiation (154.184 pm), ω–2θ scan technique, $2\theta \leqq 120°$, scan speed 4° min^{-1} (θ), scan range (1.5+0.15 tan θ)°]. Three standard reflections measured every 100 reflections showed no significant X-ray damage or crystal decay. Unique 3031 (for **2j**) and 2792 (for **3c**) reflections were used for structure determination. The structure was solved by direct methods with MULTAN 78[24] (with atomic scattering factors from International Tables for X-ray Crystallography)[25] and refined by block-diagonal least squares[26] with anisotropic thermal parameters for non-hydrogen atoms and isotropic for hydrogen atoms. **2j**: R=0.0754 and R_2=0.0681, where ω=1.0 for Fobs≠0, ω=0.8 for Fobs=0.0, **3c**: R=0.0589 and R_2=0.0656 where ω=1.0 for Fobs≠0, ω=0.8 for Fobs=0.0. Crystal data are as follows; **2j**: a=1150.0 (1), b=1163.0 (1), c=815.4 (1) pm, α=106.31 (1), β=89.33 (1), γ=116.29 (1)°, space group=P-1 (triclinic) (Z=2). V=9.303×10^8 (1) pm^3, D_c/g cm^{-3}=1.366 (1). **3c**: a=891.4 (1), b=1489.0 (1), c=733.8 (1) pm, α=90.67 (1), β=110.36 (1), γ=104.00 (1)°, space group=P-1 (triclinic) (Z=2). V=8.812×10^8 (1) pm^3, D_c/g cm^{-3}=1.336 (1).

We are grateful to Professor Yukiteru Katsube and his co-worker at Institute for Protein Research, Osaka University, for the measurement of X-ray analyses.

References

1) A. F. Garito and A. J. Heeger, *Acc. Chem. Res.*, **7**, 232 (1974). J. H. Perlstein, *Angew. Chem., Int. Ed. Engl.*, **16**, 519 (1977). J. B. Torrance, *Acc. Chem. Res.*, **12**, 79 (1979). F. Wudl, "The Physics and Chemistry of Low Dimensional Solids," ed by L. Alcácer and D. Reidel, Dordrecht, Holland (1980). D. O. Cowan, A. Kini, L-Y. Chiang, K. Lerstrup, D. R. Talham, T. O. Poehler, and A. N. Bloch, *Mol. Cryst. Liq. Cryst.*, **86**, 1 (1982). "Dendōusei Teizigen Busshitsu no Kagaku," Kagaku Sosetsu, No. 42, Gakkai Shuppan Center, Tokyo (1983). F. Wudl, *Acc. Chem. Res.*, **17**, 227 (1984). J. M. Williams, M. A. Beno, H. H. Wang, P. C. W. Leung, T. J. Emge, U. Geiser, and K. D. Carlson, *Acc. Chem. Res.*, **18**, 261 (1985), and references therein.

2) U. Schubert, S. Hünig, and A. Aumüller, *Liebigs Ann. Chem.*, **1985**, 1216. C. Kabuto, Y. Fukazawa, T. Suzuki, Y. Yamashita, T. Miyashi, and T. Mukai, *Tetrahedron Lett.*, **27**, 925 (1986).

3) T. Mukai, T. Suzuki, and Y. Yamashita, *Bull. Chem. Soc. Jpn.*, **58**, 2433 (1985). Y. Nishizawa, T. Suzuki, Y. Yamashita, T. Miyashi, and T. Mukai, *Nippon Kagaku Kaishi*, **1985**, 904.

4) A. Aumüller and S. Hünig, *Ann. Chem.*, **1984**, 618.

5) B. S. Ong and B. Keoshkerian, *J. Org. Chem.*, **49**, 5002 (1984).

6) Y. Yamashita, T. Suzuki, and T. Mukai, *Nippon Kagaku Kaishi*, **1986**, 268.

7) A. M. Kini, D. O. Cowan, F. Gerson, and R. Möckel, *J. Am. Chem. Soc.*, **107**, 556 (1985).

8) Since the UV measurements were carried out in 10^{-4}—10^{-5} mol dm^{-3}, the possibility of intermolecular CT interaction could be eliminated.

9) E. M. Kosower, "An Introduction to Physical Organic Chemistry," Wiley, New York (1968).

10) R. L. Myers and I. Shain, *Anal. Chem.*, **41**, 980 (1969).

11) F. Gerson, R. Heckendorn, D. O. Cowan, A. M. Kini, and M. Maxfield, *J. Am. Chem. Soc.*, **105**, 7017 (1983).

12) We attempted to observe radical anion and radical trianion of **3c** by ESR method, but none of the spectra could be unequivocally be attributed to them because of the complicated ESR signals.

13) B. Rosenau, C. Krieger, and H. A. Staab, *Tetrahedron Lett.*, **26**, 2081 (1985).

14) A. Kini, M. Mays, and D. O. Cowan, *J. Chem. Soc., Chem. Commun.*, **1985**, 286.

15) J. Silverman and N. F. Yannoni, *J. Chem. Soc. B*, **1967**, 194.

16) R. P. Ferrier and J. Iball, *Acta Crystallogr.*, **16**, 269 (1963).

17) F. Iwasaki, *Acta Crystallogr., Sect. B*, **27**, 1360 (1971).

18) S. Yamaguchi, T. Hanafusa, T. Tanaka, M. Sawada, K. Kondo, M. Irie, H. Tatemitsu, Y. Sakata, and S. Misumi, *Tetrahedron Lett.*, **27**, 2411 (1986).

19) G. M. Muschik, J. E. Tomaszewski, R. I. Sato, and W. B. Manning, *J. Org. Chem.*, **44**, 2150 (1979).

20) M. P. Cava, A. A. Deana, and K. Muth, *J. Am. Chem. Soc.*, **81**, 6458 (1959).

21) K. Maruyama, T. Otsuki, and S. Tai, *J. Org. Chem.*, **50**, 52 (1985).
22) D. S. Acker and W. R. Hertler, *J. Am. Chem. Soc.*, **84**, 3370 (1962).
23) J. P. Ferraris, T. O. Poehler, A. N. Bloch, and D. O. Cowan, *Tetrahedron Lett.*, **27**, 2553 (1973).
24) P. Main, S. E. Hull, L. Lessinger, G. Germain, J. -P. Declercq, and M. M. Woolfson, "A System of Computer Programs for the Automatic Solution of Crystal Structures from X-ray Diffraction Data, MULTAN 78," University of York (England) and Louvain (Belgium) (1978).
25) "International Tables for X-ray Crystallography," Vol. 4, ed by J. A. Ibers and W. C. Hamilton, Birmingham, Kynoch Press (1974).
26) T. Ashida, HBLS 5 "The Universal Crystallographic Computing System Osaka," The Computation Center, Osaka University, 53 (1979).

Facile Synthesis of AM-Toxin II

Kazuo UEDA, Michinori WAKI,* Yoshio TERUYA,† and Nobuo IZUMIYA†
Laboratory of Biochemistry, Faculty of Science, Kyushu University 33, Higashi-ku, Fukuoka 812
†Laboratory of Chemistry, Kurume Institute of Technology, Kurume, Fukuoka 830
(Received December 2, 1988)

In a search for a more effective synthetic route for AM-toxins (cyclic tetradepsipeptides), the syntheses of [L-Phe³]AM-toxin II as a preliminary peptide and AM-toxin II as a target were attempted. The cyclization of H-L-Ser(Bzl)-L-Ala-L-Hmb-L-Phe-ONSu (Hmb, 2-hydroxy-3-methylbutanoic acid) in pyridine gave a cyclic monomer in high yield (59%). The removal of *O*-Bzl in the cyclopeptide and a subsequent dehydration of Ser with carbodiimide-CuCl afforded [L-Phe³]AM-toxin II in 24% yield. AM-Toxin II was synthesized in similar yield as in the case of the analog. The characteristic features of synthetic AM-toxin II were identical to those of the natural one.

AM-Toxins are host-specific phytotoxins and cause a spot disease on apple leaves. The structures of three congeners (I, II, and III) of AM-toxins were determined to be cyclotetradepsipeptides, the structure of the II being shown in Fig. 1. AM-Toxin I and III contain L-Amp and L-Ahp, respectively, instead of L-App residue at position 3.[1] We have already synthesized three congeners in order to confirm their structures, and also various analogs to clarify the structure-activity relationship. However, the synthetic yield has still been unsatisfactory from the standpoints of two crucial steps involving preferential monomeric cyclization from linear tetrapeptides and effective ΔAla formation in cyclotetrapeptide. Therefore, it has been our continuing interest to search for more facile synthetic routes for AM-toxins.

We previously found that the cyclization of a linear tetrapepetide containing an L-Ser residue at N-terminus gave a considerable amount of cyclic polymers in addition to the desired cyclic monomer (see, Table 1),[2,3] while a linear peptide with a D-Ser residue gave a cyclic monomer exclusively.[2] However, the subsequent conversion of the D-Ser residue in cyclotetrapeptide into ΔAla with Tos-Cl, followed by Et_2NH (Photaki method), was impossible because of a steric hindrance of the D-Ser (see, Table 2).[2] On the contrary, the L-Ser in cyclopeptide was converted into ΔAla, even though yields were poor (15% and 2% in Table 2).[3,4]

In the present study, we first attempted an easier

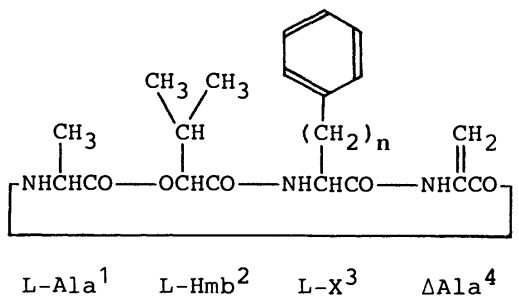

	n	X
AM-Toxin II	3	App
[L-Phe³]AM-Toxin II	1	Phe

Fig. 1. Structure of AM-toxin II and [L-Phe³]AM-toxin II.

Table 1. Formation of Cyclic Monomer and Cyclic Polymers after Cyclization of Linear Tetrapeptide Active Ester

Linear tetrapeptide active ester[a]	Formation of cyclic peptides		Ref.
	Yield(%)[b] of cyclic monomer	Formation of cyclic polymers	
H-Ser-Ala-Hmb-Phe-ONSu	11	+++	2
H-Ser-Ala-Hmb-Amp-ONSu	18	+++	3
H-D-Ser-Ala-Hmb-Phe-ONSu	52	−	2
H-D-Ser-Ala-Hmb-App-ONSu	51	−	2
H-Ser(Bzl)-Ala-Hmb-Phe-ONSu	59	±	This study
H-Ser(Bzl)-Ala-Hmb-App-ONSu	57	±	This study
H-D-Dpr(Z)-Ala-Hmb-Amp-ONSu	57	−	9

a) Initial concentration, 3 mM in pyridine; reaction time, 2 d at 20 °C. b) Isolated yield based on Boc-tetradepsipeptide-ONSu.

Table 2. ΔAla Formation from Ser or Dpr Residue in Cyclic Tetrapeptide

Cyclic tetrapeptide	Method[a]	Product	Yield(%)[b] of the product	Ref.
Cyclo(-Ser-Ala-Hmb-Tyr(Me)-)	Photaki	[L-Tyr(Me)^3]AM-toxin I	15	4
Cyclo(-Ser-Ala-Hmb-Amp-)	Photaki	AM-toxin I	2	3
Cyclo(-D-Ser-Ala-Hmb-Phe-)	Photaki	[L-Phe^3]AM-toxin II	trace	2
ditto	Modified Photaki	ditto	4	
Cyclo(-D-Ser-Ala-Hmb-App-)	Photaki	AM-toxin II	trace	2
ditto	Modified Photaki	ditto	6	
Cyclo(-Ser-Ala-Hmb-Phe-)	Photaki	[L-Phe^3]AM-toxin II	6.5	This study
ditto	Miller	ditto	24	This study
Cyclo(-Ser-Ala-Hmb-App-)	Miller	AM-toxin II	20	This study
Cyclo(-D-Dpr-Ala-Hmb-Amp-)	Shiba	AM-toxin I	26	9

a) Photaki method, Tos-Cl and Et_2NH; Shiba method, CH_3I and $KHCO_3$; Miller method, EDC·HCl and CuCl; modified Photaki method, Ms-Cl and Et_2NH.

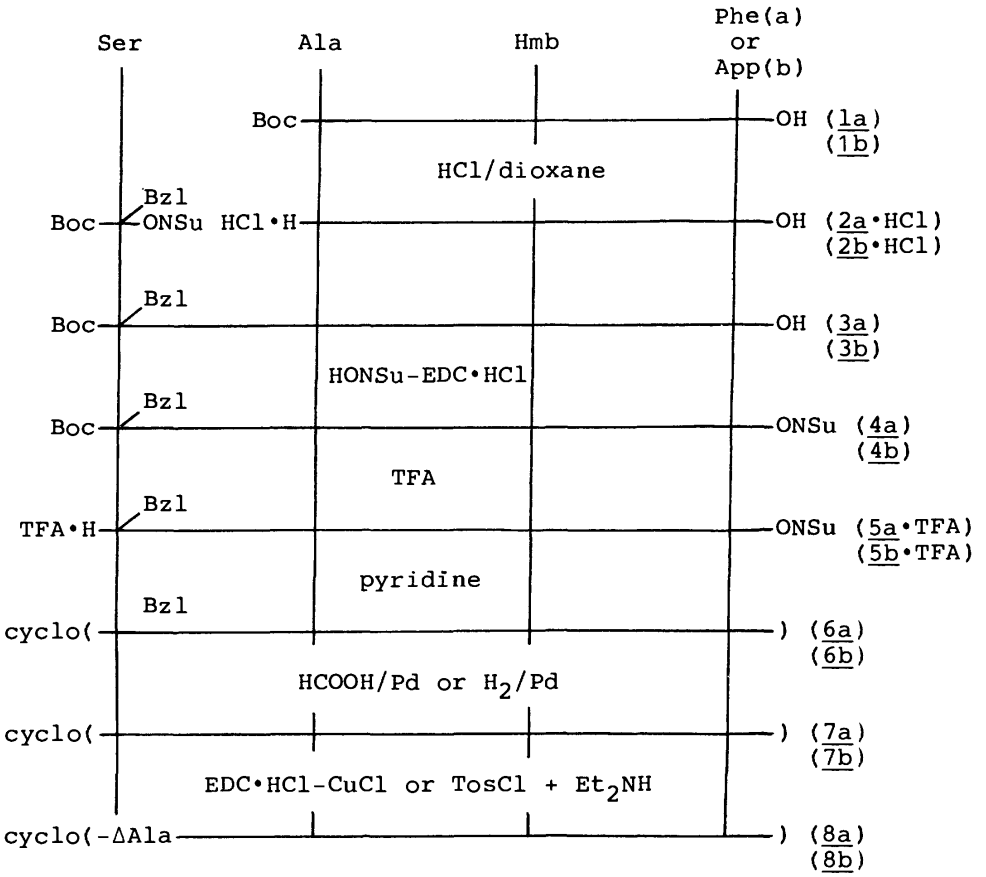

Fig. 2. Synthesis of [L-Phe^3]AM-toxin II (**8a**) and AM-toxin II (**8b**).

synthesis of cyclopeptide with the L-Ser residue from a linear peptide precursor. In a peptide synthesis, there is a tendency that a peptide with an L-Ser(Bzl) residue is obtained as a better crystalline product than a peptide with L-Ser. We therefore chose H-Ser(Bzl)-Ala-Hmb-Phe-ONSu (**5a**) as a preliminary precursor, the synthetic route of **5a** being shown in Fig. 2. Then, the cyclization of **5a** was carried out in pyridine at a concentration of 3 mM (1 M=1 mol dm^{-3}) at 20 °C for 2 d. Unexpectedly, the TLC of the reaction mixture showed the presence of a major cyclic monomer (**6a**) and a trace cyclic polymer. Indeed, an isolated solid was almost **6a**; and pure **6a** was obtained in good yield (59%) after simple recrystallization. The results indicate that the cyclization-mode of a linear tetrapeptide precursor is influenced by not only the configuration, but also the side-chain nature of the N-terminal amino acid residue in the precursor. For the synthesis of AM-toxin II, the cyclization of **5b** with L-App was carried out similarly in pyridine, and pure

6b was obtained in 57% yield.

The removal of the *O*-Bzl group in **6a** and **6b** was achieved by catalytic transfer hydrogenation[5] using Pd black and formic acid in almost quantitative yield after 2 h to produce the desired **7a** and **7b**. The **6a** was subjected to conventional hydrogenation in a solvent of DMF with Pd black; **7a** was obtained after 7d in 76% yield.

Secondly we attempted an easier formation of the ΔAla residue from L-Ser in **7a**. Recently, Miller reported an efficient one-pot dehydration of the Ser derivative to form the ΔAla derivative using carbodiimide and CuCl.[6] Thus, we examined the applicability of the Miller method for the synthesis of [L-Phe[3]]AM-toxin II (**8a**) from cyclotetrapeptide (**7a**) containing the L-Ser residue. The **7a** was treated with hydrochloride of water-soluble carbodiimide (EDC·HCl) in the presence of CuCl. In this case, more reagents and a longer time than reported in the literature[6] were needed for the completion of the reaction; however, we could obtained pure **8a** in 24% yield. When the Photaki method[7] was applied to **7a**, the yield of pure **8a** was 6.5%. We applied the procedure of the Miller method for **7b**, and could isolate pure AM-toxin II (**8b**) in 20% yield. The physicochemical properties of **8b** were identical to those reported for natural AM-toxin II, and the minimum toxic activity of the **8b** and natural II was the same for the induction of necrosis on apple leaves.

For the syntheses of natural AM-toxins and their analogs, a route using the D-Dpr residue[8] has been giving the best yield; the yields for the cyclization of the linear peptide and dehydration in cyclotetrapeptide are approximately 57%[9] (Table 1) and 26%[9] (Table 2), respectively. Yields in the present study are comparable with those in the D-Dpr route; it should be further noted that the preparation of an amino acid, L-Ser(Bzl), is easier than that of D-Dpr(Z). Thus, we believe that the present study gives a facile method for synthesizing AM-toxin II and other related cyclotetrapeptides.

Experimental

Optical rotations were measured with a JASCO polarimeter Model DIP-140. Mass spectra were taken on a Jeol mass spectrometer Model JMS-01SG operating at 75 eV. IR spectra were recorded with KBr disks on a JASCO IRA-2 spectrophotometer. UV spectra were taken on a Hitachi 124 spectrophotometer. TLC was performed on silica gel 60 F_{254} pre-coated plates (Merck) with the following solvent systems: R_f^1, $CHCl_3$–MeOH (5:1); R_f^2, $CHCl_3$–MeOH–AcOH (95:5:1); R_f^3, *n*-BuOH–AcOH–H_2O (4:1:1); R_f^4, *n*-BuOH–AcOH–pyridine–H_2O (15:3:10:12); R_f^5, EtOAc–$CHCl_3$ (1:1).

Boc-Ala-Hmb-Phe-OH (1a). Boc-Ala-Hmb-Phe-OBzl (5.27 g, 10 mmol)[2] dissolved in THF (20 ml) was hydrogenated in the presence of Pd black at 20 °C for 5 h. After removal of the catalyst, the filtrate was evaporated in vacuo and the residual oil was solidified by the addition of hexane. The resulting solid was recrystallized from EtOAc-ether-hexane: yield, 3.99 g (91%); mp 145 °C; $[\alpha]_D^{25}$ −6.9° (*c* 1, $CHCl_3$); R_f^1 0.49, R_f^2 0.33.

Found: C, 60.58; H, 7.37; N, 6.40%. Calcd for $C_{22}H_{32}O_7N_2$: C, 60.53; H, 7.39; N, 6.42%.

Boc-Ala-Hmb-App-OH (1b). Boc-Ala-Hmb-ONSu (2.07 g, 5.4 mmol)[10] was added to a suspension of H-L-App-OH (1.14 g, 5.9 mmol)[11] and Et_3N (0.83 ml, 5.9 mmol) in DMF (40 ml) at 0 °C. The mixture was stirred at 4 °C for 24 h, and the filtrate was evaporated. The residue was dissolved in EtOAc (80 ml) and washed with 10% citric acid and water, and dried over $MgSO_4$. After evaporation, the residual oil was solidified by the addition of petroleum ether, and the resulting solid was recrystallized from EtOAc–ether–petroleum ether: yield, 2.10 g (84%); mp 113 °C; $[\alpha]_D^{20}$ −10.2° (*c* 1, $CHCl_3$); R_f^1 0.56.

Found: C, 61.84; H, 7.81; N, 6.00%. Calcd for $C_{24}H_{36}O_7N_2$: C, 62.05; H, 7.81; N, 6.03%.

H-Ala-Hmb-Phe-OH·HCl (2a·HCl). Compound **1a** (3.49 g, 8 mmol) was dissolved in dioxane (13 ml) and treated with 6 M HCl in dioxane (13.3 ml, 80 mmol) at 20 °C for 3 h. The solvent was evaporated, and the residual solid was triturated with ether and collected: yield, 2.96 g (99%); mp 206—208 °C; $[\alpha]_D^{25}$ −18.5° (*c* 1, DMF); R_f^3 0.33.

H-Ala-Hmb-App-OH·HCl (2b·HCl). This compound was prepared from **1b** (1.86 g, 4 mmol) as described for **2a**·HCl: yield, 1.60 g (100%); mp 198—199 °C; $[\alpha]_D^{25}$ −17.3° (*c* 1, DMF); R_f^3 0.38.

Boc-Ser(Bzl)-Ala-Hmb-Phe-OH (3a). Boc-L-Ser(Bzl)-ONSu (2.88 g, 7.4 mmol)[12] was added to a solution of **2a**·HCl (2.61 g, 7 mmol) and Et_3N (1.96 ml, 14 mmol) in DMF (30 ml) at 0 °C. The mixture was stirred at 0 °C for 1 h and at 20 °C overnight. The mixture was treated as described for **1a**: yield, 4.20 g (98%); mp 103 °C; $[\alpha]_D^{25}$ −4.3° (*c* 1, $CHCl_3$); R_f^1 0.43.

Found: C, 62.40; H, 6.99; N, 6.79%. Calcd for $C_{32}H_{43}O_9N_3$: C, 62.62; H, 7.06; N, 6.85%.

Boc-Ser(Bzl)-Ala-Hmb-App-OH (3b). This compound was prepared from Boc-L-Ser(Bzl)-ONSu (1.57 g, 4 mmol) and **2b**·HCl (1.73 g, 4.3 mmol) as described for **3a**: yield, 2.07 g (81%); mp 114 °C; $[\alpha]_D^{20}$ −0.4° (*c* 1, $CHCl_3$); R_f^1 0.48.

Found: C, 62.79; H, 7.37; N, 6.64%. Calcd for $C_{34}H_{47}O_9N_3 \cdot 1/2H_2O$: C, 62.75; H, 7.44; N, 6.46%.

Boc-Ser(Bzl)-Ala-Hmb-Phe-ONSu (4a). To a stirred solution of **3a** (3.68 g, 6 mmol) and HONSu (1.04 g, 9 mmol) in DMF was added EDC·HCl (1.50 g, 7.8 mmol) at 0 °C. The mixture was stirred at 4 °C for 24 h. After evaporation, the residue was solidified by the addition of cold water and dried in vacuo over P_2O_5: yield, 4.30 g (100%); R_f^1 0.83, R_f^2 0.37. This was used to the next step without further purification.

Boc-Ser(Bzl)-Ala-Hmb-App-ONSu (4b). This compound was prepared from **3b** (1.60 g, 2.5 mmol) as described for **4a**: yield, 1.85 g (100%); R_f^1 0.73.

Cyclo(-Ala-Hmb-Phe-Ser(Bzl)-) (6a). A solution of **4a** (711 mg, 1 mmol) in TFA (4 ml) was allowed to stand at 0 °C for 30 min. After evaporation, the residual oil was solidified by the addition of ether to afford H-Ser(Bzl)-Ala-Hmb-Phe-ONSu·TFA (**5a**·TFA). This was dissolved in DMF (13 ml) and the solution was added dropwise into dry pyridine (320 ml) with stirring at 20 °C. The stirring was

continued at 20 °C for 2 d and the mixture was evaporated. The resulting solid was collected with the aid of cold water, washed with 10% citric acid and dried over P_2O_5. This was recrystallized from DMF-EtOAc: yield, 292 mg (59% from **4a**); mp 288—289 °C (decomp); $[\alpha]_D^{25}$ −140° (*c* 0.5, DMF); MS, *m/z* 495 (M^+); R_f^1 0.79, R_f^2 0.24.

Found: C, 64.43; H, 6.73; N, 8.49%. Calcd for $C_{27}H_{33}O_6N_3 \cdot 1/2H_2O$: C, 64.27; H, 6.79; N, 8.33%.

Cyclo(-Ala-Hmb-App-Ser(Bzl)-) (6b). This compound was prepared from **4b** (739 mg, 1 mmol) as described for **6a**: yield, 299 mg (57% from **4b**); mp 233—234 °C (decomp); $[\alpha]_D^{20}$ −187° (*c* 0.5, DMF); MS, *m/z* 523 (M^+); R_f^1 0.80, R_f^2 0.32.

Found: C, 65.49; H, 7.15; N, 7.97%. Calcd for $C_{29}H_{37}O_6N_3 \cdot 1/2H_2O$: C, 65.39; H, 7.19; N, 7.89%.

Cyclo(-Ala-Hmb-Phe-Ser-) (7a). This compound was prepared by catalytic transfer hydrogenation as follows. To a stirred solution of **6a** (130 mg, 0.26 mmol) in DMF (10 ml) were added Pd black and HCOOH (0.5 ml) at 20 °C. The stirring was continued at 20 °C for 2 h. The filtrate was evaporated and the residual solid was recrystallized from DMF-EtOAc: yield, 103 mg (97%); mp 219 °C; $[\alpha]_D^{25}$ −221° (*c* 0.5, DMF); MS, *m/z* 405 (M^+); R_f^1 0.31, R_f^2 0.10.

Found: C, 57.04; H, 6.58; N, 10.19%. Calcd for $C_{20}H_{27}O_6N_3 \cdot 4/5H_2O$: C, 57.21; H, 6.87; N, 10.01%.

The same compound was obtained by conventional hydrogenation. Compound **6a** (53 mg, 0.11 mmol) in DMF (4 ml) was hydrogenated in the presence of Pd black at 20 °C for 7 d. The filtrate was treated as above: yield, 34 mg (76%); mp 218 °C; $[\alpha]_D^{25}$ −220° (*c* 0.5, DMF); R_f^1 0.31, R_f^2 0.10.

Cyclo(-Ala-Hmb-App-Ser-) (7b). This compound was prepared from **6b** (236 mg, 0.45 mmol) by catalytic transfer hydrogenation as described for **7a**: yield, 182 mg (93%); mp 199—200 °C; $[\alpha]_D^{20}$ −248° (*c* 0.5, DMF); MS, *m/z* 433 (M^+); R_f^1 0.44.

Found: C, 58.99; H, 7.13; N, 9.48%. Calcd for $C_{22}H_{31}O_6N_3 \cdot 4/5H_2O$: C, 58.99; H, 7.34; N, 9.38%.

Cyclo(-Ala-Hmb-Phe-ΔAla-) ([L-Phe³]AM-toxin II, 8a). This compound was prepared by Miller method as follows. To a suspension of **7a** (41 mg, 0.1 mmol) in CH_2Cl_2 (10 ml) were added CuCl (5 mg, 0.05 mmol) and EDC·HCl (38 mg, 0.2 mmol). The mixture was refluxed with stirring in the dark. After 2 d, the same amounts of CuCl and EDC·HCl were added, the stirring being continued for further 4 d. Then, the solution was evaporated, and the residue was dissolved in $CHCl_3$ (3 ml). The solution was applied to a silica-gel column (0.9×9 cm, Wako silica gel C-200, 100—200 mesh) and eluted with a solvent of $CHCl_3$–acetone (4:1). The fractions (9—42 ml) were evaporated and the residual solid was recrystallized from EtOAc–petroleum ether: yield, 9.3 mg (24%); mp 230—232 °C; MS, *m/z* 387 (M^+); IR (KBr) 1740, 1655, 1630, 1520, 1040 cm^{-1}; R_f^2 0.24, R_f^3 0.81, R_f^4 0.86, R_f^5 0.24. Reported value,[2] mp 231—232 °C.

Found: C, 61.12; H, 6.65; N, 10.65%. Calcd for $C_{20}H_{25}O_5N_3 \cdot 1/3H_2O$: C, 61.05; H, 6.58; N, 10.68%.

Same **8a** was prepared by the Photaki method as follows. To a chilled solution of **7a** (80 mg, 0.2 mmol) in pyridine (2 ml) was added Tos-Cl (76 mg, 0.4 mmol) at 0 °C. After 24 h, the solution was evaporated and the solid was collected by the aid of cold water. The solid was washed with a mixture of ether–petroleum ether to remove excess Tos-Cl: yield of cyclo(-Ala-Hmb-Phe-Ser(Tos)-), 105 mg (94%); R_f^5 0.64. This tosylated cyclopeptide (105 mg, 0.19 mmol) in DMF (1 ml) was treated with 1 M Et_2NH in dioxane (0.38 ml, 0.38 mmol) at 20 °C. After 6 h the solution was evaporated and the solid was collected with cold water. The solid was suspended in EtOAc (4 ml), and the filtrate was subjected to purification by preparative TLC on silica gel 60 F_{254} precoated plate (layer thickness: 2 mm, Merck) using a solvent EtOAc–$CHCl_3$ (1:1). A portion of R_f^5 0.16 on the plate was extracted with EtOAc, evaporated and the solid was recrystallized from EtOAc–ether–petroleum ether: yield, 4.7 mg (6.5% from **7a**); mp 228—230 °C; R_f^2 0.24, R_f^4 0.86.

Cyclo(-Ala-Hmb-App-ΔAla-) (AM-toxin II, 8b). This compound was prepared from **7b** (43 mg, 0.1 mmol) by the procedure of Miller as described for **8a**: yield, 8.2 mg (20%); mp 212—213 °C; MS, *m/z* 415 (M^+); IR (KBr) 1656, 1630, 1519, 1040 cm^{-1}; UV λ_{max} (MeOH) 202 nm (ε 5500), 208 (11300), 224 (6000), 267 (800); R_f^2 0.30, R_f^3 0.83, R_f^4 0.87, R_f^5 0.30. Reported values; mp 213—214 °C,[13] 212—213 °C.[2]

Bioassays. Bioassays on apple leaves (susceptible cultivar, Indo) was carried out as described in the literature.[13] Compound **8b** and natural AM-toxin II possessed the same minimum toxic activity for the induction of necrosis at 0.02 μg ml^{-1}, where [L-Phe³]AM-toxin II (**8a**) showed the activity at 20 μg ml^{-1} level.

References

1) Abbreviations: Ahp, 2-amino-5-(*p*-hydroxyphenyl)-pentanoic acid; Amp, 2-amino-5-(*p*-methoxyphenyl)pentanoic acid; App, 2-amino-5-phenylpentanoic acid; Bzl, benzyl; ΔAla, 2,3-dehydroalanine; DMF, *N*,*N*-dimethylformamide; Dpr(Z), 3-benzyloxycarbonyl-2,3-diaminopropanoic acid; EDC, 1-ethyl-3-(3-dimethylaminopropyl)carbodiimide; Hmb, 2-hydroxy-3-methylbutanoic acid; HONSu, *N*-hydroxysuccinimide; Ms-Cl, methanesulfonyl chloride; TFA, trifluoroacetic acid; THF, tetrahydrofuran; Tos-Cl, *p*-toluenesulfonyl chloride. Amino acid symbols except D-amino acids denote the L-configuration unless otherwise indicated.

2) Y. Shimohigashi and N. Izumiya, *Int. J. Pept. Protein Res.*, **12**, 7 (1978).

3) Y. Shimohigashi, S. Lee, H. Aoyagi, T. Kato, and N. Izumiya, *Int. J. Pept. Protein Res.*, **10**, 323 (1977).

4) Y. Shimohigashi, S. Lee, H. Aoyagi, T. Kato, and N. Izumiya, *Int. J. Pept. Protein Res.*, **10**, 197 (1977).

5) B. ElAmin, G. M. Anantharamaiah, G. P. Royer, and G. E. Means, *J. Org. Chem.*, **44**, 3442 (1979).

6) M. J. Miller, *J. Org. Chem.*, **45**, 3131 (1980).

7) I. Photaki, *J. Am. Chem. Soc.*, **85**, 1123 (1963).

8) S. Nomoto, A. Sano, and T. Shiba, *Tetrahedron Lett.*, **1979**, 521.

9) H. Mihara, H. Aoyagi, S. Lee, M. Waki, T. Kato, and N. Izumiya, *Int. J. Pept. Protein Res.*, **23**, 447 (1984).

10) T. Kanmera and N. Izumiya, *Int. J. Pept. Protein Res.*, **19**, 79 (1982).

11) Y. Shimohigashi, S. Lee, and N. Izumiya, *Bull. Chem. Soc. Jpn.*, **49**, 3280 (1976).

12) D. A. Laufer and E. R. Blout, *J. Am. Chem. Soc.*, **89**, 1246 (1967).

13) T. Ueno, T. Nakashima, Y. Hayashi, and H. Fukami, *Agric. Biol. Chem.*, **39**, 1115 (1975).

Synthesis of a Functionalized Carbocyclic Skeleton of Ptaquilosin, the Aglycone of a Bracken Carcinogen Ptaquiloside Based on an Intramolecular Diels-Alder Reaction

Hideo KIGOSHI, Akihiko SAWADA, Haruki NIWA, and Kiyoyuki YAMADA*
Department of Chemistry, Faculty of Science, Nagoya University, Chikusa, Nagoya 464
(Received December 10, 1988)

A tricyclic compound **13** possessing the carbocyclic skeleton of ptaquilosin (**2**), the aglycone of a bracken carcinogen ptaquiloside (**1**) has been synthesized by the intramolecular Diels-Alder reaction of trienes **12a** and **12b**.

Since the carcinogenicity of bracken fern (*Pteridium aquilinum*: "warabi" in Japanese) was found in 1960,[1] studies in search for the carcinogen(s) have been carried out intensively: we isolated ptaquiloside (**1**) as a carcinogenic principle from bracken in 1983, determined the structure,[2] and proved its potent carcinogenicity.[3] Ptaquilosin (**2**),[4] the aglycone of **1** is a norsesquiterpene of the illudane-type. Illudin-S (**3**)[5] and -M (**4**)[5] are the representative members of the illudane-type sesquiterpenes and the total synthesis of **3** and **4** was reported.[6] Some synthetic studies on this class of sesquiterpenes have been reported.[7]

In connection with the synthesis of ptaquilosin (**2**), we have synthesized the functionalized carbocyclic skeleton of **2** based on the intramolecular Diels-Alder reaction. The Diels-Alder reaction of allylidenecyclopropane with various dienophiles to form spiro[2.5]-oct-4-enes was reported by Krief and Zutterman.[8] We attempted to utilize the Diels-Alder reaction of this type intramolecularly for a triene **11a** and for a stereoisomeric mixture of **12a** and **12b** toward the construction of the tricyclic carbon skeleton of **2**.

The triene **11a** was prepared as follows. Diethyl cyanomethylphosphonate[9] was alkylated with the iodide **5**[10] to afford the phosphonate **6** (91%), the reaction of which with the aldehyde **7**[11] provided the diene **8**[12,13] (54%, $Z:E=8:1$).[14] After removal of the tetrahydropyranyl protecting group in **8**, the resulting alcohol **9**[12,13] was oxidized to give the aldehyde **10**[12,13] (68% overall), which on reaction with diethyl (1-cyanoethyl)phosponate[9] furnished two stereoisomeric trienes **11a**[12,13] (42%) and **11b**[12,13] (29%). When **11a** was heated, the intramolecular Diels-Alder reaction did not occur, but a mixture of dimeric products resulted. Although the intramolecular Diels-Alder reaction of **11a** in the presence of $AlCl_3$ was examined, again a mixture of the dimers was obtained. The fail-

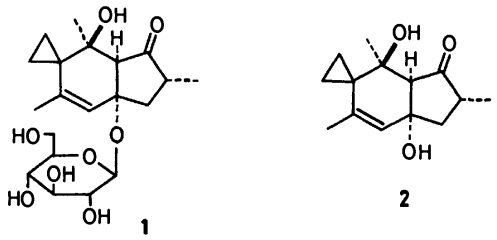

1 **2**

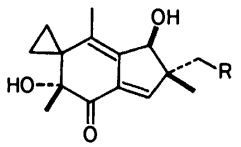

3 R = OH
4 R = H

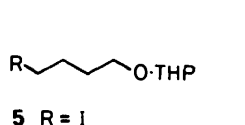

5 R = I
6 R = CH(CN)P(O)(OEt)$_2$

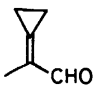

7

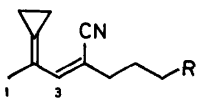

8 R = CH_2O·THP
9 R = CH_2OH
10 R = CHO

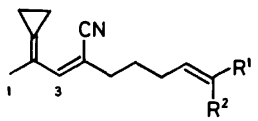

11a R^1=Me, R^2=CN
11b R^1=CN, R^2=Me
12a R^1=H, R^2=CN
12b R^1=CN, R^2=H

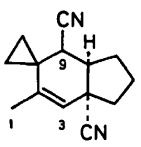

13

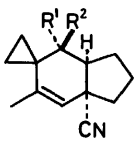

14a R^1=Me, R^2=CN
14b R^1=CN, R^2=Me

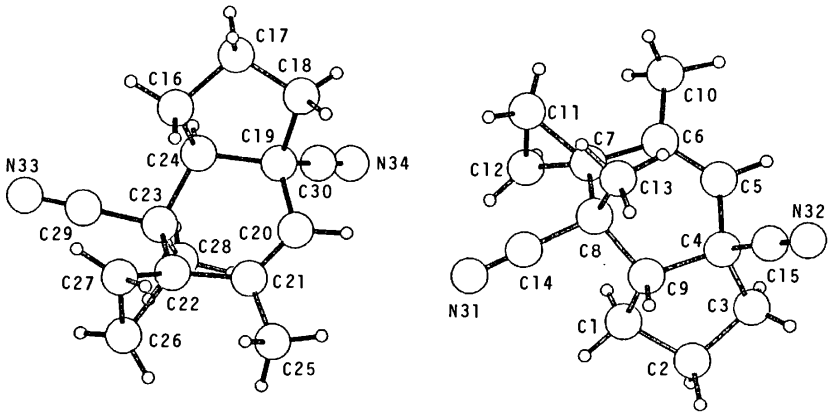

Fig. 1. Perspective drawing of the compound **14a**.

ure of the intramolecular Diels-Alder reaction of **11a** is presumably due to the steric hindrance in the transition state caused by the vinyl methyl group in the dienophilic part. Thus, the intramolecular Diels-Alder reaction of the trienes **12a** and **12b** was examined, the preparation of which follows: the reaction of **10** with diethyl cyanomethylphosphonate[9] afforded an inseparable 1:1 mixture of **12a**[12,13] and **12b**[12,13] (66%). On heating the trienes **12a** and **12b** in toluene (190—210 °C, 20 h) the tricyclic compound **13** was obtained as a single isomer (15%) together with a mixture of dimeric products (83%). The stereochemistry of **13** except for C-9 was established after conversion to the methylated derivative **14a**. The carbanion generated from **13** was methylated with methyl iodide to give two diastereomers, **14a** (mp 84—86 °C, 36%) and **14b** (mp 113—114 °C, 47%), and **14a** was subjected to X-ray crystallographic analysis. A perspective drawing of the final X-ray model of **14a** is shown in Fig. 1.[15] The result of the X-ray crystallographic analysis of **14a** reveals that the tricyclic compound **13** possesses the spirocyclopropane-containing *cis*-hexahydroindene skeleton desired for the synthesis of ptaquilosin (**2**). In summary, a functionalized tricyclic compound **13** potentially useful for the synthesis of ptaquilosin (**2**) has been synthesized, although in low yield, based on the intramolecular Diels-Alder reaction.

Experimental

Melting points are uncorrected. IR spectra were obtained in $CHCl_3$ with a JASCO IR-810 or a JASCO IR-S spectrophotometer. ^1H and ^{13}C NMR spectra were recorded on a JEOL FX-90QE spectrometer in $CDCl_3$, unless otherwise stated: chemical shifts (δ) are reported in ppm downfield from internal Me_4Si, and coupling constants are given in herz. The low-resolution mass spectra were recorded on a Hitachi RMU-6C spectrometer. The high-resolution mass spectra (HRMS) were measured on a JEOL JMS-DX300 or a JEOL JMS-LG2000 instrument. Fuji-Davison silica gel BW-820 MH was used for column chromatography. Merck precoated silica gel 60 F_{254} plates, 0.25 mm thickness, were used for thin-layer chromatography. Toluene was distilled from Na under nitrogen. Dichloromethane was distilled from CaH_2 under nitrogen. 1,2-Dimethoxyethane (DME) and tetrahydrofuran (THF) were distilled from Na-benzophenone ketyl under nitrogen. Hexamethylphosphoric triamide (HMPT) and dimethyl sulfoxide (DMSO) were distilled from CaH_2 under reduced pressure. Organic solutions were washed with saturated NaCl solution, dried over anhydrous Na_2SO_4, and concentrated under reduced pressure by a rotary evaporator.

Phosphonate 6. To a solution of diethyl cyanomethylphosphonate[9] (378 mg, 2.14 mmol) in DME (4 ml) was added KH (35% dispersion in mineral oil, 0.24 g, 2.10 mmol) under nitrogen. The suspension was stirred at room temperature for 1.5 h and then a solution of **5**[10] (582 mg, 2.05 mmol) in DME (2 ml) was added. The reaction mixture was stirred at room temperature for 2 h, diluted with the 0.25 M phosphate buffer solution (pH 7.0, 15 ml) (1 M=1 mol dm^{-3}), and extracted with EtOAc (3×20 ml). The combined extracts were washed with saturated NaCl solution, dried, and concentrated. The crude product was purified by chromatography on silica gel (15 g, EtOAc) to give **6** (644 mg, 91%) as a colorless oil: IR 2250, 1265, and 1025 cm^{-1}; ^1H NMR (90 MHz) δ=1.20—2.10 (12H, m), 1.39 (6H, t, J=7.0 Hz), 2.92 (1H, m), 3.20—4.00 (4H, m), 4.24 (4H, m), and 4.59 (1H, m); MS m/z (rel intensity) 333 (M^+; 2), 304 (2), 278 (3), 250 (40), 249 (40), 233 (60), 232 (60), 219 (30), 204 (50), 176 (75), and 165 (100). HRMS Found: m/z 333.1692. Calcd for $C_{15}H_{28}NO_5P$: M, 333.1705.

Diene 8. To a solution of **6** (2.17 g, 6.52 mmol) in DME (22 ml) was added KH (35% dispersion in mineral oil, 0.76 g, 6.65 mmol) under nitrogen. The mixture was stirred at room temperature for 1.5 h and then a solution of **7**[11] (0.99 g, 10.3 mmol) in DME (4 ml) was added. After being stirred at room temperature for 1 h, the reaction mixture was poured into the 0.25 M phosphate buffer solution (pH 7.0, 50 ml) containing hydroquinone (40 mg). The mixture was extracted with EtOAc (3×50 ml) and the combined extracts were washed with saturated NaCl solution, dried, and concentrated. The residue was separated by chromatography on silica gel (30 g, hexane/EtOAc=10:1) to afford an 8:1 mixture of (*Z*)-**8**[12] and (*E*)-**8**[12] (974 mg, 54%) as a colorless oil: IR 3010, 2210, 1735, and 1605 cm^{-1}; MS m/z (rel intensity) 275 (M^+; 2), 191 (20), 118 (20), and 85 (100). HRMS Found: m/z 275.1886. Calcd for $C_{17}H_{25}NO_2$: M, 275.1885.

^{1}H NMR (90 MHz) of (*Z*)-**8**:[16] δ=1.22 (4H, m), 1.35—1.90 (10H, m), 2.25 (3H, m), 2.10—2.50 (2H, m), 3.20—4.00 (4H, m), 4.56 (1H, m), and 6.71 (1H, br s). The *Z*/*E* ratio of **8** was determined by ^{1}H NMR spectral analysis.

Alcohol 9. A solution of **8**[13] (974 mg, 3.54 mmol) and hydroquinone (9 mg) in AcOH (30 ml)–H_2O (10 ml) was stirred at 45 °C for 1 h under nitrogen and then concentrated. The residue was dissolved in toluene (10 ml) and the solution was concentrated under reduced pressure. The residue was purified by chromatography on silica gel (20 g, hexane/EtOAc=2:1) to provide **9**[12,13] (513 mg, 76%) as a colorless oil: IR 3620, 3450 (broad), 3010, 2210, 1735, and 1605 cm^{-1}; MS *m*/*z* (rel intensity) 191 (M^+; 15), 176 (4), and 118 (100). HRMS Found: *m*/*z* 191.1289. Calcd for $C_{12}H_{17}NO$: M, 191.1310. ^{1}H NMR (90 MHz) of (*Z*)-**9**:[16] δ=1.23 (4H, m), 1.45—1.85 (5H, m), 2.25 (3H, m), 2.10—2.50 (2H, m), 3.67 (2H, br t, *J*=6.5 Hz), and 6.71 (1H, br s).

Aldehyde 10. To a solution of oxalyl dichloride (0.31 ml, 3.56 mmol) in CH_2Cl_2 (7 ml) was added a solution of DMSO (0.50 ml, 7.18 mmol) in CH_2Cl_2 (1.5 ml) at −65 °C under nitrogen. The mixture was stirred at −65 °C for 2 min, and then a solution of **9**[13] (0.34 g, 1.78 mmol) and hydroquinone (4 mg) in CH_2Cl_2 (4 ml) was added. The mixture was stirred at −60 °C for 15 min and Et_3N (2.5 ml, 18.0 mmol) was added. After stirring at −50 °C for 5 min, the reaction mixture was allowed to warm to room temperature and was kept for 1 h. Water (20 ml) was added to the mixture and the resulting mixture was extracted with CH_2Cl_2 (3×20 ml). The combined extracts were washed with saturated NaCl solution, dried, and concentrated. The residue was separated by chromatography on silica gel 10 g, hexane/EtOAc=6:1) to give **10**[12-13] (0.30 g, 89%) as a colorless oil: IR 3020, 2210, 1725, and 1625 cm^{-1}; MS *m*/*z* (rel intensity) 189 (M^+; 5), 174 (1), 160 (5), and 118 (100). HRMS Found: *m*/*z* 189.1147. Calcd for $C_{12}H_{15}NO$: M, 189.1154. ^{1}H NMR (90 MHz) of (*Z*)-**10**:[16] δ=1.25 (4H, m), 1.50—2.10 (2H, m), 2.27 (3H, m), 2.15—2.65 (4H, m), 6.71 (1H, br s), and 9.79 (1H, t, *J*=1.5 Hz).

Trienes 11a and 11b. To a solution of diethyl (1-cyanoethyl)phosphonate[9] (151 mg, 0.791 mmol) in DME (3 ml) was added KH (35% dispersion in mineral oil, 86 mg, 0.753 mmol) under nitrogen. The suspension was stirred at room temperature for 1.5 h and then a solution of **10**[13] (113 mg, 0.592 mmol) and hydroquinone (2 mg) in DME (1 ml) was added. The mixture was stirred at room temperature for 2.5 h and then to this mixture was further added the carbanion solution, prepared from diethyl (1-cyanoethyl)phosphonate (54 mg, 0.28 mmol) and KH (35% dispersion in mineral oil, 33 mg, 0.29 mmol) in DME (0.5 ml) as described above. After stirring at room temperature for further 30 min, the mixture was diluted with H_2O (5 ml) and extracted with EtOAc (4×5 ml). The combined extracts were washed with saturated NaCl solution and dried. Hydroquinone (23 mg) was added to the EtOAc solution, which was concentrated. The oily residue was purified by chromatography on silica gel (10 g, hexane/ether=8:1) to provide **11a**[12,13] (colorless oil, 56.9 mg, 42%) and **11b**[12,13] (colorless oil, 37.5 mg, 29%), respectively.

11a: IR 3020, 2220, 1735, 1645, and 1605 cm^{-1}; MS *m*/*z* (rel intensity) 226 (M^+; 10), 211 (8), and 118 (100). HRMS Found: *m*/*z* 226.1477. Calcd for $C_{15}H_{18}N_2$: M, 226.1470. ^{1}H NMR (90 MHz) of (3*Z*)-**11a**:[16] δ=1.26 (4H, m), 1.50—2.00 (2H, m), 1.94 (3H, d, *J*=1.5 Hz), 2.20—2.55 (4H, m), 2.27 (3H, m), 6.13 (1H, tq, *J*=7.5, 1.5 Hz), and 6.54 (1H, br s).

11b: IR 3020, 2220, 1735, 1640, and 1605 cm^{-1}; MS *m*/*z* (rel intensity) 226 (M^+; 10), 211 (15), and 118 (100). HRMS Found: *m*/*z* 226.1490. Calcd for $C_{15}H_{18}N_2$: M, 226.1470. ^{1}H NMR (90 MHz) of (3*Z*)-**11b**:[16] δ=1.25 (4H, m), 1.40—2.00 (2H, m), 1.88 (3H, d, *J*=1.5 Hz), 2.00—2.55 (4H, m), 2.27 (3H, m), 6.34 (1H, tq, *J*=7.5, 1.5 Hz), and 6.72 (1H, br s).

Trienes 12a and 12b. To a solution of diethyl cyanomethylphosphonate[9] (434 mg, 2.45 mmol) in DME (5 ml) was added KH (35% dispersion in mineral oil, 0.27 g, 2.36 mmol) under nitrogen. The suspension was stirred at room temperature for 50 min, and then a solution of **10**[13] (300 mg, 1.59 mmol) and hydroquinone (3 mg) in DME (4 ml) was added. The mixture was stirred at room temperature for 1 h, diluted with H_2O (20 ml), and extracted with EtOAc (4×10 ml). The combined extracts were washed with saturated NaCl solution, dried, and concentrated. The oily residue was separated by chromatography on silica gel (10 g, hexane/EtOAc=6:1) to afford an inseparable 1:1 mixture[14] of **12a**[12,13] and **12b**[12,13] (268 mg, 66%) as a colorless oil: IR 3030, 3020, 2230, 2210, 1735, 1635, and 1605 cm^{-1}; MS *m*/*z* (rel intensity) 212 (M^+; 5), 197 (3), and 118 (100). HRMS Found: *m*/*z* 212.1300. Calcd for $C_{14}H_{16}N_2$: M, 212.1313. ^{1}H NMR (90 MHz) of (3*Z*)-**12a**[16] and (3*Z*)-**12b**:[16] δ=1.26 (4H, m), 1.50—2.00 (2H, m), 2.00—2.65 (4H, m), 2.27 (3H, m), 5.37 (1H, m), and 6.35—6.90 (2H, m).

Tricyclic Compound 13. A solution of the 1:1 mixture of **12a**[13] and **12b**[13] (23 mg, 0.11 mmol) and hydroquinone (1 mg) in toluene (1 ml) in a Pyrex sealed tube under nitrogen was heated at 190—210 °C for 20 h. The solution was concentrated and the residue was separated by chromatography on silica gel (2 g, hexane/EtOAc=6:1) to give **13** (3.4 mg, 15%) and a mixture of dimeric products (19 mg, 83%).

13: colorless oil; IR 3020, 2230, 1655, and 1450 cm^{-1}; ^{1}H NMR (90 MHz) δ=0.75—1.25 (4H, m), 1.50 (3H, d, *J*=1.5 Hz), 1.70—2.40 (6H, m), 2.76 (1H, m), 3.34 (1H, d, *J*=4.0 Hz), and 5.33 (1H, br s); ^{13}C NMR (22.5 MHz, C_6D_6) δ=8.2 (t), 10.6 (t), 18.1 (s), 18.2 (q), 22.8 (t), 26.4 (t), 35.8 (d), 38.9 (t), 41.8 (s), 45.7 (d), 118.5 (s), 121.8 (d), 122.6 (s), and 137.7 (s); MS *m*/*z* (rel intensity) 212 (M^+; 65), 197 (30), 185 (35), 170 (100), and 155 (75). HRMS Found: *m*/*z* 212.1283. Calcd for $C_{14}H_{16}N_2$: M, 212.1313. The mixture of dimeric products: colorless oil; IR 3020, 2220, and 1635 cm^{-1}; ^{1}H NMR (90 MHz) δ=−0.10—1.00 (8H, m), 1.30—1.90 (6H, m), 1.50 (6H, br s), 2.10—2.65 (6H, m), 5.25—5.50 (3H, m), and 6.25—6.90 (3H, m); MS *m*/*z* (rel intensity) 424 (M^+; 35), 409 (30), 358 (20), 344 (30), and 330 (100).

Methylation of 13. To a stirred solution of diisopropylamine (0.35 ml, 2.50 mmol) in THF (8.35 ml) at 0 °C was added dropwise a 1.64 M solution of *n*-BuLi in hexane (1.3 ml, 2.1 mmol) under nitrogen, and the solution was stirred for 10 min. The 0.2 M solution of LDA described above (1.0 ml, 0.2 mmol) was added to a solution of **13** (11 mg, 0.052 mmol) in THF (0.06 ml) at 0 °C and the mixture was stirred at 0 °C for 40 min under nitrogen. To this mixture was added a solution of MeI (13 μl, 0.21 mmol) and HMPT (18 μl, 0.10 mmol) in THF (0.17 ml). The mixture was stirred at 0 °C for 1 h, diluted with 1 M HCl (2 ml), and extracted with ether (3×5 ml). The combined extracts were washed with saturated $NaHCO_3$ solution and saturated NaCl solution successively, dried, and concentrated. The

residue was separated by chromatography on silica gel (2 g, hexane/EtOAc=10:1 to 4:1) to afford **14a** (4.2 mg, 36%) and **14b** (5.5 mg, 47%).

14a: mp 84—86 °C (hexane); IR 3020, 2230, 1650, and 1450 cm^{-1}; ^1H NMR (90 MHz) δ=0.55—1.20 (4H, m), 1.20—2.50 (6H, m), 1.50 (3H, d, J=1.5 Hz), 1.65 (3H, s), 2.73 (1H, br t, J=8.5 Hz), and 5.33 (1H, br s); MS m/z (rel intensity) 226 (M^+; 80), 211 (70), 199 (35), 197 (35), and 184 (100). HRMS Found: m/z 226.1488 . Calcd for $C_{15}H_{18}N_2$: M, 226.1470.

14b: mp 113—114 °C (hexane-benzene); IR 3020, 2230, 1650, and 1450 cm^{-1}; ^1H NMR (90 MHz) δ=0.75—1.10 (4H, m), 1.21 (3H, s), 1.54 (3H, d, J=1.5 Hz), 1.60—2.50 (6H, m), 2.77 (1H, br t, J=8.5 Hz), and 5.45 (1H, br s); MS m/z (rel intensity) 226 (M^+; 90), 211 (85), 199 (80), and 184 (100). HRMS Found: m/z 226.1481. Calcd for $C_{15}H_{18}N_2$: M, 226.1470.

X-Ray Crystallographic Analysis of 14a. Crystals of **14a** were obtained by slow crystallization from hexane. D_m was measured by floatation. Crystal data of **14a** were as follows: $C_{15}H_{18}N_2$, M=226.32; monoclinic, space group $P2_1/n$, a=16.770(2) Å, b=11.076(1) Å, c=15.745(1) Å, β=117.91(1)°, V=2584.6(4) $Å^3$; D_c=1.163 g cm^{-3}, D_m=1.163 g cm^{-3}; Z=8; μ=4.565 cm^{-1}; crystal size 0.30×0.25×0.20 mm. Total 4764 reflections with $2\theta \leqq 126°$ were collected on a RIGAKU ARC-5R automated four-circle diffractometer using graphite monochromated Cu $K\alpha$ radiation (1.54178 Å). Structure was solved by Monte-Carlo direct method[17] with the aid of MULTAN 78 program system[18] using 4097 unique reflections with $|F_o| \geqq \sigma(|F_o|)$ and refined by full-matrix least-square program. Non-H atoms were assigned with anisotropic thermal parameters. All H atoms were located in a difference Fourier map and refined with the equivalent isotropic thermal parameters to those for the bonded atoms. The final unweighted R factor was 0.09 after minimizing $\sum\omega(|F_o|^2-|F_c|^2)^2$ with $\omega=1/\sigma^2(F_o^2)$; R_w=0.13, S=3.8. Atomic scattering factors were from Ref. 19. PLUTO 78 program[20] was employed in drawing the computer-generated molecular structure. All crystallographic calculations were performed on a FACOM M-382 computer, operated by Computation Center of Nagoya University, using the library program of CRYSTAN system.

References

1) I. A. Evans, "Chemical Carcinogens, Second Edition," ed by C. E. Searle, American Chemical Society, Washington, D.C. (1984), Vol. 2, Chap. 18. I. Hirono and K. Yamada, "Naturally Occurring Carcinogens of Plant Origin," ed by I. Hirono, Kodansha-Elsevier, Tokyo-Amsterdam (1987), Chap. 4.

2) H. Niwa, M. Ojika, K. Wakamatsu, K. Yamada, I. Hirono, and K. Matsushita, *Tetrahedron Lett.*, **24**, 4117 (1983). H. Niwa, M. Ojika, K. Wakamatsu, K. Yamada, S. Ohba, Y. Saito, I. Hirono, and K. Matsushita, *ibid.*, **24**, 5371 (1983). S. Ohba, Y. Saito, I. Hirono, H. Niwa, M. Ojika, K. Wakamatsu, and K. Yamada, *Acta Crystallogr., Sect. C*, **40**, 1877 (1984). M. Ojika, K. Wakamatsu, H. Niwa, and K. Yamada, *Tetrahedron*, **43**, 5261 (1987).

3) I. Hirono, K. Yamada, H. Niwa, Y. Shizuri, M. Ojika, S. Hosaka, T. Yamaji, K. Wakamatsu, H. Kigoshi, K. Niiyama, and Y. Uosaki, *Cancer Lett.*, **21**, 239 (1984). I. Hirono, S. Aiso, T. Yamaji, H. Mori, K. Yamada, H. Niwa, M. Ojika, K. Wakamatsu, H. Kigoshi, K. Niiyama, and Y. Uosaki, *Gann*, **75**, 833 (1984). I. Hirono, H. Ogino, M. Fujimoto, K. Yamada, Y. Yoshida, M. Ikagawa, and M. Okumura, *J. Natl. Cancer Inst.*, **79**, 1143 (1987).

4) Natural ptaquilosin (**2**) was prepared from natural **1** by chemical transformation: H. Kigoshi, A. Sawada, Y. Imamura, H. Niwa, and K. Yamada, unpublished result.

5) T. C. McMorris and M. Anchel, *J. Am. Chem. Soc.*, **87**, 1594 (1965). K. Nakanishi, M. Ohashi, M. Tada, and Y. Yamada, *Tetrahedron*, **21**, 1231 (1965). T. Matsumoto, H. Shirahama, A. Ichihara, Y. Fukuoka, Y. Takahashi, Y. Mori, and M. Watanabe, *Tetrahedron*, **21**, 2671 (1965). A. Furusaki, H. Shirahama, and T. Matsumoto, *Chem. Lett.*, **1973**, 1293.

6) T. Matsumoto, H. Shirahama, A. Ichihara, H. Shin, S. Kagawa, F. Sakan, S. Matsumoto, and S. Nishida, *J. Am. Chem. Soc.*, **90**, 3280 (1968). T. Matsumoto, H. Shirahama, A. Ichihara, H. Shin, S. Kagawa, and F. Sakan, *Tetrahedron Lett.*, **1970**, 1171. T. Matsumoto, H. Shirahama, A. Ichihara, H. Shin, S. Kagawa, F. Sakan, and K. Miyano, *ibid.*, **1971**, 2049.

7) Y. Ohfune, S. Misumi, A. Furusaki, H. Shirahama, and T. Matsumoto, *Tetrahedron Lett.*, **1977**, 279. J. Furukawa, N. Morisaki, H. Kobayashi, S. Iwasaki, S. Nozoe, and S. Okuda, *Chem. Pharm. Bull.*, **33**, 440 (1985). N. Morisaki, J. Furukawa, H. Kobayashi, S. Iwasaki, A. Itai, S. Nozoe, and S. Okuda, *ibid.*, **33**, 2783 (1985).

8) F. Zutterman and A. Krief, *J. Org. Chem.*, **48**, 1135 (1983).

9) B. Deschamps, G. Lefebvre, and J. Seyden-Penne, *Tetrahedron*, **28**, 4209 (1972).

10) K. Oshima, H. Takahashi, H. Yamamoto, and H. Nozaki, *J. Am. Chem. Soc.*, **95**, 2693 (1973).

11) F. Huet, A. Lechevallier, and J. M. Conia, *Tetrahedron Lett.*, **1977**, 2521.

12) This compound is air-sensitive and must be stored under argon in the presence of 5 percent of hydroquinone at −20 °C.

13) This material is an 8:1 mixture of (3*Z*)- and (3*E*)-isomers. Depicted is the structural formula corresponding to the major (3*Z*)-isomer.

14) The ratio was determined by ^1H NMR spectral analysis.

15) The tables of the atomic parameters and bond distances and angles and F_o—F_c table are deposited at the Chemical Society of Japan (Document No. 8873).

16) Signals due to the minor (3*E*)-isomer are omitted.

17) A. Furusaki, *Acta Crystallogr., Sect. A*, **35**, 220 (1979).

18) P. Main, S. E. Hull, L. Lessinger, G. Germain, J. P. Declercq, and M. M. Woolfson, MULTAN 78, (1978). Univ. of York, England, and Louvain, Belgium.

19) "International Tables for X-ray Crystallography," Kynoch Press, Birmingham (1974), Vol. IV.

20) W. D. S. Motherwell, PLUTO 78, (1978). Univ. of Cambridge, England.

Immobilized β-Cyclodextrins. Preparation with Various Crosslinking Reagents and the Guest Binding Properties

Izuru SUGIURA, Makoto KOMIYAMA,† Naoki TOSHIMA,* and Hidefumi HIRAI††
Department of Industrial Chemistry, Faculty of Engineering, The University of Tokyo, Hongo, Bunkyo-ku, Tokyo 113
(Received November 2, 1988)

β-Cyclodextrin (β-CyD) was immobilized by crosslinking with 1,2-ethanediol diglycidyl ether, 1,4-buthanediol diglycidyl ether, 1,6-hexanediol diglycidyl ether, 1,3-butadiene diepoxide, 1,7-octadiene diepoxide, and epichlorohydrin. The molar ratio of the crosslinking residue to β-CyD (degree of crosslinking) for each macromolecular product was determined by the corresponding elemental analysis. The equilibrium constant K of complex formation of each crosslinking macromolecule for cresols, phenol, nitrophenols, and 2-naphthol was determined, respectively, by the use of electronic absorption spectroscopy in pH 4 and 10 (or 11) buffer solutions. The concept of a hydrophobic enhancement coefficient R was introduced in order to compare the effect of a hydrophobic crosslinking residue upon the complex formation of the immobilized CyD.

Cyclodextrin (CyD), a cyclic oligomer of the 6—8 glucose units, forms an inclusion complex with various kinds of guest compounds.[1] The complex formation, however, proceeds selectively, since it includes guest compounds in various ways of binding. From the viewpoint of selective complexation, CyD has been studied as an enzyme model, a selective catalyst for organic synthesis, a device for separation of mixtures, and so on.

Recently, the selective "host-guest" complex formation of β-CyD has been studied by many investigators with an interest in its utilization for the stationary phase of HPLC.[2a-d] Since CyDs are composed of natural D-glucose units and, therefore, are optically active, they are expected to be utilized as the stationary phase for the optical resolution of racemic compounds.[2b] Few investigations, however, have been made concerning the effect of the supporting groups of the stationary phase on the property of CyDs to include a guest compound. Furthermore, some kinds of these stationary phases which were investigated contain nitrogen atoms (amines and/or amides) to combine the CyD residue to the supporting gel. This existence of =NH groups is considered to result in complicated interactions between the guest molecules and the CyD residues. For instance, a hydrogen bonding of an =NH group should be very sensitive to pH and the structure of a guest molecule. It could therefore be difficult to analyze the mechanism of complex formation[2c] and, in consequence, to design an efficient stationary phase.

β-CyD forms inclusion complexes selectively with many kinds of aromatic compounds. They have been studied mainly as models of hydrolysis enzymes.[1,3,4] On the other hand, many investigators have already reported that β-CyD is very effective as a selective catalyst for bond formation.[5-7] Previously, we reported the selective synthesis of 4-hydroxybenzoic acid from phenol and carbon tetrachloride in β-CyD.[7] Moreover, we have succeeded in the immobilization of β-CyD by crosslinking with epichlorohydrin and its utilization as an immobilized catalyst for the selective synthesis of 4-hydroxybenzoic acid without any decrease in the catalytic activity.[8] An immobilized catalyst is expected to have the advantage to simplify the system by easy removal from a reaction system and repeated usage, in spite of the usual observation that the activity of the immobilized catalyst tends to decrease by immobilization.[9]

On the basis of these studies, we have prepared the immobilized β-CyD with various kinds of crosslinking reagents and have investigated the property of the inclusion phenomena.[10]

Here, we report the syntheses of various immobilized β-CyD macromolecules without nitrogen atoms, and their characteristic features to form inclusion complexes with phenol, nitrophenols, cresols, and 2-naphthol under various pH conditions. The effects of crosslinking residues on the formation of inclusion complexes are discussed from the viewpoint of hydrophobic interaction. A hydrophobic enhancement coefficient R is introduced, which indicates the contribution of the crosslinking residue to the hydrophobicity of the binding site in the immobilized CyD. The correlation between a crosslinking residue and a guest molecule is discussed by use of R.

Experimental

Materials. β-CyD from Nakarai Chemical Co. was purified by recrystallization from water. The crosslinking reagents, 1,2-ethanediol diglycidyl ether, 1,4-buthanediol diglycidyl ether, 1,6-hexanediol diglycidyl ether, 1,3-butadiene diepoxide, 1,7-octadiene diepoxide, and epichlorohydrin (Tokyo Kasei Kogyo Co.) were used without further purification. (See Fig. 1 for the structures.) Cresols, phenol, nitrophenols, 2-naphthol, and all other chemicals were

† Present address: Institute of Materials Science, University of Tsukuda, Tennodai, Tsukuba-shi, Ibaraki-ken 305.

†† Present address: Department of Industrial Chemistry, Faculty of Engineering, Science University of Tokyo Kagurazaka, Shinjuku-ku, Tokyo 162.

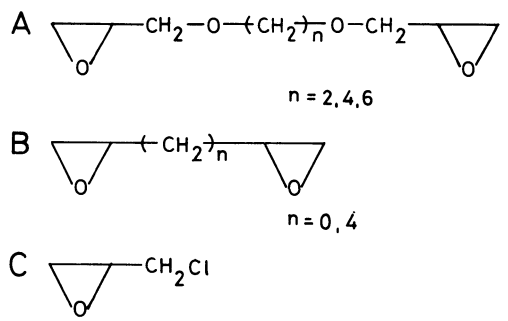

Fig. 1. Crosslinking reagents used for preparation of immobilized β-CyD.

purified by the usual methods, respectively.

Preparation of Immobilized β-CyD. Immobilized β-CyDs were prepared according to the modified method we reported previously.[10] Fifty grams (44 mmol) of β-CyD were completely dissolved in 80 ml of a 50 wt% aqueous sodium hydroxide solution, to which 440 mmol of a crosslinking reagent was added dropwise. The mixtures were kept at 50 °C which being vigorously stirred with a mechanical stirrer. As the crosslinking reaction proceeded, the viscosity of the solution increased. After several hours the solid gel appeared. Then, 150 ml of acetone was added. The resulting solids were repeatedly washed with acetone and water, and were dried in vacuo at 60 °C for 24 h.

Evaluation of the Equilibrium Constants for Complex Formation of the Immobilized β-CyDs with Guest Molecules. The equilibrium constants (K) of complex formation of the immobilized β-CyD were measured for cresols, phenol, nitrophenols, and 2-naphthol. Each K value was measured at pH 4 for all guest molecules, at pH 10 for nitrophenols and 2-naphthol, and at pH 11 for phenol and cresols. The experiments were performed by incubating 200 mg of the immobilized macromolecules and the guest compounds in 10 cm^3 of buffer solutions under pH 4, 10, or 11 at 25 °C. The charged concentrations of the guest compounds ($[G]_0$) and the ionic strength were 1.0×10^{-3} and 1.0 mol dm^{-3}, respectively. After 40 h the concentrations of the solutes in the liquid phase ($[G]_{free}$) were determined by electronic absorption spectroscopy. Completions of the equilibria were confirmed by the consistency of the concentration measured after a 60 h incubation with that after 40 h. During the long-term incubation, especially in a pH 4 buffer solution, a very slow fragmentation of one part of the immobilized macromolecule was observed, probably due to the hydrolysis of the macromolecule, resulting in a dispersion of microparticles. In order to compensate the scattering by dispersion, a blank test was performed by incubation of the immobilized macromolecules in a pH 4 buffer solution for 40 h without guest compounds. The scattering absorption caused by the microparticles was measured and subtracted from the corresponding absorption in the presence of the guest compounds.

The equilibrium constants (K) for the complex formation were calculated by

$$K = \frac{[\text{Complex}]}{[\beta\text{-CyD}]_{free}\,[G]_{free}}$$

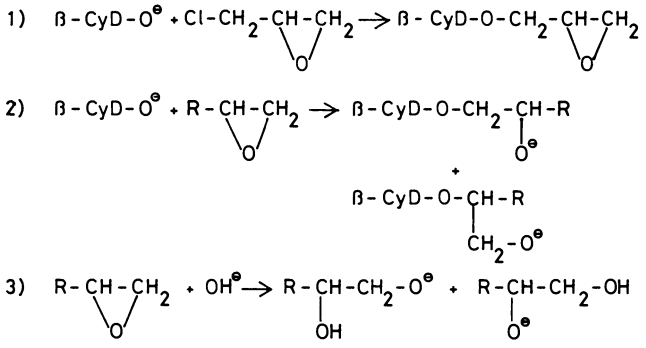

Scheme 1.

$$= \frac{[G]_0 - [G]_{free}}{([\beta\text{-CyD}]_0 - [G]_0 + [G]_{free})[G]_{free}}, \quad (1)$$

where $[G]_0$, $[G]_{free}$, and $[\beta\text{-CyD}]_0$ refer to the concentrations of the guest molecule in an initial solution, the guest molecule in the filtrate after the complex formation, and the CyD residue in the macromolecule matrix, respectively.

Equation 1 was defined on the basis of 1:1 complex formation between CyD and a guest molecule.[1] The numerator of Eq. 1 ($[G]_0-[G]_{free}$) indicates the concentration of the complex.

Evaluation of the Equilibrium Constant for Complex Formation of Free β-CyD with Guest Molecules. The equilibrium constants of the complex formation of free β-CyD with the guest molecules were evaluated according to the method reported by VanEtten et al. by using electronic absorption spectroscopy.[3b]

Results

Preparation and Characterization of Immobilized β-CyDs. Immobilization of β-CyD was carried out by a substitution or ring-opening reaction between the hydroxyl groups of β-CyD and the chlorine atoms of epichlorohydrin or the epoxide rings of the crosslinking reagents in an alkaline solution at 50 °C according to the reaction shown in Scheme 1. As shown in Scheme 1, the first step of the crosslinking reaction is a nucleophilic attack by the $-O^-$ group of β-CyD to the crosslinking reagent.[11] The spontaneous ring-opening reaction by free hydroxide OH^- proceeds at the same time (the 3rd reaction in Scheme 1), followed by the propagation reaction by the nucleophilic $-O^-$ group newly produced.

The immobilized β-CyD was obtained as a white to pale-yellow solid in sponge or beads of 1—3 mm in diameter. They are insoluble in water, methanol, ethanol, acetone, and chloroform.

The IR spectra of free β-CyD, epichlorohydrin-immobilized CyD, and 1,6-hexanediol diglycidyl ether-immobilized CyD were measured by a KBr pellet method, giving the following results: 1) The IR spectra of the immobilized CyDs maintain the specific absorptions due to free CyD. 2) The new absorption

derived from a $-(CH_2)_n-$ residue (2860—2875 cm^{-1}) appears for the immobilized CyDs. 3) The specific absorption derived from an epoxy ring (ca. 1250 cm^{-1}) is not observed for the immobilized CyDs. 4) The specific absorption derived from a $-CH_2Cl$ group (735—720 cm^{-1}) does not appear for the epichlorohydrin-immobilized CyD. 5) The absorption derived from a C-O-C stretching vibration (1070—1150 cm^{-1}) for free CyD is sharp, while that for the immobilized CyD is broad because of the crosslinkage. A new absorption derived from the C-O-C stretching vibration of the crosslinking residue (1110 cm^{-1}) appears for the 1,6-hexanediol diglycidyl ether-immobilized CyD.

The immobilized macromolecules prepared are listed in Table 1 with the results of an elemental analysis, the degree of crosslinking, and reaction conditions. The degree of crosslinking m, a molar ratio of a crosslinking residue to a β-CyD residue, is determined by calculation according to Eq. 2, by using the results of the elemental analysis of carbon in the case of the immobilized macromolecule crosslinked by diol diglydidyl ethers:

$$C(\%) = \frac{12.011[42 + (6 + n)m] \times 100}{(\text{MW of a crosslinking reagent})m + (\text{MW of } \beta\text{-CyD})}, \quad (2)$$

where m and n are the degree of crosslinking and the number of the methylene moiety of the crosslinking reagent shown in Fig. 1, respectively. The numerator of Eq. 2 intends the summation in atomic weight of the whole carbon atoms of the immobilized β-CyD per β-CyD residue. The degree of crosslinking m for the epichlorohydrin-immobilized β-CyD is calculated by a similar method.

The crosslinking reagents are not so much soluble in an aqueous solution that the reaction time required for the crosslinkage increases with the number of the hydrophobic methylene units in a reagent molecule.

The degree of crosslinking in the present system was determined to be 3—6, as shown in Table 1. Even by using the same crosslinking reagent and under the similar reaction conditions, the resulting immobilized macromolecules exhibited different values in the degree of crosslinking, depending on the lot (cf. I-3a, -3b, and -3c).

Evaluation of the Equilibrium Constants for Complex Formation of the Immobilized β-CyDs with Guest Molecules. The equilibrium of the complex formation between a β-CyD residue of the immobilized macromolecule and a guest molecule is completed by incubating the aqueous mixtures for 40 h. Since the equilibrium constant K refers the ratio of the concentration of the inclusion complex to the mathe-

Table 1. Immobilization of β-CyD by Various Crosslinking Reagents[a]

Immobilized β-CyD	Crosslinking reagent[b]	Reaction time/h	Elemental analysis		m[c]
			C/%	H/%	
I-1	A (n=2)	2.2	48.80	7.28	4.5
I-2	A (n=4)	2.2	51.20	7.77	4.6
I-3a	A (n=6)[d]	6.4	53.12	8.19	4.5
I-3b	A (n=6)[d]	7.5	53.47	8.44	5.0
I-3c	A (n=6)[d]	5.8	54.25	8.70	5.8
II-1	B (n=0)	0.4	47.82	6.93	5.6
II-2	B (n=4)	4.1	51.68	7.57	3.6
III	C	0.8	47.35	6.88	3.9

a) The molar ratio of the charged crosslinking reagent to β-CyD is 10 except I-3b. Detail reaction conditions are described in Experimental of the text. b) The structure of the crosslinking reagents are illustrated in Fig. 1. c) The degree of crosslinking calculated by the results of the elemental analysis. d) The stirring and adding rates are different because of the difficulty in completely the same operation in a heterogeneous system.

Table 2. The Equilibrium Constant (K) of the Complex Formation of the Free and Immobilized β-CyD with Cresols and Phenol at 25 °C

Immobilized β-CyD[a]	Crosslinking reagent[b]	m[c]	K/mol^{-1} dm^3							
			Cresol						Phenol	
			ortho		meta		para			
			pH 4	pH 11	pH 4	pH 11	pH 4	pH 11	pH 4	pH 11
I-1	A (n=2)	4.5	89	21	28	14	108	23	58	6
I-2	A (n=4)	4.6	165	24	23	17	193	37	117	11
I-3a	A (n=6)	4.5	167	56	167	21	165	29	68	9
III	C	3.9	300	40	70	42	704	103	331	23
β-CyD	—	—	82	81	635	176	461	135	101	17

a) See Table 1 for abbreviation. b) See Fig. 1 for the chemical structures. c) m: Degree of crosslinking.

matical product of the concentration of a free β-CyD residue and that of a free guest molecule, the practical K value can be evaluated by Eq 1. The equilibrium constants for the 1 : 1 complex formation of the β-CyD residues in the immobilized macromolecules with *o*-, *m*-, and *p*-cresols, and phenol (Table 2), with *o*-, *m*-, and *p*-nitrophenols (Table 3), and with 2-naphthol (Table 4) were obtained at 25 °C and are shown in tables, respectively. The 1 : 1 complex formation is confirmed by the independence of the K value from the charged amount of the immobilized CyDs in the range of 30—200 mg. The reproducibility of K was checked by using the immobilized beads of I-3a at various diameters. The equilibrium constants for *m*-nitrophenol at pH 4, for example, were 264, 268, and 254 $mol^{-1}\,dm^3$ for the small (1—3 mm in size, 2 mm in an average diameter), medium (2—7 mm in size, 4 mm in an average diameter), and large (4—7 mm in size, 6 mm in an average diameter) macromolecular beads, respectively. The result of these series of K values indicates that the reproducibility for the K measurement is fairly excellent and, in addition, the macromolecules employed here swell sufficiently for the measurement of the equilibrium constants in a limited time.

As shown in Tables 2—4, the equilibrium constant K depends on the crosslinking reagents. This suggests that the interaction between the crosslinking residue and the guest molecule exists in the complex formation of the immobilized β-CyD with the guest molecule. The effect of the degree of crosslinking on the complex formation constant K was examined by

Table 3. The Equilibrium Constant (K) of the Complex Formation of the Free and Immobilized β-CyD with Nitrophenols at 25 °C

Immobilized β-CyD[a]	Crosslinking reagent[b]	m[c]	$K/mol^{-1}\,dm^3$					
			ortho		meta		para	
			pH 4	pH 10	pH 4	pH 10	pH 4	pH 10
I-1	A (n=2)	4.5	432	12	115	35	142	128
I-2	A (n=4)	4.6	294	12	87	40	112	149
I-3a	A (n=6)	4.5	897	10	268	27	262	50
III	C	3.9	215	33	151	114	161	646
β-CyD	—	—	338	826	204	238	218	164

a) See Table 1 for abbreviation. b) See Fig. 1 for the chemical structures. c) m: Degree of crosslinking.

Table 4. The Equilibrium Constant (K) of the Complex Formation of the Free and Immobilized β-CyD with 2-Naphthol at 25 °C

Immobilized β-CyD[a]	Crosslinking reagent[b]	m[c]	$K/mol^{-1}\,dm^3$	
			2-Naphthol	
			pH 4	pH 10
I-1	A (n=2)	4.5	339	269
I-2	A (n=4)	4.6	324	100
I-3a	A (n=6)	4.5	1460	883
III	C	3.9	159	211
β-CyD	—	—	721	459

a) See Table 1 for abbreviation. b) See Fig. 1 for the chemical structures. c) m: Degree of crosslonking.

Table 5. The Equilibrium Constant (K) of the Complex Formation of the Three Kinds of Immobilized β-CyD (I-3) Prepared by Crosslinking with 1,6-Hexanediol Diglycidyl Ether with Three Isomers of Cresol as the Guest Molecules at 25 °C

Immobilized β-CyD[a]	m[b]	$K/mol^{-1}\,dm^3$					
		ortho		meta		para	
		pH 4	pH 11	pH 4	pH 11	pH 4	pH 11
I-3a	4.5	167	56	167	21	165	29
I-3b	5.0	169	40	149	32	150	40
I-3c	5.8	385	58	252	17	289	29

a) See Table 1 for abbreviation. b) m: Degree of crosslinking.

using the immobilized β-CyDs which are crosslinked by 1,6-hexanediol diglycidyl ether and cresols as a guest molecule. The results are summarized in Table 5.

Discussion

Preparation of Immobilized β-CyDs. Immobilization of β-CyD was successfully performed by using various crosslinking reagents. These macromolecules involve no nitrogen atoms (amines and/or amides) in the linkage. The results of the IR spectra of the immobilized CyDs are in good agreement with the immobilizing reactions shown in Scheme 1. The specific absorptions of the CyD residue in the IR spectra indicate that the structure of CyD is maintained in the immobilized CyD macromolecule. The absence of the absorption bands due to an epoxy ring and a chloromethyl group indicates that the immobilizing reaction proceeds the nucleophilic attack by the hydroxyl group of β-CyD to the epoxy ring and the chloromethyl group. The insolubility of the immobilized CyD in water suggests that the macromolecule has a tangly network composed of crosslinking residues and CyD residues. Since the CyD residues have many hydroxyl groups, in fact the strong IR absorptions due to the hydroxyl groups are observed, the crosslinked macromolecules are able to swell in water.

The number of the crosslinking residues which can bind to one CyD residue (m) is 3—6, as shown in Table 1. Harada et al. reported that the substitution of the secondary hydroxyl groups by the crosslinking residues was observed in the ^{13}C NMR spectrum of the epichlorohydrin-immobilized CyD.[11] In general, however, the reactivity of the primary hydroxyl group of CyD is thought to be much higher than that of the secondary hydroxyl group of CyD.[12] In the immobilizing reactions examined here, some parts of the crosslinking residue probably bind to the secondary hydroxyl group of CyD (as the case reported before[11]), besides the primary one, because of the present severe reaction conditions with extraordinarily high concentration of sodium hydroxide. The immobilized β-CyDs I-3a, 3b, and 3c shown in Table 1 were prepared by the same crosslinking reagent (1,6-hexanediol diglycidyl ether). The charged molar ratio of the crosslinking reagent to β-CyD is the same for I-3a and I-3c, and other reaction conditions are similar to each other. The resulting immobilized β-CyDs, however, exhibit different values of the degree of crosslinking. This is probably due to the heterogeneity of the reaction system. For instance the addition rate of the crosslinking reagents and the stirring rate of the mixtures may be effective for the constitution of the macromolecules in the heterogeneous system. In case of the macromolecule I-3b, the charged molar ratio of the crosslinking reagent was 7.5 times to CyD, and less than those for I-3a and I-3c. The degree of crosslinking, however, exhibits 5.0 which is higher than that of I-3a. This reverse phenomena would be explained by the longer reaction time for I-3b. The difference in their inclusion properties will be discussed later.

Complex Formation of the Immobilized β-CyD. From the data in Tables 2, 3, and 4, one can conclude the general tendency for the complex formation. 1) The different crosslinking residues result in a different equilibrium constant K. This indicates that the crosslinking residues affect the complex formation. 2) The long crosslinking residue which has long hydrophobic moieties (A n=6) results in a large equilibrium constant, especially at pH 4. This indicates that the hydrophobic residue plays an important role in complex formation. 3) The equilibrium constant K at pH 4 is generally larger than that at pH 10 or 11. In a pH 4 buffer solution, the guest molecules are electrically neutral, while in pH 10 or 11 they are anionic, since the pK_a values of nitrophenols, cresols, and phenol are 8.0—9.3, 10.0—10.3, and 9.8, respectively. The hydroxyl group of CyD cannot dissociate into ionic species under these conditions since the pK_a of CyD is more than 12.[1] Therefore, the present result of the larger K value at pH 4 than at pH 10 or 11 indicates that the immobilized CyDs include the neutral guest molecule strongly in its hydrophobic cavity and do the anionic molecule weakly. In other words, the hydrophobic interaction is very important for inclusion complex formation.

In order to clarify the importance of the hydrophobic interaction between the crosslinking residues and guest molecules, the relation between the degree of crosslinking and the equilibrium constant K was investigated. Three types of immobilized CyDs exhibiting different degrees of crosslinking were synthesized by using 1,6-hexanediol diglycidyl ether as a crosslinking reagent. The equilibrium constants were measured for these three kinds of immobilized CyDs against cresols as guest molecules, since cresol is considered to be a proper guest molecule in order to examine the hydrophobic interaction between the guest molecule and the new binding site composed of the CyD cavity and the crosslinking residue.

In general, the hydrophobic modifying residue of CyD can affect the inclusion complex formation of the modified CyD with a guest molecule in various ways. From a micro point of view, two kinds of effects can be reasonably considered: 1) The hydrophobic modifying residue is competitively included in the cavity of CyD[13,14] so as to inhibit the inclusion of a guest molecule, resulting in the decrease of the equilibrium constant K. 2) The hydrophobic modifying residue forms a cap and/or a floor of the CyD cavity[15] so as to promote the inclusion complex formation by the

cavity, resulting in the increase of K. From a macro point of view, the other two kinds of effects are also considered: 3) The modifying residue can reduce the flexibility of the CyD residue and the movement of the guest molecule near the CyD cavity by the steric hindrance so as to hinder the inclusion complex formation,[1] resulting in the decrease of K. 4) The hydrophobic environment composed of the modifying residue can interact with a hydrophobic guest molecule so as to increase the local concentration of the guest molecule or the frequency factor of the complex formation,[16] resulting in the increase of K.

As shown in Table 5, the K value of I-3c (m=5.8) at pH 4 is much larger than those of I-3a and I-3b (m=4.5 and 5.0, respectively). From the general considerations described above, this result can be explained by the larger contribution of 2) and/or 4) than 1) and/or 3). In other words, the hydrophobic crosslinking residues in the macromolecules do enhance the complex formation with the hydrophobic guest molecules in the micro and/or macro ways.

In a preliminary communication,[10a] we reported that the K values of the 1,2-ethanediol diglycidyl ether-immobilized CyDs with the different degree of crosslinking (m=3.1 and 5.9) for p-nitrophenol are not so different from each other (K=130 and 119 mol^{-1} dm^3, respectively). This is considered to be a rather special case, since p-nitrophenol is known to interact with the CyD cavity[1] in a special way, for instance, the dipole–dipole interaction[1,17] and the crosslinking residue of 1,2-ethanediol diglycidyl ether is rather hydrophilic.

Evaluation of the Hydrophobic Coefficients of the Immobilized β-CyD. As described above, the CyD residue and the crosslinking residue in the immobilized CyD coopetate to form an inclusion complex. The crosslinking residue can affect the complex formation not only by the so-called "general polymer effect" but also by altering the quality of the binding site. To distinguish these two factors, further analysis of the equilibrium constant K was attempted by comparing the complex formation property of free CyD with that of the immobilized CyD.

A direct comparison of the K values of free and immobilized CyD for the same guest molecule under the same pH condition reflects not only the effect of the crosslinking residue to alter the complex formation ability of the CyD residue but also the other contribution of the crosslinking or "general polymer effect," for example, the effect on the diffusion of the guest molecule to access to the binding site of the CyD residue, the swelling property of the immobilized CyD, the degree of freedom of the CyD residue, and so on. These varieties of "general polymer effects" by the crosslinking residue conceal the pure property of the binding site in the immobilized CyD. To compensate this disturbance, a concept of the hydrophobic enhancement coefficient R is introduced.

The hydrophobicities of the free CyD and the immobilized CyDs can be estimated by the ratio of the corresponding K value at pH 4 to that at pH 10 (or 11), since the guest molecule is neutral or hydrophobic at pH 4 and anionic or hydrophilic at pH 10 (or 11). The influence of the crosslinking residue to the complex formation property of the CyD residue can be evaluated by the increase of the hydrophobicity by crosslinking.

On the basis of the above consideration, the hydrophobic enhancement coefficient R is defined by

$$R = \frac{K_{imm}(\text{pH 4})}{K_{imm}(\text{pH 10 of 11})} \Big/ \frac{K_{free}(\text{pH 4})}{K_{free}(\text{pH 10 or 11})}, \quad (3)$$

where K_{imm} and K_{free} are the equilibrium constants of complex formation of the immobilized β-CyDs and the free β-CyD, respectively. The ratio K_{imm}(pH 4)/K_{imm}(pH 10 or 11) indicates the ability of the immobilized CyD to discriminate a neutral guest molecule from an anionic one, reflecting the property of the hydrophobic field composed of the crosslinking residues and the CyD residue. (This hydrophobic field binds the hydrophobic part of guest molecule and repulses the anionic part of guest molecule.) In the similar way, the ratio K_{free}(pH 4)/K_{free}(pH 10 or 11) indicates the ability of free CyD to discriminate a neutral from an anionic. (This original property will be altered by the crosslinking.) In short, the ratios K_{imm}(pH 4)/K_{imm}(pH 10 or 11) and K_{free}(pH 4)/K_{free}(pH 10 or 11) reflect the hydrophobicity of the immobilized and free CyD, respectively. Thus, the ratio of these two ratios is the hydrophobic enhancement coefficient by crosslinking (R), which indicates how the crosslinking affects on

Table 6. The Hydrophobic Enhancement Coefficient (R) for Cresols and Phenol

Immobilized β-CyD[a]	Crosslinking reagent[b]	R[c]			
		Cresol			Phenol
		ortho	meta	para	
I-1	A (n=2)	4.2	0.6	1.4	1.7
I-2	A (n=4)	6.9	0.4	1.5	1.9
I-3a	A (n=6)	3.0	2.2	1.7	1.3
III	C	7.5	0.5	2.0	2.4

a) See Table 1 for abbreviation. b) See Fig. 1 for the chemical structures. c) The coefficient R is calculated by the Eq. 3 in the text.

the property of the CyD binding site.

Table 6 lists the enhancement coefficients R which are calculated by using the K values listed in Table 3 according to the Eq. 3. It is surprising that the actual R values change to a great extent depending on the kind of the guest molecule but do not change with the kind of the crosslinking residues. In fact, they are 3.0—7.5 for *o*-cresol, 0.4—0.6 for *m*-cresol (except I-3a), 1.4—2.0 for *p*-cresol, and 1.3—2.4 for phenol. The coefficients Rs for *o*-cresol are largest among these, which means that the immobilization enhances the hydrophobicity of the CyD binding site so that the ability of CyD to discriminate *o*-cresol from *o*-cresolate is strengthened by the immobilization. For *p*-cresol and phenol, the Rs are larger than 1 but smaller than those for *o*-cresol, which means that the above ability is strengthened a little. For *m*-cresol, in contrast with other three guests, the Rs are smaller than 1 (except for I-3a), meaning that the ability of CyD to discriminate *m*-cresol from *m*-cresolate is weakened by the crosslinking. This large dependence of the R values on the guest molecule and the slight dependence of the crosslinking residue suggest that the quality of the effect of the crosslinking residue on the binding site alters with the structure of a guest molecule. In other words, the interaction between the crosslinking residue and the guest molecule may vary with the steric structure of the included guest molecule.

This might be explained in, for example, the following way: the crosslinking residue can form a cap and/or a floor of the CyD residue in the immobilized CyD.[11,15] The main interaction between the immobilized CyDs and cresols is a hydrophobic interaction. The most hydrophobic part of a cresol molecule is the methyl group and, then, the benzene ring.[18] Under the condition of pH 4, the CyD cavity includes these hydrophobic parts of a guest molecule, and the hydroxyl groups of the host and the guest molecules may interact with each other through hydrogen bonding. At pH 11 the hydrophobic interaction works in a similar way as that described above, even though the difference between the strengths of the interactions at pH 4 and at pH 11 is unknown. However, repulsion may arise between the anionic oxygen of cresolate and the hydrophobic field composed of the CyD residue and the crosslinking residue. The former hydrophobic interaction can promote a deep inclusion of cresolates into the CyD cavity at the position of the methyl group and the benzene ring. The latter repulsion, however, can make the anionic oxygen of the cresolates far from the CyD cavity or the hydrophobic crosslinking residue.

If these two effects, a hydrophobic interaction and a repulsion, cooperatively work to make the actual R value different from each other, depending on the isomers of cresolate, the structures of the inclusion complexes of the isomers are possibly illustrated as shown in Fig. 2. In the case of *o*-cresolate ($R \gg 1$), the methyl group of *o*-cresolate inhibits a deep inclusion of the benzene ring because of a steric hindrance, so that the anioic oxygen may be compelled to locate near the hydrophobic crosslinking residue which forms a cap or a floor for the CyD cavity. This situation can induce a strong repulsion between the anionic oxygen and the crosslinking residue, which results in the large R values for *o*-cresol. For *p*-cresolate, and phenolate ($R>1$), the inclusion may be deeper than that of *o*-cresolate so that the repulsion may exist but being weaker than that for *o*-cresolate. This results in the larger R values for *p*-cresol and phenol than 1, but smaller than those for *o*-cresol. On the contrary, the inclusion of *m*-cresolate ($R<1$) may be achieved by the structure shown in Fig. 2(b), where the methyl group of *m*-cresolate is deeply included in the CyD cavity. However, the anionic oxygen may be able to avoid the hydrophobic crosslinking residue. In this structure, the interaction between the benzene ring of the guest molecule and the hydrophobic crosslinking residue of the immobilized CyD may become favorable, resulting in the strengthening of the inclusion of the guest molecule by capping the CyD cavity with the crosslinking residue. These interactions, as a whole, result in the small R values for *m*-cresol. In the case of macromolecule I-3a (crosslinked by 1,6-hexanediol diglycidyl ether), the R for *m*-cresol is 2.2, which is exceptionally large. This peculiarity is probably derived from a strong hydrophobic field composed of a long hydrophobic residue of this macromolecule, resulting in the strong repulsion between the anionic oxygen of *m*-cresolate and the binding site of the immobilized CyD. The hydrophobic field may be so large that even for *m*-cresol R is larger than 1.

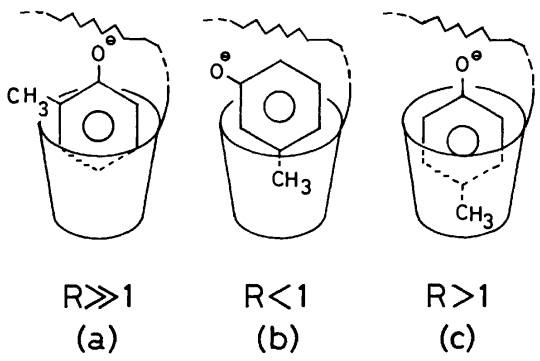

Fig. 2. Proposed structures of the complexes of the immobilized β-CyD, with *o*-, *m*-, and *p*-cresol.

The hydrophobic enhancement coefficients Rs for nitrophenols and 2-naphthol are listed in Table 7, respectively. Here again, the R value changes with the guest molecule and not so much with the crosslinking reagent. In the case of nitrophenols, the R values for the ortho-isomer is quite large in the order of the

Table 7. The Hydrophobic Enhancement Coefficient (R) for Nitrophenols and 2-Naphthol

Immobilized β-CyD[a]	Crosslinking reagent[b]	R[c]			
		Nitrophenol			2-Naphthol
		ortho	meta	para	
I-1	A (n=2)	90	3.7	0.9	0.8
I-2	A (n=4)	61	2.4	0.6	2.1
I-3a	A (n=6)	225	11.0	4.0	1.1
III	C	16	1.4	0.2	0.5

a) See Table 1 for abbreviation. b) See Fig. 1 for the chemical structures. c) The coefficient R is calculated by the Eq. 3 in the text.

magnitude of R, ortho≫meta>1>para, except for the case of the macromolecule I-3a (crosslinked by 1,6-hexanediol diglycidyl ether) for *p*-nitrophenol. It is known that a nitro group is deeply included in a CyD cavity and, in consequence, plays an important part for the inclusion complex formation.[1,17] According to the results of two-dimensional NMR studies using a nuclear Overhauser effect (NOESY), the nitro groups of *m*- and *p*-nitrophenol are suggested to be included in the CyD cavity from the secondary hydroxyl side (the wide side) of the CyD cavity; in contrast with these two guests, the nitro group of *o*-nitrophenol will be included in the cavity from the primary hydroxyl side (the narrow side) of the CyD cavity.[19] This suggests that in the immobilized CyD *o*-nitrophenol may locate near the narrow side of a CyD residue which is connected by the crosslinking residues to form a crowded and strong hydrophobic field; in consequence there may be a strong repulsion resulting in the very large R values.

For *m*- and *p*-nitrophenol, the order of the R values is reverse to that for *m*- and *p*-cresol. Though the reason is unknown there may be a special participation of the nitro group, since the interaction of the nitro group with CyD cavity can not be explained only by hydrophobic interaction and hydrogen bonding.[17]

For 2-naphthol the R is rather near unity. This might be due to the fact that the main interaction between the binding site and 2-naphthol is a hydrophobic interaction.

Conclusion

1. Many kinds of immobilized β-CyDs can be successfully synthesized as solid products by crosslinking β-CyD with six kinds of crosslinking reagents. The immobilized β-CyD prepared in the present investigations involves no nitrogen atoms (amines and/or amides) in the linkage. The degree of crosslinking was 3.6—5.8 on the basis of the elemental analysis.

2. The equilibrium constants Ks of the immobilized β-CyDs were determined for cresols, phenol, nitrophenols, and 2-naphthol. The independence of K from the amount of immobilized CyD indicates 1:1 complex formation between the CyD residue and the guest molecule.

3. The K values measured at pH 4 (a neutral guest) are generally larger than those measured at pH 10 or 11 (an anionic guest). The K values reflect the property of the crosslinking residue, indicating the participation of the crosslinking residue to the inclusion complex formation. Macromolecules containing the long crosslinking residues (I-3a, 3b, and 3c) exhibit large K values, which indicate the existence of a hydrophobic interaction between the crosslinking residue and the guest molecule. A high degree of crosslinking results in the large K values, indicating that the crosslinking residue promotes complex formation but does not inhibit it.

4. A hydrophobic enhancement coefficient R has been introduced. The R values indicate how the crosslinking residue effects on the property of the binding site for complex formation. The R values calculated from the K constants are independent of the crosslinking reagents, but dependent on the structure of the guest molecule, suggesting the expected potential for high guest selectivity of the immobilized CyD.

The authors would like to thank Mr. Katagiri for his technical assistance. The author (I. S.) would like to express his grateful thanks for the Fellowship of the Japan Society for the Promotion of Science for Japanese Junior Scientists.

References

1) M. L. Bender and M. Komiyama. "Cyclodextrin Chemistry," Springer-Verlag, Berlin (1978).

2) a) D. W. Armstrong, W. DeMond, and B. P. Czech, *Anal. Chem.*, **57**, 481 (1985), and the references cited therein; b) A. Harada, M. Furue, and S. Nozakura, *J. Polym. Sci., Polym. Chem. Ed.*, **16**, 189 (1978); c) M. Tanaka, Y. Mizobuchi, T. Sonoda, and T. Shono, *Anal. Lett.*, **14(A4)**, 281 (1981); d) K. Takahashi, S. Nakada, M. Mikami, and K. Hattori, *Nippon Kagaku Kaishi*, **1986**, 1032.

3) a) R. L. VanEtten, G. A. Clowes, J. F. Sebastian, and M. L. Bender, *J. Am. Chem. Soc.*, **89**, 3253 (1967); b) R. L. VanEtten, J. F. Sebastian, G. A. Clowes, and M. L. Bender, *ibid.*, **89**, 3242 (1967).

4) a) T. Ikeda, R. Kojin, C-J. Yoon, H. Ikeda, M. Iijima, K. Hattori, and F. Toda, *J. Incl. Phenom.*, **2**, 669 (1984); b) C-J. Yoon, H. Ikeda, R. Kojin, T. Ikeda, and F. Toda, *J. Chem. Soc., Chem. Commun.*, **1986**, 1080.

5) R. Breslow and P. Campbell, *J. Am. Chem. Soc.*, **91**, 3085 (1969).

6) a) I. Tabushi, K. Fujita, and H. Kawakubo, *J. Am. Chem. Soc.*, **99**, 6456 (1977); b) I. Tabushi, K. Yamamura, K. Fujita, and H. Kawakubo, *ibid.*, **101**, 1019 (1979).

7) M. Komiyama and H. Hirai, *J. Am. Chem. Soc.*, **106**, 174 (1984).

8) a) M. Komiyama, I. Sugiura, and H. Hirai, *J. Incl. Phenom.*, **2**, 823 (1984); b) M. Komiyama, I. Sugiura, and H. Hirai, *Polym. J.*, **17**, 1225 (1985); c) M. Komiyama, I. Sugiura, and H. Hirai, *J. Mol. Catal.*, **36**, 271 (1986).

9) a) C. U. Pittman, Jr., L. R. Smith, and R. M. Hanes, *J. Am. Chem. Soc.*, **97**, 1742 (1975); b) T. Mukaiyama and H. Iwakiri, *Chem. Lett.*, **1985**, 1363; c) H. Hirai and N. Toshima Ed. "Kobunshi Sakutai Shokubai, (Macromolecular Complex Catalysts)," Japan Scientific Societies Press, Tokyo (1982).

10) a) M. Komiyama and H. Hirai, *Polym. J.*, **19**, 773 (1987); b) M. Komiyama, I. Sugiura, and H. Hirai, *J. Coord. Chem.*, **18**, 181 (1988); c) I. Sugiura, K. Kawamura, N. Toshima, and K. Komiyama, *Polymer Preprints, Japan* **37**, No. 10, 3423 (1988).

11) A. Harada, M. Furue, and S. Nozakura, *Polym. J.*, **13**, 777 (1981).

12) For example, S. Umezawa and K. Tatsuta, *Bull. Chem. Soc. Jpn.*, **41**, 464 (1968).

13) H. Schlenk and D. M. Sand, *J. Am. Chem. Soc.*, **83**, 2312 (1961).

14) A. Ueno, F. Moriwaki, T. Osa, F. Hamada, and K. Murai, *J. Am. Chem. Soc.*, **110**, 4323 (1988).

15) a) J. Emert and R. Breslow, *J. Am. Chem. Soc.*, **97**, 670 (1975); b) I. Tabushi, K. Shimokawa, N. Shimizu, H. Shirakata, and K. Fujita, *J. Am. Chem. Soc.*, **98**, 7855 (1976).

16) a) I. Sakurada, Y. Sakaguchi, T. Ono, and T. Ueda, *Makromol. Chem.*, **91**, 243 (1966); b) S. Yoshikawa and O-K. Kim, *Bull. Chem. Soc. Jpn.*, **39**, 1515 (1966); c) C. G. Overberger, R. Corett, J. C. Salamone, and S. Yaroslavsky, *Macromolecules*, **1**, 331 (1968); d) T. Kunitake, F. Shimada, and C. Aso, *J. Am. Chem. Soc.*, **91**, 2716 (1969).

17) M. Kitagawa, H. Hoshi, M. Sakurai, Y. Inoue, and R. Chujo, *Carbohydr. Res.*, **163**, C1 (1987).

18) I. Sanemasa and Y. Akamine, *Bull. Chem. Soc. Jpn.*, **60**, 2059 (1987).

19) K. Kawamura, N. Toshima, and H. Hirai, 57th National Meeting of the Chemical Society of Japan, Sendai, September 1988, Abstr. I, No. 1G215.

Oxidation of Methoxy- and/or Methyl-Substituted Benzenes and Naphthalenes to Quinones and Phenols by H_2O_2 in HCOOH

Hideo ORITA,* Masao SHIMIZU, Takashi HAYAKAWA, and Katsuomi TAKEHIRA
National Chemical Laboratory for Industry, Tsukuba, Ibaraki 305
(Received November 25, 1988)

The oxidation of a number of arenes (methoxybenzenes, methylbenzenes, and naphthalenes) to quinones and phenols by H_2O_2 in HCOOH has been examined. Methoxybenzenes were much more easily oxidized to *p*-benzoquinones than methylbenzenes (e.g., 1,3,5-trimethoxybenzene was oxidized to 2,6-dimethoxy-*p*-benzoquinone in a 75% yield and 1,2,4-trimethylbenzene to 2,3,5-trimethyl-*p*-benzoquinone in a 16% yield). Electron-withdrawing substituents, such as nitro, cyano, and chloro groups, lowered the conversion of reactants and changed the product selectivity from quinones to phenols. Methoxybenzonitriles were oxidized to corresponding phenols in a moderate yield (e.g., 2,6-dimethoxybenzonitrile to 3-hydroxy-2,6-dimethoxybenzonitrile in a 39% yield and a 64% selectivity).

Hydrogen peroxide is an economical and clean oxidant whose waste product is only water, and can oxidize a variety of organic substrates including arenes in the presence of catalysts. However, there are few applications to organic synthesis, excepting some examples such as the manufacturing of catechol and hydroquinone from phenol.

Some of quinones are naturally occurring materials with biological activities,[1] and are the key intermediates of medicines. For example, trimethyl-*p*-benzoquinone is key compound in synthesis of vitamin E, and 2,3-dimethoxy-5-methyl-*p*-benzoquinone is useful for production of coenzyme Q, and 2-methyl-1,4-naphthoquinone is the simplest synthesized vitamin K (vitamin K_3) and used for producing vitamin K_1.[2] On the other hand, there are few papers on the direct oxidation of arenes to quinones by H_2O_2.[3-5] Ito et al.[3] reported that $RuCl_3$ catalyzed the oxidation of trimethylphenol in acidic medium to trimethyl-*p*-benzoquinone in a high yield. In this case, the high cost of $RuCl_3$ requires its recovery for practical use, which is difficult in homogeneous system. Matsumoto et al.[4] showed that trimethoxybenzenes were oxidized to dimethoxy-*p*-benzoquinones by H_2O_2 in the presence of hexacyanoferrate(II or III) ion, which is harmful. A palladium catalyst supported on sulfonated polystyrene type resins was used for the oxidation of methylbenzenes and naphthalenes.[5] Naphthalenes were oxidized to naphthoquinones in fairly good yields, but methylbenzenes gave *p*-benzoquinones in poor yields of 3—8%.

In the present work, we have investigated the oxidation of arenes (methoxybenzenes, methylbenzenes, and naphthalenes) by H_2O_2 in HCOOH. The reaction rates and selectivity were very dependent on the substituents on aromatic ring. Electron-withdrawing substituents slowed down the reaction and changed the product selectivity from quinones to phenols.

Experimental

Reagents and Apparatus. 3,5-Dimethoxytoluene was prepared by the published procedure.[6] All other reagents were commercial products of the highest purity obtainable. Infrared (IR) spectra were measured by a JASCO FT/IR-7000 spectrometer. Mass spectra were recorded at 70 eV on a Shimadzu GCMS-QP 1000 mass spectrometer. A Hitachi R-40 (90 MHz) spectrometer was used to obtain ^1H nuclear magnetic resonance (NMR) spectra.

General Procedure for Oxidation of Arenes by H_2O_2. Aqueous hydrogen peroxide (31%, 2 ml, ca. 20 mmol) was added to a solution of an arene (4 mmol) in formic acid (10 ml). The reaction mixture was stirred for 1—24 h (usually 2 h) at a desired temperature (30—50 °C) under nitrogen atmosphere. The solution was poured into water and the products were extracted with CH_2Cl_2. The organic layer was washed with water, and dried with $MgSO_4$. Generally, the products were analyzed by gas chromatography using a Thermon 3000 column (10% on Celite 545, 1 m, thermal conductivity detector) and *o*-dichlorobenzene as an internal standard. Some quinones (e.g., 2,5- and 2,6-dimethoxy-*p*-benzoquinone) are not well soluble in either H_2O or CH_2Cl_2. In these cases, the extracted organic solution was evaporated and the residue was rinsed with methanol or hexane to separate crystals of a quinone. The organic solution was analyzed by gas chromatography to determine the conversion of a reactant. The identification of products was carried out by means of ^1H NMR and/or FT-IR after separation by column (Merck, silica gel 60) and/or thin-layer (Whatman, silica gel 150A, PLK5F) chromatography. The products were also identified by GC-MS.

Results and Discussion

Oxidation of Methoxybenzenes. Various methoxybenzenes (methoxytoluenes, dimethoxybenzenes, dimethoxytoluenes, trimethoxybenzenes, and trimethoxytoluenes) were oxidized by H_2O_2 in HCOOH, and the results are tabulated in Table 1. Generally, *p*-benzoquinones were obtained as main products in relatively good yields, but some phenols were produced occasionally in small yields (Runs 3 and 8). When the para-position for methoxyl group is not substituted, a *p*-benzoquinone which has one less methoxyl group than the starting methoxybenzene is obtained as a main product. 3,4,5-Trimethoxyphenol was oxidized to 2,6-dimethoxy-*p*-benzoquinone under the same re-

Table 1. Oxidation of Methoxybenzenes by H_2O_2 in HCOOH

No.	Temp	Time	H_2O_2 aq.		Reactant	Conv.	Product	Yield	Sel.
	°C	h	wt%	ml		%		%	%
1	40	2	31	2	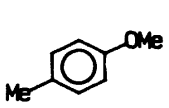	85	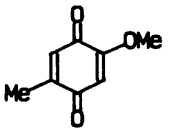	40	47
2	40	2	31	1	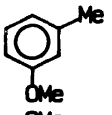	83	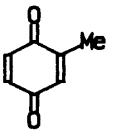	30	36
3	40	2	31	1	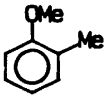	68	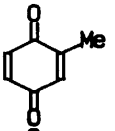	11	16
							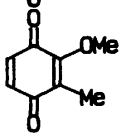	6	9
							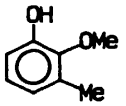	7	10
4	40	2	31	2	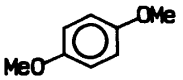	98	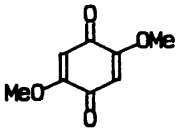	29	30
5	40	2	31	1	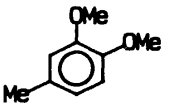	96	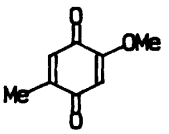	68	70
							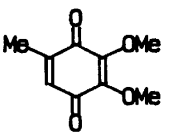	3	3
6	40	2	31	2	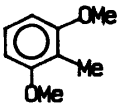	100	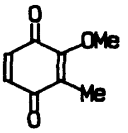	12	12
7	40	2	31	2	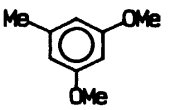	100	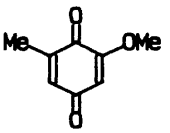	65	65

action conditions (Run 16). Therefore, the oxidation yielding quinones probably proceeds through the corresponding phenols which are produced by the hydroxylation of benzene ring at the para-position for methoxyl group, as proposed previously.[4] If the para-position for methoxyl group is substituted (Runs 1 and 4), a corresponding *p*-benzoquinone without loss of methoxyl group is obtained. It is considered that these quinones are produced through the hydroxylation of benzene ring at the ortho-position for methoxyl group followed by the further oxidation of phenols. Under the present reaction conditions, 1,2,3-substituted benzenes gave a poor yield of quinones (Runs 6, 8, and 11). These poor yields of quinones can be explained as follows: two hydroxyl groups can be introduced very easily at the para-positions for the two methoxyl groups before the oxidation to a quinone occurs, because these positions are not crowded sterically, and the further oxidation of these hydroxylated compounds proceeds rapidly. In Run 8, 2-hydroxy-5-methoxy-3-

Table 1. (Continued)

No.	Temp °C	Time h	H_2O_2 aq. wt%	H_2O_2 aq. ml	Reactant	Conv. %	Product	Yield %	Sel. %
8	40	2	31	1	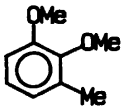	63	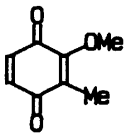	4	6
							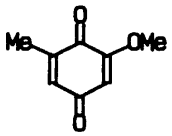	9	14
							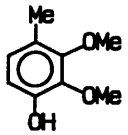	5	8
							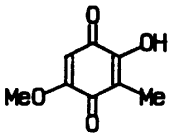	27	42
9	40	2	31	1	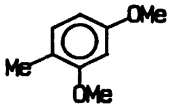	93	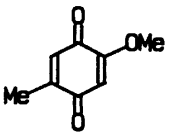	72	77
10	40	2	31	2	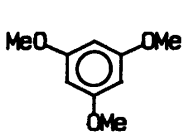	100	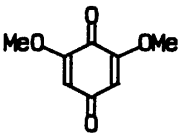	75	75
11	30	2	31	1	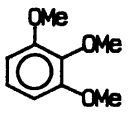	83	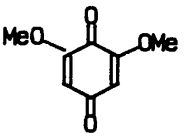	10	12
							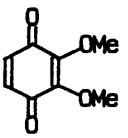	6	7
12	40	2	31	2	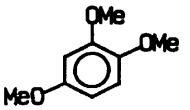	100	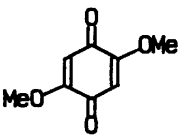	45	45

methyl-*p*-benzoquinone was obtained in a moderate yield, which is considered to form through the oxidation of 2,3-dihydroxy-5,6-dimethoxytoluene as the intermediate. On the other hand, 1,2,4-, 1,3,4-, or 1,3,5-substituted benzenes gave a good yield of corresponding *p*-benzoquinones (Runs 5, 7, 9, 10, and 12). In these cases, it is considered that only one hydroxyl group can be introduced into benzene ring, because the para-positions for methoxyl groups are crowded, and that the oxidation yielding quinones proceeds smoothly. When the reaction was carried out in methanol or acetonitrile, no quinone was obtained. The oxidation of 3,4,5-trimethoxytoluene in acetic acid gave only a 4% yield of 2,3-dimethoxy-5-methyl-*p*-benzoquinone at a 40% conversion (cf. Run 13). The active species of this reaction system is not clear at the present stage, but the most probable candidate is performic acid which is produced in situ from the reaction with H_2O_2.

Oxidation of Methylbenzenes and Naphthalenes. Oxidation of methylbenzenes and naphthalenes by H_2O_2 in HCOOH was also examined, and the results are shown in Table 2. Methylbenzenes were oxidized to

Table 1. (Continued)

No.	Temp	Time	H_2O_2aq.		Reactant	Conv.	Product	Yield	Sel.
	°C	h	wt%	ml		%		%	%
13	30	1	31	1	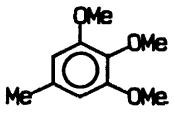	97	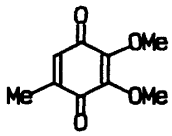	48	49
14	40	2	31	1	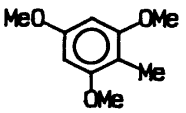	97	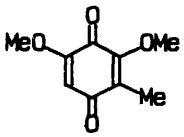	46	47
15	40	1	31	1	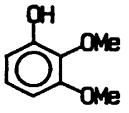	80	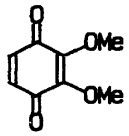	27	34
16	40	1	31	1	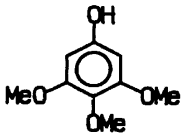	—[a]	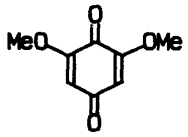	61	—[a]

Reactant 4 mmol, HCOOH 10 ml. a) Not measured.

Table 2. Oxidation of Methylbenzenes and Naphthalenes to Quinone by H_2O_2 in HCOOH

No.	Temp	Time	H_2O_2aq.		Reactant	Conv.	Product	Yield	Sel.
	°C	h	wt%	ml		%		%	%
1	50	6	60	2	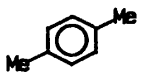	96	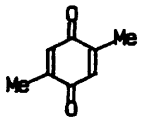	19	20
2	50	4	60	1	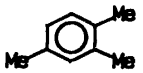	100	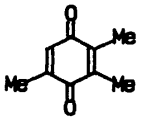	16	16
3	50	5	31	2	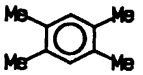	96	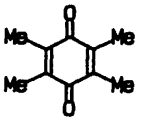	19	20
4[a]	40	4.5	31	2		43	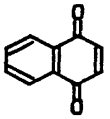	12	28
5[a]	40	4	31	2		86	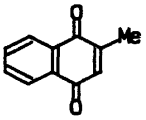	22	26
6[a]	40	2	31	2	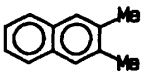	92	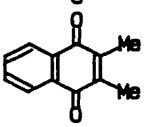	52	57

Reactant 4 mmol, HCOOH 10 ml. a) HCOOH 10 ml+AcOH 10 ml.

Table 3. Oxidation of Methoxybenzonitriles to Phenols by H_2O_2 in HCOOH

No.	Temp	Time	H_2O_2 aq.		Reactant	Conv.	Product	Yield	Sel.
	°C	h	wt%	ml		%		%	%
1	40	4	31	2	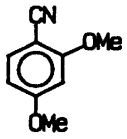	59	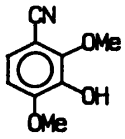	10	17
							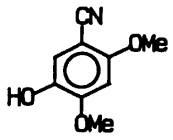	18	31
2	40	2	31	1	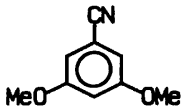	35	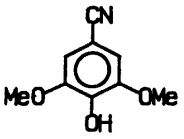	4	11
							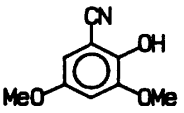	10	29
3	40	2	31	2	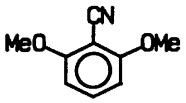	61	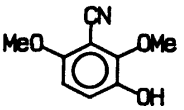	39	64
4	40	2	31	2	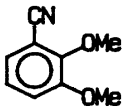	0	—		
5	40	24	31	2	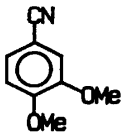	0	—		
6	40	4	31	2	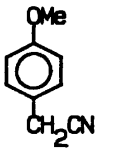	17	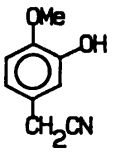	7	41

Reactant 4 mmol, HCOOH 10 ml.

corresponding quinones, but the yields were rather poor, and higher temperature and concentration of H_2O_2 were required. Many unidentified by-products which probably formed through the oxidation of methyl groups were observed with GC-MS. The yield of quinones was not dependent on the number of methyl groups in benzenes, but increased with the number of methyl groups in naphthalenes (the solubility of naphthalenes in HCOOH is small, and so the mixed solvent of formic and acetic acid was used).

Oxidation of Benzenes Substituted with Electron-Withdrawing Groups. The effect of electron-withdrawing groups such as cyano, nitro, and chloro groups on the reaction was investigated, and Table 3 lists the results of oxidation of methoxybenzonitriles. In these cases, phenols were obtained as main products, but quinones were not. When one cyano group is introduced into benzene ring, the conversion of reactants decreased up to about 60% (e.g., compare Runs 5, 9, and 12 in Table 1 with Run 1 in Table 3). Some dimethoxybenzonitriles did not give phenols in a yield more than 1% and the conversion of benzonitriles was negligible (Runs 4 and 5). The hydroxyl group is introduced only at the positions where resonance effect of both two methoxyl groups is working (i.e., the ortho- and ortho-, or para- and ortho-position for either methoxyl group). Therefore, it is considered that cyano group reduces the reactivity of methoxybenzenes by decreasing electron density of benzene ring (one cyano group effectively cancels the reactivity en-

hancement originated from resonance effect of one methoxyl group), and it inhibits the further oxidation of phenols to quinones.

Nitro group also retarded the oxidation greatly and only a trace of phenols was obtained. In the case for chloro group, which is a weak electron-withdrawing substituent and shows ortho-para-orientation in electrophilic aromatic substitutions, chloroanisoles were oxidized to phenols. For example, *m*-chloroanisole was oxidized to three isomers of phenols in a 19% yield at a 35% conversion (hydroxyl group is introduced at two ortho- and one para-positions for methoxyl group at approximate ratio of 1:1:1). Accordingly, the electron-withdrawing substituents decrease the reactivity of benzene ring with H_2O_2 in HCOOH and inhibits the further oxidation of phenols to quinones.

References

1) H. Otsuka, T. Komiya, S. Fujioka, M. Goto, Y. Hiramatsu, and H. Fujimura, *Yakugaku Zasshi*, **101**, 1108 (1981).

2) S. Yamada, T. Takeshita, and J. Tanaka, *Yuki Gosei Kagaku Kyokai Shi*, **40**, 268 (1982).

3) S. Ito, K. Aihara, and M. Matsumoto, *Tetrahedron Lett.*, **24**, 5249 (1983).

4) M. Matsumoto, H. Kobayashi, and Y. Hotta, *J. Org. Chem.*, **50**, 1766 (1985).

5) S. Yamaguchi, M. Inoue, and S. Enomoto, *Bull. Chem. Soc. Jpn.*, **59**, 2881 (1986).

6) R. N. Mirrington and G. I. Feutrill, *Org. Synth.*, **53**, 90 (1973).

The Determination of the Selectivity Coefficient of Na^+ versus Li^+ on Prussian Blue Thin Film in Propylene Carbonate by Means of a Quartz Crystal Microbalance

Katsunori AOKI, Takeshi MIYAMOTO, and Yasuhiko OHSAWA*
Materials Research Laboratory, Central Engineering Laboratories, Nissan Motor Co., Ltd.,
1, Natsushima-cho, Yokosuka, Kanagawa 237
(Received November 12, 1988)

Synopsis. The cation selectivity on a Prussian Blue (PB) modified electrode in propylene carbonate was examined by means of a quartz crystal microbalance. It was found that the selectivity coefficient of Na^+ versus Li^+ on the PB film was about 15.

Since Neff established the redox and electrochromic (EC) behavior of a Prussian Blue (PB) electrode[1] and Itaya et al. reported an electroplating method of PB,[2] many works on Prussian Blue (PB) modified electrodes have appeared.[3] Much attention has been paid to the Prussian Blue thin films not only because of their potential use as electrochromic devices,[4,5] batteries,[6] and catalysts,[7] but also because of their use as model compounds for such basic research as electron-hopping kinetics study.[8] It has been shown that Prussian Blue electrodes could be electrochemically reduced to Prussian White reversibly by means of a mechanism which involves the injection of both cations and electrons. The cations with Stokes radii of smaller sizes could penetrate the PB lattice more easily. In fact, it has been reported that, in aqueous media, K^+, Rb^+, and Cs^+ can smoothly penetrate the lattice, while repeated redox cycles are blocked in the presence of Li^+ or Na^+.[2] In an organic solvent of propylene carbonate, however, the redox reaction of PB in the presence of Li^+ or Na^+ is very stable.[4,9] Although the mechanism of ion transport has not yet been completely elucidated in detail, one of the applications of the PB modified electrode would be ion-separation making use of the different selectivities of the cations. It has been reported, that is, that the electrochemical redox cycles of the PB electrode could make it possible to separate alkali metal ions.[10]

The quartz crystal microbalance (QCM) in solution[11-13] offers a direct way of measuring the mass change of the PB film during electrochemical reduction and oxidation,[14] which would lead to quantitative estimations of the cation selectivities.

This paper will describe a new method for the determination of the selectivity coefficient of a cation versus another one on the PB film by using QCM.

Experimental

Indium tin oxide (ITO) was sputtered (ca. 20 Ω/□) on one side of a 6-MHz AT-cut quartz crystal (Inficon) with gold film electrodes on both sides. ITO was sputtered in order to prevent a chemical deposition of PB on the gold substrates.[2] The oscillating surface area was about 0.33 cm^2. Films of PB on ITO-coated crystals were electrochemically deposited under galvanostatic conditions of 5 $\mu A\ cm^{-2}$ in a freshly prepared solution of an equivolume mixture of 10 mM† $FeCl_3$ and 10 mM $K_3[Fe(CN)_6]$ aqueous solutions. The charge passed through for electroplating was 9 $mC\ cm^{-2}$. After the deposition of the PB, the film was thoroughly rinsed with distilled water and then mounted in a Teflon-made electochemical cell using O-rings. The frequency of the oscillating circuit, made up by following the method in the literature,[15] was monitored with a frequency counter. Cyclic voltammetry was conducted under a nitrogen atmosphere. Unless otherwise noted, a scan rate of 10 $mV\ s^{-1}$ was used. Simultaneously the charge passed through was recorded with a coulometer. A Pt wire and an Ag/AgCl electrode were used as the counter and the reference electrodes respectively. A propylene carbonate (PC) solution of 1 M $LiClO_4$, $NaClO_4$, or a mixture of them with 1.5 wt% H_2O[4] was used as the electrolyte solution. The mass change of the PB film upon reduction was calculated from the frequency change according to Sauerbrey's equation. The equation held within a 5% error, which was confirmed by the galvanostatic electrodeposition of Ag on Au quartz crystal electrodes.

† 1 M=1 mol dm^{-3}.

Results and Discussion

Figure 1 shows typical cyclic voltammetric (A) and frequency-potential(B) curves of the PB thin film in the $NaClO_4$/PC system, the latter illustrating that the observed mass change is reversible. It is clear that, when PB is reduced to Prussian White (PW), the weight of the film increases, while the succeeding oxidation of PW to PB is accompanied by a mass loss. The ratio of the mass change to the charge passed through (molar mass) was 21.9 $g\ mol^{-1}$, indicating that the sodium ion penetrates into the PB film upon reduction and exits from it upon oxidation.

In contrast with the $NaClO_4$/PC system, the molar

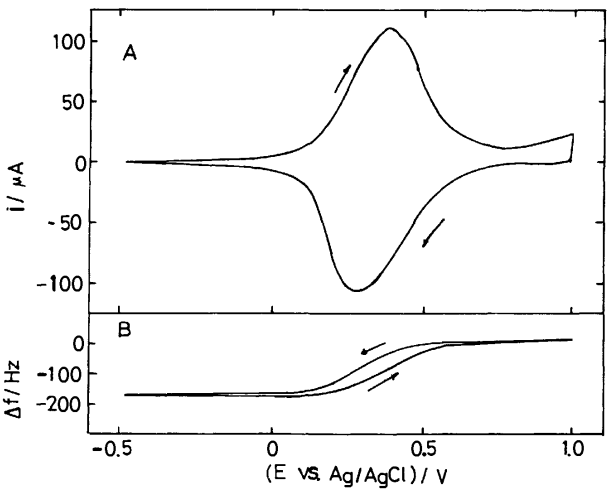

Fig. 1. Cyclic voltammetric (A) and potential-frequency curves (B) for a Prussian Blue modified quartz crystal electrode in 1M $NaClO_4$ of propylene carbonate. v=10 $mV\ s^{-1}$.

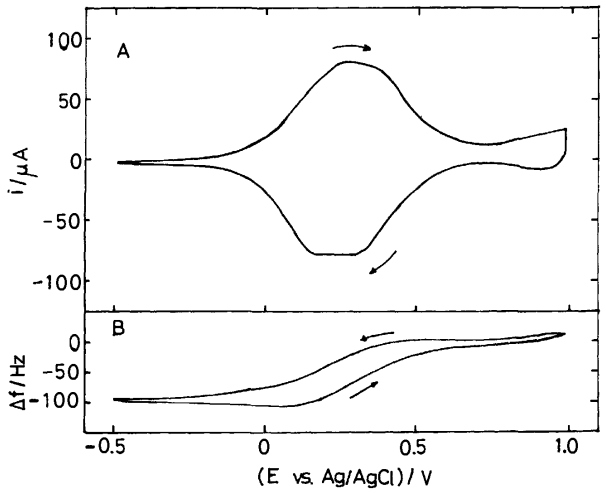

Fig. 2. Cyclic voltammetric (A) and potential-frequency curves (B) for a Prussian Blue modified quartz crystal electrode in 1M $LiClO_4$ of propylene carbonate. v=10 mV s^{-1}.

mass for PB in $LiClO_4$/PC of 10.9 g mol^{-1}, somewhat larger than that expected for Li^+ (6.9 g mol^{-1}), suggests that some water molecules are also incorporated into the PB film with Li^+ upon reduction. Typical cyclic voltammetric (A) and frequency-potential(B) curves in this system are shown in Fig. 2.

Figure 3 shows the relationship between the molar fraction of Na^+ and the molar mass in Na^+/Li^+ mixed electrolyte solutions. The molar mass was calculated for the reduction process of PB. The experimental curve indicates that Na^+ is more favorably intercalated into the PB lattice than is Li^+; this is consistent with the qualitative result in Ref. 9.

Since the molar mass was not much influenced by the scan rate, which ranged from 2 to 100 mV s^{-1}, it may be safe to conclude that distribution equilibrium of ions between the PB thin film and the electrolyte solution is established. The selectivity coefficient of Na^+ against Li^+ on the PB film (α) can be defined as:

$$\alpha = \frac{Y(1-X)}{X(1-Y)} \tag{1}$$

where X is the molar fraction of Na^+ in the solution and Y, the molar fraction of Na^+ in the PB film. The molar mass (Mm) in a Na^+/Li^+ mixed solution is the average of the Mm's for Na^+(ca. 22) and Li^+(ca. 11) obtained as above:

$$Mm = 22Y + 11(1-Y) \tag{2}$$

From Eqs. 1 and 2, we obtain:

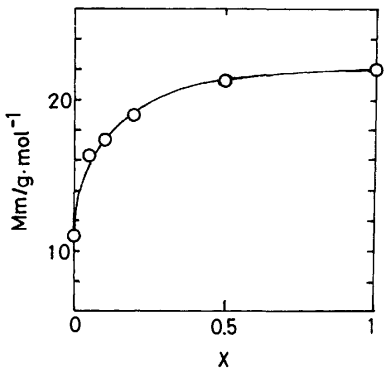

Fig. 3. Relationship between molar fraction of Na^+ in solution (X) and the molar mass (Mm) in Na^+/Li^+ mixed propylene carbonate solutions.

$$Mm = \frac{22X\alpha + 11(1-X)}{X\alpha + (1-X)} \tag{3}$$

which gives a good fit with the experimental curve provided that α is about 15. Consequently, when both ions are incorporated into the PB film, the concentration of Na^+ in the film is almost equal to that of Li^+, even in a solution with a Na^+ molar fraction lower than 0.1.

In conclusion, the quartz crystal microbalance can offer a direct and in situ measurement of ion selectivity on the PB thin film; this method may also be useful for other ion exchangers.

References

1) V. D. Neff, *J. Electrochem. Soc.*, **125**, 886 (1978).
2) K. Itaya, T. Ataka, and S. Toshima, *J. Am. Chem. Soc.*, **104**, 4767 (1982).
3) K. Itaya, I. Uchida, and V. D. Neff, *Acc. Chem. Res.*, **19**, 162 (1986) and the references cited therein.
4) T. Kase, M. Kawai, and M. Ura, *SAE paper*, 861362.
5) K. Itaya, K. Shibayama, H. Akahoshi, and S. Toshima, *J. Appl. Phys.*, **53**, 804 (1982).
6) V. D. Neff, *J. Electrochem. Soc.*, **132**, 1382 (1985).
7) K. Itaya, N. Shoji, and I. Uchida, *J. Am. Chem. Soc.*, **106**, 3423 (1984).
8) B. J. Feldman and R. W. Murray, *Inorg. Chem.*, **26**, 1702 (1987).
9) A. L. Crumbliss, P. S. Lugg, and N. Morosoff, *Inorg. Chem.*, **23**, 4701 (1984).
10) T. Ikeshoji, *J. Electrochem. Soc.*, **133**, 2108 (1986).
11) T. Nomura and O. Hattori, *Anal. Chim. Acta*, **142**, 281 (1982).
12) S. Bruckenstein and M. Shay, *Electrochim. Acta*, **30**, 1295 (1985).
13) H. Masuda and N. Baba, *Chem. Lett.*, **1987**, 1877.
14) B. J. Feldman and O. R. Melroy, *J. Electroanal. Chem.*, **234**, 213 (1987).
15) O. Melroy, K. Kanazawa, J. G. Gordon II, and D. Buttry, *Langmuir*, **2**, 697 (1986).

Flow Chemiluminescent Determination of Catecholamines Based on Permanganate Oxidation

Harumi IKKAI, Tatsuro NAKAGAMA, Masaaki YAMADA,* and Toshiyuki HOBO
Department of Industrial Chemistry, Faculty of Technology, Tokyo Metropolitan University, Setagaya, Tokyo 158
(Received November 30, 1988)

Synopsis. Luminous oxidation with acidic permanganate was found to be usable for chemiluminescent determination of catecholamines and other polyhydroxybenzenes at picomol levels. The sensitivity is high enough to determine catecholamines in urine. The present CL method is expected to be applicable to the post-column detection of these compounds in high-performance liquid chromatography.

Analytical methods using solution chemiluminescence (CL) as detection means are unique in being capable of low detection limits with simple instrumentation and have been applied to a variety of analytes of clinical and environmental significance.[1-3] The combination with flow injection method[4] and high-performance liquid chromatography[5] have made CL techniques more attractive. However, limited CL reaction system has caused the slow recognition of CL analysis, despite of other advantages including wide linear dynamic range, simplicity, rapidity, low cost per analysis, etc. In order to overcome this shortcoming, for the past several years our effort has been directed toward searching for new CL systems usable for analysis.[6-8] As a part of the investigations, we have reported on the screening of CL systems for determination of some biologically important organic compounds and made it clear that acidic permanganate oxidation may draw intense CL from many of the organic compounds tested, especially catecholamines and other polyhydroxyphenols.[8] Acidic permanganate is a strong oxidizing agent and has been used for CL determination of some drugs.[9]

In this paper, we describe the details of acidic permanganate CL system for the determination of catecholamines and other polyhydroxybenzenes by means of flow injection technique. This has been undertaken for aiming at the post-column detection of these compounds in high performance liquid chromatography.

Experimental

Apparatus. Prior to flow experiments, batch experiments were performed as described previously[10] in order to know luminescent characteristics through the measurements of time course of CL.

A schematic diagram of the flow system is illustrated in Fig. 1. An acidic permanganate solution is delivered through a flow line R_1 and water as a carrier solution through R_2 by a peristaltic pump P, respectively. Catecholamines and other organic compounds are injected by means of a 70-μl rotary value injector S. In order to block stray light, black Teflon tubing (1-mm i.d.) is used for the flow line except pump tubes and a detection flow cell D. For D a spiral flow cell (ca. 450-μl inner volume) made of flexible, transparent Teflon tubing (0.8-mm i.d.) is assembled as before.[11] The distance between S and D is about 4 cm, the minimum distance achieved. The light emitted is detected directly by a photomultiplier tube (Hamamatsu Photonics R376) with no wavelength discrimination. The signal from the photomultiplier tube is fed to picoammeter (Advantest TR-8651) and then recorded on a strip chart recorder. Peak height of the signal recorded is measured as CL signal.

Reagent. Chemicals of reagent grade were used as received. The water used was prepared by deionization of distilled water from a stainless steel apparatus. Each reagent solution was prepared daily from 10^{-1} M (permanganate) or 10^{-2} M (catecholamines and other organic compounds) stock solution (1 M=1 mol dm^{-3}). The permanganate stock solution was standardized with oxalate and stored in a dark room. Each catecholamine stock solution was prepared by dissolving its hydrochloride into and diluted with 10^{-2} M hydrochloric acid.

Results and Discussion

Batch Experiments. CL reaction often proceeds in different ways depending on the mixing order of reagent solution. This may cause considerable retardation of CL reaction and sometimes complete disappear-

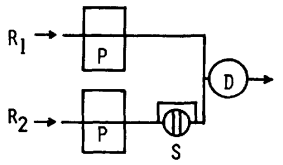

Fig. 1. Schematic diagram of the flow system (for key, see text). Recommended conditions: R_1= 1×10^{-3} M $KMnO_4$/1 M H_2SO_4, 3.2 ml min^{-1}; R_2= water, 4.5 ml min^{-1}.

Table 1. Effect of the Mixing Order of Reagent on the CL Signal for Catecholamines

Mixing order[a]			Relative CL signal[b]		
1 +	2 +	3	Dopamine	Noradrenaline	Adrenaline
$KMnO_4$[c]	H_2SO_4[c]	CA[d]	200	100	400
$KMnO_4$	CA	H_2SO_4	40	130	400
CA	H_2SO_4	$KMnO_4$	220	30	320

a) 0.1 ml of each solution was mixed in that order. b) Normalized with respect to the CL signal (=100) for noradrenaline. c) 10^{-3} M. d) 10^{-4} M catecholamines.

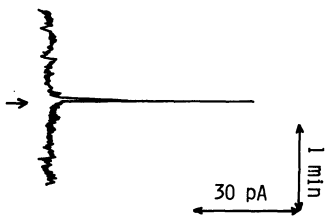

Fig. 2. Time course of CL signal for dopamine obtained by batch method. Arrow indicates the mixing of reagent (10^{-3} M $KMnO_4$/1 M H_2SO_4, 10^{-6} M dopamine).

ance of CL. And also how fast CL reaction occurs is a dominant factor which decides sensitivity in flow CL analysis because transient light emission is monitored. Accordingly, the exploration of the dependency of mixing order is of significant importance for the design of flow system. Thus, time courses of CL were measured on varying mixing orders of the reagent (permanganate, sulfuric acid, catecholamine) by the batch method. The results are shown in Table 1, indicating that the best mixing is in the order, permanganate, sulfuric acid, and catecholamines. Such a mixing order allows us to mix permanganate with sulfuric acid in advance. Consequently, this appears to permit the design of flow system consisting of a single flow line, namely, a sample injection into the stream of acidic permanganate solution. Unfortunately, a single line-flow system may not be assembled owing to a poor matching of the flow system with the speed of CL reaction. That is to say, as can be seen from the time course of CL in Fig. 2, the present CL reaction proceeds very fast and the light emission comes flashingly, resulting in an occurrence of most of light emission before the flow cell. Hence a dual line-flow system was assembled as shown in Fig. 1; the carrier stream of water into which a sample is injected enables the sample to join the stream of acidic permanganate solution just before the flow cell so that the light emission occurs mostly inside the flow cell.

Optimization. In order to determine optimum operating conditions, the CL signal for noradrenaline was taken with respect to reaction variables, i.e., the concentrations of permanganate and sulfuric acid and the flow rates of both streams. As expected, the CL signal was strongly dependent on both reagent concentrations because the oxidizing power of permanganate increases with an increase in the sulfuric acid concentration. The permanganate concentration above the concentration (1×10^{-3} M) providing the highest signal caused a decrease in the signal which was mainly due to the intense color of the permanganate solution, showing absorption maxima at 527 and 546 nm. The higher the sulfuric acid concentration, the higher the CL signal, but the higher the noise level. The highest signal-to-noise ratio was obtained at 1 M sulfuric acid. Other acids such as hydrochloric acid, phosphoric acids ($H_{n+2}P_nO_{3n+1}$, n=1, 2, 4), and monocarboxylic acids (C_1—C_4) were also examined, but none of them surpassed sulfuric acid with regard to the signal-to-noise ratio. The flow rate of the acidic permanganate solution provided a maximum signal at ca. 3 ml min^{-1}, but the increasing flow rate of carrier solution (water) gave an gradually increasing signal under any flow rates of the permanganate solution. For subsequent experiments, the optimum operating conditions were chosen as specified in Fig. 1.

Table 2. CL Signal for Catecholamines and Other Polyhydroxybenzenes

Compound (10^{-5} M)	Relative CL signal[a]
Dopamine	1.3
Noradrenaline	1.0
Adrenaline	1.0
L-Dopa	1.3
3,4-Dihydroxybenzylamine	1.5
Normethanephrine	1.0
Hydroquinone	2.1
Resorcinol	0.5
Catechol	2.1
4-Methylcatechol	1.5
4-*t*-Butylcatechol	5.6
Phloroglucinol	0.8
Pyrogallol	2.9
Gallic acid	0.4
Ethyl gallate	0.4
Tannic acid	0.6

a) Normalized with respect to the CL signal (=1.0) for noradrenaline.

Characteristics of the System. Under the optimum conditions, the background signal is 9×10^{-12} A, comparing with a noise current of 3×10^{-12} A. This high background, and consequently high noise are conceivably based on the luminous oxidation of organic impurities in the water used or from the flow line due to the use of highly acidic and concentrated permanganate solution. In a previous work,[12] the mild conditions (2×10^{-6} M permanganate at pH 2.5) gave much lower background and noise current (10^{-13} A levels), despite the presence of a fluorescent organic compound as sensitizer in the system. Calibration graphs for dopamine, noradrenaline, and adrenaline exhibited straight lines over the concentration ranges of 10^{-7} to 10^{-4} M with a slope of unity and signal ratio of 1.3:1.0:1.0, respectively. The limit of determination (S/N=3) is 7 pmol (70-μl injection of 10^{-7} M solution) for each catecholamine. This sensitivity is high enough to detect catecholamines in urine at 10^{-6} M levels. The relative standard deviation (n=10) for adrenaline (70 pmol) is 2.3%. The good reproducibility is based on an effective mixing caused by the fast flow of solution in the flow cell. The sampling rate can be as high as 500 h^{-1}.

It is known that some polyhydroxybenzenes give rise to light emission by permanganate oxidation under basic conditions.[13] Thus thirteen polyhydroxybenzenes were subjected to test in the present CL system, and CL signals obtained are summarized in Table 2 along with those for catechloamines. It can be roughly said from Table 2 that the unsubstituted phenols with a hydroxyl group at the ortho- or para-position provides higher signals and that the substituted phenols with an electron-donating group provides higher

Table 3. Effect of the Mobile Phase Used for Chromatographic Separation of Catecholamines on the CL Signal for Noradrenaline[a]

Mobile phase[b]	CL signal[c]	S/N[d]
0.2 M sodium formate	460	15
0.05 M citric acid (300 ml)+0.05 M disodium hydrogenphosphate (160 ml)+sodium dodecyl sulfate (15 mg)	140	5
Citric acid (10.5 g)+acetic acid (2.1 ml)+sodium hydroxide (4.8 g)+sodium acetate (8.2 g)	140	4
45% methanol/0.05 M sodium dihydrogenphosphate	120	5
Methanol+0.08 M acetic acid (1:1)	110	3
Water+methanol (28:72)	110	3
0.075 M citric acid	100	1
Ethyl acetate+cyclohexane (3:7)	70	4
0.12 M succinic acid+0.35 M boric acid +0.002 M EDTA (1:1:1)	60	15
0.2 M sodium acetate	50	25
0.15 M sodium dihydrogenphosphate	50	25
0.5 M sodium dihydrogencitrate	50	6
0.17 M acetic acid	40	5
6% acetonitrile/0.03 M sodium dihydrogenphosphate	10	5
0.1 M tris/HCl buffer (pH 8.5)+acetonitrile (87:13)	6	6
Water	50	17

a) 10^{-6} M. b) Flown to R_2 in place of water. c) 10^{-12} A. d) Signal-to-noise ratio.

signals, but those with an electron-withdrawing group lower signals. These trends were not observed in the above basic permanganate system. At any rate, the polyhydroxybenzenes are detected with sensitivity not so much different as those for catecholamines. This implies that these compounds can also be determined by means of the acidic permanganate CL system.

Applicability to Post-Column Detection. It is expected that the present CL system may be applied to the determination of catecholamines and other polyhydroxybenzenes in biological and clinical samples, drugs, foods, beverages, etc. after chromatographic separation. In that case, it should be noted that the constituents of mobile phase might inhibit the CL reaction. Accordingly, various kinds of mobile phases used for the elution of catecholamines were flown to R_2 in place of water, in order to know to what extent the CL signal for noradrenaline was affected. The results are shown in Table 3; the comparison of signal-to-noise ratio indicates that sodium formate, succinic acid/boric acid/EDTA, sodium acetate, and sodium phosphate may be utilized as eluent. The use of mobile phase containing alcohols seems to be undesirable because alcohols increase not only signal itself but also background noise, resulting in a deterioration of the signal-to-noise ratio. This was confirmed by the dependency of organic solvent on the signal for adrenaline. The presence of 20% methanol and ethanol in the carrier water gave about 2 and 18 times higher signal than in the absence of alcohol, but 10 and 100 times increased noise reduced both signal-to-noise ratios to one-sixth, respectively. Acetonitrile and acetone may not also be recommended as the constituent of mobile phase since they reduce signal itself to ca. 1/24 and signal-to-noise ratio to ca. 1/4, respectively.

References

1) A. Tsuji and M. Maeda, *Rinshō Byōri*, **36**, 408 (1988).
2) S. Kamei, *Rinshō Byōri*, **36**, 397 (1988).
3) M. Yamada and S. Suzuki, *Bunseki*, **1985**, 104.
4) A. Townshend, *Anal. Proc.*, **22**, 370 (1985).
5) K. Imai, "Methods in Enzymology," ed by M. A. DeLuca and W. D. McElroy, Academic Press, Inc., New York (1986), 133, p. 435.
6) M. Yamada, T. Hobo, and S. Suzuki, *Anal. Lett.*, **21**, 1887 (1988) and references therein.
7) Q. Xue-Xin, G. Yue-Ying, M. Yamada, E. Kobayashi, and S. Suzuki, *Talanta*, **36**, 505 (1989).
8) T. Nakagama, M. Yamada, and S. Suzuki, *Anal. Chim. Acta*, **217**, 371 (1989).
9) R. W. Abbot, A. Townshend, and R. Gill, *Analyst (London)*, **111**, 635 (1986).
10) M. Yamada, H. Kanai, and S. Suzuki, *Bull. Chem. Soc. Jpn.*, **58**, 1137 (1985).
11) S. Nakahara, M. Yamada, and S. Suzuki, *Anal. Chim. Acta*, **141**, 255 (1982).
12) M. Yamada, T. Nakada, and S. Suzuki, *Anal. Chim. Acta*, **147**, 401 (1983).
13) D. F. Marino and J. D. Ingle, Jr., *Anal. Chim. Acta*, **124**, 23 (1981).

Revised Structures, Benz[*cd*]indol-2(1*H*)-ones, for the Ring-Contracted Cycloadducts from 1-Substituted Cyclohepta[*b*]pyrrol-2(1*H*)-ones with Acetylenes

Akira MORI,* Guan Rong TIAN,† Hitoshi TAKESHITA,* Toshiyuki TAKEHIRO,†† and Noritaka ABE††
Institute of Advanced Material Study, 86, Kyushu University, Kasuga-koen, Kasuga, Fukuoka 816
††Department of Chemistry, Faculty of Science, Yamaguchi University, Yamaguchi 753
(Received June 27, 1988)

Synopsis. Formerly-proposed structures, cyclopent[*de*]-isoquinolin-3(4*H*)-ones, for ring contracted by-products obtained from 1-substituted cyclohepta[*b*]pyrrol-2(1*H*)-ones and acetylenes, were revised to benz[*cd*]indol-2(1*H*)-ones on the basis of spectroscopic analysis.

In our recent study of the cycloaddition of 1-substituted cyclohepta[*b*]pyrrol-2(1*H*)-ones (**1**) to electron-deficient acetylenes, dimethyl butynedioate (DMBD) and dibenzoylacetylene (DBA),[1,2] we have isolated, other than the predicted azulenes and Michael-type adducts, a series of ring-contracted compounds. We have given them isoquinoline structures (**X**) mainly from an appearance of singlet signals around δ=8.8, which, we thought, might be ascribable to H-5 of **X**. However, after reconsideration, we came to a view that benz[*cd*]indol-2(1*H*)-one structures were more plausible than the previously-proposed **X** in the ^{1}H NMR and UV spectral points of view. In this paper, we wish to correct the structures.

Results and Discussion

In the previous paper, we described the characterization of a series of compounds: the reaction of cyclohepta[*b*]pyrrol-2(1*H*)-one (**1a**) and DMBD after refluxing in acetonitrile for 45 h gave five products (**2**, **Xa**, and **3a**—**5a**) in good combined yields. However, a doubt has arisen concerning the isoquinoline structure of **Xa**.[1,2] Namely, the structure **Xa** possesses a quinodimethane structure, and the formation of **Xa** from the protoadduct (**Pa**) involves an autooxidative dehydrogenation step. The occurrence of such a process to lead non-aromatic compounds seems unlikely. Moreover, in the ^{1}H NMR spectrum[3] of **X**, the singlet signals, which were ascribed to H-5 signals, showed only a slight variation on changing the substituent on the nitrogen atom. In this paper, we revise the structures of **X** to **6**, benz[*cd*]-indol-2(1*H*)-one derivatives, from the following evidence.

To provide more information on the structures of **X** and **6**, we extended the reaction of DMBD to 1-phenacylcyclohepta[*b*]pyrrol-2(1*H*)-one (**1b**). From **1b**, only two products (**2** and **6b**) were isolated in 12 and 14% yields, respectively. The latter, **6b**, was identical with the sample prepared by the condensation of phenacyl bromide with **6a**. In the same time, **6a** was converted to an acetyl derivative (**6c**).[2,4] The **6c** was identical with one of the cycloadducts by the reaction of *N*-acetylcyclohepta[*b*]pyrrol-2(1*H*)-one with 2,3-bis(methoxycarbonyl)-7-oxabicycloheptadiene under high-pressure conditions (3000 bar).[5]

Since the UV spectra of **6a** and **6c** were almost superimposable on those of corresponding dimethyl naphthostyril-4,5-dicarboxylates (**7a** and **7c**),[6] the same structural units in both compounds are strongly

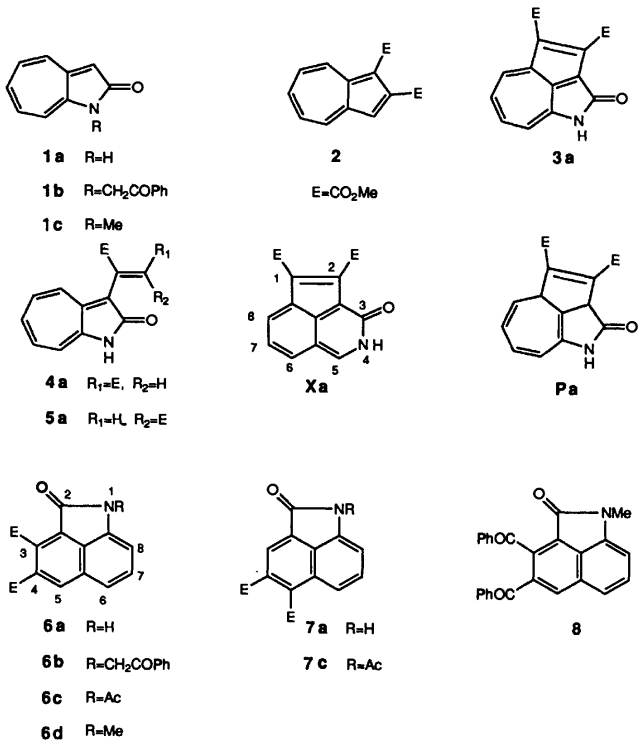

Scheme 1.

Table 1. The UV Spectral Data of **6a**, **6c**, and the Related Compounds **7a** and **7c**[a]

6a	6c	7a	7c
222 (41900)	221 (23400^{sh})	222 (46000)	233 (41800)
272 (14100)	232 (29000)	271 (13850)	255 (17880)
	255 (12600^{sh})	350 (2420)	
378 (3100)	349 (1900)	383 (3190)	346 (3850)

a) Solvent: **6a** and **6c** were measured in MeOH, and **7a** and **7c** were reported as in EtOH.

† On leave from Yabian University, Yanji, Jilin, People's Republic of China.

Table 2. Selected NMR Data of **6** and **8**

	6a	6b	6c	6d	8
H-5	8.81	8.81	8.92	8.73	8.30
H-6	7.63	7.45	7.83	7.45	7.4
		∫		∫	∫
H-7	7.56	7.7	7.71	7.6	7.9
H-8	7.11	6.89	8.32	6.95	7.03
C-5	134.7	134.0	135.6	134.0	
C-6	120.9	121.0	123.3	120.6	
C-7	130.5	130.3	131.1	130.2	
C-8	108.6	107.8	116.7	106.9	

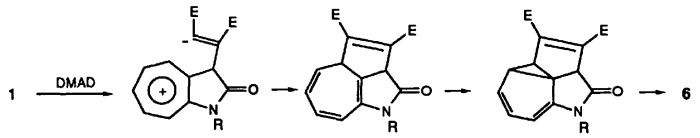

Scheme 2.

suggested (Table 1). This UV similarity is reasonable; since in both **6a, c** and **7a, c**, one of the methoxycarbonyl groups at C-4 or C-6, which is in an extended ortho- or para-position of the nitrogen-carrying carbon. This must largely influence the UV maxima, while the rest of methoxycarbonyl groups at C-5 in **6a, c** and **7a, c** are in the extended meta-position, having less affective on the UV maxima. Therefore, **6** are naphthostyril derivatives. For the vicinal bis(methoxycarbonyl) naphthostyrils having three consecutive hydrogens and one isolated hydrogen, only four structures are feasible.

The ^{1}H NMR spectra provide diagnostic information to select the correct structure, **6**. Thus, the ^{1}H NMR spectra of **6a** to **6b** and the corresponding derivative (**8**) derived from DBA and 1-methylcyclohepta-[*b*]pyrrol-2(1*H*)-one (**1d**) revealed characteristic features; i.e., they showed a singlet at δ=8.3—8.9 and aromatic proton signals at δ=6.9—8.3 (Table 2). Among them, a doublet signal, part of the three consecutive proton system, appeared at relatively high field. It was close to a substituent on the nitrogen atom, since the chemical shifts at ca. δ=6.9 or lower field were largely dependent on the *N*-substituents. The chemical shift difference, $\Delta\delta$, caused by acetylation of **6a** to **6c** was 7.11−8.32=−1.21 in chloroform-*d*. Therefore, it must be ascribable to H-8.

As has already been noticed, the singlet signals were slightly sensitive to the *N*-substituents and moved to a larger extent on changing the carbonyl substituents. Therefore, the singlet signals were close to one of the methoxycarbonyl groups, and could be assigned to H-5. Accordingly, only two possibilities remain for **6**; one is the 4,5-bis(methoxycarbonyl) structure and the other the 3,4-bis(methoxycarbonyl) structure. However, the former is already known to be **7**, and the latter remaining must be **6**.

The mechanism of formation of **6** is straightforward: a valence-bond isomerization of the initial [8+2]cycloadducts to norcaradiene derivatives and a subsequent dehydrogenative aromatization. It is difficult to explain the formation of any other naphthostyril derivatives from protoproducts of **1** and DMBD.

In conclusion, cyclopent[*de*]isoquinolin-3(4*H*)-one structures, **X**, were revised to benz[*cd*]indol-2(1*H*)-one (naphthostyril) structures, **6**, from the UV- and NMR-spectral analyses as well as the mechanistic considerations.

Experimental

Preparation of 1b. To an EtOH solution (50 cm^3) of **1a** (1.08 g) was added concd NaOH (4 cm^3) and the mixture was kept at room temperature for 4 h. A yellow sodium salt of **1a** (1.20 g, 97%; mp 300 °C) was collected by filtration. An anhydrous benzene suspension (50 cm^3) of sodium salt (836 mg) and phenacyl bromide (995 mg) was refluxed for 12 h. The mixture was poured into water and extracted with benzene. The benzene solution was washed with dil NaOH solution, dried over Na_2SO_4, and evaporated. The residue was chromatographed on a silica-gel column to give 560 mg (43%) of **1b**: yellow needles; mp 172—173 °C; ^{1}H NMR[3] δ=5.50 (2H, s), 6.17 (1H, s), 6.66 (1H, d, J=9.2 Hz), 6.86 (1H, t, J=9.2 Hz), 7.02 (1H, t, J=9.2 Hz), 7.05 (1H, t, J=9.2 Hz), 7.51 (1H, d, J=9.2 Hz), 7.52 (2H, t, J=7.3 Hz), 7.64 (1H, t, J=7.3 Hz), and 8.08 (2H, d, J=7.3 Hz); IR ν: 1698, 1680, 802, 760, 754, and 692 cm^{-1}.

Found: C, 77.47; H, 5.01; N, 5.26%. Calcd for $C_{17}H_{13}NO_2$: C, 77.55; H, 4.98; N, 5.32%.

Reaction of 1b with DMBD. An anhydrous MeCN solution (30 cm^3) of **1b** (500 mg) and DMBD (540 mg) was refluxed for 2 d. The solvent was evaporated and the residue chromatographed on a silica-gel column to give 56 mg (12%) of **2**,[2] 110 mg (14%) of **6b**, and 149 mg (30%) of unreacted **1b**. **6b**: yellow needles; mp 151—153 °C; ^{1}H NMR δ=4.00 (3H, s), 4.10 (3H, s), 5.33 (2H, s), 6.89 (1H, d, J=6.7 Hz), 7.45—7.7 (5H, m), 8.07 (2H, d, J=7.9 Hz), and 8.81 (1H, s); ^{13}C NMR δ=46.5, 52.9, 53.1, 107.8, 121.0, 123.5, 126.4, 127.9, 128.1 (2C), 128.3, 128.9 (2C), 130.3, 130.9, 134.0, 134.4 (2C), 139.1, 165.4, 165.5, 166.8, and 192.2; IR ν: 1730, 1710, 1690, 1636, 790, 757, and 685 cm^{-1}.

Found: C, 68.55; H, 4.32; N, 3.32%. Calcd for $C_{23}H_{17}NO_6$: C, 68.48; H, 4.25; N, 3.47%.

Reaction of 6a and Phenacyl Bromide. An anhydrous benzene (30 cm^3) of **6a** (18 mg), diazabicycloundecene (30 mg),

and phenacyl bromide (40 mg) was refluxed for 7 h. After removing the solvent, the residue was chromatographed on a silica-gel column to give 9 mg (35%) of **6b** and 11 mg (61%) of unreacted **6a**.

References

1) N. Abe and T. Takehiro, *Heterocycles*, **26**, 1727 (1987).
2) N. Abe and T. Takehiro, *Bull. Chem. Soc. Jpn.*, **61**, 1225 (1988).
3) All the NMR spectra were measured in $CDCl_3$.
4) In the previous paper,[2] we assigned the acetylation product (**Xc**) of **Xa** as an *O*-acetyl derivative. However, the identity of **Xc** with **6c** was proven by direct comparisons. The observed similarity of the UV spectra of **6c** and **7c** supported to have the same naphthostyril structures.
5) As the result, previous assignment of **Xc** as the *O*-acetyl derivative should also be revised as an *N*-acetyl derivative. The high-pressure investigation will be a matter of an independent report.
6) P. Bamfield, A. W. Johnson, and A. S. Katner, *J. Chem. Soc. C*, **1966**, 1028.

Synthetic Photochemistry. L.[1] Isolation and the X-Ray Structure Determination of Photocyclodimers Formed by UV-Light Irradiation of Alkyl 2,4-Dioxopentanoates

Akira MORI,* Nobuaki NISHIYAMA,† Yukiko KOHGUCHI, Hisayo SHINKA, and Hitoshi TAKESHITA*
Institute of Advanced Material Study, 86, Kyushu University, Kasuga-koen, Kasuga, Fukuoka 816
†Instrumental Analyses Center, Kyushu University, Kasuga-koen, Kasuga, Fukuoka 816
(Received October 19, 1988)

Synopsis. Upon UV-light irradiation with a high-pressure mercury lamp, methyl 2,4-dioxopentanoate in a mixture of benzene and cyclohexane afforded a crystalline head-to-head-[2+2]cyclodimer. Its structure was elucidated by a single-crystal X-ray analysis, as well as ^{1}H and ^{13}C NMR spectroscopy. Ethyl 2,4-dioxopentanoate also gave a cyclodimer.

The de Mayo reaction[2] has been regarded as one of the most synthetically useful photocycloaddition reactions. Among the previously-studied β-diketone photocycloaddends, alkyl 2,4-dioxoalkanoates,[3] being fully enolized in various solvents, have a characteristic reactivity to form regiospecific [2+2]cycloadducts with conjugated olefins, and to give useful intermediates for natural product syntheses.[4] Herein, we wish to report the isolation and structure determination of head-to-head-[2+2]dimers.

When methyl 2,4-dioxopentanoate (**1a**) was irradiated by means of a 400-W high-pressure mercury lamp through a Pyrex glass filter in a mixture of benzene and cyclohexane, a colorless crystalline product (**2a**) was formed and isolated by filtration. Its mass spectrum indicated its molecular composition to be dimeric, and the ^{1}H and ^{13}C NMR strongly suggested the presence of a symmetry element in the molecule. Presumably, **2a** is, therefore, a [2+2]cyclodimer. From the mechanism of photoaddition, the cis relationship for the acet l and hydroxy groups was expected,[5,6] though the syn- or anti-stereochemistry could not be determined. Unfortunately, spectroscopic differentiation at this point failed; i.e., an ^{1}H NMR satellite band due to the ^{13}C-H coupling could not be detected, or an attempt to measure lanthanoid-induced chemical shift change caused a decompostion of **2a**.

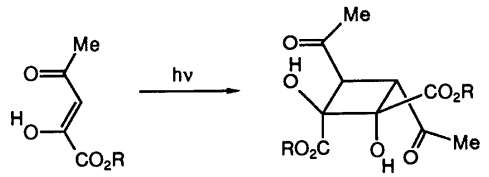

1a R=Me
b R=Et

2a R=Me
b R=Et

Scheme 1.

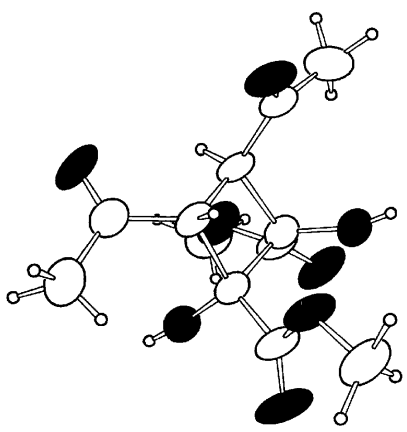

Fig. 1. The ORTEP drawing of **2a**. Dark atoms denote the oxygen atoms.

Therefore, an X-ray structure analysis with a single crystal of **2a** was carried out (see Experimental): The molecular structure obtained by the analysis was displayed as a computer-generated drawing (Fig. 1).

Similar irradiation of ethyl 2,4-dioxopentanoate (**1b**) gave a homologous cyclodimer (**2b**) in 10% yield. From the ^{1}H NMR spectral similarity it is certain that **2b** and **2a** have the same stereochemistry.

Previously, no dimer of free enolized β-diketones have been detected, although a cyclodimer of dehydroacetic acid reacted at the β-acyloxy enone moiety.[7] This is particularly interesting since none of the proto-photoadducts from ordinary 2,4-diketoalkanes with olefins has been known. On the other hand, from the 2,4-dioxoalkanoates, several proto-cycloadducts have been characterized; i.e., a) the [2+4]- and [2+6]photocycloadducts, from conjugated olefins, were normally stable and not dealdolyzed under mild conditions[6,8] and b) as a [2+2]cycloadduct, the protoadduct from *p*-isopropenyltoluene with **1a** was obtained in a trace amount after silica-gel column chromatography.[9] The present case, the isolation of stable compounds having two aldol groups as parts of a strained cyclobutane ring, seems to be quite extraordinary.

Experimental

Photodimerization of 1a. A mixed solution of benzene (6.5 cm^3) and cyclohexane (4.5 cm^3) of **1a** (884 mg) was irradiated through a Pyrex-glass filter with a 400-W high-pressure mercury lamp cooled with an ice-water for 12 h. Crystalline solid separated out was collected by filtration, and recrystallized from benzene to give **2a** [colorless needles, mp 135—136 °C, 153.4 mg; 17%. Found: C, 50.05; H, 5.71%. Calcd for $C_{12}H_{16}O_8$: C, 50.00; H, 5.50%. ^{1}H NMR δ[10]=2.20 (6H, s), 3.89 (6H, s), 4.24 (2H, s), and 4.58 (2H, s). ^{13}C NMR δ=29.3 (2C), 48.6 (2C), 53.4 (2C), 79.3 (2C), 169.9 (2C), and 205.3 (2C). *m/z*, 288 (M^+, 0.7), 271 (4), 201 (8), 169 (12), 159 (14), 145 (23), 143 (9), 141 (23), 99 (33), 84 (37), and 43 (100)].

Photodimerization of 1b. Similarly, irradiation of **1b** (349 mg) gave **2b** [colorless crystals, mp 114—115 °C, 35 mg; 10%. Found: C, 52.78; H, 6.55%. Calcd for $C_{14}H_{20}O_8$: C,

53.16; H, 6.33%. ^{1}H NMR δ=1.34 (6H, t, J=7 Hz), 2.28 (6H, s), 4.22 (2H, s), 4.32 (4H, q, J=7 Hz), and 4.45 (2H, br s). ^{13}C NMR (acetone-d_6) δ=14.3 (2C), 49.4 (2C), 62.5 (2C), 81.3 (2C), 169.8 (2C), and 203.7 (2C)].

X-Ray Analysis of 2a. Crystal and intensity data were collected on an Enraf-Nonius CAD 4 Diffractometer using Graphite monochromated Mo $K\alpha$ radiation. Crystal data: $C_{12}H_{16}O_8$, M.W., 288.25; monoclinic, Space group, $C_{2/c}$; a=15.6873(9), b=6.4078(4), c=14.6453(8) 10^{-8} cm, β=116.23(5)°. D_c=1.450 g cm^{-3} for Z=4. The intensities of 3195 reflections were measured and 603 independent reflections within a 2θ angle range of 2° through 54° were used for analysis. The structure was solved by MULTAN 78 and the positional and thermal parameters were refined by a full-matrix least-square method; anisotropic thermal parameters for all non-H atoms and fixed isotropic thermal parameters for H atoms (4.0×10^{-16} cm^2). The final R values were found to be 8.1%.[11]

The authors with to thank Dr. Hiroaki Mametsuka for his elaboration on a preliminary survey of this work.

References

1) Part XLIX: G. R. Tian, A. Mori, H. Takeshita, M. Higashi, and H. Yamaguchi, *Bull. Chem. Soc. Jpn.*, **62**, 1567 (1989).

2) P. de Mayo and H. Takeshita, *Can. J. Chem.*, **41**, 440 (1963); P. de Mayo, *Acc. Chem. Res.*, **4**, 41 (1971); S. W. Baldwin, *Org. Photochem.*, **5**, 123 (1981).

3) H. Takeshita and S. Tanno, *Bull. Chem. Soc. Jpn.*, **46**, 880 (1973).

4) H. Takeshita and N. Kato, *Yuki Gosei Kagaku Kyokai Shi*, **44**, 1081 (1986), and the references cited therein.

5) Regioselective formation of the photocycloadducts from the exclusive tautomeric form of **1a**, methyl 2-hydroxy-4-oxo-2-pentenoate, can be interpreted that even the γ-hydrogen abstraction process by the excited carbonyl of the chelated hydroxyl, a chemical reaction, acuses the deactivation. Under such circumstances, an anti-Franck-Condon geometrical change should not be involved in the dimerization.

6) Indeed, the proto-photocycloadducts isolated from cyclopentadiene and **1a** have been established to have this cis relationship. See H. Takeshita, A. Mori, and Y. Toyonaga, *Bull. Chem. Soc. Jpn.*, **48**, 307 (1975).

7) H. Takeshita, Y. Shoji, and R. Kikuchi, *Bull. Chem. Soc. Jpn.*, **46**, 690 (1973); N. Sugiyama, T. Sato, H. Kataoka, and C. Kashima, *ibid.*, **44**, 555 (1971).

8) H. Takeshita, A. Mori, and S. Ito, *Bull. Chem. Soc. Jpn.*, **47**, 1767 (1974).

9) H. Takeshita, A. Mori, and S. Nakamura, *Bull. Chem. Soc. Jpn.*, **57**, 3152 (1984).

10) The NMR spectra were measured with a GSX 270 H Spectrometer, JEOL, in $CDCl_3$ solution unless otherwise specified.

11) The complete F_o-F_c data are deposited as Document No. 8865 at the Office of the Editor of Bull. Chem. Soc. Jpn.

A Convenient Synthesis of Diketones via Alkylation of Alkyl Methyl Ketone Dimethylhydrazones

Masakazu YAMASHITA,* Kaoru MATSUMIYA, Hiroko MORIMOTO, and Rikisaku SUEMITSU
Department of Applied Chemistry, Doshisha University, Kamikyo-ku, Kyoto 602
(Received July 18, 1988)

Synopsis. Symmetrical diketones were prepared by the reaction of the lithium salts of alkyl methyl ketone dimethylhydrazones with dibromoalkanes.

We previously reported a facile synthesis of unsymmetrical ketones by successive alkylation of acetone dimethylhydrazone,[1] and the application of this reaction to the synthesis of jasmones and the sex pheromone of the peach fruit moth.[1,2]

In this paper we wish to report a simple and convenient synthesis of the symmetrical diketones by alkylation of alkyl methyl ketone dimethylhydrazones[3] with dibromoalkanes. By the use of this method, 2,15-hexadecanedione, a precursor of muscone,[4] was also prepared in good yield.

The symmetrical diketones (**4**) were synthesized from a variety of alkyl methyl ketones (**1**) according to Scheme 1. For example, 2-octanone dimethylhydrazone (**2c**), readily available from 2-octanone and *N,N*-dimethylhydrazine using trifluoroacetic acid as a catalyst, was allowed to react with 1 equiv of butyllithium in THF at −5 °C under argon, followed by half equiv of 1,4-dibromobutane to give 7,14-icosanedione (**4f**) in 83% yield after hydrolysis. The results are listed in Table 1. 2,15-Hexadecanedione (**4b**) is a precursor of muscone,[4] which is one of the famous perfume materials.

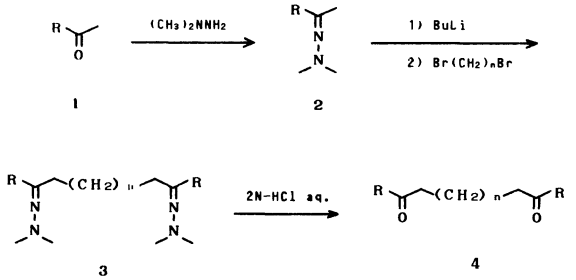

Scheme 1.

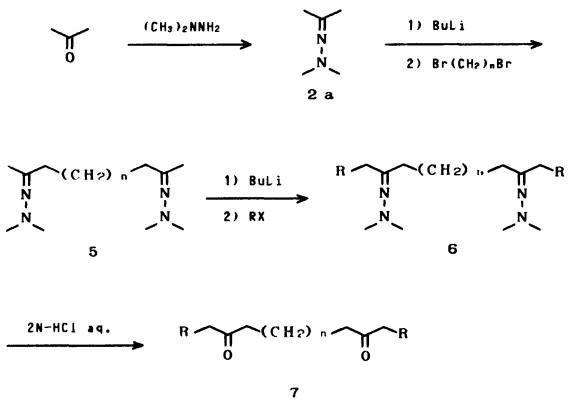

Scheme 2.

Furthermore, diketones (**7**) were also prepared by an alternative route starting from acetone dimethylhydrazone (**2a**), as shown in Scheme 2. For example, to the THF solution of the hydrazone (**2a**), 1 equiv of butyllithium and a half equiv of 1,6-dibromohexane was added successively. Then, dihydrazone was dilithiated by butyllithium, and 1-bromobutane was added to form dibutylated hydrazone, which was hydrolyzed using hydrochloric acid to afford 6,15-icosanedione (**7b**) in 84% yield. The other results are presented in Table 2.

By the methods described above, a variety of symmetrical diketones were prepared in satisfactory yields. No isomeric ketones were detected by TLC.

Table 1. Synthesis of Symmetrical Diketones (**4**) from Alkyl Methyl Ketone Dimethylhydrazones (**2**)

Run	Hydrazone	$Br(CH_2)_nBr$	Product	Yield/%[a]
1	**2a**	$n=3$	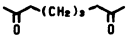 **4a**	54
2		$n=10$	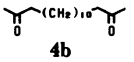 **4b**	66
3	**2b**	$n=6$	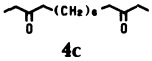 **4c**	67
4		$n=10$	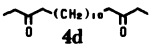 **4d**	84
5		$n=12$	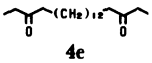 **4e**	77
6	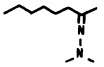 **2c**	$n=4$	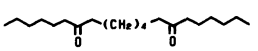 **4f**	83
7	**2d**	$n=5$	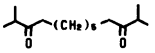 **4g**	76
8	**2e**	$n=4$	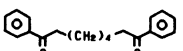 **4h**	91
9	**2f**	$n=8$	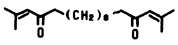 **4i**	76
10	**2g**	$n=4$	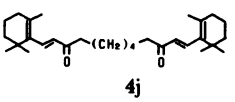 **4j**	68

a) Isolated yields.

In conclusion, this synthetic method for symmetrical diketones has been found to be a prominent procedure in terms of good product yield, high regioselectivity of the alkylations, facile operations, and mild reaction conditions.

Experimental

The NMR spectra were measured on a Hitachi R-600 FT-NMR Spectrometer at 60 MHz using tetramethylsilane (δ=0.00) as an internal standard; chemical shifts are given in ppm. The IR spectra were recorded on a Hitachi 260-10 Infrared Spectrophotometer. The mass spectra (MS) were recorded on a Hitachi RM-50 GC-MS spectrometer. The GLC analysis was carried out on a Shimadzu GC-14A gas chromatograph, and the column chromatography was performed on Merck silica gel (230—400 mesh). Melting points were taken on a Yanagimoto micro melting point apparatus. No correction was made for melting and boiling points, and all the yields were isolated ones.

Table 2. Synthesis of Symmetrical Diketones (**7**) by the Successive Alkylation of Acetone Dimethylhydrazone (**2a**)

Run	$Br(CH_2)_nB$	RX	Product	Yield/%[a]
1	$n=3$	CH_3I	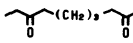 **7a**	77
2	$n=6$		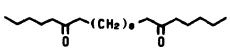 **7b**	84
3	$n=6$		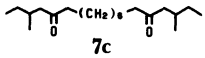 **7c**	24

a) Isolated yields.

Preparation of Ketone Dimethylhydrazone (2). A typical procedure is as follows: a mixture of 2-octanone (50 mmol, 7.8 ml), *N,N*-dimethylhydrazine (75 mmol, 4.0 ml), trifluoroacetic acid (0.05 ml) and benzene (20 ml) was placed in a flask equipped with a trap used to remove water and refluxed for 2 h. After cooling to room temperature, the reaction mixture was added to brine and extracted with ethyl acetate. The organic layer was dried over anhydrous magnesium sulfate. The solvent was removed under reduced pressure and residual liquid was distilled to give 2-octanone dimethylhydrazone (**2c**) (7.47 g, 88% yield), bp 87 °C/20 Torr (1 Torr≈ 133.322 Pa).

^{1}H NMR, IR, and mass spectral data and boiling points of new hydrazones (**2**) are shown in Table 3.

General Procedure for the Preparation of Symmetrical Diketones (4). Butyllithium (4.4 mmol) was added via a syringe at −5 °C with stirring under argon to a solution of methyl ketone dimethylhydrazone (**2**) (4 mmol) in THF (15

Table 3. ^{1}H NMR, IR, and Mass Spectral Data of Dimethylhydrazones (**2**)

Compound	^{1}H NMR ($CDCl_3$, δ)	IR/cm^{-1}	MS m/z (M^+)	Bp/°C[a]
2f	1.83 (3H, s, CH_3), 1.92 (3H, s, CH_3), 2.04 (3H, s, CH_3), 2.51 (6H, s, NCH_3), 5.65—6.18 (1H, m, CH=)	2960, 1658, 1445, 1380, 1026	140	64 (20 Torr)
2g	1.06 (6H, s, CH_3), 1.20—1.28 (2H, m, CH_2), 1.54 (4H, d, CH_2), 1.73 (3H, s, $=CCH_3$), 2.13 (3H, s, $NCCH_3$), 2.50 (3H, s, NCH_3), 2.56 (3H, s, NCH_3), 6.12 (1h, d, CH=), 6.60 (1H, d, CH=)	1620, 1580, 1210, 1155, 1030, 980	234	Oil

a) Uncorrected boiling point.

Table 4. ^{1}H NMR, IR, and Mass Spectral Data of Diketones (**4** and **7**)

Compound	^{1}H NMR ($CDCl_3$, δ)	IR/cm^{-1}	MS m/z (M^+)	Bp/°C[a]
4d	1.05 (6H, t, CH_3), 1.18—1.86 (20H, m, CH_2), 2.39 (4H, t, $COCH_2$), 2.44 (4H, q, CH_2CH_3)	2930, 1710, 1465, 1380, 1120	282	86—87
4e	1.05 (6H, t, CH_3), 1.17—1.85 (24H, m, CH_2), 2.39 (4H, t, $COCH_2$), 2.44 (4H, q, CH_2CH_3)	2920, 1705, 1465, 1380, 1120	310	91—92
4f	0.90 (6H, t, CH_3), 1.07—1.95 (24H, m, CH_2), 2.40 (8H, t, $COCH_2$)	2940, 1710, 1475, 1390, 1090	310	82—83
4g	1.10 (12H, d, CH_3), 1.20—1.85 (10H, m, CH_2), 2.46 (4H, t, $COCH_2$), 2.30—2.95 (2H, m, CH)	2930, 1710, 1470, 1385, 1045	240	Oil
4i	1.16—2.05 (16H, m, CH_2), 1.88 (6H, s, CH_3), 2.14 (6H, s, CH_3), 2.40 (4H, t, $COCH_2$), 6.07 (2H, broad s, CH=)	2930, 1688, 1620, 1440, 1115, 1028	306	58—59
4j	1.08 (12H, s, CH_3), 1.35—1.88 (16H, m, CH_2), 1.78 (6H, s, $=CCH_3$), 2.10 (4H, m, $=CCH_2$), 2.60 (4H, t, $COCH_2$), 6.11 (2H, d, J=16Hz, =CH), 7.32 (2H, d, J=16Hz, =CH)	2925, 1695, 1665, 1610, 1460, 1365, 980		Oil
7a	1.05 (6H, t, CH_3), 1.27—1.85 (6H, m, CH_2), 2.40 (4H, t, $COCH_2$), 2.42 (4H, q, CH_2CH_3)		184	
7b	0.90 (6H, t, CH_3), 1.10—1.90 (24H, m, CH_2), 2.40 (8H, t, $COCH_2$)	2920, 1700, 1465, 1380, 1085	310	76—77
7c	0.88 (6H, t, CH_3), 0.89 (6H, d, CH_3), 1.10—2.15 (18H, m, CH_2 and CH), 2.20—2.56 (8H, m, $COCH_2$)	2930, 1710, 1465, 1375, 1145, 1050	310	Oil

a) Uncorrected melting point.

ml). After 1 h dibromoalkane (2 mmol) was added at −5 °C; the reaction mixture was stirred for 15 h at room temperature before the addition of 2 mol dm^{-3} hydrochloric acid (15 ml). After standing for 15 h, the solution was diluted with water and extracted with ethyl acetate. The organic layer was washed with brine, dried over anhydrous magnesium sulfate, filtered and concentrated. The residure was purified by column chromatography over silica gel (hexane:ethyl acetate=8:2).

^{1}H NMR, IR, and mass spectral data and melting points of new diketones (**4**) are given in Table 4.

Preparation of Symmetrical Diketones (7) by Successive Alkylation Procedure. According to a method similar to that described above, using dibromoalkane and alkyl halide, the successive alkylations of acetone dimethylhydrazone (**2a**) and the hydrolysis were carried out. After the usual work up, column chromatography (hexane:ethyl acetate=9:1) gave the desired diketone.

^{1}H NMR, IR, and mass spectra data and melting points of new diketones (**7**) are given in Table 4.

References

1) M. Yamashita, K. Matsumiya, M. Tanabe, and R. Suemitsu, *Bull. Chem. Soc. Jpn.*, **58**, 407 (1985).

2) M. Yamashita, K. Matsumiya, K. Murakami, and R. Suemitsu, *Bull. Chem. Soc. Jpn.*, **61**, 3368 (1988).

3) Synthesis of Monoketone by alkylation of methyl ketone dimethylhydrazones has been reported; E. J. Corey and D. Enders, *Tetrahedron Lett.*, **1976**, 3; E. J. Corey, D. Enders, and M. G. Bock, *ibid.*, **1976**, 7; E. J. Corey and D. Enders, *ibid.*, **1976**, 11; E. J. Corey and D. Enders, *Chem. Ber.*, **111**, 1337 (1978); E. J. Corey and D. Enders, *ibid.*, **111**, 1362 (1978).

4) J. Tsuji, M. Kaito, and T. Takahashi, *Bull. Chem. Soc. Jpn.*, **51**, 547 (1978); J. Tsuji, T. Yamada, M. Kaito, and T. Mandai, *ibid.*, **53**, 1417 (1980).

Solubilization of β-Carotene in Water by Water-Soluble Linear Macromolecules

Isamu INAMURA,* Masayuki ISSHIKI, and Takeo ARAKI
Department of Chemistry, Faculty of Science, Shimane University, Matsue 690
(Received September 21, 1988)

Synopsis. β-Carotene was solubilized in water by the water-soluble linear macromolecules of poly(*N*-vinylpyrrolidone) (PVP), polyethylene glycol (PEG), poly(vinyl alcohol) (PVA), and dextran. Absorption of β-carotene in aqueous macromolecular solutions were red-shifted. The rate of photobleaching of β-carotene in water depended on the polymer species.

It is well-known that carotenoids are soluble in oragnic solvents but insoluble in water. Therefore, these have been studied in vivo and in organic solvents by many investigators,[1,2] but not in water. However, Shibata et al.[3] recently solubilized β-carotene in water by forming complexes with egg albumin. As shown in this report, we have succeeded in solubilizing β-carotene in water by means of water-soluble linear polymers of PVP, PEG, PVA and dextran.

Experimental

Materials. β-Carotene manufactured by Kanto Chemical Co., Inc. was used without further purification. PVP: molecular weight (mol wt), 40000 and PEG: mol wt, 20000 were purchased from Kishida Chemical Co., Ltd. PVA; PVA-117: mol wt, 77000, degree of saponification, 98.5 mol%, was kindly donated by Kuraray Co., Ltd. Dextran: mol wt, 75000 was purchased from Wako Pure Chemical Industries, Ltd. PVP, PEG, PVA, and dextran were purified by reprecipitation of them in solvent-nonsolvent, namely in water-acetone, benzene-petroleum ether, water-methanol, and water-ethanol, respectively. Bovine serum albumin (BSA) manufactured by Armour Pharmaceutical Company was used without further purification.

Method for Solubilization of β-Carotene. β-Carotene was solubilized in water as follows. An organic solvent containing β-carotene was added to a polymer/org. solv. or water solution. (The compositions of raw materials are shown in Table 1 for all the samples). The solution was evaporated to a dry β-carotene/polymer film under a reduced pressure at room temperature. A small amount of water was added onto the film, and stirred gently at room temperature until a homogeneous paste was formed. The paste was diluted with water to a given concentration of β-carotene. In the same way, β-carotene was solubilized in water by BSA or Triton X-100.

Analytical Methods. Absorption spectra at room temperature were measured with a double beam spectrophotometer, UVIDEC-510 (Japan Spectroscopic Co., Ltd.). Photobleaching experiments of β-carotene in different states were done under while light (2.7×10^2 J m^{-2} s^{-1}) from a projector lamp.

Results and Discussion

Figure 1 shows the absorption spectra of β-carotene in different states. β-Carotene in acetone had three ab-

Table 1. Composition of Raw Materials and Visible Light Absorption Maxima of β-Carotene in Aqueous Macromolecular Solutions

Sample No.	Composition of raw materials: Polymer-Solvent (g) (ml)	Car[a]-Solvent (mg) (ml)	Poly/Car[b]	Absorption maxima[d] (nm)
1	PEG 0.15-benzene 5	Car 4-benzene 5	1	412 439 459 490 535
2	PEG 0.15-benzene 5	Car 4-benzene 5	1	(432)[c] 460 494 540
3	PEG 0.15-benzene 5	Car 4-benzene 5	1	416 439 (466) (500)
4	PEG 0.44-benzene 5	Car 4-benzene 5	3	(427) 452 483 524
5	PEG 0.11-benzene 5	Car 0.5-benzene 5	6	(422) 448 477 518
6	PEG 0.89-benzene 10	Car 4-benzene 5	6	(423) 454 478 (515)
7	PEG 1.18-benzene 10	Car 0.5-benzene 5	64	(425) 443 470 513
8	PEG 1.18-benzene 10	Car 0.5-benzene 5	64	(425) 440 (470) 512
9	PVP 0.30-chloroform 5	Car 4-chloroform 5	1	(412) (437) 460 494 543
10	PVP 0.30-chloroform 5	Car 4-chloroform 5	1	(416) 440 (465) (500)
11	PVP 0.60-chloroform 5	Car 4-chloroform 5	2	(424) 443 (473) 514
12	PVP 1.48-chloroform 10	Car 4-chloroform 5	5	(418) 434 (467) (501)
13	PVP 0.19-chloroform 5	Car 0.5-chloroform 5	5	(418) 435 (461) (498)
14	PVP 1.18-chloroform 10	Car 0.5-chloroform 5	32	(425) 441 (470) 510
15	PVP 1.18-chloroform 10	Car 0.5-chloroform 5	32	(420) 439 (470) (510)
16	PVP 1.18-chloroform 10	Car 0.5-chloroform 5	32	(418) 436 (460) (500)
17	PVA 1.5-water 10	Car 0.5-acetone 5	21	(416) 450 478 (515)
18	PVA 1.5-water 10	Car 0.5-acetone 10	21	(414) 438 462 (495)
19	dextran 1.5-water 10	Car 0.5-acetone 5	22	410 437 (467) (502)
20	dextran 1.5-water 10	Car 0.5-acetone 5	22	412 434 (460) (495)
21	BSA 0.62-water 9	Car 0.5-ethanol 1	10	419 (437) (467) (508)
22	BSA 0.62-water 9	Car 0.5-ethanol 1	10	410 (434) (462) (502)
23	Triton X-100 1-acetone 5	Car 0.5-acetone 5		(410) (436) 460 486

a) β-Carotene. b) Mole ratio polymer/β-catotene. c) The number in parenthesis indicates an absorption maximum of a shoulder. d) Concentrations of β-carotene are 2×10^{-5} mol dm^{-3}.

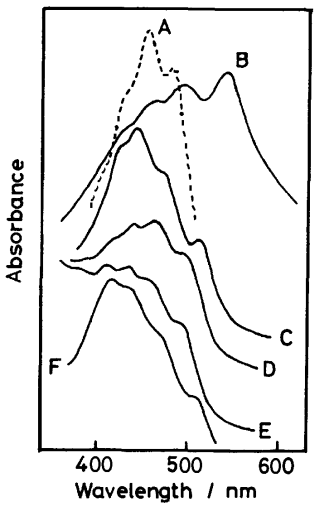

Fig. 1. Absorption spectra of β-carotene in different states. Concentrations of β-carotene are 2×10^{-5} mol dm^{-3}. The sample numbers indicated in Table 1 are shown in parentheses. (A) β-carotene in acetone, (B) β-carotene in aqueous PEG solution (No. 2), (C) β-carotene in aqueous PVP solution (No. 14), (D) β-carotene in aqueous PVA solution (No. 18), (E) β-carotene in aqueous dextran solution (No. 20), (F) β-carotene in aqueous BSA solution (No. 21).

sorption bands at 430, 450, and 481 nm. On the other hand, β-carotene in aqueous solutions of the water-soluble linear polymers and BSA had a red-shifted absorption band at the wavelength longer than 495 nm, in addition to the other three bands of shorter wavelength.

Also in Table 1, there was observed a red-shifted absorption band at the wavelength longer than 495 nm, in addition to the three or four bands of shorter wavelength, for all the β-carotene in aqueous macromolecular solutions. The red-shifted absorption appeared in the 495—543 nm range with different samples. The mole ratio polymer/β-carotene of raw material did not affect the wavelength of red-shifted absorption. It is noted, however, that the absorption bands of longer wavelength than 535 nm were observed only for the solutions with the mole ratio polymer/β-carotene of 1:1. Further, it was ascertained that the absorption spectra of β-carotene in aqueous PVP and PEG solutions were almost identical with those of the β-carotene/PVP and PEG films described in the Experimental section, respectively (data not shown).

Figure 2 shows the time-dependent spectral change of β-carotene in aqueous PVP solution caused by irradiation of white light. The intensity of red-shifted peak at 510 nm decreased at the same rate as the other bands of shorter wavelength. Such a spectral change was observed for all the β-carotene in aqueous macromolecular solutions shown in Fig. 3, suggesting that the red-shifted bands have the same origin as the other bands of shorter wavelength.

Figure 3 shows the results of photobleaching of β-carotene in different states by irradiation of while light. The rate of photobleaching of β-carotene in

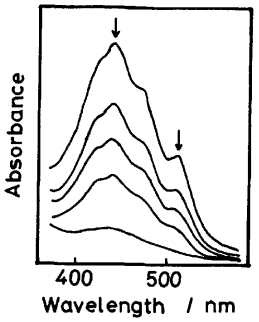

Fig. 2. Time-dependent spectral change of β-carotene in aqueous PVP solution (No. 14) caused by irradiation of white light. (Time=0, 60, 120, 360 and 900 min.)

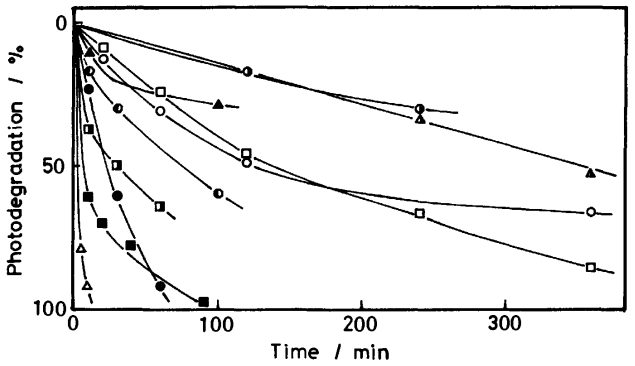

Fig. 3. Photobleaching of β-carotene in different states by irradiation of white light. The wavelengths monitoring the photobleaching were those of absorption peaks in the 440—465 nm range. The initial concentrations of β-carotene were 2×10^{-5} mol dm^{-3}. ▲, β-carotene in acetone; ◑, β-carotene in hexane; ▲, β-carotene in benzene; ◧, β-carotene in aqueous acetone (80%) solution; ◐, β-carotene in aqueous Triton X-100 solution (No. 23); ○, β-carotene in aqueous PVP solution (No. 14); □, β-carotene in aqueous PEG solution (No. 8); ■, β-carotene in aqueous PVA solution (No. 17); △, β-carotene in aqueous dextran solution (No. 19); ●, β-carotene in aqueous BSA solution (No. 22).

aqueous macromolecular solutions depended on the polymer species; the order of the rate of photobleaching was dextran>PVA>BSA>PEG>PVP. β-Carotene in aqueous dextran solution was photobleached almost completely after 10 min irradiation, while β-carotene in aqueous PVP solution remained unphotobleached by 35% after 360 min irradiation.

It should be also noted in Fig. 3 that β-carotene in acetone, hexane and benzene was more stable against light irradiation than that in aqueous macromolecular solutions. This result is unexpected because chlorophyll in the macromolecular complexes in water was more stable against light irradiation than chlorophyll in organic solvents.[4] Since β-carotene in aqueous acetone (80%) solution, having three absorption bands at 432, 457, and 483 nm, was photobleached at a higher rate than that in acetone as shown in Fig. 3, it is considered that the medium of water or organic solvents

was an important factor in the stabilization of β-carotene under light irradiation, in addition to the presence of polymer.

Recently, Wloch et al.[5-7] investigated a long-wavelength absorbing form (LWAF) of β-carotene and believed that it represents a fine-crystalline form of the pigment where head-to-tail aggregation occurs. According to them, it can be inferred that the linear macromolecules formed complexes with the fine-crystalline form of β-carotene, resulting in solubilization of the pigment in water. The polymers probably bound it within random coil of the chain. The difference in position of the red-shifted absorption bands may reflect the variation in size of the crystals of β-carotene.

References

1) D. Siefermann-Harms, *Physiol. Plantarum*, **69**, 561 (1987).

2) B. H. Davies, "Chemistry and Biochemistry of Plant Pigments," ed by T. W. Goodwin, Academic Press, London (1976), Vol. 2, p. 38.

3) H. Shibata, C. Kurosaki, T. Kawashima, and H. Ochiai, *Agric. Biol. Chem.*, **51**, 3261 (1987).

4) I. Inamura, T. Araki, M. Shei, T. Nishikawa, H. Shibata, and H. Ochiai, *Biochim. Biophys. Acta*, **932**, 335 (1988).

5) S. Wieckowski, E. Wloch, and B. Broniowska, "Advances in Photosynthesis Research," ed by C. Sybesma, Martinus Nijhoff/Dr W. Junk Publishers, The Hague/Boston/Lancaster (1984), Vol. 2, p. 1.

6) E. Wloch and S. Wieckowski, *Bull. Pol. Acad. Sci.: Biol. Sci.*, **34**, 263 (1986).

7) E. Wloch, S. Wieckowski, and A. M. Turek, *Photosynthetica*, **21**, 2 (1987).

Formation of Solvent-Separated Ion Pairs in Calixarene Ester-Alkali Picrate Complexes

Takashi ARIMURA, Michio KUBOTA, Tsutomu MATSUDA, Osamu MANABE,† and Seiji SHINKAI*
Department of Organic Synthesis, Faculty of Engineering, Kyushu University, Fukuoka 812
†Department of Industrial Chemistry, Faculty of Engineering, Nagasaki University, Nagasaki 852
(Received December 5, 1988)

Synopsis. Association constants (K_a) of calix[n]arene esters ($\mathbf{1}_n$: n=4, 6, 8) for alkali picrates have been determined in tetrahydrofuran and compared with the $\mathbf{1}_n$-induced bathochromic shifts of the absorption maxima of alkali picrates. It has been established that (1) $\mathbf{1}_n$'s mostly form the 1:1 complexes with alkali metal cations, (2) the K_a values for $\mathbf{1}_n$ are generally smaller than those for crown ethers, and (3) the certain M^+-$\mathbf{1}_n$ complexes are considerably solvent-separated because of the "encapsulation effect" of the calixarene cavity. This is the first example for the systematic investigation on the relation between K_a and the geometry of the calixarene ester complexes.

Calixarenes are cyclic oligomers made up of phenol units. It has been found that the ester derivatives ($\mathbf{1}_n$'s) show the ionophoric nature and capable of binding alkali metal, alkaline earth metal, and diazonium ions are crown ethers do.[1-6] In particular, the tetramer ($\mathbf{1}_4$) exhibits the markedly high Na^+ selectivity.[1-5,7] Arduini et al.[2] proposed on the basis of the ^1H NMR measurements that Na^+ is "encapsulated" in the cavity constructed with the ionophoric -OCH_2COO- groups (Fig. 1). Here, two questions occur to us which are both related to the essential behaviors of $\mathbf{1}_n$ as ionophores: that is, if $\mathbf{1}_n$ really forms the encapsulated complexes as illustrated in Fig. 1, then (i) do they form only the 1:1 metal/$\mathbf{1}_n$ complexes but not the 1:2 metal/$\mathbf{1}_n$ sandwich complexes as seen for certain crown ethers? and (ii) do they show the characteristics of solvent-separated ion pairs? Recently, Inoue et al.[8] suggested an interesting idea that the bathochromic shift of the absorption band of the picrate anion, extracted into the organic phase with a macrocyclic ligand from aqueous metal picrate solutions, serves as a convenient measure for evaluating the ion pair tightness in solution. We thus studied the spectroscopic behaviors of alkali picrates (M^+Pic^-) in tetrahydrofuran (THF) in the absence and the presence of $\mathbf{1}_n$ and estimated the stoichiometry and the nature of the ion pairs.

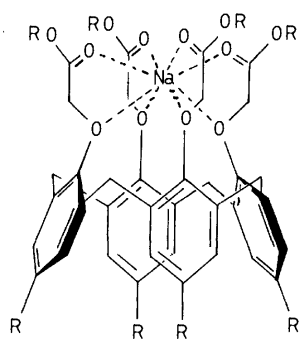

Fig. 1. Encapsulation of Na^+ by $\mathbf{1}_4$.

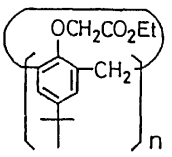

$\mathbf{1}_n$

Experimental

Preparations of $\mathbf{1}_4$ (25,26,27,28-tetrakis(ethoxycarbonylmethoxy)-*p*-*t*-butylcalix[4]arene), $\mathbf{1}_6$ (37,38,39,40,41,42-hexakis(ethoxycarbonylmethoxy)-*p*-*t*-butylcalix[6]arene), and $\mathbf{1}_8$ (49,50,51,52,53,54,55,56-octakis(ethoxycarbonylmethoxy)-*p*-*t*-butylcalix[8]arene) were described elsewhere.[1-6] All the spectroscopic measurements were carried out at 30 °C in THF.

Results and Discussion

The λ_{max} of M^+Pic^- shifted to longer wavelengths with a few isosbestic points with increasing $\mathbf{1}_n$ concentrations. The spectral change is similar to that in the presence of crown ethers.[9] From a plot of the absorbance for the new λ_{max} vs. $\mathbf{1}_4$ concentration we could determine the stoichiometry (by the molar ratio method) and the K_a (by the Benesi-Hildebrand plot). When the spectral change was relatively small, we employed the continuous variation method (absorbance for the new λ_{max} vs. $[M^+Pic^-]/([M^+Pic^-]+[\mathbf{1}_n])$ to determine the stoichiometry. However, the spectral changes observed for Li^+-$\mathbf{1}_n$(n=4, 6, 8), K^+-$\mathbf{1}_4$ and Cs^+-$\mathbf{1}_4$ were still too small to determine the stoichiometry. The results are summarized in Tables 1—3.

It is seen from Table 1 that $\mathbf{1}_n$'s mostly form the 1:1 complexes with alkali metal cations. This implies that metal cations are bound deeply in the cavity, the complexes being classified as a "nest-in-type". In crown ether chemistry, "perch-on-type" complexes, which frequently lead to the formation of 1:2 metal/crown sandwich complexes, result when the size of metal cations is greater than the cavity size. The metal selectivity in Table 3 suggests that the cavity

Table 1. Stoichiometry of $\mathbf{1}_n$-Alkali Picrate (M^+Pic^-) Complexes

$\mathbf{1}_n$	M^+Pic^-			
	M^+=Li^+	Na^+	K^+	Cs^+
n=4	a)	1:1	a)	a)
n=6	a)	1:1	1:1	1:1
n=8	a)	1:1	1:1	1:1

a) The spectral change was too small to determine the stoichiometry.

Table 2. Bathochromic Shifts ($\Delta\lambda$, nm) of λ_{max}[a)]

Ionophore	M^+Pic^-			
	M^+=Li^+	Na^+	K^+	Cs^+
$\mathbf{l}_4$	1	31	2	0
$\mathbf{l}_6$	1	6	25	20
$\mathbf{l}_8$	1	1	11	6
18-Crown-6	1	29	13	5
Cryptand 222	—	31	29	25

a) The λ_{max} values of M^+Pic^- in the absence of $\mathbf{l}_n$ are 343 nm for Li^+, 351 nm for Na^+, 357 nm for K^+, and 362 nm for Cs^+.

Table 3. Association Constants (K_a)

Ionophore	log K_a for M^+Pic^-[b)]			
	M^+=Li^+	Na^+	K^+	Cs^+
$\mathbf{l}_4$	3.00	3.95	3.08	1.60
$\mathbf{l}_6$	2.78	3.15	4.13	4.52
$\mathbf{l}_8$	2.08	2.61	3.11	3.08
18-Crown-6[a)]	3.72	4.29	5.33	4.91
Cryptand 222	—	6.69	8.38	6.61

a) The measurements were carried out mainly at [18-crown-6]/[M^+Pic^-]<2.0 so that the K_a values reflect those for the 1:1 complexes. b) K_a=[$M^+Pic^-\cdot\mathbf{l}_n$]/[$M^+Pic^-$][$\mathbf{l}_n$].

sizes of $\mathbf{l}_4$ and $\mathbf{l}_6$ are comparable with those of 15-crown-5 and 18-crown-6, respectively. Hence, the formation of the sandwich complex with $\mathbf{l}_n$ is expected, if it exists, for Cs^+-$\mathbf{l}_4$. Although the stoichiometry for this complex could not be determined even by the continuous variation method, the Benesi-Hildebrand plot (at [$\mathbf{l}_4$]/[Cs^+Pic^-]=10—100) used assuming the formation of the 1:1 complex gave a good linear relationship (r>0.98). Probably, this complex also consists of 1:1 $Cs^+/\mathbf{l}_4$. It is known that calix[8]arene derivatives having a large cavity are capable of including two guest molecules.[10,11] In the present system, however, we could not find any evidence for the formation of 2:1 $M^+/\mathbf{l}_8$ complexes.

The λ_{max} for M^+Pic^- in the absence of $\mathbf{l}_n$ shifted to longer wavelengths in the order of Li^+<Na^+<K^+<Cs^+. This order reflects the looseness of the ion pairs. The bathochromic shifts of λ_{max} induced by the addition of $\mathbf{l}_n$ are recorded in Table 2. The largest shift (31 nm) was attained for Na^+-$\mathbf{l}_4$. This shift is comparable with that induced by cryptand 222 and even greater than that induced by 18-crown-6, supporting the formation of the solvent-separated ion pair.[9,12] The significant bathochromic shifts were also observed for K^+, Cs^+-$\mathbf{l}_6$ (20—25 nm). In contrast, the shifts induced by $\mathbf{l}_8$ were generally small. Presumably, even though M^+ is entrapped in the cavity of $\mathbf{l}_8$, the M^+-Pic^- interaction can still exist because of the flexible, large cavity.

Comparison of Table 2 with Table 3 reveals that these two recognition patterns are surprisingly similar: that is, the greater the K_a, the larger bathochromic shift occurs. This means that the stable $\mathbf{l}_n$ complex encapsulates M^+ deeply in the cavity resulting in the solvent-separated ion pair. The largest K_a was attained for Cs^+-$\mathbf{l}_6$ but not for Na^+-$\mathbf{l}_4$. This implies that

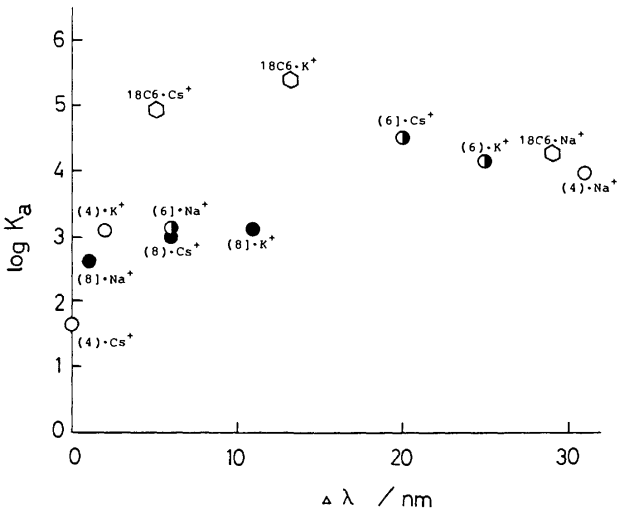

Fig. 2. log K_a vs. $\Delta\lambda$ map. In the figure $\mathbf{l}_n$'s are abbreviated with [n].

Na^+Pic^- bound to $\mathbf{l}_4$ is considerably solvent-separated but the complex is not so stable as that of Cs^+-$\mathbf{l}_6$. The discrepancy is probably related to the rigid nature of the calix[4]arene skeleton which is the origin of the sharp Na^+ selectivity: that is, the cavity of $\mathbf{l}_4$ is so small and so rigid that the Na^+-Pic^- interaction is efficiently shut down by the encapsulation of Na^+. On the contrary, $\mathbf{l}_6$ having the moderately rigid skeleton rather gives the stable complexes although the metal selectivity becomes inferior to that of $\mathbf{l}_4$.

Based on these foregoing findings, we illustrated a log K_a vs. $\Delta\lambda$ map (Fig. 2). The map explicitly clarifies several novel facets of the M^+-$\mathbf{l}_n$ complexes. Firstly, 18-crown-6 forms the considerably stable K^+ and Cs^+ complexes but they are less solvent-separated. In contrast, the K_a for Na^+ is smaller than these but the ion pair is much more solvent-separated. Secondly, the K_a values for $\mathbf{l}_n$ are generally smaller than those for 18-crown-6. Nevertheless, certain complexes (e.g., Na^+-$\mathbf{l}_4$, K^+-$\mathbf{l}_6$, and Cs^+-$\mathbf{l}_6$) result in the solvent-separated ion pairs in which the bathochromic shifts greater than 20 nm are observed. This indicates that the solvent-separatedness of these complexes is comparable with that of the cryptand complexes. The unusual power of $\mathbf{l}_n$ is ascribed to the "encapsulation effect", which appears most clearly in $\mathbf{l}_n$ having the small, rigid skeleton. Thirdly, the $\mathbf{l}_8$ complexes give the log K_a=2.8±0.3 for Na^+, K^+, and Cs^+. The nonselective nature suggests that the ion complexation with $\mathbf{l}_8$ occurs according to an "induced-fit" manner. Lastly, the Cs^+-$\mathbf{l}_4$ complex, a combination of the large alkali metal cation and the small calixarene cavity, did not cause any bathochromic shift but slightly increased the absorbance. The K_a estimated from this absorbance increase was only 40 $dm^3\,mol^{-1}$. The data visualize the Cs^+-$\mathbf{l}_4$ complex geometry: $\mathbf{l}_4$ weakly interacts with Cs^+ but cannot encapsulate Cs^+ enough to interfere with the Cs^+-Pic^- interaction.

In conclusion, the present study systematically demonstrated that (i) calixarene esters $\mathbf{l}_n$'s mostly form the 1:1 complexes with alkali metal cations and (ii)

they have a tendency to produce the solvent-separated ion pairs. Thus, small Na^+ ion is easily encapsulated leading to the solvent-separated ion pairs, whereas large Cs^+ ion is exposed to solvent media leading to the contact ion pairs. Further investigation on the reactivities and the geometries of these solvent-separated ion pairs is currently continued in our laboratories.

This research was supported by the Grant-in-Aid from the Ministry of Education, Science and Culture. We thank Miss Sayuri Edamitsu (Nagasaki University) and Miss Tomoko Nakane (Kyushu University) for technical assistance.

References

1) R. Ungaro, A. Pochini, and G. D. Andreetti, *J. Inclusion Phenom.*, **2**, 199 (1984).

2) A. Arduini, A. Pochini, S. Reverberi, R. Ungaro, G. D. Andreetti, and F. Ugozzoli, *Tetrahedron*, **42**, 2089 (1986).

3) S.-K. Chang and I. Cho, *Chem. Lett.*, **1984**, 474.

4) S.-K. Chang and I. Cho, *J. Chem. Soc., Perkin Trans. 1*, **1986**, 211.

5) M. A. McKervey, E. M. Seward, G. Ferguson, B. Ruhl, and S. Harris, *J. Chem. Soc., Chem. Commun.*, **1985**, 388.

6) S. Shinkai, S. Edamitsu, T. Arimura, and O. Manabe, *J. Chem. Soc., Chem. Commun.*, **1988**, 1622.

7) K. Kimura, M. Matsuo, and T. Shono, *Chem. Lett.*, **1988**, 615.

8) Y. Inoue, C. Fujiwara, K. Wada, A. Tai, and T. Hakushi, *J. Chem. Soc., Chem. Commun.*, **1987**, 393.

9) M. Bourgoin, K. H. Wong, J. Y. Hui, and J. Smid, *J. Am. Chem. Soc.*, **97**, 3462 (1975).

10) B. M. Furphy, J. M. Harrowfield, D. L. Kepert, B. W. Skelton, A. H. White, and F. R. Wilner, *Inorg. Chem.*, **26**, 4231 (1987).

11) S. Shinkai, K. Araki, and O. Manabe, *J. Am. Chem. Soc.*, **110**, 7214 (1988).

12) In order to obtain a further insight into the $\mathbf{l}_n \cdot M^+Pic^-$ ion pairs we measured the ^{23}Na NMR in THF/THF-d_8 mixed solvent at 30 °C. We unexpectedly found that the peak for Na^+ (added as M^+Pic^- (6.8×10^{-3} mol dm^{-3})) is invariably broadened in the presence of $\mathbf{l}_n$: for example, the T_2 values, which can be directly calculated from the peak width ($T_2=(\pi\delta_{\nu 1/2})^{-1}$ where $\delta_{\nu 1/2}$ denotes the half height line width in Hz) are 7.08×10^{-4} s in the absence of $\mathbf{l}_n$, 1.62×10^{-5} s in $\mathbf{l}_4$ (140 mmol dm^{-3}), 2.11×10^{-5} s in $\mathbf{l}_6$ (470 mmol dm^{-3}), and 3.18×10^{-5} s in $\mathbf{l}_8$ (340 mmol dm^{-3}). Such a broadening effect was not found for Na^+ bound to cyclic polyethers: $T_2=8.85\times10^{-4}$ s in 18-crown-6 (340 mmol dm^{-3}) and 1.47×10^{-3} s in cryptand 222 (670 mmol dm^{-3}). The similar observation was reported by Jin and Ichikawa: paper presented at the 57th Annual Meeting of the Chemical Society of Japan, Sendai, 1988, September.

Synthesis and Molecular Structure of Hexacarbonyl(tropone)diiron

Noboru MORITA, Chizuko KABUTO,† and Toyonobu ASAO*
Department of Chemistry, College of General Education, Tohoku University, Kawauchi, Sendai 980
†Instrumental Analysis for Chemistry, Faculty of Science, Tohoku University, Aramaki, Sendai 980
(Received December 5, 1988)

Synopsis. Molecular structure of hexacarbonyl(tropone)-diiron has been investigated by X-ray diffraction studies.

Previously, tricarbonyl(tropone)iron has been obtained by the reaction of acetylene with $Fe_2(CO)_9$,[1] or of tropone with $Fe(CO)_5$,[2] $Fe_2(CO)_9$,[3,4] or $Fe_3(CO)_{12}$,[5] and the complexes of tropone derivatives have also been obtained by the reaction of substituted tropones with $Fe_2(CO)_9$.[4]

Dodge reported in 1964[6] the X-ray analysis of the complex to clarify the structure of tricarbonyl[(2,3,4,5-η)-2,4,6-cycloheptatrienone]iron. Furthermore, many interesting chemical properties have been explored for the complexes.[7] Recently we have succeeded in optical resolution of the complex,[8] although partial resolution has been reported,[9] and kinetic data of 1,3-haptotropic rearrangement,[8] absolute configuration[10] of the complex and the related complexes have been reported.

In the course of our studies on synthesis and properties of tricarbonyl iron complex of tropone and its derivatives, we have isolated new hexacarbonyl diiron complexes along with tricarbonyl iron complexes. We have tentatively proposed a structure of hexacarbonyl-[μ-[(2,3,4-η:5,6,7-η)-2,4,6-cycloheptatrienone]]diiron for the new complex of tropone based on the spectroscopic data.[11]

Recently, we have investigated a molecular structure of the new complex by X-ray diffraction and we have found our proposed structure is correct, the results of which will be reported herein.

In the synthetic study of tricarbonyl(tropone)iron **1** by the reaction of tropone with excess of $Fe_2(CO)_9$ in refluxing ether, we isolated a new complex **2** as dark reddish crystals in 14% yield besides known complex **1** in 56% yeild.[11] Some substituted tropones also afforded mixtures of type **1** and type **2** complexes.[12] The complex **2** was also obtained from **1** by the reaction with $Fe_2(CO)_9$ in 25—30% yeild, and it was also found that **2** gradually decomposed by heating in benzene to give **1** and tropone itself.

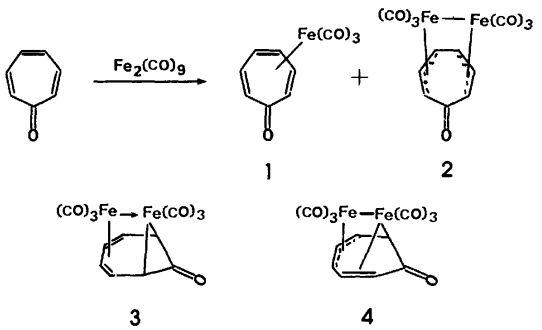

Mass spectrum of the new complex **2** by FD method showed a molecular ion peak at m/z 386 corresponding to $C_7H_6OFe_2(CO)_6$, coincided with the results of elemental analysis, and the abundant fragment ions by electron impact mode were observed at m/z 274 (1), 246 (1), 218 (5), 106 (58), and 78 (100). The infrared spectrum of **2** in KBr disk showed absorptions at 2060, 2025, 2010, 1995, 1980, 1960, 1955, and 1599 cm^{-1}, the ultraviolet absorption spectrum in ethanol showed maxima at 224 nm (log ε 4.26), 341 (3.94), and 432 (3.49), and ^1H NMR in $CDCl_3$ at 90 MHz showed signals at δ=3.33 (d, J=7.15 Hz, H-2,7), 4.40—4.67 (m, H-3,6), and 4.67—4.99 (m, H-4,5), ^{13}C NMR in $CDCl_3$ at 22.5 MHz showed signals at δ=209.50 (s, C-1), 191.96 (s, Fe-CO), 74.10 (d, J=161.6 Hz, C-3,6), 63.69 (d, J=156.2 Hz, C-2,7), and 62.49 (d, J=161.9 Hz, C-4,5).

From these sepctroscopic data we assigned a structure of hexacarbonyl[μ-[(2,3,4-η:5,6,7-η)-2,4,6-cycloheptatrienone]]diiron for the complex **2**, similar to hexacarbonyl(cycloheptatriene)diiron.[13] However, we could not exclude other structures such as **3** and **4**. Therefore, we carried out an X-ray crystallographic analysis of **2**. The molecular structure and atom labeling scheme for the complex **2** are presented in Fig. 1.

The crystallographic result shows that the structure **2** is indeed correct for this complex. Two independent

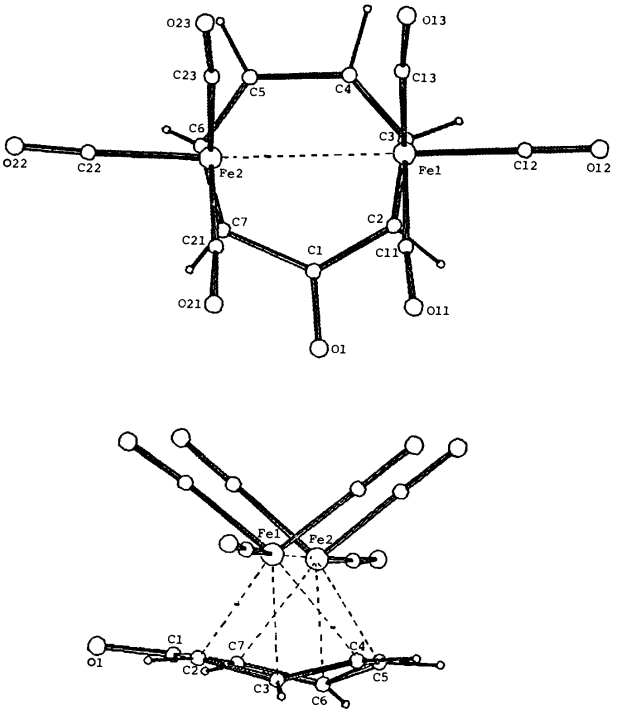

Fig. 1. Two perspective views of the $C_7H_6OFe_2(CO)_6$ molecule.

Table 1. Interatomic Bond Distances (Å) and Angles (deg) for Selected Bond in $C_7H_6OF_2(CO)_6$[a)]

Fe1-Fe2	2.894	
Fe1-C2, Fe2-C7	2.123	
Fe1-C3, Fe2-C6	2.040	
Fe1-C4, Fe2-C5	2.177	
C1-O1	1.230	
C1-C2, C1-C7	1.456	
C2-C3, C6-C7	1.414	
C3-C4, C5-C6	1.394	
C4-C5	1.447	
C11-C21	2.821	
C13-C23	2.830	
O11-O21	2.973	
O13-O23	3.023	
C2-C1-O1, C7-C1-O1		118.6
C2-C1-C7		122.8
C1-C2-C3, C1-C7-C6		129.3
C2-C3-C4, C5-C6-C7		124.3
C3-C4-C5, C4-C5-C6		126.1
Fe2-Fe1-C2, Fe1-Fe2-C7		85.4
Fe2-Fe1-C3, Fe1-Fe2-C6		92.7
Fe2-Fe1-C4, Fe1-Fe2-C5		70.6
Fe2-Fe1-C11, Fe1-Fe2-C21		84.4
Fe2-Fe1-C12, Fe1-Fe2-C22		174.9
Fe2-Fe1-C13, Fe1-Fe2-C23		92.9
C11-Fe1-C12, C21-Fe2-C22		93.1
C12-Fe1-C13, C22-Fe2-C23		89.6
C11-Fe1-C13, C21-Fe2-C23		101.6

a) The values are averaged over the equivalent bonds for mirror symmetry of the structure between two independent molecules. The e.s.d.'s are 0.003, 0.017, 0.023 Å for Fe-Fe, Fe-C, C-C bonds and 0.5, 0.8, 1.6° for Fe-Fe-C, C-Fe-C, C-C-C angles.

complexes of **2** exist in the crystalline state; however there is no essential difference in the structure of tropone ligand as well as in the way of coordination. As shown in perspective views of complex **2** (Fig. 1), the structure has an approximate mirror plane within the experimental errors. Table 1 lists the average values over the geometrically equivalent bond distances and angles for the two molecules. Tropone ligand is bent in a similar way to the case of cycloheptatriene complex, though the planarity is more retained. Somewhat longer distance of Fe_1-Fe_2 (2.894 Å) in **2** compared to that in the latter (2.866 Å) may be due to the difference of the planarity.

Experimental

Reaction of Tropone and $Fe_2(CO)_9$. A slurry of tropone (0.9 g, 8.5 mmol) and $Fe_2(CO)_9$ (8 g, 22 mmol) in 60 ml of anhydrous ether was heated at reflux under argon atmosphere for ca. 7 h. The reaction mixture was chromatographed on silica gel. The first eluent with a mixture of ether and benzene (1:9) gave green-colored $Fe_3(CO)_{12}$. From the next orange colored band eluted with a mixture of benzene and CH_2Cl_2 (1:9), complex **1** (1.18 g, 56%) was obtained as orange solid. From the successive reddish colored band eluted with ethyl acetate, complex **2** (466 mg, 14%) was obtained as dark reddish crystals. Recrystallization of **2** from benzene afforded an analytical sample, mp 118—120 °C as dark reddish prisms. Found: C, 39.92; H, 1.44%. Calcd for $C_7H_6OFe_2(CO)_6$; C, 40.45; H, 1.57%.

Reaction of 1 and $Fe_2(CO)_9$. A slurry of **1** (500 mg, 2.0 mmol) and $Fe_2(CO)_9$ (1.25 g, 3.4 mmol) in 60 ml of anhydrous ether was heated at reflux for 2 h. The reaction mixture was separated by chromatography on silica gel to afford **1** (186 mg, 37%) and **2** (247 mg, 29%).

Crystal Measurements, Data Collection, and X-Ray Structure Refinement for 2. A redish crystal with the sizes of 0.2×0.2×0.23 mm was used for data collection on a Rigaku automated four-circle diffractometer with a rotating anode (40 kV, 150 mA) using graphite monochromated Cu $K\alpha$ radiation (1.5418 Å). Crystal data are as follows: M.F.=$C_7H_6OFe_2(CO)_6$, M.W.=385.88, triclinic, space group $P\bar{1}$, a=14.660(3), b=12.919(3), c=9.086(3) Å, α=92.50(2), β=115.20(2), γ=112.00(2)°, V=1400.7(9) Å^3, Z=4, $D_{calcd.}$=1.83 g cm^{-3}. A total of 4250 reflections within 2θ=128° were collected by the θ-2θ scan mode. The structure determination was rather difficult, but finally succeeded by the direct method in consideration of pseudo-symmetrical location for eigth Fe atoms in the unit cell. The structure, thus obtained, were refined by the block diagonal least-squares method to prove the correct space group of $P\bar{1}$. After the Fe, C, and O atoms were refined anisotropically and the calculated H atoms were included, the final R value was 0.082 (R_w=0.093) for 3074 reflections with $F_o > 3\sigma(F_o)$.

Tables of positional and anisotropic thermal parameters of heavy atoms, and observed and calculated structural factors are kept at the Chemical Society of Japan, Document No. 8872. The details of crystallographic data should be requested to the author.

The authors are grateful to Dr. Hideo Sotokawa, Research Institute of Non-aqueous Solutions, Tohoku University for the technical asistant in X-ray diffraction analysis.

References

1) E. Weiss and W. Hübel, *Chem. Ber.*, **95**, 1179 (1962).
2) M. Franck-Newmann, F. Brion, and D. Martina, *Tetrahedron Lett.*, **1978**, 5033.
3) D. F. Hunt, G. L. Farrant, and G. T. Rodeheaver, *J. Organomet. Chem.*, **38**, 349 (1972).
4) A. Eisenstadt, *J. Organomet. Chem.*, **97**, 443 (1975).
5) R. B. King, *Inorg. Chem.*, **2**, 807 (1963).
6) R. P. Dodge, *J. Am. Chem. Soc.*, **86**, 5429 (1964).
7) Z. Goldschmidt, H. E. Gottlieb, and D. Cohen, *J. Organomet. Chem.*, **294**, 219 (1985); Z. Goldschmidt, H. E. Gottlieb, and A. Almadhoun, *ibid.*, **326**, 405 (1987), and references cited therein.
8) A. Tajiri, N. Morita, T. Asao, and M. Hatano, *Angew. Chem., Int. Ed. Engl.*, **24**, 329 (1985).
9) S. Litman, A. Gedanken, Z. Goldschmidt, and Y. Bakal, *J. Chem. Soc., Chem. Commun.*, **1978**, 983.
10) H. Sotokawa, A. Tajiri, N. Morita, C. Kabuto, M. Hatano, and T. Asao, *Tetrahedron Lett.*, **28**, 5873 (1987); A. Tajiri, H. Sotokawa, N. Morita, C. Kabuto, M. Hatano, and T. Asao, *Tetrahedron Lett.*, **28**, 6465 (1987).
11) N. Morita and T. Asao, *Chem. Lett.*, **1982**, 1575.
12) N. Morita, T. Asao, A. Tajiri, H. Sotokawa, and M. Hatano, *Chem. Lett.*, **1985**, 1879.
13) F. A. Cotton, B. G. DeBoer, and T. J. Marks, *J. Am. Chem. Soc.*, **93**, 5069 (1971); W. P. Fehlhammer and H. Stolzenberg, "Comprehensive Organometallic Chemistry," ed by G. Wilkinson, F. G. A. Stone, and E. W. Abel; Pergamon: Oxford, 1982; Vol. 4, p. 513.

Reactions of Metal Benzoylacetonates and Acetylacetonates with Formaldehyde

Tsutomu TAKEICHI,* Hiroaki OKUMURA, Yoshihiro SAKURADA, and Yuzi TAKAYAMA
School of Materials Science, Toyohashi University of Technology, Toyohashi 440
(Received December 13, 1988)

Synopsis. The reaction of cobalt benzoylacetonate with formaldehyde in water or methanol gave benzoic acid along with 4-hydroxy-3,3-bis(hydroxymethyl)-2-butanone or 4-methoxy-3,3-bis(hydroxymethyl)-2-butanone, respectively. The result suggests the formation of acetic acid in the reaction of metal acetylacetonate.

"Formose Reaction",[1] by which a complex mixture of sugars and sugar alcohols is formed by the base-catalyzed condensation of formaldehyde, has been attracting much attention in connection with the prebiotic synthesis of carbohydrates,[2] the possibility of the production of edible sugars from a simple materials, and the establishment of a metabolic cycle system of carbon resources in sustained space flight.[3] In general, however, the reaction results in complex products mixture, which hinders the utility of the attractive reaction. Selective formation of specific product is actively explored by using inorganic[4] or organic bases[5] as catalyst, or by photo- and γ-irradiation.[6]

During our attempt for a selective formose reaction using metal complexes, it was found out that a variety of metal acetylacetonates afforded 4-hydroxy-3,3-bis(hydroxymethyl)-2-butanone, **1**, and 4-methoxy-3,3-bis(hydroxymethyl)-2-butanone, **2**, selectively in water and methanol, respectively.[7] It was considered that **1** and **2** were formed from C-C bond cleavage of the ligand and the condensation with formaldehyde and the solvent.[7] But the fate of the other half of the ligand remained unknown. To clarify the feature of this reaction, the reaction of cobalt benzoylacetonate, instead of metal acetylacetonates, with formaldehyde was examined.

Experimental

Measurement. The gas chromatography (GC) was carried out with an OKURA Model 103 or a SHIMADZU Model GC-7AG equipped with a glass capillary column (i.d. 0.28 mm, 10 m) containing OV-1 or SE-30, the temperature of which was programmed from 100 °C to 260 °C at 6 °C min^{-1}. IR analyses were observed by JASCO Infrared Spectrophotometer Model A-3 or by JEOL JIR-40X FT-IR Spectrophotometer. ^1H NMR spectra were taken by JEOL JNM-GX 270 FT-NMR Spectrometer. Consumption of formaldehyde was determined by the method of Bricker[8] at 579 nm with HIRATA model 6B.

Formaldehyde Solution. Paraformaldehyde (1.20 g, 0.400 mol) was added into 200 ml of distilled water or anhydrous methanol and dissolved by heating to reflux for 6 h under N_2 atmosphere.

Reaction of Cobalt Benzoylacetonate with Formaldehyde. Into 30 ml of above prepared solution containing 1.80 g (60 mmol) of formaldehyde was added 1.0 mmol (0.3813 g) of cobalt benzoylacetonate,[9] and the mixture was stirred at 60 °C for 20 h under N_2 atmosphere. A 2 ml of aliquot was taken out to measure the formaldehyde consumption.

GC Analysis of the Products. After the removal of solvent and the unreacted formaldehyde, the products were trimethylsilylated[10] and analyzed by GC. Quantitative analysis of the silylated products was performed using tetradecane as an internal standard.

Isolation of the Products. The reaction mixture was treated with cation-exchange resin (Amberlite IR 118), followed by the removal of water and the unreacted formaldehyde, and then purified by column chromatography on silica gel (acetone/chloroform).

From the reaction of cobalt benzoylacetonate (3.813 g, 10 mmol) with formaldehyde (18.0 g, 600 mmol) in 300 ml of water, 0.50 g (4.1 mmol) of benzoic acid was obtained as white or pale-yellow crystal.

Results and Discussion

Reaction of Cobalt Benzoylacetonate with Formaldehyde in Water. Cobalt benzoylacetonate was reacted with formaldehyde in water at 60 °C for 20 h under N_2 atmosphere. The GC pattern of the trimethylsilylated products, as shown in Fig. 1a, was simple and a major peak, **A** in Fig. 1a, appeared, which was not observed in the case of metal acetylacetonates as shown in Fig. 1b.[7] It is to be noticed that a peak **B**, corresponding to **1**, was observed in the GC.

The reaction mixture treated with cation-exchange resin and purified by column chromatography to give the major product, corresponding to **A**, as a colorless or yellow crystal, which was identified to be benzoic acid by ^1H NMR, IR, and GC. The formation of **1** was also confirmed. Accordingly, equation shown below will be given for this reaction.

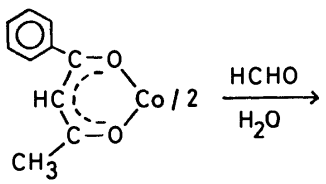

(1)

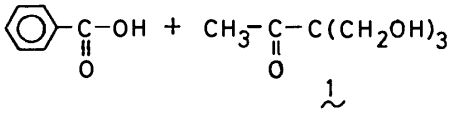

1

Quantitative analysis of the silylated products by GC using tetradecane as an internal standard gave 53 mg (0.43 mmol) of benzoic acid and 7 mg (0.05 mmol) of **1** from 1.0 mmol of cobalt benzoylacetonate. The conversion of formaldehyde was 8.0%, which means that 4.8 mmol of formaldehyde was consumed.

In the case of benzoylacetone complex, two mode of cleavage of ligand is possible as shown in Scheme 1. Route X leads to the formation of benzoic acid and **1**, and route Y to acetic acid and another polyol. Route X was confirmed here. The possible formation of other

products by route Y can not be neglected, but selective formation of benzoic acid and **1**, as shown in Fig. 1a, suggest that Route X is favored in this reaction.

Reaction of Cobalt Benzoylacetonate with Formaldehyde in Methanol. The same procedure was followed using methanol as solvent. The gas chromatogram of the trimethylsilylated products, as shown in Fig. 2a, suggests the formation of benzoic acid in the peak **A**. A peak **C**, corresponding to **2**, also appeared on the gas chromatogram. Benzoic acid was confirmed by isolating it following the above mentioned procedure, giving equation 2, shown below, for this reaction.

The quantitative analysis of the product by GC using tetradecane gave 33 mg (0.27 mmol) of benzoic acid and 2 mg (0.01 mmol) of **2** from 1.0 mmol of cobalt benzoylacetonate. The conversion of form-

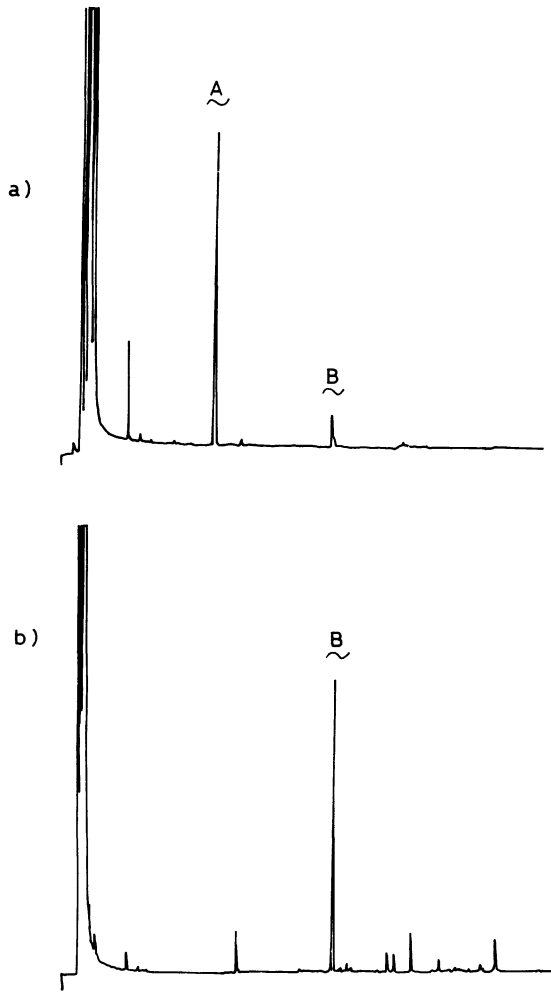

Fig. 1. The gas chromatogram of the TMS derivatives of the products. Column temperature was programmed from 100 to 260°C at 6°C min^{-1}. a) TMS-products obtained from cobalt benzoylacetonate/formaldehyde/H_2O at 60°C for 20 h. b) TMS-products obtained from cobalt acetylacetonate/formaldehyde/H_2O at 60°C for 20 h.

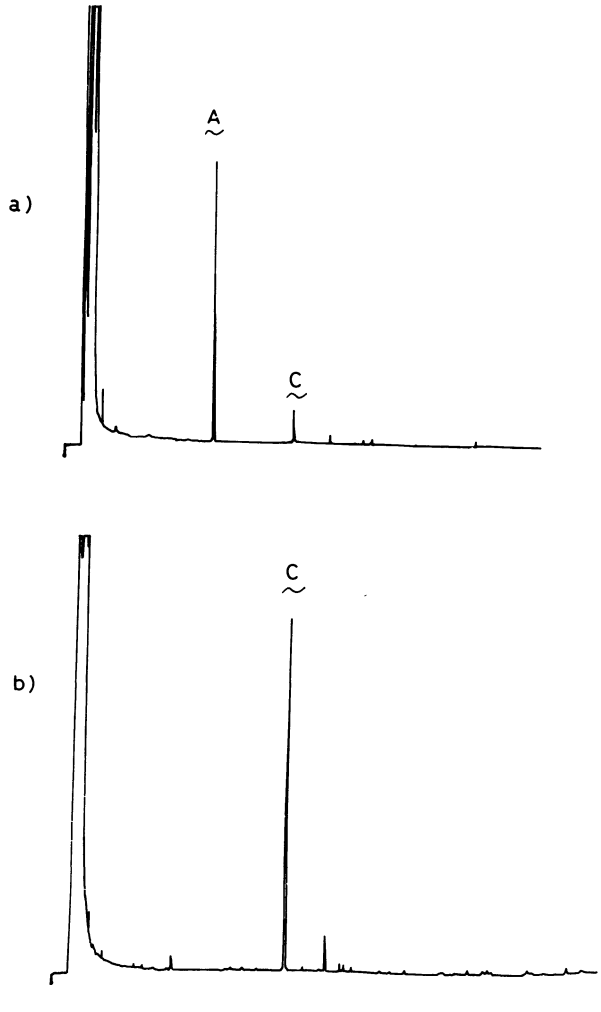

Fig. 2. The gas chromatogram of the TMS derivatives of the products. Column temperature was programmed from 100 to 260°C at 6°C min^{-1}. a) TMS-products obtained from cobalt benzoylacetonate/formaldehyde/methanol at 60°C for 20 h. b) TMS-products obtained from manganese(III) acetylacetonate/formaldehyde/methanol at 60°C for 20 h.

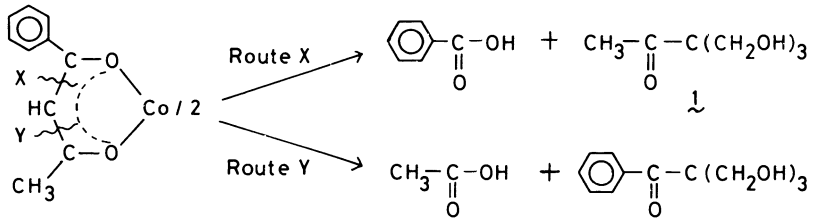

Scheme 1.

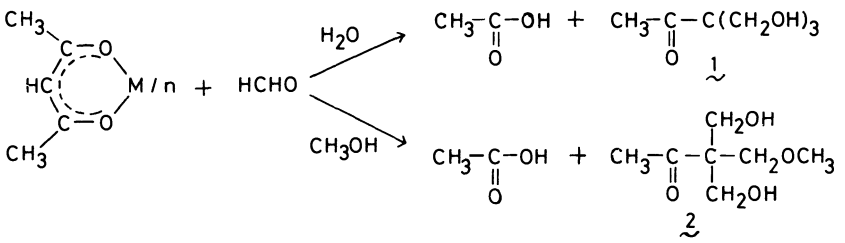

Scheme 2.

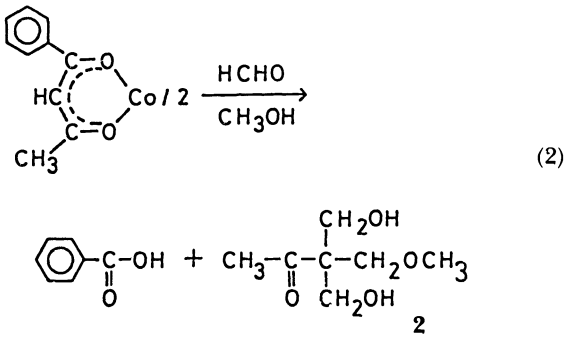

(2)

aldehyde was 1.9%, which correspond to 1.1 mmol of formaldehyde consumption.

Reaction of Metal Acetylacetonates. As menthioned before, the reaction of metal acetylacetonate with formaldehyde in water and methanol gave **1** and **2**, respectively, but the fate of the other half of the acetylacetone ligand was unknown. From the similarity of the reactions of acetylacetone and benzoylacetone complexes, the formation of benzoic acid in the reaction of metal benzoylacetone with formaldehyde, in turn, suggests the structure of the other half of the acetylacetone in the reaction of metal acetylacetonates, as acetic acid, which could not be isolated due to the volatility.

References

1) T. Mizuno, *Kagaku No Ryoiki*, **26**, 762 (1972); Y. Uchida, *Kagaku To Kogyo*, **28**, 77 (1975); Y. Shigemasa, *Yuki Gosei Kagaku Kyokai Shi*, **36**, 667 (1978); T. Matsumoto and S. Inoue, *Kagaku*, **37**, 383 (1982).

2) N. W. Gabel and C. Ponnamperuma, *Nature (London)*, **216**, 453 (1967); C. Leid and L. E. Orgel, *Nature (London)*, **216**, 455 (1967).

3) A. H. Weiss and J. Shapira, *Hydrocarbon Processing*, **49**, 119 (1972).

4) Y. Shigemasa, O. Nagae, C. Sakazawa, R. Nakashima, and T. Matsuura, *J. Am. Chem. Soc.*, **100**, 1309 (1978); Y. Shigemasa, Y. Sasaki, N. Ueda, and R. Nakashima, *Bull. Chem. Soc. Jpn.*, **57**, 2761 (1984).

5) T. Matsumoto, H. Yamamoto, and S. Inoue, *J. Am. Chem. Soc.*, **106**, 4829 (1984); T. Matsumoto, M. Yamae, and S. Inoue, *Chem. Lett.*, **1984**, 1819.

6) S. Irie, *Chem. Lett.*, **1984**, 2153.

7) T. Takeichi, Y. Sakurada, Y. Hieda, and Y. Takayama, *Chem. Lett.*, **1987**, 1301.

8) C. E. Bricker and H. R. Johnson, *Ind. Eng. Chem.*, **17**, 400 (1945); M. Lambert and A. C. Neish, *Can. J. Research*, **28B**, 83 (1950).

9) E. W. Berg and J. T. Truemper, *J. Chem. Soc.*, **64**, 487 (1960).

10) C. C. Sweeley, R. Bentley, M. Makita, and W. W. Wells, *J. Am. Chem. Soc.*, **85**, 2497 (1963); A. Nahrstedt, *J. Chromatogr.*, **50**, 518 (1970).

Selective Reduction of α,β-Unsaturated Carbonyl Compounds with Carbon Monoxide and Water Assisted by Selenium

Yutaka NISHIYAMA,* Yasuhiko MAKINO, Sawako HAMANAKA, Akiya OGAWA,† and Noboru SONODA†,*
Department of Applied Chemistry, Faculty of Engineering, Kansai University, Suita, Osaka 564
†Department of Applied Chemistry, Faculty of Engineering, Osaka University, Suita, Osaka 565
(Received December 22, 1988)

Synopsis. Carbon–carbon double bond of α,β-unsaturated carbonyl compounds can be reduced selectively with hydrogen selenide, generated in situ by the reaction of elemental selenium with carbon monoxide and water in the presence of strongly basic tertiary amine.

Recently we have developed a new reduction system, in which hydrogen selenide or its amine salt, formed in situ by the reaction of selenium with carbon monoxide and water, acts as an active reducing species.[1] The advantage of the utilization of this reduction system is to use strongly toxic hydrogen selenide[2] safely for reduction of organic compounds.[3] Now we have found that the Se–CO–H_2O reaction system is successfully usable for the selective reduction of the olefinic linkage of various α,β-unsaturated carbonyl compounds (Eq. 1).

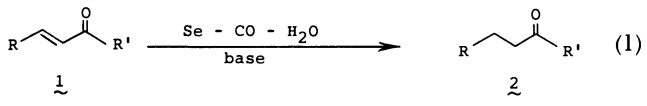

(1)

When benzylideneacetone (**1a**) was treated with carbon monoxide, water, and an equivalent amount of selenium in the presence of 1,8-diazabicyclo[5.4.0]-undec-7-ene (DBU)[4] at 50 °C, reduction of the carbon–carbon double bond took place selectively to give 4-phenyl-2-butanone (**2a**) in 82% yield. It was confirmed that similar reduction was widely applicable for the reduction of various α,β-unsaturated carbonyl compounds, and the results are summarized in Table 1. Enones having furyl or thienyl group undergo selective reduction without affecting the furyl or thienyl group (Runs 3 and 4). Reduction of α,β-unsaturated carboxylic acid (Run 5), ester (Run 6), and nitrile (Run 7) also proceeds at somewhat higher temperatures (80—100 °C). In the case of α,β-unsaturated aldehydes such as cinnamaldehyde, the similar reduction did not take place under the conditions employed.[5] Interestingly, enone (**1i**), which has no aromatic ring at the β position, underwent reduction of only conjugated C–C double (Run 9).[6] β-Ionone was reduced to 4-(2,6,6-trimethyl-

Table 1. Selective Reduction of α,β-Unsaturated Carbonyl Compounds[a]

Run	Substrate		Product	Yield/%[b]
	$PhCH{=}CHCR$ (O)		$PhCH_2CH_2CR$ (O)	
1	R=CH_3	(**1a**)	(**2a**)	82 (84)[c]
2	R=Ph	(**1b**)	(**2b**)	87
	$ArCH{=}CHCCH_3$ (O)		$ArCH_2CH_2CCH_3$ (O)	
3	Ar=	(**1c**)	(**2c**)	75 (74)[c]
4	Ar=	(**1d**)	(**2d**)	71
	$PhCH{=}CH{-}X$		$PhCH_2CH_2X$	
5[d]	X=COOH	(**1e**)	(**2e**)	93
6[e]	X=$COOC_2H_5$	(**1f**)	(**2f**)	89
7[f]	X=CN	(**1g**)	(**2g**)	72
8	$C_2H_5OCCH{=}CHCOC_2H_5$ (O, O) (**1h**)		$C_2H_5OCCH_2CH_2COC_2H_5$ (O, O) (**2h**)	86
9	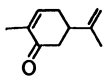 (**1i**)		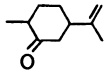 (**2i**)	85
10	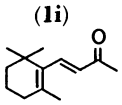 (**1j**)		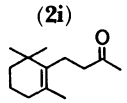 (**2j**)	83

a) Reaction conditions described in the text was used. b) Isolated yield. c) The yields in the parentheses obtained by the reaction using *N*-methylpyrrolidine (20 mmol) at 80 °C for 24 h. d) DBU (10 mmol), 100 °C. e) H_2O (10 mmol), 80 °C. f) 80 °C.

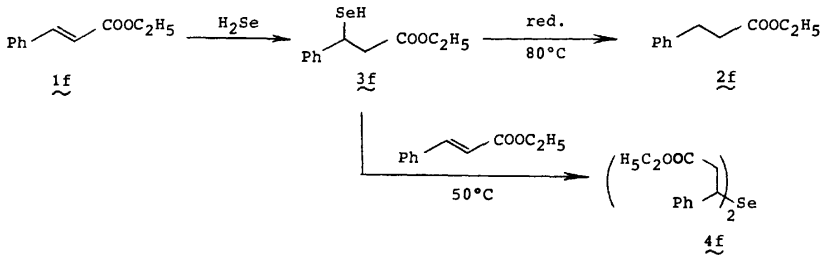

Scheme 1.

1-cyclohexenyl)-2-butanone (**2j**) in good yield (Run 10). This method is effective for the conversion of yakuchinone B (**1k**) to yakuchinone A (**2k**), both of which are linear diarly heptanoids with high pungency (Eq. 2).

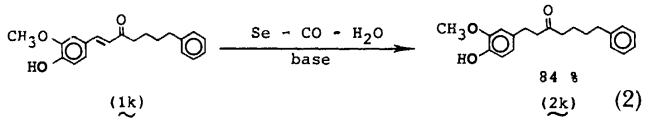

(2)

Although the mechanism of the reduction is not fully clarified, the reaction proceeds most probably through the Michael adduct **3** formed in situ by the

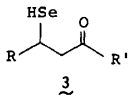

addition of hydrogen selenide to α,β-unsaturated carbonyl compound **1**. The formation of **3** is supported by the following observation: when the reaction of ethyl cinnamate (**1f**) with carbon monoxide, water, and selenium was carried out under controlled conditions (see Experimental section), the selenide **4f** was mainly formed probably through the Michael adduct **3f** (Scheme 1).

A number of methods have been reported for selective reduction of α,β-unsaturated carbonyl compounds: for example, catalytic hydrogenation using metal catalysts,[7] reduction with metal hydrides,[8] and reduction with metal or metal alloy.[9] However, high functional selectivity demonstrated in the text makes the present method more attractive.

Experimental

Instruments. The Instruments Used Were as Follows: ^{1}H NMR JEOL JNM-PS-100 and JEOL JNM-GXS-400; ^{13}C NMR Hitachi R-90H; IR, JASCO A-202; MS, Hitachi RMU-6A and JEOL JMS-QH100; melting points, Yanagimoto micro melting point apparatus.

Materials. Metallic selenium (99%) of Wako Chem. Co. and carbon monoxide (99.9%) of Seitetsu Chem. Co. were used. α,β-Unsaturated ketones (**1b**,[10] **1c**,[11] and **1k**[12]) were prepared according to the literatures. Preparation of **1d** was described below. Tetrahydrofuran (THF), amines, and other α,β-unsaturated carbonyl compounds were all purchased from commercial sources and purified by distillation or recrystallization.

4-(2-Thienyl)-3-buten-2-one (1d). To a mixture of 2-thiophenecarbaldehyde (22.4 g, 200 mmol), acetone (26.3 g, 453 mmol), and water (150 mL) was added 33% sodium hydroxide solution (3.8 mL) at 0 °C, and the mixture was stirred for 4 h at room temperature. The reaction mixture was neutralized with dilute sulfuric acid (10%). The organic layer was separated and dried over $MgSO_4$. The solvent was evaporated and the resulting liquid was distilled to give 24.1 g (79%) of 4-(2-thienyl)-3-buten-2-one (**1d**): bp 103—104 °C/6 mmHg (1 mmHg≈133.322 Pa). IR (NaCl) 1660, 1610, 960, 700 cm^{-1}; ^{1}H NMR δ=2.24 (s, 3H), 6.40 (d, J=16 Hz,1H), 6.84—7.40 (c, 3H), 7.53 (d, J=16 Hz,1H); MS (m/z) 152 (M^+).

Typical Procedure for Reduction of α,β-Unsaturated Carbonyl Compounds. A stirred mixture of benzylideneacetone (1.46 g, 10 mmol), selenium (0.79 g, 10 mmol), water (1.8 mL, 100 mmol), DBU (3.0 mL, 20 mmol), and THF (5 mL) sealed in a 50 mL stainless steel autoclave was heated under the pressure of carbon monoxide (30 atm; initial pressure at 25 °C) at 50 °C for 24 h. After the reaction was complete, carbon monoxide was purged in a well-ventilated hood, and air was blown into the solution for 10 min in order to oxidize the remaining hydrogen selenide to elemental selenium. Selenium deposited was filtered off and the filtrate was acidified with aqueous hydrochloric acid (2 M; 1 M=1 mol dm^{-3}) to pH 1—2, followed by extracted with diethyl ether (4×50 mL) and benzene (50 mL). The combined extracts were dried over $MgSO_4$. After the filtration, the solvent was evaporated in vacuo to leave yellow oil of crude material, which was chromatographed on silica gel (benzene/Et_2O=1:1) to give 1.22 g (82%) of 4-phenyl-2-butanone (**2a**): IR (neat) 1700, 740, 700 cm^{-1}; ^{1}H NMR δ=1.96, (s, 3H), 2.62 (t, J=7 Hz, 2H), 2.68 (t, J=7 Hz, 2H), 6.96—7.10 (m, 5H); MS (m/z) 148 (M^+).

Reduction of other α,β-unsaturated carbonyl compounds (**1b—1k**) and the following isolation were performed with the similar procedure described above, and the spectral data of the reduced products (**2b—2k**) were shown below. All products were identified by comparison of their ^{1}H NMR, IR, and mass spectra with those of samples commercially available or synthesized independently.

1,3-Diphenyl-1-propanone (2b). IR (neat) 1675, 740, 690 cm^{-1}; ^{1}H NMR (CCl_4) δ=2.76—3.17 (c, 4H), 6.90—7.40 (c, 8H), 7.78 (dd, J=8 and 2 Hz, 2H); MS (m/z) 210 (M^+); mp 71.5—73 °C (lit,[7a] 72—73 °C).

4-(2-Furyl)-2-butanone (2c). IR (neat) 1715, 730 cm^{-1}; ^{1}H NMR (CCl_4) δ=2.03 (s, 3H), 2.72 (t, J=8 Hz, 2H), 2.79 (t, J=8 Hz, 2H), 5.85—5.98 (m, 1H), 6.10—6.24 (m, 1H), 7.15—7.29 (m, 1H); MS (m/z) 138 (M^+).

4-(2-Thienyl)-2-butanone (2d). IR (neat) 1710, 695 cm^{-1}; ^{1}H NMR (CCl_4) δ=2.10 (s, 3H), 2.62 (t, J=8 Hz, 2H), 2.94 (t, J=8 Hz, 2H), 6.60—7.00 (c, 3H); MS (m/z) 154 (M^+).

3-Phenylpropionic Acid (2e). IR (KBr) 3500—2800, 1710, 735, 695 cm^{-1}; ^{1}H NMR (CCl_4) δ=2.50 (t, J=7 Hz, 2H), 2.82 (t, J=7 Hz, 2H), 7.02—7.24 (m, 5H), 11.68 (s, broad, 1H); MS (m/z) 150 (M^+); mp 47—48.5 °C (lit,[13] 47—49 °C).

Ethyl 3-Phenylpropionate (2f). IR (neat) 1720, 1180, 740, 695 cm^{-1}; ^{1}H NMR (CCl_4) δ=1.12 (t, J=8 Hz, 3H), 2.45 (t, J=8 Hz, 2H), 2.82 (t, J=8 Hz, 2H), 3.99 (q, J=8Hz, 2H), 7.00—7.35 (m, 5H); MS (m/z) 178 (M^+).

3-Phenylpropiononitrile (2g). IR (neat) 2240, 745, 695 cm^{-1}; ^1H NMR (CCl_2) δ=2.30 (t, J=8 Hz, 2H), 2.68 (t, J=8 Hz, 2H), 6.94—7.26 (m, 5H); MS (m/z) 131 (M^+).

Diethyl Succinate (2h). IR (neat) 1720, 1150 cm^{-1}; ^1H NMR (CCl_4) δ=1.34 (t, J=12 Hz, 6H), 2.54 (s, 4H), 4.18 (q, J=12 Hz, 4H); MS (m/z) 174 (M^+).

Dihydrocarvone (2i). IR (neat) 1710, 1650 cm^{-1}; ^1H NMR (CCl_4) δ=1.00—1.20 (m, 3H), 1.35—2.10 (c, 8H), 2.15—2.85 (m, 3H), 4.80—4.95 (m, 2H); MS (m/z) 152 (M^+).

4-(2,6,6-Trimethyl-1-cyclohexenyl)-2-butanone (2j). IR (neat) 1720, 1365, 1165 cm^{-1}; ^1H NMR (CCl_4) δ=1.00 (s, 6H), 1.40—2.15 (c, 8H), 1.57 (s, 3H), 2.15 (s, 3H), 2.25—2.55 (m, 2H); MS (m/z) 194 (M^+).

1-(3-Hydroxy-4-methoxyphenyl)-7-phenyl-3-heptanone (Yakuchinone A) (2k). IR (neat) 3560, 1710, 1275 cm^{-1}; ^1H NMR ($CDCl_3$) δ=1.51—1.62 (m, 4H), 2.38 (t, J=8 Hz, 2H), 2.58 (t, J=8 Hz, 2H), 2.60—2.90 (m, 4H), 3.82 (s, 3H), 5.50 (s, broad, 1H), 6.61 (dd, J=2,8 Hz, 1H), 6.73 (d, J=2 Hz, 1H), 6.78 (d, J=8 Hz, 1H), 7.00—7.40 (m, 5H); MS (m/z) 312 (M^+).

Isolation of Monoselenide (4f). A stirred mixture of ethyl cinnamate (**1f**) (1.76 g, 10 mmol), selenium (10 mmol), water (10 mmol), *N*-methylpyrrolidine[14] (20 mmol), and THF (5 mL) was heated under CO (30 atm) at 50 °C for 24 h. By a similar workup and purification as described above, the selenide (**4f**) was obtained in 84% yield as a mixture of its diastereoisomers whose IR, ^1H NMR, ^{13}C NMR, and mass spectrum are listed. Owing to thermal instability of the selenide, confirmation of their structures by elemental analyses was unsuccessful. IR (neat) 1730 (C=O), 1250, 1180 cm^{-1}; ^1H NMR (CCl_4) δ=1.10 (t, J=7.1 Hz, 3.6H), 1.15 (t, J=7.1 Hz, 2.4H), 2.76—2.98 (m, 2H), 3.94—4.07 (m, 4H), 4.18 (dd, J=7.3 and 8.4 Hz, 1.2H), 4.43 (dd, J=7.8 and 8.1 Hz, 0.8H), 7.11—7.29 (m, 10H); ^{13}C NMR ($CDCl_3$) δ=13.9 ($\underline{C}H_3CH_2$–), 39.3 and 39.5 ($\underline{C}$–C=O), 41.5 and 41.8 ($\underline{C}$–Se), 60.2 (O–$\underline{C}$). 126.8, 127.0, 127.3, 127.6, 128.2, 141.6 (Ph), 170.1 and 170.2 ($\underline{C}$=O); MS (m/z) 434 (M^+,^{80}Se).

References

1) N. Sonoda, K. Kondo, K. Nagano, N. Kambe, and F. Morimoto, *Angew. Chem., Int. Ed. Engl.*, **19**, 308 (1980). T. Miyata, K. Kondo, S. Murai, T. Hirashima, and N. Sonoda, *ibid.*, **19**, 1008 (1980).

2) Hydrogen selenide is regarded to be high toxic and unstable against air. To overcome these inconvenience, in situ formation and utilization without isolation are available. Cf. V. I. Cohen, *Synthesis*, **1978**, 668. D. L. Klayman and T. G. Griffin, *J. Am. Chem. Soc.*, **95**, 197 (1973). T. S. Woods and D. L. Klayman, *J. Org. Chem.*, **39**, 3716 (1974). A. Ogawa, J. Miyake, Y. Karasaki, S. Murai, and N. Sonoda, *ibid.*, **50**, 384 (1985). A. Ogawa, J. Miyake, N. Kambe, S. Murai, and N. Sonoda, *Bull. Chem. Soc. Jpn.*, **58**, 1448 (1985).

3) Y. Nishiyama, H. Hamanaka, A. Ogawa, S. Murai, and N. Sonoda, *Synthetic Commun.*, **16**, 1059 (1986). Y. Nishiyama, S. Hamanaka, A. Ogawa, N. Kambe, and N. Sonoda, *J. Org. Chem.*, **53**, 1326 (1988). A. Ogawa, Y. Nishiyama, N. Kambe, S. Murai, and N. Sonoda, *Tetrahedron Lett.*, **28**, 3271 (1987).

4) The reduction also proceeded in the presence of tertiary amine such as *N*-methylpyrrolidine.

5) When the reduction of cinnamaldehyde was carried out under the similar conditions as described in the text, side reactions took place to afford a complex mixture.

6) In the case of methyl vinyl ketone, the Michael adduct [bis(3-oxo-butyl) selenide] was formed as a main product.

7) See for example: R. Adams, J. W. Kern, and R. L. Shriner, *Org. Synth.*, Coll. Vol. 1, 101 (1956). H. Adkins and R. Connor, *J. Am. Chem. Soc.*, **53**, 1091 (1931). C. Djerassi and J. Gutzwiller, *ibid.*, **88**, 4537 (1966). R. E. Harmon, J. L. Parsons, D. W. Cooke, S. K. Gupta, and J. Schoolenberg, *J. Org. Chem.*, **34**, 3684 (1969). R. L. Augustine, D. C. Migliorine, R. E. Foscante, C. S. Sodano, and M. J. Sisbarro, *ibid.*, **34**, 1075 (1969).

8) See for example: R. W. Goetz and M. Orchin, *J. Am. Chem. Soc.*, **85**, 2782 (1963). J. P. Collman, R. G. Finke, P. L. Matlock, R. G. Wahren, and J. I. Brauman, *ibid.*, **100**, 1119 (1978). R. Noyori, I. Umeda, and T. Ishigami, *J. Org. Chem.*, **37**, 1542 (1972). M. F. Semmelhack and R. D. Stauffer, *ibid.*, **40**, 3619 (1975). M. Yamashita, Y. Kato, and R. Suemitsu, *Chem. Lett.*, **1980**, 847.

9) See for example: M. Contento, D. Saroia, C. Trombini, and A. Umani-Ronochi, *Synthesis*, **1979**, 30. N. A. Cortese and R. F. Heck, *J. Org. Chem.*, **43**, 3985 (1978). G. A. Page and D. S. Tarbell, *Org. Synth.*, Coll. Vol. 4, 136 (1963).

10) S. Wattanasin and W. S. Murphy, *Synthesis*, **1980**, 647.

11) G. J. Leuck and L. Cejka, *Org. Synth.*, Coll. Vol. 1, 283 (1956).

12) H. Itokawa, R. Aiyama, and A. Ikuta, *Chem. Pharm. Bull.*, **31**, 2491 (1983).

13) Catalog Handbook of Fine Chemicals, Aldrich; Aldrich Chemical Company: 1986—1987; p. 739.

14) Monoselenide was also formed in the case using DBU as a base.

 © 1989 The Chemical Society of Japan Bull. Chem. Soc. Jpn., 62, 1685—1691 (1989)

Novel Ferroelectric Liquid Crystals Derived from *n*-Alkyl Esters of (*R*)-3-Hydroxybutanoic Acid (II), the Correlation between Their Ferroelectric Properties and Their Molecular Structure

Jun NAKAUCHI,* Yoshitaka KAGEYAMA, Seiji HAYASHI, and Keiichi SAKASHITA
Tokyo Research Laboratories, Mitsubishi Rayon Co., Ltd., Noborito, Tama-ku, Kawasaki, Kanagawa 214
(Received September 16, 1988)

The temperature dependence of the spontaneous polarization (*Ps*) and the optical tilt angle (θ) of the following series of novel ferroelectric liquid crystals, derived from normal alkyl esters of (*R*)-3-hydroxybutanoic acid, have been investigated.

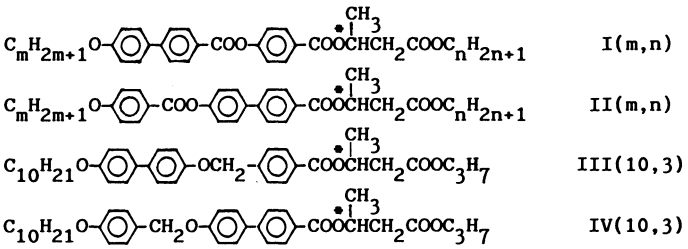

The magnitude of *Ps* and θ depends on the kind of linkage groups and their position in the core moiety as well as on the lengths of both terminal chains. The *Ps*'s for **I**(*m*,*n*) and **II**(*m*,*n*) show a maximum at (*m*,*n*)=(10, 3), whereas their θ's increase with the *m* and do not change very much with *n*. In comparison with four analogues (**I**(**10**,**3**), **II**(**10**,**3**), **III**(**10**,**3**), and **IV**(**10**,**3**)), which have the same terminal chains, but which show a different phase sequence, the magnitudes of *Ps* and θ are in the orders of: **III**(**10**,**3**)>**IV**(**10**,**3**)>**I**(**10**,**3**)~**II**(**10**,**3**) and **III**(**10**,**3**)>**I**(**10**,**3**)>**II**(**10**,**3**)>**IV**(**10**,**3**) respectively. Among all the compounds, the **III**(**10**,**3**) shows the maximum *Ps* as high as 1100 μC m^{-2} in the chiral smectic C phase and as high as 1750 μC m^{-2} in the chiral smectic I phase.

Ferroelectric liquid crystals are of great interest because of their application in a new type of high-speed switching device.[1] In the practical use of the liquid crystals, several smectogens have been blended in order to obtain a composition with properties suitable for the divice. For this purpose, it is necessary to know the material constants, such as the transition temperatures, the porality, the magnitude of spontaneous polarization (*Ps*), the optical tilt angle (θ), and the refractive index, and to understand the correlation between these physical properties and the molecular structure. Especially, it is important, not only from the practical point of view but also from the fundamental point of view, to elucidate the relationship between the two material constants (*Ps*,θ) and the molecular structure.

Ph. Martinot-Lagarde et al. showed simple formulae for the temperature dependence of *Ps* and θ for the compounds with a smectic A(SmA)-chiral smectic C(Sm*C) transition:[2]

$$Ps(T)=Ps^{\circ}(T_c-T)^a \quad (1)$$

$$\theta(T)=\theta^{\circ}(T_c-T)^b \quad (2)$$

where *Ps*(*T*) is the spontaneous polarization at temperature *T* °C, T_c is the SmA-Sm*C transition temperature, *T* is the actual temperature, $\theta(T)$ is the tilt angle at temperature *T* °C, and *Ps*°, θ°, *a*, and *b* are constants. These equations have been used in many papers; however, recent studies have shown that some materials do not exhibit the usual tendency in the temperature dependency of θ and *Ps* and that, therefore, the equations cannot be accepted as embodying general principles.[3-6] Furthermore, it has been recognized that the temperature dependency of θ in the SmC phase depends on the kind of phases adjacent to the Sm C phase.[7,8] In order to obtain a better understanding of the correlation between these material constants and the molecular structure, it is necessary to measure the material constants for various compounds and to accumulate data relating to the structural factors concerned with the ferroelectric properties.

We have synthesized the following series of novel ferroelectric liquid crytals, derived from *n*-alkyl esters of (*R*)-3-hydroxybutanoic acid, and investigated their physical properties:

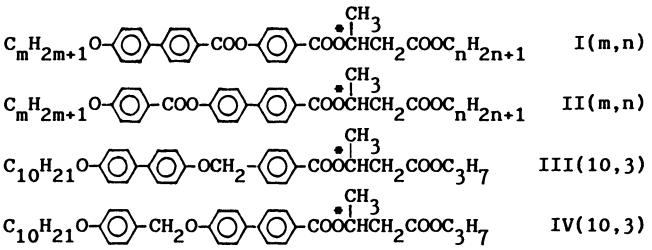

One of these compounds **I**(**8**,**2**) has already been synthesized, and the temperature dependence of its *Ps* has been reported by Taniguchi et al.[9] However, no systematic investigation of the ferroelectric properties

of the homologous series has yet been done.

In a previous paper,[10] we reported a synthetic method and the mesomorphic properties of these homologous series. In this paper, we wish to report the temperature dependency of θ and *Ps* for these compounds and discuss the correlation between their ferroelectric properties and the molecular structures.

Experimental

Measurement of Physical Properties. Miscibility tests for the unidentified smectic phase below the Sm*C phase were carried out by mixing the compounds with standard materials whose phase sequences has been assigned and by observing the microscopic textures by means of a Nikon polarizing microscope equipped with a Mettler FP52 heating stage. The spontaneous polarization (*Ps*) was determined by a triangular-wave method reported by Miyasato et al.[11] The frequency, the maximum amplitude, and the cell thickness were 10 Hz, ±150 V, and 50 μm, respectively. The optical tilt angle (θ°) and the polarity(the direction of *Ps*) were determined by applying a d.c. field to a specimen placed between crossed polarizers and by observing the direction of extinction by rotating the stage. The helical twist sense was determined by observing the variation in pitch in the Sm*C phase upon mixing with the reference compound.

Results and Discussion

The mesomorphic transition temperatures and the phase sequences of the compounds used in the experiments are summarized in Table 1. In order to assign the unidentified smectic phases below the Sm*C, we carried out miscibility tests for the analogues, **I(10,3)**, **II(10,3)**, and **III(10,3)**, by mixing them with the following standard materials:

Terephthalidene-bis-4-n-decylaniline (TBDA)

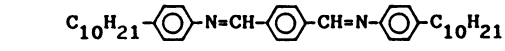

Iso→SmA→SmC→SmI→SmF→SmG

4-n-Hexyloxyphenyl 4'-n-octyloxybiphenyl-4-carboxylate (HPOBC)

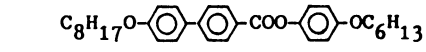

Iso→Ne→SmA→SmC→SmB

The miscibility diagrams of the binary mixtures, **I(10,3)**-TBDA, **II(10,3)**-HPOBC, and **III(10,3)**-TBDA, are shown in Figs. 1, 2, and 3 respectively. As can be seen in the figures, the Sm3 phases of **II(10,3)** and **III(10,3)** are smectic B(SmB) and chiral smectic I(Sm*I), respectively. The Sm3 phase of **I(10,3)**, which was speculated in the previous paper to be the Sm*I phase from the microscopic texture, is really chiral smectic G(Sm*G) or chiral smectic J(Sm*J). These two phases cannot be distinguished by only miscibility tests.

All the compounds used in the experiments show a

Table 1. Phase Sequences and Transition Temperatures for the **I**(*m*,*n*) and **II**(*m*,*n*) Homologous Series, and the **III**(10,3) and **IV**(10,3) Analogues

Homologous Series	Carbon No. (*m*,*n*)	Phase-transition temperature (°C)[a]										
		Mp	Sm4		Sm3		Sm*C		SmA		Iso	
I(*m*,*n*)	(7,3)	91.8					(74.9)[B]	*	105.0	*	154.3	*
	(8,3)	96.8					(66.6)	*	112.0	*	147.0	*
	(9,3)	84.5					(57.1)	*	110.0	*	146.1	*
	(10,3)	78.6					(52.5)	*	110.5	*	137.9	*
	(11,3)	81.2							115.9	*	140.6	*
	(12,3)	81.3							114.1	*	136.1	*
	(14,3)	86.3							110.5	*	130.1	*
	(16,3)	87.2							108.2	*	126.9	*
	(10,1)	78.5			(64.0)	*	102.8	*	120.0	*	155.7	*
	(10,2)	88.1					(58.0)	*	120.0	*	146.1	*
	(10,4)	68.0					(50.2)	*	111.1	*	136.5	*
	(10,5)	70.9					(49.2)	*	95.9	*	129.6	*
	(10,8)	74.5							83.5	*	123.7	*
II(*m*,*n*)	(9,3)	92.2							(80.0)	*	129.2	*
	(10,3)	85.8					(56.6)	*	(84.0)	*	126.5	*
	(12,3)	77.2							93.0	*	122.8	*
	(14,3)	72.1					(49.3)	*	96.1	*	118.7	*
	(16,3)	72.2							96.5	*	116.0	*
	(10,2)	75.8					(46.3)	*	(62.5)	*	110.5	*
	(10,7)	76.3					(46.3)	*	(62.5)	*	110.5	*
III(*m*,*n*)	(10,3)	85.4			85.4	*	110.5[c]	*			127.0	*
IV(*m*,*n*)	(10,3)	90.0							(84.0)	*	93.6	*

a) Mp; melting point, Sm3, Sm4; unidentified smectic phase, Sm*C chiral smectic C, SmA; smectic A, Iso; isotropic liquid. b) ( ); monotropic transition. c) This transition was designated as Sm2-Sm*C in a previous paper.[10]

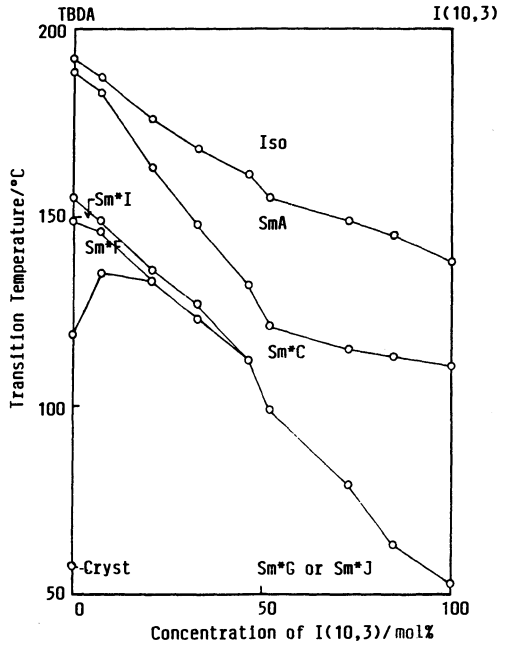

Fig. 1. Phase diagram for the binary mixtures of **I(10,3)** with TBDA.

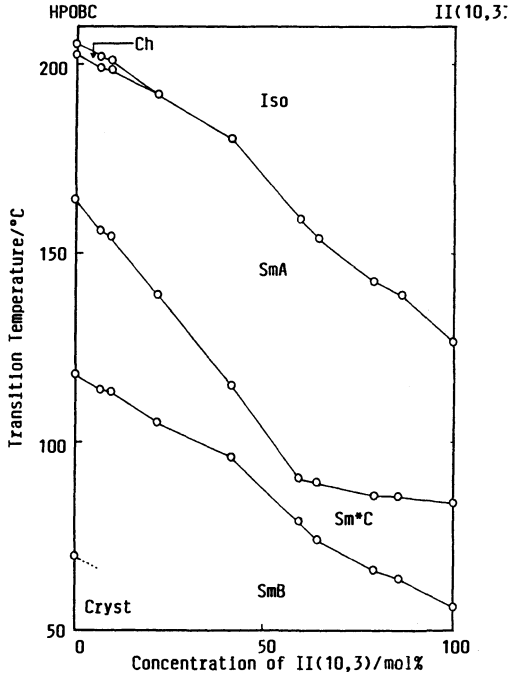

Fig. 2. Phase diagram for the binary mixtures of **II(10,3)** with HPOBC.

negative polarity and have a left-hand helix in the Sm*C phase. This tendency is consistent with the empirical rule about the relation between the absolute spatial configuration of a chiral group and the polarity and helical twist sense reported by Goodby et al.[12,13]

Figures 4(a,b) and 5(a,b) show the tempereature dependence of θ and *Ps* for the **I(*m*,3)** and **I(10,*n*)**

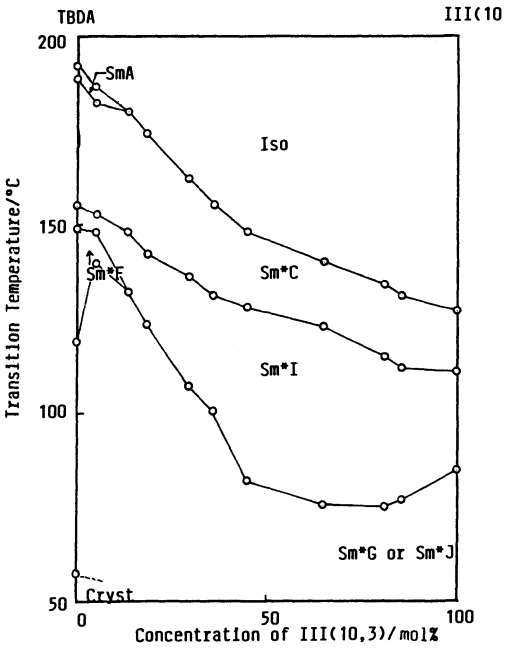

Fig. 3. Phase diagram for the binary mixtures of **III(10,3)** with TBDA.

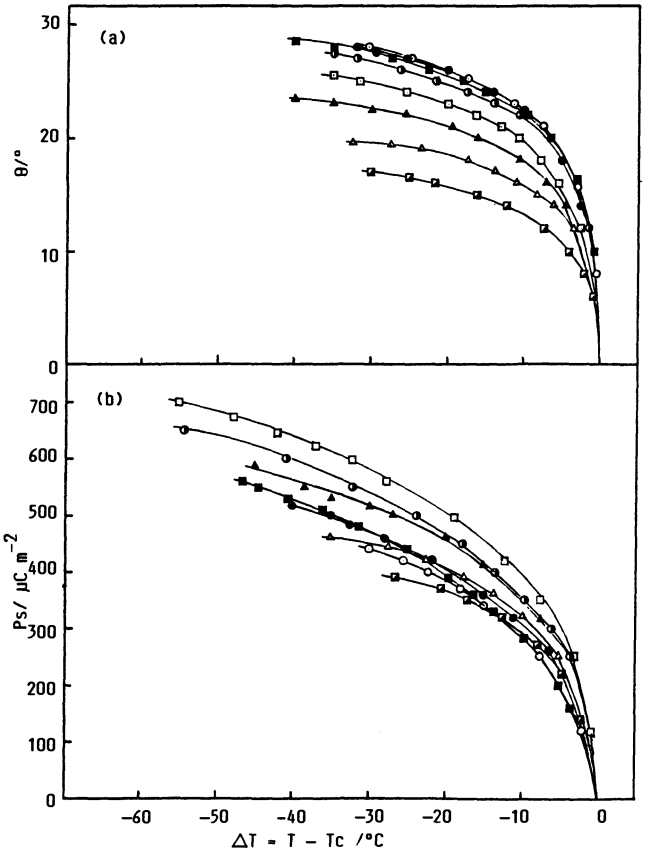

Fig. 4. Temperature dependence of the optical tilt angle (θ°) (a) and the spontaneous polarization (*Ps*) (b) for the homologous series **I(*m*,3)**: *m*=7 (—◪—); *m*=8 (—△—); *m*=9 (—▲—); *m*=10 (—□—); *m*=11 (—◑—); *m*=12 (—□—); *m*=14 (—●—); *m*=16 (—○—).

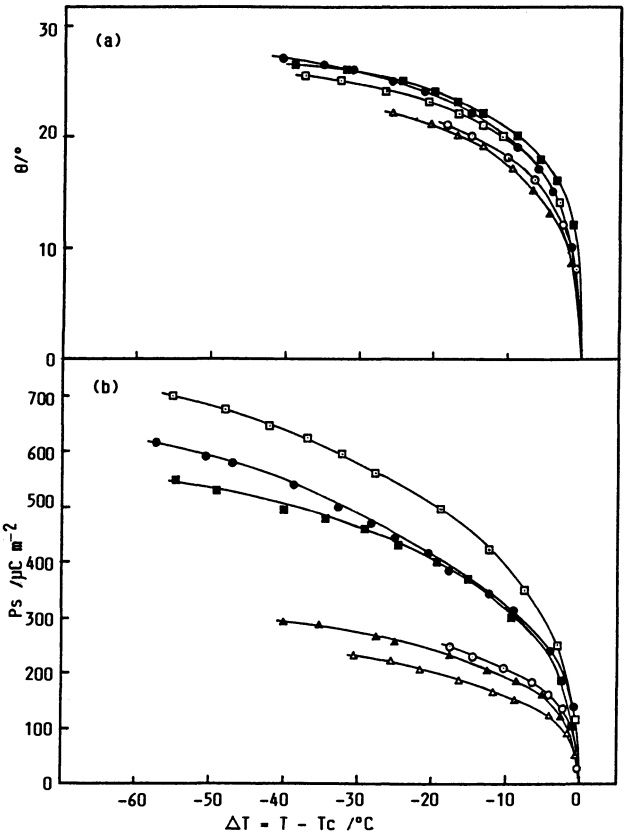

Fig. 5. Temperature dependence of the optical tilt angle (θ°) (a) and the spontaneous polarization (Ps) (b) for the homologous series **I(10,*n*)** n=1 (—○—); n=2 (—●—); n=3 (—□—); n=4 (—■—); n=5 (—▲—); n=8 (—△—).

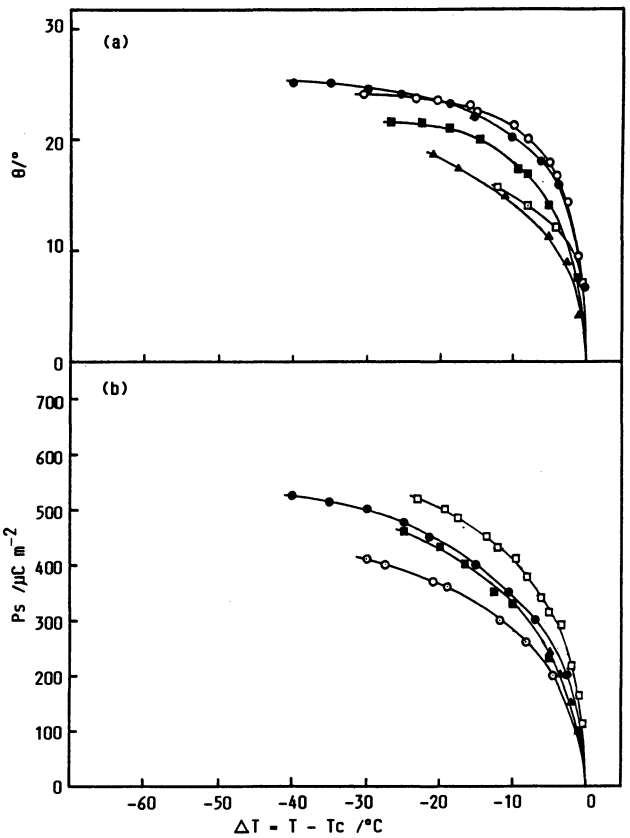

Fig. 6. Temperature dependence of the optical tilt angle (θ°) (a) and the spontaneous polarization (Ps) (b) for the homologous series **II(*m*,3)**: m=9 (—▲—); m=10 (—□—); m=12 (—■—); m=14 (—●—); m=16 (—○—).

homologous series, respectively. As is evident from the figures, the θ for **I(*m*,3)** increases with the number of carbon atoms (m) in the terminal alkoxyl chain and approaches a constant value (ca. 28°), whereas the Ps for **I(*m*,3)** increases with m up to m=10 and then decreases with m. The maximum Ps value (700 μC m^{-2}) was observed in the **I(10,3)** at ΔT=−55°C. On the other hand, the θ for **I(10,*n*)** slightly increases with n up to n=4 and then gradually decreases with n, whereas the Ps for **I(10,*n*)** abruptly increase with n up to n=3 and then rapidly decrease with n. Figures 6(a,b) and 7(a,b) show the temperature dependence of the θ and Ps values for the **II(*m*,3)** and **II(10,*n*)** homologous series, respectively. These series have the same linkage group (-COO-) as the **I(*m*,3)** and **I(10,*n*)** except for its position in the core moiety. We could not measure the θ and Ps values for all the homologues because the majority of their Sm*C phases were unstable monotropic phases and because recrystallization often occurred during the measurements. The θ for **II(*m*,3)** also increases with m and approaches a constant value (ca. 25 °C), whereas the Ps for **II(*m*,3)** increases with m up to m=3 and then decreases with m. The maximum Ps (520 μC m^{-2} was observed in the **II(14,3)** at ΔT=−40 °C. In the case of **II(10,*n*)** (Fig. 7(a,b)), the effect of the chain length (n) on the temperature dependency of θ and Ps cannot be clarified because the θ and Ps have been measured in only a few of the **II(10,*n*)**.

In order to elucidate the effect of the length of the terminal chains (m,n) on the θ and Ps for **I(*m*,*n*)** and **II(*m*,*n*)**, the values of θ and Ps at ΔT=−10 °C were plotted against the carbon number (m and n) in the terminal chains (Figs. 8A(a,b) and 8B(a,b)). As can be seen in the figures, in the case of **I(*m*,*n*)**, the dependencies of the lengths of the two terminal chains (m,n) on the θ and Ps are significantly different from one another. The θ for **I(*m*,3)** increases with m, whereas that for **I(10,*n*)** does not change very much with n. On the other hand, the Ps values for **I(*m*,3)** and **I(10,*n*)** show maxima at m=10 and n=3, respectively. Moreover, the effect of n on the magnitude of Ps is stronger than that of m on the magnitude of Ps. A similar tendency can be seen in the **II(*m*,*n*)** except for the dependency of n on the θ for **II(10,*n*)** whose θ is much smaller than that of **I(10,*n*)**; that is, the effect of m on the θ and Ps for **II(*m*,3)** is almost the same as that for **I(*m*,3)**. The effect of n on the Ps for **I(10,*n*)**, although there are only two data plotted on the figure.

These results indicate that the structural factors

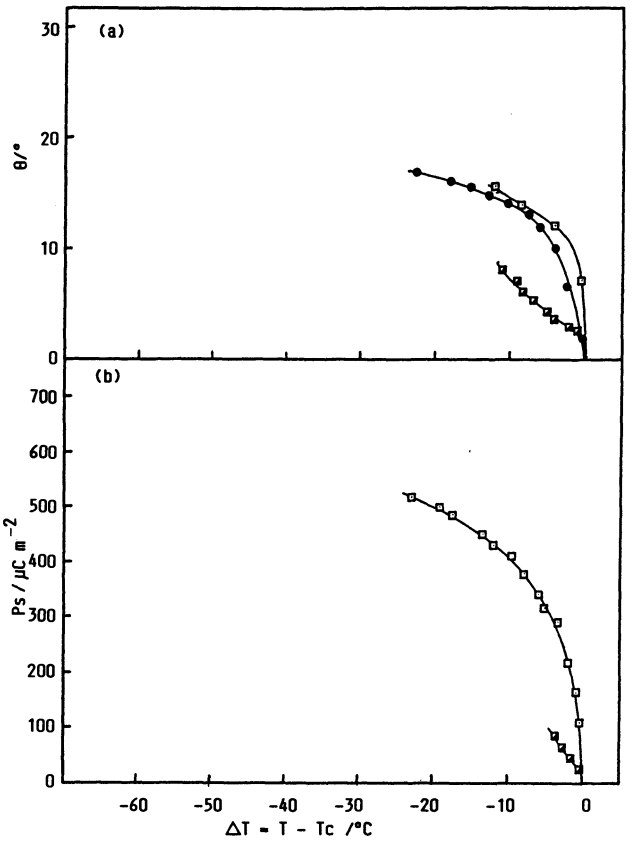

Fig. 7. Temperature dependence of the optical tilt angle (θ°) (a) and the spontaneous polarization (*Ps*) (b) for the homologous series **II**(**10**,*n*): n=2 (—●—); n=3 (—□—); n=7 (—◪—).

concerned with the temperature dependency of the terminal chains on the *Ps* are quite different from those concerned with the temperature dependency of the terminal chains on the θ and that the constants, *a* and *b*, in Eqs. 1 and 2 are generally not equal. Additionally, judging from these data, the magnitude of *Ps* seems to be independent of the position of the linkage group -COO- in the core.

For the purpose of investigating more closely the effect of the core structure on the *Ps* and θ, the temperature dependence of *Ps* and θ for four analogues, **I**(**10**,**3**), **II**(**10**,**3**), **III**(**10**,**3**), and **IV**(**10**,**3**), were examined (Fig. 9). It is noteworthy that these analogues have different phase sequences. As is evident from the figures, the magnitudes of *Ps* and θ depend strongly on the core structures, that is, the kind and position of the linkage group in the core, and are in the orders of **III**(**10**,**3**)>**IV**(**10**,**3**)>**I**(**10**,**3**)~**II**(**10**,**3**) and **III**(**10**,**3**)>**I**(**10**,**3**)>**II**(**10**,**3**)>**IV**(**10**,**3**), respectively. Among all the compounds used in the experiments, the **III**(**10**,**3**) with a -OCH_2- linkage shows the largest values of *Ps* and θ. Especially, the magnitude of *Ps* is as high as 1100 $\mu C m^{-2}$ in the Sm*C phase and 1750 $\mu C m^{-2}$ in the Sm*I phase.

Generally, the magnitude of *Ps* is considered to depend on the perpendicular component of the dipole moment of the polar group adjacent to the chiral part. These four analogues have the same group adjacent to the same chiral group; therefore, the origin of the *Ps* is considered to be same. Even if we take into consideration the difference in other factors (θ and T_c) con-

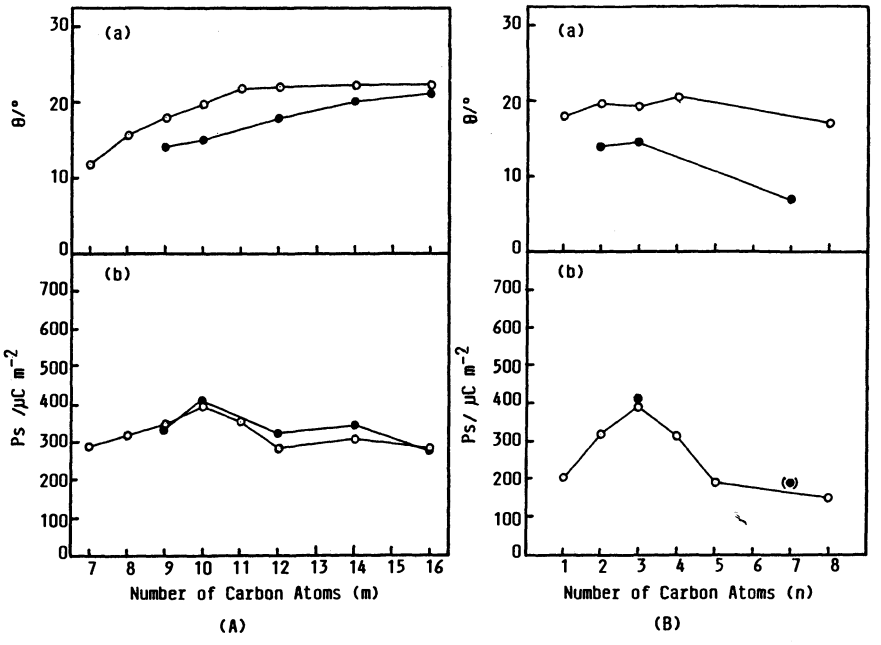

Fig. 8. Plots of the θ (a) and *Ps* (b) measured at ΔT=−10 °C against the number of carbon atoms (*m*) in the alkoxyl chain (n=3) (A) and the number of the carbon atoms (*n*) in the alkyl ester chain (m=10) (**B**): **I**(*m*,*n*) homologues (—○—); **II**(*m*,*n*) homologues (—●—). *( ): extrapolated value.

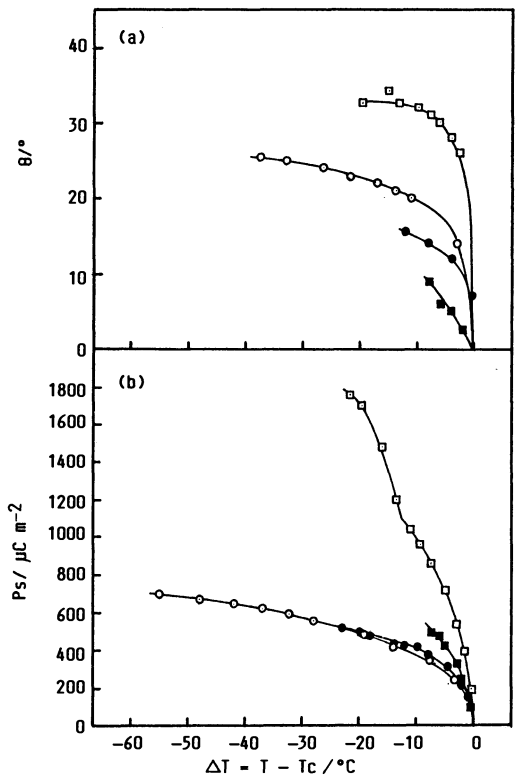

Fig. 9. Temperature dependence of the θ (a) and the *Ps* (b) for four analogues: **I(10,3)** (—○—); **II(10,3)** (—●—); **III(10,3)** (—□—); **IV(10,3)**.

nected to the magnitude of *Ps*, we cannot explain the reason for the difference in the magnitude of *Ps* among these analogues.

Taniguchi et al. investigated the effect of linkage groups (-COO- and -CH_2O-) in the core on the *Ps* for four couples, each of which was a pair of analogues with the same chiral group, and showed that the compounds with the -COO- linkage had larger *Ps* values than those with the -CH_2O- linkage, except for one couple.[14] They speculated that the -COO- linkage enhanced the *Ps* more than the -CH_2O- linkage because of its larger dipole moment, although they did not measure the effect of θ on the *Ps*. Taking the effect of θ on the magnitude of *Ps* into consideration, among the four analogues investigated in this study, the **III(10,3)** and **IV(10,3)** with the -CH_2O- linkage show much larger *Ps* value than of the **I(10,3)** and **II(10,3)**; therefore, in this case, the -CH_2O- linkage seems to enhance the *Ps* more than the -COO- linkage. Similar results were also obtained in the mesogenic compounds with -CH_2O- linkage in the same core as that of **III(10,3)**.[15]

There is another difference in the natures of the -CH_2O- and -COO- bonds. Compared with the -CH_2O- bond, the -COO- bond is conjugated to the phenyl or biphenyl moiety in the core, leading to the production of induced dipole moments parallel to the molecular axis, as is shown in the following picture:

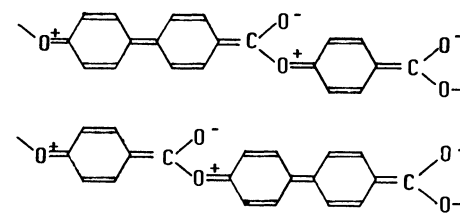

As has been pointed out by Goodby,[16] these induced dipoles cannot contribute to the *Ps*, but they do promote the following anti-parallel paking among the core moiety:

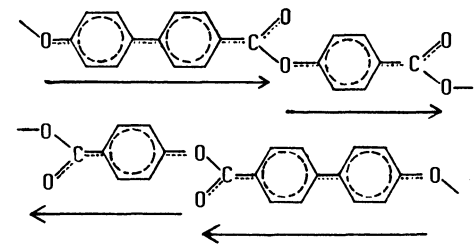

The formation of an anti-parallel pair could enhance the thermal stability of the Sm*C phase and also affect the temperature dependencies of *Ps* and θ in the Sm*C phase because of the intermolecular force attributed to the induced dipoles could suppress the interaction between the out-board dipoles and disturb the arrangement of the dipoles, thus contributing to the magnitude of *Ps*. Such difference in the intermolecular interactions may also affect the formation of higher-order smectic phases; that is, the packing state of the molecules in the Sm*C phase may some relation to the kinds of smectic phase below the Sm*C phase.

More detailed studies of the higher-order structures in smectic mesophase, including the effect of induced dipoles in the core, will be necessary to elucidate the correlation between the ferroelectric properties and the molecular structure.

The authors would like to thank Dr. Hiroshi Sato for his hearty encouragement throughout this work and also Dr. Toshio Yoshihara for his useful suggestions. The authors also wish to thank to Mr. Yoshihiro Sako for his assistance with the experiments.

References

1) N. A. Clark and S. T. Lagerwall, *Appl. Phys. Lett.*, **36**, 899 (1980).

2) Ph Martinot-Lagarde, R. Duke, and G. Durand, *Mol. Cryst. Liq. Cryst.*, **75**, 249 (1981).

3) S. Dumrongratta, C. C. Huang, G. Nouness, S. C. Lien, and J. M. Viner, *Phys. Rev. A*, **34**, 5010 (1986).

4) N. Mikami, R. Higuchi, T. Sakurai, M. Ozaki, and K. Yoshino, *Jpn. J. Appl. Phys.*, **25**, L833 (1986).

5) J. S. Patel and J. W. Goodby, *J. Phys. Chem.*, **91**, 5838 (1987).

6) J. W. Goodby, E. Chin, J. M. Geary, J. S. Patel, and P. L. Finn, *J. Chem. Soc., Faraday Trans. 1*, **83**, 3429 (1987).

7) T. Inukai, S. Saitoh, H. Inoue, K. Miyazawa, K.

Terashima, and K. Furukawa, *Mol. Cryst. Liq. Cryst.*, **141**, 251 (1986).

8) E. Fanelli, S. Melone, G. Torquati, V. G. K. M. Pisipati, and N. V. S. Rao, *Mol. Cryst. Liq. Cryst.*, **146**, 235 (1987).

9) H. Taniguchi, M. Ozaki, and K. Yoshino, *Jpn. J. Appl. Phys.*, **26**, Suppl. 26—2, 101 (1987).

10) J. Nakauchi, K. Sakashita, Y. Kageyama, S. Hayashi, and K. Mori, *Bull. Chem. Soc. Jpn.*, in press.

11) K. Miyasato, S. Abe, H. Takezoe, A. Fukuda, and E. Kuze, *Jpn. J. Appl. Phys.*, **22**, L661 (1983).

12) J. W. Goodby, E. Chin, T. M. Leslie, J. M. Geary, and J. S. Patel, *J. Am. Chem. Soc.*, **108**, 4729 (1986).

13) J. M. Goodby and E. Chin, *J. Am. Chem. Soc.*, **108**, 4736 (1986).

14) H. Taniguchi, M. Ozaki, K. Nakano, K. Yoshino, N. Yamasaki, and K. Satoh, *Jpn. J. Appl. Phys.*, **27**, 452 (1988).

15) K. Terashima, M. Ichihashi, M. Kikuchi, K. Furukawa, and T. Inukai, *Mol. Cryst. Liq. Cryst.*, **141**, 237 (1986).

16) J. W. Goodby, *Mol. Cryst. Liq. Cryst.*, **75**, 179 (1981).

Basicity of Water in Hydrogen-Bonded Networks of Methanol-1,2-Dichloroethane Mixtures Using the [(1*R*,4*S*,8*R*,11*S*)-1,4,8,11-Tetramethyl-1,4,8,11-tetraazacyclotetradecane]nickel(II) Cation as a Probe of Electron-Pair Acceptance

Etsuro IWAMOTO, Shoji YAMASAKI, and Takahiro KUMAMARU*
Department of Chemistry, Faculty of Science, Hiroshima University, Higashisenda-machi, Naka-ku, Hiroshima 730
(Received September 22, 1988)

The basicity of water in methanol (MeOH) and MeOH-1,2-dichloroethane (DCE) mixtures was examined by using spectral data of the title square planar chelate cation ([Ni(tmc)]$^{2+}$). Although MeOH molecules are hardly coordinated to the chelate, the water molecules hydrogen-bonded with MeOH are easily coordinated to the cation, depending on the degree of hydrogen-bonded networks of MeOH. A fitting method showed that in the MeOH-rich mixtures the dimerization of water occured and only the terminal monomeric water molecule in the MeOH oligomer could be coordinated. The equilibrium constant K_{NiWl}=[Ni(tmc)(H$_2$O)$^{2+}$]/[Ni(tmc)$^{2+}$][H$_2$O] was 3.2 in the 0.1 MeOH mole fraction mixture, 3.0 in 0.3, 3.2 in 0.5, 6.2 in 0.7, 9.5 in 0.9, 10.0 in 1.0. Linear relationships of ^{1}H chemical shift of the OH group for MeOH in various solvents with the K_{NiWl} values and Gutmann's donor number (DN) were found and DN values were estimated for the DCE-MeOH mixtures. The enhancement of basicity of the water molecules was discussed from the viewpoints of the charge transfer effect through hydrogen bonding and the development of hydrogen-bonded networks.

In our previous papers,[1,2] effects of intermolecular interactions between water and dipolar aprotic solvent molecules on the basicity of water have been studied by using spectral data of [(1*R*,4*S*,8*R*,11*S*)-1,4,8,11-tetramethyl-1,4,8,11-tetraazacyclotetradecane]nickel(II) ([Ni(tmc)]$^{2+}$) with an 1*R*,4*S*,8*R*,11*S*- set of nitrogen configurations as a probe of electron pair acceptance. Although it is known that the red, square planar chelate cation forms a green, five-coordinate square pyramidal complex by axial ligation with a donor solvent or ion,[3-5] we found that oxygen donor coordinating molecules such as H$_2$O, MeOH, acetone (AC), and 1,2-propanedyl carbonate (PDC) of which DNs are less than 20, were not coordinated to the nickel cation in nitrobenzene (NB) as a diluent.[1,6] However, the water molecules in pure water and in hydrogen bonding acceptor solvents such as AC, PDC, and *N*,*N*-dimethylacetamide (DMA) can be coordinated and furthermore the dimerization of water in nitromethane (NM), PDC, and AC leads to coordination of water, of which the equilibrium constant increases with increasing the basicity of the bulk solvent molecules, i.e. in the order NM<PDC<AC. The basicity of water was related with the formation constant (K_{NiW}) of the aqua chelate cation in Reaction 1

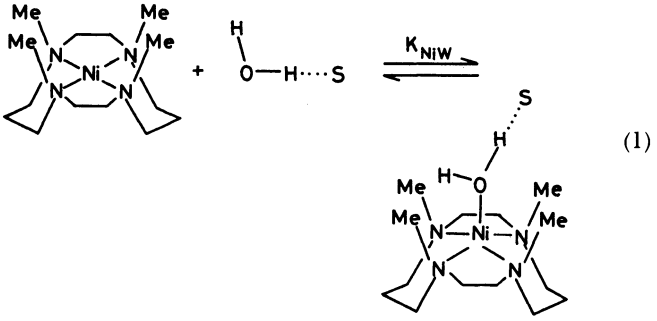

(1)

where S is hydrogen-bonding acceptors or basic solvents.

The above phenomena are explained by the increase in the charge density on the oxygen atom of water due to hydrogen bonding with such basic molecules. Thus, the donor number 18 of water proposed by Gutmann[7,8] is ascribed to the isolated water molecules of the lowest basicity, for example, dissolved in much lower basic DCE and NB. Mayer and Gutmann[9] also introduced the term "bulk donicity" to characterize the basic properties of water. The basicity of water greatly depends on the strength of hydrogen bonding and little is known concerning the nature of water basicity, especially, in protic solvents. The water molecule in aqueous mixtures is the solute or the solvent that takes our major interest.

The purpose of this work is to study the effect of network structure of MeOH on the basicity of water in DCE-MeOH mixtures. The two- or three-dimensional cross-linked polymer for the amphiprotic solvent, unlike aprotic solvents, make it more difficult to understand the water-solvent interactions. However, mixtures of MeOH with inert DCE give information concerning the network structure which is relatively easily obtained using IR and NMR data. Hydrogen-bonded networks of MeOH are promoted with increasing the MeOH fraction and the K_{NiW} value for the water molecules present in the DCE-MeOH mixtures is expected to increase with growing hydrogen bonds among MeOH molecules.

Experimental

The metal chelate electrolyte (*R*,*S*,*R*,*S*)-[Ni(tmc)](ClO$_4$)$_2$ was prepared as described previously.[1-3] DCE, MeOH, pyridine (Py), hexamethylphosphoric triamide (HMPA),

N,N-dimethylformamide (DMF), DMA, dimethyl sulfoxide (DMSO), AC, and PDC (Reagent grade, Wako Pure Chemical Industries Ltd.) were purified by fractional distillation through a 1.2-m column without washing. NB (Reagent grade, Wako Pure Chemical Industries Ltd.) was purified by fractional distillation under reduced pressure after washing with 1.5 mol dm^{-3} H_2SO_4 and 1 mol dm^{-3} $NaHCO_3$. Tetrahydrofuran (THF) (Wako Pure Chemical Industries Ltd.) and benzonitrile (BN) (Aldrich Chemical Company) were used without further purifications. All solvents were used after standing over molecular sieves (Type 4A) for one week.

The apparatus and the procedures used for measurements of the water content, the high-resolution proton chemical shift, and infrared spectra have been described earlier.[1,2]

Results and Discussion

Typical visible spectra of the chelate cation in a mixture of the 0.7 MeOH mole fraction with DCE containing water are shown in Fig. 1. The absorption peak at 520 nm is referred to the four-coordinate planar complex, and the peaks at 396 nm and ca. 660 nm are referred to the five-coordinate square pyramidal complex. When the water content is 8.30×10^{-3} mol dm^{-3}, the chelate is almost four-coordinate. The absorbance at 520 nm decreases with increasing the water concentration. This shows that the bulk solvent molecules can not be coordinated to the chelate, but the water molecules in this solution can be coordinated. The dependence of the absorbance on the water concentration in various DCE-MeOH mixtures is shown in Fig. 2 together with the results for Py. Although highly basic Py (DN=33.1[7]) molecules can not be coordinated due to steric hindrance,[6] it is seen that the water in Py can become much easily coordinated.

Ionic association of the nickel complex with the perchlorate ion may occur in mixtures containing DCE with a low dielectric constant. In our previous study,[6] ionic association effects on coordination were hardly observed even in AC solution with a first association constant of 12200. Since the basicity of the perchlorate ion is very weak, it is reasonably assumed that there is no ionic association effect on the water coordination.

IR and NMR of Water and MeOH in DCE-MeOH Mixtures. As the coordination ability of water mole-

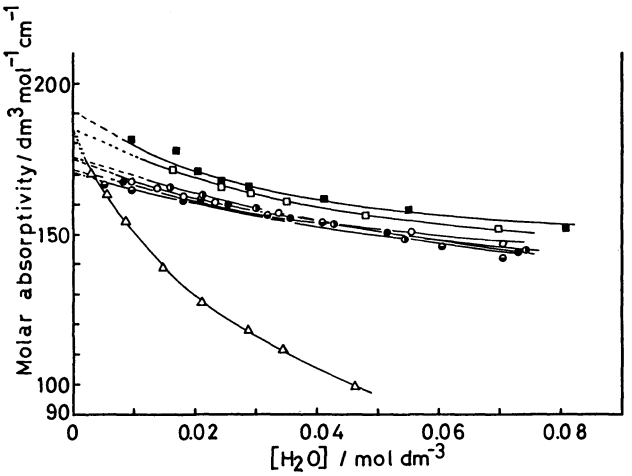

Fig. 2. Variation of molar absorptivity at 520 nm with the water concentration in various solvents at 25 °C. Δ, Py; DCE-MeOH mixtures (MeOH mole fraction): □, 1.0; ■, 0.9; ○, 0.7; ●, 0.5; ◒, 0.3; ◑, 0.1.

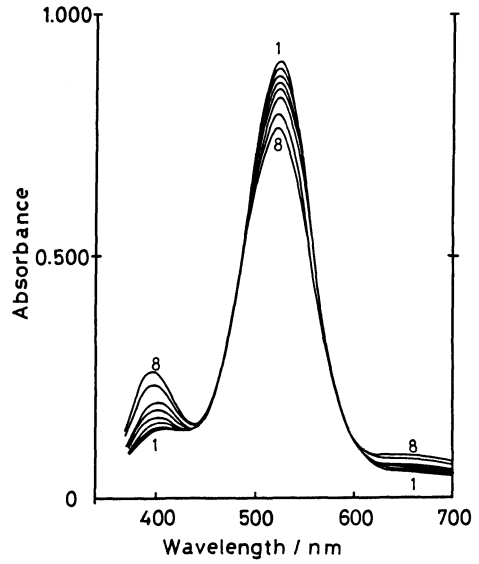

Fig. 1. Visible spectrum variation with the concentration of water of a 1.12×10^{-3} mol dm^{-3} solution of [Ni(tmc)](ClO$_4$)$_2$ at the 0.7 MeOH mole fraction and 25 °C. Water concentration (mol dm^{-3}): 1, 0.00830; 2, 0.0125; 3, 0.0153; 4, 0.0206; 5, 0.0278; 6, 0.0348; 7, 0.0561; 8, 0.0739.

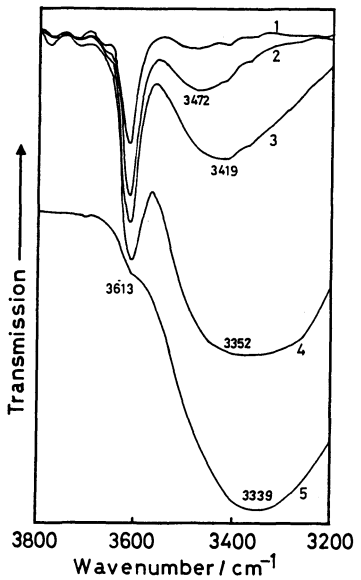

Fig. 3. IR spectra of MeOH in DCE-MeOH mixtures. MeOH mole fraction: 1, 0.03; 2, 0.07; 3, 0.10; 4, 0.30; 5, 0.70. CaF_2 cell (0.25 mm) for 1, 2, 3, and 4, and CaF_2 demountable cell for 5.

cules to the cation depends on the degree of complex formation of water with solvent molecules or self-association,[1,2] it is necessary to consider the structure of water complexes and MeOH net works.

Figure 3 shows IR spectra for MeOH in DCE-MeOH mixtures. A sharp band at 3613 cm^{-1} and a broad band at 3472 cm^{-1} exist below the 0.1 MeOH mole fraction (spectra 1, 2, and 3). The sharp high-frequency band and the broad low frequency band are assigned to the free O-H oscillator of MeOH molecules and to the bonded O-H oscillator in MeOH dimers, respectively, comparing with IR spectra of MeOH in dichloromethane (DCM) by Symons and Thomas.[10] Dependence of the IR spectrum on the MeOH fraction below the 0.1 mole fraction is predominantly elucidated by dimerization equilibrium for MeOH. As the MeOH fraction increases, the broad band is shifted to lower frequency region (toward 3300 cm^{-1} of polymer) and the band of the freee O-H group relatively decreases, and moreover, the free O-H group almost disappeared at the 0.7 MeOH mole fraction.

Chemical shifts of the O-H proton resonance of MeOH are shown as a function of the MeOH mole fraction in Fig. 4. There is a linear relationship between them below the 0.2 MeOH mole fraction. This can be explained by dimerization of MeOH, as supported by the IR results in Fig. 3. The dimer model yields a simple expression for the chemical shift ν which is referenced to TMS as inner standard at low MeOH concentrations

$$\nu=(1-2x)\nu_m+2x\nu_d \quad (1)$$

$$x=(4+1/K_{M2}C)-[(4+1/K_{M2}C)^2-16]^{1/2}/8 \quad (2)$$

where ν_m is the chemical shift of the monomer protons, ν_d is the hypothetical mean chemical shift of the dimer protons, K_{M2} is the dimer formation constant in molar unit and C is a molar concentration of MeOH. A ν_m value of 75.2 Hz at the 0.03 MeOH mole fraction where the MeOH monomers are predominant was used for evaluating the K_{M2} value. A K_{M2} value of 0.29 and a ν_d value of 175 Hz were obtained. At the 0.1 MeOH mole fraction (1.4 mol dm^{-3}), for example, the K_{M2} value indicates that 34% of MeOH is dimerized.

However, the IR and NMR results could not give information as to whether the electron pairs of the oxygen atom of water remains free or not, and whether the water molecules dimerizes or not.

Estimation of K_{NiW} Values. The K_{NiW} value was estimated at each concentration of water for the data given in Fig. 2 using the equation

$$K_{NiW}=(\varepsilon_0-\varepsilon)/(\varepsilon-\varepsilon_s)[W] \quad (3)$$

where ε is the apparent molar absorptivity at 520 nm, ε_0 is the molar absorptivity at the zero water concentration, ε_s is the molar absorptivity of the water coordinate-chelate cation and [W] is the analytical concentration of water. A constant value of ε_s=10 $dm^3 mol^{-1} cm^{-1}$ obtained in the oxygen-atom donor solvent, *N,N*-diethylformamide[6] was used. The K_{NiW} values are plotted as a function of the water concentration in Fig. 5.

The K_{NiW} values in the 0.1 and 0.3 MeOH mole fraction mixtures do not depend on the water concentration, but those in mixtures above the 0.5 MeOH mole fraction decrease with increasing the water concentration, showing a decrease in activity of water molecules. Since the isolated monomeric water which is not hydrogen-bonded to bulk solvents is hardly coordinated to the nickel,[1,2] the results in Fig. 5 show that the water molecules in the mixed solvents are hydrogen bonded to MeOH and suggest that the heterodimer with MeOH is dominant in the MeOH poor region and additional species of water leading to a decrease in activity of water appear in the MeOH rich region.

As shown in Fig. 3, in the MeOH rich region the free OH group for MeOH was hardly found, the oligomerization being enhanced. This may make it

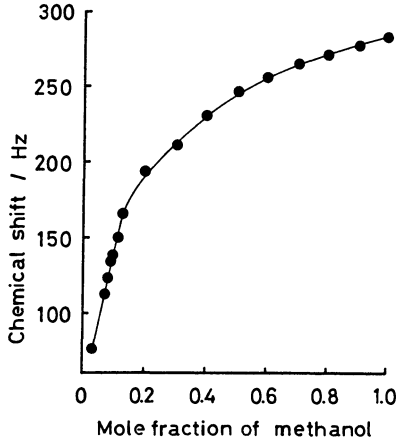

Fig. 4. Dependence of ^1H NMR chemical shift for hydroxyl group of MeOH referenced to TMS on the mole fraction of MeOH in DCE-MeOH mixtures.

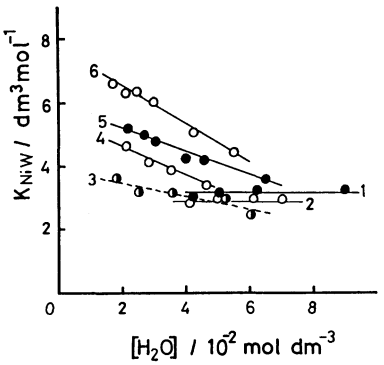

Fig. 5. Dependence of K_{NiW} on the water concentration in DCE-MeOH mixtures at 25 °C. Mole fraction of MeOH: 1, 0.1; 2, 0.3; 3, 0.5; 4, 0.7; 5, 0.9; 6, 1.0. K_{NiW} values were estimated by Eq. 3 at each concentration of water.

difficult for MeOH to act as a proton donor to water, and so it is assumed that the possibility of dimerization of water is present.

When the dimerization of water occurs, the apparent coordination constant of water $K_{NiW(app)}$ can be written by

$$K_{NiW(app)} = (K_{NiW1} + K_{NiW2}K_{W2}[H_2O])/(1 + K_{W2}[H_2O]) \quad (4)$$

where K_{NiW1} and K_{NiW2} are the coordination constants for the monomeric water (heterodimer) and dimeric water, respectively, K_{W2} is the dimerization constant of water, and $[H_2O]$ is the concentration of the monomeric water. Therefore, the apparent molar absorptivity ε is expressed by

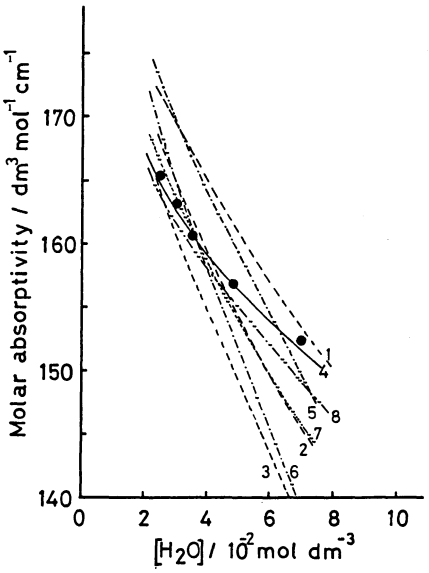

Fig. 6. Variation of molar absorptivities (●) at 520 nm and lines calculated using Eq. 4 (ε_0=183.7 and ε_s=10) with various K_{NiW1} with the water concentration in pure MeOH at 25 °C. 1, K_{NiW1}=3.0, K_{NiW2}=0, K_{W2}=0; 2, 4.0, 0, 0; 3, 5.0, 0, 0; 4, 10.3, 0, 50; 5, 0.0, 10, 50; 6, 0.0, 14, 50; 7, 6.0, 6, 50; 8, 10.3, 0, 40.

$$\varepsilon = (\varepsilon_0 + \varepsilon_s K_{NiW(app)}[H_2O'])/(1 + K_{NiW(app)}[H_2O']) \quad (5)$$

where $[H_2O']$ is the sum of concentrations of the monomeric and dimeric water.

It is assumed that all the water species are hydrogen-bonded to the MeOH oligomers, and that these are terminal water molecules with the free electron pairs except water molecules which are the proton acceptor in the dimer. Typical results for the fitness in the pure MeOH are shown in Fig. 6. It should be noted that the best fitness was obtained when only the monomeric water was regarded as a coordinated species with a K_{W2} value of 50 dm³ mol⁻¹ and a K_{NiW1} value of 10.3 dm³ mol⁻¹ and the dimeric water is hardly coordinated. In this connection protic MeOH in the hydrogen-bonded networks is remarkably contrastive with aprotic solvents such as AC and PDC in which the dimeric water is coordinated. Since the dimeric water is more basic and more acidic than the monomeric water,[1,2,11-16] it seems that the strengthened basicity and acidity of the dimer allow itself to be a member of the oligomers of MeOH which mask the electron pair effective for coordination. This is compatible with the suggestion from Symons[17] that the linear dimer of MeOH in DCM-MeOH mixtures should be more basic and more acidic than the monomer, and this would lead to a less of dimers and a gain of oligomers.

In the same way, the best fitting values for K_{W2} and K_{NiW1} were obtained in the 0.5—0.9 MeOH fractions and the results are given in Table 1. Both the values of K_{NiW1} and K_{W2} increase with increasing the MeOH fraction, that is, the hydrogen-bond energy of networks for MeOH.

In Py,[18] water forms the 1:1 and 1:2 water-Py species below 0.1 mol dm⁻³ of water. The K_{NiW1} values were estimated at each concentration of water using Eq. 3, and the average value 21±2 was obtained.

Figure 7 shows a correlation of logarithm of K_{NiW} with ^1H chemical shift (ν_{OH}) of the hydroxyl group for

Table 1. Equilibrium Constants (K_{NiW1}) for Monomeric Water Coordination to $[Ni(tmc)]^{2+}$, Dimerization Constant (K_{W2}) of Water, and Donor Number (DN) of Mixtures in DCE-MeOH Mixtures at 25 °C

X_{MeOH}	K_{NiW1} / dm³ mol⁻¹		K_{W2}[a] / dm³ mol⁻¹	Water[b] Monomer (%)	Water[b] Dimer (%)	Donor species	DN
0.1	3.4±0.2	3.2±0.1	0	100	0	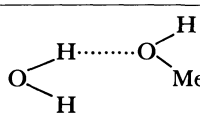	—
0.3	3.0±0.1		0	100	0		23
0.5	3.2±0.1	3.1±0.1	1±1	83	17		29
0.7	6.6±0.1	5.7±0.1	16±1	42	58	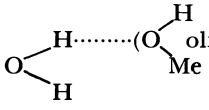	33
0.9	9.1±0.2	9.9±0.3	19±1	40	60		35
1.0	9.7±0.1	10.3±0.2	50±1	27	73		36

a) Average of two determinations. b) Water concentration is 0.1 mol dm⁻³.

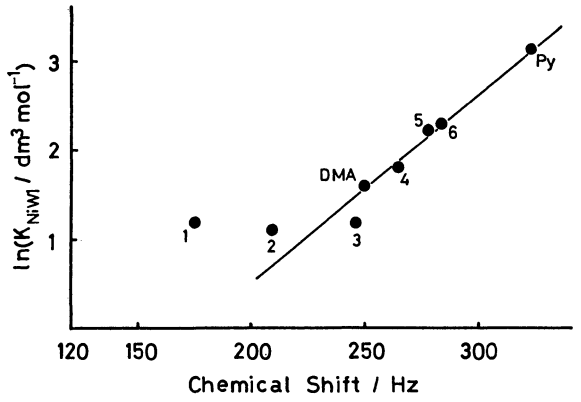

Fig. 7. Relationship of the K_{NiWI} value with ^{1}H NMR chemical shift (Hz) of hydroxyl group of MeOH in DMA, Py, and the DCE-MeOH mixtures. Dimeric MeOH: 1, 0.1 MeOH mole fraction; oligomers: 2, 0.3; 3, 0.5; 4, 0.7; 5, 0.9; 6, 1.0.

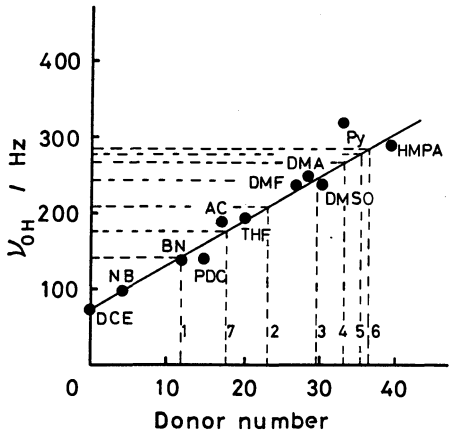

Fig. 8. Relationship between the ^{1}H NMR chemical shift (Hz) in MeOH complexes and donor number of the donor component. The apparent chemical shift of MeOH in various mixtures with DCE: 1, 0.1 mole fraction of MeOH; 2, 0.3; 3, 0.5; 4, 0.7; 5, 0.9; 6, 1.0. The hypothetical mean chemical shift of the MeOH dimer protons: 7.

MeOH in DCE-MeOH mixtures, DMA, and Py. The ν_{OH} for DCE-MeOH mixtures are mean values for protons under various circumstances in MeOH oligomers, but there is a good linear relationship between ln K_{NiWI} and ν_{OH}, indicating that the ν_{OH} mean values reflect the basicity of the oxygen atom for terminal water molecules attached to MeOH oligomers. Thus, it can be said that the basicity of the terminal waters increases with increasing the hydrogen bond energy for the oligomer. This property of basicity of protic solvents is agreement with that expected by the theoretical calculations.[11-16]

^{1}H NMR chemical shifts of the O-H group for MeOH in various organic solvents were plotted as a function of their donor number (DN) (Fig. 8). The ν_{OH} values for DCE, NB, BN, and PDC were obtained by extrapolating observed ν_{OH} values at the zero concentration of MeOH. There was found a good linear relationship expressed with Eq. 5

$$DN = 0.167\ \nu_{OH} - 11.7 \quad (5)$$

where ν_{OH} is the ^{1}H NMR chemical shift in Hz of the O-H group of MeOH.

Since the ν_{OH} value for the 0.1 MeOH mole fraction mixture is a mean value for the monomer and dimer of MeOH, the corresponding DN value only indicates a mean DN value for DCE and the monomeric MeOH. In spite of the equal number of the hydrogen-bonding proton and the free proton for dimeric MeOH, its hypothetical mean ν_{OH} value 175 gives a DN value of 18 which is very close to 19[7] for MeOH. Therefore, it is reasonably assumed that ν_{OH} values in the higher MeOH mole fraction mixtures in which the number of the free proton is much less, give meaningful DN values.

The chemical shift and K_{NiWI} in the 0.5 MeOH mole fraction mixture are nearly the same as those in DMA (DN=27.8[7]). This means that the charge transfer among MeOH molecules in the mixture is the same as that from the DMA molecule to the MeOH molecule, and moreover, the charge-transfer effect of MeOH on the water basicity is closely similar to that from DMA to the water molecules. Therefore, a DN value of 29 is reasonable for the 0.5 MeOH mole fraction mixture. In the same way, DN values 23, 33, 35, and 36 were evaluated for the MeOH mole fractions 0.3, 0.7, 0.9, and 1.0, respectively. The K_{NiWI} value for the heterodimer of water and MeOH which is between those for the water dimer (DN=26[2]) in PDC and that (DN=27[2]) in AC, gives a DN value of 26.5 for the heterodimer. The DN value for the pure MeOH is higher than DNs estimated by using other methods (DN=24—33.5).[19-22] In view of the linear relationships of ln K_{NiW}-ν_{OH} and ν_{OH}-DN plots (Figs. 7 and 8), DN of Py should be 42 in place of 33.1 with respect to charge transfer for hydrogen bonding.

This work was supported by a Grant-in-Aid for Scientific Research No. 61134043 from the Ministry of Education, Science and Culture.

References

1) S. Yamasaki, Y. Yanai, E. Iwamoto, T. Kumamaru, and Y. Yamamoto, *J. Chem. Soc., Faraday Trans. 1*, **83**, 1641 (1987).

2) S. Yamasaki, E. Iwamoto, and T. Kumamaru, *J. Chem. Soc., Faraday Trans. 1*, **84**, 1679 (1988).

3) M. J. D'Aniello, Jr., M. J. Mocella, F. Wagner, E. K. Barefield, and I. C. Paul, *J. Am. Chem. Soc.*, **97**, 192 (1975).

4) S. F. Lincoln, T. W. Hambley, D. L. Pisaniello, and J. H. Coatses, *Aust. J. Chem.*, **37**, 713 (1984).

5) I. S. Crick, B. F. Hoskins, and P. A. Tregloan, *Inorg. Chim. Acta*, **114**, L33 (1986).

6) E. Iwamoto, T. Yokoyama, S. Yamasaki, T. Yabe, T. Kumamaru, and Y. Yamamoto, *J. Chem. Soc., Dalton*

Trans., **1988**, 1935.
7) V. Gutmann, "The Donor-Acceptor Approach to Molecular Interaction," Plenum, New York (1987).
8) V. Gutmann and E. Wychera, *Inorg. Nucl. Chem. Lett.*, **12**, 257 (1966).
9) U. Mayer and V. Gutmann, *Struct. Binding (Berlin)*, **12**, 113 (1972).
10) M. C. R. Symons and V. K. Thomas, *J. Chem. Soc., Faraday Trans. 1*, **77**, 1883 (1981), and references therein.
11) P. Schuster, *Z. Chem.*, **13**, 41 (1973).
12) R. E. Furton and J. Daly, *Trans. Faraday Soc.*, **67**, 1219 (1971).
13) J. E. Del Bene, *J. Chem. Phys.*, **55**, 4633 (1971).
14) J. E. Del Bene, *J. Chem. Phys.*, **62**, 1314 (1975).
15) P. A. Kollmann and L. C. Allen, *J. Chem. Phys.*, **51**, 3286 (1969).
16) P. A. Kollmann and L. C. Allen, *J. Am. Chem. Soc.*, **92**, 4108 (1970).
17) M. C. R. Symons, *Chem. Soc. Rev.*, **12**, 1 (1983).
18) S. C. Mohr, W. D. Wilk, and G. M. Barrow, *J. Am. Chem. Soc.*, **87**, 3048 (1965).
19) R. H. Erlich, E. Roach, and A. I. Popov, *J. Am. Chem. Soc.*, **92**, 4989 (1970).
20) T. Ogata, T. Fujisawa, N. Tanaka, and H. Yokoi, *Bull. Chem. Soc. Jpn.*, **49**, 2759 (1976).
21) Y. Marcus, *J. Solution Chem.*, **13**, 599 (1984) and references therein.
22) V. Gutmann, "Coordination Chemistry in Nonaqueous Solutions," Springer-Verlag, Berlin (1968).

The Preparation of Stable Colloidal Poly(vinyl alcohol) Composites of Cu_2O and Cu

Hiroshi YOKOI,* Akihide KADOWAKI, and Shuji IKOMA
Department of Applied Chemistry, Faculty of Engineering, Shizuoka University, Hamamatsu 432
(Received September 30, 1988)

Stable colloidal particles of reddish brown Cu_2O-PVA and grayish black Cu-PVA composites have been prepared by the reduction of green Cu^{2+}-PVA complexes in aqueous solutions with hydrazine, at the [hydrazine]/[Cu^{2+}] ratios of 1—3 and 15 or more respectively, where PVA represents poly(vinyl alcohol). The average diameters of the Cu_2O and Cu particles in these composites have been estimated to be about 200 and 300 Å respectively from the half widths of the X-ray diffraction peaks for the corresponding powder samples.

There have been several papers on the preparation of copper sols by the chemical reduction of copper(II) salts in aqueous solutions in the presence and absence of polymer-protecting agents.[1-4] These colloidal dispersions have found interesting applications. Cu^{2+} ions and poly(vinyl alcohol) (PVA) react at pH$\gtrsim$6 to form green Cu^{2+}-PVA complexes, which have been identified as polynuclear $Cu(OH)_2$ complexes hydrophobically included by PVA.[5,6] In this work, the chemical reduction of these green Cu^{2+}-PVA complexes has been investigated in an effort to obtain some useful materials. The resulting reduction products have been characterized in some detail, with special interest taken in the role of PVA in them.

Experimental

Materials. Hydrolyzed (100%) PVAs with the average molecular weight of 14000 were purchased from the Aldrich Chemical Co. The concentration of PVA in this work was expressed as [PVA polymer residue], in terms of monomeric residues. All the other reagents were of a reagent grade or higher and were used without further purification. Aqueous solutions of green Cu^{2+}-PVA complexes containing 0.20 M PVA and 10 or 20 mM Cu^{2+} ions were prepared by dissolving the required amounts of $CuSO_4 \cdot 5H_2O$ and PVA in aqueous solutions and by then adjusting the pH to 8.0 with NaOH without any buffer (1 M=1 mol dm^{-3}). Chemical reductions of the complexes in aqueous solutions with sodium tetrahydroborate, hydrazine, hydroxylamine, hydroquinone, and ascorbic acid gave variously colored hydrosols. These sols, except those prepared by hydrazine reduction, were not stable in air, resulting in color changes and precipitations within a day. Hydrazine was found to reduce the Cu^{2+}-PVA complexes to differently colored hydrosols according to the value of R_r=[hydrazine]/[Cu^{2+}]. The colors of these hydrosols were reddish brown, bright yellow, and grayish black at the R_r values of 1—3, 4—15, and >15 respectively. Powder samples were obtained from these hydrosols and their original Cu^{2+}-PVA solutions by pouring them into acetone and by washing the resulting precipitates with acetone several times, as in the recovery of PVA powder from its aqueous solutions. Surprisingly, it has been found that these powder samples include microcrystals of Na_2SO_4 as will be seen in the X-ray diffraction measurements; details will be reported elsewhere.[7] Quantitative analyses of the SO_4^{2-} in these samples by means of an ion chromatograph Model HCL-601 (Tosoh Co., Ltd.) showed that 6.5, 6.2, and 6.2% of SO_4^{2-} are included in the powder samples obtained from the Cu^{2+}-PVA solution at R_p=[PVA Polymer residue]/[Cu^{2+}]=20, the reddish brown hydrosol at R_r=1, and the grayish black hydrosol at R_r=20 respectively. These SO_4^{2-} contents remarkably decreased upon dialysis with cellophane membranes. Elemental analyses for the last two powder samples gave similar results near to C 40.5, H 7.8, and Cu 5.5% (determined by atomic-absorption spectroscopy); these results were not yet useful for the identification of these complicated samples. Strictly speaking, the first sample, whose elemental analysis has already been reported,[6] was analogous. After all, elemental analyses of this kind of complicated polymer are a subject for further investigation.

Measurements. X-Ray diffraction measurements of powder samples were carried out by a Geigerflex recording X-ray diffractometer Model D-3F (Rigaku Denki Co., Ltd.). The visible absorption spectra of hydrosols were measured by means of a Hitachi U-2000 spectrophotometer using a 5-mm quartz cell. Far-infrared spectra of powder samples were recorded with a grating infrared spectrophotometer, Model IR-F (Japan Spectroscopic Co., Ltd.). Magnetic-susceptibility measurements of powder samples were carried out at room temperature by the usual Gouy method, where the contents of the copper or copper-ion species required for the calculation of the effective magnetic moments (μ_{eff}) were determined by means of an atomic absorption and flame-emission spectrophotometer Model AA-782 (Nippon Jarrel-Ash Co., Ltd.).

Results and Discussion

Reduction products of copper(II) salts in aqueous solutions are generally unstable in air, even in the presence of poly(*N*-vinyl-2-pyrrolidone) as a protective polymer.[3,4] Interestingly, however, the reduction of the green Cu^{2+}-PVA complexes in aqueous solutions by hydrazine gave stable hydrosols in air. Powder samples prepared as precipitates by pouring these hydrosols into acetone were also stable in air. All the copper or copper-ion species in the hydrosols were included in the powder samples, since such species could not be detected in the filtrates. This fact, together with the extremely high stability of the reduction products in air, indicates that copper or copper-ion species are bound to PVA and, furthermore, that

particles of these species may be protectively coated with PVA. This also seems to be responsible for the stable formation of hydrosols. At present, however, the reason why only hydrazine produces this kind of hydrosol is still obscure.

Figure 1 shows the X-ray diffraction patterns of two powder samples. In both patterns, peaks with the following 2θ values are due to Na_2SO_4: 33.8 (33.9), 31.6 (32.1), 29.7 (29.0), 23.4 (23.1), and 19.2 (19.0), where the numbers in parentheses are the values cited from the literature.[8] In addition, the following peaks assignable to Cu_2O and Cu are observed in the A and B patterns respectively:[9,10] 73.6 (73.5), 61.4 (61.3), 52.2 (52.4), 42.2 (42.3), 36.4 (36.4), and 29.7 (29.6) for the A pattern, and 73.8 (73.9), 50.2 (50.3), and 43.0 (43.3) for the B pattern. Accordingly, these results show the formation of Cu_2O and Cu microcrystals in the reddish brown and grayish black powder samples respectively. X-Ray diffraction patterns for the other powder samples obtained from hydrosols at R_r=4—15 were made up by the superposition of the A and B patterns at varying intensity ratios.

The existence of Cu_2O microcrystals in the reddish brown sample was also supported by the observation of a far-infrared absorption at 615 cm^{-1} assignable to ν_{Cu-O} in Cu_2O crystals.[11] Figure 2 shows the visible absorption spectra of hydrosols corresponding to the two powder samples in Fig. 1. The absorption maxima at 510 and 590 nm for the reddish brown and grayish black hydrosols are characteristic of Cu_2O and Cu polycrystals respectively.[12]

All the results of the magnetic-susceptibility measurements for the powder samples obtained from hydrosols at various R_r values are summarized in Fig. 3, which shows a plot of the μ_{eff} values of the samples against their R_r values. The μ_{eff} value of the Cu^{2+}-PVA complexes corresponding to R_r=0 is 1.49±0.01 B.M.[6] The errors of the other μ_{eff} values are ±0.05 or so. The fact that μ_{eff}=0 B.M. for the reddish brown samples at R_r=1—3, as is shown in Fig. 3, indicates that the addition of hydrazine at these R_r values completely reduces all the Cu^{2+} ions in the Cu^{2+}-PVA complexes to diamagnetic Cu^+ ions. The μ_{eff} value tends to increase with an increase in R_r in the range of R_r>3 and then finally to level off at R_r>15. The implication of this final μ_{eff} value of about 0.8 B.M. is now being considered.

It is important to obtain information on the sizes of Cu_2O and Cu particles in the hydrosols or powder samples. We can approximately estimate these sizes from the half widths of the X-ray diffraction peaks, using the Debye equation of $B=0.9\lambda/(t\cos\theta)$,[13] where B, t, and θ are the half width of a X-ray diffraction peak, the average diameter of crystalline particles, and the diffraction angle respectively, and where λ=

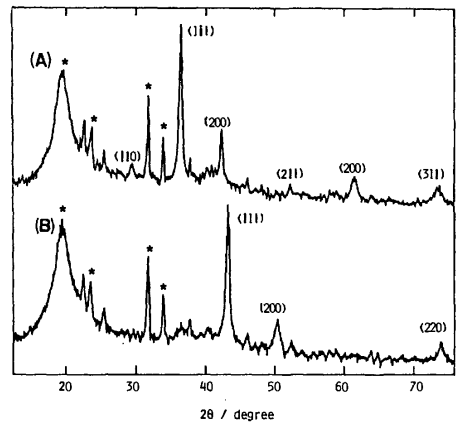

Fig. 1. X-Ray diffraction diagrams: (A) the reddish brown powder sample obtained from the hydrosol which was prepared by the reduction of Cu^{2+}-PVA complexes with hydrazine at R_r=[hydrazine]/[Cu^{2+}]=1; (B) the grayish black powder sample similarly obtained except at R_r=20 (the Cu^{2+}-PVA complexes were prepared at R_p=[PVA polymer residue]/[Cu^{2+}]=20). Peaks with asterisks are due to Na_2SO_4, and some peaks are marked with the Miller indices of Cu_2O crystals in (A) and Cu crystals in (B).

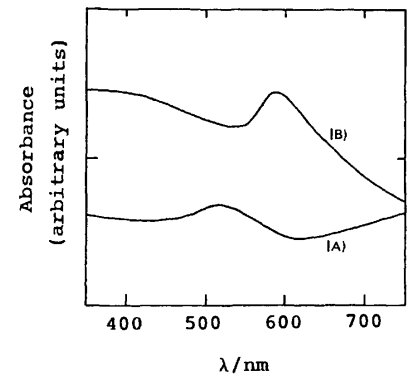

Fig. 2. Visible absorption spectra of the hydrosols corresponding to the (A) and (B) powder samples in Fig. 1.

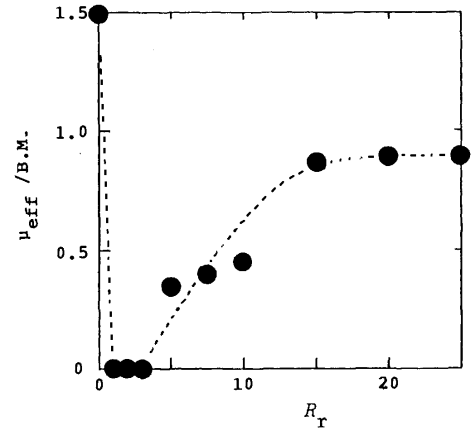

Fig. 3. A plot of the effective magnetic moment (μ_{eff}) against R_r for the powder samples obtained from hydrosols prepared at varying R_r values (see the caption of Fig. 1 as to R_r).

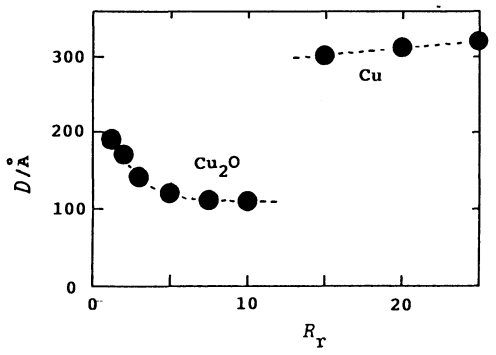

Fig. 4. A plot of the average diameters (D) of Cu_2O and Cu particles included in the powder samples against R_r (see the caption of Fig. 1 as to R_r).

1.54178 Å for Cu $K\alpha$ radiation. In this work, a strong X-ray diffraction peak for the (111) plane in every particle species was used for the purpose mentioned above. The results, summarized in Fig. 4, indicate that the average diameter of Cu particles in the grayish black samples of $R_r>15$ are almost constantly about 300 Å, while that of Cu_2O particles in the reddish brown sample of $R_r=1$ is about 200 Å. Further, there is a tendency for the diameter to decrease with the increase in R_r. We have a plan on hand for reinvestigating these particle sizes in the cast films of the present colloidal solutions by the use of a transmission electron microscope. It has been reported that the particle size of $Cu(OH)_2$ in the Cu^{2+}-PVA complexes may be extremely small, as small as less than 20 Å.[6] From this result and Fig. 4, it is concluded that there is a gathering process of small particles and, therefore, a growing process of particle size during the reductions of $Cu(OH)_2$ to Cu_2O and of Cu_2O to Cu by hydrazine in the presence of PVA, suggesting a reorganization in the interaction of such particles with PVA at every stage of reduction.

References

1) E. Sauer and D. Steiner, *Kolloid-Z*, **72**, 35 (1935).
2) G. C. Papavassiliou and T. Kokkinakis, *J. Phys. F*, **4**, L67 (1974).
3) H. Hirai, H. Wakabayashi, and M. Komiyama, *Chem. Lett.*, **1983**, 1047; *Bull. Chem. Soc. Jpn.*, **59**, 367 (1986).
4) A. C. Curtis, D. G. Duff, P. P. Edwards, D. A. Jefferson, B. F. G. Johnson, A. I. Kirkland, and A. S. Wallace, *J. Phys. Chem.*, **92**, 2270 (1988).
5) H. Yokoi, S. Kawata, and M. Iwaizumi, *J. Am. Chem. Soc.*, **108**, 3358 (1986).
6) H. Yokoi, S. Kawai, A. Kadowaki, and S. Ikoma, *Nippon Kagaku Kaishi*, **1989**, 872.
7) H. Yokoi and T. Hayakawa, to be published.
8) JCPDS, 5-631.
9) JCPDS, 5-667.
10) JCPDS, 4-836.
11) J. R. Ferraro, "Low-Frequency Vibration of Inorganic and Coordination Compounds," Plenum Press, New York (1971), p. 73.
12) N. Takezawa and H. Kobayashi, *Hyomen*, **20**, 555 (1981); S. Robert, *Phys. Rev.*, **118**, 1506 (1960); D. Beaglehole, *Proc. Phys. Soc., London*, **85**, 1007 (1965).
13) P. Sherrer, *Göttinger Nachrichten.*, **2**, 98 (1918).

The IR Photochemistry of Organic Compounds. II.[1] The IR Photochemistry of Ethers: The Decomposition Patterns[2]

Tetsuro MAJIMA,* Tadahiro ISHII,† and Shigeyoshi ARAI††
The Institute of Physical and Chemical Research, Hirosawa 2-1, Wako, Saitama 351-01
†Science University of Tokyo, Kagurazaka, Shinjukuku, Tokyo 162
††Kyoto Institute of Technology, Matsugasaki, Sakyoku, Kyoto 606
(Received October 7, 1988)

The infrared multiple-photon decomposition (IRMPD) of saturated open-chain ethers has been systematically investigated with the intention of establishing their decomposition patterns. The main products in the IRMPD of ethers (**1a—f**, **2**) are H_2CO, CO, H_2, and lower hydrocarbons. Acetaldehyde is additionally formed in the IRMPD of **1b** and **1d**, while acetone is formed in the IRMPD of **1d**. The observed results are explained on the basis of the decomposition of the highly vibrationally excited ethers produced in the IRMP excitation. The initial process is the homolytic cleavage of a C-O bond to yield the corresponding alkyl and alkoxyl radicals. The alkyl radicals are trapped by Br_2. Sequential splitting and addition reactions of the radicals yield primary products with a high internal energy. The primary products also decompose sequentially into stable products, in part. The sequential processes compete with collisional deactivation. Therefore, the branching ratio depends on the internal energy of the radicals and the primary products.

The infrared multiple-photon decomposition (IRMPD) of organic compounds induced by a TEA CO_2 laser irradiation has been extensively investigated, especially with relation to laser isotope separation.[3] The laser isotope separation of oxygen has received relatively little attention compared with the separation of hydrogen and carbon isotopes using Freon compounds.[4] Ethers absorb at 900—1150 cm^{-1} because of the C-O stretching vibration, and the absorption usually falls in the tunable range of a TEA CO_2 laser. Moreover, ethers have relatively high vapor pressures and a large isotopic shift of oxygen in the C-O stretching vibration among various oxygen-containing organic compounds. Therefore, ether is very suitable as the starting material in the oxygen-isotope separation by means of a TEA CO_2 laser. In fact, the ^{18}O separation in the IRMPD of dimethyl ether has been studied by Vizhin et al.[5] and Kutschke et al.[6] We have recently studied the ^{18}O separation in the IRMPD of perfluorodimethyl ether.[1] The separation selectivity was found to be 2.5 in the irradiation of 3.5 Torr (1 Torr=133.322 Pa) of perfluorodimethyl ether with the CO_2 laser radiation at 940.55 cm^{-1}, 15 J cm^{-2}, and room temperature, where the conversion was 1.4%. No other work on oxygen-isotope separation in the IRMPD of ethers has been reported, although a number of studies have been published with respect to the kinetics and dynamics in the IRMPD of ethyl vinyl ether,[7] allyl methyl ether,[8] dialkoxyalkanes,[9] 2,5-dihydrofuran,[7d] tetrahydrofuran,[10] methylated tetrahydrofuran,[11] oxetanes,[12] and tetramethyldioxetane.[13]

In order to find a suitable compound for the laser isotope separation of oxygen, it is important to study the mechanism and final products in the IRMPD of oxygen-containing compounds. In the present work we wish to report on the decomposition mechanism on the IRMPD of saturated open-chain ethers; dimethyl (**1a**), diethyl (**1b**), dipropyl (**1c**), diisopropyl (**1d**), dibutyl (**1e**), and *t*-butyl methyl (**1f**) ethers, and 1,2-dimethoxyethane (**2**). We have analyzed the stable decomposition products. Several radical intermediates are trapped by Br_2. On the basis of the results, suitable ethers for oxygen-isotope separation using a TEA CO_2 laser are suggested.

Experimental

Material. The saturated open-chain ethers (**1a—f**, **2**) were purchased from Tokyo Kasei Kogyo or Nakarai Chemicals. Each ether was distilled and degassed by several freeze (−196 °C)-pump-thaw cycles. Gas-chromatographic analyses of the ethers showed their purities to be over 99.5% and revealed no trace of possible decomposition products. All the other reagents and chemicals were commercially available and were used after distillation and degassing.

Apparatus and Procedure. A schematic diagram of the experimental set-up is shown in Fig. 1. A conventional glass vacuum system with an oil diffusion pump was used for the gas handling. The pressures were measured with a MKS Baratron-type 222B (0—10 Torr) gauge. The irradiation cell was a cross-type Pyrex tube equipped with four KBr windows (5 mm thick). The dimensions were 2 cm in diameter, 10 cm in the direction of the laser irradiation, and 5 cm in the direction of the infrared spectroscopic measurements. The IR absorption spectra were measured before and after irradiation by using a Japan Spectroscopic A-102 spectrophotometer.

A Lumonics 103-2 TEA (transversely excited atmospheric) CO_2 laser was operated using a mixture of CO_2 and He as flowing gases at a repetition rate of 0.7 Hz. The pulse width was about 80 ns FWHM without tailing. The laser lines were checked with an Optical Engineering CO_2 spectrum analyzer. The laser beam was passed through an aperture 1.0 cm in diameter and then tightly focused into the center of the cell using a BaF_2 lens with a focal length of 7.5 cm. The incident laser energy was attenuated by inserting one or more polyethylene films perpendicular to the beam path, and it was calibrated with a Scientech 364 disk calo-

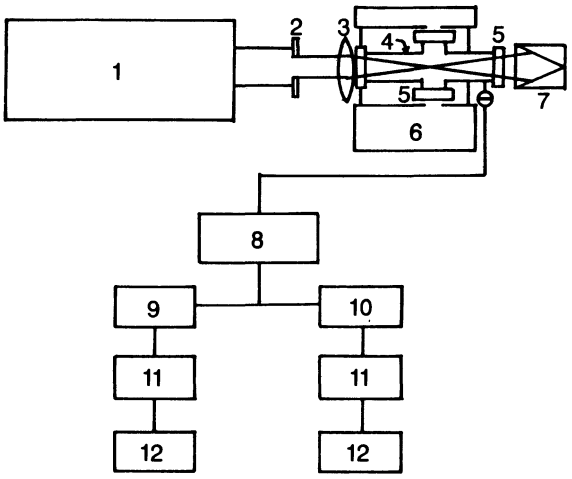

Fig. 1. Schematic diagram of the experimental set-up. 1: TEA CO_2 laser, 2: aperture, 3: BaF_2 lens, 4: reaction cell, 5: KBr window, 6: IR spectrometer, 7: power meter, 8: Toepler pump, 9: condensable gas at −196 °C, 10: non-condensable gas at −196 °C, 11: gas chromatograph, 12: mass spectrometer.

rimeter. The laser fluence at the focus corresponds to the incident pulse energy divided by the focus area (7.1×10^{-4} cm^2), which can be calculated from the aperture diameter, the focal length, and the beam divergence of 2 mrad.

Analysis. After the IR spectral measurements, sample mixtures were separated into two components, condensable gases and non-condensable gases, at −196 °C (H_2, CO, and CH_4) by using a Toepler pump. Both components were analyzed with gas chromatography (Shimadzu GC-7A, Hitachi 163, or Gasukuro Kogyo 373 gas chromatographs) using a flame-ionization or thermal-conductivity detector. Each gas chromatograph was connected to a sample injector and a integration recorder (Shimadzu Chromatopac C-R1B, Hewlett-Packard Integrator 3380, or SIC Chromatocorder 11). The lower hydrocarbons were analyzed on a Porapak Q 50/80 mesh column. The conditions were as follows: column length and diameter (L×ϕ), 6 m×3 mm; column temperature (CT), 150 °C; injection temperature (IT), 170 °C; detector (D), flame-ionization detector at 150 °C; carrier gas (CG), N_2; flow rate (FR), 50 $cm^3\,min^{-1}$. The lower hydrocarbons were also analyzed on a Sebaconitrile 10%-Uniport C 60/80 mesh column (L×ϕ, 10 m×3 mm; CT, 30 °C; IT, 50 °C; D, flame-ionization detector at 50 °C; CG, N_2; FR, 20 cm^3 min^{-1}). The ethers and bromine-containing compounds were analyzed on a PEG-20 M column (L×ϕ, 7 m×3 mm; CT, 90 °C; IT, 100 °C; D, flame-ionization detector at 100 °C; CG, N_2; FR, 30 cm^3 min^{-1}). The aldehydes were analyzed on a TSR-1 10%-Flusin T 30/60 mesh column (L×ϕ, 2 m×3 mm; CT, 100 °C; IT, 120 °C, D; thermal-conductivity detector at 100 °C; CG, He; FR, 27 cm^3 min^{-1}). The non-condensable gases (H_2, CO, CH_4) were analyzed on an Unibeads C 80/10 mesh column (L×ϕ, 3 m×3 mm; CT, 40—100 °C; IT, 100 °C; D, thermal-conductivity detector at 100 °C; CG, He; FR, 50 cm^3 min^{-1}).

A typical chromatogram of each irradiated ether showed that the peaks were fully resolved and reproducible. Standard mixtures were prepared to calibrate the gas chromatograms. The identification of the products by gas-chromatograph was based on a comparison of the product-retention times with those of the standards. The quantitative amounts of products and reactants were calibarted using gas-chromatographic sensitivity factors which had been determined by measuring the peak areas of pure standards on a integration recorder.

A mass spectrometer (Japan Electron Optics JMS-01SG) and GC-MS system (a NEVA TE-150 mass spectrometer combined with a Shimadzu GC-7A gas chromatograph) were also used to identify products, especially bromine-containing products, in the IRMPD of ether-Br_2 mixtures.

Results

The irradiation of ethers at 3.0 Torr with TEA CO_2 laser pulses caused the IRMPD to yield various products, as is shown in Tables 1—4. The laser line was tuned to the frequency coinciding with the strong absorption of the ether. The numbers of laser pulses were 100—500, and the conversions were 10—20%. The absorption coefficient (ε) of ether at the laser line changes from ether to ether in the range of 1.0×10^{-3}—7.5×10^{-2} $Torr^{-1}cm^{-1}$, while the decomposition yield ($Y_d=(1-P/P_0)/$(number of laser pulses)) varies slightly in the range of 3.7×10^{-4}—8.0×10^{-4} $pulse^{-1}$ (Table 1), where P_0 (=3.0 Torr) and P are the ether pressures before and after irradiation respectively.

The main decomposition products were H_2, CO,

Table 1. Irradiation Parameters in the IRMPD of **1a—f** and **2**

Ether	λ[a]	ε[b] $\times10^3$	E_p[c]	F[d]
	cm^{-1}	$Torr^{-1}cm^{-1}$	J $pulse^{-1}$	J cm^{-2}
1a	1079.90	70.6	0.193	271
1b	1078.59	2.45	0.253	356
1c	1085.75	1.92	0.198	279
1d	1035.74	3.96	0.186	262
1e	1046.85	1.02	0.212	299
1f	1084.64	75.0	0.176	248
2	1039.37	1.23	0.203	286

a) Laser wavenumber. b)Absorption coefficient at the laser wavenumber. c) Incident pulse energy. d) Laser fluence at the focus.

Table 2. Product Yields in the IRMPD of **1a—f** and **2**

Ether	Y_d[a] $\times10^4$	Y[b] $\times10^4$ ($pulse^{-1}$)			MB[c]
	$pulse^{-1}$	H_2	O-compnd.[d]	Hydrocarbons	%
1a	7.87	4.10	5.50	2.07	70
1b	3.97	1.71	2.22	4.77	60
1c	6.83	3.80	4.67	4.93	68
1d	3.77	3.08	3.21	3.93	85
1e	5.43	2.00	3.23	19.3	60
1f	7.40	9.93	4.57	6.53	62
2	5.87	2.08	8.02	10.5	70

a) Decomposition yield of ether. b) Yield of product. c) Material balance based on oxygen atom: MB=($\sum$ (oxygen-containing products)/(consumed **1**))×100 for **1** and MB=($\sum$(oxygen-containing products)/2 (consumed **2**))×100 for **2**. d) Oxygen-containing products.

Table 3. Relative Yields of Oxygen-Containing Products

Product	Relative yields of product[a](%)						
	1a	**1b**	**1c**	**1d**	**1e**	**1f**	**2**
CO	37	25	35	34	23	15	17
H_2CO	63	66	65	8	77	85	83
CH_3CHO	0	9	0	54	0	0	0
CH_3COCH_3	0	0	0	4	0	0	0

a) Relative yield of product to total yield of oxygen-containing products.

Table 4. Relative Yields of Hydrocarbon Products

Product	Relative yields of product[a] (%)						
	1a	**1b**	**1c**	**1d**	**1e**	**1f**	**2**
CH_4	14	38	8	12	12	0	18
C_2H_6	57	17	16	14	13	14	51
C_2H_4	18	27	6	13	49	6	30
C_2H_2	2	4	0.1	2	0.1	0.3	0.6
C_3H_8	6	14	15	1	12	0.3	0.6
C_3H_6	1	0	38	52	3	2	0.1
CH_3CCH	0	0	0	1	0	0	0
CH_2CCH_2	0	0	0	1	0	2	0
n-C_4H_{10}	3	0	11	0	3	0	0
Δ^1-C_4H_8	0	1	2	3	7	0	0.3
i-C_4H_8	0	0	0	0	0	75	0
$\Delta^{1,3}$-C_4H_6	0	0	0	0.3	0	0	0
n-C_5H_{12}	0	0	3	0	1	0	0

a) Relative yield of product to total yield of hydrocarbon products.

H_2CO, and lower hydrocarbons. Additionally, acetaldehyde (CH_3CHO) and acetone (CH_3COCH_3) were formed in the IRMPD of **1b** and **1d** and of **1d**. The yields (Y=(pressure of product)/(P_0×(number of laser pulses)) of H_2, oxygen-containing compounds, and hydrocarbons are shown in Tables 2 and 3. Neither alcohol nor aldehyde containing more than three carbon atoms was detected. The material balance based on the oxygen atoms were very good—60—85%, as is shown in Table 2. The material balance is defined as {∑(pressures of oxygen-containing products)/(consumed ether) (number of oxygen atoms in ether)}×100%. Thus, the oxygen atoms in the decomposed ether were found mostly in CO, H_2CO, or CH_3CHO.

On the other hand, the distributions of the hydrocarbons were dependent on the ethers. The yield of a hydrocarbon relative to the total yield of hydrocarbons is presented for each ether in Table 4. The main hydrocarbons reflected the structures of the alkyl groups of the ethers: ethane (C_2H_6) and ethylene (C_2H_4) for **1a**, **1b**, and **2**; propylene (C_3H_6) for **1c** and **1d**; C_2H_4 for **1e**; isobutene for **1f**.

The value of Y_d increased with the increase in the laser fluence at the focus (F); Y_d was proportional to $F^{1.3-1.7}$. In addition, the product distributions also changed with F. The relationships between Y_d and F and the product distribution vs. F in the IRMPD of **1a**

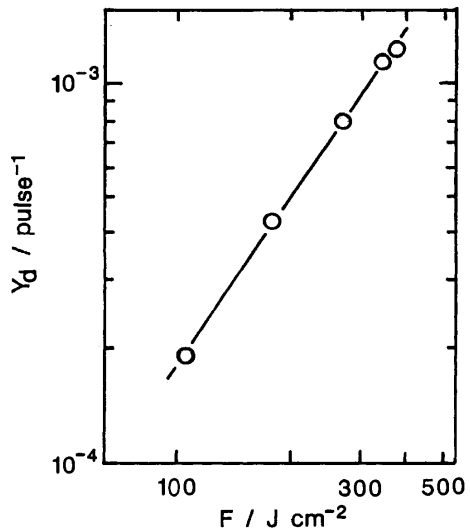

Fig. 2. Log-log plot of the decomposition yield (Y_d) vs. laser fluence at the focus (F) in the IRMPD of **1a** of 3.0 Torr.

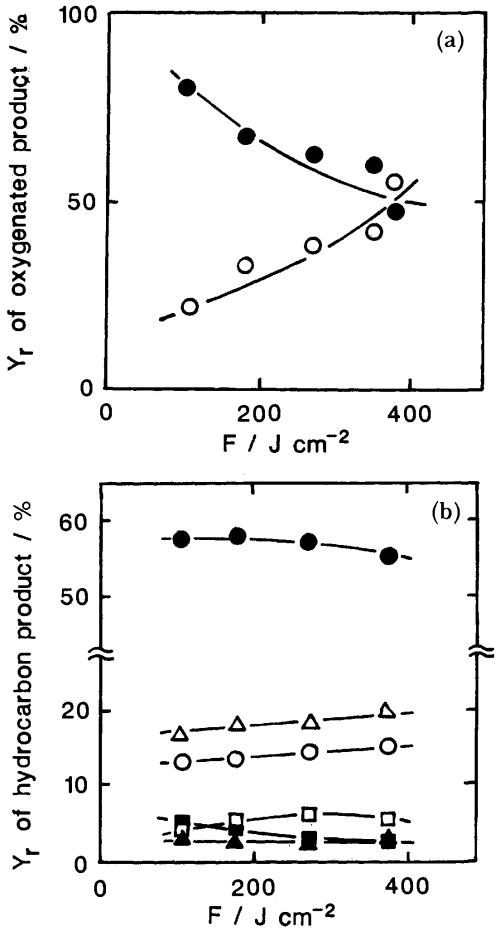

Fig. 3. Effects of F on the distribution (a) of oxygen-containing products: CO (○) and H_2CO (●) and (b) of hydrocarbon products: CH_4 (○), C_2H_6 (●), C_2H_4 (△), C_2H_2 (▲), C_3H_8 (□), and n-C_4H_{10} (■) in the IRMPD of **1a** at 3.0 Torr. The ordinate, Y_r, indicates relative yields of an oxygen-containing product and of a hydrocarbon product to the total yields of oxygen-containing products and of hydrocarbon products respectively.

Table 5. Relative Yields of Bromine-Containing Products in the IRMPD of Ether-Br_2 Mixtures

Ether	Relative yields of bromine-containing product[a](%)					
	CH_3Br	CH_2Br_2	C_2H_5Br	$C_2H_4Br_2$	C_3H_7Br	t-C_4H_9Br
1a	95	5	0	0	0	0
1b	46	1	54	2	0	0
1c	23	2	10	1	64	0
1f	12	0	0	0	0	88

a) Relative yield of product to total yield of bromine-containing products.

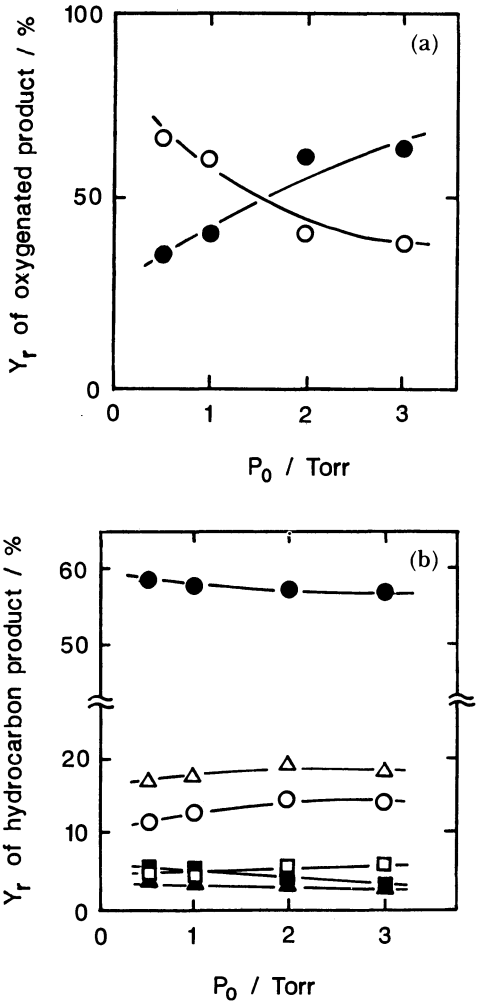

Fig. 4. Effects of P_0 on the distribution (a) of oxygen-containing products: CO (○) and H_2CO (●) and (b) of hydrocarbon products: CH_4 (○), C_2H_6 (●), C_2H_4 (△), C_2H_2 (▲), C_3H_8 (□), and n-C_4H_{10} (■) at F=271 J cm^{-2} in the IRMPD of **1a**.

are shown in Figs. 2 and 3 respectively. With the increase in F, H_2CO decreased, while CO increased in its relative yield, as is shown in Fig. 3a. On the other hand, the distribution of hydrocarbon products was hardly affected by F, as is shown in Fig. 3b.

The pressure dependence on the product distribution was examined in the range of 0.5—3.0 Torr at the same F in the IRMPD of **1a**. With the increase in the P_0 of **1a**, the relative yield of H_2CO increased, while that of CO decreased, as is shown in Fig. 4a. On the other hand, the distribution of hydrocarbon products did not significantly change with the P_0, as is shown in Fig. 4b.

When 3.0 Torr of ether was irradiated in the presence of 3.0 Torr of Br_2, bromine-containing compounds were formed with the decreases in the decomposition products (Table 5). Methyl bromide (CH_3Br) was the main product in the IRMPD of the **1a**-Br_2 mixture. A small amount of dibromomethane (CH_2Br_2) was also formed. Both CH_3Br and ethyl bromide (C_2H_5Br) in the ratio of 46 : 54 were formed in the IRMPD of the **1b**-Br_2 mixture, while t-butyl bromide (t-C_4H_9Br) and CH_3Br in the ratio of 88 : 12 were formed in the IRMPD of the **1f**-Br_2 mixture.

Discussion

Infrared multiple-photon excitation is different from UV excitation into an electronically excited state or thermal excitation, although there are similarities among the products formed in the IRMPD, vacuum-UV photolysis,[14] and thermolysis.[14a,15] The irradiation of ether using a TEA CO_2 laser yields highly vibrationally excited ether, E*, through IRMP excitation, with the asterisk denoting vibrational excitation.[3,4,16,17] The distribution of vibrational energy is usually approximated by the Boltzmann law.[16] Thus, the IRMPD can be well-explained by the statistical unimolecular decomposition according to the RRKM theory.[17,18] At high fluences, however, most of the molecules absorb more energy than is required for the dissociation of a bond.

Generally the weakest bond is broken in highly vibrationally excited molecules.[17] The cleavage of a C-O bond is obviously the lowest dissociation channel; the dissociation energy (E_{diss}) has been reported to be 81 kcal mol^{-1} in **1a**. A decomposition mechanism involving the initial cleavage of the C-O bond has been proposed in the IRMPD of **1a**.[5,6] Vacuum-UV photolysis and conventional thermolysis of ether in a vapor phase have also been explained on the basis of the initial cleavage of a C-O bond. The product distributions in the IRMPD of ethers are similar to those in UV-photolysis and thermolysis. Therefore, it is strongly suggested that the initial process in E* is the homolytic cleavage of the C-O bond, yielding

alkyl (R·) and alkoxyl radicals (R'O·) according to Eq. 1 (all the products are postulated to arise from the radicals):

$$\text{R-O-R}' \xrightarrow{nh\nu} \text{R}\cdot + \cdot\text{OR}' \quad (1)$$

1a—f, 2 (R, R'=alkyl)

The energy absorbed by ethers (E_{abs}) must be as large as the E_{diss} of the C-O bond in ethers. Since the E_{abs} of decomposing ether is generally much larger than the E_{diss} at high fluences, R· and R'O· are formed with a high internal energy and decompose into the primary products either sequentially or via secondary IRMPD. The primary products are also formed with a high internal energy and, therefore, decompose into stable products or are stabilized via collisional deactivation. It has previously been pointed out that the sequential decomposition or secondary IRMPD of radical intermediates and primary products with a high internal energy occurs favorably in the IRMPD of organic compounds, even if their $1\leftarrow0$ absorptions are not resonant with the laser radiation.[10,19]

In the IRMPD of ethers, radicals are formed spatially at a higher concentration by using a tightly focused laser beam. The relationship of $Y_d \propto F^{1.3-1.7}$ (shown in Fig. 2) means that the decomposition yield in the IRMPD of **1** and **2** approximately follows the 1.5-power rule; the fluence is much higher than the threshold one, and all the molecules in the region around a focal point decompose completely and yield radicals at high concentrations. Therefore, radical-radical reactions occur, while reactions between radicals and starting ethers are not involved. In fact, all the products in the IRMPD of ethers were either decomposition fragments or radical-radical reaction products. There were no detectable products originating from the reactions between radicals and ethers.

1a. From the distribution of decomposition fragments, the reaction processes of the radicals are considered to be as follows. The cleavage of the C-O bond in **1a*** gives primarily a methyl radical (CH_3·) and a methoxyl radical (CH_3O·). The radicals then react each other via coupling and disproportionation (Scheme 1).

Since methanol was not detected, disproportionation between two CH_3O· or H-abstraction from **1a** by CH_3O· did not occur. Thus, CH_3O· reacts with CH_3· via H-abstraction to yield H_2CO and CH_4 or decomposes into H_2CO and H. The activation energy (E_a) for the latter process has been reported to be 30 kcal mol^{-1}.[20] When the E_{diss} of decomposing **1a*** is higher than the summation of E_{diss} for the C-O bond plus E_a for the decomposition of CH_3O· into H $+H_2CO$ (i.e., $E_{abs}>E_{diss}+E_a=111$ kcal mol^{-1}), the internal energy of CH_3O· is so high that CH_3O· decomposes sequentially. Alternatively, there is a possibility that the secondary IRMPD of CH_3O· occurs within a laser pulse, if CH_3O· is formed in highly excited vibrational states and absorbs further laser radiation. The primary product H_2CO is probably formed with a high internal energy. Therefore, $H_2CO^\dagger$ may, at least in part, decompose sequentially or via the secondary IRMPD into $CO+H_2$. (The dagger denotes a high internal energy.) This decomposition is strongly suggested because the heat of reaction is only 1.3 kcal mol^{-1}.[21] Alternatively the decomposition of $H_2CO^\dagger$ into HCO+H may occur to yield CO as the final product. It is not clear whether the molecular pathway or the radical pathway is involved in the sequential decomposition of $H_2CO^\dagger$. However, CO is the final product in both pathways.

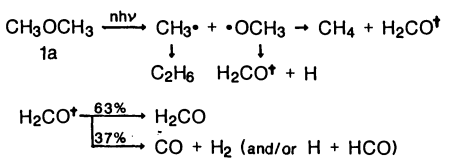

Scheme 1.

The sequential decomposition of $H_2CO^\dagger$ competes with the collisional deactivation process to give H_2CO in the ground state. The ratio of the sequential decomposition of $H_2CO^\dagger$ to the deactivation process depends on the internal energy and can be estimated from the ratio of CO to H_2CO. At higher F values, a faster IRMP excitation leads to higher internal energies of **1a*** and $H_2CO^\dagger$ and accelerates the sequential decomposition. At lower P_0 values, the collisional deactivation decreases, while the sequential decomposition increases. In fact, we observed that the ratio increased from 20 to 50% with the increase in F from 105 to 375 J cm^{-2} (Fig. 3a) and that the ratio increased from 37 to 65% with the decrease in P_0 from 3 to 0.5 Torr (Fig. 4a).

Since CH_3· is also produced with a high internal energy, such primary products as CH_4 and C_2H_6 are probably formed with high internal energies. However, the primary hydrocarbon products are mostly stabilized by the collisional deactivation processes because of the higher E_a values for the cleavage of C-H and C-C bonds, 102 and 85 kcal mol^{-1} respectively[22] in CH_4 and C_2H_6 compared with those in $H_2CO^\dagger$.[21] This is consistent with the absence of any effect of F and P_0 on the distribution of hydrocarbon products in the range of 105—375 J cm^{-2} of F (Fig. 3b) and in the range of 0.5—3 Torr (Fig. 4b). The formation of C_2H_4, C_2H_2, C_3H_8, and other hydrocarbons is explained by the following sequence of reactions (Eqs. 2—12), which are all involved in high-temperature chemistry:[23]

$$\text{CH}_3\cdot + \text{CH}_3\cdot \rightarrow \text{C}_2\text{H}_6 \quad (2)$$

$$\text{CH}_3\cdot + \text{C}_2\text{H}_6 \rightarrow \text{CH}_4 + \text{C}_2\text{H}_5\cdot \quad (3)$$

$$\text{C}_2\text{H}_5\cdot \rightarrow \text{C}_2\text{H}_4 + \text{H} \quad (4)$$

$$\text{H} + \text{C}_2\text{H}_6 \rightarrow \text{H}_2 + \text{C}_2\text{H}_5\cdot \quad (5)$$

$$\text{CH}_3\cdot + \text{C}_2\text{H}_5\cdot \rightarrow \text{C}_3\text{H}_8 \quad (6)$$

$$CH_3\cdot + C_2H_5\cdot \rightarrow CH_4 + C_2H_4 \quad (7)$$

$$H + C_2H_4 \rightarrow H_2 + C_2H_3 \quad (8)$$

$$CH_3\cdot + C_2H_4 \rightarrow CH_4 + C_2H_3 \quad (9)$$

$$C_2H_3 \rightarrow H + C_2H_2 \quad (10)$$

$$H + C_2H_5\cdot \rightarrow 2CH_3\cdot \quad (11)$$

$$H + C_2H_3 \rightarrow C_2H_4 \quad (12)$$

According to Scheme 1, the total yield of oxygen-containing products is expected to be equal to the total yield of C_n hydrocarbon products multiplied by n. The actual ratio of the two yields was, however, 1 : 0.74; several oxygen-containing products have not been detected. The value of $[CO]/([CO]+[H_2CO])=0.37$ means that H_2CO^+ decomposes into $CO+H_2$ in a 37% yield and is stabilized into H_2CO in a 63% yield. The ratio of $[H_2]/[CO]=2.0$ suggests that H_2 is formed not only via the decomposition of H_2CO^+ but also via other reactions of the alkyl radicals.

Similar mechanisms involving the sequential decomposition of primary products into final products have been proposed in the IRMPD of organic molecules.[10,19] The sequential decomposition process competes with the collisional deactivation process and, therefore, occurs more easily with smaller E_a and larger E_{abs} values. The sequential (and/or secondary) process distinguishes the IRMPD from thermolysis and shock-wave decomposition, although the sequential decomposition process sometimes occurs in thermolysis at extremely high temperatures.[24]

1b. A similar mechanism is proposed for the IRMPD of **1b** (Scheme 2). The initial cleavage of the C-O bond yields $C_2H_5\cdot$ and $C_2H_5O\cdot$. The disproportionation of $C_2H_5\cdot$ gives C_2H_4 and C_2H_6. The β-fission of $C_2H_5O\cdot$ yields H_2CO^+ and $CH_3\cdot$, while $C_2H_5O\cdot$ decomposes partly into CH_3CHO^+ by the splitting of H. The energy requirement for the cleavage of the C-C bond is considerably less in the decomposition of $C_2H_5O\cdot$.[25] Therefore, the cleavage of the C-C bond must occur favorably; the yield of H_2CO^+ is then higher than that of CH_3CHO^+.

The sequential decomposition of CH_3CHO^+ with a high internal energy yields CH_4+CO (and/or $CH_3\cdot$ +HCO) in a manner similar to that found with H_2CO^+ (Scheme 1). Even if $CH_3\cdot$ and HCO are formed, CH_4, C_2H_6, and CO are mainly formed. Therefore, CH_4 and CO are the final products in the sequential decomposition of CH_3CHO^+.

On the basis of the value of [CO]/[oxygen-containing products]=0.25 and the value of $[CH_3CHO]/([H_2CO]+[CH_3CHO])=0.12$, the branching ratios in the decomposition of $C_2H_5O\cdot$ and in the decomposition of H_2CO^+ and CH_3CHO^+ can be roughly estimated. When x, y, and z denote the ratios of the decomposition of $C_2H_5O\cdot$ into H_2CO^+ plus $CH_3\cdot$, and those of the deactivations of H_2CO^+ into H_2CO and of CH_3CHO^+ into CH_3CHO, respectively, Eqs. 13 and 14 are derived (see Scheme 2):

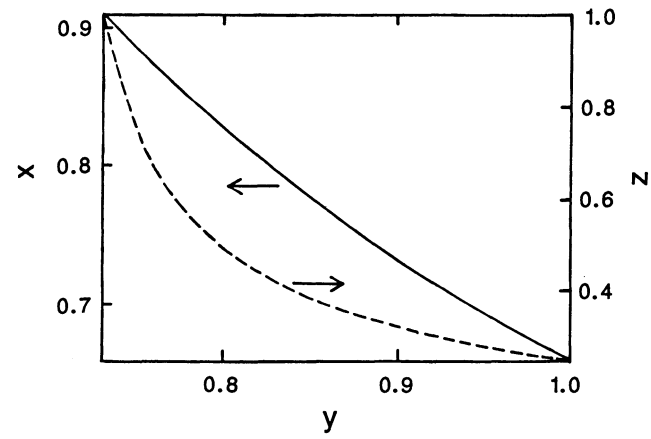

Fig. 5. Relationships of x, y, and z. Values of x and z are calculated as a function of y. For x, y, and z, see the text.

$$x = 1/(1 + 0.136y/z) \quad (13)$$

$$z = 1/(11.1 - 7.33/y) \quad (14)$$

The values of x and z are calculated as a function of y, as is shown in Fig. 5.

A higher branching ratio of the decomposition of $C_2H_5O\cdot$ into H_2CO^+ and $CH_3\cdot$ than that into CH_3CHO^+ and H can easily be expected from the energy difference between the cleavages of the β C-C and β C-H bonds in $C_2H_5O\cdot$. When the branching ratios of the sequential decomposition to collisional deactivation are equivalent in H_2CO^+ and CH_3CHO^+, one can obtain $y=z=0.75$ and $x=0.88$. However, the sequential decomposition is considered to be much more favored in CH_3CHO^+ than in H_2CO^+. It is expected that a small fragment H does not remove the excess energy, while the excess energy remains mainly in a large fragment. Therefore, CH_3CHO^+ has a higher internal energy and decomposes sequentially in a higher yield than does H_2CO^+. This means that $y>0.75$ and $z<0.75$ and that, therefore, $x<0.88$. If y is close to unity, one can obtain $x=0.67$ and $z=0.27$. The ranges of x, y, and z are determined to be as shown in Scheme 2.

The formation of hydrocarbon products is also explained by these reactions (Eqs. 2—12) and similar reactions involving $C_2H_5\cdot$. Since a considerable

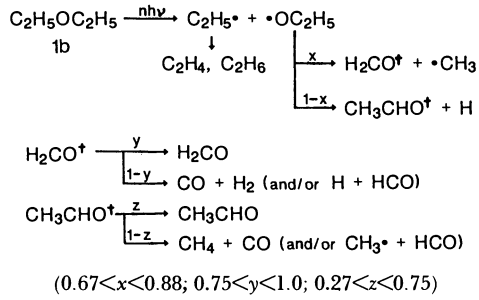

$(0.67<x<0.88;\ 0.75<y<1.0;\ 0.27<z<0.75)$

Scheme 2.

amount of propane (C_3H_8) is formed, the coupling reaction between C_2H_5· and CH_3· (Eq. 6) is particularly important.

1c and 1e. The cleavage of the C-O bond produces propyl (n-C_3H_7·) and propoxyl radicals (n-C_3H_7O·) in the IRMPD of **1c**, and butyl (n-C_4H_9·) and butoxyl radicals (n-C_4H_9O·) in the IRMPD of **1e** (Scheme 3).

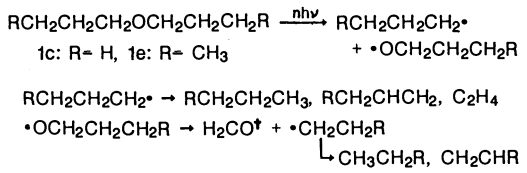

Scheme 3.

n-C_3H_7· disproportionates into C_3H_8 and C_3H_6, while n-C_4H_9· decomposes into C_2H_4 and C_2H_5· via β-fission. Since CO and H_2CO were the only detectable products containing an oxygen atom, it can be said that the cleavage of the β C-C bond in n-C_3H_7O· and n-C_4H_9O· occurs predominantly to form $H_2CO^{\dagger}$+C_2H_5· and $H_2CO^{\dagger}$+n-C_3H_7· respectively. It is well-established that the elimination of an alkyl redical from alkoxyl radicals occurs much faster than that of a hydrogen atom in thermolyses and UV photolyses.[25,26]

1d. The isopropoxyl radical (i-C_3H_7O·) formed in the IRMPD of **1d** decomposes mostly into $CH_3CHO^{\dagger}$+CH_3· and slightly into $CH_3COCH_3^{\dagger}$+H (Scheme 4). The estimation of the branching ratio

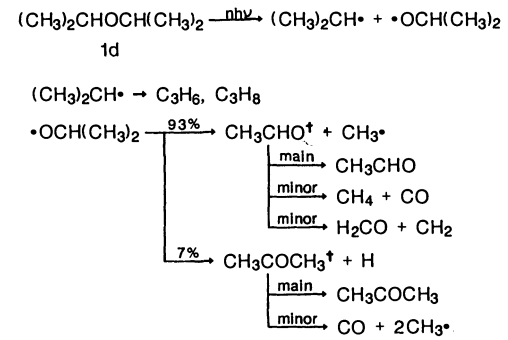

Scheme 4.

between the two processes from the value of $[CH_3COCH_3]/([CH_3COCH_3]+[CH_3CHO])$ shows that the latter process produces only in a 7% yield. It is assumed in the estimation that the branching ratios of stabilization and decomposition for $CH_3CHO^{\dagger}$ and $CH_3COCH_3^{\dagger}$ are similar to each other. The selective decomposition of i-C_3H_7O· into CH_3CHO+CH_3· is due to the smaller value of E_a=11.8 kcal mol^{-1}.[27] Additionally, H_2CO is formed in an 8% yield relative to the total yield of the oxygen-containing products. Therefore, $CH_3CHO^{\dagger}$ is mainly deactivated into CH_3CHO and slightly decomposes into CH_4+CO and H_2CO+CH_2. Similarly, $CH_3COCH_3^{\dagger}$ is mostly stabilized to CH_3COCH_3 and partly decomposes into 2CH_3·+CO, probably via the secondary IRMPD.

1f. In contrast to **1a—d**, **1f** does not have a symmetric structure; rather it has two different alkyl groups separated by an oxygen atom. Therefore, it is interesting to see which C-O bond cleaves initially in the IRMPD of **1f**. The oxygen-containing products are CO and H_2CO, while isobutene (i-C_4H_8) is formed in a 75% yield relative to the total yield of hydrocarbon products. Thus, the cleavage of the C-O bond of a t-butyl group occurs selectively to form the t-butyl radical ($(CH_3)_3C$·) and CH_3O· (Scheme 5). The

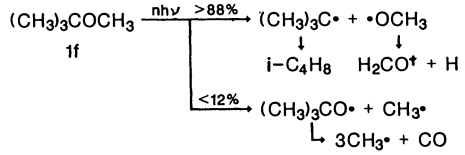

Scheme 5.

minor cleavage of the other C-O bond gives the t-butoxyl radical (t-C_4H_9O·) and CH_3·. Since neither CH_3CHO nor CH_3COCH_3 was detected, t-C_4H_9O· may be scarcely formed at all, or it may decompose into small fragments. If i-C_4H_8 is formed in the main channel and C_2 hydrocarbons are formed from the CH_3· produced in the minor channel, the selectivity for the main cleavage can be estimated to be 88% from $[i\text{-}C_4H_8]/([i\text{-}C_4H_8]+0.5\times[C_2\text{ hydrocarbons}])=0.88$. This value probably corresponds to the lower limit, because CH_3· may be produced from t-C_4H_9O·. The selectivity is due to the considerably smaller value of E_{diss} for a t-C_4H_9-O bond (ca. 60 kcal mol^{-1})[28] than that for a CH_3-O bond (81 kcal mol^{-1}).[17]

2. On the other hand, the cleavages of two different C-O bonds are involved in the IRMPD of **2**. One process gives $CH_3OCH_2CH_2$·+CH_3O·, while the other gives $CH_3OCH_2CH_2$·+CH_3·, as is shown in Scheme 6. Both $CH_3OCH_2CH_2$· and $CH_3OCH_2CH_2O$· de-

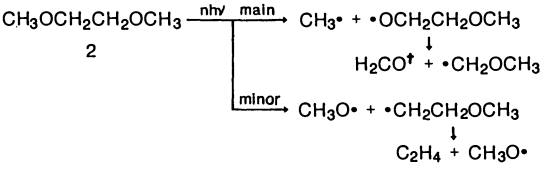

Scheme 6.

compose mainly via β-fission. Since C_2H_6 is formed in a higher yield than is C_2H_4 (1.7 : 1), the C-O cleavage to form CH_3· occurs more preferentially than that to form CH_3O·. However, the selectivity of the cleavage is small because of the similar values of E_{diss} for the two C-O cleavages.

On the basis of the distributions of the products in the IRMPD of open-chain ethers, the decomposition

mechanisms discussed above may be summarized as follows. The homolytic cleavage of the C-O bond in E* occurs primarily to form alkyl and alkoxyl radicals. Since radicals are formed with high internal energies, they further decompose and rearrange sequentially or via the secondary IRMPD. The primary products are mainly formed through β-fission. Since the primary products are also considered to be formed with high internal energies, further decomposition into the stable products occurs, at least in part. The stable products are mostly decomposition fragments, plus a few radical-radical reaction products. No product from any reactions between redicals and ethers was detected. These results are attributable to either the properties of E* in the high vibrational states or to the geometrical specificities of the reaction field in the focused laser beam.

It has been demonstrated that Br_2 is an efficient scavenger of radicals, but it does not initiate chain reactions.[29] The formation of CH_3Br has already been reported in the IRMPD of a mixture of **1a** and Br_2 by Vizhin et al.[5] We have also studied the IRMPD of mixtures of several ethers and Br_2 in order to elucidate the radical intermediates (Table 5). The predominant formation of CH_3Br in the IRMPD of mixture of **1a** and Br_2 clearly shows the intermediary of $CH_3\cdot$ (Scheme 1). The formation of a small amount of CH_2Br_2 suggests that CH_2 is trapped by Br_2. Comparable amounts of CH_3Br and C_2H_5Br were formed in the IRMPD of a mixture of **1b** and Br_2. This suggests a comparable formation of $CH_3\cdot$ and $C_2H_5\cdot$. Therefore, $C_2H_5O\cdot$ splits mainly into $H_2CO+CH_3\cdot$ (Scheme 2). The ratio of $[t\text{-}C_4H_9Br]:[CH_3Br]=88:12$ was obtained in the IRMPD of a mixture of **1f** and Br_2. This shows that the cleavage of a $t\text{-}C_4H_9\text{-}O$ bond occurs selectively in an 88% yield to produce $t\text{-}C_4H_9\cdot+\cdot OCH_3$. The value of the selectivity is equal to the value estimated from the product ratio of $[i\text{-}C_4H_8]/([i\text{-}C_4H_8]+0.5\times[C_2 \text{ hydrocarbons}])=0.88$ (Scheme 5). On the other hand, no bromine-containing compounds of alkoxyl radicals were observed because of the instability of an O-Br bond, even at room temperature.[30]

We have discussed the mechanism of the IRMPD of ethers on the basis of the distribution of the products. However, it has been pointed out that the distribution of the products is generally changed by variations in the irradiation parameters in the IRMPD of organic compounds.[3,4] The sequential processes and the secondary IRMPD of the intermediates compete with collisional deactivation. The branching ratio depends on the internal energies of the radicals and the primary products. Therefore, the branching ratios obtained in the present study are limited to the irradiation conditions of the present experiment. Other competitive processes might produce lower yields under different conditions. However, the main decomposition products are always the same, as is shown in Schemes 1—6, because the initial process is always the cleavage of a C-O bond.

There is a notable finding with respect to the values of ε and Y_d in Tables 1 and 2. **1a** and **1f** have larger ε and Y_d values compared with the other ethers. This result suggests that the $1\leftarrow0$ absorption is very important in IRMP excitation. On the other hand, **1c** has a relatively smaller ε value but a larger Y_d value. The dissociation energy of the bond cleavage and the activation energy of a sequential reaction process probably change with **1a—f** and **2**. Therefore, the decomposition efficiency is dependent not only on the $1\leftarrow0$ absorption, but also on the dissociation and the activation energies for the reaction processes.

Ethers have several advantages as starting materials for the oxygen-isotope separation by use of a TEA CO_2 laser. Firstly, the initial step is the cleavage of a C-O bond. Secondly, the resulting alkoxyl radicals sequentially split into H_2CO or CH_3CHO, which further decompose partly into CO as a stable oxygen-containing product. Since no reactions of alkoxyl radicals with ethers are involved, the isotope selectivity in the cleavage of a C-O bond is predicted to be retained even in the final product, CO. Although the sequential decomposition processes of alkoxyl radicals complicate hydrocarbon products, CO is always the main product among the oxygen-containing products.

When ^{18}O-ether decomposes into alkyl and alkoxyl racicals through selective IRMP excitation, the ^{18}O-alkoxyl radical decomposes sequentially into CO and also reacts partly with ^{16}O-ether in the reaction volume. The bimolecular reactions, together with the vibrational energy transfer between ^{18}O- and ^{16}O-ethers during IRMP excitation, decreases the isotope selectivity. Practically, a lower pressure and a lower F value are used to obtain higher selectivities. The addition of a radical scavenger sometimes effectively prevents isotope-scrambling processes.

The material balance based on oxygen atoms is high enough for it to be concluded that the oxygen atoms in decomposed ethers are found mostly in CO, H_2CO, or CH_3CHO. However, approximately 10—30% of the oxygen-containing products have not been detected. This is probably because of the adsorption of H_2CO and CH_3CHO on the cell wall. It may, alternatively, be suggested that low-volatile oxygen-containing products, including a large number of carbon and oxygen atoms, are formed on the cell wall through the complicated reactions between the radicals and the starting ether.

From the observed results, the criteria for a suitable ether for oxygen-isotope separation by means of IRMPD are considered to be as follows. A higher selectivity of oxygen-isotopes in the cleavage of a C-O bond is, of course, the most important factor. Moreover, it is necessary for a good candidate (1) that the ether have a large Y_d, (2) that a highly selective

decomposition process occur, and (3) that simple products be formed. On the basis of these factors, **1a** and **1f** may be said to be the most suitable ethers among the saturated open-chain ethers. In fact, the ^{18}O enrichment induced by a TEA CO_2 laser has been demonstrated in **1a**[5,6] and $(CF_3)_2O$.[1]

The ^{18}O enrichment by the IRMPD of **1a** and **1f** is now under investigation. We are also studying the IRMPD of cyclic ethers for the ^{18}O enrichment.

Thanks are due to Mr. Masahiro Toyoda, undergraduate student of Science University of Tokyo in 1982—1983, for his collaboration in the course of this experiment.

References

1) Part I: T. Majima, T. Igarashi, and S. Arai, *Nippon Kagaku Kaishi*, **1984**, 1490.

2) This work was partly reported at the 11th Int. Conf. on Photochem., Maryland (1983); T. Majima, S. Arai, T. Ishii, M. Toyoda, and T. Handa, Abstr. p. 27.

3) V. S. Letokhov, "Non-linear Laser Chemistry," Springer-Verlag, Berlin (1983).

4) W. C. Danen and J. C. Jang, "Laser-Induced Chemical Processes," ed by J. I. Steinfeld, Plenum Press, New York (1981), p. 45.

5) V. V. Vizhin, Y. N. Molin, A. K. Petrov, and A. R. Sorokin, *Appl. Phys.*, **17**, 385 (1978).

6) K. O. Kutschke, C. Willis, and P. A. Hackett, *J. Photochem.*, **21**, 207 (1983).

7) a) R. N. Rosenfeld, J. I. Brauman, J. R. Barker, and D. M. Golden, *J. Am. Chem. Soc.*, **99**, 8063 (1977); b) D. M. Brenner, *Chem. Phys. Lett.*, **57**, 357 (1978); c) P. Avouris, I. Y. Chan, and M. M. T. Loy, *J. Chem. Phys.*, **72**, 3522(1980); d) D. M. Brenner, *J. Phys. Chem.*, **86**, 41 (1982); e) F. Huisken, D. Krajnovich, Z. Zhang, Y. R. Shen, and Y. Y. Lee, *J. Chem. Phys.*, **78**, 3806 (1983).

8) D. Gutman, W. Braun, and W. Tsang, *J. Chem. Phys.*, **67**, 4291 (1977).

9) J. E. Kuder and D. R. Holcomb, *Chem. Phys. Lett.*, **86**, 11 (1982).

10) J. Kramer, *J. Phys. Chem.*, **86**, 26 (1982).

11) J. Kramer, *J. Photochem.*, **24**, 11 (1984).

12) W. E. Farneth and D. G. Johnson, *J. Am. Chem. Soc.*, **106**, 1875 (1984).

13) S. Ruhman, O. Anner, S. Gershuni, and Y. Haas, *Chem. Phys. Lett.*, **99**, 281 (1983); S. Ruhman, O. Anner, and Y. Haas, *J. Phys. Chem.*, **88**, 5162 (1984); Y. Haas, S. Ruhman, G. D. Greeblatt, and O. Anner, *J. Am. Chem. Soc.*, **107**, 5068 (1985).

14) a) S. Braslausky and J. Heicklen, *Chem. Rev.*, **77**, 473 (1977); b) C. Sonntag and H. -P. Schuchmann, *Adv. Photochem.*, **10**, 59 (1979).

15) G. R. Freeman, C. J. Danby, and C. Hinshelwood, *Proc. Roy. Soc. A*, **245**, 28 (1958); S. W. Benson and D. V. S. Jain, *J. Chem. Phys.*, **31**, 1008 (1959).

16) N. Bloembergen and E. Yablonovitch, *Phys. Today*, **31**, 23 (1978).

17) P. A. Schultz, A. S. Sudbo, D. J. Krajnovich, H. S. Kwok, Y. R. Shen, and Y. T. Lee, *Annu. Rev. Phys. Chem.*, **30**, 379 (1979).

18) M. Quack, *J. Chem. Phys.*, **69**, 1282 (1978); J. Troe, *ibid.*, **73**, 3205 (1980); A. C. Baldwin and J. R. Berker, *ibid.*, **74**, 3823 (1981).

19) W. E. Farneth and M. W. Thomsen, *J. Am. Chem. Soc.*, **105**, 1843 (1983).

20) F. D. Green, M. L. Savile, F. D. Osterholtz, H. H. Lau, W. N. Smith, and P. M. Zanet, *J. Org. Chem.*, **28**, 55 (1963).

21) S. W. Benson, "Thermochemical Kinetics." 2nd ed., Wiley, New York (1976).

22) B. S. Rabinovitch and D. W. Setser, *Adv. Photochem.*, **3**, 1 (1964).

23) D. L. Allara and R. Shaw, *J. Phys. Chem. Ref. Data*, **9**, 523 (1980); Th. Just, "Shock Waves in Chemistry," ed by A. Lifshitz, Marcel Dekker, New York (1981); G. B. Skinner, *ibid.*; N. C. Peterson, T. Ishii, and W. Braun, "Fast Reactions in Energetic Systems," ed by C. Capellos, R. F. Walker, D. Reidel Publishing, Dordrecht, Holland (1981), pp. 531—539.

24) R. F. C. Brown, "Pyrolytic Methods in Organic Chemistry," Academic Press, New York (1980).

25) J. A. Gray and D. W. G. Style, *Trans. Faraday Soc.*, **49**, 52 (1983).

26) H. Hershenson and S. W. Benson, *J. Chem. Phys.*, **37**, 1889 (1962).

27) T. Berces and A. F. Trotman-Dickerson, *J. Chem. Soc.*, **1961**, 348.

28) N. J. Daley and C. Wentrup, *Aust. J. Chem.*, **21**, 1535 (1968).

29) R. J. S. Morrison and E. R. Grant, *J. Chem. Phys.*, **71**, 3537 (1979); R. J. S. Morrison, R. F. Loring, R. L. Farley, and E. R. Grant, *ibid.*, **75**, 148 (1981).

30) R. T. Sanderson, "Chemical Bonds and Bond Energy," 2nd ed, Academic Press, New York (1976).

Gas Sensitivities of Polypyrrole Films to Electron Acceptor Gases

Tetsuro HANAWA and Hiroshi YONEYAMA*
Department of Applied Chemistry, Faculty of Engineering, Osaka University, Yamada-oka 2-1, Suita, Osaka 565
(Received November 29, 1988)

Electropolymerized polypyrrole films exhibited noticeable gas sensitivities to electron acceptor gases such as PCl_3, SO_2, and NO_2 at room temperature only when they were reduced electrochemically, and the resistance decrease was larger with the gas of larger electron affinity. It was also found that the resistance decrease obeyed the Elovich equation in an early stage of the gas exposure.

Conducting polymers such as polypyrrole and polyaniline have a characteristic feature that anion-doping reactions occur reversibly, and this property has been utilized in several applications such as rechargeable batteries,[1-3] electrochromic displays[4-6] and electronic devices.[7,8] The use of conducting polymers as gas-sensing elements has also been reported in the case of polypyrrole for ammonia,[9] nitrogen dioxide,[10] and alcohols.[11] We previously investigated[12] the NO_2 sensing mechanism of polypyrrole films and found that the NO_2 sensitivity was mainly indebted to chemical doping of NO_2 to give NO_2^-, as in the case of polyacetylene with iodine and bromine etc.[13,14] and of polypyrrole with iodine vapor.[15,16] The present study was intended to investigate comparatively the gas sensitivity of polypyrrole to several electron acceptor gases such as O_2, PCl_3, SO_2, NO_2, and I_2.

Experimental

Film Preparation. Electropolymerization of pyrrole was performed in acetonitrile containing 1 vol% twice distilled water, 0.1 mol dm^{-3} $LiClO_4$ and 0.1 mol dm^{-3} pyrrole under N_2 atmosphere. Distilled pyrrole, reagent grade $LiClO_4$, and acetonitrile were used for the preparation of the electrolyte solution, and prior to electrolysis N_2 was bubbled into the solution for more than 20 min to purge dissolved oxygen. An electrode used for gas sensitivity measurements is illustrated in Fig. 1. Two pieces of Pt wires (d=0.5 mm) were connected to a Pyrex male ground glass joint with 0.3 mm distance which was provided by inserting a thin adhesive tape between the Pt electrodes. The separation of the Pt electrode was fixed with epoxy resin in such a manner as to leave 3 mm bare portion of the Pt wires in their ends which served as electrodes. The polypyrrole deposition was made with the electrolysis at 1 mA for 20 min. By the electrolysis, polypyrrole was deposited in such a manner as to connect the two Pt wire electrodes with each other.

The preparation of polypyrrole films for elemental analyses and for EPMA was made using a rectangular ITO glass electrode (4.0×1.5 cm^2) and a circular ITO glass electrode with 10 mm diameter, respectively. The electrolysis was carried out at 0.5 mA cm^{-2} for 30 min for both cases.

Polypyrrole films used for an multireflectance FT-IR measurement were prepared on a Pt-sputtered rectangular ITO glass electrode (4.0×1.5 cm^2) which provided a flat reflective surface, and those for optical absorption spectrometry were prepared on a rectangular ITO glass electrode

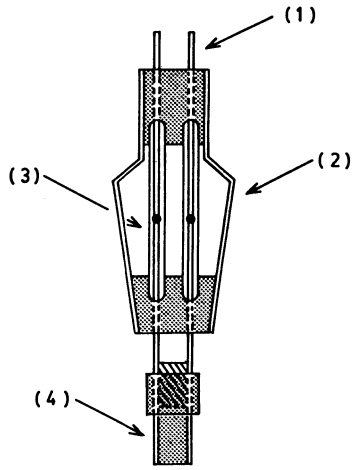

Fig. 1. Schematic illustrations of electrode used for the polypyrrole electrodeposition, designed for the gas sensitivity measurement. Dotted part and slash-lined part denote epoxy resin and adhesive tape, respectively.
(1) Cu lead wire, (2) ground pyrex glass male joint, (3) glass tube, (4) Pt wire (d=0.5 mm).

(2.5×1.5 cm^2) covered with a very thin Pt layer which assisted in homogeneous reduction of the deposited polypyrrole film. The covered Pt was thin enough to allow light penetration in the absorption measurements. In both cases, the current density of 0.2 mA cm^{-2} was used and the quantities of electricity chosen for the former and the latter were 200 mC cm^{-2} and 100 mC cm^{-2}, respectively.

After thoroughly rinsed with acetonitrile, the electropolymerized polypyrrole films were transferred into a N_2-saturated dry box, and subjected to electrochemical reduction in distilled acetonitrile containing 0.1 mol dm^{-3} $LiClO_4$ at −400 mV (vs. Ag/AgCl) for longer than 15 min. Immediately after the reduction, the polypyrrole films were rinsed with distilled acetonitrile and then transferred into a vacuum vessel having a ground female joint which allowed the connection to a vacuum line. These procedures were conducted in the dry box. The polypyrrole samples were vacuum dried at ca. 10^{-4} Torr (1 Torr=133.322 Pa) for more than 1 h.

Measurements of Gas Sensitivities. The electrode shown in Fig. 1 was connected to a branch of a three way tubing. The branch contained a stopcock and a fitted female joint for connecting the electrode. Another branch of the tubing contained a stopcock through which a gas reservoir was connected. The gas reservoir contained an injection port like

that of a gas chromatograph for the injection of test gases. The third branch of the tubing was connected to a vacuum line. Before measurements, the electrode housing and the gas reservoir were evacuated, stopcocks of them were then closed, and the test gas was introduced into the gas reservoir using a gas syringe so as to give 300 Pa in the whole cell. In the measurements of gas sensitivity to iodine vapor, however, solid iodine was first placed in the gas reservoir which was cooled by liquid N_2, and then the electrode housing and the gas reservoir were evacuated. The iodine vapor of ca. 27 Pa in the whole cell was prepared by warming the gas reservoir to room temperature. By opening the stopcock of the electrode housing part, the electrode was exposed to the test gas. Gas sensing behaviors of the polypyrrole films were obtained by measuring current transients under application of 100 mV. In this paper, the gas sensing behaviors will be shown by resistance-time relations. Oxygen, PCl_3, SO_2, NO_2, and iodine vapor which have electron affinities of 0.45 eV, 0.8 eV, 1.1 eV, between 2.1 and 2.5 eV and between 2.5 and 2.6 eV, respectively[17] were used as sample gases.

Spectral Measurements. Polypyrrole films were vacuum dried in the vessel connected to the vacuum line as in the case of the gas sensitivity measurements, and then exposed to sample gases for more than 1 h. After the vacuum evacuation of the gas-exposed films for more than 1 h, spectral measurements were carried out.

Electron probe X-ray microanalysis (EPMA) was performed using an energy dispersive X-ray analyzer EMAX-1800E (Horiba) connected to a scanning electron microscope S-450 (Hitachi). A FT-IR spectrometer FT/IR-3 (JASCO) and an UV-visible spectrometer MPS-5000 (Shimadzu) were used for multireflectance FT-IR measurements and the optical absorption measurements, respectively. The latter two measurements were performed in air.

Results and Discussion

Gas Sensitivities of Reduced Polypyrrole Films to Electron Acceptor Gases. The resistance of the polypyrrole films prepared in the electrode assembly shown in Fig. 1 was ca. 10 Ω and it increased to several kiloohms by electrochemical reduction. When the reduced polypyrrole films were exposed to either one of PCl_3, SO_2, or NO_2 in 300 Pa, or ca. 27 Pa I_2 vapors at room temperature, the resistance of the films was decreased as shown in Fig. 2, and the decreased resistance was not recovered by the subsequent vacuum evacuation. The O_2 sensitivity was also examined, but the exposure of the reduced polypyrrole film to 300 Pa O_2 did not result in any remarkable resistance change. This observation might be related to the finding reported by Scott et al. that the O_2 exposure of reduced polypyrrole films resulted in the conductivity of 10^{-2} $S\,cm^{-1}$ at most,[18] the conductivity being the same order as that of reduced polypyrrole films used in this study.

It is shown in Fig. 2 that the initial resistance of reduced polypyrrole films were different. The scatter seems to have resulted from rather ill-reproducible connections of two Pt wire electrodes with the deposited polypyrrole, but it is believed that the difference

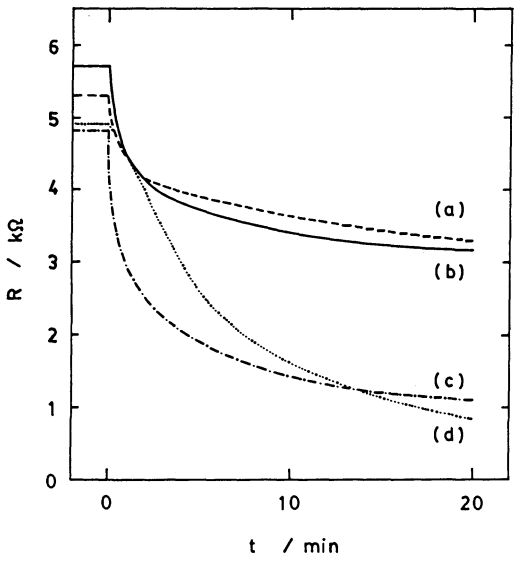

Fig. 2. Resistance changes of electrochemically reduced polypyrrole films caused by the exposure to electron acceptor gases:
(a) 300 Pa PCl_3, (b) 300 Pa SO_2, (c) 300 Pa NO_2, (d) ca. 27 Pa iodine vapor at room temperature.

in the initial resistances did not bring about any serious problem in qualitative analysis of the gas sensitivities of polypyrrole films which will be described below. It is seen in Fig. 2 that the gas sensitivities to iodine and NO_2 are larger than those to SO_2 and PCl_3. This was true even for the gas exposure for long term such as for more than 10 h. The resistance decrease rapidly occurred within initial ca. 2 hours of the gas exposure, followed by a gentle decrease. The resistance attained at the 10 h-gas exposure was 10^2 Ω for the iodine vapor, 1.8×10^2 Ω for NO_2, 1.8×10^3 Ω for SO_2 and 2.0×10^3 Ω for PCl_3. Considering that the electron affinity of NO_2 and I_2 is very near to each other and is more than 1 eV greater than those of PCl_3 and SO_2, the electron affinity seems to play an important role in determining the gas sensitivity of polypyrrole films.

Gas-Sensing Mechanisms. To analyze the resistance changes as shown in Fig. 2, FT-IR and optical absorption spectra of reduced polypyrrole films were measured before and after the gas exposure. Spectra of the reduced film, that of a film first reduced and then exposed to the sample gases, and that of an as-grown film are shown in Fig. 3. The reduced film gave a spectrum (a), while the as-grown film (b). Spectra (c), (d), and (e) concern polypyrrole films that were first reduced and then exposed to NO_2, SO_2, and PCl_3, respectively. It is shown for all cases that by the gas exposure the absorption around 1 eV was enhanced, while that around 3 eV was decreased. It is well-established that absorption having its maximum around 1 eV is related to bipolaron-related transition which is dominant in anion-doped polypyrrole, and that around 3 eV is related to π-π^* transition which is

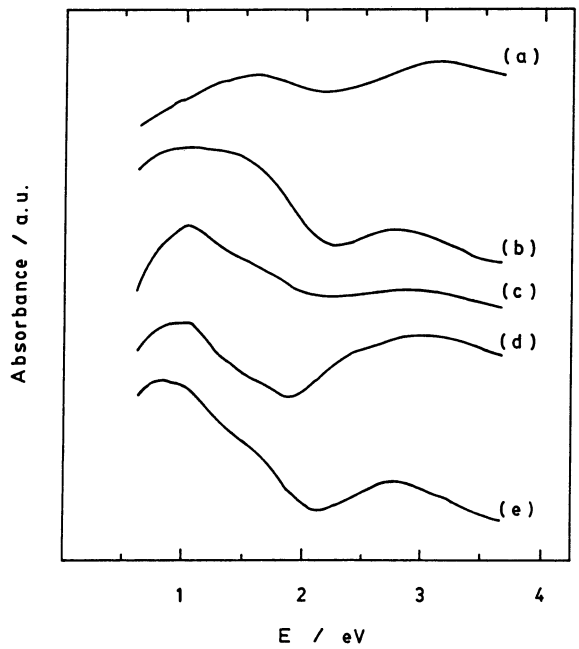

Fig. 3. Optical absorption spectra of polypyrrole films:
(a) reduced, (b) as-grown, (c) reduced and then exposed to NO_2, (d) reduced and then exposed to SO_2, (e) reduced and then exposed to PCl_3.

Table 1. Elemental Analyses of Various Polypyrrole Films[a)]

Sample	Molar ratio to carbon (C=4)				
	C	H	N	Cl	I
As-grown	4	3.03	0.96	0.33	—
Reduced	4	2.83	0.97	0.11	—
Reduced and then exposed to iodine vapor	4	3.20	1.00	0.11[b)]	0.36[c)]
Reduced and then exposed to NO_2	4	3.03	1.11	0.08	—
Reduced and then exposed to PCl_3	4	3.78	0.95	0.33	—

a) The exposure to each gas was carried out for 12 h at room temperature. The gas pressure was 300 Pa for NO_2 and PCl_3, and ca. 27 Pa for iodine vapor. b) Based on the results obtained for the reduced film. c) Estimated by subtracting the chlorine content from the total halogen content (see text).

dominant in reduced polypyrrole.[18,19)] Then it is concluded that the resistance change of polypyrrole films caused by the exposures to SO_2 and PCl_3 results from the doping reactions, as already reported for iodine[15,16)] and NO_2[12)] exposures.

Figure 4 shows FT-IR spectra for reduced films before and after SO_2-exposure. It is recognized that new absorption peaks appeared at 493, 634, 930, 940, 976, and 987 cm^{-1} with the SO_2-exposure. If polypyrrole reacts with SO_2 to give sulfur compounds like sulfone, sulfate and sulfonate, absorption should appear between 1100—1400 cm^{-1},[21)] being in contradiction to the obtained results. It is known that SO_2 gives absorption peaks at 1147, 517, and 1351 cm^{-1},[21)] SO_2^- at 984.8, 495.6, and 1042 cm^{-1},[21)] SO_3 at 484, 1391, and 536 cm^{-1},[21)] SO_2^{2-} at 967, 620, 933, and 469 cm^{-1},[21)] and SO_4^{2-} at 981 and 1104 cm^{-1}.[21)] Judging from these published data, new peaks which appeared in the spectrum (b) are attributable to doped SO_2^- and SO_3^{2-}. Multireflectance FT-IR spectrum of reduced and then PCl_3-exposed polypyrrole film was also measured. The spectrum showed the absorption around 500 cm^{-1} which is related to P-Cl stretching. However, due to lacking of published absorption data of compounds containing P and Cl, the identification of the doped anion species has not yet been done.

Table 1 shows results obtained by elemental analyses of as-grown films, reduced films, and films reduced and then exposed to one of the sample gases used. The data are given as the relative molar ratio of each elements to carbon which is fixed to 4, the number being equal to that of carbon atoms of a pyrrole ring. It was found that the reduced polypyrrole films contained 0.11 moles of ClO_4^- per unit mole of pyrrole probably due to difficulty of complete undoping in a thick film used for elemental analysis. Since the elemental analysis of halogens gives information not on each kind of halogen but on the sum of all kinds of halogens included in the polypyrrole film, the amount of iodine of iodine-exposed polypyrrole films was deduced by subtracting the amount of chlorine content of the reduced polypyrrole films from the total halogen content determined. The sulfur content could not be determined, because the analysis is unsuccessful in the presence of both chalcogen and halogen.

By counting the difference in nitrogen content between the reduced film and the reduced and then NO_2-exposed one, the amount of nitrogen species doped by the NO_2-exposure is deduced to be 0.14 atoms per pyrrole ring. The doped nitrogen species must be NO_2^-.[12)] In the case of iodine-exposed film, the amount of doped anionic species would be 0.12 per pyrrole ring, because it is highly probable that the doped iodine species is I_3^-.[20)] When the reduced polypyrrole film was exposed to PCl_3, chlorine was increased by 0.22 atoms per pyrrole ring. Though the doped anionic species produced by the PCl_3-exposure has not yet been known, the number of doped anions would be 0.07 per pyrrole ring if a single ionization to give PCl_3^- is assumed to take place on the doping. The finding that the doped ionic species was smaller in the PCl_3-doped film than in the iodine-doped films and NO_2-doped one correlates well with the resistance decrease caused by the gas exposure (Fig. 2). It is then concluded that the degree of anion doping caused by the gas exposure is primarily controlled

by the electron affinity of the exposed gas.

Chemisorption Kinetics of Exposed Gases. It was found that the resistance changing behavior as shown in Fig. 2 follows to the Elovich equation (Eq. 1), which is applicable to slow kinetics of chemisorption under a constant gas pressure,[22]

$$\frac{dv}{dt} = a \exp(-bv) \quad (1)$$

where v is the amount of an adsorbed species, a and b represent the rate of adsorption at $v=0$ and the relative rate of disappearance of active sites for chemisorption, respectively. Integration of Eq. 1 gives Eq. 2.

$$v = \frac{1}{b} \ln\left(t + \frac{1}{ab}\right) + \frac{1}{b} \ln(ab) \quad (2)$$

It is thought that the conductivity of gas-exposed polypyrrole film is proportional not to the amount of adsorbed gas but to the amount of ionized dopants. Then the v of the Elovich equation should be read to be the amount of ionized dopant. Since it is believed that the anion doping in polypyrrole occurs like adsorption on polymer fibrils, the establishment of the Elovich equation in the doping process is not strange provided that the ionization is rate-determining in the gas sensing. It is of significance to remark here that the resistance change was observed only when components of the exposed gases were detected in the polypyrrole films.

If it is assumed that the film conductance is proportional to the amount of doped anionic species,[23] then Eq. 3 holds,

$$\frac{1}{R} = Kv \quad (3)$$

where R is the resistance of polypyrrole films and K is a proportional constant. It seems important to remark here that Eq. 3 is not always valid; electrostatic interaction between dopants and positive charges induced in polypyrrole may sometimes greatly influence the conductivity.[24] However, the assumption of Eq. 3 seems to be valid as long as the results obtained at least for NO_2, SO_2, and PCl_3-exposure, as will be shown below. By combining Eq. 3 with Eq. 2, Eq. 4 is derived,

$$\frac{1}{R} = \frac{K}{b} \ln(t + t_0) - \frac{K}{b} \ln(t_0) \quad (4)$$

where t_0 is an adjustable variable to establish a linear relation between $1/R$ and logarithms of the gas exposure time and satisfies $t_0 = 1/ab$. The application of this equation to the time course of the resistance change shown in Fig. 2 gives Fig. 5 for NO_2, SO_2, and PCl_3 in an initial stage of the gas exposure, if t_0 values as given in Table 2 are used. In the case of the iodine vapor, however, the choice of any t_0 values failed to give a linear relation. In Table 2, K/b and Ka values which were determined from $t_0 = 1/ab$ and the slope of the linear relations are also given. The Ka gives a measure of the easiness of the ionization in an initial stage of gas exposure, because the a concerns the rate of adsorption at $v=0$, and K is the proportional constant in Eq. 3 which is believed to be eventually the same among the kind of gases used as long as this equation is valid. Then the results in Table 2 clearly shows that the gas having larger electron affinity has a

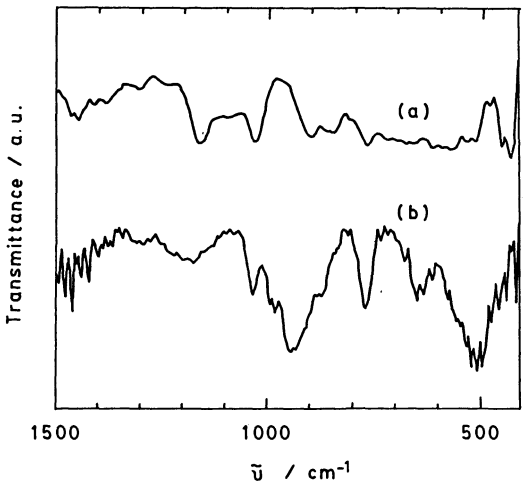

Fig. 4. Multireflectance FT-IR spectra of polypyrrole films:
(a) reduced, (b) reduced and then exposed to SO_2.

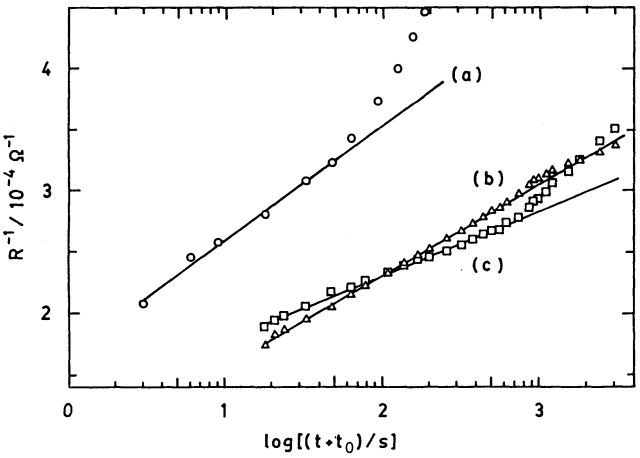

Fig. 5. Elovich plots of the resistance changes shown in Fig. 2.
(a) 300 Pa NO_2, (b) 300 Pa SO_2, (c) 300 Pa PCl_3.

Table 2. Parameters Related to the Adsorption of Electron Acceptor Gases in Polypyrrole films

	E_a[a]	K/b	t_0	Ka
	eV	$s^2A^2m^{-2}kg^{-1}$	S	$sA^2m^{-2}kg^{-1}$
NO_2	2.1<, <2.5	4.06×10^{-5}	3	1.35×10^{-5}
SO_2	1.1	3.19×10^{-5}	18	1.77×10^{-6}
PCl_3	0.8	2.29×10^{-5}	18	1.27×10^{-6}

a) Electron affinity.

higher tendency to be ionized.

This work was supported by Grant-in-Aid for Scientific Research, No. 63470066, from the Ministry of Education, Science and Culture.

References

1) R. J. Waltman, A. F. Diaz, and J. Bargon, *J. Electrochem. Soc.*, **131**, 1452 (1984).
2) B. Scrosati and B. B. Owens, *Solid State Ionics*, **23**, 275 (1987).
3) L. W. Shacklette, M. Maxfield, S. Gould, J. F. Wolf, T. R. Jow, and R. H. Baughman, *Synth. Met.*, **18**, 611 (1987).
4) F. Garnier, G. Tourillon, M. Gazard, and J. C. Dubois, *J. Electroanal. Chem.*, **148**, 299 (1983).
5) T. Kobayashi, H. Yoneyama, and H. Tamura, *J. Electroanal. Chem.*, **177**, 281 (1984).
6) H. Yashima, M. Kobayashi, K. B. Lee, D. Chung, A. J. Heeger, and F. Wudl, *J. Electrochem. Soc.*, **134**, 46 (1987).
7) O. Inganäs and I. Lundstrom, *J. Electrochem. Soc.*, **131**, 1129 (1984).
8) S. Chao and M. S. Wrighton, *J. Am. Chem. Soc.*, **109**, 6627 (1987).
9) G. Gustafsson and I. Lundström, *Synth. Met.*, **21**, 203 (1987).
10) J. J. Miasik, A. Hooper, and B. C. Tofield, *J. Chem. Soc., Faraday Trans. 1*, **82**, 1117 (1986).
11) M. Josowicz and J. Janata, *Anal. Chem.*, **58**, 514 (1986).
12) T. Hanawa, S. Kuwabata, and H. Yoneyama, *J. Chem. Soc., Faraday Trans. 1*, **84**, 1587 (1988).
13) C. K. Chiang, Y. W. Park, A. J. Heeger, H. Shirakawa, E. J. Louis, and A. G. MacDiarmid, *J. Chem. Phys.*, **69**, 5098 (1978).
14) A. G. MacDiarmid and A. J. Heeger, *Synth. Met.*, **1**, 101 (1979/1980).
15) G. B. Street, T. C. Clarke, M. Krounbi, K. Kanazawa, V. Lee, P. Pfluger, J. C. Scott, and G. Weiser, *Mol. Cryst. Liq. Cryst.*, **82**, 253 (1982).
16) H. S. Nalwa, J. G. Rabe, W. F. Schmidt, and L. R. Dalton, *Makromol. Chem., Rapid Commun.*, **7**, 533 (1986).
17) M. T. Bowers, "Gas Phase Ion Chemistry," Academic Press, New York (1979), Vol. 2, pp. 78—82.
18) J. C. Scott, J. L. Bredas, K. Yakushi, P. Pfluger, and G. B. Street, *Synth. Met.*, **9**, 165 (1984).
19) J. L. Bredas, J. C. Scott, K. Yakushi, and G. B. Street, *Phys. Rev. B*, **30**, 1023 (1984).
20) H. Shirakawa, T. Sasaki, and S. Ikeda, *Chem. Lett.*, **1978**, 1113.
21) K. Nakamoto, "Infrared and Raman Spectra of Inorganic and Inorganic and Coordination Compounds," 4th ed, Wiley, New York (1986), pp. 108—125.
22) H. A. Taylor and N. Thon, *J. Am. Chem. Soc.*, **74**, 4169 (1952).
23) A. Wilson and R. A. Collins, *Phys. Stat. Sol. A*, **98**, 633(1986).
24) S. Kuwabata, J. Nakamura, and H. Yoneyama, *J. Chem. Soc., Chem. Commun.*, **1988**, 779.

 © 1989 The Chemical Society of Japan Bull. Chem. Soc. Jpn., 62, 1715—1724 (1989)

Direct Determination of Hyperfine Coupling Constants from Complex and Poorly Resolved ESR Spectra with Numerical Decoupling Analysis

Koichi Nozaki, Akira Naito, Hiroyuki Hatano, and Satoshi Okazaki*
Department of Chemistry, Faculty of Science, Kyoto University, Sakyo-ku, Kyoto 606
(Received November 4, 1988)

Numerical decoupling analysis (NDA) has been developed as a useful analytical method for determining accurate hyperfine coupling constants (hfccs) involved in isotropic ESR spectra with constant linewidths. NDA was found to have a number of advantages over other methods developed for the extraction of hfccs from ESR spectra. For example, the nuclear spin (e.g., $I=1/2$ or 1) can easily be distinguished and hfccs as small as a linewidth can be determined. Furthermore, false hfccs which often appear and lead to confusion in obtaining the true values in other methods are largely eliminated. Owing to these advantages NDA has enabled us to interpret not only complex but also poorly resolved ESR spectra. The practical use of NDA could be demonstrated by analyzing the ESR spectra of *t*-butyl 4-nitrophenyl nitroxide and *t*-butyl 2-chlorophenyl nitroxide radicals.

While a computer simulation method has usually been used as a suitable means of interpreting complicated ESR spectra, it is tedious to determine the ESR parameters with increasing numbers. Furthermore, when an ESR spectrum is poorly resolved it is rather difficult to accurately determine the parameters. Thus, in any case, some degree of experience is required to analyze such an ESR spectrum.

In order to help with the computer simulation analysis of ESR spectra various useful techniques have been reported. For an automatic improvement in the initially estimated set of parameters, a large number of curve-fitting methods are available.[1-4] Most of them employ nonlinear least-squares techniques which generally require a finely tuned data set as the initial parameters. Without such parameters they may not converge or be trapped in an undesirable local minimum of the error function. However, new methods using Simplex[5] or Monte Carlo[6] techniques have proven to be very reliable, especially in systems involving many parameters since they enable one to search for the minimum globally.

On the other hand, if accurate parameters can be independently determined from the hyperfine structure (hfs) of an observed ESR spectrum, one could readily interpret the ESR spectrum without relying on any experience or prejudices, which sometimes cause incorrect interpretations. For this purpose, an autocorrelation method[7-10] as well as Cepstral[11] and Fourier analyses[12,13] have been applied. More recently, Dračka obtained proton and nitrogen hfccs from a complex ESR spectrum by using a 'contraction' method.[14] Motten introduced a simple method using a concept similar to those of Dračka and Newton[15] in order to extract proton hfccs.[16] Lüders determined the hfcc as small as a linewidth by means of a symmetry development transformation.[17] It is, however, still difficult to obtain parameters from poorly resolved and complex ESR spectra, since most of these methods suffer from the appearance of false hfcc peaks, such as ghosts[11,17] or odd harmonics,[15,16] and some methods can only be applied to well-resolved ESR spectra.[14]

Numerical decoupling analysis (NDA), as described in this paper, has been developed as a convenient method to determine hfccs from poorly resolved and complex ESR spectra. The basic principle of NDA involves a search for hfccs by trial and error using a micro-computer. The procedure contains two steps. The first step is a trial to remove the splittings of a given value using the least-squares method. We call this procedure 'numerical decoupling'. The second step involves an evaluation of the results of the numerical decoupling using a specific index function, ascertaining whether the value is one of the hfccs.

NDA possesses some advantages over the other methods. For example, NDA enables one to determine hfccs as small as a linewidth and to distinguish the nuclear spin. Moreover, false hfccs, which sometimes disturb the determination of the hfccs, were largely discriminated.

This paper describes the theory of NDA and its practical applications to several systems.

Theory

Numerical Decoupling Analysis for Nuclei with $I=1/2$. When one nucleus with nuclear spin, I, of 1/2 and a hfcc of **a** contributes to an isotropic ESR spectrum with a constant linewidth, $R(\omega)$, it can be represented by the following form:

$$R(\omega)=F(\omega+\mathbf{a}/2)+F(\omega-\mathbf{a}/2), \quad (1)$$

where $F(\omega)$ is the ESR spectrum without the contribution of this nucleus. We call it a *sub-spectrum*. Furthermore, at least some of the x values at which $R(\omega)$ can be written in the same form as Eq. 1 must be the hfccs involved in $R(\omega)$:

$$R(\omega)=S(\omega+x/2)+S(\omega-x/2). \quad (2)$$

Here $S(\omega)$ is a certain function.

First, these x values are obtained through the following procedures. An error function, $d(x)$ is defined by

$$d(x)\equiv\int_{-\infty}^{\infty}[R(\omega)-S(\omega+x/2)-S(\omega-x/2)]^2\,d\omega, \quad (3)$$

where $R(\omega)$ is an observed ESR spectrum. Actually, $R(\omega)$ is represented by a series of data sampled under a magnetic field that is increasing with a constant increment. Thus, Eq. 3 can be rewritten as Eq. 4 for numerical calculation:

$$d(x)\equiv\sum_{i=1+x/2}^{N-x/2}[R(i)-S(i+x/2)-S(i-x/2)]^2, \quad (4)$$

where N is the number of data points of $R(\omega)$ and $x/2$ must be an integer having a value between 0 and N.

According to the basic theory of the least-squares method, the following simultaneous equations are obtained under the conditions $\partial d(x)/\partial S(i)=0$ ($i=x+1,x+2,\cdots,N-x$):

$$\begin{aligned}
&S(1)+2S(1+x)+S(1+2x)=R(1+x/2)+R(1+3x/2)\\
&S(2)+2S(2+x)+S(2+2x)=R(2+x/2)+R(2+3x/2)\\
&\qquad\vdots\qquad\qquad\qquad\vdots\\
&S(N-2x)+2S(N-x)+S(N)=R(N-3x/2)+R(N-x/2).
\end{aligned} \quad (5)$$

In addition, Eq. 6 is obtained as the result of the reasonable assumption that the intensities at the far ends of the tails of an observed ESR spectrum are regarded as zero:

$$\begin{aligned}
&S(1)=S(2)=\cdots S(x)=0.0,\\
&S(N-x+1)=\cdots=S(N)=0.0.
\end{aligned} \quad (6)$$

Thus, $S(i)$, ($i=1,2,\cdots N$) and $d(x)$ can be calculated from Eqs. 5 and 4, respectively. Since the error function $d(x)$ is equal to 0 when Eq. 2 holds, one can readily determine the x value at which $d(x)$ becomes 0 in a plot of $d(x)$ against x.

Second, we considered the relationship between these x values and the hfccs. When $R(\omega)$ is represented by Eq. 1, namely, the hfcc of **a** is involved in $R(\omega)$, $d(\mathbf{a})$ is obviously equal to 0 and $S(\omega)$ is identical to the *sub-spectrum* $F(\omega)$. However, in this case, $d(\mathbf{a}/3)$, $d(\mathbf{a}/5)$, $d(\mathbf{a}/7)\cdots$ are also found to values of 0. The x values at which $d(x)=0$ can be represented by

$$x_n=\mathbf{a}/(2n+1) \qquad (n=0,1,2,3\cdots), \quad (7)$$

and $S_n(\omega)$ corresponding to the x_n values can be expressed by

$$S_n(\omega)=\sum_{i=-n}^{n}(-1)^{i+n}F(\omega-ix_n). \quad (8)$$

These x values (except for $n=0$) are not hfccs but are recognized as false hfccs. Therefore, the x values leading to $d(x)=0$ consist not only of the true hfccs but also of many false hfccs. If a number of hfccs are involved in an ESR spectrum, it is impossible to select the true values from the infinite number of these x values.

Finally, we discriminated the true hfccs from the false ones. An index function defined by Eq. 9 was found to be the best for this purpose:

$$I_2(x)\equiv\left[\frac{\int_{-\infty}^{\infty}|R(\omega)-R(\omega-\delta)|\,d\omega}{\sum_{j=1}^{2}\int_{-\infty}^{\infty}|R(\omega)-S(\omega-x/2)-S(\omega+x/2+(-1)^j\delta)|\,d\omega}\right]^2, \quad (9)$$

where δ is a very small value. It is replaced by 1 or 2 in actual calculations, which is sufficiently small when compared to N. The subscript in $I_2(x)$ indicates the multiplicity of the nuclear spin of $I=1/2$, namely, $2I+1=2$. The numerator of $I_2(x)$ is used for normalization. Squaring the bracket in this equation is performed for an enhancement of the resolution. Since the denominator of $I_2(x)$ is one of the error functions, such as $d(x)$, it also approaches 0, namely, $I_2(x)$ gives a maximum value when x is equal to **a**. From Eqs. 1, 7, 8, and 9, $I_2(\mathbf{a})$ can be represented by

$$I_2(\mathbf{a})=\left[\frac{\int_{-\infty}^{\infty}|F'(\omega+\mathbf{a}/2)+F'(\omega-\mathbf{a}/2)|\,d\omega}{2\int_{-\infty}^{\infty}|F'(\omega+\mathbf{a}/2)|\,d\omega}\right]^2, \quad (10)$$

where $F'(\omega)$ represents $[F(\omega)-F(\omega+\delta)]/\delta$ or $[F(\omega)-F(\omega-\delta)]/\delta$, which is a form of the derivative of $F(\omega)$. If each line in $F'(\omega+\mathbf{a}/2)+F'(\omega-\mathbf{a}/2)$, that is, in the spectrum obtained from the differentiation of $R(\omega)$, is well resolved and there is no overlap between $F'(\omega+\mathbf{a}/2)$ and $F'(\omega-\mathbf{a}/2)$, the numerator of Eq. 10 can be approximately represented by Eq. 11. Hence, $I_2(\mathbf{a})$ is nearly equal to unity.

$$\begin{aligned}
\int_{-\infty}^{\infty}|F'(\omega+\mathbf{a}/2)+F'(\omega-\mathbf{a}/2)|\,d\omega &\approx\int_{-\infty}^{\infty}|F'(\omega+\mathbf{a}/2)|\,d\omega\\
&+\int_{-\infty}^{\infty}|F'(\omega-\mathbf{a}/2)|\,d\omega=2\int_{-\infty}^{\infty}|F'(\omega)|\,d\omega.
\end{aligned} \quad (11)$$

Since the lines in most of the observed ESR spectra are more or less overlapped, $I_2(\mathbf{a})$ is usually smaller than unity. However, it should be pointed out that the line shape in the ESR spectrum, $R(\omega)$, was not specified in this analysis. If one analyzes the differentiated ESR spectrum, i.e., the 2nd or 3rd derivatives, $I_2(\mathbf{a})$ increases and shows a value closer to unity because the separation of each line becomes better. This distinctive feature is very useful, especially in the analysis of poorly resolved ESR spectra.

If the large second-order effects contribute in the ESR spectra the intensity of $I_2(\mathbf{a})$ will decrease since the basic assumption of NDA, represented by Eq. 1, is not fulfilled.

To discuss the relative intensities of the false and true peaks, the ratio $I_2(\mathbf{a}/3)/I_2(\mathbf{a})$ represented by Eq. 12 is derived from Eqs. 1,7,8, and 9:

$$\frac{I_2(a/3)}{I_2(a)}=\left[\frac{\int_{-\infty}^{\infty}|F'(\omega+a/2)|d\omega}{\int_{-\infty}^{\infty}|F'(\omega+a/2)-F'(\omega+a/6)+F'(\omega-a/6)|d\omega}\right]^2,$$

$$=\left[\frac{\int_{-\infty}^{\infty}|F'(\omega)|d\omega}{\int_{-\infty}^{\infty}|F'(\omega+a/3)-F'(\omega)+F'(\omega-a/3)|d\omega}\right]^2 \quad (12)$$

The results described in the Appendix indicate that this ratio changes between 1/9 to 1, depending on the degree of overlap of the following three functions: $F'(\omega+a/3)$, $F'(\omega)$, and $F'(\omega-a/3)$. When the overlap is small, in other words, the ESR spectrum is well resolved, the intensity of $I_2(a/3)$ is only one-ninth that of $I_2(a)$. $I_2(a/3)$ increases with decreasing the resolution of the spectrum, but is still less than $I_2(a)$, even in the worst case. Therefore, $I_2(a/3)$ is always less than $I_2(a)$. In a similar way, other false hfccs appearing at a/5, a/7,··· are found to be much less than $I_2(a)$.

The reason why these false hfccs can be distinguished by the index function $I_2(x)$ is explained as follows: Though $S_1(\omega)$ represented by Eq. 8 is quite different from the real *sub-spectrum* $F(\omega)$, $S_1(\omega+a/6)+S_1(\omega-a/6)$ becomes identical to $R(\omega)$ due to a partial canceling between $S_1(\omega+a/6)$ and $S_1(\omega-a/6)$ (Fig. 1b). This suggests that these false hfccs can not be distinguished from real values by simply using the error function $d(x)$. However, the index function $I_2(a)$ contains a small distortion of δ which interferes with the canceling, as illustrated in Fig. 2b. Therefore, false values can readily be eliminated by this index function.

Thus, the hfccs contributing to $R(\omega)$ can be readily determined by inspecting the peaks near to unity in a plot of $I_2(x)$ against x.

Numerical Decoupling Analysis for Nuclei with I=1. In the case of a nucleus of I=1, Eqs. 1 and 5 can be substituted by Eqs. 13 and 14, respectively:

$$R(\omega)=F(\omega+a)+F(\omega)+F(\omega-a), \quad (13)$$

$$\begin{aligned}&S(1)+2S(1+x)+3S(1+2x)+2S(1+3x)+S(1+4x)\\&\quad=R(1+x)+R(1+2x)+R(1+3x)\\&S(2)+2S(2+x)+3S(2+2x)+2S(2+3x)+S(2+4x)\\&\quad=R(2+x)+R(2+2x)+R(2+3x)\\&\qquad\vdots\\&S(N-4x)+2S(N-3x)+3S(N-2x)+2S(N-x)+S(N)\\&\quad=R(N-3x)+R(N-2x)+R(N-x).\end{aligned} \quad (14)$$

Some false hfccs appear at

$$x_n=a/(3n+1)\ (n=1,2,\cdots), \quad (15)$$

or

$$x_m=a/(3m+2)\ (m=0,1,2,\cdots). \quad (16)$$

S_n and S_m corresponding to x_n and x_m, respectively, can be represented by

$$S_n=\sum_{i=-3n}^{3n} c(|i|)\cdot F(\omega-ix_n), \quad (17)$$

and

$$S_m=\sum_{i=-3m-1}^{3m+1} c(|i|+2)\cdot F(\omega-ix_m), \quad (18)$$

where

$$\begin{aligned}c(k)&=1 \quad k=3p\\&=0 \quad k=3p+1\\&=-1 \quad k=3p+2,\ p=0,1,2,\cdots.\end{aligned} \quad (19)$$

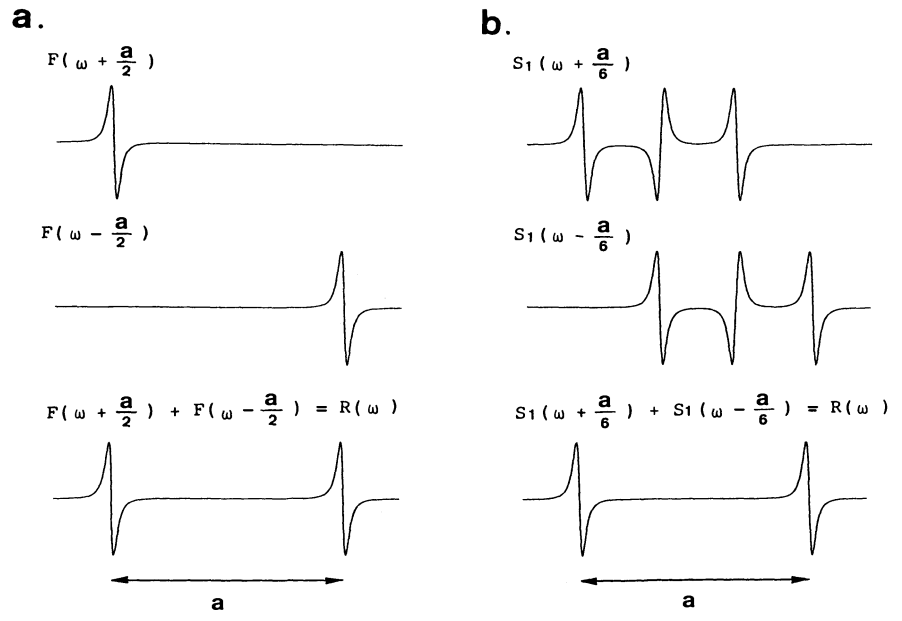

Fig. 1. The illustration of the relationship between the *sub-spectra* and the original ESR spectra (a) at the real hfcc of a and (b) at a/3, one of the false hfccs.

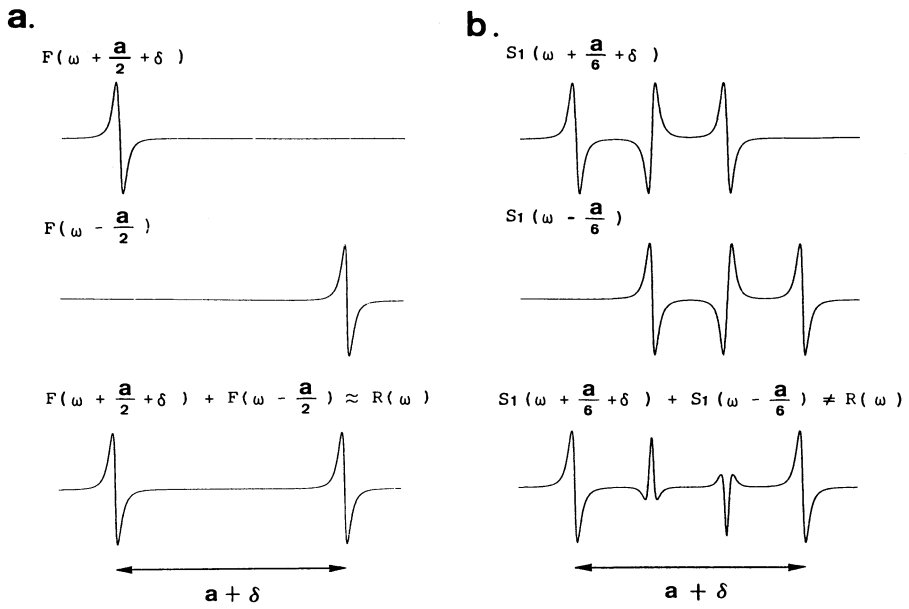

Fig. 2. An illustration showing why false hfccs can be distinguished from the real hfcc by introducing the small distortion δ. (a) The synthesized spectrum from $F(\omega)$ is almost same as the original, $R(\omega)$. (b) The synthesized spectrum from $S_1(\omega)$ is quite different from $R(\omega)$.

The index function for $I=1$ is defined by Eq. 20:

$$I_3(x)=\left[\frac{2\int_{-\infty}^{\infty}|R(\omega)-R(\omega-\delta)|d\omega}{3\sum_{j=1}^{2}\int_{-\infty}^{\infty}|R(\omega)-S(\omega+x)-S(\omega+(-1)^j\delta)-S(\omega-x)|d\omega}\right]^2 \quad (20)$$

In a similar manner as with $I=1/2$, one can show that a plot of $I_3(x)$ against x also gives a maximum value close to unity at $x=\mathbf{a}$.

The ratio $I_3(\mathbf{a}/2)/I_3(\mathbf{a})$ can be represented by

$$\frac{I_3(\mathbf{a}/2)}{I_3(\mathbf{a})}=\left[\frac{\int_{-\infty}^{\infty}|F'(\omega)|d\omega}{\int_{-\infty}^{\infty}|F'(\omega+\mathbf{a}/2)-F'(\omega)+F'(\omega-\mathbf{a}/2)|d\omega}\right]^2 \quad (21)$$

From the results described in the Appendix, the ratio is also found to change between 1/9 to 1, depending on the degree of overlap of the following three functions: $F'(\omega+\mathbf{a}/2)$, $F'(\omega)$, and $F'(\omega-\mathbf{a}/2)$. Therefore, the hfccs of nuclei with $I=1$ can be obtained from a plot of $I_3(x)$ against x in the same way as with $I=1/2$.

Experimental

The preparation of *t*-butyl 4-nitrophenyl nitroxide radical was as follows: 4-nitrophenyl radical produced by the reduction of 4-nitrobenzenediazonium salt with iodide in acetonitrile was trapped by 2-methyl-2-nitrosopropane. After evaporation of the solvent, the nitoxide radical obtained as a spin adduct was separated and purified on a silica-gel column using benzene as an eluent. *t*-Butyl 2-chlorophenyl nitroxide radical was prepared from 2-chlorobenzenediazonium salt in a similar way.

Before ESR measurements benzene solutions of nitroxide radicals in sample tubes were carefully deoxygenated by nitrogen gas bubbling and by several freeze-pump-thaw cycles.

ESR spectra were measured using a JEOL PE-3E, X band ESR spectrometer. ESR spectra were digitized using a 16bit A/D converter (Nippon Protec, Co., Ltd.) of which the acquisition time was 78 ms.

Numerical analyses and calculations of ESR spectra were performed on a PC9801 VX2 micro-computer equipped with a 80286 CPU, and a 80287 co-processor, at a CPU clock cycle of 10 MHz (NEC). Data of a calculated ESR spectrum comprised 1500 points and those of an observed ESR spectrum comprised 1500—2500 points after appropriate treatments, such as digital filtering, centering, and corrections of the offset of the amplifier. These programs for the spectrum treatment, NDA and the calculation of ESR spectra were written in FORTRAN 77. The required computing time for the $I_2(x)$ plot was about 5 minutes and that of the $I_3(x)$ plot was about 10 minutes.

Results and Discussion

Discrimination of the Nuclear Spin of I=1/2 and 1. The plots of $I_2(x)$ in Fig. 3b and $I_3(x)$ in Fig. 3c were obtained for the calculated ESR spectrum (Fig. 3a) from the parameters of $I=1/2$, hfcc=0.06 and a linewidth=0.01 mT. A Lorentzian line shape function was used to obtain all of the calculated spectra in this work. In the $I_2(x)$ plot (Fig. 3b), one well-defined peak of unity height appeared at 0.06 mT. Several additional peaks also appeared at 0.02, 0.012 mT, etc., which were assigned to be false peaks. The ratio

$I_2(\mathbf{a}/3)/I_2(\mathbf{a})$ was calculated to be 0.17, slightly larger than the lowest value predicted by Eq. 12, i.e., 1/9=0.11, since the two lines in the ESR spectrum in Fig. 3a slightly overlapped. However, $I_2(\mathbf{a}/3)$ is still considerably less than $I_2(\mathbf{a})$.

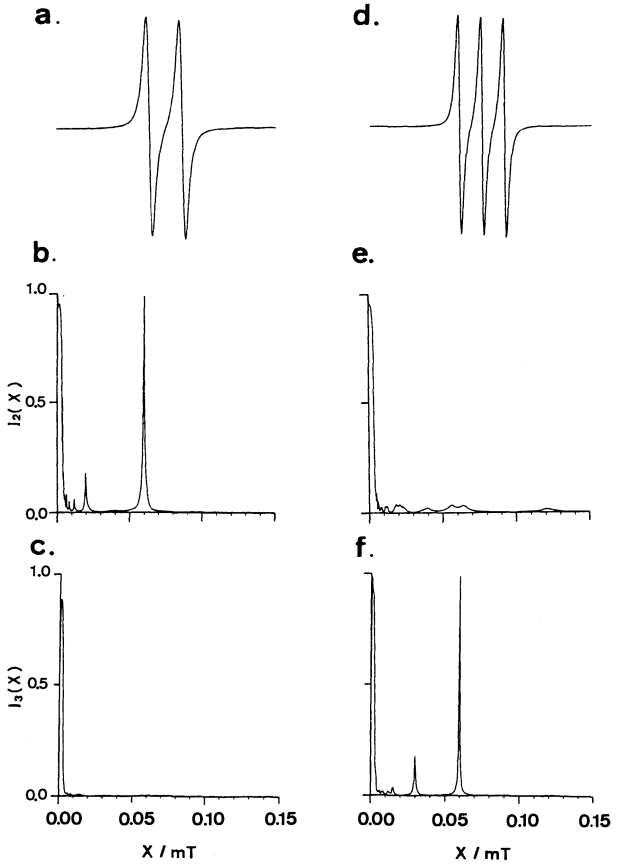

Fig. 3. (a) Simple ESR spectrum calculated using I=1/2, hfcc=0.06 and linewidth=0.01 mT. (b) The $I_2(x)$ plot and (c) $I_3(x)$ plot for the spectrum (a) calculated with δ=1. (d) Simple ESR spectrum; I=1, hfcc=0.06, linewidth=0.01 mT. (e) The $I_2(x)$ plot and (f) $I_3(x)$ plot for the spectrum (d) with δ=1.

A peak with nearly unity height appeared at 0 mT because it was regarded as a hfcc in NDA. This peak is also attributed to the overlap of an infinite number of false peaks. The singularity very near to 0 mT can not be considered as hfcc since it appears at an x value much less than the linewidth (0.01 mT). On the other hand, it is of particular interest to note that the $I_3(x)$ plot (Fig. 3c) did not show any peaks, except that at 0 mT.

Figures 3e and 3f show $I_2(x)$ and $I_3(x)$ plots for the calculated ESR spectrum (Fig. 3d) with I=1, hfcc= 0.06 and linewidth=0.02 mT. In the $I_3(x)$ plot, one well-defined peak of unity height appeared at 0.06 mT and several false peaks at 0.03 and 0.015 mT, etc. The ratio $I_3(\mathbf{a}/2)/I_3(\mathbf{a})$ was also evaluated to be 0.17. No peak appeared, except at 0 mT in the $I_2(x)$ plot in this case also.

As indicated by these results, both the nuclear spin and each hfcc involved in an ESR spectrum are readily determined by NDA without interference by any false peaks.

Determination of Small hfcc. The ESR spectra shown in Figs. 4a and 4b were calculated from the hfcc value of 0.06 (5H) and linewidths of 0.02 and 0.05 mT, respectively. When the hfcc was larger than the linewidth, it was readily determined from the position of the peak appearing in the $I_2(x)$ plots (Figs. 4a′ and 4b′). When the linewidth became 0.06 mT, which is the same as the hfcc, the hfs almost disappeared (Fig. 4c) and, hence, it was difficult to determine the hfcc from the ESR spectrum. Even in such a case, one broad peak appeared in the $I_2(x)$ plot (Fig. 4c′), while its peak position shifted slightly to a smaller hfcc value. The accuracy in determining the hfccs by NDA will be discussed later.

Since the line shape is not specified in this analysis, a 2nd-derivative spectrum can also be analyzed. One

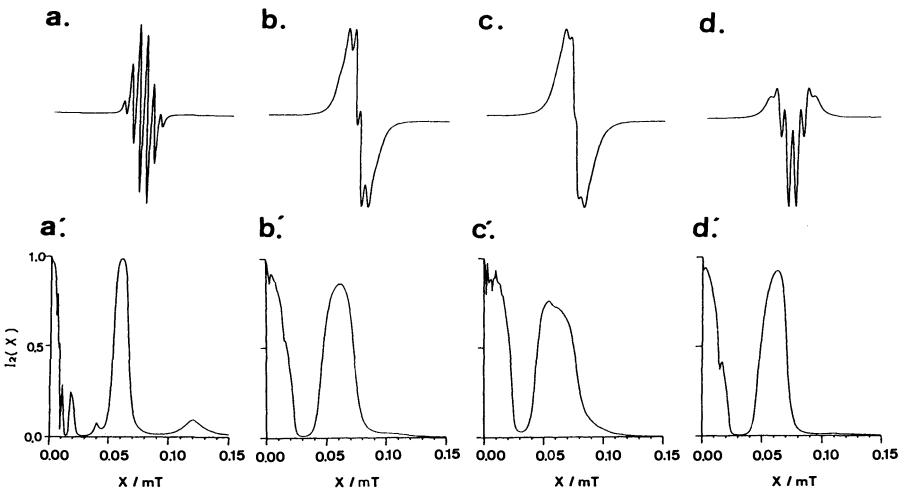

Fig. 4. ESR spectra calculated with hfcc=0.06 mT (5H) and various linewidths of (a) 0.02 (b) 0.05 (c) 0.06 and (d) 0.06 mT (2nd-derivative). (a′), (b′), (c′), and (d′) are respective $I_2(x)$ plots which were obtained with δ=1.

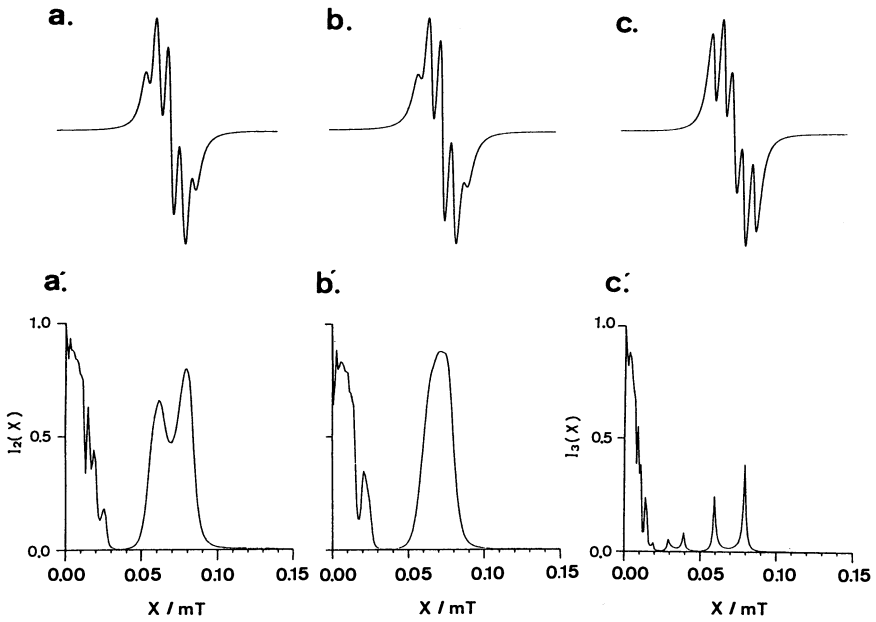

Fig. 5. (a) Calculated ESR spectrum; hfccs=0.06 (2H), 0.08 (2H), linewidth=0.04 mT. (b) hfcc=0.07 (4H), linewidth=0.045 mT. (c) hfccs=0.06 (1N), 0.08 (1N), linewidth=0.04 mT. (a′) and (b′) are the $I_2(x)$ plots for (a) and (b) with δ=1. (c′) was the $I_3(x)$ plot for (c) with δ=1.

sharp peak appeared at 0.06 mT in the $I_2(x)$ plot (Fig. 4d′) for the 2nd-derivative spectrum (Fig. 4d) obtained by differentiating the ESR spectrum in Fig. 4c. Thus, the application of NDA to a higher derivative spectrum permits one to determine accurate hfccs involved in poorly resolved ESR spectra.

The lower limit of the hfcc values for I=1 was also found to be almost the same as for I=1/2 when the first-derivative ESR spectra were analyzed with NDA.

Resolution for Small Difference between hfccs. Next, the resolution for small differences between hfccs was demonstrated. Figure 5a shows the ESR spectrum calculated with a hfcc of 0.06 (2H) and 0.08 (2H), and a linewidth of 0.04 mT. Though the linewidth was twice as large as the difference between the two hfccs, they were completely separated in the $I_2(x)$ plot (Fig. 5a′). On the other hand, this ESR spectrum closely resembled that calculated with hfcc of 0.07 mT (4H) (Fig. 5b). Thus, the hfcc of 0.07 mT would be accidentally obtained if the ESR spectrum in Fig. 5a is analyzed with ordinary methods. It is, however, very interesting to note that the $I_2(x)$ plots shown in Figs. 5a′ and 5b′ obtained for the ESR spectra in Figs. 5a and 5b, respectively, were quite different.

Figure 5c shows an $I_3(x)$ plot for the ESR spectrum calculated from hfccs of 0.06 (1N) and 0.08 (1N), and a linewidth of 0.04 mT. Though two peaks at 0.06 and 0.08 mT were fairly small, they were well resolved.

Effect of Equivalent Nuclei and Delta. Figures 6a and 6d show the ESR spectra calculated from the hfccs of 0.07 (1H) and 0.02 (10H), and linewidth of 0.005 and 0.015 mT, respectively. Figure. 6b shows the $I_2(x)$ plot obtained for the spectrum in Fig. 6a when

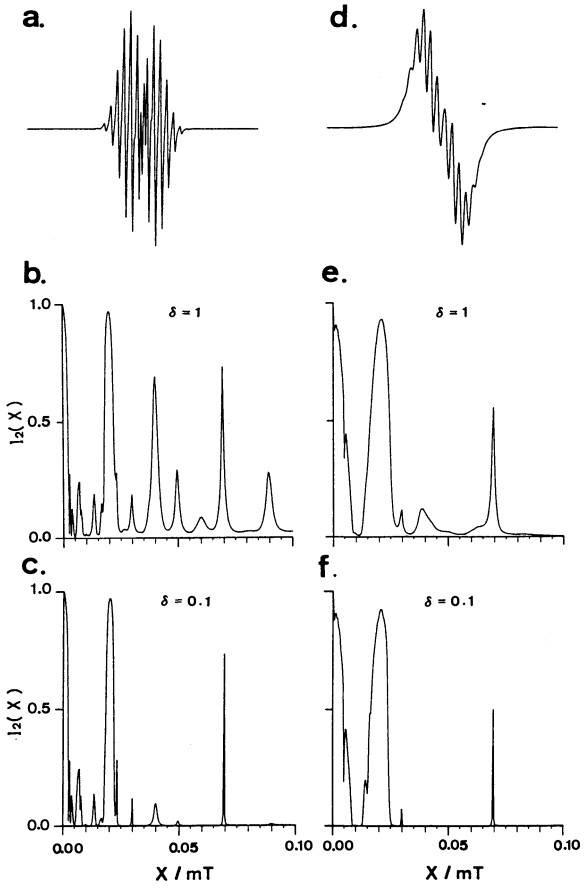

Fig. 6. (a) Calculated ESR spectrum; hfccs=0.02 (10H), 0.07 (1H), linewidth=0.005 mT. (b) The $I_2(x)$ plot for (a) with δ=1 and (c) with δ=0.1. (d) Calculated ESR spectrum with the same parameters as (a) except for a linewidth of 0.015 mT. (e) The $I_2(x)$ plot for (d) with δ=1, and (f) with δ=0.1.

δ=1, which was equal to 0.00035 mT in this calculation. Several peaks appeared in the $I_2(x)$ plot in addition to the hfcc peaks (at 0.02, 0.07 mT) and their false peaks (at 0.014, 0.007 mT). The peaks, which appeared at 0.05 and 0.09 mT, corresponded to 0.07—0.02 and 0.07+0.02 mT, respectively. Those at 0.04 and 0.06 mT seemed to be overtone peaks corresponding to 2×0.02 and 3×0.02 mT, respectively. We call these peaks *sub-peaks*, which differ from false peaks. They sometimes appear when many equivalent nuclei contribute to the hfs. On the other hand, when the linewidth was 0.015 mT, these *sub-peaks* were very small (Fig. 6e), while the hfcc peaks at 0.02 and 0.07 mT were substantially unchanged.

These results indicate that the intensities of the *sub-peaks* are closely related to the ratio of δ to the linewidth. The intensities of the *sub-peaks* increased when the value of δ was not small compared with the linewidth. To suppress the *sub-peaks*, the δ value should be chosen to be less than about 1/40 of the linewidth. Consequently, if the δ value is equal to the sampling interval of the data, each line in an observed ESR spectrum must be composed of more than 100 data points. However, when an observed ESR spectrum includes many lines this condition may be difficult to achieve on a micro-computer with limited memory space and, hence, *sub-peaks* will prohibit obtaining the exact parameters.

In order to calculate Eq. 9 for a δ value less than 1 the following approximations are used:

$$R(\omega-\delta)\approx R(\omega)-[R(\omega)-R(\omega-1)]\delta, \quad (22)$$

and

$$S(\omega\pm\delta)\approx S(\omega)-[S(\omega)-S(\omega\pm1)]\delta. \quad (23)$$

Substitution of Eqs. 22, 23 into Eq. 9 yields Eq. 24.

$$I_2(x)=\left[\frac{\delta\int_{-\infty}^{\infty}|R(\omega)-R(\omega-1)|\,d\omega}{\sum_{j=1}^{2}\int_{-\infty}^{\infty}|R(\omega)-S(\omega-x/2)-S(\omega+x/2)(1-\delta)-S(\omega+x/2+(-1)^j)\delta|\,d\omega}\right]^2. \quad (24)$$

Figures 6c and 6f show $I_2(x)$ plots calculated from Eq. 24 when δ=0.1. The heights of the *sub-peaks* decreased dramatically and the two hfccs of 0.02 and 0.07 mT were readily determined without any ambiguity. It was also realized that the linewidths of the peaks in the $I_2(x)$ plot obtained from the δ value of 0.1 were narrower than those for δ=1. The linewidths of the peaks in $I_2(x)$ and $I_3(x)$ plots seem to depend on the following factors: the linewidth of an ESR spectrum, the number of nuclei, the nuclear spin, and the δ value. The detailed relationship between them is not presently understood.

Effect of Noise. The value of the numerator in Eq. 10, which is equal to $\delta\int_{-\infty}^{\infty}|R(\omega)-R(\omega-\delta)|d\omega$, increases as the noise in $R(\omega)$ increases. In particular, it is greatly affected by the noise of which frequencies higher than those of the signals in $R(\omega)$. Although the value of the denominator in Eq. 10 also becomes large with increasing noise, it may be larger than that of the numerator since the signal-to-noise ratio in the *sub-spectrum* is always worse than that of the original

Table 1. Hfcc Detected by NDA at Various Linewidths

		Linewidth/mT						
		0.1	0.5	1.0	2.0	3.0	4.0	5.0
I=1/2, N=1, hfcc=1.00 mT								
$I_2(x)$	δ=1	1.0000	1.00	1.00	1.00	1.00	1.00	1.00
	δ=0.1	1.0000	1.00	1.00	1.00	1.00	1.00	1.00
$d(x)$		1.0000	1.00	1.00	1.00	1.00	1.00	1.00
mT/point		0.0025	0.01	0.01	0.01	0.01	0.02	0.02
I=1/2, N=4, hfcc=1.00 mT								
$I_2(x)$	δ=1	1.000	1.02	0.94	0.84	0.96		
	δ=0.1	1.000	1.00	1.00	1.00	1.00		
$d(x)$		0.995	1.00	1.00	1.00	1.00		
mT/point		0.005	0.01	0.02	0.02	0.02		
I=1, N=1, hfcc=1.00 mT								
$I_3(x)$	δ=1	1.000	1.00	1.00	1.00	0.88		
	δ=0.1	1.000	1.00	1.00	1.00	0.88		
$d(x)$		1.000	1.00	1.00	1.00	0.88		
mT/point		0.005	0.01	0.01	0.02	0.02		
I=1 ,N=3, hfcc=1.00 mT								
$I_3(x)$	δ=1	1.00	1.01	0.98	0.88			
	δ=0.1	1.00	1.00	0.98	0.88			
$d(x)$		1.00	1.00	0.98	0.88			
mT/point		0.01	0.01	0.02	0.02			

ESR spectrum. Therefore, the value of I_2(a) decreases with increasing noise in the original ESR spectrum. In order to avoid this problem it is advisable that a noisy ESR spectrum is treated with a smoothing filter before being examined by NDA.

Accuracy of hfcc Determined by NDA. Hfcc values determined by NDA from the calculated ESR spectra with hfcc=1.00 mT and various linewidths are given in Table 1. The 1st-derivative Lorentzian function was used in the calculation of all the ESR spectra. Table 1 also contains the values determined from the positions of minima of the error function, $d(x)$ (Eq. 4). In the cases of ESR spectra with a nucleus of I=1/2, the hfcc at 1.00 mT could be determined even at a linewidth of 5.0 mT, whereas a hfcc as small as the linewidth may be the smallest which can be determined by NDA in an actual ESR spectrum containing some noise and distortions. As described in the previous section, hfcc smaller than the linewidth can be determined with the aid of numerical differentiation. However, it must be considered that the calculation of a higher derivative of an observed ESR spectrum usually increases the noise, which leads to a decrease in the intensities of the hfcc peaks in the $I(x)$ plot.

It should be pointed out that when linewidths are large, the hfccs values obtained from the $I_2(x)$ plots with δ=1 become less accurate with increasing number of equivalent nuclei, or probably with increasing number of lines in the hfs. However, hfcc values could be accurately determined either from an $I_2(x)$ plot with δ=0.1 or from $d(x)$. Therefore, exact hfccs should be determined either from the index function $I(x)$ calculated with a smaller δ value or from minima of the error function $d(x)$, especially in interpreting poorly resolved ESR spectra.

When the ESR spectra involving the nuclear spin of 1 was examined less accurate values could be obtained, even from $d(x)$ or $I_3(x)$ with δ=0.1 at the larger linewidth (2 and 3 mT). This is because both tails of the ESR spectrum did not decrease to zero and, therefore, the assumption leading to Eq. 6 was not fulfilled.

Analysis of the ESR Spectrum of *t*-Butyl 4-Nitrophenyl Nitroxide Radical. Figure 7a shows the expanded ESR spectrum of the M_I=+1 components due to the nitrogen nucleus of the nitroxide group in *t*-butyl 4-nitrophenyl nitroxide radical (the entire ESR spectrum was depicted in Fig. 7). In the plots of $I_2(x)$ in Fig. 7b and $I_3(x)$ in Fig. 7c one can readily distinguish the hfcc peaks from the false peaks. Values of 0.090 and 0.223 mT as the proton hfcc and 0.0555 mT as the nitrogen hfcc were obtained, though their intensities were less than unity. The peak at 0.074 mT in Fig. 7b is a false peak for 0.223 mT and those at 0.018 and 0.030 mT are false peaks for 0.090 mT.

The simulated spectrum in Fig. 7d using hfccs of 0.090 (2H, *m*), 0.223 (2H, *o*) and 0.0555 mT(1N, NO_2) is in excellent agreement with that of Fig. 7a.

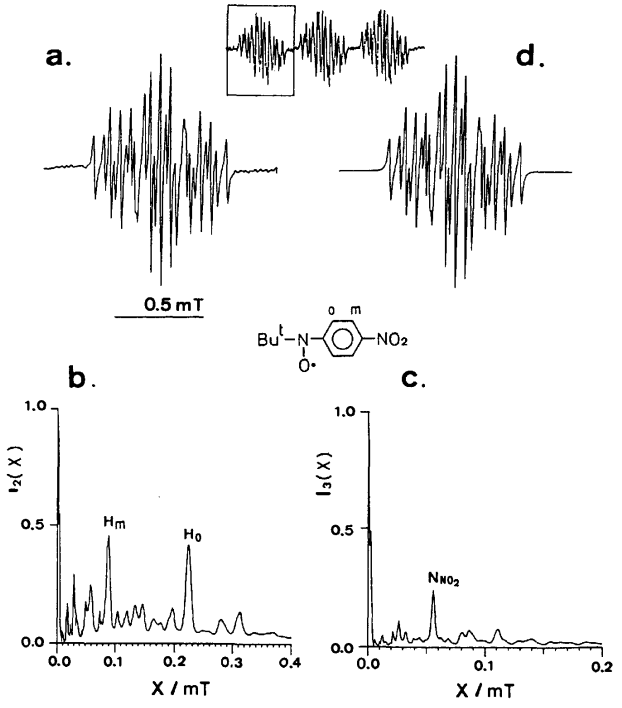

Fig. 7. (a) Expanded ESR spectrum of the M_I=+1 components of *t*-butyl 4-nitrophenyl nitroxide radical (inserted the entire ESR spectrum) measured in a benzene solution. (b) The $I_2(x)$ plot and (c) $I_3(x)$ plot for the spectrum (a) obtained with δ=1. (d) The simulated ESR spectrum using the parameters determined by NDA, i.e., 0.090 (2H, *m*), 0.223 (2H, *o*) and 0.0555 mT (1N, NO_2).

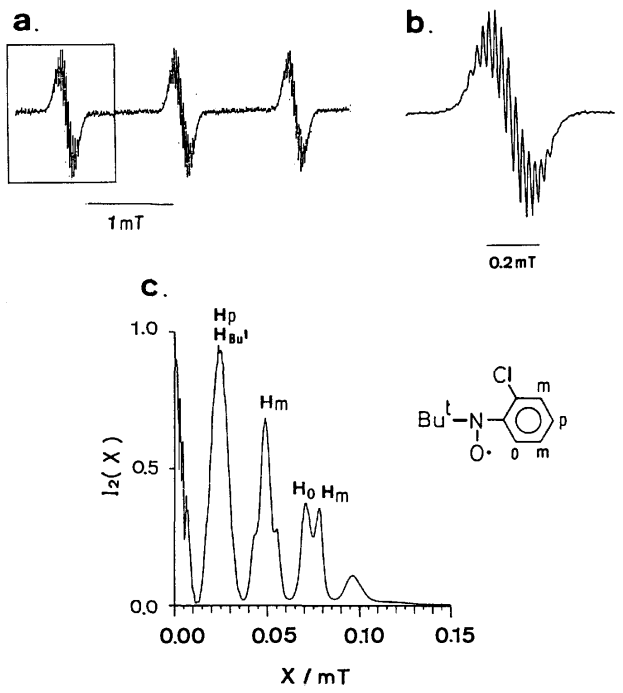

Fig. 8. (a) ESR spectrum of *t*-butyl 2-chlorophenyl nitroxide radical measured in a benzene solution. (b) Expanded spectrum of the M_I=+1 components in (a). (c) The $I_2(x)$ plot for (b) obtained with δ=1.

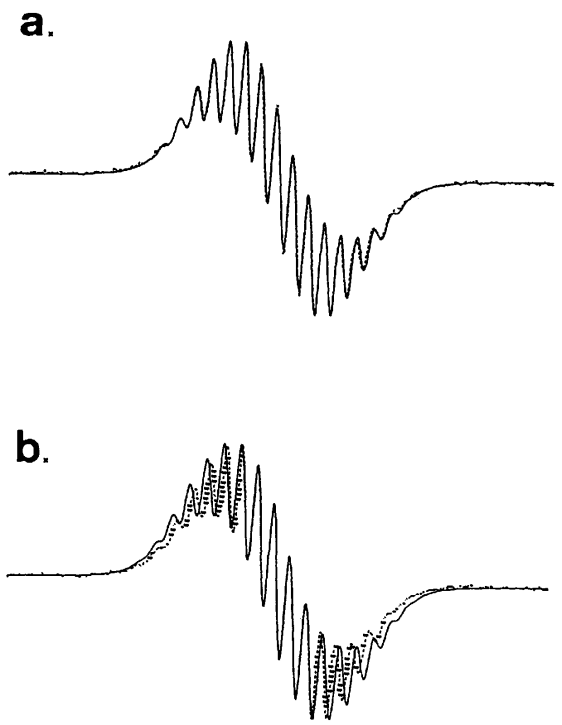

Fig. 9. (a) The simulated spectrum (solid line) using the parameters determined by NDA and (b) using those from NMR data. Experimental ESR spectra were superimposed in both figures with a dotted line (see text).

As indicated here, the nuclear spins and the hfcc values could be obtained from $I_2(x)$ and $I_3(x)$ plots without difficulty, although they were not easily obtained directly from the ESR spectrum (Fig. 7a). Furthermore, since accurate hfccs were determined with the aid of NDA, a computer simulation could be performed only by adjusting the linewidth, and the time for analysis of the ESR spectrum was greatly shortened.

Analysis of the Low-Resolved and Complex ESR Spectrum of *t*-Butyl 2-Chlorophenyl Nitroxide Radical. Figure 8b shows an expanded ESR spectrum of the M_I=+1 components in the ESR spectrum (Fig. 8a) of *t*-butyl 2-chlorophenyl nitroxide radical in benzene. It is obvious that the interpretation of the ESR spectrum is very difficult by ordinary analytical methods since no characteristic pattern appeared in the hfs. It should be noted that four peaks clearly appeared in the $I_2(x)$ plot (Fig. 8c) and, hence, the four hfccs could be precisely determined from these positions. The peak at 0.096 mT, which is nearly equal to 0.024+ 0.0705 mT, seems to be a *sub-peak*. Many peaks appearing in the region from 0 to 0.015 mT could be attributed to the overlap of false peaks for each hfcc. These peaks were excluded because they appear at x values that are much smaller than the linewidth, which is about 0.02 mT in this case.

The ESR spectrum represented by the solid line in Fig. 9a was simulated using hfccs of 0.0240 (10H), 0.0490 (1H), 0.0705 (1H) and 0.0785 (1H), and a linewidth of 0.018 mT. It is in good agreement with the experimental spectrum (superimposed using a dotted line). The hfccs determined by NDA are slightly inconsistent with those obtained from an NMR study of synthesized radicals,[18] which are 0.024 (9H, *t*-butyl), 0.078 (1H, *o*), 0.082 (1H, *m*), 0.049 (1H, *m*), and 0.028 mT (1H, *p*). The small differences between their values and ours can probably be attributed to the large difference in the concentration of radicals (> 1 mol dm^{-3} for NMR and 0.1—1mmol dm^{-3} for ESR observation). These NMR data were obviously inadequate for the analysis of the present ESR spectrum since the simulated spectrum using the NMR data was not in good agreement with the experimental one (Fig. 9b).

These results demonstrate the excellent potentialities of NDA, namely, high resolution for hfcc and an effective elimination of false hfccs.

Conclusion

The general characteristics of NDA can be summarized as follows:

1. One peak in the $I_2(x)$ or $I_3(x)$ plot essentially corresponds to one hfcc.
2. The peak height at the hfcc is nearly equal to unity, but decreases in a poorly resolved ESR spectrum.
3. The height of each hfcc peak does not depend on the number of equivalent nuclei.
4. The nuclear spin can readily be discriminated. For example, nuclei with I=1/2 give peaks in an $I_2(x)$ plot. However, other nuclei, such as nitrogen with I=1, give no peaks.
5. A hfcc as small as a linewidth can be detected.
6. The difference between hfccs as small as about half of the linewidth can be resolved.
7. The line shape in an ESR spectrum is not specified.
8. The δ value used for the calculation of $I(x)$ should be as small as possible, approximately less than 1/30—1/40 of the linewidth. Otherwise, the peak heights of *sub-peaks* usually increase.
9. A noisy ESR spectrum should be treated with a smoothing filter before being examined by NDA.

Among these characteristics, 1, 4, 5, 6, and 7 were better than those of the other numerical methods. In particular, NDA was found to be a valuable tool in analyses of poorly resolved and complex ESR spectra. Since most of these ESR spectra give fewer characteristic patterns in the hfs's, it is very difficult to obtain hfccs from the spectra with ordinary methods. As is demonstrated in Fig. 7, NDA enables one to determine the hfccs exactly, even from spectra showing poorly resolved and monotonous hfs's.

NDA is applicable to the analysis of isotropic ESR spectra with constant linewidths, in which the spectra the basic assumptions represented by Eqs. 1 and 13 are

fulfilled. The deviation from the isotropic spectrum arising, for example, from alternating linewidths, restricted motions, anisotropic interactions, or large second-order effects leads to a decrease of the peak heights in an $I(x)$ plot.

NDA is not a suitable method for analyzing ESR spectra of mixtures of paramagnetic species or those of anisotropic polycrystalline powders.

The well-developed method of electron nuclear double resonance (ENDOR) is better than NDA for the determination of hfccs. However, the ENDOR spectra can be obtained only in limited temperature ranges and, moreover, it costs much more than a micro-computer.

Appendix

Let the areas surrounded by the functions $y=f(\omega+c)$, $y=f(\omega)$ and $y=f(\omega-c)$, and by $y=0$ be $S1$, $S2$, and $S3$, respectively:

$$S1=\int_{-\infty}^{\infty}|f(\omega+c)|\,d\omega, \tag{A-1}$$

$$S2=\int_{-\infty}^{\infty}|f(\omega)|d\omega, \tag{A-2}$$

$$S3=\int_{-\infty}^{\infty}|f(\omega-c)|d\omega. \tag{A-3}$$

Moreover, let the shared area among $S1$, $S2$, and $S3$ be $S123$, and those between $S1$, and $S2$, be $S12$ and between $S2$ and $S3$ be $S23$. Let the unshared areas in $S1$, $S2$, and $S3$ be $S1r$, $S2r$ and $S3r$, respectively.

Using these notations, $S1$, $S2$, and $S3$ can be represented by Eqs. A-4, A-5, and A-6, respectively:

$$S1=S123+S12+S1r, \tag{A-4}$$

$$S2=S123+S12+S23+S2r, \tag{A-5}$$

$$S3=S123+S23+S3r. \tag{A-6}$$

From the relation of $S1=S2=S3$ and Eqs. A-4, A-5, and A-6, one obtains:

$$S1r = S23 + S2r, \tag{A-7}$$

$$S3r = S12 + S2r. \tag{A-8}$$

The denominator of Eq. 12 can be represented by Eq. A-9 by replacing $F'(\omega)$ with $f(\omega)$ and $\mathbf{a}/3$ with c as follows:

$$\begin{aligned}\int_{-\infty}^{\infty}&|F'(\omega+\mathbf{a}/3)-F'(\omega)+F'(\omega-\mathbf{a}/3)|d\omega\\ &=\int_{-\infty}^{\infty}|f(\omega+\mathbf{a}/3)-f(\omega)+f(\omega-\mathbf{a}/3)|d\omega,\\ &=S123+S1r+S2r+S3r.\end{aligned} \tag{A-9}$$

That of Eq. 21 can also be represented by Eq. A-10:

$$\begin{aligned}\int_{-\infty}^{\infty}&|F'(\omega+\mathbf{a}/2)-F'(\omega)+F'(\omega-\mathbf{a}/2)|d\omega\\ &=\int_{-\infty}^{\infty}|f(\omega+\mathbf{a}/2)-f(\omega)+f(\omega-\mathbf{a}/2)|d\omega,\\ &=S123+S1r+S2r+S3r.\end{aligned} \tag{A-10}$$

Substitution of Eqs. A-7 and A-8, and then A-5 into Eq. A-9 yields:

$$\begin{aligned}S123+S1r+S2r+S3r&=S123\\ &+3S2r+S12+S23=S2+2S2r.\end{aligned} \tag{A-11}$$

Since both numerators of Eqs. 12 and 21 are equal to S2, the value of Eqs. 12 and 21 can be represented by

$$\frac{I_2(\mathbf{a}/3)}{I_2(\mathbf{a})}=\frac{I_3(\mathbf{a}/2)}{I_3(\mathbf{a})}=\left[\frac{S2}{S2+2S2r}\right]^2. \tag{A-12}$$

If there is no overlap between $S1$, $S2$ and $S3$, $S2r$ equals $S2$ and the value of Eq. A-12 is 1/9. With increasing the overlap between them, $S2r$ decreases and the value of Eq. A-12 approaches 1:

$$\frac{1}{9}<\left[\frac{S2}{S2+2S2r}\right]^2<1. \tag{A-13}$$

This work was supported in part by a Grant-in-Aid for Scientific Research No. 62540436 from the Ministry of Education, Science and Culture.

Thanks are also due to the Murata Science Foundation for financial assistance.

References

1) D. W. Marquardt, R. G. Bennett, and E. J. Burrell, *J. Mol. Spectrosc.*, **7**, 269 (1961).
2) A. Bauder and R. J. Myers, *J. Mol. Spectrosc.*, **27**, 110 (1968).
3) L. Fischer, *J. Mol. Spectrosc.*, **40**, 414 (1971).
4) M. Barzaghi and M. Simonetta, *J. Magn. Reson.*, **51**, 175 (1983).
5) A. L. J. Beckwith and S. Brumby, *J. Magn. Reson.*, **73**, 252 (1987).
6) B. Kirste, *J. Magn. Reson.*, **73**, 213 (1987).
7) E. Ziegler and E. G. Hoffmann, *Fresenius' Z. Anal. Chem.*, **240**, 145 (1968).
8) K. D. Bieber and T. E. Gough, *J. Magn. Reson.*, **21**, 285 (1976).
9) G. Grampp and C. A. Schiller, *Anal. Chem.*, **53**, 560 (1981).
10) A. Motten and J. Schreiber, *J. Magn. Reson.*, **67**, 42 (1986).
11) D. W. Kirmse, *J. Magn. Reson.*, **11**, 1 (1973).
12) W. R. Dunham, J. A. Fee, L. J. Harding, and H. J. Grande, *J. Magn. Reson.*, **40**, 351 (1980).
13) R. H. Silsbee, *J. Chem. Phys.*, **45**, 1710 (1966).
14) O. Dračka, *J. Magn. Reson.*, **45**, 187 (1985).
15) R. Newton, K. F. Schultz, and R. M. Elofson, *Can. J. Chem.*, **44**, 752 (1966).
16) A. G. Motten, D. R. Duling, and J. Schreiber, *J. Magn. Reson.*, **71**, 34 (1987).
17) K. Lüders, *J. Magn. Reson.*, **73**, 1 (1987).
18) J. A. Pedersen and K. Torssell, *Acta. Chem. Scand.*, **25**, 3151 (1971).

Gel Filtration Chromatographic Study on the Micelle Formation of Triton X-100

Noriaki FUNASAKI,* Sakae HADA, and Saburo NEYA
Kyoto Pharmaceutical University, Yamashina-ku, Kyoto 607
(Received November 17, 1988)

The aggregation properties of Triton X-100 are investigated by frontal gel (Sephadex G-200) filtration chromatography (GFC) at 25 °C and considered in the framework of the monomer-m-mer equilibrium on the basis of both asymptotic and plate theories. The analysis of GFC data by asymptotic theory yields an equilibrium constant of $K=1.3\times10^{68}$ (mmol dm^{-3})$^{-138}$ and a micellar elution volume of $V_m=15.30$ cm^3. By using this V_m value, we calculate a micellar hydrodynamic radius of 4.6 nm and the monomer concentration C_1 for Triton X-100. Values of cmc=0.30 mmol dm^{-3} (UV at 245 nm) and 0.31 mmol dm^{-3} (UV at 265 nm and GFC) are determined and are very close to the cmc value theoretically calculated by using Phillips' definition of the cmc. The C_1 value above the cmc is larger than these cmc values by about 0.06 mmol dm^{-3}. The derivative elution pattern at the trailing boundary exhibits two maxima and a minimum (V_{min}), and indicates the formation of small micelles near the cmc. The concentration at V_{min} on the elution curve, C_{min}, is close to the cmc, as we have already predicted by both asymptotic and plate theories. The present work demonstrates the utility of these theories for analyzing the GFC pattern of self-associating systems and will serve to understand the actions of Triton X-100 on membrane bound proteins and on lipid bilayers.

Triton X-100 is a commercial, polydisperse preparation of polyethylene glycol mono[p-(1,1,3,3-tetramethylbutyl)phenyl] ethers, containing an average of 9.6 oxyethylene units per molecule. This surfactant is very frequently used in the isolation and study of membrane bound proteins and water insoluble lipids. Furthermore, this interaction of membrane proteins with Triton X-100 monomers and micelles can provide information on the mechanism whereby they are attached within membranes.[1,2] Micelle formation of Triton X-100 in aqueous solution has been studied by light scattering,[3-5] viscosity,[5,6] ultracentrifugation,[5-8] fluorescence,[8] gel filtration chromatography (GFC),[5,9] and small-angle X-ray scattering measurements.[5]

For the quantitative investigation of self-associating systems by GFC, the large sample size (frontal) method is superior to the small sample size (zonal) method.[10-14] Recently, we developed a plate theory based on mass action model for micelle formation,[13,14] but this theory has rarely been used for analysis of GFC data on surfactants. Furthermore, asymptotic theory provides analytical solutions for GFC patterns, but most of them have not yet been used for surfactants.[10-14]

In this work, we report the frontal GFC elution curve and its derivative for Triton X-100 as a function of concentration at 25 °C. These data are analyzed with the above-mentioned theories. The aggregation properties obtained of Triton X-100 are compared with those by other workers.

Theoretical Basis

For the sake of simplicity, we regarded the micelle formation of a nonionic surfactant as the following equilibrium:

$$\underset{C_1}{m \text{ monomers}} \overset{K}{\rightleftharpoons} \underset{C_m}{\text{micelle}}, \qquad (1)$$

where C_1 and C_m denote the molarities of monomer and m-mer of the surfactant on a monomer basis. The equilibrium constant K of this reaction may be written as

$$K=C_m/C_1^m. \qquad (2)$$

The total molarity C_0 of surfactant can be written as

$$C_0=C_1+C_m=C_1+KC_1^m. \qquad (3)$$

When a large volume of a sample with the concentration C_0 is charged in a column, a plateau region with the same concentration appears on the elution curve, e.g., as shown in Fig. 1a. Approximately, we may assume that the equivalent sharp boundary for the solute zone leading or trailing boundary is the first moment (centroid) of the elution profile and satisfies the relationships:[10]

$$V_c=\int_0^{C_0} V\mathrm{d}C/C_0 \qquad \text{(leading boundary)} \qquad (4)$$

and

$$V_c'=\int_0^{C_0} V\mathrm{d}C/C_0+S \qquad \text{(trailing boundary)}, \qquad (5)$$

where S is the charged volume of the sample. For these determinations the volume coordinate V is assigned a zero value when the leading boundary of the charged sample enters the column bed. According to this approximation (called asymptotic theory), the elution curve for a nonassociable solute is expected as a rectangle of C_0 in height and of S in width.

Above the cmc (for the case of $m\geqq3$)[10,13] the second "plateau region" generally appears at the trailing boundary. This region is clearly shown in its derivative, e.g., as shown in Fig. 1b. According to the asymptotic theory we can expect the derivative pattern shown by the dot-dash line and the following equations:[10,13,14]

$$m=(3V_{min}-V_1-2V_m)/(3V_{min}-2V_1,-V_m), \qquad (6)$$

$$K=(m-2)[2(m^2-1)]^{m-1}/[m(2m-1)]^m/(C_{min})^{m-1}, \qquad (7)$$

$$V_c=C_1V_1/C_0+C_mV_m/C_0, \quad (8)$$

and

$$V_c=(V_1-V_m)^{(m-1)/m}C_0^{(1-m)/m}(V_1-V_C)^{1/m}/K^{1/m}+V_m. \quad (9)$$

Here V_1 and V_m denote the centroid elution volumes of the monomer and the micelle and C_{min} may be taken as the concentration corresponding to the minimum V_{min} on the derivative curve (Fig. 1). Both V_{min} and C_{min} are expected to be independent of C_0 from Eqs. 6 and 7.

According to plate theory, a gel column may be assumed to be composed of n plates and each plate consists of the mobile and stationary phases. The total volume of the mobile phase equals to the void volume of the column. The partition ratio, P, of a solute between these phases may be written as

$$P=(V_e-V_0)/V_0, \quad (10)$$

where V_e is the elution volume of the solute and V_0 the void volume. Assuming appropriate values for V_0, n, V_1, V_m, K, m, and C_0, we can simulate the theoretical elution curve and its first-derivative curve. The plate theory predicts more realistic elution and derivative patterns than the asymptotic theory. The computer simulation procedure of the plate theory has been reported in detail elsewhere.[14]

In the both theories, micelle formation and partition equilibrium of surfactant are assumed to be instantaneously established.[14]

Experimental

Materials. Triton X-100 was purchased from Tokyo Kasei Organic Chemicals. Sephadex G-200 was obtained from Pharmacia Fine Chemicals and used as suggested by the manufacturer.[15] Four proteins whose hydrodynamic radii R_h (nm) are known[15,16] were used as standards for the determination of R_h of the Triton X-100 micelle. From Sigma are whale myoglobin type II (R_h=1.9), bovine serum albumin (R_h=3.5), yeast alcohol dehydrogenase (R_h=4.6), and thyroglobulin (R_h=8.5). The ion-exchanged water was twice distilled and degassed before use.

Methods. A gel column of an inner diameter of 1 cm and a total gel volume of V_t=26.94 cm^3 was jacketed to maintain a constant temperature at 25±0.2 °C. A sample or eluent was flown into the column at a constant flow rate of about 8 cm^3 h^{-1} by using a mini-pump. The concentration of Triton X-100 in eluate was continuously monitored with a Shimadzu SPD-2A spectrophotometric detector and recorded with a Shimadzu Chromatopac C-R1B data processor. A wavelength of 265 nm or 245 nm was used for absorbance measurements. The absorbance was converted to concentration by using the absorbances of several Triton X-100 solutions at known concentrations.

Computer simulation was carried out with an NEC PC-9801 VX personal computer.

Results and Discussion

Frontal GFC Patterns of Triton X-100. The elution curve, like Fig. 1a, was determined at 10 concentrations (C_0=0.203—10.048 mmol dm^{-3}). From the leading and trailing boundaries, we can determine the centroid volumes, V_c and V_c'. Since these values were in a agreement with each other within experimental errors, we used the average of them hereafter. As Fig. 2 shows, V_c rapidly decreased with an increase of C_0 above the cmc (Table 1). These V_c values were plotted against $1/C_0$ in Fig. 3. From the intersection of two straight lines drawn above and below the cmc, we determined a cmc value of 0.31 mmol dm^{-3}. This value is very close to the cmc values obtained from the absorbance-C_0 plots at 265 nm and 245 nm, as well as

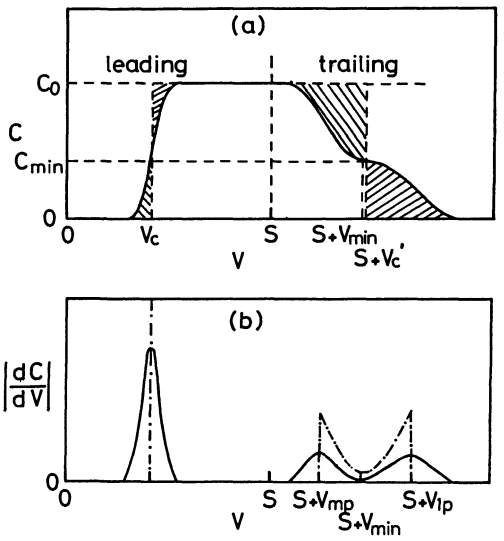

Fig. 1. Schematic elution curve (a) and its derivative (b) for a micellar system and definitions of characteristic parameters. The shaded areas around V_c and V_c' are related to Eqs. 4 and 5. The dot-dash line shows the derivative curve predicted by asymptotic theory and the solid lines show the observed results and those predicted by plate theory.

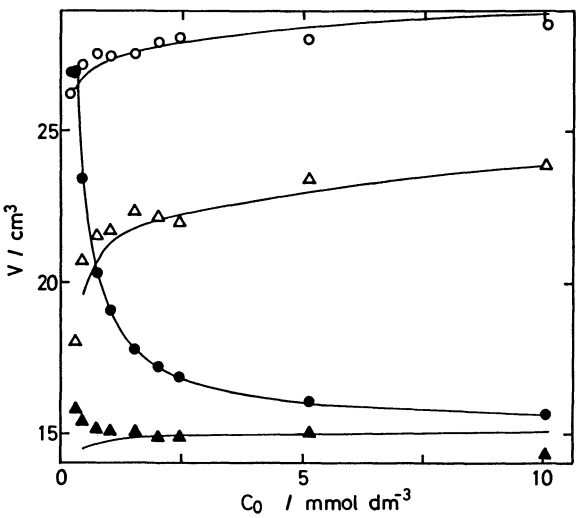

Fig. 2. Characteristic elution volume parameters as a function of total concentration for Triton X-100: ○; V_{1p}, △; V_{min}, ●; V_c, ▲; V_{mp}. The solid lines show the computer-simulated values.

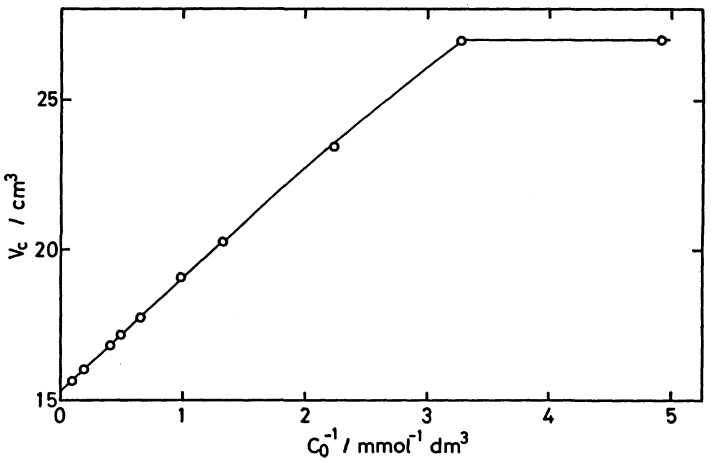

Fig. 3. Centroid volumes as a function of reciprocal concentration for Triton X-100. The solid line shows the computer-simulated values.

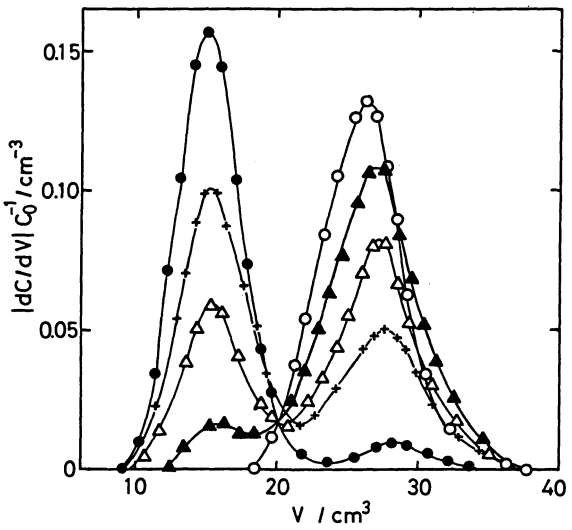

Fig. 4. Reduced derivative elution curves for Triton X-100 at five concentrations (mmol dm^{-3}): ○; 0.203, ▲; 0.305, △; 0.448, +; 0.753, ●; 5.123.

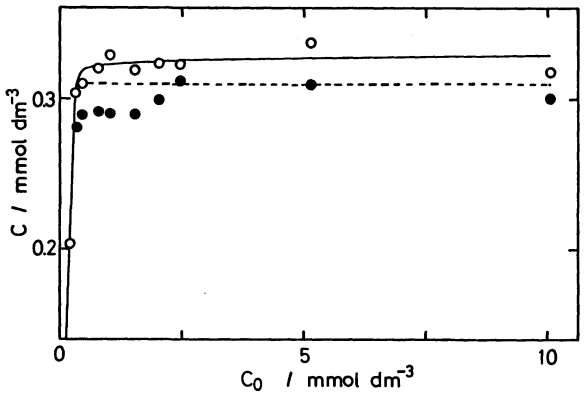

Fig. 5. Values of monomer concentration C_1 (○) and C_{min} (●) as a function of total concentration for Triton X-100. The solid line was calculated from Eq. 3 and the dashed line was computer-simulated for C_{min}.

to the literature value.[17]

Figure 4 shows the reduced derivative profiles for the trailing boundary at five concentrations, where the volume coordinate V is assigned a zero value when eluent enters the column bed. At C_0=0.305 mmol dm^{-3} a small peak of the micelle appears together with a large peak of the monomer. From the elution and derivative profiles we can determine values of V_{1p}, V_{mp}, V_{min}, and C_{min}. In Fig. 2 are shown V_{1p}, V_{mp}, and V_{min} as a function of C_0. Values of C_{min} are shown in Fig. 5.

Triton X-100 is not a pure substance, but a lot of data have been analyzed with the assumption that it was a pure surfactant.[3-8] A number of m values near 25 °C have been reported; m=139 (room temperature)[3] and 135 (25 °C)[4] by light scattering, m=134 (20 °C),[6] 100 (25 °C),[7] and 125 (25 °C, 10 mmol dm^{-3} phosphate buffer)[8] by ultracentrifugation, m=121 (25 °C, 10 mmol dm^{-3} phosphate buffer) by fluorescence titration,[8] and m=147 (20 °C) and 231 (30 °C) by small-angle X-ray scattering.[5] For the purpose of analysis of our GFC data, we used a value of m=139. When m is a large value like this, analyzed results little change with variation in m.

Figure 6 shows the plot according to Eq. 9 by employing m=139 and V_1=27.00 cm^3. This V_1 value was taken from V_e at C_0=0.203 mmol dm^{-3}, the lowest concentration used herein. From this plot we can estimate values of K=1.3×10^{68} (mmol dm^{-3})$^{-138}$ and V_m=15.30 cm^3. By using the linear relationship between $\{(-\log[(V_e-V_0)/(V_t-V_0)]\}^{1/2}$ and R_h for the proteins described in the Experimental section, we estimated a value of R_h=4.6 nm for the Triton X-100 micelle from this V_m value. This R_h value is consistent with the literature values shown in Table 1.[5,6,9]

From Eq. 8 we can estimate the monomer concentration C_1 by using the above values of V_1 and V_m. The C_1 values thus obtained are shown in Fig. 5.

Table 1. Values of Cmc and R_h for Triton X-100 Micelles at 25 °C

Method	Cmc / mmol dm^{-3}	R_h(temp) / nm	Reference
GFC	0.309		This work
UV	0.30(245nn)		This work
UV	0.31(265nm)		This work
Calcd[a)]	0.309		This work
Dialysis	0.3		17
GFC		4.6	This work
GFC		4.1(20 °C)	9
GFC		4.0(20 °C)	5
GFC		5.5(30 °C)	5
DLS[b)]		4.2(20 °C)	5
DLS[b)]		5.6(30 °C)	5
SV[c)]		4.8(20 °C)	6

a) Calculated from Eq. 11. b) Dynamic light scattering. c) Sedimentation velocity.

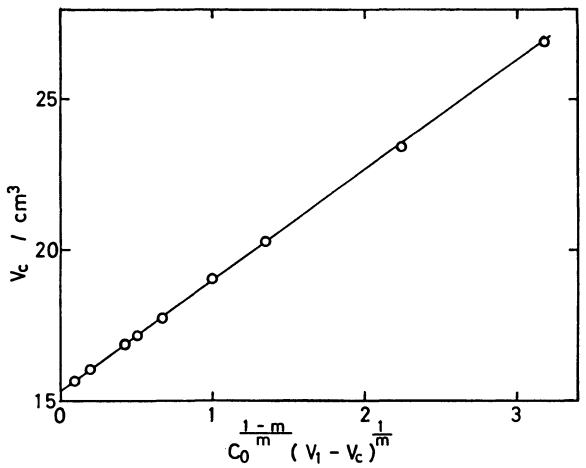

Fig. 6. Centroid volumes plotted according to Eq. 9. The straight line was fitted to the seven high-concentration data by the least-squares method.

The monomer concentration above the cmc is usually assumed to be equal to cmc. As Fig. 5 shows, C_1 is slightly larger than cmc. This is an important result when one considers various actions of Triton X-100.

Comparison between Theory and Experiment. By using the estimated values of V_1, V_m, and m, we can calculate a value of V_{min}=23.13 cm^3 from Eq. 6, regardless of C_0. This value is close to the observed values of V_{min} shown in Fig. 2, but Eq. 6 cannot explain the observed increase of V_{min} with increasing C_0. By using the estimated values of K and m, we can calculate a value C_{min}=0.309 mmol dm^{-3} from Eq. 7, regardless of C_0. This value is similar to the observed C_{min} values shown in Fig. 5, and practically the same to the cmc values shown in Table 1. Recently, by using Phillips' definition of the cmc,[18] we could derive the equation:[14]

$$\text{cmc}=[Km(2m-1)/(m-2)]^{1/(1-m)}. \quad (11)$$

When m is large enough, we can obtain from Eqs. 7 and 11

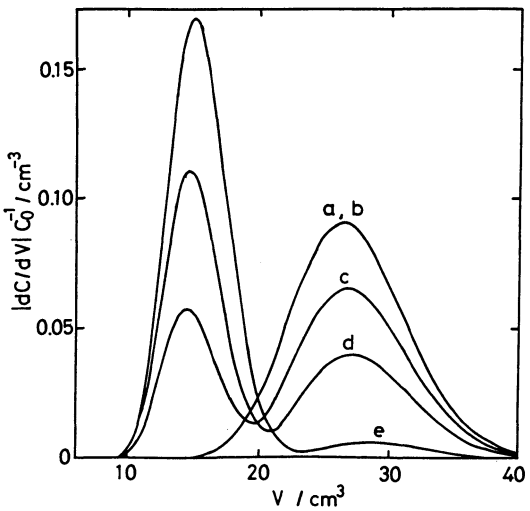

Fig. 7. Computer-simulated derivative patterns at five concentrations (mmol dm^{-3}): a; 0.203, b; 0.305, c; 0.448, d; 0.753, e; 5.123.

$$C_{min}=\text{cmc}=(2Km)^{1/(1-m)}. \quad (12)$$

Substitution of the estimated values of m and K yields a value of C_{min}=cmc=0.309 mmol dm^{-3}. This result explains the experimental observation that C_{min} is close to cmc.

Based on the plate theory, we can computer-simulate the elution curve and its derivative by assuming appropriate values for V_0, n, V_1, V_m, K, m, and C_0. For V_1, V_m, K, and m we used the values estimated above, and regarded V_0 and n as fitting parameters; we used V_0 =5.0 cm^3 and n=30.

The solid lines for V_c shown in Figs. 2 and 3 were computed by the plate theory and are very close to the observed values, as expected; for many m values we have theoretically shown that the plate theory and Eq. 8 predict the same value for V_c.[13,14] Figure 7 shows the derivative elution profiles at the five concentrations, corresponding to Fig. 4. These figures show similar results, except the results at C_0=0.305 mmol dm^{-3}. At this concentration the micellar peak experimentally observed do not appear on the theoretical curve. This discrepancy will be considered below. As Fig. 2 shows, the plate theory explains the increase of V_{1p} and V_{min} with increasing C_0, whereas it predicts a minor increase of V_{mp} with increasing C_0. As Fig. 5 shows, the comupted C_{min} values (dashed line) decreased only slightly with increasing C_0 and are very close to the cmc values shown in Table 1.

Aggregation Properties of Triton X-100. Triton X-100 is an important surfactant for the investigation of biological membranes.[1,2] To consider the action of Triton X-100 on biological membranes, we need to estimate the concentrations of the monomer and the micelle. In most cases the monomer concentration C_1 is taken as the cmc. From the analysis of our GFC data, we determined C_1 as a function of C_0. As Fig. 5 shows, C_1 is larger than the cmc by about 0.06 mmol

dm^{-3}. From Eq. 12 we can estimate the K value by using the cmc and m values and subsequently we can estimate the C_1 value from Eq. 3 by using these m and K values. The estimated C_1 value may be used, when no observed C_1 value is available. Another reason why we chose this surfactant is that its concentration can be very accurately determined by ultraviolet spectroscopy (UV). Most surfactants do not absorb ultraviolet or visible light. Therefore the refractive index (RI) measurement is usually used for monitoring their concentrations.[12] Generally speaking, UV is a more accurate method than the RI method, since the UV absorbance is less temperature-dependent than RI. An accurate concentration determination is essential for obtaining the derivative elution curve.

According to Makino et al.[17] typical samples of Triton X-100 consist of 93% polyethylene glycol mono(octylphenyl) ether and 7% of polyethylene glycol bis(octylphenyl) ether. Most of it is *p*-substituted, but about 10% of the monooctyl ether and the second alkyl group of the dioctyl ether are *o*-substituted. The presence of these impurities must be taken into consideration.

Zonal GFC,[5,9] viscosity,[5,6] and ultracentrifugation[5,8] measurements have all suggested that the size of Triton X-100 micelles little changes with variation of C_0 around 25 °C (it should be noted that these measurements were not carried out at low concentrations). This result is consistent with the data of Tanford et al.[19] They showed that micelles of dodecyl ethers possessing eight or more oxyethylene units do not grow with increasing C_0 at 25 °C.

Assuming only the micelle with an aggregation number of 139, we have applied the asymptotic and plate theories to our frontal GFC data. Taking into consideration inaccuracies of both these data and theories, agreement between theory and experiment in Figs. 2—5 and 7 is generally good except at low concentrations near the cmc. As Fig. 4 shows, a micellar peak appears at C_0= 0.305 mmol dm^{-3}. At the same concentration, however, no micellar peak is observed on the computer-simulated curve (Fig. 7). Furthermore, as Fig. 2 shows, the observed V_{mp} values at low concentrations are larger than those predicted by the plate theory. These results indicate the presence of small micelles at low concentrations and are consistent with light scattering data at low concentrations.[3] The formation of the small micelles may result in negative deviations of the observed V_1 and C_{min} values from the theoretical values at low concentrations (Fig. 5). These small micelles will contain the dioctyl ether preferentially, since the dioctyl ether is expected to be more surface-active than the monooctyl ether.

In this work, the micelle formation of Triton X-100 was analyzed in terms of the monomer-m-mer equilibrium, but we showed that smaller micelles are formed near the cmc. When attempting to take into consideration the concentration dependence of m, we encounter the difficulty that Triton X-100 contains the above-mentioned impurities. Therefore we must consider the concentration dependences of m and the micellar composition for this surfactant. Prior to overcoming this difficulty, we must understand the concentration dependence of m. This may be possible for pure surfactants.[20] Furthermore, from the theoretical view-point, the concentration of the micelle should be expressed as the "true"molarity, viz., C_m/m, and then the equilibrium constant should be denoted as K/m.

Conclusion

The monomer concentration C_1 for Triton X-100 was determined as a function of total concentration from the concentration dependence of the centroid volume by using the asymptotic theory. This C_1 value was close to that expected from the monomer-m-mer equilibrium with values of m=139 and K= 1.3×10^{68} (mmol dm^{-3})$^{-138}$. Observed values of cmc= 0.30 mmol dm^3 (UV) and 0.31 mmol dm^{-3} (UV and GFC) were smaller than the C_1 value by about 0.06 mmol dm^{-3}. The above-mentioned K value was determined from the concentration dependence of the centroid volume. The hydrodynamic radius of the Triton X-100 micelle was determined to be 4.6 nm from the elution volume V_m of the micelle. The derivative elution pattern showed the formation of small micelles near the cmc. The plate theory and asymptotic theory were useful for analyzing the elution curve and its derivative for Triton X-100. These results will serve to understand the mechanism of actions of Triton X-100 on biological membranes.

Thanks are due to Professor J. Paiement, Laval University, Canada, for helpful discussion and to Ms. A. Ohtani and Mr. M. Tanigawa for technical assistance.

References

1) A. Helenius and K. Simons, *Biochim. Biophys. Acta*, **415**, 29 (1975).
2) C. Tanford and J. A. Reynolds, *Biochim. Biophys. Acta*, **457**, 133 (1976).
3) L. M. Kushner and W. D. Hubbard, *J. Phys. Chem.*, **58**, 1163 (1954).
4) A. M. Mankowich, *Ind. Eng. Chem.*, **47**, 2175 (1955).
5) H. H. Paradies, *J. Phys. Chem.*, **84**, 599 (1980).
6) S. Yedgar, Y. Barenholz, and V. G. Cooper, *Biochim. Biophys. Acta*, **363**, 98 (1974)
7) C. W. Dwiggins, R. J. Bolen, and H. N. Dunning, *J. Phys. Chem.*, **64**, 1175 (1960).
8) C. J. Biaselle and D. B. Millar, *Biophys. Chem.*, **3**, 355 (1975).
9) R. J. Robson and E. A. Dennis, *Biochim. Biophys. Acta*, **573**, 489 (1979).
10) G. K. Ackers, *Adv. Protein Chem.*, **24**, 343 (1970).
11) T. Sasaki, *Yukagaku*, **16**, 49 (1967).

12) N. Funasaki, S. Hada, and S. Neya, *J. Phys. Chem.*, **92**, 3488 (1988).
13) N. Funasaki, S. Hada, and S. Neya, *Bull. Chem. Soc. Jpn.*, **61**, 2961 (1988).
14) N. Funasaki, S. Hada, and S. Neya, *Bull. Chem. Soc. Jpn.*, **62**, 380 (1989).
15) Pharmacia technical bulletin "Gel Filtration. Theory and Practice."
16) L. M. Siegel and K. J. Monty, *Biochim. Biophys. Acta*, **112**, 346 (1966).
17) S. Makino, J. A. Reynolds, and C. Tanford, *J. Biol. Chem.*, **248**, 4926 (1973).
18) J. N. Phillips, *Trans. Faraday Soc.*, **51**, 561 (1951).
19) C. Tanford, Y. Nozaki, and M. F. Rohde, *J. Phys. Chem.*, **81**, 1550 (1977).
20) N. Funasaki, S. Hada, and S. Neya, manuscript in preparation.

Catalysis by Heteropoly Compounds. XIII.† An Infrared Study of Ethanol and Diethyl Ether in the Pseudoliquid Phase of 12-Tungstophosphoric Acid

Kwan Young LEE, Noritaka MIZUNO, Toshio OKUHARA, and Makoto MISONO*
Department of Synthetic Chemistry, Faculty of Engineering, The University of Tokyo, Hongo, Bunkyo-ku, Tokyo 113
(Received November 24, 1988)

Ethanol, diethyl ether, and water absorbed in, and their thermal desorption from, the pseudoliquid phase of 12-tungstophosphoric acid have been studied by means of infrared spectroscopy. For all three molecules, the state of the absorption of 6 molecules per anion, $H_3PW_{12}O_{40}\cdot 6R_2O$ (R; C_2H_5 or H), was quite stable and the secondary structures were similar. The intensities of the C-H vibrations indicated that the methyl group of the ethanol molecules interacted with the anions and that its interaction became stronger as the amount of absorbed molecules decreased. In the thermal desorption of absorbed ethanol or diethyl ether, a protonated monomer and dimer as well as an ethoxy group were detected by means of infrared spectroscopy. These species are reaction intermediates of the dehydration of ethanol which were assumed previously (*J. Am. Chem. Soc.*, **109**, 5535 (1987)). It was also found that, upon the dehydration of $H_3PW_{12}O_{40}\cdot 6H_2O$, the proton which had been hydrogen-bonded to the oxygen atom of the water molecule ($(H_2O)_2H^+$) migrated onto the bridging oxygen of the heteropoly anion ($PW_{12}O_{40}^{3-}$).

Heteropoly acids such as $H_3PW_{12}O_{40}$ and their salts have been used as both heterogeneous solid catalysts[1-3] and homogeneous solution catalysts.[4] It has been reported that polar molecules are readily absorbed into the bulk of certain heteropoly acids[5] and that some catalytic reactions take place in the "pseudoliquid phase".[1,6] Since the whole protons in the bulk $H_3PW_{12}O_{40}$ can take part in the reactions, it shows a very high catalytic activity for the dehydration of alcohol or ether at low temperatures.[7,8] We recently demonstrated that the unusual pressure dependencies of the rate and selectivity of the dehydration of ethanol over $H_3PW_{12}O_{40}$ were closely correlated with the amount and the chemical state of the ethanol present in the bulk.[9] Thus, it is very important, for an understanding of the heterogeneous catalysis of heteropoly compounds, to elucidate at the molecular level the activated state of the molecules absorbed in the pseudoliquid phase.

In the case of heteropoly compounds, it is possible to investigate the reacting molecules and the polyanions simultaneously by means of spectroscopy. The primary structure of the heteropoly anion can be monitored by means of IR, as has been described by Rocchiccioli-Deltcheff et al.[10] and other groups.[11] The thermal desorption and transformation processes of acetone and ethanol in $H_3PW_{12}O_{40}$ have been studied with IR by Misono et al.[5] and Moffat et al.[12] Solid-state NMR is also useful for the study of heteropoly acid.[13] The present authors have previously investigated, by the use of solid-state NMR (^{31}P, ^{13}C, ^{1}H), the activated states of ethanol in the pseudoliquid phase of $H_3PW_{12}O_{40}$[14] and demonstrated the presence of protonated ethanols and the ethoxy group. Farneth et al. have observed a methoxy intermediate formed on the polyanion of $K_{3-x}H_xPW_{12}O_{40}$ by ^{13}C CP-MAS NMR.[13b]

In the present study, we have investigated the structure and the thermal transformation of activated ethanol and ether, mainly on the basis of the IR spectral changes brought about by heating. The local position of the protons of $H_3PW_{12}O_{40}$ during the dehydration process of $H_3PW_{12}O_{40}\cdot 6H_2O$ was also examined. These processes were then further discussed in relation to the catalytic dehydration.

Experimental

Materials. The $H_3PW_{12}O_{40}$ was purchased from the Nippon Inorganic Color and Chemical Co., Ltd., and was used after purification by ether extraction and recrystallization from water. The stoichiometric cesium salt ($Cs_3PW_{12}O_{40}$) was prepared using a Cs_2CO_3 aqueous solution as has been described previously.[15]

The C_2H_5OH (Amakasu Chemical Ind.; 99.5%), $(C_2H_5)_2O$ (Showa Ether Co. Inc., Research Grade), C_2H_5OD (Aldrich; 99.5%D), and D_2O (Aldrich; 99.8%D) were degassed by several freeze-pump-thaw cycles. The Al_2O_3 (Reference Catalyst of Catalysis Society of Japan, ALO-4, 170 m^2g^{-1}) and SiO_2 (Cabosil, 200 m^2g^{-1}) were pretreated in a vacuum at 400 °C for 2 h.

The deuterated 12-tungstophosphoric acid ($D_3PW_{12}O_{40}$) was obtained by exchange with D_2O as follows. After $H_3PW_{12}O_{40}\cdot nH_2O$ had been evacuated at room temperature (n=6), it was exposed to D_2O (15 Torr; 1 Torr ≈ 133.322 Pa) and reevacuated. This procedure was repeated several times. After the complete change of ν(O-H) to ν(O-D) had been confirmed by IR, the sample was treated at 130 °C in a vacuum for 1 h to obtain $D_3PW_{12}O_{40}$.

Absorption and Desorption Measurements. The absorption amounts of water, ethanol, and diethyl ether into $H_3PW_{12}O_{40}$ were measured by the use of a thermal gravimeter (Shimadzu TG-30) connected directly to a vacuum system. After the evacuation of the $H_3PW_{12}O_{40}$ (ca. 40 mg) for 1 h at 130 °C, ethanol (20 Torr) or diethyl ether (50 Torr)

† Part XII: T. Okuhara, S. Tatematsu, K. Y. Lee, and M. Misono, *Bull. Chem. Soc. Jpn.*, **62**, 717 (1989).

was introduced at room temperature. The thermal desorption, in which temperature was raised step-by-step, was carried out in the same system.

The content of the crystallization water was measured by the TG. After evacuation at room temperature, the amount of water which remained was 6 molecules per anion; by further evacuation at 100 °C and 200 °C, it became 1 and 0.5 molecules per anion respectively.

Thermal Desorption. The thermal desorption of ethanol and diethyl ether absorbed in $H_3PW_{12}O_{40}$ was carried out in a closed circulation system connected to a gas chromatograph. After about 0.5 g of the catalyst was evacuated at 130 °C for 1 h, the gas was added at 25 °C. Then, the temperature of the catalyst was raised step-by-step. Gases desorbed at each temperature were collected in a trap kept at the temperature of liquid nitrogen and analyzed with a gas chromatograph (Shimadzu GC 8A, TCD, Porapak Q and/or Yanaco G 2800, FID, VZ-10).

IR Measurements. The heteropoly compounds (2—7 mg) were dispersed on a thin silicon plate and were pretreated by the same method as in the thermal desorption. Their IR spectra were recorded in an in situ IR cell,[16] connected to a closed circulation system, by means of an FT-IR spectrometer (JEOL, JIR-10, MCT detector, 4 cm^{-1} resolution).

NMR Measurements. The samples for the NMR measurements were prepared using the closed circulation system or a quartz spring balance connected to the vacuum system. The amount of ethanol absorbed into $H_3PW_{12}O_{40}$ (ca. 0.5—1 g) was determined by measuring the pressure decrease or the change in weight.

High-resolution solid-state MAS NMR spectra were obtained on a Fourier Transform pulsed NMR spectrometer (JEOL JNM-GX270) equipped with a CP-MAS unit (JEOL NM-GSH27MU). The instrumental conditions were the same as those previously described.[14]

Results

IR Spectra of $H_3PW_{12}O_{40}\cdot nH_2O$ ($n\leq 6$). The infrared spectra of $H_3PW_{12}O_{40}\cdot nH_2O$ and $D_3PW_{12}O_{40}\cdot nD_2O$, evacuated at various temperatures, are shown in Figs. 1 and 2 respectively. The spectrum of $H_3PW_{12}O_{40}\cdot 6H_2O$ after evacuation at room temperature was quite similar to that in the literature (Fig. 1a).[10] The bands were assigned as follows, with reference to the structure in Fig. 3a. The band at 1080 cm^{-1} is attributed to the asymmetric stretching vibration of the central PO_4 tetrahedron (ν_{as}(P-O)), and the band at 976 cm^{-1}, to a stretching vibration of W=Ot, where Ot is the terminal oxygen. The other two bands, 887 and 795 cm^{-1}, are assigned to the stretching of the W-Oc-W bridges between corner-shared WO_6 octahedra (ν_{as}(W-Oc-W)), and to the stretching of the W-Oe-W bridges between edge-shared WO_6 octahedra (ν_{as}(W-Oe-W)), respectively.

As is shown in Fig. 1, the IR spectrum changed remarkably upon evacuation above 100 °C (Fig. 1b—d). The intensity of the ν(W=Ot) band at 976 cm^{-1} decreased, and a new band at 1007 cm^{-1} appeared. After the evacuation at 300 °C, the band at 1007 cm^{-1} remained, while the band at 976 cm^{-1} disappeared. In the ν_{as}(W-Oe-W) region, the band at 795 cm^{-1} split into two bands (798 and 768 cm^{-1}) after the 100 °C-evacuation. It was confirmed that the addition of

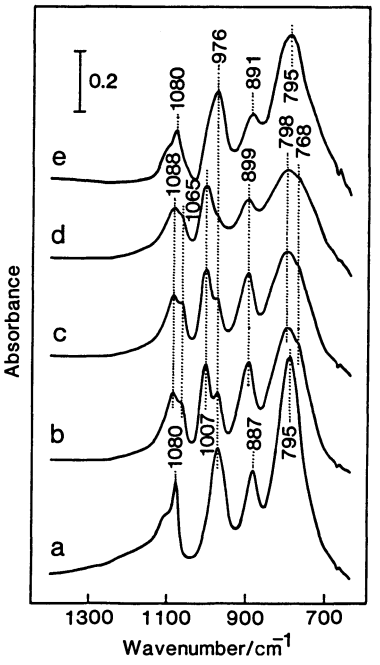

Fig. 1. Infrared spectra of $H_3PW_{12}O_{40}\cdot nH_2O$ during dehydration process; evacuated at (a) room temperature (n=6), (b) 100 °C, (c) 200 °C, (d) 300 °C, and (e) after (d), the sample was exposed to H_2O (15 Torr) and was evacuated at room temperature.

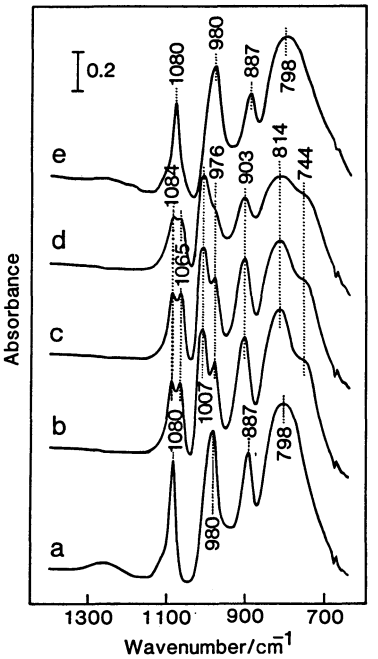

Fig. 2. Infrared spectra of $D_3PW_{12}O_{40}\cdot nD_2O$ during dehydration process; evacuated at (a) room temperature (n=6), (b) 100 °C, (c) 200 °C, (d) 300 °C, and (e) after (d), the sample was exposed to D_2O (15 Torr) and was evacuated at room temperature.

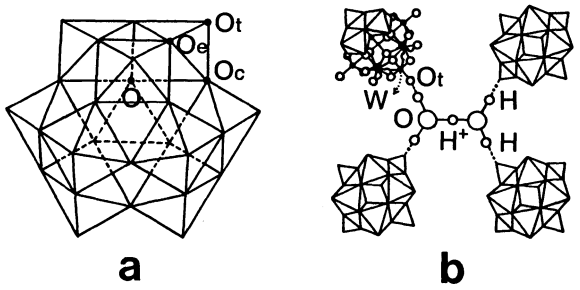

Fig. 3. Structure of (a) the primary structure of heteropoly anion ($PW_{12}O_{40}^{3-}$) and (b) the secondary structure of $H_3PW_{12}O_{40}\cdot 6H_2O$.

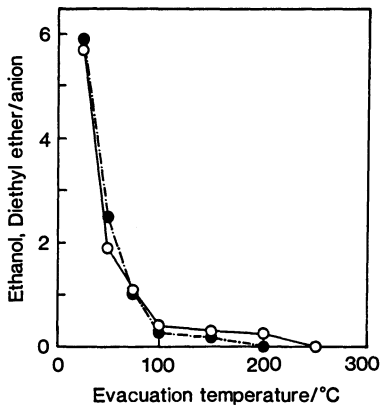

Fig. 4. The amount of ethanol (●) and diethyl ether (○) remained in the bulk of $H_3PW_{12}O_{40}$ during step-by-step thermal desorption.

water (15 Torr) to the 300 °C-evacuated sample and subsequent evacuation at room temperature completely recovered the original spectrum (Fig. 1e).

The infrared spectrum (Fig. 2a) of $D_3PW_{12}O_{40}\cdot 6D_2O$ was similar to that of $H_3PW_{12}O_{40}\cdot 6H_2O$ (Fig. 1a). During heating, the ν(W=Ot) band showed the same changes as that of $H_3PW_{12}O_{40}$. However, it was noted that the ν_{as}(W-Oe-W) band at 798 cm^{-1} split into two bands (814 and 744 cm^{-1}) which were distinctly different from the two bands observed for $H_3PW_{12}O_{40}$ (798 and 768 cm^{-1}). Also, in this case, the original IR spectrum (Fig. 2a) was recovered by the treatment with D_2O (Fig. 2e).

Amounts of Diethyl Ether and Ethanol Absorbed. Figure 4 shows the amounts of diethyl ether and ethanol which remained after the step-by-step thermal desorption. When diethyl ether vapor (150 Torr) was introduced at room temperature, the amount of diethyl ether absorbed became 6 molecules per anion after 30 min. This amount remained unchanged upon the evacuation at room temperature,[17] suggesting that the state of 6 molecules of diethyl ether per polyanion is stable, as in the case of water. The amounts of diethyl ether held were about 2 and 0 molecules per anion after 50 °C and 250 °C-evacuation respectively, as is shown in Fig. 4.

In the case of ethanol,[17] the absorption amount

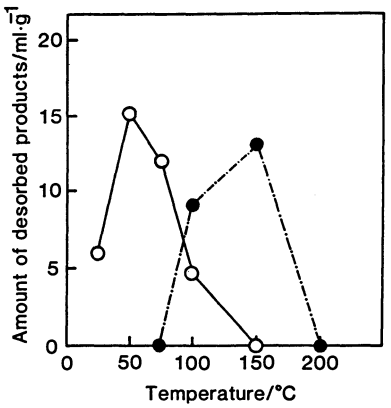

Fig. 5. Variation of products for thermal desorption of diethyl ether from $H_3PW_{12}O_{40}$. ○: $(C_2H_5)_2O$, ●: C_2H_4.

reached about 14 molecules per anion at 20 Torr. It decreased to 6, 2.5, and about 0 molecules per anion after evacuation at room temperature, 50 °C, and 200 °C respectively. At 45 °C, 9 and 6 molecules of ethanol per anion were absorbed when the pressures of ethanol were 40 and 5 Torr respectively. This value decreased to 3 molecules per anion upon the evacuation at 45 °C. In this way, the stable states of 3, 6, and 9 molecules of ethanol per anion could be obtained by controlling the pressure at 45 °C.

Figure 5 shows the products of the thermal desorption of diethyl ether from $H_3PW_{12}O_{40}$. Below 75 °C, only diethyl ether was desorbed. Ethylene was evolved in the range of 75—150 °C. Ethylene showed a maximum at 150 °C, but above 200 °C it was not detected. At 150—300 °C, small amounts of ethane, propane, and butane were detected in the gases desorbed. The total amount of these saturated hydrocarbons was about one-tenth that of the ethylene formed. The carbon balance in the absorption-desorption (up to 300 °C) was confirmed to be close to 100%.

As has been reported previously,[7b] ethanol was desorbed below 100 °C in the case of the thermal desorption of ethanol. The amount of ethylene desorbed reached a maximum at about 100 °C. Above 150 °C, ethane, propane, and methane were produced instead of ethylene.

IR Spectra of $H_3PW_{12}O_{40}\cdot n(C_2H_5)_2O$ ($n\leq 6$) during Thermal Desorption. The changes in the IR spectra of diethyl ether present in $H_3PW_{12}O_{40}$ during step-by-step heating in a vacuum are shown in Fig. 6. After the evacuation at room temperature (6 molecules of diethyl ether per anion), four bands appeared, at 2985, 2939, 2900, and 2873 cm^{-1}, which corresponded to the ν(C-H) bands (Fig. 6a). The bands at 2985 and 2939 cm^{-1} are attributed to the degenerate stretching vibrations of CH_3, while the bands at 2900 and 2873 cm^{-1} are assigned to the symmetric stretching vibrations of CH_3 and CH_2 respectively.[18] After heating up to 75

°C, these bands became weaker, without any shifts in their positions. The evacuation at 100 °C broadened these bands and produced new, weak bands at 2954, 2924, 2897, and 2870 cm^{-1}. After 150 °C-evacuation, only the latter four bands remained. These bands completely disappeared after evacuation at 300 °C, however.

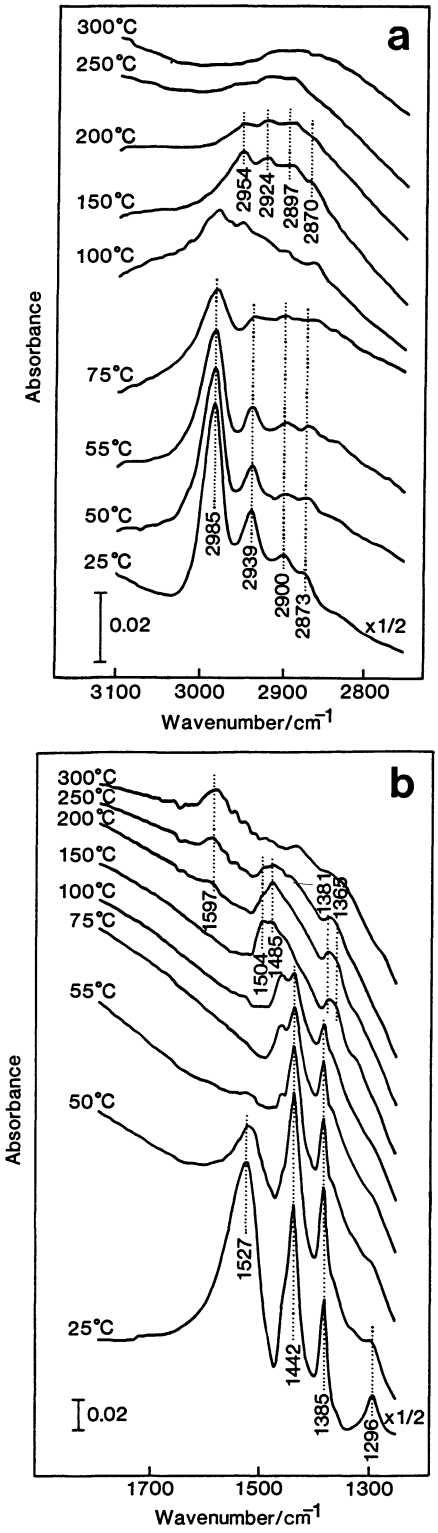

Fig. 6. Changes of IR spectra of diethyl ether absorbed in $H_3PW_{12}O_{40}$ during stepwise heating in vacuum; (a) in the ν(C-H) region; 3100—2750 cm^{-1}, (b) in the deformation region; 1800—1250 cm^{-1}.

The bands in the deformation region (1800—1250 cm^{-1}) are shown in Fig. 6b. The band at 1442 cm^{-1} is a characteristic band of the CH_3 degenerate deformation, and the shoulder at 1468 cm^{-1} is assignable to the CH_2 deformation band.[18] The 1385 cm^{-1} band is due to both the CH_3 symmetric deformation and the CH_2 wagging vibration.[18] It was notable that the band at 1527 cm^{-1} was present for $H_3PW_{12}O_{40} \cdot 6(C_2H_5)_2O$. This band was absent in the spectra of the gaseous and liquid diethyl ether[18] and for diethyl ether adsorbed on Al_2O_3 and SiO_2. In addition, when diethyl ether was introduced over $D_3PW_{12}O_{40}$, the 1527 cm^{-1} band was not observed. It probably shifted to about 1100 cm^{-1} (isotope shift), but this band was not obvious because of the presence of the strong IR bands of the heteropoly anion. As is shown in Fig. 6b, the intensity of the band at 1527 cm^{-1} decreased upon heating at 55 °C in a vacuum, in preference to the 1385 and 1442 cm^{-1} bands.

Upon heating at 150 °C, new bands at 1504, 1485, 1381, and 1365 cm^{-1} appeared, instead of the bands at 1442 and 1385 cm^{-1}. After the 200 °C-evacuation, a broad band at 1597 cm^{-1} appeared, and this band became intense at higher temperatures.

IR Spectra of $H_3PW_{12}O_{40} \cdot nC_2H_5OH$ (n=3, 6, 9). Figure 7a—d shows the IR spectra of ethanol absorbed in $H_3PW_{12}O_{40}$ or $D_3PW_{12}O_{40}$. In the case of the C_2H_5OD-$D_3PW_{12}O_{40}$ system, the O-D stretching band shifted from 2553 to 2345 cm^{-1} as the amount of C_2H_5OD decreased from 9 to 3 molecules per anion. In the ν(C-H) region (Fig. 7a), the $\nu_{deg}(CH_3)$ bands at 2981 and 2935 cm^{-1}, the $\nu_s(CH_3)$ band at 2904 cm^{-1}, and the $\nu_s(CH_2)$ band at 2870 cm^{-1} appeared. These bands were quite similar to those of absorbed diethyl ether. The integrated intensities of the 2981 cm^{-1} band ($\nu_{deg}(CH_3)$) decreased from 1.00 to 0.53 and 0.30 as the amounts of C_2H_5OD absorbed decreased from 9 to 6 and 3 molecules per anion respectively.

The IR spectra of $H_3PW_{12}O_{40} \cdot nC_2H_5OH$ in the deformation region (1800—1150 cm^{-1}) are shown in Fig. 7b. There was a broad band around 1630 cm^{-1} for the state of 9 molecules per anion. This band shifted to 1527 cm^{-1} for 6 molecule per anion; this position was in good agreement with that for 6 molecules of diethyl ether per anion. This band disappeared at 3 molecules per anion, however. Those bands at 1700—1500 cm^{-1} (Fig. 7b) shifted to about 1200 cm^{-1} upon the substitution of D for H in the OH group of C_2H_5OH, as is shown in Fig. 7c ($D_3PW_{12}O_{40} \cdot nC_2H_5OD$). For the states of 9, 6, and 3 molecules of C_2H_5OD per anion, the relative integrated intensities of the bands at 1442 cm^{-1} were 1.00, 1.17, and 0.77, while those at 1388 cm^{-1} were 1.00, 1.23, and 0.70.

Figure 7d shows the IR bands of the heteropoly anion of $D_3PW_{12}O_{40}$ absorbing different amounts of

C_2H_5OD. There was little difference in the IR spectra of the anion between 6 and 9 molecules of C_2H_5OD per anion. For 3 molecules per anion, the ν(W-Oe-W) band tended to split into 814 and 764 cm^{-1} and the ν(W=Ot) band, into 991 and 980 cm^{-1}.

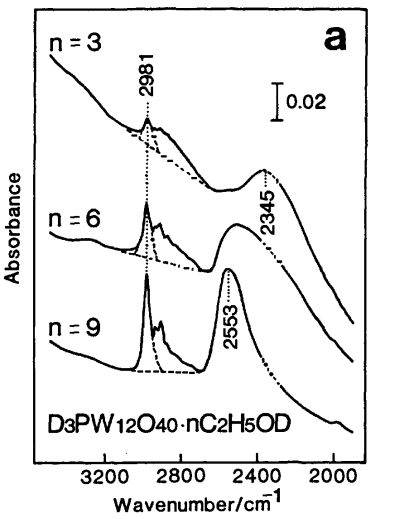

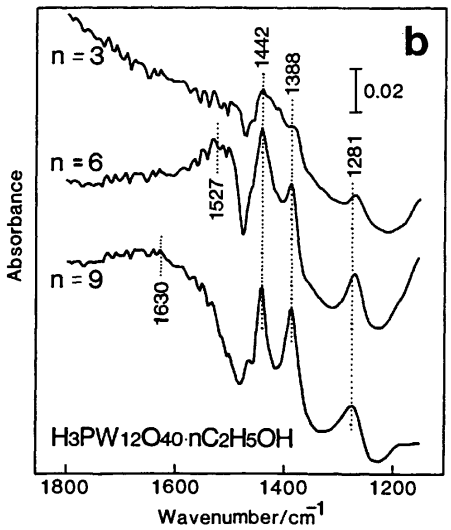

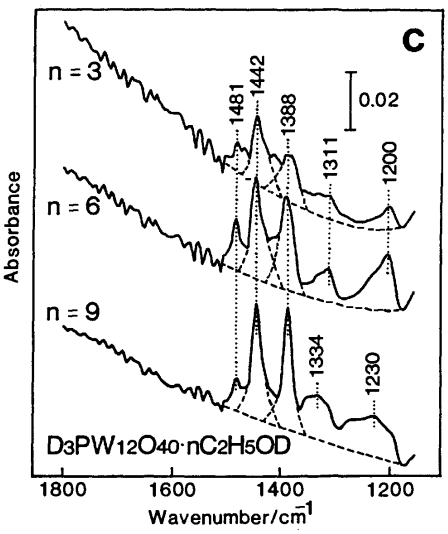

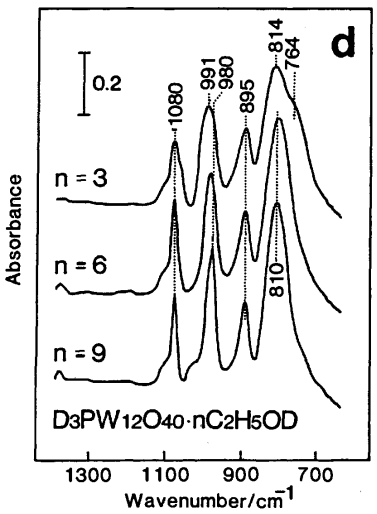

Fig. 7. IR spectra of ethanol absorbed in $H_3PW_{12}O_{40}$ or $D_3PW_{12}O_{40}$; (a) $D_3PW_{12}O_{40}\cdot n C_2H_5OD$, in the region of ν(C-H) and ν(O-D) (3500—1900 cm^{-1}), (b) $H_3PW_{12}O_{40}\cdot n C_2H_5OH$, in the region of δ(C-H), ν(O-H), and δ(O-H) (1800—1150 cm^{-1}), (c) $D_3PW_{12}O_{40}\cdot n C_2H_5OD$, in the region of δ(C-H), ν(O-D), and δ(O-D) (1800—1150 cm^{-1}), (d) $D_3PW_{12}O_{40}\cdot n C_2H_5OD$, in the region of characteristic bands of heteropoly anion (1400—633 cm^{-1}).

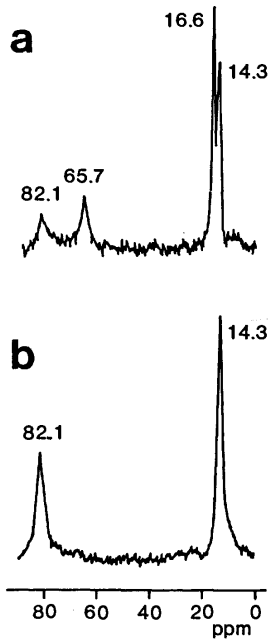

Fig. 8. The change of ^{13}C CP-MAS NMR spectra of $H_3PW_{12}O_{40}\cdot n C_2H_5OH$ by heating; (a) after evacuation at 45 °C (n=2.2), (b) after heating at 150 °C.

It was noted that there were little differences between the spectral changes of $H_3PW_{12}O_{40}\cdot n C_2H_5OH$ and $H_3PW_{12}O_{40}\cdot n(C_2H_5)_2O$ during thermal desorption.

^{13}C CP-MAS NMR of Ethanol Absorbed into $H_3PW_{12}O_{40}$. The ^{13}C CP-MAS NMR spectra of $H_3PW_{12}O_{40}\cdot 2.2C_2H_5OH$ are shown in Fig. 8a. As has been described previously,[14] the peaks at δ 16.6 (CH_3) and

65.7 (CH_2) were assigned to the protonated ethanol monomer ($C_2H_5OH_2^+$), and the signal at δ 14.3 and 82.1, to the ethoxy group on the heteropoly anion (C_2H_5O). In addition, a protonated dimer (($C_2H_5OH)_2H^+$) has been detected with ^{13}C peaks at δ 17.2 and 61.9 for $H_3PW_{12}O_{40}\cdot 6C_2H_5OH$.[14] After heating at 150 °C, the peaks at δ 16.6 and 65.7 disappeared, leaving only the peaks at δ 14.3 and 82.1.

Discussion

Location of H^+ in the Heteropoly Anion. The primary structure (Keggin structure)[19] and the secondary structure[20] of $H_3PW_{12}O_{40}\cdot 6H_2O$ are illustrated in Fig. 3. $H_3PW_{12}O_{40}\cdot 6H_2O$ has a stable structure, which has been established by X-ray and neutron diffraction.[20] The polyanions are packed in a bcc structure, in which the protonated water dimer, $(H_2O)_2H^+$, is connected to four anions by hydrogen bonding at the terminal oxygen atoms (Ot) of the anions, as is shown in Fig. 3b. Therefore, the band at 976 cm^{-1} (Fig. 1a) can firmly be assigned to the stretching vibration of the W=Ot bond, the Ot atom of which is bonded to the protonated water molecules, as is shown in Fig. 3b, and the 887 and 795 cm^{-1} bands, to the asymmetric stretching vibrations of W-Oc-W and W-Oe-W, which are not connected to either water or proton.

As the sample was dehydrated, the 976 cm^{-1} band decreased and the band at 1007 cm^{-1} grew correspondingly (Fig. 1a—d), as in the case of $H_3PMo_{12}O_{40}$.[16] The 1007 cm^{-1} band observed for dehydrated $H_3PW_{12}O_{40}$ may reasonably be assigned to W=Ot, which is not coordinated with either a free proton, water, or $(H_2O)_2H^+$. The shift of the W=Ot band to a wavenumber higher by 31 cm^{-1} is consistent with the disappearance of hydrogen bonding.[21]

The substitution of D for H caused no change in the wavenumber of the W=Ot band (compare $H_3PW_{12}O_{40}\cdot 6H_2O$ (Fig. 1a) and $D_3PW_{12}O_{40}\cdot 6D_2O$ (Fig. 2a)). The absence of the isotope shift for the W=Ot band indicates that the hydrogen bonding between the terminal oxygen and the hydrogen of the water molecules is weak. It is known that the O-H bond becomes longer as the hydrogen bonding becomes stronger.[22] The O-H bond distance of the water molecule in $H_3PW_{12}O_{40}\cdot 6H_2O$ is 0.951 Å,[20] which is close to the O-H bond length (0.958 Å) of the water molecule in the gas phase. Therefore, the hydrogen bonding between W=Ot and $(H_2O)_2H^+$ is considered to be weak.

As for the dehydration process (Figs. 1b—d and 2b—d), a significant difference was noted in the W-Oe-W band (795 cm^{-1}) between $H_3PW_{12}O_{40}$ and $D_3PW_{12}O_{40}$; the W-Oe-W band split into 798 and 768 cm^{-1} for $H_3PW_{12}O_{40}$, but it split into 814 and 744 cm^{-1} for $D_3PW_{12}O_{40}$. In contrast, there was no difference detected for the W=Ot band. This fact shows that, after dehydration, the proton interacts with the bridging oxygen (Oe), but not with the terminal oxygen (Ot). The above-mentioned shift of W=Ot to a higher wavenumber after dehydration is consistent with this idea. This is also in agreement with the fact that the bridging oxygen is more basic than the terminal oxygen.[23-25] For example, Knoth et al. have reported that the methyl cation in $CH_3OPMo_{12}O_{39}^{2-}$ is located on the bridging oxygen atom,[24] and Tonomura et al. observed a shift of the W-Oe-W band which was presumably due to the interaction with tetrahydrofuran through a proton located on the bridging oxygen atom.[25]

Since there are twelve Oe's and three protons per $PW_{12}O_{40}^{3-}$, the band at 814 cm^{-1}, which was stronger (Fig. 2b—d), may be assigned to nine W-Oe-W (non-protonated) bonds, and the 744 cm^{-1} band, to three W-OeD$^+$-W (protonated) bonds. The shift to a lower wavenumber for the latter is consistent with the presence of hydrogen-bonding.[21]

On the basis of these results, the following dehydration scheme for $H_3PW_{12}O_{40}\cdot 6H_2O$ is proposed. This process is reversible upon dehydration-hydration.

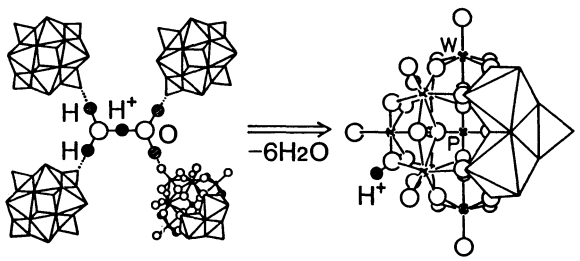

Dehydration scheme

States of Molecules in $H_3PW_{12}O_{40}\cdot nC_2H_5OH$ and $H_3PW_{12}O_{40}\cdot n(C_2H_5)_2O$ (n=3, 6, and 9). The amounts of molecules absorbed in $H_3PW_{12}O_{40}$ showed discrete values—for example, 3, 6, and 9 molecules per anion for ethanol and 6 molecules per anion for diethyl ether.[17]

First, we will discuss the absorption state of 6 molecules per anion for ethanol, diethyl ether, and water. The states of $H_3PW_{12}O_{40}\cdot 6C_2H_5OH$ and $H_3PW_{12}O_{40}\cdot 6(C_2H_5)_2O$ (Fig. 7b and 6b) exhibited a characteristic band at 1527 cm^{-1}. Klages et al. observed the same band for the 2:1 complex of diethyl ether and $HSbCl_6$.[26] It is probably assignable to a ν(O-H) mode of $[(C_2H_5)_2O\cdots H\cdots O(C_2H_5)_2]^+SbCl_6^-$ by analogy with a protonated water dimer.[27] This band was absent for the 1:1 complex ($[(C_2H_5)_2OH]^+SbCl_6^-$). Therefore, the band at 1527 cm^{-1} is considered to be a characteristic band of the protonated dimer species, **1**.

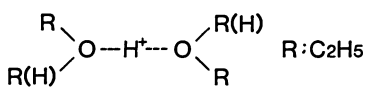

1

The presence of the protonated dimer species, $(C_2H_5OH)_2H^+$, has previously been indicated by the solid-state MAS NMR study of the present authors.[14] Note that six ether or ethanol molecules per anion correspond to two molecules per proton. The fact that this band was not observed for ethanol adsorbed on $Cs_3PW_{12}O_{40}$ as for diethyl ether adsorbed on Al_2O_3 or SiO_2 is reasonable, since these oxides do not have Bronsted-acid sites. The absence (because of a shift to a lower wavenumber) of the 1527 cm^{-1} band for $D_3PW_{12}O_{40}\cdot 6C_2H_5OD$ and $D_3PW_{12}O_{40}\cdot 6(C_2H_5)_2O$ is also consistent with the above assignment.

The positions of the ν(C-H) bands (2985, 2939, 2900, and 2873 cm^{-1}) observed for $H_3PW_{12}O_{40}\cdot 6(C_2H_5)_2O$ were very similar to those of $(C_2H_5)_2O$ in CCl_4 (2980, 2935, 2897, and 2868 cm^{-1})[18] and in the $(C_2H_5)_2O$-$AlCl_3$ complex (2983, 2940, and 2877 cm^{-1}).[28] However, the relative intensities of these bands were quite different. The $\nu_s(CH_2)$ band (2868 cm^{-1}) is more intense than the $\nu_{deg}(CH_3)$ band (2980 cm^{-1}) for $(C_2H_5)_2O$ in CCl_4, while the $\nu_{deg}(CH_3)$ band is stronger for $(C_2H_5)_2O$-$AlCl_3$. The suggested reason why $\nu_s(CH_2)$ in $(C_2H_5)_2O$-$AlCl_3$ is weak is a stronger electron-withdrawing effect of $AlCl_3$, which destabilizes the dipolar contribution to the C-H bond of the CH_2 group.[29] In the case of $H_3PW_{12}O_{40}\cdot 6(C_2H_5)_2O$, the relative intensity was similar to $(C_2H_5)_2O$-$AlCl_3$ (Fig. 6a). This supports the formation of $[(C_2H_5)_2O]_2H^+$. From these results, we can propose the following model.

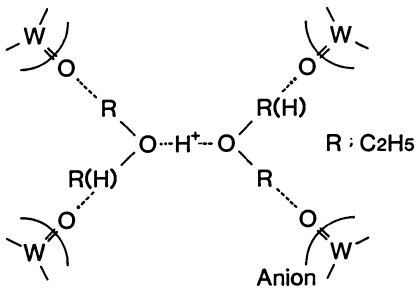

Dimer model

Since the XRD pattern, which mainly reflects the secondary structure of the polyanion packing, was very similar for $H_3PW_{12}O_{40}\cdot 6C_2H_5OH$ and $H_3PW_{12}O_{40}\cdot 6H_2O$,[14] the structure of $H_3PW_{12}O_{40}\cdot 6C_2H_5OH$ indicated above may be reasonable.

The δ(C-H), ν(O-D), and δ(O-D) region of $D_3PW_{12}O_{40}\cdot nC_2H_5OD$ can be examined in more detail because there is no overlapping of the bands in this region. The intensities of the ν(C-H) band and the δ(C-H) bands were not proportional to the concentrations of ethanol (Fig. 7a, c). Moreover, the intensities of the bands at 1442 cm^{-1} ($\delta_{deg}(CH_3)$) and 1388 cm^{-1} ($\delta_s(CH_3)$ $+w(CH_2)$) relative to the 2981 cm^{-1} band ($\delta_{deg}(CH_3)$) changed significantly with the n, as is shown in Fig. 9. Higuchi et al. have reported that the

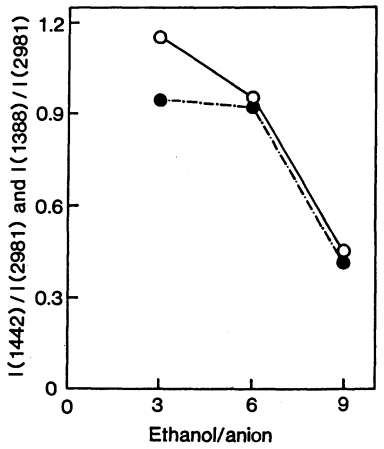

Fig. 9. Changes of the peak intensity of the 1442 (○) and 1388 (●) cm^{-1} relative to the 2981 cm^{-1} band as a funtion of the amount of C_2H_5OD absorbed into $D_3PW_{12}O_{40}$. I(1388), I(1442), and I(2981) are the integrated peak intensities of the bands at 1388, 1442, and 2981 cm^{-1}, respectively.

intensities of ν(C-H) and δ(C-H) of the methyl group of CH_3I varied greatly depending on the polarities of the solvents.[30] The changes in Fig. 9, together with the nonproportionality (Fig. 7a, c), suggest that the CH_3 group interacts with heteropoly anions and that the interaction becomes stronger as the amount of the absorption of ethanol decreases.

Transformations of Molecules during Thermal Desorption. When $H_3PW_{12}O_{40}\cdot 6(C_2H_5)_2O$ was heated at 55—75 °C in a vacuum, the characteristic band of $[(C_2H_5)_2O]_2H^+$ (at 1527 cm^{-1}) disappeared, while the frequencies of the δ(C-H) bands did not change (Fig. 6b). The species formed is probably a monomer of protonated diethyl ether, since the IR spectrum was very similar to that of $[(C_2H_5)_2OH]^+SbCl_6^-$.[26] Therefore, it is concluded that $[(C_2H_5)_2O]_2H^+$ (dimer) was transformed to $(C_2H_5)_2OH^+$ (monomer) upon the heat treatment at 55 °C.

As is shown in Fig. 6b, the evacuation at 100—150 °C brought about significant changes in the δ(C-H) bands, indicating that the monomer of protonated ether was transformed to another species. Correspondingly, the $\nu_{deg}(CH_3)$ band distinctly shifted from 2985 cm^{-1} (75 °C) to 2954 cm^{-1} (Fig. 6a). These spectral changes are due to the formation of ethoxide formed on the polyanion (C_2H_5O), which was previously detected by NMR.[14] The large shift of the $\nu_{deg}(CH_3)$ band from 2980 cm^{-1} to a lower frequency is often observed upon the formation of alkoxide—for example, the shifts of C_2H_5O-Mg to 2950 cm^{-1},[31] of C_2H_5O-Al to 2959 cm^{-1},[32] and of C_2H_5O-Ca to 2945 cm^{-1}.[31]

This assignment is confirmed by ^{13}C NMR. As is shown in Fig. 8, only one species (14.3 and 82.1 ppm) remained after $H_3PW_{12}O_{40}\cdot nC_2H_5OH$ was heated at 150 °C, and the ^{13}C chemical shifts are close to those of

$-OCH_2CH_3$ in $(CO)_5WC(OCH_2CH_3)CH_3$: δ 80.4 for α-carbon (CH_2) and δ 14.6 for β-carbon (CH_3).[33] Moffat et al. have claimed, on the basis of the IR data, the formation of an isopropyl group during the thermal desorption of ethanol from $H_3PW_{12}O_{40}$.[12] The bands at 2954, 2924, and 2897 cm^{-1} (Fig. 6a) are also consistent with the isopropyl group (2950, 2936 cm^{-1})[34] and with tertiary CH (2890 cm^{-1}).[35] However, the species responsible for the spectrum b in Fig. 8 may not be an isopropyl group, for the following reasons. First, it is not probable that isopropyl group, which is a polymerization-decomposition product of ethanol, was formed as a single species. Secondly, the ^{13}C chemical shifts of CH_3 of ethanol and diethyl ether (δ 17.6 and 16.4, respectively) are much closer to that in Fig. 8b than are those of isopropyl alcohol and diisopropyl ether (δ 25.1 and 24.3, respectively).[36] It must be considered that the CH_3 group usually shows much smaller shifts than the CH_2 group.[36] Therefore, the species formed by heating at 150 °C is assignable to ethoxide on the heteropoly anion.

It should be noted that this species showed the peak of α-carbon (δ 82.1) downfield from tungsten ethoxide, $W(OC_2H_5)_6$ (δ 69.8).[37] Olah et al. reported that the isopropyl cation in a superacid solution showed a peak at δ 320.6,[38] while the peak of $W(O\text{-}i\text{-}Pr)_6$ appeared at δ 76.1.[37] This suggests that the ethyl cation should have a peak greatly downfield from the ethoxide, although it has not been detected by NMR. Thus, the species at δ 82.1 is considered to be the ethoxy group, the ethyl group of which has a more cationic character than does ordinary ethoxide.

On the basis of these results, we propose the following scheme for the thermal desorption of ethanol absorbed in $H_3PW_{12}O_{40}$.

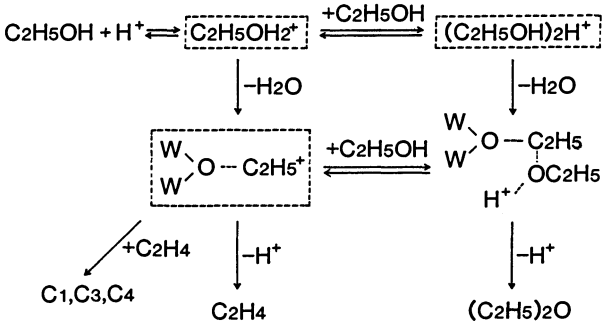

Reaction scheme

The authors wish to thank Drs. Shin-ichi Nakata and Sachio Asaoka (Chiyoda Chemical Engineering & Construction Co., Ltd.) for the solid-state NMR measurements and for their helpful discussions. The present work was supported in part by a Grant-in-Aid for Scientific Research (No. 6247007) from the Ministry of Education, Science and Culture and the Asahi Glass Foundation.

References

1) M. Misono, *Catal. Rev.-Sci. Eng.*, **29**, 269 (1987) and the references cited therein.

2) M. Otake and T. Onoda, *Shokubai (Catalyst)*, **18**, 169 (1976).

3) a) T. Baba, J. Sakai, H. Watanabe, and Y. Ono, *Bull. Chem. Soc. Jpn.*, **55**, 2555 (1982); b) H. Hayashi and J. B. Moffat, *J. Catal.*, **77**, 473 (1982).

4) Y. Izumi, K. Matsuo, and K. Urabe, *J. Mol. Catal.*, **18**, 299 (1983).

5) M. Misono, N. Mizuno, K. Katamura, A. Kasai, Y. Konishi, K. Sakata, T. Okuhara, and Y. Yoneda, *Bull. Chem. Soc. Jpn.*, **55**, 400 (1982).

6) Y. Saito and H. Niiyama, *J. Catal.*, **106**, 329 (1987).

7) a) N. Hayakawa, T. Okuhara, M. Misono, and Y. Yoneda, *Nippon Kagaku Kaishi*, **1982**, 356; b) T. Okuhara, A. Kasai, N. Hayakawa, Y. Yoneda, and M. Misono, *J. Catal.*, **83**, 121 (1983).

8) T. Hibi, K. Takahashi, T. Okuhara, M. Misono, and Y. Yoneda, *Appl. Catal.*, **24**, 69 (1986); T. Okuhara, T. Hibi, K. Takahashi, S. Tatematsu, and M. Misono, *J. Chem. Soc., Chem. Commun.*, **1984**, 697.

9) M. Misono, T. Okuhara, T. Ichiki, T. Arai, and Y. Kanda, *J. Am. Chem. Soc.*, **109**, 5535 (1987).

10) C. Rocchiccioli-Deltcheff, R. Thouvenot, and R. Franck, *Spectrochim. Acta, Part A*, **32**, 587 (1976); C. Rocchiccioli-Deltcheff, M. Fournier, R. Franck, and R. Thouvenot, *Inorg. Chem.*, **22**, 207 (1983).

11) E. g., D. H. Brown, *Spectrochim. Acta*, **19**, 585 (1963); T. J. R. Weakley, *Structure and Bonding*, **18**, 131 (1974).

12) J. G. Highfield and J. B. Moffat, *J. Catal.*, **98**, 245 (1986).

13) a) W. H. Knoth and R. D. Farlee, *Inorg. Chem.*, **23**, 4765 (1984); b) W. E. Farneth, R. H. Staley, P. J. Domaille, and R. D. Farlee, *J. Am. Chem. Soc.*, **109**, 4018 (1987); c) J. B. Black, N. J. Clayden, P. L. Gai, J. D. Scott, E. M. Serwicka, and J. B. Goodenough, *J. Catal.*, **106**, 1 (1987).

14) Y. Kanda, K. Y. Lee, S. Nakata, S. Asaoka, and M. Misono, *Chem. Lett.*, **1988**, 139; K. Y. Lee, Y. Kanda, N. Mizuno, T. Okuhara, M. Misono, S. Nakata, and S. Asaoka, *Chem. Lett.*, **1988**, 1175.

15) S. Tatematsu, T. Hibi, T. Okuhara, and M. Misono, *Chem. Lett.*, **1984**, 865.

16) M. Furuta, K. Sakata, M. Misono, and Y. Yoneda, *Chem. Lett.*, **1979**, 31.

17) T. Okuhara, S. Tatematsu, K. Y. Lee, and M. Misono, *Bull. Chem. Soc. Jpn.*, **62**, 717 (1989).

18) H. Wieser, W. G. Laidlaw, P. J. Krueger, and H. Fuhrer, *Spectrochim. Acta, Part A*, **24**, 1055 (1968).

19) J. F. Keggin, *Proc. R. Soc., London, Ser. A*, **144**, 75 (1934).

20) G. M. Brown, M.-R. Noe-Spirlet, W. R. Bushing, and H. A. Levy, *Acta Crystallogr., Sect. B*, **33**, 1038 (1977).

21) K. Nakamoto, "Infrared Spectra of Inorganic and Coordination Compounds," John Wiley & Sons, New York, London (1963), pp. 185 and 186.

22) G. C. Pimentel and A. L. McClellan, "The Hydrogen Bond," W. H. Freeman and Company, San Francisco and London (1960), p. 89.

23) M. Filowitz, W. G. Klemperer, L. Messerle, and W. Shum, *J. Am. Chem. Soc.*, **98**, 2345 (1976); L. P. Kazansky, I. V. Potapova, and V. I. Spitsyn, Climax 3rd Int. Conf. Chem.

Uses of Molybdenum (1979), p. 67.
24) W. H. Knoth and R. L. Harlow, *J. Am. Chem. Soc.*, **103**, 4265 (1981).
25) S. Tonomura and A. Aoshima, *Shokubai (Catalyst)*, **27**, 389 (1985).
26) F. Klages, J. E. Gordon, and H. A. Jung, *Chem. Ber.*, **98**, 3748 (1965).
27) A. C. Pavia and P. A. Giguere, *J. Chem. Phys.*, **52**, 3551 (1970).
28) H. Arai, Y. Saito, and Y. Yoneda, *J. Catal.*, **10**, 128 (1968).
29) S. H. Pine and D. R. Steele, *Spectrochim. Acta, Part A*, **23**, 1509 (1967).
30) S. Higuchi, S. Tanaka, and H. Kamada, *Spectrochim. Acta, Part A*, **24**, 1929 (1968); S. Higuchi, E. Kuno, S. Tanaka, and H. Kamada, *Spectrochim. Acta, Part A*, **28**, 1335 (1972).
31) N. Takezawa and H. Kobayashi, *J. Catal.*, **25**, 179 (1972); **28**, 335 (1973).
32) R. G. Greenler, *J. Chem. Phys.*, **37**, 2094 (1962).
33) G. M. Bodner, S. B. Kahl, K. Bork, B. N. Storhoff, J. E. Wuller, and L. J. Todd, *Inorg. Chem.*, **12**, 1071 (1973).
34) D. C. McKean, S. Biedermann, and H. Burger, *Spectrochim. Acta, Part A*, **30**, 845 (1974).
35) L. J. Bellamy, "The Infra-red Spectra of Complex Molecules," 3rd ed., Chapman and Hall, London (1975), pp. 13—36.
36) E. Breitmaier and W. Voelter, "Carbon-13 NMR Spectroscopy," 3rd ed., VCH Publishers (1987), pp. 206—215.
37) D. C. Bradley, M. H. Chisholm, M. W. Extine, and M. E. Stager, *Inorg. Chem.*, **16**, 1794 (1977).
38) G. A. Olah, G. K. S. Prakash, and J. Sommer, "Superacids," John Wiley and Sons, New York (1985), p. 80.

Novel Effects of K-Addition to Ru/SiO_2 on Conversion of Cyclohexane

Zheng-Zhong LIN,† Toshiyuki ENOMOTO,†† Toshio OKUHARA,* and Makoto MISONO
Department of Synthetic Chemistry, Faculty of Engineering, The University of Tokyo, Hongo, Bunkyo-ku, Tokyo 113
†Department of Chemistry, Xiamen University, Xiamen, Fujian, China
(Received December 5, 1988)

The effects of the addition of alkalis to a Ru/SiO_2 catalyst upon the conversion (hydrogenolysis and dehydrogenation) of cyclohexane, hydrogenolysis of butane, and hydrogenations of benzene and CO were studied. The addition of K or Cs slightly enhanced the catalytic activity for the hydrogenolysis of cyclohexane, whereas dehydrogenation to benzene was markedly suppressed. This result is contrary to the effect of the addition of Cu or Au to group-VIII metals, as reported in the literature. Changes in the activities became less significant as the atomic number of the added alkali decreased. From a systematic examination by varying the alkali content, it was revealed that dehydrogenation and CO hydrogenation were very sensitively suppressed by an electronic effect imposed by the alkalis, whereas changes in the activities of hydrogenolysis and benzene hydrogenation were not great.

Practically important heterogeneous catalysts are often modified by alkali metals.[1,2] K_2O in doubly promoted Fe catalysts for ammonia synthesis and Cs in a Ag catalyst for the epoxidation of ethylene are typical examples.[2] There have been many fundamental studies on the enhancement of the activities and selectivities by the addition of alkali. Regarding activity, K to Ru in ammonia synthesis,[3] Na or K to Ni/SiO_2-Al_2O_3 in methanation reaction,[4] and Li to Pd/SiO_2 in methanol synthesis[5,6] were effective.

The selectivity is also improved by the addition of alkali. In a Fischer-Tropsch synthesis, the modification of Ru by alkali greatly increased the olefin/paraffin ratios in the product hydrocarbons.[7,8] K to Rh/TiO_2[9] or Mo/SiO_2 increased C_2-oxygenated products[10] or higher alcohols[11] from the $CO+H_2$ reaction.

Alloying also brings about changes in both the activity and selectivity. Sinfelt et al.[12] reported that the addition of Cu to Ni markedly suppressed the hydrogenolysis of ethane, but did not change the rate of dehydrogenation of cyclohexane. Also, it has been shown by Ponec et al.[13] that the hydrogenolysis reaction was sensitively affected by the Pt content of the $Pt-Au/SiO_2$ catalyst. SMSI (Strong Metal-Support Interaction) caused a change in the activities of hydrogenolysis and dehydrogenation. Resasco and Haller[14] found that hydrogenolysis was suppressed by a high-temperature reduction, while dehydrogenation was only slightly influenced.

IR[7,15] and XPS[16] studies have shown that K (probably as K_2O) on Ru/Al_2O_3 or Ru/SiO_2 acts as a base capable of electron-donating to Ru. On the other hand, Li exhibited a different effect from K;[17] the addition of Li to Ru/SiO_2 effectively suppressed methane formation in CO hydrogenation without any great decrease in activity, while K significantly decreased the activity while not suppressing methane formation. It was concluded that a Li compound on Ru particles brought about a geometrical effect similar to an ensemble effect, rather than an electronic effect.

Contrary to CO hydrogenation, so far there are very few reports about the effect of alkali on the conversion of hydrocarbons, such as hydrogenolysis and dehydrogenation. We have preliminarily reported that K to Ru/SiO_2 appreciably enhances the activity for the hydrogenolysis of cyclohexane, but completely suppresses dehydrogenation.[18] Since it has been reported that the addition of Au to Pt,[19] Ru to Pt,[20] and Cu to Ru[21] preferentially enhances the dehydrogenation of cyclohexane, the effect of K observed here is novel. In order to elucidate this novel effect, we systematically examined the effects of various alkalis added to a Ru/SiO_2 catalyst on several reactions such as the conversion of cyclohexane, the hydrogenolysis of butane, and hydrogenations of benzene and CO.

Experimental

Materials. Silica (Aerosil 200, 160 $m^2 \cdot g^{-1}$) was used as a support after being calcined at 773 K in air for 20 h. The Ru/SiO_2 catalyst, which contained 2.5 wt% of Ru, was prepared by incipient-wetness impregnation with an aqueous solution of $RuCl_3$. It was then dried at 373 K for 10 h and reduced at 723 K in flowing H_2 for 2 h. Alkali-promoted Ru/SiO_2 catalysts were prepared in two different ways, as described previously.[17] The first catalysts were obtained as follows. SiO_2 was impregnated with an aqueous solution of an alkali carbonate. It was then calcined at 773 K for 10 h in air, and was again impregnated with an aqueous solution of $RuCl_3$. The product was dried at 373 K and reduced at 723 K in flowing H_2 for 2 h. The loading amount of Ru was fixed to 2.5 wt%, and the alkali content (defined as M/(M+Ru) in atom basis, M=alkali) was changed from 0.20 to 0.82. Hereafter, these catalysts will be designated as, e.g., Ru-Li(0.20)/SiO_2, where the figure in the parenthesis is the alkali content. The second catalysts were obtained by impregnating the reduced Ru/SiO_2 with an aqueous solution of alkali carbonate. These were dried at 373 K and reduced at 723 K in flowing H_2. These will be

† Present address: Nippon Oil Company, Ltd., 8 Chidoricho, Naka-ku, Yokohama, Kanagawa 231.

designated as, e.g., K(0.2)-Ru/SiO_2. As references, 1 wt% K/SiO_2 and 0.18 wt% Li/SiO_2 were prepared from K_2CO_3 and Li_2CO_3, respectively.

Butane and CO in a glass cylinder were obtained from Takachiho Chem. Co., Ltd. The butane was purified by a freeze-thaw cycle prior to the reaction. The cyclohexane and benzene were purchased from Nakarai Chemicals, Co. and used without any treatment.

Apparatus and Procedure. The adsorption of H_2 was volumetrically measured after the catalysts were reduced with H_2 at 723 K for 2 h, as in the previous work.[22] A chemisorption measurement was carried out at room temperature in a static system (60 cm^3). The total uptakes of hydrogen were measured after the H_2 pressure became constant (in about 1.5 h). The equilibrium H_2 pressure was adjusted to about 60 Torr (1 Torr=133.3 Pa). Hydrogenations of benzene and the conversion of cyclohexane (hydrogenolysis and dehydrogenation) were carried out in a conventional flow reactor under 1 atm. In the case of benzene hydrogenation, a mixture of benzene and hydrogen (1:6 in molar ratio) was supplied at 358 K just after the catalysts were reduced at 723 K for 2 h in flowing H_2. The benzene and cyclohexane produced were analyzed by using a Methoxy PEG column (4 m, 4 mm of inside diameter, 473 K).

In the case of the conversion of cyclohexane, a mixture of cyclohexane and hydrogen (1:5) was introduced to the catalysts at 573 K. Benzene was analyzed by a Methoxy PEG column; the C_1—C_6 hydrocarbons produced were analyzed by an FID gas chromatograph (Yanagimoto GC 2800) using a Porapak R column (1.5 m, 2 mm of inside diameter), the temperature of which was increased from 323 to 473 K at a rate of 2 K s^{-1}.

The hydrogenolysis of butane was carried out in a closed circulation system (volume; 250 cm^3). Prior to the reaction, the catalysts were reduced at 723 K in H_2 (300 Torr) for 2 h. A mixture of butane (50 Torr) and H_2 (100 Torr) was introduced to the catalysts at 373 K. The product hydrocarbons were analyzed by a gas chromatograph with a VZ-10 column. Hydrogenation of CO was performed in a flow reactor under 1 atm pressure at 533 K, as described previously.[17]

Results

Adsorption of H_2. Data regarding H_2 adsorption are given in Table 1. No H_2 was adsorbed on SiO_2, K/SiO_2, and Li/SiO_2. Here, the dispersion of Ru is expressed by H/Ru (the amount of hydrogen atom adsorbed divided by the amount of Ru atom in the catalyst), assuming that one H atom is adsorbed on one exposed Ru atom. It was observed that the dispersion decreased as the content of alkali increased for the Ru-M/SiO_2 systems (M=alkali).[17] For example, the dispersion of Ru on Ru-Li(0.82)/SiO_2 was one-third that of Ru/SiO_2. K-addition caused greater decreases in the dispersion than Li-addition.

Hydrogenolysis of Butane. The hydrogenolysis of butane was carried out over Ru/SiO_2 and Ru-Li/SiO_2. The product composition was independent of the conversion levels (<80%) over these catalysts, showing that the distributions of the carbon number of the products are of the primary products. The influence of the Li content on the activity and selectivity are given in Table 2. The catalytic activity per unit weight of Ru was almost independent of the Li content, although H/Ru decreased as the Li content increased (Table 1). For all the catalysts given in Table 2, the main product was ethane, which constituted about 50 mol% of the products; the mole fraction of methane slightly increased as the Li content increased.

Hydrogenation of Benzene. The product was only cyclohexane at 358 K for all catalysts. The conversion of benzene gradually decreased with the reaction time and reached stationary values after 1.5 h, which were about one half of the initial conversions. The catalytic activities were calculated from the stationary conversions. The conversions were adjusted to be less than 40% by controlling the flow rate and the catalyst weight. Table 3 shows the effects of Li, Na, and K on the activity. The reaction rate decreased as the contents of alkali increased. The effect of K was

Table 1. H_2 Adsorption on Ru-M/SiO_2 (M=alkali)

Alkali content[a]	Dispersion[b]			
	Li	Na	K	Cs
0	0.17	0.17	0.17	0.17
0.20	0.12	0.09	0.08	0.10
0.60	0.12	—	0.06	—
0.82	0.06	—	0.04	—
1.0	—	0	0	—

a) M/(M+Ru) in atom basis (M=alkali). b) H/Ru; the amount of hydrogen atom adsorbed divided by the amount of Ru in the catalyst.

Table 2. Effect of Li-Addition on Hydrogenolysis of Butane

Li/(Li+Ru)	Activity[a]	Selectivity/mol%		
		CH_4	C_2H_6	C_3H_8
0	22.3	31.7	52.7	15.6
0.60	17.6	38.2	50.8	11.0
0.82	20.0	40.1	49.4	10.5

a) 10^{-2} mol g-Ru^{-1} h^{-1}. The reaction was carried out at 373 K and 150 Torr (H_2/C_4H_{10}=2).

Table 3. Effect of Alkali-Addition on Hydrogenation of Benzene

Alkali content[a]	Activity[b]		
	Li	Na	K
0	30	30	30
0.20	26	25	17
0.60	18	—	15
0.82	15	—	1.3

a) 10^{-2} mol g-Ru^{-1} min^{-1}. b) M/(M+Ru); M=alkali. The reaction was carried out at 358 K and 1 atm (H_2/benzene=6).

Table 4. Effect of Alkali-Addition on Conversion of Cyclohexane

Content of alkali	Activity[a]							
	Li		Na		K		Cs	
	H	D	H	D	H	D	H	D
0	0.70	0.30	0.70	0.30	0.70	0.30	0.70	0.30
0.20	0.65	0.20	0.60	0.15	2.70	0	3.00	0
0.60	0.70	0.15	—	—	0.80	0	—	—
0.82	0.70	0.05	—	—	0.35	0	—	—

a) 10^{-2} mol g-Ru^{-1} min^{-1}; H: hydrogenolysis, D: dehydrogenation. The reaction was carried out at 573 K and 1 atm (H_2/cyclohexane=5).

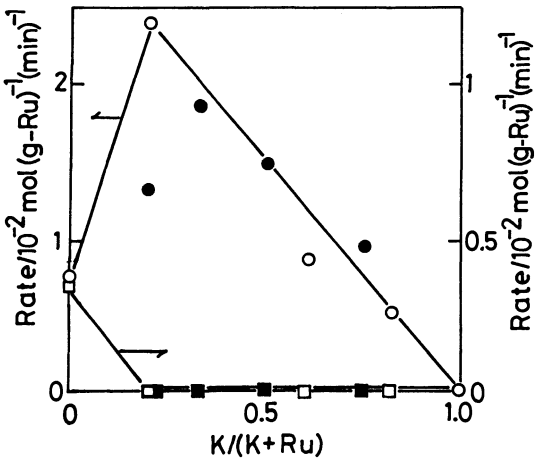

Fig. 1. Effect of K content on activity for conversion of cyclohexane at 573 K.
○: Hydrogenolysis, □: dehydrogenation over Ru-K/SiO_2 (Ru was added to K/SiO_2), ●: Hydrogenolysis, ■: deydrogenation over K-Ru/SiO_2 (K was added to reduced Ru/SiO_2).

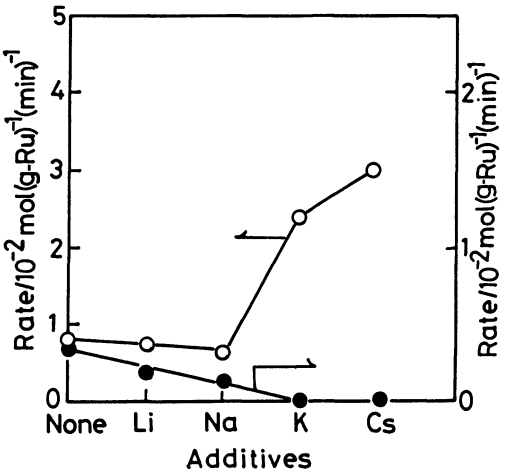

Fig. 2. Effect of kinds of alkali to Ru/SiO_2 on conversion of cyclohexane at 573 K. The content of alkali was 0.20.
○: Hydrogenolysis of cyclohexane, ●: dehydrogenation of cyclohexane.

not significant when the K content was less than 0.60. However, the activity decreased to 1/20 at a K content of 0.82. This decrease caused by Li was not significant, even at a Li content of 0.82.

Conversions of Cyclohexane. At 573 K, Ru/SiO_2 produced both benzene (dehydrogenation) and C_1—C_6 hydrocarbons (hydrogenolysis) in this reaction. The main product of the hydrogenolysis was methane (about 90%). The conversions of both reactions gradually decreased with the reaction time without marked changes in selectivity. Then, the conversions reached stationary values (about half that of the initial conversion) after about 1.5 h. Similar changes in the conversions were obtained for alkali-added catalysts.

Table 4 shows the activities and selectivities obtained at the stationary states. For all catalysts, the selectivity was measured at a conversion level of less than 30%. As shown in Table 4, the activities for hydrogenolysis were almost independent of the Li content, which is the same trend as was observed for the hydrogenolysis of butane (Table 2). On the other hand, dehydrogenation to benzene decreased significantly as the Li content increased. Contrary to this, the presence of K or Cs enhanced the hydrogenolysis. It is remarkable that the formation of benzene was completely suppressed by K or Cs.

In Fig. 1, the effects of K on the conversions of cyclohexane are given; the results of K-Ru/SiO_2 as well as Ru-K/SiO_2 are plotted. It is clear that hydrogenolysis was accelerated by the addition of K at a content level varying from 0.2 to 0.5. This trend was the same in the two different preparation methods.

The effects of the kinds of alkali are illustrated in Fig. 2, where the content of alkali was 0.2. The addition of Cs accelerated the hydrogenolysis, while Li and Na showed little effect. In contrast, the activity for benzene formation decreased monotonically as the atomic number of alkali increased.

Figure 3 shows the effects of the K content on TOF (turnover frequency), where TOF was defined as the number of molecules reacted per exposed Ru atom per second. The TOF of CO hydrogenation, obtained previously,[17] is also plotted in this figure. From Fig. 3, the reactions may be classified into two groups. The first group includes the hydrogenation of benzene and the hydrogenolysis of cyclohexane. In this group the changes of TOF were not significant, that is, within one order of magnitude. The dehydrogenation of

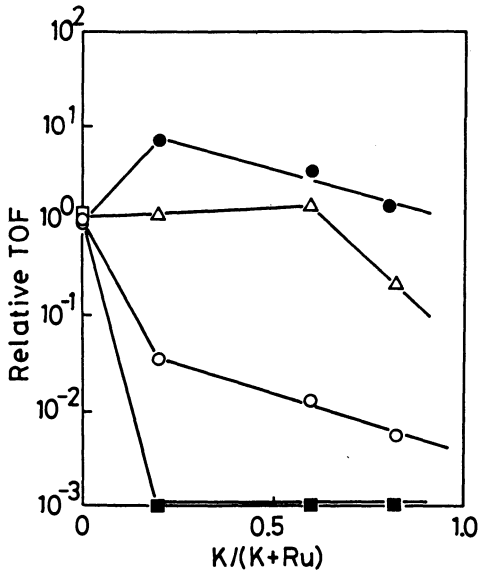

Fig. 3. Changes of TOF of various reactions as a function of K content in Ru-K/SiO_2.
O: $CO+H_2$ at 533 K, ●: hydrogenolysis of cyclohexane at 573 K, ■: dehydrogenation of cyclohexane at 573 K, △: hydrogenation of benzene at 358 K.

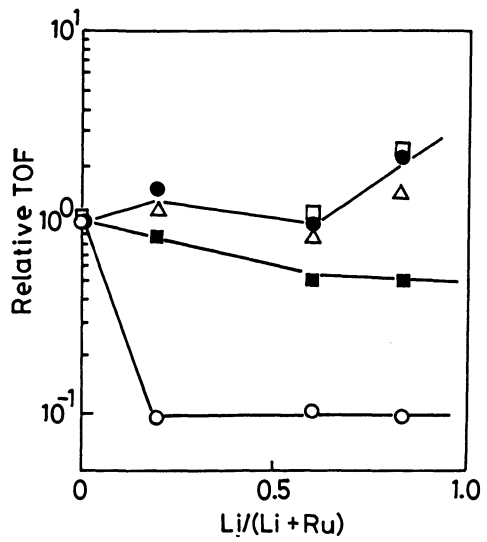

Fig. 4. Changes of TOF of various reactions as a function of Li content in Ru-Li/SiO_2.
O: $CO+H_2$, ●: hydrogenolysis of cyclohexane, ■: dehydrogenation of cyclohexane, △: hydrogenation of benzene, □: hydrogenolysis of butane.

cyclohexane and the CO hydrogenation belong to the second group. The rates of these reactions were markedly suppressed by the addition of K.

In Fig. 4, the effects of Li are summarized. Similarly to the case of K, the TOF's of CO hydrogenation and dehydrogenation of cyclohexane decreased and those of hydrogenolysis of cyclohexane and butane increased as the alkali content increased. However, these changes in both reaction groups were distinctly smaller than in the case of K.

Discussion

The dehydrogenation of cyclohexane is an important reaction involved in the reforming process. Recent studies have shown that the addition of Au to Pt[19] or Cu to Ru(0001)[23] results in enhanced catalytic activities for the formation of benzene from cyclohexane. Miura et al.[20] also observed an enhancement in dehydrogenation and a suppression of hydrogenolysis upon Pt-addition to Ru/SiO_2. However, there has been no report on the effect of alkali-addition for this reaction.

Notable points concerning the present results are (1) the addition of K or Cs enhanced the activity for the hydrogenolysis of cyclohexane, while dehydrogenation to benzene was completely suppressed and (2) the activity changes caused by the alkali depended markedly on both the kinds of alkali and the kinds of reaction. The first result is in contrast with those of the bimetallic catalysts described above.

Effect of K on Conversion of Cyclohexane. Goodman et al.[23] reported that the dehydrogenation of cyclohexane over Ru was enhanced by surface overlayers of carbon or Cu. Over fresh Ru(0001) surface, only hydrogenolysis took place, and benzene (dehydrogenation) began to be formed after an induction period. During this period, a surface layer of carbon was gradually formed, and the dehydrogenation rates increased, indicating that the carbonaceous layer is necessary for benzene formation. On the other hand, the hydrogenolysis rates decreased as the amount of carbon increased. Therefore, the carbonaceous layer effectively suppresses the C-C bond scission of cyclohexane. Goodman et al.[23] also showed that Cu on Ru(0001) played a role similar to that of the carbonaceous layer. Over Cu/Ru(0001), of which Ru(0001) was precovered with submonolayer quantities of Cu, benzene was formed from the beginning of the reaction and the hydrogenolysis reaction did not take place.

If, as described above, the carbonaceous layer is necessary for benzene formation and acts as a poison for the hydrogenolysis reaction, it may be concluded that K suppresses the formation of the carbonaceous layer.

Acceleration of C-C Bond Scission. As shown in Table 1, the addition of K or Cs gave rise to a decrease in dispersion. Therefore, an increase in the activity for the hydrogenolysis (in the unit of per weight of Ru) is not due to an increase in the number of active sites. A certain step of the hydrogenolysis reaction must have been accelerated by the addition of K or Cs. It is accepted for the hydrogenolysis reaction that a hydrogen-deficient species is formed in the initial step by a scission of the C-H bond; subsequently, the C-C bond is broken, and finally the hydrocarbon fragments, thus formed, are hydrogenated.[24-27] Over metallic catalysts, the scission of the C-H bond and

the hydrogenation of hydrocarbon fragments are considered to be rapid. Therefore, the rate-determining step is presumably the C-C bond breaking.[27,28] Since K really increased the rates of hydrogenolysis, K must have accelerated the C-C bond breaking step. Probably the carbonaceous layer was not formed on Ru/SiO_2 promoted by K due to the rapid C-C bond breaking.

Effect of Kinds of Alkali. As shown in Fig. 2, the suppression of dehydrogenation and the enhancement of hydrogenolysis became more significant as the atomic number of alkali increased. If one considers the fact that the ability of electron donation of the alkali cation M^+ and/or M_2O, increases as the atomic number increases,[1,2] the results in Fig. 2 may be considered to be mainly brought about by the electronic effects of the alkali. As a matter of fact, the IR band positions of the CO adsorbed on Ru/SiO_2 were not affected by the addition of Li, but these shifted considerably to lower frequencies upon the addition of K.[17] In addition, electron transfer from K to Ru in XPS measurements of Ru/SiO_2[16] and by the IR band positions of the CO or NO adsorbed on Ru/Al_2O_3.[7,15]

A comparison of Figs. 3 and 4 makes clear the influence of the electronic effect on the various kinds of reactions. Although the TOF of the CO hydrogenation decreased by the addition of both Li and K, the decrease was remarkable for K, showing that CO hydrogenation was strongly influenced by an electronic effect.[7] Since H_2 adsorption data indicated that Li and K covered the Ru particles to a similar extent,[17] these alkalis probably bring about similar ensemble effects. Actually, the addition of Cu to Ru also resulted in a great decrease in the rate of CO hydrogenation by the ensemble effect.[29] Thus, the greater effect of K may be due to its stronger electronic effect.

References

1) W. D. Mross, *Catal. Rev.*, **25**, 591 (1983).
2) S. T. Thompson, *J. Chem. Soc., Faraday Trans. 1*, **83**, 1893 (1987).
3) K. Aika, K. Shimazaki, Y. Hattori, A. Ohya, S. Ohshima, K. Shirota, and A. Ozaki, *J. Catal.*, **92**, 296 (1986).
4) G. Chai and J. L. Falconer, *J. Catal.*, **93**, 152 (1985).
5) Y. Kikuzono, S. Kagami, S. Naito, and K. Tamaru, *Faraday Discuss. Chem. Soc.*, **72**, 135 (1981).
6) H. Delligianni, R. L. Mielle, and J. B. Peri, *J. Catal.*, **95**, 465 (1985).
7) T. Okuhara, H. Tamura, and M. Misono, *J. Catal.*, **95**, 41 (1985).
8) M. M. Maclory and R. D. Gonzalez, *J. Catal.*, **89**, 392 (1984).
9) S. C. Chuang, J. G. Goodwin, and I. Wender, *J. Catal.*, **95**, 435 (1985).
10) M. Logan, G. Gellmen, and G. A. Somorjai, *J. Catal.*, **94**, 60 (1985).
11) A. Muramatsu, T. Tatsumi, and H. Tominaga, *Bull. Chem. Soc. Jpn.*, **60**, 3157 (1987).
12) J. H.Sinfelt, J. L. Carter, and D. J. C. Yates, *J. Catal.*, **24**, 283 (1972).
13) J. R. Van Schaik, R. P. Dessing, and V. Ponec, *J. Catal.*, **38**, 273 (1974).
14) D. E. Resasco and G. L. Haller, *J. Catal.*, **82**, 279 (1983).
15) D. L. King and J. B. Peri, *J. Catal.*, **79**, 164 (1983).
16) J. Z. Shyu, J. G. Goodwin, Jr., and D. M. Hercules, *J. Phys. Chem.*, **89**, 4983 (1985).
17) T. Enomoto, K. Kata, T. Okuhara, and M. Misono, *Bull. Chem. Soc. Jpn.*, **60**, 1237 (1987).
18) Z. Z. Lin, T. Okuhara, and M. Misono, *Chem. Lett.*, **1987**, 2212.
19) J. W. A. Sachtler and G. A. Somorjai, *J. Catal.*, **89**, 35 (1984).
20) H. Miura, M. Osawa, T. Suzuki, K. Sugiyama, and T. Matsuda, *Chem. Lett.*, **1982**, 1803.
21) C. H. Peden and D. W. Goodman, *J. Catal.*, **100**, 520 (1986).
22) T. Okuhara, T. Kimura, K. Kobayashi, M. Misono, and Y. Yoneda, *Bull. Chem. Soc. Jpn.*, **57**, 938 (1984).
23) C. H. F. Peden and D. W. Goodman, *J. Catal.*, **104**, 347 (1987).
24) G. A. Martin, *J. Catal.*, **60**, 345 (1979).
25) J. H. Sinfelt, *J. Catal.*, **27**, 468 (1972).
26) A. Frennet, L. Degols, G. Lienard, and F. Crucq, *J. Catal.*, **35**, 18 (1974).
27) K. Tanaka, T. Miyazaki, and K. Aomura, *J. Catal.*, **81**, 328 (1983).
28) S. Kristyan and J. Szamosi, *J. Chem. Soc., Faraday Trans. 1*, **80**, 1645 (1984).
29) G. C. Bond and B. D. Turnham, *J. Catal.*, **45**, 128 (1976).

 © 1989 The Chemical Society of Japan Bull. Chem. Soc. Jpn., 62, 1745—1750 (1989)

Interactions between the Tris(1,10-phenanthroline)iron(II) Cation and Anionic Surfactants: Diffusion and Conductance Studies

Toshihiro TOMINAGA,* Toru MARUYAMA, Takayuki KOSHIBA, and Yuroku YAMAMOTO†
Department of Applied Chemistry, Okayama University of Science, 1-1 Ridai-cho, Okayama 700
†Environmental and Safety Engineering Department, Fukui Institute of Technology, 3-6-1 Gakuen, Fukui 910
(Received December 7, 1988)

Tracer diffusion coefficients for the $[Fe(phen)_3]^{2+}$ cation (phen=1,10-phenanthroline) have been measured in aqueous solutions of sodium 1-hexane-, 1-octane-, 1-decane-, and 1-dodecanesulfonate (NaDSO) in concentration ranges below the critical micelle concentrations of the surfactants and at 298.2 K. The diffusion coefficient decreases with an increase in the concentration of the surfactants. At a fixed concentration, the diffusion coefficient decreases with an increase in the carbon number of the surfactants. The results are compared with our previous results in sodium dodecyl sulfate (NaDS) solutions. The conductivities of the NaDSO and NaDS solutions were also measured at 298.2 K in the presence and absence of $[Fe(phen)_3]SO_4$. In the presence of $[Fe(phen)_3]SO_4$, the molar conductivities of the surfactants first decrease, then increase, and finally decrease again with an increase in the concentration of the surfactants.

Metal chelate ions of 1,10-phenanthroline (phen) and 2,2′-bipyridine (bpy) are known to be hydrophobic.[1,2] When counter ions are hydrophobic, such ions are extracted into water-immiscible organic solvents. Particularly, the red-colored chelate ions of iron(II) have been used extensively in analytical chemistry.[3] In recent years, there has been considerable interest in the reactions of these ions in aqueous surfactant media, i.e., racemization and dissociation reactions,[4] photochemical reactions,[5-8] and electron-transfer or electrochemical reactions.[9]

The elucidation of the solute-solute interactions between these metal chelate ions and other hydrophobic ions is important for an understanding of the reactions of these ions. Our previous study of the tracer diffusion of $[Fe(phen)_3]^{2+}$ in aqueous solutions showed that the hydrophobic interaction between $[Fe(phen)_3]^{2+}$ and $[Ni(phen)_3]^{2+}$ reduced the translational diffusivity of $[Fe(phen)_3]^{2+}$.[10] Furthermore, we found that the tracer diffusion coefficient of $[Fe(phen)_3]^{2+}$ in water decreases greatly in the presence of sodium dodecyl sulfate (NaDS), even when the concentration of the latter is below its critical micelle concentration (cmc).[11]

We wish to report here the tracer diffusion coefficients for $[Fe(phen)_3]^{2+}$ in aqueous solutions of sodium 1-hexane-, 1-octane-, 1-decane-, and 1-dodecanesulfonate (NaHSO, NaOSO, NaDeSO, and NaDSO respectively), and the results will be compared with those in NaDS solutions. We also wish to report the conductivities of the $[Fe(phen)_3]SO_4$-NaDSO and $[Fe(phen)_3]SO_4$-NaDS systems.

Experimental

Materials. Reagent-grade Mohr's salt $[FeSO_4(NH_4)_2SO_4 \cdot 6H_2O]$, 1,10-phenanthroline monohydrate, $NiSO_4 \cdot 6H_2O$, $NaClO_4 \cdot H_2O$ (Wako Pure Chemicals), NaHSO, NaOSO, NaDeSO, (Tokyo Chemical Industry), and NaDS (BDH)[12,13] were used as received. The NaDSO (Tokyo Chemical Industry; ion-pair-chromatography grade) was recrystallized from an ethanol-methanol (5:1) mixture. The water was distilled twice. A stock solution of $[Ni(phen)_3]SO_4$ was prepared by mixing $NiSO_4 \cdot 6H_2O$ and phen$\cdot H_2O$ in water. A stock solution of $[Fe(phen)_3]SO_4$ was prepared by mixing $[Fe(phen)_3](ClO_4)_2$ with the sulfate form of an anion exchanger in water, after $[Fe(phen)_3](ClO_4)_2$ had been prepared from Mohr's salt, phen$\cdot H_2O$, and $NaClO_4 \cdot H_2O$.[10]

Measurements. The diffusion measurements were made by the Taylor dispersion method.[14] In this method, a small amount of a solution is injected into a solvent flowing through a capillary tube. The solute is dispersed along the tube as a result of a combination of convection and molecular diffusion. By detecting the concentration profile at the end of the stream, we can calculate the diffusion coefficient. The solvent contained a specified amount of a surfactant plus 0.1 mM (1 M=1 mol dm^{-3}) $[Ni(phen)_3]SO_4$, while the solution contained the same amount of the surfactant plus 0.1 mM $[Fe(phen)_3]SO_4$. The concentration profile of $[Fe(phen)_3]^{2+}$ was detected by the absorption at 510 nm using a spectrophotometric detector for HPLC (either Japan Spectroscopic Co., Model UVIDEC-100-IV or Waters, Model 490). The other details have been described elsewhere.[10,11,15]

The conductivities of the solutions were measured at 5 kHz by means of a linear-bridge conductometer[16] (Huso, Model 360B) in an oil thermostat controlled to ± 0.005 K. Two conductivity cells were used: either a 500-cm^3 Kraus-type cell[17] with a cell constant of 0.3575 cm^{-1} or a 10-cm^3 cell with a cell constant of 2.464 cm^{-1}. Most of the measurements were made with the 500-cm^3 cell. A solvent was introduced into the cell, nitrogen gas was bubbled through when the solvent was pure water, and the cell with a solvent was weighed. A weighed amount of a solid solute was added after each resistance measurement under a nitrogen atmosphere. Some of the measurements on the concentrated solutions were, however, made by using the 10-cm^3 cell, where solutions were prepared by weight separately and transferred into the cell. The densities of some of the solutions were measured by means of a single-neck pyc-

nometer to calculate the molar concentrations.

Results

Table 1 shows the diffusion coefficients of the $[Fe(phen)_3]^{2+}$ ion in sodium 1-alkanesulfonate solutions. Each value is the average of more than five measurements. The diffusion coefficients we measured are the interdiffusion coefficients between $[Fe(phen)_3]^{2+}$ and $[Ni(phen)_3]^{2+}$. If we assume that the diffusion coefficients of $[Fe(phen)_3]^{2+}$ and $[Ni(phen)_3]^{2+}$ are essentially the same, the results may be taken as the intradiffusion coefficients[18] of $[M(phen)_3]^{2+}$, M being Fe or Ni. Because the concentration of the $[M(phen)_3]^{2+}$ ions (0.1 mM) is low compared to those of the surfactants, the results obtained can be considered as the tracer diffusion coefficients.

In Fig. 1, the diffusion coefficient is plotted as a function of the surfactant concentration. Our previous results in NaDS solutions[11] are included in the figure. As the surfactant chain length increases, the diffusion coefficient decreases, reflecting the interactions between $[Fe(phen)_3]^{2+}$ and the surfactant anions. Note that the concentrations of the surfactants are no greater than their cmc values except for the two solutions of NaDS (10 and 20 mM).[19,20] Figure 2 shows the Stokes radius, which was calculated from

$$r_S = \frac{kT}{6\pi\eta D}, \quad (1)$$

where k is Boltzmann's constant, T is the absolute temperature, and η is the viscosity of the solvent, for which we used the value for pure water.[21] Many workers have studied the NaDS diffusion coefficient using different techniques; the Stokes radius for the micelles at cmc is 2.2—2.5 nm.[22] Although we do not have data for NaDeSO, the Stokes radius for sodium decyl sulfate (NaDeS) micelles at the cmc has been reported to be 1.98 nm in 0.1 M NaCl.[23] Thus, even in the premicellar concentration range, in NaDS and NaDSO solutions, the Stokes radius of $[Fe(phen)_3]^{2+}$ is larger than that of the NaDS micelles; in 30 and 40 mM NaDeSO solutions, the Stokes radius of $[Fe(phen)_3]^{2+}$ is close to that of the NaDeS micelles.

In order to obtain more information, we measured the conductance of solutions. The molar conductivities of NaDSO and NaDS in water and $[Fe(phen)_3]SO_4$ solutions were calculated from

Table 1. Tracer Diffusion Coefficients of $[Fe(phen)_3]^{2+}$ in Aqueous Sodium 1-Alkanesulfonate Solutions at 298.15 K

[Surfactant]/mM	$D/10^{-10}m^2s^{-1}$
In $NaC_6H_{13}SO_3$	
4	4.31±0.05
10	4.24±0.02
20	4.13±0.05
In $NaC_8H_{17}SO_3$	
4	4.12±0.06
10	3.92±0.02
20	3.69±0.04
In $NaC_{10}H_{21}SO_3$	
4	3.83±0.04
10	2.99±0.02
20	1.79±0.02
30	1.37±0.01
40	1.23±0.03
In $NaC_{12}H_{25}SO_3$	
2	1.420±0.030
3	0.961±0.010
4	0.841±0.012
5	0.790±0.015
6	0.754±0.010
7	0.755±0.029

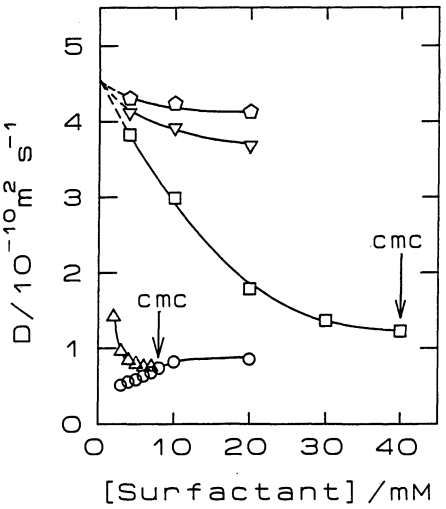

Fig. 1. Tracer diffusion coefficients of $[Fe(phen)_3]^{2+}$ in aqueous surfactant solutions. ⬠, In NaHSO; ▽, in NaOSO; □, in NaDeSO; △, in NaDSO; ○, in NaDS.[11] Arrows indicate cmc's for NaDeSO and NaDS.

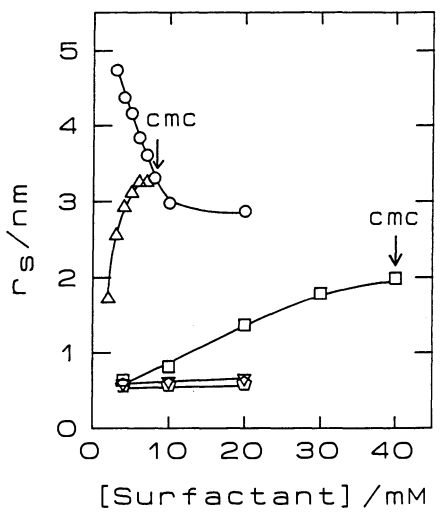

Fig. 2. The Stokes radii of $[Fe(phen)_3]^{2+}$ in aqueous surfactant solutions. Symbols are the same as in Fig. 1.

Table 2. Molar Conductivities of Sodium 1-Dodecanesulfonate in Water and in Aqueous $Fe[(phen)_3]SO_4$ Solutions at 298.15 K

C/mM	Λ/S cm^{2}mol^{-1}	C/mM	Λ/S cm^{2}mol^{-1}
In water		6.241	55.31
($10^6\kappa_0$/S cm^{-1}=0.21)		6.994	55.45
0.857	69.84	7.739	55.68
1.785	68.84	8.505	55.32
2.776	68.08	9.180	55.21
3.878	67.39		
5.148	66.63	In 1.0 mM $[Fe(phen)_3]SO_4$	
6.064	66.27	($10^6\kappa_0$/S cm^{-1}=204.47)	
7.089	65.82	0.389	50.68
8.018	65.57	0.771	49.21
		1.166	42.68
In 0.21 mM $[Fe(phen)_3]SO_4$		1.560	40.00
($10^6\kappa_0$/S cm^{-1}=45.75)		1.928	39.11
0.386	63.50	2.339	38.64
0.776	63.83	2.712	38.98
1.164	62.85	3.157	39.57
1.535	60.68	3.517	40.93
1.927	59.92	3.991	42.11
2.315	59.83	4.696	44.13
2.689	60.03	5.499	45.92
3.072	60.30	6.249	47.32
3.784	60.85	7.017	48.03
4.538	61.15	7.825	48.55
5.355	61.31	8.768	49.04
6.144	61.57	9.530	48.94
6.860	61.18		
7.567	60.97	In 2.0 mM $[Fe(phen)_3]SO_4$	
8.342	60.71	($10^6\kappa_0$/S cm^{-1}=391.65)	
9.103	60.31	0.401	41.41
9.878	59.70	0.790	37.43
		1.198	34.19
In 0.5 mM $[Fe(phen)_3]SO_4$		1.611	31.64
($10^6\kappa_0$/S cm^{-1}=106.87)		2.000	31.52
0.414	57.81	2.416	30.71
0.827	57.60	2.794	30.59
1.208	51.90	3.197	30.89
1.665	49.21	3.620	31.27
2.043	48.85	4.425	31.32
2.408	49.33	5.213	32.45
2.757	50.12	6.010	33.85
3.147	51.04	6.772	35.76
3.930	52.75	7.528	37.39
4.692	54.03	8.360	38.40
5.471	54.78	9.184	39.66

$$\Lambda = \frac{1000(\kappa - \kappa_0)}{C}, \quad (2)$$

where κ is the conductivity of the solution, κ_0 is the conductivity of the solvent (i.e., either water or a $[Fe(phen)_3]SO_4$ solution without surfactant), and C is the molarity of the surfactant. The molar conductivities of NaDSO and NaDS are listed in Tables 2 and 3 respectively; they are plotted as a function of the surfactant concentration in Fig. 3.

In the presence of $[Fe(phen)_3]SO_4$, the molar conductivity of NaDSO decreases, passes through a minimum, and increases again with an increase in the concentration of NaDSO. This tendency becomes more marked with an increase in the concentration of $[Fe(phen)_3]SO_4$. Measurement in higher concentrations of NaDSO was not possible because the Krafft temperature of NaDSO is high (306 K).[20] In the case of NaDS, when we add the surfactant to a solution of $[Fe(phen)_3]SO_4$, a precipitate of $\{[Fe(phen)_3](DS)_2\}_n$

Table 3. Molar Conductivities of Sodium Dodecyl Sulfate in Water and in Aqueous $[Fe(phen)_3]SO_4$ at 298.15 K

C/mM	Λ/S cm^{2}mol^{-1}	C/mM	Λ/S cm^{2}mol^{-1}
In water		12.051	48.09
($10^6\kappa_0$/S cm^{-1}=0.10)		13.102	46.70
1.575	69.48		
3.083	68.41	($10^6\kappa_0$/S cm^{-1}=102.19)	
4.498	67.67	9.387	51.13
5.101	67.39	10.915	49.25
6.059	67.03	12.566	47.09
8.110	64.67	14.261	44.85
9.276	61.04	16.322	42.50
10.642	56.78	18.257	40.67
11.858	53.58	20.575	39.23
12.623	52.01		
13.213	50.61	In 1.0 mM $[Fe(phen)_3]SO_4$	
		($10^6\kappa_0$/S cm^{-1}=198.91)	
($10^6\kappa_0$/S cm^{-1}=0.55)		4.811	42.14
8.480	64.35	5.482	43.85
10.814	56.66	6.109	44.69
14.388	48.58	6.780	45.23
14.477	48.30	7.445	45.52
		8.178	45.53
($10^6\kappa_0$/S cm^{-1}=1.5)		8.958	45.37
10.109	58.22[a]	9.609	45.22
19.181	42.10[a]	10.848	44.48
29.845	35.81[a]	12.095	43.66
39.218	33.28[a]		
		($10^6\kappa_0$/S cm^{-1}=196.07)	
In 0.20 mM $[Fe(phen)_3]SO_4$		12.161	44.04
($10^6\kappa_0$/S cm^{-1}=42.10)		13.852	42.85
2.662	59.30	15.632	41.27
3.687	60.32	17.119	40.08
4.922	60.70	18.867	38.89
5.531	60.40	20.399	37.95
6.664	59.80	22.382	36.81
7.944	58.84	23.867	36.02
9.287	56.82		
10.502	54.35	In 2.0 mM $[Fe(phen)_3]SO_4$	
11.797	51.59	($10^6\kappa_0$/S cm^{-1}=391.43)	
13.093	49.11	8.133	36.54
14.660	46.55	8.882	37.52
16.217	44.42	9.621	37.65
18.057	42.27	10.348	38.04
		11.125	38.15
In 0.50 mM $[Fe(phen)_3]SO_4$		11.993	38.20
($10^6\kappa_0$/S cm^{-1}=105.26)		14.504	37.76
3.698	51.01		
4.434	52.28	($10^6\kappa_0$/S cm^{-1}=385.87)	
5.181	52.97	20.280	36.36[a]
5.945	53.30	23.278	35.32[a]
6.714	53.24	26.307	34.40[a]
7.486	52.97	29.627	33.71[a]
8.252	52.44	33.918	32.33[a]
9.011	51.82	36.409	32.31[a]
9.752	51.04	42.894	31.51[a]
10.939	49.56		

a) These measurements were made using a 10-cm^3 cell. See text for more details.

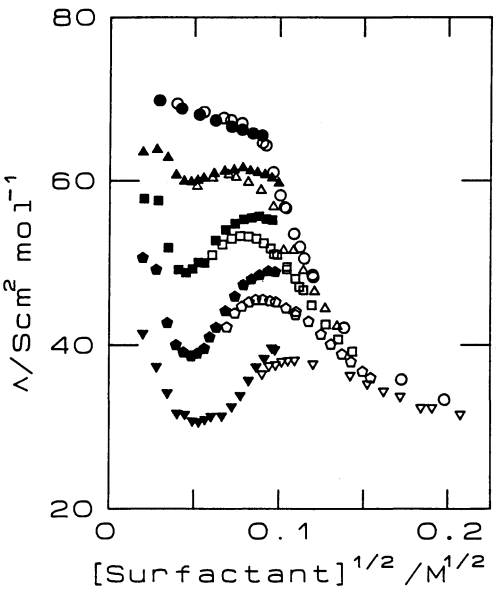

Fig. 3. Molar conductivities of NaDSO (closed symbols) and NaDS (open symbols) in water and aqueous $[Fe(phen)_3]SO_4$. Concentrations of $[Fe(phen)_3]SO_4$ are 0 mM (● and ○), 0.2 mM (▲ and △), 0.5 mM (■ and □), 1 mM (⬟ and ⬠), and 2 mM (▼ and ▽).

appears; this precipitate is then resolubilized by the further addition of NaDS.[24,25] For example, in the case of 0.2 mM $[Fe(phen)_3]SO_4$, we found that a precipitate appears when the NaDS concentration is 0.13 mM and that it is resolubilized when the NaDS concentration reaches 2.1 mM. The results shown in Fig. 3 are in NaDS concentration ranges higher than the resolubilization points. In this case, we made measurements also in the NaDS concentrations above the cmc. With an increase in the concentration of NaDS, the molar conductivity increases, passes through a maximum, decreases, and finally approaches that in pure water.

Discussion

When $[Fe(phen)_3]SO_4$ and a surfactant NaA are mixed, the reaction which takes place may be written as:

$$x[Fe(phen)_3]^{2+} + yA^- + zNa^+ \leftrightarrows Na_z[Fe(phen)_3]_xA_y^{(y-2x-z)-}. \quad (3)$$

As we noted earlier, in 3—8 mM NaDS and 3—7 mM NaDSO the Stokes radius of $[Fe(phen)_3]^{2+}$ is larger than that of the NaDS micelles. However, the conductance results do not show the existence of normal micelles in these concentration ranges. As may be seen in Fig. 3, even in 0.2 mM $[Fe(phen)_3]SO_4$ the molar conductivities of NaDS and NaDSO are much higher than that of NaDS above the cmc. (Note that the concentration of $[M(phen)_3]^{2+}$ was 0.1 mM in the diffusion measurements.) A similar conclusion has been reached on the basis of surface-tension and light-scattering measurements.[24]

The Stokes radius may reflect electrostatic interactions as well as the size of the premicellar aggregates. The electrostatic interaction is reduced when a salt is added. Even when Na_2SO_4 was added to 3 mM NaDS, the Stokes radius of $[Fe(phen)_3]^{2+}$ was still larger than that of the NaDS micelles.[11] In a 3 mM surfactant solution, the molar ratio of the surfactant to $[Fe(phen)_3]^{2+}$ is 30. If the size of an aggregate is larger than that of an NaDS micelle which contains 60 monomers, the value of x in Eq. 3 has to be larger than 2. From a luminescence-quenching study, it has been reported that $[Ru(bpy)_3]^{2+}$ forms premicellar "clusters" with NaDS which contain several $[Ru(bpy)_3]^{2+}$.[5]

The fact that there is precipitate-formation between $[Fe(phen)_3]^{2+}$ and DS^-, but not between $[Fe(phen)_3]^{2+}$ and DSO^-, together with the fact that there is a lower diffusion coefficient for $[Fe(phen)_3]^{2+}$ in NaDS than in NaDSO (Fig. 1), suggests a stronger interaction between $[Fe(phen)_3]^{2+}$ and DS^- than between $[Fe(phen)_3]^{2+}$ and DSO^-. Just above those concentrations, where the precipitate $\{[Fe(phen)_3](DS)_2\}_n$ is resolubilized, the molar conductivities of NaDS are only slightly lower than those of NaDSO, as if the system has lost the memory that it has had a precipitate. This is in contrast to the definitely smaller diffusion coefficient of $[Fe(phen)_3]^{2+}$ in NaDS than in NaDSO (Fig. 1). In the case of diffusion, we are looking at the movement of $[Fe(phen)_3]^{2+}$ ions. Because the concentration of $[Fe(phen)_3]^{2+}$ is small almost all $[Fe(phen)_3]^{2+}$ ions are considered to be in premicellar aggregates, and the diffusion coefficient of $[Fe(phen)_3]^{2+}$ is essentially that of the aggregates; thus, it is sensitive to the aggregate size.

In the case of conductivity, the situation is more complicated. Below the cmc of a surfactant NaA, the molar conductivity of the surfactant can be expressed by

$$\begin{aligned}\Lambda(\mathrm{NaA}) = \{&[C_t(\mathrm{NaA}) - \Delta C(\mathrm{Na^+})]\lambda(\mathrm{Na^+}) \\ &+ [C_t(\mathrm{NaA}) - \Delta C(\mathrm{A^-})]\lambda(\mathrm{A^-}) \\ &- 2[\Delta C([\mathrm{Fe(phen)_3}]^{2+})]\lambda([\mathrm{Fe(phen)_3}]^{2+}) \\ &+ (y-2x-z)[\Delta C(\mathrm{A^-})/y]\lambda(\mathrm{aggregate})\}/[C_t(\mathrm{NaA})], \end{aligned} \quad (4)$$

where "aggregate" refers to the right-hand side of Eq. 3, $C_t(X)$ means the total molar concentration of X in the solution, $\Delta C(X)$ means the molar concentration of X in the aggregates, and $\Lambda(X)$ or $\lambda(X)$ means the molar conductivity of X, expressed as the (X/valency) molar unit, i.e., the equivalent conductivity. In other words, the molar conductivity of NaA, as calculated from Eq. 2, has contributions from: 1) the free ions of Na^+ and A^-, 2) the $[Fe(phen)_3]^{2+}$ ions which were used to form the aggregate (negative contribution), and 3) the aggregates themselves. In Fig. 3, the initial part of the decrease in Λ of NaDSO may be attributed to

aggregate formation, which reduces the concentrations of the free Na^+, DSO^-, and $[Fe(phen)_3]^{2+}$ ions. After passing through the minima, A increases because the concentration of $[Fe(phen)_3]^{2+}$ is fixed and the aggregate formation is saturated. This is the concentration region where the precipitate $\{[Fe(phen)_3](DS)_2\}_n$ is resolubilized, and the system has sufficient free ions of Na^+ and DS^-. This is why the conductance results do not differ drastically between NaDS and NaDSO. After passing through the maxima, the conductivities decrease because normal micelles are formed.

Although DSO^- and DS^- differ from each other by only one oxygen atom, there is a large difference between their behavior when the solid state or a highly condensed state is involved, i.e., 1) DS^- forms a precipitate with $[Fe(phen)_3]^{2+}$ but DSO^- does not, 2) NaDSO is stable in a solid state rather than micelles at 298 K (the Krafft temperature is high) but NaDS forms micelles at the same temperature. Also, there are differences between their premicellar aggregates, as seen in the differences in their diffusion coefficients (Fig. 1).

Comparison with Other Studies. It is of interest to compare the above results with those in the previous work of others. Tachiyashiki and Yamatera have found that the reaction rates for the racemization and dissociation of $[M(phen)_3]^{2+}$ (M=Fe or Ni) increase significantly when anionic surfactants are added.[4] They start increasing below the cmc's of the surfactants: 20, 1—2, and 0.3—0.4 mM for NaDeSO, NaDSO, and NaDS respectively. It is worth noting that, at these concentrations, the diffusion coefficient is significantly lowered, i.e., to ca. 2×10^{-10} m^2 s^{-1} or lower (Fig. 1). Tachiyashiki and Yamatera could explain their results by assuming the formation of $1:m$ premicellar aggregates between the metal chelate cations and surfactant anions, i.e., 1 : 8 aggregates for NaDeSO, and 1 : 3 or 1 : 4 plus 1 : 8 aggregates for NaDSO and NaDS. They could also explain the result for $[Fe(bpy)_3]^{2+}$ in NaDS in terms of 1 : 3 or 1 : 4 plus 1 : 8 aggregates.

Baxendale and Rodgers found that the luminescence quenching rate of $[Ru(bpy)_3]^{2+}$ is increased by 9-methylanthracene (MeA) in a NaDS solution, even when the concentration of NaDS is below the cmc.[5] They interpreted this result as being due to the formation of premicellar clusters which incorporate the emitter and quencher molecules. The quenching rate constant is larger in 6 mM NaDS than in 3 mM NaDS (both below the cmc). This led them to state, "The higher value of k_1 (the rate constant) for 6 mM NaDS probably reflects the smaller cluster size which could put quencher and emitter in closer proximity." This is in conformity with the smaller Stokes radius of $[Fe(phen)_3]^{2+}$ in 6 mM than in 3 mM NaDS (Fig. 2). They also found that the quenching rate constant is larger in micellar systems than in premicellar solutions; they stated that this "may arise from a higher mobility of the species on the micelle surface." However, from the data presented in Fig. 2, an alternative interpretation would be that the smaller size of the micelles puts emitter and quencher in closer proximity, thereby increasing the quenching rate. The quenching of $[Ru(bpy)_3]^{2+}$ fluorescence by the 1,1′-dimethyl-4,4′-bipyridinium cation (MV^{2+}) has also been reported to be enhanced in NaDS solutions below the cmc.[6-8]

Bruhn and Holzwarth have found that the rates of electron-transfer reaction between the $[Os(bpy)_3]^{3+}/[Mo(CN)_8]^{4-}$, $[Os(bpy)_3]^{3+}/[Fe(CN)_6]^{4-}$, and $[Ir(CN)_6]^{2-}/[Os(bpy)_3]^{2+}$ ions decrease when NaDS is added; they start decreasing when the NaDS concentration is still below the cmc.[9a] This may be interpreted as a result of the interaction between the $[Os(bpy)_3]^{n+}$ (n=2 or 3) and DS^- ions, which prevents $[Os(bpy)_3]^{n+}$ ions from coming in contact with the hydrophilic anions.

Thus, although there are some exceptions,[9c,25] there are many observations of different kinds which support the formation of premicellar aggregates when $[M(phen)_3]^{2+}$ or $[M(bpy)_3]^{2+}$ cations and anionic surfactants are mixed together. The detailed picture of the aggregates, however, still differs from one observation to another; especially, our finding of a large premicellar aggregate size is unique.

This work was partially supported by a Grant-in-Aid for Scientific Research No. 62124039 from the Ministry of Education, Science and Culture.

References

1) Y. Yamamoto, T. Tominaga, and S. Tagashira, *Inorg. Nucl. Chem. Lett.*, **11**, 825 (1975); E. Iwamoto, Y. Hiyama, and Y. Yamamoto, *J. Solution Chem.*, **6**, 371 (1977).

2) Y. Masuda and H. Yamatera, *Bull. Chem. Soc. Jpn.*, **57**, 58 (1984); *J. Phys. Chem.*, **88**, 3425 (1984).

3) Y. Yamamoto, *Bunseki Kagaku*, **21**, 418 (1972).

4) S. Tachiyashiki and H. Yamatera, *Bull. Chem. Soc. Jpn.*, **57**, 1061; 1067; 1070 (1984).

5) J. H. Baxendale and M. A. J. Rodgers, *Chem. Phys. Lett.*, **72**, 424 (1980); *J. Phys. Chem.*, **86**, 4906 (1982).

6) M. A. J. Rodgers and J.C. Becker, *J. Phys. Chem.*, **84**, 2762 (1980).

7) S. J. Atherton, J. H. Baxendale, and B.M. Hoey, *J. Chem. Soc., Faraday Trans. 1*, **78**, 2167 (1982).

8) H. Sato, M. Kawasaki, K. Kasatani, and T. Ban, *Chem. Lett.*, **1982**, 1139; H. Sato, M. Kawasaki, M. Haga, K. Kasatani, T. Ban, H. Suenaga, and N. Kitamura, *Nippon Kagaku Kaishi*, **1984**, 51.

9) a) H. Bruhn and J. Holzwarth, *Ber. Bunsenges. Phys. Chem.*, **82**, 1006 (1978); b) Y. Ohsawa, Y. Shimazaki, and S. Aoyagui, *J. Electroanal. Chem.*, **114**, 235 (1980); c) D. Lemordant, *J. Electroanal. Chem.*, **219**, 125 (1987); d) J. Ouyang and A. J. Bard, *Bull. Chem. Soc. Jpn.*, **61**, 17 (1988).

10) T. Tominaga, S. Matsumoto, T. Koshiba, and Y. Yamamoto, *J. Chem. Soc., Faraday Trans. 1*, **84**, 4261 (1988).

11) T. Tominaga, S. Matsumoto, T. Koshiba, and Y.

Yamamoto, *Chem. Lett.*, **1988**, 1427.

12) K. S. Birdi, *Anal. Biochem.*, **74**, 620 (1976).

13) T. Tominaga, T. B. Stem, and D. F. Evans, *Bull. Chem. Soc. Jpn.*, **53**, 795 (1980); T. Tominaga, S. Muraoka, T. Ishii, and Y. Yamamoto, *J. Solution Chem.*, **16**, 615 (1987).

14) G. I. Taylor, *Proc. R. Soc. London, Ser. A*, **219**, 186 (1953); **225**, 473 (1954); H. J. V. Tyrrell and K. R. Harris, "Diffusion in Liquids. A Theoretical and Experimental Study," Butterworths, London (1984), p. 193.

15) T. Tominaga, S. Yamamoto, and J. Takanaka, *J. Chem. Soc., Faraday Trans. 1*, **80**, 941 (1984); T. Tominaga, S. Matsumoto, and T. Ishii, *J. Phys. Chem.*, **90**, 139 (1986); T. Tominaga, K. Tanabe, and J. Takanaka, *J. Solution Chem.*, **13**, 563 (1984).

16) S. Katayama, *Bull. Chem. Soc. Jpn.*, **46**, 106 (1973); K. Takahashi, S. Katayama, and R. Tamamushi, *Rep. I. P. C. R.*, **49**, 13 (1973); H. Yokoyama, *Bull. Chem. Soc. Jpn.*, **57**, 1304 (1984).

17) D. F. Evans and M. A. Matesich, "Techniques of Electrochemistry," ed by E. Yeager and A. J. Salkind, Wiley-Interscience, New York (1973), Vol. 1, Chap. 1.

18) R. Mills, *J. Phys. Chem.*, **69**, 3116 (1965); J. G. Albright and R. Mills, *ibid.*, **69**, 3120 (1965).

19) P. Mukerjee and K. J. Mysels, "Critical Micelle Concentrations of Aqueous Surfactant Systems," Natl. Stand. Ref. Data Ser., Natl. Bur. Stand. (1971).

20) Y. Moroi, R. Sugi, C. Akine, and R. Matsuura, *J. Colloid Interface Sci.*, **108**, 180 (1985).

21) In these concentrations, the viscosities of the surfactant solutions are not very different from that of pure water. Although we do not have data for NaDeSO, the viscosity of the 40 mM NaDeS solution is only 3% larger than that of pure water: M. Tanaka, S. Kaneshina, W. Nishimoto, and H. Takabatake, *Bull. Chem. Soc. Jpn.*, **46**, 364 (1973).

22) D. Stigter, R. J. Williams, and K. J. Mysels, *J. Phys. Chem.*, **59**, 330 (1955); J. Clifford and B. A. Pethica, *ibid.*, **70**, 3345 (1968); M. Corti and V. Degiorgio, *ibid.*, **85**, 711 (1981); R. M. Weinheimer, D. F. Evans, and E. L. Cussler, *J. Colloid Interface Sci.*, **80**, 357 (1981); J. P. Kratohvil and T. M. Aminabhavi, *J. Phys. Chem.*, **86**, 1254 (1982).

23) P. J. Missel, N. A. Mazer, G. B. Benedek, and M. C. Carey, *J. Phys. Chem.*, **87**, 1264 (1983).

24) S. Ozeki, S. Tachiyashiki, S. Ikeda, and H. Yamatera, *J. Colloid Interface Sci.*, **91**, 430 (1983).

25) D. Lemordant and R. Gaboriaud, *Fluid Phase Equilibria*, **20**, 269 (1985).

 © 1989 The Chemical Society of Japan Bull. Chem. Soc. Jpn., 62, 1751—1757 (1989)

Relationships between Mesophase Behavior and Crystal Structures of Chiral Smectogenic 4-[(*S*)-2-Methylbutyl]phenyl 4′-Alkoxybiphenyl-4-carboxylates

Kayako Hori,* Miho Takamatsu, and Yuji Ohashi
Department of Chemistry, Ochanomizu University, Otsuka, Bunkyo-ku, Tokyo 112
(Received December 8, 1988)

Interlayer distances of Sm*C and Sm A phases of the title series were measured as functions of temperature by X-ray diffraction. With increase in temperature, molecular tilt angles in Sm*C decrease from 22—25 to 0°. Crystal structures of the heptyl (**1**) and octyl (**2**) homologues have been determined by X-ray analysis. (**1**): 4-[(*S*)-2-Methylbutyl]phenyl 4′-heptyloxybiphenyl-4-carboxylate, monoclinic, $P2_1$, a=26.929(4), b=5.4249(5), c=9.2607(9) Å, β=96.78(1)°, Z=2. (**2**): 4-[(*S*)-2-Methylbutyl]phenyl 4′-octyloxybiphenyl-4-carboxylate, orthorhombic, $P2_12_12_1$, a=9.249(1), b=56.259(9), c=5.412(1) Å, Z=4. Final R were 0.076 and 0.121, respectively. Both crystals have distinct layer structures similar to those of Sm*C. In the former crystal, the molecules tilt to one direction uniformly throughout layers, while in the latter, they take two opposite directions alternately from layer to layer. However, structures within a layer are very similar to each other. Each molecule has a coplanar biphenyl moiety and a twisted paraffin chain. Mesophase behavior was interpreted very well by the molecular interaction revealed in the crystal structures.

In the preceding paper,[1] we reported crystal structures of 4-pentyloxyphenyl and 4-heptyloxyphenyl 4′-[(*S*)-2-methylbutyl]biphenyl-4-carboxylates (series I crystals, abbreviated as I-5 and I-7, respectively) and discussed a relationship between the crystal structures and Sm*C phase characteristics. In order to make the relationship clearer, we extended the study to 4-[(*S*)-2-methylbutyl]phenyl 4′-alkoxybiphenyl-4-carboxylate series, $C_nH_{2n+1}O$-C_6H_4-C_6H_4-COO-C_6H_4-$CH_2CH(CH_3)C_2H_5$ (Series II, abbreviated as II-n), which is one of the isomeric series of the series I. While the series I has a Sm*C phase between crystalline and cholesteric phases, the series II has a Sm*C which transforms to a Sm A phase.[2] It has been pointed out that temperature dependence of the molecular tilt angles and behavior of transition to a higher temperature phase are different between the two kinds of Sm C, one which transforms to a nematic and the other to a Sm A.[3] This suggests different intermolecular interactions between the two Sm C. Therefore, it is considered to be very useful to find a relationship between crystal structures and mesophase behavior of the series II, and compare the relationship with that of the series I, in order to elucidate the intermolecular interaction.

This paper describes the mesophase behavior of the series II (n=6, 7, 8, 10, and 12) and the crystal structures of II-7 and II-8. Finally, relationships between the mesophase behavior and the crystal structures are discussed.

Experimental

Compounds. All the members were synthesized in a similar way to that described previously[4] from commercially available 4-alkoxy-4′-cyanobiphenyl (BDH Chemicals Ltd.) and 4-[(*S*)-2-methylbutyl]phenol supplied by BDH Chemicals Ltd., and purified by repeated crystallization from ethanol. All the crystalline samples thus obtained showed sharp melting (cryst-mesophase) peaks in the DSC measurements.

Studies of Mesophase Characteristics. Transition temperatures were measured using a Mettler TA 3000 DSC and an Olympus POM polarizing microscope equipped with a Mettler FP82. Interlayer distances were measured on a Rigaku 2001 diffractometer with Cu $K\alpha$ (λ=1.5418 Å) and Cr $K\alpha$ (λ=2.2902 Å). Helical pitches were measured as described previously.[4]

Crystal Structure Analysis. Transparent long parallelepiped crystals were grown from a methanol-chloroform solution. Crystals of approximate dimensions, 0.2×0.2×0.05 mm of II-7 and II-8 were used. The unit cell dimensions and space groups were determined from oscillation and Weissenberg photographs. Accurate cell parameters were determined by a least-squares fit for 15 reflections within the ranges 33°<2θ<58° (II-7) and 37°<2θ<50° (II-8), measured on a Rigaku AFC-4 diffractometer with Cu $K\alpha$ radiation (λ=1.54184 Å) monochromated by graphite.

Crystal Data. II-7, M_r=458.61, $C_{31}H_{38}O_3$, monoclinic, $P2_1$, a=26.929(4), b=5.4249(5), c=9.2607(9) Å, β=96.78(1)°, V=1343.4(3) Å^3, Z=2, d_x=1.134 g cm^{-3}, μ=4.84 cm^{-1}, $F(000)$=496; II-8, M_r=472.64, $C_{32}H_{40}O_3$, orthorhombic, $P2_12_12_1$, a=9.249(1), b=56.259(9), c=5.412(1) Å, V=2816(1) Å^3, Z=4, d_x=1.123 g cm^{-3}, μ=4.73 cm^{-1}, $F(000)$=1024. Reflection data were collected on a 2θ-ω scan mode, up to 2θ=125°, with scan widths of $\Delta\omega$=(1.0+0.15 tan θ) for II-7 and $\Delta\omega$=(0.7+0.15 tan θ) for II-8. Backgrounds were counted for 5 s at both ends of a scan. Three standard reflections were recorded after every 50 reflections. No significant intensity variations were observed. For II-7, a total of 2412 reflections were collected at the rate of 4° (2θ) min^{-1}, of which 1874 were treated as significant ($|F_o|>3\sigma(|F_o|)$). For II-8, 2691 reflections were collected at the rate of 4° (2θ) min^{-1}, of which 1540 were treated as significant. The data were corrected for Lorentz and polarization factors but not for absorption.

The structures were determined by applying the program MULTAN78[5] and refined by constrained block-matrix least-squares using SHELX76.[6] The quantity minimized

Table 1. Final Atomic Coordinates of II-7 with Their Estimated Standard Deviations, Multiplied by 10^4 for All the Atoms Except for C(25′) and 10^3 for C(25′)

Atom	x	y	z	B_{eq}/Å$^{2a)}$
O(1)	7116(2)	11163(12)	617(5)	7.1
O(2)	6857(1)	8063(9)	−864(4)	4.9
O(3)	3528(1)	8810(10)	4155(5)	5.8
C(1)	3991(2)	9016(10)	3711(5)	4.2
C(2)	4338(2)	10831(10)	4129(6)	5.2
C(3)	4795(2)	10864(11)	3583(7)	5.3
C(4)	4914(1)	9071(10)	2614(5)	4.0
C(5)	4562(2)	7213(11)	2208(6)	5.4
C(6)	4115(2)	7179(11)	2764(7)	5.2
C(7)	5411(1)	9159	1992(5)	3.5
C(8)	5764(2)	10955(12)	2444(7)	6.1
C(9)	6204(2)	11120(13)	1828(8)	6.7
C(10)	6316(2)	9435(10)	785(5)	4.1
C(11)	5972(2)	7576(11)	372(6)	5.2
C(12)	5530(2)	7440(10)	966(6)	5.0
C(13)	6800(2)	9649(13)	210(6)	4.5
C(14)	7324(2)	8017(11)	−1398(6)	4.9
C(15)	7453(2)	9841(11)	−2326(7)	5.4
C(16)	7916(2)	9797(12)	−2828(7)	5.9
C(17)	8246(2)	7877(12)	−2444(7)	5.6
C(18)	8109(2)	6011(12)	−1548(7)	6.1
C(19)	7649(2)	6102(11)	−1008(7)	5.5
C(21)	8754(2)	7884(21)	−3008(10)	6.9
C(22)	9124(3)	9786(21)	−2372(11)	8.3
C(23)	9600(4)	9690(33)	−3090(17)	12.3
C(24)	9916(7)	11966(39)	−2918(38)	20.3
C(25)[c)]	9262(9)	8946(73)	−835(17)	20.5
C(31)	3370(2)	10606(15)	5113(7)	5.2
C(32)	2840(2)	9952(15)	5389(7)	5.0
C(33)	2686(3)	11526(18)	6618(9)	6.6
C(34)	2130(2)	11513(17)	6757(10)	7.3
C(35)	1905(3)	8978(19)	6910(10)	7.8
C(36)	1366(3)	9222(23)	7236(14)	10.0
C(37)	1122(4)	6756(27)	7407(20)	15.0
C(25′)[c)]	949(4)	930(40)	−73(15)	29.7[b)]

a) $B_{eq}=(4/3)\sum_{ij}\beta_{ij}(a_i\cdot a_j)$. b) Isotropic temperature factor. c) Occupation factors are fixed as 0.7 and 0.3 for C(25) and C(25′), respectively.

was $\sum w(|F_o|-|F_c|)^2$, where $w=(\sigma(F_o)^2+0.004|F_o|^2)^{-1}$. Atomic scattering factors were taken from the International Tables for X-ray Crystallography.[7] All the non-hydrogen atoms except for the disordered C(25′) atom of II-7 were refined anisotropically. Hydrogen atoms found in the difference Fourier maps and derived geometrically were refined isotropically. Max. Δ/σ and max. $\Delta\rho$ in the final difference map were 0.21 and 0.15 e Å^{-3} for II-7, and 0.45 and 0.27 e Å^{-3} for II-8. Final R (and R_w) were 0.076 (0.090) and 0.121 (0.141) for II-7 and II-8, respectively. Considerably large R value for II-8 is due to somewhat poor crystallinity. In spite of the repeated attempts of crystallization, the best crystal still showed broad rocking-curve along the ω direction. Data collected by ω-scan mode did not improve the ratio, $|F_o|/\sigma(|F_o|)$ and hence the final R-value, probably because of the wide-based peaks. The final coordinates of non-hydrogen atoms are given in Tables 1 (II-7) and 2 (II-8).[8] Computations were carried out on a HITAC M-280H computer at the Computer Center of the University of Tokyo.

Table 2. Final Atomic Coordinates of II-8 with Their Estimated Standard Deviations, Multiplied by 10^4 for x and y, and 10^3 for z Coordinates

Atom	x	y	z	B_{eq}/Å$^{2a)}$
O(1)	7560(8)	8996(2)	648(2)	8.2
O(2)	8960(9)	9119(1)	345(2)	6.3
O(3)	2854(8)	10704(1)	424(2)	7.1
C(1)	3440(11)	10483(2)	442(2)	5.2
C(2)	3147(15)	10325(2)	632(2)	6.9
C(3)	3839(12)	10106(2)	622(2)	6.0
C(4)	4844(10)	10043(2)	443(2)	5.9
C(5)	5046(14)	10207(2)	249(2)	6.9
C(6)	4426(13)	10431(2)	257(2)	6.6
C(7)	5634(11)	9810(2)	458(2)	4.8
C(8)	5234(16)	9643(2)	633(3)	7.9
C(9)	6028(15)	9433(2)	643(3)	9.3
C(10)	7128(9)	9375(2)	479(2)	4.5
C(11)	7431(14)	9538(2)	294(2)	5.3
C(12)	6741(12)	9756(2)	288(2)	5.7
C(13)	7874(15)	9150(2)	509(2)	5.7
C(14)	9650(11)	8896(2)	344(2)	5.6
C(15)	9370(11)	8752(2)	143(2)	7.0
C(16)	10028(14)	8529(2)	128(2)	7.1
C(17)	10994(12)	8457(2)	307(2)	6.7
C(18)	11326(11)	8608(2)	504(2)	6.6
C(19)	10639(12)	8825(2)	524(2)	6.6
C(21)	11747(15)	8221(2)	311(3)	8.5
C(22)	11118(15)	8039(2)	491(3)	11.2
C(23)	11950(23)	7806(3)	469(4)	14.2
C(24)	11721(41)	7658(4)	694(6)	23.9
C(25)	9555(15)	7999(3)	434(5)	14.7
C(31)	1780(13)	10782(2)	604(3)	6.6
C(32)	1402(12)	11027(2)	542(3)	6.5
C(33)	71(14)	11105(2)	686(3)	7.4
C(34)	−142(19)	11369(2)	709(3)	10.3
C(35)	−463(18)	11486(2)	463(4)	12.9
C(36)	−1058(31)	11734(3)	505(5)	19.7
C(37)	−733(54)	11899(3)	295(5)	23.7
C(38)	−983(36)	12156(2)	367(7)	21.1

a) $B_{eq}=(4/3)\sum_{ij}\beta_{ij}(a_i\cdot a_j)$.

Results

Phase Sequences. In order to discuss a relationship between a crystal structure and mesophase behavior, it is necessary to know to which mesophase the crystal transforms. While the series I has a relatively simple phase sequence, cryst.-Sm*C-chol.-isotropic, the series II was reported to have more complicated ones depending on the paraffin chain lengths and thermal history.[2] For example, it was reported that II-8 exhibits a phase sequence, cryst.-Sm*I-Sm*C SmA-chol.-iso., while the II-7 crystal transforms directly to Sm*C. Besides, as supercooled phases, Sm*K and Sm*J for II-8 and Sm*K, Sm*J, and Sm*I for II-7 were reported. In the present DSC measurements, mesophase-mesophase or mesophase-isotropic transition temperatures were in good agreement with those reported for all the members, while cryst.-mesophase transition behavior for some members were slightly different from the reported one. For II-8, a solid sample obtained from a melt showed a complex curve corresponding to the reported supercooled

phase sequence, while the crystals obtained from a solution showed a simple and sharp melting curve similar to that of II-7, as shown in Fig. 1. This indicates that the crystal structures determined in this work transform directly to Sm*C. The enthalpy changes are 24.5 kJ mol^{-1} (II-7) and 25.5 kJ mol^{-1} (II-8).

Interlayer Distances and Helical Pitches in the Mesophase. Figure 2 shows the temperature dependence of the interlayer distances, d, in Sm*C and Sm A phases. The bending points are Sm*C-Sm A phase transition points. With increase in temperature, the d-values increase rapidly near the Sm*C-Sm A transition point in the Sm*C phase, while they decrease slightly in Sm A. Similar rapid dependence was observed for Sm C of 4'-octyloxybiphenyl-4-carboxylic acid[9] and attributed to the change of the molecular tilt angle in the Sm C phase. Figure 3 shows the relationship of the d-values at the transition points with the chain lengths, n. Good linearlity is obtained except for the member n=6 at the solid-Sm*C transition point. This exception is due to the extremely narrow temperature range for this member. Applying the equation, $d=d_r+n\times d_m$, to each line, the contribution to the layer thickness per methylene group, d_m, is obtained to be 0.90 (at the solid or other Sm-Sm*C), 0.77 (at Sm*C-Sm A) and 0.75 Å (at Sm A-chol. or isotropic transition point), showing that the contribution of the paraffin chain to the interlayer distances decreases slightly with increase in temperature throughout the two phases. On the other hand, the d_r value, i.e., that of the rest moiety of the molecule involving the core part and the bulky 2-methylbutyl group, is estimated to be 20.2 (at the solid or other Sm-Sm*C), 24.1 (at Sm*C-Sm A), and 23.9 Å (at Sm A-chol. or isotropic transition point). The latter two values are almost the same and attributed to the value for a molecule oriented vertically, on average, to the layer plane.

The tilt angle is estimated for each member, assuming that the layer thickness change is only due to the change of the average tilt angle of a whole molecule, since the change of the interlayer distances due to the

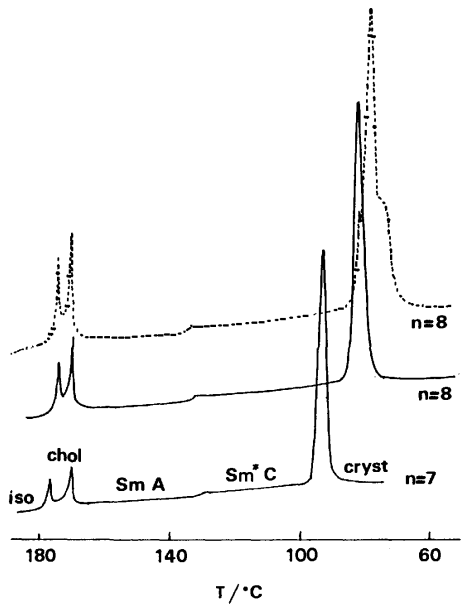

Fig. 1. DSC curves of 4-[(*S*)-2-methylbutyl]phenyl 4'-heptyloxybiphenyl-4-carboxylate (II-7) and 4-[(*S*)-2-methylbutyl]phenyl 4'-octyloxybiphenyl-4-carboxylate (II-8). A broken line denotes a curve for the solid of II-8 obtained from a melt. For II-7, DSC curves were almost independent of thermal history.

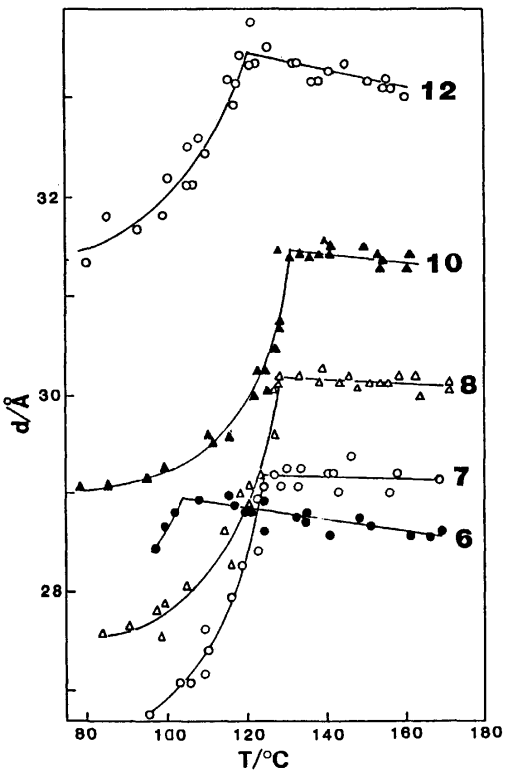

Fig. 2. Temperature dependence of interlayer distances of II-n (n=6, 7, 8, 10, and 12).

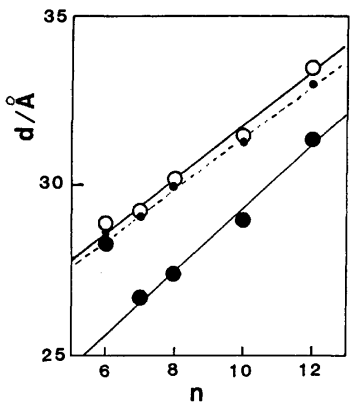

Fig. 3. Dependence of interlayer distances on the chain lengths. Open, filled (large), and filled (small) circles denote the d-values at solid (or Sm)-Sm*C, Sm*C-Sm A, and Sm A-chol. (or iso.), respectively.

paraffin chain is small, as mentioned above. The results are shown in Fig. 4. For the members with sufficiently wide temperature range of Sm*C, tilt angles are estimated to vary from 22—25 to 0° (assumed) with increase in temperature, approximately in accordance with a relation, $\theta \propto (T_c - T)^{\alpha}$, where T_c is Sm*C-Sm A transition temperature and α is estimated from the slope of relatively linear portions of the log-log plots ($T_c - T < 10$ K) to be 0.5±0.1. Similar temperature dependence of θ was generally observed for other Sm C or Sm*C adjacent to Sm A.[10]

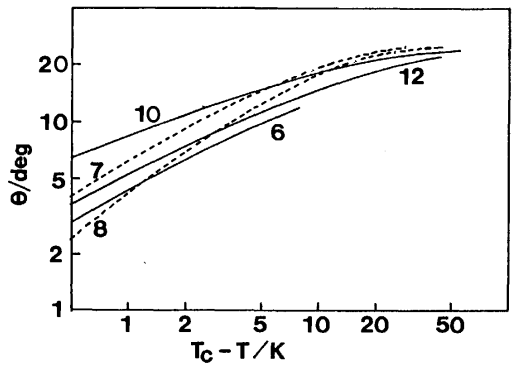

Fig. 4. Temperature dependence of tilt angles. T_c is Sm*C-Sm A transition temperature.

Selective reflection wavelengths were also measured to estimate helical pitches from the relation, $\lambda = \bar{n}p$, where λ is the wavelength, $\bar{n}$ is the average refractive index and p is the pitch. They are located in the IR region, while those of the series I were in the wavelengths of visible light.[11] Furthermore, they are less dependent on the chain lengths, especially in the lower temperature range (<100 °C), as shown in Fig. 5, than in the case of the series I with a remarkable

Table 3. Bond Lengths (Å) and Angles (°) of II-7 and II-8

Atom	II-7	II-8	Atom	II-7	II-8
O(1)-C(13)	1.209(9)	1.182(18)	C(1)-C(2)-C(3)	120.5(5)	116.9(12)
O(2)-C(13)	1.337(8)	1.352(16)	C(2)-C(3)-C(4)	120.7(5)	123.9(12)
O(2)-C(14)	1.406(8)	1.407(13)	C(3)-C(4)-C(5)	118.4(5)	116.3(11)
O(3)-C(1)	1.363(7)	1.363(15)	C(3)-C(4)-C(7)	120.4(5)	120.6(10)
O(3)-C(31)	1.417(10)	1.457(20)	C(5)-C(4)-C(7)	121.2(5)	123.0(10)
C(1)-C(2)	1.381(8)	1.380(17)	C(4)-C(5)-C(6)	120.4(5)	121.1(11)
C(1)-C(6)	1.395(8)	1.384(17)	C(1)-C(6)-C(5)	121.0(5)	119.0(11)
C(2)-C(3)	1.384(8)	1.391(19)	C(4)-C(7)-C(8)	120.6(5)	119.8(11)
C(3)-C(4)	1.386(8)	1.390(17)	C(4)-C(7)-C(12)	121.4(4)	120.5(10)
C(4)-C(5)	1.404(8)	1.408(17)	C(8)-C(7)-C(12)	117.9(5)	119.7(11)
C(4)-C(7)	1.518(7)	1.505(16)	C(7)-C(8)-C(9)	120.8(6)	117.4(11)
C(5)-C(6)	1.363(8)	1.388(18)	C(8)-C(9)-C(10)	120.9(7)	124.2(15)
C(7)-C(8)	1.391(8)	1.383(19)	C(9)-C(10)-C(11)	118.4(6)	117.0(11)
C(7)-C(12)	1.396(7)	1.407(16)	C(9)-C(10)-C(13)	118.3(6)	118.9(11)
C(8)-C(9)	1.378(10)	1.394(23)	C(11)-C(10)-C(13)	123.2(5)	124.2(11)
C(9)-C(10)	1.389(10)	1.388(20)	C(10)-C(11)-C(12)	120.6(5)	120.7(11)
C(10)-C(11)	1.392(8)	1.385(16)	C(7)-C(12)-C(11)	121.2(5)	120.7(11)
C(10)-C(13)	1.470(9)	1.453(17)	O(1)-C(13)-O(2)	122.1(7)	120.5(13)
C(11)-C(12)	1.371(8)	1.385(18)	O(1)-C(13)-C(10)	124.1(6)	126.4(13)
C(14)-C(15)	1.382(9)	1.384(16)	O(2)-C(13)-C(10)	113.7(6)	112.9(11)
C(14)-C(19)	1.379(8)	1.393(15)	O(2)-C(14)-C(15)	120.5(5)	116.2(9)
C(15)-C(16)	1.381(9)	1.393(17)	O(2)-C(14)-C(19)	119.2(5)	123.6(9)
C(16)-C(17)	1.389(9)	1.381(18)	C(15)-C(14)-C(19)	120.3(6)	120.1(10)
C(17)-C(18)	1.386(9)	1.389(17)	C(14)-C(15)-C(16)	120.0(6)	119.7(11)
C(17)-C(21)	1.520(13)	1.501(21)	C(15)-C(16)-C(17)	120.2(6)	120.2(12)
C(18)-C(19)	1.390(9)	1.383(16)	C(16)-C(17)-(18)	119.6(6)	120.1(11)
C(21)-C(22)	1.505(16)	1.525(23)	C(16)-C(17)-C(21)	119.0(7)	124.8(12)
C(22)-C(23)	1.513(21)	1.528(28)	C(18)-C(17)-C(21)	121.4(7)	115.1(12)
C(22)-C(25)	1.499(41)	1.496(31)	C(17)-C(18)-C(19)	120.1(6)	119.7(11)
C(23)-C(24)	1.498(40)	1.489(45)	C(14)-C(19)-C(18)	119.8(6)	120.2(10)
C(31)-C(32)	1.521(11)	1.462(23)	C(17)-C(21)-C(22)	116.6(9)	115.2(13)
C(32)-C(33)	1.520(13)	1.522(22)	C(21)-C(22)-C(23)	111.1(11)	109.6(15)
C(33)-C(34)	1.517(14)	1.499(23)	C(21)-C(22)-C(25)	104.0(17)	109.9(15)
C(34)-C(35)	1.516(14)	1.516(26)	C(23)-C(22)-C(25)	106.2(18)	109.8(17)
C(35)-C(36)	1.524(17)	1.515(35)	C(22)-C(23)-C(24)	115.2(18)	110.3(22)
C(36)-C(37)	1.508(23)	1.499(58)	O(3)-C(31)-C(32)	107.6(6)	107.1(13)
C(37)-C(38)	—	1.513(65)	C(31)-C(32)-C(33)	109.8(7)	110.3(13)
C(22)-C(25′)	1.73(12)	—	C(32)-C(33)-C(34)	114.8(8)	115.7(13)
C(13)-O(2)-C(14)	117.3(5)	116.8(9)	C(33)-C(34)-C(35)	114.9(8)	112.5(14)
C(1)-O(3)-C(31)	119.1(5)	119.9(11)	C(34)-C(35)-C(36)	109.9(9)	109.9(17)
O(3)-C(1)-C(2)	125.9(5)	124.2(11)	C(35)-C(36)-C(37)	112.4(12)	112.7(27)
O(3)-C(1)-C(6)	115.3(5)	113.6(10)	C(36)-C(37)-C(38)	—	111.7(37)
C(2)-C(1)-C(6)	118.8(5)	122.2(11)	C(21)-C(22)-C(25′)	121(7)	—

Table 4. Torsion Angles (°)

	II-7	II-8
Phenyl ring		
Ring(C 1—C 6)-Ring(C 7—C12)	4.1	6.7
Ring(C 7—C12)-Ring(C14—C19)	68.2	69.4
Alkyl chain		
O(3)-C(31)-C(32)-C(33)	190.4	180.1
C(31)-C(32)-C(33)-C(34)	194.3	179.9
C(32)-C(33)-C(34)-C(35)	−55.2	66.5
C(33)-C(34)-C(35)-C(36)	187.3	164.8
C(34)-C(35)-C(36)-C(37)	179.7	151.9
C(35)-C(36)-C(37)-C(38)	—	194.7

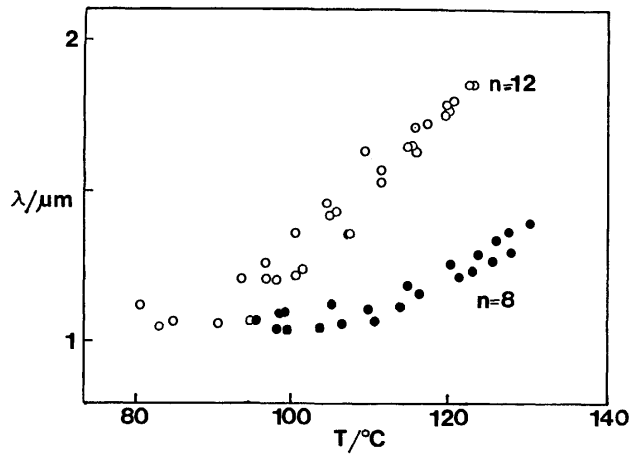

Fig. 5. Temperature dependence of selective reflection wavelengths of II-8 and II-12.

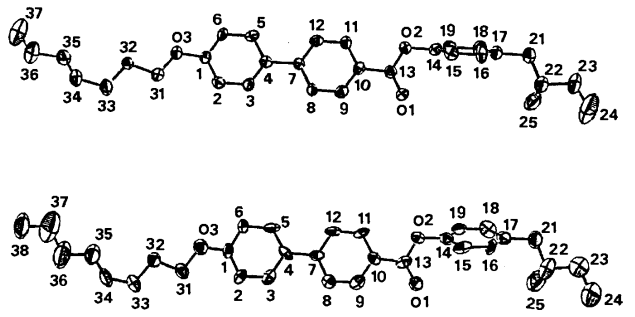

Fig. 6. ORTEP views of the molecules of II-7 (upper) and II-8 (lower) with 50% probability thermal ellipsoids. Only one of the two conformers of the disordered part is shown for simplicity.

dependence on the chain length.[4] A pitch increases with increase in temperature near the Sm*C-Sm A transition point and the increase is more rapid for a longer member.

Molecular Conformations in the Crystals. The ORTEP drawings[12] of the molecular conformations with numbering schemes are shown in Fig. 6. All the bond lengths and angles are compatible with those found in other mesogens,[1] as shown in Table 3. All the phenyl rings are planar within the experimental error. Table 4 shows torsion angles. The conformations of II-7 and II-8 are very similar to each other:

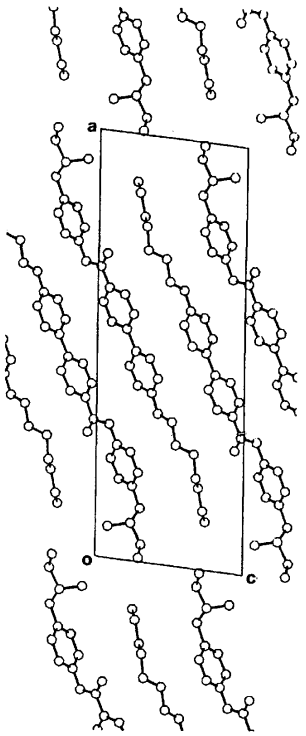

Fig. 7. Crystal structure of 11-7 viewed along the b axis.

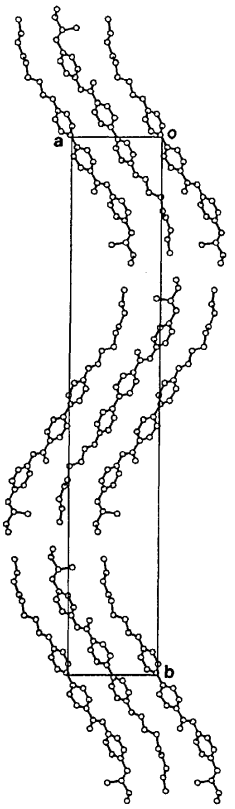

Fig. 8. Crystal structure of II-8 viewed along the c axis.

approximately coplanar biphenyl moieties and paraffin chains with the twisted C(32)-C(33)-C(34)-C(35) moieties. The twisted chains result in straight rod-

shaped molecules as a whole. For II-7, the C(25) atom is slightly disordered.

Crystal Packing. Figures 7 and 8 show the crystal structures of II-7 and II-8, respectively. Both crystals have distinct layer structures, whose layer planes are parallel to (100) plane (II-7) and (010) plane (II-8). Such layer structures were also observed in other smectogens. Structures within a layer are also strikingly similar, composed of the rod-shaped molecules described above. Intermolecular relation except the "extra" C(38) is almost the same in spite of the difference in the chain length. The whole molecule including a normal paraffin chain relates to the lateral packing in the layer, in contrast to the case of the series I, in which paraffin chains have contacts with each other between layers.[1] These facts suggest that interaction between core parts is more dominant in the crystal packing of the series II than that of the series I. This results in a large extent of molecular overlapping within a layer, leading to distinct layer structures with a small tilt angle (30°).

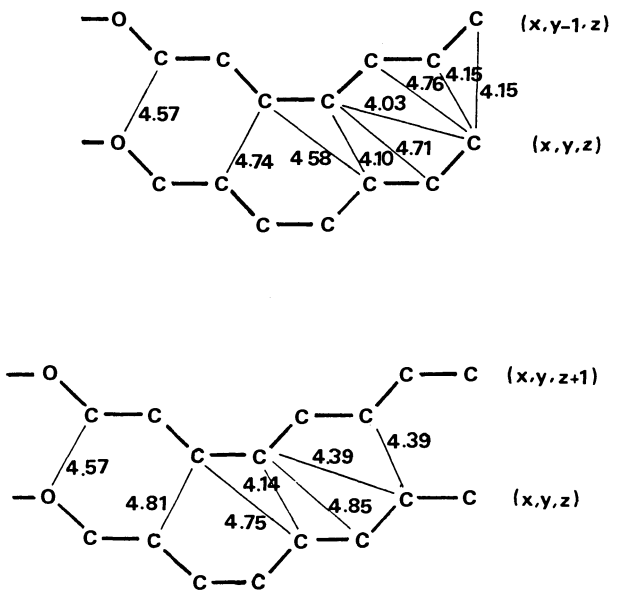

Fig. 9. Interchain distances (Å) of II-7 (upper) and II-8 (lower). Symmetry codes are shown in parentheses.

Figure 9 shows interchain distances. The chains make contacts each other only within a layer. Most of the distances are remarkably longer than those of interlayer chain contacts in the series I. This also suggests that interaction between cores is dominant in the series II.

The phenyl rings of adjacent molecules have nonparallel contacts as found in the I crystals. The angles between the mean planes are 67° (II-7) and 66° (II-8).

The II-7 crystal has a uniform direction of molecular tilt throughout layers, while in the II-8 crystal molecules have two opposite tilt direction alternately from layer to layer. This difference is regarded as induced by a small interlayer interaction in these crystals, since the two crystals of the series I with close contacts of paraffin chains between layers showed similar modes of layer stacking to each other. Both arrangements are known as polytypes for normal long-chain compounds and energy difference is reported to be very small; an alternate arrangement was evaluated to be more stable than a uniform one by 0.73 kJ mol^{-1} for octadecanoic acid.[14] In the present case, less penetration of chains into an adjacent layer in II-8 means less interlayer interaction than in II-7, corresponding to the lower melting point as described above.

Discussion

A relationship between the mesophase structures and the crystal structures are shown schematically in Fig. 10. The tilt angle in the crystals (30°) is closely related to that (22—25°) at the lowest temperature in Sm*C. This suggests that molecular rearrangements at the cryst.-Sm*C transition point are not large in spite of the large enthalpy of transition, as in the case of the series I. Nonparallel contacts of the phenyl rings would enable the molecules to begin to rotate at the melting points, leading to the direct transition to Sm*C. The transition is supposed to be caused by loosening of the core-core interaction, because the contacts of normal alkyl chains within a layer are

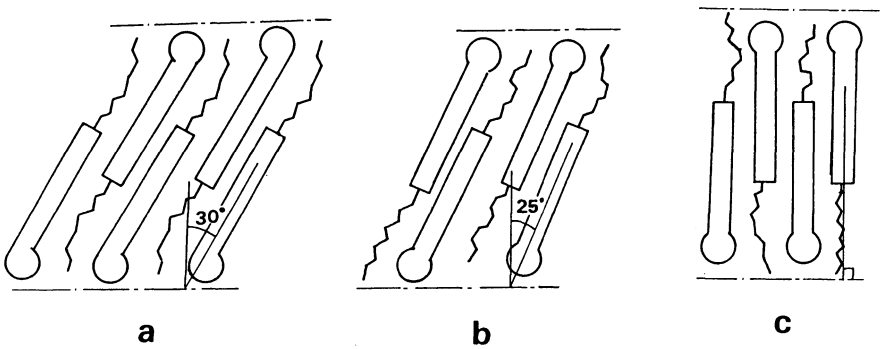

Fig. 10. Schematic diagrams of the structures of the crystal (a), Sm*C (b), and Sm A (c).

loose enough in the crystalline states. On the other hand, molecular overlapping in the layer is much larger than that in the series I. Besides, the interlayer aggregation of the paraffin chains observed in the series I, which was proposed to keep the tilt angles constant, is not found in the series II. Therefore, the molecules gradually change the tilt angles to zero with keeping layer structures; i.e. Sm*C transforms to Sm A. Paraffin chains have a twisted form even in the crystalline states. This corresponds to the small change of their contribution to the layer thickness throughout the Sm*C and Sm A phases, while in the series I, the large change of the paraffin chain organization in the Sm*C was interpreted as the melting process of the chains which are regularly organized in the crystalline states.

Interlayer interaction in the series II is found to be much less than in the series I. This fact seems to be related to the fact that helical pitches in the series II are larger than those in the series I and they are less dependent on the chain lengths. However, further investigation for more variety of compounds would be required to confirm the relationship between the helical pitch and the interlayer interaction.

It is concluded that the mesophase behavior of Sm*C between crystalline and Sm A phases is well interpreted by the intermolecular interaction revealed in the crystal sturctures, as in the case of Sm*C between crystalline and cholesteric phases.

The authors express their thanks to Professor Naoyuki Koide of Science University of Tokyo for DSC measurements and BDH Chemicals Ltd. for supplying the chiral phenol. This work was partially supported by a Grant-in-Aid for Scientific Research No. 60540280 from the Ministry of Education, Science and Culture.

References

1) K. Hori and Y. Ohashi, *Bull. Chem. Soc. Jpn.*, **61**, 3859 (1988).

2) J. W. Goodby and T. M. Leslie, *Mol. Cryst. Liq. Cryst.*, **110**, 175 (1984).

3) G. W. Gray and J. W. Goodby, "Smectic Liquid Crystals," Leonard Hill, Glasgow (1984), p. 54.

4) K. Hori, *Mol. Cryst. Liq. Cryst.*, **123**, 321 (1985).

5) P. Main, S. E. Hull, L. Lessinger, G. Germain, J.-P. Declercq, and M. M. Woolfson, MULTAN78. A System of Computor Programs for the Automatic Solution of X-ray Diffraction Data. Univs. of York, England and Louvain, Belgium (1978).

6) G. M. Sheldrick, SHELX76. A Program for Crystal Structure Determination. Univ. of Cambridge (1976).

7) "International Tables for X-ray Crystallography," Birmingham, Kynoch Press (1974), Vol. IV.

8) The tables for the anisotropic temperature factors for non-hydrogen atoms, the tables for the atomic parameters for the hydrogen atoms and the F_o-F_c list are deposited as Document No. 8875 at the Office of the Editor of the Bulletin of the Chemical Society of Japan.

9) G. W. Gray and J. W. Goodby, *Mol. Cryst. Liq. Cryst.*, **37**, 157 (1976).

10) J. Doucet, A.-M. Levelut, and M. Lanbert, *Mol. Cryst. Liq. Cryst.*, **24**, 317 (1973); Ph. Martino-Lagarde, R. Duke, and G. Durand, *Mol. Cryst. Liq. Cryst.*, **75**, 249 (1981).

11) G. W. Gray and D. G. McDonnell, *Mol. Cryst. Liq. Cryst.* **37**, 189 (1976).

12) C. Johnson, ORTEP. Report ORNL-3794, Oak Ridge National Laboratory, Tennessee (1965).

13) P. Mandal, S. Paul, H. Shenk, and K. Goubitz, *Mol. Cryst. Liq. Cryst.*, **135**, 35 (1986).

14) M. Kobayashi, T. Kobayashi, Y. Cho, and F. Kaneko, *Makromol. Chem., Macromol. Symp.*, **5**, 1 (1986).

Metal Colloids Produced by Means of Gas Evaporation Technique. V. Colloidal Dispersion of Au Fine Particles to Hexane, Poor Dispersion Medium for Metal Sol

Naoki SATOH† and Keisaku KIMURA*
Instrument Center, Institute for Molecular Science, Myodaiji, Okazaki, Aichi 444
†Kao Institute for Fundamental Research, 1334 Minato, Wakayama, Wakayama 644
(Received December 14, 1988)

Metal fine particles are not dispersed at all in pure solvents with a low dielectric constant, such as hexane. The gas flow-cold trap method combined with surfactants was found to be effective in stabilizing ultrafine metal particles in solvents with a low dielectric constant. Ultrafine gold particles can be stably dispersed in hexane in a colloidal state by this method. It was found that the stabilizability of the colloid depends on the ionic types of the surfactant. Thus, a cationic surfactant such as dimethyldioctadecylammonium chloride (DOAC) shows good dispersibility, whereas an anionic surfactant such as 1,2-bis(2-ethylhexyloxycarbonyl)ethanesulfonate (AOT) dose not. The optical spectra of colloid solutions suggest a difference in the local colloidal state between two types of surfactants. Colloidal solutions of a gold fine particle/DOAC/hexane system are so stable against heating or drying that the solvents are easily substituted.

In a coagulated metal ultrafine particle (UFP), the wave function of conduction electrons is presumed to diffuse between metal UFP's. The physical characteristics resulting from the electronic state of each metal UFP can be modified through this contact and be changed close to that of bulk materials according to the degree of contact.[1] On the contrary, metal UFP's in dispersions are expected to give physical properties and structural information concerning individual metal UFP more delicately than that in coagulation. We initiated a series of studies[2-5] in order to characterize the features of isolated metal UFP's dispersed into the liquid phase. In general, however, the preparation of stable dispersions of metal UFP in an organic liquid is difficult.

Some approaches to obtain stable dispersions of metal UFP have already been reported by several authors. The vacuum evaporation on running oil substrate (VEROS) method[6] is one of the available approaches for the preparation of dispersions of metal UFP. However, a severe restriction is imposed on the selection of solvents, i.e. oil with a very low vapor pressure must be selected. The chemical reaction method in a liquid phase is also a well-known technique in colloid chemistry for obtaining metal UFP dispersions.[7] However they are restricted to being almost only aqueous dispersions. Furthermore, several kinds of by-product, such as ions, remain in the solutions. The surface of metal UFP in these dispersions cannot be clearly defined because of considerable modifications, such as oxidation or chemisorption of several kinds of compounds. These techniques are, hence, not suitable for our purpose.

The authors have reported on methods for obtaining stable dispersions of UFP in pure organic liquids.[2] These methods were based on the evaporation technique in flow gas combined with matrix isolation techniques using frozen organic solvents (the gas flow-cold trap method) or cooled organic liquids (the gas flow-solution trap method) as a matrix. According to the combination of solvents with a high dielectric constant and metals with a high electron affinity, stable colloidal dispersions can be obtained by this method.[8] However, it is difficult to prepare stable dispersions for solvents with a low dielectric constant. We report here a method for obtaining stable colloidal dispersions of metal UFP in organic solvents with a low dielectric constant, employing the gas flow-cold trap method with the cationic surfactant of dimethyldioctadecylammonium chloride (DOAC). We tested the validity of this method with gold fine particles and hexane as the dispersed phase and dispersion medium, respectively. The surfaces of gold fine particles are considered to be free from oxidation, and hexane is one of the most poor solvents with respect to the formation of stable colloidal dispersions of metal UFP.[8] The colloidal solutions obtained by this method were found to be quite stable against such thermal processing as increasing temperature or freezing. Further, it was found that stable colloidal solutions are readily reproduced by exchanging the dispersion media after the drying process.

Experimental

Materials. Pure (99.99%) pieces of gold were purchased from Tanaka Kikinzoku Kougyou company. The dispersibility of the fine particles was examined for different types of surfactants, i.e. DOAC as a cationic surfactant and AOT (Aerosol OT, sodium 1,2-bis(2-ethylhexyloxycarbonyl)-ethanesulfonate) as an anionic surfactant. Both surfactants were of guaranteed grade and purchased from Tokyo Kasei Ltd. AOT was purified by a method reported by Kunieda et al.[9] A benzene solution of 15% AOT was washed three times with distilled water to remove water-soluble impurities. After evaporating benzene, AOT was dissolved into a 25% aqueous methanol solution and washed three times with petroleum ether to remove oil-soluble impurities. The solvents were removed by evaporation for 12

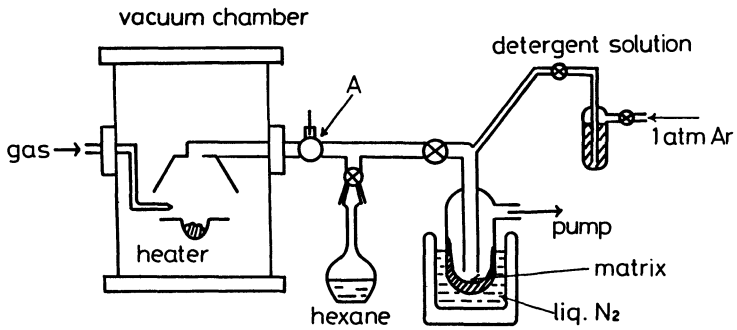

Fig. 1. The apparatus for the gas flow-cold trap method. Gas phase sampling of fine particles was performed at the point A by exposing Cu mesh with evaporated carbon film to the flow of carrier gas.

hours. AOT was then dissolved into methanol and shaken with hexane. Finally, AOT in the hexane phase was extracted and evacuated again for 12 hours. DOAC was recrystallized three times from dehydrated acetone and evacuated to dryness for 12 hours. Hexane solutions of both 0.1 wt% AOT and 0.01 wt% DOAC were prepared for the experiments. Since DOAC was hardly soluble in hexane, a cationic surfactant of (2-dodecylhexadecyl)trimethylammonium chloride (g-C28TAC)[10] was used for concentrated samples after the same purification process as DOAC. The solubility of g-C28TAC is sufficiently high due to a branched alkyl chain in this compound. g-C28TAC was kindly supplied by Mr. Kazuyuki Yahagi of Tokyo research laboratories, Kao corporation.

Preparation of Au UFP/Hexane Colloidal Solution. Au fine particles were formed and collected by the gas flow-cold trap method.[2] Figure 1 shows a schematic diagram of this method. The chamber was evacuated to 5.0×10^{-6} Torr prior to the introduction of inert gases (1 Torr≈133.322 Pa). The constant flow of He as a surrounding gas and Ar as a carrier gas were supplied around the heater. The particles in the gas stream were led to the trap which was cooled by liquid N_2. The partial pressures of He and Ar were 8 and 2 Torr, respectively. Purified and degassed hexane was vaporized into the gas stream from the chamber to the trap. Under an atmosphere of constant-flow inert gases, pieces of gold were heated in a tungsten wire heater and the UFP's produced were led to a frozen hexane matrix in the trap. After the accumulation of a sufficient amount of gold fine particles, liquid N_2 was removed. As soon as the matrix surface began to melt, a detergent solution was introduced on the matrix surface and the trap was filled with Ar gas at atmospheric pressure. Then, the trap was irradiated by ultrasonic waves. This ultrasonic wave treatment was continued for more than 5 minutes after a full melting of the matrix.

Characterization of Colloidal Solutions. The size distributions and the states of contact of UFP's were determined by a Hitachi H-500H type transmission electron microscope (TEM) of the laboratory of electron microscopy, the National Institute for Physiological Sciences at Okazaki. Specimens for TEM were obtained by dropping sample solutions on Cu grids coated by carbon film of 8 nm thickness. In order to obtain the size distribution of Au fine particles in the gas phase, Au fine particles were sampled at point A in Fig. 1, the location of which was the midpoint of the vacuum chamber and the solvent pool. A sample mesh for the electron microscope was exposed to the flow of the fine particles for about 1 second. The size distributions of Au fine particles were determined by TEM photographs using an Image analyzer (Kontron IBAS-1 of the Center for Analytical Instrument, the National Institute for Basic Biology at Okazaki).

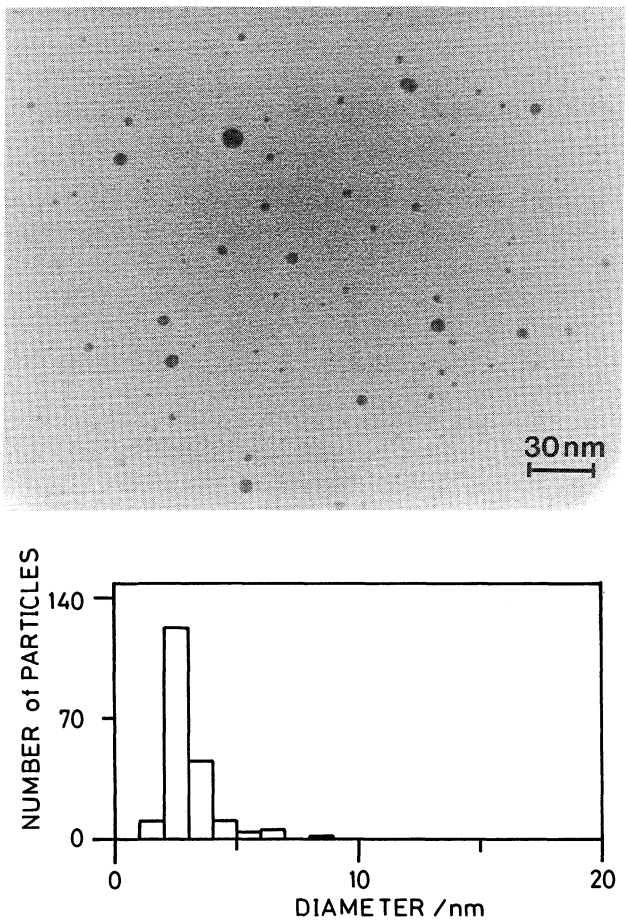

Fig. 2. (a) TEM micrograph of Au UFP's sampled in gas phase. The exposure time was about 1 second. (b) Size distribution of picture (a).

Optical measurements were carried out using a Varian Cary 2300 spectrophotometer. The absorption spectra were

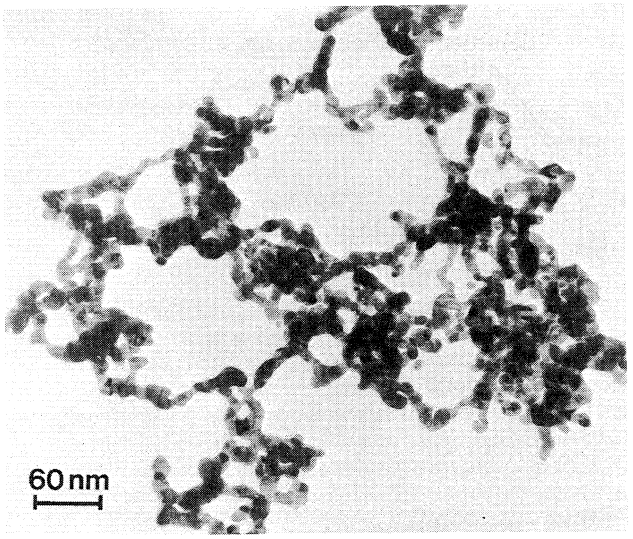

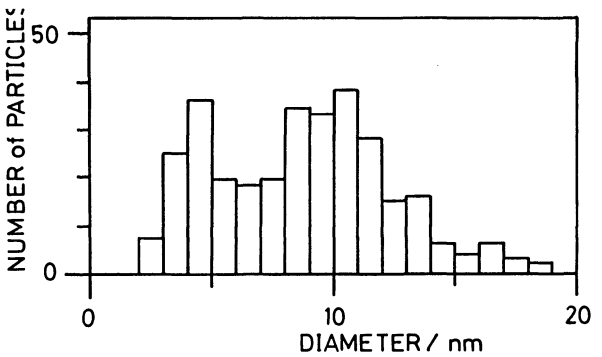

Fig. 3. (a) TEM micrograph of precipitates of Au UFP's deposited from hexane. (b) Size distribution of picture (a).

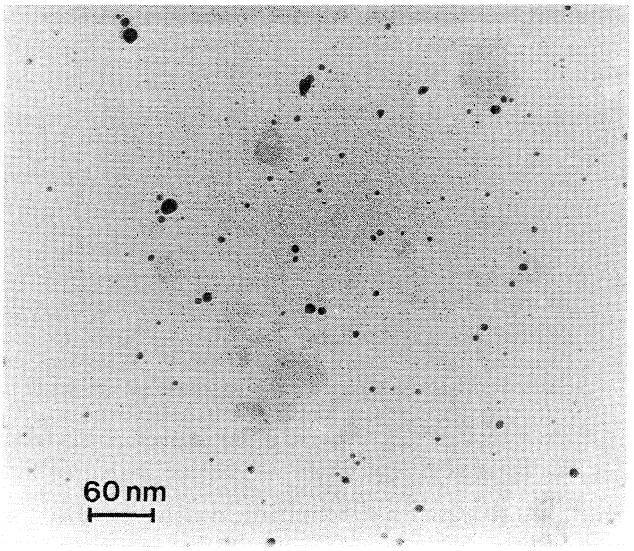

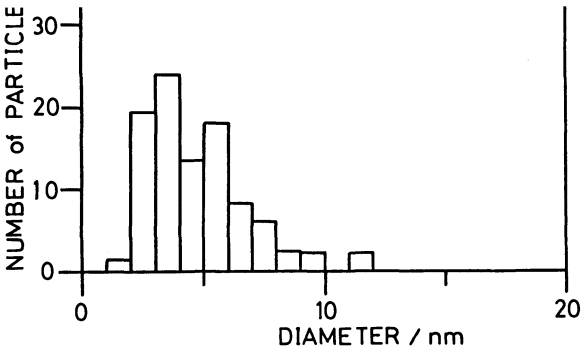

Fig. 4. (a) TEM micrograph of Au UFP's deposited from colloid solution of Au UFP's/DOAC/hexane system. (b) Size distribution of picture (a).

recorded at room temperature just after the preparation of a colloidal solution. A conventional quartz cell was used.

Results

Figure 2(a) shows an electron micrograph of the particles sampled in the gas phase. A number of particles of about 2.5 nm in diameter can be seen in the photograph. The smallest particles are less than 1.0 nm. Figure 2(b) shows the size distribution determined from this picture. It can be seen that the evaporation method with a flow gas provides a size distribution with a sharp single peak. The maximum of this distribution curve was 2.5 nm. As reported in Ref. 5, almost all kinds of metallic fine particles, including Au, do not disperse in hexane at all without surfactants. Au fine particles coagulated as soon as the melting of a matrix and precipitated and were deposited within a few minutes. Figure 3(a) shows a TEM picture of these precipitates just after an ultrasonic treatment. Fine particles come into contact with each other to form larger aggregates. The boundaries of constituent particles become indistinct. It seems that particles coalesce to each other to some extent. A typical size-distribution curve of the system of Au UFP/hexane is shown in Fig. 3(b). Compared with a size histogram of these particles with those in the gas phase, it is easy to realize that further growth by coalescence proceeded in complex ways.

The effect of DOAC on the dispersibility of Au UFP is apparent. The colloidal solution prepared by the method described in the experimental section was colored rose-red and transparent, and scattering light through the solution was hardly observable in the visible region. A TEM picture of this solution is shown in Fig. 4(a). Most of the fine particles are observed in isolation in any photogram image. The diameter of the smallest particle observed in this figure is less than 1.0 nm, which is comparable to the size of particles sampled in the gas phase. Figure 4(b) shows a typical size histogram of Au fine particle/DOAC/hexane system. The maximum peak of this histogram is located at nearly the same place as those in the gas phase; however, the width of this histogram is somewhat larger. This fact means that coalescence growth can not be completely avoided, even when

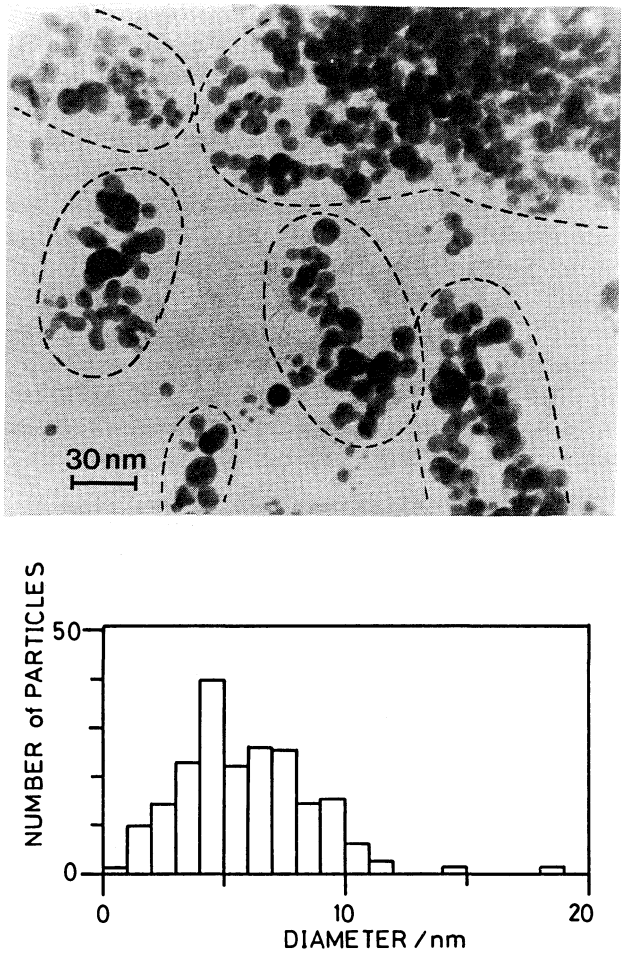

Fig. 5. (a) TEM micrograph of Au fine particles deposited from colloid solution of Au UFP's/AOT/hexane system. The encircled regions by broken lines represent the examples of aggregation unit of densely packed Au UFP's. (see discussion). (b) Size distribution of picture (a).

using the present method.

The effect of surfactants on the dispersibility of Au UFP depends on the ionic types of the hydrophilic part. The solution of the Au fine particle/AOT/hexane system is colored blue and is transparent just after the melting of the matrix. However, the colloidal dispersion of this solution is not stable. The Au UFP/AOT complexes fully precipitate within a few hours. Figure 5(a) shows a TEM picture of this system, sampled just after an ultrasonic treatment. The fine particles in this picture are anisotropic and irregular in shape more than those in Fig. 4(a). As is discussed later, this fact implies that the original Au UFP coalesce in an AOT/hexane system to a greater degree than in a DOAC/hexane system. However, it is worth noting that coalescent growth stopped at some stage. The boundaries of grown Au UFP can clearly be seen. From the size distribution of this colloidal system (Fig. 5(b)), one recognizes that AOT is also effective in preventing the coalescence growth process of fine particles to some extent, though coagulation does takes place.

Discussion

The size distributions of UFP strongly depend on the particle growth mechanism. Two growth processes have been proposed, i.e., the absorption and the coalescence growth processes.[5,11] In the absorption process, particle nuclei grow along with the absorption of metal atoms. The size distribution curve in this case is the normal distribution. In the coalescence growth process, however, particles grow by collisions of small clusters and the size distribution is the log-normal distribution. Graphical analyses make it possible to determine which mechanism takes place. Figure 6 shows logarithmic probability analyses of our samples. If the size distribution of particles is a log-normal one, a linear correlation is obtained between the cumulative percentage of particles with a certain size and the logarithm of the size of particles in a logalithmic probability plot. The size distribution of the gas-phase-particles by the gas-flow method is found to follow a log-normal distribution, as shown in Fig. 6. This is a rather surprising fact, since the coalescence growth process was derived by assuming a stationary state, whereas in the gas-flow method particles grow within a turbulent gas stream. The size distribution of a Au UFP/DOAC/hexane system also provides a linear correlation in the log-probability plot. In this case, the original features of the size distribution basically remained unchanged. The size distribution of a Au UFP/AOT/hexane system, how-

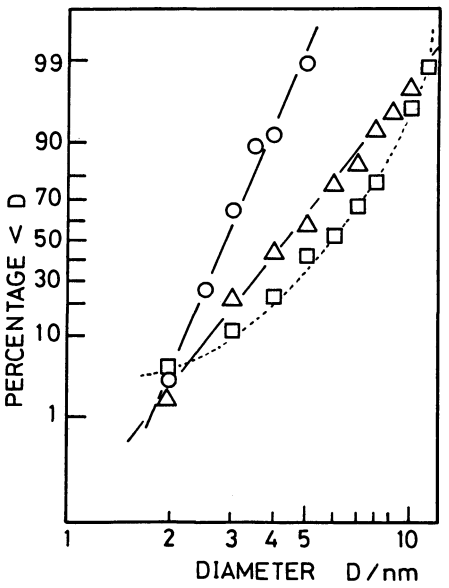

Fig. 6. Logarithmic probability plot of the size distribution of Au UFP's sampled from the gas phase (○), Au UFP/DOAC/hexane solution (△), Au UFP/AOT/hexane solution (□). The ordinate indicates the cumulative percentage of particles with diameters smaller than *D*.

ever, changes slightly from the log-normal distribution. This implies that particles in a Au UFP/AOT/hexane system grew in a more complex manner than in the Au UFP/DOAC/hexane system.

The optical properties of a colloidal solution sensitively reflect the dispersion state of the colloid, as was fully described by Kreibig.[12] He discussed and analyzed the visible absorption spectra of Au UFP taking into account the topography of the particle assembly, and introduced the fractal dimension as a relevant parameter for characterizing the metal UFP aggregate system.[13] Figure 7 shows the absorption spectra of (a) Au UFP/DOAC/hexane and (b) Au UFP/AOT/hexane solutions (those in Figs. 4 and 5, respectively) measured just after the ultrasonic treatment. The absorption spectra were characterized by a peak at 520 nm for (a) and 600 nm for (b), whereas a shoulder at 270 nm and an abrupt rise below 210 nm for both. The absorption spectrum in the visible region is mainly attributed to the surface plasma absorption of free electrons,[14] which has been well studied and is understood[15,16] in terms of Mie's scattering theory,[17] combined with Drude's free electron model. The ultraviolet spectrum reflects d-s interband transitions, the threshold of which is 2 eV.[14,15,18,19] The theoretical absorption spectra of a Au colloid solution was calculated according to the method of Doremus, in which the homogeneous dispersion was treated[15] within the framework of Mie's theory. Good agreement between the calculated and experimental absorption spectra was obtained in the case of the Au UFP/DOAC/hexane colloidal solution. This implies that DOAC is capable of dispersing Au UFP's ideally in hexane. This is not true for AOT. In the light of the classical free electron model for metal UFP, the maximum wavelength of a plasma absorption peak does not shift with the size of UFP when the size of the particles are sufficiently smaller than the wavelength, while the height and width of the peak are sensitive to the size.[15] Therefore, the differences in the average sizes and or the size distributions between Au UFP's of Au UFP/DOAC/hexane and of Au UFP/AOT/hexane systems could not explain the shift of the peak position from 520 to 600 nm (Fig. 7). A surface plasma peak is known to shift to the longer wavelength and to broaden when a volume fraction of colloid particles increases due to a dipolar interaction.[16,20,21] Since the total volume fraction of Au particles was nearly the same for both samples, the peak shift and broadening of the spectra must be explained in terms of the difference in the local colloidal state of the solutions. Actually, it is reported that a plasma resonance peak shifts to a longer wavelength and broadens when the colloid systems consist of well separated aggregates of densely packed particles.[12] In the TEM images of a Au UFP/AOT/hexane system, most particles are observed in aggregates of several tens or several hundreds of nanometers. An example of these units of aggregate is shown in Fig. 5(a). In the Au UFP/AOT/hexane colloidal system it is reasonably understood from the instability of the colloidal state that Au UFP's tend to form aggregates including AOT, even immediately after the matrix melts. The specificity to the ionic type of surfactants (i.e., the cationic surfactant disperses Au UFP's well, while the anionic surfactant does not) suggests a difference in the affinities of the surfactant to the surfaces of the Au UFP's between a cationic and an anionic surfactant. However, it is not clear at present why Au UFP's prefer DOAC to AOT. Further experiments for understanding the microscopic mechanism of the adsorption of the surfactants to the surfaces of Au UFP's are currently under way.

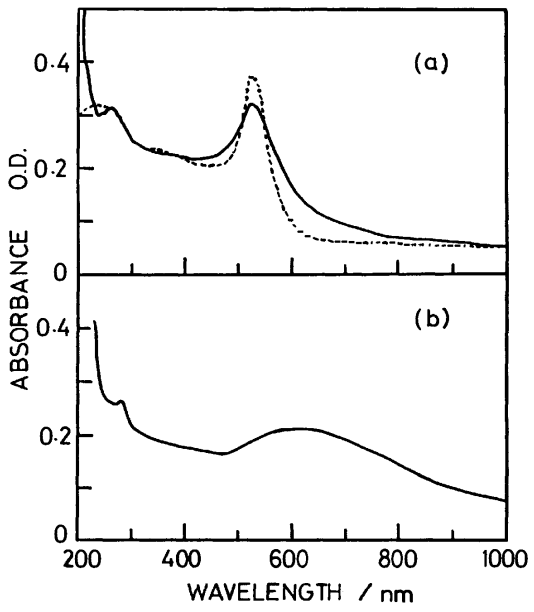

Fig. 7. (a) Optical absorption spectra of calculated (broken line) and Au UFP/DOAC/hexane colloidal solution (solid line). The calculated line was obtained from the first approximation of Mie's theory ($D \ll \lambda$; where D is diameter of UFP, λ, wavelength of light) using complex dielectric constants of Ref. 14.[15] (b) Absorption spectrum of Au UFP/AOT/hexane colloidal solution obtained just after the ultrasonic treatment.

When a Au UFP/DOAC/hexane solution is concentrated by evaporation, a phase separation occurs and Au UFP's precipitate with DOAC. It seems that the maximum concentration of Au UFP's in hexane is determined by the solubility of the surfactant into hexane. g-C28TAC, which has a much higher solubility in hexane than does DOAC due to the branched alkyl chain, is capable of stabilizing Au UFP's with more than a 100-times higher concentration.

The colloidal solutions stabilized by these cationic surfactants are quite stable against the passage of time, thermal processes (to the boiling point of hexane) and drying. In particular, the stability against drying makes it possible to exchange the type of solvent.

Hexane can be substituted for organic solvents with a dielectric constant less than ca. 10. The remarkable features of a colloidal solution of metal UFP's using a cationic surfactant for both the stability and changeability of the solvents are advantageous for future applications.

References

1) K. Kimura, *Jpn. J. Appl. Phys.*, series 1 Superconducting Materials., **1988**, 140.
2) K. Kimura and S. Bandow, *Bull. Chem. Soc. Jpn.*, **56**, 3578 (1983).
3) K. Kimura, *Bull. Chem. Soc. Jpn.*, **57**, 1683 (1684).
4) K. Kimura and S. Sako, *Chem. Lett.*, **1984**, 973.
5) K. Kimura, *Bull. Chem. Soc. Jpn.*, **60**, 3093 (1987).
6) S. Yatsuya, T. Hayashi, H. Akoh, E. Nakamura, and A. Tasaki, *Jpn. J. Appl. Phys.*, **17**, 355 (1978).
7) For example, B. Jirgensons, and M. E. Straumanis, "A Short Textbook of Colloid Chemistry," 2nd ed., Pergamon Press Ltd., England (1962).
8) N. Satoh, S. Bandow, and K. Kimura, *J. Colloid Interface Sci.*, in press (1989).
9) H. Kunieda and K. Shinoda, *J. Colloid Interface Sci.*, **70**, 577 (1979).
10) K. Yahagi, N. Hoshino, and H. Hirota, Preprint of 15th IFSCC International Congress, **1**, 71 (1988).
11) G-Hanne Comsa, *J. Phys. (Paris)*, **C2**, 185 (1977).
12) U. Kreibig, *Z. Phys.*, **D3**, 239 (1986).
13) D. Schonauer and U. Kreibig, *Surf. Sci.*, **156**, 100 (1985).
14) H. Abe, K.-P. Charle, B. Tesche, and W. Schulze, *Chem. Phys.*, **68**, 137 (1982).
15) R. H. Doremus, *J. Chem. Phys.*, **40**, 2389 (1964).
16) G. C. Papavassiliov, *Prog. Solid State Chem.*, **12**, 185 (1979).
17) G. Mie, *Ann. Phys.*, **25**, 377 (1908).
18) P. B. Johnson and R. W. Christy, *Phys. Rev. B*, **6**, 4370 (1972).
19) R. Lasser, N. V. Smith, and R. L. Benbow, *Phys. Rev. B*, **24**, 1895 (1981).
20) J. C. Maxwell-Garnett, *Philos. Trans. Royal Soc. London.*, **203**, 385 (1904); **205**, 237 (1906).
21) R. W. Cohen, G. D. Cody, M. D. Coutts, and B. Abeles, *Phys. Rev. B*, **8**, 3689 (1973).

Light-Induced Oxidative Deposition of Polypyrrole on the Back Surface in the Dark of n-Type Silicon Wafer Photocatalysts

Hiroshi YONEYAMA,* Yoshihiro SHOJI, and Kei-ichi SUZUKI
Department of Applied Chemistry, Faculty of Engineering, Osaka University,
Yamada-oka 2-1, Suita, Osaka 565
(Received December 22, 1988)

A variety of surface conditions of n-type Si wafers were prepared by etching for different time damaged surfaces that were prepared by lapping with emery papers, and the effect of flaws in the wafer surfaces on photocatalytic deposition behaviors of polypyrrole and silver from acetonitrile containing pyrrole and $AgClO_4$ was investigated. It was found that if the front surface of the wafer to be illuminated contained a fairly high amount of defects and the back surface in the dark was defect-free, oxidative polymerization of pyrrole occurred on the back surface in the dark with the simultaneous deposition of silver on the front surface as long as the diffusion length of positive holes is greater than the thickness of Si wafers.

Flaws in semiconductor surfaces play an important role in semiconductor photocatalysis.[1-3] For example, high photocatalytic activities of n-type single crystal wafers appear when their illuminated surfaces are well-etched and their back surfaces in the dark are heavily damaged. The flaws have both favorable and unfavorable effects in semiconductor photocatalysis. The favorable effect is that the flaws produce in the forbidden zone of semiconductors intermediate energy states which serve as channels for transferring photogenerated electrons from the conduction band to electron scavengers in solution under upward bending of the bands,[1,4] while the unfavorable effect is that the flaws work as the recombination centers.[5-7]

Then it will be of interest to investigate how greatly the apparent photocatalytic activities of semiconductors are affected by changing the abundance of flaws either in illuminated front surfaces or in the back surfaces in the dark, or in both. The present study has been initiated to investigate this subject using n-type Si wafers. The reaction system chosen here was simultaneous deposition of polypyrrole and silver from acetonitrile containing pyrrole and silver perchlorate.[2,8] By using this reaction system, the effective cathodic sites and photoanodic sites of semiconductor surfaces can be recognized by observing the places where the silver and polypyrrole deposition take place, respectively. It will be shown that under special configurations of the front and back surfaces of the n-type Si wafers the positive hole-consuming polypyrrole deposition evidently takes place on the back surface of n-type Si wafers in the dark as a result of effective supply of the positive holes by diffusion only.

Experimental

n-type Si single crystal wafers were purchased from Osaka Titanium Co. Except where specially noted, the experiments were carried out using wafers of 0.6 mm thickness and of 2.4 Ω cm resistivity. The surface of the wafers was polished to mirror finish by the manufacturer. This surface is denoted here as mirror-finished surface. The mirror-finished surface was lapped with No. 500 emery papers when it was intended to prepare defect-containing surfaces. The surface prepared by this damaging is denoted here as damaged surface. The flaws produced in this way must have had the depth comparable to the particle size of the abrasives which was judged to be 34 μm on average.[9] The damaged surface was etched in a mixture of 1 part of 46% HF and 20 parts of 61% nitric acid for different time to remove the defects to different degrees. The etching rate was reported to be 13 $\mu m\ min^{-1}$ [10] for this etchant.

For the photocatalytic deposition experiments, edges and undesired parts of the Si wafers were coated with polyfluoroethylene oligomer (Difloil, #200, Daikin Industries), and after mounting in a flexible plastic frame, the Si wafers were hung in a deposition bath which consisted of 0.1 M pyrrole and 0.1 M $AgClO_4$ (1 M=1 $mol\ dm^{-3}$) dissolved in acetonitrile. For electrochemical experiments, the back face of the Si wafers was pasted by a Ga-In alloy to make ohmic contact where an electrical lead wire was attached with Dupont conducting silver paint. The Si wafer was then mounted in a Teflon electrode holder. The surface exposed to electrolyte solutions was 7 mm diameter.

Just prior to both photocatalytic experiments and photoelectrochemical experiments, the Si was immersed in 46% HF for more than 30 min to remove surface oxide films, followed by washing in a stream of deionized water. The electrolyte solutions and the deposition bath were bubbled by argon for more than 20 min to purge dissolved oxygen. The electrolytic cell had one compartment with a quartz window for illumination of the electrode. Cyclic voltammograms were obtained with the use of a potentiostat (Nikko Keisoku, DPGP-1), a potential sweeper (Nikko Keisoku, NPS-2) and an X-Y recorder (Yokogawa, Type 3077). The electrolyte solutions were prepared from re agent grade chemicals.

Illumination of the Si wafers was carried out using either a 500 W xenon lamp (Ushio, ULX-500-O) or a 25 mW He-Ne laser (NEC, GLG-5700). In the former case light from the lamp was passed through a Toshida glass filter L-39 to cut off wavelengths shorter than 390 nm. The illumination intensity was usually 0.45 $W\ cm^{-2}$.

The rate of simultaneous deposition of polypyrrole and silver was evaluated by determining the amount of the deposited silver as a function of the illumination time. For this purpose the deposited silver was dissolved with nitric

acid, neutralized with sodium hydroxide, and determined colorimetrically at 620 nm using dithizone as a complexing agent.

Results

Photoelectrochemical Properties of n-Type Si Having a Variety of Damages. The mirror-finished surface had smooth surface as judged from pictures taken by a scanning electron microscope (SEM) with magnification of 20000, while the damaged surface had irregular ditches with sharp edges as shown in Fig. 1(a). With increasing the etching time the sharp edges of the flaws became smooth as Figs. 1(b) to (d) show. Considering the depth of flaws of the dam-

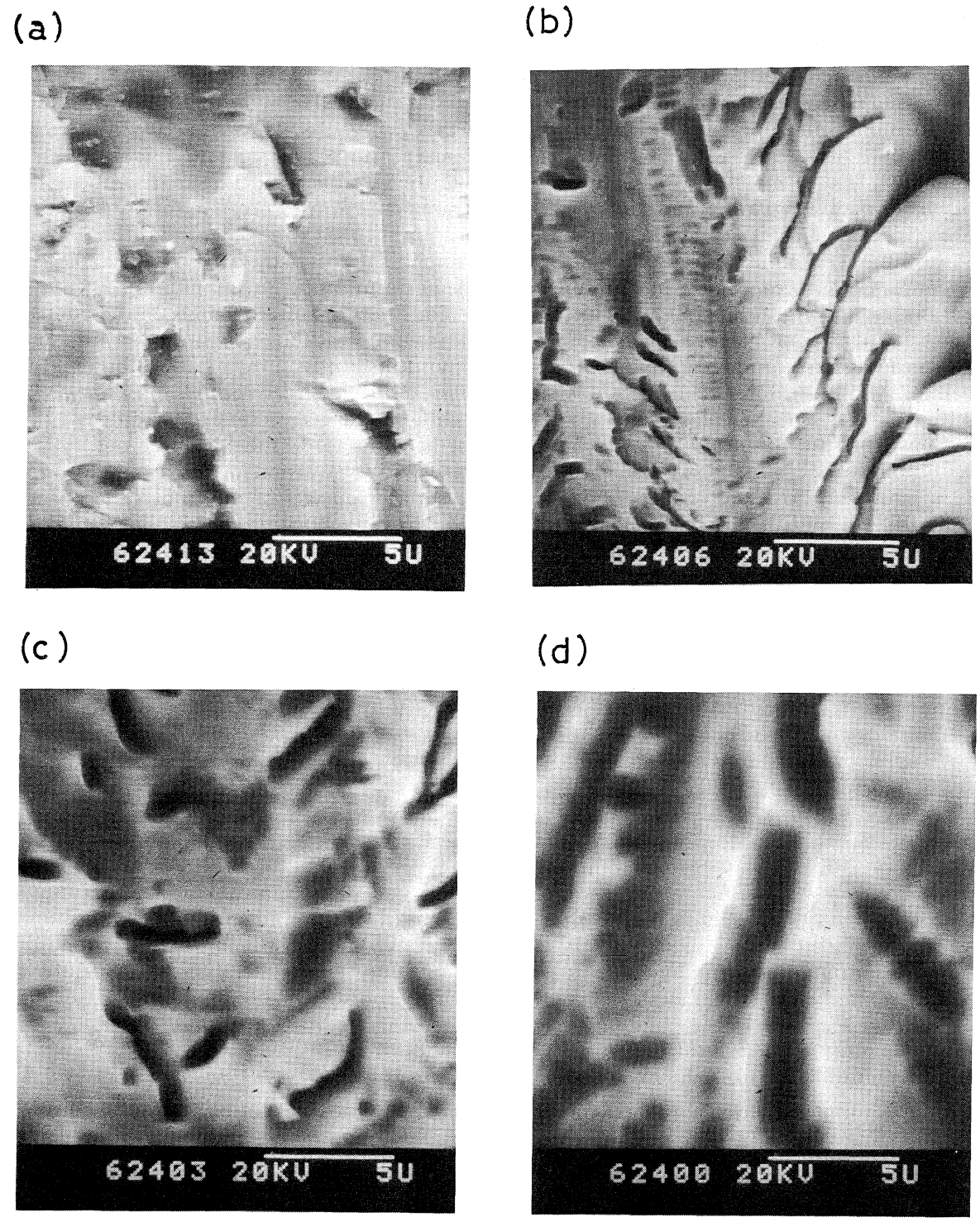

Fig. 1. Pictures of n-type Si surfaces containing a variety of damages. (a) Abraded with No. 500 emery papers (damaged surface), (b) etched of the damaged surface for 30 s, (c) etched for 60 s, and (d) etched for 5 min.

aged surface (34 μm) and the etching rate (13 μm min^{-1}), the flaws should be eliminated by the 3 min etching if the etching proceeds at the flaws only. However, the etching occurred not only in the flaws but also in the mirror-finished surfaces, it took much greater time to eliminate completely the flaws from the surface. According to the SEM pictures shown in Fig. 1, the 5 min etching of the damaged surface gave fairly smooth surface, and its electrochemical properties were found to be very close to those of the mirror-finished surface, as will be shown below.

Cyclic voltammograms of four kinds of n-type Si electrodes having different surface conditions, taken at an initial potential scan in propylene carbonate containing 10 mM ferrocene, are shown in Fig. 2. Illumination by the xenon lamp did not affect the shape of cyclic voltammograms at the damaged electrode, which behaved as if it were a metal electrode. In contrast, illumination caused photosensitized oxidation of ferrocene at the mirror-finished electrode, as shown in Fig. 2(d), though this electrode in the dark showed no appreciable reactivity for oxidation of ferrocene, as expected for n-type semiconductor electrodes.

The electrodes having different degrees of surface damages showed intermediate voltammetric behaviors between the mirror-finished and the damaged electrodes, depending on the degree of the surface damages. The onset potential of anodic photocurrents shifted negatively with increasing the etching of the damaged surface as shown in Fig. 3, and simultaneously anodic currents in the dark decreased; the onset potentials were not, however, affected by the etching. On the other hand, if the electrode contained a relatively high amount of defects in the electrode surface, the cathodic current was eventually the same as that at Pt electrodes, while if a large parts of surface flaws were eliminated, the onset potential was shifted towards negative potentials finally to reach the onset potential at the mirror-finished electrodes.

It is concluded from the results shown in Figs. 2 and 3 that the electrode surface prepared by etching the damaged surface for 15 s to 1 min possessed both semiconductor and metal electrode properties, because illumination caused negative shifts of anodic current onsets, but the onset potential of both anodic and cathodic currents in the dark were the same as those at the Pt electrodes.

The Effect of Surface Defects on the Photocatalytic Deposition Reactions. Figure 4 shows the amount of deposited silver with the illumination time, obtained when the front surface of the wafer was prepared by etching the damaged surface for different times and the back surface was the damaged one. The rate of the deposition reaction increased with the elimination of surface damages of the front surface, suggesting that the recombination of the photogenrated charge carriers in the illuminated surface controlled the rate of the deposition reaction. The silver deposition preferentially took place in the back damaged surfaces in the dark, and the polypyrrole deposited on the illuminated surfaces irrespective of whether this surface was mirror-finished or defective.

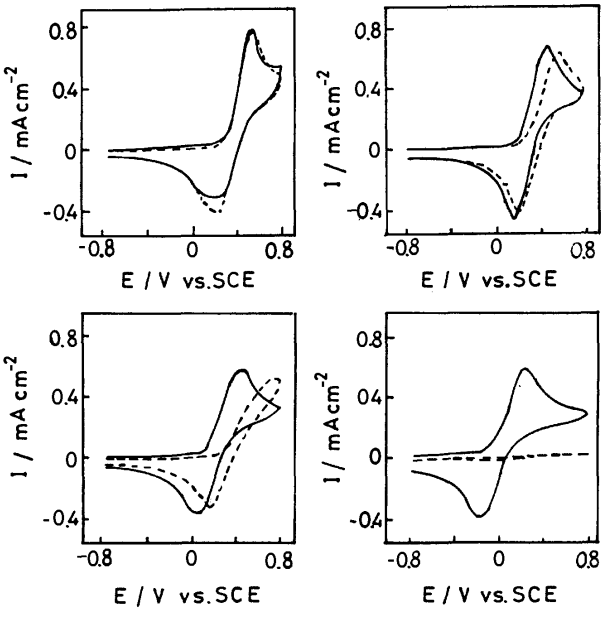

Fig. 2. Cyclic voltammograms of n-type Si electrodes in propylene carbonate containing 10 mM ferrocene and 0.1 M tetrabutylammonium perchlorate. The illumination intensity by the xenon lamp was 10 mW cm^{-2}. dE/dt=50 mV s^{-1}. Solid line: taken under illumination. Dashed line: taken in the dark. The electrodes were prepared by etching the damaged surface for (a) zero s, (b) 30 s, (c) 1 min, and (d) 5 min.

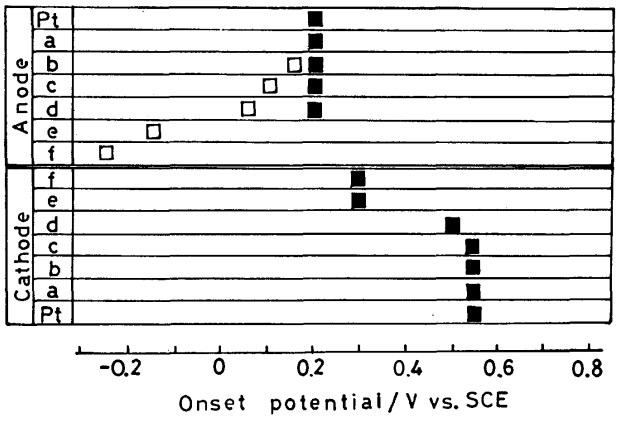

Fig. 3. The onset potential of anodic currents and cathodic currents, evaluated from cyclic voltammograms taken in a solution containing 10 mM ferrocene as shown in Fig. 1. (□) the onset potential of anodic currents under illumination of the electrode. (■) the onset potential in the dark. The etching time of the damaged Si electrode was (a) zero, (b) 15 s, (c) 30 s, (d) 1 min, (e) 5 min, (f) mirror-finished surface.

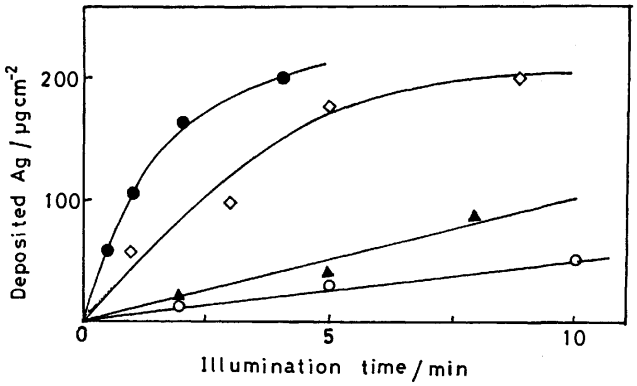

Fig. 4. Time course of silver deposition obtained when the front surface of n-type Si wafers contained flaws of different degrees, and the back surface was damaged. Solution: acetonitrile containing 0.1 M pyrrole and 0.1 M silver perchlorate. Illumination: 0.45 W cm^{-2} xenon light. The etching time of the damaged surface to prepare the front surface was (○) 1 min, (▲) 3 min, and (◇) 5 min. (●) well-etched front surface.

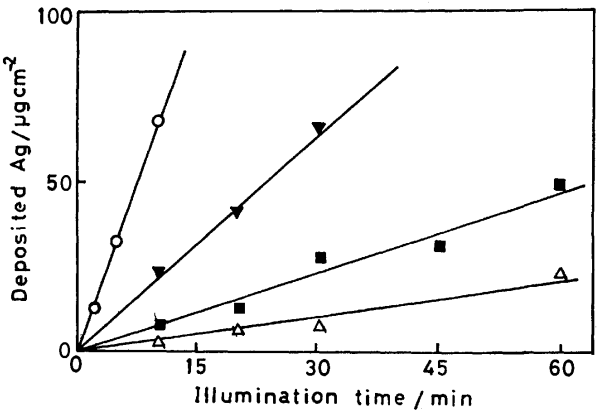

Fig. 5. As in Fig. 3, but for cases when both front and back surfaces of n-type Si wafer were in the same surface conditions. The etching time of the damaged surface for the preparation of each surface was (△) 30, s, (■) 1 min, and (▼) 5 min. (○) the well-etched surface.

Figure 5 shows the time course of silver deposition obtained when both the front and back surfaces were the same with respect to the defects. In such cases, the rate of the deposition reaction was increased by eliminating the surface damage. As shown in the figure, the highest rate was achieved when both the front and back surfaces were mirror-finished. However, the rate obtained was by far lower than that achieved when the front surface was mirror-finished and the back surface was damaged, as will be recognized by comparing Fig. 5 with Fig. 4. The deposition of both silver and polypyrrole took place in the illuminated front surface for the cases of 30 to 60 s etching of the damaged surfaces, but with further increase in the etching time, the silver deposition occurred on the back surface.

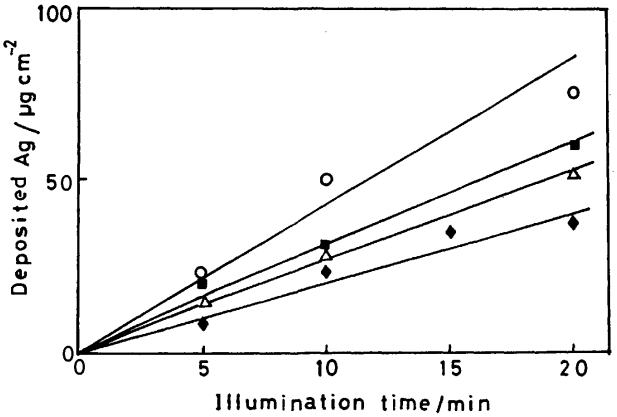

Fig. 6. As in Fig. 4, but for such surface conditions that the back surface was well-etched and the front surface was prepared by changing the etching time of the damaged surface for (■) 1 min, (△) 3 min, (◆) 5 min, and (○) 10 min.

Figure 6 shows the amount of deposited silver with illumination time for the case when the front surface was that prepared by etching the damaged surface for different time and the back surface was mirror-finished. The rate of silver deposition in that case was not so greatly influenced by the etching time of the damaged surface as that shown in Figs. 4 and 5. The interesting result obtained here is that the polypyrrole deposition took place on the mirror-finished back surface if the front surface was prepared by 30 to 60 s etching of the damaged surface, though the deposition on the front surface also took place with a less extent, as will be noticed from Fig. 7. In those cases, the silver deposition took place on the illuminated defective surface. With an increase in the etching time of the front surfaces, however, the polypyrrole deposition became to occur on the illuminated front surface. Simultaneously, the silver deposition became to take place on the back surface. It was found that the etching for 5 min was enough to change the major deposition place in such a manner as described above.

Figure 7 shows an example showing the occurrence of the polypyrrole deposition on the mirror-finished back surfaces as well as on the illuminated defective surface that was prepared by etching the damaged surface for 1 min. The illumination was made in that case by a He-Ne laser beam of ca. 0.5 mm diameter. According to this figure, there is a remarkable difference in the deposited patterns between the front surface and the back surface. In the front surface, the size of the deposition was near to that of the laser beam, but in the back surface the deposited polypyrrole occupied a much greater area. It seems important to remark here that if the front surface was unchanged but the back surface was changed from the mirror-finished surface to the damaged one, the polypyrrole deposition took place exclusively on the front

surface. Figure 8 shows the time course of the Ag deposition onto two kinds of n-type Si wafers whose front surfaces were the same and prepared by 1 min etching of the damaged surface, but whose back surfaces were different; one was mirror-finished and the other damaged. The deposition reaction at the Si wafer whose back surface was damaged stopped occurring at earlier illumination time than that at the wafer whose back surface was mirror-finished. The reason for this is that the photodeposition reaction does not proceed anymore when the deposited polypyrrole on the front surface becomes thick enough to absorb completely the incident photons, and such events are achieved more easily when the back surface of the wafer was damaged, because in that case the polypyrrole deposition took place exclusively on the front surface.

(a)

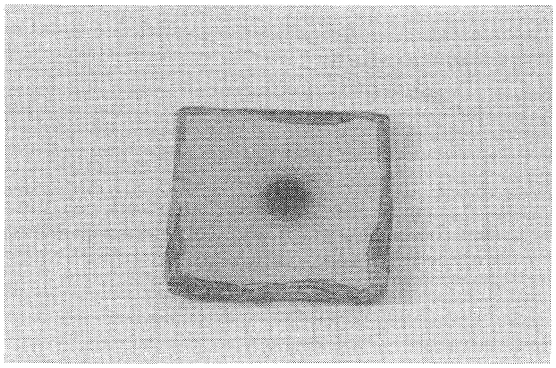

(a′)

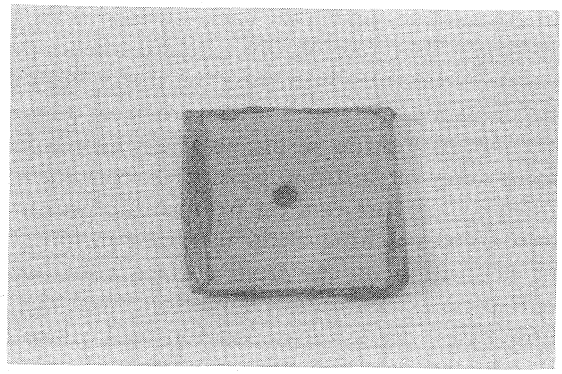

Fig. 7. Pictures showing the polypyrrole deposition on the well-etched back surface in the dark of n-type Si wafers of 0.6 mm thickness and of the resistivity of 2.4 Ωcm. The front surface was prepared by etching the damaged surfaces for 1 min, while the back surface was well-etched. Illumination was made by ca. 0.5 mm diameter He-Ne laser beam. (a) The back surface in the dark after illumination for 20 min, and (a′) the front surface at the same time.

The deposition of polypyrrole on the back surface in the dark of Si wafers was further investigated by using Si wafers of different resistivity and thickness. The experiments were carried out with almost the same surface configuration as that employed in the experiments whose results are given in Fig. 7; the front surface of the wafer was prepared by etching the damaged surface for 30 s and the back surface was mirror-finished. All the results including those shown in Fig. 7 are given in Table 1. It is recognized

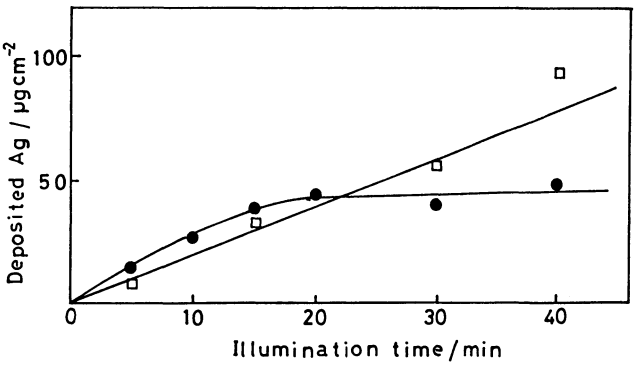

Fig. 8. Time course of the Ag deposition onto n-type Si wafers having different surface conditions in the back surfaces. The front surface was prepared by etching the damaged surface for 1 min for both cases, but the back surface was (□) well-etched and (●) damaged. Illumination: 0.45 W cm^{-2} xenon lamp.

Table 1. The Occurrence of Positive Hole-Consuming Polypyrrole Deposition on n-Type Si Wafers of Varous Resistivities and Thickness

Resistivity	Thickness	Deposition of polypyrrole		Diffusion length of positive hole
ohm cm	mm	Illuminated front surface	Back surface in the dark	mm
0.77	0.4	Occurred	Occurred	0.45
2.8	1.1	Occurred	Not occurred	0.63
2.8	0.9	Occurred	Not occurred	0.63
2.8	0.3	Occurred	Occurred	0.63
2.4	0.6	Occurred	Occurred	0.61

The front surface was prepared by etching the damaged surface for 30 s, while the back surface was well-etched. Illumination was made by a 25 mW He-Ne laser of ca. 0.5 mm beam diameter.

from the results shown in the table that the polypyrrole deposition on the mirror-finished back surface did not always take place.

Discussion

The most interesting result obtained in this study is that the oxidative deposition of polypyrrole occurred on the mirror-finished back surface if the front surface was prepared by etching the damaged surface for 30 to 60 s. Discussion on this result will be made first for the case of using the He-Ne laser as a light source.

The light penetration depth estimated from the inverse of the absorption coefficient at 632 nm is ca. 3.2 μm,[11] while the flaws in the surface prepared by ething the damaged surface for 30 to 60 s would leave the flaws of ca. 28 to 21 μm depth on average based on the assumption that the damaged surface originally contained flaws of 34 μm depth and the etching rate was 13 μm min^{-1}.[10] Accordingly, illumination of such surface will result in photogeneration of charge carriers in a surface region containing defects. Such speculation seems valid, judging from the SEM pictures of the electrode surfaces shown in Figs. 1(b) and (c), where fairly deep ditches are seen in the surfaces prepared by 30 to 60 s etching of the damaged surface. Photocurrent-potential bahaviors given in Figs. 2 and 3 also suggest that in cases of etching the damaged surface for 30 to 60 s the photogeneration of charge carriers occurred in the surface containing defects, because the onset potential of anodic photocurrens at the electrodes preprared by 30 to 60 s etching of the damaged surface was more positive than that at the mirror-finished surface.

The thickness of the space charge layer of n-type Si wafer having 2.4 ohm cm resistivity in the deposition bath is estimated to be 0.45 μm by using an well-established equation[12] under the assumption that the band bending is 0.4 V[2,3] and 2.4 Ωcm n-type Si contains 2.4×10^{15} cm^{-3} donors which is estimated from a donor concentration (N_d) vs. resistivity relation published as Fig. 5 of Ref. 13. The estimated space charge thickness is valid for well-etched surfaces and the values become small with an increase in the defect concentration.[5,7] The reviewer questioned why N_d was not determined by the Mott-Shottky plots of differential capacitances of the semiconductor electrodes. The Mott-Shottky plots may be a convenient way to determine N_d, but in many cases frequency dispersions appear in the plots, giving inaccurate determination of it. It has been shown for TiO_2 electrodes[14,15] that special surface treatments are necessary to eliminate the frequency dispersion in the plots.

It is known from the above estimation that the thickness of the Si wafers used in the present study was much greater than the sum of the light penetration depth and the space charge layer. Accordingly, positive holes must be supplied to the back surface by diffusion to cause the polypyrrole deposition there. To confirm this view, the diffusion length of positive holes (L_h) is estimated by inserting into Eqs. 1 and 2 the published data on the life time (τ_h)[16] and the mobility (μ_h)[17] both of which are available as a function of N_d.

$$L_h = (\tau_h D_h)^{1/2} \quad (1)$$

$$D_h = \mu_h kT/q \quad (2)$$

where D_h is the diffusion constant of positive holes. To estimate τ_h and μ_h, knowledge on N_d was required, and this was done from the resistivity values of the wafers using the published N_d vs. resistivity relation.[13] The estimated τ_h and μ_h of 2.4 Ω cm n-type Si, for example, were 3.4×10^{-4} s and 430 cm^2 V^{-1} s^{-1}, respectively. By using τ_h and μ_h estimated as a function of resistivities the diffusion length of positive holes is obtained also as a function of the resistivities, as shown in Fig. 9. In Table 1, the diffusion length of positive holes estimated in this manner is given. It is noticed from this table that the polypyrrole deposition took place on the mirror-finished back surface when the diffusion length of positive holes was greater than the thickness of the Si wafers used.

According to the above analysis, the thickness of Si samples used in the experiments whose results are given in Figs. 4 to 6 was shorter than the diffusion length of positive holes. Nevertheless, the polypyrrole deposition did not occur on the back surface if it was either damaged or contained a relatively high amount of defects. The main reason for this is that the presence of flaws in the back surface in the dark results in the annihilation of positive holes there. On the other hand, the presence of flaws is favorable for the silver deposition, as already described above. Furthermore, it must be remarked here that the polypyrrole deposition did not occur on the mirror-

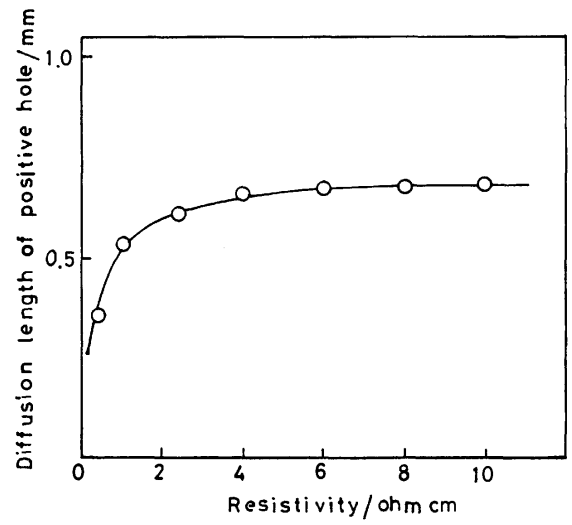

Fig. 9. The diffusion length of positive holes as a function of resistivity of n-type Si single crystals at 25 °C.

finished back surface if the front surface was also mirror-finished. Main reason for this is as follows. Since the bands are bent upward in the deposition bath, the energy structure of the illuminated mirror-finished surface is suited for the polypyrrole deposition there, but the photogenerated electrons are forced to move towards the bulk, where they recombine with positive holes that are supplied by diffusion. According to the results, the silver deposition took place on the back surface if both front and back surface were mirror-finished. Adsorbed silver ions may generate surface states which contribute to the silver deposition.[18] However, it is noticed that the rate was relatively low in that case, compared to that obtained when the front surface was mirror-finished and the back surface was damaged.

It is quite reasonable to consider that charge carriers supplied by diffusion contribute to heterogeneous reactions, but the present study have made clear that the contribution becomes appreciable under a special configuration of semiconductor surfaces; the back surface is mirror-polished and the front surface contains both anodic and cathodic sites. It is believed that the same should hold in photocatalysis of semiconductor powders.

This work was supported by Grant-in-Aid for Special Project, Nos. 62213020 and 63104005 from the Ministry of Education, Science and Culture.

References

1) H.Yoneyama, H. Shiotani, N. Nishimura, and H. Tamura, *Chem. Lett.*, **1981**, 157.

2) T. Kobayashi, Y. Taniguchi, H. Yoneyama, and H. Tamura, *J. Phys. Chem.*, **87**, 768 (1983).

3) H. Yoneyama, N. Matsumoto, and H. Tamura, *Langmuir.* **2**, 377 (1986).

4) S. R. Morrison and T. Freund, "Elechrocatalysis on Non-Metallic Surfaces," NBS Spec. Publ. No. 455, ed by A. D. Franklin, (1975), p. 137.

5) H. Gerischer, F. Fein, M. Lübke, E. Meyer, B. Pettinger, and R. Schöppel, *Ber. Bunsenges. Phys. Chem.*, **77**, 284 (1973).

6) R. L. Van Meirhaeghe, F. Cardon, and W. P. Gomes, *Ber. Bunsenges. Phys. Chem.*, **83**, 236 (1979)

7) D. M. Tench and H. Gerischer, *J. Electrochem. Soc.* **124**, 1612 (1977).

8) H. Yoneyama and M. Kitayama, *Chem. Lett.*, **1986**, 657; H. Yoneyama, K. Kawai, and S. Kuwabata, *J. Electrochem. Soc.*, **135**, 1699 (1988).

9) Japan Industrial Standards (JIS), R-6001.

10) H. Robbins and B. Schwartz, *J. Electrochem. Soc.*, **106**, 505 (1959).

11) H. A. Weakliem and D. Redfield, *J. Appl. Phys.*, **50**, 1491 (1879).

12) See, for example, H. Gerischer, *J. Electroanal. Chem. Interfacial Electrochem.*, **58**, 263 (1975) Eq. 6.

13) J. C. Irvin, *Bell System Tech. J.*, **41**, 387 (1962).

14) G. Cooper, J. A. Turner, and A. J. Nozik, *J. Electrochem. Soc.*, **129**, 1933 (1982).

15) H. O. Finklea, *J. Electrochem. Soc.*, **129**, 2003 (1982).

16) F. G. Fossum and D. S. Lee, *Solid State Electronics*, **25**, 741 (1982).

17) M. B. Prince, *Phys. Rev.*, **93**, 1204 (1954).

18) B. Ohtani, Y. Okugawa, S. Nishimoto, and T. Kagiya, *J. Phys. Chem.*, **91**, 3550 (1987).

 © 1989 The Chemical Society of Japan Bull. Chem. Soc. Jpn., 62, 1771—1776 (1989)

Quantitative Mapping of Metal-Centered Dipolar Field in Hemin Dicyano Complex by Solution NMR

Yasuhiko YAMAMOTO,* Norishige NANAI, Yoshio INOUE, and Riichirô CHÛJÔ
Department of Biomolecular Engineering, Tokyo Institute of Technology, 12-1, 2-Chome, O-okayama, Meguro-ku, Tokyo 152
(Received December 23, 1988)

The metal-centered pseudo-contact shift contribution in the hyperfine shift of NMR resonance of paramagnetic hemin dicyano complex ([Fe^{III}(proto)$(CN)_2$]) in solution was quantitatively determined from the combined use of ^1H and ^{13}C NMR data. Taking advantage of the axially symmetric magnetic property for [Fe^{III}(proto)$(CN)_2$] in solution, the paramagnetic metal-centered dipolar field was quantitatively mapped. The highly solvent-dependent magnetic anisotropy, $(g^2_{//}-g^2_{\perp})$, of this complex in CD_3OD was estimated to be 7.2 and the obtained value is placed between the values in D_2O (4.4) and in $CDCl_3$ (9 .7).

Heme occupies the active sites of various hemoproteins and its electronic structure is crucially related to the functional properties of these proteins.[1] NMR presents potentially one of the most powerful spectroscopic techniques to investigate the structure-function relationship of hemoproteins in solution.[2-8] In the case of paramagnetic hemoproteins and hemin complexes, the hyperfine field due to the unpaired electron(s) of the heme iron provides a unique probe to characterize the electronic/molecular structure of the heme, because the hyperfine shifted NMR resonances arising from the heme and/or the surrounding amino acid residues in paramagnetic hemoproteins are extremely sensitive to the change in the heme molecular environments. The observed chemical shift of a hyperfine shifted resonance (δ_{obs}) is composed of three terms;[9,10] $\delta_{obs}=\delta_{dia}+\delta_c+\delta_{pc}$($\delta_c+\delta_{pc}$ is called the hyperfine shift (δ_{hf})), where δ_{dia} is the chemical shift of a suitable diamagnetic complex and δ_c and δ_{pc} are the contact and the metal-centered pseudo-contact shifts, respectively, which stem from the interaction of the nucleus with the unpaired electron(s). The δ_c value reflects the unpaired electron density delocalized into the s orbital of that nucleus and the δ_{pc} value can be interpreted in terms of the spatial relationship between that nucleus and the unpaired electron localized at the heme iron. Therefore the relative contributions of δ_c and δ_{pc} to δ_{hf} have to be determined in order to quantitatively analyze the δ_c value in terms of the unpaired spin delocalization, i.e., electronic structure of the heme, and the heme molecular structure.

Several procedures for separating δ_{hf} to δ_c and δ_{pc} have been proposed.[9,11-13] Those procedures usually start with the determination of magnetic anisotropy and the location of magnetic axes and, therefore, generally rely on the g-tensor measurements of either single crystal or frozen sample.[14-16] Even for ideal magnetic behavior, questions must remain about the application of those solid data to interpret solution NMR results. Goff[13,17] has demonstrated an approach to estimate the metal-centered pseudo-contact shift of fourfold symmetric iron(III) tetraphenylporphyrin derivative-imidazole complexes using solution NMR measurements with the assumption that the resonances from the peripheral phenyl groups experience predominantly metal-centered pseudo-contact shifts and, hence, their contact shifts are neglected. Since cyanide ion is the most frequently used as an external ligand for iron(III) hemoproteins to ensure a stable low-spin complex and the NMR spectral properties of iron(III) hemoprotein-cyano (met-cyano) complex are considerably different from those of iron(III) hemoprotein-imidazole (met-imidazole) complex, it is of interest to investigate the metal-centered dipolar field in met-cyano complex and to compare it with that in met-imidazole complex.

We present herein a novel method to quantitatively characterize the paramagnetic metal-centered dipolar field in paramagnetic low-spin hemin dicyano complex by making use of the difference in the δ_{pc} value between heme methyl carbon and attached proton nuclei. Since it has been proved that in-plane magnetic anisotropy of hemin dicyano complex in solution is averaged to zero,[18] the assumption of axially symmetric dipolar field can be confidently applied to analyze the metal-centered dipolar field of this complex. The proposed method can be useful to map the metal-centered dipolar field in paramagnetic low-spin hemin complexes and hemoproteins with insignificant in-plane magnetic anisotropy.

Experimental

Material; Hemin chloride and (protoporphyrinato IX) zinc(II) were purchased from Sigma Chemical Co. and Aldrich Chemical Co., respectively, and were dissolved in methanol-d_4(CD_3OD) with 5-fold excess of KCN and pyridine-d_5(C_5D_5N), respectively, for the NMR measurements. Concentration of both samples are ca. 20 mM.

Instrumentation; NMR spectra were recorded on a JEOL GX-270 FT NMR spectrometer operating in the quadrature mode (^1H and ^{13}C frequencies are 270 and 67.9 MHz, respectively). Typical ^1H spectra consisted of 256 transients with 32K data points over 5000 and 10000 Hz for

Zn and Fe complexes, respectively. Proton noise decoupled ^{13}C NMR spectra were recorded using a 10 mm diameter tunable probe, about 5000 transients, 16K data points over 30 kHz. The obtained free induction decay was apodized at 1—10 Hz. ^{1}H-^{13}C heteronuclear chemical shift correlated spectrum (^{1}H-^{13}C COSY spectrum) of (protoporphyrinato IX)zinc(II) ([Zn^{II}(proto)]) in C_5D_5N was recorded using the standard pulse sequences.[19] The time domain data matrix, 2K(^{13}C-15000 Hz)×128(^{1}H-4000 Hz) was expanded to the final matrix size 2K×512 by zero filling. The data matrix was apodized with a sine bell function in both dimensions and the spectrum is presented in the absolute value mode. Chemical shifts are given in parts per million (ppm) downfield from 2,2-dimethyl-2-silapentane-5-sulfonate (DSS).

Results and Discussion

Resonance Assignment in ^{1}H and ^{13}C NMR Spectra of [Zn^{II}(proto)]. ^{1}H-^{13}C COSY spectrum of diamagnetic [Zn^{II}(proto)] in C_5D_5N at 29 °C, together with the ^{1}H and ^{13}C NMR spectra attached along the F_1 and F_2 axes, respectively, is illustrated in Fig. 1. The individual ^{1}H signal assignment is obtained by a combined use of ^{1}H-^{1}H chemical shift correlated and nuclear Overhauser effect correlated spectroscopies (results not shown) and is shown with the ^{1}H spectrum in the figure. From the known ^{1}H assignment, the ^{13}C assignment is clearly established by the ^{1}H-^{13}C connectivities in the ^{1}H-^{13}C COSY spectrum. The resonances from the quaternary β-pyrrole carbon nuclei were assigned using the long-range ^{1}H-^{13}C COSY experiment (results not shown) and no attempt was made for assigning the quaternary α-pyrrole carbon resonances. The present assignments on both ^{1}H and ^{13}C spectra confirm the partial assignment previously reported[2,20] and are summarized in Table 1. Because of the presence of a pseudo-C_2 symmetry in [Zn^{II}(proto)] molecular structure, C_2 symmetric nature of its electronic structure with respect to the α,γ-meso axis is clearly reflected in the NMR spectra. The chemical shift values of [Zn^{II}(proto)] are used as the diamagnetic reference shift (δ_{dia}) in the analysis on the shifts of the paramagnetic hemin dicyano complex([Fe^{III}(proto)$(CN)_2$]) (see below).

Temperature Dependence Study of [Fe^{III}(proto)$(CN)_2$] NMR Spectra. ^{13}C NMR spectra of [Fe^{III}(proto)$(CN)_2$] measured at various temperatures are given in Fig. 2. The individual ^{13}C signal assignment of this

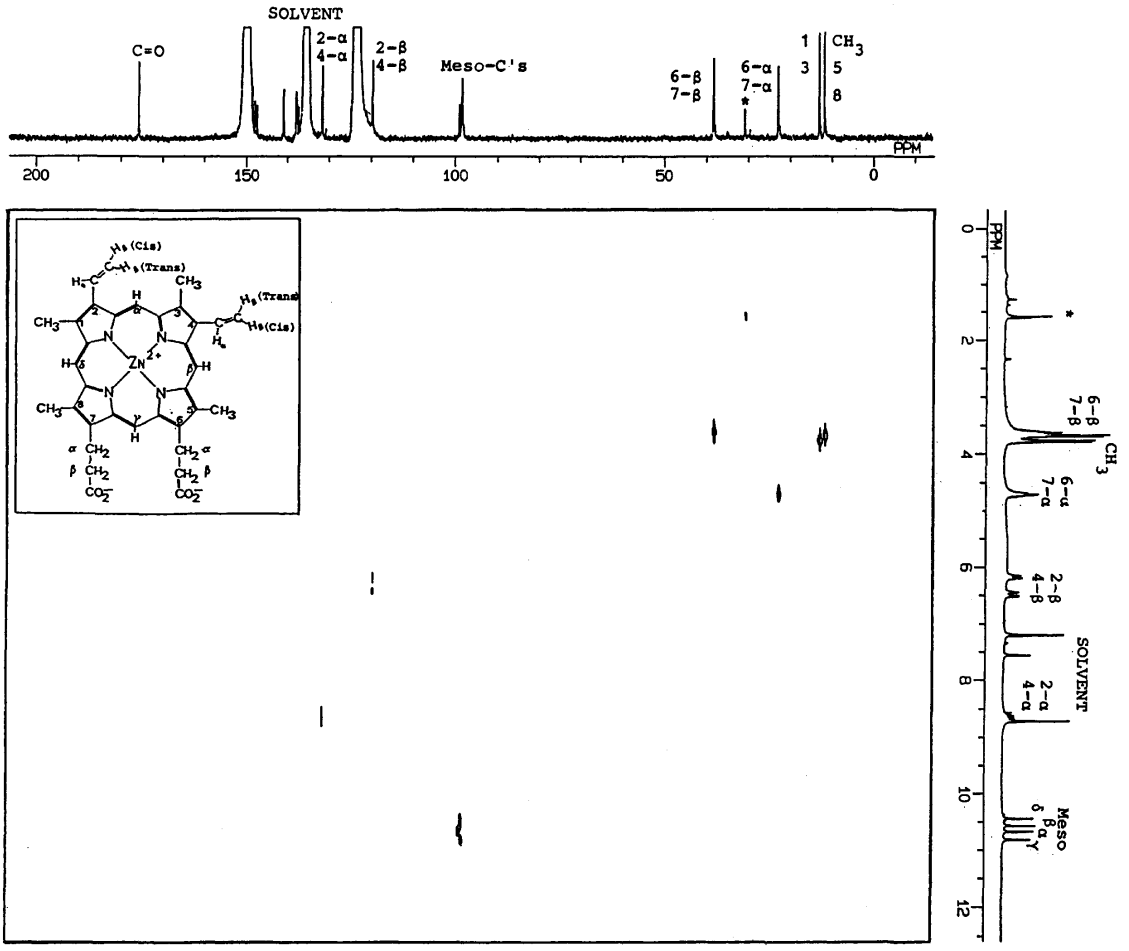

Fig. 1. ^{1}H-^{13}C COSY spectrum of [Zn^{II}(proto)] in C_5D_5N at 29 °C. The ^{1}H and ^{13}C signal assignments are shown with the corresponding spectra attached along F_1 and F_2 axes, respectively. The structure of [Zn^{II}(proto)] is shown in the inset.

Table 1. Chemical Shifts[a] of Heme ^1H and ^{13}C Resonances

^1H	$[Fe^{III}(proto)(CN)_2]$[b]	Intercept[c] at $T^{-1}=0$	$[Zn^{II}(proto)]$[d]	^{13}C	$[Fe^{III}(proto)(CN)_2]$[b]	Intercept[c] at $T^{-1}=0$	$[Zn^{II}(proto)]$[d,e]
1-CH_3	12.80	5.9	3.79	1-CH_3	−24.4	11.6	13.0
3-CH_3	13.88	7.3	3.77	3-CH_3	−26.7	8.6	13.0
5-CH_3	16.82	7.2	3.67	5-CH_3	−33.7	9.8	11.7
8-CH_3	17.22	7.0	3.70	8-CH_3	−34.3	9.2	11.7
2-α	13.21	12.6	8.64	2-α	71.7	134.1	131.5
4-α	12.67	12.7	8.64	4-α	73.3	135.6	131.5
2-β(Trans)	−0.82	8.1	6.48	2-β	ca.165[f]	119.2	119.6
2-β(Cis)	−1.37	8.6	6.17	4-β	162.6	118.4	119.6
4-β(Trans)	−0.61	8.2	6.48	6-α	−14.9	23.1	22.8
4-β(Cis)	−1.22	8.9	6.17	7-α	−13.5	24.4	22.8
6-α	8.10	9.1	4.71	6-β	93.6	41.9	38.3
7-α	7.70	8.7	4.71	7-β	91.1	39.7	38.3
6-β	0.99	4.8	3.62	α	83.2	76.7	98.9
7-β	0.99	4.8	3.62	β	66.1	127.6	98.4
α	0.60	12.5	10.67	γ	55.0	n.d.	98.2
β	1.69	13.0	10.57	δ	73.3	82.7	98.4
γ	3.43	11.9	10.82	C=O	180.2	180.2	175.6
δ	1.21	12.2	10.44				

a) Chemical shifts are given in ppm and referenced to DSS through the residual solvent signal. b) Measured in CD_3OD at 40 °C. c) Linear least-square fitting procedure on the Curie plots were used. d) Measured in C_5D_5N at 29 °C. e) The values were found to be 1.5 ppm smaller than the previous results.[20] f) Resonating under free CN^- signal. n.d.; Not determined.

complex has been reported previously.[21] The observed shifts for the heme methyl, meso, and quaternary β-pyrrole carbon resonances are plotted against reciprocal of absolute temperature in Fig. 3. Curvatures of the plots, especially in the plots of β-pyrrole carbon resonances, are apparently like the Curie plots for the ^{13}C resonances of iron(III) tetraphenylporphyrin derivative-imidazole complexes,[13,17] and, as reported previously,[2] ^1H data also exhibit some curvature in their Curie plots (results not shown). Nonlinear temperature dependence of the pseudo-contact shift[17] does not simply account for the degree of the curvature in their Curie plots because the curvature of the β-pyrrole carbon resonances is greater than that of the meso carbon resonances although the latter carbon nuclei are closer to the heme iron. Therefore the effects of aggregation[22] at low temperature might be responsible for the non-linear Curie plot. But the observed shifts of $[Fe^{III}(proto)(CN)_2]$ NMR resonances at 40 °C were essentially independent of concentration from 5 to 50 mmol dm^{-3}. The intercepts (at $T^{-1}=0$) of the Curie plots for all the resonances were calculated from the least-square fitting of the plots and are given in Table 1. The difference between the chemical shift value in $[Zn^{II}(proto)]$ and the intercept of the Curie plot, for the corresponding resonances, is relatively small for the heme side-chain carbon resonances and is large for the ^1H resonances, although the intercepts are close with each other among the resonances for the ^1H nuclei of same type.

Quantitative Mapping of Paramagnetic Metal-Centered Pseudo-Contact Field in $[Fe^{III}(proto)(CN)_2]$. The observed shifts of the heme methyl carbon resonances are plotted against those of the attached proton

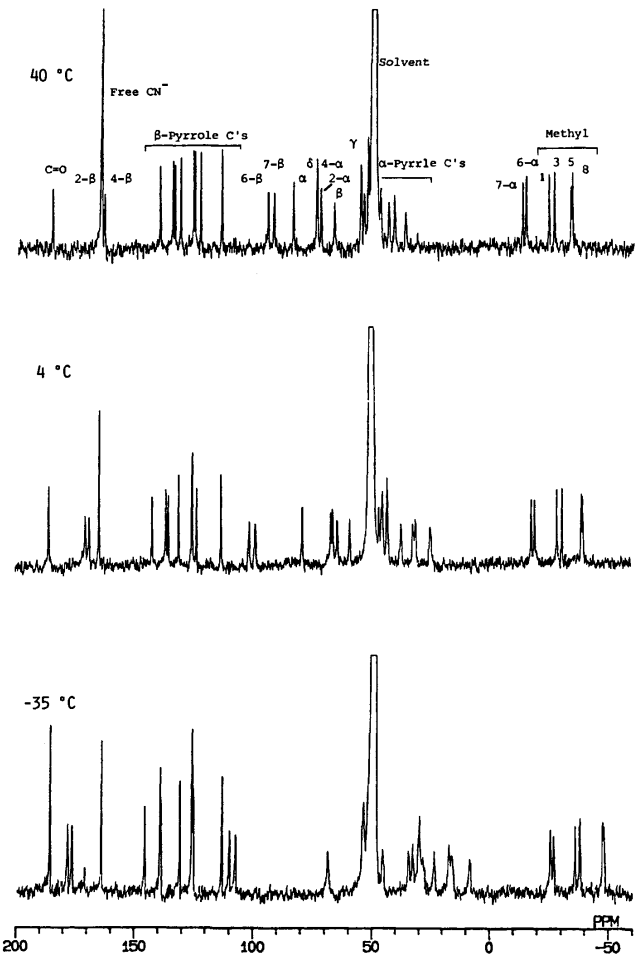

Fig. 2. Proton-noise decoupled ^{13}C NMR spectra of $[Fe^{III}(proto)(CN)_2]$ in CD_3OD at the indicated temperatures. The assignment of the resonances has been reported previously.[21]

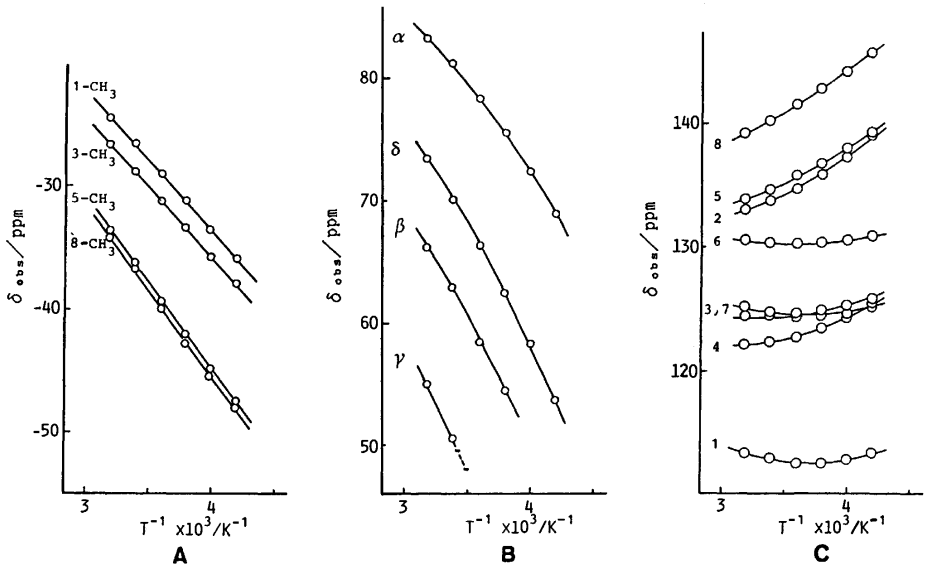

Fig. 3. Curie plot, the observed shift (δ_{obs}) vs. reciprocal of absolute temperature, for the heme methyl (A), meso (B), and β-pyrrole (C) carbon resonances. The curvature of the plots is most significant for the β-pyrrole resonances.

resonances, at various temperatures, in Fig. 4. As previously reported,[23] those plots give straight lines with a slope of $Q^{C}_{C'C}\gamma_H/Q^{H}_{CCH_3}\gamma_C$ for the system of axial symmetry ($Q^{C}_{C'C}$ and $Q^{H}_{CCH_3}$ are the parameters that account for the transfer of the unpaired spin density in the π orbital of the pyrrole carbon to directly-bonded carbon nucleus via the spin polarization and to the heme methyl proton nuclei through the hyperconjugation, respectively, and γ_H and γ_C are the gyromagnetic ratios of the proton and the carbon nuclei, respectively). The plots in Fig. 4 are straight and exhibit almost same slope over the temperature range examined, indicating $Q^{C}_{C'C}/Q^{H}_{CCH_3}$ is independent of temperature from −35—40 °C. The value of $Q^{C}_{C'C}=-39$ MHz reported for π-radical system[24] combined with the slope of the plots(=1.90) yield 82 MHz for $Q^{H}_{CCH_3}$.

For the limiting case of axial symmetry, δ_{pc} is expressed by Eq. 1,[10]

$$\delta_{pc}=\frac{(\chi_{//}-\chi_{\perp})}{3N}\frac{(3\cos^2\theta-1)}{r^3} \qquad (1)$$

where N is Avogadro's number. $\chi_{//}$ and $\chi_{\perp}$ are the components of the molecular susceptibility parallel and perpendicular to z axis of the hemin molecule (z axis is defined along the normal to the porphyrin plane). The quantity, $(3\cos^2\theta-1)/r^3$, is called axial geometric factor which defines the spatial position of the observed nucleus with respect to z axis and iron center of the hemin. Our procedure for mapping the paramagnetic metal-centered dipolar field relies on the assumption of axial symmetry in the magnetic property of [Fe^{III}(proto)$(CN)_2$]. But it has been verified for [Fe^{III}(proto)$(CN)_2$] that the in-plane anisotropy, which is present in the frozen glass state, is

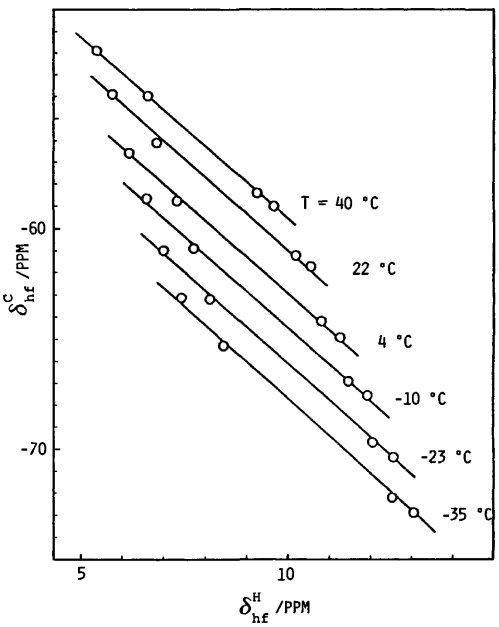

Fig. 4. The plots of heme methyl carbon hyperfine shift against the attached proton hyperfine shift at various temperatures. The plots strongly support that the in-plane magnetic anisotropy of [Fe^{III}(proto)$(CN)_2$] in solution is not significant and the $Q^{C}_{C'C}/Q^{H}_{CCH_3}$ is independent of temperature.

averaged to zero in solution.[18] The linear plots shown in Fig. 4 also prove the insignificant in-plane anisotropy of this complex.

Since the δ_c values of the heme methyl carbon and the attached proton resonances are proportional to the unpaired electron density in the π orbital of the pyrrole carbon to which the methyl group is attached, they vanish simultaneously as the density becomes

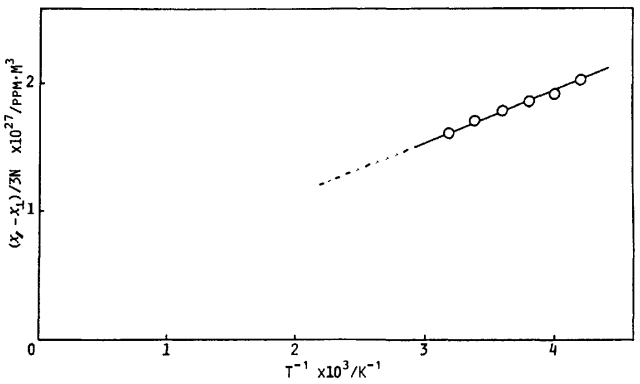

Fig. 5. The plots of $(\chi_{/\!/}-\chi_\perp)/3N$ against T^{-1}. The linear relationship indicates that the magnetic anisotropy is independent of temperature over the temperature range examined. Non-zero intercept would arise from unknown temperature dependence of $(\chi_{/\!/}-\chi_\perp)$ $(3\cos^2\theta-1)/r^3$.

0. Therefore the slope and intercept of the plots in Fig. 4 combined with the axial geometric factors[25] of heme methyl carbon and proton nuclei yield the coefficient of Eq. 1, $(\chi_{/\!/}-\chi_\perp)/3N$, and hence the axial metal-centered dipolar field given in Eq. 1 can be determined. δ_{pc} value of a given nucleus can be calculated from its axial geometric factor using the obtained equation.

The $(\chi_{/\!/}-\chi_\perp)/3N$ values are calculated at different temperatures and are plotted against T^{-1} in Fig. 5. The plot exhibits a straight line over the temperature range studied, supporting the validity of the present method for estimating δ_{pc}. The magnetic anisotropy appears to be essentially independent of temperature over the temperature range examined. If we assume that there is only a single spin state with insignificant second-order Zeeman contribution, $(\chi_{/\!/}-\chi_\perp)/3N$ is rewritten in terms of the g-factor as $\beta^2S(S+1)(g_{/\!/}^2-g_\perp^2)/9kT$ (β, S, and k are the Bohr magneton, total spin and Boltzmann constant, respectively).[10] The slope of the plot in Fig. 5 yields the value of 7.2 for the quantity, $g_{/\!/}^2-g_\perp^2$. It has been demonstrated that the magnetic anisotropy, $g_{/\!/}^2-g_\perp^2$, for [Fe^{III}(proto)$(CN)_2$] is highly solvent sensitive and is 4.4($g_{/\!/}\approx2.9$, $g_\perp\approx2.0$) in D_2O[26] and 9.7($g_{/\!/}\approx3.6$, $g_\perp\approx1.6$) in $CDCl_3$.[27] The value of 7.2 for CD_3OD solvent, obtained in the present study, is between those values and yields the δ_{pc} value of −14 ppm for the meso protons at 40 °C that is relatively large compared with the value previously estimated (−10 ppm) for met-imidazole complex,[13] but is comparable to the earlier estimation for [Fe^{III}(proto)(C_5H_5N)(CN)] complex.[11] Using −14 ppm for the δ_{pc} of meso proton resonances, the π-electron density(in percent) of −0.25, −0.33, −0.42, and −0.33(minus sign indicates negative spin density.) are calculated for the α, β, γ, and δ meso carbon nuclei, respectively, and +0.83, +0.88, +1.03, and +1.04 for 1, 3, 5, and 8-pyrrole carbons, respectively. Non-zero intercept of the plot shown in Fig. 5 would arise from unknown temperature dependence of $(\chi_{/\!/}-\chi_\perp)(3\cos^2\theta-1)/r^3$.

The present method can be applied to any paramagnetic low-spin iron(III) porphyrin complexes including hemoproteins for mapping the paramagnetic metal-centered dipolar field as long as their in-plane magnetic anisotropy is not so significantly large. The heme methyl carbon resonances have been observed in various paramagnetic low-spin hemoproteins.[23,28]

This work was supported by a Grant-in-Aid for Scientific Research (No. 63750846) from the Ministry of Education, Science and Culture.

References

1) S. Sano,"The Porphyrin," ed by D. Dolphin, Academic Press, New York (1979), Vol. VII, Chap. 8.
2) K. Wüthrich, *Struc. Bonding*, **8**, 53 (1970).
3) J. S. Morrow and F. R. N. Gurd, *CRC Crit. Rev. Biochem.*, **3**, 221 (1975).
4) R. G. Shulman, "ESR and NMR of Paramagnetic Species in Biological and Related Systems," ed by I. Bertini and R. S. Drago, D. Reidel Publishing Company (1979), p. 135.
5) G. N. La Mar, "Biological Application of Magnetic Resonance," ed by R. G. Shulman, Academic Press, New York (1979), p. 305.
6) C. Ho and I. M. Russu, *Methods Enzymol.*, **76**, 275 (1981).
7) I. Bertini and C. Luchinat, "NMR of Paramagnetic Molecules in Biological Systems," The Benjamin/Cummings Publishing Company, Inc., (1986), p. 165.
8) J. D. Satterlee, *Ann. Rep. NMR Spec.*, **17**, 79 (1986); *Met. Ion. Biol. Syst.*, **21**, 121 (1986).
9) K. Wüthrich, "NMR in Biological Research: Peptides and Proteins," North-Holland Publishing Company (1976), Chap. 6.
10) O. Jardetzky and G. C. K. Roberts, "NMR in Molecular Biology," Academic Press, New York (1981), Chap. III.
11) R. G. Shulman, S. H. Glarum, and M. Karplus, *J. Mol. Biol.*, **57**, 93 (1971).
12) W. D. Horrocks, Jr., "NMR of Paramagnetic Molecules: Principles and Application," ed by G. N. La Mar, W. D. Horrocks, Jr., and R. H. Holm, Academic Press, New York (1973), p. 127.
13) H. M. Goff, *J. Am. Chem. Soc.*, **103**, 3714 (1981).
14) H. Hori and H. Morimoto, *Biochim. Biophys. Acta*, **200**, 581 (1970).
15) H. Hori, *Biochim. Biophys. Acta*, **251**, 227 (1971).
16) G. N. La Mar and A. Walker, "The Porphyrins," ed by D. Dolphin, Academic Press, New York (1979) Vol. IV, Chap. 2.
17) H. M. Goff, "Iron Porphyrins," ed by A. B. P. Lever and H. B. Gray, Addison-Wesley Publishig Company, Reading, Massachusetts (1983), Part I, p. 237.
18) G. N. La Mar, J. Del Gaudio, and J. S. Frye, *Biochim. Biophys. Acta*, **498**, 422 (1977).
19) R. Freeman and G. A. Morris, *J. Chem. Soc., Chem. Commun.*, **1974**, 648.
20) K. Wüthrich and R. Baumann, *Helv. Chim. Acta*, **57**,

336 (1974).
21) Y. Yamamoto and N. Fujii, *Chem. Lett.*, **1987**, 1703.
22) W. I. White, "The Porphyrins," ed by D. Dolphin, Academic Press, New York (1978), Vol.V, Chap. 7.
23) Y. Yamamoto, N. Nanai, Y. Inoue, and R. Chûjô, *Biochem. Biophys. Res. Commun.*, **151**, 262 (1988).
24) M. Karplus and G. K. Fraenkel, *J. Chem. Phys.*, **35**, 1312 (1961).
25) The center of the mass of the methyl protons was used to calculate the geometric factor of heme methyl H's.
26) G. N. La Mar and F. A. Walker, *J. Am. Chem. Soc.*, **95**, 1782 (1973).
27) J. S. Frye and G. N. La Mar, *J. Am. Chem. Soc.*, **97**, 3561 (1975).
28) Y. Yamamoto, *FEBS Lett.*, **222**, 115 (1987).

Thermal Isomerization of 1′,3′,3′-Trimethyl-8-nitrospiro-[2*H*-1-benzopyran-2,2′-indoline]-6-carboxylic Acid

Norio NISHIMURA,* Jun'ichi MIYAKE, and Yoshimi SUEISHI
Department of Chemistry, Faculty of Science, Okayama University, Tsushima, Okayama 700
(Received January 5, 1988)

The rates of thermal isomerization of 1′,3′,3′-trimethyl-8-nitrospiro[2*H*-1-benzopyran-2,2′-indoline]-6-carboxylic acid (6-COOH-8-NO_2-SP) from its spiro form (SP) to its merocyanine form (MC) have been measured in some solvents and at high pressures. The equilibrium constants between these isomers at atmospheric pressure and at 30 °C are in the range of 0.25 to 2.52 depending on solvents. The activation volumes are 0.2—3.4 $cm^3 mol^{-1}$, while the reaction volumes are −7.9—−22.3 $cm^3 mol^{-1}$. Thus the volume profile was found to have a maximum, as predicted previously.

Thermochromic materials have attracted attention for many years. Recently, interest has been stimulated due to their practical applications to thermal copies, optical switches and displays. Spiropyrans belong to the most important class of the organic photochromic compounds which are used as light-sensitive materials. In spite of their practical interests, a little work focused on the mechanism of the photo and thermal isomerization of spiropyrans between SP and MC has been done.[1-5]

Recently we have studied the solvent and pressure effects on the rate of thermal conversion of 1′,3′,3′-trimethyl-6-nitrospiro[2*H*-1-benzopyran-2,2′-indoline] (6-NO_2-SP)[6] from MC to SP, and of 1′,3′,3′-trimethyl-spiro[2*H*-1-benzopyran-2,2′-indoline]-8-carboxylic acid (8-COOH-SP)[7] from SP to MC. The role of solvent-induced solute (MC) dipole has been discussed. The volume profile predicted with the help of these compounds has a maximum which is rarely found in chemical reactions. It has been concluded that these compounds probably isomerize via the same reaction path, i.e., via a transition state involving homolytic bond fission or bond formation, rather than via a heterolytic transition state.

The present work has been undertaken to ascertain if such a maximum really exists in the volume profile. We have used 6-COOH- 8-NO_2-SP for which SP and MC are in thermal equilibrium in the dark, and this made the estimation of equilibrium constant possible at any temperatures and pressures. The kinetic and thermodynamic quantities for the isomerization reaction are presented and the energy and volume profiles drawn.

Experimental

Materials. Utilizing the Reimer-Tiemann reaction, 3-formyl-4-hydroxybenzoic acid was prepared according to the method of Wynberg:[8] 4-hydroxybenzoic acid (0.1 mol) was refluxed for an hour with water (90 cm^3), KOH (1 mol), and chloroform (0.125 mol). After acidification and ether extraction, a brown solid 3-formyl-4-hydroxybenzoic acid was obtained. Nitration of this compound was carried out at temperatures between −5 and −10 °C. The precipitate, 3-formyl-4-hydroxy-5-nitrobenzoic acid, was recrystallized from 2-propanol; mp 217—219 °C. Equimolar amounts of this compound and 1,3,3-trimethyl-2-methylene indoline were dissolved into ethanol and the solution was refluxed for two hours. A dark precipitate 6-COOH-8-NO_2-SP was collected and dried. This compound is sparingly soluble in most solvents, and no further purification has been tried. However, its ^1H NMR spectrum in DMSO-d_6 showed that this compound is clearly an isomeric mixture of SP and MC in solution; δ=1.12, 1.25 (s, 3′-CH_3), 2.67 (s, >N-CH_3) for SP; δ=1.74 (s, 3′-CH_3), 3.91 (s, >N-CH_3) for MC. For spectral assignments, a report of Toppet et al. was referred.[9] Solvents used are of reagent grade and purified and dried in the usual manner.

Procedure. High pressure techniques and procedures for kinetic measurements were almost the same as those described before.[10] A sample solution (ca. 10^{-4} mol dm^{-3}) flushed with nitrogen gas was irradiated for a few seconds with a projection lamp. The thermal return from SP to MC was followed by monitoring the change in the absorbance in the vicinity of 560 nm using a Hitachi 139 spectrophotometer. The half life of the reaction was of the order of 10^3 s, and the absorbance at $t=\infty$ was estimated so that the first-order plot produced a best straight line. The photo and thermal isomerizations could be carried out reproducibly, and the apparent first-order rate constants (see Eq. 2 below) agreed within 5% error.

Results

Although conformational problems[3-5,11] remain for MC, the thermal equilibrium of 6-COOH-8-NO_2-SP between SP and MC can simply be represented as

$$\mathrm{SP} \underset{k_b}{\overset{k_f}{\rightleftarrows}} \mathrm{MC} \qquad (1)$$

Upon irradiation of the visible light, the equilibrium shifts to SP, and it returns to the original state in the dark.

In order to determine the concentrations of the isomers, it is necessary to know the molar absorptivity of MC. First, the equilibrium constant at 25 °C in DMSO-d_6 was estimated by means of ^1H NMR technique; the ratio of the integrated intensities of 3′-methyl protons in MC snd SP was regarded as the equilibrium constant (K=2.83 at 25 °C). From this

Table 1. Equilibrium Constants of 6-COOH-8-NO_2-SP between MC and SP at Various Pressures and Volumes of Reaction

Solvent	λ_{max}/nm	K (30 °C)						$\Delta V°$	ΔV_{solv}	$10^{11}q_p$ [a]	ΔV_{solv} [b]
	p/kgf cm^{-2} [c]	1	200	400	600	800	1200	cm^{3}mol^{-1}	cm^{3}mol^{-1}	Pa^{-1}	cm^{3}mol^{-1}
$CHCl_3$	573	0.250		0.312		0.383	0.454	−15.6	−30.6	15.9(30 °C)	−32.5
1,2-Dichloroethane	566	0.299		0.389		0.484	0.571	−18.6	−33.6	12.1(30 °C)	−24.7
Acetone	565	0.314		0.431		0.546	0.653	−22.3	−37.3	6.02(35 °C)	−12.3
DMSO	555	2.52	2.62	2.80	2.84			−7.9	−22.9	1.2 [d]	−1.8

a) Original q_p-values (Refs. 14,15) calculated on the basis of the Tait-type equation, $q_p=A/(B+p)$, are about twice as large as ours. We have estimated $(\partial\varepsilon/\partial p)_{T,p=0.1\ MPa}$ from the quadratic regression equation, $\varepsilon=ap^2+bp+c$. b) Calculated by using Eq. 7. c) 1 kgf cm^{-2}=9.81×10^4 Pa. d) Estimated by assuming $(\partial\varepsilon/\partial p)$= 3×10^{-8} Pa^{-1} (see text).

K-value and the absorbace at 555 nm (λ_{max} of MC), the molar absorptivity was estimated to be 33000 dm^{3}mol^{-1}cm^{-1}. This value could be used for other solvents without substantial danger, since the spectral shapes in the visible region in different solvents are almost the same.

It was found that the return rate follows the first-order kinetics, as expressed by Eq. 2.

$$d[MC]/dt = k_{obsd}([MC]_\infty - [MC]) \quad (2)$$

where $[MC]_\infty$ is the concentration of MC at equilibrium and k_{obsd} ($=k_f+k_b$) is the apparent rate constant. The equilibrium constant K is given by

$$K=[MC]_\infty/[SP]_\infty = k_f/k_b \quad (3)$$

Using K and k_{obsd}, k_f and k_b were calculated. These values at various pressures and temperatures are given in Tables 1—3.

The pressure dependence of the equilibrium constant was approximated by the following quadratic equation:

$$\ln K = ap^2+bp+c \quad (4)$$

Discussion

The reaction volumes ($\Delta V°$) at atmospheric pressure were estimated by

$$\Delta V° = (\partial \ln K/\partial P)_T \cong -bRT \quad (5)$$

and they are given in Table 1. The activation volumes for the forward and backward reactions (Eq. 1) estimated by similar equations are given in Table 2. Using the data in Tables 1—3, $\ln K$, $\ln k_f$, and $\ln k_b$ were plotted against $1/T$ in accordance with the van't Hoff and Arrhenius equations (Fig. 1, r=0.998 each). From these plots, thermodynamic parameters were estimated and they are given in Table 4. The equilibrium constant in DMSO, compared with those in other solvents (Table 1) is greater by about a factor of ten, indicating the increased stabilization of MC relative to SP. The band in the visible region shifts to a shorter wavelength as the solvent polarity increases (blue shift). This inclination was also observed for 6-NO_2-SP.[6] There are some spiropyrans which exhibit

Table 2. Pressure Dependence of the Rate Constants for the Forward and Backward Reactions at 30 °C

Solvent	10^4k_f / s^{-1}						$\Delta V^{\neq}$ / cm^{3}mol^{-1}
P/kgf cm^{-2}	1	200	400	600	800	1200	
$CHCl_3$	3.52		3.45		3.38	3.28	1.0
$C_2H_2Cl_2$	2.07		2.11		2.09	2.04	−1.7(3.4) [a]
Acetone	1.87		1.85		1.82	1.76	0.2
DMSO	6.25	6.07	5.96	5.85			3.8
	10^4k_b / s^{-1}						
$CHCl_3$	14.1		11.1		8.83	7.22	16.2
$C_2H_2Cl_2$	6.93		5.44		4.33	3.58	16.7
Acetone	5.96		4.30		3.34	2.70	22.3
DMSO	2.48	2.32	2.13	2.06			11.5

a) Obtained by the linear regression equation.

Table 3. Temperature Dependence of K, k_f/s^{-1}, and k_b/s^{-1}

Solvent		25 °C	30 °C	35 °C	40 °C	45 °C
$CHCl_3$	K	0.275	0.256	0.228	0.210	0.192
	10^4k_f	1.64	3.08	6.29	10.3	16.8
	10^4k_b	5.95	12.0	27.6	49.1	87.2
DMSO	K	2.83	2.53	2.38	2.22	2.06
	10^4k_f	3.11	5.65	11.4	20.8	35.9
	10^4k_b	1.10	2.23	4.79	9.35	17.4

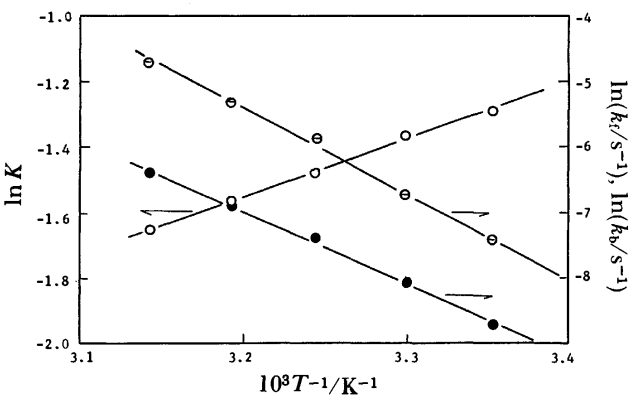

Fig. 1. The van't Hoff and Arrhenius plots for the thermal equilibration process of 6-COOH-8-NO_2-SP in $CHCl_3$: $\ln K$–$1/T$ (○); $\ln k_f$–$1/T$ (●); $\ln k_b$–$1/T$ (⊖).

Table 4. Thermodynamic Quantities (303.2 K) for the Reaction SP ⇄ MC

Solvent	ΔH°	ΔS°	ΔV°	E_a	$\Delta S^{\neq}$	$\Delta V^{\neq}$	Remark
	kJ mol^{-1}	J mol^{-1} K^{-1}	cm^3 mol^{-1}	kJ mol^{-1}	J mol^{-1} K^{-1}	cm^3 mol^{-1}	
$CHCl_3$	−14.5	−59	−15.6	92.9	−13.9	1.0	Forward
				107.4	45.1	16.2	Backward
DMSO	−12.0	−32	−7.9	98.1	8.7	3.8	Forward
				109.7	40.3	8.3	Backward

the red shift.[12] Although this band may be assigned to the conjugation band (intramolecular charge-transfer band) through one of the possible conformations of MC,[5] the blue shift is contrary to the general trend of the π-π^* transition which exhibits the red shift. Therefore, the ground state of MC must be more polar than the excited state. In fact, the dipole moments of 6-NO_2-SP in the ground and excited states are reported to be 12.7 and 3.5 Debye (1 Debye= 3.34×10^{-30} mC), respectively.[13] A substantial contribution of the following zwitterionic structures in the ground state may be responsible for the above findings.

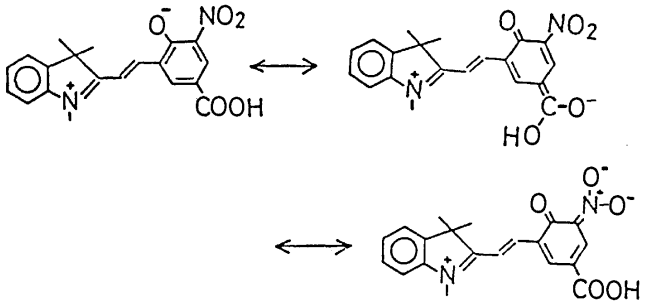

The Volume of Reaction. Volume change accompanied by chemical reactions is conventionally divided into two terms: an intrinsic volume change (ΔV_{int}) and a volume change arising from reorganization of solvent molecules (ΔV_{solv}), i.e.,

$$\Delta V^\circ = \Delta V_{int} + \Delta V_{solv} \quad (6)$$

Recent theoretical approach to the partial molar volume developed by Yoshimura and Nakahara,[14] enables us to understand its significance at the molecular level. However, the separate estimations of ΔV_{int} and ΔV_{solv} are rather critical, and must be done with great care.

Walling and Naiman[15] estimated the activation volumes of the Claisen rearrangement reaction in several solvents, and found that they fell in the range of −10—−15 cm^3 mol^{-1} with no obvious solvent dependence. They interpreted the results as consistent with rather tightly bonded cyclic transition state. This volume change could formally be ascribed to a 6-membered-ring-closure process. If we tentatively allot 15 cm^3 mol^{-1} for ΔV_{int} in the present case, then the "relative" values of ΔV_{solv} could be calculated. They are given in the 3rd column from the right in Table 1.

On the basis of the Kirkwood equation, ΔV_{solv} could be given by Eq. 7.

$$\Delta V_{solv} = N_A\left(\frac{\mu_{MC}^2}{r_{MC}^3} - \frac{\mu_{SP}^2}{r_{SP}^3}\right) q_P \quad (7)$$

where q_P is defined by Eq. 8.

$$q_P = \frac{3}{(2\varepsilon+1)}\left(\frac{\partial\varepsilon}{\partial p}\right)_{T,p=0.1\,MPa} \quad (8)$$

Using available ε-p data,[16,17] q_P-values were estimated (Table 1). Then, likely μ and r values(μ_{MC}=15 Debye, μ_{SP}=3 Debye, $r_{MC}=r_{SP}$=0.4 nm) were substituted into Eq. 7, together with the q_P-values (Table 1). The discrepancy between the observed ΔV_{solv} ($=\Delta V^\circ - \Delta V_{int}$) and calculated ΔV_{solv} becomes remarkable in the order chloroform <1,2-dichloroethane< acetone. This could be attributed to the enhanced polarization (increase of μ) within merocyanine molecule as the solvent polarity increases. Previously, we discussed this enhancement effect in some detail.[6,18,19] Unfortunately, no ϵ-p data are available for DMSO. However, judging from the $(\partial\varepsilon/\partial p)_T$-values for acetone and methanol[16,17] as polar solvents, $(\partial\varepsilon/\partial p)_T$-value for DMSO may not be far from 3×10^{-8} Pa^{-1}. Thus ΔV_{solv} in DMSO is presumed to be ca. −1.8 cm^3 mol^{-1}. It

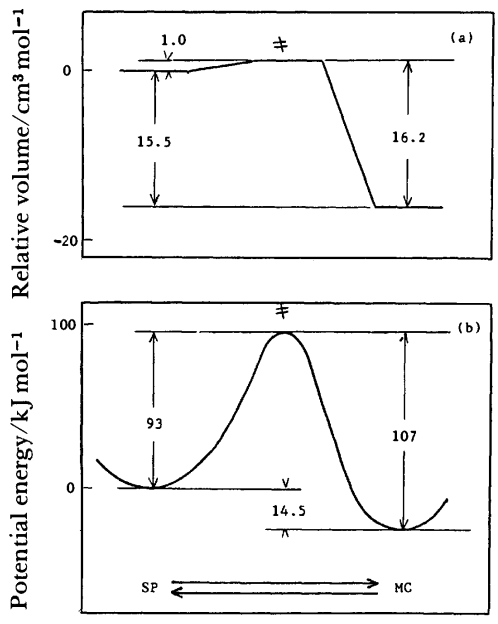

Fig. 2. Volume (a) and energy (b) profiles for the isomeric reaction of 6-COOH-8-NO_2-SP in $CHCl_3$.

could be said that the remarkable enhancement effect is involved in the case of DMSO, too.

Energy and Volume Profiles. In simple one-step reactions, the volume profiles are those having no extremum. This is in sharp contrast to the energy profile which has a maximum inevitably. According to le Noble,[20] extrema are usually the rule for stepwise reactions. However, there are some exceptions: sigmatropic shifts such as the Claisen rearrangement show minina.[21] Diels-Alder reactions participated by maleic anhydride as a dienophile also show minima.[22-24] The reaction of *p*-methoxystyrene with TCNE is another example which involves minima in the volume profile.[25] A maximum was observed in the degenerate Wagner-Meerwein shift[26] and the amide rotation of dipeptides.[27]

The energy and volume profiles are shown in Fig. 2. The activation volumes for the forward reaction are positive and small, while the reaction volumes are negative (Table 2). Therefore, it is hard to imagine a dipolar transition state where the second term in Eq. 6 would overwhelm the first one. A transition state which involves a homolytic bond stretching may be acceptable; a small volume increment is expected in this process. Therefore, it could be said that the transition state is located near the initial state in the sense that the nuclei are near the initial positions.

If the data in Table 4 are inspected, one may notice that both ΔH° and ΔS° are smaller in $CHCl_3$ than in DMSO. The same is true for E_a and ΔS^*, and ΔS° (ΔS^*) and ΔV° (ΔV^*) for the forward reaction. Although the reason is not clear, this compensation effect observed for $CHCl_3$ and DMSO are in line with the previous results.[7] It is notable that the entropy factor is as important as the enthalpy factor in determining the equilibrium. Leffler[28] exemplified the compensation effect for a variety of reaction series, and for reactions in solvents of varying polarity. The existence of the isokinetic temperature predicted from the linear free energy relationship was demonstrated by us.[29] Similarly, a rough linear correlation between $\Delta S^\circ(\Delta S^*)$ and $\Delta V^\circ(\Delta V^\circ)$ was also reported,[30-32] and the reason discussed by Kondo and Tokura.[33] Our results in this and previous investigations are in line with the findings of the above reports.

References

1) R.Heiligmen-Rim, Y. Hirshberg, and E. Fisher, *J. Phys. Chem.*, **66**, 2465 (1962).

2) J. Arnaud, G. Wippler, and F. Beaure D'augeres, *J. Chim. Phys.*, **64**, 1165 (1967).

3) I. Shimizu, H. Kadota, and E. Inoue, *Bull. Chem. Soc. Jpn.*, **42**, 1730 (1967).

4) S. A. Krysanov and M. V. Alfimov, *Laser Chem.*, **4**, 129 (1983).

5) K. Tamagake, Y. Kohno, Y. Shiota, and Y. Fujita, *Nippon Kagaku Kaishi*, **1984**, 82.

6) Y. Sueishi, M. Ohcho, and N. Nishimura, *Bull. Chem. Soc. Jpn.*, **58**, 2608 (1985).

7) Y. Sueishi, M. Ohcho, S. Yamamoto, and N. Nishimura, *Bull. Chem. Soc. Jpn.*, **59**, 3668 (1986).

8) H. Wynberg, *J. Am. Chem. Soc.*, **76**, 4998 (1954).

9) S. Toppet, W. Quintens, and G. Smets, *Tetrahedron*, **31**, 1957 (1975).

10) Y. Sueishi and N. Nishimura, *Bull. Chem. Soc. Jpn.*, **56**, 2598 (1983).

11) J. B. Flannery, Jr., *J. Am. Chem. Soc.*, **90**, 5660 (1968).

12) I. Ya. Kasparova, O. P. Shmakova, M. V. Mel'nik, B. M. Gutsulyak, and P. P. Kisilitsa, *Zh. Fiz. Khim.*, **60**, 504 (1986).

13) D. Lapienis-Grochowska, M. Kryszewski, and B. Nadolski, *J. Chem. Soc., Faraday Trans. 2*, **75**, 312 (1979).

14) Y. Yoshimura and M. Nakahara, *Ber. Bunsenges. Phys. Chem.*, **92**, 46 (1988), and references therein.

15) C. Walling snd M. Naiman, *J. Am. Chem. Soc.*, **84**, 2628 (1962).

16) H. Hartmann, A. Neumann, and G. Rinck, *Z. Phys. Chem. N. F.*, **44**, 204 (1965).

17) H. Hartmann and A. P. Schmidt, *Ber. Bunsenges. Phys. Chem.*, **72**, 875 (1968).

18) N. Nishimura, S. Kosako, and Y. Sueishi, *Bull. Chem. Soc. Jpn.*, **57**, 1617 (1984).

19) N. Nishimura, T. Tanaka, M. Asano, and Y. Sueishi, *J. Chem. Soc., Perkin Trans. 2*, **1986**, 1839.

20) W. J. le Noble, *Rev. Phys. Chem. Jpn.*, **50**, 207 (1980).

21) K. R. Brower, *J. Am. Chem. Soc.*, **83**, 4370 (1961).

22) R. A. Grieger and C. A. Eckert, *J. Am. Chem. Soc.*, **92**, 2918, 7149 (1970).

23) K. Seguchi, A. Sera, and K. Maruyama, *Bull. Chem. Soc. Jpn.*, **47**, 2242 (1974).

24) J. R. McCabe and C. A. Eckert, *Ind. Eng. Chem., Fundam.*, **13**, 168 (1978).

25) Y. Uosaki, M. Nakahara, and J. Osugi, *Int. J. Chem. Kinet.*, **15**, 805 (1983).

26) W. J. le Noble, S. Bitterman, P. Staub, F. K. Meyer, and A. E. Merbach, *J. Org. Chem.*, **44**, 3263 (1978).

27) H. Hauer, H. D. Ludemann, and R. Jaenicke, *Z. Naturforsch.*, **37**, 51 (1982).

28) J. E. Leffler, *J. Org. Chem.*, **20**, 1202 (1955), and references therein.

29) N. Nishimura, Y. Sueishi, and S. Yamamoto, *Chem. Lett.*, **1979**, 429.

30) K. J. Laidler and D. T. Y. Chen, *Can. J. Chem.*, **37**, 599 (1959).

31) L. G. Hepler, *J. Phy. Chem.*, **69**, 965 (1965).

32) S. D. Hamann snd M. Linton, *J. Chem. Soc., Faraday Trans. 1*, **1975**, 485.

33) Y. Kondo and N. Tokura, *Bull. Chem. Soc. Jpn.*, **42**, 1660 (1969).

Ionic Partial Molar Volumes of Alkali Halides in Methanol as Evaluated from the Sedimentation Potentials

Hiromitu HIRAKAWA,* Hiroyasu NOMURA,† and Fumio KAWAIZUMI†
Department of Electronics, Faculty of Engineering, Kagoshima University, Kagoshima-shi 890
†Department of Chemical Engineering, School of Engineering, Nagoya University, Chikusa-ku, Nagoya-shi 464
(Received December 3, 1988)

Sedimentation potential (SP) measurements were carried out for solutions of alkali halides dissolved in methanol. With the SP data thus obtained, the partial molar volumes V_2^∞ of alkali halide MX, V_2^∞ (MX), were divided into cationic V_2^∞ (M^+) and anionic V_2^∞ (X^-) parts. The ionic partial molar volumes evaluated showed a reasonable agreement with each other. These values of V_2^∞ (M^+) and V_2^∞ (X^-) are numerically compatible with those reported earlier by Kawaizumi and Zana using the ultrasonic vibration potential method and those given more recently by French and Criss based on the apportionment of the estimated V_2^∞ value for the large complex [Ph_4PBPh_4] (*J. Solution Chem.*, **11**, 625 (1982).) The magnitude of the concentration dependence of SP was evaluated theoretically by expressing the apparent molar volume, the transport number, and the density of a solution as functions of the solute concentration.

The evaluation of the anionic and cationic contributions to the properties of an electrolyte which consists of these ions has been one of the most important tasks in the physical chemistry of electrolytes and the goal of many studies. A thorough comparison of the properties of various ions is possible only after individual ionic properties have been evaluated in a convincing manner. For aqueous solvent media, the numerical values of the thermodynamic properties of ions evaluated by many investigators based on different methods are in good, or at least fair, agreement.

Conway[1] reviewed the earlier work related to the evaluation of ionic properties and discussed the reliability of the various methods and assumptions adopted up to that time for the assessment of the contribution of each ionic species to the physicochemical properties of the electrolyte as a whole. In his review, Conway judged that, in water, both the ultrasonic vibration potential (abbreviated hereafter as UVP) method[2-4] and the extrapolation method[5] can lead to excellent results for the division of the partial molar volume V_2^∞ of an electrolyte MX, V_2^∞ (MX), into cationic V_2^∞ (M^+) and anionic V_2^∞ (X^-) parts. Contrary to the other methods, the UVP method has been the only one that is completely free from any kind of extrathermodynamic assumption. However, because of the technical difficulty in the UVP method, no widespread use of this important method has yet been made.

For individual ionic properties in nonaqueous solvent systems, marked differences have often been observed among the reported values. These large differences may be attributed to the following three factors. First, the thermodynamic properties of an electrolyte are themselves determined less accurately in nonaqueous media than in aqueous media; hence, the ionic molar quantities derived from them necessarily contain much uncertainty. Second, in evaluating ionic contributions we are forced to rely upon assumptions and semiempirical relations that are physically questionable. Third, the paucity of various kinds of fundamental data prevents us from comparing the numerical values of individual ionic properties given by different authors. For these reasons, we are not certain which results are the more correct.

To date, the ionic division of the partial molar volume of an electrolyte in nonaqueous media using the UVP technique has been done by Zana and his co-workers for methanol,[6] ethanol,[7] DMF,[7] and DMSO.[8] An alternative to the UVP method is the sedimentation potential (abbreviated hereafter as SP) method. In the first paper[9] of this series, the present authors described an apparatus for measuring the SP designed by one of them (H. H) and the results of the SP measurements of a number of inorganic salts dissolved in water. With this apparatus we have previously measured the SP of aqueous solutions of bola-form electrolytes[10] and nitroamminecobalt(III) complexes,[11] as well as solutions of LiCl, NaCl, and KCl in mixed water-methanol solvents.[12]

In this paper, the results of the SP measurement of alkali halides in methanol will be presented. As has just been mentioned, the ionic partial molar volumes in methanol based on the UVP method[6] are available. More recently, French and Criss[13] compared the numerical values of the partial molar volume for the Br^- ion, V_2^∞ (Br^-), in water and in methanol; these values had been obtained by various methods. Based on the apportionment of the estimated V_2^∞ value for the large complex [Ph_4PBPh_4] between cationic and anionic parts in view of the charge effect, they suggested that V_2^∞ (Br^-)=19.7±2 $cm^3 mol^{-1}$ in methanol; their conclusion was that the V_2^∞ (Br^-) in methanol is between 17 and 20 $cm^3 mol^{-1}$. The method of apportionment gives results compatible with those of the UVP method, not only in aqueous systems but also in methanol systems. However, the values of V_2^∞ (Br^-) considered in the paper of French and Criss[13] are almost incredibly scattered, ranging from −30.5 to 21.7 $cm^3 mol^{-1}$. In view of this, it is of considerable inter-

est to measure the SP of simple electrolyte alkali halides in methanol and to determine the individual partial molar volumes of alkali metal ions and halide ions from the SP data

Experimental

Specimens. The solvent methanol used was of an extra pure grade, and it was used without further purification. Commercial products of alkali halide (guaranteed or extra-pure-grade regent) were dissolved in this methanol to prepare a stock solution at the concentration of 0.1 mol dm^{-3}. Sample solutions at each concentration were prepared by the dilution of the stock solution.

Sometimes the solution properties of nonaqueous solvent systems are significantly affected by the presence of a trace quantity of water. Fortunately, the SP measurements carried out in the mixed water-methanol solvents[12] indicate that it is unnecessary to use absolute methanol as solvent, so long as the water content in the solvent methanol is sufficiently low. In fact, in the UVP measurement,[6] the water in the methanolic electrolyte solution gave rise to no appreciable change in the potentials up to a water content of 1%.

Apparatus and Measurements. The experimental set-up and the procedures of the SP measurement are identical with those described before.[9] The SP measurements were carried out at 23 °C—25 °C.

Results and Discussion

SP Values Observed. Figure 1 shows the results of the SP measurements for alkali chlorides and bromides. The fluorides and iodides also showed a similar concentration dependence. The variation in SP with the salt concentration will be analyzed below. It will be seen there that the use of the logarithmic concentration scale in describing the concentration dependence of SP is acceptable.

The SP values at concentration ranges from 10^{-3} to 10^{-2} mol dm^{-3} were taken as the limiting SP values, and the partial molar volumes of the ions were calculated using these limiting values.

Partial Molar Volumes of Alkali Halides in Methanol. In the introduction, we mentioned that very large differences can be found in the literature values of the physical parameters of electrolytes in nonaqueous solvent systems. For the case of the partial molar volume, for example, the reported values of V_2^∞ for NaCl in methanol are scattered between −5.5[14] $cm^3 mol^{-1}$ and 2.0[15] $cm^3 mol^{-1}$. Such differences seem to arise from the facts that the density of a pure nonaqueous solvent varies during density measurements, because of the atmospheric humidity and that extrapolation to an infinite dilution is seldom carried out as is required by the Debye-Hückel theory.

In order for the evaluated ionic partial molar volumes to be reliable and comparable with other reported values on a common basis, we must rely upon the most reliable and "normalized" values of the partial molar volumes, V_2^∞, for which the additivity rule $V_2^\infty = V_+^\infty + V_-^\infty$ should hold (hereafter the subscripts + and − refer to the cation and the anion respectively). For this reason we adopted principally the V_2^∞ of the electrolyte obtained by adding the V_+^∞ and V_-^∞ values listed in the latest publication of French and Criss.[13] These V_2^∞ values generally agree with those given by different authors, within a precision of

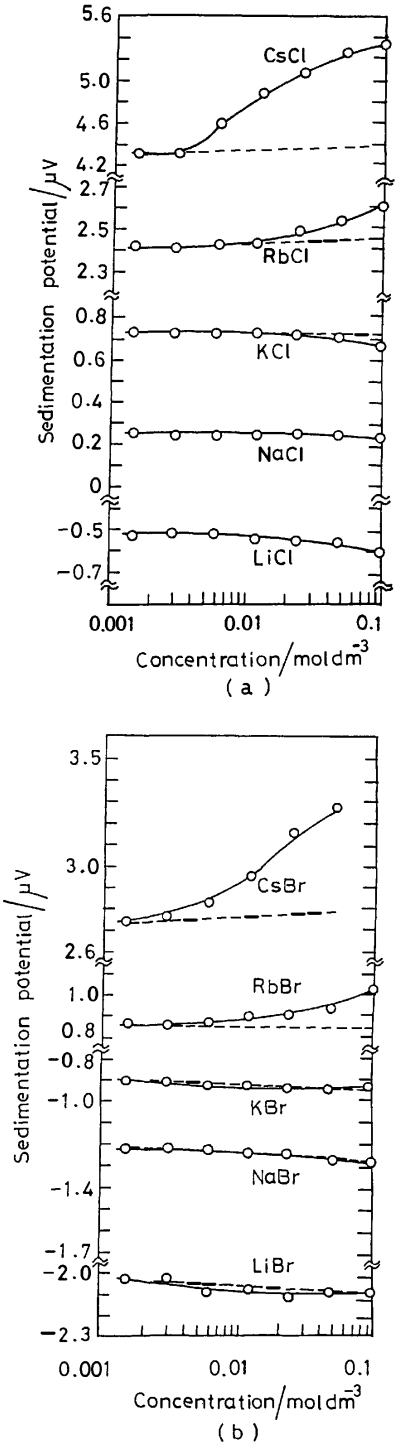

Fig. 1. Sedimentation potential in methanol for (a) chloride and (b) bromide as a function of concentration; —○— experimental; --------- calculated values obtained as explained in the text.

2 $cm^3 mol^{-1}$ or better. Only for CsCl does the difference in V_2^∞ value amount to 3.1 $cm^3 mol^{-1}$ (14.7 $cm^3 mol^{-1}$ by the additivity rule, while the value of 17.8 $cm^3 mol^{-1}$ is found in the literature[6]). Even for this case, we have used the value based on the results of French and Criss[13] in order to maintain the internal consistency of this work. However, they gave no value for the V_2^∞ of the Rb^+ ion, V_2^∞ (Rb^+), so this value was estimated by subtracting V_2^∞ (Cl^-), (Br^-), and V_2^∞ (I^-) from the respective values for rubidium salts found in the literature[6] and by then averaging the three resultant V_2^∞ (Rb^+) values.

Ionic Partial Molar Volumes in Methanol. As was done in our previous papers,[9-12] by solving simultaneously the additivity relation $V_2^\infty = V_+^\infty + V_-^\infty$ and Eq. 1; we can obtain numerical values of V_+^∞ and V_-^∞ which are free from any extrathermodynamic assumptions:

$$E = (ad/F)\cdot[(t_+/z_+)\cdot(m_+ - V_+^\infty\rho) - (t_-/z_-)\cdot(m_- - V_-^\infty\rho)] \quad (1)$$

Here, E is the SP; a, the acceleration; d, the distance between the two electrodes; F the Faraday constant; t, the transport number; z, the charge number; m, the molar mass of the ion, and ρ, the density. In our SP measurements the acceleration a is given as $\omega^2 x$, where ω is the angular frequency, and x, the amplitude of the oscillation generated in the SP apparatus. The partial molar volumes of the cation $V_+^\infty = V_2^\infty$ (M^+) and of the anion $V_-^\infty = V_2^\infty$ (X^-) evaluated for each alkali halide MX are summarized in Table 1, along with the values of t_+, t_-, and V_2^∞ used in the calculation.

Apparently the numerical values of V_2^∞ (M^+) and V_2^∞ (X^-) shown in Table 1 agree within the precision of SP measurements. The ionic partial molar volumes V_2^∞ (M^+) and V_2^∞ (X^-) given in Table 1 were averaged to give, respectively, the values for the M^+ and X^- ions in methanol. The results are shown in Table 2. In methanol, the transport numbers are known less accurately than in water. Differences of 5 units in the third decimal place of t_+ or t_- appear in different sources; this uncertsinty in the transport number alone will effect the ionic partial molar volumes by a little less than 1 $cm^3 mol^{-1}$. Therefore, Table 2 shows that the ionic partial molar volumes in methanol, as evaluated by three completely different methods agree well. Especially for V_2^∞ (Br^-), which was taken by French and Criss as a reference for ionic division, the agreement is better than we expected.

Analysis of the Concentration Dependence of SP. The experimental concentration dependences of the SP of the salts may be classified into three groups:
(1) salts with small concentration dependences; LiCl, NaCl, KCl, LiBr, NaBr, KRr, KI, RbI, and CsI.
(2) salts with moderate concentration dependences; NaF, KF, RbF, RbCl, RbBr, LiI, and NaI.
(3) salts with large concentration dependences; CsF, CsCl, and CsBr.

In our previous papers,[9-12] no attempt has been made to analyze the concentration dependence of SP. This has been done first in this work as follows: Equation 1 should describe the variation in SP with the concentration of the salts provided that the terms t_+, t_-, V_+, V_-, and d involved in Eq. 1 are given as functions of the solute concentration. As is well-known, these terms are satisfactorily expressed by the following relations:

$$t_\pm = \frac{\lambda_\pm^\infty - \frac{1}{2}B_2\sqrt{c}/(1+\kappa a_0)}{\Lambda^\infty - B_2\sqrt{c}/(1+\kappa a_0)} \quad (2)$$

$$V_\pm = V_\pm^\infty + \frac{3}{4}S_v\cdot c^{1/2} \quad (3)$$

and

Table 1. Sedimentation Potential, E, Alkali Halides, and Calculated Ionic Partial Molar Volumes for Cations and Anions in Methanol at 23 °C—25 °C

Sample	E	t_+[a]	t_-[a]	V_2^∞[b]	V_+^∞	V_-^∞
	μV			$cm^3 mol^{-1}$	$cm^3 mol^{-1}$	$cm^3 mol^{-1}$
NaF	0.72	0.520	0.480	−16.3	−16.24	−0.06
KF	1.15	0.557	0.443	−6.8	−5.23	−1.57
RbF	2.88	0.573	0.427	−1.5[c]	3.16	−4.66
CsF	5.10	0.593	0.407	2.0	6.10	−4.10
LiCl	−0.53	0.431	0.569	−4.9	−14.79	10.89
NaCl	0.25	0.463	0.537	−3.6	−16.75	13.15
KCl	0.73	0.500	0.500	5.9	−6.88	12.78
RbCl	2.40	0.516	0.484	11.2[c]	−0.30	11.60
CsCl	4.30	0.538	0.462	14.7	5.01	9.69
LiBr	−2.03	0.412	0.588	2.3	−20.80	23.10
NaBr	−1.23	0.445	0.555	3.6	−20.79	24.39
KBr	−0.90	0.482	0.518	13.1	−6.89	19.99
RbBr	0.86	0.498	0.502	18.4[c]	−2.09	20.49
CsBr	2.73	0.519	0.481	21.9	3.71	18.20
LiI	−3.76	0.387	0.613	11.5	−25.64	37.14
NaI	−3.14	0.419	0.581	12.8	−21.65	34.45
KI	−2.84	0.455	0.545	22.3	−5.67	27.97
RbI	−1.03	0.471	0.529	27.6[c]	−2.33	29.93
CsI	0.83	0.493	0.507	31.1	3.27	27.83

a)Calculated from the molar conductivities given in"Physical Chemistry of Origanic Solvents Systems," ed by A. K. Covington and T. Dickson, Plenum Press, New York (1973), p. 673. b) Ref. 13. c) See text.

Table 2. Ionic Partial Molar Volumes/($cm^3 mol^{-1}$) in Methanol at 25 °C

Ion	K-Z[a]	F-C[b]	This work
Li^+	−17.9	−17.5	−20.7±4.0
Na^+	−17.1	−16.2	−19.9±2.4
K^+	−7.3	−6.7	−6.2±0.7
Rb^+	−1.7	—	−0.4±2.2
Cs^+	4.8	2.1	4.5±1.1
F^-	−1.3	−0.1	−2.6±1.9
Cl^-	13.0	12.6	11.6±1.3
Br^-	18.3	19.8	21.2±2.2
I^-	28.2	29.0	31.5±3.7

a) Ref. 6. b) Ref. 13.

$$\rho = \rho^0 + \frac{M - \rho^0 V_2^\infty}{1000} c + \frac{S_v \rho^0}{1000} c^{3/2} \quad (4)$$

In the above equations, the subscript ± is used instead of using separately the + or − sign to refer to a cation or an anion. The parameters have the following meanings; $\Lambda_\pm^\infty$ and $\lambda_\pm^\infty$ are, respectively, the limiting molar electric conductivities of an electrolyte and that of ions constituting the electrolyte; B_2 is a constant depending on the viscosity, the dielectric constant and the temperature of the solvent; κ is the reciprocal length of the ionic atmosphere; a_0 is the distsnce of the closest approach of two ions; S_v is the coefficient derived from the Debye-Hückel theory; c is the molar concentration (mol dm^{-3}) of the electrolyte; M is the molar mass, and the superscript 0 refers to a pure solvent. The a_0's in Eq. 2 were set equal to the sum of the hydrodynamic Stokes radius of cation and that of anion, which can be calculated from the ionic molar conductivities found in the literature.[16] For S_v, we adopted the value of 14.19[14] cm^3 mol$^{-3/2}$ dm$^{3/2}$. By inserting Eqs. 2—4 into Eq. 1 and using the V_+^∞ and V_-^∞ values listed in Table 1, we can see theoretically how the SP varies with the concentration. The results of this evaluation are represented in Fig. 1 by the dotted lines. As the $V_\pm^\infty$'s are calculated with the SP values at low concentrations, the dotted lines in Fig. 1 agree with the experimental observations in the lower concentration regions. For the salts with small cations (i.e., lithium, sodium, and potassium salts), the evaluated and observed SP variations agree well, while for rubidium salts the experimental SP values deviate upwards from the theoretical curve, and this deviation becomes much larger still for the largest cationic salts, CsCl and CsBr. Any further attempts at the analysis of the behavior of CsCl and CsBr seem to be speculative at present. The significance of the present analysis is that an increase or decrease in the SP with the salt concentration can be predicted in a qualitative manner from a combination of Eqs. 1 through 4. At any rate, the magnitude of the variation in the SP with the salt concentration is small; hence, the problem of selecting a concentration scale (an ordinary concentration scale or logarithmic concentration one) for representing the concentration dependence of SP is reduced to a matter of convenience.

Conclusion

The division of the partial molar volumes into cationic and anionic parts based on the results of SP measurements carried out for 1-1 type inorganic electrolytes dissolved in methanol leads to results which are completely in agreement with those of the UVP method used by Kawaizumi and Zana[6] and the apportionment between ionic parts of a complex salt with a large volume proposed by French and Criss.[13]

References

1) B. E. Conway, *J. Solution Chem.*, **7**, 721 (1978).
2) P. Debye, *J. Chem. Phys.*, **1**, 13 (1933).
3) R. Zana and E. Yeager, *J. Phys. Chem.*, **71**, 521 (1967).
4) R. Zana and E. Yeager, *J. Phys. Chem.*, **71**, 4241 (1967).
5) B. E. Conway, J. E. Desnoyers, and R. E. Verrall, *Trans. Faraday Soc.*, **62**, 2738 (1966).
6) F. Kawaizumi and R. Zana, *J. Phys. Chem.*, **78**, 627 (1974).
7) F. Kawaizumi and R. Zana, *J. Phys. Chem.*, **78**, 1099 (1974).
8) K. M. Kale and R. Zana, *J. Solution Chem.*, **6**, 733 (1977).
9) H. Hirakawa, *J. Phys. Chem.*, **91**, 3452 (1987).
10) H. Hirakawa, H. Nomura, and F. Kawaizumi, *Bull. Chem. Soc. Jpn.*, **61**, 3316 (1988): In Refs. 9 and 10, the parameter x was called the "velocity amplitued," but this is not correct, as is discussed in this paper.
11) H. Hirakawa, H. Nomura, and F. Kawaizumi, 172nd Meeting of The Electrochemical Society, Inc., cosponsored by The Japan Society of Applied Physics, Honolulu, Hawaii October (1987); *J. Solution Chem.*, submitted for publication.
12) H. Hirakawa, H. Nomura, and F. Kawaizumi, *J. Phys. Chem.*, in press.
13) R. N. French and C. M. Criss, *J. Solution Chem.*, **11**, 625 (1982).
14) A. J. Pasztor and C. M. Criss, *J. Solution Chem.*, **7**, 27 (1987).
15) C. H. Rochester and B. Rossall, *Trans. Faraday Soc.*, **65**, 992 (1969).
16) R. A. Robinson and R. H. Stokes, "Electrolyte Solutions," 2nd Rev., Butterworths, London (1959).

 © 1989 The Chemical Society of Japan Bull. Chem. Soc. Jpn., 62, 1785—1790 (1989)

Comparison between Optical Properties of Sulfates and Hydrogensulfates in Halogen-Bridged Mixed-Valence Platinum(II, IV) Complexes

Nobuyuki MATSUSHITA,* Norimichi KOJIMA, Toshiro BAN, and Ikuji TSUJIKAWA
Department of Chemistry, Faculty of Science, Kyoto University, Kitashirakawa, Sakyo-ku, Kyoto 606
(Received January 17, 1989)

Syntheses and optical properties of some new halogen-bridged mixed-valence platinum complexes analogous to Wolffram's Red Salt, $[Pt(en)_2][PtBr_2(en)_2](HSO_4)_4$ (PBHS), $[Pt(en)_2][PtI_2(en)_2](HSO_4)_4 \cdot 4H_2O$ (PIHS), and $[Pt(en)_2][PtX_2(en)_2](SO_4)_2 \cdot 6H_2O$ {X=Br(PBSW), I(PISW)}, are reported. The powder X-ray diffraction pattern shows that PBHS is isomorphous with $[Pt(en)_2][PtCl_2(en)_2](HSO_4)_4$ (PCHS), and that PBSW and PISW are isomorphous. The hydrogensulfates PBHS and PIHS crystallize from an aqueous sulfuric acid solution, whereas the sulfates PBSW and PISW crystallize from an aqueous solution. The single crystal absorption spectra of PBHS, PIHS, PBSW, and PISW have been investigated at 4.2 K. The intense optical absorption due to intervalence charge-transfer transition from Pt(II) to Pt(IV) has been observed for the light polarized parallel to the Pt chain axis (E//chain). From the comparison of the energy of the intervalence charge-transfer absorption edges in PBHS, PBSW, and PISW, one can conclude that the influence of the substitution of the counterions HSO_4^- with SO_4^{2-} on the Pt(II)-Pt(IV) mixed-valence state is no less better than that of the substitution of the bridging halogen. The role of the counterion on the mixed-valence state is explained by the hydrogen bond network (Pt-NH···counterion···HN-Pt) on individual chains.

In recent years,[1-3] one-dimensional halogen-bridged mixed-valence complexes analogous to Wolffram's Red Salt (WRS) $[Pt(C_2H_5NH_2)_4][PtCl_2(C_2H_5NH_2)_4]Cl_4 \cdot 4H_2O$ have been investigated from viewpoints of physics and chemistry as a model of one-dimensional mixed-valence compounds. Many Wolffram's Red Salt Analogues (WRA) have ever been synthesized and studied, through the substitution of the in-plane ligand amines, bridging halogen and counterions. They comprise elongated octahedral $[Pt^{IV}X_2(AA)_2]^{2+}$ and square-planar $[Pt^{II}(AA)_2]^{2+}$ units alternately stacked along an axis, and counterions supporting the platinum complex columns, where AA denotes a bidentate amine or two monodentate amines etc., and X denotes a bridging halogen. Consequently, they comprise infinite platinum chains (···Pt^{II}···X-Pt^{IV}-X···) bridged by halogens which are not at the middle point between Pt(II) and Pt(IV), but closer to Pt(IV) than Pt(II). There is a charge-transfer interaction between an electronic state of Pt(II) and that of Pt(IV) through the bridging halogen.[4] The XPS measurement[5] suggests that the electronic state of Pt is not strictly divalence or tetravalence, and approaches that of Pt(III) by the medium of this interaction.

In WRS[4,6] and WRA,[6] the intervalence charge-transfer transition from an electronic state containing mainly d_{z^2} orbitals of Pt(II) to a state containing mainly d_{z^2} orbitals of Pt(IV) causes an intense optical absorption. This absorption appears in the spectral region from the visible to near-infrared, for light polarized parallel to the Pt chain axis (E//chain). Therefore, the single crystal spectrum for E//chain is a good probe of the Pt(II)-Pt(IV) mixed-valence state attributed to the charge-transfer interaction. Theoretical and experimental analyses of the above mentioned phenomena have been carried out on the basis of the extended Peierls-Hubbard model.[7,8]

The solid state properties in WRS and WRA have been investigated, mainly through the substitution of the metal atom (Pt, Pd, Ni) and the bridging halogen (Cl, Br, I).[8] Clark and Kurmoo[9] suggest that the hydrogen bond between a counterion and an in-plane ligand amine affects both the Pt(II)-Pt(IV) distances and the intervalence charge-transfer transition energies. Nevertheless, the influence of the hydrogen bond on the Pt mixed-valence state has not been investigated in detail by means of the substitution of the counterion. In order to elucidate the influence of the hydrogen bond on the Pt mixed-valence state we have investigated the WRA mixed-valence complexes comprising SO_4^{2-} and HSO_4^- as the counterions. Since the composition ratio of counterions for a platinum atom in the hydrogensulfate is twice as much as that in the sulfate, we can expect that the mixed-valence state of the complexes comprising SO_4^{2-} is clearly different from that of the complexes comprising HSO_4^-.

Layek and Papavassiliou[10] also reported the syntheses and Raman spectra of single crystals in WRA comprising SO_4^{2-} and HSO_4^-, $[Pt(en)_2][PtCl_2(en)_2](HSO_4)_4$ and $[Pt(en)_2][PtX_2(en)_2](SO_4)_2$ (X=Br, I), where en denotes ethylenediamine. We were able to prepare similar mixed-valence complexes, $[Pt(en)_2][PtBr_2(en)_2](HSO_4)_4$ (PBHS), $[Pt(en)_2][PtI_2(en)_2](HSO_4)_4 \cdot 4H_2O$ (PIHS), and $[Pt(en)_2][PtX_2(en)_2](SO_4)_2 \cdot 6H_2O$ {X=Br (PBSW), I (PISW)} which have different counterion composition and contain water of crystallization. In this paper, we report the syntheses and the optical properties of single crystals in PBHS, PIHS, PBSW, and PISW, and discuss the influence of the hydrogen bond on the Pt mixed-valence state.

Experimental

Preparation of the Constituent Complexes. The Pt(II) constituent complex $[Pt(en)_2]Cl_2$ was prepared by the procedure of Basolo et al.[11] The Pt(IV) constituent complexes $[PtBr_2(en)_2]Cl_2$ and $[PtI_2(en)_2]Cl_2$ were obtained by oxidation of $[Pt(en)_2]Cl_2$ in ethanol–water with Br_2 and I_2, respectively.

Preparation of the Mixed-Valence Complexes. The Pt(II)–Pt(IV) mixed-valence complexes were prepared by a procedure similar to that of Bekaroglu et al.[12] for $[Pt(en)_2][PtX_2(en)_2](ClO_4)_4$ (X=Br, I).

$[Pt(en)_2][PtBr_2(en)_2](HSO_4)_4$ (PBHS): $[Pt(en)_2]Cl_2$ (1.2 g) was dissolved in water (ca. 40 mL). This solution was divided into two equal parts. Water (ca. 100 mL) and ethanol (ca. 20 mL) were added into one of them, and Br_2 (ca. 0.1 mL) was dissolved in this solution with stirring. The color of the solution became pale yellow. The volume slowly reduced to ca. 70 mL on a hot plate. The solution, which had no odor of bromine, was then cooled and mixed with the other part of $[Pt(en)_2]Cl_2$ solution. A 62% aqueous sulfuric acid (ca. 3 mL) was then added. This solution was concentrated to ca. 10 mL on a water bath (ca. 40 °C) and then cooled. Green metallic lustrous needle-like crystals were obtained. They were filtered off and washed with diethyl ether; yield 1.6 g (87%). The single crystals were obtained by recrystallization from a dilute sulfuric acid solution. Found: C, 8.10; H, 3.00; N, 9.49; O, 21.96; S, 10.98; Br, 13.48%. Calcd for $C_8H_{36}Br_2N_8O_{16}Pt_2S_4$: C, 8.15; H, 3.08; N, 9.51; O, 21.72; S, 10.88; Br, 13.56%.

$[Pt(en)_2][PtI_2(en)_2](HSO_4)_4 \cdot 4H_2O$ (PIHS): $[Pt(en)_2]Cl_2$ (2.01 g) was dissolved in water (ca. 100 mL). This solution divided into two equal parts. An ethanol solution of I_2 (1.06 g/50 mL) was added to one of them. This solution was stirred overnight and evaporated to dryness by rotary evaporator to remove excess I_2. The residue was dissolved in water. This solution of Pt(IV) complex was added to the other part of $[Pt(en)_2]Cl_2$ solution, and the mixture was concentrated to ca. 40 mL on a hot plate. A 62% aqueous sulfuric acid (15 mL) was gradually added to the concentrated solution with stirring on an ice bath. Then, golden fine powdery solids were rapidly formed. This powder was filtered off, washed successively with a diethyl ether and sulfuric acid mixture (2:1, v/v), diethyl ether, and etanol; yield 2.59 g (74.2%). Plate-like single crystals were obtained by recrystallization from a dilute sulfuric acid solution. Found: C, 7.15; H, 3.06; N, 8.07; O, 23.87; I, 17.96%. Calcd for $C_8H_{44}I_2N_8O_{20}Pt_2S_4$: C, 7.15; H, 3.30; N, 8.33; O, 23.80; I, 18.87%.

$[Pt(en)_2][PtBr_2(en)_2](SO_4)_2 \cdot 6H_2O$ (PBSW): A solution, which contains a mixture of $[Pt(en)_2]Cl_2$ and $[PtBr_2(en)_2]Cl_2$, was prepared by the same procedure employed for the preparation of PBHS, using $[Pt(en)_2]Cl_2$ (3.66 g) and Br_2 (ca. 0.3 mL). An aqueous solution of Na_2SO_4 (2.0 g/20 mL) was added to the Pt(II)–Pt(IV) solution. This was concentrated on a steam bath to ca. 120 mL and then cooled. Reddish-brown plate-like crystals were obtained. They were filtered off and washed with ethanol; yield 4.41 g (85.4%). Single crystals were obtained by recrystallization from an aqueous solution. Found: C, 8.93; H, 4.10; N, 10.35; O, 20.44; S, 5.93; Br, 14.63%. Calcd for $C_8H_{44}Br_2N_8O_{14}Pt_2S_2$: C, 8.81; H, 4.07; N, 10.27; O, 20.54; S, 5.88; Br, 14.65%.

$[Pt(en)_2][PtI_2(en)_2](SO_4)_2 \cdot 6H_2O$ (PISW): A solution of $[Pt(en)_2]Cl_2$ and $[PtI_2(en)_2]Cl_2$ was prepared by the same procedure employed for the preparation of PIHS, using $[Pt(en)_2]Cl_2$ (3.17 g) and I_2 (2.0 g). To this solution, an aqueous solution of $NaHSO_4$ (1.9 g/10 mL) was added, and the mixture solution was concentrated on a steam bath to ca. 75 mL and then cooled. Golden lustrous plate-like crystals were obtained. They were filtered off and washed with a small amount of water; yield 3.13 g (64.4%). Single crystals were obtained by recrystallization from an aqueous solution. Found: C, 8.15; H, 3.70; N, 9.44; O, 18.77; I, 21.12%. Calcd for $C_8H_{44}I_2N_8O_{14}Pt_2S_2$: C, 8.11; H, 3.74; N, 9.46; O, 18.91; I, 21.43%.

$[Pt(en)_2][PtCl_2(en)_2](HSO_4)_4$ (PCHS): $[PtCl_2(en)_2]Cl_2$ (327 mg), which was obtained by oxidation of $[Pt(en)_2]Cl_2$ with an aqueous hydrogen peroxide solution, and $[Pt(en)_2]Cl_2$ (285 mg) were dissolved in water (ca. 20 mL). To this solution a 30% aqueous surfuric acid (ca. 2 mL) was added. This solution was slowly concentrated to a few milliliters at ca. 30 °C on a water bath. Red needle-like crystals obtained, were filtered off and dried in a desiccator containing silica gel. Yield 0.39 g (48%). Found: C, 8.78; H, 3.29; N, 9.82; O, 24.17; S, 11.77; Cl, 6.53%. Calcd for $C_8H_{36}Cl_2N_8O_{16}Pt_2S_4$: C, 8.82; H, 3.33; N, 10.28; O, 23.49; S, 11.77; Cl, 6.51%.

Elemental analysis was carried out by "The Laboratory for Organic Elemental Microanalysis" of Kyoto University.

Instrumental Measurements. Powder X-ray diffraction patterns were recorded at room temperature on a Rigaku diffractometer using the θ–2θ scan technique and graphite-monochromated Cu $K\alpha$ radiation (λ=1.5418 Å). For PBHS, PBSW, and PISW, lattice constants were obtained on a Rigaku four-circle diffractometer.

The TGA was performed on a Rigaku TG DTA 8112S apparatus in the temperature region from room temperature to 200 °C.

The absorption spectra of single crystals were measured at 4.2 K with a Jasco CT-100 spectrometer using a tungsten lamp for the light source and a Glan-Taylar prism for polarizing light. A lock-in system working with HTV R376 and R316 photomultipliers and a PbS photoconductive cell was used for detection. The sample was placed in glass Dewar's vessel and immersed in liquid helium to cool. The typical sizes of measured samples are 2×1×0.2 (mm^3) for PBHS, 3×2×0.06 (mm^3) for PIHS, 3×2×0.4 (mm^3) for PBSW, and 4×3×0.04 (mm^3) for PISW.

The absorption spectra of solutions were measured at room temperature with a Hitachi model 356 Double Beam Spectrophotometer.

Results and Discussion

Compounds. The complexes PBHS and PIHS are recrystallized from an aqueous sulfuric acid solution, and the PBSW and PISW are recrystallized from an aqueous solution. The result shows that the concentration of SO_4^{2-} and HSO_4^-, namely, the pH of the crystallizing solution dominates whether the hydrogensulfate or the sulfate crystallizes.

Table 1 shows the appearance of the single crystals of PCHS, PBHS, PIHS, PBSW, and PISW. Both the iodo-bridged mixed-valence complexes, PIHS and PISW, are golden in color. However, the bromo-

Table 1. Crystal Appearance of Mixed-Valence Complexes

Complex		Color		Shape
		Crystal	Powder	
$[Pt(en)_2][PtCl_2(en)_2](HSO_4)_4$	PCHS	Dull red	Red	Needle
$[Pt(en)_2][PtBr_2(en)_2](HSO_4)_4$	PBHS	Metallic green	Green	Needle
$[Pt(en)_2][PtI_2(en)_2](HSO_4)_4 \cdot 4H_2O$	PIHS	Golden	Black	Plate
$[Pt(en)_2][PtBr_2(en)_2](SO_4)_2 \cdot 6H_2O$	PBSW	Reddish brown	Orange	Plate
$[Pt(en)_2][PtI_2(en)_2](SO_4)_2 \cdot 6H_2O$	PISW	Golden	Black	Plate

Table 2. Lattice Constants of PCHS, PBHS, PBSW, and PISW

Complex	a/Å	b/Å	c/Å	β/°
PCHS[a]	9.27	14.43	10.94[c]	—
PBHS[a]	9.263(1)	14.317(3)	11.036(5)[c]	—
PBSW[b]	14.012(2)	11.494(2)[c]	9.217(1)	102.08(1)
PISW[b]	14.044(2)	11.662(1)[c]	9.292(1)	103.16(1)

a) Orthorhombic. b) Monoclinic. c) Pt chain axis.

Table 3. Results of TGA in the Temperature Range from Room Temperature to 200 °C

Complex	Exp.		Calcd wt(%)[a]
	Wt loss (%)	Temp range (°C)	
PIHS	1.4	24—48	
	3.1	60—84	
	1.1	90—122	
	5.6	(Total)	5.4
PBSW	9.8	87—148	9.9
PISW	9.0	86—178	9.1

a) Weight percentages of water of crystallization in chemical formulas estimated from the elemental analysis.

bridged complexes, PBHS and PBSW, are different in color. Although PBHS and other bromo-bridged mixed-valence platinum complexes analogous to WRS are all metallic lustrous green in color, PBSW is similar to chloro-bridged complexes in color.

The powder X-ray diffraction pattern shows that PCHS and PBHS are isomorphous, and that PBSW and PISW are isomorphous. The X-ray pattern of PIHS is different from that of PCHS, PBHS, PBSW, and PISW. These results are consistent with the results of the elemental analysis.

Table 2 shows the lattice constants of PCHS,[13] PBHS,[14] PBSW,[15] and PISW.[15] The distance between Pt atoms on the chain can be preliminary estimated from the lattice constant of the Pt chain axis. The Pt-Pt distances of PCHS and PBHS are as long as that of other chloro- and bromo-bridged complexes with a univalence counterion.[16-18] On the other hand, the Pt-Pt distance of PBSW (5.747(2) Å) is longer than that of PBHS (5.518(5) Å), and that of PISW (5.831(1) Å) are also slightly longer than that of the iodo-bridged complexes with a univalence counterion and a bidentate amine.[18-20] The results show that the Pt-Pt distance of the complexes with a bivalence counterion is longer than that of the complexes with a univalence counterion.

For the WRA halogen-bridged mixed-valence complexes of which the structures were known, the chloro- and bromo-bridged complexes[16-18,21-25] are isomorphous each other, but are different from the corresponding iodo-bridged complex[19,20,26] in structure. The structures of the hydrogensulfates are classified into two groups in structure as same as above mentioned, namely the group of the chloro- and bromo-bridged complexes and the group of the iodo-bridged complex. For the sulfates, however, the bromo- and iodo-bridged complexes are isomorphous. It is the first example of the corresponding bromo- and iodo-bridged complexes belonging to the same group in structure, according to our knowledge.

Table 3 shows the results of TGA obtained from room temperature to 200 °C. The weight loss on heating of PIHS, PBSW, and PISW is consistent with the weight percentage of the water of crystallization in chemical formulas estimated from the elemental analysis. Thus, the complexes PIHS, PBSW, and PISW contain water of crystallization. In the hydrogensulfates PCHS, PBHS, and PIHS, only the iodo-bridged complex PIHS contains water of crystallization, which can be explained by the following considerations. The Pt-Pt distance of the iodo-bridged complexes is longer than that of the chloro- and bromo-bridged complexes, because iodide ion is the largest among the halide ions, (Cl^-, Br^-, and I^-). Thus, in the case that the framework of the halogen-bridged Pt complex column are only retained in the crystal structure of the halogen-bridged mixed-valence complexes, the cavity size between the halogen-bridged Pt chains of PIHS is larger than that of PCHS and PBHS. The water of crystallization of PIHS, therefore, is needed to occupy a free space which the counterions cannot occupy in the cavity between the Pt chains. Since the complexes PCHS and PBHS will not have the free space, they don't contain the water of crystallization. Similar mixed-valence complexes, $[Pt(NH_3)_4][PtX_2(NH_3)_4](HSO_4)_4$ (X=Cl,[16] Br[22,23]) and $[Pt(NH_3)_4][PtI_2(NH_3)_4](HSO_4)_4 \cdot 2H_2O$[26] were previously reported. For the hydrogensulfates of the ammonia complexes, equally, only the iodo-bridged complex contains the water of crystallization. For the water of crystallization in the sulfates PBSW and PISW, the

same explanation is given. Because the sulfates contain one-half of the counterions in the hydrogensulfates, the free space which the counterions don't occupy in the cavity between the Pt chains of the sulfates is larger than that of the hydrogensulfates. The sulfates PBSW and PISW, therefore, contain six molecules of water of crystallization per a chemical formula. We consider that whether or not the WRA mixed-valence complexes contain water of crystallization depends on the free space, namely, the relation between the volume of the counterion and the cavity between the Pt chains.

Similar WRA, $[Pt(en)_2][PtCl_2(en)_2](HSO_4)_4$, and $[Pt(en)_2][PtX_2(en)_2](SO_4)_2$ (X=Br, I) were previously reported by Layek and Papavassiliou.[10] Our chloro-bridged complex PCHS is the same as their chloro-bridged complex from the elemental analysis, whereas our bromo-bridged complexes PBHS and PBSW, and our iodo-bridged complexes PIHS and PISW are different from their bromo- and iodo-bridged complexes, respectively. Thus, our complexes PBHS, PIHS, PBSW, and PISW are new WRA halogen-bridged mixed-valence platinum complexes.

Spectra. Figures 1, 2, 3, and 4 show the absorption spectra of the single crystal in PBHS, PIHS, PBSW and PISW at 4.2 K and the corresponding spectra of aqueous solutions at room temperature, respectively.

The solution spectrum of PBHS is the same as that of PBSW, and that of PIHS is the same as that of PISW. In the solution, thus, an electronic state of the platinum complex in the hydrogensulfate is the same as that in the sulfate. This is consistent with the fact that the recrystallization of the hydrogensulfate and the sulfate depends on the pH of the recrystallizing solution as above mentioned.

The single crystal absorption spectra of the WRA mixed-valence complexes with univalence anions have been reported.[4,6,27] The single crystal absorption spectra of the WRA mixed-valence complexes with bivalence anions, however, have not yet been reported, except for our previous paper.[28] The absorption spectra of the single crystal in PBSW and PISW are reported for the first time in the WRA mixed-valence complexes with bivalence counterions.

Single crystals of PBHS, PIHS, PBSW, and PISW showed the strong absorption spectra in the region from visible to near-infrared. These spectra are attributed to the intervalence charge-transfer transition from Pt(II) to Pt(IV), which is a common feature of the WRA mixed-valence complexes, namely the class II mixed-valence compounds.[29] The single crystal spectra in this region showed a remarkable dichroism.

The strong absorption spectra for E//chain are due to the charge-transfer transition from the d_{z^2} of Pt(II) to the d_{z^2} of Pt(IV),[4,27] which is only allowed by selection rule for the light polarized parallel to the Pt chain axis. Absorption coefficients of the strong

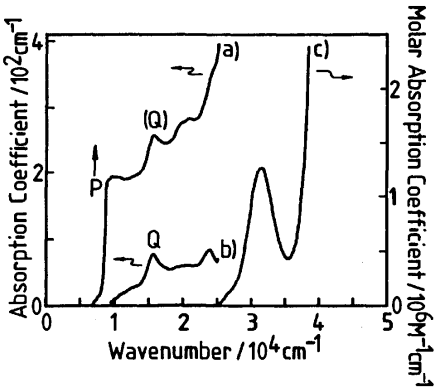

Fig. 1. Single crystal absorption spectra at 4.2 K and solution absorption spectrum at room temperature (R.T.) of $[Pt(en)_2][PtBr_2(en)_2](HSO_4)_4$ (PBHS). Curve a) is single crystal spectrum for the light polarized parallel to the Pt chain axis (E//chain). Curve b) is single crystal spectrum for the light polarized perpendicular to the Pt chain axis ($E\perp$chain). Curve c) is solution spectrum.

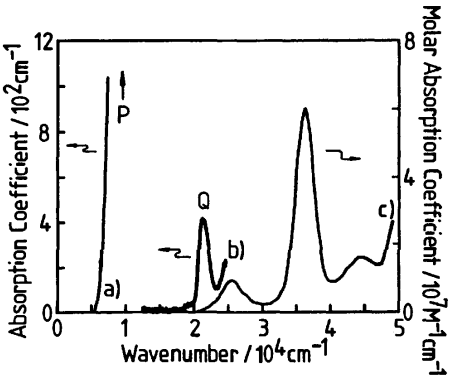

Fig. 2. Single crystal absorption spectra at 4.2 K and solution absorption spectrum at R.T. of $[Pt(en)_2][PtI_2(en)_2](HSO_4)_4 \cdot 4H_2O$ (PIHS). Curve a) is single crystal spectrum for E//chain. Curve b) is single crystal spectrum for $E\perp$ chain. Curve c) is solution spectrum.

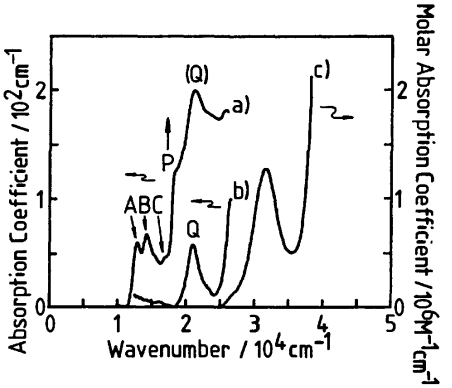

Fig. 3. Single crystal absorption spectra at 4.2 K and solution absorption spectrum at R.T. in $[Pt(en)_2][PtBr_2(en)_2](SO_4)_2 \cdot 6H_2O$ (PBSW). Curve a) is single crystal spectrum for E//chain. Curve b) is single crystal spectrum for $E\perp$chain. Curve c) is solution spectrum.

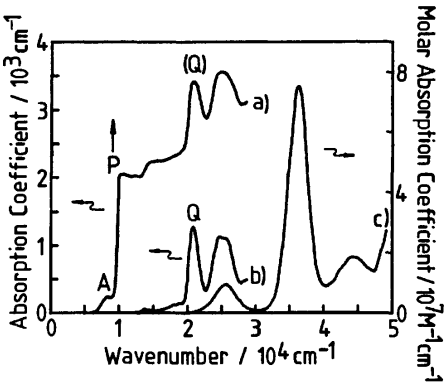

Fig. 4. Single crystal absorption spectra at 4.2 K and solution absorption spectrum at R.T. in $[Pt(en)_2][PtI_2(en)_2](SO_4)_2 \cdot 6H_2O$ (PISW). Curve a) is single crystal spectrum for E//chain. Curve b) is single crystal spectrum for $E\perp$chain. Curve c) is solution spectrum.

absorption region in these single crystal spectra are saturated. The notation P in Figs. 1—4 shows the absorption edge of the low energy side of the absorption band due to the charge-transfer transition from the d_{z^2} of Pt(II) to the d_{z^2} of Pt(IV). The absorption band Q is due to the charge-transfer transition from an electronic state consisting mainly of d_{xz} and d_{yz} orbitals of Pt(II) to a state consisting mainly of d_{z^2} of Pt(IV).[27] This is allowed only for the light polarized perpendicular to the Pt chain axis ($E\perp$chain). However, this absorption band Q appears also in the spectrum with E//chain. We consider that the structure in the region of the saturated absorption coefficient for E//chain is attributed to a leakage of the spectrum for $E\perp$chain by a slight optical inhomogeneity, as previously reported.[8] Table 4 shows the energy of the absorption edges P and the bands Q of PBHS, PIHS, PBSW, and PISW. In the case of hydrogensulfates whose counterion is univalence, the energy of P of PBHS is higher than that of PIHS. Equally, in the case of sulfates whose counterion is bivalence, the energy of P of PBSW is higher than that of PISW. In both univalence and bivalence salts the energy of P of the bromo-bridged complex is higher than that of the iodo-bridged complex.

Comparison between PBHS and PBSW, and comparison between PBSW and PISW show that the energy shift of P by substituting counterion (i.e. PBSW → PBHS) is comparable to that by substituting bridging halogen (i.e. PBSW → PISW). Namely, the energy of the absorption edge of the iodo-bridged sulfate PISW with the bivalence counterion is as much as that of the bromo-bridged hydrogensulfate PBHS with the univalence counterion. Thus, one can conclude that an influence of the substitution of the univalence counterion HSO_4^- with the bivalence counterion SO_4^{2-} on the Pt(II)-Pt(IV) mixed-valence state is comparable to that of the substitution of the bridging halogen. The energy of the absorption edge of the bromo-bridged sulfate PBSW is comparable to WRS[4] and $[Pt(en)_2][PtCl_2(en)_2](ClO_4)_4$.[27]

Table 4. The Energy of the Intervalence Charge-Transfer Absorption Edges P and Bands Q at 4.2 K

Complex	P/10^3 cm^{-1}	Q/10^3 cm^{-1}
PBHS	8.4	15.6
PIHS	6.4	21.4
PBSW	17.7	21.1
PISW	9.5	20.9

We consider that the influence of substituting the counterion on these charge-transfer absorption edges is explained by the network of the hydrogen bonds which play a role of the bond between a platinum atom and an adjacent platinum on a chain by way of the amine (NH_2) and the counterion (Y) as shown in Fig. 5. The hydrogensulfates with the univalence counterion have more hydrogen bonds than the sulfates with the bivalence counterion, because the molar ratio of the counterions for a platinum atom in the hydrogensulfates is twice the ratio in the sulfates. Thus, the bond between a platinum atom and an adjacent platinum atom on a chain in the univalence counterion complexes is more strongly supported by the outerchain bridge of the hydrogen bond than that in the bivalence counterion complexes. The energy difference between the electronic states of Pt(II) and those of Pt(IV) in the univalence counterion complexes is smaller than that in the bivalence counterion complexes. Consequently, the energy of the absorption edge due to the charge-transfer transition from the d_{z^2} of Pt(II) to the d_{z^2} of Pt(IV) in the univalence counterion complexes is lower than that in the bivalence counterion complexes.

Furthermore, the result that the influence of the substitution of the counterion on the Pt mixed-valence state is comparable to the influence of the substitution of the bridging halogen, suggests that the formation of the WRA mixed-valence complexes can be interpreted by two contributions, as follows. (1)

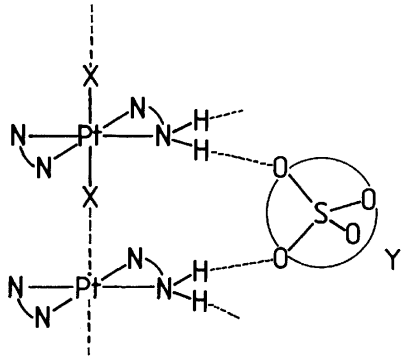

Fig. 5. The linkage between Pt(II) and Pt(IV) on a chain by hydrogen bonds through amines and counterions.

The charge-transfer interaction between the Pt(II) and Pt(IV) atoms becomes stronger in order of Cl, Br, and I which are the bridging halogen, because the energy of the intervalence charge-transfer absorption bands[7] and the energy distinction between the Pt(II) and Pt(IV) peaks in the XPS measurement[5] decrease in order of Cl, Br, and I. These results are in accordance with that the overlap integral between Pt(II) and Pt(IV) increase in the order of Cl, Br, and I. Accordingly, the ability to form the mixed-valence complexes increases in the order of Cl, Br, and I. (2) The charge-transfer interaction between the Pt(II) and Pt(IV) in the mixed-valence complexes having more counterions per a platinum atom is stronger than that in the complexes having less counterions, because the counterions link $[Pt^{IV}X_2(en)_2]^{2+}$ with $[Pt^{II}(en)_2]^{2+}$ on a chain by hydrogen bonds as shown in Fig. 5. Consequently, the charge-transfer interaction between the Pt(II) and Pt(IV) in the hydrogensulfates is stronger than that in the sulfates. In other words, the ability to form the mixed-valence complexes in the hydrogensulfates is larger than that in the sulfates.

In the energy region below the charge-transfer absorption edge P, weak absorption bands have been observed in the single crystal spectra of the sulfates PBSW and PISW for *E*//chain. This weak absorption band of PISW is noted by A in Fig. 4, and the weak absorption bands of PBSW are noted by A, B, and C in Fig. 3. The weak absorption band A of PISW, which has been recently reported partially in our previous paper,[28] and the weak absorption bands A, B, and C of PBSW will be attributed to the transition related to some kinds of defects, namely, Pt(III), Pt(IV)Pt(II)Pt(II)Pt(IV), and Pt(II)Pt(IV)Pt(IV)Pt(II) on individual Pt chains. In the case of the hydrogensulfats PBHS and PIHS, however, these weak absorption bands could not be observed. This result can be explained by the following consideration. In the hydrogensulfates, it is difficult to produce these defects, because the hydrogen bond network strongly links $[Pt^{IV}X_2(en)_2]^{2+}$ to $[Pt^{II}(en)_2]^{2+}$ on individual chains. On the other hand, in the sulfates, the defects are easily produced, because the hydrogen bond network weakly links the Pt atoms. Investigation of the dependence of the weak absorption bands on compounds will be also necessary.

The authors wish to thank Professor Tooru Taga of Kyoto University for obtaining the lattice constants of PBHS, and Dr. Koshiro Toriumi of I.M.S. for obtaining those of PBSW and PISW on a four-circle diffractometer. We are also indebted to Dr. Naohilo Watanabe of Kyoto University for his kind help and advice for data processing computer programs. This study was supported by the Grant-in-Aid for Scientific Research No. 63540485 from the Ministry of Education, Science, and Culture.

References

1) H. J. Keller, "Extended Linear Chain Compounds," ed by J. S. Miller, Plenum, New York (1982), p. 357.
2) R. J. H. Clark, "Mixed-Valence Compounds," ed by D. B. Brown, Reidel, Dordrecht (1980), p. 271.
3) K. Nasu, M. Yamashita, T. Mitani, and S. Kurita, *Butsuri*, **41**, 317 (1986).
4) P. Day, "Low-Dimensional Cooperative Phenomena," ed by H. J. Keller, Plenum, New York (1974), p. 191.
5) M. Yamashita, N. Matsumoto, and S. Kida, *Inorg. Chim. Acta*, **31**, L381 (1978).
6) S. Yamada and R. Tsuchida, *Bull. Chem. Soc. Jpn.*, **29**, 894 (1956).
7) K. Nasu, *J. Phys. Soc. Jpn.*, **52**, 3865 (1983); **53**, 302 (1984); **53**, 427 (1984).
8) Y. Wada, T. Mitani, M. Yamashita, and T. Koda, *J. Phys. Soc. Jpn.*, **54**, 3143 (1985).
9) R. J. H. Clark and M. Kurmoo, *Inorg. Chem.*, **19**, 3522 (1980).
10) D. Layek and G. C. Papavassiliou, *Z. Naturforsch.*, **36b**, 83 (1981).
11) F. Basolo, J. C. Bailar, Jr., and B. R. Tarr, *J. Am. Chem. Soc.*, **72**, 2433 (1950).
12) O. Bekaroglu, H. Breer, H. Endres, H. J. Keller, and H. Nam-Gung, *Inorg. Chim. Acta*, **21**, 183 (1977).
13) The lattice constants of PCHS were determined from the powder X-ray diffraction pattern.
14) N. Matsushita, T. Taga, N. Kojima, T. Ban, and I. Tsujikawa, manuscript in preparation for all crystal structure analysis of PBHS.
15) N. Matsushita, K. Toriumi, N. Kojima, T. Ban, and I. Tsujikawa, manuscript in preparation for all crystal structure analyses of PBSW and PISW.
16) N. Matsumoto, M. Yamashita, and S. Kida, *Mem. Fac. Sci., Kyushu Univ., Ser.C*, **11**, 209 (1978).
17) M. Cannas, M. B. Lucchesini, and G. Marongiu, *Acta Crystallogr., Sect.C*, **39**, 1514 (1983).
18) H. Endres, H. J. Keller, R. Martin, U. Traeger, and M. Novotny, *Acta Crystallogr., Sect. B*, **36**, 35 (1980).
19) H. Breer, H. Endres, H. J. Keller, and R. Martin, *Acta Crystallogr., Sect.B*, **34**, 2295 (1978).
20) H. Endres, H. J. Keller, R. Martin, H. Nam-Gung, and U. Traeger, *Acta Crystallogr., Sect. B*, **35**, 1885 (1979).
21) P. E. Fanwick and J. L. Huckaby, *Inorg. Chem.*, **21**, 3067 (1982).
22) M. Tanaka, I. Tsujikawa, K. Toriumi, and T. Ito, *Acta Crystallogr., Sect. B*, **38**, 2793 (1982).
23) R. J. H. Clark, M. Kurmoo, A. M. R. Galas, and M. B. Hursthouse, *J. Chem. Soc., Dalton Trans.*, **1982**, 2505.
24) A. L. Beauchamp, D. Layek, and T. Theophanides, *Acta Crystallogr., Sect. B*, **38**, 1158 (1982).
25) M. Yamashita, K. Toriumi, and T. Ito, *Acta Crystallogr., Sect. C*, **41**, 876 (1985).
26) M. Tanaka, I. Tsujikawa, K. Toriumi, and T. Ito, *Acta Crystallogr., Sect. C*, **42**, 1105 (1986).
27) M. Tanaka, S. Kurita, T. Kojima, and Y. Yamada, *Chem. Phys.*, **91**, 257 (1984).
28) N. Matsushita, N. Kojima, T. Ban, and I. Tsujikawa, *J. Phys. Soc. Jpn.*, **56**, 3808 (1987).
29) M. B. Robin and P. Day, *Adv. Inorg. Chem. Radiochem.*, **10**, 247 (1967).

Anomalous Peak Intensities in the EXAFS of Polynuclear Molybdenum Compounds

Takafumi MIYANAGA, Takashi FUJIKAWA,† Nobuyuki MATSUBAYASHI,†† Takao FUKUMOTO, Kunihiko YOKOI,††† Iwao WATANABE,* and Shigero IKEDA††††
Department of Chemistry, Faculty of Science, Osaka University, Toyonaka, Osaka 560
†Faculty of Engineering, Yokohama National University, Yokohama 240
††National Chemical Laboratory for Industry, Yatabe, Ibaraki 305
†††Department of Chemistry, Osaka Kyoiku University, Ikeda, Osaka 563
††††Institute of Science and Technology, Ryukoku University, Fushimi-ku, Kyoto 612
(Received June 17, 1988)

EXAFS (Extended X-ray Absorption Fine Structure) experiments on various polynuclear molybdate and tungstate compounds revealed the unusual phenomenon that Mo-O peaks which should appear at around 1.9 Å in Fourier transforms of the EXAFS spectra for $Mo_6O_{19}^{2-}$ and $PMo_{12}O_{40}^{3-}$ are hardly discernible, while the tungstates and other molybdates give the metal-oxygen peaks normally. It is concluded that the Debye-Waller factors for the metal-bridging oxygen bonds in $Mo_6O_{19}^{2-}$ and $PMo_{12}O_{40}^{3-}$ are exceptionally large ($\geqq$ 0.08 Å). The shape of the Raman bands for the $Mo_6O_{19}^{2-}$ pertaining to the vibration involving the bridging oxygens supports the large σ values estimated. EXAFS measurements were also performed for $AsMo_{12}O_{40}^{3-}$, $SiMo_{12}O_{40}^{4-}$, and $PMo_{12}O_{40}^{3-}$. The compounds with large Debye-Waller factors seem to be unstable against reductants.

EXAFS studies of molybdenum compounds have been attempted because of their interesting structures[1,2] and their reactivity as catalysts.[3]

The hexavalent molybdenum ion exists as a monomeric form of MoO_4^{2-} in a neutral or alkaline solution. In an acidic solution, the ion exists in the form of either $Mo_7O_{24}^{6-}$, $Mo_8O_{26}^{4-}$, or $Mo_6O_{19}^{2-}$, depending on the acidity of the solution. Heteropoly complexes of the Keggin structure, e.g., $PMo_{12}O_{40}^{3-}$, also exist in the presence of the PO_4^{3-} ion. Other heteropoly complexes are also known in which the P atom is replaced with Si, As, or Ge. Some of the Mo(VI) atoms in the polynuclear complexes can be reduced to form so-called molybdenum-blue. The polytungstates, e.g., $W_6O_{19}^{2-}$ and $PW_{12}O_{40}^{3-}$, with structures similar to those of the corresponding molybdenum complexes, are also known.

These molybdates and tungstates have been isolated as crystals, and their structures have been determined by the X-ray diffraction method. According to the literature, molybdenum in MoO_4^{2-} is coordinated by four oxygen atoms with the Mo-O distances of 1.75—1.78 Å.[4] $Mo_7O_{24}^{6-}$ and $Mo_6O_{19}^{2-}$ are composed of seven and six MoO_6 distorted octahedral units, respectively. In $Mo_6O_{19}^{2-}$ (Fig. 1a), the Mo-O bond distances have been reported to be 1.68 Å for terminal double bonds, 1.86—2.01 Å for bridging oxygens, and 2.32 Å for a central bridging oxygen.[5] The heteropoly compound, $PMo_{12}O_{40}^{3-}$ (Fig. 1b), has similar octahedral units around a central phosphorous atom.[6] Although the interatomic distances in the compounds of tungstates are not exactly the same as those in molybdates, the geometrical structures of the molybdenum and tungsten polynuclear compounds are quite similar to each other, e.g., $Mo_6O_{19}^{2-}$/$W_6O_{19}^{2-}$, and $PMo_{12}O_{40}^{3-}$/$PW_{12}O_{40}^{3-}$.

During the course of the EXAFS studies of these

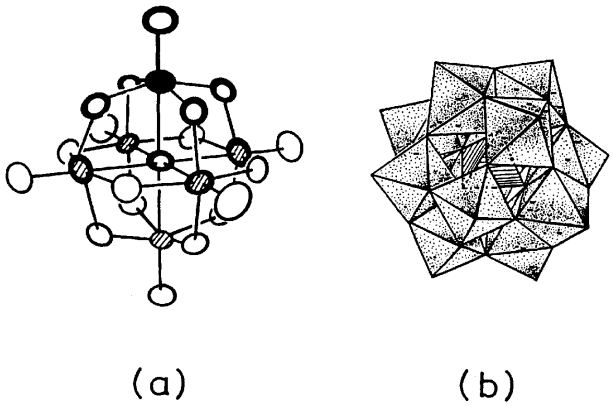

Fig. 1. (a) The structure of $Mo_6O_{19}^{2-}$ complex. The atoms circled with heavy line are included in the multiple scattering calculations. ◎ Molybdenum, ○ oxygen, and ● X-ray absorbing molybdenum atom. (b) The structure of Keggin type complex. Each octahedron represents MO_6 unit.

complexes in solution, we found the unusual phenomenon that the Mo-O peaks are hardly discernible in Fourier transforms for $Mo_6O_{19}^{2-}$ and $PMo_{12}O_{40}^{3-}$, while other molybdenum and tungsten compounds give normal peak intensities.[7] It is extremely important to know why the first shell atoms, which are normally the most easily detectable atoms by the EXAFS method, give almost no EXAFS peaks. Our lack of knowledge of the cause makes the use of the EXAFS technique too dangerous for structure analysis.

Since the anomalous peak intensities appear only for the samples of highly symmetrical $Mo_6O_{19}^{2-}$ and $PMo_{12}O_{40}^{3-}$, and not for low-symmetry samples (e.g., $Mo_7O_{24}^{6-}$), it is possible that this phenomenon is connected only to specified geometrical configurations. We must introduce a multiple-scattering the-

ory for the EXAFS analysis in order to discriminate between geometrical configurations, because the single-scattering theory treats only interatomic distances from the X-ray absorbing atom, i.e., the Mo-O and Mo-Mo distances. As far as Mo-O bonds are concerned, the single-scattering theory regards these complex polymers as simple MoO_6 octahedra. There is no room in the theory for the consideration of the symmetries of the complexes as to how the octahedral units are connected.

In the present paper, the origin for those anomalous peak intensities will be discussed from the points of view of the multiple-scattering effect and the Debye-Waller factor, which, of course, is a key parameter determining the peak intensities. Consequently, the large Debye-Waller factor for several molybdenum complexes are inferred and confirmed by the Raman spectroscopy.

Experimental

The $Na_2MoO_4 \cdot 2H_2O$, $(NH_4)_6Mo_7O_{24} \cdot 4H_2O$, and $Na_2WO_4 \cdot 2H_2O$ were purchased from Wako Pure Chemical Industries, Ltd., and the MoO_3, from the Merck Company. The $[(C_4H_9)_4N]_2Mo_6O_{19}$,[8] $[(C_4H_9)_4N]_2W_6O_{19}$,[9] $PMo_{12}O_{40}^{3-}$-TBA ($(C_4H_9)_4N^+$) salt, $AsMo_{12}O_{40}^{3-}$-TBA salt, $SiMo_{12}O_{40}^{4-}$-TBA salt, and $PW_{12}O_{40}^{3-}$-TEA($(C_2H_5)_4N^+$) salt were prepared according to the literature.[10] A partially reduced species of $PMo_{12}O_{40}^{3-}$, molybdenum-blue, was prepared by the reduction with ascorbic acid. The X-ray absorption spectra of Mo K-edge and W L_{III}-edge were obtained at BL-7C and 10B of the Photon Factory of the National Laboratory for High Energy Physics (KEK). The storage ring was operated at 2.5 GeV, and the ring current was between 150—200 mA. A Si(111) double-crystal monochromator and a Si(311) channel-cut crystal monochromator were used. The solid samples were powdered and loaded on adhesive tapes. The liquid samples were placed in a polyethylene pouch.

The Raman spectra of the powdered samples were measured with an Ar ion laser (5145 Å) at room temperature and at 88 K.

Data Analysis and Calculations

The EXAFS data treatments have been described in detail elsewhere,[11] and so they will be only briefly treated in this section. The EXAFS oscillation $\chi(k)$ is extracted from the absorption spectrum $\mu(k)$ as follows:

$$\chi(k)=[\mu(k)-\mu_0(k)]/\mu_0(k). \quad (1)$$

The background absorption $\mu_0(k)$ is obtained from the least-square fitting of the pre-edge region (about 300 eV) to the Victoreen formula, $a\lambda^3-b\lambda^4+c$, where a, b, and c are the constants and where λ is the wavelength of the incident X-ray. The c constant is introduced in order to correct the difference in the sensitivities of the ionization detectors for I and I_0. In order to remove low-frequency noises from $\chi(k)$, the following method is used. The second-order seven-point smoothing is applied to the $\chi(k)$ data until only the lowest-frequency component of significant signals remains. Subsequently, a base line is obtained by using a third-order natural spline method with which the center points of the oscillation in the smoothed spectrum are connected. Thus, the low-frequency noises are removed from $\chi(k)$ by subtracting the base line obtained. In the single-scattering approximation, the extracted EXAFS is described as:

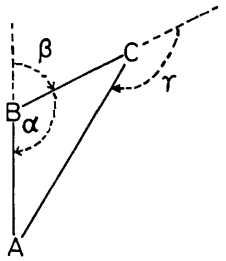

Fig. 2. Schematic representation of a triatomic system. A is the X-ray absorbing atom, and B and C are the scattering atoms.

$$\chi(k)=\sum_j S_j k^{-1} N_j r_j^{-2} f_j(k) \exp(-2r_j/\eta) \exp(-2k^2\sigma_j^2) \times \sin[2kr_j+\psi_j(k)], \quad (2)$$

where k is the photoelectron wave vector defined as:

$$k=[2m(E-E_0)]^{1/2}/\hbar. \quad (3)$$

E and E_0 are the photon energy and the threshold energy, respectively. S_j is the damping factor by the multielectron effect, m is the mass of an electron, N_j is the number of atoms located at distance r_j, η is the mean free path of the photoelectron, and σ_j is the root-mean-square displacement of r_j (the RMSRD or Debye-Waller factor). The backscattering amplitude $f_j(k)$ and the phase shift $\psi(k)$ calculated by Teo and Lee[12] are used for the Fourier transforms. The energy at the half height of the edge jump is used as the value of E_0.

The multiple-scattering calculations for EXAFS are performed according to the following equation for the triatomic model (A,B,C) shown in Fig. 2:[13,14]

$$\begin{aligned}\chi_{AC}(k)=&[(-1)^l/k]\{f_C(\pi)\exp(-2\sigma_{AC}^2k^2)\\ &\times\sin[2kr_{AC}+2\delta_l+\psi_C(\pi)]/r_{AC}^2+[2\cos(\gamma-\alpha)f_B(\beta)f_C(\gamma)/\\ &(r_{AB}r_{BC}r_{AC})]\exp[-(1-\cos\beta)^2k^2\sigma_{AB}^2/2]\\ &\times\exp[-(1-\cos\gamma)^2k^2\sigma_{AC}^2/\\ &2]\sin[k(r_{AB}+r_{BC}+r_{AC})+2\delta_l+\psi_B(\beta)\psi_C(\gamma)]+[f_B(\beta)^2f_C(\pi)/\\ &(r_{AB}^2r_{BC}^2)]\exp[-(1-\cos\beta)^2k^2\sigma_{AB}^2]\exp(-2k^2\sigma_{BC}^2)\\ &\times\sin[2k(r_{AB}+r_{BC})+2\delta_l+2\psi_B(\beta)+\psi_C(\pi)]\},\end{aligned} \quad (4)$$

where δ_l is the phase shift of the central atom with an angular momentum l and where ψ is that of the scattering atom. The muffin-tin potential of atoms with a neutral charge is assumed for the scattering field.

Results

EXAFS Spectra. Figure 3 shows the Fourier transforms of the Mo K-edge EXAFS for molybdenum com-

pounds and of the W L_{III}-edge EXAFS for tungsten compounds. The peak corresponding to Mo-O is present at 1.77 Å in the spectrum for MoO_4^{2-} (Fig. 3a). In the spectrum for MoO_3 (Fig. 3b), two peaks corresponding to Mo-O and Mo-Mo appear at 1.79 Å and 3.60 Å, respectively. Although several Mo-O bonds with different lengths are present in $Mo_7O_{24}^{6-}$, the bonds give only a single peak at 1.75 Å in the Fourier transform, and the Mo-Mo peak lies at 3.20 Å in the spectrum (Fig. 3c).

To our great surprise, we find quite an unusual phenomenon in the Fourier transform spectrum for $Mo_6O_{19}^{2-}$ (Fig. 3d). That is, the Mo-O peaks for the complex which should appear at somewhere around 1.9 Å are hardly discernible, while a high and sharp peak corresponding to the oxygen-bridged Mo-Mo distance appears at 3.26 Å. The X-ray diffraction results predict that both the Mo-O and Mo-Mo peaks for $Mo_6O_{19}^{2-}$ should be higher than those for $Mo_7O_{24}^{6-}$, since the structure of $Mo_6O_{19}^{2-}$ is highly symmetrical compared to $Mo_7O_{24}^{6-}$.[15] The EXAFS measurements were repeated at 20 K in order to study the effect of thermal vibration on the peak height for the Mo-O bonds. The result, shown as a broken line in Fig. 3d, is essentially the same as that obtained at room temperature. This indicates that the disappearance of the peak is not caused by the thermal vibration. In contrast to the result for $Mo_6O_{19}^{2-}$, the spectrum for $W_6O_{19}^{2-}$ is quite normal (Fig. 3f); there are two peaks corresponding to the terminal W=O (1.66 Å) and the bridging W-O (1.96 Å) bonds in addition to a W-W peak (3.45 Å).

An analogous phenomenon appears in heteropoly acids, as is shown in Fig. 4. The Mo-O peaks are very much obscured in the spectrum for $PMo_{12}O_{40}^{3-}$ (a), while peaks corresponding to W=O (1.60 Å) and W-O (1.98 Å) appear in that for $PW_{12}O_{40}^{3-}$(b). However, the Mo-O peak appears at 1.92 Å in the spectrum for the reduced $PMo_{12}O_{40}$ species (c).

$AsMo_{12}O_{40}^{3-}$ and $SiMo_{12}O_{40}^{4-}$ form the same structure as $PMo_{12}O_{40}^{3-}$. In the spectrum for $AsMo_{12}O_{40}^{3-}$ (d), the Mo-O peaks are poorly characterized, in a manner similar to that found for $PMo_{12}O_{40}^{3-}$ (a), whereas the Mo-O peak appears rather clearly at 1.85 Å in the spectrum for $SiMo_{12}O_{40}^{4-}$ (e).

Multiple-Scattering Calculation. The EXAFS analysis are normally done using a single-scattering theory. In this section we will study whether a photoelectron standing wave can be diminished for the system taking a special geometrical arrangement of scattering atoms due to a multiple-scattering effect, thus causing the peak in the Fourier transform to disappear. Figure 5 shows the calculated EXAFS oscillation spectra and their Fourier transforms, which were obtained by the use of the single-scattering (solid line) and multiple-scattering (broken line) theories. The atoms marked with a heavy line in Fig.

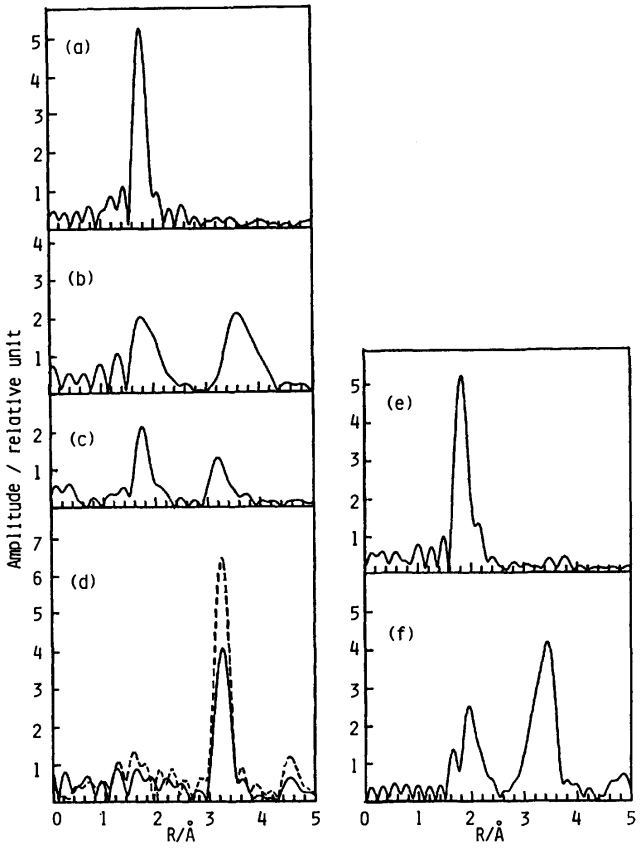

Fig. 3. Fourier transforms of Mo K-edge EXAFS for (a) $Na_2MoO_4 \cdot 2H_2O$, (b) MoO_3, (c) $(NH_4)_6Mo_7O_{24} \cdot 4H_2O$, (d) $[(C_4H_9)_4N]_2Mo_6O_{19}$, and WL_{III}-edge EXAFS for (e) $Na_2WO_2 \cdot 2H_2O$, and (f) $[(C_4H_9)_4N]_2W_6O_{19}$. Broken line in (d) represents that measured at 20 K.

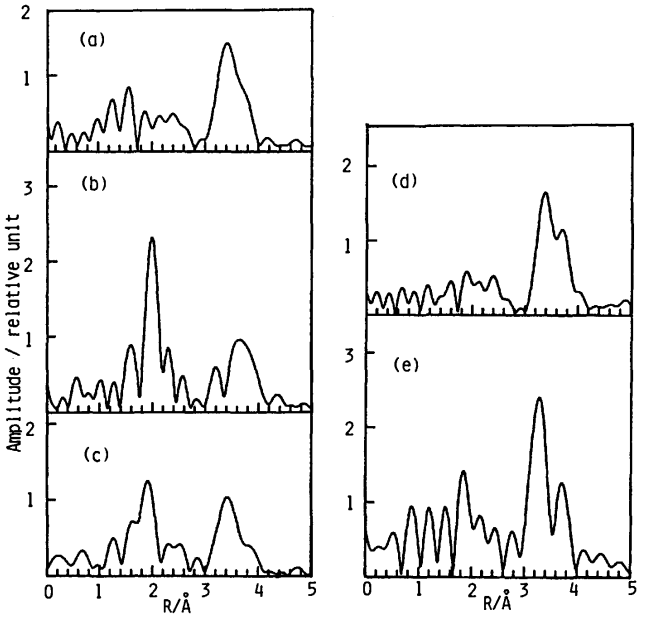

Fig. 4. Fourier transforms of Mo K-edge and W L_{III}-edge EXAFS for (a) $PMo_{12}O_{40}^{3-}$, (b) $PW_{12}O_{40}^{3-}$, (c) the reduction product from $PMo_{12}O_{40}^{3-}$, (d) $AsMo_{12}O_{40}^{3-}$ and (e) $SiMo_{12}O_{40}^{4-}$.

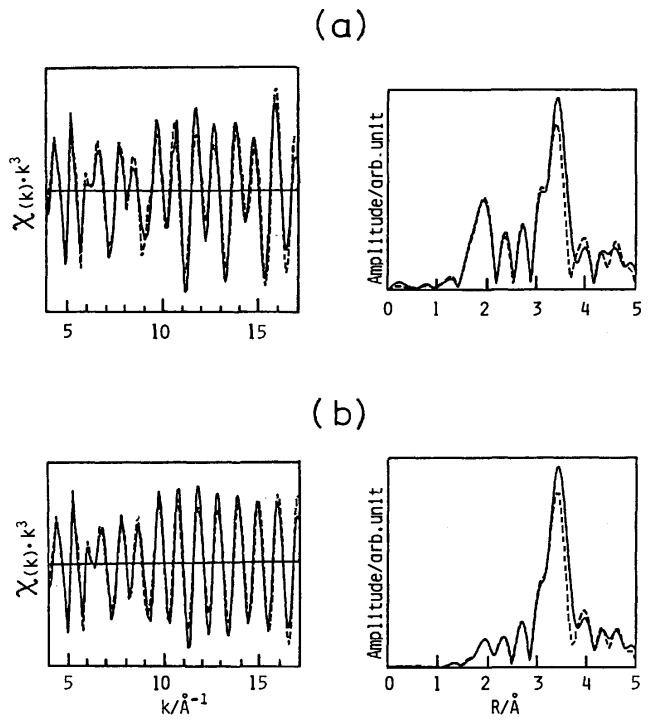

Fig. 5. Calculated EXAFS spectra and their Fourier transforms for the model compound for $Mo_6O_{19}^{2-}$. The σ values used for Mo-O are (a) 0.04 Å and (b) 0.08 Å. Solid line and broken line represent the result of the single scattering and multiple scattering calculations, respectively.

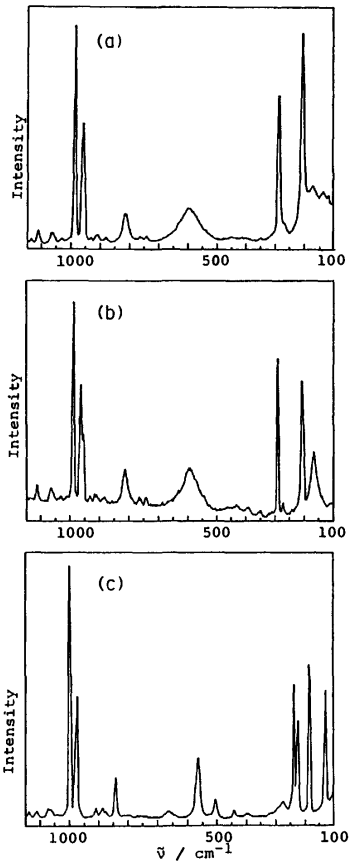

Fig. 6. Raman spectra for (a) $[(C_4H_9)_4N]_2Mo_6O_{19}$ at room temperature, (b) at 88 K, and (c) $[(C_4H_9)_4N]_2W_6O_{19}$ at room temperature.

1a constitute the MoO_6Mo_4 cluster used for the calculations of the model of $Mo_6O_{19}^{2-}$. The positions of the atoms are given from the crystallographic data.[5] Figure 5a shows the results obtained using the Debye-Waller factor σ of 0.04 Å for both Mo-O and Mo-Mo bonds. The value of 0.04 Å has been determined by Cramer et al.[1] in the case of the Mo(V) dimer. No significant difference can be observed between the single-scattering and multiple-scattering results. The calculations predict the Mo-O peaks at 1.7—2.0 Å and the Mo-Mo peak at 3.3 Å, as normal. Since the peak intensity depends upon the Debye-Waller factor, the simulation calculations were also performed using different σ values. Figure 5b shows the results for the case in which the σ value of 0.08 Å for the Mo-O bond is used. The value of 0.08 Å was selected according to the results of a Raman study, which will be discussed in the Discussion section below. The Mo-O peak at about 2.0 Å can no longer be distinguished from the ripple peaks.

Raman Spectra. A noteworthy difference in the Raman spectra is observed in the shape of the peak corresponding to the vibration involving the metal-bridging oxygen bond between the samples of $Mo_6O_{19}^{2-}$ and $W_6O_{19}^{2-}$. The Raman spectrum for $Mo_6O_{19}^{2-}$ at room temperature has a very broad peak at ca. 600 cm^{-1}, as is shown in Fig. 6a. Cooling the sample down to 88 K causes only a small reduction in the width of the peak, as is shown in Fig. 6b. According to the literature,[16] the peaks at ca. 600 cm^{-1} for $Mo_6O_{19}^{2-}$ and 570 cm^{-1} in Fig. 6c for $W_6O_{19}^{2-}$ have been assigned to correspond to the symmetrical stretching vibration of the bridging M-O-M bond (M=metal). It is remarkable that this peak for $Mo_6O_{19}^{2-}$ is significantly broader than that for $W_6O_{19}^{2-}$, while the peaks at ca. 1000 cm^{-1} due to the terminal M=O bonds are quite similar to each other. The peak at 167 cm^{-1} which has been assigned to the Mo-O-Mo bending vibration in the $Mo-O_4$ plane is also broad, and its width changes with the temperature.

Discussion

Our results definitely show that the anomalously low peak intensity for $Mo_6O_{19}^{2-}$ arises from the large Debye-Waller factor of the Mo-O bond in this compound. The theoretical calculations do not predict that the multiple-scattering effect works on the very specified symmetrical geometry of $Mo_6O_{19}^{2-}$ complex to diminish certain peaks. The calculations predict, instead, that the disappearance of the peaks can easily occur with larger σ values. The large σ value of the bond seems to be related to the anomalous peak shapes

in its Raman spectrum.

The σ value in the theory of EXAFS is given by:

$$\sigma^2 = \sigma^2_{stat} + \sigma^2_{vib.} \quad (5)$$

Thus, it is divided into static and vibronic contributions. The static factor represents the distribution of interatomic distances. As is obvious from the low symmetry of $Mo_7O_{24}^{6-}$, it is known from the X-ray diffraction study that the complex has Mo-O_{bridge} bonds with various lengths in it.[15] The bond lengths of Mo-O spread from 1.8 to 2.5 Å in $Mo_7O_{24}^{6-}$, while those in $Mo_6O_{19}^{2-}$ spread from 1.86 to 2.01 Å.[17] Therefore, the static factor must be much larger for $Mo_7O_{24}^{6-}$ than for $Mo_6O_{19}^{2-}$. Consequently, the present EXAFS results indicate that the apparent large σ value for $Mo_6O_{19}^{2-}$ comes not from the static part, but from the vibronic one. As for $W_6O_{19}^{2-}$, there are two reports which are inconsistent with each other with respect to the W-O bond lengths.[18,19]

Recently, the relationship between the Raman spectrum and the EXAFS Debye-Waller factor was studied by Lottici.[20] From his study of the nearest neighbor central force (NNCF) model, which is more exact than the Einstein model, he reported that the Debye-Waller factor can be related to the relative (or projected) density of vibrational states ρ_R. According to the Einstein model, the calculated σ_{vib} values of the M-O bond for $Mo_6O_{19}^{2-}$ and $W_6O_{19}^{2-}$ must be nearly equal because the vibrational frequencies for the M-O bonds in the two compounds are nearly equal. Thus, this model is not adequate for an attempt to find the cause of the difference in the character of the M-O bonds. The value of σ_{vib} is expressed[20] in terms of $\rho_R(\omega)$ according to the NNCF model as follows:

$$\sigma^2_{vib} = (\hbar/2\mu)\int[\rho_R(\omega)/\omega]\coth(\hbar\omega/2k_BT)d\omega. \quad (6)$$

The $\rho_R(\omega)$ is approximately related to the Raman scattering intensity $I(\omega)$ as follows:

$$I(\omega) = C\,\rho_R(\omega), \quad (7)$$

where C is the normalization constant. Now, using the above two relations, we can calculate the ratio of the σ_{vib} value of $Mo_6O_{19}^{2-}$ against that of $W_6O_{19}^{2-}$ with respect to the metal-bridging oxygen bonds from the Raman peaks of symmetrical stretching vibration at ca. 600 cm^{-1} and 570 cm^{-1}, respectively. The Raman intensities of the corresponding peaks are normalized by using one of the peaks due to the tetrabutylammonium ion at ca. 1060 cm^{-1}. The result of the calculation for the bridging oxygen gives a value of about 2 for the $\sigma_{vib}[Mo]/\sigma_{vib}[W]$ ratio. Therefore, once the σ_{vib} value of 0.04 Å for the W-O bond in $W_6O_{19}^{2-}$, which is a very typical value for metal complexes, is adopted for the EXAFS simulation calculation, the σ_{vib} value of 0.08 Å must be employed for the calculation of $Mo_6O_{19}^{2-}$. The EXAFS simulation calculations using these σ values show that the σ value of 0.04 Å is small enough to present the M-O peak in the Fourier transform, while the value of 0.08 Å is too large to present the peak, as is indicated in Fig. 5.

The EXAFS spectrum taken at 20 K for $Mo_6O_{19}^{2-}$ (Fig. 3d) indicates that the apparent σ value does not depend on the temperature. The same is true for the σ_{vib} value estimated from the Raman spectra taken at room temperature (Fig. 6a) and at 88 K (Fig. 6b). Equation 6 shows that, even at $T=0$, σ_{vib} has a finite value proportional to $\rho_R(\omega)/\omega$. The present study concludes that the Mo-O bond in $Mo_6O_{19}^{2-}$ has a large σ_{vib} value in which the temperature-independent contribution dominates. (As a matter of fact, for the vibration of ω=600 cm^{-1}, the value of $\coth(\hbar\omega/2k_BT)$ is almost 1 throughout all the range from $T=0$ to room temperature.)

We speculate that the large σ value for Mo-O bond is related to the rotational vibration on the axis of $O_{terminal}$-Mo-O_{center} (the rotation of the plane including four O_{bridge}'s); thus, the vibrational peaks corresponding to the Mo-O_{bridge} stretching vibration (at ca. 600 cm^{-1}) and the O_{bridge}-Mo-O_{bridge} bending (at ca. 160 cm^{-1}) are broad in the Raman spectrum because of the coupling of these vibrations to the rotational vibration. This interpretation is compatible with the EXAFS result of the clear appearance of the distant bond, Mo-Mo, in $Mo_6O_{19}^{2-}$ inspite of the disappearance of the shorter bond Mo-O_{bridge}, because the rotation does not change the Mo-Mo, but the Mo-O distance.

In concluding this section, it should be mentioned that there is something puzzling in the results of the X-ray diffraction analyses (XDA) of the complexes. None of the reported values of thermal parameters in XDA for Mo and W complexes contain any indication which can be connected to either the large σ values inferred from the EXAFS analyses or the broad band shapes in the Raman spectra. In either case in which static or vibronic disorder causes the peak disappearance in EXAFS of $Mo_6O_{19}^{2-}$, the values of the thermal parameters in XDA for O_{bridge} in it can be expected to be large. The incompatibility between the results of EXAFS and XDA requires further study in this regard.

Reactivity as Oxidants. It is interesting to note that $Mo_6O_{19}^{2-}$, $PMo_{12}O_{40}^{3-}$, and $AsMo_{12}O_{40}^{3-}$, for which the Mo-O peaks disappear in the Fourier transforms, are the most easily reducible species among the molybdenum complexes. According to the empirical classification by Pope,[21] the reactivity of $Mo_6O_{19}^{2-}$ as the oxidant is higher than that of $Mo_7O_{24}^{6-}$. Judging from the electrochemical redox potentials, the orders of reactivities are $PMo_{12}O_{40}^{3-} > PW_{12}O_{40}^{3-}$,[22] and $AsMo_{12}O_{40}^{3-} > PMo_{12}O_{40}^{3-} > SiMo_{12}O_{40}^{4-}$.[23] This is perfectly in accordance with the fact that $Mo_7O_{24}^{6-}$, $PW_{12}O_{40}^{3-}$, and $SiMo_{12}O_{40}^{4-}$ show the Mo-O peaks in their Fourier transforms. Thus, the compounds with high redox potentials are electrically unstable, even though they take highly symmetrical structures. It has also been reported that the redox reaction of

$PMo_{12}O_{40}^{3-}$ with hydrogen and isotopically labeled oxygen exchanges bridging oxygen atoms far more easily than the terminal oxygens.[24] Further, the Raman[24] and IR[25] spectroscopic studies and the Xα MO calculation[26] have indicated that the bridging oxygen atoms are more reactive than the terminal oxygens. From the point of view of reactivity as the oxidant, the intensity of the M-O peak in the Fourier transform seems to be small for a species with highly reactive bridging oxygen atoms. From the evidence in the present study, the M-O bonds in highly reactive molybdenum complexes can be considered to be "strained bonds" which may be created by the stress of the large framework of the polynuclear compounds. It has been reported that there is a correlation between the Debye-Waller factors determined from EXAFS experiments on aqua metal complexes and their ligand-water exchange-reaction rates.[27] The present study provides another example of the correlation between the Debye-Waller factor and the chemical reactivity.

Conclusion

Some of the molybdenum polynuclear compounds show almost no peaks corresponding to metal-oxygen bonds in their Fourier transforms of the EXAFS spectra. This very strange fact is the result of the large Debye-Waller factor of the corresponding bonds. This conclusion is supported by the theoretical simulation calculations and the results of the Raman spectroscopy. The metal-bridging oxygen bonds in those compounds must be deformed to make these compounds reactive toward a redox reaction.

The present authors wish to thank Drs. Tadashi Matsushita and Masaharu Nomura of the National Laboratory for High Energy Physics (KEK) for their help with the X-ray absorption measurements. This work was supported by a Grant-in-Aid for Special Project Research (No.62124039) from the Ministry of Education, Science and Culture.

References

1) S. P. Cramer, P. K. Eiden, M. T. Paffett, J. R. Winkler, Z. Dori, and H. B. Gray, *J. Am. Chem. Soc.*, **105**, 799 (1983).
2) K. Yokoi, N. Matsubayashi, T. Miyanaga, I. Watanabe, K. Murata, and S. Ikeda, *Chem. Lett.*, **1987**, 1453.
3) Y. Iwasawa, K. Asakura, H. Ishii, and H. Kuroda, *Z. Phys. Chem. Neue Folge*, **144**, 105 (1985).
4) K. Matsumoto, A. Kobayashi, and Y. Sasaki, *Bull. Chem. Soc. Jpn.*, **48**, 1009 (1975).
5) O. Nagano and Y. Sasaki, *Acta Crystallogr., Sect. B*, **35**, 2387 (1979).
6) R. Strandberg, *Acta Chem. Scand., Ser. A*, **29**, 359 (1975).
7) T. Miyanaga, N. Matsubayashi, T. Fukumoto, K. Yokoi, I. Watanabe, K. Murata, and S. Ikeda, *Chem. Lett.* **1988**, 487.
8) K. Murata, E. Yamamoto, and S. Ikeda, *Bull. Chem. Soc. Jpn.*, **56**, 941 (1983).
9) M. Boyer and B. L. Meur, *C. R. Acad. Sci. Paris*, **1975**, 281.
10) A. Rosenheim and J. Jaenicke, *Z. Anorg. Allog. Chem.*, **101**, 248 (1917).
11) N. Matsubayashi, Thesis, Osaka University (1986).
12) B. K. Teo and P. A. Lee, *J. Am. Chem. Soc.*, **101**, 2815 (1979).
13) B. K. Teo, *J. Am. Chem. Soc.*, **103**, 3990 (1981).
14) T. Fujikawa, *J. Phys. Soc. Jpn.*, **54**, 2747 (1985).
15) H. T. Evans, B. M. Gatehouse, and P. Leverett, *J. Chem. Soc., Dalton Trans.*, **1975**, 505
16) R. Mattes, H. Bierbusse, and J. Fuchs, *Z. Anorg. Allg. Chem.*, **385**, 230 (1971).
17) H. R. Allcock, E. C. Bissell, and E. T. Shawl, *Inorg. Chem.*, **12**, 2963 (1973).
18) G. Henning and A. Hüllen, *Z. Kristallogr.*, **30**, 162 (1969).
19) J. Fuchs, W. Freiwald, and H. Hartl, *Acta Crystallogr., Sect. B*, **34**, 1764 (1978).
20) P. P. Lottici, *Phys. Rev. B*, **35**, 1236 (1987).
21) M. T. Pope, *Inorg. Chem.*, **11**, 1973 (1972).
22) M. Otake and T. Onoda, *Shokubai*, **18**, 169 (1976); K. Katamura, T. Nakamura, K. Sakata, M. Misono, and Y. Yoneda, *Chem. Lett.*, **1981**, 89.
23) K. Eguchi, T. Seiyama, N. Yamazoe, S. Katsuki, and H. Taketa, *J. Catal.*, **111**, 336 (1988).
24) H. Tsuneki, H. Niiyama, and E. Echigoya, *Chem. Lett.*, **1978**, 1183.
25) K. Eguchi, Y. Toyozawa, K. Furuta, N. Yamazoe, and T. Seiyama, *Chem. Lett.*, **1981**, 1253.
26) H. Taketa, S. Katsuki, K. Eguchi, T. Seiyama, and N. Yamazoe, *J. Phys. Chem.*, **90**, 2959 (1986).
27) T. Miyanaga, I. Watanabe, and S. Ikeda, *Chem. Lett.*, **1988**, 1073.

The Syntheses of Ortho-, Meta-, and Paracyclophane-Type Thiacrown Compounds and Their Characteristics as Extractive-Spectrophotometric Reagents for Class *b* Metals–Silver and Copper

Motoho MUROI,* Teruo KAMIKI, and Eiichi SEKIDO†
Public Health Research Institute of Kobe City, Minatojima-nakamachi, Chuo-ku, Kobe 650
†Department of Chemistry, Faculty of Science, Kobe University, Rokkodai, Nada-ku, Kobe 657
(Received June 30, 1988)

Ortho-, meta-, and paracyclophane-type thiacrown compounds bearing 4-(4-nitrophenylazo)phenol as a chromogenic group were synthesized, and their characteristics as extractive-spectrophotometric reagents for the class *b* metals, consisting of soft Lewis acids such as silver and copper(I), were examined. Silver and copper(I) were well extracted into chloroform with all of three reagents, though especially with the metacyclophane-type reagent. The absorption maxima of silver and copper(I) complexes with the orthocyclophane-type reagents are at the longest wavelengths among the three reagents. The orthocyclophane-type reagent is adequate for the extraction and spectrophotometric measurement of copper(I), and the metacyclophane-type reagent is suitable for that of silver. The extraction behavior of copper(II) with these three reagents has been studied in order to know if the hydroxyl group participates in the formation of the metal-thiacrown complexes.

Thiacrown ethers act as soft Lewis bases and react selectively with the class *b* metals of soft Lewis acids. The resulting thioether complex cations form ion pairs with appropriate anions, such as perchlorate and picrate, which are then extracted into suitable organic solvents.[1-7] The extractive-spectrophotometric determination of silver and copper with thiacrown ethers by the use of dye anions as the pairing anions has been reported.[8]

If a thiacrown ether compound itself has a chromogenic group which can function as a counter anion, that compound can be used as an extractive-spectrophotometric reagent for metal ions. Thus, the extraction with chromogenic thiacrown ethers, such as 4′-(pycrylamino)benzo-1,4,8,11-tetrathiacyclopentadec-13-ene (4′-PicNHBz-TTCP)[9] and those in which a nitro group in 4′-PicNHBz-TTCP is replaced by a trifluoromethyl group,[10] as well as thiacrown ethers containing a phenylazo group as a chromophore, have been reported.[11]

In the present study, in order to obtain more selective and sensitive thiacrown reagents, which contain the chromogenic group also functioning as a counter anion, new ortho-, meta-, and paracyclophane-type thiacrown ether reagents were synthesized, and their characteristics as extractive-spectrophotometric reagents for class *b* metals, such as silver and copper(I), were examined. Furthermore, as it seemed interesting to know how the hydroxyl groups of the ortho-, meta-, and paracyclophane-type thiacrown ethers participate in the formation of the metal-thiacrown complexes, the extraction behavior of copper(II) has been studied.

Results and Discussion

Syntheses of Reagents. Thiacrown ether containing a hyroxyl group may be expected to be obtained by the reaction of dithiol and bis(halogenomethyl)-phenol protected with a hydroxyl-protecting group such as tetrahydropyranyl ether. However, the synthesis of each isomer of bis(chloromethyl)phenol by chloromethylation into phenol or the direct bromination of dimethylphenol into the α position was very difficult. Fortunately, thiacrown ether containing a hydroxyl group **2** was obtained by the reaction of bis-(bromomethyl)phenyl acetate **1** and 3,7-dithianonane-1,9-dithiol, as shown in Scheme 1.

The cyclization reaction was achieved by the drop-by-drop addition of a benzene solution containing 1 molar equivalent of dibromide **1** and 1.5 molar equi-

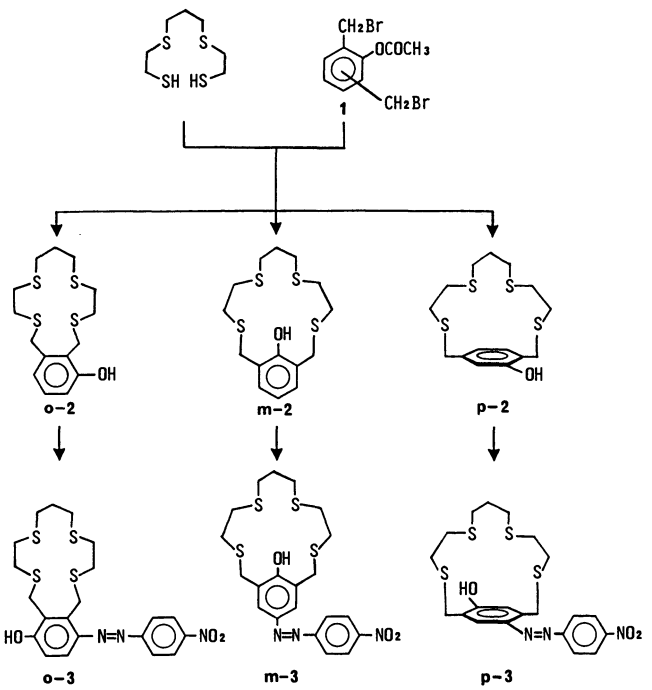

Scheme 1.

valents of 3,7-dithianonane-1,9-dithiol to a sodium ethoxide solution by means of the high-dilution method. The cyclizations of *o*-, *m*-, and *p*-substituted dibromides with dithiol all produced satisfactory yields.

The reaction of hydroxy-substituted cyclophane **2** and *p*-nitrobenzenediazonium tetrafluoroborate was carried out in a dioxane-water solution under slightly alkaline conditions. The reaction mixture was acidified. A large quantity of water was added and then extracted with ethyl acetate. The solvent was removed, the residue was chromatographed on a silica-gel column, and the pure product was obtained by the recrystallization of the major band.

The orthocyclophane-type thiacrown ether **o-3** is moderately soluble in such organic solvents as chloroform, ethyl acetate, and acetone. The reagents **m-3** and **p-3** are soluble in chloroform or acetone. The proton NMR spectra of **o-3** and **m-3** are similar to each other except for that of aromatic protons, but that of **p-3** is very different from that of **o-3** or **m-3**. The benzyl proton signal of **p-3** separates into two quartets, indicating a two-AB pattern, although that of **o-3** is a doublet and that of **m-3** is a singlet. The protons of the thioether ring of **p-3** are shielded by a benzene ring and are probably affected by azo-group electrons. These proton NMR spectra are consistent with the desired configuration for each isomer; **m-3** is a symmetrical structure in which the thioether ring is coplanar for the benzene ring. **o-3** has an unsymmetrical thioether ring which is coplanar for the benzene ring. The thioether ring of **p-3** is an unsymmetrical structure and exists at the upper space of the benzene ring. It seems that the difference in the configuration of **p-3** from that of **o-3** or **m-3** causes the decrease in metal extraction to be described below.

Absorption Spectra of Three Reagents (o-3, m-3, and p-3) and of Their Silver Complexes in a 50% (v/v) Dioxane-Water Mixture. In Table 1, the absorption-spectra data for three reagents (**o-3**, **m-3**, and **p-3**), in a 50% (v/v) dioxane-water mixture are shown, along with those for their silver complexes. The absorption maxima of the three reagents in acidic media, which are present in the range of 384—400 nm, shift to longer wavelengths (537—545 nm) in alkaline media, and their molar absorptivities (ε) increase from 22000—24000 in acidic media to 34400—35800 in alkaline. These changes in the absorption spectra with the increase in the pH are almost the same as those of 4-(4-nitrophenylazo)phenol with the dimethyl substituent (2,3-dimethyl-; HL 394 nm, L^- 548 nm: 2,6-dimethyl-; HL 393 nm, L^- 556 nm: 2,5-dimethyl-; HL 398 nm, L^- 547 nm).

Table 1. Absorption Spectra Data of Reagents **3** and of Their Silver Complexes in a 50% (v/v) Dioxane-Water Mixture

	HL		L^-		AgL	
	λ_{max}/nm	ε	λ_{max}/nm	ε	λ_{max}/nm	ε
o-3	394	24400	537	35400	525	33400
m-3	384	22000	545	35800	531	36200
p-3	400	23600	538	34400	528	31200

Concentration of **3** and silver ions: 2.5×10^{-5} M.

In the presence of the silver ion, the absorption maxima of all three reagents shift to wavelengths shorter by 10—14 nm than those of L^-. It seems that the shift shows the decrease in the resonance of the azobenzene moiety by the shift of electrons from that of *p*-nitrobenzene to the thioether ring as a result of the coordination of the silver ion to the sulfur atoms. It is interesting that the molar absorptivities for **o-3** and **p-3** silver complexes decrease, but that for **m-3** increases, compared with L^-. This seems to indicate that the phenolate ion not only functions as a counter ion, but also takes part in the bonding of the silver ion.

Proton-Dissociation Constant. The acid dissociation constants of the reagents **3** were determined spectrophotometrically in a 50% (v/v) dioxane-water mixture, the effects of the silver ion on their pK_a values were also examined. The results are shown in Table 2. The pK_a values of **o-3** and **p-3** are similar, but that of **m-3** is somewhat small. In the presence of silver ions, the apparent pK_a value of every reagent decreases. Probably this is a result of the decrease in electron density on the phenolic oxygen atom when the electrons are shifted from the azobenzene moiety by the coordination of the silver ion. The large decrease in pK_a value for **m-3** suggests that the silver ion interacts directly with the hydroxyl group and

Table 2. Proton-Dissociation Constants of Reagents **3** in a 50% (v/v) Dioxane-Water Mixture

HL : Ag	o-3	m-3	p-3
1 : 0	9.0	8.15	8.7
1 : 1	7.55	5.3	7.2

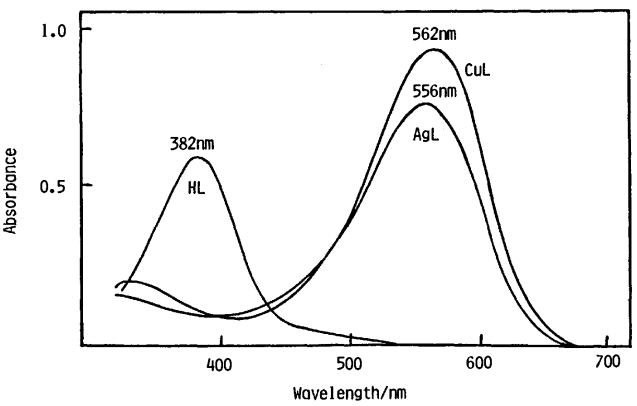

Fig. 1. Absorption spectra of **o-3** and of their silver and copper(I) complexes in chloroform. Concentration of **o-3** and metal ions: 2.5×10^{-5} M.

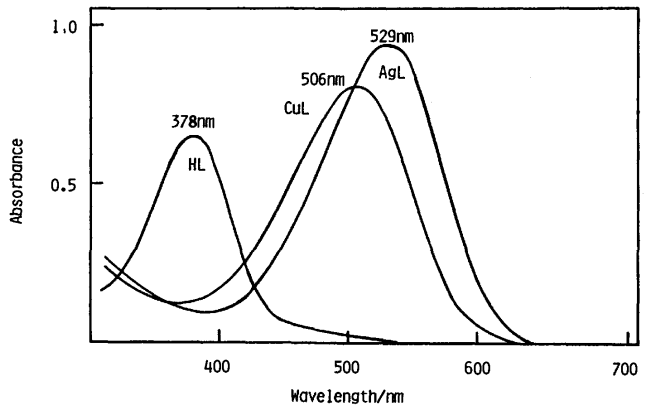

Fig. 2. Absorption spectra of **m-3** and of their silver and copper(I) complexes in chloroform. Concentration of **m-3** and metal ions: 2.5×10^{-5} M.

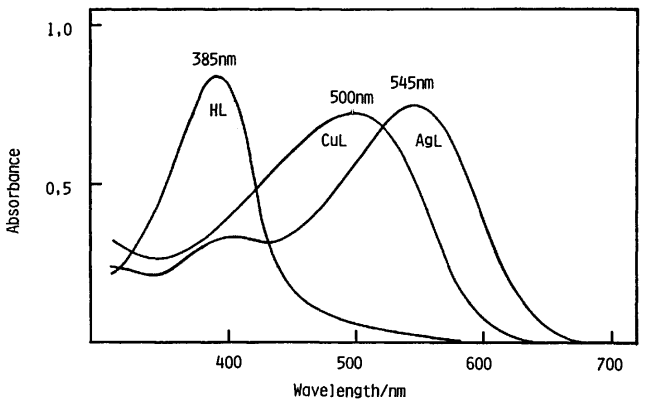

Fig. 3. Absorption spectra of **p-3** and of their silver and copper(I) complexes in chloroform. Concentration of **p-3** and metal ions: 4×10^{-5} M.

Table 3. Absorption Maxima of the Silver Complexes in Various Extraction Solvents

	λ_{max}/nm		Dielectric constant
	o-3	**m-3**	
$CHCl_3$	556	529	4.8
CH_2ClCH_2Cl	561	540	10.7
$CH_2ClCH_2Cl : C_6H_5NO_2$ = 1 : 1	565	548	22.7
$C_6H_5NO_2$	571	554	34.8

Concentration of **3** and silver ions : 2×10^{-5} M. **o-3** : pH 10.05 and **m-3** : pH 8.95.

Table 4. Percentages of Extraction of Silver and Copper(I) into Chloroform

	Ag (%)	Cu(I)
o-3	99.2	99.4
m-3	99.4	99.2
p-3	99.0	99.2

Concentration of **3** : 6×10^{-4} M. Concentration of metal ions: 3×10^{-5} M. pH 8.3.

Table 5. Percentages of Extraction of Silver and Copper(I) into Chloroform

	Ag (%)	Cu(I)
o-3	86.3	94.2
m-3	98.7	97.3
p-3	51.4	52.7

Concentration of **3** and metal ions : 3×10^{-5}M. pH 8.95.

that, consequently, the proton is excluded by proton-silver ion repulsion.

Liquid-Liquid Extraction Behavior of Silver and Copper(I). (i) Absorption Spectra of Silver and Copper(I) Complexes for Reagents 3: The absorption spectra of **o-3**, **m-3**, and **p-3** and of those silver and copper(I) complexes extracted into chloroform are shown in Figs. 1—3.

The absorption bands of HL have their maxima at 378—385 nm (ε=21000—25000). The absorption maxima of silver complexes for **o-3** and **p-3** exist at 556 nm and 545 nm, which are longer than those of the corresponding silver complexes in a 50% (v/v) dioxane-water solution. However, that for **m-3** in chloroform exists at a shorter wavelength than those in a 50% (v/v) dioxane-water solution. This may be attributed to the larger decrease in the resonance of the azobenzene moiety by the coordination of silver. This influence may be weakened by a polar solvent, and the effect may be larger for **m-3** than for **o-3** and **p-3**. As shown in Table 3, the absorption maxima of silver complexes for **o-3** and **m-3** are shifted to the longer wavelengths with the increase in the solvent polarity and the shift for **m-3** is larger than that for **o-3**.

(ii) The Percentage of the Extraction of Silver and Copper(I) Complexes: The percentage of the extraction of silver and copper(I) with three reagents was also examined. The results are shown in Table 4. As has been reported in previous papers,[3,9,11] silver and copper(I) were well extracted with these thiacrown compounds. Similarly, those two metals were well extracted with these three reagents **3** at 20 times the metal concentration into chloroform, as shown in Table 4. Also, as shown in Table 5, these were well extracted with **m-3** in the same concentration is that of metal ions at pH 8.95. It seems that **m-3** has an intraannular hydroxyl group; therefore, a dissociated hydroxyl group exists at a preferable position compared with that of **o-3**. The extraction with **p-3** decreases to about a half. This decrease is presumed to be accounted for as follows: two sulfur atoms of the para-substituted benzyl group exist far apart, consequently, the silver or copper(I) ion can not be coordinated by those sulfur atoms-only two sulfur atoms bonded to the trimethylene group can be coordinated. In fact, it is obvious that the internal cavity of

Table 6. Extraction Behavior of Copper(II) Complexes with 3

	Absorption maximum/nm	% Extraction Cu(II) : HL	
		1 : 2	1 : 20
o-3	558	29	94
m-3	498	35	97
p-3	—	8	81

Concentration of Cu(II): 3×10^{-5}M. pH 8.3

p-3 is too small for silver or copper(I), as assumed by CPK model of the space-field type.

Liquid-Liquid Extraction of Copper(II). Among the metals belonging to class *ab* metals, Co^{2+}, Ni^{2+}, and Zn^{2+} were scarcely extracted at all with 4′-(2-hydroxy-5-chlorophenylazo)Bz-TTCP[11] and 4′-PicNHBz-TTCP.[9] Only Cu^{2+} was extracted appreciably with 4′-(2-hydroxy-5-chlorophenylazo)Bz-TTCP and not with 4′-PicNHBz-TTCP. It seemed interesting to determine whether or not copper(II) can be extracted with these three reagents **3**. The absorption spectra data of copper(II) complexes for the reagents **3** in chloroform are shown in Table 6. The percentage of extraction was examined, it is also shown in Table 6. Although the percentage of the extraction of copper(II) is less than those of silver or copper(I), copper(II) is extracted in an appreciable amount. In the previous paper, we presumed that the extraction of copper(II) with 4′-(2-hydroxy-5-chlorophenylazo)Bz-TTCP is performed by the complex formation of adjacent azo and hydroxyl groups, rather than the thioether ring. However, the results of the extraction with these reagents **3** strongly suggest the formation of copper(II) complexes with the thioether ring.

Experimental

Syntheses of Reagents. Bis(bromomethyl)phenyl Acetate 1: Dimethylphenyl acetate (8.2 g, 0.05 mol) was dissolved in carbon tetrachloride (100 ml) and *N*-bromosuccinimide (17.5 g, 0.1 mol), and then benzoyl peroxide (0.2 g) was added. The reaction mixture was refluxed for 2—3 h. After cooling, the precipitate was filtered and washed with a small amount of ether. The filtrate and the washings were combined, and the solvent was removed in vacuo. The solid was recrystallized from ethanol.

2,3-Bis(bromomethyl)phenyl Acetate: Mp 100—101 °C; yield, 5.6 g (34.6%). Found: C, 37.46; H, 3.19%. Calcd for $C_{10}H_{10}Br_2O_2$: C, 37.30; H, 3.13%. IR(KBr) 1760, 1220, 1210, 1190, 620 cm^{-1}. MS (70 eV) *m/z* (rel intensity) 324 (M+2, 28), 322 (M^+, 58), 320 (29), 280 (98), 243 (98), 241 (98), 119 (100). ^1H NMR ($CDCl_3$) δ=2.35 (3H, s, CH_3), 4.60 (4H, s, CH_2Br), 6.95—7.35 (3H, m, aromatic H).

2,6-Bis(bromomethyl)phenyl Acetate: Mp 119—120 °C; yield, 7.3 g (45.6%). Found: C, 37.42; H, 3.10%. IR (KBr) 1760, 1220, 1210, 1180, 590 cm^{-1}. MS (70 eV) *m/z* (rel intensity) 324 (M+2, 6), 322 (M^+, 12), 320 (6), 280 (88), 201 (100), 199 (98). ^1H NMR ($CDCl_3$) δ=2.40 (3H, s, CH_3), 4.35 (4H, s, CH_2Br), 7.00—7.50 (3H, m, aromatic H).

2,5-Bis(bromomethyl)phenyl Acetate: Mp 99—100 °C; yield, 4.9 g (30.1%). Found: C, 37.07; H, 3.00%. IR (KBr) 1760, 1230, 1200, 1190, 625 cm^{-1}. MS (70 eV) *m/z* (rel intensity) 324 (M+2, 5), 322(M^+, 9), 320 (5), 243 (44), 241 (45), 199 (100). ^1H NMR ($CDCl_3$) δ=2.35 (3H, s, CH_3), 4.30—4.50 (4H, d, CH_2Br), 7.05—7.35 (3H, m, aromatic H).

Hydroxy-Substituted Cyclophane (Compounds o-2, m-2, and p-2). In absolute ethanol (360 ml) under nitrogen, sodium metal (0.83 g, 36 mmol) was dissolved. To this solution, an anhydrous benzene solution (450 ml) containing dibromide **1** (3.86 g, 12 mmol) and 3,7-dithianonane-1,9-dithiol (4.10 g, 18 mmol) was added dropwise during a 6-h period at 10—15 °C. After the mixture had then been stirred overnight, the solvent was removed until the volume has only about 100 ml, and then water was added. The mixture was acidified with dilute hydrochloric acid, extracted with ethyl acetate, washed with water, and dried. The solvent was then removed, and the residue was chromatographed on a silica-gel column with chloroform-ethyl acetate (20:1 v/v) (for ortho- and paracyclophanes) or benzene (for metacyclophane) as a eluting solvent. The major band was collected. The product was pure enough for the next process. Recrystallization gave an every purer product.

o-2: Yield, 3.11 g (74.9%). Recrystallization from methanol-methyl acetate (1 : 1); mp 112—113 °C. Found: C, 51.75; H, 6.30%. Calcd for $C_{15}H_{22}OS_4$: C, 51.98; H, 6.40%. IR (KBr) 3425, 1580, 1465, 1200, 765 cm^{-1}. MS (70 eV) *m/z* (rel intensity) 348 (M+2, 5), 346 (M^+, 26), 211 (17), 167 (92), 107 (100). ^1H NMR ($CDCl_3$) δ=1.55—2.10 (2H, m, CH_2-CH_2CH_2), 2.50—3.10 (12H, overlapping t and s, CH_2-CH_2CH_2, CH_2CH_2), 3.75—4.10 (4H, d, CH_2Ar), 6.55—7.20 (3H, m, aromatic H).

m-2: Yield, 3.58 g (86.2%). Recrystallization from ethanol; mp 94—95 °C. Found: C, 51.99; H, 6.18%. IR(KBr) 3325, 1460, 1410, 1200, 750 cm^{-1}. MS (70 eV) *m/z* (rel intensity) 348 (M+2, 22), 346 (M^+, 100), 286 (15), 184 (50), 120 (88), 91 (82). ^1H NMR ($CDCl_3$) δ=1.40—1.90 (2H, m, CH_2CH_2-CH_2), 2.30—2.75 (12H, overlapping t and s, $CH_2CH_2CH_2$, CH_2CH_2), 3.80 (4H, s, CH_2Ar), 6.65—7.30 (3H, m, aromatic H).

p-2: Yield, 3.49 g (84.0%). Recrystallization from acetonitrile; mp 96—97 °C. Found: C, 51.91; H, 6.31%. IR (KBr) 3245, 1580, 1430, 1230, 720 cm^{-1}. MS (70 eV) *m/z* (rel intensity) 348 (M+2, 20), 346 (M^+, 97), 286 (8), 198 (16), 167 (96), 107 (100). ^1H NMR ($CDCl_3$) δ=1.25—1.80 (2H, m, $CH_2CH_2CH_2$), 2.15—2.65 (12H, overlapping t and s, $CH_2CH_2CH_2$, CH_2CH_2), 3.60—3.85 (4H, d, CH_2Ar), 6.80—7.25 (3H, m, aromatic H).

***p*-Nitrophenylazo Reagents 3 (Compounds o-3, m-3, and p-3).** Phenolic cyclophane **2** (1.04 g, 3.0 mmol) was dissolved in dioxane (60 ml), and then 0.05 M sodium hydroxide solution (60 ml) was added. To this solution, *p*-nitrobenzenediazonium tetrafluoroborate (0.77 g, 3.3 mmol) dissolved in water (150 ml) was added dropwise at 5—10 °C. During this addition, the reaction mixture was kept homogeneously at pH 8—9 by the use of dioxane and a dilute sodium hydroxide solution. Then the solution was stirred at room temperature for 1 h and acidified with dilute hydrochloric acid. A large quantity of water was added, the mixture was extracted with ethyl acetate and dried. The solvent was removed, and the residue was chromatographed on a silica-gel column with chloroform-ethyl ace-

tate (20:1 v/v) (for ortho- and paracyclophanes) or chloroform (for metacyclophane) as a eluting solvent. The major band was collected and recrystallized.

o-3: Recrystallization from acetonitrile; yield, 0.87 g (58.5%). Mp 219—220 °C. Found: C, 50.73; H, 4.90; N, 8.59%. Calcd for $C_{21}H_{25}N_3O_3S_4$: C, 50.88; H, 5.08; N, 8.48%. IR (KBr) 3280, 1580, 1330, 1280, 1240 cm^{-1}. MS (70 eV) *m/z* (rel intensity) 495 (M^+, 3), 301 (16), 267 (32), 167 (68), 61 (100). ^1H NMR ($CDCl_3$:DMSO-d_6=1:1) δ=1.75—2.10 (2H, m, $CH_2CH_2CH_2$), 2.70—3.10 (12H, overlapping t and s, $CH_2CH_2CH_2$, CH_2CH_2), 4.10 (2H, s, CH_2Ar), 4.55 (2H, s, CH_2Ar), 6.85—6.95 (1H, d, aromatic H), 7.60—7.70 (1H, d, aromatic H), 7.95—8.20 (4H, q, aromatic H).

m-3: Recrystallization from acetonitrile; yield, 0.35 g (23.4%). Mp 162—163 °C. Found: C, 51.00; H, 4.97; N, 8.56%. IR (KBr) 3300, 1510, 1345, 1295, 1285 cm^{-1}. MS (70 eV) *m/z* (rel intensity) 495 (M^+, 5), 269 (15), 194 (13), 107 (65), 61 (100). ^1H NMR ($CDCl_3$) δ=1.30—1.85 (2H, m, $CH_2CH_2CH_2$), 2.35—2.80 (12H, overlapping t and s, $CH_2CH_2CH_2$, CH_2CH_2), 3.90 (4H, s, CH_2Ar), 7.80—8.50 (6H, m, aromatic H).

p-3: Recrystallization from acetonitrile and water; yield, 0.49 g (33.0%). Mp 145—146 °C. Found: C, 50.77; H, 5.00; N, 8.57%. IR (KBr) 3450, 1525, 1340, 1280, 1260 cm^{-1}. MS (70 eV) *m/z* (rel intensity) 495 (M^+, 17), 301 (35), 268 (100), 167 (98), 107 (99). ^1H NMR (pyridine-d_5) δ=1.50—1.70 (2H, m, $CH_2CH_2CH_2$), 2.20—2.95 (12H, m, $CH_2CH_2CH_2$, CH_2CH_2), 3.78 and 4.48 (2H, AB-q, J=13.9, CH_2Ar), 3.80 and 5.17 (2H, AB-q, J=14.0, CH_2Ar), 7.51 (1H, s, aromatic H), 8.11 and 8.41 (4H, q, aromatic H), 8.25 (1H, s, aromatic H).

Reagent and Apparatus. Metal solution: Copper(II) sulfate, an analytical-grade reagent, was used to prepare the 1×10^{-2} M stock solution, which was then standardized by EDTA titration. A 1×10^{-2} M stock solution of silver nitrate commercially available for volumetric analysis was used.

The other reagents and all of the apparatus used were the same as have been described in a previous paper.[11]

Proton-Dissociation Constant. The proton dissociation constants of thiacrown ether reagents were determined spectrophotometrically in a 50% (v/v) dioxane-water mixture by means of a method similar to that described in the previous paper.[11] The ionic strength was adjusted to 0.1 with sodium sulfate.

Extraction of Metals. An aliquot (10 ml) of an aqueous solution containing the metal ion and the buffer solution was placed in a 20-ml cylindrical glass tube equipped with a stopper. The ionic strength was kept at 0.1 with sodium sulfate. To obtain a copper(I) solution, enough hydroxylamine sulfate was added to the copper(II) sulfate solution.

After the addition of 10 ml of the reagent **3** solution, the mixture was shaken for 30 min at 200 strokes/min and centrifuged for 5 min. The absorbance of the organic phase was measured at the wavelength of each absorption maximum against a reagent blank. The metal concentrations in the organic phase were determined as follows: 5 ml of the organic phase was taken and allowed to evaporate. The residue was dissolved with a small amount of concentrated nitric acid and diluted adequately with water, and then the metal ion was determined by means of atomic absorption spectrometry.

The authors wish to thank Professor Jun-ichi Oda, Dr. Yukio Yamamoto, and Dr. Naomichi Baba, Institute for Chemical Research, Kyoto University, for their useful suggestions for the syntheses of reagents and for obtaining the NMR spectra.

References

1) D. Sedvic and H. Meider-Gorican, *J. Inor. Nucl.*, **43**, 153 (1981).
2) M. Ōue, A. Ishigaki, Y. Matsui, T. Maeda, K. Kimura, and T. Shono, *Chem. Lett.*, **1982**, 275.
3) K. Saito, Y. Masuda, and E. Sekido, *Anal. Chim. Acta*, **151**, 447 (1983).
4) A. Ohki and M. Takagi, *Anal. Chim. Acta*, **159**, 245 (1984).
5) E. Sekido, K. Saito, Y. Naganuma, and H. Kumazaki, *Anal. Sci.*, **1**, 363 (1985).
6) E. Sekido, K. Suzuki, and K. Hamada, *Anal. Sci.*, **3**, 505 (1987).
7) K. Chayama and E. Sekido, *Anal. Sci.*, **3**, 535 (1987).
8) K. Saito, Y. Masuda, and E. Sekido, *Bull. Chem. Soc. Jpn.*, **57**, 189 (1984).
9) E. Sekido, K. Chayama, and M. Muroi, *Taranta*, **32**, 797 (1985).
10) E. Sekido and K. Chayama, *Nippon Kagaku Kaishi*, **1986**, 907.
11) M. Muroi, A. Hamaguchi, and E. Sekido, *Anal. Sci.*, **2**, 351 (1986).

Preparation and Properties of the σ-Picolyl Complexes of Palladium(II), [{PdCl(C_5H_4N-2-CH_2)$PPh_{3-n}Me_n$}$_2$] (n=0, 1, and 2)

Kiyoshi Isobe,*,† Yukio Nakamura,† and Shinichi Kawaguchi††
Department of Applied Molecular Science, Institute for Molecular Science, Myodaiji, Okazaki 444
†Department of Chemistry, Faculty of Science, Osaka City University, Sumiyoshi-ku, Osaka 558
††School of Medicine (Premedical Bldg.), Kinki University, Osaka-sayama 589
(Received September 19, 1988)

The oxidative addition of 2-(chloromethyl)pyridine to tetrakis(triphenylphosphine)palladium(0) in toluene at 100 °C gave [{PdCl(C_5H_4N-2-CH_2)PPh_3}$_2$] (**1a**), which was characterized by analytical, molecular-weight, and IR data as well as ^1H, ^{31}P, and ^{13}C NMR spectroscopy. The chloride ligand was readily replaced by other halides, whereas tertiary phosphines such as diphenylmethyl-, phenyldimethyl-, and triethylphosphines cleaved the bridge after substitution of triphenylphosphine to result in the monomeric *trans*-[PdCl(C_5H_4N-2-CH_2)(PR_3)$_2$] complexes. Reactions of **1a** with carbon monoxide and other reagents are also reported. The corresponding 3-picolyl complex [{PdCl(C_5H_4N-3-CH_2)PPh_3}$_n$] was also prepared, but could not be well characterized because of lower stability and solubility.

Organopalladium complexes have been investigated extensively,[1] since they play important parts in organic synthesis as catalysts and/or intermediates.[2] The benzylpalladium(II) complexes prepared by oxidative addition of benzyl halides to palladium(0)[3] have attracted special attention of many workers. Thus Stille and his collaborators revealed the S_N2 nature of the oxidative addition of benzyl chloride and related compounds to $Pd(PPh_3)_4$ and $PdCO(PPh_3)_3$ based on the stereochemical investigations.[4] Carbon monoxide is readily inserted into the Pd-C bond,[5] leading to synthesis of ketones[6] and esters.[7] Oxidative addition of benzyl chloride to palladium atoms yielded dimeric η^3-benzylchloropalladium(II),[8] and the same η^3-benzylpalladium(II) structure was also realized by the reaction of *trans*-benzylchlorobis(triethylphosphine)palladium(II) with sodium tetraphenylborate in ethanol.[9]

The benzylpalladium(II) complexes have thus been studied extensively, but investigation of the picolylpalladium(II) complexes are rather few, although several papers have appeared in reporting the picolyl complexes of Cr,[10] Co,[11] and other metals such as Mn, Mo, and Fe,[12] and their reactions with various electrophiles.[13] Roberts and Klabunde[8] obtained a picolylpalladium(II) complex by cocondensation of 2-(chloromethyl)pyridine with palladium vapors, but the exact structure has not been clarified. Recently Hiraki and his collaborators reported several 2-picolylpalladium(II) complexes.[14] As an extension of our studies on the σ-pyridyl complexes,[15-17] this paper reports on the properties and structures of some picolyl-palladium(II) complexes. A preliminary account and X-ray molecular structure of the 2-picolylpalladium(II) complex have previously been reported.[18]

Experimental

Air-sensitive compounds were handled in an atmosphere of nitrogen using solvents and reagents which had been redistilled under and purged with nitrogen, respectively. Tetrakis(triphenylphosphine)palladium(0), $Pd(PPh_3)_4$, was prepared according to literature.[19] 3-(Chloromethyl)-pyridine was prepared by treating the hydrochloride commercially available with triethylamine in diethyl ether. Tertiary phosphines and other reagents were purchased and used without further purification.

Preparation of the [Chloro(2- and 3-picolyl)(triphenylphosphine)palladium(II)] Complexes, [{PdCl(C_5H_4N-2-CH_2)PPh_3}$_2$] (1a) and [{PdCl(C_5H_4N-3-CH_2)PPh_3}$_n$] (4). To a solution of $Pd(PPh_3)_4$ (3.15 g, 2.73 mmol) in toluene (50 cm^3) was added 2- or 3-(chloromethyl)pyridine (3.48 g, 27.3 mmol) and the mixture was heated to 100 °C for 30 min. The mixture was then left standing at room temperature for 4 h to deposit a yellow-green precipitate, which was filtered and dissolved in dichloromethane (50 cm^3). After filtration, the solvent was distilled away under reduced pressure to obtain a yellow solid of **1a** or **4** in 73 and 15% yields, respectively, which was recrystallized from a mixture of dichloromethane and methanol (1 : 5 by volume).

Preparation of the Bis[chloro(2-picolyl)(diphenylmethyl- and phenyldimethylphosphine)palladium(II)] Complexes, [{PdCl(C_5H_4N-2-CH_2)PPh_2Me}$_2$] (1b) and [{PdCl(C_5H_4N-2-CH_2)$PPhMe_2$}$_2$] (1c). To a solution of **1a** (0.28 g, 0.28 mmol) in dichloromethane (10 cm^3) was added PPh_2Me (0.43 g, 2.2 mmol) or $PPhMe_2$ (0.30 g, 2.2 mmol) to change the color of solution from yellow to pale orange-yellow. After the reaction at room temperature for 3 h, the solution was concentrated to ca. 3 cm^3 by evaporation under reduced pressure. The concentrate was charged onto a column (30 cm×1.5 cm d) of Aluminiumoxid 60 PF_{254} (Type E, Merck). Petroleum ether (150 cm^3) was passed through the column to elute the excess phosphine, and dichloromethane (70 cm^3) was used as the developing solvent. The eluate was concentrated to 10 cm^3 again, and petroleum ether (50 cm^3) was added to the concentrate to precipitate yellow crystals of **1b** or **1c** in 62 and 45% yields, respectively, which were recrystallized from a mixture of dichloromethane and diethyl ether (1 : 6 by volume).

Preparation of the Bis[bromo- and iodo(2-picolyl)-(triphenylphosphine)palladium(II)] Complexes, [{PdX-(C_5H_4N-2-CH_2)PPh_3}$_2$], X=Br (1d) and I (1e). A methanol

solution (15 cm^3) of sodium bromide (0.309 g, 3.00 mmol) or iodide (0.450 g, 3.00 mmol) was added to a dichloromethane solution (30 cm^3) of **1a** (0.15 g, 0.15 mmol). The mixture was allowed to react at room temperature for 3 h and then concentrated to ca. 20 cm^3 by evaporation under reduced pressure to deposit a yellow (**1d**) or deep yellow (**1e**) precipitate in 80 and 65% yields, respectively. They were recrystallized from a mixture of dichloromethane and methanol (1 : 5 by volume).

Preparation of the *trans*-Chloro(2-picolyl)bis(triethylphosphine and phenyldimethylphosphine)palladium(II) Complexes, *trans*-[PdCl(C_5H_4N-2-CH_2)(PR_3)$_2$], PR_3= PEt_3 (2a) and $PPhMe_2$ (2b). To a solution of **1a** (0.35 g, 0.35 mmol) in dichloromethane (10 cm^3) was added PEt_3 (0.50 g, 4.2 mmol) or $PPhMe_2$ (0.59 g, 4.3 mmol), when color of the solution changed from yellow to pale orange-yellow. After the reaction at room temperature for 3 h, the solution was concentrated to ca. 1 cm^3 by evaporation under reduced pressure. Diethyl ether (30 cm^3) was added to the concentrate and the mixture was cooled to −78 °C to precipitate white to pale yellow crystals in 15 (**2a**) and 62% (**2b**) yields, respectively. They were recrystallized at the Dry Ice-methanol temperature from a mixture of dichloromethane and diethyl ether (1 : 10 by volume) containing a small amount of free phosphine.

Preparation of Chloro(2-pyridylacetyl-*C,N*)(triphenylphosphine)palladium(II), [PdCl(C_5H_4N-2-CH_2CO-*C,N*)PPh_3] (3). Carbon monoxide was bubbled at ambient temperature and pressure for 8 h through a suspension of **1a** (0.15 g, 0.15 mmol) in tetrahydrofuran (THF) (50 cm^3) to result in a pale yellow clear solution. Then the vessel was stoppered and the reaction was allowed to continue for further 4 h. Then the slightly reddish solution was concentrated to ca. 10 cm^3 by evaporation under reduced pressure to precipitate white crystals in a 47% yield. A mixture of dichloromethane and diethyl ether (1 : 5 by volume) was used for recrystallization.

Reaction of 1a with Phenyldimethylphosphine. Four different quantities of phenyldimethylphosphine (0.009 g (0.065 mmol), 0.027 g (0.0195 mmol), 0.032 g (0.23 mmol), and 0.054 g (0.39 mmol)) were added to four tubes of which each contained a solution of **1a** (0.065 g, 0.065 mmol) in CD_2Cl_2 (0.3 cm^3). Concentrations of $PPhMe_2$ were 0.22, 0.65, 0.77, and 1.3 mol dm^{-3}, respectively, **1a** being 0.217 mol dm^{-3} in each solution. These solutions were subjected to ^1H NMR assay of **1c** and **2b** formed.

Reaction of 1a with Hydrogen Chloride. A dichloromethane solution (15 cm^3) of hydrogen chloride (0.07 mol dm^{-3}) was added dropwise to a solution of **1a** (0.23 g, 0.23 mmol) in dichloromethane (20 cm^3) and the mixture was stirred at room temperature for 2 h. The solvent was then evaporated to dryness under reduced pressure and the residue was extracted with CD_3OD (0.7 cm^3). The solution was subjected to ^1H NMR measurement to identify 2-methylpyridine hydrochloride. No other organic compounds except triphenylphosphine were detected. The residue was further extracted with chloroform. The extract was evaporated to dryness to leave an orange solid, which was identified to be trans-[$PdCl_2(PPh_3)_2$] by IR spectroscopy[20] and elemental analysis (Found: C, 60.93; H, 4.08%. Calcd for $C_{36}H_{30}Cl_2P_2Pd$: C, 61.60; H, 4.31%) and the yield was 36%.

Reaction of 1a with Silver Acetate. Silver acetate (0.12 g, 0.72 mmol) was added to a suspension of la (0.29 g, 0.29 mmol) in benzene (20 cm^3) and the mixture was allowed to react at 40 °C for 3 h. The solvent was evaporated to dryness under reduced pressure. The residue was treated with dichloromethane (20 cm^3), and silver chloride and remaining silver acetate were filtered off. The yellow filtrate was again evaporated to dryness and the residue was extracted with diethyl ether (20 cm^3). The solvent was vaporized and the residue was dissolved in $CDCl_3$ (0.5 cm^3). A small amount of 2-picolyl acetate was identified on the ^1H NMR spectrum (CH_3, 2.16 s; CH_2, 5.27 s; H^6 of pyridine, δ 8.66 d). On the other hand the IR spectrum of residue suggests the presence of triphenylphosphine, picolyl and acetoxyl groups, and the elemental analysis (C, 52.03; H, 4.10; N, 2.47%) is near the values calculated for [{$PdOCOCH_3(C_5H_4N$-$CH_2)PPh_3$}$_2$] (C, 60.07; H, 4.65; N, 2.69%). The yield was 43%. Purification was not successful.

Reaction of 1a with Phenylacetyl Chloride. To a solution of **1a** (0.32 g, 0.32 mmol) in CD_2Cl_2 (0.5 cm^3) were added C_6D_6 (4 cm^3) and phenylacetyl chloride (0.10 g, 0.65 mmol), and the mixture was heated to 80 °C for 3 h, color of the solution changing from yellow to red. Then the solution was cooled and evaporated to ca. 2 cm^3 under reduced pressure. Red-orange crystals were filtered and the filtrate was subjected to ^1H NMR spectrometry. The organic compound giving proton signals at 3.83 d and 4.17 s ppm could not be identified. The crystals were identified as $Pd_2Cl_4(PPh_3)_2$ by elemental analysis (Found: C, 48.76; H, 3.29%. Calcd for $C_{36}H_{30}P_2Cl_4Pd_2$: C, 49.18; H, 3.44%) and comparison of the IR spectrum with that of an authentic sample and literature.[21] The yield of the dinuclear complex in the present reaction was 73%.

Derivation of Methyl 2-Pyridylacetate from 1a. Carbon monoxide was passed slowly through a suspension of **1a** (0.18 g, 0.18 mmol) in THF (30 cm^3) for 7 h. A methanol solution (5 cm^3) of sodium methoxide (0.023 g, 0.43 mmol) was added to the reaction mixture and CO bubbling was continued for further 2 h. The solvent was evaporated to dryness under reduced pressure and the residue was extracted with diethyl ether (20 cm^3), which was again vaporized. The residue was dissolved in $CDCl_3$ (0.5 cm^3) and shown by ^1H NMR assay to contain a small amount of methyl 2-pyridylacetate (CH_3 and CH_2 overlapping, 3.77 broad: H^6 of pyridine, δ 8.40).

Measurements. Infrared spectra were recorded in Nujol on a JASCO DS-701G spectrophotometer. A JEOL JNM MH-100 instrument was used to obtain ^1H NMR spectra at 100 MHz with tetramethylsilane as internal reference. ^{13}C NMR spectra were taken at 25.0 MHz on a JEOL JNM FX-100 spectrometer with tetramethylsilane as external reference and ^{31}P NMR spectra were recorded at 40.25 MHz on the same instrument with phosphoric acid as external reference. The molecular weight was determined in dichloromethane at 25 °C by vapor pressure osmometry with an instrument manufactured by Knauer in West Berlin, West Germany.

Results and Discussion

Although $Ni(PPh_3)_4$ reacted readily with 2-, 3-, and 4-(chloromethyl)pyridines, the expected picolylnickel(II) complexes could not be isolated, On the other hand, the reactions of $Pd(PPh_3)_4$ with these pyridine

Table 1. Analytical Data for the Picolyl Palladium(II) Complexes

Complex		Found (Calcd)			
		C/%	H/%	N/%	Mol wt
$[\{PdCl(C_5H_4N\text{-}2\text{-}CH_2)PPh_3\}_2]$	**1a**	58.01	4.30	2.94	924
		(58.09)	(4.29)	(2.82)	(993)
$[\{PdCl(C_5H_4N\text{-}2\text{-}CH_2)PPh_2Me\}_2]$	**1b**	52.71	4.42	3.11	851
		(52.56)	(4.41)	(3.23)	(868)
$[\{PdCl(C_5H_4N\text{-}2\text{-}CH_2)PPhMe_2\}_2]$	**1c**	45.17	4.58	3.65	733
		(45.19)	(4.61)	(3.76)	(744)
$[\{PdBr(C_5H_4N\text{-}2\text{-}CH_2)PPh_3\}_2]$	**1d**	52.70	4.02	2.50	1065
		(53.31)	(3.91)	(2.59)	(1081)
$[\{PdI(C_5H_4N\text{-}2\text{-}CH_2)PPh_3\}_2]$	**1e**	48.23	3.51	2.24	1083
		(49.05)	(3.60)	(2.38)	(1175)
$[PdCl(C_5H_4N\text{-}2\text{-}CH_2)(PEt_3)_2]$	**2a**	45.77	7.42	2.75	447
		(45.97)	(7.72)	(2.98)	(470)
$[PdCl(C_5H_4N\text{-}2\text{-}CH_2)(PPhMe_2)_2]$	**2b**	51.88	5.57	2.46	501
		(51.78)	(5.53)	(2.74)	(510)
$[PdCl(C_5H_4N\text{-}2\text{-}CH_2CO)PPh_3]$	**3**	57.09	4.14	2.70	518
		(57.28)	(4.04)	(2.67)	(524)
$[\{PdCl(C_5H_4N\text{-}3\text{-}CH_2)PPh_3\}_n]$	**4**	57.41	4.11	2.61	
		(58.09)	(4.27)	(2.82)	

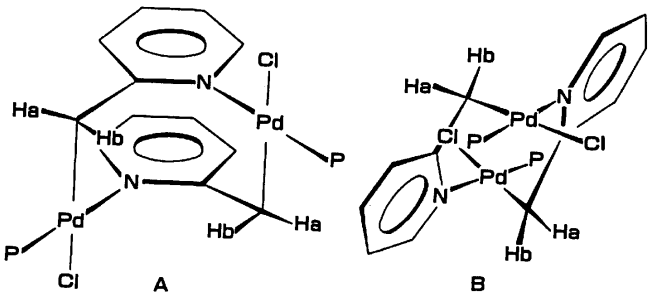

Fig. 1. Two possible dinuclear structures for $[\{PdCl(C_5H_4N\text{-}2\text{-}CH_2)PPh_3\}_2]$ (**1a**).

Table 2. Some Far IR Data in cm^{-1}

Complex	ν(Pd-X)	ν(Pd-P)
1a	284m	420m
1b	280m	430m
1c	268m	420m
1d	181m	420m
1e	153m	420w
2b	278m	415m
3	292w	427m
4	265w	420w

derivatives did not take place at room temperature, but occurred at 100 °C to finish after 30 min. The 2- and 3-picolylpalladium(II) complexes were isolated, but stability and solubility of the latter were not enough to allow full characterization. The 4-picolyl complex was not even isolated. Thus the stability of the picolylpalladium(II) complexes varies remarkably with the site of substitution on the pyridine ring.

Characterization of the Dinuclear Picolyl Complexes. The analytical and molecular-weight data in Table 1 indicate that complexes **1a** and **1b—1e** which were derived from **1a** by the ligand substitution reactions are dinuclear. As a dinuclear structure for the palladium(II) complexes the di-μ-chloro structure is most common.[21] However, X-ray analysis revealed that $[\{PdBr(C_5H_4N\text{-}C^2)PPh_3\}_2]$ has the pyridyl(C^2, N)-bridged structure.[22] If the picolyl ligand in the present dinuclear complexes also functions as a similar bridging ligand, the two structures depicted in Fig. 1 are conceivable. Structure A has a C_2 axis, while B being shown in the 2-litiomethyl-6-methylpyridine-tetramethylethylenediamine dimer[23] has a center of inversion. Hiraki and his co-workers proposed structure B,[14] but molecular models indicate that A is more favorable, since the bulky triphenylphosphine ligands experience a serious steric interference by the picolyl ligand in structure B. In fact X-ray analysis has confirmed that compound **1a** has structure A.[18]

The ν(Pd-Cl) frequencies observed for **1a—1c** (Table 2) are rather low for the terminal chloride, but are reasonable when located at the coordination site trans to carbon.[5] Table 3 lists ^1H NMR data for complexes **1a—1c**. The pyridyl ring protons are readily assigned by reference to the data for free 2-picoline[24] except the H^6 atoms of **1a** and **1b** of which signals are indiscernible because of overlapping with those for the phenyl-ring protons. Thus, the triplet signal at about δ 6.5 is assigned to H^5 and the doublet in the δ 6.7—7.0 region to H^3 which resonates at lower field than H^5 because of the anisotropic effect of the $(PPh_3)ClPdCH_2$ substituent.[25,17] The remaining triplet in the δ 7.0—7.3 region is attributed to H^4, H^6 of **1c** appearing as a doublet at δ 7.84.

Each of the pyridyl-ring protons except H^4 of the picolyl ligands resonates at a remarkably higher field than that of 2-(chloromethyl)pyridine (H^3 and H^5, around δ 7.6; H^4, 7.13; H^6, 8.56).[12a] In the case of $Fe(C_5H_4N\text{-}2\text{-}CH_2)(\eta^5\text{-}C_5H_5)(CO)_2$, the pyridyl-ring

protons show similar upfield shifts (H^3 and H^5, δ 6.90; H^4, 7.32; H^6, 8.28),[12a] which were considered to be caused by the electron-donating effect of the CH_2ML_n moiety.[11,12b] The phenyl-ring protons in **1a**, **1b**, and **1c** exhibit two multiplets at about δ 7.5 and 7.9, the former being assigned to the meta and para protons and the latter to the ortho protons.[26] The methyl protons of the phosphine in **1b** resonate as a doublet at δ 2.22 with ^2J(P-H)=ca. 12.5 Hz, but those in **1c** exhibit two doublets at δ 1.88 and 1.91 both with ^2J(P-H)=ca. 11 Hz (Fig. 2), showing that the two methyl groups of phenyldimethylphosphine in **1c** differ in their time-averaged magnetic environments. This indicates that there is no plane of symmetry through the Pd-P bond[27] in accordance with the dinuclear structure A in Fig. 1.

The methylene protons of the picolyl ligand in **1a**—**1c** are not equivalent as is seen in Fig. 1, but exhibit two separate signals in the δ 2.42—2.52 and 3.72—3.81 regions, respectively (Fig. 2 and Table 3). The higher-field signal is a triplet and the lower-field one doublet, both having the same coupling constant of about 9 Hz. Irradiation at the frequency of the triplet reduced the lower-field doublet to a singlet, and irradiation at the latter frequency reduced the triplet to a doublet, confirming the geminal coupling (J=ca. 9 Hz) of the methylene protons. The ^{31}P NMR spectrum of **1a** exhibits a signal at δ 36.06 downfield from H_3PO_4. Irradiation only at the region for the phenyl-ring protons gave a doublet shown in Fig. 3. The coupling constant is ca. 9 Hz, indicating that the phosphorus atom couples to one of the methylene protons which resonates as a triplet. As is seen in Fig. 2, the low-field doublet for **1c** splits due to ca. 3 Hz coupling to phosphorus. Thus one of the methylene protons in **1c** strongly couples to ^{31}P with J=ca. 9 Hz, while the other weakly with J=ca. 3 Hz.

Table 4 lists the ^{13}C chemical shifts and J(P-C) values for complex **1a** together with the corresponding data for uncoordinated triphenylphosphine[28] and 2-ethylpyridine[29] for comparison. Assignment for the phenyl carbons in **1a** was made on the basis of J(P-C)

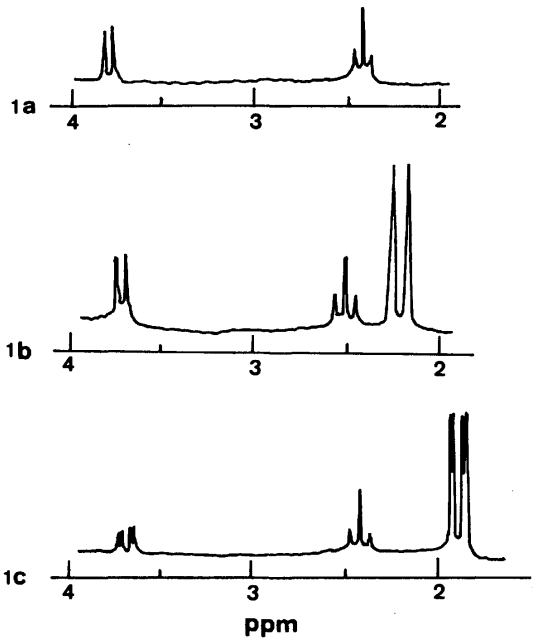

Fig. 2. Methyl and methylene signals in ^{1}H NMR spectra of [{PdCl(C_5H_4N-2-CH_2)L}$_2$] with PPh_3 (**1a**), PPh_2Me (**1b**) and $PPhMe_2$ (**1c**) as L.

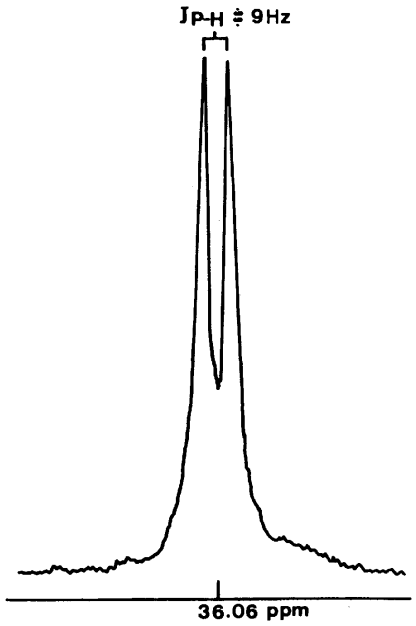

Fig. 3. ^{31}P NMR signal from [{PdCl(C_5H_4N-2-CH_2)PPh_3)$_2$] (**1a**) under irradiation at the phenyl-ring proton resonances.

Table 3. Proton Chemical Shifts in ppm from Internal Tetramethylsilane at Room Temperature

Complex	Solvent	Pyridyl-ring proton				CH_2	Phenyl-ring proton		CH_3
		H^3	H^4	H^5	H^6		meta and para	ortho	
1a	CD_2Cl_2	6.95d	7.26t	6.53t	a)	2.44t 3.81d	7.55m	7.89m	
1b	$CDCl_3$	6.80d	7.15t	6.47t	a)	2.52t 3.72d	7.51m	7.85m	2.22d
1c	$CDCl_3$	6.74d	7.09t	6.46t	7.84d	2.42t 3.75dd	7.53m	7.97m	1.88d, 1.91d
2b	CD_2Cl_2	7.13d	6.77t	6.53br	8.15d	2.78s,br	7.43m	7.65m	1.80s
3	$CDCl_3$	a)	a)	a)	9.57d	4.11s	7.45m	7.75m	

a) Indiscernible because of overlapping with signals from the phenyl-ring proton.
s: singlet, d: doublet, t: triplet, dd: doublet of doublets, m: multiplet, br: broad.

values and by reference to uncoordinated PPh_3 and $[\{PdBr(C_5H_4\text{-}C^2)PPh_3\}_2]$.[16] The methylene carbon of the picolyl ligand in **1a** resonates at δ 28.47 and appears as a triplet of doublets under the off-resonance condition, ^2J(P-C) being ca. 7 Hz. The small coupling constant suggests that the methylene and phosphine ligands are mutually cis. Assignments for the pyridyl-ring carbons were made based on the off-resonance data and referring to $[\{PdBr(C_5H_4N\text{-}C^2)PPh_3\}_2]$.[16] As is shown by Table 4, the shielding of each carbon is quite similar to that of the corresponding ring carbon in 2-ethylpyridine, indicating that the $(PPh_3)ClPdCH_2$ moiety is functioning as an electron-donating group, but the effect is weaker than that of the $(PPh_3)BrPd$ group directly attached to the pyridyl ring in $[\{PPdBr(C_5H_4N\text{-}C^2)PPh_3\}_2]$.[16]

Table 4. ^{13}C Chemical Shifts δ (in ppm from external Me_4Si) and Coupling Constants J (in Hz) in CD_2Cl_2 at Room Temperature

Phenyl carbon in **1a**			Phenyl carbon in free PPh_3		
	δ	J(P-C)		δ	J(P-C)
C^1	130.98	51.5	C^1	138.3	21
C^2	135.13	11.8	C^2	134.4	20
C^3	128.60	11.8	C^3	129.2	7
C^4	131.01	0	C^4	129.3	<1
Picolyl carbon in **1a**			2-Ethylpyridine		
	δ	J(P-C)		δ	
CH_2	28.47	ca. 7	CH_2	32.0	
C^2	169.83		C^2	163.9	
C^3	123.48		C^3	121.9	
C^4	136.01		C^4	136.3	
C^5	117.7		C^5	121.9	
C^6	151.72		C^6	149.8	

Although the 3-picolyl complex **4** was prepared and isolated, it is less stable and less soluble in organic solvents than the 2-picolyl complex **1a** and its characterization has not been enough to allow the structure assignment. Results of the elemental analysis indicate that the complex is not mononuclear but may be polynuclear, since a dinuclear structure seems difficult.

Characterization of the Mononuclear Picolyl Complexes. The mononuclear picolyl complexes **2a** and **2b** were prepared by the reactions of **1a** with excess amounts of PEt_3 and $PPhMe_2$, respectively and isolated at low temperature. The analytical and molecular-weight data in Table 1 indicate that they are mononuclear and the ν(Pd-Cl) frequency of **2b** in Table 2 is quite similar to that recorded for *trans*-$[PdCl(CH_2Ph)(PPh_3)_2]$.[3] The ^1H NMR data for **2b** are included in Table 3. Contrary to the case of **1c**, the methyl protons of the phosphine ligands in **2b**

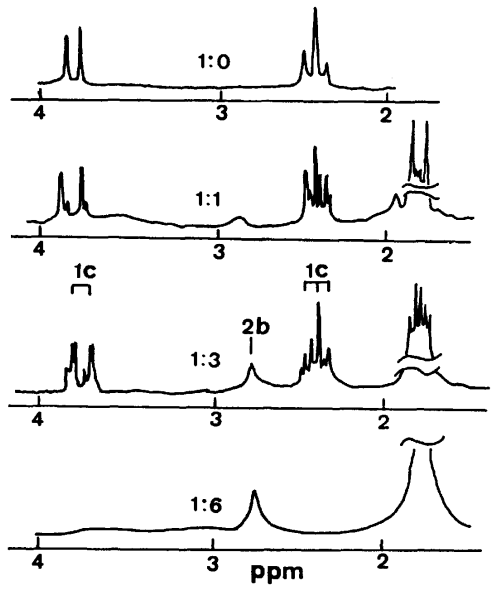

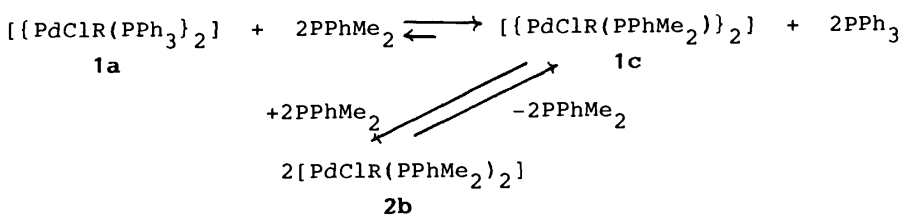

Fig. 4. The methylene-proton signals from $[\{PdCl(C_5H_4N\text{-}2\text{-}CH_2)PPh_3\}_2]$ (**1a**) in CD_2Cl_2 at room temperature in the absence and in the presence of one equivalent, three times, and six times molar amount of phenyldimethylphosphine. In the reaction scheme R represents the 2-picolyl ligand.

resonate as a singlet at δ 1.80 with no coupling to phosphorus, and the picolylic protons also exhibit a broad singlet at δ 2.78. The benzylic protons in *trans*-[PdCl(CH_2Ph)(PPh_3)$_2$] also lack coupling to phosphorus and the behavior was rationalized by the rapid phosphine exchange between the mononuclear complex and PPh_3 freed by the equilibrium $2[PdCl(CH_2Ph)(PPh_3)_2] \rightleftarrows [\{PdCl(CH_2Ph)PPh_3\}_2]+2PPh_3$.[3] Similar situation seems to be realized for **2b**. In fact the ^{1}H NMR spectrum of **2b** in CD_2Cl_2 at −40 °C exhibits two triplets at δ 1.83 and 2.74 assignable to the phosphine methyl (J=ca. 3 Hz) and picolyl methylene (J=ca. 8 Hz) protons, respectively, indicating that the rapid phosphine exchange is prohibited at lower temperature and that **2b** has the trans structure.[30]

The Phosphine Substitution and Bridge Cleavage Reactions of 1a with Phenyldimethylphosphine. Figure 4 compares the methylene-proton signals exhibited by solutions of **1a** in CD_2Cl_2 at room temperature containing various amounts of $PPhMe_2$. An equimolar mixture of **1a** and $PPhMe_2$ shows signals assignable mainly to **1a** and **1c** accompanied by a small amount of **2b** giving the signal at δ 2.78. When a three times molar amount of $PPhMe_2$ is added to **1a**, the predominant species is **1c** and the amount of **2b** is also increased. The last spectrum in Fig. 4, which is given by a 1:6 mixture of **1a** and $PPhMe_2$, is composed of broad signals assignable solely to **2b**. Such a sequence of spectra indicates that the phosphine substitution reaction of **1a** with $PPhMe_2$ to produce **1c** takes place prior to the bridge cleavage to result in a mononuclear complex **2b**.

As was described in the Experimental section, the mononuclear complexes **2a** and **2b** were obtained upon direct crystallization from the reaction mixture, but the dinuclear complexes **1b** and **1c** were isolated by virtue of the chromatographic separation of the mixture.

Characterization of the 2-Pyridylacetyl Complex 3. Complex **1a** reacted readily with carbon monoxide in THF to afford white crystals of **3**, which is shown to be mononuclear by the analytical and molecular-weight data in Table 1. A very strong IR band at 1690 cm^{-1} is assigned to the ν(C=O) vibration and a weak band at 330 cm^{-1} may be tentatively assigned to the ν(Pd-N) vibration. The ^{1}H NMR spectrum shows the methylene signal as a sharp singlet at δ 4.11. These spectral data for **3** conform with the following (*C,N*) chelate structure.

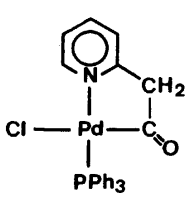

3

In this structure the pyridyl ring lies on the coordination plane and the methylene protons experience equal magnetic environment. Although the signals from the pyridyl-ring protons except H^6 are indiscernible because of overlapping with those from the phenyl-ring protons, H^6 resonates at δ 9.57. Such a remarkable downfield shift of H^6 may be caused by the deshielding anisotropic effect of the carbonyl group. Similar 2-pyridylacetyl complexes (C_5H_4N-2-CH_2CO)$Mn(CO)_4$ and (C_5H_4N-2-CH_2CO)$Mo(CO)_2$-(η^5-C_5H_5), to both of which the (C,N) chelate structure is proposed, show the methylene singlet at δ 4.00 and the pyridyl-ring H^6 doublet at δ 8.99 and 8.96, respectively.[12a]

Reactions of the Picolyl Ligand with Some Reagents. As was described in the Experimental section, reactions of the picolyl ligand with some reagents were examined. Hydrogen chloride decomposed **1a** in dichloromethane to produce 2-picoline hydrochloride and *trans*-$PdCl_2(PPh_3)_2$. The reaction of **1a** with silver acetate in benzene gave a small amount of 2-picolyl acetate and a complex which was presumed to be [{$PdOCOCH_3(C_5H_4N$-2-CH_2)-PPh_3}$_2$]. The acetato complex may be formed by the ligand substitution of **1a** and function as an intermediate for production of 2-picolyl acetate. Production of benzyl acetate by the reaction of *trans*-benzylchlorobis(triphenylphosphine)palladium(II) with silver acetate was similarly presumed to be preceded by replacement of chloride with acetate.[3] The reaction between **1a** and phenylacetyl chloride was tried with the aim of getting 2-picolyl benzyl ketone, but identification of organic products was unsuccessful, although [{$PdCl_2(PPh_3)$}$_2$] was obtained in a high yield. Carbonylation of **1a** followed by the reaction with methoxide gave methyl 2-pyridylacetate. This is analogous to the reactions reported for the benzylpalladium(II) complex.[4,7] Thus complex **1a** is a useful intermediate for preparation of various pyridine derivatives.

We wish to thank Mr. Junichi Gohda for elemental analysis and Mr. Tetsu Hinomoto of JEOL Co. Ltd. for measurements of the ^{13}C and ^{31}P NMR spectra.

References

1) P. M. Maitlis, "The Organic Chemistry of Palladium," Vol. I, Academic Press, New York (1971); F. R. Hartley, "The Chemistry of Platinum and Palladium," Applied Science Publishers, London (1973).

2) J. Tsuji, *Acc. Chem. Res.*, **2**, 144 (1969); P. M. Maitlis, "The Organic Chemistry of Palladium," Vol. II, Academic Press, New York (1971); B. M. Trost, *Tetrahedron*, **33**, 2615 (1977); R. F. Heck, *Acc. Chem. Res.*, **12**, 146 (1979).

3) P. Fitton, J. E. McKeon, and B. C. Ream, *Chem. Commun.*, **1969**, 370.

4) K. S. Y. Lau, R. W. Fries, and J. K. Stille, *J. Am. Chem. Soc.*, **96**, 4983 (1974); K. S. Y. Lau, P. K. Wong, and J. K. Stille, *ibid.*, **98**, 5832 (1976); Y. Becker and J. K. Stille,

ibid., **100**, 838 (1978).

5) R. Ros, M. Lenarda, T. Boschi, and R. Roulet, *Inorg. Chim. Acta*, **25**, 61 (1977).

6) G. Carturan, M. Graziani, R. Ros, and U. Belluco, *J. Chem. Soc., Dalton Trans.*, **1972**, 262.

7) J. K. Stille and K. S. Y. Lau, *J. Am. Chem. Soc.*, **98**, 5841 (1976).

8) J. S. Roberts and K. J. Klabunde, *J. Am. Chem. Soc.*, **99**, 2509 (1977).

9) Y. Becker and J. K. Stille, *J. Am. Chem. Soc.*, **100**, 845 (1978).

10) R. G. Coombes, M. D. Johnson, and N. Winterton, *J. Chem. Soc.*, **1965**, 7029.

11) M. D. Johnson, M. L. Tobe, and L. Y. Wong, *J. Chem. Soc. A*, **1968**, 923.

12) a) R. B. King and M. B. Bisnette, *Inorg. Chem.*, **5**, 293 (1966); b) M. D. Johnson and N. Winterton, *J. Chem. Soc. A*, **1970**, 507.

13) M. D. Johnson, *Acc. Chem. Res.*, **11**, 57 (1978).

14) M. Onishi, K. Hiraki, K. Maeda, and T. Itoh, *J. Organomet. Chem.*, **188**, 245 (1980).

15) K. Isobe, Y. Nakamura, and S. Kawaguchi, *Chem. Lett.*, **1977**, 1383; *Bull. Chem. Soc. Jpn.*, **53**, 139 (1980); K. Isobe and S. Kawaguchi, *Heterocycles*, **16**, 1603 (1981).

16) K. Isobe, K. Nanjo, Y. Nakamura, and S. Kawaguchi, *Bull. Chem. Soc. Jpn.*, **59**, 2141 (1986).

17) K. Isobe, E. Kai, Y. Nakamura, K. Nishimoto, T. Miwa, S. Kawaguchi, K. Kinoshita, and K. Nakatsu, *J. Am. Chem. Soc.*, **102**, 2475 (1980); K. Isobe, Y. Nakamura, T. Miwa, and S. Kawaguchi, *Bull. Chem. Soc. Jpn.*, **60**, 149 (1987).

18) K. Nakatsu, K. Kafuku, H. Yamaoka, K. Isobe, Y. Nakamura, and S. Kawaguchi, *Inorg. Chim. Acta*, **54**, L69 (1981).

19) D. R. Coulson, *Inorg. Synth.*, **13**, 121 (1972).

20) Pale yellow crystals of $[PdCl_2(PPh_3)_2]$ were reported to have the cis configuration based on the ν(Pd-Cl) bands at 327 and 300 cm^{-1} [D. C. Goodall, *J. Chem. Soc. A*, **1968**, 887], but a recent paper [J. J. MacDougall and J. H. Nelson, *Inorg. Nucl. Chem. Lett.*, **15**, 315 (1979)] concluded that the complex is trans by ^{13}C and ^{31}P NMR spectroscopy and assigned the 357 cm^{-1} band to the ν(Pd-Cl) vibration. K. Shobatake and K. Nakamoto [*J. Am. Chem. Soc.*, **92**, 3332 (1970)] also assigned the 360 cm^{-1} band to the ν(Pd-Cl) vibration in *trans*-$[PdCl_2(PPh_3)_2]$ based on the metal isotope effect. *cis*-$[PdCl_2(PPh_3)_2]$ seems to have not been prepared as yet [D. T. Clark, K. B. Dillon, H. R. Thomas, and T. C. Waddington, *J. Chem. Soc., Dalton Trans.*, **1979**, 250].

21) R. J. Goodfellow, P. L. Goggin, and L. M. Venanzi, *J. Chem. Soc. A*, **1967**, 1897.

22) K. Nakatsu, K. Kinoshita, H. Kanda, K. Isobe, Y. Nakamura, and S. Kawaguchi, *Chem. Lett.*, **1980**, 913.

23) P. R. Schleyer, R. Hacker, H. Dietrich, and W. Mahdi, *J. Chem. Soc., Chem. Commun.*, **1985**, 622.

24) T. J. Batterham, "NMR Spectra of Simple Heterocycles," Wiley, New York (1973).

25) H. C. Clark and J. E. H. Ward, *J. Am. Chem. Soc.*, **96**, 1741 (1974); D. R. Coulson, *ibid.*, **98**, 3111 (1976).

26) R. Keat, *Chem. Ind. (London)*, **1968**, 1362.

27) W. B. Jennings, *Chem. Rev.*, **75**, 307 (1975).

28) O. A. Gansow and B. Y. Kimura, *Chem. Commun.*, **1970**, 1621.

29) J. B. Stothers, "Carbon-13 NMR Spectroscopy," Academic Press, New York (1972), p. 250.

30) J. M. Jenkins and B. L. Shaw, *J. Chem. Soc. A*, **1966**, 770.

 © 1989 The Chemical Society of Japan Bull. Chem. Soc. Jpn., 62, 1809—1816 (1989)

Syntheses, and Crystal and Molecular Structures of Tetramethylammonium [Aquamethanolhexakis(isothiocyanato)lanthanoidates(III)], $[(CH_3)_4N]_3[M(NCS)_6(CH_3OH)(H_2O)]$ (M=La, Ce, Pr, Nd, Sm, Eu, Gd, Tb, Dy, Er), and Tetramethylammonium [Heptakis(isothiocyanato)lanthanoidates(III)], $[(CH_3)_4N]_4[M(NCS)_7]$(M=Dy, Er, Yb)

Fumiko Matsumoto,† Naomi Matsumura,† and Akira Ouchi*

Department of Chemistry, College of Arts and Sciences, The University of Tokyo, Komaba, Meguro-ku, Tokyo 153
†Department of Chemistry, School of Hygienic Sciences, Kitasato University, Kitasato, Sagamihara-shi, Kanagawa 228
(Received October 4, 1988)

The title complexes were synthesized and their crystal and molecular structures were determined by the X-ray diffraction method using their single crystals. The crystals of the former ten hexakis(isothiocyanato) complexes of lanthanum through dysprosium(III) and erbiun(III) are isomorphous with each other: monoclinic, space group $P2_1$, $Z=2$. The central metal atom is octa-coordinated, in a square-antiprism geometry, to six nitrogen atoms of thiocyanato (SCN) ions and two oxygen atoms of methanol and water molecules. The two oxygen atoms take the positions of the most approaching apexes of two squares. The latter three heptakis(isothiocyanato) complexes of dysprosium, erbium, and ytterbium are in another isomorphous form with each other: orthorhombic, space group $P2_1nb$, $Z=4$. The central metal atom is hepta-coordinated, in a deformed pentagonal-bipyramidal geometry, to seven nitrogen atoms of SCN ions.

The study of the molecular structures of the metal complexes of thiocynate (SCN) is one of the very interesting fields due to their variety of coordinated forms and bridging structures. The structure of tetrabutylammonium [hexakis(isothiocyanato)lanthanoidates(M)] (M=Pr—Yb, and Y) has already been elucidated by Martin and others.[1] It has a coordination number of six, although almost all lanthanoids have a coordination number 8—9 in almost all of thier complexes.

On the other hand, in anionic complexes of tetrapotassium [tetraaquatetrakis(isothiocyanato)lanthanoidates(M)] thiocyanates (M=Nd, Eu), reported by Lazarev, the coordination number of the central metal atom is eight (square-antiprism geometry).[2] The authors have already shown that in tetraethylammonium [aquaheptakis(isothiocyanato)lanthanoidates(M)] (M=La—Pr and Nd—Er) the central metal atom is in a cubic octa-coordination geometry.[3]

In this line of the study, the authors have tried to synthesize other types of thiocyanato complexes of lanthanoids, and have obtained the two series of the anionic complexes shown in the title. From now on, the former ten hexakis(isothiocyanato) complexes are called **A**-type complexes, while the latter three heptakis(isothiocyanato) complexes are called **B**-type.

In many cases a series of the isomorphous lanthanoid complexes were obtained only for a limited range of the members of the following series: for example, Sm—Yb for $[M(CH_3C_6H_4SO_3)_2(H_2O)_6](CH_3C_6H_4SO_3)\cdot 3H_2O$,[4] La—Gd for $[M\{(C_2H_5O)_2PS_2\}_2(C_6H_5CONH_2)_3][(C_2H_5O)_2PS_2]$,[5] La—Eu for $[\{M(ClCH_2CO_2)_3\}_3(H_2O)_5]$,[6] Gd—Yb for $[M_3(ClCH_2CO_2)_9(H_2O_4)]_n\cdot nH_2O$.[7] In a series of isomorphous lanthanoid complexes it was found that some structural detail changed, depending on the metal atomic number.[6,8,9] Since we had obtained ten members of isomorphous **A**-type complexes, we had planned to compare their detailed structures with each other. Moreover, by almost the same synthetic technique, the other type, **B**-type, complexes were obtained from the heavier lanthanoids. Therefore, a comparison of the **A**- and **B**-type complexes was also thought to be interesting.

Therefore, the authors investigated the crystal structures of the title two series of complexes by single-crystal X-ray diffraction.

Experimental

Synthesis of the A-Type Complexes: Tetramethylammonium [Aquamethanolhexakis(isothiocyanato)lanthanoidates(III)], $[(CH_3)_4N]_3[M(NCS)_6(CH_3OH)(H_2O)]$(M=La—Er). Lanthanoid(III) thiocyanates and tetramethylammonium thiocyanate were obtained by the metathetical reaction between lanthanoid(III) chlorides or tetramethylammonium chloride and potassium thiocyanate in methanolic medium, respectively (as reported previously), to obtain cadmium and other metal thiocyanates.[10,11] The obtained lanthanoid thiocyantes were stored as their methanolic solution (0.5 mol dm^{-3}) without drying.

To synthesize the lanthanum(III) complex, to the methanolic solution (7 cm^3) of lanthanum thiocyanate (1.0 mmol), tetramethylammonium thiocyanate (0.41 g, 3.1 mmol), and water (0.1 cm^3, 6 mmol) were added. The mixture was then warmed and stirred until complete dissolution occured. The solution was left standing for several days in a silica gel desiccator for drying to about 1 cm^3 at room temperature. A square plate form crystals were deposited. Yield: 0.55 g (0.72 mmol, 72 %).

Crystals were also obtained when the above-mentioned starting solution was left standing in chlorobenzene vapor. Yield, 0.25 g, 0.33 mmol, 33%, started from 1 mmol of the

Table 1. Elemental Analyses (*n*/%)

A. **A**-type Complexes, $[(CH_3)_4N]_3[M(SCN)_6(CH_3OH)(H_2O)]$, $MC_{19}H_{42}N_9O_2S_6$ (The Calculated Values Are Shown in Parentheses)

M	M	C	H	N
La	18.10	29.85	5.55	16.60
	(18.28)	(30.03)	(5.57)	(16.59)
Ce	18.50	29.69	5.50	16.57
	(18.41)	(29.99)	(5.56)	(16.56)
Pr	18.45	29.55	5.50	16.75
	(18.50)	(29.95)	(5.56)	(16.55)
Nd	18.80	29.55	5.47	16.67
	(18.85)	(29.82)	(5.53)	(16.47)
Sm	19.19	29.39	5.46	16.01
	(19.49)	(29.59)	(5.49)	(16.34)
Eu	19.80	29.27	5.49	15.96
	(19.66)	(29.53)	(5.48)	(16.31)
Gd	19.92	29.01	5.27	16.17
	(20.21)	(29.32)	(5.44)	(16.20)
Tb	20.40	29.06	5.41	16.10
	(20.38)	(29.26)	(5.43)	(16.16)
Dy	20.50	28.82	5.36	15.80
	(20.74)	(29.13)	(5.40)	(16.09)
Er	21.40	28.67	5.29	16.19
	(21.22)	(28.95)	(5.37)	(15.99)

B. **B**-type Complexes, $[(CH_3)_4N]_4[M(SCN)_7]$, $MC_{23}H_{48}N_{11}S_7$ (The Calculated Values Are Shown in Parentheses)

M	M	C	H	N
Dy	18.34	31.69	5.54	17.55
	(18.77)	(31.91)	(5.59)	(17.80)
Er	18.90	31.41	5.45	17.48
	(19.22)	(31.74)	(5.56)	(17.70)
Yb	19.51	31.37	5.44	17.32
	(19.75)	(31.53)	(5.52)	(17.59)

metal salt.

The Ce through Dy complexes were obtained by the same technique in almost the same yield; even in the case of the Dy salt, only the **A**-type complex crystals were deposited, unless the starting solution was severely dried. (By the latter method, the **B**-type Dy complex was obtained.)

Both of the above-mentioned methods did not give the **A**-type erbium complex; only hexagonal thick plate crystals of the **B**-type complex were deposited within several days. The erbium complex was obtained by using a starting solution containing a little more water (0.5 cm^3 in place of 0.1 cm^3). The solvent was evaporated very slowly, over several months, at room temperature. Yield: 0.3 g (0.38 mmol, 38%) starting from 1.0 mmol of erbium thiocyanate.

All attempts to synthesize the **A**-type complex of ytterbium were unsuccessful. Even when more water was added to the starting solution, the **B**-type complex was always deposited.

Synthesis of the B-Type Complex: Tetramethylammonium Heptakis(thiocyanato)dysprosium(III), $[(CH_3)_4N]_4[M(SCN)_7]$ (M=Er, Yb). The dysprosium complex was synthesized as follows. To the methanol solution (10 cm^3) of dysprosium thiocyanate (2.0 mmol) and tetramethylammonium thiocyanate (1.06 g, 8.0 mmol), 10 cm^3 of ethanol and 10 cm^3 of benzene were added, and the mixture was evaporated to dryness by a vacuum rotary evaporator at about 80 °C. The same process was repeated three times so as to remove the water completely. The residue was dissolved into 10 cm^3 of methanol (GR grade reagent of Wako Pure Chemicals Industry Ltd.: it contains at most 0.3% of water). The solution was dried to 2 cm^3 by standing in a silica gel desiccator for several days: crystals were deposited. These were washed with a small portion of ethanol and dried in a silica gel desiccator. Yield: 1.21 g, 1.40 mmol 70%. By the same synthetic method **B**-type Er and Yb complexes were also obtained in almost the same yield.

B-type complexes of terbium and the lighter lanthanoids

Table 2. Crystallographic Data and Various Experimental Conditions for the **A**-Type Complexes, $[(CH_3)_4N]_3[M(SCN)_6(CH_3OH)(H_2O)]$, $MC_{19}H_{42}N_9O_2S_6$, Monoclinic, Space Group, $P2_1$, Z=2

M	La	Ce	Pr	Nd	Sm	Eu	Gd	Tb	Dy	Er
F. W.	759.87	761.09	761.87	765.21	771.33	772.93	778.22	779.89	783.47	788.23
a(*l*/Å)	9.082(7)	9.061(2)	9.047(3)	9.044(2)	9.011(4)	8.999(4)	8.993(4)	8.980(4)	8.967(2)	8.948(3)
b(*l*/Å)	22.59(6)	22.545(14)	22.542(17)	22.524(12)	22.497(15)	22.47(3)	22.460(13)	22.459(18)	22.43(5)	22.399(17)
c(*l*/Å)	8.963(9)	8.950(4)	8.928(6)	8.929(4)	8.901(4)	8.899(3)	8.893(5)	8.874(5)	8.867(4)	8.846(4)
β(ϕ/°)	91.29(8)	91.19(3)	91.18(4)	91.06(2)	91.15(4)	91.11(4)	91.01(5)	91.09(5)	90.96(3)	90.98(3)
U(v/Å^3)	1838(5)	1827.9(15)	1820.4(19)	1818.6(12)	1804.0(17)	1798(2)	1795.8(16)	1789.4(19)	1783(4)	1772.8(16)
D_m(d/g cm^{-3})	1.35(3)	1.37(3)	1.37(3)	1.38(3)	1.42(3)	1.43(3)	1.43(3)	1.46(3)	1.45(3)	1.48(3)
D_x(d/g cm^{-3})	1.37	1.38	1.39	1.40	1.42	1.43	1.44	1.45	1.46	1.48
μ(Mo $K\alpha$) (n/cm^{-1})	15.41	16.16	17.00	18.05	20.14	21.21	22.69	23.89	25.43	28.29
N_m[a]	6041	6004	5474	5691	5439	5918	6712	5871	5372	6621
N_c[b]	4569	3957	3393	4397	4511	4661	4553	4277	4447	4461
R[c]	0.081	0.077	0.078	0.052	0.052	0.051	0.066	0.060	0.052	0.059
V_c[d](v/mm^3)	0.35×0.33 ×0.33	0.28×0.25 ×0.25	0.21×0.21 ×0.20	0.30×0.30 ×0.22	0.35×0.32 ×0.23	0.33×0.33 ×0.33	0.32×0.31 ×0.30	0.30×0.30 ×0.20	0.33×0.33 ×0.35	0.30×0.30 ×0.29
S_w[e] (ω/°)	1.16+ 0.5tanθ	1.25+ 0.35tanθ	1.15+ 0.5tanθ	1.12+ 0.5tanθ	1.15+ 0.5tanθ	1.20+ 0.35tanθ	1.30+ 0.5tanθ	1.30+ 0.35tanθ	1.25+ 0.35tanθ	1.16+ 0.5tanθ
S_R[f](2θ/°)	3—62	3—62	3—60	3—60	3—60	3—62	3—65	3—62	3—60	3—65

a) Number of reflections measured. b) Number of reflections used for the calculation (reflections of $|F_o|>3\sigma(|F_o|)$ were used). c) $R=\sum||F_o|-|F_c||/\sum|F_o|$. d) The size of the crystal (approximately parallelepiped). e) Scan width. f) Scanned range.

Table 3. Crystallographic Data and Various Experimental Conditions for the **B**-Type Complexes, $[(CH_3)_4N]_4[M(SCN)_7]$, $MC_{23}H_{48}N_{11}S_7$, Orthorhombic, Space Group, $P2_1nb$, $Z=4$

M	Dy	Er	Yb
F. W.	865.68	870.44	876.22
a(l/Å)	12.800(5)	12.775(5)	12.762(2)
b(l/Å)	26.180(9)	26.154(19)	26.119(5)
c(l/Å)	12.715(8)	12.693(3)	12.674(2)
U(v/Å^3)	4261(3)	4242(4)	4224.7(12)
D_m(d/g cm^{-3})	1.36(3)	1.36(3)	1.35(3)
D_x(d/g cm^{-3})	1.35	1.36	1.38
μ(Mo $K\alpha$) (n/cm^{-1})	21.79	24.15	26.90
N_m[a]	6402	6011	6144
N_C[b]	3101	3053	3495
R[c]	0.067	0.061	0.058
V_c[d] (v/mm^3)	0.32×0.28×0.30	0.35×0.30×0.30	0.32×0.30×0.28
S_w[e] (ω/°)	1.23	1.30	1.15
S_R[f] (2θ/°)	3—55	3—57	3—57.5

a—f) See the footnotes of Table 2.

were not obtained, even when a strictly dried starting solution was used.

The results of elemental analyses of the **A**- and **B**-type complexes are shown in Table 1.

X-Ray Structure Analysis. Crystallographic data and various experimental conditions for collecting intensity data are listed in Tables 2 and 3.

Reflections were collected on a Rigaku AFC-6A automated four-circle X-ray diffractometer with graphite monochromated Mo $K\alpha$ radiation (λ=0.71073 Å). In the case of the **A**-type complexes a ω-2θ scan technique was used, while for the **B**-type complexes a ω-scan was adopted. The intensities were corrected for the Lorentz and polarization factors, but not for absorption and extinction.

Structure Determination. The structure of the Nd complex in the **A**-type and that of the Yb complex in the **B**-type were solved by the heavy-atom method, respectively. The positions of the metal and some sulfur atoms were deduced from their three-dimensional Patterson maps; the other non-hydrogen atoms were located by successive Fourier syntheses. Their positional and thermal parameters were refined by a block-diagonal least-squares method. No hydrogen atoms were included in the structure factor calculations.

The structures of the other **A**-type complexes, Ce—Er complexes, were determined by starting from the final parameters of the neodymium complex. The structures of the **B**-type Dy and Er complexes were determined by starting from the final parameters of the ytterbium complex. In all cases, at the final cycle of the refinement the shifts of all the parameters were less than one third of the respective standard deviations.

Some thermal parameters of tetramethylammonium carbon atoms are relatively large in the **A**-type complexes, especially when the atomic number of the central lanthanoid atom is small. In the **B**-type complex the thermal parameters of some tetramethylammonium carbon atoms as well as the S(7) atom were large: the isotropic temperature factor was applied to the S(7) atom. Such large temperature factors of some atoms are also found in some other lanthanoid complexes, especially for their sulfur and carbon atoms, when they are loosely packed in the crystal.[12]

All calculations were carried out on a HITAC M-682H computer at the Computer Center of the University of Tokyo using a local version of the UNICS program.[13] The atomic scattering factors were taken from Ref. 14.

Infrared Absorption Spectrum Measurements. The infrared absorption spectra were obtained by means of a JASCO 202-A grating infrared spectrophotometer using paraffin oil and hexachloro-1,3-butadiene mull.

Results and Discussion

The final atomic positional and thermal parameters

Table 4. Final Atomic Coordinates (×10^4, for Er ×10^5) and Equivalent Isotropic Temperature Factors (B_{eq}/Å^2) of the Atoms of Tetramethylammonium [Aquamethanolhexakis-(isothiocyanato)erbate(III)] with Estimated Standard Deviations in Parentheses

Atom	x	y	z	B_{eq}/Å^2[a]
Er	15240(4)	25000	44128(4)	2.7
S(1)	3410(4)	412(2)	2899(5)	5.9
S(2)	862(5)	810(2)	8253(5)	6.1
S(3)	2947(5)	3556(2)	9410(4)	5.6
S(4)	−3564(4)	1683(2)	2621(4)	5.5
S(5)	−3338(4)	3357(2)	6565(5)	6.5
S(6)	2670(6)	4615(2)	2416(5)	7.8
0(1)	4188(7)	2561(7)	4287(9)	5.7
0(2)	1553(11)	2589(7)	1697(8)	6.4
N(1)	2489(11)	1554(4)	3540(12)	4.6
N(2)	1036(12)	1794(4)	6360(11)	4.6
N(3)	2480(11)	2964(5)	6686(10)	4.2
N(4)	−734(11)	2043(5)	3413(12)	5.0
N(5)	−595(11)	3020(5)	5414(12)	5.1
N(6)	1981(12)	3509(5)	3651(11)	5.0
N(7)	5643(13)	1374(6)	7947(13)	6.2
N(8)	7410(14)	3965(6)	1486(15)	6.8
N(9)	8871(11)	22(4)	3133(11)	4.2
C(1)	2872(11)	1091(5)	3267(12)	3.6
C(2)	981(12)	1380(5)	7117(13)	3.9
C(3)	2675(12)	3187(5)	7829(12)	3.8
C(4)	−1935(12)	1906(5)	3074(12)	3.8
C(5)	−1730(13)	3155(5)	5938(13)	4.2
C(6)	2286(14)	3959(6)	3141(13)	4.7
C(21)	1145(22)	2175(7)	560(15)	7.9
C(71)	4800(20)	1915(8)	8452(22)	8.5
C(72)	5048(23)	1071(11)	6449(18)	9.6
C(73)	7265(20)	1516(14)	8026(33)	15.0
C(74)	5305(29)	904(8)	9119(18)	10.1
C(81)	6375(21)	3396(8)	1677(20)	7.9
C(82)	6697(20)	4351(8)	340(19)	7.8
C(83)	8913(22)	3860(16)	1088(34)	15.9
C(84)	7533(40)	4303(14)	2981(23)	15.6
C(91)	7208(13)	−70(8)	3193(17)	5.9
C(92)	9250(16)	305(7)	1640(14)	5.6
C(93)	9339(16)	450(7)	4386(14)	5.5
C(94)	9704(15)	−563(6)	3334(16)	5.4

a) The equivalent isotropic temperature factors were computed using the following expression: B_{eq}= 4/3 ($B_{11}a^2+B_{22}b^2+B_{33}c^2+B_{13}ac\cos\beta$). The B_{ij}'s are defined by: T=exp[−($h^2B_{11}+k^2B_{22}+l^2B_{33}+2hkB_{12}+2hlB_{13}+2klB_{23}$)].

Table 5. Final Atomic Coordinates ($\times10^4$, for Yb $\times10^5$) and Equivalent Isotropic Temperature Factors (B_{eq}/Å^2) of the Atoms of the Tetramethylammonium Heptakis(isothiocyanato)-ytterbate with Estimated Standard Deviations in Parentheses

Atom	x	y	z	B_{eq} or B_{iso}/Å$^{2a,b)}$	Atom	x	y	z	B_{eq} or B_{iso}/Å$^{2a,b)}$
Yb	25000	11954(4)	19922(4)	3.9	N(11)	6288(13)	2275(7)	482(14)	9.6
S(1)	3249(7)	3076(2)	2492(6)	10.8	N(21)	4457(13)	−484(5)	4519(12)	7.4
S(2)	1428(7)	−640(2)	2489(7)	11.9	N(31)	5683(10)	2107(5)	5163(10)	5.5
S(3)	−1176(4)	1678(3)	3092(5)	8.9	N(41)	8536(11)	5061(5)	4064(10)	6.3
S(4)	3025(7)	1018(3)	5946(4)	13.5	C(11)	5460(21)	2257(12)	1190(21)	13.8
S(5)	6344(4)	907(3)	2775(5)	8.2	C(12)	7283(21)	2254(13)	789(28)	16.8
S(6)	3768(8)	1736(3)	−1605(5)	12.6	C(13)	6068(27)	2679(9)	−298(19)	13.4
N(1)	2916(11)	2037(4)	2329(10)	6.0	C(14)	6333(27)	1740(13)	−1(30)	17.2
N(2)	2198(11)	327(5)	2151(11)	6.8	C(21)	3368(21)	−421(13)	4951(27)	16.7
N(3)	870(11)	1441(5)	2603(10)	6.0	C(22)	5182(21)	−362(12)	5369(22)	14.4
N(4)	2685(16)	1118(4)	3830(8)	5.9	C(23)	4337(24)	−135(14)	3650(25)	17.5
N(5)	4265(10)	939(5)	2201(10)	5.5	C(24)	4657(37)	−1024(10)	4199(24)	16.9
N(6)	3339(12)	1433(6)	429(10)	6.7	C(31)	5890(21)	1573(7)	5583(23)	12.7
N(7)	1350(12)	1031(6)	592(10)	6.8	C(32)	5264(19)	2418(8)	6097(16)	9.4
C(1)	3085(13)	2463(6)	2386(12)	5.4	C(33)	4872(16)	2078(7)	4329(15)	7.9
C(2)	1865(13)	−73(6)	2316(13)	5.5	C(34)	6592(19)	2339(9)	4706(17)	10.2
C(3)	−1(13)	1540(6)	2819(11)	5.1	C(41)	7754(19)	5300(11)	4706(18)	13.5
C(4)	2836(12)	1073(5)	4700(11)	5.6	C(42)	7959(21)	4671(9)	3507(26)	13.8
C(5)	5110(11)	919(5)	2441(12)	4.3	C(43)	8972(21)	5420(10)	3336(21)	11.7
C(6)	3451(14)	1577(5)	−414(12)	5.7	C(44)	9328(22)	4818(7)	4787(18)	10.5
C(7)	837(15)	1104(8)	−73(15)	8.1	S(7)[b]	18(11)	1222(4)	−1028(10)	17.91(4)

a) The equivalent isotropic temperature factors were computed using the following expression: $B_{eq}=4/3(B_{11}a^2+B_{22}b^2+B_{33}c^2)$. The B_{ij}'s are defined by: $T=\exp[-(h^2B_{11}+k^2B_{22}+l^2B_{33}=2hkB_{12}+2hlB_{13}+2klB_{23})]$. b) The isotropic temperature factor was used for S(7) in the refinement. c) C (11—14; 21—24; 31—34, and 41—44) are the methyl carbon atoms bonded to the N(11, 21, 31, and 41) atoms, respectively.

(B_{eq}(Å)) of the **A**-type erbium(III) and of the **B**-type ytterbium(III) complexes are listed in Tables 4 and 5, and the selected bond lengths and bond angles of the **A**- and **B**-type complexes are given in Tables 6 and 7, respectively. Perspective drawings of the **A**-type Er complex as well as that of the **B**-type Yb complex are shown in Figs. 1 and 2, together with a numbering scheme of their atoms.

The crystal structures of the **A**-type Er and the **B**-type Yb complexes projected along the b-axis are shown in Figs. 3 and 4.[15]

The Structure of the A-Type Complexes. In the **A**-type erbium complex the central metal atom is octa-coordinated, in a square-antiprism geometry, to six nitrogen atoms of SCN ions, and two oxygen atoms of one water and one methanol molecules. The two ligated oxygen atoms take positions at the most approaching apexes of the respective bottom squares, obeying the empirical rule that the same kind of ligating atoms preferably take the neighboring posi-

Table 6. Selected Bond Lengths and Bond Angles of the **A**-Type Complexes, $[(CH_3)_4N]_3[M(SCN)_6\cdot(CH_3OH)(H_2O)]$, with the Standard Deviations in Parentheses

A. Bond lengths (l/Å) M	La	Ce	Pr	Nd	Sm
M-O(1)	2.530(9)	2.537(8)	2.526(9)	2.498(6)	2.466(6)
M-O(2)	2.547(12)	2.558(11)	2.522(13)	2.496(8)	2.472(19)
M-O (Sum of Shannon's ionic radii)	2.51	2.49	2.48	2.46	2.43
M-N(1)	2.589(14)	2.514(12)	2.466(15)	2.531(9)	2.504(9)
M-N(2)	2.554(15)	2.477(14)	2.465(16)	2.484(9)	2.470(10)
M-N(3)	2.536(15)	2.567(14)	2.551(14)	2.514(9)	2.495(19)
M-N(4)	2.561(15)	2.498(13)	2.476(16)	2.504(9)	2.493(9)
M-N(5)	2.587(14)	2.599(13)	2.569(15)	2.508(10)	2.478(10)
M-N(6)	2.540(16)	2.622(14)	2.603(14)	2.515(9)	2.468(9)
M-N(n) (n=1—6) (average)	2.561	2.546	2.522	2.509	2.485
M-N (Sum of Shannon's ionic radii)	2.62	2.60	2.59	2.57	2.54
N(n)-C(n) (n=1—6) (average)	1.15 (1.09(2)—1.21(2))	1.14 (1.11(2)—1.18(2))	1.15 (1.12(2)—1.22(2))	1.146 (1.125(13)—1.166(14))	1.138 (1.101(13)—1.166(13))
C(n)-S(n) (n=1—6) (average)	1.612 (1.563(15)—1.647(15))	1.618 (1.578(14)—1.639(15))	1.614 (1.539(17)—1.662(18))	1.616 (1.593(10)—1.638(10))	1.623 (1.587(10)—1.655(10))

A. Bond lengths (l/Å) M	Eu	Gd	Tb	Dy	Er
M-O(1)	2.452(6)	2.434(8)	2.424(7)	2.408(7)	2.393(6)
M-O(2)	2.468(8)	2.444(11)	2.439(10)	2.410(9)	2.411(9)
M-O (Sum of Shannon's ionic radii)	2.42	2.40	2.40	2.38	2.35
M-N(1)	2.424(9)	2.478(12)	2.468(11)	2.439(12)	2.419(10)
M-N(2)	2.393(10)	2.449(13)	2.410(12)	2.410(11)	2.385(10)
M-N(3)	2.507(9)	2.465(12)	2.429(10)	2.449(11)	2.407(10)
M-N(4)	2.434(9)	2.461(12)	2.442(11)	2.428(10)	2.419(10)
M-N(5)	2.508(10)	2.438(12)	2.459(11)	2.430(11)	2.407(11)
M-N(6)	2.530(9)	2.444(12)	2.427(11)	2.417(11)	2.395(11)
M-N(n) (n=1—6) (average)	2.466	2.456	2.439	2.429	2.405
M-N (Sum of Shannon's ionic radii)	2.53	2.51	2.50	2.49	2.46
N(n)-C(n) (n=1—6) (average)	1.147 (1.131(13) 1.161(13))	1.144 (1.138(17) 1.172(18))	1.147 (1.125(16) 1.170(17))	1.143 (1.113(15) 1.160(15))	1.143 1.120(15) 1.163(16))
C(n)-S(n) (n=1—6) (average)	1.620 (1.592(10)— 1.632(12))	1.622 (1.601(14)— 1.654(16))	1.620 (1.593(14)— 1.655(15))	1.623 (1.589(12)— 1.650(14))	1.623 (1.585(12)— 1.642(14))

B. Bond angles (ϕ/°) M	La	Ce	Pr	Nd	Sm
O(1)-M-O(2)	88.3(3)	84.9(3)	84.6(4)	85.8(2)	85.5(2)
O(1)-M-N(1)	71.7(4)	72.4(3)	72.7(4)	71.5(3)	70.7(3)
O(1)-M-N(6)	76.6(4)	75.0(4)	74.2(4)	75.7(2)	75.9(2)
O(2)-M-N(1)	77.7(4)	75.8(4)	75.7(5)	74.8(3)	73.5(3)
N(1)-M-N(2)	71.6(4)	74.2(4)	73.8(5)	73.8(3)	74.8(3)
N(1)-M-N(3)	122.0(4)	122.6(4)	122.0(5)	121.8(3)	122.2(3)
N(1)-M-N(4)	79.8(5)	82.4(4)	82.4(5)	80.1(3)	79.4(3)
N(1)-M-N(5)	145.9(4)	147.4(4)	147.5(5)	145.8(3)	147.0(3)
M-N(n)-C(n) (n=1—6) (average)	168.1 (164.4(13)— 171.8(14))	168.9 (164.4(12)— 172.0(11))	169.3 (165.1(14)— 171.5(13))	168.7 (166.3(9)— 171.8(8))	167.6 (164.6(9)— 170.7(9))
N(n)-C(n)-S(n) (n=1—6) (average)	174.6 (168.9(16)— 178.7(17))	174.5 (173.5(14)— 176.9(17))	175.8 (173.5(17)— 177.6(16))	177.3 (175.7(9)— 178.0(11))	177.1 (176.9(10)— 178.3(10))

B. Bond angles (ϕ/°) M	Eu	Gd	Tb	Dy	Er
O(1)-M-O(2)	85.4(2)	84.3(3)	85.5(3)	8 5.1(3)	85.5(3)
O(1)-M-N(1)	71.7(3)	70.8(3)	71.2(3)	70.4(3)	71.0(3)
O(1)-M-N(6)	74.8(2)	76.2(3)	75.6(3)	76.5(3)	76.0(3)
O(2)-M-N(1)	75.8(3)	74.2(4)	75.1(3)	74.3(3)	75.2(3)
N(1)-M-N(2)	75.7(3)	74.3(4)	74.2(4)	74.4(4)	73.8(3)
N(1)-M-N(3)	122.9(3)	122.3(4)	121.9(4)	122.4(4)	121.4(3)
N(1)-M-N(4)	81.3(3)	79.5(4)	79.4(4)	79.2(4)	79.2(3)
N(1)-M-N(5)	148.1(3)	145.8(4)	146.1(4)	146.3(4)	146.0(4)
M-N(n)-C(n) (n=1—6) (average)	168.6 (165.1(9)— 171.2(9))	168.5 (168.4(11)— 170.5(12))	168.9 (166.6(11)— 171.8(11))	168.7 (165.2(10)— 171.1(10))	168.7 (165.9(10)— 172.8(10))
N(n)-C(n)-S(n) (n=1—6) (average)	175.5 (175.5(11)— 179.7(11))	176.5 (175.0(13)— 177.7(13))	177.0 (175.1(12)— 178.3(12))	177.6 (176.7(11)— 178.8(12))	177.3 (175.8(11)— 178.8(11))

tions.[17] A schematic presentation which shows the coordinating positions of the ligating atoms around the erbium atom is given in Fig. 5.

The complex, where an alcohol and a water molecules are coordinated to the same metal atom, had already been found in neodymium(III) 1-hydroxy-2-naphthoate;[16] however, it was readily decomposed in open air, missing the alcohol ligand. The crystal used for the intensity collection had to be sealed in a glass capillary. On the other hand, these **A**-type complexes are more stable in the open, and do not decompose in open air during the intensity collection process (about one week) without a cover.

Angle O(1)-Er-O(2) is 85.5°, and the Er-O(1) and Er-O(2) bonds are approximately directed to the next metal atoms in the a- and c-axis directions, respectively.

As shown in Table 6, the Er-O distance is 2.402 Å

Table 7. Selected Bond Lengths and Bond Angles of the **B**-Type Complexes, $[(CH_3)_4N]_4[M(SCN)_7]$, with the Standard Deviations in Parentheses

A. Bond length (l/Å) M	Dy	Er	Yb
M-N(1)	2.394(15)	2.361(14)	2.302(12)
M-N(2)	2.307(14)	2.277(14)	2.310(13)
M-N(3)	2.363(18)	2.294(17)	2.311(14)
M-N(4)	2.376(16)	2.383(15)	2.350(12)
M-N(5)	2.394(15)	2.412(14)	2.364(13)
M-N(6)	2.344(19)	2.363(18)	2.336(14)
M-N(7)	2.354(19)	2.345(17)	2.343(15)
M-N(av.)[a]	2.362	2.348	2.331
N(n)-C(n) (n—7) (av.)[a]	1.136 (1.05(3)—1.19(3))	1.126 (1.07(3)—1.18(3))	1.133 (1.08(3)—1.17(2))
C(n)-S(n) (n=1—7) (av.)[a]	1.611 (1.53(2)—1.68(2))	1.618 (1.57(2)—1.69(2))	1.612 (1.581(17)—1.631(14))

B. Bond angle (ϕ/°) M	Dy	Er	Yb
N(1)-M-N(2)	162.8(5)	163.3(5)	163.9(5)
N(1)-M-N(3)	83.8(6)	83.3(5)	83.1(5)
N(2)-M-N(3)	96.6(6)	96.9(5)	95.4(5)
N(3)-M-N(4)	76.8(6)	77.2(6)	77.5(5)
N(4)-M-N(5)	77.0(5)	76.6(5)	76.7(4)
N(5)-M-N(6)	75.6(6)	74.4(6)	74.5(5)
N(6)-M-N(7)	71.8(7)	72.0(6)	72.2(5)
N(3)-M-N(7)	75.6(6)	76.7(6)	74.9(5)
M-N(n)-C(n) (n=1—7)(av .)[a]	166.6 (160.8(18)—172.8(8))	166.9 (158.1(17)—173.0(14))	167.2 (159.3(16)—175.8(13))
N(n)-C(n)-S(n) (n=1—7)(av.)[a]	175.4 (173(2)—177.5(17))	175.7 (171.2(19)—178.7(19))	176.9 (176.4(15)—179.1(15))

a) Average of the seven values of the all SCN ions.

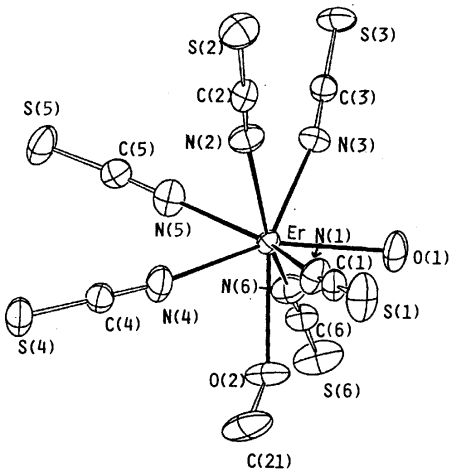

Fig. 1. A perspective drawing of the **A**-type erbium(III) complex around the metal atom, with the numbering scheme of the atoms.

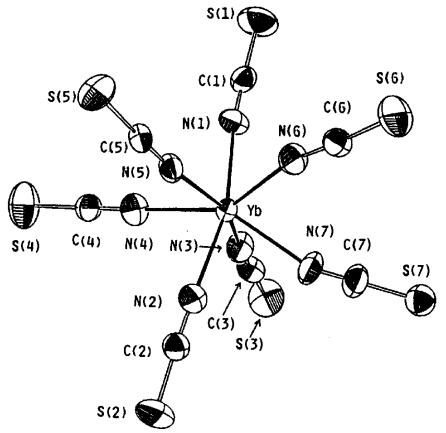

Fig. 2. A perspective drawing of the **B**-type ytterbium(III) complex around the metal atom, with the numbering scheme of the atoms.

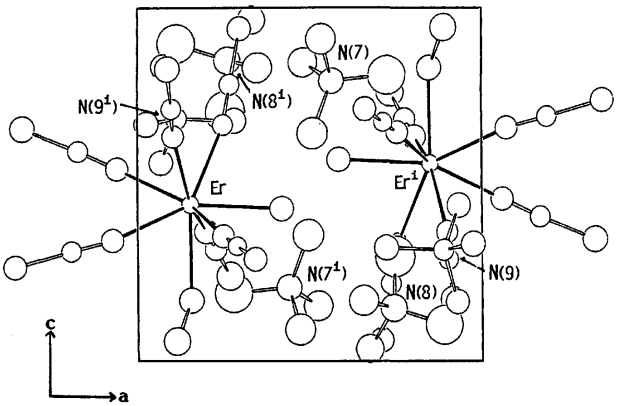

Fig. 3. A projection of the unit cell of the **A**-type erbium(III) complex along b-axis.

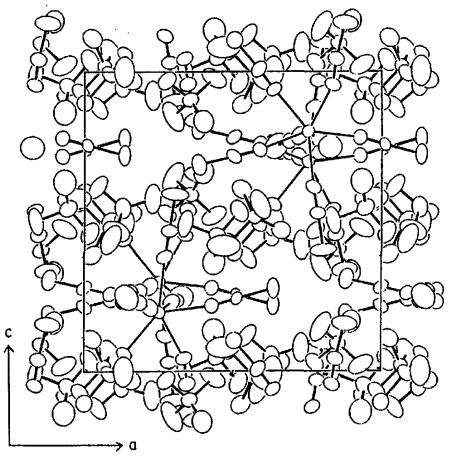

Fig. 4. A projection of the unit cell of the **B**-type ytterbium(III) complex along b-axis.

(on the average), where Er-O(water) is 0.018 Å shorter than Er-O(methanol). Judging from these bond lengths, although methanol is coordinated to the metal atom more weakly than water, the diffence in the bond strengths does not seem to be great.

Although the Er complex is the last member of the **A**-type isomorphous complexes, the Er-N bond lengths are in the range 2.385(10)—2.419(10) Å (2.405 Å on the average): abnormally long bonds, which were found in some carboxylato complexes of lantha-

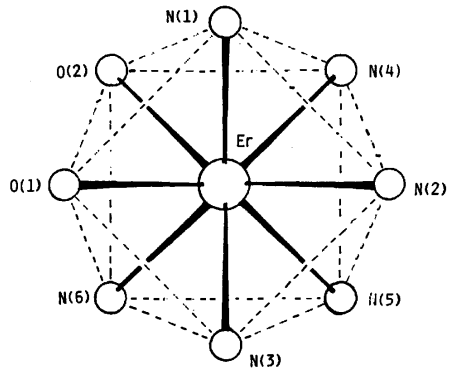

Fig. 5. Schematic presentation of the A-type erbium-(III) complex to show the coordination geometry around the metal atom.

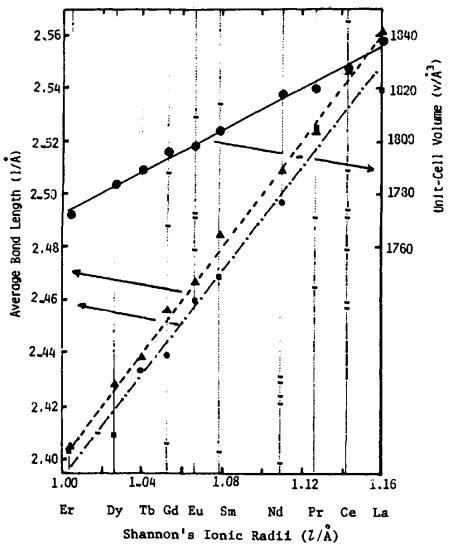

Fig. 6. The relation between the interatomic distances, M-N and M-O, as well as the unit cell volumes, and the Shannon's ionic radii of the central metal atom of the A-type complexes (unit cell volume (—●—); M-N bond length (---▲---); and average M-O bond length (-·-■-·-).

noids, do not exist.[6,18]

The sums of the Shannon's ionic radii are 2.35 and 2.46 Å for Er-O and Er-N (coordination number of Er is 8), respectively.[19] Therefore, the observed Er-O is longer and the observed Er-N, is shorter than the sums of the Shannon's ionic radii, respectively. In many carboxylato complexes of lanthanoids the M-O bond lengths are not much different from the sums of Shannon's ionic radii.[6,7,18] Therefore, in these complexes, the M-O bonds are a little weaker than those of the usual oxygen donor complexes. In the other aqua-isothiocyanato mixed complex, $K_4[M(SCN)_4(H_2O)_4](SCN)_3 \cdot nH_2O$ (M=Nd, Eu), the average Nd-O and Eu-O bonds are reported to be 2.60 and 2.51 Å, respectively, which are much longer than the sums of the Shannon's ionic radii, 2.46 and 2.42 Å.[2] The shortening of the Er-N bonds are also found in the

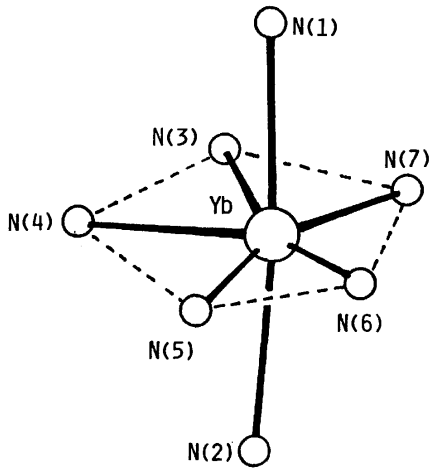

Fig. 7. Schematic presentation of the B-type ytterbium (III) complex to show the coordination geometry around the metal atom.

other isothiocyanato complexes. For example, the sums of the Shannon's ionic radii and the observed bond lengths of $[(C_2H_5)_4N]_4[Er(SCN)_7(H_2O)]$ are 2.46 and 2.36(3) Å, respectively.[3] However, in $[(C_4H_9)_4N]_3[Er(SCN)_6]$, these values are 2.35 and 2.34(2) Å, respectively, not much different from each other.[1]

The bond angles of Er-N-C and of N-C-S are 168.7° on the average (165.9(10)—172.8(10)°), and 177.3° on the average (175.8(11)—178.8(11)), respectively. They are not very far from 180°.

The relations between the Shannon's ionic radii of the central metal atom and the unit cell volume, as well as the average M-O and M-N bond lengths of the A-type complexes, are shown in Fig. 6. No irregular changes were found among the series of isomorphous complexes. However, the earlier members decomposed more easily than the later member ones when left standing in open air.

The Structure of the B-Type Coiplexes. In the B-type ytterbium complex, the central metal atom is hepta-coordinated in a deformed pentagonal-bipyramidal geometry to seven nitrogen atoms of SCN ions, as shown schematically in Fig. 7. The deviations of the atomic positions from the mean-square plane of the six atoms, five equatorially ligated SCN nitrogen atoms and the central metal atom, are 0.344 Å on the average (0.037—0.927 Å). The plane is approximately parallel to the ac-plane. The axis angle, N(1)-Yb-N(2), is 163.9(5)°, and the axis of the complex is directed approximately parallel to the b-axis.

The tetramethylammonium ions are approximately sandwitched between pentagon planes consisting of five equatorially coordinated SCN ions of the complexes, where the central nitrogen atoms of the cations are arranged on several layers parallel to the ac-plane and between the pentagon planes. Consequently, layers of the complexes and of the cations are piled up alternately in the b-axis direction.

The M-N bond lengths of the ytterbium complex are, as shown in Table 7, 2.331 Å on the average (2.302(12)—2.364(13) Å), which is much shorter than the sum of the Shannon's ionic radii, 2.39 Å,[19] as in the case of the **A**-type complexes.

The Yb-N-C and N-C-S bond angles are, on the average, 167.2 and 176.9°, respectively.

There are no systematic changes of the respective bond lengths and bond angles through the series of the **B**-type three complexes, except for the change of the M-N bond length due to a decrease in the metal ionic radii, depending on the metal atomic number. The three **B**-type complexes can be considered to have the same type structure. All members of the three **B**-type complexes are stable in open air for at least several weeks.

General Remark. Though the 6N-hexa-coordinated hexakis(thiocyanato) lanthanoidate(III) ion was found in its tetrabutylammonium salt,[1] deduced from the results of this and several related studies, the central metal atoms of thiocyanato complexs are not always in the hexa-coordination. Their coordination number can be seven or eight, depending on the kinds of counter cations, and of the included guest molecule, such as benzene, in the crystal,[20] or of the ligands other than the SCN ions of the complex.

Infrared Spectra. The general feature as well as the maximum wavenumbers of the infrared spectra of the **A**- and **B**-type complexes are not much different from each other, except for the strong ν(O-H) bands of the **A**-type complexes caused by including methanol and water, which appeared at about 3320—3350 cm^{-1}. The bands due to the N-bonded SCN ion appear almost in the same region as the other metal complexes:[21] ν(CN)(s), 2060 and 2100 cm^{-1} for the **A**-type, and 2060 and 2070 cm^{-1} for the **B**-type complexes; ν(CS), 730 cm^{-1}, and δ(SCN), 480 cm^{-1} for both type complexes. The bands due to the tetramethylammonium ion appear at 1488(s), 1433(m), 1163(m), 942(s), and 720(m) cm^{-1}. These bands are approximately the same as those found in the spectra of the other tetramethylammonium salts.

The authors wish to thank Shin-Etsu Chemical Ind. Co., Ltd., for presenting us the highly pure lanthanoid oxides.

References

1) J. L. Martin, L. C. Thompson, L. J. Radonovich, and M. D. Glick, *J. Am. Chem. Soc.*, **90**, 4493 (1968).

2) P. I. Lazarev, L. A. Aslanov, V. M. Ionov, and M. A. Porai-Koshits, *Koord. Khim.*, **1**, 710 (1975); *Structure Report*, **41A**, 210 (1975).

3) Y. Tateyama, Y. Kuniyasu, Y. Suzuki , and A. Ouchi, *Bull. Chem. Soc. Jpn.*, **61**, 2805 (1988).

4) Y. Ohki, Y. Suzuki, T. Takeuchi, and A. Ouchi, *Bull. Chem. Soc. Jpn.*, **61**, 393 (1988).

5) R. Nakamura, K. Nagai, M. Shimoi, and A. Ouchi, *Bull. Chem. Soc. Jpn.*, **57**, 2979 (1984).

6) T. Imai, M. Shimoi, and A. Ouchi, *Bull. Chem. Soc. Jpn.*, **60**, 159 (1987)

7) Y. Sugita and A. Ouchi, *Bull. Chem. Soc. Jpn.*, **60**, 171 (1987).

8) J. W. Moore, M. D. Glick, and W. A. Baker Jr., *J. Am. Chem. Soc.*, **94**, 1858 (1972).

9) K. Prout, J. M. Marin, and C. A. Hutchison Jr., *Acta Crystallogr., Sect. C*, **41**, 201 (1985).

10) I. S. Ahuja and A. Garg, *J. Inorg. Nucl. Chem.*, **34**, 1929 (1972).

11) M. Taniguchi, M. Shimoi, and A. Ouchi, *Bull. Chem. Soc. Jpn.*, **59**, 2299(1986).

12) T. Imai, M. Nakamura, K. Nagai, Y. Ohki, Y. Suzuki, M. Shimoi, and A. Ouchi, *Bull. Chem. Soc. Jpn.*, **59**, 2115 (1986).

13) "The Universal Crystallographic Computation Program System(UNICS)," ed by T. Sakurai, Crystallographic Society of Japan, Tokyo (1967).

14) "International Tables for X-Ray Crystallography," Kynoch Press, Birmingham (1974), Vol. IV, pp. 72, 150.

15) The atomic coordinates, the anisotropic thermal parameters, the F_o-F_c tables and some additional bond lengths and bond angles data of the all **A**- and **B**-type complexes, except for the data listed in this paper, are deposited as Document No. 8870 at the Office of the Editor of Bull. Chem. Soc. Jpn.

16) Y. Ohki, Y. Suzuki, T. Takeuchi, M. Shimoi, and A. Ouchi, *Bull. Chem. Soc. Jpn.*, **59**, 1015 (1986).

17) M. E. Silver, H. K. Chun, and R. C. Fay, *Inorg. Chem.*, **21**, 3765 (1982).

18) H. Sawase, Y. Koizumi, Y. Suzuki, M. Shimoi, and A. Ouchi, *Bull. Chem. Soc. Jpn.*, **57**, 2730 (1984).

19) R. D. Shannon, *Acta Crystallogr. Sect. A*, **32**, 751 (1976). According to this paper, the ionic radii of the tervalent metal ions are:(Coordination number=8), La, 1.160; Ce, 1.143; Pr, 1.126; Nd, 1.109; Sm, 1.079; Eu, 1.066; Gd, 1.053; Tb, 1.040; Dy, 1.027; Er 1.004; Yb, 0.985 Å, (Coordination number=7) , Tb, 0.98; Dy, 0.97; Er, 0.945; Yb, 0.925 Å. The ionic radii of O (Valence=2−, Coordination number=2), 1.35; and that of N (Valence=3−, Coordination number=4), 1.46 Å.

20) F. Matsumoto, T. Takeuchi, and A. Ouchi, *Bull. Chem. Soc. Jpn.*, **62**, 2078 (1989).

21) K. Nakanishi, "Infrared and Raman Spectra of Inorganic and Coordination Compounds," 4th ed, John & Wiley, New York (1986), p. 283.

 © 1989 The Chemical Society of Japan Bull. Chem. Soc. Jpn., 62, 1817—1821 (1989)

Solvent Extraction of Indium with 3-Hydroxy-2-methyl-1-phenyl-4-pyridone

Hajime Ishii,* Shinji Numao,† and Tsugikatsu Odashima
Chemical Research Institute of Non-Aqueous Solutions, Tohoku University, Katahira, Sendai, Miyagi 980
(Received September 17, 1988)

Extraction behavior of indium has been investigated with 3-hydroxy-2-methyl-1-phenyl-4-pyridone (HMPP) at 25 ± 0.1 °C and an ionic strength of 0.2. The values of the proton-dissociation constants, pK_{a1} and pK_{a2}, of HMPP were determined spectrophotometrically to be 3.02 and 9.56. The value of the partition coefficient, $\log K_D$, of HMPP between 1,2-dichloroethane and water was determined to be 1.35. Indium(III) was extracted into 1,2-dichloroethane by forming a 1 : 3 (metal : ligand) complex with HMPP. The extraction constant, K_{ex}, the overall formation constant, β_3, and the distribution constant, K_{DC}, of the indium(III)-HMPP complex were determined, their values being as follows: $\log K_{ex}=2.16$, $\log \beta_3=32.63$, and $\log K_{DC}=2.26$.

Since Herak and his co-workers[1] used 2-ethoxycarbonyl-5-hydroxyl-1-phenyl-4-pyridone and its analogues to the extraction and separation of tantalum(V) and niobium(V), 4-pyridones including 1-aryl-2-ethoxycarbonyl-5-hydroxy-4-pyridones and 1-aryl-3-hydroxy-2-methyl-4-pyridones[2,3] were synthesized and proposed as chelating and extracting reagents for various metal ions. As is apparent from their structures, these pyridones are *O,O*-donating chelating reagents, so they seem to be promising chelating and/or extracting reagents for metal ions classified into the hard acids including indium(III), gallium(III), and aluminium(III), investigations on the extraction of gallium(III) with some of these pyridones having already been done.[4,5]

On the other hand, indium is an element widely dispersed in nature, about 0.1 ppm of indium being contained in the earth's crust. Minerals containing indium as a major constituent are not known. Indium is usually recovered as a by-product in the zinc industry. Taking into consideration that indium is used not only as a constituent of corrosion-resisting alloys for bearings and a semi-conductor but also in many fields such as non-ferrous metallurgy, electric contacts and reflectors and so on, the separation and/or concentration of indium by solvent extraction with the above 4-pyridones are much attractive as well as of practical and theoretical importance.

Thus to start with, we investigated the extraction of indium(III) with 3-hydroxy-2-methyl-1-phenyl-4-pyridone (HMPP), the results of which are described in this paper.

Experimental

Reagents. All reagents used were of analytical-reagent grade unless stated otherwise. All aqueous solutions were prepared with distilled, deionized water.

HMPP solutions. Prepared by dissolving HMPP in 1,2-dichloroethane or 1,4-dioxane. The HMPP was synthesized by heating a mixture of 3-hydroxy-2-methyl-4-pyrone, aniline and water in a sealed, thick-walled glass tube for 46 h at 150 °C.[3]

Standard indium(III) solution, 5.0×10^{-2} M (1M=1 mol dm^{-3}). Prepared by dissolving the required mass of metallic indium (99.99 % pure), with heating, in a sufficient volume of nitric acid (1+1) to give an acidity of 0.1 M in the final solution. Working solutions were prepared by diluting this solution with water.

Buffer solutions. Buffers consisting of 1 M chloroacetic acid-1 M sodium chloroacetate, 1 M acetic acid-1 M sodium acetate, (0.2 M boric acid+0.05 M sodium chloride)-0.05 M sodium borate, 0.2 M tris(hydroxymethyl)aminomethane-0.2 M hydrochloric acid or 0.2 M sodium hydrogencarbonate-0.2 M sodium carbonate system was used according to the pH values required.

Apparatus. The following instruments were used: a Hitachi 139 spectrophotometer and a Hitachi 340 automatic recording spectrophotometer with 10-mm quartz cells, a Toa HM-5B pH meter, an Iwaki KM shaker and a Haake FK-2 thermoelectric circulating bath. All extractions were performed by shaking samples in 50-cm^3 separating funnels jacketed so that the system could be kept at a constant temperature (25±0.1 °C) by means of water circulated from the thermostatic bath.

Procedures. Proton Dissociation Constants: The proton dissociation constants of HMPP were determined spectrophotometrically[6] in aqueous dioxane of various concentrations (8—32% v/v) at 25±0.1 °C and at an ionic strength of 0.2. The ionic strength was adjusted with sodium chloride. Values of pH measured in aqueous dioxane solutions were not corrected because logarithmic values of U_H were very small (−0.03 at a dioxane concentration of 32% v/v), where U_H is a conversion factor in the equation proposed by Uitert et al.[7]

Partition of HMPP: A 10-cm^3 aliquot of an aqueous solution containing 2.7—5.3 cm^3 of 0.1 M sodium hydroxide solution and sodium nitrate to maintain the ionic strength to 0.2 was placed in a 50-cm^3 separating funnel along with 10 cm^3 of a 1.1×10^{-4} M HMPP solution in 1,2-dichloroethane. The funnnel was shaken for 30 min and allowed to stand for 15 min for the phase separation. The organic phase was transferred into a flask containing about 1 g of anhydrous sodium sulfate in order to dehydrate it. The absorbance of the organic phase was measured at 292 nm against 1,2-dichloroethane, the concentration of HMPP being calculated by using the molar absorptivity of HMPP in 1,2-dichloroethane, obtained beforehand. The equilibrium concentration of HMPP in the aqueous phase was calculated by subtracting the organic equilibrium concen-

† Present address: Research and Development Department, Showa Aluminum Corp., 6-224, Kaisan-cho, Sakai-shi, Osaka 590.

tration from the initial concentration.

Distribution of Indium: The distribution of indium between 1,2-dichloroethane and aqueous phases was determined as a function of the hydrogen ion concentration.

A 10-cm^3 aliquot of an aqueous solution containing 14.9 μg of indium (III), dilute perchloric acid to adjust the pH to the required value and potassium nitrate to maintain the ionic strength to 0.2 was placed in a 50-cm^3 separating funnel along with 10 cm^3 of 4.1×10^{-4} M HMPP solution in 1,2-dichloroethane. The funnel was shaken for 30 min and then allowed to stand for 15 min for the phase separation. The equilibrium concentration of indium in the organic phase was determined by measuring the absorbance of the extract at 319 nm against a reagent blank prepared under the identical conditions. The equilibrium concentration of indium in the aqueous phase was calculated by subtracting the organic equilibrium concentration from the initial concentration.

Formation Constant: To an aliquot containing 1.50 mg of indium(III) in a 25-cm^3 calibrated flask were added 10 cm^3 of a dilute nitric acid solution of 2.5×10^{-4} M HMPP, dilute perchloric acid to adjust the pH to the required value and sodium chloride to maintain the ionic strength to 0.2. Then the solution was diluted to the mark with water. After allowing to stand for 30 min at 25±0.1 °C, the absorbance of the solution was measured at 315 nm against water as a reference.

Results and Discussion

Proton Dissociation Constants, Species Distribution Diagram and Absorption Spectra of HMPP. HMPP is insoluble in water and practically insoluble in nonpolar organic solvents such as benzene and hexane, but very soluble in ethanol, dioxane, chloroform and 1,2-dichloroethane. It is also soluble in weakly acidic and alkaline solutions, but it decomposes in solutions of pH below 1 and above 12.5.

As is evident from the structure of HMPP shown in **I**, at least 3 species, H_2L^+, HL, and L^-, are involved in

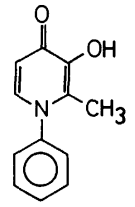

(I)

its acid-base equilibria, the probable equilibria being as follows:

$$H_2L^+ \overset{K_{a1}}{\rightleftharpoons} HL \overset{K_{a2}}{\rightleftharpoons} L^- \qquad (1)$$

where L denotes the undissociable part of HMPP and, K_{a1} and K_{a2} are the proton dissociation constants. The value of K_{a2} is already determined by Herak et al.,[7] but that of K_{a1} is not determined yet. So both proton dissociation constants were determined by extrapolating the linear plot of apparent pK_a values obtained by the procedure stated already versus dioxane concentrations (8—32% v/v) to the intercept. The result was shown in Fig. 1. Values of apparent pK_{a1} decrease, whereas those of apparent pK_{a2} increase, with increasing the dioxane concentration. The values of pK_{a1} and pK_{a2} thus obtained were 3.02 and

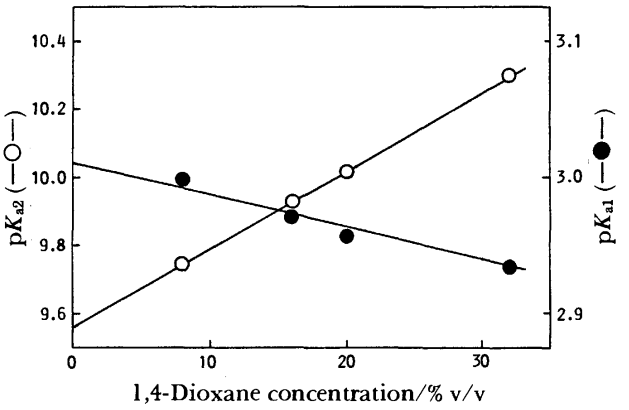

Fig. 1. Plots of pK_a values vs. 1,4-dioxane concentration.

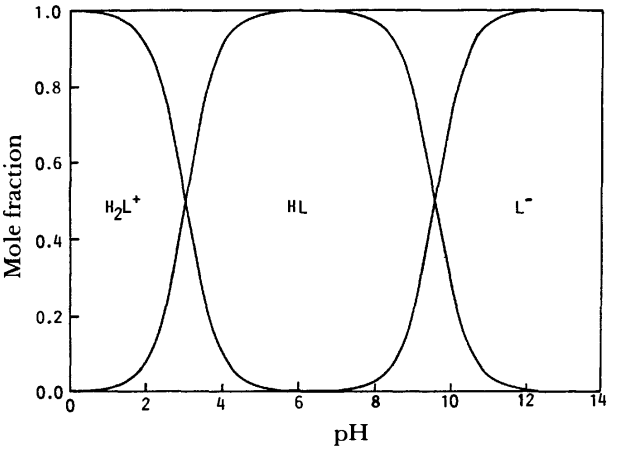

Fig. 2. Species distribution diagram.

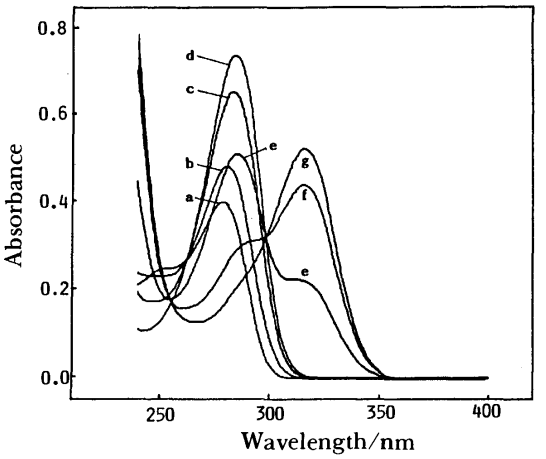

Fig. 3. Absorption spectra of HMPP in 8% v/v 1,4-dioxane. HMPP, 4.1×10^{-5} M; reference, 8% v/v 1,4-dioxane; pH—a, 1.1; b, 2.7; c, 3.7; d, 6.0; e, 9.6; f, 10.5; g, 12.0.

9.56, respectively. The latter value is near to the pK_{a2} value (9.88) reported by Herak et al.[8] K_{a1} and K_{a2} are considered to correspond to the deprotonations of the protonated pyridone-nitrogen and the hydroxyl group, respectively.

Figure 2 shows the species distribution diagram of HMPP prepared on the basis of the above results.

Figure 3 indicates absorption spectra of HMPP in 8% v/v dioxane solutions of various pHs. Spectra a, d, and g correspond to species of H_2L^+, HL, and L^-, respectively. The absorption maximum, λ_{max}, and the molar absorptivity, ε, of each species and the isosbestic points are summarized in Table 1.

Partition Coefficient of HMPP. The distribution ratio, D_L, of HMPP between an aqueous and a 1,2-dichloroethane phase can be expressed as Eq. 2 and is rewritten as Eq. 3 by using the proton dissociation constants and the partition coefficient K_D:

$$D_L = \frac{[HL]_{org}}{[H_2L^+]+[HL]+[L^-]} \quad (2)$$

$$D_L = \frac{K_D}{\frac{[H^+]}{K_{a1}} + 1 + \frac{K_{a2}}{[H^+]}} \quad (3)$$

where the subscript org denotes the concentration in the organic phase. When $[H^+] \ll K_{a1}, K_{a2}$, Eq. 3 can be approximated by Eq. 4 and rewritten as Eq. 5

$$D_L = \frac{K_D}{K_{a2}}[H^+] \quad (4)$$

$$\log D_L = \log K_D + pK_{a2} - pH \quad (5)$$

Equation 5 implies that the plot of $\log D_L$ against the pH gives a straight line with a slope of -1, the value of K_D being calculated from the intercept of this line. Such a relation was experimentally obtained as shown in Fig. 4, from which the value of 1.35 was obtained as $\log K_D$. This value is close to that (1.69) obtained in the chloroform-water system.[8]

Table 1. Spectral Characteristics of HMPP in 8% v/v 1,4-Dioxane

	H_2L^+	HL	L^-
Absorption maximum/nm	279	285	316
Molar absorptivity/M^{-1} cm^{-1}	9900	18000	13000
Isosbestic point/nm	264	256, 299	

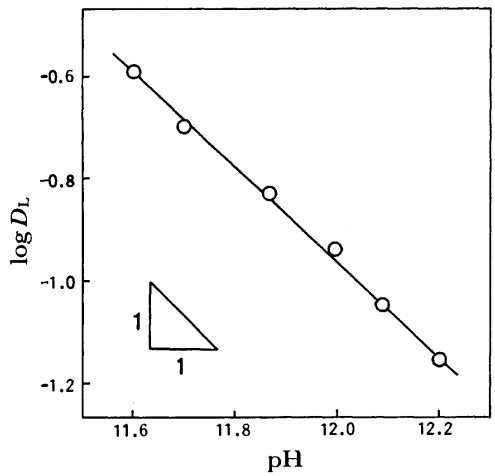

Fig. 4. Plot of $\log D_L$ vs. pH for the partition of HMPP between 1,2-dichloroethane and water at an ionic strength of 0.2 and at 25±0.1 °C. HMPP, 1.1×10^{-4} M; $V_{aq}/V_{org}=1$ ($V_{org}=10$ cm^3); shaking time, 30 min.

Absorption Spectra. Absorption spectra of HMPP and its indium(III) complex extracted into 1,2-dichloroethane are shown in Fig. 5 along with those of aluminium(III) and gallium(III) complexes measured for comparison. The absorption maxima of indium(III), gallium(III), and aluminium(III) complexes lie at nearly the same wavelengths, i.e., 319, 319, and 318 nm, respectively. The absorption maxima and the shape of the spectra did not vary in the pH range 2—12 and the molar ratio range of metal to ligand of 1:10—10:1, which suggests that only one species of each complex is extracted.

Shaking Time and Stability of the Extract. In general, as the shaking time needed to attain the extraction equilibrium increases with decreasing the pH, the influence of the shaking time on the extraction of the indium(III)-HMPP complex was examined at indium(III) and HMPP concentration of 1.3×10^{-5} and 4.1×10^{-4} M, respectively, and at pHs 2.7

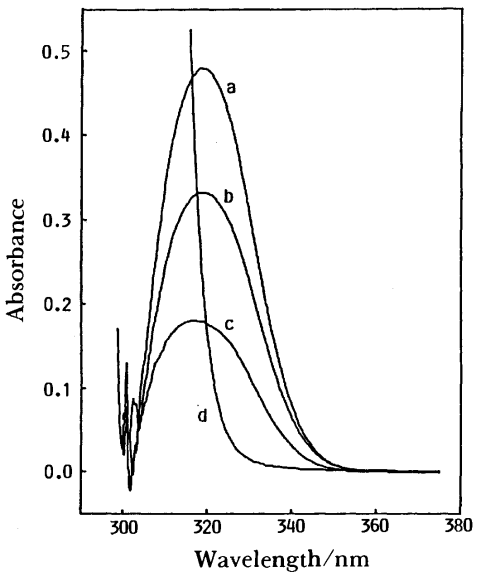

Fig. 5. Absorption spectra of HMPP and its metal complexes in 1,2-dichloroethane. HMPP, 4.1×10^{-4} M; In(III), 1.3×10^{-5} M; Ga(III), 1.1×10^{-5} M; Al(III), 9.9×10^{-6} M; a, In(III) complex; b, Ga(III) complex; c, Al(III) complex; d, HMPP alone (Reagent blank); reference—a,b,c, reagent blank; d, 1,2-dichloroethane.

and 1.9, by varying the shaking time from 15 to 60 min. The results revealed that shaking for 15 min is sufficient at either pH. The complex, once extracted, was very stable, the absorbance of the extract remaining unchanged for more than 2 h.

Influence of pH on Extraction. The degree of extraction of indium(III) with HMPP dissolved in 1,2-dichloroethane, as à function of the pH, is shown in Fig. 6 together with results on the extraction of gallium(III) and aluminium(III) carried out for comparison. Indium(III), gallium(III), and aluminium(III) were quantitatively extracted at pH above 2.6, 2.8, and 4.3, respectively, within 30 min, except for the extraction of indium(III) in the pH range 5—7 and that of gallium(III) in the pH range 4—6, where more than 14 hour's shaking was needed to attain equilibrium presumably because of hydrolysis of these ions. Values of half-extraction pHs, $pH_{1/2}$, for indium(III) and aluminium(III) were 2.16 and 3.15, respectively, but that for gallium(III) could not be obtained because no reliable extraction curve for gallium(III) was obtained below pH 1.7.

Extraction Constant of Indium. The overall reaction in the extraction of indium(III) with HMPP may be expressed as

$$In^{3+} + n\,HL_{org} \rightleftarrows InL_{n,org} + n\,H^+ \quad (6)$$

The extraction constant, K_{ex}, is defined as Eq. 7 and is rewritten as Eq. 8 by using the distribution ratio of indium, D_{In}, if it is assumed that (a) indium(III) forms no appreciable amounts of hydrolysis or anion coordination complexes, (b) the complex concentration in the aqueous phase is negligible, (c) the concentrations of intermediate complex species are negligible and (d) the volume of the organic phase is equal to that of the aqueous phase.

$$K_{ex} = \frac{[InL_n]_{org}[H^+]^n}{[In^{3+}][HL]^n_{org}} \quad (7)$$

$$\log D_{In} = \log K_{ex} + n \log [HL]_{org} + n\,pH \quad (8)$$

Equation 8 implies that the plot of $\log D_{In}$ against the pH at a constant HMPP concentration gives a straight line with a slope of n for indium(III), the value of K_{ex} being calculated from the intercept of this line. In fact, a linear relationship with a slope of about 3 was obtained experimentally as shown in Fig. 7, from which it can be concluded that only a 1:3 complex, InL_3, is extracted into 1,2-dichloroethane in this extraction system. The logarithmic value of K_{ex} was calculated to be 2.16 from the intercept of the line in Fig. 7.

Formation Constant of the Complex. Since HMPP and its indium(III) complex have enough solubilities in slightly and/or weakly acidic solution to investigate the complexation reaction in aqueous solution and in addition, the formation constant of the complex was expected to be large, the formation constant was determined in aqueous solution according to the same method as was used by Musha et al.[9]

On the basis of the results stated above, the overall complexation reaction may be written as

$$In^{3+} + 3\,HL \rightleftarrows InL_3 + 3\,H^+ \quad (9)$$

The equiliblium constant, K_{eq}, is defined as Eq. 10

$$K_{eq} = \frac{[InL_3][H^+]^3}{[In^{3+}][HL]^3} \quad (10)$$

In the pH region 2.5—3.5, where the experiment was carried out, HMPP exists as species of HL and

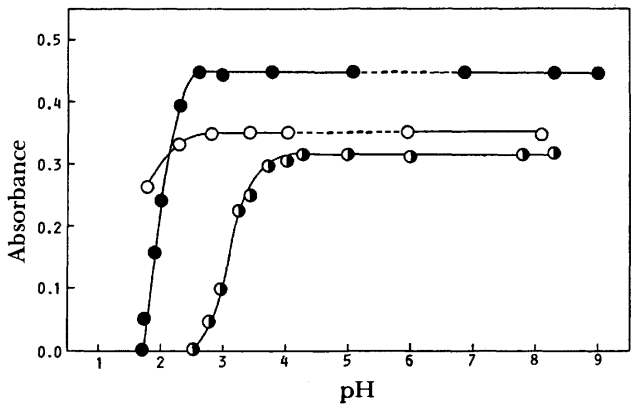

Fig. 6. Extraction curves for In(III)-, Ga(III)-, and Al(III)-HMPP complexes. HMPP, 4.1×10^{-4} M; $V_{aq}/V_{org}=1$ ($V_{org}=10$ cm^3); shaking time, 30 min; reference, reagent blank.

	Concentration/M	Wavelength/nm
—●— In(III)	1.3×10^{-5}	319
—○— Ga(III)	1.1×10^{-5}	319
—◑— Al(III)	9.9×10^{-6}	318

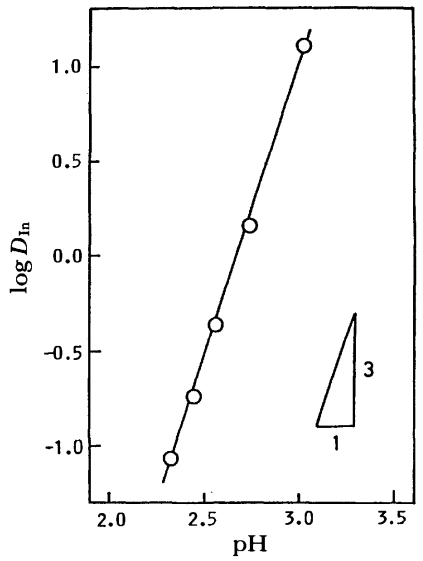

Fig. 7. Plot of $\log D_{In}$ vs. pH for the extraction of indium(III) with HMPP into 1,2-dichloroethane at an ionic strength of 0.2 and at 25±0.1 °C. In(III), 1.3×10^{-5} M; HMPP, 4.1×10^{-4} M; shaking time, 30 min; $V_{aq}/V_{org}=1$ ($V_{org}=10$ cm^3).

H_2L^+. So if the initial concentration of indium(III), C_{In}, is much higher than that of HMPP, C_{HL}, Eq. 10 can be expressed as

$$K_{eq}=x[H^+]^3\left(1+\frac{[H^+]}{K_{a1}}\right)^3/C_{In}(C_{HL}-3x)^3 \qquad (11)$$

where x is the equilibrium concentration of the complex formed. At a specified wavelength where the ligand, HMPP, shows no absorption, Eqs. 12 and 13 exist.

$$A=\varepsilon x \qquad (12)$$

$$A_\infty=\frac{1}{3}\varepsilon C_{HL} \qquad (13)$$

where ε is the molar absorptivity of the complex, A is the absorbance at a given pH of the solution containing indium(III) and HMPP and A_∞ is the limiting absorbance when all of the HMPP is complexed quantitatively with indium(III) at a higher pH. From Eqs. 11, 12, and 13, Eq. 14 can finally be obtained:

$$\log\frac{A}{27(A_\infty-A)^3}=\log C_{In}-2\log\varepsilon-pK_{eq}+3\log\frac{K_{a1}}{[H^+]^2+K_{a1}[H^+]} \qquad (14)$$

Equation 14 implies that at a constant value of C_{In} a plot of $\log A/27(A_\infty-A)^3$ vs. $\log K_{a1}/\{[H^+]^2+K_{a1}[H^+]\}$ should yield a straight line with a slope of 3. Such a relation was experimentally obtained as shown in Fig. 8. The pK_{eq} value was evaluated to be -3.95 by entering the value of $\log K_{a1}/\{[H^+]^2+K_{a1}[H^+]\}$ obtained when $\log A/27(A_\infty-A)^3$ is equal to zero in Eq. 14.

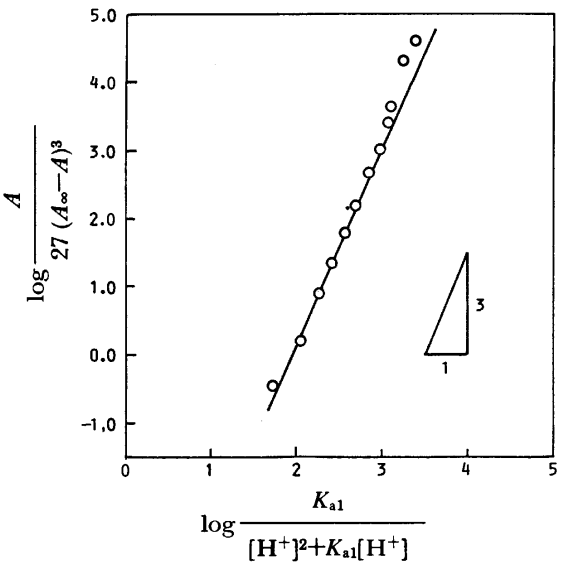

Fig. 8. Plot of $\log A/27(A_\infty-A)^3$ vs. $\log k_{a1}/\{[H^+]^2+K_{a1}[H^+]\}$ for the determination of the equilibrium constant, K_{eq}, at an ionic strength of 0.2 and 25±0.1 °C. In(III), 5.2×10^{-4} M; HMPP, 1.0×10^{-4} M; wavelength, 315 nm.

The overall formation constant, β_3, of this complex defined by

$$In^{3+}+3L^-\rightleftarrows InL_3$$
$$\beta_3=[InL_3]/[In^{3+}][L^-]^3 \qquad (15)$$

can be calculated from the values of K_{eq} and K_{a2} as follows:

$$\log\beta_3=3\,pK_{a2}-pK_{eq}=3\times9.56-(-3.95)=32.63 \qquad (16)$$

Distribution Constant of the Complex. The distribution constant of the indium(III) complex, K_{DC}, is defined by

$$InL_3\rightleftarrows InL_{3,org}$$
$$K_{DC}=[InL_3]_{org}/[InL_3] \qquad (17)$$

and K_{ex} is finally represented by

$$K_{ex}=K_{DC}K_{a2}^3\beta_3/K_D^3 \qquad (18)$$

From Eq. 18 the value of K_{DC} is calculated as follows:

$$\log K_{DC}=\log K_{ex}+3\log K_D-3\log K_{a2}-\log\beta_3=2.16+3(1.35)-3(-9.56)-32.63=2.26$$

Conclusion

From the results described above, it is concluded that the value of the overall formation constant of the indium(III)-HMPP complex is very large, but those of the partition coefficient of HMPP and the distribution constant of the complex are not so large as expected. So it is desirable to increase these two values, for example, by introducing a hydrophobic group into the HMPP molecule and enhance the practical usefulness of HMPP as an extractant, which is now in progress.

References

1) M. J. Herak, M. Janko, and K. Blazevic, *Croat. Chem. Acta*, **41**, 85 (1969).
2) B. Tamhina, K. Jakopcic, F. Zorko, and M. J. Herak, *J. Inorg. Nucl. Chem.*, **36**, 1855 (1974).
3) K. Jakopcic, B. Tamhina,, F. Zorko, and M. J. Herak, *J. Inorg. Nucl. Chem.*, **39**, 1201 (1977).
4) M. J. Herak, B. Tamhina, and K. Jakopcic, *J. Inorg. Nucl. Chem.*, **35**, 1665 (1973).
5) B. Tamhina, M. J. Herak, and K. Jakopcic, *J. Less-Common Metals*, **33**, 289 (1973).
6) G. P. Hildebrand and C. N. Reilley, *Anal. Chem.*, **29**, 258 (1957).
7) L. G. Van Uitert and C. G. Haas, *J. Am. Chem. Soc.*, **75**, 451 (1953).
8) M. J. Herak and Z. Kolarik, *Solv. Extr. Ion Exch.*, **3**, 427 (1985).
9) S. Musha and K. Ogawa, *Bunseki Kagaku*, **8**, 161 (1959).

Single Crystal X-Ray and Optical Studies on Bis(1,5-diazacyclooctane)-copper(II) Nitrate, a Thermochromic Copper(II) Complex Involving Hydrogen Bonds between the Ligand and the Counter Ion

Naomi HOSHINO,† Yutaka FUKUDA,* Kozo SONE, Kiyoaki TANAKA,†† and Fumiyuki MARUMO††
Department of Chemistry, Faculty of Science, Ochanomizu University, Otsuka, Bunkyo-ku, Tokyo 112
†† Research Laboratory of Engineering Materials, Tokyo Institute of Technology, Nagatsuta, Midori-ku, Yokohama 227
(Received September 27, 1988)

A thermochromic copper(II) complex of 1,5-diazacyclooctane (daco), $[Cu(daco)_2](NO_3)_2$, has been subjected to single-crystal X-ray and optical studies. This complex is orange as isolated, but it turns violet discontinuously when heated above 90 °C and returns to orange on cooling. Crystal structure of the low-temperature form has been determined at room temperature; the complex crystallizes in the monoclinic space group $P2_1/n$ with a=7.9040(7), b=15.694(1), c=7.0886(7) Å, β=95.36(1)°; V=875.5(1) Å^3, and Z=2. The CuN_4 chelate plane is planar and Cu-N coordination bonds are rather short. The structure has revealed the presence of weak hydrogen bonds bridging imino groups of the ligands with the nitrate ions and forming a macrocycle-like ring system, which results in enhancement of the ligand field strength. Single-crystal visible and infrared spectra for both low- and high-temperature forms have heen obtained and compared. A high-energy d-d transition band(s) causing the orange color at room temperature is in contrast to an extremely flattened broad band(s) for the violet form. The IR spectra of the two forms clearly differ in the intensity of ν_{NH} stretching peak, implying that the thermochromic phase transition involves a change in the nature of the hydrogen bonds of the imine ligands. On the basis of these observations and comparison to reported studies on a similarly thermochromic copper(II) complex, a mechanism is suggested involving dynamic fluctuation of the ligand field and geometry due to thermal motion of the anion/ligand hydrogen bond system.

Thermochromism and related chromotropic behaviors of inorganic compounds have been recently reviewed.[1] There exist a number of examples of thermochromic metal complexes and origins of the color changes are quite diverse. A certain class of materials show gradual color change over a wide temperature range, which is called continuous thermochromism.[2] Discontinuous thermochromism,[2] on the other hand, is a more abrupt or clearly visible color change over a small temperature range and manifests the onset of a first- or second-order phase transition. This latter phenomenon is not only interesting in its own right but also provides information on various factors determining coordination geometries and crystal structures of transition metal complexes.

We have previously reported that a copper(II) complex of 1,5-diazacyclooctane (daco), $[Cu(daco)_2](NO_3)_2$, shows reversible thermochromism between orange (at room temperature) and violet (above 90 °C) in solid state.[3] It was suggested at the moment that coordination of the nitrate ions to the copper center at elevated temperatures is responsible for the color change. On the other hand, Musker and Hussain have previously studied on bis(daco) complexes of copper(II) and nickel(II) and stated that the boat-chair conformation of the mesocyclic chelate ring would more or less shield the axial site of the central metal atom.[4,5] It was revealed later [6] that the nitrate ion in $[Cu(daco)_2](NO_3)_2$ is indeed far from accessible to the copper atom in the axial direction, and is rather interacting laterally with the daco ligands via a pair of hydrogen bonds. Thus the thermochromic mechanism appears to involve such ligand-anion interaction rather than the metal-anion bonding.

The purpose of this paper is to shed new light on the role of ligand-anion hydrogen bonding interaction in determining the structure, the ligand field strength, and the resulting physical properties of transition metal chelates. The crystal structure and optical spectra of $[Cu(daco)_2](NO_3)_2$, obtained for single crystals, are reported herein to show that the daco-nitrate interaction is really a key factor in the thermochromic phase transition of this complex.

Experimental

Materials. Synthesis of daco and $[Cu(daco)_2](NO_3)_2$ has been reported elsewhere.[3,7] Single crystals of the latter were grown by slow evaporation from an ethanol solution.

Physical Measurements. Single-crystal infrared absorption spectra were measured using an optical system consisting of a JASCO infrared radiation source, a JASCO CT-25C monochromator, an SBRC HgCdTe detector, and a PAR Model 124A lock-in amplifier. Visible absorption spectra were obtained with a similar system comprising a halogen-gas-filled tungsten incandescent lamp, an ISA Jobin Yvon Type HR1000 monochromator, and a Hamamatsu R376 photomultiplier. Polarized spectra were not obtained since the crystal faces were ill-defined.

The thermochromic transition temperature and enthalpy were determined using a Rigaku Thermoflex differential scanning calorimeter at a heating rate of 5 K min^{-1}.

X-Ray Analysis. An orange crystal was shaped into a sphere with a diameter of 0.22 mm on a wet filter paper under a microscope. Weissenberg photographs were taken with Cu$K\alpha$ radiation (λ=1.54184 Å) and the crystal was found to be monoclinic and has the space group $P2_1/n$.

† Present address: Department of Chemistry, Faculty of Science, Hokkaido University, Sapporo 060.

Diffraction data were collected on a Philips automated four-circle diffractometer PW1100 having a maximum 2θ value of 90° with graphite monochromated Mo $K\alpha$ radiation (λ= 0.71073 Å). Cell constants (Table 1) were obtained from least-squares refinement, on the basis of setting angles of 67 reflections in the range $52° < 2\theta < 74°$, where separation of the $K\alpha$ doublet was clear and only the Mo $K\alpha_1$ reflections were used. A total of 3963 independent reflections were collected, and 2948 reflections (h=−13 to 13, k=0 to 29, and l=0 to 18) met the condition $I > 3\sigma(I)$ to be used for subsequent analysis. Three standard reflections (hkl=400, 080, and 004) were measured every 50 reflections and no significant variation was detected. Each reflection was measured up to 8 times until the total peak count exceeded 40000. Lorentz-polarization correction and absorption correction (factors ranging between 1.245 and 1.250) were applied to the data.

The structure was solved by the direct method with MULTAN78,[8] which yielded positions of all the nonhydrogen atoms. The structure was refined by the full-matrix least-squares method with the program LINKT80,[9] which minimizes the function $\sum(|F_o|-|F_c|)^2$; unit weight was assigned to each reflection. Hydrogen atoms were located on difference Fourier maps and their positions were refined with isotropic temperature factors, while anisotropic temperature factors were refined for nonhydrogen atoms. Anisotropic Type I extinction parameters were also refined.[10] The final values for R and R_w were 0.0311 and 0.0315, respectively. The maximum shift in the final cycle of the least-squares refinement was 0.15 for the isotropic temperature factor of H(12). The final difference Fourier map was featureless. Atomic scattering factors and dispersion terms were taken from the literature.[11] Tables of temperature factors and structure factors are deposited as Document No.8878 at the Office of the Editor of Bull. Chem Soc. Jpn.

Table 1. Crystallographic Data for $[Cu(daco)_2](NO_3)_2$

Formula	$CuC_{12}H_{28}N_6O_6$
Fw	415.94
Space group	$P2_1/n$
a/Å	7.9040(7)
b/Å	15.694(1)
c/Å	7.0886(7)
β/deg	95.36(1)
V/Å^3	875.5(1)
Z	2
d_{calcd}/g cm^{-3}	0.7889
$F(000)$	438
μ/cm^{-1} (Mo $K\alpha$)	13.42

Results and Discussion

Crystal Structure of $[Cu(daco)_2](NO_3)_2$ at Room Temperature. This is the first example of bis(daco) complex of copper(II) for which the crystal structure has been solved. Figure 1 shows the structure, determined at room temperature, together with the numbering scheme. A stereoview showing crystal packing is given in Fig. 2. Table 2 lists atomic positional parameters, and selected interatomic distances and bond lengths and angles are summarized in Table 3.

The structure is centrosymmetric with the center of symmetry on the site of Cu and the CuN_4 chelate plane is planar. But it is not precisely square since two Cu-N coordination bonds of a daco ligand differ in length significantly (1.997(1) Å for Cu-N(1) and 2.034(1) Å for Cu-N(2)). These bond lengths, particularly of the former, are rather short for a Cu(II)-N(secondary amine) bond.[12] These facts agree with an enhanced ligand field strength suggested by the orange color which is rarely encountered among copper(II) com-

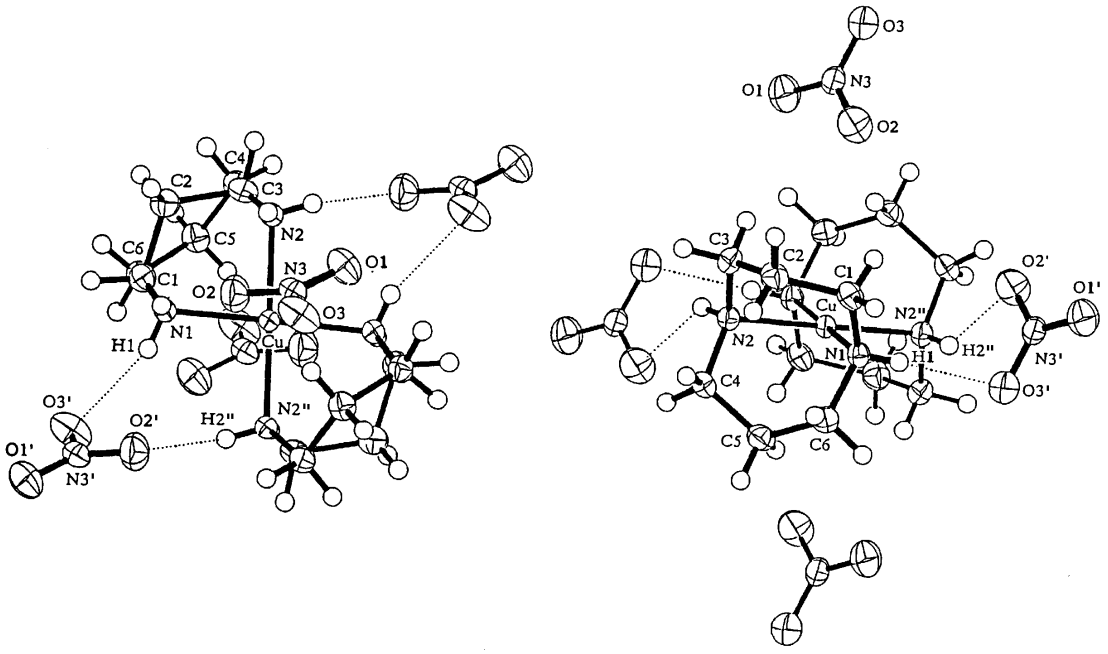

Fig. 1. Perspective drawings of $[Cu(daco)_2](NO_3)_2$ with thermal ellipsoids scaled to 40% probability and atomic numbering scheme. The atoms labeled by ′ and ″ are generated by symmetry operations, $(-x, -y, 1-z)$ and $(-x, -y, -z)$, respectively.

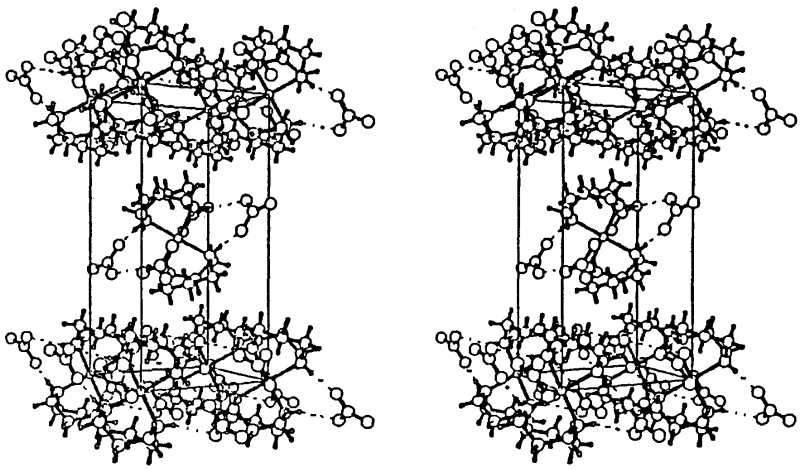

Fig. 2. Stereoview of crystal packing for $[Cu(daco)_2](NO_3)_2$.

Table 2. Fractional Atomic Coordinates and Equivalent Thermal Parameters, B_{eq}(Å^2), for $[Cu(daco)_2](NO_3)_2$

$$B_{eq} = \frac{4}{3}\sum_i\sum_j B_{ij}a_ia_j$$

Atom[a]	x	y	z	B_{eq}/Å^2
Cu	0.0	0.0	0.0	1.791(5)
N(1)	0.0663(2)	−0.11025(7)	0.1266(2)	2.20(3)
N(2)	−0.2147(2)	−0.06144(7)	−0.1058(2)	2.15(3)
N(3)	−0.3582(2)	0.09057(9)	0.4851(2)	2.88(3)
O(1)	−0.4166(2)	0.1162(1)	0.3279(2)	5.03(7)
O(2)	−0.2716(2)	0.02510(9)	0.5014(2)	4.71(7)
O(3)	−0.3820(2)	0.1316(1)	0.6316(2)	5.37(9)
C(1)	−0.0543(2)	−0.1298(1)	0.2699(2)	2.87(4)
C(2)	−0.2329(2)	−0.1499(1)	0.1852(3)	3.12(4)
C(3)	−0.3161(2)	−0.0820(1)	0.0555(3)	2.87(4)
C(4)	−0.1794(2)	−0.1371(1)	−0.2244(2)	2.60(8)
C(5)	0.0081(3)	−0.1587(1)	−0.2091(3)	2.97(4)
C(6)	0.0874(2)	−0.1806(1)	−0.0118(3)	2.74(4)
H(1)	0.156(3)	−0.105(1)	0.185(3)	3.12(5)
H(2)	−0.271(3)	−0.028(1)	−0.171(3)	3.3(1)
H(3)	−0.009(3)	−0.179(2)	0.347(3)	3.78(6)
H(4)	−0.054(3)	−0.082(2)	0.348(3)	3.80(6)
H(5)	−0.235(3)	−0.202(1)	0.121(3)	3.13(5)
H(6)	−0.301(3)	−0.158(2)	0.288(3)	4.05(7)
H(7)	−0.332(3)	−0.032(2)	0.122(3)	3.59(6)
H(8)	−0.429(3)	−0.099(1)	0.008(3)	3.75(6)
H(9)	−0.213(3)	−0.123(2)	−0.356(4)	4.17(7)
H(10)	−0.244(3)	−0.184(1)	−0.186(3)	3.31(5)
H(11)	0.071(3)	−0.113(2)	−0.259(4)	4.29(8)
H(12)	0.021(3)	−0.208(2)	−0.292(4)	4.71(8)
H(13)	0.041(3)	−0.231(1)	0.035(3)	3.27(5)
H(14)	0.211(3)	−0.189(1)	−0.010(3)	3.52(6)

a) Hydrogen atoms H(3) through H(14) are numbered in the order of attached carbon atoms C(1) through C(6).

plexes. An important feature to note is that each $[Cu(daco)_2]^{2+}$ unit carries two NO_3^- ions which are hydrogen bonded to the amino nitrogens. These hydrogen bonds form a macrocycle-like ring system including a pair of N(1)-H(1)-[O(3)′-N(3)′-O(2)′]-H(2)″-N(2)″ bridges (dotted lines in Fig. 1). But these bonds are relatively weak; the interatomic distances 2.912(2) Å (N(1)···O(3)′) and 3.093(2) Å (N(2)″···O(2)′) are both in the range of weak hydrogen bond distances.[13] The positions of the hydrogen atoms which have been determined clearly demonstrate that these hydrogen bonds are not equivalent; the plane of NO_3^- is tilted by 68.2° relative to the CuN_4 chelate plane within which the O(3)′ atom and both of the hydrogen atoms H(1) and H(2)″ reside (Fig. 1, right), and so the N(1)-H(1)-O(3)′ hydrogen bond is rather straight (161(2)°) while the N(2)″-H(2)″-O(2)′ bond is bent (136(2)°). As a consequence of this unsymmetrical interaction of the anion to the ligand, not only the symmetry of the NO_3^- ion deviates from D_{3h} but also the two coordination bond lengths are significantly different as mentioned above; more linear and shorter hydrogen bond N(1)-H(1)-0(3)′ makes the related coordination bond Cu-N(1) shorter than the other.

Although the axial nitrate ions in Fig. 2 appear to have a close contact to the metal centers to form one-dimensional arrays of the chelate cations, such axial coordination does not exist, since even the shortest axial distance is 4.338(2) Å for Cu···O(2). This situation is well illustrated in the side view of the complex shown on the right in Fig. 1. The axial coordination appears to be precluded by chair and boat conformations of the chelate rings involving C(1)-C(2)-C(3) and C(4)-C(5)-C(6), respectively.

It is interesting to compare the structure with those of analogous species. Boeyens and Fox determined the structure of $[Ni(daco)_2](B(C_6H_5)_4)_2 \cdot 2DMSO$ and stated that the two solvent molecules, located aside the chelate plane, are interacting with the diamine nitrogen atoms through hydrogen bonding.[14] In addition, redetermination of the crystal structure of $[Ni(daco)_2](ClO_4)_2 \cdot 2H_2O$ by Boeyens et al. revealed that the water molecules also act as bridges between neighboring chelate cations through a set of O-H-N hydrogen bonds.[15] Thus the hydrogen bonding in crystals of daco complexes seems to be not uncom-

Table 3. Selected Interatomic and Bond Distances (Å) and Bond Angles (deg) in $[Cu(daco)_2](NO_3)_2$

Cu-N(1)	1.997(1)	N(3)'H···(2)"	3.10(2)
Cu-N(2)	2.034(1)	O(2)'···H(2)"	2.47(2)
Cu···N(3)	4.866(2)	O(3)'···H(1)	2.15(2)
Cu···O(1)	4.583(2)	C(1)-C(2)	1.515(3)
Cu···O(2)	4.338(2)	C(1)-C(6)	2.508(3)
Cu···N(3)'	4.629(1)	C(1)-H(3)	0.99(2)
Cu···O(2)'	3.980(2)	C(1)-H(4)	0.93(2)
Cu···O(3)'	4.328(2)	C(2)-C(3)	1.517(3)
N(1)-C(1)	1.488(2)	C(2)-H(5)	0.94(2)
N(1)-C(6)	1.496(2)	C(2)-H(6)	0.95(3)
N(1)-H(1)	0.79(2)	C(3)-H(7)	0.93(2)
N(1)···O(3)'	2.912(2)	C(3)-H(8)	0.96(2)
N(2)-C(3)	1.491(2)	C(4)-C(5)	1.514(3)
N(2)-C(4)	1.496(2)	C(4)-H(9)	0.97(2)
N(2)-H(2)	0.80(2)	C(4)-H(10)	0.95(2)
N(2)"···O(2)'	3.093(2)	C(5)-C(6)	1.517(2)
N(3)-O(1)	1.233(2)	C(5)-H(11)	0.95(3)
N(3)-O(2)	1.234(2)	C(5)-H(12)	0.99(3)
N(3)-O(3)	1.251(2)	C(6)-H(13)	0.95(2)
N(3)'···H(1)	2.72(2)	C(6)-H(14)	0.99(2)
N(1)-Cu-N(2)	85.98(5)	C(3)-C(2)-H(6)	108(2)
Cu-N(1)-C(1)	109.1(1)	H(5)-C(2)-H(6)	106(2)
Cu-N(1)-C(6)	112.67(9)	N(2)-C(3)-C(2)	112.6(1)
Cu-N(1)-H(1)	109(2)	N(2)-C(3)-H(7)	108(1)
C(1)-N(1)-C(6)	114.4(1)	N(2)-C(3)-H(8)	110(1)
C(1)-N(1)-H(1)	106(2)	C(2)-C(3)-H(7)	111(1)
C(6)-N(1)-H(1)	106(2)	C(2)-C(3)-H(8)	111(1)
Cu-N(2)-C(3)	108.0(1)	H(7)-C(3)-H(8)	104(2)
Cu-N(2)-C(4)	112.98(9)	N(2)-C(4)-C(5)	111.8(1)
Cu-N(2)-H(2)	108(2)	N(2)-C(4)-H(9)	108(1)
C(3)-N(2)-C(4)	113.6(1)	N(2)-C(4)-H(10)	109(1)
C(3)-N(2)-H(2)	106(2)	C(5)-C(4)-H(9)	107(1)
C(4)-N(2)-H-(2)	108(2)	C(5)-C(4)-H(10)	111(1)
O(1)-N(3)-O(2)	120.9(2)	H(9)-C(4)-H(10)	110(2)
O(1)-N(3)-O(3)	120.6(2)	C(4)-C(5)-C(6)	115.7(2)
O(2)-N(3)-O(3)	118.4(2)	C(4)-C(5)-H(11)	110(2)
N(3)'-O(2)'···H(2)"	108.9(6)	C(4)-C(5)-H(12)	107(2)
N(3)'-O(3)'···H(1)	102.7(6)	C(6)-C(5)-H(11)	109(2)
N(1)-C(1)-C(2)	113.9(1)	C(6)-C(5)-H(12)	108(2)
N(1)-C(1)-H(3)	108(1)	H(11)-C(5)-H(12)	106(2)
N(1)-C(1)-H(4)	106(2)	N(1)-C(6)-C(5)	112.1(1)
C(2)-C(1)-H(3)	110(1)	N(1)-C(6)-H(13)	109(1)
C(2)-C(1)-H(4)	111(2)	N(1)-C(6)-H(14)	105(1)
H(3)-C(1)-H(4)	108(2)	C(5)-C(6)-H(13)	112(1)
C(1)-C(2)-C(3)	115.4(2)	C(5)-C(6)-H(14)	111(1)
C(1)-C(2)-H(5)	110(1)	H(13)-C(6)-H(14)	107(2)
C(1)-C(2)-H(6)	107(2)	N(1)-H(1)···O(3)'	161(2)
C(3)-C(2)-H(5)	110(1)	N(2)"-H(2)"···O(2)'	136(2)

mon; as will be discussed below, we believe that the subtleness of this interaction is closely related to the thermochromic phase transition in the case of $[Cu(daco)_2](NO_3)_2$.

It would be desirable to have crystal structure of the high temperature form as well, but it has not been possible to date due to crystal disintegration on prolonged heating.

Optical and EPR Spectral Changes Associated with Thermochromism of $[Cu(daco)_2](NO_3)_2$. The reversible thermochromism of $[Cu(daco)_2](NO_3)_2$ can be visually observed as a distinct color change of a powdered

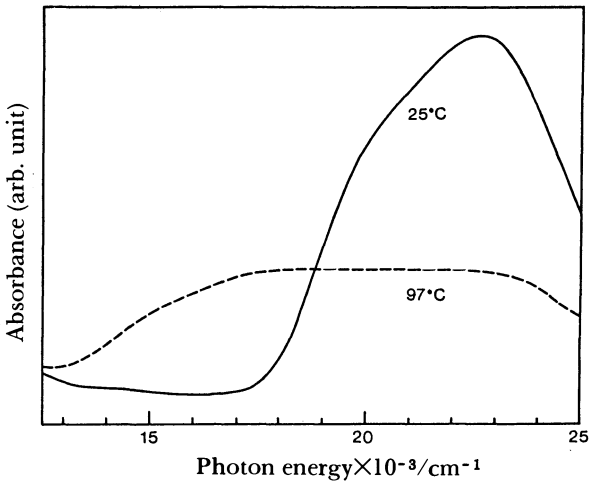

Fig. 3. Single-crystal visible spectral change associated with thermochromism of $[Cu(daco)_2](NO_3)_2$.

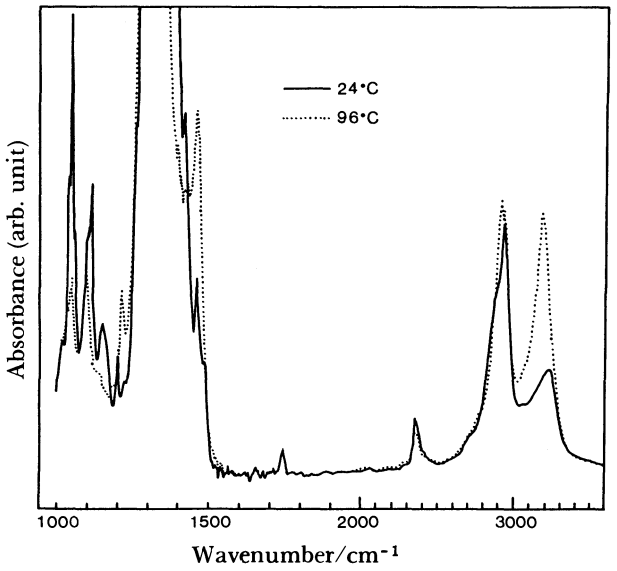

Fig. 4. Single-crystal infrared spectral change upon thermochromic transition of $[Cu(daco)_2](NO_3)_2$.

sample between orange and violet, as mentioned above. Powder reflectance spectral changes corresponding to this behavior were previously reported.[3] Single crystals have been used in this work in order to obtain absorption data which can be directly compared with each other. The results are shown in Figs. 3 and 4 for visible and infrared regions, respectively.

The visible absorption spectrum of $[Cu(daco)_2](NO_3)_2$ recorded at 25 °C exhibits a broad hand which peaks at 22.7×10^3 cm^{-1} and shows a shoulder at 20.0×10^3 cm^{-1}. As the crystal is heated with the peak intensity monitored, this band slightly diminishes at first and then suddenly drops to about one third of the original intensity at around 90 °C. The spectrum recorded at 97 °C indicates also that the absorption band is now widely spread (Fig. 3).

Royer et al. have investigated single-crystal polar-

ized spectra of $[Cu(daco)_2](ClO_4)_2 \cdot 2H_2O$, and deduced with some assumptions that the d-orbital energy order is $b_{1g} \gg b_{2g} > e_g > a_{1g}$ under D_{4h} symmetry.[16] According to their Gaussian resolution of the spectra, the visible band of this perchlorate salt is composed of three components; $^2B_{1g} \rightarrow {}^2B_{2g}$ at 18.2×10^3 cm^{-1}, $^2B_{1g} \rightarrow {}^2E_g$ at 20.8×10^3 cm^{-1}, and $^2B_{1g} \rightarrow {}^2A_{1g}$ at 23.1×10^3 cm^{-1}. Polarization experiments were not performed in this study, but it seems that the Gaussian fitting would become more arbitrary; it requires four components, since at least the crystal structure at room temperature has shown that the effective ligand field symmetry in $[Cu(daco)_2](NO_3)_2$ is no higher than D_{2h}. However, we can still apply the fundamental scheme obtained for the perchlorate analogue that strong σ interaction of the daco ligand raises the energy of $d_{x^2-y^2}$ orbital up high, while the rest of d-orbitals are lying low and relatively close to each other. It is notable in Fig. 3 that, regardless of possible spectral resolution, even the lowest energy transition component with significant intensity should appear at the energy no lower than ca. 20×10^3 cm^{-1} for the room temperature spectrum. This suggests that the σ-interaction of the ligand is stronger in the nitrate salt than in the perchlorate salt. This could well be due to the ligand-nitrate hydrogen bonds enhancing rigidity of the planar coordination geometry and also basicity of the donor nitrogen atoms.

On the other hand, the spectrum recorded at 97 °C indicates at least that some of the d-d transition components have shifted towards lower energy. This can be interpreted as a result of weakening of the ligand field and/or a change in its symmetry; not only is the energy of $d_{x^2-y^2}$ orbital lowered but also the relative spacings among the rest of d-orbitals must have changed, as suggested by the spectral breadth.

A piece of evidence for correlation of the hydrogen bonding to the thermochromic phase transition was obtained from infrared measurements. Comparison of the IR spectra of $[Cu(daco)_2](NO_3)_2$ at 24 °C and at 96 °C, shown in Fig. 4, reveals that most drastic change occurs in the absorption peaks assignable to ν_{NH} stretching mode, which should be sensitive to the nature of the hydrogen bond. Intensification of the peak at 3200 cm^{-1} upon heating can be viewed as release of the intensity of this mode which has been supressed in the low-temperature phase. However, the shift in its energy is minimal, suggesting that the "average" hydrogen bond strength is not much changed in the two phases. Another noticeable intensification upon heating occurs to a peak at 1460 cm^{-1}, which may be assigned to δ_{NH} deformation. Stretching absorption of the NO_3^- ion is too intense to assess a change with temperature on this side of the hydrogen bond. It is noted, however, that a small peak at 1747 cm^{-1}, which can be a combination band of NO_3^- modes, shows no detectable change in shape.

If this complex nitrate is ground together with KBr, resulting powder mixture is colored violet and the IR spectrum of this KBr disk is identical to that of $[Cu(daco)_2]Br_2 \cdot H_2O$,[17] with a characteristic sharp peak at 1649 cm^{-1}, indicating that NO_3^- can be easily relaced by Br^-. It is likely that one of the bromide ions is coordinated to copper in the violet bromide salt,[17] and this inclines one to assume a similar anion coordination in the high-temperature violet form of nitrate salt which is apparently similar in color. However, an EPR evidence has shown that the two violet species are different in terms of the ligand field strength and symmetry. Figure 5 compares the powder EPR spectra of low- and high-temparature forms of $[Cu(daco)_2](NO_3)_2$ and $[Cu(daco)_2]Br_2 \cdot H_2O$. The g-values for the former are $g_{//}=2.142$ and $g_{\perp}=2.033$, which are practically constant from room temperature up to the transition temperature (orange form, Fig. 5a) and change to $g_{//}=2.122$ and $g_{\perp}=2.046$ (violet form, Fig. 5b). Those for the bromide salt, on the other hand, are $g_{//}=2.169$ and $g_{\perp}=2.031$ (Fig. 5c). Thus the thermochromic transition of the nitrate salt is associated with decreases in the $g_{//}$ value and in the anisotropy of the g-values at the elevated temperatures. This behavior is opposite to what would be expected if the anion coordinates axially to the metal center upon heating.[18] What then would be the cause for the color change of the nitrate salt?

On the Mechanism of Thermochromism. The thermochromic phase transition of $[Cu(daco)_2](NO_3)_2$ occurs endothermically at 85.5 °C (at a heating rate of 5 K min^{-1}, $\Delta H=7.61$ kJ mol^{-1}). Solid-state thermochromism has been observed among other metal complexes of daco ligand,[4,5] but in these cases (e.g., $Co(daco)_2I_2 \cdot EtOH$[5] and $Cu(daco)_2X_2 \cdot H_2O$ (X=Br, Cl)[17]) the observed color changes involve dehydration

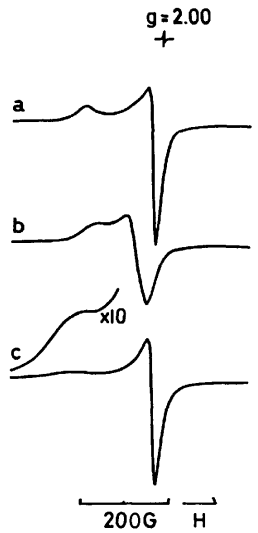

Fig. 5. Powder EPR spectra for (a) orange form and (b) violet form of $[Cu(daco)_2](NO_3)_2$, and (c) $Cu(daco)_2]Br_2 \cdot H_2O$ (violet). Spectra were recorded at the apparent cavity temperatures of 99.7 °C for (a) and (c) and of 120 °C for (b).

or desolvation at relatively high temperatures. On the other hand, there exists a broader class of materials containing *N,N*-diethylethylenediamine (deen) which exhibit thermochromic phase transition, and among them $[Cu(deen)_2](ClO_4)_2$ has been most extensively investigated. Bloomquist and Willett has reviewed[2] the work on this compound including crystal structure determination for both low- and high-temperature forms.[12] A short summary will be given below to facilitate comparison between $[Cu(daco)_2](NO_3)_2$ and $[Cu(deen)_2](ClO_4)_2$ that follows.

This compound is red at room temperature, and changes to deep blue-purple at T_{th}=43 °C (ΔH= 8.91 kJ mol^{-1}) returning to red upon cooling. Mechanistic interpretation for this behavior based on EPR and IR spectroscopies ascribed it to axial interaction of the perchlorate ion, since the evidences suggested an increase in the in-plane ligand field at lower temperatures. However, X-ray crystallographic analyses revealed that the perchlorate ions are isolated from the Cu(II) coordination sphere in both phases; the closest Cu···O distance is 3.65(1) Å and 4.16(2) Å in the low- and high-temperature form, respectively. It was thus concluded that the thermochromic change in $[Cu(deen)_2](ClO_4)_2$ must be due to a sudden change of the in-plane ligand field strength caused by conformational changes in the $Cu(en)_2$ ring system.[12] Bloomquist and Willett noticed that each perchlorate ion is involved in two N-H···O hydrogen bonds with chelate cations (here also) at room temperature and stated further that, "as the temperature is raised, a point is reached at which the thermal motion energy sufficiently weakens the hydrogen bonding network to allow the two Cu-diamine ring systems to begin rapid conformational interconversion." A puzzling part of the results of the above crystallographic study is that the Cu-N bond lengths hardly differ between the two phases, raising a question as to why the change in the in-plane ligand field strength is not reflected in these parameters. This, however, was explained in terms of the ligand disorder, dynamic in nature, preventing optimal Cu-N overlap in the high-temperature blue modification.

Returning to the present case of $[Cu(daco)_2](NO_3)_2$, it is not possible to fully delineate the thermochromic mechanism at the present stage without a complete set of structural evidences. However, the data available at present seem to indicate that this picture of "dynamic" disorder will apply to the case of $[Cu(daco)_2](NO_3)_2$ just as well or even better. It should be emphasized that the visible absorption spectral change accompanying the phase transition of $[Cu(daco)_2](NO_3)_2$ is not a simple shift of a certain d-d transition. It has been conveniently and perhaps reasonably assumed for $[Cu(deen)_2](ClO_4)_2$ that the visible absorption can be ascribed to the d_{xz}, $d_{yz} \rightarrow d_{x^2-y^2}$ transition with the effective ligand field symmetry D_{4h} and that this band shifts up and down according to the variation in the in-plane ligand field. However, the discontinuous absorption spectral change with temperature for $[Cu(daco)_2](NO_3)_2$ appears to involve a rather drastic change in d-orbital energy scheme. The very broad and flat shape of the visible absorption band for the high-temperature form implies that mixing among the d-orbitals has become extensive. The infrared spectral change also suggests that the hydrogen bond strength in a static sense does not change on heating. Thus a simple picture of weakening of the in-plane ligand field due to thermal motion of the ligand and/or to weakening of the ligand/anion hydrogen bonds is not sufficient to explain the thermochromic transition in $[Cu(daco)_2](NO_3)_2$.

Therefore, we would like to point out the possibility that the anions play an active role as a source of disorder in the thermochromic transition of this complex, as suggested in the case of $[Cu(deen)_2](ClO_4)_2$.[2] It can be easily imagined that the thermal motion of the anions would create dynamical fluctuation in the hydrogen bond strength, with protons shifting back and forth, and in the electron density on the ligand nitrogen atoms. It is recalled that the perchlorate group in $[Cu(deen)_2](ClO_4)_2$ (blue) showed anisotropic temperature factors no smaller than those of the ligand.[12] In the case of $[Cu(daco)_2](NO_3)_2$, extensive librational movements of the nitrate ions within the macrocycle-like chelate ring would also induce some distortion in the planar coordination geometry.

Thus the thermochromism of $[Cu(daco)_2](NO_3)_2$ seems to have much part of its origin in the anion/ligand hydrogen bond system. Little attention has been paid to the ability of the anions in metal complexes to form hydrogen bonds to the ligands, and to influence the mode and strength of their coordination, while a number of cationic chelates with ligands which are bulky enough to preclude coordination of the anions to the metal center are known. It certainly deserves more studies to exploit this type of interaction, in order to generate novel physical properties of coordination compounds in solid state.

This work was partially supported by a Grant-in-Aid for Scientific Research from Ministry of Education, Science and Culture (No. 59430009). The authors thank the Computer Center, Institute for Molecular Science (IMS), Okazaki National Institutes for the use of HITAC M-680H. We also thank Dr. Takenaka and Prof. Yoshio Sasada of Tokyo Institute of Technology for the drawing program DCMS82 used in the preparation of Figs. 1 and 2. Assistance of Prof. Tadaoki Mitani of IMS in the single crystal optical measurements is greatly appreciated.

References

1) K. Sone and Y. Fukuda, "Inorganic Thermochrom-

ism," Springer, Heidelberg (1987).

2) D. R. Bloomquist and R. D. Willett, *Coord. Chem. Rev.*, **47**, 125 (1982).

3) S. Yamaki, Y. Fukuda, and K. Sone, *Chem. Lett.*, **1982**, 269.

4) W. K. Musker and M. S. Hussain, *Inorg. Chem.*, **5**, 1416 (1966).

5) W. K. Musker and M. S. Hussain, *Inorg. Chem.*, **8**, 528 (1969).

6) K. Tanaka, F. Marumo, Y. Fukuda, and K. Sone, The 31st Conference on Coordination Chemistry, Sendai, 1981, Abstr., No. 3C09.

7) E. L. Buhle, A. M. Moore, and F. Y. Wiseloge, *J. Am. Chem. Soc.*, **65**, 29 (1943).

8) P. Main, S. E. Hull, L. Lessinger, G. Germain, J. -P. Declercq, and M. M. Woolfson, MULTAN78, Univ. of York, England, and Univ. of Louvain, Belgium (1978).

9) K. Tanaka and F. Marumo, *Acta Crystallogr., Sect. A*, **39**, 631 (1983).

10) P. J. Becker and P. Coppens, *Acta Crystallogr., Sect. A*, **30**, 129 (1974); **30**, 148 (1974); **31**, 417 (1975);

11) Atomic scattering factors for nonhydrogen atoms were taken from "International Tables for X-Ray Crystallography," ed by J. A. Ibers and W. C. Hamilton, Kynoch Press, Birmingham (1974), Vol. IV and those for hydrogen atoms from R. F. Stewart, E. R. Davidson, and W. T. Simpson, *J. Chem. Phys.*, **42**, 3185 (1965).

12) I. Grenthe, P. Paoletti, M. Sandstroem, and S. Glikberg, *Inorg. Chem.*, **18**, 2687 (1979).

13) G. H. Stout and L. H. Jensen, "X-Ray Structure Determination: A Practical Guide," MacMillan, New York (1968).

14) J. C. A. Boeyens and C. C. Fox, *S. Afr. J. Chem.*, **37**, 1 (1984).

15) J. C. A. Boeyens, C. C. Fox, and R. D. Hancock, *Inorg. Chim. Acta*, **87**, 1 (1984).

16) D. J. Royer, V. H. Schievelbein, A. R. Kalyanaraman, and J. A. Bertrand, *Inorg. Chim. Acta*, **6**, 307 (1972).

17) N. Hoshino, J. Kawashima, S. Yamaki, Y. Fukuda, and K. Sone, unpublished results.

18) H. Yokoi, M. Sai, and T. Isobe, *Bull. Chem. Soc. Jpn.*, **42**, 2232 (1969).

Orientation of Isomeric Phthalic Acids on Alumina and Magnesia Surface Observed by Inelastic Electron Tunneling Spectroscopy

Morihide HIGO,* Sinichi MIZUTARU,† and Satsuo KAMATA
Faculty of Engineering, Kagoshima University, Korimoto, Kagoshima 890
(Received November 4, 1988)

The vibrational spectra of phthalic, isophthalic, and terephthalic acid adsorbed onto alumina and magnesia surfaces from the gas phase have been measured by inelastic electron tunneling spectroscopy. The analysis of the tunneling spectra shows that phthalic and isophthalic acid react with the surface OH groups on Al_2O_3 and MgO to give the adsorbed dicarboxylate ions on both surfaces. Phthalic acid is adsorbed with its benzene ring perpendicular to the surfaces, while isophthalic acid is adsorbed parallel to the surfaces. However, terephthalic acid is adsorbed predominantly as the monocarboxylate ion almost perpendicular to the alumina surface, while it is adsorbed as the dicarboxylate ion parallel to the magnesia surface. These results suggest the different properties of the surface OH groups on Al_2O_3 and MgO. There are more than one type of OH group on the alumina surface and they interact with each other through hydrogen bonding. The magnesia surface has an isolated and a hydrogen-bonding OH group. The OH groups on MgO are more basic than those on Al_2O_3, and thus have higher reactivity. The different properties and basicity of the OH groups cause the different orientation and reactivity of the adsorbed terephthalic acid on the alumina and magnesia surfaces.

Recently there has been an increased interest in a new technique for investigating a metal surface and adsorbed species on it. Inelastic electron tunneling spectroscopy (IETS) is a relatively new and a unique technique using the phenomena of electron tunneling through a metal-oxide-metal tunneling junction at cryogenic temperatures. It reveals the vibrational spectrum of the oxide surface and the adsorbed species on it. The high sensitivity and wide spectral range inherent in IETS enable us to analyze the surface and the adsorbed species in detail.[1]

Alumina has been widely used as the oxide of the tunneling junction for its chemical, physical, and electric stability, in addition to its ease of formation.[1-3] Few IETS studies, however, have utilized magnesia.[4-14] The surfaces of alumina and magnesia have been studied by infrared spectroscopy,[15-17] and their surface models have been proposed.[18-20] These oxides are used as catalysts or catalyst supports in chemical engineering. Alumina is an amphoteric oxide and magnesia is a basic one; thus, these oxides have interesting and sometimes different catalytic properties. However, their surface states and their chemical interaction with adsorbed species are not well understood.[21,22] Thus, the measurement and analysis of the tunneling spectra of Al_2O_3 and MgO and the adsorbed species on both surfaces are important and interesting.

The isomeric phthalic acids have two carboxyl groups bonded to a single benzene ring. The important information on their structures and orientations on oxide surfaces can be obtained by examining the characteristic C=O group. Oxley et al.[23] measured the tunneling spectra of the isomeric phthalic acids on Al_2O_3. They reported that these acids are adsorbed as the dicarboxylate ions. In our previous papers,[24,25] however, we have shown that phthalic and isophthalic acid are adsorbed as the dicarboxylate ions, while terephthalic acid is adsorbed predominantly as the monocarboxylate ion onto Al_2O_3. Lewis and Field[26] also measured the tunneling spectra of these acids on Al_2O_3, however, they reported that these acids are adsorbed as the monocarboxylate ions. The geometry of the isomeric phthalic acids on colloidal silver particles was studied by surface-enhanced Raman spectroscopy.[27] Adsorption of terephthalic acid and terephthalic-d_4 acid onto alumina surfaces has been investigated by external reflection infrared spectroscopy.[28]

In this study, the tunneling spectra of the isomeric phthalic acids adsorbed onto Al_2O_3 and MgO from the gas phase have been obtained. The analysis and comparison of these spectra and the tunneling spectra of isomeric phthalic acids adsorbed onto Al_2O_3 from alcohol solutions clarify the discrepancy of the previous results. These results also give important information on the properties of both surfaces and the chemical interaction with the adsorbed species. The properties of the alumina and magnesia surfaces, and the orientation and reactivity of the isomeric phthalic acids on both surfaces are discussed.

Experimental

The junctions were prepared in a bell jar of a vacuum evaporator evacuated with a liquid nitrogen-trapped 4-inch diffusion pump (ANELVA CDP-600A). The pressure in the bell jar was measured with an ionization gauge (DAIA VACUUM IT-10P) or a Pirani gauge (DAIA VACUUM PT-9P). The base pressure was 6×10^{-7} Torr (1 Torr=133.322 Pa).

Aluminium (Mituwa Chemicals, 99.999%) or magnesium (Rare Metallic Co., 99.99%) was evaporated from a resistively heated molybdenum boat onto a clean glass slide (13×37×1 mm) to form three strips (1 mm wide) at a pressure of 10^{-6} Torr. Magnesium was evaporated from a molybdenum boat with a cover which has a slit in order to prevent the

† Present address: Toshiba Electronic Device Engineering Co., 72, Horikawa-chou, Saiwai-ku, Kawasaki 210.

dispersion of the chips from the boat. The surfaces of the strips were oxidized in an oxygen-DC glow discharge (400—800 V, 75 mTorr, 5 mA, 15—30 s) in the bell jar. For the undoped alumina and magnesia junctions, the longer oxidation time of 1.5—2 and 8—10 min was used, respectively.

The sample molecules were adsorbed onto the oxide surfaces from the gas phase (60—320 mTorr, 60 min) by evaporating the acid from a molybdenum boat at 80—100 °C in the bell jar. Phthalic, isophthalic, and terephthalic acid (Kanto Chemicals, >99.5%) and *p*-acetylbenzoic acid (Aldrich Chemicals, 99.4%) were used without further purification.

The junctions (1×1 mm area) were completed with an evaporated Pb (Wako Chemicals, 99.999%) cross strip (1 mm wide). These operations were done in a class 10000 clean room (Airtech Japan AER-233C).

The tunneling spectrum was obtained by measuring the second derivative of the tunneling current through the junction at liquid-helium temperature (4.2 K). The circuit was of the bridge type developed by Adler and Jackson. The details have been described before.[24,25] A 500 Hz AC modulation signal (2—3 mV_{pp}) and a slowly varying DC voltage were applied to the junction. The aluminium or magnesium electrode was negatively biased with respect to the Pb electrode. The second harmonic signal through a notch filter (NF Electronic Instruments 2BE) and a bandpass filter (NF 3BP) was detected with a lock-in amplifier (NF LI-574A).

The performance of the apparatus and procedures were tested by measuring the tunneling spectrum of benzoic acid on Al_2O_3.[25] The peak positions of the spectrum were corrected by −1 meV (−8 cm^{-1}) owing to the energy gap of the superconducting Pb electrode.[1,29] The resolution was estimated to be 2.5 meV (20 cm^{-1}) by measuring the narrowest peak width in the spectrum. The accuracy of the peak position is estimated to be ±0.5 meV (± 4 cm^{-1}).

Results

Tunneling Spectra of Alumina and Magnesia. The tunneling spectra of the undoped Al-Al_2O_3-Pb and Mg-MgO-Pb junction are shown in Fig. 1. The peak positions and features of the spectra agree well with those previously reported.[1-6,11,25] The peaks at 300 and 930 cm^{-1} of the tunneling spectrum of the alumina junction are assigned to the aluminium phonon and the vibrational mode of the aluminium oxide, respectively. The broad peak at 3610 cm^{-1} is assigned to the stretching mode of the surface OH groups. The broadness and asymmetric tailing toward lower frequencies are typical features of hydrogen-bonding hydroxyl groups. The very weak peak at about 2900 cm^{-1} is due to the CH stretching mode of a hydrocarbon contamination; however, the weakness of this peak indicates that the amount of contamination is negligible.

The peaks at 430 and 640 cm^{-1} of the tunneling spectrum of the magnesia junction are due to the vibrational modes of MgO. The peak at 260 cm^{-1} arises from the magnesium phonon mode. The strong peak at 3650 cm^{-1} and the shoulder at 3590 cm^{-1} are caused by the stretching vibrations of the surface OH groups. These peaks indicate that there are two types of OH groups on the magnesia surface: An isolated OH and a hydrogen-bonding OH group. These peaks of the spectra of magnesia junctions vary in intensity from sample to sample. There is no peak near 2900 cm^{-1}, and these junctions show no organic contamination. Magnesia junctions doped from water or alcohols gave very noisy tunneling spectra. This instability of the spectrum is probably caused by a change of the surface state of the junction due to the dissolution of the magnesia surface.

Tunneling Spectra of Isomeric Phthalic Acids. The tunneling spectra of phthalic, isophthalic, and terephthalic acid doped onto the alumina and magnesia surfaces from the gas phase are shown in Figs. 2—4, respectively. Their peak assignments are shown in

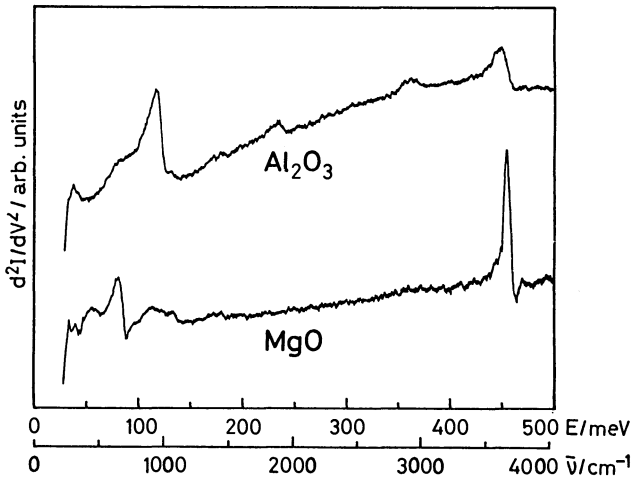

Fig. 1. Tunneling spectra of the undoped Al-Al_2O_3-Pb and Mg-MgO-Pb junction. The oxides were made by an oxygen glow discharge.

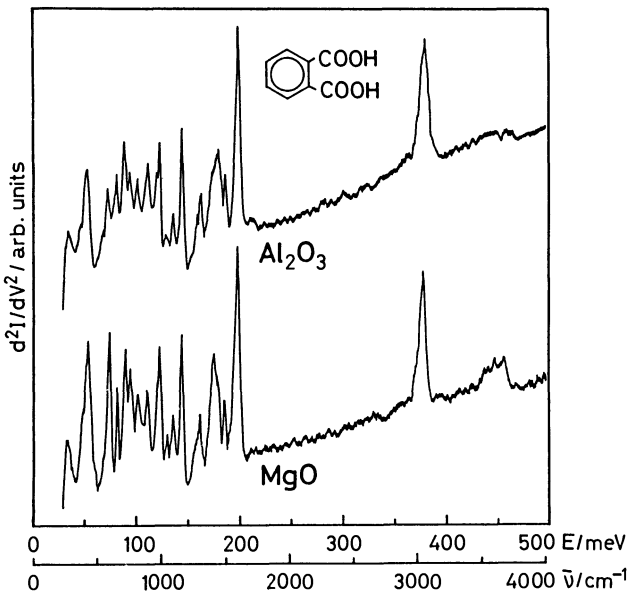

Fig. 2. Tunneling spectra of phthalic acid on Al_2O_3 and MgO doped from the gas phase.

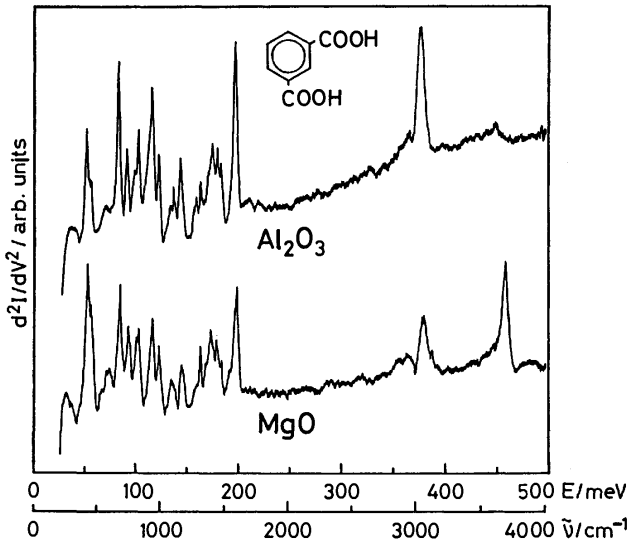

Fig. 3. Tunneling spectra of isophthalic acid on Al_2O_3 and MgO doped from the gas phase.

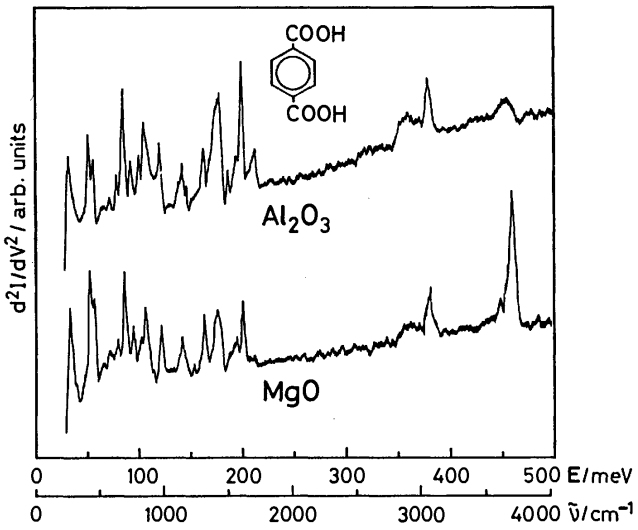

Fig. 4. Tunneling spectra of terephthalic acid on Al_2O_3 and MgO doped from the gas phase.

Table 1. Vibrational Frequencies (cm^{-1}) and Mode Assignments for Phthalic Acid on Al_2O_3 and MgO Doped from Gas Phase Measured by IETS

MgO	Al_2O_3	Al_2O_3[a)]	Assignment
3630 m b	3619 w b	3596 w b	νOH (surface)
3038 s	3037 s	3037 s	νCH (20b)
		2894 w b	(contamination)
	1697 vw	1704 vw	νC=O
1588 vs	1585 vs	1588 vs	νCC (8a)
1573 sh			ν_{as}COO$^-$
1484 m	1484 m	1486 m	νCC (19b)
1429 sh			ν_sCOO$^-$
1406 s b	1425 s b	1422 s b	ν_sCOO$^-$
1296 m	1295 m	1296 m	βCH (3)
1264 sh	1268 sh	1260 w	νCX (7a)
1155 s	1151 s	1149 s	βCH (15)
1085 m	1082 m	1081 m	βCH (9b)
1040 m	1036 m	1035 m	βCH (18b)
978 s	980 s	980 s	γCH (5)
957 sh	954 sh	957 sh	γCH (10a)
880 m	886 m	881 m	γCH (10b)
808 m	803 m	802 m	νCC (1)
743 m	743 m	744 m	γCH (11)
708 s	707 m	702 m	γCC (4)
649 m	645 m	644 m	γ_sCOO$^-$
587 s	580 m	582 m	βCC (6b)
548 sh	545 sh		βCC (6a)
422 s	416 s	422 s	β_{as}COO$^-$
382 sh	377 sh	374 sh	?
	295 m	285 w	Al phonon
255 m	267 sh	259 m	βCX (9a)

vs=very strong, s=strong, m=medium, w=weak, vw=very weak, sh=shoulder, b=broad. a) Doped from ethanol solution in Ref. 25.

Table 2. Vibrational Frequencies (cm^{-1}) and Mode Assignments for Isophthalic Acid on Al_2O_3 and MgO Doped from Gas Phase Measured by IETS

MgO	Al_2O_3	Al_2O_3[a)]	Assignment
3687 s			νOH (surface)
3616 sh	3617 w b	3621 w b	νOH (surface)
3040 m	3039 s	3038 s	νCH (7a)
2894 w b	2916 w b	2888 w b	(contamination)
	1703 vw	1684 vw	νC=O
1591 s	1586 s	1587 s	νCC (8b)
1544 sh			ν_{as}COO$^-$
1465 vw	1469 w	1467 sh	νCC (19b)
1441 s	1444 s	1441 s	νCC (19a)
1394 s b	1404 s b	1402 s b	ν_sCOO$^-$
1312 m	1309 w	1311 w	νCC (14)
1272 w	1278 w	1281 vw	βCH (3)
1160 m	1156 m	1151 m	βCH (9b)
1095 m	1100 m	1088 w	βCH (18b)
1070 vw	1075 vw	1061 vw	βCH (18a)
989 m	982 m	980 m	γCH (5)
934 m	932 s	930 s	νCX (7b)
827 m	826 m	824 m	νCC (1)
809 sh	799 sh	801 sh	?
744 m	735 m	737 m	β_sCOO$^-$
674 s	670 s	672 s	γCC (4)
597 m b	572 w b	582 w b	βCC (6b)
447 sh	440 sh	440 sh	?
420 s	417 s	418 s	β_{as}COO$^-$
	299 m b	294 m b	Al phonon
251 m			Mg phonon

a) Doped from ethanol solution in Ref. 25.

Tables 1—3. The tunneling spectra of the isomeric phthalic acids doped from alcohol solutions onto the alumina surfaces have been measured, and their detailed assignments and comparison with their infrared and Raman spectra have been shown in our previous paper.[25] The peak positions of the spectra doped from ethanol solutions are shown in each table for the sake of comparison. In these tables, stretching, in-plane bending, and out-of-plane bending vibrations are denoted by ν, β, and γ, respectively. The symmetric or asymmetric vibration is indicated by the subscript s or as, respectively. Of the bending

Table 3. Vibrational Frequencies (cm^{-1}) and Mode Assignments for Terephthalic Acid on Al_2O_3 and MgO Doped from Gas Phase Measured by IETS

MgO	Al_2O_3	Al_2O_3[a)]	Assignment
3681 vs			νOH (surface)
	3622 m b	3623 m b	νOH
3605 sh			νOH (surface)
3043 m	3041 m	3042 m	νCH (20b, 7b)
2872 w b	2876 w b	2873 w b	(contamination)
	1698 m	1699 m	νC=O
1598 m	1598 s	1594 s	νCC (8b)
1558 m	1556 sh	1550 sh	$\nu_{as}COO^-$
1497 sh	1498 w	1493 w	νCC (19a)
1410 s b	1426 s b	1423 s b	βOH, ν_sCOO^-
1301 m	1305 m	1302 m	νCX (13)
1136 m	1137 m	1136 m	βCH (9a)
1096 sh	1096 w		?
1006 vw	1006 vw	1003 vw	βCH (18a)
966 m	962 m	963 m	γCH (17a)
		916 vw	γCH (10b)
865 sh	871 sh	867 sh	β_sCOO, β_sCOO^-
842 s	842 s	839 s	νCC (1)
818 w	803 w	797 vw	βCH-βCX (18b-15)
731 m	737 m	736 m	βCC (12)
679 s	676 s	677 s	γCC (4)
626 w	627 w	619 w	γ_sCOO, γ_sCOO^-
560 w b	556 w b	540 w b	γCC (16b)
437 sh	435 s	436 s	$\beta_{as}COO$, $\beta_{as}COO^-$
409 s	407 s	400 s	$\gamma_{as}COO^-$ +γCH (5)
	284 sh	298 sh	Al phonon
250 m	254 m	242 m	γCX (5)

a) Doped from ethanol solution in Ref. 25.

modes of the COO^- group, β_s designates the scissoring, β_{as} denotes the rocking and γ_s the wagging mode. The Wilson number for the normal vibration of the benzene ring is shown in parenthesis.

The peak positions of the tunneling spectra doped from the gas phase and ethanol solution agree well with each other within the measurement accuracy. This agreement shows that our apparatus and procedures are suitable for the accurate measurement of tunneling spectra. It also shows that there is no contribution from the solvent to our previous tunneling spectra.

When phthalic acid is adsorbed onto the Al_2O_3 and MgO surfaces, the peak intensities of the surface OH groups decrease, and the weak and broad peaks remain in both spectra. In contrast, the clear and characteristic peaks of the adsorbed phthalic acid appear. The relative intensities of the peaks in both spectra on Al_2O_3 and MgO are similar except for those of βCC(6b) and γCC(4). This similarity suggests the same molecular structure and orientation of the adsorbed phthalic acid on both surfaces. The tunneling spectrum of phthalic acid on MgO has no νC=O peak, while that on Al_2O_3 has a very weak peak at 1697 cm^{-1}. The tunneling spectra on both surfaces have strong and broad ν_s, medium γ_s and strong β_{as} peaks of the COO^- groups. The peak position of the ν_sCOO^- mode on MgO shifts from that of the mode on Al_2O_3 about 20 cm^{-1} toward lower frequencies. The peak of the $\nu_{as}COO^-$ mode appears as a shoulder on the very strong peak at 1588 cm^{-1} in the spectrum on MgO. These results show that phthalic acid reacts with the surface OH groups on both surfaces by loosing the protons of the COOH groups and is adsorbed as the benzenedicarboxylate ion onto the surface cations (Lewis-acid sites). The peak shift of the ν_sCOO^- mode may relate to the difference in the interaction between the COO^- groups and the surface cations as suggested by Walmsley et al.[6)]

The tunneling spectra of isophthalic acid on Al_2O_3 and MgO have strong and broad ν_s, medium β_s and strong β_{as} peaks of the COO^- groups. The peak position of the ν_sCOO^- mode on MgO also shifts 10 cm^{-1} toward lower frequencies. The peak of the $\nu_{as}COO^-$ mode appears as a shoulder on the strong peak at 1591 cm^{-1} in the spectrum on MgO. The surface OH groups remain on the MgO surface. These results show that isophthalic acid is also adsorbed onto both surfaces as the dicarboxylate ion. The remainder of the surface OH groups on MgO may relate to the orientaion and the surface coverage of the adsorbed isophthalic acid as discussed later.

The tunneling spectrum of terephthalic acid on Al_2O_3 doped from the gas phase has a medium νC=O peak in addition to the νCOO^- peaks. The spectrum is identical with that doped from the ethanol solution,[25)] and it is concluded that terephthalic acid doped from the gas phase is also predominantly adsorbed onto Al_2O_3 as the monocarboxylate ion. On the other hand, the spectrum on MgO has the COO^- peaks with no νC=O peak and it shows that terephthalic acid is adsorbed onto the magnesia surface as the dicarboxylate ion. Because terephthalic acid is adsorbed as the dicarboxylate ion, its benzene ring must be parallel to the surface. The surface OH groups remain as in the case of isophthalic acid. The peak position of the ν_sCOO^- mode on MgO also has a shift of 16 cm^{-1} toward lower frequencies. The features and the relative peak intensities of both spectra on Al_2O_3 and MgO are independent of the doping conditions of the gas pressure: 60—240 mTorr, and the exposure: 10—60 min.

Comparison of Tunneling Spectra of Isomeric Phthalic Acids. The tunneling spectra of the isomeric phthalic acids adsorbed onto Al_2O_3 have previously been measured by Oxley et al.[23)] They concluded that these acids are adsorbed as the dicarboxylate ions onto Al_2O_3. A comparison of their spectra showed that most of the peak positions and the features of their spectra of phthalic and isophthalic acid agreed with those of our spectra. However, their spectrum of terephthalic acid has no νC=O peak, and disagreed with ours. We examined the experimental conditions in detail and found that the peak intensity and the features of the spectrum of

terephthalic acid strongly depend on the solvent used. The spectrum of terephthalic acid doped from a solution of methanol, ethanol, or 1-propanol onto Al_2O_3 has the νC=O peak. However, it has a very weak νC=O peak in the case of an aqueous solution. The weakness of the νC=O peak indicates that terephthalic acid is adsorbed onto Al_2O_3 predominantly as the dicarboxylate ion. The spectra of phthalic and isophthalic acid have no such solvent dependence.[25]

The reason of this discrepancy between our spectrum of terephtalic acid and that measured by Oxley et al. is not clear. However, it seemed to us that the amount of the terephthalic acid adsorbed onto the alumina surface was so small that the νC=O peak disappeared in their spectrum. We concluded that the tunneling spectrum of terephthalic acid doped from the gas phase onto Al_2O_3 also has the νC=O peak, and that terephthalic acid is adsorbed predominantly as the monocarboxylate ion as in the case of the alcohol solutions.[25]

Lewis and Field[26] have also reported the tunneling spectra of the isomeric phthalic acids on Al_2O_3 doped from an ethanol solution. They concluded that these acids are adsorbed as the monocarboxylate ions. We compared the peak positions in their tunneling spectra with those in ours and found that all the peak positions in their spectra have shifts of 15—225 cm^{-1} to higher frequencies. This comparison of the peak positions in the tunneling spectra of terephthalic acid on Al_2O_3 is shown in Table 4. Their assignments for the peaks are completely different from ours. For example, they assigned the strong peak at 1638 cm^{-1} to the νC=O peak, which corresponds to the νCC (8b) peak at 1598 cm^{-1} in our spectrum. No assignment was given to the weak peak at 1735 cm^{-1}, which corresponds to the νC=O peak in our assignment. These peak shifts in their tunneling spectra may be caused by parasitic resistances in the tunneling junctions as indicated by Oxley et al.[23] A comparison between the spectra of terephthalic and *p*-acetylbenzoic acid adsorbed onto Al_2O_3 and MgO clearly shows the presence of the νC=O peak in the tunneling spectrum of the adsorbed terephthalic acid on Al_2O_3 and the absence of the νC=O peak in that on MgO as is shown in Fig. 5.

Table 4. Comparison of Vibrational Frequencies (cm^{-1}) for Terephthalic Acid on Al_2O_3 Measured by IETS

This work		Lewis and Field[a]		Oxley et al.[b]	
3622	m b			3621	s
3041	m	3266	m	3052	m
		3112	s		
		2966	s		
2876	w b	2928	s	2931	s
1698	m	1735	w		
1598	s	1638	s	1605	s
1556	sh			1582	sh
1498	w			1518	sh
1426	s b	1462	s	1427	s
				1380	sh
1305	m	1349	m	1300	s
		1249	w	1211	m
1137	m			1152	m
1096	w	1146	w	1112	sh
1006	vw	1083	w	1022	sh
962	m	982	m	946	m
871	sh			888	sh
842	s	871	s	835	s
803	w			774	m
737	m	763	w		
676	s	705	m	695	s
627	w			635	m
556	w b				
435	s			472	s
407	s			410	s
287	sh				
254	m				

a) Ref. 26. b) Ref. 23.

Discussion

Surface Structure of Alumina and Magnesia. Knözinger and Ratnasamy[20] have proposed the surface models of the ideal planes of γ- and η-Al_2O_3. Though the oxygen lattice is more densely packed in γ-Al_2O_3 than in η-Al_2O_3, both aluminas have defect spinel lattices and the local ionic configurations of the Al^{3+} cations are identical. The preferentially exposed faces are considered to be the (110)- and (111)-faces of γ- and η-Al_2O_3, respectively. Because the net charge

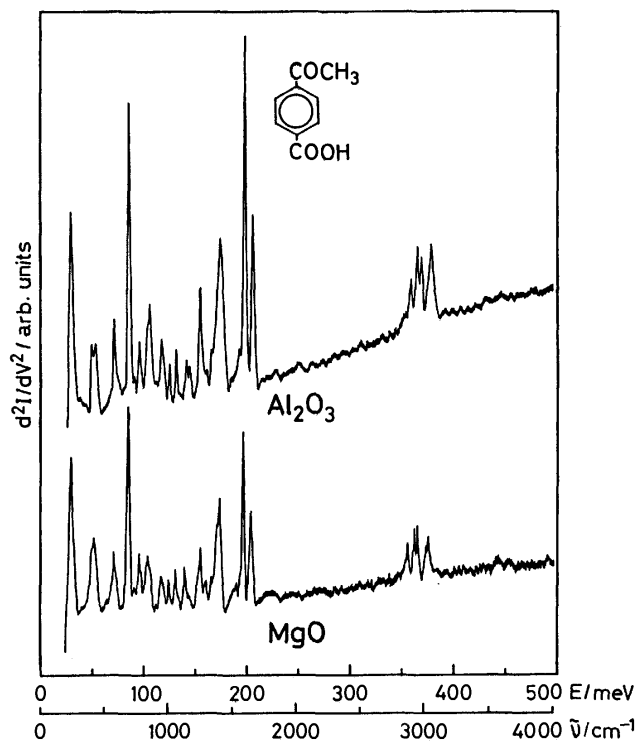

Fig. 5. Tunneling spectra of *p*-acetylbenzoic acid on Al_2O_3 and MgO doped from the gas phase.

in a stable ionic structure should be equal or nearly equal to zero, OH anions are favorable to terminate these faces. From a consideration of the configuration of the aluminium cations and the OH anions, and the coordination numbers of the OH anions, they have shown that there are five types of OH groups on the (111)-face and three types of OH groups on the (110)-face.

The surface OH groups on these faces have different net charge and relate to their different acidity and basicity. The protonic acidity of the OH groups decreases as the net charge on them becomes more negative, while their basicity increases at the same time. The infrared spectra of alumina surfaces have five bands in frequency range 3700—3800 cm^{-1}. They have assigned the band of highest frequency (3800 cm^{-1}) to the most negative OH group with the highest basicity, while the band of lowest frequency (3700 cm^{-1}) is attributed to the most positive OH group with the lowest basicity. The remaining three bands are assigned with decreasing frequency to the corresponding configurations with increasingly positive net charge. Hydrogen bonding between adjacent OH groups perturbs the acidity and basicity, and thus the frequencies of the OH groups to some extent at high OH densities.

The tunneling spectrum of the alumina surface shows the νOH mode in the frequency range 3500—3700 cm^{-1}. The frequency is shifted downward by about 100 cm^{-1}. This shift is due to the image dipole effect of the top lead electrode.[1,29] Using several top metal electrodes and an image dipole theory, Kirtley and Hansma[29] have shown that the νOH mode of hydroxide ions on Al_2O_3 has a shift of approximately 15 meV (120 cm^{-1}), however, the shifts of the vibrational modes of the adsorbed benzoate ion are less than 0.5 meV (4 cm^{-1}). Judging from the broadness and asymmetric tailing toward lower frequencies, there seems to be more than one type of surface OH group on the alumina surface. These appear to interact with each other through hydrogen bonding. The surface model proposed by Knözinger and Ratnasamy[20] is useful to explain the surface structure of the tunneling junction of Al_2O_3.

Magnesia has the structure of NaCl and the external surface of its crystal is predominantly the (100)-face. It has a more ionic character than Al_2O_3 because the electronegativity difference is larger between Mg and O than between Al and O. According to the hydration characteristics and the infrared spectra, Anderson et al.[16] proposed a simple model for the chemisorption of H_2O on this face; the (100)-face consists of a collection of an isolated OH group coordinated on a surface magnesium cation and a second set of OH group formed by the remaining protons and adjacent O^{2-} ions. The second type of OH group interacts with their neighbors through hydrogen bonding. A sharp band at 3752 cm^{-1} has been assigned to the νOH mode of the first OH group, whereas a broad band at 3610 cm^{-1} has been attributed to the second group.[16]

The tunneling spectrum of MgO also shows a strong and sharp peak at 3650 cm^{-1} and a broad peak at 3590 cm^{-1}, these correspond to the isolated and hydrogen-bonding OH group suggested by Anderson et al.[16] The peak positions are shifted downward due to the effect of the top Pb electrode as in the case of the OH groups on Al_2O_3. It is expected that the isolated OH group has higher reactivity and basicity because it is isolated and has the more negative net charge.

Orientation of Adsorbed Isomeric Phthalic Acids. The vibrational spectra of the adsorbed isomeric phthalic acids on metal surfaces have been measured by surface-enhanced Raman spectroscopy (SERS),[27] external reflection infrared spectroscopy (RAIR),[28] and IETS.[25] Moskovits and Suh[27] used SERS to investigate the surface geometry of the adsorbed isomeric phthalic acids on colloidal silver particles from aqueous solutions. The SERS spectra of the isomeric phthalic acids had peaks of the COO^- groups but no C=O group and showed that these acids are adsorbed as the dicarboxylate ions onto the surfaces. However, the spectral features of phthalic acid were quite different from those of the others. They attributed this difference to different surface-bonding geometry, and concluded that phthalic acid is adsorbed with its benzene ring perpendicular to the surface, while isophthalic and terephthalic acid are adsorbed parallel to the surface.

Boerio et al.[28] investigated the adsorption of terephthalic acid and terephthalic-d_4 acid onto aluminium mirrors from dilute solutions in ethanol by RAIR. The spectra of both terephthalic acids showed a strong and characteristic νC=O band of the undissociating COOH group near 1700 cm^{-1} in addition to the bands of the COO^- groups. Because the ν_s and ν_{as} mode of the COO^- groups were observed, they have concluded that terephthalic acids are adsorbed as the monocarboxylate ions with a vertical conformation in which the benzene rings are perpendicular to the surface but the twofold symmetry axes are inclined at least several degrees from the normal to the surface.

The adsorption and orientation of isomeric phthalic acids on Al_2O_3 from alcohol solutions have been studied in our previous paper using IETS.[25] It was found that these acids are adsorbed onto the alumina surface with their own molecular structures and orientations at saturation coverage; phthalic and isophthalic acid are adsorbed as the dicarboxylate ions with their benzene rings almost perpendicular and parallel to the surface, respectively. Terephthalic acid is adsorbed as the monocarboxylate ion almost perpendicular to the surface. Hydrogen bonding through the COOH groups of the adsorbed hydrogen terephthalate ions was observed.

Ogawa et al.[30] have reported the selective monomethyl esterification of dicarboxylic acids adsorbed onto Al_2O_3. Terephthalic and isophthalic acid adsorbed onto Al_2O_3 reacted with diazomethane to give predominantly the monomethyl esters, however, the reaction of phthalic acid was unsuccessful. They have suggested that terephthalic and isophthalic acid are adsorbed onto Al_2O_3 as the monocarboxylate ions, and the unreacting COOH groups are preferentially esterified. The lack of reactivity of phthalic acid was explained by the close proximity of the two COOH groups and the forced orientation of the second COOH group.

Though reactivity is not necessarily a measure of surface orientation of adsorbed species, the orientations and molecular structures of phthalic and terephthalic acid on Al_2O_3 suggested by Ogawa et al.[30] are identical with those observed by IETS. It seems that isophthalic acid which is only weakly bonded to the surface as the monocarboxylate ion may react to give predominantly the monoester. These results indicate that IETS is useful to investigate the surface reactions on an alumina catalyst, and also show that the orientation of the adsorbed species plays an important role to determine the reactivity and selectivity of the surface reaction.

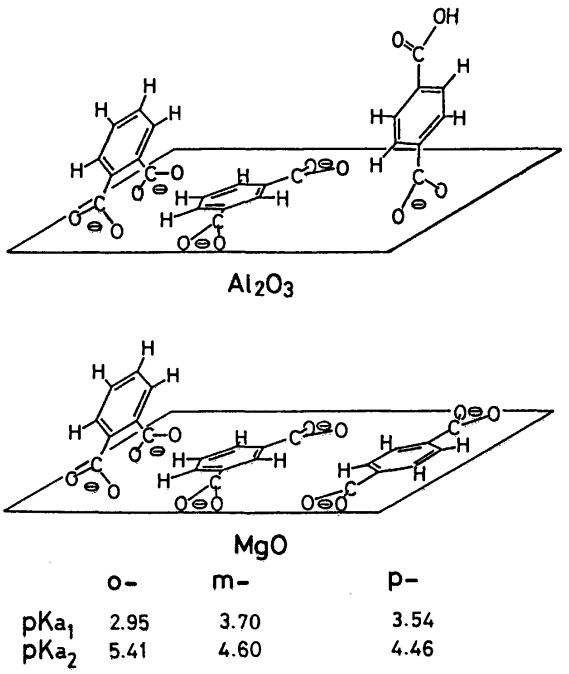

	o-	m-	p-
pKa_1	2.95	3.70	3.54
pKa_2	5.41	4.60	4.46

Fig. 6. Schematic representation of the adsorbed isomeric phthalic acids on Al_2O_3 and MgO. Their dissociation constants in water are also shown.

The similarity of the spectral features of the tunneling spectra of phthalic and isophthalic acid adsorbed onto Al_2O_3 and MgO from the gas phase indicates that these acids are adsorbed in the same molecular structure and orientation onto both surfaces. Thus, it can be concluded that phthalic acid is adsorbed as the dicarboxylate ion with its benzene ring perpendicular to the alumina and magnesia surface, while isophthalic acid is adsorbed as the dicarboxylate ion parallel to the alumina and magnesia surface. However, the tunneling spectra of terephthalic acid adsorbed onto Al_2O_3 and MgO show different molecular structure and orientation on both surfaces. It is adsorbed as the monocarboxylate ion onto Al_2O_3; however, it is adsorbed as the dicarboxylate ion onto MgO. A schematic representation of the isomeric phthalic acids adsorbed onto alumina and magnesia surfaces is shown in Fig. 6. Also shown are their dissociation constants in water.

Judging from the dissociation constants of the isomeric phthalic acids, one would expect that phthalic acid is adsorbed predominantly as the monocarboxylate ion because the difference between the two dissociation constants is largest. However the tunneling spectra show that both phthalic and isophthalic acid are adsorbed as the dicarboxylate ions onto Al_2O_3 and MgO. It is clear that the structures and the orientations of these acids on the surfaces are not explained by their dissociation constants. In the case of phthalic and isophthalic acid, when they are adsorbed at one of the COOH groups, the other COOH group seems to be very close to the surface. Thus, the COOH group dissociates more easily than would be expected from their second dissociation constants. According to the molecular models, phthalic acid is adsorbed with its benzene ring almost perpendicular to both surfaces, while isophthalic acid is parallel to the surfaces. The molecular structures and the orientations are identical to those observed on silver colloidal surface by SERS.[27]

The difference in the molecular structure and orientation of the adsorbed terephthalic acid on Al_2O_3 and MgO seems to be caused by the different structures and reactivity of the surface OH groups on both surfaces. The surface OH groups on Al_2O_3 interact with each other through hydrogen bonding. This hydrogen bonding seems to some extent to prevent the reaction between the COOH groups and the surface OH groups. On the other hand, MgO has the isolated OH group on the surface. The OH groups on MgO are expected to have higher reactivity than the OH groups on Al_2O_3. When terephthalic acid is adsorbed onto MgO, both COOH groups easily dissociate to give the dicarboxylate ion with its benzene ring parallel to the surface because of the high reactivity and basicity of the surface OH groups. The remainder of the OH groups on the magnesia surface may relate to the surface coverage; the coverage of the surface by the adsorbed terephthalate ion may make some surface OH groups inactive because of the hindrance of the benzene ring. On the other hand, it seems that the undissociating COOH group of the adsorbed hydrogen terephthalate ion can not interact with the surface OH groups on Al_2O_3 because of the

medium reactivity and the hydrogen bonding of the surface OH groups. Thus, the adsorbed terephthalic acid on Al_2O_3 remains as the monocarboxylate ion with its benzene ring almost perpendicular to the surface at saturation coverage. The hydrogen bonding through the undissociating COOH groups of the adsorbed hydrogen terephthalate ions seems to make them stable on the alumina surface.

Concluding Remarks

IETS is a useful analytical tool for investigating the alumina and magnesia surfaces and the adsorbed species on them. It reveals the different orientations of terephthalic acid adsorbed onto Al_2O_3 and MgO. This difference is caused by the different surface properties of both oxides.

The authors wish to thank Professors Kerry Wayne Hipps and Ursula Mazur of Washington State University for their critical reading of the manuscript and for the valuable comments. The present study was partially supported by a Reseach Aid of the Inoue Foundation for Science No.025.

References

1) P. K. Hansma, "Tunneling Spectroscopy," Plenum, New York (1982).
2) W. M. Bowser and W. H. Weinberg, *Surf. Sci.*, **64**, 377 (1977).
3) S. Gauthier, S. de Cheveigné, J. Klein, and M. Belin, *Phys. Rev. B*, **29**, 1748 (1984).
4) J. G. Adler, *Solid State Commun.*, **7**, 1635 (1969).
5) J. Klein, A. Léger, M. Belin, D. Défourneau, and M. J. L. Sangster, *Phys. Rev. B*, **7**, 2336 (1973).
6) D. G. Walmsley, W. J. Nelson, N. M. D. Brown, and R. B. Floyd, *Appl. Surf. Sci.*, **5**, 107 (1980).
7) N. M. D. Brown, W. J. Nelson, R. J. Turner, and D. G. Walmsley, *J. Chem. Soc., Faraday Trans. 2*, **77**, 337 (1981).
8) D. G. Walmsley, W. J. Nelson, N. M. D. Brown, S. de Cheveigné, S. Gauthier, J. Klein, and A. Léger, *Spectrochim. Acta, Part A*, **37**, 1015 (1981).
9) W. Plesiewicz and J. G. Adler, *Phys. Rev. B*, **34**, 4583 (1986).
10) M. C. Gallagher, Y. B. Ning, and J. G. Adler, *Phys. Rev. B*, **36**, 6651 (1987).
11) S. Kamata, M. Higo, S. Mizutaru, and Y. Owaki, *Rep. Asahi Glass Found. Ind. Technol.*, **49**, 191 (1986).
12) S. Kamata, M. Higo, Y. Owaki, and H. Hayashi, *Rep. Asahi Glass Found. Ind. Technol.*, **51**, 263 (1987).
13) M. Higo, Y. Owaki, and S. Kamata, *Chem. Lett.*, **1987**, 1567.
14) M. Higo, Y. Owaki, and S. Kamata, *Chem. Lett.*, **1987**, 2009.
15) J. B. Peri, *J. Phys. Chem.*, **69**, 211 (1965).
16) P. J. Anderson, R. F. Horlock, and J. F. Oliver, *Trans. Faraday Soc.*, **61**, 2754 (1965).
17) T. Ito, K. Kanehori, and T. Tokuda, *Z. Phys. Chem. N. F.*, **103**, 203 (1976).
18) J. B. Peri, *J. Phys. Chem.*, **69**, 220 (1965).
19) A. A. Tsyganenko and V. N. Filimonov, *J. Mol. Struct.*, **19**, 579 (1973).
20) H. Knözinger and P. Ratnasamy, *Catal. Rev. Sci. Eng.*, **17**, 31 (1978).
21) K. Tanabe, "Solid Acids and Bases," Kodansha, Tokyo (1970).
22) H. Knözinger, *Adv. Catal.*, **25**, 184 (1976).
23) D. P. Oxley, A. J. Bowles, C. C. Horley, A. J. Langley, R. G. Pritchard, and D. L. Tunnicliffe, *Surf. Interface Anal.*, **2**, 31 (1980).
24) S. Kamata and M. Higo, *Chem. Lett.*, **1984**, 2017.
25) M. Higo, S. Mizutaru, and S. Kamata, *Bull. Chem. Soc. Jpn.*, **58**, 2960 (1985).
26) D. M. Lewis and B. O. Field, *Spectrochim. Acta, Part A*, **41**, 477 (1985).
27) M. Moskovits and J. S. Suh, *J. Phys. Chem.*, **88**, 1293 (1984).
28) F. J. Boerio, J. P. Boerio, and R. C. Bozian, *Appl. Surf. Sci.*, **31**, 42 (1988).
29) J. Kirtley and P. K. Hansma, *Phys. Rev. B*, **13**, 2910 (1976).
30) H. Ogawa, T. Chihara, and K. Taya, *J. Am. Chem. Soc.*, **107**, 1365 (1985).

 © 1989 The Chemical Society of Japan Bull. Chem. Soc. Jpn., 62, 1837—1843 (1989)

Studies of the Hydrous Silicon(IV)-Titanium(IV) Oxide Ion Exchanger. I. A Method of Synthesis and Some Properties

Hiromichi YAMAZAKI, Yasuhito KANNO, and Yasushi INOUE*
Department of Nuclear Engineering, Faculty of Engineering, Tohoku University, Aramaki, Sendai 980
(Received December 1, 1988)

Hydrous silicon(IV)-titanium(IV) oxide ion exchanger was prepared by using $TiCl_4$ and Na_2SiO_3 solutions. From a detailed examination of the dependency of the compositions and the acid-base properties of the products on the conditions for precipitation, a reproducible synthetic procedure was established. The exchangers with 37 to 67 mol% of titanium to metallic elements possess much larger ion-exchange capacities and are more stable to highly alkaline solutions than simple mixtures of hydrous silicon(IV) oxide and hydrous titanium(IV) oxide. The dependency of the ion-exchange capacity on the composition can be explained by the difference in the structure of the matrix as evidenced from the thermal analysis, X-ray diffraction, and infrared absorption studies.

Hydrous metal oxides are a group of promising materials for use in the processing of radioactive liquid wastes. This is on account of their unique ion-exchange selectivity produced by the metallic elements forming the materials.[1] However, amorphous hydrous metal oxides are liable to lose their ion-exchange capacity at high temperatures and their use is limited at elevated temperatures. On the other hand, it is conceivable that thermally stable hydrous metal oxides possessing various ion-exchange characteristics may be synthesized by combining more than two kinds of metallic elements.

Kaneko et al. investigated a silica-titania mixed oxide gel,[2,3] but did not clarify the relation between the ion-exchange properties of this material and those of simple hydrous metal oxides. In the investigation of this group of ion-exchange materials, it is indispensable to examine the synthetic conditions for establishing a reproducible method because of the difficulty in reproducible synthesis due to thermodynamical metastability of the materials.

The present paper deals with an investigation undertaken to establish the best conditions for the synthesis of hydrous silicon(IV)-titanium(IV) oxide ion exchanger, laying emphasis on the dependence of ion-exchange properties on the composition of the materials.

Experimental

Reagents and Apparatus. Sodium metasilicate and titanium(IV) chloride were of reagent grade supplied by Wako Pure Chemical Industries, Ltd., and their purities were checked before use. Hydrofluoric acid was obtained from Hirota Kagaku Kogyo Kaisha, Ltd. The other chemicals were of the highest purity grade supplied by Wako Pure Chemical Industries, Ltd.

Thermal analysis was undertaken using a Shimadzu micro thermal analyzer, Model DT-20B, connected to a thermal balance, Model TGC-20H, for thermogravimetric analysis (TGA), and a high-temperature sample holder, Model MDH-20B, for differential thermal analysis (DTA). The reference material for DTA was α-alumina. The measurement was performed in air at a heating rate of 10 °C min^{-1}. The infrared (IR) absorption spectra were measured with a Hitachi infrared spectrometer, Model 2650-50, using the KBr disk method. The specific surface areas of the samples were determined by the BET method (N_2 adsorption at −196 °C) using a Yanagimoto Surface Area Measuring Apparatus, Model GSA-10. Atomic absorption measurements were made with a Nippon Jarrell-Ash atomic-absorption and flame-emission spectrophotometer, Model AA-782. Spectrophotometric analysis was carried out with a Hitachi Model 557 double wavelength spectrophotometer with a 1 cm-glass cell. X-Ray diffraction patterns were obtained by means of Shimadzu X-ray diffraction unit, Model XD-3A, using Ni-filtered Cu $K\alpha$-radiation.

Synthesis of Ion Exchangers. The starting solution of $TiCl_4$ was prepared by dissolving a desired amount of unhydrated titanium(IV) chloride in distilled water, followed by dilution to a desired volume with either HCl solution or distilled water. The starting solution of Na_2SiO_3 was obtained by dissolving a desired amount of $Na_2SiO_3 \cdot 9H_2O$ in 1M NaOH solution (1 M=1 mol dm^{-3}), followed by dilution to a desired volume with either distilled water or NaOH solution. Hydrous silicon(IV)-titanium(IV) oxide was precipitated at various pH and different concentrations of metal ions by mixing an equal volume of the $TiCl_4$ and the Na_2SiO_3 solutions. After being separated from the mother liquor by decantation and filtration through Toyo No.1 filter paper under suction, the precipitate was uniformly dispersed into distilled water and filtered again after being sedimented. The precipitate was then dried at 70 °C or at room temperature. The product was immersed in distilled water to break it down into fine particles, which were subsequently dried at room temperature. The particles were then ground in a porcelain mortar and sieved to obtain required particle sizes (63 to 210 μm). Hydrous silicon(IV) oxide was precipitated by mixing an equal volume of 0.50 M Na_2SiO_3 solution in 1.0 M NaOH and 1.85 M HCl solution. Hydrous titanium(IV) oxide was precipitated at pH 7 by adding 0.98 M NaOH solution into 0.95 M $TiCl_4$ solution. These precipitates were washed in the same manner described above, until no Cl^- was detected in the filtrate, and then dried at room temperature.

Conditioning. The exchanger of a desired particle size was washed with distilled water to remove any adherent powder. The slurry was poured into a glass tube with glass-wool plugging for column support, and 0.05 M HCl was passed through the column until the pH of the effluent

approached that of the influent. The column was then washed with distilled water until no Cl^- was detected in the effluent and its pH became constant (pH=5.5). The exchangers, thus prepared, were air-dried at room temperature and stored in a desiccator containing a saturated NH_4Cl solution (relative humidity; 79% at 25 °C).

Total Analysis of the Exchanger. A sample of 0.2 g was ignited at 850 °C, and the water content was calculated from the weight loss. The validity of the procedure had been confirmed thermogravimetrically. The oxide thus formed was dissolved in 1 cm^3 of concentrated H_2SO_4 and 2 cm^3 of 46% HF solutions. This solution was gently heated in order to vaporize SiF_4 and HF, followed by dilution to 50 cm^3 with 9 M H_2SO_4 solution. Titanium was assayed by a complexiметric titration: back titration using PAN(1-(2-pyridylazo)-2-naphthol) as an indicator. The amount of TiO_2 thus determined was subtracted from the mass of the calcined exchanger to obtain the amount of SiO_2.

Ion-Exchange Capacity. The ion-exchange capacity for Na^+ was measured as follows. The exchanger (0.10 g) in the H^+ form was immersed in 15 cm^3 of various solutions, prepared by the desired combinations of 0.10 M NaCl and 0.10 M NaOH solutions, for 7 d at room temperature with intermittent shaking. This was followed by pH measurements and by determination of the sodium ions. The sodium ions were converted to an equivalent amount of sodium chloride and indirectly determined by titrating the chloride ions (the Fajans' method). The amount of the ions taken up by the exchanger was evaluated from the difference between the initial and the final concentrations of the ions in the solutions.

Results and Discussion

(I) Synthesis of Hydrous Silicon(IV)-Titanium(IV) Oxides. In order to establish a reproducible synthetic method, the composition and the acid-base property of hydrous silicon(IV)-titanium(IV) oxides (hereafter called the composite exchanger) were studied as a function of the conditions for precipitation, as mentioned below.

(a) Effect of pH at Precipitation. As the solubility of Si^{4+} largely depends on the pH of the solution, in contrast to Ti^{4+} which is precipitated nearly quantitatively from solutions of pH higher than 1, the yield of silicon was examined as a function of pH. The hydrous metal oxides were precipitated at various pH by mixing 0.25 M $TiCl_4$ solution in HCl and 0.25 M Na_2SiO_3 solution in NaOH. Here, the concentrations of HCl and NaOH were adjusted to give the desired pH. After the precipitate had been completely sedimentated, the concentration of SiO_3^{2-} in the supernatant solution was determined spectrophotometrically, using 10% ammonium molybdate as a coloring reagent.[4] As seen in Fig. 1, the concentration of SiO_3^{2-} in the supernatant increases sharply on both sides of pH 7 to 9. Therefore, the pH at precipitation was controlled to be 7.6±0.3 in the subsequent experiments.

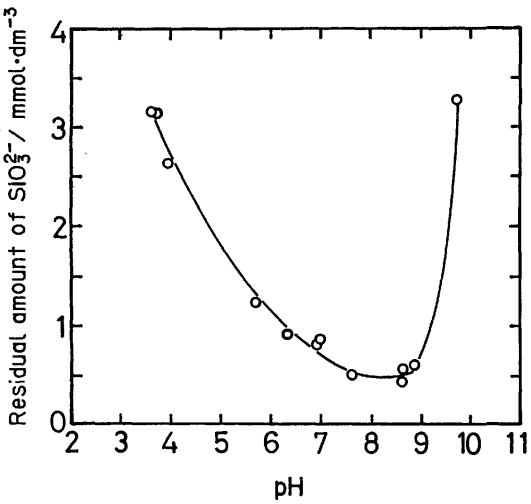

Fig. 1. Dependence of SiO_3^{2-} concentration in supernatant solution on pH at precipitation.

(b) Effect of the Methods of Mixing the Solutions. The ion-exchange capacity and physical strength were studied on the composite exchangers, which were prepared by the following three methods;

Method I: the Na_2SiO_3 solution was added to the $TiCl_4$ solution,

Method II: the $TiCl_4$ solution was added to the Na_2SiO_3 solution,

Method III: the $TiCl_4$ and the Na_2SiO_3 solutions were simultaneously poured into a beaker with vigorous stirring.

For each method, the rate of addition of the solutions was from 5 to 3000 $cm^3\,min^{-1}$. After aging for 2 d, the precipitate was washed in a manner described in the experimental section, and then dried at 70 °C for 50 h. Irrespective of the addition rates, the composite exchangers prepared by methods I and II were glassy or chalky opaque particles large enough to be used for

Table 1. Effect of Addition Rates of Na_2SiO_3 Solution into $TiCl_4$ Solution on Ion-Exchange Capacity and Composition (Method II)

Addition rate	Ti-mol%		Water content	Ion-exchange capacity for Na^+ ions at pH 13
	mol TiO_2	×100	mol H_2O	
$cm^3\,min^{-1}$	mol(SiO_2+TiO_2)		mol(SiO_2+TiO_2)	mmol g^{-1}
3000	50±1		2.19±0.01	3.54±0.06
67	50±1		2.13±0.01	3.62±0.06
16	50±1		1.96±0.01	3.70±0.06
6	50±1		2.03±0.01	3.68±0.06

column operation. In method III, the physical strength of the particles was weak, except with the addition rate of 3000 $cm^3 min^{-1}$. As the precipitate could not be completely washed without suffering from peptization, it was washed only once to avoid wasteful loss. Table 1 shows the effect of the addition rate of the solution in method II on the ion-exchange capacity and the composition of the composite exchangers. The water content increased slightly with the addition rate, but the titanium content (titanium content refers to mol% of Ti/(Si+Ti)) and the ion-exchange capacity were not significantly affected by this factor.

(c) Effect of Concentrations of the Solutions. The hydrous metal oxides were precipitated by mixing the $TiCl_4$ solution and the Na_2SiO_3 solution in 1.0 M NaOH with varying concentration. The addition rates of the solutions were 5 $cm^3 min^{-1}$ for methods I and II, and 3000 $cm^3 min^{-1}$ for method III. Figure 2 shows the Na^+-uptake curves of the materials, indicating that the difference in the ion-exchange capacities is 0.4 mmol g^{-1} (less than 5% of the total exchange capacity) at the largest. Thus, the acid-base properties of the exchangers are not significantly affected by the method of mixing, nor by the concentration of the solutions.

(d) Effect of Titanium Content. The exchange capacities for Na^+ at pH 13 were measured as a function of the titanium content in the exchangers which were precipitated by methods I and III under the best conditions of a constant total concentration of metal

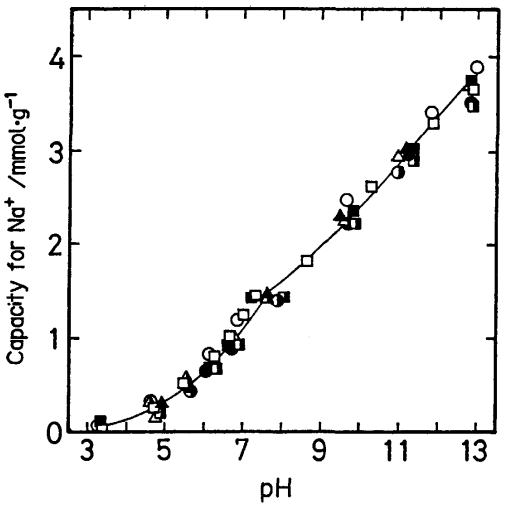

Fig. 2. Uptake curves for Na^+ ions (effect of concentrations of metal solutions used at precipitation).
Concentration of metal solution/M; ◑: 0.10, ○: 0.25, ●: 1.0 (Method I); ▲: 0.10, △: 0.25, ▲: 1.0 (Method II); ◧: 0.10, □: 0.25, ■: 1.0 (Method III).

Table 2. Synthetic Conditions and Compositions of the Exchangers

Sample No.	Method	Drying temp.	Ti-mol% in solution: mol Ti^{4+} / mol(Si^{4+}+Ti^{4+}) ×100	Ti-mol% in exchanger: mol TiO_2 / mol(SiO_2+TiO_2) ×100		Water content: mol H_2O / mol(SiO_2+TiO_2)	
1			35	37		1.77	
2			40	42		1.62	
3			45	46		1.75	
4			50	51		1.80	
5			55	57		1.76	
6	I	70 °C	60	62	±1	1.64	±0.02
7			65	67		1.75	
8[a)]			50	52		1.94	
9[a)]			50	51		1.82	
10[a)]			50	53		1.90	
11[a)]			50	52		1.75	
12			11	10		1.84	
13			11	10		1.75	
14			11	11		1.83	
15			32	34		2.04	
16			52	56		2.45	
17	III	Room	52	57	±1	2.61	±0.02
18		temperature	52	56		2.48	
19			72	76		2.51	
20			91	89		1.92	
21			91	90		1.97	
22			91	90		2.03	
23	Hydrous silicon(IV) oxide			$SiO_2 \cdot 1.27H_2O$			
24	Hydrous titanium(IV) oxide			$TiO_2 \cdot 2.35H_2O$			

a) Exchangers were prepared in a large amount by the recommended procedure.

ions (0.5 M). These conditions were realized by using desired combinations of 0.5 M $TiCl_4$ solutions in HCl and 0.5 M Na_2SiO_3 solutions in NaOH, where the concentrations of HCl and NaOH were suitably adjusted for providing pH 7.6 at precipitation. The gels thus prepared by method I were dried at 70 °C, while those by method III were dried at room temperature. As is shown in Table 2, the composite exchangers thus prepared have nearly the same titanium content as the solution mixed. The composite exchangers contained appreciably less water than the hydrous titanium(IV) oxide, but much more than the hydrous silicon(IV) oxide.

Figure 3 shows the ion-exchange capacities of the composite exchangers. For comparison, the exchange capacities were measured for simple mixtures of the hydrous silicon(IV) oxide and the hydrous titanium(IV) oxide (the mixed exchanger), as is shown in the same figure (dotted line). The measurement for the mixed exchangers was made at pH 12.2 instead of pH 13 because the dissolution of a part of the hydrous silicon(IV) oxide in the mixed exchangers limited the applicable maximum pH. The line shows that the ion-exchange capacities of the mixed exchangers are the algebraical sums of those of the component simple hydrous oxides. Based on this observation, we can estimate the hypothetical capacities at pH 13 of the mixed exchangers (a chain line). This figure indicates that the exchangers with 37 to 67 mol% titanium have nearly the same ion-exchange capacities, much larger than the mixed exchangers. The exchanger with 90 mol% titanium has a much smaller capacity than the mixed exchanger of the similar titanium content. This figure also indicates that the exchange capacities were not affected by the method of mixing the solutions or the drying temperature.

Figure 4 shows uptake curves for Na^+ of the exchangers with various titanium contents, along with those of the simple hydrous metal oxides. The decrease of the capacities of the exchanger with 10 mol% titanium in pH regions beyond 11.5, similar to the hydrous silicon(IV) oxide, is ascribed to the partial dissolution of the exchanger. This phenomenon is not observed in the other exchangers, which suggests the stabilization of the matrix in highly alkaline solution in spite of the large silicon content. The minimum pH at which sodium ions were adsorbed was significantly lower for the exchangers with 10 to 76 mol% titanium than for the simple hydrous oxides. These findings suggest the formation of a compound, basically different in properties from the hydrous silicon(IV) oxide and the hydrous titanium(IV) oxide.

(e) Effect of Drying Temperature. If no excessive decrease in the capacity occurs, heating is preferable for rapid drying of the hydrous oxide gel. From this standpoint, the acid-base property and the water content were compared between the exchangers dried at 70 °C (Nos. 8—11 in Table 2) and those at room temperature (Nos. 16—18 in Table 2). Although the water content is smaller in the materials dried at 70 °C than in those at room temperature, little difference in the Na^+ uptake curves was observed between them, when it was normalized to the number of moles of Na^+ taken up per mole of metals composing the materials. Hence, drying at 70 °C does not affect the acid-base property of the exchanger.

Recommended Procedure. The composite ex-

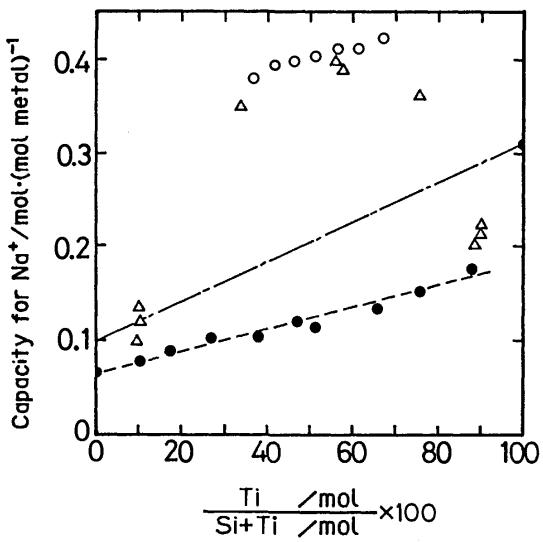

Fig. 3. Dependence of ion-exchange capacity on titanium content.
Exchangers; O: Nos. 1—7 in Table 2, Δ: Nos. 12—22 in Table 2, ●: Mixture of $SiO_2 \cdot 1.27H_2O$ and $TiO_2 \cdot 2.35H_2O$, -·-·-: Estimated exchange capacity of the mixed exchanger at pH 13.

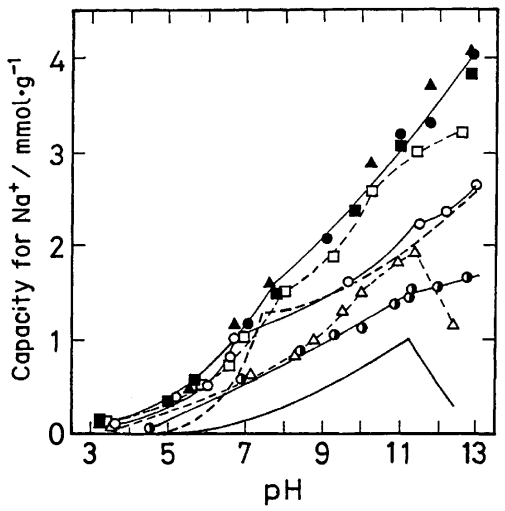

Fig. 4. Uptake curves for Na^+ ions (Effect of titanium content).
Exchangers; ■: No. 1, ▲: No. 4, ● : No. 7, Δ: No. 12, □: No. 15, O: No. 19, ◑: No. 21, ——: No. 23, ------: No. 24. The numbers are the same as those in Table 2.

changers with 37 to 67 mol% titanium possess ion-exchange capacity larger than those with other compositions. In this study, the exchanger with 50 mol% titanium was selected as the best choice for easy control of the composition. Method I was chosen because it produced particles hard and large enough to be used for column operation. The concentrations of $TiCl_4$ and Na_2SiO_3 solutions were 0.5 M, which was as high as practicable to prepare a large amount of the exchanger in one batch. The recommended procedure is as follows: In 2 dm^3 of 0.5 M $TiCl_4$ solution, 2 dm^3 of 0.5 M Na_2SiO_3 solution in 1.0 M NaOH are added at a rate of 16 cm^3/min with vigorous stirring, followed by adjusting pH to 7.6±0.3 by adding a small amount of concentrated HCl or NaOH solutions. After aging for 2 d, the precipitate thus formed is separated from the mother liquor by filtration under suction, and is then uniformly dispersed into 5 dm^3 of water. The precipitate is filtered again after being completely sedimentated, and is dried at 70 °C for 50 h. The resulting product is ground to a desired particle size, and is then converted to the H^+ form by the procedure described in the experimental section. As a result of four independent syntheses, the uptake curves and the compositions agreed well with each other, except for a little larger fluctuation of water content which is susceptible to the environmental conditions (Table 2). The synthetic procedure, therefore, is considered to be highly reproducible. The yield, calculated on the basis of the metallic element used, exceeded 99 percent.

(II) Structural Analysis of the Exchangers. In order to obtain structural information, (a) specific surface area, (b) infrared spectra, (c) thermal analytical curves, and (d) X-ray diffraction patterns were measured on the samples with various titanium content and the simple hydrous metal oxides. Their compositions are shown in Table 2.

(a) Specific Surface Area. Figure 5 shows the specific surface areas of the samples. It is nearly the same as that of the hydrous silicon oxide up to 57 mol% titanium content and decreased with titanium content; reaching to about one-half of the hydrous silicon oxide in the hydrous titanium oxide. As the ion-exchange capacity (Fig. 3) does not increase in keeping with the specific surface area, the uptake of Na^+ in the exchangers cannot be explained by the sorption only on the internal surface of the materials. The change in the ion-exchange capacities with the composition of the exchanger may be ascribed to the variation in the number of exchange sites in the whole sample.

(b) IR Spectra. Figure 6 shows IR spectra of the composite exchangers, along with the simple hydrous metal oxides. The asymmetric absorption band near 3400 cm^{-1} is attributable to the sum of the contributions from water and hydroxyl groups bonding to the metal in the materials; the former at the lower-, and the latter at the higher-wavenumber sides. The absorption band near 1630 cm^{-1} is due to the bending mode of water and the absorption in the wavenumber region below 1500 cm^{-1}, to the metal-oxygen bond in the matrix. The absorption peak due to the hydroxyl groups is larger for the exchanger with 57 mol% titanium than for the others. This result is compatible with the change in the ion-exchange capacities with the composition (Fig. 3), as the hydroxyl groups

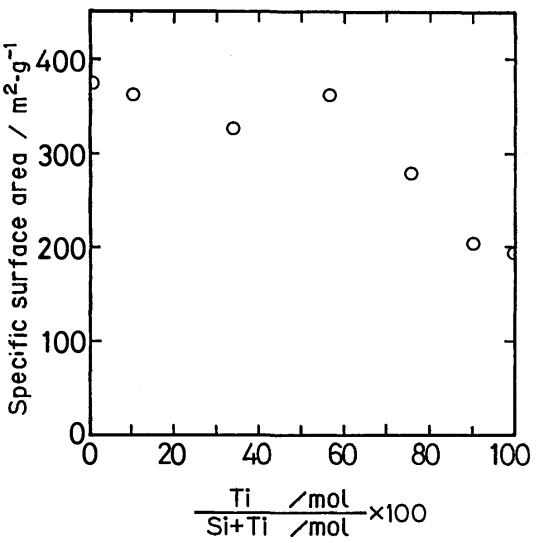

Fig. 5. Dependence of surface area of the exchangers on titanium content.

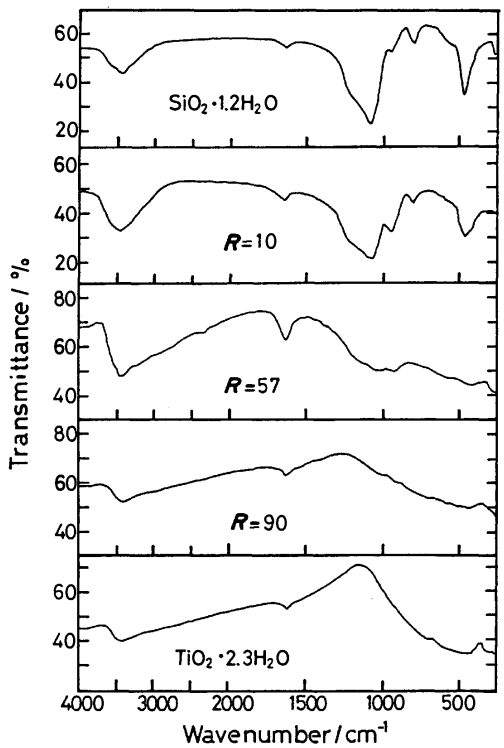

Fig. 6. IR spectra of the exchangers. *R* refers to mol% of Ti/(Si+Ti).

function as ion-exchange sites. In the wavenumber region below 1500 cm^{-1}, the exchangers with 10 and 90 mol% titanium, respectively, showed absorption spectra similar to hydrous silicon oxide and hydrous titanium oxide, while the spectrum of the exchanger with 57 mol% titanium differed from that of the simple hydrous metal oxides.

(c) Thermal Analysis. The TGA and the DTA curves were measured on the same samples as were used in the IR spectrum measurements. In the DTA curves, the large endothermic peak appearing in the range below 250 °C is due to loss of water. A combination of peaks at 90 °C and 125 °C indicates that the exchangers have at least two kinds of water having different binding energies. Figure 7 shows the percentile weight loss at various temperatures. As the fraction of water lost below 100 °C was smaller for the composite exchangers than for the simple hydrous metal oxides, the ratio of water of high binding energy to total is larger in the former than in the latter oxides. As had been discussed previously,[5-7] the water of lower binding energy is zeolitic or adherent, while the water of higher binding energy is present as either hydroxyl groups or water bound thereto. Accordingly, the large amount of bound water accounts for a large ion-exchange capacity of the exchanger with 57 mol% titanium, being compatible with the IR observations. The water lost during drying at 70 °C is mainly zeolitic or adherent and irrelevant to the ion-exchange capacity.

(d) X-Ray Analysis. Figure 8 shows X-ray diffraction patterns of the exchangers with various titanium contents. All exchangers have poor crystallinity. The broad peak at low angle, characteristic of the hydrous silicon oxide, shifts to higher angle and broadens further with the increase of titanium content up to 67 mol%. An increase in titanium content from 67 to 76 mol% results in a sudden change in the matrix; the X-ray diffraction pattern of the exchanger with 76 mol% titanium closely resembles that of the anatase form of the titanium oxide, as compared with the diffuse pattern of the composite exchanger with 67 mol% titanium. The peaks sharpen with titanium content, becoming most clear for the exchanger with 90 mol% titanium, indicating an enhanced crystallization of the matrix. The exchangers with 37 to 67 mol% titanium are amorphous because of the diffuse diffraction patterns.

From the observations described above, the change in the ion-exchange capacity with titanium content can be summarized as follows. The matrices of the exchangers with 37 to 67 mol% titanium are amorphous and contained a large number of hydroxyl groups compared to the exchangers with other compositions, so that these amorphous compounds have large ion-exchange capacity. While the exchanger with 10 mol% titanium possesses much more ion-exchange sites of higher acidity than those of the

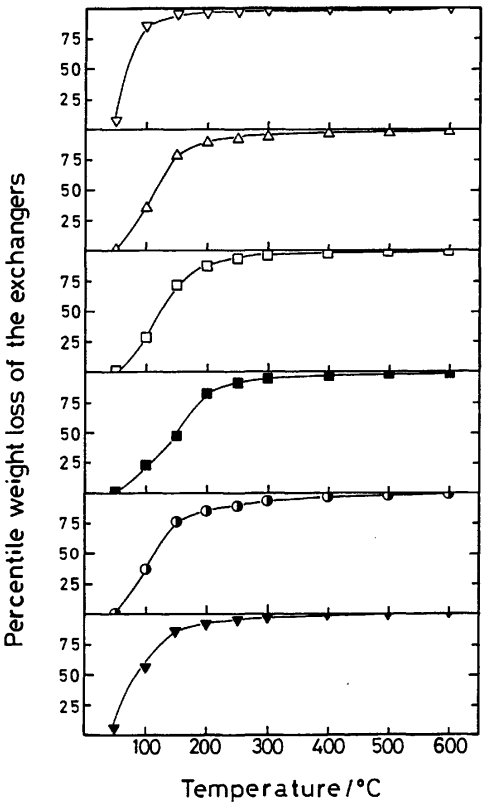

Fig. 7. Weight losses of the exchangers by heat treatment.
Exchangers; ▽: No. 23, △: No. 12, □: No. 17, ■: No. 8, ◑: No. 21, ▼: No. 24. The sample numbers are the same as those in Table 2.

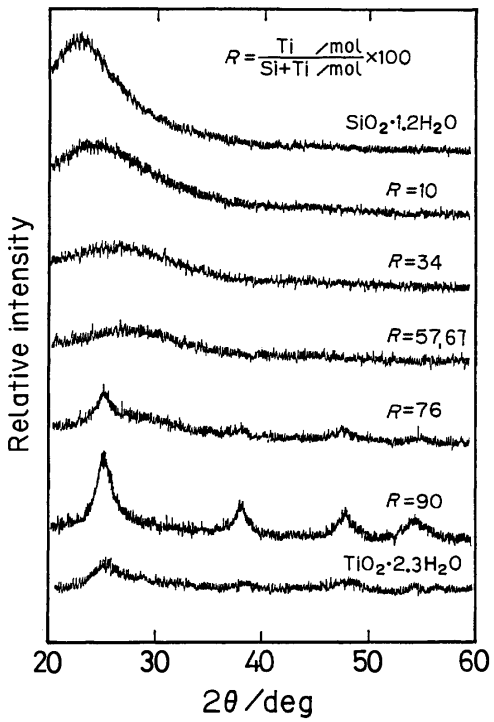

Fig. 8. X-Ray diffraction patterns of the exchangers.

hydrous silicon(IV) oxide, it is unstable to highly alkaline solutions because of the similarity in the structure to the hydrous silicon(IV) oxide. The smaller ion-exchange capacity of the exchanger with 90 mol% titanium than the hydrous titanium(IV) oxide is attributable to better crystallinity of the former than the latter.

This research was supported in part by a grant from Tohoku Radiological Science Center.

References

1) Y. Inoue and H. Yamazaki, *J. Nucl. Sci. Technol.*, **24**, 462 (1987).
2) S. Kaneko, S. Okuda, M. Nakamura, and Y. Kubo, *Chem. Lett.*, **1980**, 1621.
3) S. Kaneko and K. Tsukamoto, *Chem. Lett.*, **1983**, 1425; **1984**, 505.
4) JIS K-0101-1986 (1986).
5) Y. Inoue and M. Tsuji, *Bull. Chem. Soc. Jpn.*, **51**, 479 (1978).
6) Y. Inoue, H. Yamazaki, and H. Nakamizo, *Bull. Chem. Soc. Jpn.*, **58**, 1292 (1985).
7) Y. Inoue, H. Yamazaki, and Y. Matsuda, *Bull. Chem. Soc. Jpn.*, **58**, 3225 (1985).

Preparation of Superconductive Films by Fume Pyrolysis

Takao OGAWA, Seiji YAMADA, Takeshi MIKI, Hideyasu TSUIKI, Noriyoshi KAKUTA, Akifumi UENO,* Yasuji SUZUKI,† Kuniyuki KOYAMA,† Seiichiro NOGUCHI,† and Mamoru YAMADA††

Department of Materials Science, Toyohashi University of Technology, Tempaku, Toyohashi, Aichi 440
†Department of Electronic Engineering, Toyohashi University of Technology, Tempaku, Toyohashi, Aichi 440
††Government Institute for Industry at Nagoya, Kitaku, Nagoya, Aichi 462

(Received December 2, 1988)

Superconductive films composed of $Ba_2YCu_3O_{7-\delta}$ were prepared by fume pyrolysis with a temperature programmed electric furnace. Fumes generated from an aqueous solution of Ba, Y, and Cu nitrates with an aid of supersonicant were introduced into the furnace with flowing O_2. Fine particles consisting of Ba, Y, and Cu ions were formed in the furnace and deposited on the surface of a YSZ substrate placed at the top of the furnace. Films thus prepared and annealed at 1273 K showed superconductive properties below 90 K and zero resistivity was observed at 80 K with 100 μA of the current.

Since the announcements of possible high-T_c superconductive oxides[1] and subsequent studies on relating systems,[2-5] numerous works on the structures and the electronic properties of these compounds have been reported.[6-8] Several problems for practical use have been pointed out and among them the developments of the techniques to prepare materials with high-J_c have been strongly desired to be achieved promptly. Since the J_c values have been suggested to depend on the size of powder particles, evenly sized fine particles are prefered to be employed as starting materials. One of the useful methods to produce fine oxide particles is fume pyrolysis with a supersonic nebulizer,[9] and Tohge et al.[10] have adopted this method for the preparation of superconductive bulk materials. The improvement in J_c values was not mentioned in the paper. Studies on the development of superconductive thin films have been of current interest, since high-J_c materials have been expected to be readily achieved with thin films. Films prepared by an epitaxial growth of $Ba_2YCu_3O_{7-\delta}$ on a $SrTiO_3$ substrate or those produced by an ion cluster beame (ICB) method using a MgO substrate have been reported to exhibit a J_c value of higher than 10^6 A cm^{-2} at 77 K.[11] Spray pyrolysis is also a useful method for superconductive films,[12] though sufficiently high-J_c values have not yet been reported.

In the present work, superconductive films were prepared by fume pyrolysis techniques aided by supersonicant with an aqueous solution of Ba, Y, and Cu nitrates. Fumes generated were brought into an electric furnace with flowing oxygen and turned out to be fine oxide or nitrate particles, which accumulated on the surface of a ceramic substrate (Yttrium Stabilized Zirconia, YSZ), placed at the top of furnace. The direct deposition of fine particles on the substrate is a feature of this work and is quite different from the spray pyrolysis, where fumy droplets are spreaded over a hot substrate and, subsequently, small particles are generated. Films mainly composed of a superconductive phase, $Ba_2YCu_3O_{7-\delta}$, were prepared with annealing the accumulated particles at 1273 K in oxygen atmosphere. The superconductive properties of films were discussed with the surface morphorogies of films observed by a scanning electron microscope (SEM).

Experimental

Apparatus. In Fig. 1 is shown the apparatus employed for fume pyrolysis. The apparatus mainly consists of two parts; in part A fumes are generated by a supersonicant mounted at the bottom of a vessel, including an aqueous solution of Y, Ba, and Cu nitrates with a molar ratio of 1 : 2 : 3; the concentration of metal ions was 0.02 mol L^{-1}. The frequency of the supersonicant employed was always 1.5 MHz. The part B is an electric furnace, equipped with 3 heaters located at the top, middle, and bottom of the furnace, respectively. These 3 heaters are independently controlled to give an appropriate temperature distribution in the furnace. At the radial center of the furnace is placed a reaction tube, made of quartz, directly connected with the part A. The fumes generated were introduced into the tube with flowing O_2, the flow rate being 3 L min^{-1}. A YSZ plate (2×7×0.3 mm) was placed at the top of the tube and fine oxide and/or nitrate particles formed in the furnace deposited on the surface of YSZ to be a thin film. In this experiment the temperature was controlled to be 1073 K at any parts of the tube during fume pyrolysis for 2 h. The films thus produced were annealed at 1273 K for 5, 10, 15, and 30 min, respectively, in flowing oxygen and then cooled to 673 K with the rate of 150 K h^{-1} and then to 473 K with the rate of 120 K h^{-1}, still in O_2 atmosphere.

Resistivity Measurements. The electrical resistivity of films was measured by a four-probe DC method with the current of 100 μA in the temperature range of 300—50 K. The resistivity was calculated by measuring the voltage generated between the middle 2 points on the sample film. The film thickness was estimated to be 5 μm in average by an electron probe microanalyzer (EPMA, JEOL Superprobe 733). The sample film was attached on a holder made of metallic copper and was placed in a cryostat available at liquid He temperature. The film temperatures were monitored by an Au(Fe)-Ag thermocouple.

Magnetization Measurements. Magnetization of the sample film was measured by SQUID equipment (Susceptometer 900, SHE Co.,) with an external magnetic field of 100 Öe; the sample films are placed in parallel with the magnetic field. During the measurement the sample film was vibrated with a frequency rate of 500 mm min^{-1}.

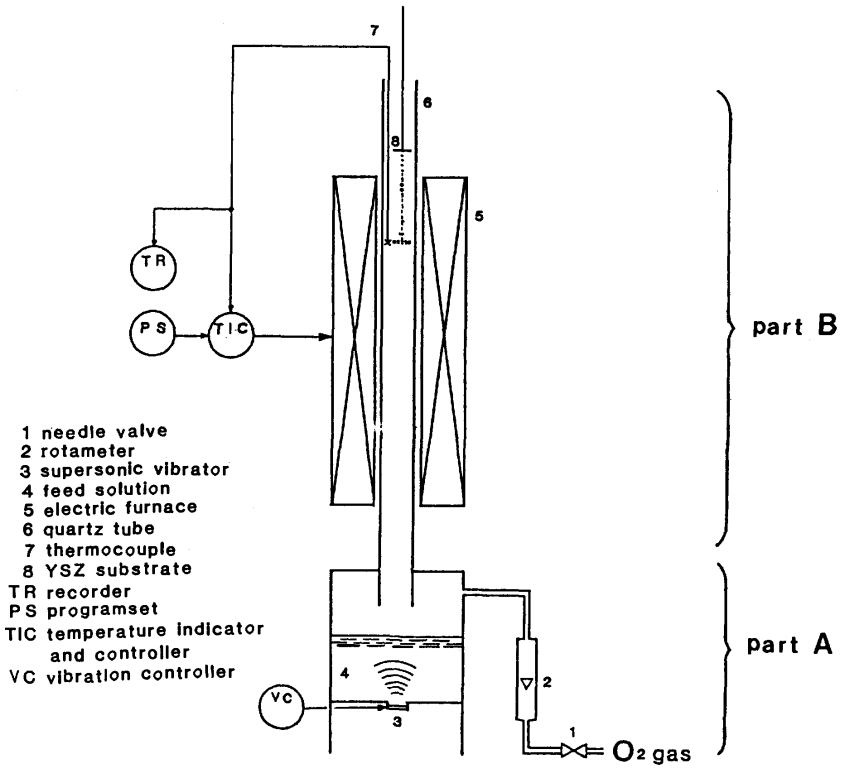

Fig. 1. Apparatus for fume pyrolysis.

Temperature dependencies of magnetization for the films, treated at 1273 K for 5, 10, 15, and 30 min in flowing O_2, respectively, were measured and the volume fractions of superconductive phases in the films were estimated.

X-Ray Diffraction Measurements. The sample film was subjected to X-ray diffraction (XRD) analysis. Since the conventional diffractometer showed peaks due to YSZ substrate as well as those due to $Ba_2YCu_3O_{7-\delta}$, a reflection X-ray diffractometer (Rigaku Denki Co., Rotaflex) was used at 50 kV with a filament current of 40 mA and carbon filter for Cu $K\alpha$ radiation. An incident X-ray angle to the sample film was settled at 0.5 degree from the horizontal plane.

SEM and EPMA Measurements. The surface structures and metal ions distributions on the sample films were observed by EPMA, operated at an accelerating voltage of 15 kV with an energy dispersive detector. The depth profiles of metal ions were also monitored by EPMA with samples mounted in polyethylene supports. All the samples submitted to EPMA measurements were covered with carbon films to prevent the charge-up phenomenon.

TEM Measurements. Particles accumulated on YSZ substrate during fume pyrolysis were removed and suspended in ethanol with the aid of a supersonicant to be submitted to a transmission electron microscope (TEM, Hitachi H-800), operated at an accelerating voltage of 200 kV with a magnification of 10^5. Thus, the size and shape of the fine particles were observed and the compositions of particles were also analyzed by an element analyzer (EMAX, Horiba Co.), equipped with an energy dispersive detector.

Results

Resistivity Measurements. In Fig. 2 are shown the changes in the resistivity of the superconductive films,

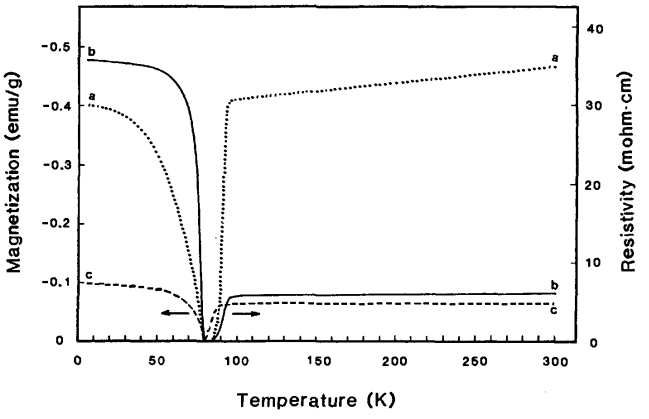

Fig. 2. Temperature dependences of resistivity and magnetization of $Ba_2YCu_3O_{7-\delta}$ films annealed at 1273 K for 5 (a), 10 (b) and 30 min (c).

treated at 1273 K for 5, 10, and 30 min in O_2 atmosphere, with temperatures varied from 50 to 300 K. The film employed was 5 μm in thickness in average. Resistivities with 100 μA of the current were almost constant (3 mohm cm) at temperatures higher than 90 K and decreased to zero at 80 K. The resistivity curves were well-reproducible for samples formed under the similar conditions; T_c=90 K, $T_{c(zero)}$=80 K, ΔT=10 K.

Magnetization Measurements. In Fig. 2 are also shown the temperature dependencies of magnetization for the films treated at 1273 K for 5, 10, and 30 min, respectively. From the saturation magnetizations

thus obtained, the volume fractions of superconducting phases formed in the films were estimated (see Fig. 3).

XRD Measurements. The reflection XRD patterns of the films annealed at 1273 K for 10 and 30 min are given in Figs. 4c and d, indicating the significant crystal growth along with c-axis of $Ba_2YCu_3O_{7-\delta}$ during the oxygen treatment at 1273 K. On the otherhand, the diffraction patterns due to $Ba(NO_3)_2$ were observed for the unannealed film (see Fig. 4a), though the decomposition temperature of $Ba(NO_3)_2$ is described at 871 K.[13] For comparison, X-ray diffraction patterns of the films annealed at 1223 K for 2 h are shown in Fig. 4b. From the slight changes in the diffraction angles of superconductive phases, changes in the lattice constants with annealing time were calculated and listed in Table 1. Oxygen contents in the superconductive unit cell were estimated from the difference between a and b-axial lengths, according to the previous paper[14] and are also given in Table 1.

SEM and EPMA Measurements. Typical SEM photographs showing the changes in surface morphorogies of the films are given in Figs. 5a to 5e with magnification of ×1600, where 5a represents the surface of the unannealed film and 5b to 5e show the surfaces of films annealed at 1273 K for 5, 10, 15, and 30 min, respectively. A SEM photograph of the films annealed at 1223 K for 2 h is shown in Fig. 5f to be compared with those of the films annealed at 1273 K. The depth profiles of Y, Ba, and Cu ions in the film annealed at 1273 K for 10 min are demonstrated in Fig. 6 and X-ray images of Y, Ba, and Cu ions on the films annealed at 1273 K for 30 min are given in Fig. 7.

TEM Photograph. In Fig. 8 are shown the TEM photographs of fine particles deposited on the substrate, particles unannealed. Particles deposited on

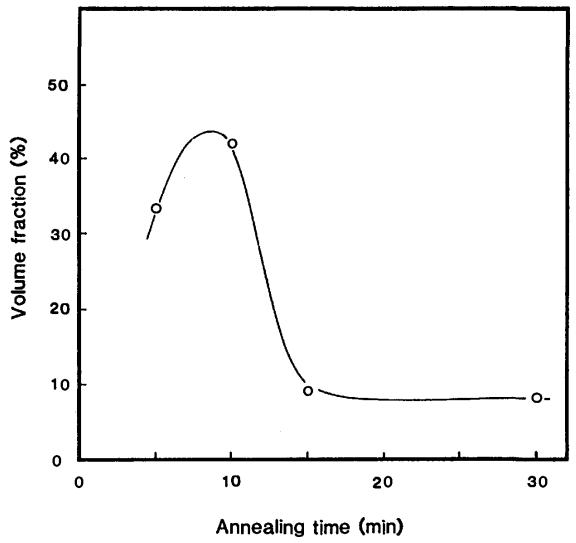

Fig. 3. Change in the volume fraction of superconductive phases in films treated at 1273 K with the annealing time.

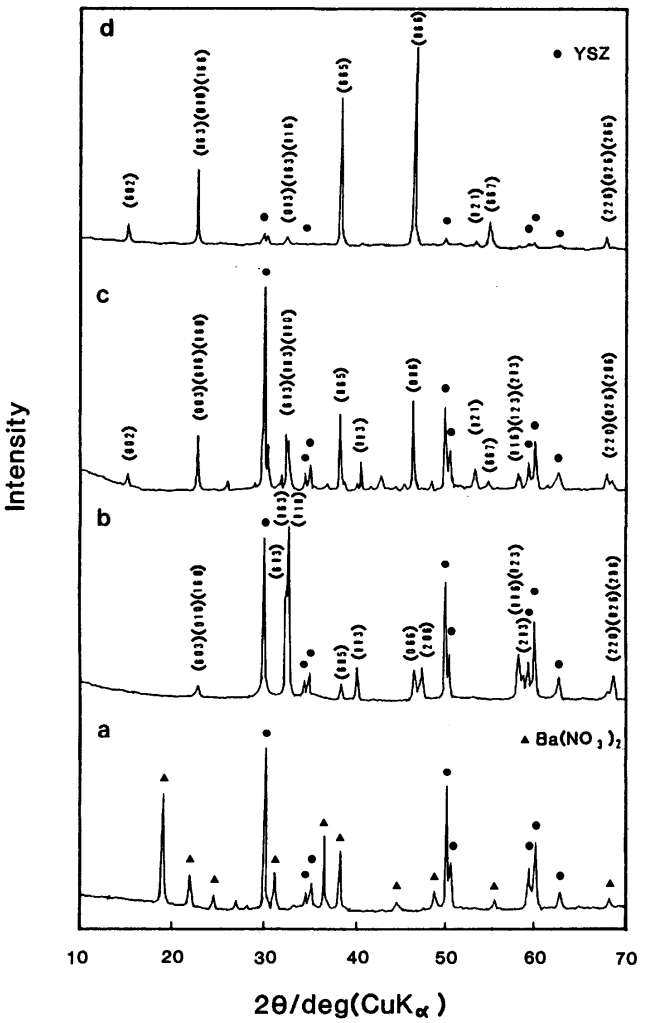

Fig. 4. XRD patterns of the films annealed at 1273 K for 10 (c) and 30 min (d), annealed at 1223 K for 2 h (b) and the unannealed films (a).

Table 1. Characterazation of Films Annealed at 1273 K for Various Times

annealed time	T_c(zero)	Volume fraction	Lattice constant (Å)			Oxygen content
min	K	%	c-axis	a-axis	b-axis	
5	84	33	11.68	3.82	3.88	6.74
10	85	42	11.67	3.81	3.87	6.65
15	—	9	11.68	3.81	3.88	6.83
30	78	8	11.66	3.82	3.84	6.29

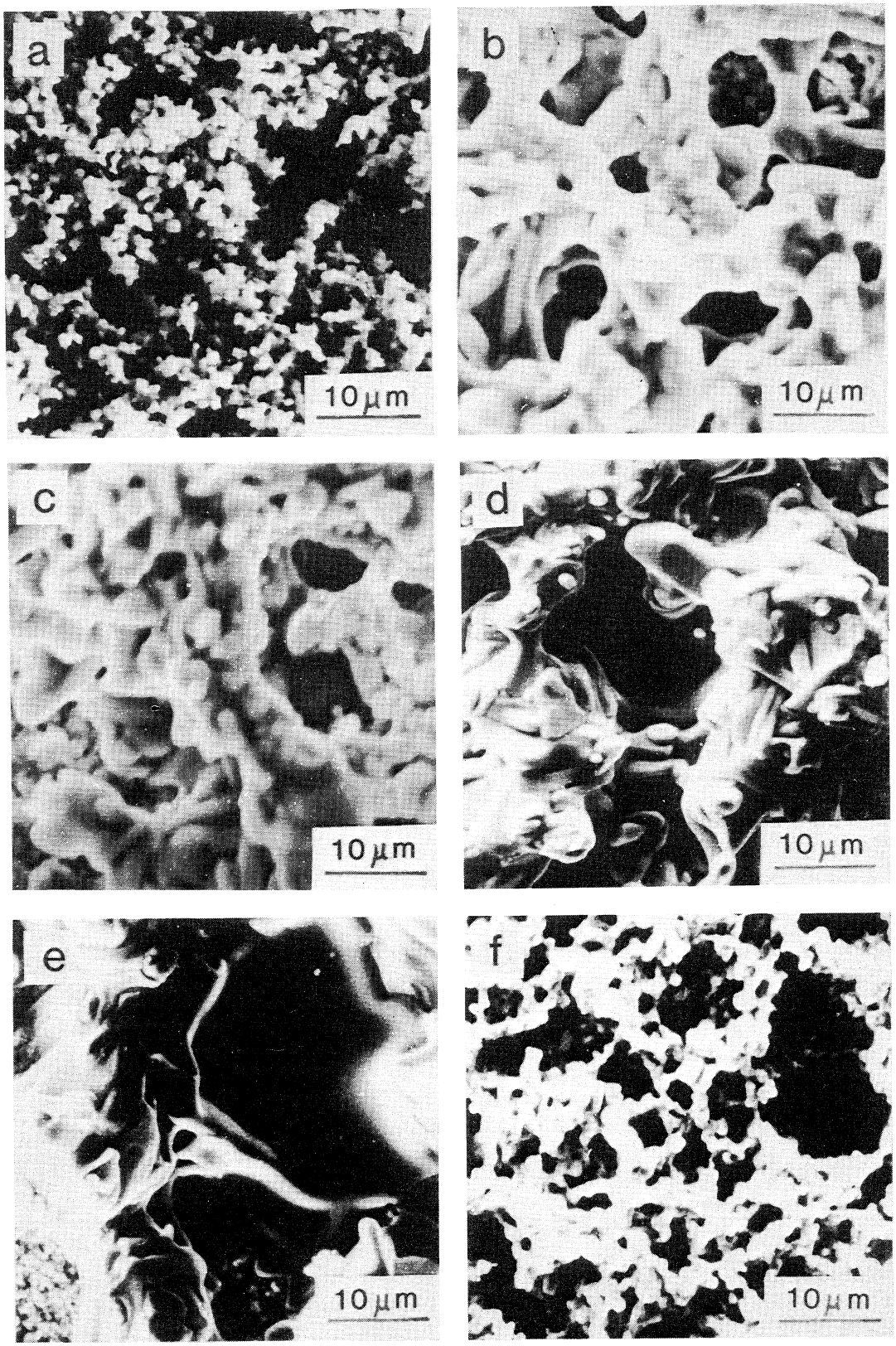

Fig. 5. SEM photographs with the magnification of ×1600; the unannealed films (a), and the films annealed at 1273 K for 5 min (b), 10 min (c), 15 min (d), and 30 min (e) and the films annealed at 1223 K for 2 h (f).

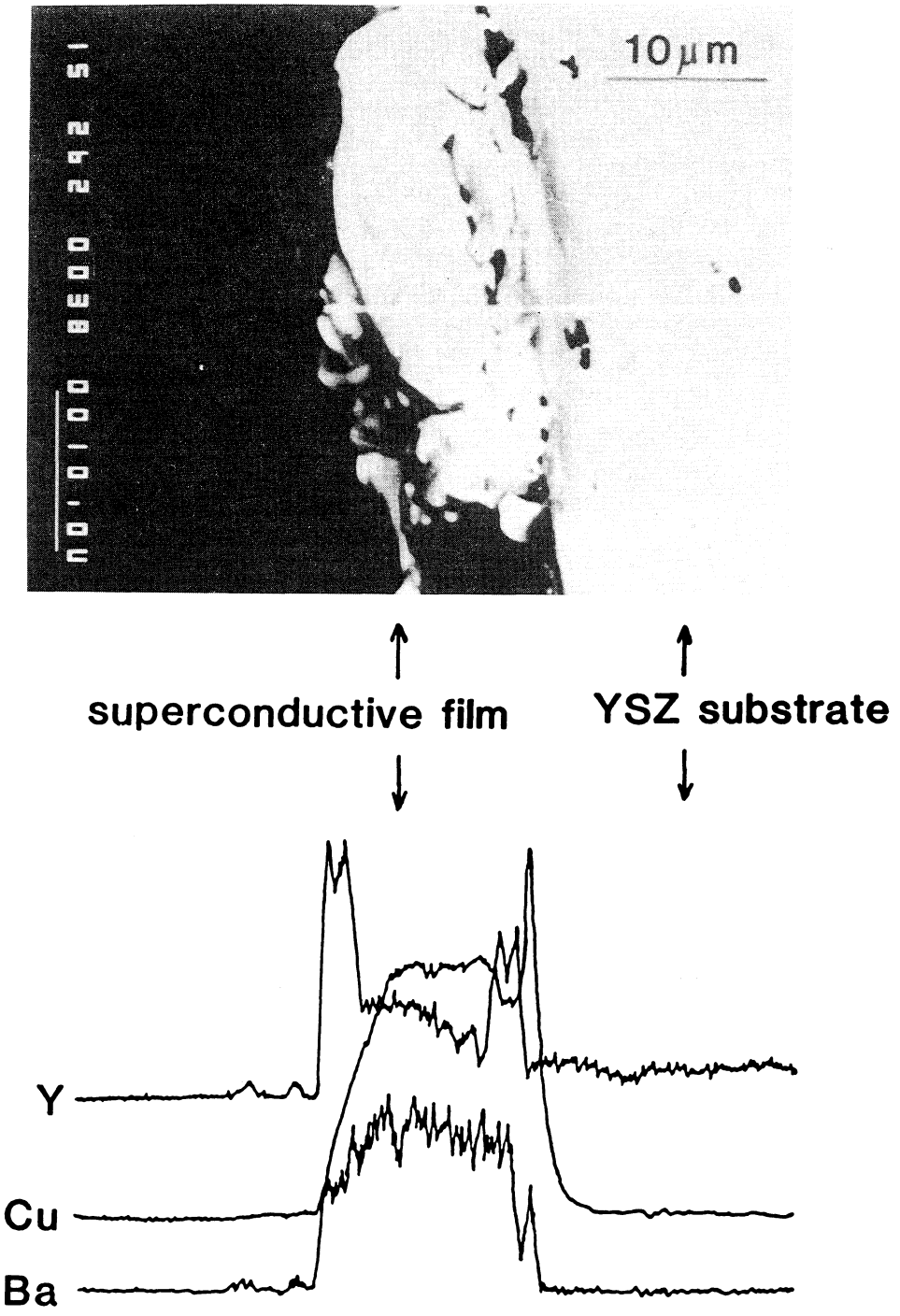

Fig. 6. Depth profilms of Y, Ba and Cu in the films annealed at 1273 K for 15 min, measured by EPMA.

the substrate seem to be spheres with the diameter of 0.5 μm, almost evenly. The composition analysis of particles is also depicted in Fig. 8, suggesting the particle consists of Y, Ba, and Cu ions though Cu ions were rather enriched in the particle than were expected to be 1/2/3 for Y/Ba/Cu.

Discussion

Particles Depositing on YSZ. Fume pyrolysis techniques with an aid of supersonication[15] have been used for the preparation of oxide particles and the particle size will be controlled by the size of droplets in fumes. A droplet size can be estimated by the following equation;[16]

$$d = 0.34\left(\frac{8\pi\gamma}{\rho f^2}\right)^{1/3} \quad (1)$$

where d is the average size of droplets, f means the

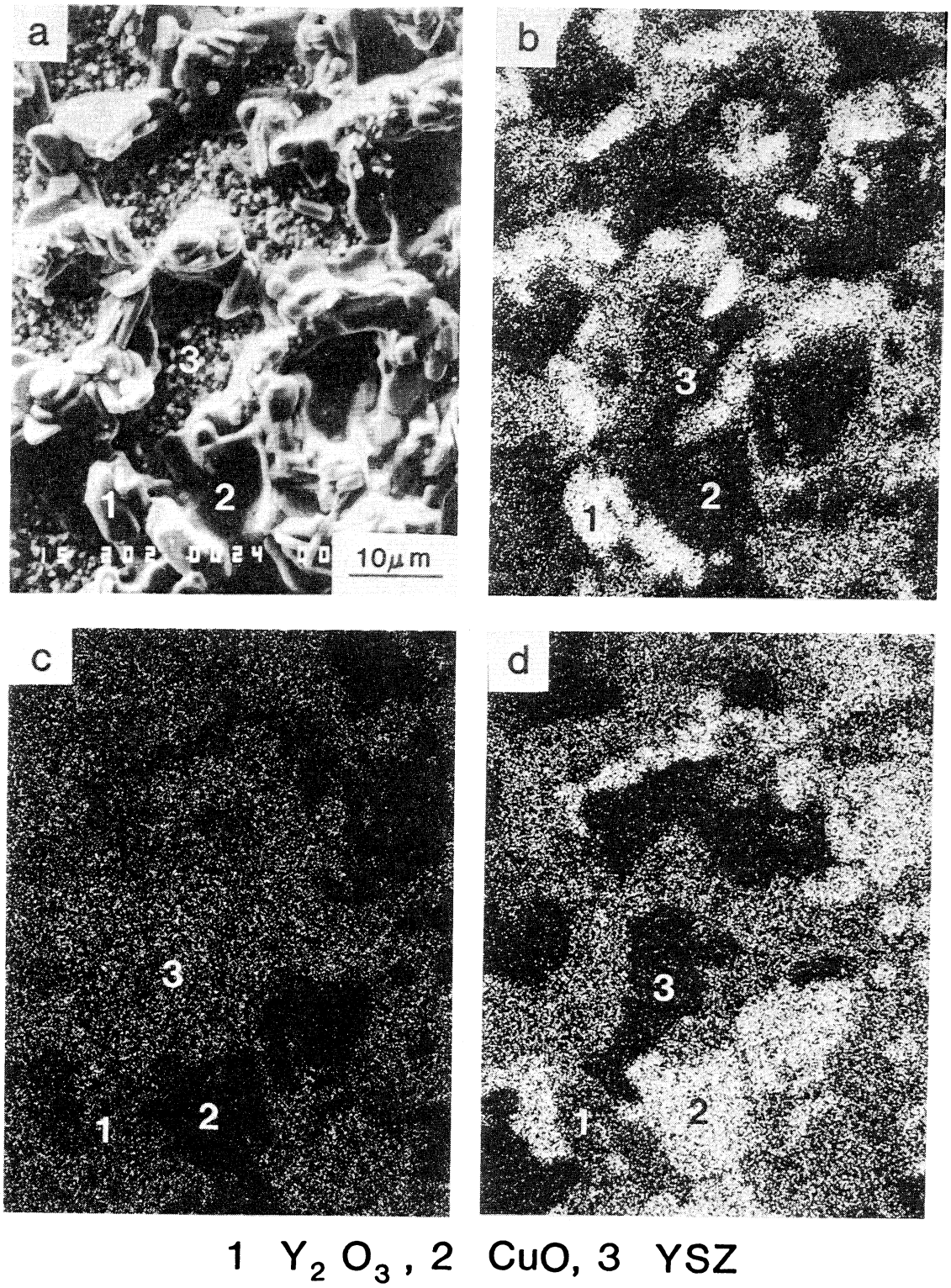

Fig. 7. SEM photograph (a) and X-ray image of Y (b), Ba (c), and Cu (d) in the films annealed at 1273 K for 30 min, measured by EPMA with a magnification of ×1600.

frequency of supersonication (1.5 MHz) and γ and ρ are the surface tension and density of droplets, respectively. In this work, metal nitrates employed are so diluted with water that the surface tension and density of droplets might be approximately the same as those of water. Thus, the average size of droplets in fumes was calculated ca. 3.2 μm and the size of particles formed during pyrolysis was estimated to be ca. 0.41 μm, since the concentration of metal ions in a droplet is 0.02 mol L^{-1}; more than 99 wt% of a droplet is water, volatilized during pyrolysis. As can be seen in Fig. 8 the size of particles depositing on the substrate is ca.

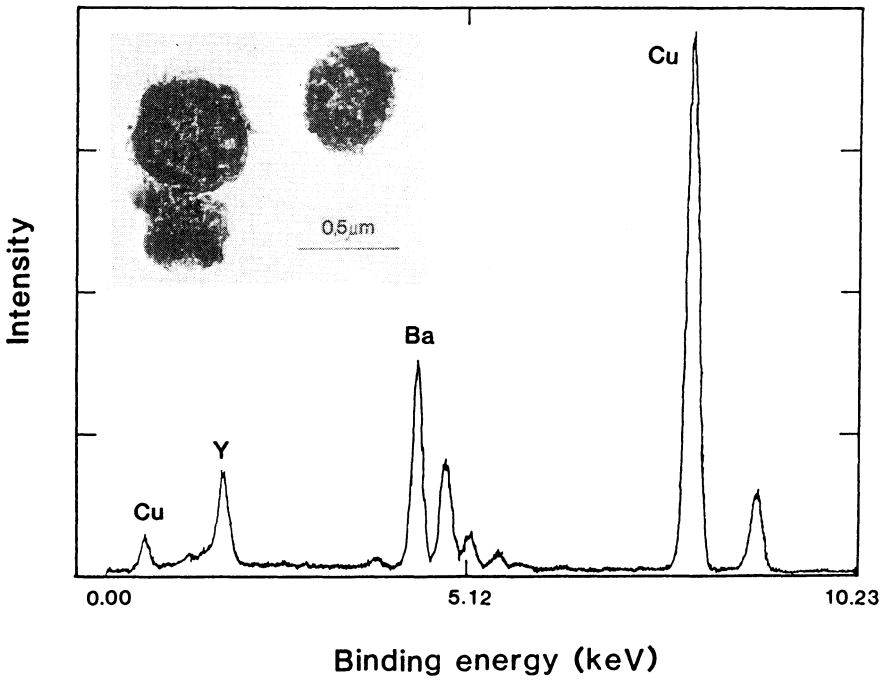

Fig. 8. TEM photograph and composition analysis of the particles depositing on the substrate during fume pyrolysis.

0.5 μm, in good accordance with the estimated size of 0.41 μm, suggesting that a droplet in fumes turned out a particle during pyrolysis. A particle, hence a droplet, was proved to be composed of Y, Ba, and Cu ions although an excess amount of Cu ions was observed (see Fig. 8). In Fig. 4a is shown an XRD spectrum of the particles depositing on the substrate and almost all of the peaks are assigned to $Ba(NO_3)_2$. By annealing the particles at 1223 K for 2 h, the peaks attributed to $Ba(NO_3)_2$ disappeared and those due to $Ba_2YCu_3O_{7-\delta}$ were observed (see Fig. 4b).

SEM Observation and Superconductivity of the Annealed Films. SEM observations of the unannealed films are given in Fig. 5a, where the films are proved to consist of spherical particles sized ca. 0.5 μm. Sintering of the particles are demonstrated in Figs. 5b to 5e, when the films were annealed at 1273 K for 5, 10, 15, and 30 min in flowing O_2. From Figs. 5d and 5e, it will be found that $Ba_2YCu_3O_{7-\delta}$ seems to be sintered by a prolonged annealing at 1273 K. The XRD spectrum of the sintered films is given in Fig. 4d, suggesting the crystalline growth of $Ba_2YCu_3O_{7-\delta}$ with the heat treatments in O_2 atmosphere at 1273 K. Although the photographs given in Figs. 5a to 5e emphasize uneven structures of the films, zero resistivities and Meissner effects were clearly confirmed at 80 K for the annealed films (see Fig. 2). A SEM photograph of the films annealed at 1223 K for 2 h showed unsintered particles mainly composed of $Ba_2YCu_3O_{7-\delta}$ (see Figs. 4b and 5f). The resistivities of this film were proved to decrease gradually below 90 K but did not reach zero even at 50 K with a small current of 10 μA.

Volume Fractions of Superconductive Phases. The saturation magnetiaztions and, consequently, the volume fractions of the superconductive phases in the annealed films strongly depend upon, the annealing time at 1273 K, as shown in Figs. 2 and 3. Thus, the volume fraction as high as 45% was achieved for the films annealed at 1273 K for 10 min but with a prolonged annealing the superconductive phases seem to decompose. In Fig. 7 are shown the X-ray images of Y, Ba, and Cu ions on the films treated at 1273 K for 15 min in O_2 atmosphere, indicating the deposition of copper oxides by the decomposition of superconductive phases. Copper oxides thus yielded were spreaded and covered over YSZ substrate, evidenced by disappearance of diffraction peaks due to YSZ of the films treated at 1273 K for 30 min (see Fig. 4d). As can be seen in Table 1, nevertheless the prolonged annealing the axial lengths of unit cell did not change so much. The difference between a and b-axial length became so small, however, when films were annealed at 1273 K for 30 min, resulting in the decrease of oxygen content in a superconducive unit cell (see Table 1).

The current used in the resistivity measurements was 100 μA and the average thickness of films annealed at 1273 K for 10 min was ca. 5 μm, as is shown in Fig. 6. Accordingly, the J_c value was estimated to be in the order of 10^2 A cm^{-2}. Unfortunately, high-J_c values in the order of 10^6 A cm^{-2} could not be achieved with the present films, probably because of uneven structures of films. Thus, one of the most important

factors to improve J_c value must lie in the homogeneous structures of films. The films with homogeneous structures will depend on the size of particles depositing on the substrate during pyrolysis. To prepare smaller particles, supersonicant with a high frequency should be used, as suggested by the Eq. 1.

Conclusion

1) A feature of fume pyrolysis is a direct accumulation of fine particles over substrate surface and was first applied here to the preparation of superconductive films.

2) With annealing the films at 1273 K, they exhibited superconductive properties below 90 K, but with a prolonged annealing the superconductive phases decomposed, probably, to the respective oxides. Thus, the relationship between annealing time at 1273 K and the volume fraction of superconductive phases in films were revealed.

3) Because of uneven structure of the films, high-J_c could not be achieved in this work. However, it was suggested that films with a homogeneous structure might be posible when fine sized droplets are employed for a fume pyrolysis. Such droplets can be generated by a supersonicant with higher frequency.

The authors express their thanks to Dr. Keizou Masuda at Toray Co. for supplying the YSZ substrates. Thanks are also to Professor Masatoshi Satoh at Institute for Molecular Science for measurements of magnetization at liquid He temperature.

References

1) J. B. Bednorz and K. A. Muller, *Z. Phys.*, **B64**, 189 (1986).

2) C. W. Chu, P. H. Hor, R. L. Meng, L. Gao, Z. J. Huang, and Y. Q. Wang, *Phys. Rev. Lett.*, **58**, 405 (1987).

3) K. Kishio, K. Kitazawa, S. Kanbe, I. Yasuda, N. Sugii, H. Takagi, S. Uchida, K. Fueki, and S. Tanaka, *Chem. Lett.*, **1987**, 429.

4) K. Kishio, K. Kitazawa, N. Sugii, S. Kanbe, K. Fueki, H. Takagi, and S. Tanaka, *Chem. Lett.*, **1987**, 635.

5) M. K. Wu, J. R. Ashburn, C. J. Torng, P. H. Hor, R. L. Meng, L. Gao, Z. J. Huang, Y. Q. Wang, and C. W. Chu, *Phys. Rev. Lett.*, **58**, 908 (1987).

6) F. Izumi, H. Asano, T. Ishigaki, E. Takayama-Muromachi, Y. Uchida, N. Watanabe, and T. Nishikawa, *Jpn. J. Appl. Phys.*, **26**, L649 (1987).

7) E. M. Engler, V. Y. Lee, A. I. Nazzal, R. B. Bayers, P. M. Grant, G. Lim, S. S. P. Parkin, N. L. Ramierz, J. E. Vazquez, and R. T. Sovoy, *J. Am. Chem. Soc.*, **109**, 2848 (1987).

8) A. Ourmazd, J. A. Rentschled, J. C. H. Spence, M. O'Keeffe, R. J. Graham, D. W. Johnson, Jr., and W. W. Rhodes, *Nature (London)*, **327**, 308 (1987).

9) K. Okuyama, Y. Kousaka, N. Tohge, and M. Adachi, *J. Mater. Sci. Lett.*, **6**, 1466 (1987); H. Imai, *Hyoumen*, **21**, 741 (1983).

10) N. Tohge, M. Tatsumisago, T. Ninami, K. Okuyama, M. Adachi, and Y. Kousaka, *Jpn. J. Appl. Phys.*, **27**, L1086 (1988).

11) Y. Bando, Powder and Powder Metallurgy, **35**, 305 (1988); A. Yamaji, Y. Enomoto, T. Murakami, and M. Suzuki, *ibid.*, **34**, 567 (1987); Y. Bando, T. Terashima, K. Iijima, K. Yamamoto, K. Hirata, and H. Mazaki, MRS Intern. Confr., Tokyo, May 30-June 3, 1988.

12) M. Kawai, T. Kawai, H. Masuhira, and M. Takahasi, *Jpn. J. Appl. Phys.*, **26**, L1740 (1987).

13) Kagaku-Binran, Kiso-Hen, I, (Table for Chemistry, Fundamentals), ed by Chem. Soc. Jpn., Maruzen, Tokyo (1984), p. 110.

14) K. Nakamura and K. Ogawa, *Jpn. J. Appl. Phys.*, **27**, 577 (1988); R. J. Cava, B. Batlogg, C. H. Chen, E. A. Rietman, S. M. Zahurak, and D. Werder, *Phys. Rev. B*, **36**, 5719 (1987).

15) Y. Hirata and A. Katoh, *Nippon Kagaku Kaishi*, **1980**, 1703; M. L. Nielsen, P. M. Hamilton, and R. J. Walsh, "Ultrafine Particles," ed by W. E. Kuhn, Wiley, New York (1963), p. 181.

16) R. J. Lang, *J. Acoustic Soc. Am.*, **34**, 6 (1962).

Variable-Temperature and Variable-Pressure Nitrogen-14 NMR Studies on the Exchange Reaction of Different Nitriles at the Nickel(II) Ion

Masao Ishii, Shigenobu Funahashi,* Koji Ishihara,† and Motoharu Tanaka
Laboratory of Analytical Chemistry, Faculty of Science, Nagoya University, Chikusa, Nagoya 464-01
(Received December 5, 1988)

The activation parameters for the exchange reaction of several nitriles at the nickel(II) ion have been determined for the nickel(II) trifluoromethanesulfonate solutions by means of the ^{14}N NMR line broadening method at various temperatures and pressures up to 220 MPa. Values of activation enthalpy ($\Delta H^{\ddagger}$/kJ mol^{-1}), activation entropy ($\Delta S^{\ddagger}$/J mol^{-1} K^{-1}), and activation volume at zero pressure ($\Delta V_0^{\ddagger}$/cm^3 mol^{-1}) for the exchange of various nitriles are respectively as follows: 41.4±0.5, −30±2, and +12.0±0.4 in acetonitrile; 42.0 ±0.4, −25±2, and +13.7±0.5 in propionitrile; 43.3±0.7, −23±2, and +13.1±0.5 in butyronitrile; 43.3±0.5, −19±2, and +12.4±0.6 in isobutyronitrile; 47.1±1.2, −10±4, and +14.4±0.4 in valeronitrile; 51.6±1.9, +4±6, and +13.1±0.6 in benzonitrile. The activation volume varies little in spite of the large variation of the molar volume of nitriles. The activation energy (E_Q/kJ mol^{-1}) and the activation volume at zero pressure ($\Delta V_q^{\ddagger}$/cm^3 mol^{-1}) for the reorientation of nitrile molecules around the axis perpendicular to the C≡N bond were also determined to be respectively as follows: 7.4±0.1 and +8.3±0.4 for acetonitrile; 8.1±0.1 and +9.5±0.2 for propionitrile; 9.2±0.1 and +9.7±0.3 for butyronitrile; 9.1±0.1 and +11.3±0.2 for isobutyronitrile; 10.7±0.2 and +11.9±0.2 for valeronitrile; 12.5±0.2, and +13.5±0.2 for benzonitrile. Both E_Q and $\Delta V_q^{\ddagger}$ increase with increasing bulkiness of the substituent to the cyano group.

The volume of activation $\Delta V^{\ddagger}$ is one of the useful parameters for elucidating the reaction mechanisms.[1-4] The discussion of the reaction mechanism on the basis of $\Delta V^{\ddagger}$, however, is sometimes still ambiguous, since the effect of the bulkiness of reactants including solvent on the activation volume has not been thoroughly understood.

For the limiting associative (A) mechanism and the limiting dissociative (D) mechanism in the solvent exchange at metal ions, one would expect that the absolute value of the limiting activation volume $|\Delta V^{\ddagger}_{\mathrm{lim}}|$[3,4] is roughly equal to the molar volume of the solvent V°. Interchange mechanisms (Ia, I, and Id) will give smaller $|\Delta V^{\ddagger}|$ values. Therefore, not only $\Delta V^{\ddagger}_{\mathrm{lim}}$ but also $\Delta V^{\ddagger}$ for Ia and Id mechanisms would be anticipated to vary with the molar volume of solvent even for the same mechanism.

This work has been designed to elucidate the effect of the molar volume of solvent upon the value of $\Delta V^{\ddagger}$ for the solvent-exchange reaction. We report $\Delta V^{\ddagger}$ for the exchange of various nitriles at the nickel(II) ion. The utilized nitriles include acetonitrile, propionitrile, butyronitrile, isobutyronitrile, valeronitrile, and benzonitrile. We propose a model for the solvent-exchange reaction based on the volume of activation. In addition, we discuss some microscopic properties of the liquid nitriles obtained from the temperature and pressure dependence of the ^{14}N transverse relaxation time of the neat nitriles.

Experimental

Solvents. Reagent grade acetonitrile (Wako Pure Chemical Industries Co.), propionitrile (Wako), butyronitrile (Tokyo Chemical Industry Co.), isobutyronitrile (Tokyo Chemical), valeronitrile (Tokyo Chemical) were distilled twice after refluxing for 1 h in the presence of P_2O_5 (<2g dm^{-3}). Benzonitrile (Wako) was dried over P_2O_5 for 12 h and distilled twice under reduced pressure.

$[Ni(H_2O)_6](CF_3SO_3)_2$. Trifluoromethanesulfonic acid (50 g, Wako) was added dropwise to basic nickel(II) carbonate (20 g, $NiCO_3 \cdot 2Ni(OH)_2 \cdot 4H_2O$, Wako) suspended in 50 cm^3 water. The resulting mixture was heated to complete the reaction and to concentrate the solution. Finally, the green salt yielded by cooling the solution was recrystallized from water and dried under vacuum at room temperature. Found: C, 5.20; H, 2.63%. Calcd for $[Ni(H_2O)_6](CF_3SO_3)_2$: C, 5.17; H, 2.60%.

Sample Preparation. Nitrile solutions of nickel(II) trifluoromethanesulfonate were prepared by dissolving the hydrated nickel(II) trifluoromethanesulfonate (ca. 4 g) in respective nitriles (ca. 60 cm^3) and removing the water under reflux for about 5 h in the modified Soxhlet extractor with Molecular Sieves 4A in the thimble.[5,6] The reflux was repeated two or three times with freshly activated molecular sieves. The nickel(II) concentration of each stock solution was determined by EDTA titration with TAMSMB (2-(2-thiazolylazo)-4-methyl-5-(sulfomethylamino)benzoic acid) as an indicator.[7] The content of water in sample solutions as determined by the Karl-Fischer titration was less than 5×10^{-3} mol kg^{-1} that corresponded to at most less than 0.05 mol/mol of Ni^{2+}.

The dilution of the stock solution and the transfer of the sample solution into an NMR tube were carried out under dry nitrogen gas in a dry box. The sample solutions for variable-temperature NMR measurement were degassed and sealed on a standard vacuum line. The nickel(II) concentrations of the NMR sample solutions were ranged over 2×10^{-2}—2×10^{-1} mol kg^{-1}.

Variable-Temperature ^{14}N NMR Measurement. ^{14}N NMR measurements were performed at various temperatures on a JEOL JNM-GX270 FT-NMR spectrometer operating at 19.51 MHz. The pulse width was 31 μs (90°) and

† Present address: Department of Chemistry, School of Science and Engineering, Waseda University, Okubo, Shinjuku, Tokyo 160.

pulse repetition time was typically 0.15 s. The number of scans was varied between 300 and 30000 depending on the line width. An 8 mm o.d. NMR sample tube was inserted into a 10 mm o.d. NMR tube containing a lock solvent (CD_3OD or D_2O) and nitromethane as a chemical shift standard. The temperature was measured by a substitution technique using a thermistor (D111-1031 or D641, Takara Thermistor Co.). About 15 to 30 min were required for the temperature equilibration of the sample solution and the temperature stability was ±0.2 K.

Variable-Pressure ^{14}N NMR Measurement. For variable-pressure NMR experiments, a multinuclear NMR probe designed for a wide-bore superconducting magnet (6.34 Tesla) of a JEOL JNM-GX270 FT-NMR spectrometer has been newly constructed. The pressure vessel consisting of four separable parts is illustrated in Fig. 1A. The pressure pipe (1) is made of nonmagnetic titanium alloy, around which spiral is cut. A Dewar vessel (e) covers it to insulate the heat. The thermostating gas is flowed along the spiral in order to adjust the temperature in the pressure vessel. An adapter (2) made of titanium alloy is attached to facilitate insertion and withdrawal of the sample tube. Four leading wires for a saddle-shaped coil and a copper-constantan thermocouple are introduced into the electrical terminal (3). The pressure seal at this part is achieved with the cone-type seal using small copper cones covered with Daiflon (poly(chlorotrifluoroethylene), Daikin-Kogyo Co.) for insulation, and at other parts the pressure sealing is accomplished with standard cone-type seals and O-ring seals. The internal housing (4) made of titanium alloy is the guide for the sample tube and also reduces the volume of pressure-transmitting liquid filled in the pressure vessel. The pressure vessel is connected through the flexible tube (a) to a pressure-generating system[8] consisting of a high-pressure generating pump (KBP56, Hikarikouatsu) and Heise Bourdon gauges. The pressure-transmitting liquid used in this work was Daifloil #1 (poly(chlorotrifluoroethylene), Daikin-Kogyo Co.).

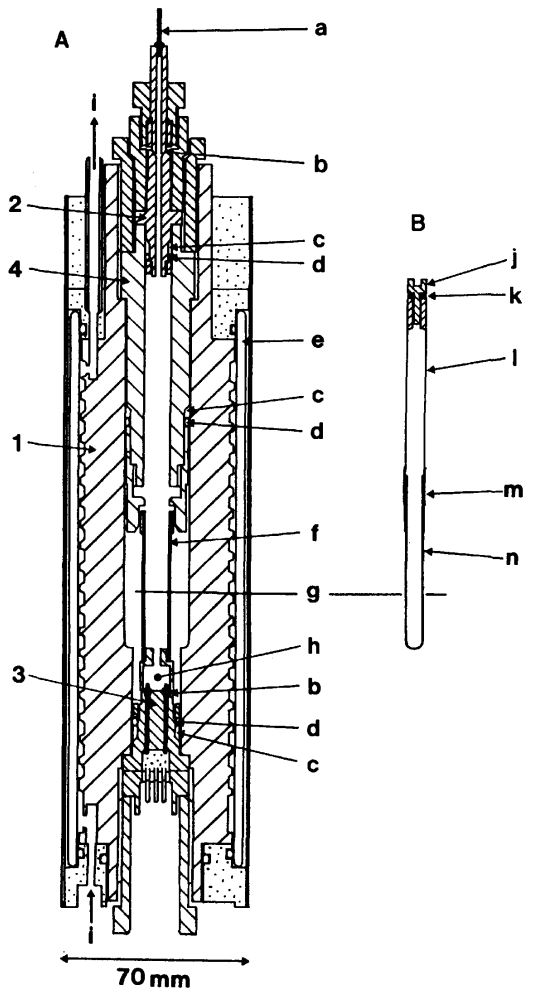

Fig. 1. High-pressure vessel and NMR sample tube for high-pressure NMR experiments.
(A) High-pressure vessel. 1, pressure pipe (titanium alloy); 2, adapter (titanium alloy); 3, electrical terminal; 4, internal housing (titanium alloy); a, flexible tube (SUS316); b, cone-type seal; c, backup ring (Teflon); d, O-ring (Viton); e, Dewar vessel; f, bobbin (glass); g, r.f. coil center; h, copper-constantan thermocouple; i, thermostating gas flow. (B) Sample tube. j, screw (Teflon); k, O-ring (silicone); l, flexible Teflon cap; m, contractive Teflon tube; n, 7 mm o.d. glass tube.

The sample tube, illustrated in Fig. 1B, is filled with the sample solution. It consists of a 7 mm o.d. glass tube and a flexible Teflon cap, both of which are connected with a contractive Teflon tube. At the top a silicone O-ring and Teflon screw are attached.

Before carrying out the high-pressure experiment, the temperature of the sample was measured by a substitution technique using a thermistor, and monitored with a thermocouple introduced into the pressure vessel during the high-pressure experiments. About 5 h were required for the complete temperature equilibration and the temperature stability over several hours was ±0.2 K.

Results and Discussion

Structure of Solvated Ni(II) Ion in Nitrile. The crystal structure of $[Ni(CH_3CN)_6](SbF_6)_2$[9] and $[Ni(CD_3CN)_6](SbF_6)_2$[10] has been determined by the X-ray diffraction method; the nickel(II) ion is octahedrally coordinated by six acetonitrile molecules with the Ni-N-C angle of 175°. The electronic absorption spectra of $Ni(BF_6)_2$,[11] $Ni(MF_6)_2$ (M=Sb, Bi),[10] and $Ni(ClO_4)_2$[6] in acetonitrile are characteristic of an octahedrally coordinated Ni^{2+} ion. The solvation number of 6 for nickel(II) ion in acetonitrile has also been confirmed by means of ^1H NMR.[12,13]

In Fig. 2 are shown the electronic absorption spectra of solutions of $Ni(CF_3SO_3)_2$ in various nitriles which were recorded on a UV-265FW spectrophotometer (Shimadzu) and a U-3400 spectrophotometer (Hitachi). The spectrum of acetonitrile solution is very similar to those reported,[6,10,11] and the spectra of the other nitrile solutions are also characteristic of the octahedrally coordinated Ni^{2+} ion, although the slight band shift is observed. Therefore, we can safely state that Ni^{2+} ion is octahedrally coordinated by the nitrile molecules in all solutions investigated.

Transverse Relaxation Time of ^{14}N in Neat Nitrile. Transverse relaxation time T_2 of nitrogen-14 in neat

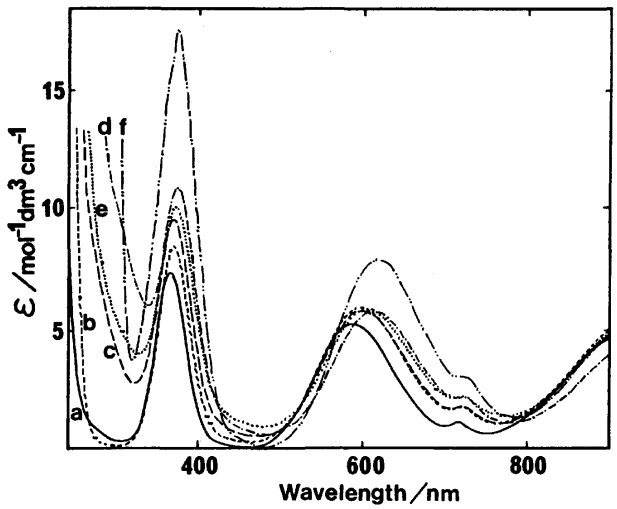

Fig. 2. Electronic absorption spectra of $Ni(CF_3SO_3)_2$ nitrile solutions. a (———), acetonitrile solution; b (·····), propionitrile solution; c (— — —), butyronitrile solution; d (— · —), isobutyronitrile solution; e (·····), valeronitrile solution; f (—··—), benzonitrile solution.
The values of ε are somewhat ambiguous, since the concentrations of the solution in the unit of mol kg^{-1} are transformed into the unit of mol dm^{-3} using the density of the neat solvent.

nitrile is evaluated from the half-height width of the ^{14}N NMR spectrum ($T_2=(\pi\Delta\nu)^{-1}$). Since reorientation of acetonitrile molecules around the axis perpendicular to the C≡N bond in the liquid state is very rapid, ^{14}N ($I=1$) transverse relaxation rate (T_2^{-1}) of acetonitrile is equal to the longitudinal relaxation rate (T_1^{-1}),[14] and these are expressed as follows:

$$T_1^{-1}=T_2^{-1}=\frac{3}{2}\pi^2\chi^2\left(1+\frac{1}{3}\xi^2\right)\tau_q \qquad (1)$$

where χ/Hz is the quadrupole coupling constant ($\chi=e^2Qq/h$), τ_q/s is the correlation time characterizing the reorientation about the axis perpendicular to the C≡N bond and ξ is the asymmetry parameter. This equation is valid for the ^{14}N nuclear relaxation in all the studied nitriles. The temperature and pressure dependence of the relaxation time may be attributable to the variation of τ_q.[14,15]

The temperature dependences of T_2 for ^{14}N of nitriles are shown in Fig. 3. The data were conventionally analyzed by using Eq. 2:

$$\ln T_2=\ln T_2^{298.2}-E_Q(1/T-1/298.2)/R \qquad (2)$$

where $T_2^{298.2}$ and E_Q refer to T_2 at 298.2 K and the activation energy for the reorientation, respectively. The values of $T_2^{298.2}$ and E_Q for acetonitrile are in good agreement with the literature values.[6,14,16] The obtained parameters are listed in Table 1.

By using Eq. 1, we can estimate values of the rate constant (τ_q^{-1}) of the reorientation for some nitriles of which the values of χ and ξ are available; values of τ_q^{-1}

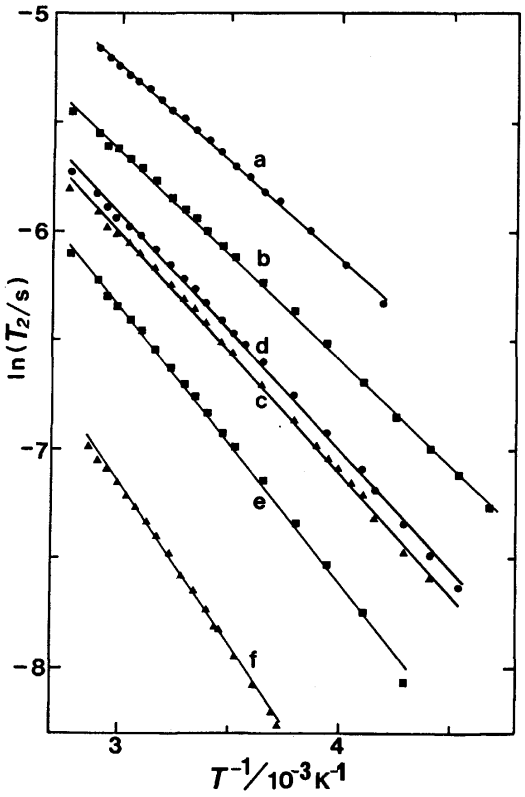

Fig. 3. Temperature dependences of T_2/s for ^{14}N of nitriles. a, acetonitrile; b, propionitrile; c, butyronitrile; d, isobutyronitrile; e, valeronitrile; f, benzonitrile.

Table 1. Transverse Relaxation Time of ^{14}N and Activation Parameters for Reorientation of Nitrile[a]

Solvent	$T_2^{298.2}$	E_Q	$\Delta V_q^{\neq}$		$10^2\Delta\beta_q^{\neq}$	$V^{ob)}$
	s	kJ mol^{-1}	cm^3 mol^{-1}		cm^3 mol^{-1} MPa^{-1}	cm^3 mol^{-1}
Acetonitrile	3.88×10^{-3}	7.4±0.1	+8.3±0.4	(332 K)	+2.0±0.4	52.9
Propionitrile	2.56×10^{-3}	8.1±0.1	+9.5±0.2	(330 K)	+2.0±0.2	70.9
Butyronitrile	1.66×10^{-3}	9.2±0.1	+9.7±0.3	(329 K)	+1.5±0.3	87.9
Isobutyronitrile	1.82×10^{-3}	9.1±0.1	+11.3±0.2	(328 K)	+2.2±0.2	90.3
Valeronitrile	1.12×10^{-3}	10.7±0.2	+11.9±0.2	(329 K)	+2.4±0.2	104.6
Benzonitrile	4.59×10^{-4}	12.5±0.2	+13.5±0.2	(332 K)	+2.0±0.2	103.1

a) Errors quoted are standard deviations. b) Molar volume at 298.2 K. Calculated using the data taken from J. A. Riddick, W. B. Bunger, and T. K. Sakano, "Organic Solvents," 4th ed, Wiley-Interscience, New York (1986).

at 298.2 K and corresponding $\Delta H^{\ddagger}$ and $\Delta S^{\ddagger}$ are 8.0×10^{11} s^{-1}, 5.0±0.1 kJ mol^{-1}, and −0.3±0.4 J mol^{-1} K^{-1} (χ=3.738 MHz, $\xi=0.46\times10^{-2}$)[17] for acetonitrile, 5.4×10^{11} s^{-1}, 5.8±0.1 kJ mol^{-1}, and −1.0±0.4 J mol^{-1} K^{-1} (χ=3.776 MHz, $\xi=2.08\times10^{-2}$)[17] for propionitrile, and 1.0×10^{11} s^{-1}, 9.9±0.2 kJ mol^{-1}, and −1.0±0.6 J mol^{-1} K^{-1} (χ=3.885 MHz, $\xi=10.73\times10^{-2}$)[18] for benzonitrile. It is to be noted that the reorientation of these nitriles is characterized by very small entropy values. Since χ values in different nitriles change no more than a few percent and the contribution of $\xi^2/3$ is negligibe,[14] the difference of τ_q is considered to be exclusively responsible for the difference of T_2. Therefore the rate of reorientation is in the order: acetonitrile > propionitrile > isobutyronitrile≈butyronitrile > valeronitrile > benzonitrile.

Plots of $\ln T_2$ vs. pressure are shown in Fig. 4. Since all plots are slightly curved, the data were analyzed according to the quadratic equation:

$$\ln T_2 = \ln T_2^0 - \Delta V_q^{\ddagger} P/RT + \Delta\beta_q^{\ddagger} P^2/2RT \quad (3)$$

where $\Delta V_q^{\ddagger}$ is the activation volume for the reorientation by rotation about the axis perpendicular to the C≡N bond at zero pressure and $\Delta\beta_q^{\ddagger}$ is the compressibility coefficient of activation. The parameters obtained are listed in Table 1 together with the molar volume of the solvent V°. The value of $\Delta V_q^{\ddagger}$ for acetonitrile (+8.3±0.4 cm^3 mol^{-1}) is in excellent agreement with that (+8.5±1.4 cm^3 mol^{-1}) obtained by Bull and Jonas[15] and the agreement is fair with the value (+6.4±0.2 cm^3 mol^{-1}) obtained by Swaddle et al.[6] There is a trend that $\Delta V_q^{\ddagger}$ increase slightly with the increase of V°. In conclusion, correlation time, activation energy, and activation volume for reorientation increase with increasing bulkiness of substituent to the cyano group.

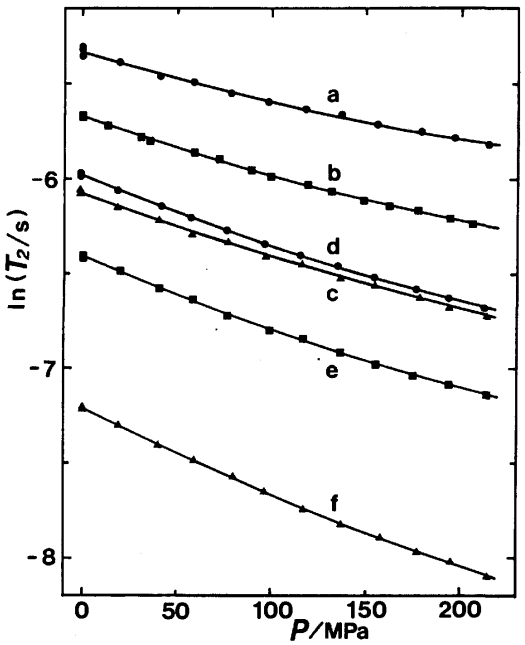

Fig. 4. Pressure dependences of T_2/s for ^{14}N of nitriles. a, acetonitrile; b, propionitrile; c, butyronitrile; d, isobutyronitrile; e, valeronitrile; f, benzonitrile.

Solvent Exchange at the Nickel(II) Ion in Nitrile. The rate for rapid solvent exchange between the bulk and the coordination site of a paramagnetic metal ion can be derived from the transverse relaxation rate of the bulk solvent nuclei.[19-21] The nitrile ^{14}N line broadening, $(T_{2P}P_M)^{-1}$, caused by the interaction with the nickel(II) ion can be expressed as Eq. 4:

$$(T_{2P}P_M)^{-1} = \pi(\Delta\nu_{obsd} - \Delta\nu_{solv})P_M^{-1} \quad (4)$$

where P_M is the ratio of the number of nitrile molecules bound to nickel(II) to that in the bulk, $\Delta\nu_{obsd}$ and $\Delta\nu_{solv}$ are the full widths at half-height of the ^{14}N NMR signal for the bulk nitrile of the nickel(II) nitrile solution and of the neat nitrile, respectively. For $P_M \ll 1$, $(T_{2P}P_M)^{-1}$ is given by the modified Swift-Connick equation (Eq. 5):[19-21]

$$\frac{1}{T_{2P}P_M} = \frac{1}{\tau_M}\frac{T_{2M}^{-2} + (T_{2M}\tau_M)^{-1} + \Delta\omega_M^2}{(T_{2M}^{-1} + \tau_M^{-1})^2 + \Delta\omega_M^2} + \frac{1}{T_{2O}} \quad (5)$$

in which symbols have their usual meaning.[22] We measured the NMR spectra of sample solutions with two or three different concentrations of nickel(II) trifluoromethanesulfonate at various temperatures. The observed line widths ($\Delta\nu_{obsd} - \Delta\nu_{solv}$) are excellently proportional to the P_M value. The temperature dependences of $(T_{2P}P_M)^{-1}$ for the nitrile solutions of $Ni(CF_3SO_3)_2$ are shown in Fig. 5. Since $\Delta\omega_M^2 \gg \tau_M^{-2}$, T_{2M}^{-2} over the temperature range of our experiment, Eq. 5 is simplified to Eq. 6:

$$(T_{2P}P_M)^{-1} = \tau_M^{-1} + T_{2O}^{-1} \quad (6)$$

where τ_M^{-1} is equivalent to the rate constant k_{ex} for the solvent-exchange reaction ($k_{ex} = k_B T/h \exp(-\Delta H^{\ddagger}/RT + \Delta S^{\ddagger}/R)$) and T_{2O}^{-1} ($= C_O/T \exp(E_O/RT)$) is the relaxation term due to the interaction in the outer sphere of the nickel(II) ion. We analyzed the data according to Eq. 6 by a least-squares fitting and obtained the kinetic parameters listed in Table 2.

The variable-pressure ^{14}N NMR experiments have been performed at about 330 K where the outer-sphere contribution T_{2O}^{-1} is negligible so that $(T_{2P}P_M)^{-1}$ is exclusively ascribed to the solvent-exchange contribution τ_M^{-1}. The pressure dependences of $k_{ex(p)}$ ($=\tau_M^{-1} = (T_{2P}P_M)^{-1}$ at a given temperature) are presented in Fig. 6. $k_{ex(p)}$ can be expressed as Eq. 7:

$$\ln k_{ex(p)} = \ln k_{ex(0)} - \Delta V_0^{\ddagger} P/RT + \Delta\beta^{\ddagger} P^2/2RT \quad (7)$$

where $k_{ex(0)}$ is the rate constant at zero pressure, $\Delta V_0^{\ddagger}$ is the volume of activation at zero pressure, and $\Delta\beta^{\ddagger}$ is the compressibility coefficient of activation. The kinetic parameters are evaluated by a least-squares fitting of the data to Eq. 7 and are listed in Table 2. The $\Delta V_0^{\ddagger}$ value for the reaction in acetonitrile is in good agreement with that obtained by Merbach et

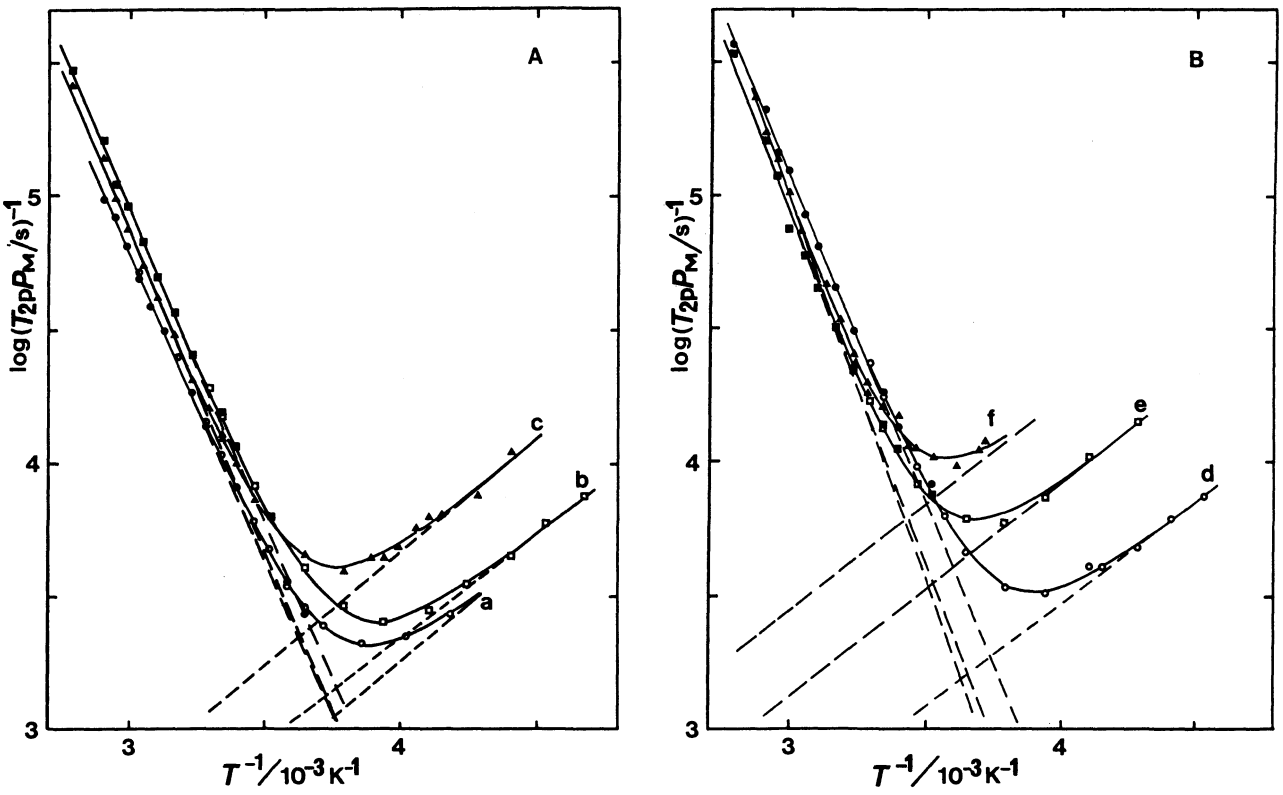

Fig. 5. Temperature dependences of $(T_{2P}P_M)^{-1}/s^{-1}$.
(A) a, acetonitrile solution (●: P_M=1.49×10^{-2}, ◐: P_M=3.19×10^{-2}, ○: P_M=4.39×10^{-2}); b, propionitrile solution (■: P_M=2.27×10^{-2}, □: P_M=5.73×10^{-2}); c, butyronitrile solution (▲: P_M=2.12×10^{-2}, △: P_M=4.24×10^{-2}). (B) d, isobutyronitrile solution (●: P_M=2.06×10^{-2}, ○: P_M=3.80×10^{-2}); e, valeronitrile solution (■: P_M=2.07×10^{-2}, □: P_M=4.19×10^{-2}); f, benzonitrile solution (▲: P_M=1.63×10^{-2}, △: P_M=4.505×10^{-2}). Dashed lines show the contribution of τ_M^{-1} and T_{2O}^{-1}.

Table 2. Kinetic Parameters for Nitrile Exchange at Nickel(II)[a)]

Solvent	$k_{ex}^{298.2}$	$\Delta H^{\ddagger}$	$\Delta S^{\ddagger}$	$\Delta V_0^{\ddagger}$	$10^2\Delta\beta^{\ddagger}$
	s^{-1}	kJ mol^{-1}	J mol^{-1} K^{-1}	cm^3 mol^{-1}	cm^3 mol^{-1} MPa^{-1}
Acetonitrile	6.24×10^3	41.4±0.5	−30±2	+12.0±0.4 (332 K)	4.0±0.3
Propionitrile	1.33×10^4	42.0±0.4	−25±2	+13.7±0.5 (330 K)	2.3±0.2
Butyronitrile	1.04×10^4	43.3±0.7	−23±2	+13.1±0.5 (329 K)	4.1±0.4
Isobutyronitrile	1.59×10^4	43.3±0.5	−19±2	+12.4±0.6 (328 K)	3.8±0.6
Valeronitrile	9.99×10^3	47.1±1.2	−10±4	+14.4±0.4 (329 K)	5.0±0.4
Benzonitrile	9.38×10^3	51.6±1.9	+4±6	+13.1±0.6 (332 K)	6.3±0.6

a) Errors quoted are standard deviations.

al. (+11.3±1.0 cm^3 mol^{-1}).[23)]

In spite of the large variation of V° of the nitriles (53—105 cm^3 mol^{-1}), little change is observed in the activation volumes for the solvent exchange at nickel(II) (12.0—14.4 cm^3 mol^{-1}): the molar volume of solvent itself has little influence upon $\Delta V^{\ddagger}$ for the exchange reaction of nitriles.

In order to consider the activation volume for the solvent exchange at a metal ion, we now define the inner sphere of the solvated metal ion as the sphere into which the solvent molecules in the bulk can not penetrate at the initial state (see Fig. 7). The activation volume for the solvent exchange is thought to be the difference between the volume V_d that the leaving solvent loses in the inner sphere and the volume V_a that the entering solvent gets in the inner sphere at the transition state, as illustrated in Fig. 7. According to the molecular model constructed with van der Waals's radii of atoms, the nitrile molecules in the bulk can penetrate into the gaps among the bound nitriles without any steric hindrance regardless of the bulkiness of the substituent: the inner sphere does not include the substituent to cyano group and its size does not depend on the bulkiness of the nitrile. In fact the $\Delta V^{\ddagger}$ value is positive and varies little from solvent to solvent. Therefore both V_a and V_d are

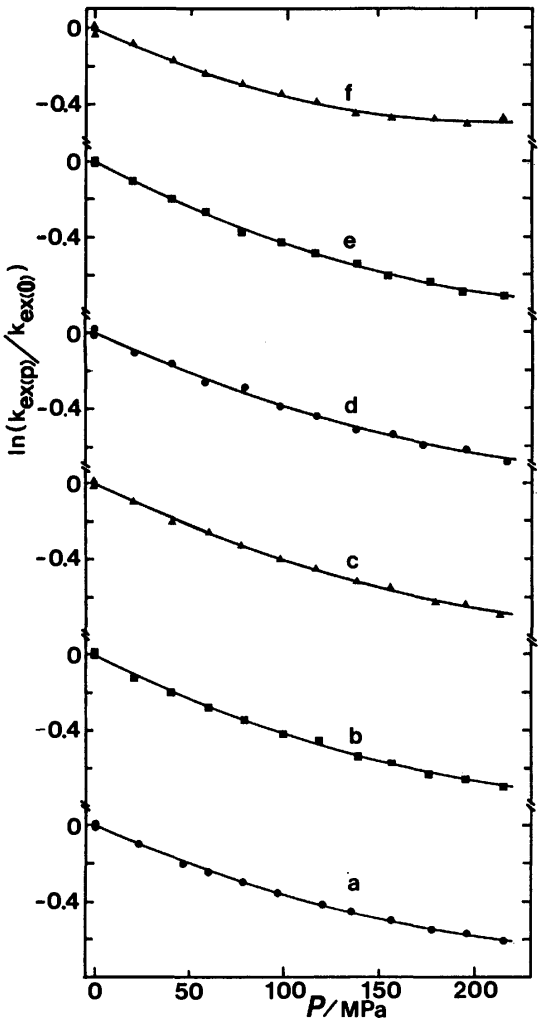

Fig. 6. Pressure dependences of $k_{ex(p)}/k_{ex(0)}$ for solvent exchange at Ni^{2+} in nitriles.
a, acetonitrile solution (P_M=1.76×10^{-2}); b, propionitrile solution (P_M=2.07×10^{-2}); c, butyronitrile solution (P_M=2.39×10^{-2}); d, isobutyronitrile solution (P_M=2.02×10^{-2}); e, valeronitrile solution (P_M=3.02×10^{-2}); f, benzonitrile solution (P_M=4.05×10^{-2}).

expected to be almost the same for all the studied nitriles. After all, the mechanism of the nitrile exchange at the nickel(II) ion is of the similar dissociative character for different nitriles of different bulkiness.

There is no parallel relation between $\Delta S^{\ddagger}$ and $\Delta V_0^{\ddagger}$ in the present systems (Table 2). The activation volume reflects the difference in nuclear positions between reactants and transition state, while the alternative concept of activation entropy seems to reflect the difference in both nuclear positions and energy.[24] Thus the solvent-solvent interaction may contribute considerably to values of $\Delta S^{\ddagger}$.[25] In the present system, acetonitrile liquid is highly structured due to strong dipole-dipole interactions, and the coordination sphere of the central nickel(II) ion has a definite octahedral structure. There should be the less ordered secondary sphere between the coordination sphere and the bulk solvent (B region according to the Frank-Wen model).[26] Therefore the leaving acetonitrile molecule in the activation process may strongly interact with the solvent molecules in the secondary sphere, and then the entropy of activation should become largely negative. Thus we anticipate a trend that the solvent interaction in the transition state should become smaller, and accordingly $\Delta S^{\ddagger}$ values may become larger with increasing size of solvent molecules. We notice such a trend for values of $\Delta S^{\ddagger}$ in Table 2. In conclusion, the sign of $\Delta V^{\ddagger}$ is useful for diagnosing the mechanism, whereas the interpretation of $\Delta S^{\ddagger}$ in terms of mechanism is likely to be complicated by the solvent-solvent interactions.

This work was supported by a Grant-in-Aid for Scientific Research (No. 62470041) from the Ministry of Education, Science and Culture. We thank Professor Jiri Jonas (University of Illinois) for his useful advice and Mr. Sadao Kanbe (JEOL) for his technical assistance on the construction of our high-pressure NMR probe.

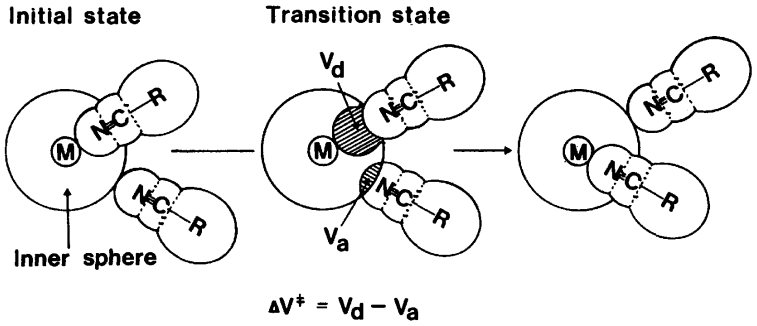

Fig. 7. Illustration for solvent exchange at a metal ion. The non-exchanging solvent molecules are omitted for simplicity; V_d, the volume that the leaving solvent molecule loses from the inner sphere in the activation process; V_a, the volume that the entering solvent molecule gets in the inner sphere in the activation process. The activation volume $\Delta V^{\ddagger}$ is represented as $\Delta V^{\ddagger}=V_d-V_a$.

References

1) A. E. Merbach, *Pure Appl. Chem.*, **54**, 1479 (1982).
2) T. W. Swaddle, *Adv. Inorg. Bioinorg. Mech.*, **2**, 95 (1983).
3) A. E. Merbach, *Pure Appl. Chem.*, **59**, 161 (1987).
4) "Inorganic High Pressure Chemistry : Kinetics and Mechanisms" ed by R. van Eldik, Elsevier, Amsterdam (1986).
5) P. Arthur, W. M. Haynes, and L. P. Varga, *Anal. Chem.*, **38**, 1630 (1966).
6) Y. Yano, M. T. Fairhurst, and T. W. Swaddle, *Inorg. Chem.*, **19**, 3267 (1980).
7) T. Ishizuki, H. Wada, and G. Nakagawa, *Bunseki Kagaku*, **28**, 535 (1979).
8) M. Ishii, S. Funahashi, and M. Tanaka, *Inorg. Chem.*, **27**, 3192 (1988).
9) I. Leban, D. Gantar, B. Frlec, D. R. Russell, and J. H. Holloway, *Acta Crystallogr., Sect. C. Cryst. Struct. Commun.*, **34**, 1888 (1987).
10) R. Bougon, P. Charpin, K. O. Christe, J. Isabey, M. Lance, M. Nierlich, J. Vigner, and W. W. Wilson, *Inorg. Chem.*, **27**, 1389 (1988).
11) B. J. Hathaway and D. G. Holah, *J. Chem. Soc.*, **1964**, 2400.
12) K. E. Newman, F. K. Meyer, and A. E. Merbach, *J. Am. Chem. Soc.*, **101**, 1470 (1979).
13) S. Chopra, R. E. D. McClung, and R. B. Jordan, *J. Magn. Reson.*, **59**, 361 (1984).
14) W. B. Moniz and H. S. Gustowsky, *J. Chem. Phys.*, **38**, 1155 (1963).
15) T. E. Bull and J. Jonas, *J.Chem. Phys.*, **53**, 3315 (1970).
16) T. T. Bopp, *J. Chem. Phys.*, **47**, 3621 (1967).
17) P. A. Casabella and P. J. Bray, *J. Chem. Phys.*, **29**, 1105 (1958).
18) H. Negita and P. J. Bray, *J. Chem. Phys.*, **33**, 1876 (1960).
19) T. J. Swift and R. E. Connick, *J. Chem. Phys.*, **37**, 307 (1962).
20) Z. Luz and S. J. Meiboom, *J. Chem. Phys.*, **40**, 1058 (1964).
21) L. L. Rusnak and R. B. Jordan, *Inorg. Chem.*, **15**, 709 (1976).
22) A. Hioki, S. Funahashi, and M. Tanaka, *J. Phys. Chem.*, **89**, 5057 (1985).
23) F. K. Meyer, K. E. Newman, and A. E. Merbach, *Inorg. Chem.*, **18**, 2142 (1979).
24) S. Funahashi, K. Ishihara, and M. Tanaka, *Inorg. Chem.*, **22**, 2070 (1983).
25) E. F. Caldin and H. P. Bennetto, *J. Solution Chem.*, **2**, 217 (1973); H. P. Bennetto and E. F. Caldin, *J. Chem. Soc. A*, **1971**, 2198.
26) H. S. Frank and W.-Y. Wen, *Discuss. Faraday Soc.*, **24**, 133 (1957).

 © 1989 The Chemical Society of Japan Bull. Chem. Soc. Jpn., 62, 1859—1863 (1989)

Synthesis and Properties of Copper(II) Perchlorate Complexes with Imino Oximes

Songping WAN, Wasuke MORI, Shoichiro YAMADA, and Shun-Ichi MURAHASHI*
Faculty of Engineering Science and College of General Education, Osaka University, Toyonaka 560
(Received December 23, 1988)

Three types of imino oxime copper(II) complexes were obtained by the reactions of copper(II) perchlorate with imino oximes (3-[2-[(alkylamino)ethyl]imino]-2-butanone oximes or 3-[2-[(dialkylamino)ethyl]imino]-2-butanone oximes, abbreviated as Hdox-enRR′). One type contains the dinuclear complexes $[Cu_2(dox\text{-}enRR')_2]^{2+}$ and uncoordinated perchlorate anions. The magnetic susceptibilities measured over the temperature range 77—320 K indicate that there exists a strong antiferromagnetic spin coupling interaction through the N-O bridge in these complexes. The magnetic behavior can be explained by using the Bleaney-Bowers equation. Complexes of the second type probably contain a square-tetranuclear complex. The copper(II) ions assume a penta-coordinated configuration with perchlorate anion coordinated at the axial coordination site. It is assumed that the dinuclear and mononuclear magnetic units coexist in the complexes of the third type. The plot of the magnetic susceptibilities versus temperature is linear in the two temperature ranges ($T>250$ K, <100 K).

Previous reports on the metal complexes with imino oximes **1** have shown a variety of structural and magnetic properties, which depend upon the substituents R and R′, metal ions and counter anions.[1-5] For example, the reactions of

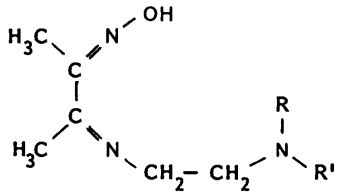

1a Hdox-enR(R′ = H, R = alkyl)
1b Hdox-enR$_2$(R′ = R = alkyl)
1

nickel(II) salts with imino oximes **1** gave two types of complexes, namely hexa-coordinated octahedral and tetra-coordinated planar nickel(II) complexes. Significant effects of the counter anions[1] are also found in these studies. We have extended similar studies to copper(II) complexes. In the copper(II) thiocyanato complexes, imino oximes **1** are coordinated to copper (II) ion as a bridging quadridentate ligand, and the thiocyanate anion is coordinated through nitrogen atom to form a group of penta-coordinated dinuclear copper(II) complexes.[4] In copper(II) halide complexes with imino oximes, the main skeleton of complexes is similar to that of the copper(II) thiocyanato complexes, in which imino oximes act as a bridging quadridentate ligand. However, halide anions are not coordinated, in contrast to the thiocyanato complexes, showing their weaker coordination ability than that of thiocyanate anion.[5] Although some copper(II) perchlorate complexes with this ligand which were concluded to have a penta-coordinated dinuclear structure have been reported previously,[6] there remain important problems about related complexes with ligands having different steric conditions. In the present work more detailed examination has been carried out on copper(II) perchlorate complexes with a series of imino oximes. The study has shown that tetranuclear complexes and complexes consisting of mononuclear and dinuclear magnetic units, in addition to simple dinuclear one, occur in these copper(II) perchlorate complexes. Reported here are the results of our work on the polynuclear copper(II) perchlorate complexes with imino oximes.

Experimental

Materials. Biacetyl monoxime, *N*-alkylethylenediamine, *N*,*N*-dialkylethylenediamine, and copper(II) perchlorate hexahydrate were commercially available and used as received.

Synthesis. Cu(Hdox-enMe)(ClO$_4$)$_2$ (R′ = H, R = Me; 4a). A mixture of biacetyl monoxime (1.01 g, 0.01 mol) and *N*-methylethylenediamine (0.74 g, 0.01 mol) in 2-propanol (20 cm^3) was heated at 70 °C for 2 h. The resulting solution was added to a suspension of copper(II) perchlorate (3.70 g, 0.010 mol) in ethanol (30 cm^3) at 50 °C and stirred for 2 h. Filtration and subsequent washing with ethanol gave green powder of complex (2.52 g) in 56% yield. Mp: 217 °C. Found: C, 22.85; H, 4.07; N, 9.19%. Calcd for $C_7H_{15}N_3OCu(ClO_4)_2 \cdot 1/2PrOH$: C, 22.70; H, 4.26; N, 9.34%.

Cu(Hdox-enPr)(ClO$_4$)$_2$ (R′=H, R=Pr; 4b). A mixture of biacetyl monoxime (1.01 g, 0.010 mol) and *N*-propylethylenediamine (1.02 g, 0.01 mol) in ethanol(30 cm^3) was heated at 60 °C for 1.5 h. The resulting solution was added to a solution of copper(II) perchlorate (3.70 g, 0.01 mol) in 2-propanol (20 cm^3) at room temperature, and the mixture was stirred for several hours. Slow evaporation of the reaction mixture at room temperature gave green powder of complex (1.18 g) in 24% yield. Mp>300 °C. Found: C, 26.74; H, 5.13; N, 8.92%. Calcd for $C_7H_{15}N_3OCu(ClO_4)_2 \cdot EtOH$: C, 26.75; H, 5.10; N, 8.51%.

Cu(dox-enRR′)ClO$_4$ (R′=H, R=Ph, 2a; R′=R=Pr^i, 2b). These complexes were prepared by a similar method to that for Cu(dox-enPr)ClO$_4$ (**4b**), except that *N*-phenylethylenediamine (1.36 g, 0.01 mol) or *N*,*N*-diisopropylethylenediamine (1.44 g, 0.01 mol) was used in place of *N*-

propylethylenediamine. Dark-green crystalline complexes **2a** (2.83 g) and **2b** (1.40 g) were obtained in 72% yield and 36% yield respectively. Mp: **2a**, 254 °C and **2b**, 229 °C (all accompanied by explosion). Found: C, 38.08; H, 4.25; N, 10.85%. Calcd for $C_{12}H_{16}N_3OCuClO_4 \cdot 1/4EtOH$ (**2a**): C, 38.16; H, 4.48; N, 10.68%. Found: C, 37.08; H, 6.15; N, 10.64%. Calcd for $C_{12}H_{24}N_3OCuClO_4$ (**2b**): C, 37.02; H, 6.21; N, 10.79%.

Cu(dox-enMe)ClO$_4$ (R′=H, R=Me; 3a). This complex was prepared by a similar method to that for Cu(dox-enPr)ClO$_4$ (**4b**), except that *N*-methylethylenediamine (0.74 g, 0.01 mol) was used in place of *N*-propylethylenediamine. Complex **3a** (0.76 g) as dark green crystals was obtained in 23% yield. Mp: 225 °C. Found: C, 26.89; H, 4.57; N, 12.58%. Calcd for $C_8H_{16}N_3OCuClO_4 \cdot 1/4EtOH$: C, 27.24; H, 4.72; N, 12.71%.

Cu(dox-enEt)ClO$_4$ (R′=H, R=Et; 3b). This complex was prepared by a method similar to that for complex Cu(dox-enMe)ClO$_4$, except that *N*-ethylethylenediamine was used instead of *N*-propylethylenediamine. Filtration and recrystallization with ethanol gave dark-green crystals of complex **3b** (1.90 g) in 57% yield. Mp: 240 °C. Found: C, 28.93; H, 4.76; N, 12.78% Calcd for $C_8H_{16}N_3OCuClO_4$: C, 28.83; H, 4.84; N, 12.61%.

Measurements. Electronic absorption spectra were measured at room temperature with a Shimadzu MPS 5000 spectrophotometer. Infrared absorption spectra were recorded as Nujol mulls on a Perkin-Elmer 938G infrared spectrophotometer. Room temperature magnetic moments were determined by the Gouy method using H_2O as a susceptibility standard, and magnetic susceptibilities at temperatures 4 K to 320 K were measured by the Faraday method in a manner as described previously.[11] Pascal's constants were used to estimate the diamagnetic corrections for imino oximes, ClO_4, and Cu.[12]

Results and Discussion

Synthesis of the Copper(II) Perchlorate Complexes with Imino Oximes. In the present work, two types of copper(II) complexes were obtained, depending upon the nature of R and R′, by reactions of copper (II) perchlorate with one equivalent of imino oximes (Hdox-enRR′, **1**). From their magnetic properties, as discussed later in more detail, these complexes can be classified into the following three groups:

i) Cu(dox-enRR′)ClO$_4$ (**2**; R′=H, R=Ph; R′=R=Pr^i)
ii) Cu(dox-enR)ClO$_4$ (**3**; R=Me, Et)
iii) Cu(Hdox-enR)(ClO$_4$)$_2$ (**4**; R=Me, Pr)

Characterization of the Copper(II) Perchlorate Complexes 2. In these complexes **2**, the copper(II) ion is assumed to have a quadri-coordinated square-planar geometry, similar to that in copper(II) halide complexes.[5] The composition determined by the elemental analysis indicates that the imino oximes lose a proton on coordination to the copper(II) ion.

Infrared spectra of the complexes **2** exhibit no vibrations in 3140—3253 cm^{-1}, showing that the deprotonated imino oxime monoanions are coordinated to the copper(II) ion, in agreement with the assumption that the complexes **2** are copper(II) complexes. Moreover,

Table 1. The Main Data for Copper(II) Perchlorate Complexes of Imino Oximes

Complex	R	R′	μ/BM	d-d/10^{3}cm^{-1}	$\nu_{C=N}$/cm^{-1}
2a	Ph	H	0.51	17.0	1654
2b	Pr^i	Pr^i	0.68	16.8	1642
3a	Me	H	1.62	16.1	1637
3b	Et	H	1.62	15.2	1636
4a	Me	H	1.43	15.9	1642
4b	Pr	H	1.34	15.7	1641

the bands due to imino oxime C=N (Table 1) are shifted from the vibration of the free ligand at 1623—1630 cm^{-1}, indicating that the nitrogen atom of imino oxime C=N is bound to the copper(II) ion. The perchlorate anion is not bound to the copper(II) ion, since an unsplit band due to the perchlorate anion appears at about 1080 cm^{-1}.

Electronic absorption spectra of the copper(II) complexes **2** show one broad band in the visible region (Table 1), where d-d bands of square planar copper(II) complexes are expected to occur.[13,14] Since the magnetic moments of these copper(II) complexes at room temperature are subnormal, the spin-coupling interaction between copper(II) ions is presumed to be present. In the light of previous studies on the corresponding copper(II) halide complexes,[5] a similar dinuclear structure [Cu$_2$(dox-enRR′)$_2$]$^{2+}$ (shown in **2**) may also be proposed for the copper(II) perchlorate complexes **2** in the present work. This is supported by the finding in the present work that d-d bands, like those of copper(II) halide complexes,[5] are shifted to higher energy region, as compared with those of thiocyanato copper(II)

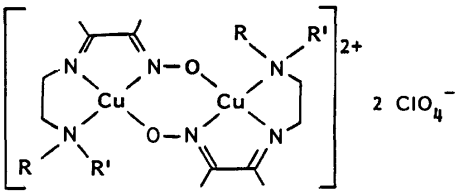

2a, R′=H, R=Ph
2b, R′=Pr^i
[Cu$_2$(dox-enRR′)$_2$]$^{2+}$
2

complexes.[4] It is well known that the d-d bands of the square-planar copper(II) complex undergo a bathochromic shift when the fifth ligand is bound to the planar copper(II) ion.[13,14]

Consistent with the assumption about the dinuclear structure, the temperature dependence of the magnetic susceptibilities of copper(II) perchlorate complexes shows that there exists a spin-coupling interaction between two copper(II) ions of dinuclear complexes. Magnetic susceptibilities of complexes **2** measured over the temperature range 77—320 K, which are shown in Fig. 1, indicate the presence of a

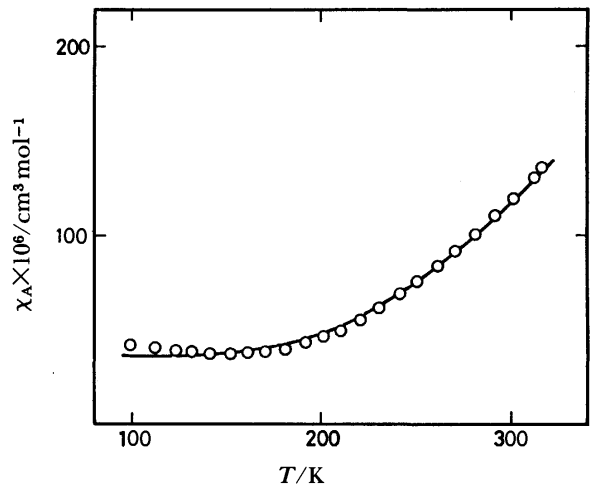

Fig. 1. Temperature dependence of the magnetic susceptibilities for Cu(dox-enPh)ClO_4 (**2a**). The solid line was calculated from Eq. 1 with g=2.29, $2J/k$=−1300 K, $N\alpha$=35×10^{-6} cm^3 mol^{-1}.

strong spin-coupling interaction between copper(II) ions in these dinuclear complexes, in the same way as in copper(II) thiocyanato and copper(II) halide complexes. The magnetic behaviors can be explained using the Bleaney-Bowers equation (Eq. 1)

$$\chi_A = \frac{Ng^2\beta^2}{kT}\frac{1}{3+\exp(-2J/kT)} + N\alpha \quad (1)$$

The symbols in Eq. 1 have their usual meanings. Figure 1 exhibits good agreement between the experimental and calculated values. The exchange parameters for the copper(II) perchlorate complexes **2** are given in Table 2. The values of $-2J$ of the copper(II) perchlorate complexes **2**, just like the copper(II) halide complexes, are greater than those of the thiocyanato copper(II) complexes. This result implies that the spin-coupling interaction between two copper(II) ions is stronger in the perchlorate complexes than that in the thiocyanato complexes, and may be considered to arise from the apical bonding of the thiocyanate anion to the copper(II) ion in the latter. Thus all the findings combined are consistent with the assumption that the complexes **2** adopts a dinuclear structure $[Cu_2(dox\text{-}enRR')_2]^{2+}$ and that there exists a strong antiferromagnetic interaction between two copper(II) ions through two bridging N-O groups.

Table 2. Magnetic Susceptibilities at Room Temperature and Magnetic Parameters of Copper(II) Perchlorate Complexes of Imion Oximes

Complex	χ_g / cm^3 g^{-1}	g	$-2Jk^{-1}$ / K	$N\alpha\times10^6$ / cm^3 mol^{-1}
2a	0.18	2.29	1300	35
2b	−0.09	2.33	1300	50
3a	3.05	2.00	128	60
3b	2.84	2.17	180	60
4a	1.55	2.10	960	60
4b	1.14	2.00	860	60

Characterization of Copper(II) Perchlorate Complexes 3. The composition of the elemental analysis shows the same empirical formula as that of complexes **2** though, the magnetic moments (1.62 BM) at room temperature are much higher than those of complexes **2**, indicating that the structure of complexes **3** is significantly different from that of complexes **2**. Similar to complexes **2**, infrared spectra of complexes **3** show that deprotonated imino oximate monoanion is coordinated to the copper(II) ion. A perchlorate anion is coordinated to copper(II) ion (Table 1), which is different from complexes **2**. The d-d bands of complexes **3** (Table 1) appear at a lower wavenumber than those of the copper(II) halides complexes. Therefore, it is likely that copper(II) ion in complexes **3** may be penta-coordinated, in a similar way to copper(II) thiocyanato complexes.

Although the subnormal magnetic moments of complexes **3** indicate the presence of antiferromagnetic spin-interaction, their variable temperature magnetic susceptibilities do not obey the Bleaney-Bowers equation for the dinuclear model. Investigation of variable temperature magnetic susceptibilities shows that complexes **3** have a tetranuclear structure, in which there exist an antiferromagnetic interactions. Over the temperature range 4—300 K, the best fit curve of susceptibilities versus temperature shows a clear peak at about 100 K (Fig. 2). The magnetic behaviors can be explained using Eq. 2 for the square-tetranuclear structure:[15]

$$\chi_A = \frac{Ng^2\beta^2}{2kT}\frac{2+5\exp(-2x)+\exp(2x)}{7+5\exp(-2x)+3\exp(2x)+\exp(4x)} + N\alpha \quad (2)$$

$$(x=-J/kT)$$

where g, J, and $N\alpha$ are g factor, exchange integral, and T. I. P. respectively. The exchange parameters for the copper(II) perchlorate complexes **3** are given in

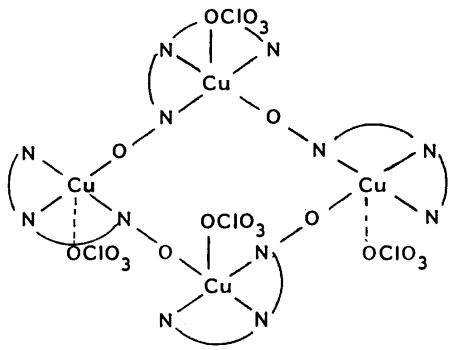

3a, R′=H, R=Me
3b, R′=H, R=Et
$[Cu_4(dox\text{-}enR)_4(ClO_4)_4]$
3

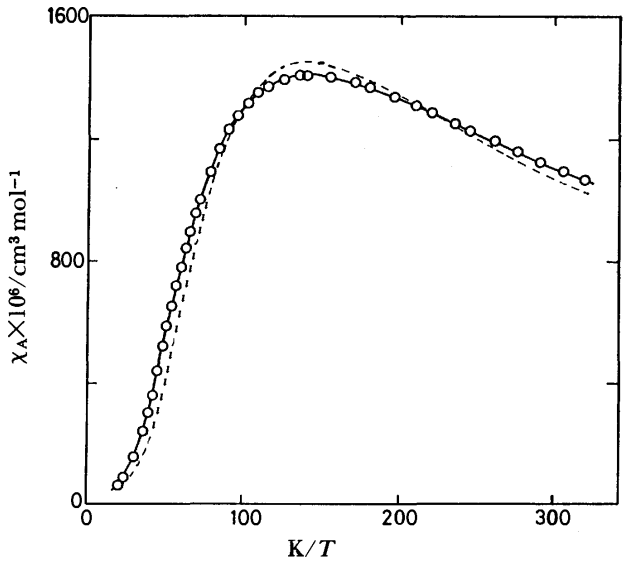

Fig. 2. Temperature dependence of the magnetic susceptibilities for Cu(dox-enEt)ClO_4 (**3b**). The solid line was calculated from Eq. 2 with g=2.17, $2J/k$=−180 K, $N\alpha$=60×10^{-6} cm^3 mol^{-1}. The broken line shows the best fit curve for dinuclear structure with g=2.04, $2J/k$=−255 K, $N\alpha$=60×10^{-6} cm^3 mol^{-1}.

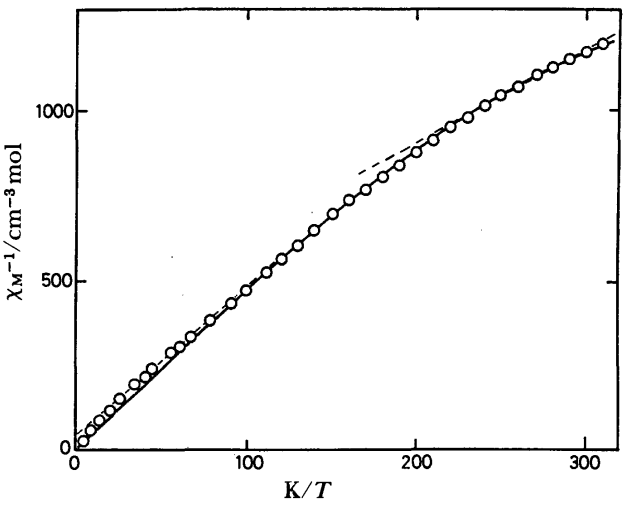

Fig. 3. Reciprocal susceptibility vs. temperature for Cu(Hdox-enMe)$(ClO_4)_2$ (**4a**). The solid line shows the theoretical susceptibilities calculated from Eq. 4 with g=2.10, $2J/k$=−960 K, $N\alpha$=60×10^{-6} cm^3 mol^{-1}. The broken lines show the Curie-Weiss law.

Table 2. Figure 2 exhibits good agreement between the experimental and calculated values, giving support to the assumption that complexes **3** consist of tetranuclear units.[16] One of most possible structures is shown in **3**.

Characterization of Copper(II) Perchlorate Complexes 4. The elemental analysis leads to the empirical formula Cu(Hdox-enR)$(ClO_4)_2$, which is significantly different from those of the complexes **2** and **3**. This formulation, requires that molecules of the imino oximes are coordinated to copper(II) ion in complexes **4**. Infrared spectra show that perchlorate anion, as in complexes **3**, is coordinated to the copper(II) ion. The d-d bands (Table 1) indicate that the coordination geometry around copper(II) ion is pentacoordinated. The magnetic moment calculated per copper(II) ion (1.34—1.43 BM) is smaller than the spin-only value, showing the presence of spin-coupling interaction between copper(II) ion in these complexes **4**. Magnetic susceptibilities were measured over the temperature range 4—300 K. The plot of reciprocal susceptibility versus temperature is linear in two temperature ranges, namely, T<100 K and T>250 K (Fig.3). The data fit to the Curie-Weiss law (Eq.3) with C_h=0.313 emu K mol^{-1} and θ_h=−140 K, C_l=0.226 emu K mol^{-1} and θ_l=−10 K for complex **4a**, and C_h=0.302 emu K mol^{-1} and θ_h=−100 K, C_l=0.185 emu K mol^{-1} and θ_l=−10 K for complex **4b**, where C_h and θ_h are Curie and Weiss constant of the high temperature range, and C_l and θ_l are Curie and Weiss constant of the low temperature range.

$$\chi^{-1}=C^{-1}(T-\theta) \quad (3)$$

It is thus clear that there exists a strong antiferromagnetic interaction between copper(II) ions in these complexes **4**. The ratio C_h/C_l (1.6 for **4a** and 1.4 for **4b**) suggests centered-triangular tetranuclear unit or coexistence of dinuclear and mononuclear magnetic units (1:1 ratio) in complexes **4**. The magnetic susceptibility for the model of coexisting dinuclear and mononuclear copper(II) complexes in 1:1 ratio can be formulated as Eq. 4:

$$\chi_A=\frac{1}{2}\frac{Ng^2\beta^2}{kT}\frac{1}{3+\exp(-2J/kT)}+\frac{1}{2}\frac{Ng^2\beta^2}{4kT}+N\alpha \quad (4)$$

This equation reproduces the observed susceptibilities well with $2J/k$=−960 K, g=2.10 and $N\alpha$=60×10^{-6} cm^3 mol^{-1} for complex **4a** (Fig.3), and $2J/k$=−860 K, g=2.00 and $N\alpha$=60×10^{-6} cm^3 mol^{-1} for complex **4b**. The agreement between calculated and observed susceptibility for the centered-triangular tetranuclear model is much poorer than for the model of coexisting dinuclear and mononuclear units. Therefore, the latter models more likely for complexes **4**. It may be possible that there exists an antiferromagnetic spin interaction between two copper(II) ions in the tetranuclear clusters, but the third and fourth copper(II) ions in the cluster are not involved in spin-coupling with the other copper(II) ions.** Although the precise structure can be determined by the single crystal X-ray study, attempts to grow crystals of the complexes suitable for X-ray studies have not so far been successful.

As discussed above, the present work has revealed

** A referee has questioned whether there would be bridging groups in the proposed formula. It is true that the alcoholato oxygen atom most frequently occurs as a bridge. However, it may also be possible that the alcoholic hydroxyl group functions as a bridge.

that various skeletal structures have been found in copper(II) perchlorate complexes with imino oximes, the result which shows that the structure of copper(II) complexes is quite versatile. It is noteworthy that according to the nature of ligand and the steric condition, copper(II) ion forms various complexes with a different coordination number and a different structure. In consequence of the Jahn-Teller effect, copper(II) complexes show various structures which rarely occur in the corresponding nickel(II) complexes.

References

1) S. P. Wan, H. Kuma, and S. Yamada, *Synth. React. Met.-Org. Chem.*, **16**, 1049 (1986).

2) S. P. Wan, W. Mori, and S. Yamada, *Synth. React. Met.-Org. Chem.*, **16**, 1273 (1986).

3) H. Tanaka, H. Kuma, and S. Yamada, *Synth. React. Met.-Org. Chem.*, **15**, 699 (1985).

4) S. P. Wan, W. Mori, S. Yamada, and S.-I. Murahashi, *Bull. Chem. Soc. Jpn.*, **61**, 2833 (1988).

5) S. P. Wan, H. Kuma, S. Yamada, and S.-I. Murahashi, *Bull. Chem. Soc. Jpn.*, **62** (1989) in press.

6) S. Baral and A. Chakravorty, *Proc. Indian Acad. Sci.*, **86A**, 45 (1977).

7) L. Walz, H. Paulus, and W. Haase, *J. Chem. Soc., Dalton Trans.*, **1985**, 913. L. Schwabe and W. Haase, *J. Chem. Soc., Dalton Trans.*, **1985**, 1909.

8) M. Mikuriya, M. Nakamura, H. Okasawa, and S. Kida, *Inorg. Chim. Acta*, **68**, 111 (1983).

9) L. Strinna Erre, G. Micera, P. Piu, F. Cariati, and G. Ciani, *Inorg. Chem.*, **24**, 2297 (1985).

10) G. A. Nicholson, C. R. Lazarus, and B. J. McCormick, *Inorg. Chem.*, **19**, 192 (1980).

11) W. Mori, M. Kishita, and M. Inoue, *Inorg. Chim. Acta*, **42**, 11 (1980).

12) A. Earnshaw, "Introduction to Magnetochemistry," Academic Press Inc., New York (1968).

13) A. B. P. Lever, "Inorganic Electronic Spectroscopy," Elsevier, Amsterdam (1984). S. Yamada, "Structural Coordination Chemistry," Kagakudojin, Kyoto (1980), p.155.

14) B. J. Hathaway and A. A. G. Tomlinson, *Coord. Chem. Rev.*, **5**, 1 (1970).

15) L. Dubicki, G. A. Kakos, and G. Winter, *Aust. J. Chem.*, **21**, 1461, (1968).

16) Y. Nakao, W. Mori, N. Okuda, and A. Nakahara, *Inorg. Chim. Acta*, **35**, 1 (1979).

Microbiosensing Device for Real Time Determination

Yoshihito IKARIYAMA,*,† Naoki SHIMADA, Tomoaki YUKIASHI,††
Masuo AIZAWA,††† and Shigeru YAMAUCHI
Research Institute of National Rehabilitation Center, Namiki 4-1, Tokorozawa, Saitama 359
††Central Research Laboratory, Sumitomo Cemment Co., Ltd., Toyotomi 5-8-5, Funabashi, Chiba 274
†††Department of Bioengineering, Tokyo Institute of Technology, O-okayama 2-12-1, Meguro-ku, Tokyo 152
(Received December 24, 1988)

A microbiosensing device fabricated by assembling an enzyme-embodied microelectrode with a counter electrode and a reference electrode was applied to the real time determination of trace droplet of glucose sample. The microdevice demonstrated unique properties such as real time response, independence of sample volume, unnecessity of sample mixing by the rendezvous of microfabricated biosensing device with pulse voltammetry. A linear relationship between sensor output and glucose concentration was obtained in the concentration range from 10^{-3} to 10^{-1} mol L^{-1}. The sensing device responded to every glucose sample of different concentration in 2 ms, and the coefficient of variation for 10 mM glucose determination was within 5%.

Microfabrication is one of the common trends in science and technology of our age, since microfabricated sensors will play indispensable roles for the construction of very small sophisticated instrument as well as the microinstrumentation of analytical tools.[1] Being small has many advantages in electrochemical analysis of trace substances of biological importance with biosensors. In the early step of biosensor research many enzyme-immobilized membranes have been attached to Clark-type oxygen electrodes.[2-6] In recent years further application of enzyme electrodes has been extended by the microfabrication of electrode-based biosensors, since multifuctional biosensors can be developed by taking advantages of silicon technology.[7-9] Recent photolithographic techniques for deposition and patterning of thin noble metal films (50—300 nm) have been developed for the purposes of fabrication of planar integrated circuits.[10] These techniques are also promising for the preparation of microtransducer for miniaturized biosensors. However, new favorable techniques for immobilizing enzyme onto microtransducers are strongly required for the fabrication of microenzyme electrodes, which sizes are in the μm range, because the conventional enzyme immobilization techniques are not necessarily compatible with miniaturized transducers as long as enzymes are employed in polymer matrix-supported forms.

In previous papers we have reported fundamental properties of microenzyme electrodes with diameters in the range from 10 to 200 μm prepared by incorporating enzyme molecules onto a platinized surface of microplatinum electrode.[11,12] It was the platinization technique that enabled the microfabrication of the biosensor. It is a well-known fact that platinized platinum, porous microparticles of platinum, possesses very large surface area and high catalytic activities for electrolytic processes. By employing a microelectrode as a base electrode for platinization and simultaneous enzyme immobilization, a microenzyme sensor can be easily fabricated.[13] Enzyme molecules are stably retained in the porous platinum particles.[14] In other words, the platinum particles play the dual roles of transducer of enzyme electrode and matrix for enzyme immobilization.

The fabricated microbiosensors for glucose demonstrates high performances such as low detection limit of 5×10^{-7} mol L^{-1}, wide dynamic range from 5×10^{-7} to 2×10^{-2} mol L^{-1}, rabid response of 3 s, satisfactory coefficient of variation [2%], and time stability of over one month.[14,15]

Here we described a unique microbiosensing device for the real time determination of droplet glucose sample. As the operation mode of the microdevice is a voltammetry driven by the application of pulsed potential, stationary trace glucose sample can be determined in 2 ms.

Experimental

A microplatinum wire having a diameter from 10 to 200 μm, a platinum wire (200 μm diameter), and a silver wire (500 μm diameter) were sealed in a Teflon casing (2.5-mm inner diameter) with polyester resin, ground, and polished to leave exposed a circular surface. Electrodes were polished with Imperial™ wrapping films of alumina powders of different particle sizes. At the final stage of polishing 0.1 μm Al_2O_3 was used as the finish and only the microplatinum electrode for enzyme immobilization was cycled between −0.25 and +1.28 V vs. a silver-silver chloride electrode (reference electrode) in 0.5 M H_2SO_4 (1 M=1 mol dm^{-3}) prior to platinization with a conventional three electrode system. The silver electrode was anodized in 1 M NaCl solution for the preparation of a silver-silver chloride electrode. The microplatinum electrode was platinized in a mixed solution of hexachloroplatinate and lead acetate by following the procedure described previously.[14] After the platinization high purity glucose oxidase (EC 1.1.3.4) (from A. *niger*, 120 units/mg) was embodied with the porous surface of microplatinum electrode, following which crosslinking of the enzyme molecules with glutaraldehyde was performed.[14] Figure 1 shows a schematic illustration of

† Present address: Department of Bioengineering, Tokyo Institute of Technology, O-okayama 2-12-1, Meguro-ku, Tokyo 152.

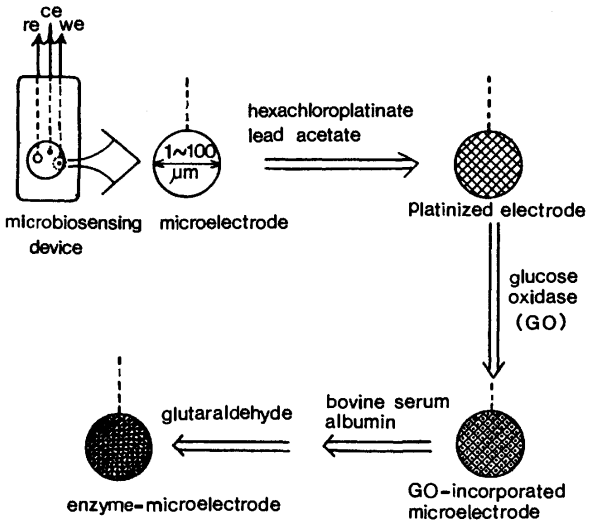

Fig. 1. Schematic illustration of electrochemical fabrication technique.
After the preparation of microplatinum electrode in a Teflon casing, platinization is performed by electrochemical reduction of hexachloroplatinate in the presence of lead acetate, following which enzyme incorporation is carried out. The electrode is immersed in an albumin solution and then treated with glutaraldehyde.

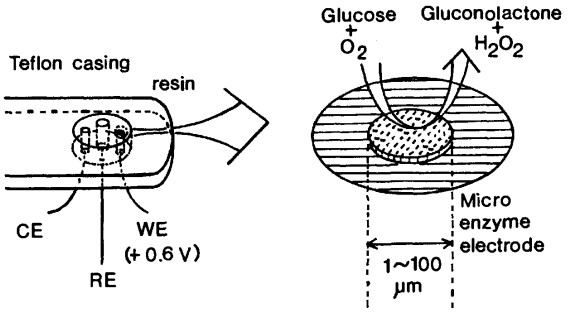

Fig. 2. Schematic drawing of microbiosensing device.
Glucose oxidase immobilized in the porous surface of platinized microelectrode oxidizes glucose in a droplet sample, and the generated hydrogen peroxide is electrochemically oxidized to give anodic sensor signal.

electrochemical microfabrication techniques. The measuring principle of the microbiosensing device thus prepared is schematically shown in Fig. 2.

A stock buffer solution of pH 6.8 was prepared from phosphate salts (50 mM) and NaCl (50 mM) as working electrolyte.

Experimental assays of droplet glucose sample were carried out with a potentiostat in a three-electrode configuation with the Ag/AgCl reference electrode of the microbiosensing device. The potentiostat was operated in on-off potential application mode. A potential of +0.6 V vs. Ag/AgCl was applied to the enzyme-embodied working electrode. The resulting amperometric signals were recorded by using an x-y-t recorder or a memory scope (MOS static RAM=4×12 bit×4096 word). The response time of the x-y-t recorder was 200 ms. In the later case each recorded datum was stored in a floppy disk, and then recorded on an x-y-t recorder. A schematic diagram of the microbiosensing principle is shown in Fig. 3. Glucose determination was performed by addition of aliquot of glucose stock solution. Potential was applied at 10 s aftter the addition of a droplet glucose sample.

Results and Discussion

Typical Responses of Microbiosensing Device. The effectiveness of the microbiosensing device, pulse voltammetry combination was evaluated in glucose sample by loading aliquot of standard glucose sample (10 mM). Every glucose sample (10 μL) was dropped on the three-electrode biosensing device, and a potential of +0.6 V was applied at 10 s after sample loading. Figure 4 shows typical data recorded on the x-y-t recorder. Also shown is the response curve of a blank

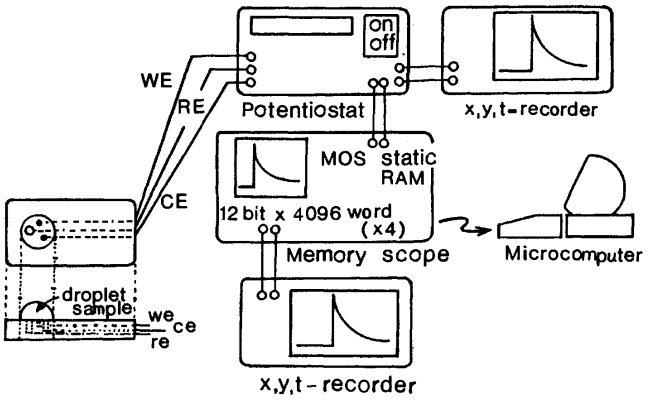

Fig. 3. Schematic diagram of the sensing principle of microbiosensing device.
After the addition of a droplet glucose sample on the three-electrode biosensing device, a potential of +0.6 V is applied to the microdevice and the resulting transient response is recorded on an x-y-t recorder or on a memory scope.

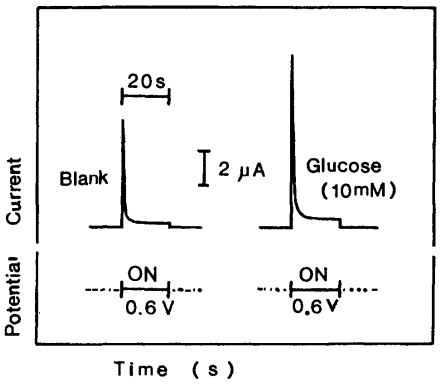

Fig. 4. Typical responses of microbiosensing device.
The responses of the biosensing device to a blank sample (the phosphate-buffered NaCl solution) and a 10 mM glucose sample (in the same buffered solution) were recorded on an x-y-t recorder whose response time is 200 ms.

sample (the phosphate-buffered NaCl solution). After the initial sharp peak, gradually decaying curve was observed. As the response time of the x-y-t recorder is 200 ms, the initial peak seems to the sums of capacitive and faradaic currents. The difference between the peak height of glucose sample and that of blank sample was plotted to the concentration of glucose sample, whose result gave a linear relationship between the peak height current and the glucose concentration in the range from 1 mM to 20 mM against a double logarithmic expression. The calibration curve was a straight line with slope equaled to ca. one-third. Since the slope of the curve seemed worth remarking, we applied a platinized microplatinum electrode to the pulse voltammetric determination of hydrogen peroxide, whose result gave a linear relation against a double logarithmic expression, with a slope of +1, between the initial peak height and the H_2O_2 concentration in the range of 1—100 mM hydrogen peroxide. These results explain the distinction between the enzyme-embodied and the platinized (non-enzyme) electrodes.

The above results make it apparent that in order to measure faradaic current a sufficient recording instrument of fast electrodic process will significantly separate faradaic current from capacitive one.

A sufficiently equipped memory scope was employed to investigate the transient response of the microdevice in further detail. In chronoamperometry current as a function of time is not the response of the microbiosensing devise described in this report but that of the recording system, as long as the x-y-t recorder whose response time is 200 ms is taken. Figure 5 shows a detailed response of the microbiosensing device to 10 mM droplet glucose sample (10 μL). In addition to a blank sample, we employed a fructose sample of the same volume and concentration to know the specificity of the microdevice. All three samples demonstrated similar responses in the rapid decay of initial peak, however, considerable difference among three samples was observed after the decay of charging current. The potential application initiated an instantaneous current as a result of the oxidation of hydrogen peroxide. The resulting current decreases as the electrodic reaction proceeds. In the faradaic process, therefore, the charge passed across the electrode interface is related to the amount of material that has been converted, and the generated current is related to the instantaneous rate at which the oxidation of hydrogen peroxide produced by the immobilized glucose oxidase occurs. In general monitored response to the potential excitation signal for a solution containing supporting electrolyte only is the background response (capacitive current) which should decay rapidly when the electrode has been charged to the applied potential. However, the response to a blank sample shows the faradaic current even after the decay of capacitive current. It should be noted that when platinum electrode is used as a transducer electrode, faradaic current is observed due to the formation of surface oxide of platinum.[16,17] After the anodic polarization the faradaic current for the surface oxide formation decreases significantly.[18] With respect to the response curve of the sensing device in Fig. 5, the difference in the transient response between a glucose sample and a blank sample can be a reasonable sensor signal of the pulse voltammetric biosensing device. As the behavior of the device to a fructose sample was almost similar to that to a blank sample, the microdevice was regarded to have specificity to glucose.

Relation between Transient Response and Glucose Concentration. As the greater difference in the tran-

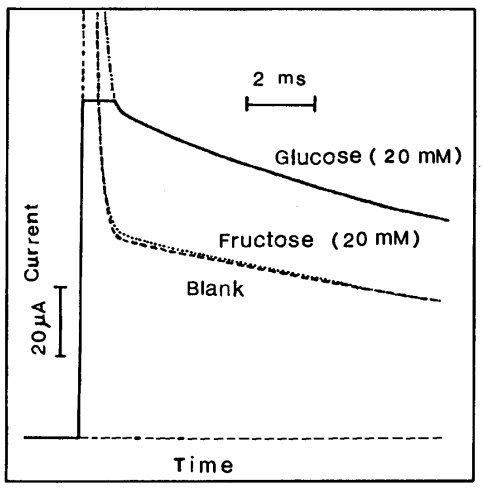

Fig. 5. Transient responses of microbiosensing device.
The responses of the microdevice were obtained by applying a potential of 0.6 V after a glucose sample (20 mM), a fructose sample and a blank sample were separately loaded on the device surface.

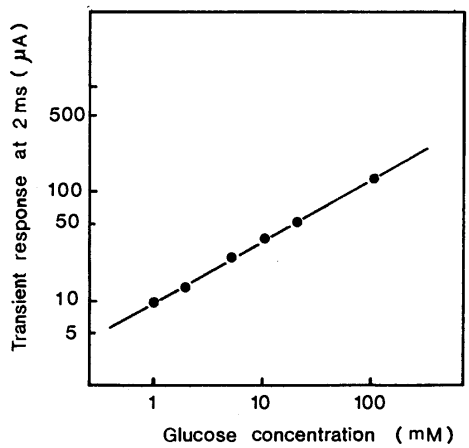

Fig. 6. Calibration curve for real time determination of glucose.
The difference in transient response at 2 ms between glucose sample and blank sample is plotted to the glucose concentration.

sient current between a glucose sample and a fructose sample was observed at 2 ms after the application of +0.6 V to the three-electrode device, the relation between the difference in sensor output and glucose concentration was investigated. Figure 6 shows a linear calibration curve for real time determination of glucose in the range from 1 mM to 100 mM. We have also here a linear relation with a slope of one-third. So far we can not find a resonable explanation for the slope of the calibration curve. In the case of glucose determination in a batch system[14] and a flow system[15] where samples are in hydrodynamic state, we have obtained a linear calibration with a slope of +1. In the determination with the present pulse voltammetric device, droplet samples are in hydrostatic conditions where the flux of hydrogen peroxide to the microelectrode is diffusion control. It is noteworthy that the enzyme reaction is also diffusion-controlled process in the stationary solution. A microplatinized electrode was applied for the pulse-voltammetric determination of hydrogen peroxide in a similar manner, and the resulting calibration curve showed a linear relationship with a slope of +1 in the concentration range from 1 mM to 100 mM hydrogen peroxide, as shown in Fig. 7. A complicated mass transfer process in the enzyme-embodied electrode is reflected on this experimental fact. With this in mind one can easily understand that the transient response seemed to reflect the non-steady state of the enzyme reaction as well as the electrodic reaction. The reasonable explanation for this intriguing phenomenon still remains to be studied in further detail.

Relation between Sensor Output and Sample Volume. The responses of the microbiosensing device to 10 mM glucose sample of different sample volume were obtained to know the relation between sensor output and sample volume. Almost identical responses were observed in this series of measurements where sample volume was varied from 1 to 20 μL. When the sample volume was less than 1 μL, the three-electrode microbiosensing device was not covered with the sample droplet. On the other band, the sample droplet more than 20 μL spilt from the device surface. Table 1 shows the relation between sensor output and sample volume. It should be noted that the sensing principle is independent of sample volume, which is one of the advantages for the microinstrumentation in clinical situations, because the pulse voltammetric device does not require any attached stirring machines.

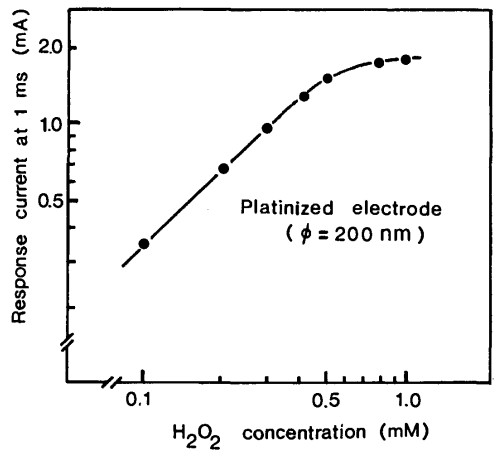

Fig. 7. Relation between transient response and hydrogen peroxide concentration.
The difference in transient responce at 1 ms between hydrogen peroxide sample and blank sample is plotted to the H_2O_2 concentration. The electrode employed here was a platinized microelectrode.

Table 1. Relation between Sensor Output and Sample Volume

Volume (μL)	1	2	5	10	15	20
Sensor output (μA)	29	30	31	31	30	30

The sensor output taken here is the difference in transient response at 1 ms between droplet glucose sample and droplet blank sample.

As the conventional voltammetry such as pulse voltammetry is independent of solution volume being tested, the results in Table 1 are consistent with typical data obtained by pulse voltammetric techniques. It is also worth noting that almost all the measurements with chemical sensors are also independent of sample volume. To our knowledge, however, this is the first experimental demonstration that biosensors are applicable to hydrostatic samples without paying attention to the volume of the sample being tested. Although the present work is in the early stage of experimentation, we examined the accuracy of the pulse voltammetric biosensing device by using 10 mM glucose sample (10 μL). The resulting coefficient of variation was calculated to be +4.4% (N=10).

Conclusion

The microbiosensing device demonstrated several performance characteristics such as real time determination, unnecessity of stirring equipment, and unnecessity of sampling tool. These advantages will allow several design criteria for microinstrumentation of clinical analyzers. The performance characteristics of the platinized platinum microelectrode-based biosensors in batch system, flow system, and pulse voltammetric measurements are summarized in the table.

By combining three microelectrodes into a single sensing unit, we have succeeded in fabricating a miniaturized biosensing device. Therefore, very small amount of sample can be applied to the microdevice, even if the droplet sample volume is a few μL. The microsensing device described here has

a couple of advantages over the dry chemistry-based clinical test papers. Microinstrumentation can be easily performed, because the device does not require additional equipments for the sampling of exact sample and for the stirring of sample solution. Furthermore, the microbiosensing device can be repeatedly used because of the stable, intact immobilization of enzyme molecules in the porous platinized electrode matrix. In addition to these advantages, another most important performance characteristic is that every sample can be determined instantaneously by taking advantage of pulse voltammetric technique. Finally, while we have focused on the fabrication of microbiosensing device which can be operated in the real time determination of analytes, the principle described here will also be a useful means of the microinstrumentation of portable-type biosensors for the daily surveillance of diabetic patients, especially of diabetic blind patients.

References

1) G. Haugen and H. Hieftze, *Anal. Chem.*, **60**, 23A (1988).
2) L. C. Clark Jr. and C. Lyons, *Ann. N. Y. Acad.*, **102**, 29 (1962).
3) S. J. Updike and G. P. Hicks, *Nature (London)*, **214**, 986 (1967).
4) M. Aizawa, I. Karube, and S. Suzuki, *Anal. Chim. Acta*, **69**, 431 (1974).
5) M. Nanjo and G. G. Guilbault, *Anal. Chim. Acta*, **73**, 367 (1974).
6) Y. Ikariyama, M. Furuki, and M. Aizawa, *Anal. Chem.*, **57**, 496 (1985).
7) S. Caras and J. Janata, *Anal. Chem.*, **52**, 1935 (1980).
8) Y. Miyahara, T. Moriizumi, and K. Ichimura, *Sensors and Actuators*, **7**, 1 (1985).
9) Y. Hanazato, M. Nakano, and S. Shiono, IEEE Trans. Electron Devices, ED-33, 47 (1986).
10) S. M. Sze, VLSI Technology, McGraw Hill Book Co., New York (1983).
11) Y. Ikariyama, S. Yamauchi, T. Yukiashi, and H. Ushioda, *Anal. Lett.*, **20**, 1407 (1987).
12) Y. Ikariyama, S. Yamauchi, T. Yukiashi, and H. Ushioda, *Anal. Lett.*, **20**, 1791 (1987).
13) Y. Ikariyama, S. Yamauchi, T. Yukiashi, and H. Ushioda, *J. Electrochem. Soc.*, **136**, 702 (1989).
14) Y. Ikariyama, S. Yamauchi, M. Aizawa, T. Yukiashi, and H. Ushioda, *Bull. Chem. Soc. Jpn.*, **61**, 3525 (1988).
15) Y. Ikariyama, S. Yamauchi, T. Yukiashi, and H. Ushioda, *Bull. Chem. Soc. Jpn.*, **62**, 1869 (1989).
16) J. A. Polta and D. C. Johnson, *Anal. Chem.*, **57**, 1373 (1985).
17) G. Neuberger and D. C. Johnson, *Anal. Chem.*, **59**, 204 (1987).
18) Y. Ikariyama, S. Yamauchi, T. Yukiashi, and H. Ushioda, *J. Electroanal. Chem.*, **251**, 267 (1988).

Micro-Enzyme Electrode as a High-Performance Detector of Flow Injection Analysis

Yoshihito IKARIYAMA,*,† Shigeru YAMAUCHI, Tomoaki YUKIASHI,††
Hiroo USHIODA,†† and Masuo AIZAWA†††
Research Institute of National Rehabilitation Center, Namiki 4-1, Tokorozawa, Saitama 359
††Central Research Laboratory, Sumitomo Cemment Co., Ltd., Toyotomi 5-8-5, Funabashi, Chiba 274
†††Department of Bioengineering, Tokyo Institute of Technology, O-okayama 2-12-1, Meguro-ku, Tokyo 152
(Received January 20, 1989)

The advantages of miniaturized enzyme electrode have been applied to flow injection analysis for the development of a rapid and selective method for the continuous determination of glucose. By assembling a micro-enzyme electrode having a diameter of 10 μm for an amperometric flow-through detector, at least 600 glucose samples can be determined in one hour. And micro-enzyme electrodes are satisfactorily stable for over 4 weeks even after 1000 glucose injections.

Miniaturization is one of the common trends in science and technology of our age. As far as chemistry is concerned, miniaturization is closely related to the microinstrurmentation of analytical tools. As Haugen et al. pointed out in a recent journal,[1] microfabricated sensors will play indispensable roles for the construction of very small sophisticated instruments.

A great number of approaches for microfabrication of chemical sensors are currently under way, particularly in the areas of field effect transistor (FET)-based chemical sensors, metal oxide gas sensors, and biosensors. Since Janata et al. reported the first micro-enzyme electrodes based on FET,[2] a number of groups have been taking microfabrication techniques such as semiconductor technology and photolithography for fabricating micro-enzyme electrodes. Despite enormous efforts of many groups the FET-based micro-enzyme electrodes of practical use have not been realized yet, because this potentiometric method lacks fast response, high sensitivity, and wide dynamic range.

Over several years, microelectrodes having diameters less than 20 μm have been introduced as the in vivo chemical sensors of neurotransmitter.[3-5] Because of their nonselective voltammetric principle, microelectrodes of high selectivity have been earnestly desired to be developed.

Obviously selective membrane layers such as enzyme membranes exhibit for the target substances affinities by taking advantages of specificity and selectivity to enzymes' substrates.

In our previous papers we have successfuly fabricated amperometric micro-enzyme electrodes having diameters from 10 μm to 500 μm by the embodiment of enzyme molecules with platinized microelectrode.[6,7] We have taken two approaches for the construction of micro-enzyme electrodes. One of them is to incorporate enzyme molecules to an platinized microelectrode,[8] and the other is to make enzyme molecules adsorb electrochemically on the surface of an electrochemically growing platinized electrode matrix.[9]

Here we describe an effectiveness of the smallness of enzyme (glucose oxidase, GO) electrodes whose diameters from 10 μm 500 μm by applying them to amperometric detectors of flow injection analysis (FIA) of glucose. In addition to the fundamental characteristics of micro-enzyme electrodes as high-performance detectors for FIA, the authors would like to mention the importance of anodic polarization of the platinized electrodes for the improvement of the selectivity of the enzyme electrodes. The benefits of miniaturization of enzyme-electrodes are also discussed in this paper with respect to the microinstrumentation of FIA.

Experimental

Reagents and Materials. Hexachloroplatinic acid and lead(II) acetate were the products of Wako Chem. Co. (Osaka). Glucose was obtained from Nakarai Chem. Co. (Kyoto), and glucose oxidase (EC 1.1.3.4, 110 u/mg) was the product of Toyobo (Osaka). Bovine serum albumin (Grade V) and glutaraldehyde (50% water solution) were purchased from Tokyo Kasei (Tokyo). All the other reagents were of analytical grade; their solutions were prepared with glass-distilled water.

Platinum wires having diameters from 10 μm to 500 μm were manufactured by Sanwa Metal Co. (Tokyo). Imperial™ wrapping films of alumina powders of different particle sizes from 0.1 μm to 30 μm were obtained from Sumitomo 3M Co. (Tokyo).

Apparatus. The flow-through cell used for a transducer electrode in the FIA system is shown in Fig. 1. The working electrode (WE) was a platinized platinum whose diameter is from 10 μm to 500 μm, the reference electrode (RE) was an Ag/AgCl electrode, and the auxiliary electrode (AE) was a stainless steel upper cell for a thin-layer transducer cell for LCEC (BAS, West Lafayette, IN). Every microelectrode was fixed in an acrylic block bottom cell with a polyester resin. The reference electrode was positioned downstream from the biosensing cell. Potential application and the generated current observation were carried out by a Potentiostat/Galvanostat (Model

† Present address: Department of Bioengineering, Tokyo Institute of Technology, O-okayama 2-12-1, Meguro-ku, Tokyo 152.

2090 with Low Noise of TOHO Technical Research, (Tokyo). The output current was recorded with an X-t recorder (Model R-302V of RIKADENKI, Tokyo). A double plumger pump (Model NF-EX-2 of NIHON SEIMITSU KAGAKU Co., Tokyo) was employed with a pulse damper (NIHON SEIMITSU KAGAKU Co.). A 5 μL sample loop was used for all experiments. The length of the connective tube (inner diameter=200 μm) from the injection valve to the detector was 50 cm. The flow rate of the pump was controlled at 0.8 mL min^{-1}. The electrode potential of micro-enzyme electrode was 0.6 V, and all the electrode potentials are reported vs. an Ag/AgCl reference electrode. All the experiments were carried out at room temperature (23 °C).

Preparation of Micro-Enzyme Electrode in an Electrode-Assembled Transducer Cell. A microplatinum electrode (diameter=10 μm—500 μm) in an acrylic block bottom cell for the thin-layer transducer cell concerned was platinized with a conventional three-electrode system using a platinum wire electrode (diameter=1 mm, l=10 mm) and an Ag/AgCl reference electrode. Electrolytic reduction of hexachloroplatinate (33 mg mL^{-1}) was carried out in the presence of lead acetate (0.6 mg mL^{-1}) at a potential of −0.08 V for 5 min. After the reductive deposition of platinum particles, the platinized electrode was thoroughly rinsed in 0.1M phosphate buffer (pH 6.8). Incorporation of GO molecules in the platinized electrode was carried out by immersing the electrode in an enzyme solution for 10 min before assembling the three electrode detector cell. The solution contained 50 mg of GO in one mL of 0.1 M phosphate buffer (pH 6.8). The electrode was then kept in a bovine serum albumin (20 mg) in 1 mL of 0.1 M phosphate buffer of pH 6.8 for 10 min. The albumin-incorporated platinized microelectrode was treated with a 2% glutaraldehyde solution buffered with 0.1 M phosphate of pH 6.8 for 10 min for the preparation of thin-layer albumin film over the porous electrode surface, following which thorough washing of the electrode was performed overnight. A gasket having a thickness of 100 μm was employed between the upper stainless steel cell and the enzyme electrode-embedded acrylic bottom cell as shown in Fig. 1. Also is shown a schematic diagram of instrumentation.

Anodic polarization of the micro-enzyme electrode was performed before enzyme incorporation by applying +1.2 V to the electrode for 10 min in 0.1 M phosphate buffer (pH 6.8).

Results

Responses of Enzyme-Electrode to the Repeated Injection of Glucose Sample. A glucose sample (10 mM, 5 μl) was repeatedly injected to the transducer assembly. Figure 2 illustrates the typical responses of the detector system. Every response reached a peak within 2 or 3 s and decayed to the baseline within a few seconds. Each peak was highly reproducible, and gave ca. 200 nA maximum peak to 10 mM glucose sample. The micro-enzyme electrode having a diameter of 100 μm demonstrated responses neither to blank samples (0.1 M phosphate buffer of pH 6.80 nor to fructose and galactose samples after the anodic polarization of the platinized transducer electrode at 1.2 V for 10 min. Without anodic polarization the platinized electrodes as well as the enzyme-embodied platinized electrodes demonstrated responses not only to glucose but to galactose, fructose, and maltose. Before anodic polarization, the relative responses of the enzyme electrode were 7.7%, 6.2%, and 3.8% for galactose, fructose, and maltose, respectively, when the responses were normalized to that of glucose. After the anodic treat-

§ 1 M=1 mol dm^{-3}.

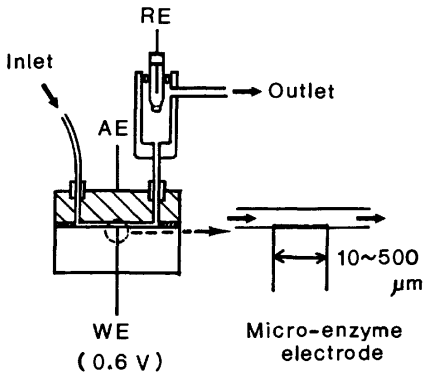

Fig. 1. Schematic diagram of instrumentation for FIA with micro-enzyme electrode.
The upper stainless steel cell is employed as an auxiliary electrode. The micro-enzyme electrode (WE) is embedded with a polyester resin in an acrylic bottom cell. The potential of the enzyme electrode is controlled at 0.6 V vs. Ag/AgCl reference electrode.

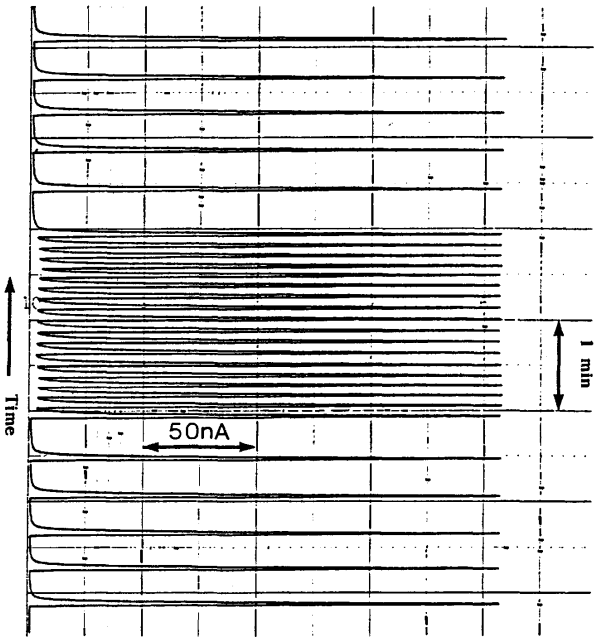

Fig. 2. Typical responses of micro-enzyme sensor system.
A micro-enzyme electrode having a diameter of 100 μm was used at a flow rate of 0.8 mL min^{-1}. Glucose (10 mM) samples were repeatedly injected. The flow-through detector showed no responses to fructose and galactose after anodic polarization.

ment the platinized enzyme electrodes showed no responses to these carbohydrates, and the enzyme electrodes demonstrated selective response to glucose. On the other hand, the anodically polarized platinized electrodes showed no responses to any carbohydrates. However, gradual polarization was observed at 0.6 V when the enzyme electrode was kept at the potential for a few hours. After the gradual oxide formation on the electrode surface at the potential, the enzyme electrode demonstrated selective response to glucose. Since a double plumger pump with a pulse damper was employed, the baseline slightly showed typical behavior of peristaltic wave.

The Relation between the Glucose Concentration and the Peak Current. A series of glucose samples whose concentrations varied from 200 μM to 20 mM were injected to the thin-layer transducer cell consisted of a 100 μm micro-enzyme electrode. Figure 3 shows the responses for the repeated injections. All the responses showed sharp peaks, reaching the peak heights in 2 or 3 s, and returned to the steady state current (residual current) in 7 or 8 s. Every glucose sample was injected 3 times, and all of the resulting three peak heights were almost same. The micro-enzyme electrode demonstrated little response to the injection of blank samples (0.1 M phosphate mobile buffer of pH 6.2). Figure 4 shows a linear relationship between the glucose concentration injected and the peak height in the glucose concentration range from 50 μM to 20 mM. As was already reported,[6,7] the micro-enzyme electrode showed high sensitivity (lowest detection limit: 0.5 μM), and wide dynamic range (0.5 μM—20 mM) in a batch system measurement, however, in this flow type measurement the detection limit still remained to be 50 μM range because of the sample dilution in the tube from the injection value to the transducer cell and of the poor signal to noise ratio due to a peristaltic wave caused by the double plunger pump. The improvement of the sensitivity seems to be easily attained by the employment of a nonperistaltic pump, by which mass transfer process from the mobile phase to the electrode is kept constant.

Figure 5 shows the relationship between the flow rate of the system and the peak height for a glucose sample of 10 mM. In the hydrodynamic voltammetry the transducer output is a function of the thickness of diffusion layer. As far as the electrochemistry between an electrode and an analyte is diffusion-controlled process, a greater response is anticipated at

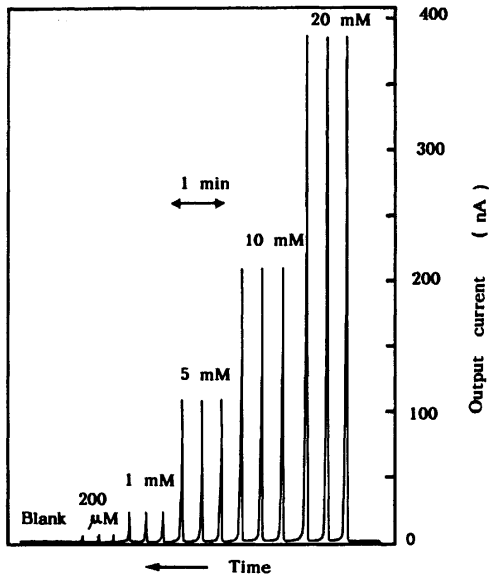

Fig. 3. Responses of micro-enzyme detector system to a series of glucose samples.
A series of glucose samples were injected to a detector system composed of a 100 μm micro-enzyme electrode at a flow rate of 0.8 mL min^{-1}.

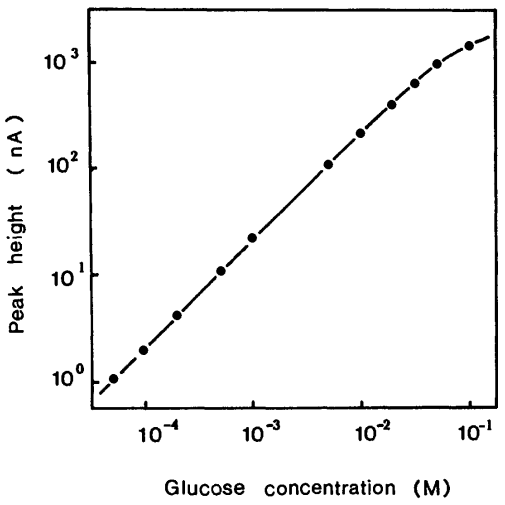

Fig. 4. Relationship between glucose concentration and peak height.

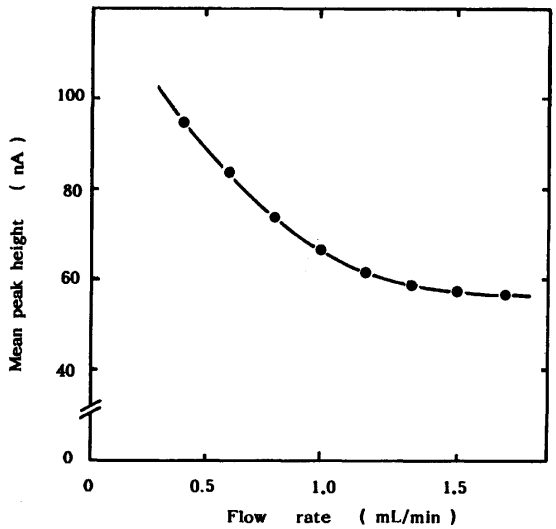

Fig. 5. Relationship between flow rate and peak height.
Micro-emyme electrode having a diameter of 50 μm and glucose sample of 10 mM was employed.

a higher flow rate.[11,12] In the case of highly porous transducer bioelectrode such as the platinized enzyme electrode being concerned, however, there are mainly three processes for the generation of sensor output: mass transfer process, enzyme reaction, and electrochemical reaction (charge transfer process). The mass transfer process in a porous electrode can be divided into two processes, i.e., mass transfer from mobile bulk solution to the apparent surface of electrode by convective flow and that within the crevasses of platinized microparticles. Both the enzyme reaction of glucose oxidase and the electrochemical oxidation of the produced hydrogen peroxide seem to be high enough to generate sensor output, since apparent K_m value (ca. 50 mM) for the enzyme electrode was much greater than the analyte concentration (10 mM), and the applied potential (0.6 V) was higher than the oxidation potential (ca. 0.45 V) of hydrogen peroxide, respectively. Therefore, it would be the mass transfer within the porous particles mainly by diffusion that determines the relation in Fig. 5.

Relation of the Micro-Enzyme Electrode Diameter to the Processing Speed. A variety of enzyme electrodes whose diameters were from 10 μm to 3 mm were prepared to study the relationship between the size of enzyme-microelectrodes and the measuring performance of the detecting system. An enzyme electrode having a diameter of 3000 μm was here employed as a reference to know the effect of miniaturization of enzyme electrode. The flow rate for this experimentation was 0.8 mL min^{-1}. Figure 6 shows the relationship of enzyme electrode diameter and the time required for the measurement of every glucose sample (10 mM). The solid line shows the time when each sample peak returns completely to the baseline, and the dotted one shows the time in which every sample peak has no interaction with each other in the continuous injections of glucose sample. One can easily understand that the smaller the enzyme electrode is employed, the faster measurement is carried out. Figure 6 shows one of the most beneficial characteristics of the microfabricated enzyme electrodes, because smaller electrodes are in shorter contact time with the injected samples.

Table 1 lists the relation of sensor diameter to coefficient of variation. Also listed are the mean sensor response of the respective electrode and the number of injection. Although the mean sensor response was related to the size of micro-enzyme electrode, the enzyme-electrode size was not reflected on the coefficient of variation as long as the enzyme-electrode diameter was in this range. On the other hand, in the case of a macro-enzyme electrode having a diameter of 3000 μm, the coefficient of variation was 1.1% for N=10.

Table 1. Coefficients of Variations of a Series of Micro-Enzyme Sensor Systems

Diameter	Mean sensor response	CV	N
μm	nA	%	
10	13.0	0.61	20
50	75.5	0.59	20
100	205	0.73	20
200	260	0.40	20
500	610	0.61	20

Precision and Reproducibility of the Micro-Enzyme Electrode for FIA of Glucose. A micro-enzyme electrode having a diameter of 100 μm was assembled in a transducer assembly for the repeated injections of 10 mM glucose. The flow rate for this time stability checking in FIA of glucose was 0.8 mL min^{-1}. The micro-enzyme electrode embedded in an acrylic bottom cell was kept in a refrigerator (4 °C) when the electrode was not used. One hundred glucose samples were injected every three days in order to evaluate precision and reproducibility. On the first and fourth days, however, fifty glucose samples were repeatedly injected. Table 2 lists the accuracy of the micro-enzyme electrode. The precision and reproducibility are here expressed as coefficient of variation (CV,%) and relative activity (%) of the micro-enzyme electrode. It is noted that the microfabricated enzyme electrodes demonstrated satisfactory precision in the FIA of glucose.

In another series of experimentations six hundred samples were injected to the flow-through enzyme electrode having a diameter of 100 μm at room temperature, and the coefficient of variation was then calculated. The mean response to 10 mM glucose sample was 252 nA at a flow rate of 0.8 mL min^{-1}. The CV was 1.9 (%) for the six hundred sample injections. One can easily notice the discrepancy that the CV for N=600 is larger than that for N=100 as listed in Table 2. Although all the experimentations were carried out at a room temperature of 23±2 °C, subtle change of the room temperature in one hour seemed to have affected the output of the flow-through enzyme electrodes. We are convinced that the CV for a great number of sample injections can be improved to be

Table 2. Precision and Reproducibility of Micro-Enzyme Sensor in FIA

Time	Relative activity	CV	N
day	%	%	
0	100	1.00	50
4	99	0.73	50
7	100	1.30	100
9	103	0.62	100
12	105	0.51	100
15	100	0.74	100
18	100	1.30	100
21	95	1.10	100
24	99	1.30	100
27	101	0.83	100
30	100	0.75	100

much smaller if the system is strictly thermostated. In the one hundred injections in ca. 10 min the subtle influence of the temperature change seemed to be negligible.

Discussion

The rapid responses of the enzyme (GO)-incorporated platinized microelectrodes can be explained by the properties of the porous platinum surface where sufficient amount of the enzyme molecules (GO) can be embodied with the highly porous platinum, and electrolytic oxidation of hydrogen peroxide proceeds smoothly on the highly catalytic surface of platinized electrode. The asymmetric shape of the response of every electrode can also be interpreted by the porous structure where a part of glucose sample can be retained within the micropores for a relatively long time, although the sample solution was throughly washed away by the mobile buffer.

The surface conditions of the platinized electrodes, both bare platinized electrodes and enzyme (GO)-embodied electrodes, play very important roles in the selective detection of glucose. The improvement of the enzyme electrode selectivity may be elucidated by the surface oxide formation at an anodic potential of ca. 1.2 V. The surface oxide formation of platinum has been uniquely utilized by Johnson et al.[13-15] for the amperometric detection of electroinactive species. In the present study, the hydrogen peroxide to be detected at the electrode seems to promote the surface oxide formation, because the enzyme-incorporated microelectrodes gradually became irresponsive to other sacccharides than glucose after several glucose injections even without anodic polarization at a potential of 0.6 V for 10 min.

One of the benefits of hydrodynamic voltammetry is the impressive detection limit,[16] however, in the FIA of glucose described here we have not succeeded in the sensitive determination of the analyte, which may have been caused mainly by the low signal-to-noise ratio due to the peristaltic wave, as long as a double plumger pump is adopted. Current and future developments are certain to improve detection limits.

A couple of literatures concerning thin-layer electrochemical cells have recently confirmed that the electrode output current depends on the solution velocity to the one-third power. The major reason why the micro-enzyme transducer cell does not obey this theoretical and experimental evidence would be the porous electrode matrix structure where diffusion-controlled as well as convection-controlled mass transfers contribute the output current. From the relationship between the output peak current and the flow rate, it may be stated that there are a few complicated processes until the peak current is generated. In the flow-through electrode like the enzyme electrode being considered, the diffusion process within the crevasses of porous matrix seems to be a rate-determining process, because the output current decreased when the flow rate increased.

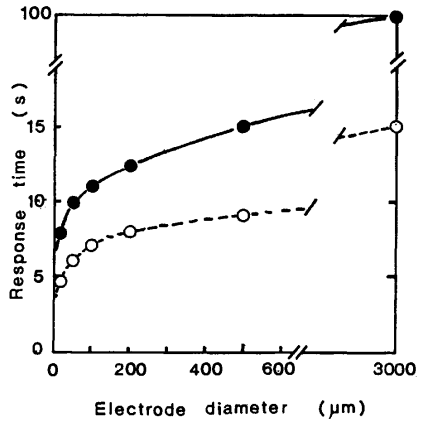

Fig. 6. Relation of micro-enzyme electrode diameter to response time.
The response times in single injection and repeated injections are represented by a solid and dotted lines, respectively.

The most remarkable benefit of miniaturization is the high processing speed of the microfabricated channel electrodes. The evidence is clear in Fig. 6. Another advantage may be the development of microinstrumentation by combining the microsensors with a micropump fabricated by silicon technology.[17]

The satisfactory precision and reproducibility of the FIA electrodes reflect the intact immobilization of enzyme (GO) molecules. Although the GO-entrapped electrode was treated in a glutaraldehyde solution for the preparation of a thin film of albumin, the enzyme molecules within the electrode matrix seemed to be kept as intact as possible.

Coating with anion membrane such as Nafion™ can be a promising approach to make the amperometric enzyme electrode irresponsive to concomitant oxidizable substances such as uricate and ascorbate,[18] however, usage of two electrodes, an enzyme-deactivated electrode and an enzyme-embodied electrode is a general strategy in practical situations, because by measuring the difference between two electrodes the FIA analyzer for glucose would be unaffected by those undesired ingredients. This approach is now under progress.

References

1) G. Haugen and G. Hieftze, *Anal. Chem.*, **60**, 23A (1988).
2) S. Caras and J. Janata, *Anal. Chem.*, **52**, 1935 (1980).
3) R. M. Wightman, *Anal. Chem.*, **53**, 1125A (1981).
4) K. Ishii and T. Kato, *Brain Res.*, **359**, 260—266 (1985).
5) E. M. Kristensen, W. G. Kuhr, and M. R. Wightman, *Anal. Chem.*, **59**, 1752 (1987).
6) Y. Ikariyama, S. Yamauchi, T. Yukiashi, and H. Ushioda, *Anal. Lett.*, **20**, 1407 (1987).

7) Y. Ikariyama, S. Yamauchi, T. Yukiashi, and H. Ushioda, *Anal. Lett.*, **20**, 1791 (1987).
8) Y. Ikariyama, S. Yamauchi, T. Yukiashi, and H. Ushioda, *Bull. Chem. Soc. Jpn.*, **61**, 3525 (1988).
9) Y. Ikariyama, S. Yamauchi, T. Yukiashi, and H. Ushioda, *Electrochem. Soc.*, **136**, 702 (1989).
10) S. G. Weber and W. C. Purdy, *Anal. Chim. Acta*, **100**, 531 (1978).
11) S. G. Weber, *J. Electroanal. Chem.*, **145**, 1 (1983).
12) J. A. Polta and D. C. Johnson, *J. Liq. Chromatogr.*, **6**, 1727 (1983).
13) J. A. Polta and D. C. Johnson, *Anal. Chem.*, **57**, 1373 (1985).
14) G. G. Neuburger and D. C. Johnson, *Anal. Chem.*, **59**, 203 (1987).
15) P. T. Kissinger and W. R. Heineman, Laboratory Techniques in Electroanalytical Chemistry, Marcel Dekker, New York (1984).
16) Y. Hirata, P. T. Lin, M. Novotny, and R. M. Wightman, *J. Chromatogr.*, **181**, 287 (1980).
17) M. Esashi, S. Shoji, and T. Matsuo, Proc. Symp. Chem. Sensors, Proc. Vols. 87—9 (Electrochem. Soc.) 31—38 (1987).
18) G. A. Gerhardt, A. F. Oke, G. Nagy, B. Moghaddam, and R. N. Adams, *Brain Res.*, **290**, 390 (1984).

 © 1989 The Chemical Society of Japan Bull. Chem. Soc. Jpn., 62, 1875—1879 (1989)

An X-Ray Diffraction Study on the Structure of Solvated Cadmium(II) Ion and Tetrathiocyanatocadmate(II) Complex in *N,N*-Dimethylformamide

Kazuhiko OZUTSUMI,§ Toshiyuki TAKAMUKU, Shin-ichi ISHIGURO,* and Hitoshi OHTAKI†
Department of Electronic Chemistry, Tokyo Institute of Technology at Nagatsuta, Nagatsuta-cho 4259, Midori-ku, Yokohama 227
†Coordination Chemistry Laboratories, Institute for Molecular Science, Myodaiji, Okazaki 444
(Received December 27, 1988)

The structure of solvated cadmium(II) ion and the tetrathiocyanatocadmate(II) complex in *N,N*-dimethylformamide (DMF) has been determined by means of X-ray diffraction at 25 °C. The radial distribution curve for a cadmium(II) perchlorate DMF solution is well explained in terms of the presence of the octahedral $[Cd(dmf)_6]^{2+}$ complex with the Cd-O bond length of 229.6(4) pm, which is practically the same as that within $[Cd(dmso)_6]^{2+}$ in DMSO and $[Cd(H_2O)_6]^{2+}$ in H_2O. It is also found that the tetrathiocyanatocadmate(II) complex has a tetrahedral structure, $[Cd(NCS)_3(SCN)]^{2-}$, with three Cd-N and one Cd-S bonds, the distances being 223(2) and 257(2) pm, respectively. The coordination structure of the complex in DMF is different from that found in aqueous solution, $[Cd(NCS)_2(SCN)_2]^{2-}$.

Thiocyanate ion binds to metal ions through either the nitrogen or sulfur atom depending on the nature of metal ions. According to the X-ray, Raman, and NMR studies, relatively hard zinc(II) and soft mercury(II) ions form $[Zn(NCS)_4]^{2-}$ and $[Hg(SCN)_4]^{2-}$ in aqueous solution, respectiveiy.[1] Similar coordination geometry has also been reported for the tetrathiocyanato complexes of zinc(II) and mercury(II) ions in dimethyl sulfoxide (DMSO).[2] On the other hand, cadmium(II) ion, which has intermediate hard and soft characters between zinc(II) and mercury(II) ions, forms $[Cd(NCS)_2(SCN)_2]^{2-}$ with coordinating two nitrogen and two sulfur atoms of thiocyanate ions in aqueous solution.[1] It is suggested from Raman spectroscopic and thermodynamic data that the coordination of other thiocyanato complexes of cadmium(II) ion ($[Cd(SCN)_n]^{(2-n)+}$, $n=1-3$) changes with the number of ligand ions, $[Cd(NCS)]^+$, $[Cd(NCS)(SCN)]$ and $[Cd(NCS)_2(SCN)]^-$, in aqueous solution.[3]

The complex formation between cadmium(II) and thiocyanate ions occurs extensively in *N,N*-dimethylformamide (DMF), and a different coordination mode of thiocyanate ions in the complexes in DMF from that in water has been suggested.[4] However, no direct structural information on the thiocyanato complexes has so far been given in DMF. Therefore, in this work we aimed at determining the structure of the tetrathiocyanatocadmate(II) complex in DMF by the X-ray diffraction method. In aqueous and DMSO solutions cadmium(II) ion is octahedrally coordinated with relevant solvent molecules through oxygen atoms.[5,6] Since the corresponding structure of cadmium(II) DMF solvate has been revealed neither in solution nor in the solid state, we also determined the solvation structure of cadmium(II) ion in DMF.

§ Present address: Department of Chemistry, The University of Tsukuba, Tsukuba, Ibaraki 305.

Experimental

Preparation of Sample Solutions. All chemicals used were of reagent grade. *Cadmium(II) perchlorate DMF solvate* was prepared by dissolving cadmium(II) perchlorate hydrate crystals in DMF and recrystallized three times from DMF and finally from acetone. Crystals thus obtained were dried at room temperature in a vacuum oven for several days. The analysis of the cadmium(II) perchlorate DMF solvate by EDTA titration showed the composition of $Cd(ClO_4)_2(dmf)_6$. *Cadmium(II) thiocyanate* was obtained by mixing stoichiometric amounts of aqueous cadmium(II) perchlorate and ammonium thiocyanate solutions. Crystals thus obtained were washed by suspending them in hot water and finally dried at 80 °C under atmospheric pressure. *Ammonium thiocyanate* was used without further purification and dried at room temperature in vacuum. *N,N*-Dimethylformamide was purified by the same method as described elsewhere.[4,7]

X-Ray diffraction measurements were performed for three test solutions A, B, and C (Table 1). Solution A was prepared by dissolving cadmium(II) perchlorate DMF solvate crystals in DMF. Solutions B and C were prepared by dissolving suitable amounts of cadmium(II) and ammonium thiocyanates in DMF so as to involve the tetrathiocyanatocadmate(II) complex as the main species in the solutions. Concentrations of cadmium(II) and thiocyanate ions in the sample solutions were determined by EDTA

Table 1. The Composition (mol dm^{-3}), Stoichiometric Volumes V, and Densities ρ of the Sample Solutions

	A	B	C
Cd^{2+}	0.9738	0.9854	0.9433
SCN^-	—	5.009	5.996
NH_4^+	—	3.038	4.110
ClO_4^-	1.948	—	—
DMF	12.28	9.624	8.872
ρ/g cm^{-3}	1.201	1.160	1.160
$V/10^9$ pm^3	1.705	1.685	1.760
C_{SCN}/C_{Cd}	—	5.083	6.356

titration and by gravimetry as AgSCN, respectively. Densities of the solutions were determined pycnometrically.

X-Ray Diffraction Measurements. X-Ray diffraction data were obtained on a JEOL θ-θ type diffractometer and an Mo tube (λ=71.07 pm) was used as the X-ray source. The observed range of scattering angle 2θ was from 2° to 140° and the data were recorded at least twice over the whole angle range. Corrections for absorption, polarization, and multiple scatterings of X-rays to the observed intensities were made by a usual manner as described elsewhere.[8]

The reduced intensities $i(s)$ are given as

$$i(s)=K\cdot I(s)-\sum_j n_j\cdot f_j^2(s), \qquad (1)$$

were K represents a normalization factor of the observed intensities $I(s)$ to the absolute unit, n_j the number of atom j in a stoichiometric volume and $f_j(s)$ the atomic scattering factors of atom j corrected for anomalous dispersion. The reduced intensities multiplied by s ($=4\pi\ \lambda^{-1}\ \sin\theta$) for the sample solutions are depicted in Fig. 1. The $s\cdot i(s)$ values are converted into the radial distribution function $D(r)$ as

$$D(r)=4\pi r^2\rho_o+\frac{2r}{\pi}\int_0^{s_{max}} s\cdot i(s)\cdot M(s)\cdot\sin(rs)ds. \qquad (2)$$

ρ_o ($=\{\sum n_j\cdot f_j(0)\}^2/V$) stands for the average scattering density in a stoichiometric volume V per cadmium atom of the sample solution and s_{max} the maximum s-value available in the measurement ($s_{max}=16.6\times10^{-2}$ pm^{-1}). The modification function $M(s)$ has the form of $[\sum n_j\cdot f_j^2(0)/\sum n_j\cdot f_j^2(s)]\cdot\exp(-ks^2)$, the damping factor k being chosen as 100 pm^2 in the present case. The radical distribution curves in the form of $D(r)-4\pi r^2\rho_o$ for the test solutions are shown in Fig. 2.

A least-squares refinement for determining the structure parameters was carried out by comparing the observed and theoretical reduced intensities so as to minimize the error-square sum U,

$$U=\sum_{s_{min}}^{s_{max}} s^2\{i(s)_{obsd}-i(s)_{calcd}\}^2. \qquad (3)$$

The theoretical intensities $i(s)_{calcd}$ resulting from the interatomic interactions in the solutions are calculated as

$$i(s)_{calcd}=\sum_{p}\sum_{\substack{q\\ p\neq q}} n_{pq}f_p(s)f_q(s)\frac{\sin(r_{pq}s)}{r_{pq}s}\exp(-b_{pq}s^2), \qquad (4)$$

where r_{pq}, b_{pq}, and n_{pq} stand for the distance, the temperature factor, and the frequency factor of the atom-pair p-q, respectively.

All calculations were performed by using programs KURVLR[9] and NLPLSQ.[10]

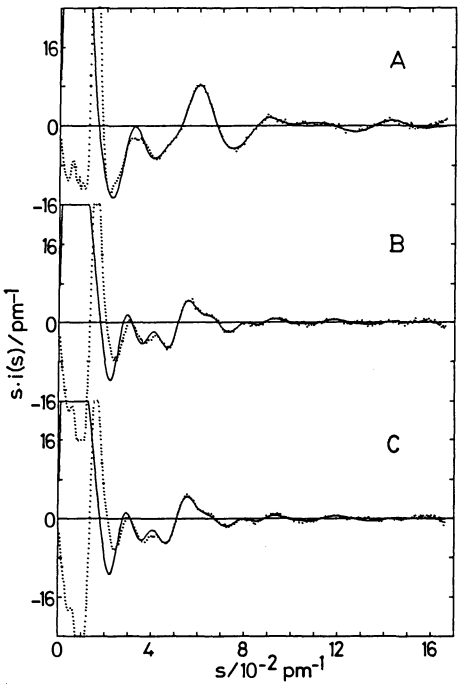

Fig. 1. The reduced intensities multiplied by s for solutions A, B, and C. The observed $s\cdot i(s)$ values are drawn by the dotted lines and calculated ones by the solid lines.

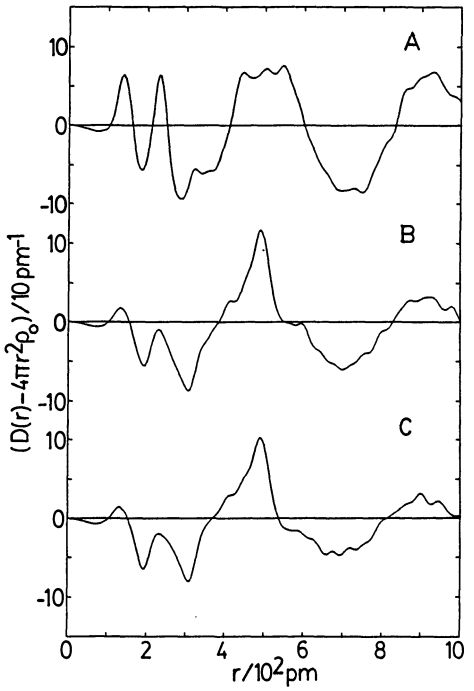

Fig. 2. The radial distribution curves in the form of $D(r)$-$4\pi r^2\rho_o$ for solutions A, B, and C.

Results and Discussion

Structure of Solvated Cadmium(II) Ion. Figure 3 shows the ($D(r)-4\pi r^2\rho_o$) curve of solution A. In the curve six peaks are observed at 140, 230, 320, 440, 500, and 550 pm. The last two peaks are originated from long distant intermolecular interactions which are not analyzed in the present study. The first peak at 140 pm is ascribable to the C-H, C-N, and C=O bonds within DMF molecules and the Cl-O bonds within perchlorate ions. The second peak at 230 pm is expected to be due to the Cd-O(dmf) bond similar to the Cd-O(H_2O) and Cd-O(dmso) bonds within the $[Cd(H_2O)_6]^{2+}$ and $[Cd(dmso)_6]^{2+}$ complexes, respectively.[5,6] The nonbonding C···C, C···O, and N···O interactions within DMF molecules and the O···O contacts within perchlorate ions also contribute to the

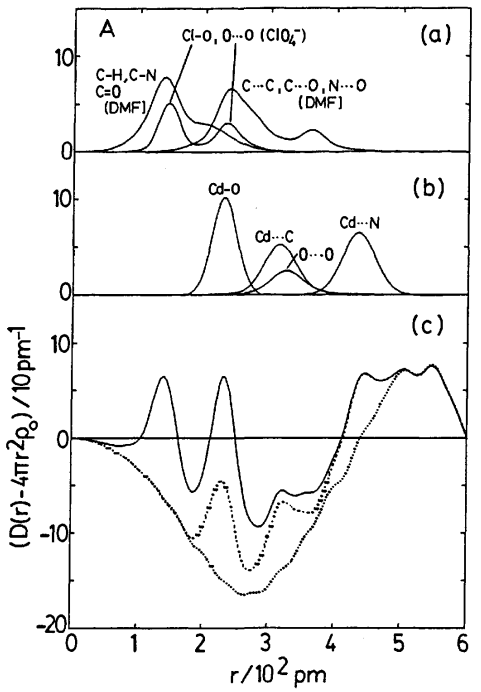

Fig. 3. The $(D(r)-4\pi r^2\rho_0)$ curve for solution A. (a) The theoretical peak shapes for intramolecular interactions within DMF molecule and perchlorate ion. (b) The peak shapes calculated for the Cd-O, Cd···C, O···O, and Cd···N interactions within the $[Cd(dmf)_6]^{2+}$ ion. (c) The chain and dotted lines represent the residual curves after subtraction of the theoretical peaks in (a) and (b), respectively, from the original one (solid line).

peak. The third and fourth peaks at 320 and 440 pm may be attributed to the nonbonding Cd···C(dmf) and Cd···N(dmf) interactions, respectively, the corresponding peaks having also been observed for the solvated copper(II) ion in DMF.[11]

In order to evaluate the structure parameters of the solvated cadmium(II) ion in DMF, the theoretical peak shapes due to the intramolecular interactions within DMF and perchlorate (Fig. 3a) are subtracted from the observed radial distribution function. The parameter values are taken from the literature.[12,13] The residual curve thus obtained (chain line in Fig. 3c) shows a large peak at 230 pm, which is ascribed to the Cd-O bonds within the solvated cadmium(II) ion. The area under the peak corresponds to six Cd-O bonds. Thus the solvated cadmium(II) ion in DMF is concluded to have an octahedral structure. Subtraction of the peaks due to the Cd-O, Cd···C, Cd···N, and O···O interactions based on the octahedral $[Cd(dmf)_6]^{2+}$ structure leads to a smooth background curve (dotted line) with no distinct peak over the range $r<450$ pm.

The least-squares method was applied to the high-angle region of $s\cdot i(s)$ values ($s>4\times10^{-2}$ pm^{-1}) to refine the structure parameters of the $[Cd(dmf)_6]^{2+}$, where the intramolecular interactions within DMF molecule, perchlorate and $[Cd(dmf)_6]^{2+}$ ions mainly contribute to the intensity values. In the course of the refinement, the structure parameters for DMF molecule and perchlorate ion were fixed at the literature values,[12,13] and the interatomic distances and the corresponding temperature factors arising from atom-pairs based on the $[Cd(dmf)_6]^{2+}$ structure were optimized. The interligand O···O distance was calculated from the Cd-O distance. The results thus obtained are summarized in Table 2, together with the structure parameters for the $[Cd(H_2O)_6]^{2+}$ and $[Cd(dmso)_6]^{2+}$ complexes. The Cd-O bond distance within the $[Cd(dmf)_6]^{2+}$ finally determined is 229.6(4) pm, and the Cd···C distance is 315(1) pm. The Cd-O-C bond angle is thus calculated to be 123°.

The structure parameters of the octahedrally solvated cadmium(II) ion in DMF, DMSO, and water in Table 2 show that the Cd-O distance within the solvated ion is not largely different within the limit of experimental uncertainties. However, the observed Cd-O bond length seems to be lengthened in the order Cd-O(H_2O)>Cd-O(dmf)>Cd-O(dmso), i.e., the decreasing order of the solvent donicity DMSO>DMF>water.[14]

Structure of $[Cd(SCN)_4]^{2-}$. According to the formation constants of cadmium(II)-thiocyanato complexes in DMF,[4] the tetrathiocyanatocadmate(II) complex is present as the main species in solutions B and C. The radial distribution curves of solutions B and C depicted in Fig. 2 were analyzed by the similar procedure to that employed for solution A. In the following discussion we describe only the result for solution C because the same conclusion was obtained for solution B. The peaks owing to the C-H, C-N, and C=O bonds within DMF molecule, the C-S and C≡N bonds within thiocyanate ion and the N-H bonds within ammonium ion appear around 100 pm, and those of the nonbonding C···C, C···O, and N···O interactions within DMF molecule and N···S interactions within thiocyanate ion give a composite peak at 200—300

Table 2. Structure Parameters for the Solvated Cadmium(II) Ion in DMF, DMSO, and Water

Interaction	Parameter	DMF	DMSO[a]	Water[b]
Cd-O	r/pm	229.6(4)	229.4	231
	b/10 pm^2	6.3(5)	4.4	2
	n	6[c]	6	6
O···O	r[d]/pm	325	—	—
	b/10 pm^2	10[c]	—	—
	n	12[c]	—	—
Cd···C	r/pm	315(1)	342.2[e]	—
	b/10 pm^2	20(2)	15.4[e]	—
	n	6[c]	6[e]	—
Cd···N	r/pm	434(2)	—	—
	b/10 pm^2	20(2)	—	—
	n	6[c]	—	—

Standard deviations are given in parentheses.
a) Ref. 6. b) Ref. 5. c) The values were kept constant during the calculation. d) $r_{O\cdots O}=\sqrt{2}\,r_{Cd\text{-}O}$. e) Cd···S (dmso) interaction.

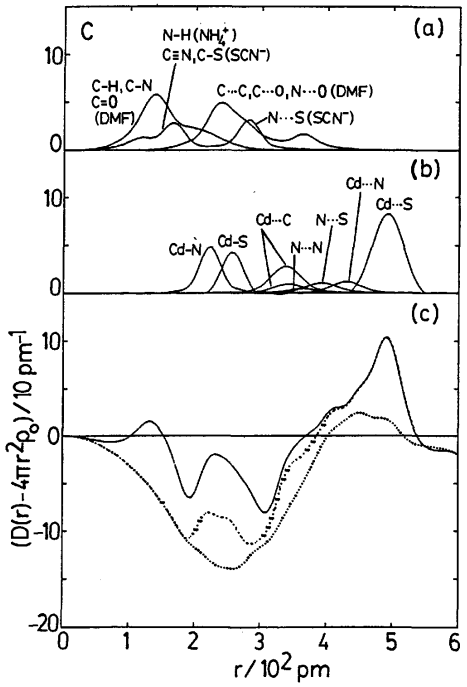

Fig. 4. The $(D(r)-4\pi r^2\rho_0)$ curve for solution C. (a) The theoretical peak shapes calculated for intramolecular interactions within DMF molecule and ammonium and thiocyanate ions. (b) The peak shapes for the intramolecular interactions within the $[Cd(NCS)_3(SCN)]^{2-}$ complex. (c) The chain and dotted lines represent the residual curves after subtracting the theoretical peaks in (a) and (b), respectively, from the original one (solid line).

pm. Subtraction of these peaks leads to the residual curve shown by the chain line in Fig. 4c. The peaks in the curve may mainly be ascribed to the intramolecular interactions within the tetrathiocyanatocadmate(II) complex.

The peak at 200—270 pm is doublet and thus consists of at least two kinds of interactions, probably the Cd-N and Cd-S bonds within the tetrathiocyanatocadmate(II) complex. The hump around 340 pm may be due to the intramolecular Cd···C, Cd···N, N···N, and N···S interactions within the complex. The large peak at about 500 pm is mainly due to the nonbonding Cd···S interaction between cadmium(II) ion and sulfur atom of N-bonding thiocyanate ion which has been seen also in aqueous solution.[1]

In the course of the analysis of the tetrathiocyanatocadmate(II) in DMF, we assumed as a first approximation that the distances of atom-pairs within the complex are the same as those in aqueous solution,[1] and the coordination numbers of cadmium(II) ion with nitrogen and sulfur atoms are searched by analyzing the areas under the doublet peak, the hump and the large and sharp peak at about 500 pm. The best result was obtained when we assumed the coordination numbers of three and one for the Cd-N and Cd-S bonds, respectively (Fig. 4b and c). No solvent molecule coordinates to cadmium(II) ion. Thus, we concluded that the tetrathiocyanatocadmate(II) complex has a four-coordinated tetrahedral structure, $[Cd(NCS)_3(SCN)]^{2-}$.

The structure parameters for the tetrahedral $[Cd(NCS)_3(SCN)]^{2-}$ complex in DMF were finally optimized by the least-squares method using the $s\cdot i(s)$ data in the high-angle region ($s>4\times10^{-2}$ pm^{-1}) at the fixed coordination structure. The interligand N···N and N···S distances are calculated from the Cd-N and Cd-S bond lengths and the tetrahedral structure. Since the contribution of the nonbonding Cd···C and Cd···N interactions arising from the S-bonding thiocyanate ion with cadmium(II) ion to the overall intensity is rather small, the distances are calculated from the Cd-S bond length and the Cd-S-C and Cd-S-N bond angles found in aqueous solution (106°)[1] and no significant error could be introduced by this treatment. The parameter values thus refined are given in Table 3, together with those obtained in aqueous solution.[1]

The Cd-N and Cd-S bond distances are finally determined to be 223(2) and 257(2) pm, respectively.

The tetrathiocyanatocadmate(II) complex has the

Table 3. Structure Parameters for the Tetrathiocyanatocadmate(II) Complex in DMF and Water

Interaction	Parameter	DMF B	DMF C	Water[a]
Cd-N	r/pm	224(1)	222(1)	224.6
	b/10 pm²	4(1)	2(1)	2.5
	n	3[b]	3[b]	2
Cd···C	r/pm	333(3)	337(3)	328
	b/10 pm²	15[b]	15[b]	15
	n	3[b]	3[b]	2
Cd···S	r/pm	491(1)	491(1)	486.7
	b/10 pm²	16(1)	22(2)	18
	n	3[b]	3[b]	2
Cd-S	r/pm	257(2)	256(1)	264.9
	b/10 pm²	18(4)	4(1)	7.7
	n	1[b]	1[b]	2
Cd···C	r/pm	341[c]	340[c]	349
	b/10 pm²	15[b]	15[c]	15
	n	1[b]	1[b]	2
Cd···N	r/pm	429[c]	428[c]	435
	b/10 pm²	15[b]	15[b]	14
	n	1[b]	1[b]	2
N···N	r/pm	360[d]	362[d]	367
	b/10 pm²	8[b]	8[b]	8
	n	3[b]	3[b]	1
S···N	r/pm	388[d]	390[d]	400
	b/10 pm²	15[b]	15[b]	15
	n	3[b]	3[b]	4
S···S	r/pm	—	—	433
	b/10 pm²	—	—	17
	n	—	—	1

Standard deviations are given in parentheses.
a) Ref. 1. b) The values were kept constant during the calculation. c) Assumed ∠Cd-S-C=∠Cd-S-N=106°. d) Assumed ∠N-Cd-N=∠S-Cd-N=109.5°.

different coordination structures of $[Cd(NCS)_3(SCN)]^{2-}$ and $[Cd(NCS)_2(SCN)_2]^{2-}$ in DMF and water, respectively. The difference may be ascribed to different solvation tendency of thiocyanate ion in the two solvents. As discussed in a previous paper,[4] thiocyanate ion is strongly solvated at the hydrogen bonding N-site in water, but much weakly at the S-site. Solvation of the thiocyanate ion is much weaker in aprotic DMF with a smaller acceptor number than water, and the solvation at the N-site may be especially weakened and consequently solvation at the S-site may become even relatively stronger than that at the N-site.[15] Therefore, the formation of the Cd-N bond may become more favorable in DMF than in water and the $[Cd(NCS)_3(SCN)]^{2-}$ structure may be formed in the DMF solutions. The coordination geometry of $[Cd(NCS)_3(SCN)]^{2-}$ may be favorable rather than that of $[Cd(NCS)_2(SCN)_2]^{2-}$ in DMF in the respect of solvation of the complex itself, because the former complex exposes more S atoms of ligating SCN^- ions into the bulk DMF solvent, which may be able to better solvate than the N atoms[15] in the ligand.

The work has been financially supported by the Grant-in-Aid for Scientific Research No. 63612005 (Macromolecular Complexes) from the Ministry of Education, Science and Culture. Computer calculations were carried out at the computer center of the Institute for Molecular Science in Okazaki.

References

1) Y. Yamaguchi , K. Yamamoto, and N. Ohtaki, *Bull. Chem. Soc. Jpn.*, **58**, 3235 (1985).
2) I. Persson, Å. Iverfeldt, and S. Ahrland, *Acta Chem. Scand., Ser. A*, **35**, 295 (1981).
3) S. Ishiguro, K. Yamamoto, and N. Ohtaki, *Bull. Chem. Soc. Jpn.*, **59**, 1009 (1985).
4) S. Ishiguro, T. Takamuku, and H. Ohtaki, *Bull. Chem. Soc. Jpn.*, **61**, 3901 (1988).
5) H. Ohtaki, M. Maeda, and S. Ito, *Bull. Chem. Soc. Jpn.*, **59**, 1009 (1985).
6) M. Sandström, I. Persson, and S. Ahrland, *Acta Chem. Scand., Ser. A*, **32**, 607 (1978).
7) S. Ishiguro, B. G. Jeliazkova, and H. Ohtaki, *Bull. Chem. Soc. Jpn.*, **58**, 1143 (1985).
8) H. Ohtaki, *Rev. Inorg. Chem.*, **4**, 103 (1982).
9) G. Johansson and M. Sandström, *Chem. Scr.*, **4**, 195 (1973).
10) T. Yamaguchi, Doctor Thesis, Tokyo Institute of Technology, March (1978).
11) K. Ozutsumi, S. Ishiguro, and H. Ohtaki, *Bull. Chem. Soc. Jpn.*, **61**, 945 (1988).
12) H. Ohtaki, S. Itoh, T. Yamaguchi, S. Ishiguro, and B. M. Rode, *Bull. Chem. Soc. Jpn.*, **56**, 3406 (1983).
13) H. Ohtaki and M. Maeda, *Bull. Chem. Soc. Jpn.*, **47**, 2197 (1974).
14) V. Gutmann, "The Donor-Acceptor Approach to Molecular Interactions," Prenum, New York (1978).
15) P. Bacelon, J. Corset, and C. de Loze, *J. Solution Chem.*, **12**, 1, 13, 23 (1983).

Oxidation of Lipids. XVI. Inhibition of Autoxidation of Methyl Linoleate by Diarylamines

Mareyuki TAKAHASHI, Jyunichi TSUCHIYA, and Etsuo NIKI*
Department of Reaction Chemistry, Faculty of Engineering, University of Tokyo, Hongo, Tokyo 113
(Received September 21, 1988)

The inhibition of oxidation of methyl linoleate in homogeneous solution and in aqueous dispersions by diarylamines has been studied. Diphenylamines with electron-donating substituents exhibited antioxidant activities, while those having electron-withdrawing substituents such as niflumic acid and flufenamic acid did not suppress the oxidation appreciably. When both 4,4′-dimethoxydiphenylamine and α-tocopherol were present as antioxidants, only α-tocopherol was consumed at first and when α-tocopherol was almost completely depleted, 4,4′-dimethoxydiphenylamine began to be consumed to give nitroxide radical, which further acted as antioxidant.

Oxygen is a double-edged sword: various useful and important chemicals are synthesized from the oxidations of organic compounds by molecular oxygen, but at the same time, oxygen is responsible for oxidative degradation and deterioration of plastics, rubber, oils, foods and even biological membranes and tissues.[1,2] Various kinds of both natural and synthetic antioxidants have been explored and used to protect biological, chemical, and industrial molecules from the oxygen toxicity.[3] Especially, phenols and amines have been used extensively as antioxidants.[4] The inhibition of oxidation by secondary amines has been studied by several groups.[4] Amines scavenge the chain-carrying peroxyl radicals to interrupt the chain propagation reaction giving N-centered aminyl radicals, which may dimerize, disproportionate, react with a second peroxyl radical on nitrogen to give a nitroxide or on carbon to give quinonoid products.[4-10] The diaryl nitroxides may react not only with carbon radical but also with peroxyl radicals to give quinone imine *N*-oxides.[11] Diaryl nitroxides react also with hydroperoxides. Thus, the amines are transformed by several competing reactions into various products which may also act as antioxidants. The relative importance of the above competing reactions depends on the reaction conditions and variables and hence the mechanism for antioxidant action by amines and stoichiometry also depends on the conditions.

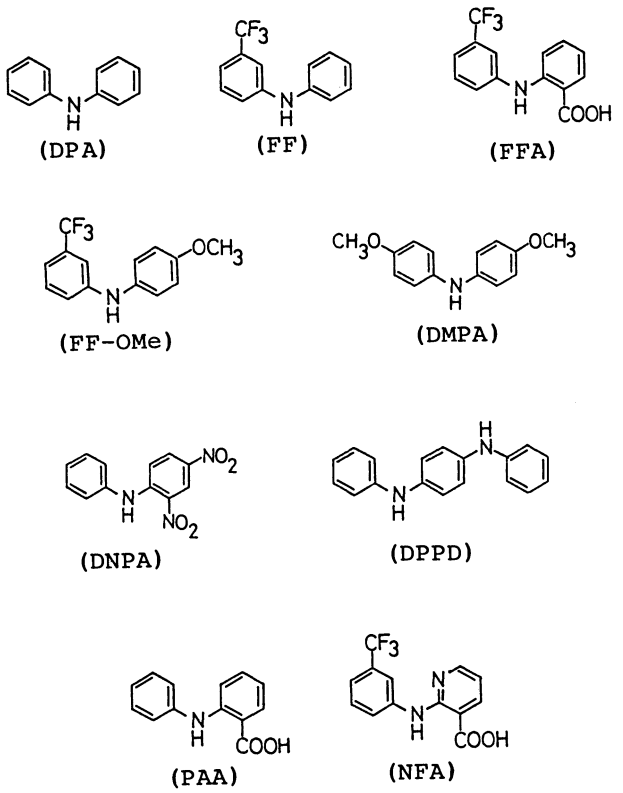

Fig. 1. Diarylamines used in this study and their abbreviations.

We have recently found that disodium 4-chloro-2,2′-iminodibenzoate and disodium 4-chloro-3′,6′-dimethyl-2,2′-iminodibenzoate, the water-soluble derivatives of diphenylamine, function as chain-breaking antioxidants in the oxidations of methyl linoleate micelles and phosphatidylcholine liposomes, oxidative hemolysis of red blood cells and in free radical-mediated damage of biological tissues.[12] The objective of the present work is to study the inhibition of oxidation of methyl linoleate by several types of lipophilic diarylamines. Figure 1 shows the diarylamines used in this study.

Experimental

Commercial methyl linoleate was purified by silica-gel column before use. 2,2′-Azobis(2,4-dimethylvaleronitrile) (AMVN) and 2,2′-azobis(2-amidinopropane) dihydrochloride (AAPH) were obtained from Wako Pure Chemical Ind. and used as lipid-soluble and water-soluble radical initiators respectively. Di-*t*-butyl diperoxyoxalate (DBPO), used as a *t*-butoxyl radical source, was prepared and purified as described in the literatures.[13,14] Commercial diarylamines, galvinoxyl and 2,2-diphenyl-1-picrylhydrazyl (DPPH) were used as received. RRR-α-tocopherol was kindly supplied by Eisai Co., Ltd.

Methyl linoleate micelles were prepared as reported previously[15] by mixing methyl linoleate and aqueous solution of 10 mM Triton X-100 vigorously with Vortex mixer for 2 minutes. The oxidation was carried out at 37 °C under air. The rate of oxygen uptake was followed with either a

pressure transducer or an oxygen electrode.[15] The rates of consumption of α-tocopherol and diarylamines were followed with a high-performance liquid chromatography. Electron spin resonance (ESR) spectra were recorded on a X-band JEOL FE1X spectrometer.

Results and Discussion

Inhibition of Oxidation of Methyl Linoleate by Diarylamines. The oxidation of methyl linoleate by molecular oxygen induced by a radical initiator proceeds by a free radical chain mechanism and gives four isomeric, conjugated diene hydroperoxides quantitatively as primary products.[16-19] Therefore, the rate of oxidation can be measured quantitatively by following the rate of either oxygen uptake or conjugated diene hydroperoxides formation.[19] In the presence of AMVN but absence of diarylamine, the oxidation proceeded without induction period and a constant rate of oxygen uptake was observed. As observed previously,[15] α-tocopherol (vitamin E) suppressed the oxidation markedly and after some inhibition period, the oxidation proceeded at the similar rate as that without α-tocopherol. α-Tocopherol was consumed linearly with time and when it was depleted the inhibition period was over. Similarly, DPPD, DPA, FF-OMe, and DMPA suppressed the oxidation, but FF, FFA, PAA, DNPA, and NFA did not suppress the oxidation. The pertinent results are summarized in Table 1. It can be seen that electron-donating substituent such as methoxy group on the aromatic ring promotes the antioxidant activity of diarylamine while electron-withdrawing substituent such as trifluoromethyl and nitro group reduces its antioxidant activity. Table 1 shows that DMPA, DPPD, and α-tocopherol act as strong antioxidants and suppress the oxidation markedly, while FF-OMe and DPA function less efficiently and reduce the rate of oxidation (R_{inh}/R_p) to one half to one fourth. Niflumic acid (NFA)[20] and flufenamic acid (FFA)[21] known as anti-inflammatoires had little antioxidant activities.

Table 1. Inhibition of Oxidation of Methyl Linoleate (MeLH) in Benzene by Diarylamines (IH) at 37 °C under Air

MeLH	AMVN	IH		t_{inh}[a]	10^7R_{inh}[b]	10^7R_p[c]
mM	mM		μM	s	M s^{-1}	M s^{-1}
159	10.5	None	0	0		3.04
151	16.1	α-TOC	50.0	1620	0.62	3.16
151	16.1	DPPD	50.0	1950	0.19	3.00
159	10.5	DMPA	50.0	2940	0	2.78
151	16.1	DMPA	50.0	1800	0	2.81
159	10.5	DPA	31.1	1800		2.50
159	10.5	DPA	50.1	3663	1.21	2.66
151	16.1	DPA	50.0	2220	1.70	3.05
159	10.5	FF-OMe	32.5	1800	0	2.28
159	10.5	FF-OMe	100	5280	0.87	3.60
152	10.1	FF-OMe	50.0	3120	0.82	3.12
151	16.1	FF-OMe	50.0	2040	0.34	3.09
159	10.4	FF	50.0	0		2.79
159	10.5	FFA	50.0	0		2.84
151	16.1	FFA	50.0	0		2.81
116	12.4	PAA	115	0		1.78
151	16.1	PAA	50.0	0		3.09
116	12.4	NFA	115	0		2.30
151	16.1	NFA	50.0	0		2.96
159	10.5	DNPA	50.0	0		2.78

a) Induction period. b) Rate of oxidation during the induction period. c) Rate of oxidation without antioxidant or after induction period.

Figure 2 shows the plot of inhibition period as a function of [IH]/[AMVN], where IH is an antioxidant such as diarylamine and α-tocopherol. As observed previously, the inhibition period was proportional to the antioxidant concentration and inversely proportional to the rate of chain intiation.[15,22-27]

Figure 3 shows the rates of disappearance of α-tocopherol and FF-OMe during the oxidation of methyl linoleate in benzene in the presence of both antioxidants. Interestingly, α-tocopherol was consumed first, while FF-OMe remained constant at first and it began to be consumed after substantially all of α-tocopherol disappeared. Fast oxidation took place when both antioxidants were depleted.

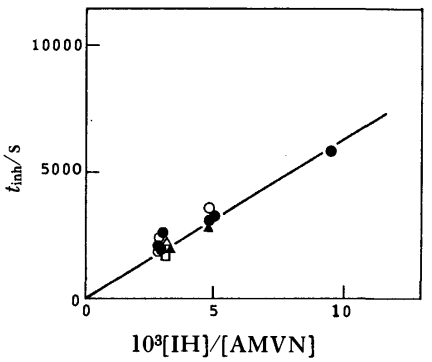

Fig. 2. Plot of inhibition period as a function of [IH]/[AMVN] in the oxidation of methyl linoleate in benzene at 37 °C initiated with AMVN and inhibited by α-tocopherol and diarylamines.
□: α-Tocopherol, ○: DPA, ●: FF-OMe, ▲: DMPA, △: DPPD.

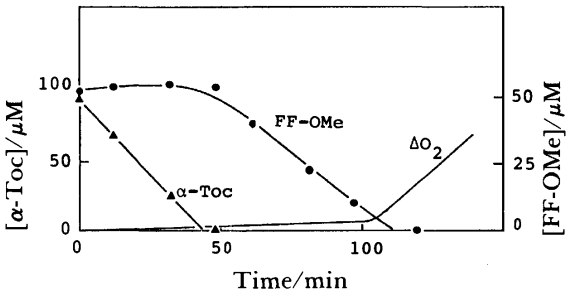

Fig. 3. Rates of disappearance of α-tocopherol and FF-OMe during the oxidation of 151 mM methyl linoleate in benzene initiated with 16.1 mM AMVN at 37 °C under air in the presence of both antioxidants. [α-TOC]=100 μM, [FF-OMe]=50 μM.

Inhibition of Oxidation of Methyl Linoleate Micelles. The oxidation of methyl linoleate micelles in Triton X-100 aqueous dispersions proceeds similarly and gives conjugated diene hydroperoxides quantitatively.[15] AAPH dissolved in water produces free radicals in the aqueous phase and they attack methyl linoleate and induce free radical chain oxidation. Table 2 shows some pertinent results of the oxidation of methyl linoleate micelles induced by AAPH in the presence of diarylamines or α-tocopherol. DPA, DPPD, DMPA, and α-tocopherol inhibited the oxidation, but FFA and PAA did not. As shown in Fig. 4, the inhibition period was again proportional to the antioxidant concentration and inversely proportional to the rate of chain initiation.

Figure 5 shows the rates of consumption of antioxidants during the oxidations of methyl linoleate micelles in aqueous dispersions inhibited by both α-tocopherol and DMPA. As observed in the homogeneous solution, α-tocopherol was consumed first and after all of α-tocopherol disappeared, DMPA was consumed. When both antioxidants were depleted, a fast oxidation proceeded.

Table 2. Oxidation of Methyl Linoleate (MeLH) Micelles in 10 mM Triton X-100 Aqueous Dispersions at 37 °C in the Presence of Diarylamines and α-Tocopherol

MeLH	AAPH	IH		t_{inh}	10^7R_{inh}
mM	mM		μM	s	M s^{-1}
151	10.1	α-TOC	50.0	8040	0.24
151	9.9	DPPD	10.0	1800	0
151	10.0	DPPD	50.0	8400	0
137	17.2	DMPA	10.0	960	1.03
151	10.0	DMPA	10.0	2110	0.65
137	8.54	DMPA	10.0	2180	0.71
151	10.1	DMPA	50.0	8940	0
151	10.2	DPA	10.0	550	3.3
151	10.1	FFA	10.0	0	
151	10.9	PAA	50.0	0	

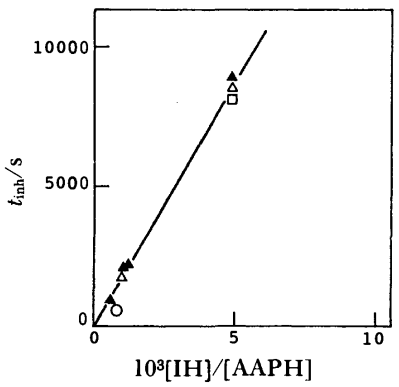

Fig. 4. Plot of inhibition period as a function of [IH]/[AAPH] in the oxidation of methyl linoleate micelles in 10 mM Triton X-100 aqueous dispersions initiated with AAPH and inhibited by α-tocopherol and diarylamines at 37 °C under air.
□: α-Tocopherol, ○: DPA, ▲: DMPA, △: DPPD.

ESR Spectra of Radicals Derived from Diarylamines. Figure 6 shows the ESR spectra observed in the oxidations of methyl linoleate in benzene and in aqueous dispersions inhibited with DMPA. Figure 7 shows the relative amount of radicals observed in the oxidation of methyl linoleate micelles initiated with AAPH and inhibited by both α-tocopherol and DMPA. The ESR spectrum of α-tocopheroxyl radi-

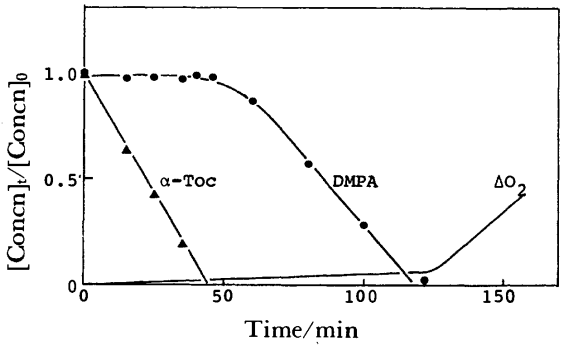

Fig. 5. Rates of disappearance of α-tocopherol and DMPA during the oxidation of 116 mM methyl linoleate micelles in aqueous dispersions initiated with 21.5 mM AAPH and inhibited by 50 μM α-tocopherol and 50 μM DMPA at 37 °C.

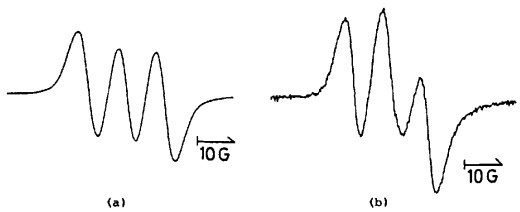

Fig. 6. ESR spectra observed (a) in the oxidation of 151 mM methyl linoleate in benzene at 37 °C under air initiated with 72 mM AMVN in the presence of 204 μM DMPA and (b) in the oxidation of 302 mM methyl linoleate micelles in 10 mM Triton X-100 aqueous dispersions at 37 °C under air initiated with 92.3 mM AAPH in the presence of 600 μM DMPA.

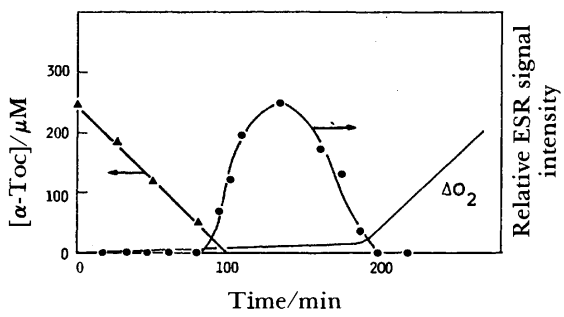

Fig. 7. Relative amount of radical observed during the oxidation of 302 mM methyl linoleate micelles in aqueous dispersions initiated with 92.3 mM AAPH and inhibited by both 204 μM DMPA and 244 μM α-tocopherol at 37 °C under air.

cal (phenoxyl radical from α-tocopherol) is well characterized,[28] but the ESR signal for α-tocopheroxyl radical was not observed, probably because it reacted rapidly with peroxyl radical to give a stable adduct.[29] As Fig. 7 shows, little ESR signal was observed at the initial stage, when only α-tocopherol was consumed. After α-tocopherol was depleted and when DMPA began to be consumed, ESR signal intensity increased and after passing a maximum it decreased. When most of ESR signal disappeared, the rapid oxidation took place.

These results suggest that DMPA scavenges peroxyl radical to give intermediate radical which gives ESR signal and then reacts with another radical to give a stable product. The identification or assignment of the ESR signal observed is difficult at present. It has been reported that 4,4′-dimethoxydiphenylaminyl radical and its *N*-oxyl radical have coupling constants of $a^N=0.849$ mT and $a^N=1.006$ mT, respectively.[30] Since the coupling constant for the radicals observed in this study was 1.0 mT, the radicals shown in Fig. 6 may be ascribed to *N*-oxyl radical **1**.

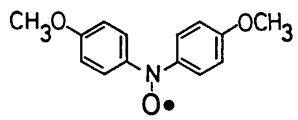

1

DPA, FFA, and PAA do not react with galvinoxyl nor with DPPH, suggesting that the diarylaminyl radicals derived therefrom are less stable than galvinoxyl and DPPH. However, when these amines were dissolved in benzene containing DBPO, ESR signals were observed and the solution was colored to brown. Figure 8 shows the ESR spectra observed for DPA, FFA, and PAA, respectively.

$$(CH_3)_3COOC(=O)C(=O)OC(CH_3)_3 \rightarrow 2(CH_3)_3CO^{\cdot}+2CO_2 \quad (1)$$

$$(CH_3)_3CO^{\cdot}+Ar_2NH \rightarrow (CH_3)_3COH+Ar_2N^{\cdot} \quad (2)$$

$$(CH_3)_3CO^{\cdot} \rightarrow (CH_3)_2C=O+CH_3^{\cdot} \quad (3)$$

$$CH_3^{\cdot}+O_2 \rightarrow CH_3O_2^{\cdot} \quad (4)$$

$$CH_3O_2^{\cdot}+Ar_2N^{\cdot} \rightarrow CH_3O^{\cdot}+Ar_2NO^{\cdot} \quad (5)$$

When these amines were dissolved in benzene containing both DBPO and *t*-butyl hydroperoxide, the same ESR spectra were observed and the solution became brown similarly. This system generates *t*-butylperoxyl radical[31] and the *N*-oxyl radical must be formed by a sequence of reactions 1, 6, 7, and 8.

$$(CH_3)_3CO^{\cdot}+(CH_3)_3COOH \rightarrow (CH_3)_3COH+(CH_3)_3COO^{\cdot} \quad (6)$$

$$(CH_3)_3COO^{\cdot}+Ar_2NH \rightarrow (CH_3)_3COOH+Ar_2N^{\cdot} \quad (7)$$

$$(CH_3)_3COO^{\cdot}+Ar_2N^{\cdot} \rightarrow (CH_3)_3CO^{\cdot}+Ar_2NO^{\cdot} \quad (8)$$

The ESR spectrum shown in Fig. 8(a) obtained for DPA is the same as that of diphenyl nitroxide radical reported by Mukai et al.[32] Furthermore, the same ESR spectrum was observed as that of Fig. 8(a) when phenylazotriphenylmethane was decomposed thermally under vacuum in benzene containing nitrosobenzene, oxygen was added, and then evacuated again: $a^N=0.990$ mT, $a^H_{o,p}=0.184$ mT, $a^H_m=0.078$ mT.

Thus the results of the present study and those reported in the literature suggest that diarylamines such as DPA, FF-OMe, and DMPA suppress the oxidation mainly by the following sequence:

$$LO_2^{\cdot}+Ar_2NH \rightarrow LOOH+Ar_2N^{\cdot} \quad (9)$$

$$LO_2^{\cdot}+Ar_2N^{\cdot} \rightarrow LO^{\cdot}+Ar_2NO^{\cdot} \quad (10)$$

(or ketone + hydroxylamine)

$$L\cdot(LO_2^{\cdot})+Ar_2NO^{\cdot} \rightarrow \text{stable product} \quad (11)$$

On the other hand, *N*,*N*′-dipheyl-1,4-phenylenediamine (DPPD) behaves differently. DPPD donates hydrogen atom to a peroxyl radical and the resulting aminyl radical must donate one more hydrogen atom to another peroxyl radical to give benzoquinone diimines without generating nitroxide radical.

$$LO_2^{\cdot}+Ph\text{-}NH\text{-}Ph\text{-}NH\text{-}Ph \rightarrow LOOH+Ph\text{-}\dot{N}\text{-}Ph\text{-}NH\text{-}Ph \quad (12)$$

$$LO_2^{\cdot}+Ph\text{-}\dot{N}\text{-}Ph\text{-}NH\text{-}Ph \rightarrow LOOH+Ph\text{-}N{=}\langle\bigcirc\rangle{=}N\text{-}Ph \quad (13)$$

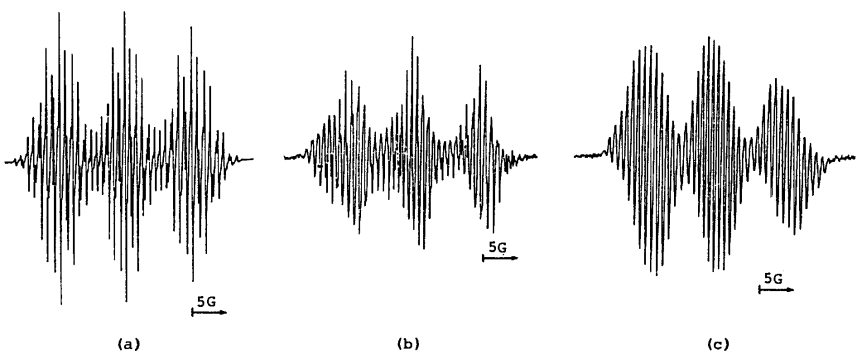

Fig. 8. ESR spectra observed when diarylamines were dissolved in benzene containing DBPO under vacuum at room temperature.
(a) DPA; (b) FFA; (c) PAA.

Under these conditions, each molecule of diarylamines scavenges two molecules of radicals and, as shown in Figs. 2 and 4, they produce similar inhibition period as α-tocopherol which also scavneges two molecules of peroxyl radicals.[22]

This study was supported in part by Grant-in-Aid for Scientific Research No. 62470078 from the Ministry of Education, Science and Culture.

References

1) "The Role of Oxygen in Chemistry and Biochemistry," ed by W. Ando and Y. Moro-oka, Elsevier, Amsterdam (1988).
2) "Medical, Biochemical and Chemical Aspects of Free Radicals," ed by O. Hayaishi, E. Niki, M. Kondo, and T. Yoshikawa, Elsevier, Amsterdam (1989).
3) E. Niki, *Chem. Phys. Lipids*, **44**, 227 (1987), and the references cited therein.
4) J. Pospisil, "Developments in Polymer Stabilization," ed by G. Scott, Applied Sci. Pub., Barking, (1984), Vol. 7, Chap. 1.
5) O. L. Harle and J. R. Thomas, *J. Am. Chem. Soc.*, **79**, 2973 (1957).
6) J. R. Thomas, *J. Am. Chem. Soc.*, **82**, 5955 (1960).
7) D. F. Bowman, B. S. Middleton, and K. U. Ingold, *Can. J. Chem.*, **45**, 2419 (1967).
8) K. Adamic, M. Dunn, and K. U. Ingold, *Can. J. Chem.*, **47**, 287 (1969).
9) K. Adamic and K. U. Ingold, *Can. J. Chem.*, **47**, 295 (1969).
10) A. R. Forrester, J. D. Fullerton, and G. McConnachie, *J. Chem. Soc., Perkin Trans. 1*, **1983**, 2711.
11) A. Calder, A. R. Forrester, and G. McConnachie, *J. Chem. Soc., Perkin Trans. 1*, **1974**, 2198.
12) E. Niki, M. Takahashi, J. Tsuchiya, E. Komuro, E. Ito, and K. Terao, *Chem.-Biol. Interactions*, **67**, 81 (1988).
13) P. D. Bartlett, E. P. Benzing, and R. E. Pincock, *J. Am. Chem. Soc.*, **82**, 1762 (1960).
14) E. Niki and Y. Kamiya, *J. Am. Chem. Soc.*, **96**, 2129 (1974).
15) Y. Yamamoto, S. Haga, E. Niki, and Y. Kamiya, *Bull. Chem. Soc. Jpn.*, **57**, 1260 (1984).
16) H. W. S. Chan and G. Levett, *Lipids*, **12**, 99 (1977).
17) N. A. Porter, *Acc. Chem. Res.*, **19**, 262 (1986); *Adv. Free Rad. Biol. Med.*, **2**, 283 (1986), and references cited therein.
18) E. N. Frankel, *J. Am. Oil Chem. Soc.*, **61**, 1908 (1984); *Prog. Lipid Res.*, **23**, 197 (1985).
19) Y. Yamamoto, E. Niki, and Y. Kamiya, *Bull. Chem. Soc. Jpn.*, **55**, 1548 (1982); *Lipids*, **17**, 870 (1982).
20) J. R. Biossier, J. Fichelle-Pagny, and Z. Horakova, *Therapie*, **22**, 157 (1967).
21) C. V. Winder, J. Wax, V. Burn, M. Been, and C. E. Rosiere, *Arch. Int. Pharmacobyn.*, **116**, 26, (1958).
22) E. Niki, T. Saito, A. Kawakami, and Y. Kamiya, *J. Biol. Chem.*, **259**, 4177 (1984).
23) E. Niki, J. Tsuchiya, Y. Yoshikawa, Y. Yamamoto, and Y. Kamiya, *Bull. Chem. Soc. Jpn.*, **59**, 497 (1986).
24) E. Niki, M. Saito, Y. Yoshikawa, Y. Yamamoto, and Y. Kamiya, *Bull. Chem. Soc. Jpn.*, **59**, 471 (1986).
25) L. R. C. Barclay, S. J. Locke, J. M. MacNeil, J. Van Kessel, G. W. Burton, and K. U. Ingold, *J. Am. Chem. Soc.*, **106**, 2479 (1984).
26) L. R. C. Barclay, D. Kong, and J. Van Kessel, *Can. J. Chem.*, **64**, 2103 (1986).
27) W. A. Pryor, T. Strickland, and D. F. Church, *J. Am. Chem. Soc.*, **110**, 2224 (1988).
28) K. Mukai, N. Tsuzuki, K. Ishizu, S. Ouchi, and K. Fukuzawa, *Chem. Phys. Lipids*, **29**, 129 (1981).
29) S. Matsumoto, M. Matsuo, Y. Iitaka, and E. Niki, *J. Chem. Soc., Chem. Commun.*, **1986**, 1076.
30) H. Ueda, S. Kuri, and S. Shida, *J. Chem. Phys.*, **36**, 1676 (1962).
31) E. Niki, S. Yokoi, J. Tsuchiya, and Y. kamiya, *J. Am. Chem. Soc.*, **105**, 1498 (1983).
32) K. Mukai, H. Nishiguchi, K. Ishizu, Y. Deguchi, and H. Takaki, *Bull. Chem. Soc. Jpn.*, **40**, 2731 (1967).

Oxidation of Lipids. XVII. Crossover Effect of Tocopherols in the Spontaneous Oxidation of Methyl Linoleate†

Mareyuki TAKAHASHI, Yasuyuki YOSHIKAWA, and Etsuo NIKI*
Department of Reaction Chemistry, Faculty of Engineering, University of Tokyo, Hongo, Tokyo 113
(Received September 21, 1988)

Tocopherols suppressed the spontaneous, thermal oxidation of methyl linoleate and produced a clear induction period. During the induction period, small amounts of *cis,trans*-hydroperoxides were formed but the formation of *trans,trans*-hydroperoxides was almost completely inhibited. Tocopherols were consumed and when they were depleted, the induction period was over and a fast oxidation proceeded to give more *trans,trans*-hydroperoxides than *cis,trans*-hydroperoxides. However, tocopherols, especially α-tocopherol, acted as prooxidants when their concentrations were extraordinarily high and the rate of initial radical formation was low. The reducing agent such as ascorbic acid diminished the prooxidant action of α-tocopherol. This prooxidant effect of tocopherols was ascribed to the spontaneous formation of tocopheroxyl radical followed by the hydrogen atom abstraction by the tocopheroxyl radical from the hydroperoxide to give a peroxyl radical.

Lipids are readily oxidized by molecular oxygen. There is an increasing number of evidence that shows the deleterious effects of the oxidation of lipids and its products in foods and in biological systems, and, accordingly, the inhibition of the oxidation of lipids has received much attention recently.[1-11] The aerobic organisms are protected against such oxygen toxicity by an array of defense systems: the preventive antioxidants such as glutathione peroxidase and catalase suppress or reduce the formation of active free radicals by decomposing without generation of free radicals lipid hydroperoxides and/or hydrogen peroxide which are precursors to free radicals, while the chain-breaking antioxidants such as vitamin E and vitamin C scavenge the radicals and interrupt the chain propagation. On the other hand, various kinds of natural and synthetic antioxidants are added to the edible oils and fats to suppress their oxidations. Tocopherols (vitamin E) are known as natural, potent chain-breaking antioxidants. In fact, it has been shown that tocopherols, especially α-tocopherol, scavenge the peroxyl radicals faster than any synthetic, phenolic antioxidants such as 2,6-di-*t*-butyl-4-methylphenol (BHT).[7-11] On the other hand, however, it has been also observed that α-tocopherol can act as a prooxidant under certain conditions.[12-23] For example, Olcott and Einset[13] found that the addition of α-tocopherol into the stabilized oil induced the oxidation during the induction period. Cillard and Cillard[15-17,19,20,22,23] have also observed that tocopherols can act as prooxidants depending on the conditions. More recently, Terao and Matsushita[21] reported the similar effect of α-tocopherol in the oxidation of methyl linoleate. A prooxidant effect of α-tocopherol quinone has been also reported.[24] The detailed mechanism for such a "crossover effect" of α-tocopherol is not well understood. In the course of our study on the oxidation of lipids and its inhibition, we have studied in the present work the prooxidant effect of tocopherols in the spontaneous oxidation of methyl linoleate. Methyl linoleate was chosen as a substrate since the mechanism of its oxidation is well established to give quantitatively four isomeric conjugated diene hydroperoxides, 13-hydroperoxy-9-*cis*,11-*trans*-, 13-hydroperoxy-9-*trans*,11-*trans*-, 9-hydroperoxy-10-*trans*,12-*cis*-, and 9-hydroperoxy-10-*trans*,12-*trans*-octadecadienoic acid methyl esters.[25-29] Thus, it is possible to follow the oxidation quantitatively by measuring either the oxygen uptake, substrate disappearance, hydroperoxide formation or conjugated diene formation.[29] This study confirms some of the previous observations, adds some new data and render a conclusion on the crossover effect of tocopherols.

Experimental

Natural *R,R,R*-α-, *R,R,R*-β-, *R,R,R*-γ-, and *R,R,R*-δ-tocopherols were kindly supplied by Eisai Co., Ltd. Commercial ascorbic acid and its esters were used as received. Methyl linoleate purchased from Daigo Chemical Co. was purified by a silica-gel column before use. *t*-Butyl hydroperoxide kindly supplied by Nippon Oil and Fats Co. was distilled under reduced pressure, 42 °C/24 Torr (1Torr=133.322 Pa). Commercial 2,2-diphenyl-1-picrylhydrazyl (DPPH) was used as received.

Methyl linoleate and additives were dissolved in methyl decanoate and placed in the dark or under laboratory light at room temperature or at 37 °C in air. Sample size was 5 ml. Aliquots of the sample were taken out at regular intervals and analyzed as follows.

The methyl linoleate hydroperoxides were analyzed as their corresponding alcohol, after reduction of the product solution with triphenylphosphine, by high-pressure liquid chromatography (HPLC) using a silica-gel column and hexane/isopropyl alcohol/acetic acid (1000:10:1, v/v/v) as the eluent. The rate of consumption of tocopherols was followed by HPLC with a Finepak SIL 18 column. Methanol was delivered as an eluent at 1 ml min^{-1} and the eluent was monitored at 290 nm. ESR spectrum was

† This work was presented at the 24th General Meeting of the Japan Oil Chemists' Society, October, 1985, Osaka.

recorded on X-band JEOL FE1X spectrometer at room temperature.

Results

Tocopherols are active radical scavengers and efficiently suppress the oxidations of methyl linoleate initiated by a radical initiator.[7,11,29-31] Tocopherols are consumed by the reactions with peroxyl radicals and, when they are depleted, a fast oxidation proceeds.[30] It was found that polyunsaturated fatty acids such as linoleic acid and its esters were oxidized spontaneously even in the absence of any radical initiator. Figure 1 shows the results of spontaneous oxidation of methyl linoleate at room temperature under normal laboratory light in air in the absence and presence of α-tocopherol. In the absence of α-tocopherol, methyl linoleate was slowly oxidized without any noticeable induction period and the conjugated diene hydroperoxides accumulated with time. When 0.25 mM (1 M=1 mol dm^{-3}) of α-tocopherol was added, the oxidation was suppressed and little accumulation of hydroperoxides was observed in about 10 days. α-Tocopherol decreased at roughly constant rate and it was depleted in 14 days. The hydroperoxides were gradually formed as α-tocopherol disappeared. Figure 1 also shows the effect of initial amount of methyl linoleate hydroperoxide. As the initial concentration of methyl linoleate hydroperoxide was increased, the rate of consumption of α-tocopherol increased and the duration of induction period was shortened. In every case, fast oxidation proceeded when α-tocopherol disappeared.

Other tocopherols also suppressed the spontaneous oxidation of methyl linoleate similarly. When α-, β-, γ-, and δ-tocopherols were added simultaneously into methyl linoleate and the solution was stood at room temperature in air under laboratory light, tocopherols were consumed as shown in Fig. 2. As observed previously[30] in the oxidation of methyl linoleate initiated with a radical initiator, α-tocopherol was consumed first, β- and γ-tocopherols decreased after most of α-tocopherol disappeared, and finally δ-tocopherol was consumed. These results may be ascribed partly to the different reactivities of tocopherols (α>β>γ>δ) toward peroxyl radials[7,11,32] and also to the interactions between tocopheroxyl radical (oxyl radical from tocopherol) and tocopherol.[30] For example, α-tocopherol reacts with β-, γ-, and δ-

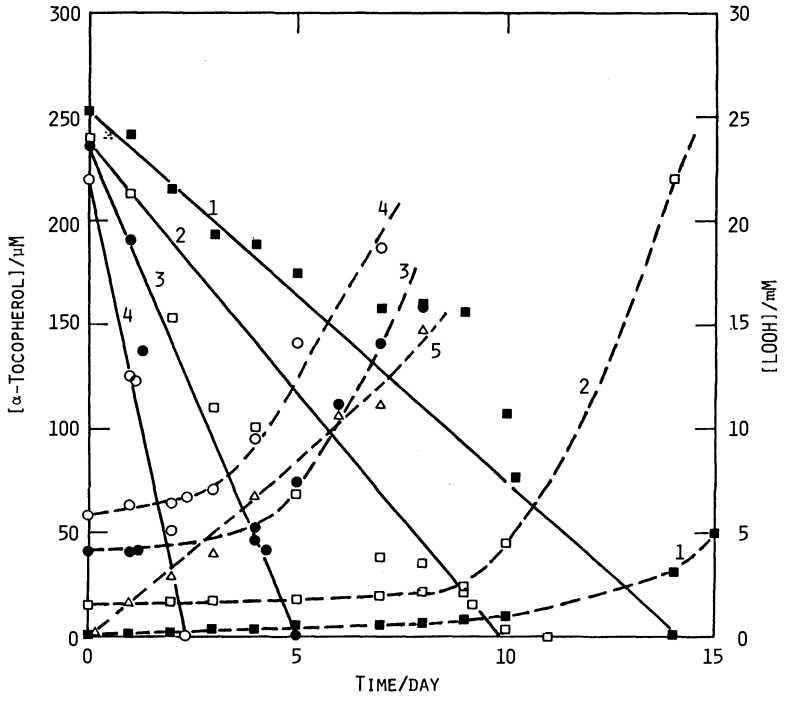

Fig. 1. Rate of accumulation of hydroperoxides (------) and α-tocopherol disappearance (———) in the spontaneous oxidation of methyl linoleate at room temperature under laboratory light.

Line	Mark	[α-Toc]/μM	$[LOOH]_0$/mM
1	■	251	0
2	□	241	1.22
3	●	249	3.95
4	○	229	5.92
5	△	0	0

tocopheroxyl radicals to give α-tocopheroxyl radical and corresponding tocopherols. Mukai has also observed that the reactivities toward phenoxyl radical decreased in the order of α->β-=γ->δ- tocopherols.[33]

Figure 3 shows the distribution of *cis,trans*- and *trans,trans*-hydroperoxides formed in the spontaneous oxidation of methyl linoleate in air under laboratory light in the presence of α-tocopherol. As described above, α-tocopherol suppressed the oxidation and when it was consumed completely, the oxidation proceeded rapidly. Interestingly, when α-tocopherol was present, only *cis,trans*-hydroperoxides were formed and little *trans,trans*-hydroperoxides were observed, whereas more *trans,trans*-hydroperoxides were formed

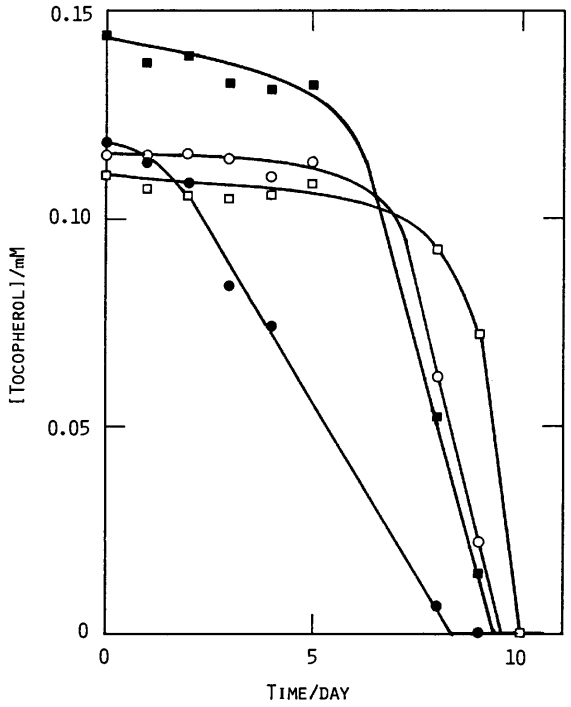

Fig. 2. Rate of disappearance of α-(●), β-(○), γ-(■), and δ-(□) tocopherols during spontaneous oxidation of methyl linoleate at room temperature under laboratory light.

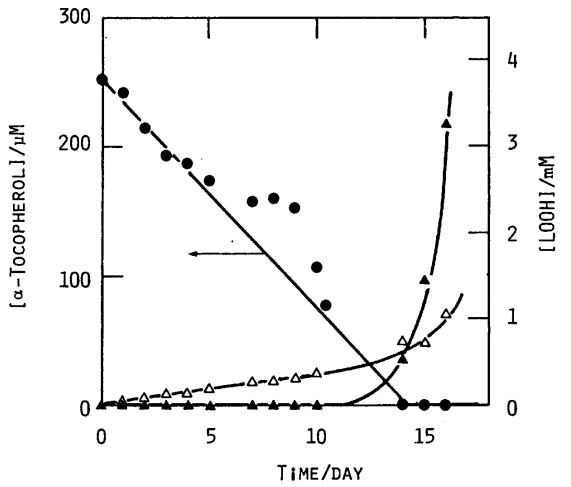

Fig. 3. Rate of hydroperoxide formation and α-tocopherol disappearance in the spontaneous oxidation of methyl linoleate at room temperature under laboratory light.
△: 13-Hydroperoxy-9-*cis*,11-*trans*-octadecadienoic acid methyl ester. ▲: 13-Hydroperoxyl-9-*trans*,11-*trans*-octadecadienoic acid methyl ester.

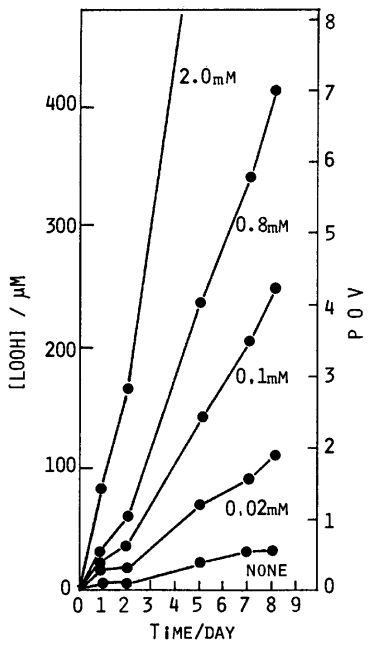

Fig. 4. Rate of spontaneous oxidation of methyl linoleate at 37 °C in the dark in the presence of α-tocopherol.

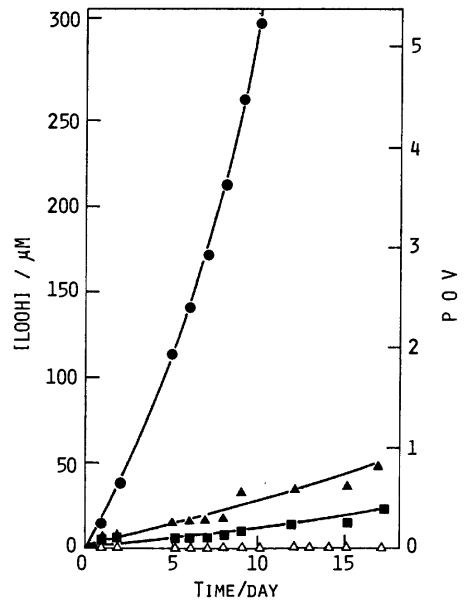

Fig. 5. Rate of accumulation of methyl linoleate hydroperoxide in the spontaneous oxidation of methyl linoleate at room temperature in the dark.
●: α-Toc 9.86 mM; ▲: β-Toc 10.5 mM; ■: γ-Toc 11.3 mM; △: none.

than *cis,trans*-ones after α-tocopherol was depleted.

Thus, α-tocopherol generally acts as an antioxidant and suppresses the spontaneous oxidation of methyl linoleate as well as the oxidation initiated with a radical initiator. However, when the rate of oxidation is quite slow or when the concentration of tocopherol is extraordinarily high, it may act as a prooxidant. When methyl linoleate was stood in air under laboratory light in the presence of 0.296, 2.43, and 18.3 mM α-tocopherol, the rate of hydroperoxide formation increased with increasing concentration of α-tocopherol (data not shown).

When methyl linoleate was stood at 37 °C in the dark, it was oxidized much slower than that stood under laboratory light. Under these conditions, α-tocopherol had a prooxidant effect even at relatively low concentrations. Figures 4 and 5 show the results observed when methyl linoleate was stood in the dark. The addition of tocopherols increased the initial rate of hydroperoxide accumulation with increasing α-tocopherol concentration (Fig. 4) and α-tocopherol had more profound effect than β- and γ-tocopherols (Fig. 5).

Discussion

α-Tocopherol acts as an antioxidant by scavenging chain-carrying peroxyl radical and breaking a chain propagation sequence. In fact, it is known that α-tocopherol scavenges peroxyl radicals much faster than the synthetic, hindered phenols often used commercially as antioxidants.[7,34,35] α-Tocopherol also suppresses the formation of *trans,trans*-hydroperoxide from methyl linoleate. The oxidation of methyl linoleate proceeds by a scheme shown in Fig. 6.[26,27] When the concentrations and/or activities of hydrogen donors are high, the peroxyl radical **1** rapidly abstracts a hydrogen atom to give *cis,trans*-hydroperoxide **2**, while the peroxyl radical **1** has more chance to release oxygen and yield the peroxyl radical **3** which eventually gives *trans,trans*-hydroperoxide **4** when the concentrations of active hydrogens are low. Thus, α-tocopherol acts as a strong hydrogen donor and gives *cis,trans*-hydroperoxide exclusively.[26,27,36-38]

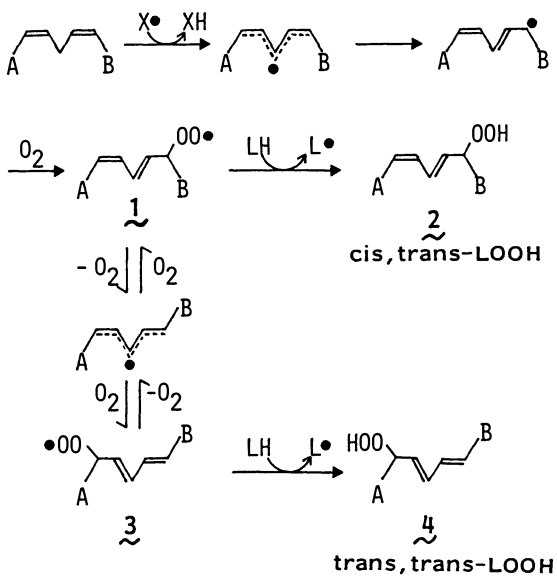

Fig. 6. Scheme for the oxidation of methyl linoleate.
A, B: $CH_3(CH_2)_4$-, $CH_3OC(O)(CH_2)_7$-.

However, as reported previously by other investigators[12-23] and as observed in this study, α-tocopherol can act as a prooxidant under certain circumstances, for example, when the rate of chain initiation is quite low and when the concentration of α-tocopherol is quite high. The prooxidant effect of α-tocopherol must stem from the hydrogen atom abstraction from hydroperoxide by α-tocopheroxyl radicals **5** (reaction 1),

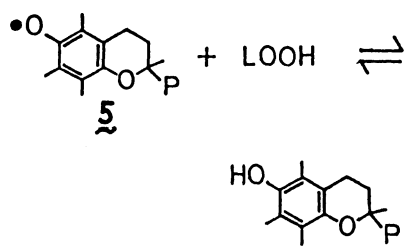

(1)

where P is a phytyl side chain, $C_{16}H_{33}$. This reaction may proceed rapidly. In fact, as shown in Fig. 7, when *t*-butyl hydroperoxide was added to the benzene solution containing α-tocopheroxyl radical, tocopheroxyl radical disappeared quite rapidly. The rate constants for the hydrogen atom abstraction from

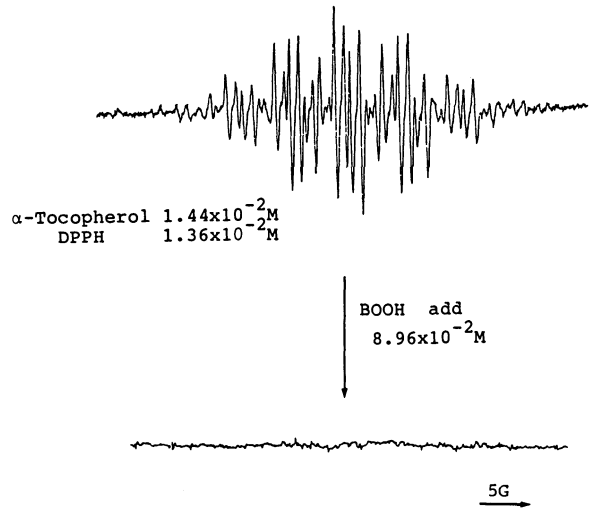

Fig. 7. ESR spectra observed when *t*-butyl hydroperoxide was added to the benzene solution containing α-tocopheroxyl radical.
A: ESR spectrum observed when 14.4 mM α-tocopherol was reacted with 13.6 mM DPPH in benzene. The spectrum was taken under vacuum. B: ESR spectrum observed under vacuum when 89.6 mM *t*-butyl hydroperoxide was added into the solution A.

hydroperoxide by phenoxyl radicals have been reported.[39-41] Mukai et al.[42] reported quite recently the rate constant for the hydrogen atom abstraction from *t*-butyl hydroperoxide by 5,7-diisopropyl-6-chromanoxyl radical as 0.365 $M^{-1}s^{-1}$ at 25 °C. Considering the steric effect involved in the hydrogen atom transfer from hydroperoxide to a phenoxyl radical,[39,43,44] the hydrogen atom abstraction from lipid hydroperoxide by α-tocopheroxyl radical must be larger than that. The peroxyl radical formed in the reaction 1 must attack lipid and induce the chain oxidation. The direct attack of α-tocopheroxyl radical on the methyl linoleate can not be ruled out, although it must be much less favorable than the reaction 1.

As reported previously,[30,32,33] the stabilities of tocopheroxyl radicals decrease in the order of $\alpha>\beta=\gamma>\delta$, suggesting that α-tocopheroxyl radical is formed most easily among the four tocopheroxyl radicals. This must explain why α-tocopherol has the most profound prooxidant activity among the four tocopherols. Terao and Matsushita[21] found that BHT did not act as prooxidant for methyl linoleate. This must be because the phenoxyl radical derived from BHT is much less resonance-stabilized[32] and the spontaneous formation of the phenoxyl radical from BHT is quite slow.

In consistent with the above assumption, the prooxidant effect of α-tocopherol was diminished by a reducing agent such as ascorbic acid and its esters. As observed previously by Terao,[21] little prooxidant effect of α-tocopherol was observed in the presence of ascorbic acid esters such as 6-ascorbyl palmitate. Ascorbic acid added to the methyl linoleate as an ethanol solution also had a similar effect. It has been previously observed by pulse radiolysis[45] and ESR[46] studies that α-tocopheroxyl radical is reduced by ascorbic acid to regenerate α-tocopherol. Packer, Slater and Willson[45] obtained a value of 1.55×10^6 $M^{-1}s^{-1}$ as rate constant for the reaction 2. Mukai et al.[47] has recently obtained a rate constant of 549 $M^{-1}s^{-1}$ for the interaction between ascorbic acid and 5,7-diisopropyltocopheroxyl radical.

The crossover effect of α-tocopherol depends on the relative importance of the first step and the following competing reactions 2 and 3, which is determined by the ratio of the concentration of lipid peroxyl radical to that of lipid hydroperoxide. When this ratio is high as in the oxidations initiated with an added initiator, under light, or at high temperature, α-tocopherol functions as an antioxidant, while it acts as a prooxidant when this ratio is low. The higher the α-tocopherol concentration, the more α-tocopheroxyl radical must be formed spontaneously. Furthermore, α-tocopherol must give its radical most easily than any other tocopherols and synthetic phenols.

The prooxidant effect of vitamin E in vivo has not been reported. This may be because the concentration of vitamin E is usually low and/or because the vitamin E radical is reduced readily by, for example, vitamin C in biological systems.

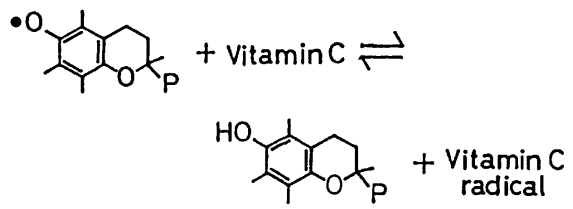

In conclusion, α-tocopherol functions in general as a chain-breaking antioxidant, but it may also act as a prooxidant under certain conditions, for example, when its concentration is quite high or when the rate of oxidation (that is, the rate of chain initiation) is very low. It may be said that the antioxidant, like oxygen molecule, is also a double-edged sword.

This study was supported by Grant-in-Aid for Scientific Research No. 62470078 from the Ministry of Education, Science and Culture.

References

1) "Tocopherol, Oxygen, and Biomembranes," ed by C. de Duve and O. Hayaishi, Elsevier, Amsterdam (1978).
2) L. A. Witting, "Free Radicals in Biology, IV," ed by W. A. Pryor, Academic Press, (1980), pp. 295—319.
3) "Vitamin E. A Comprehensive Treatise," ed by L. J. Machlin, Marcel Dekker, New York (1980).
4) "Vitamin E: Biochemical, Hematological, and Clini-

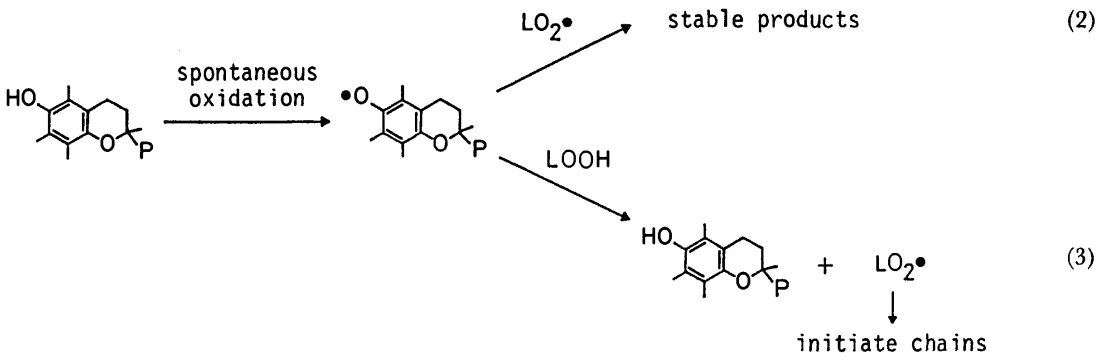

cal Aspects," ed by B. Lubin and L. J. Machlin, Ann. N. Y. Acad. Sci., (1982), Vol. 393.
5) "Biology of Vitamin E," (Ciba Foundation Symp. 101), Pitman, London (1983).
6) "Clinical and Nutritional Aspects of Vitamin E," ed by O. Hayaishi and M. Mino, Elsevier, Amsterdam (1987).
7) G. W. Burton and K. U. Ingold, *Acc. Chem. Res.*, **19**, 194(1986).
8) P. B. McCay, *Annl. Rev. Nutr.*, **5**, 323 (1985).
9) G. W. Burton, D. O. Foster, B. Perly, T. F. Slater, I. C. P. Smith, and K. U. Ingold, *Phil. Trans. R. Soc. Lond.*, **B311**, 565 (1985).
10) A. Bendich, L. J. Machlin, O. Scandurra, G. W. Burton, and D. D. M. Wayner, *Adv. Free Rad. Biol. Med.*, **2**, 419 (1986).
11) E. Niki, *Chem. Phys. Lipids*, **44**, 227 (1987); *Ann. N. Y. Acad. Sci.*, **498**, 186 (1987).
12) W. O. Lundberg, "Autoxidation and Antioxidants, Vol. II," ed. by W. O. Lundberg, Interscience, New York (1962), pp. 451—476.
13) H. S. Olcott and E. Einset, *J. Am. Oil Chem. Soc.*, **35**, 159(1958).
14) C. Kanno, K. Yamauchi, and T. Tsugo, *Agr. Biol. Chem.*, **34**, 886 (1970).
15) J. Cillard and P. Cillard, *J. Am. Oil Chem. Soc.*, **57**, 39(1980).
16) J. Cillard, P. Cillard, and M. Cormier, *J. Am. Oil Chem. Soc.*, **57**, 252 (1980).
17) J. Cillard, P. Cillard, and M. Cormier, *J. Am. Oil Chem. Soc.*, **57**, 255 (1980).
18) H. Kamematsu, M. Aoyama, T. Maruyama, I. Niiya, and T. Matsumoto, *J. Jpn. Oil Chem. Soc.*, **33**, 241 (1984).
19) B. Bazin, J. Cillard, J. P. Koskas, and P. Cillard, *J. Am. Oil Chem. Soc.*, **61**, 1212(1984).
20) J. P. Koskas, J. Cillard, and P. Cillard, *J. Am. Oil Chem. Soc.*, **61**, 1466 (1984).
21) J. Terao and S. Matsushita, *Lipids*, **21**, 255(1986).
22) J. Cillard and P. Cillard, *J. Am. Oil Chem. Soc.*, **63**, 1165(1986).
23) S. R. Husain, J. Cillard, and P. Cillard, *J. Am. Oil Chem. Soc.*, **64**, 109 (1987).
24) J. A. Lindsey, H. Shang, H. Kaseki, N. Morisaki, T. Sato, and D. G. Comwell, *Lipids*, **20**, 151 (1985).
25) H. W. S. Chan and G. Levett, *Lipids*, **12**, 99 (1977).
26) N. A. Porter, B. A. Weber, H. Weener, and J. A. Khan, *J. Am. Chem. Soc.*, **102**, 5597 (1980).
27) N. A. Porter, *Acc. Chem. Res.*, **19**, 262 (1986); *Adv. Free Rad. Biol. Med.*, **2**, 283 (1986).
28) E. N. Frankel, *J. Am. Oil Chem. Soc.*, **61**, 1908 (1984); *Prog. Lipid Res.*, **23**, 197 (1985).
29) Y. Yamamoto, E. Niki, and Y. Kamiya, *Lipids*, **17**, 870 (1982).
30) E. Niki, J. Tsuchiya, Y. Yoshikawa, Y. Yamamoto, and Y. Kamiya, *Bull. Chem. Soc. Jpn.*, **59**, 497 (1986).
31) L. R. C. Barclay, S. J. Locke, J. M. MacNeil, G. W. Burton, and K. U. Ingold, *J. Am. Chem. Soc.*, **106**, 2479 (1984).
32) G. W. Burton, T. Doba, E. J. Gabe, L. Hughes, F. L. Lee, L. Prasad, and K. U. Ingold, *J. Am. Chem. Soc.*, **107**, 7053 (1985).
33) K. Mukai, Y. Watanabe, Y. Uemoto, and K. Ishizu, *Bull. Chem. Soc. Jpn.*, **59**, 3133 (1986).
34) G. W. Burton and K. U. Ingold, *J. Am. Chem. Soc.*, **103**, 6472 (1981).
35) E. Niki, R. Tanimura, and Y. Kamiya, *J. Jpn. Petrol. Inst.*, **27**, 21 (1984).
36) H. Weenen and N. A. Porter, *J. Am. Chem. Soc.*, **104**, 5216 (1982).
37) K. E. Peers, D. T. Coxon, and H. W. S. Chan, *J. Sci. Food Agric.*, **32**, 898 (1981).
38) K. E. Peers and D. T. Coxon, *Chem. Phys. Lipids*, **32**, 49 (1983).
39) J. R. Thomas, *J. Am. Chem. Soc.*, **86**, 4807 (1964).
40) L. R. Mahoney and M. A. DaRooge, *J. Am. Chem. Soc.*, **98**, 5619 (1967).
41) A. P. Griva, *Int. J. Chem. Kinet.*, **V**, 869 (1973).
42) K. Mukai, Y. Kohno, and K. Ishizu, *Biochem. Biophys. Res. Commun.*, **155**, 1046 (1988).
43) J. A. Howard and K. U. Ingold, *Can. J. Chem.*, **41**, 2800 (1963).
44) L. R. Mahoney, *Angew. Chem., Int. Ed. Engl.*, **8**, 547 (1969).
45) J. E. Packer, T. F. Slater, and R. L. Willson, *Nature (London)*, **278**, 737(1979).
46) E. Niki, J. Tsuchiya, R. Tanimura, and Y. Kamiya, *Chem. Lett.*, **1982**, 789.
47) K. Mukai, K. Fukuda, K. Ishizu, and Y. Kitamura, *Biochem. Biophys. Res. Commun.*, **146**, 134 (1987).

The Ei Reaction of Substituted *threo*- and *erythro*-1-Phenylethyl Phenyl Sulfoxides

Toshiaki YOSHIMURA,* Eiichi TSUKURIMICHI, Yukihiko IIZUKA, Hironobu MIZUNO, Hiroshi ISAJI, and Choichiro SHIMASAKI
Department of Industrial Chemistry, Faculty of Engineering, Toyama University, Gofuku, Toyama 930
(Received September 24, 1988)

Substituted (*RS,SR*)-1-phenylethyl phenyl sulfoxides (threo) ($XC_6H_4S(O)CH(CH_3)C_6H_4Y$) and some substituted (*RR,SS*)-sulfoxides (erythro) were prepared and kinetic investigation for the thermal decomposition was carried out at 80.0, 90.0, and 100.0 °C in dioxane. Hammett plots for *threo*-$XC_6H_4S(O)CH(CH_3)C_6H_5$ gave positive ρ-values (ρ_X=0.60—0.64 at three temperatures), while those for *threo*- and *erythro*-$C_6H_5S(O)CH(CH_3)C_6H_4Y$ showed V-shape lines with bottoms at the *m*-OCH_3 substituent though the effects of the substituents are small. Meanwhile, large kinetic isotope effects for *threo*- and *erythro*-$C_6H_5S(O)CH(CD_3)C_6H_4Y$ (Y=H, *p*-OMe, *m*-Cl) (k_H/k_D=4—6) were observed at all temperatures. The activation energies were in the range of 104—121 kJ mol^{-1} for all sulfoxides, while the activation entropies were relatively large (7—−37 J K^{-1} mol^{-1}) and were correlated with Hammett σ-values to give small negative trend. Reactions of all erythro-isomers examined were 2—3 times faster than those of the corresponding threo-isomers. From these results, it is suggested that the pyrolysis of 1-arylethyl aryl sulfoxides proceeds via a concerted mechanism in which the transition state is variable from an E1-like to a conjugated one. In the latter transition state, conjugation of the phenyl group bearing the electron-withdrawing substituent with the developing π-bond electron acidifies the β-proton.

Thermolysis of sulfoxides bearing at least one β-hydrogen atom has been shown to proceed via an intramolecular cis elimination[1] affording olefins[2-8] and sulfenic acids which are dimerized to thiosulfinic S-esters or can be trapped by activated olefins.[9-16] Cram et al.[1] prposed a radical mechanism based on the observation of loss of stereospecificity for the pyrolysis of 1,2-diphenyl-1-propyl phenyl sulfoxides at high temperatures. However, no evidence suggesting the radical mechanism has been reported ever since. Though the Ei-reaction of sulfoxides is generally regarded as a concerted process, some kinetic investigations using aryl propyl sulfoxides[17] or aryl *t*-butyl sulfoxides[8] reveal that electron-withdrawing substituents on the phenyl ring accelerate the reaction suggesting the polarization of the carbon-sulfur bond and development of partially negative charge on the sulfinyl group in the transition state. From these results, development of partially positive charge on the α-carbon atom, i.e., E1-like mechanism, has been assumed. However, we recently proposed a carbanion-like mechanism for the pyrolysis of 2-phenylethyl phenyl sulfoxide which showed positive trends for Hammett substituent effects on both phenyl groups (ρ_X=0.76 for $XC_6H_4S(O)CH_2CH_2Ph$, ρ_Y=0.32 for $PhS(O)CH_2CH_2C_6H_4Y$). These results reveal that partial charge on the α-carbon atom in the transition state cannot be determined without an examination of the substituent effect on the α-position.

Meanwhile, Oae et al. reported the mechanistic investigation of Ei-reaction of sulfilimines which have isoelectronic structure to the sulfoxides. They suggested cis-concerted E1-like mechanism.[18-21]

In order to clarify the transition state of the Ei-reaction of sulfoxides and to compare with that of sulfilimines, kinetic investigation of the thermolysis of substituted *threo*- and *erythro*-1-phenylethyl phenyl sulfoxides was carried out.

Results

Preparation of Substituted 1-Phenylethyl Phenyl Sulfoxides and Their Diastereoisomer. The substituted *threo*- and *erythro*-1-phenylethyl phenyl sulfoxides were prepared from the corresponding sulfides by oxidation with hydrogen peroxide in acetic acid. The mixture of threo- and erythro-isomers obtained were separated by fractional crystallization and repeated column chromatography. The *threo*- and *erythro*-sulfoxides obtained were tentatively assigned as follows. ^1H NMR chemical shifts of methine protons of the sulfoxides were plotted against Hammett σ-values as shown in Fig. 1.

Apparently, two series of methine signals were observed. The higher field one could be assigned as that of threo isomer by comparing with that of 1-phenylethyl phenyl and 1-phenylethyl *p*-tolyl sulfoxides whose absolute configurations[22,23] are known. A similar series of ^1H NMR methine signals of 1-phenylethyl (*p*-substituted phenyl) sulfoxides and their lanthanoid-induced shifts, solvent effects, and assignments of their absolute configurations were reported.[24,25]

Upon heating the sulfoxides in carbon tetrachloride at 100 °C for 15—20 min, formation of the substituted styrenes were observed by NMR and liquid chromatography. If the reaction should be accompanied by a possible threo-erythro isomerization due to a pyramidal inversion[30] on sulfur atom or a homolytic cleavage like in the racemization of benzyl *p*-tolyl sulfoxide at 135—165 °C,[31] the kinetic behavior should be complicated. But the NMR spectra showed no contamination of the threo-erythro isomerization, also sug-

gesting that the radical mechanism is unlikely.

Kinetics. The reaction was followed by measuring the decreasing peak area of the sulfoxide in liquid chromatography using diphenyl ether, diphenyl sulfide or methyl phenyl sulfide as an internal standard. The process of the reactions was found to follow good first-order kinetics and the rate constants had no dependence on initial concentration of the sulfoxides. The results obtained are listed in Table 1 and Hammett substituent effects are compiled in Table 2.

Effects of X-substituents for the threo-isomer gave positive ρ-values suggesting that departure of leaving group is important in the transition state. However, both the electron-withdrawing and -releasing Y-substituents were found to accelerate the reaction to give concave curves in which a series of substituents from the *p*-OCH_3 to *m*-OCH_3 groups gave negative ρ-values, while the *m*-OCH_3 to *p*-NO_2 groups afforded

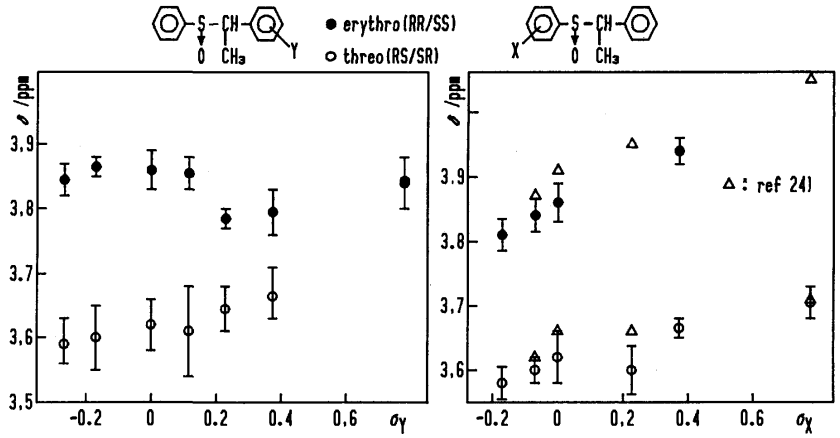

Fig. 1. Dependence of ^1H NMR methine signals of *threo*- and *erythro*-1-arylethyl aryl sulfoxides on Hammett σ-values.

Table 1. The Kinetic Data for Pyrolysis of Substituted 1-Phenylethyl Phenyl Sulfoxides in Dioxane

XC_6H_4-S-CHC_6H_4Y
↓ |
O $CH_3(CD_3)$

Sulfoxides			Rate constants[a]			Activation parameters		
X	Y	Isomer	$k\times10^5$ / s^{-1}			ln *A*	E_a / kJ mol^{-1}	ΔS^* / J K^{-1} mol^{-1}
			80.0 °C	90.0 °C	100.0 °C			
H	*p*-OMe	th[b]	6.92 ±0.07	22.4 ±0.4	57.7 ±0.8	30.1±1.8	116±5	−5±15
H	*p*-OMe	er[c]	18.1 ±0.9	55.2 ±0.9	137 ±4	29.2±1.6	111±5	−12±13
H	*p*-OMe	th(β-d_3)[d]	1.60 ±0.06	4.91±0.12	13.2 ±0.2	28.4±0.8	116±2	−19±6
H	*p*-Me	th	6.04 ±0.02	18.5 ±0.5	48.7 ±0.6	29.3±1.0	114±3	−12±8
H	*p*-Me	th(β-d_3)	1.20 ±0.04	3.65±0.23	9.77±0.44	27.8±0.7	115±2	−24±6
H	H	th	5.15 ±0.18	14.5 ±0.4	43.5 ±1.6	29.9±1.3	117±4	−6±11
H	H	er	10.2 ±0.5	30.4 ±0.6	83.9 ±3.0	30.1±0.2	115±1	−4±2
H	H	th(β-d_3)	1.00 ±0.02	2.92±0.05	9.12±0.14	29.7±1.3	121±4	−8±11
H	H	er(β-d_3)	2.30 ±0.05	6.12±0.07	17.9 ±0.2	27.6±1.6	112±5	−26±13
H	*m*-OMe	th	4.98 ±0.18	15.8 ±0.6	40.2 ±1.1	29.1±1.7	114±5	−13±14
H	*m*-OMe	er	12.8 ±1.8	35.6 ±0.4	96.0 ±1.4	28.6±0.3	110±1	−17±2
H	*p*-Cl	th	5.47 ±0.22	14.7 ±0.6	43.1 ±1.0	28.7±1.5	113±5	−17±13
H	*p*-Br	th	4.40 ±0.16	13.1 ±0.2	34.9 ±1.1	28.6±0.6	113±2	−17±5
H	*m*-Cl	th	5.21 ±0.10	15.1 ±0.5	39.9 ±0.8	28.1±0.4	112±1	−21±3
H	*m*-Cl	er	15.0 ±0.3	42.4 ±0.9	104 ±3	27.4±0.9	106±3	−27±8
H	*m*-Cl	th(β-d_3)	0.858±0.008	2.53±0.09	7.09±0.36	27.7±0.1	116±1	−24±1
H	*p*-NO_2	th	6.97 ±0.33	19.3 ±0.9	47.5 ±4.5	26.3±0.7	105±2	−37±6
H	*p*-NO_2	er	20.6 ±1.1	49.4 ±2.0	138 ±5	26.9±2.2	104±6	−31±18
p-Me	H	th	4.21 ±0.05	12.2 ±0.2	34.1 ±1.4	29.0±0.2	115±1	−14±2
m-Me	H	th	4.91 ±0.05	13.2 ±0.4	37.5 ±0.5	28.0±1.2	111±4	−22±10
p-Cl	H	th	6.05 ±0.22	15.2 ±0.4	46.6 ±1.6	28.3±2.7	112±8	−20±22
m-Cl	H	th	6.61 ±0.34	20.2 ±0.6	53.5 ±2.8	29.4±0.9	115±3	−10±7
p-NO_2	H	th	17.5 ±0.3	47.3 ±1.1	151 ±2	31.5±2.4	118±7	7±20

a) The rate constants and activation parameters were calculated by the least-squares method and the errors are standard deviations. b) Threo-isomer. c) Erythro-isomer. d) β-Deuterated sulfoxide.

Table 2. Hammett ρ-Values (vs. σ) for Pyrolysis of 1-(Substituted phenyl)ethyl Phenyl Sulfoxides and 1-Phenylethyl (Substituted phenyl) Sulfoxides in Dioxane

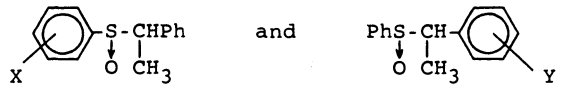

Temp °C	ρ_X(threo)	ρ_{Y1}(threo)[a]	ρ_{Y2}(threo)[a]	ρ_{Y1}(erythro)	ρ_{Y2}(erythro)
80.0	0.61(0.96)	−0.38(0.98)[b]	0.24(0.86)	−0.49(0.75)	0.31(0.99)
90.0	0.60(0.96)	−0.43(0.88)	0.19(0.78)	−0.58(0.85)	0.21(0.99)
100.0	0.64(0.95)	−0.39(0.97)	0.13(0.68)	−0.47(0.84)	0.24(0.98)

a) ρ_{Y1}, *p*-OMe≈*m*-OMe; ρ_{Y2}, *m*-OMe≈*p*-NO_2. b) The numbers in the parentheses are correlation coefficients.

Table 3. Isotope Effects for 1-Arylethyl-2,2,2-d_3 Phenyl Sulfoxides

X	Y	Isomer	Isotope effects (k_H/k_D)			$E_{aD}-E_{aH}$	A_H/A_D
			80.0 °C	90.0 °C	100 °C	kJ mol^{-1}	
H	*p*-OMe	th	4.33±0.17	4.56±0.14	4.37±0.09	0±7	5.5
H	H	th	5.15±0.21	4.97±0.16	4.77±0.19	4±8	1.2
H	H	er	4.43±0.24	4.97±0.11	4.69±0.18	3±6	12
H	*m*-Cl	th	6.07±0.13	5.97±0.29	5.63±0.31	4±2	1.49

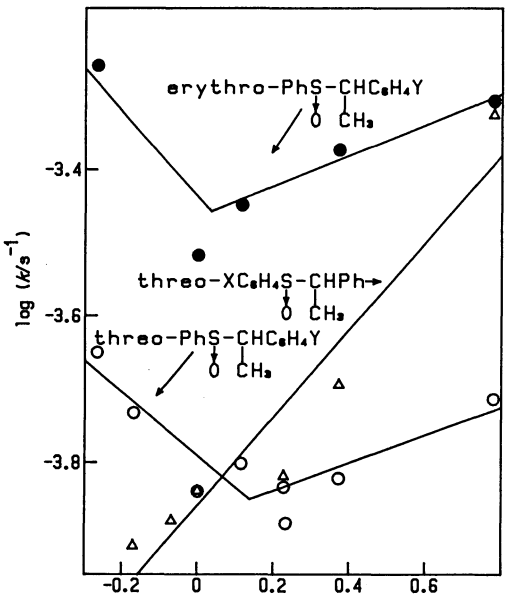

Fig. 2. Hammett plots for the rates of pyrolysis of *threo*- and *erythro*-1-arylethyl aryl sulfoxides at 90.0 °C in dioxane.

positive ρ-values for both the threo- and erythro-isomers as the example at 90.0 °C shown in Fig. 2. Though some Hammett correlations are not very good and the reflecting point is not clear, all of the correlations for different temperatures and different isomers have the same tendencies. The bottoms of the Hammett plots for Y-substituent effects for the threo-isomers seem to be deviated to a positive side at all temperatures unlike the erythro-isomers whose bottom positions are not clear due to only a few measured points. The Hammett plots for the threo- and the erythro-isomers gave the separated parallel lines suggesting that the present assignments of the isomers are valid, especially for 1-(*p*-nitrophenyl)ethyl phenyl sulfoxides ^{1}H NMR methine signals of which cannot be distinguished the isomers.

Large kinetic isotope effects using β,β,β-d_3 sulfoxides were observed as shown in Table 3 for both the *erythro*- and the *threo*-sulfoxides bearing both the electron-withdrawing and -releasing Y-substituents (*p*-OCH_3, *p*-CH_3, H, *m*-Cl), suggesting an involvement of a proton transfer from the β-carbon to the oxygen and no radical cleavage of the C-S bond in the transition state, since the free radical mechanism involving the rate-determining C-S bond cleavage is not in accord with the large kinetic isotope effect. These results reveal that both the C-S bond cleavage and the proton transfer are important in the transition state namely the reaction proceeds via a concerted process.

Activation parameters were calculated for all the sulfoxides (Table 1). The activation entropies are all in the range of 7 to −37 J K^{-1} mol^{-1}. These values are of positively deviated compared to those for primary alkyl aryl sulfoxides (phenyl propyl sulfoxide −63 J K^{-1} mol^{-1},[17] 2-phenylethyl phenyl sulfoxide −45 J K^{-1} mol^{-1}.[26] The activation entropies correlate with the Hammett σ-values giving a negative correlation for Y-substituents as shown in Fig. 3, though the correlation for X-substituents is not clear. Namely, the activation entropy for the reaction of the sulfoxide having more electron-withdrawing Y-substituent is more negative.

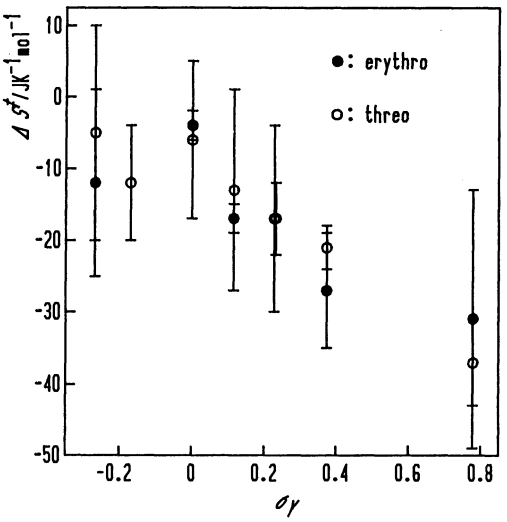

Fig. 3. Dependence of activation entropies on Hammett σ-values for the pyrolysis of *threo*- and *erythro*-1-arylethyl phenyl sulfoxides.

Table 4. Solvent Effect on Pyrolysis of *threo*-1-Phenylethyl Phenyl Sulfoxide at 90.0 °C

Solvent	Dielectric constant	Rate constant $k\times10^5$ / s^{-1}	Relative rates
Dioxane	2.21	14.5 ±0.4	1
DMSO	48.9	7.48±0.09	0.52
Acetonitrile	37.5	5.59±0.25	0.39
Ethanol	24.3	2.31±0.09	0.16

Pyrolysis of the sulfoxide in other solvents was carried out as shown in Table 4. The pyrolysis was not much affected by the solvent change, the rates of pyrolysis are not correlated to the dielectric constants, and the relative rates are very similar to those for the pyrolysis of 2-phenylethyl phenyl sulfoxide[26] and sulfilimines[19] suggesting that the transition state of the reaction is not ionic but concerted one like other sulfoxides and sulfilimines. Namely, the more solvation in the starting state by a dipole-dipole interaction between sulfoxides and dipolar aprotic solvents or by a hydrogen bonding to the sulfoxide oxygen than in the transition state causes the reduction of the reaction rate as described in the previous paper.[26]

Discussion

Though Ei-reaction of sulfoxides are generally recognized as a concerted process, a balance of extent of the C-S bond cleavage and the proton migration from the β-carbon to the oxygen causes the deviation to an E1-like or a carbanion-like mechanism in the five-membered cyclic transition state. Namely, in the E1-like mechanism the departure of leaving group progresses more than the proton abstraction developing a partially positive charge at the α-carbon while in the carbanion-like mechanism the reverse relation develops a partially negative charge at the β-carbon in the transition state.

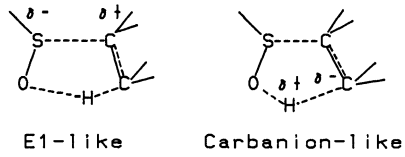

Fig. 4. E1-like and carbanion-like cyclic transition states.

However, unlike E2-reactions the development of charge at the α- or β-carbon should be small, because the stretching of the C-S bond can lead to an enhancement of both the basicity of the oxygen atom and the acidity of the β-proton which would facilitate the proton transfer resulting a neutralization of the positive charge at the α-carbon atom, similarly the progress of the proton transfer would promote the C-S bond cleavage neutralizing the negative charge at the β-carbon. In fact, relative yields of 1-butene to the 2-butene are nearly equal to those on the statistical basis of the numbers of the β-hydrogens in the pyrolysis of ethyl *s*-butyl and propyl *s*-butyl sulfoxides,[4] suggesting that the orientation of elimination has no tendency of Saytzeff or Hofmann rule. Nevertheless, examinations of a Hammett substituent effect have shown to some extent the development of the partial charge in the transition state of the pyrolysis of sulfoxides.[8,17,26] In many variations of Hammett σ-values, use of the usual σ-values for the correlations is considered to be enough to examine such small charge distributions in the concerted transition state, and has been done in these literatures.

Hammett Substituent Effect. The positive Hammett ρ-values for X-substituents appears to be consistent with an E1-like mechanism. Various examples of ρ-values for the pyrolysis of other alkyl aryl sulfoxides and sulfilimines are compiled in Table 5. The effects of X-substituents generally show a positive trend for both sulfoxides and sulfilimines except for 2-cyanoethyl phenyl sulfoxide.[26] However, the pyrolysis proceeding via a carbanion-like mechanism for 2-cyanoethyl phenyl and aryl 2-phenylethyl sulfoxides shows negative or small positive ρ-values. The posi-

Table 5. Representative Hammett ρ-Values of Pyrolysis of Sulfoxides and Sulfilimines

Substrate	Solvent	Temp / °C	ρx	Ref.
$XC_6H_4S(O)CH_2CH_2CH_3$	PhOPh	170—180	0.51	17
$XC_6H_4S(O)C(CH_3)_3$	$PhCH_3$	101.3	0.695	8
$XC_6H_4S(O)CH_2CH_2Ph$	Dioxane	120.0	0.33	26
$XC_6H_4S(O)CH_2CH_2CN$	Dioxane	100.0	−0.49	26
$XC_6H_4S(NTs)CH_2CH_3$	Benzene	80.3	0.90	20
$XC_6H_4S(NTs)CH(CH_3)Ph$	Benzene	25.0	0.90	19

tive trend for the pyrolysis of aryl 2-phenylethyl sulfoxides via even a carbanion-like mechanism is attributed to the substituent effect on the *S*-phenyl group being more susceptible to C-S bond cleavage than proton abstraction.[26] Therefore, from the examination of only the substituent effect on the *S*-phenyl group the mechanism can not be clarified. The substituent effect on the α-phenyl group showed negative Hammett ρ-values from the *p*-OCH_3 group to the *m*-OCH_3 group suggesting apparently development of partially positive charge on the α-position in the transition state, i.e., an E1-like mechanism. However, the ρ-values turned from negative to positive from the *m*-OCH_3 group to the *p*-NO_2 group to give V-shaped Hammett plots. A similar Hammett substituent effect is known in the nucleophilic substitution at substituted benzyl chlorides by trimethylamine which is interpreted in a change of the transition state from S_N1-like to S_N2-like.[29] The present results can also be explained in the same way. Namely, the transition state of the elimination presumably varies from E1-like in the case of the sulfoxides bearing electron-releasing Y-substituents into a conjugated system as shown in Fig. 5 in the case of electron-withdrawing groups.

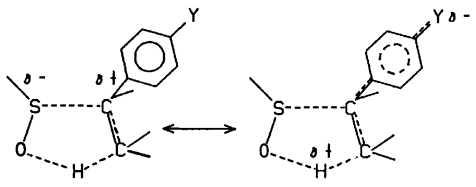

Fig. 5. Conjugated transition state of the pyrolysis of 1-(electron-withdrawing group-substituted phenyl)-ethyl phenyl sulfoxides.

The conjugation with electron-withdrawing groups is advantageous for the elimination, because it acidifies the β-proton effectively, assists the C-H bond cleavage, and stabilizes the transition state. Meanwhile, the conjugation with electron-releasing substituents interferes the development of C-C π-bond formation, instead, stabilizes the partially positive charge at the α-carbon, assisting the extension of the C-S bond to increase the basicity of the sulfoxide oxygen which also accelerates the elimination. Figure 2 shows that the position of 1-phenylethyl phenyl sulfoxide is on the negative line suggesting that the transition state of its Ei is El-like.

Activation Parameters. Activation parameters for pyrolysis of sulfoxides are usually in the range of 106—125 kJ mol^{-1} for activation enthalpies and −71—+30 J K^{-1} mol^{-1} for activation entropies.[1,4,8,17,26] The activation entropy of the slowest type of such simple sulfoxides as phenyl propyl is large negative (−63 J K^{-1} mol^{-1})[17] suggesting that the transition state is more rigid than the starting state due mainly to a cyclization. However, the present system shows a nearly zero activation entropy which is presumably a result of a relatively large contribution of the extension of the C-S bond in the cyclic transition state compared to the small contribution of the progress of the proton transfer according to the following reason. The contribution of extent of the proton transfer to the activation entropy is probably small, because the contribution of looseness of the C-H bond is canceled by that of development of the O-H bond formation. Therefore the increase of the activation entropy to the positive direction in the present system is mainly based on the contribution of the looseness of the C-S bond in the transition state. In the case of the pyrolysis via a carbanion-type transition state such as that of 2-phenylethyl phenyl sulfoxide, the C-S bond is not so loose as compared with the progress of the proton transfer resulting a relatively large negative activation entropy.[26] Therefore, the positively deviated activation entropy for the present system is consistent with the El-like mechanism. The fact that the plot of activation entropies for Y-substituents vs. Hammett σ-values gave the negative trend is probably due to the increase of an El-like character by electron-releasing substituents.

Isotope Effect. Kinetic isotope effects for the Ei-reaction of β-deuterated sulfoxides, sulfilimines, and tertiary amine oxides are usually small (k_H/k_D=2—3.5)[19,20,27] due to the cyclic transition state. However, the present system shows relatively large kinetic isotope effects. Meanwhile, Kwart et al. reported a usual magnitude of kinetic isotope effect for the thermolysis of heptyl-2-*d* phenyl sulfoxide (k_H/k_D=2.3—3.1)[27,28] and a relatively large effect for *t*-butyl-d_9 ethyl sulfoxide (k_H/k_D=3.3—6).[11] They examined a temperature dependence of k_H/k_D to result that the activation energy difference and the frequency factor ratio between hydrogen and deuterium for the cis-elimination of heptyl phenyl sulfoxide ($E_{a_D}-E_{a_H}$=4.81 kJ mol^{-1} A_H/A_D=0.76)[27] are in the range of zero-point energy controlled isotope effect ($E_{a_D}-E_{a_H}<5.9$ kJ mol^{-1}, $0.6<A_H/A_D<1.4$),[28] but those for *t*-butyl ethyl sulfoxide ($E_{a_D}-E_{a_H}$=13 kJ mol^{-1}, A_H/A_D=0.07) are out of that range suggesting the incursion of hydrogen tunneling.[11] The temperature dependences of the isotope effects for the present system were examined as shown in Table 3. Though it is difficult to discuss about the involvement of the tunnel effect from the data for only one sample because of unavoidable large errors in the differences of the activation parameters measured in the narrow temperature range, in total view of data for all samples, the parameter differences do not seem to be deviated so much from the range of the zero-point energy differences. Though the ratios of the frequency factors are scattered, the values do not fit to tunneling since smaller values ($0<A_H/A_D \ll 1$) can be expected for the tunnel effect.[28] Assuming the isotope effect to be controlled by a zero point energy, the large kinetic isotope effects for the present system (the

isotope effects are larger than that for heptyl phenyl sulfoxide[27] even though the values are extrapolated to the same temperatures) should be explained by a change of the structure of the transition state. In general, a maximum magnitude of the hydrogen-deuterium isotope effect controlled by a zero-point energy is known to be ca. 8 for linear hydrogen transfer reactions.[28] Therefore, small isotope effects for Ei reactions have been attributed to their non-linearity. The relatively large activation entropies for the present system are the result of the C-S bond loosened transition state which allows the linear hydrogen transfer to show the large isotope effect.

The substituent effect on the magnitude of the isotope effects is also interesting. There might be two geometric factors in the transition state to affect the isotope effect. One is the linearity of the hydrogen transfer as described above. The C-S bond in the transition state might be more loosened for the sulfoxide having more electron-releasing Y-substituent as discussed in the activation parameters section expecting the more linear hydrogen transfer and larger isotope effect. The other factor is a symmetry of the hydrogen transfer which shows a maximum primary isotope effect. In view of that the hydrogen transfer is performed by a low basic sulfoxide oxygen, the position of the hydrogen atom in the transition state is considered to be nearer to the starting state. In this situation, the more acidic β-proton the sulfoxide has, the more symmetric hydrogen transfer can be expected. Contrary to the former factor, the more electron-withdrawing Y-substituent will show the larger isotope effect. The present results show that the latter effect could be more important than the former in the substituent effect on the kinetic isotope effects.

Reactivity of Isomers. The ratios of pyrolytic rates of threo-erythro-isomers (k_{er}/k_{th}) are listed in Table 6. The pyrolysis of erythro-isomers is 2—3 times faster than that of threo-isomers for all substituents and at all three temperatures.

In 1982, Kobayashi et al.[25] reported that there is some attractive interaction between *S*-phenyl and α-phenyl group (CH-π interaction) in the conformation of both *threo*- and *erythro*-1-phenylethyl aryl sulfoxides, and the most stable conformers are as shown in Fig. 6 for the threo- and the erythro-isomers, respectively. The most stable conformer of the erythro-isomer in the starting state is advantageous for the Ei-reaction compared to that of the threo-isomer since the sulfoxide oxygen and the methyl group is close. Assuming the phenyl-phenyl attractive interaction still remained in the transition state for the erythro-isomer, the activation free energy for the threo-isomer would be larger than that for the erythro-isomer because of an unavoidable breaking of the interaction for the threo-isomer. Thus the pyrolysis results in the faster elimination for the erythro-isomers. Inspection of the data in the Table 6 reveals that there are similar tendencies between k_{er}/k_{th} and σ-values of Y-substituents at all temperatures, though

Table 6. The Ratios of Pyrolysis Rates of Erythro-Threo Isomers (k_{er}/k_{th}) of 1-Arylethyl Phenyl Sulfoxides in Dioxane

Ph-S-CHC$_6$H$_4$Y
↓ |
O CH$_3$

Y	80.0 °C	90.0 °C	100.0 °C
p-OMe	2.62	2.46	2.37
H	1.98	2.07	1.93
H(β-d$_3$)	2.30	2.10	1.96
m-OMe	2.57	2.25	2.39
m-Cl	2.88	2.81	2.61
p-NO$_2$	2.96	2.56	2.91

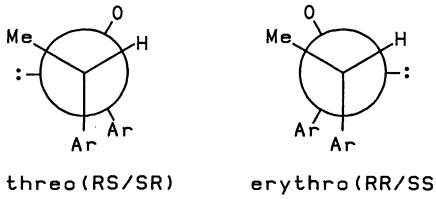

Fig. 6. The most favorable conformations of *threo*- and *erythro*-1-arylethyl aryl sulfoxides.

Table 7. Effects of the Phenyl Group on the α -and β-Positions of Ethyl Phenyl Sulfoxide and Sulfilimine

	Solvent	Temp °C	$k\times10^5$ s^{-1}	Rel rate	Ref.
PhS(O)CH$_2$CH$_3$	Dioxane	100	0.165	1	
PhS(O)CHCH$_3$ threo	Dioxane	100	43.5	264	
Ph erythro	Dioxane	100	83.9	508	
PhS(O)CH$_2$CH$_2$Ph	Dioxane	100	1.41	12.8[a]	26
PhS(NTs)CH$_2$CH$_3$	Benzene	80.3	1.08	1	19,20
PhS(NTs)CHCH$_3$	Benzene			10^3	19
Ph					
PhS(NTs)CH$_2$CH$_2$Ph	Benzene			1.5[a]	19

a) Corrected with number of β-hydrogens.

the data are scattered. The tendencies that both the electron-withdrawing and -releasing substituents enlarge the ratios (k_{er}/k_{th}) are similar to those for log k vs. σ. Though the reason for this observation is not clear, it might be explained by the stronger CH-π interaction for the more polar sulfoxides.

Effect of the α-Phenyl Group on the Rate of the Pyrolysis. The pyrolysis of *threo*- and *erythro*-1-phenylethyl phenyl sulfoxides was found to be 264 and 508 times faster than that of ethyl phenyl sulfoxide at 100 °C in dioxane. The effects of the phenyl substituent on the α- and β-positions of ethyl phenyl sulfoxide and sulfilimine are compared in Table 7. Introduction of a phenyl group at the α-position results in much more acceleration than that at the β-position suggesting that the C-S bond cleavage is more important than the proton transfer in the transition state of pyrolysis for both sulfoxides and sulfilimines.

Conclusion

From these results the following conclusion can be obtained. The large β-hydrogen kinetic isotope effect rules out a radical pair mechanism and an ionic mechanism is also ruled out because of the small solvent effect and the relatively small Hammett substituent effects. The reaction mechanism is thus considered to be a concerted process through a five-membered cyclic transition state. The large activation entropies reveal a C-S bond loosened transition state to make possible to more linear proton transfer and to give the large hydrogen kinetic isotope effect compared to primary alkyl sulfoxides. The V-shaped Hammett plot for the rates and the negative trend for the substituent effect for the activation entropies on the 1-phenyl group indicate that the transition state changes as follows. Electron-releasing substituents on the 1-phenyl group change the transition state to a C-S bond loosened E1-like type, while electron-withdrawing ones change that to C-S bond not so stretched conjugated type in which the acidity of the β-proton is increased. These results suggest that the transition state is on a broad potential energy surface. The higher reactivity of erythro-isomers than threo-isomers can be attributed to a 1-phenyl-*S*-phenyl attractive interaction (CH-π interaction)[25] of the sulfoxide in both the ground and the transition states. The larger enhancement by a 1-phenyl group on the rate of pyrolysis of ethyl phenyl sulfoxide than that by a 2-phenyl group suggests that the Ei-reaction of sulfoxides essentially tend to take an E1-like transition state.

Experimental

General. All melting points were uncorrected. IR spectra were taken on a JASCO IRA-1 spectrometer. NMR spectra were recorded with a Hitachi R-24B spectrometer (60 MHz) using TMS as an internal standard.

Preparation of 1-Arylethyl Aryl Sulfoxides. All sulfoxides were prepared by oxidation of the corresponding 1-arylethyl aryl sulfides with hydrogen peroxide in acetic acid at room temperature. Most of the threo-isomers were obtained by repeated recrystallization from ether, ether-hexane, or methanol except for 1-phenylethyl phenyl, 1-(*m*-methoxyphenyl)ethyl phenyl, and 1-(*m*-chlorophenyl)ethyl phenyl sulfoxides, instead the erythro-isomers of which were isolated by recrystallization. The threo-isomers of the latter three sulfoxides and other erythro-isomers were obtained by repeated silica-gel column chromatography using chloroform or ether-hexane (3 : 1) as an eluent. The sulfoxides thus obtained have the following physical properties.

$XC_6H_4S(O)CH(CH_3)C_6H_4Y$: X,Y, Threo or Erythro: H, *p*-MeO, Threo: Mp 92 °C (from ether-hexane); IR (KBr) 1051 cm^{-1} (S-O); ^{1}H NMR (CCl_4) δ=1.52 (3H, d, J=7 Hz, CH_3), 3.59 (1H, q, J=7 Hz, CH), 3.73 (3H, s, OCH_3), 6.5—7.1 (4H, AB, J=9 Hz, Ar), 7.1—7.5 (5H, s-like, Ph). Found: C, 69.59; H, 6.19%. Calcd for $C_{15}H_{16}O_2S$: C, 69.20, H, 6.19%.

H,*p*-MeO, Erythro: Mp 83—84 °C (from ether-hexane); IR (KBr) 1040 cm^{-1} (S-O); ^{1}H NMR (CCl_4) δ=1.49 (3H, d, J=7 Hz, CH_3), 3.82 (1H, q, J=7 Hz, CH), 3.69 (3H, s, OCH_3), 6.68 (4H, s-like, Ar), 6.9—7.4 (5H, s-like, Ph). Found: C, 69.39; H, 6.09%. Calcd for $C_{15}H_{16}O_2S$: C, 69.20; H, 6.19%.

H,*p*-Me, Threo: Mp 99—100 °C (ether-hexane); IR (KBr) 1051 cm^{-1} (S-O); ^{1}H NMR (CCl_4) δ=1.56 (3H, d, J=7 Hz, CH_3), 3.59 (1H, q, J=7 Hz, CH), 2.31 (3H, s, *p*-CH_3), 6.7—7.2 (4H, m, Ar), 7.2—7.5 (5H, s-like, Ph). Found: C, 73.72; H, 6.58%. Calcd for $C_{15}H_{16}OS$: C, 73.73; H, 6.60%.

H,H,Threo: Mp 67.5—68.5 °C (ether-hexane); IR (KBr) 1049 cm^{-1} (S-O); ^{1}H NMR (CCl_4) δ=1.59 (3H, d, J=7 Hz, CH_3), 3.66 (1H, q, J=7 Hz, CH), 6.7—7.5 (10H, m, Ph); ($CDCl_3$) δ=1.66 (3H, d, J=7 Hz, CH_3), 3.78 (1H, q, J=7 Hz, CH), 6.8—7.6 (10H, m, Ph).[22,25]

H,H, Erythro: Mp 111—112 °C (ether); IR (KBr) 1050 cm^{-1} (S-O); ^{1}H NMR (CCl_4) δ=1.55 (3H, d, J=7 Hz, CH_3), 3.88 (1H, q, J=7 Hz, CH), 6.7—7.4 (10H, m, Ph); ($CDCl_3$) δ=1.58 (3H, d, J=7 Hz, CH_3), 3.99 (1H, q, J=7 Hz, CH), 6.8—7.5 (10H Ph).[22,25]

H,*m*-OMe, Threo: Oil; IR (neat) 1046 cm^{-1} (S-O). ^{1}H NMR (CCl_4) δ=1.58 (3H, d, J=7 Hz, CH_3), 3.55 (1H, q, J=7 Hz, CH), 3.65 (3H, s, OCH_3), 6.3—7.3 (9H, m, Ar); ($CDCl_3$) δ=1.64 (3H, d, J=7 Hz, CH_3), 3.74 (1H, q, J=7 Hz, CH), 3.64 (3H, s, OCH_3), 6.4—7.5 (9H, m, Ar). Found: C, 68.59; H, 6.29%. Calcd for $C_{15}H_{16}O_2S$: C, 69.20; H, 6.19%.

H,*m*-OMe, Erythro: Mp 115 °C; IR (KBr) 1051 cm^{-1} (S-O); ^{1}H NMR (CCl_4) δ=1.53 (3H, d, J=7 Hz, CH_3), 3.85 (1H, q, J=7 Hz, CH), 3.65 (3H, s, OCH_3), 6.2—7.4 (9H, m, Ar); ($CDCl_3$) δ=1.56 (3H, d, J=7 Hz, CH_3), 4.00 (1H, q, J=7 Hz, CH), 3.66 (3H, s, OCH_3), 6.4—7.5 (9H, m, Ar). Found: C, 68.94; H, 6.36%. Calcd for $C_{15}H_{16}O_2S$: C, 69.20; H, 6.19%.

H,*p*-Cl, Threo: Mp 122.5 °C; IR (KBr) 1045 cm^{-1} (S-O); ^{1}H NMR (CCl_4) δ=1.49 (3H, d, J=7 Hz, CH_3), 3.63 (1H, q, J=7 Hz, CH), 6.7—7.7 (9H, m, Ar). Found: C, 63.78; H, 5.08%. Calcd for $C_{14}H_{13}ClOS$: C, 63.51; H, 4.95%.

H,*p*-Br, Threo: Mp 137.5 °C; IR (KBr) 1047 cm^{-1} (S-O); ^{1}H NMR (CCl_4) δ=1.45 (3H, d, J=7 Hz, CH_3), 3.61 (1H, q, J=7 Hz, CH), 6.7—7.7 (9H, m, Ar). Found: C, 54.46; H, 4.26%. Calcd for $C_{14}H_{13}BrOS$: C, 54.38; H, 4.24%.

H,*m*-Cl, Threo: Oil; IR (neat) 1049 cm^{-1} (S-O); ^{1}H NMR (CCl_4) δ=1.51 (3H, d, J=7 Hz, CH_3), 3.67 (1H, q, J=7 Hz, CH), 6.7—7.5 (9H, m, Ar). Found: C, 62.79; H, 5.29%.

Calcd for $C_{14}H_{13}ClOS$: C, 63.51; H, 4.95%.

H,*m*-Cl,Erythro: Mp 81.5 °C; IR (KBr) 1047 cm^{-1} (S-O); ^1H NMR (CCl_4) δ=1.56 (3H, d, J=7 Hz, CH_3), 3.79 (1H, q, J=7 Hz, CH), 6.6—7.4 (9H, m, Ar). Found: C, 63.28; H, 4.84%. Calcd for $C_{14}H_{13}ClOS$: C, 63.51; H, 4.95%.

H,*p*-NO_2,Threo: Mp 119—120 °C (MeOH); IR (KBr) 1353, 1523 (NO_2) and 1048 cm^{-1} (S-O); ^1H NMR (CCl_4) δ=1.55 (3H, d, J=7 Hz, CH_3), 3.84 (1H, q, J=7 Hz, CH), 7.1—8.2 (9H, m, Ar); ($CDCl_3$) δ=1.64 (3H, d, J=7 Hz, CH_3), 3.99 (1H, q, J=7 Hz, CH), 7.1—8.3 (9H, m, Ar). Found: C, 61.17; H, 4.93; N, 5.22%. Calcd for $C_{14}H_{13}NO_3S$: C, 61.07; H, 4.76; N, 5.09%.

H,*p*-NO_2,Erythro: Mp 100 °C (ether); IR (KBr) 1322, 1490 (NO_2) and 1047 cm^{-1} (S-O); ^1H NMR (CCl_4) δ=1.73 (3H, d, J=7 Hz, CH_3), 3.82 (1H, q, J=7 Hz, CH), 6.8—8.1 (9H, m, Ar); ($CDCl_3$) δ=1.75 (3H, d, J=7 Hz, CH_3), 3.94 (1H, q, J=7 Hz, CH), 6.9—8.2 (9H, m, Ar). Found: C, 61.21; H, 4.88; N, 5.21%. Calcd for $C_{14}H_{13}NO_3S$: C, 61.07; H, 4.76; N, 5.09%.

***p*-Me,H,Threo:** Mp 136.8 °C; IR (KBr) 1052 cm^{-1} (S-O); ^1H NMR(CCl_4) δ=1.58 (3H, d, J=7 Hz, CH_3), 3.58 (1H, q, J=7 Hz, CH), 2.35 (3H, s, CH_3), 6.8—7.4 (9H, m, Ar); ($CDCl_3$) δ=1.64 (3H, d, J=7 Hz, CH_3), 3.73 (1H, q, J=7 Hz, CH), 2.30 (3H, s, CH_3), 6.8—7.4 (9H, m, Ar).[25] Found: C, 73.74; H, 6.50%. Calcd for $C_{15}H_{16}OS$: C, 73.73; H, 6.60%.

***m*-Me,H,Threo:** Mp 82.5 °C (from ether-hexane); IR (KBr) 1049 cm^{-1} (S-O); ^1H NMR (CCl_4) δ=1.56 (3H, d, J=7 Hz, CH_3), 3.59 (1H, q, J=7 Hz, CH), 2.27 (3H, s, CH_3), 6.8—7.3 (9H, m, Ar). Found: C, 73.52; H, 6.56%. Calcd for $C_{15}H_{16}OS$: C, 73.73; H, 6.60%.

***p*-Cl,H,Threo:** Mp 128.7 °C; IR (KBr) 1056 cm^{-1} (S-O); ^1H NMR (CCl_4) δ=1.60 (3H, d, J=7 Hz, CH_3), 3.61 (1H, q, J=7 Hz, CH), 6.7—7.4 (9H, m, Ar); ($CDCl_3$) δ=1.60 (3H, d, J=7 Hz, CH_3), 3.69 (1H, q, J=7 Hz, CH), 6.8—7.5 (9H, m, Ar). Found: C, 63.38; H, 4.87%. Calcd for $C_{14}H_{13}ClOS$: C, 63.51; H, 4.95%.

***m*-Cl,H,Threo:** Mp 73.5—74.5 °C (from ether-hexane); IR (KBr) 1052 cm^{-1} (S-O); ^1H NMR (CCl_4) δ=1.58 (3H, d, J=7 Hz, CH_3), 3.66 (1H, q, J=7 Hz, CH), 6.7—7.5 (9H, m, Ar). Found: C, 63.49; H, 5.07%. Calcd for $C_{14}H_{13}ClOS$: C, 63.51; H, 4.95%.

***p*-NO_2,H,Threo:** Mp 124—125.5 °C (methanol-ether); IR (KBr) 1338, 1522 (NO_2) and 1054 cm^{-1} (S-O); ^1H NMR (CCl_4) δ=1.68 (3H, d, J=7 Hz, CH_3), 3.68 (1H, q, J=7 Hz, CH), 6.8—8.3 (9H, m, Ar); ($CDCl_3$) δ=1.72 (3H, d, J=7 Hz, CH_3), 3.72 (1H, q, J=7 Hz, CH), 6.9—8.4 (9H, m, Ar). Found: C, 61.17; H, 4.78; N, 5.04%. Calcd for $C_{14}H_{13}NO_3S$: C, 61.07; H, 4.76; N, 5.09%.

Preparation of 1-(Substituted phenyl)ethyl-2,2,2-d_3 Phenyl Sulfoxides. To a stirred solution of methyl-d_3-magnesium iodide (0.06 mol) in dry ether (20 ml) was added dropwise substituted benzaldehyde (0.05 mol) in dry ether (20 ml). After usual work-up process, α-methyl-d_3-benzyl alcohol obtained was converted to the corresponding chloride which was then allowed to react with sodium benzenethiolate to give the corresponding sulfide-β,β,β-d_3 in ca. 85% yield. The obtained sulfide was oxidized with 35% H_2O_2 in acetic acid to afford the sulfoxide in ca. 67% yield.

Kinetics. Pyrolysis of the sulfoxides was carried out at 80.0±0.1 °C, 90.0±0.1 °C, and 100.0±0.1 °C in sealed capillary tubes, which contain 50 μl of 2.7 mmol dm^{-3} dioxane solution of each sulfoxide and 32 mmol dm^{-3} diphenyl ether or 5.4 mmol dm^{-3} diphenyl sulfide as an internal standard depending on the retention time of olefin formed in liquid chromatography. A sealed tube was taken out at several time intervals and was cooled in an ice bath to stop the reaction. The decreasing sulfoxide was followed by means of JASCO FAMILIC-100N liquid chromatograph with UV monitor UVIDEC 100II at 256 nm using TAKEDA RIKEN-TR-2217 Automatic Integrator. The rate of the reaction was found to fit nicely with a first-order rate equation and the rate constant was calculated by a least-squares method.

The authors are grateful to Professor Shigeru Oae of Okayama University of Science, and Professor Naomichi Furukawa, the University of Tsukuba, for their helpful discussions. We also would like to thank Dr. Motohiro Nishio, Meiji Seika Kaisha, for his helpful suggestions to assign threo- and erythro-isomers and their favorable conformations of 1-phenylethyl aryl sulfoxides.

References

1) C. A. Kingsbury and D. J. Cram, *J. Am. Chem. Soc.*, **82**, 1810 (1960).
2) C. A. Walling and L. Bollyky, *J. Org. Chem.*, **29**, 2699 (1964).
3) D. N. Jones, A. C. F. Edmons, and S. D. Knox, *J. Chem. Soc., Perkin Trans. 1*, **1976**, 459.
4) D. W. Emerson, A. R. Craig, and J. W. Potts, Jr., *J. Org. Chem.*, **32**, 102 (1967).
5) J. L. Kice and J. D. Campbell, *J. Org. Chem.*, **32**, 1631 (1967).
6) B. M. Trost and R. A. Kunz, *J. Org. Chem.*, **39**, 2648 (1974).
7) B. M. Trost, T. N. Salzmann, and K. Hiroi, *J. Am. Chem. Soc.*, **98**, 4887 (1976).
8) J. R. Shelton and K. E. Davis, *Int. J. Sulfur Chem.*, **8**, 197 (1973).
9) J. R. Shelton and K. E. Davis, *J. Am. Chem. Soc.*, **89**, 718 (1967).
10) J. R. Shelton and K. E. Davis, *Int. J. Sulfur Chem.*, **8**, 205 (1973).
11) J. W. A. M. Janssen and H. Kwart, *J. Org. Chem.*, **42**, 1530 (1977).
12) D. N. Jones, D. R. Hill, D. A. Lewton, and C. Sheppard, *J. Chem. Soc., Perkin Trans. 1*, **1977**, 1574.
13) D. N. Jones, P. D. Cotton, and J. Davies, *Tetrahedron Lett.*, **1979**, 4977.
14) F. A. Davis, R. H. Jenkins, Jr., S. Q. A. Rizvi, and S. G. Yocklovich, *J. Org. Chem.*, **46**, 3467 (1981).
15) F. A. Davis and R. H. Jenkins, Jr., *J. Am. Chem. Soc.*, **102**, 7967 (1980).
16) F. A. Davis, S. G. Yocklovich, and G. S. Baker, *Tetrahedron Lett.*, **1978**, 97.
17) D. W. Emerson and T. J. Korniski, *J. Org. Chem.*, **34**, 4115 (1969).
18) K. Tsujihara, K. Harada, N. Furukawa, and S. Oae, *Tetrahedron*, **27**, 6101 (1971).
19) S. Oae, K. Harada, K. Tsujihara, and N. Furukawa, *Bull. Chem. Soc. Jpn.*, **46**, 3482 (1973).
20) K. Tsujihara, N. Furukawa, and S. Oae, *Tetrahedron*, **27**, 4921 (1971).
21) N. Furukawa, T. Hatanaka, K. Harada, and S. Oae,

Bull. Chem. Soc. Jpn., **49**, 2337 (1976).
22) G. Modena, V. Quintily, and G. Scorrano, *J. Am. Chem. Soc.*, **94**, 202 (1972).
23) M. Nishio and K. Nishihata, *J. Chem. Soc., Chem. Commun.*, **1970**, 1485. K. Nishihata and M. Nishio, *J. Chem. Soc., Perkin Trans. 2*, **1973**, 758.
24) M. Nishio, *J. Chem. Soc., Chem. Commun.*, **1969**, 51, 560. K. Nishihata and M. Nishio, *Tetrahedron Lett.*, **1977**, 1041.
25) K. Kobayashi, Y. Kodama, M. Nishio, T. Sugawara, and H. Iwamura, *Bull. Chem. Soc. Jpn.*, **55**, 3560 (1982).
26) T. Yoshimura, M. Yoshizawa, and E. Tsukurimichi, *Bull. Chem. Soc. Jpn.*, **60**, 2491 (1987).
27) H. Kwart and T. J. George, R. Louw, and W. Ultee, *J. Am. Chem. Soc.*, **100**, 3927 (1978).
28) R. P. Bell, *Chem. Soc. Rev.*, **3**, 513 (1974).
29) C. G. Swain, W. P. Langsdorf, *J. Am. Chem. Soc*, **73**, 2813 (1951).
30) D. R. Rayner, A. J. Gordon, and K. Mislow, *J. Am. Chem. Soc.*, **90**, 4854 (1968).
31) E. G. Miller, D. R. Rayner, H. T. Thomas, and K. Mislow, *J. Am. Chem. Soc.*, **90**, 4861 (1968).

Synthesis of a Protected Sperm Whale Myoglobin-(77—96)-Eicosapeptide and Circular Dichroism Spectra of the Related Peptides

Chikao HASHIMOTO* and Ichiro MURAMATSU†
Department of Chemistry, The Jikei University School of Medicine, 8-3-1, Kokuryo-Cho, Chofu-Shi, Tokyo 182
†Department of Chemistry, College of Science, Rikkyo University, Nishi-Ikebukuro, Tokyo 171
(Recevied October 1, 1988)

A protected sperm whale myoglobin-(77—96)-eicosapeptide (**23**) was synthesized by a solution method. The protected peptide **23** could be effectively purified by silica-gel column chromatography with 1-butanol-acetic acid-water as the eluate. The CD spectra of protected fragment peptides were measured in a solution of 2,2,2-trifluoroethanol. A protected sperm whale myoglobin-(85—96)-dodecapeptide and **23** showed CD profiles characteristic of a helical structure.

Myoglobin is a globular heme protein which plays a role in the storage of oxygen in the cells of muscle. The myoglobin molecule of higher animals is composed of a globin chain containing 153 amino acid residues (mol wt 17000) and a protoheme. A higher-order structure of sperm whale myoglobin was elucidated by means of an X-ray analysis by Kendrew et al.[1] The E and F regions of sperm whale myoglobin include distal (E7) and proximal (F8) histidine residues which coordinate a heme iron atom, and are important sites for producing physiological functions. It is of interest to synthesize a peptide of the E-EF-F region and to investigate the structure and functional properties of the peptide in comparison with those of myoglobin. However, few studies have been carried out on the synthesis of those regions of the myoglobin. In the past Eckstein and Bayer[2] tried to synthesize the sperm whale myoglobin-(81—94)-peptide using two methods involving fragment condensation: between positions 81—82 and 83—94, and between positions 81—88 and 89—94. However, they could not obtain the desired peptide.

As an initial approach regarding the subject mentioned above, we synthesized a protected sperm whale myoglobin-(77—96)-eicosapeptide (**23**). Peptide **23** consists of EF and F segments of the myoglobin and includes the important proximal histidine residue. The synthesis of **23** carried out by a solution method which makes it possible to obtain some protected intermediate peptides of various size. Various problems in the synthesis are described in "Results and Discussion". The CD spectra of **23** and the fragment peptides were measured in order to investigate whether those protected peptides can form a helical structure. The helical property deduced from the CD spectra of each peptide was correlated with the secondary structure, shown by X-ray analysis,[1] of the corresponding part of myoglobin.

Results and Discussion

The protected eicosapeptide **23** was built up from four fragment peptides by the route illustrated in Fig. 6. These four fragment peptides were prepared by a stepwise elongation method, according to the routes showed in Figs. 1—5.

Peptide in Positions 91—96. Figure 1 illustrates the synthesis of fragment (**5**), Boc-Gln-Ser(Bzl)-His-Ala-Thr-Lys(Z)-OBzl.[3] Boc-His(Boc)-Ala-Thr-Lys(Z)-OBzl (**3**) was constructed stepwise with Boc-Thr-OH, Boc-Ala-OH, and Boc-His(Boc)-OH using H-Lys(Z)-OBzl as starting material by a mixed anhydride (MA) method.[4] Boc-Thr-Lys(Z)-OBzl (**1**) was purified by chromatography on a silica-gel column with CH_2Cl_2-MeOH systems as eluates. Compound **3** was contaminated with a small amount of impurities, but used for the following coupling without further purification. After the treatment of **3** with trifluoroacetic acid (TFA), the tetrapeptide ester was condensed with Boc-Ser(Bzl)-OH using EDC[5] in the presence of HOBt[6] to give Boc-Ser(Bzl)-His-Ala-Thr-Lys(Z)-OBzl (**4**). The pentapeptide ester derived from **4** was coupled with Boc-Gln-ONp by an active ester method.[7] Product **5** was purified into a chromatographyically homogeneous form by gel filtration on Sephadex LH-20.[8]

Peptide in Positions 85—90. Figure 2 shows the synthesis of fragment (**11**), Boc-Glu(OBzl)-Leu-

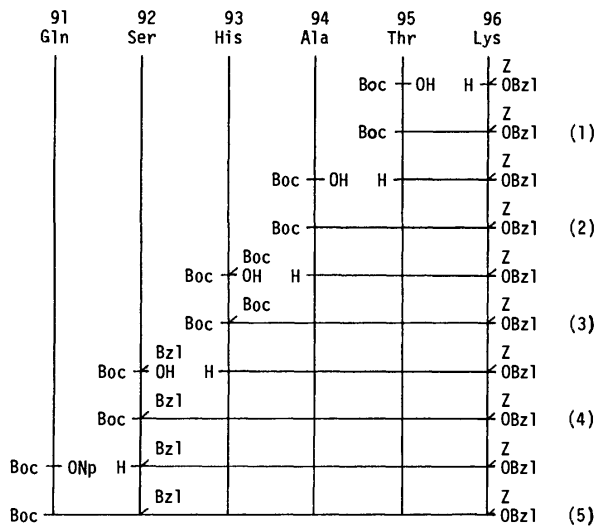

Fig. 1. Synthetic scheme of positions 91—96.

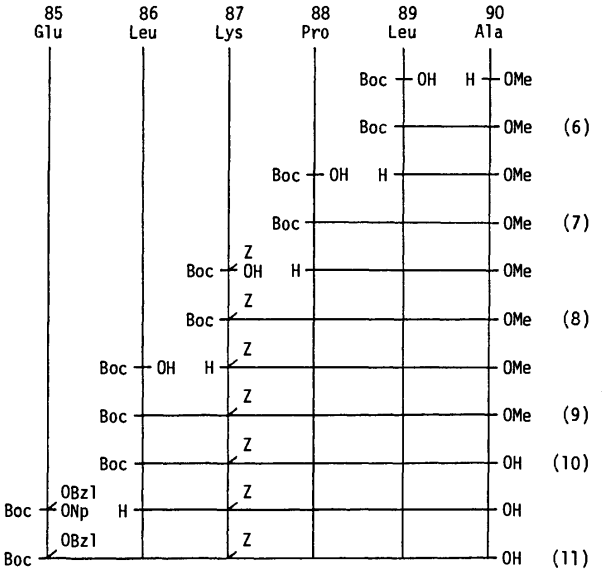

Fig. 2. Synthetic scheme of positions 85—90.

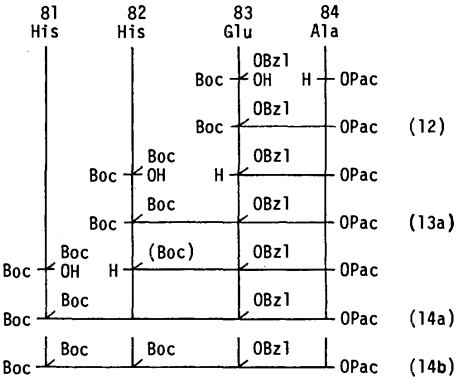

Fig. 3. Synthetic scheme of positions 81—84.

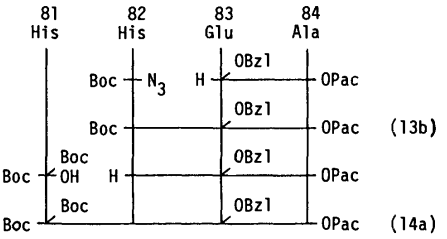

Fig. 4. Alternative synthetic scheme of positions 81—84.

Lys(Z)-Pro-Leu-Ala-OH. In the synthesis of Boc-Leu-Lys(Z)-Pro-Leu-Ala-OMe (**9**), the starting material, H-Ala-OMe, was elongated stepwise with Boc-Leu-OH, Boc-Pro-OH, Boc-Lys(Z)-OH, and Boc-Leu-OH by means of the MA or EDC-HOBt method. Compound **9** was purified by the use of a Sephadex LH-20 column. The methyl ester **9** was hydrolyzed to give Boc-Leu-Lys(Z)-Pro-Leu-Ala-OH (**10**). After removing the N-terminal protecting group of **10**, the resulting partially protected pentapeptide, TFA·H-Leu-Lys(Z)-Pro-Leu-Ala-OH, was neutralized and, then, coupled with Boc-Glu(OBzl)-ONp by an active ester method to afford **11**. Fragment **11** was purified by gel filtration.

Peptide in Positions 81—84. Figures 3 and 4 illustrate the routes employed in the preparation of fragment (**14a**), Boc-His(Boc)-His-Glu(OBzl)-Ala-Opac. The coupling of H-Ala-Opac with Boc-Glu(OBzl)-OH proceeded in yields 43—56% by the MA method, and in an yield of 74% by the EDC-HOBt procedure. Compound **12** was treated with TFA and the dipeptide ester was condensed with Boc-His(Boc)-OH by the MA method to give Boc-His(Boc)-Glu(OBzl)-Ala-Opac (**13a**). After the treatment of **13a** by TFA for 70—340 min at room temperature, the product showed two spots on TLC. The treatment of **13a** with 4 M† HCl/dioxane for 3 h at room temperature also gave a similar result. The two components seemed to be peptides in which, respectively, one and two Boc groups were removed with an acid-treatment. Therefore, the mixture containing the two components was coupled without purification with Boc-His(Boc)-OH by the EDC-HOBt method to yield **14a**. The crude product, including two components (A and B), was chromatographed on a silica-gel column and the two components were separately isolated. Component A was identified as Boc-His(Boc)-His(Boc)-Glu(OBzl)-Ala-Opac (**14b**), and component B as the desired compound **14a** by elemental and FAB mass analyses. Fragment **14a** was also synthesized by another route, illustrated in Fig. 4. The Boc-His-N_3 derived from corresponding hydrazide was coupled with the H-Glu(OBzl)-Ala-Opac to prepare Boc-His-Glu(OBzl)-Ala-Opac (**13b**) by the Honzl and Rudinger method.[9] After the deprotection of **13b** with TFA, the tripeptide ester was condensed with Boc-His(Boc)-OH by the MA method to yield **14a**. Analytical data regarding component B agreed with that of **14a** synthesized by the route shown in Fig. 4.

Peptide in Positions 77—80. Figure 5 outlines the synthesis of fragment (**18**), Boc-Lys(Z)-Lys(Z)-Lys(Z)-Gly-OH. The starting material, H-Gly-OEt, was succesively elongated by Boc-Lys(Z)-OH with the MA method to produce fragment (**17**), Boc-Lys(Z)-Lys(Z)-Lys(Z)-Gly-OEt. Product **17** was converted to the corresponding acid **18** by saponification. The synthesis of **18** proceeded smoothly and requires no additional comments.

Peptide in Positions 77—84. The removal of the Boc group of **14a** was carried out smoothly by treating with TFA under the usual conditions. The resulting peptide gave a single spot on TLC and was confirmed to be 3TFA·H-His-His-Glu(OBzl)-Ala-Opac (**19**) by elemental analysis. The tetrapeptide ester **19** was coupled with **18** in the presence of HOBt by EDC to yield protected octapeptide **20**. The product **20** was reduced over zinc powder in acetic acid[10] to afford fragment (**21**), Boc-Lys(Z)-Lys(Z)-Lys(Z)-Gly-His-

† 1 M=1 mol dm^{-3}.

His-Glu(OBzl)-Ala-OH.

Peptide in Positions 85—96. Several methods were investigated for the synthesis of fragments (positions 85—96 or 87—96). Acyl components, Boc-Glu(OBu^t)-Leu-Lys(Z)-Pro-Leu-Ala-N_3 and Boc-Lys(Z)-Pro-Leu-Ala-N_3, respectively, were condensed with an amino component, H-Gln-Ser-His-Ala-Thr-Lys(Z)-OH. The yields of both couplings were very low. Also, the coupling of the former azide with an amino component, H-Gln-Ser-His-Ala-Thr-Lys(Z)-OBzl, did not give a satisfactory result. The low yield in these coupling reactions seems to be attributed to a conversion of the N-terminal residue to pyroglutamyl, since the glutamine residue of a free hexapeptide, H-Gln-Ser-His-Ala-Thr-Lys-OH, easily changed to the pyroglutamyl residue. This reaction was catalyzed by the imidazole ring of the neighboring histidine residue.[11] Therefore, the hydroxyl group of serine was protected by a benzyl group, as one carrying a steric hindrance in order to suppress the effect of the imidazole ring. Also, the coupling method was changed to the EDC-HOBt procedure, a more reactive compared to the azide method. As illustrated in Fig. 6, fragment **5** was treated with TFA and the corresponding hexapeptide ester was coupled with **11** by the EDC-HOBt procedure to prepare fragment (**22**), Boc-Glu(OBzl)-Leu-Lys(Z)-Pro-Leu-Ala-Gln-Ser(Bzl)-His-Ala-Thr-Lys(Z)-OBzl. The yield was 86% and was extremely high compared with those of the three methods described above. The improvement in the yield may be attributed to the use not only of **5**, but also of the reactive EDC-HOBt procedure. Namely, the slower condensation should cause the formation of a greater amount of pyroglutamic acid residue from the N-terminal glutamine residue of the hexapeptide, H-Gln-Ser-His-Ala-Thr-Lys(Z)-[OH or OBzl].

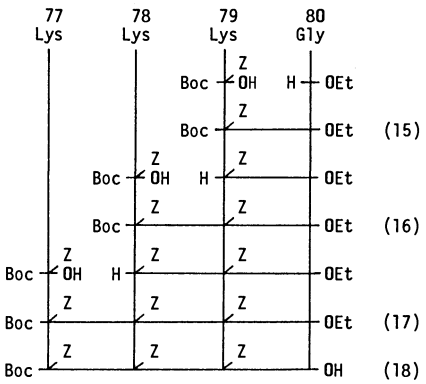

Fig. 5. Synthetic scheme of positions 77—80.

Peptide in Positions 77—96. After removing the Boc group of **22**, the dodecapeptide ester was coupled with **21** in the presence of HOBt by EDC to afford fragment (**23**), Boc-Lys(Z)-Lys(Z)-Lys(Z)-Gly-His-His-Glu(OBzl)-Ala-Glu(OBzl)-Leu-Lys(Z)-Pro-Leu-Ala-Gln-Ser(Bzl)-His-Ala-Thr-Lys(Z)-OBzl. After the purification of **23** by gel filtration, it still contained small amounts of impurities. A part of **23** was further purified by a silica-gel column with 1-butanol-acetic acid-water solvent system as the eluate. The recovery of pure **23** was 24%. The cause of the low recovery is most likely based on adsorption on the silica gel.

As mentioned above, the improvement in fragment condensation between **5** and **11** has enabled the syn-

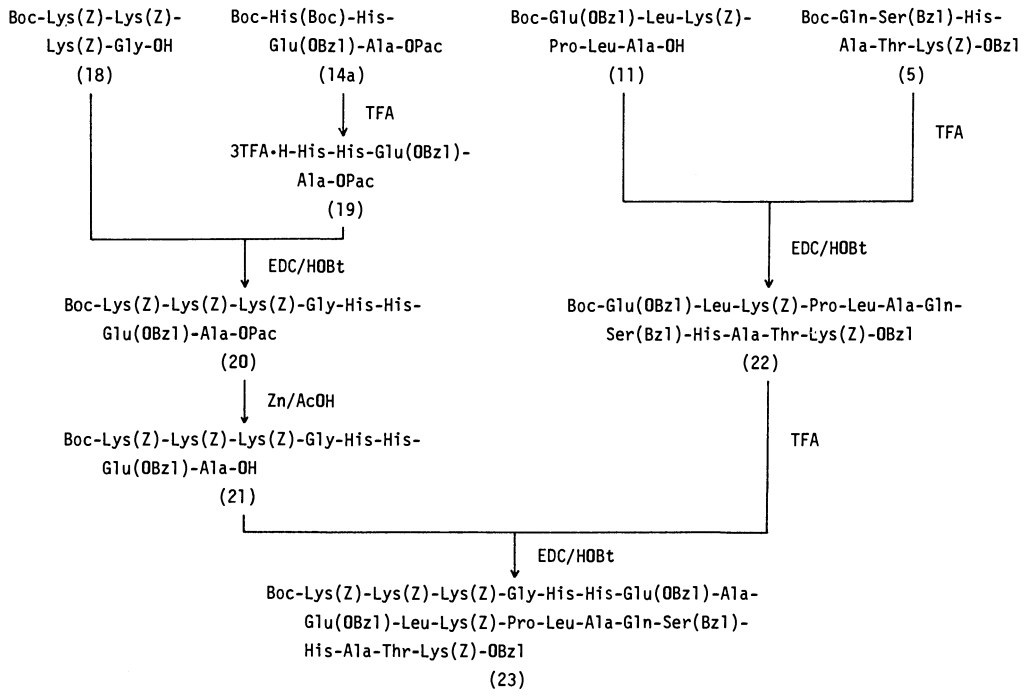

Fig. 6. Synthetic scheme of positions 77—96.

Table 1. Yields, Physical Properties and Analytical Data of Intermediate Protected Peptides[a)]

Compound	Yield/%	Mp θ_m/°C	$[\alpha]_D^{24}$/° (c 1.0, MeOH)	Molecular formula	Elemental analysis/% Found (F:), Calcd (C:)			R_f[b)]				
					C	H	N	R_f^1	R_f^2	R_f^5	R_f^6	R_f^7
1[c)]	91	85—90	−19.2	$C_{30}H_{41}O_8N_3$	F: 62.89	7.39	7.40	0.55	0.77			
					C: 63.03	7.23	7.35					
2	76	115—116	−37.5	$C_{33}H_{46}O_9N_4 \cdot H_2O$	F: 60.29	7.32	8.48	0.38	0.67			
					C: 59.99	7.32	8.48					
3	74	113—118	−4.2 (DMF)	$C_{44}H_{61}O_{12}N_7 \cdot H_2O$	F: 58.41	7.16	10.70	0.43	0.77			
					C: 58.85	7.07	10.92					
4	75	141—143	−13.2 (DMF)	$C_{49}H_{64}O_{12}N_8 \cdot H_2O$	F: 60.40	6.84	11.48	0.12	0.40			
					C: 60.36	6.82	11.49	0.02	0.18	(trace)		
6[d)]	94	114—114.5	−45.7	$C_{15}H_{28}O_2N_2$	F: 56.72	9.11	8.71	0.83	0.86			0.90
					C: 56.94	8.92	8.85					
7	95	89—90	−95.6	$C_{20}H_{35}O_6N_3$	F: 57.79	8.40	9.99	0.60	0.83			
					C: 58.09	8.53	10.16					
8	82	77—79	−78.3	$C_{34}H_{53}O_9N_5$	F: 59.93	8.00	10.23	0.47	0.78			0.86
					C: 60.43	7.90	10.36					
9	76	79—81.5	−86.1	$C_{40}H_{64}O_{10}N_6 \cdot 1/2H_2O$	F: 60.31	8.30	10.60	0.52	0.72			
					C: 60.21	8.21	10.53					
12	74	128—129	−38.0	$C_{28}H_{34}O_8N_2$	F: 63.68	6.59	5.30	0.79		0.70		
					C: 63.87	6.51	5.32					
13a	94	130—131	−25.2	$C_{39}H_{49}O_{11}N_5$	F: 61.21	6.56	9.07	0.49	0.91			
					C: 61.33	6.47	9.17	0.57	(trace)			
13b	68	79—83	−41.4	$C_{34}H_{41}O_9N_5 \cdot 1/2H_2O$	F: 61.10	6.53	10.02		0.41			
					C: 60.70	6.29	10.41		0.33	(trace)		
14a[e)]	44	101—104 (decomp)	−31.8	$C_{45}H_{56}O_{12}N_8 \cdot 1/2H_2O$	F: 59.16	6.31	12.21		0.40			
					C: 59.40	6.31	12.31					
15[f)]	93	66—68	−12.8	$C_{23}H_{35}O_7N_3$	F: 59.33	7.80	9.00	0.57	0.82	0.42		
					C: 59.34	7.58	9.03					
16	92	145.5—147	−21.1	$C_{37}H_{53}O_{10}N_5$	F: 60.98	7.35	9.53	0.40	0.73	0.12		
					C: 61.06	7.34	9.62					
18	99	166—168	−13.4 (DMF)	$C_{49}H_{67}O_{13}N_7$	F: 61.08	7.11	10.14				0.35	0.83
					C: 61.17	7.02	10.19					

a) The amino acid composition of the acid hydrolyzate of each compound agreed well with that of theoretical values. b) The solvent systems of R_f were showed in experimental section. c) Mp 82—83 °C in lit.[15)] d) Mp 113—115 °C in lit.[16)] e) This compound was synthesized by the procedure of Fig. 4; FAB mass: m/z 901 (MH^+, $C_{45}H_{57}O_{12}N_8$). f) Mp 68 °C in lit.[17)]

thesis of the protected eicosapeptide **23**; it will further be helpful in the syntheses of longer peptides. Also, it has been found that a solvent system, 1-butanol-acetic acid-water, well dissolves protected peptides and, accordingly, it is very useful in silica-gel chromatography of protected long peptides.

The purity of all the protected compounds was confirmed by TLC, amino acid analysis of acid hydrolyzate and elemental analysis.

Circular Dichroism Spectra. The CD spectra of protected fragment peptides were recorded in the region of approximately 190 to 270 nm. In the CD measurement the protected fragment peptides and sperm whale myoglobin were dissolved in TFE and in 60% TFE, respectively. The CD data were reported as mean residue ellipticity, $[\theta]$, which were expressed in degree square centimeter per decimole. For calculations of helical contents, the value of $[\theta]_{222}$ for completely helical structure was taken as −32000.[12)] The theoretical helicity of a fragment peptide is expressed by the proportion of amino acid residues participating in the helical structure in the known three-dimensional structure of sperm whale myoglobin to the total residues in the fragment peptide. In order to compare the helicity of fragment peptides of different size, the relative helical contents of the fragment peptides were expressed by the helical ratio,[13)] which is the ratio of the observed helical content vs. that expected from the position of the fragment peptide in sperm whale myoglobin. In the amino acid sequence of sperm whale myoglobin-(77—96)-peptide, -Lys-Lys-Lys-Gly-His-His-Glu-Ala-Glu-Leu-Lys-Pro-Leu-Ala-Gln-Ser-His-Ala-Thr-Lys-, the underlined amino acid residues take part in the helical structure according to the result of X-ray analysis.

Figure 7 illustrates the CD spectra of four protected fragment peptides in TFE. The spectrum of **11** shows a shoulder at 228 nm and a negative band at 200 nm. The spectra of **20** and **21** exhibits a negative band near 230 nm and a positive band near 210 nm. Fragments **11**, **20**, and **21** do not exhibit the distinguishing CD profiles for a helical structure. The parts corresponding to fragments **20** and **21** scarcely contributed to the helical structure in the sperm whale

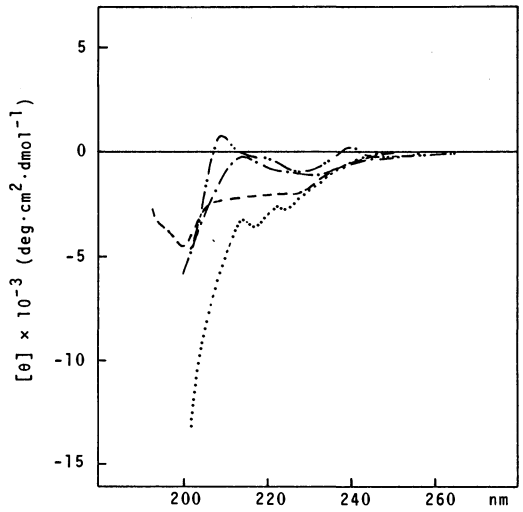

Fig. 7. CD spectra of **5** (·····), **11** (———), **20** (—·—), and **21** (—··—) in TFE.

myoglobin; it is therefore expected that those two peptides do not take a helical structure. Fragment **11** includes a part of the F helical region, though its spectrum did not suggest the exsistence of a helical structure. Fragment **5** also contains a fraction of the F helical region. The spectrum of **5** revealed negative bands at 226 and 217 nm, and suggested the presence of a helical structure, in spite of the small peptide. The helicity of **5** was calculated as 8.4% on the basis of the assumption that its $[\theta]_{222}$ value (−2700) depends only on the helical structure. The theoretical helicity was calculated according to the method stated above. That is, the part corresponding to fragment **5**, within the sperm whale myoglobin, has 4 residues in the helical structure out of 6 residues (theoretical helicity; 67%). Fragment **5**, containing part of a helical segment, is apt to form a helical structure compared with **20** and **21**, including a large portion of a nonhelical segment. However, fragment **11**, containing a helical segment, did not show the presence of a helical structure.

Figure 8 exhibits the CD spectra of two fragments, **22** and **23**, in TFE and sperm whale myoglobin in 60% TFE. The spectra of **22** and **23** showed negative bands at 220 and 205 nm, a cross overpoint at 200 nm and a positive band near 195 nm, and are very similar to that of the myoglobin. These two fragments exhibited conspicuous helical CD profiles. The values of $[\theta]_{222}$ of **22** and **23** were −10400 and −12000, respectively, and the helicity of the two fragments were calculated as being 33% (theoretical helicity; 75%) and 38% (theoretical helicity; 50%), respectively, from those data. It is well-known that TFE used as a solvent stabilizes a helical structure of peptide or protein.

Figure 9 shows the CD spectra of **23** in TFE and TFE containing water. The values of $[\theta]_{222}$ of **23** in TFE, 80% TFE-water, and 60% TFE-water were −12000 (helicity; 38%), −10200 (helicity; 32%), and

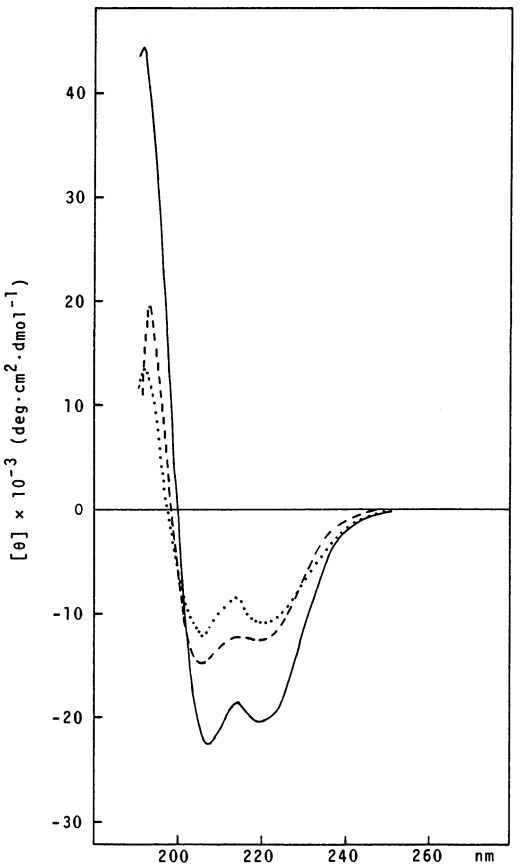

Fig. 8. CD spectra of **22** (·····) and **23** (———) in TFE, and myoglobin (———) in 60% TFE-water.

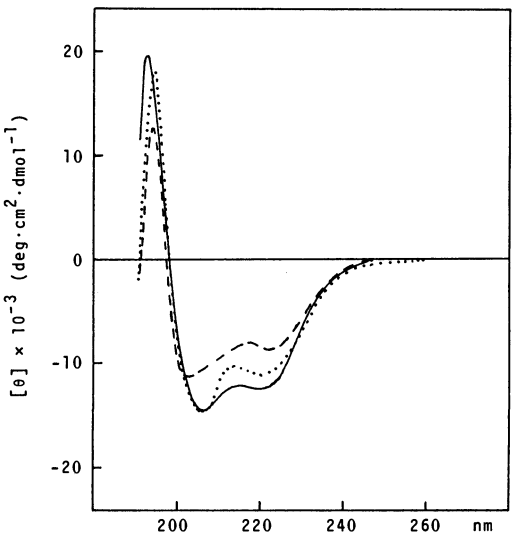

Fig. 9. CD spectra of **23** in TFE (———), 80% TFE-water (·····), and 60% TFE-water (———).

−8300 (helicity; 26%), respectively. The increment of water content diminished the helical content. These results revealed that the helical structure of **22** and **23** are stabilized in TFE solution. Those two fragments possess hydrophobic protecting groups on the side chains of amino acid residues. The helicities

of protecting-group-free peptides derived from **22** and **23** were very small in aqueous solution, and were rather smaller than those of the protected peptides, even in 60% TFE.[14]

In peptides **22** and **23**, the protection of some residues by hydrophobic groups seems to enhance the helical property of these peptides. The disappearance of the ionic property of the side chains of some residues by protection may also affect the helicity. Fragment **23** was formed by the addition of **21**, including almost nonhelical region to **22**. In spite of the addition of an almost nonhelical segment, the helical content of **23** was somewhat larger than that of **22**. This result implied that the helical structure is stabilized by the interaction among amino acid residues remote in the primary sequence. The helical ratios of **5**, **22**, and **23** were 0.13, 0.44, and 0.76, respectively. The ratios increased with the elongation of the peptide chain. The increase of the helical ratios also suggested the importance of the interaction among remote amino acid residues.

In conclusion, the CD study revealed that fragment peptides **5**, **22**, and **23** have helical structures, even though to various extents. The structures of those compounds seem to be stabilized by the effect of TFE and the hydrophobic interaction among hydrophobic protecting groups and side chains arranged spatially near to each other. This result also suggests that the hydrophobic interaction may be an important factor for the formation of a helical structure in myoglobin. Values of the helical ratio suggest that peptides **22**, and particularly **23**, probably possess a structure similar to the corresponding parts of myoglobin. The suggestion of the existence of a helical structure in peptides **22** and **23** is significant as a prerequisite of the formation of a complex between synthesized peptides and a protoheme in a similar way to that in myoglobin.

Experimental

Melting points were measured by the capillary method and are given as uncorrected values. Optical rotations were determined with a DIP-140 type (Jasco) polarimeter. Amino acid analyses were performed on a JLC-6AS automatic analyzer (JEOL) after acid hydrolysis with 6 M HCl in a sealed tube at 110 °C for 20—21 h. The theoretical values of amino acid ratios are shown in parentheses after each results.

In synthetic procedures, the imidazole functional group of histidine was temporarily protected by the Boc group on the occasion of incorporation of a histidine residue into a peptide chain. The functional groups of side chains, other than the hydroxyl group of threonine, were protected. The N^{α}- and N^{im}-Boc protecting groups were removed by TFA in the presence of anisole, or TFA at room temperature for 45—180 min. After evaporation of the solvents, the residue was triturated with diethyl ether to give a product. The removal of Boc groups of compounds **1**, **2**, **3**, **6**, **7**, **8**, **12**, **13b**, and **15** were carried out by a method similar to this method. Compounds **1**, **2**, **3**, **6**, **7**, **9**, **13a**, **14a** in Fig. 4, **15**, and **16** were synthesized by the MA method, compounds **4**, **8**, and **12** by the EDC-HOBt method and compound **13b** by the azide method. After couplings, the organic layers were washed successively with water, 5% citric acid, water, 5% sodium hydrogencarbonate, and water, and then dried over anhydrous sodium sulfate except when noted otherwise. Compound **18** was prepared from **17** by saponification. The evaporation of solvents was carried out under reduced pressure. Unless stated otherwise, residues and crystals were dried over NaOH pellets and P_2O_5 in vacuo at room temperature. Silica gel 60 (Merck and Co.) was used in column chromatography if not mentioned otherwise.

Thin-layer chromatography was performed on TLC plates silica gel 60 F_{254} and HPTLC plates silica gel 60 F_{254} with a concentration zone, (Merck and Co.), using the following solvent systems (volume ratios): R_f^1, chloroform-methanol (95 : 5); R_f^2, chloroform-methanol (9 : 1); R_f^3, chloroform-methanol (2 : 1); R_f^4, chloroform-methanol (1 : 1); R_f^5, chloroform-ethyl acetate (1 : 1); R_f^6, chloroform-methanol-acetic acid (95 : 5 : 5); R_f^7, chloroform-methanol-acetic acid (9 : 1 : 1); R_f^8, 1-butanol-acetic acid-water (3 : 1 : 1); R_f^9, 1-butanol-acetic acid-water (4 : 1 : 1); R_f^{10}, 1-butanol-pyridine-acetic acid-water (4 : 1 : 1 : 2), R_f^{11}, 1-butanol-pyridine-acetic acid-water (16 : 10 : 3 : 12).

Analytical data of compounds **1**, **2**, **3**, **4**, **6**, **7**, **8**, **9**, **12**, **13a**, **13b**, **14a** in Fig. 4, **15**, **16**, and **18** are given in Table 1.

CD measurements were performed using a J-500 spectropolarimeter with a DP-500N Data Processor. The temperature was kept constant at 24 °C. Cells with light paths of 0.1 and 0.5 mm were used. Measurements of fragment peptides and myoglobin were carried out in solutions at concentrations of 5×10^{-4} M and 5×10^{-5} M, respectively. Sperm whale myoglobin was purchased from Sigma and used without further purification.

Boc-Gln-Ser(Bzl)-His-Ala-Thr-Lys(Z)-OBzl (5). Compound **4** (6.410 g) was treated with TFA (25 ml) and anisole (1.45 ml) in the usual manner and yielded a solid. Boc-Gln-ONp (2.952 g) was dissolved in DMF (10 ml); to this solution was added a solution containing the above-mentioned solid and Et_3N (1.86 ml) in DMF (25 ml). The mixture was stirred for 4.5 d at room temperature and then concentrated. The product was dissolved in MeOH (80 ml), and the solution was applied to a Sephadex LH-20 column (3.6×139 cm). The product was eluted with DMF. Fractions of 10 g each were collected. Fractions 53—77 were combined and the solvent was evaporated. The residue was recrystallized from methanol-diethyl ether; 5.816 g (80%), mp 181—183 °C, $[\alpha]_D^{24}$ −13.3° (*c* 1.0, DMF), R_f^2 0.10, R_f^9 0.69. Amino acid ratios in acid hydrolyzate: Thr 0.95 (1), Ser 0.89 (1), Glu 1.07 (1), Ala 1.01 (1), His 1.04 (1), Lys 1.03 (1), NH_3 1.28 (1). Found: C, 57.12; H, 6.53; N, 12.14%. Calcd for $C_{54}H_{72}O_{14}N_{10}\cdot3H_2O$: C, 56.93; H, 6.90; N, 12.29%.

Boc-Leu-Lys(Z)-Pro-Leu-Ala-OH (10). To an ice-chilled solution of **9** (13.587 g) in methanol (15 ml) was added 1.98 M NaOH (9.57 ml). The mixture was stirred for 170 min at room temperature; then, 1 M HCl (18.95 ml) was added to this solution in an ice-bath. After evaporation of the methanol, the residual solution was dissolved in 1-butanol (ca. 150 ml) saturated with water, and the organic layer was washed with water (10 ml×3). After removing the solvent, the product was recrystallized from ethyl acetate-diethyl ether; 12.300 g (92%), mp 105—114 °C, $[\alpha]_D^{24}$

$-77.2°$ (c 1.0, MeOH), R_f^6 0.44, R_f^7 0.81. Amino acid ratios in acid hydrolyzate: Pro 0.97 (1), Ala 0.98 (1), Leu 2.03 (2), Lys 1.02 (1). Found: C, 56.54; H, 7.80; N, 10.07%. Calcd for $C_{39}H_{62}O_{10}N_6 \cdot 3H_2O$: C, 56.51; H, 8.27; N, 10.14%.

Boc-Glu(OBzl)-Leu-Lys(Z)-Pro-Leu-Ala-OH (11). Compound **10** (3.100 g) was treated with TFA (20 ml)–anisole (0.87 ml) to give a solid. The solution of Boc-Glu(OBzl)-ONp (2.847 g) in DMF (10 ml) was mixed with the solution of the above-mentioned solid and Et_3N (1.11 ml) in DMF (20 ml). The mixture was stirred for 69 h at room temperature and then condensed. The residue was dissolved in 1-butanol saturated with water and the 1-butanol layer was washed with 5% citric acid (30 ml×1) and water (10 ml×1). After removing the solvent, the product was dissolved in DMF (ca. 20 ml) and the solution was applied to a Sephadex LH-20 column (2.7×140.5 cm) employing the same solvent as the eluate. Fractions of 10 g each were collected. Fractions 30—38, including the desired peptide, were combined and the solvent was removed. After the residue was extracted with ethyl acetate (200 ml), the organic layer was further washed in the same manner mentioned above and concentrated. Fractions 39—46, containing impurity, were combined and concentrated. After the addition of ethanol to the residue, the resulting precipitate was removed by filtration. An additional crop was obtained from the filtrate by rechromatography on the same column. The combined product was crystallized from diethyl ether; 3.433 g (86%), mp 92—96 °C, $[\alpha]_D^{24}$ $-74.6°$ (c 1.0, MeOH), R_f^6 0.45, R_f^7 0.84, R_f^9 0.87. Amino acid ratios in acid hydrolyzate: Glu 1.05 (1), Pro 1.02 (1), Ala 0.93 (1), Leu 2.04 (2), Lys 0.97 (1). Found: C, 60.94; H, 7.72; N, 9.69%. Calcd for $C_{51}H_{75}O_{13}N_7 \cdot 1/2H_2O$: C, 61.06; H, 7.64; N, 9.77%.

Boc-His(Boc)-His-Glu(OBzl)-Ala-Opac (14a) in Fig. 3. Compound **13a** (3.914 g) was treated with TFA (22 ml) in the presence of anisole (2.23 ml). The solid obtained by the usual method showed two spots (R_f^{10} 0.73, 0.79) on TLC in an approximately equal proportions. The crude product was employed for the following coupling without purification. To an ice-cooled solution of Boc-His(Boc)-OH (2.185 g) in DMF (9.0 ml) were added HOBt (1.246 g), EDC·HCl (1.297 g), and the ice-chilled solution of the above solid and Et_3N (1.42 ml) in DMF (23 ml). The mixture was stirred for 44.5 h in an ice-bath and then at room temperature. After evaporation of the solvent the residue was extracted with ethyl acetate (200 ml), and the organic layer was washed using the usual procedure. The residue obtained after removing the solvent showed two spots on TLC (components A and B). This crude residue was dissolved in chloroform (30 ml) and the solution was subjected to a silica-gel column (2.2×35.0 cm) which was eluted with chloroform–methanol solvent systems. The fractions containing component A, Boc-His(Boc)-His-(Boc)-Glu(OBzl)-Ala-Opac (**14b**), were combined and the solvent was evaporated. The residue was triturated with diethyl ether; 1.305 g, mp 90—91 °C, $[\alpha]_D^{24}$ $-22.0°$ (c 1.0, MeOH), R_f^1 0.47 (trace 0.26, 0.36), R_f^2 0.79 (trace 0.36, 0.66). Amino acid ratios in acid hydrolyzate: Glu 1.06 (1), Ala 1.01 (1), His 1.94 (2). Found: C, 59.80; H, 6.47; N, 11.15%. Calcd for $C_{50}H_{64}O_{14}N_8$: C, 59.99; H, 6.44; N, 11.19%. FAB mass: m/z 1001 (MH^+, $C_{50}H_{65}O_{14}N_8$). Component B, corresponding to the desired peptide, **14a**, was isolated from other fractions in the same chromatography described above; 0.965 g (21%), mp 86—87.5 °C, $[\alpha]_D^{24}$ $-30.0°$ (c 1.0, MeOH), R_f^1 0.11 (trace 0.36), R_f^2 0.40 (trace 0.79). Amino acid ratios in acid hydrolyzate: Glu 1.04 (1), Ala 1.00 (1), His 1.96 (2). Found: C, 58.80; H, 6.40; N, 11.97%. Calcd for $C_{45}H_{56}O_{12}N_8 \cdot H_2O$: C, 58.81; H, 6.36; N, 12.19%. FAB mass: m/z 901 (MH^+, $C_{45}H_{57}O_{12}N_8$).

Boc-Lys(Z)-Lys(Z)-Lys(Z)-Gly-OEt (17). Compound **16** (24.047 g) was treated with TFA (30 ml)–anisole (3.59 ml), in the usual method, to give a solid. Boc-Lys(Z)-OH prepared from its dicyclohexylammonium salt (22.297 g) was dissolved in DMF (50 ml) and the solution was cooled below -20 °C. NMM (4.37 ml) and ECC (3.81 ml) were added to this solution with stirring. The mixture was stirred for 5 min at -14—-16 °C, and then cooled below -20 °C. To the mixture was added the ice-cooled solution of the above solid and Et_3N (4.60 ml) in DMF (50 ml). The mixture was stirred for 20.5 h in an ice-bath and then at room temperature. After the solvent was evaporated, the residue was extracted with ethyl acetate (300 ml). The solution was washed with water (300 ml×1). The precipitation brought about by the washing was dissolved by warming. The solution was dried and concentrated. The residue was recrystallized from methanol–chloroform–diethyl ether and chloroform–diethyl ether; 25.670 g (78%). For the purpose of analysis, a part of the product (0.320 g) was further purified by a silica-gel column (1.7×35.2 cm) with chloroform–methanol solvent systems as eluates. The obtained product was recrystallized from chloroform–methanol; 0.297 g (93%), mp 148.5—151.5 °C, $[\alpha]_D^{24}$ $-14.3°$ (c 1.0, DMF), R_f^1 0.51, R_f^2 0.78. Amino acid ratios in acid hydrolyzate: Gly 1.00 (1), Lys 3.01 (3). Found: C, 61.26; H, 7.29; N, 9.80%. Calcd for $C_{51}H_{71}O_{13}N_7 \cdot 1/2H_2O$: C, 61.31; H, 7.26; N, 9.81%.

Boc-Lys(Z)-Lys(Z)-Lys(Z)-Gly-His-His-Glu(OBzl)-Ala-Opac (20). Compound **14a** (1.367 g) was treated with TFA (15 ml) and anisole (0.659 ml), in the usual way, to yield a solid (**19**), 3TFA·H-His-His-Glu(OBzl)-Ala-OPac; R_f^9 0.13, R_f^{10} 0.55, R_f^{11} 0.57. Found: C, 46.40; H, 4.01; N, 10.71%. Calcd for $C_{41}H_{43}O_{14}N_8F_9 \cdot H_2O$: C, 46.42; H, 4.28; N, 10.56%. The ice-chilled solution of **18** (1.824 g) in DMF (4.5 ml) was mixed with HOBt (0.384 g), EDC·HCl (0.436 g), and an ice-cooled solution of **19** and Et_3N (0.633 ml) in DMF (7.0 ml). The mixture was stirred for 18.5 h in an ice-bath and then at room temperature. The residue yielded, after removing the solvent, was dissolved in 1-butanol saturated with water. The organic layer was washed in the routine manner. After the solution was concentrated, the residue was recrystallized from methanol; 2.195 g (88%), mp 170 °C (decomp), $[\alpha]_D^{24}$ $-18.8°$ (c 1.0, DMF), R_f^4 0.90, R_f^9 0.60. Amino acid ratios in acid hydrolyzate: Glu 1.08 (1), Gly 0.98 (1), Ala 0.97 (1), His 1.96 (2), Lys 3.00 (3). Found: C, 60.61; H, 6.57; N, 12.54%. Calcd for $C_{84}H_{105}O_{20}N_{15} \cdot H_2O$: C, 60.67; H, 6.49; N, 12.63%.

Boc-Lys(Z)-Lys(Z)-Lys(Z)-Gly-His-His-Glu(OBzl)-Ala-OH (21). Compound **20** (6.239 g) was dissolved in acetic acid (27 ml). Zinc powder (8.00 g) was added to this solution. The mixture was stirred for 4.5 h at 40 °C. After removing the catalyst, the filtrate was evaporated and the residue was triturated with water. The precipitates were collected and recrystallized from methanol–ethyl acetate; 4.861 g (84%), mp 176 °C (decomp), $[\alpha]_D^{24}$ $-15.3°$ (c 1.0, DMF), R_f^9 0.53 (trace 0.44). Amino acid ratios in acid hydrolyzate: Glu 1.03 (1), Gly 1.01 (1), Ala 0.98 (1), His 1.98 (2), Lys 3.00 (3). Found: C, 59.04; H, 6.69; N, 13.52%. Calcd for $C_{76}H_{99}O_{19}N_{15} \cdot H_2O$: C, 59.09; H, 6.59; N, 13.60%.

Boc-Glu(OBzl)-Leu-Lys(Z)-Pro-Leu-Ala-Gln-Ser(Bzl)-His-Ala-Thr-Lys(Z)-OBzl (22). Compound **5** (4.070 g) was treated with TFA (40 ml)–anisole (0.815 ml) in the usual manner to produce a solid. To an ice-cooled solution of **11** (4.847 g) in DMF (12.5 ml) were added HOBt (0.988 g), EDC·HCl (1.028 g) and the ice-chilled solution of the above solid and Et_3N (1.04 ml) in DMF (17.5 ml). The mixture was stirred for 72 h in an ice-bath and then at room temperature. The solvent was evaporated, the residue was dissolved in 1-butanol (ca. 150 ml) saturated with water and the organic layer was washed in the usual method. After concentration in vacuo, the crude product was dissolved in DMF (10 ml) and the solution was subjected to a Sephadex LH-60 column (2.2×143.8 cm) using the same solvent as the eluate. Fractions of 10 g each were collected. Fractions 28—53 were combined and the solvent was evaporated. The residue was recrystallized from methanol; 6.300 g (86%), mp 192 °C (decomp), $[\alpha]_D^{24}$ −31.8° (*c* 1.0, DMF), R_f^4 0.99 (HPTLC), R_f^9 0.75 (HPTLC). Amino acid ratios in acid hydrolyzate: Thr 0.84 (1), Ser 0.79 (1), Glu 2.11 (2), Pro 1.16 (1), Ala 1.91 (2), Leu 2.31 (2), His 0.91 (1), Lys 1.98 (2), NH_3 1.07 (1). Found: C, 60.19; H, 7.31; N, 11.71%. Calcd for $C_{100}H_{137}O_{24}N_{17}\cdot 2H_2O$: C, 60.14; H, 7.12; N, 11.92%.

Boc-Lys(Z)-Lys(Z)-Lys(Z)-Gly-His-His-Glu(OBzl)-Ala-Glu(OBzl)-Leu-Lys(Z)-Pro-Leu-Ala-Gln-Ser(Bzl)-His-Ala-Thr-Lys(Z)-OBzl (23). Compound **22** (3.000 g) was treated with TFA-CH_2Cl_2 (1:1) (40 ml) containing anisole (0.498 ml) in the usual procedure to afford a solid. Compound **21** (2.803 g) was dissolved in DMF (12 ml) and the solution was cooled in an ice-bath. The solution was mixed with HOBt (0.372 g), EDC·HCl (0.387 g), and the ice-cooled solution of the above solid and Et_3N (0.475 ml) in DMF (19 ml). The mixture was stirred for 65 h in an ice-bath and then at room temperature. The solvent was evaporated and the residue was dissolved in 1-butanol saturated with water. The 1-butanol layer was washed using the routine method. After removing the solvent, the product was dissolved in DMF (20 ml), and the solution was applied to a column (2.2×140 cm) of Sephadex LH-60 using the same solvent as the eluate. Fractions of 10 g each were collected. Fractions 26—42 were combined and the solvent was evaporated. The residue was repeatedly chromatographed on the same column, and recrystallized from methanol. However, the product still contained minor impurities; 2.856 g (55%). For the sake of further purification for analysis, the product (0.500 g) was dissolved in 1-butanol–acetic acid–water (4:1:1) (2.0 ml) and applied to a column (1.5×38.5 cm) of silica gel (Silica gel 100; Merck and Co.), which had been equilibrated with the same solvent system. It was eluted with the same solvent. Fractions of 5.0 g each were collected. Fractions 17—29 were combined and the solvent was removed. The recrystallization of the residue from methanol afforded a pure product; 0.122 g (24%), mp 198 °C (decomp), $[\alpha]_D^{24}$ −15.9° (*c* 1.0, DMF), R_f^3 0.83, R_f^8 0.67, R_f^9 0.60. Amino acid ratios in acid hydrolyzate: Thr 0.91 (1), Ser 0.87 (1), Glu 3.04 (3), Pro 1.19 (1), Gly 1.00 (1), Ala 2.95 (3), Leu 2.03 (2), His 2.99 (3), Lys 5.01 (5), NH_3 1.19 (1). Found: C, 59.55; H, 6.81; N, 12.93%. Calcd for $C_{171}H_{226}O_{40}N_{32}\cdot 4H_2O$: C, 59.67; H, 6.85; N, 13.02%.

The authors wish to thank Professor Machiko Tozawa, Associate Professor Tomoyoshi Takahashi and emeritus Professor Tsunetaka Kushimoto of The Jikei University School of Medicine, Professor Shosuke Sofuku of Rikkyo University for continuing interest and encouragement, and Associate Professor Sukekatsu Nozaki of Josai University for many discussions. They also thank the members of the Radiochemical Laboratory of Rikkyo University for CD measurements, the Research Laboratory of Toyo Jozo Co. Ltd. for elemental and FAB mass analyses.

References

1) J. C. Kendrew, R. E. Dickerson, B. E. Strandberg, R. G. Hart, D. R. Davies, D. C. Phillips, and V. C. Shore, *Nature (London)*, **185**, 422 (1960).

2) H. Eckstein and E. Bayer, *Justus Liebigs Ann. Chem.*, **1978**, 1607.

3) The amino acids except glycine used are of L-configuration. The abbreviations used are those recommended by IUPAC-IUB Joint Commission on Biochemical Nomenclature (JCBN): *Eur. J. Biochem.*, **138**, 9 (1984). The following additional abbreviations are used: EDC·HCl, 1-ethyl-3-(3-dimethylaminopropyl)carbodiimide hydrochloride; HOBt, 1-hydroxybenzotriazole; Pac, phenacyl; DMF, *N,N*-dimethylformamide; Et_3N, triethylamine; NMM, *N*-methylmorpholine; ECC, ethyl chloroformate; FAB, Fast Atom Bombardment.

4) G. W. Anderson, J. E. Zimmerman, and F. M. Callahan, *J. Am. Chem. Soc.*, **88**, 1338 (1966).

5) J. C. Sheehan, J. Preston, and P. A. Cruickshank, *J. Am. Chem. Soc.*, **87**, 2492 (1965).

6) W. König and R. Geiger, *Chem. Ber.*, **103**, 788 (1970).

7) M. Bodanszky and V. du Vigneaud, *J. Am. Chem. Soc.*, **81**, 5688 (1959).

8) M. Joustra, B. Söderqvist, and L. Fischer, *J. Chromatogr.*, **28**, 21 (1967).

9) J. Honzl and J. Rudinger, *Collect. Czech. Chem. Commun.*, **26**, 2333 (1961).

10) J. B. Hendrickson and C. Kandall, *Tetrahedron Lett.*, **1970**, 343.

11) E. Schnabel, H. Klostermeyer, J. Dahlmans, and H. Zahn, *Justus Liebigs Ann. Chem.*, **707**, 227 (1967); M. Bodanszky and J. Martinez, "Side Reactions in Peptide Synthesis," in "The Peptides, Analysis, Synthesis, Biology," ed by E. Gross and J. Meienhofer, Academic Press, New York (1983), Vol. 5, "Special Methods in Peptide Synthesis, Part B", Chap. 3, pp. 152—156.

12) R. M. Epand and H. A. Scheraga, *Biochemistry*, **7**, 2864 (1968).

13) R. P. Singhal and M. Z. Atassi, *Biochemistry*, **9**, 4252 (1970).

14) C. Hashimoto and I. Muramatsu, 55th National Meeting of the Chemical Society of Japan, Fukuoka, October 1987, Abstr., No. 2W26.

15) D. E. Nitecki, B. Halpern, and J. W. Westley, *J. Org. Chem.*, **33**, 864 (1968).

16) H. Kinoshita and H. Kotake, *Bull. Chem. Soc. Jpn.*, **50**, 280 (1977).

17) K. Khodadadeh, K. Heppenheimer, and E. R. Heidemann, *Makromol. Chem.*, **178**, 1897 (1977).

The Preparation of Poly(3-methoxy-2,5-thiophenediyl) with Iron(III) Chloride and Its Properties

Susumu TANAKA* and Kyoji KAERIYAMA
Research Institute for Polymers and Textiles, 1-1-4, Higashi, Tsukuba, Ibaraki 305
(Received October 18, 1988)

Soluble and conductive poly(3-methoxy-2,5-thiophenediyl) was obtained by the chemical oxidation of 3-methoxythiophene with iron(III) chloride. The resulting polymer was found to be in a doped state, since it contained 0.1—0.2 counterions ($FeCl_4^-$ and Cl^-) per monomeric unit. This means that the oxidation is a convenient method for preparing conductive polymers in one step. We also obtained a poly-MOT solution and film in a state doped to a great extent, showing no π-π^* transition band and a high stability in air. An undoped polymer film was prepared by the electrochemical reduction of the doped film. The undoped film had a π-π^* transition band at 2.3 eV, indicating that the effective conjugation length of the polymer could be assumed to be the same as that of the poly(3-methoxythiophene) prepared electrochemically.

Electrochemical polymerization has been found to be an advantageous method for preparing conductive polyheterocycles, such as polythiophene[1] and polypyrrole,[2] since it permits polymers to be obtained on the surface of an electrode as films. In electrochemical polymerization, film thickness is proportional to the amount of charge flowed. However, film conductivity has been found to decrease extremely when the thickness becomes great.[3] Heterocyclic conductive polymers can be prepared not only by the electrochemical means, but also by the chemical method using transition metal salts.[4] By this method, the polymers are obtained as powdery products, but the amounts of polymers obtained increase in proportion to the feed of the starting materials.

We have previously prepared poly(3-methoxythiophene)(poly-MOT) electrochemically and found it to be soluble in organic solvents.[5] The doped state of poly-MOT was stable in air. In this paper, we wish to report on the preparation of poly-MOT with iron (III) chloride and its properties. The polymer obtained is soluble in organic solvents and in a doped state, as in the case of the electrochemically prepared one. This is a convenient method for preparing conductive polymers in one step.

Experimental

Materials. MOT[6] was prepared as reported previously. It was then distilled in vacuo: bp 62 °C (30 mmHg; 1 mmHg≈133.322 Pa) (lit,[6] bp 80—82 °C (65 mmHg)). Iron(III) chloride was used without any further purification. Chloroform was washed five times with about half its volume of water, dried with anhydrous calcium chloride, and distilled over calcium hydride under argon; bp 62 °C. Methanol was distilled and dried with Zeolite; bp 65—66 °C. Benzene was dried with anhydrous calcium chloride and distilled over calcium hydride; bp 80.0—80.5 °C. Nitromethane and acetonitrile were purified as reported previously.[3]

Polymerization. The typical polymerization procedures were as follows. In a three-necked flask equipped with a stirrer, a condenser, and an argon inlet, chloroform and iron(III) chloride were placed. Prior to polymerization, argon was bubbled, and bubbling was continued up to the end of the polymerization. The resulting yellowish green suspension was stirred at 30 °C, and MOT was added. A rapid color change into dark red took place. When benzene was used as the solvent, the brown suspension was changed into a dark red one by the addition of MOT. After stirring for 2 h, the reaction mixture was poured into methanol to remove the unreacted iron(III) chloride and iron(II) chloride. The precipitate was collected on a filter, washed with methanol, and dried in vacuo.

Reprecipitated poly-MOT was obtained by adding 100 ml of benzene to a solution of 0.1 g of poly-MOT in 20 ml of dimethyl sulfoxide (DMSO).

An undoped polymer was prepared by the electrochemical reduction of the doped film cast on an indium-tin oxide glass (ITO).

A cast film was obtained from a solution of 20 mg of the polymer in 4 ml of DMSO. About 20 mg of the solution was cast on ITO (1 cm×1 cm=1 cm^2) and dried in vacuo at 120 °C for 1 h.

Electrochemical Doping. A cast film on ITO was used as a working electrode. The counter electrode was a platinum plate or wire. A reference electrode consisting of Ag/Ag^+ was connected to the cell by means of a salt bridge. Acetonitrile was used as the solvent, and $NaClO_4$ (0.1 mol l^{-1}) as the electrolyte. The electrochemical data were obtained using a Hokuto Denko HA-501 potentiostat/galvanostat and an HB-104 function generator.

Measurements. The electrical conductivity was measured on pressed pellets by Van der Pauw's four probe method. Fourier transform IR and VIS-near IR spectra were recorded on a Perkin-Elmer Model 1720 spectrometer and a Hitachi U-3400 spectrometer respectively. The spectral change and cyclic voltammograms were measured according to the method described in a previous paper.[5]

Results and Discussion

Polymerization. The results of the polymerization of MOT are summarized in Table 1. Among the four kinds of solvents shown in Table 1, iron(III) chloride is soluble in nitromethane and methanol, while it is almost insoluble in benzene and chloroform. Considering the color change described in the Experimental section, iron(III) chloride is slightly soluble in benzene and chloroform, and polymerization should

Table 1. Preparation of Poly-MOT with Iron(III) Chloride[a)]

Exp. No.	Solvent	$FeCl_3$ mol l^{-1}	Temp °C	Yield[b)] mg	Conductivity S cm^{-1}
1	PhH	0.4	30	58.8	2.8×10^{-4}
2	$MeNO_2$	0.2	30	48.8	8.2×10^{-4}
3	$CHCl_3$	0.2	30	54.5	9.3×10^{-3}
4	MeOH	0.4	30	—	—
5	$CHCl_3$	0.2	−30	8.0	4.2×10^{-4}
6	$CHCl_3$	0.2	0	50.1	1.7×10^{-3}
7	$CHCl_3$	0.2	45	84.7[c)]	1.3×10^{-2}
8	$CHCl_3$	0.2	60	109.5[c)]	3.1

a) The concentration of MOT was 0.1 mol l^{-1}. b) The feed of MOT was 100 mg. c) Partly soluble in DMSO. Elemental analyses of poly-MOT obtained in Exp. No. 3: Before reprecipitation: C, 39.94; H, 2.82; S, 20.54; Fe, 5.76; Cl, 17.06. After reprecipitation: C, 44.21; H, 3.49; S, 20.61; Fe, 4.40; Cl, 10.97.

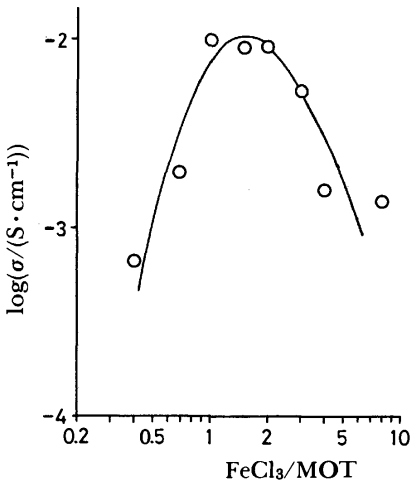

Fig. 1. Effect of the molar ratio of iron(III) chloride to MOT on conductivity of poly-MOT.

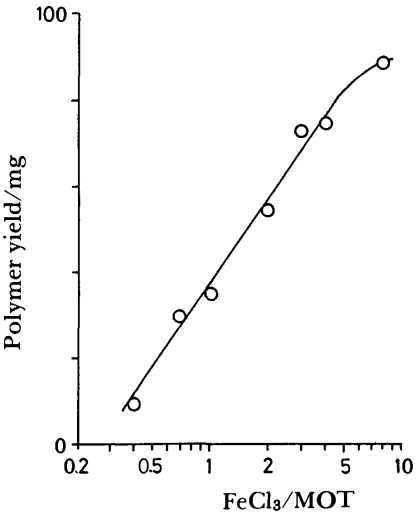

Fig. 2. Effect of the molar ratio of iron(III) chloride to MOT on polymer yield.

occur in a solution of iron(III) chloride. In Exps. Nos. 1—3, a black powdery product was obtained. The highest conductivity was obtained when chloroform was used as the solvent. In the case of methanol, no polymer was obtained as a precipitate from the solution nor by adding benzene or chloroform to the solution. In Exps. Nos. 3 and 5—8, the conductivity of the pressed pellet and polymer yield increased with the increase in the polymerization temperature. However, the polymer obtained above 45 °C was partly soluble in DMSO, although that obtained below 30 °C was soluble in DMSO. Figure 1 shows the effect of the molar ratio of iron(III) chloride to MOT on the conductivity of poly-MOT when MOT was polymerized at 30 °C in chloroform. The conductivity was highest when the ratio was in the range of 1—2. Figure 2 shows the effect of the ratio on the polymer yield when polymerization was done at 30 °C in chloroform. The yield increased with the increase in the ratio.

The above results show that a conductive and soluble product is obtained in a high yield when MOT is polymerized at 30 °C in chloroform with a molar ratio of 2. Thereafter, the polymerization was carried out under these conditions except otherwise mentioned. Elemental analyses showed the resulting poly-MOT to contain 0.16 and 0.11 counterions ($FeCl_4^-$ and Cl^-) per monomeric unit respectively, judging from the ratios of iron to sulfur and of chlorine to iron. However, reprecipitated poly-MOT contained 0.12 counterions ($FeCl_4^-$), indicating that reprecitipation brought about the removal of Cl^-. As to a polythiophene and its derivatives prepared by this method, they have been obtained in the undoped state. The reaction of thiophene with iron(III) perchlorate gave an insulating polymer.[7)] Using iron(III) chloride, soluble polythiophene derivatives were prepared from alkylthiophene monomers ($n\geqq4$), but the polymers were in an undoped state.[8)] Only a small number of papers on a one-step synthesis of doped polythiophenes have been published. Inoue et al. reported that the reaction of 2,2′-bithiophene with copper(II) perchlorate yielded doped polythiophene in one step.[9)] 2,2′-Bithiophene was polymerized more easily than thiophene, since the oxidation potentials of the former and the latter were 1.26 and 1.65 V vs. SCE respectively.[10)] MOT was also polymerized easily because of its low oxidation potential.[11)] The oxidation potential of polythiophene was lower by 0.55 V than that of the thiophene monomer. Therefore, the polymerization of thiophene should be followed by the oxidation of polythiophene in view of the thermodynamic data, but in fact polythiophene was obtained in an undoped state. We have to consider, therefore, that the reaction was not simply controlled thermodynamically.

IR Spectra. Figure 3 shows the Fourier transform IR spectra of doped and undoped poly-MOT. Both

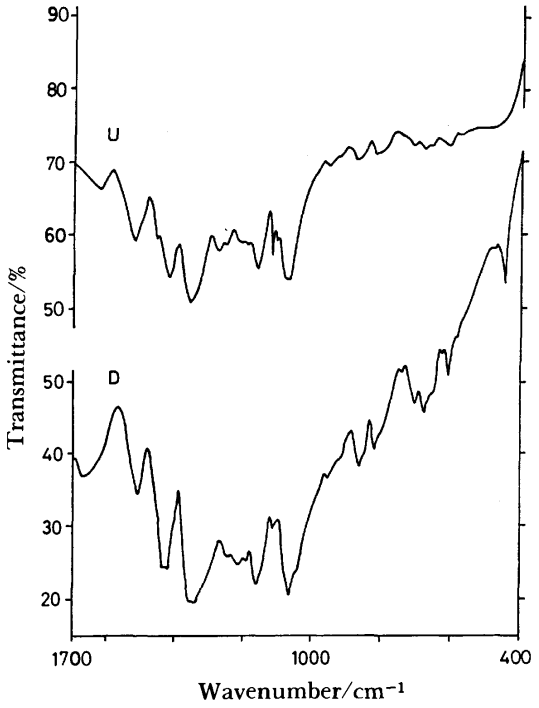

Fig. 3. IR spectra of poly-MOT.
U: an undoped polymer, D: a $FeCl_4^-$ doped polymer.

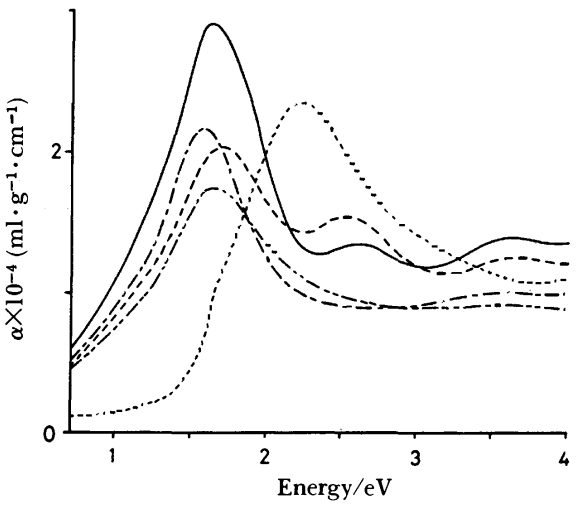

Fig. 4. VIS-near IR spectra of poly-MOT in DMSO.
———: Just after preparation, ----: After 4 days in air, — — —: Just after preparation (reprecipitated), ——·——: After 4 days in air (reprecipitated), ·····: an undoped polymer solution (reprecipitated).

polymers had two peaks, at 820 and 1260 cm^{-1}, assigned to the C-H deformation vibration of the 2,3,5-trisubstituted thiophene ring[12] and the C-O-C stretching vibration of the methoxyl group respectively. Neither had a peak at 795 cm^{-1} assignable to the C-H deformation vibration of the 2,5-disubstituted thiophene ring. Therefore, the structure of poly-MOT was consistent with that of poly(3-methoxy-2,5-thiophenediyl). In the 3000—3100 cm^{-1} frequency range,[12] no peak could be observed. We have previously reported the IR spectra of doped and undoped poly-MOT prepared electrochemically.[5] There was no difference between the spectra of the two undoped poly-MOT. As to the spectra of the two doped poly-MOT, some differences were observed; electrochemically prepared poly-MOT had two bands at 560 and 845 cm^{-1}, possibly due to the supporting electrolyte (Bu_4NPF_6), since the electrolyte had these peaks. The peaks at 445, 610, 870, and 1425—1440 cm^{-1} were observed only in the present poly-MOT.

VIS-Near IR Spectra. As has been mentioned above, poly-MOT was soluble in DMSO. Other polar solvents, such as 1-methyl-2-pyrrolidinone (NMP) and propylene carbonate (PC), were found to dissolve poly-MOT. Figure 4 shows the VIS-near IR spectra of poly-MOT in DMSO. The solid line had three absorption bands, at 1.6, 2.6, and 3.6 eV. The absorbance at 3.6 eV decreased in a broken line, suggesting that the band at 3.6 eV was not due to a π-π^* transition, since the doped state of poly-MOT should gradually change to the undoped state in air.[5] On the contrary, the band at 2.6 eV was considered to be due to a π-π^* transition, judging from the increase in the absorbance at 2.6 eV of the broken line.

To confirm the above estimation, the reprecipitation of poly-MOT was carried out. The spectra of reprecipitated poly-MOT are presented in the same figure. The spectrum of an undoped poly-MOT solution had only one band, at 2.2 eV, assigned to a π-π^* transition. The spectrum of a doped poly-MOT solution had two bands, at 1.6 and 3.6 eV. No band was observed around 2.2 eV, indicating that the reprecipitation brought about the removal of the poly-MOT containing undoped sites.

In the case of the poly-MOT prepared electrochemically, the spectrum of a doped polymer solution had a small π-π^* transition band at 2.3 eV in addition to the two bands at 1.0 and 1.5 eV,[5] suggesting that a slight undoping occurred in this case. These three characteristic bands were also observed in a doped poly-MOT film cast on ITO. On the other hand, the spectrum of the present poly-MOT film had only one band, at 1.6 eV, and no band was exhibited around 2.2 eV (Fig. 5). Thus, we obtained a poly-MOT solution and film in a state doped to a great extent. These results indicate that the doped state of the present poly-MOT was more stable in air than that of the electrochemical one.

As for the two bands at 1.6 and 3.6 eV shown in Fig. 4, further discussion will be given below.

The change in the VIS-near IR spectra during the doping of the film of poly-MOT is shown in Fig. 5. Cast films on the ITO anode were electrochemically doped at different voltages, and in situ spectra were recorded. At −0.7 V, the film had two bands, at 2.3 and 3.4 eV. The doping level became higher as the applied voltage was increased. At 0.3 V, a band at 1.9 eV was observed. When the voltage decreased to −0.7

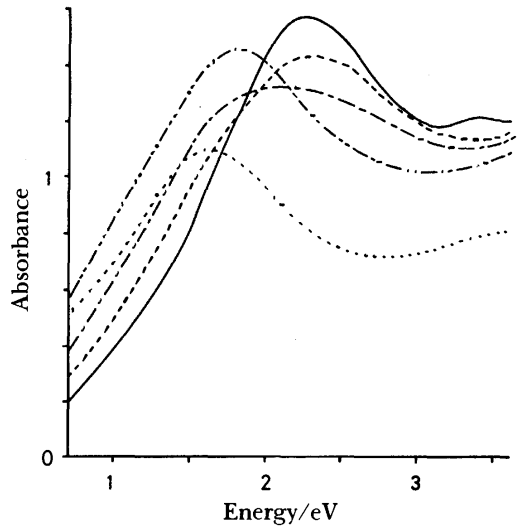

Fig. 5. VIS-near IR spectrum of reprecipitated poly-MOT film cast on ITO (------) and spectral change during electrochemical doping of poly-MOT. Electrolyte: $NaClO_4$ (0.1 mol l^{-1}). Applied voltage: ——: −0.7V; ----: −0.3V; — - —: −0.1V; —·—: 0.3V.

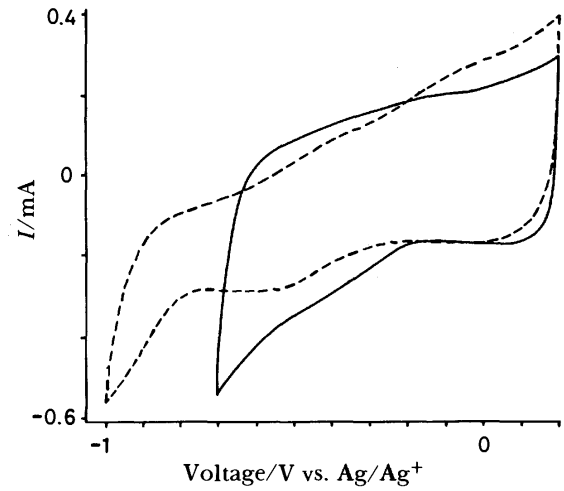

Fig. 6. Cyclic voltammograms of poly-MOT. In every case, current was calculated under the conditions that 1 mg of the polymer was deposited on ITO (1×1=1 cm^2). Electrolyte: $NaClO_4$ (0.1 mol l^{-1}). Sweep rate: 2 mV s^{-1}.

V again, the film had only one band, at 2.3 eV, and the band at 3.4 eV disappeared completely. These results indicate that the band at 2.3 eV is to be assigned to a π-π^* transition, while the band at 3.4 eV might be caused by a contamination. The low-molecular-weight part of poly-MOT should be more soluble than the other part. Moreover, the solubility of undoped poly-MOT was higher than that of doped poly-MOT. Accordingly, at the lower applied voltage, acetonitrile might dissolve the low-molecular-weight part. The band at 1.9 eV observed in the doped film could be attributed to Würster-type radical cations produced by the oxidation of poly-MOT, as has been discussed in the previously reported paper.[5]

Concerning the change in the VIS-near IR spectra of the reprecipitated poly-MOT film, as a whole it was the same as that presented in Fig. 5, including that the band at 3.4 eV, observed initially at −0.7 V, disappeared on the second sweep. The undoped film had a band at 2.3 eV, and the doped one, one at 1.55 eV. The effective conjugation length of the undoped poly-MOT was assumed to be the same as that of the poly-MOT prepared electrochemically, since the latter showed a π-π^* transition band at 2.3 eV.[5]

Cyclic Voltammetry. Figure 6 shows the cyclic voltammograms of cast films of poly-MOT with $NaClO_4$. On the sweep ranging from −0.7 V to 0.2 V, an anodic shoulder was observed at −0.2 V and a cathodic shoulder at −0.5 V, as is shown by the solid line. The film was blue above the oxidation potential and red-purple below the reduction potential. On another sweep ranging from −1.0 V to 0.2 V, the anodic shoulder could be observed more clearly than before, as is shown by the broken line. However, in this case, the anodic and cathodic currents decreased gradually when the sweep was carried out repeatedly, suggesting that poly-MOT deteriorates at applied voltages lower than −0.7 V. Electrochemically prepared poly-MOT presented an anodic peak and a cathodic peak quite clearly at −0.20—−0.18 V and at −0.50—−0.48 V respectively. The present polymer had the anodic and cathodic shoulders in the same regions, but no clear peak was observed. The same results were found in the cyclic voltammograms of the cast films of reprecipitated poly-MOT. The ambiguity of the oxidation and reduction peaks should be mainly explainable by the finding that the background current was about 10 times as high as that in poly-MOT prepared electrochemically.[5]

References

1) V. L. Afanas'ev, I. B. Naznrova, and M. L. Khidekel, *Izv. Akad. Nauk SSSR. Ser. Khim.*, **1980**, 1687. K. Kaneto, K. Yoshino, and Y. Inuishi, *Jpn. J. Appl. Phys.*, **21**, L567 (1982).

2) A. F. Diaz and K. K. Kanazawa, *J. Chem. Soc., Chem. Commun.*, **1982**, 635.

3) S. Tanaka, M. Sato, and K. Kaeriyama, *Makromol. Chem.*, **185**, 1295 (1984).

4) a) T. H. Chao and J. March, *J. Polym. Sci., Polym. Chem. Ed.*, **26**, 743 (1988). b) S. Rapi, V. Bocchi, and G. P. Gardini, *Synth. Met.*, **24**, 217 (1988).

5) S. Tanaka, M. Sato, and K. Kaeriyama, *Synth. Met.*, **25**, 277 (1988).

6) S. Gronowitz, *Ark. Kemi*, **12**, 239 (1958).

7) N. M. -Thevenin and G. Bidan, *Mol. Cryst. Liq. Cryst.*, **118**, 227 (1985).

8) R. Sugimoto, S. Takeda, H. B. Gu, and K. Yoshino, *Chem. Express*, **1**, 635 (1986).

9) M. B. Inoue, E. F. Velazquez, and M. Inoue, *Synth. Met.*, **24**, 223 (1988).

10) G. Tourillon and F. Garnier, *J. Electroanal. Chem.*, **161**, 51 (1984).
11) R. L. Blankespoor and L. L. Miller, *J. Chem. Soc., Chem. Commun.*, **1985**, 90.
12) M. Akiyama, *J. Mol. Spectrosc.*, **43**, 226 (1972). T. Yamamoto, K. Sanechika, and A. Yamamoto, *Bull. Chem. Soc. Jpn.*, **56**, 1497 (1983). G. Tourillon and F. Garnier, *J. Phys. Chem.*, **87**, 2289 (1983). S. Hotta, T. Hosaka, M. Soga, and W. Shimotsuma, *Synth. Met.*, **9**, 87 (1984).

On the Reaction of *N*-Vinyliminophosphoranes. 9.[1] The Synthesis and Reaction of *N*-(1,3,5-Cycloheptatrienyl)iminophosphoranes to Provide a Novel Route to 1-Azaazulenes

Yukio Iino, Eijiro Hara, and Makoto Nitta*
Department of Chemistry, School of Science and Engineering, Waseda University, Shinjuku-ku, Tokyo 169
(Received November 5, 1988)

The first syntheses of *N*-(2,4,6-cycloheptatrienyl)iminophosphoranes (**3a, b**) and their thermal conversion to *N*-(1,3,5-cycloheptatrienyl)iminophosphoranes (**5a,b**) have been studied. The kinetic study of the 1,5-hydrogen migration of **3a,b** to *N*-(1,3,6-cycloheptatrienyl)iminophosphoranes (**4a,b**) has also been investigated. The reaction of **5b** with α-bromoacetophenone derivatives has provided a novel route to the 1-azaazulene ring system, albeit in low yields.

The reaction of a tertiary phosphine with an organic azide to produce an iminophosphorane after nitrogen evolution is known as the Staudinger reaction.[2] Many intermolecular[3] and intramolecular[4] Wittig-type (aza-Wittig) reactions with carbonyl compounds to construct a carbon-nitrogen double bond have been reported. However, the synthetic versatility of iminophosphoranes has still not been fully explored compared with that of methylenephosphoranes.[5] This fact can be ascribed in part to the poor variation of the substituent on the nitrogen atom of iminophosphoranes. Previously, we demonstrated the simple preparation of novel *N*-(1-phenylvinyl)iminophosphorane,[6] *N*-vinyliminotriphenylphosphorane,[7] and *N*-(1-butylvinyl)iminotriphenylphosphorane[7] by the Staudinger reaction of the corresponding organic azides with tertiary phosphines. *N*-Vinyliminophosphoranes were found to react with α-bromo ketones, α,β-unsaturated ketones, and tropone derivatives in an enamine alkylation process followed by an aza-Wittig reaction to provide a convenient route to phenyl-substituted pyrroles,[8,9] pyridines,[7,9] and 1-azaazulenes.[6,10] However, the potential value of *N*-vinyliminophosphoranes bearing cycloalkene on the nitrogen atom remains unexplored. We describe here the preparation of novel *N*-(1,3,5-cycloheptatrienyl)iminophosphoranes (**5a, b**) and their reactions with α-bromoacetophenone derivatives to give 2-aryl-1-azaazulene derivatives.

Results and Discussion

The reaction of 7-azido-1,3,5-cycloheptatriene (**1**)[11] with triphenylphosphine (**2a**) and tributylphosphine (**2b**) in dry benzene at room temperature afforded *N*-(2,4,6-cycloheptatrienyl)iminotriphenylphosphorane (**3a**) and *N*-(2,4,6-cycloheptatrienyl)iminotributylphosphorane (**2b**), respectively. Compound **3a** is a crystalline compound, which could be easily purified by recrystallization. On the other hand, compound **3b** is not stable on silica gel and it could not be purified. Thus, oily **3b** was used for further reactions. However, the structures of **3a** and **3b** were easily deduced on the basis of spectral data. The ^{13}C NMR

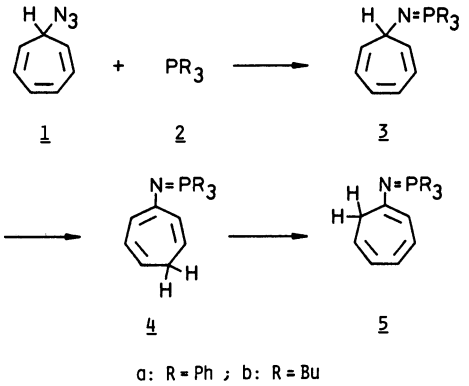

Scheme 1.

Table 1. ^{13}C and ^{31}P NMR Chemical Shifts (ppm) of Iminophosphoranes[a]

Compound	C1	C2	C3	C4	C5	C6	C7	Remaining signal	^{31}P[b]
3a	132.51	119.55	129.95				54.61	131.77(9.0), 131.51(95.3)	11.7
	(15.2)	(1.4)					(1.4)	130.44(2.8), 127.59(11.8)	
3b	131.29	117.72	128.40				52.38	25.08, 22.40, 22.05,[d]	23.9
	(12.7)						(2.8)	21.18, 21.79, 11.49	
5a	143.14	107.15		130.55	126.66[c]		39.55	132.18(9.7), 131.29(2.8)	3.5
	(6.2)	(13.8)		119.89	115.20		(19.3)	129.69(94.7), 128.11(11.7)	
5b	144.29	102.72		129.19	125.44[c]		39.20	25.10, 23.06, 22.66,[d]	24.8
	(9.0)	(12.4)		117.43	113.39		(20.0)	22.48, 12.26	

a) The numerical values in parentheses denote the coupling constants with ^{31}P. b) Downfield relative to external 85% H_3PO_4 standard. c) Each of the chemical shifts for C3—C6 are not assigned distinctly. d) Butyl groups appear as multiplets because of its coupling with ^{31}P.

and ^{31}P NMR spectral data are summarized in Table 1.

In general, the cycloheptatrienes undergo sequential 1,5-hydrogen migration and the equilibrium shifts to the side of the most stable isomer bearing a substituent at C1, although the formation of other isomers has been detected. Therefore, the thermal reaction of **3a, b** is probably a useful method for the attempted preparation of *N*-(1,3,5-cycloheptatrienyl)iminophosphoranes **5a, b**. When **3a** was heated in toluene under reflux, isomer **4a** was formed at first. Progress of the reaction could be followed by ^{1}H NMR spectroscopy. After prolonged heating, only the desired product **5a** was obtained in 89% yield after recrystallization. Similarly, compound **3b** was isomerized in benzene under reflux for 7 h to give **5b** in good yield. The ^{1}H NMR spectra of **5a, b** exhibited a typical pattern of the 1-substituted cycloheptatriene. The ^{13}C NMR and ^{31}P NMR spectral data, which are summarized in Table 1, and other spectral data are in good accordance with the proposed structures, **5a, b**.

6a-c 7a-c

a: R=Me ; b: R=OMe ; c: R=Ph

Scheme 2.

A kinetic study of the rearrangement (**3a**→**4a** and **3b**→**4b**) was carried out at temperatures ranging from 68.0 °C to 99.0 °C and from 60.3 °C to 79.5 °C, respectively, to establish the mechanistic aspects. Further rearrangement of **4a, b** to **5a, b** was not observed during the kinetic studies of the early stage of the reactions. A plot of the logarithm of the concentration of unchanged **3a, b** against the reaction time was linear. The rate constants, thus obtained, are shown in Table 2. Arrhenius plots of the data for **3a** and **3b** (Table 2) provided straight lines, from which the kinetic parameters were calculated. These parameters as well as those of the thermal 1,5-hydrogen shift of 7-substituted cycloheptatrienes **6a—c** to 3-substituted cycloheptatrienes **7a—c** are summarized in Table 3.

Table 2. The First-Order Rate Constants k of **3a** and **3b**

	Temp/ °C	$10^5 \times k/s^{-1}$		Temp/ °C	$10^5 \times k/s^{-1}$
3a	68.0	1.04	**3b**	60.3	0.96
	79.5	3.60		68.0	3.04
	86.5	9.25		76.0	6.04
	99.0	27.56		79.5	8.83

Table 3. The Kinetic Parameters of 1,5-Hydrogen Shift of 7-Substituted Cycloheptatrienes

Compound	E_a/kcal mol^{-1}	log A	$\Delta S^{\neq}$/cal mol^{-1}deg^{-1}
3a	26.6	12.1	−5.0[a]
3b	26.3	12.3	−6.1[a]
6a	33.25±0.19	12.6±0.2	−4.9[b]
6b	26.407	10.04	−15.0[c]
6c	27.6	10.8	−11.7[d]

a) At 80 °C. b) Ref. 12. c) Ref. 13. d) Ref. 14.

The preexponential factors obtained, $10^{12.1}$ and $10^{12.3}$ for **3a** and **3b**, respectively, correspond to the negative entropy of activation, i.e., −5.0 and −6.1 eu (at 80 °C). These values are intermediate between that of **6a**[12] and those of **6b, c**.[13,14] These facts clearly suggest that the 1,5-hydrogen shift of **3a, b** is sigmatropic in character and proceeds via a rigid transition state such as **8**. The activation energies for **3a** and **3b**

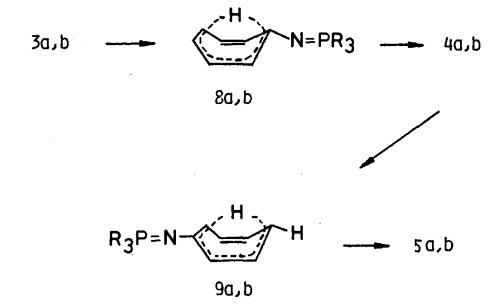

Scheme 3.

are similar to those of **6b**[13] and **6c**.[14] Thus, the steric or electronic effect of the phosphoranylideneamino group seems also to accelerate the 1,5-hydrogen shift in **3a, b**. Compounds **4a, b** further undergo a 1,5-hydrogen shift via a transition state **9**; the equilibrium are almost shifted to the side of the most stable isomers, **5a, b**.

The thermal reaction of **5a** with α-bromoacetophenone (**10a**) in benzene in the presence of triethylamine under reflux afforded no isolable products. However, compound **5b** reacted with **10a** to afford 1,8-dihydrocyclohepta[*b*]pyrrole (**11a**)[6,10] in 28% yield. Compound **11a** is not very stable, and it was dehydrogenated by NiO_2[15] in benzene to afford 2-phenyl-1-azaazulene (**12a**) in 44% yield. When a series of annelation reactions giving **11a** and the subsequent dehydrogenation by NiO_2 was carried out without rigorous purification of **11a**, compound **12a** was also obtained in 12% yield (Table 4, entry 1) (see Experimental). Similarly, reactions of **5b** with **10b—d** were carried out

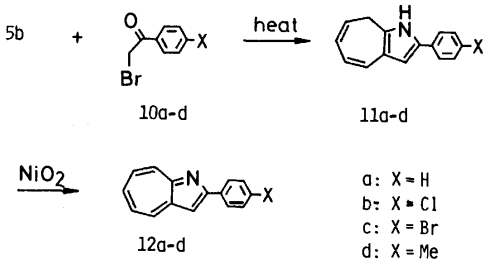

10a-d 11a-d

12a-d

a: X=H
b: X=Cl
c: X=Br
d: X=Me

Scheme 4.

Table 4. Annelation Reaction of *N*-(1,3,5-Cycloheptatrieneyl)iminophosphorane **5b** with α-Bromoacetophenones (**10a—d**) and Subsequent Dehydrogenation

Annelation reaction[a]			Dehydrogenation[b]		
Entry	Compound **10**	Reaction time/h	Reaction time/h	Product **12**	Yield/%
1	**10a**	22	15	**12a**	12
2	**10b**	15	15	**12b**	11
3	**10c**	5	15	**12c**	8
4	**10d**	15	15	**12d**	11

a) All the reactions were carried out in benzene under refluxing. b) Reactions were carried out at room temperature.

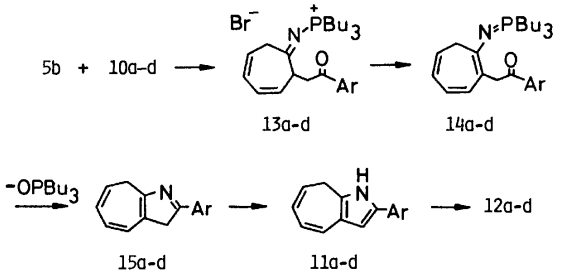

Scheme 5.

in dry benzene under reflux to give plausible intermediates **11b—d**, which were subsequently dehydrogenated by NiO_2 to give the 2-aryl-1-azaazulene derivatives **12b—d**. The detailed reaction conditions and the yields of the products are summarized in Table 4. Product **12a**[16] is a known compound, and the other 1-azaazulenes **12b—d** were characterized on the basis of spectral data.

The plausible reaction pathways for the formation of 1-azaazulenes **12a—d** are summarized in Scheme 5. By analogy with the reaction of *N*-vinyliminophosphorane[8,9] with α-bromoketones, the initial step is the formation of a C-C bond between **5b** and **10a—d** to give intermediates **13a—d**, which undergo hydrogen migration to give **14a—d**. The intramolecular aza-Wittig reaction followed by hydrogen migration constructing the pyrrole ring gives **11a—d**. The oxidation of **11a—d** with NiO_2 results in the formation of 1-azaazulenes **12a—d**.

Thus, the desired *N*-(1,3,5-cycloheptatrienyl)iminophosphoranes **5a, b** were easily prepared, and were reacted with α-bromoacetophenones to give arylsubstituted 1-azaazulenes albeit in low yields. Further synthetic applications of the iminophosphoranes are in progress.

Experimental

The IR spectra were recorded on a Shimadzu IR-400 spectrometer. The ^1H NMR and ^{13}C NMR spectra were recorded on Hitachi R-24 and Hitachi R-90H spectrometers, and the chemical shifts are given in ppm (δ) relative to the internal $SiMe_4$ standard. The ^{31}P NMR spectra were recorded on a Hitachi R-90H spectrometer and the chemical shifts are given in ppm (δ) relative to the external 85%-H_3PO_4 standard. Mass spectral and high-resolution mass spectral studies were conducted using Shimadzu GCMS-QP1000 and JEOL DX-300 spectrometers. All the melting points were measured on a Büch apparatus and are uncorrected.

Preparation of *N*-(2,4,6-Cycloheptatrienyl)iminophosphoranes 3a, b. A solution of tropylium tetrafluoroborate (5 g, 28 mmol) and sodium azide (10 g, 154 mmol) in water (50 cm^3) was stirred for 5 min at room temperature. The reaction mixture was extracted with benzene and the benzene extract was dried over $MgSO_4$ and then concentrated to 50 cm^3. To this solution of 7-azidocycloheptatriene (**1**)[11] thus obtained was added to triphenylphosphine (**2a**) (6.5 g, 25 mmol) or tributylphosphine (**2b**) (5 g, 25 mmol) at room temperature and stirred for 2 h or 5 h. After the benzene was evaporated, the resulting residue was crystallized from benzene-hexane to give yellow crystals of **3a** (3.1 g, 89%): mp 109—110 °C (from benzene-hexane); ^1H NMR ($CDCl_3$) δ=3.00 (1H, dm, *J*=19.5 Hz), 5.50 (2H, dd, *J*=4.6, 9.2 Hz), 5.80—6.10 (2H, m), 6.52 (2H, t, *J*=2.6 Hz), 7.30—7.85 (15H, m); IR ($CHCl_3$) 3004, 1591, 1485, 1441, 1393, 1304, 1180, 1105, 908, 697 cm^{-1}; MS, *m/z* (rel intensity) 367 (M^+, 16), 261 (100). Found: C, 81.99; H, 6.19; N, 3.60%. Calcd for $C_{25}H_{22}NP$: C, 81.72; H, 6.04; N, 3.81%. In the case of **3b**, the benzene was evaporated in vacuo and the resulting oily residue was used for further reaction, because of its instability to heat and chromatography on silica gel. For **3b**: ^1H NMR ($CDCl_3$) δ=0.75—1.15 (9H, m), 1.15—1.85 (18H, m), 2.55 (1H, dm, *J*=20.5 Hz), 5.25 (2H, dd, *J*=8.5, 4.5 Hz), 5.70—6.15 (2H, m), 6.54 (2H, t, *J*=3.0 Hz); IR ($CHCl_3$) 2955, 2929, 2866, 1468, 1391, 1305, 1184, 1094 cm^{-1}. HRMS Found: *m/z* 307.2431. Calcd for $C_{19}H_{34}NP$: M, 307.2429.

Thermal Isomerization of 3a,b to *N*-(1,3,5-Cycloheptatrienyl)-iminophosphoranes 5a,b. (A) A solution of **3a** (3.5 g, 9.5 mmol) in toluene (10 cm^3) was heated under reflux for 7 h. After the toluene was evaporated in vacuo, the resulting residue was crystallized from hexane to give yellow crystals of **5a** (3.1 g, 89%): mp 131—132 °C (from EtOH); ^1H NMR ($CDCl_3$) δ=2.65 (2H, dd, *J*=7.8, 1.0 Hz), 4.90—5.40 (2H, m), 5.83—6.30 (3H, m), 7.30—7.91 (15H, m); IR ($CHCl_3$) 2995, 1574, 1496, 1441, 1328, 1174, 1107, 1026 cm^{-1}; MS, *m/z* (rel intensity) 367 (M^+, 75), 366 (100). Found: C, 81.83; H, 6.22; N, 3.60%. Calcd for $C_{25}H_{22}NP$: C, 81.72; H, 6.04; N, 3.81%.

(B) A solution of **3b** in benzene, which was prepared as described above, was heated under reflux for 7 h. After the benzene was evaporated, the resulting residue was distilled under reduced pressure to give **5b** (6.15 g, 81% based on tropylium cation used). For **5b**: bp 137 °C/11 Pa. ^1H NMR (CCl_4) δ=0.75—1.20 (9H, m), 1.20—2.10 (18H, m), 2.23 (2H, dd, *J*=7.2, 1.6 Hz), 4.80—5.15 (2H, m), 5.55—6.40 (3H, m); IR ($CHCl_3$) 2964, 2934, 2871, 1567, 1486, 1441, 1333, 1204, 1026 cm^{-1}. HRMS Found: *m/z* 307.2413. Calcd for $C_{19}H_{34}NP$: M, 307.2429.

Reaction Rate of 1,5-Hydrogen Migration of 3a, b to 4a, b. The solution of **3a** (0.5 mol dm^{-3}) in CCl_2CCl_2 was placed in six reaction tubes (5 mm in outer diameter and 30 mm long), which were fitted in the neck of a 500 cm^3 flask with six necks and a reflux condenser, which contained a suitable solvent. Six tubes were heated at the same time by vapor of boiling solvent such as dioxane (99.0 °C), trichloroethylene

(86.5 °C), benzene (79.5 °C), or hexane (68 °C). During heating, each tube was periodically withdrawn from the flask and cooled quickly with ice bath to quench the reaction. The ^{1}H NMR spectrum was measured by a Hitachi R-24 spectrometer. The concentration ratios of the isomerized product, **4a** and **3a**, were calculated from the proton area of the signal ascribed to the 7H-proton of cycloheptatriene of the corresponding compounds.

The solution of **3b** (3.0 mol dm^{-3}) in CCl_2CCl_2 with 1/6 molar equivalent amounts of anisole was placed in six reaction tubes, which were fitted in the same apparatus described above. Six tubes were heated at the same time by vapor of boiling solvent such as *i*-PrOH (79.5 °C), CCl_4 (76.0 °C), hexane (68 °C), or $CHCl_3$ (60.3 °C). The ^{1}H NMR spectrum was measured, and the concentration ratios of the remaining **3b** was determined by the proton area of the signals ascribed to the 7H-proton of **3b** and the methyl proton of anisole used as the internal standard. From this concentration ratio, the product ratio of **4b** was calculated.

The Reaction of *N*-(1,3,5-Cycloheptatrienyl)iminotributylphosphorane (5b) with α-Bromoacetophenone (10a). A solution of the iminophosphorane (**5b**) (307 mg, 1 mmol), α-bromoacetophenone (**10a**) (199 mg, 1 mmol), and triethylamine (202 mg, 2 mmol) in benzene (5 cm^3) was heated under reflux for 22 h. After the reaction was completed, the reaction mixture was chromatographed on Florisil. The fractions eluted with benzene afforded 1,8-dihydro-2-phenylcyclohepta[*b*]pyrrole (**11a**) (58 mg, 28 %), which was identified by comparison of the spectral data of the authentic specimen.[6]

General Procedure for the Reaction of *N*-(1,3,5- Cycloheptatrienyl)iminotributylphosphorane (5b) with α-Bromoacetophenones (10a—d) and Subsequent Dehydrogenation. A solution of the iminophosphorane (**5b**) (307 mg, 1 mmol), α-bromoacetophenone (**10**) (1 mmol), and triethylamine (202 mg, 2 mmol) in benzene (5 cm^3) was heated under reflux for a period indicated in Table 4. After the reaction was completed, the reaction mixture was chromatographed on Florisil. The fractions eluted with benzene was concentrated to 20 cm^3. To this solution was added NiO_2 (910 mg, 10 mmol); and the mixture was then stirred for 10—15 h at room temperature. After the reaction mixture was filtered through Celite to remove insoluble materials, the filtrate was concentrated and the resulting residue was purified by TLC on Silica gel using hexane-ethyl acetate (1/1) to give 1-azaazulene derivatives (**12**) in the yields indicated in Table 4. 2-Phenyl-1-azaazulene (**12a**): mp 148—149.5 °C (from EtOH) (lit, 157—159 °C); ^{1}H NMR ($CDCl_3$) δ=7.22—7.72 (7H, m), 8.19—8.48 (3H, m), 8.48—8.74 (1H, m); IR ($CHCl_3$) 2906, 2857, 1586, 1466, 1445, 1412, 1030 cm^{-1}; *m/z* (rel intensity) 205 (M^+, 100); UV (EtOH, log ε) 205 (4.33), 237 (4.20), 287 (4.59), 310 (4.45), 355 (4.09), 372 (4.04), 497 (3.44), 529 (3.16) nm; (EtOH-TFA, log ε) 260 (4.30), 282 (4.33), 306 (4.57), 340 (3.90), 446 (4.06) nm. 2-(4-Chrolophenyl)-1-azaazulene (**12b**): mp 165—165.9 °C (from EtOH); ^{1}H NMR ($CDCl_3$) δ=7.24—7.78 (6H, m), 8.06—8.82 (4H, m); IR ($CHCl_3$) 2985, 2955, 1602, 1464, 1437, 1413, 1087, 1012 cm^{-1}; MS, *m/z* (rel intensity) 242 (M^++1, 5), 241 (M^+, 28), 240 (M^++1, 18), 239 (M^+, 100); UV (EtOH, log ε) 205 (4.26), 237 (4.18), 287 (4.50), 312 (4.41), 356 (4.09), 372 (4.06), 496 (3.45), 527 (3.25) nm; (EtOH-TFA, log ε) 263 (4.26), 280 (4.23), 310 (4.49), 345 (3.93), 446 (4.03) nm. Found: C, 75.49; H, 4.35; N, 6.09%. Calcd for $C_{15}H_{10}NCl$: C, 75.16; H, 4.20; N, 5.84%. 2-(4-Bromophenyl)-1-azaazulene (**12c**): mp 169—171.5 °C (from EtOH); ^{1}H NMR ($CDCl_3$) δ=7.27—7.83 (6H, m), 8.02—8.73 (4H, m); IR ($CHCl_3$) 2985, 2955, 1597, 1464, 1437, 1411, 1070, 1009 cm^{-1}; MS, *m/z* (rel intensity) 286 (M^++1, 11), 285 (M, 58), 284 (M^++1, 11), 283 (M^+, 59), 204 (100); UV (EtOH, log ε) 206 (4.39), 248 (4.30), 288 (4.65), 313 (4.58), 356 (4.25), 373 (4.23), 496 (3.56), 527 (3.32) nm; (EtOH-TFA, log ε) 263 (4.43), 279 (4.36), 311 (4.63), 345 (4.09), 447 (4.20) nm. Found: C, 63.37; H, 3.59; N, 4.81%. Calcd for $C_{15}H_{10}NBr$: C, 63.40; H, 3.55; N, 4.93%. 2-(4-Methylphenyl)-1-azaazulene (**12d**): mp 146.5—147.5 °C (from EtOH); ^{1}H NMR ($CDCl_3$) δ=2.33 (3H, s), 7.09—7.64 (6H, m), 8.04—8.30 (3H, m), 8.41—8.65 (1H, m); IR ($CHCl_3$) 2990, 2940, 1615, 1467, 1438, 1413 cm^{-1}; MS *m/z* (rel intensity) 220 (M^++1, 27), 219 (M, 100); UV (EtOH, log ε) 206 (4.25), 240 (4.12), 288 (4.43), 315 (4.36), 361 (4.04), 377 (4.02), 497 (3.34), 529 (3.00) nm; (EtOH-TFA, log ε) 262 (4.27), 278 (4.16), 314 (4.43), 349 (3.82), 450 (4.05) nm. Found: C, 87.21; H, 5.85; N, 6.21%. Calcd for $C_{16}H_{13}N$: C, 87.64; H, 5.98; N, 6.39%.

This work was supported by an Annual Project organized by Waseda University 1987.

References

1) Part 8. N. Kanomata and M. Nitta, *Tetrahedron Lett.*, **29**, 5957 (1988).

2) Yu. G. Gololobov, I. N. Zhmurova, and L. F. Kasukhin, *Tetrahedron*, **37**, 437 (1981).

3) J. A. Kloek and K. L. Leschinsky, *J. Org. Chem.*, **43**, 1460 (1978); O. Tsuge, S. Kanemasa, and K. Matsuda, *J. Org. Chem.*, **49**, 2688 (1984); T. Saito, M. Nakane, M. Endo, H. Yamashita, Y. Oyamada, and S. Motoki, *Chem. Lett.*, **1986**, 135; P. Molina, M. Alajarín, and A. Vidal, *Tetrahedron Lett.*, **29**, 3849 (1988).

4) P. H. Lambert, M. Vaultier, and R. Carrié, *J. Chem. Soc., Chem. Commun.*, **1982**, 1224; T. Sasaki, S. Eguchi, and T. Okano, *J. Am. Chem. Soc.*, **105**, 5912 (1983); D. M. B. Hickey, A. R. MacKenzie, C. J. Moody, and C. W. Rees, *J. Chem. Soc., Chem. Commun.*, **1984**, 776; L. Bruche, L. Garanti, and G. Zecchi, *Synthesis*, **1985**, 304; H. R. Stegmann, D. Klotz, and J. E. Weiss, *Chem. Ber.*, **118**, 4632 (1985).

5) K. B. Becker, *Tetrahedron*, **36**, 1717 (1980).

6) M. Nitta and T. Kobayashi, *Chem. Lett*, **1986**, 463.

7) Y. Iino and M. Nitta, *Bull. Chem. Soc. Jpn.*, **61**, 2235 (1988).

8) Y. Iino, T. Kobayashi, and M. Nitta, *Heterocycles*, **24**, 2437(1986).

9) T. Kobayashi, Y. Iino, and M. Nitta, *Nippon Kagaku Kaishi*, **1987**, 1237.

10) M. Nitta, Y. Iino, E. Hara, and T. Kobayashi, *J. Chem. Soc., Perkin Trans. 1*, **1989**, 51.

11) J. J. Looker, *J. Org. Chem.*, **30**, 638 (1965).

12) K. W. Egger, *J. Am. Chem. Soc.*, **89**, 3688 (1967).

13) T. Nozoe and K. Takahashi, *Bull. Chem. Soc. Jpn.*, **38**, 665 (1965).

14) A. P. ter Borg and H. Kloosterziel, *Recl. Trav. Chim. Pays-Bas*, **82**, 741 (1962).

15) K. Nakagawa, R. Konaka, and T. Nakata, *J. Org. Chem.*, **27**, 1597 (1962).

16) Y. Sugiyama, N. Soma, and Y. Kishida, *Bull. Chem. Soc. Jpn.*, **45**, 3174 (1972).

The Selective Claisen and Dieckmann Ester Condensations Promoted by Dichlorobis(trifluoromethanesulfonato)titanium(IV)

Yoo Tanabe
Takatsuki Research Laboratory, Sumitomo Chemical Co., Ltd., Takatsuki, Osaka 569
(Received November 7, 1988)

Inter and intramolecular condensations (the Claisen and the Dieckmann condensations) between ester functions have been performed by the combined use of dichlorobis(trifluoromethanesulfonato)titanium(IV) (= dichlorobis(triflato)titanium(IV)) and tertiary amine under mild reaction conditions. These results led to the development of the selective (crossed) Claisen and Dieckmann ester condensation between methoxymethyl ester and methyl ester, in that, dichlorobis(triflato)titanium(IV) contribute to control the direction of the reaction.

The Claisen and the Dieckmann ester condensations are the most fundamental and useful carbon-carbon bond forming reactions in organic synthesis.[1] However, the utility of these reactions have been limited by the several problems. Basic labile functional groups could be hardly introduced in the substrates employed, because these reactions are conventionally carried out in basic media. And, it is more of critical that it has been difficult in controlling the direction of the reaction, namely when the condensation is carried out between two different esters, each of which possesses α-hydrogen, a mixture of all four products is generally obtained.[2] To evade the problem, esters lacking α-hydrogen such as benzoates, carbonates, and oxalates are commonly employed as acylating agents.

In the preceding communications,[3] we have reported the Claisen and the Dieckmann ester condensation between alkyl esters and the crossed type of the ester condensation between methoxymethyl ester and methyl ester could be performed under mild reaction conditions by using dichlorobis(trifluoromethanesulfonato)titanium(IV)[4] (=dichlorobis(triflato)titanium(IV)). In this paper, the author describe the results of the studies on them in detail.

Results and Discussion

The characteristic properties of the metal triflates (trifluoromethanesulfonates) system had led to the development of significant carbon-carbon bond forming reactions in organic synthesis.[5] In particular, dialkylboryl triflates and tin(II) triflates mediated synthetic processes enjoyed highly regio-, stereo-controlled aldol type[5a-f] and the Michael type[5g,h] reactions. In connection with the progress, we paid our attention to the utilization of titanium(IV) triflates species, which were known in inorganic chemistry.[4,6] Among the four feasible titanium(IV) spesies, we chose the most stable and accessible dichlorobis(trifluoromethanesulfonato)titanium(IV) (=dichlorobis(triflato)titanium(IV)).[7]

Firstly, we studied the ability of dichlorobis(triflato)-titanium(IV) ($TiCl_2(OTf)_2$) to generate the enolate from ester, because tin(II) triflate or dialkylbolyl triflate fail to promote the reaction perhaps due to the low acidity of α-proton of ester. The addition reaction of methyl propionate with benzaldehyde in the presence of $TiCl_2(OTf)_2$ and triethylamine (molar ratio of ester : aldehyde : $TiCl_2(OTf)_2$: Et_3N=1.0 : 1.1 : 1.1 : 1.1) was found to give not even a trace amount of the β-hydroxy ester **1**, but unexpectedly methyl 2-methyl-3-oxovalerate (**2**) as a main product in 36% yield. Meanwhile, treatment of the β-hydroxy ester **1** with $TiCl_2(OTf)_2$ and triethylamine under the same conditions did not take place the retro-aldol reaction and the ester **1** was recoverd quantitatively. The cross-over experiment showed that the aldol-type reaction did not occured at all in this system (Scheme 1).

Based on these results, the different type of Claisen ester condensation under nonbasic media were studied. To optimize the conditions, intramolecular cyclization (the Dieckmann condensation) of dimethyl adipate was examined. Among several solvents screened, dichloromethane gave the best result in yield (Table 1). Tertiary amines such as triethylamine or *N,N*-diisopropylethylamine was found to give good results. As molar ratio, the combined use of 1.5 equivalent of $TiCl_2(OTf)_2$ and 2.2 equivalent of triethylamine gave

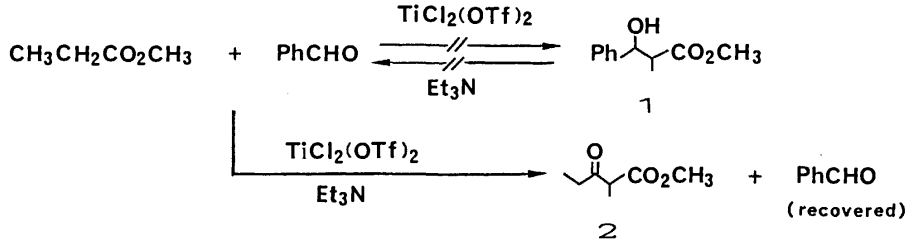

Scheme 1.

Table 1. Effect of the Solvent on the Dieckmann Condensation of Dimethyl Adipate[a]

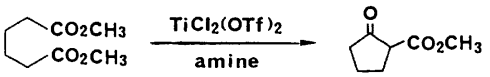

Solvent	Yield of 2-methoxycarbonyl-1-cyclopentanone/%	Recovery of dimethyl adipate/%
Toluene	32	55
Tetrahydrofuran[b]	0	—
Ether	17	75
Dichloromethane	55	42
1,2-Dichloroethane	35	55

a) The reaction was carried out at 0 °C for 2 h employing triethylamine as base. Molar ratio of dimethyl adipate: $TiCl_2(OTf)_2$: Et_3N=1.0 : 1.1 : 1.5. b) Tetrahydrofuran was polymerized in this condition.

Table 2. Effect of Bases and Molar Ratio on the Dieckmann Condensation of Dimethyl Adipate[a]

Entry	Base(equiv)		Equiv of $TiCl_2(OTf)_2$	Yield/%[b]
1	Pyridine	(2.2)	1.1	5>
2	Cesium Fluoride	(2.2)	1.1	0
3	*N*-Ethylpiperidine	(2.2)	1.1	30
4	Diisopropylethylamine	(2.2)	1.1	45
5	DBU	(2.2)	1.1	0
6	2,6-Lutidine	(2.2)	1.1	10
7	Triethylamine	(1.1)	1.1	35
8	Triethylamine	(2.2)	1.1	55
9	Triethylamine	(2.2)	1.5	71
10	Triethylamine	(3.3)	1.1	38
11	Triethylamine	(3.3)	1.5	48
12	Triethylamine[c]	(2.2)	1.5	80

a) The reaction was carried out at 0 °C for 2 h employing dimethyl adipate as substrate. b) Isolated yield. c) In the presence of Molecular Sieves 4A.

the best yield (Table 2). The tendency of these conditions is similar to those of other metal (tin(II) and boryl) triflates systems. A somewhat excess of $TiCl_2(OTf)_2$ was required to complete the reaction perhaps owing to compensate the reagent decomposed by an equimolar amount of methanol produced during the condensation. The addition of Molecular Sieves 4A to catch the methanol slightly effected the yield.

Analogous types of titanium complexes such as dichlorobis(fluorosulfonato)titanium(IV) ($TiCl_2(SO_3F)_2$),[8] titanium(IV) chloride ($TiCl_4$), and bis(η-cyclopentadienyl)bis(trifluoromethanesulfonato)titanium(IV) ($TiCp_2(OTf)_2$)[9] were also applied to expect the same reaction. However, their titanium(IV) reagents failed to proceed the condensation reaction, probably because $TiCl_2(SO_3F)_2$ could be hardly soluble in dichloromethane during the reaction and $TiCl_4$, $TiCp_2(OTf)_2$ are less reactive compared with $TiCl_2(OTf)_2$ as Lewis acid.

Methyl 5-(chloroformyl)valerate was examined as substrate to compare the reactivity with dimethyl adipate, but no reaction occured at all under the same conditions. The results suggest that the capture of the methoxyl group by $TiCl_2(OTf)_2$ correlates the driving force of the reaction.

Several examples of the condensation under the optimum conditions were depicted in Table 3. α-unsubstituted esters could be subjected to self ester condensation (Entries 1—3), whereas no desired compound was obtained in the case of α-alkyl-substituted ester such as methyl isobutyrate (Entry 5). The result reflected on the regioselective cyclization of diethyl 2-methyladipate to afford only 2-ethoxycarbonyl-5-methylcyclopentanone (Entry 6). Benzoylation, formylation, and oxalylation were similarly performed employing third fold excess of the corresponding acylating reactants (Entries 7—11).

A plausible mechanism is illustrated in Scheme 2. Small amount of the enolate of an ester in the system, which is successively generated from the ester on equilibrium, immediatly transformed into more stable titanium salt of the enol of the corresponding β-keto ester. The resultant titanium salt of the β-keto ester is quenched by water to give the product. This speculation could be supported by the following facts; (1) the aldol-type reaction did not proceeded under this condition, (2) also in the usual Claisen condensation α-alkyl-substituted ester required more harsh basic conditions.[1a]

In due consideration of the dichlorobis(triflato)titanium(IV) promoted Claisen ester condensation, we studied the direct and the crossed (regiocontrolled) type-Claisen ester condensation which was hitherto enable to be realized under commonly known basic conditions.[10,11] To answer the problem, we planned regioselective enolate formation of one of the two different ester functions. In the hope that titanium(IV) species exhibit the strong chelating ability toward oxygen or sulfur atom adjacent to ester functions, methoxymethyl ester **13**, methylthiomethyl ester **14**, and 2-methoxyethyl ester **15** were examined to produce the enolate predominantly against methyl ester through intramolecular (the Dieckmann) condensa-

Table 3. Several Types of Ester Condensation[a)]

Entry	Ester(substrate)	Acylating reagent[b)]	Conditions	Yield/%[c)]	Product	
1	$CH_3CH_2CO_2Me$	—	0 °C, 2 h	72	$EtCOCH(CH_3)CO_2Me$	3
2	$CH_3CH_2CO_2Et$	—	0 °C, 2 h	70	$EtCOCH(CH_3)CO_2Et$	4
3	$PhCH_2CH_2CO_2Me$	—	0 °C—r.t., 10 h	55	$PhCH_2\underset{\displaystyle COCH_2CH_2Ph}{\underset{\vert}{C}}HCO_2Me$	5
4	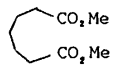	—	0 °C—r.t., 10 h	51	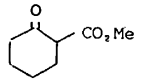	6
5	*i*-$PrCO_2Me$	—	0 °C—r.t., 10 h	0	—	
6	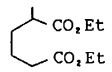	—	0 °C—r.t., 10 h	56	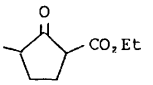	7
7	$PhCH_2CH_2CO_2Me$	$PhCO_2Me$	0 °C—r.t., 10 h	71	$PhCH_2\underset{\displaystyle COPh}{\underset{\vert}{C}}HCO_2Me$	8
8	$PhCH_2CH_2CO_2Me$	HCO_2Et	0 °C—r.t., 10 h	59	$PhCH_2\underset{\displaystyle CHO}{\underset{\vert}{C}}HCO_2Me$	9
9	$PhCH_2CH_2CO_2Me$	$HCOCO_2Et$	0 °C—r.t., 10 h	62	$PhCH_2\underset{\displaystyle COCHO}{\underset{\vert}{C}}HCO_2Me$	10
10	γ-Butyrolactone	$PhCO_2Me$	0 °C—r.t., 10 h	70	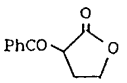	11
11	γ-Butyrolactone	HCO_2Et	0 °C—r.t., 10 h	52	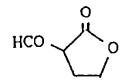	12

a) The reaction was carried out in CH_2Cl_2 in the presence of M.S. 4A. Molar ratio of $TiCl_2(OTf)_2$: Et_3N : ester (substrate)=1.5 : 2.2 : 1.0. b) Three equiv of acylating reagents vs. esters (substates) were used. c) Isolated yield.

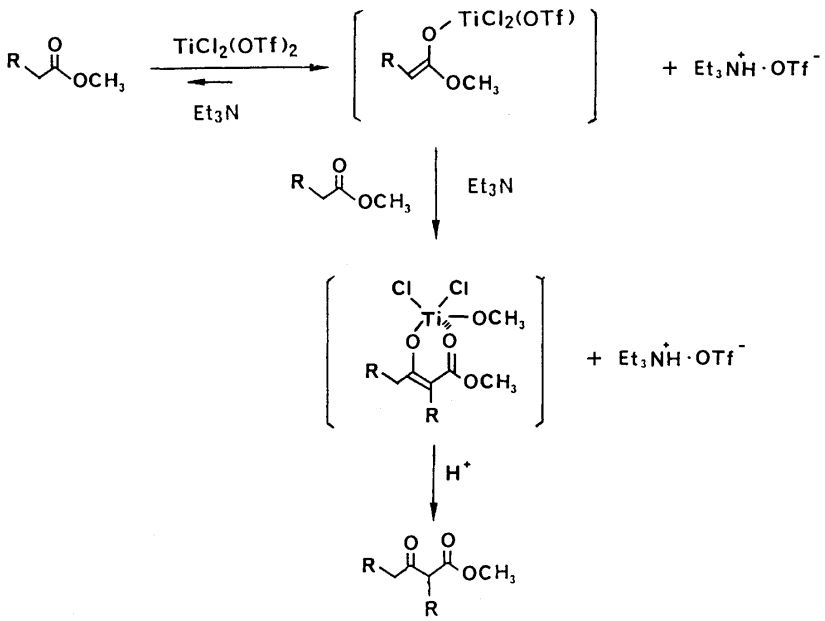

Scheme 2.

tion as depicted in Scheme 3.[12] Among them, methoxymethyl methyl adipate (**13**) was found the appropriate substrate: methoxymethyl 2-oxocyclopentanecarboxylate (**16**), the desired β-keto ester was obtaied as the main product along with a trace amount (<3%) of 2-(methoxycarbonyl)cyclopentanone. Other alkoxymethyl esters such as isopropoxymethyl methyl adipate (**19**), benzyloxymethyl methyl adipate (**20**), 1-

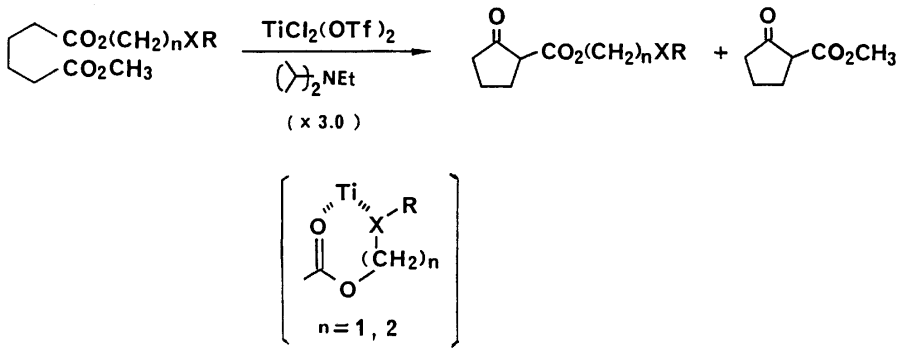

	n	XR			
13	1	OCH_3	16	83%	
14	1	SCH_3	17	22%	14%
15	2	OCH_3	18	32%	25%

Scheme 3.

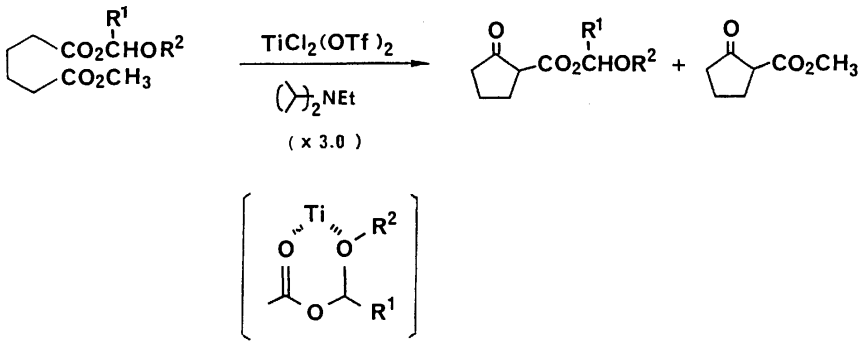

	R^1	R^2			
19	H	*i*-Pr	22	55%	5%
20	H	CH_2Ph	23	62%	12%
21	CH_3	Et	24	--	5%

Scheme 4.

Table 4. Condensation of Methoxymethyl Methyl Adipate (**13**)[a]

Entry	Aminine (equiv) vs. **13**	Conditions	Yield of **16**/%	Recovery of **13**/%
1	Triethylamine (3.0)	0 °C, 1h	31	52
2	Triethylamine (3.0)	−23 °C, 1h	45	41
3	*N*,*N*-Diisopropylethylamine (2.0)	−23 °C, 1h	69	22
4	*N*,*N*-Diisopropylethylamine (3.0)	−23 °C, 1h	83	3
5	*N*,*N*-Diisopropylethylamine (3.5)	−23 °C, 1h	82	0
6	Tributylamine (3.0)	−23 °C, 1h	62	18
7	*N*-Methylpiperidine (3.0)	−23 °C, 1h	71	7
8	*N*-Ethylpiperidine (3.0)	−23 °C, 1h	77	5
9	*N*-Ethylpiperidine (3.0)	−23 °C, 3h	83	5

a) The reaction was carried out in dichloromethane and the molar ratio of $TiCl_2(OTf)_2$: **13**=1.3 : 1.0. 2-Methoxycarbonyl-1-cyclopentanone was produced with only a trace amount in every conditions.

Table 5. Self Condensation of Methyl 3-Phenylpropionate[a)]

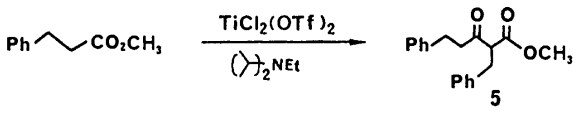

Entry	Conditions	Yield of 5/%
1	0 °C—r.t., 10 h	37
2	0 °C, 3h	15
3	−23 °C, 3h	trace

a) The reaction was carried out in CH_2Cl_2 and the molar ratio of $TiCl_2(OTf)_2$: diisopropylethylamine : methyl 3-phenylpropionate=1.3 : 3.0 : 2.0.

(ethoxymethyl)ethyl methyl adipate (**21**) were attempted, but more fruitful results were not obtaied both in yield and with selectivity (Scheme 4). The use of *N,N*-diisopropylethylamine (the Hünig base) or *N*-ethylpiperidine at −23 °C gave the best results in yield and with selectivity as shown in Table 4.

Before the investigation of intermolecular condensation, the temperature to control the undesirable self condensation of methyl esters was fixed using methyl 3-phenylpropionate as a substrate , and −23 °C was found sufficient to the purpose (Table 5). Intermolecular condensations between a variety of methyl esters and methoxymethyl esters were examined under the optimum conditions found for the intramolecular reactions (Table 6). As controlled experiments, commonly employed bases such as potassium hydride (Entry 4) and sodium methoxide (Entry 5) were examined in the same reaction,[13)] however, the condensation products were obtained in poor yield with low selectivity.

It is notable that the present method could be successfully applied to esters containing base-sensitive functional groups such as α, β-unsaturated, α-chloro, and β-siloxy esters as substrates giving the β-keto esters without the loss of their functionalities (Entries 1, 2, 9, and 10).

In summary, the present method provides the first example of the crossed type-Claisen ester condensation between two different esters (methyl ester and methoxymethyl ester) under mild acidic conditions, and that the resulting methoxymethyl esters of β-keto acids could have wider applicability in organic syntheses.

Experimental

All the melting points and the boiling points are uncorrected. The IR spectra were determined on a Hitachi Model 260-30 spectrometer. The ^1H NMR spectra were recorded with a Hitachi R-24B and a JEOL FX-90Q spectrometers with tetramethylsilane as an internal standard. The ^{19}F NMR spectra were recorded with a Hitachi R-20B spectrometer. MS and HRMS spectra were obtained with a Hitachi GC/MS M-80 instrument. Purification of products was performed by distillation or column chromatography on silica gel (Wakogel C-200 or Merck, Art. 7734), preparative TLC on silica gel (Wakogel B-5F or Merck Art. 11798).

Preparation of Dichlorobis(trifluoromethanesulfonato)-titanium(IV) (=Dichlorobis(triflato)titanium(IV)). A modified procedure of the reported method[4a)] for large scale preparation: To a stirred solution of trifluoromethanesulfonic acid (35.6 g, 0.237 mol) was added titanium(IV) chloride (5.0 g, 0.026 mol) at −50 °C with stirring under an argon atmosphere. The reaction mixture was allowed to warm to room temperature during 3 h with stirring (HCl gas was evolved). Then, sulfuryl chloride (25 ml) was

Table 6. Intermolecular Ester Condensation between Methyl Ester and Methoxymethyl Ester[a)]

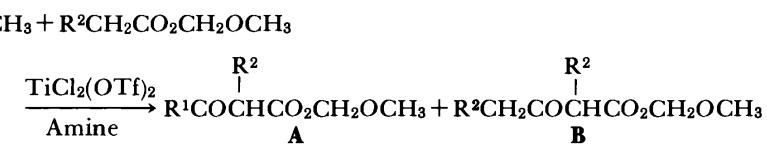

Entry	R^1	R^2	Base	Yield of	A/%	Yield of	B/%
1	PhCH=CH	Et	C[b)]	82	**24**	5	**25**
2	PhCH=CH	Et	D[c)]	76	**24**	8	**25**
3	$PhCH_2CH_2$	Et	C	83	**26**	7	**25**
4	$PhCH_2CH_2$	Et	KH[d)]	18	**26**	13	**25**
5	$PhCH_2CH_2$	Et	$NaOCH_3$[d)]	Trace		12	**25**
6	Et	Pr	C	67	**27**	8	**28**
7	*s*-Bu	Et	C	57	**29**	Trace	
8	$PhCH_2CH_2$	$BrCH_2CH_2$	C	72	**30**	15	**31**
9	$PhCH_2CH_2$	Cl	C	45	32	7	**33**
10	$PhCH_2CH_2$	*t*-Bu$(Me)_2SiOCH_3$	C	66	**34**	5	

a) The reaction was carried out in CH_2Cl_2 at −23 °C for 3 h and at 0 °C for 1 h and the molar ratio of methyl ester : methoxymethyl ester : $TiCl_2(OTf)_2$: amine=1 : 1 : 1.3 : 3.0. b) C; *N,N*-diisopropylethylamine. c) D; *N*-ethylpiperidine. d) Potassium hydride or sodium methoxide was used as a promoter in place of $TiCl_2(OTf)_2$ and amine.

added and filtered the liquid portion under an inert atmosphere. The resultant yellow powder was washed with another sulfuryl chloride (25 ml× 2) and dried up with vacumn to give 9.6 g (89%) of $TiCl_2(OTf)_2$ as powdered yellow crystals; ^{19}F NMR (hexamethylphosphoric triamide) ϕ=77.5 (6F, s, trichlorofluoromethane as an external standard). The quality was checked by the comparison with hexafluorobenzene as an internal standard.

Preparation of Methyl 3-Hydroxy-2-methyl-3-phenylpropionate (1). To a stirred solution of diisopropylamine (1.11 g, 11 mmol) in THF (20 ml) was added 6.9 ml of BuLi in hexane (1.60 M; 1 M=1 mol dm^{-3}) at 0 °C under an nitrogen atmosphere. After 15 min, the resultant mixture was cooled to −78 °C, and methyl propionate (0.88 g, 10 mmol) in THF (5 ml) was added dropwise, followed by stirring at the same temperature for 30 min. Then, benzaldehyde (1.17 g, 11 mmol) in THF (5 ml) was added dropwise and stirred for 1 h at −78 °C. The reaction mixture was poured onto 1 M HCl aq (20 ml) and extracted with ether (20 ml×2). The combined extracts were washed with water and brine and dried ($MgSO_4$). Removal of the solvent under reduced pressure and distilled gave 1.33 g (66%) of **1**: bp 125 °C (oven temp)/0.60 mmHg (1mmHg=133.3Pa), (lit,[14] 100—103 °C/0.50 mmHg); IR (neat) 3300, 1690 cm^{-1}; ^1H NMR ($CDCl_3$) δ=0.90, 1.05 (total 3H, d, d, J=7.0, 6.0 Hz), 2.40—2.90 (1H, m), 3.45, 3.53 (total 3H, s, s), 4.55, 5.85 (total 1H, d, d, J= 9.0, 5.0 Hz). 6.80—7.25 (5H, m).

Intramolecular Condensation of Dimethyl Adipate: A Typical Procedure. To a stirred suspension of $TiCl_2(OTf)_2$ (415 mg, 0.99 mmol) and Molecular Sieves 4A (1.0 g) in dichloromethane (2.0 ml) was added dimethyl adipate (116 mg, 0.66 mmol) in dichloromethane (0.5 ml) at 0 °C under an argon atmosphere. Then, triethylamine (220 mg, 2.18 mmol) in dichloromethane (1 ml) was added dropwise to the mixture. After being stirred at room temperature for 2 h, the reaction was quenched with phosphate buffer (pH 7.0). The organic phase was separated by Celite filtration and washed with water and dried (Na_2SO_4). Removal of the solvent under reduced pressure and purified with column chromatography using hexane–ethyl acetate (5 : 1) gave 81 mg (80%) of 2-(methoxycarbonyl)cyclopentanone. IR (neat) 1720, 1750 cm^{-1}; ^1H NMR ($CDCl_3$) δ=1.60—2.50 (6H, m), 3.00—3.50 (1H, m), 3.75 (3H, s,).

2-(Methoxycarbonyl)cyclohexanone[16] (6): IR (neat) 1700 cm^{-1}; ^1H NMR ($CDCl_3$) δ=1.50—2.60 (8H, m), 3.10—3.50 (1H, m), 3.75 (3H, 2).

2-Ethoxycarbonyl-5-methylcyclopentanone[17] (7): IR (neat) 1720, 1750 cm^{-1}; ^1H NMR ($CDCl_3$) δ=0.85—1.30 (6H, m), 1.50—2.40 (5H, m), 2.95—3.40 (1H, m), 4.00 (2H, q, J=7.0 Hz).

Intermolecular Ester Condensation. A similar procedure of intramolecular condensation of dimethyl adipate except the following conditions; (1) the mixture of the substrates and acylating reagents were added spontaneously to the suspension of $TiCl_2(OTf)_2$, (2) the temperature and the reaction time were shown in Table 3.

Methyl 2-Methyl-3-oxovalerate[15] (3): IR (neat) 1720 cm^{-1}; ^1H NMR ($CDCl_3$) δ=1.00 (3H, t, J=7.0 Hz), 1.25 (3H, d, J=7.0 Hz), 2.45 (2H, q, J=7.0 HZ), 3.55 (1H, q, J=7.0 Hz), 3.80 (3H, s).

Ethyl 2-Methyl-3-oxovalerate[16] (4): IR (neat) 1720 cm^{-1}; ^1H NMR ($CDCl_3$) δ=1.00 (3H, J=7.0 Hz), 1.15—1.50 (6H, m), 2.45 (2H, q, J=7.0 Hz), 3.55 (1H, q, J=7.0 Hz), 4.25 (2H, q, J=7.0 Hz).

Methyl 2-Benzyl-5-phenyl-3-oxovalerate (5): IR (neat) 1715, 1740 cm^{-1}; ^1H NMR ($CDCl_3$) δ=2.55—2.75 (4H, m), 3.00 (2H, d, J=8.0 Hz), 3.45 (3H, s), 3.60 (1H, t, J= 8.0 Hz), 6.80—7.10 (10H, m); HRMS, Found: m/z 296.1427. Calcd for $C_{19}H_{20}O_3$:M, 296.1414.

Methyl 2-Benzyl-3-oxo-3-phenylpropionate (8): IR (neat) 1690, 1720 cm^{-1}; ^1H NMR ($CDCl_3$) δ=3.15 (2H, d, J=7.0 Hz), 3.45 (3H, s), 4.40 (1H, t, J=7.0 Hz), 6.80—7.80 (10 H, m); HRMS, Found: m/z 268.1096. Calcd for $C_{17}H_{16}O_3$: M, 268.1100.

Methyl 2-Formyl-3-phenylpropionate (9): IR (neat) 1720 cm^{-1}; ^1H NMR ($CDCl_3$) δ=2.90—3.35 (2H, m), 3.45—3.55 (0.3 H, m; methylene), 3.55 (3H, s), 6.80—7.20 (5.7H, m), 9.50 (0.3H, d, J=2.0 Hz; aldehyde), 11.30 (0.7H, d, J=12.0 Hz; enol); HRMS, Found: m/z 191.9951. Calcd for $C_{11}H_{12}O_3$: M, 191.9942.

Methyl 2-Benzyl-3,4-dioxobutyrate (10): IR (neat) 1720 cm^{-1}; ^1H NMR ($CDCl_3$) δ=2.90—3.35 (2H, m), 3.40—3.55 (1H, m), 3.55 (3H, s), 6.80—7.20 (5H, m), 10.05 (1H, s); HRMS, Found: m/z 220.0720. Calcd for $C_{12}H_{12}O_4$: M, 220.0735.

2-Benzoyl-γ-butyrolactone (11): Mp 54—56 °C, (lit,[18] 57 °C); IR (Nujol) 1680, 1760 cm^{-1}; ^1H NMR ($CDCl_3$) δ=2.10—3.10 (2H, m), 4.10—4.60 (3H, m), 7.10—8.10 (5H, m).

2-Formyl-γ-butyrolactone (12): Mp 72 °C, (lit,[19] 72.5—73.5 °C); IR (neat) 1740 cm^{-1}; ^1H NMR ($CDCl_3$) δ=2.20—3.20 (2H, m), 4.20—4.55 (2H, m), 6.80 (1H, d, J=12.0 Hz), 11.50 (1H, d, J=12.0 Hz).

Methoxymethyl Methyl Adipate (13): To a stirred solution of methyl hydrogen adipate (3.20 g, 20 mmol) and triethylamine (2.45 g, 24 mmol) in *N,N*-dimethylformamide (50 ml) chloromethyl methyl ether (1.93 g, 24 mmol) was added at 0 °C. After being stirred at room temperature for 10 h, the reaction mixture was quenched with water and extracted with ether (50 ml×2). The combined extracts were washed with water and brine, dried (Na_2SO_4), and condensed under reduced pressure. The crude product was distilled to give 3.30 g (81 %) of **13**. Bp 145 °C (oven temp)/0.07 mmHg; IR (neat) 1740, 1140 cm^{-1}; ^1H NMR ($CDCl_3$) δ=1.50—1.85 (4H, m), 2.05—2.50 (4H, m), 3.35 (3H, s), 3.55 (3H, s), 5.10 (2H, s); HRMS, Found: m/z 204.1016. Calcd for $C_9H_{16}O_5$: M, 204.0999.

Methylthiomethyl Methyl Adipate (14): By a similar procedure of preparation of **13**, the reaction of methyl hydrogen adipate (3.20 g, 20 mmol) and chloromethyl methyl sulfide (2.12 g, 22 mmol) gave 3.74 g (85%) of **14**. Bp 180 °C (oven temp)/0.1 mmHg; IR (neat) 1740, 1140 cm^{-1}; ^1H NMR ($CDCl_3$) δ= 1.45—1.85 (4H, m), 2.00 (3H, s), 2.10—2.55 (4H, m), 3.55 (3H, s), 4.95 (2H, s); HRMS, Found: m/z 220.0786. Calcd for $C_9H_{16}O_4S$: M, 220.0771.

2-Methoxylethyl Methyl Adipate (15): By a similar procedure of preparation of **13**, the reaction of methyl hydrogen adipate (3.20 g, 20 mmol) and iodoethyl methyl ether (4.09 g, 22 mmol) gave 3.83 g (88%) of **15**. Bp 150 °C (oven temp)/0.1 mmHg; IR (neat) 1720, 1120 cm^{-1}; ^1H NMR ($CDCl_3$) δ=1.45—1.90 (4H, m), 2.05—2.55 (4H, m), 3.35 (3H, s), 3.50—3.70 (2H, m), 3.55 (3H, s), 4.20—4.40 (2H, m); HRMS, Found: m/z 218.1141. Calcd for $C_{10}H_{18}O_5$: M, 218.1156.

The Selective Intramolecular Dieckmann Condensation: A Typical Procedure. To a stirred suspension of $TiCl_2$-

$(OTf)_2$ (417 mg, 1.00 mmol) in dichloromethane (2.0 ml) was added *N,N*-diisopropylethylamine (297 mg, 2.3 mmol) in dichloromethane (1 ml) at −23 °C under an argon atmosphere. Then methoxymethyl methyl adipate **13** (157 mg, 0.77 mmol) in dichloromethane (1.0 ml) was added dropwise to the mixture. After being stirred at −23 °C for 1 h, the reaction was quenched with phosphate buffer (pH 7.0). The organic phase was separated by Celite filtration and washed with water and dried (Na_2SO_4). Removal of the solvent under reduced pressure and purified with thin layer chromatography using hexane-ethyl acetate (3 : 1) gave 110 mg (83%) of methoxymethyl 2-oxocyclopentanecarboxylate **16**, and 4.7 mg (3%) of **13** which was recovered. IR (neat) 1750, 1720, 1140 cm^{-1}; ^1H NMR ($CDCl_3$) δ=1.90—2.50 (6H, m), 2.90—3.30 (1H, m), 3.35 (3H, s), 5.15 (2H, s); HRMS, Found: *m/z* 172.0731. Calcd for $C_8H_{12}O_4$: M, 172.0735.

Methylthiomethyl 2-Oxocyclopentanecarboxylate (17): IR (neat) 1750, 1140 cm^{-1}; ^1H NMR ($CDCl_3$) δ=1.80—2.50 (6H, m), 2.05 (3H, s), 2.90—3.30 (1H, m), 5.00 (2H, s); HRMS, Found: *m/z* 188.0880. Calcd for $C_8H_{12}O_3S$: M, 188.0892.

2-Methoxyethyl 2-Oxocyclopentanecarboxylate (18): IR (neat) 1750, 1140 cm^{-1}; ^1H NMR ($CDCl_3$) δ=1.90—2.55 (6H, m), 2.90—3.30 (1H, m), 3.55 (3H, s), 3.55—3.70 (2H, m), 4.20—4.45 (2H, m); HRMS, Found: *m/z* 186.0899. Calcd for $C_9H_{14}O_4$: M, 186.0892,

Isopropoxymethyl Methyl Adipate (19): By a similar procedure of preparation of **13**, the reaction of methyl hydrogen adipate (3.20 g, 20 mmol) and chloromethyl isopropyl ether (2.60 g, 24 mmol) gave 3.85 g (83%) of **19**. IR (neat) 1740, 1130 cm^{-1}; ^1H NMR ($CDCl_3$) δ=1.15 (6H, d, *J*=7.0 Hz), 1.30—1.80 (4H, m), 2.00—2.40 (4H, m), 3.55 (3H, s), 3.60 (1H, m), 5.10 (2H, s); HRMS, Found: *m/z* 232.1332. Calcd for $C_{11}H_{20}O_5$: M, 232.1312,

Benzyloxymethyl Methyl Adipate (20): By a similar procedure of preparation of **13**, the reaction of methyl hydrogen adipate (3.20 g, 20 mmol) and chloromethyl benzyl ether (3.75 g, 24 mmol) gave 4.60 g (83%) of **20**. Bp 155—159 °C/0.3 mmHg; IR (neat) 1740, 1130 cm^{-1}; ^1H NMR ($CDCl_3$) δ=1.30—1.70 (4H, m), 2.00—2.30 (4H, m), 3.50 (3H, s), 4.50 (2H, s), 5.15 (2H, s), 7.00—7.20 (5H, m); HRMS, Found: *m/z* 280.1330. Calcd for $C_{15}H_{20}O_5$: M, 280.1312.

1-Ethoxyethyl Methyl Adipate (21): To a stirred solution of methyl hydrogen adipate (3.20 g, 20 mmol) and a catalytic amount of *p*-toluenesulfonic acid (ca. 20 mg) in ether (40 ml) was added ethyl vinyl ether (1.59 g, 22 mmol) at room temperature. After 1 h the reaction mixture was quenched with saturated $NaHCO_3$ aq and extracted with ether (50 ml). The extract was washed with water and brine, dried (Na_2SO_4), and condensed under reduced pressure. The crude product was distilled to give 3.11 g (67%) of **21**. Bp 180 °C (oven temp)/0.15 mmHg; IR (neat) 1720 cm^{-1}; ^1H NMR ($CDCl_3$) δ=1.10 (3H, t, *J*=7.0 Hz), 1.30 (3H, d, *J*=7.0 Hz), 1.30—1.65 (4H, m), 2.00—2.45 (4H, m), 3.20—3.60 (2H, m), 3.50 (3H, s), 5.75 (1H, q, *J*=7.0 Hz); HRMS, Found: *m/z* 232.1318. Calcd for $C_{11}H_{20}O_5$: M, 232.1312.

Isopropoxymethyl 2-Oxocyclopentanecarboxylate (22): IR (neat) 1740, 1715, 1140 cm^{-1}; ^1H NMR ($CDCl_3$) δ=1.50 (6H, d, *J*=7.0 Hz), 1.90—2.50 (6H, m), 2.90— 3.30 (1H, m), 3.70—4.10 (1H, m), 5.20 (2H, s); HRMS, Found: *m/z* 200.1052. Calcd for $C_{10}H_{16}O_4$: M, 200.1049.

Benzyloxymethyl 2-Oxocyclopentanecarboxylate (23): IR (neat) 1720, 1140 cm^{-1}; ^1H NMR ($CDCl_3$) δ=1.80—2.50 (6H, m), 2.80—3.20 (1H, m), 4.50 (2H, s), 5.25 (2H, s), 7.10—7.30 (5H, m); HRMS, Found: *m/z* 248.1044. Calcd for $C_{14}H_{16}O_4$: M, 248.1049.

Preparation of Methoxymethyl Esters: By a similar procedure of the preparation of **13**.

Methoxymethyl Butyrate: IR (neat) 1730 cm^{-1}; ^1H NMR δ=0.80 (3H, t, *J*=7.0 Hz), 1.10—1.80 (2H, m), 1.90—2.30 (2H, m), 3.30 (3H, s), 5.10 (2H, s); HRMS, Found: *m/z* 132.0777. Calcd for $C_6H_{12}O_3$: M, 132.0786.

Methoxymethyl Valerate: IR (neat) 1730 cm^{-1}; ^1H NMR δ=0.80 (3H, t, *J*=7.0 Hz), 1.00—2.35 (6H, m), 3.30 (3H, s), 5.10 (2H, s); HRMS, Found: *m/z* 146.0955. Calcd for $C_7H_{14}O_3$: M, 146.0943.

Methoxymethyl 4-Bromovalerate: Bp 135 °C (oven temp)/19 mmHg; IR (neat) 1730 cm^{-1}; ^1H NMR δ=1.90—2.70 (4H, m), 3.30 (3H, s), 3.50 (2H, t, *J*=7.0 Hz), 5.10 (2H, s); HRMS, Found: *m/z* 209.9881. Calcd for $C_7H_{14}BrO_3$: M, 209.9891.

Methoxymethyl 2-Chloroacetate: Bp 135 °C (oven temp)/19 mmHg. IR (neat) 1730 cm^{-1}; ^1H NMR δ=3.55 (3H, s), 4.00 (2H, s), 5.25 (3H, s); HRMS, Found: *m/z* 138.0088. Calcd for $C_4H_7ClO_3$: M, 138.0084.

Methoxymethyl 3-(*t*-Butyldimethylsiloxy)propionate: IR (neat) 1715, 1140 cm^{-1}; ^1H NMR δ=0.15 (6H, s), 0.80 (9H, s), 2.55 (2H, t, *J*=7.0 Hz), 3.60 (2H, t, *J*=7.0 Hz), 3.30 (3H, s), 5.10 (2H, s); HRMS, Found: *m/z* 248.1441. Calcd for $C_{11}H_{24}O_4Si$: M, 248.1444.

The Selective Intermolecular Condensation between Methoxymethyl Ester and Methyl Ester: A similar method of the intramolecular condensation except the point that the mixture of methoxymethyl ester and methyl ester was added.

Methoxymethyl 2-Ethyl-3-oxo-5-phenyl-4-pentenoate (24): IR (neat) 1715, 1140 cm^{-1}; ^1H NMR δ=0.75 (3H, t, *J*=7.0 Hz), 1.35—2.00 (2H, m), 3.55 (3H, s), 3.70 (1H, t, *J*=7.0 Hz), 5.15 (2H, s), 6.75 (1H, d, *J*=16 Hz), 6.90—7.60 (5H, m); HRMS, Found: *m/z* 262.1222. Calcd for $C_{15}H_{18}O_4$: M, 262.1206.

Methoxymethyl 2-Ethyl-3-oxohexanoate (25): IR (neat) 1720, 1140 cm^{-1}; ^1H NMR δ=0.60—1.00 (3H, t, *J*=7.0 Hz), 1.05—2.00 (2H, m), 3.15 (1H, t, *J*=7.0 Hz), 3.55 (3H, s), 5.10 (2H, s); HRMS, Found: *m/z* 188.1057. Calcd for $C_9H_{16}O_4$: M, 188.1049.

Methoxymethyl 2-Ethyl-3-oxo-5-phenylvalerate (26): IR (neat) 1720, 1140 cm^{-1}; ^1H NMR δ=0.75 (3H, t, *J*=7.0 Hz), 1.35—2.00 (2H, m), 2.70 (4H, brs), 3.15 (1H, t, *J*=7.0 Hz), 3.55 (3H, s), 5.10 (2H, s), 6.90—7.30 (5H, m); HRMS, Found: *m/z* 264.1348. Calcd for $C_{15}H_{20}O_4$: M, 264.1363.

Methoxymethyl 3-Oxo-2-propylvalerate (27): IR (neat) 1720, 1140 cm^{-1}; ^1H NMR δ=0.60—1.05 (5H, m), 1.10—1.90 (5H, m), 2.05—2.50 (2H, m), 3.15 (1H, t, *J*= 7.0 Hz), 3.55 (3H, s), 5.10 (2H, s); HRMS, Found: *m/z* 202.1994. Calcd for $C_{10}H_{18}O_4$: M, 202.1205.

Methoxymethyl 3-Oxo-2-propylheptanoate (28): IR (neat) 1720, 1140 cm^{-1}; ^1H NMR δ=0.60—1.90 (14H, m), 2.05—2.55 (2H, m), 3.15 (1H, t, *J*=7.0 Hz), 3.55 (3H, s), 5.10 (2H, s); HRMS, Found: *m/z* 230.1496. Calcd for $C_{12}H_{22}O_4$: M, 230.1519.

Methoxymethyl 2-Ethyl-4-methyl-3-oxohexanoate (29): IR (neat) 1720, 1140 cm^{-1}; ^1H NMR δ=0.60—1.90 (14H, m), 2.05—2.55 (2H, m), 3.15 (1H, t, *J*=7.0 Hz), 3.55 (3H, s), 5.10 (2H, s); HRMS, Found: *m/z* 230.1505. Calcd for $C_{12}H_{22}O_4$: M, 230.1519.

Methoxymethyl 2-(2-Bromoethyl)-3-oxo-5-phenylvalerate (30): IR (neat) 1720, 1140 cm^{-1}; ^1H NMR δ=2.10—2.40

(2H, m), 2.70 (4H, brs), 3.15 (1H, t, J=7.0 Hz), 3.55 (3H, s), 3.60—3.85 (2H, m), 5.10 (2H, s), 6.90—7.30 (5H, m); HRMS, Found: m/z 343.0483. Calcd for $C_{15}H_{19}O_4Br$: M, 343.0468.

Methoxymethyl 6-Bromo-2-(2-bromoethyl)-3-oxohexanoate (31): IR (neat) 1720, 1140 cm^{-1}; ^{1}H NMR δ=1.90—3.90 (11H, m), 3.55 (3H, s), 5.10 (2H, s); HRMS, Found: m/z 358.9508. Calcd for $C_{10}H_{16}O_4Br_2$: M, 358.9494.

Methoxymethyl 2-Chloro-3-oxo-5-phenylvalerate (32): IR (neat) 1720, 1140 cm^{-1}; ^{1}H NMR δ=2.70 (4H, brs), 3.55 (3H, s), 4.80 (1H, s), 5.15 (2H, s), 6.90—7.30 (5H, m); HRMS, Found: m/z 270.0675. Calcd for $C_{13}H_{15}O_4Cl$: M, 270.0660.

Methoxymethyl 2,4-Dichloro-3-oxobutyrate (33): IR (neat) 1720, 1140 cm^{-1}; ^{1}H NMR δ=3.55 (3H, s), 4.30 (2H, s), 4.80 (1H, s), 5.15 (2H, s); HRMS, Found: m/z 213.9813. Calcd for $C_6H_8O_4Cl$: M, 213.9801.

Methoxymethyl 2-(*t*-Butyldimethylsiloxy)-3-oxo-5-phenylvalerate (34): IR (neat) 1720, 1140 cm^{-1}; ^{1}H NMR δ=0.15 (6H, s), 0.80 (9H, s), 2.70 (4H, brs), 3.55 (1H, m), 3.20—3.90 (2H, m), 3.55 (3H, s), 5.10 (2H, s), 6.90—7.30 (5H, m); HRMS, Found: m/z 364.2055. Calcd for $C_{20}H_{32}O_4Si$: M, 364.2071.

The author wish to express his thanks to Professor Teruaki Mukaiyama of Science University of Tokyo for his helpful discussions throughout this work.

References

1) a) J. March, "Advanced Organic Chemistry," 3rd ed, McGrawhill, Inc., New York (1985), pp. 437—443; b) H. O. House, "Modern Synthetic Reaction," 2nd ed, W. A. Benjamin, Inc., Menlo Park, California (1972), pp. 740—745; c) C. R. Hauser and B. E. Hudson Jr., *Org. React.*, **1**, 266 (1942) (the Claisen condensation); d) J. P. Schaefer and J. J. Bloomfield, *Org. React.*, **15**, 1 (1967) (the Dieckmann condensation).

2) One feasible solution to these complexities could be found in the reaction between ketene silyl acetals and acid chlorides which afford the desired β-keto esters. For example, see: M. W. Rathke and D. F. Sullivan, *Tetrahedron Lett.*, **1973**, 1297. This method, however, requiers preceding preparation of ketene silyl acetals, and in addition, it is difficult to conduct the reaction in the case of intramolecular (the Dieckmann) condensation.

3) Preliminary work of these reactions has been reported as communications: Y. Tanabe and T. Mukaiyama, *Chem. Lett.*, **1984**, 1867; Y. Tanabe and T. Mukaiyama, *ibid.*, **1986**, 1813.

4) a) R. E. Noftle and G. H. Cady, *Inorg. Chem.*, **5**, 2182 (1966); b) M. Schmei β er, P. Sartori, and B. Lippsmeier, *Chem. Ber.*, **103**, 868 (1970).

5) Dialkylboryl triflate: a) T. Mukaiyama and T. Inoue, *Chem. Lett.*, **1976**, 559; b) S. Masamune, H. Hirama, S. Mori, S. A. Ali, and D. S. Garvey, *J. Am. Chem. Soc.*, **103**, 1568 (1981). Tin(II) triflate: c) T. Mukaiyama, R. W. Stevens, and N. Iwasawa, *Chem. Lett.*, **1982**, 353; d) T. Mukaiyama, N. Iwasawa, R. W. Stevens, and T. Haga, *Tetrahedron*, **40**, 1381 (1984); e) T. Mukaiyama and N. Iwasawa, *Chem. Lett.*, **1984**, 753; f) T. Yura, N. Iwasawa, and T. Mukaiyama, *Chem. Lett.*, **1986**, 187; g) T. Mukaiyama, N. Iwasawa, T. Yura, and R. S. J. Clark, *Tetrahedron*, **43**, 5003 (1987); h) T. Yura, N. Iwasawa, K. Narasaka, and T. Mukaiyama, *Chem. Lett.*, **1988**, 1025. For other application using metal triflates, see: i) E. J. Corey and K. Shimoji, *Tetrahedron Lett.*, **24**, 169 (1983). (zinc triflate and magnesium triflate); j) M. P. Doyle and M. L. Trudell, *J. Org. Chem.*, **49**, 1196 (1984). (cupric triflate); k) E. J. Corey and E. M. Eckrich, *Tetrahedron Lett.*, **25**, 2415 (1984), G. E. Keck, E. J. Enholm, and D. F. Kachensky, *ibid.*, **25**, 1867 (1984). (tributylstannyl triflate); l) N. Minowa and T. Mukaiyama, *Chem. Lett.*, **1987**, 1719. (aluminum triflate).

6) R. D. Howells and J. D. McCown, *Chem. Rev.*, **77**, 69 (1977).

7) Dichlorobis(triflato)titanium(IV) was prepared by the reported procedure according to Ref. 4a. It is easy to handle lemon yellow powder that can be prepared in large quantity and be stored for many weeks under an inert atmosphere.

8) J. R. Daliziel, R. D. Klett, P. A. Yeats, and F. Aubke, *Can. J. Chem.*, **52**, 231 (1974).

9) U. Thewalt and H. P. Klein, *Z. Kristallografiya*, **153**, 307 (1980).

10) Recently an another approach to the site-selective Claisen condensation employing polyanions of β-keto esters has been explored: a) Y. Yamaguchi, K. Shibato, and I. Hirao, *Chem. Lett.*, **1985**, 1145. b) Y. Yamaguchi, *Yuki Gosei Kagaku Kyokai Shi*, **45**, 969 (1987).

11) An another method of the regiocontrolled Dieckmann condensation employing half thiol esters was reported: a) Y. Yamada, T. Ishii, M. Kimura, and K. Hosaka, *Tetrahedron Lett.*, **22**, 1353 (1981); b) M. Hatanaka, Y. Yamamoto, H. Nitta, and T. Ishimaru, *ibid.*, **22**, 3883 (1981); c) Y. Nagao, T. Nakamura, M. Ochiai, K. Fuji, and E. Fujita, *Chem. Lett.*, **1987**, 1861.

12) Alkoxymethyl esters could be prepared easily from the corresponding carboxylic acids and chloromethyl alkyl ethers. For example, see: T. W. Green, "Protective Groups in Organic Synthesis," John Wiley and Sons, New York (1981), pp. 159—160. Other methods are cited therein.

13) These reactions were carried out according to the known procedure: D. C. Roberto and S. M. McElvain, *J. Am. Chem. Soc.*, **59**, 2007 (1937) (sodium methoxide); C. A. Brown, *Synthesis*, **1975**, 326 (potassium hydride).

14) P. L. Creger, *Tetrahedron Lett.*, **1972**, 79.

15) E. E. Royals, *J. Am. Chem. Soc.*, **70**, 489 (1948).

16) G. Stork, A. Brizzolara, H. Landesman, J. Szmuszkovics, and R. Terrell, *J. Am. Chem. Soc.*, **85**, 207 (1963).

17) L. Nicole and L. Berlinguet, *Can. J. Chem.*, **40**, 353 (1962).

18) H. O. House and J. W. Blaker, *J. Org. Chem.*, **23**, 334 (1958).

19) F. Korte and H. Machleidt, *Chem. Ber.*, **88**, 136 (1955).

Reactions of Sodium Salts of Tosylhydrazones of 2- and 3-Thiophenecarbaldehydes, 1-Methyl-2-pyrrolecarbaldehyde, and Furfural with Acrylonitrile

Katsuhiro SAITO,* Tatsuji SATO, Hiraku ISHIHARA, and Kensuke TAKAHASHI
Department of Applied Chemistry, Nagoya Institute of Technology, Gokiso-cho, Showa-ku, Nagoya 466
(Received November 11, 1988)

Reactions of the sodium salts of tosylhydrazones of several heteroaromatic aldehydes with an equimolar amount of acrylonitrile afforded the corresponding cyclopropane derivatives as the major products accompanied by small amounts of pyrazole derivatives. On the other hand, reactions using ten-molar equivalents of acrylonitrile gave pyrazole derivatives as major products.

Much effort has been devoted to the investigation of the reactivities of tosylhydrazones which generate carbenes via diazo compounds. It is known that the reactivities of the diazo compounds or the carbenes are influenced by conjugation with unsaturated moieties.[1] Many papers have been published on the chemistry of tosylhydrazones conjugated with olefinic, aromatic, or carbonyl moieties, while detailed reports on the chemistry of tosylhydrazones conjugated with heterocyclic moieties have been relatively few.[2]

Previously, Shechter reported that the carbenes generated from the tosylhydrazones of furfural or thiophenecarbaldehyde inserted into the C-H bonds of alkanes or rearranged into unstable acetylene derivatives.[3] Maas[4] has documented the addition reactions of olefins with carbenes conjugated with furan, thiophene, or pyridine moieties to give cyclopropanes. The authors have investigated the reactivities of tosylhydrazones conjugated with heterocyclic moieties and reported 1,3 N-C migration of the tosyl group or nucleophilic and stereospecific additions of the carbenes generated from the tosylhydrazones.[5] As one part of our these studies, we investigated the reactions of tosylhydrazones conjugated with thiophene, pyrrole, and furan moieties with acrylonitrile. Here, the results are discussed.

Results and Discussion

The reaction of sodium salt of 2-thiophenecarbaldehyde tosylhydrazone (**1a**) with an equimolar amount of acrylonitrile (**2**) was carried out in anhydrous diglyme at 120 °C for 20 min. A thin-layer chromatographic separation and purification of the reaction mixture afforded a 1 : 1 mixture of *cis*-**3a** and *trans*-cyclopropane **4a** derivatives and a pyrazoline derivative **5a** in 65.0 and 9.1% yields, respectively. A similar reaction, but using ten-molar equivalents of **2**, afforded a pyrazoline derivative **6a** and a pyrazole derivative **7a** in 45.1 and 6.1% yields, respectively. A

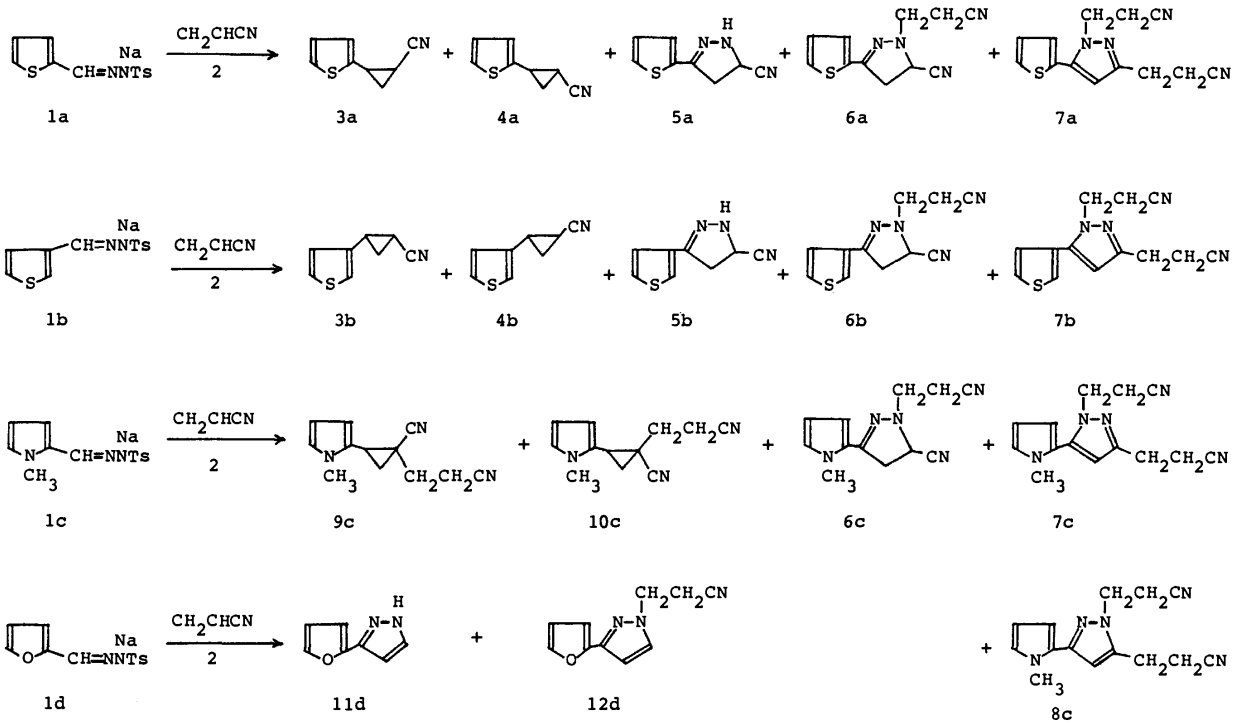

Fig. 1.

reaction with sodium salt of 3-thiophenecarbaldehyde tosylhydrazone (**1b**) gave almost the same result as mentioned above; a reaction of **1b** with an equimolar amount of **2** afforded a 1 : 1 mixture of cyclopropanes, **3b** and **4b**, and a pyrazoline derivative **5b** in 67.3 and 19.7% yields, respectively. A reaction of **1b** with ten-molar equivalents of **2** gave a pyrazoline derivative **6b** and a pyrazole derivative **7b** in 50.1 and 8.9% yields, respectively.

The same type of reaction using sodium salt of 1-methyl-2-pyrrolecarbaldehyde tosylhydrazone (**1c**) with an equimolar amount of **2** afforded no isolatable product. However, the employment of a large excess amount of acrylonitrile gave a better result, as follows. A reaction of **1c** with ten-molar equivalents of **2** yielded a cyclopropane derivative **9c**, a pyrazoline derivative **6c**, and pyrazole derivatives, **7c** and **8c**, in 6.5, 5.6, 3.1, and 4.9% yields, respectively. A reaction with twenty-molar equivalents of **2** promoted the product yields to give **9c**, **10c**, **6c**, **7c**, and **8c** in 18.8, 6.6, 18.6, 4.0, and 3.9% yields, respectively.

No cyclopropane derivatives were detected in the reaction of sodium salt of furfural tosylhydrazone (**1d**). A reaction of **1d** with an equimolar amount of **2** afforded pyrazole derivatives, **11d** and **12d**, each in 1.1% yield; these yields were improved by using ten-molar equivalents of **2** to 2.2 and 11.1%, respectively.

The structures of the products were deduced on the basis of their spectral properties and a comparison of the NMR spectra with those of the analogous compounds.[6] The absorption maxima in the UV spectra of **5a**, **b** and **6a**, **b** (ca. 290 nm), which appear at longer wavelengths than those of **3a**, **b** and **4a**, **b** (238 nm) or thiophene (231 nm), show that these pyrazoline derivatives have double bonds conjugated with the heterocyclic moieties.

The structures of **7c** and **8c** were deduced by measurements of the nuclear overhauser effect in their NMR spectra, as follws. Irradiation of the methylene protons of the *N*-substituted cyanoethyl group of **7c** caused a 10% growth of the signal of the 3-position proton of the pyrrole ring, though the peak of the other cyanoethyl group showed no change, as shown in Fig. 2. On the other hand, a corresponding irradiation of **8c** resulted in a 15% enhancement of the peak of the other cyanoethyl moiety but did not effect on the ring protons. The structures of **7a** and **7b** were assigned on the basis of a comparison of their ^{1}H NMR and ^{13}C NMR spectra with those of **7c** and **8c**.

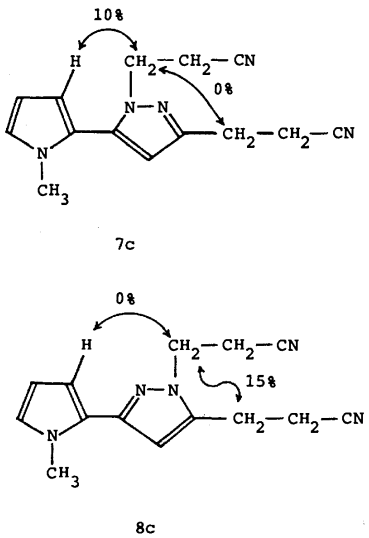

Fig. 2.

The stereochemistries of **9c** and **10c** are not clear, but considering the steric size of cyanoethyl and cyano groups, the major product **9c** is thought to have a pyrrole group and a cyanoethyl group as a trans-configuration, as shown in the figure.

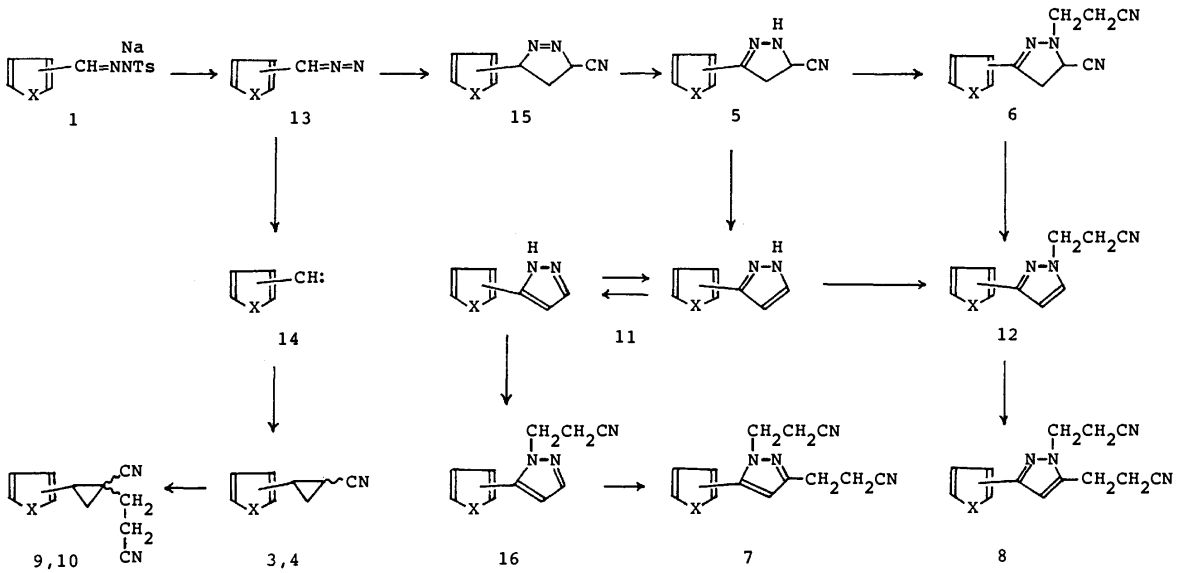

Fig. 3.

The reaction is considered to proceed as follows.[7] The thermolysis of **1** generates the diazo compound **13**, which further decomposes to carbene **14**, and adds to **2** to give **3** and **4**.[8] The cyclopropane derivatives, **9** and **10**, are considered to be formed through reactions of **3** and **4** with **2**. A 1,3-dipolar addition of **13** to **2** gives **5** via an intermediate **15**. An aromatization of **5**, leaving hydrogen cyanide, forms **11**. A nucleophilic attack of **5** to **2** can give **6**, which then aromatizes to **12** leaving hydrogen cyanide. The pyrazole derivatives **7** and **8** are considered to be derived through **11** and **12**, respectively.

There is a possibility of the formation of cyclopropane derivatives (**3**, **4**) from **15** via a loss of nitrogen. In order to examine this possibility, a reaction of **1b** with ten-molar equivalents of **2** was carried out in a five-fold diluted concentration. The products were a 38.0% yield of **6b** and a 21.3% yield of **7b**; no cyclopropane derivatives were detected at all. This fact shows that the cyclopropane derivatives were formed via a reaction of carbene **14** but not via **15**.

In the presence of an excess amount of acrylonitrile, the diazo compound **13** reacts with acrylonitrile to give pyrazoline- or pyrazole-type products. If there is no such excess amount of acrylonitrile, **13** further decomposes to the carbene to give cyclopropane-type products.

It has been reported that in a reaction of **1** with stilbene, dimethyl fumarate, dimethyl maleate, or styrene derivatives, neither pyrazoline nor pyrazole derivatives were detected; only cyclopropane derivatives were afforded.[5] The difference between the above-mentioned result and the present result can be considered to be attributable to the high reactivity of acrylonitrile to diazo compounds.

The product yields of the reaction of **1d** were poor. One of the reasons for this phenomenon is considered to be the liability of the furyl ring to ring opening. Shechter reported that the ring in carbene **14d** can very easily be opened and rearranged to a very unstable acetylene derivative.[3] In the present reaction, **1d** is thought to generate the unreactive diazo compound **13d**, which then forms carbene; it then decomposes to resinous materials via an unstable acetylene derivative.

Experimental

Melting points were recorded on a Yanagimoto Micro Melting Point Apparatus and are uncorrected. NMR spectra were measured with a Varian XL 200 or a Hitachi R-20B spectrometer with tetramethylsilane as an internal standard. UV and IR spectra were measured with Hitachi 220A and JASCO A-102 spectrometers, respectively. Mass spectra were measured with a Hitachi M-52 or a JMS-DX300 spectrometer. Wako gel B5F was used for thin-layer chromatography. Diglyme was distilled from calcium hydride and stored on Molecular Sieves 3A 1/16.

Reaction of 1a with an Equimolar Amount of 2. A typical reaction procedure: To a solution of **1a** (2.80 g, 10 mmol) in anhydrous diglyme (30 ml) was added sodium hydride (50% in mineral oil, 0.72 g, 15 mmol). After the evolution of hydrogen gas had ceased **2** (0.53 g, 10 mmol) was added. The mixture was then heated at 120 °C for 20 min to evolve a nitrogen gas (170 ml, 76%). The reaction mixture was poured into water and extracted with diethyl ether. The ether was washed with water and brine and dried over anhydrous sodium sulfate. The solvent was removed on a rotary evaporator and the residue was subjected to thin-layer chromatography on silica gel by using chloroform as a developing solvent to give an oily mixture of **3a** and **4a** (970 mg, 65.0%, R_f=0.70) and crystals **5a** (169 mg, 9.1%, R_f=0.24).

3a or 4a: Found: *m/z* 149.0279. Calcd for C_8H_7NS: M, 149.0299. MS *m/z* (rel intensity): 149 (M^+, 100) and 121 (40). IR (oil): 2240 cm^{-1}. UV (EtOH): 238 nm (log ε, 3.78). ^1H NMR ($CDCl_3$) δ=1.38 (m, 1H), 1.53 (m, 2H), 2.72 (m, 1H), 6.84 (m, 1H), 6.91 (m, 1H), and 7.12 (m, 1H).

4a or 3a: Found: *m/z* 149.0311. Calcd for C_8H_7NS: M, 149.0299. MS *m/z* (rel intensity): 149 (M^+, 100) and 121 (48). IR (oil): 2240 cm^{-1}. UV (EtOH): 238 nm (log ε, 3.78). ^1H NMR ($CDCl_3$) δ=1.42 (m, 2H), 1.70 (m, 1H), 2.52 (m, 1H), 6.93 (m, 2H), and 7.18 (m, 1H).

5a: Mp 53—54 °C. Found: *m/z* 177.0322. Calcd for $C_8H_7N_3S$: M, 177.0335. MS *m/z* (rel intensity): 177 (M^+, 100), 143 (35), and 121 (15). IR (KBr): 2230 cm^{-1}. UV (EtOH): 285 nm (log ε, 3.99). ^1H NMR ($CDCl_3$) δ=2.99 (dd, 1H, *J*=18 and 10 Hz), 3.34 (dd, 1H, *J*=18 and 12 Hz), 5.31 (dd, 1H, *J*=18 and 10 Hz), 6.60 (s, 1H), 7.02 (m, 2H), and 7.31 (m, 1H).

Reaction of 1a with Ten-Molar Equivalents of 2. A mixture of **1a** (2.50 g, 9 mmol), sodium hydride (50%, 0.65 g, 14 mmol), and **2** (4.78 g, 90 mmol) in diglyme (30 ml) was heated at 130 °C for 1 h to evolve nitrogen gas (100 ml, 45%). The reaction mixture was treated as usual by using benzene-diethyl ether 6:4 as a developing solvent to give crystals **6a** (926 mg, 45.1%, R_f=0.60) and an oil **7a** (140 mg, 6.1%, R_f=0.37).

6a: Mp 90—91 °C. Found: *m/z* 230.0620. Calcd for $C_{11}H_{10}N_4S$: M, 230.0626. MS *m/z* (rel intensity): 230 (M^+, 85), 189 (100), and 163 (26). IR (KBr): 2260 and 2220 cm^{-1}. UV (EtOH): 291 nm (log ε, 3.99). ^1H NMR ($CDCl_3$) δ=2.71 (t, 2H, *J*=7 Hz), 3.03 (dd, 1H, *J*=18 and 12Hz), 3.36 (m, 3H), 5.00 (dd, 1H, *J*=12 and 11 Hz), 7.02 (m, 1H), 7.24 (m, 1H), and 7.37 (m, 1H).

7a: Found: *m/z* 256.0774. Calcd for $C_{13}H_{12}N_4S$: M, 256.0728. MS *m/z* (rel intensity): 256 (M^+, 100), 215 (69), and 202 (47). IR (oil): 2243 cm^{-1}. ^1H NMR ($CDCl_3$) δ=2.91 (m, 6H), 4.35 (t, 2H, *J*=7 Hz), 6.24 (s, 1H), 7.36 (m, 1H), and 7.43 (m, 2H). ^{13}C NMR ($CDCl_3$) δ=17.0, 18.7, 24.4, 44.7, 106.7, 116.9, 119.4, 127.6, 127.9, 128.1, 129.6, 138.0, and 149.4.

Reaction of 1b with an Equimolar Amount of 2. A mixture of **1b** (2.80 g, 10 mmol), sodium hydride (50%, 0.72 g, 15 mmol), and **2** (0.53 g, 10 mmol) in diglyme (30 ml) was heated at 120 °C for 20 min to evolve nitrogen gas (98 ml, 44%). The usual work up using chloroform as a developing solvent gave a mixture of **3b** and **4b** (1004 mg, 67.3%, R_f=0.65) and an oil **5b** (349 mg, 19.7%, R_f=0.30).

Mixture of 3b and 4b: Found: *m/z* 149.0312. Calcd for C_8H_7NS: M, 149.0299. MS *m/z* (rel intensity): 149 (M^+, 100) and 121 (45). IR (oil): 2240 cm^{-1}. UV (EtOH): 238 nm (log ε, 3.72). ^1H NMR ($CDCl_3$) δ=1.2—1.8 (m, 3H), 2.3—2.8 (m, 1H), and 6.7—7.4 (m, 3H).

5b: Found: *m/z* 177.0348. Calcd for C_8H_7NS: M, 177.0335. MS *m/z* (rel intensity): 177 (M^+, 1), 148 (100), and 122 (46). IR (oil): 2230 cm^{-1}. UV (EtOH): 282 nm (log ε, 3.85). ^1H NMR ($CDCl_3$) δ=2.90 (dd, 1H, *J*=18 and 10 Hz), 3.31 (dd, 1H, *J*=18 and 12 Hz), 5.16 (dd, 1H, *J*=18 and 10 Hz), 6.63 (s, 1H), 7.04 (m, 1H), and 7.32 (m, 2H).

Reaction of 1b with Ten-Molar Equivalents of 2. A mixture of **1b** (2.52 g, 9 mmol), sodium hydride (50%, 0.65 g, 14 mmol), and **2** (4.78 g, 90 mmol) in diglyme (30 ml) was heated at 130 °C for 20 min to evolve nitrogen gas (90 ml, 45%). The reaction mixture was treated as usual by using chloroform–diethyl ether 8 : 2 as a developing solvent to give crystals **6b** (2070 mg, 50.1%, R_f=0.70) and an oil **7b** (202 mg, 8.9%, R_f=0.33).

6b: Mp 108—109 °C. Found: *m/z* 230.0625. Calcd for $C_{11}H_{10}N_4S$: M, 230.0626. MS *m/z* (rel intensity): 230 (M^+, 74), 189 (100), 163 (21). IR (KBr): 2250 and 2230 cm^{-1}. UV (EtOH): 291 nm (log ε, 4.05). ^1H NMR ($CDCl_3$) δ=2.65 (m, 2H), 2.97 (dd, 1H, *J*=18 and 13 Hz), 3.30 (m, 3H), 4.87 (dd, 1H, *J*=13 and 11 Hz), 7.16 (m, 1H), and 7.42 (m, 2H).

7b: Found: *m/z* 256.0763. Calcd for $C_{13}H_{12}N_4S$: M, 256.0782. MS *m/z* (rel intensity): 256 (M^+, 93), 215 (83), and 202 (100). IR (oil): 2240 cm^{-1}. ^1H NMR ($CDCl_3$) δ=2.74 (t, 2H, *J*=7 Hz), 2.95 (m, 4H), 4.34 (t, 2H, *J*=6 Hz), 6.22 (s, 1H), 7.19 (m, 1H), and 7.45 (m, 2H). ^{13}C NMR ($CDCl_3$) δ=17.0, 18.7, 24.4, 44.6, 105.6, 117.1, 119.4, 124.9, 127.0, 127.8, 129.7, 140.4, and 149.4.

Reaction of 1c with Ten-Molar Equivalents of 2. A mixture of **1c** (2.77 g, 10 mmol), sodium hydride (50%, 0.66 g, 14 mmol), and **2** (5.31 g, 10 mmol) in diglyme (50 ml) was heated at 95 °C for 25 min to evolve nitrogen gas (180 ml, 80%). The usual work up using benzene–diethyl ether 7 : 3 as a developing solvent gave oils **9c** (130 mg, 6.5%, R_f=0.45), **6c** (126 mg, 5.6%, R_f=0.36), **7c** (78 mg, 3.1%, R_f=0.60), and **8c** (125 mg, 4.9%, R_f=0.55).

6c: Found: *m/z* 227.1178. Calcd for $C_{12}H_{13}N_5$: M, 227.1170. MS *m/z* (rel intensity): 227 (M^+, 19), 226 (100), 158 (90), and 145 (48). IR (oil): 2250 and 2220 cm^{-1}. UV (EtOH): 290 nm (log ε, 3.96). ^1H NMR ($CDCl_3$) δ=2.62 (ddd, 1H, *J*=17, 6, and 6 Hz), 2.71 (ddd, 1H, *J*=17, 8, and 6 Hz), 3.01 (dd, 1H, *J*=17 and 14 Hz), 3.27 (ddd, 1H, *J*=13, 6, and 6 Hz), 3.28 (dd, 1H, *J*=17 and 12 Hz), 3.35 (ddd, 1H, *J*=13, 8, and 6 Hz), 3.63 (s, 3H), 4.79 (dd, 1H, *J*=14 and 12 Hz), 6.08 (dd, 1H, *J*=4 and 3 Hz), 6.16 (dd, 1H, *J*=4 and 2 Hz), and 6.66 (dd, 1H, *J*=3 and 2 Hz).

7c: Found: *m/z* 253.1348. Calcd for $C_{14}H_{15}N_5$: M, 253.1327. MS *m/z* (rel intensity): 253 (M^+, 100), 213 (53), 200 (49), and 173 (26). IR (oil): 2265 cm^{-1}. UV (EtOH): 253 nm (log ε, 3.96). ^1H NMR ($CDCl_3$) δ=2.73 (t, 2H, *J*=7 Hz), 2.85 (t, 2H, *J*=7 Hz), 2.99 (t, 2H, *J*=7 Hz), 3.54 (s, 3H), 4.29 (t, 2H, *J*=7 Hz), 6.19 (s, 1H), 6.21 (dd, 1H, *J*=4 and 3 Hz), 6.25 (dd, 1H, *J*=4 and 2 Hz), and 6.69 (dd, 1H, *J*=3 and 2 Hz). ^{13}C NMR ($CDCl_3$) δ=17.0, 18.8, 24.4, 34.5, 44.3, 106.6, 108.1, 111.4, 117.1, 119.5, 120.7, 124.5, 136.5, and 149.2.

8c: Found: *m/z* 253.1355. Calcd for $C_{14}H_{15}N_5$: M, 253.1326. MS *m/z* (rel intensity): 253 (M^+, 21), 252 (100), 212 (55), 200 (52), and 173 (33). IR (oil): 2265 and 2210 cm^{-1}. UV (EtOH): 271 nm (log ε, 4.12). ^1H NMR ($CDCl_3$) δ=2.58 (t, 2H, *J*=7 Hz), 2.83 (t, 2H, *J*=6 Hz), 2.86 (t, 2H, *J*=7 Hz), 3.83 (s, 3H), 4.13 (t, 2H, *J*=6 Hz), 6.10 (dd, 1H, *J*=4 and 3 Hz), 6.21 (s, 1H), 6.36 (dd, 1H, *J*=4 and 3 Hz), and 6.62 (dd, 1H, *J*=3 and 2 Hz). ^{13}C NMR ($CDCl_3$) δ=16.9, 18.8, 21.2, 36.3, 44.0, 103.4, 107.6, 108.8, 117.7, 118.8, 124.4, 126.3, 140.0, and 145.8.

9c: Found: *m/z* 199.1084. Calcd for $C_{12}H_{13}N_3$: M, 199.1108. MS *m/z* (rel intensity): 199 (M^+, 19), 198 (35), and 158 (100). IR (oil): 2240 and 2220 cm^{-1}. UV (EtOH): 225 nm (log ε, 4.01). ^1H NMR ($CDCl_3$) δ=1.43 (dd, 1H, *J*=9 and 6 Hz), 1.71 (dd, 1H, *J*=7 and 6 Hz), 1.82 (dd, 1H, *J*=15 and 7 Hz), 2.05 (dd, 1H, *J*=15 and 7 Hz), 2.21 (dd, 1H, *J*=4 and 3 Hz), 6.04 (dd, 1H, *J*=4 and 2 Hz), and 6.64 (dd, *J*=3 and 2 Hz).

Reaction of 1c with Twenty-Molar Equivalents of 2. A mixture of **1c** (2.77 g, 10 mmol), sodium hydride (50%, 0.66 g, 14 mmol), and **2** (10.62 g, 200 mmol) in diglyme (50 ml) was heated at 100 °C for 10 min to evolve nitrogen gas (195 ml, 87%). The same treatment as above gave oils **9c** (374 mg, 18.8%), **10c** (131 mg, 6.6%), **6c** (423 mg, 18.6%), **7c** (101 mg, 4.0%), and **8c** (98 mg, 3.9%).

10c: Found: *m/z* 199.1094. Calcd for $C_{12}H_{13}N_3$: M, 199.1108. MS *m/z* (rel intensity): 199 (M^+, 23), 159 (100), and 145 (31). IR (oil): 2230 cm^{-1}. UV (EtOH): 227 nm (log ε, 3.84). ^1H NMR ($CDCl_3$) δ=1.38 (m, 2H), 1.79 (m, 2H), 2.43 (m, 2H), 2.62 (dd, 1H, *J*=10 and 7 Hz), 3.62 (s, 3H), 5.83 (dd, 1H, *J*=4 and 3 Hz), 6.01 (dd, 1H, *J*=4 and 2 Hz), and 6.63 (dd, 1H, *J*=3 and 2 Hz).

Reaction of 1d with an Equimolar Amount of 2. A mixture of **1d** (7.89 g, 30 mmol), sodium hydride (50%, 2.16 g, 45 mmol), and **2** (1.59 g, 30 mmol) in diglyme (70 ml) was heated at 90 °C for 20 min to evolve nitrogen gas (600 ml, 89%). The usual work up using benzene–diethyl ether 1 : 1 as a developing solvent gave oils **11d** (45 mg, 1.1%, R_f=0.38) and **12d** (61 mg, 1.1%, R_f=0.25).

11d: Found: *m/z* 134.0467. Calcd for $C_7H_6N_2O$: M, 134.0480. MS *m/z* (rel intensity): 134 (M^+, 100), 115 (25), and 105 (53). IR (oil): 3140 cm^{-1}. UV (EtOH): 262 nm (log ε, 4.08). ^1H NMR ($CDCl_3$) δ=6.46 (dd, 1H, *J*=3 and 2 Hz), 6.54 (d, 1H, *J*=2 Hz), 6.65 (dd, 1H, *J*=3 and 1 Hz), 7.26 (s, 1H), 7.45 (dd, 1H, *J*=2 and 1 Hz), and 7.62 (d, 1H, *J*=2 Hz).

12d: Found: *m/z* 184.0740. Calcd for $C_{10}H_9N_3O$: M, 187.0746. MS *m/z* (rel intensity): 187 (M^+, 79), 147 (100), and 119 (26). IR (oil): 2240 cm^{-1}. UV (EtOH): 266 nm (log ε, 4.58). ^1H NMR ($CDCl_3$) δ=2.98 (t, 2H, *J*=7 Hz), 4.41 (t, 2H, *J*=7 Hz), 6.47 (dd, 1H, *J*=3 and 2 Hz), 6.50 (d, 1H, *J*=2 Hz), 6.66 (dd, 1H, *J*=3 and 1 Hz), 7.46 (dd, 1H, *J*=2 and 1 Hz), and 7.50 (d, 1H, *J*=2 Hz).

Reaction of 1d with Ten-Molar Equivalents of 2. A mixture of **1d** (2.64 g, 10 mmol), sodium hydride (50%, 0.66 g, 14 mmol), and **2** (5.31 g, 100 mmol) in diglyme (30 ml) was heated from 90 °C to 160 °C in a period of 50 min. No nitrogen gas was evolved. The usual work up using benzene–diethyl ether 1 : 9 as a developing solvent gave oils **11d** (29 mg, 2.2%, R_f=0.55) and **12d** (208 mg, 11.1%, R_f=0.46).

Reaction of 1a with Ten-Molar Equivalents of 2 in Diluted Conditions. A mixture of **1a** (2.80 g, 10 mmol), sodium hydride (50%, 0.72 g, 15 mmol), and 2 (5.3 g, 100 mmol) in diglyme (150 ml) was heated at 140 °C for 25 min to evolve nitrogen gas (70 ml, 31%). The reaction mixture was chromatographed on silica gel to give **6a** (873 mg, 38.0%, benzene–diethyl ether 8 : 2) and **7a** (545 mg, 21.3%, benzene–diethyl ether 1 : 1).

References

1) W. Kirms, "Carbene Chemistry," Academic Press (1964); J. Hine, "Divalent Carbon," Ronald Press (1964); W.

R. Bambord and T. S. Stevens, *J. Chem. Soc.*, **1952**, 4735; W. M. Jones and C. L. Ennis, *J. Am. Chem. Soc.*, **89**, 3069 (1967); K. Saito, T. Toda, and T. Mukai, *Bull. Chem. Soc. Jpn.*, **57**, 1567 (1984); K. Saito, *ibid.*, **60**, 2105 (1987); K. Saito and H. Ishihara, *ibid.*, **60**, 4447 (1987).

2) R. Huisgen, *Angew. Chem.*, **75**, 604 (1963); E. Ciganek, *ibid.*, **78**, 1979 (1966); W. J. Lenoble, Tatsukami, H. F. Morris, *J. Am. Chem. Soc.*, **92**, 5681 (1970); M. Jones, Jr., W. J. Baron, and Y. H. Shen, *ibid.*, **92**, 4745 (1970).

3) R. V. Hoffman and H. Shechter, *J. Am. Chem. Soc.*, **93**, 5940 (1971); R. V. Hoffman, G. G. Orphanide, and H. Shechter, *ibid.*, **100**, 7934 (1978); R. V. Hoffman and H. Shechter, *ibid.*, **100**, 7937 (1978).

4) G. Maas and C. Hummel, *Chem. Ber.*, **113**, 3679 (1980).

5) K. Saito and H. Ishihara, *Heterocycles*, **24**, 1291 (1986); *idem*, *ibid.*, **26**, 1891 (1987); K. Saito, H. Ishihara, T. Murase, Y. Horie, and E. Maekawa, *Bull. Chem. Soc. Jpn.*, **60**, 4317 (1987); K. Saito, H. Ishihara, and K. Takahashi, *Heterocycles*, **27**, 1141 (1988).

6) N. S. Bacca, D. P. Hollis, L. F. Johnson, and E. A. Pier, "NMR Spectra Catalog," The National Press (1985); C. J. Powchert and J. R. Campbell, "The Aldrich Library of NMR Spectra," Aldrich Chemical Company Inc. (1974); A. R. Katritzky, "Handbook of Heterocyclic Chemistry," Pergamon Press (1985).

7) K. Bowden and M. J. Price, *J. Chem. Soc. B*, **1970**, 1466; E. K. Launio and T. G. Frey, *J. Org. Chem.*, **36**, 345 (1971); K. Saito, *Bull. Chem. Soc. Jpn.*, **60**, 2105 (1987).

8) The referee suggested a possibility of an existence of the following diazo intermediate. We are indebted to the referee for this suggestion.

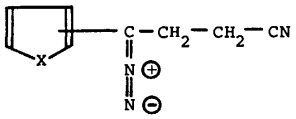

Fig. 4.

The Formation Pathway of 3,5-Bis(methoxymethyl)perhydro-1,3,5-oxadiazin-4-one

Ryuichi SHIBA,* Miyuki TAKAHASHI, Toichi EBISUNO,† and Michiaki TAKIMOTO†
Department of Applied Science, Faculty of Technology, Tokyo Denki University, Kanda Chiyoda-ku, Tokyo 101
†Department of Chemistry, Faculty of Science, Toho University, Miyama 2-2-1, Funabashi, Chiba 274
(Received November 14, 1988)

The investigation of the reactions of urea and its methyl derivatives with formaldehyde elucidated the formation pathway of 3,5-bis(methoxymethyl)perhydro-1,3,5-oxadiazin-4-one. 1) The addition of formaldehyde to urea became increasingly difficult according to the increase of the number of added formaldehyde molecules, probably because of the steric hindrance of the hydroxymethyl groups. 2) 3,5-Bis(methoxymethyl)perhydro-1,3,5-oxadiazin-4-one was concluded to be derived from urea via tris(hydroxymethyl)urea and 3-(hydroxymethyl)perhydro-1,3,5-oxadiazin-4-one but not via tetrakis(hydroxymethyl)urea or perhydro-1,3,5-oxadiazin-4-one.

Urea-formaldehyde resins have been commercially available as important adhesives in the wood industry because of their low cost. However, previous works on their chemical structure and reaction mechanisms are not necessarily adequate. The maximal number of formaldehyde molecules added to urea has been considered to be 4, because the formation of 3,5-bis(methoxymethyl)perhydro-1,3,5-oxadiazin-4-one (U-2Mcyc2F) has been reported.[1] Although there are several reports[1-4] on the preparations of tris- and tetrakis- substituted products from urea and formaldehyde, the basic problem of the formation pathway of U-2Mcyc2F remained uncertain. Until now, two different pathways for the formation of U-2Mcyc2F have been proposed. Kadowaki[1] proposed that U-2Mcyc2F was produced from urea and formaldehyde via tetrakis(hydroxymethyl)urea (U-4F). Alternatively, Takahashi[4] proposed the formation pathway via perhydro-1,3,5-oxadiazin-4-one (Ucyc2F). These proposals have remained hypothetical partly because of the uncertain confirmation of U-4F.

Ito[2] analyzed the reaction products from urea and a large excess of formaldehyde in the presence of a strong base at 50 °C by two-dimensional paper chromatography. He considered one of the spots to be U-4F. However, Tomita and Hirose[3] assigned it to U-2Mcyc2F by its ^{1}H NMR spectrum and published a negative report on the production of U-4F.

In order to obtain a clue for the elucidation of the formation pathway of U-2Mcyc2F, urea or its methyl derivatives were allowed to react with formaldehyde under various conditions. In our present report, we wish to propose a new formation pathway for U-2Mcyc2F.

Results snd Discussion

Several reports[5-8] on the selective preparation of mono- and bis(hydroxymethyl)urea (U-1F and U-2F) have been published. They suggested that the number of added formaldehyde molecules could be controlled by the feed ratio of urea/formaldehyde and the reaction temperature. U-1F and U-2F have been reported to be easily isolated from the reaction solution. However, tris(hydroxymethyl)urea (U-3F) and U-4F were difficult to isolate, probably because of their lability to heat, acids or bases. In order to isolate these products, all the hydroxymethylated products were converted to their methyl ethers under the optimal conditions described in the Experimental section. The methylation conditions used were such that the amount of HCl was 50—100 times greater than in the conventional method and the reaction temperature was lowered from 64—65 °C of the conventional method to 0—5 °C. Under these conditions, the condensation and acid hydrolysis of the hydroxymethylated products did not occur and the hydroxymethylated products were stoichiometrically converted to their methyl ethers.

The optimal preparation conditions of mono-, bis-, tris-, and tetrakis-substituted products from urea and formaldehyde are shown in Scheme 1 together with their reaction equations and their highest yields. Although Zigeuner[9] reported the production of the asym-type of U-2F as well as that of the sym-type, the amount of U-2F obtained was speculated not to contain the former from its ^{1}H NMR spectrum. The optimal temperatures were raised from 0—5 °C to 25—30, 60—80, and 95 °C with the increase of the number of added formaldehyde molecules, respectively. Furthermore, the preparation of tris(methoxymethyl)-urea (U-3M) or U-2Mcyc2F necessitated the large excess of formaldehyde in addition to high temperatures. In order to examine the production of tetrakis-(methoxymethyl)urea (U-4M), the products from urea and formaldehyde under appropriate reaction conditions between the optimal conditions for U-3M and U-2Mcyc2F were analyzed by gas-liquid chromatography, but no other products than U-3M and U-2Mcyc2F were detected.

These results suggest that the addition of formaldehyde to urea becomes increasingly difficult according to the increase of the number of added formaldehyde molecules. This is probably due to steric hindrance

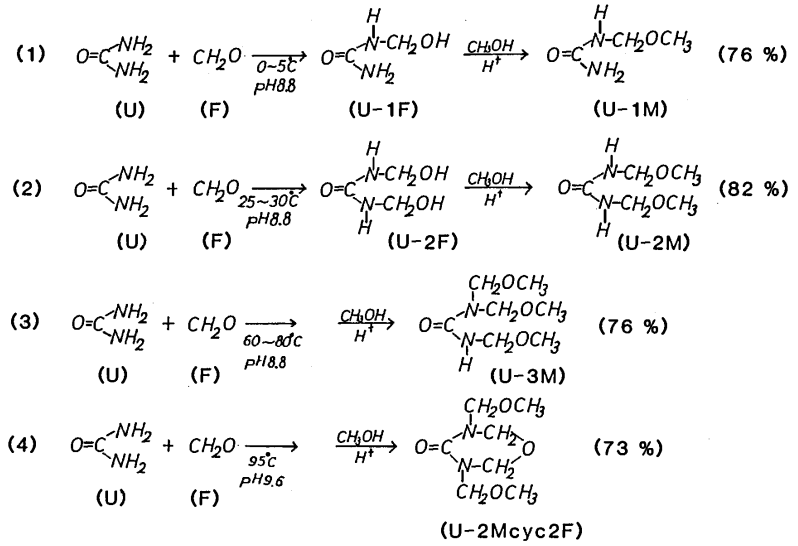

Scheme 1.

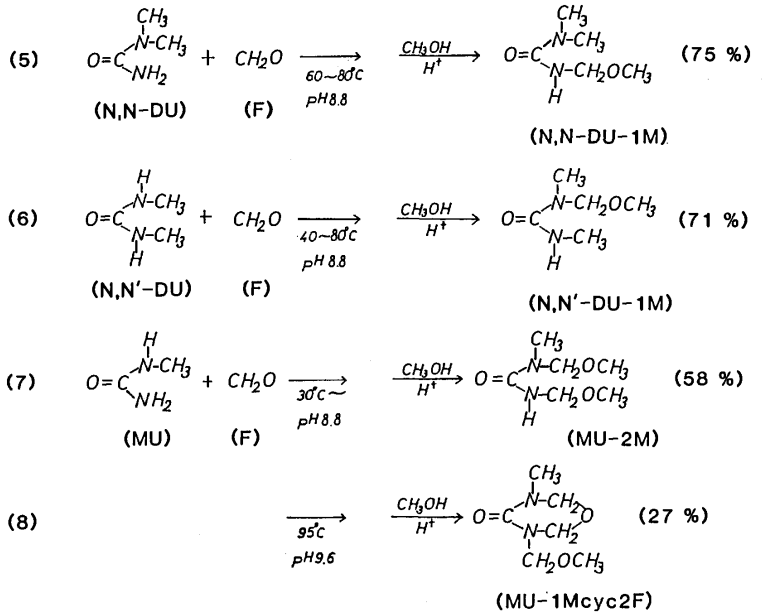

Scheme 2.

by the hydroxymethyl groups. This speculation is supported by the fact that sym-U-2F is prepared more easily than asym-U-2F by a factor of about ten.[3] U-2Mcyc2F is speculated to be produced via another pathway than those proposed by Kadowaki[1] and Takahashi[4] because neither U-4M nor Ucyc2F was detected. From these facts, the formation pathway of U-2Mcyc2F is proposed as follows:

$$\text{Urea} \rightarrow \text{U-3F} \rightarrow \text{U-1Fcyc2F} \rightarrow \text{U-2Mcyc2F}$$

Under such strong alkaline conditions that the binding of the dimethylene ether may be formed.[10-11] The oxadiazine ring may feasibly be formed from the two hydroxymethyl groups in sym-position of U-3F and this ring formation may be a rate-limiting step in the formation of U-2Mcyc2F. This speculation is supported by the results of the reaction of methyl derivatives of urea with formaldehyde.

The optimal preparation conditions for methoxymethylated products from methylurea (MU), 1,1-dimethylurea (*N,N*-DU), and 1,3-dimethylurea (*N,N'*-DU) with formaldehyde are shown in Scheme 2 together with their reaction equations and their highest yields. By comparison of the optimal temperatures for the highest yields of **MU** → **MU-2M**, *N,N*-DU → *N,N*-DU-1**M**, and *N,N'*-DU → *N,N'*-DU-1**M** with those for urea → U-3**M**, it is seen that the nitrogen atoms in methyl derivatives of urea are equally or more easily attacked by $CH_2(OH)_2$ than those in urea itself because of the electron-donating nature of the

methyl group. Its electron-donating nature is partly compensated by its bulkiness. Although the optimal conditions of MU → MU-1Mcyc2F were closely identical with those of urea → U-2Mcyc2F, the yield of MU-1Mcyc2F was lower than that of U-2Mcyc2F. This may be explained by the probability of the formation of an oxadiazine ring.

Even in the reaction of *N,N*-DU or *N,N'*-DU with a large excess of formaldehyde at high temperatures under strong alkaline conditions, no 1,1-dimethyl-3,3-bis(methoxymethyl)urea or 1,3-dimethyl-1,3-bis(methoxymethyl)urea could be obtained. These results can be understood if two methyl groups and one hydroxymethyl group of 1,1-dimethyl-1-hydroxymethylurea or 1,3-dimethyl-1-hydroxymethylurea interfere with the further addition of formaldehyde and if they cannot form an oxadiazine ring. As an oxadiazine ring can be formed from two hydroxymethyl groups of 1-methyl-1,3-bis(hydroxymethyl)urea (MU-2F), MU-1Mcyc2F can be derived from MU-2F via 3-methylperhydro-1,3,5-oxadiazin-4-one.

Experimental

Preparation of Tris(methoxymethyl)urea (U-3M). Twelve grams of urea and 88.7 g of formalin were mixed and the pH of the mixture was maintained at 8.8 by the successive addition of a 0.1 M (1 M=1 mol dm^{-3}) NaOH solution. While the solution was stirred for 30 min, its temperature was kept at 65 °C. The reaction mixture was then evaporated to dryness under reduced pressure below 40 °C. The desiccated products were dissolved in 400 ml of MeOH. Keeping the temperature of the solution below −15 °C in a Dry Ice-MeOH bath, 5 ml of concd HCl was added dropwise to the solution. The solution was stirred for 10 min at 0—5 °C. After neutralization with 6 M NaOH solution and evaporation of MeOH, the methoxymethylated products were extracted with EtOH, then with dichloromethane, finally with diethyl ether. The solvent was distilled off. The resulting viscous solution was distilled at 1 Torr (1 Torr=133.322 Pa), and a distillate of 128—131 °C containing U-3M was collected (yield : 76%). Found; C, 43.66; H, 8.45; N, 14.49%: Calcd for $C_7H_{16}N_2O_4$; C, 43.75; H, 8.33; N, 14.58%: ^{1}H NMR(DMSO-d_6): δ=7.34 (1H, t, J=6 Hz, -NH-), 4.69 (4H, s,-CH_2-), 4.49 (2H, d, J=6 Hz, -CH_2-), 3.21 (6H,s,-CH_3), and 3.17 (3H, s, -CH_3): ^{13}C NMR (DMSO-d_6): δ=162.43 (O=C<), 82.25, 77.70 (-CH_2-), and 59.98, 59.85 (-CH_3): MS(FD): m/z =192(M^+).

The by-products were U-2M and condensation polymers. With rise in the hydroxymethylation temperature above 65 °C, a decrease of U-2M and an increase of condensation polymers resulted and a trace amount of U-2Mcyc2F was produced.

Preparation of U-2Mcyc2F. U-2Mcyc2F was prepared by the virtually identical procedure described in the preparation of U-3M except for a reaction temperature of 95 °C with the pH of the reaction solution of 9.6. The resulting viscous solution was placed on an alumina column. U-2Mcyc2F was eluted with a hexane-dichloromethane (7:3) mixture (yield: 73%). Found; C, 44.14; H, 7.45; N, 14.60%: Calcd for $C_7H_{14}N_2O_4$; C, 44.21; H, 7.37; N, 14.74%: ^{1}H NMR($CDCl_3$): δ=4.93 (4H, s, -CH_2-), 4.79 (4H, s, -CH_2-) and 3.34 (6H, s, -CH_3): ^{13}C NMR($CDCl_3$): δ=152.25 (O=C<), 76.67, 74.34 (-CH_2-) and 54.24 (-CH_3): MS (FD): m/z= 190(M^+).

All of the remainder other than U-2Mcyc2F in the distillate was elucidated to be U-3M by gas-liquid chromatography on a column of PEG-20M (ϕ 3 mm×2 m) at 190 °C. However, its content was as low as 10%.

Without the successive addition of a 0.1 M NaOH solution, the pH of the reaction solution fell from 9.6 to 7.0—7.2 and the yield of U-2Mcyc2F decreased into 16% and those of U-3M and condensation polymers increased.

Preparation of 1,1-Dimethyl-3-methoxymethylurea (*N,N*-DU-1M). The pH of the reaction mixture of 17.6 g of 1,1-dimethylurea (*N,N*-DU) and 40.3 g of formalin was adjusted to 8.8. The solution was stirred for 30 min at 70 °C. The procedures of methoxymethylation and extraction were the same as described above. The resulting viscous solution was permitted to stand for at least 2—3 days. The deposited crystals were recrystallized from EtOH as white rod-like crystals (yield: 75%). Mp 54.0—55.0 °C: Found; C, 45.32; H, 9.14; N, 21.15%; Calcd for $C_5H_{12}N_2O_2$; C, 45.45; H, 9.09: N, 21.21%: ^{1}H NMR (DMSO-d_6): δ=7.26 (1H,t, J=6Hz, -NH-), 4.49 (2H, d, J=6Hz, -CH_2-), 3.15 (3H, s, -OCH_3), and 2.81 (6H, s, -CH_3): ^{13}C NMR (DMSO-d_6): δ=157.41 (O=C<), 72.49 (-CH_2-), 54.10 (-OCH_3), and 35.54 (-CH_3): MS (FD): m/z=132(M^+).

Preparation of 1,3-Dimethyl-1-methoxymethylurea (*N,N'*-DU-1M). A mixture of 17.6 g of 1,3-dimethylurea (*N,N'*-DU) and 40.3 g of formalin was stirred at 50 °C for 30 min while the pH of the solution was kept at 8.8. The methoxymethylation and extraction procedures were the same as descrived above. A distillate of 95—99 °C at 1 Torr was collected (yield: 71%). Found; C, 45.31; H, 9.14; N, 21.14%: Calcd for $C_5H_{12}N_2O_2$; C, 45.45; H, 9.09; N, 21.21%: ^{1}H NMR (DMSO-d_6): δ=6.43 (1H, m, -NH-), 4.60 (2H, s, -CH_2-), 3.14 (3H, s, -OCH_3), 2.82 (3H, s, -CH_3), and 2.58 (3H, d, J=4Hz, -CH_3), ^{13}C NMR (DMSO-d_6): δ=158.18 (O=C<), 79.15 (-CH_2-), 54.15 (-OCH_3), 33.10 (-CH_3), and 26.84 (-CH_3): MS (FD): m/z=132 (M^+).

Preparation of 1-Methyl-1,3-bis(methoxymethyl)urea (MU-2M). The mixture of 14.8 g of methylurea (MU) and 40.3 g of formalin (F/MU=5) was stirred at 50 °C for 30 min while the pH of the mixture was kept at 8.8. The methoxymethylation and extraction procedures were the same as described above. A distillate of 137—142 °C at 1 Torr was collected (yield: 58%). Found; C, 44.34; H, 8.75; N, 17.14%: Calcd for $C_6H_{14}N_2O_3$; C, 44.44; H, 8.64; N, 17.28%: ^{1}H NMR (DMSO-d_6): δ=6.36 (1H, m, -NH-), 4.63 (4H, s, -CH_2-), 3.20 (6H, s, -OCH_3), and 2.63 (3H, d, J=4Hz, -CH_3): ^{13}C NMR (DMSO -d_6): δ=157.45 (O=C<), 77.94 (-CH_2-), 54.37 (-OCH_3), and 26.85 (-CH_3): MS(FD): m/z=162 (M^+).

The optimal temperature in the preparation of MU-2M was above 30 °C, and over a broad range of temperature the major product from MU and formaldehyde was MU-2M.

Preparation of 3-Methyl-5-methoxymethyl-perhydro-1,3,5-oxadiazin-4-one (MU-1Mcyc2F) The mixture of 7.4 g of MU and 80.6 g of formalin (F/MU =10) was stirred at 95 °C for 30 min while the pH of the solution was kept at 9.6. The methoxymethylation and extraction procedures were the same as described above. The resulting viscous solution was placed on an alumina column and MU-1Mcyc2F was eluted with a hexane-dichloromethane (7:3) mixture

(yield: 27%). Found; C, 44.87; H, 7.61; N, 17.41%: Calcd for $C_6H_{12}N_2O_3$; C, 45.00; H 7.50; N, 17.50%: ^{1}H NMR (DMSO-d_6): δ=4.87, 4.78, 4.63 (2H, s, -CH_2-), 3.17 (3H, s, -OCH_3) and 2.74 (3H, s, -CH_3): ^{13}C NMR (DMSO-d_6): δ=153.09 (O=C<), 79.18, 77.56, 75.31 (-CH_2-), 54.62(-OCH_3), and 30.07 (-CH_3): MS(FD): m/z=160(M^+).

References

1) H. Kadowaki, *Bull. Chem. Soc. Jpn.*, **11**, 248 (1936).
2) Y. Ito, *Kogyo Kagaku Zasshi*, **64**, 382, 385 (1961).
3) B. Tomita and Y. Hirose, *J. Polym. Sci.*, **14**, 387 (1976).
4) A. Takahashi, "Thermosetting Plastics and Their Manufacturing," ed. by Kobunshi Gakkai, Chijinshokan, Tokyo (1964), p. 217.
5) A. Einhorn and A. Hamburger, *Ber.*, **41**, 24 (1908).
6) A. Ninagawa, *Nippon Kagaku Zasshi*, **77**, 1633 (1956).
7) P. R. Ludlam, *Analyst London*, **98**, 107 (1973).
8) H. Kadowaki, *Repts. Imp. Ind. Res. Lab. Osaka, Jpn.*, **14**, 37, 44 (1933).
9) G. Zigeuner, *Kuntstoffe*, **41**, 221 (1951).
10) A. Takahashi and I. Yamazaki, *Kobunshi Kagaku*, **15**, 232, 327 (1958).

Molecular Structures of Diarylcyclobutanes Associated with Reactivities in Ring-Cleavage Reactions: Implications of Conformationally Controlled Through-Bond Coupling

Kensuke SHIMA,* Jun KIMURA, Kouhei YOSHIDA, Masahide YASUDA, Kiyohisa IMADA, and Chyongjin PAC*,†
Department of Industrial Chemistry, Faculty of Engineering, Miyazaki University, Miyazaki 889-21
†Department of Chemical Process Engineering, Faculty of Engineering, Osaka University, Suita, Osaka 565
(Received November 17, 1988)

Molecular structures of diarylcyclobutanes (**1**—**6**) have been determined by single-crystal X-ray analyses. Although the distances and angles of the cyclobutane rings are relatively normal, the torsional angles between the aryl ring and the plane involving the ipso carbon and the aryl-substituted carbons of cyclobutane ring are close to 90° in cases of **1**—**4**, but very small (2.3—11.3 °) in cases of **5** and **6**; conformations of the aryl substituents are highly restricted by the rigid tricyclic structure or by nonbonding interactions between the vicinal substituents in the cis configuration. Restricted conformations are closely related to the different reactivities of the cyclobutane in photochemical, thermal, and radiation-induced ring-splitting reactions. The structure-reactivity relationships are discussed in terms of the conformation-controlled π-σ orbital interactions associated with the capabilities of the π electron systems in through-bond coupling.

The chemistry of cyclobutanes has been of stereochemical significance as a suitable probe for the exploration of both steric and electronic effects on chemical reactivities and as a prototype for theoretical investigations of chemical reaction courses. It can be expected that the chemical behavior of cyclobutanes is remarkably susceptible to a variety of steric and electronic perturbations, since the cyclobutane rings are relatively rigid with small conformational mobilities,[1] and since the molecular-orbital of the ring σ framework shows a small, but significant, π-bonding character.[2] Indeed, we found that aryl-substituted cyclobutanes reveal remarkable structure dependences in photochemical,[3-7] radiation-induced,[8] and thermal[9] ring-splitting reactions as well as in electrochemical oxidation potentials.[3] For instance, the head-to-head transoid cyclobutane dimer of indene (**1**) and related diarylcyclobutanes of "head-to-head" structure are efficiently split into the corresponding olefins by the redox photosensitization that proceeds by way of the π complex with the cation radical of aromatic hydrocarbons (Fig. 1). By contrast, no redox-photosensitized ring splitting occurs at all for the head-to-tail transoid dimer of indene (**2**), other "head-to-tail" diarylcyclobutanes, and monoarylcyclobutanes. Similarly, the head-to-head cisoid dimers of 1,3-dimethylthymine and 1,3-dimethyluracil are efficiently monomerized by redox photosensitization, while the head-to-tail isomers are not at all.[10]

These observations have been interpreted as the consequences of the structure-controlled capabilities of the two π or n electron systems in electronic coupling through the ring σ orbitals, since the "head-to-head" structures are requisite for efficient through-bond coupling. Through-bond coupling has been investigated from theoretical[11] and spectroscopic[12] points of view and has been suggested to play important roles in the photochemical and thermal reactions of some rigid polycyclic compounds with separated π chromophores which are perpendicular to each other.[13] It is, however, predicted that if through-bond coupling is essential in chemistry of diarylcyclobutanes,

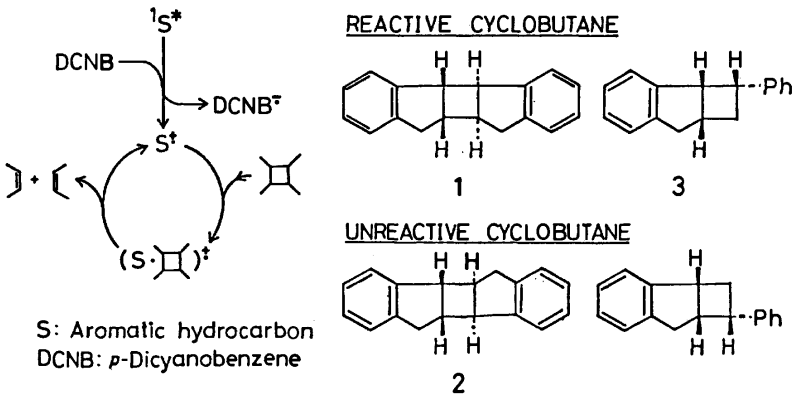

Fig. 1. Redox-photosensitized splitting of the cyclobutane ring; typical "head-to-head" diarylcyclobutanes which are reactive and typical "head-to-tail isomers which are unreactive

conformations of the aryl substituents should control the stereochemical reaction courses. However, little has been known on what relationships exist between the conformational effects on the chemical reactivities and stereochemical requirements for through-bond coupling. Another important expectation is that through-bond coupling would bring about an unusual elongation of a cyclobutane-ring σ bond to activate the "head-to-head" cyclobutanes[14,15] or may stabilize transition states of the ring-splitting reactions by extended electronic conjugation over relevant orbital arrays. From the above-mentioned points of view, we have performed X-ray crystallographic analyses of diarylcyclobutanes **1—6** in order to determine the exact molecular structure. In this paper we wish to report on the results and to discuss the implications of molecular structures in the through-bond coupling associated with the reactivities of the cyclobutanes.

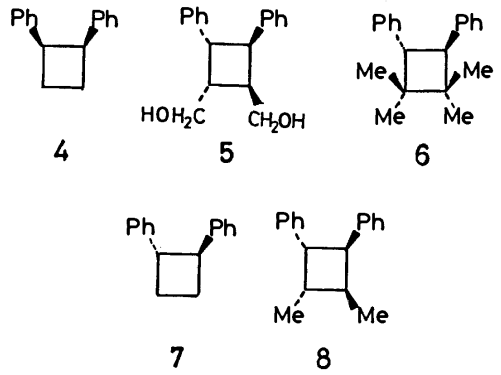

Experimental

Materials. The preparation of the cyclobutanes was carried out according to reported methods; *cis-transoid-cis*-cyclobuta[1,2-*a*;4,3-*a'*]diindene (**1**),[16] *cis-transoid-cis*-cyclobuta[1,2-*a*;3,4-*a'*]diindene (**2**),[3] *endo*-2-phenyl-2,2a,7,7a-tetrahydro-1*H*-cyclobut[*a*]indene (**3**),[3] *cis*-1,2-diphenylcyclobutane (**4**),[17] *r*-1,*t*-2-bis(hydroxymethyl)-*t*-3, *c*-4-diphenylcyclobutane (**5**),[5] 1,1,2,2-tetramethyl-*trans*-1,2-diphenylcyclobutane (**6**),[18] *trans*-1,2-diphenylcyclobutane (**7**),[17] and *r*-1,*t*-2-dimethyl-*t*-3,*c*-4-diphenylcyclobutane (**8**).[5] Single crystals for X-ray analyses were obtained by recrystallization from methanol for **1—5** and from hexane for **6**. On the other hand, all attempts failed in obtaining single crystals of **7** and **8**; these cyclobutanes remained oily at room temperature.

Single-Crystal X-Ray Analysis. Crystal structure analyses were carried out on an Enraf Nonius automated four-circle X-ray diffractometer (CAD 4) using graphite-monochromated Mo $K\alpha$ radiation (λ=0.71073 Å). Intensity data were collected by ω-2θ scan upto 50° for **1**, **4**, and **6**, 60° for **2**, 54° for **3**, and 56° for **5** in 2θ. The crystallographic data are shown in Table 1.

Structure Determination. All of the calculations were carried out on a DEC PDP 11/34 system using a SDP and SDP-Plus programs. The structures were solved by the direct method (MULTAN 82) and refined by a full-matrix least-squares method.

In the last cycle of the refinement with anisotropic temperature factors for nonhydrogen atoms, all of the parameter shifts were less than one-third of the corresponding standard deviations. After the refinement hydrogen atoms were located in positions calculated for a C–H bond length = 0.950 Å. Tables of the observed and calculated structure factors, anisotropic temperature factors, and bond distances and angles have been deposited to the Chemical Society of Japan (Document No. 8874).

^{1}H NMR spectra were taken on a JEOL JNM-PS-100 spectrometer for a $CDCl_3$ solution using tetramethylsilane as the internal standard.

Results and Discussion

Molecular Structures. Table 2 lists the final atomic parameters. The crystal packing diagrams and computer-generated molecular structures of **1—6** are shown in Figs. 2 and 3, respectively. For the present investigation, the essential structure parameters are the bond distances and angles of the cyclobutane ring,

Table 1. Crystallographic Data and Experimental Conditions

	1	2	3	4	5	6
Formula	$C_{18}H_{16}$	$C_{18}H_{16}$	$C_{17}H_{16}$	$C_{16}H_{16}$	$C_{18}H_{20}O_2$	$C_{20}H_{24}$
Formula wt	232.33	232.33	220.32	208.31	268.36	264.42
Crystal system	Orthorhombic	Monoclinic	Monoclinic	Monoclinic	Monoclinic	Monoclinic
Space group	*Pbca*	$P2_1$	$P2_1/c$	$P2_1/c$	$P2_1/c$	$P2_1/n$
a/Å	12.510(2)	7.162(2)	13.290(2)	7.013(12)	6.392(1)	10.014(3)
b/Å	13.805(9)	6.320(3)	5.842(11)	12.193(3)	15.783(3)	16.749(2)
c/Å	14.897(4)	13.647(2)	17.003(2)	14.302(6)	14.721(3)	19.671(4)
β/deg	—	97.60(8)	109.44(1)	88.56(9)	89.13(5)	76.68(6)
V/Å^3	2572.7	612.4	1244.8	1222.6	1484.8	3210.5
D_{obsd}/g cm^{-3}	1.200	1.260	1.176	1.132	1.200	1.094
D_{calcd}/g cm^{-3}	1.18	1.250	1.16	1.13	1.18	1.10
Z	8	2	4	4	4	8
R_w	0.077	0.071	0.120	0.106	0.096	0.083
R	0.072	0.060	0.085	0.105	0.080	0.070
No. refl. obsd.	8783	1624	2495	1416	1529	3981
No. unobsdly weak refl.	5404	1950	1691	699	970	5162

Table 2. Final Atomic Coordinates with Their Estimated Standard Deviations and Temperature Factors

Atom	x	y	z	B_{eq}/Å^{2} [a]
cis-transoid-cis-Cyclobuta[1,2-*a*; 4,3-*a'*]diindene (**1**)				
C1	0.3337(9)	0.5671(8)	0.0220(8)	4.3(3)
C2	0.3367(10)	0.6686(8)	−0.0226(8)	4.3(3)
C3	0.2129(9)	0.6810(8)	−0.0043(7)	3.8(3)
C4	0.2080(9)	0.5697(7)	0.0191(7)	3.9(3)
C5	0.2604(11)	0.3915(9)	−0.1618(8)	5.4(3)
C6	0.1603(13)	0.3826(10)	−0.2007(8)	7.4(4)
C7	0.0701(11)	0.4342(9)	−0.1724(8)	6.1(4)
C8	0.0785(10)	0.4963(9)	−0.1012(8)	5.0(3)
C9	0.1780(9)	0.5071(8)	−0.0599(7)	4.1(3)
C10	0.2693(12)	0.4565(8)	−0.0891(7)	5.2(3)
C11	0.3245(10)	0.8492(9)	0.1664(8)	5.0(3)
C12	0.2324(13)	0.8683(9)	0.2154(8)	7.0(4)
C13	0.1303(11)	0.8319(9)	0.1980(8)	5.9(4)
C14	0.1215(9)	0.7685(8)	0.1272(8)	4.8(3)
C15	0.2098(9)	0.7475(9)	0.0759(7)	4.1(3)
C16	0.3123(8)	0.7829(8)	0.0950(8)	3.9(3)
C17	0.3691(10)	0.4809(9)	−0.0382(9)	5.6(3)
C18	0.3947(8)	0.7480(10)	0.0311(8)	4.9(3)
cis-transoid-cis-Cyclobuta[1,2-*a*; 3,4-*a'*]diindene (**2**)				
C1	0.1569(8)	0.6744(9)	0.7969(4)	3.2(1)
C2	0.3556(6)	0.7162(9)	0.7642(4)	2.54(9)
C3	0.3387(7)	0.5114(8)	0.7004(4)	2.8(1)
C4	0.1421(9)	0.4701(7)	0.7303(5)	3.5(1)
C5	−0.2452(9)	0.774(1)	0.6024(5)	4.3(1)
C6	−0.3105(9)	0.639(1)	0.5199(4)	4.6(1)
C7	−0.2355(9)	0.450(1)	0.5081(5)	4.3(1)
C8	−0.0910(8)	0.384(1)	0.5739(5)	4.0(1)
C9	−0.0127(7)	0.5035(8)	0.6531(4)	3.0(1)
C10	−0.1018(7)	0.7081(8)	0.6640(4)	2.60(9)
C11	0.5860(8)	0.8000(9)	0.9244(4)	3.2(1)
C12	0.7403(8)	0.726(1)	0.9905(4)	3.9(1)
C13	0.8230(7)	0.528(1)	0.9791(5)	3.9(1)
C14	0.7531(7)	0.4062(9)	0.9026(4)	3.3(1)
C15	0.5954(8)	0.4746(9)	0.8310(5)	3.6(1)
C16	0.5244(7)	0.6668(9)	0.8448(4)	3.0(1)
C17	−0.0018(8)	0.8199(9)	0.7556(4)	3.3(1)
C18	0.5054(8)	0.363(1)	0.7432(5)	4.0(1)
endo-2-Phenyl-2,2a,7,7a-tetrahydro-1*H*-cyclobut[*a*]-indene (**3**)				
C1	0.8891(4)	−0.0304(8)	0.8705(3)	3.7(1)
C2	0.9543(4)	−0.2607(9)	0.8917(4)	4.6(1)
C3	0.8659(5)	−0.3499(9)	0.9266(3)	5.0(1)
C4	0.8244(4)	−0.1026(9)	0.9290(3)	3.9(1)
C5	0.7096(4)	−0.0550(8)	0.9052(3)	3.5(1)
C6	0.6758(5)	0.1375(9)	0.9371(3)	4.8(1)
C7	0.5667(5)	0.187(1)	0.9162(4)	6.3(2)
C8	0.4892(5)	0.048(1)	0.8623(4)	5.8(1)
C9	0.5246(5)	−0.142(1)	0.8302(4)	5.9(2)
C10	0.6326(4)	−0.1929(9)	0.8504(3)	4.7(1)
C11	0.8319(3)	−0.0483(7)	0.7785(3)	3.22(9)
C12	0.7560(4)	0.0997(8)	0.7280(3)	3.7(1)
C13	0.7124(4)	0.055(1)	0.6432(3)	4.8(1)
C14	0.7440(5)	−0.136(1)	0.6086(3)	5.4(1)
C15	0.8211(4)	−0.2864(9)	0.6595(3)	5.1(1)
C16	0.8655(4)	−0.2405(8)	0.7446(3)	3.9(1)
C17	0.9533(4)	−0.3644(9)	0.8101(4)	5.2(1)
cis-1,2-Diphenylcyclobutane (**4**)				
C1	0.3663(8)	−0.0064(5)	0.1706(4)	5.2(1)
C2	0.2070(9)	−0.0943(5)	0.1806(4)	5.2(1)
C3	0.079(1)	−0.0227(6)	0.1228(5)	6.6(2)
C4	0.256(1)	0.0369(6)	0.0870(5)	7.1(2)
C5	0.3815(8)	0.0697(5)	0.2524(4)	4.8(1)
C6	0.5002(9)	0.0404(5)	0.3262(4)	5.5(1)
C7	0.517(1)	0.1051(6)	0.4019(5)	6.7(2)
C8	0.418(1)	0.2021(6)	0.4088(5)	7.1(2)
C9	0.3000(9)	0.2297(5)	0.3397(5)	6.6(2)
C10	0.2807(9)	0.1655(5)	0.2610(4)	5.4(1)
C11	0.1517(8)	−0.1338(5)	0.2781(4)	4.8(1)
C12	0.2354(9)	−0.2248(5)	0.3135(4)	5.4(1)
C13	0.188(1)	−0.2599(6)	0.4025(6)	7.6(2)
C14	0.058(1)	−0.2063(6)	0.4587(5)	6.7(2)
C15	−0.025(1)	−0.1172(6)	0.4202(5)	7.0(2)
C16	0.0145(9)	−0.0788(5)	0.3341(4)	5.7(2)
r-1,*t*-2-Bis(hydroxymethyl)-*t*-3,*c*-4-diphenyl-cyclobutane (**5**)				
C1	0.737(1)	0.5445(3)	0.2372(3)	2.9(2)
C2	0.788(1)	0.4492(3)	0.2344(3)	2.9(1)
C3	0.779(1)	0.4474(3)	0.3396(3)	2.8(1)
C4	0.795(1)	0.5450(3)	0.3393(3)	3.3(2)
C5	0.856(1)	0.6058(3)	0.1755(3)	3.5(2)
C6	0.786(1)	0.6888(3)	0.1705(4)	4.1(2)
C7	0.890(1)	0.7480(4)	0.1166(4)	5.0(2)
C8	1.065(1)	0.7247(4)	0.0674(4)	5.0(2)
C9	1.128(1)	0.6427(5)	0.0698(5)	5.4(2)
C10	1.028(1)	0.5818(4)	0.1236(4)	4.7(2)
C11	0.655(1)	0.3893(3)	0.1822(3)	3.1(1)
C12	0.492(1)	0.4163(4)	0.1305(4)	4.6(2)
C13	0.367(1)	0.3582(5)	0.0829(4)	6.0(2)
C14	0.410(1)	0.2726(4)	0.0865(4)	4.8(2)
C15	0.577(1)	0.2456(4)	0.1360(4)	4.2(2)
C16	0.698(1)	0.3037(4)	0.1830(4)	3.8(2)
C17	0.572(1)	0.4129(3)	0.3767(3)	4.0(2)
C18	1.006(1)	0.5785(4)	0.3595(3)	4.1(2)
O1	0.5632(9)	0.4208(2)	0.4731(2)	5.4(1)
O2	1.048(1)	0.5738(3)	0.4537(3)	6.9(1)
1,1,2,2-Tetramethyl-*trans*-3,4-diphenylcyclobutane (**6**)				
C1	−0.2758(5)	0.1093(3)	0.5525(2)	4.2(1)
C2	−0.1927(5)	0.0883(3)	0.6101(2)	4.1(1)
C3	−0.0714(5)	0.1374(3)	0.5654(2)	3.4(1)
C4	−0.1742(5)	0.1798(3)	0.5314(2)	3.9(1)
C5	0.0246(5)	0.1815(3)	0.6006(2)	3.7(1)
C6	0.1134(6)	0.1388(3)	0.6326(3)	4.6(1)
C7	0.2013(6)	0.1769(4)	0.6670(3)	6.0(2)
C8	0.2042(6)	0.2585(4)	0.6694(3)	6.7(2)
C9	0.1201(7)	0.3025(3)	0.6378(3)	6.1(2)
C10	0.0295(6)	0.2644(3)	0.6026(3)	4.9(1)
C11	−0.1328(5)	0.2102(3)	0.4567(2)	3.7(1)
C12	−0.2327(5)	0.2363(3)	0.4229(3)	4.5(1)
C13	−0.1947(6)	0.2625(3)	0.3543(3)	5.1(1)
C14	−0.0602(6)	0.2651(3)	0.3203(3)	5.4(1)
C15	0.0395(6)	0.2411(3)	0.3533(3)	5.2(1)
C16	0.0021(5)	0.2130(3)	0.4214(2)	4.5(1)
C17	−0.2594(6)	0.0473(3)	0.4951(3)	5.9(1)
C18	−0.4258(6)	0.1278(4)	0.5774(3)	6.6(2)
C19	−0.2521(6)	0.1268(3)	0.6798(3)	5.3(1)
C20	−0.1649(6)	0.0014(3)	0.6226(3)	5.5(1)

a) $B_{eq}=4/3\ \sum_i\sum_j B_{ij}\boldsymbol{a}_i\boldsymbol{a}_j$.

Table 3. Bond Distances, Bond Angles, and Dihedral Angles (ϕ) of the Cyclobutane Rings and Torsional Angles (θ)[a]

Compd.	Bond distance/Å		Bond angle/deg		ϕ/deg	θ/deg
1	C_A-C_B	1.576(9)	C_A-C_B-C_C	88.4(6)	18	73.1 (C8-C9-C4-C3)
	C_A-C_D	1.573(10)	C_B-C_C-C_D	90.0(6)		74.6 (C14-C15-C3-C4)
	C_B-C_C	1.581(10)	C_C-C_D-C_A	89.5(7)		
	C_C-C_D	1.551(10)	C_D-C_A-C_B	89.4(6)		
2	C_A-C_B	1.57(2)	C_A-C_B-C_C	88(1)	3	79.9 (C8-C9-C4-C3)
	C_A-C_D	1.56(2)	C_B-C_C-C_D	91(1)		78.5 (C11-C16-C2-C1)
	C_B-C_C	1.57(2)	C_C-C_D-C_A	90(1)		
	C_C-C_D	1.54(2)	C_D-C_A-C_B	90.8(9)		
3	C_A-C_B	1.575(6)	C_A-C_B-C_C	87.9(3)	22	77.4 (C12-C11-C1-C4)
	C_A-C_D	1.578(6)	C_B-C_C-C_D	90.9(3)		81.5 (C10-C5-C4-C1)
	C_B-C_C	1.551(6)	C_C-C_D-C_A	87.0(3)		
	C_C-C_D	1.574(6)	C_D-C_A-C_B	89.9(3)		
4	C_A-C_B	1.548(8)	C_A-C_B-C_C	89.4(5)	28	89.5 (C6-C5-C1-C2)
	C_A-C_D	1.531(9)	C_B-C_C-C_D	87.9(5)		86.5 (C16-C11-C2-C1)
	C_B-C_C	1.514(8)	C_C-C_D-C_A	89.9(5)		
	C_C-C_D	1.517(9)	C_D-C_A-C_B	86.2(5)		
5	C_A-C_B	1.539(6)	C_A-C_B-C_C	89.6(3)	23	8.3 (C10-C5-C1-C2)
	C_A-C_D	1.554(6)	C_B-C_C-C_D	88.3(3)		4.2 (C12-C11-C2-C1)
	C_B-C_C	1.550(6)	C_C-C_D-C_A	89.3(4)		
	C_C-C_D	1.544(6)	C_D-C_A-C_B	88.3(4)		
6	C_A-C_B	1.523(5)	C_A-C_B-C_C	88.4(3)	30	11.3 (C16-C11-C4-C3)
	C_A-C_D	1.549(5)	C_B-C_C-C_D	87.3(3)		2.3 (C10-C5-C3-C4)
	C_B-C_C	1.557(5)	C_C-C_D-C_A	86.3(3)		
	C_C-C_D	1.590(5)	C_D-C_A-C_B	90.0(3)		

a) See Fig. 4.

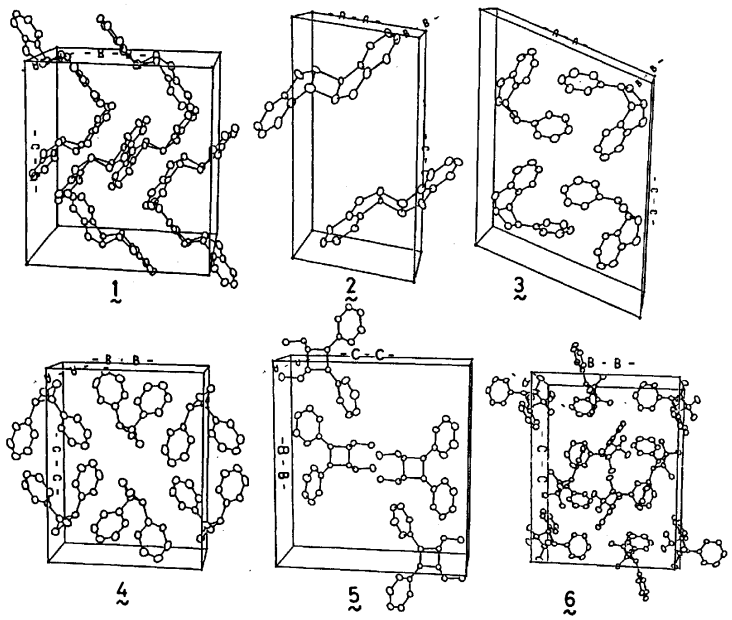

Fig. 2. Crystal-packing diagrams of **1**—**6**.

dihedral angles (ϕ) between the $C_AC_BC_D$ and $C_BC_CC_D$ planes of the cyclobuatne rings, and torsional angles (θ) between the planar ring of the aryl substituent and the plane involving ipso carbon of the aryl group and the C_A-C_B bond. Figure 4 shows the relevant angles, together with notation of the cyclobutane-ring carbon atoms, which are used in further discussion for convenience. These data are shown in Table 3.

The bond distances of the cyclobutane ring of **1**—**3** are slightly longer than the normal distances of monocyclic cyclobutanes (1.52—1.56 Å),[1] perhaps due to the fused tricyclic or bicyclic structure. However, it is important to note that the C_A-C_B bond of **1** and **3** is not unusually longer than the cyclobutane-ring bonds of head-to-tail cyclobutane **2**. The C_B-C_C and C_C-C_D bonds of **4** are relatively short, suggesting a slight distortion of the cyclobutane ring which might arise from steric repulsion between the vicinal phenyl

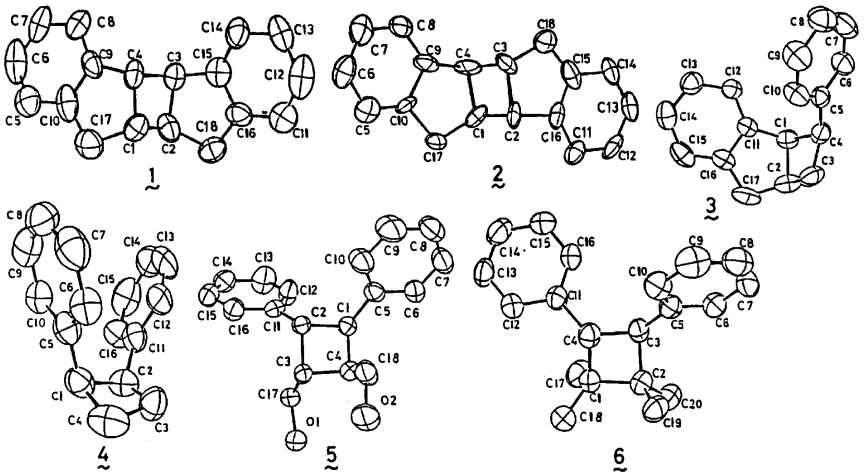

Fig. 3. ORTEP drawing of molecular structures of **1**—**6**.

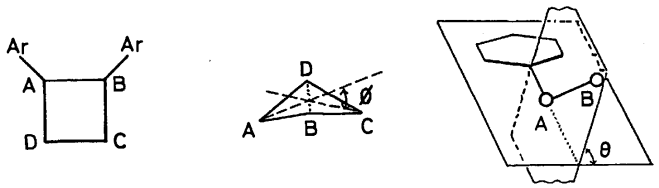

Fig. 4. Notation of each carbon atom of the cyclobutane ring, dihedral angle (ϕ), and torsional angle (θ).

groups in the cis configuration, as shown by the molecular structure in Fig. 1 as well as by molecular models. Similarly, the long C_C-C_D distance of **6** can be attributed to nonbonding interactions between the methyl substituents at C_C and C_D. However, it should be noted that the C_A-C_B distances of **4**—**6** fall within the normal values. The cyclobutane rings of **1**—**6** commonly take puckering forms, in which the $C_AC_BC_D$ and $C_BC_CC_D$ planes meet at the C_B-C_D line with normal dihedral angles (3—30°).[1] The bond angles of the cyclobutane rings are also normal, very close to 90°. It is, therefore, appropriate to conclude that these cyclobutanes are not unusually distorted but, rather, relatively normal.

Of particular related significance regarding through-bond coupling is that the θ values are close to 90° in the cases of **1**, **3**, and **4** but very small (2.3—11.3°) in the cases of **5** and **6**. The solid-state conformations of the aryl substituents should be virtually preserved in solution as well, since the rotational motions of the aryl rings are almost frozen by the rigid tricyclic structures of **1** and **2**, and are largely restricted by nonbonding interactions between the phenyl ring and the vicinal cis substituents in **3**—**6**. This is strongly supported by comparisons of the C_A-H chemical shifts in ^{1}H NMR using **1** as a reference compound with an almost fixed conformation. The resonance of C_A-H of **1** appears at δ 3.50, being considerably higher in field than that of **3** (the methine proton of the indan moiety, δ 3.98) and also than that of **4** (PhC-H, δ 3.92). This is clearly due to shielding of C_A-H by the opposite aryl ring at C_B facing to this proton, while the cis configuration of the two aryl substituents of **3** and **4** prohibits such magnetic anisotropic effects on $C_A(C_B)$-H. The aromatic resonances of **3** and **4** are spread over a wider range of field, δ 6.03—7.8 for **3** and δ 6.61—7.3 for **4** compared with those of **1** (δ 6.8—7.3) and **5**—**8** (δ 6.8—7.4), thus indicating that the aryl rings of **3** and **4** take face-to-face conformations, i.e., $\theta \approx 90°$. On the other hand, the C_A-H resonance of **5** (δ 4.22) is much lower in field than that of **1**, irrespective of similar configurational situations and even lower than that of **4**. This is in line with the solid-state conformation of **6** in Fig. 3, since $C_A(C_B)$-H should be deshielded by the phenyl ring at $C_B(C_A)$. In the case of **6**, however, the deshielding effects of the phenyl ring should be counterbalanced by the shielding effects of the methyl group at $C_D(C_C)$ facing to $C_A(C_B)$-H, whereas one of the geminal ring facing to this group. As a result, **6** reveals a C_A-H(C_B-H) resonance at δ 3.55 and two methyl signals at δ 0.80 and 1.13.

Structure-Dependent Orbital Interactions Associated with Through-Bond Coupling. Figure 5 shows qualitative molecular-orbital diagrams of 1,2-diphenylcyclobutane with $\theta = 90°$ using Salem's σ orbital of cyclobutane[2a] and combinations of the π orbitals of benzene and toluene as the basis-set orbitals, which are symmetric or antisymmetric with respect to two-fold rotation or reflection. As shown in Fig. 6, the π orbitals of "head-to-head" diarylcyclobutanes may interact with the C_A-C_B σ orbitals or with the C_A-C_D and C_B-C_C σ orbitals, depending on the conformations of aryl substituents. The rigid tricyclic structure of **1** or the cis configurations of the vicinal aryl substituents of **3** and **4** almost freeze the conformations of the aryl groups favorable to maximum orbital overlapping of the π orbitals with the C_A-C_B σ orbitals, as demonstrated by the observed

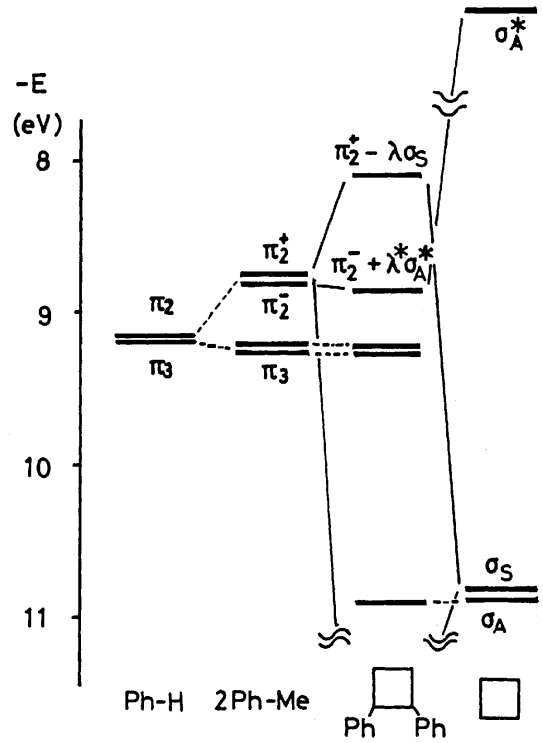

Fig. 5. Schematic molecular-orbital diagrams of 1,2-diphenylcyclobutane with θ=90°; the energy levels of the isolated π and σ orbitals are those of benzene, toluene, and parent cyclobutane, whereas that of $\pi_2^+ - \lambda\sigma_S$ is estimated from the reported ionization potential of *trans*-1,2-diphenylcyclobutane.

torsional angles (θ) being very close to 90°. In the cases of these cyclobutanes (group (i)), the symmetric π_2 combination (π_2^+) can interact with symmetric σ_S to give the highest-occupied molecular orbital (HOMO), $\pi_2^+ - \lambda\sigma_S$, whereas the antisymmetric combination (π_2^-) may interact with σ_A^* to give a bonding MO, $\pi_2^- + \lambda^*\sigma_A^*$.[11,12]

On the other hand, the θ values of **5** and **6** (group (ii)) are very small (2.3—11.3°) because of steric repulsion between the phenyl groups and the vicinal methyl or hydroxymethyl substituents in the cis configuration, demonstrating that the π orbitals can not overlap with the orthogonal C_A-C_B σ orbitals but can do so favorably with the C_A-C_D and C_B-C_C σ orbitals. Such restricted conformations should allow only π_2^--σ_A and π_2^+-σ_S^* interactions, which are certainly ineffective to through-bond coupling. Similarly, the orbital interactions of head-to-tail cyclobutane **2** are ineffective regarding through-bond coupling.

Probably, **7** falls in group (i), since the phenyl substituents can take conformations of $\theta \approx 90°$ without steric repulsion. In this regard, it should be noted that the chemical shift of C_A-H (C_B-H) of **7** (δ 3.50) in the ^{1}H NMR spectrum is the same as that of **1**, but higher in field than that of **4**. This suggests that the phenyl rings of **7** assume stable conformations similar to the structure of **1**. On the other hand, **8** belongs to group (ii), as indicated by the C_A-H (C_B-H) chemical shift (δ 4.10) which is very similar to that of **5** (δ 4.22), but lower in field than that of **1**.

Since the reported ionization potential of **7** (8.2 eV)[19] is considerably lower than those of alkylbenzenes (8.7—8.8 eV),[20,21] through-bond coupling substantially occurs in group (i) cyclobutanes, i.e., $\lambda > 0$. Furthermore, the group (i) cyclobutanes show oxidation waves in cyclic voltammetry at considerably lower potentials than the others; the observed half-peak oxidation potentials ($E_{p/2}^{ox}$ vs. Ag/$AgNO_3$ in CH_3CN) are 1.32 V for **1**, 1.29 V for **4**, and 1.33 V for **7** compared with 1.49 V for **2**, with 1.53 V for **6**, and with 1.63 V for **8**.[3,5] Although all the cyclobutanes reveal irreversible waves in cyclic voltammetry, the irreversible oxidation potentials would be linearly correlated with the energy levels of the HOMO's of the cyclobutanes, as demonstrated for the oxidation potentials of

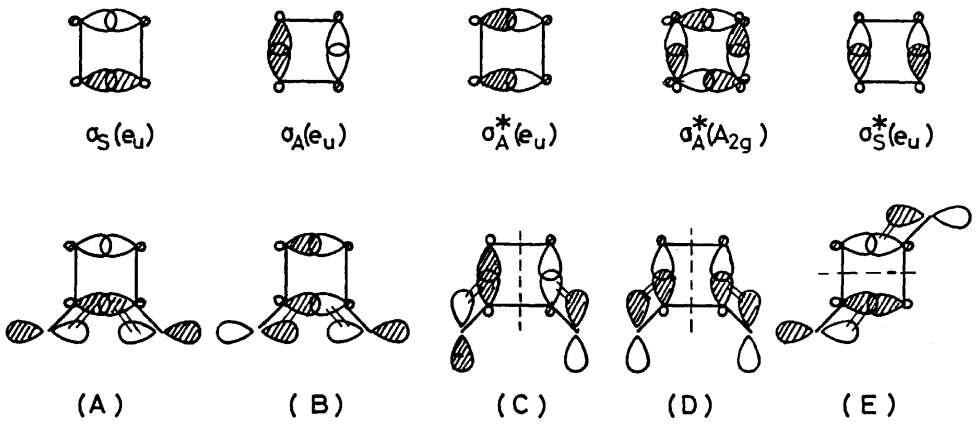

Fig. 6. Top: Salem's σ and σ^* orbitals of cyclobutane. Bottom: (A) π_2^+-σ_S and (B) π_2^--σ_A^* interactions in "head-to-head" cyclobutanes with $\theta \approx 90°$; (C) π_2^--σ_A and (D) π_2^+-σ_S^* interactions in "head-to-head" cyclobutanes with $\theta \approx 0°$ which are ineffective to through-bond coupling; (E) π-σ interactions in "head-to-tail" cyclobutane **2** which are ineffective to through-bond coupling.

homoleptic alkylmetals and various organic compounds.[22] It might, thereforee, be reasonable to conclude that the π_2 orbitals can significantly couple through interactions with σ_S for the group (i) cyclobutanes while through-bond coupling of π_2 is negligible or inefficient in the other cases, as predicted.

In cases of the group (i) cyclobutanes, the π orbitals may again couple through π_2^--σ_A^* interactions to result in a mixing of the σ^* character in a bonding MO which should bring about a specific elongation of the C_A-C_B bond.[13,14] However, the C_A-C_B bond is normal in the case of **4** or not particularly longer in the cases of **1** and **3** than the other bonds nor than the cyclobutane-ring bonds of **2**. This indicates that π_2^--σ_A^* interactions are not important below room temperature, i.e., $\lambda^* \approx 0$. This is again true for the group (ii) cyclobutanes, as demonstrated by the observed cyclobutane-ring distances. Presumably, the energy levels of σ^*'s are too high for appreciable π-σ^* interactions to occur without any vibrational activation of the relevant σ bond. However, such orbital interactions should play important roles in the transition states of the thermal ring-splitting reactions where σ bonds are vibrationally perturbed (vide infra).

Implications of Through-Bond Coupling in Bond-Cleavage Reactions. The selective C_A-C_B bond cleavage of the group (i) cyclobutanes is effected by redox photosensitization,[3] by exciplex[5] or electron-transfer[6] photosensitization with electron acceptors, and by γ-radiolysis in butyl chloride,[8] giving the corresponding olefins in most cases, as shown in Scheme 1. By contrast, no chemical change of the other cyclobutanes occurs at all by these reactions. The different chemical behavior of the diarylcyclobutanes is certainly in parallel with capabilities of the π-electron systems in coupling through the cyclobutane-ring σ framework.

A key chemical event in the reactions shown in Scheme 1 is the population of a positive charge on the cyclobutanes by charge resonance with a cation radical species and by charge-transfer interactions with or electron transfer to an excited-state electron acceptor. The positive charge population on the group (i) cyclobutanes should be delocalized over the π_2-σ_S-π_2 orbital array, thus leading to decreases in both the C_A-C_B bonding character and the C_A-C_D (C_B-C_C) antibonding character of σ_S, resulting in both a weakening of the C_A-C_B bond and a shortening of the C_A-C_D and C_B-C_C bonds.[23] This is the driving force for the selective bond cleavage of the group (i) cyclobutanes. In the cases of the other cyclobutanes, however, the positive charge should be mostly localized on the isolated-π_2 orbital to cause only minor or slight perturbation of the cyclobutane-ring σ framework, since through-bond coupling is much weaker or disallowed to occur. This is clearly ineffective to bond-cleavage reactions.

Thermal ring-splitting reactions of the "head-to-head" cyclobutanes reveal interesting features in regiochemistry as well as in reactivities, depending on the stable conformations associated with different orbital interactions (Scheme 2).[9] Exclusive or dominant C_A-C_B cleavage occurs upon heating **1**, **4**, or **7** to give

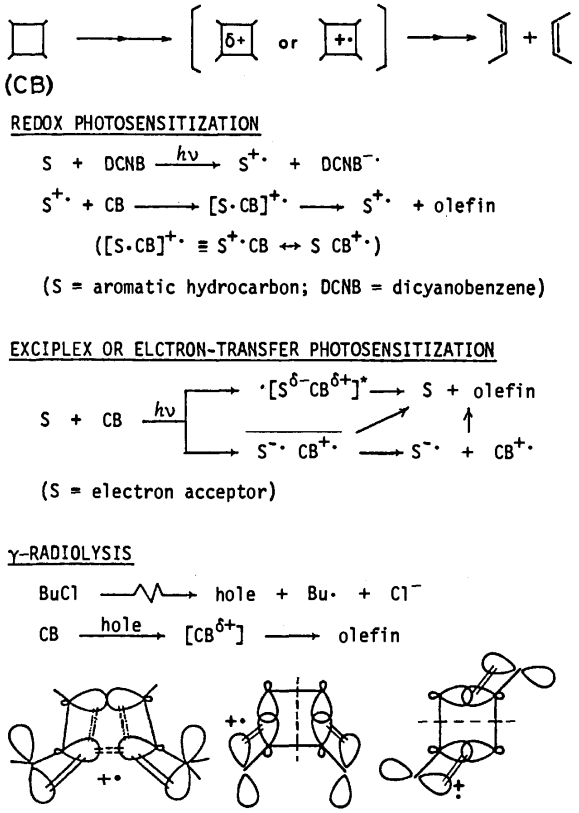

Scheme 1.

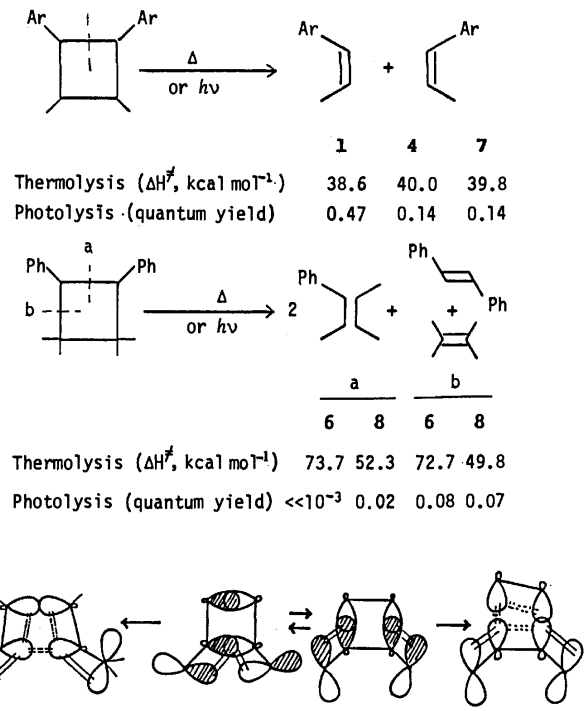

Scheme 2.

indene or styrene with activation enthalpies of ca. 40 kcal mol^{-1},[9,24] while **6** and **8** undergo nonselective cleavages of both the C_A-C_B and C_A-C_D bonds with higher activation enthalpies (50—74 kcal mol^{-1}).[9] These observations can be interpreted in terms of conformation-controlled π-σ^* interactions.

Although π-σ^* interactions are negligeble below room temperature, extensive vibrations at elevated temperatures bring about a skeletal distortion of the cyclobutane ring, which should perturb the σ^* levels to allow π-σ^* interactions. Since mixing of the σ_A^* character by π_2^--σ_A^* interactions is inherently more efficient than that of the σ_S^* character by π_2^+-σ_S^* interactions, the activation barriers for the C_A-C_B cleavage should be lower than those for the C_A-C_D (C_B-C_C) cleavage unless the relevant orbital interactions are sterically inhibited. Consequently, the C_A-C_B bond is selectively cleaved in cases of group (i) cyclobutanes where π_2^--σ_A^* interactions are coformationally allowed. On the other hand, nonbonding interactions between the phenyl and the methyl substituents in **6** and **8** inhibit the phenyl rings from taking conformations for π_2^--σ_A^* interactions, thus imposing additional rotational barriers for the C_A-C_B cleavage. This might be the reason why the thermal reactions of **6** and **8** nonselectively occur with higher activation barriers.

The above arguments imply that the effects of through-bond coupling are not static but, rather, dynamic in nature in the control of stereochemical reaction courses in the ring splitting of the diarylcyclobutanes. This is more explicitly shown in photochemistry. The absorption and fluorescence spectra of the cyclobutanes are essentialy identical with those of indan or toluene, independently of the different conformations of the aryl groups,[7] thus demonstrating that the spectroscopic ground and excited singlet states of the cyclobutanes are the same as those of the isolated π chromophores with slight electronic perturbation. Nevertheless, both regioselectivities and efficiencies in the photolytic ring-cleavage reactions are apparently controlled by different orbital interactions, depending on the restricted stable conformations,[7,25] through π^*-σ^* interactions should be taken into consideration when considering the photochemistry.

Conclusion

Among the molecular-structure parameters of the "head-to-head" diarylcyclobutanes which have been determined by X-ray crystallographic analyses, torsional angles (θ) between the aryl ring and the ipso C-C_A-C_B plane are directly related to the different reactivities of the group (i) and group (ii) cyclobutanes in various types of ring-splitting reactions. With $\theta \approx 90°$, through-bond coupling can occur by π-σ_S interactions to give the HOMO and by π-σ_A^* interactions which result in the mixing of the σ_A^* character in a bonding MO. On the other hand, restricted conformations of the aryl groups with $\theta \approx 0°$ allow only π-σ_A and π-σ_S^* interactions which are ineffective to through-bond coupling. The efficient regioselective cleavage of the C_A-C_B bond of the group (i) cyclobutanes can, thus, be interpreted in terms of the delocalization of a positive charge over the π-$C_A(\sigma)$-$C_B(\sigma)$-π orbital array upon partial or complete removal of an electron, in terms of stabilization of the transition state of thermal reaction due to mixing of σ_A^* character at elevated temperature, and in terms of π^*-σ_A^* interactions in direct photolysis. Such effects of through-bond coupling might not be effective regarding the bond-cleavage reactions of group (ii) cyclobutanes. The through-bond coupling concept might provide a general rationale for interpreting the steric control of chemical reaction courses in the cleavage of a C-C bond with vicinal π or n substituents.

This research was supported by a Grant-in-Aid for Scientific Research from the Ministry of Education, Science and Culture (No. 62550616). We express our hearty thanks to the Research Center for Material Analysis in Miyazaki University for the use of the X-ray diffractometer and also to Professor Emeritus Hiroshi Sakurai and Professor Shozo Yanagida of Osaka University for their encouragement throughout this work.

References

1) R. M. Moriarty, *Top. Stereochem.*, **8**, 271 (1974).
2) a) L. Salem and J. S. Wright, *J. Am. Chem. Soc.*, **91**, 5947 (1969). b) R. Hoffman and R. B. Davidson, *ibid.*, **93**, 5699 (1971).
3) T. Majima, C. Pac, and H. Sakurai, *J. Am. Chem. Soc.*, **102**, 5265 (1980).
4) T. Majima, C. Pac, and H. Sakurai, *J. Chem. Soc., Perkin Trans. 1*, **1980**, 2705.
5) a) C. Pac, T. Ohtsuki, Y. Shiota, S. Yanagida, and H. Sakurai, *Bull. Chem. Soc. Jpn.*, **59**, 1133 (1986). b) C. Pac, *Pure Appl. Chem.*, **58**, 1249 (1986).
6) C. Pac, T. Fukunaga, Y. Go-An, T. Sakae, and S. Yanagida, *J. Photochem. Photobiol. A: Chemistry*, **41**, 37 (1987).
7) C. Pac, Y. Go-An, and S. Yanagida, *Bull. Chem. Soc. Jpn.*, **62**, 1951 (1989).
8) a) T. Majima, C. Pac, S. Takamuku, and H. Sakurai, *Chem. Lett.*, **1979**, 1149. b) C. Pac, T. Majima, S. Takamuku, and H. Sakurai, *Nippon Kagaku Kaishi*, **1984**, 1880.
9) M. Yasuda, K. Yoshida, K. Shima, and C. Pac, *Bull. Chem. Soc. Jpn.*, **62**, 1943 (1989).
10) C. Pac, J. Kubo, T. Majima, and H. Sakurai, *Photochem. Photobiol.*, **36**, 2773 (1982).
11) R. Hoffman, *Acc. Chem. Res.*, **1**, 1 (1971).
12) a) R. Gleiter, K. Gubernator, and W. Grimme, *J. Org. Chem.*, **46**, 1247 (1981). b) P. Bischof, R. Gleiter, K. Gubernator, R. Haider, H. Musso, W. Schwarz, W. Trautman, and H. Hopf, *Chem. Ber.*, **114**, 994 (1981). c) R. Gleiter and K. Gubernator, *ibid.*, **115**, 3811 (1982). d) R.

Gleiter, P. Bischof, K. Gubernator, M. Christl, L. Schwager, and P. Vogel, *J. Org. Chem.*, **50**, 5064 (1985). e) R. Gleitor, W. Sander, and I. Butler-Ransohoff, *Helv. Chim. Acta*, **69**, 1872 (1986).

13) J. Dressel and L. A. Paquette, *J. Am. Chem. Soc.*, **109**, 2857 (1987) and references cited therein.

14) K. Harano, T. Ban, M. Yasuda, E. Osawa, and K. Kanematsu, *J. Am. Chem. Soc.*, **103**, 2310 (1981).

15) a) D. A. Dougherty, H. B. Schlegel, and K. Mislow, *Tetrahedron*, **34**, 1411 (1978). b) D. A. Dougherty, W. D. Hounshell, H. B. Schlegel, R. A. Bell, and K. Mislow, *Tetrahedron Lett.*, **1976**, 3479.

16) W. Metzner and D. Wendisch, *Justus Liebigs Ann. Chem.*, **730**, 111 (1969).

17) R. M. Dodson and A. G. Zielske, *J. Org. Chem.*, **32**, 28 (1967).

18) O. L. Chapman and W. Adams, *J. Am. Chem. Soc.*, **90**, 2333 (1968).

19) G. S. Groenwald, E. K. Chess, and M. L. Gross, *J. Am. Chem. Soc.*, **106**, 539 (1984).

20) K. Watanabe, T. Nakayama, and J. Mottle, *J. Quant. Spectrosc. Radiat. Transfer*, **2**, 369 (1962).

21) K. Kimura, S. Katsumata, Y. Achiba, T. Yamazaki, and S. Iwata, *Handbook of Hel Photoelectron Spectra of Fundamental Organic Molecules*, Japan Scientific Societies Press, Tokyo, (1981).

22) a) R. J. Klingler and J. K. Kochi, *J. Am. Chem. Soc.*, **102**, 4790 (1980). b) L. L. Miller, G. D. Nordblom, and E. Myeda, *J. Org. Chem.*, **37**, 916 (1972).

23) P. Bischoff, E. Haselbach, and E. Heilbronner, *Angew. Chem.*, **82**, 952 (1970).

24) G. Jones, II and V. L. Chow, *J. Org. Chem.*, **39**, 1447 (1974).

25) G. Kaupp and M. Stark, *Chem. Ber.*, **110**, 3084 (1977).

Thermal Ring-Splitting Reactions of Diarylcyclobutanes: Significance of Steric Effects on Orbital Interactions in Transition States and Biradical Intermediates

Masahide YASUDA,* Kouhei YOSHIDA, Kensuke SHIMA, Chyongjin PAC,*,† and Shozo YANAGIDA†
Department of Industrial Chemistry, Faculty of Engineering, Miyazaki University, Gakuen-Kibanadai, Miyazaki 889-21
†Department of Chemical Process Engineering, Faculty of Engineering, Osaka University, Yamadaoka, Suita, Osaka 565
(Received November 17, 1988)

Regiochemistry and reactivities in the thermal ring-splitting reactions of diarylcyclobutanes (**1**—**5**) have been studied and shown to depend on the stable conformations and rotational mobilities of the aryl substituents. The reactions of **1** and **2** result in a regiospecific symmetric cleavage to give indene or styrene along with significant isomerization of **2** to **3**. In the cases of **3**—**5** both the symmetric and unsymmetric cleavages competitively occur with decreasing symmetric-to-unsymmetric ratios with an increase in methyl substitution. The olefin products from **4** are mixtures of *cis*- and *trans*-2-butene, *cis*- and *trans*-β-methylstyrene, and *trans*-stilbene. Thermochemical analyses combined with product analyses indicate that the symmetric cleavage of **1** and the unsymmetric cleavage of **3** proceed with a concerted mechanism, whereas 1,4-biradicals are involved in the other reactions. Structure-reactivity relationships of the present reactions are discussed in terms of mixing of the σ* character in a bonding MO by specific π-σ* interactions, depending on the conformational situations of the aryl groups and in terms of the steric effects which destabilize 1,4-biradicals as well as transition states of the biradical fragmentation to the olefins.

Ring-splitting reactions of cyclobutanes have beeen providing an excelent diagnosis method for exploring the steric and electronic factors controlling chemical reaction courses.[1-3] Theories predict that concerted $[_\sigma 2_s + _\sigma 2_s]$ cycloreversions are forbidden in the ground state.[4] A considerable body of stereochemical and thermochemical evidence indeed supports mechanisms involving 1,4-biradicals in thermal ring-splitting and stereomutation reactions of cyclobutanes with no particular π substituents such as parent cyclobutane,[5,6] alkylcyclobutanes,[7] divinylcyclobutane,[8] and other substituted cyclobutanes,[9] as shown by molecular-orbital considerations.[10,11]

On the other hand, much less has been investigated concerning mechanistic details of thermal reactions of cyclobutanes with large π substituents. It can be presumed that the chemical behavior must be remarkably susceptible to steric and electronic effects of such π substituents, since the cyclobutane rings are small in size and conformationally rigid[12] and since the π-bonding character contributes to the ring σ framework.[13] Since vibrational motions of a C-C bond with a large substituent are very slow, the rate-determining step for the ring cleavage of such cyclobutanes may be not scisson of a C-C bond but rotation or other motions.

It was reported that thermolyses of substituted tetrahydrocyclobuta[*a*]naphthalenes[14] and [4.4.2]propelladienes[15] result in regiospecific ring cleavages to give aromatized products and olefin fragments with high stereoretention. Although the high stereoselectivities would be attributable to steric inhibition of bond rotaion in 1,4-biradicals, an attractive alternative is the participation of a concerted mechanism that would occur as the consequence of extended π conjugation in transition states. This was suggested for thermal reactions of phenylated oxetanes[16] and *cis*-3,6-diphenyl-1,2-diazacyclohexene.[17] Of another stereochemical interest in bond cleavages of π-substituted cyclobutanes are regioselectivities, which would reflect the relative stabilities of different biradicals or which would be controlled by interactions of the π orbitals with each of the σ orbitals of the cyclobutane ring along the reaction coordinate.[1,18]

From the above points of view, we have investigated thermal ring-splitting reactions of diarylcyclobutane (**1**—**5**). It can be expected that the stereochemical features and reactivities of the reactions are controlled by complex combinations of steric and electronic effects of the aryl substituents. We report here mechanistic details concerning the ring-splitting reactions and the significance of steric control of orbital interactions in the stereochemical reaction courses.

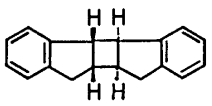

1

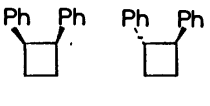

2 3

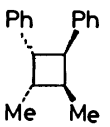

4

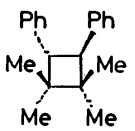

5

Experimental

The cyclobutanes were prepared according to methods described in the literature; *cis-transoid-cis*-cyclobuta[1,2-*a*; 4,3-*a'*]diindene (**1**),[19] *cis*-1,2-diphenylcyclobutane (**2**),[20] *trans*-1,2-diphenylcyclobutane (**3**),[20] *r*-1, *t*-2-dimethyl-*t*-3, *c*-4-diphenylcyclobutane (**4**),[18b] and 1,1,2,2-tetramethyl-*trans*-3,4-diphenylcyclobutane (**5**).[21] Purification was carried out by repeated recrystallization from methanol for **1** and **2** or from hexane for **5**, whereas **3** and **4** were distilled in vacuo. Diphenyl ether was used after vacuum distillation.

Aliquot portions (2 cm^3) of a diphenyl ether solution of **1—5** (0.02 mol dm^{-3}) were introduced into Pyrex tubes (8 mm i.d.), thoroughly degassed by three freeze-pump-thaw cycles under $<10^{-3}$ Torr, and then heated in a Shimadzu GC-6AM electric furnace that had been preheated at given temperatures (±<1 °C). The reactions were followed by vapor-phase chromatography on a Shimadzu GC-8A machine using a 3-m column of 5% OV-17 on Chromosorb W AW-DMCS.

Results

Thermal reactions of **1—5** were performed by heating a degassed diphenyl ether solution (0.02 mol dm^{-3}) at 160—360 °C. The products were exclusively the corresponding olefins, except for the case of **2** where the isomerization to **3** significantly occurred, as shown in Scheme 1. In the cases of **1** and **2**, the ring cleavage is regiospecific in the symmetric (*a*) direction, whereas **3—5** are cleaved in both the symmetric (*a*) and the unsymmetric (*b*) directions in *a*:*b* ratios decreasing with an increase in methyl substitution. Although the formation of ethylene, 2-butene, and 2,3-dimethyl-2-butene was confirmed, their yields were not determined because of analytical difficulties. However the yields of the other products accounted for the conversions of the cyclobutanes within experimental errors (≤5%). It was confirmed that no isomerization of **3** to **2** occurs at all. Similarly, the stereomutation of **4** should be negligible, if any, since no product other than the olefins was detected at all by vapor-phase chromatography (VPC), and since the combined yields of β-methylstyrene and stilbene virtually equaled the amounts of **4** consumed. Although the stilbene formed from **3—5** was only the trans isomer, **4** gave a mixture of *cis*- and *trans*-2-butene in a ca. 35 : 65 ratio independently of temperature and mixtures of *cis*- and *trans*-β-methylstyrene in ratios increasing with an increase in the temperature from 15 : 85 at 280 °C to 27 : 73 at 320 °C. It was confirmed that each isomer of either stilbene or β-methylstyrene is not isomerized at ≤360 °C.

The total rate constants (k_t) for the thermal reactions at various temperature were determined from linear plots of $\ln(C/C_0)$ vs. the reaction time in seconds; C_0 and C represent the concentrations of each cyclobutane before thermolysis and at a given reaction time, respectively. Although k_t equals the rate constant (k_a) for the symmetric cleavage of **1**, each rate constant (k_a, k_b, or k_i) for the symmetric or the unsymmetric cleavage of **2—5** or for the isomerization of **2** to **3** at a given temperature was obtained from k_t multiplied by the molar proportion of the relevant product, styrene product/(styrene product+2×stilbene or 2×**3**), 2×stilbene/(styrene product+2×stilbene), or 2×**3**/(styrene+2×**3**). Table 1 summarizes the calculated rate constants at various temperatures. Figure 1 shows Arrhenius plots of ln k_a, ln k_b, and ln k_i vs. T^{-1} from which the activation enthalpies ($\Delta H_a^{\neq}$, $\Delta H_b^{\neq}$, and $\Delta H_i^{\neq}$) and the frequency factors (A_a, A_b, and A_i) were obtained, as listed in Table 2. In the case of **5**, the unusually high activation barriers and frequency factors appear to involve large experimental errors, because of the very slow reaction occurring even at very high temperatures. Nevertheless, the observed values should indicate that the thermochemical parameters are much larger than those of the other cyclobutanes, thus being of mechanistic significance. Figure 2 shows a plot of ln (cis-trans ratio) vs. T^{-1} for the β-methylstyrene formation from **4**, which gives an activation enthalpy difference of 44.3 kJ mol^{-1}

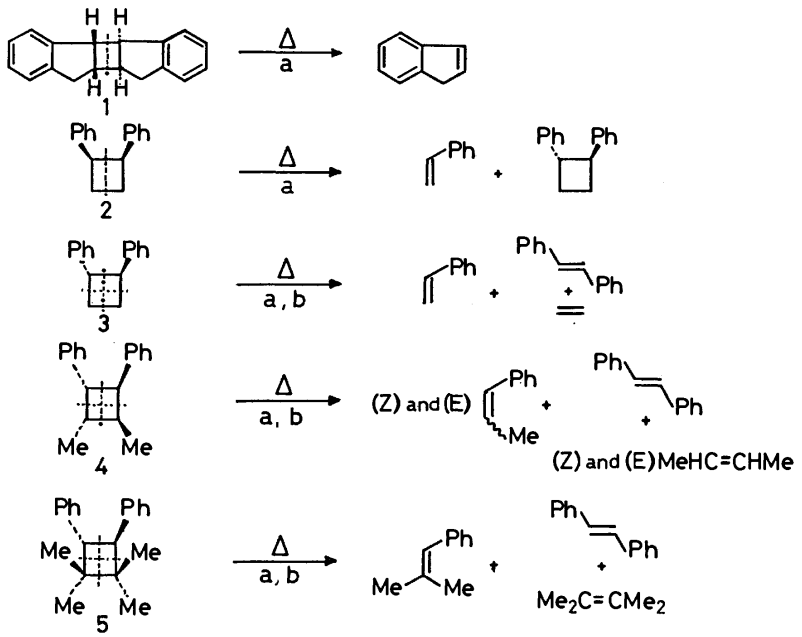

Scheme 1.

Table 1. Rate Constants for Thermal Reactions of **1**—**5**[a)]

1	T/K	493	503	513	523		
	$k_t=k_a$/s^{-1}	1.46×10^{-5}	4.27×10^{-5}	8.73×10^{-5}	1.41×10^{-4}		
2	T/K	433	443	453	463	473	
	k_t/s^{-1}	8.63×10^{-7}	2.65×10^{-6}	6.45×10^{-6}	1.87×10^{-5}	4.44×10^{-5}	
	k_a/s^{-1}	6.13×10^{-7}	1.98×10^{-6}	4.98×10^{-6}	1.43×10^{-5}	3.42×10^{-5}	
	k_i/s^{-1}	2.50×10^{-7}	6.77×10^{-7}	1.47×10^{-6}	4.36×10^{-6}	1.02×10^{-5}	
3	T/K	493	503	513	523		
	k_t/s^{-1}	2.37×10^{-5}	5.83×10^{-5}	1.10×10^{-4}	2.55×10^{-4}		
	k_a/s^{-1}	2.27×10^{-5}	5.64×10^{-5}	1.06×10^{-4}	2.47×10^{-4}		
	k_b/s^{-1}	9.67×10^{-7}	1.88×10^{-6}	4.04×10^{-6}	7.48×10^{-6}		
4	T/K	553	558	563	568	573	578
	k_t/s^{-1}	4.60×10^{-6}	6.13×10^{-6}	9.44×10^{-6}	1.52×10^{-5}	2.32×10^{-5}	3.20×10^{-5}
	k_a/s^{-1}	3.40×10^{-6}	4.39×10^{-6}	6.75×10^{-6}	1.16×10^{-5}	1.68×10^{-5}	2.39×10^{-5}
	k_b/s^{-1}	1.20×10^{-6}	1.74×10^{-6}	2.70×10^{-6}	3.57×10^{-6}	6.37×10^{-6}	8.10×10^{-6}
	T/K	583	588	593	598	603	
	k_t/s^{-1}	4.56×10^{-5}	5.71×10^{-5}	8.55×10^{-5}	1.63×10^{-4}	2.42×10^{-4}	
	k_a/s^{-1}	3.47×10^{-5}	4.22×10^{-5}	6.25×10^{-5}	1.24×10^{-4}	1.88×10^{-4}	
	k_b/s^{-1}	1.10×10^{-5}	1.49×10^{-5}	2.31×10^{-5}	3.88×10^{-5}	5.38×10^{-5}	
5	T/K	603	613	623	633		
	k_t/s^{-1}	3.14×10^{-6}	1.11×10^{-5}	2.78×10^{-5}	6.15×10^{-5}		
	k_a/s^{-1}	4.36×10^{-7}	1.58×10^{-6}	3.95×10^{-6}	9.05×10^{-6}		
	k_b/s^{-1}	2.70×10^{-6}	9.47×10^{-6}	2.38×10^{-5}	5.24×10^{-5}		

a) k_t, rate constant for the consumption of **1**—**5**; k_a, rate constant for the symmetric cleavage of **1**—**5**; k_b, rate constant for unsymmetric cleavage of **3**—**5**; k_i, rate constant for the isomerization of **2** to **3**.

Table 2. Thermochemical Parameters for Thermal Reactions of **1**—**5**[a)]

	1	**2**		**3**		**4**		**5**	
	a	a	i	a	b	a	b	a	b
$\Delta H^{\neq}$/kJ mol^{-1}	161.5	167.4	161.1	166.5	148.1	218.8	208.4	308.4	304.2
$\log A$	12.4	14.0	12.8	13.0	9.7	15.2	13.7	20.6	21.0
$\Delta S^{\neq b)}$/e.u.	−3.8	+3.5	−2.0	−1.1	−16.2	+9.0	+2.2	+37.0	+37.9

a) The letters a, b, and i refer the symmetric ring cleavage, the unsymmetric one, and the isomerization of **2** to **3**. b) Values at 300 K obtained by assuming that the transmission coefficient (κ) is unity.

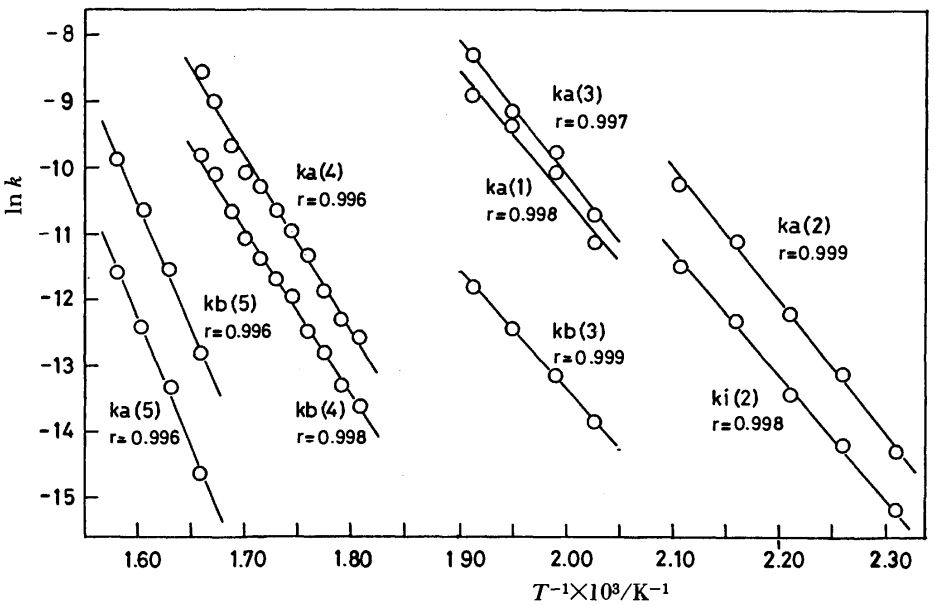

Fig. 1. Arrhenius plots for the thermal reactions of **1**—**5**. k_a, k_b, and k_i are the rate constants for the symmetric cleavage, the unsymmetric cleavage, and the isomerization of **2** to **3**, respectively. Data are from Table 1.

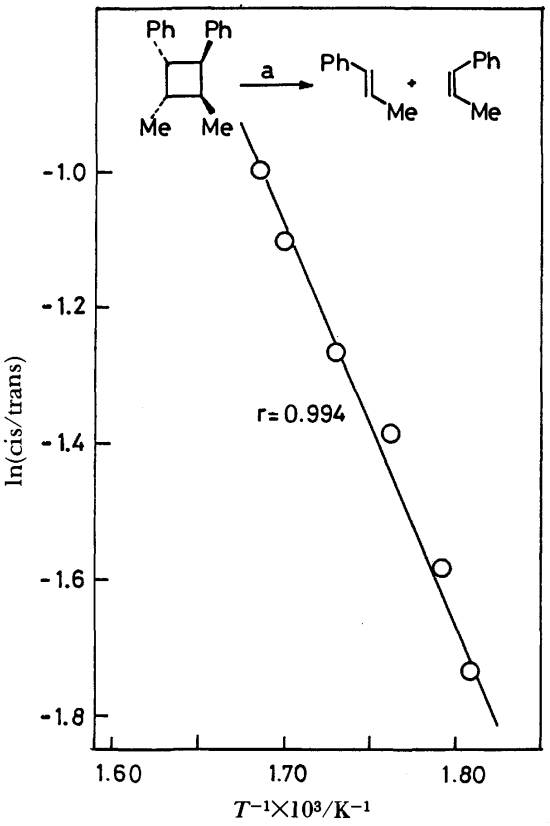

Fig. 2. Plot of ln(cis-trans ratio of β-methylstyrene) vs. T^{-1} for the symmetric cleavage of **4**

and log (A_{cis}/A_{trans}) of 3.4.

Discussion

Mechanisms. The significant isomerization of **2** to **3** and the losses of stereointegrity in the olefin formation from **4** strongly suggest the intervention of 1,4-biradicals in these reactions. The activation barriers for the symmetric cleavage of **1**—**3** are lower by 94—96 kJ mol^{-1} than that of parent cyclobutane.[6] The differences are similar to the energy gained by the benzylic stabilization of 1,4-butanediyl, 2×54 kJ mol^{-1}. Similarly, $\Delta H_b^{\neq}$ of **4** is a value which is expected for a biradical mechanism for unsymmetric cleavage. Furthermore, the frequency factor for the symmetric cleavage of **3** is very similar to those for the isomerization of *trans*-1,2-divinylcyclobutane which proceeds by way of 1,4-biradicals.[8] The high activation barriers and the large frequency factors for the symmetric cleavage of **4** and, in particular, for both the symmetric and the unsymmetric cleavages of **5** are not accommodated with a concerted mechanism, but with considerable structure changes from the relatively rigid cyclobutanes to very loose transition states.

It is of mechanistic significance to note that log A_a of **1** is unusually low for such a two-bond splitting reaction by way of a discrete 1,4-biradical from a very rigid molecule. Since the transition state should be very tight, as shown by the negative entropy change, the symmetric cleavage of **1** appears to proceed by a concerted or concerted-like mechanism. The rigid tricyclic structure is certainly favorable for efficient orbital overlap between the C-C bonds being broken with minimum molecular motions. By the same token, the unsymmetric cleavage of **3** should be concerted since $\Delta S_b^{\neq}$ at 300 K is −16.2 e.u., still more negative than the entropy change for the concerted Cope rearrangement of *cis*-1,2-divinylcyclobutane to 1,5-cyclooctadiene.[8] Futhermore, $\Delta H_b^{\neq}$ of **3** is much smaller than that of **4** and even smaller than a calculated enthalpy difference (≈163 kJ mol^{-1}) between **3**

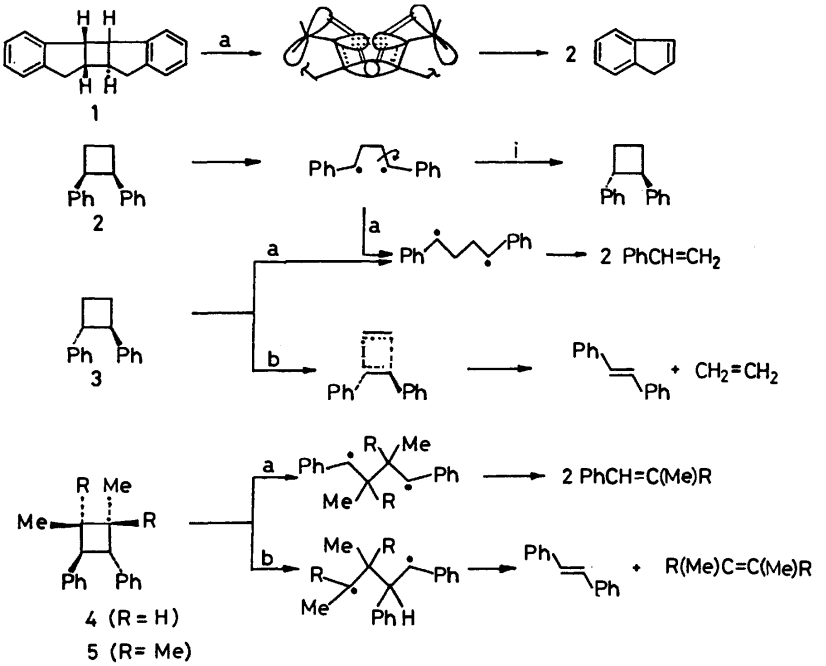

Scheme 2.

and 1,2-diphenyl-1,4-butanediyl.[2,23] Effective vibrational motions are probably not inhibited by any steric interactions in **3**, thus realizing the simultaneous cleavage of the C1-C4 and C2-C3 bonds. Scheme 2 summarizes the mechanisms for the thermal reactions of **1**—**5**.

Stereoelectronic Effects on Regioselectivities and Reactivities. The present thermal reactions can not be interpreted in terms of simple steric and electronic effects, e.g., steric assistance of bond breaking by nonbonding interactions between the substituents or benzylic stabilization of 1,4-biradicals. For instance, $\Delta H_a^{\neq}$ of **4** is higher than $\Delta H_b^{\neq}$, even though the 1,4-biradical intermediate for the symmetric cleavage is evidently more stable than that for the unsymmetric one. Another interesting observation is that $\Delta H_a^{\neq}$ of **2** is almost identical with that of **3** irrespective of large steric repulsion between the cis phenyl groups expected for **2**. It appears that both the regioselectivities and the reactivities are controlled by restricted conformations and torsional mobilities of the aryl substituents associated with specific orbital interactions, as demonstrated for photochemical reactions of the cyclobutanes.[1,18]

Figure 3 shows different stable conformations of the aryl substituents, case (i) and case (ii), with respect to each of the ring C-C bonds; the arylated carbon atoms

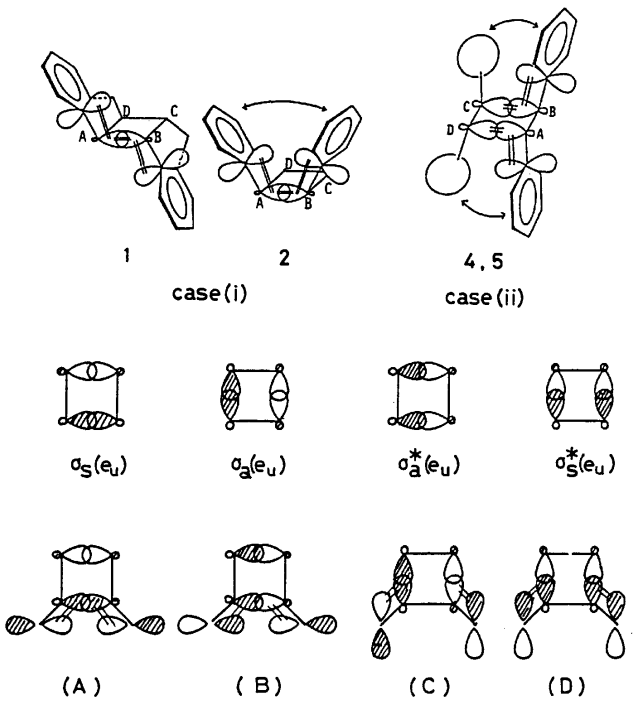

Fig. 3. Top: Different situations for stable rotameric conformations of the aryl rings, case (i) for **1** and **2** and case (ii) for **4** and **5**, associated with specific orbital interactions. Middle: Salem's σ and σ^* orbitals relevant for interactions with the π combinations. Bottom: (A) π_s-σ_s and (B) π_a-σ_a^* interactions occurring in case (i) and (C) π_a-σ_a and (D) π_s-σ_s^* interactions in case (ii)

are abbreviated as C_A and C_B and the others as C_C and C_D for convenience. In order to elucidate implications of orbital interactions in the present reactions, we consider conformation-controlled interactions of Salem's σ and σ^* orbitals of the cyclobutane ring[24] with combinations of the π orbitals, $\pi_s=\pi_A+\pi_B$ and $\pi_a=\pi_A-\pi_B$; subscript s or a denotes the symmetric or antisymmetric character with respect to two-fold rotation or reflection. In case (i), π_s-σ_s (A in Fig. 3) and π_a-σ_a^* (B) interactions can occur to give the highest occupied MO, $\pi_s-\lambda_1\sigma_s$ and a lower bonding MO, $\pi_a+\lambda_1^*\sigma_a^*$, respectively.[25] Similarly, π_a-σ_a (C) and π_s-σ_s^* (D) interactions may occur in case (ii) to give the bonding MO's, $\pi_a-\lambda_2\sigma_a$ and $\pi_s+\lambda_2^*\sigma_s^*$. The π-σ^* interactions should result in mixing of the σ_a^* or σ_s^* character to bring about a weakening of the relevant C-C bonds of the cyclobutane ring, while such bond-weakening effects can not be expected for the π-σ interactions. It is, therefore, reasonable to presume that the π_a-σ_a^* and π_s-σ_s^* interactions are responsible for the symmetric and the unsymmetric cleavages respectively.

It was reported that significant mixing of σ^* character in a bonding MO occurs by through-bond coupling between two π orbitals separated by a C-C bond to bring about unusual elongation of this bond.[26,27] Although the cyclobutane-ring C-C bonds of **1**, **2**, and **5** are not particularly long in common,[28] extensive vibrational and puckering motions of the cyclobutane ring might perturb the σ^* orbitals to allow significant π-σ^* interactions. It should be noted that the π_a-σ_a^* interactions are inherently more effective to through-bond coupling between π_A and π_B than the π_s-σ_s^* interactions. It can, therefore, be predicted that the symmetric cleavage selectively occurs unless there is particular steric inhibition in the orbital interactions. On the other hand, the unsymmetric cleavage may compete with the symmetric one in cases where π_a-σ_a^* interactions are sterically inhibited. This prediction is in good accord with the observed regioselectivities in the reactions of **1**—**5**.

On the basis of these arguments, the reason why $\Delta H_a^{\neq}$ of **3** is almost identical with that of more congested **2** can be easily interpreted by assuming that π_a-σ_a^* interactions are essential in the transition state of the symmetric cleavage of **2** and **3**. Furthermore, the lower-frequency factor for the symmetric cleavage of **3** than that of **2** indicates that a net loss of the rotational motions of the phenyl groups is required for the π_a-σ_a^* interactions in the transition state of **3**, while the orbital interactions are realized with least rotational motions in the case of **2**. Similarly, the thermochemical parameters reveal that the unsymmetric cleavage of **4** proceeds without either significant steric hindrance or large structure changes, being accommodated with the process from stable case (ii) conformations to the π_s-σ_s^* transition state. On the other hand, the relatively large values of $\Delta H_a^{\neq}$ and $\log A_a$ for

the symmetric cleavage of **4** are attributable to steric inhibition of case (i) conformations required for the π_a-σ_a* in transition state. In the case of **5**, the very high activation barriers and the unusually large frequency factors are certainly accommodated with very loose transition states, thus suggesting that the rate-determining step is no longer the orbital interactions but, perhaps, bond breaking of 1,4-biradicals.

Steric Effects on Reactivities of 1,4-Biradicals. Activation enthalpies for cyclization and fragmentation of 1,4-biradicals are usually ca. 30 kJ mol^{-1} in the absence of particular steric inhibition.[2] The cyclization of 1,4-diphenylbutanediyl must suffer a remarkable steric hindrance by the phenyl substituents at the radical centers to require a high activation barrier. Calculations according to the additivity of bond and group properties[2,23] allow us to estimate the heat of formation of **3** or 1,4-diphenylbutanediyl (**3**-BR$_a$) which is 245.8 kJ mol^{-1} or 353.6 kJ mol^{-1} each. The activation enthalpy for the cyclization of **3**-BR$_a$ is, therefore, calculated from the estimated values of the heat of formation and $\Delta H_a^{\neq}$ to be ca. 58 kJ mol^{-1}, a relatively large value in accord with the prediction of remarkable steric hindrance. Moreover, the relatively low value of log A_i of **2** is comparable to that for the isomerization of *cis*-1,2-diphenylcyclopropane.[22] Consequently, the significant isomerization of **2** to **3** is not attributable to the cyclization of a thermally equilibrated 1,4-biradical but, rather, to torsion about PhC-C of a non-streched 1,4-biradical followed by efficient bonding with least motion. On the other hand, the biradical fragmentation of **2** or **3** to styrene appears to proceed with a lower activation barrier since an orbital overlap between each of the radical centers and the C$_C$-C$_D$ bond is easily achieved without steric inhibition.

In the cases of **4** and **5**, however, steric hindrance should be significant for both the ring closure and the fragmentation of 1,4-biradicals because of the substitution of the methyl or the phenyl group at each carbon, as shown in Fig. 4. Extensive gauche interactions in the biradical (**4**-BR$_a$) for the symmetric cleavage of **4** certainly destabilize the biradical to contribute, at least in part, to the high value of $\Delta H_a^{\neq}$, while such steric interactions are less in **4**-BR$_b$, the biradical for the unsymmetric cleavage. Provided that the biradical fragmentation requires orbital overlap between each of the radical centers and the C-C bond being broken,[2,29] the transition state for the *cis*-β-methylstyrene from **4**-BR$_a$ should require much greater vibrational motions than that for the trans-olefin formation. This is in line with the observed difference in either the activation enthalpy or the frequency factor for the formation of *cis*- and *trans*-β-methylstyrene. The rotation of the massive PhCH group is perhaps rate determining. On the other hand, the temperature-independent cis-trans ratio in the 2-butene formation from **4** implies that the rate-determining step is the initial cleavage of C$_A$-C$_D$ (C$_B$-C$_C$) of the cyclobutane ring, since the rotation of the light MeCH group of **4**-BR$_b$ should be very rapid.

In particular, the biradicals of **5** (**5**-BR$_a$ and **5**-BR$_b$) are clearly very crowded and perhaps destabilized by large nonbonding interactions between the substituents.[30] The radical centers of **5**-BR$_a$ suffer large steric repulsion with the bulky substituents at quarter-

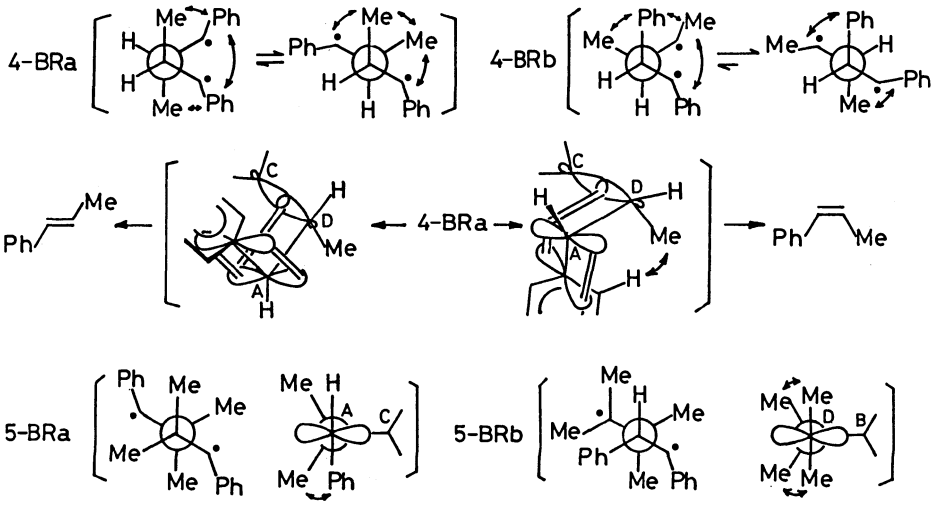

Fig. 4. Top: Newman projection formulas of **4**-BR$_a$ and **4**-BR$_b$ showing that the former is sterically more crowded than the latter. Middle: Perspective illustration of hypothetical transition states for the biradical fragmentation of **4**-BR$_a$ to *cis*- and *trans*-β-methylstyrene. Bottom: Newman projection formulas of **5**-BR$_a$ and **5**-BR$_b$ showing that either of the biradicals is sterically very crowded and that the radical centers are sterically hindered either in taking a planar conformation or in overlapping between the p orbitals and the C-C σ orbitals being broken.

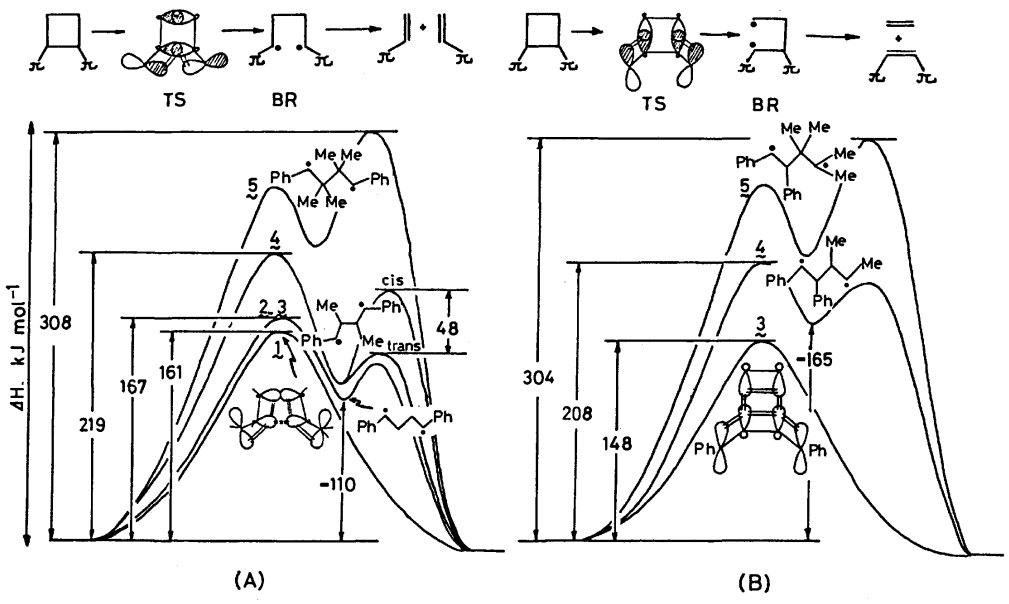

Fig. 5. Schematic potential surface diagrams for (A) the symmetric cleavage of **1**—**5** and (B) the unsymmetric cleavage of **3**—**5**. The numerals are enthalpy differences in kJ mol^{-1}.

nary carbon to inhibit the phenyl rings from taking the coplaner conformations required for benzylic stabilization. Similarly, large nonbonding interactions might destabilize **5**-BR$_b$ by a possible distortion of the Me_2C radical center from a planar conformation. More importantly, such large nonbonding interactions again impede the maximum overlap between the p orbitals of the radical centers and the C-C σ orbitals being broken. Such large steric effects on the destabilization of biradicals as well as on the biradical fragmentation should contribute to the very high values of $\Delta H_a^{\neq}$ and $\Delta H_b^{\neq}$. It is therefore suggested that the biradical fragmentation is rate determining in either the symmetric or the unsymmetric cleavage of **5**. Since the frequency factors are unusually large, extensive vibrational and rocking motions of C-Me are probably important in relieving large steric hindrance in the transition state.

Conclusion

Figure 5 shows schematic potential surface diagrams for the thermal reactions of the diarylcyclobutanes as a summary. The symmetric cleavage of **1** and the unsymmetric cleavage of **3** proceed by a concerted or concerted-like mechanism because of the small steric perturbation in realizing a "pericyclic" transition state, whereas 1,4-biradicals are involved in the other reactions. The net regiochemistry and the reactivities are controlled by both stable conformations and rotational mobilities of the aryl substituents associated with the π_a-σ_a* and π_s-σ_s* interactions occurring by thermal activation. Since the σ_a* character is more efficiently mixed in a bonding MO by through-bond coupling than the σ_s* character, the specific or selective symmetric cleavage of **1**—**3** should arise from the π_a-σ_a* interactions which are allowed without steric inhibition. In the cases of **4** and **5**, where the π_s-σ_s* interactions are sterically favorable, unsymmetric cleavage can occur competitively with the symmetric type. In conclusion, the steric-controlled orbital interactions are essential in the transition states of both the symmetric and the unsymmetric cleavage of the diarylcyclobutanes. For the reaction of **5**, however, the rate-determining step is the biradical fragmentation since nonbonding interactions are very large to destabilize both the biradicals and the transition states of the biradical fragmentation.

This research was supported in part by a Grant-in-Aid for Scientific Research from the Ministry of Education, Science and Culture (No. 62550616).

References

1) C. Pac, *Pure Appl. Chem.*, **58**, 1249 (1986).
2) S. W. Benson,"Thermochemical Kinetics, Methods for the Estimation of Thermochemical Data and Rate Parameters," 2nd ed., John Wiley and Sons, New York (1976).
3) E. Schaumann and R. Ketcham, *Angew. Chem., Int. Ed. Engl.*, **21**, 225 (1982).
4) R. B. Woodward and R. Hoffman, "The Conservation of Orbital Symmetry," Verlag Chemie, Weinheim/Bergstr., (1970).
5) J. S. Chikos, A. Annamalai, and T. A. Keiderling, *J. Am. Chem. Soc.*, **108**, 4398 (1986).
6) R. W. Carr, Jr. and W. D. Walters, *J. Phys. Chem.*, **67**, 1370 (1963).
7) H. R. Gerberich and W. D. Walters, *J. Am. Chem.*

Soc., **83**, 4884 (1961). J. A. Berson, D. C. Tompkins, and G. Jones, II, *ibid.*, **92**, 5879 (1970). Also see references cited in Refs. 2 and 3.

8) G. S. Hammond and C. D. DeBoer, *J. Am. Chem. Soc.*, **86**, 899 (1964). D. J. Trecker and D. H. Henry, *ibid.*, **86**, 902 (1964).

9) G. Jones, II, *J. Chem. Educ.*, **51**, 175 (1974). W. H. Richardson, M. B. Yelvington, and H. E. O'Neal, *J. Am. Chem. Soc.*, **94**, 1619 (1972). G. Jones, II and M. H. Williamson Jr., *ibid.*, **96**, 5617 (1974). L. M. Stephenson and T. A. Gibson, *ibid.*, **96**, 5624 (1974). Also see references cited in Refs. 2 and 3.

10) M. J. S. Dewar and S. Kirschner, *J. Am. Chem. Soc.*, **96**, 5246 (1974). G. A. Segal, *ibid.*, **96**, 7892 (1974).

11) R. Hoffman, S. Swaminathan, B. G. Odell, and R. Gleiter, *J. Am. Chem. Soc.*, **92**, 7091 (1970).

12) R. M. Moriarty, *Top. Stereochem.*, **8**, 271 (1974).

13) R. Hoffman and R. B. Davidson, *J. Am. Chem. Soc.*, **93**, 5699 (1971).

14) C. Pac, K. Mizuno, and H. Sakurai, *Bull. Chem. Soc. Jpn.*, **51**, 329 (1978).

15) L. A. Paquette and G. L. Thompson, *J. Am. Chem. Soc.*, **94**, 7127 (1972).

16) T. Imai and S. Nishida, *Chem. Lett.*, **1980**, 41.

17) G. Jones, II and V. L. Chow, *J. Org. Chem.*, **39**, 1447 (1974).

18) T. Majima, C. Pac, and H. Sakurai, *J. Am. Chem. Soc.*, **102**, 5265 (1980). C. Pac, T. Ohtsuki, Y. Shiota, S. Yanagida, and H. Sakurai, *Bull. Chem. Soc. Jpn.*, **59**, 1133 (1986). C. Pac, T. Fukunaga, Y. Go-An, T. Sakae, and S. Yanagida, *J. Photochem. Photobiol., A: Chemistry*, **41**, 37 (1987). C. Pac, Y. Go-An, and S. Yanagida, *Bull. Chem. Soc. Jpn.*, **62**, 1951 (1989).

19) W. Metzner and D. Wendisch, *Justis Liebigs Ann. Chem.*, **730**, 111 (1969).

20) R. M. Dodson and A. G. Zielsske, *J. Org. Chem.*, **32**, 28 (1967).

21) O. L. Chapman and W. Radams, *J. Am. Chem. Soc.*, **90**, 2333 (1968).

22) L. D. Rodewald and C. H. dePuy, *Tetrahedron Lett.*, **1964**, 2951.

23) The heat of formation of **3** and 1,4-biradicals can be calculated according to the additivity rules of bond and group properties listed in tables of Ref. 2; ΔH_f^0 (**3**)=245.8 kJ mol^{-1}, ΔH_f^0 (PhĊHCH$_2$CH$_2$ĊHPh)=353.6 kJ mol^{-1}, and ΔH_f^0 (PhĊHCH(Ph)CH$_2$ĊH$_2$)=408.7 kJ mol^{-1}.

24) L. Salem and J. S. Wright, *J. Am. Chem. Soc.*, **91**, 5947 (1969).

25) R. Hoffman, *Acc. Chem. Res.*, **1**, 1 (1971).

26) K. Harano, T. Ban, M. Yasuda, E. Osawa, and K. Kanematsu, *J. Am. Chem. Soc.*, **103**, 2310 (1981).

27) a) D. A. Dougherty, H. B. Schlegel, and K. Mislow, *Tetrahedron*, **34**, 1411 (1978). b) D. A. Dougherty, W. D. Hownshell, H. D. Schlegel, R. A. Bell, and K. Mislow, *Tetrahedron Lett.*, **1976**, 3479.

28) K. Shima, J. Kimura, K. Yoshida, M. Yasuda, K. Imada, and C. Pac, *Bull. Chem. Soc. Jpn.*, **62**, 1934 (1989).

29) C. Steel, R. Zand, P. Hurwitz, and S. G. Cohen, *J. Am. Chem. Soc.*, **86**, 679 (1964).

30) Alternatively the C_C-C_D bond breaking would initially occur for the symmetric cleavage to generate 1,1,4,4-tetramethyl-2,3-diphenyl-1,4-butanediyl, which should be again unstable by large nonbonding interactions.

Photochemical Reactions of Aromatic Compounds. XLVI.[1] Stereochemical Reaction Courses in the Photolytic Ring-Cleavage Reactions of Diarylcyclobutanes: Implications of Conformation-Controlled Orbital Interactions in the Excited-State Chemistry

Chyongjin PAC,* Kazuyoshi GO-AN, and Shozo YANAGIDA
Department of Chemical Process Engineering, Faculty of Engineering, Osaka University, Suita, Osaka 565
(Received November 14, 1988)

The photolyses of *cis-transoid-cis*-cyclobutadiindene (**1**), *cis*-2-phenylcyclobut[*a*]indene (**2**), *cis*-1,2-diphenylcyclobutane (**3**), the trans isomer (**4**), and its dimethyl (**5**) and tetramethyl (**6**) derivatives have been investigated to explore stereoelectronic factors controlling the excited-state reaction courses for the ring cleavages. The symmetric ring cleavage occurs regiospecifically in the cases of **1**—**3** and with 98% specificity in the case of **4**. The photolysis of **5** results in both the symmetric and the asymmetric cleavages in a ca. 1 : 3 ratio accompanied by substantial losses of stereointegrity in the olefin formation, and the regiospecific asymmetric cleavage occurs in the case of sterically more congested **6**. The ring-cleavage efficiencies systematically decrease in the order **1**>**2**>**3**>**4**>**5**>**6** and reveal negative temperature dependences, particularly in the cases of **1**, **5**, and **6**. The features of the reactions are in parallel with stable conformations and conformational mobilities of the aryl groups associated with different π-σ orbital interactions, while the spectroscopic properties of the cyclobutanes are essentially identical with those of benzene chromophores with little electronic perturbation. The photolytic ring-cleavage reactions are discussed in terms of crossing from the localized $^1\pi,\pi^*$ state to a σ^* hypersurface, in which conformation-controlled orbital interactions play important roles. The final products are formed via a pericyclic minimum which might be biradicaloid in nature.

Splitting of the cyclobutane rings has been providing an excellent probe for mechanistic and stereochemical studies[2-4] as well as a typical prototype for theoretical understanding of chemical reaction courses[5,6] because of simplicity of the net chemistry. Theories predict that [2+2] cycloreversions of cyclobutanes with stereoretention are forbidden in the ground state but are allowed in the σ,σ^* state of the ring framework.[5,6] Extensive thermochemical and stereochemical data of thermal ring-splitting reactions of parent cyclobutane and alkyl derivatives are indeed accomodated with stepwise mechanisms involving 1,4-biradicals.[3,4] By contrast, little has been known on mechanistic and stereochemical aspects in the photochemistry of simple cyclobutanes bearing no particular chromophore, since no suitable methods are available to achieve the selective population of the ring σ,σ^* state.[7]

Photochemical studies have therefore been carried out with chromophore-substituted cyclobutanes capable of being photoexcited by usual light sources. It was found that a few π-chromophore substituted cyclobutanes undergo the photolytic cycloreversions with complete stereoretention[8] or with only a minor loss of stereointegrity.[9,10] Another interesting observation of stereochemical significance is that the photolysis of π-substituted cyclobutanes results in the regiospecific or regioselective cleavage of a ring C-C bond in cases where a π chromophore and a substituent vicinally attach to each end of this bond in the *cis configuration*. This is called "cis effect".[11]

A crucial question should emerge as to why the photo-excitation of a π substituent can effect the specific or selective cleavage of the ring σ framework that should proceed by way of a reaction hypersurface correlating with the ring σ,σ^* state. Presumably, energy migration might occur from the photoexcited π substituent to a specific C-C bond of the cyclobutane ring to bring about a surface crossing to the σ,σ^* reaction hypersurface. However, there have been presented no convincing experimental data to explicate possible mechanisms and stereoelectronic requirements for such a surface crossing. Another important question is whether or not the photolytic ring cleavage of π-substituted cyclobutanes generally occurs with stereoretention. Systematic studies are certainly required to explore controlling factors in stereochemical reaction courses of photolytic ring-cleavage reactions of π-substituted cyclobutanes. The present paper deals with stereochemical and mechanistic details of the photolytic ring-cleavage reactions of diarylcyclobutanes **1**—**6**. We have found that the cyclobutanes reveal unique dependences of both the fluorescence bahavior and the reaction features on either stable conformations of the aryl substituents or temperature.

Results

Spectroscopic Properties. Table 1 lists the absorption and fluorescence spectra in cyclohexane and the fluorescence quantum yields and lifetimes in acetonitrile at 20 °C together with the relevant quantities of toluene and indane used as reference compounds. The fluorescence spectra of **1**—**4** were taken by means of a photon-counting method, since the

Table 1. Spectroscopic Properties of the Cyclobutanes

Compound	λ_{max}[a]/nm ($10^{-3}\varepsilon$)	λ^{F}_{max}[b]/nm	ϕ_F[c]	τ_F[d]/ns
1	275 (4.3), 268 (4.0)	276	ca. 0.006	e)
2	275 (1.3), 267 (1.4)	277	ca. 0.007	e)
3	271 (0.3), 267 (0.4)	272	ca. 0.002	e)
4	270 (0.5), 262 (0.7)	272	ca. 0.01	e)
5	271 (0.6), 263 (0.7)	271	ca. 0.070	23
6	271 (0.8), 265 (0.9)	271	0.14	22
Indane	274 (1.3), 267 (1.3)	277	f)	f)
Toluene	270 (0.2), 263 (0.3)	270	0.14	25

a) Absorption maxima in cyclohexane. b) Fluorescence maxima in cyclohexane. c) Fluorescence quantum yields in cyclohexane at 20 °C calculated from fluorescence intensities relative to that of toluene as standard. See Ref. 14. d) Fluorescence lifetimes in acetonitrile at 20 °C. e) The lifetimes were not be able to be determined, being presumably shorter than 1 ns; see text. f) Not determined.

Table 2. Temperature Dependences of Fluorescence Lifetimes[a]

T/°C	τ_F/ns		
	5	**6**	Cumene
−196[b]	30	34	
−20	40	40	44
2	30	28	28
20	23	22	18
30	20	19	14
40	18	16	11
50	14	13	8
60	12	10	6

a) Measured for degassed acetonitrile solution. b) In EPA (5:5:2 diethyl ether-isopentane-ethanol mixture) glasses. The lifetimes of **1**, **3**, and **4** in EPA glasses at 77 K are 10 ns, 9 ns, and 9 ns, respectively, but are presumed to be < 1 ns at ≥ -20 °C; see text.

fluorescence efficiencies are very low and since usual measurements resulted in substantial contamination of the fluorescence from indene or styrene formed by the photolysis during the measurements. The absorption and fluorescence spectra of the cyclobutanes are essentially identical with those of indane or toluene, while the fluorescence quantum yields largely vary from $<10^{-2}$ for **1**—**3** to 0.14 for **6**, a value identical with that of toluene.

The fluorescence lifetimes were measured by means of single photon counting after deconvolution. In the cases of **1**—**4**, however, we obtained no reliable lifetime data at room temperature and even at −20 °C, probably because of very low emission efficiencies and very short lifetimes. At 77 K, the lifetimes could be determined to be 9—10 ns but are substantially shorter than those of **5**, **6**, and toluene (35 ns) at this temperature. Table 2 shows the fluorescence lifetimes of **5**, **6**, and cumene at various temperatures, which commonly decrease with the increase of temperature from −20 °C.

Photolysis. Irradiation of deaerated acetonitrile or cyclohexane solution of **1**—**6** at 254 nm gave exclusively the olefins formed by the symmetric (*a*) and/or

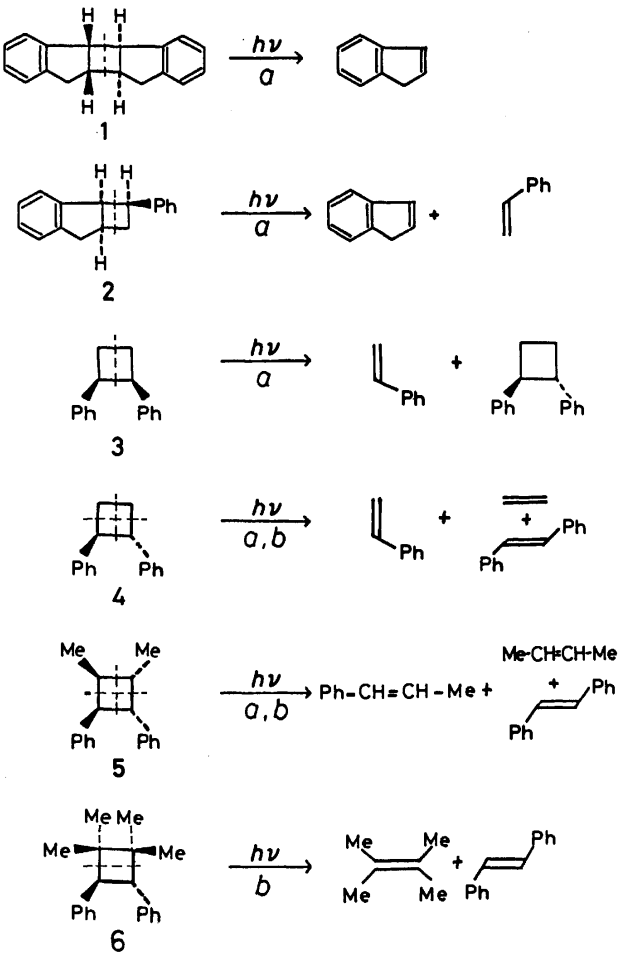

Scheme 1.

the asymmetric (*b*) ring cleavages (Scheme 1); the isomerization of **3** to **4** occurred in a low efficiency. Material balances were well over 95% at <5% conversions and no other product was detected at all. Table 3 lists the reaction quantum yields (ϕ_a and ϕ_b) and the $a:b$ ratios at 20 °C. It was found that the reaction efficiencies vary with reaction temperature from 2 °C to 70 °C, particularly in the cases of **1**, **5**, and **6**, as shown in Table 4. The $a:b$ ratios in the photolysis

Table 3. Reaction Quantum Yields for Photolysis of **1**—**6** at 254 nm[a]

Cyclobutane	ϕ_a	ϕ_b[b]	$a:b$
1	0.47		100:0
2	0.37[c]		100:0
	0.32[d]		
3	0.17		100:0
	0.006[c]		
	(0.17, 0.014[e])		100:0)
4	0.14	0.002	98:2
	(0.14	0.006	96:4)
5	0.025	0.070	26:74
	(0.020	0.070	22:78)
6		0.080	0:100

a) Obtained for acetonitrile and cyclohexane solution at 20 °C unless otherwise stated. In parentheses are the values for cyclohexane solution only in cases where they are different from those for acetonitrile solution. The quantum yields for the olefin formation from the symmetric cleavages of **1**, **3**, **4**, and **5** are the double of the listed values. b) For the stilbene formation. c) For the indene formation. d) For the styrene formation. e) For the isomerization to **4**.

Table 4. Temperature Dependences of Quantum Yields[a]

T/°C	ϕ_a			ϕ_a	ϕ_b	ϕ_b
	1	**3**	**4**	**5**		**6**
2	0.50	0.20	0.15	0.025	0.130	0.075
20	0.47	0.17	0.14	0.025	0.080	0.080
30	0.42			0.025	0.060	0.082
50	0.39			0.020	0.040	0.052
70	0.27	0.15	0.14	0.020	0.020	0.010

a) See footnotes in Table 3.

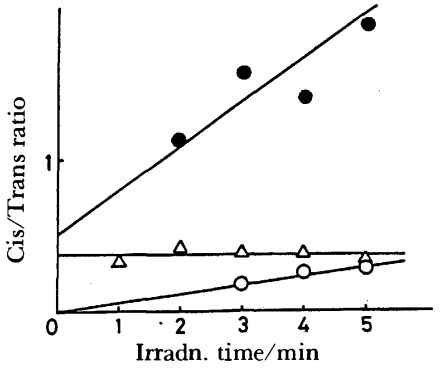

Fig. 1. Plots of cis-trans ratio vs. irradiation time for the formation of 1-phenylpropene (—●—), stilbene (—○—), and 2-butene (—△—) in the photolysis of **5** in acetonitrile at 20 °C; irradiation at 254 nm; [**5**]=0.01 M.

of **5** increase with an increase of temperature to reach 1:1 at 70 °C. In the case of **4**, the asymmetric cleavage is too minor to allow reliable determination of temperature-dependent $a:b$ ratios.

The olefin products from the photolysis of **5** are mixtures of the cis and trans isomers. The cis/trans ratios were determined at various irradiation times under keeping conversions below 3%. As shown in Fig. 1, the isomer ratios in formation of stilbene and 1-phenylpropene increase with irradiation time, probably due to secondary photoisomerization of the primary products. The values obtained by extrapolation of the plots to zero irradiation time should give the primary cis:trans ratios which are 0:100 in the stilbene formation and ca. 2:1 in the 1-phenylpropene formation. On the other hand, 2-butene was formed in a ca. 2:5 cis-trans ratio independently of irradiation time. Similarly *trans*-stilbene was confirmed to be the primary photoproduct from **6**.

Discussion

Mechanism. The isomerization of **3** to **4** and the loss of stereointegrity in the olefin formation from **5** strongly suggest that the photolytic reactions of **3** and **5** proceed by way of a state or an intermediate susceptible to bond rotation. The acetone-photosensitized reaction of **3** gives styrene and **4** in respective quantum yields of 0.15 and 0.04[12] and the styrene: **4** ratio in the thermal reaction of **3** is 2.3:1 at 300 K.[13] Calculations using these values and the data in Table 3 indicate that the participation of either the triplet state of **3** or thermally equilibrated 1,4-diphenylbutane-1,4-diyl should be very minor, 15% or less the total reaction at best, provided that all the formation of **4** would arise only from triplet **3** or from the 1,4-biradical. Similarly, the involvement of a 1,4-biradical in the photolysis of **5** should be negligible since the cis:trans ratio in the 1-phenylpropene by the thermal reaction of **5** is 1:9 at 550 K and is calculated to be ca. 0:100 at 300 K.[13] Furthermore, it was reported that either *trans*-2-heptene or dimethyl maleate does not affect the photolytic reaction of **3**.[12b] We also confirmed that air saturation of solution exerts no effect on the photoreactions of **1**—**4** at all and slightly quenches those of **5** and **6**, probably due to oxygen quenching of the excited singlet state of the cyclobutanes.

The above arguments suggest that the photolytic ring-cleavage reactions of the cyclobutanes are not concerted but involve a reactive state responsible for the product formation, presumably a biradicaloid pericyclic minimum,[6] which should be different from either the triplet state of the cyclobutanes or discrete 1,4-biradicals; this state is denoted as "X" for convenience. Since the absorption and fluorescence spectra of the cyclobutanes are essentially identical with those of alkylbenzenes, the spectroscopic excited state is the $^1\pi,\pi^*$ state of the aryl substituent in which little electronic perturbation by the cyclobutane ring occurs. The basic mechanistic pathways of the photoreactions are shown in Eqs. 1—6 where Eq. 3 involves temperature-independent photophysical processes (e.g., internal conversion and intersystem crossing) and an activated nonradiative process. The reaction quan-

tum yield (ϕ_r) is represented by Eq. 7 where α is the partition coefficient for the product formation from X.

$$M \xrightarrow{h\nu} {}^1M^*({}^1\pi,\pi^*) \quad (1)$$

$${}^1M^* \xrightarrow{k_F} M + h\nu_F \quad (2)$$

$${}^1M^* \xrightarrow{k_d} M \quad (3)$$

$${}^1M^* \xrightarrow{k_r} X \quad (4)$$

$$X \xrightarrow{\alpha} \text{product} \quad (5)$$

$$X \xrightarrow{1-\alpha} M \quad (6)$$

$$\phi_r = \alpha k_r/(k_F + k_d + k_r) = \alpha k_r \tau_s \quad (7)$$

Analysis of Temperature Dependence. It is known that fluorescence lifetimes of benzene and alkylbenzenes decrease with an increase of temperature as the consequence arising from the involvement of an activated pathway in the nonradiative decay.[14] This pathway is attributed to a surface crossing from the excited singlet state to an isomer surface, from which the starting ground-state arene is mostly regenerated along with very inefficient formation of an isomer such as fulvene. At any rate this mechanism should be responsible for the temperature dependence of fluorescence lifetimes of **5** and **6** since k_r appears to be smaller by an order of magnitude than τ_s^{-1}, as calculated by Eq. 7. The temperature dependence can therefore be analyzed by the use of Eq. 8 in which k_d^0 represents the rate constant for overall temperature-independent photophysical processes.

$$1/\tau_s = k_d^0 + A_d \exp(-\Delta H_d^{\neq}/RT) \quad (8)$$

Figure 2 shows best-fit plots of $\log(\tau_s^{-1} - k_d^0)$ vs. $1/T$ for cumene, **5**, and **6**, from which A_d and $\Delta H_d^{\neq}$ are

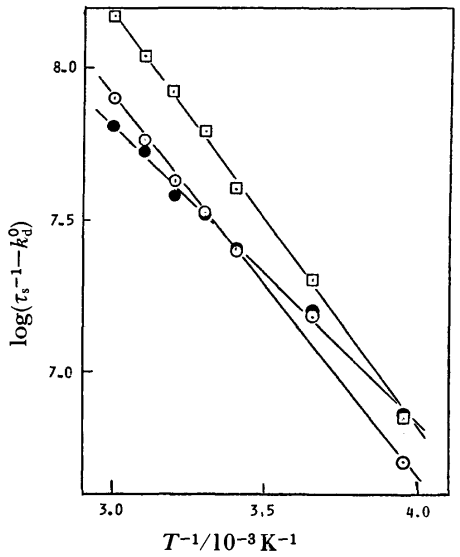

Fig. 2. Best-fit plots of $\log(\tau_s^{-1} - k_d^0)$ vs. T^{-1} for **5** (—●—), **6** (—○—), and cumene (—□—); data are from Table 2.

Table 5. Preexponential Factor A_d and Activation Barrier $\Delta H_d^{\neq}$ for Activated Nonradiative Decay[a]

Compound	$k_d^0/10^7\,s^{-1}$	$A_d/10^{11}\,s^{-1}$	$\Delta H_d^{\neq}$/ kcal mol^{-1}
Cumene	1.6	21.0	6.3
5	1.8	0.65	4.6
6	2.0	2.6	5.3
c-t-c-TPCB[b,c]	1.5	4.2	3.8
all-t-TPCB[b,d]	1.5	0.14	2.4

a) Obtained by analysis of the data in Table 2; see Fig. 2 and text. b) Reported values for tetraphenylcyclobutane; see Ref. 15. c) *r*-1,*c*-2,*t*-3,*t*-4-Tetraphenylcyclobutane. d) All-trans isomer.

obtained. Table 5 lists the values of k_d^0, A_d, and $\Delta H_d^{\neq}$ together with the reported quantities for the cis-trans-cis and all-trans isomers of tetraphenylcyclobutane[15] for comparison. These values fall in those reported for benzene and toluene.[14] It is therefore evident that the spectroscopic excited singlet state of **5** and **6** is just the ${}^1\pi,\pi^*$ state of an isolated phenyl substituent not only in the electronic properties but also in the dynamic decay pathways, Eqs. 2 and 3. This appears to be again true for **1**—**4**, since the electronic spectra reveal no perturbation of the ${}^1\pi,\pi^*$ state of the aryl substituent; the very low emission efficiencies should be due to large k_r.

Analysis of the temperature dependences of quantum yield might provide a clue to explore the dynamic reaction pathways from the ${}^1\pi,\pi^*$ state. It can be presumed that no activated pathways participate after the decay from X to the ground-state surface, since a 1,4-biradical minimum is unlikely to be involved in the ring-cleavage reactions as already mentioned. Calculations according to Eq. 7 using the observed lifetimes and quantum yields give the αk_r values at 2—70 °C for **5** and **6**; the lifetimes at 70 °C were estimated from the plots in Fig. 2. Plots of $\log(\alpha k_r)$ vs. $1/T$ give positive slopes for the asymmetric clevage of **5** and for the ring cleavage of **6** at ≥50 °C, whereas the symmet-

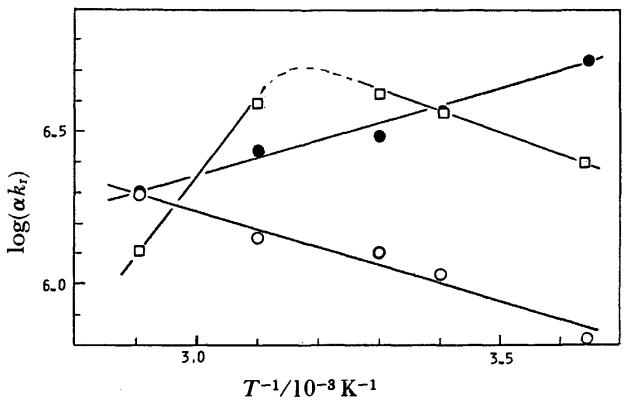

Fig. 3. Plots of $\log(\alpha k_r)$ vs. T^{-1} for the symmetric (—○—) and asymmetric (—●—) cleavages of **5** and for the asymmetric cleavage of **6** (—□—); data are from Tables 2 and 4.

ric cleavage of **5** and the ring cleavage of **6** at lower temperatures reveal plots of usual negative slopes, as shown in Fig. 3.

The negative temperature dependences might arise from α or from k_r as the consequence of increasing regeneration of the starting cyclobutane with the increase of temperature through an activated pathway along the excited-state potential surface. We can assume two possibilities, i.e., (1) thermal regeneration of $^1M^*$ from another intermediate state "Y" involved prior to X in the mechanistic sequence and (2) pseudo equilibrium between an early pericyclic minimum X_1 and another more stable one X_2 which decay to the starting cyclobutane and to the olefin products respectively. In the latter case, X_1 is thermally repopulated from X_2 in which losses of stereo-integrity should occur. It can therefore be presumed that the isomerization of **5** might increasingly occur with the increase of temperature. In order to confirm possible formation of an isomer of **5** (e.g., *r*-1,*c*-2-dimethyl-*c*-3,*t*-4-diphenylcyclobutane), we extensively carried out VPC analyses using different columns for photolysates of **5** irradiated at 60 °C and ^1H NMR analyses for cyclobutane fractions obtained by column chromatography of the photolysates. However, no indication was obtained for the formation of any isomer of **5**.

Accordingly, we choose the former mechanism to analyze the observed temperature dependences under the assumption that α is independent of temperature, though there is no direct evidence to discard the other mechanism. On the basis of this assumption, Eq. 4 is replaced by Eqs. 9 and 10, and k_r is represented by Eq. 11. The positive slopes of the plots in Fig. 3 imply that $k_{-r}>k_c$, thus giving lower limits of the difference between the enthalpy change of Eq. 9

$$^1M^* \underset{k_{-r}}{\overset{k_r'}{\rightleftarrows}} Y \qquad (9)$$

$$Y \xrightarrow{k_c} X \qquad (10)$$

$$k_r = k_r'[k_c/(k_{-r}+k_c)] = k_c[k_r'/(k_{-r}+k_c)] \qquad (11)$$

and the activation enthalpy of Eq. 10, $(\Delta H_{-r}^{\neq} - \Delta H_r^{\neq}) - \Delta H_c^{\neq}$, which are 3±1 kcal mol^{-1} (1 kcal=4.184 kJ) for the asymmetric cleavage of **5** and roughly 10—12 kcal mol^{-1} for the ring cleavage of **6**. On the other hand, the plots of negative slope in Fig. 3 indicate that $(\Delta H_{-r}^{\neq} - \Delta H_r^{\neq}) \gg \Delta H_c^{\neq}$ or $\Delta H_c^{\neq}=0$, giving $\Delta H_r^{\neq}$ and the preexponential factor A_r for the symmetric cleavage of **5** and lower limits of $\Delta H_r^{\neq}$ and A_r for the ring cleavage of **6**, which are listed in Table 6 together with the relevant values reported for the photolysis of tetraphenylcyclobutane.[15]

In the cases of **1—4**, it is reasonable to presume that $k_r \geq 5\times10^8$ s$^{-1} \gg (k_F+k_d)$. In this regard, it should be noted that the fluorescence lifetimes of **1**, **3**, and **4** are 9—10 ns at 77 K, still much shorter than those of **5** and **6** which are similar to that of toluene. Moreover, we confirmed that irradiation of **1—4** in EPA glasses at 77 K gives the corresponding olefins[11] while little photolytic ring cleavage of **5** and **6** occurs under similar conditions. It is therefore implied that $\Delta H_r^{\neq}<3$ kcal mol^{-1} and $A_r>10^{11}$ s^{-1} for the symmetric cleavage of **1—4**. Since $k_r \gg k_d$, the negative temperature dependence of ϕ_r in the photolysis of **1** can be analyzed according to Eq. 12. A best-fit plot of $\log[(\alpha-\phi_r)/\phi_r]$ vs. $1/T$ obtains by assuming α=0.55 as shown in Fig. 4, thus giving the value of $(\Delta H_{-r}^{\neq} - \Delta H_c^{\neq})$ which is 7±1 kcal mol^{-1}.

Table 6. Preexponential Factor A_r and Activation Barrier $\Delta H_r^{\neq}$ for the $^1M^*\rightarrow Y$ Process[a]

Cyclobutane	A_r/s^{-1}	$\Delta H_r^{\neq}$/kcal mol^{-1}
1—4	$>10^{11}$	<3
5[b]	$(7\pm2)\times10^{7}$[c]	2.4±0.2
6	$\geq4\times10^{8}$[c]	≥3
c-t-c-TPCB[d]	2.0×10^{11}	3.5
all-t-TPCB[d]	7.9×10^{10}	3.8

a) Obtained by analysis of the data in Tables 2 and 3; see text. b) For the symmetric cleavage. c) Calculated by assuming α=0.5. d) Reported values for tetraphenylcyclobutanes; see footnote in Table 5 and Ref. 15.

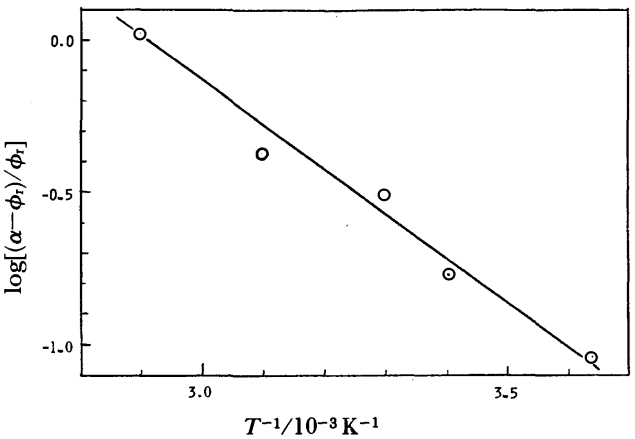

Fig. 4. A best-fit plot of $\log[(\alpha-\phi_r)/\phi_r]$ vs. T^{-1} obtained by assuming α=0.55 for the photolysis of **1**; data are from Table 4.

$$(\alpha-\phi_r)/\phi_r = k_{-r}/k_c \qquad (12)$$

Stereochemical Reaction Courses Associated with π-σ Orbital Interactions. We previously reported that through-bond coupling between vicinal π electron systems across the cyclobutane-ring σ framework plays essential roles in ring-splitting reactions of diarylcyclobutanes by redox photosensitization,[16] by exciplex photosensitization,[17] by electron-transfer photosensitization,[18] and by γ radiolysis.[19] Although an essential mechanistic event in those reactions is commonly the population of a positive charge by the complete or partial removal of an electron, it can be presumed that the regiochemistry and reactivities in the present photolytic reactions of the cyclobutanes are controlled by different π-σ orbital interactions.

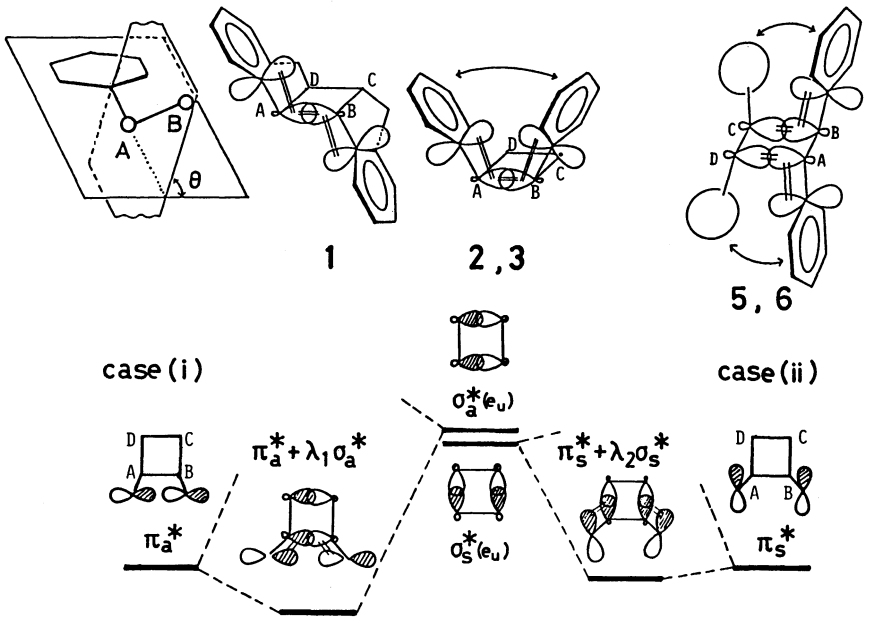

Fig. 5. Top: Stable conformations of the aryl substituents associated with favorable orbital interactions; $\theta \approx 90°$ for case (i) and $\theta \approx 0°$ for case (ii). Bottom: Schematic representation of π_a^*-σ_a^* and π_s^*-σ_s^* interactions.

Figure 5 shows different conformational situations of the aryl ring for π-σ orbital interactions (case (i) and case (ii)) together with the notation of the carbon atoms of the cyclobutane ring.

In case (i) where torsional angles (θ) between the aryl ring and the ipso C-C_A-C_B plane are ca.90°, the π orbitals can maximally overlap with the C_A-C_B σ orbitals. Such conformational situations are indeed realized in **1** by the rigid tricyclic structure as well as in **2** and **3** by steric repulsion between the bulky vicinal aryl substituents in the cis configuration, as demonstrated by the X-ray crystallographic analysis[20] as well as by molecular models. It is evident that conformational rigidity decreases in the order of **1**>**2**>**3**. In case (ii) where $\theta \approx 0°$, the π orbitals can not overlap with the orthogonal C_A-C_B σ orbitals but favorably with the C_A-C_D and C_B-C_C σ orbitals. The X-ray crystallographic analysis of **6** and *r*-1,*t*-2-bis(hydroxymethyl)-*t*-3,*c*-4-diphenylcyclobutane, an analogue of **5**, demonstrates that $\theta \leq 11.3°$ due to nonbonding interactions between the cis substituents.[20] It is therefore evident that conformations of **5** and **6** fall in case (ii) though **5** is more mobile than the very rigid cyclobutane, **6**. On the other hand **4** can take either case (i) or case (ii) conformations. These conformational situations of the cyclobutanes associated with orbital interactions are well in parallel with the observed regiochemistry in the photolytic ring-cleavage reactions. However, effects of orbital interactions on the present photochemistry should be dynamic in nature since the spectroscopic properties of the cyclobutanes are essentially identical with those of alkylbenzenes with little electronic perturbation. It can be presumed that π-σ orbital interactions play important roles in the mechanistic sequence, $^1M^* \rightarrow Y \rightarrow X$.

For qualitative considerations on roles of orbital interactions in the stereochemical reaction courses, we use Salem's σ_s^* and σ_a^* orbitals of cyclobutane[21] and the π^* combinations, $\pi_s^* \equiv (\pi_A^*, \pi_B) + (\pi_A, \pi_B^*)$ and $\pi_a^* \equiv (\pi_A^*, \pi_B) - (\pi_A, \pi_B^*)$; subscript s or a represents the symmetric or antisymmetric character with respect to two-fold rotation or reflection. Orbital interactions can occur between π_a^* and σ_a^* or between π_s^* and σ_s^* to give a half-filled molecular orbital, $\pi_a^*+\lambda_1\sigma_a^*$ or $\pi_s^*+\lambda_2\sigma_s^*$ each,[22] as shown in Fig. 5. It should be however noted that the π_a^*-σ_a^* interactions lead to through-bond coupling between the vicinal π electron systems without large molecular distortions to stabilize $\pi_a^*+\lambda_1\sigma_a^*$, i.e., $\lambda_1 > 0$. In other words the π_a^*-σ_a^* interactions can efficiently occur along the reaction coordinate to bring about delocalization of the photoexcitation of $^1M^*$ over the π_A-σ_A-σ_B-π_B orbital array involved in through-bond coupling, thus facilitating the crossing from $^1M^*$ to a σ,σ^* reaction hypersurface for the symmetric cleavage. On the other hand the π_s^*-σ_s^* interactions are ineffective to through-bond coupling because of little overlap between the C_A-C_D and the C_B-C_C σ orbitals in σ_s^*, i.e., $\lambda_2 \approx 0$ without large structure changes. It can therefore be predicted that the crossing from $^1M^*$ to a reaction hypersurface for the asymmetric cleavage is slow, since energy migration from the photoexcited aryl group to the cyclobutane-ring σ framework through the $^*\pi_s$-σ_s^* interactions should be inefficient.

The above molecular-orbital arguments provide a

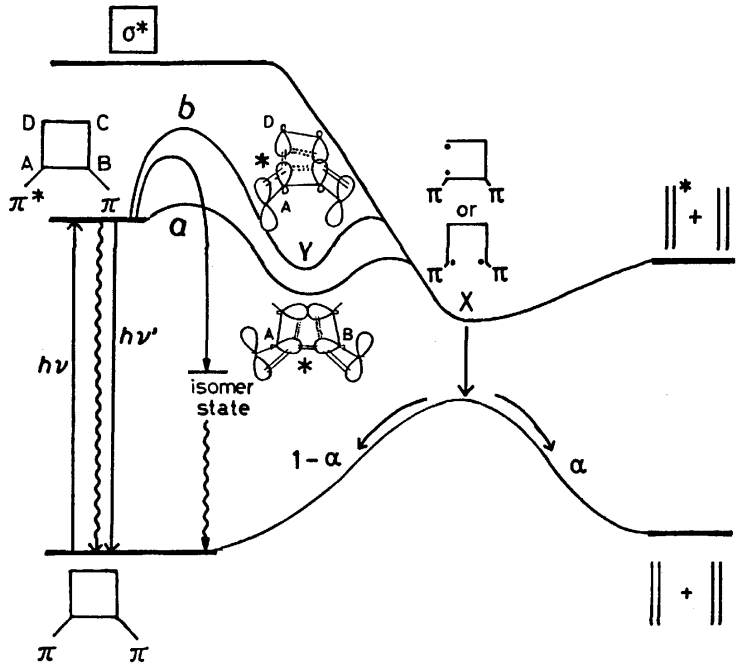

Fig. 6. Schematic reaction surfaces for the photolytic ring cleavages of diarylcyclobutanes in *a* and *b* directions involving the sequential pathways $^1M^*$ (localized $^1\pi,\pi^*$ state)→Y(π^*-σ^* state)→σ,σ^* reaction hypersurface→X(biradicaloid state)→product.

rational to interpret the conformation-controlled regiochemistry and the different reactivities of the symmetric and asymmetric cleavages. In the cases of **1**—**3** where only the π_a^*-σ_a^* interactions are conformationally allowed, the low activation barriers and the large A_r values for the $^1M^*$→Y process suggest that the σ_a^* character should be significantly mixed in the transition state without large structure changes. On the other hand, the slow ring cleavage of **6** in *b* direction suggests that mixing of the σ_s^* character should be inefficient even though only the π_s^*-σ_s^* interactions are conformationally allowed. Since $\Delta H_r^{\neq}>3$ kcal mol^{-1} and $A_r \ll 10^{11}$ s^{-1} for **6**, significant mixing of the σ_s^* character would require highly restricted molecular motions in the transition state of the $^1M^*$→Y process, e.g., elongation of the C_A-C_D and C_B-C_C bonds and concurrent shortening of the C_A-C_B bond with keeping $\theta \approx 0°$. In the cases of **4** and **5**, therefore, more effective mixing of the σ_a^* character may allow the regioselective cleavage of **4** in *a* direction irrespective of mobile conformations and may counterbalance the conformational disadvantage of the π_a^*-σ_a^* interactions in **5**. The low A_r value for the symmetric cleavage of **5** indeed demonstrates that vibrational and rotational motions are extremely restricted in the transition state. Although details of Y still remain unknown, stabilization by the π_a^*-σ_a^* or π_s^*-σ_s^* orbital interactions might be important in Y where structures of the cyclobutanes would be different from those in $^1M^*$. In this regard it should be noted that $\Delta H_r^{\neq}<\Delta H_c^{\neq}$ for **1** and **6** but $\Delta H_r^{\neq} \approx \Delta H_c^{\neq}$ for **3** and **4**. Presumably the rigid structures of **1** and **6** might freeze maximum orbital overlaps to stabilize Y to substantial degrees. On the other hand conformational mobilities of **3** and **4** would be unfavorable for stabilization of Y since the orbital interactions can slip out with small molecular motions, e.g., rotational and rocking motions of the phenyl rings and puckering motions of the cyclobutane ring. At any rate significant mixing of the σ_a^* or σ_s^* character in Y is certainly favorable for the crossing from Y to a σ,σ^* reaction hypersurface for a molecule to reach a biradicaloid pericyclic minimum X,[6] in which the C_A-C_B or the C_A-C_D (or C_B-C_C) bond is elongated enough for substantial bond rotation to occur.

Conclusion

Figure 6 shows schematic reaction surfaces for the photolytic ring cleavages of **1**—**6** as a summary. The mechanism involves the sequential pathways, $^1M^*$ (localized $^1\pi,\pi^*$ state) → Y (π_a^*-σ_a^* or π_s^*-σ_s^* state) → σ,σ^* reaction hypersurface → X (biradicaloid state) → product. The net regiochemistry is determined in the $^1M^*$ → Y process depending on conformations of the aryl substituents associated with the orbital interactions. Since the σ_a^* character is effectively mixed by through-bond interaction without large structure changes, the $^1M^*$→Y→X processes can efficiently occur in cases where the π_a^*-σ_a^* interactions are con-

formationally allowed. On the other hand, the asymmetric cleavage is inherently slow as the consequence of inefficient mixing of the σ_s* character. In other words the specific or selective asymmetric ring cleavage can occur only in cases where the aryl rings are sterically inhibited to take case (i) conformations. In short the "cis effect" should be the consequence arising from steric control of the different orbital interactions.

The present investigation may provide a general concept for the understanding of both regioselectivities and reactivities in photolytic bond-cleavage reactions of various π-substituted cyclobutanes[11,23-25] and, perhaps, of diarylethane-type compounds. Synthetic implications of the present investigation may be given by elegant preparation of bullvalene,[26] pentalene derivatives,[27] cyclobutadiene,[28] and azetidinone[29] from photolyses of rigid polycyclic cyclobutanes with π chromophores, since the regiochemistry is that expected from specific orbital interactions imposed by the rigid structures.

Experimental

Ultraviolet absorption spectra were recorded on a Hitachi 220-A UV spectrophotometer and fluorescence measurements were performed on a Hitachi 850 spectrofluorometer after correction for the spectral response of the instrument. Fluorescence lifetimes were determined on a Horiba NAES-1100 time-resolved spectrofluorometer. Vapor-phase chromatographic analyses were performed on a Shimadzu GC-7A gas chromatograph using a 2-m column of 10% PEG 20M on Shimalite NAW-101, a 3-m column of 2% OV 17 on Chromosorb W AW-DMCS, and a 5-m column of 25% ODPN on Shimalite NAW-101.

Materials. Spectrograde cyclohexane (Wako Pure Chemicals) was used after distillation. Reagent-grade acetonitrile was refluxed over P_2O_5 and then distilled. This procedure was repeated three times, and then the acetonitrile was distilled from CaH_2 prior to use. The cyclobutanes were prepared according to the literature methods; *cis-transoid-cis*-cyclobuta[1,2-*a*;4,3-*a'*]diindene (**1**),[30] *endo*-2-phenyl-2,2a,7,7a-tetrahydro-1*H*-cyclobut[*a*]indene (**2**),[16] *cis*-1,2-diphenylcyclobutane (**3**),[31] *trans*-1,2-diphenylcyclobutane (**4**),[31] *r*-1,*t*-2-dimethyl-*t*-3,*c*-4-diphenylcyclobutane (**5**),[17] and 1,1,2,2-tetramethyl-*trans*-3,4-diphenylcyclobutane (**6**).[32] Purification was achieved by repeated recrystallization from methanol for **1**, **2**, and **3** or from hexane for **6**, whereas **4** and **5** were distilled in vacuo. Vapor-phase chromatographic analyses of the purified cyclobutanes revealed that **4** includes the cis isomer in ca. 5% whereas the other cyclobutanes are virtually pure (> 99%).

Photolysis. A cyclohexane or acetonitrile solution of **1**—**6** (0.01 mol dm^{-3}) in a quartz cuvette was flushed with a gentle stream of Ar, placed in a temperature-regulated water bath, and then irradiated with an Eikosha POL-100 low-pressure mercury arc lamp through a Toshiba UV-D 25 glass filter which cuts off the 185-nm emission from the light source. The progress of the photoreaction was followed by vapor-phase chromatography. A potassium trioxalatoferrate(III) actinometer was used for the determination of quantum yields. It was confirmed that the observed quantum yields for the photoreactions of **1** and **5** are almost constant within experimental errors (± 5%) independently of concentration from 5×10^{-3} to 5×10^{-2} mol dm^{-3}.

This work was partly supported by Grant-in-Aid for Special Project Research from the Ministry of Education, Science and Culture (Nos. 61113001 and 62113001). We thank to Professors Kensuke Shima and Masahide Yasuda of Miyazaki University for helpful discussions on structure-reactivity relationships in the ring-cleavage reactions of the cyclobutanes.

References

1) Part XLV. C. Pac, T. Fukunaga, Y. Go-An, T. Sakae, and S. Yanagida, *J. Photochem. Photobiol. A: Chemistry*, **41**, 37 (1987).
2) C. Pac, *Pure Appl. Chem.*, **58**, 1249 (1986).
3) S. W. Benson, "Thermochemical Kinetics, Methods for the Estimation of Thermochemical Data and Rate Parameters," 2nd ed., John Wiley & Sons, New York (1976).
4) E. Schaumann and R. Ketcham, *Angew. Chem., Int. Ed. Engl.*, **21**, 225 (1982).
5) R. B. Woodward and R. Hoffmann,"The Conservation of Orbital Symmetry," Verlag Chemie, Weinheim/Bergstr (1970).
6) W. Gerharts, R. D. Poshusta, and J. Michl, *J. Am. Chem. Soc.*, **98**, 6427 (1976); J. Michl, *Photochem. Photobiol.*, **25**, 141 (1977).
7) W. Adam and T. Oppenlander, *Angew. Chem., Int. Ed. Engl.*, **23**, 641 (1984).
8) C. Pac, K. Mizuno, and H. Sakurai, *Bull. Chem. Soc. Jpn.*, **51**, 329 (1978).
9) R. A. Caldwell and D. Creed, *Acc. Chem. Res.*, **13**, 45 (1980).
10) L. A. Paquette and G. L. Thompson, *J. Am. Chem. Soc.*, **94**, 7172 (1972).
11) G. Kaupp, *Angew. Chem.*, **84**, 741 (1974); G. Kaupp and M. Stark, *Chem. Ber.*, **110**, 3084 (1977).
12) a) Our quantum yields for the present direct photolysis of **3** and **4** and for the acetone-photosensitized reactions are larger by an order of magnitude than the values reported by Jones and Chow.[12b] b) G. Jones, II and V. L. Chow, *J. Org. Chem.*, **39**, 1447 (1974).
13) a) M. Yasuda, K. Yoshida, K. Shima, and C. Pac, *Bull. Chem. Soc. Jpn.*, **62**, 1943 (1989). b) For the thermal reaction of **3**, $\Delta H^{\neq}$=40.0 kcal mol^{-1} and $\log A$=14.0 for the styrene formation and $\Delta H^{\neq}$=38.5 kcal mol^{-1} and $\log A$=12.8 for the isomerization to **4**, and ($\Delta H_{cis}^{\neq}-\Delta H_{trans}^{\neq}$) =10.6 kcal mol^{-1} and $\log(A_{cis}/A_{trans})$=3.4 for the 1-phenylpropene formation from **5**.[13a]
14) J. B. Birks, "Photophysics of Aromatic Molecules," Wiley-Interscience, London (1970), Chap. 5 and pp. 240—248.
15) H. Shizuka, I. Seki, T. Morita, and T. Iizuka, *Bull. Chem. Soc. Jpn.*, **52**, 2074 (1979).
16) T. Majima, C. Pac, and H. Sakurai, *J. Am. Chem. Soc.*, **102**, 5265 (1980) and *J. Chem. Soc., Perkin Trans. 1*, **1980**, 2705; C. Pac, J. Kubo, T. Majima, and H. Sakurai, *Photochem. Photobiol.*, **36**, 2773 (1982).
17) C. Pac, T. Ohtsuki, Y. Shiota, S. Yanagida, and H. Sakurai, *Bull. Chem. Soc. Jpn.*, **59**, 1133 (1986).

18) C. Pac, T. Ohtsuki, T. Fukunaga, Y. Yanagida, and H. Sakurai, *Chem. Lett.*, **1985**, 1855. Also see Refs. 1 and 2.
19) C. Pac, T. Majima, S. Takamuku, and H. Sakurai, *Chem. Lett.*, **1979**, 1149; *Nippon Kagaku Kaishi*, **1984**, 1880.
20) K. Shima, J. Kimura, K. Yoshida, M. Yasuda, and C. Pac, *Bull. Chem. Soc. Jpn.*, **62**, 1943 (1989).
21) L. Salem and J. S. Wright, *J. Am. Chem. Soc.*, **91**, 5947 (1969).
22) R. Hoffmann, *Acc. Chem. Res.*, **1**, 1 (1971).
23) G. Kaupp and E. Jostkleigrewe, *Angew. Chem., Int. Ed. Engl.*, **15**, 779 (1976).
24) S. Takamuku and W. Schnabel, *Chem. Phys. Lett.*, **69**, 399 (1980).
25) N. Yonezawa, T. Yoshida, and M. Hasegawa, *J. Chem. Soc., Perkin Trans. 1*, **1983**, 1083.
26) G. Schröder, *Chem. Ber.*, **97**, 3140 (1964).
27) K. Hafner, R. Dönges, E. Goedecke, and R, Kaiser, *Angew. Chem.*, **85**, 362 (1973).
28) S. Masamune, M. Suda, H. Ona, and L. M. Leichter, *J. Chem. Soc., Chem. Commun.*, **1972**, 1268.
29) G. Kretschner and R. N. Warrener, *Tetrahedron Lett.*, **1975**, 1335.
30) W. Metzner and D. Wendisch, *Liebigs Ann. Chem.*, **1980**, 1583.
31) R. M. Dodson and A. G. Zielske, *J. Org. Chem.*, **32**, 28 (1967).
32) O. L. Chapman and W. Radams, *J. Am. Chem. Soc.*, **90**, 2333 (1968).

Nonstabilized Azomethine Ylides Generated by Decarboxylative Condensation of α-Amino Acids. Structural Variation, Reactivity, and Stereoselectivity

Shuji KANEMASA,* Kazushige SAKAMOTO, and Otohiko TSUGE*
Institute of Advanced Material Study, and Department of Molecular Science and Technology, Interdisciplinary Graduate School of Engineering Sciences, Kyushu University, Kasugakoen, Kasuga 816
(Received December 2, 1988)

A variety of aldehydes, containing enolizable aldehydes other than acetaldehyde can be used in the generation method of nonstabilized azomethine ylides by decarboxylative condensation of α-amino acids. Reactivity of the nonstabilized ylides was examined in intermolecular and intramolecular cycloadditions with olefins; stereoselectivity of the intramolecular cycloaddition using nonstabilized ylides was compared with that of ester-stabilized ylides.

Condensation of α-amino esters or related derivatives with carbonyl compounds[1-4] and decarboxylative condensation of α-amino acids[2,4-11] offer a direct and general generation method for carbonyl-stabilized and nonstabilized azomethine ylides, respectively. These two methods can be termed "a deprotonation route" and "a decarboxylation route" for the generation of azomethine ylide 1,3-dipoles.[12]

It was observed in the previous work that two competitive deprotonations took place from the iminium intermediates **A** when an enolizable aldehyde was used in the deprotonation route.[3] One was deprotonation at the α-position (path a in Fig. 1) leading to azomethine ylides **B** and the other at the β′-position leading to enamines **C** (path b). The condensation of ethyl (methylamino)acetate (R=Me) with acetaldehyde exclusively led to enamine **C** (R″=H), and with propanal the **B** : **C** ratio (R″=Me) was 73 : 27.[3]

In the decarboxylation route, the iminium carboxylate betaines **D** must undergo a rapid cyclization into 5-oxazolidinone intermediates, which then lose carbon dioxide to generate nonstabilized azomethine ylides **E**.[2,11] It is therefore expected that a side reaction forming enamine intermediates would be effectively suppressed. However, only limited examples are known for the use of enolizable aldehydes in the decarboxylation route.[5,7,10] In most preceding cases, only aromatic aldehydes and formaldehyde were employed.

Ester-stabilized azomethine ylides, generated from

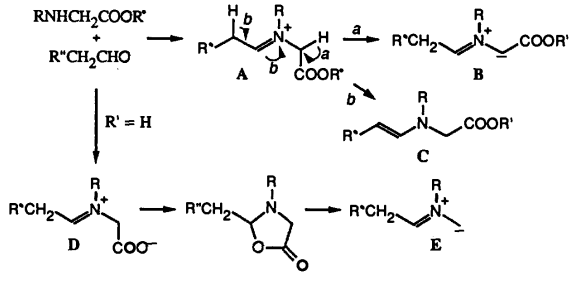

Fig. 1. Generation of azomethine ylides by the deprotonation route and the decarboxylation route.

the deprotonation route, have been well studied in terms of ylide structure, reactivity of ylide, and regio- and stereoselectivity of their cycloaddition.[3] However such chemical properties of nonstabilized azomethine ylides, generated by the decarboxylation route, remain unsolved. In most cases, nonstabilized ylides were applied to the reaction with highly activated dipolarophiles such as maleimides and showed a satisfactory reactivity.[5,6,9-11] It is very exceptional that *C*-unsubstituted ylides and its *C*-phenyl derivative reacted with less reactive olefins.[9] In intramolecular versions, however, nonstabilized ylides can be successfully trapped even with nonactivated olefin dipolarophiles.[2,5-7]

In the present article, several aldehydes are used in the decarboxylation route of azomethine ylide generation to see the scope and limitation of this method, and the reactivity of the resulting nonstabilized ylides both in inter- and intramolecular cycloadditions. Stereochemical selectivity is also briefly discussed.

Results and Discussion

Three *N*-substituted aminoacetic acids, (methylamino)- (**1a**) (benzylamino)- (**1b**), and (*p*-methoxybenzylamino)acetic acid (**1c**), were employed in the decarboxylation route. The benzyl and *p*-methoxybenzyl *N*-protecting groups were selected because they would be readily removed, after cycloaddition by hydrogenation and quinone oxidation, respectively. These α-amino acids were heated with a variety of aldehydes under reflux in toluene and the resulting ylides were trapped with *N*-(*p*-tolyl)maleimide, a highly reactive dipolarophile (Scheme 1 and Table 1).

Though the condensation reaction of (methylamino)acetic acid **1a** with benzaldehyde was previously reported,[9] the result is again listed in Table 1 in order to compare it with other results. Use of crotonaldehyde and paraformaldehyde in the condensation with **1b** and **1c**, respectively, gave no difficulty to generate the corresponding azomethine ylides **F** (R′=MeCH=CH(*E*) and H), while the yield of cycloadduct **2c** from the α,β-unsaturated aldehyde was

Table 1. Decarboxylative Condensation of α-Amino Acids **1a**—c with Aldehydes and Trap of the Resulting Nonstabilized Azomethine Ylides with Olefins

1	Aldehyde	Dipolarophile	Conditions[a]	Product	Yield/%[b]	endo:exo
1a	PhCHO	*N*-(*p*-Tolyl)maleimide	1 h	**2a**	86	5:2[c,d]
1a	EtCHO	*N*-(*p*-Tolyl)maleimide	2 h	**2b**	86	38:48[e]
1b	MeCH=CHCHO(*E*)	*N*-(*p*-Tolyl)maleimide	2 h	**2c**	58	23:35[e]
1b	MeCHO	*N*-(*p*-Tolyl)maleimide	30 min	**2c+3**	72+18	2:3[c,d]
1b	EtCHO	*N*-(*p*-Tolyl)maleimide	2 h	**2d**	84	3:2[c,d]
1c	HCHO	*N*-(*p*-Tolyl)maleimide	10 min	**2e**	100	—
1c	EtCHO	*N*-(*p*-Tolyl)maleimide	50 min	**2f**	74	33:41[e]
1c	EtCHO	Dimethyl fumarate	30 min	**4**	80	52:48[f]
1c	EtCHO	Dimethyl maleate	2 h	**5**	28	20:8[e]
1c	EtCHO	Methyl acrylate	2 h	**6**	39	f,g)

a) Under reflux in dry toluene. b) Yield of isolated products. c) Isomer ratio was determined by ^{1}H NMR. d) Each isomer was separated through column chromatograhy. e) Ratio of isolated isomers. f) Determined by GLC. g) An inseparable mixture of more than three isomers.

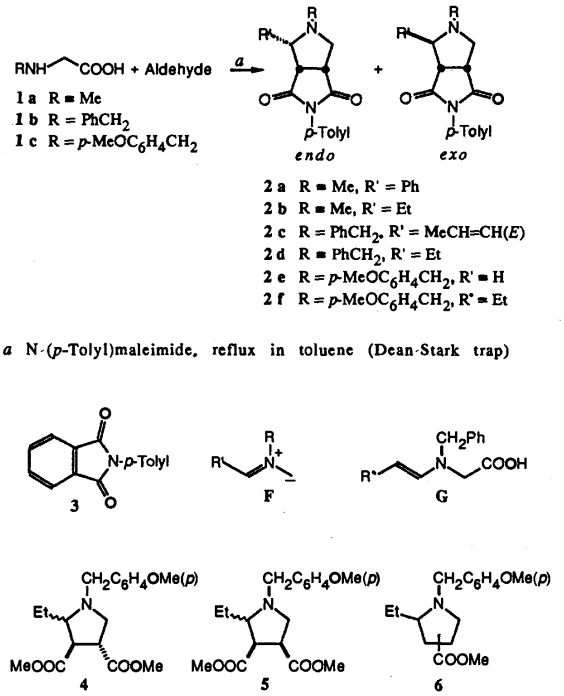

Scheme 1.

rather low.

The reaction of α-amino acid **1b** with acetaldehyde, the simplest enolizable aldehyde, under similar conditions resulted in the exclusive formation of enamine intermediate **G** (R″=H), which then underwent further condensation with another molecule of acetaldehyde to generate (1-propenyl)-substituted azomethine ylide **F** (R′=MeCH=CH(*E*)) or dienamine **G** (R″=CH_2=CH). The ylide **F** reacted with *N*-(*p*-tolyl)-maleimide to give cycloadduct **2c** (54%) while the diene **G** underwent a Diels-Alder reaction with the maleimide to afford phthalimide **3** (18%) after deamination and aromatization. A similar Diels-Alder reaction leading to the dihydro derivative of **3** was previously observed in the deprotonation route using acetaldehyde and ethyl (methylamino)acetate.[3]

In contrast with the above disappointing result, a promising feature of the decarboxylation route was unveiled in the reaction of **1a**—**c** with propanal, the second simplest enolizable aldehyde. The only products **2b**, **d**, **f** obtained in better than 80% yields were the cycloadducts of ethyl-substituted azomethine ylide **F** (R′=Et), no enamine intermediate being even detected. This indicates that any alkyl groups except methyl may be directly introduced from aldehyde to nonstabilized azomethine ylides, and this must be a very important synthetic advantage of the decarboxylation route over the deprotonation route.

The maleimide cycloadducts **2a**—**f** were all mixtures of endo (or 3a,4-cis) and exo (or 3a,4-trans) isomers, however they could be separated from each other by column chromatography over silica gel.

The stereostructures of **2a**—**f** were determined mainly on the basis of ^{1}H NMR spectra. A stereostructural inspection using molecular models indicates that the substituent at 4-position of both 3a,4-cis and 3a,4-trans isomers of **2** would occupy an equatorial position so that $J_{6\text{-}6a}$ (trans) of the 3a,4-cis isomers becomes zero. It was found that, in addition, difference of the chemical shifts between two nonequivalent hydrogens of *N*-benzyl and *N*-(*p*-methoxybenzyl) moieties was much smaller in the 3a,4-trans isomers (0.28—0.34 ppm) than that in the cis isomers (0.94—0.99 ppm).

Since only a little is known on the reactivity of azomethine ylides bearing an alkyl moiety as the only *C*-substituent,[7,9] ethyl-substituted ylide **F** (R=*p*-$MeOC_6H_4$, R′=Et) was allowed to react with several olefin dipolarophiles (Scheme 1 and Table 1). With highly activated dipolarophiles such as *N*-(*p*-tolyl)-maleimide and dimethyl fumarate, satisfactory yields of cycloadducts **2d** (74%, 41:33) and **4** (80%, 52:48 (by GLC)) were obtained under mild reaction conditions. However, this ylide **F** showed only a poor reactivity toward dimethyl maleate and methyl acrylate; low yields of cycloadduct **5** (28%, 20:8) and **6** (39%, more than three isomers) resulted, respectively. Although

Table 2. Intramolecular Cycloadditions of Azomethine Ylides Generated by the Decarboxylation Route

Amine	Aldehyde	Conditions[a]	Product	Yield/%[b]
1c	*o*-(CH_2=$CHCH_2O$)C_6H_4CHO	4 h	**7a**	53
1c	*o*-(PhCH=$CHCH_2O$)C_6H_4CHO	5 h[c]	**7b+8**	33+16[d]
1c	*o*-(MeOOCCH=$CHCH_2O$)C_6H_4CHO	1 h	**7c**	87
1d	*o*-(MeOOCCH=$CHCH_2O$)C_6H_4CHO	4 h	**9**	70
1e	*o*-(MeOOCCH=$CHCH_2O$)C_6H_4CHO	2 h	**10+11**	68+22[d]
1d	*o*-(CH_2=$CHCH_2O$)C_6H_4CHO	2 h	**12**	51

a) Under reflux in dry toluene. b) Yield of isolated prducts. c) Under reflux in xylene. d) Yield of separated products.

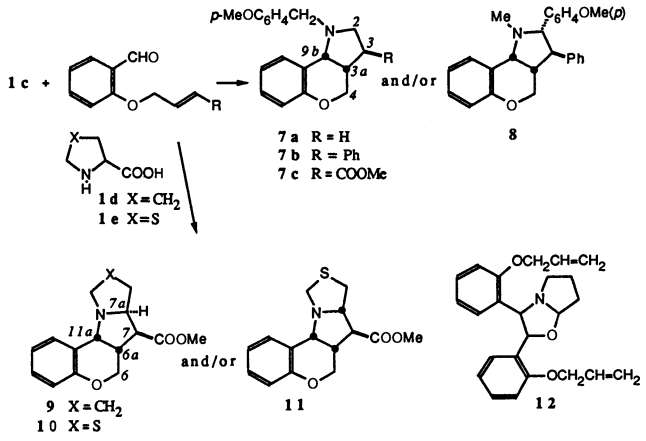

Scheme 2.

the structure of each isomer was not specified, both regio- and stereoselectivity were very poor in the latter case.

Thus, the reactivity of nonstabilized azomethine ylides and the stereoselectivity of their cycloaddition were not sufficient enough for the decarboxylation route to be utilized effectively in organic synthesis. Therefore, application of these ylides to intramolecular cycloaddition reaction was investigated next.

Three benzaldehydes having an internal olefin dipolarophile were selected as partners of (*p*-methoxybenzylamino)acetic acid (**1c**). It was not surprsing that the ester-activated olefin showed a high reactivity toward an internal nonstabilized ylide to give cycloadduct **7c** in a regio- and stereoselective manner (Scheme 2 and Table 2). Both nonsubstituted and phenyl-substituted olefins were also sufficiently reactive to produce the cis-fused cycloadducts, **7a**, **b** and **8**.[5-7]

2-Pyrrolidine- (**1d**) and 4-thiazolidinecarboxylic acid (**1e**) similarly reacted with methyl (*E*)-4-(2-formylphenoxy)-2-butenoate to produce the cis-fused cycloadducts **9**—**11** in satisfactory yields. However, a nonactivated internal olefin failed to trap the nonstabilized ylide,[5] an aldehyde cycloadduct **12** being obtained instead as a single stereoisomer.

Stereostructures of cycloadducts **7**—**11** were determined on the basis of coupling constants and the rule of stereospecificity of 1,3-dipolar cycloaddition.[12,13] Especially two medium couplings $J_{3a\text{-}4}$ (5.1 and 8.4 Hz for **7c**) and a medium coupling of $J_{3a\text{-}9b}$ (6.0 for **7c**) of **7**—**8** were informative. The 6a,11a-cis structures of **9**—**11** and the 6a,7a-cis structure of **11** were assigned on the basis of $J_{6a\text{-}6}$ (3.7 and 4.8 Hz for **9**) and a magnetic shielding of 10-Hs (δ=3.76 and 3.99 for **11**; 4.27 and 4.46 for **10**) by the fused benzene ring, respectively.

Cycloadduct **8** corresponds to the product of ylide **I**. The initially generated ylide **H** presumably isomerized into the more stabilized ylide **I** by a 1,3-proton migration (Fig. 2). This indicates that nonstabilized azomethine ylides may behave as bases and may abstract a proton from acidic molecules around if no reactive dipolarophile exists.

Although the intramolecular trap of 1,3-dipole with an (*E*)-olefin dipolarophile is not known so far, the exclusive formation of cis-fused cycloadducts **7a**—**c** must have resulted from the sterically least crowded transition state **J**. Similar selectivity was previously observed in the intramolecular cycloadditions using a terminal olefin.[4-7]

Products **9** and **10** are the cis-fused cycloadducts of

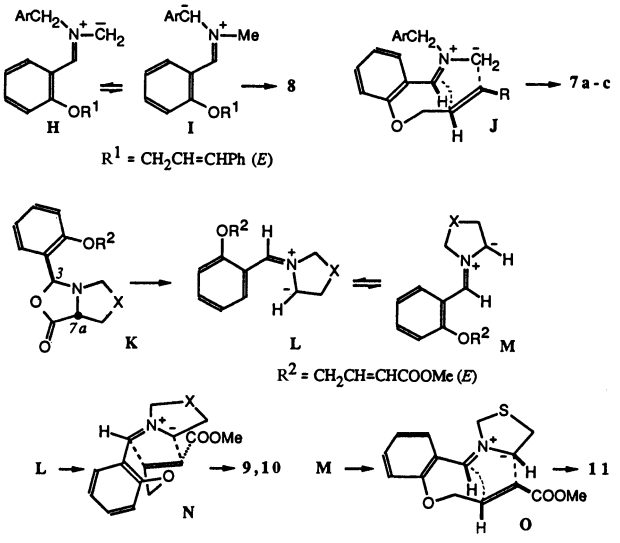

Fig. 2. Stereoselectivity of intramolecular cycloaddition of the nonstabilized azomethine ylides generated by the decarboxylation route.

anti ylides **L** (X=CH_2 and S). Exclusive involvement of **L** (X=CH_2) in the reaction of **1d** was conceivable because of the expected stereospecific extrusion of carbon dioxide from the most favorable 3,7a-trans bicyclic lactone intermediate **K** (X=CH_2).[11] However, there should be a significant steric repulsion between the ester moiety and the five-membered heterocycle in its approach **N** (X=CH_2).

If internal trap of anti ylide **L** is sluggish, **L** equilibrates with syn ylide **M**, which then undergoes a cycloaddition via **O**. The formation of **11**, as a side product, in the reaction of **1e** is the case.[10,11]

Intramolecular cycloadditions of ester-stabilized azomethine ylides were next investigated in order to compare their reactivity and stereoselectivity with those of nonstabilized azomethine ylides. Thus, reaction of ethyl (methylamino)acetate with three benzaldehydes above employed were carried out under similar conditions (Scheme 3). The reactions with unsubstituted and phenyl-substituted internal olefins gave the cis-fused cycloadducts as single isomers, **13c** and **13d**, respectively, of anti forms of ester-stabilized azomethine ylides (Table 3).[4,6]

On the other hand, the reaction with a more reactive ester-activated internal olefin furnished two isomeric cyloadducts **13a** and **14a** in comparable yields.

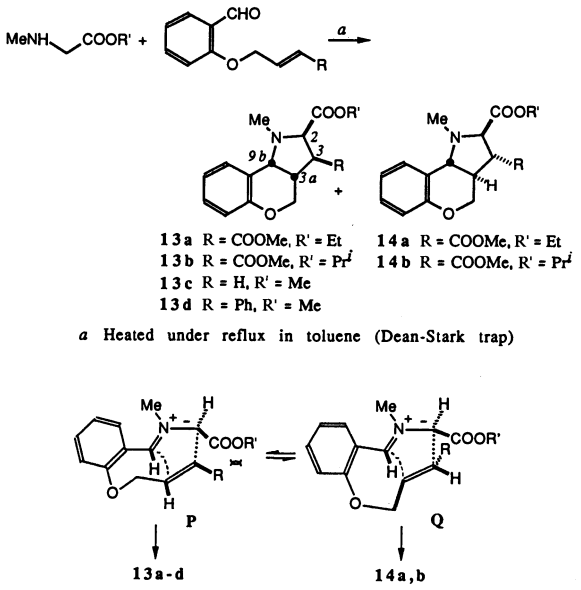

13a R = COOMe, R' = Et
13b R = COOMe, R' = Pr^i
13c R = H, R' = Me
13d R = Ph, R' = Me

14a R = COOMe, R' = Et
14b R = COOMe, R' = Pr^i

a Heated under reflux in toluene (Dean-Stark trap)

Scheme 3.

One product **13a** (42%) is cis fused cycloadduct of anti ylide and the other **14a** (44%) trans-fused isomer of anti ylide. A similar result was obtained from the reaction of isopropyl (methylamino)acetate.

These isomeric cycloadducts **13** and **14** were separated from each other by column chromatography over silica gel. The stereostructures of **13a—d** were determined on the basis of two small coupling constants of $J_{3a\text{-}4}$, a magnetic shielding of 2-COOMe by the adjacent phenyl for **13d**, and medium couplings of $J_{2\text{-}3}$ for **13a,b**, and **13d**.

According to a molecular model inspection, 3a-H of isomeric cycloadducts **14a,b** is located antiperiplanar to 3-H, one of 4-Hs, and 9b-H. The observed large couplings among these hydrogens accord with the model structure. A medium coupling of $J_{2\text{-}3}$ confirmed the 2,3-trans stereochemistry.

It was already reported that ester-stabilized azomethine ylides bearing an *N*-substituent participated in cycloadditions in anti forms.[3] In an approach depicted in **P** which leads to the cis-fused cycloadducts **13a—d**, the ester moiety COOR′ derived from α-amino acids and the olefin substituent R close to each other. This approach **P** becomes sterically more favored if R is either small (R=H) or can interact attractively (R=Ph) with the ester moiety. When a steric repulsion exists between COOR′ and R (R=COOMe), the other ring fusion via **Q** competes with **P**.

Formation of trans-fused [5.6] ring systems by intramolecular cycloadditions is quite rare.[14] The competitive participation of such energetically disfavored approach **Q** may be due to a tight structure of the anti forms of ester-stabilized azomethine ylides. This makes a striking contrast with the ready isomerization of nonstabilized ylides, which was shown above in the isomerization example of **N** into **O**.

Thus, it is concluded that (1) the decarboxylation route offers a general preparation method for nonstabilized azomethine ylides, (2) nonstabilized ylides can be effectively trapped intermolecularly by highly activated olefin dipolarophiles such as maleimides and fumarates, (3) nonstabilized ylides can be trapped by nonactivated and phenyl-substituted internal olefins and ester-activated olefins, (4) cis-fused cycloadducts are exclusively produced in intramolecular reaction, (5) the isomerization of nonstabilized ylides can be sufficiently suppressed by the intramolecular cycload-

Table 3. Intramolecular Cycloadditions of Azomethine Ylides Generated by the Deprotonation Route

Amine	Aldehyde	Conditions[a]	Producrt	Yield/%[b]
$MeNHCH_2COOEt$	*o*-($MeOOCCH{=}CHCH_2O$)C_6H_4CHO	40 min	**13a+14a**	42+44[c]
$MeNHCH_2COOPr^i$	*o*-($MeOOCCH{=}CHCH_2O$)C_6H_4CHO	6 h	**13b+14b**	36+39[c]
$MeNHCH_2COOMe$	*o*-($CH_2{=}CHCH_2O$)C_6H_4CHO	1 h	**13c**	53
$MeNHCH_2COOMe$	*o*-($CH_2{=}CHCH_2O$)C_6H_4CHO	3 h	**13d**	69

a) Under reflux in dry toluene. b) Yield of isolated products. c) Yield of separated isomers.

ditions using an ester-activated olefin dipolarophile.

Experimental

General. Melting points were determined on a Yanagimoto melting point apparatus and are uncorrected. IR spectra were taken with a JASCO IRA-1 or a JASCO A-702 spectrometer. ^{1}H and ^{13}C NMR spectra were recorded on a JEOL GSX-270 (270 MHz for ^{1}H and 67.94 MHz for ^{13}C) and a JEOL FX-100 instrument (100 MHz for ^{1}H and 25.05 MHz, for ^{13}C). Chemical shifts are expressed in parts per million downfield from tetramethylsilane as an internal standard. Mass spectra and high resolution mass spectra (HRMS) were measured with a JEOL-01SG-2 spectrometer at 70 eV of ionization energy. Elemental analyses were performed on a Hitachi 026 CHN analyzer. Wakogel C-200, C-300 (Wako), and Silica gel 60 (Merck) were employed for preparative column chromatography. Flash chromatography was carried out on an EYELA EF-10 apparatus using a column (20×180 mm) packed with Silica gel 60 (Merck, size: 0.04—0.063 mm). Gas liquid chromatography (GLC) was accomplished on a Yanaco G-2800 gas chromatograph (Yanagimoto) with an ionization flame detector using a glass column (SE-30, 3×2000 mm) or a glass capillary column (Silicone GE, SE-30, 0.25×50000 mm).

Materials. (Methylamino)acetic acid (**1a**) is commercially available. (Benzylamino)acetic acid (**1b**) and (*p*-methoxybenzylamino)acetic acid (**1c**) were prepared through the condensation of ethyl aminoacetate and aldehydes followed by a reduction with sodium borohydride:[15] The ethyl esters of **1b** and **1c** were first purified by silica-gel chromatography (ethyl acetate-ethanol= 4 : 1 v/v as an eluent) and then hydrolyzed with sodium hydroxide (half an equivalent of the ester used) in aqueous ethanol (75%) at room temperature for 1 h. After 1 M hydrochloric acid (1 M=1 mol dm^{-3}) was added to pH 7, the mixture was evaporated in vacuo and the residue was dried on calcium chloride under vacuum. The resulting α-amino acids **1b** and **1c** containing sodium chloride were used without separation. (3a*R**, 6a*S**)-5-Methyl-4-phenyl-2-(*p*-tolyl)perhydropyrrolo[3,4-*c*]pyrrole-1,3-dione (**2a**)[9] was previously reported.

General Procedure for the Condensations of α-Amino Acids 1a—c with Aldehydes and Trap of the Resulting Azomethine Ylides. A mixture of **1** (2 mmol as a mixture with sodium chloride), an aldehyde (paraformaldehyde and propanal: 5 mmol; crotonaldehyde: 1.5 mmol), and an olefin (1 mmol) was heated under reflux in dry toluene (10—20 ml) with continuous removal of water with the aid of a Dean-Stark trap. Only in the reaction with methyl acrylate, a mixture of **1** (1 mmol), propanal (5 mmol), and methyl acrylate (5 mmol) was employed. After the reaction was complete (checked by TLC), all volatile materials were evaporated in vacuo. The residue was extracted with boiling chloroform (20 ml×2). The chloroform was evaporated and the residue was chromatographed over silica gel by using hexane-ethyl acetate (10 : 1 v/v for **2b**,c; 4 : 1 for **2e**, f; 3 : 1 for **2d**) to give **2a—f** and **3—6**. The reaction conditions and results are summarized in Table 1.

(3a*R,6a*S**)-4-Ethyl-5-methyl-2-(*p*-tolyl)perhydropyrrolo-[3,4-*a*]pyrrole-1,3-dione (2b): 3a,4-*cis*-2b:** Colorless solid; mp 79—81 °C; IR (KBr) 1775, 1700, 1390, and 1200 cm^{-1}; ^{1}H NMR ($CDCl_3$) δ=1.14 (3H, t, J=7.0 Hz, Et), 2.4—2.8 (2H, m, Et), 2.21 (1H, m, 4-H), 2.26, 2.37 (each 3H, s, NMe and *p*-Me), 2.40 (1H, dd, J_{gem}=9.5 and J_{6-6a}=7.7 Hz, one of 6-H), 3.22 (1H, dd, J_{3a-4}=8.0 and J_{3a-6a}=7.7 Hz, 3a-H), 3.35 (1H, t, J_{6a-3a}=J_{6a-6}=7.7 Hz, 6a-H), 3.48 (1H, d, J_{gem}=9.5 Hz, the other of 6-H), and 7.1—7.3 (4H, m, Ar); MS *m/z* (rel intensity, %) 272 (M^+, 8), 244 (16), 243 (base peak), and 82 (51). Found: C, 70.57; H, 7.40; N, 10.29%. Calcd for $C_{16}H_{20}N_2O_2$: C, 70.72; H, 7.47; N, 10.19%. **3a,4-*trans*-2b**: Colorless solid; mp 84—86 °C; IR (KBr) 1780, 1705, 1385, and 1190 cm^{-1}; ^{1}H NMR ($CDCl_3$) δ=1.05 (3H, t, J=7.5 Hz, Et), 1.48 (1H, ddq, J_{gem}=15.7, J= 7.5, and 7.5 Hz, one of Et), 1.84 (1H, ddq, J_{gem}=15.7, J=7.5, and 3.2 Hz, the other of Et), 2.34, 2.38 (each 3H, s, NMe and *p*-Me), 2.6—2.7 (2H, m, 3a- and 4-H), 3.15 (1H, dd, J_{gem}=8.6 and J_{6-6a}=5.4 Hz, one of 6-H), 3.38 (1H, t, J_{gem}=J_{6-6a}=8.6 Hz, the other of 6-H), 3.44 (1H, dt, J_{6a-6}=J_{6a-3a}=8.6 and J_{6a-6}=5.4 Hz, 6a-H), 7.15 and 7.27 (each 2H, d, J=8.4 Hz, Ar); MS *m/z* (rel intensity, %) 272 (M^+, 7), 243 (base peak), 82 (46), and 57 (59). Found: C, 70.61; H, 7.45; N, 10.38%. Calcd for $C_{16}H_{20}N_2O_2$: C, 70.57; N, 7.40; H, 10.29%.

(3a*R,6a*S**)-5-Benzyl-4-[(*E*)-1-propenyl]-2-(*p*-tolyl)perhydropyrrolo[3,4-*a*]pyrrole-1,3-dione (2c): 3a,4-*cis*-2c:** Pale yellow liquid; IR (neat) 1780 and 1700 cm^{-1}; ^{1}H NMR ($CDCl_3$) δ=1.78 (3H, d, J=6.5 Hz, MeCH=CH), 2.38 (3H, s, *p*-Me), 3.03 (1H, d, J_{gem}=13.9 Hz, one of $PhCH_2$), 3.13 (1H, dd, J_{gem}=9.2 and J_{6-6a}=8.0 Hz, one of 6-H), 3.22 (1H, dd, J_{3a-6a}=8.0 and J_{3a-4}=7.3Hz, 3a-H), 3.33 (1H, t, J_{6a-3a}=J_{6a-6}=8.0 Hz, 6a-H), 3.42 (1H, d, J_{gem}=9.2 Hz, the other of 6-H), 4.02 (1H, J_{gem}=13.9 Hz, the other of $PhCH_2$), 5.41 (1H, m, =CH), 5.85 (1H, dq, J=15.4 and 6.5 Hz, =CH), and 7.0—7.4 (9H, m, Ph and Ar); MS *m/z* (rel intensity, %) 360 (M^+, 4), 91 (45), 86 (50), 84 (68), 59 (22), and 49 (base peak). HRMS Found: *m/z* 360.1839. Calcd for $C_{23}H_{24}N_2O_2$: M, 360.1838. **3a,4-*trans*-2c:** Pale yellow liquid; IR (neat) 1770 and 1715 cm^{-1}; ^{1}H NMR ($CDCl_3$) δ=1.76 (3H, dd, J=6.3 and 1.5 Hz, MeCH=CH), 2.38 (3H, s, *p*-Me), 3.01 (1H, dd, J_{gem}=9.7 and J_{6-6a}=3.9 Hz, one of 6-H), 3.16 (1H, dd, J_{gem}=9.7 and J_{6-6a}=8.3 Hz, the other of 6-H), 3.3—3.9 (3H, m, 3a-, 4-, and 6a-H), 3.48 (1H, J_{gem}=13.5 Hz, one of $PhCH_2$), 3.76 (1H, J_{gem}=13.5 Hz, the other of $PhCH_2$), 5.5—5.9, 6.0—6.4 (each 1H, CH=CH), and 7.1—7.4 (9H, m, Ph and Ar); MS *m/z* (rel intensity, %) 360 (M^+, 5), 239 (28), 210 (29), 108 (28), 107 (25), 106 (31), 105 (20), 91 (base peak), 86 (45), 84 (72), 79 (38), and 77 (32). HRMS Found: *m/z* 360.1837. Calcd for $C_{23}H_{24}N_2O_2$: M, 360.1836.

(3a*R,6a*S**)-5-Benzyl-4-ethyl-2-(*p*-tolyl)perhydropyrrolo-[3,4-*a*]pyrrole-1,3-dione (2d): 3a,4-*cis*-2d:** Colorless needles (hexane); mp 98—99 °C; IR (KBr) 1700, 1385, and 1190 cm^{-1}; ^{1}H NMR ($CDCl_3$) δ=1.16 (3H, t, J=7.2 Hz, Et), 1.4—2.1 (2H, m, Et), 2.34 (1H, dd, J_{gem}=9.6 and J_{6-6a}=7.5 Hz, one of 6-H), 2.38 (3H, s, *p*-Me), 2.56 (1H, ddd, J_{4-Et}=9.8, 3.2, and J_{4-3a}=7.4 Hz, 4-H), 3.12 (1 H, d, J_{gem}=13.5 Hz, one of $PhCH_2$), 3.19 (1H, dd, J_{3a-6a}=8.0 and J_{3a-4}=7.4 Hz, 3a-H), 3.38 (1H, d, J_{gem}=9.6 Hz, the other of 6-H), 3.39 (1H, dd, J_{6a-3a}=8.0 and J_{6a-6}=7.5 Hz, 6a-H), 4.08 (1H, d, J_{gem}=13.5 Hz, the other of $PhCH_2$), and 7.0—7.4 (9H, m, Ph and Ar); ^{13}C NMR ($CDCl_3$) δ=10.70, 21.17 (each Et), 21.79 (*p*-Me), 42.95 (6a-C), 46.71 (3a-C), 56.24 (6-C), 68.98 (4-C), 126.30, 127.11, 128.30, 129.56, 138.51, 138.80 (each Ph and Ar), 176.00, and 178.45 (each CON); MS *m/z* 348 (M^+, 7), 320 (23), 319 (95), and 91 (base peak). Found: C, 75.93; H, 6.93; N, 8.09%. Calcd for $C_{22}H_{24}N_2O_2$: C, 75.84; H, 6.94; H, 8.04%. **3a,4-*trans*-2d:** Pale yellow prisms (hexane); mp 112—113 °C;

IR (KBr) 1770, 1700, 1370, and 1170 cm^{-1}; ^1H NMR ($CDCl_3$) δ=1.04 (3H, t, J=7.2 Hz, Et), 1.3—2.0 (2H, m, Et), 2.38 (3H, s, *p*-Me), 2.84 (1H, dd, J_{gem}=9.7 and $J_{6\text{-}6a}$=4.0 Hz, one of 6-H), 3.0—3.5 (4H, m, 3a-, 4-, 6a-H, and the other of 6-H), 3.50, 3.86 (each 1H, d, J_{gem}=13.3 Hz, $PhCH_2$), and 7.0—7.4 (9H, m, Ph and Ar); ^{13}C NMR ($CDCl_3$) δ=9.69 (q, Et), 21.14 (t, Et), 43.94 (d, 6a-C), 49.19 (d, 3a-C), 53.95 (t, 6-C), 55.28 (t, $PhCH_2$), 67.33 (d, 4-C), 126.22, 127.18, 128.28, 128.39, 129.77 (each d, Ar), 138.40, 138.54 (each s, Ar), 177.79, and 178.12 (each s, CON); MS *m/z* (rel intensity, %) 348 (M^+, 4), 319 (85), and 91 (base peak). Found: C, 75.81; H, 6.92; N, 8.01%. Calcd for $C_{22}H_{24}N_2O_2$: C, 75.84; H, 6.94; H, 8.04%.

(3a*R,6a*S**)-5-(*p*-Methoxybenzyl)-2-(*p*-tolyl)perhydropyrrolo[3,4-*a*]pyrrole-1,3-dione (2e):** Colorless prisms (benzene-hexane); mp 139—140 °C; IR (KBr) 1770, 1695, 1505, 1380, 1240, and 1185 cm^{-1}; ^1H NMR ($CDCl_3$) δ=2.39 (3H, s, *p*-Me), 2.44, 2.45 (each 1H, dd, J_{gem}=9.9 and J=6.2 Hz, one of 4-H and one of 6-H), 3.29, 3.33 (each 1H, t, $J_{3a\text{-}6a}$=6.2 and J=6.2 Hz, 3a- and 6a-H), 3.38 (2H, d, J_{gem}=9.9 Hz, the other of 4-H and the other of 6-H), 3.56 (2H, s, $ArCH_2$), 3.79 (3H, *p*-OMe), and 6.8—7.3 (8H, m, Ar); MS *m/z* (rel intensity, %) 350 (M^+, 16), 122 (22), and 121 (base peak). Found: C, 72.06; H, 6.25; N, 7.98%. Calcd for $C_{21}H_{22}N_2O_3$: C, 71.98; H, 6.33; N, 7.99%.

(3a*R,6a*S**)-4-Ethyl-5-(*p*-methoxybenzyl)-2-(*p*-tolyl)-perhydropyrrolo[3,4-*a*]pyrrole-1,3-dione (2f): 3a,4-*cis*-2d:** Pale yellow liquid; IR (neat) 1780, 1715, 1510, 1460, and 1240 cm^{-1}; ^1H NMR ($CDCl_3$) δ=1.18 (3H, t, J=7.5 Hz, Et), 1.4—2.1 (2H, m, Et), 2.2—2.7 (2H, m, 4-H and one of 6-H), 2.40 (3H, s, *p*-Me), 3.10 (1H, d, J_{gem}=13.0 Hz, one of $ArCH_2$), 3.18 (1H, dd, $J_{3a\text{-}4}$=8.0 and $J_{3a\text{-}6a}$=7.5 Hz, 3a-H), 3.37 (1H, d, J_{gem}=9.3 Hz, the other of 6-H), 3.47 (1H, t, $J_{6a\text{-}3a}$=$J_{6a\text{-}6}$=7.5 Hz, 6a-H), 3.78 (3H, s, *p*-MeO), 4.04 (1H, d, J_{gem}=13.0 Hz, the other of $ArCH_2$), and 6.7—7.4 (8H, m, Ar), MS *m/z* (rel intensity, %) 378 (M^+, 6), 349 (10), 121 (base peak), and 109 (13). HRMS Found: *m/z* 378.1949. Calcd for $C_{23}H_{26}N_2O_3$: M, 378.1942. **3a,4-*trans*-2d:** Pale yellow liquid; IR (neat) 1780, 1710, 1510, 1380, and 1240 cm^{-1}; ^1H NMR ($CDCl_3$) δ=1.04 (3H, t, J=7.5 Hz, Et), 1.4—2.0 (2H, m, Et), 2.40 (3H, s, *p*-Me), 2.83 (1H, dd, J_{gem}=9.8 and $J_{6\text{-}6a}$=4.3 Hz, one of 6-H), 3.0—3.5 (4H, m, 3a-, 4-, 6a-H, and the other of 6-H), 3.46 (1H, d, J_{gem}=12.9 Hz, one of $ArCH_2$), 3.78 (3H, s, *p*-MeO), 3.80 (1H, J_{gem}=12.9 Hz, the other of $ArCH_2$), and 6.7—7.6 (8H, m, Ar); MS *m/z* (rel intensity, %) 378 (M^+, 3), 349 (16), and 121 (base peak). HRMS Found: *m/z* 378.1951. Calcd for $C_{23}H_{26}N_2O_3$: M, 378.1942.

Dimethyl (3*R,4*R**)-2-Ethyl-1-(*p*-methoxybenzyl)-3,4-pyrrolidinedicarboxylate (4):** Obtained as an inseparable mixture of two stereoisomers (48:51 by GLC). Pale yellow liquid; IR (neat) 1730, 1615, 1510, 1440, and 1250 cm^{-1}; ^1H NMR ($CDCl_3$) δ=0.91 and 0.95 (each 1/2×3H, t, J=7.3 Hz, Et), 1.2—1.8 (2H, m, Et), 2.4—3.9 (5H, m, 2-, 3-, 4-, and 5-H), 3.14, 3.88 (each 1/2×2H, d, J_{gem}=13.2 Hz, $PhCH_2$), 3.36, 3.86 (each 1/2×2H, d, J_{gem}=12.8 Hz, $PhCH_2$), 3.66, 3.67, 3.71, 3.72 (each 1/2×3H, s, COOMe), 3.79, 3.80 (each 1/2×3H, s, *p*-MeO), and 6.8—7.3 (4H, m, Ar); MS *m/z* (rel intensity, %) 335 (M^+, 9), 306 (31), and 121 (base peak). Found: C, 64.47; H, 7.51; N, 4.18%. Calcd for $C_{18}H_{25}NO_5$: C, 64.62; H, 7.62; N, 4.10%.

Dimethyl (3*R,4*S**)-2-Ethyl-1-(*p*-methoxybenzyl)-3,4-pyrrolidinedicarboxylate (5):** Two stereoisomers were obtained in 20 and 8% yields, but the stereostructures could not be determined. The major isomer: Pale yellow liquid; IR (neat) 1730, 1610, 1430, and 1240 cm^{-1}; ^1H NMR ($CDCl_3$) δ=0.96 (3H, t, J=7.5 Hz, Et), 1.4—1.9 (2H, m, Et), 2.5—3.2 (5H, m, 2-, 3-, 4-, and 5-H), 3.24 (1H, d, J_{gem}=12.5 Hz, one of $ArCH_2$), 3.60, 3.64 (each 3H, s, COOMe), 3.76 (3H, s, *p*-MeO), 3.93 (1H, d, J_{gem}=12.5 Hz, the other of $ArCH_2$), and 6.7—7.4 (4H, m, Ar); MS *m/z* (rel intensity, %) 335 (M^+, 4), 121 (base peak), 78 (21), and 77 (45). HRMS Found: *m/z* 335.1728. Calcd for $C_{18}H_{25}NO_5$: M, 335.1731. The minor isomer: Pale yellow liquid; IR (neat) 1730, 1610, 1510, 1430, and 1240 cm^{-1}; ^1H NMR ($CDCl_3$) δ=1.00 (3H, t, J=7.0 Hz, Et), 1.1—2.0 (2H, m, Et), 2.6—3.5 (5H, m, 2-, 3- 4-, and 5-H), 3.36 (1H, d, J_{gem}=13.5 Hz, one of $ArCH_2$), 3.60, 3.68 (each 3H, s, COOMe), 3.77 (3H, s, *p*-MeO), 3.95 (1H, d, J_{gem}=13.5 Hz, the other of $ArCH_2$), and 6.7—7.3 (4H, m, Ar); MS *m/z* (rel intensity, %) 335 (M^+, 8), 138 (67), 137 (36), 121 (base peak), 109 (42), and 77 (26). HRMS Found: *m/z* 335.1729. Calcd for $C_{18}H_{25}NO_5$: M, 335.1731.

Methyl 2-Ethyl-1-(*p*-methoxybenzyl)-3(or 4)-pyrrolidinecarboxylate (6): An inseparable mixture of more than three isomers was obtained as colorless liquid. Only ^1H NMR and mass spectra were taken. ^1H NMR ($CDCl_3$) δ=0.9—1.0 (3H, m, Et), 1.3—2.0 (2H, m, Et), 2.2—3.0 (6H, m, 2-, 3-, 4-, and 5-H), 3.1—3.2 (1H, m, one of $ArCH_2$), 3.65, 3.68, 3.69 (3H, each s, COOMe), 3.79, 3.81 (3H, each s, *p*-MeO), 3.9—4.1 (1H, m, the other of $ArCH_2$), and 6.8—7.3 (4H, m, Ar); MS *m/z* (rel intensity, %) 277 (M^+, 6), 248 (24), and 121 (base peak).

General Procedure for the Reactions of α-Amino Acids 1c—e with *o*-(2-Alkenyloxy)benzaldehydes. A mixture of **1c** (2 mmol as a mixture with sodium chloride) or **1d, e** (1.2 mmol) and an aldehyde (1 mmol) was heated under reflux in dry toluene or xylene (15 ml) with continuous removal of water with the aid of a Dean-Stark trap. After the completion of reaction (checked by TLC), the solvent was removed. The residue was washed with boiling chloroform (20 ml×2). The chloroform was evaporated in vacuo and the residue was chromatographed over silica gel with hexane-ethyl acetate (15:1 v/v for **7b**; 10:1 for **7a**; 6:1 for **7c**; 3:1 for **9—12**) to give **7a—3c**, **8**, and **9—12**. The reaction conditions and results are summarized in Table 2.

(3a*R,9b*S**)-1-(*p*-Methoxybenzyl)-1,2,3,3a,4,9b-hexahydro-[1]benzopyrano[4,3-*b*]pyrrole (7a):** Pale yellow liquid; IR (neat) 1610, 1580, 1460, and 1250 cm^{-1}; ^1H NMR ($CDCl_3$) δ=1.37, 2.01 (each 1H, m, 3-H), 2.15 (1H, br q, J_{gem}=9.7 and $J_{2\text{-}3}$=9.7 Hz, one of 2-H), 2.42 (1H, m, 3a-H), 2.84 (1H, dt, J_{gem}=9.7, $J_{2\text{-}3}$=9.7, and 2.7 Hz, the other of 2-H), 3.15 (1H, d, J_{gem}=12.1 Hz, $ArCH_2$), 3.22 (1H, d, $J_{9b\text{-}3a}$=5.5 H, 9b-H), 3.77 (3H, s, *p*-MeO), 4.01 (1H, dd, J_{gem}=10.0 and $J_{4\text{-}3a}$=5.5 Hz, one of 4-H), 4.07 (1H, dd, J_{gem}=10.0 and $J_{4\text{-}3a}$=9.9 Hz, the other of 4-H), 4.32 (1H, d, J_{gem}=12.1 Hz, $ArCH_2$), and 6.8—7.3 (8H, m, Ar); MS *m/z* (rel intensity, %) 295 (M^+, 24), 174 (22), 131 (17), 122 (14), and 121 (base peak). Found: C, 77.08; H, 6.96; N, 4.32%. Calcd for $C_{19}H_{21}NO_2$: C, 77.26; H, 7.17; N, 4.74%.

(3*R,3a*S**,9b*R**)-1-(*p*-Methoxybenzyl)-3-phenyl-1,2,3,3a,4,9b-hexahydro[1]benzopyrano[4,3-*b*]pyrrole (7b):** Pale yellow liquid; IR (neat) 1600, 1580, and 1440 cm^{-1}; ^1H NMR ($CDCl_3$) δ=2.30 (1H, dd, J_{gem}=9.5 and $J_{2\text{-}3}$=9.2 Hz, one of 2-H), 2.55 (1H, dddd, $J_{3a\text{-}4}$=7.6, 5.3, $J_{3a\text{-}9b}$=7.0, and $J_{3a\text{-}3}$=5.4 Hz, 3a-H), 2.93 (1H, ddd, $J_{3\text{-}2}$=9.2, 8.4, and $J_{3\text{-}3a}$=5.4 Hz, 3-H), 3.21 (1H, dd, J_{gem}=9.5 and $J_{2\text{-}3}$=8.4 Hz, the other of 2-H), 3.30 (1H, d, J_{gem}=12.5 Hz, $ArCH_2$), 3.66 (1H, d, $J_{9b\text{-}3a}$=7.0 Hz, 9b-H), 3.72 (3H, s, *p*-MeO), 4.07 (1H, dd J_{gem}=10.6 and

$J_{4\text{-}3a}$=5.3 Hz, one of 4-H), 4.09 (1H, dd, J_{gem}=10.6 and $J_{4\text{-}3a}$=7.6 Hz, the other of 4-H), 4.33 (1H, d, J_{gem}=12.5 Hz, $ArCH_2$), and 6.8—7.4 (13H, m, Ph and Ar); ^{13}C NMR ($CDCl_3$) δ=44.10 (3-C), 44.69 (3a-C), 55.10 ($ArCH_2$), 57.31 (*p*-MeO), 61.14 (2-C), 61.64 (9b-C), 67.07 (4-C), 113.55, 117.16, 120.27, 122.57, 126.52, 127.61, 128.58, 128.69, 129.82, 131.44, 143.34, 155.63, and 158.60 (each Ph and Ar); MS *m/z* (rel intensity, %) 371 (M^+, 4), 370 (14), 267 (26), 238 (34), 150 (25), 131 (38), 121 (base peak), 117 (61), 115 (32), 105 (29), 91 (50), and 76 (36). Found: C, 80.83; H, 6.78; N, 3.77%. Calcd for $C_{25}H_{25}NO_2$: C, 80.83; H, 6.78; N, 3.77%.

Methyl (3*R,3a*R**,9b*S**)-1-(*p*-Methoxybenzyl)-1,2,3,3a,4,9b-hexahydrohydro[1]benzopyrano[4,3-*b*]pyrrole-3-carboxylate (7c):** Pale yellow liquid; IR (neat) 1740, 1460, and 1240 cm^{-1}; ^1H NMR ($CDCl_3$) δ=2.46 (1H, dd, J_{gem}=10.0 and $J_{2\text{-}3}$=8.0 Hz, one of 2-H), 2.67 (1H, ddd, $J_{3\text{-}2}$=9.0, 8.0, and $J_{3\text{-}3a}$=4.0 Hz, 3-H), 2.77 (1H, m, 3a-H), 3.06 (1H, dd, J_{gem}=10.0 and $J_{2\text{-}3}$=9.0 Hz, the other of 2-H), 3.27 (1H, d, J_{gem}=12.3 Hz, one of $ArCH_2$), 3.51 (1H, d, $J_{9b\text{-}3a}$=6.0 Hz, 9b-H), 3.69 (3H, s, COOMe), 3.76 (3H, s, *p*-MeO), 4.08 (1H, dd, J_{gem}=10.6 and $J_{4\text{-}3a}$=5.1 Hz, one of 4-H), 4.12 (1H, dd, J_{gem}=10.6 and $J_{4\text{-}3a}$=8.4 Hz, the other of 4-H), 4.24 (1H, d, J_{gem}=12.3 Hz, the other of $ArCH_2$), and 6.8—7.2 (8H, m, Ar); ^{13}C NMR ($CDCl_3$) δ=39.37 (d, 3a-C), 43.20 (d, 3-C), 51.92 (q, *p*-MeO), 52.01 (q, COOMe), 54.43 (t, 2-C), 55.17 (t, $ArCH_2$), 60.70 (d, 9b-C), 66.68 (t, 4-C), 113.59, 117.00, 120.24, 121.46, 128.82, 129.69, 131.26 (each d, Ar), 131.53, 155.42, 158.64 (each s, Ar), and 174.42 (s, COOMe); MS *m/z* (rel intensity, %) 353 (M^+, 35), 232 (28), 131 (54), and 121 (base peak). HRMS *m/z* 353.1648. Calcd for $C_{21}H_{23}NO_4$: M, 353.1620.

(2*R,3*S**,3a*R**,9b*S**)-2-(*p*-Methoxyphenyl)-1-methyl-3-phenyl-1,2,3,3a,4,9b-hexahydro[1]benzopyrano[4,3-*b*]-pyrrole (8):** Colorless prisms (benzene); mp 169—171 °C; IR (KBr) 1605, 1450, 1240, and 1030 cm^{-1}; ^1H NMR ($CDCl_3$) δ=2.33 (3H, s, NMe), 3.26 (1H, dddd, $J_{3a\text{-}9b}$=9.1, $J_{3a\text{-}3}$=8.0, $J_{3a\text{-}4}$=2.9, and 1.1 Hz, 3a-H), 3.70 (3H, s, *p*-MeO), 3.91 (1H, dd, $J_{3\text{-}3a}$=8.0 and $J_{3\text{-}2}$=7.7 Hz, 3-H), 3.97 (1H, dd, J_{gem}=11.4 and $J_{4\text{-}3a}$=2.9 Hz, one of 4-H), 4.08 (1H, dd, J_{gem}=11.4 Hz and $J_{4\text{-}3a}$=1.1 Hz, the other of 4-H), 4.11 (1H, d, $J_{2\text{-}3}$=7.7 Hz, 2-H), 4.59 (1H, d, $J_{9b\text{-}3a}$=9.1 Hz, 9b-H), and 6.6—7.4 (13H, m, Ph and Ar); MS *m/z* (rel intensity, %) 371 (M^+, 47), 254 (36), 222 (61), 148 (37), 131 (base peak), 121 (77), 107 (35), and 91 (27). Found: C, 81.08; H, 6.76; N, 3.88%. Calcd for $C_{25}H_{25}NO_2$: C, 80.83; H, 6.78; N, 3.77%.

Methyl (6a*R,7*R**,7a*R**,11a*S**)-6a,7a,8,9,10,11a-Hexahydro-6*H*,7*H*-[1]benzopyrano[4′,3′:2,3]pyrrolo[1,5-*a*]pyrrole-7-carboxylate (9):** Colorless liquid; IR (neat) 1730, 1610, 1590, 1490, and 1220 cm^{-1}; ^1H NMR ($CDCl_3$) δ=1.3—1.5, 1.8—2.0, 2.8—3.0 (1H, 3H, and 2H, m, 8-H, 9-H, and 10-H, respectively), 3.25 (1H, t, $J_{7\text{-}6a}$=$J_{7\text{-}7a}$=8.8 Hz, 7-H), 3.38 (1H, dddd, $J_{6a\text{-}7}$=8.8, $J_{6a\text{-}11a}$=7.3, $J_{6a\text{-}6}$=4.8, and 3.7 Hz, 6a-H), 3.71 (3H, s, COOMe), 3.81 (1H, dt, $J_{7a\text{-}7}$=8.8, $J_{7a\text{-}8}$=8.8, and 6.7 Hz, 7a-H), 4.03 (1H, d, $J_{11a\text{-}6a}$=7.3 Hz, 11a-H), 4.15 (1H, dd, J_{gem}=10.0 and $J_{6\text{-}6a}$=3.7 Hz, one of 6-H), 4.20 (1H, dd, J_{gem}=10.0 and $J_{6\text{-}6a}$=4.8 Hz, the other of 6-H), and 6.8—7.4 (4H, m, Ar); MS *m/z* (rel intensity, %) 273 (M^+, 23), 174 (35), 145 (45), 144 (28), 132 (41), 131 (base peak), 115 (43), 91 (32), and 77 (20). HRMS Found: *m/z* 273.1360. Calcd for $C_{16}H_{19}NO_3$: M, 273.1364.

Methyl (6a*R,7*R**,7a*S**,11a*S**)-6a,7a,8,11a-Tetrahydro-6*H*,7*H*,10*H*-[1]benzopyrano[4′,3′:2,3]pyrrolo[1,5-*c*]-thiazole-7-carboxylate (10):** Colorless prisms (diethyl ether-hexane); mp 118—119 °C; IR (KBr) 1730, 1440, 1250, and 1230 cm^{-1}; ^1H NMR ($CDCl_3$) δ=2.67 (1H, dd, J_{gem}=10.6 and $J_{8\text{-}7a}$=8.8 Hz, one of 8-H), 3.00 (1H, dd, J_{gem}=10.6 and $J_{8\text{-}7a}$=7.3 Hz, the other of 8-H), 3.09 (1H, dddd, $J_{6a\text{-}7}$=$J_{6a\text{-}11a}$=8.8, $J_{6a\text{-}6}$=4.4, and 4.0 Hz, 6a-H), 3.61 (1H, dd, $J_{7\text{-}6a}$=8.8 and $J_{7\text{-}7a}$=6.6 Hz, 7-H), 3.76 (3H, s, COOMe), 3.84 (1H, ddd, $J_{7a\text{-}8}$=8.8, 7.3, and $J_{7a\text{-}7}$=6.6 Hz, 7a-H), 3.91 (1H, d, $J_{11a\text{-}6a}$=8.8 Hz, 11a-H), 3.99 (1H, dd, J_{gem}=11.4 and $J_{6\text{-}6a}$=4.4 Hz, one of 6-H), 4.15 (1H, dd, J_{gem}=11.4 and $J_{6\text{-}6a}$=4.0 Hz, the other of 6-H), 4.27, 4.46 (each 1H, d, J_{gem}=10.4 Hz, 10-H), and 6.9—7.3 (4H, m, Ar); ^{13}C NMR ($CDCl_3$) δ=33.62 (8-C), 38.92 (6a-C), 47.64 (7-C), 52.14 (COOMe), 56.95 (11a-C), 58.47 (10-C), 67.79 (6-C), 70.08 (7a-C), 117.68, 121.88, 128.84, 129.20, 136.02, 155.91 (each Ar), and 172.03 (COOMe); MS *m/z* (rel intensity, %) 291 (M^+, 31), 232 (39), 186 (35), 145 (20), 132 (76), 131 (base peak), 115 (32), 91 (21), and 77 (24). Found: C, 62.00; H, 6.10; N, 4.74%. Calcd for $C_{15}H_{17}NO_3S$: C, 61.84; H, 5.88; N, 4.81%.

Methyl (6a*R,7*R**,7a*R**,11a*S**)-6a,7a,8,11a-Tetrahydro-6*H*,7*H*,10*H*-[1]benzopyrano[4′,3′:2,3]pyrrolo[1,5-*c*]-thiazole-7-carboxylate (11):** Pale yellow liquid; IR (neat) 1730, 1600, 1580, 1450, and 1220 cm^{-1}; ^1H NMR ($CDCl_3$) δ=2.56 (1H, dd, $J_{7\text{-}7a}$=7.7 and $J_{7\text{-}6a}$=5.1 Hz, 7-H), 2.69 (1H, dd, J_{gem}=9.9 and $J_{8\text{-}7a}$=7.7 Hz, one of 8-H), 3.09 (1H, dddd, $J_{6a\text{-}6}$=10.0, 5.0, $J_{6a\text{-}11a}$=7.3, and $J_{6a\text{-}7}$=5.1 Hz, 6a-H), 3.13 (1H, dd, J_{gem}=9.9 and $J_{8\text{-}7a}$=5.1 Hz, the other of 8-H), 3.57 (1H, dt, $J_{7a\text{-}7}$=7.7, $J_{7a\text{-}8}$=7.7, and 5.1 Hz, 7a-H), 3.76 (1H, d, J_{gem}=10.0 Hz, one of 10-H), 3.76 (3H, s, COOMe), 3.92 (1H, dd J_{gem}=10.7 and $J_{6\text{-}6a}$=10.0 Hz, one of 6-H), 3.93 (1H, d, $J_{11a\text{-}6a}$=7.3 Hz, 11a-H), 3.99 (1H, d, J_{gem}=10.0 Hz, the other of 10-H), 4.19 (1H, dd, J_{gem}=10.7 and $J_{6\text{-}6a}$=5.0 Hz, the other of 6-H), and 6.9—7.3 (4H, m, Ar); MS *m/z* (rel intensity, %) 291 (M^+, 28), 245 (26), 132 (74), 131 (base peak), 115 (26), 109 (28), 95 (35), 91 (34), 83 (27), 81 (36), and 77 (30). Found: C, 61.46; H, 5.92; H, 4.34%. Calcd for $C_{15}H_{17}NO_3S$: C, 61.84; H, 5.88; N, 4.81%.

2,3-Bis[*o*-(2-propenyloxy)phenyl]perhydropyrrolo[2,1-*b*]-oxazole (12): Colorless liquid; IR (neat) 1640, 1600, 1585, 1490, 1450, and 1240 cm^{-1}; ^1H NMR ($CDCl_3$) δ=1.7—2.3 (4H, m, 6- and 7-H), 2.8—3.3 (2H, m, 5-H), 4.1—4.3 (4H, m, *O*-allyl), 4.46 (1H, d, $J_{2\text{-}3}$=7.8 Hz, 2-H), 4.9—5.2 (4H, m, *O*-allyl), 5.32 (1H, d, $J_{3\text{-}2}$=7.8 Hz, 3-H), 5.2—5.8 (3H, m, 7a-H and *O*-allyl), 6.4—7.4 (6H, m, Ar), and 7.58 (2H, d, *J*=8.0 Hz, Ar); ^{13}C NMR ($CDCl_3$) δ=24.33 (6-C), 31.56 (7-C), 56.26 (5-C), 68.96, 69.05 (each *O*-allyl), 71.45 (3-C), 81.23 (2-C), 98.44 (7a-C), 111.80 (*O*-allyl), 116.84, 116.95, 121.03, 127.03, 127.93, 128.39, 128.44, 133.37, 133.63, 156.26, and 156.45 (each Ar and *O*-allyl); MS *m/z* (rel intensity, %) 377 (M^+, 3), 215 (47), 214 (20), 174 (base peak), 146 (23), 145 (23), 132 (28), 131 (38), 91 (24), and 77 (23). HRMS Found: *m/z* 377.1986. Calcd for $C_{24}H_{27}NO_3$: M, 377.1989.

General Procedure for the Reactions of α-Amino Esters with *o*-(2-Alkenyloxy)benzaldehydes. A mixture of the hydrochloride of an ester of (methylamino)acetic acid (1.5—2 mmol), an aldehyde (1 mmol), and triethylamine (1.5—2 mmol) was heated under reflux in dry toluene (10 ml) with continuous removal of water with the aid of a Dean-Stark trap. The solvent was removed in vacuo and the residue was chromatographed over silica gel by using hexane-ethyl acetate (7 : 1 v/v for **13c, d**; 4 : 1 for **13a, b** and **14a, b**) to give **13a—d** and **14a, b**. The reaction conditions and results are summarized in Table 2.

Ethyl (2*R,3*S**,3a*S**,9b*R**)-3-Methoxycarbonyl-1-methyl-1,2,3,3a,4,9b-hexahydro[1]benzopyrano[4,3-*b*]pyrrole-2-car-**

boxylate (13a): Pale yellow liquid; IR (neat) 1730, 1600, 1580, 1450, and 1250 cm^{-1}; ^1H NMR ($CDCl_3$) δ=1.30 (3H, t, J=7.5 Hz, Et), 2.40 (3H, s, NMe), 3.38 (1H, dddd, J_{3a-9b}=9.2, J_{3a-3}=9.1, J_{3a-4}=3.7, and 1.3 Hz, 3a-H), 3.47 (1H, dd, J_{3-3a}=9.1 and J_{3-2}=7.0 Hz, 3-H), 3.71 (3H, s, COOMe), 3.87 (1H, dd, J_{gem}=11.4 and J_{4-3a}=3.7 Hz, one of 4-H), 4.01 (1H, d, J_{2-3}=7.0 Hz, 2-H), 4.03 (1H, d, J_{9b-3a}=9.2 Hz, 9b-H), 4.19 (1H, dd, J_{gem}=11.4 and J_{4-3a}=1.3 Hz, the other of 4-H), 4.20 (2H, q, J=7.5 Hz, COOEt), and 6.9—7.3 (4H, m, Ar); ^{13}C NMR ($CDCl_3$) δ=14.43 (Et), 35.58 (NMe), 41.71 (3a-C), 47.70 (3-C), 51.94 (COOMe), 59.84 (2-C), 60.47 (COOEt), 67.66 (9b-C), 69.76 (4-C), 118.02, 121.44, 125.18, 128.62, 129.87, 157.24 (each Ar), 170.98, and 171.77 (COOMe and COOEt); MS m/z (rel intensity, %) 319 (M^+, 6), 246 (base peak), 186 (23), and 131 (21). HRMS Found: m/z 319.1340. Calcd for $C_{17}H_{21}NO_5$: M, 319.1418.

Isopropyl (2*R,3*S**,3a*S**,9b*R**)-3-Methoxycarbonyl-1-methyl-1,2,3,3a,4,9b-hexahydro[1]benzopyrano[4,3-*b*]pyrrole-2-carboxylate (13b):** Colorless liquid; IR (neat) 1730, 1610, 1580, and 1210 cm^{-1}; ^1H NMR ($CDCl_3$) δ=1.28, 1.29 (each d, J=6.3 Hz, *i*-Pr), 2.40 (3H, s, NMe), 3.40 (1H, dddd, J_{3a-3}=9.2, J_{3a-9b}=8.8, J_{3a-4}=3.5, and 2.2 Hz, 3a-H), 3.47 (1H, dd, J_{3-3a}=9.2 and J_{3-2}=6.6 Hz, 3-H), 3.71 (3H, s, COOMe), 3.88 (1H, dd, J_{gem}=11.5 and J_{4-3a}=3.5 Hz, one of 4-H), 3.98 (1H, d, J_{2-3}=6.6 Hz, 2-H), 4.00 (1H, d, J_{9b-3a}=8.8 Hz, 9b-H), 4.20 (1H, dd, J_{gem}=11.5 and J_{4-3a}=2.2 Hz, the other of 4-H), 5.10 (1H, m, *i*-Pr), and 6.8—7.4 (4H, m, Ar); MS m/z (rel intensity, %) 333 (M^+, 7), 246 (base peak), 186 (27), 131 (28), 85 (27), and 83 (43). HRMS Found: m/z 333.1575. Calcd for $C_{18}H_{23}NO_5$: M, 333.1575.

Methyl (2*R,3a*S**,9b*R**)-1-Methyl-1,2,3,3a,4,9b-hexahydro-[1]benzopyrano[4,3-*b*]pyrrole-2-carboxylate (13c):** Pale yellow liquid; IR (neat) 1730, 1610, 1590, 1490, and 1200 cm^{-1}; ^1H NMR ($CDCl_3$) δ=1.96 (1H, ddd, J_{gem}=13.5, J_{3-2}=8.1, and J_{3-3a}=3.9 Hz, one of 3-H), 2.18 (1H, ddd, J_{gem}=13.5, J_{3-3a}=8.1, and J_{3-2}=3.3 Hz, the other of 3-H), 2.45 (3H, s, NMe), 2.64 (1H, m, 3a-H), 3.72 (3H, s, COOMe), 3.74 (1H, dd, J_{2-3}=8.1 and 3.3 Hz, 2-H), 3.88 (1H, dd, J_{gem}=11.0 and J_{4-3a}=8.4 Hz, one of 4-H), 3.96 (1H, dd, J_{gem}=11.0 and J_{4-3a}=4.7 Hz, the other of 4-H), 3.97 (1H, d, J_{9b-3a}=7.0 Hz, 9b-H), and 6.9—7.2 (4H, m, Ar); ^{13}C NMR ($CDCl_3$) δ=30.40 (3-C), 35.02 (3a-C), 35.54 (NMe), 51.29 (COOMe), 58.72 (2-C), 64.00 (9b-C), 68.10 (4-C), 117.20, 120.21, 121.94, 128.63, 131.30, 155.75 (Ar), and 174.31 (COOMe); MS m/z (rel intensity, %) 274 (M^+, 8), 189 (12), 188 (base peak), and 131 (20). HRMS Found: m/z 247.1209. Calcd for $C_{14}H_{17}NO_3$: M, 247.1207.

Methyl (2*R,3*R**,3a*S**,9b*R**)-1-Methyl-3-phenyl-1,2,3,3a,4,9b-hexahydro[1]benzopyrano[4,3-*b*]pyrrole-2-carboxylate (13d):** Colorless prisms (diethyl ether-hexane); mp 148 °C; IR (KBr) 1710, 1580, 1440, and 1160 cm^{-1}; ^1H NMR ($CDCl_3$) δ=2.51 (3H, s, NMe), 3.37 (3H, s, COOMe), 3.38 (1H, dddd, J_{3a-3}=9.9, J_{3a-9b}=9.5, J_{3a-4}=3.6, and 2.2 Hz, 3a-H), 3.86 (1H, dd, J_{gem}=11.4 and J_{4-3}=3.6 Hz, one of 4-H), 3.93 (1H, dd, J_{3-3a}=9.9 and J_{3-2}=7.7 Hz, 3-H), 3.96 (1H, dd, J_{gem}=11.4 and J_{4-3a}=2.2 Hz, the other of 4-H), 4.00 (1H, d, J_{2-3}=7.7 Hz, 2-H), 4.40 (1H, d, J_{9b-3a}=9.5 Hz, 9b-H), and 6.9—7.4 (9H, m, Ph and Ar); ^{13}C NMR ($CDCl_3$) δ=35.98 (NMe), 43.48 (3a-C), 48.58 (3-C), 50.67 (COOMe), 60.11 (9b-C), 68.39 (4-C), 72.37 (2-C), 117.99, 121.42, 125.91, 127.41, 128.39, 128.46, 128.55, 129.77, 137.17, 156.80 (each Ph and Ar), and 172.22 (COOMe); MS m/z (rel intensity, %) 323 (M^+, 3), 265 (20), 264 (base peak), and 132 (11). Found: C, 74.22; H, 6.56; N, 4.45%. Calcd for $C_{20}H_{21}NO_3$: C, 74.29; H, 6.55; N, 4.33%.

Ethyl (2*R,3*R**,3a*R**,9b*R**)-3-Methoxycarbonyl-1-methyl-1,2,3,3a,4,9b-hexahydro[1]benzopyrano[4,3-*b*]pyrrole-2-carboxylate (14a):** Pale yellow liquid; IR (neat) 1730, 1610, 1490, 1460, and 1210 cm^{-1}; ^1H NMR ($CDCl_3$) δ=1.31 (3H, t, J=7.0 Hz, Et), 2.54 (3H, s, NMe), 2.66 (1H, dq, J_{3a-3}=J_{3a-9b}=11.0, J_{3a-4}=11.0, and 4.4 Hz, 3a-H), 3.13 (1H, dd, J_{3-3a}=11.0 and J_{3-2}=6.0 Hz, 3-H), 3.74 (3H, s, COOMe), 3.98 (1H, d, J_{9b-3a}=11.0 Hz, 9b-H), 4.15 (1H, d, J_{2-3}=6.0 Hz, 2-H), 4.18 (1H, dd, J_{gem}=10.3 and J_{4-3a}=11.0 Hz, one of 4-H), 4.24 (2H, q, J=7.0 Hz, COOEt), 4.64 (1H, J_{gem}=10.3 and J_{4-3a}=4.4 Hz, the other of 4-H), and 6.8—7.4 (4H, m, Ar); ^{13}C NMR ($CDCl_3$) δ=14.23 (Et), 38.51 (NMe), 41.45 (3a-C), 48.98 (3-C), 52.50 (COOMe), 61.37 (COOEt), 64.58 (2-C), 69.77 (4-C), 71.70 (9b-C), 116.58, 120.23, 123.29, 125.83, 128.23, 154.12 (each Ar), 172.62, and 172.41 (COOMe and COOEt); MS m/z (rel intensity, %) 319 (M^+, 10), 246 (base peak), and 135 (28). HRMS Found: m/z 319.1418. Calcd for $C_{17}H_{21}NO_5$: M, 319.1418.

Isopropyl (2*R,3*R**,3a*R**,9b*R**)-3-Methoxycarbonyl-1-methyl-1,2,3,3a,4,9b-hexahydro[1]benzopyrano[4,3-*b*]-pyrrole-2-carloxylate (14b):** Pale yellow liquid; IR (neat) 1730, 1610, 1490, and 1220 cm^{-1}; ^1H NMR ($CDCl_3$) δ=1.28, 1.31 (each 3H, d, J=6.2 Hz, *i*-Pr), 2.56 (3H, s, NMe), 2.66 (1H, dq, J_{3a-2}=J_{3a-9b}=11.4, J_{3a-4}=11.4, and 4.4 Hz, 3a-H), 3.07 (1H, dd, J_{3-3a}=11.4 and J_{3-2}=6.0 Hz, 3-H), 3.75 (3H, s, COOMe), 3.99 (1H, d, J_{9b-3a}=11.4 Hz, 9b-H), 4.12 (1H, d, J_{2-3}=6.0 Hz, 2-H), 4.19 (1H, dd, J_{gem}=9.9 and J_{4-3a}=11.4 Hz, one of 4-H), 4.64 (1H, dd, J_{gem}=9.9 and J_{4-3a}=4.4 Hz, the other of 4-H), 5.08 (1H, m, *i*-Pr), and 6.8—7.4 (4H, m, Ar); MS m/z (rel intenity, %) 333 (M^+, 9), 290 (40), 246 (base peak), 214 (20), 187 (22), 186 (54), 161 (20), 131 (42), and 115 (24). HRMS Found: m/z 333.1573. Calcd for $C_{18}H_{23}NO_5$: M, 333.1575.

The present work was financially supported by a Grant-in-Aid for Scientific Research (No. 63550652) from the Ministry of Education, Science and Culture.

References

1) P. N. Confalone and E. H. Huie, *J. Org. Chem.*, **48**, 2994 (1983).

2) P. N. Confalone and E. M. Huie, *J. Am. Chem. Soc.*, **106**, 7175 (1984).

3) O. Tsuge, S. Kanemasa, H. Ohe, K. Yorozu, S. Takenaka, and K. Ueno, *Chem. Lett.*, **1986**, 1271; O. Tsuge, S. Kanemasa, H. Ohe, S. Takenaka, and K. Ueno, *Bull. Chem. Soc. Jpn.*, **60**, 4067 (1987).

4) P. N. Confalone and R. A. Earl, *Tetrahedron Lett.*, **27**, 2695 (1986).

5) R. Grigg and S. Thianpatanagul, *J. Chem. Soc., Chem. Commun.*, **1984**, 180.

6) R. Grigg, M. F. Aly, V. Sridharan, and S. Thianpatanagul, *J. Chem. Soc., Chem. Commun.*, **1984**, 182.

7) D.-L. J. Wang, W. C. Ripka, and P. N. Confalone, *Tetrahedron Lett.*, **25**, 4613 (1984).

8) M. Joucla and J. Mortier, *J. Chem. Soc., Chem. Commun.*, **1985**, 1566.

9) O. Tsuge, S. Kanemasa, H. Ohe, and S. Takenaka, *Chem. Lett.*, **1986**, 973; O. Tsuge, S. Kanemasa, M. Ohe, and S. Takenaka, *Bull. Chem. Soc. Jpn.*, **60**, 4079 (1987).

10) R. Grigg, S. Surendrakumar, S. Thianpatanagul, and D. Vipond, *J. Chem. Soc., Chem. Commun.*, **1987**, 47.
11) R. Grigg, J. Idle, P. McMeekin, and D. Vipond, *J. Chem. Soc., Chem. Commun.*, **1987**, 49.
12) O. Tsuge and S. Kanemasa, "Recent Advances in Azomethine Ylide Chemistry," in "Advances in Heterocyclic Chemistry," ed by A. R. Katritzky, Academic Press, Inc., San Diego (1989), Vol. 45, pp. 232—349.
13) A. Padwa, "1,3-Dipolar Cycloaddition Chemistry," in "General Heterocyclic Chemistry Series," ed by E. C. Taylor and A. Weissberger, John Wiley and Sons, New York, Chichester, Brisbane, Toronto, Simgapore (1984), Chap. 1, pp. 61—75.
14) O. Tsuge, K. Ueno, and I. Ueda, *Heterocycles*, **16**, 1503 (1981).
15) G. R. Brown, A. J. Foubister, and D. Stribling, *J. Chem. Soc., Perkin Trans. 1*, **1987**, 547.

 © 1989 The Chemical Society of Japan Bull. Chem. Soc. Jpn., 62, 1969—1975 (1989)

Stopped-Flow Kinetics of Reactions of 1-Ethoxy-2,4-dinitronaphthalene with Pyrrolidine and Piperidine in Dimethyl Sulfoxide Solution[1)]

Hajime FUJINUMA, Masaru HOSOKAWA, Tohru SUZUKI, Mitsuo SATO, and Shizen SEKIGUCHI*
Department of Synthetic Chemistry, Gunma University, Ten-jin cho, Kiryu, Gunma 376
(Received December 3, 1988)

The reaction of 1-ethoxy-2,4-dinitronaphthalene (**1**) with pyrrolidine or piperidine in dimethyl sulfoxide occured in two stages (Stages I and II). In the stage I, a σ-adduct forms at such a rate as is measured by a stopped-flow technique, and in the stage II it decays at a slower and spectrophotometrically measurable rate. The pyrrolidine system is more reactive than the piperidine system in the stages I and II, with the former reactivity in the stage II being ca. 11000 times higher than the latter. This huge difference was found by NMR evidence to stem from the structure of transition state in the stage II. Further, the activation parameters were determined, which corresponded to such difference in reactivity very well.

Previously we carried out the kinetics of the reaction of 1-ethoxy-2,4-dinitronaphthalene (**1**) with pyrrolidine or piperidine in dimethyl sulfoxide (DMSO) and determined the reaction sequence (Scheme 1).[2)] The

Stage I

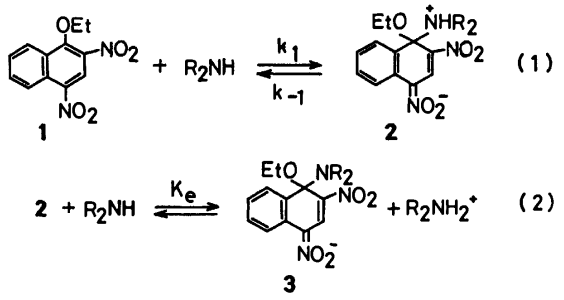

Stage II

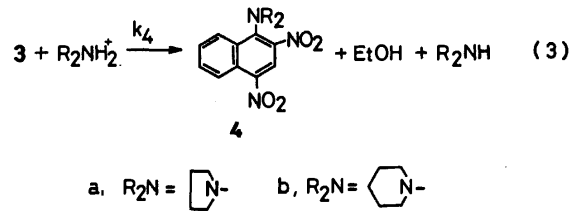

Scheme 1.

reaction occurs in two distinct stages (Stages I and II), in which the stage I is relatively fast and the stage II is slow. As the k_4 stage is rate-determining as shown in Table 5 and general acid catalyzed,[2)] the present reaction can be considered to proceed via the SB-GA (special base [R_2NH]-general acid [$R_2NH_2^+$] catalysis) mechanism.[3,4)] Several aromatic nucleophilic substitution reactions (S_NAr) via the SB-GA mechanism have been observed[5-8)] since Orvik and Bunnett[9)] confirmed the SB-GA mechanism in the reaction of **1** with butylamine and *t*-butylamine in DMSO. In this paper we determined the activation parameters of the reaction in Scheme 1 and reconsidered such huge difference in the k_4 step between the pyrrolidine and piperidine systems [k_4(pyrrolidine)/k_4(piperidine)= ca. 11000], using ^{1}H NMR evidence.

Results

General Features. Upon addition of excess piperidine to a DMSO solution of in the presence of piperidinium chloride, the solution instantly turned red, indicating the formation of a σ adduct, which corresponded to the first spectral change from curve a, attributable to **1**, to curve b, attributable to **3b** (Fig. 1).[2,9-11)] The second spectral change of curve b → c → d → e was much slower, in which curve e was attributable to **4b** (NR_2=$C_5H_{10}N$).

Therefore, the reaction consists of the I and II stages: the stage I is the fast formation of **3** (Eqs. 1 and 2) and the stage II is the relatively slow decomposition of **3**, giving **4**.

Stage I Kinetics. Let us rewrite Scheme 1 in a fashion more useful for the derivation of rate equations as Scheme 2. Under the conditions studied, the reaction occurs rapidly to establish the equilibrium between **1** and **3** (Fig. 1 and Eqs. 4 and 5).

$$1 + R_2NH \underset{k_{-1}}{\overset{k_1}{\rightleftharpoons}} 2, \qquad (4)$$

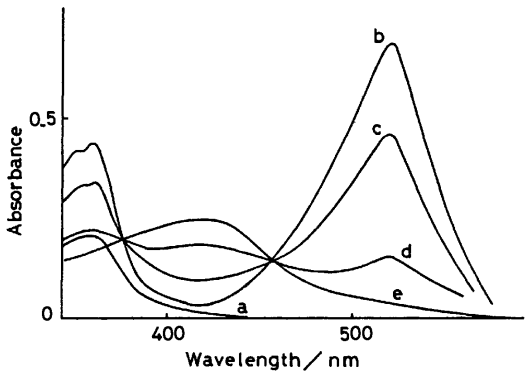

Fig. 1. Time-dependent absorption spectra relevant to the reaction of 1-ethoxy-2,4-dinitronaphthalene (**1**, 2.87×10^{-5}M) with piperidine (1.01 M) in the presence of piperidinium chloride (8.08×10^{-2}) in DMSO at 25 °C: a **1** before addition of piperidine; b, c, d, and e immediately, 60, 240, and 1200 min, respectively, after addition of piperidine.

$$2 + R_2NH \overset{K_e}{\rightleftharpoons} 3 + R_2\overset{+}{N}H_2, \quad (5)$$

$$3 + R_2\overset{+}{N}H_2 \overset{k_4}{\rightleftharpoons} 4 + C_2H_5OH + R_2NH, \quad (6)$$

Scheme 2.

Accordingly the pseudo-first-order rate constant (k_ψ) for attainment of the equilibrium is the sum of those for the foward and reverse reactions, and Eq. 7 holds (see the reference[12] about its derivation).

$$k_\psi = k_1[R_2NH] + \frac{k_{-1}[R_2\overset{+}{N}H_2]}{K_e[R_2NH]} \quad (7)$$

Multiplying each side by [R_2NH],

$$k_\psi[R_2NH] = k_1[R_2NH]^2 + \frac{k_{-1}}{k_e}[R_2\overset{+}{N}H_2]. \quad (8)$$

This kinetic measurements on the stage I were shown in Tables 1 and 2, and a linear plot of $k_\psi[R_2NH]$ against $[R_2NH]^2$, at constant piperidinium chloride concentration, is compatible with Eq. 8 (Fig. 2). From the slope and intercept, k_1 and k_{-1}/K_e can be obtained. The similar relationship was obtained for the pyrrolidine system too (not shown).

As a result, one can evaluate the equilibrium constant, K_i, for the overall stage I by using k_1 and k_{-1}/K_e [$K_i = k_1/(k_{-1}/K_e)$].

The best K_i value, however, was determined as follows: the K_i value derived from the stage I kinetics was put into the rate equation for the stage II (Eq. 9) as an initial value and its best value was evaluated by using a nonlinear least squares method (refer to the next paragraph about the detailed procedure). From the best K_i value and the k_1 values, obtained accurately from the slope in a plot of $k_\psi[R_2NH]$ vs. $[R_2NH]^2$, k_{-1}/K_e was recalculated. These values are summarized in Table 5 together with the activation and thermodynamic parameters obtained from the temperature-dependence of these constants. The calculated k_ψ values, obtained by using these k_1 and k_{-1}/K_e, are in good agreement with the observed k_ψ values (Table 1 and 2).

Table 1. Reaction of **1** with Pyrrolidine in DMSO: Stage I Kinetics[a]

$[C_4H_8NH]$ M	k_ψ s^{-1}	k_ψ(calcd)[b] s^{-1}	$[C_4H_8NH]$ M	k_ψ s^{-1}	k_ψ(calcd)[b] s^{-1}
	35 °C			45 °C	
0.011	236	231	0.015	470	470
0.020	139	138	0.021	345	346
0.031	101	104	0.038	210	216
0.045	90.5	91.1	0.051	177	183
0.058	91.6	89.7	0.069	171	166
0.071	92.3	92.7	0.080	167	163
0.093	110	110	0.091	163	163
0.111	115	113	0.102	165	166
0.121	116	119	0.135	182	182
	50 °C				
0.028	403	404			
0.042	298	295			
0.058	251	244			
0.069	228	277			
0.078	222	219			
0.099	217	214			
0.113	223	217			
0.135	227	226			

a) [**1**]$_0$ ca. 5.0×10^{-5} M; $[C_4H_8\overset{+}{N}H_2Cl^-]_0$ 4.27×10^{-3} M; measurement at 522 nm; all k_ψ are average of duplicate runs, differing by <3.5%. b) Calculated by substituting the k_1 and (k_{-1}/K_e) values in Table 5 into Eq. 7.

Table 2. Reaction of **1** with Piperidine in DMSO: Stage I Kinetics[a]

$[C_5H_{10}NH]$ M	k_ψ s^{-1}	k_ψ[b] s^{-1}	$[C_5H_{10}NH]$ M	k_ψ s^{-1}	k_ψ[b] s^{-1}
	35 °C			45 °C	
0.014	182	187	0.013	572	571
0.025	111	111	0.028	276	276
0.032	90.9	91.2	0.049	176	174
0.049	69.5	69.2	0.065	142	145
0.065	60.4	62.2	0.081	127	131
0.082	60.3	60.0	0.095	121	124
0.098	59.5	60.6	0.112	120	121
0.117	61.9	63.0	0.127	121	120
0.130	65.9	65.4			
	50 °C				
0.025	506	507			
0.043	312	311			
0.062	236	234			
0.083	194	195			
0.092	184	186			
0.120	172	170			
0.135	168	167			
0.147	166	167			

a) [**1**]$_0$ ca. 5.0×10^{-5} M; $[C_5H_{10}\overset{+}{N}H_2Cl^-]_0$ 5.10×10^{-3} M; measurement at 522 nm; all k_ψ are average of duplicate runs, differing by <2.4%. b) Calculated by substituting the k_1 and (k_{-1}/K_e) values in Table 5 into Eq. 7.

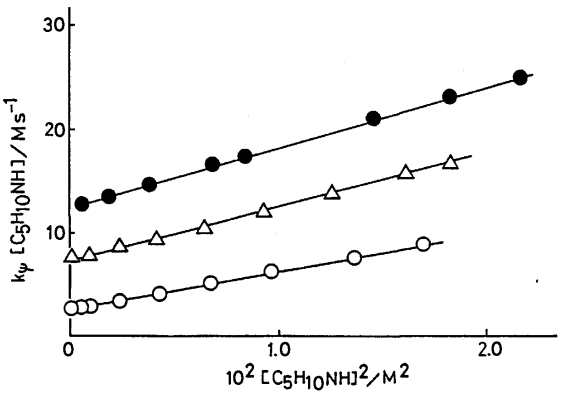

Fig. 2. Relationship between k_ψ $[C_5H_{10}NH]/M\,s^{-1}$ and $[C_5H_{10}NH]^2/M^2$ (Stage I): ○ 35; △ 45; ● 50 °C.

Stage II Kinetics. As the overall stage I is a mobile fast equilibrium (K_i) on the time scale of the stage II under the present conditions, the substrate is considered substantially to be split between **1** and

3. Letting $[\mathbf{1}]_{st}=[\mathbf{1}]+[\mathbf{3}]$, and letting K_i be the equilibrium constant for the overall stage I, one derives Eq. 9 (K_{obsd}; pseudo-first-order rate constant for the stage II,[9]

$$k_{obsd}=\frac{k_4K_i[R_2NH]^2[R_2\overset{+}{N}H_2]}{K_i[R_2NH]^2+[R_2\overset{+}{N}H_2]} \quad (9)$$

in which k_{obsd} depends on amine and amine hydro-

Table 3. Reaction of **1** with Pyrrolidine in DMSO; Stage II Kinetics[a]

$[C_4H_8NH]$	10^2k_{obsd}	10^2k_{obsd}(calcd)[b]	$[C_4H_8NH]$	10^2k_{obsd}	10^2k_{obsd}(calcd)[b]
M	s^{-1}	s^{-1}	M	s^{-1}	s^{-1}
	35 °C			45 °C	
0.011	0.48	0.49	0.010	0.36	0.36
0.016	0.91	0.90	0.021	1.39	1.39
0.027	1.86	1.87	0.034	2.83	2.84
0.032	2.23	2.24	0.041	3.58	3.57
0.036	2.51	2.50	0.052	4.53	4.54
0.041	2.76	2.78	0.060	5.10	5.11
0.054	3.32	3.30	0.071	5.73	5.74
0.064	3.57	3.56	0.083	6.24	6.24
0.082	3.85	3.86	0.103	6.82	6.82
0.102	4.05	4.40	0.114	7.04	7.04
0.123	4.16	4.16	0.123	7.20	7.19
	50 °C				
0.021	1.32	1.34			
0.039	3.55	3.56			
0.049	4.74	4.73			
0.059	5.74	5.76			
0.068	6.56	6.54			
0.078	7.27	7.25			
0.088	7.81	7.83			
0.105	8.59	8.58			
0.117	8.98	8.97			
0.122	9.13	9.11			

a) $[\mathbf{1}]_0$ ca. 2.3×10^{-5} M; $[C_4H_8\overset{+}{N}H_2Cl^-]_0$ 1.45×10^{-3} M; measurement at 522 nm; all k_{obsd} are average of duplicate runs, differing by <2.4%. b) Calculated by substituting the k_4 and K_i values in Table 5 into Eq. 9.

Table 4. Reaction of **1** with Piperidine in DMSO: Stage II Kinetics[a]

$[C_5H_{10}NH]$	10^5k_{obsd}	10^5k_{obsd}(calcd)[b]	$[C_5H_{10}NH]$	10^5k_{obsd}	10^5k_{obsd}(calcd)[b]
M	s^{-1}	s^{-1}	M	s^{-1}	s^{-1}
	35 °C			45 °C	
0.100	2.66	2.67	0.110	4.35	4.38
0.261	12.3	12.2	0.150	7.78	7.81
0.342	16.6	16.6	0.251	18.9	18.8
0.381	18.3	18.4	0.292	23.5	23.5
0.430	20.4	20.3	0.361	31.9	31.8
0.500	22.6	22.6	0.460	42.3	42.4
0.572	24.4	24.3	0.531	48.8	48.7
0.673	26.0	26.1	0.672	58.7	58.7
0.780	27.8	27.7	0.750	63.1	63.2
	50 °C				
0.120	5.94	6.02			
0.201	14.4	15.3			
0.261	24.2	24.5			
0.292	29.5	29.3			
0.350	38.7	39.1			
0.440	53.5	53.4			
0.582	73.2	73.1			
0.671	83.6	83.5			
0.840	98.7	98.8			

a) $[\mathbf{1}]_0$ ca. 5.0×10^{-5} M; $[C_5H_{10}\overset{+}{N}H_2Cl^-]_0$ 8.00×10^{-2} M; measurement at 522 nm; all k_{obsd} are average of duplicate runs, differing by <2%. b) Calculated by substituting the k_4 and K_i values in Table 5 into Eq. 9.

chloride concentrations (Tables 3 and 4), and involves K_i, mentioned in the preceding paragraph.

The best K_i and k_4 values were determined as follows: first, the K_i values, derived from the stage I kinetics, were used to calculate k_4, that is, for pyrrolidine K_i=1.32, 0.53, and 0.35, and for piperidine 0.77, 0.33_8 and 0.35 M^{-1} (M=mol dm^{-3}, and so forth) at 35, 45, and 50 °C, respectively; second, by substituting these K_i values and the experimental values ([R_2NH], k_{obsd}, and [R_2NH_2Cl]) of the top line at each temperature in Tables 3 and 4 into Eq. 9, the following k_4 values were calculated, that is, for pyrrolidine 33.4, 69.6, and 94.6, and for piperidine 4.07×10^{-3}, 11.1×10^{-3}, and 18.1×10^{-3} $M^{-1}s^{-1}$ at 35, 45, and 50 °C, respectively; third, by substituting these K_i and k_4 values into Eq. 9 as initial values and using a nonlinear least squares method (Gauss-Newton method), the best K_i and k_4 values were obtained, which are listed in Table 5. The k_{-1}/K_e values in Table 5 were calculated, therefore, by using these K_i values and the k_1 ones (obtained in the stage I kinetics).

Agreement between observed and calculated k_{obsd}, derived by substituting the K_i and k_4 values into Eq. 9, was found to be fairly good (Tables 3 and 4).

Equation 9 is converted to Eq. 10 by rearranging and taking logarithms. To check the validity of Eq. 10, we plotted the quantity on the left side against that on the right side of Eq. 10 by using the pyrrolidine or piperidine concentrations, and the K_i and k_4 values in Table 5 (Fig. 3). The slopes are 1.99 ± 0.02,

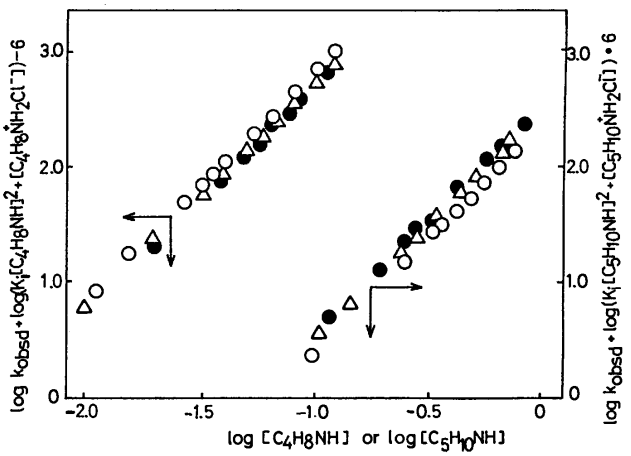

Fig. 3. Relationships between $\log k_{obsd}+\log(K_i[C_4H_8NH]^2+[C_4H_8\overset{+}{N}H_2Cl^-])-6$ and $\log[C_4H_8NH]$, and between $\log k_{obsd}+\log(K_i[C_5H_{10}NH]+[C_5H_{10}\overset{+}{N}H_2Cl^-])+6$ and $\log[C_5H_{10}NH]$ (Stage II).

Table 5. Summary of Rate Constants, Equilibrium Coefficients, Activation and Thermodynamic Parameters

Reaction	Parameter[a]	Temp °C	Reaction with pyrrolidine	Reaction with piperidine
1 → 2	$k_1/M^{-1}s^{-1}$	25[b]	6.5×10^2	2.4×10^2
		35	$8.22\pm0.10\times10^2$	$3.52\pm0.05\times10^2$
		45	$9.77\pm0.16\times10^2$	$4.92\pm0.05\times10^2$
		50	$11.0\pm0.2\times10^2$	$5.67\pm0.06\times10^2$
	$\Delta H^{\ddagger}$		3.3 ±0.4	5.6 ±05
	$\Delta S^{\ddagger}$		−34.5 ±1.5	−27.7 ±1.6
	$\Delta G^{\ddagger}$		13.6 ±0.6	14.2 ±0.7
1 ⇄ 3	K_i/M^{-1}	25[b]	3.44±0.05	1.55±0.02
		35	1.44±0.01	0.70±0.01
		45	0.61±0.01	0.34±0.01
		50	0.44±0.01	0.23±0.01
	ΔH^0		−15.8 ±0.8	−14.4 ±0.6
	ΔS^0		−50.5 ±2.3	−39.6 ±2.1
	ΔG^0		−0.74±1.06	−2.59±2.1
3 → 1	$k_{-1}/K_e/s^{-1}$	25[b]	-1.89 ± 10^2	1.54 ± 10^2
		35	$5.11\pm0.10\times10^2$	$5.02\pm0.13\times10^2$
		45	$1.60\pm0.03\times10^3$	$1.44\pm0.02\times10^3$
		50	$2.54\pm0.05\times10^3$	$2.42\pm0.06\times10^3$
	$\Delta H^{\ddagger}$		8.9 ±1.1	20.3 ±1.1
	$\Delta S^{\ddagger}$		15.4 ±3.8	19.4 ±3.7
	$\Delta G^{\ddagger}$		14.4 ±1.6	14.5 ±1.5
3 → 4	$k_4/M^{-1}s^{-1}$	25[b]	15.7	$1.40\pm0.01\times10^{-3}$
		35	30.6 ±0.3	$4.11\pm0.02\times10^{-3}$
		45	56.8 ±1.1	$1.12\pm0.01\times10^{-2}$
		50	76.6 ±2.0	$1.84\pm0.02\times10^{-2}$
	$\Delta H^{\ddagger}$		11.4 ±0.5	18.9 ±0.7
	$\Delta S^{\ddagger}$		−14.6 ±1.6	−8.2 ±3.1
	$\Delta G^{\ddagger}$		15.8 ±0.7	21.4 ±1.2

a) Units of $\Delta H^{\ddagger}$, ΔH^0, $\Delta G^{\ddagger}$, and ΔG^0(25 °C) are $kcal_{th}$ dm^{-3};units of $\Delta S^{\ddagger}$ and ΔS^0 (25 °C) are cal_{th} K^{-1} dm^{-3}. b) Cited from the Ref. 2. These values are almost the same as those in the present reaction, differing by <3.0%.

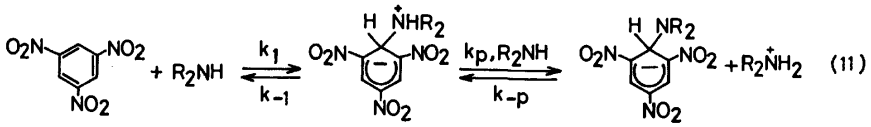

Scheme 2.

1.96±0.01, and 2.00±0.01 for pyrrolidine, and 2.00±0.01, 2.01±0.01, and 2.00±0.01 for piperidine at 35, 45, and 50 °C, indicating the validity of Eq. 10.

$$\log k_{obsd} + \log (K_1[R_2NH]^2 + [R_2\overset{+}{N}H_2]) = \log k_4K_i + 2\log[R_2NH] + \log[R_2\overset{+}{N}H_2] \quad (10)$$

Discussion

Stage I. Rate and Equilibrium Constants. The pyrrolidine system is a little more reactive than the piperidine one at the k_1 step, depending on $\Delta H^{\neq}$ rather than on $\Delta S^{\neq}$ (Table 5). Further, much more difference is seen between the $\Delta S^{\neq}$ values than between the $\Delta H^{\neq}$ ones, although difference between the $\Delta G^{\neq}$ values is much less, which could arise from the steric or stereoelectronic origin, as discussed in the later paragraph, by considering similar properties for these two amines, such as their pK_a values.[2,15] For the nucleophilic attack of pyrrolidine on **1**, electron delocalization would be considered to be somewhat larger between the unshared electron on the nitrogen atom of pyrrolidinyl group and the naphthalene moiety (**1**) than that for piperidine,[2] which would increase, to a larger extent, the repulsion between α-methylene group of the pyrrolidinyl ring and 2-nitro group of **1** (refer to later discussion).

The pyrrolidine/piperidine reactivity ratios at the step are 2.7, 2.3, 2.0, and 1.9 at 25, 35, 45, and 50 °C, respectively, which are close to the corresponding ratios in K_i, overall stage I equilibrium constant: 2.2, 2.1, 1.8, and 1.9 at 25, 35, 45, and 50 °C, respectively. These results naturally stems from the similar k_{-1}/K_e values for the two amine systems. The present kinetics can not tell whether these values (k_{-1}/K_e) arise from each almost same k_{-1} and K_e values or from appropriate balance of their different ones for the two amines (see the next paragraph).

Proton Transfer in K_e Step. The results in Tables 1—4 are fairly consistent with the reaction sequence in Scheme 1. It is well-known, however, that whether the K_e step is a fast mobile equilibrium or a proton transfer is sophisticated or controvertial.[3,4,10,11] A relatively slow proton-transfer reaction has been found in the reactions of methyl 4-methoxy-3,5-dinitrobenzoate with pyrrolidine[5] or butylamine[6] in DMSO, of 1-ethoxy-2,4,6-trinitrobenzene with butylamine,[7] and of 1-phenoxy-2,4-dinitro- and 1-phenoxy-6-methyl-2,4-dinitrobenzene with pyrrolidine and piperidine in 60% dioxane-40% water,[8] from which it is evident that in the case of secondary amines a proton transfer is relatively slow on account of steric effects.

In addition, Bernasconi et al.[13] and Crampton and Greenhalgh[14] determined the rate and equilibrium constants for the reactions of 1,3,5-trinitrobenzene (**5**) with pyrrolidine and piperidine in 30% DMSO-70% water[13] (hereafter abbreviated to DMSO-water) or in DMSO[14] (Scheme 2). From these results k_p and k_{-p} are as follows: k_1 ($M^{-1}\,s^{-1}$), k_{-1} ($M^{-1}\,s^{-1}$), k_p ($M^{-1}\,s^{-1}$), k_{-p}, ($M^{-1}\,s^{-1}$), K_p and K (M^{-1}, overall equilibrium constant) are 9.00×10^3, 6.2×10^5, 1.7×10^7, 5.1×10^4, 3.3×10^2, and 4.7 for the pyrrolidine system and 4.10×10^3, 1.0×10^6, 1.6×10^7, 3.9×10^4, 4.1×10^2, and 1.2 for the piperidine system at 20 °C in 30% DMSO-70% water, whereas 7.5×10^5, 1.0×10^5, 1.5×10^6, 3.0×10^3, 500, and 3.5×10^3 for the pyrrolidine system and $>2\times10^5$, $>1.44\times10^4$, 1.4×10^5, 2.8×10^2, 500, and 2.14×10^3 for the piperidine system at 25 °C in DMSO.

As a result, k_{-1}/K_p, corresponding to k_{-1}/K_e in the present reaction, is calculated to be 1.9×10^3 and $2.4\times10^3\ s^{-1}$ in DMSO-water, and 2×10^2 and $>2.9\times10^{-1}\ s^{-1}$ in DMSO for pyrrolidine and piperidine respectively, in which $(k_{-1}/K_p)_{pyr}/(k_{-1}/K_p)_{pip}$ is 0.8 in DMSO-water and ca. 6.8 in DMSO. The one thing to be commented at this point is that the K_p values in DMSO are presumed ones (see the reference[14] for the details), and therefore a little uncertain. By considering these results, our ratio, mentioned just above, is 1.2, which can be believed to be similar to their values,[13,14] although their magnitudes are reversed or different, probably depending on solvent compositions and structures of substrates.

In addition, we assumed that K_e step is an equilibrium. In some reactions,[5,7,8,13,14] however, rate-limiting or partly rate-limiting proton transfer has been advocated, which can be estimated from the effect of added bases, such as DABCO (1,4-diazabicyclo-[2.2.2]octane), on k_ψ. In the preliminary experiment, we found that in the presence of **1** (2.46×10^{-5} M) and pyrrolidine (2.15×10^{-2} M) k_ψ changed from 10.3±0.5 to 12.5±0.3 s^{-1} at [DABCO]=1.90×10^{-2} to 1.90×10^{-1} M (10-fold change), whereas in the presence of **1** (2.46×10^{-5} M) and piperidine (3.95×10^{-1} M) k_ψ changed from 3.13±0.61 to 3.62±0.116 s^{-1} at [DABCO]=1.40×10^{-2} to 1.76×10^{-1} M (ca. 17-fold change). An increase in k_ψ is 21% for the former and 15.6% for the latter, which is much less than those found already.[5,7,8,13,14] These results indicates that pK_a of **2** is less than that of **6** partly due to an electron-withdrawing character of the ethoxyl group. It would be reasonable, therefore, that the K_e step is

treated as an equilibrium.

Huge Difference in Reactivities of Stage II. It was already described that pyrrolidinium or piperidinium ion catalyzes the explusion of ethoxide ion from **3** (general acid catalysis).[2] Huge difference in k_4 at 25 °C corresponds to $\Delta\Delta G^{\ddagger}$ of 5.6 kcal mol^{-1} (1 cal_{th}=4.184 J) (Table 5). In view of the similarity of the two amines in the stage I behavior and their pK_a [11.27 (H_2O)[15] and 11.42% (30% DMSO-70% water)[13] for pyrrolidine; 11.22 (H_2O)[15] and 11.42 (30% DMSO-70% water)[13] for piperidine] this huge difference is very surprising. We concluded by examination of Dreiding models that some steric, stereoelectronic or conformational effect concerning the carbon-bound amino moiety in the transition state for the k_4 step is the source of this huge stage II reactivity difference [about detailed discussion, refer to the reference[2]].

We have recnetly found the NMR evidence supporting the discussion described just above (Fig. 4).

Interestingly the signal pattern of aromatic protons of 1-dimethylamino-2,4-dinitronaphthalene (**4c**), in which the singlet at δ 8.81 and the multiplets centered at ca. δ 8.68 and ca. δ 7.88 are attributed to H^3, $H^{5,8}$, $H^{6,7}$ respectively, was found to be similar to those of 1-diethylamino- (**4d**), 1-(*N*-methylbutylamino)- (**4e**), and **4b** (about numbering of protons see Fig. 5A). The pattern (Fig. 4C) was obtained in 64 days after piperidine (3 equivalents) were added into a DMSO-d_6 solution of **4b** (NR_2; piperidino). The downfield shift of H^3 singlet of **4b** from δ 8.63 to 9.30 is characteristic for its conversion to an adduct.[10] The signal pattern of **4a** is similar, if anything, to 1,1-dipiperidino-substituted 2,4-dinitronaphthalene anionic σ complex, in which the NR_2 (piperidino) group is substituted in place of the ethoxyl group in **3**, that is, two piperidino groups are attached to C_1. These results show that in the case of **4a** such conjugation as **4** (Fig. 5A) is larger than in the case of **4b** and **4c—d**, suggesting comparatively small steric interaction between α-methylene group of the pyrrolidinyl ring and 2-nitro group. This implies that when the ethoxyl group is expelled from **3** (k_4 step), the pyrrolidinyl ring can more easily keep its plane coplanar to the naphthalene moiety at a certain angle and that its unshared electron pair can assume a configuration antiperiplanar to the rupturing C-O bond with respect to the C_1-N (piperidino nitrogen) bond in the transition state (Fig. 5B). Although in this transition state the pyrrolidinyl ring is drawn as a plane, the conformation with C_2 symmetry is greatly preferred for substituted pyrrolidines.[17] Backside assistance of this electron pair to expulsion of the ethoxyl group would cause a huge increase in reactivity at the k_4 step for the pyrrolidine system.[16]

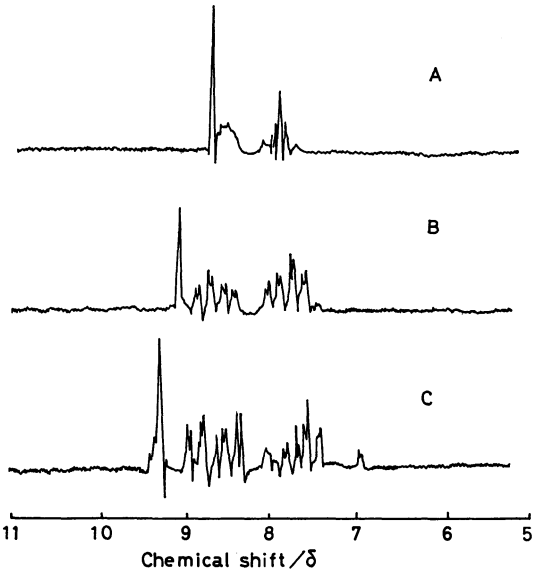

Fig. 4. ^{1}H NMR spectra for 1-dimethylamino- (**4c**, A), 1-pyrrolidino-2,4-dinitronaphthalene (**4a**, B), and 1,1-dipiperidino-substituted 2,4-dinitronaphthalene anionic a complex (C) in DMSO-d_6.

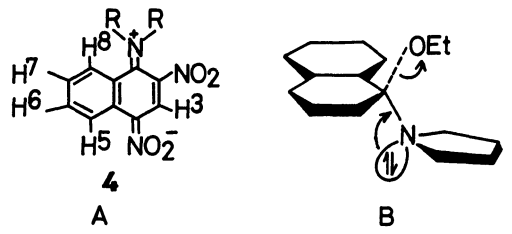

Fig. 5. Canonical structure of 1-(disubstituted amino)-2,4-dinitronaphthalene (A), and transition state at the k_4 step for the pyrrolidine system, in which 2- and 4-nitro groups are omitted for simplicity (B).

Experimental

NMR spectra were recorded on a Varian A-60D spectrometer and UV-VIS absorption spectra on a Hitachi Model 200-10 spectrophotometer. All the melting points were uncorrected.

Materials. Dimethyl sulfoxide, pyrrolidine, piperidine, diethylamine, *N*-methylbutylamine were purified as previously described.[2] Commerical dimethylamine was used without further purification. Pyrrolidinium and piperidinium chloride, and 1-ethoxy-2,4-dinitronaphthalene (**1**) were prepared as previously described.[2]

1-(Disubstituted amino)-2,4-dinitronaphthalene (**4a—e**) were prepared from 1-chloro-2,4-dinitronaphthalenes and corresponding amine as previously described.[18] The yield was higher than 80% and the elemental analysis was within (calculated value ±0.3%) in each case. The physical properties were shown in the following except for **4b**.[18] All mp, λ, ε, and δ were in DMSO.

(1-Pyrrolidinyl)-2,4-dinitronaphthalene (4a): Mp 201.5—202 °C; λ_{438} (ε 2.1×10^4); ^{1}H NMR δ=1.93 [4H, m, NC_4H_8 (2β-CH_2)] and 3.73 [4H, t, NC_4H_8 (2α-CH_2)].

1-Dimethylamino-2,4-dinitronaphthalene (4c): Mp 87—87.5 °C; λ_{419} (ε 8.8×10^3); ^{1}H NMR δ=3.07 [6H, s, $N(CH_3)_2$], 7.87 (2H, m, $H^{6,7}$), 8.67 (1H, s, H^3), and 8.53 (2H, m, $H^{5,8}$).

1-Dimethylamino-2,4-dinitronaphthalene (4d): Mp 87.5—88.5 °C; λ_{430} (ε 1.5×10^4); ^{1}H NMR δ=1.13 [6H, t, $N(CH_2CH_3)_2$], 3.40 [(4H, q, $N(CH_2CH_3)_2$], 7.93 (2H, m, $H^{6,7}$), 8.67 (1H, s, H^3), and 8.53 (2H, m, $H^{5,8}$).

1-(*N*-Methylbutylamino)-2,4-dinitronaphthalene (4e): Mp 66—67 °C; λ_{425} (ε 7.4×10^3); ^{1}H NMR δ=0.80 [3H, t, $N(CH_2)_3CH_3$], 1.50 [4H, m, $N(CH_2)_3CH_3$ (β- and γ-CH_2)], 3.09 (3H, s, NCH_3), 3.21 [2H, t, $N(CH_2)_3CH_3$ (α-CH_2)], 7.95 (2H, M, $H^{6,7}$), 8.53 (2H, m, $H^{5,8}$), and 8.73 (1H, s, H^3).

Rate Measurement. As regards the kinetics of formation of σ adduct (**3**) (Stage I), an increase in the absorbance at 522 nm, due to **3** was followed in order to estimate the apparent first-order rate constant (k_ψ) with a thermostatted stopped-flow spectrophotometer (Otsuka Denshi Co.).[2] In order to estimate k_{obsd} (Stage II) a decrease in the absorbance at 522 nm was followed with a thermostatted Hitachi Model 200-10 spectrophotometer.[2]

References

1) Aromatic Nucleophilic Substitution. 25; for part 24, see H. Takahashi, T. Hirade, Y. Hashida, and S. Sekiguchi, *Bull. Chem. Soc. Jpn.*, in press.

2) J. F. Bunnett, S. Sekiguchi, and L. A. Smith, *J. Am. Chem. Soc.*, **103**, 4865 (1981).

3) C. F. Bernasconi, *MTP Int. Rev. Sci.: Org. Chem. Ser. One*, **3**, 33 (1973).

4) C. F. Bernasconi, *Acc. Chem. Res.*, **11**, 147 (1978).

5) Y. Hasegawa, *J. Org. Chem.*, **50**, 649 (1985).

6) Y. Hasegawa, *J. Chem. Soc., Perkin Trans. 2*, **1984**, 547.

7) M. R. Crampton and P. J. Routledge, *J. Chem. Soc., Perkin Trans. 2*, **1984**, 573.

8) J. F. Bunnett and A. V. Cartano, *J. Am. Chem. Soc.*, **103**, 4861 (1981).

9) A. Orvik and J. F. Bunnett, *J. Am. Chem. Soc.*, **92**, 2410 (1970).

10) M. J. Strauss, *Chem. Rev.*, **70**, 667 (1970).

11) F. Terrier, *Chem. Rev.*, **82**, 77 (1982).

12) K. J. Laidler, "Chemical Kinetics," McGraw-Hill, New York (1965), p. 24.

13) C. F. Bernasconi, M. C. Muller, and P. Schmid, *J. Org. Chem.*, **44**, 3189 (1979).

14) M. R. Crampton and C. Greenhalgh, *J. Chem. Soc., Perkin Trans. 2*, **1983**, 1175.

15) A. Albert and E. P. Serjeant, "Ionization Constants of Acids and Bases," Methuen and Co., London (1962), p. 141.

16) S. Sekiguchi, T. Horie, and T. Suzuki, *J. Chem. Soc., Chem. Commun.*, **1988**, 698.

17) E. L. Eliel, "Stereochemistry of Carbon Compounds," McGraw-Hill Book Co., New York (1962), Chap. 9.

18) S. Sekiguchi, T. Itagaki, T. Hirose, K. Matsui, and K. Sekine, *Tetrahedron*, **29**, 3527 (1973).

Design of the Synthetic Route for Helical Peptides.[1] Synthesis and Solubility of Model Peptides Having a Helical Structure

Mitsuaki NARITA,* Yoshihisa KOJIMA, and Shizuko ISOKAWA
Department of Industrial Chemistry, Faculty of Technology, Tokyo University of Agriculture and Technology, Koganei 184
(Received December 6, 1988)

Fragment condensations between amino- and carboxyl-components of hydrophobic decapeptides, which have a β-sheet structure in the solid state and are insoluble in DMF, NMP, and DMSO, were examined in a mixture of CH_2Cl_2 and TFE (4/1, v/v) using various coupling reagents. By the use of DCC and HOBt as coupling reagents, the reaction proceeded smoothly in moderate yield to give eicosapeptides. These have a stable helical structure in the solid state and are easily soluble in a variety of organic solvents. The hydrophobic eicosapeptides obtained were subjected to a successive coupling reaction in CH_2Cl_2 alone to give helical tetracontapeptides in high yield, which also have high solubility in various organic solvents of low polarity. The solubility of hydrophobic helical peptides presents a solubility feature of helical peptides which are obtained as peptide intermediates in protein synthesis. The synthetic strategy for helical peptides and proteins is discussed in connection with the solubility prediction method.

One of the most serious obstacles in peptide and protein syntheses is the insolubility of protected peptides in organic solvents, which causes difficulty regarding successive reactions. In previous papers[2,3] we proposed the solubility prediction method for protected peptides and showed its usefulness for the design of synthetic routes for peptides and proteins. In this method, peptides which were to be made an object of the prediction were as long as or larger than an octapeptide. Solvents to be done were such as DMF, DMA, NMP, DMSO, and HMPA, which are commonly used for peptide and protein synthesis. Furthermore, the prediction method was practically based on the following four assumptions: (1) a tertiary peptide bond, such as an X-Pro, separates a peptide to peptide segments with respect to the peptide structure (peptide segment separation); (2) the insolubility of protected peptides is caused by a β-sheet aggregation consisting of peptide segments as long as or larger than an octa- or nonapeptide sequence; (3) peptides having helical and/or coiled structures have high solubility in organic solvents; and (4) the potential of peptide segments for a β-sheet formation is estimated using their average coil conformation $\langle P_c \rangle$ values when a peptide is smaller than the critical chain length for the development of a stable helix in the solid state.

In a solubility prediction for protected peptides,[2] the average coil conformation $\langle P_c \rangle$ value was practically applied to a whole peptide instead of a peptide segment, and the adequacy of the above assumptions was widely supported by the application of the solubility prediction method to various kinds of oligopeptides.[4-10] Especially, the potential of protected peptides for β-sheet formation was relevantly estimated using their $\langle P_c \rangle$ values rather than their average β-sheet conformation $\langle P_\beta \rangle$ values when they were smaller than the critical chain length for the development of a stable helix in the solid state. In agreement with the estimation, octa- to tetradecapeptides having a high potential for a helix formation actually had a β-sheet structure in the solid state and were insoluble in DMF, DMA, NMP, DMSO, and HMPA. On the other hand, eicosapeptides having a high potential for helix formation were assumed to be larger than the critical size for the development of a stable helix in the solid state,[11] and were expected to be easily soluble in various organic solvents. Therefore, it is quite important how peptide intermediates larger than the critical chain length for the development of a stable helix in the solid state are prepared.

We recently found that a mixture of CH_2Cl_2 and a strong electron-acceptor solvent such as HFIP, TFE, or phenol have a high solubilizing potential for protected octa- to tetradecapeptides to be insoluble in DMF, DMA, NMP, DMSO, and HMPA.[12,13] This fact suggests that their fragment condensation in a mixture of CH_2Cl_2 and TFE is excellent for the preparation of peptide intermediates larger than the critical chain length for the development of a stable helix in the solid state. In the present study we practically examined fragment condensation between amino and carboxyl components of hydrophobic decapeptides in a mixture of CH_2Cl_2 and TFE (4/1, v/v) using various coupling reagents and demonstrated the usefulness of the mixture for fragment condensation. Here, we also discuss the solubility of helical peptides in organic solvents, and a synthetic strategy for helical peptides and proteins is proposed.

Results

Fragment Condensations between Amino and Carboxyl Components of Decapeptides. Two hydrophobic decapeptides (Boc-$Leu_2Ala_2Leu_6$-OBzl, **1** and Boc-$Leu_2Phe_2Leu_6$-OBzl, **2**) were prepared by the usual method, as shown in Scheme 1, and were used for the present study. Since they are smaller than the

critical chain length for the development of a stable helix in the solid state, they actually have a β-sheet structure in the solid state and are insoluble in DMF, NMP, and DMSO. Due to their insolubility in a mixture of MeOH and AcOH, the removal of their Bzl group was performed by hydrogenolysis in a mixture of HFIP and AcOH using Pd/C as a catalyst to give carboxyl components **1b** and **2b**. The liberation of their amino groups was carried out by treatment with TFA/anisole (9/1, v/v), followed by treatment with NMM to give amino components **1a** and **2a**. These products were used as amino and carboxyl components of decapeptides in order to prepare three eicosapeptides, **3—5**, as shown in Scheme 1. The amino and carboxyl components of decapeptides were also insoluble in DMF, NMP, and DMSO. Their fragment condensation in these solvents was difficult. On the other hand, they were readily soluble in a mixture of CH_2Cl_2 and TFE (4/1, v/v) and their fragment condensation proceeded smoothly in moderate yield using DCC and HOBt as coupling reagents. As a coupling reagent in the reaction of **2a** with **1b**, DCC was superior to EEDQ, DEPC, and DPPA, and the combination of DCC and HOBt gave the highest yield (Table 1).

Fragment Condensations between Amino and Carboxyl Components of Eicosapeptides. Eicosapeptides **3—5** were easily soluble in a variety of organic solvents, and the liberation of their amino groups was readily performed using the same method as described for the decapeptides to give amino components **3a—5a**. The removal of the Bzl group from the eicosapeptide **3** was also readily performed by hydrogenolysis in a mixture of MeOH and AcOH using Pd/C as a catalyst to give the carboxyl component **3b**. Successive fragment condensation between amino and carboxyl components of eicosapeptides were smoothly carried out in CH_2Cl_2 alone using DCC and HOBt as coupling reagents to produce the corresponding tetracontapeptides **6—8** in high yield (Scheme 1).

Table 1. Results of Fragment Condensation between Amino and Carboxyl Components of Decapeptides

Amino component	Carboxyl component (equivalent)	Coupling reagent (equivalent)	Product	Yield %
1a	**1b** (3)	DCC, HOBt (3)	**3**	58
1a	**2b** 3)	DCC, HOBt (3)	**4**	35
2a	**1b** (3)	DCC, HOBt (3)	**5**	48
2a	**1b** (3)	DCC, HOSu (3)	**5**	11
2a	**1b** (3)	DCC, HONB (3)	**5**	23
2a	**1b** (3)	EEDQ (3)	**5**	32
2a	**1b** (3)	DEPC (3)	**5**	below 2
2a	**1b** (3)	DPPA (3)	**5**	below 2

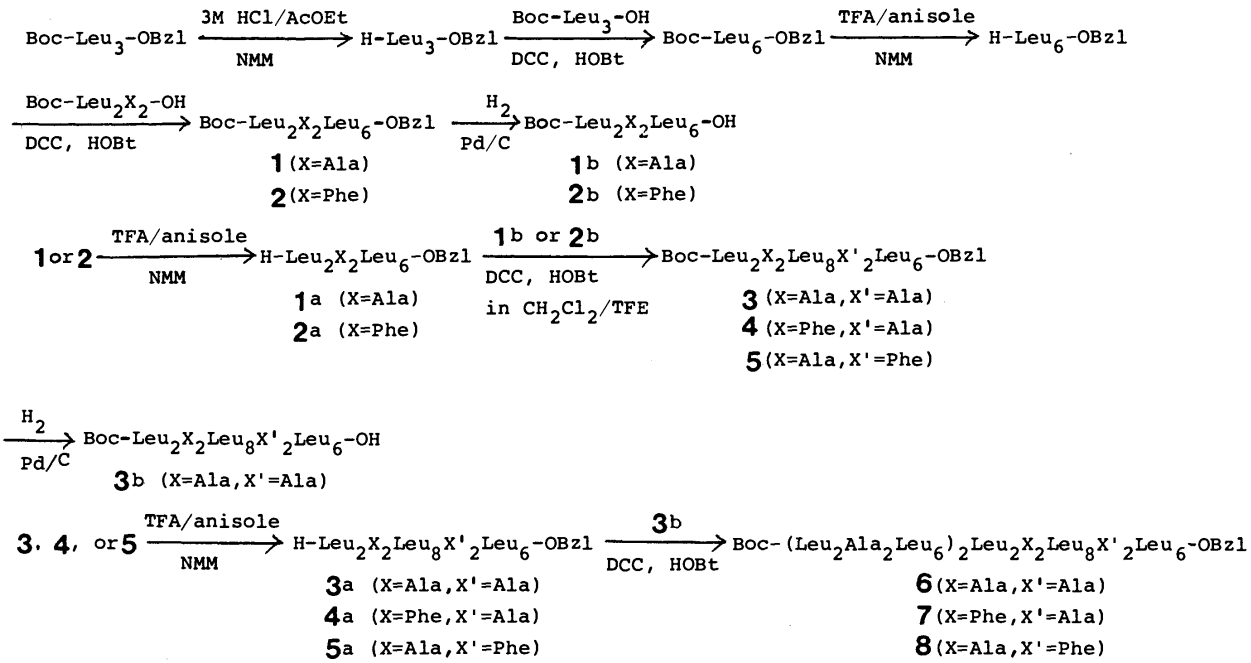

Scheme 1.

Table 2. Solubility Properties[a] of the Peptides (c=1.0 g dl^{-1}).

Compound ( )[c]	Solvent[b]												
	HMPA	DMSO	DMF	NMP	MeOH EtOH	DCM THF $CHCl_3$	AC	AcOEt	AN	TFE	DCM -TFE (4:1)	HFIP	DCM -HFIP (4:1)
1 (10)	A	C	D	C	D	D	D	D	D	A	A	C	A
2 (10)	C	C	D	C	D	D	D	D	D	D	A	A	A
3 (20)	A	D	A	A	A	A	A	B	B	A	A	A	A
4 (20)	B	D	A	A	C,[d] B[e]	A	B	B	B	A	A	A	A
5 (20)	A	D	A	A	B	A	A	B	B	A	A	A	A
6 (40)	A	D	D	B	D	A	B	B	D	C	A	C	A
7 (40)	A	D	D	B	D	A	B	B	D	C	A	C	A
8 (40)	A	D	D	B	D	A	B	B	D	C	A	C	A

a) Solubility: A, soluble at room temperature; B, soluble at 80 °C or refluxing temperature; C, partially soluble at 80 °C or refluxing temperature; D, practically insoluble at 80 °C or refluxing temperature. b) Abbreviations: DCM, dichloromethane; THF, tetrahydrofuran; AC, acetone; AN, acetonitrile. Others, see Ref. 1. c) Number of amino acid residues of the peptide. d) In the case of MeOH. e) In the case of EtOH.

Conformations and Solubility Properties of the Peptides 1—8. The IR absorption spectra of decapeptides **1** and **2** in the solid state showed strong bands at 3280 cm^{-1} in the amide A region and at 1630 cm^{-1} in the amide I region, indicating a β-sheet structure in the solid state.[14] On the other hand, those of eicosapeptides **3**—**5** and tetracontapeptides **6**—**8** in the solid state showed strong bands at 3330—3320 cm^{-1} in the amide A region and at 1660—1650 cm^{-1} in the amide I region, indicating a helical structure in the solid state.[14]

Table 2 shows the solubility properties of peptides **1**—**8** in a variety of organic solvents. As expected from their conformations, decapeptides **1** and **2**, having a β-sheet structure, were practically insoluble in various organic solvents, while eicosapeptides **3**—**5** and tetracontapeptides **6**—**8**, having a stable helix, were easily soluble in various organic solvents. As reported for octa- to tetradecapeptides having a β-sheet structure in the solid state,[12,13] decapeptides **1** and **2** were also easily soluble in mixtures of CH_2Cl_2 and TFE and of CH_2Cl_2 and HFIP since TFE and HFIP have a high potential for a β-sheet structure disruption due to their strong electron-accepting property. In fact, the IR absorption spectra of the amino and carboxyl components of decapeptides **1a** and **1b** in a mixture of CH_2Cl_2 and TFE showed a sharp, strong band around 1660 cm^{-1} in the amide I region, suggesting a large contribution of a helical or unordered structure and to be free from a β-sheet structure in the solution. Those of the amino and carboxyl components of eicosapeptides **3a** and **3b** in CH_2Cl_2 alone showed bands around 3320 cm^{-1} in the amide A region and around 1655 cm^{-1} in the amide I region, indicating that they have a stable helical structure in CH_2Cl_2.

Discussion

It was shown that the synthetic strategy used for the preparation of helical eicosa- and tetracontapeptides overcame the obstacle of the insolubility of peptide intermediates having a high potential for helix formation. A mixture of CH_2Cl_2 and TFE has a high solubilizing potential for decapeptides to be insoluble in highly polar solvents which are commonly used in peptide and protein syntheses. Fragment condensations between amino- and carboxyl-components of hydrophobic decapeptides in the mixture could be smoothly carried out using DCC and HOBt as coupling reagents. Although the yield was not so high due to the high nucleophilicity of TFE, as exhibited in peptide bond formation in TFE and HFIP,[15] the result indicates that the mixture was excellent for a coupling reaction between deca- to tetradecapeptides having a high potential for a helix formation. As expected from the solubility prediction method,[2] the eicosapeptides obtained were easily soluble in a variety of organic solvents (listed in Table 2). As a result, fragment condensation between eicosapeptides could be readily performed in CH_2Cl_2 alone to give the corresponding tetracontapeptides in high yield, indicating that peptides having a stable helical structure in the solid state can be coupled in CH_2Cl_2 to achieve further peptide chain elongation without any difficulty. Concerning the critical chain length of protected peptides for the development of a stable helix in the solid state, the solubility and conformational behavior of eicosapeptides **3**—**5** indicate that it is sufficient at an eicosapeptide level when protected peptides have a high potential for the formation of a helical structure.

Here, it becomes important to know how to estimate the helix-forming potential of protected peptides. In previous papers[16-18] we showed that the potential can be pertinently estimated using their average helix conformation $\langle P_\alpha \rangle$ values. In fact, $\langle P_\alpha \rangle$ and $\langle P_\beta \rangle$ values of protected peptides were useful for estimating their potential for the β-sheet $\rightarrow$ helix transformation with an increase in the peptide chain length or on the application of strong shear stress.

Both values were also useful for estimating the potential of protected peptides for a β-sheet structure-disruption by the adding of strong electron-acceptor solvents. The $\langle P_\alpha \rangle$ and $\langle P_\beta \rangle$ values of the decapeptide **1** are obtained by taking conformational parameters of P_α and P_β to be 1.36 and 1.17, respectively, and those of decapeptide **2** to be 1.30 and 1.23, respectively. Therefore, the amino and carboxyl components of decapeptides **1** and **2** are estimated to have high potentials for a helix formation and for a β-sheet-structure disruption by strong electron-acceptor solvents. In fact, the β-sheet structure of decapeptides **1a** and **1b** was disrupted in a mixture of CH_2Cl_2 and TFE, and fragment condensation between amino and carboxyl components of decapeptides proceeded smoothly in the mixture using DCC and HOBt as coupling reagents to give helical eicosapeptides in moderate yield. Although the $\langle P_\alpha \rangle$ and $\langle P_\beta \rangle$ values of protected peptides are useful for estimating their helix-forming potential, we should make an effort to establish how to estimate a helix-forming potential of protected peptides exactly, since the conformational behaviors of protected peptides must reflect the individuality of amino acid residues in protected peptides.[17]

With respect to the conformation and solubility of protected peptides, the results of the peptide solubility (shown in Table 2) strongly indicate the adequacy of the assumption in the solubility prediction method. The solubility behavior of the β-sheet-forming decapeptides was the same as that discussed before.[12,13] Furthermore, the solubility behavior of the helix-forming eicosapeptides was similar to that of Aib-containing oligoleucines,[8] which have a stable helix in the smaller peptide size due to a helix-promoting potential of Aib. Actually, hydrophobic eicosapeptides **3—5** were easily soluble in a variety of organic solvents. On the other hand, hydrophobic tetracontapeptides **6—8** were less soluble in highly polar solvents and easily soluble only in solvents of low polarity. Namely, the eicosapeptides were more easily soluble in DMF, NMP, EtOH, and MeOH than the tetracontapeptides. This can clearly be attributed to a large contribution of polar N- and C-termini of a helix to solvation of the eicosapeptides. The high solubilizing potential of HMPA for the hydrophobic tetracontapeptides may be due to the richness of hydrocarbon moieties in HMPA. For the same reason, the solubilizing potential of NMP is higher than that of DMF.

The solubility data of hydrophobic helical peptides illustrate a solubility feature of helical peptides which are obtained as peptide intermediates in protein synthesis. Especially, the solubility of the hydrophobic tetracontapeptides indicates that the solubility depends on the side chain moieties of the helix and that interactions between intermolecular side chain moieties are not strong, even at a tetracontapeptide level. The helical peptides obtained as peptide intermediates in protein synthesis contain various kinds of amino acid residues. Thus, they are probably easily soluble in a variety of organic solvents. The results in the present study strongly suggest that the synthetic strategy for helical peptides **3—8** is applicable to the synthesis of proteins which consist of a few long helical structures. *E. coli* acidic ribosomal protein L12[19] is presumed to be an example.

Experimental

General. Uncorrected capillary melting points will be reported. The optical rotations were taken in a 1 cm-path length cell on a JASCO model ORD/UV-5 optical rotatory dispersion recorder. The amino acid compositions of acid hydrolysates were determined with a Shimadzu HPLC LC-3A all amino acid analysis system. The acid hydrolyses of the peptides were carried out with propionic acid/12 M† HCl (2/1, v/v) for 2 days at 115 °C in evacuated sealed tubes. The IR spectra in the solid state were measured on KBr disks using a JASCO DS 403 G IR spectrophotometer. It was observed that shear stress on peptides examined here scarcely affected the IR spectra. The IR spectra in solution were recorded with a JEOL JIR-100 FTIR spectrophotometer by employing 0.1 mm path length cells with potassium bromide windows.

Preparation of Boc-Leu$_2$Ala$_2$Leu$_6$-OBzl 1 and Boc-Leu$_2$Phe$_2$Leu$_6$-OBzl 2. Boc-Leu$_2$Ala$_2$-OBzl, Boc-Leu$_2$-Phe$_2$-OBzl, and Boc-Leu$_3$-OBzl were prepared by the usual stepwise elongation under the conditions previously described.[4] The Bzl group of these peptides was removed by the usual hydrogenolysis using Pd/C as a catalyst to obtain Boc-Leu$_2$Ala$_2$-OH, Boc-Leu$_2$Phe$_2$-OH, and Boc-Leu$_3$-OH, respectively. Boc-Leu$_6$-OBzl was obtained by fragment condensation of H-Leu$_3$-OBzl (obtained from Boc-Leu$_3$-OBzl by treatment with 3 M HCl/AcOEt, followed by treatment with NMM) with Boc-Leu$_3$-OH in CH_2Cl_2 using DCC and HOBt as coupling reagents.

Boc-Leu$_6$-OBzl 15 g (16.9 mmol) was treated with TFA/anisole (4/1, v/v) (30 ml) at 0 °C for 2 h. Then, the mixture was concentrated in vacuo. The addition of a small portion of hexane to the mixture and its removal were repeated several times. DMF (65 ml) was added to the residue, and the mixture was poured into water (400 ml). The resulting precipitate was filtered, washed with water, and dried. Yield of TFA·H-Leu$_6$-OBzl was 14 g (91%). To NMP (200 ml) solution of TFA·H-Leu$_6$-OBzl, NMM (5 equiv) was added and the mixture was stirred for 10 min at room temperature. Then, the mixture was poured into water (700 ml), and the precipitate was filtered, washed with water, and dried. Yield of H-Leu$_6$-OBzl was 13 g (97%).

To the ice-chilled NMP (50 ml) solution of H-Leu$_6$-OBzl 4 g obtained above, Boc-Leu$_2$Ala$_2$-OH (1.5 equiv) and HOBt (1.5 equiv), was added DCC (1.5 equiv) and the mixture was stirred at 0 °C for 3 h and then at room temperature overnight. The mixture was poured into water and the precipitate was filtered, washed successively with 5% $NaHCO_3$ and water, and dried. The crude product was treated twice with refluxing methanol. Yield of **1**; 4.9 g (76%). mp 273.5—274.5 °C, $[\alpha]_D^{20}=-170°$ (c=1, in CH_2Cl_2-

† 1 M=1 mol dm^{-3}.

TFE(4/1, v/v)). Found: C, 62.18; H, 9.20; N, 11.02%. Calcd for $C_{66}H_{114}O_{13}N_{10}\cdot H_2O$: C, 62.24; H, 9.18; N, 11.00%. Amino acid analysis; Ala 2.00; Leu 8.13.

The peptide **2** was obtained by the same procedure as described above using Boc-Leu$_2$Phe$_2$-OH in place of Boc-Leu$_2$Ala$_2$-OH. Yield of **2**: 82%. mp>300 °C, $[\alpha]_D^{20}=-70°$ (c=1, in CH_2Cl_2-TFE(4/1, v/v)). Found: C, 65.70; H, 8.73; N, 9.86%. Calcd for $C_{78}H_{122}O_{13}N_{10}\cdot H_2O$: C, 65.70; H, 8.77; N, 9.82%. Amino acid analysis: Leu, 7.63; Phe, 2.00.

Preparation of H-Leu$_2$Ala$_2$Leu$_6$-OBzl 1a and H-Leu$_2$-Phe$_2$Leu$_6$-OBzl 2a. The peptide **1a** and **2a** were obtained from **1** and **2**, respectively, by their treatment with TFA/anisole (4/1, v/v) as described for preparation of H-Leu$_6$-OBzl. Yield of **1a**: 94%. Yield of **2a**: 94%.

Preparation of Boc-Leu$_2$Ala$_2$Leu$_6$-OH 1b and Boc-Leu$_2$Phe$_2$Leu$_6$-OH 2b. To the HFIP (5 ml) solution of **1** (1.5 g, 1.2 mmol) was added 10% Pd/C 0.15 g with acetic acid 3 ml and the mixture was stirred under hydrogen at atmospheric pressure for 3 days. After removing Pd/C by filtration and washing with a small amount of a mixture of HFIP and CH_2Cl_2, the joined filtrate and washings were poured into water (100 ml). The resulting precipitate was filtered, washed with water, and dried. Yield of **1b**: 1.35 g (97%). The peptide **2b** was prepared from **2** by the same procedure. Yield of **2b**: 99%.

Fragment Condensation between Amino and Carboxyl Components of Decapeptides. To the ice-chilled solution of an amino component decapeptide (**1a** or **2a**) 100 mg, a carboxyl component decapeptide (**1b** or **2b**) (3 equiv), and an additive (HOBt, HOSu, or HONB) (3 equiv) in CH_2Cl_2-TFE (4/1, v/v) (5 ml) was added DCC (3 equiv) with CH_2Cl_2-TFE (4/1, v/v) (5 ml). The mixture was stirred at 0 °C for 3 h and then at room temperature for 45 h. After removing *N,N*-dicyclohexylurea by filtration, the filtrate was concentrated in vacuo, and water (25 ml) was added to the residue. The resulting precipitate was filtered, washed successively with water, 10% citric acid, water, 5 % $NaHCO_3$, and water, and dried. The crude product was treated with refluxing dichloromethane (15 ml). After allowing the mixture to stand and cool to room temperature, the resulting precipitate was filtered off, and the filtrate was concentrated. The residue was treated with refluxing ethyl acetate (20 ml) in the same manner, and the product was obtained as a residue. A coupling reaction using EEDQ, DEPC, or DPPA was carried out essentially in the same manner as described above. Yields of the peptides **3**—**6** are listed in Table 1. Peptide **3**: mp>300 °C, $[\alpha]_D^{20}=-80°$ (c=1, in CH_2Cl_2). Found: C, 62.06; H, 9.02; N, 12.13%. Calcd for $C_{120}H_{212}O_{23}N_{20}\cdot H_2O$: C, 62.10; H, 9.29; N, 12.07%. Amino acid analysis: Ala, 4.00; Leu 15.70. Peptide **4**: mp>300 °C, $[\alpha]_D^{20}=0°$ (c=1, in CH_2Cl_2). Found: C, 62.89; H, 8.98; N, 11.30%. Calcd for $C_{132}H_{220}O_{23}N_{20}\cdot 3H_2O$: C, 63.18; H, 9.08; N, 11.16%. Amino acid analysis: Ala, 2.19; Leu 15.98; Phe, 2.00. Peptide **5**: mp>300 °C, $[\alpha]_D^{20}=0°$ (c=1, in CH_2Cl_2). Found: C, 64.37; H, 9.08; N, 11.30%. Calcd for $C_{132}H_{220}O_{23}N_{20}$: C, 64.10; H, 9.05; N, 11.33%. Amino acid analysis: Ala, 1.86; Leu, 16.01; Phe, 2.00.

Fragment Condensations between Amino and Carboxyl Components of Eicosapeptides. H-(Leu$_2$Ala$_2$Leu$_6$)$_2$-OBzl, H-Leu$_2$Phe$_2$Leu$_8$Ala$_2$Leu$_6$-OBzl, and H-Leu$_2$Ala$_2$Leu$_8$Phe$_2$-Leu$_6$-OBzl were prepared by the same procedure used for preparation of **1a** and **2a**, from the peptides **3**—**5** in 86, 80, and 89% yield, respectively. Boc-(Leu$_2$Ala$_2$Leu$_6$)$_2$-OH was also prepared from **3** by the usual hydrogenolysis in MeOH-AcOH in 93% yield.

To an ice-chilled solution of an amino component peptide 120 mg, Boc-(Leu$_2$Ala$_2$Leu$_6$)$_2$-OH (1.2 equiv), and HOBt (1.2 equiv) in CH_2Cl_2 (5 ml), was added DCC (1.2 equiv) with CH_2Cl_2 (3 ml), and the mixture was stirred at 0 °C for 3 h, and then at room temperature overnight. After the addition of a small amount of CH_2Cl_2, the mixture was filtered and the filtrate was concentrated in vacuo. The residue was washed successively with water, 10% citric acid, water, 5% $NaHCO_3$, and water, and dried. The crude product was treated with refluxing MeOH (20 ml). After standing, the mixture cooled to room temperature and the precipitate was filtered and recrystallized with ethyl acetate. Yields of the peptides **6**—**8** were 48, 60, and 54%, respectively. Peptide **6**: mp>300 °C, $[\alpha]_D^{20}=-40°$ (c=1, in CH_2Cl_2). Found: C, 61.07; H, 9.14; N, 12.02%. Calcd for $C_{228}H_{408}O_{43}N_{40}\cdot 5H_2O$: C, 61.02; H, 9.39; N, 12.48%. Amino acid analysis: Ala, 8.19; Leu, 32.00. Peptide **7**: mp>300 °C, $[\alpha]_D^{20}=0°$ (c=1, in CH_2Cl_2). Found: C, 62.41; H, 8.97; N, 11.71%. Calcd for $C_{240}H_{416}O_{43}N_{40}\cdot 5H_2O$: C, 62.12; H, 9.25; N, 12.07%. Amino acid analysis: Ala, 6.15; Leu 32.00; Phe, 1.83. Peptide **8**: mp>300 °C, $[\alpha]_D^{20}=0°$ (c=1, in CH_2Cl_2). Found: C, 62.02; H, 8.91; N, 11.62%. Calcd for $C_{240}H_{416}O_{43}N_{40}\cdot 5H_2O$: C, 62.12; H, 9.25; N, 12.07%. Amino acid analysis: Ala, 6.11; Leu 32.00, Phe, 1.86.

The authors wish to thank Central Glass Co., Ltd., Mitsubishi Kasei Co., Ltd., and Ajinomoto Co., Ltd., for the generous gift of reagents.

References

1) The abbreviations for amino acids are those recommended by the IUPAC-IUB Commission on Biochemical Nomenclature, *J. Biol. Chem.*, **247**, 977 (1972). Amino acid symbols except for Gly denote the L-configuration. Additional abbreviations used are the following: DMF, *N,N*-dimethylformamide; NMP, *N*-methylpyrrolidone; DMSO, dimethyl sulfoxide; TFE, 2,2,2-trifluoroethanol; DCC, dicyclohexylcarbodiimide; HOBt, 1-hydroxy-1*H*-benzotriazole; DMA, *N,N*-dimethylacetamide; HMPA, hexamethylphosphoric triamide; HFIP, 1,1,1,3,3,3-hexafluoro-2-propanol; Boc, *t*-butoxycarbonyl; OBzl, benzyl ester; MeOH, methanol; AcOH, acetic acid; TFA, trifluoroacetic acid; NMM, *N*-methylmorpholine; AcOEt, ethyl acetate; HOSu, *N*-hydroxysuccinimide; HONB, *N*-hydroxy-5-norbornene-2,3-dicarboximide; EEDQ, *N*-ethoxycarbonyl-2-ethoxy-1,2-dihydroquinoline; DEPC, diethoxyphosphoryl cyanide; DPPA, diphenylphosphoryl azide; IR, infrared; EtOH, ethanol.

2) M. Narita, K. Ishikawa, J.-Y. Chen, and Y. Kim, *Int. J. Peptide Protein Res.*, **24**, 580 (1984).

3) M. Narita, T. Ogura, K. Sato, and S. Honda, *Bull. Chem. Soc. Jpn.*, **59**, 2433 (1986).

4) M. Narita, T. Fukunaga, A. Wakabayashi, K. Ishikawa, and H. Nakano, *Int. J. Peptide Protein Res.*, **23**, 306 (1984).

5) M. Narita, J.-Y. Chen, H. Sato, and Y. Kim, *Bull. Chem. Soc. Jpn.*, **58**, 2494 (1985).

6) M. Narita, M. Doi, T. Nakai, and H. Takegahara, *Int. J. Peptide Protein Res.*, **32**, 200 (1988).

7) M. Narita, S. Nagasawa, J.-Y. Chen, H. Sato, and Y. Tanaka, *Makromol. Chem.*, **185**, 1069 (1984).

8) M. Narita, M. Doi, H. Sugasawa, and K. Ishikawa, *Bull. Chem. Soc. Jpn.*, **58**, 1473 (1985); M. Narita, K. Ishikawa, H. Sugasawa, and M. Doi, *ibid.*, **58**, 1731 (1985); S. Isokawa, M. Doi, R. Wakita, H. Sugasawa, T. Asakura, and M. Narita, *Macromolecules*, **20**, 1227 (1987).

9) M. Narita, M. Doi, K. Kudo, and Y. Terauchi, *Bull. Chem. Soc. Jpn.*, **59**, 3553 (1986).

10) M. Narita, S. Honda, and H. Umeyama, *Bull. Chem. Soc. Jpn.*, **60**, 4127 (1987).

11) R. Katakai, *Macromolecules*, **14**, 613 (1981).

12) M. Narita, S. Honda, H. Umeyama, and S. Obana, *Bull. Chem. Soc. Jpn.*, **61**, 281 (1988).

13) M. Narita, S. Honda, and S. Obana, *Bull. Chem. Soc. Jpn.*, **62**, 342 (1989).

14) T. Miyazawa and E. R. Blout, *J. Am. Chem. Soc.*, **83**, 712 (1961); T. Miyazawa, "Poly-α-Amino Acids," ed by G.D. Fasman, Marcel Dekker, New York (1967), pp. 69—103; S. Krimm and Y. Abe, *Proc. Natl. Acad. Sci. U.S.A.*, **69**, 2788 (1972); Y. N. Chirgadze and N. A. Nevskaya, *Biopolymers*, **15**, 607 (1976).

15) A. M. Felix, C.-T. Wang, and T. J. Lambros, Peptides Structure and Function, Proc. Ninth American Peptide Symposium, ed by C. M. Deber, V. J. Hruby, and K. D. Kopple, Pierce Chemical Co., Rockford IL (1985), pp. 389—396; L. S. Trzupek, A. Go and K. D. Kopple, *J. Org. Chem.*, **44**, 4577 (1979); C. Toniolo, G. M. Bonora, E. P. Hermer, and A. M. Felix, *Int. J. Peptide Protein Res.*, **30**, 232 (1987).

16) M. Narita, T. Ogura, K. Sato, and S. Honda, *Bull. Chem. Soc. Jpn.*, **59**, 2439, 2445 (1986); M. Narita, M. Doi, and T. Nakai, *ibid.*, **60**, 3255 (1988); M. Narita, M. Doi, and H. Takegahara, *ibid.*, **60**, 2445 (1987).

17) M. Narita, S. Isokawa, S. Honda, H. Umeyama, H. Kakei, and S. Obana, *Bull. Chem. Soc. Jpn.*, **62**, 773 (1989).

18) M. Narita, H. Umeyama, S. Isokawa, S. Honda, C. Sasaki, and H. Kakei, *Bull. Chem. Soc. Jpn.*, **62**, 780 (1989).

19) M. Dzionara, S. M. L. Robinson, and B. Wittmnn-Leibold, *Hoppe-Seyler's Z. Physiol. Chem.*, **358**, 1003 (1977).

Stereochemistry of a Chiral Germyl Radical in the Reaction of Carbon Tetrachloride

Kunio MOCHIDA,* Takato YAMAUCHI, and Hideki SAKURAI†
Department of Chemistry, Faculty of Science, Gakushuin University, 1-5-1 Mejiro, Tokyo 171
†Department of Chemistry, Faculty of Science, Tohoku University, Aoba, Sendai 980
(Received December 13, 1988)

A chiral germyl radical produced from an optically active hydrogermane, 1-NpPhMeGe*H, abstracted a chlorine atom from CCl_4 to give the corresponding chlorogermane with retention of configuration. Progressive dilution of CCl_4 with cyclohexane demonstrated that the chiral germyl radical could also undergo inversion. A mechanism in which inversion of the chiral germyl radical competed with chlorine abstraction was proposed and the relative rate of chlorine abstraction to inversion (k_{Cl}/k_{inv}) of the chiral germyl radical was found to be (0.52±0.13) $mol^{-1}dm^3$ at 80 °C. The rate constant for the chlorine abstraction (k_{Cl}) by germyl radicals with CCl_4 was determined to be $(6.6\pm1.0)\times10^8$ $s^{-1}mol^{-1}dm^3$ by laser-photolysis experiments. By using this rate constant, the k_{inv} value for the chiral germyl radical was estimated to be ca. 2×10^9 s^{-1}.

In a former paper, we have reported that 1-naphthylphenylmethylgermyl radical, 1-NpPhMeGe*, produced from an optically active 1-NpPhMeGe*H undergoes chlorine abstraction mostly with retention of configuration.[1] Thus, the chiral germyl radical exists in a pyramidal form which is in harmony with ESR parameters[2-6] and IR data[7-10] of germyl radicals, and retains asymmetry for the abstraction of a chlorine atom with CCl_4.

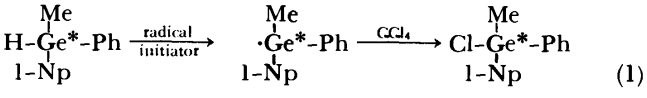

(1)

The inversion process of this germyl radical must be slow in comparison with the chlorine abstraction from CCl_4 since the germyl radical undergoes retention.

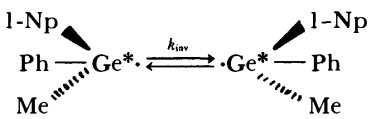

(2)

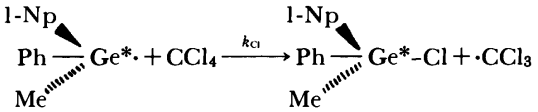

(3)

$$k_{inv} < k_{Cl}[CCl_4]$$

However, racemic or partially racemized products may be obtained from the chiral germyl radical, if product-forming chlorine abstraction is slow enough for the inversion process.

In this paper, we report the benzoyl peroxide (BPO)-catalyzed and uncatalyzed chlorination of optically active 1-NpPhMeGe*H with CCl_4 and the capacity of the chiral germyl radical produced from the optically active hydrogermane in the reaction (1) to invert under conditions of progressively greater dilution of CCl_4 with cyclohexane. Laser-photolysis studies of the photochemical primary processes of hydrogermanes are also described. A mechanism that induces inversion of the chiral germyl radical competes with chlorine abstraction is discussed, and the k_{inv} value for the chiral germyl radical is estimated by using the rate constant for chlorine abstraction, k_{Cl} obtained by laser-photolysis experiments.

Results and Discussion

BPO-Catalyzed Chlorination of an Optically Active Hydrogermane, (+)-1-NpPhMeGe*H. The reaction of (+)-1-NpPhMeGe*H (≡(+)-R_3Ge^*H), $[\alpha]_{589}$ +27.0± 0.9° (*c* 4.3, cyclohexane),[11] with CCl_4 diluted cyclohexane at various concentrations was carried out in sealed and degassed tubes using BPO as an initiator at 80 °C The optically active hydrogermane, (+)-R_3Ge^*H, afforded the corresponding chlorogermane quantitatively in all reactions. The products, obtained after evaporation of CCl_4 and cyclohexane followed by recrystallization from pentane, was identified by comparing IR and NMR spectra, and retention time on GLC (SE30 5% l m) with those of the racemic R_3Ge^*Cl compound. The results are summarized in Table 1. The (+)-R_3Ge^*H and (−)-R_3Ge^*Cl have the same stereochemical configuration, since optical rotation correlated with the configuration of the optically active hydrogermane, R_3Ge^*H, and the optically active chlorogermane, R_3Ge^*Cl.[12] Therefore, it can be concluded that the free-radical chlorination of the optically active hydrogermane, (+)-R_3Ge^*H, with CCl_4 without dilution should proceed with retention of configuration.

$$(+)\text{-}R_3Ge^*H \xrightarrow[\text{BPO, 80 °C}]{CCl_4} (-)\text{-}R_3Ge^*Cl \xrightarrow{LiAlH_4} (-)\text{-}R_3Ge^*H \quad (4)$$

$[\alpha]_{589}$+27.0± 0.9° $[\alpha]_{589}$−4.6±1.1° $[\alpha]_{589}$−17.8±1.2°

The optical purity of the product (−)-R_3Ge^*Cl, $[\alpha]_{589}$ −4.6±1.1° (*c* 3.9, cyclohexane)[12], was about 73%. Furthermore, (−)-R_3Ge^*Cl was converted to (−)-R_3Ge^*H, $[\alpha]_{589}$−17.8±1.2°, again by reduction with lithium aluminum hydride. Thus, the rate of abstraction of a chlorine atom from CCl_4 with the chiral germyl radical is fast in the reaction of the

Table 1. Effects of Cyclohexane Dilution on the Stereospecificity of Reaction of (+)-R_3Ge^*H with CCl_4 at 80 °C

Run	Reactant[a]			Reaction time/h	Product, R_3Ge^*Cl	
	(+)-R_3Ge^*H (mmol)	CCl_4 (mmol·dm^{-3})	BPO (mmol)		Yield/%[b]	$[\alpha]_{589}$
1	1.12	10.4	0.08	5	100	−4.6±1.1
2	1.21	8.17	0.06	5	100	−3.4±0.4
3	1.10	6.06	0.04	5	99	−2.0±0.5
4	1.08	0.90	0.04	5	95	0

a) A value of $[\alpha]_{589}$ of the (+)-R_3Ge^*H is $[\alpha]_{589}$+27.0±0.9°. b) Isolated yield.

optically active R_3Ge^*H with CCl_4. However, the optical purity of the product (−)-R_3Ge^*Cl was decreased as CCl_4 was diluted with cyclohexane as shown in Table 1. Thus, the rate of chlorine abstraction competes with the rate of inversion under conditions of dilution of CCl_4 with cyclohexane.

Optically active hydrosilanes[13,14] and hydrostannane[15] also react stereoselectively with CCl_4 to give the corresponding chlorides, respectively, with retention of configuration.

Uncatalyzed Chlorination of an Optically Active Hydrogermane, (+)-1-NpPhMeGe*H. The reaction of (+)-R_3Ge^*H, $[\alpha]_{589}$+27.0±0.9° (*c* 4.3, cyclohexane), with CCl_4 was carried out without any catalyst in a sealed and degassed tube at 80 °C for 5 h. The product, $[\alpha]_{589}$+11.9±1.0°, (*c* 4.3, cyclohexane), obtained after evaporation of CCl_4, contained unreacted hydrogermane. The conversion of the hydrogermane to the chlorogermane was determined to be 40% by GLC by an internal standard method. The (+)-R_3Ge^*H and (−)-R_3Ge^*Cl have the opposite optical rotation in spite of the same configuration.[12] The value of $[\alpha]_{589}$ of the product, a mixture of (+)-R_3Ge^*H and (−)-R_3Ge^*Cl, by accounting for the concentration of the unreacted optically active hydrogermane is estimated to be +20°, if all the chlorogermane racemizes completely. A test of the optical stability of the R_3Ge^*Cl will be discussed in the next section. From the observed $[\alpha]_{589}$ of the product, the value of the optical rotation of (−)-R_3Ge^*Cl produced in this uncatalyzed chlorination is estimated to be about −6.0°. Therefore, uncatalyzed chlorination of the optically active hydrogermane proceeded mostly with retention of configuration. Since the free-radical mechanism for uncatalyzed chlorination of hydrogermanes with CCl_4 has been established,[16] this result is consistent with that for BPO-catalyzed chlorination of the optically active hydrogermane.

A Test of the Optical Stability of a Chlorogermane, (+)-1-NpPhMeGe*Cl. The optical stability of (+)-R_3Ge^*Cl was investigated in CCl_4, cyclohexane, and $CHCl_3$ under the reaction conditions.

The optically active chlorogermane, (+)-R_3Ge^*Cl, $[\alpha]_{589}$+6.0±1.0° (*c* 4.3, cyclohexane), was heated in CCl_4 in a sealed and degassed tube at 80 °C for 5 h. The value of $[\alpha]_{589}$ of the optically active chlorogermane, (+)-R_3Ge^*Cl, recovered after evaporation of CCl_4 followed by recrystallization from pentane, was +6.0±1.0°. Therefore, no change in the optical purity was observed. Similarly, the optically active chlorogermane, (+)-R_3Ge^*Cl, was heated in both cyclohexane and $CHCl_3$ at 80 °C for 5 h. The optical purity of the chloride, (+)-R_3Ge^*Cl, was also unchanged within experimental error. Thus, the optically active chlorogermane, R_3Ge^*Cl, is configurationally stable in CCl_4, cyclohexane, and $CHCl_3$ under the reaction conditions.

Laser-Photolysis Study of a Hydrogermane, 1-NpPhMeGeH. Laser-photolysis (ca. 0.1 mol·dm^{-3}) in a mixture of benzene and di-*t*-butyl peroxide (DTBP) was carried out at 28.5±2 °C.[17] The laser-photolysis apparatus and measuring system were similar to those published elsewhere.[18] As expected, the rise of the absorption due to the germyl radical was observed in R_3GeH solution. As an example, the time dependence of the probe light intensity, $I(t)$, observed in the R_3GeH solution at 400 nm is shown by curve (a) in Fig. 1. This curve shows the initial rise and the following slow decay of $R_3Ge\cdot$. The time-resolved absorption spectrum corresponding to the rise of $R_3Ge\cdot$ was also measured. The spectrum observed at 50 and 150 ns after excitation of the R_3GeH solution is shown in Fig. 2. As shown in Fig. 2, the transient spectrum observed with the solution of R_3GeH has a peak at 390 nm.

As is shown by curve (a) in Fig. 1, the decay of $R_3Ge\cdot$ was found to be slow. In the presence of CCl_4, how-

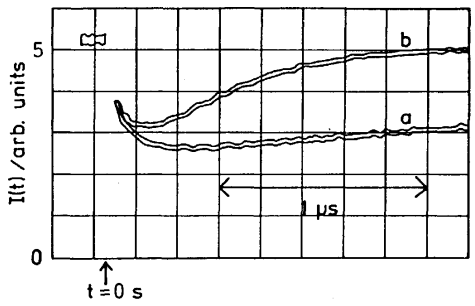

Fig. 1. Ocsilloscope traces of the $I(t)$ curves observed at 400 nm for 1-NpPhMeGeH (0.1 mol·dm^{-3}) in a mixture of benzene and DTBP (a) in the absence and (b) presence of CCl_4 (3.35×10^{-3} mol·dm^{-3}).

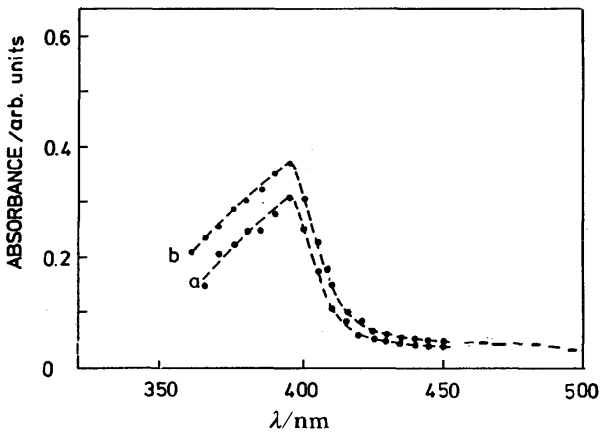

Fig. 2. Transient absorption spectra of 1-NpPhMeGeH (0.1 mol dm^{-3}) in a mixture of benzene and DTBP observed at (a) 50 ns and (b) 150 ns and after excitation with an N_2 laser.

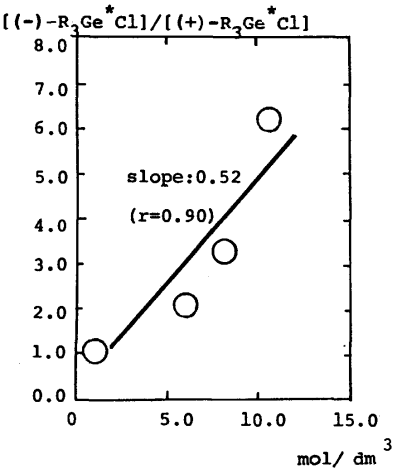

Fig. 3. Correlation between the product ratio and concentrations of CCl_4.

ever, the decay became fast. $R_3Ge\cdot$ was observed to decay with first-order kinetics in the presence of CCl_4, and the rate constant of chlorine abstraction (k_{Cl}) was obtained to be $(6.6\pm1.0)\times10^8$ s^{-1} mol^{-1} dm^3. The k_{Cl} value in a mixture of cyclohexane-DTBP was not changed within experimental error. Recently, Ingold and co-workers have also obtained a similar k_{Cl} value of $Bu_3Ge\cdot$ with CCl_4 using DTBP and an N_2 laser.[19]

Stereochemistry of a Chiral Germyl Radical in the Reaction with CCl_4. The chiral germyl radical produced from an optically active hydrogermane, (+)-R_3Ge^*H, abstracts a chlorine atom from CCl_4 to give the (−)-R_3Ge^*Cl predominantly with retention of configuration. However, the optical purity of the product, (−)R_3Ge^*Cl, decreased as the CCl_4 is diluted with cyclohexane. Since (−)-R_3Ge^*Cl is configurationally stable under these conditions, optically active chlorogermane was produced. Thus, the loss of optical activity in the product must be due to the fact that the rate of abstraction of a chlorine atom from CCl_4 diluted with cyclohexane may be comparable to the rate of inversion of the germyl radical.

Net stereochemistry of the chiral germyl radical with CCl_4 depends on relative rates of chlorine abstraction (k_{Cl}) and inversion (k_{inv}) as shown in the following scheme.

$$\begin{array}{ccccc} (+)\text{-}R_3Ge^*H & \rightarrow & (+)\text{-}R_3Ge^*\cdot & \underset{k_{inv}}{\rightleftharpoons} & (-)\text{-}R_3Ge^*\cdot \\ & & \downarrow{\scriptstyle k_{Cl}}\ CCl_4 & & \downarrow{\scriptstyle k_{Cl}}\ CCl_4 \\ & & (-)\text{-}R_3Ge^*Cl & & (+)\text{-}R_3Ge^*Cl \end{array} \quad \leftarrow (-)\text{-}R_3Ge^*H$$

From this scheme using the relevant rate constants shown above, the product ratio can be expressed by the formula

$$\frac{d[(-)\text{-}R_3Ge^*Cl]}{d[(+)\text{-}R_3Ge^*Cl]} = \frac{[(+)\text{-}R_3Ge^*\cdot]}{[(-)\text{-}R_3Ge^*\cdot]} \quad (5)$$

where [(+)-$R_3Ge^*\cdot$] and [(−)-$R_3Ge^*\cdot$] are the concentrations of each chiral germyl radical, respectively. The product ratio from (+)-R_3Ge^*H can be derived as following by assuming the steady state concentration of (−)-$R_3Ge^*\cdot$ radical.

$$d[(-)\text{-}R_3Ge^*\cdot]/dt = k_{inv}[(+)\text{-}R_3Ge^*\cdot] - k_{inv}[(-)\text{-}R_3Ge^*\cdot] - k_{Cl}[(-)\text{-}R_3Ge^*\cdot][CCl_4] = 0 \quad (6)$$

Combination of Eqs. 5 and 6 yields

$$[(-)\text{-}R_3Ge^*Cl]/[(+)\text{-}R_3Ge^*Cl] = 1 + (k_{Cl}/k_{inv})\times[CCl_4]. \quad (7)$$

Thus, the product ratio depends on the concentration of CCl_4.[20,21]

The relationship between the product ratio and concentrations of CCl_4 are shown in Fig. 3. The k_{Cl}/k_{inv} value was calculated to be (0.52±0.13) mol dm^3.

Taking the k_{Cl} value at 28.5 °C into consideration, it may be assumed that the k_{Cl} value at 80 °C for $R_3Ge^*\cdot$ is less than 1×10^9 s^{-1} mol^{-1} dm^3. Thus the k_{inv} value for $R_3Ge^*\cdot$ at 80 °C may be less than 2×10^9 s^{-1}. If we assume that inversion at the germanium center has a normal pre-exponential factor (i.e., ca. $10^{13.3}$ s^{-1}), it is possible to estimate the activation barrier for the inversion process as ca. 5.7 kcal·mol^{-1}. This value is almost the same as that of the silyl radical inversions previously reported.[22]

In conclusion, the rate of inversion of the chiral germyl radical is comparable to that of chlorine abstraction from CCl_4 and the remarkable configurational stability of the chiral germyl radical in the reaction resulted partly from the rapid chlorine abstraction.

Experimental

Polarimetric analyses of optically active organogermanium compounds were carried out on a Hitachi EPU-2A photoelectric Spectrometer. Laser-photolysis experiments were performed on degassed solutions using a Molectron UV-24 N_2 laser (337 nm, pulse width 10 ns) as an exciting light source.

Materials. Optically active 1-naphthylphenylmethylger-

mane, R_3Ge^*H, and 1-naphthylphenylmethylchlorogermane, R_3Ge^*Cl, were prepared according to the literature.[11,16] (+)-R_3Ge^*H, $[\alpha]_{589}$+27.0±0.9°, mp 74—75 °C; (−)-R_3Ge^*H, $[\alpha]_{589}$−26.6±0.9°, mp 74—75 °C. (+)-R_3Ge^*Cl, $[\alpha]_{589}$+6.0±1.0°, mp 67—69 °C.

Reaction of (+)-R_3Ge^*H with CCl_4 at Various Concentrations. A representative example is described. In a small Pyrex tube were placed 0.36 g (1.21 mmol) of (+)-R_3Ge^*H, $[\alpha]_{589}$+27.0±0.9°, 2.51 g (16.3 mmol) of CCl_4, and 0.02 g (0.06 mmol) of BPO. The reaction mixture was diluted with cyclohexane to 4.0 dm^3. The Pyrex tube was degassed, sealed and immersed in an oil bath kept at 80 °C for 5 h. After completion of the reaction, volatile materials were removed. The chlorogermane, $[\alpha]_{589}$−3.4±0.4°, was purified by recrystallization from pentane. The chlorogermane was identified by comparing IR and NMR spectra and the retention time on GLC (SE30 5% 1 m) with those of an authentic sample.

A Test of Optical Stability of (+)-R_3Ge^*Cl under the Reaction Conditions. In a small Pyrex tube were placed 0.40 g (1.22 mmol) of (+)-R_3Ge^*Cl, $[\alpha]_{589}$+6.0±1.0°, and 4.0 dm^3 of CCl_4. The tube was degassed, sealed and immersed in an oil bath kept at 80 °C for 5 h. After removal of CCl_4, the chlorogermane, $[\alpha]_{589}$=6.0±1.0° was recovered and purified by recrystallization from pentane.

The authors wish to thank Dr. Hisaharu Hayashi of the Institute of Physical and Chemical Research for measuring the laser-photolysis of the hydrogermanes. We also thank Professor Tadashi Suehiro of Gakushuin University for providing the Hitachi EPU-2A photoelectric Spectrometer and the Varian FT-80A NMR Spectrometer.

References

1) H. Sakurai and K. Mochida, *Chem. Commun.*, **1971**, 1581.
2) R. L. Morehouse, J. J. Christiansen, and W. Gordy, *J. Chem. Phys.*, **45**, 1751 (1969).
3) G. S. Jakel, J. J. Christiansen, and W. Gordy, *J. Chem. Phys.*, **47**, 4274 (1967).
4) J. Roncin and R. Debuyst, *J. Chem. Phys.*, **51**, 577 (1969).
5) R. V. Lyloyd and M. T. Rogers, *J. Am. Chem. Soc.*, **95**, 2459 (1973).
6) M. Geoffroy, L. Ginet, and E. A. C. Lucken, *Chem. Phys. Lett.*, **38**, 321 (1976).
7) L. Andrews and D. L. Fredrick, *J. Am. Chem. Soc.*, **92**, 775 (1970).
8) R. J. Isabel and W. A. Guillory, *J. Chem. Phys.*, **55**, 1197 (1971); **57**, 1116 (1972).
9) W. A. Guillory and E. C. Smith, *J. Chem. Phys.*, **56**, 1661 (1972).
10) G. R. Smith and W. A. Guillory, *J. Chem. Phys.*, **56**, 1423 (1972).
11) A. G. Brook and G. J. D. Peddle, *J. Am. Chem. Soc.*, **85**, 1869 (1963).
12) A. G. Brook and G. J. D. Peddle, *J. Am. Chem. Soc.*, **85**, 2338 (1963).
13) H. Sakurai, M. Murakami, and M. Kumada, *J. Am. Chem. Soc.*, **91**, 319 (1969).
14) L. H. Sommer and L. A. Ulland, *J. Org. Chem.*, **37**, 3878 (1972).
15) M. Gielen and Y. Tonduer, *J. Organomet. Chem.*, **169**, 265 (1979).
16) H. Sakurai, K. Mochida, A. Hosomi, and F. Mita, *J. Organomet. Chem.*, **38**, 275 (1972).
17) H. Hayashi and K. Mochida, *Chem. Phys. Lett.*, **101**, 307 (1983).
18) H. Hayashi and S. Nagakura, *Bull. Chem. Soc. Jpn.*, **53**, 2419 (1980); Y. Sakaguchi, S. Nagakura, A. Minoh, and H. Hayashi, *Chem. Phys. Lett.*, **82**, 213 (1981).
19) K. U. Ingold, J. Lusztky, and J. C. Scaiano, *J. Am. Chem. Soc.*, **106**, 343 (1984).
20) S. Kobayashi and O. Simamura, *Chem. Lett.*, **1973**, 695.
21) H. Sakurai and M. Murakami, *Bull. Chem. Soc. Jpn.*, **50**, 3384 (1977).
22) C. Chatgilialoglu, K. U. Ingold, and J. C. Scaiano, *J. Am. Chem. Soc.*, **104**, 5123 (1982).

A New Method for Determination of Disulfide Pairing in Peptides†

Yuji HIDAKA and Yasutsugu SHIMONISHI*
Institute for Protein Research, Osaka University, Yamada-oka 3-2, Suita, Osaka 565
(Received December 21, 1988)

A new method was developed for determination of disulfide pairings in peptides. This method consisted in the synthesis of peptides with deuteriocysteine residues at given positions and the analysis of deuteriocystine generated in the acid hydrolyzates of the synthetic peptides by fast atom bombardment mass spectrometry. The availability of this method was confirmed by its application for determining the positions of disulfide linkages in a heat-stable enterotoxin of enterotoxigenic *Escherichia coli*.

Many biologically interesting peptides contain several Cys residues joined intramolecularly through disulfide bonds.[1-3] The roles of these disulfide linkages in the biological effects of these peptides are not yet clear, but these linkages are known to be important for stabilizing the native conformations of the peptides essential for expression of their biological activity.[4] The mismatching of disulfide pairs during construction of the spatial structure may change the native conformations of peptides and result in marked reduction or loss of their biological activities. Therefore, information on the disulfide pairing in peptides is very useful for understanding of the bioactive conformations of peptides, the mechanisms of a peptide-to-peptide or peptide-to-protein interaction, etc.

In general, the disulfide pairing of cystine residues in peptides is determined by isolation and sequencing of peptides containing cystine, which are generated by either partial acid or enzymatic hydrolysis of the original peptides.[1] Recently a method was reported for measurement of the molecular weights of peptides containing cystine, by direct analysis of the enzymatic digest of peptides by FAB mass spectrometry, resulting in determination of disulfide pairing in the original peptides.[5] These methods are useful for determination of disulfide pairing in peptides that contain Cys residues at interspersed positions in the peptide chain and that release peptides containing cystine with one disulfide linkage, but they are not suitable for peptides in which Cys residues are located in vicinal positions in the peptide chain and from which peptides containing cystines with multiple-disulfide linkages are generated by hydrolysis, because of the difficulty in cleaving peptide bonds between vicinal Cys residues. Another method to determine disulfide pairing in peptides is synthesis of peptides with disulfide linkages at given positions using selectively removable protecting groups at Cys residues and then comparison of the synthetic peptides with the natural one.[6,7] However, this method is very tedious and time-consuming, because peptides with all possible disulfide pairings must be synthesized for comparison with the natural peptide. Furthermore disulfide exchange reaction may occur under the experimental conditions used.

In this paper, we report a new method for determining disulfide pairing in a peptide by synthesizing a peptide with the same sequence as that of the natural peptide but with deuterio-Cys residues and then analyzing hydrolyzates of the peptide by FAB mass spec-

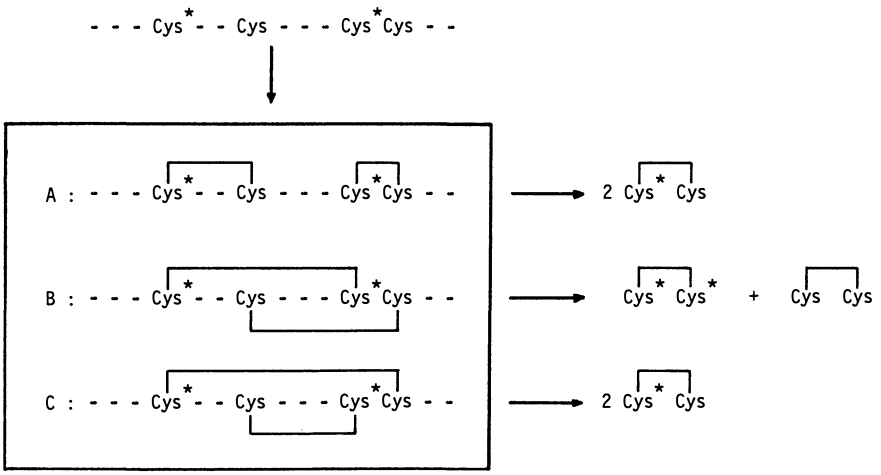

Fig. 1. Strategy for determination of disulfide pairings in a peptide.

† We dedicate this paper to Professor Haruaki Yajima on the occation of his retirerment from Kyoto University.

trometry. The application of this method to confirm the positions of disulfide bonds that were previously determined by chemical synthesis[7] in a heat-stable enterotoxin produced by enterotoxigenic *Escherichia coli*[8] is also described.

Method

The strategy of the present method is as follows: A protected peptide with deuterio-Cys residues (denoted as Cys* in this paper) at given positions is first synthesized by a solid-phase or solution method, and after removal of the protecting groups, the resulting peptide is oxidized to form intramolecular disulfide linkages between Cys residues, as shown in Fig. 1. The oxidized peptide is then purified by HPLC to isolate the fraction with the same retention time on HPLC as that of its corresponding natural or standard peptide, which has one of the possible disulfide pairings shown in Fig. 1. The purified peptide is then hydrolyzed to constituent amino acids including cystine in acidic medium. If no disulfide-exchange reaction occurs during this hydrolysis, the hydrolyzate contains one kind of cystine (Cys*,Cys) from peptide A or C and two kinds of cystines ((Cys)$_2$ and (Cys*)$_2$) from peptide B. In the case of deuterio-Cys (Cys*) in which two hydrogens are replaced by two deuteriums, the three kinds of cystines should have the theoretical mass spectra shown in Fig. 2. The hydrolyzate from peptide B, consisting of two kinds of cystines ((Cys)$_2$ and (Cys*)$_2$) should show the mass spectrum of a mixture of equal amounts of these two cystines, whereas the hydrolyzates of peptides A or C should

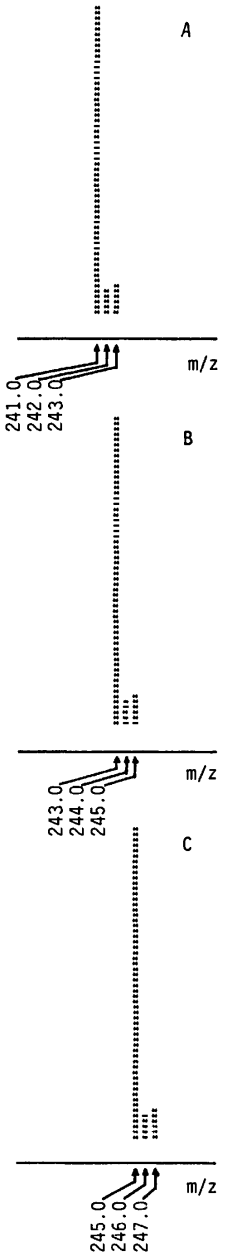

Fig. 2. Theoretical molecular ion distribution of A) (Cys)$_2$, B) (Cys*, Cys), and C) (Cys*)$_2$ (two hydrogens are replaced by two deuteriums in Cys*).

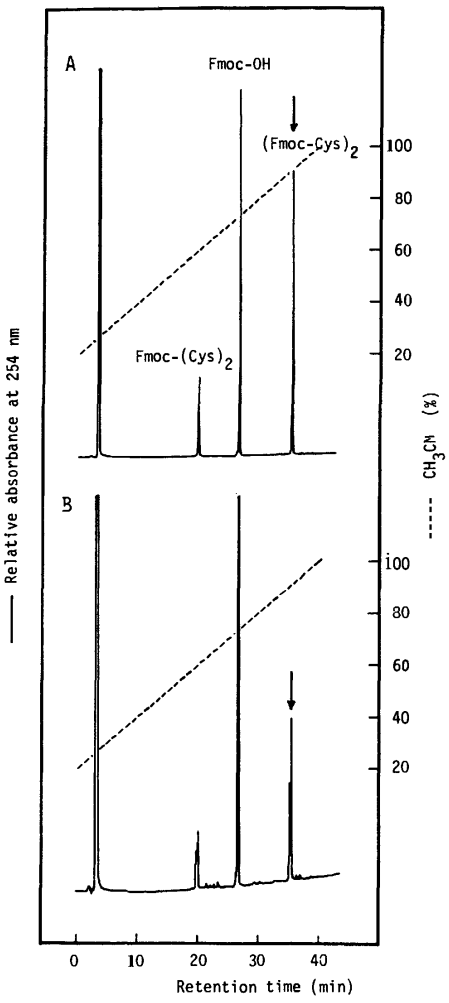

Fig. 3. HPLC profiles of the reaction products of cystine with Fmoc-Cl on a reversed-phase column (Cosmosil C_{18}) with a linear gradient of CH_3CN in 0.05% TFA with increase of 2% min^{-1} at 30 °C: A) without previous treatment and B) after treatment with 5.7 M HCl at 110 °C for 24 h.

exhibit mass spectra consisting of Cys and Cys*. Thus, if the mass spectrum of the hydrolyzate can be measured with similar accuracy to that of the theoretical mass spectrum, the types of cystine present in the hydrolyzate, and so the disulfide pairing in a peptide can be determined. This method has the characteristics that only one kind of the protecting group is used for cysteine residues and disulfide linkages are formed simultaneously after removal of the protecting group but not stepwisely, whereas intermediates with fewer numbers of disulfide linkages than those of peptides should be purified and identified in the method for determination of disulfide pairings using selectively removable protecting groups.[6,7] This theoretical treatment can be extended to complex peptides containing more cystine residues than those in Fig. 1.

Results and Discussion

Detection of Cystine by Fast Atom Bombardment (FAB) Mass Spectrometry: For this strategy, we tried to find suitable conditions for analysis of cystine in hydrolyzates of peptides by FAB mass spectrometry. First we examined a mixture of amino acids including cystine instead of an acid hydrolyzate of a peptide by FAB mass spectrometry, because we considered that direct analysis of an acid hydrolyzate of a peptide was simple and time-saving. However, we could not detect signal of cystine with a satisfactory signal to noise ratio by mass spectrometry, because the signal intensity of cystine was much smaller than those of other amino acids.[9] Consistent with these findings, the hydrophobicity indices of amino acids[10] suggest that ionization of cystine is difficult in an amino acid mixture including amino acids with hydrophobic side chains. Therefore, we tried to compensate for the hydrophilic character of cystine by adding a substituent with a hydrophobic character to it. For this we treated the amino acid mixture with Fmoc-Cl, and then examined it by FAB mass spectrometry. However, we could not detect the signal of the reaction product of cystine in the FAB mass spectrum due to the intense noise signals derived from the excess reagents. Then, we tried to isolate the reaction product of cystine ((Fmoc-Cys)$_2$) from the reaction mixture and examined it alone by FAB mass spectrometry. Fmoc-amino acids are known to be easily

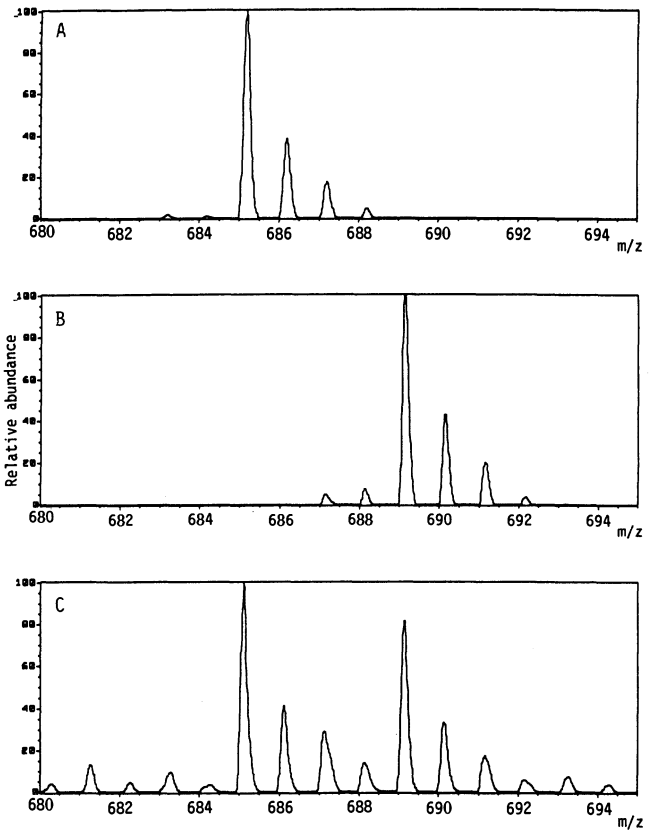

Fig. 4. FAB mass spectra in the molecular ion region of A) (Fmoc-Cys)$_2$, B) (Fmoc-Cys*)$_2$, C) a mixture of A) and B).

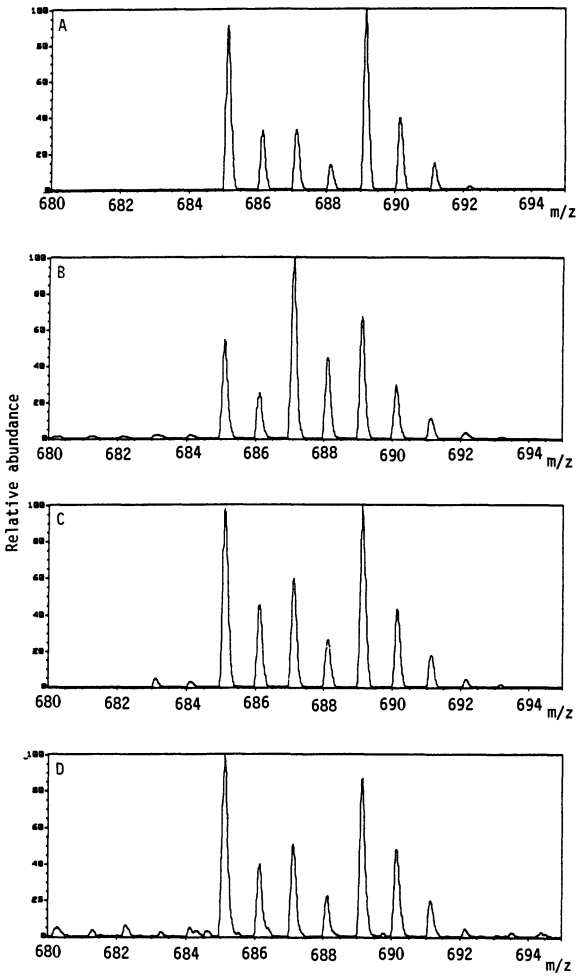

Fig. 5. FAB mass spectra in the molecular ion region of (Fmoc-Cys)$_2$ fractions separated from the reaction products of a mixture of equal amounts of cystine and cystine* with Fmoc-Cl: A) without previous treatment, and after incubation at 110 °C for 24 h in B) 5.7 HCl, C) 4M CH_3SO_3H, and D) 4M TFA.

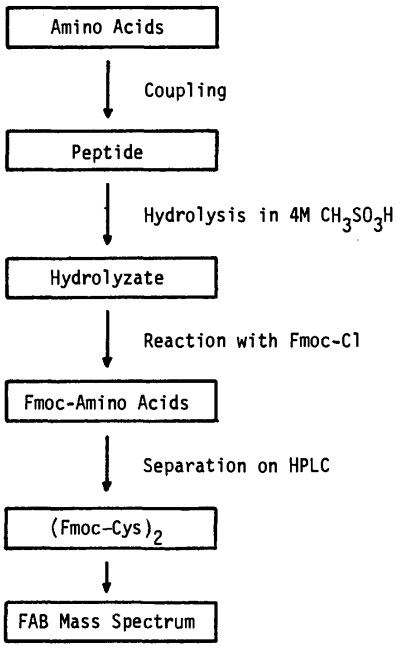

Fig. 6. Flow sheet for detection of cystine in a peptide.

separated by HPLC with a mixture of organic solvents and phosphate buffer as a mobile phase.[11] However, as solvent containing an inorganic salt is not suitable for mass measurement of amino acids and peptides,[12] we used volatile CH_3CN containing 0.05% aq TFA instead of the above mixture as a mobile phase for separation of $(Fmoc-Cys)_2$ from other Fmoc-amino acids by HPLC, as shown in Fig. 3. We found that the $(Fmoc-Cys)_2$ separated in this way could easily be detected in the FAB mass spectrum, as shown in Fig. 4A. These results indicated that cystine could be detected by FAB mass spectrometry of an acid hydrolyzate of a peptide that had been treated by the procedures as shown in Fig. 6.

Conditions for Reaction of Cystine with Fmoc-Cl: As shown in Fig. 4A, $(Fmoc-Cys)_2$ could easily be detected by FAB mass spectrometry. Then we examined the conditions for generating $(Fmoc-Cys)_2$ from cystine in satisfactory yield as a model of the reaction of the hydrolyzate of a peptide with Fmoc-Cl. The reaction was not completed at pH 6.8, but proceeded well at pH 7.8 in 1% aqueous ammonium hydrogen carbonate and $(Fmoc-Cys)_2$ was obtained mainly, as shown in Fig. 3A.

Differentiation of Cystine and Deuteriocystine by Mass Spectrometry: To determine whether cystine could be distinguished from deuteriocystine by mass spectrometry, we examined $(Fmoc-Cys)_2$ and its deuterio derivative ($(Fmoc-Cys^*)_2$), synthesized by the procedure described above, and their mixture by FAB mass spectrometry. In this experiment, we used 3,3,3′,3′-tetradeuteriocystine (denoted as cystine*), which was synthesized as a mixture of the (*S,S*)-, (*R,R*)-, and (*R,S*)-isomers by the procedure described below, as a deuteriocystine. Figures 4A—4C show the FAB mass spectra of $(Fmoc-Cys)_2$, $(Fmoc-Cys^*)_2$, and their mixture. Their mass distributions were very similar to the theoretical molecular ion distributions of these compounds (data not shown), indicating that cystine* can be distinguished from cystine and implying that (Fmoc-Cys, Fmoc-Cys*), which consists of half-cystine and half-deuteriocystine, gives signals between the mass values of Fmoc derivatives of cystine and cystine* and so can easily be distinguished from these cystines.

Conditions for Acid Hydrolysis of Peptides: Another important premise for the present approach was to find conditions for hydrolysis of a peptide without accompanying disproportionation of disulfide linkages. If a marked disulfide-exchange reaction takes place in this hydrolysis, determination of disulfide pairing in a peptide is impossible. For examination of this possibility, we used a model system in which cystine, cystine*, and their mixture were each treated under the usual conditions for acid hydrolysis of a peptide and allowed to react with Fmoc-Cl as described above. Cystine or cystine* treated with 5.7 M† HCl, 4 M CH_3SO_3H, or 4 M TFA at 110 °C for 24 h gave the same HPLC profile as that shown in Fig. 3B, in which the two peak fractions, indicated by arrows, contained $(Fmoc-Cys)_2$ and $(Fmoc-Cys^*)_2$, respectively, while the reaction product of cystine with Fmoc-Cl gave a single peak without prior acid treatment (Fig. 3A). The reason why after this treatment $(Fmoc-Cys)_2$ gave two peak fractions will be discussed later. These two peak fractions were isolated together and examined by FAB mass spectrometry. The reaction products from cystine and cystine* exhibited mass spectra with signals of monoisotope masses at m/z=685 and 689, respectively, with signals of isotope masses that were identical with those of cystine and cystine* without acid treatment, as shown in Figs. 4A and 4B, respectively.

On the other hand, when a mixture of equimolar amounts of cystine and cystine* was treated directly with Fmoc-Cl without previous acid treatment, it gave the mass spectrum shown in Fig. 5A, which was slightly different from that seen in Fig. 4C: the peak height of the ion signal at m/z=687 was slightly increased. The mass value of this ion signal was 2 amu more than that of $(Fmoc-Cys)_2$ (m/z=685) and 2 amu less than that of $(Fmoc-Cys^*)_2$ (m/z=689). This finding suggested that this ion signal was derived from (Fmoc-Cys, Fmoc-Cys*), which was formed by rearrangement of disulfide linkages of cystine and cystine* during the reaction with Fmoc-Cl and consisted of half-cystine and half-cystine*. The degree of this disulfide-exchange reaction was calculated by subtraction of the peak height of the isotope

† 1 M=1 mol dm^{-3}.

mass of (Fmoc-Cys)$_2$ at m/z=687 from the observed peak height at this mass value, as shown in Table 1.

When a mixture of equimolar amounts of cystine and cystine* was treated in 5.7 M HCl, 4 M CH_3SO_3H or 4 M TFA at 110 °C for 24 h and then with Fmoc-Cl, it showed the FAB mass spectra depicted in Figs. 5B—5D, respectively. The mass spectrum (Fig. 5B) of the mixture of cystine and cystine* treated with 5.7 M HCl differed from that seen in Fig. 5A in showing decreased intensities of the ion signals at m/z=685 and 689 and increased intensity of the ion signal at m/z=687. As most of the ion signal at m/z=687 was considered to be due to Fmoc-half-cystine and Fmoc-half-cystine* as described above, treatment of cystine with 5.7 M HCl was concluded to cause considerable rearrangement of its disulfide linkages. The degree of this disulfide-exchange reaction was estimated to be about 60% by a similar calculation to that described above (Table 1). On the contrary, treatment of the mixture of cystine and cystine* with 4 M CH_3SO_3H or 4 M TFA gave the similar mass spectra (Figs. 5C and 5D, respectively) to that without acid treatment seen in Fig. 5A. The amounts of the disulfide-exchange reaction during these treatments were estimated to be as shown in Table 1, suggesting that the disulfide pairings of cystine residues in a peptide were rearranged slightly, but not significantly, during treatment with 4 M CH_3SO_3H or 4 M TFA. The recoveries of amino acids from the hydrolyzate of a peptide with 4M CH_3SO_3H were excellent, but rather low with 4 M TFA (data not shown), indicating that the hydrolysis of a peptide with 4 M CH_3SO_3H is better than that with 4 M TFA. These results show that cystine can be recovered with slight disulfide disproportionation by hydrolysis of a peptide with 4 M CH_3SO_3H at 110 °C for 24 h, a treatment that is generally used for peptide hydrolysis.[13]

Racemization of Cystine in Acid Hydrolysis: When cystine was kept under the conditions for acid hydrolysis of a peptide and then treated with Fmoc-Cl, the reaction product gave two peak fractions, which were eluted very close to each other on HPLC, as shown in Fig. 3B, while a mixture of cystine with Fmoc-Cl gave only one peak fraction, as shown in Fig. 3A. Coelution of the reaction product (Fmoc-Cys)$_2$ in Fig. 3A with these two peak fractions indicated that the second of these two peak fractions was that of (Fmoc-Cys)$_2$. Moreover, these two peak fractions had the same molecular weight as that of (Fmoc- Cys)$_2$, as shown in Figs. 7A and 7B. These results suggested that cystine was partially racemized under the conditions for acid hydrolysis of a peptide, and that the first of these two peaks was that of the meso-isomer of cystine and that the second was that of the D- and L-isomers. This was confirmed by keeping cystine under the same conditions as those described above but in 5.7 M DCl in D_2O and then treating it with 1 M HCl to remove deuterium attached to amino and carboxyl groups. The resulting cystine gave a similar HPLC profile to that in Fig. 3B, but its mass spectrum showed increments of ion signals at mass values by 1 and 2 amu more than that of cystine at m/z=685, as shown in Fig. 7C. This finding indicates that cystine was deuterated at its α,α'-positions during incubation in acidic conditions; that is, cystine was racemized by replacement of protons on its 2,2′-carbons by deuterium from D_2O under the conditions for acid hydrolysis of a peptide. The degree of racemization was calculated to be about 40% from the mass distributions as shown in Figs. 7A and 7C.

Preparation of a Derivative of 3,3-Dideuteriocysteine for Peptide Synthesis: As described above, the protons on the 2,2′-carbons of cystine are replaced

Table 1. Interchange Reaction of the Disulfide Linkage in Cystine under Various Conditions for Acid Hydrolysis of Peptides

Acid	Reaction with Fmoc-Cl	Disulfide-exchange reaction (%)
–	+	4.8
5.7 M HCl	+	62.4
4 M CH_3SO_3H	+	14.0
4 M TFA	+	9.8

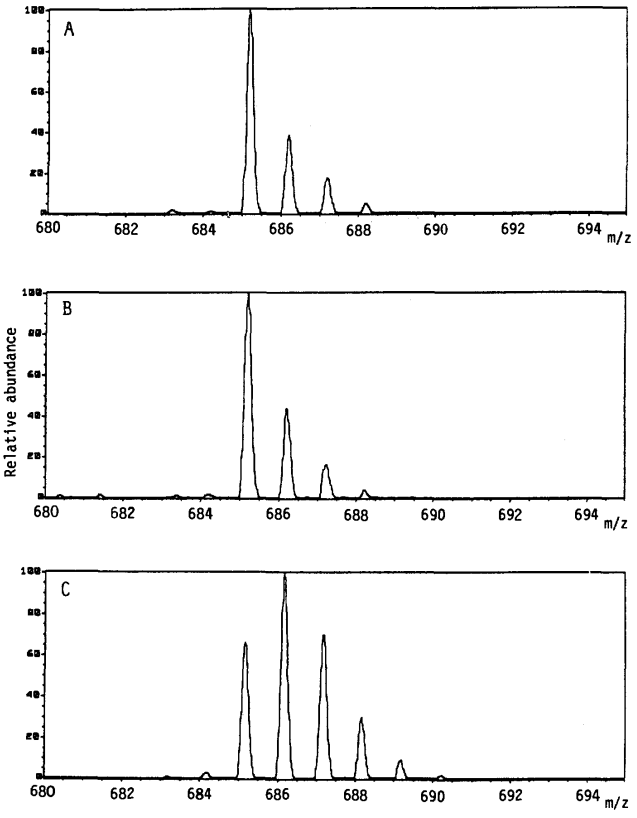

Fig. 7. FAB mass spectra: A) and B) peak fractions indicated by arrows in Figs. 3A and 3B, respectively, and C) (Fmoc-Cys)$_2$ prepared by treatment of cystine with 5.7 M DCl in D_2O at 110 °C for 24 h and with Fmoc-Cl.

by protons derived from a solvent during acid treatment, indicating that a deuteriocysteine with a deuterium substitution on its 2-carbon is not suitable for peptide synthesis by the present method. Moreover, with increase in the mass difference between cystine and deuteriocystine, differentiation of their mass spectra becomes easier. Therefore, we synthesized a cysteine derivative in which two deuteriums were incorporated at the 3,3-positions. The synthesis and use in a peptide of this compound have been reported,[14,15] but we synthesized a 3,3-dideuteriocysteine derivative, *N*-Boc-*S*-(4-methylbenzyl)-3,3-dideuterio-DL-cysteine by the scheme shown in Fig. 8, because this is a rapid and simple procedure for synthesis of this cysteine derivative. Moreover, as separation of the L-isomer from the synthetic racemic compound did not seem necessary, we used the DL-cysteine derivative for peptide synthesis, as described below.

Use of the Method to Establish the Disulfide Pairings in a Heat-Stable Enterotoxin: A heat-stable enterotoxin produced by a porcine strain of enterotoxigenic *Escherichia coli* has the amino acid sequence shown in Fig. 9.[8] The positions of the three intramolecular disulfide pairings were recently determined by chemical synthesis of the enterotoxin using selectively removable protecting groups on Cys residues.[7] To confirm the validity of the present method, we used this method to establish the positions of the disulfide linkages of the enterotoxin and compared them with those determined previously. Thus, we synthesized protected peptides with the sequence from position 5 to 17 of the enterotoxin with Cys* at two positions, which had been determined to be linked or not to be linked in the enterotoxin previously;[7] that is 5 and 10 or 6 and 14 or 5 and 14 or 9 and 17. These peptides were synthesized by a solid-phase method, oxidized by air to form intramolecular disulfide linkages after removal of the protecting groups, and purified by HPLC. The HPLC profile of the synthetic peptide with two Cys* at positions 6 and 14 is

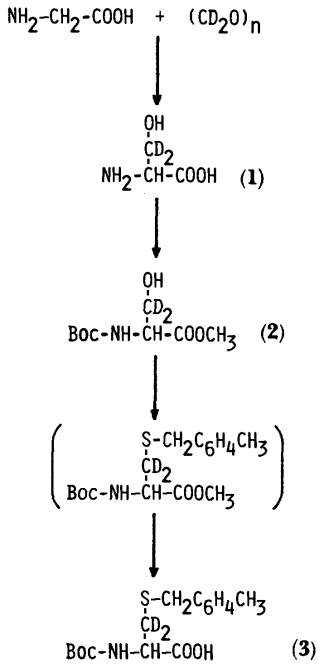

Fig. 8. Scheme for synthesis of *N*-Boc-*S*-(4-methylbenzyl)-3,3-dideuterio-DL-cysteine.

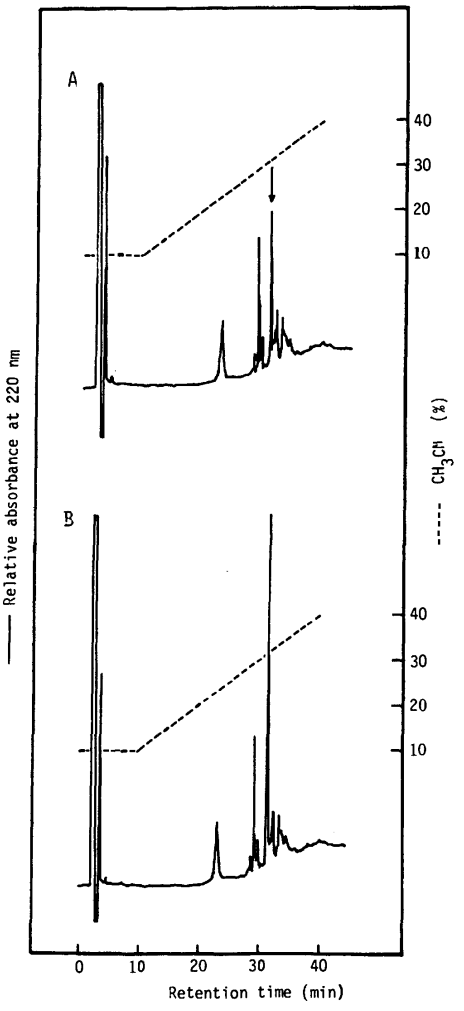

Fig. 10. HPLC profiles of A) a crude synthetic heat-stable enterotoxin with the sequence from position 5 to 17 shown in Fig. 9 and with two Cys* at positions 6 and 14 and B) a mixture of A) and a standard peptide.[16c]

1 5 10 15 18
Asn-Thr-Phe-Tyr-Cys-Cys-Glu-Leu-Cys-Cys-Asn-Pro-Ala-Cys-Ala-Gly-Cys-Tyr

Fig. 9. Amino acid sequence of a heat-stable enterotoxin (ST_P) produced by a porcine strain of enterotoxigenic *Escherichia coli*.[8]

shown in Fig. 10. The peak fraction, which had the same retention time as that of the standard peptide shown by an arrow, was isolated. The purified peptide had almost the same biological activity as that of the standard peptide. Analytical data of synthetic peptides are summarized in Table 2. The peptide with Cys* at positions 6 and 14 was hydrolyzed under the conditions described above and treated with Fmoc-Cl, and the (Fmoc-Cys)$_2$ fractions were isolated by HPLC and analyzed by FAB mass spectrometry. The mass spectrum (Fig. 11A) was similar to the theoretical mass spectrum of a mixture of (Fmoc-Cys)$_2$ and (Fmoc-Cys*)$_2$ (w/w, 2/1), as shown in Fig. 11C. The mass spectra from peptides with Cys* at positions 5 and 10, and 9 and 17 were also quite similar to that in Fig. 11A. However, the spectrum of the peptide with Cys* at positions 5 and 14 was quite different from the theoretical spectrum in Fig. 11C, but almost the same as the theoretical mass spectrum of a mixture of (Fmoc-Cys)$_2$ and (Fmoc-Cys, Fmoc-Cys*) (w/w, 1/2), as shown in Figs. 11B and 11D, respectively. These results indicated that the disulfide pairings of the enterotoxin were present between positions 5 and 10, 6 and 14, and 9 and 17, but not between positions 5 and 14. These findings were compatible with the positions of the disulfide linkages of the enterotoxin determined previously.[7] Thus it was demonstrated that this method is applicable for determination of disulfide pairings in peptides.

Table 2. Amino Acid Compositions,[a] Mass Values,[b] and Yields of Synthetic Peptides

	Cys*$_{5,10}$	Cys*$_{6,14}$	Cys*$_{9,17}$	Cys*$_{5,14}$	Theoretical value
Asp	1.01	1.04	1.38	1.22	1
Glu	1.04	0.99	1.02	1.00	1
Gly	0.99	1.02	1.02	1.07	1
Ala	2	2	2	2	2
Cys	5.50	3.79	4.57	4.18	6
Leu	0.95	0.81	0.96	0.84	1
Pro	0.97	1.05	1.09	1.04	1
$[M+H]^+$	1287.1	1286.9	1287.0	1286.7	1287.3
Yield (%)	6.0	7.5	6.9	6.9	

a) Values were calculated as mol/mol of Ala. b) $[M+H]^+$, mass value of quasi-molecular ion.

In summary, we developed a new method for determining disulfide pairings in peptides. This method involves the following procedures: i) synthesis of a peptide with the same sequence as that of the native or a standard peptide and with deuterio-Cys residues at given positions, ii) hydrolysis of the peptide in 4 M CH_3SO_3H at 110 °C for 24 h, and reaction of the hydrolyzate with Fmoc-Cl, and iii) HPLC separation and FAB mass analysis of the (Fmoc-Cys)$_2$ fraction including deuteriocystine. The method was applied to confirm the positions of the three intramolecular disulfide linkages in a heat-stable enterotoxin.

Experimental

The general and analytical methods used were as described previously.[7,16] All chemicals used for synthetic experiments were of reagent grade, while those used for analysis were of guaranteed grade. All amino acids except glycine and deuteriocysteine were of the L-configuration and Boc-amino acid derivatives were purchased from the Peptide Institute Inc. (Minoh, Osaka) unless otherwise mentioned. A reversed-phase column (Cosmosil C_{18}, 4×250 mm) was obtained from Nacalai Tesque Inc. (Kyoto). ^1H NMR spectra were recorded with a JEOL JNM-GX-400 spectrometer. Mass spectra were taken with an FAB mode on a JEOL HX-100 mass spectrometer. The abbreviations used in this paper are those recommended by the IUPAC-IUB [*J. Biol. Chem.*, **261**, 1 (1986)]. Additional abbreviations are: FAB, fast atom bombardment; Fmoc, 9-fluorenylmethoxycarbonyl; Fmoc-Cl, 9-fluorenylmethyl chloroformate; HPLC, high-performance liquid chromatography;

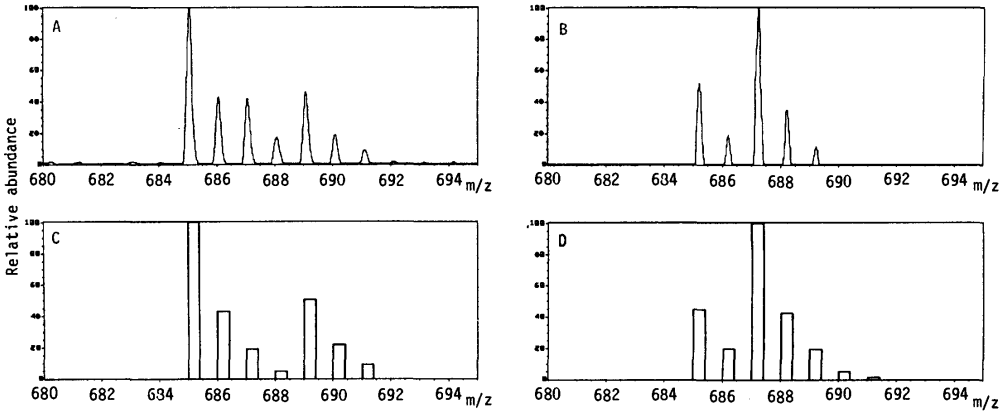

Fig. 11. A) and B), FAB mass spectra of (Fmoc-Cys,)$_2$ fractions isolated from hydrolyzates of heat-stable enterotoxin peptides with the sequence from position 5 to 17 and with two Cys* at positions 6 and 14 and 5 and 14, respectively. C) and D), theoretical molecular ion distributions of mixtures of (Fmoc-Cys)$_2$ and (Fmoc-Cys*)$_2$ (2/1) and (Fmoc-Cys)$_2$ and (Fmoc-Cys, Fmoc-Cys*) (1/2), respectively.

TFA, trifluoroacetic acid; amu, atomic mass unit.

3,3-Dideuterio-DL-serine (1). The title compound was synthesized from glycine (540 mg, 7.2 mmol) in 1 M Na_2CO_3 (30 ml), 0.2 M $CuSO_4$ (0.36 ml), and paraformaldehyde-d_2 (1.73 g, 36 mmol) by the procedure described in Ref. 17 with some modifications. Yield, 235 mg (31% based on the amount of glycine); MS m/z=108.0 (theoretical for $[M+H]^+$ 108.1); ^1H NMR (D_2O), δ=3.82 (1H, s, CH); Found: C, 33.52; H+D, 6.69; N, 13.00%. Calcd for $C_3H_5D_2NO_3$: C, 33.64; H+D, 6.59; N, 13.08%.

Boc-3,3-dideuterio-DL-Ser-OMe (2). Compound **1** (107 mg, 1 mmol) was dissolved in a mixture of dioxane and water (3 ml, v/v: 2/1), and mixed with Boc_2O (262 mg, 1.2 mmol) and triethylamine (140 μl, 1 mmol) under cooling in an ice-water bath. The mixture was stirred for 3 h at room temperature and then concentrated to a syrup under reduced pressure. The syrup was redissolved in MeOH (3 ml), treated with diazomethane, and concentrated to an oily residue under reduced pressure. The residue was dissolved in AcOEt, and washed with 0.2 M HCl, 5% aq $NaHCO_3$, and water. The washed solution was dried over Na_2SO_4 and concentrated to a syrup; 210 mg (95%); MS, m/z=222.0 (theoretical for $[M+H]^+$, 222.1); ^1H NMR ($CDCl_3$), δ=1.46 (9H, s, $(CH_3)_3C$), 3.79 (3H, s, OCH_3), 4.37 (1H, d, CH), 5.52 (1H, d, NH); Found: C, 48.38; H+D, 7.90; N, 6.17%. Calcd for $C_9H_{15}D_2O_5N$: C, 48.86; H+D, 7.74; N, 6.33%.

N-Boc-3,3-dideuterio-DL-Cys(MBzl)-OH (3). Compound **2** (800 mg, 3.6 mmol) was treated with 1.2 equiv each of Ph_3P, 4-methylphenylmethanethiol, and diethyl azodicarboxylate in dry toluene (18 ml) by the method described in Ref. 18. The reaction product was applied to a silica-gel column with ether as an eluent to remove the resulting Ph_3P=O. The eluate was concentrated to a solid under reduced pressure, redissolved in MeOH (36 ml), and saponified by mixing it with 1 M NaOH (4.3 ml). The solution was concentrated to dryness under reduced pressure, and the residue was dissolved in water (100 ml), adjusted to pH 2.0 by adding 1 M HCl, and extracted with AcOEt. The extract was washed with water, dried over anhydrous Na_2SO_4, and concentrated to a residue under reduced pressure. The residue was purified by chromatography on a silica-gel column with a mixture of $CHCl_3$, MeOH, and AcOH (v/v/v, 100/3/1) as eluent; Yield, 775 mg (66% based on the amount of compound **2**); mp 135 °C; MS, m/z=328.0 (theoretical for $[M+H]^+$ 328.1); ^1H NMR (DMSO-d_6/$CDCl_3$, v/v, 1/1), δ=1.46 (9H, s, $(CH_3)_3C$), 2.32 (3H, s, Ar-CH_3), 3.71 (2H, s, Ar-CH_2), 4.36 (1H, d, CH), 5.93 (1H, d, NH), 7.10—7.20 (4H, d,d, ArH); Found: C, 58.36; H+D, 7.20; N, 4.29; S, 9.59%. Calcd for $C_{16}H_{21}D_2O_4NS$: C, 58.69; H+D, 7.08; N, 4.28; S, 9.79%.

Synthesis of Peptides. Peptides were synthesized manually by the solid-phase method.[19,20] Briefly, Boc-Cys (MBzl)- or Boc-Cys* (MBzl)-polystyrene (2% divinylbenzene) (0.2—0.3 mmol of amino acid per 1 g of resin) was used as starting material. The γ-carboxyl group of glutamic acid was protected by Bzl. All couplings were carried out with 5-fold excess of Boc-amino acid and DCC except that of Boc-Cys*(MBzl)-OH (3 equiv). Boc-Asn-OH was coupled repeatedly twice with 2 equiv of 1-hydroxybenzotriazole. After coupling all the amino acid derivatives, peptides were liberated from the resin by treatment with anisole in anhydrous hydrogen fluoride at 0 °C for 1 h, extracted with 10% formic acid in an ice-water bath, and washed three times with hexane. The extract was diluted with water to a final peptide concentration of 5×10^{-5} M. The solution was adjusted to pH 8.0 and stood at room temperature until no free mercapto groups were detectable. The crude peptides were purified by high-performance liquid chromatography, as described below.

High-Performance Liquid Chromatography (HPLC). The synthetic peptide was purified on a reversed-phase column using a high-performance liquid chromatography system consisting of a Waters M600 multisolvent delivery system (Milford, MA) and Hitachi 655A variable wavelength UV monitor and D-2000 chromatointegrator (Tokyo). The peptide was eluted with a linear gradient of CH_3CN in 0.05% TFA or 0.01 M ammonium acetate (pH 5.7) with increase of 1% min^{-1} at a flow rate of 1 ml min^{-1}. Fractions of the eluate were monitored for absorbance at 220 nm.

Hydrolysis of Peptides. Amino acids or peptides were hydrolyzed at 110 °C for 24 h in a Waters pico-TAG™ workstation by either one of the following three methods: 1) The sample amino acid or peptide (ca. 2 nmol) was put into a vial and mixed with 5.7 M HCl (200 μl). 2) The sample (ca. 2 nmol) was put into a vial containing 4 M CH_3SO_3H (20 μl). 3) The sample (ca. 2 nmol) was put into a small test tube containing 4 M TFA (200 μl) and sealed in vacuo.

Reaction of Hydrolyzates of Peptides with Fmoc-Cl. The sample (ca. 50 nmol) was dissolved in 1% ammonium hydrogencarbonate (100 μl) at pH 7.8 and treated with 16 mM Fmoc-Cl in acetone (100 μl) at room temperature for 30 min. The solution was washed three times with hexane, insoluble materials were filtered off, and the filtrate was subjected to HPLC.

Amino Acid and Fast Atom Bombardment (FAB) Mass Spectrometric Analyses. The amino acid compositions of synthetic peptides were examined by amino acid analysis, and the molecular weights of synthetic peptides and deuteriocystine derivative were measured by FAB mass spectrometry, as described in Refs. 20 and 21, respectively.

This work was supported in part by a Grant-in-Aid from the Ministry of Education, Science and Culture (Scientific Research Grant No. 62470022). We deeply thank Drs. Tadao Harada and Hiroshi Ozaki of the Institute for Protein Research, Osaka University for helpful discussions. We are also indebted to Prof. Akira Tai (Basic Research Laboratory, Himeji Institute of Technology) for facilitating use of an NMR spectroscopy instrument, to Mrs. Aiko Kobatake for elemental analysis, and to Mrs. Aiko Kobatake and Miss Yumiko Kuhara for preparation of the manuscript.

References

1) A. P. Ryle, F. Sanger, L. F. Smith, and R. Kitai, *Biochem. J.*, **60**, 541 (1955).

2) W. R. Gray, A. Luque, B. M. Olivera, J. Barrett, and L. J. Cruz, *J. Biol. Chem.*, **256**, 4734 (1981).

3) S. Aimoto, T. Takao, Y. Shimonishi, S. Hara, T. Takeda, Y. Takeda, and T. Miwatani, *Eur. J. Biochem.*, **129**, 257 (1982).

4) R. Wetzel, *Trends in Biol. Sci.*, **12**, 478 (1987).

5) T. Takao, M. Yoshida, Y.-M. Hong, S. Aimoto, and

Y. Shimonishi, *Biomed. Mass Spectrom.*, **11**, 549 (1984).
6) Y. Nishiuchi and S. Sakakibara, *FEBS Lett.*, **148**, 260 (1982).
7) Y. Hidaka, H. Kubota, S. Yoshimura, H. Ito, Y. Takeda, and Y. Shimonishi, *Bull. Chem. Soc. Jpn.*, **61**, 1265 (1988).
8) T. Takao, T. Hitouji, S. Aimoto, Y. Shimonishi, S. Hara, T. Takeda, Y. Takeda, and T. Miwatani, *FEBS Lett.*, **152**, 1 (1983).
9) A. Wada, Y. Hidaka, T. Takao, and Y. Shimonishi, unpublished data.
10) H. B. Bell and K. Breese, *Arch. Biochem. Biophys.*, **161**, 665 (1974).
11) S. Einarsson, B. Josefsson, and S. Lagerkvist, *J. Chromatogr.*, **282**, 609 (1983).
12) S. A. Martin, C. E. Costello, and K. Biemann, *Anal. Chem.*, **54**, 2362 (1982).
13) R. J. Simpson, M. R. Neuberger, and T.-Y. Liu, *J. Biol. Chem.*, **251**, 1936 (1976).
14) D. A. Upson and V. J. Hruby, *J. Org. Chem.*, **41**, 1353 (1976).
15) H. S. Beilan, D. T. Browne, and G. L. Kenyon, *Bioorg. Chem.*, **15**, 109 (1987).
16) a) S. Yoshimura, T. Takao, H. Ikemura, S. Aimoto, Y. Shimonishi, S. Hara, T. Takeda, Y. Takeda, and T. Miwatani, *Bull. Chem. Soc. Jpn.*, **57**, 1381 (1984); b) H. Ikemura, S. Yoshimura, S. Aimoto, Y. Shimonishi, S. Hara, T. Takeda, Y. Takeda, and T. Miwatani, *Bull. Chem. Soc. Jpn.*, **57**, 2550 (1984); c) S. Yoshimura, H. Ikemura, H. Watanabe, S. Aimoto, Y. Shimonishi, S. Hara, T. Takeda, T. Miwatani, and Y. Takeda, *FEBS Lett.*, **181**, 138 (1985).
17) S. Akabori, T. T. Otani, R. Marshall, M. Winitz, and J. P. Greenstein, *Arch. Biochem. Biophys.*, **83**, 1 (1959).
18) H. Loibner and E. Zbiral, *Helv. Chim. Acta*, **59**, 2100 (1976).
19) R. B. Merrifield, *J. Am. Chem. Soc.*, **85**, 2149 (1963).
20) Y. Shimonishi, Y. Hidaka, M. Koizumi, M. Hane, S. Aimoto, T. Takeda, T. Miwatani, and Y. Takeda, *FEBS Lett.*, **215**, 165 (1987).
21) T. Takao, T. Hitouji, Y. Shimonishi, T. Tanabe, S. Inouye, and M. Inouye, *J. Biol. Chem.*, **259**, 6105 (1984).

 © 1989 The Chemical Society of Japan Bull. Chem. Soc. Jpn., 62, 1995—2001 (1995)

Synthesis of Nonadeca- and Octadecaribonucleotides Using the Solid-Phase Phosphotriester with Tetrahydropyranyl Groups as the 2′-Hydroxyl-Protecting Group

Ichiro HIRAO, Masahide ISHIKAWA, Hiroyuki HORI, Kimitsuna WATANABE,† and Kin-ichiro MIURA*
Department of Industrial Chemistry, Faculty of Engineering, The University of Tokyo, Hongo, Tokyo 113
(Received December 27, 1988)

Nonadeca- and octadecaribonucleotides corresponding to the D-loop of $tRNA^{Phe}$ from yeast and the leader sequence of phage f1 coat protein mRNA were synthesized by the activated phosphotriester method. Coupling yield in the synthesis of oligoribonucleotides depended on the extent of nucleosides loaded on controlled pore glass beads (CPG). *N*-Acyl-5′-*O*-dimethoxytrityl-2′-*O*-tetrahydropyranyl derivatives were used as fully protected ribonucleotide monomer units. The 18mer and 19mer corresponding to the D-loop did not serve as substrates for tRNA (guanosine-2′-)methyltransferase from *T. thermophilus*, but inhibited methylation of the 5′-half fragment of $tRNA^{Phe}$. This indicates that both fragments possess some affinity with the enzyme.

The synthesis of long-chain oligoribonucleotides up to about the icosamer (20mer) has recently been achieved by the solid phase approach: 19mer[1] was synthesized by the chlorophosphite method, 15mer,[2] 11mer,[3] 43mer,[4] 19mer,[5] and 13mer,[6] 77mer[7] by the phosphoramidite method, 21mer[8] and 24mer[9] by the H-phosphonate method, 13mer[10] by the triester method and 9mer[11] and 8mer[12] by the phosphoro-*p*-anisidate method. However, the phosphotriester approach though easy to conduct, is attended by various problems such as the long time required for the coupling reaction, its low yield and the occurrence of side reactions on the uracil and guanine moieties.[13] The synthesis of long-chain oligoribonucleotides (about 20mer) by the phosphotriester solid-phase method has not been reported so far.

The starting materials, 5′-*O*-dimethoxytrityl-2′-*O*-tetrahydropyranyl-*N*-acylribonucleosides[14] were prepared from 3′,5′-*O*-(tetraisopropyldisiloxane-1,3-diyl) derivatives[15] on a large scale. We previously reported the selective deprotection of the 5′-*O*-dimethoxytrityl group of oligoribonucleotides by treatment with 1% dichloroacetic acid in dichloromethane at room temperature without removal of the 2′-*O*-tetrahydropyranyl (THP) group,[16] followed by the synthesis of undecaribonucleotides (11mers)[17] on a polystyrene support using 2-chlorophenyl-*O*,*O*-bis(1-benzotriazolyl) phosphate, initially reported by van Boom et al.[18] Recently, Kierzek et al. have reported the synthesis of oligoribonucleotides by the phosphoramidite approach, using our method in combination with the THP group.[19]

However, we were unable to synthesize nonadecaribonucleotides (19mers) by this method, possibly since long-chain oligoribonucleotides were easily adsorbed on the polystyrene resin, used for the solid support, during the synthesis. We thus attempted the solid-phase synthesis using controlled pore glass (CPG), a well-known support for nucleic acids synthesis,[20] instead of a polystyrene resin. When the coupling reaction was carried out on the long-chain ω-aminoalkyl CPG resin using acetonitrile as the solvent, with a loading amount less than 20 $\mu mol\,g^{-1}$ the average coupling yields exceeded 95% during a 15 min reaction period.

In the present study, the simple solid-phase synthesis of nonadeca- and octadecaribonucleotides corresponding to the D-loop of yeast $tRNA^{Phe}$ and the leader sequence of phage f1 coat protein mRNA were carried out by the phosphotriester approach.

Results and Discussion

For preparation of guanosine or adenosine bound to the CPG resin, 5′-*O*-dimethoxytrityl-N^2-isobutyryl-2′-*O*-tetrahydropyranylguanosine **1a** or N^6-benzoyl-5′-*O*-dimethoxytrityl-2′-*O*-tetrahydropyranyladenosine **1b** was succinylated at the 3′-hydroxyl group, followed by its activation with 1-hydroxybenzotriazole and dicyclohexylcarbodiimide (DCC) applying the same procedure as that for preparing, the 2′-*O*-deoxyribonucleoside resin.[21] The activated ester of guanosine derivative was subsequently allowed to react with various CPG resins such as 3-aminopropyl (AP)-, aminoaryl (AA)-, and long-chain aminoalkyl (LCA)-CPG. Unreacted amino groups on the CPG resin were capped with a mixture of 5% acetic anhydride, 3.5% 4-dimethylaminopyridine, and 5% 2,6-lutidine in dry tetrahydrofuran or pyridine.

We first tested the effects of solvents on the condensation reaction of a AA-CPG resin covering a guanosine derivative with 3′-*O*[(1-benzotriazolyloxy)(2-chlorophenoxy)phosphinyl]-5′-*O*-dimethoxytrityl-N^2-isobutyryl-2′-*O*-tetrahydropyranylguanosine **3a**: When 1,4-dioxane, benzene, dichloromethane, or acetonitrile were used as the solvents for promoting the condensation reaction on the polystyrene resin. 1,4-Dioxane was found to be effective solvent. While in case of the CPG resin, a reaction conducted in acetonitrile, provided the highest coupling yield (data not shown).

The condensation reaction was thus carried out in

† Present address: Department of Life Chemistry, Tokyo Institute of Technology, Nagatsuta, Yokohama 227.

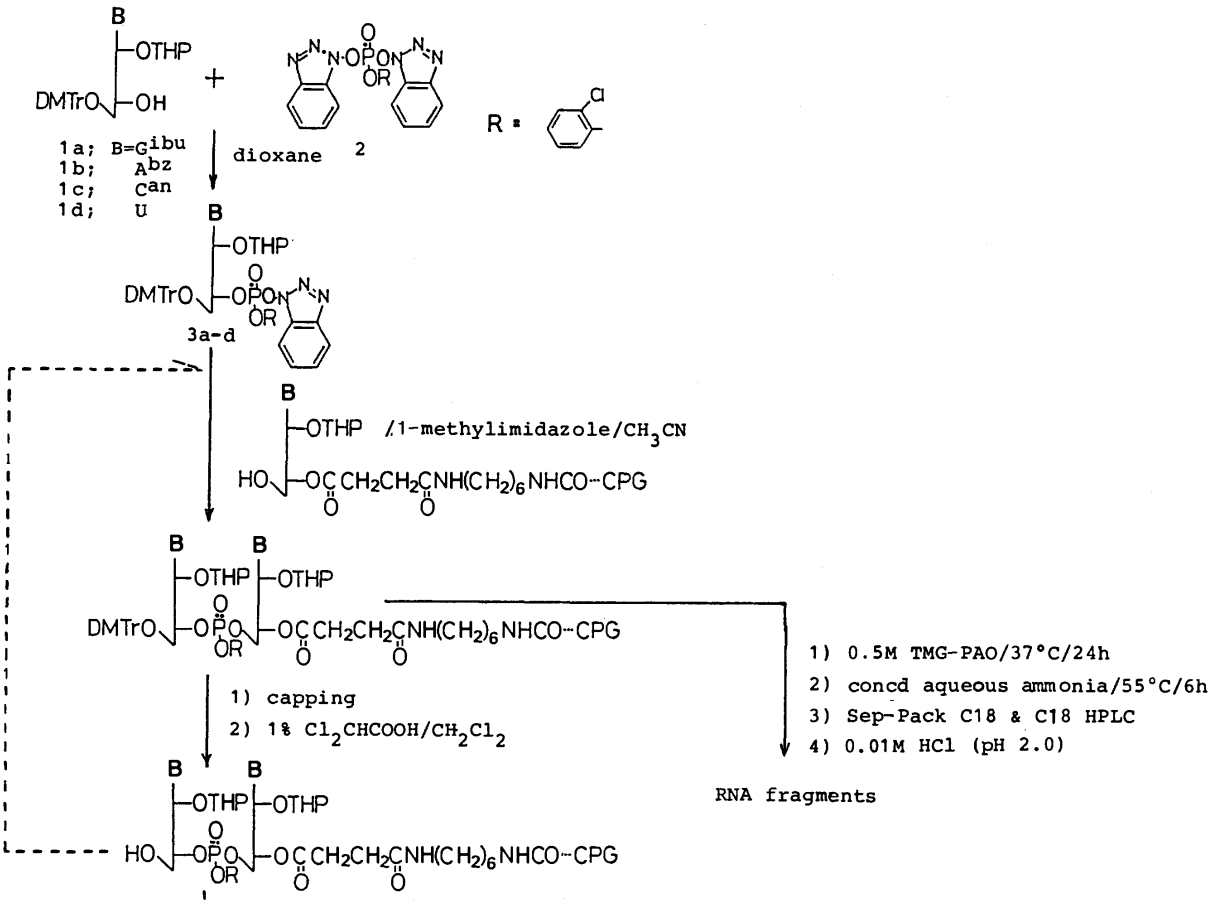

Scheme 1.

Table 1. Yields of Coupling Reactions on Various CPG-Resins

Entry	2c in CH_3CN		CPG[a]	Time	Base[b]	Coupling yield/%
	Volume/ml	Concn/mol dm^{-3}	mg	min		
1	0.5	0.1	AP (21.2)	20	1-MeIm	66
2	0.5	0.1	AA (20.0)	20	1-MeIm	51
3	0.5	0.1	LCA (80.9)	20	1-MeIm	91
4	0.4	0.125	AA (20.0)	20	1-MeIm	67
5	0.4	0.125	AA (20.0)	20	1-MeMo	52
6	0.4	0.125	LCA (50.0)	15	1-MeIm	101

a) AA, aminoaryl-; LCA, long-chain ω-aminoalkyl-; AP, 3-aminopropyl-. b) 1-MeIm, 1-methylimidazole; 1-MeMo, 1-methylmorpholine.

acetonitrile on three different CPG resins (AA, AP, and LCA) each having a guanosine derivative. To obtain the 5′-free hydroxyl group, the CPG resins were first treated with 1% dichloroacetic acid in CH_2Cl_2 for 1.5 min. N^4-Anisoyl-5′-*O*-dimethoxytrityl-2′-*O*-tetrahydropyranylcytidine **1c** (1.1 mole equiv) was phosphorylated with *O*,*O*-bis(benzotriazolyl)-phosphate **2** (1.0 mole equiv) according to the procedure reported by van Boom.[18] The condensation reaction was conducted with a ZEON Genet manual DNA synthesizer (NIPPON ZEON Co., Ltd.). The resulting N^4-anisoyl-3′-*O*-[(1-benzotriazolyloxy)(2-chlorophenoxy)phosphinyl]-5′-*O*-dimethoxytrityl-2′-*O*-tetrahydropyranylcytidine **3c** and a base catalyst were added to the CPG resin in the reaction vessel. The condensation yields were estimated on the basis of the colorimetric determination of the released dimethoxytrityl cation (Scheme 1 and Table 1).

The LCA-CPG resin (Table 1, Entries 3 and 6) was found to give a dimer in satisfactory yield and lessen the reaction time (15 min). The AA-CPG resin with the highest content of the guanosine derivative provided only a low yield of 50—70% (Table 1, Entries 2 and 5). Next, clarification was made of the relationship between coupling yield and amount of nucleoside loaded on the CPG resin. Coupling efficiency

Table 2. Yield of Each Fragment

Sequence no.	Sequence (5′—3′)	Average coupling yields/%	Yields of pure oligomers($OD_{260}U$)
RNA 1	UAGCUCAGUUGGGAGAGCG	93	0.76
RNA 2	AGCUCAGUUGGGAGAGCG	97	0.50
RNA 3	ACUGGAAACUUCCUCAUG	95	2.33
RNA 4	ACUAAAAACUUCCUCAUG	97	1.81
RNA 5	ACUCCAAACUUCCUCAUG	94	0.96
RNA 6	UAAGGAAACUUCCUCAUG	93	0.64

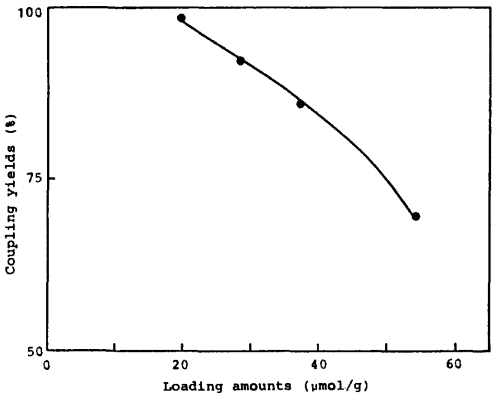

Fig. 1. Coupling yields plotted against loading amounts of the nucleoside on the LCA-CPG resin.

Table 3. Synthetic Cycle

Step	Reagent or solvent	Time/min
1	1% $Cl_2CHCOOH$-CH_2Cl_2	1.5(A,U,C) 1.0(G)
2	CH_3CN×4	3.0
3	0.26M Nucleotide-CH_3CN (0.3 ml),1-methylimidazole (0.03 ml), 30 °C	15.0
4	CH_3CN×3	2.0
5	5% $(CH_3CO)_2O$-3.5% DMAP -5% 2,6-lutidine-THF	1.0
6	CH_3CN×3	2.0

Synthesizer: ZEON Genet H-6 DNA manual synthesizer. Total time for cycle: 25—25.5 min.

was assessed using activated cytidine 3′-phosphotriester unit **3c** (0.27 M††, 0.27 ml) and LCA-CPG resins bound to the protected adenosin derivative at various loading amounts, [Weight of the LCA-CPG resin (g)=0.66 (μmol)/loading amount ($\mu mol\,g^{-1}$)], with 1-methylimidazole (0.027 ml) at 30 °C for 10 min. In Fig. 1, the coupling yield has increased with decrease in the amount of nucleoside loaded on the resin. This is possible due to steric hindrance of a nucleoside present on the CPG resin. Therefore the LCA-CPG resin derivatized with a 5′-*O*-dimethoxytrityl ribonucleoside, at a loading amount less than 20 $\mu mol\,g^{-1}$ used.

On the basis of the results obtained above, the 19mer including the D-stem and loop of yeast $tRNA^{Phe}$ and the 18mer lacking the 5′-terminal uridine in the 19mer were synthesized. Two dihydrouridine residues in the D-loop were replaced with uridine in both the 18mer and 19mer (RNA 1 and 2 in Table 2). Synthesis was made also of the sequence of the phage f1 coat protein mRNA (18mer) as well as the AUG initiation codon (RNA 3 in Table 2) and several 18mers in each of which two guanosine residues in the Shine-Dalgarno sequence[22] were replaced by different nucleosides (RNA 4—6 in Table 2).

As protected ribonucleoside monomers, N^2-isobutyrylguanosine **1a**, N^6-benzoyladenosine **1b**, N^4-anisoylcytidine **1c**, and uridine **1d**, each protected at both the 5′- and 2′-hydroxyl groups with the 4,4′-dimethoxytrityl and tetrahydropyranyl groups, respectively[14] were used. These protected ribonucleosides **1** (0.088 mmol/coupling reaction) were converted to *O*-benzotriazolyl phosphate derivatives **3** by treatment with *O*,*O*-bis(benzotriazolyl) 2-chlorophenyl phosphate **2**[18] (0.08 mmol/coupling reaction). In order to perform the reaction of **2** with **1**, a slight excess of **2** was used. By TLC-analysis of the reaction mixture, the resulting **3** was detected along with small amounts of 3′,3′-dinucleotide and remaining **1**. The trityl group of **1a** was removed by treatment with 1-hydroxybenzotriazole in acetonitrile for few hours. Following preparation of the activated ribonucleotide units as the key intermediates **3**, a small amount of pyridine was added to neutralize the resulting slightly acidic species 1-hydroxybenzotriazole and excess pyridine was evapolated off. However, this treatment caused considerable decomposition resulted from hydrolysis of **3** catalyzed by a trace amount of pyridine still remaining. Thus, for the synthesis of long-chain oligoribonucleotides, fresh ribonucleotide units **3** must be prepared within five hours.

Guanosine-bound-LCA-CPG (20—50 mg, 0.3—0.8 μmol) was detritylated by 1% dichloroacetic acid in dichloromethane at 30 °C. To the LCA-CPG resin in the reaction vessel were added **3** in acetonitrile (0.250 ml) and 1-methylimidazole (0.025 ml). The condensation was carried out for 15 min at 30 °C. Fully protected oligoribonucleotides were prepared in the same way. One cycle of the synthesis required 25 min for a coupling yield more than 90% (see Scheme 1 and Table 2). The synthesis cycle is shown in Table 3.

†† 1 M=1 mol dm^{-3}.

Following their synthesis, deprotection of the fully protected oligoribonucleotides was carried out according to the general procedure (see experimental section). 5′-*O*-DMTr-2′-*O*-THP oligomers were purified first by Sep-Pak C-18 (Waters) and then by high-performance liquid chromatography (HPLC) with a reversed-phase C-18 column (M&S Co.) (Fig 2). The eluted oligomers were treated with 0.01 M HCl (pH 2.0) to remove the 2′-*O*-tetrahydropyranyl and 5′-*O*-dimethoxytrityl groups. These crude oligomers were purified by HPLC at 55 °C or room temperature (Fig. 3), and the fractions corresponding to the main peak were collected. The HPLC profiles of the purified oligomers are shown in Fig. 3.

The purity of the oligomers was assessed by electrophoresis on a 20% polyacrylamide gel containing 7M urea, and when a single band could not be detected, purification was conducted again by polyacrylamide gel electrophoresis (Fig. 4). Yields of pure fragments are shown in Table 2. One reason for the low yields is that each fragment was partially lost through the purification process used for increasing the purity.

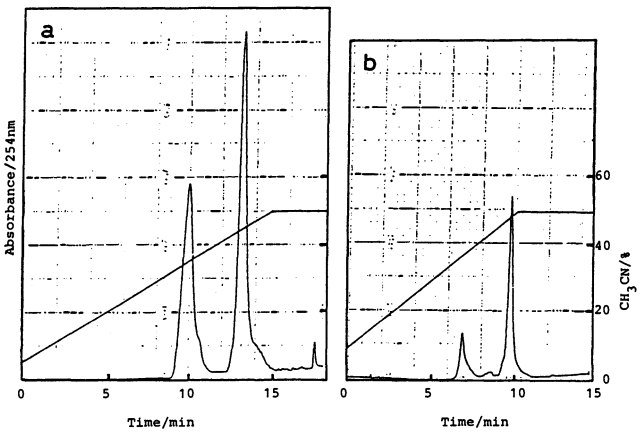

Fig. 2. Separation of 5′-*O*-dimethoxytrityl-2′-*O*-tetrahydropyranyl r-18mer (RNA 3) (a) and r-19mer (RNA 1) (b) by reversed-phase C-18 HPLC.

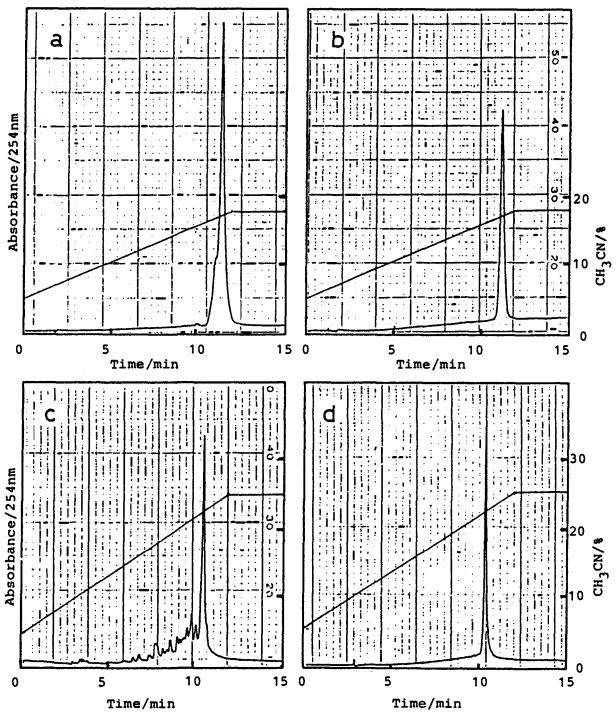

Fig. 3. Reversed-phase HPLC profiles for purification and analysis; the crude product mixture containing r-18mer (RNA 3) (a) and r-19mer (RNA 1) (c), and the elution profiles of the main peaks of RNA 3 (b) and RNA 2 (d).

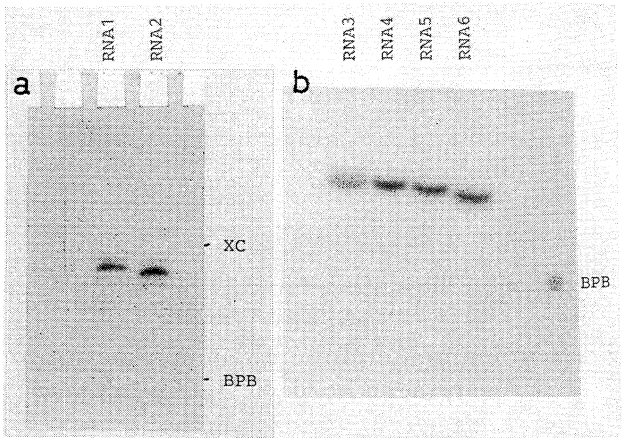

Fig. 4. 20% Polyacrylamide-7 M urea gel electrophoresis of RNA 1 and RNA 2, followed by dying with 0.02% Methylene Blue (a); ^{32}P-labeled RNA 3—6 (b).

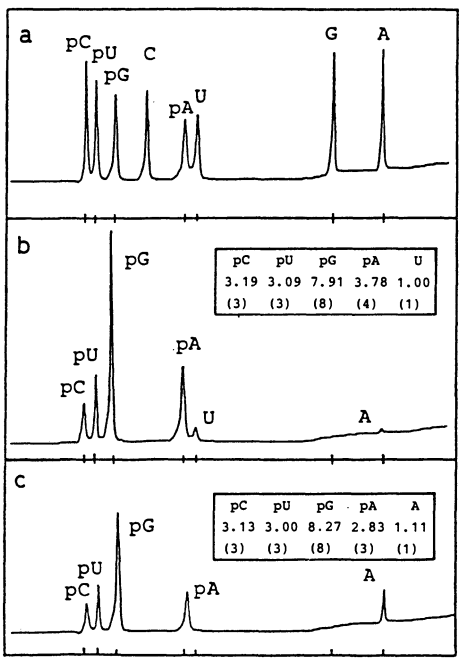

Fig. 5. Reversed-phase HPLC profiles for composition analysis of RNA 1 (b) and RNA 2 (c) both digested with nuclease P1, and authentic ribonucleosides and ribonucleotides (a). The insets show the ratios of their nucleoside and nucleotide compositions, as determined from peak area.

Base compositions were determined by enzymatic digestion using nuclease P1 (Fig. 5). It was observed that the initial digestion product, adenosine 5′-phosphate, underwent simultaneous hydrolysis to adenosine with nuclease P1 but only to a slight degree. The base sequences of the synthesized oligomers were confirmed by partial enzymatic degradation of the 5′-end-labeled oligomers in polyacrylamide gel electrophoresis (Fig. 6).

A convenient method has been presented above for the synthesis of oligoribonucleotides. Compared with the phosphoramidite or H-phosphonate method, our synthetic cycle (see Table 3) is simple owing to elimination of an oxidation step. Side reactions due to the use of 1-hydroxybenzotriazole have been reported,[23] but no other products was detected in the purified oligomers. However, the by-products shown in Figs. 3a and 3c may possibly resulted from base modification or release of the tetrahydropyranyl group; the latter was not observed in our previous paper on the synthesis of the 11mer.[17]

The synthesized 18mer and 19mer corresponding to the D-loop of yeast $tRNA^{Phe}$ (Table 2, RNA 1 and RNA 2) were examined for their ability to be methylated with tRNA (guanosine-2′)-methyltransferase (Gm-methylase) isolated from an extreme thermophile, *Thermus thermophilus* HB 27.[24-26] It has been already elucidated that the D-loop-and-stem structure of tRNA is a minimal prerequisite for recognition with Gm-methylase (Matsumoto et al., unpublished), and that s^4U8 of *E. coli* $tRNA^{fMet}$ is involved in the recognition with Gm-methylase.[27] Therefore, regarding on the substrate ability for Gm-methylase, comparison of the 18mer (RNA 2) having no 5′-terminal U corresponding to U8 of tRNA, with the 19mer (RNA 1) having the U, would be useful to confirm importance of the U residue.

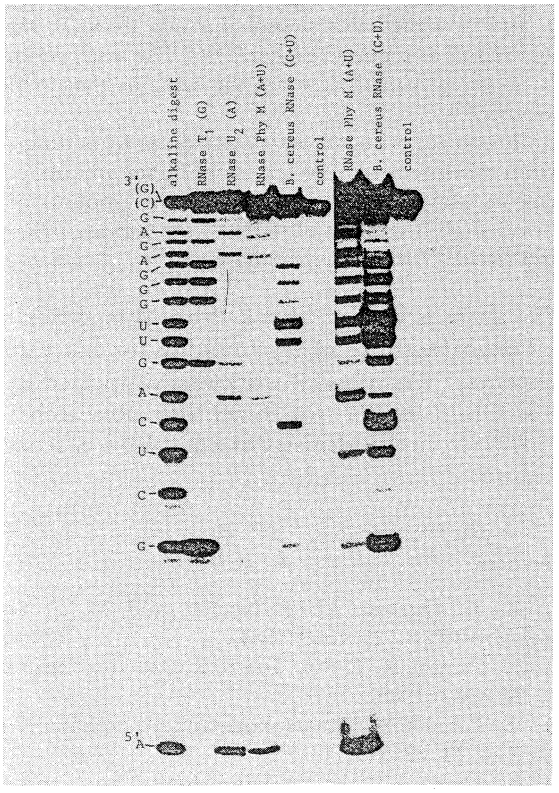

Fig. 6. Autoradiogram of electrophoresis on a 23% polyacrylamide gel containing 7 M urea for RNA sequencing. The 5′-end-^{32}P-labeled RNA 1 was partially digested with ribonucleases according to the method of Donis-Keller.[30]

Table 4. Inhibitory Effect of the Synthetic 18mer and 19mer to the Methylation of the 5′-Half Fragment of $tRNA^{Phe}$ with Gm-methylase (a) and of $tRNA^{fMet}$ with m^1-methylase (b)

	Conditions	Methylation activity/%
(a)	5′-Half fragment	100
	Plus 18mer	31±3
	Plus 19mer	43±5
(b)	$tRNA^{fMet}$	100
	Plus 18mer	95
	Plus 19mer	97

19mer, 18mer, 5′-half fragment and $tRNA^{fMet}$; 0.05 OD_{260} unit.

However, the result was negative, showing that neither 19mer nor 18mer was methylated with the enzyme, instead both fragments inhibited to a great extent methylation of the 5′-half fragment of yeast $tRNA^{Phe}$ which is known as a good substrate for the enzyme (Matsumoto et al., unpublished) as shown in Table 4. A possibility that the inhibition was caused by an impurity which may have been contaminated in the fragment preparations was avoided by the fact that both fragments did not inhibit the methylation of *E. coli* $tRNA^{fMet}$ with tRNA(1-methyladenosine)-methyltransferase (m^1A-methylase)[27] (Table 4). Therefore, it is concluded that the minimal fragment for the substrate with Gm-methylase is longer than the 19mer (RNA 1) synthesized here and it has to take a special tertiary structure which may be supported by other parts in a complete tRNA molecule. The 18mer corresponding to the leader sequence of phage f1 coat protein mRNA is now being examined for its binding efficiency to ribosomes.

Experimental

Reagents and solvents were purified and dried according to the procedure reported by van Boom et al.[8] 1-Hydroxybenzotriazole was purchased from DOJINDO and coevaporated with pyridine just before use.

HPLC was conducted by the Gilson gradient chromatography system with a C-18 column (M&S Co.) for reversed-phase HPLC and the elution buffer was a mixture of CH_3CN and 0.1 M triethylammonium acetate (pH 7.0).

RNase P1 was purchased from Seikagaku Kogyo (a product of Yamasa Co.), RNase U_2 from Sankyo Co., and

RNase T1, RNase Phy M and *B. cereus* RNase, from Pharmacia Co.

Preparation of Fully Protected Nucleosides: The 5′-*O*-dimethoxytrityl-2′-*O*-tetrahydropyranyl derivatives of N^2-isobutyrylguanosine **1a**, benzoyladenosine **1b**, N^4-anisoylcytidine **1c**, and uridine **1d** were prepared from 3′,5′-*O*-(tetraisopropyldisiloxane-1,3-diyl) derivatives according to the methods described previously.[14]

The starting material, N^2-isobutyryl-3′,5′-*O*-(tetraisopropyldisiloxane-1,3-diyl)guanosine **1a**, was synthesized as follows. To a solution of guanosine (14.2 g, 50 mmol) in an anhydrous mixture of *N*,*N*-dimethylformamide (250 ml) and pyridine (100 ml) was added 1,3-dichloro-1,1,3,3-tetraisopropyldisiloxane (18 ml). The mixture was stirred overnight at room temperature, followed by the addition of trimethylchlorosilane[28] (25 ml) and stirring for 1 h. Isobutyric anhydride (45 ml) was then added and stirring was continued for another 3 h at room temperature. The mixture thus obtained was hydrolyzed with water (60 ml) for 15 min at 0 °C, followed by treatment with aqueous ammonia (65 ml) for 15 min at 0 °C. It was concentrated under reduced pressure and the resulting residual oil was dissolved in CH_2Cl_2 (500 ml). The CH_2Cl_2 layer was followed by washing with 1 M sodium hydrogencarbonate, drying with magnesium sulfate and concentrating under reduced pressure. The residue was dissolved in a small amount of CH_2Cl_2 and precipitated into a rapidly stirred mixture of hexane (750 ml) and ethyl acetate (250 ml). The precipitate was crystallized from ethyl acetate, to give **1a** (18.4 g, 60% yield from guanosine).

Preparation of CPG Resins Carrying Nucleosides: Nucleoside-containing CPG resins were prepared according to the literatures.[21] The condensation reaction of fully protected nucleoside 3′-succinate with the CPG resin was carried out at 37 °C for 10—20 min.

Preparation of *N*-Acyl-3′-*O*-[(1-benzotriazolyloxy)(2-chlorophenoxy)phosphinyl]-5′-*O*-dimethoxytrityl-2′-*O*-tetrahydropyranylnucleoside (3): The method of van Boom[18] was applied as follows with slight modification.

To dried *N*-acyl-5′-*O*-dimethoxytrityl-2′-*O*-tetrahydropyranylnucleoside **1a**, **1b**, **1c**, or **1d** (0.088 mmol/one coupling reaction) was added a 0.2 M solution (0.4 ml) of **2** in dioxane followed by stirring at room temperature for 30 min. The solution was then evaporated, the residue dissolved in pyridine (0.1 ml) and evaporation was continued to dryness. The residue thus obtained was dissolved in acetonitrile (0.3 ml) which was used within 5 h following the synthesis of oligoribonucleotides.

Synthesis of Oligonucleotides: The fully protected nucleoside derived LCA-CPG resin (50 mg, 0.76 μmol) was introduced into a reaction vessel of the ZEON Genet DNA manual synthesizer (NIPPON ZEON Co.). The cycle for synthesis is shown in Table 3. At the time of the condensation reaction, a solution (0.4 ml) of **3** and 1-methylimidazole (0.04 ml) was added followed by shaking at 30 °C for 15 min.

Following completion of the above cycle, the resin was treated with 0.5 M 2-pyridinecarbaldehyde oxime-tetramethylguanidinium in a mixture of pyridine and water (9 : 1 v/v) (0.2 ml) at 37 °C for 24 h, filtered and then washed with a mixture of pyridine and water (9 : 1 v/v) (1 ml×3). The filtrate was evaporated, and the residue was applied on a Sep Pak C18 (Waters Associates) after treatment with concd aqueous ammonia (55 °C, 1 h) and washed successively with 10 ml of 0.1 M triethylammonium hydrogencarbonate (TEAB) and 20 ml of 15% acetonitrile in 0.1 M TEAB. The 5′-*O*-dimethoxytrityl-2′-*O*-tetrahydropyranyl oligoribonucleotide was finally eluted with 10 ml of 35% acetonitrile in 0.1 M TEAB and then this oligomer was applied on a reversed-phase C18 column (M&S Pack C18, M&S Co.). Elution was conducted with a linear gradient from 5% or 9.5% CH_3CN in 0.1 M triethylammonium acetate (TEAA, pH 7.0) to 50% CH_3CN in 0.1 M TEAA (Fig. 2). The desired product fraction was pooled and evaporated to dryness. The residue was treated with 0.01 M HCl (pH 2.0, 5 ml) at room temperature for 48 h. The solution was neutralized with dil. aqueous ammonia, washed with ethyl acetate (10 ml×5), and evaporated.

Crude oligomers were purified by a reversed-phase C-18 column. Elution was performed with a linear gradient of 5%—25% CH_3CN in 0.1 M TEAA (Fig. 3). Slightly crude oligomers were purified by 20% polyacrylamide gel electrophoresis in the usual manner.[29]

Enzyme Digestion and Nucleotide Sequencing: The above oligomers (0.1 A_{260} units) were treated with Nuclease P1 (1 μg) in 0.1 M ammonium acetate (pH 5.3) at 37 °C for 20 min. The mixtures thus produced were analyzed by HPLC on a C-18 column (elution buffer: CH_3CN-50 mM $NH_4H_2PO_4$, pH 5.2) (Fig 5).

The labeled oligomers were partially digested with RNases or alkali and sequenced by the 20—23% polyacrylamid-7M urea gel electrophoresis developed by Donis-Keller[30] for distinguishing G, A, A+U, and C+U from each other.

Preparation of Methyltransferases and the Enzyme Assay: Gm- and m^1A-methylases were purified from *T. thermophilus* HB 27 as reported earlier.[24,25] The assay conditions for Gm- or m^1A-methylase are the same as those reported previously.[25]

Inhibition experiments were carried out by adding to the reaction mixture several to ten times larger amounts of the fragments (the 18mer or 19mer) than the amounts of substrates (5′-half fragments of $tRNA^{Phe}$ for Gm-methylase and *E. coli* $tRNA^{fMet}$ for m^1A-methylase).

The authors wish to thank Prof. Mitsuo Sekine of the Tokyo Institute of Technology for his valuable comments. The present work was supported in part by a Grant-in-Aid for Scientific Research (No. 62750777) from the Ministry of Education, Science and Culture.

References

1) K. K. Ogilvie, M. J. Nemer, and M. F. Gillen, *Tetrahedron Lett.*, **25**, 1669 (1984).

2) N. Usman, R. T. Pon, and K. K. Ogilvie, *Tetrahedron Lett.*, **26**, 4567 (1985).

3) T. Tanaka, S. Tamatsukuri, and M. Ikehara, *Nucleic Acids Res.*, **14**, 6265 (1986).

4) N. Usman, K. K. Ogilvie, M.-Y. Jiang, and R. J. Cedergren, *J. Am. Chem. Soc.*, **109**, 7845 (1987).

5) T. S. Rao, C. B. Reese, H. T. Serafinowska, H. Takaku, and G. Zappia, *Tetrahedron Lett.*, **28**, 4897 (1987).

6) H. Tanimura, T. Fukazawa, M. Sekine, T. Hata, and J. William, *Tetrahedron Lett.*, **29**, 577 (1988).

7) K. K. Ogilvie, N. Usman, K. Nicoghosian, and R. J. Cedergren, *Proc. Natl. Acad. Sci. U.S.A.*, **85**, 5764 (1988).
8) P. J. Garegg, I. Lingvar, T. Regberg, J. Stawinski, and R. Strömberg, *Tetrahedron Lett.*, **27**, 4055 (1986).
9) T. Tanaka, S. Tamatsukuri, and M. Ikehara, *Nucleic Acids Res.*, **15**, 7235 (1987).
10) G. A. van der Marel, G. Wille, and J. H. van Boom, *Recl. Trav. Chim. Pays-Bas*, **101**, 241 (1982).
11) S. Iwai, M. Asaka, H. Inoue, and E. Ohtsuka, *Chem. Pharm. Bull.*, **33**, 4618 (1985).
12) T. Tanaka, K. Fujino, S. Tamatsukuri, and M. Ikehara, *Chem. Pharm. Bull.*, **34**, 4126 (1986).
13) S. S. Jones, B. Rayner, C. B. Reese, A. Ubasawa, and M. Ubasawa, *Tetrahedron*, **36**, 3075 (1980).
14) J. H. van Boom and C. T. J. Wreesmann, "Oligonucleotide Synthesis," ed by M. J. Gait, IRL Press, Oxford (1981), pp. 153—183.
15) W. T. Markiewicz, *J. Chem. Res. (S)*, **1979**, 24.
16) I. Hirao, M. Ishikawa, and K. Miura, *Nucleic Acids Res., Symp. Ser.*, **1985**, 173.
17) I. Hirao, M. Ishikawa, and K. Miura, *Chem. Lett.*, **1986**, 1929.
18) G. van der Marel, C. A. A. van Boeckel, G. Mrs Wille, and J. H. van Boom, *Tetrahedron Lett.*, **22**, 3887 (1981); J. H. Marugg, N. Piel, L. W. McLaughlin, M. Tromp, G. H. Veeneman, G. A. van der Marel, and J. H. van Boom, *Nucleic Acids Res.*, **12**, 8639 (1984); E. de Vroom, A. Fidder, C. P. Saris, G. A. van der Marel, and J. H. van Boom, *Nucleic Acids Res.*, **15**, 9933 (1987).
19) R. Kierzek, M. H. Caruthers, C. E. Longfellow, O. Swinton, D. H. Turner, and S. M. Freier, *Biochemistry*, **25**, 7840 (1986).
20) H. Köster, A. Stumpe, and A. Wolter, *Tetrahedron Lett.*, **24**, 747 (1983).
21) J. E. Marugg, N. Piel, L. W. McLaughlin, M. Tromp, G. H. Veeneman, G. A. van der Marel, and J. H. van Boom, *Nucleic Acids Res.*, **12**, 8639 (1984).
22) J. Shine and L. Dalgarno, *Proc. Natl. Acad. Sci., U.S.A.*, **71**, 1342 (1974).
23) C. B. Reese and K. H. Richards, *Tetrahedron Lett.*, **26**, 2245 (1985); E. de Vroom, A. Fidder, J. E. Marugg, G. A. van der Marel, and J. H. van Boom, *Nucleic Acids Res.*, **14**, 5885 (1986).
24) T. Kumagai, K. Watanabe, and T. Oshima, *Proc. Natl Acad Sci., U.S.A.*, **77**, 1922 (1980).
25) I. Kumagai, K. Watanabe, and T. Oshima, *J. Biol. Chem.*, **257**, 7388 (1983).
26) T. Matsumoto, T. Ohta, I. Kumagai, T. Oshima, K. Murao, T. Hasegawa, H. Ishikura, and K. Watanabe, *J. Biochem.*, **101**, 1191 (1987).
27) H. Hori, K. Watanabe, M. Saneyoshi, I Kumagai, I. Hirao, and K. Miura, *Nucleic Acids Res., Symp. Ser.*, **1986**, 175.
28) G. S. Ti, B. L. Gaffney, and R. A. Jones, *J. Am. Chem. Soc.*, **104**, 1316 (1982).
29) T. Maniatis, E. F. Fritsch, and J. Sambrook, Molecular Cloning: A Laboratory Manual, pp. 180—181, Cold Spring Harbor Laboratory, Cold Spring Harbor, NY (1982).
30) H. Donis-Keller, A. M. Maxam, and W. Gilbert, *Nucleic Acids Res.*, **4**, 2527 (1977).

High-Resolution Nuclear Magnetic Resonance Study of 6-*O*-α-D-Glucopyranosyl-α-cyclodextrin–*p*-Nitrophenol Inclusion Complex in Aqueous Solution

Yoshihiro KANDA, Yasuhiko YAMAMOTO, Yoshio INOUE,* Riichirô CHÛJÔ, and Shôichi KOBAYASHI†
Department of Biomolecular Engineering, Tokyo Institute of Technology, O-okayama 2-chome, Meguro-ku, Tokyo 152
†National Food Research Institute, Ministry of Agriculture, Forestry, and Fisheries, Kannondai, Tsukuba, Ibaraki 305
(Received December 28, 1988)

6-*O*-α-D-Glucopyranosyl-α-cyclodextrin (G_1-α-CD)–*p*-nitrophenol (pNP) inclusion complex has been characterized by high resolution ^1H and ^{13}C NMR. From ^1H NMR measurements it is concluded that G_1-α-CD forms a 1:1 inclusion complex with pNP at both pD 7 and 10, and the dissociation constants for their complexation are quite similar to those for α-CD–pNP complexation, suggesting that G_1-α-CD and α-CD have a similar ability of complexation with pNP. The geometry of G_1-α-CD–pNP complex was found to be similar to that of α-CD–pNP complex. Analysis on the NMR spectral parameters of G_1-α-CD have revealed that the asymmetric nature of G_1-α-CD molecule is enhanced by complexation with pNP.

6-*O*-α-D-Glucopyranosyl-α-cyclodextrin (G_1-α-CD), is a branched α-cyclodextrin (α-CD), produced by limited action of *Bacillus macerans* cyclodextrin glucanotransferase on waxy corn starch.[1,2] It can be isolated and purified from the other sugar by-products using procedures of Kobayashi et al.[1,2] As shown in Fig. 1, G_1-α-CD has one branching glucopyranosyl residue attached to one of glucopyranosyl residues constituting α-CD through (1→6)-α-glucosidic linkage and due to this branch G_1-α-CD is more water-soluble and more resistant to enzymic degradation than the parent α-CD.[3] It is well-documented that CDs trap various substances as guests in their cavities to form inclusion complexes in solution and because of this property CD has received a considerable attention from a variety of field.[4-6] Although it is expected that G_1-α-CD forms inclusion complexes with guest molecules in solution in a manner similar to α-CD, neither the interaction between G_1-α-CD and guest molecule nor the structure of its inclusion complexes has been characterized in detail.

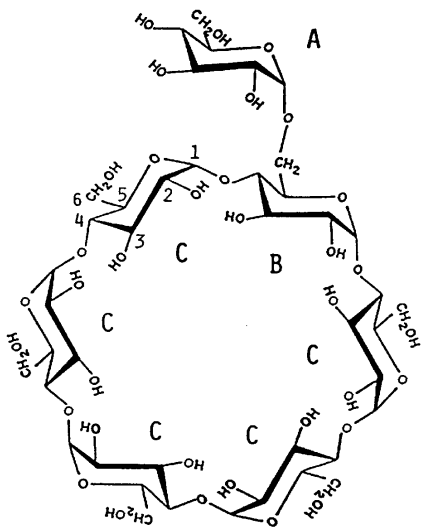

Fig. 1. The structure of G_1-α-CD. The glucopyranose residues are divided into three different groups, **A**—**C**, on the basis of ^1H NMR spectrum.

NMR spectroscopy is one of the most useful techniques for studying CD inclusion complexes in solution because of its sensitivity.[7,8] The interaction of guest molecule with CD is clearly reflected in changes on various NMR spectral parameters.[9,10] Although ^1H NMR spectra of CD derivatives exhibit severely overlapped resonances in the narrow chemical shift range of about δ 3 to 4 from Me_4Si, combined use of various modern two-dimensional NMR spectroscopic techniques can be quite effectively utilized to obtain unambiguous resonance assignments which is essential for detailed structural analysis on CD complexes by NMR.

We report herein the results of 500 MHz ^1H and 125 MHz ^{13}C NMR study of the interaction between G_1-α-CD and *p*-nitrophenol (pNP) in aqueous solution which not only reveal that pNP is indeed inserted into the cavity of G_1-α-CD in a manner similar to α-CD, but also indicate that a considerable conformational change is induced on both the macrocyclic ring structure and constituents of G_1-α-CD upon complexation with pNP.

Results and Discussion

Interpretation of the ^1H Spectra. The 500 MHz ^1H NMR spectra of G_1-α-CD and the mixture of G_1-α-CD and pNP in D_2O at pD 7.0 and 30 °C are illustrated in traces A and B of Fig. 2, respectively. G_1-α-CD exhibits severely overlapped ^1H spectrum in the chemical shift region δ 3.4 to 4.0 and two-dimensional NMR techniques were utilized to assign all the resonances in the spectra of G_1-α-CD.[11] In trace A there are three sets of independent spin net-work systems arising from three different types of glucopyranose residues, which can be assigned to **A**—**C** units illustrated in Fig. 1, respectively. Due to the presence of the C_6 symmetry axis on α-CD molecule in solution, only single set of NMR signal pattern corresponding to a gluco-

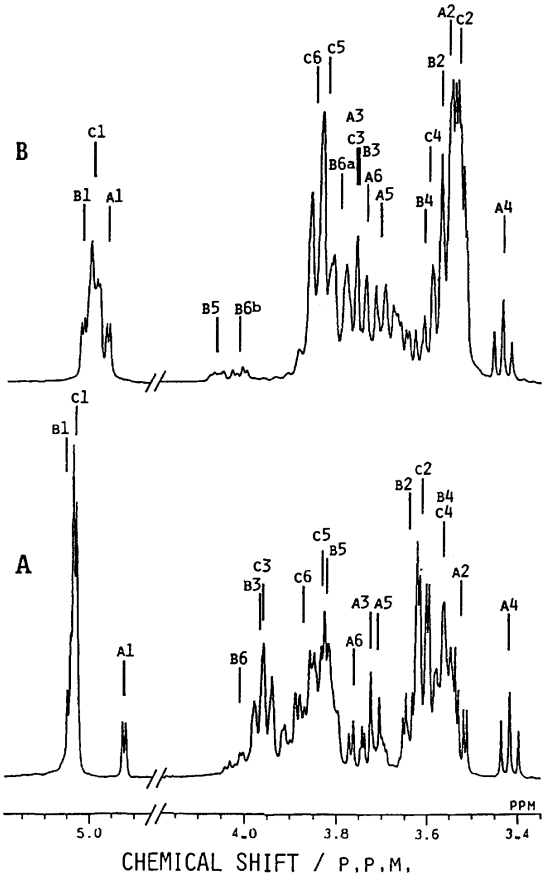

Fig. 2. 500 MHz ^{1}H NMR spectra of (A) 0.04 M G_1-α-CD, (B) 0.04 M G_1-α-CD mixed with 0.08 M pNP, in D_2O at pD 7 and 30 °C. The signals around δ 5 arise from the anomeric protons of the host.

pyranose constituent is observed.[9] Such symmetric property of α-CD is conserved even in the complexed state with pNP owing to the fast averaging of the spatial orientation of pNP with respect to α-CD, although the chemical shifts of α-CD resonances are influenced by the addition of pNP.

On the other hand, in G_1-α-CD the symmetry-breaking constituent, **A** unit, perturbs the C_6 symmetric property of the macrocyclic ring consists of **B** and **C** units, resulting in shifting the resonances of **B** unit relative to those of **C** units, but only single set of NMR signal pattern corresponding to a glucopyranose constituent is observed from **C** units. The observed ^{1}H shifts of the signals of **C** units agree very closely with those of the corresponding resonances of α-CD, suggesting that the substitution of **A** unit perturbs the electronic structure only of **B** unit and all **C** units exist in α-CD-like state.

The complexation of α-CD with pNP in solution leads to a perturbation of NMR spectra of α-CD[9,12] and the ^{1}H resonances of G_1-α-CD are also similarly and even more dramatically perturbed by addition of two-molar excess of pNP as shown in Fig. 2B. The combined use of various 2D NMR techniques (DQF COSY, C-H COSY,[11] HOHAHA,[13] ROESY[14]) makes possible to assign those resonances and their assignment are given with the spectrum in Fig. 2B. Although the resonances arising from **C** units degenerate in only single set of NMR signal pattern, that degeneracy is partially removed by the addition of pNP and the proton resonances, especially H(1) resonance, of **C** unit are split into several peaks.[10]

The resonances of the H(5), H(6a), and H(6b) protons of **B** unit overlap with other proton resonances in Fig. 2A and the individual observation of the spectral patterns of these three proton resonances is difficult. But the H(5) and one of the H(6) resonances are clearly resolved around δ 4.1 in Fig. 2B and the spectral analysis by simulation of these resonances has been carried out to obtain their coupling constants (see below).

Inclusion Complexation between G_1-α-CD and pNP. The induced chemical shift changes of the H(1) and H(3) proton resonances of **C** unit due to the pNP addition are plotted against the molar ratio of pNP to G_1-α-CD in Fig. 3, together with those of α-CD for comparison. Since the H(3) and H(5) protons are located inside the cavity, their resonances are most likely to be influenced by the guest trapped in the cavity. A large upfield shift of H(3) resonance due to the ring-current effect of pNP provides one of the most direct evidence to indicate that pNP is included into the cavity of α-CD,[12] whereas H(1) resonance is slight-

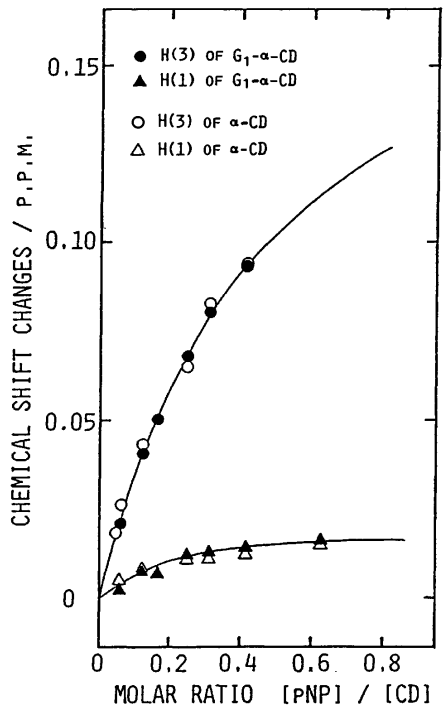

Fig. 3. Effects of *p*-nitrophenol (pNP) on the ^{1}H NMR spectra of G_1-α-CD and α-CD at pD 7 and 30 °C. The pNP-induced changes in chemical shifts of H(1) and H(3) protons of both CDs are plotted relative to the molar ratio [pNP]/[CD]. (▲, ●) G_1-α-CD system; (△, ○) α-CD system.

ly affected and their chemical shift changes are correlated with the conformational changes of the (1→4)-α-linkage and the glucopyranose ring.[10] When pNP was added to G_1-α-CD, H(3) resonances of **C** units as well as **B** unit shift toward upfield considerably due to the ring current effect of aromatic moiety of pNP and the patterns of the chemical shift changes are similar in both G_1-α-CD and α-CD systems, confirming that pNP is inserted into the cavity of G_1-α-CD as in the case of α-CD. The ^{1}H NMR resonances of pNP in free and complexed states can not be observed separately due to a fast exchange process of pNP between the two states and therefore, only single set of pNP resonances, as time-averaged signals, is observed with G_1-α-CD as in the case of α-CD (result not shown).

The chemical shift changes of ortho and meta proton resonances of pNP in aqueous solution of pD 7 are plotted against the molar ratio of G_1-α-CD to pNP and α-CD to pNP in Fig. 4. Downfield shifts are induced for both resonances by G_1-α-CD as well as by α-CD and the meta-proton resonance shifts more significantly in both host-guest systems. The curve indicates a predominant 1 : 1 complexation and the dissociation constant (K_d) of the inclusion complex can be calculated using the chemical shift changes of the meta-proton resonance induced by the host by applying a modified Benesi-Hildebrand equation.[15] Similar procedures were carried out on G_1-α-CD and α-CD-pNP complexes at 30 °C and pD 7 or 10, and the same trend in proton chemical shift changes was also observed in alkaline solution. From these shifts, the

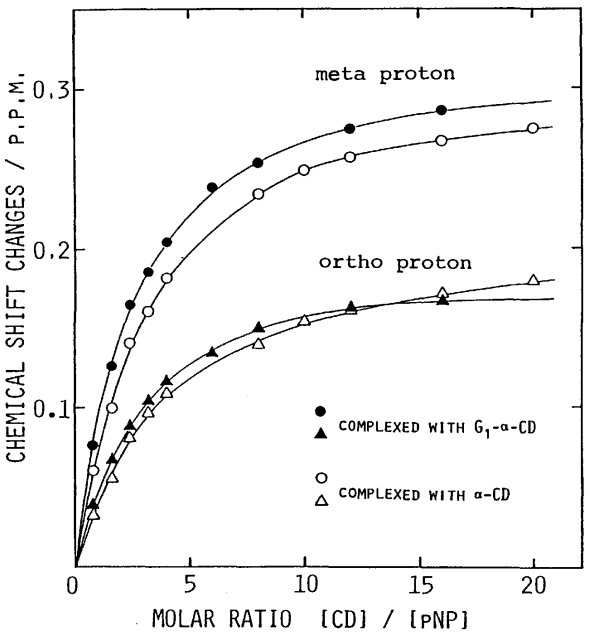

Fig. 4. Effects of G_1-α-CD and α-CD on the ^{1}H NMR spectra of *p*-nitrophenol (pNP) at pD 7 and 30 °C. The CD-induced shifts are plotted as a function of the molar ratio [CD]/[pNP], and [pNP] is constant (2.5 mM).

Table 1. Observed Changes in the Chemical Shift of the ^{1}H Resonances of G_1-α-CD and α-CD Induced by Complexation with pNP

Unit	Chemical shift[a] δ/ppm					
	H(1)	H(2)	H(3)	H(4)	H(5)	H(6)
G_1-α-CD						
A	0.04	0.02	0.03	0.02	0.02	−0.01[b]
B	−0.02	−0.05	−0.22[b]	0.04	0.24[b]	0.00, 0.19[b]
C	−0.03[b]	−0.08[b]	−0.20	0.00	−0.01	−0.03[b]
α-CD	−0.04	−0.07	−0.25	0.00	0.01	−0.04,−0.01

a) Obtained for the solution ([pNP]/[CD]=0.08 M/0.04 M) at pD 7; positive values indicate the downfield shifts. b) Rough estimates due to low resolution of resonances or peak splittings.

K_d values for complexation were estimated to be 4.6×10^{-3}M†† (G_1-α-CD-pNP) and 6.0×10^{-3}M (α-CD-pNP) at pD 7, and 5.1×10^{-4}M (G_1-α-CD-pNP) and 6.1×10^{-4}M (α-CD-pNP) at pD 10. Considering the pK_a value for pNP, the stability of the CD-pNP inclusion complex seems to depend on the ionization state of pNP, and pNP^- ion appears to be more stable than neutral pNP inside the cavity of CD.[16] The K_d values for G_1-α-CD-pNP complex at pD 7 and 10 are markedly close to those of α-CD-pNP complex at corresponding pD values, suggesting that G_1-α-CD and α-CD have a similar ability for complexation with pNP and pNP^-.

Host-Guest Geometry in G_1-α-CD-pNP Inclusion Complex. The orientation of pNP molecule insertion with respect to the cavity of CD can be deduced from the chemical shift changes induced on the resonances of pNP.[17] ^{1}H NMR NOE studies clearly indicated that pNP was preferentially inserted into the α-CD cavity from the 2,3-hydroxyl side with the nitro group first and the respective large and small downfield shifts of the meta- and ortho-proton resonances, respectively, are indicative of inclusion with this orientation.[18,19] The same trend of the chemical shift changes of pNP proton resonances was observed in both G_1-α-CD- and α-CD-pNP complexes, clearly suggesting similar insertion of pNP into the G_1-α-CD cavity as has been suggested for the α-CD-pNP complex. The observed chemical shift differences for the proton resonances of G_1-α-CD between free and complexed states (traces A and B in Fig. 2, respectively) are listed in Table 1, together with the corresponding data of α-CD-pNP complex. The resonances arising from **C** unit of G_1-α-CD are influenced by the addition of pNP like the corresponding resonances of α-CD, and it is consistent with the identical orientation of the pNP insertion in both complexes.

The insertion depth of the guest aromatic molecule into the cavity is determined by using the Johnson-Bovey theory from the chemical shift changes induced by the ring-current effect on the resonances of the H(3)

†† 1 M=1 mol dm^{-3}.

and H(5) protons. The Johnson-Bovey curves for the α-CD-pNP inclusion complex have been reported.[16] Insertion depth is defined as the distance between the center of the benzene ring of pNP and the plane comprised of six H(3) protons and the positive sign representative of the center of the benzene ring lying on the H(5) proton side with respect to the plane of H (3) protons. The depth was found to be 0.8±0.1 Å for α-CD-pNP complex. Assuming the close similarlity of the structural nature of the cavity between both hosts in complexed state, in the case of G_1-α-CD-pNP complex at pD 7 the induced shift changes of the H(3) and H(5) protons of **C** unit, δ −0.22 and −0.01 respectively, suggest that the depth is 0.7±0.2 Å. From these values, the depth of the pNP insertion into the G_1-α-CD cavity is almost the same with that into the α-CD cavity.

Conformation of G_1-α-CD in Complexed State with pNP. The degeneracy of proton resonances of **C** units is removed by complexation with pNP. As already discussed, since the H(1) protons are oriented outside of the cavity, their chemical shift changes may not be explained based on the aromatic ring current effect of pNP. The dispersion of their chemical shift values would be interpreted in terms of small differences in the conformation around the glucosidic bond among the (1→4)-α-linkages of G_1-α-CD in the complexed state with pNP because the magnetic anisotropy effect arising from the lone-pair electrons of the glucosidic oxygen is known to account for the chemical shift of the anomeric proton resonance in glucose derivatives.[20] Conformational changes are presumed to be induced to the different extent among the (1→4)-α-linkages of the macrocyclic ring, and more apparent indications of these conformational changes can be observed on ^{13}C NMR spectra (see below). In addition, the analysis of the vicinal coupling constant, J_{12}, revealed that the structural changes of the glucopyranose C_1 chair conformation of **B** and **C** units appear to be induced by the complexation to the different extent.[10]

It is interesting to investigate where the branch residue is located relative to the macrocyclic ring. The useful information on this location can be obtained from the analysis on the population of the rotamers around C(5)-C(6) bond of **B** unit. Although the spectral parameters for the H(5) and H(6) protons of **B** unit were not easily obtained in the spectrum of G_1-α-CD because of severe overlapping of resonances, two of those proton resonances are resolved in the spectrum of the complexed state with pNP. ^1H vicinal coupling constants, i.e. $^3J_{56a}$ and $^3J_{56b}$, in the spin-network of the glucopyranose residue provide the fractional rotamer populations about the C(5)-C(6) bond[21] and were accurately determined using the LAOCN spin simulation program[22] for **B** unit in the complexed state G_1-α-CD. The obtained spectral parameters are listed in Table 2. The three staggered rotamers, gg, gt, and tg (Fig.5) are considered around the C(5)-C(6) bond of **B** unilt.[23] The

Table 2. ^1H NMR Data for **B** Unit Included in G_1-α-CD Complexed with pNP

Chemical shift δ/ppm	Coupling constant $^3J_{HH}$/Hz	Rotamer population[b]/%
H(5) 4.06		P_{gg} 66 (63)
	J_{56a} 1.8	
H(6a) 3.82[a]		P_{gt} 32 (1)
	J_{56b} 4.6	
H(6b) 4.01[a]		P_{tg} 2 (35)

a) Assignment of H(6a) and H(6b) are interchangeable. The other assignment gives different rotamer populations which are designated in parentheses. b) Calculated with the following equations.[21] $1.7P_{gg}+1.9P_{gt}+11.1P_{tg}=J_{56a}$, $1.5P_{gg}+11.1P_{gt}+2.1P_{tg}=J_{56b}$, $P_{gg}+P_{gt}+P_{tg}=1$.

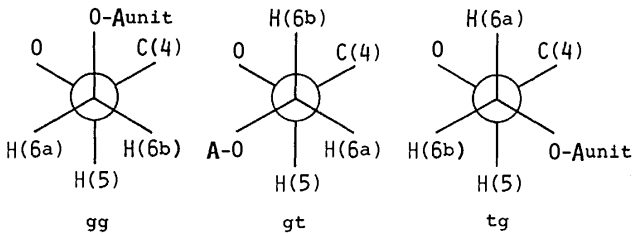

Fig. 5. Stable conformations gg, gt, and tg around C(5)-CH_2O-**A** unit group in **B** unit of G_1-α-CD.

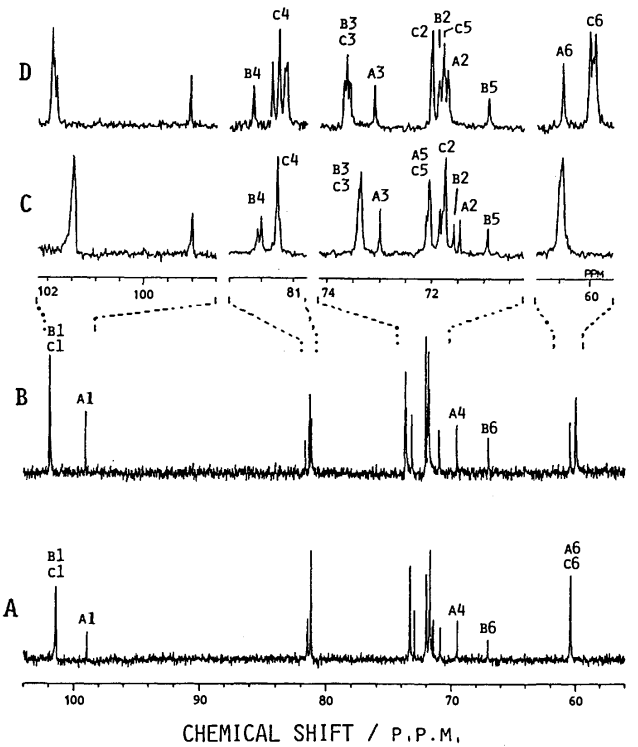

Fig. 6. 125 MHz ^{13}C NMR spectra of (A), (C) 0.04 M G_1-α-CD; (B), (D) 0.04 M G_1-α-CD mixed with 0.08 M pNP, in D_2O at pD 7 and 30 °C.

observed J_{56a} and J_{56b} are expressed with the rotamer populations p_{gg}, p_{gt}, and p_{tg} of the three rotamers by employing the equations in Ref. 21. The assignments of H(6a) and H(6b) are interchangeable, so two alternatives are obtained. In D-glucopyranose units, tg rotamer was very disfavored due to the 1,3-syn repulsion between OR(4) and OR(6).[21] Therefore the data listed in Table 2 represents the most probable rotamer populations for **B** unit. The caluculation indicated predominance of gg rotamer for the **B** unit (p_{gg}=66, p_{gt}=32, and p_{tg}=2), suggesting that the branch residue, **A** unit, is oriented away from the cavity of G_1-α-CD.

Interpretation of the ^{13}C Spectra. The 125 MHz ^{13}C NMR spectra of G_1-α-CD and its complex with two molar excess of pNP in D_2O at pD 7.0 and 30 °C are illustrated in traces A and B of Fig. 6, respectively. From the assignment of the ^1H resonances, the ^{13}C resonances can be assigned using ^1H-^{13}C COSY spectra.[10] The ^{13}C COSY contour plot of G_1-α-CD complexed with pNP, together with ^1H and ^{13}C NMR spectra, are shown in Fig. 7.

In agreement with the results of ^1H NMR, only single set of NMR signal pattern arising from **C** units is observed on ^{13}C NMR spectrum of G_1-α-CD (Fig. 6C), and the observed ^{13}C shifts of the resonances of **C** units are close to those of the corresponding resonances of α-CD (with the differences less than ±0.09 ppm).

Although C_6 symmetric property of α-CD is conserved in the complexed state as described above with the ^1H data, in the case of G_1-α-CD complexed with pNP most of ^{13}C resonances of **C** units are split into several peaks in addition to the shifts of their peaks (Fig. 6D). This indicates that the degeneracy of ^{13}C resonances from **C** units is removed by complexation with pNP, similar to their ^1H resonances, and the splitting of the C(1) and C(4) resonances of **C** units would be interpreted in terms of small differences in the electronic structure of their glucopyranose ring and the conformation of the glucosidic bond among the (1→4)-α-linkages of G_1-α-CD in the complexed state with pNP. It is partly because ^{13}C NMR chemical shifts of the anomeric and aglycone carbon atoms can be correlated with one of the glycoside tortion angles,[23] and partly because conformational distor-

Table 3. Observed Changes in the Chemical Shift of the ^{13}C Resonances of G_1-α-CD and α-CD Induced by Complexation with pNP

Unit	Chemical shift[a] δ/ppm					
	C(1)	C(2)	C(3)	C(4)	C(5)	C(6)
G_1-α-CD						
A	0.06	0.25	0.12	−0.06	n.d.[b]	0.00
B	0.45	0.29	0.28	0.13	−0.02	−0.13
C	0.45	0.26	0.28	−0.01	−0.26	−0.53
	0.41		0.32	−0.14		−0.50
	0.34		0.23	0.09		−0.44
α-CD	0.49	0.27	0.28	−0.07	−0.27	−0.54

a) Obtained for the solution ([pNP]/[CD]=0.08M/0.04 M) at pD 7: positive values indicate the downfield shift. b) Not detected.

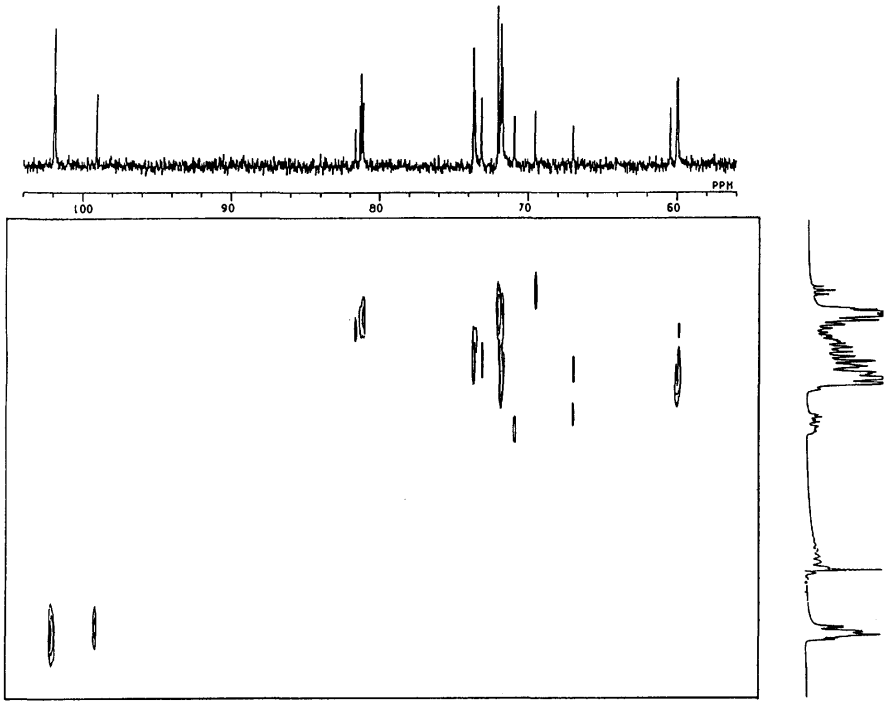

Fig. 7. ^1H-^{13}C COSY spectrum of G_1-α-CD complexed with pNP in D_2O at pD 7 and 30 °C. The ^1H and ^{13}C NMR spectra are attached along F_1 and F_2 axes, respectively.

tion of glucopyranose ring of **C** unit may occur. Due to the lack of C_6 symmetry on G_1-α-CD molecular structure, such conformational changes are not necessarily induced to the same extent among the (1→4)-α-glucosidic linkages of the macrocyclic ring. It is not possible at present to characterize the extent of conformational change of the individual (1→4)-α-linkages. The measurements of long-range C-H J resolved NMR spectra would provide the value of heteronuclear spin-spin coupling constants, $^3J_{COCH}$, which can be interpreted quantitatively in terms of dihedral angles, ϕ, ψ, of the individual(1→4)-α-linkages of G_1-α-CD.[24]

The observed ^{13}C chemical shift differences obtained from the spectra in Fig. 6 are listed in Table 3 with the related data for α-CD. The values for the resonances of **C** unit in G_1-α-CD complex are similar to those of the corresponding resonances of α-CD complex (with differences less than ±0.15 ppm), suggesting that the overall electronic structures are similar between both hosts in complexed state, but the conformational distortions might be induced to the different extent in each (1→4)-α-linkage and each **C** unit as was indicated by the analysis based on the ^1H coupling constant J_{12}. The smaller perturbation induced on the ^{13}C resonances of **A** unit than those of **C** units by the pNP addition indicates that no significant interaction between the branch residue, **A** unit, and pNP inserted into the cavity. This result consistents with those obtained from the analysis on the fractional rotamer populations which lead the conclusion that **A** unit is oriented away from the cavity of G_1-α-CD in complexed state. Although the C(1)-C(3) carbon resonances of **B** unit exhibit almost the same pattern of chemical-shift changes with those of the corresponding resonances of α-CD (with differences less than 0.04 ppm) , those of the resonances of the C(4), C(5), and C(6) carbons are different from those of α-CD (with differences 0.20 to 0.41 ppm). The latter carbons are located nearer the branch residue and the glucopyranose ring conformation of **B** unit is considered to be influenced by the movement of **A** unit. It might be assumed that the difference in the chemical shift changes between **B** unit and others was correlated with some changes of the orientation of **A** unit relative to the macrocyclic ring of G_1-α-CD, and further characterization of this difference and the conformational change is needed.

Experimental

Apparatus and Procedures. The ^1H spectra were recorded at 30 °C on either a JEOL GX-500 (500MHz) or a GX-270 (270 MHz) spectrometers, operating in the quadrature mode. The ^{13}C spectra (125 MHz) and 2D NMR specra were recorded at 30 °C on a GX-500 spectrometer. ^1H and ^{13}C chemical shifts δ are given in parts per million (ppm) downfield from that of Me_4Si with an accuracy of about 0.005 and 0.01 ppm, respectively.

The ^1H-^{13}C COSY spectrum was recorded using the pulse sequence [PD-90° (^1H)-t_1/2-180°(^{13}C)-t_1/2-D_1-90°(^1H, ^{13}C)-D_2-t_2 (with ^1H decoupling)].[25] The delay times D_1 and D_2 were set to 3.4 and 1.7 ms, respectively. A total of 128 transients was accumulated per t_1 value with a pulse delay of 1 s. The initial data matrix was 2K(^{13}C-10000 Hz)×128(^1H-3000 Hz) in the ω_2 and ω_1 dimensions, respectively, and was expanded to the final matrix size 2K×512 by zero filling. The data matrix was apodised with sine bell function and absolute value mode spectrum is presented. DQF-COSY spectra were recorded using the standard procedures.[11]

Spectrum simulations were run on an NEC PC-9801VM personal computer using a LAOCN spin-simulation program.[22]

Materials. G_1-α-CD was prepared using the procedures of Kobayashi et al.[1,2] α-CD was a generous gift from Nihon Shokuhin Kako Co., Ltd. pNP was commercial materials and was purified by high-vacuum sublimation. D_2O with isotopic purity of 99.7% was purchased from Merck Co.

^1H NMR Determination of Dissociation Constants for the Inclusion Complexes. The 270 MHz ^1H NMR spectra were recorded on a GX-270 spectrometer at 30 °C. The change in chemical shift of the pNP aromatic proton resonances was measured as a function of host to guest molar ratio. The pNP and its ionized state, p-nitrophenolate (pNP^-), were prepared in D_2O solution at pD 7.0 and 10.0, respectively. The concentrations of pNP and pNP^- were held constant at 2.5 mM each, and the concentrations of α-CD and G_1-α-CD were varied between 2—50 mM. The data were treated according to a modified Benesi-Hildebrand equation,[15] and linear least-squares analysis were performed on all data.

This work was partially supported by a Grant-in-Aid for Scientific Research from the Ministry of Education, Science and Culture (No. 62430019).

References

1) S. Kobayashi, N. Shibuya, B. M. Young, and D. French, *Carbohydr. Res.*, **26**, 215 (1984).
2) S. Kobayashi, K. Kainuma, and S. Suzuki, *Agric. Biol. Chem.*, **51**, 691 (1977).
3) S. Kobayashi, K. Maruyama, and K. Kainuma, *Denpun Kagaku*, **30**, 231 (1983).
4) W. Saenger, *Angew. Chem., Int. Ed. Engl.*, **19**, 344 (1980).
5) J. Szejtli, "Cyclodextrins and Their Inclusion Complexes," Akademiai Kiado, Budapest (1982).
6) Y. Inoue, *Kagaku(Iwanami)*, **55**, 710 (1985).
7) Y. Inoue, *JEOL NEWS*, **23A**, 36 (1987).
8) Y. Yamamoto and Y. Inoue, *J. Carbohydr. Chem.*, **8**, 29 (1989).
9) D. J. Wood, F. E. Hruska, and W. Saenger, *J. Am. Chem. Soc.*, **99**, 1735 (1977).
10) Y. Yamamoto, Y. Kanda, Y. Inoue, R. Chûjô, and S. Kobayashi, *Chem. Lett.*, **1988**, 495.
11) Y. Yamamoto, Y. Inoue, R. Chûjô, and S. Kobayashi, *Carbohydr. Res.*, **166**, 156 (1987).
12) R. J. Bergeron, M. A. Channing, G. J. Gibeily, and D. M. Pillor, *J. Am. Chem. Soc.*, **99**, 5146 (1977).
13) D. G. Davis and A. Bax, *J. Am. Chem. Soc.*, **107**, 2820

(1985).
14) A. Bax and D. G. Davis, *J. Magn. Reson.*, **63**, 207 (1985).
15) R. J. Bergeron, M. A. Channing, K. A. McGovern, and W. P. Roberts, *Bioorg. Chem.*, **8**, 263 (1979).
16) Y. Yamamoto, M. Onda, Y. Takahashi, Y. Inoue, and R. Chûjô, *Carbohydr. Res.*, **182**, 41 (1988).
17) Y. Inoue, Y. Takahashi, and R. Chûjô, *Carbohydr. Res.*, **144**, c9 (1985).
18) R. Bergeron and R. Rowan, III, *Bioorg. Chem.*, **5**, 425 (1976).
19) Y. Yamamoto, M. Onda, M. Kitagawa, Y. Inoue, and R. Chûjô, *Carbohydr. Res.*, **167**, c11 (1987).
20) B. Casu, M. Reggiani, G. G. Gallo, and A. Vigevani, *Tetrahedron*, **24**, 803 (1968).
21) D. G. Streefkerk, M. J. A. de Bie, and J. F. G. Vliegenthart, *Tetrahedron*, **29**, 833 (1973).
22) K. Satake, *Kagaku (Kyoto)*, **39**, appendix (1984).
23) K. Bock, A. Brignole, and B. B. Sigurskjord, *J. Chem. Soc., Perkin Trans. 2*, **1986**, 1171.
24) M. J. Gidley and S. M. Bociek, *J. Chem. Soc., Chem. Commun.*, **1985**, 220.
25) R. Freeman and G. A. Morris, *J. Chem. Soc., Chem. Commun.*, **1978**, 648.

No Electron-Donating Substituent Effect on the Singlet Excited State Formation from the 5-(5-Aryl-2-pyrazinylamino)-1,2,4-trioxanes in Dimethyl Sulfoxide Triggered by Potassium *t*-Butoxide

Katsunori TERANISHI and Toshio GOTO*
Laboratory of Organic Chemistry, Faculty of Agriculture, Nagoya University, Chikusa, Nagoya 464
(Received January 11, 1989)

5-(5-Phenyl-2-pyrazinylamino)-1,2,4-trioxane derivatives having a substituent on the 4 position of the phenyl group gave chemiluminescence in dimethyl sulfoxide by addition of potassium *t*-butoxide. No electron-donating substituent effect was observed on the yield of singlet excited state formation. This may be explained by the negative charge formed on the nitrogen atom next to the transient dioxetane moiety, which may produce singlet excited-state molecule by the intramolecular CIEEL mechanism.

Simple, isolable dioxetanes such as tetramethyl-1,2-dioxetane are relatively stable at room temperature and afford predominantly triplet excited-state molecules on thermolysis,[1] whereas singlet excited products were efficiently produced in the case of bioluminescent systems such as firefly and *Cypridina*[2] (Scheme 1). In the latter cases, the transient 1,2-dioxetane intermediate produced must be extremely unstable[3] so as in the case of efficiently chemiluminescent compounds. The high efficiency of singlet excited state production and the instability of the intermediate dioxetanes in bioluminescence and efficient chemiluminescence may come from the conjugation of an electron-donating (easily oxidizable) and highly fluorescent chromophore with the excited-state carbonyl group to be formed.[4]

Koo et al.[5] explained these effects in terms of the chemically initiated intramolecular electron-exchange luminescence (intramolecular CIEEL) mechanism. In the firefly case, for example (Scheme 2), electron transfer from the easily oxidizable phenoxide anion to the highly energized dioxetanone moiety to cause a heterolytic O-O bond fission followed by rapid decarboxylation with electron exchange generates an excited state product (emitter). Thus, the phenoxide anion formation would accelerate strongly the dioxetane decomposition[6] and singlet state formation.

This is further supported by the observation of Schaap and Gagnon[7] in chemiluminescence of some dioxetanes. Dioxetane **7b** having a *p*-hydroxyphenyl substituent is fairly stable at room temperature in *o*-xylene (tau 1/2 at 25 °C, 57 h), but addition of *t*-BuOK/18-crown-6 dramatically accelerates the rate of decomposition (4.4×10^6 times) of **7b** with produc-

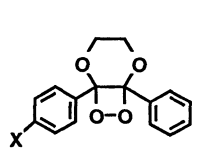

(7a) X=H
(7b) X=OH

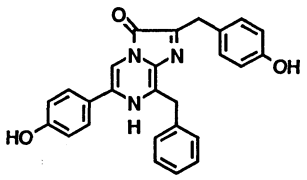

(8)

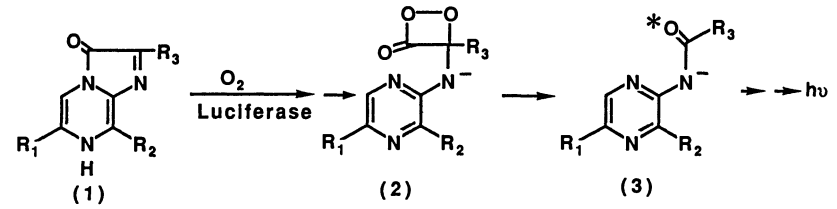

(1)
R_1=3-Indolyl
R_2=$CH_2CH_2CH_2NHC(NH)NH_2$
R_3=2-methylpropyl

(2) (3)

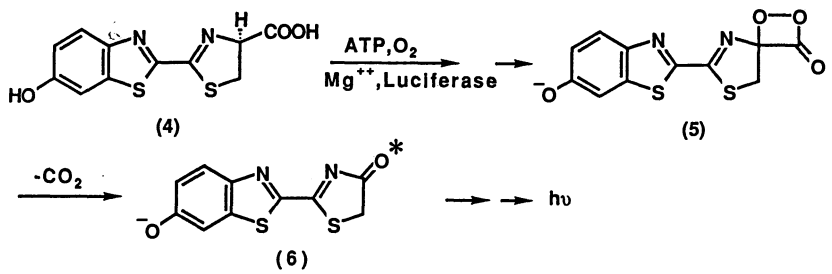

(4) (5)

(6)

Scheme 1. Mechanism of *Cypridina* and firefly bioluminescence.

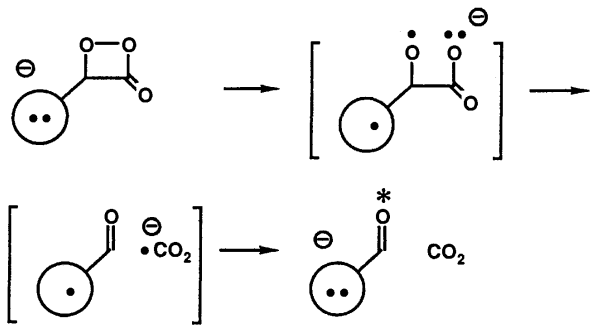

Scheme 2. Schematic presentation of intramolecular CIEEL mechanism.

tion of singlet excited molecules ca. 160 times more than that formed from the neutral molecules. An amino group also has a strongly electron-donating ability and hence is expected to have the effect similar to $-O^-$.[4,8-10]

Coelenterazine (*Oplophorus* luciferin) (**8**)[2] which is a luminescent chromophore of a photoprotein, aequorin, has a *p*-hydroxyphenyl substituent on the 3,7-dihydroimidazo[1,2-*a*]pyrazin-3-one chromophore, which is transformed to a dioxetane intermediate during bioluminescent oxidation (see Scheme 1). Shimomura et al.[11] previously suggested that the phenolic hydroxyl group must be dissociated in the photoprotein. It might indicate that the phenoxide anion, as in the firefly luciferin case, contributes to the quantum yield of singlet excited state formation, but very recently Shimomura et al.[12] also suggested that such an anion formation in aequorin would not be important. To see whether this dissociation of the phenolic hydroxyl group is necessary or not to produce a high-quantum-yield luminescence similar to the case of firefly bioluminescence, we have examined the trioxane **9e** in comparison with those having other substituents, since such the trioxanes **9** have been found to give strong chemiluminescence with base[13,14] and are regarded as a luminescent system similar to coelenterazine (**8**) and *Cypridina* luciferin (**1**) (Scheme 3).[15]

As shown in Table 1, the *p*-hydroxyphenyl-substituted trioxane **9e** gave a slightly higher chemiluminescence quantum yield than the phenyl or methoxyphenyl trioxane, **9a** or **9c**, but quantum yield of singlet excited-state molecules was rather decreased since the fluorescence quantum yield of the product **10e** was better than that of others. In this case the phenolic hydroxyl group was dissociated to form phenoxide anion, which has almost no effect on the formation of the singlet excited molecule. 4-Dimethylaminophenyl and 3-indolyl derivatives, **9f** and **9g**, behave

Table 1. Chemiluminescence Properties of the Trioxanes in DMSO Containing *t*-BuOK

Compound	$\phi_{CL}\times10^2$	$\phi_F\times10^2$	$\phi_S^*\times10^2$	λ_{max}/nm	Reference
9a	0.10	15	0.67	450	16
9b	0.049	8.1	0.60	465	16
9c	0.14	21	0.67	454	16
9d	0.13	20	0.65	454	16
9e	0.21	63	0.33	545	This work
9f	0.13	50	0.26	471	This work
9g	0.22	52	0.42	545	16

ϕ_{CL}=quantum efficiency of chemiluminescence. ϕ_F=quantum efficiency of fluorescence of the corresponding amide anion **10**. ϕ_S^*=quantum efficiency of excited singlet state formation calculated from an equation $\phi_{CL}=\phi_S^*\times\phi_F$.

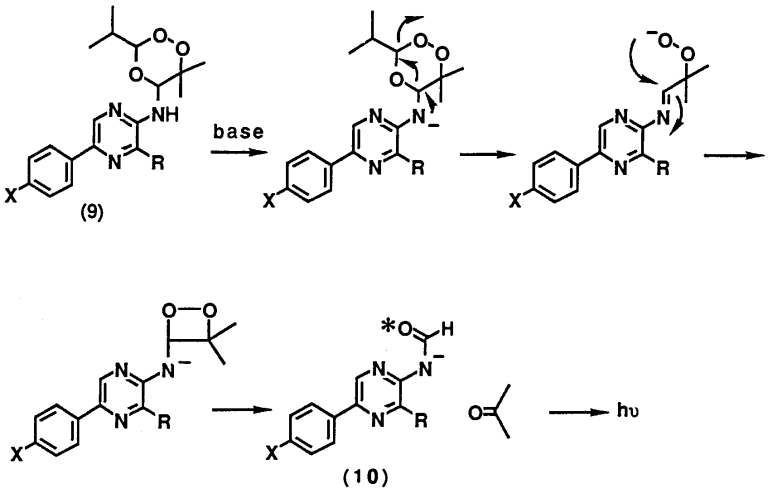

(9a) X=R=H
(9b) X=Br R=H
(9c) X=CH_3O R=H
(9d) X=CH_3O R=benzyl
(9e) X=OH R=benzyl
(9f) X=NMe_2 R=benzyl

Scheme 3. Chemiluminescence reaction of the 5-amino-1,2,4-trioxanes.

similarly. The difference in the behavior between the Schaap's compound **7** and the present case may be explained as follows. In the present case, cyclization of the intermediate hydroperoxide anion forms the dioxetane having a negative charge on the nitrogen atom next to the dioxetane moiety. The negative charge donates enough electrons to the dioxetane moiety to produce singlet excited state molecule **10** so

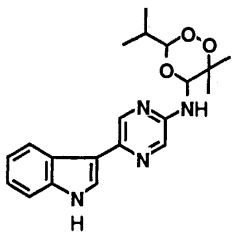

(9g)

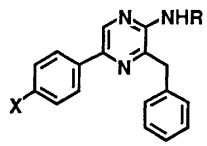

(10e) R=CHO X=OH
(10f) R=CHO X=NMe_2
(11e) R=H X=OH
(11f) R=H X=NMe_2

that no other electron-donating moiety would be necessary. On the other hand, firefly luciferin (**4**) and the Schaap's compound **7a** without a phenoxide anion on the molecule have insufficient electrton-donating ability to the intermediate dioxetane moiety so that only triplet state produces predominantly. Thus, ionization of the phenolic hydroxyl group in the firefly luciferin (**4**) and **7b** dramatically changes the yield of singlet excited state molecules, whereas no such a change is observed in the present case. This explanation may also be extended to the luminescence of *Cypridina* luciferin (**1**), since the initially produced excited molecule was proven to be anion of the oxyluciferin (**3**).[16]

Experimental

All melting points were measured on a Mitamura Riken mp aparatus and uncorrected. ^{1}H NMR spectra were recorded on a JNM-FX200 spectrometer. Chemical shifts are given in ppm from internal TMS and coupling constants in Hz. IR spectra were taken on a JASCO IR-700 infrared spectrometer. UV spectra were obtained on a Hitachi 228 spectrometer. Mass spectra were measured on a JEOL JMS-DX300 instrument. Chemiluminescence and fluorescence spectra were recorded on an Otsuka Electronics MCPD-110A and JASCO FP-770 spectrometers, respectively. Dimethyl sulfoxide was distilled from calcium hydride under reduced pressure. The other solvents were of reagent grade.

5-(4-Dimethylaminophenyl)-3-benzyl-2-aminopyrazine (11f): To a solution of *p*-dimethylaminophenylglyoxal oxime[17] (3.0 g) and 2-amino-3-phenylpropionitrile (3.0 g) in pyridine (50 ml) was added $TiCl_4$ (2.0 ml) dropwise under argon at 0 °C. After being allowed to stand for 10 min, the mixture was heated at 50 °C for 30 min. To this reaction mixture was added slowly 10% aq $NaHCO_3$ at 0 °C to neutralize it and the resulting mixture was filtered through Celite bed. The filtrate was diluted with water and extracted three times with ethyl acetate. The organic layer was washed with water and sat. NaCl solution, dried over anhydrous Na_2SO_4, and evaporated to dryness. The residue was crystallized from ethyl acetate to give the *N*-oxide of **11f** (2.8 g). The *N*-oxide was dissolved in MeOH (100 ml) and CH_2Cl_2 (20 ml) and reduced with Raney Ni (W2) at 50 °C under hydrogen atmosphere for 5 h with stirring, and the mixture was filtered. The filtrate was concentrated to a small volume and diluted with diethyl ether to give the aminopyrazine **11f** (2.5 g, 52%); slightly brownish needles (from methanol), mp 175—176 °C; IR (KBr) cm^{-1} 3478, 3294, 3134, 1610, 1463; UV (MeOH) λ_{max}/nm (ε) 304 (24800), 366 (10500); MS *m/z* 304 (M^+); ^{1}H NMR ($CDCl_3$) δ (*J*) 3.00 (6H, s), 4.30 (2H, s), 4.40 (2H, br. s), 6.80 (2H, d, 9.0), 7.30 (5H, s), 7.84 (2H, d, 9.0), 8.30 (1H, s). Calcd for $C_{19}H_{20}N_4$: C, 74.97; H, 6.62; N, 18.41%. Found: C, 75.00; H, 6.70; N, 18.63%.

5-[5-(4-Dimethylaminophenyl)-3-benzyl-2-pyrazinylamino]-3-isopropyl-6,6-dimethyl-1,2,4-trioxane (9f): A solution of the aminopyrazine **11f** (400 mg) and isobutyraldehyde (5.0 ml) in hexane (10 ml) was heated at 90 °C for 3 h and then stirred at 20 °C for 3 days with a $CaCl_2$ tube. The mixture was poured in 5% aq $NaHCO_3$ and extracted twice with ethyl acetate. The organic layer was dried over anhydrous Na_2SO_4 and evaporated. The residue was chromatographed on a silica-gel column with ethyl acetate–hexane (1 : 20) to give a mixture of two diastereomers of **9f** (350 mg, 58%), which was crystallized from hexane. Recrystallizations of the mixture from hexane gave a main isomer of **9f** as slightly brownish needles, mp 129—130 °C; IR (KBr) cm^{-1} 1611, 1499; UV (MeOH) λ_{max}/nm (ε) 306 (23900), 362 (12700); MS *m/z* 462 (M^+); ^{1}H NMR ($CDCl_3$) δ (*J*) 0.80 (3H, s), 0.90 (3H, d, 7), 0.91 (3H, s, 7), 1.12 (3H, s) 1.79 (1H, m), 3.00 (6H, s), 4.13 (1H, d, 16), 4.30 (1H, d, 16), 4.42 (1H, br. d, 10), 5.12 (1H, d, 5.0), 5.58 (1H, d, 10), 6.84 (2H, br. d, 9.0), 7.25 (5H, m), 7.86 (2H, d, 9.0), 8.40 (1H, s). Calcd for $C_{27}N_{34}O_3N_4$: C, 70.10; H, 7.41; N, 12.11%. Found: C, 70.23; H, 7.46; N, 12.39%.

5-[5-(4-Hydroxyphenyl)-3-benzyl-2-pyrazinylamino]-3-isopropyl-6,6-dimethyl-1,2,4-trioxane (9e): The trioxane **9e** was prepared from the aminopyrazine **11e**[18] (170 mg), isobutyraldehyde (5.0 ml) and hexane (20 ml) according to the procedure described in the preparation of **9f**. After chromatography was obtained **9e** (180 mg, 70%) as a 4 : 1 mixture of diastereomers; slightly yellowish amorphous solid (from ether–hexane); mp 65—67 °C; IR (KBr) cm^{-1} 3430, 1498; UV (MeOH) λ_{max}/ nm (ε) 280 (22200), 346 (10500); MS *m/z* 435 (M^+). Calcd for $C_{25}N_{29}O_4N_3$: C, 68.94; N, 6.71; N, 9.65%. Found: C, 68.89; N, 6.84; N, 9.58%. ^{1}H NMR ($CDCl_3$) δ (*J*): **major isomer** (20 °C) 0.80 (3H, s), 0.90 (6H, d, 6.8), 1.12 (3H, s), 1.75 (1H, m), 4.14 (1H, d, 16), 4.30 (1H, d, 16), 4.50 (1H, d, 10), 5.12 (1H, d, 4.5), 5.58 (1H, d, 10), 5.80 (1H, br. s), 6.90 (2H, d, 8.7), 7.20—7.40 (5H, m), 7.80 (2H, d, 8.7), 8.38 (1H, s); **minor isomer** (60 °C) : 0.77 (3H, d, 7), 0.78 (3H, d, 7), 0.90 (3H, s),1.60 (3H, s) 1.7 (1H, m), 4.14 (1H, d, 15), 4.29 (1H, d, 15), 4.40, (1H, d, 5.0) 5.42 (1H, d, 9.0), 5.58 (1H, d, 9.0), 6.90 (2H, d, 9.0), 7.4 (5H, m), 7.86 (2H, d, 9.0), 8.41 (1H, s).

5-(4-Dimethylaminophenyl)-3-benzyl-2-(formylamino)-pyrazine (10f): To a solution of the aminopyrazine **11f** (50 mg) in pyridine (0.8 ml) was added acetic formic anhydride (0.2 ml) dropwise at 0 °C. After being stirred further 2 h, the mixture was evaporated to dryness to give the amide **10f**

(45 mg) as yellow needles from methanol; mp 200—202 °C; IR (KBr) 1681 cm^{-1}; UV (MeOH) λ_{max}/nm (ε) 328 (996), 370 (11400); MS m/z 332 (M^+); ^1H NMR ($CDCl_3$-CD_3OD, 80 °C) δ (*J*) 3.00 (6H, s), 4.24 (2H, s), 6.80 (2H, d, 9.5), 7.25 (5H, s), 7.87 (2H, d, 9.5), 8.50 (1H, s), 9.04 (1H, br.s). Calcd for $C_{20}N_{20}ON_4$: C, 72.27; N, 6.07; N, 16.86%. Found: C, 72.23; N, 6.05; N, 17.03%.

5-(4-Hydroxyphenyl)-3-benzyl-2-formylaminopyrazine (10e): To a solution of the aminopyrazine **11e** (50 mg) in pyridine (0.8 ml) was added acetic formic anhydride (0.2 ml) at 0 °C. After being stirred further 2 h, the reaction mixture was evaporated to dryness and the residue purified by silica gel TLC to give **10e** (20 mg, 36%) as colorless needles from methanol; mp 208—210 °C; IR (KBr) cm^{-1} 3368, 1674; UV (MeOH) λ_{max}/nm (ε) 277 (18000), 294 (15800), 341 (15600); MS m/z 305 (M^+); ^1H NMR ($CDCl_3$-acetone-d_6) δ (*J*) 4.30 (2H, s), 6.96 (2H, d, 8.0), 7.28 (5H, s), 7.88 (2H, d, 8.0), 8.20 (1H, br.d, disappeared with D_2O), 8.30 (1H, s, diappeared with D_2O), 8.52 (1H, s), 9.3 (1H, br.s). Calcd for $C_{18}N_{15}O_2N_3$: C, 70.80; H, 4.95; N, 13.76%. Found: C, 70.83; H, 4.95; N, 13.95%.

Chemiluminescence and Fluorescence Measurements. To a solution of a trioxane (concn 1×10^{-5} mol l^{-1}) in dimethyl sulfoxide (2 ml) was added a solution of *t*-BuOK (0.25 mol l^{-1}) in *t*-BuOH (0.1 ml) at 25 °C. The resulting light emission was recorded with a luminometer. Quantum yields of chemiluminescence and fluorescence were determined as described previously.[4]

This work was supported by a Grant-in-Aid for Special Project Research of the Ministry of Education, Science and Culture, to which our thanks are due.

References

1) W. H. Richardson, J. H. Anderegg, M. E. Price, and R. Crawford, *J. Org. Chem.*, **43**, 4045 (1978) and references cited therein.

2) (Review) T. Goto, "Marine Natural Products," ed by P. Scheuer, Academic Press, Inc., New York (1980), pp. 179—222.

3) J. E. Lloyd, "Bioluminescence in Action," ed by P. J. Herring, Academic Press, New York (1978), p. 264.

4) T. Goto and H. Nakamura, *J. Chem. Soc., Chem. Commun.*, **1978**, 781; H. Nakamura and T. Goto, *Photochem. Photobiol.*, **30**, 27 (1979).

5) J.-Y. Koo, S. P. Schmidt, and G. B. Schuster, *Proc. Natl. Acad. Sci., USA*, **75**, 30 (1978); J.-Y. Koo and G. B. Schuster, *J. Am. Chem. Soc.*, **99**, 5403 (1977). See also F. McCapra, *J. Chem. Soc., Chem. Commun.*, **1977**, 946.

6) E. H. White, H. Worther, H. H. Seliger, and W. D. McElroy, *J. Am. Chem. Soc.*, **88**, 2015 (1966).

7) A. P. Schaap and S. D. Gagnon, *J. Am. Chem. Soc.*, **104**, 3504 (1982); see also A. P. Schaap, S. D. Gagnon, and K. A. Zaklika, *Tetrahedron Lett.*, **23**, 2943 (1982); K. A. Zaklika, T. Kissel, A. L. Thayer, P. A. Burns, and A. P. Schaap, *Photochem. Photobiol.*, **30**, 35 (1979).

8) C. Lee and L. A. Singer, *J. Am. Chem. Soc.*, **102**, 3823 (1980); K. A. Zaklika, A. L. Thayer, and A. P. Schaap, *ibid.*, **100**, 4916 (1978).

9) E. H. White, H. Worther, G. F. Field, and W. D. McElroy, *J. Org. Chem.*, **30**, 2344 (1965).

10) K. A. Zaklika, T. Kissel, A. L. Thayer, P. A. Burns, and A. P. Schaap, *Photochem. Photobiol.*, **30**, 35 (1979).

11) O. Shimomura, F. H. Johnson, and H. Morise, *Biochemistry*, **13**, 3278 (1974).

12) O. Shimomura, B. Musick, and Y. Kishi, *Biochem. J.*, **251**, 405 (1988).

13) T. Goto and H. Nakamura, *Tetrahedron Lett.*, **1976**, 4627.

14) H. Nakamura and T. Goto, *Bull. Chem. Soc. Jpn.*, **61**, 3776 (1988).

15) T. Goto, "New Synthetic Methodology and Functionally Interesting Compounds," ed by Z. Yoshida, Kodansha Ltd., Tokyo (1986), pp. 285—306.

16) T. Goto, S. Inoue, K. Sugiura, K. Nishikawa, M. Isobe, and Y. Abe, *Tetrahedron Lett.*, **1968**, 4035.

17) J. J. Norman, R. M. Heggie, and J. B. Larose, *Can. J. Chem.*, **40**, 1547 (1962).

18) Y. Kishi, H. Tanino, and T. Goto, *Tetrahedron Lett.*, **1972**, 2747.

Synthesis of *S*-Methyl 2-Hydroxyalkanethioates, 2-Hydroxyalkanoic Acids and Related Compounds via the Addition Reaction of Tris(methylthio)methanide Ion to Alkanals

Kazuhiko ORITO,* Yoshikatsu SEKI, Hiroshi SUGINOME, and Tsukasa IWADARE†
Department of Chemical Process Engineering, Hokkaido University, Sapporo 060
†Research Laboratory, Sakura Finetechnical Co., Ltd., 3-1-8, Hikawadai, Nerima-ku, Tokyo 176
(Received January 11, 1989)

In connection with the studies on biological activities on myrmicacin and related compounds, the synthetic method for 2-hydroxyalkanoic acids and the corresponding 1,2-diols was studied. The addition reaction of tris(methylthio)methyllithium to the aldehydes (propanal—dodecanal) gave the corresponding 1,1,1-tris-(methylthio)-2-alkanols **1a—j**. Treatment of **1** with mercury(II) chloride-mercury(II) oxide in water-acetone afforded *S*-methyl 2-hydroxyalkanethioates **2a—j**, and in methanol methyl 2-hydroxyalkanoates **3c—j** were obtained. Reduction of the thioates **2** with lithium aluminium hydride gave 1,2-diols **4c—j** and saponification produced the corresponding 2-hydroxyalkanoic acids **5c—j**.

Myrmicacin was isolated from the secretion of South American leaf-cutting ants, *Atta sexdens*, and identified as (*R*)-(−)-3-hydroxydecanoic acid by Schildeknecht and Koob in 1971.[1] It is understood that this substance prevents germination of collected seeds and intruding spores, as a herbicide, in the ant's nest. Recent studies revealed that it had a reversible inhibitory effect on pollen growth.[2-6] The activity of myrmic acids[7] on cleavage of fertilized sea urchin eggs,[8,9] HeLa cells,[10] human erythrocytes,[11] and propagation of pathogenic bacteria in silk worm, *larvae*[12] has been reported. A close relationship between intensity of inhibitory activity and degree of lipophilicity of myrmicacin analogues has recently been found.[13,14] Strong inhibitory activity of 2-hydroxyalkanoic acids on pollen germination has also been observed.[15]

In view of the above-stated facts, it seemed of significance for further study on biological activity of myrmicacin and related compounds to establish the synthetic method of 2-hydroxyalkanoic acids[16a,17] as well as 1,2-diols[16b,17] with a common starting material and to obtain their physical properties and spectral data. Thus the present study was undertaken.

Results and Discussion

To a solution of tris(methylthio)methanide ion, generated by interaction of tris(methylthio)methane with butyllithium at −78 °C,[18-20] was slowly added the tetrahydrofuran solution of the appropriate aldehydes (C_3—C_{12}). By warming the mixture to room temperature, the corresponding tris(methylthio)methyl adducts (**1a—j**) were obtained in good yields, as shown in Table 1. Preliminary attempts to prepare the straight-chain 2-hydroxyalkanoic acids **5** were made by treating the adducts **1** with mercury(II) chloride or mercury(II) oxide in aqueous solution, according to the procedure described by Seebach.[18] In each case the main product was not the 2-hydroxyalkanoic acid but the *S*-methyl 2-hydroxyalkanethioates **2**.[19a] When stirred in a suspension with mercury(II) chloride-mercury(II) oxide[20] (2.5 : 1.0 mol) in water-acetone (1 : 5) at room temperature for 2 h, the adducts **1** were efficiently converted to the thioates **2** in the yields ranging in 75—95%, as summarized together with boiling and melting points of the analytical samples in Table 2.[21] When heated to reflux for 1 h, the thioates **2** were obtained also in good yield. Longer heating did not give much effect on further hydrolysis (desulfurization) to the acids. Boron trifluoride etherate-mercury(II) oxide[19] worked well and gave **2** in the yields comparable to those given for the aforementioned reactions in the presence of mercury(II) chloride-mercury(II) oxide. Similarly, when the adducts **1** were refluxed with mercury(II) chloride-mercury(II) oxide (2.5 : 1.0 mol) in methanol for 2 h, the ready formation of the methyl esters **3** took place. However, the esters with lower molecular weights were isolated in the lesser yields due to their water-soluble character (Table 3). Treatment of the *S*-methyl thioates **2** with excess

Table 1. Synthesis of 1,1,1-Tris(methylthio)-2-alkanols **1**

$CH_3(CH_2)_nCHO + LiC(SCH_3)_3 \longrightarrow CH_3(CH_2)_nCH(OH)C(SCH_3)_3$ (**1**)
−78 °C—r.t. in THF

Entry	*n*	Products **1** Bp(°C/Torr)	Yield (%)
a:	1	154—155/14	75
b:	2	160—162/14	76
c:	3	171—173/14[a]	88
d:	4	180—181/14	89
e:	5	121—122/0.2	91
f:	6	127—128/0.2	89
g:	7	144—146/0.4	85
h:	8	142—145/0.2	87
i:	9	165—166/0.2	87
j:	10	176—177/0.2	95

a) Lit,[18] mp 60—63 °C.

Table 2. Synthesis of *S*-Methyl Thioesters **2** from **1**
$CH_3(CH_2)_nCH(OH)C(SCH_3)_3$ (**1**) ⟶ $CH_3(CH_2)_nCH(OH)COSCH_3$ (**2**)
$HgCl_2$-HgO (2.5 : 1.0 mol) in H_2O-acetone (1 : 5) at r.t. for 2 h

Entry *n*	Products **2**		
	Bp(°C/Torr)	Mp (°C)	Yield (%)
a: 1	91/14		56
b: 2	104/14		63
c: 3	115/10		85
d: 4	119/7		87
e: 5	124/5		89
f: 6	95/0.2		83
g: 7	105/0.2	38	82
f: 8	118/0.2	34	81
g: 9	135/0.5	48	83
h: 10	144/0.6	41	83

Table 3. Synthesis of Methyl 2-Hydroxyalkanoates **3** from **1**
$CH_3(CH_2)_nCH(OH)C(SCH_3)_3$ (**1**) ⟶ $CH_3(CH_2)_nCH(OH)COOCH_3$ (**3**)
$HgCl_2$-HgO(2.5 : 1.0 mol) in MeOH refluxing for 2 h

Entry *n*	Products **3**		
	Bp(°C/Torr)	Mp (°C)	Yield (%)
c: 3	111/50		50
d: 4	127/50		57
e: 5	110/13		67
f: 6	108/5		75
g: 7	122/5		75
h: 8	105/1		78
i: 9	117/1	36—37	77
j: 10	128/1	39—42	80

Table 4. Synthesis of 1,2-Alkanediols **4** by $LiAlH_4$ Reduction of *S*-Methyl Thioesters **2**
$CH_3(CH_2)_nCH(OH)COSCH_3$ (**2**) ⟶ $CH_3(CH_2)_nCH(OH)CH_2OH$ ($LiAlH_4$ in ether refluxing for 2 h)

Entry *n*	Products **4**		
	Bp(°C/Torr)	Mp (°C)	Yield (%)
c: 3	78—79/0.6[a]		90
d: 4	77—81/0.1[b]		90
e: 5	81—85/0.1	30[c]	91
f: 6	92—93/0.1	35	90
g: 7	93—96/0.05	46—47[d]	95
h: 8		46—48	92
i: 9		55—56[e]	94
j: 10		61—62[f]	96

a) Lit,[24] bp 96—98 °C/1.0;[25] bp 75—80 °C/0.3;[26] bp 119—120 °C/13.5. b) Lit,[26] bp 122.5 °C/10. c) Lit,[24] bp 103—105 °C/0.5, mp 29—30 °C;[26] bp 131—132 °C/10;[27] mp 30—30.5 °C. d) Lit,[24] mp 48—49 °C;[27] mp 48—49 °C. e) Lit,[24] mp 56—58 °C;[26] mp 60—60.5 °C;[27] mp 60—61 °C. f) Lit,[28] mp 61.2—62.4 °C.

Table 5. Saponification of *S*-Methyl Thioesters **2**
$CH_3(CH_2)_nCH(OH)COSCH_3$ (**2**) ⟶ $CH_3(CH_2)_nCH(OH)COOH$
5% NaOH-aq. MeOH refluxing for 1 h

Entry *n*	Products **5**	
	Mp (°C)	Yield (%)
c: 3	60—61[a]	90
d: 4	65—66	87
e: 5	68—69[b]	85
f: 6	69—70[c]	87
g: 7	70—71[d]	88
h: 8	72—73[e]	86
i: 9	73—74	90
j: 10	76—77	91

a) Lit,[29] mp 61—62 °C;[25] mp 60—62.5 °C. b) Lit,[30] mp 69—70 °C;[31] mp 69 °C. c) Lit,[31] mp 70 °C. d) Lit,[31] mp 70.5 °C. e) Lit,[31] mp 75 °C.

lithium aluminium hydride in boiling tetrahydrofuran gave the 1,2-diols **4** in essentially quantitative yields (Table 4). Saponification of the thioates **2** in the usual manner furnished the corresponding crystalline 2-hydroxyalkanoic acids **5** in good yields as well (Table 5).

Experimental

Melting points were determined on a Laboratory Devices MEL-TEMP, and are uncorrected. Boiling points are uncorrected. IR spectra were recorded using the neat samples, unless otherwise stated, on a Hitachi-Perkin Elmer Model 125 spectrophotometer. ^1H NMR spectra were run in $CDCl_3$ solutions with Me_4Si as an internal reference at ambient temperature and resistered on a 90 MHz Hitachi R-22 spectrometer.

General Procedure for the Addition Reaction of Tris(methylthio)methyllithium to Aldehydes. A stirred solution of tris(methylthio)methane (4.62 g, 0.03 mol)[20] in dry THF (50 ml) under an atmosphere of nitrogen was cooled at −78 °C, *n*-BuLi (0.029 mol, 18.5 ml) of 10 w/v% hexane solution was dropwise added at such a rate that the temperature did not rise more than −15 °C (10 min or more). An additional stirring at −78 °C for 15 min gave a white suspension, probably, due to partly precipitated lithium salt of tris(methylthio)methane. A solution of the freshly distilled appropriate aldehyde (0.025 mol) in dry THF (20 ml) was gradually added in the course of 20 min and the mixture was kept stirring at −78 °C for further 1 h. The cooling bath was removed and the mixture was allowed to warm to room temperature (1 h). To this, saturated NH_4Cl solution (20 ml) was added, and the mixture was shaken. The aqueous layer was extracted with ether (20 ml×2). The combined organic layers were washed with saturated brine (20 ml) and dried over anhydrous Na_2SO_4. Evaporation of the solvent left an oil, which was distilled in vacuo to give the pure alcohol.

1,1,1-Tris(methylthio)-2-butanol (1a). 4.0 g. IR 3460 cm^{-1}; ^1H NMR δ=1.03 (3H, br. t, J=7.0 Hz, CH_3), 1.75 (2H, m, CH_2), 2.18 (9H, s, 3×SCH_3), 2.74 (1H, d, J=4.0 Hz, OH),[22] 3.62 (1H, ddd, J=9.5, 4.0, 3.0 Hz, C<u>H</u>OH[23]→dd,

J=9.5, 3.0 Hz). Found: C, 39.61; H, 7.50; S, 45.29%. Calcd for $C_7H_{16}OS_3$: C, 39.59; H, 7.59; S, 45.29%.

1,1,1-Tris(methylthio)-2-pentanol (1b). 4.3 g. IR 3470 cm^{-1}; ^1H NMR δ=0.92 (3H, br. t, J=7.0 Hz, CH_3),1.1—1.9 (4H, m, 2×CH_2) 2.19 (9H, s, 3×SCH_3), 2.74 (1H, d, J=4.0 Hz, OH),[22] 3.72 (1H, m, C<u>H</u>OH[23]→dd, J=8.5, 3.0 Hz). Found: C, 42.22; H, 7.90; S, 42.59%. Calcd for $C_8H_{18}OS_3$: C, 42.44; H, 8.01; S, 42.48%.

1,1,1-Tris(methylthio)-2-hexanol (1c). 5.3 g. IR 3430 cm^{-1}; ^1H NMR δ=0.87 (3H, br. t, J=7.0 Hz, CH_3), 1.20 (4H, m, 2×CH_2), 1.71 (2H, m, CH_2), 2.19 (9H, s, 3×SCH_3), 2.72 (1H, d, J=4.0 Hz, OH),[22] 3.71 (1H, m, C<u>H</u>OH[23]→dd, J=8.5, 2.5 Hz). Found: C, 44.69; H, 8.27; S, 39.83%. Calcd for $C_9H_{20}OS_3$: C, 44.69; H, 8.38; S, 40.00%.

1,1,1-Tris(methylthio)-2-heptanol (1d). 5.65 g. IR 3450 cm^{-1}; ^1H NMR δ=0.87 (3H, br. t, J=7.0 Hz, CH_3), 1.32(6H, m, 3×CH_2), 1.71 (2H, m, CH_2), 2.18 (9H, s, 3×SCH_3), 2.75 (1H, d, J=4.0 Hz, OH),[22] 3.71 (1H, m, C<u>H</u>OH[23]→dd, J=8.5, 2.5 Hz). Found: C, 47.11; H, 8.65; S, 37.61%. Calcd for $C_{10}H_{22}OS_3$: C, 47.20; H, 8.71; S, 37.80%.

1,1,1-Tris(methylthio)-2-octanol (1e). 6.1 g. IR 3470 cm^{-1}; ^1H NMR δ=0.85 (3H, br. t, J=6.0 Hz, CH_3), 1.29 (8H, m, 4×CH_2), 1.71 (2H, m, CH_2), 2.18 (9H, s, 3×SCH_3), 2.74 (1H, d, J=4.0 Hz, OH),[22] 3.70 (1H, m, C<u>H</u>OH[23]→dd, J=8.5, 2.5 Hz). Found: C, 49.14; H, 9.01; S, 35.66%. Calcd for $C_{11}H_{24}OS_3$: C, 49.21; H, 9.01; S, 35.82%.

1,1,1-Tris(methylthio)-2-nonanol (1f). 6.3 g. IR 3450 cm^{-1}; ^1H NMR δ=0.84 (3H, br. t, J=6.0 Hz, CH_3), 1.28 (10H, m, 5×CH_2), 1.72 (2H, m,CH_2), 2.17 (9H, s, 3×SCH_3), 2.73 (1H, d, J=4.0 Hz, OH),[22] 3.71 (1H, m, C<u>H</u>OH[23]→dd, J=8.5, 2.5 Hz). Found: C, 51.02; H, 9.13; S, 34.16%. Calcd for $C_{12}H_{26}OS_3$: C, 51.02; H, 9.28; S, 34.04%.

1,1,1-Tris(methylthio)-2-decanol (1g). 6.5 g. IR 3460 cm^{-1}; ^1H NMR δ=0.85 (3H, br. t, J=6.0 Hz, CH_3), 1.28 (12H, m, 6×CH_2), 1.72 (2H, m, CH_2), 2.18 (9H, s, 3×SCH_3), 2.73 (1H, d, J=4.0 Hz, OH),[22] 3.71 (1H, m, C<u>H</u>OH[23]→dd, J=8.5, 2.5 Hz). Found: C, 52.54; H, 9.46; S, 32.57%. Calcd for $C_{13}H_{28}OS_3$: C, 52.65; H, 9.52; S, 32.43%.

1,1,1-Tris(methylthio)-2-undecanol (1h). 6.8 g. IR 3460 cm^{-1}; ^1H NMR δ=0.84 (3H, br. t, J=6.0 Hz, CH_3), 1.25 (14H, m, 7×CH_2), 1.72 (2H, m, CH_2), 2.18 (9H, s, 3×SCH_3), 2.73 (1H, d, J=4.0 Hz, OH),[22] 3.71 (1H, m, C<u>H</u>OH[23]→dd, J=8.0, 2.0 Hz). Found: C, 54.10; H, 9.76; S, 30.96%. Calcd for $C_{14}H_{30}OS_3$: C, 54.14; H, 9.74; S, 30.97%.

1,1,1-Tris(methylthio)-2-dodecanol (1i). 7.1 g. IR 3450 cm^{-1}; ^1H NMR δ=0.84 (3H, br. t, J=6.0 Hz, CH_3), 1.24 (16H, m, 8×CH_2), 1.71 (2H, m, CH_2), 2.18 (9H, s, 3×SCH_3), 2.73 (1H, d, J=4.0 Hz, OH),[22] 3.71 (1H, m, C<u>H</u>OH[23]→dd, J=8.5, 2.5 Hz). Found: C, 55.76; H, 9.96; S, 29.81%. Calcd for $C_{15}H_{34}OS_3$: C, 55.50; H, 9.96; S, 29.63%.

1,1,1-Tris(methylthio)-2-tridecanol (1j). 8.05 g. IR 3470 cm^{-1}; ^1H NMR δ=0.84 (3H, br. t, J=6.0 Hz, CH_3), 1.24 (18H, m, 9×CH_2), 1.71 (2H, m, CH_2), 2.18 (9H, s, 3×SCH_3), 2.73 (1H, d, J=4.0 Hz, OH),[22] 3.71 (1H, m, C<u>H</u>OH[23]→dd, J=8.5, 2.5 Hz). Found: C, 56.73; H, 10.15; S, 28.48%. Calcd for $C_{16}H_{34}OS_3$: C, 56.75; H, 10.15; S, 28.40%.

General Procedure for Preparation of *S*-Methyl 2-Hydroxyalkanethioates (2). A mixture of each orthothiocarboxylic acid trimethyl ester (**1**, 1 mmol), $HgCl_2$ (5 mmol), and HgO (red, 2 mmol) in a solution of H_2O–acetone (1 : 5, 30 ml) was refluxed with stirring for 2 h. Precipitates were filtered, and acetone was evaporated at room temperature. The residue was dissolved in CH_2Cl_2, washed with saturated NH_4Cl solution (2 ml), and dried over anhydrous Na_2SO_4. Evaporation of the solvent gave the crude product, which was distilled in vacuo to afford the pure *S*-methyl 2-hydroxyalkanethioate **2**. Analytical samples of **2g—j** were prepared on crystallization from petroleum ether.

***S*-Methyl 2-Hydroxybutanethioate (2a).** 150 mg. IR 3400, 1660 cm^{-1}; ^1H NMR δ=1.00 (3H, br. t, J=7.5 Hz, CH_3), 1.82 (2H, m, CH_2), 2.23 (3H, s, SCH_3), 3.05 (1H, d, J=6.0 Hz, OH),[22] 4.28 (1H, m, C<u>H</u>OH[23]→dd, J=8.0, 4.5 Hz). Found: C, 44.69; H, 7.57; S, 23.67%. Calcd for $C_5H_{10}O_2S$: C, 44.75; H, 7.51; S, 23.89%.

***S*-Methyl 2-Hydroxypentanethioate (2b).** 186 mg. IR 3400, 1660 cm^{-1}; ^1H NMR δ=0.97 (3H, br. t, J=7.0 Hz, CH_3), 1.53 (2H, m, CH_2), 1.71 (2H, m, CH_2), 2.35 (3H, s, SCH_3), 3.01 (1H, d, J=6.0 Hz, OH),[22] 4.33 (1H, m, C<u>H</u>OH[23]→dd, J=6.0, 4.0 Hz). Found: C, 48.76; H, 8.22; S, 21.44%. Calcd for $C_6H_{12}O_2S$: C, 48.62; H, 8.16; S, 21.62%.

***S*-Methyl 2-Hydroxyhexanethioate (2c).** 275 mg. IR 3400, 1660 cm^{-1}; ^1H NMR δ=0.92 (3H, br. t, J=7.0 Hz, CH_3), 1.43 (4H, m, 2×CH_2), 1.78 (2H, s,CH_2), 2.33 (3H, s, SCH_3), 3.09 (1H, d, J=5.5 Hz, OH),[22] 4.33 (1H, m, C<u>H</u>OH[23]→dd, J=7.0, 4.0 Hz). Found: C, 51.79; H, 8.68; S, 19.83%. Calcd for $C_7H_{14}O_2S$: C, 51.83; H, 8.99; S, 19.76%.

***S*-Methyl 2-Hydroxyheptanethioate (2d).** 306 mg. IR 3400, 1660 cm^{-1}; ^1H NMR δ=0.89 (3H, br. t, J=6.0 Hz, CH_3), 1.33 (6H, m, 3×CH_2), 1.78 (2H, m, CH_2), 2.33 (3H, s, SCH_3), 3.01 (1H, d, J=7.0 Hz, OH),[22] 4.33 (1H, m, C<u>H</u>OH[23]→dd, J=8.0, 4.5 Hz). Found: C, 54.49; H, 9.17; S, 18.16%. Calcd for $C_8H_{16}O_2S$: C, 54.51; H, 9.15; S, 18.19%.

***S*-Methyl 2-Hydroxyoctanethioate (2e).** 338 mg. IR 3400, 1660 cm^{-1}; ^1H NMR δ=0.89 (3H, br. t, J=6.0 Hz, CH_3), 1.33 (8H, m, 4×CH_2), 1.75 (2H, m, CH_2), 2.33 (3H, s, SCH_3), 3.02 (1H, d, J=5.0 Hz, OH),[22] 4.33 (1H, m, C<u>H</u>OH[23]→dd, J=8.0, 4.5 Hz). Found: C, 56.85; H, 9.66; S, 16.73%. Calcd for $C_9H_{18}O_2S$: C, 56.80; H, 9.53; S, 16.85%.

***S*-Methyl 2-Hydroxynonanethioate (2f).** 339 mg. IR 3400, 1660 cm^{-1}; ^1H NMR δ=0.87 (3H, br. t, J=6.0 Hz, CH_3), 1.30 (10H, m, 5×CH_2), 1.75 (2H, m, CH_2), 2.32 (3H, s, SCH_3), 3.26 (1H, d, J=5.0 Hz, OH),[22] 4.30 (1H, m, C<u>H</u>OH[23]→dd, J=7.0, 4.5 Hz). Found: C, 58.64; H, 9.88; S, 15.517%. Calcd for $C_{10}H_{20}O_2S$: C, 58.78; H, 9.87; S, 15.69%.

***S*-Methyl 2-Hydroxydecanethioate (2g).** 357 mg. IR (Nujol) 3470, 1670 cm^{-1}; ^1H NMR δ=0.90 (3H, br. t, J=6.0 Hz, CH_3), 1.30 (12H, m, 6×CH_2), 1.75 (2H, m, CH_2), 2.33 (3H, s, SCH_3), 2.95 (1H, d, J=5.0 Hz, OH),[22] 4.33 (1H, m, <u>C</u>HOH[23]→dd, J=7.5, 4.0 Hz). Found: C, 60.37; H, 10.09; S, 14.87%. Calcd for $C_{11}H_{22}O_2S$: C, 60.50; H, 10.16; S, 14.68%.

***S*-Methyl 2-Hydroxyundecanethioate (2h).** 376 mg. IR (Nujol) 3470, 1665 cm^{-1}; ^1H NMR δ=0.89 (3H, br. t, J=6.0 Hz, CH_3), 1.26 (14H, m, 7×CH_2), 1.75 (2H, m, CH_2) , 2.34 (3H, s, SCH_3), 2.92 (1H, br. s, OH), 4.32 (1H, dd, J=7.5, 4.0 Hz, CHOH). Found: C, 61.93; H, 10.32; S, 13.77%. Calcd for $C_{12}H_{24}O_2S$: C, 62.02; H, 10.42; S, 13.80%.

***S*-Methyl 2-Hydroxydodecanethioate (2i).** 408 mg. IR (Nujol) 3470, 1665 cm^{-1}; ^1H NMR δ=0.88 (3H, br. t, J=6.0 Hz, CH_3), 1.25 (16H, m, 8×CH_2), 1.75 (2H, m, CH_2) , 2.32 (3H, s, SCH_3), 2.65 (1H, br. s, OH), 4.32 (1H, d, J=6.5, 4.0 Hz, C<u>H</u>OH). Found: C, 63.28; H, 10.52; S, 12.99%. Calcd for $C_{13}H_{26}O_2S$: C, 63.37; H, 10.63; S, 13.01%.

***S*-Methyl 2-Hydroxytridecanethioate (2j).** 430 mg. IR (Nujol) 3470, 1665 cm^{-1}; ^1H NMR δ=0.90 (3H, br. t, J=6.0 Hz, CH_3), 1.24 (18H, m, 9×CH_2), 1.75 (2H, m, CH_2) , 2.32 (3H, s, SCH_3), 2.65 (1H, br. s, OH), 4.32 (1H, dd, J=6.5, 4.0

Hz, CHOH). Found: C, 64.46; H, 10.69; S, 12.38%. Calcd for $C_{14}H_{28}O_2S$: C, 64.57; H, 10.84; S, 12.31%.

General Procedure for Preparation of Methyl Esters 3 from 1. A mixture of **1** (2 mmol), $HgCl_2$ (5 mmol), and HgO (red, 2 mmol) in a solution of 99% MeOH (20 ml) was refluxed for 1 h, and worked up in the same manner as noted for **2**. The crude oily product was distilled in vacuo.

Methyl 2-Hydroxyhexanoate (3c). 171 mg. IR 3450, 1730 cm^{-1}; ^1H NMR δ=0.89 (3H, br. t, J=7 Hz, CH_3), 1.40 (4H, m, 2×CH_2), 1.71 (2H, m, CH_2), 2.90 (1H, d, J=6.0 Hz, OH),[22] 3.82 (3H, s, OCH_3), 4.26 (1H, m, CHOH[23]→dd, J=6.5, 4.5 Hz). Found: C, 57.52; H, 9.53%. Calcd for $C_7H_{14}O_3$: C, 57.51; H, 9.65%.

Methyl 2-Hydroxyheptanoate (3d). 181 mg. IR 3460, 1730 cm^{-1}; ^1H NMR δ=0.89 (3H, br. t, J=7.0 Hz, CH_3), 1.34 (6H, m, 3×CH_2), 1.71 (2H, m, CH_2), 3.04 (1H, d, J=6.0 Hz, OH), 3.82 (3H, s, OCH_3),[22] 4.21 (1H, m, CHOH[23]→dd, J=6.5, 6.0 Hz). Found: C, 60.03; H, 10.16%. Calcd for $C_8H_{16}O_3$: C, 59.98; H, 10.07%.

Methyl 2-Hydroxyoctanoate (3e). 234 mg. IR 3450, 1732 cm^{-1}; ^1H NMR δ=0.88 (3H, br. t, J=7.5 Hz, CH_3), 1.33 (8H, m, 4×CH_2), 1.71 (2H, m, CH_2), 2.94 (1H, d, J=5.5 Hz, OH),[22] 3.83 (3H, s, OCH_3), 4.25 (1H, m, CHOH[23]→dd, J=6.6, 6.0 Hz). Found: C, 61.90; H, 10.32%. Calcd for $C_8H_{16}O_3$: C, 62.04; H, 10.41%.

Methyl 2-Hydroxnonanoate (3f). 282 mg. IR 3450, 1735 cm^{-1}; ^1H NMR δ=0.88 (3H, br. t, J=6.0 Hz, CH_3), 1.32 (10H, m, 5×CH_2), 1.72 (2H, m, CH_2), 2.98 (1H, d, J=5.5 Hz, OH),[22] 3.82 (3H, s, OCH_3), 4.25 (1H, m, CHOH[23]→dd, J=6.6, 6.0 Hz). Found: C, 63.70; H, 10.75%. Calcd for $C_9H_{18}O_3$: C, 63.79; H, 10.71%.

Methyl 2-Hydroxydecanoate (3g). 302 mg. IR 3460, 1730 cm^{-1}; ^1H NMR δ=0.88 (3H, br. t, J=6.0 Hz, CH_3), 1.30 (12H, m, 6×CH_2), 1.73 (2H, m, CH_2), 2.94 (1H, d, J=5.5 Hz, OH),[22] 3.85 (3H, s, OCH_3), 4.25 (1H, m, CHOH[23]→dd, J=6.5, 5.5 Hz). Found: C, 65.42; H, 10.87%. Calcd for $C_{10}H_{20}O_3$: C, 65.31; H, 10.96%.

Methyl 2-Hydroxyundecanoate (3h). 337 mg. IR 3460, 1735 cm^{-1}; ^1H NMR δ=0.88 (3H, br. t, J=6.0 Hz, CH_3), 1.27 (14H, m, 7×CH_2), 1.73 (2H, m, CH_2), 2.97 (1H, br. s, OH), 3.85 (3H, s, OCH_3), 4.25 (1H, br. t, J=6.5 Hz, CHOH). Found: C, 66.69; H, 11.30%. Calcd for $C_{11}H_{22}O_3$: C, 66.63; H, 11.18%.

Methyl 2-Hydroxydodecanoate (3i). 355 mg. IR 3440, 1720 cm^{-1}; ^1H NMR δ=0.87 (3H, br. t, J=6.5 Hz, CH_3), 1.27 (16H, m, 8×CH_2), 1.73 (2H, m, CH_2), 2.84 (1H, br. d, J=5.5 Hz, OH),[22] 3.85 (3H, s, OCH_3), 4.23 (1H, m, CHOH[23]→dd, J=6.0, 5.5 Hz). Found: C, 67.88; H, 11.50%. Calcd for $C_{12}H_{24}O_3$: C, 67.78; H, 11.38%.

Methyl 2-Hydroxytridecanoate (3j). 391 mg. IR 3450, 1722 cm^{-1}; ^1H NMR δ=0.87 (3H, br. t, J=6.0 Hz, CH_3), 1.25 (18H, m, 9×CH_2), 1.73 (2H, m, CH_2), 2.87 (1H, d, J=6.5 Hz, OH),[22] 3.83 (3H, s, OCH_3), 4.23 (1H, m, CHOH[23]→dd, J=6.0, 5.5 Hz). Found: C, 68.77; H, 11.46%. Calcd for $C_{14}H_{28}O_3$: C, 68.81; H, 11.55%.

Preparation of 1,2-Alkanediols (4) by $LiAlH_4$ Reduction of *S*-Methyl 2-Hydroxyalkanethioates (2). A stirred suspension of the appropriate thioate (**2**, 2 mmol) and $LiAlH_4$ (8 mmol, 300 mg) in dry ether (20 ml) was heated. After refluxing for 3 h, the mixture was cooled and water (about 2 ml) was added. The resulting white precipitates were filtered through a thin pad of powdered anhydrous $MgSO_4$. The filtrate and ether washings were combined, and evaporated to leave the crude diol, which was distilled under reduced pressure or crystallized from petroleum ether.

1,2-Hexanediol (4c). 213 mg. IR 3350 cm^{-1}; ^1H NMR δ=0.92 (3H, br. t, J=6.0 Hz, CH_3), 1.39 (6H, m, 3×CH_2), 2.46 (2H, s, 2×OH), 3.28—3.85 (3H, m, CHOHCH$_2$OH). Found: C, 60.87; H, 11.99%. Calcd for $C_6H_{14}O_2$: C, 60.98; H, 11.98%.

1,2-Heptanediol (4d). 238 mg. IR 3350 cm^{-1}; ^1H NMR δ=0.89 (3H, br. t, J=6.0 Hz, CH_3), 1.35 (8H, m, 4×CH_2), 2.48 (2H, s, 2×OH), 3.25—3.80 (3H, m, CHOHCH$_2$OH). Found: C, 63.41; H, 12.23%. Calcd for $C_7H_{16}O_2$: C, 63.59; H, 12.20%.

1,2-Octanediol (4e). 266 mg. IR (Nujol) 3350 cm^{-1}; ^1H NMR δ=0.88 (3H, br. t, J=6.0 Hz, CH_3), 1.30 (8H, m, 4×CH_2), 1.38 (2H, m, CH_2), 2.01 (2H, s, 2×OH), 3.28—3.85 (3H, m, CHOHCH$_2$OH). Found: C, 65.67; H, 12.43%. Calcd for $C_8H_{18}O_2$: C, 65.71; H, 12.41%.

1,2-Nonanediol (4f). 266 mg. IR (Nujol) 3300, 3230 cm^{-1}; ^1H NMR δ=0.88 (3H, br. t, J=6.0 Hz, CH_3), 1.29 (10H, m, 5×CH_2), 1.39 (2H, m, CH_2), 2.00 (2H, s, 2×OH), 3.30—3.85 (3H, m, CHOHCH$_2$OH). Found: C, 67.62; H, 12.53%. Calcd for $C_9H_{20}O_2$: C, 67.45; H, 12.58%.

1,2-Decanediol (4g). 288 mg. IR (Nujol) 3310, 3220 cm^{-1}; ^1H NMR δ=0.88 (3H, br. t, J=6.0 Hz, CH_3), 1.27 (12H, m, 6×CH_2), 1.38 (2H, m, CH_2), 1.93 (2H, s, 2×OH), 3.25—3.85 (3H, m, CHOHCH$_2$OH). Found: C, 67.62; H, 12.53%. Calcd for $C_{10}H_{22}O_2$: C, 68.91; H, 12.72%.

1,2-Undecanediol (4h). 331 mg. IR (Nujol) 3310, 3220 cm^{-1}; ^1H NMR δ=0.88 (3H, br. t, J=6.0 Hz, CH_3), 1.27 (14H, m, 7×CH_2), 1.38 (2H, m, CH_2), 1.93 (2H, s, 2×OH), 3.25—3.85 (3H, m, CHOHCH$_2$OH). Found: C, 70.22; H, 12.93%. Calcd for $C_{11}H_{24}O_2$: C, 70.16; H, 12.85%.

1,2-Dodecanediol (4i). 354 mg. IR (Nujol) 3310, 3220 cm^{-1}; ^1H NMR δ=0.88 (3H, br. t, J=6.0 Hz, CH_3), 1.26 (16H, m, 8×CH_2), 1.38 (2H, m, CH_2), 2.14 (2H, br.s, 2×OH), 3.25—3.85 (3H, m, CHOHCH$_2$OH). Found: C, 71.31; H, 13.11%. Calcd for $C_{12}H_{26}O_2$: C, 71.23; H, 12.95%.

1,2-Tridecanediol (4j). 388 mg. IR (Nujol) 3310, 3210 cm^{-1}; ^1H NMR δ=0.88 (3H, br. t, J=6.0 Hz, CH_3), 1.26 (18H, m, 9×CH_2), 1.39 (2H, m, CH_2), 1.86 (2H, br s, 2×OH), 3.25—3.85 (3H, m, CHOHCH$_2$OH). Found: C, 72.89; H, 12.42%. Calcd for $C_{13}H_{26}O_2$: C, 72.84; H, 12.23%.

Preparation of 2-Hydroxyalkanoic Acids (5). A solution of the appropriate thioate (**2**, 2 mmol) in 90% MeOH (10 ml) containing 5% NaOH was refluxed for 1 h. MeOH was removed under reduced pressure. To the redidue water (10 ml) was added and the resulting solution was extracted with ether (10 ml). Water layer was acidified with diluted HCl and extracted with CH_2Cl_2 (10 ml×2). The CH_2Cl_2 extracts were dried over anhydrous Na_2SO_4, and evaporated to leave a solid. Recrystallization from petroleum ether gave the pure 2-hydroxyalkanoic acid.

2-Hydroxyhexanoic Acid (5c). 238 mg. IR (Nujol) 3600—2300, 3440, 3390, 1710 cm^{-1}; ($CHCl_3$) 3600—2400, 1715 cm^{-1}; ^1H NMR δ=0.92 (3H, br. t, J=6.0 Hz, CH_3), 1.43 (4H, m, 2×CH_2), 1.78 (2H, m, CH_2), 4.28 (1H, dd, J=5.5, 4.4 Hz, CHOH), 4.65 (2H, br. s, OH and COOH). Found: C, 54.46; H, 9.07%. Calcd for $C_6H_{12}O_3$: C, 54.53; H, 9.15%.

2-Hydroxyheptanoic Acid (5d). 254 mg. IR (Nujol) 3600—2300, 3440, 3390, 1710 cm^{-1}; ($CHCl_3$) 3600—2400, 1715 cm^{-1}; ^1H NMR δ=0.90 (3H, br. t, J=6.5 Hz, CH_3), 1.34 (6H, m, 3×CH_2), 1.72 (2H, m, CH_2), 4.28 (1H, dd, J=5.5, 4.5 Hz, CHOH), 5.82 (2H, br. s, OH and COOH). Found: C,

57.44; H, 9.51%. Calcd for $C_7H_{14}O_3$: C, 57.51; H, 9.65%.

2-Hydroxyoctanoic Acid (5e). 272 mg. IR (Nujol) 3600—2300, 3430, 3380, 1705 cm^{-1}; ($CHCl_3$) 3600—2400, 1715 cm^{-1}; ^1H NMR δ=0.89 (3H, br. t, J=6.0 Hz, CH_3), 1.33 (8H, m, 4×CH_2), 1.78 (2H, m, CH_2), 4.28 (1H, dd, J=5.5, 5.0 Hz, CHOH), 5.58 (2H, br. s, OH and COOH). Found: C, 59.91; H, 10.02%. Calcd for $C_8H_{16}O_3$: C, 59.98; H, 10.07%.

2-Hydroxynonanoic Acid (5f). 303 mg. IR (Nujol) 3600—2300, 3430, 3380, 1705 cm^{-1}; ($CHCl_3$) 3600—2400, 1715 cm^{-1}; ^1H NMR δ=0.88 (3H, br. t, J=6.0 Hz, CH_3), 1.30 (10H, m, 5×CH_2), 1.78 (2H, m, CH_2), 4.28 (1H, dd, J=6.5, 5.0 Hz, CHOH), 5.76 (2H, br. s, OH and COOH). Found: C, 61.91; H, 10.62%. Calcd for $C_9H_{18}O_3$: C, 62.04; H, 10.41%.

2-Hydroxydecanoic Acid (5g). 331 mg. IR (Nujol) 3600—2300, 3450, 1740 cm^{-1}; ($CHCl_3$) 3600—2400, 3510, 1715 cm^{-1}; ^1H NMR δ=0.88 (3H, br. t, J=6.0 Hz, CH_3), 1.28 (12H, m, 6×CH_2), 1.78 (2H, m, CH_2), 4.28 (1H, dd, J=6.5, 5.0 Hz, CHOH), 6.19 (2H, br. s, OH and COOH). Found: C, 63.72; H, 10.76%. Calcd for $C_{10}H_{20}O_3$: C, 63.79; H, 10.71%.

2-Hydroxyundecanoic Acid (5h). 350 mg. IR (Nujol) 3600—2300, 3550, 1690 cm^{-1}; ($CHCl_3$) 3600—2400, 3510, 1715 cm^{-1}; ^1H NMR δ=0.88 (3H, br. t, J=6.0 Hz, CH_3), 1.27 (14H, m, 7×CH_2), 1.78 (2H, m, CH_2), 4.27 (1H, dd, J=6.5, 4.5 Hz, CHOH), 5.52 (2H, br. s, OH and COOH). Found: C, 65.20; H, 10.99%. Calcd for $C_{11}H_{22}O_3$: C, 65.31; H, 10.96%.

2-Hydroxydodecanoic Acid (5i). 389 mg. IR (Nujol) 3600—2400, 3540, 1745, 1690 cm^{-1}; ($CHCl_3$) 3600—2400, 3510, 1715 cm^{-1}; ^1H NMR δ=0.88 (3H, br. t, J=6.5 Hz, CH_3), 1.26 (16H, m, 8×CH_2), 1.78 (2H, m, CH_2), 4.27 (1H, dd, J=6.5, 5.0 Hz, CHOH), 4.57 (2H, br. s, OH and COOH). Found: C, 66.44; H, 11.23%. Calcd for $C_{12}H_{24}O_3$: C, 66.63; H, 11.18%.

2-Hydroxytridecanoic Acid (5j). 491 mg. IR (Nujol) 3600—2400, 3540, 1745, 1690; ($CHCl_3$) 3600—2400, 3510, 1715 cm^{-1}; ^1H NMR δ=0.88 (3H, br. t, J=6.0 Hz, CH_3), 1.26 (18H, m, 9×CH_2), 1.78 (2H, m, CH_2), 4.27 (1H, dd, J=6.5, 5.5 Hz, CHOH), 4.47 (2H, br. s, OH and COOH). Found: C, 67.72; H, 11.31%. Calcd for $C_{13}H_{26}O_3$: C, 67.78; H, 11.38%.

References

1) H. Schildeknecht and K. Koob, *Angew. Chem., Int. Ed. Engl.*, **10**, 129 (1971).

2) Y. Iwanami and T. Iwadare, *Bot. Gaz.*, **139**, 42 (1978).

3) Y. Iwanami and T. Iwadare, *Bot. Gaz.*, **140**, 1 (1979).

4) Y. Iwanami, M. Iwamatsu, I. Okada, and T. Iwadare, *Experientia*, **35**, 1311 (1979).

5) Y. Iwanami, I. Okada, M. Iwamatsu, and T. Iwadare, *Cell Struct. Funct.*, **4**, 135 (1979).

6) Y. Iwanami, S. Nakamura, H. Miki-Hiroshige, and T. Iwadare, *Protoplasma*, **104**, 341 (1979).

7) The term of myrmic acid has been proposed for a group of growth inhibitors. See Ref. 3.

8) Y. Iwanami, E. Tazawa, and T. Iwadare, *Cell Struct. Funct.*, **4**, 67 (1979).

9) Y. Iwanami, E. Tazawa, and T. Iwadare, *J. Yokohama City Univ.*, **7**, 1 (1982).

10) Y. Iwanami, E. Fukuyasu, K. Kawakami, and K. Kazuno, *J. Yokohama City Univ.*, **6**, (Biol), 1 (1981).

11) Y. Kanaho, T. Sato, T. Fujii, Y. Iwanami, I. Iwadare, and K. Orito, *Chem. Pharm. Bull.*, **29**, 3063 (1981).

12) T. Iizuka, T. Iwadare, and K. Orito, *J. Fac. Agr. Hokkaido Univ.*, **59-2**, 262 (1979).

13) K. Orito, Y. Seki, A. Watanabe, M. Matsumoto, and T. Iwadare, *Phytochemistry.*, **25**, 941 (1986).

14) K. Orito, Y. Seki, Y. Iwanami, M. Murase, and T. Iwadare, *Japan. J. Palynol.*, **32**, 1 (1986).

15) K. Orito, T. Iwadare, and Y. Iwanami, *Phytochemistry*, **22**, 2316 (1983).

16) a) 2-Hydroxyalkanoic acids with the carbon number 12, 14, 16, 18, have been obtained from the saponifiable fraction of wool wax. see D. H. S. Horn, F. W. Hougen, E. von Rudloff, and D. A. Sutton, *J. Chem. Soc.*, **1954**, 177. b) The unsaponifiable fraction gave 1,2-diols of higher molecular weight. see D. H. Horn and F. W. Housgen, *J. Chem. Soc.*, **1953**, 3533.

17) 2-Hydroxyalkanoic acids have been known to be highly active on growth of *Lactobacillus Casei* 280-16. see M. N. Camien and M. S. Dunn, *J. Biol. Chem.*, **221**, 593 (1956). 1,2-Diols are also markedly growth-promoting. see M. N. Camien, M. S. Dunn, and E. Geller, *J. Biol. Chem.*, **220**, 169 (1961).

18) D. Seebach, *Angew. Chem., Int. Ed. Engl.*, **6**, 442 (1967).

19) a) R. E. Damon, T. Luo, and R. H. Schlessinger, *Tetrahedron Lett.*, **1976**, 2749. b) R. E. Damon and R. E. Schlessinger, *ibid.*, **1976**, 1561.

20) O. D. Dailey, Jr. and P. L. Fuchs, *J. Org. Chem.*, **45**, 216 (1980).

21) The *S*-alkyl or *S*-phenyl thioesters have been known to be excellent acylating agents and to react efficiently with ester enolates. see H-J. Liu and H. K. Lai, *Tetrahedron Lett.*, **1979**, 1193; Y. Yamada, T. Ishii, M. Kimura, and K. Hosaka, *ibid.*, **22**, 1353 (1981); M. Hatanaka, Y. Yamamoto, H. Nitta, and T. Ishimura, *ibid.*, **22**, 3883 (1981) and Ref. 19.

22) This signal disappeared by addition of deuterium oxide.

23) These multiplet or double double doublet signal became double doublet by addition of deuterium oxide, as shown by the arrow mark.

24) W. D. Emmons, A. S. Pagano, and J. P. Freeman, *J. Am. Chem. Soc.*, **76**, 3472 (1954).

25) E. von Rudloff, *Can. J. Chem.*, **36**, 486 (1958).

26) R. Criegee and E. Hoger, *Justus Liebigs Ann. Chem.*, **599**, 81 (1956).

27) D. Swern, G. N. Billen, and J. T. Scanlan, *J. Am. Chem. Soc.*, **68**, 1504 (1946).

28) I. A. Baser, *Fitte Seifen Anstrich.*, **74**, 524 (1972).

29) C. S. Maevel, D. W. MacCorquodale, F. E. Kendall and W. A. Lazier, *J. Am. Chem. Soc.*, **46**, 2838 (1924).

30) D. A. Konen, L. S. Silbert and P. E. Pfeffer, *J. Org. Chem.*, **40**, 3253 (1975).

31) T. Haga, *Nippon Kagaku Zasshi*, **81**, 948 (1960).

Uranyl Ion as a Highly Effective Catalyst for Internucleotide Bond Formation

Hiroaki SAWAI,* Kensei KURODA, and Takashi HOJO
Department of Chemistry, Faculty of Technology, Gunma University, Kiryu, Gunma 376
(Received January 12, 1989)

Uranyl ion catalyzes the polymerization of adenosine-5′-phosphorimidazolide very efficiently in aqueous solution. Up to 95% of the input adenosine-5′-phosphorimidazolide is converted to oligoadenylates from dimer to hexadecamer when 1 mM of UO_2^{2+} is used as a catalyst. The oligomeric products are predominantly 2′-5′ linked. The chain length and the regioselectivity of the resulting oligoadenylates varies greatly with the concentration of the UO_2^{2+} ion catalyst and the pH of the reaction medium. A high total yield of oligouridylates up to dodecamer is also obtained by UO_2^{2+} ion catalyst with high 2′-5′regioselectivity. The oligonucleotide formation is mediated by UO_2^{2+}-nucleotide complex.

An efficient procedure for the nonenzymatic synthesis of oligonucleotides from an activated nucleotide in aqueous solution has been interesting subjects of prebiotic chemistry[1,2] and biomimetic chemistry of nucleic acid biosynthesis,[3] and may provide a new synthetic methodology for the oligonucleotides. Nucleoside-5′-phosphorimidazolide is an activated nucleotide and hydrolyzes to nucleoside-5′-phosphate in the absence of a template or a catalyst. Previously we reported that metal ions such as Pb^{2+} and Zn^{2+}catalyze the oligomerization of nucleoside-5′-phosphorimidazolide to yield short oligonucleotides even in the absence of a template.[3] Pb^{2+} ion has been the most active catalyst. Most of the resulting oligomers are 2′-5′ internucleotide linked. The Pb^{2+}-ion catalyzed oligomerization was applied to the convenient synthesis of 2′-5′ linked oligonucleotides.[5] The mechanistic role of the metal ion catalyst on the oligonucleotide formation is unclear. However, we tentatively believe that the metal ion could organize the nucleoside-5′-phosphorimidazolide by coordination so as to promote internucleotide bond formation. The metal ion may also enhance the nucleophilicity of a OH group of the nucleotide. We have explored other efficient metal ion catalysts which can possibly play such roles, and found that uranyl ion is a highly effective catalyst for the oligonucleotide formation. Here we wish to report the uranyl ion-catalyzed oligonucleotide formation under various reaction conditions.

Experimental

Materials. Adenosine-5′-monophosphate and uridine-5′-monophosphate were purchased from Seikagaku Kogyo. *N*-Ethylmorpholine, from Tokyo Kasei was distilled before use. Imidazole, from Tokyo Kasei, was recrystallized from benzene. Uranyl nitrate was from Yoneyama Chemicals. Reagent grade triethylamine, triphenylphosphine, di-2-pyridyl disulfide, and lead nitrate were obtained commercially. Nuclease P1 (N.P1) was from Yamasa and venom phosphodiesterese (VPDase) from Worthington. Adenosine-5′-phosphorimidazolide was prepared from adenosine-5′-monophosphate and imidazole using triphenylphosphine and di-2-pyridyl disulfide as a condensing agent as described previously.[5a,6] Uridine-5′-phosphorimidazolide (ImpU) was prepared from uridine-5′-monophosphate and imidazole by a similar procedure.[5b]

Standard Procedure for the Polymerization of ImpA. Reactions were carried out in an Eppendorf tube. The reaction mixture was prepared on an ice bath by the addition of compounds in the following order; buffer solution, ImpA solution and finally uranyl nitrate solution. Samples of the mixture were agitated vigorously and kept at 20 °C for various periods of times. A typical reaction mixture (200 μl) contained ImpA (50 mM) and a catalytic amount of uranyl nitrate (10 μM—12.5 mM) in *N*-ethylmorpholine-HNO_3 buffer (0.2 M, pH 7.3) or imidazole-HNO_3 buffer (0.2 M^+, pH 6.0—8.0). When the reaction was carried out at pH 5.5 and 8.9, the pH of the reaction mixture was adjusted to the appropriate value with 0.1 M HCl or 0.1 M NaOH. The reactions were stopped by adding of 20 μl of 0.25 M EDTA solution. Samples were analyzed by high performance liquid chromatography (HPLC).

High-Performance Liquid Chromatograhpy on RPC-5. HPLC was taken with a Hitachi 638 apparatus with a stainless steel column (4 mm×25 cm) packed with RPC-5 material. The RPC-5 was prepared from Adogen 464 and granular polychlorotrifluoroethylene (2—10 μm) by a modification of the method described by Pearson et al.[7] The elution was carried out with a linear gradient of $NaClO_4$ solution (0—0.05 M) buffered with 2.5 mM Tris-acetate (pH 7.5) and 0.1 mM EDTA in 60 min at a flow rate of 1.0 ml min^{-1}. The eluate was monitored by UV absorption at 260 nm. Linkage isomers of oligoadenylates and oligouridylates with 2′-5′ and 3′-5′ internucleotide bonds were separated very well by HPLC on the RPC-5 column. Yields were calculated from peak integrals of the oligonucleotides on the HPLC chromatogram, after allowing for the hyperchromicity of each oligonucleotide. The hyperchromicity of the oligonucleotides up to the octamer was estimated by the ratio of UV absorption at 260 nm after and before alkaline hydrolysis as described previously.[5] We made no estimate of the hyperchromicity of the long oligonucleotides with chain length more than eight, using instead the value of the octamer for the calculation of the yield.

Characterization of Oligonucleotides. Identification of the resulting oligonucleotides was carried out by comparing the HPLC chromatogram with that of the authentic sample and by sequential enzyme and alkaline digestions. Authentic oligonucleotides up to the pentamer were

† 1 M=1 mol dm^{-3}.

obtained as described previously.[5a] When no authentic sample was available, oligonucleotides were identified by degradation with enzymes, alkaline or acidic medium.

The enzyme nuclease P1(N. P1) degrades 3′-5′ internucleotide linkage and is inactive to the 2′-5′ linkage. Thus digestion of the oligonucleotides with N. P1 distinguishes between 2′-5′ and 3′-5′ linked products. After treatment of a total sample with Chelex-100 to remove uranyl ion, digestion of the resulting oligonucleotides with N. P1 gave a series of fully 2′-5′ linked oligonucleotides. Digestion with N. P1 was performed at 37 °C for 2.5 h in a mixture (50 μl) containing the oligonucleotide (0.1—1.0 ODU), 0.03 M Veronal-acetate buffer (pH 5.75) and an enzyme solution (5 μg in 50 μl).

Venom phosphodiesterase (VPDase) degrades both 3′-5′ and 2′-5′ internucleotide linkage to give nucleoside-5′-monophosphate. It also cleaves a pyrophosphate bond. Degradation with VPDase was carried out at 37 °C for 2.5 h in a mixture (50 μl) containing the substrate (0.1—0.3 ODU), 0.01 M Tris-acetate (pH 8.8) 0.01 M $MgCl_2$ and enzyme solution (0.02 unit).

Alkaline hydrolysis of the oligonucleotides was carried out at room temperature for 1 d in a 0.5 M NaOH solution. The hydrolysis of a $(pA)_n$ oligomer containing both 2′-5′ and 3′-5′ linkage yielded on equivalent each of pAp and A and n-2 equivalent of Ap. The ratio of the resulting mononucleotides was determined by HPLC, which permits one to estimate the chain length. The HPLC of the mononucleotides was performed on a modified RPC-5 column with a linear gradient elution of $NaClO_4$ solution (0—0.01 M) buffered with 2.5 mM Tris-acetate (pH 7.5) and 0.1 mM EDTA in 15 min at flow rate of 1.0 ml min^{-1}.

Oligonucleotide-5′-phosphorimidazolide ($Im(pA)_n$, $Im(pU)_n$; n=2, 3, 4) was identified by conversion of the phosphorimidazolide with 1 M acetate buffer (pH 4.5) to the corresponding oligonucleotide-5′-monophosphate by acidic hydrolysis for 1 d. The compounds ImpA2′p5′A and Imp A2′p5′A2′p5′A were further confirmed by comparing the HPLC chromatogram with those of the authentic samples which were prepared from pA2′p5′A and pA2′p5′A2′p5′A in a way similar to that of ImpA.[5a]

Results and Discussion

ImpA was gradually hydrolyzed to pA in neutral aqueous solution in the absence of a template or metal ion catalyst. Addition of a catalytic amount of uranyl nitrate enhanced the polymerization of ImpA greatly and gave a good yield of long, predominantly 2′-5′ linked oligomers. A HPLC elution profile of the reaction mixture, in which 1 mM of uranyl ion ([ImpA]/[UO_2^{2+}]=50) was used as a catalyst, is shown in Fig. 1. The formation of the simple hydrolyzed product, pA was less than 1%. Oligoadenylates from dimer to hexadecamer were obtained in more than 95% total yield. Digestion of the total reaction mixture with nuclease P1 resulted in the disappearance of the

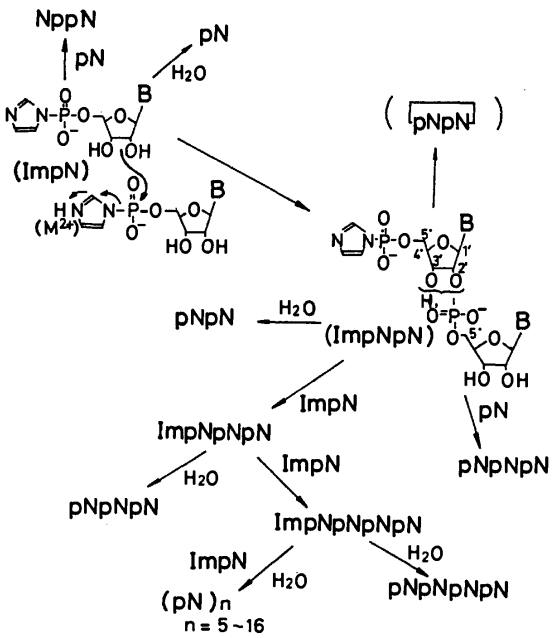

Scheme 1. Reaction scheme of the oligonucleotide formation.

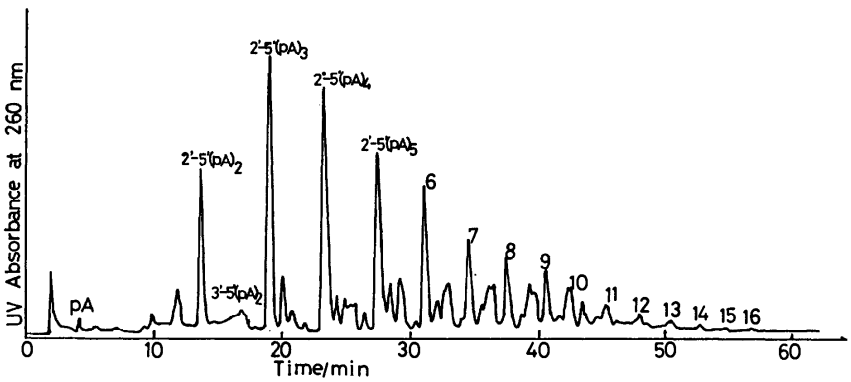

Fig. 1. HPLC elution profile of the products from the uranyl-ion catalyzed polymerization of ImpA. The reaction was run at 20 °C and pH 7.3 for 1 d. 50 mM of ImpA and 1 mM of uranyl nitrate were used for the reaction. The position of the fully 2′-5′ linked oligoadenylates from dimer to hexadecamer are indicated.

subsidary peaks, leaving only the series of main peaks, which indicates that the products are all 2′-5′ linked oligoadenylates. The subsidiary peaks to the right of the main peaks are oligomers of the same chain length containing one or more 3′-5′ linkages. The regioselectivity of the 2′-5′ internucleotide linkage decreased as the chain length of the oligomer increased. Thus the ratio of the fully 2′-5′ linked oligoadenylates was 98% in the case of dimer, and fell to 60% in the case of octamer. The yields of all 2′-5′ linked dimer, trimer, tetramer, pentamer, hexamer, heptamer and octamer were 5.6%, 13.9%, 11.9%, 10.4%, 6.9%, 4.1%, and 3.9%, respectively.

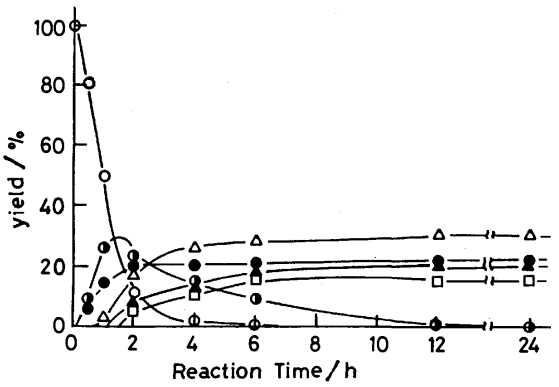

Fig. 2. Time course of the oligoadenylates formation ImpA. Reaction conditions: ImpA, 50 mM; $UO_2(NO_3)_2$, 1 mM; 20 °C; pH 7.3 ImpA, (○); $Im(pA)_2$+$Im(pA)_3$, (◑); $(pA)_2$+$(pA)_3$, (●); $(pA)_4$+$(pA)_5$, (△); $(pA)_6$—$(pA)_8$, (▲); $(pA)_9$, (□).

Figure 2 represents the time course of the polymerization of ImpA. Phosphorimidazolides of di- and triadenylate ($Im((pA)_n$, n=2, 3) formed initially in appreciable amounts, then gradually decreased. The chain length of the oligoadenylates increased with reaction time. The polymerization of ImpA in the presence of 1 mM of $UO_2(NO_3)_2$ catalyst at room temperature was almost complete in 8 h. The time course of the reaction indicates that this oligoadenylate formation proceeds stepwisely as shown in the Scheme 1.

Table 1 shows the effect of the concentration of the uranyl ion catalyst on the oligoadenylate formation. The catalyst concentration had large effect on the chain length and the internucleotide linkage of the resulting oligoadenylate. High catalyst concentration ($UO_2(NO_3)_2$=12.5 mM; [ImpA]/[UO_2^{2+}]=4) gave preferentially short-chained oligomers from dimer to pentamer in addition to small amounts of long oligomers over heptamer. The yields of long-chained oligomers increased as the catalyst concentration decreased and reached a maximum at 1 mM of $UO_2(NO_3)_2$, and fell off substantially at lower concentrations. The highest yield of total oligoadenylates was

Table 1. Oligoadenylate Formation Catalyzed by Uranyl Ion at Various Concentration

No.	$UO_2(NO_3)_2$	Time	Yield (%) (ratio of fully 2′-5′ linked oligomer)[a]											
	mM	day	ImpA	pA	AppA[b]	$Im(pA)_n$[c]	$(pA)_2$	$(pA)_3$	$(pA)_4$	$(pA)_5$	$(pA)_6$	$(pA)_7$	$(pA)_8$	$(pA)_{9-18}$
1	12.5	1	0.5	7.7	0.1	1.0	11.7 (98)	26.9 (74)	20.0 (70)	11.8 (64)	6.7 (54)	2.5	0.8	1.8[d]
2	5	1	0.9	4.2	0.1	1.1	8.7 (98)	19.5 (84)	18.0 (75)	13.6 (73)	10.7 (69)	5.1	3.0	8.9[e]
3	1	1	1.3	0.2	0.3	0.4	5.7 (98)	16.6 (83)	16.8 (71)	16.0 (65)	9.5 (73)	6.9	6.5	11.7[f]
4*	1	1	1.1	0.5	0.1	18.9	9.1 (98)	15.5 (79)	16.3 (68)	10.3 (59)	8.9 (60)	4.5	3.4	6.6[g]
5*	1	5	1.1	0.4	0.2	1.3	7.2 (97)	15.0 (82)	16.3 (72)	12.2 (62)	13.0 (57)	6.5	7.1	15.6[h]
6	0.25	1	1.4	0.5	0.4	4.3	19.8 (97)	29.0 (86)	20.8 (68)	10.7 (66)	5.1 (62)	2.9	0.8	1.7[i]
7	0.1	5	0.5	4.5	0.6	0.3	36.4 (95)	36.1 (82)	15.6 (57)	4.3 (58)	1.5			
8	0.05	5	1.3	14.3	2.0	1.9	50.8 (91)	21.0 (70)	6.1 (41)	1.1	0.3			
9	0.01	5	9.8	34.2	3.3	4.2	36.4 (70)	10.0 (35)	2.3 (25)	0.6				
10	0	14	9.2	81.8	8.0		0.9 (77)	0.1						
11	1 $Pb(NO_3)_2$[j]	5	26.1	37.9	2.7	4.1	22.3 (91)	4.3 (65)	1.0	0.2				

Reactions were run at 20 °C in 0.2 M *N*-ethylmorpholine-HNO_3 buffer (pH 7.3), except for Nos. 4 and 5 where reactions were run at 0 °C in the same buffer. 50 mM of ImpA was used in the reaction.
a) Ratio of the fully 2′-5′ linked oligomers is shown in the parenthesis below the yield data of each oligoadenylate. b) P^1,P^2-diadenosine 5′-pyrophosphate. c) $Im(pA)_2$, $Im(pA)_3$, and $Im(pA)_4$ are included. d) $(pA)_9$+$(pA)_{10}$. e) $(pA)_9$—$(pA)_{13}$. f) $(pA)_9$—$(pA)_{16}$. g) $(pA)_9$—$(pA)_{14}$. h) $(pA)_9$—$(pA)_{18}$. i) $(pA)_9$+$(pA)_{10}$. j) $Pb(NO_3)_2$ was used instead of $UO_2(NO_3)_2$.

obtained with 1—0.25 mM of $UO_2(NO_3)_2$. The proportion of the yield of the fully 2′-5′ linked oligoadenylate to that of the total oligomers with the same chain length are shown in the parenthesis in Table 1. The 2′-5′ regioselectivity of the oligoadenylates was almost the same when 12.5 mM—0.25 mM of uranyl ion was used as a catalyst. Hydrolysis of phosphorimidazolide competes with the internucleotide bond formation and decreases the chain length of the oligoadenylate at lower catalyst concentrations. Thus the yield of short-chained oligoadenylates reached a maximum at 0.25—0.05 mM of the uranyl ion catalyst. 0.05 mM of the uranyl ion gave the 2′-5′ diadenylate in 46.2% yield. The 2′-5′ linked trimer and tetramer were formed in significant yields at 0.1—0.25 mM of uranyl ion catalyst. The catalytic effect of $UO_2(NO_3)_2$ was still significant at concentrations as low as 0.01 mM, though a significant degree of hydrolysis of ImpA took place. Concentration of the catalyst below 0.1 mM decreased the 2′-5′ regioselectivity. The lower the concentration, the lower the proportion of the 2′-5′ linkage of the resulting oligoadenylates. Thus 0.01 mM of the uranyl ion gave 2′-5′ and 3′-5′ linked dimers in 25.4% and 11.0% yield, respectively.

We carried out the polymerization at 0 °C in the presence of 1 mM of uranyl nitrate. The low temperature suppressed the hydrolysis of the phosporimidazolide bond more strongly than the internucleotide bond formation. Therefore, completion of the reaction required long reaction time at 0 °C. On the other hand the yield of long-chained oligoadenylates increased at 0 °C, and oligoadenylates up to octadecamer were obtained at 0 °C for 1 day.

Table 2 presents the effect of pH of the medium on the oligoadenylate formation. The reaction was carried out in the presence of 1 mM $UO_2(NO_3)_2$ catalyst in imidazole buffer between pH 6.0 and 8.0. Replacement of *N*-ethylmorpholine buffer with imidazole buffer at pH 7.3 did not change the total yield of the oligoadenylate, but effected a small decrease in long-chained oligoadenylates. Imidazole coordinates to the UO_2^{2+} ion, which might suppress the UO_2^{2+}-ion catalyzed internucleotide bond formation to some extent. The reactions were also conducted at pH 5.5 and 8.9. At pH 5.5 and 6.0, only small amounts of dimer and trimer were formed with low 2′-5′ regioselectivity. Instead, P^1,P^2-diadenosine 5′-pyrophosphate formed in addition to the hydrolysis of ImpA to pA. The oligoadenylate formation was markedly enhanced at pH 6.5 and increased with the higher of pH of the medium. Optimum pH for the polymerization to obtain 2′-5′ linked oligoadenylates was around pH 7.5. When the reaction was carried out at pH 8.9, both the rate of hydrolysis of phosphorimidazolide and the internucleotide bond formation slowed down, resulting in the low yield of oligoadenylates after 1 day.

In a similar way, the UO_2^{2+} ion catalyzes the oligomerization of ImpU, giving oligouridylates from dimer to dodecamer in high total yields, as shown in Table 3. The resulting oligouridylates contained mainly 2′-5′ internucleotide linkage. Cyclic dimer and trimer were obtained in substantial amounts in addition to the linear oligomer.

The effective catalytic activity of the UO_2^{2+} ion for the internucleotide bond formation is surprising. Without a template or an enzyme, no long-chained oligonucleotide has been obtained in aqueous solution. The UO_2^{2+} ion catalyzes the oligonucleotide-bond formation far more effectively than the Pb^{2+} ion

Table 2. Effect of pH of Medium on Oligoadenylates Formation Catalyzed by Uranyl Ion

pH	Yield (%) (Percentage of fully 2′-5′ linked oligomer)[a]												
	ImpA	pA	AppA	Im(pA)$_2$	(pA)$_2$	Im(pA)$_3$	(pA)$_3$	(pA)$_4$	(pA)$_5$	(pA)$_6$	(pA)$_7$	(pA)$_8$	(pA)$_{9-14}$
5.5		63.6	24.3		8.8		3.2						
					(67)		(47)						
6.0		48.7	26.6		12.1		5.8						
					(66)		(48)						
6.5	0.1	0.8	0.1		13.3		24.5	21.4	13.2	7.9	4.9	23.2	2.3
					(97)		(79)	(63)	(45)	(43)			
7.0	0.4	1.2	0.5		10.2		17.8	19.2	14.0	9.4	7.0	4.8	5.4
					(96)		(77)	(63)	(51)	(46)			
7.5	0.1	0.2	0.5	0.3	5.8	0.2	16.5	17.3	13.3	9.7	6.9	6.3	8.5
					(98)		(73)	(60)	(51)	(40)			
8.0	0.5	0.3	0.3	3.1	5.7	3.5	16.0	18.5	13.6	9.2	6.3	5.7	6.8
					(98)		(67)	(62)	(52)	(42)			
8.9	15.9	0.1	tr	31.2	9.1	7.6	18.2[b]	9.3[c]	4.9	1.7	0.4	0.2	
					(98)		(41)	(52)	(43)				

Reactions were run at 20 °C for 1 day in 0.2 M-imidazole-HNO_3 buffer. At pH 5.5 and 8.9, pH of the reaction mixture was adjusted with 1 M HCl or 1 M NaOH solution 50 mM of ImpA and 1 mM of uranyl nitrate were used in the reaction.

a) Ratio of the fully 2′-5′ linked oligomer is shown in the parenthesis below the yield data of each oligoadenylate. b) Small amount of Im(pA)$_4$ is included. c) Small amount of Im(pA)$_5$ is included.

Table 3. Oligouridylates Formation Catalyzed by Uranyl Ion

$UO_2(NO_3)_2$	Time	Yield (%) (ratio of fully 2′-5′ linked oligomer)[a]										
mM	day	PU+ImpUUppU		$\lceil pU_2 \rfloor$	$(pU)_2$	$\lceil pU_3 \rfloor$	$(pU)_3$	$(pU)_4$	$(pU)_5$	$(pU)_6$	$(pU)_7$	$(pU)_{8-12}$[b]
1	1	5.1	tr	14.6	3.6 (97)	4.6	13.3 (65)	12.1 (62)	11.8 (36)	8.2	6.2	14.8
0.25	1	7.2	0.1	14.3	6.0 (98)	3.1	17.3 (69)	15.2 (59)	10.8 (29)	4.6	3.2	6.2
0.05	5	10.4	0.7	12.1	30.0 (94)	2.0	19.6 (64)	11.5 (36)	5.9 (27)	2.5		
0.01	5	44.1	1.6	4.9	29.7 (77)	1.0	9.1 (41)	3.1 (35)				

Reactions were run at 20 °C in 0.2 M imidazole-HNO_3 buffer (pH 7.5). ImpU (50 mM) was used in the reaction. a) Ratio of the fully 2′-5′ linked oligomer is shown below the yield data of each oligouridylate in the parenthesis. b) Oligouridylates with chain length eight to twelve are included.

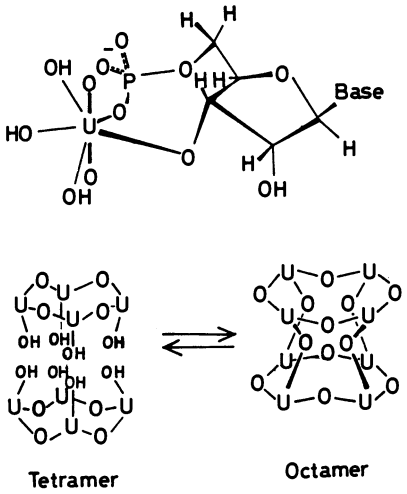

Fig. 3. Structure of the uranyl complex of 5′-nucleotide proposed by Kainosho et al.

which has been considered the most efficient catalysis.[4] High concentration of Pb^{2+} ion is required for its catalytic activity. 0.1 mM of Pb^{2+} ion has a negligible effect on the oligoadenylate formation. 12.5 mM of Pb^{2+} ion catalyst gives oligoadenylates up to hexamer.[4]

Our results do not permit us to draw any conclusions about the reaction mechanism. However the oligoadenylate formation is probably mediated by a uranyl complex of ImpA. The structure of the UO_2^{2+}-ImpA complex remains unclear, but probably is similar to that of the uranyl complex of pA. Two unique structures for the UO_2^{2+}-pA complex have been proposed from NMR studies.[8,9] In an early study, Feldman et al. proposed a dimeric structure in which 2′- and 3′-hydroxyl groups of ribose ring coordinate to the uranyl ion with removal of protons.[8] The 3′-oxo group coordinates to both uranyl ions working as a bridging ligand. Later Kainosho et al. reported a revised structure from the study of 500 MHz NMR and C-13 NMR of the complex from [N^{15}]pA.[9] They claimed that the uranyl complex of nucleoside-5′-monophosphate is composed of several oligomeric species with hydroxo or oxo bridges. Each species has a common structural unit as shown in Fig. 3. The primary coordination sites are phosphate and 3′-hydroxyl group with a removal of a proton.

We tentatively postulate that the uranyl complex of ImpA could form a polymeric structure similar to that claimed for the UO_2^{2+}-pA complex.[9] The activation of 2′-OH of the ribose moiety in the complex by hydrogen bond with 3′-oxo group may be responsible for the efficient 2′-5′ internucleotide bond formation. The formation of polymeric UO^{2+} complex of ImpA could be favorable for the long oligoadenylates formation, since ImpA could line up on uranyl ions in the polymeric complex. The polymeric uranyl ion probably works as a kind of a template. The detailed discussion of the mechanistic roles of UO^{2+} ion for the oligonucleotide formation needs further study of the uranyl complex of ImpA and other nucleotides.

The uranyl ion-catalyzed oligoadenylate synthesis from ImpA has a potent synthetic utility. Since the isolation of 2′-5′ linked triadenylate (2-5A) from interferon-treated cells and the discovery of its strong biological activity,[10] 2—5A and its analogues have been synthesized by a number of groups.[11] Recently, Torrence et al. reported that 2′-5′ linked hexadenylate inhibits DNA topoisomerase reaction.[2] They suggested that 2′-5′ linked oligoadenylates of sufficient chain length may be involved in mediating the interferon-induced translational regulation by an inhibition of DNA topoisomerase. The oligoadenylate synthesis with UO^{2+} ion catalysts seems to provide the most efficient and convenient method for making the 2′-5′ linked oligoadenylates with desired chain length. Any chain length of the oligomer from dimer to decamer can be obtained by changing the catalyst concentration or pH of the medium.

Finally we mention the significance of this reaction in the context of prebiotic chemistry. Egami has suggested that the metal ion which is abundant in seawater was incorporated into protoenzymes, which have evolved to contemporary metalloenzymes.[13] The abundant metal ions in seawater are generally

essential for life. The UO^{2+} ion is more abundant in seawater than the Co^{2+} ion which is essential for many living organisms.[13] No long-chained oligonucleotide has been obtained in the model reactions of prebiotic synthesis without a template. The UO^{2+} might have worked as a catalyst for oligonucleotide formation in the stage of chemical evolution, though its function disappeared during the later evolution.

This work was supported partially by a Grant-in-Aid from the Ministry of Education, Science and Culture.

References

1) L. E. Orgel and R. Lohrmann, *Acc. Chem. Res.*, **7**, 368 (1974).

2) a) R. Lohrmann, P. K. Bridson, and L. E. Orgel, *Science*, **208**, 1464 (1980). b) J. H. G. Van Roode and L. E. Orgel, *J. Mol. Biol.*, **144**, 579 (1980).

3) a) T. Inoue and L. E. Orgel, *J. Mol. Biol.*, **162**, 201 (1982). b) T. Inoue and L. E. Orgel, *Science*, **219**, 856 (1983).

4) H. Sawai, *J. Am. Chem. Soc.*, **98**, 7037 (1976).

5) a) H. Sawai, T. Shibata, and M. Ohno, *Tetrahedron*, **37**, 481 (1981). b) H. Sawai and M. Ohno, *Chem. Pharm. Bull.*, **29**, 2237 (1981). c) H. Sawai and M. Ohno, *Bull. Chem. Soc. Jpn.*, **58**, 361 (1985).

6) R. Lohrmann and L. E. Orgel, *Tetrahedron*, **34**, 853 (1978).

7) R. L. Pearson, J. F. Weiss, and A. D. Kelmers, *Biochim. Biophys. Acta*, **228**, 770 (1971).

8) a) R. P. Agarwal and I. Feldman, *J. Am. Chem. Soc.*, **90**, 6635 (1968). b) I. Feldman and K. E. Rich, *ibid.*, **92**, 4559 (1970).

9) M. Kainosho and M. Takahashi, *Nucleic Acids Res. Symp. Ser.*, **12** 181 (1983).

10) a) I. M. Kerr and R. E. Brown, *Proc. Natl. Acad. Sci. U. S. A.*, **75**, 256 (1978). b) L. A. Ball and C. White, *ibid.*, **75**, 1167 (1978). c) P. Lengyel, "Interferon," ed by I. Gresser, Academic Press, New York (1981), ed by pp. 78—99.

11) a) M. Ikehara, K. Oshie, and E. Ohtsuka, *Tetrahedron Lett.*, **1979**, 3677. b) H. Sawai, T, Shibata, and M. Ohno, *ibid.*, **1979**, 4573 c) J. A. J. den Hertog, J, Doornbos, R. Crea, and J. H. Van Boom, *Recl. Trav. Chim. Pays-Bas*, **98**, 469 (1979). d) S. S. Jones and C. Reese *J. Am. Chem. Soc.*, **101**, 7399 (1979). e) K. K. Ogilvie and N. Y. Theriault, *Tetrahedron Lett.*, **1979**, 211. f) J. Engels and U. Krahmer, *Angew. Chem.*, **91**, 1007 (1979). g) R. Charubara and W. Pfleiderer, *Tetrahedron Lett.*, **21**, 1933 (1980). h) C. Gioele, M. Kwiatowski, B. Oberg, and J. B. Chattopdhyaya, *Tetrahedron Lett.*, **22**, 1741 (1981). i) Y. Hayakawa, M. Uchiyama, T. Nobori, and R. Noyori, *Tetrahedron Lett.*, **26**, 761 (1985).

12) F. J. Castora and P. F. Torrence, Abstracts of the ISIR Meeting on the Interferon system, Washington D. C., November, 1987, p. 727.

13) F. Egami, *J. Mol. Evol.*, **4**, 113 (1974).

Ring-Opening Fluorination and Ring-Expansion Fluorination of Cyclopropanemethanols with Amine/Metal Fluoride/ Poly(hydrogen fluoride)-Pyridine Complex

Shigekazu KANEMOTO, Makoto SHIMIZU,* and Hirosuke YOSHIOKA*
The Institute of Physical and Chemical Research (RIKEN), Wako, Saitama 351-01
(Received January 20, 1989)

Treatment of cyclopropanemethanols with pyridinium poly(hydrogen fluoride) in the presence of diisopropylamine and KHF_2 gave selectively homoallylic fluorides or fluorocyclobutanes according to the mode of substitution of the starting cyclopropanemethanols. Cyclopropanemethanols with no substitution at 1-position of the cyclopropane ring gave homoallylic fluorides in a stereoselective manner. While, 1-methylcyclopropanemethanol gave the fluorocyclobutane in high stereoselectivity. Fluorocyclobutanes containing hydroxymethyl group were also prepared from 2-(1-methylcyclopropyl)oxiranes. The amine and the metal fluoride were necessary as additives for the best results. Influencing factors involving solvents and temperature for the reactions are also described.

Organic synthons containing a single fluorine atom have been increasingly attracting attentions of chemists in agricultural, and pharmaceutical research areas because of their unique chemical and biological characters useful for the molecular design works.[1] For example, certain monofluorinated steroids[2] are selectively metabolized by insects to generate highly toxic fluoroacetic acid revealing potentiality as new insecticide. Some amino acids containing a fluoromethyl group have been known to be potent suicide inhibitors to enzymatic decarboxylation.[3]

There are two approaches to synthesize monofluorinated compounds. The first is an introduction of a fluorine atom onto a molecule by fluorination of alcohols or halides, and even hydrides. DAST,[4] HFP-DA,[5] quaternary ammonium fluorides,[6] or specifically modified metal fluorides[7] with crown ethers,[8] are recently developed for the nucleophilic fluorination, and F_2,[9] CF_3OF,[10] XeF_2,[11] or other modified hypofluorite reagents are for direct fluorination. The second is to make use of fluorinated building blocks or their equivalents.[12]

Among them, homoallylic fluorides are the most versatile intermediates for synthesis of a variety of monofluorinated bioactive compounds. However, there has been no pertinent method for selective fluorination leading to homoallylic fluorides. Attempts to prepare homoallylic fluorides by nucleophilic substitution of corresponding alcohols or their derivatives often results in troublesome contaminations of by-products. Particularly, fluorination of tertiary hydroxyl groups is hardly successful. For example, fluorination of 4-phenyl-3-buten-1-ol with a common fluorinating reagent such as DAST, gave only dehydrated ethers and dienes.

Thence, we attempted to use cyclopropanemethanols as better precursors to homoallylic fluorides, since a cyclopropylmethyl cation generated from a cyclopropanemethanol or its derivative with pyridinium poly(hydrogen fluoride) will be possibly rearranged to a homoallylic cation, that is promptly quenched with a fluoride anion. Here we wish to report a selective preparation of homoallylic fluorides by the ring-opening fluorination of cyclopropanemethanol derivatives. In addition, selective synthesis of monofluorocyclobutanes containing a *tertiary* fluorine atom is also described for 1-substituted cyclopropanemethanols and corresponding epoxides.[13]

Synthesis of Homoallylic Fluorides Using Modified Pyridinium Poly(hydrogen fluoride) by Ring-Opening Fluorination. Ring opening halogenation of cyclopropanemethanols with aqueous hydrogen bromide or hydrogen chloride has been known as Julia rearrangement, that gives the corresponding homoallylic bromides or chlorides.[14] However, application of this method for fluorination of cyclopropanemethanols with aqueous hydrogen fluoride was not successful at all. Nucleophilicity of water is much stronger than that of fluoride anion, and this gave rise to only homoallylic alcohols and ethers due to self-condensation. In order to make the reaction media anhydrous, we employed the Olah's reagent[15] as fluoride anion source. Olah's reagent, or pyridinium poly(hydrogen fluoride): $(HF)_n \cdot Py$ is widely used, known to be the most useful for halo- or hydro-

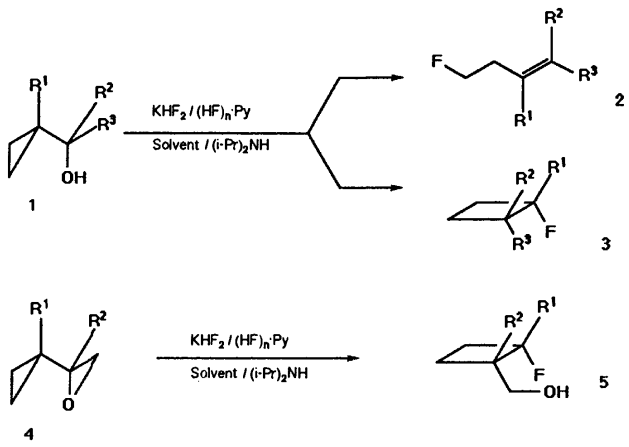

Scheme 1.

fluorination of olefins as well as fluorination of alcohols. However, the attempted fluorination of cyclopropanemethanols with the reagent afforded a homoallylic fluoride in poor yield with major contamination of homoallylic alcohols, ethers, and other by-products. It was obvious that poly(hydrogen fluoride) behaved majorly as acid catalyst for ring opening and self-condensation, and not as a reagent for nucleophilic fluorination. This result indicated that it was necessary to activate the fluoride anion more than ever. In order to control the acidity of the system and to activate fluoride anion, we tried certain additives with co-solvents. Various aromatic and aliphatic amines were employed as co-solvent together with inorganic fluorides, NaF, KF, KHF_2, CsF, and quaternary ammonium fluorides for additives. A number of combinations of an amine with a fluoride salt were screened for better result and selectivity using α-phenylcyclopropanemethanol (**6**) as a model substrate. The role of these additives may be explained as follows. These amines diminish the degree of aggregation of poly(hydrogen fluoride), and activate the fluoride anion as nucleophile giving "ammonium fluoride" type reaction species which is more reactive than fluoride anion in Olah's reagent. Second, fluoride salts increase the concentration of fluoride anion and its nucleophilicity. Among them, a combination of diisopropylamine with KHF_2 dried up in a microwave oven gave the best result. Dried KHF_2 has an additional advantage to behave as dehydrant and to avoid the attack of water which was generated from dehydration of an alcohol moiety. The choice of solvents is also essentially important. For example, ethereal solvents such as diethyl ether, or tetrahydrofuran, which are commonly used with $(HF)_n \cdot Py$, were not applicable at all for this reaction. These solvents behaved as nucleophile giving complex products.[16] Only chloroalkanes and chlorobenzene gave acceptable results. Their stability together with lipophilicity and polarity appears to be critical for the reaction. A variety of substituted cyclopropanemethanols were treated in this reaction system, and the results are summarized in Tables 1 and 2. We employed the procedure to add the $(HF)_n \cdot Py$ into a mixture of substrate, KHF_2, and diisopropylamine in dichloromethane or chlorobenzene at 0 °C. Addition of a solution of substrate into a reagent mixture always decreased the yields of the products. In the presence of a certain functional group(s) such as phenyl, vinyl, and alkynyl group which stabilize α-carbocation, the reaction generally proceeds in good yield and selectivity. On the other hand, an α,α-dialkyl-substituted substrate gave the homoallylic fluoride in poor yield (Run 4, Table 1), and majorly yielded diene products. Attack of a fluoride anion generally occurred at the more substituted carbon atom (Runs 1 and 6, Table 2). In the case of the substrate (**28**), only a ring opened and condensed product was obtained under the standard reaction conditions. Among the condi-

Table 1. Formation of Primary Homoallylic Fluorides with Modified Hydrogen Fluoride

Run	Substrate	Product	Yield(%)[a,b]
1	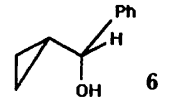 **6**	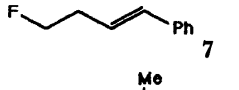 **7**	73(100/0)
2	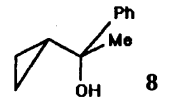 **8**	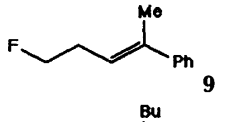 **9**	65 (95/5)
3	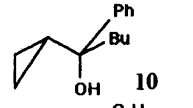 **10**	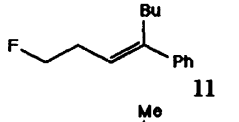 **11**	55(85/15)
4	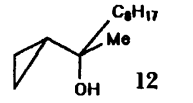 **12**	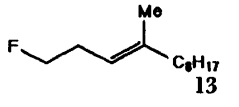 **13**	37(65/35)
5	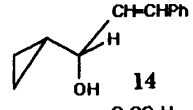 **14**	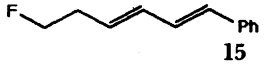 **15**	70(100/0)
6	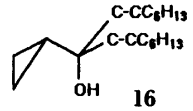 **16**	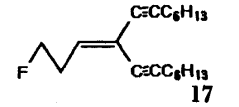 **17**	62

a) Isolated yield. b) Figures in parentheses were *E/Z* ratio of products. Major isomers are shown in the table.

Table 2. Ring-Opening Fluorination of Substituted or Functionalized Cyclopropanemethanols

Run	Substrate	Product	Yield(%)
1	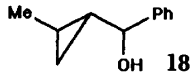 **18**	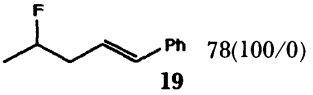 **19**	78(100/0)
2	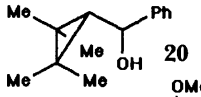 **20**	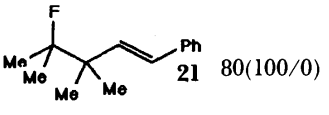 **21**	80(100/0)
3	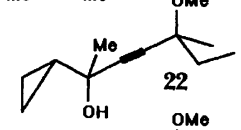 **22**	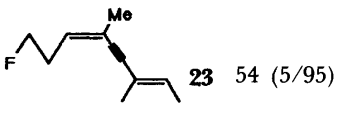 **23**	54 (5/95)
4	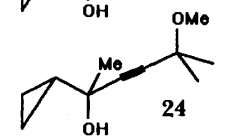 **24**	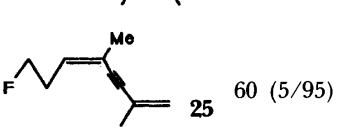 **25**	60 (5/95)
5	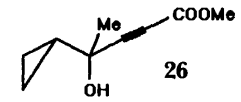 **26**	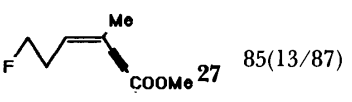 **27**	85(13/87)
6	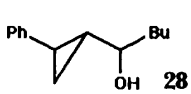 **28**	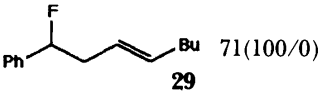 **29**	71(100/0)

a) Isolated yield. b) Figures in parentheses were *E/Z* ratio of products. Major isomers are shown in the table.

tions tried, the best result was obtained in an inverse addition mode. Dropwise addition of a THF solution of the substrate into the mixture of KHF_2, and $(HF)_n \cdot Py$ in THF with $(i\text{-}Pr)_2NH$ gave the desired fluoride (**29**) in 71% yield.

Stereochemistry of the resultant olefin was highly dependent on the steric factor of the substituent at the α-carbon, and a more bulky group is always at trans position to the 2-fluoroethyl group in the resultant olefin. The tertiary ethers (**22**, **24**), could not stand the reaction conditions. Elimination to yield the corresponding olefin was predominant. On the other hand, ester moiety was not affected (Run, 5, Table 2).

These homoallylic fluorides have wide applicability as substrate to the synthesis of monofluorinated analogues of known bioactive compounds as prototype. For example, fluorinated fenvalerate (**31**) was first prepared from α-methyl-α-phenylcyclopropanemethanol (**30**) in good overall yield, and juvenile hormone mimic (**32**) and anti-juvenile hormone mimic (**33**) have been also prepared in a few steps. These compounds showed similar activities as those of the prototypes.[17]

Synthesis of Fluorocyclobutanes Using 1-Substituted Cyclopropanemethanol Derivertives by Ring-Expansion Fluorination. In the course of experiments dealing with ring opening fluorination, we wish to expand it to a synthesis of fluorocyclobutanes. A cyclopropylmethyl cation can be smoothly rearranged to a homoallylic cation with release of ring strain. When a cyclopropane ring has a substituent at 1-position, generation of tertiary cyclobutyl cation by ring expantion would be preferred to rearrangement to primary homoallylic cation, although cyclobutane still has certain ring strain.[18] Then a fluoride anion would immediately attack the cyclobutyl cation to form fluorocyclobutane. Based on the hypothesis, we examined the reaction of 1-methyl-α-phenylcyclopropanemethanol (**34**) with $(i\text{-}Pr)_2NH\text{-}KHF_2\text{-}(HF)_n \cdot Py$ complex in dichloromethane at 0 °C, and it gave fluorocyclobutane in moderate yield. Ring expantion fluorination of α,1-dimethyl-α-phenylcyclopropanemethanol (**36**) gave selectively 1-fluoro-1,2-dimethyl-*trans*-2-phenylcyclobutane (**37**) in 75% yield, but the similar treatment without $(i\text{-}Pr)_2NH$ and/or KHF_2

Table 3. Ring-Expansion Fluorination of 1-Substituted Cyclopropanemethanols

Run	Substrate	Product	Yield(%)
1	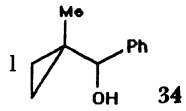 **34**	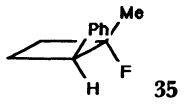 **35**	71 (95/5)
2	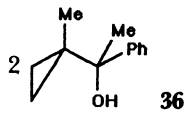 **36**	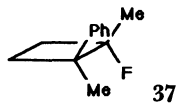 **37**	75 (95/5)
3	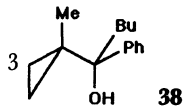 **38**	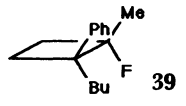 **39**	64 (95/5)
4	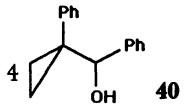 **40**	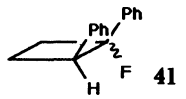 **41**	62(45/55)[c]
5	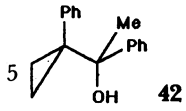 **42**	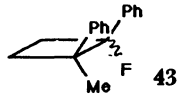 **43**	68(59/41)[c]
6	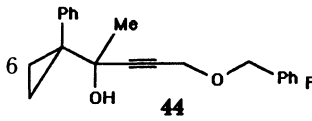 **44**	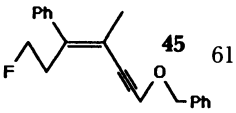 **45**	61

a) Isolated yield. b) Figurs in parentheses are trans/cis ratio of products. Major isomers are shown unless otherwise noted. c) Phenyl-F trans/cis ratio.

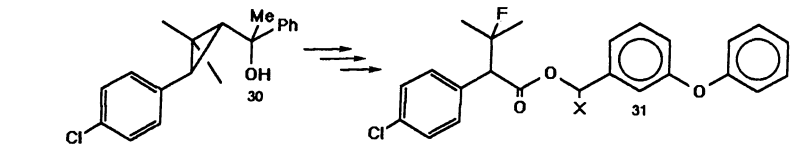

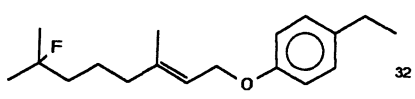

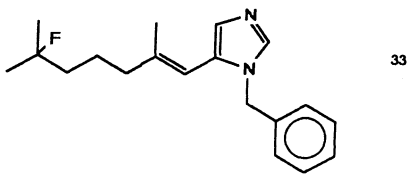

Fig. 1.

failed to give the fluorocyclobutane.

Usually poly- and perfluorocyclobutanes are synthesized via thermal,[19] photochemical,[20] or Michael type[21] [2+2] cycloaddition of polyfluoroolefins, which do not appear to be applicable to the synthesis of monofluorocyclobutanes.[22] Besides, regio- and stereochemistry would not be controlled during the cycloaddition if monofluoroolefins were available at all.

This ring expansion reaction was also sensitively affected by solvent for reaction, and we found dichloromethane or chlorobenzene to be the best solvents. The reaction temperature is also crucial to the yield of the fluorocyclobutane. For example, the substrate (**34**) gave the fluorinated cyclobutane (**35**) in 77% yield at −20 °C, whereas the yield decreased to 40% at 0 °C.

The stereoselectivity in fluorine introduction to the cyclobutane ring is highly dependent on the substituent "R^1" on the cyclopropane ring. The substrates containing methyl group for R^1 generally gave the cyclobutanes in high stereoselectivity. Fluorine was introduced in "trans" orientation to the bulkier group at the α-position of the cyclobutane in over 95% stereoselectivity (determined by HPLC, Runs 1, 2, and 3, Table 3). However, the substrates with phenyl group as R^1 gave the trans-products in the lower stereoselectivities (Runs 4 and 5). This may be explained in terms of the fixed geometry of the initially formed carbocation (**46**) due to the steric conflict between the endo hydrogen atoms and R^2, and this results in the observed high stereoselectivity (Fig. 2). When R^1 and R^2 are phenyl groups (Runs 4 and 5), each conformation (**46a**, **46b**) is equally possible and this may cause the formation of cis and trans fluorides. Another possible explanation of the low stereoselectivities observed for formation of **41** and **43** seems to be due to the cyclobutyl cation (**47**) stabilized by an extra phenyl group. The resultant plane sp^2 carbon would reduce the selectivity.[23]

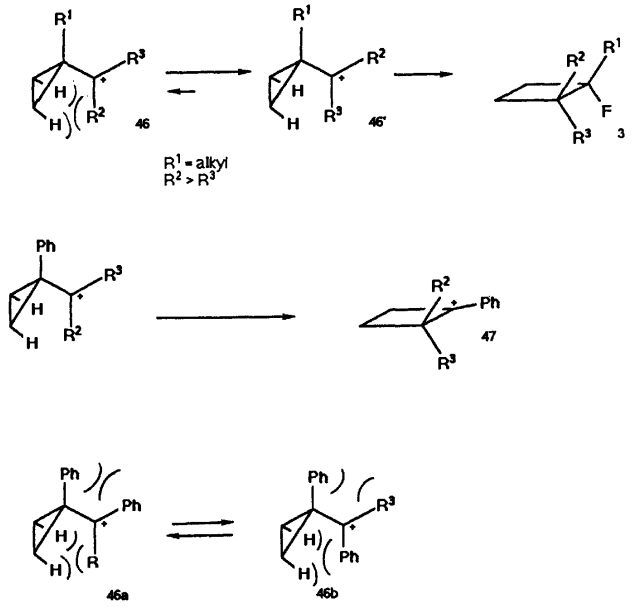

Fig. 2.

Initial formation of the carbocation is supported by the following result. Chiral (*R*)-(+)-1-methyl-α-phenylcyclopropanemethanol (**34**) as prepared from (*R*)-(+)-mandelic acid in three steps, gave the racemic fluorocyclobutane (**35**) losing perfectly its optical integrity.

The reaction pathway is controlled in accordance with the substituent R^1 on the cyclopropane and R^2 at the α-position of the hydroxyl group. No ring rearrangement occurred when substrates having an electron withdrawing group such as acyl or cyano group as R^1 on the cyclopropane ring were applied. These groups appear to prevent the formation of the rearranged carbocation.[24] As for R^2, in sharp contrast to the alkyl or phenyl substituents, the substrates containing the α-acetylenic or olefinic functions were converted exclusively to the corresponding homoallylic fluorides (Run 6, Table 3). The distinct control on the selection of these alternative pathways can be attributed to an electronic effect of acetylenic or olefinic group in the substituent R^2.

Parallel Ring Rearrangement of 2-(1-Substituted cyclopropyl)oxirane to Hydroxymethyl-Substituted Fluorocyclobutanes. It was necessary to seek a group of new substrates in order to provide fluorocyclobutanes whose substituent is variously functionalized for

Table 4. Synthesis of Hydroxymethyl-Substituted Fluorocyclobutanes Using Epoxycyclopropanes

Run	Substrate	Product	Yield(%)[a,b]
1	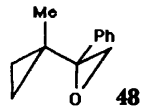 **48**	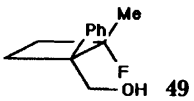 **49**	83 (5/95)
2	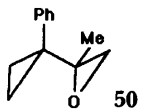 **50**	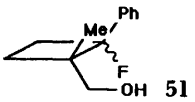 **51**	87(46/54)[c]
3	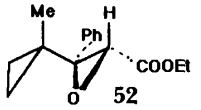 **52**	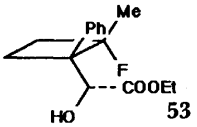 **53**	60 (5/95)
4	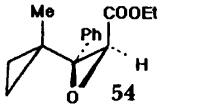 **54**	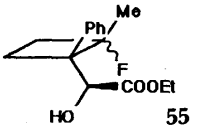 **55**	26(45/55)[d]

a) Isolated yield. b) Figures in parentheses are trans/cis ratio of products. Major isomers are shown unless otherwise noted. c) Hydroxymethyl-F trans/cis ratio. d) Phenyl-F trans/cis ratio.

further transformation. Cyclopropyloxirane was expected to generate fluorocyclobutanes containing hydroxymethyl group at the adjacent position of the fluorinated carbon atom upon the ring-expansion fluorination. Moreover, this parallel three-membered ring system, a cyclopropane connected with oxirane ring, has certain advantages over cyclopropanemethanols. That is, the substrate has highly strained ring system and appear to be more favored to form carbocation. Moreover, on the contrary to the cyclopropanemethanol substrates, oxiranes do not generate water that is adverse to the reaction media under the current fluorination conditions.

Under similar reaction conditions as before, the cyclopropyloxirane (**48**) was transformed stereoselectively into the fluorocyclobutane (**49**) in 83% yield (Table 4). The product has a "trans" configuration with respect to the fluorine and the phenyl groups. As it is similar to the case of the cyclopropanemethanols, the stereoselectivity decreased with the 1-phenylcyclopropyl counterpart (**50**) resulting in nearly a 1 : 1 stereoisomeric mixture (**51**) in moderate yields. Interestingly, the 2-(ethoxycarbonyl)oxirane (**52**) gave the geometrically pure fluorocyclobutane (**53**) in 60% yield (see Table 4). We assume that the oxirane (**52**) can easily take the conformation necessary for the anti-displacement of the C_1-C_2 bond of the cyclopropane when attacked by fluoride anion. In contrast, the stereoisomer (**54**) gave an isomeric mixture of fluorocyclobutane (**55**) in poor yield. Main product was an α-hydroxy-γ-lactone via intramolecular ring formation. The influencing factor over the reaction course may be ascribed for the conformation of the ethoxycarbonyl group in **54**, where the generated cyclobutyl cation and the ethoxycarbonyl group were situated closely. As result, intramolecular attack of oxygen occurred much faser than intermolecular attack of fluoride anion. These cyclobutanes containing a hydroxymethyl group may serve as useful intermediates for further functionalization. Using this ring-expansion fluorination method, we synthesized (±)-2-fluorograndisol (**57**) from the sulfonate (**56**).[25]

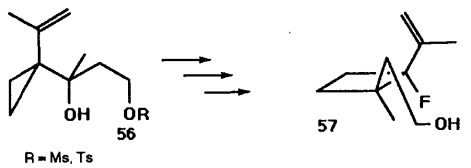

Fig. 3.

In conclusion, homoallyl fluorides or fluorocyclobutanes with multiple substituents or functional groups, which are difficult to provide by any other methods, were selectively synthesized by the current new methods we have developed. Its wide applicability is expected in the selective synthesis of functionalized homoallylic fluorides as well as fluorocyclobutanes.

Experimental

Infrared spectra of neat liquid film samples (unless otherwise noted) were determined on a Shimadzu infrared spectrophotometer IR-430, mass spectra on a Hitachi RMU-6M. and exact mass on a Hitachi M-80. ^{1}H NMR spectra were recorded on a JEOL FX-90Q or EX-90 spectrometer using TMS as an internal standard. ^{19}F NMR spectra were recorded on a JEOL EX-90 or Hitachi R-24F spectrometer using $CFCl_3$ as an internal standard. Multiplicity is designated as s, singlet; d, doublet; t, triplet; q, quartet; m, mutiplet. Preparative TLC plates were prepared with Merck Kiesel Gel PF_{254}. Column chromatography was carried out with silica gel (Wakogel C-300).

Preparation of Poly(hydrogen fluoride)-Pyridine Complex: The $(HF)_n \cdot Py$ was prepared from anhydrous hydrogen fluoride and pyridine according to the reported procedure.[15] All the reactions were carried out in polyethylene test tube as the reaction vessel and $(HF)_n \cdot Py$ was added through a polyethylene syringe.

General Procedure for the Ring-Opening Fluorination of Cyclopropanemethanol Derivertives with (i-Pr)$_2$NH-KHF$_2$-(HF)$_n \cdot$ Py Complex: Preparation of 4-fluoro-1-phenyl-1-butene (**7**) was representative. 25 ml polyethylene test tube fitted with magnetic stirring bar inside was connected to a nitrogen line. To a suspension of KHF_2 (0.08 g, 1.0 mmol, dried in a microwave oven) in chlorobenzene (1.0 ml) was added a solution of α-phenylcyclopropanemethanol (0.15 g, 1.0 mmol) in 1.0 ml of chlorobenzene and diisopropylamine (0.6 ml), and the whole was stirred for 5 min at 25 °C. The reaction mixture was cooled with ice-water bath and $(HF)_n \cdot Py$ (2.0 ml) was added slowly to the reaction mixture. After stirring at 0 °C for 5 min, the reaction mixture was diluted with ether (5.0 ml) and aqueous KF solution (5.0 ml). The whole was poured into water (10 ml). The water layer was extracted with ether (3×30 ml) and the combined organic layers were washed with saturated aqueous sodium hydrogencarbonate and brine successively, and dried over sodium sulfate. Concentration and purification on preparative TLC (hexane) gave the title compound, 4-fluoro-1-phenyl-1-butene (**7**) (0.11 g, 76%). IR (neat) 3040, 2910, 1595, 1490, 1445, 965, 745, and 690 cm^{-1}; ^{1}H NMR ($CDCl_3$) δ=2.61 (ddt, 2H, J=2.40, 5.66, 5.67 Hz), 4.49 (dt, 2H, J=47.30, 5.66 Hz), 6.15 (dt, 1H, J=16.40, 5.67 Hz), 6.49 (d, 1H, J=16.40 Hz), 7.0—7.4 (m, 5H); ^{19}F NMR ($CDCl_3$) δ=−219.5; MS m/z (rel intensity in %) 91 (18), 115 (39), 117 (100), 129 (7), 150 (M^+, 63). Found: C, 80.15; H, 7.47%. Calcd for $C_{10}H_{11}F$: C, 79.97; H, 7.38%.

5-Fluoro-2-phenyl-2-pentene (9): IR (neat) 2950, 1595, 1490, 1440, 755, and 695 cm^{-1}; ^{1}H NMR ($CDCl_3$) δ=2.06 (d, 3H, J=1.54 Hz), 2.61 (ddt, 2H, J=22.72, 6.48, 6.48 Hz), 4.50 (dt, 3H, J=47.50, 6.48 Hz), 5.77 (tq, 1H, J=6.48, 1.54 Hz), 7.1—7.4 (m, 5H); ^{19}F NMR ($CDCl_3$) δ=−219.0; MS m/z (rel intensity in %) 78 (8), 117 (19), 118 (100), 164 (M^+, 13); exact mass spectrum m/z 164.1014. Calcd for $C_{11}H_{13}F$: M, 164.1002.

***trans*-1-Fluoro-4-phenyl-3-octene (11) (Major Isomer):** IR (neat) 2995, 1590, 1490, 1405, 750, and 695 cm^{-1}; ^{1}H NMR ($CDCl_3$) δ=0.86 (t, 3H, J=5.40 Hz), 1.1—1.4 (m, 4H), 2.44 (t, 2H, J=7.20 Hz), 2.73 (ddt, 2H, J=22.30, 6.83, 6.84 Hz), 4.49 (dt, 2H, J=47.50, 6.84 Hz), 5.60 (t, 1H, J=6.83 Hz), 7.1—7.4

(m, 5H); ^{19}F NMR ($CDCl_3$) δ=−219.0; MS m/z (rel intensity in %) 91 (8), 117 (18), 118 (100), 164 (26), 206 (M^+, 4); exact mass spectrum m/z 206.1468. Calcd for $C_{14}H_{19}F$: M, 206.1471.

***cis*-1-Fluoro-4-phenyl-3-octene (11) (Minor Isomer):** IR (neat) 2955, 1595, 1495, 1400, 760, and 695 cm^{-1}; ^{1}H NMR ($CDCl_3$) δ=0.86 (t, 3H, J=5.40 Hz), 1.1—1.4 (m, 4H), 2.3—2.6 (m, 4H), 4.38 (dt, 2H, J=46.80, 6.83 Hz), 5.54 (t, 1H, J=6.83 Hz); ^{19}F NMR ($CDCl_3$) δ=−219.0; MS m/z (rel intensity in %) 91 (7), 117 (19), 118 (100), 164 (28), 206 (M^+, 4); exact mass spectrum m/z 206.1468. Calcd for $C_{14}H_{19}F$: M, 206.1471.

1-Fluoro-4-methyl-3-dodecene (13): IR (neat) 2800, 2700, 1455, 1370, 1000, and 910 cm^{-1}; ^{1}H NMR ($CDCl_3$) δ=0.87 (t, 3H, J=5.76 Hz), 1.0—1.5 (m, 12H), 1.61 (bs, 3H), 1.9—2.1 (m, 2H), 2.30 (ddt, 2H, J=22.40, 6.48, 6.80 Hz), 4.36 (dt, 2H, J=47.90, 6.48 Hz), 5.65 (t, 1H, J=6.80 Hz); ^{19}F NMR ($CDCl_3$) δ=−218.0; MS m/z (rel intensity in %) 97(29), 102(100), 112(18), 171(1), 200(M^+, 1).

***trans,trans*-6-Fluoro-1-phenyl-1,3-hexadiene (15):** IR (neat) 2910, 1670, 1485, 1445, 740, and 690 cm^{-1}; ^{1}H NMR ($CDCl_3$) δ=2.60 (ddt, 2H, J=24.40, 6.84, 6.84 Hz), 4.47 (dt, 2H, J=47.20, 6.84 Hz), 5.6—6.1 (m, 1H), 6.1—7.0 (m, 3H), 7.0—7.5 (m, 5H); ^{19}F NMR ($CDCl_3$) δ=−215.2; MS m/z (rel intensity in %) 91 (46), 115 (43), 128 (67), 129 (100), 141 (18), 143 (22), 176 (M^+, 30).

1-Fluoro-4-(1-octynyl)-3-dodecen-5-yne (17): IR (neat) 2900, 2850, 2250, 1715, 1460, 1380, and 735 cm^{-1}; ^{1}H NMR ($CDCl_3$) δ=0.84 (t, 3H, J=6.84 Hz), 1.0—1.7 (m, 16H), 2.1—2.4 (m, 4H), 2.70 (ddt, 2H, J=23.80, 6.84, 6.84 Hz), 4.44 (dt, 2H, J=46.80, 6.84 Hz), 6.11 (t, 1H, J=6.84 Hz), ^{19}F NMR ($CDCl_3$) δ=−219.0; MS m/z (rel intensity in %) 67 (36), 95 (28), 117 (37), 131 (42), 145 (28), 159 (24), 177 (22), 191 (23), 290 (M^+, 100); exact mass spectrum m/z 290.2431. Calcd for $C_{20}H_{31}F$: M, 290.2411.

4-Fluoro-1-phenyl-1-pentene (19): IR (neat) 3000, 2880, 1600, 1495, 1450, 1385, 1130, 965, 740, and 690 cm^{-1}; ^{1}H NMR ($CDCl_3$) δ=1.34 (dd, 3H, J=23.40, 6.50 Hz), 2.48 (dt, 1H, J=20.20, 6.50 Hz), 2.50 (dt, 1H, J=19.90, 6.50 Hz), 4.70 (dtq, 1H, J=48.20, 6.50, 6.50 Hz), 6.15 (dt, 1H, J=16.60, 6.50 Hz), 6.46 (d, 1H, J=16.60 Hz), 7.0—7.4 (m, 5H); ^{19}F NMR ($CDCl_3$) δ=−173.2; MS m/z (rel intensity in %) 69 (43), 83 (37), 91 (34), 115 (46), 117 (100), 129 (10), 149 (7), 164 (M^+, 22).

4-Fluoro-1-phenyl-3,3,4-trimethyl-1-pentene (21): IR ($CHCl_3$) 2950, 1600, 1490, 1380, and 970 cm^{-1}; ^{1}H NMR ($CDCl_3$) δ=1.18 (d, 6H, J=0.70 Hz), 1.35 (d, 6H, J=22.00 Hz), 6.3—6.5 (m, 2H), 7.2—7.5 (m, 5H); ^{19}F NMR ($CDCl_3$) δ=−147.7; MS m/z (rel intensity in %) 91 (35), 117 (32), 129 (17), 145 (100), 171 (25), 186 (12), 206 (M^+, 15). Found: C, 81.35; H, 9.28%. Calcd for $C_{14}H_{19}F$: C, 81.51; H, 9.31%.

9-Fluoro-3,6-dimethyl-2,6-nonadien-4-yne (23): IR (neat) 2970, 1440, 1360, and 1020 cm^{-1}; ^{1}H NMR ($CDCl_3$) δ=1.6—1.9 (m, 9H), 2.67 (ddt, 2H, J=24.20, 6.84, 6.84 Hz), 4.46 (dt, 2H, J=47.90, 6.84 Hz), 5.5—5.8 (m, 2H); ^{19}F NMR ($CDCl_3$) δ=−217.5; MS m/z (rel intensity in %) 77 (17), 79 (17), 91 (51), 105 (58), 133 (77), 151 (18), 166 (M^+, 100); exact mass spectrum m/z 166.1133. Calcd for $C_{11}H_{15}F$: M, 166.1158.

8-Fluoro-2,5-dimethyl-1,5-octadien-3-yne (25): IR (neat) 2970, 1440, 1360, and 1020 cm^{-1}; ^{1}H NMR ($CDCl_3$) δ=1.8—2.0 (m, 6H), 2.67 (ddt, 2H, J=23.80, 7.20, 7.20 Hz), 4.49 (dt, 2H, J=47.90, 7.20 Hz), 5.2—5.4 (m, 2H), 5.72 (tq, 1H, J=7.20, 1.10 Hz); ^{19}F NMR ($CDCl_3$) δ=−204.0; MS m/z (rel intensity in %) 77 (16), 91 (31), 104 (11), 119 (64), 137 (11), 152 (M^+, 100).

Methyl (*Z*)-7-Fluoro-4-methyl-4-hepten-2-ynoate (27) (Major Isomer): IR (neat) 2940, 2210, 1715, 1700, 1430, 1250, 1020, and 745 cm^{-1}; ^{1}H NMR ($CDCl_3$) δ=1.9—2.1 (m, 3H), 1.70 (ddt, 2H, J=25.60, 6.50, 7.20 Hz), 3.82 (s, 3H), 4.48 (dt, 2H, J=47.10, 6.50 Hz), 6.06 (tq, 1H, J=7.20, 1.40 Hz); ^{19}F NMR ($CDCl_3$) δ=−218.8; MS m/z (rel intensity in %) 79 (77), 91 (68), 109 (72), 139 (100), 149 (12), 170 (M^+, 26). Found: C, 63.67; H, 7.10%. Calcd for $C_9H_{11}O_2F$: C, 63.52; H, 6.51%.

Methyl (*E*)-7-Fluoro-4-methyl-4-hepten-2-ynoate (27) (Minor Isomer): IR (neat) 2970, 2220, 1710, 1435, 1260, 1010, and 745 cm^{-1}; ^{1}H NMR ($CDCl_3$) δ=1.8—1.9 (m, 3H), 1.54 (ddt, 2H, J=24.50, 6.50, 6.50 Hz), 3.79 (s, 3H), 4.46 (dt, 2H, J=46.80, 6.50 Hz), 6.19 (tq, 1H, J=6.50, 1.80 Hz); ^{19}F NMR ($CDCl_3$) δ=−218.4; MS m/z (rel intensity in %) 69 (100), 91 (84), 109 (58), 139 (94), 149 (39), 170 (M^+, 3). Found: C, 63.36; H, 6.53%. Calcd for $C_9H_{11}O_2F$: C, 63.52; H, 6.51%.

1-Fluoro-1-phenyl-3-octene (29): 25 ml polyethylene test tube, fitted with magnetic stirring bar inside was connected to a nitrogen line. $(HF)_n$·Py (1.0 ml), KHF_2 (0.12 g, 1.5 mmol), and diisopropylamine (0.3 ml) were mixed in THF (1.0 ml) and the mixture was stirred for 30 min at 0 °C. A solution of α-butyl-2-phenylcyclopropanemethanol (**28**) (0.10 g, 0.5 mmol) in THF (1.0 ml) was slowly added to the reaction mixture at 0 °C and the whole mixture was stirred for additional 1 h at 25 °C. After the consumption of the substrate (monitored with TLC), the reaction mixture was diluted with ether (5.0 ml) and aqueous potassium fluoride solution (5.0 ml). Extraction, and concentration gave an oil, which was purified by column chromatography to give 1-fluoro-1-phenyl-3-octene (**29**) (0.07 g, 73%). IR (neat) 3000, 2940, 2900, 2830, 1490, 1445, and 965 cm^{-1}; ^{1}H NMR ($CDCl_3$) δ=0.86 (t, 3H, J=6.10 Hz), 1.0—1.4 (m, 6H), 1.8—2.1 (m, 2H), 2.55 (ddd, 2H, J=26.90, 6.84, 6.84 Hz), 5.38 (dt, 1H, J=43.90, 6.50 Hz), 5.44 (dt, 2H, J=4.30, 6.50 Hz), 7.2—7.4 (m, 5H); ^{19}F NMR ($CDCl_3$) δ=−171.1; MS, m/z 91 (15), 109 (100), 129 (25), 143 (11), 186 (7), 206 (M^+, 7); exact mass spectrum m/z 206.1462. Calcd for $C_{14}H_{19}F$: M, 206.1466.

5-(4-Fluorobutyloxy)-2-phenyl-2-pentene:[16] 25 ml polyethylene test tube fitted with magnetic stirring bar inside was connected to a nitrogen line. To a suspension of KHF_2 (0.12 g, 1.5 mmol dried with microwave oven) in THF (0.5 ml) was added 1-cyclopropyl-1-phenylethanol (0.08 g, 0.5 mmol) in 0.5 ml of THF and the suspension was stirred for 10 min at 25 °C. $(HF)_n$·Py was added slowly to the suspension at 0 °C and the whole was stirred for 1 h at that temperature. The reaction mixture was diluted with ether (5.0 ml) and aqueous potassium fluoride (5.0 ml) and the entire mixture was poured into ice water. The organic layer was separated and the water layer was extracted with ethyl acetate (3×30 ml) then the combined organic layers were washed with aqueous sodium hydrogencarbonate and brine successively. The organic layer was dried over sodium sulfate and concentrated. Purification of the crude oil gave the title compound as colorless oil (0.07 g, 65%). IR (neat) 2950, 2870, 1595, 1480, 1445, 1360, 1110, 755, and 695 cm^{-1}; ^{1}H NMR ($CDCl_3$) δ=1.5—1.9 (m, 4H), 2.0—2.1 (m, 3H), 2.48 (dt, 2H, J=6.84, 6.84 Hz), 3.49 (t, 2H, J=4.68 Hz), 3.51 (t, 2H, J=6.84 Hz), 4.46 (dt, 2H, J=47.50, 5.94 Hz), 5.77 (tq, 1H, J=6.84, 1.81 Hz), 7.1—7.4 (m, 5H); ^{19}F NMR ($CDCl_3$) δ=−218.7; MS m/z (rel intensity in %) 55(46),

74(27), 91(13), 118(70), 131(100), 146(20), 236(M^+, 5); exact mass spectrum m/z 236.1585. Calcd for $C_{15}H_{21}OF$: M, 236.1577.

General Procedure for the Ring-Expansion Fluorination of 1-Substituted Cyclopropanemethanol Derivatives with (i-Pr)$_2$NH-KHF$_2$-(HF)$_n$·Py-Complex: Preparation of 1-fluoro-1,2-dimethyl-t-2-phenylcyclobutane (**37**) was representative. 25 ml polyethylene test tube fitted with magnetic stirring bar inside was connected to a nitrogen line. To a suspension of KHF_2 (0.12 g, 1.5 mmol dried in microwave oven) in dichloromethane (0.5 ml) was added α,1-dimethyl-α-phenylcyclopropanemethanol (**36**) (0.09 g, 0.5 mmol) in 0.5 ml of dichloromethane and diisopropylamine (0.3 ml), and the suspension was stirred for 10 min at 25 °C. The suspension was cooled to −20 °C and (HF)$_n$·Py (1.0 ml) was slowly added into the mixture with cooling. The reaction completed within 5 min and the mixture was diluted with ether (5.0 ml) and aqueous potassium fluoride solution (5.0 ml). The water layer was extracted with ether (3×30 ml), and the combined organic layers were washed with aqueous sodium hydrogencarbonate and brine successively. Drying and concentration followed by chromatographic purification gave the r-1-fluoro-1,2-dimethyl-t-2-phenylcyclobutane (**37**) (0.06 g, 62%). IR (neat) 3000, 1495, 1445, 1380, 1260, and 705 cm^{-1}; ^{1}H NMR ($CDCl_3$) δ=1.12 (d, 3H, J=22.70 Hz), 1.51 (d, 3H, J=2.20 Hz), 1.5—2.8 (m, 4H), 7.0—7.5 (m, 5H), ^{19}F NMR ($CDCl_3$) δ=−136.9; MS m/z (rel intensity in %) 78 (8), 103 (11), 117 (22), 118 (100), 150 (6), 178 (M^+, 1). Found: C, 80.72; H, 8.55%. Calcd for $C_{12}H_{15}F$: C, 80.86; H, 8.48%.

1-Fluoro-1-methyl-t-2-phenylcyclobutane (35): IR (neat) 3000, 1605, 1495, 1380, 1255, 1115, 920, and 700 cm^{-1}; ^{1}H NMR ($CDCl_3$) δ=1.06 (d, 3H, J=22.30 Hz), 1.0—2.6 (m, 4H), 3.80 (dt, 1H, J=20.90, 10.40 Hz), 7.0—7.4 (m, 5H); ^{19}F NMR ($CDCl_3$) δ=−116.7; MS m/z (rel intensity in %) 78 (4), 104 (100), 136 (7), 164 (M^+, 2).

2-Butyl-1-fluoro-1-methyl-t-2-phenylcyclobutane (39): IR (neat) 2950, 2850, 1605, 1450, 1380, 1175, and 705 cm^{-1}; ^{1}H NMR ($CDCl_3$) δ=0.79 (t, 3H, J=7.90 Hz), 0.7—1.4 (m, 6H), 1.09 (d, 3H, J=21.60 Hz), 1.6—2.8 (m, 4H), 7.0—7.5 (m, 5H); ^{19}F NMR ($CDCl_3$) δ=−138.7; MS m/z (rel intensity in %) 58 (57), 77 (18), 83 (22), 91 (19), 118 (100), 160 (10), 220 (M^+, 2). Found: C, 81.56; H, 9.63. Calcd for $C_{15}H_{21}F$: C, 81.77; H, 9.61%.

1-Fluoro-1,c-2-diphenylcyclobutane (41) (Major Isomer): IR ($CHCl_3$) 3050, 2970, 1605, 1500, 1450, 890, and 695 cm^{-1}; ^{1}H NMR ($CDCl_3$) δ=2.0—3.0 (m, 4H), 3.6—4.2 (m, 1H), 7.1—7.6 (m, 10H); ^{19}F NMR ($CDCl_3$) δ=−163.7; MS m/z (rel intensity in %) 78 (11), 91 (9), 104 (100), 122(12), 226 (M^+, 3).

1-Fluoro-1,t-2-diphenylcyclobutane (41) (Minor Isomer): IR ($CHCl_3$) 3050, 2970, 1600, 1495, 1445, 1070, 750, and 695 cm^{-1}; ^{1}H NMR ($CDCl_3$) δ=1.8—2.9 (m, 4H), 4.16 (ddd, 1H, 20.90, 9.00, 9.40 Hz), 6.7—7.3 (m, 10H); ^{19}F NMR ($CDCl_3$) δ=−118.2; MS m/z (rel intensity in %) 58 (73), 83 (25), 91 (15), 104 (100), 122 (13), 226 (M^+, 3).

1-Fluoro-2-methyl-1,t-2-diphenylcyclobutane (43) (Major Isomer): IR (neat) 2980, 1600, 1495, 1445, 760, and 700 cm^{-1}; ^{1}H NMR ($CDCl_3$) δ=1.70 (d, 3H, J=3.60 Hz), 2.0—3.2 (m, 4H), 6.8—7.5 (m, 10H); ^{19}F NMR ($CDCl_3$) δ=−144.8; MS m/z (rel intensity in %) 78 (7), 117 (36), 118 (100), 204 (13), 205 (7), 220 (4), 240 (M^+, 2). Found: C, 85.29; H, 7.11%. Calcd for $C_{17}H_{17}F$: C, 84.96; H, 7.13%.

1-Fluoro-2-methyl-1,c-2-diphenylcyclobutane (43) (Minor Isomer): IR ($CHCl_3$) 2990, 1605, 1495, 1445, 770, and 700 cm^{-1}; ^{1}H NMR ($CDCl_3$) δ=1.22 (s, 3H), 2.6—3.2 (m, 4H), 7.1—7.6 (m, 5H); ^{19}F NMR ($CDCl_3$) δ=−149.1; MS m/z (rel intensity in %) 78 (9), 117 (29), 118 (100), 205 (8), 220 (40), 40 (M^+, 1). Found: C, 84.86; H, 7.15%. Calcd for $C_{17}H_{17}F$: C, 84.96; H, 7.13%.

1-Fluoro-c-2-hydroxymethyl-1-methyl-2-phenylcyclobutane (49): IR (neat) 3630, 3450, 3000, 2890, 1605, 1495, 1380, 1030, 880, and 700 cm^{-1}; ^{1}H NMR ($CDCl_3$) δ=1.20 (dd, 3H, J=23.60, 1.20 Hz), 1.2—2.8 (m, 5H), 3.97 (d, 2H, J=5.70 Hz), 7.0—7.4 (m, 5H); ^{19}F NMR ($CDCl_3$) δ=−138.6; MS m/z (rel intensity in %) 55 (100), 69 (56), 95 (31), 105 (27), 129(15), 193(M^+−1, 6). Found: C, 74.03; H, 7.87%. Calcd for $C_{12}H_{15}OF$: C, 74.20; H, 7.78%.

1-Fluoro-c-2-hydroxymethyl-1-phenylcyclobutane (51) (Major Isomer): IR (neat) 3640, 3400, 2980, 1500, 1450, 1300, 1025, 760, and 695 cm^{-1}; ^{1}H NMR ($CDCl_3$) δ=0.74 (s, 3H), 1.2—3.0 (m, 4H), 3.60 (bs, 1H), 3.67 (d, 1H, J=11.60 Hz), 4.03 (d, 1H, J=11.60 Hz), 7.2—7.5 (m, 5H); ^{19}F NMR ($CDCl_3$) δ=−144.8; MS m/z (rel intensity in %) 83(27), 91(20), 105(22), 115(29), 122(100), 129(41), 193 (M^+−1, 2). Found: C, 73.91; H, 7.90%. Calcd for $C_{12}H_{15}OF$: C, 74.20; H, 7.78%.

1-Fluoro-t-2-hydroxymethyl-2-methyl-1-phenylcyclobutane (51) (Minor Isomer): IR (neat) 3600, 3400, 2980, 2500, 1500, 1450, 1030, 1005, 765, and 700 cm^{-1}; ^{1}H NMR ($CDCl_3$) δ=1.38 (d, 3H, J=3.10 Hz), 1.40 (bs, 1H), 1.6—3.0 (m, 4H), 3.24 (bs, 2H), 7.2—7.5 (m, 5H); ^{19}F NMR ($CDCl_3$) δ=−143.7; MS m/z (rel intensity in %) 55 (100), 83 (53), 115 (37), 122 (41), 129 (40), 144 (18), 193 (M^+−1, 4). Found: C, 73.84; H, 7.86%. Calcd for $C_{12}H_{15}OF$: C, 74.20; H, 7.78%.

Ethyl (2R*)-2-(2-Fluoro-2-methyl-1-phenylcyclobutyl)-2-hydroxyacetate (53): IR (neat) 3570, 3000, 1730, 1605, 1495, 1450, and 705 cm^{-1}; ^{1}H NMR ($CDCl_3$) δ=1.11 (t, 3H, J=7.20 Hz), 3.72 (d, 3H, J=20.60 Hz), 1.8—2.2 (m, 2H), 2.4—2.8 (m, 2H), 3.00 (dd, 1H, J=5.40, 4.30 Hz), 4.01 (q, J=7.20 Hz), 4.93 (d, 1H, J=5.40 Hz), 7.1—7.4 (m, 5H); ^{19}F NMR ($CDCl_3$) δ=−132.8; MS m/z (rel intensity in %) 105 (34), 133 (100), 160 (31), 189 (35), 203 (26), 246 (M^+−20, 29). Found: C, 67.87; H, 7.23. Calcd for $C_{15}H_{19}O_2F$: C, 67.65; H, 7.19%.

Ethyl (2S*)-2-(2-Fluoro-2-methyl-1-phenylcyclobutyl)-2-hydroxyacetate (55) (Inseparable Isomeric Mixture.): IR (neat) 3570, 3000, 1725, 1600, 1490, 1450, and 700 cm^{-1}; ^{1}H NMR ($CDCl_3$) δ=0.84 (t, 3H, J=7.00 Hz), 1.32 (d, 3H, J=25.1 Hz), 1.8—2.3 (m, 2H), 2.4—2.8 (m, 2H), 2.9—3.0 (m, 1H), 3.6—3.9 (m, 2H), 4.7—4.8 (m, 1H), 7.0—7.5 (m, 5H), ^{19}F NMR ($CDCl_3$) δ=−135.7 and −132.8; MS m/z (rel intensity in %) 70 (34), 105 (100), 129 (71), 132 (47), 133 (47), 143 (52), 151 (44), 186 (77), 189 (73), 246 (M^+−20, 15).

References

1) "Biochemical Aspects of Fluorine Chemistry," ed by R. Filler and Y. Kobayashi, Kodansha Ltd., Elsevier Biochemical Press: Tokyo, New York (1982); "Synthesis and Function of Fluorinated Compounds," ed by N. Ishikawa, C.M.C. Ltd., Tokyo (1987); R. Filler, "Biochemistry Involving Carbon-Fluorine Bonds," American Chemical Society, Washington DC (1976); J. T. Welch, *Tetrahedron*, **43**, 3123 (1987).

2) J. Kollonitsch, L. M. Perkins, A. A. Patchett, G. A. Doldouras, S. Marburg, D. E. Duggan, A. L. Maycock, and S. D. Aster, *Nature (London)*, **274**, 906 (1978).

3) G. D. Prestwich and S. Phirwa, *Tetrahedran Lett.*, **24**,

2461 (1983).

4) C. M. Sharts and W. A. Sheppard, *Org. React.*, **21**, 125 (1974).

5) A. Takaoka, H. Iwakiri, and N. Ishikawa, *Bull. Chem. Soc. Jpn.*, **52**, 3377 (1979).

6) M. Shimizu, Y. Nakahara, and H. Yoshioka, *Tetrahedron Lett.*, **26**, 4207 (1985).

7) M. M. Boudakian, *J. Heterocycl. Chem.*, **5**, 683 (1968); **4**, 381 (1967); G. C. Finger, L. D. Starr, D. R. Dickerson, H. S. Tutowsky, and J. Hamer, *J. Org. Chem.*, **28**, 1666 (1963); N. Ishikawa, T. Kitazume, T. Yamazaki, Y. Mochida, and T. Tatsuno, *Chem. Lett.*, **1981**, 761.

8) K. Makino and H. Yoshioka, *J. Fluorine Chem.*, **35**, 677 (1987).

9) M. Hudlicky, "Chemistry of Organic Fluorine Compounds: A Laboratory Manual," Ellis Horwood: Chichester, England (1976); pp. 67—73; S. Misaki, *J. Fluorine Chem.*, **17**, 159 (1981); T. Tsushima, K. Kawada, and T. Tsuji, *J. Org. Chem.*, **47**, 1107 (1982).

10) D. H. R. Barton, *Pure Appl. Chem.*, **49**, 1241 (1977); R. H. Hesse, *Isr. J. Chem.*, **17**, 60 (1978).

11) R. Filler, *Isr. J. Chem.*, **17**, 71 (1978).

12) Y. Takeuchi, *Yuki Gosei Kagaku Kyokai Shi*, **46**, 145 (1988).

13) The preliminary results of this work gave already been published: S. Kanemoto, M. Shimizu, and H. Yoshioka, *Tetrahedron Lett.*, **28**, 663, 6313 (1987).

14) M. Julia, S. Julia, and R. Guegan, *Bull. Soc. Chim. Fr.*, **1960**, 1072; M. Julia, S. Julia, and S. Y. Tchen, *ibid.*, **1961**, 1849; "Concepts of Organic Synthesis," ed by B. Marcel Dekker, Inc.: New York and Basel 1979, Chap. 15—2; "Carbonium Ions," ed by G. A. Olah and P. von R. Schleyer, John Wiley & Sons, Inc., New York (1972), Chaps. 25 and 26.

15) G. A. Olah, J. T. Welch, Y. D. Vankar, M. Nojima, I. Kerekes, and J. A. Olah, *J. Org. Chem.*, **44**, 3872 (1979).

16) Treatment of 1-cyclopropyl-1-phenylethanol with $(HF)_n$·Py in THF gave 5-(4-fluorobutyloxy)-2-phenyl-2-pentene in 65% yield under optimum conditions. Spectral data were available in experimental section.

17) Z.-H. Qian, M. Shimizu, and H. Yoshioka, unpublished results.

18) Solvolysis of 1-substituted cyclopropanemethanol derivatives to give cyclobutanes has been previously reported, a) J. W. Wilt and D. D. Roberts, *J. Org. Chem.*, **27**, 3430 (1962); b) D. D. Roberts, *ibid.*, **30**, 23 (1965); c) *Idem, ibid.*, **31**, 2000 (1966); d) E. F. Cox, M. C. Caserio, M. S. Silver, and J. D. Roberts, *J. Am. Chem. Soc.*, **83**, 2719 (1961).

19) J. D. Roberts and C. M. Sharts, *Org. React.*, **12**, 1 (1962), and references cited therein.

20) Y. Yamada, H. Uda, and K. Nakanishi, *J. Chem. Soc., Chem. Commun.*, **1966**, 423; R. L. Cargill, J. R. Damewood, and M. M. Cooper, *J. Am. Chem. Soc.*, **88**, 1330 (1966); C. M. Cimarusti and J. Wolinsky, *ibid.*, **90**, 113 (1968); W. C. Agosta and W. W. Lowrance Jr., *Tetrahedron Lett.*, **1969**, 3053; R. Zurfluh, L. L. Dunham, V. L. Spain, and J. B. Siddall, *J. Am. Chem. Soc.*, **92**, 425 (1970).

21) E. D. Bergmann and S. Szinai, *J. Chem. Soc.*, **1956**, 1521.

22) S. Hoz, D. Aurbach, and C. Avivi, *Tetrahedron Lett.*, **24**, 1639 (1983).

23) Reaction of 1-(1-vinylcyclopropyl)-1-phenylethanol also gave a mixture of *r*-1-fluoro-2-methyl-*c*-2-phenyl-1-vinylcyclobutane (cis-product) and its trans-isomer in 65% yield (cis : trans=4 : 6).

24) Only substitution of hydroxyl group occurred and gave cyclopropylmethyl fluorides.

25) S. Kanemoto, M. Shimizu, and H. Yoshioka, *J. Chem. Soc., Chem. Commun.*, in press.

Photolysis of Alcohols and Alkanones in Acetone Solutions. Photochemical [2+2]Cycloaddition Reaction between Acetone and Aliphatic Enols

Nobujiro SHIMIZU,* Toru MIYAHARA, Masaaki MISHIMA, and Yuho TSUNO
Department of Chemistry, Faculty of Science, Kyushu University, Fukuoka 812
(Received January 20, 1989)

Transient enols including those of acetaldehyde, acetone, cyclopentanone, 3-pentanone, 2,4-dimethyl-3-pentanone, 2-butanone, and 2-methyl-3-pentanone were trapped photochemically with acetone via a [2+2]cycloaddition and isolated as corresponding 3-oxetanols in reasonable yields in the photolysis of six different secondary alcohols and two alkanones, 3-octanone and hexanal, in acetone solutions. The trapping experiments indicated the photodehydrogenation of unsymmetrical alcohols, 2-butanol and 2-methyl-3-pentanol, in acetone to be highly regioselective in preference for the formation of the less alkylated enol.

The chemistry of simple enols has received wide attention in recent years from structural and mechanistic interests.[1-4] A number of short-lived enols[1-3,5] have been prepared and characterized directly by spectral analyses including microwave,[6] IR,[7] and NMR.[2,8,9] CIDNP technique is particularly useful for identification of transient enol species which may often be involved in photochemical processes.[10,11] This method, however, does not always provide quantitative information on the formation of such species. In this connection, trapping experiments seem important. Although there have been extensive studies on ketonization of enols via protonation and halogenation,[3,12,13] works on reactions other than ketonization are surprisingly few. Cycloaddition reaction is especially attractive for chemical proof of transient enols. There have been reported several [2+4]-type cycloaddition reactions for some dienols such as photo enols of *o*-alkylated phenyl ketones,[14,15] however, successful trapping of simple enols like vinyl alcohol via a cycloaddition reaction is rare. An interesting observation, in this connection, is the formation of a small amount of 2,2,3-trimethyl-3-oxetanol (**1a**) in the photolysis of acetone in the liquid phase reported by Kagan et al.[16] Although mechanism for the formation of **1a** has not been established yet, a photocycloaddition between acetone and its enol would probably be involved.[17] Accordingly, an excited molecule of acetone seems to be a good candidate for a trapping agent for enol intermediates which are formed in photochemical reactions. We report here our results on the photolysis of eight different alcohols and two alkanones carried out in acetone solutions and show photochemical trapping of various enols with acetone.

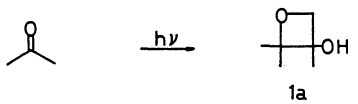

1a

Results and Discussion

Photocycloaddition of Acetone with Acetone Enol. We first examined the photolysis of acetone in the liquid phase in the presence of a hydrogen-donating substrate with a view to understanding the mechanism for the formation of the oxetane **1a**. Table 1 shows the results of irradiation of acetone (100 cm^3) with or without a hydrogen-donating substrate (RH, 35 mmol) including cyclohexane, 2-propanol, 3-pentanol, 2-trimethylsiloxypropane, and triethylsilane under the same photolysis conditions (0—5 °C, 2 h under argon) using a 100 W low-pressure mercury lamp. In agreement with the earlier observation,[16] these photolysis reactions gave a mixture of **1a** and several other major compounds including 4-hydroxy-4-methyl-2-pentanone (**2**), pinacol (**3**), 2,5-hexanedione (**4**), and a coupling product **5** between acetone and RH as a low-boiling

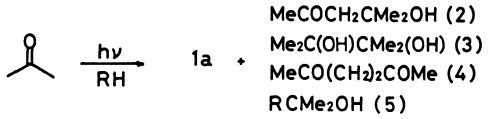

liquid distilling under vacuum. Obviously, **1a** is formed much more efficiently in the photolysis of acetone in the presence of a hydrogen donor than in the photolysis of pure acetone. For example, the yield of **1a** increased by a factor of more than nine when acetone was irradiated with 2-propanol instead of acetone alone. Cyclohexane shows a similar effect, although less pronounced. It is worth stating that the photolysis of acetone in cyclohexane has been reported to give a coupling product **5a** (R=cyclohexyl) but not **1a**.[18] The presence of a good hydrogen donor greatly favored the formation of **2** and **3** as well. In contrast, it little affected or in some cases reduced significantly the formation of 2,5-hexanedione. It is also informative that the irradiation of acetone containing 2-propanol and trace *p*-toluenesulfonic acid gave pinacol but not **1a** at all. Although **1a** readily rearranges to 4-hydroxy-3,3-dimethyl-2-butanone under acidic conditions,[19] we could not find the rearranged product either. Thus, the presence of trace acid completely prohibits the formation of **1a**. All these findings are consistent with a mechanism for the formation of **1a** outlined in Scheme 1. An excited molecule

Table 1. Effects of a Hydrogen-Donating Substrate (RH) on the Liquid-Phase Photolysis of Acetone[a)]

Substrate (RH)	Low-boiling fraction/g[b)]	Products/mmol[c)]					
		1a	**2**	**3**	**4**	**5**	Others
None	0.094	0.41	0.19	0.08	0.18		
Cyclohexane	0.584	1.89	0.86	0.59	0.20	1.13	
2-Propanol	1.02	3.71	1.98	2.59	0.25		
2-Propanol/*p*-TsOH	0.303	d)	d)	2.58	d)		
2-Trimethylsiloxypropane	1.36	3.36	1.72	1.20	0.15	1.26	e)
Triethylsilane	3.75	3.80	0.85	3.39	d)		f)
3-Pentanol	4.52[g)]	9.66	3.45	3.60	d)	4.38	h)

a) All the photolysis reactions were carried out under the same irradiation conditions (0—5 °C, 2 h) using a 100 W low-pressure mercury lamp by taking 35 mmol of a substrate (RH) and 100 cm^3 of acetone. b) Amount of low-boiling liquid distilling below 70 °C at 0.5 Torr after fractionation of crude photolysate. c) Determined by GLC using appropriate internal standards. d) Could not be observed. e) 2,2,3-Trimethyl-3-trimethylsiloxyoxetane (**10**) was also formed. f) 2-Triethylsiloxypropane, 3-triethylsiloxy-2,2,3-trimethyloxetane, pinacol mono(triethylsilyl) ether, and triethylsilanol (**14**—**17**) were also formed. g) Irradiation for 4 h. h) 3-Ethyl-2,2,4-trimethyl-3-oxetanol (**1b**) and 3-ethyl-2-methyl-2,3-pentanediol (**20b**) were also formed.

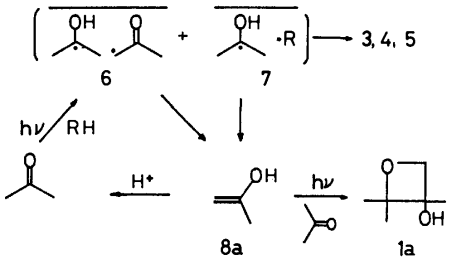

Scheme 1.

of acetone abstracts a hydrogen from solvent acetone or from a hydrogen donor RH yielding radical pairs **6** and **7** which can terminate to **3**—**5** via coupling reactions or to acetone enol **8a** via disproportionation.[20)] The enol thus generated can be trapped with another excited molecule of acetone as **1a** prior to complete ketonization. Under acidic conditions, the ketonization must be so rapid that **8a** cannot be trapped as oxetane. Table 1 clearly indicates that a hydrogen abstraction process leading to **6** which accounts for the formation of **4** does not contribute appreciably to the formation of **8a**, **2**, and **3** when a better hydrogen donor than acetone like 2-propanol is present. The product **2** may be formed directly from **6** or from **8a** via 2,4,4-trimethyl-2-oxetanol (**9**) which is a regioisomer of **1a**.[16,17)] The former is not the major route because

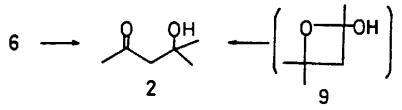

such the pathway should yield **2** in proportion to the formation of **4** against the observation. Both fairly constant **2**/**1a** ratios irrespective of photolysis conditions and the fact that **2** as well as **1a** were not formed at all under acidic conditions are more in accord with the latter pathway.

The photolysis of acetone with 2-trimethylsiloxypropane gave pinacol mono(trimethylsilyl) ether **5b** and 2,2,3-trimethyl-3-trimethylsiloxyoxetane (**10**) in 22 and 33% yields based on the substrate added besides **1a**—**4**. The formation of these products is consistent with the intervention of a pair of radicals, 1-hydroxy-1-methylethyl radical (**11a**) and 1-trimethylsiloxy-1-methylethyl radical (**12**), which terminates to **5b** or disproportionates affording a mixture of **8a** and its trimethylsilyl ether **13**. Noteworthy is the fact that **1a** was formed predominantly over **10** (**1a**/**10**=1.8) in

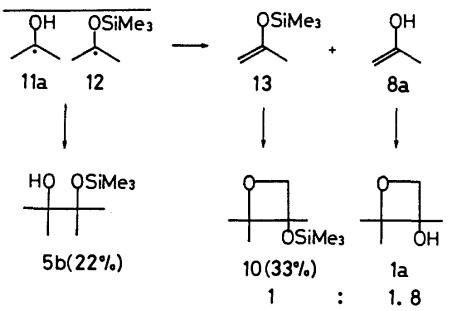

this photolysis reaction. Although the disproportionation step would give **8a** and **13** in comparable amounts, **8a** must remain in a very low concentration throughout the irradiation because of its short lifetime,[21)] while the concentration of **13** must accumulate during the irradiation. The preferential formation of **1a** therefore suggests that an enol can be trapped efficiently as oxetane as soon as it is generated.

In the case of triethylsilane as a hydrogen donor, four major products, 2-triethylsiloxypropane (**14**), 3-triethylsiloxy-2,2,3-trimethyloxetane (**15**), pinacol mono(triethylsilyl) ether (**16**), and triethylsilanol (**17**) were obtained in 26, 10, 3, and 45% yields, respectively, besides **1**—**3**. Probably, the reaction involves the formation of 1-triethylsiloxy-1-methylethyl radical which accounts for the formation of **14**—**16**.[22)]

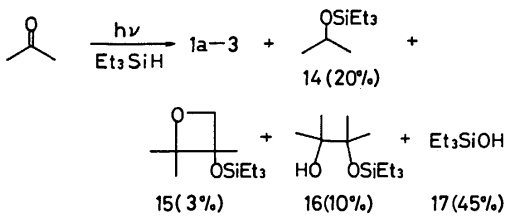

Mechanism for the formation of **17** is not clear.

Photocycloaddition of Acetone with Other Aliphatic Enols. Table 1 includes the result of the photolysis of acetone in the presence of 3-pentanol. From the discussion above mentioned, it is expected that irradiation of acetone in the presence of an alcohol (**18b—h**) may lead to formation of an enol (**8b—h**) derived from the alcohol added, hence a new 3-oxetanol (**1b—h**) according to Scheme 2, where Fd and Fc are fractions of enol formation from a hydroxyalkyl radical **11** and oxetane formation from the enol thus generated respectively. Indeed, 3-ethyl-2,2,4-trimethyl-3-oxetanol (**1b**) was obtained as a mixture of two stereoisomers (E/Z=1) in 24% yield on the basis of the consumed 3-pentanol together with 3-pentanone (**19b**, 18%) and 3-ethyl-2-methyl-2,3-pentanediol (**20b**, 25%) besides **1a—3**. Structure of **1b** was deduced from its spectral data (IR, NMR, and MS) and from its chemical property that either stereoisomer of **1b** gave 5-hydroxy-4,4-dimethyl-3-hexanone (**22b**) on treating with boron trifluoride etherate.[19,23] Provided **1b**, **19b**, and **20b** are the sole products from 3-pentanol and all **19b** is formed from an enol **8b**,[20] it follows from the result that a 63% fraction of 1-hydroxy-1-ethylpropyl

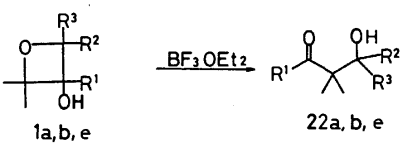

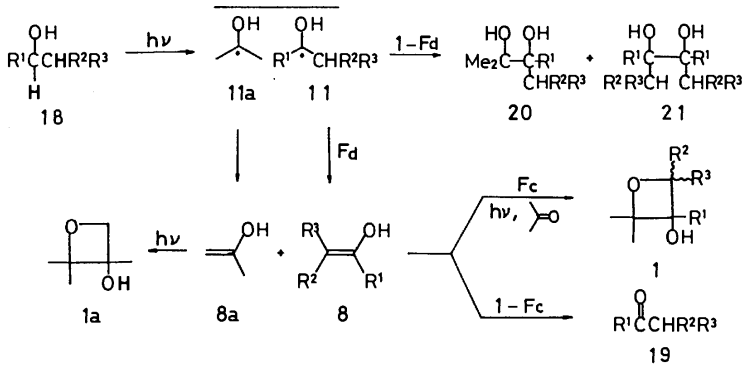

a) R¹=Me; R²=R³=H, b) R¹=Et; R²=Me; R³=H, c) R¹=i-Pr; R²=R³=Me, d) R¹,R²=-(CH₂)₃-R³=H, e) R¹=Et, R²=R³=H, f) R¹=i-Pr, R²=Me, R³=H, g) R¹=R²=R³=H, h) R¹=H, R²=R³=Me

Scheme 2.

Table 2. Photolysis of Alcohols and Alkanones (RH) in Acetone Solutions[a]

Substrate (RH)	Conversion (%)	Enol trapped	Yield/%[b,c] 1	19	20	21	F_d[d] (%)	F_c[e] (%)	1/1a
2-Propanol (**18a**)	f)	**8a**	21[g]		11[g]				
3-Pentanol (**18b**)	50	**8b**	24[h]	18	25		63	57	0.45
2,4-Dimethyl-3-pentanol (**18c**)	40	**8c**	18	23	14	4	69	44	0.33
Cyclopentanol (**18d**)	56	**8d**	5	20	12		67	20	0.18
2-Butanol (**18e**)	40	**8e**	15	d)	11	4			0.39
2-Butanol (**18e**)	22[i]	**8e**	43	d)	5	1			0.68
2-Methyl-3-pentanol (**18f**)	48	**8f**	21[h]	19	17		70	53	0.34
Ethanol (**18g**)	f,j)		k)	f)	13[g]				
Isobutyl alcohol (**18h**)	40		k)	f)	28	8			
3-Octanone (**23**)	42[l]	**8e**	34	f)					
Hexanal (**26**)	96[m]	**8g**	8	f)					

a) All the phtolysis reactions were carried out under argon at 0—5 °C for 4 h with a 100 W low-pressure mercury lamp by taking 100 cm³ of acetone and 35 mmol of a substrate RH. b) Determined by GLC. c) Based on the consumed substrate. d) (**1**+**19**)/(**1**+**19**+**20**+**21**). e) **1**/(**1**+**19**). f) Not determined. g) Based on the substrate added. h) As a mixture of two stereoisomers. i) At −70 °C for 2 h. j) 2-Methyl-3-butanone was also formded. k) Could not be detected. l) 1,2-Diethylcyclobutanol (16%) was also obtained. m) 2-Ethylcyclobutanol (24%) and 2-hydroxy-2-methyl-3-octanone (8%) were formed as well.

radical (**11b**) gave the enol **8b** and that a 57% fraction of **8b** was subsequently trapped as oxetane prior to complete ketonization to 3-pentanone. The results of the photolysis of eight different alcohols **18a—h** and two alkanones, 3-octanone (**23**) and hexanal (**26**), in acetone solutions are summarized in Table 2. Several interesting features are worth noting. First of all, a variety of ketone enols including a cyclic (**8d**) and acyclic ones with one (**8a** and **8e**), two (**8b** and **8f**), and three alkyl substituents (**8c**) were successfully trapped and isolated as corresponding oxetanes **1a—f** in the photolysis of secondary alcohols **18a—f** in fairly good yields, in most cases about 20% of the reacted alcohol. Fd and Fc values suggest that the radicals **11b—f** terminate preferentially via disproportionation to the enols and that the subsequent trapping with acetone proceeds with similar efficiencies about 50% irrespective of structure of enols except for **8d**. Since the photodehydrogenation of alcohols **18b—f** in acetone involves the formation of **8a** hence **1a** as a common side reaction, ratios of oxetanes **1b—f**/**1a**, which are listed in the last column in Table 2, also represent approximate relative efficiencies for the formation of the oxetane from each enol. The fairly constant ratios except for **1d** again suggest that the trapping efficiency does not vary appreciably with the structure of enols.

Norrish II reaction of alkanones is another effective way to generate enols,[24] and it is interesting to see whether photolysis of alkanones in an acetone solution leads to formation of expected 3-oxetanols. Irradiation of 3-octanone (**23**) in acetone gave indeed 3-ethyl-2,2-dimethyl-3-oxetanol (**1e**) in 34% yield together with 1,2-diethylcyclobutanol (**24**) in 16% yield. The formation of **24** and **1e** hence its precursory enol **8e** is

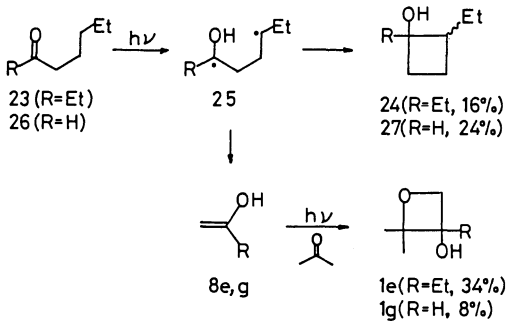

consistent with a conventional scheme for the photolysis of alkanones via an intermediate biradical **25**, although it is not clear whether excitation of 3-octanone is direct or sensitized by acetone under the present photolysis conditions. Photolysis of hexanal (**26**) in acetone was more complicated than that of 3-octanone but an expected vinyl alcohol could be isolated as the corresponding oxetanol **1g** in 8% yield along with several other products including 2-ethylcyclobutanol (**27**, 24%) and 2-hydroxy-2-methyl-3-octanone (**28**, 8%). In the photocycloaddition reactions between acetone and enols **8b—g**, regioisomeric 2-oxetanols like **9** might be formed but we could identify neither such compounds nor their decomposition products, presumably because of small amounts of their formation.

Photodehydrogenation of unsymmetrical alcohols such as 2-butanol (**18e**) and 2-methyl-3-pentanol (**18f**) is expected to produce a mixture of two regioisomeric enols **8** and **8′** which is more highly alkylated, hence thermodynamically more favorable than **8**. Indeed, the formation of **8e** and **8e′** has been confirmed by CIDNP experiments in the photochemical decomposition of *t*-butyl hydroperoxide in 2-butanol.[11] In the present experiments, however, only one of the regioisomers, i.e., the less highly alkylated isomer **8**, could be identified as oxetane in the photolyses of both alcohols **18e** and **18f**. For example, irradiation of **18e** in acetone gave **1e** in 15% yield or in 43% yield when the photolysis was carried out at −70 °C but not an isomeric oxetane **1e′** in detectable amounts. Since, as mentioned earlier, excited acetone would trap **8** and **8′** with similar trapping efficiencies, the above results strongly suggest that the formation of enols from unsymmetrical radicals **11e** and **11f** is highly regioselective in preference for the formation of **8e** and **8f** to their regioisomers **8e′** and **8f′**. Probably, in a disproportionation step, β-hydrogen abstraction from **11e** or **11f** by a partner radical **11a** would predominantly occur at the sterically less hindered site to yield a thermodynamically less favorable enol **8** as the major component in contrast to expectation from acid-catalyzed enolization of ketones.

Oxetanes **1b** and **1f** were obtained as two stereoisomeric mixtures in the ratios 1 : 1 and 4 : 1, respectively. These results appear interesting in relation to the stereochemical structure of the enols **8b** and **8f**; however, the stereochemistry of these oxetanes does not seem to provide meaningful information on the geometry of the enols in view of the fact that the

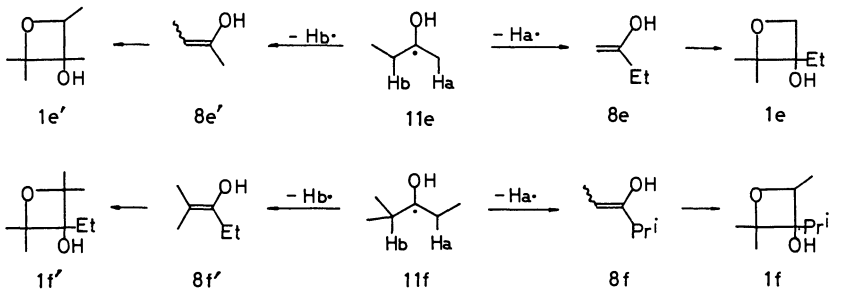

photo-oxetane formation between acetone and electron rich alkenes such as vinyl ethers is a nonstereospecific process.[25]

Temperature significantly affected the formation of oxetane and coupling products. Thus, irradiation of **18e** in acetone at 0—5 °C gave **1e**, **20e**, and **21e** in 15, 11, and 4% yields, while at −70 °C, in 43, 5, and 1% yields, respectively. A marked increase in the yield of the oxetane probably arises from retardation of the rate of ketonization of **8e** and partly from an increase in the fraction of disproportionation from **11e**.

Finally, in contrast to the photolysis of secondary alcohols, we could not detect the formation of aldehyde enols **8g** and **8h** as corresponding oxetanols in

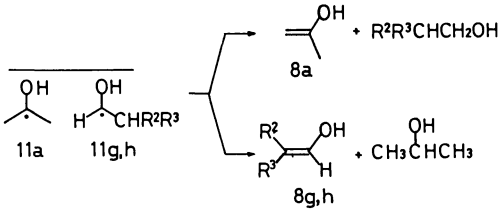

the photolysis of two primary alcohols, ethanol (**18g**) and isobutyl alcohol (**18h**), although CIDNP experiments indicate the formation of these enols under similar conditions.[26] In both cases, there were obtained considerable amounts of coupling products but not expected oxetanols **1g** and **1h** in detectable amounts. There seems to be no reason for that excited acetone traps aldehyde enols much less effectively than it does ketone enols. Indeed, vinyl alcohol could be trapped as **1g** in the photolysis of hexanal in acetone. It is therefore conceivable that aldehyde enols are formed in very low concentrations in the photolysis of primary alcohols in acetone solutions. Presumably, disproportionation of a pair of radicals such as **11a** and **11g** would preferentially occur in such a way that **11g** abstracts a hydrogen from **11a** affording acetone enol rather than it loses a β-hydrogen yielding vinyl alcohol, since **11g** is sterically less hindered and probably more reactive than its partner radical **11a**.

The present results indicate that aliphatic enols generated by photodehydrogenation of alcohols and by Norrish II reaction of alkanones can be isolated as corresponding 3-oxetanols when these photolysis reactions are carried out in acetone solutions, providing a rare example of [2+2]cycloadditions of simple enols.

Experimental

IR spectra were recorded on a Hitachi R-215 spectrophotometer. NMR spectra were recorded in carbon tetrachloride on a Hitachi R-20B spectrometer. Mass spectra were taken with a Hitachi M-60 mass spectrometer or an ion cyclotron resonance (ICR) mass spectrometer.[27] GLC were performed with a Hitachi 163 gas chromatograph equipped with glass columns (6 mm×1.5, 2.0, and 3 m) packed with 10% Silicone oil SE-30 on Chamelite CS (SE-30), 25% silicon oil DC-550 on Chamelite CS (SIDC), 25% Apiezon grease L on Chromosorb W (AGL), 15% Carbowax 20M on Chamelite CS (CW), or 10% diethylene glycol succinate polyester on Chamelite CS (DGS). Acetone was purified by refluxing with potassium permanganate followed by fractionation.

2,2,3-Trimethyl-3-(trimethylsiloxy)oxetane (10). A solution of 2-(trimethylsiloxy)propene (4.61 g) in acetone (100 cm³) was irradiated with a 100 W low-pressure mercury lamp under argon for 2 h, during which period 56% starting material was consumed. Fractionation of crude photolysate gave **10** as a colorless oil (1.68 g, 55%): bp 66—68 °C (22 Torr; 1 Torr=133.3 Pa); IR (neat) 1255, 1025, and 845 cm⁻¹; ^{1}H NMR δ=0.09 (9H, s), 1.18 (3H, s), 1.30 (3H, s), 1.43 (3H, s), 3.94 (1H, d, J=6.0 Hz), and 4.32 (1H, d, J=6.0 Hz). Found: C, 57.25; H, 10.70%. Calcd for $C_9H_{20}O_2Si$: C, 57.40; C, 10.71%. A foregoing fraction, bp 35—58 °C (28 Torr) contained another component which was shown to be 4-hydroxy-4-methyl-2-pentanone (**2**). GLC analysis (SE-30, 100 °C) of the crude photolysate indicated the formation of **10** and **2** in the ratio 86:14. **10** gave quantitatively 2,2,3-trimethyl-3-oxetanol (**1a**) on treatment with methanol.

Photolysis of Acetone in the Presence of a Hydrogen-Donating Substrate. General Procedure. Acetone (100 cm³) was directly irradiated under argon with or without a hydrogen donating substrate (35 mmol) using a 100 W low-pressure mercury lamp (Eikosha Halos PIH-100) in a 200 cm³ photolysis vessel which was immersed in an ice bath. After irradiation, acetone was first removed by distillation under reduced pressure (ca. 120 Torr) and resulting oil was fractionated under vacuum from 6 to 0.5 Torr. Each fraction was analyzed directly by GLC using an appropriate internal standard. In most cases, products were isolated by GLC and characterized from their spectral data.

Photolysis of Acetone. Irradiation of acetone (100 cm³) for 2 h gave 0.094 g of an oil, bp 42—58 °C (6 Torr), besides high-boiling material (0.212 g) after fractionation of photolysate. The former oil was shown to be a mixture of 2,2,3-trimethyl-3-oxetanol (**1a**), 4-hydroxy-4-methyl-2-pentanone (**2**), pinacol (**3**), and 2,5-hexanedione (**4**) in the ratio 51:23:9:17 in agreement with the earlier observation.[16]

Photolysis of Acetone with 2-Propanol (18a). Irradiation of acetone (100 cm³) containing 2-propanol (2.19 g, 35.5 mmol) for 2 h gave a mixture of **1a—4** in the ratio 42:23:31:3 [1.016 g, bp 48—58 °C (6 Torr)] besides 0.246 g of a high boiling material.

Photolysis of Acetone with 2-Propanol in the Presence of p-Toluenesulfonic Acid. A solution of 2-propanol (2.14 g), p-toluenesulfonic acid (99 mg), and acetone (100 cm³) was irradiated for 2 h. Most acetone was removed by distillation at 110 Torr. Residue was dissolved in ether, washed with aq. $NaHCO_3$, and dried. Solvent was removed to give a solid (303 mg) which was shown to be almost pure pinacol hydrate.

Photolysis of Acetone with Cyclohexane. Irradiation of an acetone solution of cyclohexane (2.99 g) for 2 h gave 0.583 g of an oil, bp 49—53 °C (6 Torr), besides 0.381 g of a high-boiling material. The former oil consisted of **1a—4** and another major component which was shown to be 2-cyclohexyl-2-propanol (**5a**) by comparison with an authentic sample: IR 3400 cm⁻¹; ^{1}H NMR δ=1.08 (6H, s), 0.9—2.0 (11H, m). GLC analysis of the crude photolysate indicated the formation of **1a—4** and **5a** in the ratio 40:18:13:4:24.

Photolysis of Acetone with 2-Trimethylsiloxypropane. Irradiation of an acetone solution of 2-trimethylsiloxypropane (4.73 g) for 2 h led to 16% consumption of 2-trimethylsiloxypropane to give 1.361 g of an oil distilling below 49 °C at 2 Torr besides 0.136 g of a high-boiling material. GLC analysis (2 m, SE-30, 80 °C) indicated the former oil to be a mixture of **1a—4** and two other major components (t_R=10.7 and 11.4 min), which were isolated by GLC and assigned to 2,3-dimethyl-3-(trimethylsiloxy)-2-butanol (**5b**) and **10**, respectively. **5b**: ^{1}H NMR δ=0.13 (9H, s), 1.08 (6H, s), 1.21 (s, 6H). On treatment with methanol **5b** cleanly gave pinacol. GLC analysis indicated the formation of **5b** and **10** in 22 and 33% yield, respectively on the basis of 2-trimethylsiloxypropane consumed. The relative yields of **1a—4**, **5b**, and **10** were 36 : 19 : 11 : 1 : 13 : 20.

Photolysis of Acetone with Triethylsilane. An acetone solution of triethylsilane (2.35 g) was irradiated for 2 h. Distillation of photolysate gave two fractions, I (2.22 g) distilling below 90 °C at 17 Torr and II (1.51 g), bp 123—135 °C (3 Torr). The fraction I contained **1a—3** and two other components. They were identified as triethylisopropoxysilane (**14**) and triethylsilanol (**17**) by comparison with authentic specimens. The fraction II consisted of two major components and they were assigned to 3-triethylsiloxy-2,2,3-trimethyloxetane (**15**) and 2,3-dimethyl-3-triethylsiloxy-2-butanol (**16**) from their spectral data. **15**: ^{1}H NMR δ=0.4—1.1 (15H, m), 1.18 (3H, s), 1.32 (3H, s), 1.42 (3H, s), 3.95 (1H, d, J=6.0 Hz), 4.29 (1H, d, J=6.0 Hz). On treatment with methanol **15** cleanly gave **1a**. **16**: IR 3430, 1020, and 740 cm^{-1}; ^{1}H NMR δ=0.45—1.1 (15H, m), 1.09 (6H, s), 1.22 (6H, s), 1.97 (1H, s, disappeared on adding D_2O). GLC analysis indicated the formation of **14**, **15**, **16**, and **17** in 26, 3, 10, and 45% yields, respectively. The relative yields for **1a—3**, **14**, **15**, **16**, and **17** were 15 : 3 : 14 : 21 : 2 : 8 : 36, respectively.

Photolysis of Acetone with 3-Pentanol (18b). Irradiation of 3-pentanol (3.10 g) in acetone (100 cm^3) for 2 h resulted in 46% consumption of 3-pentanol to give an oil (3.18 g) distilling below 60 °C at 2 Torr besides a high-boiling residue (0.51 g). The distilled oil was shown to be a mixture of three major components besides **1a—3**, unchanged **18b**, and 3-pentanone (**19b**). They were assigned to (*E*)- and (*Z*)-stereoisomers of 3-ethyl-2,2,4-trimethyl-3-oxetanol (**1b**) and 3-ethyl-2-methyl-2,3-pentanediol (**20b**) from their spectral data. (*E*)-**1b** (tentative stereochemical assignment): MS (ICR) m/z 145 (M^+ +1); IR 3420, 1150, 1055, 1010, and 905 cm^{-1}; ^{1}H NMR δ=0.84 (3H, t, J=7.2 Hz), 1.19 (3H, d, J=6.6 Hz), 1.24 (3H, s), 1.28 (3H, s), 1.65 (2H, q, J=7.2 Hz), 1.85 (1H, s, OH), and 4.30 (1H, q, J=6.6 Hz). On treatment with boron trifluoride etherate in dichloromethane (−15 °C, 30 min), this compound was smoothly converted into a single product which was shown to be 5-hydroxy-4,4-dimethyl-3-hexanone (**22b**): IR 3460 and 1700 cm^{-1}; ^{1}H NMR δ=0.99 (3H, t, J=7.2 Hz), 1.03 (3H, d, J=6.6 Hz), 1.10 (6H, s), 2.46 (2H, q, J=7.2 Hz), 2.32 (1H, OH), 3.80 (1H, q, J=6.6 Hz). Found: C, 66.50; H, 11.25%. Calcd for $C_8H_{16}O_2$: C, 66.68; H, 11.18%. (*Z*)-**1b** (tentative stereochemical assignment): MS (ICR) m/z 145 (M^+ +1); IR 3450, 1060, and 1015 cm^{-1}; ^{1}H NMR δ=0.89 (3H, t, J=7.2 Hz), 1.18 (3H, d, J=6.6 Hz), 1.20 (3H, s), 1.30 (3H, s), 1.69 (2H, q, J=7.2 Hz), and 4.35 (1H, q, J=6.6 Hz). On treatment with boron trifluoride etherate, this isomer also gave **22b** as a single product. An attempt at isolation of **1b** by GLC (3m, DGS) at 130 °C resulted in collection of **22b**. **20b**: IR 3450, 1380, 1125, and 950 cm^{-1}; ^{1}H NMR δ=0.77—1.5 (10H, m), 1.16 (s, 6H), and 1.63 (2H, s, disappeared on adding D_2O). GLC analysis of crude photolysate indicated the formation of **1a—3**, **1b**, **19b**, and **20b** in the ratio 34 : 12 : 13 : 15 : 11 : 15. The yield of the last three products were shown to be 24 (*E*/*Z*=1.0), 25, and 18%, respectively, based on 3-pentanol reacted.

Photolysis of Acetone with 2,4-Dimethyl-3-pentanol (18c). Irradiation of a solution of **18c** (4.14 g) in acetone (100 cm^3) for 4 h resulted in 40% consumption of **18c** to give two fractions, I [2.524 g, bp 25—46 °C (6 Torr)] and II [2.364 g, bp 52—64 °C (1 Torr)], besides a high-boiling residue (0.378 g) after fractionation of photolysate. The fraction I contained mainly **1a—3** (in the ratio 61 : 24 : 15), unchanged **18c**, and 2,4-dimethyl-3-pentanone (**19c**). The fraction II contained two major components and three minor ones besides small amounts of **1a—3**. The former two were shown to be 3-isopropyl-2,2,4,4-tetramethyl-3-oxetanol (**1c**) and 3-isopropyl-2,4-dimethyl-2,3-pentanediol (**20c**) by their spectral data. **1c**: mp 99—100 °C; MS (ICR) m/z 173 (M^+ +1); IR (Nujol) 3440, 1020 cm^{-1}; ^{1}H NMR δ=0.82 (6H, d, J=6.0 Hz), 1.20 (6H, s), 1.37 (6H, s), 1.60 (1H, s, OH), and 1.88—2.63 (m, 1H). **20c**: IR 3420 cm^{-1}; ^{1}H NMR δ=1.05 (12H, d, J=6.0 Hz), 1.27 (6H, s), 1.8—2.4 (2H, m), and 1.80 (2H, broad s, disappeared on adding D_2O). One of the three minor components in II was assigned to 3,4-diisopropyl-2,5-dimethyl-3,4-hexanediol (**21c**) from its spectral properties: IR 3470 cm^{-1}; ^{1}H NMR δ=0.93 (24H, d, J=6.6 Hz), 1.7—2.3 (2H, m), and 2.0 (2H, broad s, OH). The rest two components were not identified yet. GLC analysis (1.5 m, AGL, 130 °C) of crude photolysate indicated the formation of **19c**, **1c**, **20c**, and **21c** in 23, 18, 14, and 4% yields, respectively.

Photolysis of Acetone with Cyclopentanol (18d). Irradiation of a solution of cyclopentanol (3.10 g) in acetone for 4 h resulted in 34% consumption of the alcohol to yield two liquid fractions, I (1.23 g, distilling below 48 °C at 1 Torr) and II [0.36 g, bp 63—70 °C (0.5 Torr)], besides a high-boiling residue (1.09 g) after fractionation of crude photolysate. The fraction I contained mainly **1a—3**, cyclopentanol, and cyclopentanone (**19d**). The fraction II contained mainly two components. They were isolated by GLC and assigned to 1-hydroxy-7,7-dimethyl-6-oxabicyclo[3.2.0]heptane (**1d**) and 1-(2-hydroxyprop-2-yl)cyclopentanol (**20d**). **1d**: MS (ICR) m/z 143 (M^+ +1); IR 3430 cm^{-1}; ^{1}H NMR δ=1.17 (3H, s), 1.38 (3H, s), 1.5—2.1 (m, 6H), 2.36 (1H, disappeared on adding D_2O), and 4.62 (1H, d, J=2.5 Hz). **20d**: IR 3500 cm^{-1}; ^{1}H NMR δ=1.19 (6H, s), 1.47—1.87 (8H, m), and 2.35 (2H, disappeared on adding D_2O). GLC analysis (1.5 m, AGL, 130 °C) of crude photolysate indicated the formation of **1a—4**, **19d**, **1d**, and **20d** in the ratio 31 : 12 : 14 : 3 : 21 : 6 : 13. The yields of the last three components were 20, 5.2, and 12%, respectively, based on the consumed **18d**.

Photolysis of Acetone with 2-Butanol (18e). Irradiation of a solution of 2-butanol (2.71 g) in acetone for 4 h resulted in 37% consumption of 2-butanol to give two liquid fractions, I (1.1 g, distilling below 62 °C at 6 Torr) and II [0.89 g, bp 80—88 °C (2 Torr)], besides a high-boiling residue (0.3 g). I contained mainly **1a—4** (in the ratio 48 : 20 : 23 : 9). GLC analysis (2 m, SE-30, 130 °C) showed II to be a mixture of three major components (t_R 4.7, 5.1, and 7.8 min). They were assigned to 3-ethyl-2,2-dimethyl-3-oxetanol (**1e**), 2,3-dimethyl-2,3-pentanediol (**20e**), and 3,4-dimethyl-3,4-

hexanediol (**21e**) from their spectral data. **1e**: MS (ICR) *m/z* 131 (M+1); IR 3420 cm^{-1}; ^1H NMR δ=0.90 (3H, t, J=6.0 Hz), 1.26 (3H, s), 1.33 (3H, s), 1.44—1.91 (2H, m), and 4.16 (2H, almost s). On treatment with boron trifluoride etherate, **1e** was converted into 1-hydroxy-2,2-dimethyl-3-pentanone (**22e**): ^1H NMR δ=1.00 (3H, t, J=7.2 Hz), 1.11 (6H, s), 1.81 (1H, disappeared on addition of D_2O), and 3.43 (2H, s). The NMR spectrum was in agreement with that reported.[28] **22e** was also obtained when **1e** was passed through a 3 m DGS column at 130 °C. **20e**: IR 3430 cm^{-1}; ^1H NMR δ=0.92 (3H, t, J=6.6 Hz), 1.07 (3H, s), 1.15 (6H, s), 1.43 (2H, q, J=6.6 Hz), and 1.65 (2H, OH). The IR spectrum was superimposable with that reported.[29] The NMR spectrum of **21e** [δ=0.91 (6H, complicated), 1.06 (6H, s), 1.8 (2H, OH)] was in agreement with that reported.[30] GLC analysis of crude photolysate indicated the formation of **1a—4**, **1e**, **20e**, and **21e** in the ratio 36:15:17:14:8:3. The yields of the last three components were 15, 11, and 4%, respectively, based on 2-butanol reacted.

Photolysis of Acetone with 2-Butanol at Low Temperature. Irradiation of 2-butanol (2.71 g) in acetone (100 cm^3) at Dry Ice temperature for 2 h resulted in 14% consumption of 2-butanol to give 1.18 g of an oil distilling below 57 °C at 3 Torr. GLC analysis indicated the oil to be a mixture of **1a—4**, **1e**, **20e**, and **21e** in the ratio 38:16:4:10:26:3:1. The yields of the last three components were 43, 5, and 1%, respectively, on the basis of 2-butanol consumed.

Photolysis of Acetone with 2-Methyl-3-pentanol (18f). Irradiation of 2-methyl-3-pentanol (3.63 g) in acetone for 4 h resulted in 42% consumption of the alcohol to give two liquid fractions, I (3.13 g, distilling below 48 °C at 2 Torr) and II [1.0 g, bp 55—70 °C (1.5 Torr)]. Fraction I contained mainly **1a—3**, unchanged **18f**, and 2-methyl-3-pentanone (**19f**). GLC analysis (1.5 m, SIDC, 130 °C) indicated the fraction II to be a mixture of two major components (t_R 15.2 and 28 min) together with two minor ones (t_R 17.2 and 18.8 min) besides small amounts of **1a—3**. The major two products were shown to be 3-isopropyl-2,2,4-trimethyl-3-oxetanol (**1f**) and 3-ethyl-2,4-dimethyl-2,3-pentanediol (**20f**). **1f**: MS (ICR) *m/z* 159 (M^++1); IR 3430 cm^{-1}; ^1H NMR δ=0.76 (3H, d, J=7.2), 0.80 (3H, d, J=7.2 Hz), 1.15 (3H, d, J=6.0 Hz), 1.21 (3H, s), 1.35 (3H, s), 1.97 (1H, disappeared on addition of D_2O), 1.9—2.4 (1H, m), and 4.40 (1H, q, J=6.0 Hz). **20f**: IR 3440 cm^{-1}. ^1H NMR δ=0.93 (3H, d, J=6.6 Hz), 0.99 (3H, d, J=7.2 Hz), 0.8—1.0 (3H), 1.21 (6H, s), 1.4—2.1 (2H, m), and 2.2 (2H, disappeared on addition of D_2O). One of the two minor products was assigned to a stereoisomer of **1f** from the following spectral data: IR 3430 cm^{-1}; ^1H NMR δ=0.82 (3H, d, J=6.6 Hz), 0.85 (3H, d, J=6.6 Hz), 1.16 (3H, d, J=7.2 Hz), 1.22 (3H, s), 1.36 (3H, s), 1.9—2.4 (1H, m), and 4.24 (1H, q, J=7.2 Hz). The rest one components was not identified yet. GLC analysis indicated the formation of **1a—3**, **19f**, **1f** (4:1 mixture of stereoisomers), and **20f** in the ratio 39:17:11:12:13:11. The yields of the last three products were 19, 21, and 17%, respectively, on the basis of 2-methyl-3-pentanol consumed.

Photolysis of Acetone with Ethanol (18g). Irradiation of ethanol (1.67 g) in acetone for 4 h gave 2.134 g of an oil distilling below 63 °C at 2 Torr besides a high-boiling residue (0.323 g). GLC analysis (1.5 m, SIDC, 100 °C) indicated the oil to be a mixture of two major products (t_R 3.6 and 6.0 min) besides **1a—3**. They were shown to be 3-hydroxy-3-methyl-2-butanone and 2-methyl-2,3-butanediol (**20g**) by comparison with the authentic specimens. **20g**: IR 3420 cm^{-1}; ^1H NMR δ=1.13 (6H, s), 1.14 (3H, d, J=7.2 Hz), 3.50 (1H, q, J=7.2 Hz), and 3.61 (2H, disappeared on addition of D_2O). GLC analysis showed the formation of **1a—3**, 3-hydroxy-3-methyl-2-butanone, and **20g** in the ratio 38:17:18:5:22.

Photolysis of Acetone with Isobutyl Alcohol (18h). Irradiation of isobutyl alcohol (2.70 g) in acetone for 4 h resulted in 40% consumption of the alcohol to give 1.85 g of an oil distilling below 53 °C at 2 Torr besides a high-boiling residue (0.467 g). GLC analysis (2 m, SE-30, 80 °C) indicated the oil to be a mixture of two major components (t_R 10.6 and 26 min) besides **1a—4**. They were assigned to 2,4-dimethyl-2,3-pentanediol (**20h**) and 2,5-dimethyl-3,4-hexanediol (**21h**, mostly as meso form) from their spectral data which were in agreement with those reported.[29] GLC analysis indicated the formation of **1a—4**, **20h**, and **21h** in the ratio 32:14:13:7:27:8. The yields of the last two products were 28 and 8%, respectively, based on isobutyl alcohol consumed.

Photolysis of Acetone with 3-Octanone (23). Irradiation of 3-octanone (4.66 g) in acetone (100 cm^3) for 4 h resulted in 42% consumption of 3-octanone to give, after fractionation of crude photolysate, two liquid fractions, I (4.04 g, distilling below 33 °C at 0.5 Torr) and II [0.67 g, bp 42—64 °C (0.5 Torr)], besides a high-boiling residue (1.09 g). Fraction I contained mainly **1a** and **2** other than **23**. Fraction II contained two major components which were assigned to **1e** and 1,2-diethylcyclobutanol (**24**) from their spectral properties. **24**: MS *m/z* 129 (M^++1); IR 3430 cm^{-1}; ^1H NMR δ=0.87 (6H, complicated), 1.2—2.07 (9H, m), 1.17 (1H, disappeared on adding D_2O). GLC analysis (2 m, SE-30, 80 °C) indicated the formation of **1a**, **2**, **1e**, and **24** in the ratio 46:19:24:11. The yields of the last two products were 34 and 16%, respectively, on the basis of 3-octanone consumed.

Photolysis of Acetone with Hexanal (26). Irradiation of hexanal (3.64 g) in acetone (100 cm^3) for 4 h resulted in 96% consumption of hexanal to give, after fractionation of photolysate, two liquid fractions, I (1.54 g distilling below 30 °C at 0.5 Torr) and II [0.80 g, bp 54—67 °C (0.5 Torr)], besides a high-boiling residue (0.26 g). GLC analysis (1.5 m, SIDC, 70 °C) indicated the fraction I to contain three major components (t_R 27.6, 32.8, and 40.4 min) other than **1a** and **2** (t_R 44.4 and 35.2 min, respectively). They were characterized as (*E*)- and (*Z*)-stereoisomers of 2-ethylcyclobutanol (**27**) and 2,2-dimethyl-3-oxetanol (**1g**) from their spectral properties. (*E*)-**27** (tentative stereochemical assignment): IR 3350 and 1105 cm^{-1}; ^1H NMR δ=0.87 (3H, t, J=6.6 Hz), 1.08—2.27 (7H, m), 2.07 (1H, disappeared on adding D_2O), and 3.69 (1H, m). (*Z*)-**27** (tentative stereochemical assignment): IR 3330 and 1120 cm^{-1}; ^1H NMR δ=0.87 (3H, t, J=6.6 Hz), 1.06—2.6 (7H, m), 1.54 (1H, disappeared on adding D_2O), and 4.27 (1H, m). These NMR spectra were in agreement with those reported.[31] **1g**: MS *m/z* 103 (M^++1), 72, and 59; IR 3400, 1150, 1120, 1045, 975, 955, and 825 cm^{-1}; ^1H NMR δ=1.29 (3H, s), 1.32 (3H, s), 4.0—4.62 (3H, m). Fraction II contained two major components. One of them was assigned to 2-hydroxy-2-methyl-3-octanone (**28**): IR 3450 and 1715 cm^{-1}; ^1H NMR δ=0.91 (3H, t, J=6.5 Hz), 1.29 (6H, s), 1.07—1.64 (6H, m), 2.46 (2H, t, J=6.6 Hz), and 3.4 (1H, OH). GLC analysis indicated the formation of **1a**, **2**, **27** (2:1 stereoisomeric mixture), **1g**, and **28** in the ratio 14:6:48:16:16. The yields of the last three products were 24, 8,

and 8%, respectively, on the basis of hexanal consumed.

References

1) H. Hart, *Chem. Rev.*, **79**, 515 (1979).

2) B. Capon, B-Z. Guo, F. C. Kwok, A. K. Siddhanta, and C. Zucco, *Acc. Chem. Res.*, **21**, 135 (1988).

3) J. P. Keeffe, A. Kresge, and N. P. Schepp, *J. Am. Chem. Soc.*, **110**, 1993 (1988); Y. Chiang, M. Hojatti, J. R. Keeffe, A. J. Kresge, N. P. Schepp, and J. Wirz, *ibid.*, **109**, 4000 (1987); Y. Chiang, A. J. Kresge, and Y. S. Tang, and J. Wirz, *ibid.*, **106**, 460 (1984); Y. Chiang, A. J. Kresge, and J. Wirz, *ibid.*, **106**, 6392 (1984).

4) E. B. Nadler and Z. Rappoport, *J. Am. Chem. Soc.*, **109**, 2112 (1987) and references cited therein.

5) E. A. Schmidt and H. M. R. Hoffmann, *J. Am. Chem. Soc.*, **94**, 7832 (1972); S. M. Rosenfeld, R. G. Lawlor, and H. R. Ward, *J. Am. Chem. Soc.*, **95**, 946 (1973); P. Haspra, A. Sutter, and J. Wirz, *Angew. Chem., Int. Ed. Engl.*, **18**, 617 (1979); M-C. Lasne and J-L. Ripoll, *Tetrahedron Lett.*, **23**, 1587 (1982); B. Capon, A. K. Siddhanta, and C. Zucco, *J. Org. Chem.*, **50**, 3580 (1985); B. Capon and G. Bozhang, *J. Am. Chem. Soc.*, **110**, 5144 (1988).

6) S. Saito, *Chem. Phys. Lett.*, **42**, 399 (1976).

7) J-L. Ripoll and T-C. Wang, *J. Am. Chem. Soc.*, **91**, 1146 (1969).

8) A. Henne and H. Fischer, *Angew. Chem., Int. Ed. Engl.*, **15**, 435 (1976).

9) B. Capon, D. S. Rycroft, and T. W. Watson, *J. Am. Chem. Soc.*, **103**, 1761 (1981).

10) B. Blank and H. Fischer, *Helv. Chim. Acta*, **56**, 506 (1973); J. Bargon and K-G. Seifert, *Chem. Ber.*, **108**, 2073 (1975).

11) W. B. Moniz, S. A. Sojka, C. F. Poranski, Jr., and D. L. Birkle, *J. Am. Chem. Soc.*, **100**, 7940 (1978).

12) J. R. McNesby and A. S. Gordon, *J. Am. Chem. Soc.*, **80**, 261 (1958); G. R. McMillan, J. G. Calvert, and J. N. Pitts, Jr., *ibid.*, **86**, 3602 (1964).

13) J. Toullec and J. E. Debois, *J. Am. Chem. Soc.*, **98**, 5518 (1976); J. E. Dubois, M. El-Alaoui, and J. Toullec, *ibid.*, **103**, 5393 (1981); R. R. Gallucci and R. Going, *J. Org. Chem.*, **46**, 2532 (1981); J. P. Guthrie, J. Cossar, and A. Klym, *J. Am. Chem. Soc.*, **106**, 1351 (1984).

14) P. G. Sammes, *Tetrahedron*, **32**, 405 (1976) and the references cited therein.

15) G. Quinkert, W-D. Weber, U. Schwartz, and G. Durner, *Angew. Chem., Int. Ed. Engl.*, **19**, 1027 (1980).

16) J. T. Przybytek, S. P. Singh, and J. Kagan, *J. Chem. Soc. D*, **1969**, 1224.

17) H. A. J. Carless, "Synthetic Organic Photochemistry," ed by W. M. Horspool, Plenum Press, New York and London (1984). Chap. 8.

18) N. C. Yang and D. H. Yang, *J. Am. Chem. Soc.*, **80**, 2913 (1950).

19) J. Kagan and J. T. Przybytek, *Tetrahedron*, **29**, 1163 (1969).

20) G. P. Laroff and H. Fischer, *Helv. Chim. Acta*, **56**, 2011 (1973).

21) The lifetime of **8a** is reported 14 s in acetonitrile, see Ref. 20.

22) H. Gilman and D. Wittenberg, *J. Org. Chem.*, **23**, 50 (1958); H-D. Becker, *ibid.*, **34**, 2469 (1969).

23) N. Shimizu, S. Yamaoka, and Y. Tsuno, *Bull. Chem. Soc. Jpn.*, **56**, 3853 (1983).

24) P. J. Wagner, *Acc. Chem. Res.*, **4**, 168 (1971); A. Henne and H. Fischer, *Angew. Chem., Int. Ed. Engl.*, **15**, 435 (1976); P. Haspra, A. Sutter, and J. Wirz, *Angew. Chem., Int. Ed. Engl.*, **18**, 617 (1979).

25) N. J. Turro and P. A. Wriede, *J. Am. Chem. Soc.*, **90**, 6863 (1968); J. C. Dalton, P. A. Wried, and N. J. Turro, *ibid.*, **92**, 1318 (1970); N. J. Turro, C. Lee, N. Schore, J. Barltrop, and H. A. J. Carless, *ibid.*, **93**, 3079 (1971).

26) J. Bargon and K-G. Seifert, *Chem. Ber.*, **108**, 2073 (1975).

27) M. Mishima, M. Fujio, and Y. Tsuno, *Mem. Fac. Sci., Kyushu Univ., Ser. C*, **14(2)**, 365 (1984).

28) H. Reinheckel and G. Sonnek, *Z. Chem.*, **1975**, 50.

29) M. Stiles and R. Mayer, *J. Am. Chem. Soc.*, **81**, 1497 (1959).

30) R. E. Balsells and A. R. Frasca, *Tetrahedron*, **38**, 245 (1982).

31) J. D. Coyle, *J. Chem. Soc. B*, **1971**, 2254.

An Efficient Preparation and Reactions of [5,6′-Biguaiazulene]-3,3′(5*H*,6′*H*)-dione and 5-Isopropylidene-3,8-dimethyl-1(5*H*)-azulenone: Key Intermediates for the Autoxidation Products of Guaiazulene[1)]

Yoshiharu MATSUBARA, Shuichi MATSUI, Shin-ichi TAKEKUMA,* Yan Pin QUO,†
Hiroshi YAMAMOTO,††,* and Tetsuo NOZOE†††
Department of Applied Chemistry, Faculty of Science and Engineering, Kinki University, Kowakae, Higashi-Osaka 577
††Department of Chemistry, Okayama University, Okayama 700
†††Tokyo Research Laboratories, Takasago Corporation, Kamata, Ohta-ku, Tokyo 144
(Received January 27, 1989)

Oxidation of guaiazulene (**1**) with peracetic acid in hexane at 25 °C afforded as high as an 80% yield of the title biguaiazulenedione (**12**), which upon heating at 60 °C under nitrogen gave the title 1-azulenone (**13**) quantitatively. Oxidation of **12** and **13** was studied under various conditions, and these compounds were shown to be highly important key intermediates for a large number of the complex products obtained by autoxidation of **1**.

For the past several years we have undertaken a systematic investigation on autoxidation of various azulenic hydrocarbons and isolated a wide variety of interesting products, whose structures were mostly elucidated.[2-11)] These products can be classified mainly into four groups according to their structural type: i) oxidative coupling products (dimers and trimers), ii) side-chain oxidation products, iii) nucleus-oxidation products (azulenequinones, indenones, naphthalenoids, and benzenoids), and iv) one- carbon-transfer products (formylazulenes, diazulenylmethanes, and ketones). Compounds coupled with substrate azulenes have also been obtained as the secondary products.

In particular, autoxidation of guaiazulene (**1**), which possesses a high, redox potential (E_{pa} 0.71 V vs. SCE),[12)] has been intensively studied under various conditions as a model compound for investigation of oxidation of azulenic hydrocarbons, and a preliminary view on the possible pathways for the extremely complex, competitive reactions has been proposed;[5,11)] see Scheme 1 for intermediates and products **2**—**11** as well as paths i—iv corresponding to the classified structural type mentioned above. We now wish to report herein our study on the reaction of **1** with peracetic acid in hexane, which enabled us to efficiently isolate unique compounds that are considered to be highly important in view of further clarification of complex mechanisms of oxidation of azulenic hydrocarbons.

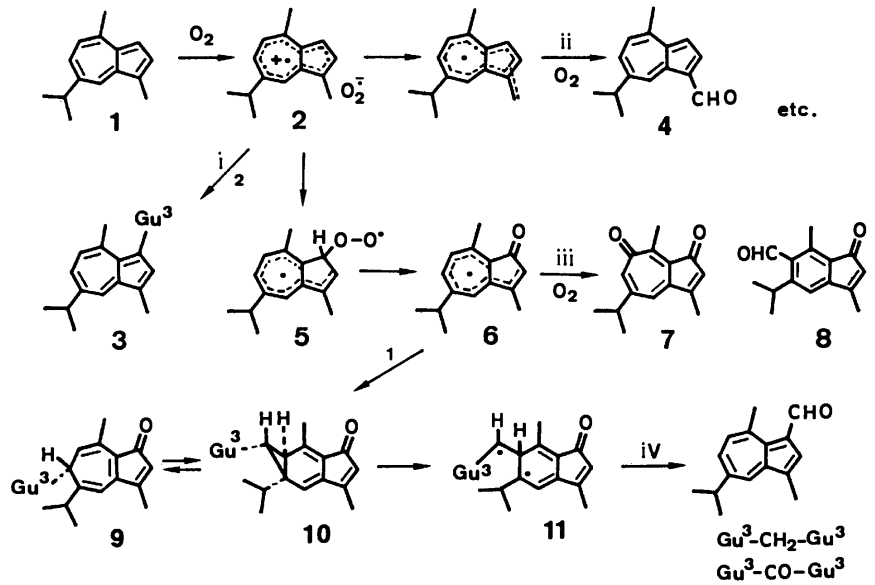

Scheme 1. Autoxidation of guaiazulene (**1**):[5,11)] Gu^3=3-guaiazulenyl.

† Present address: Guangzhou Institute of Chemistry, Academica Sinica, P.O.Box 122, Guangzhou, China.

Results and Discussion

It was briefly reported[10] that treatment of **1** with equimolar peracetic acid in acetic acid at 15 °C for 3 min gave [5,6′-biguaiazulene]-3,3′(5*H*,6′*H*)-dione (**12**, 18% isolated yield) together with **9**[4,11] (20%), **10**[4,11] (10%), and other minor products. However, we have now found out that when the same reaction was carried out in hexane using an excess of 30% peracetic acid at 25 °C for 1 h, **12** was exclusively produced on the evidence of TLC and HPLC; see the reaction conditions summarized in Table 1. Addition of saturated aq sodium carbonate to the reactant afforded **12** as a precipitate in an 80% isolated yield; see the Experimental section for additional spectroscopic data (FAB-MS and ^{13}C NMR) obtained presently to confirm the asymmetrically coupled dimeric structure. The rest of the products isolated from the hexane filtrate and purified by chromatography were **4**,[2,5] **7**,[2,5] **8**,[2,5] **9**, **10**, and 5-isopropylidene-3,8-dimethyl-1(5*H*)-azulenone (**13**), besides a polar resinous substance that remained unidentified (Scheme 2). The yields of these isolated products are summarized in Table 2. Among these products, **13** was newly obtained here in an extremely low yield, but it was prepared efficiently from **12** (see below).

Table 1. Reaction Conditions of Peroxy Acid Oxidation of **1** in Hexane

Expt	Temp/ °C	Time/ h	Mole equiv of peracid[a]	Recovered **1**/%
I	25	1	1	70
II	25	1	3	42
III	25	1	6	13

a) Mol equiv of 30% peracetic acid in 40 parts of hexane.

Table 2. Isolated Yield[a]/% of the Oxidation Products from **1**

Product	Expt (reaction conditions)[b]		
	I	II	III
4	0.7	0.2	0.2
7	0.3	0.2	0.1
8	0.7	0.5	0.2
9	1.3	1.6	0.5
10	0.7	0.2	1.3
12	70.5	70.2	80.1
13	0.3	0.2	0.1
RS[c]	20.1	23.3	15.2

a) The yield of each product is based on the consumed **1**. b) Expts I—III correspond to those in Table 1. c) Polar resinous substance.

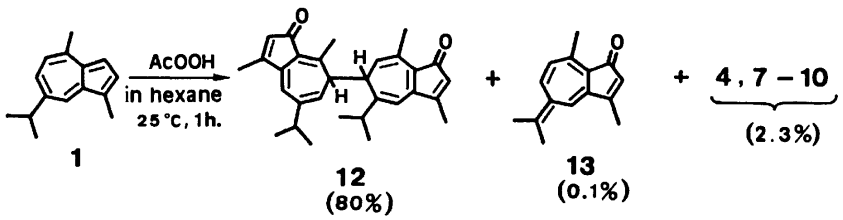

Scheme 2. Oxidation of **1** with peracetic acid.

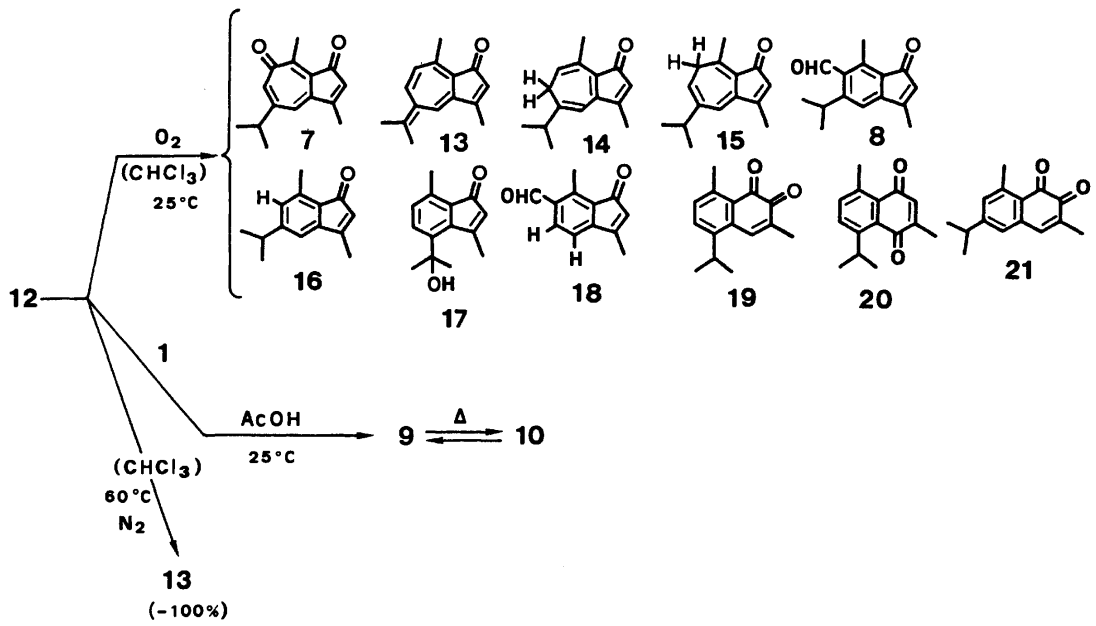

Scheme 3. Reactions of **12**.

The dimer **12** is a pale yellow powder and stable at 25 °C as long as it is kept as a solid. When **12** was, however, dissolved in chloroform and allowed to stand at 25 °C under aerobic conditions, it was found to give many products, a majority of which was obtained by autoxidation of **1** (through path iii). The isolated products were various azulenones [**7**[2,5] (0.4% yield), **13** (30%), **14** (24%), **15** (5%)], indenones [**8**[2,5] (6%), **16**[2,5] (22%), **17** (1%), **18**[11] (2%)], and naphthoquinones [**19**[13] (2%), **20**[2,5] (3%), **21** (5%)] (see Scheme 3). In contrast, when dissolved in degassed chloroform[14] and heated at 60 °C for 1 h under nitrogen, **12** turned out to undergo disruption to afford **13** almost quantitatively.

Compound **13** having a unique structure of quinonemethide is isolable as orange needles but rather unstable. Thus, when dissolved in chloroform and set aside at 25 °C for 1 d in open air, **13** yielded several 1-indenone derivatives **8** (3%), **16** (8%), **17** (1%), **18** (54%), **22** (5%), **23** (1%), **24** (4%), and **25** (1%) (see Scheme 4), some of which had also been produced by autoxidation of **1** (path iii).

The structures of the hitherto unreported compounds **13**—**15**, **17**, and **21**—**25** mentioned above were established by the mass spectrometry and ^{1}H NMR and IR spectroscopy. These spectral data and their assignments are given in the Experimental section. The most probable pathways particularly of the unusual reactions of **13** are then proposed in Scheme 4. It is especially of interest that compounds missing the isopropyl side chain (**18**, **23**) or having an oxidized side chain (**17**, **22**, **24**, **25**) are derived under such extremely mild conditions as those employed presently. This suggests that, at initial stage, **13** is likely to behave like diradical **26** and to react with oxygen competitively at C-6 and the isopropylidene side chain. Then, a series of degradative transformations involving presumably intramolecular hydrogen transfer, acetone cleavage, and decarbonylation proceed to afford various 1-indenones, as illustrated in Scheme 4.

Furthermore, the dimer **12** was shown to react with guaiazulene (**1**) in acetic acid at 25 °C to afford exclusively, at the initial stage, a mixture of **9** (50% yield) and **10** (50%) (Scheme 3). This also provides an important suggestion of a reaction pathway of oxidation of **1**, because both **9** and **10** have been shown[4,11] to give most of the same one-carbon-transfer products as those directly obtained by autoxidation of **1** (see path

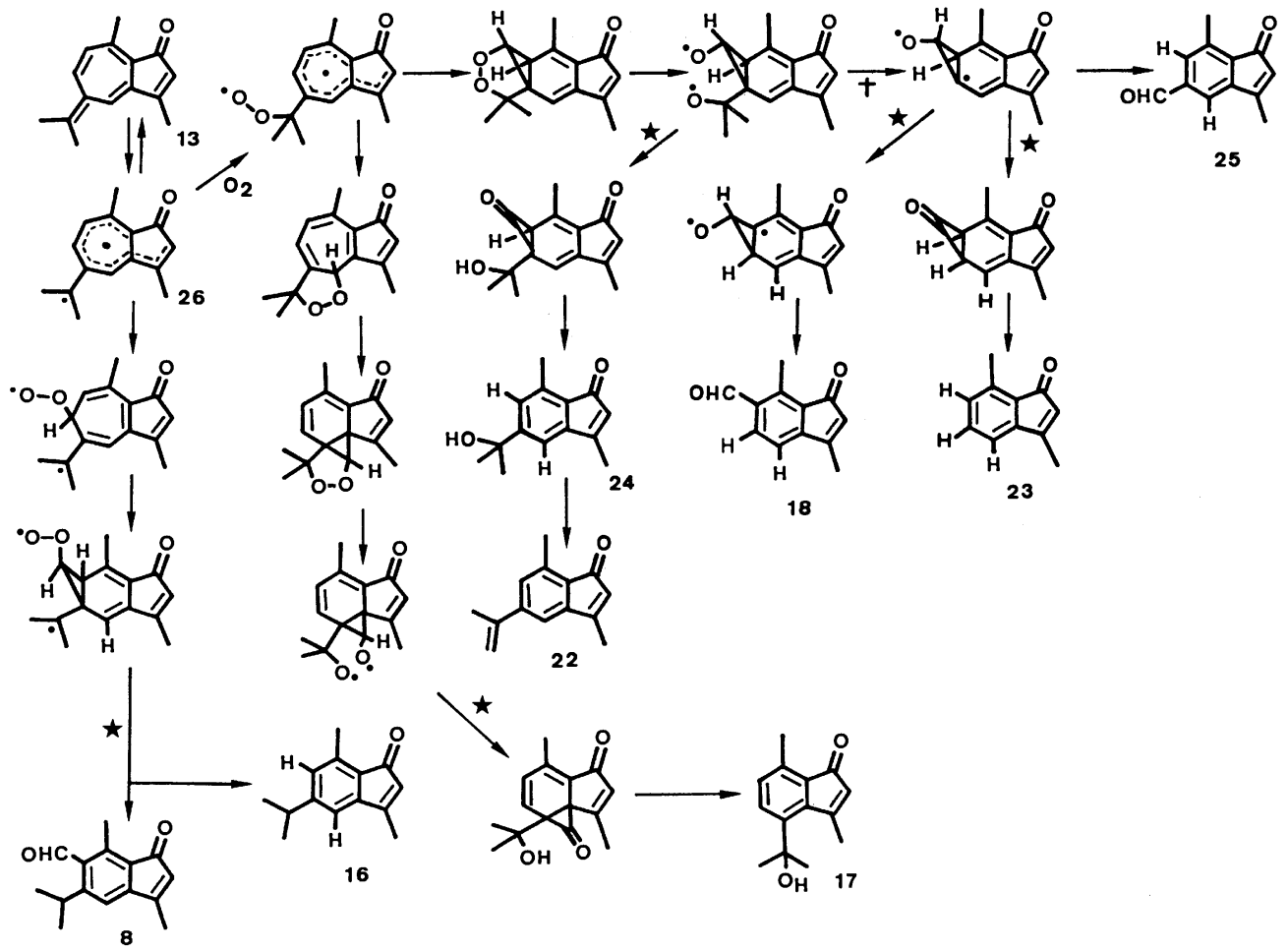

Scheme 4. Autoxidation of **13** in chloroform and possible reaction pathways for the products: *Intramolecular H· transfer; †acetone cleavage.

iv in Scheme 1).

These pieces of evidence described so far are indicative of the 3-guaiazulenone dimer **12** (and presumably the dissociated monomeric radical ketone **6**) and 3-azulenone **13** to be very important key intermediates for the two major reaction pathways (iii and iv in Scheme 1) for the autoxidation of guaiazulene (**1**) and apparently other azulenic hydrocarbons as well. Further studies (including theoretical calculation of the reactivities of these compounds) with regard to the exact reaction mechanisms and selective preparations of desired oxidation products are currently under intensive investigation.

Experimental

Melting points were determined with a Yanagimoto MP-S3 instrument and are uncorrected. Column chromatography was performed with Wako C-300 silica gel. TLC was conducted on plates precoated with silica gel 60F-254 (0.25 mm, Merck) by using 15:85 AcOEt–hexane as eluant. HPLC was carried out with Hitachi gel #3011 packed in a Pyrex column (ϕ 5 mm, 500 mm length) with 1:9 hexane–MeOH as solvent.

The UV and IR spectra were taken on a Hitachi 323 spectrophotometer and a JASCO IR-A-202 Grating spectrometer, respectively. Mass spectra were taken on a JEOL JMS-HX100 (with a JEOL JMA-DA5000 mass data system) high-resolution instrument and are given in terms of *m/z* (rel intensity) compared with the base peak. NMR spectra were recorded in $CDCl_3$ with a JEOL FX-200 (200 MHz for ^1H and 50 MHz for ^{13}C) or JEOL GSX-270 cryospectrometer at 27 °C. The assignments of all signals were made by employing a first-order analysis with the aid of decoupling technique and the parameters were confirmed by a computer-assisted simulation analysis.

Oxidation of Guaiazulene (1). **1**[15] (0.50 g) was added to a stirred solution of peracetic acid [30% aq, 0.64 cm^3, 1.0 mol equiv (for Expt I described in Table 1)] in hexane (20 cm^3). The mixture was stirred at 25 °C for 1 h and then saturated aq sodium carbonate was added. The precipitated solid was filtered off and washed well with water, then with hexane, and finally with ethyl acetate, thus giving pure **12** (105 mg, 71% theoretical yield). The above hexane filtrate and the organic washings were combined, washed thoroughly with water, dried (Na_2SO_4), and evaporated in vacuo. The residue (390 mg) was purified by silica-gel column chromatography first with hexane (to recover unreacted **1**), then with hexane–ethyl acetate (to separate various products), and finally with methanol (to eluate the polar substance) as the eluants. Then, each fraction of the products was further purified by preparative HPLC; when necessary, this chromatographic procedure was repeated.

Expts II and III (Table 1) were conducted under exactly the same procedures as those described above except for using 1.92 and 3.86 cm^3 of 30% peracetic acid in 20 cm^3 of hexane. The yield of each product based on the consumed starting material is summarized in Table 2.

[5,6'-Biguaiazulene]-3,3'(5*H*,6'*H*)-dione (12):[10] A pale yellow powder, mp 138—142 °C (decomp) (lit,[10] 138—142 °C decomp); although some spectral data for this compound were reported[10] the following data to confirm the structure have been obtained in the present study, FAB-MS (matrix, 3-mercapto-1,2-propanediol+NaI) *m/z* 449 (M+23; 3), 427 (M+1; 2), 343 (15), 319 (6), 236 (M/2+23; 20), and 213 (M/2; 100); ^{13}C NMR δ=194.12, 193.57 (C-3, 3'), 162.89, 162.64, 147.90, 147.28, 144.40, 143.66, 141.53, 141.42, 130.29, 129.37, 128.58, 122.87, 122.64, 121.23, 120.35, 45.91, 45.80, 35.55, 22.99, 22.63, 22.45, 22.27, 21.96, 13.73, and 13.69.[16]

5-Isopropylidene-3,8-dimethyl-1(5*H*)-azulenone (13): Orange needles, mp ca. 135 °C (darkened); R_f 0.30; UV λ_{max} (MeOH) 209, 244sh, 265, 300sh, 389, 400sh, and 488sh nm; IR ($CHCl_3$) 1680 cm^{-1} (C=O); EI-MS *m/z* 212 (M$^+$; 100), 197 (95), 183 (5), 169 (17), 153 (12), 141 (14), 128 (9), and 115 (6); ^1H NMR δ=1.89, 1.92 (3 H each, 2 s, Me_2C-5), 2.18 (3 H, d, $J\simeq$1.0 Hz, Me-3), 2.37 (3 H, s, Me-8), 5.62 (1 H, d, J=13.0 Hz, H-7), 6.15 (1 H, qd, $J\simeq$1.0, 0.3 Hz, H-2), 6.43 (1 H, dd, J=13.0, 2.0 Hz, H-6), and 6.52 (1 H, dd, J=2.0,$\simeq$0.3 Hz, H-4). Found: *m/z* 212.1210. Calcd for $C_{15}H_{16}O$: M, 212.1201.

Reactions of 12. A. Under Aerobic Conditions: A solution of **12** (100 mg) in chloroform (10 cm^3) was allowed to stand at 25 °C for 1 d in open air. After evaporation of the solvent and purification of the residue by chromatography, the following products were obtained: **7**[2,5] (0.4% yield), **8**[2,5] (5.7%), **13** (30.4%), **14** (24.1%), **15** (5.1%), **16**[2,5] (21.5%), **17** (1.0%), **18**[11] (1.7%), **19**[13] (2.2%), **20**[2,5] (3.2%), and **21** (4.8%).

3(6*H*)-Guaiazulenone (14): Pale yellow needles; R_f 0.55; EI-MS *m/z* 214 (M$^+$; 100) 199 (46), 184 (6), 172 (80), 171 (80), 156 (28), 143 (62), 129 (37), 128 (34), and 115 (8), the fragmentation pattern closely resembled that of **15** (see below); ^1H NMR, the sample was not stable enough for the measurement of the spectrum.

3(5*H*)-Guaiazulenone (15): Pale yellow needles; R_f 0.55; EI-MS *m/z* 214 (M$^+$; 46), 199 (45), 184 (5), 172 (38), 171 (100), 156 (12), 143 (18), 128 (12), and 115 (5). ^1H NMR δ=1.07 (6 H, d, J=7.0 Hz, Me_2C-7), 2.196 (3 H, d, J=1.5 Hz, Me-1), 2.41 (3 H, s, Me-4), 2.484 (1 H, sept, J=7.0 Hz, CH-7), 2.73 (2 H, d, J=7.0 Hz, H-7), 5.40 (1 H, td, J=7.0, 2.0 Hz, H-6), 5.91 (1 H, q, J=1.5 Hz, H-2), and 6.34 (1 H, d, J=2.0 Hz, H-8). Found: *m/z* 214.1366. Calcd for $C_{15}H_{18}O$: M, 214.1357.

4-(1-Hydroxy-1-methylethyl)-3,7-dimethyl-1*H*-inden-1-one (17): Pale yellow oil; R_f 0.18; IR ($CHCl_3$) 3600—3200 (OH) and 1700^{-1}(C=O); EI-MS 216 (M$^+$; 22), 201 (35), 198 (100), 183 (83), 173 (6), 169 (6), 159 (74), 155 (31), 141 (6), 128 (22), 115 (15), 100 (6), 93 (11), 77 (6), 59 (6), 51 (5), and 43 (34); ^1H NMR δ=1.69 (6 H, s, Me_2C-4), 1.728 [1 H, s, C(OH)-4], 2.51 (3 H, br s, Me-7), 2.61 (3 H, d, J=1.5 Hz, Me-3), 5.75 (1 H, q, J=1.5 Hz, H-2), 6.95 (1 H, br d, J=8.0 Hz, H-6), and 7.216 (1 H, d, J=8.0 Hz, H-5). Found: *m/z* 216.1089. Calcd. for $C_{14}H_{16}O_2$: M, 216.1150.

6-Isopropyl-3,8-dimethyl-1,2-naphthoquinone (21): Pale yellow needles; R_f 0.55; EI-MS *m/z* 228 (M$^+$; 18), 185 (100), 157 (22), and 128 (8); ^1H NMR δ=1.225 (6 H, d, J=7.0 Hz, Me_2C-6), 2.27 (3 H, d, J=1.5 Hz, Me-3), 2.58 (3 H, br s, Me-8), 3.52 (1 H, sept, J=7.0 Hz, CH-6), 5.76 (1 H, q, J=1.5 Hz, H-4), 7.48 (1 H, d, J=2.0 Hz, H-5), and 7.61 (1 H, br d, J=2.0 Hz, H-7). Found: *m/z* 228.1148. Calcd for $C_{15}H_{16}O_2$: M, 228.1150.

B. Under Anaerobic Conditions: A solution of **12** in degassed chloroform was heated at 60 °C for 1 h under nitrogen, followed by the same work-up, giving **13** quatitatively (by TLC and HPLC).

C. In the Presence of 1: A solution of **12** (166 mg) and **1** (300 mg) in acetic acid (15 cm^3) was allowed to stand at 25 °C for 1 h, followed by the same work-up, giving **9**[4] (50% yield)

and **10**[4] (50%).

Reaction of 13. A solution of **13** (100 mg) in chloroform (10 cm^3) was allowed to stand at 25 °C for 1 d in open air, followed by the same work-up as above, giving **8**[2,5] (3.0% yield), **16**[2,5] (7.8%), **17** (1.0%), **18**[11] (53.8%), **22** (5.0%), **23** (1.0%), **24** (4.4%), and **25** (1.0%).

5-Isopropenyl-3,7-dimethyl-1*H*-inden-1-one (22): Pale yellow needles; R_f 0.78; EI-MS *m/z* 198 (M^+; 100), 183 (98), 169 (11), 155 (86), 139 (8), 128 (18), and 115 (13).

3,7-Dimethyl-1*H*-inden-1-one (23): Pale yellow needles, R_f 0.78; EI-MS *m/z* 158 (M^+; 100), 129 (37), and 115 (44).

5-(1-Hydroxy-1-methylethyl)-3,7-dimethyl-1*H*-inden-1-one (24): Pale yellow oil; R_f 0.18; EI-MS *m/z* 198 ($M^+ - H_2O$; 100), 183 (98), 169 (11), 155 (86), 139 (8), 128 (18), and 115 (13).

3,7-Dimethyl-1-oxo-1*H*-indene-5-carbaldehyde (25): Pale yellow needles; R_f 0.49; EI-MS *m/z* 186 (M^+; 100), 157 (20), 143 (3), 129 (30), and 115 (30).

References

1) A part of the results were presented at the 56th Meeting of Japan Chemical Society, Tokyo, April 1988, Abstr. No. 4XIG14 and at the 57th Meeting, Sendai, September 1988, Abstr. No. 1E214.

2) T. Nozoe, S. Takekuma, M. Doi, Y. Matsubara, and H. Yamamoto, *Chem. Lett.*, **1984**, 627.

3) Y. Matsubara, S. Takekuma, K. Yokoi, H. Yamamoto, and T. Nozoe, *Chem. Lett.*, **1984**, 631.

4) Y. Matsubara, S. Takekuma, H. Yamamoto, and T. Nozoe, *Chem. Lett.*, **1987**, 455.

5) Y. Matsubara, S. Takekuma, K. Yokoi, H. Yamamoto, and T. Nozoe, *Bull. Chem. Soc. Jpn.*, **60**, 1415 (1987).

6) S. Takekuma, Y. Matsubara, H. Yamamoto, and T. Nozoe, *Bull. Chem. Soc. Jpn.*, **60**, 3721 (1987).

7) Y. Matsubara, S. Takekuma, K. Ibata, H. Yamamoto, and T. Nozoe, *Nippon Kagaku Kaishi*, **1987**, 1555.

8) S. Takekuma, Y. Matsubara, H. Yamamoto, and T. Nozoe, *Nippon Kagaku Kaishi*, **1988**, 157.

9) S. Takekuma, Y. Matsubara, S. Matsui, H. Yamamoto, and T. Nozoe, *Nippon Kagaku Kaishi*, **1988**, 923.

10) Y. Matsubara, S. Matsui, S. Takekuma, H. Yamamoto, and T. Nozoe, *Nippon Kagaku Kaishi*, **1988**, 1704.

11) S. Takekuma, Y. Matsubara, H. Yamamoto, and T. Nozoe, *Bull. Chem. Soc. Jpn.*, **61**, 475 (1988).

12) J. Bargon, S. Mohmand, and R. J. Waltman, *IBM J. Res. Develop.*, **27**, 330 (1983).

13) M. T. Dumas, G. M. Strunz, M. Hubbes, and R. S. Jeng, *Experientia*, **39**, 1089 (1983).

14) On setting aside this solution at room temperature, a well-resolved, hyperfine ESR spectrum became observable, suggesting a splitting of **12** into a certain radical species, probably the monomeric radical **6**, under anaerobic conditions. We are very grateful to Dr. Yozo Miura (Osaka City Univ.) for the measurement of the ESR spectrum. Full analysis of the spectrum for the structural proof is currently in progress and the result will be reported in a future paper.

15) Guaiazulene (**1**) is commercially available from Konan Kako, Co. (Osaka): Blue-violet prisms, mp 31 °C.

16) In addition to these data, we were puzzled to observe optical activity for **12**:$[\alpha]_D^{21}$ −6.98 ($CHCl_3$, *c*=0.5). Details of this unexpected fact is currently being studied and the result will be reported elsewhere.

Note added to Proof. After this paper was accepted for publication, Professor Toyonobu Asao (Tohoku University, Sendai) has kindly informed us that his newly synthesized 3-guaiazulenol gives, on being allowed to stand in ether, an oxidative dimeric product which he considers identical with our specimen **12**. On the basis of 600 MHz ^1H NMR (with 2D mode, in C_6D_6) data, he has assigned the product to be a ca. 10:8 mixture of meso and enantiomers of [5,5′-biguaiazulene]- 3,3′(5*H*,5′*H*)-dione. For the NMR measurement the specimen was dissolved in C_6D_6 (sparingly soluble) by prolonged heating and the IR spectrum (KBr) of his specimen appears to be slightly different from ours. Nevertheless, we are further checking our structure proposed for **12**.

 © 1989 The Chemical Society of Japan Bull. Chem. Soc. Jpn., 62, 2045—2049 (1989)

Substrate Selectivity of Artificial Transaminase Constituted with Functionalized Bilayer Membrane†

Yukito MURAKAMI,* Jun-ichi KIKUCHI,§ and Nobuyuki SHIRATORI
Department of Organic Synthesis, Faculty of Engineering, Kyushu University, Hakozaki, Higashi-ku, Fukuoka 812
(Received February 2, 1989)

The transamination reactions of α-amino acid derivatives with α-keto acids as catalyzed by an artificial transaminase were examined in aqueous media under mild conditions. The present artificial holoenzyme was constituted with a combination of a cationic peptide lipid having a L-histidyl residue, a hydrophobic pyridoxamine derivative, and copper(II) ions, and found to exercise marked substrate selectivity which came from the molecular recognition in the course of formation of the aldimine Schiff-base chelates composed of the hydrophobic pyridoxal derivative, α-amino acids, and copper(II) ions. The transamination reaction of the hydrophobic β-benzyl L-aspartate with the hydrophilic pyruvate was most effectively catalyzed among 18 combinations of substrate species employed here. Enantioselectivity was observed for the catalytic transamination of phenylalanine with pyruvate.

Biomimetic approaches to constitution of artificial enzymes have been attracting current attention.[1] Nature has adopted α-amino acids as the main building blocks for enzymes and often cofactors, such as coenzymes and metal ions, are incorporated into their catalytic sites. Meanwhile, lipids are major constituents of biomembranes but do not directly participate in enzymatic functions. In our current approaches, we have been using the synthetic lipids having an α-amino acid residue as molecular building blocks for artificial enzymes, and demonstrated that functionalized bilayer membranes formed with the peptide lipids provide appropriate reaction sites for simulation of various enzymatic reactions.[2-4]

When a hydrophobic vitamin B_6 derivative was introduced into the bilayer membrane, the transamination reaction of an α-amino acid with an α-keto acid proceeded catalytically in the presence of copper(II) ions under mild conditions.[5] In a previous study,[6] we have modified the active site of our artificial transaminase by employing various combinations of peptide lipids and hydrophobic vitamin B_6 derivatives and investigated their catalytic performance in the transamination reaction of L-phenylalanine with pyruvate. As a result, the highest catalytic activity has been observed with the bilayer aggregates composed of a peptide lipid having a L-histidyl residue (N^+C_5-His2C_{16}) and a hydrophobic pyridoxamine derivative (PM2C_{16}) in the presence of copper(II) ions. In the present work, we studied on catalytic efficiency of the identical artificial transaminase in detail with primary emphasis on the substrate selectivity.

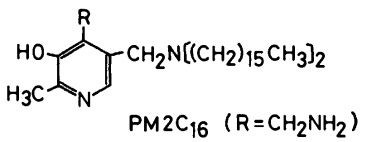

PM2C_{16} (R=CH_2NH_2)
PL2C_{16} (R=CHO)

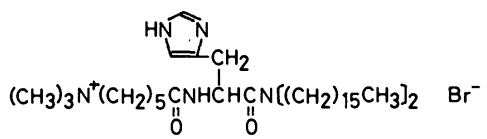

N^+C_5His2C_{16}

Experimental

Materials. The following α-amino acids and their derivatives were obtained from commercial sources as guaranteed reagents and used without further purification: DL-2-aminobutanoic acid, DL-norvaline, DL-norleucine, DL-2-aminooctanoic acid, D-phenylalanine, methyl L-phenylalaninate, L- and D-glutamic acid, L-aspartic acid (these were from Nakarai Chemicals), L-phenylalanine, benzyl L-phenylalaninate, γ-benzyl L-glutamate, α,γ-dibenzyl L-glutamate, β-benzyl L-aspartate, and α,β-dibenzyl L-aspartate (these were from Protein Research Foundation). α-Benzyl L-aspartate was prepared by selective hydrolysis of α,β-dibenzyl L-aspartate in a manner similar to that reported previously[7] (Found: C, 58.96; H, 5.91; N, 6.29%. Calcd for $C_{11}H_{13}NO_4$: C, 59.19; H, 5.87; N, 6.27%). Three kinds of α-keto acids which were coupled with the above α-amino acids were commercially available as guaranteed reagents: sodium pyruvate (Wako Pure Chemical Industries), 2-oxobutanoic acid (Nakarai Chemicals), and 3-hydroxypyruvic acid (Sigma Chemical Co., Missouri, U.S.A.). Preparation and characterization of 4-aminomethyl-5-[(dihexadecylamino)methyl]-2-methyl-3-pyridinol (PM2C_{16})[6] and *N*,*N*-dihexadecyl-N^{α}-[6-(trimethylammonio)hexanoyl]-L-histidinamide bromide (N^+C_5-His2C_{16})[8] have been reported elsewhere. Dansyl chloride [5-(dimethylamino)-1-naphthalenesulfonyl chloride] for fluorescent labeling of amino acids was obtained from Nakarai Chemicals as a guaranteed reagent. Copper(II) perchlorate (Kishida Chemical Co.) was dissolved in deionized water and standardized by conventional chelatometric titration.

Analyses and Measurements. Elemental analyses were performed at the Microanalysis Center of Kyushu Univer-

† Contribution No. 898 from this Department.
§ Present address: Department of Applied Chemistry, Faculty of Science and Engineering, Saga University, Honjo-machi, Saga 840.

sity. A Beckman Φ71 pH meter equipped with a Beckman 39505 combined electrode was used for pH measurements after calibration with a combination of appropriate standard aqueous buffers. Single-walled covesicles composed of the peptide lipid and the hydrophobic vitamin B_6 derivative were prepared upon sonication of an aqueous dispersion sample of these species by a probe-type sonicator (W-220F, Heat Systems-Ultrasonics) in a manner similar to that reported previously.[5] Progress of the transamination reaction of an α-amino acid with an α-keto acid, as catalyzed by the vesicular catalyst composed of $N^+C_5His2C_{16}$, $PM2C_{16}$, and copper(II) ions in an aqueous acetate buffer (25 mmol dm^{-3}) at pH 5.0, μ 0.10 with KCl, and 30.0 °C, was monitored by measuring amounts of an amino acid produced. An amino acid derived from the corresponding α-keto acid was dansylated, separated by liquid chromatography on a column of TSK gel ODS-120T (length, 250 mm; internal diameter, 4.6 mm) with a Hitachi 655A high performance liquid chromatograph, and eluting fractions were monitored by a Hitachi F-1000 fluorescence spectrophotometer: flow rate, 1.0 mL min^{-1}; mobile phase, mixtures of Tris buffer (10 mmol dm^{-3}, pH 8.0) and methanol at volume ratios of 2:1, 13:7, and 7:3 for the dansylated alanine, 2-aminobutanoic acid, and serine, respectively. The analytical procedure in detail was similar to that reported elsewhere.[5]

Results and Discussion

On the basis of our current studies on the functionalized bilayer vesicles having vitamin B_6 activity,[5,6,8,9] the reaction cycle for the catalytic transamination of an α-amino acid with an α-keto acid in the $PM2C_{16}$-$N^+C_5His2C_{16}$-Cu^{II} vesicular system is schematically shown in Fig. 1. In order to clarify the mechanistic implication in substrate selectivity exercised by the present artificial transaminase, its catalytic activity for various sets of substrates was examined under comparable kinetic conditions: $PM2C_{16}$, 5.0×10^{-5} mol dm^{-3}; $N^+C_5His2C_{16}$, 1.0×10^{-3} mol dm^{-3}; $Cu(ClO_4)_2$, 5.0×10^{-5} mol dm^{-3}; α-amino acid derivatives, 5.0×10^{-3} mol dm^{-3}; α-keto acids, 5.0×10^{-3} mol dm^{-3}; in an aqueous acetate buffer (25 mmol dm^{-3}) at pH 5.0, μ 0.10 with KCl, and 30.0 °C.

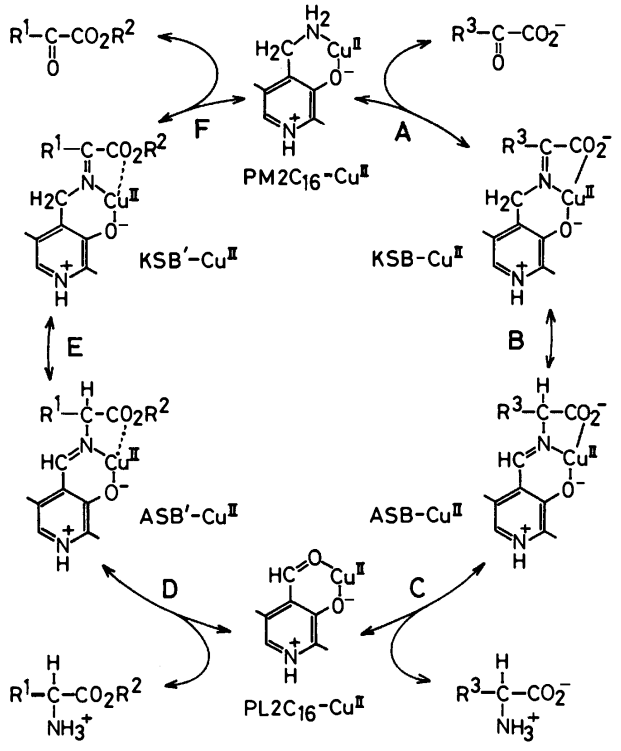

Fig. 1. Schematic representation of transamination cycle with an α-amino acid and an α-keto acid as substrates, as catalyzed by $PM2C_{16}$ and copper(II) ions in functionalized bilayer membrane.

Time courses for the transamination reactions of various DL-α-amino acids, having different normal alkyl side chains, with pyruvate are shown in Fig. 2. The reactivity increased sensitively along with increase in hydrophobicity of the amino acid. Thus, the reaction cycle for the amino group transfer from DL-2-aminooctanoic acid to pyruvate proceeded 47 times faster than that from DL-2-aminobutanoic acid to pyruvate in the present catalytic system (Table 1, Entries 2 and 16, respectively). The transamination reaction of L-phenylalanine (L-Phe) with the hydrophilic pyruvate was also effectively catalyzed by the present vesicular catalyst, as previously reported.[6] However, for a combination of L-Phe and a slightly

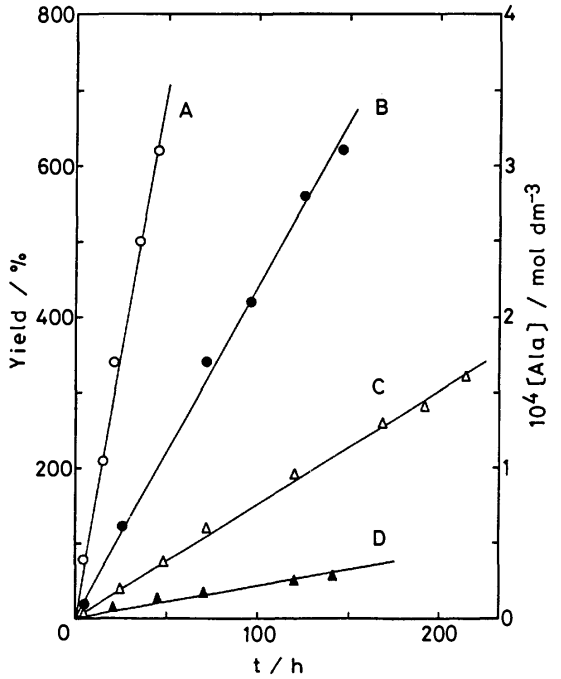

Fig. 2. Time courses for transamination catalyzed by an artificial transaminase formed with $PM2C_{16}$ (5.0×10^{-5} mol dm^{-3}), $N^+C_5His2C_{16}$ (1.0×10^{-3} mol dm^{-3}), and copper(II) ions (5.0×10^{-5} mol dm^{-3}) in an aqueous acetate buffer (25 mmol dm^{-3}) at pH 5.0, μ 0.10 with KCl, and 30.0 °C with combinations of pyruvic acid and the following α-amino acids (5.0×10^{-3} mol dm^{-3} each): A, DL-2-aminooctanoic acid; B, DL-norleucine; C, DL-norvaline; D, DL-2-aminobutanoic acid.

Table 1. Substrate Selectivity of an Artificial Transaminase Formed with $PM2C_{16}$ (5.0×10^{-5} mol dm^{-3}), $N^+C_5His2C_{16}$ (1.0×10^{-3} mol dm^{-3}), and Copper(II) Ions (5.0×10^{-5} mol dm^{-3}) at 30.0 °C[a]

Entry	α-Amino acid derivative [$R^1CH(NH_2)CO_2R^2$]			α-Keto acid (R^3COCO_2H)	Reactivity	
					h	
	R^1	R^2	Chirality	R^3	Turnover	Relative rate
1	$PhCH_2O_2CCH_2$	H	L	CH_3	5	100
2	$CH_3(CH_2)_5$	H	DL	CH_3	6	83
3	$PhCH_2O_2C(CH_2)_2$	H	L	CH_3	9	56
4	$PhCH_2$	H	D	CH_3	12	42
5	$PhCH_2$	H	L	CH_3	16	31
6	$CH_3(CH_2)_3$	H	DL	CH_3	22	23
7	$PhCH_2$	H	L	CH_3CH_2	44	11
8	$PhCH_2O_2CCH_2$	CH_2Ph	L	CH_3	52	9.6
9	$CH_3(CH_2)_2$	H	DL	CH_3	65	7.7
10	$PhCH_2O_2C(CH_2)_2$	CH_2Ph	L	CH_3	65	7.7
11	$PhCH_2$	CH_2Ph	L	CH_3	84	6.0
12	$PhCH_2$	CH_3	L	CH_3	90	5.6
13	HO_2CCH_2	H	L	CH_3	100	5.0
14	$HO_2C(CH_2)_2$	H	L	CH_3	190	2.6
15	$HO_2C(CH_2)_2$	H	D	CH_3	190	2.6
16	CH_3CH_2	H	DL	CH_3	280	1.8
17	HO_2CCH_2	CH_2Ph	L	CH_3	322	1.6
18	$PhCH_2$	H	L	$HOCH_2$	—[b]	0

a) In an aqueous acetate buffer (25 mmol dm^{-3}) at pH 5.0 and μ 0.10 with KCl. b) Turnover behavior was not observed.

more hydrophobic α-keto acid, 2-oxobutanoate, the reactivity was ca. one-third of that for a combination of L-Phe and pyruvate (Fig. 3). Thus, the present vesicular system requires a combination of a hydrophobic α-amino acid and a hydrophilic α-keto acid to achieve high catalytic performance. Such marked substrate selectivity supports our mechanistic concept previously proposed: the overall transamination reaction is controlled by the distribution behavior of substrates between bilayer and bulk aqueous phases and not by the isomerization rate between the aldimine Schiff-base chelate and the ketimine Schiff-base chelate; the former chelate is composed of the hydrophobic pyridoxal derivative ($PL2C_{16}$), an α-amino acid, and the copper(II) ion, while the latter composed of $PM2C_{16}$, an α-keto acid, and the copper(II) ion.[6] In addition, the substrate selectivity evidently comes from the molecular recognition exercised during the course of forming the aldimine Schiff-base chelates (steps C and D in Fig. 1) and the reaction steps for formation of the ketimine Schiff-base chelates (steps A and F in Fig. 1) are not responsible for the selectivity in the overall reaction cycle. On the other hand, the transamination reaction of L-Phe with 3-hydroxypyruvate, a more hydrophilic α-keto acid than pyruvate, did not proceed catalytically (Fig. 3, line C). In this case, the reaction behavior, exhibiting high reactivity in the initial stage followed by gradual inactivation, suggests consumption of the α-keto acid via a certain side reaction because of its labile 3-hydroxyl moiety.

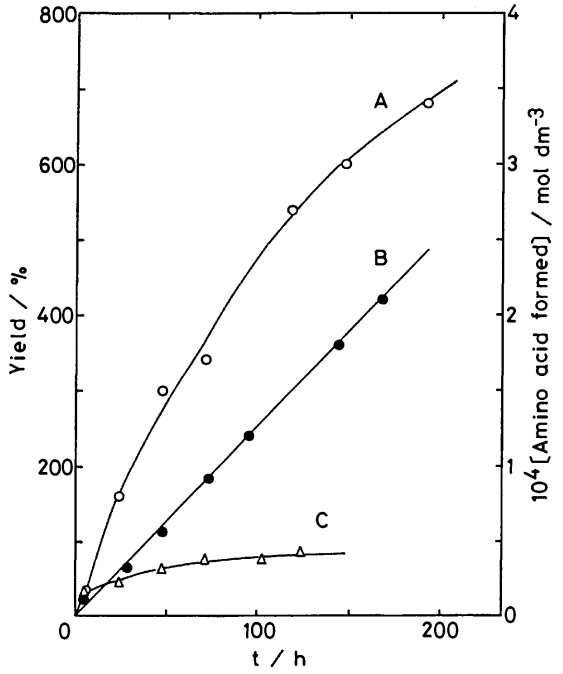

Fig. 3. Time courses for transamination catalyzed by an artificial transaminase formed with $PM2C_{16}$ (5.0×10^{-5} mol dm^{-3}), $N^+C_5His2C_{16}$ (1.0×10^{-3} mol dm^{-3}), and copper(II) ions (5.0×10^{-5} mol dm^{-3}) in an aqueous acetate buffer (25 mmol dm^{-3}) at pH 5.0, μ 0.10 with KCl, and 30.0 °C with combinations of L-Phe and the following α-keto acids (5.0×10^{-3} mol dm^{-3} each): A, pyruvic acid; B, 2-oxobutanoic acid; C, 3-hydroxypyruvic acid.

The substrate selectivity was also much affected by modification of the α-carboxyl moiety of an α-amino acid. As shown in Fig. 4, the transamination reactivity of L-Phe with pyruvate was much depressed upon conversion of the α-carboxylato group into its methyl

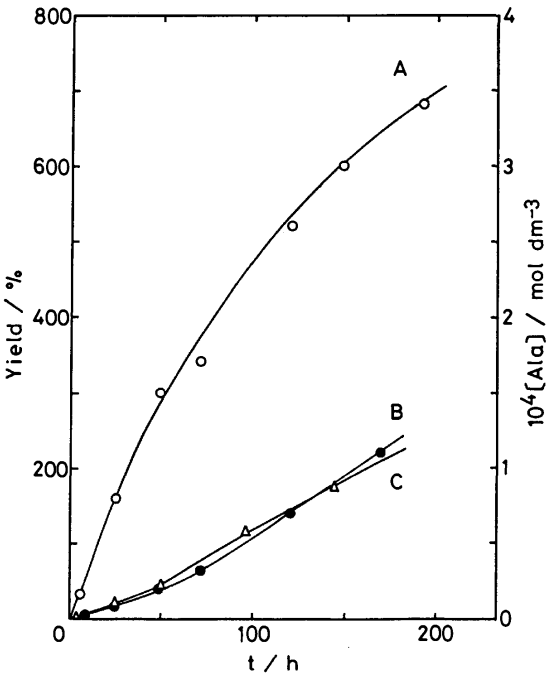

Fig. 4. Time courses for transamination catalyzed by an artificial transaminase formed with $PM2C_{16}$ (5.0×10^{-5} mol dm^{-3}), $N^+C_5His2C_{16}$ (1.0×10^{-3} mol dm^{-3}), and copper(II) ions (5.0×10^{-5} mol dm^{-3}) in an aqueous acetate buffer (25 mmol dm^{-3}) at pH 5.0, μ 0.10 with KCl, and 30.0 °C with combinations of pyruvic acid and the following L-Phe analogs (5.0×10^{-3} mol dm^{-3} each): A, L-Phe; B, methyl L-phenylalaninate; C, benzyl L-phenylalaninate.

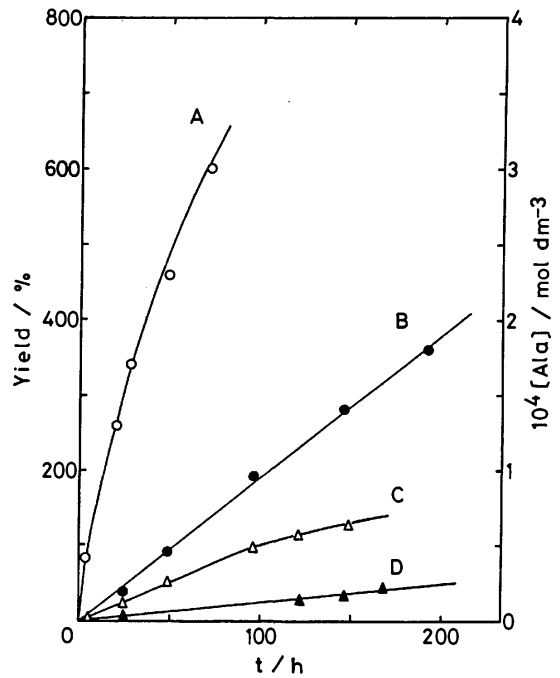

Fig. 5. Time courses for transamination catalyzed by an artificial transaminase formed with $PM2C_{16}$ (5.0×10^{-5} mol dm^{-3}), $N^+C_5His2C_{16}$ (1.0×10^{-3} mol dm^{-3}), and copper(II) ions (5.0×10^{-5} mol dm^{-3}) in an aqueous acetate buffer (25 mmol dm^{-3}) at pH 5.0, μ 0.10 with KCl, and 30.0 °C with combinations of pyruvic acid and the following L-aspartate analogs (5.0×10^{-3} mol dm^{-3} each): A, β-benzyl L-aspartate; B, α,β-dibenzyl L-aspartate; C, L-aspartate; D, α-benzyl L-aspartate.

or benzyl ester, in spite of increased hydrophobicity of the α-amino acid species. This seems to reflect the fact that the stability of the copper(II) complex of the terdentate aldimine Schiff-base formed with the former α-amino acid and $PL2C_{16}$ is much enhanced relative to that of the Schiff-base chelate derived from the latter amino acid ester; the alkoxycarbonyl group is a weaker ligand than the carboxylato for copper(II) ions. Consequently, the substrate selectivity is of thermodynamic origin; the higher stability the aldimine Schiff-base chelate attains, the greater overall reactivity is observed.

To confirm this mechanistic implication on the substrate selectivity, the transamination reactions of various L-aspartate and L-glutamate analogs with pyruvate were investigated. Time courses for the transamination of four L-aspartate analogs with pyruvate are shown in Fig. 5. The L-asparate-pyruvate couple is 2.8 times more reactive than the DL-2-aminobutanoate-pyruvate couple (Table 1, Entries 13 and 16, respectively). Although the transamination reactivity was increased by two-fold upon conversion of L-aspartic acid into the corresponding dibenzyl ester due to increased hydrophobicity of the latter substrate, the highest reactivity was observed for the β-benzyl L-aspartate-pyruvate couple among these L-aspartate analogs. In contrast, the α-benzyl L-aspartate-pyruvate couple is markedly less reactive than the β-benzyl L-aspartate-pyruvate couple, even though both α-amino acid derivatives possess comparable hydrophobicity (Table 1, Entries 1 and 17, respectively). This seems to come from the difference in thermodynamic stability between the aldimine Schiff-base chelate composed of β-benzyl L-aspartate, $PL2C_{16}$, and the copper(II) ion (**A**) and the corresponding aldimine chelate of α-benzyl L-aspartate (**B**); the former forms a five-membered chelate ring, while the latter a six-membered one with the carboxylate moiety. Figure 6 shows time courses for the transamination reactions of three L-glutamate analogs with pyruvate. The reaction behavior is analogous to that for combinations of the L-aspartate analogs with pyruvate. Lower reactivity of the L-glutamate analog-pyruvate couples in comparison with the corresponding L-aspartate

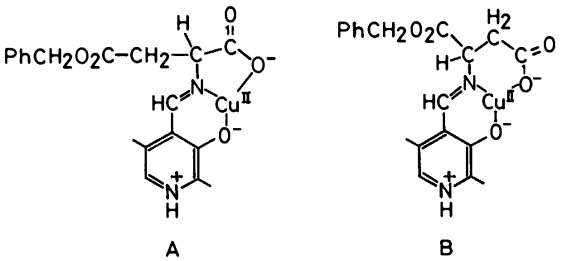

A B

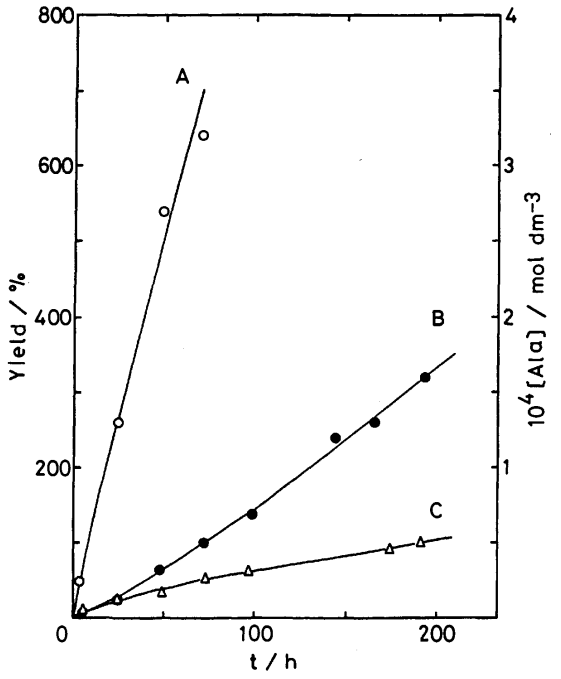

Fig. 6. Time courses for transamination catalyzed by an artificial transaminase formed with $PM2C_{16}$ (5.0×10^{-5} mol dm^{-3}), $N^+C_5His2C_{16}$ (1.0×10^{-3} mol dm^{-3}), and copper(II) ions (5.0×10^{-5} mol dm^{-3}) in an aqueous acetate buffer (25 mmol dm^{-3}) at pH 5.0, μ 0.10 with KCl, and 30.0 °C with combinations of pyruvic acid and the following L-glutamate analogs (5.0×10^{-3} mol dm^{-3} each): A, γ-benzyl L-glutamate; B, α,γ-dibenzyl L-glutamate; C, L-glutamate.

analog-pyruvate couples are also explained primarily from the viewpoint of the chelate effect; the aldimine Schiff-base chelates formed with the former couples are lower in stability relative to those formed with the latter.

As regards the transamination reaction catalyzed by the present vesicular system, the general acid-base catalysis by the imidazolyl group introduced into the peptide lipid is essential to exhibiting the turnover behavior, since the sequential reactions shown in Fig. 1 did not cycle in the vesicle of *N,N*-dihexadecyl-N^{α}-[6-(trimethylammonio)hexanoyl]-L-alaninamide bromide in which the L-histidyl residue of $N^+C_5His2C_{16}$ is replaced by the L-alanyl residue.[6] In addition, the reaction site is provided in the hydrogen-belt domain of the highly organized and chiral bilayer membrane.[8] We have previously observed enantioselective catalysis by the chiral L-histidyl moiety of an analogous synthetic peptide lipid in ester hydrolysis.[2] Thus, one can expect to observe enantioselectivity for the transamination reaction catalyzed by the $PM2C_{16}$-$N^+C_5His2C_{16}$-Cu^{II} vesicular system. In fact, we observed that the amino group transfer from D-Phe to pyruvate was accelerated to a 33% extent relative to that from L-Phe to pyruvate (Table 1, Entries 4 and 5, respectively), presumably due to favorable thermodynamic stability of the aldimine Schiff-base chelate of D-Phe. On the other hand, there was no significant difference in transamination reactivity between the L-glutamate-pyruvate and D-glutamate-pyruvate couples (Table 1, Entries 14 and 15, respectively). This seems to arise from the weaker coordination effect by the γ-carboxylato moiety of glutamate for the development of enantioselectivity as discussed above.

In conclusion, it became apparent that the artificial transaminase composed of $PM2C_{16}$, $N^+C_5His2C_{16}$, and copper(II) ions exhibits marked substrate selectivity in the catalytic transamination reactions of α-amino acids with α-keto acids under mild conditions. The substrate recognition exercised in the course of formation of the aldimine Schiff-base chelates in the pseudo-hydrophobic domain of the bilayer membrane is responsible for such selectivity. Although further modification of the present artificial holoenzyme is required for performing high enantioselectivity, it is noteworthy that a simple system composed of three molecular components, a synthetic peptide lipid, a hydrophobic vitamin B_6 derivative, and metal ions, readily undergoes self-organization in aqueous media to form the supramolecular bilayer assembly capable of mimicking the catalytic functions of vitamin B_6-dependent transaminase.

The present work was supported in part by a Grant-in-Aid for Special Project Research from the Ministry of Education, Sciences and Culture (No. 63107002).

References

1) J. H. Fendler, "Membrane Mimetic Chemistry," John Wiley, New York (1982), Chap. 10; R. Breslow, *Adv. Enzymol. Relat. Areas Mol. Biol.*, **58**, 1 (1986).

2) Y. Murakami, A. Nakano, A. Yoshimatsu, and K. Fukuya, *J. Am. Chem. Soc.*, **103**, 728 (1981).

3) Y. Murakami, J. Kikuchi, K. Nishida, and A. Nakano, *Bull. Chem. Soc. Jpn.*, **57**, 1371 (1984).

4) Y. Murakami, Y. Hisaeda, and T. Ohno, *Bull. Chem. Soc. Jpn.*, **57**, 2091 (1984); Y. Murakami, Y. Hisaeda, T. Ohno, and Y. Matsuda, *Chem. Lett.*, **1986**, 731; Y. Murakami, Y. Hisaeda, and T. Ohno, *ibid.*, **1987**, 1357.

5) Y. Murakami, J. Kikuchi, K. Akiyoshi, and T. Imori, *J. Chem. Soc., Perkin Trans. 2*, **1985**, 1919.

6) Y. Murakami, J. Kikuchi, K. Akiyoshi, and N. Shiratori, *Isr. J. Chem.*, **28**, 23 (1987/1988).

7) P. M. Bryant, R. H. Moore, P. J. Pimlott, and G. T. Young, *J. Chem. Soc.*, **1959**, 3868.

8) Y. Murakami, J. Kikuchi, and K. Akiyoshi, *Bull. Chem. Soc. Jpn.*, **58**, 1200 (1985).

9) Y. Murakami, A. Nakano, and K. Akiyoshi, *Bull. Chem. Soc. Jpn.*, **55**, 3004 (1982); Y. Murakami, J. Kikuchi, A. Nakano, K. Akiyoshi, and T. Imori, *ibid.*, **57**, 1116 (1984); Y. Murakami, J. Kikuchi, and K. Akiyoshi, *Chem. Lett.*, **1984**, 1185; Y. Murakami, J. Kikuchi, T. Imori, and K. Akiyoshi, *J. Chem. Soc., Chem. Commun.*, **1984**, 1434; Y. Murakami, J. Kikuchi, K. Akiyoshi, and T. Imori, *J. Chem. Soc., Perkin Trans. 2*, **1986**, 1445.

One-Pot Synthesis of Tetrahydrofuran Derivatives from Allylic Alcohols and Vinyl Ethers by Means of Palladium(II) Acetate

Keigo FUGAMI,† Koichiro OSHIMA,* and Kiitiro UTIMOTO*
Department of Industrial Chemistry, Faculty of Engineering, Kyoto University, Sakyo-ku, Kyoto 606
(Received December 12, 1988)

Reaction of allylic alcohol with vinyl ether in the presence of $Pd(OAc)_2$ afforded furan derivatives in good yield. $Pd(OAc)_2$ was essential for the reaction. $PdCl_2$ complex did not afford cyclized product but gave acetal exclusively. Three components were combined at once to produce 4-(3-butenyl)-2-butoxy-4-methyltetrahydrofuran upon treatment of a mixture of 2-methyl-2-propen-1-ol, butyl vinyl ether, and allyl bromide. The reaction could successfully be extended to the synthesis of nitrogen containing heterocycles by use of *N*-tosyl allylic amines in place of allylic alcohols.

We now report here the reaction between allylic alcohols and vinyl ethers promoted by $Pd(OAc)_2$. Treatment of (*E*)-2-buten-1-ol in butyl vinyl ether with $Pd(OAc)_2$ gave unexpected cyclic products **1** and **2** in 74% combined yield (Scheme 1). Hydrogenation

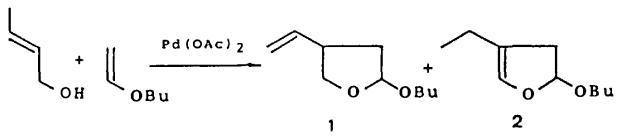

Scheme 1.

of the products **1** and **2** followed by oxidation[1] provided 3-ethyl-γ-butyrolactone which was identical with the authentic sample[2] (Scheme 2).

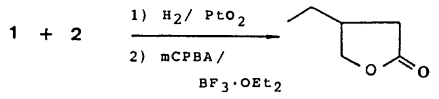

Scheme 2.

Other results are summarized in Table 1. Five-membered rings were formed in preference to six-membered rings with an exception of the reaction of cinnamyl alcohol which gave a dihydropyran derivative solely (Entries 6 and 7). As shown in Scheme 3, the formation of furan derivatives could be explained by assuming an intermediary palladium compound **3**,

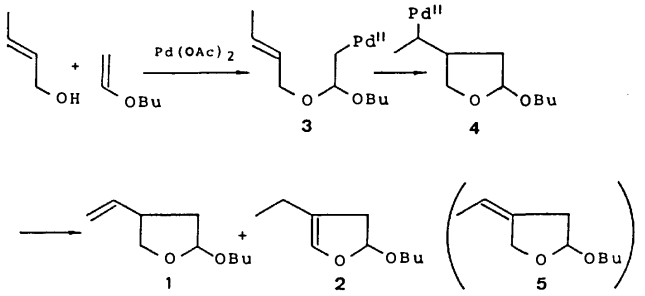

Scheme 3.

† Recipient of the Fellowships of the Japan Society for the Promotion of Science for Japanese Junior Scientists.

Table 1. Palladium(II)-Promoted Tetrahydrofuran Synthesis[a]

Entry	Allylic alcohol (mmol)	Vinyl ether (mmol)	Product	Yield[b] %
1	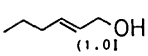		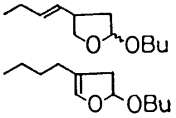	82 12
2	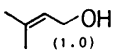	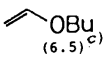	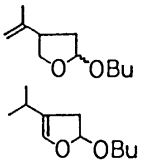	58 23
3	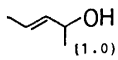		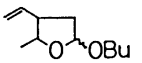	75
4	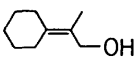	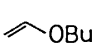	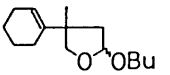	55
5	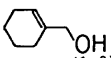	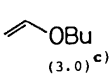	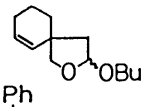	47
6	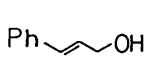	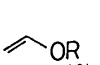	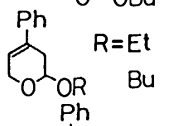	R=Et 88 Bu 63
7	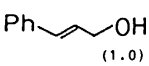	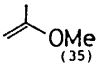	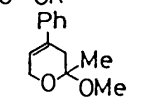	54
			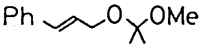	27

a) Reactions were performed at 25 °C using one mmol of $Pd(OAc)_2$. b) Isolated yield based on $Pd(OAc)_2$ employed. c) Toluene was used as solvent. In other cases, CH_2=CH-OR was used as solvent.

which undergoes intramolecular olefin insertion followed by β-elimination of palladium hydride from palladium complex **4** to afford vinyltetrahydrofuran **1** as a major product along with dihydrofuran derivative **2**. 4-Ethylidenetetrahydrofuran **5** could not be detected in the reaction mixture.

In the reaction of methallyl alcohol, two molar

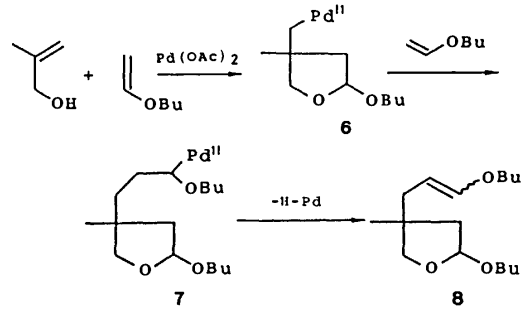

Scheme 4.

equivalents of butyl vinyl ether were consumed per one 2-methyl-2-propen-1-ol to afford 2-butoxy-4-(3-butoxy-2-propenyl)-4-methyltetrahydrofuran (**8**) (Entry 1 in Table 2).[3] In this case, β-elimination of palladium hydride could not occur from the intermediary palladium complex **6**, then the complex added to the second molecule of butyl vinyl ether to give **7** which was converted into the final product **8** by β-elimination (Scheme 4). It was anticipated that olefins such as vinyl acetate, allyl bromide, and methyl acrylate act as the third component in place of the second butyl vinyl ether. This was indeed the case and these olefins reacted with the complex **6** through the addition-elimination process to give the corresponding coupling products as shown in Table 2. In Entry 3, it was supposed that Pd(II) species would be regenerated in the course of the reaction, but the amount of $Pd(OAc)_2$ could not be reduced.[4] In the case of (*E*)-2-buten-1-ol, the third component such as allyl bromide did not participate in the reaction and the ordinary product **1** was obtained in good yield. Thus, the β-elimination of palladium hydride from the complex **4** took place much faster than the addition of Pd-C bond to the olefinic double bond of allyl bromide.

The reaction of simple allyl alcohol which cannot give vinyltetrahydrofuran derivative resulted in the formation of a complex mixture.

Palladium(II) acetate is essential for the construction of furan or pyran rings. The use of $PdCl_2(CH_3CN)_2$ gave acetal without any contamination by desired cyclized product.[5] It turned out, however, that an addition of an appropriate base to the reaction mixture is effective to give the furan or pyran derivatives. Treatment of a *t*-BuOH solution of 2-methyl-2-propen-1-ol, butyl vinyl ether, and allyl bromide with $PdCl_2(CH_3CN)_2$ in the presence of potassium acetate gave the cyclized product, 4-(3-butenyl)-2-butoxy-4-methyltetrahydrofuran as a single product. The reaction between lithium alkoxide, $PhCH{=}CHCH_2OLi$, and ethyl vinyl ether also enabled us to use $PdCl_2(CH_3CN)_2$ instead of $Pd(OAc)_2$ and provided the corresponding dihydropyran derivative in 99% yield.[6] The $Pd(OAc)_2$-promoted reactions sometimes gave a small amount of noncyclized acetal as a by-product. The extent of the acetal formation seemed to depend on the quality of $Pd(OAc)_2$ employed. In such cases, an addition of one molar equivalent of potassium acetate perfectly suppressed the acetal formation and gave the desired heterocycle exclusively, although the reaction rate was somewhat retarded.

The amount of $Pd(OAc)_2$ could be reduced to 0.3 molar equivalent when $Cu(OAc)_2$ was added as a co-

Table 2. Three Component Combination Reaction[a]

Entry	Allylic alcohol (mmol)	Vinyl ether (mmol)	Olefin (mmol)	Product	Yield[b] %
1	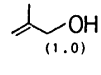 (1.0)	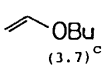 (3.7)[c]		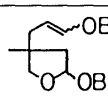	31
2	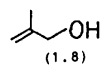 (1.8)	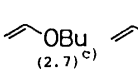 (2.7)[c]	(14)	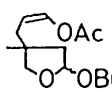	90
3	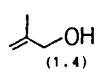 (1.4)	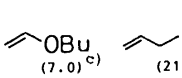 (7.0)[c]	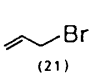 (21)	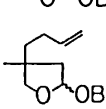	81
4	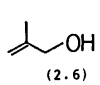 (2.6)	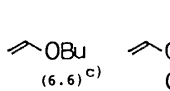 (6.6)[c]	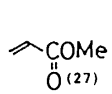 (27)	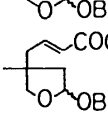	95
5	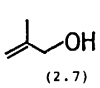 (2.7)	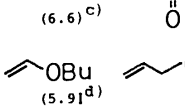 (5.91[d])	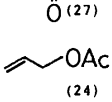 (24)	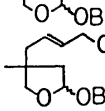	98

a) Reactions were performed at 25 °C using one mmol of $Pd(OAc)_2$. b) Isolated yield based on $Pd(OAc)_2$ employed. c) Toluene was used as solvent. d) Allyl acetate was used as solvent.

Table 3. Palladium(II)-Mediated Pyrrolidine Synthesis[a]

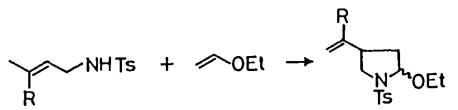

Entry	*N*-Tosyl allylic amine (mmol)	Vinyl ether (mmol)	Product	Yield[b] %
1	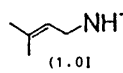 (1.01)	(5.6)	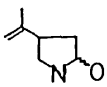	77
2	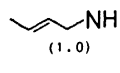 (1.0)	(6.0)	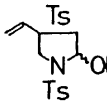	94
3	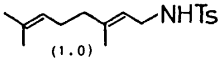 (1.0)	(6.7)	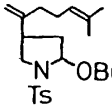	86
4	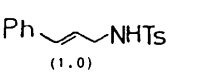 (1.0)	(8.2)	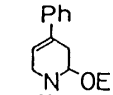	82

a) Reactions were performed at 25 °C using one mmol of $Pd(OAc)_2$ in toluene. b) Isolated yield based on $Pd(OAc)_2$ employed.

oxidizer.[7] For instance, stirring of an acetonitrile solution of 2-hexen-1-ol (1.0 mmol) and butyl vinyl ether (3.4 mmol) at 25 °C for 20 h under the coexistence of $Pd(OAc)_2$ (0.3 mmol) and $Cu(OAc)_2$ (2.5 mmol) provided 4-(1-butenyl)-2-butoxytetrahydrofuran in 90% yield.

The reaction was successfully extended to the synthesis of pyrrolidine or piperidine derivatives from the corresponding *N*-tosyl allylic amine.[8] The typical results were summarized in Table 3. The presence of tosyl group on nitrogen atom was essential for the successful reaction. Desired heterocycles were not obtained from the reaction of free allylic amines.

Experimental

Distillations of the products were performed by use of Kugelrohr (Büchi), and boiling points are indicated by an air-bath temperature without correction. All melting points were obtained on a Yanaco MP-50929 melting point apparatus and are uncorrected, too. ^1H NMR spectra were taken on a Varian XL-200 spectrometer, $CDCl_3$ was used as solvent, chemical shifts being given in δ with tetramethylsilane as an internal standard. IR spectra were determined on a JASCO IR-810 spectrometer. The analyses were carried out by the staff at the Elemental Analyses Center of Kyoto University. Tetrahydrofuran (THF) was freshly distilled from sodium benzophenone ketyl.

Synthesis of *N*-Tosyl Allylic Amines. These compounds were prepared according to a reported procedure.[9,10] Preparation of *N*-geranyl-*p*-toluenesulfonamide is representative. Sodium (0.87 g, 38 mmol) was dissolved in ethanol (20 ml) and ethyl *N*-tosylcarbamate (11 g, 45 mmol) was added at room temperature under an argon atmosphere. After stirring for half an hour, geranyl bromide (5.0 g, 23 mmol) was added to the resulting clear solution. A white precipitate appeared after stirring for an additional hour. Resulting white suspension was stirred over night. White precipitate was filtered off, and the filtrate was poured into aqueous ammonium chloride solution and extracted twice with dichloromethane. Organic layer was dried over anhydrous sodium sulfate and the residue after evaporation of solvent under reduced pressure was submitted to a silica-gel column chromatography to afford 4.0 g (45% yield) of ethyl *N*-geranyl-*N*-tosylcarbamate. A THF solution (10 ml) of *N*-geranyl-*N*-tosylcarbamate (4.0 g, 10 mmol) was added to a 50% aqueous solution of sodium hydroxide (10 ml) and then 10 ml of methanol was added in order to make the reaction mixture homogeneous. After stirring for 12 h, the reaction mixture was poured into aqueous ammonium chloride solution and extracted with dichloromethane. Organic layer was concentrated and purification by silica-gel column chromatography of the residue gave 3.1 g (99% yield) of *N*-geranyl-*p*-toluenesulfonamide: bp 132 °C/2 Torr (1 Torr= 133.322 Pa); IR (neat) 3276, 2920, 2852, 1599, 1496, 1438, 1328, 1160, 1095, 1050, 814, 662 cm^{-1}; ^1H NMR δ=1.54 (br.s, 3H), 1.57 (br.s, 3H), 1.67 (br.s, 3H), 1.9—2.1 (m, 4H), 2.44 (s, 3H), 3.56 (dd, J=6.4, 6.3 Hz, 2H), 4.25 (t, J=6.3 Hz, 1H), 5.0—5.2 (m, 2H), 7.32 (d, J=8.2 Hz, 2H), 7.76 (d, J=8.2 Hz, 2H); Found: C, 66.40; H, 8.16; N, 4.39%. Calcd for $C_{17}H_{25}NO_2S$: C, 66.41; H, 8.20; N, 4.56%.

General Procedure for the Reaction of Allylic Alcohol or *N*-Tosyl Allylic Amine with Vinyl Ether in the Presence of $Pd(OAc)_2$. Typical procedure is as follows. To a solution of (*E*)-2-buten-1-ol (72 mg, 1.0 mmol) in butyl vinyl ether (3 ml, 10 mmol), $Pd(OAc)_2$ (0.23 g, 1.0 mmol) was added and the resulting mixture was stirred at 25 °C for 2 h. The mixture was diluted with hexane (10 ml) and pyridine (0.1 g) was added. After stirring for an additional 10 min, the precipitated palladium residue was filtered off and filtrate was concentrated in vacuo. Purification of the residual oil by silica-gel column chromatography gave 2-butoxy-4-vinyltetrahydrofuran (**1**) (0.13 g, cis:trans=1:1) in 74% yield: bp 75 °C/25 Torr; IR (neat) 2954, 2932, 2869, 1643, 1459, 1347, 1098, 1070, 1032, 1011, 994, 916 cm^{-1}; ^1H NMR δ=0.92 (t, J=7.1 Hz, 3H), 1.3—1.9 (m, 5H), 2.07 (dd, J=12.5, 7.8 Hz, 0.5H), 2.30 (ddd, J=13.4, 9.4, 5.4 Hz, 0.5H), 2.7—3.0 (m, 0.5H), 3.0—3.3 (m, 0.5H), 3.3—3.5 (m, 1H), 3.5—3.8 (m, 2H), 3.95 (t, J=8.0 Hz, 0.5H), 4.07 (t, J=8.1 Hz, 0.5H), 5.0—5.2 (m, 3H), 5.7—6.0 (m, 1H); Found: C, 70.80; H, 10.86%. Calcd for $C_{10}H_{18}O_2$: C, 70.55; H, 10.66%.

2-Butoxy-4-(1-butenyl)tetrahydrofuran (60:40 Mixture of Diastereomers): Bp 104 °C/21 Torr; IR (neat) 2956, 2930, 2870, 1641, 1459, 1443, 1345, 1097, 1069, 1030, 1005, 968, 918 cm^{-1}; ^1H NMR δ=0.8—1.0 (m, 6H), 1.2—2.5 (m, 8H), 2.6—2.9 (m, 0.6H), 2.9—3.2 (m, 0.4H), 3.3—3.8 (m, 4H), 5.0—5.2 (m, 1H), 5.2—5.7 (m, 2H); Found: C, 72.67; H, 11.42%. Calcd for $C_{12}H_{22}O_2$: C, 72.68; H, 11.18%.

2-Butoxy-4-isopropenyltetrahydrofuran (2:1 Mixture of Diastereomers): Bp 74 °C/20 Torr; IR (neat) 2956, 2932, 2870, 1648, 1458, 1378, 1345, 1181, 1103, 1047, 890 cm^{-1}; ^1H NMR δ=0.92 (t, J=7.2 Hz, 3H), 1.2—2.1 (m, 8.67H, including two singlets at 1.69 ppm (1.0H) and 1.72 ppm (2.0H)), 2.2—2.4 (m, 0.33H), 2.7—3.0 (m, 0.33H), 3.0—3.3 (m, 0.67H), 3.3—3.5 (m, 1H), 3.6—3.8 (m, 2H), 3.93 (t, J=8.1 Hz, 0.33H), 4.05 (t, J=8.4 Hz, 0.67H), 4.74 (br.s, 1.33H), 4.76 (br.s, 0.67H), 5.1—5.2 (m, 1H); Found: C, 71.74; H, 11.02%. Calcd for $C_{11}H_{20}O_2$: C, 71.70; H, 10.94%.

2-Butoxy-4-isopropyl-2,3-dihydrofuran: Bp 94 °C/20 Torr; IR (neat) 2956, 2930, 2870, 1735, 1656, 1459, 1364, 1283, 1187, 1103, 1056, 939, 852 cm^{-1}; ^1H NMR δ=0.92 (t, J=7.2 Hz, 3H), 1.03 (d, J=6.8 Hz, 3H), 1.05 (d, J=6.8 Hz, 3H), 1.2—1.8 (m, 4H), 2.2—2.5 (m, 2H, including d, at δ=2.36, J=16.3 Hz, 1H), 2.73 (dddd, J=16.3, 7.3, 2.5, 1.2 Hz, 1H), 3.47 (dt, J=9.6, 6.8 Hz, 1H), 3.76 (dt, J=9.6, 6.6 Hz, 1H), 5.48 (dd, J=7.3, 2.8 Hz, 1H), 6.04 (br.s, 1H); Found: C, 71.64; H, 11.11%. Calcd for $C_{11}H_{20}O_2$: C, 71.70; H, 10.94%.

2-Butoxy-5-methyl-4-vinyltetrahydrofuran (1:1 Mixture of Diastereomers): Bp 92 °C/21 Torr; IR (neat) 2958, 2930, 2868, 1643, 1459, 1445, 1379, 1095, 996, 936, 915, 658 cm^{-1}. ^1H NMR δ=0.92 (t, J=7.1 Hz, 3H), 1.23 (d, J=6.1 Hz, 1.5H), 1.29 (d, J=6.1 Hz, 1.5H), 1.2—2.8 (m, 7H), 3.3—3.5 (m, 1H, including ddd at δ=3.36, J=13.8, 9.5, 6.5 Hz), 3.6—3.9 (m, 2H, including ddd at δ=3.70, J=16.3, 6.8, 2.1 Hz, and dq at δ=3.82, J=6.1, 3.0 Hz), 5.0—5.3 (m, 3H), 5.67 (ddd, J=17.1, 10.1, 8.1 Hz, 0.5H), 5.74 (ddd, J=17.9, 9.0, 7.6 Hz, 0.5H); Found: C, 71.44; H, 11.23%. Calcd for $C_{11}H_{20}O_2$: C, 71.70; H, 10.94%.

2-Butoxy-4-(1-cyclohexenyl)-4-methyltetrahydrofuran (1:1 Mixture of Diastereomers): Bp 130 °C/1 Torr; IR (neat) 3020, 2958, 2928, 2862, 1456, 1437, 1358, 1325, 1122, 1097, 1028, 931, 669, 638 cm^{-1}; ^1H NMR δ=0.92 (t, J=7.3 Hz, 3H), 0.97 (s, 1.5H), 0.98 (s, 1.5H), 1.2—2.3 (m, 14H), 3.3—3.8 (m, 4H), 5.2—5.3 (m, 1H), 5.7—5.8 (m, 1H); Found: C, 75.70; H, 11.17%. Calcd for $C_{15}H_{26}O_2$: C, 75.58; H, 10.99%.

9-Butoxy-8-oxaspiro[5.4]dec-1-ene (Mixture of Diastereomers): bp 120 °C/1 Torr; IR (neat) 3018, 2956, 2928, 2864, 1440, 1347, 1180, 1094, 1031, 931, 731, 656 cm^{-1}; ^1H NMR δ=0.92 (t, J=7.2 Hz, 3H), 1.3—2.2 (m, 12H), 3.3—3.5 (m, 1H), 3.6—3.8 (m, 3H), 5.1—5.2 (m, 1H), 5.5—5.8 (m 2H); Found: C, 74.31; H, 10.82%. Calcd for $C_{13}H_{22}O_2$: C, 74.24; H, 10.54%.

2-Ethoxy-4-phenyl-3,6-dihydro-2*H*-pyran: Bp 105 °C/1 Torr; IR (neat) 2960, 2915, 2855, 1733, 1592, 1486, 1442, 1419, 1339, 1179, 1092, 1043, 1028, 993, 741, 689 cm^{-1}; ^1H NMR δ=1.21 (t, J=7.1 Hz, 3H), 2.71 (dm, J=16.5 Hz, 1H), 2.94 (dm, J=16.5 Hz, 1H), 3.51 (dq, J=9.8, 7.1 Hz, 1H), 3.78 (dq, J=9.8, 7.1 Hz, 1H), 4.69 (d, J=2.2 Hz, 1H), 4.71 (d, J=2.2 Hz, 1H), 5.24 (dd, J=5.0, 0.7 Hz, 1H), 6.4—6.5 (m, 1H), 7.1—7.5 (m, 5H); Found: C, 76.36; H, 7.95%. Calcd for $C_{13}H_{16}O_2$: C, 76.44; H, 7.90%.

2-Butoxy-4-phenyl-3,6-dihydro-2*H*-pyran: Bp 130 °C/2 Torr; IR (neat) 2948, 2922, 2860, 1660, 1594, 1488, 1445, 1420, 1340, 1175, 1095, 1032, 920, 743, 689 cm^{-1}; ^1H NMR δ=0.92 (t, J=7.1 Hz, 3H), 1.2—1.7 (m, 4H), 2.70 (br.d, J=16.4 Hz, 1H), 2.91 (dm, J=16.4 Hz, 1H), 3.43 (dt, J=9.6, 6.7 Hz, 1H), 3.72 (dt, J=9.6, 6.8 Hz, 1H), 4.82 (br.s, 2H), 5.19 (d, J=4.9 Hz, 1H), 6.29 (br.s, 1H), 7.1—7.4 (m, 5H); Found: C, 77.54; H, 8.82%. Calcd for $C_{15}H_{20}O_2$: C, 77.55; H, 8.68%.

2-Methoxy-2-methyl-4-phenyl-3,6-dihydro-2*H*-pyran: Bp 80 °C/2 Torr; IR (neat) 2984, 2938, 2906, 2850, 2824, 1665, 1599, 1492, 1449, 1422, 1381, 1324, 1309, 1203, 1157, 1131, 1061, 1025, 933, 838, 775, 749, 694 cm^{-1}; ^1H NMR δ=1.52 (s, 3H), 2.7—2.9 (m, 2H), 3.26 (s, 3H), 4.65 (ddd, J=13.9, 4.2, 2.3 Hz, 1H), 4.73 (ddd, J=13.9, 4.1, 2.1 Hz, 1H), 6.3—6.4 (m, 1H), 7.1—7.5 (m, 5H); Found: C, 76.53; H, 8.08%. Calcd for $C_{13}H_{16}O_2$: C, 76.44; H, 7.90%.

2-Butoxy-4-(3-butoxy-2-propenyl)-4-methyltetrahydrofuran (*E*:*Z*=1:1): Bp 96 °C/2 Torr; IR (neat) 2956, 2930, 2868, 1664, 1653, 1458, 1376, 1187, 1104, 1030, 928, 737 cm^{-1}; ^1H NMR δ=0.92 (t, J=7.2 Hz, 6H), 1.06 (s, 3H), 1.2—1.8 (m, 9H, including dd, at δ=1.68 J=13.3, 3.4 Hz, 1H), 1.89 (dd, J=13.3, 5.7 Hz, 1H), 2.0—2.2 (m, 1H), 2.2—2.3 (m, 1H), 3.3—3.6 (m, 2H), 3.6—3.8 (m, 4H), 4.9—5.1 (m, 1H), 5.16 (dd, J=5.7, 3.4 Hz, 1H), 5.82 (ddt, J=16.9, 10.3, 5.7 Hz, 1H); Found: C, 71.08; H, 11.45%. Calcd for $C_{16}H_{30}O_3$: C, 71.07; H, 11.18%.

(*Z*)-4-(3-Acetoxy-2-propenyl)-2-butoxy-4-methyltetrahydrofuran (65:35 Mixture of Diastereomers): Bp 130 °C/1 Torr; IR (neat) 2956, 2932, 2870, 1757, 1672, 1459, 1444, 1370, 1215, 1153, 1098, 1032, 934 cm^{-1}; ^1H NMR δ=0.92 (t, J=7.1 Hz, 3H), 1.05 (s, 1.95H), 1.06 (s, 1.05H), 1.3—2.0 (m, 6H), 2.12 (s, 1.95H), 2.15 (s, 1.05H), 2.15 (br.s, 0.65H), 2.19 (br.s, 0.65H), 2.31 (br.s, 0.35H), 2.35 (br.s, 0.35H), 3.3—3.8 (m, 4H), 5.1—5.2 (m, 1H), 5.40 (dt, J=12.4, 8.1 Hz, 1H), 7.11 (dm, J=12.4 Hz, 1H); Found: C, 65.34; H, 9.58%. Calcd for $C_{14}H_{24}O_4$: C, 65.60; H, 9.44%.

4-(3-Butenyl)-2-butoxy-4-methyltetrahydrofuran: Bp 110 °C/2 Torr; IR (neat) 2956, 2930, 2866, 1642, 1459, 1379, 1098, 1032, 911 cm^{-1}; ^1H NMR δ=0.92 (t, J=7.3 Hz, 3H), 1.06 (s, 3H), 1.2—2.2 (m, 10H, including dd, at δ=1.69, J=13.4, 3.3 Hz, 1H, and ddd, at δ=1.88, J=13.4, 5.7, 0.7 Hz, 1H), 3.3—3.8 (m, 4H), 4.9—5.1 (m, 2H), 5.15 (dd, J=5.7, 3.3 Hz, 1H), 5.82 (ddt, J=17.1, 10.2, 6.5 Hz, 1H); Found: C, 73.38; H, 11.52%. Calcd for $C_{13}H_{24}O_2$: C, 73.54; H, 11.39%.

Methyl 4-(4-Butoxy-3-methyltetrahydrofuran-3-yl)-2-butenoate: Bp 105 °C/2 Torr; IR (neat) 2956, 2868, 1727, 1656, 1437, 1341, 1272, 1195, 1096, 1033, 926 cm^{-1}; ^1H NMR δ=0.91 (t, J=7.1 Hz, 3H), 1.08 (s, 3H), 1.2—1.7 (m, 4H), 1.78 (dd, J=13.4, 2.9 Hz, 1H), 1.87 (dd, J=13.4, 5.4 Hz, 1H), 2.3—2.4 (m, 2H), 3.37 (dt, J=9.5, 6.4 Hz, 1H), 3.52 (d, J=8.2 Hz, 1H), 3.6—3.8 (m, 5H, including s at δ=3.74, 3H), 5.15 (dd, J=5.4, 2.9 Hz, 1H), 5.88 (dt, J=15.5, 1.4 Hz, 1H), 6.93 (dt, J=15.5, 7.8 Hz, 1H); Found: C, 65.82; H, 9.69%. Calcd for $C_{14}H_{24}O_4$: C, 65.60; H, 9.44%.

4-(4-Butoxy-3-methyltetrahydrofuran-3-yl)-2-butenyl Acetate: Bp 130 °C/2 Torr; IR (neat) 2956, 2930, 2868, 1742, 1458, 1444, 1380, 1363, 1231, 1196, 1029, 971, 926 cm^{-1}; ^1H NMR δ=0.92 (t, J=7.1 Hz, 3H), 1.05 (s, 3H), 1.2—1.7 (m, 4H), 1.73 (dd, J=13.5, 3.2 Hz, 1H), 1.87 (dd, J=13.5, 5.4 Hz, 1H), 2.07 (s, 3H), 2.22 (br.s, 1H), 2.25 (br.s, 1H), 3.36 (dt, J=9.5, 6.6 Hz, 1H), 3.48 (d, J=8.4 Hz, 1H), 3.6—3.8 (m, 2H, including d at δ=3.68, J=8.4 Hz, 1H), 4.53 (d, J=5.7 Hz, 1H), 5.14 (dd, J=5.4, 3.2 Hz, 1H), 5.5—5.8 (m, 2H); Found: C, 66.55; H, 9.86%. Calcd for $C_{15}H_{26}O_4$: C, 66.64; H, 9.69%.

(*E*)-3,3-Dimethyl-7-phenyl-2,4-dioxahept-6-ene. This compound was obtained by the following procedure. $PdCl_2(CH_3CN)_2$ (26 mg, 0.1 mmol) was added to a benzene solution (2 ml) of cinnamyl alcohol (134 mg, 1.0 mmol) and 2-propenyl methyl ether (0.7 g, 10 mmol) at room temperature under an argon atmosphere. The reaction mixture was stirred for 1 h and diluted with hexane and several drops of pyridine was added. Precipitated palladium species was filtered off and solvent was evaporated. Residual oil was purified by preparative thin-layer chromatography on silica gel to afford (*E*)-3,3-dimethyl-7-phenyl-2,4-dioxahept-6-ene (190 mg) in 95% yield: bp 83 °C/2 Torr; IR (neat) 2988, 2936, 1494, 1459, 1450, 1380, 1368, 1258, 1212, 1184, 1151, 1101, 1072, 1034, 965, 862, 824, 734, 690 cm^{-1}; ^1H NMR δ=1.41 (s, 6H), 3.25 (s, 3H), 4.13 (dd, J=5.8, 1.4 Hz, 2H), 6.30 (dt, J=15.9, 5.8 Hz, 1H), 6.63 (br.d, J=15.9 Hz, 1H), 7.2—7.5 (m, 5H); Found: C, 75.49; H, 8.79%. Calcd for $C_{13}H_{18}O_2$: C, 75.69; H, 8.80%.

The Reaction in the Presence of KOAc. Noncyclized acetal was major by-product in the reaction of allylic alcohol with vinyl ether mediated by $Pd(OAc)_2$. Though the by-product was hardly separable from the desired product, the formation of noncyclized acetal could be completely suppressed by an addition of base such as KOAc to the reaction mixture. Potassium acetate (98 mg, 1.0 mmol) was added to a benzene (2 ml) solution of cinnamyl alcohol (134 mg, 1.0 mmol) and 2-propenyl methyl ether (1.4 g, 19 mmol) and then $Pd(OAc)_2$ (450 mg, 2.0 mmol) was added to this suspension at room temperature under an argon atmosphere. The reaction mixture gradually turned black and was stirred for 15 h. The mixture was diluted with hexane and several drops of pyridine was added. Precipitated solid was filtered off and solvent was removed under reduced pressure. The residual oil was submitted to silica-gel column chromatography to afford 2-methyl-2-methoxy-4-phenyl-3,6-dihydro-2*H*-pyran (108 mg) in 53% yield along with 27% yield of cinnamaldehyde. (*E*)-3,3-Dimethyl-6-phenyl-2,4-dioxahex-5-ene, which was obtained in 27% yield in the experiment without KOAc, was not observed in this case. The rate of reaction was remarkably retarded and yield was usually slightly lower than that without base.

2-Ethoxy-4-isopropenyl-1-tosylpyrrolidine: Bp 135 °C/2 Torr; IR (neat) 2972, 2930, 1649, 1598, 1442, 1343, 1165 1110, 1085, 1064, 986, 897, 814, 707, 670 cm^{-1}; ^1H NMR δ=1.20 (t, J=7.1 Hz, 3H), 1.37 (dd, J=12.6, 5.2 Hz, 1H), 1.56 (s, 3H), 1.91 (dd, J=12.6, 5.8 Hz, 1H), 2.43 (s, 3H), 2.93 (dd, J=10.3,

9.0 Hz, 1H), 3.0—3.3 (m, 1H), 3.4—3.7 (m, 2H), 3.7—4.0 (m, 1H), 4.63 (br.s, 1H), 4.71 (br.s, 1H), 5.2—5.3 (m, 1H), 7.32 (d, J=8.1 Hz, 2H), 7.74 (d, J=8.1 Hz, 2H); Found: C, 62.07; H, 7.61; N, 4.39%. Calcd for $C_{16}H_{23}NO_3S$: C, 62.11; H, 7.49; N, 4.53%.

2-Butoxy-1-tosyl-4-vinylpyrrolidine (75:25 Mixture of Diastereomers): Bp 133 °C/2 Torr; IR (neat) 2956, 2930, 2868, 1644, 1598, 1458, 1347, 1164, 1082, 998, 921, 814, 708, 673 cm^{-1}; ^1H NMR δ=0.91 (t, J=7.2 Hz, 0.75H), 0.92 (t, J=7.2 Hz, 2.25H), 1.22 (dd, J=12.4, 5.0 Hz, 0.75H), 1.2—1.8 (m, 4.25H), 1.94 (dd, J=12.4, 5.9 Hz, 0.75H), 1.9—2.0 (m, 0.25H), 2.44 (s, 3H), 2.87 (dd, J=9.7, 9.6 Hz, 0.75H), 2.9—3.1 (m, 1H), 3.2—3.7 (m, 2.25H), 3.76 (dt, J=9.6, 6.6 Hz, 1H), 4.9—5.2 (m, 2H), 5.18 (d, J=5.0 Hz, 0.75H), 5.29 (dd, J=6.1, 2.7 Hz, 0.25H), 5.50 (ddd, J=17.1, 10.1, 7.4 Hz, 0.75H), 5.78 (ddd, J=17.5, 9.8, 8.1 Hz, 0.25H), 7.32 (d, J=8.4 Hz, 2H), 7.74 (d, J=8.4 Hz, 2H); Found: C, 63.33; H, 7.91; N, 4.30%. Calcd for $C_{17}H_{25}NO_3S$: C, 63.13; H, 7.79; N, 4.33%.

2-Butoxy-4-(5-methyl-1-methylene-4-hexenyl)-1-tosylpyrrolidine (70:30 Mixture of Diastereomers): Bp 174 °C/2 Torr; IR (neat) 2954, 2926, 2868, 1643, 1598, 1495, 1449, 1347, 1164, 1108, 1083, 1024, 990, 892, 815, 708, 670, 596 cm^{-1}; ^1H NMR δ=0.91 (t, J=7.1 Hz, 0.9H), 0.92 (t, J=7.1 Hz, 2.1H), 1.2—2.4 (m, 15.7H), 2.43 (s, 3H), 2.63 (t, J=7.1 Hz, 0.3H), 2.8—3.0 (m, 1H), 3.0—3.3 (m, 1H), 3.4—3.9 (m, 3H), 4.64 (br.s, 0.7H), 4.73 (br.s, 1H), 4.76 (br.s, 0.3H), 5.03 (br.t, J=6.8 Hz, 1H), 5.19 (d, J=4.8 Hz, 1H), 7.31 (d, J=8.4 Hz, 2H), 7.74 (d, J=8.4 Hz, 2H); Found: C, 68.25; H, 8.89; N, 3.36%. Calcd for $C_{23}H_{35}NO_3S$: C, 68.11; H, 8.70; N, 3.45%.

2-Ethoxy-4-phenyl-1-tosyl-1,2,3,6-tetrahydropyridine: Bp 180 °C/2 Torr; IR (neat) 2974, 2926, 1735, 1598, 1493, 1448, 1345, 1164, 1097, 1071, 1045, 1025, 1011, 912, 814, 759, 716, 666, 590 cm^{-1}; ^1H NMR δ=1.17 (t, J=7.0 Hz, 3H), 2.41 (s, 3H), 2.5—2.6 (m, 2H), 3.54 (dq, J=9.6, 7.0 Hz, 1H), 3.78 (dq, J=9.6, 7.0 Hz, 1H), 4.1—4.4 (m, 2H), 5.33 (dd, J=4.7, 1.5 Hz, 1H), 6.3-6.4 (m, 1H), 7.1—7.5 (m, 7H), 7.44 (d, J=8.3 Hz, 2H); Found: C, 67.44; H, 6.48; N, 3.85%. Calcd for $C_{20}H_{23}NO_3S$: C, 67.20; H, 6.49; N, 3.92%.

The present work was partially supported by a Grant-in-Aid for Encouragement of Young Scientists No. 63790320 from the Ministry of Education, Science and Culture.

References

1) P. A. Grieco, T. Oguri, and Y. Yokoyama, *Tetrahedron Lett.*, **1978**, 419.

2) J. Surzur and P. Teissier, *Bull. Soc. Chim. Fr.*, **1970**, 653.

3) Alkylpalladium which cannot undergo β-hydride elimination adds to olefinic double bond: M. M. Abelman and L. E. Overman, *J. Am. Chem. Soc.*, **110**, 2328 (1988). See also Ref. 4.

4) K. Iritani, S. Matsubara, and K. Utimoto, *Tetrahedron Lett.*, **29**, 1799 (1988).

5) $PdCl_2$(COD)-catalyzed reaction of alcohol and 2-benzyloxy-1-propene has been reported for the synthesis of acetal as a protecting method of hydroxyl group: T. Mukaiyama, M. Ohshima, and M. Murakami, *Chem. Lett.*, **1984**, 265; T. Mukaiyama, M. Ohshima, H. Nagaoka, and M. Murakami, *ibid.*, **1984**, 615.

6) K. Iritani, N. Yanagihara, and K. Utimoto, *J. Org. Chem.*, **51**, 5501 (1986); N. Yanagihara, C. Lambert, K. Iritani, K. Utimoto, and H. Nozaki, *J. Am. Chem. Soc.*, **108**, 2753 (1986).

7) Y. Ito, H. Aoyama, T. Hirao, A. Mochizuki, and T. Saegusa, *J. Am. Chem. Soc.*, **101**, 494 (1979).

8) Palladium(II)-catalyzed intramolecular cyclizations of *N*-tosyl amine derivatives with a pendant olefinic moiety are known: Y. Tamaru, T. Kobayashi, S. Kawamura, H. Ochiai, and Z. Yoshida, *Tetrahedron Lettt.*, **26**, 4479 (1985); L. S. Hegedus and M. S. Holden, *J. Org. Chem.*, **51**, 1171 (1986).

9) Preparation of ethyl *N*-(*p*-toluenesulfonyl)carbamate: F. J. Marshall and M. V. Sigal, Jr., *J. Org. Chem.*, **23**, 927 (1958).

10) Transformation of ethyl *N*-(*p*-toluenesulfonyl)-carbamate into *N*-alkyl sulfonamides: W. J. Gensler, F. J. Frank, S. K. Dheer, and J. W. Lauher, *J. Org. Chem.*, **36**, 4102 (1971).

The Electrolytic Reduction of *p*-Substituted α-(Methylsulfinyl)-α-(methylthio)acetophenones in Acetonitrile

Akira KUNUGI,* Norimasa TAKAHASHI,† Kyo ABE,†† and Taketsugu HIRAI†
Department of Chemical Science and Technology, Faculty of Engineering, Tokushima University, Minamijosanjima, Tokushima 770
†Department of Applied Chemistry, Faculty of Engineering, Osaka City University, Sumiyoshi-ku, Osaka 558
††Department of Chemistry, Faculty of Science, Osaka City University, Sumiyoshi-ku, Osaka 558
(Received September 28, 1988)

Synopsis. *p*-Substituted α-(methylsulfinyl)-α-(methylthio)-acetophenones (**1**) exhibit, on polarographic reduction, three waves. The two last waves correspond to the reductions of *p*-substituted α-(methylthio)acetophenones (**2**) and *p*-substituted acetophenones respectively. The macroelectrolysis at the first wave potential results in the formation of **2** in good yields in the presence of benzoic acid. The electrolytic reduction of **1** is characterized by the elimination of the methylsulfinyl group rather than by the deoxygenative reduction of the sulfoxide to the sulfide or the reduction of the carbonyl group.

Methylthiomethyl sulfoxide (FAMSO), which is a kind of sulfoxide bearing methylthio group at the α-position, is utilized in a wide variety of organic-synthesis processes. One of the title compounds, α-(methylsulfinyl)-α-(methylthio)acetophenone (**1a**), synthesized with facility from FAMSO and ethyl benzoate, is reduced with sodium tetrahydroborate to afford the corresponding hydroxy compound,[1] while the reaction with copper(II) chloride in 1,2-dimethoxyethane gives PhCOCOSMe.[2]

The present paper is concerned with the electrolytic reduction of the title compounds, *p*-substituted α-(methylsulfinyl)-α-(methylthio)acetophenones (**1**) at mercury, platinum, and lead electrodes in acetonitrile (MeCN). The electrolytic reduction of **1** afforded desulfinylated compounds, *p*-substituted α-(methylthio)acetophenones (**2**), in good yields in the presence of an efficient proton donor. A similar desulfinylation occurs in the electrolytic reduction of 1-methylsulfinyl-1-methylthio-2-arylethenes, which are synthesized from FAMSO and the corresponding aldehydes.[3] Phenacyl phenyl sulfide[4] and sulfoxide[5] also favor the cathodic cleavage of the carbon-sulfur bond, whereas the electrolytic reduction of the carbonyl group predominates for the organosulfur compound bearing the COOH group on the carbon adjacent to the carbonyl group ($HOOCCOCH_2SC_2H_5$).[6] Recently, the electrolytic reduction of diphenyl sulfoxide in nonaqueous media has been reported to afford diphenyl sulfide, together with the benzenesulfinate ion.[7] The above examples show that the cathodic cleavage of the carbon-sulfur bond does not necessarily occur for all the organosulfur compounds.

The substrates, **1**, and the related compounds investigated in this work are as follows.

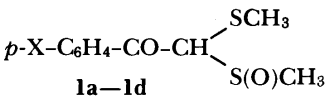

1a—1d

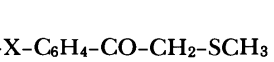

2a—2d

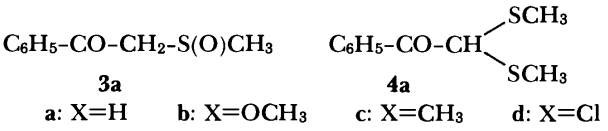

3a **4a**

a: X=H **b**: X=OCH_3 **c**: X=CH_3 **d**: X=Cl

Experimental

The compounds, **1a—1d**, were prepared from FAMSO and ethyl *p*-substituted benzoates according to the published method.[1] The compounds, **1a—1d**, were purified by repeated recrystallizations from a mixture of methanol and water; they showed ^{1}H NMR spectra consistent with the structures assigned.

Polarography and controlled potential macroelectrolysis were carried out, using the experimental set-up and procedure which were reported in a previous paper.[8] All the polarograms were taken in MeCN containing 0.1 (M = mol dm^{-3}) tetrabutylammonium perchlorate (TBAP), the potential being measured against a Ag/0.1 M $AgNO_3$ in MeCN reference electrode (Ag/Ag^+). In the controlled potential macroelectrolysis, tetrabutylammonium tetrafluoroborate (TBAB) were used as the supporting electrolyte, and mercury, platinum, and lead, as the cathode material. After the macroelectrolysis had virtually been completed, the catholyte was carefully concentrated (ca. 3 cm^3), poured into NaCl-saturated water (50 cm^3), and extracted with diethyl ether (3×50 cm^3). After ether-extraction and the usual work-up, the crude mixture and the major product isolated by TLC were subjected to ^{1}H NMR in order to characterize the products.

Results and Discussion

The results of polarography with **1a—1d** are summarized in Table 1. The dc polarogram of **1a** in the absence of proton donors exhibited three waves. In the presence of phenol and benzoic acid, the half-wave potentials ($E_{1/2}$) and wave heights (i_d) of these polarograms were varied, as Table 1 shows. That is, the addition of phenol and benzoic acid caused all the wave heights to increase. On the other hand, the $E_{1/2}$ of the first reduction wave was not changed by adding phenol and benzoic acid, but those of the second and third waves were shifted to more positive potentials. The other substrates, **1b—1d**, exhibited polarographic behavior similar to **1a**. Plots of $E_{1/2}$ vs. the substituent constant sigma gave a good straight line with a slope of 0.50 V for the first reduction wave, indicating that a substrate with a strongly electron-withdrawing group such as Cl is easier to reduce than a substrate with an electron-donating group such as CH_3O.

Controlled potential macroelectrolyses of **1a—1d** at the potential of the first reduction wave were con-

Table 1. Polarographic Half-Wave Potential ($E_{1/2}$) and Wave Height (i_d) of **1a—1d** at a Dropping Mercury Electrode in MeCN Containing 0.1 M TBAP in the Absence and Presence of a Proton Donor

Substrate	Proton donor	$-E_{1/2}$/V vs. Ag/Ag$^+$ [i_d/mA M^{-1}]		
1a	None	1.76	2.29	2.43
		[2.8]	[0.6]	[0.2]
	Phenol (4 equiv)	1.76	2.19	2.34
		[5.3]	[2.4]	[1.5]
	Benzoic acid (2.2 equiv)	1.76	2.19	2.35
		[10.2]	[4.5]	[3.0]
1b	None	1.90	2.38	2.53
		[2.8]	[0.7]	[0.3]
	Phenol (4 equiv)	1.90	2.26	2.35
		[5.4]	[2.3]	[1.5]
	Benzoic acid (2.2 equiv)	1.90	2.25	2.34
		[10.0]	[4.7]	[3.0]
1c	None	1.83	2.32	2.49
		[2.7]	[0.6]	[0.2]
	Phenol (4 equiv)	1.83	2.18	2.30
		[5.3]	[2.5]	[1.6]
	Benzoic acid (2.2 equiv)	1.83	2.19	2.32
		[10.1]	[4.9]	[2.8]
1d	None	1.65	2.12	2.30
		[2.7]	[0.6]	[0.2]
	Phenol (4 equiv)	1.65	1.99	2.28
		[5.3]	[2.5]	[1.6]
	Benzoic acid (2.2 equiv)	1.65	1.97	2.25
		[10.1]	[4.3]	[2.9]

ducted at various cathodes (Hg, Pt, and Pb) in the absence and in the presence of proton donors at room temperature. The substrates, **1a—1d**, were found to undergo the cathodic cleavage of a carbon-sulfur bond to yield *p*-substituted α-(methylthio)acetophenones (**2a—2d**). However, the corresponding hydroxides, *p*-substituted α-(methylsulfinyl)acetophenones (**3**), and *p*-substituted α,α-bis(methylthio)-acetophenones (**4**) were not obtained. Table 2 summarizes the isolated yields of **2a—2d**, along with the coulometric *n*-values (electrons per molecule). The *n*-values were obtained from the amount of the substrate added and the quantity of electricity passed through before the termination of the electrolysis. The yield of **2a** was low in the absence of the proton donor and even in the presence of excess phenol. The addition of benzoic acid caused the yield of **2a** to increase considerably (82%). Therefore, the use of benzoic acid as the proton donor was found to be desirable to improve the yield of **2a**. The kinds of *p*-substituents (X) of the compounds, **1**, and the cathode material (Hg, Pt, and Pb) do not appear to have had a significant influence on the yield of **2**.

Table 3 summarizes the $E_{1/2}$ and i_d values of α-(methylthio)acetophenone (**2a**), α-(methylsulfinyl)acetophenone (**3a**), α,α-bis(methylthio)acetophenone (**4a**), and acetophenone (**5a**) in the presence of proton donors, such as phenol and benzoic acid, together with those of **1a**. If **4a** is an intermediate in the electrolytic reduction of **1a**, the polarographic wave corresponding to the reduction of **4a** must be observed on the polarogram of **1a** because the $E_{1/2}$ value of **4a** is more negative by about 0.17 V than that of **1a**. Such a polarographic wave was not, however, obtained as is shown in Table 3. Furthermore, there was no detectable amount of **4a** in the macroelectrolysis of **1a**. Therefore, it may be concluded that the deoxygenated reduction of the oxygen-sulfur bond in the electrolytic reduction of **1a** does not take place, i.e., the electrolytic redurtion of **1a** does not proceed through **4a**. Similarly, **3a** must also be ruled out as an intermediate in the reductive conversion of **1a** to **2a**, because the polarogram of **1a** did not exhibit the polarographic wave corresponding to the reduction of **3a** and **3a** was not detected in the macroelectrolysis of **1a**. Moreover, Table 3 suggests that the first wave of **1** in the presence of benzoic acid corresponds to a four-electron reduction, since the i_d for the first wave of **1a** was about twice that of **4a** and also, since the i_d for the first wave of **3a**[9] was about twice that of **2a**, when benzoic acid was used as the proton donor.

Tables 2 and 3 indicate that the second and third polarographic waves of **1a** correspond to the reductions of **2a** and **5a** respectively.

On the basis of the above-mentioned results and discussion, it is concluded that the electrolytic reduction of **1** at the potential of the first reduction wave proceeds through neither **3** nor **4**, but through the elimination of the methylsulfinyl group. Also, the reduction of the carbonyl group was found not to occur in the electrolysis of **1**. Furthermore, taking into account the fact that none of the $E_{1/2}$ values of the first reduction wave of **1a—1d** were changed by adding the proton donor, the following scheme may be proposed for the electrolytic reduction of **1** to **2** in the

Table 2. Controlled Potential Electrolyses of **1a—1d** at the Potential of the First Reduction Wave in MeCN Containing 0.1 M TBAB

Substrate	Cathode	Potential vs. Ag/Ag$^+$/V	Proton donor (equiv)	*n*-Value	Product (Yield/%)
1a	Hg	−1.80	None	0.8	**2a** (24)
	Hg	−1.80	Phenol (4.0)	2.3	**2a** (58)
	Hg	−1.80	Benzoic acid (2.0)	2.5	**2a** (82)
	Pt	−1.80	Phenol (4.0)	2.2	**2a** (65)
	Pb	−1.70	Phenol (4.0)	2.8	**2a** (50)
1b	Hg	−1.93	Benzoic acid (2.0)	2.9	**2b** (86)
1c	Hg	−1.85	Benzoic acid (2.0)	2.7	**2c** (83)
1d	Hg	−1.68	Benzoic acid (2.0)	2.3	**2d** (80)

Table 3. Polarographic Harf-Wave Potentials ($E_{1/2}$) and Wave Height (i_d) of **1a** and Related Compouds in MeCN Containing 0.1 M TBAP in the Presence of a Proton Donor

Substrate	Proton donor	$-E_{1/2}$ vs. Ag/Ag$^+$/V [i_d/mA M^{-1}]		
1a	Phenol (4.0 equiv)	1.76 [5.3]	2.19 [2.4]	2.34 [1.5]
	Benzoic acid (2.2 equiv)	1.76 [10.2]	2.19 [4.5]	2.35 [3.0]
2a	Phenol (4.0 equiv)		2.18 [4.9]	2.32 [1.6]
	Benzoic acid (2.2 equiv)		2.18 [5.6]	2.33 [1.6]
3a	Phenol (4.0 equiv)	1.89 [5.4]		2.34 [3.3]
	Benzoic acid (2.2 equiv)	1.89 [10.3]		2.35 [3.3]
4a	Phenol (4.0 equiv)	1.93 [4.8]	2.15 [2.9]	2.31 [1.4]
	Benzoic acid (2.2 equiv)	1.93 [5.0]	2.15 [2.9]	2.32 [1.4]
5a	Phenol (4.0 equiv)			2.31 [5.1]
	Benzoic acid (2.2 equiv)			2.32 [5.8]

presence of an efficient proton donor:

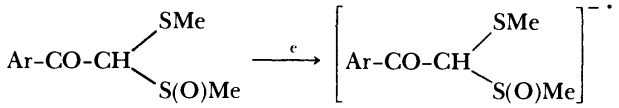

1

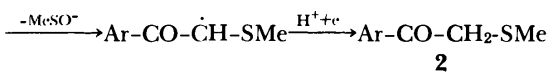

2

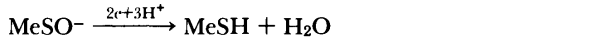

It is not clear whether or not the methylsulfinyl anion resulting from the cleavage of the carbon-sulfur bond undergoes further reduction to yield methanethiol, since the formation of methanethiol has not yet been ascertained and since the above mechanism indicates that **1** is reduced in an overall four-electron process (the coulometric n-values obtained were 2.2—2.9 for **1a—1d**, even in the presence of the proton donor). However, the polarographic n-value for the first reduction wave of **1** was 4, suggesting that the reduction of methylsulfinyl anion to methanethiol occurs at the reduction potential of **1**. Furthermore, it has been reported that the electrolytic reduction of 1-methyl-sulfinyl-1-methylthio-2-phenylethene afforded desulfinylated compounds, 1-methylthio-2-phenylethene and methanethiol, with the consumption of 3.6 electrons per molecule.[3] Accordingly, from the evidence that the coulometric n-values were more than 2 in the presence of the proton donor, as is shown in Table 2, together with above considerations, it seems reasonable to conclude that a part of the methylsulfinyl anions are electrochemically reduced to afford methanethiol. The remainder will be converted chemically to methanethiol etc., since methane sulfenic acid, if formed at all, is very unstable.

References

1) K. Ogura, S. Furukawa, and G. Tsuchihashi, *Chem. Lett.*, **1974**, 659.

2) K. Ogura, *Yuki Gosei Kagaku Kyokai Shi*, **37**, 903 (1979).

3) A. Kunugi, K. Abe, T. Hagi, and T. Hirai, *Bull. Chem. Soc. Jpn.*, **59**, 2009 (1986).

4) H. Lund, *Acta Chem. Scand.*, **14**, 1927 (1960).

5) A. Kunugi and N. Kunieda, *Electrochim. Acta*, **28**, 715 (1983).

6) M. B. Fleury, J. Tohier, and P. Zuman, *J. Electroanal. Chem.*, **143**, 253 (1983) and the references cited therein.

7) N. Djeghigjegh and J. Simonet, *Electrochim. Acta*, **33**, 541 (1988).

8) A. Kunugi, T. Hagi, T. Hirai, and K. Abe, *Electrochim. Acta*, **39**, 1049 (1985).

9) The macroelectrolysis of **3a** gave **5a** in a 70% yield.

Photooxidation of Bis[1,2-diphenylethanedithione]nickel(0)-tetrabutylamine with α-Tocopherol

Koe ENMANJI
Materials and Electronic Devices Laboratory, Mitsubishi Electric Co., Tsukaguchi-Honmachi, Amagasaki-shi 661
(Received October 24, 1988)

Synopsis. The photooxidation of a nickel dithiolate complex by α-tocopherol was found for the development of a recording medium which can be used to read by a laser diode. The mechanism was analyzed. As a result, it was found that α-tocopherol produced oxygen adducts by light; the oxygen adducts oxidized bis[1,2-diphenylethanedithione]-nickel(0)tetrabutylamine.

The development of recording medium for a laser diode is desirable since a laser diode is small in size and conventional. Because of the character of high-density recording and rewritability, photon-mode recording was hopeful and the appearence of a recording dye for the laser diode was desired. A Schrauzer complex was one of the dithiolate complexes; it was synthesized in 1962 by Schrauzer and Mayweg.[1] It was reported by them that some complexes have absorption peaks at 700—900 nm,[2] and that the development of a recording medium which can be read by a laser diode is possible if redox reaction can be induced by light. We obtained the reductant (bis[1,2-diphenylethanedithione]nickel(0)tetrabutylamine=BDNH) of bis[1,2-diphenylethanedithione]nickel(0) (BDN) and investigated its properties, finding that BDNH was oxidized by UV light in the presence of α-tocopherol (αT) and produced the BDN. We thus recognized the possibility for developing a photo-recording medium. We now report on our investigation of the effect of various factors on the photooxidation of BDNH to BDN as well as the mechanism.

Experimental

BDNH was purchased from Midori Chem. Co. and used without purification. α-Tocopherol was purchased from Nakarai Chem. Co., and toluene was purchased from Wako Chem. Co.

The monochromatic light was irradiated by a Ushio-500 type super-high-pressure mercury lamp equipped with a Toshiba KL-28 filter. The light intensity was measured by a method described in the literature.[3] The optical absorption spectra were measured by a Shimadzu MPS-5000.

A Hückel molecular orbital calculation was carried out with Otsuka's program[4] by using a Multi 16 computer.

Results and Discussion

BDNH (5.13×10^{-5} mol dm^{-3}) was dissolved into toluene and α-tocopherol (0.100 mol dm^{-3}) was added. The irradiation of this solution made the peak at 975 nm disappear and new peak appeared at 875 nm (Fig. 1). Also, the color changed from brown to green. It was found that BDN was produced. These phenomena were considered by the following mechanism. The oxygen adduct of α-tocopherol was produced by the irradiation of α-tocopherol under aerobic conditions; this adduct substructs a $(C_4H_9)_4N^+$ group from

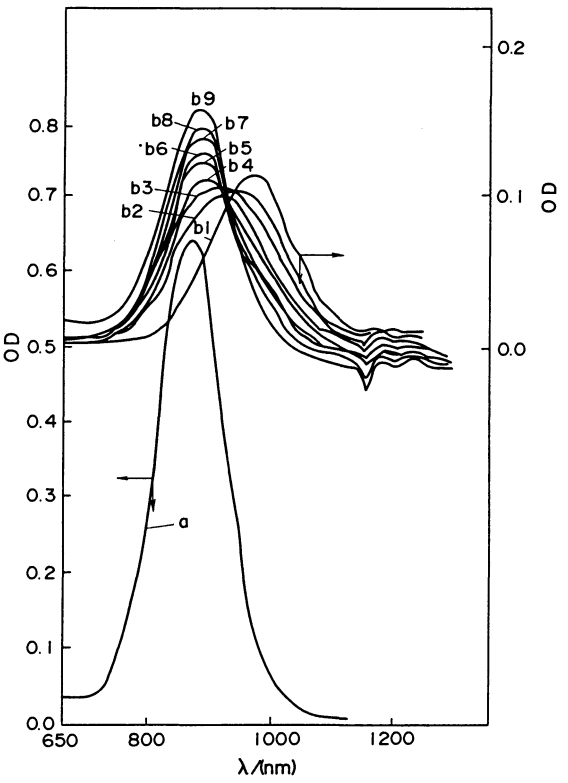

Fig. 1. Change in absorption spectra of BDNH containing α-tocopherol during photo-illumination.
a: BDN, b1: after 0 minutes, b2: 1 min, b3: 2 min, b4 4 min, b5: 9 min, b6: 14 min, b7: 24 min, b8: 34 min, b9: 79 min.
[BDNH]=5.13×10^{-5} mol dm^{-3}, [αT]=0.1 mol dm^{-3}, I=3.24 mol dm^{-3} s^{-1}

BDNH and oxidizes to BDN as the same mechanism as the initiation reaction of the polymerization of methyl methacrylate.[5] The assumed mechanism can be described as in the following equations:

$$\alpha T \xrightarrow{h\nu} \alpha T\cdot, \quad (1)$$

$$\alpha T\cdot + O_2 \xrightarrow{k_i} \alpha TO_2\cdot, \quad (2)$$

$$\alpha TO_2\cdot \xrightarrow{k_q} Q(\alpha T\text{-}O_2\text{-}\alpha T), \quad (3)$$

$$\alpha TO_2\cdot + BDNH \xrightarrow{k_i} \alpha TO_2{=}N(C_4H_9)_4 + BDN \quad (4)$$

Here, the existence of αT· is assured by the flash-photolysis of an α-tocopherol toluene solution in air.[5] The reaction rate is given by

$$v_i = \frac{k_i C_{BDNH}}{(k_i C_{BDNH}+k_q)} \Phi I[1-10^{-\varepsilon C_{\alpha T} l}]/l, \quad (5)$$

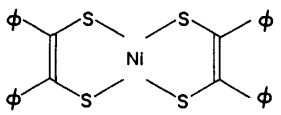

BDN

Scheme 1.

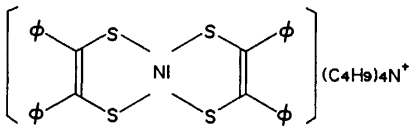

BDNH

Scheme 2.

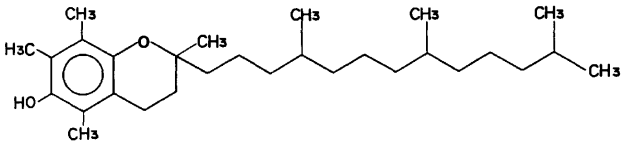

α-Tocopherol

Scheme 3.

where Φ is the quantum yield for the production of $\alpha T\cdot$, Q is the subproduct, l(cm) is the length of the reaction champer, ε ($1\,mol^{-1}\,cm^{-1}$) is the molecular extinction constant of α-tocopherol, and I (einstein $cm^{-2}s^{-1}$) is the light intensity. When $\varepsilon C_{\alpha T} l$ is sufficiently small, i.e. light is not completely absorbed, $10^{-\varepsilon C}\ \alpha T^{l}$ becomes $1-\varepsilon C_{\alpha T} l$, and Eq. 5 reduces to Eq. 6,

$$v_i = \frac{2.303\ k_i C_{BDNH}}{(k_i C_{BDNH} + k_q)} \Phi I \varepsilon C_{\alpha T}, \qquad (6)$$

if $k_i C_{BDNH} \ll k_q$

$$v_i = \frac{2.303 k_i}{k_q} C_{BDNH}\ \Phi I C_{\alpha T}. \qquad (7)$$

On the contrary, when $\varepsilon C_{\alpha T}$ is sufficiently large, i.e. light is completely absorbed, $10^{-\varepsilon C_{\alpha T} l}$ becomes zero and Eq. 5 can be reduced to Eq. 8.

$$v_i = \frac{2.303\ k_i C_{BDNH}}{(k_i C_{BDNH} + k_q)} \Phi I / l, \qquad (8)$$

If $k_i C_{BDNH} \ll k_q$ holds, Eq. 8 can be reduced to Eq. 9 and the reaction rate is proportional to the first order of the BDNH concentration.

$$v_i = \frac{2.303\ k_i}{k_q} C_{BDNH} \Phi I / l. \qquad (9)$$

Here, for $\varepsilon_{280}=71$ and $C_{\alpha T}>0.02$ mol dm^{-3} Eq. 9 holds and for $C_{\alpha T}<0.001$ mol dm^{-3} Eq. 7 holds. It was found that $k_i\Phi/k_q=\Phi'=0.373$. A plot of logarithm optical density at 975 nm was proportional to the irradiation time. It was found that the reaction is the mechanism of first order of BDNH i.e. $k_i C_{BDNH} \ll k_q$ holds.

The dependence of the concentration of α-tocopherol on the photooxidation of BDNH is shown in Fig. 2. As can be seen in Fig. 2, v_i becomes constant when $C_{\alpha T}$ is larger than 10^{-3} mol dm^{-3}. Consequently, when $C_{\alpha T}$ is larger than 10^{-3} mol dm^{-3} the condition of the $10^{-\varepsilon}\ C_{\alpha T}{}^{l}$ is nearly equal zero holds as well as Eq. 9. The dependence of the light intensity on the photooxidation of BDNH is shown in Fig. 3. As can be seen, since the reaction rate is proportional to the first order of the light intensity, Eq. 5 holds.

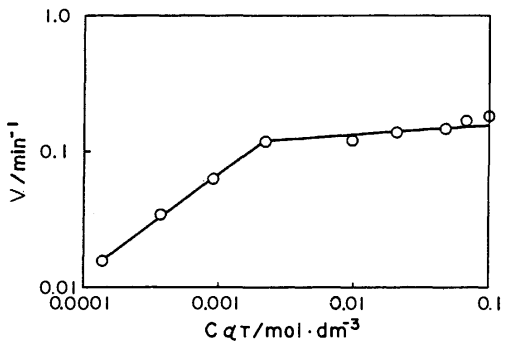

Fig. 2. Dependence of the rate of photooxidation of BDNH on the concentration of α-tocopherol. [BDNH]=5.13×10^{-5} mol dm^{-3}, I=3.24 M s^{-1}

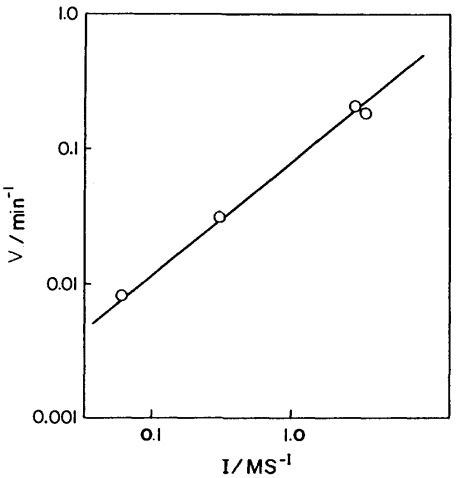

Fig. 3. Dependence of the rate of photooxidation of BDNH on light intensity. [BDNH]=5.13×10^{-5} mol dm^{-3}, [αT]=0.1 mmol dm^{-3}.

Table 1. Effect of Addition of Various Tocopherols on Photo oxidation Rate of BDNH

Tocopherol	v/min^{-1}	$E(E)$ of C_5
α	0.123	3.8985
β	0.146	2.9472
γ	0.351	2.5352
δ	0.904	2.0469

The rates of photooxidation of BDNH are shown in Table 1 under the condition that the concentration of α-tocopherol, β-tocopherol, γ-tocopherol, and δ-tocopherol are 7.74×10^{-3} mol dm^{-3}. As can be seen in Table 1, the photooxidation rate increases according to the order of the action property of vitamine E.[6] Because it was found that tocopherols form a radical at C_5,[7] the delocalization energies of α-tocopherol, β-tocopherol, γ-tocopherol, and δ-

tocopherol to an electrophilic reagent (which are calculated by HMO method) are shown in Table 1. As can be seen, the lower the delocalization energy the larger is the rate of photooxidation of BDNH. The calculation satisfied the experimental results.

The possibility of a photorecording medium was assumed for a BDNH-α-tocopherol system. Increasing the α-tocopherol concentration was not effective for increasing the recording speed, though increasing the light intensity was. In a solid medium this reaction can occur. A device using this reaction will be developed by the present author.

References

1) G. N. Schrauzer and V. Mayweg, *J. Am. Chem. Soc.*, **84**, 3221 (1962)
2) G. N. Schrauzer and V. Mayweg, *Z. Naturforsch.*, **19**, 192 (1964).
3) E. Kokubu, "Zikken Kagaku Koza, Light(2)" ed by Jpn. Chem. Soc., Maruzen, Tokyo (1976), p. 241.
4) Kozo Ohtsuka, "Learning Chemistry with Microcomputer," p.118 (1984), Tokyo Kagaku Dojin.
5) K. Enmanji, *Bull. Chem. Soc. Jpn.*, **58**, 2181 (1985).
6) H. Masugi and T. Nakamura, *Tampakushitu Kakusan Koso*, **21**, 855(1976).
7) S. Urano and M. Matsuo, *Lipids*, **11**, 380 (1976).

ENDOR Studies of the Complexation Reaction between Spin-Labeled Crown Ether and Alkali Metal Salts

Kunihiko TAJIMA,* Masanao MIYOSHI, Masahiro FURUTANI, Yasushi FUJIMURA, Kazuo MUKAI, and Kazuhiko ISHIZU

Department of Chemistry, Faculty of Science, Ehime University, Matsuyama 790

(Received November 30, 1988)

Synopsis. A new crown ether spin-labeled by the phenoxyl radical moiety was prepared. Intramolecular odd-π electron delocalization was investigated by means of ENDOR spectroscopy. On the basis of ENDOR spectrometric titration, the equilibrium constant for Na^+-labeled crown-ether-complex formation was evaluated to be $pK_{Na^+}=3.5$ in 2-propanol at −30 °C.

The spin-labeling technique has been applied to obtain information about the molecular structures of both labeled crown ether and its metal complexes. For example, the molecular structure of 2 : 1 sandwich type complexes of labeled crown ethers were characterized on the basis of detailed analyses of the triplet ESR spectra.[1-3] In addition, the dihedral angles of the vibrating crown methylene protons were estimated by means of temperature-dependent ENDOR measurements.[4] In the previous studies, however, the details of the metal-complexation reaction between these labeled crown ethers and metal cations have not been fully compiled. Here, a stable spin-labeled crown ether bearing the phenoxyl radical moiety (CR-O·) was newly prepared and isolated as pure crystals in order to obtain an improved view of the host-guest chemistry relating to this crown ether. The conformational change in the benzylic methylene protons upon metal chelation was investigated in detail by ENDOR. In addition, the equilibrium constants of alkali metal complex formation were also estimated.

Experimental

The spin labeled crown ether CR-O· (Fig. 1) was synthesized by the usual procedures,[3,5] (Found: C, 69.99, H, 8.79%. Calcd for $C_{31}H_{46}O_7$: C, 70.16; H, 8.79%. Mp 135—136 °C). The purity of the CR-O· was estimated to be above 98% by means of magnetic susceptibility measurements at 25 °C. The ENDOR spectra were recorded by a JEOL ES EDX-1 spectrometer in the temperature range from −50 to +10 °C in dry 2-propanol. All the measurements were performed at the Advanced Instrumental Center for Chemical Analysis, Ehime University.

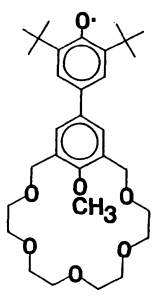

Fig. 1. The molecular structure of the phenoxyl radical crown ether CR-O·.

Results and Discussion

Figure 2 shows the higher half frequency field of the ENDOR spectra observed for metal free CR-O· (1.0 m M†) in 2-propanol. The ENDOR fine structures were safely assigned with reference to the results of previous report[6] as summarized in Table 1. The benzylic methylene protons, H_1 and H_2, revealed a nonequivalence in the magnitude of proton hfcc at −30 °C (Fig. 2-3), as has already been noted for other spin-labeled crown ethers.[4] On raising the temperature, the distance between these two lines began to decrease, finally they collapsed together into a single

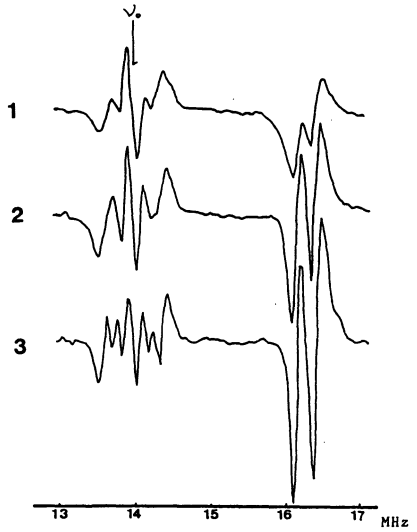

Fig. 2. The higher frequency half of ENDOR spectra observed in the absence of alkaline metal salts at (1) +10 °C, (2) −20 °C, and (3) −30 °C.

Table 1. Observed Proton Hyperfine Coupling Constants (hfcc in mT) of CR-O· and Its Alkaline Metal Complexes

Position	CR-O· 10 °C	CR-O· −30 °C	Na^+-CR-O· −30 °C	K^+-CR-O· −30 °C
2	0.0107	0.0076	0.0086	0.0080
3	0.1610	0.1601	0.1682	0.1704
4	0.0270	0.0290	0.0482	0.0392
H_1,H_2	0.0268	0.0167 0.0293	0.0482	0.0394

† 1 M=1 mol dm^{-3}.

line above +10 °C (Fig. 2-1). Based on the proton hfcc of the benzylic methylene protons H_1 and H_2 at the maximum separation, the equilibrium dihedral angles were estimated to be 55 ° and 61 ° in terms of the McConnell-Heller equation,[7] as illustrated in Fig. 3. A restricted movement, as demonstrated in the benzylic methylene protons, may be attributed to a steric repulsion occurring between the crown ether chain and the methoxyl group. The activation energy for the vibrating benzylic methylene protons were evaluated to be 14 kJ mol^{-1} after Gutowsky and Holm's treatment.[8]

The ENDOR spectra were measured in the presence of a ten-fold molar equivalent of alkali metal salts: Li^+-, Na^+- and K^+ClO_4. No important ENDOR spectral change was detected, even after the mixing of $LiClO_4$ with the CR-O· (Fig. 4-1), indicating that no complex formation occurs between $LiClO_4$ and the radical crown ether. On the other hand, both Na^+ and K^+ salts showed a drastic variation upon the ENDOR fine structure recorded at −30 °C, as shown in Fig. 4-2 and -3. A nonequivalence in the benzylic-methylene-proton splitting disappeared in the temperature range from −30 °C to +10 °C upon the addition of Na^+ and K^+ salts. This implies that the thermal motion occurring in the benzylic-methylene protons is tightly locked by metal chelation in the crown ether cavity. Interestingly, the ENDOR signal of the metal-free CR-O· was again recorded, after the addition of a 20 molar excess of 18-CR-6, which had a pronounced affinity for Na^+ and K^+ ions. These findings, therefore, indicate that marked conformational changes in the crown ether moiety take place upon the complex formation with Na^+ and K^+ ions.

In order to evaluate the equilibrium constant for Na^+-complex formation, ENDOR spectrometric titration was carried out by changing the initial concentration ratio, R_0=[$NaClO_4$]/[CR-O·$_0$], as is shown in Fig. 5. When a two-fold excess amount of $NaClO_4$ was added to CR-O·, the observed ENDOR spectrum (Fig. 5-2) showed mixed fine structures consisting of the metal-free CR-O· and of the Na^+-CR-O· complex. The ENDOR signal intensity ascribable to Na^+ complex gradually increased, and eventually the ENDOR signals of metal free CR-O· completely disappeared at R_0=6.0 (Fig. 5-4). This ENDOR fine structure recorded during the titration from R_0=0 to 6.0 was adequately simulated by means of the computer superposition of the ENDOR fine structures of CR-O· and its Na^+ complex, as demonstrated in Fig. 5. An excellent agreement was seen between the observed spectra and those simulated, which were obtained after trial-and-error calculations by changing the mixing ratio, R'=[Na^+-CR-O·]/[CR-O·]. In

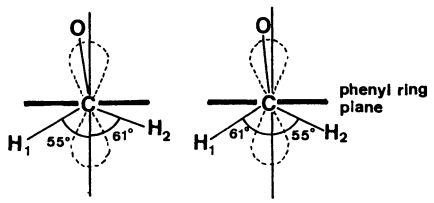

Fig. 3. The equilibrium dihedral angle of the vibrating benzylic methylene protons H_1 and H_2.

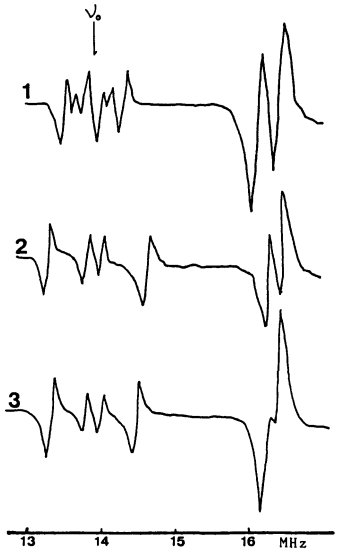

Fig. 4. ENDOR spectra observed at −30 °C in 2-propanol in the presence of ten fold excess amount of (1) $LiClO_4$, (2) $NaClO_4$, and (3) $KClO_4$.

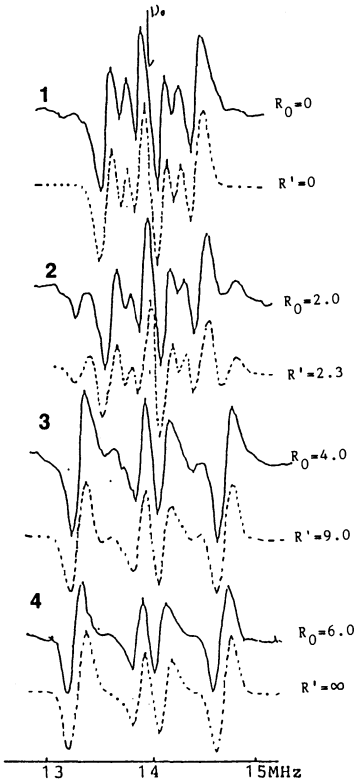

Fig. 5. ENDOR spectral changes observed (solid line) during the $NaClO_4$-titration at −30 °C and the calculated ENDOR fine structure (broken line). R_0 is initial mixing molar ratio [$NaClO_4$]/[CR-O·$_0$] and R' is the estimated molar ratio [Na^+-CR-O·]/[CR-O·] by means of computer superposition using Eq. 1.

terms of the R_0 and R' values, the equilibrium constant $pK_{Na}+$ was calculated using Eq. 1:

$$pK_{Na}+=\log(R'(1+R')/[Na^+_0]+R'[Na^+_0]-R'[CR\text{-}O\cdot_0]) \quad (1)$$

The values of $pK_{Na}+$ at −20 °C and −10 °C were also evaluated to be 3.5 and 3.3 by means of similar procedures. Based on the temperature dependence of the $pK_{Na}+$ values, the thermodynamic parameters of ΔH and ΔS were estimated to be 1.4 kJ mol^{-1} and −1.5 J mol^{-1} deg^{-1}. By a similar ENDOR titration carried out for the K^+-CR-O· system, the $pK_K{}^+$ value was estimated to be above 6.0 at −30 °C. This implies that the labeled crown ether CR-O· possesses a pronounced affinity to the K^+ ion rather than to the Na^+ ion. Further investigations to evaluate the $pK_K{}^+$ value of the K^+-CR-O· complex formation are now in progress.

References

1) K. Ishizu, K. Kohama, and K. Mukai, *Chem. Lett.*, **1978**, 227.
2) K. Mukai, N. Iida, and K. Ishizu, *Bull. Chem. Soc. Jpn.*, **55**, 1362 (1982).
3) K. Mukai, M. Yamashita, K. Ueda, K. Tajima, and K. Ishizu, *J. Phys. Chem.*, **87**, 1338 (1980).
4) K. Tajima, H. Shimizu, H. Tomoda, K. Mukai, and K. Ishizu, *Org. Mag. Reson.*, **21**, 376 (1983).
5) K. Tajima, T. Mita, Y. Fujimura, K. Mukai, and K. Ishizu, *Nippon Kagaku Kaishi*, **1987**, 283; K. E. Koeing, G. M. Lein, P. Stuckler, T. Kaneda, and D. J. Cram, *J. Am. Chem. Soc.*, **101**, 3533 (1979).
6) K. Mukai and N. Inagaki, *Bull. Chem. Soc. Jpn.*, **53**, 2695 (1980).
7) J. S. Hyde, R. Bleslow, and C. DeBore, *J. Am. Chem. Soc.*, **88**, 4763 (1966).
8) H. S. Gutowsky and C. H. Holm, *J. Chem. Phys.*, **25**, 1182 (1956).

Metastable Dissociations of $CH_3NO_2^+$ and $CD_3NO_2^+$ Ions. Isotope Effects of the Loss of a Hydroxyl Radical

Ryuichi ARAKAWA
College of Biomedical Technology, Osaka University, 1-1 Machikaneyama-cho, Toyonaka, Osaka 560
(Received December 21, 1988)

Synopsis. A large kinetic isotope effect has been observed for the metastable transitions of $CX_3NO_2^+ \rightarrow CX_2NO^+ + OX$ (X=H, D). The large effect was explained by assuming a rate-determining isomerization to an *aci*-nitromethane ion and the quantum mechanical tunneling of a hydrogen atom.

The dissociation of a nitromethane ion has been studied by a variety of experimental techniques.[1-7] The dissociation mechanism has been discussed in terms of the participation of an *aci*-nitromethane tautomer, $CH_2=N(OH)O^+$, and a methyl nitrite ion, CH_3ONO^+. In particular, isomerization to an *aci*-nitromethane ion, followed by the formation of CH_2NO^+ and OH, has been established by recent studies of the appearance energy and metastable-ion fragmentations using MS/MS and photoionization experiments.[6,7] On the other hand, the NO^+ formation from the nitromethane ion has been explained by its isomerization to the methyl nitrite ion prior to dissociation.[3,4] Moreover, it has been reported that the dissociations of the nitromethane ion at the near threshold are all competing processes.[7] However, no quantitative interpretation accounting for the metastably slow dissociations, including CH_2NO^+ and NO^+ paths, has been presented based on a usual RRKM/QET treatment.

In the system of a methyl nitrite ion, it is of much interest that the dissociation involves non-interconverting excited states or structures. The CH_2OH^+ formation from CH_3ONO^+ appears with a rate constant of $k(E)\approx 10^5$ s^{-1}, while the rate of NO^+ is $k(E)\gg 10^7$ s^{-1}.[3,4] There is no satisfactory interpretation of the slow CH_2OH^+ path. Recently, Ferguson[8] has suggested that a quantum mechanical tunneling for a hydrogen migration is due to the slow dissociation of CH_2OH^+ and has interpreted the large isotope effect of $k_H/k_D\approx 10$, measured previously by Gilman et al.[4] This suggests an alternative reaction path leading to D_2NO^+ for $CD_3NO_2^+$. However, more recent studies,[9,10] have excluded such a proposal.

There is a class of dissociation reactions in which ions dissociate at a rate much slower than that predicted from the RRKM/QET calculation. In such a case, the activation energy is usually less than 1 eV, so that the predicted rates are much greater than 10^7 s^{-1}, while the measured rates are in the 10^5 s^{-1} range. To overcome this difficulty, it has been proposed that the reaction involves isomerization into sufficiently stable isomers or the existence of stable ion-dipole complexes. In addition, tunneling through a potential barrier or a rotational barrier and the participation of an anharmonic interaction potential[11] have been reported to be the origin of the metastable-ion dissociations. The reaction systems of nitromethane and methyl nitrite cations lie within the category discussed above. Below we will present an isotope effect k_H/k_D for the loss of a hydroxyl radical in the nitromethane metastable dissociations. If the isomerization to the *aci*-nitromethane ion is a rate-determining step, tunneling is a probable process for explaining the slow dissociation; thus, the large isotope effect can be expected.

Figure 1 shows the metastable-ion decays for CH_2NO^+ and NO^+ as a function of the ion-storage time, as determined by the use of the ion-trapping

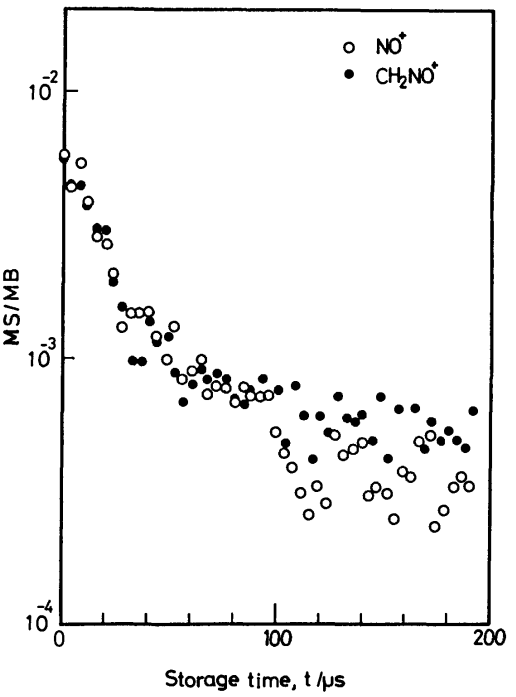

Fig. 1. Metastable-to-main-beam intensity ratio vs. the ion-storage time at the electron-impact energy of 40 eV.

Table 1. Metastable Ion (MI) and Collision-Induced Dissociation (CID) Spectra of Nitromethane Ions

Ion	$CH_3NO_2^+$		$CD_3NO_2^+$	
(m/z)	MI	CID	MI	CID
15		2		
30	27	35	44	46
34				<1
44	26	4		
46		42	1±1	37
48				2
60	47	17		
62			55	14

technique[12] utilizing the space charge of an electron beam. It indicates that slow dissociations are measured at $\leqq 10^4$ s^{-1}. The two intensities are almost the same throughout the long storage time. This is consistent with the photoionization result[7] that their appearance energies are nearly equal within the limits of experimental error. The intensities of the metastable ions and of the collision-induced dissociations (CID) at the zero storage time are listed in Table 1. The CID spectra were measured at a 20% decrease in the main beam intensity by raising the He gas pressure in a collision cell. We believed that the CID components in the metastable peaks were negligible, because there was no CID peak of NO_2^+. For $CD_3NO_2^+$ the peak at m/z 46 corresponding to CD_2NO^+ or NO_2^+ was observed with a low intensity. This peak may be CD_2NO^+, because no peak of NO_2^+ was observed for $CH_3NO_2^+$. The metastable observation is actually limited within a narrow rate range, because the present time window in the second-field-free region is between 6.8 and 10.6 μs; it corresponds to the average decay rate of 1.2×10^5 s^{-1}. Thus, the intensity ratio in Table 1 represents the relative rate constant. Consequently, the isotope effect was determined to be $k_H/k_D\approx26$ for the hydroxyl radical loss.

The tunneling correction of the unimolecular rate constants was examined in order to explain the large experimental isotope effect. The correction is given by $k(E)=p(E)k(E_0)$, where $p(E)$ is the tunneling probability and where $k(E_0)$ is the minimum rate at the threshold energy of E_0. The vibrational frequencies for a reactant and a transition state were obtained by a vibrational analysis for the assumed geometries and force fields.[13] The value of k_H/k_D may be independent of the influence of approximate vibrational frequencies resulting from the simple force field. Thus, the rough estimation of vibrational frequencies is sufficient to account for the present isotope effect. The isomerization to the *aci*-nitromethane ion probably involves a hydrogen migration to a oxygen atom prior to the OH loss. A four-center complex was employed as the transition state; the bond orders of C-H and H-O regarding the migrating hydrogen were assumed to be 0.5. The results of the vibrational analysis are shown in Table 2. The activation entropies, ΔS^*, as calculated from a set of frequencies, are $\Delta S^*=-0.20$ (X=H) and -0.63 e.u.(X=D) when $T=1000$ K. In general, rearrangements, followed by molecular elimination, exhibit "tight" transition states and low(or even negative) ΔS^* values, while simple bond cleavages have "loose" transition states and high ΔS^* values.[14] For example, HCN eliminations from pyridine[15] and benzonitrile[16] cations are specified as $\Delta S^*=-2.5$ and 0.4 e.u, respectively. In recent RRKM calculations with reference to the reaction of the methyl nitrite ion to H_2COH^++NO, Baer and Hass[17] have synthesized very tight transition-state frequencies such as -5.6 e.u. Accordingly, the present model represents a reasonable tightness as structural isomerization. Actual RRKM calculations yielded $k(E_0)=3\times10^8$ s^{-1} for $CH_3NO_2^+$, and proved that the chief origin of the large isotope effect is not the $k(E_0)$ rate, but the tunneling probability. The activation energy for CD_2NO^+ was estimated by applying a zero-point energy correction.

Tunneling has been investigated for neutral unimolecular reactions by Miller and his co-workers[18,19] and for metastable-ion dissociations of methane,[20] methanol,[21] and phenol[22] cations. Tunneling through a potential barrier is generally favored for a case of one-step hydrogen-bond cleavage. For isomerization to the aci-nitromethane ion, the barrier heights, as estimated relative to the reactants and the products, are 0.63 and 1.58 eV respectively.[6,7] The $p(E)$ values in Table 3 were calculated with the imaginary frequencies described in Table 2, based on Miller modification[18] using a generalized Eckart potential. The imaginary frequencies used here are nearly equal to those[18] in the isomerization of *trans*-formaldehyde to H_2CO. $p(E)$ depends upon imaginary frequencies and, as may be seen in Table 3, decreases more rapidly for D species than for H with a decrease in the energy. At the energy of 0.35 eV below the threshold, which represents the experimental metastable rate of 10^5 s^{-1}, the ratio of tunneling probabilities is $p_H(E)/p_D(E)\approx30$;

Table 3. The Calculated Tunneling Probabilities

$(E-E_0)$/eV	X=H	X=D
0	5.3×10^{-1}	5.2×10^{-1}
−0.1	1.2×10^{-1}	5.4×10^{-2}
−0.2	1.3×10^{-2}	2.4×10^{-3}
−0.3	1.1×10^{-3}	7.3×10^{-5}
−0.4	6.5×10^{-5}	1.5×10^{-6}
−0.5	2.3×10^{-6}	1.5×10^{-8}

Table 2. Vibrational Frequencies for the Reaction of $CX_3NO_2^+\rightarrow CX_2NO^+$+ OX(X=H,D) as Used in RRKM Calculations

a) The reactant state										
X=H	3080	3080	2960	1650	1560	1480	1330	1060	1060	840
	660	520	380	370	200					
X=D	2300	2290	2140	1640	1440	1140	1060	830	830	780
	560	410	360	350	150					
b) The transition state										
X=H	3470	3080	2980	1720	1330	1130	1090	850	820	660
	520	430	370	190	2450*i*					
X=D	2600	2290	2150	1720	1310	960	870	750	600	590
	430	380	360	140	1770*i*					

thus, it leads to $k_H/k_D \approx 100$. This is in fair agreement with the experimental isotope effect.

Finally, tunneling correction explains the large isotope effect for the hydroxyl-radical loss, assuming that the reaction involves rate-determining isomerization to the *aci*-nitromethane ion prior to dissociation. It is not unusual that an OH or H_2O loss from oxygen containing ions shows intense metastable peaks in the mass spectra in spite of a small activation energy; examples include the H_2O loss from ionized ethyl acetate[23] and the CH_2OH loss from ionized methyl acetate.[24] The reactions involving hydrogen-atom migration generally indicates a complex mechanism in the isomerization/dissociation paths.

References

1) S. Meyerson and E. K. Fields, *Org. Mass Spectrom.*, **9**, 485 (1974).
2) Y. Niwa, S. Tajima, and T. Tsuchiya, *Int. J. Mass Spectrom. Ion Phys.*, **40**, 287 (1981).
3) J. P. Gilman, T. Hsieh, and G. G. Meisels, *J. Chem. Phys.*, **78**, 1174 (1983).
4) J. P. Gilman, T. Hsieh, and G. G. Meisels, *J. Chem. Phys.*, **78**, 3767 (1983); G. G. Meisels, T. Hsieh, and J. P. Gilman, *J. Chem. Phys.*, **73**, 4126 (1980).
5) I. K. Ogden, H. Shaw, C. J. Danby, and I. Powis, *Int. J. Mass Spectrom. Ion Phys.*, **54**, 41 (1983).
6) H. Egsgaard, L. Carlsen, and S. Elbel, *Ber. Bunsenges. Phys. Chem.*, **90**, 369 (1986).
7) C. Lifshitz, M. Rejwan, I. Levin, and T. Peres, *Int. J. Mass Spectrom. Ion Processes*, **84**, 271 (1988).
8) E. E. Ferguson, *Chem. Phys. Lett.*, **138**, 450 (1987).
9) H. Egsgaard and L. Carlsen, *Chem. Phys. Lett.*, **147**, 30 (1988).
10) M. P. Irion, A. Selinger, A. W. Castleman, Jr., E. E. Ferguson, and K. G. Weil, *Chem. Phys. Lett.*, **147**, 33 (1988).
11) J.-D. Shao, T. Baer, J. C. Morrow, and M. L. F.-Monterio, *J. Chem. Phys.*, **87**, 5242 (1987).
12) A. A. Herod and A. G. Harrison, *Int. J. Mass Spectrom. Ion Phys.*, **4**, 415 (1970).
13) A frequency program in BEVOBIV-IV was used for the frequency calculations. L. B. Sims, G. W. Burton, and D. F. Lewis, BEVOBIV-IV, Quantum Chemistry Program exchange No. 337 (1977); C. W. Burton, L. B. Sims, J. C. Wilson, and A. Fry, *J. Am. Chem. Soc.*, **99**, 3371 (1977).
14) P. J. Robinson and K. A. Holbrook, "Unimolecular Reactions," Wiley-Interscience, London (1972).
15) J. H. D. Eland, J. Berkowitz, H. Schulte, and R. Frey, *Int. J. Mass Spectrom. Ion Phys.*, **28**, 297 (1978).
16) H. M. Rosenstock, R. Stockbauer, and A. C. Parr, *J. Chim. Phys.*, **77**, 745 (1980).
17) T. Baer and J. R. Hass, *J. Phys. Chem.*, **90**, 451 (1986).
18) W. H. Miller, *J. Am. Chem. Soc.*, **101**, 6810 (1979).
19) Y. Osamura, H. F. Shaefer, S. K. Gray, and W. H. Miller, *J. Am. Chem. Soc.*, **103**, 1904 (1981).
20) A. J. Illies, M. F. Jarrold, and M. T. Bowers, *J. Am. Chem. Soc.*, **104**, 3587 (1982).
21) J. H. Beynon, A. E. Fontaine, and G. R. Lester, *Int. J. Mass Spectrom: Ion Phys.*, **1**, 1 (1968).
22) C. Lifshitz, S. Gefen, and R. Arakawa, *J. Phys. Chem.*, **88**, 4242 (1984).
23) R. Arakawa, *Bull. Chem. Soc. Jpn.*, **61**, 569 (1988).
24) N. Heinrich, J. Schmidt, H. Schwarz, and Y. Apeloig, *J. Am. Chem. Soc.*, **109**, 1317 (1987); R. Arakawa, *Bull. Chem. Soc. Jpn.*, **61**, 3425 (1988).

A Molecular Orbital Study of Cyclodextrin Inclusion Complexes. II. The Structural Analysis of α-Cyclodextrin Inclusion Complex with *m*-Nitrophenol in Aqueous Solution Based on the Quantum-Chemical Solvation Theory†,††

Minoru SAKURAI,* Masaki KITAGAWA, Hajime HOSHI,††† Yoshio INOUE, and Richirô CHÛJÔ
Department of Biomolecular Engineering, Tokyo Institute of Technology, O-okayama 2-chome, Meguro-ku, Tokyo 152
(Received December 22, 1988)

Synopsis. The host-guest orientation and the position of the guest *m*-nitrophenol (MNP) in the α-cyclodextrin(α-CD)-MNP complex in aqueous solution have been determined by comparing the complexation-induced ^{13}C NMR chemical shifts of MNP with those predicted by quantum chemical calculation. The results are consistent with the X-ray data of this complex.

α-Cyclodextrins (α-CDs) is a cyclic oligosaccharide composed of six (1—4)-linked α-D-glucosyl residues and admits a variety of guest molecules into its cavity.[1-4] The inclusion of benzene derivatives has been extensively studied in both solution and solid states.[1-4] One of the most interesting phenomena observed in such inclusion complexes is the orientational specificity of the guests in the α-CD cavity. For example, in α-CD-*p*-nitrophenol complex, in both solution[5-8] and solid states[9] the nitro group is located in the cavity and the phenolic hydroxyl group protrudes from the secondary hydroxyl side of α-CD. The determination of the guest orientation is essential for identifying the main driving force stabilizing the inclusion complexes.[10]

For α-CD-*m*-nitrophenol complex, two types of guest orientations have been proposed on the basis of the observation of complexation-induced ^{13}C NMR chemical shifts of the guest MNP. Namely, the first (Fig. 2C or D) is that the nitrophenyl group is located in the cavity and the hydroxyl group is exposed to the aqueous medium.[7] The second (Fig. 2A or B) is the reverse of the first one.[11] In this report, we show that the first is more reasonable, with the aid of the quantum chemical analysis of ^{13}C chemical shift displacements of MNP.

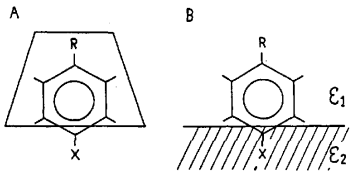

Fig. 1. (A) Schematic representation of α-CD inclusion complexes with benzene derivatives. The CD molecule is represented by bucket-like shape. (B) Double-layer model.

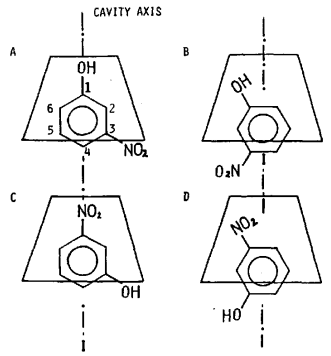

Fig. 2. Possible orientations of the guest MNP relative to the α-CD cavity. Due to the bulkiness of the substituents (NO_2 and OH), only two modes of guest-insertion are possible according to which sustituent is located in the cavity. Furthermore, each of the two is classified into two types of guest-orientations. In the type A and C orientations, the C_3-C_6 axis lies on the cavity one. In type B and D orientations, both the C_4-C_6 and the C_1-C_3 axes are parallel to the cavity axis.

Methods

In the calculation, the "double layer" model developed in a previous paper[12] is used in order to approximate the environment surrounding the guest molecule complexed with α-CD. Namely, it is assumed that a part of the guest molecule is embedded in a low dielectric medium (dielectric constant $\varepsilon_1=2$) and its residual part is exposed to the aqueous medium with higher dielectric constant ($\varepsilon_2=80$) as shown in Fig. 1B. Thus the complexation of the guest with α-CD in aqueous solution corresponds to its transfer from the aqueous medium ($\varepsilon=80$) to the double layer one. The interactions of the guest molecule with the dielectrics are formulated on the basis of Klopman's solvation theory.[13] The molecular wave functions were obtained by means of the CNDO/2 method[14] and subsequently the ^{13}C shielding constants are evaluated using Karplus and Pople's average excitation method.[15]

The geometry of MNP was determined using Pople's standard values for bond lengths and bond angles.[14]

Results and Discussion

According to the preliminary structural analysis using the CPK molecular model, four types of guest

† Previous paper in series is Ref. 10.

†† A part of this paper was presented at the 3rd International Symposium on Cyclodextrin, Lancaster, U. K., July, 1986, and the abstract was issued in *J. Inclusion Phenomena*, **5**, 55 (1987).

††† Present adress: Institute for Molecular Science, Myodaiji, Okazaki 444.

orientations are possible in the α-CD-MNP complex. They are schematically represented in Fig. 2. For each of these orientations, one can draw the borderline dividing the surrounding of the guest into the two layers and express the depth of guest inclusion as the number of atoms included in the layer of ε_1. A series of calculations of ^{13}C shielding was carried out by shifting the borderline. Then, the complexation-induced ^{13}C shift displacements are expressed as the shift changes when the guest MNP is transferred from the medium of ε=80 to the double-layer environments (ε_1=2, ε_2=80). The calculated results are reproduced in Figs. 3 and 4, where the positive and negative signs for ^{13}C displacements indicate low-field and up-field shifts, respectively and the scale in the abscissa indicates the number of the included atoms mentioned above. The observed data (bold lines) were cited from Ref. 7.

In the case of the type A and C orientations, our attention is particularly given to the carbons lying on the cavity axis: namely the C_1 and the C_4 carbons for the type A orientation and the C_3 and the C_6 carbons for the type C one. In the type B and D orientations, the data for only the C_1, C_3, C_4, and C_6 carbons are examined. These carbons are located far from the cavity interior and thus their ^{13}C shieldings are insusceptible to the so-called steric shielding effects,[12] which are not taken into account in the present theoretical model.

As can be seen from Fig. 3 a (for type A), the calculated values for the C_1 carbon deviate from the corresponding observed ones (bold lines) irrespective of the position of the borderline. Therefore it is impossible to reproduce the observed data for both C_1 and C_4 carbons simultaneously by the calculation. Similarly, in the case of the type B orientation (Fig. 3 b), the calculated values for the C_1 and the C_6 carbons always deviate from the corresponding observed data.

On the other hand, in the cases of the reversed-guest insertions with the type C orientation, the calculated values for both C_4 and C_6 carbons are in excellently good agreement with the corresponding observed ones at the position of 10—12 included-atoms (Fig. 4 a). Similarly, on the assumption of the type D orientation, the calculations simultaneously reproduce the observed trends for the C_1, C_3, C_4, and C_6 carbons at the position of 10 included-atoms, although the agreements of the magnitudes of ^{13}C displacements are not always good.

Therefore, for the α-CD-MNP inclusion complex, the observed characteristic ^{13}C displacements are reproduced only when the guest molecule is inserted into the cavity from the nitro group side (Fig. 2C and D). This orientation of the guest molecule is the same as that found in the solid state by X-ray diffraction for the α-CD-MNP complex.[16] Furthermore, it should be noted that the observed trends are reproduced only at the position of the borderline as shown in Fig. 5. If it is assumed that the borderline corresponds to the α-CD wider rim consisting of secondary hydroxyl groups, one or two carbons in the phenyl ring must protrude from the CD cavity. This finding again agrees with that in the solid state.

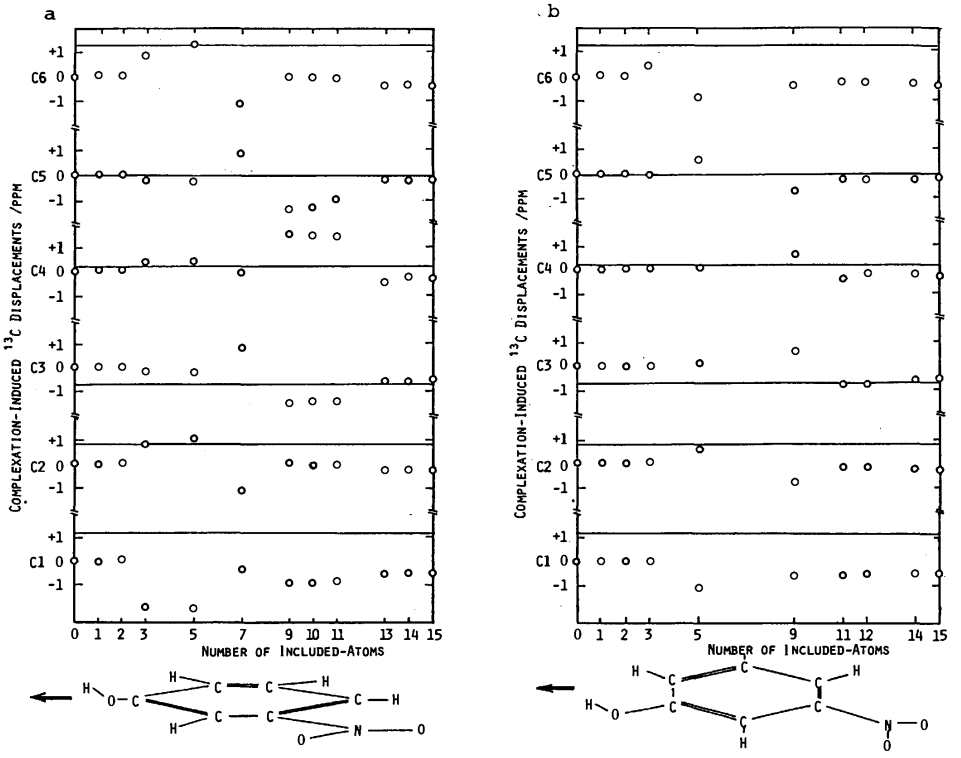

Fig. 3. Dependence of ^{13}C shift displacements of MNP on the position of the borderline. (a) and (b) show the data for the type A and B orientations shown in Fig. 2, respectively. The arrows indicate the direction of guest-insertion.

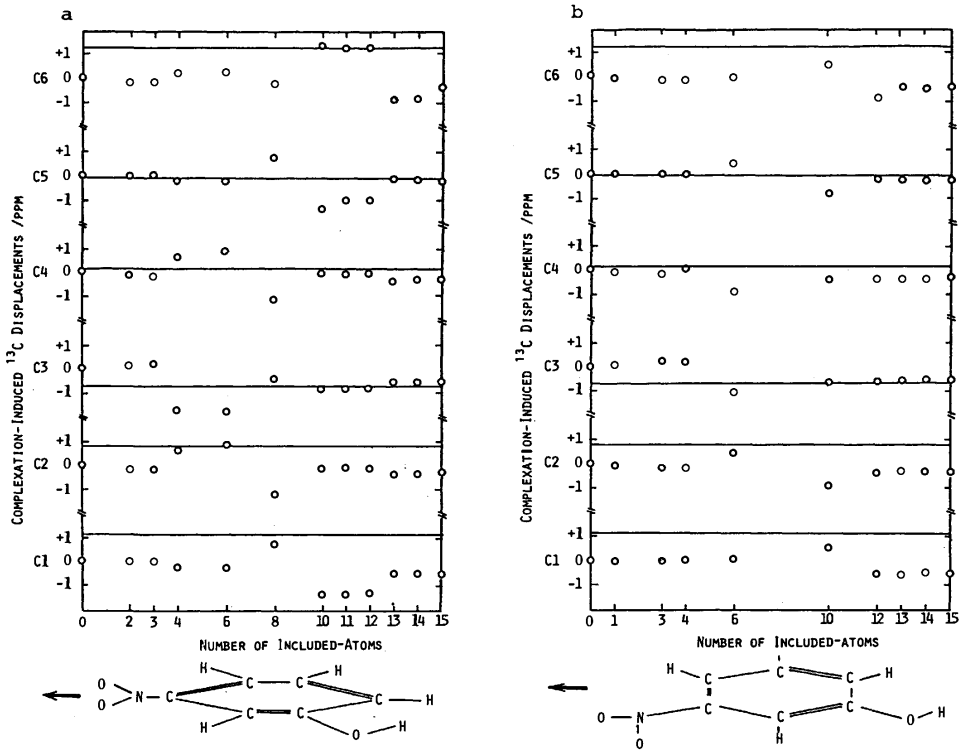

Fig. 4. Dependence of ^{13}C shift displacements of MNP on the position of the borderline. (a) and (b) show the data for the type C and D orientations, respectively.

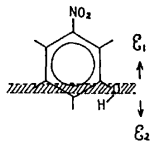

Fig. 5. The position of the borderline (shaded region) where the characteristic ^{13}C displacements are reproduced well by the calculations.

These results are inconsistent with those of Komiyama and Hirai's report.[11] They did not observe the ^{13}C displacements of the tertiary carbons, C_1 and C_3. As described above, these carbons provide decisive information about the orientation of the guest molecule, and thus the lack of these data may be responsible for the discrepancy.

In conclusion, the structure of α-CD-MNP complex in aqueous solution is consistent with that in the solid state.

One (Y. I.) of the authors wishes to thank for the partial support by a Grant-in-Aid for Scientific Research on Priority Area of "Dynamic Interactions and Electronic Processes of Macromolecular Complexes" from the Ministry of Education, Science and Culturee. The authors thank the Computer Center, Institute for Molecular Science, Okazaki National Research Institute, Japan, for the use of the HITAC M-680H and S-810/10 computer system.

References

1) M. I. Bender and M. Komiyama, "Cyclodextrin Chemistry," Springer-Verlag, New York (1978).
2) W. Saenger, *Angew. Chem., Int. Ed. Engl.*, **19**, 344 (1980).
3) I. Tabushi and Y. Kuroda, *Adv. Catal.*, **32**, 417 (1983).
4) Y. Matsui, T. Nishioka, and T. Fujita, *Top. Curr. Chem.*, **128**, 61 (1985).
5) R. J. Bergeron, M. A. Channing, B. Gibeily, and D. M. Pillor, *J. Am. Chem. Soc.*, **99**, 5146 (1977).
6) R. J. Bergeron, M. A. Channing, and K. A. McGovern, *J. Am. Chem. Soc.*, **100**, 2878 (1978)
7) R. I. Gelb, L. M. Schwartz, B. Cardelino, H. S. Fuhrman, R. F. Johnson, and D. A. Laufer, *J. Am. Chem. Soc.*, **103**, 1750 (1981).
8) Y. Yamamoto, M. Onda, M. Kitagawa, Y. Inoue, and R. Chûjô, *Carbohydr. Res.*, **167**, c11 (1987).
9) K. Harata, *Bull. Chem. Soc. Jpn.*, **50**, 1416 (1977).
10) M. Kitagawa, H. Hoshi, M. Sakurai, Y. Inoue, and R. Chûjô, *Bull. Chem. Soc. Jpn.*, **61**, 4225 (1988).
11) M. Komiyama and H. Hirai, *Bull. Chem. Soc. Jpn.*, **54**, 828(1981).
12) Y. Inoue, H. Hoshi, M. Sakurai, and R. Chûjô, *J. Am. Chem. Soc.*, **107**, 2319 (1985).
13) G. Klopman, *Chem. Phys. Lett.*, **1**, 200 (1967).
14) J. A. Pople and D. L. Beveridge, "Approximate Molecular Orbital Theory," McGraw-Hill, New York (1970).
15) M. Karplus and J. A. Pople, *J. Chem. Phys.*, **38**, 2803 (1963).
16) K. Harata, H. Uedaira, and J. Tanaka, *Bull. Chem. Soc. Jpn.*, **51**, 1627 (1978).

Aldol Addition of Butyraldehyde over Solid Base Catalysts

Geng ZHANG, Hideshi HATTORI,* and Kozo TANABE
Department of Chemistry, Faculty of Science, Hokkaido University, Sapporo 060
(Received January 20, 1989)

Synopsis. Aldol addition of butyraldehyde was investigated on alkaline earth oxides, zirconium oxide, and lanthanum oxide to compare the active site and mechanism with those for aldol addition of acetone. It is found that the active site is the surface O^{2-} and the rate-determining step is α-H abstraction.

Aldol type reaction of butyraldehyde as shown below is one of the most important reactions in organic chemistry and has been extensively studied for fundamental understanding.

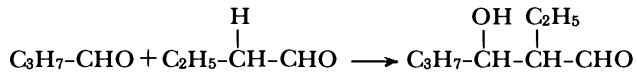

Many investigations for industrial application of catalysts to aldol addition of ketones and aldehydes were made. Although practical catalysts developed in industry are mostly heterogeneous, the fundamental studies are made primarily in homogeneous system. Recently, we studied aldol addition of acetone over several kinds of solid base catalysts, and found that the active sites for this reaction are surface basic OH groups, and that the rate-determining step is the formation of a new C-C bond between two acetone molecules rather than the abstraction of an α-H^+ ion from acetone.[1-3]

In this work, we studied aldol addition of butyraldehyde over solid base catalysts, and found that the active sites and the rate-determining step for butyraldehyde are different from those for acetone.

Experimental

Catalyst Preparation: Magnesium oxide was prepared from commercial MgO(Merck) as follows. The commercial MgO powder was added into distilled water and stirred at room temperature for 24 h followed by being dried in an oven at 100 °C for 24 h to form hydroxide. Starting material for CaO was $Ca(OH)_2$. Calcium hydroxide was also treated in distilled water in the same way as MgO. The hydroxides of magnesium and calcium were heated at various temperatures in a vacuum to form the oxides before use. Zirconium oxide and La_2O_3 were prepared from aqueous solutions of $ZrOCl_2$ and $La(NO_3)_3$, respectively, by hydrolysis with aqueous ammonia. Strontium oxide was obtained by evacuating $SrCO_3$ at high temperatures.

Reaction Procedures: Reaction was carried out in a H-type batch reactor at 0 °C as described in a previous paper.[1] The two branches were separated by a breakable seal. The catalyst sample was able to be treated in one side and the reactant in another side. One gram of reactant and 50 mg of catalyst were used as a standard procedure. Reactant was admitted to the side of catalyst by breaking the breakable seal and transferring reactant to catalyst side by cooling this side to liquid nitrogen temperature. Reaction was started by rapid melting of the reactant at reaction temperature of 0 °C. In some poisoning experiments, poison was admitted into the reactor before reaction. Products were analyzed by GLC.

Results

The main products were a dimer (namely 2-ethyl-3-hydroxyhexanal) and a trimer. The formation of the trimer was confirmed by field-ionization mass spectrometry, although its exact structure was not clear. Besides dimer and trimer, 2-ethyl-2-hexenal formed by dehydration of dimer was obtained less than 3% of the total products. The activities of several kinds of catalysts for aldol addition of butyraldehyde are summarized in Table 1. Zirconium oxide and La_2O_3 had low activities, while MgO, CaO, and SrO showed high activities. As the specific surface areas were in the order of MgO > CaO ≫ SrO (about a ratio 25 : 10 : 1,[1]) the order for the activities upon unit surface area basis is SrO > CaO > MgO ≫ La_2O_3 > ZrO_2. The activities of La_2O_3 and ZrO_2 for aldol addition of acetone were comparable to that of MgO. Considering the strength of basic site being the order MgO > La_2O_3 > ZrO_2, the activity dependency on the basic strength is higher for butyraldehyde than for acetone.

Relation between the ratio of dimer to trimer and conversion was examined with MgO and CaO by changing the reaction time although the results are not presented. The ratio with MgO declined slightly from 7.1 to 5.0 over the range of conversion from 7.8 to 84.4, while the ratio with CaO kept near an unchanged value of ca. 0.7 over a similar range of conversion as that with MgO. Variations of activity and selectivity with pretreatment temperature of MgO are shown in Fig. 1. Maximum of conversion ap-

Table 1. Activities of Various Catalysts for Aldol Addition of Butyraldehyde

Cat.	Pretreatment temp./°C	Reaction time/h	Conversion /%	Selectivity to 2EHA[a]/%	Dimer/Trimer
ZrO_2	600	2	0.9	—	—
La_2O_3	600	1	3.2	—	1.3
MgO	600	1	35.0	1.7	5.0
CaO	600	1	41.1	2.8	0.7
SrO	800	1	41.7	1.3	2.2

a) 2EHA: 2-ethyl-2-hexenal.

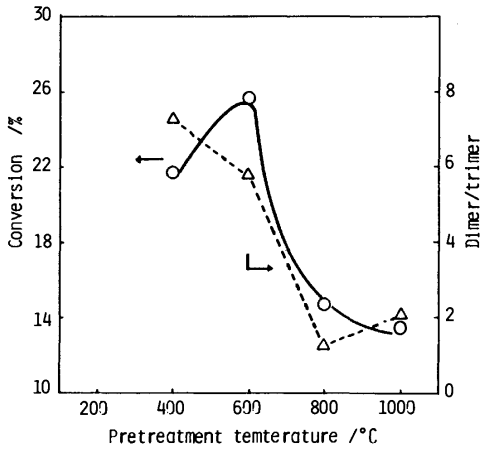

Fig. 1. Pretreatment temperature dependences of activity for aldol addition of butyraldehyde and of ratio of dimer to trimer in the reaction over MgO.

peared around the pretreatment temperature of 600 °C. The ratio of dimer to trimer decreased monotonously as the pretreatment temperature increased.

The results of poisoning experiments with MgO are summarized in Table 2. Ammonia did not poison the active sites, whereas pyridine, carbon dioxide, and water poisoned to considerable extents. Poisoning effect of water in aldol addition of butyraldehyde is in contrast to a marked promoting effect of water in aldol addition of acetone. The ratio of dimer to trimer was increased by water addition. Addition of acetone to butyraldehyde did not affect the reaction of butyraldehyde at all. Neither aldol addition of acetone nor cross aldol addition between butyraldehyde and acetone occurred.

Discussion

A good correspondence of the order of the activity for aldol addition of butyraldehyde to the basic strength of catalyst indicates that the reaction proceeds on the basic sites. Since the activity dependency on the surface basic property is stronger for butyraldehyde than that for acetone, some differences between the constitutions of active sites for aldol addition of acetone and aldehyde are suggested. Two kinds of basic sites, basic OH groups and the surface

Table 2. Preadsorption Effect of Various Additives on Aldol Addition of Butyraldehyde over MgO

Additives[a]	Conversion[b] /%	2-Ethyl-2-hexenal	Ratio of dimer to trimer
None	23.5	0.4	6.6
Pyridine	17.4	0.2	6.9
NH_3	24.5	0.4	6.6
CO_2	15.1	0.2	6.0
H_2O[c]	14.7	0.3	7.4
H_2O[d]	4.4	0.3	13.3

a) All molecules adsorbed at room temperature. b) Reaction time: 0.5 hour. c) Amount of H_2O adsorbed was 2.4 mmol/g-cat. d) Amount of H_2O adsorbed was 4.8 mmol/g-cat.

Table 3. Relative Activity with Poison or Promoting Molecules in the Aldol Additions of Butyraldehyde and Acetone

Reactant	Added molecule				
	Ammonia	Pyridine	Water	Carbon dioxide	None
Butyraldehyde	1.04	0.74	0.63	0.64	1.00
Acetone	1.38	1.15	1.69	0.86	1.00

O^{2-}, exist on the surface of solid base catalysts. The results of poisoning experiments in aldol additions of butyraldehyde and acetone suggest the relevant sites for each reaction. The poisoning and promoting effects on the aldol additions of butyraldehyde and acetone are compared in Table 3. Marked difference is observed for the effect of water; considerable promoting effect was observed for acetone while poisoning effect for butyraldehyde. If only surface O^{2-} ions were active sites, water and carbon dioxide would have completely poisoned the active sites. Complete poisoning effect with water and carbon dioxide were observed for many other base-catalyzed reactions such as double bond migration of olefin, hydrogenation of 1,3-butadiene, etc.[4] This is, however, not the observed result for aldol addition of butyraldehyde. The percentage of the activity remaining on addition of water and carbon dioxide is considered to be due to surface OH groups. No promotion effect observed on addition of water is explained by the higher efficiency for the surface O^{2-} ions than for the surface OH groups which may be weaker base than the surface O^{2-}. For aldol addition of acetone, the active sites are the surface OH groups.

Differences in the activity dependency on basic strength and the efficiency of surface O^{2-} and OH groups between aldol addition of butyraldehyde and acetone are considered to be caused by the difference in rate-determining steps for these reactions. Since the aldehyde is stronger acid than ketone, and the surface OH groups can abstract α-H from acetone, it is plausible that the basic strength of the surface OH groups is sufficient to abstract α-H from both butyraldehyde and acetone. The steric hindrance in the C-C bond formation is thought to be larger for acetone than butyraldehyde as shown below.

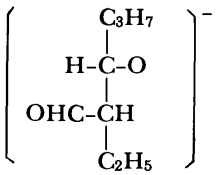

a) Intermediate for butyraldehyde.

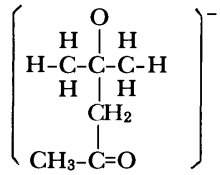

b) Intermediate for acetone.

The rate of C-C bond formation between two butyraldehyde molecules is fast as compared to an α-H abstraction, while the C-C bond formation is slower than an α-H abstraction for acetone. Therefore, the rate-determining step is suggested to be an α-H abstraction for butyraldehyde in contrast to C-C bond formation for acetone. The base strength is directly

associated with the slow step for butyraldehyde, which causes strong dependency of the activity on the basic strength.

It should be noted that the variation of ratio of dimer to trimer with conversion is very small. Nearly constant values of the ratio indicate that the dimer converts to trimer very slowly. Increase of ratio of dimer to trimer owing to the addition of water as shown in Table 2 is ascribed to the conversion of the surface O^{2-} of strong basic sites into the OH groups of weak basic sites. These results indicate that a stronger basic site facilitates the formation of trimer without desorption of dimer. The fact that the ratio of dimer to trimer obtained with MgO is higher than those for CaO and SrO coincides with the result, although a slightly opposite tendency is observed as comparing CaO with SrO.

References

1) G. Zhang, H. Hattori, and K. Tanabe, *Appl. Catal.*, **36**, 189 (1988).
2) G. Zhang, H. Hattori, and K. Tanabe, *Appl. Catal.*, **40**, 183 (1988).
3) H. Hattori, K. Kumai, K. Tanaka, G. Zhang, and K. Tanabe, Proc. National Symp. Catal. India, **1987**, Sindri., p. 243.
4) H. Hattori, *Materials of Chemistry and Physics*, **18**, 533 (1988).

Effects of Pressure on Hydrolysis of *p*-Nitrophenyl Acetate in Aerosol OT Reversed Micelles

Katsuhiro TAMURA* and Mami YOSHINARI
Department of Chemical Science and Technology, Faculty of Engineering,
The University of Tokushima, Minamijosanjima-cho, Tokushima 770.
(Received January 25, 1989)

Synopsis. Kinetic studies were made on imidazole-catalyzed hydrolysis of *p*-nitrophenyl acetate in Aerosol OT (AOT) reversed micelles (AOT/H_2O/heptane) at high pressure. The rate of the reaction was found to increase with increase in the size of the aqueous core in the reversed micelles and with increase in pressure. Micellar effects on the hydrolysis are discussed in relation with the activation parameters of the reaction.

The hydrolyses of carboxylic acid esters in micelles have often been used as examples of chemical reactions in micellar systems that are similar to enzyme reactions. Studies on micelle catalysts are important because many hydrolyses catalyzed by nucleophiles or enzymes occur in biosystems. Aerosol OT forms stable reversed micelles that can contain large amounts of water as an aqueous core, and these reversed micelles are of biochemical interest because their molecular assembly is similar to that of water pockets in bioaggregates (biomembranes, mitochondria,[1] etc.).

We have studied the effects of pressure on some chemical reactions in micellar systems.[2-6] In the present paper we report the effects of pressure on the hydrolysis of *p*-nitrophenyl acetate in AOT reversed micelles. Micellar effects on the hydrolysis are discussed in relation with activation parameters of the reaction.

Experimental

Sodium salt of bis(2-ethylhexyl) sulfosuccinate (Aerosol OT, AOT) was obtained from Tokyo Kasei. It was dissolved in methanol and filtered, and then the solvent was removed under vacuum. *p*-Nitrophenyl acetate (Tokyo Kasei) was recrystallized twice from ethanol. Imidazole (Wako) was used without further purification.

A high-pressure vessel with quartz optical windows was used to follow the reaction at high pressure directly. Sample solutions were charged into a sliding cell (inner quartz cell) to prevent contamination of the solution by the metal body and packing of the vessel. The high-pressure vessel was set in a Hitachi 100-60 UV-visible spectrophotometer and the reaction product, *p*-nitrophenol, was determined by measuring its absorbance at 400 nm. Pressures were generated by a hand-operated hydraulic pump (Hikari KP-5B) and measured with a Heise Bourdon gauge.

The reaction solution was prepared by mixing 3 wt% AOT in heptane with aqueous 5.0×10^{-2} mol dm^{-3} imidazole solution in various ratios. *p*-Nitrophenyl acetate (8.0×10^{-5} g) was added to 4 cm^3 samples of the AOT/H_2O/imidazole/heptane solutions and the mixtures were stirred for 10 min. Reaction rates in water were used as standards in evaluating micellar effects.

Results and Discussion

Pseudo-first-order rate constants (k) were deter-

Table 1. Effects of Pressure and Temperature on the Pseudo-First-Order Rate Constants of the Hydrolysis of *p*-Nitrophenyl Acetate in Aerosol-OT Reversed Micelles[a] and Water[b]

R=[H_2O]/[AOT]	$k/10^{-4}$ s^{-1}								
	P/MPa=0.1	10	20	30	60	70	80	90	100
				T/K=288.15					
5.0	0			0	0				0
12.1	1.14		1.22		1.41				1.76
23.4	1.54			1.72	2.07				2.55
aq. soln[b]	1.52			1.84	2.26				3.03
				T/K=298.15					
1.1	0			0	0				0
5.8	0			0	0				0
11.2	1.50			1.54	1.62	2.09	2.71	2.89	2.87
12.9	2.26			2.46	2.67				3.48
23.7	2.59			3.01	3.12				4.03
35.2	2.92			3.36	4.05				5.17
38.7	2.97			3.53	4.18				5.51
39.9	2.90			3.48	4.16				5.53
aq. soln[b]	3.48			3.99	4.66				5.55
				T/K=308.15					
5.0	0			0	0				0
12.2	1.95	1.88	2.06	2.31	3.24				3.32
24.6	2.79			3.20	3.60				4.29
34.4	3.52			4.32	5.63		6.29		
aq. soln[b]	5.74			7.29	8.44				

a) [Imidazole]=5.0×10^{-2} mol dm^{-3} (AOT systems). b) [Imidazole]=5.0×10^{-4} mol dm^{-3} (aq. soln).

mined by the Guggenheim method[7] and are presented in Table 1. Water contents are shown as molar ratios of water to AOT (R=[H_2O]/[AOT]). The hydrolysis of p-nitrophenyl acetate was strongly dependent on the properties of the reaction fields and pressure. For example, the reaction did not occur when the water content was less than 6 ($R<6$). This is because at $R<6$ almost all the water molecules in the reversed micelles are strongly bound to the polar heads of AOT or to sodium ions (counter ions),[8-10] and so hydrolysis does not readily occur. At $R>10$, there is a free water phase and the hydrolysis occurs. Thus we can conclude that the hydrolysis of p-nitrophenyl acetate proceeds only in the presence of free water. The size of the aqueous core also affected the reaction rate: the rate increased with increase in the size of the water pool. Over a range of water contents of $10<R<30$, the rate of p-nitrophenyl acetate hydrolysis was an almost linear function of R ([H_2O]/[AOT]) at both atmospheric and high pressures.

Pressure also promoted the hydrolysis of p-nitrophenyl acetate in AOT reversed micelles. In general, acid- and base-catalyzed hydrolyses of esters are promoted by pressure, because partial electric charges or bonds are formed during the reactions. Apparent activation volumes ($\Delta V^{\neq}_{ap}$) were calculated by the equation:

$$(\partial \ln k/\partial P)_T = -\Delta V^{\neq}_{ap}/RT$$

where R, T, and P are the gas constant, the absolute temperature and the pressure, respectively. The apparent activation volumes of the hydrolysis of p-nitrophenyl acetate are shown in Table 2. These volumes depend greatly on the nature of the reaction field. The large and irregular variations of the values from -3.2 (R=11.2) to -16.0 $cm^3 mol^{-1}$ (R=39.9) suggest that not only the nature of the water pool, but also micellar size are closely related to the effects of pressure on the reaction rate. In particular, the $\Delta V^{\neq}_{ap}$ is found to decrease rapidly at $R\approx30$. Fluorescence polarization studies of AOT reversed micelles at high pressures[11] showed that the micelles aggregated and formed polydisperse syslems at $R\approx30$ and that these changes of micellar size were greatly enhanced by pressure. This aggregation of the micelles can be considered as one reason for the increase in reaction rates with increase in pressure at $R\geqq30$. The activation volume in the aqueous solution (-11.8 cm^3 mol^{-1}) coincided exactly with that at this water content $R\approx30$ (Fig. 1).

Table 2. Apparent Activation Volumes of the Hydrolysis of p-Nitrophenyl Acetate in AOT Reversed Micelles[a] and Water[b] at Atmospheric Pressure and 298.15 K

R=[H_2O]/[AOT]	$\Delta V^{\neq}_{ap}$/$cm^3 mol^{-1}$
11.2	−3.2
12.9	−6.4
23.7	−10.4
35.2	−14.4
38.7	−15.2
39.9	−16.0
aq. soln[b]	−11.8

a) [Imidazole]=5.0×10^{-2} mol dm^{-3} (AOT systems).
b) [Imidazole]=5.0×10^{-4} mol dm^{-3} (aq. soln).

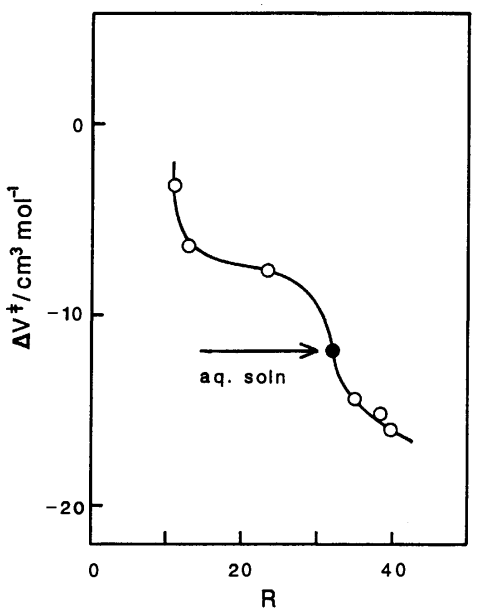

Fig. 1. Activation volumes for the hydrolysis of p-nitrophenyl acetate in AOT reversed micellar systems and aqueous solution at atmospheric pressure and 298.15 K. R=[H_2O]/[AOT].

The base-catalyzed hydrolyses of esters in water usually have activation volumes in the range of -5 to -10 $cm^3 mol^{-1}$.[12] These values are explained as follows. The coordination of OH^- ions to esters should be associated with volume reduction due to formation of new chemical bonds, although loss of electrostriction by dispersion of electric charges may result in some increase in volume. In imidazole-calalyzed hydrolysis of p-nitrophenyl acetate in AOT reversed micelles, the imidazole molecule presumably acts as a nucleophile rather than a general base as in aqueous solutions.[13]

As imidazole is insoluble in dry AOT/heptane solutions, it must be present exclusively in the water pool of AOT/H_2O/heptane reversed micelles. When p-nitrophenyl acetate is added to the AOT/H_2O/imidazole/heptane system, hydrolysis of the ester occurs in the water pool. Therefore, the partition of the ester between the heptane phase and the water phase across the surfactant boundary becomes important.[14] Accordingly, when determining reaction rates at high pressure the effect of pressure on partition coefficients should be considered. The volume change ΔV for the transfer of p-nitrophenyl acetate from the heptane to water phase can be expressed as

$$-RT(\partial \ln K/\partial P)_T = \Delta V = V_W - V_H$$
$$K = x_W/x_H$$

where K is the partition coefficient, V_W and V_H are the partial molar volumes of p-nitrophenyl acetate in the water and heptane phases, and x_W and x_H are the mole fractions in these systems. In general, esters have smaller partial molar volumes in water than in alkanes ($\Delta V<0$). This means that pressure increases

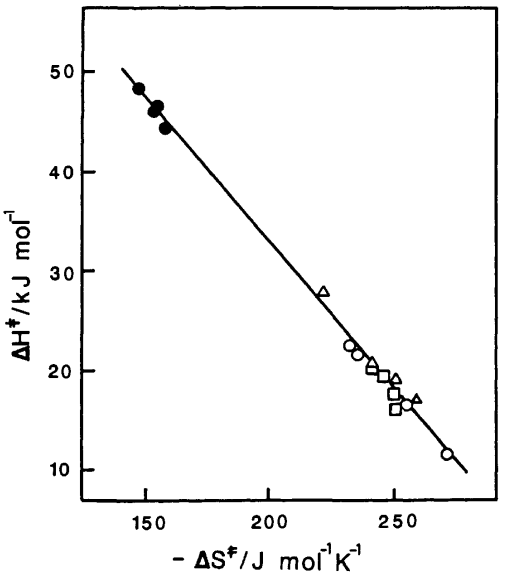

Fig. 2. Linear relationship between activation enthalpies and entropies for the hydrolysis of *p*-nitrophenyl acetate in AOT reversed micellar systems and aqueous solution at atmospheric pressure and 298.15 K.
Water contents (R): △: 12, □: 24, ○: 35, ●: aq. soln.

the partition coefficient and promotes the hydrolysis. This is another reason for acceleration of the reaction by increase in pressure. This effect is more pronounced at higher water contents ($R > 30$).

Figure 2 shows the relationship between the activation enthalpies and entropies of the hydrolysis of *p*-nitrophenyl acetate at 298.15 K. Good compensation effects between the enthalpies and the entropies are observed in the water and AOT systems. Although the activation enthalpies and entropies for the aqueous solution have much larger values than those for AOT systems, the linear relationship is very good.

References

1) B. Chance, *Proc. Natl. Acad. Sci., U.S.A.*, **67**, 560 (1970).
2) K. Tamura and M. Suminaka. *J. Chem. Soc., Faraday Trans. 1*, **81**, 2287 (1985).
3) K. Tamura and M. Aida, *J. Chem. Soc., Faraday Trans. 1*, **82**, 1619 (1986).
4) K. Tamura and M. Yoshinari, *Chem. Express*, **3**, 603 (1988).
5) K. Tamura, M. Abe, and M. Terai, *J. Chem. Soc., Faraday Trans. 1*, in press.
6) K. Tamura and S. Miyoshi, *Chem. Express*, **4**, 5 (1989).
7) A. A. Frost and P. G. Pearson, "Kinetics and Mechanisms," Wiley, New York (1961), p. 49.
8) Z. E. Zinsli, *J. Phys. Chem.*, **83**, 3223 (1973).
9) H. Kondo, I. Miwa, and J. Sunamoto, *J. Phys. Chem.*, **86**, 4826 (1982).
10) A. D'Aprano, A. Lizzio, V. T. Liveri, F. Aliotta, C. Vasi, and P. Migliardo, *J. Phys. Chem.*, **92**, 4436 (1988).
11) K. Tamura and N. Nii, *J. Phys. Chem.*, in press.
12) N. S. Issacs, "Liquid Phase High Pressure Chemistry," Wiley, New York (1981), pp. 278, 314.
13) T. C. Bruice and S. J. Benkovic, *J. Am. Chem. Soc.*, **86**, 418 (1964).
14) F. M. Menger, J. A. Donohue, and R. F. Williams, *J. Am. Chem. Soc.*, **95**, 286 (1973).

Optical Resolution of Di-2-pyridylamine Complexes of Ruthenium(II)

Takashi FUKUCHI, Noriharu NAGAO, Eiichi MIKI, Kunihiko MIZUMACHI,* and Tatsujiro ISHIMORI
Department of Chemistry, College of Science, Rikkyo University, Nishi-ikebukuro, Toshima-ku, Tokyo 171
(Received October 12, 1988)

Synopsis. Through SP-Sephadex ion exchange chromatography $[Ru(Hdpa)_3]^{2+}$ and $[Ru(bpy)_2(Hdpa)]^{2+}$ (Hdpa= di-2-pyridylamine) were resolved by the use of an aqueous sodium *d*-tartrate solution as the eluting agent. *Λ*-$[Ru(Hdpa)_3]^{2+}$ and *Λ*-$[Ru(bpy)_2(Hdpa)]^{2+}$ were eluted in the early fractions. The precipitation of diastereomers with dibenzoyl-*d*-tartrate was also successful in the resolution of $[Ru(Hdpa)_3]^{2+}$ and $[Ru(bpy)(Hdpa)_2]^{2+}$. The absolute configurations of the complexes were assigned by referring to the signs of CD spectra at around 3.2—3.8 μm^{-1}.

Synthetic and spectrochemical studies on a series of complexes $[Ru(bpy)_n(Hdpa)_{3-n}]^{2+}$ (bpy=2,2′-bipyridine, Hdpa=di-2-pyridylamine, n=0—2) have been reported by DeArmond et al.[1,2] The present work describes the resolution of the complexes through SP-Sephadex cation-exchange chromatography and the precipitation of diastereomers with sodium (*R,R*)-dibenzoyltartrate (Na_2dbt). Although $[Ru(bpy)_3]^{2+}$ and $[Ru(phen)_3]^{2+}$ can be resolved through the precipitation of diastereomers with sodium bis(*d*-tartrato)diantimonate ($Na_2Sb_2(tart)_2$),[3,4] this resolving agent failed to give precipitate with the above Hdpa-containing complexes.

Experimental

Preparation of $[Ru(bpy)(Hdpa)_2](ClO_4)_2$. A dilute hydrochloric acid solution (100 cm^3) of $RuCl_3 \cdot 3H_2O$ (Koso Chemicals, 1 g) and Hdpa (Aldrich, 200 mg) was refluxed for 8 h, and filtered. The filtrate was concentrated to about 20 cm^3 while precipitating a green product. This contained *cis*-$[RuCl_2(Hdpa)_2]Cl \cdot H_2O$, the X-ray structural study of which will be reported in a separate paper. The green product was suspended in 200 cm^3 of water with bpy (90 mg) and Hdpa (50 mg), and refluxed for 3 h in the presence of sodium phosphinate (2 g). Upon the addition of $NaClO_4$ to the reaction mixture a brown precipitate was formed. For purification it was charged on the top of an SP-Sephadex column (Na^+ form) and eluted with a 0.3 mol dm^{-3} NaCl solution. Fractions of a brown eluate were collected from which $[Ru(bpy)(Hdpa)_2](ClO_4)_2$ was precipitated. The product was washed with an aqueous solution of 0.1 mol dm^{-3} $NaClO_4$, ethanol/2-methyl-2-propanol (1 : 1 v/v), and ether, successively, and dried at 60 °C. Yield 20% (Found: C, 44.98; H, 3.23; N, 13.98%). Other members of the series $[Ru(bpy)_n(Hdpa)_{3-n}]^{2+}$ which were formed as by-products were separated off by chromatography; complexes with higher n values were eluted faster.

$[Ru(Hdpa)_3](ClO_4)_2$[1] and $[Ru(bpy)_2(Hdpa)](ClO_4)_2$[2] were prepared by methods similar to those reported by DeArmond et al., except that both complexes were purified through the chromatography described above.

Optical Resolution. a) Cation-Exchange Chromatography. $[Ru(Hdpa)_3]^{2+}$ was charged on the top of an SP-Sephadex column (ϕ 6 cm×60 cm), and eluted with 0.15 mol dm^{-3} sodium *d*-tartrate (Na_2*d*-tart) solution. Since one elution gave only partial resolution, the earlier and later fractions were collected separately, and again charged on the column. This procedure was repeated three times. From the early fractions $(+)_{\Delta\varepsilon}$-$[Ru(Hdpa)_3](ClO_4)_2$[5] was isolated. Peaks of CD: $\Delta\varepsilon_{410}$=−36.6, $\Delta\varepsilon_{314}$=207, and $\Delta\varepsilon_{283}$=−177 (cm mol $dm^{-3})^{-1}$.

$[Ru(bpy)_2(Hdpa)]^{2+}$ was also resolved almost in the same way as the above. After elutions were repeated three times $(-)_{\Delta\varepsilon}$-$[Ru(bpy)_2(Hdpa)](ClO_4)_2$ was isolated from the early fractions. Peaks of CD: $\Delta\varepsilon_{355}$=6.83, $\Delta\varepsilon_{292}$=−185, and $\Delta\varepsilon_{275}$=119 (cm mol $dm^{-3})^{-1}$. For $[Ru(bpy)(Hdpa)_2]^{2+}$ the chromatography gave only poor resolution.

b) Precipitation of the Diastereomers with Na_2dbt. Four hundred milligrams of $[Ru(Hdpa)_3](ClO_4)_2$ was converted to the chloride through anion exchange. To a 100 cm^3 chloride solution was added 100 mg of Na_2dbt. The solution was allowed to stand at room temperature for 3—4 days during which $(-)_{\Delta\varepsilon}$-$[Ru(Hdpa)_3](dbt)$ was precipitated. The diastereomer was recrystallized from water. Yield: 130 mg. This was converted to the perchlorate, $(-)_{\Delta\varepsilon}$-$[Ru(Hdpa)_3](ClO_4)_2$. CD: $\Delta\varepsilon_{410}$=36.6 (cm mol $dm^{-3})^{-1}$.

A similar procedure was applied to the resolution of $[Ru(bpy)(Hdpa)_2]^{2+}$. From 400 mg of racemic perchlorate 70 mg of the diastereomer, $(+)_{\Delta\varepsilon}$-$[Ru(bpy)(Hdpa)_2](dbt)$ was obtained. CD peaks of $(+)_{\Delta\varepsilon}$-$[Ru(bpy)(Hdpa)_2](ClO_4)_2$: $\Delta\varepsilon_{408}$=−13.7, $\Delta\varepsilon_{296}$=158, and $\Delta\varepsilon_{279}$=−133 (cm mol $dm^{-3})^{-1}$.

$[Ru(bpy)_2(Hdpa)]^{2+}$ gave no precipitate on addition of Na_2dbt.

Measurements. Electronic spectra were recorded on a Hitachi 340 Spectrophotometer, and CD spectra were on a JASCO J-500A Spectropolarimeter. The solvent was water throughout the measurements.

Results and Discussion

The electronic and CD spectra are shown in Figs. 1 and 2, respectively. The two strong bands at around 3.2—3.8 μm^{-1}, which are common to the four complexes, correspond to the intraligand π-π^* transitions in coordinated pyridine groups. The CD bands

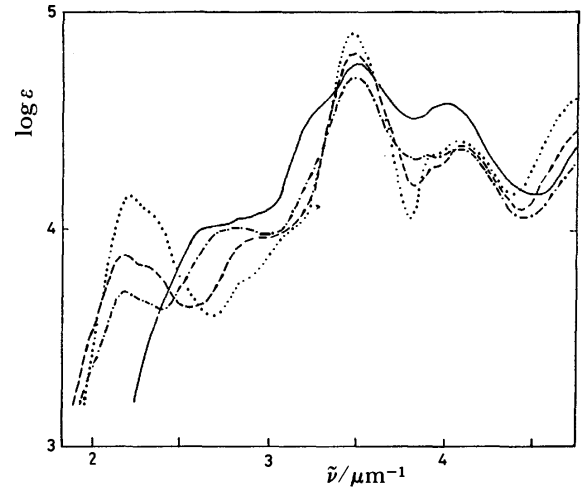

Fig. 1. Electronic spectra of $[Ru(bpy)_n(Hdpa)_{3-n}]^{2+}$. —— $[Ru(Hdpa)_3]^{2+}$;-·-· $[Ru(bpy)(Hdpa)_2]^{2+}$;--- $[Ru(bpy)_2(Hdpa)]^{2+}$; ····· $[Ru(bpy)_3]^{2+}$.

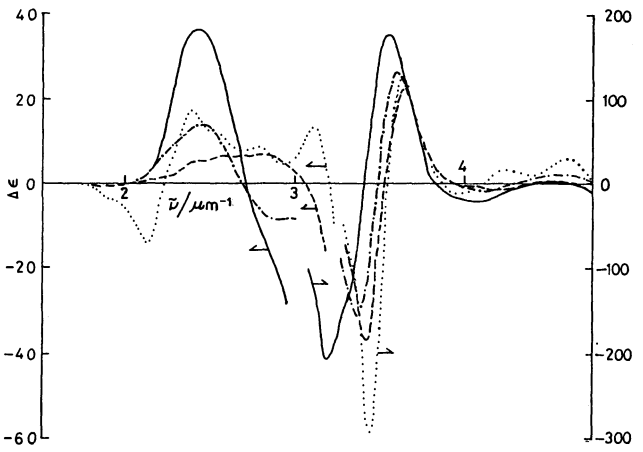

Fig. 2. CD spectra of $(-)_{\Delta\varepsilon}$-$[Ru(bpy)_n(Hdpa)_{3-n}]^{2+}$. The symbols are the same as in Fig. 1.

which are usually observed for tris- and bis(diimine) complexes such as $[M(bpy)_3]^{n+}$, $[M(phen)_3]^{n+}$, and $[M(bpy)_2(py)_2]^{n+}$ are used to assign the absolute configurations of these complexes based on exciton theory;[6-8] that is, an enantiomer whose CD bands corresponding to π-π^* transition show a minus (at lower wavenumbers)-plus (at higher wavenumbers) pattern has a *Δ* configuration. If this rule can be applied to the present system, the CD spectra shown in Fig. 2 are of *Δ* isomers.

The agreement of the absolute values of $\Delta\varepsilon$ of *act*-$[Ru(Hdpa)_3]^{2+}$ resolved by two different methods was sufficiently good to assure complete resolution.

In the precipitation procedure for $[Ru(Hdpa)_3]^{2+}$, when the filtrate after the filtration of $(-)_{\Delta\varepsilon}$-$[Ru(Hdpa)_3](dbt)$ was treated with more Na_2dbt and kept at room temperature for an additional week, often $(+)_{\Delta\varepsilon}$-$[Ru(Hdpa)_3](dbt)$ precipitated, whose optical purity was very good. The perchlorate which was derived from the diastereomer had $\Delta\varepsilon_{410}$ of -36.0 $(cm\,mol\,dm^{-3})^{-1}$. Such "post precipitation" of the other diastereomer was not observed in the resolution of $[Ru(bpy)(Hdpa)_2]^{2+}$.

The enantiomers which form less soluble diastereomers with dbt^{2-} are *Δ*-$[Ru(Hdpa)_3]^{2+}$ and *Λ*-$[Ru(bpy)(Hdpa)_2]^{2+}$. Although the mechanisms of the precipitation and the resolution were not clear, Na_2dbt was found to be a good resolving agent for these two complexes. As described in "Experimental", a single precipitation followed by a recrystallization yielded very pure diastereomers.

Table 1. Enantiomer Which was Eluted in the Early Fractions on the SP-Sephadex Column Chromatography

Complex	Eluting agent		
	Na_2*d*-tart	Na_2Sb_2(*d*-tart)$_2$	NaCl
$[Ru(bpy)_3]^{2+}$	*Δ*	*Δ*	*Δ*
$[Ru(bpy)_2(Hdpa)]^{2+}$	*Δ*	*Δ*	*Δ*
$[Ru(bpy)(Hdpa)_2]^{2+}$	*Δ*	*Δ*	*Δ*
$[Ru(Hdpa)_3]^{2+}$	*Λ*	*Δ*	*Λ*

For chromatographic resolution various reagents were tried. Table 1 shows the enantiomers of each complex which were eluted in the early fractions by three kinds of eluting agents. Among them sodium *d*-tartrate was the most efficient agent in the resolution of $[Ru(Hdpa)_3]^{2+}$ and $[Ru(bpy)(Hdpa)_2]^{2+}$. No definite conclusion could be deduced regarding the mechanism of the resolution from the data.

The optical isomers were inert in aqueous solutions against racemization in the dark. Under irradiation with a xenon lamp, however, they racemized with a very slight decomposition. Preliminary experiments showed that the quantum yield of racemization was in the order $[Ru(Hdpa)_3]^{2+} < [Ru(bpy)_3]^{2+} \approx [Ru(bpy)_2(Hdpa)]^{2+}$.

The present work was partially supported by a Grant-in-Aid for Scientific Research No. 61470048 from the Ministry of Education, Science and Culture.

References

1) D. P. Segers and M. K. DeArmond, *J. Phys. Chem.*, **86**, 3768 (1982).
2) D. E. Morris, Y. Ohsawa, D. P. Segers, M. K. DeArmond, and K. W. Hanck, *Inorg. Chem.*, **23**, 3010 (1984).
3) F. P. Dwyer and E. C. Gyarfas, *Proc. Roy. Soc. New South Wales*, **83**, 170 (1949).
4) F. P. Dwyer and E. C. Gyarfas, *Proc. Roy. Soc. New South Wales*, **83**, 174 (1949).
5) In the present paper the signs, $(+)_{\Delta\varepsilon}$ and $(-)_{\Delta\varepsilon}$, before chemical formula mean that the CD bands corresponding to the intraligand π-π^* transitions have plus-minus patterns and minus-plus patterns of $\Delta\varepsilon$ values, respectively (See "Results and Discussion").
6) B. Bosnich, *Inorg. Chem.*, **7**, 178 (1968).
7) B. Bosnich, *Acc. Chem. Res.*, **2**, 266 (1969).
8) A. J. McCaffery, S. F. Mason, and B. J. Norman, *J. Chem. Soc. A*, **1969**, 1428.

The Crystal and Molecular Structures of Tetraethylammonium [Heptakis-(isothiocyanato)lanthanate(III) and -praseodymate(III)]·Benzene, $[(C_2H_5)_4N]_4[M(SCN)_7]\cdot C_6H_6$ (M=La, Pr), in a Unicapped Trigonal Prism Geometry

Fumiko MATSUMOTO,† Toshio TAKEUCHI,†† and Akira OUCHI*

Department of Chemistry, College of Arts and Sciences, The University of Tokyo, Komaba, Meguro-ku, Tokyo 153
†Department of Chemistry, School of Hygienic Sciences, Kitasato University, Kitasato, Sagamihara-shi, Kanagawa 228
††Department of Natural Sciences, Faculty of Science and Technology, Sophia University, Kioi, Chiyoda-ku, Tokyo 102

(Received December 7, 1988)

Synopsis. The crystals of the title new lanthanum(III) complex, $LaC_{45}H_{86}N_{11}S_7$, F.W. 1144.59, are orthorhombic, space group $Bm2_1b$, a=17.438(7), b=21.507(9), c=16.616(6) Å, U=6232(4) Å^3, Z=4, D_m=1.21(3), D_x=1.22 g cm^{-3}, and μ(Mo $K\alpha$)=9.63 cm^{-1}. The central lanthanum(III) atom has a unicapped trigonal-prism 7N-hepta-coordination geometry: seven thiocyanato nitrogen atoms are ligated. There are no bridgings between the complexes and/or counter cations. Each benzene molecule is surrounded by the thiocyanate ions and ethyl groups of the cations. Although these crystals lose benzene at about 60 °C, they are stable for more than several weeks at ambient temperature, and can be regarded as a kind of inclusion compound. The isomorphous praseodymium(III) complex was also obtained.

The hexa-coordinated isothiocyanato(SCN) complexes of lanthanoids, $[(C_4H_9)_4N]_3[M(NCS)_6]$ (M=Pr—Yb), reported about 20 years ago,[1] are thought to have a specific structure, since in common complexes of lanthanoids the coordination numbers are in most cases 8, 9 or higher:[2] the SCN does not seem to be as massive as the one which should have a lower coordination number. In cases of the aqua-SCN mixed complexes, their coordination numbers were found to be eight.[3-5] The structures of the anionic thiocyanato complexes of cadmium are different from each other, depending on the kinds of their counter cations.[6,7] We recently found a new hepta-coordinated (in pentagonal bipyramidal form) isothiocyanato complexes of lanthanoids $[(CH_3)_4N]_4[M(NCS)_7]$ (M=Dy—Yb).[5] Therefore, we expected to find other types of new complexes from their tetraethylammonium salts, and obtained the title complexes. From preliminary chemical analyses, we found that they include the metal, SCN ions, and benzene in a mole ratio of 1:7:1, and were expected to have interesting structures. Therefore, their crystal and molecular structures were examined by the single-crystal X-ray diffraction method.

Experimental

Synthesis of Tetraethylammonium Heptakis(isothiocyanato)lanthanate(III)·Benzene (1). Lanthanum and tetraethylammonium thiocyanates were obtained as previously reported.[4] Into a methanolic solution (15 cm^3) containing 1.0 mmol of lanthanum(III) thiocyanate and 0.8 g (4.3 mmol) of tetraethylammonium thiocyanate, 10 cm^3 of an ethanol-benzene mixed solution (1:1=v/v) was added and dried up at about 80 °C using a rotary vacuum evaporator. The sirupy residue was dissolved into 15 cm^3 of dried methanol and was left standing in benzene vapor at ambient temperature. Although no precipitates appeared during several weeks, crystals of the title complex were deposited after several months. Yield: 0.6 g (0.52 mmol, 52%). The praseodymium complex (**2**) was also obtained by almost the same technique, and almost in the same yield. Attempts to synthesize the isomorphous neodymium or the heavier lanthanoid complexes using the same technique have not been successful. Calcd for $MC_{45}H_{86}N_{11}S_7$: M=La (**1**), La, 12.14; C, 47.22; H, 7.57; N, 13.46%; M=Pr (**2**), Pr, 12.29; C, 47.14; H, 7.56; N, 13.44%. Found: **1**, La, 12.02; C, 46.85; H, 7.42; N, 13.45%; **2**, Pr, 12.30; C, 46.91; H, 7.40; N, 13.33%.

Single Crystal X-Ray Structure Analysis. The crystal of **1** was colorless, parallelepiped (0.30×0.25×0.20 mm^3), D_m=1.21(3), and D_x=1.22 g cm^{-3}; and that of **2**, pale green in color, parallelepiped (0.30×0.20×0.12 mm^3), D_m=1.21(3), and D_x=1.23 g cm^{-3}. Intensities in the range $3<2\theta<60°$ were collected on a Rigaku AFC-6A automated 4-circle X-ray diffractometer using graphite monochromated Mo $K\alpha$ radiation (λ=0.71073Å) by means of an ω-2θ scan technique (scan speed (ω), 4° min^{-1}, and scan width (ω), 1.08+0.35 tanθ) for **1** and **2**. The intensities were corrected for Lorentz and polarization factors, but not for absorption and extinction. Of 4970 independent intensities collected, 1571 reflections with $|F_o|>3\sigma(|F_o|)$ were used for the structure determination of **1**, while 1874 in 4956 reflections for that of **2**. The crystallographic data of **2** are: a=17.412(7), b=21.468(6), c=16.612(6) Å, U=6209(4) Å^3, μ(Mo $K\alpha$)=10.51 cm^{-1}.

All the calculations were carried out on a HITAC M-682H computer at the Computer Center of the University of Tokyo using a local version of the UNICS program.[8] The scattering factors were taken from Ref. 9.

The structure of **1** was solved by the heavy-atom method (positional and thermal parameters were refined by a block-

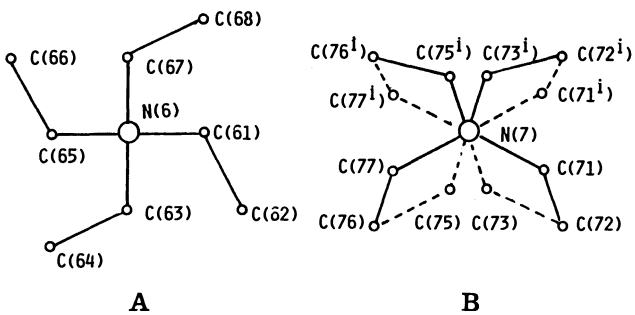

Fig. 1. Schematic presentation of the tetraethylammonium ions with the numbering scheme of the atoms.
A. The ion centered by N(6). **B**. The ion centered by N(7): the bonding and the numbering way are the same as the one centered by the N(8) atom. Key to the symmetry operation: i; $\bar{x}$, y, z.

diagonal least-squares method). No hydrogen atoms were included in the structure factor calculations. The structure of **2** was calculated starting from the final values of **1**. They were also refined. During the final stage of refinements, the movements of the respective parameters were less than one-third of the corresponding standard deviations, except for a few cases. The carbon atoms of the tetraethylammonium ions centered by N(7) and N(8) atoms are disordered, as shown in Fig. 1. The N(7) atom is bonded with four carbon atoms in two ways: with C(71), C(73^{i}), C(75^{i}), and C(77), or with C(71^{i}), C(73), C(75), and C(77^{i}), atoms (i, $-x$, y, z). The occupancy factors of both type structures are 0.5 due to symmetry. The final R and R_w (in parentheses) values[10] are: **1**, 0.091(0.071); **2**, 0.086 (0.070). Since the R and R_w values of the inversed chirality structures were, **1**, 0.093 (0.073); **2**, 0.089 (0.074), the structures were not adopted. Although the thermal parameters of some atoms were found to be large, such phenomena were sometimes found in the lanthanoid complexes, especially for the atoms relatively far from the central metal atom.[11]

The Other Measurements. Thermogravimetric (TG)-differential thermal analysis (DTA) simmultaneous measurement was carried out by the Rigaku "Thermoflex" M-8075 using samples weighing about 10 mg each at heating rate of 10 °C min^{-1} in air, α-alumina as the reference. Infrared spectra were obtained by means of a JASCO A-202 grating infrared spectrophotometer using paraffin oil and hexachloro-1,3-butadiene mull.

Results and Discussion

Selected bond lengths and bond angles are listed in Table 1. A perspective drawing of the anionic complex is shown in Fig. 2, and a projection of the unit cell along b-axis in Fig. 3.[12]

The metal atom is in a unicapped trigonal prism hepta-coordination geometry, as shown by the broken lines in Fig. 2: seven N atoms of SCN ions are ligated. The atoms of the metal and the SCN ions following N(1), N(4), and N(2) (cap position) are on planes parallel to the bc-plane; the other two pairs of the SCN ions (following N(3), and N(3^{i}); and N(5) and N(5^{i})) are at the respective mirror image positions with each other on both sides of the planes. The triangle planes of the prism are approximately parallel to the ac-plane.

The average M-N bond lengths to the three N atoms at the apexes of one bottom triangle are short (**1**, 2.46, and **2**, 2.37Å, on the average), and the other four, to the N atoms at the apexes of the other bottom triangle and at the cap position, are long (**1**, 2.58, and **2**, 2.56Å, on the average). The averages of the M-N-C and N-C-S angles are: **1**, 167 and 172; **2**, 168 and 176°, respectively. These are not much deviated from 180°.

It is an interesting fact that $[Dy(SCN)_7]^{4-}$ ion in tetramethylammonium salt has an approximately pentagonal bipyramidal geometry around its metal atom, while the present $[Pr(SCN)_7]^{4-}$ in tetraethylammonium salt a unicapped trigonal prism.

The centers of cations, N(7) and N(8) atoms, as well as the centers of benzene rings are on planes parallel to the bc-plane. The benzene ring is arranged approximately parallel to the ab-plane and is mirror-symmetrical to the bc-plane. The benzene ring is

Table 1. Selected Bond Lengths and Bond Angles of the Complexes with the Standard Deviations in Parentheses

Bond length(l/Å) M=	La	Pr	M=	La	Pr
M-N(1)	2.57(3)	2.57(2)	M-N(2)	2.56(7)	2.52(6)
M-N(3)	2.60(2)	2.58(2)	M-N(4)	2.47(3)	2.37(3)
M-N(5)	2.45(2)	2.37(2)	N(1)-C(1)	1.19(4)	1.14(3)
N(2)-C(2)	1.14(9)	1.14(9)	N(3)-C(3)	1.13(3)	1.11(2)
N(1)-C(1)	1.00(5)	1.09(5)	N(5)-C(5)	1.18(3)	1.18(3)
C(1)-S(1)	1.51(3)	1.54(3)	C(2)-S(2)	1.62(7)	1.61(6)
C(3)-S(3)	1.59(2)	1.59(2)	C(4)-S(4)	1.92(4)	1.85(5)
C(5)-S(5)	1.61(2)	1.63(2)			

Bond angl (ϕ/°) M=	La	Pr
M-N(1)-C(1)	178(2)	173(2)
M-N(2)-C(2)	164(6)	173(6)
M-N(3)-C(3)	171(2)	168(1)
M-N(4)-C(4)	151(3)	158(3)
M-N(5)-C(5)	171(2)	168(2)
N(1)-C(1)-S(1)	177(3)	179(2)
N(2)-C(2)-S(2)	163(7)	175(6)
N(3)-C(3)-S(3)	175(2)	179(2)
N(4)-C(4)-S(4)	175(4)	179(4)
N(5)-C(5)-S(5)	169(2)	170(2)

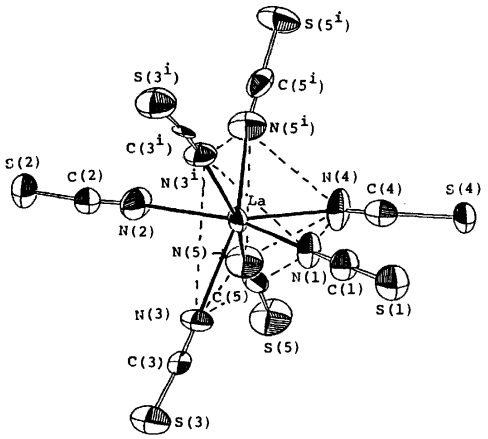

Fig. 2. The perspective drawing of the anionic complex with the numbering scheme of the atoms. (i; $\bar{x}$, y, z.)

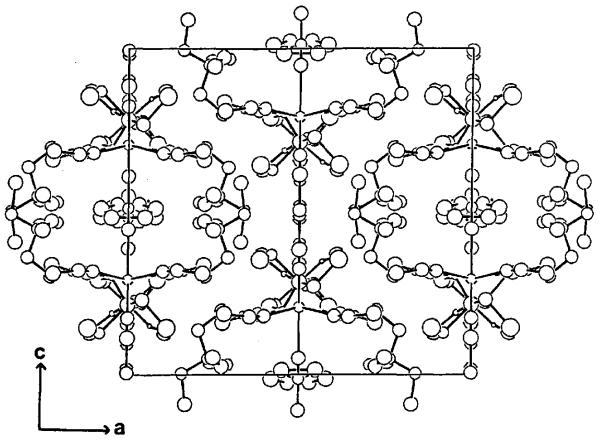

Fig. 3. Projection of the unit-cell along b-axis.

situated between two cations centered by N(7) and N(8) atoms in the c-axis direction. Moreover, on both sides of the ring along b-axis, there are the SCN ions bonded to the cap-positions of the complexes which are neighboring along [011] or [0$\bar{1}$1] axis.

The metal and a center of the cation, N(6), atoms are on planes parallel to the ac-plane intersecting the b-axis at 0 and 0.5, while the benzene molecules and the other cations (centered by N(7) and N(8) atoms) are sandwitched between the former planes: both kinds of layers are arranged alternately along b-axis.

The general feature of the TG and DTA curves of **1** and **2** are approximately the same: they decompose in two steps. At the first step of TG curve (at, **1**, 60; **2**, 103 °C) they lose benzene (corresponding DTA endothermic peaks are at, **1**, 65; **2**, 120 °C). At the second step of TG curve (at, **1**, 264; **2**, 274 °C) they seem to decompose in a one-step reaction into their oxides. However, as the corresponding DTA curve shows an endothermic followed by exothermic peaks, the reaction is likely to consist of several complicated steps.

When **1** and **2** were heated at 110 °C for several hours, they lost only benzene, judging from their mass loss. In the infrared spectra of their heating residue, peaks of SCN were found (ν(CN), 2035; ν(CS), 730(sh); δ(SCN), 482 cm^{-1}) as well as those of the $[(C_2H_5)_4N]^+$ ion (for example, strong peaks at 1490, 1395, 1364, 1170, 997, and 780 cm^{-1}). Those for benzene, found in the spectra of **1** or **2** (for example peaks at 1480, 680 (splitted into two) cm^{-1}), disappeared.

On the other hand, at room temperature, these complexes were stable, and the included benzene was not removed after, at least, several weeks (when they were kept in a stoppered glass bottle in a refrigerator, they were not decomposed even after six months).

References

1) J. L. Martin, L. C. Thompson, L. J. Radonovich, and M. D. Glick, *J. Am. Chem. Soc.*, **90**, 4493 (1968).

2) T. Moeller, "Comprehensive Inorganic Chemistry," ed by J. C. Bailar, H. J. Emeléus, R. Nyholm, and A. F. Trotman-Dickenson, Pergamon Press, Oxford, U. K. (1973), Vol. 4, p. 22.

3) P. I. Lazarev, L. A. Aslanov, V. M. Ionov, and M. A. Porai-Koshits, *Koord. Khim.*, **1**, 710 (1975); also *Struct. Report*, **41A**, 210 (1975).

4) Y. Tateyama, Y. Kuniyasu, Y. Suzuki, and A. Ouchi, *Bull. Chem. Soc. Jpn.*, **61**, 2805 (1988).

5) F. Matsumoto, N. Matsumura, and A. Ouchi, *Bull. Chem. Soc. Jpn.*, **62**, 1809 (1989).

6) Y. Kuniyasu, Y. Suzuki, M. Taniguchi, and A. Ouchi, *Bull. Chem. Soc. Jpn.*, **60**, 179 (1987).

7) M. Taniguchi and A. Ouchi, *Bull. Chem. Soc. Jpn.*, **62**, 424 (1989).

8) "The Universal Crystallographic Computation Program System (UNICS)," ed by T. Sakurai, Crystallographic Society of Japan, Tokyo (1967).

9) "International Tables for X-Ray Crystallography," Kynoch Press, Birmingham (1974), Vol. IV, pp. 72, 150.

10) $R=\sum||F_o|-|F_c||/\sum|F_o|$; $R_w=[\sum w(|F_o|-|F_c|)^2/\sum wF_o^2]^{1/2}$, where $w=1/[\{\sigma(|F_o|)\}^2+(F_w\times F_o)^2]$, $F_w=0.015$ for **1** and **2**.

11) T. Imai, M. Nakamura, K. Nagai, Y. Ohki, Y. Suzuki, M. Shimoi, and A. Ouchi, *Bull. Chem. Soc. Jpn.*, **59**, 2115 (1986).

12) The positional and isotropic equivalent as well as anisotropic temperature factors, the final F_o and F_c tables, and some additional data of bond lengths and bond angles of **1** and **2** are deposited as Document No. 8876 at the Office of the Editor of Bull. Chem. Soc. Jpn.

The Crystal and Molecular Structure of Di-μ-hydroxo-bis[pentaaquascandium(III)] Benzenesulfonate Tetrahydrate, $[\{(H_2O)_5Sc\}(OH)_2\{Sc(H_2O)_5\}](C_6H_5SO_3)_4\cdot 4H_2O$: A Dimeric Complex in Pentagonal-Bipyramidal Hepta-Coordination

Fumiko MATSUMOTO,† Yoshiyuki OHKI,†† Yasuo SUZUKI,†† and Akira OUCHI*
Department of Chemistry, College of Arts and Sciences, The University of Tokyo, Komaba, Meguro-ku, Tokyo 153
†Department of Chemistry, School of Hygienic Sciences, Kitasato University, Kitasato, Sagamihara-shi, Kanagawa 228
††Department of Industrial Chemistry, Faculty of Engineering, Meiji University, Higashi-Mita, Tama-ku, Kawasaki-shi, Kanagawa 214
(Received January 7, 1989)

Synopsis. The crystal and molecular structure of the new title complex has been determined by means of a single-crystal X-ray diffraction method. It is triclinic with the space group $P\bar{1}$, $Z=2$, $a=15.518(5)$, $b=19.827(7)$, $c=7.493(2)$ Å, $\alpha=100.90(3)$, $\beta=103.94(2)$, $\gamma=82.85(3)°$. Both of the metal atoms have almost the same coordination geometry, pentagonal bipyramidal which coordinates the oxygen atoms of five water molecules (2 axial and 3 equatorial ones) and the two hydroxide ions which bridge the both metal atoms. The Sc(1)···Sc(2) distance is 3.403(2) Å. The average Sc-O(H_2O) bond length is 2.194 Å, which is much longer than that of Sc-O(OH), 2.072 Å. Benzenesulfonate ions and the other water molecules do not coordinate to the metal atoms, though their oxygen atoms as well as those of the coordinated water are connected with each other by a network involving hydrogen bonding.

Although the structures of scandium complexes have not yet been sufficiently clarified, some of them were recently elucidated: most of them are in the octahedral hexa-coordinated geometry,[1-5] and the others are in the octa-coordination.[6-10] Some scandium salts have a layer,[7] a chain[3,4] or a dimeric structure[8] like the lanthanoid complexes.[11-14]

Previously, the authors investigated the structures of several scandium salts,[3-5] and recently were able to obtain the new title complex. Subsequently, its crystal and molecular structure was determined by the single-crystal X-ray diffraction method.

Experimental

Synthesis of Di-μ-hydroxo-bis[pentaaquascandium(III)] Benzenesulfonate Tetrahydrate. Scandium oxide (69 mg, including 1 mmol of Sc) was dissolved into hydrochloric acid (6 mol dm^{-3}, 10 cm^3) after boiling. The solution was dried up on a water bath, and the residue was dissolved into 10 cm^3 of water. To the solution sodium benzenesulfonate hydrate (610 mg, 3.1 mmol) was added, dissolved by warming, and left standing in a desiccator over silica gel at room temperature until one third of the solvent was evaporated; plate-like crystals were deposited. Yield: 92 mg (0.091 mmol as a dimer, 18%) Found: Sc, 9.14; C, 28.67; H, 4.70%. Calcd for $Sc_2C_{24}H_{50}O_{28}S_4$: Sc, 8.95; C, 28.69; H, 5.02%.

X-Ray Structure Analysis. The used crystal was colorless, approximately parallelepiped in shape (0.30×0.25×0.25 mm^3), triclinic, space group $P\bar{1}$, $Z=2$ (including four Sc atoms in a unit cell), $a=15.518(5)$, $b=19.827(7)$, $c=7.493(2)$ Å, $\alpha=100.90(3)$, $\beta=103.94(2)$, $\gamma=82.85(3)°$, $U=2190(1)$ Å, $D_m=1.51(3)$, $D_x=1.52$ g cm^{-3}, μ(Mo $K\alpha$)=5.92 cm^{-1}. The intensities were measured with graphite monochromated Mo $K\alpha$ radiation ($\lambda=0.71073$ Å), a ω-2θ scan technique being employed (the scan speed was 4° min^{-1} (ω), scan width, 1.00+0.5 tanθ (ω), and the scan range was 3—55° (2θ)). Of the 10123 independent reflections measured, 5866 reflections of $|F_o|>3\sigma(|F_o|)$ were used for its structure calculation. The intensities were corrected for both Lorentz and polarization factors, but not for absorption and extinction. The structure was solved by the heavy-atom method. The positional and thermal parameters of the atoms were refined by a block-diagonal least-squares method. The positions of the hydrogen atoms of coordinated water molecules and hydroxide ions were obtained from a difference synthesis map; they were included in the structure factor calculations (without fixing); the other hydrogen atoms were excluded from the calculations. During the final stage (in the map) almost no electron clouds could be recognized around the ligated oxygen atoms. The observed H-O bond lengths of the water molecules and the hydroxide ions are 0.91 and 0.90 Å (on the average), respectively (they were a little too short, which may be due to their large temperature factors). The H-O-H bond angles of water, and Sc-O-H of water and hydroxide ions are 110, 122, and 120° (on the average), respectively. The final R value was found to be 0.070 by applying anisotropic temperature factors for all nonhydrogen atoms.[15]

All calculations were carried out on a HITAC M-682H computer at the Computer Center of the University of Tokyo using a local version of the UNICS program system.[16] The atomic scattering factors were taken from Ref. 17.

Results and Discussion

The selected bond lengths and bond angles are shown in Table 1. A perspective drawing of the dimeric complex together with the numbering scheme of the atoms is shown in Fig. 1, and a projection of the unit cell along b-axis, together with the numbering of some metal and other atoms, in Fig. 2.[18]

Both of the scandium(III) atoms, Sc(1) and Sc(2) are approximately in the same coordination geometry, deformed pentagonal bipyramidal. The seven ligating oxygen atoms are five water oxygen atoms (two are axial and three equatorial) and two oxygen atoms of hydroxide ions (equatorial). The two hydroxide ions make bridges between the two metal atoms. The axial Sc-O(H_2O) bonds are shorter than the equatorial ones (the axial bonds are 2.146 Å on the average, and the average equatorial bond length is 2.227 Å), while the Sc-O (hydroxide) bonds are the shortest (2.072 Å on the average). The bond angles of O(hydroxide)-

Table 1. Selected Interatomic Distances and Bond Angles with Their Standard Deviations in Parentheses

Interatomic distance	(l/Å)	Interatomic distance	(l/Å)
Sc(1)···Sc(2)	3.403(2)	O(A6)···O(A7)	2.353(6)
Sc(1)-O(A1)	2.143(6)	Sc(2)-O(B1)	2.152(4)
Sc(1)-O(A2)	2.152(6)	Sc(2)-O(B2)	2.138(4)
Sc(1)-O(A3)	2.230(4)	Sc(2)-O(B3)	2.228(5)
Sc(1)-O(A4)	2.256(4)	Sc(2)-O(B4)	2.249(4)
Sc(1)-O(A5)	2.200(4)	Sc(2)-O(B5)	2.196(5)
Sc(1)-O(A6)	2.071(4)	Sc(2)-O(A6)	2.076(4)
Sc(1)-O(A7)	2.069(4)	Sc(2)-O(A7)	2.072(4)
Bond angle	**(ϕ/°)**	**Bond angle**	**(ϕ/°)**
Sc(1)-O(A6)-Sc(2)	110.3(2)	Sc(1)-O(A7)-Sc(2)	110.5(2)
O(A1)-Sc(1)-O(A2)	160.2(2)	O(B1)-Sc(2)-O(B2)	160.4(2)
O(A1)-Sc(1)-O(A3)	91.3(2)	O(B1)-Sc(2)-O(B3)	82.6(2)
O(A1)-Sc(1)-O(A4)	80.6(2)	O(B1)-Sc(2)-O(B4)	79.8(2)
O(A1)-Sc(1)-O(A5)	81.8(2)	O(B1)-Sc(2)-O(B5)	93.3(2)
O(A1)-Sc(1)-O(A6)	115.3(2)	O(B1)-Sc(2)-O(A6)	112.4(2)
O(A1)-Sc(1)-O(A7)	84.2(2)	O(B1)-Sc(2)-O(A7)	81.8(2)
O(A2)-Sc(1)-O(A6)	81.8(2)	O(B2)-Sc(2)-O(A6)	84.1(2)
O(A2)-Sc(1)-O(A7)	112.5(2)	O(B2)-Sc(2)-O(A7)	115.1(2)
O(A3)-Sc(1)-O(A4)	73.3(1)	O(B3)-Sc(2)-O(B4)	73.2(2)
O(A4)-Sc(1)-O(A5)	74.4(2)	O(B4)-Sc(2)-O(B5)	74.3(2)
O(A5)-Sc(1)-O(A6)	77.2(2)	O(B3)-Sc(2)-O(A6)	76.6(2)
O(A6)-Sc(1)-O(A7)	69.3(2)	O(A6)-Sc(2)-O(A7)	69.1(2)
O(A7)-Sc(1)-O(A3)	76.6(2)	O(A7)-Sc(2)-O(B5)	77.6(2)

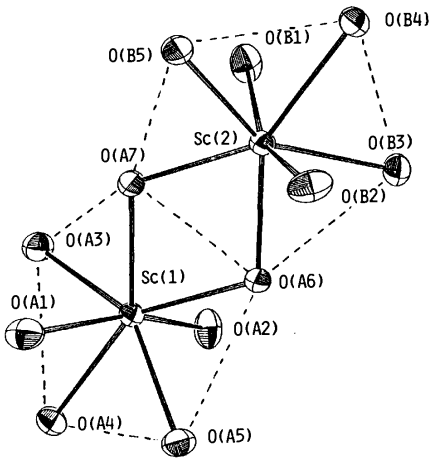

Fig. 1. The perspective drawing of the dimeric complex with the numbering scheme of the atoms: 30% probability thermal ellipsoids are shown for the nonhydrogen atoms of the complex.

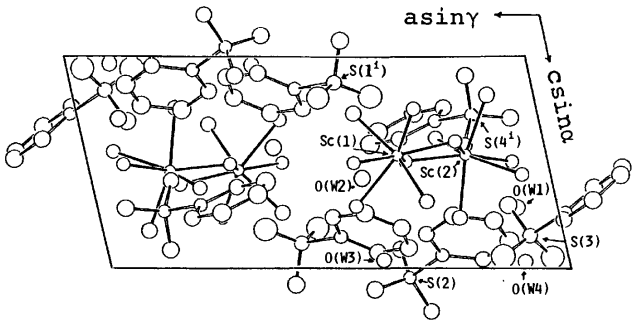

Fig. 2. Projection of the unit cell along b-axis: the numbering scheme of some atoms are also shown (i, x, y, $-1+z$).

Sc-O(hydroxide) and Sc(1)-O(hydroxide)-Sc(2) are, 69.2 and 110.4° (on the average), while the separations of Sc(1)···Sc(2) and O(A6)···O(A7) are 3.403(2) Å and 2.353(6) Å, respectively.

The size and the form of this Sc_2O_2 quadrilateral resemble the corresponding ones of the di-μ-hydroxo bridging found in the dimeric basic nitrate.[8] Moreover, from the difference synthesis map, only one hydrogen atom was found around each O(A6) and O(A7) atom, while two hydrogen atoms were found to exist around the other ligating oxygen atom, respectively. This is further support of our inference that the two bridging oxygen atoms are hydroxide ions.

Three mean-square planes are defined as **A**, **B**, and **C**, including following atoms, respectively: (**A**) Sc(1) and O(A3—A7); (**B**) Sc(1, 2) and O(A6, A7) ; and (**C**), Sc(2) and O(A6, A7, B3—B5). The average positional deviations of the atoms from the respective planes are: **A**, 0.239; **B**, 0.061; and **C**, 0.260 Å. The dihedral angles between them are: **A**-**B**, 147.1; **A**-**C**, 117.8; **B**-**C**, 29.4°, respectively.

The benzenesulfonate ions, as well as crystalline water molecules, are not directly bonded to the metal atoms. Many interatomic distances of 2.6—2.9 Å are observed between the water and sulfonato group oxygen atoms; almost all of them are expected to be hydrogen bondings.[18] Thus, in the crystal the cations, anions, and crystalline water molecules are hydrogen bonded with each other to form a network. However, the O(A6) and O(A7) atoms do not participate in the hydrogen network.

From studies of the solution chemistry of the scandium(III) ion, the existence of a dimeric ion, $[Sc_2(OH)_2]^{4+}$, has already been reported.[19-21] The structure of the present complex may be the same as the species in the above-mentioned solution.

It is an interesting fact that the crystals of scandium benzenesulfonate (**1**), *p*-toluenesulfonate (**2**), and *m*-nitrobenzenesulfonate (**3**), obtained from their aqueous solution under almost the same synthetic conditions, have structures which are much different from each other.[4,5] The very rare coordination number for scandium, 7, was only found in **1**. Moreover, the acid anion does not coordinate only in **1**, in spite of the fact that the acid ion of **1** is the smallest of the three: a minimum mutual steric hindrance is expected for the anion of **1**, even if it coordinates. This fact is also in contradiction to the consideration connecting the inductive effect of the substituents of the benzene rings of their acid anions. Since the methyl group in **2** (in *p*-position) increases, and the nitro group in **3** (in *m*-position) decreases the electron density of the sulfonato group compared with that of **1**, it is unreasonable that only the acid anion of **1** does not coordinate to the scandium atom.

References

1) T. J. Anderson, M. A. Neuman, and G. A. Melson, *Inorg. Chem.*, **12**, 927 (1973).
2) J. L. Atwood and K. D. Smith, *J. Chem. Soc., Dalton Trans.*, **1974**, 921.
3) Y. Sugita, Y. Ohki, Y. Suzuki, and A. Ouchi, *Bull. Chem. Soc. Jpn.*, **60**, 3441 (1987).

4) Y. Ohki, Y. Suzuki, T. Takeuchi, and A. Ouchi, *Bull. Chem. Soc. Jpn.*, **61**, 393 (1988).
5) Y. Tateyama, Y. Ohki, Y. Suzuki, and A. Ouchi, *Bull. Chem. Soc. Jpn.*, **61**, 2214 (1988).
6) B. Barlic, L. Golic, and F. Lazarini, *Cryst. Struct. Commun.*, **3**, 407 (1974).
7) E. Hansson, *Acta Chem. Scand.*, **26**, 1337 (1972).
8) A. Arif, F. Alan, M. B. Hursthouse, M. Thornton-Pett, and W. Zhu, *J. Chem. Soc., Dalton Trans.*, **1984**, 2449.
9) T. J. Anderson, M. A. Neuman, and G. A. Melson, *Inorg. Chem.*, **13**, 1884 (1974).
10) A. R. Davis and F. W. B. Einstein, *Inorg. Chem.*, **13**, 1880 (1974).
11) C. Favas, D. L. Kepert, B. W. Skelton, and A. H. White, *J. Chem. Soc., Dalton Trans.*, **1980**, 454.
12) T. Imai, M. Shimoi, and A. Ouchi, *Bull. Chem. Soc. Jpn.*, **60**, 159 (1987).
13) Y. Sugita and A. Ouchi, *Bull. Chem. Soc. Jpn.*, **60**, 171 (1987).
14) Y. Sugita and A. Ouchi, *Bull. Chem. Soc. Jpn.*, **61**, 1607 (1988).
15) $R=\sum||F_o|-|F_c||/\sum|F_o|$.
16) "Universal Crystallographic Computation Program System (UNICS)," ed by T. Sakurai, Crystallographic Society of Japan, Tokyo, 1967.
17) "International Tables for X-Ray Crystallography," Kynoch Press, Birmingham, U. K. (1974), Vol. IV, pp. 72, 150.
18) The final atomic positional and thermal parameters, the final F_o-F_c table, and some additional data of bond lengths, bond angles, and some interatomic distances expected to be hydrogen bonding are deposited as Document No. 8877, at the Office of the Editor of Bull. Chem. Soc. Jpn.
19) G. Biedermann, M. Kilpatrick, L. Pokras, and L. G. Sillen, *Acta Chem. Scand.*, **10**, 1327 (1956).
20) J. Aveston, *J. Chem. Soc. A*, **1966**, 1599.
21) P. L. Brown, J. Ellis, and R. N. Sylva, *J. Chem. Soc., Dalton Trans.*, **1983**, 35.

The Fluorometric Determination of Magnesium with 2,2′-Dihydroxy-4,4′-dimethylazobenzene

Izuo AOKI,*,† Atsushi SAITO, and Kunihiro WATANABE
Faculty of Science and Technology, Science University of Tokyo, 2641, Yamazaki, Noda-shi, Chiba 278
†R. & D. Laboratory for Speciality Chemicals, Nippon Soda Co., Ltd., 12-54, Goi-minamikaigan, Ichihara-shi, Chiba 290
(Received December 24, 1988)

Synopsis. In an alkaline medium, magnesium reacts with 2,2′-dihydroxy-4,4′-dimethylazobenzene to emit a strong fluorescence, which is about 5 times as intense as that obtained with its parent compound (2,2′-dihydroxyazobenzene). Nonextraction (water-ethanol-dioxane, a mixed solvent) and extraction (an isopentyl alcohol solvent) procedures for the fluorometric determination of magnesium with this reagent were established. 0.1 μg to 4.0 μg of magnesium can be rapidly determined by the nonextraction procedure. In the extraction procedure, 1000-fold excesses of calcium did not interfere even when no masking agent was used.

Among a large number of 2,2′-dihydroxy azo compounds available for use in colorimetric and fluorometric methods for metal ions, 2,2′-dihydroxyazobenzene (DHAB), which has the most fundamental structure, is an excellent fluorometric reagent for magnesium in the presence of calcium.[1] 8-Quinolinol,[2] methyl salicylate,[3] and calcein[4] give fluorescence reactions with magnesium, but they also react with calcium to emit a strong fluorescence. Dagnall et al.[5] proposed 2,3-bis(salicylideneamino)benzofuran (SABF) as a specific reagent for magnesium without any interference from calcium. Although SABF seems to be more sensitive than DHAB, DHAB is superior to SABF with regard to the stability of its magnesium complex, for SABF gradually hydrolyzes in aqueous methanol solutions.

One of the present authors has previously reported that 2,2′-dihydroxy-4,4′-dimethylazobenzene (4,4′-DDAB) is more sensitive than the parent compound, DHAB, for the fluorometric determination of gallium.[6] In this study, it was found that 4,4′-DDAB reacted quantitatively with magnesium to emit a strong fluorescence in an alkaline medium. The detection limit for magnesium with this reagent was as good as that obtained with SABF. On the other hand, the magnesium-DHAB complex is extractable into isopentyl alcohol; however, the extraction procedure is not so useful for the determination of magnesium because the distribution coefficient of the complex between isopentyl alcohol and water is only about 9.[7] The present authors have, though, found that a remarkable enhancement of the distribution coefficient could be achieved by using 4,4′-DDAB instead of DHAB.

Experimental

Apparatus. The fluorescence spectra and the intensity were measured with a Hitachi Model 204 fluorescence spectrophotometer fitted with a 150 W Xenon lamp. A Shimadzu fluorescence spectrophotometer Model RF-540 (exciting source; 150 W Xenon lamp, photomultiplier; R924F) was used for the measurements of the fluorescence quantum efficiencies.

Reagents. Standard Solution of Magnesium. A stock solution of magnesium was prepared by dissolving 0.5012 g of magnesium (99.9%) with 30 cm^3 of 6 mol dm^{-3} hydrochloric acid and then diluting the mixture to 1 dm^3 with water. The standard solution was prepared by suitable dilution with 0.1 mol dm^{-3} hydrochloric acid from the stock solution.

Synthesis of Azo Compounds. DHAB, 4,4′-DDAB, and 2,2′-dihydroxy-5,5′-dimethylazobenzene (5,5′-DDAB) were synthesized by the conventional method[8] and were identified by means of their melting points and IR spectra. These azo compounds were used as the 1,4-dioxane solution.

Rhodamine B Reference Standard Solution. 0.1 g of rhodamine B was dissolved in ethanol to give a solution containing 10 μg cm^{-3}. This solution was then diluted with water.

All the other reagents and solvents were of an analytical grade and were used without further purification.

Determination Procedure

(A) Nonextraction Procedure (Water-Ethanol-Dioxane, a Mixed Solvent). (a) Preparation of Buffer Solution. Add 20 cm^3 of ethylenediamine (en) and 10 cm^3 of 6 mol dm^{-3} hydrochloric acid to 200 cm^3 of ethanol, and then allow the mixture to cool. Dilute the solution to 500 cm^3 with 1,4-dioxane. **(b) Determination Procedure of Magnesium.** To a sample solution containing from 0.1 μg to 4 μg of magnesium, add 15 cm^3 of the buffer solution and 1 cm^3 of a 0.01% 4,4′-DDAB solution. Dilute the solution to 25 cm^3 with water and allow the mixture to stand for 10 minutes at room temperature. Measure the fluorescence intensity at 560 nm with an excitation wavelength of 465 nm by using a rhodamine B solution as the reference standard.

(B) Extraction Procedure. To a sample solution containing from 0.04 μg to 3 μg of magnesium, add 1 cm^3 of a 0.5 mol dm^{-3} sodium hydrogencarbonate aqueous solution. Adjust the pH to 11.7 with a dilute hydrochloric acid or a dilute sodium hydroxide and then add 1 cm^3 of a 0.02% 4,4′-DDAB solution. Transfer the mixture into a 100 cm^3 separatory funnel and adjust its volume about 50 cm^3 with water. Add 10 cm^3 of isopentyl alcohol to the solution and shake it for 10 minutes. Discard the aqueous layer after the separation of the layers. Centrifuge the organic layer at 2000 rpm for 10 minutes, if necessary. Measure the fluorescence intensity at 560 nm with an excitation wavelength of 480 nm by using a rhodamine B solution as the reference standard.

Results and Discussion

Fluorescence Properties of the Magnesium-4,4′-DDAB Complex. The fluorescence properties of the magnesium-4,4′-DDAB complex in several solvents were investigated and compared with those of magnesium-DHAB and -5,5′-DDAB complexes. The fluorescence properties of these three complexes are listed in Table 1.

The molar extinction coefficients at the maximum absorption wavelength (ε) of the magnesium complexes were affected by the methyl groups in the ligands (azo compounds), while they changed only slightly in different solvents. The ε value of the 4,4′-DDAB complex was the largest among the three complexes. The fluorescence quantum efficiencies (ϕ_f) of the complexes were remarkably affected by both methyl groups and solvents. The ϕ_f values of the 4,4′-DDAB complex in the mixture of water-ethanol-dioxane (volume ratio: 3 : 2 : 3) were about 4 times and 9 times larger than that of the DHAB and 5,5′-DDAB complexes in the same solvent respectively.

The above-mentioned ε and ϕ_f values shown that the absolute sensitivities ($\varepsilon \cdot \phi_f$)[10] of the magnesium-4,4′-DDAB complex in both water-ethanol-dioxane and isopentyl alcohol were about (3—5) times larger than that of the DHAB complex in these solvents.

Structure of the Magnesium-4,4′-DDAB Complex. The mole ratio of magnesium to 4,4′-DDAB in the complex was determined fluorometrically by the continuous variation method to be 1 : 1 in both the mixture of water-ethanol-dioxane and isopentyl alcohol. These results were consistent with those obtained by the equilibrium-shift method.

Knoeck et al.[11] have proposed that the fluorescence enhancement by the addition of alcohols to aqueous magnesium-DHAB complex solutions probably comes from a direct magnesium coordination by the alcohols. The present authors have determined the mole ratio of magnesium to isopentyl alcohol in the extracted 4,4′-DDAB complex by the equilibrium-shift method to be 1 : 2. The complete composition of the magnesium-4,4′-DDAB complex in isopentyl alcohol is, therefore, Mg(4,4′-DDAB)(isopentyl alcohol)$_2$, which is consistent with the five-coordinate structure proposed for the DHAB complex.[11]

Effect of Organic Solvent. In Determination Procedure A (a nonextraction procedure), the effect of adding organic solvents to aqueous solutions on the fluorescence intensity of the magnesium-4,4′-DDAB complex was investigated. A remarkable increase in the fluorescence intensity of the complex was observed upon the addition of ethanol and 1,4-dioxane, while the intensity of the reagent blanks was not changed. The maximum fluorescence intensity of the complex, which was about 5 times as intense as that of its aqueous solution, was obtained with more than 11 cm^3 for dioxane or with 20 cm^3 for ethanol in a final volume of 25 cm^3. Other organic solvents, i.e., acetone, the mixtures of ethanol-methyl isobutyl ketone (MIBK), -ethyl acetate, or -tributyl phosphate (TBP), and the mixtures of ethanol and nonpolar organic solvents, were less effective than ethanol and dioxane. For the determination procedure of magnesium, it was convenient to add these organic solvents as a buffer solution by mixing ethylenediamine (en) and hydrochloric acid. As far as the enhancement ability of the fluorescence intensity of the magnesium complex is concerned, dioxane was superior to ethanol, but dioxane caused a turbidity when en and hydrochloric acid were mixed. A mixture of dioxane and ethanol (3 : 2, v/v) was, therefore, chosen as a solvent of the buffer solution. In consideration of the volume of the sample solution, it was suitable for the determination procedure to add 15 cm^3 of this solution in a final volume of 25 cm^3.

According to Determination Procedure B, the magnesium-4,4′- DDAB complex was extracted with TBP and alcohols, such as isopentyl alcohol, pentyl alcohol, and isobutyl alcohol, but not with MIBK, ethyl acetate, and other nonpolar organic solvents, such as hexane, benzene, and chloroform. Although the extracts with TBP and the alcohols were nearly equal in fluorescence intensity, isopentyl alcohol was chosen for the extraction solvent because it is less soluble in water than the other alcohols and because TBP is inferior to isopentyl alcohol in its separability from water because of its specific gravity (0.97). The extractability of the magnesium-4,4′-DDAB complex was 91.8% (isopentyl alcohol : aqueous phase=1 : 5, v/v), and the distribution coefficient of the complex was 56.3, while the corresponding values of the magnesium-DHAB complex were 66.4% and 9.9 respectively.

Table 1. Fluorescence Properties of Magnesium Complexes with DHAB, 4,4′-DDAB, and 5,5′-DDAB[a]

Ligand	Solvent[b]	$\lambda_{ex(max)}/\lambda_{em(max)}$(nm)		ε	ϕ_f[c]	$\varepsilon \cdot \phi_f$[d]
		Apparent	Corrected	dm^3 mol^{-1} cm^{-1}		dm^3 mol^{-1} cm^{-1}
DHAB	W/E/D	465/565	480/590	1.6×10^4 (480 nm)	0.013	2.1×10^2
	I	475/570	485/595	1.6×10^4 (485 nm)	0.019	3.0×10^2
4,4′-DDAB	W	465/570	480/595	2.2×10^4 (480 nm)	0.013	2.9×10^2
	W/E/D	465/560	480/590	2.2×10^4 (480 nm)	0.049	1.1×10^3
	I	480/560	485/590	2.0×10^4 (485 nm)	0.062	1.2×10^3
5,5′-DDAB	W/E/D	490/575	505/605	1.8×10^4 (505 nm)	0.0055	1.0×10^2

a) The mole ratio of magnesium to ligands is 1 : 1. b) W/E/D: a mixture of water-ethanol-dioxane (3 : 2 : 3, volume ratio); I: isopentyl alcohol; W: water. c) Reference standard solution: 1 μg cm^{-3} rhodamine B ethanol solution (ϕ_f=0.76).[9] d) Absolute sensitivity: $\varepsilon \cdot \phi_f$.

Effect of pH. A maximum fluorescence intensity was obtained at pH values from 10.3 to 11.3 in the mixture of water-ethanol-dioxane (Fig. 1). This pH value can be adequately maintained with the buffer solution described above. In the case of isopentyl alcohol extraction, the magnesium complex showed its maximum fluorescence in the pH range from 11.5 to 12.0. A 0.5 mol dm^{-3} sodium hydrogencarbonate solution was chosen as the buffer because the buffer consisting of en and hydrochloric acid caused an unfavorable separability between isopentyl alcohol and the aqueous phase.

Effect of the 4,4′-DDAB Concentration. The effect of the variation in the 4,4′-DDAB concentration on the fluorescence intensity was also investigated. The maximum intensity was obtained in the range of $(2—4)\times10^{-7}$ mol for 1 μg (4.1×10^{-8} mol) of magnesium in the mixture of water-ethanol-dioxane, where 4×10^{-7} mol corresponded to adding 1 cm^3 of a 0.01% 4,4′-DDAB solution. The addition of 1 cm^3 of a 0.02% 4,4′-DDAB solution was suitable in the isopentyl alcohol-extraction procedure.

Effects of Standing Time and of Shaking Time. The fluorescence of the magnesium complex developed fully within a few minutes after the preparation of the solution in the nonextraction procedure and after shaking in the extraction procedure. The intensity was stable for at least 2 hours.

Calibration Curves. According to Determination Procedure A, magnesium can be determined in the range of (0.1—4.0) μg. Linear relationships are observed between the fluorescence intensity and the magnesium concentration in this range. The coefficient of variation (c.v.) for 1 μg and 0.1 μg of magnesium were 1.2% and 3.2% (n=10) respectively. In Determination Procedure B, the determinable range of magnesium is (0.04—3.0) μg. The c.v. values for 1 μg and 0.04 μg of magnesium were 2.0% and 7.3% (n=10) respectively.

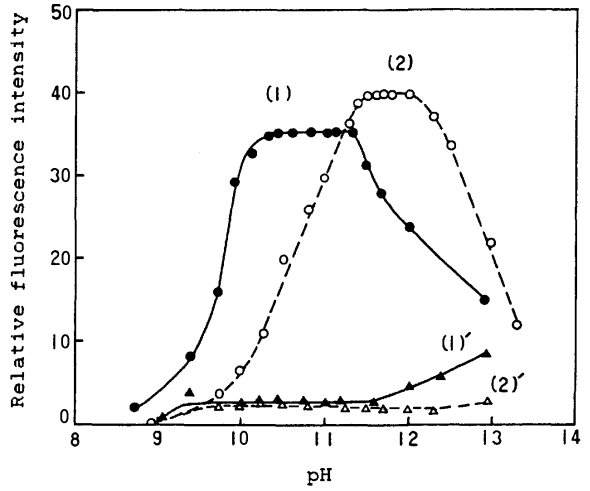

Fig. 1. Effect of pH on fluorescence intensity of magnesium-4,4′-DDAB complex.
(1) *Nonextraction procedure*; solvent: water-ethanol-dioxane (3:2:3, vol. ratio), Mg(II): 1 μg, 0.01% 4,4′-DDAB: 1 cm^3, wavelength: 465 nm/560 nm, 50 div vs. 0.5 μg cm^{-3} rhodamine B (setting 465 nm/560 nm).
(2) *Extraction procedure*; solvent: isopentyl alcohol, Mg(II): 1 μg cm^{-3}, 0.02% 4,4′-DDAB: 1 cm^3, wavelength: 480 nm/560 nm, 80 div vs. 0.5 μg cm^{-3} rhodamine B (setting 480 nm/560 nm).
(1)′ Reagent blank of (1).
(2)′ Reagent blank of (2).

Effect of Diverse Ions. The effects of diverse ions on the fluorescence intensity produced by 1 μg of magnesium were also investigated. In the nonextraction procedure, the following cations in 1000-fold excesses did not interfere: silver(I), arsenic(III), gold(III), barium(II), bismuth(III), cadmium(II), mercury(II), molybdenum(VI), nickel(II), palladium(II), antimony(III), selenium(IV), and thallium(I). Calcium(II), tin(IV), and zinc(II) caused no interference in 100-fold excesses. 1000-fold amounts of chromium(VI), indium(III), and zirconium(IV), 100-fold amounts of iron(II), lanthanum(III), and tungsten(VI), and 10-fold amounts of aluminum(III), cobalt(II), cupper(II), gallium(III), and hafnium(IV) could be tolerated by adding 3 cm^3 of 40% (2.7 mol dm^{-3}) triethanolamine as a masking agent. 1000-fold amounts of cobalt(II) and copper(II), and 500-fold amounts of iron(II) and iron(III) could be tolerated by adding 3 cm^3 of 10% (1.5 mol dm^{-3}) potassium cyanide. In the extraction procedure, 1000-fold excesses of calcium(II), 100-fold excesses of aluminum(III), and 10-fold excesses of chromium(VI), gallium(III), and titanium(IV), did not interfere even when no masking agent was used.

In conclusion, the authors recommend the nonextraction procedure (Determination Procedure A), because it is simple and rapid, and therefore yields highly reproducible results.

References

1) F. D. Snell, "Photometric and Fluorometric Methods of Analysis, Metals. Part 2," John Wiley & Sons, New York (1978), p. 1928.
2) S. Watanabe, W. Frantz, and D. Trottier, *Anal. Biochem.*, **5**, 345 (1963).
3) B. Aurivillius and P. Stenson, *Ark. Kemi.*, **23**, 551 (1965); *Chem. Abstr.*, **63**, 1680f (1965).
4) D. F. H. Wallach and T. L. Steck, *Anal. Chem.*, **35**, 1035 (1963).
5) R. M. Dagnall, R. Smith, and T. S. West, *Analyst*, **92**, 20 (1967).
6) K. Watanabe, *Bunseki Kagaku*, **32**, 698 (1983).
7) H. Diehl, R. Olsen, G. I. Spielholtz, and R. Jensen, *Anal. Chem.*, **35**, 1144 (1963).
8) D. C. Freeman, Jr., and C. E. White, *J. Org. Chem.*, **21**, 379 (1956).
9) H. V. Drushell, A. L. Sommers, and R. C. Cox, *Anal. Chem.*, **35**, 2166 (1963).
10) Y. Nishikawa and K. Hiraki, "Keikou·Rinkou Bunseki-hou (Fluorimetry and Phosphorimetry)," Kyoritsu (1984), p. 97.
11) J. Knoeck and J. A. Buchholz, *Talanta*, **18**, 895 (1971).

Deuterium Isotope Effect on the Rate of Ligand Exchange between Tetrakis-(acetylacetonato)thorium(IV) and Free Acetylacetone in CD_3CN

Naoshi FUJIWARA,*,† Tomoe NAKAGAWA, Hiroshi TOMIYASU, and Hiroshi FUKUTOMI††
Research Laboratory for Nuclear Reactors, Tokyo Institute of Technology, O-okayama 2-12-1, Meguro-ku, Tokyo 152
(Received January 6, 1989)

Synopsis. A deuterium isotope effect on the rate of acetylacetonate exchange between tetrakis(acetylacetonato)thorium(IV), $Th(acac)_4$, and free acetylacetone in CD_3CN has been examined by means of ^1H NMR technique. The second-order rate constant, k, which is expressed as a function of the observed first-order rate constant, k_{obsd}, and the concentration of acetylacetone in the enol form, $[acetylacetone]_{enol}$, by $k=k_{obsd}/[acetylacetone]_{enol}$ was determined for the reaction of deuterated acetylacetone, Dacac, as well as undeuterated acetylacetone, Hacac. The ratio of second-order rate constants for Hacac and Dacac, k_H/k_D, was approximately 9. This large deuterium isotope effect strongly supports a mechanism proposed in a previous paper that the proton transfer process is the rate determining step of the whole reaction.

Much interest has been concerned with respect to ligand exchange reactions in various acetylacetonato complexes.[1-9] In an earlier paper, we reported the study on the kinetics of acac exchange in $Th(acac)_4$ and proposed a mechanism passing through a nine coordinate intermediate, $Th(acac)_4\cdots$Hacac, where Hacac in the enol form coordinated as a unidentate ligand and a proton transferred from Hacac to one of four acac's at the rate determining step.[2]

This paper presents results of the deuterium isotope effect of the acac exchange in $Th(acac)_4$ in order to clarify the above mechanism.

Experimental

Materials. The complex $Th(acac)_4$ was synthesized by the method reported previously.[2] Acetylacetone was deuterated by the reported method.[7] The deuteration of the methine proton in coordinated acac was carried out by the following procedure: $Th(acac)_4$ (0.2 g) and deuterated acetylacetone Dacac (0.5 g) was dissolved in 2 cm^3 of dichloromethane, and the solvent involving Dacac and Hacac was removed by evaporation under reduced pressure, and then the resulted precipitate was dried in vacuo at 100 °C for one day. Acetonitrile-d_3 (Merck Co., Ltd.) was dried over Molecular Sieves 4A (Wako Pure Chemical Ltd.). Dichloromethane (Wako) was dried over anhydrous calcium chloride (Wako) for one day and distilled. Acetylacetone (Wako) and deuterated acetylacetone were dried over anhydrous calcium sulfate and distilled twice before use.

Kinetic Procedure. $Th(acac)_4$, Dacac, and CD_3CN were weighed, and sealed in a 5 mmϕ NMR sample tube. A JEOL JNM FX-100 FT NMR spectrometer equipped with a JNM-VT-3B temperature controller was used for measurements of ^1H NMR spectra. The water content of the reaction mixture was analyzed by the Karl-Fischer titration. The rate constants of the exchange reaction were determined from the line shape analysis of methine proton signals by using the two-site model.[2]

Results

Deuterium Isotope Effect on the Acac Exchange in $Th(acac)_4$. The ^1H NMR spectra of methine protons for the mixture of $Th(acac)_4$ and Hacac, and their deuterated species in CD_3CN were measured at various temperatures (Fig. 1). The deuterated fraction of acetylacetone was determined to be 86% based on the ratio of peak areas of methine and methyl protons. The signals of coordinated acac (upper field) and that of free $Hacac_{enol}$ (lower field) were observed separately at 0 °C. However, two signals tended to coalesce as the temperature was raised. Though the difference in the chemical shifts of the methine proton signals between Dacac and $Th(acac)_4$ is less than that between Hacac and $Th(acac)_4$, the coalescence temperature of 28 °C was significantly higher than that of 12 °C for the exchange between undeuterated $Th(acac)_4$ and $Hacac_{enol}$.[2] This clearly indicates that the exchange

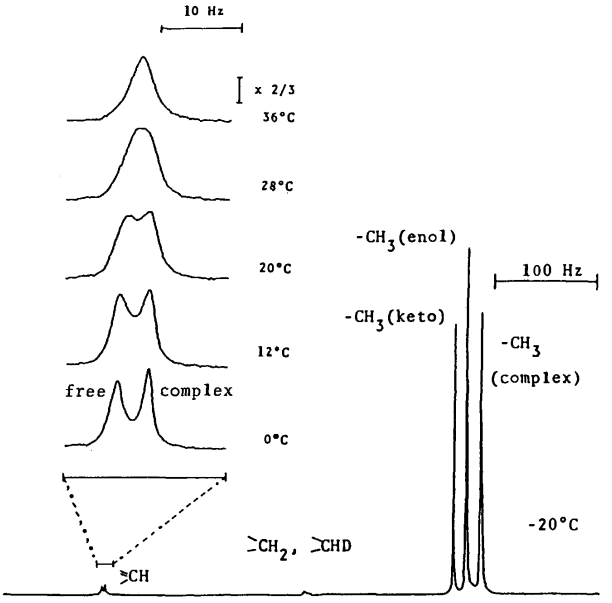

Fig. 1. ^1H NMR spectrum of the mixture of $Th(acac)_4$ and deuterated acetylacetone in CD_3CN, and the change of methine proton signals with temperatures. $[Th(acac)_4]=0.106$ mol kg^{-1}, $[Hacac]_{total}$ (deuterated fraction: 86%)=0.690 mol kg^{-1}, and $[H_2O]=0.08$ mol kg^{-1}. The observed first-order rate constant k_{obsd} was determined at various temperatures as follows.

T/°C	12.0	20.0	28.0	36.0
k_{obsd}/s^{-1}	17.2	24.0	33.4	43.0

† Present address: Department of Anesthesiology, School of Medicine, Niigata University, Asahimachi-dori 1-757, Niigata 951.

†† Present address: Department of Chemistry, Faculty of Science, Okayama University, Tushimanaka, Okayama 700.

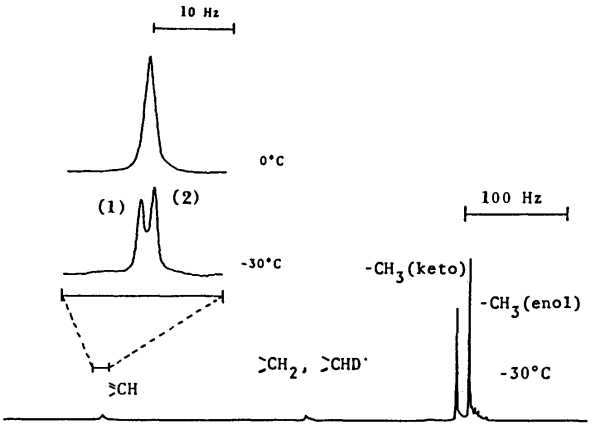

Fig. 2. ^{1}H NMR spectrum of deuterated acetylacetone in CD_3CN at −30 °C. The expanded signals of methine proton at −30 and 0 °C are also shown. $[Hacac]_{total}$ (deuterated fraction: 55%)=0.667 mol kg^{-1} and $[H_2O]$=0.06 mol kg^{-1}.

reaction in the deuterated system is much slower than in the undeuterated one.

Acac Exchange between Hacac and Dacac. The NMR spectra of the methine proton of deuterated $Hacac_{enol}$ (deuterated fraction 55%) in the absence of $Th(acac)_4$ are shown in Fig. 2. Two signals, which were observed at −30 °C, coalesced to a single peak at 0 °C. Four types of isotope isomers exist in incompletely deuterated $Hacac_{enol}$ as written below.

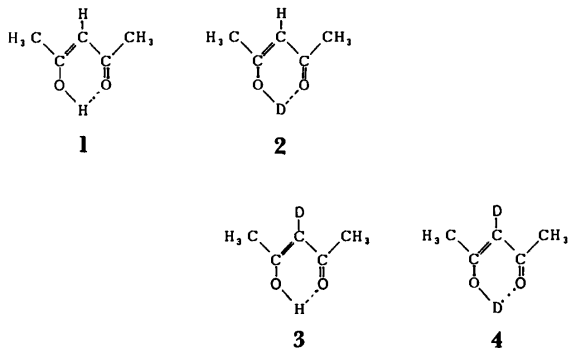

1 2

3 4

Among these isomers, only **1** and **2** give the methine proton signals. On the basis of the signal intensity, the peaks in upper and lower fields are assigned as the signals of **2** and **1**, respectively. The exchange rate between **1** and **2** was calculated by use of the two-site model. The reciprocal values of life time for **1**, which correspond to the first-order rate constant for exchange of two methine protons, were determined to be 3.63, 1.97, and 0.82 s^{-1} at 0, −10, and −20 °C, respectively. Because of the very narrow splitting between the signals of **1** and **2**, the singls coalesced at 0 °C, although the exchange rate was comparable with that of acac exchange between $Th(acac)_4$ and $Dacac_{enol}$. The broadening of the methine proton signals due to the exchange between **1** and **2**, however, was taken into account for the calculation of the exchange rates between $Th(acac)_4$ and $Dacac_{enol}$.

Discussion

In the previous paper,[2] the rate of the exchange between $Th(acac)_4$ and free Hacac was found to be first order in both $[Th(acac)_4]$ and $[Hacac]_{enol}$. Since the same rate law is expected for the exchange between $Th(acac)_4$ and Dacac, the observed first-order rate constant, k_{obsd}, is expressed by Eq. 1.

$$k_{obsd}=k[Dacac]_{enol} \quad (1)$$

where k is the second-order rate constant and $Dacac_{enol}$ consists of the four isotope isomers **1**, **2**, **3**, and **4** in the incompletely deuterated system. Therefore, Eq. 1 yields

$$k_{obsd}=k_1[\mathbf{1}]+k_2[\mathbf{2}]+k_3[\mathbf{3}]+k_4[\mathbf{4}] \quad (2)$$

where k_1, k_2, k_3, and k_4 are the second-order rate constants for **1**, **2**, **3**, and **4**, respectively.

It is reasonable to assume that $k_1=k_3(=k_H)$ and $k_2=k_4=(k_D)$, because the primary isotope effects due to O-H and O-D groups are of essential importance for the exchange rate. Then, Eq. 2 is written by

$$k_{obsd}=k_H([\mathbf{1}]+[\mathbf{3}])+k_D([\mathbf{2}]+[\mathbf{4}]). \quad (3)$$

The values of k_H were determined previously[2] and the concentrations [**1**]+[**3**] and [**2**]+[**4**] were calculated from the NMR signal intensity. These data along with Eq. 3 give the values of k_D, which are listed in Table 1. The ratio k_H/k_D is about 9. This value is close to the maximum of the kinetic isotope effect, which is estimated from the difference in the zero-point energy of O-H and O-D bonds in Hacac and Dacac, respectively.[8] The deuterium isotope effects for acac exchange reactions were reported in a variety of complexes, M^{III}=Cr^{III}, Co^{III}, Rh^{III}, Fe^{III}, and V^{III}, and $VO(acac)_2$.[3-7] The small isotope effects observed in these reactions were consistent with mechanisms that the addition of free Hacac to the complexes or the dissociation of acac from the complexes, which preceded the proton transfer step, substantially governed the whole reaction rates. An only exception was recently reported for the acac exchange in $Sc(acac)_3$, which revealed the considerably large isotope effect (k_1^H/k_1^D=5, where k_1 was related to k_{obsd} as $k_{obsd}=k_1[acac]_{enol}$).[8] In the latter case, a role of the proton transfer step was consider to be particular importance for the exchange rate.

In the present study, the deuterium isotope effect is largest of all acac exchange reactions ever studied and k_H/k_D is closed the maximum value. Morever, the rate of acac exchange between $Th(acac)_4$ and Dacac is comparable with that between Hacac and Dacac. These facts strongly supports the following

Table 1. Deuterium Isotope Effect on the Second-Order Rate Constant k for the acac Exchange Reaction in $Th(acac)_4$ in CD_3CN

T/°C	k_H/s^{-1} mol^{-1} kg	k_D/s^{-1} mol^{-1} kg	k_H/k_D
12	184	18.6	9.9
20	246	27.6	8.9
28	351	37.0	9.5

reaction mechanism proposed in the previous paper,[2]

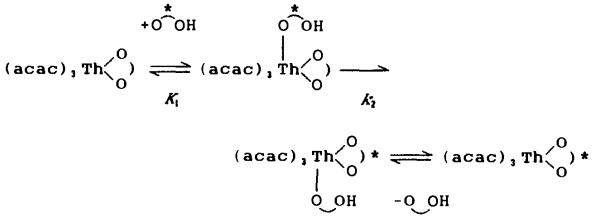

where $\overset{O}{\underset{O}{\frown}}$ and $\overset{O}{\underset{OH}{\frown}}$ represent acac and $Hacac_{enol}$, respectively and proton transfer process (k_2 path) determined the exchange rate.

A similar mechanism was also proposed for the tta (tta=2-thenoyltrifluoroacetonate) exchange in $Th(tta)_4$.[10] In this case, the addition of DMSO (dimethyl sulfoxide) to the complex forming $Th(tta)_4 \cdots$dmso was directly observed by ^1H NMR measurements and the exchange of dmso was found to be extremely fast (10^2 s^{-1} at $-92\,°C$). This fact is consistent with the above mechanism that K_1 path is in fast equilibrium prior to the proton transfer.

This work is partly supported by a Grant-in-Aid for Scientific Research No. 62470039 from the Ministry of Education, Science and Culture.

References

1) N. Fujiwara, H. Tomiyasu, and H. Fukutomi, *Chem. Lett.*, **1983**, 377.
2) N. Fujiwara, H. Tomiyasu, and H. Fukutomi, *Bull. Chem. Soc. Jpn.*, **57**, 1576 (1984).
3) M. Nishizawa and K. Saito, *Bull. Chem. Soc. Jpn.*, **51**, 483 (1978).
4) H. Kido, *Bull. Chem. Soc. Jpn.*, **53**, 82 (1980).
5) H. Kido and K. Saito, *Bull. Chem. Soc. Jpn.*, **53**, 424 (1980).
6) A. Watanabe, H. Kido, and K. Saito, *Inorg. Chem.*, **20**, 1107 (1981).
7) H. Kido and K. Saito, *Inorg. Chem.*, **16**, 397 (1977).
8) Y. Hatakeyama, H. Kido, K. Saito, M. Harada, H. Tomiyasu, and H. Fukutomi, *Inorg. Chem.*, **27**, 992 (1988).
9) H. Kido and K. Saito, *Bull. Chem. Soc. Jpn.*, **53**, 82 (1980).
10) N. Fujiwara, H. Tomiyasu, and H. Fukutomi, *Bull. Chem. Soc. Jpn.*, **58**, 1386 (1985).

Syntheses of 1β-Hydroxyvitamin D_2 and D_3

Yoji TACHIBANA
Central Research Laboratory, Nisshin Flour Milling, Co., Ltd., Tsurugaoka, Ooimachi, Irumagun, Saitama 354
(Received July 30, 1988)

Synopsis. Reduction of 1-oxo-3,5-cyclovitamin D_2 and D_3 was carried out under various conditions. $LiAlH_4$ reduction in ether preferentially afforded 1β-hydroxy-3,5-cyclovitamin D_2 and D_3, which were converted to 1β-hydroxyvitamin D_2 and D_3.

It has been established that the hydroxyl group at C-1 of vitamins D_2 and D_3 plays an important role in eliciting their biological activity.[1] In order to investigate the relationship between the molecular configuration and the physiological activity, DeLuca[2] and Mazur[3] synthesized 1β-hydroxyvitamin D_3 (**2**), the C_1 epimer of 1α-hydroxyvitamin D_3 (**1**), by oxidation of **1** followed by the reduction of the formed 1-oxo-previtamin D_3, and evaluated its biological activity.

DeLuca et al. reported that 1α-hydroxyvitamin D_2 (**3**) is about ten-times less toxic than **1**, but appears to be almost equally potent regarding vitamin D activity.[4] Thus, it is noteworthy to compare the physiological activity of the C_1 epimer of **3** with that of **1**.

In the present paper, the reduction of 1-oxo-3,5-cyclovitamin D_3 (**5**) and D_2 (**6**)[5] under various conditions and the conversion of the formed 1β-hydroxy-cyclovitamin D_3 (**8**) and D_2 (**10**) into the corresponding 1β-hydroxyvitamin D_3 (**2**) and D_2 (**4**), are described.

The 1-oxo-3,5-cyclovitamin D_3 (**5**) and D_2 (**6**) employed for the reduction were prepared from the corresponding 3,5-cyclovitamin D_3 and D_2 by modifying the procedure reported by DeLuca et al.[5] 1-Hydroxycyclovitamin D_3 and D_2 produced in the above mentioned reaction were converted to **5** and **6** by further oxidation with activated manganese oxide.

As indicated in Table 1, the stereochemistry of the reduction of **5** and **6** is highly dependent on the reagent and solvent used.[6,7] The reduction of **5** and **6** with lithium aluminum hydride ($LiAlH_4$) in ether gave 1β-hydroxy isomer (**8** and **10**) and 1α-hydroxy isomer (**7** and **9**) in a ratio of 5/1. On the other hand, the selectivity (**8/7** and **10/9**) was decreased when tetrahydrofuran (THF) was employed as solvent. The reduction with $Na[AlH_2(OCH_2CH_2OCH_3)_2]$ (sodium dihydridobis(2-methoxyethoxy)aluminate) gave similar results. These results may be well explained by assuming the coordination of the methoxyl group (at C-6) and carbonyl group (at C-1) of **5** and **6** to the Al atom of the reagent. Consequently, the approach of the hydride from the α-side of **5** and **6** appears to be hindered due to the chelation described above. Accordingly, the β-side attack of the hydride may be facilitated to yield a higher amount of 1β-hydroxy isomer (**8** and **10**). In contrast, THF may coordinate to the reducing agent, which probably makes the chelation between the Al atom and the oxygen atoms of A ring of vitamin D more difficult compared with the reduction in ether. As a result, this seems to lead to a lower ratio of 1β-hydroxy

Table 1. Reduction of 1-Oxo-3,5-cyclovitamin D_3 (**5**) and D_2 (**6**) under Various Conditions

Entry	R	Reducing reagent	Temp	Solvent	Ratio (**8/7** or **10/9**)[a]
1	R_1	$LiAlH_4$	rt[b]	Ether	5.0
2	R_1	$LiAlH_4$	rt	THF	2.5
3	R_1	$LiAlH_4$	0 °C	Ether	4.5
4	R_1	$LiAlH_4$	0 °C	THF	2.5
5	R_1	$NaBH_4$	rt	Ether-EtOH	1.8
6	R_1	$NaBH_4$	rt	Ether-THF	2.1
7	R_1	DIBAL	rt	Ether	2.0
8	R_1	DIBAL	rt	THF	1.4
9	R_1	DIBAL	rt	Ether	1.6[c]
10	R_1	DIBAL	rt	THF	1.0[c]
11	R_1	DIBAL	−20 °C	Ether	1.5[c]
12	R_2	$LiAlH_4$	rt	Ether	5.1
13	R_2	$LiAlH_4$	rt	THF	2.7
14	R_2	$NaBH_4$	rt	Ether-EtOH	1.7
15	R_2	DIBAL	rt	Ether	1.5
16	R_2	DIBAL	rt	THF	1.1
17	R_2	DIBAL	rt	Ether	1.3[c]
18	R_2	DIBAL	rt	THF	1.1[c]
19	R_2	$Na[AlH_2(OCH_2CH_2OCH_3)_2]$	rt	Ether	5.0
20	R_2	$Na[AlH_2(OCH_2CH_2OCH_3)_2]$	rt	THF	1.4

a) Formation ratio was determined by means of high pressure liquid chromatography (HPLC) after 1-hydroxycyclovitamin D_3 and D_3 (**7**—**10**) were converted to corresponding 3β-acetoxy-1-hydroxyvitamin D_3 and D_2 (**11**—**14**). b) rt: room temperature. c) DIBAL solution was added to the solution of 1-oxo-3,5-cyclovitamin D_3 (**5**) and D_2 (**6**).

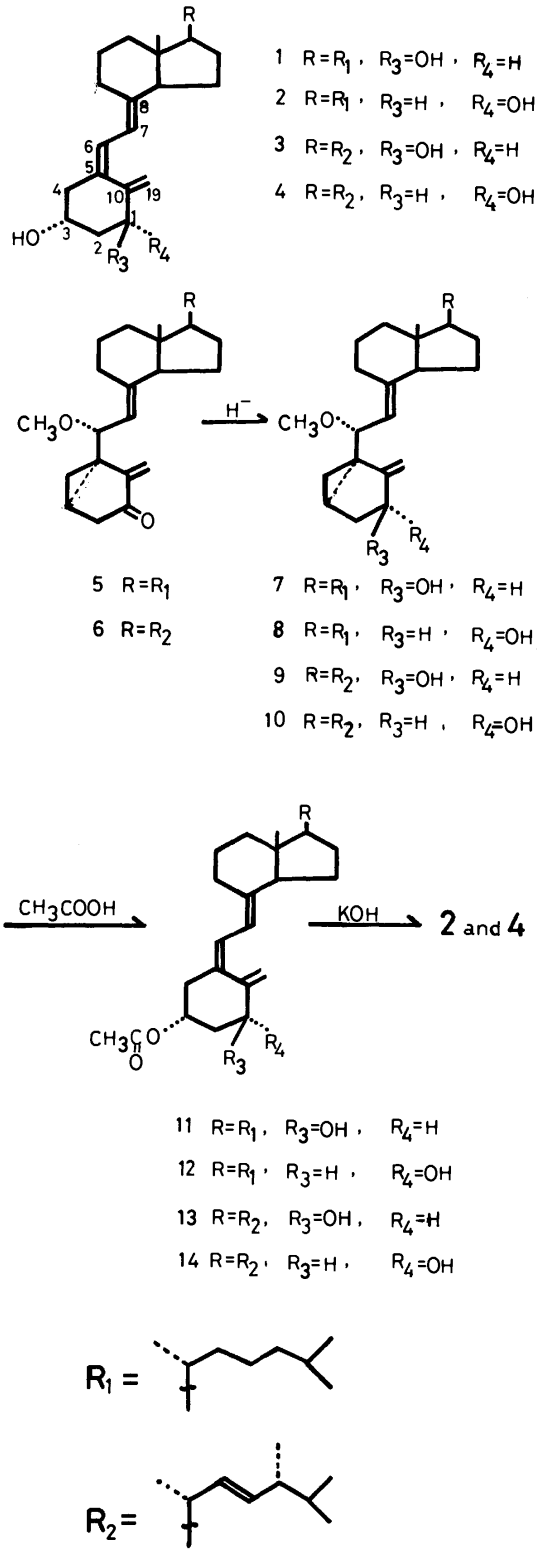

isomer (**8** and **10**) to 1α-hydroxy isomer (**7** and **9**). The effect of temperature was not relevant to the reduction selectivity.

Other reducing reagents, such as sodium borohydride ($NaBH_4$) and diisobutylaluminum hydride (DIBAL), showed no appreciable stereoselectivity in the reduction of **5** and **6** compared with $LiAlH_4$. It seems that DIBAL may be too bulky to form the chelation with the oxygen atoms of A ring moiety. Especially, the reduction with DIBAL in THF gave almost the same isomer ratio (1β-ol/1α-ol=1). However, this system (DIBAL-THF) can be an effective way to provide radioisotope labeled 1α-hydroxyvitamin D_2 and D_3 at position C-1, which seems to serve as convenient tools for a number of detailed biomedical experiments.[8,9]

Thus, the obtained 1β-hydroxy-3,5-cyclovitamin D_3 (**8**) and D_2 (**10**) were solvolyzed in acetic acid to yield 3β-acetoxy-1β-hydroxyvitamin D_3 (**12**) and D_2 (**14**), which were subsequently hydrolyzed upon treatment with ethanolic potassium hydroxide to produce 1β-hydroxyvitamin D_3 (**2**) and D_2 (**4**), respectively.

The inversion of the hydroxyl group at C-1 of **7** or **9** by a Mitsunobu reaction was not successful.[10] The procedure described here may be applied to the syntheses of other 1β-hydroxyvitamin D derivatives from the corresponding vitamin D derivatives.

Experimental

Melting points were uncorrected. UV spectra were taken on a Hitachi 320 spectrometer. ^1H NMR spectra were recorded in $CDCl_3$ on a JNF-FX200 spectrometer with TMS as an internal standard. Mass spectra were measured on a Hitachi M-80 mass spectrometer. HPLC were performed on a Hitachi 615-11 liquid chromatography equiped with a UV detector (set at 265 nm) and a Hibar column (prepacked column, LiChrosorb Si 60 (5 μm); 4 mm$\times$25 mm) with 20% hexane in dichloromethane as a mobile phase at a flow rate 1.0 ml min^{-1} (pressure: 30 kg cm^{-2}). Solvents were removed under reduced pressure.

1-Oxo-3,5-cyclovitamin D_3 (5) and D_2 (6). To a stirred suspension of SeO_2 (280 mg) in dichloromethane (100 ml), was added 4 ml of 3 M (1 M=1 mol dm^{-3}) 2,2,4-trimethylpentane solution of *t*-BuOOH. After the mixture was stirred for 1 h at room temperature, a dichloromethane solution (100 ml) of 3,5-cyclovitamin D_3[5] (1.0 g) was added dropwise. The mixture was allowed to react for 40 min at room temperature. The solution was washed with a 10% NaOH solution (40 ml). The dichloromethane solution was separated and concentrated to a heavy oil. The residue was extracted with ether, washed with brine, and dried over sodium sulfate. The ether solution was evaporated and the residue was chromatographed on silica gel. Elution with ethyl acetate/hexane (5/95, v/v) gave **5** as oil. 435 mg (42%). λ_{max} 248 nm (ε=4200, EtOH) (lit,[5] ε=3500).

Further elution with ethyl acetate/hexane (1/4, v/v) afforded 1α-hydroxycyclovitamin D_3 (**7**). 312 mg (25%). **7** (312 mg) was dissolved in dichloromethane (30 ml) and allowed to react with (activated) manganese oxide (900 mg) at room temperature for 1 h. The mixture solution was filtered on celite and concentrated. The residue was chromatographed on silica gel. Elution with ethyl acetate/hexane (5/95, v/v) gave **5**. 234 mg (75%).

Treatment of 3,5-cyclovitamin D_2[5] (1.0 g) in a similar way involving the oxidation process of 1α-hydroxycyclovitamin D_2 (**9**) provided 1-oxo-3,5-cyclovitamin D_2 (**6**). 620 mg (60%). λ_{max} 248 nm (ε=4000, EtOH).

1β-Hydroxyvitamin D_3 (2). To an ether solution (20 ml) containing $LiAlH_4$ (200 mg) was added dropwise an ether solution (10 ml) of 1-oxo-3,5-cyclovitamin D_3 (**5**) (400 mg) at room temperature. The mixture was stirred for 30 min. After decomposition of the excess $LiAlH_4$ with H_2O, the ether solution was washed with brine, dried (Na_2SO_4) and evaporated to dryness. The residue was purified by silica

gel chromatography (eluted with hexane/ethyl acetate, 4/1) to give a mixture of 1β- and 1α-hydroxycyclovitamin D_3[5] (**8**/**7**=5.0). 296 mg (74%).

The 1-hydroxycyclovitamin D_3 (296 mg) was dissolved in acetic acid (6 ml) and the mixture was stirred at 55 °C for 20 min. The mixture was extracted with ether, washed with a sat. $NaHCO_3$ solution and brine, dried (Na_2SO_4), and evaporated. The residue was chromatographed on silica gel. Elution with hexane/ethyl acetate (4/1) afforded 3β-acetoxy-1β-hydroxyvitamin D_3 (**12**). 205 mg (65%). λ_{max} 264 nm (ε=17500, EtOH) (lit,[3] ε=18000).

The actate (**12**) (205 mg) was dissolved in ethanolic potassium hydroxide (KOH 150 mg, EtOH 5 ml) and the mixture was stirred for 15 min at room temperature. The ethanol solution was extracted with ether, washed with brine, dried (Na_2SO_4) and concentrated to dryness. The residue was purified by silica gel chromatography (chloroform/ethyl acetate, 9/1) to yield 1β-hydroxyvitamin D_3 as oil. 149 mg (80%). λ_{max} 264 nm (ε=18500, EtOH) (lit,[3] ε=18000).

1β-Hydroxyvitamin D_2 (4). 1-Oxocyclovitamin D_2 (**6**) (400 mg) was reduced with $LiAlH_4$ (200 mg) in ether and treated in a similar manner described above to give 1-hydroxy-3,5-cyclovitamin D_2 (**10**/**9**=5.1). 280 mg (70%). *m/z* 426 (M^+).[5]

1-Hydroxycyclovitamin D_2 (280 mg) was treated with acetic acid (6 ml) at 60 °C for 15 min. After the usual work up, the residue was chromatographed (hexane/ethyl acetate, 4/1) to afford 3β-acetoxy-1β-hydroxyvitamin D_2 (**14**). 182 mg (61%): *m/z* 454 (M^+), 394 (M^+-CH_3COOH); ^1H NMR δ=6.33—6.00 (2H, ABq, *J*=12 Hz, H-6, H-7), 5.37 (1H, m, H-19E), 5.20 (2H, m, H-22, H-23), 5.00 (1H, m, H-19Z), 4.99 (1H, m, H-3), 4.17 (1H, bs, H-1), 2.05 (3H, s, $COCH_3$).

The acetate (**14**) (182 mg) was hydrolyzed in ethanolic potassium hydroxide (KOH 150 mg, EtOH 5 ml) at room temperature for 15 min. The solution was extracted with ether, washed with brine, dried (Na_2SO_4) and evaporated. The residue was chromatographed on silica gel (chloroform/ethyl acetate, 4/1) to produce 1β-hydroxyvitamin D_2 (**4**). 124 mg (75%): Calcd for $C_{28}H_{44}O_2$: M, 412.3339. Found: *m/z* 412.3338; ^1H NMR δ=6.01—6.42 (2H, ABq, *J*=12Hz, H-6, H-7), 5.26 (1H, m, H-19E), 5.17 (2 H, m, H-22, H-23), 4.96 (1H, m, H-19Z), 4.30 (1H, bs, H-1), 4.07 (1H, m, H-3).

1α-Hydroxyvitamin D_2 (3) from 6. A 1 M hexane solution of DIBAL (10 ml) was added to a THF solution (20 ml) of 1-oxo-3,5-cyclovitamin D_2 (**6**) (400 mg) at room temperature and the mixture was stirred for 30 min. The solution was washed with brine and filtered on Celite. The solution was dried over Na_2SO_4 and evaporated. Purification on silica gel (hexane/ethyl acetate, 4/1) gave 1-hydroxycyclovitamin D_2 (**10**/**9**=1). 180 mg (45%).

The 1-hydroxycyclovitamin D_2 (180 mg) was treated with acetic acid (5 ml) at 60 °C for 20 min. The mixture was extracted with ether. The ether solution was washed with sat. $NaHCO_3$ and brine, and concentrated to dryness. The residue was purified by silica-gel chromatography. Elution with hexane/ethyl acetate (9/1) afforded 3β-acetoxy-1β-hydroxyvitamin D_2 (**14**) (60 mg, 31%). Further elution with the same developing solvent gave 3β-acetoxy-1α-hydroxyvitamin D_2 (**13**) (65 mg, 34%).

The acetate (**13**) (65 mg) was hydrolyzed with ethanolic potassium hydroxide (KOH 40 mg, EtOH 5 ml). The solution was extracted with ether, washed with brine and evaporated. Chromatography on silica gel (chloroform/ethyl acetate, 4/1) and crystallization (hexane-ethyl acetate) yielded **3**. 26 mg (44%). mp 140—141 °C (lit, [5] 138—140 °C).

References

1) H. F. DeLuca and H. K. Schnoes, *Ann. Rev. Biochem.* **52**, 411 (1983).

2) H. E. Paaren, H. K. Schnoes, and H. F. DeLuca, *J. Chem. Soc., Chem. Commun.*, **1977**, 890.

3) M. Sheves, N. Friedman, and Y. Mazur, *J. Org. Chem.*, **42**, 3597 (1977).

4) G. Sjoden, C. Smith, U. Lindgren, and H. F. DeLuca, *Proc. Soc. Exp. Biol. Med.*, **178**, 432 (1985).

5) H. E. Paaren, H. F. DeLuca, and H. K. Schnoes, *J. Org. Chem.*, **45**, 3253 (1980).

6) L. J. Vanmaele, P. J. DeClercqc, M. Vandewalle, S. J. Halkes, and W. R. M. Overbeek, *Tetrahedron*, **40**, 1179 (1984); L. Vanmaele, D. J. DeClercq, and M. Vandewalle, *Tetrahedron*, **41**, 141(1985).

7) S. Maruyama, N. Ogihara, I. Adachi, J. Ohotawa, and M. Morisaki, *Chem. Pharm. Bull.*, **35**, 1847 (1987); J. Barluenga, J. G. Resa, B. Olano, and S. Fustero, *J. Org. Chem.*, **52**, 1425 (1987).

8) Y. Tohira, K. Ochi, I. Matsunaga, M. Fukushima, S. Takanashi, K. Hata, C. Kaneko, and T. Suda, *Anal. Biochem.*, **77**, 495 (1977).

9) M. F. Holick, T. E. Tavela, S. A. Holick, H. K. Schnoes, H. F. DeLuca, and B. M. Gallagher, *J. Biol. Chem.* **251**, 1020 (1976).

10) Treatment of 1α-hydroxycyclovitamin D_3 (**7**) (or 1α-hydroxycyclovitamin D_2, (**9**)) (1 mmol) with formic acid (or benzoic acid), triphenylphosphine and diethyl azodicarboxylate (2 mmol, each) in dry tetrahydrofuran (10 ml) at room temperature for 24 h afforded no desired product and only starting material (**7** or **9**) was recovered. (cf. W. H. Okamura and M. R. Pirio, *Tetrahedron Lett.*, **1975**, 4317).

Rotational Isomerism in Fluorene Derivatives. XVI.[1] Conformational Equilibria of 9-Substituted 9-(2′-Bromomethylphenyl)fluorene Derivatives

Akiko NISHIDA, Shinsuke SHIRAKAWA, Masuji YAMAMOTO, Shigeki WATANABE, Shizuo FUJISAKI, and Shoji KAJIGAESHI*

Department of Industrial Chemistry, Faculty of Engineering, Yamaguchi University, Tokiwadai, Ube 755

(Received September 1, 1988)

Synopsis. (Eight 9-substituted 9-(2′-bromomethylphenyl)fluorene derivatives) (**1**) were prepared. Their conformational equilibria (*ap* ⇄ *sp*) are discussed on the basis of kinetic data for internal rotation obtained by ^{1}H NMR spectroscopy.

We have recently investigated the conformational equilibria (*ap* ⇄ *sp*) of 9-(2′-substituted phenyl)fluorene derivatives having the 2′-substituents such as methyl-,[2] methoxy-,[3] methylthio-,[4] methylsulfinyl-,[4] dimethylamino-,[5] methoxymethyl-,[6] and methylamino group,[7] on the basis of their DNMR spectra. In the present paper, we wish to report on the preparation of 9-substituted 9-(2′-bromomethylphenyl)fluorene derivatives (**1**) and a study concerning the conformational equilibria of these compounds by comparing their ^{1}H NMR behavior with those of 9-substituted 9-(2′-methylphenyl)fluorene derivatives (**2**).

Results and Discussion

Preparation of 1. Fluorenes **1**, except 9-(2′-bromomethylphenyl)fluorene (**1b**), were prepared by the bromination of the corresponding 9-substituted 9-(2′-methylphenyl)fluorenes **2** with NBS in carbon tetrachloride in the presence of a small amount of BPO. Thus, 9-hydroxy- (**1a**), 9-methoxy- (**1c**), 9-methyl- (**1d**), 9-carboxy- (**1e**), 9-methoxycarbonyl- (**1f**), 9-acetyl- (**1g**), and 9-benzoyl-9-(2′-bromomethyl)fluorene (**1h**) were obtained from 9-hydroxy- (**2a**),[7] 9-methoxy- (**2c**),[8] 9-methyl- (**2d**),[2] 9-carboxy- (**2e**),[2] 9-methoxycarbonyl- (**2f**),[2] 9-acetyl- (**2g**),[2] and 9-benzoyl-9-(2′-methylphenyl)fluorene (**2h**),[2] respectively (Scheme 1). Compound **1b** was obtained by the bromination of 9-(2′-hydroxymethylphenyl)fluorene (**4**), which was prepared by the hydrolysis of 9-(2′-iodomethylphenyl)fluorene (**3**),[6] with dry hydrogen bromide. The results of the preparation of **1** and their partial ^{1}H NMR data are shown in Table 1.

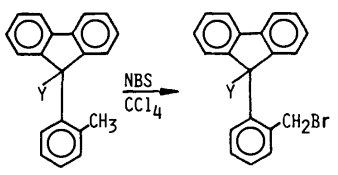

Y		Y	
a	OH	f	$COOCH_3$
c	OCH_3	g	$COCH_3$
d	CH_3	h	COPh
e	COOH		

Scheme 1.

Table 1. ^{1}H NMR Data of 9-Substituted 9-(2′-Bromomethylphenyl) fluorene Derivatives (**1**) at Room Temperature (δ, $CDCl_3$)

Compd	2′-CH_2Br	9-Substituent	6′-H
1a	4.02br.s	2.38br.s	
1b	4.96s(5.5)	5.55s(5.5)	6.42d
	3.44s(1)	5.02(1)	
1c	4.12br.s	2.76s	
1d	3.48s	1.78s	
1e	3.94br.s	—	
1f	4.06br.s	3.84s	
1g	4.16s	1.95s	
1h	4.40s	—	

a) Numerals in parentheses are ratios of signal intensities.

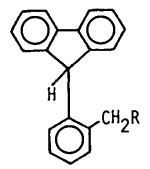

1b: R = Br 3: R = I
2b: R = H 4: R = OH

Conformational Equilibria of 1. Signals due to the two rotamers, *ap* and *sp*, of 9-(2′-substituted phenyl)fluorene derivatives were observed in their NMR spectra at room temperature or at low temperature owing to their high barriers for rotation about the C(9)-C(Ar) bond. For example, two singlets due to the bromomethyl group of *ap* and *sp* forms of **1b** were observed at δ 3.44 and 4.96 ($K(ap/sp)$=1/5.5) at room temperature. The geometries of the two rotamers, *ap* and *sp*, of **1b** are shown in Fig. 1.

Since the signal of bromomethyl group of compound **1d** appeared at 3.48 ppm, which was very close to that of the *ap*-form of **1b**, as a sharp singlet even at

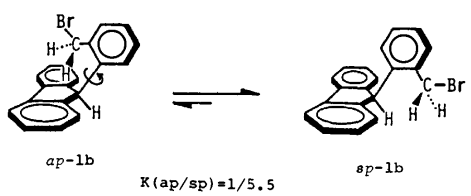

Fig. 1. The two rotamers of **1b**.

low temperature (−50 °C), this compound may exist only as the *ap*-form.

It was, however, difficult to assign the predominant conformers of the other bromomethyl series **1a**, **1c**, **1e**, **1f**, **1g**, and **1h**, by means of their ^{1}H NMR spectra at room temperature. Their DNMR spectra at low temperature (ca. −50 °C) were, therefore, measured by the usual method. The signals of the bromomethyl group in **1a**, **1c**, and **1f** were found to split at low temperature. Although the signal of **1h** broadened (T_c=−45 °C), two isomers of **1h** could not be observed until as low as −50 °C. The DNMR spectra of **1e** and **1g** could not be obtained because of their poor solubilities in $CDCl_3$ at low temperature. The equilibrium constants $K(ap/sp)$ between *ap* and *sp* forms of these compounds at room temperature or at low temperature, together with that of compound **2**,[9] are shown in Table 2. Since each *ap*- and *sp*- bromomethyl signal of **1g** and **1h** could not be observed at low temperature (−50 °C), it was assumed that these chemical shifts were the same values as those of **1b**. Then, K values of **1g** (or **1h**) were estimated from the chemical shifts of the bromomethyl group of *ap*-, and *sp*-**1b** and **1g** (or **1h**).

As shown in Table 2, though the equilibrium of **2a** was onesided in the *ap*-form, two conformers of **1a** existed in equilibrium, $K(ap/sp)$=3.9/1. In order to explain the stabillization of the *sp*-form of **1a**, we assumed the existence of intramolecular hydrogen bonding between the oxygen atom of the 9-hydroxyl group and the hydrogen atom of the 2′-bromomethyl group or the hydrogen atom of the 9-hydroxyl group and the bromine atom of the 2′-bromomethyl group in the *sp*-form (the latter hydrogen bonding has been reported in 2-haloethanol[10]). An intramolecular hydrogen bonding which controlled the equilibrium of **1a** would be influenced by a solvent effect. No expected solvent effects, which were found in the cases of 9-(2′-methoxyphenyl)-9-fluorenol[3] and 9-(2′-dimethylaminophenyl)-9-fluorenol,[5] however, were observed in the ^{1}H NMR spectra of **1a** in several solvents (DMSO-d_6, acetone-d_6, and methanol-d_4). If intermolecular hydrogen bonding between the hydrogen atom of the 9-hydroxyl group and these solvents exists, the equilibrium of **1a** would incline completely to the *ap*-form.

Table 2. Equilibrium Constant and Activation Parameter for Rotation of **1** and **2**[a]

	1			**2**[a]		
	$K(ap/sp)$ (Temp/ °C)	ΔG^*/kcal mol^{-1}		$K(ap/sp)$ (Temp/ °C)	ΔG^*/kcal mol^{-1}	
		ap→*sp*	*sp*→*ap*		*ap*→*sp*	*sp*→*ap*
a	3.9/1(−37)	13.7	12.9	*ap* only		
b	1/5.5(25)	15.5	16.5	1/1.6(25)	16.3	16.6
c	2.6/1(−50)	13.5	12.9	*ap* only		
d	*ap* only			*ap* only		
e	—[b]			—[b]		
f	1.35/1(−50)	12.9	12.7	1/1.1(−50)	12.4	12.7
g	(1/1)[b,c]			1/2.1(−50)	12.2	12.7
h	(1/2)[c,d]			1/3.5(−65)	11.7	12.4

a) Results taken from Refs. 2 and 12. b) Insoluble in $CDCl_3$ at low temperature. c) K value is estimated from the chemical shifts of the bromomethyl group of *ap*- and *sp*-**1b** and this compound. d) Coalesed at −45 °C.

Compounds **1b** and **1c** also showed a tendency to increase the *sp*-form, compared with 9-(2′-methylphenyl)fluorene (**2b**) and **2c**. Regarding compounds **1a—c**, it can be considered that a repulsive interaction between the π-electron of the fluorene ring and an unshared electron of the bromine atom of 2′-bromomethyl group or a steric repulsion between the fluorene ring and the bromomethyl group may destabilize the *ap*-form. Thus, the *ap*-forms of **1a—c** would be more unstable than those of **2a—c**.

We have already presumed that the stabilization of the *sp*-forms in **2f—h**, which are disadvantageous with respect to the steric effect, may be due to the existence of an attractive interaction between the oxygen atom of the 9-carbonyl group and the 2′-methyl group.[2] However, the *ap*-forms in **1f—h** were found to increase, compared with those of **2f—h**. It can be concluded that the equilibria of **1f—h** are controlled by a balance of the electronic repulsion and/or the steric hindrance between the 2′-bromomethyl group and the 9-carbonyl group or the fluorene ring.

Experimental

All melting points are uncorrected. The ^{1}H NMR spectra were recorded on a JEOL-MH-100 spectrometer with a JEOL model JES-VT-3 variable temperature controller (Solvent, $CDCl_3$; $SiMe_4$). Dynamic NMR spectra were analyzed by using a modified version of the computer program DNMR 3.[11] The IR spectra were measured with a IRA-1 spectrometer as potassium bromide pellets.

Bromination of 2a with NBS. Typical Procedure. To a solution of **2a** (1.0 g, 4 mmol) in CCl_4 (20 ml) was added NBS (0.7 g, 4 mmol) and a small amount of BPO, and the mixture was refluxed for 30 min. After cooling the reaction mixture the obtained succinimide was filtered off; the filtrate was then concentrated. The crude product was washed with water, dried, and recrystallized from petroleum benzine to give 9-(2′-bromomethylphenyl)-9-fluorenol (**1a**) as colorless prisms; yield 1.1 g (85%); mp 146—147 °C; IR (KBr) 3515 cm^{-1} (OH); Found: C, 68.73; H, 4.06%. Calcd for $C_{20}H_{15}OBr$: C, 68.39; H, 4.30%.

9-(2′-Bromomethylphenyl)-9-methoxyfluorene (1c). Yield 49%; colorless prisms; mp 101—103 °C; Found: C, 68.76; H, 4.75%. Calcd for $C_{21}H_{17}OBr$: C, 69.04; H, 4.69%.

9-(2′-Bromomethylphenyl)-9-methylfluorene (1d). Yield 75%; colorless prisms; mp 150—152 °C; Found: C, 72.30; H, 4.85%. Calcd for $C_{21}H_{17}Br$: C, 72.22; H, 4.91%.

9-(2′-Bromomethylphenyl)-9-fluorenecarboxylic Acid (1e). Yield 55%; colorless crystals; mp 163—164 °C; IR (KBr) 1685 cm^{-1} (C=O); Found: C, 66.25; H, 4.02%. Calcd for $C_{21}H_{15}O_2Br$: C, 66.51; H, 3.99%.

9-(2′-Bromomethylphenyl)-9-methoxycarbonylfluorene (1f). Yield 62%; colorless prisms; mp 99—101 °C; IR (KBr) 1730 cm^{-1} (C=O); Found: C, 67.05; H, 4.47%. Calcd for $C_{22}H_{17}O_2Br$: C, 67.19; H, 4.36%.

9-Acetyl-9-(2′-bromomethylphenyl)fluorene (1g). Yield 66%; colorless prisms; mp 103—105 °C; IR (KBr) 1700 cm^{-1} (C=O); Found: C, 70.30; H, 4.28%. Cacld for $C_{22}H_{17}OBr$: C, 70.04; H, 4.54%.

9-Benzoyl-9-(2′-bromomethylphenyl)fluorene (1h). Yield 78%; colorless prisms; mp 131—132 °C; IR (KBr) 1670 cm^{-1} (C=O); Found: C, 73.84; H, 4.45%. Cacld for $C_{27}H_{19}OBr$: C, 73.81; H, 4.36%.

9-(2′-Iodomethylphenyl)fluorene (3). To a solution of **1a** (1 g, 3 mmol) in acetic acid (15 ml) was added hydroiodic acid (57%, 2.1 g, 9 mmol); the mixture was refluxed for 2 h. Upon cooling to room temperature, the reaction mixture was poured into water and extracted with benzene. The benzene solution was washed with a $NaHSO_3$ solution, dried over $MgSO_4$, and concentrated in vacuo. The crude product was recrystallized from petroleum benzine to give **3** as light-yellow crystals; yield 0.52 g (47%); mp 117—119 °C; ^{1}H NMR δ=3.26, 4.75 (0.4H and 1.6H, two s, CH_2I), 4.84, 5.29 (0.8H and 0.2H, two s, 9-H), 6.12—7.78 (12H, m, $H_{arom.}$). Found: C, 62.64; H, 3.76%. Calcd for $C_{20}H_{15}I$: C, 62.84; H, 3.95%.

9-(2′-Hydroxymethylphenyl)fluorene (4). A solution of **3** (0.2 g, 0.5 mmol) in dioxane (10 ml)-water (2 ml) was refluxed for 3 h. Upon cooling to room temperature, the reaction mixture was poured into water; the deposited crude product was filtered, dried, and recrystallized from petroleum benzine to give **4** as colorless needles; yield 0.11 g (80%); mp 135—136 °C; IR (KBr); 3340 cm^{-1} (OH); ^{1}H NMR δ=3.42, 5.03 (0.6H and 1.4H, two s, CH_2OH), 5.04, 5.43 (1H, two s, 9-H), 6.34 (0.7H, d, J=8 Hz, 6′-H), 7.74 (2H, d, J=7.5 Hz, 4- and 5-H), 6.7—7.5 (9.3H, m, $H_{arom.}$). Found: C, 88.18; H, 5.79%. Calcd for $C_{20}H_{16}O$: C, 88.20; H, 5.92%.

9-(2′-Bromomethylphenyl)fluorene (1b). Into a solution of **4** (0.5 g, 1.8 mmol) in acetic acid (10 ml) was bubbled dry hydrogen bromide, which was generated by a reaction of tetralin with bromine for 5 min. The reaction mixture was poured into cold water; then, precipitated crystals were filtered, washed, and dried. The product was recrystallized from petroleum benzine to give **1b** as light-yellow needles; yield 0.54 g (88%); mp 87—88 °C; Found: C, 71.82; H, 4.35%. Calcd for $C_{20}H_{15}Br$: C, 71.66; H, 4.51%.

References

1) Part XV: A. Nishida, M. Takeshita, N. Kawano, S. Fujisaki, and S. Kajigaeshi, *Bull. Chem. Soc. Jpn.*, **62**, 1093 (1989).

2) A. Nishida, S. Watanabe, S. Fujisaki, H. Hara, and S. Kajigaeshi, *Nippon Kagaku Kaishi*, **1983**, 1148.

3) A. Nishida, S. Shiwaku, S. Fujisaki, and S. Kajigaeshi, *Nippon Kagaku Kaishi*, **1984**, 574.

4) A. Nishida, M. Takamuku, S. Fujisaki, and S. Kajigaeshi, *Bull. Chem. Soc. Jpn.*, **61**, 1195 (1988).

5) A. Nishida, M. Takeshita, S. Fujisaki, and S. Kajigaeshi, *Nippon Kagaku Kaishi*, **1987**, 1791.

6) A. Nishida, S. Shirakawa, S. Fujisaki, and S. Kajigaeshi, *Mem. Fac. Engin. Yamaguchi Univ.*, **38**, 269 (1988).

7) A. Nishida, M. Takeshita, S. Fujisaki, and S. Kajigaeshi, *Bull. Chem. Soc. Jpn.*, **61**, 3919 (1988).

8) S. Kajigaeshi, *Nippon Kagaku Zasshi*, **84**, 185 (1963).

9) T. H. Siddall, III and W. E. Stewart, *J. Org. Chem.*, **34**, 233 (1969).

10) P. Buckley, P. A. Giguere, and M. Schneider, *Can. J. Chem.*, **47**, 901 (1969); R. G. Azrak and E. B. Wilson, *J. Chem. Phys.*, **52**, 5299 (1970); T. Kobayashi, *Phys. Lett. A*, **103A**, 424 (1984).

11) G. Binsch, *J. Am. Chem. Soc.*, **91**, 1304 (1969); H, Kihara, *J. of Association of PC for Chemists*, **4**, 9 (1983).

12) M. Nakamura, N. Nakamura, and M. Ōki, *Bull. Chem. Soc. Jpn.*, **50**, 2986 (1977).

Halogenation Using Quaternary Ammonium Polyhalides. XIX.[1] Aromatic Chlorination of Arenes with Benzyltrimethylammonium Tetrachloroiodate

Shoji KAJIGAESHI,* Yasuhiro UEDA, Shizuo FUJISAKI, and Takaaki KAKINAMI†
Department of Industrial Chemistry, Faculty of Engineering, Yamaguchi University, Tokiwadai, Ube 755
†Department of Industrial Chemistry, Ube Technical College, Tokiwadai, Ube 755
(Received December 15, 1988)

Synopsis. The reaction of arenes with a calculated amount of benzyltrimethylammonium tetrachloroiodate in acetic acid at room temperature or at 70 °C gave nuclear chloro-substituted arenes in fairly good yields.

Direct aromatic chlorination of arenes (**1**) with chlorine has usually been carried out in the presence of a catalyst such as iodine, iron(III) chloride, or an aluminium-mercury couple. As the chlorinating agents which are easier to handle than toxic gaseous chlorine, sulfuryl chloride,[2] iodine trichloride,[3] titanium(IV) chloride,[4] copper(II) chloride,[5] alumina-supported copper(II) chloride,[6] antimony(V) chloride,[7] tellurium(IV) chloride,[8] trichloroisocyanuric acid,[9] and poly(*N*-chloromaleimide),[10] etc. have been used to chlorinate **1**.

As one part of our investigation concerning the halogenation of aromatic compounds with quaternary ammonium polyhalides, we have recently found that a new reagent, benzyltrimethylammonium tetrachloroiodate (BTMA ICl_4), is an effective chlorinating agent.[1,11] In this paper we wish to report on the aromatic chlorination of **1** by the use of BTMA ICl_4.

Results and Discussion

A reaction of **1** with BTMA ICl_4 in acetic acid at room temperature or at 70 °C gave aromatic chloro-substituted arenes (**2**) together with benzyltrimethylammonium dichloroiodate (BTMA ICl_2).[12] Thus, the produced BTMA ICl_2 is easily separable from the reaction mixture, since BTMA ICl_2 is hardly

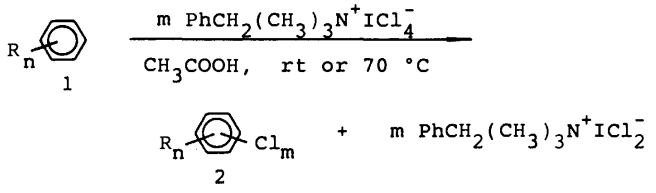

Table 1. Aromatic Chlorination of Arenes(**1**) with BTMA ICl_4 in AcOH

Substrate 1	Molar ratio BTMA ICl_4/1	Reaction conditions Time/h	Temp/ °C	Product 2	Yield[a] %	Mp(°C) or Bp(°C/mmHg) Found	Reported
(**1a**)	1.0	48	70	(**2a**)	16	132—133/760	131.65—131.66/760[13]
(**1b**)	1.0	24	70	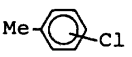 (**2b**)	88[c]	158—161/760	—
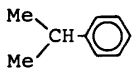 (**1c**)	1.0	20	70	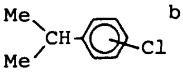 (**2c**)	30[d]	187—189/760	—
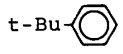 (**1d**)	1.0	20	70	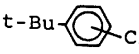 (**2d**)	66[e]	213—215/760	—
(**1e**)	1.0	20	70	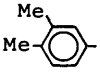 (**2e**)	70	194—196/760	193—197/760[14]
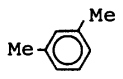 (**1f**)	1.0	20	rt	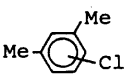 (**2f**)	90[f]	185—187/760	—
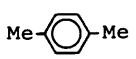 (**1g**)	1.0	20	70	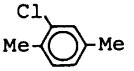 (**2g**)	66	185—187/760	186.8/760[15]

Table 1. (Continued)

Substrate 1	Molar ratio BTMA ICl_4/1	Reaction conditions Time/h	Temp/°C	Product 2	Yield[a] %	Mp(°C) or Bp(°C/mmHg) Found	Reported
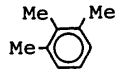 (1h)	1.0	20	rt	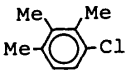 (2h)	81	218—220/760	86—87/16[16]
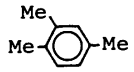 (1i)	1.0	20	rt	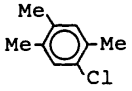 (2i)	52	67—68	70.5—71[16]
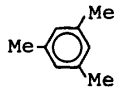 (1j)	1.0	22	rt	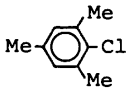 (2j-1)	90	205—206/760	86—86.8/14[17]
1j	2.0	22	70	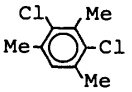 (2j-2)	95	59—60	58—59[16]
1j	3.0	24	70	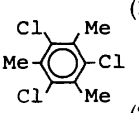 (2j-3)	98	205.5—206	204—205[18]
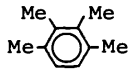 (1k)	1.0	20	rt	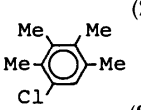 (2k-1)	76	242—244/760	131—132/24[16]
1k	2.0	20	rt	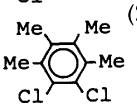 (2k-2)	96	189—191	193[19]
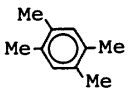 (1l)	1.0	20	rt	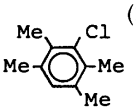 (2l-1)	73	43.5—44.5	47.5—48[16]
1l	2.0	20	rt	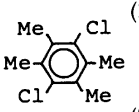 (2l-2)	94	187—190	189—189.5[16]
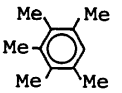 (1m)	1.0	20	rt	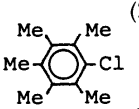 (2m)	96	152—153	155[20]
(1n)	1.0	24	70	(2n)	65	256—258/760	106.5/5[21]
(1o)	1.0	18	70	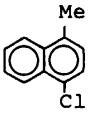 (2o)	73	271—273/760	132.5—136/12[22]
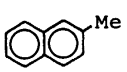 (1p)	1.0	15	70	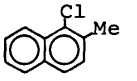 (2p)	95	273—275/760	120—122/4.5[2]
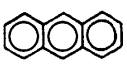 (1q)	1.0	18	rt	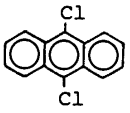 (2q-2)	40	212—213	214—215[23]
1q	2.0	24	rt	2q-2	99	212—213	214—215[23]

a) Yield of isolated product. b) Product was obtained as a mixture of 4- and 2-chloro derivatives, and its isomer ratio was determined by GC analysis and / or ^1H NMR spectrum. c) 4-Chloro deriv. / 2-chloro deriv. =3/7. d) 4-Chloro deriv. / 2-chloro deriv. =1/1. e) 4-Chloro deriv. / 2-chloro deriv. =7/3. f) 4-Chloro deriv. / 2-chloro deriv. =2/1.

soluble in acetic acid at room temperature. The results are summarized in Table 1.

The reaction of such polyalkylbenzenes as 1,3,5-trimethylbenzene (**1j**), 1,2,3,4-tetramethylbenzene (**1k**), and 1,2,4,5-tetramethylbenzene (**1l**), with equivalent weights of BTMA ICl_4 gave the desired mono-, di-, or trichloro-substituted arenes selectively. For example, the reactions of **1j** with 1.0, 2.0, and 3.0 equiv of BTMA ICl_4 gave 1-chloro- (**2j-1**), 1,3-dichloro- (**2j-2**), and 1,3,5-trichloro-2,4,6-trimethylbenzene (**2j-3**), in good yields, respectively.

We emphasize that the stable reagent BTMA ICl_4 is an excellent chlorinating agent for **1** since it can be treated safely and quantitatively in comparison with toxic gaseous chlorine. Readily separable by-product BTMA ICl_2 can be easily converted to BTMA ICl_4 by treatment with chlorine in dichloromethane.[24]

However, benzene and isopropylbenzene gave chloro-substituted products in poor yields, respectively, even with a Lewis acid-catalyst such as iron(III) chloride, titanium(IV) chloride, or zinc chloride.

Experimental

1-Chloro-2,4,6-trimethylbenzene (2j-1); General Procedure: To a solution of 1,3,5-trimethylbenzene (**1j**) (0.50 g, 4.16 mmol) in acetic acid (30 ml) was added BTMA ICl_4 (1.74 g, 4.16 mmol). The mixture was stirred for 22 h at room temperature. During the period of stirring BTMA ICl_4, which was only slightly soluble in acetic acid, gradually reacted with **1j** to give a product and a yellow precipitate. The precipitate (BTMA ICl_2, 1.02 g, 2.93 mmol) was filtered off. The filtrate was treated with 5% $NaHSO_3$ (20 ml) and then extracted with hexane (25 ml×4). The hexane solution was washed with 5% $NaHCO_3$ (30 ml) and was purified by column chromatography on alumina. The eluent was concentrated in vacuo to give an oily residue which was distilled, affording **2j-1** as a colorless liquid; yield 0.58 g (90%); bp 205—206 °C/760 mmHg (lit,[17] bp 86—86.8 °C/14 mmHg).

References

1) Part XVIII; S. Kajigaeshi, Y. Shinmasu, S. Fujisaki, and T. Kakinami, *Chem. Lett.*, **1989**, 415.

2) P. B. D. de la Mare and H. Suzuki, *J. Chem. Soc. C*, **1967**, 1586.

3) E. Campaigne and W. Thompson, *J. Am. Chem. Soc.*, **72**, 629 (1950).

4) G. K. Chip and J. S. Grossert, *Can. J. Chem.*, **50**, 1233 (1972).

5) D. C. Nonhebel, *Org. Synth.*, **43**, 15 (1963).

6) M. Kodomari, H. Satoh, and S. Yoshitomi, *J. Org. Chem.*, **53**, 2093 (1988).

7) P. Kovacic and A. K. Sparks, *J. Am. Chem. Soc.*, **82**, 5740 (1960).

8) M. Albeck and S. Shaik, *J. Chem. Soc., Perkin Trans. 1*, **1975**, 1223.

9) E. C. Juenge, D. A. Beal, and W. P. Duncan, *J. Org. Chem.*, **35**, 719 (1970).

10) C. Yaroslavsky and E. Katchalski, *Tetrahedron Lett.*, **1972**, 5173.

11) S. Kajigaeshi, T. Kakinami, H. Ikeda, and T. Okamoto, *Chem. Express*, **3**, 659 (1988).

12) S. Kajigaeshi, T. Kakinami, H. Yamasaki, S. Fujisaki, M. Kondo, and T. Okamoto, *Chem. Lett.*, **1987**, 2109.

13) R. H. Myers, M. E. Hobbs, and P. M. Gross, *J. Am. Chem. Soc.*, **76**, 4737 (1954).

14) D. R. Lyon, F. G. Mann, and G. H. Cookson, *J. Chem. Soc.*, **1947**, 662.

15) R. L. Datta and F. V. Fernandes, *J. Am. Chem. Soc.*, **38**, 1809 (1916).

16) L. I. Smith and C. L. Moyle, *J. Am. Chem. Soc.*, **58**, 1 (1936).

17) G. Illuminati and G. Marino, *J. Am. Chem. Soc.*, **78**, 4975 (1956).

18) C. P. Smith and G. L. Lewis, *J. Am. Chem. Soc.*, **62**, 949 (1940).

19) A. H. White, B. S. Biggs, and S. O. Morgan, *J. Am. Chem. Soc.*, **62**, 16 (1940).

20) L. J. Andrews and R. M. Keefer, *J. Am. Chem. Soc.*, **79**, 5169 (1957).

21) A. I. Vogel, *J. Chem. Soc.*, **1948**, 654.

22) J. Sauer, R. Huisgen, and A. Hauser, *Chem. Ber.*, **91**, 1461 (1958).

23) Y. Nagai and M. Tanabe, *Kogyo Kagaku Zasshi*, **60**, 294 (1957).

24) S. Kajigaeshi, T. Kakinami, M. Moriwaki, T. Tanaka, and S. Fujisaki, *Tetrahedron Lett.*, **29**, 5783 (1988).

Asymmetric Oxidation of Alkyl Aryl Selenides under Sharpless Oxidation Conditions

Toshio SHIMIZU, Michio KOBAYASHI, and Nobumasa KAMIGATA*
Department of Chemistry, Faculty of Science, Tokyo Metropolitan University, Fukazawa, Setagaya-ku, Tokyo 158
(Received November 26, 1988)

Synopsis. Optically active alkyl aryl selenoxides were synthesized by the asymmetric oxidation of corresponding selenides under Sharpless oxidation conditions. The absolute configurations of the optically active alkyl aryl selenoxides prepared were estimated by comparisons of their circular dichroism spectra with those of the optically active sulfoxides.

Although optically active sulfoxides were resolved in the early twenties century,[1] there had been no example of an optically active selenoxide for a long time. Recently, though, optically active alkyl aryl and dialkyl selenoxides were obtained by kinetic resolution (5—11% e.e.)[2] or by complexation with optically active diol.[3] We also obtained optically active selenoxides by the optical resolution of racemic selenoxides[4] and the asymmetric oxidation of selenide.[5] Furthermore, we found that chromatographic resolution of racemic selenoxides using an optically active column was effective for preparing optically active diaryl selenoxides.[6] However, alkyl aryl selenoxides could not be separated by this method, and there has been no report on an effective synthetic method for such optically active compounds. Very recently, the asymmetric oxidation of 2-methoxy-2,2-diphenylethyl aryl selenides to corresponding selenoxides (18—40% e.e.) under Sharpless oxidation conditions was reported by Tiecco et al.[7] We have also investigated the asymmetric synthesis of optically active alkyl aryl selenoxides by the asymmetric oxidation of the corresponding selenides under Sharpless oxidation conditions. We report here the results and an estimation of the absolute configurations of the optically active alkyl aryl selenoxides obtained by a comparison of their circular dichroism spectra with those of optically active alkyl aryl sulfoxides.

Results and Discussion

Asymmetric oxidations of methyl 2,4,6-triisopropylphenyl selenide (**1a**) were examined in dichloromethane using titanium tetraisopropoxide and (+)-diethyl tartrate ((+)-DET) under several reaction

1 2

a: R = Methyl. Ar = 2,4,6-Triisopropylphenyl
b: R = Methyl. Ar = 2,4,6-Tri-t-butylphenyl
c: R = Neopentyl, Ar = 2,4,6-Tri-t-butylphenyl
d: R = Benzyl, Ar = 2,4,6-Tri-t-butylphenyl
e: R = o-Methoxybenzyl. Ar = 2,4,6-Tri-t-butylphenyl

temperatures. The highest enantiomeric excess (e.e.) of methyl 2,4,6-triisopropylphenyl selenoxide (+)-**2a** was obtained at −15 °C. The results are summarized in Table 1 (Entries 1—4). When (−)-DET was used in place of (+)-DET, (−)-selenoxide (−)-**2a** was obtained (Entry 5). The reaction conditions of the asymmetric oxidations of **1a** were examined by using some tartrates and Lewis acids (Entries 6—9). However, only a decrease of e.e. was observed. It was observed that the most effective combination of tartrate and Lewis acid was that of diethyl tartrate and titanium tetraisopropoxide. It was reported that the addition of equimolar amounts of water increased the e.e. of optically active sulfoxides in the asymmetric

Table 1. Asymmetric Oxidation of Methyl 2,4,6-Triisopropylphenyl Selenide (**1a**)

Entry	Lewis acid	Tartrate[a]	Solvent	Condition	Selenoxide (**2a**)		
					Chem. yield /%	$[\alpha]_D$[b] /°	E.e.[c] /%
1	$Ti(OPr^i)_4$	(+)-DET	CH_2Cl_2	0 °C, 5 h	70	+7.42	11.0
2	$Ti(OPr^i)_4$	(+)-DET	CH_2Cl_2	−10 °C, 14 h	61	+7.48	11.1
3	$Ti(OPr^i)_4$	(+)-DET	CH_2Cl_2	−15 °C, 18 h	58	+19.0	28.2
4	$Ti(OPr^i)_4$	(+)-DET	CH_2Cl_2	−25 °C, 26 h	56	+16.6	24.6
5	$Ti(OPr^i)_4$	(−)-DET	CH_2Cl_2	−15 °C, 18 h	57	−14.2	21.1
6	$Ti(OPr^i)_4$	(+)-DMT	CH_2Cl_2	−15 °C, 18 h	57	+13.7	20.3
7	$Ti(OPr^i)_4$	(+)-DIPT	CH_2Cl_2	−15 °C, 18 h	74	+7.28	10.8
8	$Ti(OBu^n)_4$	(+)-DET	CH_2Cl_2	−15 °C, 18 h	53	+8.14	12.1
9	$Al(OPr^i)_3$	(+)-DET	CH_2Cl_2	−15 °C, 70 h	3.8	−0.96	1.4
10[d]	$Ti(OPr^i)_4$	(+)-DET	CH_2Cl_2	−28 °C, 40 h	27	−0.35	0.5
11	$Ti(OPr^i)_4$	(+)-DET	Et_2O	−15 °C, 20 h	51	−2.50	3.7
12	$Ti(OPr^i)_4$	(−)-DET	Et_2O	−15 °C, 20 h	47	+1.65	2.4
13	$Ti(OPr^i)_4$	(+)-DET	CH_3CN	−15 °C, 18 h	54	+5.58	8.3

a) DMT: dimethyl tartrate, DET: diethyl tartrate, DIPT: diisopropyl tartrate. b) Optical rotations were taken in chloroform. c) Determined by ^1H NMR by using optically active shift reagent, $Eu(hfc)_3$. d) Equimolar water (1 mmol) was added to the mixture of Lewis acid and tartrate.

Table 2. Asymmetric Oxidation of Alkyl 2,4,6-Tri-*t*-butylphenyl Selenide (**1b—1e**)[a]

Entry	Selenide	DET[b]	Solvent	Condition	Selenoxide	Chem. yield /%	$[\alpha]_D$[c] /°	E.e.[d] /%
1	**1b**	(+)-DET	CH_2Cl_2	−15 °C, 63 h	**2b**	12	−9.60	7.9
2	**1b**	(−)-DET	CH_2Cl_2	−15 °C, 63 h	**2b**	15	+9.17	7.5
3	**1b**	(+)-DET	Et_2O	−15 °C, 63 h	**2b**	12	−39.9	32.7
4	**1b**	(−)-DET	Et_2O	−15 °C, 63 h	**2b**	9.0	+32.1	26.3
5	**1c**	(+)-DET	CH_2Cl_2	25 °C, 160 h	**2c**	18	+2.65	2.8
6	**1c**	(+)-DET	Et_2O	25 °C, 160 h	**2c**	30	+10.8	11.4
7	**1d**	(+)-DET	CH_2Cl_2	25 °C, 72 h	**2d**	22	+5.97	6.6
8	**1e**	(+)-DET	CH_2Cl_2	25 °C, 72 h	**2e**	19	+27.8	16.7

a) Titanium tetraisopropoxide was used as the Lewis acid. b) DET: diethyl tartrate. c) Optical rotations were taken in chloroform. d) Determined by ^1H NMR by using optically active shift reagent, Eu(hfc)$_3$

oxidation of sulfides.[8] We studied the oxidation of **1a** by adding equimolar amounts of water to our reaction systems. However, the addition of water only decreased the ratio of the enantiomers (Entry 10). The oxidation of **1a** was also carried out in ether or acetonitrile (Entries 11—13). Though the e.e. decreased in both solvents, (+)-selenoxide (+)-**2a** and (−)-selenoxide (−)-**2a** were obtained by the use of (−)-DET and (+)-DET, respectively, in ether (Entries 11 and 12). The absolute configurations of **2a** obtained in ether were opposite to the results found in dichloromethane or acetonitrile. These results suggest that there is an interaction between the Lewis acid and the lone pair of oxygen atoms of solvent ether, which reverses the selectivity of the enantio-face in the oxidation of the selenide.

The asymmetric oxidations of several alkyl 2,4,6-tri-*t*-butylphenyl selenides (**1b—1e**) were carried out using diethyl tartrate and titanium tetraisopropoxide. Methyl, neopentyl, and benzyl groups were chosen as alkyl groups since the existence of β-hydrogen of selenoxide easily caused β-elimination.[9] The results are shown in Table 2. In the oxidation of **1b**, (−)-**2b** was obtained in 33% optical yield in ether using (+)-DET, although the reaction was slow and the chemical yield was 12% after 63 h (Entry 3). Similarly, (+)-**2b** were obtained in 26% optical yield by the oxidation of **1b** using (−)-DET in ether (Entry 4). Asymmetric oxidations of **1c** were also carried out in dichloromethane or ether using (+)-DET (Entries 5 and 6). A higher e.e. of **2c** was obtained in ether than in dichloromethane. However in this case, optically active (+)-selenoxide (+)-**2c** was formed in both solvents.

The solvent effects in the oxidations of **1a—1c** prompted us to study the oxidations of benzyl 2,4,6-tri-*t*-butylphenyl selenide (**1d**) and *o*-methoxybenzyl 2,4,6-tri-*t*-butylphenyl selenide (**1e**) in order to clarify the effect of the oxygen atom of the methoxyl group in **1e**. The oxidations of **1d** and **1e** gave optically active selenoxides (**2d** and **2e**) in 7 and 17% optical yields, respectively (Entries 7 and 8). The ortho methoxyl group in **1e** pretty much increased the e.e. in the oxidation of the selenides. The solvent effect and substrate dependence are very interesting, though the mechanism of the asymmetric oxidation of selenides under these conditions is not clear at the present time.

Davis et al. proposed that the absolute configurations of selenoxides (+)-**2a** and (−)-**2a** are *S* and *R* forms, respectively.[2] However, the optically active selenoxides, **2b—2e**, are new compounds and the absolute configurations are not known. We tried to estimate the optically active alkyl aryl selenoxides **2a—2e** by comparisons of the circular dichroism spectra with those of alkyl aryl sulfoxides. All (+)-selenoxides (+)-**2a—2b** showed positive first Cotton effects in the 258—301 nm region on circular dichroism spectra, as shown in Table 3. On the other hand, alkyl aryl sulfoxides, such as (+)-methyl *p*-tolyl sulfoxide, showed a positive first Cotton effect at 241 nm[10] and (+)-ethyl phenyl sulfoxide also had a positive Cotton effect at 245 nm.[11] Since both (+)-sulfoxides had been determined to be *R*-configuration, the (+)-selenoxides (+)-**2a—2e** were estimated to be of *R* form. These estimations are opposite to those absolute configurations proposed by Davis et al.[2]

Experimental

Materials. **Methyl 2,4,6-triisopropylphenyl selenide (1a)** was prepared by the reaction of 2,4,6-triisopropylphenylmagnesium bromide with dimethyl diselenide,[12] and alkyl 2,4,6-tri-*t*-butylphenyl selenides (**1b—1e**) were prepared by the reaction of 2,4,6-tri-*t*-butylphenyllithium with the corresponding dialkyl diselenides. The physical and spectral data are as follows.

1a: Mp 43—44 °C; IR (KBr) 3000—2800, 1460, 1360, and 880 cm^{-1}; ^1H NMR ($CDCl_3$) δ=1.23 (18H, d, *J*=7.2 Hz), 2.07 (3H, s), 2.86 (1H, hep., *J*=7.2 Hz), 3.84 (2H, hep., *J*=7.2 Hz), and 6.93 (2H, s); MS (70 eV) *m/z* 298 (M^+)(^{80}Se); Found: *m/z* 298.1230, Calcd for $C_{16}H_{26}{}^{80}Se$: M, 298.1200.

1b: Mp 86.5—87.0 °C; IR(KBr) 3000—2800, 1580, 1465, 1380, 1350, and 870 cm^{-1}; ^1H NMR ($CDCl_3$) δ=1.28 (9H, s),

Table 3. Circular Dichroism of Optically Active Selenoxides (+)-**2a—2e**

Selenoxide	First Cotton effect /sign (nm)
(+)-**2a**	+(258)
(+)-**2b**	+(262)
(+)-**2c**	+(263)
(+)-**2d**	+(301)
(+)-**2e**	+(290)

1.59 (18H, s), 1.93 (3H, s), and 7.31 (2H, s,); MS (70 eV) m/z 340 (M^+) (^{80}Se); Found: m/z 340.1650, Calcd for $C_{19}H_{32}{}^{80}Se$: M, 340.1669.

1c: Mp 118—119 °C; IR (KBr) 3000—2800, 1585, 1460, 1380, 1355, 1240, 1210, and 875 cm^{-1}; ^1H NMR($CDCl_3$) δ=1.02 (9H, s), 1.28 (9H, s), 1.59 (18H, s), 2.43 (2H, s), and 7.27 (2H, s); MS (70 eV) m/z 396 (M^+) (^{80}Se); Found: m/z 396.2299, Calcd for $C_{23}H_{40}{}^{80}Se$: M, 396.2295.

1d: Mp 82—83 °C; IR (KBr) 3000—2800, 1500, 1450, 1390, and 1360 cm^{-1}; ^1H NMR ($CDCl_3$) δ=1.31 (9H, s), 1.59 (18H, s), 3.65 (2H, s), 7.0—7.3 (5H, m), and 7.36 (2H, s); MS (70 eV) m/z 416 (M^+) (^{80}Se); Found: m/z 416.1989, Calcd for $C_{25}H_{36}{}^{80}Se$: M, 416.1982.

1e: Mp 132.5—133.0 °C; IR (KBr) 3000—2800, 1590, 1490, 1465, 1390, 1360, and 1250 cm^{-1}; ^1H NMR ($CDCl_3$) δ=1.31 (9H, s), 1.57 (18H, s), 3.64 (2H, s), 3.74 (3H, s), 6.6—7.2 (4H, m), and 7.27 (2H, s); MS (70 eV) m/z 446 (M^+) (^{80}Se); Found: m/z 446.2079, Calcd for $C_{26}H_{38}O{}^{80}Se$: M, 446.2088.

General Procedure for the Asymmetric Oxidation of Selenides. A typical manner for the oxidation of **1a** is described below. (+)-Diethyl tartrate (0.34 cm^3, 2.0 mmol) and titanium tetraisopropoxide (0.30 cm^3, 1.0 mmol) were dissolved in 8.0 cm^3 of dichloromethane under nitrogen, and the mixture was stirred for 30 min. Methyl 2,4,6-triisopropylphenyl selenide (**1a**) (297 mg, 1.0 mmol) was added to the mixture and cooled to −15 °C. A solution of *t*-butyl hydroperoxide (1.3 mmol), dried over magnesium sulfate prior to use, in dichloromethane (2.0 cm^3) was added to the cooled solution. Stirring was continued for 18 h at −15 °C. The reaction mixture was subjected to alumina column chromatography without evaporation of the solvent using hexane-ethyl acetate as an eluent to give 182 mg (58%) of methyl 2,4,6-triisopropylphenyl selenoxide (**2a**). $[\alpha]_D^{22}$ + 19.0° (*c* 1.17, chloroform). Enantiomeric excess (e.e.) was determined to be 28.2% by ^1H NMR using optically active shift reagent (Eu(hfc)$_3$).

(*R*)-(+)-2a: Mp 154.0—154.5 °C; $[\alpha]_D^{22}$ +19.0° (*c* 1.17, chloroform); e.e.=28.2%; IR (KBr) 820 (Se=O) cm^{-1}; ^1H NMR ($CDCl_3$) δ=1.20, 1.23, and 1.27 (18H, d, J=7.2 Hz, methyl of isopropyl), 2.74 (3H, s), 2.5—3.1 (1H, m), 3.92 (2H, hep.), and 7.03 (2H, s); UV (methanol) 261 (ε 5.03×10^3), 233 (ε 1.09×10^4), and 208 (ε 3.80×10^4) nm; CD (methanol) 258 ([θ] +5.13×10^3) and 228 ([θ] −2.21×10^3) nm; MS (30 eV) m/z 314 (M^+) (^{80}Se); Found m/z 314.1154, Calcd for $C_{16}H_{26}O{}^{80}Se$: M, 314.1149.

(*S*)-(−)-2a: 154.5—155.0 °C; $[\alpha]_D^{27}$ −14.2° (*c* 1.35, chloroform); e.e.=21.1%; IR (KBr) 820 (Se=O) cm^{-1}; ^1H NMR ($CDCl_3$) δ=1.20, 1.23, and 1.27 (18H, d, J=7.2 Hz, methyl of isopropyl), 2.74 (3H, s), 2.5—3.1 (1H, m), 3.92 (2H, hep.), and 7.03 (2H, s); UV (methanol) 261 (ε 4.70×10^3), 233 (ε 1.04×10^4), and 208 (ε 3.75×10^4) nm; CD (methanol) 258 ([θ] −3.24×10^3) and 227 ([θ] +1.50×10^3) nm; MS (30 eV) m/z 314 (M^+) (^{80}Se); Found m/z 314.1159, Calcd for $C_{16}H_{26}O{}^{80}Se$: M, 314.1149.

(*R*)-(+)-2b: Mp 123.5—124.0 °C; $[\alpha]_D^{26}$ +32.1° (*c* 0.64, chloroform); e.e.=26.3%; IR (KBr) 830 (Se=O) cm^{-1}; ^1H NMR ($CDCl_3$) δ=1.29 (9H, s), 1.55 (18H, s), 2.55 (3H, s), and 7.37 (2H, s); UV (methanol) 261 (ε 3.40×10^3), 235 (ε 1.02×10^4), and 208 (ε 3.00×10^4) nm; CD (methanol) 262 ([θ] +7.42×10^3), 237 ([θ] −1.13×10^3), and 223 ([θ] +7.41×10^3) nm; MS (30 eV) m/z 356 (M^+)(^{80}Se); Found: m/z 356.1615, Calcd for $C_{19}H_{32}O{}^{80}Se$: M, 356.1618.

(*S*)-(−)-2b: Mp 124.0—124.5 °C; $[\alpha]_D^{28}$ −39.9° (*c* 0.88, chloroform); e.e.=32.7%; IR (KBr) 830 (Se=O) cm^{-1}; ^1H NMR ($CDCl_3$) δ=1.29 (9H, s), 1.55 (18H, s), 2.55 (3H, s), and 7.37 (2H, s); UV (methanol) 262 (ε 3.61×10^3), 236 (ε 1.07×10^4), and 207 (ε 3.14×10^4) nm; CD (methanol) 262 ([θ] −9.32×10^3), 237 ([θ] +1.24×10^3), and 221 ([θ] −1.02×10^4) nm; MS (30 eV) m/z 356 (M^+)(^{80}Se); Found: m/z 356.1548, Calcd for $C_{19}H_{32}O{}^{80}Se$: M, 356.1618.

(*R*)-(+)-2c: Mp 114.5—115.0 °C; $[\alpha]_D^{22}$ +10.8° (*c* 1.24, chloroform); e.e.=11.4%; IR (KBr) 830 (Se=O) cm^{-1}; ^1H NMR ($CDCl_3$) δ=1.09 (9H, s), 1.30 (9H, s), 1.58 (18H, s), 2.08 and 3.17 (2H, ABq, J=12.0 Hz), and 7.35 (2H, s); UV (methanol) 270 (ε 3.77×10^3), 243 (ε 9.26×10^3), and 208 (ε 3.02×10^4) nm; CD (methanol) 263 ([θ] +2.78×10^3) and 232 ([θ] −3.30×10^3) nm; MS (30 eV) m/z 412 (M^+) (^{80}Se); Found: m/z 412.2208, Calcd for $C_{23}H_{40}O{}^{80}Se$: M, 412.2244.

(*R*)-(+)-2d: Mp 138 °C (decomp); $[\alpha]_D^{22}$ +5.97° (*c* 0.71, chloroform); e.e.=6.6%; IR (KBr) 840 (Se=O) cm^{-1}; ^1H NMR ($CDCl_3$) δ=1.32 (9H, s), 1.41 (18H, s), 4.0—4.2 (2H, m), 6.4—7.2 (5H, m), and 7.29 (2H, s); UV (methanol) 281 (ε 2.39×10^3), 237 (ε 1.18×10^4), and 203 (ε 4.02×10^4) nm; CD (methanol) 301 ([θ]+2.94×10^3) and 244 ([θ]+3.23×10^3) nm; MS (30 eV) m/z 432 (M^+) (^{80}Se); Found: m/z 432.1915, Calcd for $C_{25}H_{36}O{}^{80}Se$: M, 432.1931.

(*R*)-(+)-2e: Viscous oil; $[\alpha]_D^{22}$ +27.8° (*c* 0.96, chloroform); e.e.=16.7%; IR (liq. film) 840 (Se=O) cm^{-1}; ^1H NMR ($CDCl_3$) δ=1.37 (9H, s), 1.48 (18H, s), 3.81 (3H, s), 4.1—4.2 (2H, m), 6.4—7.5 (4H, m), and 7.32 (2H, s); UV (methanol) 280 (ε 3.39×10^3), 230 (ε 1.31×10^4), and 202 (ε 3.71×10^4) nm; CD (methanol) 290 ([θ]+6.99×10^3) and 238 ([θ]+1.45×10^4) nm; MS (30 eV) m/z 462 (M^+) (^{80}Se); Found: m/z 462.1992, Calcd for $C_{26}H_{38}O_2{}^{80}Se$: M, 462.2037.

References

1) P. W. B. Harrison, J. Kenyon, and H. Phillips, *J. Chem. Soc.*, **1926**, 2079.

2) F. A. Davis, J. M. Billmers, and O. D. Stringer, *Tetrahedron Lett.*, **24**, 3191 (1983); F. A. Davis, O. D. Stringer, and J. P. McCauley, Jr., *Tetrahedron*, **41**, 4747 (1985); and references cited therein.

3) F. Toda and K. Mori, *J. Chem. Soc., Chem. Commun.*, **1986**, 1357.

4) T. Shimizu and M. Kobayashi, *Chem. Lett.*, **1986**, 161; T. Shimizu, K. Kikuchi, Y. Ishikawa, I. Ikemoto, M. Kobayashi, and N. Kamigata, *J. Chem. Soc., Perkin Trans. 1*, **1989**, 597.

5) M. Kobayashi, H. Ohkubo, and T. Shimizu, *Bull. Chem. Soc. Jpn.*, **59**, 503 (1986); T. Shimizu, M. Kobayashi, and N. Kamigata, *Sulfur Lett.*, **8**, 61 (1988).

6) T. Shimizu and M. Kobayashi, *Bull. Chem. Soc. Jpn.*, **59**, 2654 (1986); *idem*, *J. Org. Chem.*, **52**, 3399 (1987).

7) M. Tiecco, M. Tingoli, L. Testaferri, and D. Bartoli, *Tetrahedron Lett.*, **28**, 3849 (1987).

8) P. Pitchen, E. Duñach, M. N. Deshmukh, and H. B. Kagan, *J. Am. Chem. Soc.*, **106**, 8188 (1984).

9) D. N. Jones, D. Mundy, and R. D. Whitehouse, *J. Chem. Soc., Chem. Commun.*, **1970**, 86; H. J. Reich, J. M. Renga, and I. L. Reich, *J. Am. Chem. Soc.*, **97**, 5434 (1975); and references cited therein.

10) K. Mislow, M. M. Green, P. Laur, J. T. Melillo, T. Simmons, and A. L. Ternay, Jr., *J. Am. Chem. Soc.*, **87**, 1958 (1965).

11) H. Takeuchi, Doctoral Thesis, Tokyo Metropolitan University, Tokyo, Japan, 1981.

12) T. W. Campbell and J. D. McCullough, *J. Am. Chem. Soc.*, **67**, 1965 (1945).

Studies on Aromatic Sesquiterpenes. XI.[1] Synthesis of 7-Isopropyl-3,5-dimethyl-1-naphthol

Juichi TANAKA and Kazuo ADACHI*
Osaka Institute of Technology, Omiya, Asahi-ku, Osaka 535
(Received December 7, 1988)

Synopsis. Starting from *m*-cresol, the title new naphthol was synthesized through 4-methyl-3-(2-methoxy-4-methylbenzoyl)pentanoic acid as a key intermediate.

Phenolic sesquiterpene curcuphenol[2] (**1**) was cyclized by treatment with acid catalysts to give 8-hydroxycalamenene (**2**) along with its structural isomer, 5-hydroxyisocalamenene (**3**).[3] The tetrahydronaphthol (**2**) and its methyl ether have been, respectively, isolated from *Dysoxylum* species (Meliaceae) and a horny coral as naturally occurring sesquiterpenes, and their absolute configuration were confirmed by chemical derivation.[4] 5-Methoxydaucalene (**4b**) derived from the methyl ether of **3** afforded 5-hydroxydaucalene (**4a**) by demethylation with BBr_3.[1] However, **4b** was refluxed in a solution of acetic acid with HBr to furnish a new naphthol, which was apparently different from **4a**. 7-Isopropyl-3,5-dimethyl-1-naphthol (**5a**) was proposed as the structure of this new naphthol on the basis of comprehensive spectral studies.[1] 4-Methoxyisocadalene (**6**) has been isolated from *Heterotheca* species (Compositae) and also synthesized.[5] However, the naphthol (**5**), having a related structure with **6**, is an unknown phenolic sesquiterpenoide as a natural product.

In this paper we report on an efficient synthesis of **5**, starting from *m*-cresol through 4-methyl-3-(2-methoxy-4-methylbenzoyl)pentanoic acid (**11**) as a key intermediate. This synthetic fashion is useful for the preparation of 7-isopropyl-1-naphthol derivatives, which are expected to occur as natural products or formation by the conversion of some sesquiterpenes.

In order to prepare the keto acid (**11**), at first the methoxyacetophenone (**8a**) obtained from *m*-tolyl acetate (**7a**) was derived to the diketo ester (**9**). Generally, the diketo esters prepared from a ketone with diethyl oxalate are readily converted into the β-keto esters by decarbonylation with heating,[6] but the pyrolysis of **9** gave a mixture of four components (**8a**, **10**, and the dimerized product including **9**), in which the desired β-keto ester (**10**) was found in low yield (32.8%). Therefore, we next attempted the bromination of isovalerophenone derivative (**8c**) obtained from *m*-tolyl isovalerate (**7c**) and successive condensation of the resulting α-bromo ketone with ethyl cyanoacetate. The crude reaction product was hydrolyzed to give a γ-keto acid (**11**), which showed in its NMR spectrum two methyl proton signals of an isopropyl group at δ=0.73 and 0.97 as a pair of doublets (J=7 Hz) and methylene proton signals as a pair of double doublets at δ=2.35 (J=17 and 4 Hz) and 2.91 (J=17 and 10 Hz). By a Clemmensen reduction the keto acid (**11**) was converted into 4-methyl-3-(2-methoxy-4-methylbenzyl)-pentanoic acid (**12**), which was cyclized with phosphoryl chloride to give the tetralone (**13**). Ketone **13** was allowed to react with methylmagnesium iodide and the dehydration of the resulting alcohol with formic acid afforded 3,4-dihydro-3-isopropyl-5-methoxy-1,7-dimethylnaphthalene (**14**), which was dehydrogenated by heating with 5% Pd-C at 240—250 °C to give 7-isopropyl-1-methoxy-3,5-dimethylnaphthalene (**5b**). 7-Isopropyl-3,5-dimethyl-1-naphthol (**5a**) was obtained by the demethylation of **5b** with HBr in a refluxing acetic acid. The spectra (^1H and ^{13}C NMR, IR and GC) of the synthesized naphthol **5a** were completely coincident with those of the naphthol obtained from the reaction of **4b** with HBr.[1] The IR and NMR spectra of the acetate of **5a** were wholly different from those of the acetate of **4a**.[1]

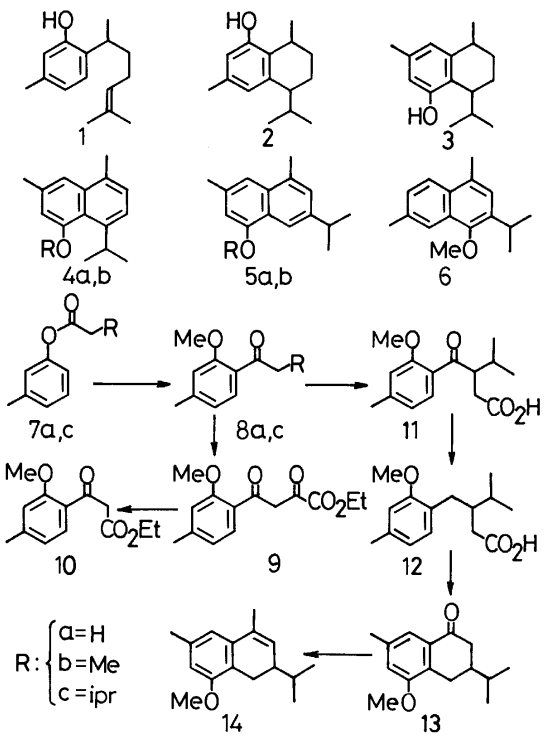

Experimental

2-Methoxy-4-methylacetophenone (8a) and 2-Methoxy-4-methylisovalerophenone (8c). A mixture of *m*-cresol (0.1 mol), acyl chloride (0.12 mol), Mg (1.2 g), and benzene (25 ml) was refluxed for 1 h to give the corresponding *m*-tolyl esters.[7]

m-Tolyl acetate (**7a**): 78.1%, bp 88 °C/11 mmHg (1 mmHg=133.322 Pa); IR (neat): 1770, 1375, 1210, and 1150 cm^{-1}.

m-Tolyl isovalerate (**7c**): 94.7%, bp 136 °C/22 mmHg; IR (neat): 1755, 1240, 1180, 1140, and 1100 cm^{-1}.

A mixture of the tolyl ester (0.1 mol), $AlCl_3$ (0.12 mol), and carbon disulfide (16 ml) was refluxed for 2 h with stirring. The solvent was removed and the residue heated at 145—150 °C for 4 h. The reaction mixture was decomposed with dil. HCl to give the *o*-hydroxy ketone.

2-Hydroxy-4-methylacetophenone: 84.0%, bp 106—108 °C/9 mmHg; IR (neat): 3600—2300, 1630, 1370, 1325, 1300, 1250, 1230, and 795 cm^{-1}; ^1H NMR ($CDCl_3$): δ=2.30 (s, 3H, CH_3), 2.53 (s, 3H, $COCH_3$), 6.65 (d, 1H, J=8 Hz), 6.71 (broad s, 1H), 7.54 (d, 1H, J=8 Hz), and 12.27 (s, 1H, OH).

2-Hydroxy-4-methylisovalerophenone: 95.3%, bp 151—152 °C/21 mmHg; IR (neat); 3500—2500, 1640, 1360, 1310, 1275, 1210, 1150, and 795 cm^{-1}; ^1H NMR ($CDCl_3$): δ=0.99 (d, 6H, J=6.5 Hz, CH_3×2), 2.26 (m, 1H, J=6.5 Hz, >CH-), 2.31 (s, 3H, CH_3), 2.78 (d, 2H, J=6.5 Hz, CH_2), 6.66 (dd, 1H, J=8, 1.5 Hz), 6.74 (broad s, 1H), 7.60 (d, 1H, J=8 Hz), and 12.50 (s, 1H, OH).

To a mixture of the *o*-hydroxy ketone (0.04 mol) and K_2CO_3 (0.06 mol) in acetone (30 ml) was added dimethyl sulfate (0.05 mol) at room temperature; the mixture was refluxed for 10 h with stirring to yield the *o*-methoxy ketone.

2-Methoxy-4-methylacetophenone (**8a**): 87.9%, bp 125—126 °C/10 mmHg; IR (neat): 1670, 1605, 1290, 1260, 1240, 1170, and 1035 cm^{-1}; ^1H NMR ($CDCl_3$): δ=2.36 (s, 3H, CH_3), 2.57 (s, 3H, $COCH_3$), 3.87 (s, 3H, OCH_3), 6.74 (broad s, 1H), 6.78 (d, 1H, J=8 Hz), and 7.66 (d, 1H, J=8 Hz).

2-Methoxy-4-methylisovalerophenone (**8c**): 96.1%, bp 146 °C/10 mmHg; IR (neat): 1670, 1610, 1470, 1410, 1300, 1280, 1255, 1170, and 1040 cm^{-1}; ^1H NMR ($CDCl_3$): δ=0.94 (d, 6H, J=6.5 Hz, CH_3×2), 2.21 (m, 1H, J=6.5 Hz, >CH-), 2.35 (s, 3H, CH_3), 2.82 (d, 2H, J=6.5 Hz, CH_2), 3.85 (s, 3H, OCH_3), 6.73 (broad s, 1H), 6.77 (d, 1H, J=8 Hz), and 7.56 (d, 1H, J=8 Hz).

Ethyl 3-(2-Methoxy-4-methylphenyl)-3-oxopropionate (10). To a mixture of methoxy ketone **8a** (5.0 g) and Na (0.8g) in ethanol (17 ml) was added diethyl oxalate (5.1 g) with cooling in an ice bath; the mixture was stirred for 3 h. The reaction mixture was decomposed by adding dil. H_2SO_4 under cooling. The precipitate was collected by filtration, (7.8 g, 97.5%) to give ethyl 4-(2-methoxy-4-methylphenyl)-2,4-dioxobutyrate (**9**) as yellow leaves (from petroleum ether), mp 73.0—74.0 °C; IR (KBr): 1745, 1605, 1500, 1295, 1250, 1230, and 1025 cm^{-1}; ^1H NMR ($CDCl_3$): δ=1.39 (t, 3H, J=7 Hz, CH_3), 2.40 (s, 3H, CH_3), 3.93 (s, 3H, OCH_3), 4.37 (q, 2H, J=7 Hz, CH_2), 6.79 (s, 1H), 6.84 (d, 1H, J=8 Hz), 7.31 (s, 1H, =CH-), 7.81 (d, 1H, J=8 Hz), and 15.42 (broad s, 1H, enol-OH, disappeared with D_2O). Found: C, 63.63; H, 6.05%. Calcd for $C_{14}H_{16}O_5$: C, 63.62; H, 6.10%.

A mixture of the diketo ester **9** (3.0 g), ground glass (0.3 g), and iron borings (0.03 g) was heated at 150 °C under reduced pressure (16 mmHg). A subsequent distillation of the reaction mixture gave an oily product, bp 157—158 °C/6 mmHg (1.3 g), which was a mixture of **8a** (22.4%), **10** (68.2%), and an unreacted **9** (9.4%) on the basis of the ^1H NMR. The β-keto ester (**10**) was purified by redistillation: (0.8 g, 28.6%), bp 157—158 °C/6 mmHg; IR (neat): 1740, 1670, 1610, 1325, 1260, 1195, and 1035 cm^{-1}; ^1H NMR ($CDCl_3$): δ=1.23 (t, 3H, J=7 Hz, CH_3), 2.36 (s, 3H, CH_3), 3.86 (s, 3H, OCH_3), 3.92 (s, 2H, CH_2), 4.17 (q, 2H, J=7 Hz, CH_2), 6.75 (s, 1H), 6.80 (d, 1H, J=8 Hz), and 7.78 (d, 1H, J=8 Hz).

The distillation residue was chromatographed on silica gel and eluted with CH_2Cl_2 to give an unidentified dimerized product (0.4 g) as yellow needles after recrystalization from benzene, mp 213.0—213.5 °C. Found: C, 69.47; H, 5.54%. Calcd for $C_{22}H_{20}O_6$: C, 69.46; H, 5.30%.

4-Methyl-3-(2-methoxy-4-methylbenzoyl)pentanoic Acid (11). The ketone **8c** (8.0 g) in ether (10 ml) was brominated in the presence of $AlCl_3$ (10 mg) with bromine (3.2 g)[8] to give 2-bromo-3-methyl-1-(2-methoxy-4-methylphenyl)-1-butanone as an oil (11.0 g, 99.1%); IR (neat): 1675, 1610, 1460, 1405, 1295, 1280, 1255, 1165, and 1035 cm^{-1}; ^1H NMR ($CDCl_3$): δ=1.05 (d, 3H, J=6.5 Hz, CH_3), 1.08 (d, 3H, J=6.5 Hz, CH_3), 2.3 (m, 1H, J=6.5 Hz, >CH-), 2.37 (s, 3H, CH_3), 3.88 (s, 3H, OCH_3), 5.33 (d, 1H, J=6.5 Hz, >CH-), 6.76 (s, 1H), 6.80 (d, 1H, J=8 Hz), and 7.61 (d, 1H, J=8 Hz).

The α-bromo ketone (11.0 g) was added to sodio-cyanoacetate prepared from ethyl cyanoacetate (4.5 g) and Na (0.9 g) in ethanol (20 ml); the mixture was refluxed for 5 h with stirring. The reaction mixture was diluted with water and extracted with benzene to give a crude condensed product (11.0 g), which was refluxed with an aqueous solution of 5% NaOH for 5 h. The solution was acidified with HCl and extracted with benzene. The extract was evaporated and recrystallized from benzene to give **11** as prisms (3.6 g, 35.3%), mp 128.5—129.5 °C; IR (KBr): 1700, 1660, 1610, 1465, 1410, 1290, 1260, 1200, 1035, and 820 cm^{-1}; ^1H NMR ($CDCl_3$): δ=0.73 (d, 3H, J=7 Hz, CH_3), 0.97 (d, 3H, J=7 Hz, CH_3), 2.1 (m, 1H, >CH-), 2.35 (dd, 1H, J=17, 4 Hz, $>C<^{H}_{H}$), 2.36 (s, 3H, CH_3), 2.91 (dd, 1H, J=17, 10 Hz, $>C<^{H}_{H}$), 3.86 (s, 3H, OCH_3), 3.9 (m, 1H, >CH-), 6.74 (broad s, 1H), 6.78 (d, 1H, J=8 Hz), 7.59 (d, 1H, J=8 Hz), and 10.58 (broad s, 1H, CO_2H). Found: C, 67.76; H, 7.87%. Calcd for $C_{15}H_{20}O_4$: C, 68.16; H, 7.63%.

When the above α-bromo ketone was condensed with diethyl malonate in place of ethyl cyanoacetate, the yield of keto acid **11** was only 17.6%.

4-Methyl-3-(2-methoxy-4-methylbenzyl)pentanoic Acid (12). The Clemmensen reduction of keto acid **11** (3.1 g) with amalgamated zinc prepared from Zn (7.6 g) and $HgCl_2$ (0.9 g) for 10 h gave **12** (1.7 g, 58.6%), bp 163—164 °C/5 mmHg, mp 96.5—97.5 °C (from petroleum ether); IR (KBr): 1700, 1610, 1505, 1460, 1450, 1410, 1320, 1300, 1290, 1260, 1155, and 1040 cm^{-1}; ^1H NMR ($CDCl_3$): δ=0.90 (d, 3H, J=6.5 Hz, CH_3), 0.94 (d, 3H, J=6.5 Hz, CH_3), 1.7 (m, 1H, >CH-), 2.2 (m, 3H, CH_2, >CH-), 2.29 (s, 3H, CH_3), 2.5 (m, 2H, CH_2), 3.76 (s, 3H, OCH_3), 6.61 (s, 1H), 6.64 (d, 1H, J=8 Hz), 6.97 (d, 1H, J=8 Hz), and 11.11 (broad s, 1H, CO_2H). Found: C, 71.54; H, 9.16%. Calcd for $C_{15}H_{22}O_3$: C, 71.97; H, 8.86%.

3,4-Dihydro-3-isopropyl-5-methoxy-7-methyl-1(2*H*)-naphthalenone (13). A solution of the carboxylic acid **12** (1.7 g) and $POCl_3$ (0.7 g) in 1,1,2,2-tetrachloroethane (25 ml) was refluxed for 2 h with stirring; the mixture was poured into an ice water. The organic layer was separated and concentrated to afford **13** (1.5 g, 93.8%), bp 165—167 °C/7 mmHg; IR (neat): 1685, 1610, 1465, 1340, 1320, 1300, 1250, 1130, and 1060 cm^{-1}; ^1H NMR ($CDCl_3$): δ=0.98 (d, 6H, J=6 Hz, CH_3×2), 1.7 (m, 1H, J=6 Hz, >CH-), 1.8—2.5 (m, 3H, CH_2, >CH-), 2.35 (s, 3H, CH_3), 2.9 (m, 2H, CH_2), 3.85 (s, 3H, OCH_3), 6.83 (d, 1H, J=1.5 Hz), and 7.44 (broad s, 1H). 2,4-Dinitrophenylhydrazone: Red microcrystals (from benzene), mp 216.0—217.0 °C. Found: C, 61.00; H, 5.70; N, 13.33%. Calcd for $C_{21}H_{24}N_4O_5$: C, 61.15; H, 5.87; N, 13.59%.

3,4-Dihydro-3-isopropyl-5-methoxy-1,7-dimethylnaphthalene (14). A solution of tetralone **13** (1.2 g) in ether (15 ml) was added to a Grignard reagent prepared from methyl iodide (2.3 g) and Mg (0.4 g) in ether (20 ml) with cooling in an ice bath. The reaction mixture was refluxed for 10 h with stirring; the mixture was then decomposed by adding ice and NH_4Cl. The resulting crude alcohol (1.3 g, IR: 3380 cm^{-1}) was dehydrated by stirring with formic acid (2.5 ml) at 80 °C for 2 h. After extraction with benzene, the resulting products were chromatographed on silica gel and eluted with CCl_4 to give **14** as an oil (1.0 g, 83.3%); IR (neat): 1605, 1570, 1460, 1280, 1140, 1060, and 830 cm^{-1}; ^1H NMR ($CDCl_3$): δ=0.93 (d, 6H, J=6 Hz, CH_3×2), 1.69 (m, 1H, J=6 Hz, >CH-), 2.04 (broad s, 3H, $\geq$-CH_3), 2.32 (s, 3H, CH_3), 2.5

(m, 2H, CH_2), 2.9 (m, 1H, >CH-), 3.79 (s, 3H, OCH_3), 5.73 (broad, 1H, =CH-), 6.59 (broad s, 1H), and 6.70 (broad s, 1H).

7-Isopropyl-3,5-dimethyl-1-naphthol (5a). The dihydronaphthalene **14** (1.0 g) was dehydrogenated by heating with 5% Pd-C (0.2 g) at 240—250 °C for 5 h. The resulting products were chromatographed on silica gel and eluted with CCl_4 to give the methoxynaphthalene **5b** as an oil (0.8 g, 80.8%), which was identical in all respects with the specimene[1] derived from **4b**. Picrate: Brown needles (from ethanol), mp 165.0—166.0 °C (lit,[1] mp 165.0—166.0 °C).

A mixture of **5b** (0.7 g) and 48% HBr (7 ml) in glacial acetic acid (7 ml) was refluxed for 2 h. The reaction mixture was diluted with water (20 ml) and extracted with benzene. The extract was evaporated and the residue recrystallized from petroleum ether to give 7-isopropyl-3,5-dimethyl-1-naphthol **5a** (0.6 g, 90.9%) as woolly crystals, mp 86.0—87.0 °C (lit,[1] mp 86.0—87.0 °C). The IR and NMR spectra of this naphthol **5a** were superimposable with those of the specimene[1] obtained from **4b** by refluxing in acetic acid with HBr. Acetate: Prisms (from petroleum ether), mp 67.5—68.5 °C; IR (KBr): 1760, 1610, 1400, 1365, 1200, 1120, 1025, and 870 cm^{-1}; ^1H NMR ($CDCl_3$): δ=1.29 (d, 6H, J=7 Hz, CH_3×2), 2.41 (s, 3H, $COCH_3$), 2.49 (s, 3H, CH_3), 2.62 (s, 3H, CH_3), 2.95 (m, 1H, J=7 Hz, >CH-), 7.04 (d, 1H, J=1.5 Hz), 7.20 (broad s, 1H), 7.43 (broad s, 1H), and 7.58 (broad s, 1H). Found: C, 79.58; H, 7.91%. Calcd for $C_{17}H_{20}O_2$: C, 79.65; H, 7.86%.

References

1) Preceeding paper: J. Tanaka and K. Adachi, *Nippon Kagaku Kaishi*, **1989**, 268.

2) F. Bohlmann and M. Lonitz, *Chem. Ber.*, **111**, 843 (1978); F. J. McEnroe and W. Fenical, *Tetrahedron*, **34**, 1661 (1978); E. L. Ghisalberti, P. R. Jefferies, and A. D. Stuart, *Aust. J. Chem.*, **32**, 1627 (1979).

3) J. Tanaka, K. Nobutani, and K. Adachi, *Nippon Kagaku Kaishi*, **1988**, 1065.

4) Y. Kashman, *Tetrahedron*, **35**, 263 (1979); J. D. Bunko, E. L. Ghisalberti, and P. R. Jefferies, *Aust. J. Chem.*, **34**, 2237 (1981); M. Nishizawa, A. Inoue, S. Sastrapradja, and Y. Hayashi, *Phytochemistry*, **22**, 2083 (1983); M. Uemura, K. Isobe, and Y. Hayashi, *Chem. Lett.*, **1985**, 91.

5) F. Bohlmann and C. Zdero, *Chem. Ber.*, **109**, 2021 (1976); F. Bohlmann and W. Mailahn, *ibid.*, **114**, 1091 (1981); K. Adachi and N. Taniguchi, *Bull. Chem. Soc. Jpn.*, **55**, 1655 (1982); K. Adachi and M. Mori, *ibid.*, **56**, 651 (1983).

6) J. Tanaka and K. Adachi, *Yuki Gosei Kagaku Kyokaishi*, **32**, 1006 (1974); K. Adachi, J. Tanaka, Y. Imai, and T. Okazaki, *Nippon Kagaku Kaishi*, **1980**, 62.

7) A. Spasov, *Ann. Univ. Sofia. II Faculté Phy-math.*, Livre 2, **35**, 289 (1938—1939); *Chem. Abstr.*, **34**, 2343 (1940).

8) R. M. Cowper and L. H. Davidson, *Org. Synth.*, Coll. Vol. II, 480 (1943).

Tellurium-Assisted Cyclopropanation and Alkylidenation of α,β-Unsaturated Carbonyl Compounds with Dibromomalonic Esters[1)]

Toshiaki MATSUKI, Nan Xing HU, Yoshio ASO, Tetsuo OTSUBO, and Fumio OGURA*
Department of Applied Chemistry, Faculty of Engineering, Hiroshima University, Saijo, Higashi-Hiroshima 724
(Received December 15, 1988)

Synopsis. Dibutyl telluride assists cyclopropanation of α,β-unsaturated ketone, ester, and nitrile with dibromomalonic esters without solvent at room temperature. In addition, it effects alkylidenation of aldehydes including α,β-unsaturated aldehyde with the same reagent.

The dehalogenation of *vic*-dibromide with diphenyl telluride giving the corresponding olefin and diphenyltellurium dibromide is the first reported transformation of an organic molecule using organotellurium compound.[2)] The halophilic nature of the divalent telluride is due to high stability of the resulting tetravalent tellurane. A recent paper has described the cyclopropanation of electron-deficient olefins with dibromomalonic ester with the aid of trialkylstibine, giving polysubstituted cyclopropanes with electron-withdrawing groups,[3)] which are very useful in organic syntheses.[4)] This has prompted us to study the utility of organotellurium species in a similar reaction as one of our interests on organotellurium chemistry. We like to report here tellurium-assisted cyclopropanation of α,β-unsaturated carbonyl compounds as well as alkylidenation of common aldehydes including α,β-unsaturated aldehydes with dibromomalonic esters. The latter provides a novel example of tellurium-based condensation, while a Wittig reaction using telluronium ylides has been already known.[5)]

Dibutyl telluride (**1**), like organostibine, induced cyclopropanation of α,β-unsaturated ester, ketone, or nitrile **3** with dibromomalonic ester **2** (Scheme 1).

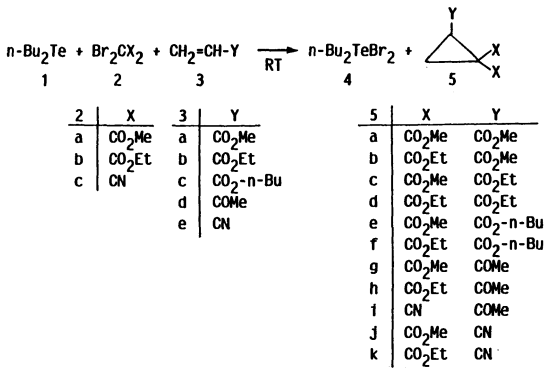

2	X
a	CO_2Me
b	CO_2Et
c	CN

3	Y
a	CO_2Me
b	CO_2Et
c	CO_2-n-Bu
d	COMe
e	CN

5	X	Y
a	CO_2Me	CO_2Me
b	CO_2Et	CO_2Me
c	CO_2Me	CO_2Et
d	CO_2Et	CO_2Et
e	CO_2Me	CO_2-n-Bu
f	CO_2Et	CO_2-n-Bu
g	CO_2Me	COMe
h	CO_2Et	COMe
i	CN	COMe
j	CO_2Me	CN
k	CO_2Et	CN

Scheme 1.

The termolecular reaction exothermically took place without solvent at room temperature to give the corresponding cyclopropane derivative **5** in moderate to high yields after 1—24 h. The main by-product was dibutyltellurium dibromide (**4**).[6)] A variety of trisubstituted cyclopropanes **5a—k** were thus obtained by appropriate combinations of reactants summarized in Table 1. When benzene or ethanol was used as a solvent, the reaction took longer time. On the other hand, a similar reaction using dibromomalononitrile (**2c**) instead of dibromomalonic ester vigorously occurred, leading to decomposition in most cases. Only from the reaction of **1**, **2c**, and vinyl methyl ketone (**3d**) in ethanol at 0 °C for 3 h, 1-acetyl-2,2-dicyanocyclopropane (**5i**) could be isolated in 85% yield. Bis(*p*-methoxyphenyl) telluride (**6**) instead of dibutyl telluride hardly promoted the reaction even at 150 °C.

Table 1. Tellurium-Assisted Cyclopropanation and Alkylidenation[a)]

Reactants	Time/h	Product	Yield/%[b)]
2a+3a	12	**5a**	52
2b+3a	12	**5b**	94
2a+3b	18	**5c**	32
2b+3b	16	**5d**	73
2a+3c	12	**5e**	39
2b+3c	24	**5f**	47
2a+3d	1	**5g**	78
2b+3d	1	**5h**	86
2c+3d	3	**5i**	85[c)]
2a+3e	12	**5j**	41
2b+3e	12	**5k**	57
2a+7a	0.5	**9a**	87
2b+7a	0.5	**9b**	79
2a+7b	1	**9c**	59
2b+7b	1	**9d**	68
2a+7c	1	**9e**	82
2b+7c	3	**9f**	47
2a+7d	1	**9g**	47
2b+7d	1	**9h**	63
2a+7e	5	**9i**	66
2b+7e	2	**9j**	53
2a+7f	2	**9k**	71
2b+7f	6	**9l**	48

a) Reaction conditions: no solvent at RT unless otherwise stated. b) Yield of isolated product. c) Reaction conditions: ethanol solvent at 0 °C.

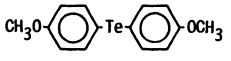

6

Although organostibine can also induce a similar cyclopropanation of α,β-unsaturated aldehydes, **1** behaves differently. It thus allowed acrylaldehyde (**7a**), crotonaldehyde (**7b**), methacrylaldehyde (**7c**), or *trans*-cinnamaldehyde (**7d**) to react at the aldehyde function with dibromomalonic ester **3**, giving a conjugated olefin **9** (Scheme 2). The optimal reaction required two equiv of **1**, as different from the above cyclopropanation using one equiv of **1**. The formation of **4** as a product from **1** was little detected. On the other hand, dibutylbromotellurium hydroxide (**8**)

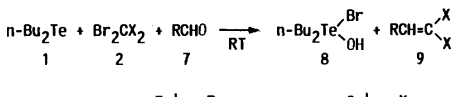

7	R
a	CH_2=CH
b	MeCH=CH
c	CH_2=CMe
d	t-PhCH=CH
e	n-C_6H_{13}
f	Ph

9	X	R
a	CO_2Me	CH_2=CH
b	CO_2Et	CH_2=CH
c	CO_2Me	MeCH=CH
d	CO_2Et	MeCH=CH
e	CO_2Me	CH_2=CMe
f	CO_2Et	CH_2=CMe
g	CO_2Me	t-PhCH=CH
h	CO_2Et	t-PhCH=CH
i	CO_2Me	n-C_6H_{13}
j	CO_2Et	n-C_6H_{13}
k	CO_2Me	Ph
l	CO_2Et	Ph

Scheme 2.

was obtained in an excellent yield after aqueous treatment of the reaction mixture. This alkylidenation is also applicable for common aldehydes such as heptanal (**7e**) and benzaldehyde (**7f**), affording simple condensed products **9** and accordingly useful as a substitute for Knoevenagel condensation of aldehyde and active methylene.[7]

Although the mechanisms are not established, these reactions are likely to proceed through pathways as shown in Scheme 3. The chemoselectivity of cyclo-

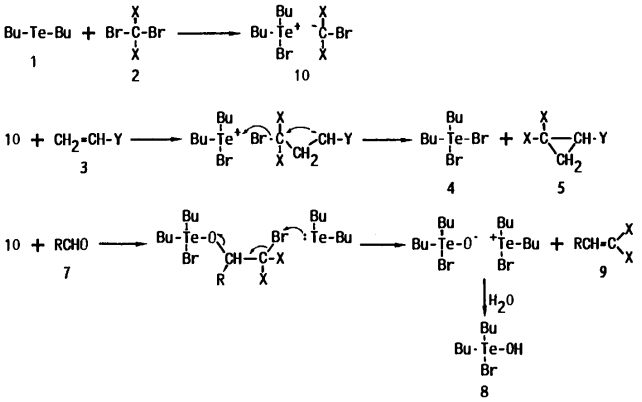

Scheme 3.

propanation and alkylidenation of α,β-unsaturated carbonyl compound **3** depends on reactivity of the initial complex **10**. Aldehydes **7** suffer ready 1,2-addition leading to alkylidenation. In contrast, ketones, esters, and nitriles are inert, and accordingly their conjugated olefins can effect Michael type addition leading to cyclopropanation.

Experimental

Melting points are uncorrected. All reactions were carried out under an argon atmosphere. Dibutyl telluride (**1**),[8] dimethyl dibromomalonate (**2a**),[9] diethyl dibromomalonate (**2b**),[9] and dibromomalononitrile (**2c**)[10] were prepared according to the reported methods. Other chemicals are commercially available. IR spectroscopy was run on a Hitachi 260-30 spectrophotometer. NMR spectra were recorded on a JEOL PMX-60 spectrometer (60 MHz) using carbon tetrachloride as a solvent. Mass spectra were measured with a Shimazu QP-1000 spectrometer.

Typical Procedure for Cyclopropanation: 1-Acetyl-2,2-bis(ethoxycarbonyl)cyclopropane (5h). Diethyl dibromomalonate (**2b**; 954 mg, 3 mmol) and methyl vinyl ketone (**3d**; 267 mg, 3.1 mmol) were placed in a 20 mL round-bottomed flask with a septum cap, which was purged with an argon gas. Dibutyl telluride (**1**; 726 mg, 3 mmol, 1 equiv) was added by a syringe and the mixture was stirred at room temperature under an inert gas. The exothermic reaction was complete within 1h. It was then chromatographed on an alumina column (70—230 mesh) with ethyl acetate as eluent to give first dibutyltellurium dibromide (**4**)[6] as a colorless oil, yield 1.012 g (84%); ^{1}H NMR (CCl_4) δ=0.88—1.21 (m, 6H, $2CH_3$), 1.21—2.60 (m, 8H, $4CH_2$), and 3.41—3.80 (m, 4H, $2TeCH_2$).

Further elution gave 1-acetyl-2,2-bis(ethoxycarbonyl)-cyclopropane (**5h**) as a colorless oil, which was further purified by bulb-to-bulb distillation; bp 88—90 °C/11 Pa (lit,[11] bp 92 °C/11 Pa); yield 587 mg (86%).

5a: colorless oil, bp 137—140 °C/15 Pa; IR (neat) 3020, 1755, 1750, 1735, and 885 cm^{-1}; ^{1}H NMR δ=1.55 (dd, 1H, J=5.5 and 8 Hz), 1.83 (dd, 1H, J=4.5 and 7 Hz), 2.46 (dd, 1H, J=7 and 8 Hz), 3.68 (s, 6H), and 3.74 (s, 3H); MS m/z (rel intensity) 216 (M^+, 0.3) and 157 (M^+-CO_2Me, 100). Anal. ($C_9H_{12}O_6$) C, H.

5b: colorless oil, bp 115—116 °C/5 Pa (lit,[12] bp 84—85 °C/1 Pa).

5c: colorless oil, bp 105—107 °C/11 Pa; IR (neat) 3000, 1760, 1750, 1730, and 865 cm^{-1}; ^{1}H NMR δ=1.25 (t, 3H, J=7 Hz), 1.56 (dd, 1H, J=4.5 and 8 Hz), 1.84 (dd, 1H, J=4.5 and 7 Hz), 2.45 (dd, 1H, J=7 and 8 Hz), 3.66 (s, 3H), 3.74 (s, 3H), and 4.10 (q, 2H, J=7 Hz); MS m/z 230 (M^+, 2.1) and 185 (M^+-OEt, 100). Anal. ($C_{10}H_{14}O_6$) C, H.

5d: colorless oil, bp 99—102 °C/8 Pa (lit,[13] bp 76—80 °C/7 Pa).

5e: colorless oil, bp 103—105 °C/11 Pa; IR (neat) 2960, 1760, 1755, 1730, and 885 cm^{-1}; ^{1}H NMR δ=0.8—1.7 (m, 7H), 1.56 (dd, 1H, J=4.5 and 8.5 Hz), 1.85 (dd, 1H, J=4.5 and 7 Hz), 2.49 (dd, 1H, J=4.5 and 8.5 Hz), 3.67 (s, 3H), 3.74 (s, 3H), and 4.07 (bt, 2H, J=6 Hz); MS m/z (rel intensity) 258 (M^+, 13) and 185 (M^+-OBu, 100). Anal. ($C_{12}H_{18}O_6$) C, H.

5f: colorless oil, bp 129—132 °C/11 Pa; IR (neat) 2990, 1755, 1750, 1745, and 860 cm^{-1}; ^{1}H NMR δ=0.8—1.7 (m, 7H), 1.30 (t, 3H, J=7 Hz), 1.33 (t, 3H, J=7 Hz), 1.51 (dd, 1H, J=4.5 and 8.5 Hz), 1.82 (dd, 1H, J=4.5 and 7 Hz), 2.47 (dd, 1H, J=7 and 8.5 Hz), 4.11 (q, 2H, J=7 Hz), 4.19 (q, 2H, J=7 Hz), and 4.31 (t, 2H, J=6 Hz), MS m/z (rel intensity) 286 (M^+, 0.04) and 185 (M^+-CO_2Bu, 100). Anal. ($C_{14}H_{22}O_6$) C, H.

5g: colorless oil, bp 117—120 °C/11 Pa; IR (neat) 3000, 1730, 1708, and 880 cm^{-1}; ^{1}H NMR δ=1.49 (dd, 1H, J=4.5 and 8.5 Hz), 1.88 (dd, 1H, J=4.5 and 7 Hz), 2.33 (s, 3H), 2.77 (dd, 1H, J=7 and 8.5 Hz), 3.62 (s, 3H), and 3.73 (s, 3H); MS m/z (rel intensity) 200 (M^+, 2.3) and 185 (M^+-Me, 100). Anal. ($C_9H_{12}O_5$) C, H.

5i: colorless oil, bp 129—132 °C/11 Pa; IR (neat) 3120, 2255, 1715, and 840 cm^{-1}; ^{1}H NMR δ=2.0—2.4 (m, 2H), 2.40 (s, 3H), and 3.10 (dd, 1H, J=7 and 8.5 Hz); MS m/z (rel intensity) 134 (M^+, 1.4) and 43 (COMe, 100). Anal. ($C_7H_6N_2O$) C, H, N.

5j: colorless oil, bp 121—123 °C/1470 Pa (lit,[14] bp 123—125 °C/1730 Pa).

5k: colorless oil, bp 99—103 °C/15 Pa (lit,[12] bp 98—100 °C/13 Pa).

Typical Procedure for Alkylidenation: Diethyl 2-Propenylidenemalonate (9b). A mixture of diethyl dibromomalonate (**2b**; 477 mg, 1.5 mmol) and acrylaldehyde (87 mg, 1.5 mmol) was treated with dibutyl telluride (**1**; 726 mg, 3 mmol, 2 equiv) as described for the preparation of **5h**. After 30 min, the mixture was taken up with chloroform (30 mL) and washed with water, dried over anhydrous magnesium sulfate, and concentrated in vacuo. The

residue was diluted with hexane (20 mL). The insoluble material was filtered off and the filtrate was chromatographed on silica-gel column (88—125 mesh) with chloroform to give first dibutyltellurium dibromide (**4**) as a colorless oil, yield 30 mg (5%), and then diethyl 2-propenylidenemalonate (**9b**) as a colorless oil, yield 258 mg (87%), which was purified by bulb-to-bulb distillation; bp 63—65 °C/16 Pa; IR (neat) 2990, 1745, 1720, 1590, and 865 cm^{-1}; ^1H NMR δ=1.27 (t, 3H, J=7 Hz), 1.30 (t, 3H, J=7 Hz), 4.18 (q, 2H, J=7 Hz), 4.20 (q, 2H, J=7 Hz), 5.49 (dd, 1H, J=2 and 9.5 Hz), 5.61 (ddd, 1H, J=9.5, 11, and 17 Hz), and 7.14 (d, 1H, J=11 Hz); MS m/z (rel intensity) 198 (M^+, 31) and 153 (M^+—OEt, 100). HRMS Found: m/z 198.0934. Calcd for $C_{10}H_{14}O_4$: M, 198.0892.

Recrystallization of the insoluble material from benzene-hexane gave white scales of dibutylbromotellurium hydroxide (**8**); yield 811 mg (80%); mp 141—142 °C; IR (KBr) 3450 (O-H) and 2970 cm^{-1}; ^1H NMR ($CDCl_3$) δ=0.84—1.20 (m, 6H, $2CH_3$), 1.20—2.33 (m, 8H, $4CH_2$), 1.69 (br s, 1H, OH), and 2.70—3.85 (m, 4H, $2TeCH_2$). Anal. ($C_8H_{19}BrOTe$) C, H.

9a: colorless oil, bp 85—87 °C/15 Pa; IR (neat) 3050, 1735, 1720, 1590, and 840 cm^{-1}; ^1H NMR δ=3.74 (s, 3H), 3.77 (s, 3H), 5.54 (dd, 1H, J=2 and 9.5 Hz), 5.67 (dd, 1H, J=2 and 17 Hz), 6.68 (ddd, J=9.5, 11, and 17 Hz), and 7.16 (d, 1H, J=11 Hz); MS m/z (rel intensity) 170 (M^+, 52) and 139 (M^+—OMe, 100). HRMS Found: m/z 170.0577. Calcd for $C_8H_{10}O_4$: M, 170.0579.

9c: colorless oil, bp 120—123 °C/147 Pa (lit,[15] bp 130—135 °C/200 Pa).

9d: colorless oil, bp 145—148 °C/2000 Pa (lit,[16] bp 143 °C/2000 Pa).

9e: colorless oil, bp 101—103 °C/10 Pa; IR (neat) 2965, 1745, 1735, 1655, and 845 cm^{-1}; ^1H NMR δ=1.89 (br s, 3H), 3.78 (s, 6H), 5.2—5.5 (m, 2H), and 7.19 (s, 1H); MS m/z (rel intensity) 184 (M^+, 100) and 153 (M^+—OMe, 52). HRMS Found: m/z 184.0746. Calcd for $C_9H_{12}O_4$: M, 184.0736.

9f: colorless oil, bp 93—95 °C/4 Pa (lit,[17] bp 85—87 °C/1.3 Pa).

9g: colorless crystals, mp 60—62 °C; IR (KBr disk) 2965, 1745, 1735, 1620, and 865 cm^{-1}; ^1H NMR δ=3.73 (s, 3H), 3.79 (s, 3H), and 6.7—7.6 (m, 8H); MS m/z (rel intensity) 246 (M^+, 42) and 215 (M^+—OMe, 100). Anal. ($C_{14}H_{14}O_4$) C, H.

9h: colorless crystals, mp 35—36 °C (lit,[18] mp 34—35 °C).

9i: colorless oil, bp 125—128 °C/40 Pa; IR (neat) 2970, 1740, 1730, 1645, and 840 cm^{-1}; ^1H NMR δ=0.7—2.5 (m, 13H), 3.70 (s, 3H), 3.75 (s, 3H), and 6.88 (t, 1H, J=8 Hz); MS m/z (rel intensity) 228 (M^+, 5.7) and 197 (M^+—OMe, 100). Anal. ($C_{12}H_{20}O_4$) C, H.

9j: colorless oil, bp 138—141 °C/67 Pa (lit,[19] bp 143—145/67 Pa).

9k: colorless oil, bp 131—134 °C/20 Pa (lit,[20] bp 143—146 °C/27 Pa).

9l: colorless oil, bp 163—165 °C/1470 Pa (lit,[21] bp 179.5 °C/1870 Pa).

This work was partially supported by a Grant-in-Aid of Scientific Research from the Ministry of Education, Science and Culture.

References

1) Organotellurium Part XVI. Part XV, T. Matsuki, N. X. Hu, Y. Aso, T. Otsubo, and F. Ogura, *Bull. Chem. Soc. Jpn.*, **61**, 2117 (1988).
2) M. M. Campos, N. Petragnani, and C. Thome, *Tetrahedron Lett.*, **1960**, No. 15, 5.
3) C. Chen, Y. Huang, and Y. Shen, *Tetrahedron Lett.*, **29**, 1033 (1988).
4) For an excellent review, see S. Danishefsky, *Acc. Chem. Res.*, **12**, 66 (1977).
5) A. Osuka, Y. Mori, H. Shimizu, and H. Suzuki, *Tetrahedron Lett.*, **24**, 2599 (1983); X. Hung, L. Xie, and H. Wu, *J. Org. Chem.*, **53**, 4862 (1988).
6) W. Hieber and T. Kruck, *Chem. Ber.*, **95**, 2027 (1962).
7) R. L. Reeves, "The Chemistry of the Carbonyl Group," ed by S. Patai, Interscience, London (1966), p. 593; G. Jones, *Org. React.* **15**, 204 (1967); H. O. House, "Modern Synthetic Reactions," 2nd ed., W. A. Benjamin Inc., Menlo Park (1972), p. 646; J. Mathieu and J. Weill-Raynal, "Formation of C-C Bonds," G. Thieme Publishers, Stuttgart (1975), Vol. 2, p. 515.
8) M. P. Balfe, C. A. Chaplin, and H. Phillips, *J. Chem. Soc.*, **1938**, 341.
9) T. Wakui, Y. Otsuji, and F. Imoto, *Nippon Kagaku Kaishi*, **1974**, 1686.
10) K. Torssell and K. Dahlqvist, *Acta Chem. Scand.*, **16**, 346 (1962).
11) D. T. Warner, *J. Org. Chem.*, **24**, 1536 (1959).
12) H. Fauduet and R. Burgada, *Synthesis*, **1980**, 642.
13) U. Schmidt, R. Schoer, and A. Hochrainer, *Justus Liebigs Ann. Chem.*, **733**, 180 (1970).
14) R. Verhe, N. D. Kimpe, L. D. Buyck, D. Courtheyn, L. V. Caenegem, and N. Schamp, *Bull. Soc. Chim. Belg.*, **92**, 386 (1983).
15) H. Meerwein, *Justus Liebigs Ann. Chem.*, **358**, 71 (1908).
16) T. Curigny and H. Normant, *Bull. Soc. Chim. Fr.*, **1961**, 2423.
17) T. Lennartz, *Ber.*, **76**, 1006 (1943).
18) H. Holmes and D. J. Currie, *Can. J. Chem.*, **47**, 4076 (1969).
19) B. Wojik and H. Adkins, *J. Am. Chem. Soc.*, **56**, 2424 (1934).
20) C. F. H. Allen and F. W. Spangler, *Org. Synth.*, **25**, 42 (1945).
21) I. Vogel, *J. Chem. Soc.*, **1928**, 2031.

Indirect Electrooxidation by Using Ruthenium Tetraoxide and Chloride Ion as Recycling Mediators. Optimization for the Oxidation of Diisopropylidene-D-glucose to the Ulose

Sigeru TORII,* Tsutomu INOKUCHI, Shigeaki MATSUMOTO, Takeaki SAEKI, and Tsunehei OKI
Department of Applied Chemistry, Faculty of Engineering, Okayama University, Okayama 700
(Received January 5, 1989)

Synopsis. Various factors related to the yield and selectivity for the indirect electrooxidation of diisopropylideneglucose (**1**) to the ulose **2** with ruthenium tetraoxide (RuO_4) and chloride ion are investigated. The following is found to be optimum conditions: pH, ca. 10: solvent system, carbon tetrachloride and *t*-butyl alcohol (ca. 9 : 1); current density, 10—40 mA cm^{-2}; temperature, 20—40 °C; catalyst amount, 2 mol% of $RuO_2 \cdot 2H_2O$ (based on **1**). The optimized electrolysis affords the desired **2** in 90% yield along with a trace of the cleavaged product **3** (0.2%) by an overoxidation.

Ruthenium tetraoxide (RuO_4) has been utilized as a versatile reagent for oxidative transformations[1] since the first example was reported by Djerassi et al.[2] In the preceding paper, we have developed an in situ regeneration of RuO_4 from $RuO_2 \cdot 2H_2O$ or $RuCl_3$ by the electrolysis in a two-phase system consisting of an aqueous sodium chloride and an appropriate organic solvent.[3-5] This electrochemical procedure involves following three reaction steps: (1) oxidation of the substrate by RuO_4, (2) regeneration of RuO_4 from RuO_2 by the action of oxidizing chlorine species, and (3) anodic oxidation of chloride ion to the oxidizing chlorine species. Optimization of the reaction by controlling the electrolysis conditions, however, has not been examined in details. We chose 1,2 : 5,6-di-*O*-isopropylidene-α-D-glucofuranose (diisopropylideneglucose, **1**), prepared from D-glucose by isopropylidenation,[6] as a substrate for the following reasons: (a) synthetic utility of the product as a chiron pool[7] and (b) structural diversity of **1**, bearing acid-labile groups, to know the range of applicability of the

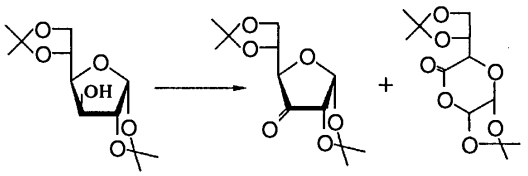

1 2 3

Scheme 1.

method.

The preparation of 1,2 : 5,6-di-*O*-isopropylidene-α-D-ribo-hexofuranos-3-ulose (**2**) by oxidation of diisopropylideneglucose **1** has been carried out by using $CrO_3 \cdot 2Py$ (yield: 6%),[8a] PCC-Molecular Sieves (yield: 85%),[8b] DMSO-Ac_2O (yield: 62%),[9] DMSO-DCC (yield: 0—70%),[10] DMSO-P_2O_5 (yield: 45—65%),[11] DMSO-TFAA (yield: 85%),[12] RuO_4-$NaIO_4$ (yield: 75—95%),[13] photochemical oxidation of pyruvic ester,[14] and others.[15] Most of these oxidizing agents suffer from one of the following disadvantages: high cost of reagents, troublesome workup, and hazardous waste products from the oxidants. In addition, the overoxidation of **2** to the corresponding δ-lactone **3** is a problem to be circumvented.[13] In this study we have investigated the influential factors which are related with the formation of **2** from **1** in the RuO_4-mediated electrochemical process.

Experimental

Material. $RuO_2 \cdot 2H_2O$ purchased from Nippon Engelhard Company was used. The starting compound **1** prepared by the known methods[6] was purified by recrystallization from cyclohexane prior to the use. Chloroform ($CHCl_3$) was washed with water to remove ethanol before use. Aqueous buffer solutions were prepared by dissolving an appropriate phosphate or carbonate in aqueous saturated sodium chloride.

Electrolysis Apparatus. Electrolyses were usually carried out in a simple 30 ml beaker-type cell (2.5 cm diameter and 10 cm height) fitted with a condenser, a stirring bar, a thermometer, and two platinum foil electrodes (3 cm^2) being placed parallel to each other 10 mm apart. The vessel was immersed in a thermostated water bath and approximately maintained at prescribed temperature.

General Procedure for the Electrooxidation of 1. 1,2 : 5,6-Di-*O*-isopropylidene-α-D-glucofuranose (**1**, 400 mg, 1.45 mmol) was dissolved in CCl_4 (5 ml) in an electrolysis vessel and then $RuO_2 \cdot 2H_2O$ (10 mg, 0.06 mmol) and saturated NaCl buffered at pH 9 with 0.03 M $NaHCO_3$ (10 ml) were added to this solution. To the upper aqueous layer of two phase mixture were immersed two platinum electrodes and then the entire mixture was electrolyzed under a constant current of 20 mA cm^{-2} at room temperature with a vigorous stirring. The electrolysis was continued until the organic phase has changed slightly to a yellow solution from greenish black. It required the passage of about 5 F mol^{-1} of electricity based on **1**. The mixture was treated with 2-propanol (0.5 ml) to deactivate the excess ruthenium tetraoxide. The CCl_4 layer was separated and the aqueous layer was extracted with $CHCl_3$. The combined extracts were washed with water, dried over Na_2SO_4, and concentrated in vacuo to give 360 mg of the crude oily products. The product yields were determined with quantitative analysis with gas chromatography. The yields of the ulose **2** and the lactone **3** were 82% and 1.2%, respectively and a small amount of the starting glucofuranose **1** was recovered (7.2%).

Similar electrolysis of 1.20 g (4.62 mmol) of **1** using 0.02 g (0.12 mmol) of $RuO_2 \cdot 2H_2O$ in the mixed solvent of CCl_4 (7 ml), *t*-butyl alcohol (1 ml), and saturated NaCl buffered at pH 10 with 0.03M $NaHCO_3$ and 0.01M Na_2CO_3 (12 ml) as above required 5.1 F mol^{-1} of electricity and then the desired ketone **2**, the lactone **3**, and **1** were obtained in 90%, 0.2%, and 7% yields, respectively.

Analysis. The starting diisopropylideneglucose **1** and the products were analyzed with gas chromatography (1 m, 10% ucone oil 50HB5100/chromosorb W-HP 80/100 mesh). The quantitative analysis was performed in an internal

standard method by gas chromatography (an internal standard: sulfolane).

Results and Discussion

The electrolyses of **1** were carried out in a two-phase system consisted of an organic solvent and an aqueous saturated sodium chloride solution. In order to find a suitable electrolysis solvent system, we first plotted the yields of the diisopropylidene ulose **2** by changing the kind of organic solvents under different pH ranges of an aqueous phase (Fig. 1). Carbon tetrachloride (CCl_4), 4-methyl-2-pentanone, and *t*-butyl alcohol were found to be useful for the present purpose. Of interest to note is that the product yield of the ulose **2** in a halogenated solvent such as carbon tetrachloride (CCl_4) and chloroform ($CHCl_3$) increases at basic pH range. On the other hand, acetone and 4-methyl-2-pentanone were preferable ones in the acidic conditions. The overoxidation of the ulose **2** to the δ-lactone **3** is a major problem to be solved in the present RuO_4-mediated electrooxidation. The formation of **3** can be suppressed to less than 5% by employing CCl_4 or $CHCl_3$.

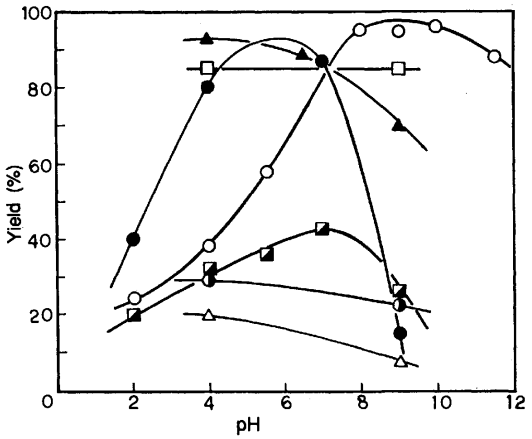

Fig. 1. Effect of pH of the aqueous phase for the formation of **2** in a two phase system consisting of a different sort of organic solvents and saturated NaCl (8 ml/12 ml). Data points of this figure were obtained by electrolysis of **1** (170 mg) in the presence of $RuO_2 \cdot 2H_2O$ (10 mg) at a current of 10 mA cm^{-2} by passing 5 F mol^{-1} of electricty. ○: CCl_4; ◑: diisopropyl ether; ●: acetone; □: *t*-butyl alcohol; ◪: $CHCl_3$; △: CH_3CN; ▲: 4-methyl-2-pentanone.

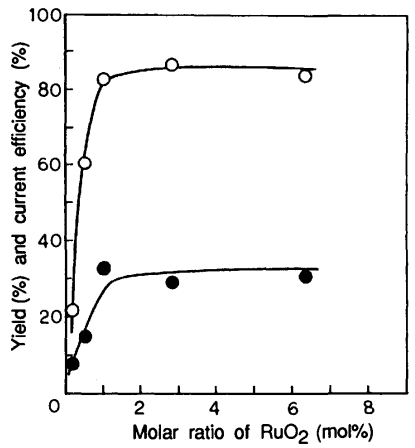

Fig. 2. Effect of molar ratio of $RuO_2 \cdot 2H_2O$ (to **1**) for the formation of **2**. Data points were obtained by electrolysis in CCl_4/saturated NaCl (8 ml/12 ml) by passing 5 F mol^{-1} of electricity. Symbols follows: product yield (○), current efficiency (●).

So far as the effect of current density and temperature is concerned, satisfactory conversion yields were obtained under the conditions of 10—40 mA cm^{-2} at 20—40 °C.

In order to visualize the correlation of the amount of ruthenium reagent for the ulose electrosynthesis, the conversion yields together with the current efficiencies with changing the amount of $RuO_2 \cdot 2H_2O$ are plotted in the Fig. 2. The results show the minimum amount of ruthenium reagent required for the oxidation of **1**. The both conversion yields and current efficiencies reach a plateau under the conditions of more than 1.5 mol% of $RuO_2 \cdot 2H_2O$ (based on the substrate **1**) at a current density of 20 mA cm^{-2}.

In order to clarify the correlation of the amount of ruthenium dioxide toward the current efficiency, the molar ratio of ruthenium dioxide vs. current density was plotted in terms of the conversion yield as well as the current efficiency of the ulose **2** as compiled in Fig. 3. Apparently, both the yields and the current efficiencies increase with increasing the value of RuO_2 amount divided by current density. The maximum points were obtained when the value reached about 0.2×10^{-2} [mol (A cm^{-2})$^{-1}$].

The conversion yields and the current efficiencies in the ulose electrosynthesis are referred to the substrate concentration in the media. The curves in Fig. 4 indicate that the current efficiencies and conversion yields of the ulose **2** decrease in proportion to the increase of the substrate concentration. Carbon tetrachloride can not be used for the large scale operation due to the limited solubility of the substrate **1** (maximum solubility in carbon tetrachloride: 4

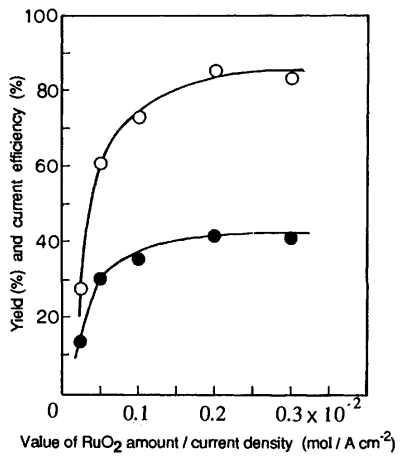

Fig. 3. Effect of value of RuO_2 amount divided by current density for the formation of **2**. Data points were obtained by the electrolysis in CCl_4/saturated NaCl (8 ml/12 ml) at a current of 20 mA cm^{-2} by passing 5 F mol^{-1} of electricity at pH 8—9. Symbols follows: product yield (○), current efficiency (●).

wt%). The co-solvent system may be a choice for the present electrooxidation in order to attain higher concentration of the substrate.

Taking the data in Fig. 1 into the account, we chose *t*-butyl alcohol as an additional solvent to carbon tetrachloride, since *t*-butyl alcohol can maintain almost same current efficiency as carbon tetrachloride. The experimental results are summarized in Fig. 5. The yields of the ulose **2** obtained in various co-solvent ratios and different pH ranges are shown as a form of contour line like as on a map. The horizontal zones are made by binding the points of the same yields. The contour lines summarize the correlation between pH values and co-solvent systems in terms of the conversion yields of the ulose **2**. Of interest to note is that two maximum zones are observed in the region of 90 vol% of carbon tetrachloride (to *t*-butyl alcohol) at about pH 10 and 10 vol% of CCl_4 (to *t*-butyl alcohol) at about pH 4. From a practical point of view, however, it is desirable to choose the electrolysis conditions of slightly basic media to prevent hydrolysis of the acetonide protecting groups.

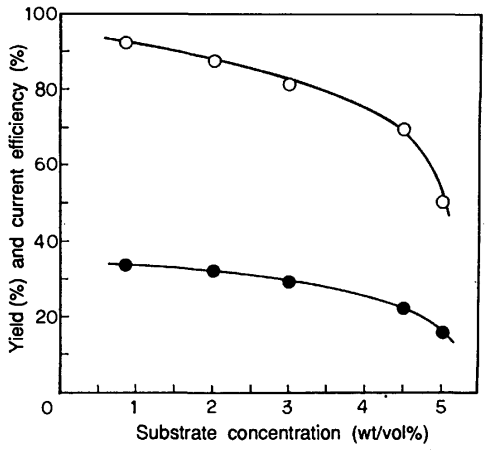

Fig. 4. Effect of substrate concentration for the formation of **2**. Data points were obtained by electrolysis in CCl_4-saturated NaCl (7 ml/14 ml) at a current density of 10 mA cm^{-2} by passing 5.5 F mol^{-1} of electricity at pH 8—9. Symbols follows: product yield (○), current efficiency (●).

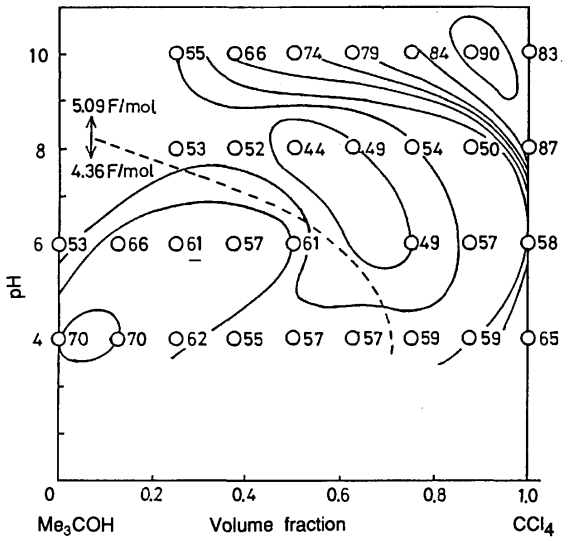

Fig. 5. Correlation between pH and CCl_4/*t*-butyl alcohol ratio for the formation of **2**. The suffix number of data points denotes the yield of **2**. These data were obtained by electrolysis at a current density of 20 mA cm^{-2} by passing 4.36 F mol^{-1} of electricity. The substrate concentration was 6 (wt/vol).

In conclusion, ruthenium tetraoxide has proven to be an efficient mediator as an oxidizing reagent in the present electrolysis system. The constant current electrolysis at 20 mA cm^{-2} of **1** (1.20 g) with 20 mg of $RuO_2 \cdot 2H_2O$ at about pH 10 in CCl_4-Me_3COH (ca. 9 : 1)-saturated NaCl-(Pt) system gives **2** (ratio of **2** to **3**=ca. 450 : 1) in about 90% yields.

This work was partially supported by the Grant-in-Aid for Developmental Scientific Research (No. 63850172) from the Ministry of Education, Science and Culture.

References

1) D. G. Lee and M. van der Engh, "Oxidation in Organic Chemistry," W. S. Trahanovsky, Academic Press, New York (1973), Part B, Chap. 4, p.117.
2) C. Djerassi and R. R. Engle, *J. Am. Chem. Soc.*, **75**, 3838 (1953).
3) S. Torii, T. Inokuchi, and T. Sugiura, *J. Org. Chem.*, **51**, 155 (1986).
4) S. Torii, T. Inokuchi, and T. Yukawa, *Chem. Lett.*, **1984**, 1064.
5) S. Torii, T. Inokuchi, and Y. Hirata, *Synthesis*, **1987**, 377.
6) C. L. Mehltretter, B. H. Alexander, R. L. Mellies, and C. E. Rist, *J. Am. Chem. Soc.*, **73**, 2424 (1951).
7) a) S. Hanessian, "Total Synthesis of Natural Products: The 'Chiron' Approach, Pergamon Press: Oxford (1983); b) T. D. Inch, *Tetrahedron*, **40**, 3161 (1984).
8) a) O. Theander, *Acta Chem. Scand.*, **18**, 2209 (1964); b) J. E. Herscovici and K. J. Antonakis, *J. Chem. Soc., Chem. Commun.*, **1980**, 561.
9) a) W. Sowa and G. H. S. Thomas, *Can. J. Chem.*, **44**, 836 (1966); b) A. Szarek, J. S. Jewel, I. Szczerk, and J. K. N. Jones, *Can. J. Chem.*, **47**, 4473 (1969).
10) a) G. H. Jones and J. G. Moffat, *Methods Carbohydr. Chem.*, **6**, 315 (1972); b) B. R. Baker and D. H. Buss, *J. Org. Chem.*, **30**, 2304 (1965).
11) a) K. Onodera, S. Hirano, and N. Kashimura, *Carbohydr. Res.*, **6**, 276 (1968); b) J. S. Brimacombe, J. G. H. Bryan, A. Husain, M. Stacey, and M. S. Tolley, *Carbohydr. Res.*, **3**, 318 (1967).
12) J. Yoshimura, K. Sato, and H. Hashimoto, *Chem. Lett.*, **1977**, 1327.
13) a) P. J. Beynon, P. M. Collins, P. T. Doganges, and W. G. Overend, *J. Chem. Soc. C*, **1966**, 1131; b) R. F. Nutt, M. J. Dickinson, F. W. Holley, and E. Walton, *J. Org. Chem.*, **33**, 1789 (1968): c) D. C. Baker, D. Horton, and C. G. Tindall, Jr., *Carbohydr. Res.*, **24**, 192 (1972).
14) R. W. Binkley, *J. Org. Chem.*, **42**, 1216 (1977).
15) R. F. Butterworth and S. Hanessian, *Synthesis*, **1971**, 70.

The Utility of *t*-Butyldimethylsilane as an Effective Silylation Reagent for the Protection of Functional Groups

Keiji YAMAMOTO* and Makoto TAKEMAE
Department of Chemical Engineering, Tokyo Institute of Technology, Meguro, Tokyo 152
(Received January 11, 1989)

Synopsis. Treatment of compounds containing functional groups, such as alcohols, amines, and carboxylic acids, with *t*-butyldimethylsilane in the presence of a catalytic amount of palladium on carbon is described to provide a new, convenient method for the introduction of a *t*-butyldimethylsilyl (TBDMS) group.

Protection of functional groups via chlorosilanes occupies a prominent place in a variety of protection techniques which are often indispensable for organic syntheses.[1] Corey and Venkateswarlu[2] have invented the use of *t*-butyldimethylsilyl chloride (TBDMSCl) to protect alcohols effectively in *N*,*N*-dimethylformamide (DMF) solution under the catalytic influence of imidazole (Im). The protection with this reagent is most widely used, mainly because of the stability of the corresponding silyl ethers towards certain oxidation, reduction, and mild solvolytic conditions and, moreover, an easy removal of the silyl group from silyl ethers by fluoride ions. Since TBDMSCl/Im/DMF method does not apply well to amines and carboxylic acids, many variations therefrom have been reported.[3]

Hazardous preparation of TBDMSCl using *t*-butyllithium[4] can be avoided on an industrial scale by a sequence of reactions of dimethoxymethylsilane with *t*-butylmagnesium chloride and with methylmagnesium chloride, followed by chlorination of the resulting *t*-butyldimethylsilane.[5] We became aware of the possibility of the selective protection of functional groups with use of the latter compound. Described herein is a convenient method for the protection of certain alcohols, amines, and carboxylic acids, which involves a simple treatment of these compounds with *t*-butyldimethylsilane in the presence of 10% palladium on carbon as a catalyst.

It has previously been documented by Sommer and Lions[6] that the group VIII metal-catalyzed solvolysis of an optically active methyl-1-naphthylphenylsilane with a wide variety of nucleophilic solvents such as alcohols and amines takes place to proceed with inversion of configuration at the silicon center.

Results and Discussion

The group VIII metals and their salts catalyze the cleavage of the silicon-hydrogen bond by certain nucleophiles containing OH and NH functions (Eq. 1). Besides the mechanistic implications of the nucleo-

$$\text{Nu-H} + \text{R}_3\text{SiH} \xrightarrow{\text{metal cat.}} \text{Nu-SiR}_3 + \text{H}_2 \qquad (1)$$

Nu-H=alcohols, amines, and carboxylic acids

philic substitution on the silicon center which is activated by the catalyst, the reaction is experimentally ideal for the selective protection of alcohols, for example, in that only hydrogen is formed as a by-product and the catalyst is easily removed by filtration.

Alcohols: Thus, when *t*-butyldimethylsilane in hexane was treated with 3-phenyl-1-propanol and 10% Pd/C (5 mol% equiv) at room temperature, hydrogen slowly evolved and the silyl ether was obtained in 96% conversion (by GLC) in 2 h. Simple filtration of the reaction mixture through a Celite plug and, if necessary, flash chromatography, provided 3-phenylpropyl *t*-butyldimethylsilyl (TBDMS) ether with satisfactory purity in 72% yield. In the protection of alcohols, rhodium on carbon (10%) worked even better than 10% Pd/C and Ru/C, although it is more expensive. More polar solvents, such as, CH_2Cl_2, THF, and benzene, retarded significantly the rate of reaction, although they are often desirable for solubility purposes.

Several alcohols were examined in this protection procedure under the same conditions (0.3 mol dm^{-3} of the substrate in hexane at 70 °C), and we have found the relative reactivity (percent conversion and reaction time in parentheses) in the order $PhCH_2OH$ (99%, 1 h) > $PhCH_2CH_2CH_2OH$ (96%, 2 h) > $C_6H_{11}OH$ (92%, 7 h) PhCHMeOH (76%, 7 h) ≫ *t*-BuOH (trace, 9 h). The reactivity pattern clearly indicates that a primary alcohol, especially benzyl alcohol, undergoes protection faster than a secondary alcohol, whereas *t*-butyl alcohol hardly reacted under the conditions employed.[4b] Selective protection of primary hydroxyl group in 1,2-propanediol and 1-phenyl-1,2-ethanediol was easily achieved with >96% selectivity. It should be mentioned that no hydrogenolysis at the benzylic position of 1-phenyl-1,2-ethanediol was observed at all under the present conditions. Taking higher reactivity of benzylic alcohols into account, we examined by GLC analysis any competitive formation of $PhCH(OSiMe_2Bu^t)CH_2OH$, an authentic sample of which was prepared separately (see, Experimental). The ratio of primary silylation to secondary silylation was efficiently 96 : 4. The reagent combination of TBDMSCl, 4-(dimethylamino)pyridine, and triethylamine can be employed as well with a pronounced kinetic preference for primary against secondary alcohols.[7]

Protection of allylic alcohols (e.g., cinnamyl alcohol and geraniol) always accompanied partial hydrogenation of the olefin moiety due to the hydrogen which formed as the protection proceeded. Attempted quenching of the by-product hydrogen with excess 1-hexene instead of hexane as a solvent resulted in little improvement. It is worthy of mention that the stoichiometric hydrogenation of certain olefins has previously been reported by employing either ethanol/hydrosilane/Pd-C[8] or methanol/$NaBH_4$/H_2PtCl_6 catalyst[9] system under ambient conditions.

Amines: In the protection of amines, palladium

on carbon was the only choice as a catalyst. Benzene was a better solvent than hexane and CH_2Cl_2. Again benzyl amine reacted faster than morpholine in benzene at 70 °C: $PhCH_2NH_2$ (100%, 1.5 h) > $PhCHMeNH_2$ (82%, 12 h); morpholine (93%, 5 h). In order to exhibit a synthetic usefulness of the procedure, optically active 4-hydroxymethyl-2-azetidinone was subjected to the present protection to provide easily an *N,O*-disilylated derivative (Eq. 2).[10]

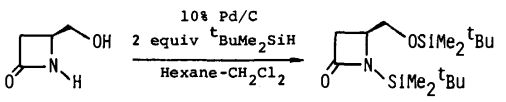

(2)

Carboxylic Acids: An expeditious synthesis of *t*-butyldimethylsilyl triflate has been reported by a direct reaction of *t*-butyldimethylsilane with a strong acid.[11] There is another precedent[12] in which $RhCl(PPh_3)_3$-catalyzed reaction of carboxylic acids with $EtMe_2SiH$ or $PhMe_2SiH$ gives the corresponding silyl esters. Hydrocinnamic acid and 2-methylbutanoic acid were reacted with *t*-butyldimethylsilane under the same conditions as those for alcohols described above to afford the silyl esters, respectively, in almost quantitative yields. Since the latter compounds are sensitive to hydrolysis, the present protection procedure is of special advantage due to its easy isolation.

Finally, (1,1,2-trimethylpropyl)dimethylsilane was prepared in a reasonable yield by the reaction of tetramethylethylene and dimethylsilane in the presence of a catalytic amount of $AlCl_3$.[13] All protection procedures presented here are equally applicable to the use of (1,1,2-trimethyl)dimethylsilane. The results will be discussed separately along with the novel mechanistic aspects of the $AlCl_3$-catalyzed hydrosilylation.

In conclusion, we propose the utility of *t*-butyldimethylsilane as an effective silylation reagent for alcohols, amines, and carboxylic acids, the method suffering from a drawback of incompatibility with olefinic functionality.

Experimental

Materials. *t*-$BuMe_2SiH$[4b] is a stable colorless liquid with a low boiling point (80 °C), being provided by Shin-Etsu Chemical Industry, Co., Ltd. and used as received. Group VIII metal catalysts (10% Pd/C, Rh/C, and Ru/C dry type) were obtained from Kawaken Fine Chemicals Co., Ltd. All substrates examined are commercial samples except a 2-azetidinone and mostly purified by distillation before use. Solvents were dried according to the standard procedure. (*S*)-4-Hydroxymethyl-2-azetidinone was prepared starting from pure L-aspartic acid in four steps.[10]

Protection Procedures. Alcohols: In a 20 mL two-necked flask, equipped with a reflux condenser topped with a nitrogen balloon, a rubber septum, and a magnetic stirring bar, were placed an alcohol (1.0 mmol), *t*-$BuMe_2SiH$ (140—174 mg, 1.2—1.5 mmol), 10% Pd/C (53.2 mg, 5 mol%), and dry hexane (3 mL) under a nitrogen atmosphere. The whole mixture was heated at 70 °C for a given time (0.5—9 h). The extent of the reaction was monitored by either GLC or TLC analysis. After the protection was completed (mostly at the conversion > 96% except for *t*-butyl alcohol), the catalyst was filtered through a short Celite plug, and the solvent and excess *t*-$BuMe_2SiH$ were evaporated under reduced pressure. The residue was purified by either column chromatography or by distillation (Kugelrohr), being practically pure for further use.[14] Selective protection of 1,2-propanediol and 1-phenyl-1,2-ethanediol was also carried out using 1.2 equiv amount of *t*-$BuMe_2SiH$ in hexane-CH_2Cl_2 (1 : 1 v/v). In the case of 1-phenyl-1,2-ethanediol, a little phenacyl alcohol was detected as a by-product during the protection. An authentic sample of the secondary silylated product, $PhCH(OSiMe_2Bu^t)CH_2OH$:[15] ^1H NMR (90 MHz, TMS, $CDCl_3$) δ=−0.10 (s, 3H), 0.06 (s, 3H), 0.91 (s, 9H), 3.58 (d, 2H, *J*=6.1 Hz), 4.76 (brt, 1H, *J*=5.9 Hz), and 7.31 (brs, 5H). GLC (Silicone DC-550, 3 m, at 200 °C, H_2 40 mL min^{-1}): T_R=2.4 min. For the primary silylated product, T_R=3.1 min. Table 1 lists ^1H NMR data

Table 1. ^1H NMR (90 MHz, $CDCl_3$, TMS) of TBDMS Derivatives of Alcohols, Amines, and Carboxylic Acids

TBDMS derivative	Chemical shifts (δ)
$PhCH_2OSiMe_2Bu^t$	0.11 (s, 6H), 0.95 (s, 9H), 4.75 (s, 2H), 7.31 (s, 5H)
$PhCH_2CH_2CH_2OSiMe_2Bu^t$	0.05 (s, 6H), 0.91 (s, 9H), 1.7—2.0 (m, 2H), 2.5—2.8 (m, 2H), 3.63 (t, 2H, *J*=6.3 Hz), 7.2—7.3 (m, 5H)
$PhCHMeOSiMe_2Bu^t$	0.03 (s, 3H), 0.05 (s, 3H), 0.90 (s, 9H), 1.40 (d, 3H, *J*=6.4 Hz) 4.86 (q, 1H, *J*=6.4 Hz), 7.29 (s, 5H)
$c\text{-}C_6H_{11}OSiMe_2Bu^t$	0.05(s, 6H), 0.89 (s, 9H), 1.1—1.9 (m, 10H), 3.4—3.8 (m, 1H)
$MeCH(OH)CH_2OSiMe_2Bu^t$	0.08 (s, 6H), 0.91 (s, 9H), 1.12 (d, 3H, *J*=6.2 Hz),3.33 (dd, 1H, *J*=9.7, 7.7 Hz), 3.60 (dd, 1H, *J*=9.7, 3.3 Hz), 3.80 (ddq, 1H, *J*=7.7, 6.2, 3.3 Hz)
$PhCH(OH)CH_2OSiMe_2Bu^t$	0.06 (s, 6H), 0.91 (s, 9H), 3.53 (dd, 1H, *J*=10.0, 8.6 Hz), 3.77 (dd, 1H, *J*=10.0, 3.7 Hz), 4.75 (dd, 1H, *J*=8.6, 3.7 Hz), 7.34 (brs, 5H)
$PhCH_2NHSiMe_2Bu^t$	0.07 (s, 6H), 0.94 (s, 9H), 3.99 (d, 2H, *J*=7.5 Hz), 7.31 (s, 5H)
$PhCHMeNHSiMe_2Bu^t$	−0.06 (s, 3H), −0.04 (s, 3H), 0.87 (s, 9H), 1.38 (d, 3H, *J*=6.6 Hz), 3.8—4.3 (m, 1H), 7.23 (s, 5H)
$CH_2CH_2OCH_2CH_2N\text{-}SiMe_2Bu^t$	0.03 (s, 6H), 0.86 (s, 9H), 2.8—3.0 (m, 4H), 3.4—3.6 (m, 4H)
$PhCH_2CH_2COOSiMe_2Bu^t$	0.26 (s, 6H), 0.93 (s, 9H), 2.5—2.8 (m, 2H), 2.8—3.1 (m, 2H), 7.25 (s, 5H)
$EtCHMeCOOSiMe_2Bu^t$	0.17 (s, 6H), 0.84 (s, 9H), 0.7—0.9 (m, 3H), 1.04 (d, 3H, *J*=7.0 Hz), 1.1—1.8 (m, 2H), 2.0—2.5 (m, 1H)

for all silyl ethers thus obtained here.

Amines and carboxylic acids were also treated in a similar manner to that for alcohols except for the use of benzene as solvent in the protection of amines. Table 1 is also for ^{1}H NMR data of the protected amines and acids examined in this paper.

a 2-Azetidinone: (*S*)-4-Hydroxymethyl-2-azetidinone (33.8 mg, 0.33 mmol) was dissolved in hexane-CH_2Cl_2 (1:1 v/v, 3.0 mL). To the solution were added *t*-$BuMe_2SiH$ (116 mg, 1.0 mmol) and 10% Pd/C (35.5 mg, 5 mol%) and the whole mixture was stirred at room temperature for 2 h. Usual workup gave an *N,O*-disilylated 2-azetidinone as a colorless oil (87 mg, 80% isolated yield): ^{1}H NMR δ=0.06 (s, 6H), 0.22 (s, 3H), 0.24 (s, 3H), 0.90 (s, 9H), 0.96 (s, 9H), 2.5—3.2 (m, 2H), and 3.4—3.8 (m, 3H).

References

1) T. W. Greene, "Protective Groups in Organic Synthesis," Academic Press, New York (1981).

2) E. J. Corey and A. Venkateswarlu, *J. Am. Chem. Soc.*, **94**, 6190 (1972).

3) J. M. Aizpurua and C. Palomo, *Tetrahedron Lett.*, **26**, 475 (1985) and references therein.

4) a) L. H. Sommer and L. J. Tyler, *J. Am. Chem. Soc.*, **76**, 1030 (1954). b) T. J. Barton and C. R. Tully, *J. Org. Chem.*, **43**, 3649 (1978).

5) M. Takamizawa, T. Ishihara, and A. Yamamoto, Jpn. Kokai, 62/22790; *Chem. Abstr.*, **107**, 198653j (1987).

6) L. H. Sommer and J. E. Lions, *J. Am. Chem. Soc.*, **91**, 7061 (1969).

7) S. K. Chaudhary and O. Hernandez, *Tetrahedron Lett.*, **1979**, 99.

8) K. Yamamoto, M. Kumada, I. Nakajima, K. Maeda, and N. Imaki, *J. Organomet. Chem.*, **13**, 329 (1968).

9) H. C. Brown and C. A. Brown, *J. Am. Chem. Soc.*, **84**, 1493 and 2827 (1962).

10) T. Kimura, M. S. Thesis, T.I.T. (1986). Also, see T. N. Saltzman, R. W. Ratcliffe, and F. A. Bouffard, *J. Am. Chem. Soc.*, **102**, 6163 (1980).

11) J. M. Aizpurua and C. Palomo, *Tetrahedron Lett.*, **26**, 6113 (1985).

12) Y. Nagai, I. Ojima, and S. Inaba, Jpn. Kokai, 74,110,634; *Chem. Abstr.*, **85**, 206415m (1975).

13) K. Oertle and H. Wetter, *Tetrahedron Lett.*, **26**, 5511 (1985).

14) It should be mentioned that Corey and his coworker[2] observed a slow hydrogenolysis of certain silyl ethers including dimethylisopropylsilyl ones using 10% Pd/C, 1 atm H_2, and ethanol solvent. However, this was not the case of TBDMS ethers under present conditions.

15) The following sequence of reactions applied: $PhCH(OH)CH_2OH \rightarrow PhCH(OH)CH_2OBz \rightarrow PhCH(OSiMe_2Bu^t)CH_2OBz \rightarrow PhCH(OSiMe_2Bu^t)CH_2OH$.

Formation of Furan Derivatives from Phenacyl Bromides and Sodium Telluride; Attempted Extension to Coumarin Synthesis

Seetharamaiyer PADMANABHAN, Takuji OGAWA, and Hitomi SUZUKI*
Department of Chemistry, Faculty of Science, Ehime University, Bunkyo-cho, Matsuyama 790
(Received January 14, 1989)

Synopsis. The enolates, generated from phenacyl bromides by sodium telluride, yield 2,4-diarylfurans in addition to the expected dehalogenation products. No 1,4-dicarbonyl compounds could be isolated even in the presence of excess oxidizing agent, copper(II) chloride. Condensation of 2-(methoxymethoxy)arenecarbaldehydes with ethyl bromoacetate in the presence of sodium telluride gave the expected α,β-unsaturated esters which resisted cyclization to yield the desired coumarin derivatives. Attempted intramolecular Reformatsky-type reaction of 2-(bromoacetoxy)-benzaldehyde gave only 6,12-epoxy-6*H*,12*H*-dibenzo[*b*,*f*]-[1,5]dioxocin as the major product.

Sodium telluride, as a reagent for effecting many functional group transformations, has been studied in our laboratory for quite some time. Many heterocyclic compounds containing tellurium as the heteroatom have been synthesized using sodium telluride,[1] while there have been no reports concerning the formation of non-tellurium heterocyclic compounds using sodium telluride. Herein we wish to report the formation of 2,4-diarylfurans (**5**) from the ketone enolates generated from phenacyl bromides (**1**) and the results of our efforts to synthesize coumarins using sodium telluride.

2,4-Diarylfurans. Ketone enolates and ester enolates have been oxidatively coupled to give synthetically important 1,4-diketones employing $CuCl_2$,[2] $FeCl_3$,[3] and $Cu(OTf)_2$.[4] Ketene silyl acetals have also been subjected to similar reaction.[5] Recently, Belletire reported the occurrence of symmetrical dimerizations of carboxylic dianions and β-keto ester dianions using molecular iodine as oxidant.[6] He also reported the C-C coupling at γ-position of the dianions from β-keto sulfones. These results prompted us to investigate whether a coupling at the active methylene of halo ketones could be achieved from the enolate generated by sodium telluride taking advantage of the affinity of telluride anion for the halogens. Such a study would enable us to see the fate of enolates generated by sodium telluride under oxidative coupling conditions.

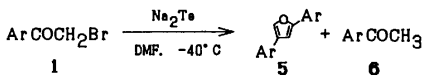

As a model compound we studied the enolate derived from phenacyl bromide **1** in the presence of iodine. Addition of a solution of **1a** in *N*,*N*-dimethylformamide (DMF) to a suspension of sodium telluride in the same solvent at −40 °C followed by the addition of iodine in DMF resulted in a dark reaction mixture which gave two fractions after chromatography. The first, hexane fraction, showed ^{1}H NMR spectrum which was completely devoid of aliphatic protons. The second one was easily identified as acetophenone (**6a**; 29%). From the elemental analysis and spectral data in combination with comparison of reported melting points of diphenylfuran derivatives, the product isolated from the hexane fraction was identified as 2,4-diphenylfuran (**5a**; 14%). When anhydrous copper(II) chloride was employed in place of iodine the furan was obtained in a slightly better yield (17%). To our surprise no oxidatively coupled product could be isolated from the reaction mixture. Isolation of furan derivative was also possible using iron(III) chloride. Similarly from other substituted phenacyl bromides were obtained 2,4-diarylfurans (**5b—5d**) in varying yields (Table 1).

The formation of furan **5** could be attributed to an intermolecular condensation between the enolate generated and the bromo ketone **1** followed by presumably a formation of an epoxide ring which underwent further cyclization (Scheme 1). Synthesis of 2,4-diarylfurans from phenacyl bromides by electrochemical reduction[7] and formation of 2,4-diarylfurans from reactions of phenacyl bromides with nickel carbonyl in DMF[8] and with copper(I) chloride in DMSO[9] have been reported. Formation of furan derivatives during the dehalogenation of halo ketones by magnesium in tetrahydrofuran (THF)[10] has also been observed. Condensation of imino ketones from 1-amino-4,6-diaryl-2-pyridone with phenacyl bromides followed by acid treatment afforded 2,4-diarylfurans having different substituents.[11]

A support for the proposed mechanism was provided by reacting excess of the enolate generated from

Table 1. 2,4-Diarylfuran Derivatives Isolated

	Ar **1**	Mp/ °C **5** (lit,[7] Mp)	Yield/%[a] **5**	 **6**
a	C_6H_5	108—110 (109—110)	17	47
b	4-BrC_6H_4	157—160 (159—160)	36	43
c	4-ClC_6H_4	127—129 (127—128)	19	47
d	4-$C_6H_5C_6H_4$	258—263 (267—268)	2	58

a) Yields refer to the products isolated using an equimolar amount of copper(II) chloride.

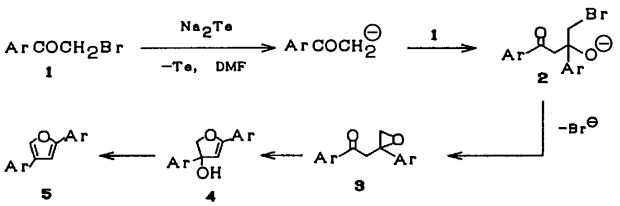

Scheme 1.

acetophenone by potassium hydride[12] with 4-chlorophenacyl bromide (**1c**) in the presence of copper(II) chloride under the similar conditions. From the reaction mixture the expected 2-phenyl-4-(4-chlorophenyl)furan was obtained in 36% yield. It was found that when the reaction was carried out in the absence of copper(II) chloride or if the formation of enolate was carried out in a short time the yield of furan derivative was considerably low. Attempts to develop an efficient method for synthesizing mixed 2,4-diarylfurans based on the above route did not give encouraging results.

To find the role of the oxidizing agent the reaction was carried out in the absence of copper(II) chloride and also in the presence of potassium iodide. Even in these cases furan derivative **5** was isolated in about 10% yield. This rules out the possibility of additives actually taking part in the reaction, but it is worth mentioning that the presence of copper(II) chloride or iron(III) chloride led to a very clean reaction mixture. In the absence of tellurium species, i.e., only in the presence of sodium hydride, 4-bromophenacyl bromide was recovered intact under similar conditions. With the view to obtain the furans in better yields the reaction was carried out deliberately using a less amount of sodium telluride. Such an attempt was, however, unsuccessful.

Finally in an attempt to isolate the oxidatively coupled product from the ketone enolate, generated from α-bromo ketone by sodium telluride, experiment was carried out using a large excess of copper(II) chloride. No oxidatively coupled product could be isolated from the reaction mixture (Table 2).

It is interesting to note the difference in behavior of both the ester enolate from ethyl bromoacetate and ketone enolates from phenacyl bromide derivatives generated by sodium telluride. In contrast to the ester enolate which has been found to be unreactive towards ketones,[13] the ketone enolates in the present study underwent intermolecular condensation and further cyclization leading to furan derivatives.

Coumarins. Recently we developed a novel route to α,β-unsaturated esters from aldehydes and ethyl bromoacetate using sodium telluride.[13] It was anticipated that extension of this reaction to salicylaldehyde derivatives would lead to coumarin derivatives. Attempted condensation of salicylaldehyde with ethyl bromoacetate resulted only in the recovery of the aldehyde. However, the desired α,β-unsaturated esters (**8a—c**) were obtained from 2-(methoxymethoxy)benzaldehydes (**7a—c**) and ethyl bromoacetate in moderate yields. Attempted cyclization of these unsaturated esters in acetic acid under reflux for 6 h resulted only in the hydrolysis of methoxymethoxy group. Cyclization using sulfuric acid or polyphosphoric acid gave a dark polymeric reaction mixture. Reluctance for cyclization could probably be attributed to the demand of sterically less favorable cis configuration of unsaturated esters for cyclization to occur.

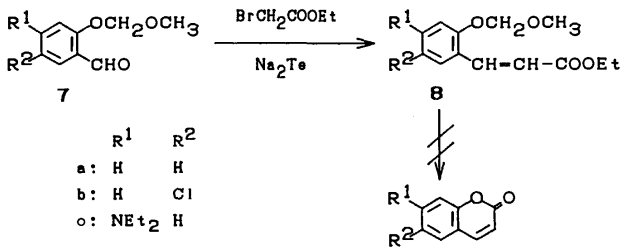

Having met with no success in the above scheme we turned our attention to an intramolecular Reformatsky-type reaction of 2-(bromoacetoxy)benzaldehyde (**9**). Fuson and coworkers observed that the Reformatsky reaction of **9** occurs only in the presence of anhydrous zinc bromide in addition to zinc.[14] The products isolated include salicylaldehyde (65%), coumarin (26%), and *trans-o*-hydroxycinnamic acid (9%). Attempted intramolecular Reformatsky-type reaction of **9** using sodium telluride gave only 6,12-epoxy-6*H*,12*H*-dibenzo[*b*,*f*][1,5]dioxocin (**10**; disalicylaldehyde) (32%) in addition to salicylaldehyde (8%). Compound **10** would result from the self-acetalization of salicylaldehyde, generated from 2-(bromoacetoxy)benzaldehyde by the elimination of ketene. Formation of this compound from reactions using salicylaldehyde has been observed earlier.[15] Thus our attempts to synthesize coumarin derivatives using sodium telluride was entirely unsuccessful.

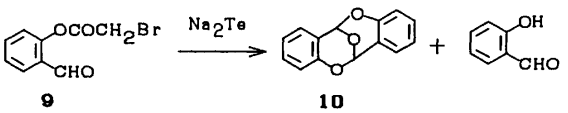

Table 2. Influence of Oxidizing Agents and the Relative Amounts of Halo Carbonyl Compounds, Na_2Te and Oxidant on the Yields of Furan Derivatives **5**

Phenacyl halide	Oxidant	Amounts employed (equiv)			Yield/%	
		Substrate **1**	Na_2Te	Oxidant	Furan **5**	Ketone **6**
4-$BrC_6H_4COCH_2Br$	—	1.0	1.0	0	10	40
	I_2	1.0	1.0	1.0	8	45
	$FeCl_3$	1.0	1.0	1.0	22	44
	$CuCl_2$	1.0	1.0	1.0	36	43
	$CuCl_2$	1.0	0	1.0	—	—[a]
	$CuCl_2$	2.0	1.0	1.0	22	34
	$CuCl_2$	1.0	1.0	5.0	22	44
4-$BrC_6H_4COCH_2I$	$CuCl_2$	1.0	1.0	1.0	11	36

a) Starting material was recovered intact.

Experimental

2-(Methoxymethoxy)arene carbaldehydes (**7a—c**) were prepared following the procedure reported by La Forge for the preparation of **7a**.[16] 2-(Bromoacetoxy)benzaldehyde (**9**) was prepared from salicylaldehyde and bromoacetyl bromide following the method reported.[14]

2,4-Diarylfurans: General Procedure: To sodium telluride (prepared from tellurium (1.0 mmol) and sodium hydride (2.2 mmol; washed with hexane prior to use))[17] in dry DMF (3 ml) at −40 °C was slowly added a solution of halo ketone (**1**: 1.0 mmol) in dry THF (3 ml) followed by the addition of anhydrous copper(II) chloride (1.0 mmol) in DMF (3 ml). Initially the reaction mixture could be stirred, but near the end of complete addition of halo ketone the mixture became very thick. Reaction mixture was kept at that temperature for 2 h and then slowly raised to room temperature. After 1 h the reaction was quenched by adding saturated aqueous ammonium chloride (10 ml) and the organic phase was extracted into benzene. The mixture was freed from insoluble inorganic materials by filtration through a thin layer of Celite. The organic layer was separated and the aqueous layer was extracted with benzene. The combined extracts were washed with 0.5 M† sulfuric acid followed by brine and dried over sodium sulfate. The crude product, obtained after evaporation, was purified by column chromatography over silica gel. Furan derivatives **5** were eluted first using hexane as eluent and then dehalogenated ketone **6** using a mixture of hexane and dichloromethane.

2-Phenyl-4-(4-chlorophenyl)furan: Acetophenone (1.0 mmol) in THF (5 ml) was added to potassium hydride (1.2 mmol; after removal of oil matrix following the procedure and precautions reported by Brown[18]) in THF (35 ml) at 20 °C and after the evolution of hydrogen ceased the reaction mixture was stirred for 24 h. The reaction mixture was cooled to −40 °C and 4-chlorophenacyl bromide (0.6 mmol) in DMF (3 ml) was added followed by the addition of copper(II) chloride (0.6 mmol) in DMF (3 ml). The dark reaction mixture was stirred at this temperature for 30 min and the reaction went to completion during this period. Water (10 ml) was added, THF was removed under vacuum, and the reaction mixture was extracted into benzene. 2-Phenyl-4-(4-chlorophenyl)furan was isolated in 36% yield. Mp 132—134 °C (lit,[11] 130 °C). IR: 1490, 1450, 1155, 1100, 1090, 1010, 930, 910, 835, 805, 770, 690 cm^{-1}; ^1H NMR: δ= 6.79 (s, 1H), 7.0—7.7 (m, 10H).

Preparation of the Unsaturated Esters (8a—c): General Procedure: To sodium telluride (4.0 mmol) in dry DMF (3 ml) at −20 °C was added, 2-(methoxymethoxy)benzaldehyde (**7a—c**) (1.0 mmol) in dry DMF (3 ml) followed by ethyl bromoacetate (4.0 mmol) in DMF (4 ml). Immediate separation of tellurium was observed and the reaction mixture was stirred at this temperature for 1 h and then at room temperature for 1 h. The reaction was quenched by the addition of 0.5 M sulfuric acid (5 ml) and the reaction mixture was extracted with benzene (10 ml). After stirring for 30 min the insolubles were removed by filtration through a bed of Celite and the aqueous layer was extracted with benzene (5 ml). The combined organic layer was washed with water and dried, and the solvent was removed under reduced pressure to give the crude unsaturated ester, which was purified by chromatography on silica gel using hexane as eluent.

8a: Yield 76%. Bp 158—160 °C/2 mmHg.†† IR: 1720, 1640, 1600, 1500, 1325, 1280, 1240, 1175, 1090, 1000 cm^{-1}; ^1H NMR: δ=1.25 (t, 3H; J=7 Hz), 3.43 (s, 3H), 4.21 (q, 2H; J=7 Hz), 5.16 (s, 2H), 6.43 (d, 1H; J=16 Hz), 6.8—7.6 (m, 4H), 8.00 (d, 1H; J=16 Hz).

8b: Yield 44%. Bp 160—165 °C/3 mmHg. IR: 1710, 1630, 1480, 1320, 1180, 1160, 1080, 990 cm^{-1}; ^1H NMR: δ=1.29 (t, 3H; J=7 Hz), 3.45 (s, 3H), 4.23 (q, 2H; J=7 Hz), 5.20 (s, 2H), 6.43 (d, 1H; J=16 Hz), 7.1—7.4 (m, 3H), 7.92 (d, 1H; J=16 Hz).

8c: Yield 60%. Bp 165—170 °C/2.5 mmHg. IR: 1700, 1595, 1510, 1410, 1360, 1220, 1160, 1000 cm^{-1}; ^1H NMR: δ=1.13 (t, 6H; J=7 Hz), 1.23 (t, 3H; J=7Hz), 3.15—3.66 (q, 4H; J=7 Hz), 3.45 (s, 3H), 4.18 (q, 2H), 5.16 (s, 2H), 6.0—6.5 (m, 2H), 6.36 (s, 1H), 7.32 (d, 1H; J=9 Hz), 7.83 (d, 1H; J=16 Hz).

Reaction of 2-(Bromoacetoxy)benzaldehyde (9) with Sodium Telluride. To a suspension of sodium telluride (1.0 mmol) in DMF (3 ml) at −40 °C was added a solution of 2-(bromoacetoxy)benzaldehyde (**9**) (1.0 mmol) in DMF (3 ml). The reaction was carried out as in the above case and the crude reaction mixture was purified by chromatography on silica gel. First, 6,12-epoxy-6*H*,12*H*-dibenzo[*b*,*f*][1,5]-dioxocin (**10**) was eluted followed by salicylaldehyde (8%) and only trace of coumarin, detectable on TLC, was eluted. Compound **10**, obtained in 32% yield, was crystallized from hexane. Mp 127—131 °C (lit,[14] 127—130 °C). MS: m/z (rel intensity) 226 (M^+, 100), 197 (24), 181 (22), 180 (10), 121 (12), 121 (67); IR: 1610, 1590, 1480, 1460, 1320, 1270, 1220, 1110, 1060, 1030, 970, 950, 760, 700 cm^{-1}. ^1H NMR: δ=6.22 (s, 2H), 6.7—7.4 (m, 8H). Found: C, 73.84; H, 4.65%. Calcd for $C_{14}H_{10}O_3$: C, 74.33; H, 4.43%.

† 1 M=1 mol dm^{-3}.

†† 1 mmHg≈133.322 Pa.

References

1) M. Renson, "The Chemistry of Organic Selenium and Tellurium Compounds," ed. by S. Patai and Z. Rappoport, John Wiley & Sons (1986), Vol. I, Chap. 13, pp. 399—516.

2) M. W. Rathke and A. Lindert, *J. Am. Chem. Soc.*, **93**, 4605 (1971); Y. Ito, T. Konoike, T. Harada, and T. Saegusa, *ibid.*, **99**, 1487 (1977).

3) R. H. Frazier, Jr. and R. L. Harlow, *J. Org. Chem.*, **45**, 5408 (1980).

4) Y. Kobayashi, T. Taguchi, and E. Tokuno, *Tetrahedron Lett.*, **1977**, 3741.

5) S. Inaba and I. Ojima, *Tetrahedron Lett.*, **1977**, 2009.

6) J. L. Belletire and E. G. Spletzer, *Synth. Commun.*, **17**, 1701 (1987).

7) F. Barba, M. D. Velasco, and A. Guirado, *Synthesis*, **1981**, 625.

8) E. Yoshisato and S. Tsutsumi, *J. Chem. Soc., Chem. Commun.*, **1969**, 33.

9) T. Shirafuji, Y. Yamamoto, and H. Nozaki, *Tetrahedron Lett.*, **1968**, 4097.

10) J. E. Dubois and J. Itzkowitch, *Tetrahedron Lett.*, **1965**, 2839.

11) P. Molina, A. Lorenzo, and P. M. Fresneda, *Synthesis*, **1983**, 49.

12) C. A. Brown, *J. Org. Chem.*, **39**, 1324 (1974).

13) H. Suzuki and M. Inouye, *Chem. Lett.*, **1986**, 403.

14) R. C. Fuson and N. Thomas, *J. Org. Chem.*, **18**, 1762 (1953).

15) R. Adams, M. F. Fogler, and C. W. Kreger, *J. Am. Chem. Soc.*, **44**, 1126 (1922); A. A. Khalaf, *Bull. Fac. Sci., Assiut Univ.*, **2**, 237 (1973); *Chem. Abstr.*, **85**, 20260t (1973).

16) F. B. La Forge, *J. Am. Chem. Soc.*, **55**, 3040 (1933).

17) H. Suzuki, H. Manabe, T. Kawaguchi, and M. Inouye, *Bull. Chem. Soc. Jpn.*, **60**, 771 (1987).

18) C. A. Brown, *J. Org. Chem.*, **39**, 3913 (1974).

Tellurodicarbonic Acid Diesters; Preparation and Properties

Hitomi SUZUKI* and Yoshinobu NISHIOKA
Department of Chemistry, Faculty of Science, Ehime University, Bunkyo-cho, Matsuyama 790
(Received January 23, 1989)

Synopsis. Title compounds were obtained as reasonably stable to labile oily substances by reacting alkyl carbonochloridates with sodium telluride under phase-transfer conditions at room temperature or in dry *N*,*N*-dimethylformamide under ice-cooling.

Tellurodicarbonic acid (**1**) is one of the tellurium isologues of dicarbonic acid, which has not hitherto been described in the literature. We now report the preparation of dialkyl 2-tellurodicarbonates (**2**) and their unique properties quite different from those of ordinary esters.

HO-C(=O)-Te-C(=O)-OH
1

RO-C(=O)-Te-C(=O)-OR
2

R	R
a: CH_3	d: $C_6H_5CH_2$
b: C_2H_5	e: C_6H_5
c: *i*-C_3H_7	

When a solution of alkyl carbonochloridates (**3**) in benzene was added slowly to an aqueous solution of sodium telluride in the presence of tetrabutylammonium bromide at room temperature, the initial reddish violet color gradually faded away and a yellow reaction mixture was obtained together with a small amount of free tellurium. After usual work-up followed by distillation of crude product under reduced pressure, compounds **2** were obtained as a pale yellow oil or low-melting colorless solid which, on standing in open air at room temperature, gradually got colored. Among four diesters **2a—2d** preparerd, diisopropyl ester **2c** is the most stable and can be stored for weeks without any appreciable change in a refrigerator. Dibenzyl ester **2d** is the most labile and begins to decompose within several hours after isolation, finally leading to a black resinous substance. Diesters **2** could be also obtained under aprotic conditions by reacting carbonochloridates **3** with sodium telluride in situ prepared from sodium hydride and tellurium in dry *N*,*N*-dimethylformamide (DMF). The yields of diesters usually ranged from 30 to 60%. Because of the instability of products under basic conditions employed, prolonged reaction time should be avoided.

Attempts to obtain diphenyl tellurodicarbonate (**2e**) under similar conditions were unsuccessful, however. The reaction with phenyl carbonochloridate (**3e**) went on smoothly, but the product isolated was not the expected dicarbonate **2e** but diphenyl carbonate (**6**). The initially formed phenyl tellurocarbonate anion (**4**) would readily collapse into phenolate ion (**5**), carbon monoxide and free tellurium, and the ion **5** thus formed would undergo further reaction with carbonochloridate **3e** to afford **6.**

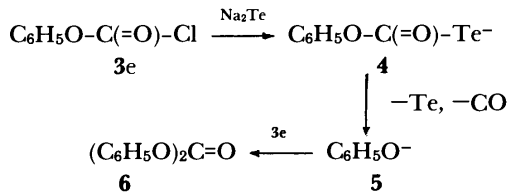

Diesters **2** possess a characteristic odor not so offensive as that of lower dialkyl tellurides. On contact with skin, they produce black stains after a few hours,

Table 1. Dialkyl Tellurodicarbonates Prepared

Compound **2**	R	Yield/%	Bp (°C/mmHg)[a] [Mp (°C)]	^{1}H NMR/δ	IR/cm^{-1}
2a	CH_3[b]	39	76/1.0	3.90 (s)	1720, 1420, 1180, 1065, 920, 790
2b	C_2H_5	48	89/1.5	1.36 (t, 6H; *J*=7 Hz), 4.37 (q, 4H; *J*=7 Hz)	1745,1690, 1440, 1380, 1070, 1000, 835, 800, 760
2c	*i*-C_3H_7[c]	69	99/1.0 [34—35]	1.33(d, 12H; *J*=7 Hz), 5.23 (sept, 2H; *J*=7 Hz)	1740, 1700, 1470, 1390, 1380, 1130, 1050, 900, 830
2d	$C_6H_5CH_2$[d]	50	163/1.0	5.24 (s, 4H), 6.9—7.2 (m, 10H)	1740, 1695, 1590, 1480, 1450, 1250, 1080, 1020, 750, 685

a) Boiling points refer to the Kugelrohr bath temperatures. b) Found: C, 19.35; H, 2.49%. Calcd for $C_4H_6O_4Te$: C, 19.55; H, 2.46%. c) Found: C, 31.52; H, 4.70%. Calcd for $C_8H_{14}O_4Te$: C, 31.84; H, 4.68%. d) Not analyzed due to rapid decomposition.

which persist for days. In marked contrast to ordinary esters, compounds **2** resist any further transformations but decomposition. Thus, attempted ester interchange with alcohols in the presence or absence of catalyst only resulted in the decomposition of diesters. Actions of sodium methoxide and diethylamine led to immediate and gradual decompositions of diesters, respectively. Reaction with excess of 4-methylphenylmagnesium bromide afforded bis(4-methylphenyl) ditelluride, which should have been formed by the reaction of the Grignard reagent with tellurium liberated from diester.

Tellurium(II) compounds bearing two carbonyl groups on the tellurium atom are known to be extremely unstable and easily decompose in open air.[1] Acyclic diacyl tellurides such as bis(2-chlorobenzoyl) telluride and di-1-naphthoyl telluride have only recently been isolated and characterized.[2] Thus it is worth mentioning here that diesters **2** in which two ester carbonyl groups attached geminally to the tellurium atom are much more stable toward oxidative degradation than diacyl tellurides.

Reaction of dimethylcarbamoyl chloride with sodium telluride under phase-transfer conditions did not lead to the expected tellurodicarbonic diamide but to bis(dimethylcarbamoyl) ditelluride in a low yield. The ditelluride is most likely to be derived from the oxidative coulpling of tellurocarbamate ion during work-up.[3,4]

Experimental

All melting and boiling points were uncorrected. Infrared spectra were measured as KBr pellets or as neat films between NaCl plates by using a Hitachi 260-10 photospectrometer and only prominent peaks between 2000 and 650 cm^{-1} are recorded. ^1H NMR spectra were determined on a Hitachi R-600 spectrometer using chloroform-*d* as solvent and TMS as internal standard. Mass spectra were obtained on a Hitachi M-80B spectrometer.

Preparation of Dialkyl Tellurodicarbonates: Typical Procedure; Method A: A mixture of tellurium (3.80 g; 30 mmol), Rongalite (9.2 g; 60 mmol) and 1 M (1 M=mol dm^{-3}) sodium hydroxide solution (180 mL) was stirred for 2 h at 60 °C under nitrogen to give sodium telluride as a wine-colored solution. After cooling an aqueous solution (5 mL) of tetrabutylammonium bromide (1.9 g; 6 mmol) followed by a solution of ethyl carbonochloridate (9.1 g; 84 mmol) in benzene (100 mL) was added dropwise with vigorous stirring. The initial color was lost within 15 min and small amounts of tellurium was liberated. The reaction mixture was then passed through a thin bed of Celite to remove the inorganic insolubles, the organic phase was separated, and dried over sodium sulfate. The solvent was evaporated under reduced pressure to leave diester **2b** as a pale yellow oil, which was further purified by Kugelrohr distillation. Bp 89 °C/1.0 mmHg (1 mmHg≈133.322 Pa). Yield, 3.9 g (48%). MS (20 eV): *m/z* (relative intensity) 274 (M^+, 4.4), 232 (7.0), 204 (95.3), 176 (100), 159 (38.7), 130 (71.6), and 73 (20.5). Found: C, 26.21; H, 3.69%. Calcd for $C_6H_{10}O_4Te$: C, 26.31; H, 3.68%.

Method B: A mixture of sodium hydride (53 mg; 2.2 mmol; washed thoroughly with hexane prior to use), tellurium (128 mg; 1 mmol) and dry DMF (1 mL) was heated at 120 ° C for 1 h under nitrogen to give sodium telluride as a pale yellow suspension. After cooling to room temperature, ethyl carbonochloridate (325 mg; 3.0 mmol) in the same solvent (1 mL) was added dropwise. The mixture turned reddish brown under evolution of white fumes. After 15 min the reaction was quenched by the addition of water and the organic phase was extracted with benzene. The extract was washed with water, filtered through a thin bed of Celite, dried over sodium sulfate, and evaporated in vacuo to leave an oil, which was purified by bulb-to-bulb distillation to give diester **2b** in 47% yield.

Reaction of Phenyl Carbonochloridate (3e) with Sodium Telluride: To a wine-colored solution of sodium telluride prepared from tellurium (128 mg; 1.0 mmol), Rongalite (310 mg; 2 mmol) and 1 M sodium hydroxide solution (6 mL) was added an aqueous solution (1 mL) of tetrabutylammonium bromide (64 mg; 0.2 mmol) followed by a solution of phenyl carbonochloridate (330 mg; 2 mmol) in benzene (5 mL) under nitrogen at room temperature. Within 15 min the initial color was lost under the separation of free tellurium. The resulting mixture was passed through a thin bed of Celite to remove the insolubles and the product was extracted with benzene. The extract was dried with sodium sulfate and evaporated under reduced pressure to leave a solid, which was crystallized from hexane to give diphenyl carbonate **6** as white crystals, mp 77—78 °c (lit,[5] 78 °C). Yield, 174 mg (77% based on carbonochloridate).

We are grateful to Professor Shinzi Kato of Gifu University for a gift of bis(2-methoxybenzoyl) ditelluride as a reference compound for spectral inspection. This work was in part supported by a Grant-in-Aid from the Ministry of Education, Science and Culture.

References

1) S. Kato, T. Murai, and M. Ishida, *Org. Prep. Proced. Int.*, **18**, 369 (1986).

2) S. Kato, T. Kakigano, and M. Ishida, *Z. Chem.*, **26**, 179 (1986); *Chem. Abstr.*, **108**, 94157e (1988); T. Severengiz, W. W. du Mont, D. Lenoir, and H. Voss, *Angew. Chem., Int. Ed. Engl.*, **24**, 1041 (1985).

3) H. Suzuki, H. Manabe, and M. Inouye, *Chem. Lett.*, **1985**, 1671.

4) R. A. Zingaro, C. Herrera, and E. A. Meyers, *J. Organomet. Chem.*, **306**, C36 (1986).

5) D. Martin and S. Rackow, *Chem. Ber.*, **98**, 3662 (1965).

Stereoselective Synthesis of 3′-Deoxy-3′-fluoroadenosine

Yoshitomi MORIZAWA,* Toshiaki NAKAYAMA, Arata YASUDA, and Keiichi UCHIDA
Research Center, Asahi Glass Co., Ltd., Hazawa, Kanagawa-ku, Yokohama 221
(Received January 27, 1989)

Synopsis. A new fluorinated nucleoside, 3′-deoxy-3′-fluoroadenosine(**1**), has been synthesized by a six-step synthesis from methyl 2-*O*-benzyl-5-*O*-*t*-butyldimethylsilyl-β-D-xylofuranoside (**2a**). Activation of O-3 by formation of a triflate followed by nucleophilic displacement allowed introduction of fluoride ion in a stereospecific manner at C-3.

Nucleoside derivatives with a fluorine atom on the sugar moiety are potential antitumor and/or antiviral agents. Extensive studies on the synthesis and biological activity of nucleosides possessing *trans*-fluorohydrin moiety at the C-2′ and C-3′ positions have been reported. Thus, 2′-deoxy-2′-fluoro-β-D-arabinofuranosyl pyrimidines have been found to exhibit selective inhibitory activity against herpes simplex viruses.[1] The synthesis of 3′-fluorinated derivatives, such as 3′-deoxy-3′-fluoro-β-D-xylofuranosyl purines/pyrimidines[2] and 3′-deoxy-3′-fluoro-β-D-arabinofuranosyl purines/pyrimidines have also been reported.[3]

However, there have been only limited reports on the synthesis of nucleosides with a *cis*-fluorohydrin moiety at the C-2′ and C-3′ positions; e.g. 2′-deoxy-2′-fluoroadenosine[4] and -thymidine.[5]

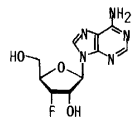

1

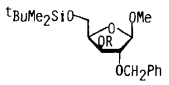

2a : R = H
2b : R = SO_2CF_3

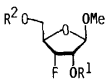

3a : $R^1=R^2=H$
3b : $R^1=CH_2Ph$, $R^2=H$
3c : $R^1=R^2=COPh$

We describe here the novel synthesis of 3′-deoxy-3′-fluoroadenosine, a new class of fluorinated nucleoside. The synthetic plan to reach the fluorinated nucleoside **1** required access to the 3-deoxy-3-fluororibofuranoside **3a**. The latter would be readily available via an appropriately blocked 3-deoxy-3-fluoroarabinofuranoside.[6] However, inversion of configuration at C-2 to give the desired ribo type product did not occur. For example, methyl 3-deoxy-3-fluoro-2-*O*-(methylsulfonyl)arabinofuranoside failed to react with CsOAc[7] and the Mitsunobu reaction[8] ($EtO_2CN=NCO_2Et$-Ph_3P-HCOOH) of methyl 3-deoxy-3-fluoroarabinofuranoside resulted only in recovery of the starting material.[9] Synthesis of the desired deoxyfluoro sugar was finally accomplished by the displacement of the trifluoromethanesulfonate at C-3 of xyloside **2b** with fluoride ion.

The C-2 hydroxyl group of methyl 3,5-*O*-isopropylidene-β-D-xylofuranoside[10] was protected with a benzyl group (100% yield). Hydrolysis of the isopropylidene group with acetic acid-H_2O (8:3) at 50 °C followed by selective protection of the primary hydroxyl group with *t*-butyldimethylsilyl chloride gave methyl 2-*O*-benzyl-5-*O*-*t*-butyldimethylsilyl-β-D-xylofuranoside (**2a**) in 87% yield. Conversion of the free 3-hydroxyl group into the trifluoromethanesulfonate (**2b**) followed by treatment with tetrabutylammonium fluoride in tetrahydrofuran at room temperature gave the desired fluorinated compound **3b** in 58% yield (from **2a**). The stereoisomer, 3-deoxy-3-fluoroxylofuranoside,[2a] could not be detected in the reaction mixture by the examination of the ^{19}F NMR spectra. By contrast, the direct fluorination of the alcohol **2a** with piperidinosulfur trifluoride[11] gave the fluorinated sugar in low yield.

Removal of the benzyl protecting group in compound **3b**, followed by protection of the resulting diol with benzoyl chloride gave the dibenzoate (**3c**) (50% yield). The methyl glycoside was converted into the glycosyl bromide with 30%-HBr-acetic acid and coupled with adenine monobenzoate in the presence of mercury(II) cyanide to give the protected adenosine in 63% yield. Deprotection of the benzoyl group with methanolic sodium methoxide afforded 3′-deoxy-3′-fluoroadenosine **1** in 90% yield.

Experimental

Melting points were determined on a Mettler FP80, the IR spectra on a JASCO IR-810 spectrophotometer, and the NMR spectra on a JEOL JNM-FX-90Q spectrometer. Chemical shifts are given in δ with tetramethylsilane as an internal standard. Ultraviolet spectra were recorded with a Shimadzu MPS-2000 spectrophotometer. Rotatory power at sodium D line was measured with a JASCO DIP-140 polarimeter. Elemental analyses were performed by the microanalytical group of Asahi Glass Co., Ltd. Research Center. Purification of products were carried out with column chromatography on silica gel (Merck, 0.063—0.200 mm or 0.040—0.063 mm).

Methyl 2-*O*-Benzyl-5-*O*-*t*-butyldimethylsilyl-β-D-xylofuranoside (2a). Benzyl bromide (108.7 g, 0.64 mol) was added to a suspension of methyl 3,5-*O*-isopropylidene-β-D-xylofuranoside[10] (63 g, 0.31 mol) and silver oxide (76 g, 0.31 mol) in *N*,*N*-dimethylformamide (DMF) (200 ml) at room temperature over a period of 20 min. After 24 h, the mixture was filtrated on Celite 545 and the solvent was evaporated. Purification by column chromatography (toluene-ethyl acetate=5:1) gave 92 g (100% yield) of benzyl ether: ^1H NMR ($CDCl_3$) δ=1.37 (6H, s), 3.41 (3H, s), 3.9—4.4 (5H, m), 4.59 (2H, s), 4.98 (1H, s), 7.32 (5H, s).

This compound was dissolved in 164 ml of acetic acid and 66 ml of water and the solution was heated in a bath at 50 °C for 1 h. Evaporation to dryness in vacuo and short column chromatography gave crude diol (65.1 g, 92% yield).

To a solution of the diol (53.8 g, 0.21 mol) in DMF (200 ml) was added imidazole (43.4 g, 0.63 mol) and *t*-butyldimethylsilyl chloride (31.9 g, 0.21 mol) at 0 °C. After 3 h, the mixture

was poured into sat. aq. sodium hydrogencarbonate (1000 ml) and the solution was extracted with chloroform. The combined extracts, dried with magnesium sulfate, were evaporated to dryness in vacuo. Purification by column chromatography (toluene-ethyl acetate=5 : 1) gave **2a** (74.4 g, 95% yield) as an oil: ^{1}H NMR ($CDCl_3$) δ=0.10 (6H, s), 0.91 (9H, s), 3.37 (3H, s), 3.9—4.1 (3H, m), 5.2—4.4 (2H, m), 4.61 (2H, s), 4.93 (1H, s), 7.32 (5H, s).

Methyl 2-*O*-Benzyl-3-deoxy-3-fluoro-β-D-ribofuranoside (3b). To a solution of **2a** (74.4 g, 0.20 mol) and 2,6-lutidine (64.6 g, 0.60 mol) in dichloromethane (250 ml) was added trifluoromethanesulfonic anhydride (113.0 g, 0.40 mol) at 0 °C over a period of 1 h. After 2 h, the mixture was washed with sat. aq. copper sulfate (200 ml×3) and purified by short column chromatography to give 106.8 g of a crude triflate (**2b**).

Tetrabutylammonium fluoride (1 M† tetrahydrofuran (THF) solution, 370 ml, 0.37 mol) was added to the solution of the crude triflate in THF (250 ml) at 0 °C. After 7 h, the solvent was evaporated under reduced pressure and the residue was purified by silica-gel column to give **3b** (30.2 g, 58% yield (2 steps)): ^{1}H NMR ($CDCl_3$) δ=3.47 (3H, s), 4.0—4.2 (2H, m), 4.55 (2H, s), 4.5—5.1 (4H, m), 5.27 (1H, s), 7.33 (5H, s); ^{19}F NMR ($CDCl_3$, relative to CCl_3F) −207.1 ppm (ddd, J=13.4, 22.0, 53.7 Hz).

Methyl 2,5-Di-*O*-benzoyl-3-deoxy-3-fluoro-β-D-ribofuranoside (3c). The benzyl ether (**3b**) (30 g, 0.12 mol) dissolved in ethanol (100 ml) was stirred in the presence of 5% palladium on charcoal (20 g) under a hydrogen atmosphere for 24 h. Removal of the catalyst by filtration and concentration gave a diol **3a**.

The diol **3a** was mixed with pyridine (80 ml) and benzoyl chloride (23 g, 0.16 mol), and allowed to react at room temperature for 24 h. All the volatile material was evaporated under reduced pressure and the residue was purified by column chromatography (toluene-ethyl acetate=100 : 1) to give **3c** (16.4 g, 50% yield (2 steps)). Mp 53.8 °C (hexane); ^{1}H NMR($CDCl_3$) δ=3.42 (3H, s), 3.4—4.0 (2H, m), 4.4—5.9 (4H, m), 7.2—8.3 (10H, m); ^{19}F NMR ($CDCl_3$, relative to CCl_3F) −211.6 ppm (ddd, J=4.89, 18.06, 53.22 Hz). Found: C, 63.94; H, 5.23%. Calcd for $C_{20}H_{19}O_6F$: C, 64.17; H, 5.12%.

3′-Deoxy-3′-fluoroadenosine (1). To a solution of **3c** (2.4 g, 6.4 mmol) in acetic acid (12 ml) and acetic anhydride (0.5 ml) was added 30%-hydrogen bromide-acetic acid (36 ml) at room temperature over a period of 20 min. After 4 h, all the volatile was evaporated under reduced pressure and the residue dissolved in nitromethane (20 ml) was added to the solution of 6-benzamidopurine (1.6 g, 6.7 mmol) and mercury(II) cyanide (2.4 g, 9.5 mmol) in nitromethane (80 ml) at 100 °C. The solution was refluxed for 1 h, and evaporated to dryness in vacuo at 50 °C, and the residue was suspended in chloroform (200 ml). After being washed with 30% aqueous potassium iodide (200 ml) and water (200 ml), the solution was dried with magnesium sulfate, evaporated, and purified by column chromatography (toluene-ethyl acetate=1 : 3), giving 6-benzamido-9-(2,5-di-*O*-benzoyl-3-deoxy-3-fluoro-β-D-ribofuranosyl)purine (2.16 g, 63% yield). ^{1}H NMR($CDCl_3$) δ=4.2—5.1 (3H, m), 6.0—6.6 (3H, m), 7.2—8.3 (16H, m), 8.34 (1H, s), 8.64 (1H, s); ^{19}F NMR($CDCl_3$, relative to CCl_3F) −200.0 ppm (ddd, J=18.5, 24.5, 53.0 Hz).

A solution of the protected 3′-deoxy-3′-fluoroadenosine (2.16 g, 3.73 mmol) in methanol (10 ml) and 1 M-methanolic sodium methoxide (3.73 ml, 3.73 mmol) was heated to reflux for 1 h, and then evaporated to dryness in vacuo. The residue was dissolved in water (30 ml) and neutralized with 2 M-acetic acid. Methyl benzoate was removed by washing with chloroform, and the aqueous layer was evaporated to dryness in vacuo. Purification by silica-gel column (ethyl acetate) gave the title compound: 0.91 g (90% yield); UV: λ_{max}^{pH14} 258 nm, λ_{max}^{pH7} 258 nm, λ_{max}^{pH2} 256 nm, λ_{min}^{pH14} 237 nm, λ_{min}^{pH7} 236 nm, λ_{min}^{pH2} 236 nm; mp 206.5 °C (decomp, ethanol); $[\alpha]_D^{25}$ −61.8° (H_2O, c=0.5); ^{1}H NMR (DMSO-d_6) δ=3.6—3.7 (2H, m, H-5′), 4.29 (1H, dt, J=27.6, 3.7 Hz, H-4′), 4.80—5.0 (1H, m, H-2′), 5.09 (1H, dd, J=54.4, 4.2 Hz, H-3′), 5.69 (1H, dd, J=7.3, 4.9 Hz, 5′-OH), 5.89 (1H, d, J=6.3 Hz, H-1′), 5.93 (1H, d, J=8.1 Hz, 2′-OH), 7.39 (1H, s), 8.13 (1H, s), 8.36 (1H, s); ^{19}F NMR (DMSO-d_6, relative to CCl_3F) −19.78 ppm (dt, J=54.4, 27.6 Hz); ^{13}C NMR (DMSO-d_6) δ=61.1 (d, J=12.2 Hz, C-5′), 72.0 (d, J=15.9 Hz, C-2′), 83.9 (d, J=22.0 Hz, C-4′), 86.9 (C-1′), 93.1 (d, J=181.8 Hz, C-3′), 119.4 (C-5), 141.1 (C-8), 149.1 (C-4), 152.4 (C-2), 156.2 (C-6); IR (KBr) 3300, 1650 cm^{-1}; Found: C, 44.61; H, 4.71; N, 25.99%. Calcd for $C_{10}H_{12}O_3N_5F$: C, 44.61; H, 4.49; N, 26.01%.

† 1 M=1 mol dm^{-3}.

References

1) a) K. Harada, J. Matulic-Adamic, R. W. Price, R. F. Schinazi, K. A. Watanabe, and J. J. Fox, *J. Med. Chem.*, **30**, 226 (1987). b) C. H. Tann, P. R. Brodfuehrer, S. P. Brundidge, C. Sapino, Jr., and. H. G. Howell, *J. Org. Chem.*, **50**, 3644 (1985). c) K. A. Schat, R. F. Schinazi, and B. W. Calnak, *Antiviral Reseearch*, **4**, 259 (1984).

2) a) J. A. Wright and N. F. Taylor, *Carbohydr. Res.*, **6**, 347 (1968). b) M. J. Robins, Y. Fouron, and R. Mengel, *J. Org. Chem.*, **39**, 1564 (1974).

3) K. Miyai, R. K. Robins, and R. L. Tolman, *J. Med. Chem.*, **15**, 1092 (1972).

4) a) M. Ikehara, A. Hasegawa, and J. Imura, *J. Carbohydrates. Nucleosides Nucleotides*, **7**, 131 (1980). b) R. Ranganathan, *Tetrahedron Lett.*, **1977**, 1291.

5) J. F. Codington, I. L. Doerr, and J. J. Fox, *J. Org. Chem.*, **29**, 558 (1964).

6) J. A. Wright and J. J. Fox, *Carbohydr. Res.*, **13**, 297 (1970).

7) Y. Torisawa, H. Okabe, and S. Ikegami, *Chem. Lett.*, **1984**, 1555.

8) O. Mitsunobu, *Synthesis*, **1981**, 1.

9) Oxidation of trans-fluorohydrin also failed to give α-fluoro ketone.

10) B. R. Baker, R. E. Schaub, and J. H. Williams, *J. Am. Chem. Soc.*, **77**, 7 (1955).

11) L. N. Markovskij, V. E. Pashinnik, and A. V. Kirsanov, *Synthesis*, **1973**, 787.

Stereoselective *syn*-Reduction of (*R*)-4-Acyl-2,2-dimethyl-1,3-dioxolanes with Metal Hydride Reagents

Hidenori CHIKASHITA,* Toshiki NIKAYA, Hiromitsu UEMURA, and Kazuyoshi ITOH
Department of Applied Chemistry, Faculty of Engineering, Kansai University, Suita, Osaka 564
(Received January 30, 1989)

Synopsis. Lithium tri-*s*-butylborohydride and lithium aluminum hydride were found to be efficient reducing agents for the stereoselective preparation of *syn*-glycerol derivatives from (*R*)-4-acyl-2,2-dimethyl-1,3-dioxolanes. The scope and limitation of the stereoselective L-Selectride reduction of (*R*)-4-acyl-2,2-dimethyl-1,3-dioxolanes were also described.

2,3-*O*-Isopropylideneglyceraldehyde is a very useful chiral starting material for the synthesis of a variety of optically active molecules including natural products[1] because of ready availability of both the (*S*)-[2] and (*R*)-forms.[3] Among the methodologies developed in this field, much interest has been concentrated on the diastereoselective addition of C-nucleophiles such as organometallic reagents to the glyceraldehyde. Although the stereochemical course in this reaction has been extensively studied in recent years, the addition of organometallic reagents usually produces *anti*-glycerol derivatives as major products with varying degree of diastereoselectivity depending on the reagents and conditions employed.[4] On the other hand, however, an efficiently controlled method for the preparation of syn-adducts based on this methodology is rare.[5] A different approach to obtain *syn*-glycerol derivatives selectively would be to employ the diastereoselective carbonyl addition of hydride to 4-acyl-2,2-dimethyl-1,3-dioxolanes.[6] We have now examined the diastereofacial selectivity of the reduction of (*R*)-4-acyl-2,2-dimethyl-1,3-dioxolanes (**1**) with a variety of metal hydride reagents and found that lithium tri-*s*-butylborohydride (L-Selectride) and lithium aluminum hydride were excellent candidates as reducing agents for the syn-selective hydride addition to **1** producing *syn*-glycerol derivatives **2**. In this paper, we describe these results including the scope and limitation of the stereoselective L-Selectride reduction of **1**.

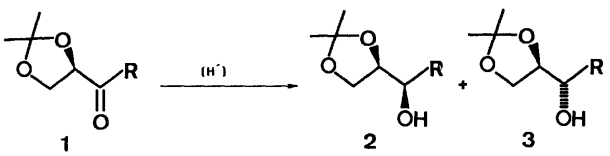

Scheme 1.

Reduction of ketone **1a** to the glycerols **2a** and **3a** was initially examined with a variety of metal hydride reagents and the results are presented in Table 1. In all cases of the reducing agents and conditions examined, the reduction proceeded in high yield and provided the syn-diastereomer **2a** as the major product. These results indicate that the β-chelation transition state A which predicts the syn selectivity should be favored over the α-chelation transition state B when chelatable reagents are employed (Entries 1—6). On the other hand, reduction with diisobutylaluminum hydride (DIBAL-H) which is known to have low chelating ability showed very low selectivity (Entry 7). Thus, non-chelation reaction which should predict the syn selectivity according to the Felkin-Ahn transition state model C is regarded to be ineffective for the present type of diastereofacial selection of **1**. Higher diastereoselectivity was obtained in the reaction with a series of lithium metal hydrides (Entries 3—5) with the following order of selectivity: LiBH(*s*-Bu)$_3$>LiAlH$_4$≫LiAlH(O*t*-Bu)$_3$. This shows the high chelation efficiency of the Li^+ counterion in the transition state A rather than the transition state B leading to the formation of the minor anti-addition product **3a**.

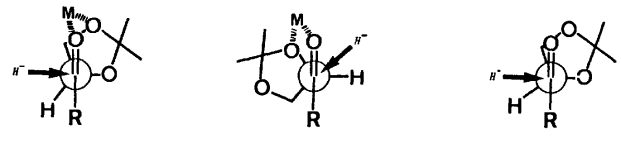

Scheme 2.

Although a similar stereochemical outcome of the L-Selectride reduction has been obtained by Macdonald et al. for a model compound,[7] the scope and limitations of the reduction have not been clari-

Table 1. Reduction of **1a** (R=Ph) with Various Metal Hydrides

Entry	Metal hydride	Solvent	Temp/°C (Time/h)	Yield/%[a]	Product ratio[b] *syn*-**2a** : *anti*-**3a**
1	$NaBH_4$	Ethanol	−78(1.5)	89	67:33
2	$Zn(BH_4)_2$	Ether	−78(1.5)	57	63:37
3	LiBH(*s*-Bu)$_3$	THF	−78(3.0)	83	97: 3
4	$LiAlH_4$	THF	−78(1.5)	87	94: 6
5	LiAlH(OBu^t)$_3$	Ether	−78(3.0)	78	73:27
6	$NaAlH_2(OCH_2CH_2OMe)_2$	Benzene	0(1.2)	98	60:40
7	AlH(*i*-Bu)$_2$	Benzene	0(3.0)	90	59:41

a) Isolated yield. b) Determined by HPLC analyses.

fied yet. Thus, to establish the generality, we examined the reduction of a variety of (*R*)-4-acyl-2,2-dimethyl-1,3-dioxolanes (**1b—h**). The results are summarized in Table 2. A variety of aromatic (Entries 1—3) and aliphatic (Entries 4,5) ketones were efficiently reduced to the corresponding *syn*-glycerols **2b—e** in high yields with excellent stereoselectivity. Keto ester **1f** and 1,3-dithian-2-yl ketone **1g** were similarly reduced in high yield with excellent syn-selectivity to give the β-hydroxy ester **2f** and the dithianyl alcohol **2g**, respectively. However, the reduction of the 1,3-dithian-2-yl ketone **1h** with L-Selectride did not proceed at all (Entry 8). This result suggests that L-Selectride can not be used for the reduction of highly hindered ketones due to the strong hindrance of the reaction because of the steric bulks of both the reducing agent and the substrate, and shows the limitation of the present L-Selectride reduction. In contrast to this, the reduction of **1h** with $LiAlH_4$, which is the another excellent candidate as shown previously (Table 1), proceeded in high yield to give the syn-product **2h** in good selectivity (Entry 8).

Table 2. Stereoselective Reduction of (*R*)-4-Acyl-2,2-dimethyl-1,3-dioxolanes (**1**) with L-Selectride[a)]

Entry	Substrate	Isolated yield/%	Product ratio[b)] *syn*-**2**:*anti*-**3**
1	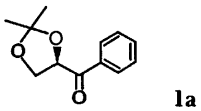 **1a**	83	97: 3
2	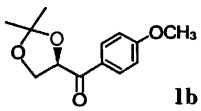 **1b**	81	97: 3
3	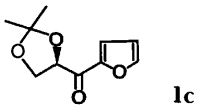 **1c**	98	>99: 1
4	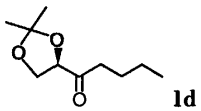 **1d**	67	96: 4
5	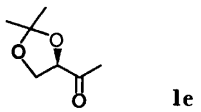 **1e**	33	85:15
6	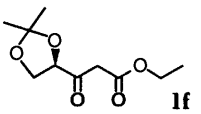 **1f**	55	96: 4
7	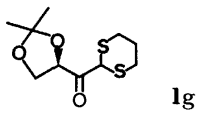 **1g**	82	>99: 1
8	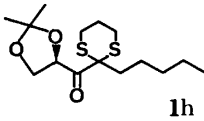 **1h**	No reaction (87)[c)]	(80:20)[c)]

a) All the reactions were carried out with 3 equiv of L-Selectride in THF at −78 °C for 3 h. b) Determined by HPLC analyses (Entries 1—3 and 7), GLC analyses (Entries 4 and 5), and 400 MHz ^{1}H NMR analyses (Entries 6 and 8). c) Reactions with 3 equiv of $LiAlH_4$ in THF at −78 °C for 3 h.

In conclusion, the L-Selectride reduction of (*R*)-4-acyl-2,2-dimethyl-1,3-dioxolanes (**1**) was found to be a fairly general method for the stereoselective preparation of *syn*-glycerol derivatives **2**. On the other hand, $LiAlH_4$ was also found to be useful as another selective reducing agent especially in the case of the reduction of highly hindered substrates.

Experimental

Optical rotations were determined with a Union Digital PM-101 polarimeter. IR spectra were obtained on a JASCO A-202 spectrometer. ^{1}H NMR spectra were measured with a JEOL JNM-GX400 spectrometer at 400 MHz with tetramethylsilane as an internal reference. GLC analyses were carried out on a Yanagimoto Gas chromatograph G2800T using glass columns (3 m) packed with 10% EG-20W on Shimalite-NAW (60/80 mesh). HPLC analyses were carried out on a Yanagimoto high-pressure liquid chromatograph L-5000. Silica gel (Merck silica gel 60, 230—400 mesh ASTM) was used for medium-pressure liquid chromatography (MPLC). TLC were carried out on Merck precoated silica gel plates (Merck silica gel 60 F_{254}).

Materials. Tetrahydrofuran (THF) was freshly distilled over $LiAlH_4$ before use. The other solvents were purified by the usual methods and were freshly distilled before use. Metal hydride reagents were supplied as high grade commercial products and used without further purification. (*R*)-4-Acyl-2,2-dimethyl-1,3-dioxolanes **1a—e** were prepared by the reaction of 1,2-*O*-isopropylidene-D-glyceraldehyde with organolithium or Grignard reagents followed by oxidation of the resulting diastereomeric mixture of glycerol derivatives. The keto ester **1f** and 1,3-dithian-2-yl ketones **1g,h** were similarly prepared by the reaction with the lithium enolate of ethyl acetate[8)] and 2-lithio-1,3-dithiane derivatives and the subsequent PCC and PDC oxidations, respectively.

General Procedure for the Reduction of (*R*)-4-Acyl-2,2-dimethyl-1,3-dioxolanes with L-Selectride. To a 1 M THF solution of L-Selectride (2 ml, 2 mmol) was added dropwise a solution of the (*R*)-4-acyl-2,2-dimethyl-1,3-dioxolanes **1** (1 mmol) in THF (2 ml) under nitrogen with stirring. The mixture was stirred for 3 h at −78 °C and the solution was allowed to warm to room temperature and then quenched by the addition of water (8 ml). The mixture was extracted with ether (30 ml×5) and the extract was washed with water (30 ml×2). The aqueous washings were again extracted with ether and the combined organic layers were dried with $MgSO_4$. The solution was filtered through silica gel (Wakogel C-300) and the filtrate was concentrated under reduced pressure to give a fairly pure (monitored by TLC and ^{1}H NMR) diastereomeric mixture of **2** and **3** as a colorless oil. The β-keto ester **1f** was similarly reduced to a mixture of **2f** and **3f** by the general procedure, except that the reaction time was 5 h and a buffer solution (pH=6.86) was used for quenching in place of water.

Identification of products was performed by spectroscopic (NMR and IR) methods. These spectral data were in satisfactory agreement with those of the corresponding authentic samples.

The relative stereochemistry of major and minor diastereoisomers **2a—f** and **3a—f** was assigned by HPLC, GLC, or ^{1}H NMR comparison with stereochemically defined authentic samples.

The syn and anti diastereoisomers **2g** and **3g** were easily distinguished by ^{1}H NMR on the basis of chemical shift values for the OH protons (δ_{syn}OH>δ_{anti}OH).[9] Full spectroscopic data of the major *syn*-**2g** and the minor *anti*-**3g** which could be separated by MPLC (benzene-ethyl acetate, 20:1 v/v) after conversion into the corresponding benzyl ethers are as follows.

***syn*-2g**: $[\alpha]_D^{24}$+5.00° (*c* 0.95, $CHCl_3$) as a benzyl ether; IR of the benzyl ether (neat) 3030, 2984, 2933, 2896, 1497, 1454, 1422, 1380, 1370, 1248, 1213, 1157, 1069, 1028, 855, 796, 737, and 699 cm^{-1}; ^{1}H NMR ($CDCl_3$) δ=1.39 (s, 3H), 1.46 (s, 3H), 1.94 (m, 1H), 2.11 (m, 1H), 2.68 (d, 1H, *J*=6.0 Hz), 2.81 (m, 2H), 2.92 (m, 2H), 3.75 (ddd, 1H, *J*=6.6, 6.0, 3.9 Hz), 3.93 (dd, 1H, *J*=8.3, 6.6 Hz), 4.10 (d, 1H, *J*=6.6 Hz), 4.12 (dd, 1H, *J*=8.3, 6.6 Hz), and 4.50 (dt, 1H, 3.9, 6.6 Hz).

***anti*-3g**: $[\alpha]_D^{23}$+24.4° (*c* 0.45, $CHCl_3$) as a benzyl ether; IR of the benzyl ether (neat) 3031, 2985, 2933, 2896, 1496, 1454, 1422, 1380, 1370, 1341, 1248, 1213, 1157, 1074, 908, 854, 786, 738, 699, and 681 cm^{-1}: ^{1}H NMR ($CDCl_3$) δ=1.37 (s, 3H), 1.44 (s, 3H), 1.94 (m, 1H), 2.11 (m, 1H) 2.35 (d, 1H, *J*=4.2 Hz), 2.93 (m, 4H), 3.88 (dt, 1H, *J*=6.6, 4.2 Hz), 4.02 (dd, 1H, *J*=8.5, 5.4 Hz), 4.09 (dd, 1H, *J*=8.5, 6.6 Hz), 4.32 (td, 1H, 6.6, 5.4 Hz), and 4.35 (d, 1H, *J*=4.2 Hz).

Reduction of 1,3-Dithian-2-yl Ketone 1h with $LiAlH_4$. To a stirred suspension of lithium aluminum hydride (39 mg, 2 mmol) in dry THF (12 ml) was slowly added the ketone **1h** (375 mg, 1 mmol) in dry THF (2 ml) at −78 °C. After stirring for 3 h at −78 °C, the mixture was quenched by the addition of water (10 ml). The aqueous mixture was extracted with ether and the ether extract was washed with water and then dried with $MgSO_4$. Concentration of the solution under reduced pressure gave the fairly pure (monitored by TLC and ^{1}H NMR) diastereomeric mixture of **2h** and **3h** as a colorless oil (323 mg, 86%).

The relative stereochemistry of the syn and anti diastereoisomers was easily distinguished by ^{1}H NMR on the basis of chemical shift values for the OH protons (δ_{syn}OH >δ_{anti}OH).[9] Full spectroscopic data of the major *syn*-**2h** and the minor *anti*-**3h** separated by MPLC (benzene-ethyl acetate, 4:1 v/v) are as follows.

***syn*-2h**: $[\alpha]_D^{25}$−7.28° (*c* 1.24, $CHCl_3$); IR (neat) 3489, 2925, 2854, 1458, 1423, 1370, 1255, 1218, 1158, 1122, 1065, 965, 909, 869, 797, and 722 cm^{-1}: ^{1}H NMR ($CDCl_3$) δ=0.88 (t, 3H, *J*=6.8 Hz), 1.26 (br, 12H), 1.42 (s, 3H), 1.46 (s, 3H), 1.56 (m, 2H), 1.76 (m, 1H), 1.84—2.06 (m, 3H), 2.71 (m, 2H), 2.89 (ddd, 1H, *J*=14.0, 10.4, 3.6 Hz), 2.95 (ddd, 1H, *J*=14.0, 10.4, 3.6 Hz), 3.02 (d, 1H, *J*=5.3 Hz), 3.83 (dd, 1H, *J*=5.3, 3.9 Hz), 3.87 (t, 1H, *J*=8.0 Hz), 4.17 (dd, 1H, *J*=8.0, 6.3 Hz), and 4.53 (ddd, 1H, *J*=8.0, 6.3, 3.9 Hz). Found: C, 60.53; H, 9.44%. Calcd for $C_{19}H_{36}O_3S_2$: C, 60.60; H, 9.63%.

***anti*-3h**: $[\alpha]_D^{25}$+11.7° (*c* 1.05, $CHCl_3$); IR (neat) 3465, 2922, 2853, 1456, 1423, 1370, 1248, 1213, 1159, 1123, 1058, 908, 856, 799, 758, 722, and 655 cm^{-1}: ^{1}H NMR ($CDCl_3$) δ=0.88 (t, 3H, *J*=7 Hz), 1.26 (br, 12H), 1.38 (s, 3H), 1.46 (s, 3H), 1.55 (m, 2H), 1.87 (m, 3H), 2.02 (m, 1H), 2.71 (m, 2H), 2.75 (d, 1H, *J*=2.2 Hz), 3.00 (ddd, 1H, *J*=3.2, 10.6, 14.1 Hz), 3.08 (ddd, 1H, *J*=3.2, 10.6, 14.1 Hz), 4.02 (dd, 1H, *J*=8.1, 6.8 Hz), 4.12 (dd, 1H, *J*=8.1, 6.8 Hz), 4.25 (dd, 1H, *J*=2.9, 2.2 Hz), and 4.59 (td, 1H, *J*=6.8, 2.9 Hz). Found: C, 60.52; H, 9.57%. Calcd for $C_{19}H_{36}O_3S_2$: C, 60.60; H, 9.63%.

References

1) S. Hanessian, *Acc. Chem. Res.*, **12**, 159 (1979); W. A. Szabo and H. T. Lee, *Aldri. Chim. Acta*, **13**, 13 (1980); S. Hanessian, "Total Synthesis of Natural Products: The 'Chiron' Approach," Pergamon, New York (1983); J. W. Scott, "Asymmetric Synthesis," ed by J. D. Morrison and J. W. Scott, Academic Press, New York, Vol. 1, Chap. 1.

2) S. B. Baker, *J. Am. Chem. Soc.*, **74**, 827 (1952); M. E. Jung and T. J. Shaw, *ibid.*, **102**, 6304 (1980).

3) E. Baer and H. O. L. Fischer, *J. Biol. Chem.*, **128**, 463 (1939).

4) As reviews, see: G. J. McGarvey, M. Kimura, T. Oh, and J. M. Williams, *J. Carbohydr. Chem.*, **3**, 125 (1984); T. Oishi and T. Nakata, *Acc. Chem. Res.*, **17**, 338 (1984); S. Masamune, W. Choy, J. S. Peterson, and L. R. Sita, *Angew. Chem., Int. Ed. Engl.*, **24**, 1 (1985); J. Jurczak, S. Pikul, and T. Bauer, *Tetrahedron*, **42**, 447 (1986).

5) A very efficient method using organocopper reagents has been recently reported: F. Sato, Y. Kobayashi, O. Takahashi, T. Chiba, Y. Takeda, and M. Kusakabe, *J. Chem. Soc., Chem. Commun.*, **1985**, 1636.

6) Stereoselective hydride reduction of different types of chiral acyl-heterocycles has been reported: K. -Y. Ko, W. J. Frazee, and E. L. Eliel, *Tetrahedron*, **40**, 1333 (1984); A. Ookawa and K. Soai, *J. Chem. Soc., Perkin Trans. 1*, **1987**, 1465.

7) K. Mead and T. L. Macdonald, *J. Org. Chem.*, **50**, 422 (1985).

8) C. H. Heathcock, S. D. Young, J. P. Hagen, M. C. Pirrung, C. T. White, and D. VanDerveer, *J. Org. Chem.*, **45**, 3846 (1980).

9) B. Landmann and R. W. Hoffmann, *Chem. Ber.*, **120**, 331 (1987).

Synthesis of Hydroxy Ketones by Chemoselective Alkylation of Keto Aldehydes with Dialkylzincs Catalyzed by Amino Alcohol, Diamine, or Dilithium Salt of Piperazine

Kenso SOAI,* Masami WATANABE, and Masashi KOYANO
Department of Applied Chemistry, Faculty of Science, Science University of Tokyo, Shinjuku-ku, Tokyo 162
(Received February 3, 1989)

Synopsis. Hydroxy ketones were obtained in high yields by the chemoselective alkylation of formyl group of keto aldehydes with dialkylzincs in the presence of such catalysts as 2-dimethylaminoethanol, *N,N,N',N'*-tetramethylethylenediamine, or dilithium salt of piperazine.

Chemoselective alkylation of aldehydes in the presence of ketones by organometallic reagents has attracted considerable attention.[1] Organolead,[1a] -lithium, -magnesium (in combination with organoaluminum),[1b] -lanthanoid (and Sc, Y, Nb, Ta),[1c] and -titanium reagents[1d] have been used for the above-mentioned reaction. However, most of the examples reported in these reports are intermolecular competitive experiments between aldehydes and ketones, and there are relatively few example of the chemoselective alkylation of keto aldehydes.

On the other hand, the addition of dialkylzincs to aldehydes without catalyst is very slow.[2] Mukaiyama et al., including one of us (K. S.), reported β-amino alcohol catalyzed addition of diethylzinc to benzaldehyde which affords 1-phenyl-1-propanol in 76%.[3]

To establish the synthetic utility of the aminoalcohol-catalyzed addition of dialkylzincs to aldehydes, we report in this paper the chemoselective alkylation of the formyl group of keto aldehydes with dialkylzincs in the presence of such catalysts as 2-dimethylaminoethanol (**4**) or diamine (Scheme 1). When 4-benzoylbenzaldehyde (**1a**)[4] was treated with dimethyl-, diethyl-, or diisopropylzinc in the presence of 5—20 mol% of **4**, formyl group of **1a** was alkylated (methylation, ethylation, or isopropylation respectively) in chemoselective manner. The results are summarized in Table 1. Isolated yields of the corresponding hydroxy ketones (**3a—c**) were very high (93—100%) (Table 1, Entries 1—3). In a similar manner, chemoselective alkylation of 3-benzoyl-2,4-dichlorobenzaldehyde (**1b**) was performed. The yields of hydroxy ketone (**3d**) were quantitative regardless of the amount of catalyst (Entries 4 and 5). The reaction of 3-benzoylpropanal (**1c**, γ-keto aldehyde)[6] with Et_2Zn using **4** afforded γ-hydroxy ketone (**3e**) in 76% (Entry 8). *N,N,N',N'*-tetramethylethylenediamine (**5**, TMEDA) and dilithium salt of piperazine (**6**)[5] were also found to be effective catalysts (Entries 6 and 7).

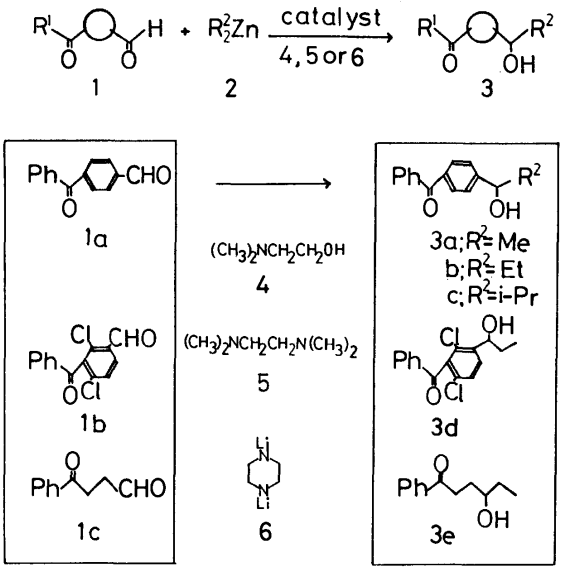

Scheme 1.

On the other hand, the reaction of 2-benzoyl-2-methylpropanal (**1d**, β-keto aldehyde)[7] with Et_2Zn using **4** as the catalyst (20 mol%) gave unexpected isopropyl phenyl ketone in 85% (Eq. 1). In addition,

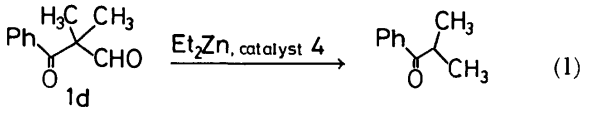

(1)

intermolecular competitive ethylation of a mixture of benzaldehyde and acetophenone using **4** (10 mol%) afforded 1-phenyl-1-propanol (75%)(as a result of the ethylation of benzaldehyde), and acetophenone was recovered (70%).

Experimental

All reactions were carried out under an argon atmosphere. Toluene was distilled from lithium aluminum hydride. 4-Benzoylbenzaldehyde (**1a**),[4] 3-benzoylpropanal (**1c**),[6] and 2-benzoyl-2-methylpropanal (**1d**)[7] were prepared according

Table 1. Synthesis of Hydroxy Ketones (**3**) from Keto Aldehydes (**1**)

Entry[a]	1	R^2	Catalyst	Mole ratio[b]	3	Yield/%
1	a	Me	4	A	a	100
2	a	Et	4	B	b	93
3	a	*i*-Pr	4	C	c	100
4	b	Et	4	B	d	100
5	b	Et	4	D	d	100
6	b	Et	5	B	d	100
7	b	Et	6	B	d	77
8[c]	c	Et	4	E	e	76

a) Unless otherwise noted, reactions were run at room temperature. b) Molar ratio of keto aldehyde (**1**) : dialkylzinc (**2**) : catalyst. A=1.0 : 4.0 : 0.2. B=1.0 : 2.2 : 0.05. C=1.0 : 2.2 : 0.2. D=1.0 : 2.2 : 1.0. E=1.0 : 4.0 : 0.1. c) Reaction was run at 0 °C.

to a method described in the literature. 2,4-Dichloro-3-benzoylbenzaldehyde and diethylzinc are commercially available. Diisopropylzinc was prepared according a method from the literature and was purified by distillation.[8] ^{1}H NMR spectra were taken on a JEOL JNM PMX-60 (TMS as the internal reference). The IR spectra were recorded on a Hitachi 260-10 spectrometer. Measurement of mass spectra were carried out on a Hitachi RMU7M spectrometer.

Typical Procedure for Chemoselective Alkylation of Keto Aldehydes with Dialkylzincs Using 2-Dimethylaminoethanol (Table 1, Entry 2): A toluene solution of 2-dimethylaminoethanol (**4**, 0.05 M,† 0.025 mmol) was added to a toluene solution (0.5 ml) of 4- benzoylbenzaldehyde (**1a**, 0.106 g, 0.50 mmol) at 0 °C. After 15 min of stirring, diethylzinc (1.1 ml, 1 M, in hexane solution) was added dropwise. The resulting mixture was stirred at room temperature for 14 h and quenched with 1 M HCl (3 ml), the organic layer was separated, and aqueous layer was extracted with dichloromethane. The combined organic layer was dried over anhydrous Na_2SO_4, then evaporated under reduced pressure. The residue was purified by silica gel TLC [$CHCl_3$: MeOH=50 : 1 v/v as eluent]. 4-(1-Hydroxypropyl)benzophenone (**3b**) was obtained in 93% yield (0.113 g, 0.47 mmol); ^{1}H NMR ($CDCl_3$) δ=0.73—1.16 (t, 3H), 1.50—2.05 (m, 2H), 2.96 (s, 1H), 3.46—4.74 (t, 3H), and 7.12—7.91 (m, 9H); IR (neat) 3430, 2970, and 1660 cm^{-1}; Found: *m/z* 240.1148. Calcd for $C_{16}H_{16}O_2$: M, 240.1151.

According to a similar procedure as that described above, the following hydroxy ketone (**3**) were synthesized from the corresponding **1** and **2** using **4** or **5** as the catalyst.

4-(1-Hydroxyethyl)benzophenone (3a, Table 1, Entry 1): Yield 100%; ^{1}H NMR ($CDCl_3$) δ=1.40—1.67 (d, 3H), 2.76—3.17 (broad, 1H), 4.67—5.01 (m, 1H), and 7.17—7.90 (m, 9H); IR (neat) 3420, 2975, and 1660 cm^{-1}; Found: *m/z* 226.0994. Calcd for $C_{15}H_{14}O_2$: M, 226.0994.

4-(1-Hydroxy-2-methylpropyl)benzophenone (3c, Table 1, Entry 3): Yield 100%; ^{1}H NMR ($CDCl_3$) δ= 0.57—1.30 (m, 6H), 1.67—2.30 (m, 1H), 2.78 (s, 1H), 4.20—4.67 (m, 1H), and 7.03—8.00 (m, 9H); IR (neat) 3450, 2960, and 1650 cm^{-1}; Found: *m/z* 254.1301. Calcd for $C_{17}H_{18}O_2$: M, 254.1307.

2,6-Dichloro-3-(1-hydroxypropyl)benzophenone (3d, Table 1, Entries 4, 5, 6, and 7): Yield 77—100%; ^{1}H NMR ($CDCl_3$) δ=0.83—1.20 (t, 3H), 1.47—2.23 (m, 3H), 4.87—5.33 (m, 1H), and 7.24—8.93 (m, 7H); IR (neat) 3370, 2920, and 1660 cm^{-1}; Found: *m/z* 308.0378. Calcd for $C_{16}H_{14}O_2Cl_2$; M, 308.0372.

† 1 M=1 mol dm^{-3}.

Dilithium salt of piperazine (**6**) was in situ prepared by the treatment of piperazine with 2 equiv of butyllithium (Entry 7).

4-Hydroxy-1-phenyl-1-hexanone (3e, Table 1, Entry 8): Yield 76%; ^{1}H NMR ($CDCl_3$) δ=0.80—1.17 (m, 3H), 1.30—2.13 (m, 5H), 3.00—3.33 (t, 2H), 3.33—3.77 (m, 1H), and 7.20—8.13 (m, 5H); IR (neat) 3450, 2970, and 1685 cm^{-1}; Found: *m/z* 192.1143. Calcd for $C_{12}H_{16}O_2$: M, 192.1151.

Reaction of 1d with Diethylzinc Using 4: The reaction of **1d** (0.174 g, 0.99 mmol) under the same reaction conditions using Et_2Zn instead of diisopropylzinc (Table 1, Entry 3) for 56 h afforded 0.125 g of isopropyl phenyl ketone in 85% yield.

We thank Tomoiki Hayasaka for his contribution during the early stage of this research, and Tri Chemical Laboratory Inc. for a generous gift of dimethylzinc.

References

1) a) Y. Yamamoto and J. Yamada, *J. Am. Chem. Soc.*, **109**, 4395 (1987); b) K. Maruoka, Y. Araki, and H. Yamamoto, *Tetrahedron Lett.*, **29**, 3101 (1988); c) T. Kauffmann, E. Antfang, B. Ennen, and N. Klas, *ibid.*, **23**, 2301 (1982); T. Kauffmann, C. Pahde, and D. Wingbermuhle, *ibid.*, **26**, 4059 (1985); T. Kauffmann, C. Pahde, A. Tannert, and D. Wingbermuhle, *ibid.*, **26**, 4063 (1985); d) M. T. Reetz, J. Westermann, R. Steinbach, B. Weneroth, R. Peter, R. Ostarek, and S. Maus, *Chem. Ber.*, **118**, 1421 (1985). For the allylation, e) with allylchromium, Y. Okude, S. Hirano, T. Hiyama, and H. Nozaki, *J. Am. Chem. Soc.*, **99**, 3179 (1977); f) with allylbismuth, M. Wada, H. Ohki, and K. Akiba, *Tetrahedron Lett.*, **27**, 4771 (1986).

2) B. Marx, E. Henry-Basch, and P. Freon, *C. R. Acad. Sci., Ser. C*, **264**, 527 (1967).

3) T. Sato, K. Soai, K. Suzuki, and T. Mukaiyama, *Chem. Lett.*, **1978**, 601; T. Mukaiyama, K. Soai, T. Sato, H. Shimizu, and K. Suzuki, *J. Am. Chem. Soc.*, **101**, 1455 (1979).

4) S. V. Lieberman and R. Connor, *Org. Synth.*, Coll. Vol. II, 441 (1966).

5) For the enantioselective alkylation of aldehydes using dilithium salt of chiral piperazine, see K. Soai, S. Niwa, Y. Yamada, and H. Inoue, *Tetrahedron Lett.*, **28**, 4841 (1987).

6) T. Sato, T. Kawara, K. Sakata, and T. Fujisawa, *Bull. Chem. Soc. Jpn.*, **54**, 505 (1981).

7) T. Inukai and R. Yoshizawa, *J. Org. Chem.*, **32**, 404 (1967).

8) L. R. Noller, *Org. Synth.*, Coll. Vol. II, 184 (1966).

The Thermodynamics of Chemical Reactions at High Pressures

Sefton Davidson HAMANN
Division of Chemicals and Polymers, Commonwealth Scientific and Industrial Research Organization, G. P. O. Box 4331, Melbourne, Victoria 3001, Australia
(Received March 24, 1988)

Synopsis. A "thermodynamic" derivation by Jee of a simple proportionality between the effects of pressure on the enthalpy change ΔH and the entropy change ΔS for a chemical reaction in solution, is shown to be erroneous.

In a recent paper,[1] J.-G. Jee has presented a derivation "from the basic thermodynamic equation(s)," of a simple proportional relationship between the influence of pressure on the molar change of enthalpy ΔH for a chemical reaction and its corresponding influence on the molar change of entropy ΔS.

Jee[1] began by applying one of the Maxwell relations to derive the formula

$$(\partial H/\partial p)_T=(T-1/\alpha)(\partial S/\partial p)_T, \quad (1)$$

where p denotes the pressure and T the absolute temperature. This is a standard thermodynamic relation [it is given, for example, by combining Guggenheim's[2] formulae (1.47.4) and (1.48.4)], linking the pressure derivatives of the total enthalpy H and the total entropy S of a closed homogeneous phase in the absence of a chemical reaction: α denotes the coefficient of thermal expansion of the phase,

$$\alpha=(\partial V/\partial T)_p/V, \quad (2)$$

where V is the total volume of the phase.

Jee[1] then assumed that a relation similar to Eq. 1 applies to a chemical equilibrium, with H and S being replaced by ΔH and ΔS, denoting changes of enthalpy and entropy accompanying the reaction. On that basis, and assuming α to be independent of p, he integrated Eq. 1 to obtain his relation (Eq. 12):

$$\Delta H^p-\Delta H^\circ=(T-1/\alpha)(\Delta S^p-\Delta S^\circ), \quad (3)$$

where the superscripts ^{p} and $^\circ$ indicate values at a high pressure and at atmospheric pressure, respectively. He took that formula to mean that there is a "theoretical" linear relationship between $\Delta H^p-\Delta H^\circ$ and $\Delta S^p-\Delta S^\circ$.

If Jee's relation were correct, it might be useful. However, it is not correct.

In dealing with a chemically reacting system we need to consider, not the total quantities H, S, and V for the mixture, but the behavior of the corresponding *partial molar* quantities for the reacting species and for the products. If, for a particular species J, we write these as H_J, S_J, and V_J, then a relation analogous to Eq. 1 holds between the partial molar functions of J in the form

$$(\partial H_J/\partial p)_T=(T-1/\alpha_J)(\partial S_J/\partial p)_T, \quad (4)$$

where α_J is defined[3] as

$$\alpha_J=(\partial V_J/\partial T)_p/V_J. \quad (5)$$

Taking the simple case of a chemical reaction equilibrium,

$$A \rightleftarrows B, \quad (6)$$

between two species A and B in a homogeneous mixture, we have

$$\Delta H=H_B-H_A \quad (7)$$

and

$$\Delta S=S_B-S_A, \quad (8)$$

where ΔH is the difference between the partial molar enthalpy (or standard partial molar enthalpy) of the product and that of the initial species; ΔS is the corresponding difference of entropy.

Combining Eqs. 4, 7, and 8, we obtain

$$(\partial\Delta H/\partial p)_T= (T-1/\alpha_B)(\partial\Delta S/\partial p)_T+(1/\alpha_A-1/\alpha_B)(\partial S_A/\partial p)_T, \quad (9)$$

and if we make an additional (usually unjustified) assumption that α_A and α_B are independent of p, we can integrate Eq. 9 to obtain

$$\Delta H^p-\Delta H^\circ= (T-1/\alpha_B)(\Delta S^p-\Delta S^\circ)+(1/\alpha_A-1/\alpha_B)(S_A^p-S_A^\circ). \quad (10)$$

More complex relations apply if more than two species take part in the reaction.

Unlike the supposed relation (Eq. 3), the correct formula (Eq. 10) does *not* represent a simple proportionality between $\Delta H^p-\Delta H^\circ$ and $\Delta S^p-\Delta S^\circ$. It would do so only if additional conditions were met—namely, either (a) that $\alpha_B=\alpha_A$, which is improbable (particularly so for ionic reactions), or (b) that S_A and S_B have the same functional dependence upon p. These are both *extra*-thermodynamic conditions, and the second resembles El'yanov's[5] assumption of a "linear free energy relation" for the effects of pressure on equilibrium constants, which enabled him to derive an expression similar to Eq. 3

Criticisms analogous to the above apply also to Jee's[1] supposed enthalpy/volume and entropy/volume relations.

Finally, when we come to examine Jee's[1] experimental evidence for linear correlations between ΔH and ΔS, we encounter a difficulty, because it is impossible to reconcile the values of ΔH, ΔS, and ΔV that he has listed in his Table 2 and plotted in Fig. 1, with the experimental values of the equilibrium constants K that he has reported in Table 1. For instance, his listed values of ΔV have both the wrong sign and the wrong magnitude [his formula (Eq. 9) for ΔV is, in any case, incorrect[6] when applied to values of K having volume concentration units ($dm^3\,mol^{-1}$)]. Also, the equilibrium constants yield values of ΔH and ΔS that show large and random scatter, with no indication whatever of the smooth trends suggested in Jee's Table 2.

Admittedly, they give good linear plots of ΔH versus ΔS, with slopes near the experimental temperature, ca. 300 K; but that is precisely the behavior that would arise from random errors in the experimental temperature dependences of the K.

References

1) J.-G. Jee, *Bull. Chem. Soc. Jpn.*, **60**, 4483 (1987).
2) E. A. Guggenheim, "Thermodynamics," North Holland, Amsterdam (1967), p. 39.
3) The derivative α_J, defined in this way, should not be confused with the 'partial molar expansivity' of J, which is conventionally defined[4] as $(\partial V_J/\partial T)_p$.
4) H. S. Harned and B. B. Owen, "The Physical Chemistry of Electrolyte Solutions," Reinhold, New York (1963), p. 370.
5) B. S. El'yanov, *Aust. J. Chem.*, **28**, 933 (1975); B. S. El'yanov and E. M. Vasylvitskaya, *Rev. Phys. Chem. Jpn.*, **50**, 169 (1980).
6) S. D. Hamann and W. J. le Noble, *J. Chem. Educ.*, **61**, 658 (1984).

A Mechanistic Study of a Gas-Phase Ion/Molecule Reaction between $CH_2NH_2^+$ and CH_4

Satoshi OKADA,* Yasuo ABE, Setsuo TANIGUCHI, Shinichi YAMABE,† and Tsutomu MINATO††
Radiation Center of Osaka Prefecture, Shinke-cho, Sakai 593
†Educational Technology Center, Nara University of Education, Takabatake-cho, Nara 630
††Institute for Natural Science, Nara University, 1500 Misasagi-cho, Nara 631
(Received October 31, 1988)

A gas-phase ion/molecule reaction starting from (CH_4^+ and N_2O)/(CH_4 and N_2O^+) is studied using a pulsed-discharge high-pressure mass spectrometer and the ab initio MO calculation. Two dominant ions, $C_2H_6N^+$ and $C_3H_8N^+$, are recognized; they are formed by the methylation of CH_4N^+. The $C_2H_6N^+$ is formed via the following two reactions:

$$CH_2NH_2^+ \text{ (or } CH_3NH^+) + CH_4 \longrightarrow (CH_3)_2NH_2^+ \quad (5)$$

$$(CH_3)_2NH_2^+ \longrightarrow CH_3NHCH_2^+ + H_2 \quad (7)$$

The methylation is composed of the heterolytic CH_3^+-H^- addition to the C=N bond of CH_4N^+ and the subsequent H_2 elimination. The growth of the ion by the methylation is largely exothermic, while the H_2 elimination has a large energy barrier on the potential energy surface.

Methane is an inert molecule and does not react in condensed media. However, in the gas phase, some unique reactions[1-3] are observed. Field[1a] and Ausloos[1c] have investigated the ionic reactions, the photolysis, and the radiolysis of CH_4. In those reports, secondary and higher-order reactions of CH_4 with the reactive species (ions, radicals, etc.) generated by these processes have been found. Moreover, Hiraoka[1f] has reported a slow ion/molecule reaction of $C_2H_5^+$ with CH_4. In CH_4/N_2O, Ryan[2] and McAllister[3] have reported the minor formation of CH_4N^+ at a low pressure. In spite of these gas-phase studies, however, the ion structure of CH_4N^+ and the reaction mechanism for the formation of this ion have not yet been made clear.

In this work, a gas-phase ion/molecule reactions in CH_4/N_2O is studied using pulsed-discharge high-pressure mass spectrometry. The time profiles of ions formed at high pressures are extensively analyzed, and these ion species are identified by using, as a labelled compound, CD_4 instead of CH_4. The purpose of this work is to clarify experimentally and theoretically why such simple and small cations as CH_4^+ and N_2O^+ may give larger cationic products in the ion/molecule reaction of (CH_4^+ and N_2O)/(CH_4 and N_2O^+).

Experimental

Apparatus and Reagents. The measurements were done with a pulsed-discharge high-pressure mass spectrometer. The primary ionization of reactant gases in an ion source of chemical ionization[4] and an atmospheric-pressure-ionization mass spectrometer[5] was performed with a Townsend-discharge ion source. In our experiment, the temperature of the ion source is easily controllable in the absence of such filaments as rhenium and tungsten. Then, in the pulsed-discharge ion source, a usual electron trap of a commercially available mass spectrometer was replaced with a discharge electrode.

Figure 1 shows schematic diagrams of the discharge-ion source and pulse circuit. The pulse-timing sequence generated by this circuit and the pulse-counting diagram are shown in the figure. The discharge ion source consists of a tip with a height of 0.1 mm on the flat surface of a stainless steel (3.5 mmϕ×1.6 mm) as the cathode and an 85% transmission gold-clad tungsten screen as the anode, while the potential is that of the ionization chamber. The distance between the cathode and anode was fixed at about 3 mm. The distance from the center of the discharge point to the ion-exit slits was 9 mm; the ion-exit slits, 2×0.01 mm, were made of two stainless steel razor blades. The potential of the

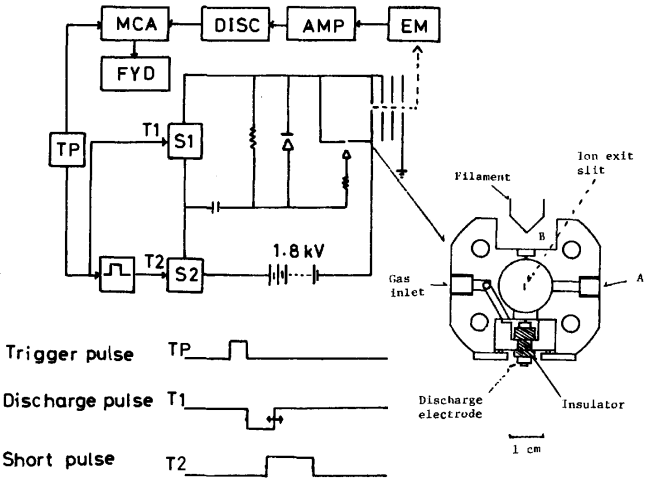

Fig. 1. Schematic diagrams of the discharge ion source and pulse circuit. The pulse timing sequence generated by this pulse circuit and pulse counting diagram are shown. EM: secondary electron multiplier; AMP: amplifier; DISC: discriminator; MCA: multichannel analyzer; FYD: floppy disk drive; TP: trigger pulse; T_1,T_2: discharge and short pulses; S_1,S_2: switching circuits.

first lens with ion-exit slits to prevent field penetration induced by the electric field of the focusing lens was identical with that of the ionization chamber. The pulsed discharge was carried out by two switching circuits (S_1, S_2) using the electric charge and discharge in the capacitor. Since the discharge pulse T_1 tailed for several hundred μs after discharge, the positive pulse T_2 was applied to the discharge electrode to exclude this tailing. In this way, the pulse width of T_1 was decreased to about 30 μs. The discharge-pulse width and the amplitude of T_1 were monitored indirectly with an oscilloscope. Under typical operating conditions, the discharge pulse width, amplitude, and repetition frequency of T_1 were 30 μs, 1.44 kV, and 200 Hz respectively.

The pressures of CH_4 and N_2O in two 10-dm^3 reservoirs were measured with an MKS Baratron model 221 A capacitance manometer. The CH_4/N_2O mixture thus obtained was introduced into the ion source through a Granville-Phillips model-203 manually variable leak. The sample pressure in the ion source was measured with an MKS manometer connected to the gas-inlet line to the ion source. This pressure was corrected with another MKS manometer connected directly to the hole A in Fig. 1 by means of a separate measurement. The correction factor was 0.923. The ion source was heated using an electron-emitting rhenium filament; the maximum temperature obtained was about 453 K. During the present experiments, the holes, A and B, were closed.

In Fig. 1, the time-resolved mass-selected ions formed in the ion source have been accumulated in a multichannel analyzer (Nuclear Data ND 100). Then, the data obtained were transferred to a floppy disk (FYD) and were analyzed with a computer.

The ion-source pressure was in the range from 226.6 to 306.6 Pa, and the flow rate of sample gas was about 0.4 $cm^3\,s^{-1}$. The gases used were methane (Takachiho research grade; 99.95% CH_4), dinitrogen monoxide (Showa Denko, Ltd.; 99.995% N_2O), and methane-d_4 (Merck Sharp and Dohme; 99.5 atom% D). The dinitrogen monoxide was purified by vacuum distillation several times through P_2O_5 chilled with liquid N_2. A trace amount of CO_2 in N_2O was decreased by the use of an Ascarite II trap (20—30 mesh) from Author H. Thomas Co. However, the experimental results obtained were not seriously affected by the Ascarite II. The contents of water and $\geqq C_2$ hydrocarbons in the methane were suppressed by passing the methane through liquid N_2 or Dry Ice-acetone cooled Molecular Sieves. The purities of the methane and dinitrogen monoxide were checked gas-chromatographically using a Pora PLOT Q column of 0.32 mmϕ×10 m at 100 °C. The contents of the $\geqq C_2$ hydrocarbons contained in those samples were less than 1 ppm.

In spite of the general complexity of electrical discharges, the Townsend discharge source[4a] afforded mass spectra that were essentially identical to those obtained with the conventional filament-operated chemical ionization sources. The mass spectra obtained with the Townsend-discharge source have contained only a low abundance of several polymeric reactant ions of a higher mass (m/z>41).

In this study, since the DC discharge was pulsed, it is possible to generate a low current of electricity. Therefore, it seems that the pulsed-discharge ion source suppresses the complexities of the discharge;[6] in fact, the reproducibility of experiments (after six months) could be confirmed.

In the present experiments, the measured total ion current decreased rapidly with a decrease in the temperature of the ion source and the content of CH_4 in the CH_4/N_2O mixture. Headley et al.[7] have reported similar phenomena when oxygen containing molecules such as NO, CO, CO_2, N_2O, and dioxane were used as the reactant gases. Therefore, the experimental conditions are controlled so that the temperature and ratio of the $[CH_4]/[N_2O]$ mixture were kept above 398 K and $\geqq$0.8 respectively. In the text and the **Appendix**,

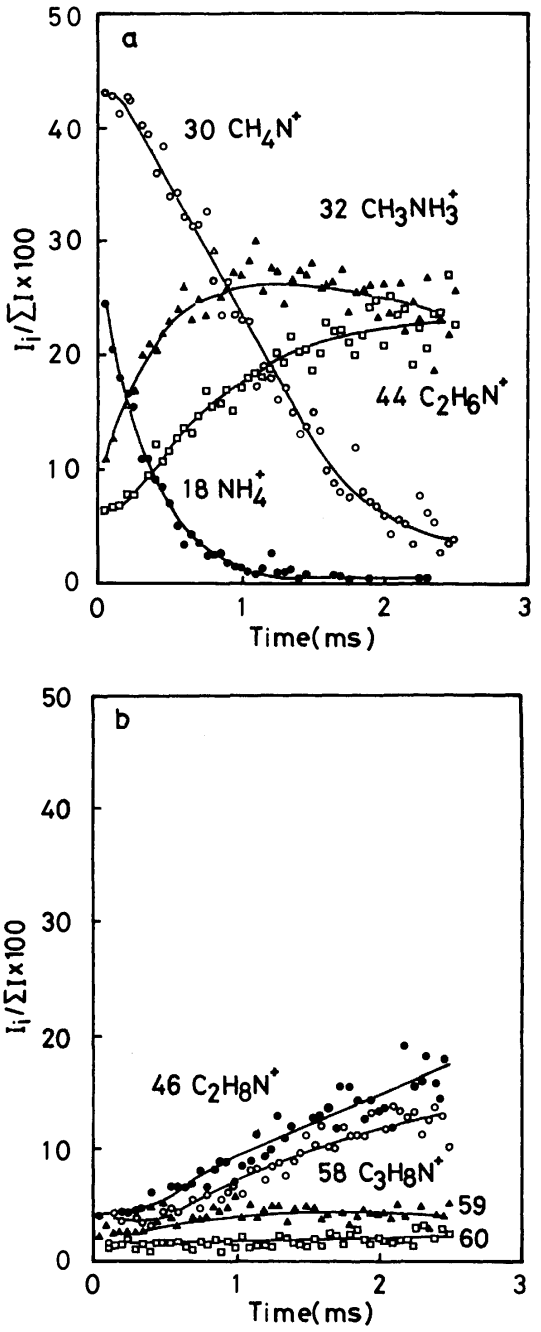

Fig. 2. Normalized ion intensities vs. reaction time observed in CH_4/N_2O mixture at $[CH_4]/[N_2O]$=1.2, T=404 K, P=275.9 Pa. In the figure, mass numbers (m/z) and possible ions are indicated. a is for ions with $m/z\leqq 44$ and b is for $m/z\geqq 46$, respectively.

Reactions (1), (2),···(7) are the major ones, while (A), (B),···(H) are side reactions.

Calculations. The ab initio MO calculation was made using the GAUSSIAN 82 program.[8] The 3-21G basis set was used for the geometry optimization. To obtain accurate energies, the single-point calculation on the 3-21G geometry was made with the third-order Møller-Plesset perturbation of the 6-31+G* basis set (MP3/6-31+G*//RHF(or UHF)/3-21G). For the transition state (**TS**) of the H_2 elimination, the vibrational analysis was performed.

Results and Discussion

Experimental. In Figs. 2 and 3, the time profiles of the relative ion intensities of the major ions observed are exhibited. In Fig. 3, CD_4 was used instead of CH_4. The decay curves in Fig. 2 (Fig. 3) are found for *m/z* 18; NH_4^+(ND_4^+(*m/z* 22)), and *m/z* 30; CH_4N^+(CD_4N^+ (*m/z* 34)). The growth curves are observed for *m/z* 32; $CH_3NH_3^+$($CD_3ND_3^+$(*m/z* 38)), *m/z* 44; $C_2H_6N^+$($C_2D_6N^+$ (*m/z* 50)), *m/z* 46; $C_2H_8N^+$ ($C_2D_8N^+$(*m/z* 54)), *m/z* 58; $C_3H_8N^+$, *m/z* 59 and 60. The reaction mechanism of *m/z* 44 and 46 and the results for the minor ions are given in the **Appendix**.

The major cations except the NH_4^+ and the *m/z* 59 ion are found to appear in three groups; (i), (ii), and (iii):

(i) *m/z* 30 CH_4N^+ and *m/z* 32 $CH_3NH_3^+$
(ii) *m/z* 44 $C_2H_6N^+$ and *m/z* 46 $C_2H_8N^+$
(iii) *m/z* 58 $C_3H_8N^+$ and *m/z* 60 $C_3H_{10}N^+$

In each group, the difference in the mass number is 2

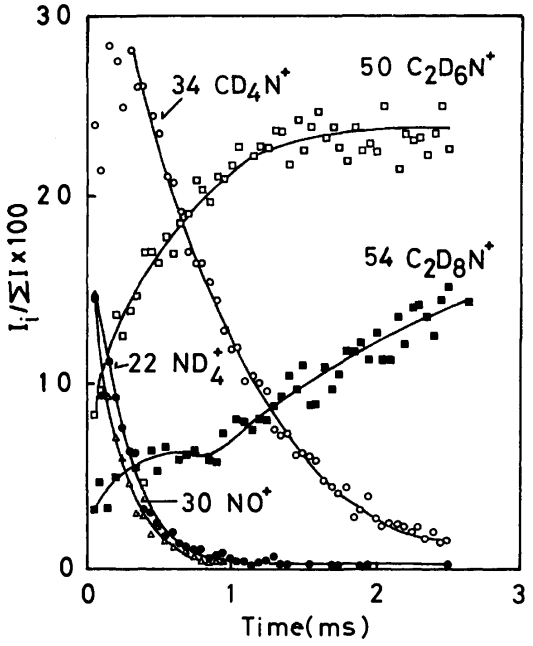

Fig. 3. Normalized ion intensities vs. reaction time observed in CD_4/N_2O mixture at $[CD_4]/[N_2O]$=0.84, *T*=403 K, *P*=295.9 Pa. In the figure, mass numbers (*m/z*) and possible ions are indicated.

(a hydrogen molecule). The growth of the ion size [(i)→(ii)→(iii)] appears to be by the methylation. The decay curve of *m/z* 30, CH_4N^+, indicates that the ion is the precursor for the methylation.

(i) It has been reported[2,3] that the CH_4N^+ was generated from CH_4^+ (*m/z* 16) and N_2O^+ (*m/z* 44) by Reactions (A) and (B). Although the ion intensity for CH_4N^+ has been reported to be very weak under a low pressure (1.3×10^{-1}—1.3×10^{-2} Pa),[3] the large intensity of CH_4N^+ in the present experiments may be due to the large collisional frequency in Reactions (A) and (B), forming intermediate complexes at high pressures (several hundred Pa):

$$CH_4^+ + N_2O \longrightarrow CH_4N^+ + NO \quad (A)$$

$$N_2O^+ + CH_4 \longrightarrow CH_4N^+ + NO \quad (B)$$

As the ion species of *m/z* 60, the association complex$(CH_4\cdot N_2O)^+$ or an intermediate **1** caused by

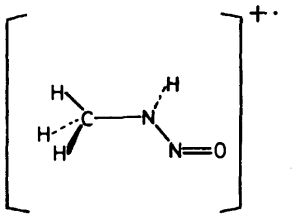

1

the insertion of N_2O into methane is likely. However, the $CD_4\cdot N_2O^+$(*m/z* 64) could not be found under our experimental conditions. Thus, the *m/z* 60 ion assigned to $C_3H_{10}N^+$ in Group (iii), to be described below. Two isomers, $CH_2NH_2^+$ (the methaniminium cation) and CH_3NH^+ (the methylimidogenium cation), appear as the CH_4N^+ (*m/z* 30).[1d,9a] The $CH_2NH_2^+$ is more stable than the CH_3NH^+ (the energy difference in the heat of formation between these ions is 121.2 or 138 kJ mol^{-1}).[10] Moreover, it has been reported[1d] that the first electronically excited state of the $CH_2NH_2^+$ is 2 eV above its ground state. The ionic species of CH_4N^+ forming $C_2H_6N^+$ and $C_2H_8N^+$ by the ion/molecule reactions with CH_4 must be the CH_3NH^+ or the electronically excited state of the $CH_2NH_2^+$.[1d]

The overall disappearance-rate constant of CH_4N^+ for CH_4 was estimated to be ca. 1×10^{-14} cm^3/molecule·s at a temperature of 391—403 K, and concentration of $[CH_4]$, from 5.60 to 13.6×10^{16} molecule/cm^3. A similar slow reaction rate constant has been found[10] in the ion/molecule reaction of $C_2H_5^+$ with CH_4 to form *s*-$C_3H_7^+$ and H_2 (*k*=ca. 10^{-14} cm^3/molecule·s at 300 K).

The $CH_3NH_3^+$ may be formed by the reaction between NH_4^+ and CH_4, but the ion is not related to the subsequent methylation. This process will be discussed as Reaction (F) in the **Appendix**.

(ii) Several isomers have been reported[9b,c,11] for

the $C_2H_6N^+$ (m/z 44) and $C_2H_8N^+$ (m/z 46). These ions were generated by the ion/molecule reaction of CH_4N^+ with CH_4. The $C_2H_6N^+$ (m/z 44) may be the $CH_3CHNH_2^+$ (ΔH_f=656.8 kJ mol^{-1})[9b] or $CH_3NHCH_2^+$ (ΔH_f=694.5 kJ mol^{-1}).[9b] As the $C_2H_8N^+$ (m/z 46) ion, the $CH_3CH_2NH_3^+$ (ΔH_f=574.8 kJ mol^{-1})[12,13] or $CH_3NH_2CH_3^+$ (ΔH_f=588.6 kJ mol^{-1})[14] is likely from the enthalpy change in the reactions.

The isomerization from $CH_3CHNH_2^+$ to $CH_3NHCH_2^+$ and that from $CH_3CH_2NH_3^+$ to $CH_3NH_2CH_3^+$ have

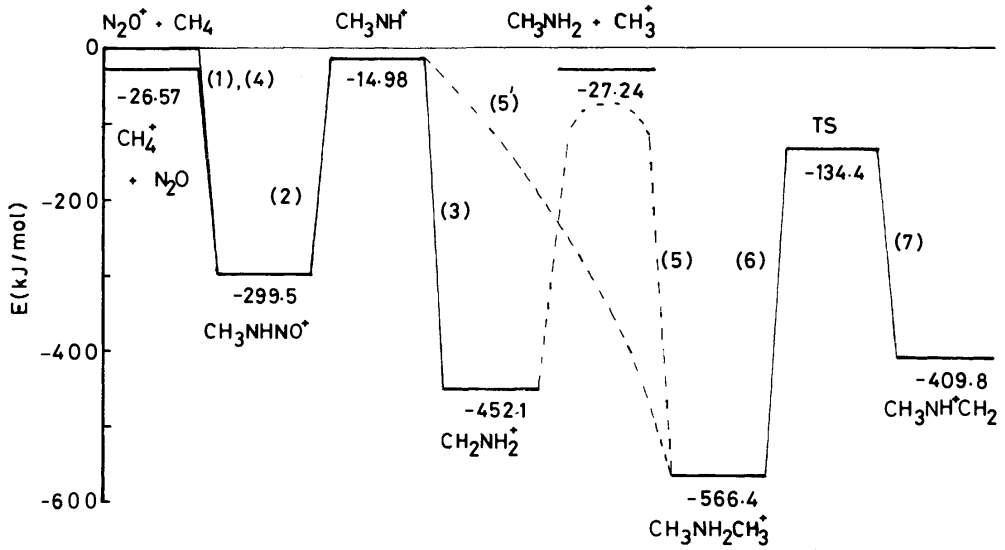

Fig. 4. The energetics of $C_2H_8N_2O^+$ evaluated with the MP3/6-31+G*//HF/3-21G method. The numbers (1)—(7) are defined in charts 1 and 2. The stabilizing energies in kJ mol^{-1} relative to the total energy of (N_2O^++CH_4+CH_4) are shown.

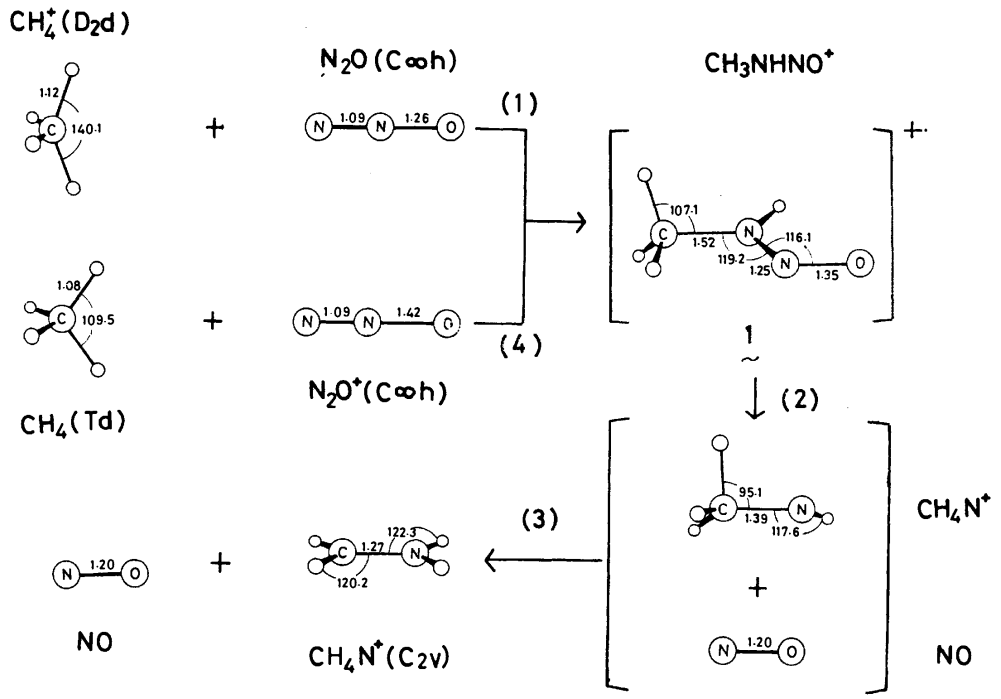

Fig. 5. 3-21G optimized geometries of neutral and cation species involved in reactions (1), (2), (3), and (4). The lengths are in Å and angles in degrees, respectively. The empty circles denote hydrogen atoms.

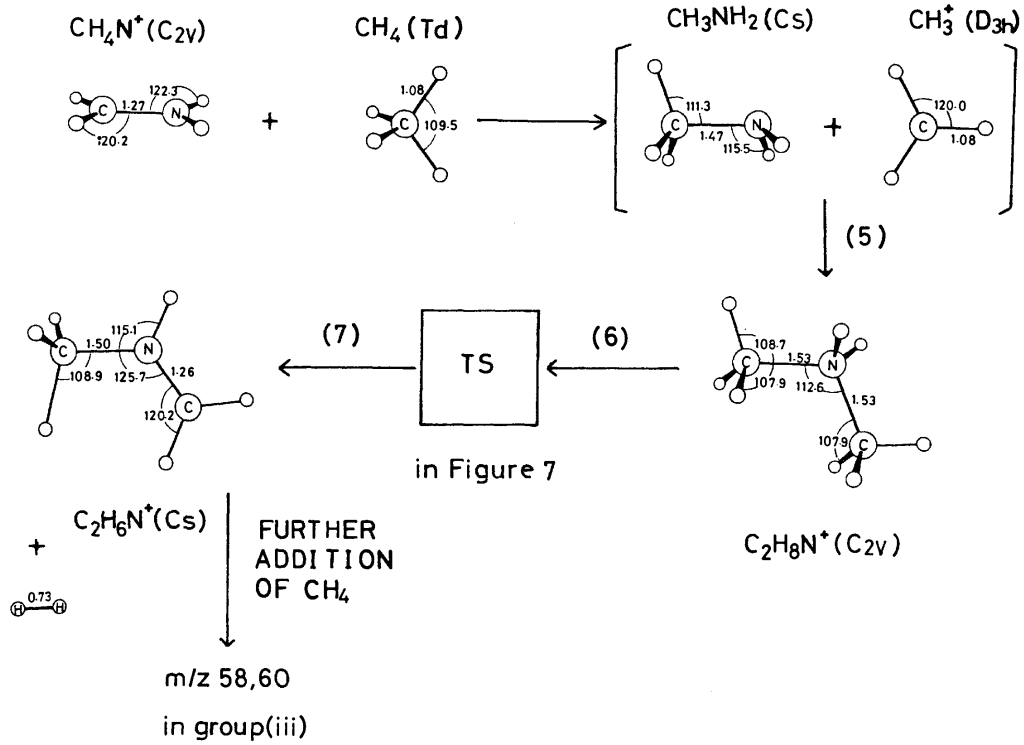

Fig. 6. 3-21G optimized geometries of neutral and cation species involved in reactions (5), (6), and (7).

very high barriers, estimated to be ΔH=ca. 401[11] and >418 kJ mol^{-1}.[15] These isomers, therefore, have been shown to be non-interconvertible under the usual mass-spectrometric conditions.

In the present experiment, the detected ions, *m/z* 30, 44, and 46, may be identified according to Bowers's result.[15] The *m/z* 30 ion is $CH_2NH_2^+$, the *m/z* 46 ion is $CH_3NH_2CH_3^+$ (and partly $CH_3CH_2NH_3^+$), and the *m/z* 44 ion is $CH_3NHCH_2^+$. The detailed discussion of this assignment will be given at the beginning of the **Appendix**.

(iii) For the $C_3H_8N^+$, several isomers have been reported;[9b] $(CH_3)_2CNH_2^+$ (ΔH_f=589.9 kJ mol^{-1}), $CH_3CHNHCH_3^+$ (ΔH_f=615 kJ mol^{-1}), $CH_3CH_2CHNH_2^+$ (ΔH_f=635.9 kJ mol^{-1}), $CH_3CH_2NHCH_2^+$ (ΔH_f=652.7 kJ mol^{-1}), and $(CH_3)_2NCH_2^+$ (ΔH_f=661 kJ mol^{-1}). Among these ions, the most stable isomer is $(CH_3)_2CNH_2^+$. However, the ion species formed by the ion/molecule reaction of $C_2H_6N^+$ with CH_4 is not clear experimentally. The formation and subsequent reactions of these ions must, therefore, be examined theoretically.

Computational. Of the three groups, the ions of (ii) and (iii) seem to be formed by a similar reaction pattern. Since the molecular size of Group (iii) is large, we will restrict ourselves to the cations in Groups (i) and (ii) for the computational analysis.

In Fig. 4, the energy diagram of Charts 1 and 2 is shown. In Figs. 5—7, the geometries of the reactants

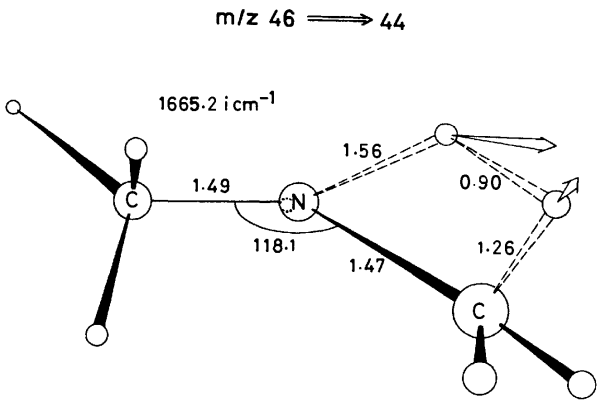

Fig. 7. The transition-state (TS) structure of H_2 elimination in reactions (6) and (7). The reaction coordinate vector corresponding to the sole imaginary frequency 1665.2i cm^{-1} is sketched. Note that a hydrogen atom ((shown by a broken circle)) stays behind the nitrogen atom.

and intermediates are displayed. In Fig. 4, the system of (CH_4^++N_2O) is only 26.56 kJ mol^{-1} more stable than that of (CH_4+N_2O^+). This small energetic difference suggests that both systems are precursors of further reactions. The potential energies vary considerably alnog with the reaction process, which suggests that all the intermediate species are quite "hot" molecules. For instance, the energy level of the transition state of the H_2 elimination is lower than that of the precursor

Chart 1. Possible Reactions (1)—(4) to Generate the CH_4N^+ Species

Reactions	ΔH_r/kJ mol^{-1} Exptl[a]	Calcd[b]
$CH_4^+ + N_2O \xrightarrow{(1)} [1] \xrightarrow{(2)} CH_3\text{-}NH^+ + NO \xrightarrow{(3)} CH_2NH_2^+ + NO$ (m/z 16 → m/z 30)	−397.1 (−413.8)	−425.5
$N_2O^+ + CH_4 \xrightarrow{(4)} [1] \xrightarrow{(2)} CH_3\text{-}NH^+ + NO \xrightarrow{(3)} CH_2NH_2^+ + NO$ (m/z 44 → m/z 30)	−420.2 (−436.9)	−454.8

a) $\Delta H_f(CH_4^+)$=1150 kJ mol^{-1} from Ref. 13a. $\Delta H_f^{298}(CH_2NH_2^+)$=744.7 kJ mol^{-1} from Ref. 9b. $\Delta H_f(N_2O^+)$=1330 kJ mol^{-1} from Ref. 13a. $\Delta H_f^{298}(N_2O)$=82.04 kJ mol^{-1}, $\Delta H_f^{298}(NO)$=90.24 kJ mol^{-1}, and $\Delta H_f^{298}(CH_4)$=−74.80 kJ mol^{-1} from Ref. 13a. The values in parenthesis were estimated using $\Delta H_f^{298}(CH_2NH_2^+)$=728 kJ mol^{-1} from Ref. 9a. b) Computed with the MP3/6-31+G* method.

$CH_4^+ + N_2O$. The sufficient kinetic and vibrational energies accumulated may make the reactions in Charts 1 and 2 likely. In Fig. 4, the energy level of CH_3NH_2 plus CH_3^+ is shown. The level is regarded as the upper boundary of the barrier energy of the hydride-ion shift and the methyl-cation migration. The cooperative mechanism will lower the barrier energy to make Reaction (5) a facile process.

The $(CH_4 \cdot N_2O)^+$ species (m/z 60) **1**, which is ruled out by the experiment using a deuterium compound, is calculated to be stable by 284.5 kJ mol^{-1} relative to CH_3-NH^+ plus NO. Under the present condition (404 K), however, the lifetime of **1** would be too short to be observed in Fig. 2. This is because the hot molecule **1** has enough energy accumulated by insertion to decompose into $CH_4N^+ + NO$.

In Chart 1, four reactions-(1), (2), (3), and (4)- are displayed. Two isomers[1d,9a,d] of CH_4N^+ are considered. One is CH_3-NH^+, while the other is CH_2=NH_2^+. Although a carbene-type form is obtained for CH_3-NH^+, the stability is sensitive to the method of computation.[16] Indeed, the ethylidene CH_3-CH, which is isoelectronic with CH_3-NH^+, has been reported by Pople et al. to be absent.[17] Therefore, CH_3-NH^+ is only a transient species, and CH_2=NH_2^+ (isoelectronic with ethylene) is the sole stable species. In Chart 1, the CH_3NH^+ is shown to be first formed by the insertion of N_2O^+/N_2O into a C-H bond of CH_4/CH_4^+ via **1**. The insertion can be explained by an orbital interaction like the insertion of CH_2 or NH into a C-H bond.[18] For instance, the interaction (in the figure of the frontier orbitals) is effective in the insertion. The charge-transfer (**CT**) interaction from the **HOMO** of the C-H bond to the **SOMO** of N_2O^+ is the driving force of the reaction. In the case of Reaction (1) in Chart 1, the **CT** from the **HOMO** of N_2O to the **SOMO** of CH_4^+ is the driving force. This CH_3-NH^+ isomerizes to CH_2=NH_2^+.

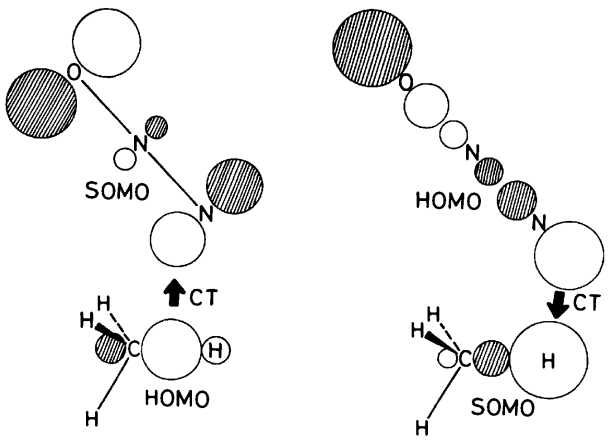

Under the present high pressure (P=275.9 Pa), the transient ion may collide with neutral molecules, H_2 and CH_4, prior to its arrival at CH_2=NH_2^+. If CH_3-NH^+ reacts with H_2, $CH_3NH_3^+$ (m/z 32) in Group (i) may be formed. If CH_3-NH^+ reacts with methane in Chart 2, the protonated dimethylamine (m/z 46) in Group (ii) is produced. The transition-state search for this route was attempted, but we failed to arrive at the energy maximum. Thus, Route (5)′ seems not to include an energy barrier. The reaction of CH_2=NH_2^+ with CH_4 in Route (5) to form the protonated dimethylamine is also likely. The CH_2=NH_2^+ stays at the electronically excited state or at a high vibrational state, as is shown by the large exothermicity in Chart 1. The energy-rich species may cause the hydride-ion shift and the subsequent methyl-cation addition.

The isolation of the methyl cation is unlikely, because the lone-pair electrons on the nitrogen atom capture the cation instantly. Once the $(CH_3)_2NH_2^+$ ion is formed, the dehydrogenation shown in Chart 2 is expected to give m/z 44 in Group (ii). From the protonated dimethylamine, the *N*-methylmethaniminium cation may be produced. The transition state (**TS**)

Chart 2. Addition Reactions to Form $C_2H_6N^+$ and $C_2H_8N^+$ from CH_4N^+

Reactions					ΔH_r/kJ mol^{-1}	
					Exptl[a]	Calcd[b]
m/z 30		*m/z* 46				
$CH_2NH_2^+$	+ CH_4	⟶	$(CH_3)_2NH_2^+$	(5)	−81.3 (−64.6)	−114.2
CH_3–NH^+	+ CH_4	⟶	$(CH_3)_2NH_2^+$	(5)′		
m/z 46						
$(CH_3)_2NH_2^+$		⟶	TS	(6)		
TS		⟶	$CH_3NHCH_2^+$ *m/z* 44	+ H_2 (7)	24.6[c] (41.3)[c]	42.3[c]

a) $\Delta H_f^{298}(CH_2NH_2^+)$=744.7 kJ mol^{-1} from Ref. 9b. $\Delta H_f^{298}(CH_4)$=−74.80 kJ mol^{-1} from Ref. 13a. $\Delta H_f^{298}((CH_3)_2NH_2^+)$=588.6 kJ mol^{-1} from Ref. 14. $\Delta H_f^{298}(CH_3NHCH_2^+)$=694.5 kJ mol^{-1} from Ref. 9b. The values in parenthesis were estimated using $\Delta H_f^{298}(CH_2NH_2^+)$=728 kJ mol^{-1} from Ref. 9a. b) Computed with the MP3/6-31+G* method. c) Experimental and calculated ΔH_r for the formation of $CH_3NHCH_2^+$ is calculated from the reaction, $CH_2NH_2^+ + CH_4 \rightarrow CH_3NHCH_2^+ + H_2$.

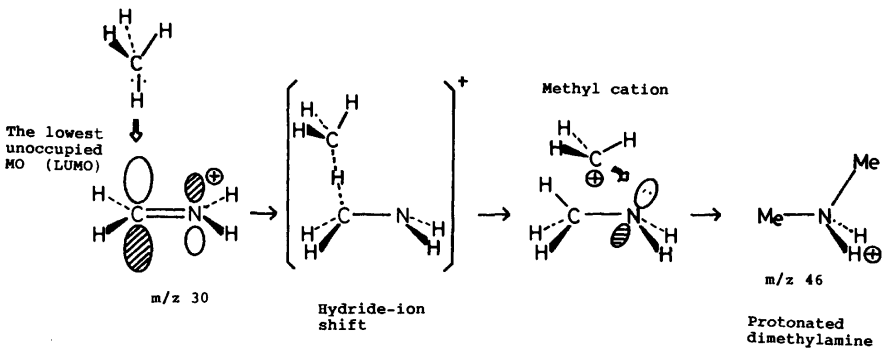

structure of the dehydrogenation is explicitly determined (It is shown in Fig. 7).

In view of the reaction patterns in Chart 2, the formation of Group (iii) may be deduced. To give the *m/z* 60 species, the H_3C–HN^+=CH_2 should be a precursor for two species in Group (iii):

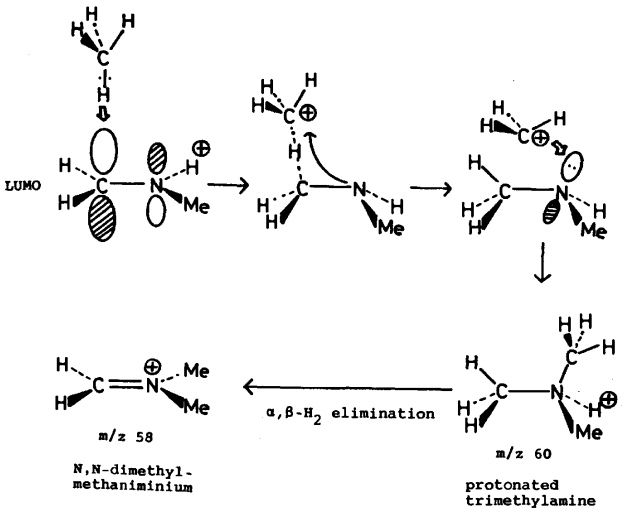

The *m/z* 60 cation is obtained by the methane addition to H_3C–HN^+=CH_2, followed by the H_2 elimination to give *m/z* 58. According to this scheme, the methane addition to CH_2=$N^+(CH_3)_2$ (*m/z* 58) can possibly give CH_3–$N^+(CH_3)_3$ (*m/z* 74), but the formation of *m/z* 72 is unlikely because of the absence of the α,β-H_2 elimination. That is, the *m/z* 74 is the end of the chain reaction of methane addition and H_2 elimination.

Bowers et al.[15] have reported that Reactions (5) and (6) in Chart 2 have the large barriers on the basis of metastable and collision-induced studies of $C_2H_8N^+$. From Fig. 4, the values for these two reactions are estimated to be below 424.9 (−27.24—(−452.2), upper boundary) and 432 (−134.4—(−566.4)) kJ mol^{-1} respectively.

Concluding Remarks

Methane is a rigid, ball-type molecule, and its reaction is improbable in the sense of organic chemistry. However, in the gas phase, specific patterns of chain-type reactions (formally, the methylation) have been observed.[1f,19,20]

The CH_4N^+ ion (*m/z* 30) is the key precursor for the growth of the ion size. The methylation is composed of the heterolytic CH_3^+–H^- addition to the C=N double bond and the subsequent α,β-H_2 elimination. That is, the methane addition is initiated by the hydride ion sharing by two cations. This is followed by the

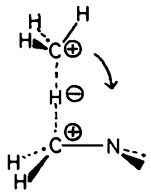

methyl-cation 1, 2 shift toward the nitrogen lone-pair electrons. The H_2 elimination occurs by a combination of the *N*-protonated hydrogen and the methyl hydrogen. The high vibrational state of the C-H stretching will make the elimination a facile process (cf. Fig. 7). The methylation is terminated when a hydrogen atom connected to the nitrogen atom is not available. That is, $N(CH_3)_4^+$ (*m/z* 74) will be the final product, although no species with this large mass number is detected here.

Thus, the growth of the mass number is the substitution process of protonated amines and imines, primary→secondary→tertiary.

As an important result, the activation energy for the H_2 elimination was quantitatively calculated.

Appendix

***m/z* 46 and 44.** The results by collision-induced dissociation[15] have indicated that, for $CH_3CH_2NH_3^+$ (*m/z* 46), only one metastable dissociation reaction (C) was observed and that there is not a significant barrier in the reverse reaction. Also, it has been shown that, for $CH_3NH_2CH_3^+$, the metastable reactions forming $CH_3NHCH_2^+$ (*m/z* 44) and $CH_2NH_2^+$ (*m/z* 30) were observed, while the reverse reactions of Eqs. (D) and (E) have large activation barriers. (The values were not estimated.)

$$\underset{(m/z\ 46)}{CH_3CH_2NH_3^+} \longrightarrow \underset{(m/z\ 18)}{NH_4^+} + C_2H_4 \qquad (C)$$

$$\underset{(m/z\ 46)}{CH_3NH_2CH_3^+} \longrightarrow \underset{(m/z\ 44)}{CH_3NHCH_2^+} + H_2 \qquad (D)$$

$$\underset{(m/z\ 46)}{CH_3NH_2CH_3^+} \longrightarrow \underset{(m/z\ 30)}{CH_2NH_2^+} + CH_4 \qquad (E)$$

In the present experiments, some ions (*m/z* 30, 44, and 46) are detected. Of these, *m/z* 46 and 44 must be formed by the reverse reaction of (E) and the forward reaction (D) respectively, although the details of these reaction mechanism are unknown.

The Minor Ions. *m/z* 18(NH_4^+). The NH_4^+ (*m/z* 18) in Fig. 2 may be yielded by the following two reactions:

i) The proton transfer from the carbonium ions[12] and hydronium ions, etc., to a trace amount of NH_3, whose ions were found by the ion/molecule reactions in CH_4. The NH_3 is contained in the reaction system as an impurity or is generated by the pulsed discharge in the CH_4/N_2O mixture.

ii) The direct routes forming NH_4^+ by means of ion/molecule reactions.

The decrease in the relative ion intensity of NH_4^+ (*m/z* 18) in the range of reaction times of 0—1 ms may be due to Reaction (F), corresponding to the increase in that of $CH_3NH_3^+$ (*m/z* 32):

$$NH_4^+ + CH_4 \xrightarrow{k} CH_3NH_3^+ + H_2 \qquad (F)$$

The overall disappearance-rate constant of $I_{18}/\sum I$, *k* (the nomalized ion intensity of NH_4^+, where I_{18} denotes the ion intensity of *m/z* 18), was determined to be $(3\pm0.5)\times10^{-14}$ cm^3/molecule·s. This slow rate constant may be due to the endothermicity (ΔH_r=55.22 kJ mol^{-1}) of Reaction (F).

***m/z* 30(NO^+) and *m/z* 46(NO_2^+).** Nitrogen monoxide, NO^+ (*m/z* 30), and NO_2^+ (*m/z* 46) ions are present as other ionic species of *m/z* 30 and 46. However, the results in Fig. 3 show that the relative ion intensity of NO^+ (*m/z* 30) decreased until the reaction time of <0.3 ms. The intensity of NO^+ decreases rapidly, which indicates that the ion reacts with some neutral molecules. A check was made to see whether or not these are higher hydrocarbons as impurities derived in the reagents. In the literature,[9-11] *m/z* and the intensities of the products of reactions between NO^+ and hydrocarbons are available. Fortunately, none of the cited ions were found in our experiment. Thus, the contribution of higher hydrocarbons (as well as ethane) to the reaction with NO^+ may be neglected.

The neutral molecule is expected to be methane, thus giving the following two reactions:

$$NO^+(a^3\Sigma^+) + CH_4 \longrightarrow CH_4^+ + NO \qquad (G)$$

$$NO^+ + CH_4 \longrightarrow \underset{N\text{-hydroxymethaniminium ion}}{CH_2{=}NH(OH)^+} \qquad (H)$$

Eq. (G) is a charge transfer-reaction with a large rate constant (k=ca. 1.0×10^{-9} cm^3/molecule·s). Eq. (H) is an insertion with a large exothermicity (ΔH_r=−180.3 kJ mol^{-1} computed with MP3/6-31+G*//RHF/3-21G). Although the result for NO_2^+ (*m/z* 46) is not shown in the figure, the relative ion intensity of NO_2^+ (*m/z* 46) was very weak (<several%) and independent of the reaction time. Therefore, the contribution of NO^+ and NO_2^+ to the decrease in CH_4N^+ (*m/z* 30) and the formation of $C_2H_8N^+$ (*m/z* 46) could be eliminated by the longer reaction time (>0.3 ms).

***m/z* 59.** The ion species of *m/z* 59 seems to be $C_3H_7O^+$ (oxygen-containing ion)[1a] for the following reasons: i) the relative ion intensity of *m/z* 59 increased with the increase in the content of H_2O in the reaction system; ii) in an experiment using CD_4, *m/z* 66 ($C_3D_7O^+$) was detected as the corresponding ion.

Nitrogen-Containing Molecules besides $C_2H_6N^+$ and $C_2H_8N^+$. If trace amounts of the nitrogen-containing molecules—NH_3, CH_3NH_2, C_2H_7N, etc.— are present in the reaction system as impurities or as products of the pulsed discharge, the formation of CH_4N^+ (*m/z* 30),[1d,e,g,25] $CH_3NH_3^+$ (*m/z* 32), and $C_2N_8N^+$ (*m/z* 46)[25-27] may be, in part, due to the contribution of these molecules. Particularly, the growth curve of $C_2D_8N^+$ (*m/z* 54) in Fig. 3 is somewhat complicated. A part of the increase in $C_2D_8N^+$ may be due to the proton transfer to a trace amount of C_2D_7N. However, the reactions for the formation of $C_2H_6N^+$ (*m/z* 44) are unlikely.[25-27] Munson[26] has reported that the rate of hydride transfer is about one-fifth that of proton transfer, judging from the ratio of the increase in the relative ion

intensities of $(CH_3)_2NCH_2^+$ (m/z 58) and $(CH_3)_3NH^+$ (m/z 60) in $(CH_3)_3N$. The ratio of the increase in the relative ion intensity of these ions in Fig. 2 is different from Munson's result. Our data show that the increase in the relative ion intensity of $C_3H_8N^+$ (m/z 58) is larger than that of $C_3H_{10}N^+$ (m/z 60). This suggests that $C_3H_8N^+$ (m/z 58) and $C_3H_{10}N^+$ (m/z 60) in Fig. 2 were formed by the ion/molecule reaction of $C_2H_6N^+$ with CH_4.

The authors wish to thank the Data Processing Center of Kyoto University for the allotment of the CPU time on the FACOM M-380 Computer. Thanks are also due to the Institute for Molecular Science for the use of the HITAC M-680H computer.

References

1) a) F. H. Field, J. L. Franklin, and M. S. B. Munson, *J. Am. Chem. Soc.*, **85**, 3575 (1963). b) F. P. Abramson and J. H. Futrell, *J. Chem. Phys.*, **45**, 1925 (1966). c) R. Gorden, Jr., and P. Ausloos, *J. Chem. Phys.*, **46**, 4823 (1967). d) W. T. Huntress, Jr., and D. D. Elleman, *J. Am. Chem. Soc.*, **92**, 3565 (1970). e) W. T. Huntress, Jr., R. F. Pinzzotto, Jr., and J. B. Landenslager, *J. Am. Chem. Soc.*, **95**, 4107 (1973). f) K. Hiraoka and P. Kebarle, *J. Chem. Phys.*, **63**, 394 (1975). g) G. P. K. Smith, M. Saunders, and R. J. Cross, Jr., *J. Am. Chem. Soc.*, **98**, 1324 (1976).

2) K. R. Ryan and P. W. Harland, *Int. J. Mass Spectrom. Ion Phys.*, **15**, 197 (1974).

3) T. McAllister, *Int. J. Mass Spectrom. Ion Phys.*, **25**, 55 (1977).

4) a) D. F. Hunt, C. N. McEwen, and T. M. Harvey, *Anal. Chem.*, **47**, 1730 (1975). b) D. F. Hunt, G. C. Stafford, Jr., F. W. Crow, and J. W. Russell, *Anal. Chem.*, **48**, 2098 (1976).

5) a) M. M. Shahin, *J. Chem. Phys.*, **45**, 2600 (1965). b) E. C. Horning, M. G. Horning, D. I. Carroll, I. Dzidic, and R. N. Stillwell, *Anal. Chem.*, **45**, 936 (1973). c) H. Kambara and I. Kanomata, *Anal. Chem.*, **49**, 270 (1977). d) I. Dzidic, D. I. Carroll, R. N. Stillwell, and E. C. Horning, *Anal. Chem.*, **48**, 1763 (1976).

6) For example, ethane (C_2H_6), etc., or the nitrogen-containing molecules (NH_3, etc.) would be formed by the discharge.

7) J. V. Headley, R. S. Mason, and K. R. Jennings, *J. Chem. Soc., Faraday Trans. 1*, **78**, 933 (1982).

8) J. S. Binkley, M. J. Frisch, D. J. DeFrees, K. Raghavachari, R. A. Whiteside, H. B. Schlegel, E. M. Fluder, and J. A. Pople, GAUSSIAN 82, Carnegie-Mellon University, Pittsburg, PA 15213 U.S.A.

9) a) J. E. Collin and M. J. Franklin, *Bull. Soc. R. Sci. Liege*, **35**, 267 (1966). b) F. P. Lossing, Y.-T. Lam, and A. Macoll, *Can. J. Chem.*, **59**, 2228 (1981). c) V. Barone, F. Lelj, P. Grande, and N. Russo, *THEOCHEM*, **124**, 319 (1985). d) M. M. Bursey, D. J. Harvan, C. E. Parker, J. A. Darden, and J. R. Hass, *Org. Mass Spectrom.*, **18**, 530 (1983).

10) $\Delta H_f^{298}(CH_2NH_2^+)$=728 and 744.7 kJ mol^{-1} were used from Refs. 9a and 9b. $\Delta H_f^{298}(CH_3NH^+)$=866 kJ mol^{-1} is taken from Ref. 9a.

11) R. D. Bowen, D. H. Williams, and G. Hvistendahr, *J. Am. Chem. Soc.*, **99**, 7509 (1977).

12) $\Delta H_f^{298}(CH_3CH_2NH_3^+)$=574.8 kJ mol^{-1} is calculated by using $\Delta H_f^{298}(CH_3CH_2NH_2)$=−47.15 kJ mol^{-1} from Ref. 13a. $PA(CH_3CH_2NH_2)$=907.9 kJ mol^{-1} and $\Delta H_f^{298}(H^+)$=1530 kJ mol^{-1} are from Ref. 13b.

13) a) *J. Phys. Chem. Ref. Data*, **6**, I-776, I-777 (1977). b) *J. Phys. Chem. Ref. Data*, **13**, 703, 709 (1984).

14) $\Delta H_f^{298}((CH_3)_2NH_2^+)$=588.6 kJ mol^{-1} is calculated by using $\Delta H_f^{298}((CH_3)_2NH)$=−18.45 kJ mol^{-1} from Ref. 13a. $PA((CH_3)_2NH)$=922.9 kJ mol^{-1} and $\Delta H_f^{298}(H^+)$=1530 kJ mol^{-1} are from Ref. 13b.

15) M. F. Jarrold, N. J. Kirchner, S. Liu, and M. T. Bowers, *J. Phys. Chem.*, **90**, 78 (1986).

16) A theoretical calculation of the H_2 elimination, $CH_4N^+ \longrightarrow CH_2N^+ + H_2$, with the 6-31G** basis set has been reported recently: K. F. Donchi, B. A. Rumpf, G. D. Willett, J. R. Christie, and P. J. Derrick, *J. Am. Chem. Soc.*, **110**, 347 (1988). The instability of the CH_3–NH^+ species has been pointed out there.

17) K. Raghavachari, M. J. Frisch, J. A. Pople, and P. von R. Schleyer, *Chem. Phys. Lett.*, **85**, 145 (1982).

18) M. S. Gordon and D. R. Gano, *J. Am. Chem. Soc.*, **106**, 5421 (1984).

19) F. H. Field and M. S. B. Munson, *J. Am. Chem. Soc.*, **87**, 3289 (1965).

20) M. Meot-Ner, *Origins of Life*, **9**, 115 (1978).

21) K. Hiraoka, K. Aoyama, and K. Morise, *Can. J. Chem.*, **63**, 2899 (1985).

22) "Gas-Phase Ion-Molecule Reaction Rate Constants Through 1986," ed by Y. Ikezoe, S. Matsuoka, M. Takebe, and A. Viggiano, Maruzen Press, Tokyo (1987).

23) D. F. Hunt and T. M. Harvey, *Anal. Chem.*, **47**, 2136 (1975).

24) R. Chal and A. G. Harrison, *Anal. Chem.*, **55**, 969 (1983).

25) E. G. Jones and A. G. Harrison, *Can. J. Chem.*, **45**, 3119 (1967).

26) M. S. B. Munson, *J. Phys. Chem.*, **70**, 2034 (1966).

27) J. M. Brupbacher, C. J. Eagle, and E. Tschuikow-Roux, *J. Phys. Chem.*, **79**, 671 (1975).

The Addition Effects of Methyl Halides on Ethane Ignition Behind Reflected Shock Waves

Kazuo TAKAHASHI, Tadaaki INOMATA,* Takao MORIWAKI, and Satiko OKAZAKI
Department of Chemistry, Faculty of Science and Technology, Sophia University,
7-1 Kioi-cho, Chiyoda-ku, Tokyo 102
(Received November 29, 1988)

Ignition delay times were measured in C_2H_6–O_2–CH_3X(X:Cl, Br or I) mixtures highly diluted with argon behind reflected shock waves. The measurements covered a temperature range of 1200—1900 K and the pressure range of 1.4—2.9 atm. The times were longer than those without CH_3X, indicating that CH_3X inhibits ethane ignition. This was contrary to the previous results which showed that CH_3X promoted methane ignition. To clarify the addition effects of CH_3X from the viewpoint of the reaction mechanism, computational analyses were performed in C_2H_6–O_2–CH_3Br and CH_4–O_2–CH_3Br mixtures. The analytical results showed that different chain cycles for Br-containing species were formed in the two mixtures. The opposite effects of CH_3Br on ethane and methane ignitions could be interpreted in terms of these different cycles.

For combustion, the effects of additives are generally divided into two types: chemical and physical effects. With respect to the addition of halogen-containing compounds (RX), the former is predominant.[1]

Most RX's decrease the burning velocity when they are added into a flame.[2] Namely, an RX acts as an inhibitor for flame propagation. Rosser et al.[2] and Westbrook[3] have reported that halogen acid (HX) generated by the decomposition of RX captures H atoms in a flame through the following reaction:

$$HX + H = H_2 + X. \quad (X5)$$

Reaction (X5) is competitive with reaction (R76), which is the most important chain-branching reaction in combustion:

$$H + O_2 = OH + O. \quad (R76)$$

However, the addition effect of RX on ignition is not always similar to that on flame propagation. In previous work,[4–6] we have shown that methyl halides (CH_3X) act as promotors for methane ignition, and discussed the promotion effect on the basis of chemical kinetics.

In this study, in order to examine the addition effect of CH_3X on ethane ignition, the ignition delay times were measured in C_2H_6–O_2–CH_3X mixtures by using a shock tube. Moreover, by means of computational analyses, the chain cycle formed in a C_2H_6–O_2–CH_3Br mixture was compared with that in a CH_4–O_2–CH_3Br mixture.

Experimental

All of the experiments were carried out behind reflected shock waves in a 6.2 cm i.d. stainless steel shock tube. The driver and test sections were 1.7 and 3.8 m long, respectively, so that dwell times above 1.5 ms could be obtained in all of the experiments. Other apparatus for measurements of the shock velocity and ignition delay time and associated procedures have already been reported.[4] Ignition delay times, defined as the time interval between the arrival of a shock wave and the onset of ignition, were obtained by rapid increases in pressure and OH emission ($X^2\Pi_i \leftarrow A^2\Sigma^+$ transition, 306.4 nm).

The compositions of test gas mixtures used are shown in Table 1. The accuracy of the composition of mixtures is better than 0.01%. The measurements were carried out over the temperature range 1200—1900 K and the pressure range 1.4—2.9 atm.

Analytical Treatment

To clarify the addition effects of CH_3X from the viewpoint of the reaction mechanism, ignition delay times were calculated in mixtures 1 (C_2H_6–O_2) and 3 (C_2H_6–O_2–CH_3Br), and sensitivity analyses were carried out. Details concerning the calculation were described previously.[5] The reaction mechanism assembled for ethane oxidation consists of the 93 elementary reactions employed in a previous study on methane oxidation (reactions (R1)—(R93)),[5,6] and 18 reactions added in this study (reactions (R94)—(R111) in Table 2). However, with respect to the rate coefficient of reaction (R38),

Table 1. The Composition of Test Gas Mixture (%)

No.	C_2H_6	O_2	Ar	CH_3Cl	CH_3Br	CH_3I
1	1.00	3.50	95.50	—	—	—
2	1.00	3.50	95.40	0.10	—	—
3	1.00	3.50	95.40	—	0.10	—
4	1.00	3.50	95.40	—	—	0.10

Table 2. Reactions Added in This Study

	Reaction	log A	n	E	Ref.
(R94)	$CH_3+OH=CH_2O+H_2$	12.60	0.00	0.00	7
(R95)	$CH_3+M=CH_2+H+M$	16.29	0.00	91.60	8
(R96)	$CH_3O+H=CH_2O+H_2$	13.30	0.00	0.00	9
(R97)	$C_2H_6+O_2=C_2H_5+HO_2$	13.00	0.00	51.00	10
(R98)	$C_2H_5+O=CH_2O+CH_3$	13.00	0.00	0.00	11
(R99)	$C_2H_5+O=CH_3CHO+H$	13.70	0.00	0.00	12
(R100)	$C_2H_5+CH_3=C_3H_8$	13.93	0.00	6.25	13
(R101)	$C_2H_5+C_2H_5=C_4H_{10}$	12.90	0.00	0.00	12
(R102)	$C_2H_5+C_2H_3=C_4H_8$	12.95	0.00	0.00	13
(R103)	$C_2H_4+C_2H_3=C_4H_6+H$	12.00	0.00	7.30	14
(R104)	$C_2H_3+CH_3=C_3H_6$	13.20	0.00	−4.08	13
(R105)	$C_2H_3+C_2H_3=C_4H_6$	12.95	0.00	0.00	13
(R106)	$C_2H_2+C_2H_2=C_4H_3+H$	13.00	0.00	45.00	15
(R107)	$C_2H_2+C_2H=C_4H_2+H$	13.60	0.00	0.00	15
(R108)	$C_4H_3+M=C_4H_2+H+M$	16.00	0.00	60.00	15
(R109)	$C_4H_2+M=C_4H+H+M$	17.54	0.00	80.00	15
(R110)	$OH+O+M=HO_2+M$	17.00	0.00	0.00	16
(R111)	$H_2O_2+H=H_2O+OH$	14.50	0.00	8.94	17

Rate constants in the form $k=AT^n\exp(-E/RT)$, in cm^3, mol, s, kcal, and K units.

Table 3. Reactions Involving Br-Containing Species

	Reaction	log A	n	E	Ref.
(B1)	$CH_3Br=CH_3+Br$	13.20	0.00	71.70	5
(B2)	$CH_3Br+H=CH_3+HBr$	14.24	0.00	6.90	3
(B3)	$CH_3Br+Br=CH_3+Br_2$	13.70	0.00	22.90	3
(B4)	$Br+CH_4=CH_3+HBr$	14.00	0.00	18.30	3
(B5)	$HBr+H=H_2+Br$	11.88	0.50	1.11	3
(B6)	$Br_2+H=HBr+Br$	12.81	0.50	1.11	3
(B7)	$Br+Br+M=Br_2+M$	16.00	0.00	0.00	3
(B8)	$Br+H+M=HBr+M$	18.00	−0.71	0.00	3
(B9)	$Br+C_2H_6=C_2H_5+HBr$	13.90	0.00	13.40	3

Rate constants in the form $k=AT^n\exp(-E/RT)$, in cm^3, mol, s, kcal, and K units.

$$C_2H_5 (+ M) = C_2H_4 + H (+ M), \qquad (R38)$$

an expression given by Warnatz,[18]

$$k_{(R38)}(\text{1st order})/s^{-1}$$

$$= 2.00 \times 10^{14}\exp(-39.67 \text{ kcal mol}^{-1}/RT),$$

was employed in this study instead of the expression in the previous one:

$$k_{(R38)}(\text{2nd order})/\text{mol}^{-1}\,\text{cm}^3\,\text{s}^{-1}$$

$$= 2.00 \times 10^{15}\exp(-30.00 \text{ kcal mol}^{-1}/RT).^{19}$$

To complete the reaction model in the presence of CH_3Br, 9 reactions (Table 3) involving Br-containing species (CH_3Br, Br, Br_2, and HBr) were added to the reactions for ethane oxidation. For a comparison, the ignition delay times in CH_4–O_2 and CH_4–O_2–CH_3Br mixtures were also calculated using the same reaction model.

The reverse rate constants were computed using the forward rate constants and the appropriate equilibrium constants. Most thermochemical and thermodynamic data were taken from Refs. 20 and 21. The data for eight species (C_2H_3, C_2H_5, C_2H_6, CH_3O, CHCO, CH_2CO, H_2O_2, and CH_3Br) were not available, and so were evaluated by a statistical method.[20] Details concerning the calculation procedure and the validity of results were descrived previously.[5]

Three methods were carried out to define calculated ignition delay times. The first of these is the time at which the OH concentration increases rapidly, and the second is the time at which C_2H_6 concentration decreases rapidly. The third is the time at which the gas temperature rises rapidly. All of these times agreed to within 7%. Finally, the calculated ignition delay times were determined from the temperature profile, since the error in reading was least.

Results and Discussion

The ignition delay time (τ) measured in mixtures 1—4 are shown in Fig. 1. The addition of CH_3X lengthens τ, i.e., CH_3X inhibits ethane ignition. This

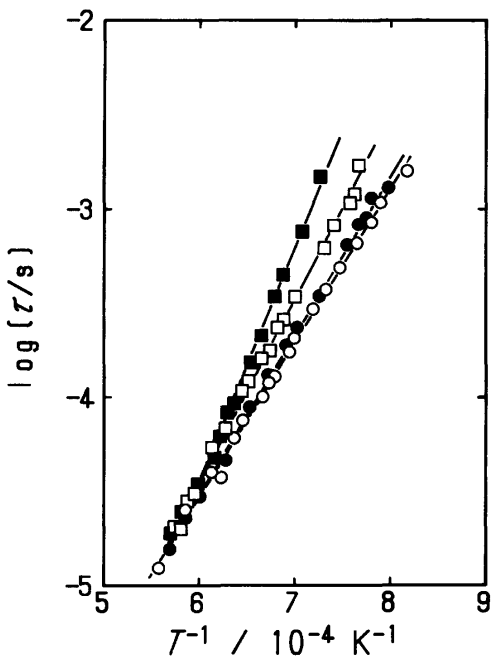

Fig. 1. Measured ignition delay times. O, Mixture 1; ●, Mixture 2; □, Mixture 3; ■, Mixture 4.

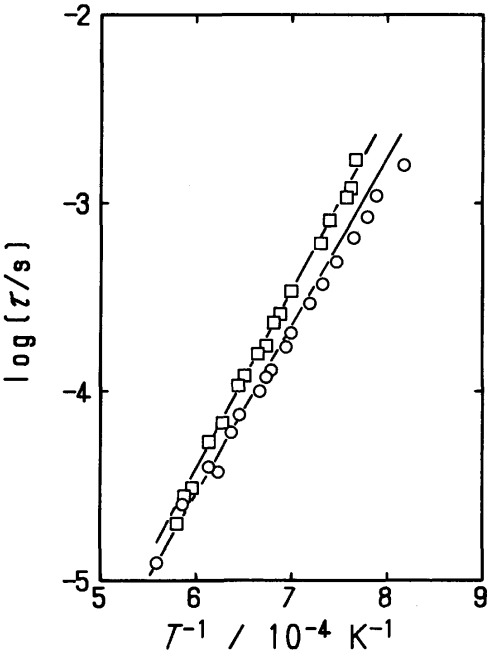

Fig. 2. Comparison between calculated and measured ignition delay times. O, Mixture 1; □, Mixture 3. Straight lines are calculated.

is contrary to the previous results in which CH_3X promoted methane ignition.[5,6] In three CH_3X compounds (CH_3Cl, CH_3Br, and CH_3I), the inhibition effect of CH_3I is the greatest, while that of CH_3Cl is the least. For all mixtures, plots of $\log \tau$ against the reciprocal of the temperature give straight lines. The slope of the line is 0.81 for mixture 1, while the slopes are 0.85, 0.98, and 1.24 for mixtures 2—4, respectively.

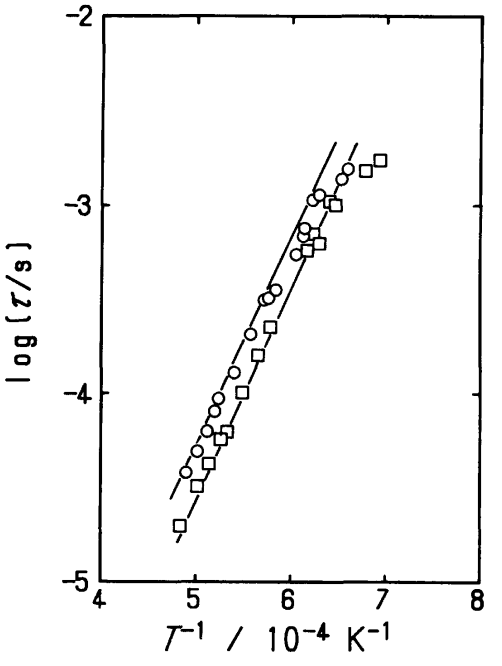

Fig. 3. Comparison between calculated and measured ignition delay times. O, CH_4–O_2 mixture; □, CH_4–O_2–CH_3Br mixture.[5] Straight lines are calculated.

These values indicate that the inhibition effect of CH_3X is remarkable at low temperature.

In Fig. 2, the ignition delay times calculated in mixtures 1 and 3 are compared with the measured ones. Although the temperature dependence of the calculated values in mixture 1 is somewhat large, the calculated ignition delay times are generally in good agreement with the measured values.

Using the same reaction model, the ignition delay times calculated in CH_4–O_2 and CH_4–O_2–CH_3Br mixtures are shown in Fig. 3. Plots in the figure express the measured values which have already been reported.[5] The ignition delay times re-calculated in this study are identical to those found in the previous one, which were calculated by using 93 reactions for methane oxidation and 8 reactions involving Br-containing species.[5] This agreement indicates that the reactions added in this study (Table 2) have no effect for methane ignition.

As is obvious from Figs. 2 and 3, the assembled reaction mechanism can express the experimental results that CH_3Br promotes methane ignition, but inhibits ethane ignition. To clarify the opposite addition effects of CH_3Br on methane and ethane ignitions, sensitivity analyses were performed on 9 reactions involving Br-containing species (Table 3). In a CH_4–O_2–CH_3Br mixture, the ignition delay times calculated by deleting reactions (B1)—(B9), one by one, are shown in Table 4 (1500 K). Similarly, the ignition delay times calculated at 1500 and 1900 K in mixture 3 (C_2H_6–O_2–CH_3Br) are also shown in Table 4.

Table 4. Calculated Ignition Delay Times

Reaction[a]	Ignition delay time/μs		
	CH_4-O_2-CH_3Br	C_2H_6-O_2-CH_3Br	
	1900 K	1500 K	1900 K
None	56.9	161	8.03
(B1) $CH_3Br=CH_3+Br$	119 (+109%)[b]	163 (+1%)	8.35 (+4%)
(B2) $CH_3Br+H=CH_3+HBr$	74.9 (+32%)	107 (−34%)	6.85 (−15%)
(B3) $CH_3Br+Br=CH_3+Br_2$	57.6 (+1%)	161 (0%)	8.09 (+1%)
(B4) $Br+CH_4=CH_3+HBr$	69.5 (+22%)	163 (+2%)	8.01 (0%)
(B5) $HBr+H=H_2+Br$	54.9 (−4%)	139 (−14%)	7.76 (−3%)
(B6) $Br_2+H=HBr+Br$	56.7 (0%)	160 (0%)	8.01 (0%)
(B7) $Br+Br+M=Br_2+M$	56.7 (0%)	160 (0%)	8.09 (+1%)
(B8) $Br+H+M=HBr+M$	57.2 (+1%)	161 (0%)	8.09 (+1%)
(B9) $Br+C_2H_6=C_2H_5+HBr$	57.7 (+1%)	166 (+3%)	8.15 (+1%)

Calculated ignition dely time is 110 μs at 1900 K in CH_4-O_2 mixture; it is 105 μs at 1500 K and 6.69 μs at 1900 K in C_2H_6-O_2 mixture. a) Reaction which is deleted from the complete mechanism. b) Percentage of change to ignition delay time calculated by using complete mechanism.

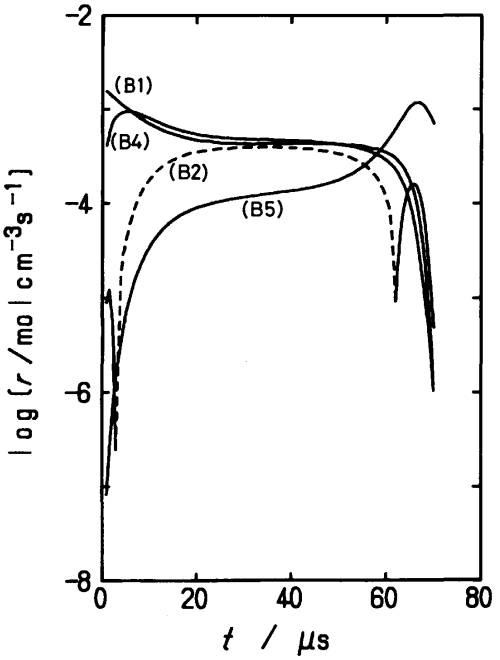

Fig. 4. Net reaction rates of (B1), (B2), (B4), and (B5) at 1900 K in CH_4-O_2 mixture. Calculated ignition delay time is 56.9 μs. t means time after the arrival of reflected shock wave. Solid line: net reaction proceeds in forward direction, dashed line: in reverse direction.

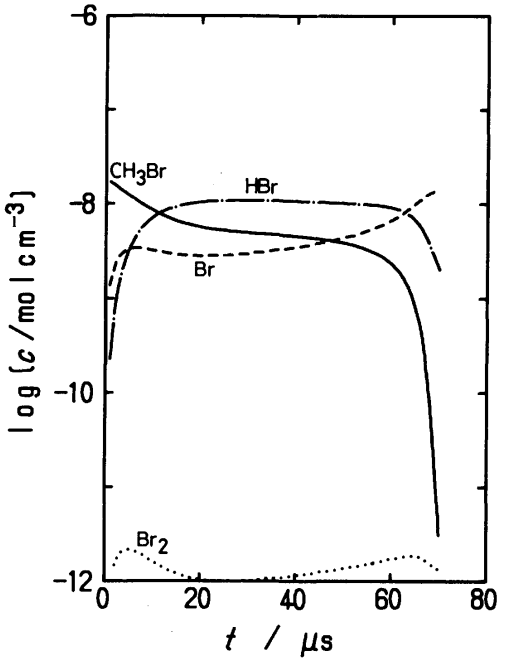

Fig. 5. Calculated concentration profiles of CH_3Br, Br, Br_2, and HBr at 1900 K in CH_4-O_2 mixture.

In a CH_4-O_2-CH_3Br mixture, reactions (B1), (B2), and (B4) greatly influence the ignition delay time (Table 4). When each of these reactions is deleted from the complete mechanism, the ignition delay time is longer than that in the complete mechanism, showing that reactions (B1), (B2), and (B4) promote methane ignition. Moreover, considering the reaction rates (Fig. 4) and the concentrations of Br-containing species (Fig. 5), we arrived at the same conclusion as in a previous study.[5] The following cycle is formed among CH_3Br, Br, and HBr:

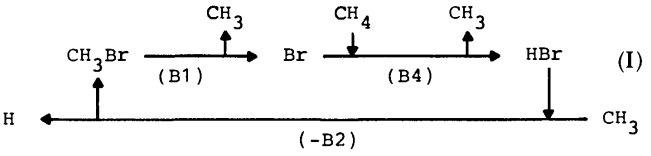

The net reaction of cycle (I) corresponds to the production of one H atom and one CH_3 radical from methane in each chain, and so methane ignition is promoted.

In mixture 3 (C_2H_6-O_2-CH_3Br), the inhibition effect of CH_3Br is remarkable at low temperature, as has been mentioned. From the calculated results at low

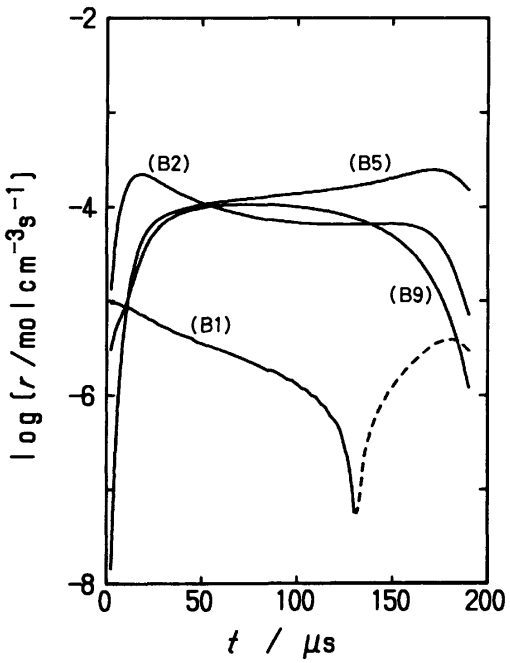

Fig. 6. Net reaction rates of (B1), (B2), (B5), and (B9) at 1500 K in Mixture 3 (C_2H_6-O_2). Calculated ignition delay time is 161 μs.

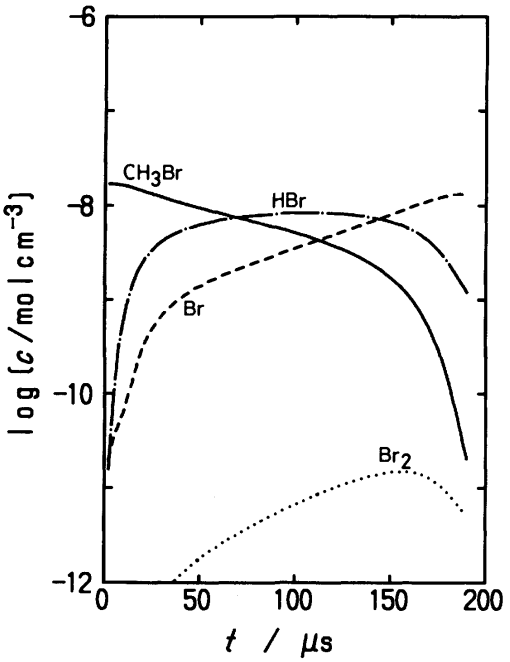

Fig. 7. Calculated concentration profiles of CH_3Br, Br, Br_2, and HBr at 1500 K in Mixture 3 (C_2H_6-O_2).

temperature (1500 K), as shown in Table 4, it is obvious that reactions (B2) and (B5) greatly influence the ignition delay time. Both reactions (B2) and (B5) inhibit ethane ignition, because deletion of these reactions makes the ignition delay time shorter. As shown in Fig. 6, the main reaction of CH_3Br consumption at low temperature is not (B1) but, rather, (B2). Reaction (B2) shows a inhibition effect, because the H atom which is the reactant of the most important chain-branching reaction (R76) controlling ignition is simultaneously consumed. Since the product HBr also mainly reacts with the H atom through reaction (B5), ethane ignition is more inhibited. The bromine atoms consume ethane through reaction (B9), and HBr is regenerated. Reaction (B9), itself, seems to show a promotion effect, because ethane is oxidized through reaction (B9). However, as HBr reproduced through reaction (B9) is the reactant of the inhibition reaction (B5), the promotion effect of reaction (B9) is compensated, as shown in Table 4. This consideration suggests that the following cycle is formed at low temperature in a C_2H_6-O_2-CH_3Br mixture:

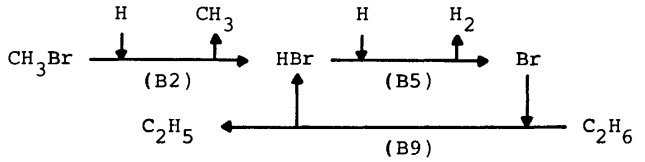

(II)

The difference between the chain cycle formed in the CH_4-O_2-CH_3Br mixture (I) and that in the C_2H_6-O_2-CH_3Br mixture (II) can also be confirmed in the concentration profiles (Figs. 5 and 7). A bromine atom appears earlier than HBr in the CH_4-O_2-CH_3Br mixture, while HBr appears earlier than Br in the C_2H_6-O_2-CH_3Br mixture.

At high temperature, where the inhibition effect of CH_3Br falls, the other channel of CH_3Br consumption, reaction (B1), is open in the C_2H_6-O_2-CH_3Br mixture. As is obvious in Table 4, the inhibition effects due to reactions (B2) and (B5) decrease at high temperature (1900 K). Instead, reaction (B1) shows a slight promotion effect. These reaction rate profiles at 1900 K are shown in Fig. 8. The rate ratio of reaction (B1) to (B2) at the half time of the induction period, $[r(B1)/r(B2)]_{\tau/2}$, is 0.027 at 1500 K, but 0.25 at 1900 K. The increase in the relative rate of reaction (B1) to (B2) is caused by a difference in activation energy between these reactions. Therefore, the cycle formed at high temperature in the C_2H_6-O_2-CH_3Br mixture is expressed as follows.

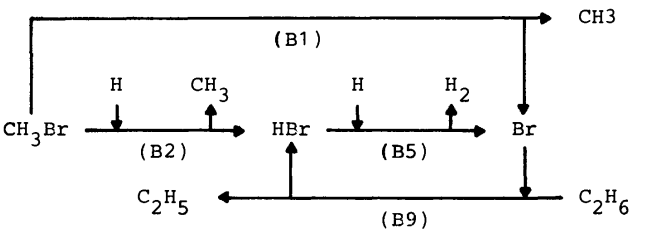

(III)

Reaction (B1), which is competitive with reaction (B2) for CH_3Br consumption, shows a promotion

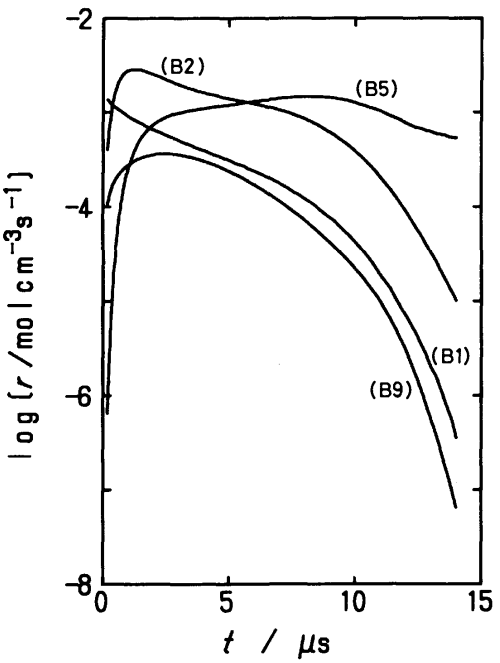

Fig. 8. Net reaction rates of (B1), (B2), (B5), and (B9) at 1900 K in Mixture 3 (C_2H_6-O_2). Calculated ignition delay time is 8.03 μs.

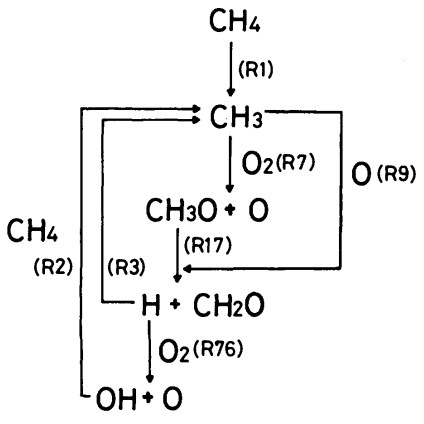

$CH_4 + M = CH_3 + H + M$ (R1)
$CH_3 + O_2 = CH_3O + O$ (R7)
$CH_3O + M = CH_2O + H + M$ (R17)
$CH_3 + O = CH_2O + H$ (R9)
$H + O_2 = OH + O$ (R76)
$CH_4 + OH = CH_3 + H_2O$ (R2)
$CH_4 + H = CH_3 + H_2$ (R3)

Fig. 9. Main process for CH_4 consumption at the early stage of induction period in CH_4-O_2 mixture (1750 K).

effect rather than an inhibition type, as shown in Table 4. The CH_3 radical produced through reaction (B1) accelerates ethane consumption through the path (Fig. 10). Moreover, the relative rates of reactions (B2) and (B5) to the chain-branching reaction (R76) are reduced with temperature, because of the difference in the activation energy between these reactions. The ratios, $[r(B2)/r(R76)]_{\tau/2}$ and $[r(B5)/r(R76)]_{\tau/2}$, are 0.20 and 0.34 at 1500 K, while they are 0.14 and 0.093 at

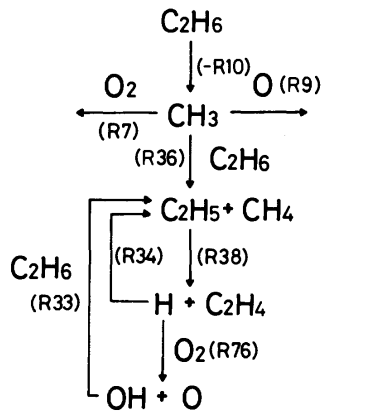

$C_2H_6 = CH_3 + CH_3$ (-R10)
$CH_3 + O_2 = CH_3O + O$ (R7)
$CH_3 + O = CH_2O + H$ (R9)
$C_2H_6 + CH_3 = C_2H_5 + CH_4$ (R36)
$C_2H_5 = C_2H_4 + H$ (R38)
$H + O_2 = OH + O$ (R76)
$C_2H_6 + OH = C_2H_5 + H_2O$ (R33)
$C_2H_6 + H = C_2H_5 + H_2$ (R34)

Fig. 10. Main process for C_2H_6 consumption at the early stage of induction period in Mixture 1 (C_2H_6-O_2, 1750 K).

1900 K. Therefore, it is concluded that competitive reactions (B1) and (R76) with inhibition reactions (B2) and (B5) lower the inhibition effect at high temperature.

In order to consider why the cycle for Br-containing species in the C_2H_6-O_2-CH_3Br mixture differs from that in the CH_4-O_2-CH_3Br mixture, the reaction rates in two CH_3Br-free mixtures were calculated at 1750 K. The main processes for methane and ethane consumption in the early stage of the induction period are summarized in Figs. 9 and 10. The initiation reaction is reaction (R1) for methane oxidation, while it is reaction (−R10) for ethane oxidation. Although both reactions involve a thermal decomposition of fuels, the initial rate of reaction (−R10) is about 2000-times (1750 K) as fast as that of reaction (R1), because of the difference in the dissociation energy. Then, chain cycles, such as shown in Figs. 9 and 10, are formed while consuming methane or ethane.

In these cycles the difference between the consuming rate of CH_3 and that of C_2H_5 is very important. The C_2H_5 radical is mainly consumed through thermal decomposition (R38), while the CH_3 radical is consumed by being reacted with O_2 (R7) or O atoms (R9). The rate coefficient of reaction (R7) is very small. Although the rate coefficient of reaction (R9) is sufficiently large, its reaction rate is not fast, since few O atoms of the reactant exist during the early stage. The rate ratios of reactions (R7) and (R9) in the CH_4-O_2 mxture to reaction (R38) in the C_2H_6-O_2 mixture at 10% of the time of induction period, $[r(R7)_{Me}/r(R38)_{Et}]_{\tau/10}$ and $[r(R9)_{Me}/r(R38)_{Et}]_{\tau/10}$, are 7.5×10^{-4} and 2.6×10^{-4} at 1750 K, respectively. Therefore, the consuming rate of the CH_3 radical is

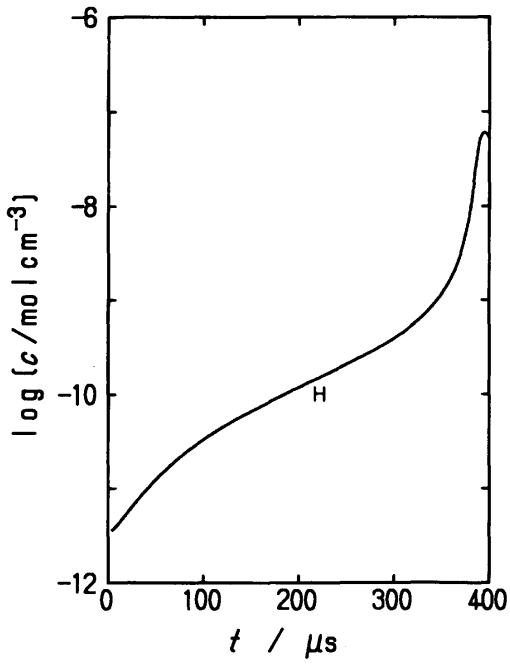

Fig. 11. Calculated concentration profile of H at 1750 K in CH_4–O_2 mixture. Calculated ignition delay time is 360 μs.

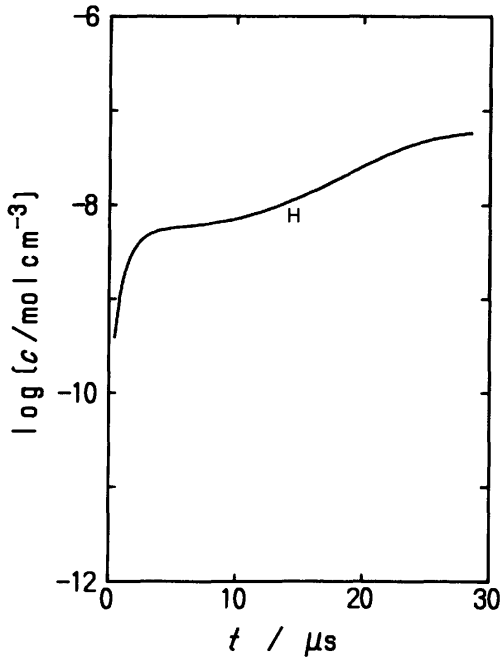

Fig. 12. Calculated concentration profile of H at 1750 K in Mixture 1 (C_2H_6–O_2). Calculated ignition delay time is 16.4 μs.

slower than that of the C_2H_5 radical. This causes a low H concentration during the induction period, as can be seen from a comparison between Figs. 11 and 12. The ratio of the H concentration in the CH_4–O_2 mxture to that in the C_2H_6–O_2 mixture at one half of the induction period, $[[H]_{Me}/[H]_{Et}]_{\tau/2}$, is 0.015 at 1750 K.

From this consideration, we can interpret the opposite effects of CH_3Br on ethane and methane ignitions. With respect to ethane oxidation, since the H concentration is higher during the induction period, reactions (B2) and (B5) are predominant instead of reactions (B1) and (−B2), resulting in an inhibition effect.

The ignition delay times in mixtures 2(C_2H_6–O_2–CH_3Cl) and 4(C_2H_6–O_2–CH_3I) were also calculated using reactions involving Cl- or I-containing species. When the reaction mechanism and the rate coefficients which we had previously used for methane ignition[5,6] were employed, the calculated ignition delay times disagreed with the observed values in both mixtures 2 and 4. The calculation overestimates the ignition delay times in mixture 2, but underestimates them in mixture 4. These disagreements indicate that the assumed reaction mechanism and/or the rate coefficients are impertinent. Thus, more research needs to be carried out in the future.

References

1) K. Akita, *J. Inst. Safty High Pressure Gas Eng.*, **15**, 151 (1978).
2) W. A. Rosser, H. Wise, and J. Miller, "Seventh Symposium (International) on Combustion," The Combustion Institute, Pittsburgh (1958), p. 175.
3) C. K. Westbrook, "Nineteenth Symposium (International) on Combustion," The Combustion Institute, Pittsburgh (1982), p. 127.
4) T. Inomata, T. Moriwaki, and S. Okazaki, *Combust. Flame*, **62**, 183 (1985).
5) K. Takahashi, T. Inomata, T. Moriwaki, and S. Okazaki, *Bull. Chem. Soc. Jpn.*, **61**, 3307 (1988).
6) K. Takahashi, T. Inomata, T. Moriwaki, and S. Okazaki, *Bull. Chem. Soc. Jpn.*, in press.
7) C. P. Fenimore, "Twelfth Symposium (International) on Combustion," The Combustion Institute, Pittsburgh (1969), p. 463.
8) P. Roth, U. Barner, and R. Lohr, *Ber. Bunsenges. Phys. Chem.*, **83**, 929 (1979).
9) K. Hoyermann, N. S. Loftfield, R. Sievert, and H. Gg. Wagner, "Eighteenth Symposium (International) on Combustion," The Combustion Institute, Pittsburgh (1981), p. 831.
10) J. E. Taylor and D. M. Kulich, *Int. J. Chem. Kinet.*, **5**, 455 (1973).
11) K. Hoyermann and R. Sievert, "Seventeenth Symposium (International) on Combustion," The Combustion Institute, Pittsburgh (1979), p. 517.
12) J. Warnatz, "Eighteenth Symposium (International) on Combustion," The Combustion Institute, Pittsburgh (1981), p. 369.
13) C. K. Westbrook and F. L. Dryer, *Prog. Energy Combust. Sci.*, **10**, 1 (1984).
14) S. W. Benson G. R. Haugen, *J. Phys. Chem.*, **71**, 1735 (1967).
15) T. Tanzawa and W. C. Gardiner, Jr., "Seventeenth Symposium (International) on Combustion," The Combustion Institute, Pittsburgh (1979), p. 563.
16) G. S. Bahn, *Pyrodynamics*, **2**, 315 (1965).

17) D. L. Baulch, D. D. Drysdale, and A. C. Lloyd, "High Temperature Reaction Rate Data," Report No. 3, Leeds University, Leeds (1969).
18) Warnats, *Combust. Sci. Tech.*, **34**, 177 (1983).
19) D. B. Olson, T. Tanzawa, and W. C. Gardiner, Jr., *Int. J. Chem. Kinet.*, **11**, 23 (1979).
20) "JANAF Thermochemical Tables," 2nd ed, NSRDS-NBS 37, ed by D. R. Stull and H. Prophet, National Bureau of Standards, Washington D. C., 1971; and later supplements.
21) G. S. Bohn, NASA-CR-2178, NASA, 1973.

 © 1989 The Chemical Society of Japan Bull. Chem. Soc. Jpn., 62, 2146—2151 (1989)

Dynamics of Exciplex Formation in Cholesteric Liquid Crystals Containing Carbazolyl and Terephthaloyl Group

Koji KAWAGUCHI, Masahiko SISIDO,*,†,†† Yukio IMANISHI, Masashi KIGUCHI,††† and Yoshio TANIGUCHI†††

Department of Polymer Chemistry, Kyoto University, Kyoto 606
†Research Center for Medical Polymers and Biomaterials, Kyoto University, Kyoto 606
†††Advanced Research Laboratory, Hitachi Ltd., Kokubunji, Tokyo 185

(Received February 2, 1989)

Dynamics of exciplex formation was studied on cholesteric liquid crystals consisting of cholesteryl 3-(9-ethyl-3-carbazolyl)propanoate (3Cz-2), cholesteryl 5-phenylpentanoate (Ph-4), and cholesteryl methyl terephthalate (CMT) with different amounts of CMT. Transient fluorescence spectrum and the analysis of fluorescence rise and decay curves of the exciplex emission indicated that two types of exciplex are present at low temperatures. Rate constants of exciplex formation were obtained at different temperatures in the cholesteric and isotropic phases. The activation energy for the rate constant was nearly zero in the cholesteric phase, but it was positive (3—6 kcal mol^{-1}) in the isotropic phase. The difference was interpreted in terms of different mechanisms of exciplex formation in the two phases.

Photophysical processes, such as excimer formation and exciplex formation in liquid crystalline mesophases have been studied.[1-8] A primary goal of these studies is to clarify the effect of liquid crystalline order on the photophysical processes, which should depend on the interchromophore distances and orientations. In our previous reports, syntheses of cholesteryl ω-arylalkanoates carrying 1- and 2-naphthyl, 1-pyrenyl, 9-anthryl, and 3- and 9-carbazolyl groups were described.[1-5] The orientations of the aromatic groups in cholesteric liquid crystalline (CLC) phases were determined by circular dichroic (CD) spectroscopy in the ground state and by circularly polarized fluorescence (CPF) spectroscopy in the excited state.[2] Studies on the dynamics of excimer formation of CLC mixtures containing cholesteryl 3-(1-pyrenyl)propanoate (Py-2)[5] revealed that the activation energy of the rate constant for excimer formation was slightly higher in the isotropic phase than in the CLC phase. The activation energy for the excimer dissociation was found to be considerably higher in the isotropic phase than in the CLC mesophase. These data were interpreted in terms of a reduced entropy of the ground state by the cholesteric order and efficient energy migrations before the excimer formation. Weiss and co-workers[7] reported an excimer formation between free pyrene molecules dispersed in a cholesteric mixture. They observed a higher activation energy for the excimer formation in the CLC phase than in the isotropic phase and explained the difference in terms of a higher viscosity of the cholesteric phase. They also observed a higher activation energy in the CLC phase on the exciplex formation in other cholesteric mixtures. The different behaviors of our systems and the Weiss's systems may be ascribed to the differences in the order of chromophore arrangement and their mobility in the CLC phases. In Py-2, the pyrenyl groups are covalently linked to the cholesteryl group and their orientation is highly ordered in the CLC phase. Also their translational diffusion may be highly restricted. Therefore the energy migration process may become more important than the diffusion in CLC phase of our system, for which less activation energy will be needed. One of the purpose of this study is to examine the activation energy for exciplex formation in the CLC mixture and in the isotropic phase containing chromophores covalently linked to cholesteryl groups.

In the present work, a cholesteryl ester carrying covalently linked carbazolyl group, i.e., cholesteryl 3-(9-ethyl-3-carbazolyl)propanoate (3Cz-2, **1**) was used as electron donor and cholesteryl methyl terephthalate (CMT, **2**) was used as an acceptor. Other cholesteryl ω-arylalkanoates carrying phenyl and naphthyl group (Ph-2, **3**; Ph-4, **4**) were used as liquid-crystalline solvents.

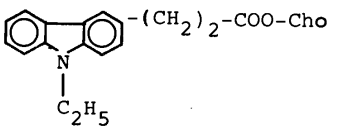

(1)

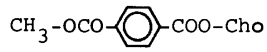

(2)

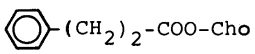

(3)

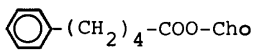

(4)

A static structure of the exciplex between cholesteryl 3-(9-carbazolyl)propanoate (9Cz-2) and CMT has been studied.[4] Fluorescence spectra showed a presence of a high-energy exciplex in the CLC phase at low temperatures. Thus, it was shown that the orientational constraints by the CLC order can alter the configuration of the exciplex. However, the high-energy exciplex was not detected in the 3Cz-2/CMT system in the stationary-state fluorescence spectrum.

†† Present address: Research Laboratory of Resources Utilization, Tokyo Institute of Technology, 4259 Nagatsuta, Midori-ku, Yokohama 227.

The second purpose of this study is to reexamine the exciplex spectra of 3Cz-2/CMT system by using the time-resolved spectroscopy.

Experimental

Preparation of the cholesteryl ω-arylalkanoates has been described.[3] The mixture was placed in an optical cell specially designed to measure surface fluorescence of the liquid crystalline sample under vacuum.[3] Before the fluorescence measurements, the liquid crystalline mixture was mechanically tilted to align the helix axis of the cholesteric texture perpendicular to the cell surface. The perpendicular alignment was confirmed by the appearance of a bright color (blue to red) of the selective reflection.

Fluorescence rise and decay curves were measured on a home-built time-correlated single-photon counting machine, using an air-discharge lamp (half width is about 2.5 ns) as an excitation source. For the measurement of fast processes, a single-photon counting instrument using a picosecond laser pulse was used. The excitation beam was a frequency-doubled laser pulse (314 nm, 13 picosecond, 4 nJ) generated from a synchronously pumped, cavity-dumped dye laser (Spectra Physics 375B dye and Spectra Physics 3000 1W mode-locked YAG lasers). An XP 2020/Q photomultiplier tube was used as a detector. The system was controlled and the data was processed with a PDP-11 minicomputer. The time-resolved fluorescence spectra were obtained by adjusting the time-to-amplitude converter to collect only stop pulses which appeared after a specified time period.

Results and Discussion

Stationary and Transient Spectra. The stationary and the transient fluorescence spectra were measured on a CLC and isotropic mixture of 3Cz-2/Ph-2/CMT (molar ratio: 18/73/9). The mixture of 3Cz-2/Ph-2 (20/80) in the absence of CMT showed little excimer emission in the stationary spectrum, although a weak excimer emission has been observed in a 3Cz-2/Ph-2 (50/50) mixture.[3] Figure 1 compares stationary and transient spectra of the CLC mixture of 3Cz-2/Ph-2/CMT (18/73/9). The transient spectra were measured using a 13 picosecond excitation pulse. The transient spectrum 0.5—1.5 ns after the excitation shows only monomer emission of carbazolyl group. The spectrum around 350 nm is distorted by a self-absorption of carbazolyl groups. The absence of exciplex emission at the early stage indicates the absence of any preformed exciplex site in the CLC mixture. The spectrum 13—18 ns after the excitation shows an exciplex emission centered at 450 nm. (An effect of the selective reflection of the CLC appears as a small trough at 480 nm.) The spectrum profile of the transient exciplex emission is sharper than that of the stationary spectrum and the transient peak locates at shorter wavelength than the stationary one by about 20 nm.

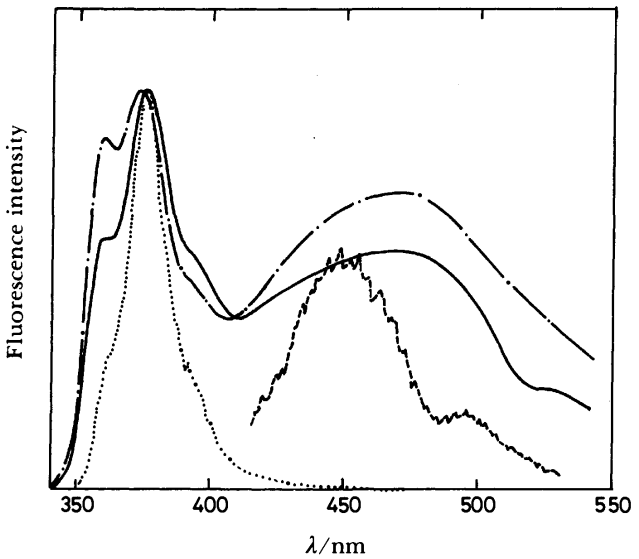

Fig. 1. Stationary and transient fluorescence spectra of 3Cz-2/Ph-4/CMT mixture (molar ratio=18/73/9). Stationary spectra: (——): 70 °C in cholesteric mesophase; (—·—): 130 °C in isotropic phase. λ_{ex}= 333 nm. Transient spectra in cholesteric phase at 76 °C, (--------): 0.5—1.5 ns after excitation; (-----): 13—18 ns after excitation. λ=314 nm. Both the stationary and the transient spectra are uncorrected.

The different profile of the transient spectrum indicates that the configuration of the exciplex at the early stage is different from that of the stationary one.

Rise and Decay Curves of the Exciplex Emission. The rise and decay curves were measured for CLC mixtures of 3Cz-2/Ph-4/CMT having four different molar ratios: (19.5/78/2.4), (19/76.2/4.8), (18.6/74.4/7.0), and (18.1/72.7/9.1). The emissions at longer wavelengths than 500 nm were collected. The curves obtained at lower temperatures than 120 °C were fitted to three component exponential functions (Eq. 1), one for the rise and two for the decay.

$$F(t) = G_1\exp(-t/T_1) + G_2\exp(-t/T_2) + G_3\exp(-t/T_3) \quad (1)$$

The χ^2 values were in most cases less than 1.2. A typical rise and decay curve is shown in Fig. 2. The rise and decay curves at higher temperatures than 120 °C were reasonably fitted to two exponential functions, one for the rise and one for the decay. The rise and decay times (T_1 for rise, T_2 and T_3 for decay) and the ratio of the preexponential factors for the two decay functions (G_2/G_3) are shown in Figs. 3—6.

The longer decay time of the exciplex emission (T_3) shown in Fig. 3 do not depend on the concentration of the acceptor (CMT). As will be discussed later, the longer decay time corresponds to the inverse of the deactivation rate of the exciplex. Therefore, the insensitiveness of the T_3 values to the acceptor concentration can be understood by the independence of the monomolecular process to the acceptor concentration. The activation energy for the deactivation process in cholesteric phase seems to differ slightly

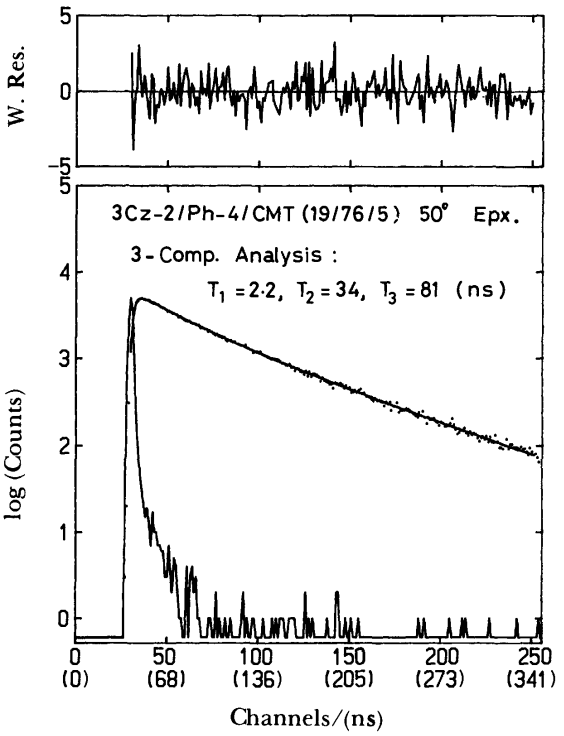

Fig. 2. Rise and decay curve for the exciplex emission from 3Cz-2/Ph-4/CMT (19/76.2/4.8) mixture. $\lambda_{em}>500$ nm. The curve fitting was made with a three-exponential function (Eq. 1), T_1=2.2, T_2=34, T_3=81 (nsec), G_1=−0.38, G_2=−0.23, G_3=0.23, χ^2=1.2.

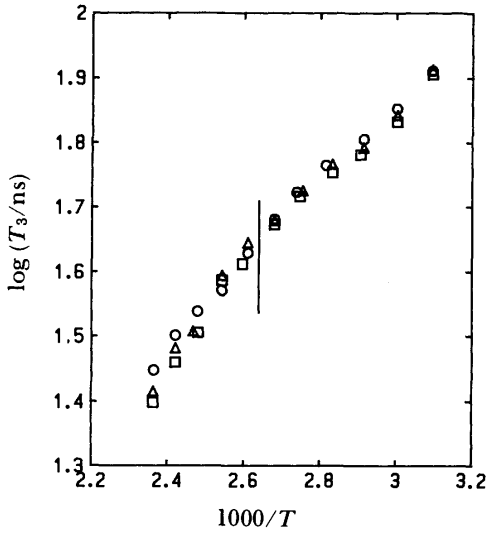

Fig. 3. Temperature dependence of the longer lifetime of the exciplex emission from 3Cz-2/Ph-4/CMT mixtures. Molar ratios are: 19.5/78.0/2.4 (○); 19.0/76.2/4.8 (□); 18.6/74.4/7.0 (△). The vertical bar indicates the cholesteric-isotropic transition point.

from that in isotropic phase.

The shorter decay time of the exciplex (T_2) (Fig. 4) and the G_2/G_3 ratio (Fig. 5) were also insensitive to the acceptor concentration, although the data points

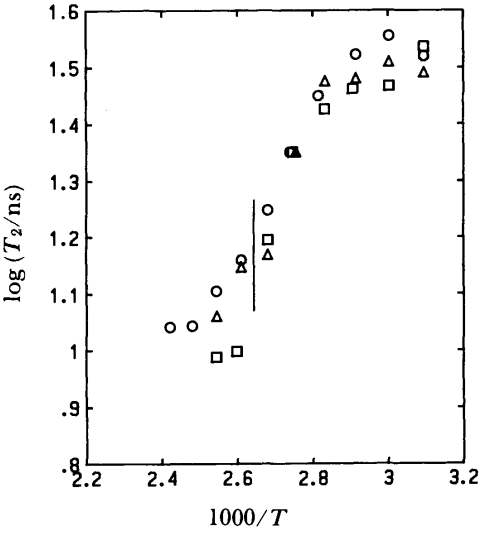

Fig. 4. Temperature dependence of the shorter lifetime of the exciplex emission from 3Cz-2/Ph-4/CMT mixtures. Notations are the same as in Fig. 3.

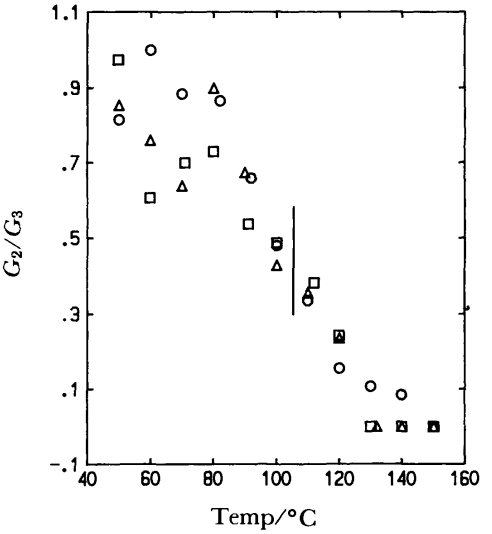

Fig. 5. Temperature dependence of the ratio of preexponential factors for the shorter and the longer lifetime components of the exciplex emission from 3Cz-2/Ph-4/CMT mixtures. Other notations are the same as in Fig. 3.

scatter to somewhat larger extent.

Contrary to other parameters, the rise time of the exciplex (T_1) becomes shorter with the increase of the CMT concentration (Fig. 6). Furthermore, the Arrhenius plot shows a turning point at the cholesteric-isotropic transition point which is shown by vertical bars in the figure.

The decay curves of the monomer emission were also measured. The decay curves consisted of essentially a single fast component with a small contribution of the slow component, which may be ascribed to the exciplex emission overlapped to the monomer emission. The decay times of monomer

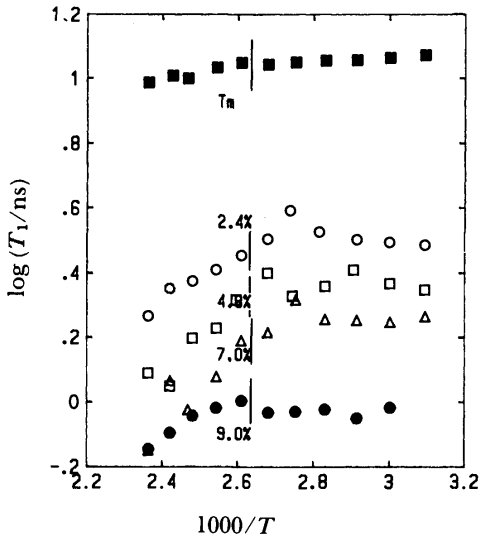

Fig. 6. Temperature dependence of the rise time of the exciplex emission from 3Cz-2/Ph-4/CMT mixtures. Molar ratios of the mixtures are: 19.5/78.0/2.4 (○); 19.0/76.2/4.8 (□); 18.6/74.4/7.0 (△); 18.1/ 72.7/ 9.1 (●). The vertical bars indicate the cholesteric-isotropic transition temperature. The monomer lifetimes observed in the 3Cz-2/Ph-4 (20/80) are also plotted (■).

emission were about the same as the corresponding rise times of the exciplex emission. However, since the former data scattered more than the latter, the latter were used in the following discussion. The decay curves of the monomer fluorescence in the absence of CMT [3Cz-2/Ph-4 (20/80)] at different temperatures were fitted to single exponential functions with a typical lifetime of 11.3 ns (80 °C, CLC) or 9.9 ns (132 °C). The lifetimes T_m are plotted in Fig. 6.

Kinetics of Exciplex Formation in the CLC Mixture. The experimental results described above are summarized as follows. (1) There are two types of exciplex, one decaying faster (typically, 30 ns at 80 °C) than the other (60 ns at 80 °C). The faster component disappears at higher temperatures than about 120 °C. (2) The decay times of the two types of exciplex are independent of the concentration of the acceptor, indicating that the decay times are determined only by monomolecular processes of the types of exciplex. (3) The rise time of the exciplex emission is shortened at higher acceptor concentrations, indicating that the rise time is determined by a bimolecular process of the exciplex formation. The rise time is also sensitive to the phase (cholesteric or isotropic) of the mixture. (4) No preformed exciplex site was detected in the in the transient spectrum.

The above results fit the following kinetic scheme which takes two types of exciplex into account. The exciplex formation process was assumed irreversible, since the monomer decay curve showed only marginal

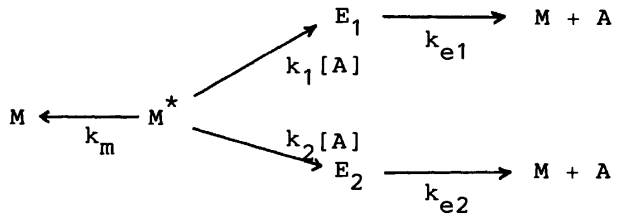

contribution of the decay component of the exciplex emission, which may be ascribed to the insufficient spectral separation. Since only a single rise time was observed in the exciplex emission, the possibility for the successive formation of two types of exciplex, i.e., $M \rightarrow E_1 \rightarrow E_2$, can be excluded. It is not possible to decide only from the kinetic results whether an interconversion between the two types of exciplex is occurring or not. However, since the two types of exciplex can be distinguished in the time scale of a few ten nanosecond, the interconversion, if it exists, should be slower than the time scale.

The relations between the decay times and the rate constants are:

$$k_{e1} = T_2(e)^{-1},\ k_{e2} = T_3(e)^{-1}. \quad (2)$$

The rise time of the exciplex is related to the rate constants for the two exciplex formation processes. Since virtually a single rise time was observed in the exciplex emission, the two rate constants should not be very different to each other. In the following discussion, the apparent rate constant of exciplex formation k_{ap}, calculated using Eq. 3 will be discussed.

$$k_{ap} = T_1(e)^{-1}/[A]. \quad (3)$$

Figure 7 shows the k_{ap} values obtained for the four different concentrations of the acceptor. It is seen that the activation energy in the cholesteric phase is nearly zero, whereas that in the isotropic phase is positive (3—6 kcal mol^{-1}).

Activation Energy for Exciplex Formation. Exciplex formation processes in highly concentrated molecular assemblies are generally governed by the following factors: (1) Diffusion of the donor groups to the acceptor. (2) Energy migration among the donor groups. (3) Population of exciplex-forming sites. (4) Molecular reorientation required for the exciplex formation in the exciplex-forming site. (5) Quenching of the excited state by bimolecular processes, such as an excimer formation, between the excited and the ground-state donor molecules. In the present case, item (5) may be neglected, since only very weak excimer emission was detected in the fluorescence spectrum of 3Cz-2/Ph-4 (20/80) mixture and the decay time of the (20/80) mixture is almost equal to that of the 3Cz-2/Ph-4/Ph-2 (1/33/66) mixture.

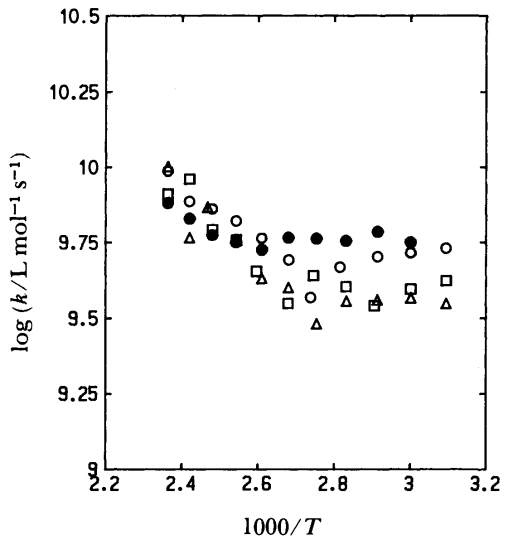

Fig. 7. Arrhenius plot of apparent rate constants for exciplex formation in 3Cz-2/Ph-4/CMT mixtures. Notations are the same as in Fig. 6.

Since cholesteric phase is known to be more viscous than isotropic phase, a higher activation energy for the exciplex formation is expected in the former phase. Actually, Weiss and co-workers reported a higher activation energy of exciplex formation between free pyrene molecules and *N,N*-dimethyl-5α-cholestan-3β-ylamine (CA) in the CLC phase (9.9—11.8 kcal mol^{-1}) than in the isotropic phase (5.3—5.4 kcal mol^{-1}). They observed higher activation energy in the CLC phase also in the excimer formation between pyrene molecules dispersed in the cholesteric mixtures. The Arrhenius plots in Fig. 7 contrast the above expectation and experimental results. The very small activation energy in the CLC phase is remarkable, but the activation energy in the isotropic phase is not mush different from that observed by Weiss and co-workers. Therefore, the low activation energy in the CLC phase cannot be interpreted only by the high concentration of carbazolyl groups in the present system. A possible reason is that the cholesteric order may align the carbazolyl groups in a manner which enhances the energy migration among carbazolyl groups and/or facilitates the exciplex formation in the exciplex-forming site. The lower activation energy in the CLC phase has been observed also in the excimer formation in cholesteric mixtures containing 3—25% of Py-2,[5] although the difference between CLC and isotropic phase is much smaller than the present case.

It was concluded that the exciplex or the excimer formation of Ar-2-type molecules requires less activation energy in the CLC phase than in the isotropic phase. This may be accounted for in terms of the high orientational order in the CLC phase which facilitates the photophysical processes, such as the energy migration and the exciplex formation.

Assignment of the Two Types of Exciplex. Two types of exciplex were suggested from the decay curves of exciplex emission. Furthermore, the exciplex at the early stage after excitation showed a shorter peak wavelength than the stationary spectrum. The early stage component should correspond to the first exciplex component with a shorter decay time. This first component (G_2) disappeared at higher temperatures than about 120 °C (Fig. 5). The second component decays more slowly and, therefore, is a major component in the stationary spectrum. A possible explanation for the first component is that the exciplex in the CLC mesophase cannot take the most stable structure due to constraints by the CLC order. The fact that the first component is still present above the transition point (Fig. 5) can be explained by a local CLC order, which is known to be remaining above the transition temperature.[11]

Similar finding has been observed in a stationary fluorescence spectra of a mixture of cholesteryl 3-(9-carbazolyl)propanoate (9Cz-2, **5**), cholesteryl 3-(2-naphthyl)propanoate (2N-2, **6**), and CMT (9Cz-2/2N-2/CMT=47.6/47.6/4.8).

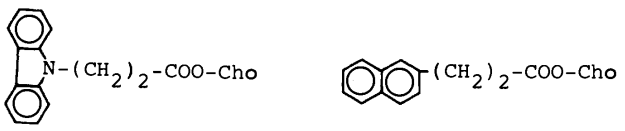

(**5**) (**6**)

In the cholesteric phase, the mixture showed a high-energy exciplex emission located around 425 nm. At elevated temperatures, the exciplex peak shifted to a longer wavelength. The presence of the high-energy exciplex in the CLC phase has been interpreted in terms of an metastable exciplex structure due to the constraints by the CLC order. The high-energy exciplex could not be found in the stationary spectra of a 3Cz-2/Ph-2/CMT mixture. The present study showed the presence of the metastable exciplex also in the latter mixture at an early stage after excitation. Therefore, it may be commonly stated for these types of CLC mixtures that a CLC order imposes constraints on the structure of exciplex.

References

1) M. Sisido, K. Takeuchi, and Y. Imanishi, *J. Phys. Chem.*, **88**, 2893 (1984).

2) M. Sisido, K. Takeuchi, and Y. Imanishi, *Chem. Lett.*, **1983**, 961.

3) K. Kawaguchi, M. Sisido, and Y. Imanishi, *J. Phys. Chem.*, **92**, 4806 (1988).

4) M. Sisido, X.-F. Wang, K. Kawaguchi, and Y. Imanishi, *J. Phys. Chem.*, **92**, 4797 (1988).

5) M. Sisido, X.-F. Wang, K. Kawaguchi, and Y. Imanishi, *J. Phys. Chem.*, **92**, 4801 (1988).

6) V. C. Anderson, B. B. Craig, and R. G. Weiss, *J. Am.*

Chem. Soc., **103**, 1169 (1981).
7) V. C. Anderson, B. B. Craig, and R. G. Weiss, *J. Am. Chem. Soc.*, **104**, 2972 (1982).
8) N. Tamai, I. Yamazaki, H. Masuhara, and N. Mataga, *Chem. Phys. Lett.*, **104**, 485 (1984).
9) M. Yamamoto, Y. Hatano, and Y. Nishijima, *Chem. Lett.*, **1976**, 351.
10) Y. Hatano, M. Yamamoto, and Y. Nishijima, *J. Phys. Chem.*, **82**, 367 (1978).
11) P. P. Crooker and W. G. Laidlaw, *Phys. Rev. A*, **21**, 2174 (1980).

^{1}H NMR Conformational Study of Viologen-Linked Porphyrins

Yasuhiko YAMAMOTO, Sumio NODA,† Norishige NANAI, Ichiro OKURA,† and Yoshio INOUE*
Department of Biomolecular Engineering, Tokyo Institute of Technology,
O-okayama, Meguro-ku, Tokyo 152
†Department of Bioengineering, Tokyo Institute of Technology,
O-okayama, Meguro-ku, Tokyo 152
(Received February 10, 1989)

Novel porphyrins to which the viologen is linked (*m*-PC*n*V) were synthesized. The linkage methylene chain between the porphyrin and the bipyridine moieties was systematically changed from $(CH_2)_3$ to $(CH_2)_6$. The molecular structure of *m*-PC*n*V was characterized by ^{1}H NMR in some detail. The orientation of the viologen with respect to the porphyrin plane in *m*-PC*n*V was semiquantitatively estimated from the porphyrin ring current induced chemical shift changes on the resonances from the viologen moiety. The NMR conformational analyses on *m*-PC*n*V in dimethyl sulfoxide and acetonitrile clearly revealed the effect of the solvent on its molecular structure.

Porphyrins to which a variety of electron acceptor units are covalently bonded have been investigated intensively to gain insight into the intramolecular electron transfer between the porphyrin and the viologen which results in the generation of a high-energy charge-separated state that has a potential of various applications.[1-7] The intramolecular electron transfer process has been clearly detected in various covalently linked porphyrin–viologen molecules by fluorescence quenching techniques or lifetime measurements[1,5,6] and more directly by resonance Raman spectroscopy.[3] Electron-transfer quenching of the photoexcited porphyrin by the linked viologen was found to depend on solvent and the length of linkage between the porphyrin and viologen.[1] Although the photoinduced electron-transfer process occurs during the lifetime of the excited state of porphyrin which is on nanosecond time scale, it would be of interest to characterize the ground state molecular structure of those porphyrin derivatives and to relate those structures to the rate of the intramolecular electron transfer.

We have synthesized novel porphyrins covalently linked to viologen (*m*-PC*n*V, Fig. 1). The length of the methylene chain ($+CH_2+_n$) between the porphyrin and bipyridine was systematically changed from n=3 to n=6 to investigate the effect of the methylene chain length on the molecular structure which in turn determines the spatial relationship between the porphyrin ring and the bipyridine moiety of the viologen. The solution structure of *m*-PC*n*V was investigated using ^{1}H NMR. The individual resonances have been completely and unambiguously assigned by the combined use of ^{1}H–^{1}H two-dimensional chemical shift correlated spectroscopy (COSY) and two-dimensional nuclear Overhauser effect spectroscopy (NOESY). Based on the porphyrin ring current induced chemical shift,[2,8-11] a spatial relationship between the porphyrin ring and the bipyridine moiety of the viologen in *m*-PC*n*V was semiquantitatively determined. Analyses on the porphyrin ring current induced shifts in terms of the position of a nucleus with respect to the porphyrin plane require appropriate model compound which, ideally, possesses all structure features present in *m*-PC*n*V but the porphyrin ring current, because the induced chemical shift change originates solely from the magnetic anisotropy due to the magnetic dipole arising from the porphyrin ring current. We therefore synthesized the compounds,

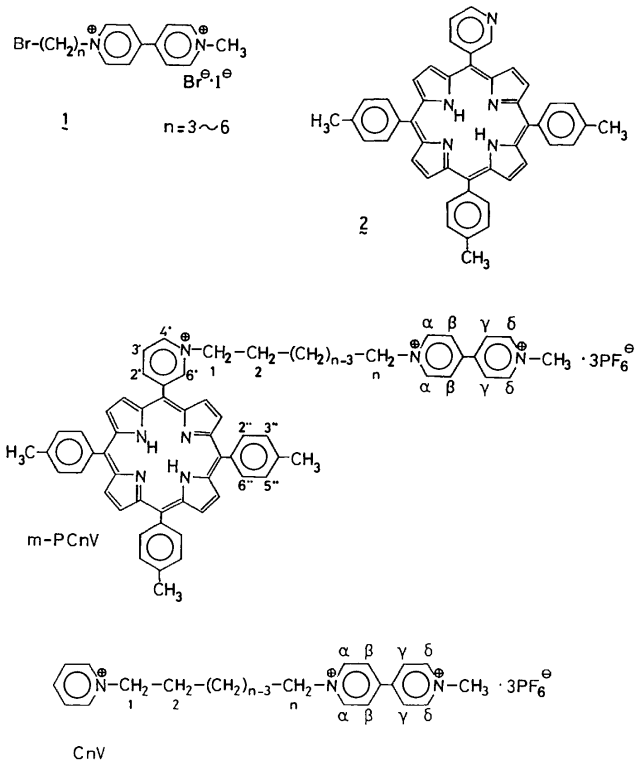

Fig. 1. Molecular structures of 1-methyl-1′-(ω-bromoalkyl)-4,4′-bipyridinium salt (**1**), 5-(3-pyridyl)-10,15,20-tritolylporphyrin (**2**), viologen-linked porphyrin synthesized (*m*-PC*n*V), and model compounds (C*n*V). The numbering systems for *m*-PC*n*V and C*n*V are shown with the structures.

C*n*V, shown in Fig. 1 as models for *m*-PC*n*V. Their NMR spectra were characterized and the difference in the observed chemical shifts between *m*-PC*n*V and C*n*V for the corresponding viologen proton resonances is discussed in terms of the spatial orientation of the viologen moiety with respect to the porphyrin plane in *m*-PC*n*V molecule. Conformational analyses were carried out in two different solvents, i.e., dimethyl sulfoxide and acetonitrile, to investigate the effect of solvent on the molecular structure of *m*-PC*n*V. The difference in conformation of *m*-PC*n*V in different solvents which in turn results in placing the bipyridine moiety of the viologen at spatially different position with respect to the porphyrin plane was clearly reflected in the porphyrin ring current induced shift changes for the viologen proton resonances. Although the linkage methylene chain is flexible, the bipyridine moiety of the viologen does not appear to fold back above the porphyrin plane in *m*-PC*n*V studied here.

Experimental

Materials; All chemicals and solvents were of reagent grade and were obtained from commercial sources.

Syntheses; The viologen-linked porphyrins with a series of methylene chain length (*m*-PC*n*V) were synthesized from the coupling reaction of **1** and **2** (Fig. 1) which were prepared using the literature procedures.[12,13] **1** (0.3 mM; 1 M=1 mol dm^{-3}) and **2** (0.6 mM) were reacted in *N*,*N*-dimethylformamide at 80 °C for 48 hours and then toluene (300 ml) was added to precipitate the product and unreacted **2**. The solids were filtered and then washed with toluene and distilled water. The products were dissolved in MeOH and NH_4PF_6 (0.2 g) was added to replace the counter anion to PF_6^-. The desired products should be insoluble in MeOH with PF_6^-. The precipitate is collected, washed with MeOH, and then dried under vacuum at room temperature for 1 hour. The yield was about 30%. The purity of the products was established from their ^{1}H NMR spectra.

Model compounds, C*n*V, were synthesized using the reaction of **1** with pyridine in MeOH for 8 hours followed by the replacement of the counter anion to PF_6^- using NH_4PF_6. C*n*V was filtered and then washed by MeOH. Solids were dried under vacuum at room temperature.

NMR Measurements; The compounds were dissolved in either dimethyl-d_6 sulfoxide (DMSO-d_6) or acetonitrile-d_3 (MeCN-d_3) for the NMR samples and the concentrations of the samples were 10 and 30 mM for *m*-PC*n*V and C*n*V, respectively. 500 MHz ^{1}H NMR spectra were recorded on a JEOL GSX-500 FT-NMR spectrometer. Typical spectra were recorded with 16 transients, 32 k data points over a 5000 Hz spectral width, and 5.3 μs 90° pulse. Chemical shifts were referenced to the residual solvent peak, which in turn was calibrated against tetramethylsilane, TMS, and are reported in parts per million, ppm, referenced to TMS.

COSY and NOESY spectra were obtained using the standard pulse sequences[14] and data processing procedures. The mixing time of 700 ms was used for NOESY.

Results and Discussion

^{1}H NMR Signal Assignment. 500 MHz ^{1}H NMR spectrum of *m*-PC4V in MeCN-d_3 at 27 °C is illustrated in Fig. 2. The spectrum indicates the purity of the sample prepared. The unambiguous ^{1}H signal assignments are obtained from ^{1}H-^{1}H COSY and NOESY spectra shown in Figs. 3 and 4, respectively. The scalar coupling connectivities in the COSY

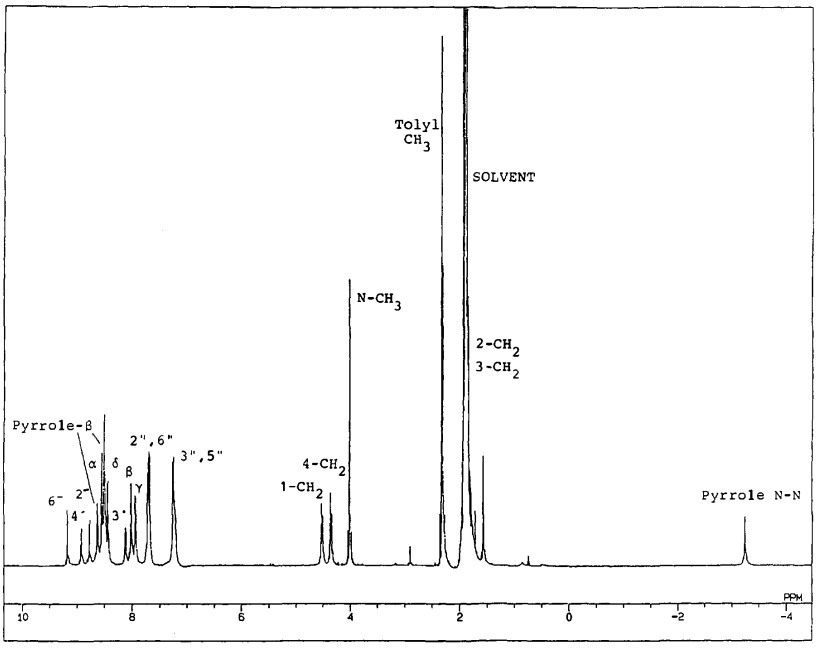

Fig. 2. 500 MHz ^{1}H NMR spectrum of *m*-PC4V in MeCN-d_3 at 27 °C. The signal assignment is attached with the spectrum.

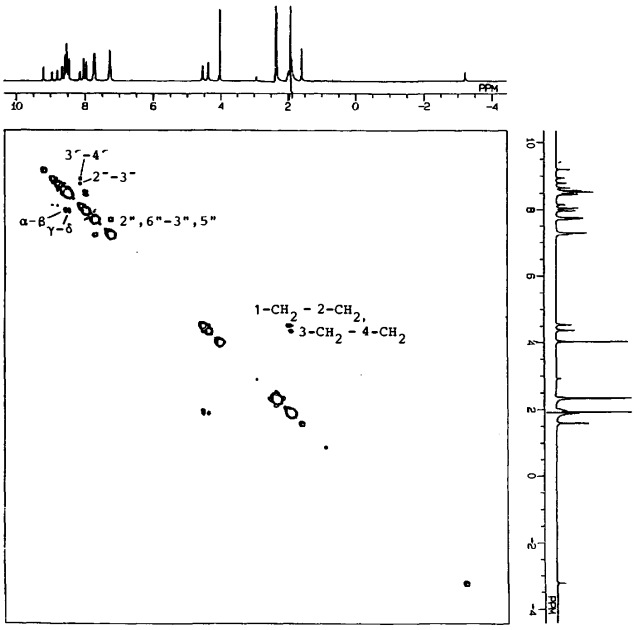

Fig. 3. COSY spectrum of *m*-PC4V in MeCN-d_3 at 27°C.

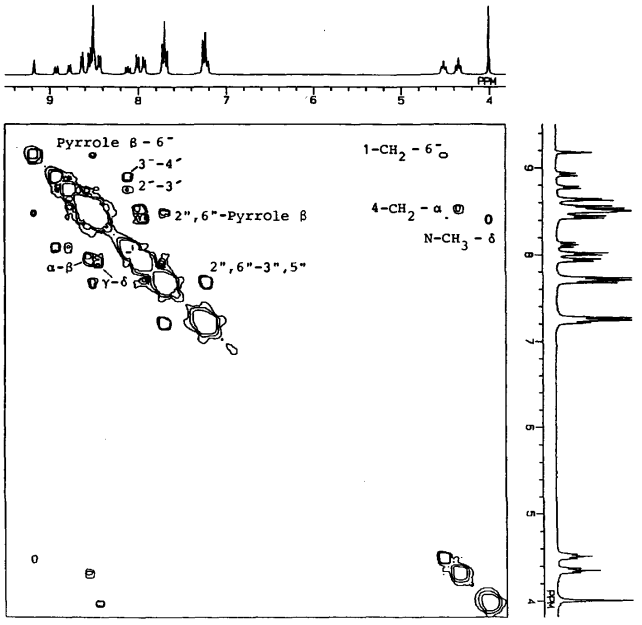

Fig. 4. A portion of NOESY spectrum of *m*-PC4V in MeCN-d_3 at 27°C.

spectrum establish most of the assignment but the differentiation of the bipyridine, terminal methylene, or tolyl proton resonances was hampered by the discontinuity of spin-spin coupling network. The dipolar coupling connectivities in NOESY spectrum allow the specific assignment of those resonances. The singlet N-CH_3 resonance at δ 4.14 exhibits a cross-peak with a doublet resonance at δ 8.57 in the NOESY spectrum, indicating the assignment of this resonance to the bipyridine δ proton. The terminal methylene

Table 1. Chemical Shifts[a] of Porphyrin and Tolyl ^{1}H Resonances of *m*-PC*n*V(*n*=3—6) in DMSO-d_6 and MeCN-d_3

Resonance[b]	DMSO-d_6	MeCN-d_3
Pyridyl		
2′	9.51	8.90
3′	8.65	8.25
4′	9.58	9.05
6′	10.09	9.31
Tolyl		
2″,6″[c]	8.10	7.84
3″,5″[c]	7.66	7.38
CH_3	2.69	2.44
Pyrrole-β	8.88, 9.02	8.63, 8.76
Pyrrole N-H	−2.92	−3.10

a) Chemical shifts are given in ppm and referenced to TMS through the residual solvent signal. Deviation of less than ±0.03 ppm among *m*-PC*n*V(*n*=3—6) prepared. b) Numbering system is shown in Fig. 1. c) Resonances exhibit multiplet structures in their line shape.

proton resonances can be differentiated using the connectivities with the pyridine 4′ or/and 6′ and bipyridine α proton resonances and the tolyl proton can be specifically assigned from the NOESY cross-peak with the singlet tolyl CH_3 resonance. The unambiguous assignments of all the resonances for the other *m*-PC*n*V prepared were similarly obtained and the chemical shift values are summarized in Tables 1 and 2. The solvent dependence of the chemical shifts of *m*-PC*n*V ^{1}H resonance is apparent. But, in a given solvent, the shifts of the pyridine resonances as well as the pyrrole N-H proton resonances were found to be essentially independent of the length of the methylene chain of *m*-PC*n*V. The fine structure of the line shape of the resonances arising from the tolyl 2″, 6″ and 3″, 5″ protons was altered by the length of the methylene chain, indicating small deviation in the chemical shift among the resonances from the three tolyl groups on the molecule. The shift values of the tolyl resonances are interpreted in terms of both the orientation of the aromatic ring with respect to the porphyrin plane and the asymmetric nature in electronic structure of the porphyrin ring. Considering that the electronic structure of the porphyrin ring in *m*-PC*n*V is essentially C_2 symmetric, the asymmetry of the porphyrin ring electronic structure does not account for the deviation of the chemical shifts of the resonances from the three tolyl ring protons of *m*-PC*n*V. But no evidence was detected for a direct interaction of those aromatic rings with the bipyridine moiety of the viologen which can be thought to perturb the chemical shifts of the tolyl ring protons.

Analyses of the Porphyrin Ring Current Induced Shift. Spatial relationship between the porphyrin and the viologen can be deduced from the analyses on the porphyrin ring current induced chemical shift changes on the resonances from the viologen.[2,11] The

Table 2. Chemical Shifts[a] of Viologen ^{1}H Resonances of *m*-PC*n*V(*n*=3—6) in DMSO-d_6 and MeCN-d_3

Resonance[b]	DMSO-d_6				MeCN-d_3			
	m-PC3V	*m*-PC4V	*m*-PC5V	*m*-PC6V	*m*-PC3V	*m*-PC4V	*m*-PC5V	*m*-PC6V
Methylene chain								
1-CH_2	5.04	4.96	4.91	4.89	4.74	4.65	4.57	4.58
2-CH_2	2.95	2.2[c]	2.28[c]	2.2[c]	2.74	1.96[c]	2.05[c]	2.00[c]
3-CH_2	4.93	2.2[c]	1.57[c]	1.5[c]	4.63	1.88[c]	1.38	1.35
4-CH_2		4.79	2.11[c]	1.5[c]		4.49	1.88[c]	1.28
5-CH_2			4.72	2.01			4.38	1.80[c]
6-CH_2				4.66				4.36
Bipyridyl								
α	9.41	9.38	9.37	9.34	8.72	8.68	8.63	8.59
β	8.81	8.77	8.77	8.74	8.19	8.14	8.09	8.09
γ	8.71	8.69	8.71	8.69	8.10	8.07	8.03	8.05
δ	9.25	9.25	9.25	9.25	8.59	8.57	8.52	8.55
N-CH_3	4.41	4.42	4.42	4.42	4.15	4.14	4.10	4.13

a) Chemical shifts are given in ppm and referenced to TMS through the residual solvent signal. b) Numbering system is shown in Fig. 1. c) Resonating under the residual solvent signal and shifts were obtained from the COSY cross-peaks.

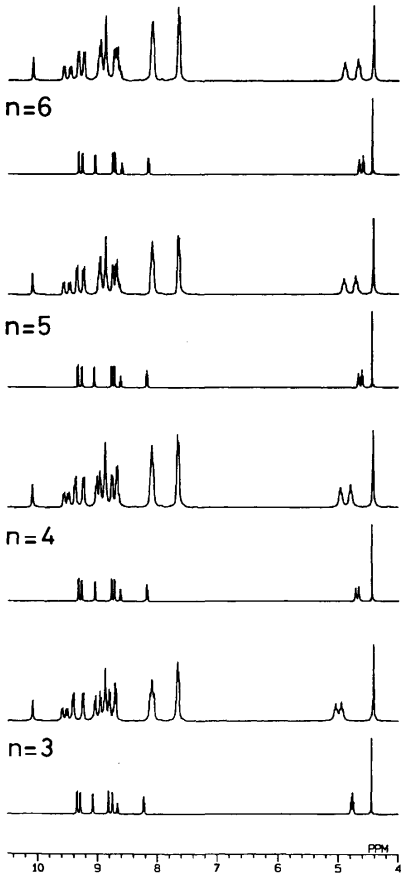

Fig. 5. 500 MHz ^{1}H NMR spectra of *m*-PC*n*V and C*n*V (*n*=3—6) in DMSO-d_6 at 27 °C. Chemical shift region of δ 4—10.5 is presented. For each set of the spectra, the lower trace is the spectrum of C*n*V.

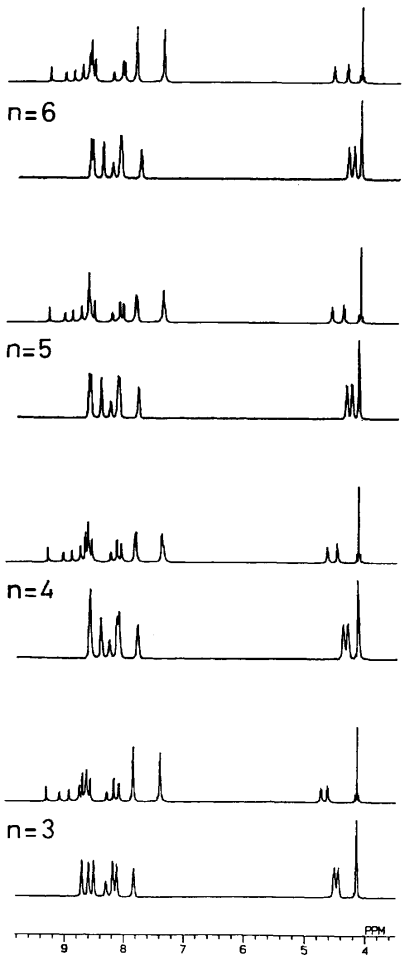

Fig. 6. 500 MHz ^{1}H NMR spectra of *m*-PC*n*V and C*n*V in MeCN-d_3 at 27 °C. Chemical shift region of δ 3.5—9.8 is presented. For each set of the spectra, the lower trace is the spectrum of C*n*V.

dipolar field arising from the ring current of the porphyrin ring π-electrons strongly influences the resonance frequencies of the nuclei which are located in the close proximity to the porphyrin and the induced chemical shift change spans up to several ppm depending on the position of the nucleus with respect to the porphyrin ring. The porphyrin ring current induced chemical shift change ($\Delta\delta$) is calculated as the difference in the observed shift between *m*-PC*n*V and appropriate model which, ideally, possesses

Table 3. Porphyrin Ring Current Induced Chemical Shift Changes[a] on Viologen ^{1}H Resonances of *m*-PC*n*V(*n*=3—6) in DMSO-d_6 and MeCN-d_3

Resonances[b]	DMSO-d_6				MeCN-d_3			
	m-PC3V	*m*-PC4V	*m*-PC5V	*m*-PC6V	*m*-PC3V	*m*-PC4V	*m*-PC5V	*m*-PC6V
Methylene Chain								
1-CH_2	+0.29	+0.30	+0.30	+0.30	+0.30	+0.33	+0.30	+0.31
2-CH_2	+0.24	+0.19[c]	+0.26[c]	+0.27[c]	+0.28	+0.15[c]	+0.21[c]	+0.29[c]
3-CH_2	+0.15	+0.19[c]	+0.21[c]	+0.16[c]	+0.14	+0.07[c]	+0.19	+0.18
4-CH_2		+0.18	+0.13[c]	+0.13[c]		+0.10	+0.08[c]	+0.11
5-CH_2			+0.05	+0.08			+0.02	+0.09[c]
6-CH_2				0.00				0.00
Bipyridyl								
α	+0.07	+0.05	+0.02	0.00	+0.01	+0.06	−0.01	−0.05
β	−0.02	−0.01	−0.01	−0.03	0.00	−0.01	−0.04	−0.06
γ	−0.05	−0.04	−0.03	−0.04	−0.03	−0.05	−0.08	−0.07
δ	−0.04	−0.03	−0.03	−0.03	−0.01	−0.04	−0.09	−0.05
N-CH_3	−0.04	−0.02	−0.02	−0.02	+0.01	−0.01	−0.05	−0.02

a) Chemical shift changes ($\Delta\delta=\delta_{m\text{-}PCnV}-\delta_{CnV}$) are given in ppm and uncertainty is ±0.01 ppm unless specified. Positive Δδ value indicates the downfield shift of *m*-PC*n*V proton with respect to the corresponding C*n*V proton. b) Numbering system is shown in Fig. 1. c) Uncertainty is ±0.03 ppm.

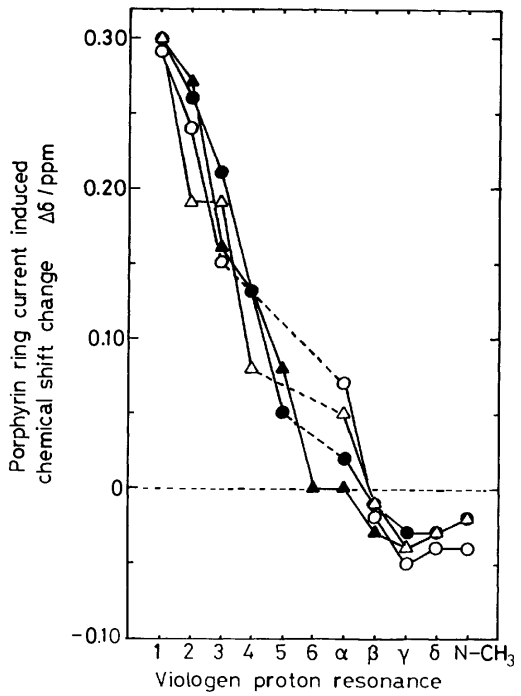

Fig. 7. Plots of the porphyrin ring current induced chemical shift change (Δδ) vs. viologen proton resonance of *m*-PC*n*V in DMSO-d_6. The viologen protons are arranged in the order of he distance away from the porphyrin ring along the covalent bond on the horizontal axis. *m*-PC3V (○), *m*-PC4V (△), *m*-PC5V (●), *m*-PC6V (▲).

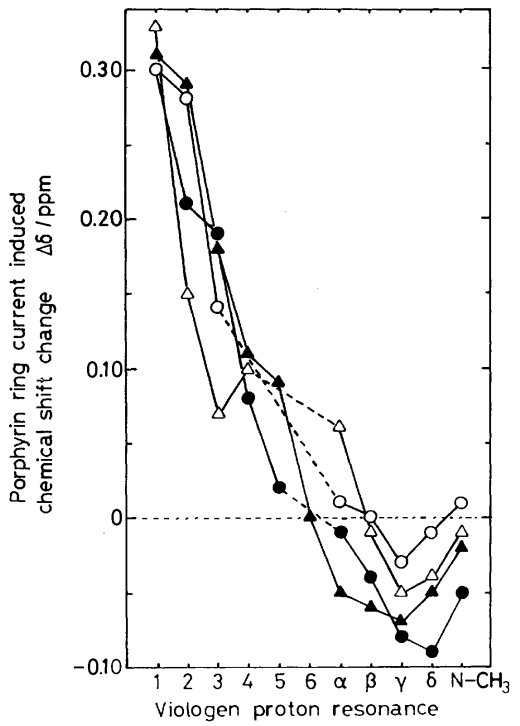

Fig. 8. Plots of the porphyrin ring current induced chemical shift change (Δδ) vs. viologen proton resonance of *m*-PC*n*V in MeCN-d_3. The viologen protons are arranged in the order of he distance away from the porphyrin along the covalent bond on the horizontal axis. *m*-PC3V (○), *m*-PC4V (△), *m*-PC5V (●), *m*-PC6V (▲).

all structure features present in *m*-PC*n*V but the porphyrin ring current. Therefore the model compounds, C*n*V, have been synthesized. Their ^{1}H NMR spectra were recorded and the signals were assigned using COSY and NOESY (results not shown). The spectra of *m*-PC*n*V in DMSO-d_6 and MeCN-d_3 are compared with those of the corresponding model C*n*V in Figs. 5 and 6, respectively. The obtained Δδ values, $\Delta\delta=\delta_{m\text{-}PCnV}-\delta_{CnV}$, for corresponding viologen proton resonances are summarized in Table 3. The Δδ values of *m*-PC*n*V in DMSO-d_6 and MeCN-d_3 are compared in Figs. 7 and 8, respectively. Although the patterns of the Δδ plots for both solvents look similar, they are

slightly and subtly different with each other (see below).

Conformational Analyses of *m*-PC*n*V. The $\Delta\delta$ value for 1-CH_2 of *m*-PC*n*V in DMSO-d_6 is about +0.3 ppm, reflecting the strong deshielding effect due to the porphyrin ring current. The $\Delta\delta$ value of methylene proton decreases as ^{1}H nucleus is oriented away from the porphyrin ring along the methylene chain of the viologen and eventually becomes nagative for the resonances from the bipyridine moiety, indicating that the viologen is oriented across the boundary expressed by the equation, $(3\cos^2\theta-1)/r^3=0$, where r is the magnitude of the vector connecting the center of the porphyrin ring and the nucleus and θ is the angle between $\vec{r}$ and the z-axis which is defined normal to the porphyrin plane; in particular, the θ is called the magic angle when θ satisfies the equation $3\cos^2\theta-1=0$, i.e., $\theta=54.7°$. The sign of the $\Delta\delta$ value changes between bipyridyl α and β protons of the viologen, dictating that the part around these nuclei of the viologen moiety is located close to the boundary expressed by $3\cos^2\theta-1=0$. Because of the difficulties arising from nonlinear averaging of the porphyrin ring current induced chemical shift changes in terms of the relative orientation of the nucleus with respect to the porphyrin plane, the flexibility in conformation of the methylene chain, and the uncertainty in the orientation of the pyridine ring with respect to the porphyrin ring, we have not attempted to determine the time averaged conformation of *m*-PC*n*V molecule. The insensitivity of the $\Delta\delta$ values for the length of the methylene chain, however, is consistent with the extended all-anti conformation and the bipyridine moiety being just across the boundary of the magic angle. Since the pyridine ring is neither coplanar nor orthogonal to the porphyrin plane but slightly tilted,[15] the length of the methylene chain linkage does not have a significant effect on the position of the bipyridine moiety of the viologen with repect to the dipolar field arising from the porphyrin ring π-electrons. With the energetically stable all-anti methylene chain conformation,[16] the closest edge-to-edge distance of the π-systems of the porphyrin and bipyridine of *m*-PC*n*V are ca. 6 to ca. 12 Å for n=3 to 6. If there is a direct relationship between that distance and the rate of the intramolecular electron transfer as Gust et al.[2] have suggested, the larger distance for the greater n value is completely consistent with the linkage length dependency of the electron-transfer rate found in viologen-linked zinc porphyrin.[1]

The patterns of the $\Delta\delta$ plots for *m*-PC*n*V in MeCN-d_3 are similar to those in DMSO-d_6, but slightly different features are observed. In the plot illustrated in Fig. 9, the sign of the value changes at bipyridine β proton for *m*-PC3V and *m*-PC4V and between α and 5- or 6-CH_2 resonances for *m*-PC5V and *m*-PC6V, respectively, suggesting either that the dihedral angle between the pyridine and porphyrin planes is closer to orthogonal in MeCN-d_3 than that in DMSO-d_6 or that the direction of the vector connecting pyridyl N and N-CH_3 is directed more toward z axis of the porphyrin ring in MeCN-d_3. These results strongly suggest that the orientations of the viologen with respect to the porphyrin ring of *m*-PC*n*V in DMSO-d_6 and MeCN-d_3 are different and the difference in the spatial relationship between the porphyrin and the viologen in different solvents could explain the solvent dependency of the rate of the intramolecular electron transfer.[1] Similar porphyrin ring current induced shift for 1-CH_2 resonance of *m*-PC*n*V in both solvents indicates that the magnetic anisotropy of the porphyrin ring current is not significantly altered by solvent. As can be seen in the $\Delta\delta$ plots, the difference in conformation between the two solvents is clearly manifested in the difference in the patterns of the $\Delta\delta$ plots. Such difference in conformation between the two solvents appears to be enhanced with the n value. But it is not easy at present to interpret the solvent

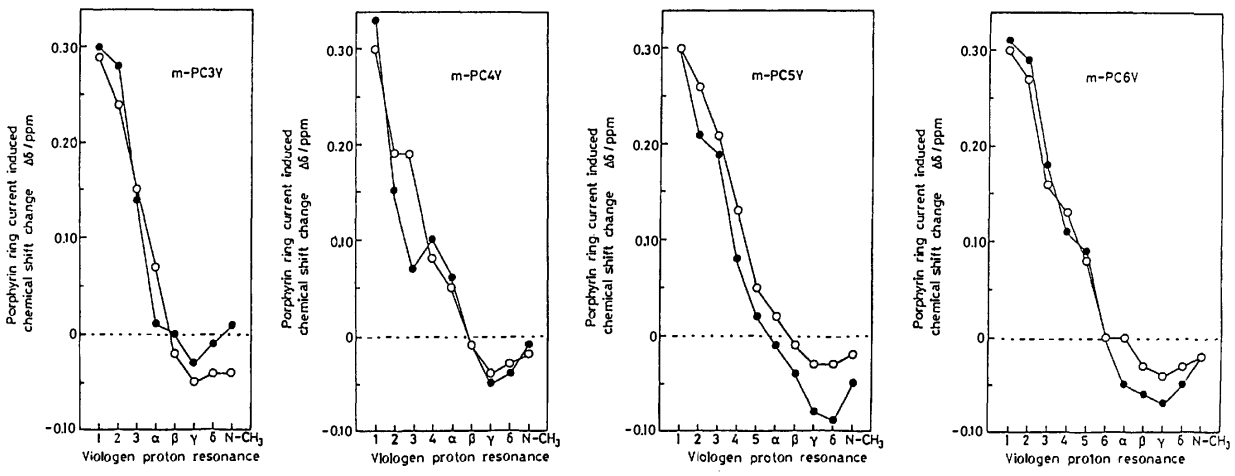

Fig. 9. Plots of the porphyrin ring current induced chemical shift change ($\Delta\delta$) vs. viologen proton resonance of *m*-PC*n*V in DMSO-d_6 (○) and MeCN-d_3 (●).

dependency of *m*-PC*n*V conformation because of the absence of the knowledge of the interaction of *m*-PC*n*V with the surrounding solvent molecules.

Conclusion

Novel porphyrins linked to viologen (*m*-PC*n*V) which are expected to serve as both a photosensitizer and an electron carrier in the same molecule have been synthesized. The flexible methylene chain was used to link the porphyrin ring and the bipyridine and the constituent methylene unit was systematically changed from 3 to 6 to observe the effect of the methylene chain length on the spatial relationship of the bipyridine moiety with respect to the porphyrin. Using the porphyrin ring current induced chemical shift change, the orientation of the viologen with respect to the porphyrin ring in *m*-PC*n*V was semiquantitatively determined and the results suggested that the viologen does not fold back in a way that the bipyridine moiety of the viologen is oriented above the porphyrin plane and that the bipyridine moiety is oriented around the boundary defined by the magic angle where the porphyrin ring current induced shift change vanishes. The conformational analyses of *m*-PC*n*V in DMSO-d_6 and MeCN-d_3 indicated that the spatial orientation of the bipyridine with respect to porphyrin ring is slightly different between the two solvents and such difference in the conformation of *m*-PC*n*V appears to be enhanced with the length of the methylene chain.

With the extended methylene chain conformation, the closest edge-to-edge distance between the π-systems of the porphyrin and the bipyridine increases with the methylene chain length. Therefore the rate of the intramolecular electron transfer of *m*-PC*n*V would be smaller with the longer methylene chain linkage, if there is a direct relationship between the electron transfer rate and the distance of two π-systems.[2] Fluorescence lifetime measurements are currently under way on these *m*-PC*n*V in DMSO and MeCN.

Two (I.O and Y.I) of authors wish to thank for the partial support by a Grant-in-Aid for Scientific Research of Priority Area, "Dynamic Interaction and Electronic Process of Macromolecular Complexes," (1988), from the Ministry of Education, Science and Culture.

References

1) A. Harriman, G. Porter, and A. Wilowska, *J. Chem. Soc., Faraday Trans. 2*, **80**, 191 (1984).

2) D. Gust, T. A. Moore, P. A. Liddell, G. A. Nemeth, L. R. Makings, A. L. Moore, D. Barrett, P. J. Pessiki, R. V. Bensasson, M. Rougee, C. Chachaty, F. C. De Schryver, M. Van der Auweraer, A. R. Holzwarth, and J. S. Connolly, *J. Am. Chem. Soc.*, **109**, 846 (1987) and the references therein.

3) R. J. McMahon, R. K. Force, H. H. Patterson, and M. S. Wrighton, *J. Am. Chem. Soc.*, **110**, 2670 (1988) and the references therein.

4) J. L. Sessler, M. R. Johnson, T.-Y. Lin, and S. E. Creager, *J. Am. Chem. Soc.*, **110**, 3659 (1988) and the references therein.

5) I. Okura, N. Kaji, S. Aono, and T. Nishisaka, *Bull. Chem. Soc. Jpn.*, **60**, 1243 (1987).

6) S. Aono, N. Kaji, and I. Okura, *J. Chem. Soc., Chem. Commun.*, **1986**, 170.

7) N. Kaji, S. Aono, and I. Okura, *J. Mol. Catal.*, **36**, 201 (1986).

8) R. G. Shulman, K. Wüthrich, T. Yamane, D. Patel, and W. E. Blumberg, *J. Mol. Biol.*, **53**, 143 (1970).

9) R. J. Abraham. G. R. Bedford, D. McNeille, and B. Wright, *Org. Magn. Reson.*, **14**, 418 (1980).

10) K. J. Cross and P. E. Wright, *J. Magn. Reson.*, **64**, 220 (1985).

11) C. Chachaty, D. Gust, T. A. Moore, G. A. Nemeth, P. A. Liddle, and A. L. Moore, *Org. Magn. Reson.*, **22**, 39 (1984).

12) C. Franco and C. McLendon, *Inorg. Chem.*, **23**, 2370 (1984).

13) T. Nakahira and M. Grätzel, *J. Phys. Chem.*, **88**, 4007 (1984).

14) K. Nagayama, "NMR in Stereochemical Analysis," VCH Publishers, Inc. (1986), Chap. 5.

15) J. W. Dirks, G. Underwood, J. C. Matheson, and D. Gust, *J. Org. Chem.*, **44**, 2551 (1979).

16) P. J. Flory, "Statistical Mechanics of Chain Molecules," Wiley-Interscience, New York (1969).

Silica-Supported Heteropoly Acid Catalyst for Liquid-Phase Friedel-Crafts Reactions

Yusuke IZUMI,* Noriko NATSUME, Harumi TAKAMINE, Ikuyo TAMAOKI, and Kazuo URABE
Department of Synthetic Chemistry, Faculty of Engineering, Nagoya University,
Furo-cho, Chikusa-ku, Nagoya 464
(Received February 20, 1989)

Silica-supported Keggin-type heteropoly acids such as 12-tungstophosphoric, molybdophosphoric, and tungstosilicic acids efficiently catalyzed Friedel-Crafts alkylation and acylation reactions of aromatic hydrocarbons with 1-octene, benzyl chloride and benzoyl chloride in the liquid phase. The catalytic activity of heteropoly acid was generally enhanced when supported on silica. Silica-supported tungstosilicic acid worked as an insoluble heterogeneous catalyst even to the acylation of *p*-xylene with benzoyl chloride or benzoic anhydride, though deactivation was observed during repeated use. Considering that supported *p*-toluenesulfonic acid, an ordinarily used typical strong protonic acid, was far less active than the supported heteropoly acid, the high catalytic efficiency revealed by heteropoly acid appears to be due to a unique property of heteropoly anion which can stabilize alkyl and acyl cations as the reaction intermediates.

Several types of insoluble heterogeneous acid catalysts have recently been proposed for liquid-phase Friedel-Crafts reactions, in order to replace the conventional homogeneous catalysts such as $AlCl_3$ and sulfuric acid which often pose difficult operational problems of corrosion, removal from products, and requirement of stoichiometric catalyst amount. These heterogeneous catalyst systems include metal ion-exchanged aluminosilicates[1,2] and sulfate-doped metal oxides.[3] Concerning the acylation with acyl halides, however, there have not been developed such heterogeneous catalysts as can endure long-term use, yet.

Keggin-type heteropoly acid, which has been known to catalyze several organic reactions much more effectively than the ordinary protonic acids,[4] has also been explored as a Friedel-Crafts catalyst in the non-supported[5,6] or supported[7] state. The present study aims to inspect the applicability of supported heteropoly acids as heterogeneous catalysts for liquid-phase Friedel-Crafts reactions through the examination on the optimal conditions of catalyst preparation and through the re-examination on a problem of deterioration of heteropoly acid which has previously been pointed out concerning the acylation using acyl halides.[6]

Experimental

Catalyst. Each supported heteropoly acid catalyst was prepared by impregnating a support in the form of powders (115 mesh pass) with an aqueous solution of heteropoly acid followed by drying at 60—70 °C. The catalyst was calcined at a given temperature under reduced pressure (3 kPa) prior to use for the reaction. The Keggin-type heteropoly acids employed were of commercially available purity; tungstophosphoric ($H_3PW_{12}O_{40}\cdot 25H_2O$), molybdophosphoric ($H_3PMo_{12}O_{40}\cdot 9.3H_2O$), and tungstosilicic ($H_4SiW_{12}O_{40}\cdot 23.8H_2O$) acids. Silica A (Fuji Davison B, surface area 585 $m^2\,g^{-1}$, pore volume 0.774 $cm^3\,g^{-1}$), silica B (Fuji Davison ID, 105 $m^2\,g^{-1}$, 1.08 $cm^3\,g^{-1}$), and active carbon (Kraray GC, 1656 $m^2\,g^{-1}$, 0.34 $cm^3\,g^{-1}$) were used as catalyst supports.

Reaction Procedure. The organic reagents used were all purified by distillation. A suspension mixture of liquid organic substrates and solid catalyst granules in a flask was heated under reflux at atmospheric pressure. In the alkylation and acylation reactions using benzyl chloride and benzoyl chloride, the hydrogen chloride evolved during the reaction was removed by a continuous flow of nitrogen.

Analysis. The reaction products were determined by GLC (SE 30 and Unisole 30T columns) using internal standards. After the recation, the structural change of the supported heteropoly acid or of the heteropoly acid dissolved out during the reaction was examined through IR measurement using a Jasco IR-810 spectrophotometer.

Results and Discussion

Alkylation. Among the heteropoly acid catalysts tested, supported tungstophosphoric acid was most active for the alkylation of benzene with 1-octene. Only less than 5 mol% of a by-product dioctylbenzene was formed even at complete conversion of olefin, provided that an excess of benzene was used at a low reaction temperature of 35 °C. The isomers of 3- and 4-phenyloctanes were formed in addition to the major product of 2-phenyloctane (50—80 mol%).

Figure 1 demonstrates a remarkable influence of pretreatment temperature of catalyst on the catalytic activity of silica A-supported tungstophosphoric acid. The maximum conversion of 1-octene was attained when the catalyst was treated at 150 °C. The pretreatment at 100 °C gave only a meager activity. This is probably due to the remains of the crystal water of heteropoly acid which may reduce its acid strength. Indeed, according to the measurement by Hammett indicators, hydrous heteropoly acid ($H_3PW_{12}O_{40}\cdot 25H_2O$) showed an acid strength of $H_0 \geqq -3.0$, but it became more acidic ($H_0 \geqq -8.2$) when dehydrated by calcination at above 150 °C. Since it was confirmed from IR measurement that the Keggin structure of tungstophosphoric acid had still been completely retained even after 300 °C treatment, the reduction in catatytic

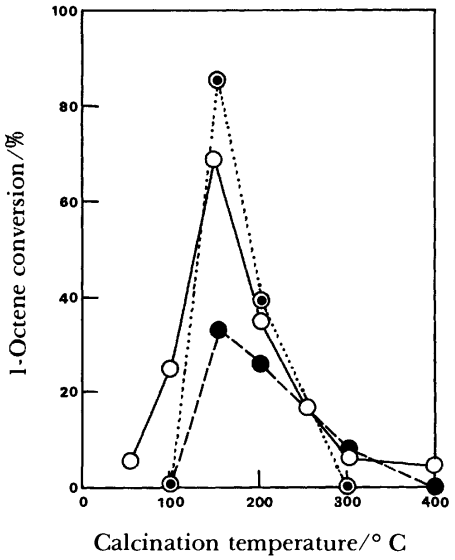

Fig. 1. Alkylation of benzene with 1-octene catalyzed by 12-tungstophosphoric acid (35 °C, 2 h). O: Supported on silica A (15 wt%, 0.01 mmol); ●: supported on silica B (15 wt%, 0.01 mmol); ⊙: non-supported (0.03 mmol); benzene: 30 mmol; 1-octene: 3 mmol.

activity of supported heteropoly acid caused by calcination at 300 °C may be due to decrease in effective surface area of the exposed crystallites of heteropoly acid through aggregation. In this context, it was observed that the surface area of non-supported tungstophosphoric acid was decreased on heating from 8.3 $m^2 g^{-1}$ (150 °C) to 4.2 $m^2 g^{-1}$ (300 °C), though the degree of activity decrease was more drastic (Fig. 1). A similar decrease in surface area on heating has already been pointed out by Misono et al.[8] about non-supported molybdophosphoric acid.

Lower dispersion of heteropoly acid on silica B support which has a relatively small surface area (105 $m^2 g^{-1}$) brought about lower catalytic activity in comparison with high surface area silica A support (585 $m^2 g^{-1}$). Tungstophosphoric acid, even in non-supported state, reasonably catalyzed the reaction, but its efficiency could be enhanced obviously when supported on silica A.

The catalytic activity increased monotonously with the loading of heteropoly acid even beyond high levels of 25 and 30 wt% over silica B and silica A supports, respectively, without any dissolution and deterioration of heteropoly acid (Fig. 2). According to our previous study on the vapor-phase alkylation of benzene with ethene over silica (319 $m^2 g^{-1}$)-supported tungstophosphoric acid catalysts,[4c] a ceiling of activity increase was observed at a lower loading of 15—20 wt% (Fig. 2, a broken line). Since the vapor-phase alkylation proceeded exclusively on the outer surface of the supported heteropoly acid, a loading of more than 15 wt% did not bring about a substantial increase in activity because of crystal growth of supported

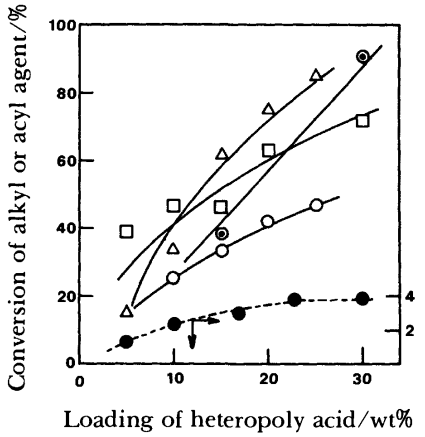

Fig. 2. Effect of loading of heteropoly acid on catalytic activities. O: Alkylation of benzene with 1-octene by 12-tungstophosphoric acid (0.01 mmol) on silica B (35 °C, 2 h); ⊙: alkylation of benzene with 1-octene by 12-tungstophosphoric acid (0.01 mmol) on silica A (35 °C, 1 h); ●: vapor-phase alkylation of benzene with ethene over silica-supported 12-tungstophosphoric acid (200 °C),[4c] △: alkylation of toluene with benzyl chloride by 12-molybdophosphoric acid (0.02 mmol) on silica B (75 °C, 2 h); □: acylation of *p*-xylene with benzoyl chloride by 12-tungstosilicic acid (0.01 mmol) on silica B (138 °C, 1 h).

Table 1. Benzylation of Benzene with Silica-Supported Acid Catalysts (80 °C, 2 h)[a]

Acid	Benzyl chloride conversion/%
$H_3PMo_{12}O_{40}$	72.2
$H_3PW_{12}O_{40}$	27.2
$H_4SiW_{12}O_{40}$	17.3
p-$CH_3C_6H_4SO_3H$	0

a) Support: silica B; acid: 0.02 mmol; loading: 15 wt%; pretreatment: 300 °C, 3 h; benzene: 100 mmol; benzyl cloride: 5 mmol.

heteropoly aicd. Therefore, the activity increase beyond 25 wt% loading observed even with a smaller surface area silica B support (105 $m^2 g^{-1}$) in the present liquid-phase alkylation reaction suggests that the reaction may involve a 'bulk-type reaction,' namely, the reaction occurs not only on the surface but also inside the bulk of the crystallites of heteropoly acid on the support.

In contrast to the case of alkylation with olefin, silica B-supported molybdophosphoric acid catalyzed the alkylation of aromatic hydrocarbons with benzyl chloride most efficiently (Table 1). Neither dissolution nor deterioration of the supported heteropoly acid was observed during the reaction. Since the acid strength of molybdophosphoric acid is weaker than that of tungstophosphoric acid,[4d] higher catalytic efficiency of molybdophosphoric acid in this acylation may reflect its stronger affinity to benzyl chloride

compared with other heteropoly acids. *p*-Toluenesulfonic acid, a typical conventional protonic acid, was inactive for this reaction. It is, therefore, suggested that heteropoly acid may exhibit Lewis acid-like catalytic function through an stabilizing effect by heteropoly anion[4d] on the benzyl cation as a reaction intermediate, although heteropoly acid itself is a protonic acid in nature.

Figure 3 illustrates the effect of pretreatment temperature of supported molybdophosphoric acid on the catalytic activity of benzylation of toluene. The maximum conversion appeared when the catalyst was preheated at 300 °C, but deactivation of catalyst occurred at higher pretreatment temperatures above 300 °C mainly because of decomposition of the heteropoly acid.

The benzylation activity increased with increasing loading of heteropoly acid beyond 25 wt% on silica B support without any dissolution and deterioration of heteropoly acid (Fig. 2), indicating that the benzylation involved a bulk-type reaction, also (vide supra). Other active alkyl halides such as bromocyclohexane could be favorably applied as an alkylating agent in the presence of the supported molybdophosphoric acid catalyst, but the catalyst was almost inactive for the alkylation reactions using primary alkyl halides.

Acylation. Figure 4 shows the result of the acylation of *p*-xylene with benzoyl chloride using silica-supported molybdophosphoric acid catalyst which was calcined beforehand at different temperatures. The catalysts which underwent milder thermal pretreatment were active, in particular (a solid line). However, the reaction proceeded still more even when the solid catalyst was removed out of the reaction medium in the course of the reaction (a broken line). In addition, molybdophosphoric acid was found almost decomposed after the reaction. These results unambiguosly indicate that the real active catalyst species was not the heteropoly acid on the support, but any other soluble species which might be formed during the reaction between heteropoly acid and benzoly chloride. Yamaguchi et al.[6] have also reported similar possibility of deterioration of non-supported molybdophosphoric acid when employed as a catalyst in the liquid-phase acylation of chloro-

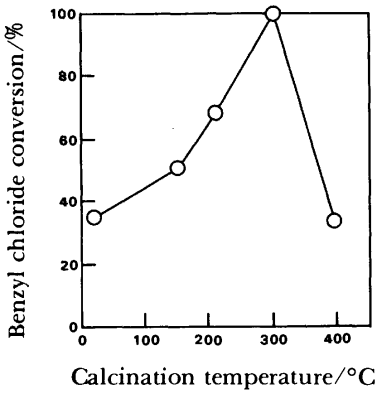

Fig. 3. Alkylation of toluene with benzyl chloride catalyzed by supported 12-molybdophosphoric acid (75 °C, 2 h). Heteropoly acid: 0.02 mmol; support: silica B (15 wt% loading); toluene: 100 mmol; benzyl chloride: 10 mmol.

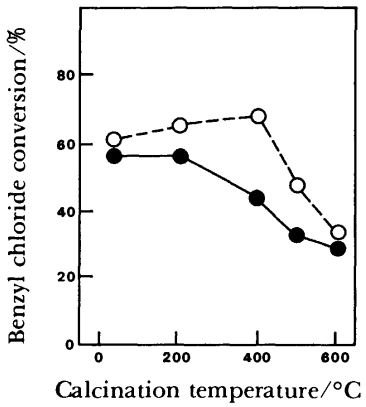

Fig. 4. Acylation of *p*-xylene with benzoyl chloride catalyzed by supported 12-molybdophosphoric acid (138°, 1 h). Heteropoly acid: 0.01 mmol; support: silica B (15 wt% loading); *p*-xylene: 30 mmol; benzoyl chloride: 3 mmol. The broken line denotes the final conversion of the reaction performed for more one hour successively after the catalyst was removed.

Table 2. Acylation of *p*-Xylene with Benzoyl Chloride Catalyzed by Supported Heteropoly Acid (138 °C, 1 h)[a]

Calcination temperature/°C	Benzoyl chloride conversion/%[b]	
	Tungstosilicic acid	Tungstophosphoric acid
Not treated	6.4 (6.4)	0 (0)
100	11.9 (11.5)	— —
200	49.0 (47.4)	11.0 (10.6)
300	46.0 (47.3)	33.2 (33.6)
400	40.7 (39.4)	17.0 (16.0)
500	0 (0)	20.2 (21.2)
600	0 (0)	0 (0)

a) Support: silica B; loading: 15 wt%; net amount of heteropoly acid: 0.01 mmol; *p*-xylene: 30 mmol; benzoyl chloride: 3 mmol. b) The values in parentheses denote the final conversions of the reaction which was performed for more one hour successively after the catalyst was removed.

benzene with *o*-chlorobenzoyl chloride.

In contrast to molybdophosphoric acid, however, it was found that tungstosilicic acid and tungstophosphoric acid were both hardly soluble and remained unchanged in the reaction medium of the acylation of *p*-xylene with benzoyl chloride, still holding their Keggin structures. Thus the supported tungstosilicic and tungstophosphoric acids proved to effectively catalyze the acylation as heterogeneous and insoluble catalysts, particularly when calcined at between 200—500 °C (Table 2). In these cases, the reaction did not proceed any more if each solid catalyst was filtrated off out of the reaction medium.

The benzoylation activity increased with increasing loading of tungstosilicic acid beyond 30 wt% on silica B support without any dissolution and deterioration of heteropoly acid (Fig. 2), indicating that the benzoylation involved a bulk-type reaction, also.

In a polar reaction medium as met in the acylation of chlorobenzene, however, even silica-supported tungstosilicic acid was gradually migrated and deteriorated in the course of the reaction like as supported molybdophosphoric acid. Thus the silica-supported tungstosilicic acid appears to be effectively applicable as an insoluble acid catalyst for an acylation reaction in which a large excess of less polar aromatic hydrocarbon is applied, as exemplified by a reaction medium which consists of benzene and benzoyl chloride in a mole ratio of between 10:1 and 3:1.

Table 3 represents the deactivation of silica-supported tungstosilicic acid catalyst in the course of the acylation reaction which was repeated several times by separating organic liquid from catalyst followed by the addition of fresh reactants whenever the reaction was performed for 3 h. A rapid decline in catalytic activity was observed from the second repeated run, but the total catalytic turnover was as much as about 300 per mole of heteropoly acid. The deactivation is probably caused by strong adsorption of the product benzophenone onto the catalyst, because it was confirmed from a separate experiment that the acylation was considerably retarded if the reaction was started in the presence of benzophenone. The detailed examination on catalyst deactivation and its regeneration are in progress.

Benzoic anhydride was also favorably employed as an acylating agent over the silica-supported tungstosilicic acid, but the acylation with benzoic acid did not proceed over this catalyst. Active carbon-supported tungstosilicic acid could catalyze the acylation, although its activity was limited to about a half of silica B-supported catalyst because of the reduction in acid strength.

Table 3. Deactivation of Silica-Supported Tungstosilicic Acid in Acylation of *p*-Xylene with Benzoyl Chloride[a)]

Repeated run number	Benzoyl chloride conversion/%
0	100
1	100
2	91
3	62
4	41
5	0

a) Support: silica B; loading: 15 wt%; net amount of heteropoly acid: 0.04 mmol; *p*-xylene: 30 mmol; benzoyl chloride: 3 mmol; reaction conditions: 138 °C, 3 h.

p-Toluenesulfonic acid was quite inactive also for this acylation reaction. This fact again indicates a peculiar function of heteropoly anion to be able to stabilize the intermediate acyl cation.

The present work was supported by a Grant-in-Aid for Scientific Research No. 62470075 from the Ministry of Education, Science and Culture.

References

1) P. Laszlo and A. Mathy, *Helv. Chem. Acta*, **70**, 577 (1987).

2) B. Chiche, A. Finiels, C. Gauthier, and P. Geneste, *J. Mol. Catal.*, **42**, 229 (1987).

3) a) K. Tanabe, *Shokubai*, **27**, 198 (1985). b) K. Arata and M. Hino, *ibid.*, **25**, 124 (1983). c) K. Arata and M. Hino, 9th International Congress on Catalysis, Calgary, June 1988, Proc., p. 1727.

4) a) Y. Izumi and K. Hayashi, *Chem. Lett.*, **1980**, 787. b) Y. Izumi and K. Urabe, *ibid.*, **1981**, 663. c) K. Matsuo, K. Urabe, and Y. Izumi, *ibid.*, **1982**, 1315. d) Y. Izumi, K. Matsuo, and K. Urabe, *J. Mol. Catal.*, **18**, 299 (1983). e) Y. Izumi, R. Hasebe, and K. Urabe, *J. Catal.*, **84**, 402 (1983).

5) K. Nomiya, T. Ueno, and M. Miwa, *Bull. Chem. Soc. Jpn.*, **53**, 827, 2089, 3389 (1980).

6) T. Yamaguchi, A. Mitoh, and K. Tanabe, *Chem. Lett.*, **1982**, 1229.

7) R. T. Sebulsky and A. M. Henke, *Ind. Eng. Chem., Process Des. Dev.*, **10**, 272 (1971).

8) M. Misono, Y. Konishi, M. Furuta, and Y. Yoneda, *Chem. Lett.*, **1978**, 709.

Electronic Spectra of Square-Planar Bis(biuretato)cobaltate(III)-Type Complexes

Takashi KOMORITA,* Masanori B. FUJITA, Kan KANAMORI,† Sawako HAYASHI, and (the late) Yoichi SHIMURA

Department of Chemistry, Faculty of Science, Osaka University, Toyonaka, Osaka 560
†Department of Chemistry, Faculty of Science, Toyama University, Gofuku, Toyama 930

(Received January 29, 1988)

Several square-planar cobalt(III) complexes of bis(biuretato)-type were synthesized with new quadridentate ligands, alkylenebis(biuret)'s, where alkylene bridging group is (*R,S*)- or (*R*)-propylene, 1,1-dimethylethylene, *cis*-1,2-cyclohexylene, or tetramethylethylene. Faraday parameters for possible CT transitions in the complexes were expressed as functions of MO coefficients and energies. From the examination of the magnetic circular dichroism, the intense absorption band observed at ca. 20×10^3 cm^{-1} was assigned to ligand-to-metal charge-transfer transitions of ligand π (a_u of D_{2h}) to metal d_{yz} and $d_{zx'}$, and the ground state was inferred to be one close to D_{4h} symmetry. The band assignment was also consistent with the resonance Raman spectrum of potassium bis(biuretato)cobaltate(III). Absorption spectra of the complexes occasionally lost intensity with decrease of temperature. Origin of the thermochromism, which was found to be reversible, was also discussed.

Bis(biuretato)cobaltate(III)-type complexes, first reported by Bour and Steggerda, are known to possess a square-planar $Co(N)_4$ coordination geometry.[1-3] Magnetic susceptibility measurements have shown that spin-triplet ground state is retained even below 10 K in crystalline state.[4] The electronic ground state and the coordination mode have been considered to be kept also in solution as judged by observed electronic spectral features. To our knowledge, no detailed investigations have ever been made, however, about the interactions of the complexes with the solvent molecules of weak electron-donor property such as dimethyl sulfoxide (DMSO), ethanol, and water, though some amines have been demonstrated to be coordinated to give usual low-spin six-coordinate cobalt(III) species in ethanol.[4] Consistently potassium bis(3-phenylbiuretato)cobaltate(III) crystallizes with two uncoordinated DMSO molecules as revealed by X-ray analysis.[3]

Furthermore, nature of electronic absorption bands in the complexes have been not so fully investigated. In the present paper, the following main points will be discussed: 1) Assignment of the relatively weak and intense absorption bands observed at 10—16 and ca. 20×10^3 cm^{-1}, respectively. 2) A remarkable thermochromism in water-containing media, which was discovered in the present study.

Scheme 1 displays the ligands used and their abbreviations. The complexes with the last two ligands are known[4] whereas complexes with the other four were newly prepared for the purpose of comparative study of their electronic spectra. Improvement of solubility properties was achieved to some extent by the modification of ligands in the complexes.

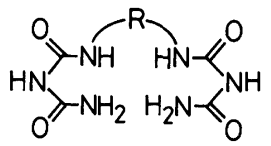

H_4bbpn	R = -CH(CH$_3$)CH$_2$-
H_4bbibn	R = -C(CH$_3$)$_2$CH$_2$-
H_4bbchxn	R =
H_4bbtmen	R = -C(CH$_3$)$_2$C(CH$_3$)$_2$-
H_4bbphen	R =
H_2bi	R/2 = H

Scheme 1.

Experimental

Materials. *o*-Phenylenebis(biuret) (H_4bbphen) and three new ligands, (*R,S*)-propylene-, 1,1-dimethylethylene-, and *cis*-1,2-cyclohexylene-bis(biuret) (H_4bbpn, H_4bbibn, and H_4*cis*-bbchxn) were prepared in a similar manner as given for H_4bbphen:[4] For the new ligands, mp 201—202, 207—208, 199.5—200.5 °C, respectively. Found for H_4bbpn·2H_2O: C, 29.78; H, 6.52; N, 29.47%. Calcd for $C_7H_{18}N_6O_6$: C, 29.79; H, 6.43; N, 29.77%. Found for H_4bbibn: C, 36.68; H, 6.16; N, 31.82%. Calcd for $C_8H_{16}N_6O_4$: C, 36.92; H, 6.20; N, 32.29%. Found for H_4*cis*-bbchxn·0.5H_2O: C, 40.79; H, 6.42; N, 28.45%. Cacld for $C_{10}H_{19}N_6O_{4.5}$: C, 40.67; H, 6.49; N, 28.46%. (*R*)-Propylenebis(biuret) was similarly derived from (*R*)-propylenediamine. Found for H_4bbpn·2H_2O: C, 29.59; H, 6.60; N, 29.44%.

Tetramethylethylenebis(biuret) (H_4bbtmen) was also obtained by a similar procedure, but we often found that *N,N*-dimethylformamide (DMF) was preferred as solvent for the syntheses of alkylbiurets,[5] especially in this case: mp 210—210.5 °C. Found for H_4bbtmen: C, 41.67; H, 7.00; N, 28.81%. Calcd for $C_{10}H_{20}N_6O_4$: C, 41.66; H, 6.99; N, 29.15%. Yields were generally 30—60% by 0.02—0.1 mole scale preparation for all the ligands.

Apart from isolation and purification procedures, potassium salts of the alkylenebis(biuretato)cobaltate(III) complexes were prepared in a similar method as that employed for the preparation of potassium ethylenebis(biuretato)-cobaltate(III).[4] In some cases active charcoal seems effective in complex formation. All the four complexes newly prepared were reprecipitated from aqueous solutions, whereas the known analogous complexes may be purified, if possible, only with organic solvents. Found for K[Co(*R,S*)-

bbpn]·H_2O: C, 23.49; H, 3.40; N, 23.43% and for the (*R*)-bbpn analog: C, 23.37; H, 3.39; N, 23.34%. Calcd for $C_7H_{12}N_6O_5CoK$: C, 23.47; H, 3.38; N, 23.46%. Found for K[Co(bbibn)]·H_2O: C, 25.89; H, 3.85; N, 22.21%. Calcd for $C_8H_{14}N_6O_5CoK$: C, 25.81; H, 3.79; N, 22.58%. Found for K[Co(*cis*-bbchxn)]·$0.5H_2O$: C, 30.56; H, 3.81; N, 21.02%. Calcd for $C_{10}H_{15}N_6O_{4.5}CoK$: C, 30.85; H, 3.88; N, 21.59%. Found for K[Co(bbtmen)]·$1.5H_2O$: C, 29.16; H, 4.57; N, 19.49%. Calcd for $C_{10}H_{19}N_6O_{5.5}CoK$: C, 29.34; H, 4.68; N, 20.53%. Yields were roughly 50, 45, 20, and 10%, respectively. The two known complexes were prepared according to the literature.[4] Found for K[Co(bbphen)]·H_2O: C, 30.69; H, 2.54; N, 20.95%. Calcd for $C_{10}H_{10}N_6O_5CoK$: C, 30.62; H, 2.57; N, 21.42%. Found for $K[Co(bi)_2]\cdot 0.5H_2O$: C, 15.78; H, 2.42; N, 27.30%. Calcd for $C_4H_7N_6O_{4.5}CoK$: C, 15.54; H, 2.28; N, 27.18%.

Measurements. The visible and ultraviolet absorption and reflectance spectra were recorded by a Hitachi 330 spectrophotometer. The CD and magnetic circular dichroism (MCD) spectra were obtained by a JASCO MOE-1 and a JASCO J-500C spectropolarimeter equipped with a 1.5-T electromagnet.

The low-temperature absorption spectra were measured with a hand-made cell and a glass Dewar provided with a light path. Body of the cell was made of a sheet of aluminum plate, on which polyacrylonitrile windows were mounted. Temperature measurements were carried out with a copper-constantan thermocouple dipped into sample solutions. With those samples that were employed for the low-temperature measurements, ambient-temperature measurements were also made for comparison.

Raman spectra were recorded on a JASCO R-800 laser Raman spectrophotometer. Exciting lines were provided by a Spectra-Physics Model 164 Ar^+ ion laser (514.5, 501.7, 496.5, 488.0, 476.5, 472.7, 465.8, and 457.9 nm) and by a Coherent Radiation Model 599 dye laser employing Rhodamine 6G (588.0 and 567.8 nm). A rotating sample technique was used to minimize thermal decomposition of the sample by laser illumination. Samples were provided by K_2SO_4 disks. Intensities were measured with respect to the 981 cm^{-1} band of K_2SO_4 as internal standard and corrected for instrumental spectral response and the ν^4 law.

Theoretical

Molecular Orbitals. The extended Hückel (EH) molecular orbital calculations with self-consistent charge were carried out on bis(biuretato)cobaltate(III) and three related complex anions: bis(biuretato)-cuprate(II) and -nickelate(II), and tris(biuretato)-cobaltate(III).[6,7] The atomic coordinates from X-ray analyses[3,8] were adapted to fit D_{2h} or D_3 symmetry. The molecular coordinate system adopted is shown in Scheme 2. Double-ζ functions of Richardson et al. for +1 ions were used for metal 3d atomic orbitals (AO),[9] and single-ζ functions of Summerville and Hoffmann for all the other valence AO's including metal 4s and 4p.[10]

Valence orbital ionization potentials (3d-VOIP's) for d^{n-1}s configurations[6b,11] were modified as below to give those results that enable a systematic explanation for the electronic spectra of the above four complexes. First, energy calculations were made for the copper(II) complex using modified *A* and *B* values (*A'* and *B'*) and the original *C*, where $A'=\eta A$, $B'=\eta B$ (η is a scaling factor), and symbols *A*, *B*, and *C* have the usual significance.[6b] A reasonable result was obtained at $\eta=0.4$.[12] Parameters *A'* and *B'* for cobalt or nickel were determined by $A'_M=A_M-0.6A_{Cu}$ and $B'_M=B_M-0.6B_{Cu}$ (M=Co or Ni); i.e., the same amount as in copper was subtracted from the relevant original value regarding each parameter, *A* or *B*. The original values of *A*, *B*, and *C* of d^{n-1}s and d^{n-1}p configurations were used for metal 4s and 4p H_{ii}'s, respectively. Constant Coulomb integrals[10] were employed for hydrogen 1s and second-row-atom 2s and 2p orbitals. The present parametrization may be partly rationalized by intramolecular Madelung energies.[13] Wolfsberg-Helmholz approximation was employed for off-diagonal H_{ij}'s; the value of the interaction constant *k* was 1.75 unless otherwise stated. Open shell configuration with two singly-occupied orbitals was assumed for bis(biuretato)-cobaltate(III) anion.

Figure 1 displays the resulting energy levels for the molecular orbitals (MO) which are largely metal d or ligand π in character. Several MO's of largely oxygen σ were neglected from Fig. 1 for simplicity, though turned out to be located at ca. -112×10^3 cm^{-1} or lower wavenumbers in all the complexes. The present calculation for bis(biuretato)cobaltate(III) ion gave the ground state with $(yz)^1(zx)^1$ configuration in contrast with $(zx)^1(x^2-y^2)^1$ given by Birker et al.,[4] where (yz), (zx), etc. denote the MO's of largely d_{yz}, d_{zx}, etc.

Faraday Parameters for Charge Transfer Transitions. For $^3B_{1g}$ ground state with $(yz)^1(zx)^1$ configuration, such charge-transfer (CT) transitions as shown in Table 1 may be allowed between metal d and ligand π

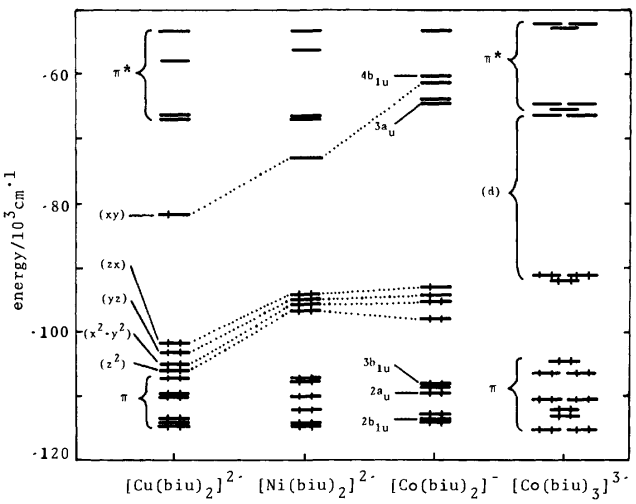

Fig. 1. Molecuar orbital energy diagram of bis-(biuretato)cobaltate(III) and related complexes. Molecular orbitals of largely ligand σ are omitted.

Table 1. Possible Types of Charge-Transfer Transitions in $[Co(bi)_2]^-$ for $^3B_{1g}$ Ground State with $(yz)^1(zx)^1$ Configuration[a)]

Excited states	LMCT	Abbrev.	MLCT	Abbrev.
$^3B_{3u}$	$b_{1u}(\pi_L) \rightarrow (yz)$	J_1	$(yz) \rightarrow b_{1u}(\pi^*_L)$	J_1'
$^3B_{2u}$	$b_{1u}(\pi_L) \rightarrow (zx)$	J_2	$(zx) \rightarrow b_{1u}(\pi^*_L)$	J_2'
$^3B_{2u}$	$a_u(\pi_L) \rightarrow (yz)$	J_3	$(yz) \rightarrow a_u(\pi^*_L)$	J_3'
$^3B_{3u}$	$a_u(\pi_L) \rightarrow (zx)$	J_4	$(zx) \rightarrow a_u(\pi^*_L)$	J_4'
^3A_u	$a_u(\pi_L) \rightarrow (xy)$	J_5	$(z^2) \rightarrow b_{1u}(\pi^*_L)$	J_5'
^3A_u	——	—	$(x^2-y^2) \rightarrow b_{1u}(\pi^*_L)$	J_6'

a) For example, the abbreviation of ligand MO $b_{1u}(\pi_L)$ represents the $nb_{1u}(\pi_L)$ with n=1, 2, or 3, so J_1 the transition from one of the three MO's.

MO's in bis(biuretato)cobaltate(III) anion. Faraday parameters $\bar{B}_0$ for all the CT transitions can be formulated, as given below, in terms of the MO coefficients and the matrix elements of operator ∇ by the standard procedure:[14)]

$$\bar{B}_0(J_1) = -\bar{B}_0(J_1') = -C(M_1/E_{3b})[M_3/(E_{32}E_{2b}) - \sqrt{3}M_4/(E_{31}E_{1b}) - M_2/(E_{43}E_{4b})], \quad (1)$$

$$\bar{B}_0(J_2) = -\bar{B}_0(J_2') = -C(M_2/E_{4b})[M_3/(E_{42}E_{2b}) + \sqrt{3}M_4/(E_{41}E_{1b}) + M_1/(E_{43}E_{3b})], \quad (2)$$

$$\bar{B}_0(J_3) = -\bar{B}_0(J_4) = C(M_5)^2/(E_{4a}E_{43}E_{3a}), \quad (3)$$

$$\bar{B}_0(J_5) = 2C(M_5M_6/E_{5a})[1/(E_{54}E_{4a}) + 1/(E_{53}E_{3a})], \quad (4)$$

$$\bar{B}_0(J_3') = -\bar{B}_0(J_3) + CM_5M_6/(E_{5a}E_{53}E_{3a}), \quad (5)$$

$$\bar{B}_0(J_4') = -\bar{B}_0(J_4) + CM_5M_6/(E_{5a}E_{54}E_{4a}), \quad (6)$$

$$\bar{B}_0(J_5') = \bar{B}_0(J_6') = 0, \quad (7)$$

where $\bar{B}_0(J)$ refers to a transition J given in Table 1; constant C is equal to 207.35 if MO energy differences E_{ij} are given in 10^3 cm^{-1} and quantities M_k in atomic unit; E_{ij} is defined by $E_i - E_j$; and the i or j values, a, b, and 1—5, denote the MO's, $na_u(\pi_L)$, $nb_{1u}(\pi_L)$ (n: ordinal number), $9a_g=(z^2)$, $10a_g=(x^2-y^2)$, $3b_{3g}=(yz)$, $4b_{2g}=(zx)$, and $8b_{1g}=(xy)$, respectively. Care must be taken especially in the MO symbols a and b, which indicate the π or π^* MO's relevant to the CT transition in question. Thus every equation connecting $\bar{B}_0(J_i)$ for a ligand-to-metal (LM) and $\bar{B}_0(J_i')$ for a metal-to-ligand (ML) CT transition in Eqs. 1, 2, 5, and 6 means only a formal resemblance between the two $\bar{B}_0$'s. In the above formulation, two-center magnetic-transition-moment integrals were ignored and the MO's of mainly metal d character were approximated by pure d orbitals.

The quantities, M_k, can be expressed as:

$$M_1 = -4\sum_{m=1}^{3} c_{bm}[\cos^2\theta_m \langle ZX|\nabla_X|Z\rangle^m + \sin^2\theta_m \langle YZ|\nabla_Y|Z\rangle^m] - 2c_{b4}\langle ZX|\nabla_X|Z\rangle^4, \quad (8)$$

$$M_2 = 4\sum_{m=1}^{3} c_{bm}[\sin^2\theta_m \langle ZX|\nabla_X|Z\rangle^m + \cos^2\theta_m \langle YZ|\nabla_Y|Z\rangle^m] + 2c_{b4}\langle YZ|\nabla_Y|Z\rangle^4, \quad (9)$$

$$M_3 = -4\sum_{m=1}^{3} c_{bm}\cos(2\theta_m)\langle X^2-Y^2|\nabla_Z|Z\rangle^m - 2c_{b4}\langle X^2-Y^2|\nabla_Z|Z\rangle^4, \quad (10)$$

$$M_4 = -4\sum_{m=1}^{3} c_{bm}\langle Z^2|\nabla_Z|Z\rangle^m - 2c_{b4}\langle Z^2|\nabla_Z|Z\rangle^4, \quad (11)$$

$$M_5 = -2\sum_{m=1}^{3} c_{am}\sin(2\theta_m)[\langle ZX|\nabla_X|Z\rangle^m - \langle YZ|\nabla_Y|Z\rangle^m], \quad (12)$$

$$M_6 = 4\sum_{m=1}^{3} c_{am}\sin(2\theta_m)\langle X^2-Y^2|\nabla_Z|Z\rangle^m, \quad (13)$$

where c_{im} is the amplitude coefficient of $2p_\pi$ AO on atom m in the relevant π-MO i [i=a or b for a_u or b_{1u}; and m=1—4 for N(terminal), C, O, and N(central) atom, respectively, of the N-CO-N group in the first quadrant of the molecular coordinate system (Scheme 2)]. The acute angle θ_m is defined by the x-axis and the position vector of atom m. Two-center integrals $\langle J|\nabla_I|K\rangle^m$, referring to metal $3d_J$ and atom-m $2p_K$ AO's, were defined relative to the local coordinate system shown in Scheme 3 and evaluated by Kral's formulas.[15)] Thus M_k's can be written by

$$M_k = \sum_{m=1}^{4} c_{im}C_{km}, \quad (14)$$

where C_{km}'s, which were evaluated as given in Table 2,

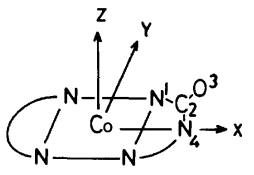

Scheme 2.

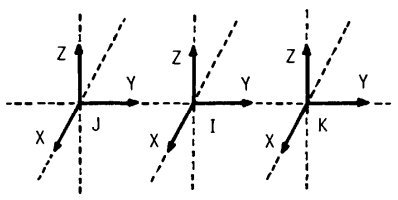

Scheme 3.

Table 2. C_{km} Values for $[Co(bi)_2]^-$

k	C_{k1}	C_{k2}	C_{k3}	C_{k4}
1	0.339	0.025	0.00055	0.0010
2	−0.339	−0.070	−0.00102	−0.0092
3	0.0	0.030	0.00028	0.0051
4	0.358	0.042	0.00058	0.0041
5	−0.198	−0.027	−0.00063	0.0
6	−0.339	−0.037	−0.00073	0.0

are dependent only on the given AO set and the molecular geometry.

The above formulation of $\bar{B}_0$ reflects mainly symmetry properties of the system, so it may be applicable to other d^6 planar complexes with a slight modification in M_k's, or Eqs. 8—13. In addition, Eqs. 1—7 need not be revised by a change in the energy order of MO's so long as it takes place within any of the doubly-occupied, the singly-occupied, and the vacant MO's.

The numerical results of $\bar{B}_0$ for several low-energy CT transitions are exemplified together with the calculated dipole strengths $\bar{D}_0$ in Table 3.

Results and Discussion

The absorption, CD, and MCD data obtained in DMSO and in aqueous solution at ambient temperature are shown in Tables 4 and 5 and Figs. 2—5. Abbreviations for intense bands, I—IV, were also denoted in Fig. 2. Spectral features in methanol solution were of intermediate between those in DMSO and aqueous solutions, although related data are not given.

Assignment of the Absorption Bands. An Intense Band at ca. 20×10^3 cm^{-1}: The bis(biuretato)cobaltate(III)-type complexes generally showed an intense absorption band ($\varepsilon\simeq7000$ in DMSO) at ca. 20×10^3 cm^{-1}. This band (band I) may be attributed to CT transitions between metal d and ligand π MO's because of the high intensities and of the relatively low energies. Numerical data of band I have once been given but not discussed at all.[3] From the absorption-band shape and the dispersion pattern of negative A-term type in this region, band I consists of at least two nearly degenerate components.

The band I for the complexes of bis(biuretato)-cobaltate(III) type was observed at much lower energies than the lowest-lying intense bands for the three related complexes.[16] The relative order of the transition energies is in agreement with the EH energy diagrams (Fig. 1) if band I is assigned to the lowest-lying LMCT transitions, whereas a different situation would be expected if it is assigned to MLCT.

Figure 6 shows the Raman spectrum (514.5 nm excitation) of the mother complex, $K[Co(bi)_2]\cdot0.5H_2O$, of the alkylenebis(biuretato) complexes discussed above. Assignment of the observed Raman bands was made based on a close correlation between the peaks in the Raman spectra of $K[Co(bi)_2]\cdot0.5H_2O$ and of $K_2[Cu(bi)_2]$[17] and summarized in Table 6.

It is well known that resonance Raman effects reflect the nature of the resonant electronic transition; that is, if a Raman band showed a strong resonance enhancement near the frequency of an electronic excitation within a certain chromophore, the equilibrium conformation of the chromophore should be considered to be distorted along the normal coordinate for the Raman band.[18] Figure 7 shows the excitation profiles of the Raman bands for which strong enhancements were observed on resonance with band I. Taking the

Table 3. The Values of $\bar{B}_0$ and $\bar{D}_0$ Parameters and Transition Energies Calculated by the EHMO Method[a] for Several Low-Energy CT Transitions in $[Co(bi)_2]^-$ with $^3B_{1g}$ Ground State

LMCT transition				
π-MO	Transition	Energy	$\bar{B}_0$	$\bar{D}_0$
		10^3 cm^{-1}	10^{-3} D^2 cm	D^2
$3b_{1u}$	J_1	13.8; 17.1	−0.43; 0.37	5.8; 3.0
$3b_{1u}$	J_2	15.0; 18.9	13.6; 4.6	4.4; 2.1
$2a_u$	J_3	15.4; 18.1	5.3; 2.3	3.3; 2.2
$2a_u$	J_4	16.6; 19.9	−5.3; −2.3	2.9; 1.8
$2b_{1u}$	J_1	19.8; 23.2	−1.3; −0.34	2.4; 1.8
$2b_{1u}$	J_2	20.9; 25.0	6.5; 3.3	2.4; 1.7
MLCT transition				
π-MO	Transition	Energy	$\bar{B}_0$	$\bar{D}_0$
		10^3 cm^{-1}	10^{-3} D^2 cm	D^2
$3a_u$	J_4'	28.4; 36.1	0.12; 0.23	0.20; 0.14
$3a_u$	J_3'	29.5; 37.9	−0.52; −0.07	0.18; 0.12
$4b_{1u}$	J_2'	32.5; 36.3	−0.011; −0.13	0.02; 0.10
$4b_{1u}$	J_1'	33.7; 38.1	−0.004; 0.06	0.0001; 0.05

a) Two set of the Wolfsberg-Helmholz constants were tested: $k_\sigma=k_\pi=1.75$, and $K_\sigma=1.75$ and $k_\pi=2.00$. The results obtained by the former and the latter set are given on the left and right of semicolon, respectively.

Table 4. Absorption Data of the Complexes[a)]

Complex	Solvent[b)]	$\tilde{\nu}_{max}/10^3$ cm^{-1} ($\log(\varepsilon/$mol^{-1} dm^3 cm^{-1}))		
K[Co((*R*,*S*)-bbpn)]·H_2O	D	11.4sh(1.8)	13.04(2.13)	18.83(3.85)
		24.3sh(3.5)	28.17(3.55)	36.66(3.79)
	W	11.21(1.35)	13.09(1.83)	20.41(3.55)
		23.8sh(3.5)	37.7sh(3.7)	
K[Co(bbibn)]·H_2O	D	11.4sh(1.8)	12.1sh(1.9)	12.82(2.16)
		18.87(3.87)	24.2sh(3.5)	28.17(3.54)
		35.84(3.78)		
	W	11.56(1.52)	12.3sh(1.9)	12.82(1.96)
		20.37(3.61)	23.8sh(3.5)	37.7sh(3.8)
K[Co(*cis*-bbchxn)]·0.5H_2O	D	≈11sh(1.7)	12.0sh(2.1)	12.76(2.72)
		18.90(3.87)	23.36(3.55)	27.93(3.59)
		35.59(3.83)		
	W	10.5sh(1.5)	12.3sh(2.0)	12.66(2.02)
		20.53(3.50)	22.9sh(3.4)	36.5sh(3.8)
K[Co(bbtmen)]·1.5H_2O	D	≈11sh(1.7)	12.0sh(2.0)	12.74(2.18)
		19.08(3.86)	23.53(3.51)	28.2sh(3.6)
		34.84(3.78)		
	W	11.3sh(1.7)	12.3sh(2.1)	12.72(2.14)
		20.70(3.65)	23.3sh(3.6)	36.50(3.76)
K[Co(bbphen)]·H_2O	D	11.17(3.03)	13.80(3.19)	19.19(3.83)
		26.8sh(3.5)	27.88(3.57)	31.0sh(3.7)
		34.1sh(4.0)		
	W	15.2sh(2.0)	22.54(2.69)	27.2sh(2.8)
		≈36br(4.22)		

a) sh denotes shoulder and br broad band. b) D and W denote DMF and water, respectively.

Table 5. MCD and CD Data of the Complexes

Complex	Solvent[a)]	$\tilde{\nu}_{ext}/10^3$ cm^{-1} ($\Delta\varepsilon_M/$mol^{-1} dm^3 cm^{-1} T^{-1})		
K[Co((*R*,*S*)-bbpn)]·H_2O	D	12.18(0.006)	13.00(−0.04)	18.20(6.75)
		20.30(−5.58)	27.07(−1.59)	33.57(0.17)
	W	13.02(−0.04)	18.41(1.10)	21.90(−1.25)
		29.20(−0.50)	39.95(−0.28)	
K[Co((*R*)-bbpn)]·H_2O[b)]	D	11.03(−0.72)	13.19(−1.81)	18.32(8.45)
		21.98(−1.07)	24.39(3.15)	30.40(−1.45)
	W	10.71(−0.51)	13.09(−1.25)	18.83(2.34)
		26.39(1.75)	30.96(−0.69)	
K[Co(bbibn)]·H_2O	D	11.42(−0.03)	12.90(−0.09)	18.24(6.99)
		20.31(−5.61)	26.78(−1.48)	33.31(0.27)
	W	12.92(−0.05)	18.42(1.14)	21.83(−1.43)
		28.92(−0.65)	39.60(−0.25)	
K[Co(*cis*-bbchxn)]·0.5H_2O	D	12.85(−0.11)	17.96(6.12)	20.19(−4.53)
		26.66(−1.36)		
	W	12.84(−0.08)	17.80(1.75)	21.45(−1.95)
		28.95(−0.99)	38.88(−0.35)	
K[Co(bbtmen)]·1.5H_2O	D	11.69(−0.10)	12.81(−0.15)	18.27(6.54)
		20.42(−4.93)	26.76(−1.53)	34.05(0.02)
		37.31(−0.29)		
	W	11.30(−0.04)	12.78(−0.29)	18.30(2.05)
		21.79(−2.39)	29.12(−1.13)	39.57(−0.20)
K[Co(bbphen)]·H_2O	D	10.08(−0.50)	12.76(−0.47)	14.30(0.22)
		18.23(5.00)	20.49(−3.49)	25.55(−1.84)
		31.03(0.12)		

a) See footnote b) in Table 1. b) For this complex, $\Delta\varepsilon_M$ is read as $\Delta\varepsilon$.

intensity of each band to be unity at 588.0 nm, the intensities of the bands at 392 and 815 cm^{-1} became ca. 30, those at 548, 1013, and 1625 cm^{-1} ca. 15, and those at 273 and 1362 cm^{-1} ca. 10, at the maximum of band I. The Raman bands arise from the skeletal stretching and deformation vibrations of the chelate ring as shown in Table 6. This observation indicates that the electron which is participating in the transitions of band I should be extensively delocalized over the ligand, being consistent with the assignment given above for band I.

As mentioned before, a marked MCD generally

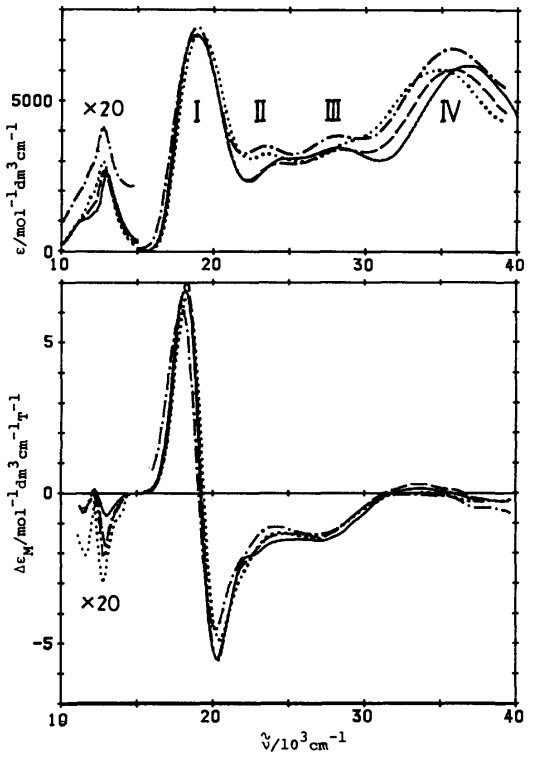

Fig. 2. Absorption and MCD spectra in DMSO solutions: K[Co((*R*,*S*)-bbpn)] (——), K[Co(bbibn)] (----), K[Co(*cis*-bbchxn)] (—·—·—), and K[Co(bbtmen)] (--------).

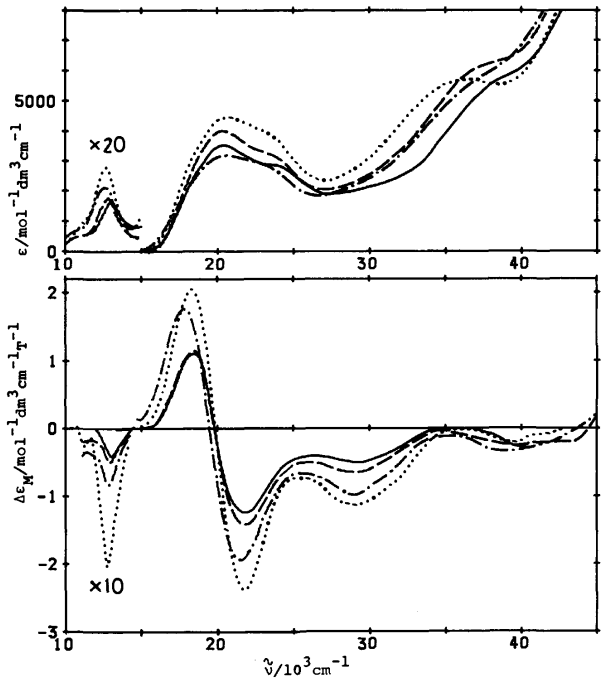

Fig. 3. Absorption and MCD spectra in aqueous solutions: K[Co((*R*,*S*)-bbpn)] (——), K[Co(bbibn)] (----), K[Co(*cis*-bbchxn)] (—·—·—), and K[Co(bbtmen)] (--------).

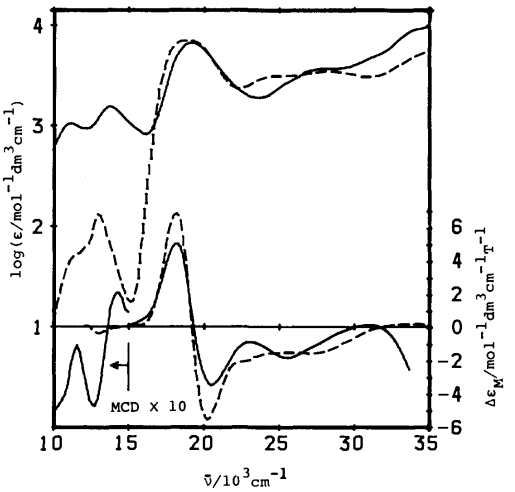

Fig. 4. Absorption and MCD spectra of K[Co(bbphen)] in DMSO solution (——). The spectra of K[Co((*R*,*S*)-bbpn)] (----) are added for comparison.

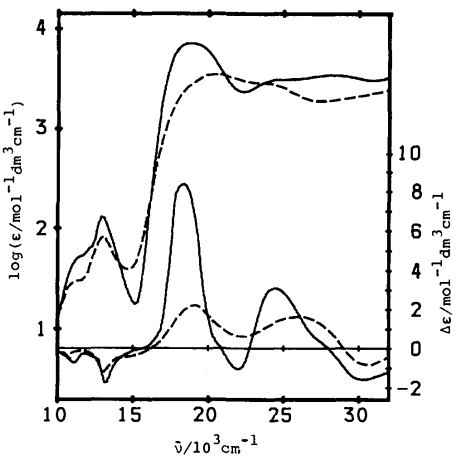

Fig. 5. Absorption and CD spectra of K[Co((*R*)-bbpn)] in DMSO (——) and in aqueous solution (----). The absorption spectra are added for comparison.

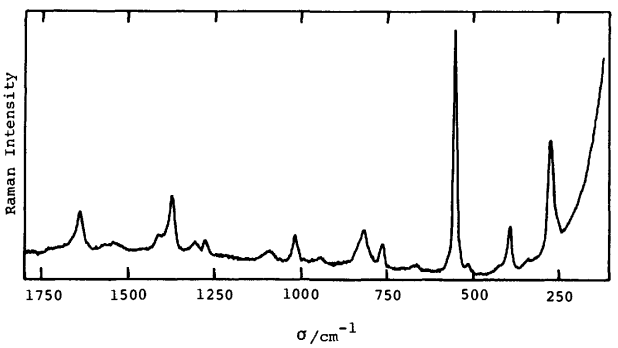

Fig. 6. Raman spectrum of $K[Co(bi)_2]\cdot 0.5H_2O$ (514.5 nm excitation).

appears in the region of band I. Its negative A-term pattern is retained among all the planar cobalt(III) complexes investigated. In Eqs. 1—3, so-called pseudo-A terms are found as couples of the B terms, i.e., of $\overline{B}_0(J_3)$ and $\overline{B}_0(J_4)$ and of the third terms in both $\overline{B}_0(J_1)$ and $\overline{B}_0(J_2)$, where each couple refers to a common ligand MO of a_u or b_{1u} symmetry. Such a couple of the B terms can be correlated by the following relation to the A term of a degenerate CT transition in square-planar model complex $[Co(NH_2)_4]^-$ with D_{4h} symmetry:

$$\overline{A}_1(J) = -\overline{B}_0(J')\Delta W = \overline{B}_0(J'')\Delta W, \quad (15)$$

where $\overline{A}_1(J)$ is the Faraday parameter defined for a degenerate transition J, J′ and J″ are the lower and the higher split components in the lower symmetry, and ΔW is the splitting between J′ and J″.[14a] For example, if transitions J_1 and J_2 are chosen as J′ and J″ and the energy difference $\Delta W = E_{43}$ is brought close to zero, the contributions from the first and the second terms of the right-hand sides of Eqs. 1 and 2 become negligible and Eq. 15 comes to hold exactly for J=an $a_{2u}(\pi_L)$-to-$e_g(d_{yz,zx})$ transition. If our $[Co(bi)_2]^-$ model is supposed to be very close to D_{4h}, only the first term $c_{i1}C_{k1}$ must survive in Eq. 14 as inferred from Table 2. Thus the influence of the non-ligating atoms on ligand π MO's disappears. Therefore the pseudo-A terms in the bis(biuretato) complexes can be discussed in terms of the square-planar model complex.

For the A terms of the latter model complex, the following relations are easily shown to hold:

$$\overline{A}_1/\overline{D}_0 = 1 \text{ for transitions between } e_g(d_{yz,zx}) \text{ and } a_{2u}(\pi_L), \quad (16)$$

$$\overline{A}_1/\overline{D}_0 = -1 \text{ for those between } e_g(d_{yz,zx}) \text{ and } b_{1u}(\pi_L), \quad (17)$$

where $\overline{D}_0$ are defined according to the literature.[14a] In addition, Eqs. 16 and 17 hold for various assumed ground states of $^3A_{2g}$ or ^3E_g. It should be noted that the a_{2u} and the b_{1u} MO's of largely ligand π in the square-planar complex correspond to a b_{1u} and an a_u MO's in the D_{2h} complex, respectively. Furthermore, the $^3A_{2g}(D_{4h})$ ground state corresponds to the $^3B_{1g}(D_{2h})$ with $(yz)^1(zx)^1$ configuration, whereas the $^3B_{2g}(D_{2h})$ ground state with $(x^2-y^2)^1(zx)^1$ is considerably different from every state of the D_{4h} model complex, because it has different occupation numbers, i.e., 2 and 1, for (yz) and (zx).

The Gaussian curve fittings were carried out for the band I region of the observed absorption and MCD spectra of the bbpn complex in DMSO (Fig. 8).[19] The $\overline{B}_0$ and $\overline{D}_0$ values were determined as given in Table 7. The $\overline{A}_1/\overline{D}_0$ value was also estimated at ca. −1.5 by use of Eq. 15 and the data in Table 7. By comparison of these results with the calculated values in Table 3 and with

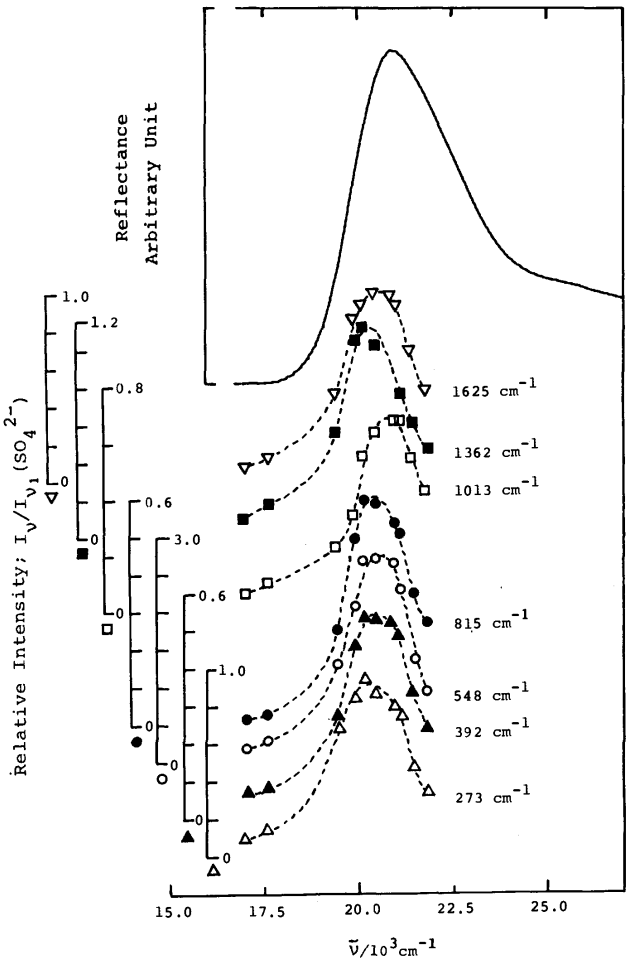

Fig. 7. Excitation profiles of the Raman bands of $K[Co(bi)_2]\cdot 0.5H_2O$ (----) together with the diffuse reflectance spectrum (——).

Table 6. Observed Raman Frequencies (cm^{-1}) and Their Assignments for $K[Co(bi)_2]\cdot 0.5H_2O$

Obsd.	Assignment	Obsd.	Assignment
1625*	ν(C=O)+ν(C-N)	1013*	ν(C-N)
1530	ν(C-N)+δ(C=O)	815*	ring def.
1400	ν(C-N)+δ(C=O)	763	δ(C=O)+ν(Co-N)
1362*	ν(C=O)+δ(N-H)	548*	ring def.+δ(C=O)+ν(Co-N)
1305	δ(N-H)	509	ring def.+δ(C=O)
1267	δ(N-H)	392*	ν(Co-N)+(C=O)+ring def.
1094	ν(C-N)	273*	ν(Co-N)

* Bands of which excitation profiles were obtained.

Table 7. The Curve Analysis Results for the Two Components of Band I of K[Co((*R*,*S*)-bbpn)] in DMSO[a)]

$\tilde{\nu}_{ext}$	δ[b)]	$(\varepsilon/\tilde{\nu})_{ext}$	$(\Delta\varepsilon_M/\tilde{\nu})_{ext}$	$\bar{D}_0$	$\bar{B}_0$
$10^3\,cm^{-1}$	$10^3\,cm^{-1}$	$mol^{-1}\,dm^3$	$10^{-3}\,mol^{-1}\,dm^3\,T^{-1}$	D^2	$10^{-3}\,D^2\,cm$
18.19	1.81	0.300	0.136	1.76	1.72
19.87	2.07	0.250	−0.098	1.69	−1.42

a) Details of the method are given in text and in Ref. 19. b) The whole width at half height.

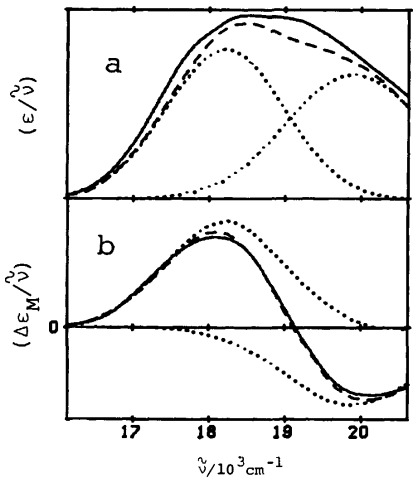

Fig. 8. Gaussian fittings of a) absorption and b) MCD spectra in the region of band I of K[Co(bbpn)] in DMSO: observed (——), calculated (----), and component curves (--------).

Eq. 17, band I may be assigned to the LMCT transitions of $a_u(\pi_L)$ to (yz) and (zx), that is, J_3 and J_4, which are derived from a b_{1u}-to-$e_g(yz,zx)$ transition in $[Co(NH_2)_4]^-$. Such a producibility of dispersion pattern in CT transitions is not specific for the $(yz)^1(zx)^1$ but in common with the $(yz,zx)^3(i)^1$ configuration, where $i=x^2-y^2$ or z^2. It should be noted in this context, however, that the energy difference of (yz) and (zx), ΔW, should be small enough only in the latter configuration, so as to secure essentially equal electron population on themselves, or to make the Boltzmann factor $\exp(-\Delta W/kT)$ unity. The situation is unlikely as in the $(zx)^1(x^2-y^2)^1$ configuration cited before.[4)]

Regarding the transition energies, however, the above band assignment is less satisfactory because in our EHMO results (Fig. 1) $3b_{1u}(\pi_L)$ lies above $2a_u(\pi_L)$ even though the energy difference is small. This point will be mentioned again in the next subsection.

Other Intense Bands: Three other intense absorption bands were generally observed at 23—24 (band II), 27—29 (band III), and ca. $35\times10^3\,cm^{-1}$ (band IV). Although many d-d bands are expected besides LMCT and MLCT bands throughout the wavenumber region, most of the absorption intensities may also be attributed to CT transitions from their high intensities.

Unfortunately, our EHMO calculations could not reproduce the transition energies and MCD intensities of bands I—IV simultaneously; the order of MO energies for k=1.75 (Fig. 1) was not altered by various k values except for the energy of (xy),[20)] and the amplitude coefficients in each MO and the calculated B terms for each CT transition (Table 3) were rather slightly dependent on k. Although any clear-cut assignment of bands II—IV cannot be made in these circumstances, it is supposed that the signs of B terms are usable as the basis for the following discussion but the transition energies are unusable since the difficulty in quantitative determination by MO method is well known.[21)]

Roughly speaking, the MCD of the bands decreases in intensity with increase in transition energies, i.e., in the order of I—IV, in line with the assignment of all these bands to CT and Eqs. 1—6. Since the MO results and Eqs. 1 and 2 predicted a net positive B term for the lowest-lying LMCT of (J_1, J_2) and a net negative one for the lowest-lying MLCT of (J_1', J_2') as seen in Table 3, bands IV and III may be tentatively assigned to the LMCT and the MLCT, respectively. Since band II seemingly resembles band III in the absorption spectra, MLCT may also be assigned to band II. The g value for a relatively strong CD accompanied by band II in the (R)-bbpn complex was one to two orders of magnitude too low for the band to be regarded as magnetically allowed. Since band II of the (R,S)-bbpn complex lost a significant amount of the intensity at liquid nitrogen temperature (Fig. 9b), some d-d character may also be suggested for band II.

Also in the region of bands II—IV the bbphen complex showed a spectral behavior slightly different from that in the other complexes.

Weak Bands in 10—16×10³ cm⁻¹ Region: The complexes of bis(biuretato)cobaltate(III)-type generally exhibited a group of weak absorption bands in this region in both DMSO and aqueous solutions. Two bands were always clearly observed at ca. 11 and $13\times10^3\,cm^{-1}$ and occasionally accompanied by a fine structure consisting of one to several very weak bands. In the region, our data in DMSO solutions nearly reproduced those for the analogous complexes reported by Birker et al.[4)] According to the latter authors the absorption bands measured both in DMSO and in ethanol solution as well as in the solid state of

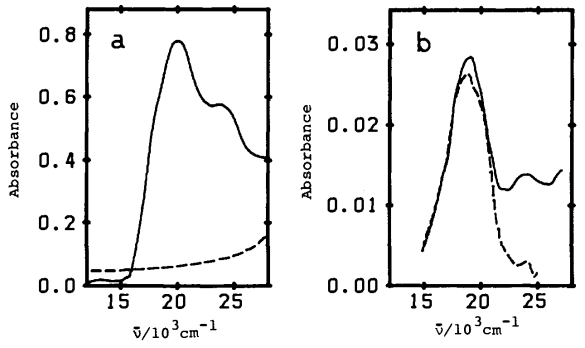

Fig. 9. Absorption spectra of K[Co((*R*,*S*)-bbpn)] at ambient temperature (——) and at 77 K (----): a) in water-glycerol (1/1 volume ratio), and b) in DMF-chloroform (1/1 volume ratio).

potassium bis(3-propylbiuretato)cobaltate(III) were quite the same; so the solvent molecules are not likely to interact with the planar $Co(N)_4$ species. It may be also the case with the complexes investigated in the present work as assumed in the preceding discussion.

The bands under discussion can be assigned to d–d transitions because of the low intensities. Furthermore, the *g* value, $|\Delta\varepsilon|/\varepsilon$, for the (*R*)-bbpn complex was roughly 1×10^{-2} in the region, indicating that the bands are magnetically allowed in agreement with the above assignment. Bour et al. assigned the 11 and $13\times10^3\,cm^{-1}$ bands to the transitions $^3B_{2g}\rightarrow{}^3A_{2g}$ and $^3B_{2g}\rightarrow{}^3E_g$, respectively.[2] This assignment, however, seems to assume an orbital energy too high for (z^2). As seen in Fig. 1, (z^2) may be lowered close to a level of (x^2-y^2), (yz), and (zx) by a configuration interaction involving metal 4s-orbital. Half-value widths of the two main bands are only $1.2—1.6\times10^3\,cm^{-1}$, being considerably narrower than those observed for the spin allowed bands due to transitions from nearly nonbonding d-orbitals[22] to strongly antibonding d_{xy} orbital; e.g., the band widths of planar bis(aminocarboxamidato)-nickel(II) complexes amount to $2.3\times10^3\,cm^{-1}$ or larger.[23] Therefore the weak bands in question would be more appropriately assigned to some transitions among the nonbonding d-orbitals rather than nonbonding d to d_{xy}. The fine structure observed on the d–d bands may reasonably be attributed to some spin-forbidden d–d transitions as judged by an angular overlap model examination of d^6 system.[24]

In agreement with the above discussion, the d–d transitions to d_{xy} orbital are located at $15\times10^3\,cm^{-1}$ or higher wavenumbers even in square-planar cobalt(II) complexes.[25] Exceptionally high intensities of the two bands of the bbphen complex in DMSO (Fig. 4) have been discussed by the previous authors.[4]

Thermochromism. We found a marked thermochromism for the five bis(biuretato)cobaltate(III)-type complexes in water-glycerol (1/1 volume ratio); with the bbphen complex, a small amount of DMSO was added to effect the dissolution. Preliminary measurements were carried out for the absorption spectra of the complexes below ambient temperature. One of the results is shown in Fig. 9a. In general the red color reversibly faded to pale yellow or pale violet when the solutions were cooled to 77 K. The bbtmen complex showed a slightly less pronounced temperature-dependence; its color was changed to bright orange at 77 K.

On the contrary the five complexes did not show any pronounced color change in DMSO or DMF solution, i.e., in nonaqueous media; as an example the temperature dependence of a nonaqueous glassy solution is shown in Fig. 9b. Some, not all, of the solutions changed the colors when a considerable amount of water was added. Red color of those solutions which remarkably faded when cooled to 77 K was darkened when heated. Thus the thermochromism was observed in a rather wide range of temperature. As an example of the detailed behavior, we observed that the decoloration of the bbpn complex was accelerated under −20 °C in the water-glycerol mixture. A hyperchromic effect was also observed when organic solvents such as alcohols and DMSO were added to aqueous solutions. Thus the thermochromism seems to occur only in water-containing media. Seemingly no thermochromism could be detected about the solid samples, however, in agreement with the knowledge that the spin-triplet ground state is retained in potassium bis(3-propylbiuretato)cobaltate(III) dihydrate even at −250 °C;[4] interestingly this substance contains water of crystallization.

While absorption, CD, and MCD spectra of the bis(biuretato)-cobaltate(III)-type complexes were appreciably deformed in aqueous solution, characteristic features exhibitied in DMSO were still retained except for the bbphen complex (Figs. 2 and 3). Dependence of both absorption and MCD spectra upon modification of the ligands was observed more remarkably in aqueous solution than in DMSO. The less the number of out-of-plane substituents are on the bridging group R in Scheme 1, the larger the observed solvent effect became. This fact implies that steric interactions between the bridging groups and water molecules dominate the spectral behavior.

All the above observations may be explained if it is supposed that each complex exists as an equilibrium mixture of the four-coordinate square-planar species and one or more five- or six-coordinate species in aqueous solution, and that any one of the non-planar species comes to dominate with lowering of temperature. This explanation may not be unreasonable in view of the residual ability of coordination in the analogous complexes.[4] Irreversible decomposition of the five complexes containing the bbphen complex seems negligible from the time-dependence of the absorption spectra. The bbpn complex in aqueous solution, for example, varied less than 1% in absorb-

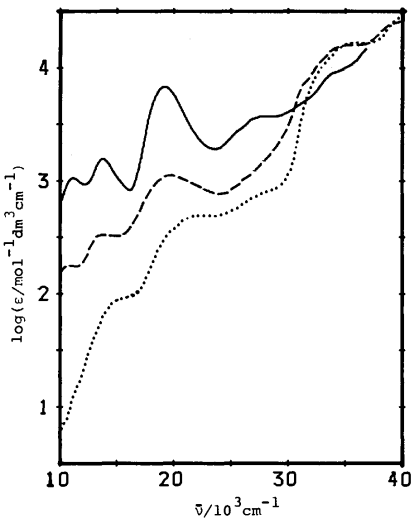

Fig. 10. Absorption spectra of K[Co(bbphen)]: in DMSO (——), in DMSO-water (1/1 volume ratio) (----), and in water (--------). The spectrum in DMSO solution is added for comparison.

ance for 8 h.

The absorption spectrum of the bbphen complex was deformed much more seriously than the other analogous complexes in aqueous solution, as shown in Fig. 10. The spectrum in the region of ca. 30×10^3 cm^{-1} or lower wavenumbers is seemingly dominated by ligand field transitions; accordingly a profound conversion of the planar species is likely to take place to give some usual low-spin cobalt(III) species. The spectral behavior of the bbphen complex should be considered, however, to be not so specific but rather general for all the five complexes since dark brown color of the bbphen complex in aqueous solution instantly turned to bright red, characteristic of the planar species, when a large amount of DMSO was added. Every absorption spectrum given in Fig. 10 obeys Beer's law almost exactly; it showed a negligible time-dependence for a few hours. The observations as a whole rule out the possibility that some associated species might play an important role in the temperature and solvent dependences of absorption spectra of the bis(biuretato)cobaltate(III)-type complexes.

References

1) J. J. Bour and J. J. Steggerda, *J. Chem. Soc., Chem. Commun.*, **1967**, 85.

2) J. J. Bour, P. T. Beurskens, and J. J. Steggerda, *J. Chem. Soc., Chem. Commun.*, **1972**, 221.

3) P. J. M. W. L. Birker and P. T. Beurskens, *Recl. Trav. Chim. Pays-Bas*, **93**, 218 (1974).

4) P. J. M. W. L. Birker, J. J. Bour, and J. J. Steggerda, *Inorg. Chem.*, **12**, 1254 (1973).

5) T. L. Davis and K. C. Blanchard, *J. Am. Chem. Soc.*, **51**, 1804 (1929).

6) a) R. Hoffmann, *J. Chem. Phys.*, **39**, 1397 (1963); b) C. J. Ballhausen and H. B. Gray, "Molecular Orbital Theory," W. A. Benjamin, Inc., New York (1964).

7) QCPE #193 program by R. M. Rawlinson and J. Fitzpatrick and some subprograms of CNINDO by J. A. Pople and D. L. Beveridge were used with some modifications.

8) H. C. Freeman, J. E. W. L. Smith, and J. C. Taylor, *Acta Crystallogr.*, **14**, 407 (1961); P. J. M. W. L. Birker, J. M. M. Smits, J. J. Bour, and P. T. Beurskens, *Recl. Trav. Chim. Pays-Bas*, **92**, 1240 (1973). The atomic coordinates for the copper complex were also used for the nickel complex.

9) J. W. Richardson, W. C. Nieuwpoort, R. R. Powell, and W. F. Edgell, *J. Chem. Phys.*, **36**, 1057 (1962).

10) R. H. Summerville and R. Hoffmann, *J. Am. Chem. Soc.*, **98**, 7240 (1976).

11) The parameters for copper were similarly derived: *A*, *B*, and *C* are 14.95, 114.75, and 86.0 for 3d; 7.6, 71.3, and 62.3 for 4s; and 8.45, 53.55, and 32.1×10^3 cm^{-1} for 4p orbitals.

12) Numerically similar parameters will be found in P. J. Hay, J. C. Thibeault, and R. Hoffmann, *J. Am. Chem. Soc.*, **97**, 4884 (1975).

13) C. K. Jørgensen, S. M. Horner, W. E. Hatfield, and S. Y. Tyree, *Int. J. Quantum. Chem.*, **1**, 191 (1967).

14) a) S. B. Piepho and P. N. Schatz, "Group Theory in Spectroscopy," John Wiley & Sons, New York (1983); b) P. H. Butler, "Point Group Symmetry Applicaions," Plenum, New York (1981).

15) M. Kral, *Collect. Czech. Chem. Commun.*, **35**, 1939 (1970); in the formula of $\langle 3d_{z^2}|\partial/\partial z|2p_z\rangle$ in Table IV, we read 9/4 instead of factor 3/4.

16) M. Kato, Y. Komuro, and K. Sone, *Nippon Kagaku Zasshi*, **78**, 896 (1957); M. Kato, *Z. Anorg. Allg. Chem.*, **300**, 84 (1959).

17) T. J. Thamann and T. M. Loehr, *Spectrochim. Acta, Part A*, **36**, 751 (1980).

18) A. Y. Hirakawa and M. Tsuboi, *Science*, **188**, 359 (1975).

19) The position and width for every component of the absorption band were treated as parameters common to the corresponding component of MCD. The agreement between the calculated and observed curves seems not so good especially in the absorption and a few minor components are likely to exist in this region. However, the results will not be arbitrary since the position of one component, 18194 cm^{-1}, is so close to that of the main CD band in this region.

20) The constant k was varied from 1.5 to 2.5 with the restriction of $k_\sigma<k_\pi$. The general trends of MO energies for various k were similar to those found in the paper: F. A. Cotton and C. B. Harris, *Inorg. Chem.*, **6**, 369 (1967).

21) R. F. Fenske, "Progress in Inorganic Chemistry," ed. by S. J. Lippard, Vol. 21, Wiley-Interscience, New York (1976), p. 179; *Pure Appl. Chem.*, **27**, 61 (1971).

22) The four d orbitals other than d_{xy} are called nonbonding for convenience.

23) T. Komorita and Y. Shimura, *Bull. Chem. Soc. Jpn.*, **52**, 1832 (1979).

24) T. Komorita, unpublished results.

25) Y. Nishida and S. Kida, *Bull. Chem. Soc. Jpn.*, **45**, 461 (1972); F. L. Ulbach, R. D. Bereman, J. A. Topich, M. Hariharan, and B. J. Kalbacher, *J. Am. Chem. Soc.*, **96**, 5063 (1974); J. -P. Barbier, Ahmed El Biyyadh, C. Kappenstein, N'Dongui Mabiala, and R. P. Hugel, *Inorg. Chem.*, **24**, 3615 (1985).

 © 1989 The Chemical Society of Japan Bull. Chem. Soc. Jpn., 62, 2173—2178 (1989)

Ionic Association of Mixed Nickel(II) Chelates in Alcohols, Ketones, and Nitrobenzene

Kazuaki ITO* and Yuroku YAMAMOTO†

Department of Environmental Science, Faculty of Engineering, Hiroshima University, Saijo, Higashi-Hiroshima 724

†Environmental and Safety Engineering Department, Fukui Institute of Technology, Gakuen, Fukui 910

(Received December 26, 1988)

The conductances of mixed nickel(II) chelates, [Ni(acac)(*N,N,N′,N′*-tmen)]X (where acac=2,4-pentanedionato, *N,N,N′,N′*-tmen=*N,N,N′,N′*-tetramethylethylenediamine, and X^-=ClO_4^- or NO_3^-), in alcohols {ethanol (EtOH), 1-propanol (*n*-PrOH), 2-propanol (*i*-PrOH), and 1-butanol (*n*-BuOH)}, ketones {acetone (Me_2CO), methyl ethyl ketone (MEK), and methyl isobutyl ketone (MIBK)}, and nitrobenzene ($PhNO_2$) were measured at 25 °C. The obtained ionic association constants (K_a) of [Ni(acac)(*N,N,N′,N′*-tmen)]ClO_4 which were derived by using the extended Fouss–Hsia function indicated that (1) the perchlorate complex is a normal type of uni-uni-valent electrolyte and (2) it is more dissociated than [Co(acac)$_2$(*N,N,N′,N′*-tmen)]ClO_4 in EtOH, *n*-PrOH, and *n*-BuOH. Walden products of the cations suggest that the nickel(II) chelate cation in the alcohols is present as an octahedral form with the coordination of two solvent molecules. On the other hand, K_a of [Ni(acac)(*N,N,N′,N′*-tmen)]NO_3 are much larger than those of [Ni(acac)(*N,N,N′,N′*-tmen)]ClO_4. This can be ascribed to the coordination of a nitrate ion to the nickel(II) ion. The effect is large and approximately the same in the ketones and $PhNO_2$, though small in EtOH, *n*-PrOH, and *n*-BuOH due to the coordination of solvent molecules.

Since the central metal ion of a quadratic-planar chelate cation is available to interact with solvents and anions, the complex offers interesting information which helps in understanding solute-solvent interactions different from those of octahedral complexes. However, very little attention have been paid to ionic association,[1] although there have been a number of studies concerning axial interaction by solvents with coordinating ability.

In this study, in order to obtain information on the ionic association of quadratic-planar complexes, the conductances of nickel(II) chelates, [Ni(acac)(*N,N,N′,N′*-tmen)]X (acac=2,4-pentanedionato, *N,N,N′,N′*-tmen=*N,N,N′,N′*-tetramethylethylenediamine, and X^-=ClO_4^- or NO_3^-) were measured in some alcohols and ketones as well as nitrobenzene. The conductance measurement is a useful tool for determining the ionic association constant and size of solvated- and coordinated-chelate cations.

It is well known that the color of the mixed nickel(II) chelate, [Ni(acac)(*N,N,N′,N′*-tmen)]ClO_4, which was prepared successfully by Fukuda and Sone,[2] changes abruptly from red to green on varying the solvent basicity. This has been ascribed to an equilibrium between two forms, one quadratic-planar (diamagnetic low-spin) and the other octahedral (paramagnetic hign-spin),

$$\underset{\text{(red)}}{[\text{Ni(acac)}(N,N,N',N'\text{-tmen})]^+} + 2\text{solvent} \rightleftharpoons \underset{\text{(green)}}{[\text{Ni(acac)}(N,N,N',N'\text{-tmen})(\text{solvent})_2]^+}. \quad (1)$$

As for the nitrate complex, on the other hand, the NO_3^- ion acts as a bidentate ligand and a counter anion in non-coordinating and strongly coordinating solvents, respectively.[2]

Since the alcohols and ketones in this study have similar basicities, but different dielectric constants and steric structures, the equilibrium of ionic association may be different from each other. Nitrobenzene, which is an inert solvent in basicity, was selected for a comparison. The obtained conductance parameters were compared in detail with those of an octahedral complex [Co(acac)$_2$(*N,N,N′,N′*-tmen)]ClO_4 in the solvents,[3–5] thus elucidating such solvent effects as solvent basicity, steric factor, and dielectric constant on ionic association.

Experimental

Material. [Ni(acac)(*N,N,N′,N′*-tmen)]ClO_4 was synthesized and recrystallized according to a published procedure,[2] followed by vacuum drying at ca. 50 °C. Calcd. for $NiC_{11}H_{23}N_2ClO_6$: C, 35.38; H, 6.21; N, 7.50%. Found: C, 35.10; H, 6.43; N, 7.67%.

Ni(acac)(*N,N,N′,N′*-tmen)(NO_3) was synthesized according to a published procedure,[2] recrystallized from 2-propanol, and then vacuum dried at ca. 50 °C. Calcd. for $NiC_{11}H_{23}N_3O_5$: C, 39.32; H, 6.90; N, 12.51%. Found: C, 39.54; H, 7.01; N, 12.50%.

Ethanol (EtOH), 1-propanol (*n*-PrOH), 2-propanol (*i*-PrOH), acetone (Me_2CO), methyl ethyl ketone (MEK), methyl isobutyl ketone (MIBK), and nitrobenzene ($PhNO_2$) of reagent grade were purified as described previously.[3–5] 1-Butanol (*n*-BuOH) was refluxed over calcium oxide and fractionally distilled.

Apparatus. The instrumentation and procedure used for the conductance measurements were described previously.[3]

Results

(A)[Ni(acac)(*N,N,N′,N′*-tmen)]ClO_4. The measured molar conductances, Λ (S cm^2 mol^{-1}) and the corresponding concentrations, C (mol dm^{-3}) are given

Table 1. Molar Concentrations (C/mol dm^{-3}) and Molar Conductances (Λ/S cm^2 mol^{-1}) of [Ni(acac)(N,N,N',N'-tmen)]ClO_4 in Alcohols, Ketones, and Nitrobenzene at 25 °C

EtOH		*n*-PrOH		*i*-PrOH		*n*-BuOH	
$C/10^{-4}$	Λ	$C/10^{-4}$	Λ	$C/10^{-4}$	Λ	$C/10^{-4}$	Λ
30.918	39.541	42.326	15.818	42.095	11.007	50.466	8.319
23.791	41.027	25.114	17.659	36.196	11.529	32.994	9.292
17.842	42.540	20.547	18.358	28.508	12.366	22.941	10.150
13.524	43.745	16.396	19.120	23.515	13.092	16.488	10.936
10.587	44.768	11.807	20.184	18.959	13.904	12.529	11.529
7.6498	46.005	7.8290	21.405	13.968	15.080	8.0525	12.565
5.8780	46.882	5.5427	22.314	9.6619	16.496	4.4196	13.784
4.9481	47.444	3.5231	23.312	6.6765	17.922	2.0132	15.092
—	—	2.4217	24.055	4.1567	19.616	—	—
Me_2CO		MEK		MIBK		$PhNO_2$	
$C/10^{-4}$	Λ	$C/10^{-4}$	Λ	$C/10^{-4}$	Λ	$C/10^{-4}$	Λ
46.640	141.58	36.869	97.267	22.376	40.685	42.344	30.104
29.550	150.66	28.905	101.64	16.698	44.162	35.410	30.570
15.930	161.47	22.970	105.62	12.430	47.850	28.594	31.090
12.212	165.69	17.164	110.51	8.9069	52.267	21.100	31.758
9.5289	169.50	13.074	115.21	5.9929	57.650	15.203	32.387
5.6724	176.12	9.3209	120.69	4.3787	62.032	10.543	33.006
4.3342	179.06	7.1014	124.74	2.9139	67.716	7.8916	33.408
—	—	4.6619	130.38	1.9400	73.186	5.1132	33.908
—	—	2.8327	136.10	0.9179	82.470	3.3470	34.323

Table 2. Solvent Parameters

Solvent	ε	η/mPa s	DN	AN
EtOH	24.33	1.082	20	37.9
n-PrOH	20.45	1.948	19.6	37.3
i-PrOH	19.41	2.078	—	33.5
n-BuOH	17.45	2.589	—	36.8
Me_2CO	20.56	0.3052	17	12.5
MEK	18.01	0.3803	—	—
MIBK	12.8	0.5478	—	—
$PhNO_2$	34.82	1.847	4.4	14.8

in Table 1. In EtOH, a slight increase in conductivity with time (ca. 0.1%/h) was observed. Therefore, a small correction was made by extrapolating to time zero. The data were analyzed by the Fuoss-Hsia function with Fernández-Prini coefficients and $E=E_1\Lambda_0-2E_2$,[6]

$$\Lambda = \gamma(\Lambda_0 - SC^{1/2}\gamma^{1/2} + EC\gamma\log C\gamma + J_1(d)C\gamma + J_2(d)C^{3/2}\gamma^{3/2}), \quad (2)$$

where the symbols have their usual meanings. The ionic association constant K_a can be expressed as

$$K_a = (1-\gamma)/\gamma^2 C f_\pm^2. \quad (3)$$

The mean ionic activity coefficient $f_\pm$ is given by the extended Debye-Hückel equation,

$$-\log f_\pm = AC^{1/2}\gamma^{1/2}/(1 + BdC^{1/2}\gamma^{1/2}). \quad (4)$$

The method for fitting in terms of Λ_0, K_a, and ion-size parameter d was described previously.[3] The standard deviation σ_Λ is defined as

$$\sigma_\Lambda = [\Sigma(\Lambda_{calcd.} - \Lambda_{obsd.})^2/(n-3)]^{1/2}, \quad (5)$$

where n is the number of experimental points. The dielectric constant (ε) and viscosity (η in mPa s) of the solvents[3,5,7-12] used in this study for analyses are given in Table 2, together with the donor number (DN) and acceptor number (AN) as measures of solvent basicity and acidity, respectively.[13] The obtained conductance parameters are given in Table 3. The limiting conductances (λ_0^+/S cm^2 mol^{-1}) and Walden products ($\lambda_0^+\cdot\eta$/S cm^2 mol^{-1} 10^{-1} Pa s) of the nickel(II) chelate cation were obtained from the limiting conductances of the perchlorate ion, λ_0^- (ClO_4^-): in EtOH, 32.04;[5] in *n*-PrOH, 16.42;[7] in *i*-PrOH, 15.24;[8] in *n*-BuOH, 11.22;[9] in Me_2CO, 118.35;[10] in MEK, 93.0;[5] in MIBK, $\lambda_0^-\cdot\eta$=0.34;[5] in $PhNO_2$, 20.9.[12]

(B)[Ni(acac)(N,N,N',N'-tmen)]NO_3. The molar conductivities of [Ni(acac)(N,N,N',N'-tmen)]NO_3 in the alcohols, the ketones, and $PhNO_2$ are given in Fig. 1. Since the conductivities are extremely small, due to a coordination of the nitrate ion to the nickel(II) ion, it is impossible to obtain Λ_0 and, consequently, K_a using the extended Fuoss-Hsia function (Eq. 2).

Thus, only K_a was estimated from Eq. 3, in which the fraction of electrolyte present as ions γ is simply expressed in the form

$$\gamma = \Lambda/(\Lambda_0 - SC^{1/2}\gamma^{1/2}), \quad (6)$$

where Λ_0 of [Ni(acac)(N,N,N',N'-tmen)]NO_3 was obtained from λ_0^+ ([Ni(acac)(N,N,N',N'-tmen)]$^+$) in Table 3 and λ_0^-(NO_3^-) from the literature.[12,14-16] The activity coefficient $f_\pm$ was estimated by using Eq. 4 and

Table 3. Conductance Results for [Ni(acac)(*N,N,N',N'*-tmen)]ClO_4 in Alcohols, Ketones, and Nitrobenzene at 25 °C

Solvent	Λ_0	λ_0^+	$\lambda_0^+ \cdot \eta$	K_a	d	σ_Λ
	S cm^2 mol^{-1}	S cm^2 mol^{-1}	S cm^2 mol^{-1} 10^{-1} Pa s	dm^3 mol^{-1}	10^{-1} nm	
EtOH	52.55±0.08	20.51	0.222	145± 10	13.8	0.05
n-PrOH	26.98±0.02	10.56	0.206	389± 11	14.3	0.02
i-PrOH	26.52±0.14	11.28	0.234	1160± 80	15.4	0.02
n-BuOH	17.58±0.03	6.36	0.165	749± 16	16.0	0.03
Me_2CO	199.0 ±0.1	80.6	0.246	162± 3	12.9	0.09
MEK	154.7 ±0.2	61.7	0.235	382± 28	13.2	0.11
MIBK	101.2 ±0.4	—	0.21	2900±100	17.5	0.15
$PhNO_2$	35.85±0.01	14.95	0.276	34± 5	7.6	0.007

Table 4. Limiting Conductances and Ionic Association Constants for [Ni(acac)(*N,N,N',N'*-tmen)]NO_3 in Alcohols, Ketones, and Nitrobenzene at 25 °C

Solvent	Λ_0	$\lambda_0^-(NO_3^-)$	K_a
	S cm^2 mol^{-1}	S cm^2 mol^{-1}	dm^3 mol^{-1}
EtOH	46.2	25.65	$(1.26\pm0.21)\times10^3$
n-PrOH	23.8	13.2	$(1.66\pm0.07)\times10^4$
i-PrOH	23.6	12.3	$(1.22\pm0.14)\times10^6$
n-BuOH	15.2	8.8	$(3.53\pm0.17)\times10^4$
Me_2CO	200.7	120.1	$(2.63\pm0.01)\times10^7$
MEK	147.7	86.0	$(3.48\pm0.23)\times10^7$
$PhNO_2$	37.6	22.6	$(3.36\pm0.26)\times10^6$

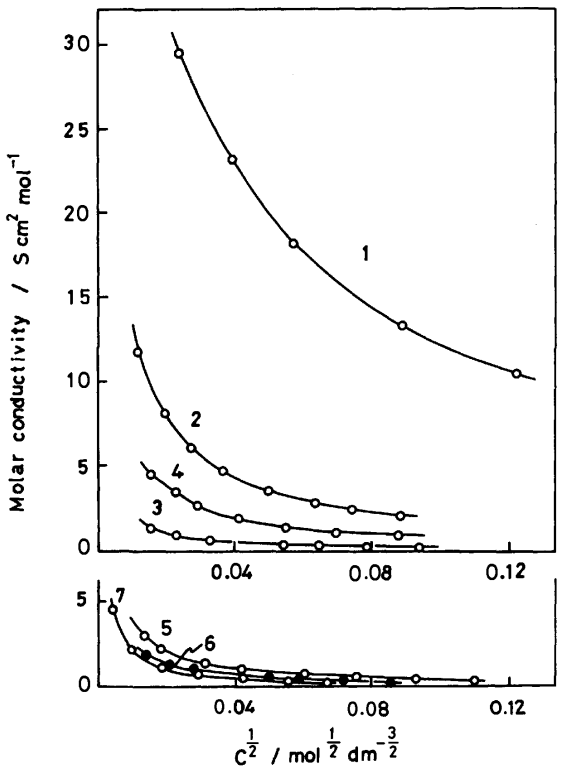

Fig. 1. Plots of the molar conductivity of [Ni(acac)-(*N,N,N',N'*-tmen)]NO_3 against the square root of the concentration in organic solvents at 25 °C. 1, EtOH; 2, *n*-PrOH; 3, *i*-PrOH; 4, *n*-BuOH; 5, Me_2CO; 6, MEK; 7, $PhNO_2$.

Bjerrum's critical distance in each solvent. The mean K_a values of a series of experimental points are given in Table 4 together with the values of Λ_0 and $\lambda_0^-(NO_3^-)$.

Discussion

(A)[Ni(acac)(*N,N,N',N'*-tmen)]ClO_4. The following classification becomes feasible toward the color change of [Ni(acac)(*N,N,N',N'*-tmen)]ClO_4 in the solvents, as described in Eq. 1:

Class I (Me_2CO, MEK, MIBK, $PhNO_2$, and *i*-PrOH) Red

Class II (EtOH, *n*-PrOH, and *n*-BuOH) Green

This indicates that the nickel(II) chelate ion is mainly present as a quadratic-planar [Ni(acac)(*N,N,N',N'*-tmen)]$^+$ for Class I and an octahedral [Ni(acac)-(*N,N,N',N'*-tmen)(solvent)$_2$]$^+$ for Class II.[2] This can be confirmed from the mobility data shown in Fig. 2. Walden products ($\lambda_0^+ \cdot \eta$) of [Ni(acac)(*N,N,N',N'*-tmen)]$^+$ should be larger than those of [Co(acac)$_2$-(*N,N,N',N'*-tmen)]$^+$ since the molal volume of the former is smaller than that of the latter due to a difference in the number of the ligand acac. This is the case for Class I, except for *i*-PrOH; the difference in $\lambda_0^+ \cdot \eta$ is particularly large in $PhNO_2$. For Class II, on the other hand, the opposite result is observed. In addition, the difference increases in the order EtOH< *n*-PrOH<*n*-BuOH.[17] This can not be explained in terms of coordination by one molecule, supporting

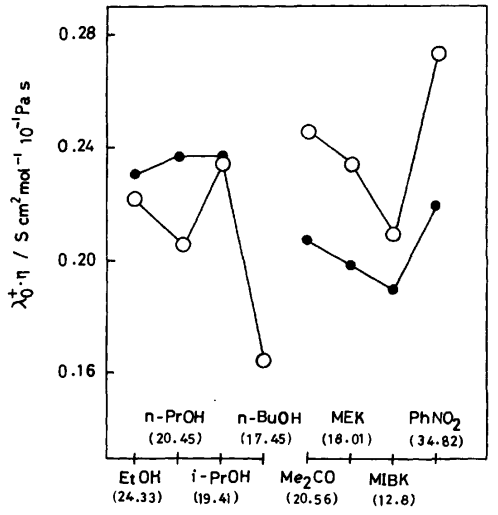

Fig. 2. Walden products of O, [Ni(acac)(*N,N,N',N'*-tmen)]$^+$ and ●, [Co(acac)$_2$(*N,N,N',N'*-tmen)]$^+$ in organic solvents at 25 °C. The values in parentheses are the dielectric constant (ε) of each solvent.

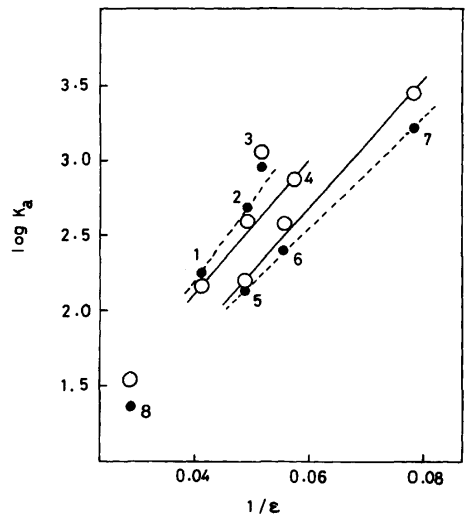

Fig. 3. Plots of $\log K_a$ with $1/\varepsilon$ for O, [Ni(acac)-(*N,N,N',N'*-tmen)]ClO_4 and ●, [Co(acac)$_2$(*N,N,-N',N'*-tmen)]ClO_4 in organic solvents at 25 °C. 1, EtOH; 2, *n*-PrOH; 3, *i*-PrOH; 4, *n*-BuOH; 5, Me_2CO; 6, MEK; 7, MIBK; 8, $PhNO_2$.

coodination by two molecules in Eq. 1.

The transfer of a quadratic-planar [Ni(acac)(*N,N,N',N'*-tmen)]$^+$ to an octahedral [Ni(acac)(*N,N,N',N'*-tmen)-(solvent)$_2$]$^+$ is influenced by solvent basicity.[2] The DN value, which is a measure of the basicity of a solvent, is 20 and 19.6 for EtOH and *n*-PrOH, respectively, suggesting that *i*-PrOH and *n*-BuOH have similar DN values (Table 2). Thus, although the configuration of the nickel(II) chelate cation in these solvents should be equal (Class II), the configuration in *i*-PrOH, which is quadratic-planar, is different from the result regarding primary alcohols. This may be due to a steric hindrance by branched methyl groups: The donor number, which was defined by Gutmann, is obtained from the solvation enthalpy of antimony pentachloride by the donor solvent in 1,2-dichloroethane. Therefore, it indicates the "bulk" donicity of the solvent and does not take into account the structural factor. However, $\lambda_0^+ \cdot \eta$ of the nickel(II) chelate ion in *i*-PrOH is compatible with that of the cobalt(III) chelate ion, suggesting that the solvation of the oxygen atom in acac (the nickel(II) chelate ion) by the OH proton occurs without steric hindrance.

The ketones do not interact with the nickel(II) ion, due to the steric hindrance, in analogy with *i*-PrOH. In addition, they have no solvation site to the nickel(II) chelate ion, resulting in an increase in mobility compared to the cobalt(III) chelate ion. However, the difference in $\lambda_0^+ \cdot \eta$ (Me_2CO=0.038, MEK=0.035, and MIBK=0.02) is small compared to that (0.054) in $PhNO_2$ which is inert in donicity, indicating the presence of a weak interaction between the ketones and the nickel(II) ion.[2] This is also confirmed from the fact that dimethyl sulfoxide (DN=29.8), which is very strong in donicity, coordinates directly to the nickel(II) ion, although the geometry of the solvent is similar to the ketones.

Figure 3 shows that $\log K_a$ of [Ni(acac)(*N,N,N',N'*-tmen)]ClO_4, in analogy with those of octahedral complex [Co(acac)$_2$(*N,N,N',N'*-tmen)]ClO_4, increases with a decrease in the dielectric constant of the solvents (increase in $1/\varepsilon$). This is expected from the coulombic theory of ionic association,[18]

$$\log K_a = e^2/akT \cdot 1/\varepsilon + \log K_a^\circ, \quad (7)$$

where a is the contact distance between the cation and the anion and other symbols (e, k, and T) have their usual meanings. K_a° contains the contribution to K_a for all factors, except for the long-range coulombic interaction. K_a is larger in the alcohols than in the ketones at the same dielectric constant. This larger K_a in the alcohols could be explained in terms of (1) diminution in the dielectric constant due to a breaking of the hydrogen-bonding structure in the vicinity of an ion pair and (2) a multiple-step association process occurring from the solvation of ClO_4^- by the alcohol molecules. This pattern is set up for other uni-uni-valent electrolytes such as [Co(acac)$_2$(en)]ClO_4 (en= ethylenediamine),[3-5] and R_4NClO_4 (R: alkyl group (C=2—4)).[7-9] Moreover, the K_a values of [Ni(acac)-(*N,N,N',N'*-tmen)]ClO_4 are not so much diferent from those of [Co(acac)$_2$(*N,N,N',N'*-tmen)]ClO_4. Thus, it is considered that [Ni(acac)(*N,N,N',N'*-tmen)]ClO_4 in the solvents behaves as a normal-type of uni-uni-valent electrolyte and that the nickel(II) ion does not interact with the ClO_4^- ion.

However, the K_a values of the nickel(II) chelate complex can be classified into two groups as described previously: (1) The K_a values of the nickel(II) complex

are larger than those of the cobalt(III) complex in the ketones, $PhNO_2$, and *i*-PrOH (Class I). (2) The reverse trend is obtained in EtOH, *n*-PrOH, and *n*-BuOH (Class II). Since the nickel(II) ion does not directly interact with the ClO_4^- ion, it seems that the classification can not be only attributed to the difference in the central metal ion {Ni(II) or Co(III)} and the number of the acac. Thus, it may be explained as follows: For Class I, since the nickel(II) chelate ion is present as a quadratic-planar ion, the entity is small compared to $[Co(acac)_2(N,N,N',N'\text{-tmen})]^+$. This suggests that K_a of $[Ni(acac)(N,N,N',N'\text{-tmen})]ClO_4$ should be larger than that of $[Co(acac)_2(N,N,N',N'\text{-tmen})]ClO_4$. For Class II, on the other hand, the reverse trend may be obtained due to the large volume of $[Ni(acac)(N,N,N',N'\text{-tmen})(alcohol)_2]^+$ compared with $[Co(acac)_2(N,N,N',N'\text{-tmen})]^+$ (Fig. 2).

(B)[Ni(acac)(*N,N,N',N'*-tmen)]NO_3. The nitrate ion, as a bidentate ligand, can coordinate directly to $[Ni(acac)(N,N,N',N'\text{-tmen})]^+$ in organic solvents.[2] This behaviour is accounted for by two association processes, outer-sphere ionic association and the formation of an inner-sphere octahedral complex,

$$[Ni(acac)(N,N,N',N'\text{-tmen})]^+ + NO_3^- \overset{K_{a1}}{\rightleftharpoons} [Ni(acac)(N,N,N',N'\text{-tmen})]^+ \cdot NO_3^- \overset{K_{a2}}{\rightleftharpoons} [Ni(acac)(N,N,N',N'\text{-tmen})(NO_3)]. \quad (8)$$

The observed association constant (K_a) can be shown to be equal to

$$K_a = K_{a1} \cdot K_{a2}. \quad (9)$$

Table 4 shows that (1) the K_a values of the nitrate complex are larger than those of the perchlorate complex and (2) may be conveniently classified into two groups; the K_a values in the ketones, $PhNO_2$, and *i*-PrOH are remarkably larger than those in EtOH, *n*-PrOH, and *n*-BuOH. This classification is in good agreement with the classification by the color change of $[Ni(acac)(N,N,N',N'\text{-tmen})]^+$ in each solvent, Classes I and II. For Class I, the nickel(II) chelate ion in Eq. 8 is present as a quadratic-planar chelate ion, resulting in an octahedral complex $[Ni(acac)(N,N,N',N'\text{-tmen})(NO_3)]$. On the other hand, for Class II the nickel(II) chelate ion is present as an octahedral chelate ion $[Ni(acac)(N,N,N',N'\text{-tmen})(alcohol)_2]$, resulting in an octahedral complex $[Ni(acac)(N,N,N',N'\text{-tmen})(NO_3)]$ accompanied by a decoordination of two alcohol molecules from the nickel(II) ion. The coordination of anions is obtained for the copper complex in nitromethane:[1] $[Cu(acac)(N,N,N',N'\text{-tmen})]^+ + X^- \rightleftharpoons [Cu(acac)(N,N,N',N'\text{-tmen})(X)]$ (where $X^- = Cl^-$, Br^-, and SCN^-). The formation constants are large compared to that from the coulombic theory of ionic association.

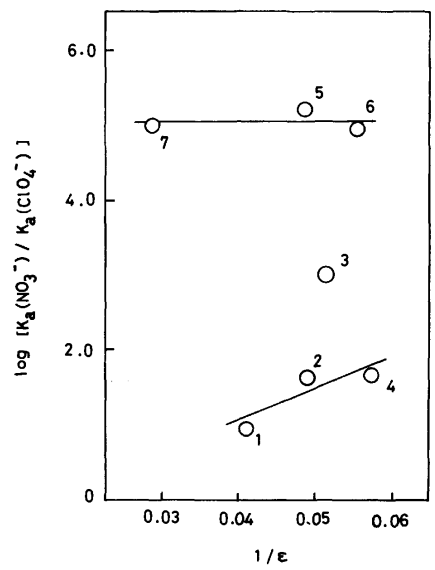

Fig. 4. The ratio of log K_a of $[Ni(acac)(N,N,N',N'\text{-tmen})]NO_3$ to $[Ni(acac)(N,N,N',N'\text{-tmen})]ClO_4$ as a function of $1/\varepsilon$ in organic solvents at 25 °C. 1, EtOH; 2, *n*-PrOH; 3, *i*-PrOH; 4, *n*-BuOH; 5, Me_2CO; 6, MEK; 7, $PhNO_2$.

The K_{a1} value in Eq. 8 seems to be roughly equal to that of the perchlorate complex, since K_a for R_4NNO_3 is similar to that for R_4NClO_4 (from the coulombic theory of ionic association) and the ClO_4^- ion does not interact with the nickel(II) ion. Thus, K_{a2} can be reasonably estimated from Eq. 9. Figure 4 shows plots of $\log K_a(NO_3^-)/K_a(ClO_4^-)$, ($\approx K_{a2}$) vs. $1/\varepsilon$. Similar K_{a2} values are obtained for Class I, indicating that coordination by solvent molecules is very weak for Class I, as discussed in a preceding section. The difference between Classes I and II is ascribed to the energy of decoordination of two alcohol molecules and the desolvation of NO_3^- by the alcohol molecules with high acidities (AN, Table 2). It is considered that the data for *i*-PrOH support the solvation of the acac by 2-propanol melecules, as shown in Fig. 2.

References

1) Y. Fukuda, H. Kimura, and K. Sone, *Bull. Chem. Soc. Jpn.*, **55**, 3738 (1982).

2) Y. Fukuda and K. Sone, *J. Inorg. Nucl. Chem.*, **34**, 2315 (1972).

3) K. Ito, *Inorg. Chem.*, **22**, 2872 (1983).

4) K. Ito, E. Iwamoto, S. Suehisa, H. Isono, and Y. Yamamoto, *Bull. Chem. Soc. Jpn.*, **59**, 3841 (1986).

5) K. Ito, H. Isono, E. Iwamoto, and Y. Yamamoto, *Bull. Chem. Soc. Jpn.*, **61**, 4077 (1988).

6) a) R. M. Fuoss and K. L. Hsia, *Proc. Natl. Acad. Sci., U.S.A.*, **57**, 1550 (1967); b) Fernández-Prini, *Trans. Faraday Soc.*, **65**, 3311 (1969).

7) D. F. Evans and P. Gardam, *J. Phys. Chem.*, **72**, 3281 (1968).

8) S. M. A. Matesich, J. A. Nadas, and D. F. Evans, *J. Phys. Chem.*, **74**, 4568 (1970).

9) D. F. Evans and P. Gardam, *J. Phys. Chem.*, **73**, 158 (1969).
10) D. F. Evans, J. Thomas, J. A. Nadas, and S. M. A. Matesich, *J. Phys. Chem.*, **75**, 1714 (1971).
11) S. R. C. Hughes and D. H. Price, *J. Chem. Soc. A*, **1967** 1093.
12) C. R. Witschonke and C. A. Kraus, *J. Am. Chem. Soc.*, **69**, 2472 (1947).
13) V. Gutmann, "The Donor-Acceptor Approach to Molecular Interactions," Plenum Press, New York (1978).
14) M. Spiro, "Physical Chemistry of Organic Solvent Systems," ed. by A. K. Covington and T. Dickson, Plenum Press, London (1973), Chap. 5.
15) M. B. Reynolds and C. A. Kraus, *J. Am. Chem. Soc.*, **70**, 1709 (1948).
16) Since a sequence of λ_0^- in the methanol and EtOH is $Cl^- < Br^- < NO_3^- < I^- < ClO_4^-$ (Ref. 14), $\lambda_0^-(NO_3^-)$ in *n*-PrOH, *i*-PrOH, and *n*-BuOH were estimated from λ_0^- of other anions (Refs. 7—9). Similarly, $\lambda_0^-(NO_3^-)$ in MEK was estimated from $\lambda_0^-(NO_3^-)$ in Me_2CO (Ref. 15) and $PhNO_2$ (Ref. 12), and λ_0^- of other anions in Me_2CO, MEK, and $PhNO_2$ (Refs. 10—12).
17) The $\lambda_0^+ \cdot \eta$ value of $[Co(acac)_2(N,N,N',N'\text{-tmen})]^+$ in *n*-BuOH, which is not available due to limited solubility may be similar to the values in EtOH, *n*-PrOH, *i*-PrOH, since the chelate ion have no specific site for solvation by the alcohols. This agrees well with the data of the bulky tetraalkylammonium ions such as Bu_4N^+ and $(i\text{-}C_5H_{11})_3BuN^+$ which indicate similar $\lambda_0^+ \cdot \eta$ values (Refs. 7—9).
18) a) W. R. Gilkerson, *J. Chem. Phys.*, **25**, 1199 (1956); b) R. M. Fuoss, *J. Am. Chem. Soc.*, **80**, 5059 (1958).

 © 1989 The Chemical Society of Japan Bull. Chem. Soc. Jpn., 62, 2179—2183 (1989)

Zone-Melting Separation of Carbazole and Anthracene from Polynuclear Aromatic Compounds Using Biphenyl as a Medium, Followed by the Synchronous Fluorometric Determination

Masaki TACHIBANA* and Motohisa FURUSAWA
Faculty of Engineering, Yamanashi University, Takeda, Kofu 400
(Received January 14, 1989)

Biphenyl is favorable as a zone-melting medium for the selective separation of small amounts of carbazole and anthracene and a subsequent determination. A definite amount (20—100 mg) of an aromatic sample was mixed with 4 g of purified biphenyl. The mixture was zone-melted 20 times. The two analytes were accumulated in the beginning part of the zone-molten ingot, but many others were eliminated from the part. After being dissolved in xylene along with the biphenyl, carbazole and anthracene could be simultaneously determined up to 10 ng ml^{-1} by measuring the synchronous fluorescence intensities at 340 and 384 nm, respectively.

Carbazole and anthracene, widely known as constituents of coal tar, can be easily found as chief impurities in many kinds of polynuclear aromatic chemicals. These two materials may, therefore, serve as significant criteria for the purity and the origin of the products made from tar. However, it is difficult to separate and determine small amounts because of the diversity and complexity of these chemicals. Although conventional chromatographic methods are effective for the general separation of a large number of polynuclear aromatic compounds, a selective and simple method for the separation of carbazole and/or anthracene in such products is of great importance.

In the initial investigation, the authors found that the two materials in dibenzofuran are unusually concentrated in the beginning part of the ingot purified by zone melting, and that they can be selectively separated from many other analogs which are normally accumulated in the end part. Consequently, after zone melting both impurities in dibenzofuran could be simultaneously determined by synchronous fluorescence spectrometry without interference of the concomitants.[1] The advanced technique using dibenzofuran as a zone-melting medium could be applied to the determination of small amounts of anthracene in several chemicals, such as fluoranthene,[2] pyrene, anthraquinone, etc.[3] Carbazole in these chemicals, however, could not be determined because of the spectral interference of a large amount of dibenzofuran.

In the present paper the zone-melting technique was further developed by using biphenyl as an alternative medium. Since biphenyl possesses an unusual zone-melting property similar to that of dibenzofuran, carbazole and anthracene can be separated from the analogs in a similar manner. In addition, biphenyl has no effect on the synchronous measurement of carbazole since it fluoresces in a shorter wavelength region than dibenzofuran. Therefore, the two analytes separated by the zone-melting technique could be simultaneously determined by subsequent synchronous fluorimetry. In terms of the separation efficiency for anthracene, however, the biphenyl medium is not as good as the dibenzofuran medium.

Experimental

Reagents. Biphenyl was purified from commercial chemicals in the same manner as dibenzofuran: the procedure was described in detail in a previous paper.[2] Some polynuclear aromatic compounds were purified in the same way as that employed in the initial investigation.[2,3] The others were either zone-refined or used without purification. Xylene of guaranteed reagent grade was used as a solvent without further purification.

Apparatus. A new-type Shibayama SS-950 high-speed zone refiner was used for any zone-melting procedure. The new-model apparatus is identical, except for the length of the molten zone, in mechanism with the old one.[4] All measurements of the synchronous fluorescence spectra were made on a Hitachi 650-40 fluorescence spectrophotometer equipped with a Hitachi 056 recorder. The excitation and emission spectral bandpasses were always set at 2 nm. A 150-W xenon lamp was used as the excitation light source. Quartz cells of 1.00 cm in path length were used.

Zone-Melting Procedure. A definite amount (20—100 mg) of a sample was mixed with 4 g of the purified biphenyl. The mixture was charged in a glass tube of 4-mm i.d. having a silicone rubber stopper. The tube was then mounted vertically in the zone-melting apparatus. Six molten zones, each approximately 40 mm long, were produced by six ring heaters placed at equal spacings on the charge. The zones were set to travel upward at a speed of 100 mm h^{-1}, and the pass was repeated 20 times. During the travel, the zones were stirred by spinning the tube at 20 s^{-1}, with a reversal of the rotation direction at intervals of 1.0 s.

Synchronous Fluorescence Spectrometry. The zone-molten ingot was cut exactly into quarters. The lower half of the ingot was used for a simultaneous determination, the lowest quarter being for the determination of carbazole alone: the half or the quarter was dissolved in 20 ml or 10 ml of xylene. The synchronous fluorescence spectrum of the solution was measured with a wavelength interval of 6 nm. Carbazole and anthracene were determined from the intensities at 340 and 384 nm, respectively, by using the baseline method. The intensities of the two analytes in a xylene

solution (both 0.200 μg ml^{-1}) were used as the standard. Both calibration curves were prepared from their xylene solutions. The incomplete recovery of anthracene was finally corrected for.

Results and Discussion

Zone-Melting Behavior in Biphenyl. Zone-melting samples for polynuclear aromatic compounds of interest were prepared by uniformly mixing small amounts of the individual compounds with the purified biphenyl. After all these samples were zone-melted under the same conditions, the variation in the concentration of particular compounds was measured for each portion of the ingot cut into segments. The relative concentration, C/C_0, was subsequently calculated from the result, where C_0 and C are the initial and final concentrations in the biphenyl, respectively. In addition, the results of these calculations were embodied in the form of a concentration profile. The resulting profiles for carbazole and anthracene are shown in Fig. 1, and the profiles for 14 different aromatic compounds are shown in Fig. 2 (A)—(N). Figure 1 indicates that carbazole and anthracene are concentrated toward the beginning part of the zone-molten ingot. On the other hand, Fig. 2 shows that all of the analogs, which have large effects on the spectrofluorometric determination of carbazole and/or anthracene, are accumulated in the end part of the ingot, and that the extent of the accumulation is dependent on not only the species but also the content. With regard to these interfering compounds, except 5*H*-benzo[*b*]carbazole (5*H*-BC), roughly speaking, the zone-melting behavior in biphenyl was similar to that in dibenzofuran. Only the accumulation of 5*H*-BC was reversed by this biphenyl medium. The behavior of these substances indicates that the use of biphenyl as the zone-melting medium is suitable, like dibenzofuran, for the selective separation of carbazole and anthracene from the interfering analogs.

Separation of Carbazole and Anthracene from Interfering Compounds. Judging from Figs. 1 and 2, carbazole and anthracene can be separated from 20 to 100 mg of the interfering compounds, except for naphthacene and 5*H*-BC, when 4 g of biphenyl is used as the medium. It is possible to separate the two analytes from less than about 800 μg of naphthacene, but impossible to separate them from 5*H*-BC completely. The recoveries of carbazole and anthracene in the

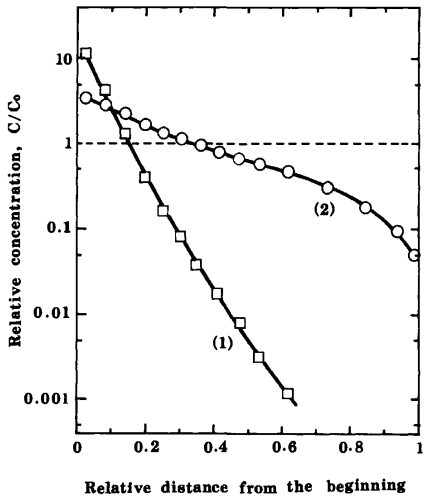

Fig. 1. Concentration profiles for carbazole and anthracene in biphenyl.
C_0 and C are initial and final concentrations of the solute, respectively; (1) carbazole, C_0=171 ppm; (2) anthracene, C_0=219 ppm.

Table 1. Recovery of Carbazole at Various Positions in Zone-Molten Biphenyl Medium

Substances added/mg		Carbazole found[a]					
		0—0.25[b]		0.25—0.5[b]		0.5—0.625[b]	
		Amount	Recovery	Amount	Recovery	Amount	Recovery
		μg	%	μg	%	μg	%
None		2.0$_5$	99.$_5$	0.0$_1$	0.$_5$	0.0$_0$	0.$_0$
None		2.0$_4$	99.$_0$	0.0$_1$	0.$_5$	0.0$_0$	0.$_0$
None		2.0$_5$	99.$_5$	0.0$_1$	0.$_5$	0.0$_0$	0.$_0$
None		2.0$_5$	99.$_5$	0.0$_1$	0.$_5$	0.0$_0$	0.$_0$
9-Fluorenone	22	2.0$_6$	100.$_0$	0.0$_1$	0.$_5$	0.0$_0$	0.$_0$
Anthraquinone	21	2.0$_6$	100.$_0$	0.0$_1$	0.$_5$	—[c]	—
9,10-Phenanthrenequinone	23	2.0$_7$	100.$_5$	0.0$_1$	0.$_5$	0.0$_0$	0.$_0$
Fluoranthene	21	2.0$_8$	101.$_0$	0.0$_1$	0.$_5$	0.0$_0$	0.$_0$
Pyrene	22	2.0$_2$	98.$_1$	0.0$_1$	0.$_5$	0.0$_0$	0.$_0$
Chrysene	21	2.0$_6$	100.$_0$	0.0$_2$	1.$_0$	0.0$_0$	0.$_0$
9-Fluorenone	103	2.0$_5$	99.$_5$	0.0$_1$	0.$_5$	0.0$_0$	0.$_0$
Acenaphthene	101	2.0$_3$	98.$_5$	0.0$_1$	0.$_5$	—[c]	—
Fluoranthene	101	2.1$_5$	104.$_4$	0.0$_1$	0.$_5$	—[c]	—
Fluoranthene	103	2.0$_5$	99.$_5$	0.0$_1$	0.$_5$	—[c]	—
Pyrene	103	2.0$_2$	98.$_1$	0.0$_1$	0.$_5$	0.0$_0$	0.$_0$

a) The total amount of carbazole added to the medium was 2.06 μg. b) These values represent relative distances from the beginning of zone-molten ingot. c) It was impossible to evaluate the amount because of imperfection of the separation.

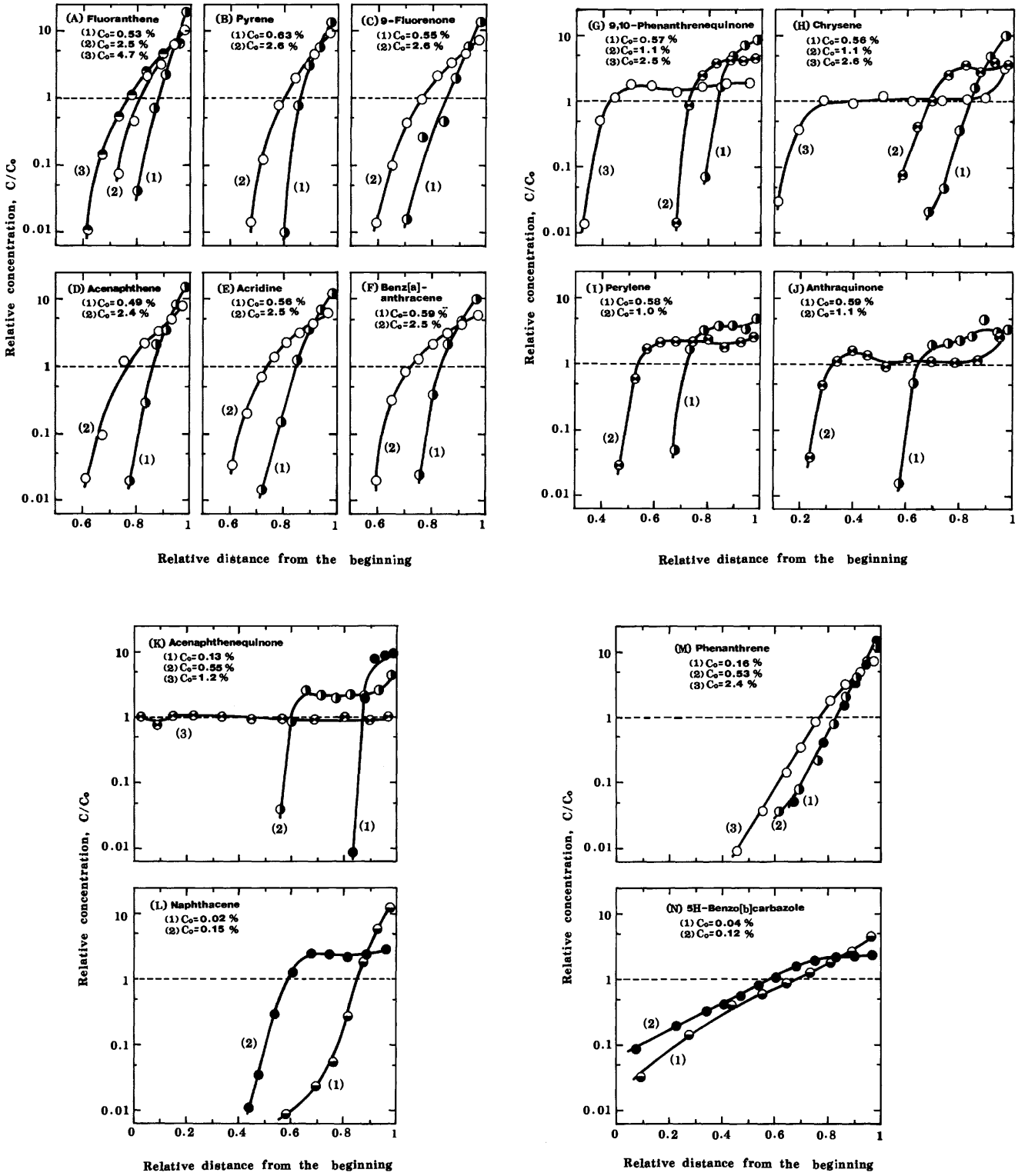

Fig. 2. Concentration profiles for 14 different polynuclear aromatic compounds in biphenyl.

zone-molten fraction of 0—0.25, 0.25—0.5, and 0.5—0.625, where the figures represent the relative distance from the beginning, are summarized as Tables 1 and 2, respectively. As is shown in Table 1, carbazole can be almost quantitatively recovered in the first quarter, even in the presence of a variety of interfering compounds. On the other hand, the recoveries of anthracene in 0—0.25, 0—0.5, and 0—0.625 range from

Table 2. Recovery of Anthracene at Various Positions in Zone-Molten Biphenyl Medium

Substances added/mg		Anthracene found[a]					
		0—0.25[b]		0.25—0.5[b]		0.5—0.625[b]	
		Amount	Recovery	Amount	Recovery[d]	Amount	Recovery[d]
		μg	%	μg	%	μg	%
None		1.54	62.9	0.56	22.9/85.7	0.15	6.1/91.8
None		1.64	66.9	0.53	21.6/88.6	0.12	4.9/93.5
None		1.61	65.7	0.56	22.9/88.6	0.13	5.3/93.9
None		1.62	66.1	0.54	22.0/88.2	0.14	5.7/93.9
9-Fluorenone	22	1.62	66.1	0.50	20.4/86.5	0.13	5.3/91.8
Anthraquinone	21	1.56	63.7	0.55	22.4/86.1	0.13	5.3/91.4
9,10-Phenanthrenequinone	23	1.60	65.3	0.54	22.0/87.3	0.13	5.3/92.7
Fluoranthene	21	1.64	66.9	0.51	20.8/87.8	0.13	5.3/93.1
Pyrene	22	1.59	64.9	0.52	21.2/86.1	0.14	5.7/91.8
Chrysene	21	1.58	64.5	0.56	22.9/87.3	0.14	5.7/93.1
9-Fluorenone	103	1.68	68.6	0.51	20.8/89.4	0.12	4.9/94.3
Acenaphthene	101	1.72	70.2	0.48	19.6/89.8	0.10	4.1/93.9
Fluoranthene	101	1.70	69.4	0.50	20.4/89.8	0.13	5.3/95.1
Fluoranthene	103	1.76	71.8	0.47	19.2/91.0	0.10	4.1/95.1
Pyrene	103	1.67	68.2	0.53	21.6/89.8	0.12	4.9/94.7

a) The total amount of anthracene added to the medium was 2.45 μg. b) These values represent relative distances from the beginning of zone-molten ingot. d) The total recovery from the beginning is also shown.

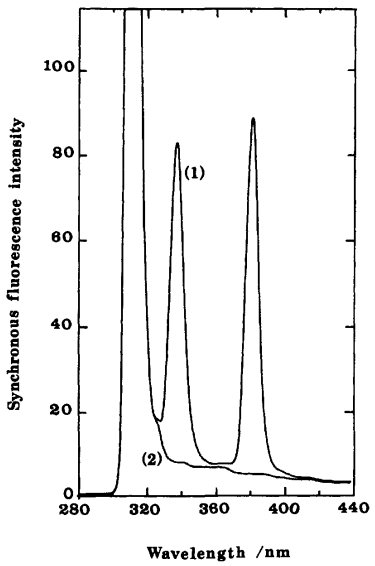

Fig. 3. Synchronous fluorescence spectra of a mixed solution of carbazole, anthracene, and biphenyl and a biphenyl solution.
Wavelength interval ($\Delta\lambda$), 6 nm; solvent, xylene; (1) carbazole (0.2 μg ml^{-1}), anthracene (0.2 μg ml^{-1}), and biphenyl (100 mg ml^{-1}); (2) biphenyl (100 mg ml^{-1}).

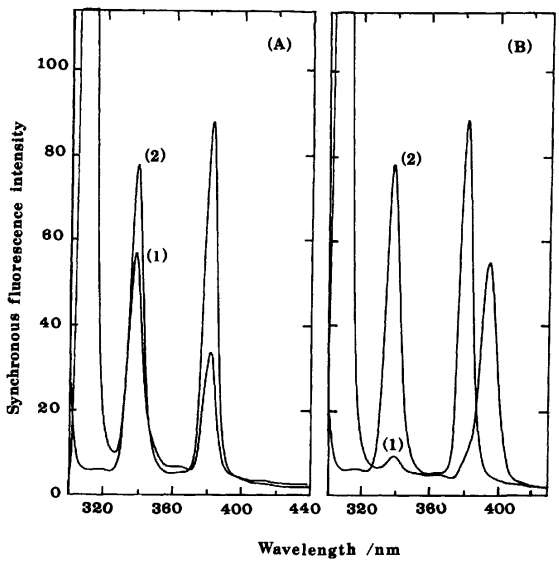

Fig. 4. Synchronous fluorescence spectra of solutions used for the determinations in the practical samples and the standard solution.
Solvent, xylene; $\Delta\lambda$, 6 nm; (A) (1) in the fluoranthene sample; (B) (1) in the chrysene sample; (A) (2) and (B) (2) the standard solution containing both carbazole and anthracene (each 0.200 μg ml^{-1}).

63 to 72% with an average of 67%, 86—91% with that of 88%, and 91—95% with that of 93%, respectively. For the reproducible recovery of anthracene, therefore, it is necessary to use at least the beginning half of the ingot. In the previous dibenzofuran medium, the recovery of anthracene had clearly increased with an increase in the content of other concomitant compounds.[2,3] In this medium, however, such an effect on the recovery could not be definitely observed.

Determinations by Synchronous Fluorescence Spectrometry. Since the simultaneous determination by synchronous fluorimetry has already been reported in the previous papers,[1,5] only the effect of biphenyl on the two analytes was studied. The synchronous fluorescence intensities of carbazole and anthracene gradually increased and decreased, respectively, with an increase in the biphenyl concentration. The variations, however, were so small that the effect of

biphenyl could almost be neglected over the wide concentration range from 0 to 180 mg ml^{-1}. Figure 3 (1) represents the spectrum of a ternary solution of biphenyl (100 mg ml^{-1}), carbazole (0.2 μg ml^{-1}), and anthracene (0.2 μg ml^{-1}). The spectrum has three peaks attributable to these three compounds, and their peaks are well-resolved from one another. Consequently, carbazole and anthracene can be successfully determined even in the presence of biphenyl. Calibration curves were prepared by using xylene solutions containing both analytes (0—0.2 μg ml^{-1}), the 0.2-μg ml^{-1} solution being used as the standard. Each of the resulting curves gave a linear relationship between the intensity and the concentration. Both analytes can be determined up to 10 ng ml^{-1} by using the calibration curves.

Application to Practical Samples. The present method was applied to commercially available fluoranthene and chrysene. The zone-molten ingot obtained by treating the fluoranthene sample (100 mg) was cut in two, and the lower half was dissolved in 20 ml of xylene. The solution was further diluted 4 times with xylene. The synchronous fluorescence spectrum of the dilute solution is illustrated in Fig. 4 (A), as well as the standard solution. The spectrum has peaks at 340 and 384 nm, which agree well with those of the standard solution: each analytical value was 106 and 59 ppm, respectively. Next, the spectrum measured for the determination of carbazole in chrysene is shown in Fig. 4 (B). It was obtained by using 20 mg of chrysene as the sample size, cutting the lowest quarter of the zone-molten ingot away, dissolving it in 10 ml of xylene, and diluting the solution 10 times. No anthracene could be determined because the 5*H*-BC contained as a concomitant impurity was inseparable and influential. For the determination of carbazole, however, the interference of 5*H*-BC could be neglected by using a sufficiently dilute solution of the zone-molten sample: the carbazole content was 40 ppm. The above solutions used for these determinations did not show absorption based on interfering impurities at the characteristic wavelengths to be measured. Therefore, the proposed method in the present paper can be applied to such practical samples.

References

1) M. Tachibana and M. Furusawa, *Bull. Chem. Soc. Jpn.*, **56**, 2254 (1983).

2) M. Tachibana and M. Furusawa, *Anal. Sci.*, **1**, 77 (1985).

3) M. Tachibana and M. Furusawa, *Anal. Sci.*, **3**, 457 (1987).

4) M. Furusawa and M. Tachibana, *Bull. Chem. Soc. Jpn.*, **54**, 2968 (1981).

5) M. Furusawa, M. Tachibana, and Y. Hayashi, *Bunseki Kagaku*, **31**, 229 (1982).

Spectroscopic and Electrochemical Characterization of 18-Molybdodisulfate(VI)(4−), $S_2Mo_{18}O_{62}^{4-}$

Sadayuki HIMENO,* Toshitaka HORI,† and Atsuyoshi SAITO
Department of Chemistry, College of Liberal Arts, Kobe University, Kobe 657
†Department of Chemistry, College of Liberal Arts and Sciences, Kyoto University, Kyoto 606
(Received October 13, 1988)

The formation conditions of a yellow Dawson-type $S_2Mo_{18}O_{62}^{4-}$ anion have been investigated as functions of the concentrations of Mo(VI), H_2SO_4, organic solvents, the nature of the organic solvents used, temperature of the solution, and the reaction time. For a 50 mM Mo(VI)/50% (v/v) acetonitrile system, the yellow $S_2Mo_{18}O_{62}^{4-}$ anion formed in 0.2—1.0 M H_2SO_4, while a pale-yellow $Mo_6O_{19}^{2-}$ anion did in 0.04—0.3 M H_2SO_4. The yellow heteropolyanion is electrochemically reduced in six successive steps to mixed-valence heteropoly blues at the glassy carbon electrode. Each of the first four waves corresponds to a reversible two-electron transfer. The mixed-valence blue species were characterized by their inherent visible and infrared (IR) spectra.

The so-called Dawson-type heteropolyanion was first reported for $P_2W_{18}O_{62}^{6-}$ by Dawson and then for $P_2Mo_{18}O_{62}^{6-}$ by Strandberg.[1,2] In addition, $As_2W_{18}O_{62}^{6-}$ and $As_2Mo_{18}O_{62}^{6-}$ anions are known to exist.[3,4] These heteropolyanions have been extensively studied with respect not only to the crystal structures and physical properties in the solid state, but also to the chemical natures in the solution state where they are electroreduced in multi-steps to mixed-valence blue species.[5–7] Nowadays, these behaviors are comprehensively explained in relation to those of the corresponding Keggin-type heteropolyanions.[8] However, there are no previous studies on heteropolyanions with SO_4^{2-} as a central tetrahedron because of the lack of proper examples except for the $S_2V_2W_{16}O_{62}^{6-}$ anion.[9]

In the presence of organic solvents such as acetone and acetonitrile, acidified Mo(VI) solutions become pale-yellow due to the formation of $Mo_6O_{19}^{2-}$.[10–13] When H_2SO_4 was used for the acidification, the yellow color became more intense by heating and the resulting orange-yellow solution changed to blue by chemical and electrochemical reductions. These results show strong promise of the formation of a heteropolymolybdosulfate because the reduction of $Mo_6O_{19}^{2-}$ yields a brown solution.[14] Actually, an orange-yellow heteropolyanion was isolated as tetraalkylammonium salts (R_4N^+ salts, R=CH_3, C_2H_5, and n-C_4H_9) from a Mo(VI)/H_2SO_4/CH_3CN system.[15] Recently, the crystal structural analysis demonstrated the existence of the Dawson-type molybdosulfate anion, $S_2Mo_{18}O_{62}^{4-}$ with SO_4^{2-} anions as central tetrahedra.[16]

The present paper describes the chemical and physicochemical properties of the yellow Dawson-type molybdosulfate anion in solutions, regarding to the optimum formation conditions, ultraviolet(UV)-visible spectroscopic characteristics, and electrochemical behaviors. In addition, mixed-valence blue species are identified by visible and IR spectroscopy.

Experimental

Voltammetric measurements were made on a PARC 174-A polarographic analyzer equipped with a Yokogawa Hokushin Electric 3023 X-Y recorder. A Tokai glassy carbon (GC-30S) with a surface area of 0.071 cm^2 was used as a working electrode. Controlled potential electrolysis (CPE) was carried out with a Hokuto Denko HA-501 potentiostat. A Hokuto Denko HF-202D coulometer was used for coulometric experiments. Glassy carbon fibers (GC-20) were employed as a working electrode. A platinum wire was used as a counter electrode and a saturated calomel electrode (SCE) served as the reference electrode. UV-visible spectra were recorded on a Hitachi 220-A spectrophotometer equipped with a constant temperature housing for the cell. UV-visible spectrophotometric and voltammetric measurements were made at 25±0.1 °C. IR spectra were recorded on a Hitachi 270-30 spectrophotometer as KBr pellets. The TG-DTA measurements were carried out with a Rigaku Denki 8002-SD thermal analyzer.

All reagents were of analytical grade and were used without further purification. Molybdenum(VI) solutions were prepared from $Na_2MoO_4 \cdot 2H_2O$.

The Et_4N^+ and n-Bu_4N^+ salts of the yellow molybdosulfate, $(Et_4N)_4S_2Mo_{18}O_{62}$ and $(n\text{-}Bu_4N)_4S_2Mo_{18}O_{62}$ prepared according to ref. 15 were purified further by recrystallization from neat CH_3CN. As already described,[16] the crystals contain the solvent molecule of CH_3CN as a constituent. The TG-DTA analysis for the crystals showed that they lost the CH_3CN molecule around 130 °C via an endothermic process. The crystals were heated at 130 °C for several hours to let the solvent molecule liberate. The fine powders thus obtained were used for preparing solutions of a given concentration of the heteropolyanion.

Results and Discussion

UV-Visible Spectroscopic Measurements. The R_4N^+ salts of the $S_2Mo_{18}O_{62}^{4-}$ anion are soluble in organic solvents such as acetonitrile, acetone, and dimethyl sulfoxide, giving rise to yellow solutions. Curve a of Fig. 1 shows a UV-visible spectrum of 1.98×10^{-5} M (M=mol dm^{-3}) $S_2Mo_{18}O_{62}^{4-}$ in CH_3CN. The complex anion shows a broad absorption band in

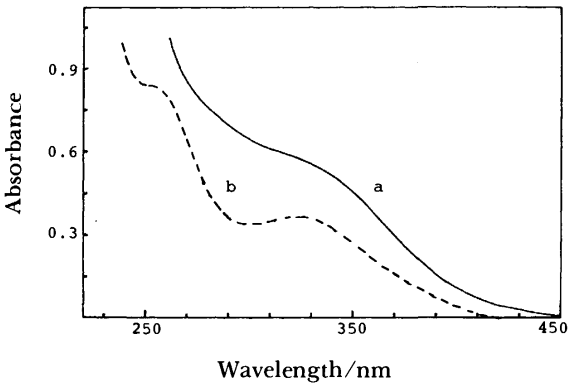

Fig. 1. UV-visible spectra of 1.98×10^{-5} M $S_2Mo_{18}O_{62}^{4-}$ in a, neat CH_3CN and b, 90% (v/v) CH_3CN–water.

the 270—450 nm range. The spectrum in neat CH_3CN was unchanged for at least one month, and conformed to Beer's law in the whole spectral region studied, the molar absorption coefficient at 330 nm being calculated as 2.71×10^3 cm^{-1} M^{-1}.

With the addition of water by more than 5% (v/v), however, the color of the solution changed gradually to pale-yellow. In the presence of 10% (v/v) water, for example, the spectrum was converged in 24 h to that shown in curve b of Fig. 1. The ultimate spectrum with absorption maxima at 257 and 325 nm is attributed not to the reformation of other-type heteropolyanions, but to the hexamolybdate, $Mo_6O_{19}^{2-}$.[11,13] The decomposition was retarded by the presence of 1.0 M $HClO_4$ in the solution, where the spectrum was unchanged for a week. On the basis of these facts, the hydrolytic decomposition of the heteropolyanion proceeds according to the reaction:

$$S_2Mo_{18}O_{62}^{4-} + 3H_2O = 3Mo_6O_{19}^{2-} + 2SO_4^{2-} + 6H^+$$

In the presence of 1.0 M HCl or 1.0 M H_2SO_4 in place of the $HClO_4$, on the other hand, the heteropolyanion decomposed within several hours to give colorless solutions, which is due to the formation of colorless molybdenum(VI)-chloro or molybdenum(VI)-sulfato complexes.[17–19]

Formation of the $S_2Mo_{18}O_{62}^{4-}$ Anion in the Mo(VI)/H_2SO_4/CH_3CN System. In order to confirm the conditions for the formation of the $S_2Mo_{18}O_{62}^{4-}$ anion, absorbance measurements were made for the Mo(VI)/H_2SO_4/CH_3CN system. Firstly, a series of 50 mM Mo(VI) solutions containing 50% (v/v) CH_3CN and various concentrations of H_2SO_4 (0.02—1.2 M) were prepared. When stood for 3 h at 25 °C, the solutions turned to pale-yellow in the H_2SO_4 concentration range 0.04—0.4 M. The absorbances at 410 nm are plotted against the H_2SO_4 concentration and shown in curve a of Fig. 2, where absorbances have a maximum around the H_2SO_4 concentration of 0.06 M. By the addition of R_4NBr to

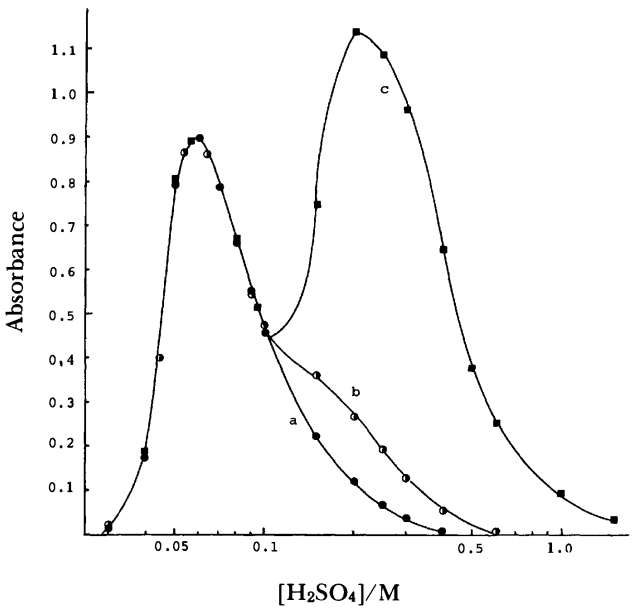

Fig. 2. Absorbances at 410 nm for 50 mM Mo(VI) in 50% (v/v) CH_3CN containing various concentrations of H_2SO_4. Measured after standing a, at 25 °C for 3 h; b, at 25 °C for 24 h; c, at 50 °C for 24 h. Path length, 1 cm.

the solution, pale-yellow precipitates were obtained, being identified as $(R_4N)_2Mo_6O_{19}$ by elemental analysis and IR spectroscopy.[13] When solutions stood for 24 h at 25 °C, absorbances in the H_2SO_4 concentration range >0.2 M were found to increase, while absorbances remained unchanged in the range <0.1 M where $Mo_6O_{19}^{2-}$ was formed. This result, which has been overlooked so far, is well illustrated in curve b. The absorbance grew rather slowly at 25 °C but the absorbance increase was remarkably accelerated by heating of the solution. Curve c shows absorbances after standing at 50 °C for 24 h. Orange-yellow precipitates occurred by the addition of R_4NBr to the yellow solutions in the H_2SO_4 concentration range 0.4—0.8 M. The IR spectrum of the precipitate is in good agreement with that of the authentic $(R_4N)_4S_2Mo_{18}O_{62}$ (vide infra), which indicates that the absorbance increase in the H_2SO_4 concentration range >0.2 M is due to the formation of the yellow $S_2Mo_{18}O_{62}^{4-}$ anion. In conclusion, the $S_2Mo_{18}O_{62}^{4-}$ anion occurs at higher acidities than $Mo_6O_{19}^{2-}$ anion, each anion being distinguishable by the region and condition of formation.

The effect of the Mo(VI) concentration on the complex formation was studied in 50% (v/v) CH_3CN containing 0.4 M H_2SO_4. Absorbances at 400 and 430 nm were measured at 25 °C after standing at 70 °C for 2 h, and plotted against the Mo(VI) concentration in Fig. 3. It was observed that the complex formation became appreciable only at Mo(VI) concentrations >30 mM. Finally, the effect of the CH_3CN concentration (0—80% (v/v)) was investigated. The presence of

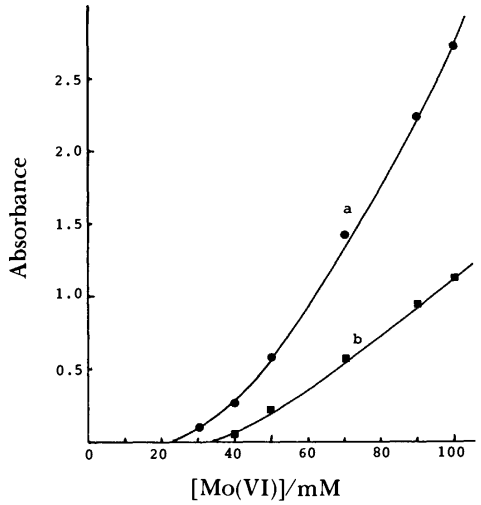

Fig. 3. Effect of Mo(VI) concentrations on absorbances after standing at 70°C for 2 h in 50% (v/v) CH_3CN containing 0.4 M H_2SO_4. Wavelength/nm; a, 400; b, 430. Path length, 1 cm.

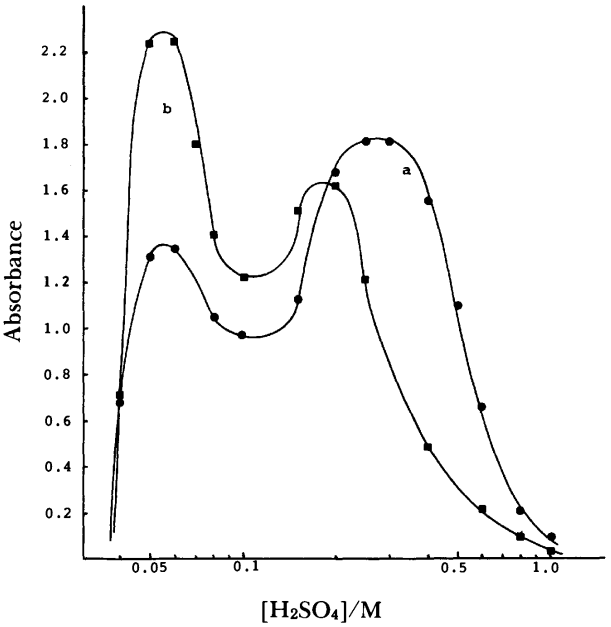

Fig. 4. Absorbances after standing at 50°C for 24 h for 50 mM Mo(VI) in 50% (v/v) a, acetone (400 nm); b, 1,4-dioxane (410 nm) containing various concentrations of H_2SO_4. Path length, a, 2 mm; b, 1 cm.

CH_3CN at concentrations <20% (v/v) had no effect but yellow solutions due to the formation of the $S_2Mo_{18}O_{62}^{4-}$ anion resulted at concentrations >30% (v/v). Adsorbance values increased as the CH_3CN concentration was increased. In the presence of CH_3CN at concentrations >60% (v/v), however, the system separated into two-phases; the $S_2Mo_{18}O_{62}^{4-}$ anion is extracted into the upper layer.

The complex formation is also facilitated in the presence of acetone and 1,4-dioxane. Similar experiments were carried out for the Mo(VI)/H_2SO_4 system containing 50% (v/v) acetone or 1,4-dioxane. The absorbances were measured at 400 nm (for the acetone system) and at 410 nm (for the 1,4-dioxane system) after standing at 50 °C for 24 h. The results are illustrated by curves a and b in Fig. 4. Both curves are similar in shape to curve c of Fig. 2, in that the heteropolyanion is formed at higher acidities than $Mo_6O_{19}^{2-}$; the $S_2Mo_{18}O_{62}^{4-}$ anion can be separated from the $Mo_6O_{19}^{2-}$ anion.

Voltammetric Measurements. Figure 5 shows a typical cyclic voltammogram of 8.33×10^{-5} M $S_2Mo_{18}O_{62}^{4-}$ in 95% (v/v) CH_3CN containing 0.1 M $HClO_4$. The voltammogram consists of six cathodic and six anodic waves under these conditions. The peak potentials (E_p's) for the cathodic waves are: +0.53, +0.43, +0.24, −0.06, −0.20, and −0.24 V. Of these, the fifth cathodic wave is observed as a shoulder and the sixth wave is rather unusual in shape. The anodic peaks occurred at +0.55, +0.45, +0.27, −0.04, and −0.18 V; the sixth anodic wave appeared only as a shoulder. The waves are numbered in the direction of more cathodic potentials. For the first four waves, each peak potential is independent of scan rate, v, and each current function $i_p/v^{1/2}$ is constant, i_p being the

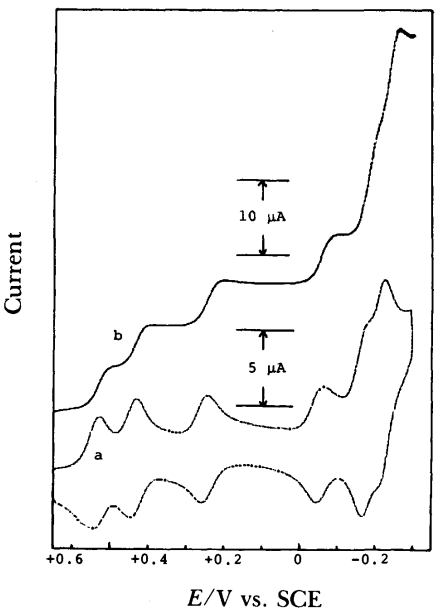

Fig. 5. A cyclic voltammogram (a) and a normal pulse polarogram (b) of 8.33×10^{-5} M $S_2Mo_{18}O_{62}^{4-}$ in 95% (v/v) CH_3CN containing 0.1 M $HClO_4$. Scan rate/mV s^{-1}; a, 100; b, 10.

peak current. The cathodic-to-anodic i_p ratio is one. These results show that each step is diffusion-controlled. The separation of the cathodic and anodic peak potentials for each couple is 28±3 mV, which indicates that these waves are reversible two-electron waves. Coulometric analysis showed that each of the first four reductions consumed two-electrons per the

$S_2Mo_{18}O_{62}^{4-}$ anion. The E_p's shifted to more positive potentials with an increase in the $HClO_4$ concentration. The E_p's for the first four reductions were measured in 95% (v/v) CH_3CN solutions with various concentrations of $HClO_4$ (0.01—0.1 M) which were kept at constant ionic strength of 0.1 with $NaClO_4$. Plots of E_p's against the logarithm of the $HClO_4$ concentration yielded straight lines with a common slope of 60±5 mV, indicating that two protons are consumed for each step of the first four reduction waves.

CPE at each of the first four steps was carried out for 1.0×10^{-4} M $S_2Mo_{18}O_{62}^{4-}$ in 95% (v/v) CH_3CN containing 0.1 M $HClO_4$. Figure 6 shows visible spectra of the solutions obtained. When CPE was made at +0.50 V, a blue solution was obtained, showing a round maximum around 760 nm (curve a). When electrolyzed at +0.35 V, the maximum shifted to 690 nm. As the degree of reduction further proceeded, the blue color became more intense. The spectrum for a 6-electron reduction species was characterized by two maxima around 670 and 790 nm (curve c). Curve d is the spectrum for a 8-electron reduction species, showing a maximum at 570 nm with a round shoulder around 700 nm. Each of 2-, 4-, 6-, and 8-electron reduction species is stable in 95% (v/v) CH_3CN containing 0.1 M $HClO_4$. When reoxidized at +0.80 V, the respective blue species were reverted to the original yellow species, which was identified by IR measurements.

As shown in Fig. 5, the peak separation between the fifth and sixth waves is so small that it is difficult to obtain the visible spectrum for the blue solution by CPE at the fifth step. However, the visible spectrum obtained by CPE at the sixth step (at −0.30 V) was identical in shape with that of the 8-electron reduction species shown in curve d. As CPE at −0.30 V progressed, the spectrum showed a gradual absorbance decrease in the range 450—900 nm. Finally a colorless solution resulted, indicating the decomposition of the heteropolyanion. These observations suggest that the 8-electron reduction species accepts further electrons with the subsequent decomposition.

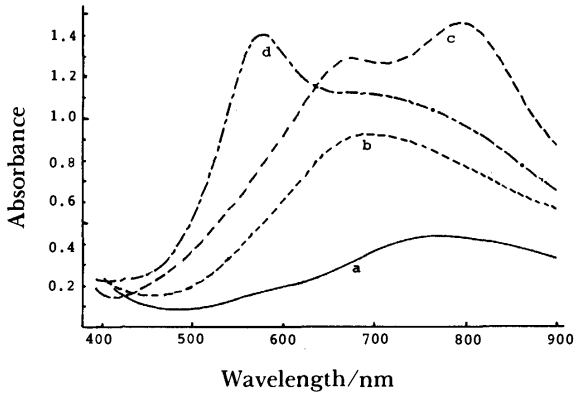

Fig. 6. Visible spectra of the reduced species for 1.0×10^{-4} M $S_2Mo_{18}O_{62}^{4-}$ in 95% (v/v) CH_3CN containing 0.1 M $HClO_4$. a, b, c, d; 2-, 4-, 6-, and 8-electron reduction species, respectively. Path length, 5 mm.

As shown in curve b of Fig. 5, six reduction waves were observed in normal pulse polarography. Their approximate current ratios are 1:1:1:1:2:2, fitting the 2:2:2:2:4:4 electron ratios. In normal pulse polarography, short potential pulses (57 ms) are applied so that the electrode is at its initial potential most of the time. Therefore the effect of the decomposition may not be observed.

The reduction process of $S_2Mo_{18}O_{62}^{4-}$ is summarized as follows:

$$S_2Mo_{18}O_{62}^{4-} + 2H^+ + 2e = H_2S_2Mo^{V}_2Mo^{VI}_{16}O_{62}^{4-}$$

$$H_2S_2Mo^{V}_2Mo^{VI}_{16}O_{62}^{4-} + 4H^+ + 4e = H_6S_2Mo^{V}_6Mo^{VI}_{12}O_{62}^{4-}$$

$$H_6S_2Mo^{V}_6Mo^{VI}_{12}O_{62}^{4-} + 2H^+ + 2e = H_8S_2Mo^{V}_8Mo^{VI}_{10}O_{62}^{4-}$$

$$H_8S_2Mo^{V}_8Mo^{VI}_{10}O_{62}^{4-} + 4e \longrightarrow \text{unstable species}$$

IR Spectroscopic Measurements. Figure 7 shows IR spectra for Et_4N^+ salts of 2- and 4-electron reduction species in addition to the yellow species. As for the yellow species, as reported previously,[15] bands in the range 1500—1350 cm^{-1} are due to the Et_4N^+ unit, and bands at 1170 and 1070 cm^{-1} can be assigned to the asymmetric and symmetric stretches of the S-O bond. In the Mo-O stretching and bending region (<1000 cm^{-1}), the strong band at 960 cm^{-1} can be assigned to $Mo{=}O_{terminal}$ bonds. In addition, a weak band at 880 cm^{-1} and a broad band at 785 cm^{-1} are observed. Thouvenot et al. have made a systematic vibrational study of $XMo_{12}O_{40}^{n-}$ salts related to the Keggin

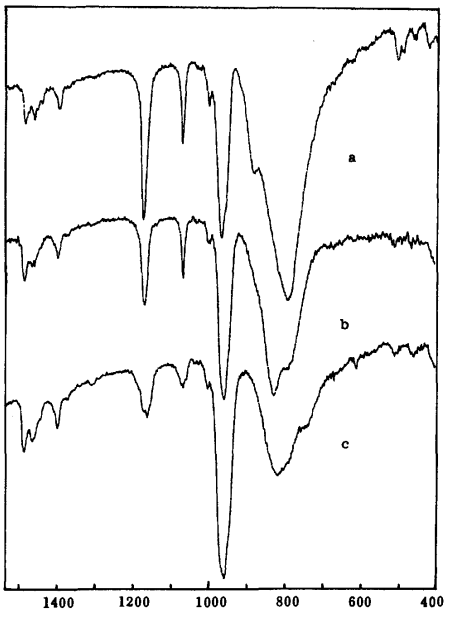

Fig. 7. IR spectra of Et_4N^+ salts of heteropolymolybdosulfates. a, the yellow species; b, 2-electron reduction species; c, 4-electron reduction species.

structure.[20] According to them, bands in the range 890—850 cm^{-1} correspond to inter Mo–O–Mo bridges between corner-sharing octahedra, and bands in the range 800—760 cm^{-1} to intra Mo–O–Mo bridges between edge-sharing octahedra. Both bands at 880 and 785 cm^{-1} are situated within the region predicted by them. In addition to these strong bands, the spectrum contains weak bands at 504, 492, 460, and 420 cm^{-1} to which no assignments can be made.

To obtain the salt of blue species, n-Bu_4N^+ salts of the yellow heteropolyanion were dissolved in 95% (v/v) CH_3CN containing 0.1 M $HClO_4$ and electrolyzed by CPE at +0.50 and +0.35 V. During the electrolysis, the solution was purged with N_2 gas to avoid possible reoxidation by dissolved oxygen. At the end of each electrolysis, Et_4NBr was added to the solution, and the Et_4N-salts of 2- and 4-electron reduction species were obtained. The 4-electron reduction species was also synthesized by CPE of the 0.1 M Mo(VI)/1.5 M H_2SO_4/40% (v/v) CH_3CN system at −0.10 V.[21] As the degree of reduction proceeded, as shown in curves b and c of Fig. 7, both bands due to the S–O bond decreased in intensity with a simultaneous shift to shorter wave numbers. Simultaneously, intensities of bands due to the Mo–O–Mo bridges decreased, while the band due to the $Mo{=}O_{terminal}$ bond remained unchanged. Similar behavior has been reported for the $PMo_{12}O_{40}^{3-}$ salt known as the Keggin structure.[22,23]

References

1) B. Dawson, *Acta Crystallogr.*, **6**, 113 (1953).
2) R. Strandberg, *Acta Chem. Scand.*, **A29**, 350 (1975).
3) F. Kehrmann, *Z. Anorg. Allgem. Chem.*, **22**, 285 (1900).
4) A. Rosenheim and A. Traube, *Z. Anorg. Chem.*, **91**, 75 (1915).
5) M. T. Pope and E. Papaconstantinou, *Inorg. Chem.*, **6**, 1147 (1967).
6) E. Papaconstantinou and M. T. Pope, *Inorg. Chem.*, **6**, 1152 (1967).
7) P. Souchay, R. Contant, and J. Fruchart, *C. R. Acad. Sci.*, **C264**, 976 (1967).
8) L. C. W. Baker and J. S. Figgis, *Inorg. Chem.*, **92**, 3794 (1970).
9) A. Botar and J. Fuchs, *Z. Naturforsch.*, **B37**, 806 (1982).
10) K. Murata, E. Yamamoto, and S. Ikeda, *Bull. Chem. Soc. Jpn.*, **56**, 941 (1983).
11) J. J. Cruywagen and T. Rypstra, *Polyhedron*, **4**, 545 (1985).
12) A. Halasz and E. Pungor, *Talanta*, **18**, 569 (1971).
13) S. Himeno, N. Ishii, M. Hasegawa, A. Saito, and T. Hori, *Inorg. Chim. Acta*, **131**, L11 (1987).
14) M. Che, M. Fournier, and J. P. Launay, *J. Chem. Phys.*, **71**, 1954 (1979).
15) T. Hori and S. Himeno, *Chem. Lett.*, **1987**, 53.
16) T. Hori, O. Tamada, and S. Himeno, *J. Chem. Soc., Dalton Trans.*, in press.
17) S. Himeno and M. Hasegawa, *Inorg. Chim. Acta*, **73**, 255 (1983).
18) S. Himeno, Y. Ueda, and M. Hasegawa, *Inorg. Chim. Acta*, **70**, 53 (1983).
19) E. F. C. H. Rohwer and J. J. Cruywagen, *J. South African Chem. Inst.*, **19**, 11 (1966).
20) R. Thouvenot, M. Fournier, R. Franck, and C. Rocchiccioli-Deltcheff, *Inorg. Chem.*, **23**, 598 (1984); C. Rocchiccioli-Deltcheff, M. Fournier, R. Franck, and R. Thouvenot, *Inorg. Chem.*, **22**, 207 (1983).
21) T. Hori, M. Sugiyama, and S. Himeno, *Chem. Lett.*, **1988**, 1017.
22) H. Tsuneki, H. Niiyama, and E. Echigoya, *Chem. Lett.*, **1978**, 645.
23) K. Eguchi, Y. Toyozawa, K. Furuta, N. Yamazoe, and T. Seiyama, *Chem. Lett.*, **1981**, 1253.

 © 1989 The Chemical Society of Japan Bull. Chem. Soc. Jpn., 62, 2189—2195 (1989)

Molecular Recognition in the Formation of Conglomerate Crystal. 2. The Role of Arenesulfonic Acid in the Conglomerate Crystals of Amino Acid Salts

Hiroki KIMOTO, Kazuhiko SAIGO,* Yuji OHASHI,† and Masaki HASEGAWA
Department of Synthetic Chemistry, Faculty of Engineering, The University of Tokyo, Hongo, Bunkyo-ku, Tokyo 113
†Department of Chemistry, Faculty of Science, Ochanomizu University, Otsuka, Bunkyo-ku, Tokyo 112
(Received December 9, 1988)

The structures of conglomerate crystals, *p*-chlorobenzenesulfonic acid salt of L-alanine, *p*-toluenesulfonic acid salt of L-serine, and benzenesulfonic acid salt of L-leucine, were determined by X-ray analysis. The crystals are built up of repeating units consisting of two amine components and two acid components to form a helical column by hydrogen bonds. The arrangements of the arenesulfonic acids are found to be similar to each other in these systems. Moreover, the arrangements have similarity to those of cinnamic acid in the crystals of cinnamic acid salts of (*R*)-1-phenylethylamine and of (*R*)-1-(4-isopropylphenyl)ethylamine, which are also conglomerates. These results suggest that our proposed criteria for the choice of an achiral derivatizing agent in the transformation of a racemic compound into a conglomerate crystal is appropriate.

The diastereomeric salt method is the most popular in the optical resolution. But, in the resolution, a stoichiometric amount of an optically pure compound is usually required as a resolving agent, and it is difficult to get both enantiomers from a racemic modification by a simple operation.[1] Although this difficulty can be solved by the preferential crystallization method, this method is applicable to only uncommon conglomerate crystals. They are ascertained by trial-and-error procedure using an achiral derivatizing agent.[1] Then, it is worthy to find the criteria for the choice of an achiral compound in the transformation of a racemic compound into a conglomerate crystal. In the previous paper,[2] we reported the structures of two conglomerate crystals, cinnamic acid salts of α-substituted benzylamine derivatives, and proposed the criteria on the structural requirement for an achiral acid in the transformation of a racemic amine into a conglomerate crystal.

On the other hand, it is already known that the arenesulfonic acid salts of some amino acids are also conglomerate crystals.[3–6] We report here the crystal structures of three conglomerate crystals, *p*-toluenesulfonic acid salt of L-serine (**1**), *p*-chlorobenzenesulfonic acid salt of L-alanine (**2**), and benzenesulfonic acid salt of L-leucine (**3**) to verify our hypotheses for the transformation.

Experimental

Crystal Structure Determination. Colorless plate-like crystals, **1**, **2**, and **3** were grown from saturated aqueous solutions of equimolar mixtures of the amino acids and the arenesulfonic acids, respectively. The specimen used was a fragment of a plate. The space group was determined by

Table 1. Crystal Data and Details of Refinement

	1	2	3
Formula	$C_3H_7NO_3 \cdot C_7H_8O_3S$	$C_3H_7NO_2 \cdot ClC_6H_5O_3S$	$C_6H_{13}NO_2 \cdot C_6H_6O_3S \cdot H_2O$
M	276.8	281.3	306.9
Crystal system	Orthorhombic	Orthorhombic	Orthorhombic
Space group	$P2_12_12_1$	$P2_12_12_1$	$P2_12_12_1$
a/Å	6.853(0)	8.806(1)	9.921(1)
b/Å	27.306(2)	26.528(9)	25.741(2)
c/Å	6.783(0)	5.247(0)	6.216(0)
V/Å^3	1269.3(2)	1225.7(2)	1587.4(2)
Z	4	4	4
D_m/g cm^{-3}	1.45	1.50	1.30
D_c/g cm^{-3}	1.449	1.525	1.285
μ(Cu $K\alpha$)/cm^{-1}	23.46	43.03	19.15
Crystal size/mm^3	0.45×0.40×0.30	0.30×0.30×0.40	0.45×0.45×0.30
No. of unique reflections	1235	1176	1505
No. of observed reflections	1199	1142	1477
No. of parameters	205	190	244
$\Delta\rho_{max}$/e Å^{-3}	+0.37	+0.93	+0.26
$\Delta\rho_{min}$/e Å^{-3}	−0.71	−0.56	−0.65
$(\Delta/\rho)_{max}$	0.226	0.109	0.017
R	0.069	0.059	0.064
R_w	0.072	0.061	0.069

Table 2. Fractional Atomic Coordinates ($\times 10^4$) and Equivalent Isotropic Thermal Parameters for **1**

Atom	x	y	z	B_{eq}[11]/Å^2
S(1)	9370(2)	3978(0)	2261(2)	2.4(0)
C(1)	5253(8)	4339(2)	−2366(8)	2.4(1)
O(1)	4740(7)	4853(2)	512(6)	3.3(1)
O(2)	8554(7)	3961(2)	4241(7)	3.8(1)
N(1)	7147(6)	4600(2)	−2595(7)	2.5(1)
O(3)	9077(7)	4443(1)	1253(6)	3.6(1)
C(2)	4373(8)	4255(2)	−4383(8)	2.7(1)
O(4)	11421(6)	3834(2)	2207(7)	3.9(1)
O(5)	4747(7)	4515(2)	−5744(6)	3.5(1)
C(3)	4866(18)	2626(3)	−3137(15)	6.4(3)
C(4)	6271(9)	3378(2)	1393(10)	3.5(1)
C(5)	3854(8)	4656(2)	−1150(8)	2.9(1)
C(6)	8121(7)	3551(2)	833(8)	2.4(1)
O(6)	3171(8)	3888(2)	−4386(8)	2.4(1)
C(7)	7808(11)	3104(2)	−2232(10)	4.2(2)
C(8)	5270(10)	3069(2)	123(13)	4.2(2)
C(9)	5992(11)	2941(2)	−1696(10)	3.9(2)
C(10)	8909(9)	3410(2)	−985(9)	3.2(1)

Table 3. Fractional Atomic Coordinates ($\times 10^4$) and Equivalent Isotropic Thermal Parameters for **2**

Atom	x	y	z	B_{eq}[11]/Å^2
S (1)	4468(1)	8227(0)	326(2)	2.6(0)
Cl(1)	5771(4)	10380(1)	−4030(5)	8.0(1)
O (1)	3181(4)	8280(1)	2033(8)	3.6(1)
O (2)	5870(4)	8102(1)	1702(8)	3.3(1)
O (3)	4184(4)	7897(1)	−1798(8)	3.8(1)
C (1)	5610(5)	6830(2)	2803(10)	2.8(1)
O (4)	3713(4)	6731(1)	−303(8)	3.6(1)
N (1)	5960(4)	7196(1)	4869(9)	2.9(1)
C (2)	4147(8)	9255(2)	221(14)	4.7(2)
C (3)	5980(8)	9368(2)	−3998(13)	4.6(2)
O (5)	3064(4)	7103(1)	3365(8)	3.6(1)
C (4)	4805(5)	8839(2)	−940(10)	2.9(1)
C (5)	5359(9)	9778(2)	−2839(14)	5.0(2)
C (6)	5838(9)	6296(2)	3753(17)	5.5(2)
C (7)	5701(6)	8896(2)	−3060(11)	3.7(1)
C (8)	4407(11)	9731(2)	−752(15)	5.7(2)
C (9)	3996(5)	6914(2)	1977(11)	2.6(1)

photographs. Data were collected up to $2\theta=125°$ on a Rigaku four-circle diffractometer using graphite-monochromated Cu $K\alpha$ (1.5418 Å) radiation by ω-2θ scan. Standard reflections showed no significant intensity change. Of unique reflections measured, those as observed with $|F_o|>3\sigma(|F_o|)$ were used. The intensities were corrected for Lorentz, polarization, but not for absorption nor extinction. The structure was solved by the direct method (MULTAN 78[7]) and was refined by the full-matrix least-squares (SHELX 76[8]). Crystal data and details of refinement are summarized in Table 1. Scattering factors were taken from "International Tables for X-ray Crystallography".[9] Computations were performed on Hitachi M-680H and M-682H in the Computer Centre of the University of Tokyo.

Results and Discussion

Fractional coordinates for the crystals of **1**, **2**, and **3** are given in Tables 2, 3, and 4, respectively.[10] Labeled

Table 4. Fractional Atomic Coordinates ($\times 10^4$) and Equivalent Isotropic Thermal Parameters for **3**

Atom	x	y	z	B_{eq}[11]/Å^2
S(1)	8214(1)	3511(0)	4327(2)	3.8(0)
O(1)	8083(5)	3519(1)	6619(7)	7.1(1)
O(2)	9292(3)	3170(1)	3580(4)	4.3(1)
N(1)	3966(3)	2345(1)	419(5)	3.5(1)
O(3)	6969(4)	3379(2)	3202(12)	8.3(2)
O(4)	6148(2)	2686(1)	−1441(5)	3.9(1)
C(1)	5247(4)	3005(1)	−1397(6)	3.5(1)
C(2)	3630(4)	3245(2)	1635(6)	3.9(1)
O(5)	5327(5)	3448(2)	−2308(8)	7.7(1)
C(3)	8664(4)	4144(1)	3519(6)	3.3(1)
C(4)	3915(3)	2898(1)	−323(6)	3.3(1)
C(5)	8296(6)	4324(2)	1530(7)	5.1(1)
C(6)	8727(9)	4824(3)	915(11)	7.6(2)
C(7)	9467(5)	4435(2)	4904(9)	5.4(1)
C(8)	9463(10)	5118(2)	2290(15)	8.5(2)
C(9)	9853(9)	4922(2)	4299(14)	8.1(2)
C(10)	3258(5)	3810(2)	1167(9)	4.9(1)
C(11)	3131(9)	4091(3)	3335(14)	8.6(2)
C(12)	1994(9)	3858(3)	−152(14)	8.4(2)
O(6)	6105(3)	2298(2)	−6526(5)	4.7(1)

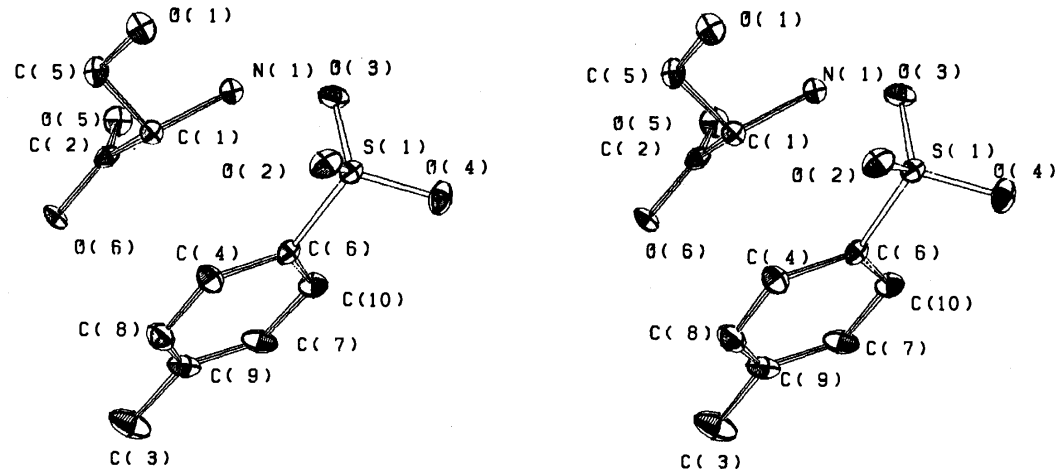

Fig. 1. Labeled stereoscopic drawing of **1**.

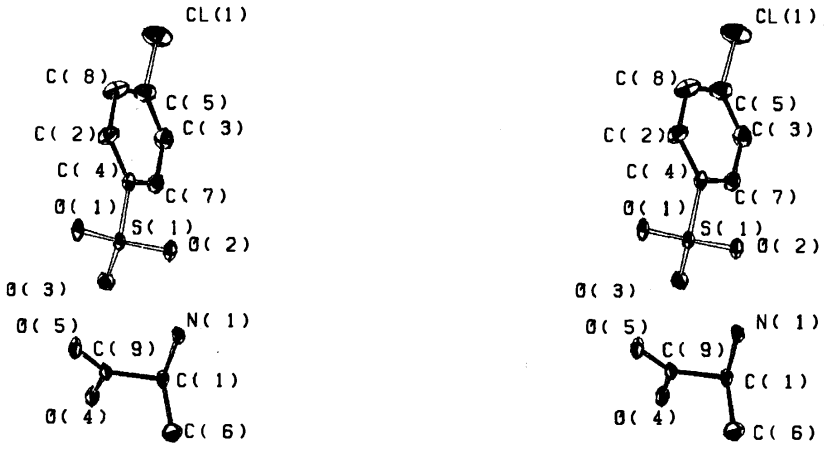

Fig. 2. Labeled stereoscopic drawing of **2**.

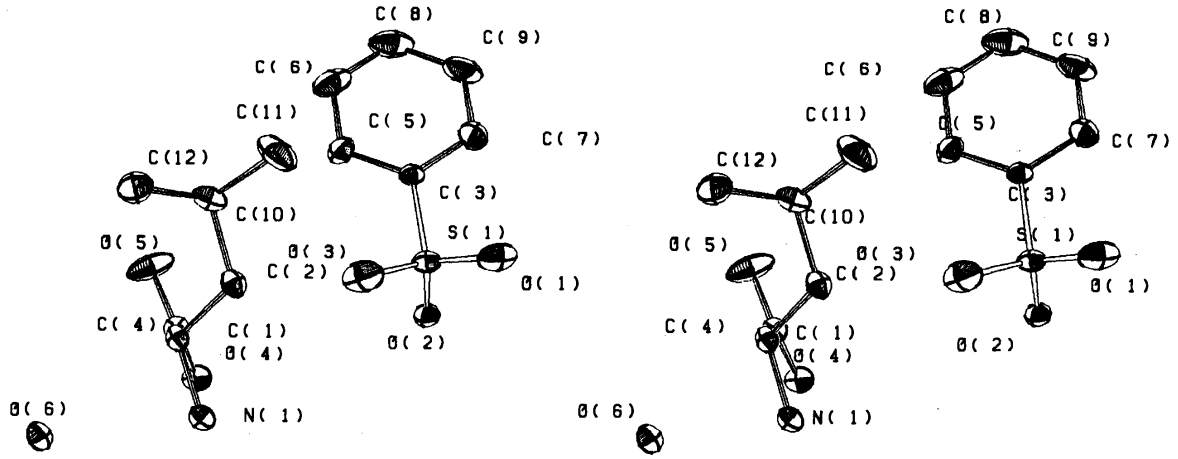

Fig. 3. Labeled stereoscopic drawing of **3**.

stereoscopic drawings of the crystals of **1**, **2**, and **3** are given in Figs. 1, 2, and 3, respectively. Their bond distances and angles are given in Tables 5, 6, and 7, respectively.

In the crystal of **1**, there are three distinct hydrogen bonds, by which two amine components and two acid components form a helical column along the *c* axis (Fig. 4). Moreover, two other hydrogen bonds exist. One links up the hydroxyl group in a molecule of serine with the carboxyl group in the neighboring molecule of serine. They are related by the operation: $x, y, -1+z$. And the other exists between the carboxyl group in serine and the oxygen atom in *p*-toluenesulfonic acid to combine two neighboring columns which are related by the operation: $-1+x, y, -1+z$. The geometries of the hydrogen bonds are listed in Table 8. There is no unusually short contact other than the hydrogen bonds.

In the crystal of **2**, two amine components and two acid components are also arranged to form a helical column by four distinct hydrogen bonds along the *a*

Table 5. Bond Distances (l/Å) and Angles (ϕ/°) of **1**

S(1)-O(2)	1.456(5)	O(2)-S(1)-O(3)	114.1(3)
S(1)-O(3)	1.456(5)	O(2)-S(1)-O(4)	112.6(3)
S(1)-O(4)	1.459(5)	O(2)-S(1)-C(6)	107.7(3)
S(1)-C(6)	1.739(5)	O(3)-S(1)-O(4)	110.8(3)
C(1)-N(1)	1.488(7)	O(3)-S(1)-C(6)	104.7(3)
C(1)-C(2)	1.512(8)	O(4)-S(1)-C(6)	106.3(3)
C(1)-C(5)	1.532(9)	N(1)-C(1)-C(2)	109.0(4)
O(1)-C(5)	1.389(8)	N(1)-C(1)-C(5)	109.4(4)
C(2)-O(5)	1.192(7)	C(2)-C(1)-C(5)	108.8(5)
C(2)-O(6)	1.298(8)	C(1)-C(2)-O(5)	121.7(5)
C(3)-C(9)	1.513(14)	C(1)-C(2)-O(6)	111.8(5)
C(4)-C(6)	1.406(8)	O(5)-C(2)-O(6)	126.5(6)
C(4)-C(8)	1.388(11)	C(6)-C(4)-C(8)	118.9(6)
C(6)-C(10)	1.401(8)	C(1)-C(5)-O(1)	112.5(5)
C(7)-C(9)	1.371(11)	S(1)-C(6)-C(4)	121.2(4)
C(7)-C(10)	1.408(10)	S(1)-C(6)-C(10)	119.0(4)
C(8)-C(9)	1.374(12)	C(4)-C(6)-C(10)	119.5(5)
		C(9)-C(7)-C(10)	121.3(7)
		C(4)-C(8)-C(9)	122.3(8)
		C(3)-C(9)-C(7)	118.4(8)
		C(3)-C(9)-C(8)	122.7(8)
		C(7)-C(9)-C(8)	118.9(7)
		C(6)-C(10)-C(7)	119.1(6)

Table 6. Bond Distances (l/Å) and Angles (ϕ/°) of **2**

S (1)-O(1)	1.451(5)	O (1)-S(1)-O(2)	112.0(2)
S (1)-O(2)	1.469(4)	O (1)-S(1)-O(3)	113.6(3)
S (1)-O(3)	1.439(4)	O (1)-S(1)-C(4)	105.9(2)
S (1)-C(4)	1.778(5)	O (2)-S(1)-O(3)	112.9(2)
Cl(1)-C(5)	1.753(8)	O (2)-S(1)-C(4)	104.5(2)
C (1)-N(1)	1.487(7)	O (3)-S(1)-C(4)	107.1(2)
C (1)-C(6)	1.515(10)	N (1)-C(1)-C(6)	110.1(5)
C (1)-C(9)	1.503(8)	N (1)-C(1)-C(9)	108.0(4)
O (4)-C(9)	1.315(7)	C (6)-C(1)-C(9)	111.0(5)
C (2)-C(4)	1.389(9)	C (4)-C(2)-C(8)	119.7(7)
C (2)-C(8)	1.379(12)	C (5)-C(3)-C(7)	119.9(7)
C (3)-C(5)	1.360(10)	S (1)-C(4)-C(2)	119.5(4)
C (3)-C(7)	1.367(9)	S (1)-C(4)-C(7)	120.0(4)
O (5)-C(9)	1.206(7)	C (2)-C(4)-C(7)	120.5(5)
C (4)-C(7)	1.372(8)	Cl(1)-C(5)-C(3)	119.0(6)
C (5)-C(8)	1.382(12)	Cl(1)-C(5)-C(8)	119.3(6)
		C (3)-C(5)-C(8)	121.6(7)
		C (3)-C(7)-C(4)	119.8(6)
		C (2)-C(8)-C(5)	118.4(8)
		C (1)-C(9)-O(4)	112.8(5)
		C (1)-C(9)-O(5)	122.1(5)
		O (4)-C(9)-O(5)	125.0(5)

Table 7. Bond Distances (l/Å) and Angles (ϕ/°) of **3**

S (1)-O(1)	1.431(5)	O(1)-S (1)-O(2)	113.1(3)
S (1)-O(2)	1.458(3)	O(1)-S (1)-O(3)	113.8(4)
S (1)-O(3)	1.460(7)	O(1)-S (1)-C(3)	107.1(3)
S (1)-C(3)	1.763(4)	O(2)-S (1)-O(3)	109.2(3)
N(1)-C(4)	1.498(5)	O(2)-S (1)-C(3)	106.2(2)
O(4)-C(1)	1.216(5)	O(3)-S (1)-C(3)	107.0(3)
C(1)-O(5)	1.274(6)	O(4)-C(1)-O(5)	123.3(4)
C(1)-C(4)	1.506(5)	O(4)-C(1)-C(4)	122.1(3)
C(2)-C(4)	1.535(5)	O(5)-C(1)-C(4)	114.5(4)
C(2)-C(10)	1.528(7)	C(4)-C(2)-C(10)	116.5(4)
C(3)-C(5)	1.370(7)	S (1)-C(3)-C(5)	120.1(3)
C(3)-O(7)	1.391(6)	S (1)-C(3)-O(7)	117.8(3)
C(5)-C(6)	1.411(11)	C(5)-C(3)-O(7)	122.0(4)
C(6)-C(8)	1.354(13)	N(1)-C(4)-C(1)	106.3(3)
O(7)-C(9)	1.364(10)	N(1)-C(4)-C(2)	108.3(3)
C(8)-C(9)	1.402(13)	C(1)-C(4)-C(2)	114.0(3)
C(10)-C(11)	1.535(10)	C(3)-C(5)-C(6)	118.2(6)
C(10)-C(12)	1.504(10)	C(5)-C(6)-C(8)	120.2(8)
		C(3)-O(7)-C(9)	119.0(6)
		C(6)-C(8)-C(9)	120.6(9)
		O(7)-C(9)-C(8)	119.9(8)
		C(2)-C(10)-C(11)	107.6(5)
		C(2)-C(10)-C(12)	112.6(5)
		C(11)-C(10)-C(12)	111.8(6)

axis (Fig. 5). The geometries of the hydrogen bonds are also listed in Table 8. Other than the hydrogen bonds, there is no unusually short nonbonding distance.

In the crystal of **3**, two amine components and two acid components show the same arrangement to form a helical column by four distinct hydrogen bonds along the *a* axis (Fig. 6). In addition, one molecule of water per one molecule of salt is included in the crystal of **3** to form two more hydrogen bonds. No unusually short contact exists other than the hydrogen bonds.

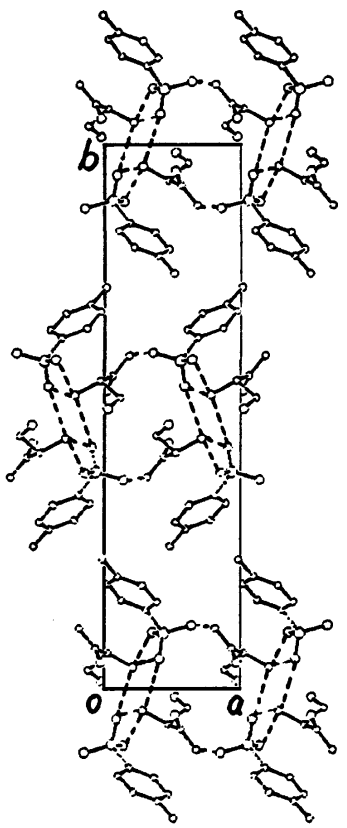

Fig. 4. The crystal structures of **1** viewed along the *c* axis. Hydrogen bonds are shown by dashed lines.

Table 8. The Distances (l/Å) of O···N or O···O, and Angles (ϕ/°) of ∠O···H-N or ∠O···H-O

	Distance	Angle
1:		
O(2)···H-N(1)^{i}	2.929(6)	155(0)
O(3)···H-N(1)^{ii}	2.764(6)	158(5)
O(3)···H-N(1)^{iii}	2.855(6)	177(0)
O(4)···H-O(6)^{iv}	2.608(7)	157(6)
O(5)···H-O(1)^{v}	2.703(6)	169(7)
2:		
O(1)···H-N(1)^{vi}	2.839(7)	168(0)
O(2)···H-N(1)^{i}	2.922(6)	162(1)
O(2)···H-O(4)^{vii}	2.646(6)	178(8)
O(3)···H-N(1)^{v}	2.995(7)	180(1)
3:		
O(6)···H-N(1)^{ii}	2.850(5)	176(0)
O(6)···H-O(3)^{ii}	2.915(8)	163(5)
O(1)···H-O(5)^{ii}	2.820(7)	154(8)
O(2)···H-O(3)^{viii}	2.836(5)	157(6)
O(2)···H-N(1)^{viii}	2.836(5)	165(0)
O(4)···H-N(1)^{viii}	2.868(5)	156(0)

The symmetry operations: i: x, y, z; ii: x, y, $1+z$; iii: $3/2-x$, $1-y$, $1/2+z$; iv: $-1+x$, y, $-1+z$; v: x, y, $-1+z$; vi: $-1/2+x$, $3/2-y$, $1-z$; vii: $1/2+x$, $3/2-y$, $-z$; viii: $1/2+x$, $1/2-y$, $-z$.

The geometries of the hydrogen bonds are listed in Table 8.

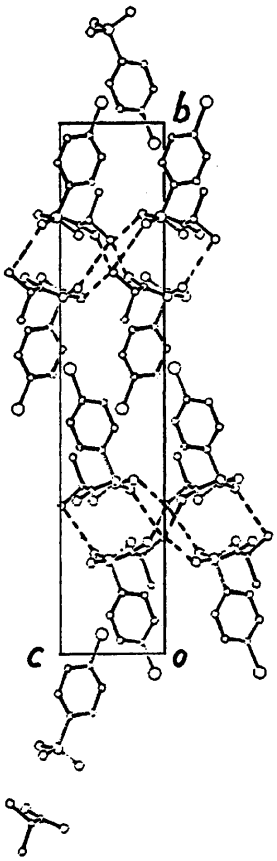

Fig. 5. The crystal structures of **2** viewed along the *a* axis. Hydrogen bonds are shown by dashed lines.

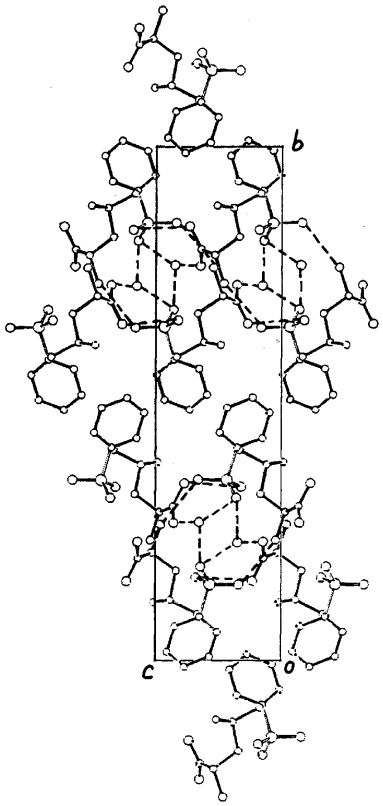

Fig. 6. The crystal structures of **3** viewed along the *a* axis. Hydrogen bonds are shown by dashed lines.

Crystals of **1**, **2**, and **3** are built up, in a similar fashion, by three distinct hydrogen bonds between two amine components and two acid components to form helical columns along the axis. This structural similarity is also observed for the crystals of cinnamic acid salts of (*R*)-1-phenylethylamine (**4**) and of (*R*)-1-(4-isopropylphenyl)ethylamine (**5**).[2] Figure 7 shows the helical columns in **1**, **2**, **3**, **4**, and **5**. Every helical column is found to be supported by repeating helical hydrogen networks.

The crystal of **1** has the same repeating unit as those of the crystals of **4** and **5**, containing one nitrogen in a molecule of the amine component and two oxygens in a molecule of the acid component. The crystal of **1** also has another hydrogen bond, which combines the amine component with the acid component, to fix the column tightly as observed in the crystals of **4** and **5**. Moreover, in the case of the crystal of **1**, one more distinct hydrogen bond exists between the carboxyl group in the amino acid component and the hydroxyl group in the neighboring acid component. They are related by the operation: x, y, $-1+z$. On the other hand, in the crystals of **2** and **3**, the repeating unit includes uniquely a part of amino acids (N-C-C-O). To support the helical hydrogen networks in each column tightly, another distinct hydrogen bond exists between two amino acid components. The repeating units and the supporting hydrogen bonds in each crystal are denoted by dashed and waved lines, respectively, in Fig. 7.

The analyses of these crystals show that conglomerate crystals of amino acid salts include a unique part of the amino acid (N-C-C-O) in the helical column, except for the case like **1** with the hydroxyl group, which can make hydrogen bonds. But, as shown in Fig. 7, the alternate arrangement of the arenesulfonic acid and the amino acid components in the crystals of **1**, **2**, and **3** is essentially the same as those of cinnamic acid and the amine components in the crystals of **4** and **5**. Moreover, arenesulfonic acid is also a rigid molecule like cinnamic acid. The rigidity would prevent the molecule of the amino acid from contacting each other by strong hydrogen bonds.

The appropriate R^1 and R^2 groups tightly pack two neighboring columns, which are related by twofold screw axis. The schematic drawing is shown in Fig. 8. The helical column is denoted by the thick line. Benzene rings in neighboring columns are arranged parallel each other to interact by π-π orbitals. The π-π interaction is denoted by dashed line. Compared with the crystal of **3**, the crystal of **2** has leucine bigger than that of alanine, and benzenesulfonic acid smaller than *p*-chlorobenzenesulfonic acid. The fact suggests that

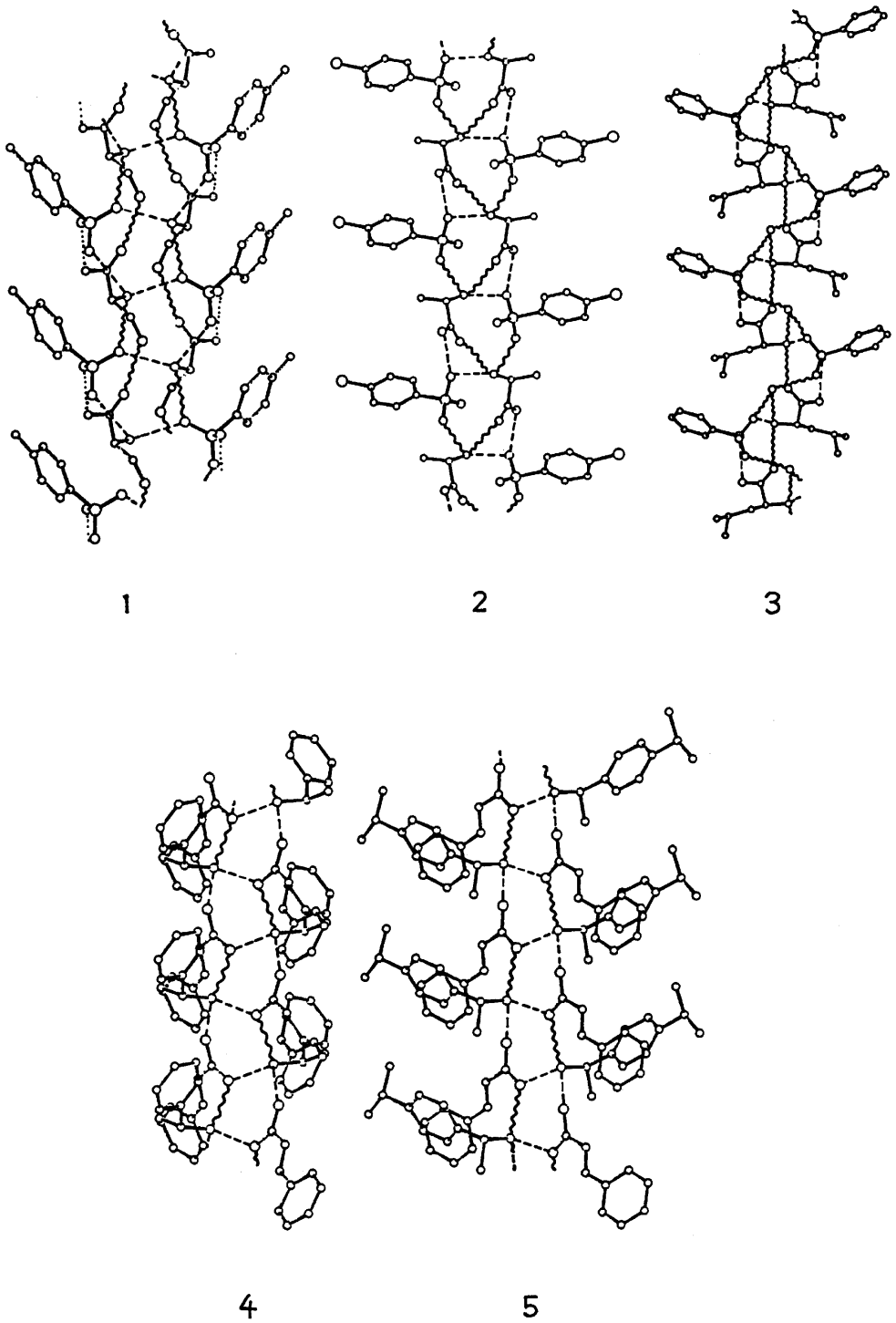

Fig. 7. A helical column in each crystal of **1**, **2**, **3**, **4**, and **5**. Hydrogen bonds are shown by dashed, waved and dotted lines. **1**: *p*-toluenesulfonic acid salt of L-serine, **2**: *p*-chlorobenzenesulfonic acid salt of L-alanine, **3**: benzenesulfonic acid salt of L-leucine, **4**: cinnamic acid salt of 1-phenylethylamine, **5**: cinnamic acid salt of 1-(4-isopropylphenyl)ethylamine.

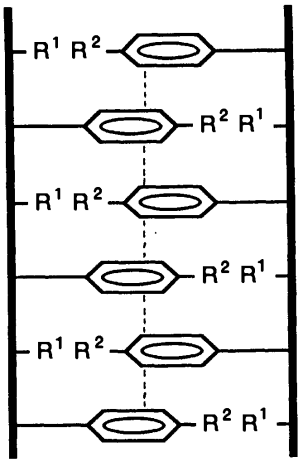

Fig. 8. The schematic drawing of the helical column. **1**: R^1=H and R^2=Me. **2**: R^1=Me and R^2=Cl. **3**: R^1=H and R^2=Pr^i. **4**: R^1=H and R^2=Ph **5**: R^1=H and R^2=$C_6H_4Pr^i$-*p*.

bigger R^1 paired with smaller R^2 makes the crystal packing close by π-π interaction. In the crystal of **1**, R^1 is rather small because hydroxymethyl group is oriented along the column by a hydrogen bond, and paired acid has methyl group bigger than hydrogen as R^2.

These results indicate that the shape of the arenesulfonic acid plays an important role to form a rigid helical arrangement and to offer suitable space for the amino acid molecule. Namely, the following criteria proposed by us are considered to be appropriate for the choice of an achiral derivatizing agent in the transformation of a racemic compound into a conglomerate crystal: (a) The achiral derivatizing agent should be able to form a helical column by hydrogen bonds with the molecule of the racemic compound; (b) The derivatizing agent should be rigid and flat to limit the orientation of the molecules of the racemic compound; (c) The sizes of the derivatizing agent and the molecule of the racemic compound should be complementary to make the crystal packing close.

A part of this work was supported by The Fujisawa Foundation, to which acknowledgment is made.

References

1) J. Jacques, A. Collet, and S. H. Wilan, "Enantiomers, Racemates, and Resolutions," John Wiley & Sons, New York (1981).

2) K. Saigo, H. Kimoto, H. Nohira, K. Yanagi, and M. Hasegawa, *Bull. Chem. Soc. Jpn.*, **60**, 3655 (1987).

3) I. Chibata, S. Yamada, M. Yamamoto, and M. Wada, *Experientia*, **24**, 638 (1968).

4) N. Sato, T. Uzuki, K. Toi, and T. Akashi, *Agr. Biol. Chem.*, **33**, 1107 (1969).

5) S. Yamada, M. Yamamoto, and I. Chibata, *Chem. Eng. (London)*, June 2, 528 (1973).

6) S. Yamada, M. Yamamoto, and I. Chibata, *J. Org. Chem.*, **38**, 4408 (1973).

7) P. Main, S. E. Hull, L. Lessinger, G. Germain, J.-P. Declercq, and M. M. Woolfson, "A System of Computer Programs for the Automatic Solution of Crystal Structures from X-ray Diffraction Data, MULTAN 78," University of York, England, and Louvain, Belgium (1978).

8) G. M. Sheldrick, "Program for Crystal Structure Determination, SHELX 76," University of Cambridge, England (1976).

9) "International Tables for X-ray Crystallography," Vol. IV, Kynoch Press, Birmingham (1974).

10) F_o–F_c tables, anisotropic thermal temperature factors and fractional atomic coordinates of hydrogen atoms are deposited as Document No. 8881 at the Office of the Editor of Bull. Chem. Soc. Jpn.

11) The equivalent isotropic temperature factors were computed using the following expression;

$$B_{eq} = 4/3(B_{11}a^2 + B_{22}b^2 + B_{33}c^2).$$

Generation of an *N*-Sodioazomethine Ylide and Its Cycloadditions with α,β-Unsaturated Esters

Shuji KANEMASA,* Manabu YOSHIOKA, and Otohiko TSUGE*
Institute of Advanced Material Study, and Department of Molecular Science and Technology, Interdisciplinary Graduate School of Engineering Sciences, Kyushu University, Kasugakoen, Kasuga 816
(Received December 21, 1988)

Treatment of methyl 2-(benzylideneamino)propanoate with sodium hydride in THF generates an *N*-sodioazomethine ylide, which shows a very poor stereoselectivity in the cycloaddition with methyl acrylate. However, addition of such a base as triethylamine or *t*-butyl alcohol improves the selectivity. Chemical properties of the ylide have been discussed on the basis of the selectivity totally different from that of *N*-lithio analogue.

N-Metalated azomethine ylides **A**, the ylide of new type, can be generated upon treatment of imines [PhCH=NCH(R)COY] of α-amino esters and amides with tertiary amines in the presence of metal halides.[1-3] These ylides show increased reactivity in their cycloadditions and high reliability in stereochemical selectivities. A variety of metals such as lithium, magnesium, zinc, aluminum, and silver can be incorporated; metal-chelated intermediates **B** are responsible for the highly stereoselective cycloadditions with carbonyl-activated olefins [$R^1CH=C(R^2)COY'$] leading to **C**.

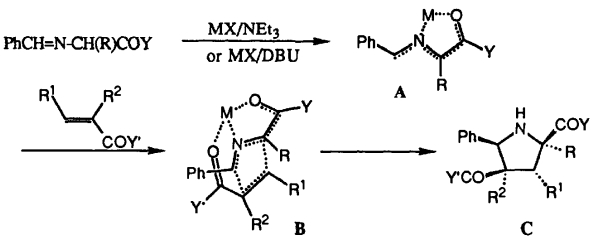

In this ylide generation scheme, ylide species **A** are always accompanied by the formation of an equimolar amount of acidic products, trialkylammonium halides, which can act as a quencher of the anionic intermediates involved. Therefore, the ylide generation using tertiary amine is a reversible process, causing the undesired formation of Michael adducts.[2]

Irreversible ylide generation would be achieved if imines of α-amino esters are treated with metallic bases such as lithium diisopropylamide, butyllithium, and sodium hydride.[4] The ylides generated in high concentration are expected to show a much more enhanced reactivity.

In the present article, reactions of an imine of α-amino ester, methyl 2-(benzylideneamino)propanoate (**1**), with a variety of olefins in the presence of sodium hydride have been examined. Although cycloaddition of the resulting *N*-sodioazomethine ylide with methyl acrylate shows a poor stereoselectivity, addition of triethylamine or *t*-butyl alcohol as a base improves the selectivity. A stepwise cyclization mechanism is proposed since metal chelation is less important. Stereoselectivities are mainly determined at the step of intramolecular nucleophilic imine addition.

Results and Discussion

It was previously reported that treatment of imine **1** with triethylamine and sodium iodide generated the *N*-sodioazomethine ylide.[2] Its reaction with methyl acrylate produced a 1:2.7 mixture of stereoselective cycloadduct **2A** and Michael adduct **3** in a combined yield of 96%, indicating highly ionic character of the transition state rather than a tightly chelated structure.

On the other hand, reaction of imine **1** with methyl acrylate in the presence of sodium hydride, in tetrahydrofuran (THF) at room temperature, gave three isomeric 1:1 cycloadducts **2A—C** in 45, 13, and 6% yields, respectively, along with the Michael adduct **3** (25%, Scheme 1 and Entry 1 in Table 1). These three isomers **2A—C** could be separated from each other through column chromatography over silica gel.

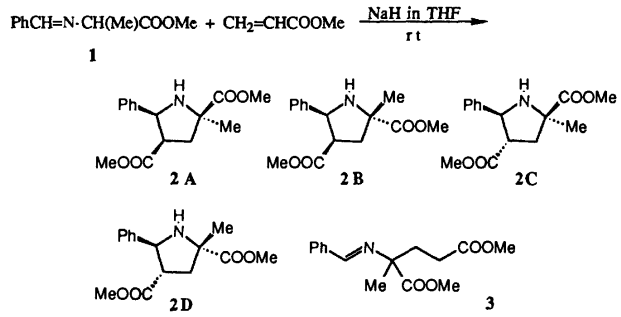

Scheme 1.

Figure 1 shows ^1H NMR spectral data of **2A—C** and the last possible isomeric cycloadduct **2D** whose formation is to be described later. Isomer **2A** is identical with 2,4-*cis*:4,5-*cis*-2,4-pyrrolidinedicarboxylate which was previously obtained as a single isomer in the reaction of **1** with methyl acrylate in the presence of lithium bromide and triethylamine.[1] Isomer **2B** was determined to be a 2,4-trans:4,5-cis structure on the basis of the following spectral data

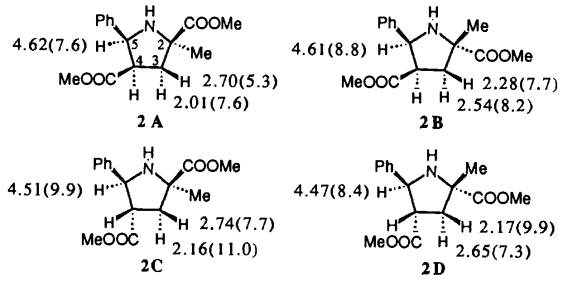

Fig. 1. Structural assignment of isomeric cycloadducts **2A—D** on the basis of ^{1}H NMR spectral data with vicinal coupling constants in Hz in parentheses.

(Fig. 1), and hence the reported 2,4-cis:4,5-cis geometry of **2A** was reconfirmed: 1) The ester methyl at the 4-position (4-COOMe, δ=3.12) is shielded by 5-Ph, 2) the difference of chemical shifts of 3-Hs (2.54−2.28=0.26 ppm) is much smaller than that of **2A** (2.70−2.01=0.69 ppm), and 3) the lower 3-H (2.70) of **2A**, which is cis to 2-COOMe, shows a small trans coupling with 4-H ($J_{3-4(trans)}$=5.3 Hz). The isomer **2B** is most likely to take an envelope conformation with two bulky substituents, 2-Me and 5-Ph, in pseudo equatorial positions. The corresponding envelope conformation of **2A** becomes less stable because the bulkier 2-Me has to occupy a pseudo axial position, the dihedral angle between 3-H (2.70) and 4-H being reduced.

Isomer **2C** has a 2,4-trans:4,5-trans structure on the basis of no shielding of 4-COOMe (δ=3.61), an NOE between one 3-H (2.16) and 2-Me, and an NOE between the other 3-H (2.74) and 4-H. Therefore, the other 4,5-trans isomer **2D** was assigned to be 2,4-cis:4,5-trans structure. Large trans couplings between the higher 3-H (2.16) and 4-H ($J_{3-4(trans)}$=11.0 Hz) and between 4-H and 5-H ($J_{4-5(trans)}$=9.9) are consistent with the assigned geometry of **2C**.

Thus, *N*-sodioazomethine ylides generated from **1** either by treating with sodium hydride or sodium iodide/triethylamine exhibited different stereoselectivities. The only differences anticipated would be 1) higher concentration of the intermediate ylide in the former case, and 2) existence of triethylammonium iodide (or together with triethylamine and sodium iodide) in the latter case.

Therefore, the *N*-sodioazomethine ylide was first generated by using sodium hydride and then treated with triethylamine (1.2 equiv). The resulting species was allowed to react with methyl acrylate. Surprisingly, the pattern of stereoselectivity changed dramatically to produce 2,4-trans:4,5-trans cycloadduct **2C** as major isomer along with 2,4-cis:4,5-trans minor isomer **2D** (Entry 2, **2C**:**2D**=6:1), no formation of either **2A**, **2B** or Michael adduct **3** being detected.

Addition of *t*-butyl alcohol or methanol (1.1—1.2 equiv), instead of triethylamine, resulted in no any deactivation of the reactive intermediate, *N*-sodioazomethine ylide; mixtures of two cycloadducts were similarly obtained (Entries 3 and 4, **2C**:**2D**=7:1). Use of water as an additive, however, furnished **2A** as the sole isomer together with Michael adduct **3** (Entry 5, **2A**:**3**=3:5). Separation of pure **2D** from the mixture with **2C** failed.

These unusual stereoselectivities of the *N*-sodioazomethine ylide in the presence of additives let us investigate further its cycloadditions with other olefinic esters. Triethylamine or *t*-butyl alcohol was employed as additive.

With methyl crotonate and triethylamine, a 7:1 mixture of two stereoisomers was obtained in a total yield of 89% (Scheme 2 and Entry 1 in Table 2). Major isomer **4A** is identical with 2,3-cis:4,5-cis cycloadduct that was previously obtained as the sole product in the lithium bromide/triethylamine-induced reaction of **1** with methyl crotonate.[1] Minor isomer **4C** was assigned to be a 2,3-trans:4,5-trans structure because of no shielding of 4-COOMe (δ=3.64), a large trans coupling of J_{4-5} (10.2 Hz),[5] and lower resonance of 2-Me (21.32, 2-Me of **4A** appears at 20.30). Addition of *t*-butyl alcohol decreased its stereoselectivity, a 2:1 mixture of **4A** and **4C** being obtained (Entry 2).

With methyl methacrylate, the reaction in the presence of triethylamine resulted in a lower isomer ratio (Entry 3, **5A**:**5B**=2.5:1) than that in the presence of *t*-butyl alcohol (Entry 4, **5A** only). The structures of **5A** and **5B** were readily determined as shown in Scheme 2 on the basis of the shielding of 4-COOMe (**5A**: δ=3.24, **5B**: 3.16) and the chemical shifts of 3-Hs (**5A**: 1.77 and 3.04, **5B**: 2.30 and 2.66).

A 1:2 mixture of two regioisomers **6A** and **7** was

Table 1. Sodium Hydride-Induced Reactions of Imine **1** with Methyl Acrylate

Entry	NaH	Additive (equivalent)	Time/h	Product (yield/%)[a]
1	1.5	None	1	**2A**(45)+**2B**(13)+**2C**(6)+**3**(25)
2	1.2	NEt_3 1.2	1	**2C**+**2D** (79) **2C**:**2D**=6:1[b,c]
3	1.2	*t*-BuOH 1.1	1	**2C**+**2D** (82) **2C**:**2D**=7:1[b,c]
4	1.2	MeOH 1.2	0.25	**2C**+**2D** (79) **2C**:**2D**=7:1[b,c]
5	1.2	H_2O 1.2	0.25	**2A**+**3** (54) **2A**:**3** =3:5[b,d]

a) Yields of isolated products. b) Determined by ^{1}H NMR of unpurified reaction mixture. c) Only **2C** could be separated by column chromatography. d) Inseparable mixture.

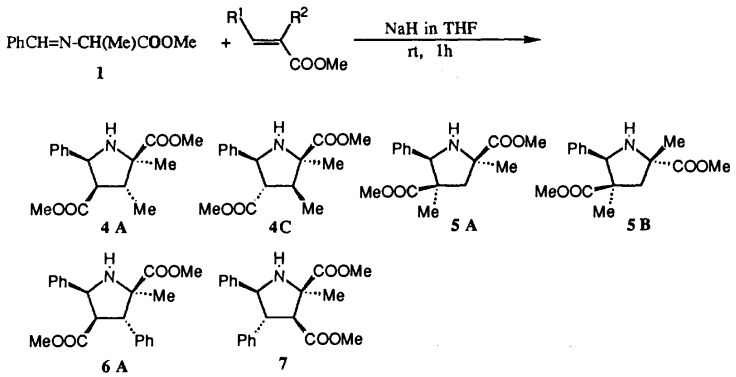

Scheme 2.

Table 2. Sodium Hydride-Induced Reactions of Imine **1** with Electron-Deficient Olefins[a]

Entry	Olefin	NaH Additive (equivalent)	Product (yield/%)[b]
1	Methyl crotonate	1.2 NEt_3 1.2	**4A**+**4C** (89) **4A**:**4C**=7:1[c,d]
2	Methyl crotonate	1.2 *t*-BuOH 1.1	**4A**+**4C** (79) **4A**:**4C**=2:1[c,d]
3	Methyl methacrylate	1.2 NEt_3 1.2	**5A**+**5B** (79) **5A**:**5B**=2.5:1[c,e]
4	Methyl methacrylate	1.2 *t*-BuOH 1.1	**5A** (79)
5	Methyl cinnamate	1.2 *t*-BuOH 1.1	**6A**+**7** (62) **6A**:**7** =1:2[c,f]

a) All reactions were carried out for 1 h at room temperature in THF. b) Yields of isolated products. c) Determined by ^1H NMR of unpurified mixture. d) Only **4A** was isolated. e) **5A** and **5B** could be separated by column chromatography. f) **6A** and **7** could be separated by column chromatography.

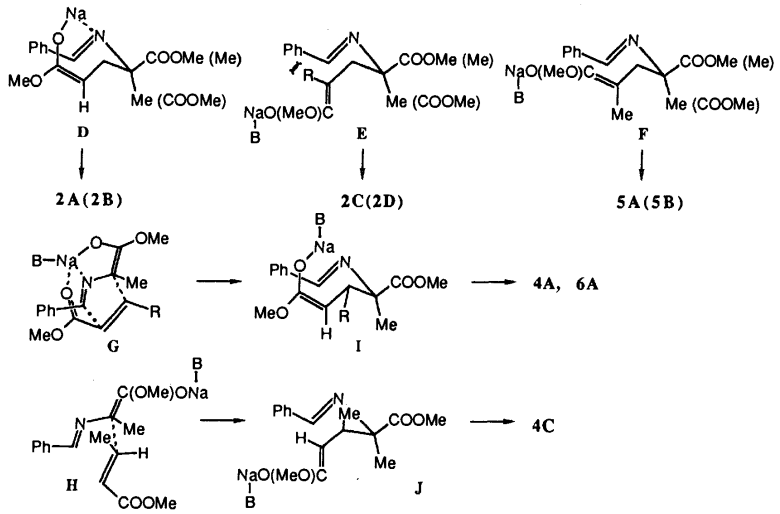

Fig. 2. Stereoselectivity in the cycloadditions of *N*-sodioazomethine ylide with esteric olefins.

obtained in the sodium hydride-induced reaction of **1** with methyl cinnamate (Entry 5). This result resembles a similar reaction induced by lithium bromide and 1,8-diazabicyclo[4.2.0]undec-7-ene (DBU) where a 2:1 mixture of **6A** and **7** was furnished in a total yield of 60%.[2]

Metal enolates containing a metal more electropositive than lithium such as sodium are most likely to undergo stepwise cycloadditions with α,β-unsaturated esters via metal enolate intermediates.[2] A concerted cycloaddition mechanism with a cyclic chelation, e.g. **B**, would be less important in these cases.

Thus, the *N*-sodioazomethine ylide of **1** reacts with methyl acrylate or methacrylate to form sodium enolate intermediates. In the reaction with methyl acrylate in the absence of additive (B), a weak interaction still working between the sodium and the imine nitrogen favors the chelation-controlled cyclization via **D** to give **2A** as major product (Fig. 2),[6] while the presence of an additive, which interacts with the

metal, not only weakens such chelation but also makes the metal bulkier. As a result, cyclization via **E** (R=H) becomes easier, the dramatic change of stereoselectivity having resulted to give **2C** as major product along with **2D**.

In the reaction of the sodium enolate intermediate from methyl methacrylate, cyclization via **E** (R=Me) becomes disfavored because these is a considerable steric repulsion between the phenyl and the methyl moieties. Thus, the cyclization via approach **F** was only observed to give **5A** and **5B**.

The Michael reaction of **1** with methyl crotonate offers an additional stereoselectivity at the newly formed bond, which finally reflects the stereochemistry of cycloadducts **4**. In the presence of a less polar additive such as triethylamine, the endo-selective cycloaddition via approach **G** (R=Me) takes place because there would still remain attractive interactions of the metal sodium to both the imine nitrogen and the ester oxygen atoms. The presence of *t*-butyl alcohol collapses the chelation **G** so that the contribution of linear transition state **H** becomes relatively more important.[7] Stereospecific cyclization of **I** and **J** leads to **4A** and **4C**, respectively.

Poor regioselectivity in the reaction of *N*-lithioazomethine ylide with methyl cinnamate is known.[2] A similar explanation would be enough for the formation of two regioisomers, **6A** and **7**.

In conclusion, 1) *N*-sodioazomethine ylides are characterized more or less as metal enolates, 2) their cycloadditions with α,β-unsaturated esters proceed through a stepwise mechanism via sodium enolate intermediates, 3) a basic additive collapses fragile metal chelations so that the stereoselectivity of cycloadditions is mainly determined by steric factors, 4) *N*-sodio ylides are synthetically complementary to other *N*-metalated ylides.

Experimental

General. Melting points were determined on a Yanagimoto melting point apparatus and are uncorrected. IR spectra were taken with JASCO IRA-1 and A-702 spectrometers. ^{1}H and ^{13}C NMR spectra were recorded on JEOL FX-100 (100 MHz for ^{1}H NMR and 25.05 MHz for ^{13}C NMR) and GSX-270 (270 MHz for ^{1}H NMR and 67.94 MHz for ^{13}C NMR) instruments. Chemical shifts are expressed in parts per million downfield from tetramethylsilane as an internal standard. Mass spectra and high-resolution mass spectra (HRMS) were measured with a JEOL-01SG-2 spectrometer at 70 eV of ionization energy. Elemental analyses were performed on a Hitachi 026 CHN analyzer. For preparative column chromatography, Wakogel C-200, C-300 (Wako), and Silica gel 60 (Merck) were employed. Flash chromatography was carried out on an EYELA EF-10 apparatus using a column (20×180 mm) packed with Silica gel 60 (Merck, size: 0.04—0.063 mm). Gas liquid chromatography (GLC) was accomplished on a Yanaco G-2800 gas chromatograph (Yanagimoto) with an ionization flame detector using a glass column (SE-30, 3×2000 mm) or a glass capillary column (Silicone GE, SE-30, 0.25×50000 mm). Micro vacuum distillation was carried out on a Sibata GTO-250R Kugelrohr distilling apparatus. Solvents were evaporated with a Tokyo Rikakikai rotary evaporator type-V at about 50 °C unless otherwise stated.

Materials. Dimethyl 2-methyl-*c*-5-phenyl-*r*-2,*c*-4-pyrrolidinedicarboxylate (**2A**),[1] dimethyl 2-(benzylideneamino)-2-methylpentanedioate (**3**),[2] dimethyl 2,*t*-3-dimethyl-*c*-5-phenyl-*r*-2,*c*-4-pyrrolidinedicarboxylate (**4A**),[1] dimethyl 2,*t*-4-dimethyl-*c*-5-phenyl-*r*-2,*c*-4-pyrrolidinedicarboxylate (**5A**),[1] dimethyl 2-methyl-*t*-3,*c*-5-diphenyl-*r*-2,*c*-4-pyrrolidinedicarboxylate (**6A**),[2] and dimethyl 2-methyl-*t*-4,*c*-5-diphenyl-*r*-2,*c*-3-pyrrolidinedicarboxylate (**7**)[2] were all previously prepared.

Reaction of Methyl 2-(Benzylideneamino)propanoate (1) with Sodium Hydride and Cycloaddition with Methyl Acrylate. Sodium hydride (suspension in mineral oil, 60 wt%, 0.06 g, 1.5 mmol) was washed with dry hexane (3 ml×3) and suspended in dry THF under nitrogen. Addition of imine **1** (0.191 g, 1 mmol) was followed by methyl acrylate (0.095 g, 1.1 mmol) after 5 min. The mixture was stirred at room temperature for 1 h, poured into saturated ammonium chloride (10 ml), and extracted with diethyl ether (40 ml×2). The combined extracts were dried over magnesium sulfate and evaporated in vacuo. The residue (0.261 g) was chromatographed over silica gel by using hexane–ethyl acetate (4:1 to 3:1 v/v) to give **2A** (0.125 g, 45%), **2B** (0.035 g, 13%), and **2C** (0.018 g, 6%). Formation of **3** was confirmed on the basis of ^{1}H NMR spectrum of the crude reaction mixture (25%).

Dimethyl 2-Methyl-*t*-5-phenyl-*r*-2,*t*-4-pyrrolidinedicarboxylate (2B): Colorless liquid; IR (neat) 3270, 1740, and 1730 cm^{-1}; ^{1}H NMR ($CDCl_3$) δ=1.61 (3H, s, 2-Me), 2.28 (1H, dd, J_{gem}=12.8 and J_{3-4}=7.7 Hz, one of 3-H), 2.54 (1H, dd, J_{gem}=12.8 and J_{3-4}=8.2 Hz, the other of 3-H), 2.66 (1H, br, NH), 3.12 (3H, s, 4-COOMe), 3.28 (1H, ddd, J_{4-3}=8.2, 7.7, and J_{4-5}=8.8 Hz, 4-H), 3.75 (3H, s, 2-COOMe), 4.61 (1H, d, J_{5-4}=8.8 Hz, 5-H), and 7.2—7.4 (5H, m, Ph); ^{13}C NMR ($CDCl_3$) δ=25.44 (2-Me), 38.11 (3-C), 49.42 (4-C), 51.13, 52.42 (each COOMe), 63.80 (2-C), 65.73 (5-C), 127.31, 127.43, 127.87, 140.46 (each Ph), 173.01, and 177.75 (each COOMe); MS *m/z* (rel intensity, %) 277 (M^+, 2), 219 (15), 218 (base peak), 158 (30), and 131 (14). Found: C, 64.94; H, 6.94; N, 4.96%. Calcd for $C_{15}H_{19}NO_4$: C, 64.96; H, 6.91; N, 5.05%.

Dimethyl 2-Methyl-*c*-5-phenyl-*r*-2,*t*-4-pyrrolidinedicarboxylate (2C): Colorless liquid; IR (neat) 3270, 1735, and 1725 cm^{-1}; ^{1}H NMR ($CDCl_3$) δ=1.53 (3H, s, 2-Me), 2.16 (1H, dd, J_{gem}=12.8 and J_{3-4}=11.0 Hz, one of 3-H, showing an NOE against 2-Me), 2.58 (1H, br, NH), 2.74 (1H, dd, J_{gem}=12.8 and J_{3-4}=7.7 Hz, the other of 3-H, showing an NOE against 4-H), 2.95 (1H, ddd, J_{4-3}=11.0, 7.7, and J_{4-5}=9.9 Hz, 4-H), 3.61 (3H, s, 4-COOMe), 3.78 (3H, s, 2-COOMe), 4.51 (1H, d, J_{5-4}=9.9 Hz, 5-H), and 7.3—7.4 (5H, m, Ph); ^{13}C NMR ($CDCl_3$) δ=26.54 (2-Me), 42.30 (3-C), 51.79, 52.57 (each COOMe), 52.63 (4-C), 65.33 (2-C), 66.06 (5-C), 126.92, 127.76, 128.58, 141.18 (each Ph), 173.44, and 176.98 (each COOMe); MS *m/z* (rel intensity, %) 277 (M^+, 3), 219 (15), 218 (base peak), 177 (15), 158 (32), and 131 (13). Found: C, 64.92; H, 7.01; N, 4.75%. Calcd for $C_{15}H_{19}NO_4$: C, 64.96; H, 6.91; N, 5.05%.

General Procedure for the Reaction of 1 with α,β-Unsaturated Esters in the Presence of Sodium Hydride and Additives. Under nitrogen, sodium hydride (60% in oil,

0.048 g, 1.2 mmol) was washed with dry hexane (3 ml×2) and suspended in dry THF (3 ml). Imine **1** (0.191 g, 1 mmol) was added, and after stirring at room temperature for 15 min was added an additive such as triethylamine (0.121 g, 1.2 mmol), *t*-butyl alcohol (0.082 g, 1.1 mmol), or water (21 mg, 1.2 mmol). After 5 min, an olefin ester (1 mmol) was added. The mixture was stirred at room temperature and then poured into saturated ammonium chloride (10 ml). Extraction with diethyl ether (40 ml×2), evaporation of the dried extract, and chromatography of the residue on silica gel gave **2—7**. The reaction conditions and results are all listed in Tables 1 and 2.

Dimethyl 2-Methyl-*t*-5-phenyl-*r*-2,*c*-4-pyrrolidinedicarboxylate (2D): This isomer could not be isolated in its pure form. Only ^{1}H NMR spectrum was recorded from the spectrum of the mixture with **2C**: ^{1}H NMR ($CDCl_3$) δ=1.50 (3H, s, 2-Me), 2.17 (1H, dd, J_{gem}=13.2 and J_{3-4}=9.9 Hz, one of 3-H), 2.30 (1H, br, NH), 2.65 (1H, dd, J_{gem}=13.2, and J_{3-4}=7.3 Hz, the other of 3-H), 2.90 (1H, ddd, J_{4-3}=9.9, 7.3, and J_{4-5}=8.4 Hz, 4-H), 3.62 (3H, s, 4-COOMe), 3.77 (3H, s, 2-COOMe), 4.47 (1H, d, J_{5-4}=8.4 Hz, 5-H), and 7.3—7.5 (5H, m, Ph).

Dimethyl 2,*c*-3-Dimethyl-*c*-5-phenyl-*r*-2,*t*-4-pyrrolidinedicarboxylate (4C): Isomer **4C** could not be separated in a pure form from the mixture with **4A**. Therefore, mixtures with two different isomer ratios were subjected to ^{1}H and ^{13}C NMR measurements, and spectra of **4C** were assigned as follows: ^{1}H NMR ($CDCl_3$) δ=1.06 (3H, d, J=7.0 Hz, 3-Me), 1.40 (3H, s, 2-Me), 2.7 (1H, br, NH), 3.64 (3H, s, 4-COOMe), 3.81 (3H, s, 2-COOMe), 4.72 (1H, d, J_{5-4}=10.2 Hz, 5-H), and 7.2—7.5 (5H, m, Ph). Both 3-H and 4-H are overlapped with the signals of **4A**. ^{13}C NMR ($CDCl_3$) δ=11.71 (3-Me), 21.32 (2-Me), 43.27 (3-C), 51.56, 52.54 (each COOMe), 56.43 (4-C), 62.33 (2-C), 68.71 (5-C), 127.11, 127.48, 127.58, 142.31 (each Ph), 172.32, and 177.46 (each COOMe).

Dimethyl 2,*c*-4-Dimethyl-*t*-5-phenyl-*r*-2,*t*-4-pyrrolidinedicarboxylate (5B): Colorless liquid; IR (neat) 3430 and 1730 cm^{-1}; ^{1}H NMR ($CDCl_3$) δ=1.33 (3H, s, 4-Me), 1.60 (3H, s, 2-Me), 2.30 (1H, d, J_{gem}=13.6 Hz, one of 3-H), 2.66 (1H, d, J_{gem}=13.6 Hz, the other of 3-H), 2.70 (1H, br, NH), 3.16 (3H, s, 4-COOMe), 3.76 (3H, s, 2-COOMe), 4.06 (1H, s, 5-H), and 7.2—7.3 (5H, m, Ph); ^{13}C NMR ($CDCl_3$) δ=23.30 (4-Me), 25.98 (2-Me), 46.62 (3-C), 51.30, 52.38 (each COOMe), 55.09 (4-C), 64.58 (2-C), 72.83 (5-C), 126.98, 127.68, 127.87, 139.22 (each Ph), 175.20, and 178.31 (each COOMe); MS *m/z* (rel intensity, %) 291 (M^+, 5), 290 (18), 233 (17), 192 (12), 191 (89), 172 (23), 131 (64), and 130 (12). Found: C, 65.96; H, 7.54; N, 4.68%. Calcd for $C_{16}H_{21}NO_4$: C, 65.96; H, 7.27; N, 4.81%.

The present work was financially supported by a Grant-in-Aid for Scientific Research (No. 63550652) from the Ministry of Education, Science and Culture.

References

1) O. Tsuge, S. Kanemasa, and M. Yoshioka, *J. Org. Chem.*, **53**, 1384 (1988).

2) S. Kanemasa, M. Yoshioka, and O. Tsuge, *Bull. Chem. Soc. Jpn.*, **62**, 869 (1989).

3) D. A. Barr, R. Grigg, H. Q. N. Gunaratune, J. Kemp, P. McMeekin, and V. Sridharan, *Tetrahedron*, **44**, 557 (1988).

4) Reaction of methyl (benzylideneamino)acetate with butyllithium resulted in no clean formation of the *N*-lithiated ylide, due to nucleophilic reactions at the ester and/or the imine moieties. This problem was solved by use of *t*-butyl ester instead of the methyl ester (S. Kanemasa and O. Uchida, unpublished results).

5) A large trans coupling of J_{4-5}=10.2 Hz can be explained only with the envelope conformation having 3-Me/4-COOMe/5-Ph all in pseudo equatorial positions. Thus, 3,4-trans:4,5-trans geometry of **4C** is confirmed.

6) O. Tsuge, K. Ueno, S. Kanemasa, and K. Yorozu, *Bull. Chem. Soc. Jpn.*, **60**, 3347 (1987).

7) As a discussion on the linear mechanism: M. Yamaguchi, *Yuki Gosei Kagaku Kyokai Shi*, **44**, 405 (1986).

The Polymerization of Toluene and Its Analogs Catalyzed by a Copper(I) Chloride-Aluminum Chloride-Oxygen System

Naoki TOSHIMA,* Keiichi KANAKA, Naoko ISHIYAMA, and Hidefumi HIRAI†
Department of Industrial Chemistry, Faculty of Engineering, The University of Tokyo, Hongo, Bunkyo-ku, Tokyo 113
(Received December 26, 1988)

The polymerization of aromatic compounds other than benzene (such as toluene, xylene, ethylbenzene, mesitylene, and biphenyl) was performed by using a copper(I) chloride–aluminum chloride–oxygen system which caused benzene to polymerize. Excess aluminum chloride, with respect to copper(I) chloride, was required for these compounds to polymerize, as was also true for benzene. For example, the treatment of toluene with aluminum chloride and copper(I) chloride (15:3:1 in molar ratio) under 1 atm of oxygen at 50 °C for 24 h gave toluene polymer in 204% yield based on copper(I) chloride. This fact suggests that copper(I) chloride also worked as a catalyst in the case of the polymerization of toluene. The toluene polymer was obtained as both solid and liquid products, both of which were soluble in various organic solvents. The solid product has a complicated, crosslinked and "quinonoid-like" structure. On the other hand, the liquid product has a structure that is nearly identical with that of methylated poly(1,4-phenylene). Other alkylbenzenes gave the only liquid polymerization products, except for *o*-xylene which gave a small amount of solid products. The polymerization of biphenyl gave a low-molecular-weight poly(1,4-phenylene).

It is well-known that the aromatic hydrocarbon polymer is thermally stable[1] and becomes electrically conductive upon doping with various dopants.[2] In particular, an investigation of poly(1,4-phenylene) (PPP), the polymer of benzene, has been intensively carried out while considering synthetic methods and properties.

A number of methods for synthesizing PPP have been invented, such as the electrolytic polymerization of benzene,[3] the dehalogenation from dihalogenated benzene in the presence of nickel complex catalysts,[4] the dehydrogenation from poly(1,3-cyclohexadiene)[5] and so on. On the other hand, for a direct synthesis of PPP from benzene, a well-known procedure is the oxidative cationic polymerization of benzene by a Lewis acid–oxidant system reported by Kovacic et al.[6] In this method, aluminum chloride and copper(II) chloride are used as a Lewis acid and an oxidant, respectively, and are most effectively used for polymerization:[7]

$$n\,C_6H_6 + 2n\,CuCl_2 \xrightarrow{AlCl_3} (C_6H_4)_n + 2n\,CuCl + 2n\,HCl. \quad (1)$$

In this method, however, the polymerization of 1 mol of benzene produces 2 mol of hydrogen chloride. Since the reaction mixtures are occupied by many insoluble metal salts which result in slurried conditions, it is difficult to stir them. Since copper(II) chloride is consumed during the reaction, the yield of PPP based on the oxidant is always less than 100%, i.e., copper(II) chloride does not work as a catalyst. The polymerization of toluene by this method gives a toluene polymer which has mainly a 1,2-phenylene backbone (**1**). Especially, by using carbon disulfide as a solvent, polynuclear polymer (**2**) is obtained which is insoluble in organic solvent.[8] In contrast, by the use of the same reagents, the other group reported that the polymerization reaction also occurs at the benzyl position of toluene molecules.[9] The polymerization of biphenyl by the Kovacic's method was also investigated.[10]

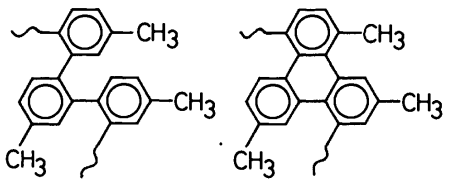

(1) (2)

Recently, the present authors have reported that the polymerization of benzene is possible using copper(I) chloride (a low-valence metal salt), aluminum chloride, and oxygen as an oxidant.[11] In this method the polymerization can be performed under considerably homogeneous conditions as copper(I) chloride becomes soluble in benzene by forming a double salt with aluminum chloride ($AlCuCl_4$);[12] no evolution of a hydrogen chloride gas occurs. Furthermore, it becomes possible to polymerize benzene in over 100% yield based on copper(I) chloride.

Since the PPP obtained in this manner is entirely insoluble in organic solvents and does not melt upon a heat treatment, it is a poor material for processing. It is expected that the introduction of alkyl groups into a highly rigid PPP molecule causes its solubility in an organic solvent to be higher while making the processing of this type polymer easy. As one method to make this kind of modification, we tried to polymerize toluene and its analogs by taking advantage of a copper(I) chloride–aluminum chloride–oxygen system. In the present paper we report on the results of

† Present address: Department of Industrial Chemistry, Faculty of Engineering, The Science University of Tokyo, Kagurazaka, Shinjuku-ku, Tokyo 162.

the polymerization of toluene and other alkylbenzenes as well as those of biphenyl, which was found to polymerize resulting in a PPP oligomer.

Experimental

Materials. The aluminum chloride (Kishida Chemical Co.) was purified by vacuum sublimation. The copper(I) chloride (Koso Chemical Co.) was reprecipitated from an aqueous hydrochloric acid solution by the addition of distilled water, followed by successive washing with ethanol and diethyl ether. It was then dried in vacuo at 100 °C for 24 h.

The toluene, *o*-xylene, *p*-xylene, ethylbenzene, and mesitylene were distilled over metallic sodium. The biphenyl was purified by recrystallization from petroleum ether.

The oxygen was dried by being passed through columns of Molecular Sieves 3A and diphosphorus pentaoxide before use.

Analysis. The ^{1}H NMR spectrum measurement was carried out with JEOL models FX90Q and GX400 spectrometers at 89.55 and 399.6 MHz, respectively. The infrared absorption spectra were measured with a JASCO model A-3 spectrometer by a KBr disk method. The GPC was recorded on a TOYO SODA model HLC-802UR chromatograph equipped with TSK-GEL G7000H, G5000H, and G3000H columns.

Polymerization of Toluene by a CuCl-AlCl$_3$-O$_2$ System. Copper(I) chloride (0.835 g, 8.43 mmol), aluminum chloride (3.38 g, 25.3 mmol), and toluene (13.5 cm^3, 127 mmol) were placed in a 100 cm^3 Kjeldahl flask, and the mixtures were stirred at room temperature for 2 h under dry nitrogen. During this stage the copper(I) chloride was completely dissolved and a highly homogeneous solution was obtained, leaving some excess aluminum chloride. The polymerization reaction was carried out by replacing the reaction atmosphere with oxygen and stirring the mixtures at 60 °C for 24 h. As the reaction proceeded, the color of the reaction mixtures changed from green to black at the end of the reaction. Polymerization was terminated by adding an 18% hydrochloric acid solution to the reaction mixtures. After the filtration of the reaction mixtures with a membrane filter (Nippon Millipore Kogyo, an SC type, pore size=8.0 μm), the remaining solid was repeatedly washed with a boiling solution of 18% hydrochloric acid and then with boiling water. The subsequent drying of the brownish black solid product at 100 °C for 24 h yielded 0.170 g (44.8% yield based on the charged copper(I) chloride) of the toluene polymer. The toluene solution was also washed several times with an 18% hydrochloric acid solution and water. After the evaporation of the toluene under reduced pressure, followed by drying for 24 h at room temperature, 0.603 g (159% yield based on the charged copper(I) chloride) of a reddish-brown oily product was obtained, which was soluble in toluene. The solid product was insoluble in benzene, acetone, and petroleum ether, though soluble in chloroform, THF, and DMF.

The results of the elemental analysis of the solid product were: C, 87.1; H, 6.3; Cl, 1.3%. Thus, the C/H ratio is 1.42, which is much higher than 1.17, the calculated value of that for $(C_6H_3(CH_3))_n$. The IR spectrum of the solid product showed bands at 810, 860 (C–H out-of-plane bending vibration of a para-disubstituted benzene ring), 1375 (C–H bending vibration of a methyl group), 1510, 1600 (C=C stretching vibration of a benzene ring), and 2920 cm^{-1} (C–H stretching vibration of a methyl group). The ^{1}H NMR spectrum in $CDCl_3$ (Fig. 2) shows peaks at δ 7.0—7.5 (m; aromatic protons), 2.2—2.5 (m; aliphatic protons of a methyl group substituted on a benzene ring), 1.25, 0.88 (m; aliphatic protons) (vide infra).

The results of the elemental analysis of the liquid product were: C, 90.2; H, 7.0; Cl, 0.6%. Thus, the C/H ratio is 1.09, which is nearly identical with the calculated value of that for $H(C_6H_3(CH_3))_4H$, 1.08. The IR spectrum has bands at 700, 730, 770 (C–H out-of-plane bending vibration of a 1,2- and 1,3-disubstituted benzene ring), 810, 890 (C–H out-of-plane bending vibration of the same species and a 1,2,4-trisubstituted benzene ring), 1375 (C–H bending vibration of a methyl group), 1510, 1600 (C=C stretching vibration of a benzene ring), 2860, 2920 (C–H stretching vibration of a methyl group), and 3020 cm^{-1} (C–H stretching vibration of a benzene ring). The ^{1}H NMR spectrum in $CDCl_3$ (Fig. 3) shows the peaks at δ 7.0—7.4 (m; aromatic protons) and 2.2—2.5 (m; aliphatic protons of a methyl group substituted on a benzene ring).

Polymerization of Biphenyl by a CuCl-AlCl$_3$-O$_2$ System. Copper(I) chloride (0.95 g, 9.60 mmol), aluminum chloride (3.85 g, 28.9 mmol), and biphenyl (14.8 g, 96.2 mmol) were placed in a 100 cm^3 Kjeldahl flask, and stirred at 80 °C for 2 h under dry nitrogen, resulting in a reddish-brown solution. Replacing the solution atmosphere with oxygen started the reaction at the same temperature for 24 h. At the end of the reaction, the color of the mixtures was purple. Reaction was terminated by the addition of an 18% hydrochloric acid solution into the reaction mixtures. The obtained solid was repeatedly washed with boiling petroleum ether, an 18% hydrochloric acid solution, and water. It was then dried at 100 °C for 24 h, resulting in 0.501 g (137% yield based on CuCl) of a brown product (poly(1,4-phenylene)).

The results of the elemental analysis for the solid product were: C, 93.1; H, 4.7; Cl, 1.2%. Thus, the C/H ratio is 1.65, while the calculated value of $(C_6H_4)_n$ is 1.50. The IR spectrum showed bands at 815 (C–H out-of-plane bending vibration of a para-disubstituted benzene ring), 1000 (C–H in-plane bending vibration of the same species), and 1480 cm^{-1} (C=C skeletal in-plane vibration).

Results and Discussion

Polymerization of Toluene by the Use of the CuCl-AlCl$_3$-Oxygen System. Table 1 shows the results of the polymerization of toluene by a copper(I) chloride–aluminum chloride–oxygen (CuCl–AlCl$_3$–O$_2$) system using excess $AlCl_3$ with respect to CuCl. Under these conditions, upon replacing the solution atmosphere by oxygen the polymerization of toluene occurred smoothly, and the toluene polymer was obtained. For example, when a threefold quantity of $AlCl_3$ with respect to that of CuCl was used and the polymerization reaction was carried out at 50 °C for 24 h, a solid polymer of toluene and liquid one were obtained in a yield of 44.8 and 159%, respectively, and no evolution of HCl was observed (run 2). In contrast

Table 1. Polymerization of Toluene Catalyzed by Copper(I) Chloride and Aluminum Chloride under Oxygen[a]

Run	Charged molar ratio[b]		Temperature /°C	Yield/%[c]		
	$AlCuCl_4$	Excess $AlCl_3$		Solid	Liquid	Total
1	1.0	2.0	15	19	52	71
2	1.0	2.0	50	45	159	204
3	1.0	2.0	91	45	369	414
4	1.0	4.5	50	192	367	559
5	2.0	4.0	50	31	155	186
6	4.0	8.0	50	86	69	155
7	1.0	2.0+2.5[d]	50	199	287	486

a) Reaction time, 24 h. b) Toluene=15.0. c) Based on CuCl. d) After the reaction with 2.0 excess molar ratio of aluminum chloride for 12 h, then adding further 2.5 excess molar ratio of aluminum chloride, the reaction was continued for further 12 h.

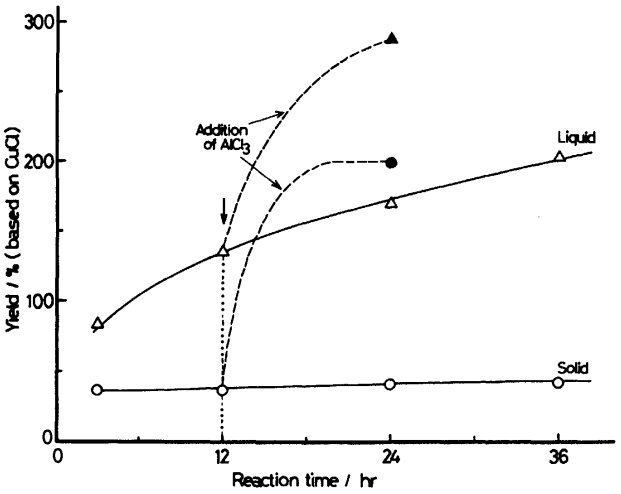

Fig. 1. Changes with the reaction time in the yields of the solid (○) and liquid (△) products of the toluene polymer by a CuCl-$AlCl_3$-O_2 system. The charged molar ratio of CuCl/$AlCl_3$/toluene was 1:3:15 and the reaction temperature was 50°C. Closed circles and triangles show the yields of the toluene polymer in the case of the extra addition of 2.5 excess molar ratio of $AlCl_3$ to CuCl after the reaction for 12 h using 3 fold of $AlCl_3$ to CuCl.

with the Kovacic's method in which $CuCl_2$ works as a reagent, it becomes apparent that toluene polymerizes catalytically with respect to CuCl in the present method.

The yield of the toluene polymer generally increased with the reaction time. The yield of the solid product, however, became saturated within a few hours in contrast with that of the liquid one (Fig. 1). This result indicates that the formation mechanisms of the solid and liquid product are different from each other (vide infra). The yield of the toluene polymer was also influenced by the reaction temperature and the quantity of excess $AlCl_3$. As shown in Table 1, the yield of the toluene polymer became higher upon raising the reaction temperature (run 3) or increasing the quantity of excess $AlCl_3$ (run 4). Furthermore, a drastic increase in the yield could be achieved by an extra addition of $AlCl_3$ in the middle of the reaction and continuous stirring for another 12 h (run 7), as shown by dashed lines in Fig. 1 (the yields of the solid and the liquid products are 199 and 287% respectively at reaction temperature of 50°C). These results indicate that the excess $AlCl_3$ is consumed during the reaction. In fact, when a half molar ratio of water to $AlCl_3$ was added to the reaction system, the polymerization reaction could be suppressed and the yield of the toluene polymer decreased by half. In addition, oxygen was consumed during the polymerization reaction. In a previous paper,[11] we reported on the result of oxygen uptake during the polymerization of benzene. In this case, the uptake of oxygen nearly corresponded to a one-half molar amount of the yield of poly(1,4-phenylene). Therefore, the deactivation of $AlCl_3$ during the reaction is considered to be due to the hydrate formation of $AlCl_3$ with the water generated by the reaction between oxygen and protons which is eliminated from toluene. On the other hand, the polymer yield increases upon rising the reaction temperature.

Structure of Toluene Polymer. Analytical data of the polymers of toluene are shown in Table 2. If the polymerization product has a disubstituted toluene structure in its polymer chain, i.e., an ideal "poly-toluene" structure (**3**), the C/H ratio of the polymer given from elemental analysis should be 1.17.

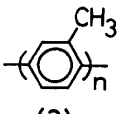

(3)

The observed value for the solid polymers, however, is about 1.4, which is higher than 1.17. This result suggests that a considerable intramolecular crosslinkage would occur after the addition reaction of toluene, instead of rearomatization by dehydrogenation. This consideration is supported by the results of a ^1H NMR spectral measurement. In the case of the solid product, the areal ratio of peaks of the aromatic protons to those

Table 2. Analytical Data of the Toluene-Polymer Prepared by a Copper(I) Chloride-Aluminum Chloride-Oxygen System

	Anal. C/H	^{1}H NMR ArH:CH$_3$	^{1}H NMR C-CH$_3$[a]	IR/cm^{-1}	GPC[b] count	UV λ_{max}/nm
Solid product	1.42	8:15	yes	810, 860, 1370, 1510, 1600, 2920	85	450
Liquid product	1.06	1;1	no	700, 730, 770, 810, 890, 1375, 1510, 1600, 2860, 2920, 3020	90	360

a) Peaks at δ 0.88 and 1.24. b) Conditions: columns, TSK-GEL G7000H+G5000H+G3000H; eluent, $CHCl_3$; temperature, 30°C.

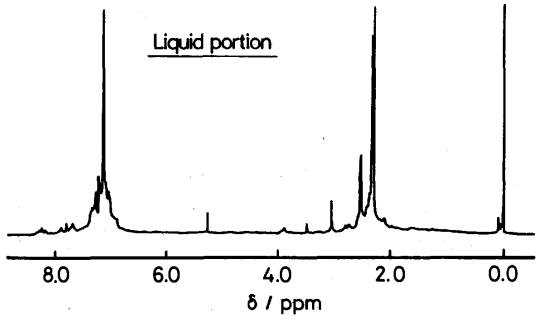

Fig. 2. ^{1}H NMR spectrum of the solid product of the toluene polymer prepared by a CuCl-$AlCl_3$-O_2 method (in $CDCl_3$ at 55°C with a JNM GX-400 spectrometer).

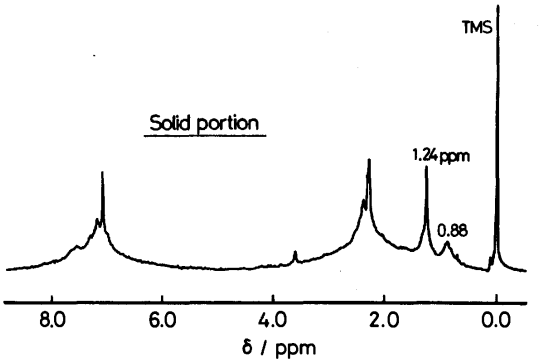

Fig. 3. ^{1}H NMR spectrum of the liquid product of the toluene polymer prepared by a CuCl-$AlCl_3$-O_2 method (in $CDCl_3$ at 25°C with a JNM FX-90Q spectrometer).

of the methyl protons is 8:15, which fairly deviates from the ideal ratio 1:1. This means that a sufficient amount of aromatic protons isn't included in this polymer structure. Furthermore, as shown in Fig. 2, unexpected peaks from the wholly aromatized toluene polymer structure, such as **1**, **2**, or **3**, were observed at δ 0.88 and 1.24 in the NMR spectra of the toluene polymer. These peaks were not found in the spectra of Kovacic's toluene polymer.[8] Since the peaks at these positions are attributed to aliphatic protons, these observations suggest that the solid polymer obtained in the present investigations arises from a nonaromatized "quinonoid-like" structure like **4**, **5**, and **6**.

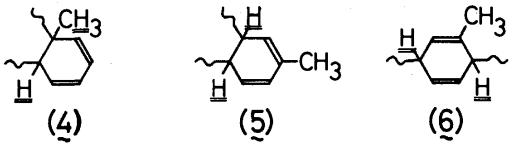

(4) (5) (6)

Therefore, the solid product is considered to have the following components in its chemical structure: (a) a highly crosslinked structure between aromatic rings, and (b) a nonaromatized "quinonoid-like" structure. Based on these considerations, an example of the structure **7** which is consistent with the observed analytical data might be depicted in order to estimate the structure of the solid toluene polymer.

On the other hand, the C/H ratio of the liquid product calculated from the elemental analytical data is about 1.1, which is near to the value of the ideal toluene polymer ($(C_6H_3(CH_3))_n$). The peaks at a high

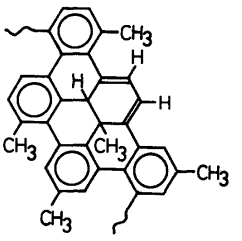

(7)

C/H=1.42
ArH:CH$_3$=8:15

magnetic field in the ^{1}H NMR spectrum, which were observed for the solid polymer, were not found in the liquid polymer (cf. Fig. 3). The areal ratio of the peaks of the aromatic and the methyl protons is almost 1:1. Therefore, the liquid product can be proved to have the ideal "polytoluene" structure (**1** or **3**), in which the framework of toluene is held in the polymer chain. The molecular weight of the toluene polymer was investigated by GPC. In the case of the liquid product, although the peaks of GPC spectrum appeared nearly at the limit of the detection area, the main component could be an oligomer, perhaps a tetramer of toluene.

It was reported that, by the use of a Kovacic's method, the polymerization reaction also occurs at the benzyl position of a toluene molecule.[9] In the present method, however, the reaction probably doesn't occur at the benzyl position because neither the liquid product nor the solid product has any peak around δ 4 in the ^{1}H NMR spectrum assigned to methylene

protons connected by two phenylene groups.

Polymerization Mechanism of Toluene. (a) Formation Mechanism of the Solid Product: The solid polymer of toluene obtained by the CuCl–$AlCl_3$–O_2 system has characteristic aliphatic protons due to a "quinonoid-like" structure. The formation of such protons requires the existence of a ring structure which is connected to another benzene ring of toluene at the carbon atom which substituted by a methyl group. In order to form this kind of structure, a cation radical on a benzene ring of toluene must attack another toluene molecule in an electrophilic way, resulting in cationic polymerization. The possible mechanism is illustrated in Scheme 1. Since the benzene ring of toluene is favorably attacked by electrophiles at the ortho- and para-positions, the toluene molecules attacked by the cation radical of toluene (**8**) would produce species **9** and **13**. When species **9** and **13** are attacked by the next toluene molecule, species **10**, **11**, **12**, **14**, and **15** could be considered to be produced, respectively, on the basis of the orientation of toluene in the substitution reaction. That is to say, the "quinonoid-like" structures (**10** and **14**) are considered to be formed by an extension of the polymer chain from the carbon atoms attached to a methyl group, since the density in positive charge on these carbon atoms is high due to the methyl group.

(b) Formation Mechanism of Liquid Product: In the polymerization of benzene using $CuCl_2$ and $AlCl_3$, Kovacic et al. already proposed a "stair-step" mechanism.[13] That is to say, it now appears the benzene cation radicals serve as the sites for coordination with an appreciable number of benzene nuclei in a propagative manner as stair steps, ranging from straight to spiral. When the chain buildup reaches a certain stage, the radical cation character on the terminal members become too small to induce further propagation. Covalent bond formation and the elimination of protons and electrons then lead to poly(1,4-phenylene). As to the mechanism for the formation of the liquid toluene polymer obtained by the present method, the "stair-step" mechanism is thought to be reasonable. This mechanism is supported by the absence of the peaks at δ 0.88 and 1.24, which appear in the solid product, in the ^1H NMR spectrum of the liquid product. This result is considered to be due to a small possibility for the formation of the aliphatic methyl group on the basis of the "quinonoid-like" structure. This is because it is almost impossible by a steric hindrance upon connecting with the stair steps that a toluene molecule can attack the carbon atom attached to a methyl group.

(c) The Effect of the Addition of Excess $AlCl_3$ in the

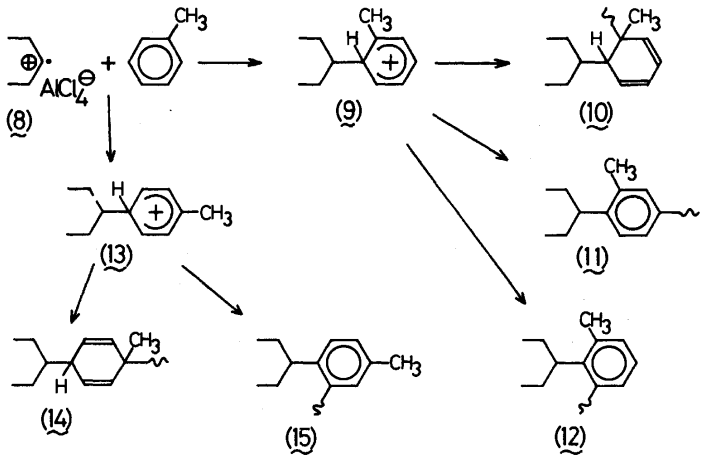

Scheme 1. The proposed mechanism for the solid toluene polymer.

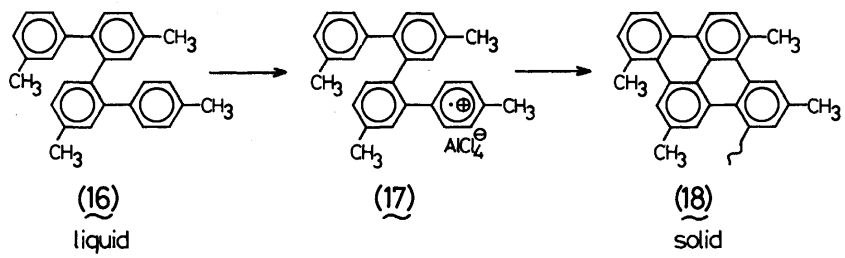

Scheme 2. The formation of the solid product from the liquid product of the toluene polymer by the addition of $AlCl_3$.

Course of the Reaction: The extra addition of excess $AlCl_3$ in the course of the reaction and further stirring of the reaction mixtures greatly increased the yield of the toluene polymer based on CuCl. When the reaction was carried out for the same period by adding the excess amount of $AlCl_3$ at once (at the beginning of the reaction), the yield of the polymer was also high. The structure of the latter polymer, however, was different from that of the polymer obtained in the former manner. The intensity of the peaks at δ 0.88 and 1.24 in the ^1H NMR spectrum of the former polymer was lower than that of the latter one. In the former case, the liquid product which formed before the extra addition of $AlCl_3$ is considered to give rise to intramolecular crosslinking and to initiate cationic polymerization again after the extra addition of $AlCl_3$, resulting in the solid product (Scheme 2). In the beginning, the liquid product does not involve the "quinonoid-like" structure. If this liquid product is crosslinked and forms a part of the solid product, the intensity of the ^1H NMR peaks at δ 0.88 and 1.24 would be relatively low in comparison with the solid product directly obtained. In fact, the treatment of the isolated liquid product by $AlCl_3$ in nitrobenzene gave the crosslinked insoluble solid product, indicating that the crosslinking reaction occurred as the result of the extra addition of $AlCl_3$ to the liquid toluene polymer and also that the liquid product had a 1,2-phenylene backbone which could be easily crosslinked (cf. **16** in Scheme 2). As shown in Fig. 1, the yield of the solid product doesn't increase with the reaction time, although the yield of the liquid product does. The reason for this is considered to be due to the deactivation of $AlCl_3$ by hydrate formation with water, since only free $AlCl_3$ could serve as a crosslinking reagent.

Table 3. Polymerization of Various Kinds of Benzene Derivatives Catalyzed by Copper(I) Chloride–Aluminum Chloride under Oxygen[a]

Aromatic compound	Yield/%[b]
o-Xylene	106[c]
p-Xylene	140
Ethylbenzene	91
Mesitylene	81

a) Reaction time, 24 h. Reaction temperature, 50 °C. CuCl : $AlCl_3$: Aromatic compound=1 : 3 : 20. b) Based on the aromatic compound. c) The total yield involving the solid product (5%).

Polymerization of Other Benzene Derivatives. The polymerization of xylenes, ethylbenzene, and mesitylene was attempted by using the present system. Every monomer gave the corresponding polymerization product. The yields of these product are summarized in Table 3. A solid product was obtained only in the case of *o*-xylene. However, no particular difference in the IR spectra was observed between the solid and liquid products of the *o*-xylene polymer. As can be seen in Table 3, the catalytic effectiveness for the present system decreases in the case of polymerizations of xylenes compared with toluene, in spite of the higher solubility of the reaction product. For the polymerization of toluene, the catalytic effectiveness is higher than that for the polymerization of benzene. Thus, the yields of the benzene polymer and the toluene polymer are 65 and 210%, respectively, at a reaction temperature of 50 °C. The decrease in the yield of the xylene polymer is thought to be the result of a steric hindrance of substituted groups. The ^1H NMR spectra showed intense peaks at higher magnetic fields (about δ 1—1.5), suggesting the existence of the "quinonoid-like" structure in these cases as well. These liquid polymerization products are thought to contain both liquid and solid products which correspond to those in the case of the polymerization of toluene, since the other benzene derivatives have many, or long, alkyl groups and the degree of polymerization would be low in these derivatives.

In the case of biphenyl, the polymerization product by the present method exhibited a lighter brown color than that of benzene. The IR spectrum suggested that the polymer involves only mono- and disubstituted benzene rings, not trisubstituted ones. The intensity ratio of the absorption peaks at 700 and 760 cm^{-1}, which were attributable to the C–H vibration of a monosubstituted benzene ring, to that at around 800 cm^{-1} (which was attributable to the C–H vibration of a para-disubstituted benzene ring), was stronger than that of poly(1,4-phenylene). These facts indicate that the polymer obtained from biphenyl is a kind of poly(1,4-phenylene), though its molecular weight is lower than that obtained from benzene. Furthermore,

Table 4. The IR Peak Attributed to the C–H Vibration of a para-Disubstituted Benzene Ring of 1,4-Phenylene Oligomers

p-Phenylene compound	Wavenumber/cm^{-1}	Reference
p-Terphenyl	842	14
p-Quaterphenyl	830	14
p-Quinquephenyl	820	14
p-Sexiphenyl	815	14
Poly(1,4-phenylene)	800	7, 11
Biphenyl-polymer	815	Present work

the peak based on the C–H vibration of a para-disubstituted benzene ring was detected at a higher-wavenumber position (815 cm^{-1}) in this polymer than that in the usual poly(1,4-phenylene) from benzene (800 cm^{-1}). It is reported that the absorption band at this area in poly(1,4-phenylene) shifts to a lower wavenumber by increasing the number of para-disubstituted benzene rings.[14] The absorption band at 815 cm^{-1} is quite similar to that reported for *p*-sexiphenyl (Table 4). Thus, the main part of the biphenyl polymer obtained in the present catalytic system is thought to be a trimer of biphenyl (a hexamer with respect to phenylene unit).

References

1) Reviews: G. K. Noren and J. K. Stille, *J. Polym. Sci., Macromol. Rev.*, **5**, 385 (1971); Y. Imai, *Yuki Gosei Kagaku Kyokai Shi*, **42**, 1061 (1984).

2) D. M. Ivory, G. G. Miller, J. M. Sowa, L. W. Shacklette, R. R. Chance, and R. H. Baughman, *J. Chem. Phys.*, **71**, 1506 (1979); R. H. Baughman, J. L. Bredas, R. R. Chance, R. L. Elsenbaumer, and L. W. Shacklette, *Chem. Rev.*, **82**, 209 (1982).

3) I Rubinstein, *J. Electrochem. Soc.*, **130**, 1506 (1983); M. Tabata, M. Satoh, K. Kaneto, and K. Yoshino, *J. Phys. Soc. Jpn.*, **55**, 1305 (1986).

4) T. Yamamoto, Y. Hayashi, and A. Yamamoto, *Bull. Chem. Soc. Jpn.*, **51**, 2091 (1978).

5) C. S. Marvel and G. E. Hartzell, *J. Am. Chem. Soc.*, **81**, 448 (1959); D. A. Frey, M. Hasegawa, and C. S. Marvel, *J. Polym. Sci., Part A*, **1**, 2057 (1963).

6) P. Kovacic and M. B. Jones, *Chem. Rev.*, **87**, 357 (1987).

7) P. Kovacic and A. Kyriakis, *J. Am. Chem. Soc.*, **85**, 454 (1963).

8) P. Kovacic and J. S. Ramsey, *J. Polym. Sci., Part A-1*, **7**, 111 (1969); C.-F. Hsing, M. B. Jones, and P. Kovacic, *J. Polym. Sci., Polym. Chem. Ed.*, **19**, 973 (1981).

9) H. Kuwata, *Mem. Fac. Eng., Hiroshima Univ.*, **2**, 55 (1965).

10) H. Guenther and P. Kovacic, *Synth. Commun.*, **14**, 413 (1984).

11) H. Hirai, N. Toshima, K. Kanaka, and A. Koshirai, *Chem. Lett.*, **1987**, 1461; N. Toshima, K. Kanaka, A. Koshirai, and H. Hirai, *Bull. Chem. Soc. Jpn.*, **61**, 2551 (1988).

12) R. W. Turner and E. L. Amma, *J. Am. Chem. Soc.*, **88**, 1877 (1966).

13) P. Kovacic and W. B. England, *J. Polym. Sci., Polym. Lett. Ed.*, **19**, 359 (1981).

14) R. C. Doss and P. W. Solomon, *J. Org. Chem.*, **29**, 1566 (1964).

Syntheses of Fluoroalkyl and Fluoroaryl Titanates

Norio YOSHINO,* Junko TOMITA, and Hidefumi HIRAI
Department of Industrial Chemistry, Faculty of Engineering, Science University of Tokyo, Kagurazaka, Shinjuku-ku, Tokyo 162
(Received January 24, 1989)

Tetrakis(1H,1H-perfluoroethyl) titanate, $Ti(OCH_2CF_3)_4$, tetrakis(1H,1H-perfluoropropyl) titanate, $Ti(OCH_2CF_2CF_3)_4$, tetrakis(2,2,2-trifluoro-1-methylethyl) titanate, $Ti[OCH(CH_3)CF_3]_4$, tetrakis(2,2,2-trifluoro-1,1-dimethylethyl) titanate, $Ti[OC(CH_3)_2CF_3]_4$, tetrakis((1H,1H,3H-perfluoropropyl) titanate, $Ti(OCH_2CF_2CF_2H)_4$, tetrakis(1H,1H,5H-perfluoropentyl) titanate, $Ti[OCH_2(CF_2CF_2)_2H]_4$, tetrakis(1H,1H,7H-perfluoroheptyl) titanate, $Ti[OCH_2(CF_2CF_2)_3H]_4$, and tetrakis(1H,1H,9H-perfluorononyl) titanate, $Ti[OCH_2(CF_2CF_2)_4H]_4$, were prepared by the reaction of titanium tetrachloride with fluoro-substituted alcohols in the presence of ammonia. Tetrakis(pentafluorophenyl) titanate, $Ti(OC_6F_5)_4$ was synthesized by the ester interchange reaction of tetraisopropyl titanate with pentafluorophenyl acetate. These compounds were characterized on the basis of chemical analysis, IR, ^1H NMR, ^{13}C NMR and ^{19}F NMR spectra. Tetrakis(2,2,2-trifluoro-1,1-dimethylethyl) titanate was the monomeric in nitrobenzene, but tetrakis(1H,1H-perfluoroethyl) titanate and tetrakis(1H,1H-perfluoropropyl) titanate were associated in the same solvent, in which the highest association numbers observed were 3.5 and 1.5, respectively. These titanates were very sensitive to moisture and easy to decompose to give titanium oxide and alcohol or phenol.

Metal alkoxides have been the subject of extensive research because of their potential as precursor materials for several applications, such as new-ceramics, adhesives and coupling agents, which are molecular bridges between the interface of an inorganic filler and an organic polymer. Many of alkyl or aryl titanates and their halogenated derivatives were prepared[1] and the reactivities of these titanates towards various types of donors such as amides, amines, ethers, and amino acids have been reported.[2] The number of worldwide commercial applications for coupling agents established using monoalkoxy-type titanates such as titanium isopropoxide tris(2-heptylundecanoyloxide) are now very substantial, as indicated by over one hundred patents.[3-6]

In recent years, dramatic developments have been made in the utilization of organofluoro compounds because of the resulting materials with high performance. However, only a few research reports concerning fluoro-substituted alkoxides of metals have appeared in the literature. Redwood and his co-workers[7,8] have prepared the trifluoromethoxides of heavier alkali metals by the reaction of carbonyl fluoride on a suspension of alkali metal fluoride in acetonitrile. Kapoor et al.[9,10] reported syntheses of 2,2,2-trifluoroethoxides and 2,2,2-trifluoro-1-(trifluoromethyl)-ethoxides of metals, such as germanium, titanium, zirconium, niobium, and tantalum, by the reaction of metal chlorides with the appropriate alcohol. Mazdiyasni et al.[11] reported syntheses of 2,2,2-trifluoro-1-(trifluoromethyl)ethoxides of aluminium, silicon, germanium, titanium, zirconium, and hafnium, through reactions of suitable metal chlorides with sodium 2,2,2-trifluoro-1-(trifluoromethyl)ethoxides. In these reports, the fluoro-substituted alkoxides of metals studied have been limited to only one or two species of low molecular weight or simple structural alcohols, as a starting material. However, the chemical and physical properties of fluoro-substituted alkoxides of metals having a longer $-CF_2-$ bonding or a bulky structure in the alkyl moiety should be important for making new type titanate coupling agents, which possess a dispersing capacity of inorganic particles in a fluorinated organic polymer. Especially, these alkoxides are expected to be stable against moisture, because many compounds having the fluorinated carbon structure possess water repellency.

In this paper, the results of the syntheses and characterizations of fluoro-substituted alkoxides of titanium are reported. The characterizations of these compounds were achieved through chemical analysis, IR, ^1H NMR, ^{13}C NMR, and ^{19}F NMR spectra. Molecular association of these compounds in nitrobenzene has been also determined.

Experimental

Special precautions were adopted to avoid any hydrolysis of the starting materials and products, and all experiments were carried out under an atmosphere of purified nitrogen to preclude oxygen and moisture.

Materials. 1H,1H-Perfluoroethanol, CF_3CH_2OH (bp 74—75 °C) (**1**), 1H,1H-perfluoro-1-propanol, $CF_3CF_2CH_2OH$ (bp 81 °C) (**2**), 1,1,1-trifluoro-2-propanol, $CF_3CH(CH_3)OH$ (bp 75—76 °C) (**3**), 2-trifluoromethyl-2-propanol, $CF_3C(CH_3)_2OH$ (bp 80—81 °C) (**4**) were commercially available. 1H,1H,3H-Perfluoro-1-propanol, $HCF_2CF_2CH_2OH$ (bp 109—110 °C) (**5**), 1H,1H,5H-perfluoro-1-pentanol, $H(CF_2CF_2)_2CH_2OH$ (bp 139—140 °C) (**6**), 1H,1H,7H-perfluoro-1-heptanol, $H(CF_2CF_2)_3CH_2OH$ (bp 169—170 °C) (**7**), and 1H,1H,9H-perfluoro-1-nonanol, $H(CF_2CF_2)_4CH_2OH$ (bp 63 °C/53 Pa) (**8**) were received as gifts from Daikin Industries, Ltd. Pentafluorophenol, C_6F_5OH (bp 143 °C) (**9**) was obtained from PCR Inc. These alcohols, except **8**, were kept over anhydrous magnesium sulfate for a few days and distilled over a small amount of calcium hydride. **8** and **9** were purified by distillation. Titanium tetrachloride (bp

136 °C) and tetraisopropyl titanate (bp 84 °C/133 Pa) were commercially available and purified by distillation. The solvents used were purified by usual methods.

Measurements. IR spectra were measured in a liquid film or by a KBr method with a Hitachi 215 Grating Spectrophotometer. Pulsed Fourier Transform 100-MHz ^{1}H and 25-MHz ^{13}C NMR were run in THF-d_8 with TMS as an internal standard using a JEOL JNR-PX-100 spectrometer at room temperature: ^{1}H NMR spectra (pulse repetition time, 5 s; number of accumulations, 4) and ^{13}C NMR spectra (pulse repetition time, 5 s; number of accumulations, 18500). The resonance peaks of the ^{13}C NMR spectra were assigned by the peak splitting pattern using the method of off-resonance. The FT mode 90-MHz ^{19}F NMR was recorded at 27 °C on a JEOL JNM-FX-90Q in THF with fluorobenzene (−113.6 ppm[12] from $CFCl_3$ in $CDCl_3$) as an external standard: pulse repetition time, 0.5 s; number of accumulations, 20. The assignments of the ^{19}F NMR spectra were referred to in the databook.[12] The molecular association numbers of some fluoro-substituted alkoxides of titanium were measured using the cryoscopic method in nitrobenzene. Gas chromatograms were performed with a Hitachi 063 (PEG-6000 supported Chromosorb A NAW 30/60 mesh 5 m packed column, TCD) or Hitachi G-3000 gas chromatograph (OV-1 25 m Fused capillary column, FID) and these intensities were measured with a Hitachi 834 chromato processor.

Analytical Methods. Titanium was determined gravimetrically as titanium oxide after the hydrolysis of titanium alkoxides. The fluoroalkoxyl group was determined by using gas chromatography after the hydrolysis of titanium alkoxide to alcohol by adding aqueous ammonia.

Synthesis of Tetrakis(1H,1H-perfluoroethyl) Titanate, $Ti(OCH_2CF_3)_4$ (T1). To a stirred 1H,1H-perfluoroethanol **1** 13.8 g (138 mmol), 5.3 g (28 mmol) of titanium tetrachloride was slowly added using a dropping funnel below 5 °C in a two-necked 200-ml flask connected with a dropping funnel and a reflux condenser. The reaction was exothermic. After 30 min, the mixture was allowed to react at 80 °C. The evolution of hydrogen chloride was observed continuously for about 5—8 h. After an addition of 100-ml benzene, dry ammonia gas was slowly introduced to the system for about 3 h at 10 °C; the mixture was reluxed for 30 min. The completion of the substitution reaction was checked by flame testing a clear solution using copper wire. After removing the ammonium chloride formed by filtration, benzene and excess **1** were evaporated using a vacuum-evaporator. A transparent colorless liquid **T1** was obtained by distillation (yield 10.2 g, 82.9%). **T1** gradually transformed into a white waxy solid: bp 114 °C/133 Pa (lit,[9] bp 94 °C/27 Pa) mp 62 °C; IR 2940, 2870, 1450, 1405, 1365, 1280, 1150, 1080, 960, 827, 695, 670 cm^{-1}; ^{1}H NMR δ=4.60 (CH_2, q, J=8.9 Hz); ^{13}C NMR δ=59.7—70.3 (b, m), 124.3 (a, q, J=279.4 Hz) for ($C^aF_3C^bH_2O)_4Ti$; ^{19}F NMR δ=36.0 (m (=multiplet)). Found: Ti, 10.7; RfO (fluoroalkoxyl group), 89.3%. Calcd for $C_8H_8F_{12}O_4Ti$: Ti, 10.8; RfO, 89.2%.

Synthesis of Tetrakis(1H,1H-perfluoropropyl) Titanate, $Ti(OCH_2CF_2CF_3)_4$ (T2). To a stirred 1H,1H-perfluoro-1-propanol **2** (29.5 g, 0.20 mol), titanium tetrachloride (7.5 g, 0.04 mol) was added below 5 °C. After removing hydrogen chloride formed, 100 ml of THF was added and dry ammonia gas was introduced into the solution. The product was purified by distillation to give **T2** (yield 19.5 g, 75.7%): bp 125 °C/1067 Pa, mp 56 °C; IR 2940, 2875, 1350, 1190, 1090, 1008, 948, 926, 800, 730, 688 cm^{-1}; ^{1}H NMR δ=4.81 (CH_2, q, J=15.1 Hz); ^{13}C NMR δ=70.4 (c, m), 114.7 (b, t(=triplet)(q(=quartet)), J=253.6(36.0) Hz), 120.4 (a, q(t), J=286.0(35.7) Hz) for ($C^aF_3C^bF_2C^cH_2O)_4Ti$; ^{19}F NMR δ=28.1 (a, m), −13.3 (b, t, J=13.4 Hz) for ($CF_3^aCF_2^bCH_4O_4$)Ti. Found: Ti, 7.29; RfO, 92.2%. Calcd for $C_{12}H_8F_{20}O_4Ti$: Ti, 7.44; RfO, 92.6%.

Synthesis of Tetrakis(2,2,2-trifluoro-1-methylethyl) Titanate, $Ti[OCH(CH_3)CF_3]_4$ (T3). The synthesis of **T3** was carried out in a similar manner to that of **T1**. The colorless liquid product was purified by distillation to give **T3** (yield 45.5%): bp 59 °C/133 Pa; IR 3000, 2920, 1458, 1385, 1282, 1180, 1130, 1108, 1030, 960, 800, 704 cm^{-1}; ^{1}H NMR δ=1.42 (CH_3, d, J=6.4 Hz), 4.62 (CH, septet, J=6.4 Hz); ^{13}C NMR δ=18.0 (b, d, J=1.5 Hz), 79.5 (c, q, J=32.1 Hz), 126.4 (a, q, J=282.3 Hz) for $[C^aF_3(C^bH_3)C^cHO]_4Ti$; ^{19}F NMR δ=31.4 (d(=doublet), J=7.3 Hz). Found: Ti, 9.73; RfO, 90.2%. Calcd for $C_{12}H_{16}F_{12}O_4Ti$: Ti, 9.58; RfO, 90.4%.

Synthesis of Tetrakis(2,2,2-trifluoro-1,1-dimethylethyl) Titanate, $Ti[OC(CH_3)_2CF_3]_4$ (T4). In a similar manner to that mentioned above, **T4** was synthesized. The white solid product was purified by distillation to give **T4** (yield 79.8%): bp 78 °C/67 Pa, mp 42 °C; IR 2990, 2945, 1460, 1385, 1320, 1155, 1120, 1013, 1000, 900, 775, 670 cm^{-1}; ^{1}H NMR δ=1.44 (CH_3, s); ^{13}C NMR δ=22.8 (b, s(=singlet)), 24.3 (small peak)(b, s), 71.8 (c, q, J=29.3 Hz), 126.5 (small peak)(a, q, J=284.3 Hz), 137.5 (a, q, J=284.3 Hz) for $[C^aF_3(C^bH_3)_2C^cO]_4Ti$; ^{19}F NMR δ=29.1(s). Found: Ti, 8.83; RfO, 91.2%. Calcd for $C_{16}H_{24}F_{12}O_4Ti$: Ti, 8.62; RfO, 91.4%.

Syntheses of Tetrakis(1H,1H,3H-perfluoropropyl) Titanate, $Ti(OCH_2CF_2CF_2H)_4$ (T5), Tetrakis(1H,1H,5H-perfluoropentyl) Titanate, $Ti[OCH_2(CF_2CF_2)_2H]_4$ (T6), Tetrakis(1H,1H,7H-perfluoroheptyl) Titanate, $Ti[OCH_2(CF_2CF_2)_3H]_4$ (T7) and Tetrakis(1H,1H,9H-perfluorononyl) Titanate, $Ti[OCH(CF_2CF_2)_4H]_4$ (T8). These procedures and purification techniques were almost the same as that for the preparation of **T2**.

T5 was colorless liquid (yield 52.4%): bp 131 °C/27 Pa; IR 2945, 2860, 1455, 1405, 1353, 1285, 1240, 1230, 1200, 1100, 1045, 945, 935, 835, 800, 750, 690 cm^{-1}; ^{1}H NMR δ=4.70 (CH_2, t, J=14.7 Hz), 5.43 (HCF_2, t(t), J=52.7(3.7) Hz); ^{13}C NMR δ=70.6 (c, t, J=24.9 Hz), 109.5 (a, t(t), J=249.0 (37.1) Hz), 115.0 (b, t(t), J=249.0(27.3) Hz) for ($HC^aF_2C^bF_2C^cH_2O)_4Ti$; ^{19}F NMR δ=−27.5 (a, d, J=53.2 Hz), −27.6 (a, d, J=53.2 Hz), −15.0 (b, m) for ($HCF_2^aCF_2^bCH_2O)_4Ti$. Found: Ti, 8.31; RfO, 91.4%. Calcd for $C_{12}H_{12}F_{16}O_4Ti$: Ti, 8.38; RfO, 91.6%.

T6; colorless liquid (yield 69.1%): bp 148 °C/27 Pa; IR 2945, 2870, 1450, 1401, 1359, 1285, 1245, 1160, 1140, 1085, 986, 948, 895, 805, 763, 710 cm^{-1}; ^{1}H NMR δ=4.94 (CH_2, t, J=14.7 Hz), 5.38 (HCF_2, t(t), J=51.4(4.0) Hz); ^{13}C NMR δ=76.7 (e, t, J=24.4 Hz), 112.5 (a, t(t), J=255.6(31.7) Hz), 113.7 (b, t(m), J=253.9 Hz), 115.9 (c, t(m), J=266.0 Hz), 120.0 (d, t(t), J=257.1(31.5) Hz) for ($HC^aF_2C^bF_2C^cF_2C^dF_2C^eH_2O)_4Ti$; ^{19}F NMR δ=−25.9 (a, d, J=53.1 Hz), −18.2 (b, s), −13.0 (c, m), −9.1 (d, m) for ($HCF_2^aCF_2^bCF_2^cCF_2^dCH_2O)_4Ti$. Found: Ti, 4.93; RfO, 95.6%. Calcd for $C_{20}H_{12}F_{32}O_4Ti$: Ti, 4.93; RfO, 95.1%.

T7; slightly brown liquid (yield 73.2%): bp 214 °C/400 Pa; IR 2950, 2885, 1455, 1403, 1365, 1290, 1265, 1195, 1140, 1095, 1000, 955, 860, 802, 763, 740, 720, 655 cm^{-1}; ^{1}H NMR δ=4.88 (CH_2, t, J=13.7 Hz), 6.48 (HCF_2, t(t), J=51.8(5.8) Hz);

^{13}C NMR δ=72.9 (g, t, J=24.0 Hz), 109.5 (a, t(t), J=253.0 (31.5) Hz), 111.6 (b, t(x(=no detectable)), J=274.4 Hz), 112.2 (c, t(x), J=272.2 Hz), 112.9 (d, t(x), J=269.8 Hz), 114.3 (e, t(x), J=270.7 Hz), 117.2 (f, t(t), J=257.9(27.8) Hz) for $(HC^aF_2C^b$-$F_2C^cF_2C^dF_2C^eF_2C^fF_2C^gH_2O)_4Ti$; ^{19}F NMR δ=−25.9 (a, d, J=53.1 Hz), −17.4 (b, s), −10.9 (c and d, m), −9.7 (e, m), −8.9 (f, m) for $(HCF_2^aCF_2^bCF_2^cCF_2^dCF_2^eCF_2^fCH_2O)_4Ti$. Found: Ti, 3.45; RfO, 96.6%. Calcd for $C_{28}H_{12}F_{48}O_4Ti$: Ti, 3.49; RfO, 96.5%.

T8; slightly brown waxy solid (yield 56.8%): bp 210 °C/1.3 Pa; IR 2950, 2870, 1455, 1403, 1370, 1352, 1290, 1200, 1140, 1017, 995, 950, 880, 830, 805, 780, 738, 710, 660 cm^{-1}; ^{1}H NMR δ=4,90 (CH_2, t, J=13.9 Hz), 6.32 (HCF_2, t(t), J=50.5(5.4) Hz); ^{13}C NMR δ=71.8 (i, t, J=24.7 Hz), 109.5 (a, t(t), J=253.3(31.7) Hz), 111.6 (b, t(m), J=264.9 Hz), 112.2 (c, t(x=no detectable), J=258.8 Hz), 112.7 (d, t(x), J=262.5 Hz), 112.7 (e, t(x), J=264.9 Hz), 113.6 (f, t(x), J=266.7 Hz), 113.8 (g, t(x), J=271.0 Hz), 117.6 (h, t(t), J=257.9(29.5) Hz) for $(HC^aF_2C^bF_2C^cF_2C^dF_2C^eF_2C^fF_2C^gF_2C^hF_2C^iH_2O)_4Ti$; ^{19}F NMR δ=−25.8 (a, d, J=51.3 Hz), −17.2 (b, s), −10.7 (c and d, m), −9.4 (e to g, m), −9.5 (h, m) for $(HCF_2^aCF_2^bCF_2^cCF_2^dCF_2^eCF_2^fC$-$F_2^gCF_2^hCH_2O)_4Ti$. Found: Ti, 2.59; RfO, 97.6%. Calcd for $C_{36}H_{12}F_{64}O_4Ti$: Ti, 2.70; RfO, 97.3%.

Synthesis of Tetrakis(pentafluorophenyl) Titanate, Ti-(OC_6F_5)$_4$ (T9). **T9** was prepared by a method involving an ester interchange. 18.4 g (0.1 mol) of pentafluorophenol **9** was allowed to react with excess potassium carbonate in 15 ml of water at room temperature. After completion of the reaction, potassium pentafluorophenolate was extracted to tetrahydrofuran (THF). A white solid potassium pentafluorophenolate was obtained after evaporating THF at room temperature under vacuum. A colorless liquid pentafluorophenyl acetate, $C_6F_5OCOCH_3$, (bp 170—172 °C) was obtained by distillation after reacting excess acetyl chloride and potassium pentafluorophenolate at 50 °C. Tetraisopropyl titanate (0.70 g, 2.5 mmol) and pentafluorophenyl acetate (2.88 g, 12.7 mmol) were mixed in a 50-ml distillation flask and heated at 100 °C for 10 h; 0.82 g (yield 42.7% vs. tetraisopropyl titanate) of dark-red solid **T9** (bp 193 °C/0.67 Pa, mp 97—99 °C) was obtained by a fractional distillation i. vac., after removing almost all isopropyl acetate formed and excess pentafluorophenyl acetate by distillation under reduced pressure (2000 Pa) at 80 °C. IR; 1600, 1510, 1487, 1350, 1515, 1190, 1175, 1165, 1090, 1030, 990, 980, 850, 735, 715, 662 cm^{-1}; ^{1}H NMR no proton; ^{13}C NMR δ=140.9 (para, d(t), J=244.7(13.9) Hz), 143.8 (meta, d(m), J=249.1 Hz), 146.1 (ortho, d(m), J=249.1 Hz); ^{19}F NMR δ=120.0 (para, t(m), J=22.0 Hz), 123.6 (meta, t, J=20.2 Hz), 129.8 (ortho, d, J=20.2 Hz). Found: Ti, 6.35%. Calcd for $C_{24}F_{20}O_4Ti$: Ti, 6.14%.

Results and Discussion

These obtained fluoro-substituted titanates were sensitive to moisture and decomposed to give titanium oxide and alcohol or phenol. Considering the hydrolytic nature of these obtained compounds, metal and fluoro-substituted alkoxyl group analyses were in fair agreement with the calculated values.

The NMR spectra of tetrakis(1H,1H,5H-perfluoropentyl) titanate, $Ti[OCH_2(CF_2CF_2)_2H]_4$, **T6** as an example are shown in Figs. 1—3. These spectrum

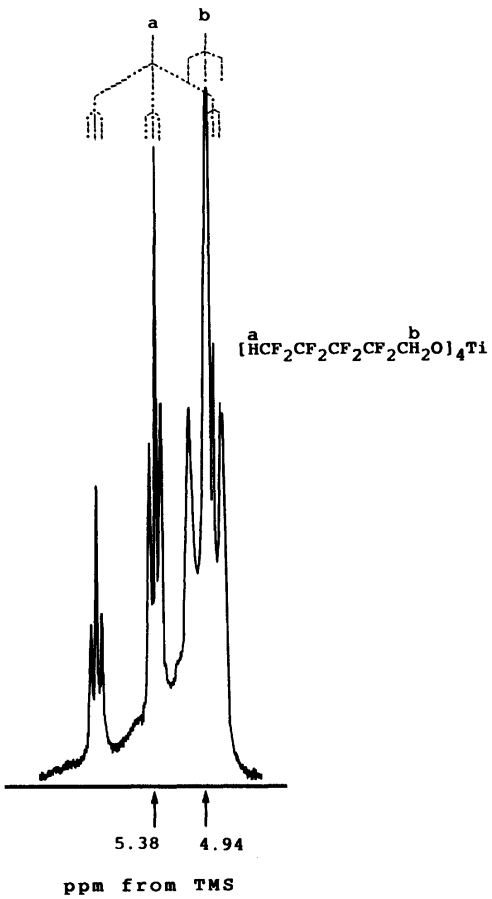

Fig. 1. Pulsed Fourier transform 100 MHz ^{1}H NMR spectrum of **[$HCF_2CF_2CF_2CF_2CH_2O$]$_4$Ti** in THF-d_8 (recorded at r.t.; internal standard, TMS; pulse repetition time, 5 s; number of accumulations, 4).

patterns resembled that of the starting alcohol, except for an absence of the OH group. The ^{13}C NMR spectrum pattern was relatively complicated (see Fig. 2). The resonance peaks of a carbon atom were coupled magnetically with the geminal and vicinal fluorine atoms. In the case of the ^{13}C NMR spectra having a fluorinated carbon atom, it is well-known that the peak intensities of a carbon bonded to a hydrogen atom, such as HCF_2-, H_2CF-, or -HCF-, are stronger than that of a carbon bonded only to fluorine atoms, such as CF_3- or -CF_2-. A group of peaks of the terminal HCF_2- (triplet(triplet)) was observed with the strongest one at 112.5 ppm from TMS in THF-d_8, and the other -CF_2- peaks were weaker and split in a complicated manner.

In ^{19}F NMR, the resonance peaks of -CF_3 of tetrakis(1H,1H-perfluoroethyl) titanate **T1**, were observed as multiplet peaks centered at 36.0 ppm from fluorobenzene in THF. However, the -CF_3 peaks of the starting alcohol, 1H,1H-perfluoroethanol **1**, were triplet at 34.7 ppm. The same difference in the ^{19}F NMR was detected between tetrakis(1H,1H-perfluoropropyl) titanate **T2** and 1H,1H-perfluoro-1-propanol

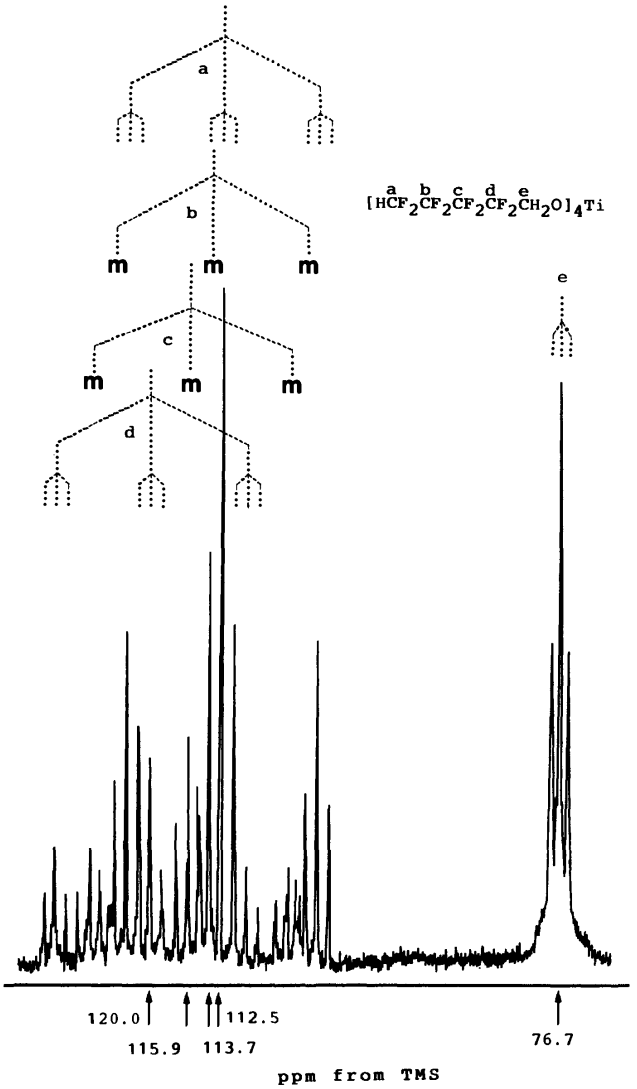

Fig. 2. Pulsed Fourier transform 25 MHz ^{13}C NMR spectrum of $[HCF_2CF_2CF_2CF_2CH_2O]_4Ti$ in THF-d_8 (recorded at r.t.; internal standard, TMS; pulse repetition time, 5 s; number of accumulations, 18500), "m" shows multiplet.

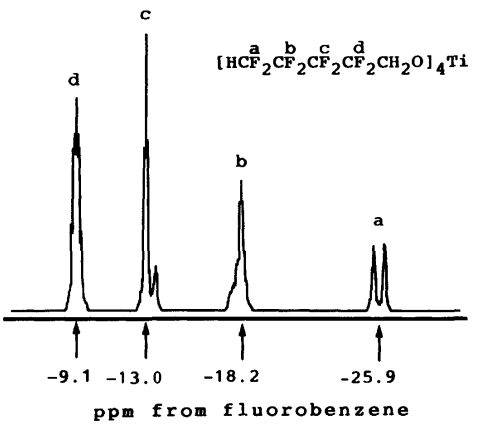

Fig. 3. Pulsed Fourier transform 90 MHz ^{19}F NMR spectrum of $[HCF_2CF_2CF_2CF_2CH_2O]_4Ti$ in THF (recorded at 27°C; external standard, fluorobenzene; rocked with benzene-d_6; pulse repetition time, 0.5 s; number of accumulations, 20).

2, though the observation could not differentiate between tetrakis(2,2,2-trifluoro-1,1-dimethylethyl) titanate **T4** and 2-trifluoromethyl-2-propanol **4**. These results suggest that the magnetic circumstances of the fluorine atoms composed of four $-CF_3$ groups in **T4** are equivalent. On the other hand, the fluorine atoms making four $-CF_3$ groups in **T1** and **T2** form a more complicated magnetic circumstances by molecular association with the mutual titanate molecules in THF. This suggestion was confirmed by measurements of the molecular association number of these three titanates (see later).

Mazdiyasni et al.[11] again tried to synthesize either aluminium or group-IV metal hexafluoro-substituted isopropoxides by an ammonia method described in the literature.[9,10] They found that the only poor yield product obtained was the fluorinated alkoxides of metal having two molecules of ammonia. They also described that the ammonia was apparently bonded strongly enough to prevent its loss during vacuum sublimation or fractional distillation at relatively high temperatures.

The present authors carried out ammonia analyses for a few products by the Kjeldal method. The ammonia contents (0.0025, 0.0127, 0.0023, and 0.0034%) were obtained from **T1**, **T2**, **T4**, and tetrakis(1H,1H,3H-perfluoropropyl) titanate **T5**, respectively. Analytical data showed that either the ammonia molecule did not form ammonia adducts of pure titanates or it dissociated from the ammonia adducts of titanates during vacuum distillation at relatively high temperatures. From these results the ammonia method for these titanate syntheses has been found to be a suitable method, since these analytical values indicate that ammonia contamination only represented one ammonia molecule per ca. 200—1500 titanate molecules.

Molecular Association Numbers of Some Titanates: The molecular association numbers of three titanates, tetrakis(1H,1H-perfluoroethyl) titanate **T1**, tetrakis-(1H,1H-perfluoropropyl) titanate **T2**, and tetrakis-(2,2,2-trifluoro-1,1-dimethylethyl) titanate **T4**, were measured by the cryoscopic method in nitrobenzene. The results are shown in Fig. 4. The bulky **T4**, which has the most bulky fluoro-substituted alkyl groups among the three titanates, shows a monomeric in nitrobenzene. The association number obtained is unity, an independent concentration in the concentration range 0.2—1.8 wt%, as shown by the open squares. The maximum molecular association numbers of **T2** and **T1** were 1.5 (closed circles) and 3.5 (open circles), respectively, and the numbers became larger as the concentration increased within the same concentration range. Considering the electronegativity of the

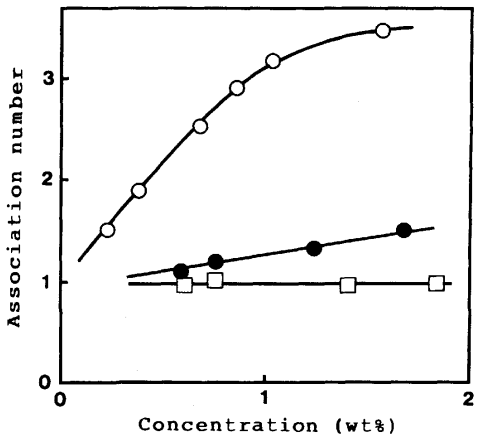

Fig. 4. Association curves of $Ti(OCH_2CF_3)_4$ (**T1**) (○), $Ti(OCH_2CF_2CF_3)_4$ (**T2**) (●), and $Ti[(OC(CH_3)_2CF_3)]_4$ (**T4**) (□): measured by the cryoscopic method in nitrobenzene. The bulky **T4** shows a monomeric in nitrobenzene and the association number is unity being concentration independently in the concentration range 0.2—1.8 wt%. The maximum molecular association numbers of **T2** and **T1** were 1.5 and 3.5, respectively, and the numbers become larger with concentration increase in the same concentration range.

fluorine atom, the partial charge density ($\delta+$) on the titanium atom of these fluoroalkyl titanates should be higher than those of the alkyl titanates. Therefore, the electronegative alkoxyloxygen ($\delta-$) of the fluoroalkyl titanate would be favorable to coordinate to the titanium atom of another fluoroalkyl titanate molecule; in other words, a fluoroalkyl titanate would be subject to form a molecular association. However, the results of the molecular association measurement indicate that the molecular association numbers of these titanates were influenced by a steric effect of the fluoro-substituted alkoxyl groups, rather than their inductive effect. These results also elucidate the difference of the magnetic circumstances of the fluorine atoms in **T1**, **T2**, and **T4** mentioned above, i.e. the magnetic circumstances of the fluorine atoms composed of four $-CF_3$ groups in the monomeric **T4** are equivalent, while the fluorine atoms making four $-CF_3$ groups in the associated **T1** and **T2** form a more complicated magnetic circumstances.

The authors are grateful to Dr. Takeo Konakahara of the Science University of Tokyo for the ^{19}F NMR measurements. We also thank Mr. Noboru Komine, Mr. Yukihide Shiraishi, and Mr. Hideo Terajima for their assistance in carrying out a part of experiment of this study.

The present work was partially supported by a Grant-in-Aid for Scientific Research No. 62550618 from the Ministry of Education, Science and Culture, to which the authors are also grateful.

References

1) a) D. C. Bradley, D. C. Hancock, and W. Wardlaw, *J. Chem. Soc.*, **1952**, 2773: b) D. C. Bradley, F. M. El-Halim, R. C. Mehrotra, and W. Wardlaw, *J. Chem. Soc.*, **1952**, 4609: c) J. S. Jennings, W. Wardlaw, and W. J. Way, *J. Chem. Soc.*, **1936**, 637.

2) a) N. Yoshino and T. Yoshino, *Kogyo Kagaku Zasshi*, **71**, 1025 (1968); **73**, 1161 (1970); **74**, 1673 (1971): b) N. Yoshino, K. Dohya, and T. Yoshino, *Kogyo Kagaku Zasshi*, **74**, 2138 (1971): c) N. Yoshino and T. Yoshino, *Bull. Chem. Soc. Jpn.*, **45**, 3172 (1972); **46**, 2899 (1973).

3) *Jpn. Kokai Tokkyo Koho* JP **59** 99616 [**84** 99616].

4) *Jpn. Kokai Tokkyo Koho* JP **59** 93741 [**84** 93741].

5) S. J. Monte and G. Surgerman, *Mod. Plast.*, **61(5)**, 74 (1984).

6) S. J. Monte and G. Surgerman, *Rubber World*, **190(1)**, 20 (1984); **190(1)**, 24 (1984).

7) D. C. Bradley, M. E. Redwood, and C. J. Willis, *Proc. Chem. Soc.*, **1964**, 416.

8) M. E. Redwood and C. J. Willis, *Can. J. Chem.*, **43**, 1893 (1965).

9) P. N. Kapoor and R. C. Mehrotra, *Chem. Ind.*, **1966**, 1034.

10) P. N. Kapoor, R. N. Kapoor, and R. C. Mehrotra, *Chem. Ind.*, **1968**, 1314.

11) K. S. Mazdiyasni, B. J. Schaper, and L. M. Brown, *Inorg. Chem.*, **10**, 889 (1971).

12) K. Kushida and A. Watanabe, "Proton and Fluorine Nuclear Magnetic Resonance Spectral Data 1988 Edition," ed by Varian Instruments Ltd. Tokyo, Japan and Japan Halon Co., Ltd. Tokyo, Japan.

 © 1989 The Chemical Society of Japan Bull. Chem. Soc. Jpn., 62, 2213—2218 (1989)

Photoisomerization of Oxime Ethers and Efficiency of Triplet Formation via Exciplexes

Yoshihiko TAKEDA, Hiroaki MISAWA, Hirochika SAKURAGI, and Katsumi TOKUMARU*
Department of Chemistry, University of Tsukuba, Tsukuba, Ibaraki 305
(Received January 28, 1989)

9,10-Dicyanoanthracene(DCA)-sensitized isomerization of (*E*)- and (*Z*)-isomers of an oxime ether of 2-acetylnaphthalene (*E*-**1** and *Z*-**1**, respectively) was investigated in benzene by means of steady irradiation and laser flash photolysis. The excited singlet DCA was effectively quenched by *E*-**1** and *Z*-**1** to afford exciplexes, decay of which gave DCA triplets or **1** triplets. The triplet state of **1** was proposed as the isomerization intermediate and the formation efficiency of **1** triplets was estimated from isomerization quantum yields.

Although photochemical geometrical isomerization of the ethylenic[1] and azo linkage[2] has been well-investigated, little work has been done on photoisomerization of the imine linkage.[3] For many imines, only one geometrical isomer, usually (*E*)-isomer, is stable and the other, usually (*Z*)-isomer, is unstable at room temperature.[4] The (*Z*)-isomers, when formed from irradiation of the (*E*)-isomers, revert quickly to the (*E*)-isomers. This situation made it difficult to work with the imines by the conventional procedures. However, introduction of a methoxyl group on the nitrogen atom of N=C bonds stabilizes effectively configurations of both isomers, enabling one to investigate photochemical geometrical isomerization of oxime ethers, particularly on triplet sensitization.[5]

Recently much effort has been done to investigate photochemical reactions proceeding through electron transfer.[6] During the course of our investigation on photochemical behavior of imines[7] as well as olefins[1c,8] on triplet and electron-transfer sensitization, we found that 9,10-dicyanoanthracene (DCA) sensitizes the isomerization of a pair of oxime ethers of 2-acetylnaphthalene, (*E*)- and (*Z*)-*N*-methoxy-1-(2-naphthyl)ethanimine (*E*-**1** and *Z*-**1**, respectively). In this paper we report in detail isomerization behavior of **1** via exciplexes with DCA.

Experimental

(*E*)- and (*Z*)-*N*-Methoxy-1-(2-naphthyl)ethanimine (*E*-**1** and *Z*-**1**, respectively).[5c] A mixture of 2-acetylnaphthalene (17 g, 0.10 mol) and *O*-methylhydroxyamine hydrochloride (9.3 g, 0.11 mol) was refluxed in ethanol (95%, 210 ml) containing sodium acetate (151 g, 1.85 mol) for 12 h. Usual work-up gave 15 g of a mixture of oxime ethers *E*-**1** and *Z*-**1** (*E*/*Z*=90:10 by GLPC); yield 75%. Crystallization from ethanol afforded pure *E*-**1**; mp 89—90 °C (lit, 89.5—90 °C).[5c]

The mixture of *E*-**1** and *Z*-**1** was dissolved in benzene (1 dm^3), and irradiated under nitrogen with a 400-W high-pressure mercury lamp (>300 nm) for several hours. Evaporation of the solvent left a solid (*E*/*Z*=44:56), which was crystallized from ethanol to give a *Z*-**1** rich filtrate (*E*/*Z*=25:75). This mixture was separated by column chromatography (silica gel, benzene) to afford an oily material, which was distilled twice under vacuum to give pure *Z*-**1**; mp 24.5—26 °C (lit, 25—26 °C).[5c]

DCA was purified by crystallization from ethanol followed by sublimation under vacuum. Benzene was distilled over calcium hydride and acetonitrile was distilled twice over phosphorus pentoxide and then over potassium carbonate.

Fluorescence spectra were obtained on a Hitachi MPF-2A or a Hitachi F-4000 fluorescence spectrophotometer. Fluorescence lifetimes were measured using a single photon counting apparatus, Applied Photophysics Model SP-3X or Horiba NAES 1100.

Laser flash photolyses were performed with 406-nm laser pulses (DPS, 10-nm fwhm) from a XeCl (308 nm) excimer laser (Lambda Physik EMG-101)-pumped dye laser (Lambda Physik FL-3002) and with a pulsed xenon arc (Wacom KXL-151, 150 W) as a monitoring light source. The monitoring light coming from a monochromator (JASCO CT-25C) was amplified by a photomultiplier (Hamamatsu Photonics R928) and stored in a storage scope (Iwatsu TS-8123), and the signals were transferred to a personal computer (NEC PC-9801E) and accumulated for 3—5 times to be averaged. The system was computer-controlled and the decay curves were analyzed by this computer system. Sample solutions containing DCA (1.2×10^{-4} M, M=mol dm^{-3}) and oxime ether *Z*-**1** (0.13 M) were deaerated by bubbling nitrogen for 30 min.

Near-infrared emission from singlet oxygen was observed by a germanium p-n junction detector (Hamamatsu Photonics B2144) with a silicon window. The element was reverse-biased (9 V) and placed in series with a load resistor (1 kΩ). The response time of this system is less than 3 μs.

Redox potentials were measured by cyclic voltammetry with a Hokuto Potentiostat-Galvanostat HA-201 and a Hokuto Function Generator HB-104. The measurements were carried out using a three-electrode cyclic voltammetric cell. The working electrode was a platinum wire and the reference electrode was SCE. Tetraethylammonium perchlorate (0.1 M) was used as a supporting electrolyte. Sample concentrations were ca. 5×10^{-3} M in acetonitrile.

For quantum yield measurements nitrogen-purged solutions of DCA and *E*-**1** or *Z*-**1** were irradiated on a merry-go-round type apparatus with 405- and 436-nm light from a 400-W high-pressure mercury lamp through a Toshiba L-39 glass filter. Light intensities were determined by potassium tris(oxalato)ferrate(III) actinometry. The solutions were analyzed at low conversion (<10%) of the substrate on a Shimadzu GC-4CM-PF gas chromatograph.

Photostationary isomer ratios were measured by irradiating benzene solutions of *Z*-**1** and *E*-**1** in the presence of optically matched concentrations of sensitizers (OD's at

irradiation wavelength=ca. 2).

Results

Quenching of DCA Fluorescene by *E*-1 and *Z*-1. The fluorescence intensity and lifetime of DCA (3×10^{-5} M) were effectively quenched by both *E*-1 (0—0.025 M) and *Z*-1 (0—0.046 M) in deaerated benzene and acetonitrile (Fig. 1 for *Z*-1 in benzene). Stern-Volmer plots are linear over the concentration range investigated. Table 1 lists the quenching rate constants (k_q) calculated from the Stern-Volmer constants ($K_{SV}=k_q\tau_S$) of intensity quenching and fluorescence lifetimes (τ_S), 12.4 ns in benzene and 14.9 ns in acetonitrile, determined by single photon counting. The k_q values are close to the diffusion-controlled rate constant in each solvent.[9]

On quenching of DCA fluorescence by *E*-1 and *Z*-1 in benzene, new weak emissions appeared at the longer wavelength region with their maxima around 520 nm for *E*-1 and 505 nm for *Z*-1. These emissions are reasonably assigned to the exciplexes formed from the excited singlet DCA and the ground-state oximes. Figure 1 indicates the profile of the exciplex emission of *Z*-1. The exciplexes decayed with lifetimes of 22.8 and 28.7 ns for *E*-1 and *Z*-1, respectively, as measured by single photon counting. In acetonitrile no exciplex emission was observed for *E*-1 or *Z*-1.

Photostationary State Isomer Ratio. Oxime ethers *E*-1 and *Z*-1 (5×10^{-3} M) were irradiated in deaerated benzene or acetonitrile solutions containing DCA (1×10^{-3} M) with 405- and 436-nm light. The irradiation resulted in nearly the same photostationary state isomer ratios $([E]/[Z])_{pss}$ around 40/60 starting with either isomer in both solvents. When typical triplet sensitizers like acetophenone and benzophenone (1×10^{-2} M) were used in benzene, similar $([E]/[Z])_{pss}$ values (44/56) were obtained. Direct irradiation of **1** with 313-nm light gave an $([E]/[Z])_{pss}$ value around 60/40. The results are listed in Table 2.

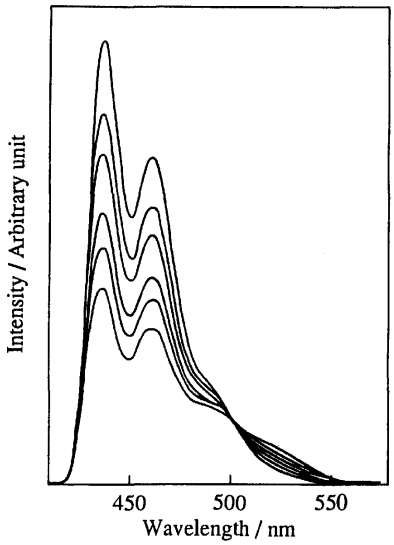

Fig. 1. Quenching of DCA fluorescence by *Z*-1 and exciplex emission in benzene.

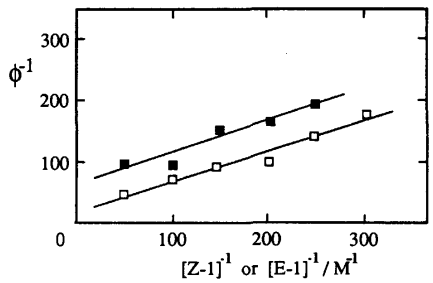

Fig. 2. Stern-Volmer plots of DCA-sensitized isomerization of *E*-1 (■) and *Z*-1 (□) in benzene.

Table 1. Rate Constants for Fluorescence Quenching of DCA by Oxime Ethers in Benzene and Acetonitrile

Oxime ether	In benzene		In acetonitrile	
	$k_q\tau_S$/M^{-1}	k_q/M^{-1} s^{-1}	$k_q\tau_S$/M^{-1}	k_q/M^{-1} s^{-1}
E-1	94	7.8×10^9	270	1.8×10^{10}
Z-1	27	2.2×10^9	420	2.8×10^{10}

Table 2. Photostationary State Isomer Ratios of Oxime Ether **1** on Direct and Sensitized Irradiation in Benzene and Acetonitrile

Sensitizer	Wavelength/nm	Solvent	Isomer ratio	
			Z	*E*
—	313	Benzene	58	42
DCA	405, 436	Benzene	41	59
Benzophenone	366	Benzene	44	56
Acetophenone	313	Benzene	44	56
—	313	MeCN	62	38
DCA	405, 436	MeCN	38	62
Benzophenone	366	MeCN	44	56

Quantum Yields for Isomerization. The quantum yields for DCA(10^{-3} M)-sensitized $E \rightarrow Z$ and $Z \rightarrow E$ isomerization ($\phi_{E \rightarrow Z}$ and $\phi_{Z \rightarrow E}$, respectively) were determined in benzene with varying concentrations (3.3×10^{-3}—2.0×10^{-2} M) of *E*-**1** and *Z*-**1** at their low conversion (<10%). Figure 2 shows Stern-Volmer plots for $E \rightarrow Z$ and $Z \rightarrow E$ isomerization. The reciprocal of the intercept and the ratio of intercept/slope in the plot for $Z \rightarrow E$ isomerization give, respectively, 0.062 as a limiting quantum yield ($\phi_{Z \rightarrow E}^{lim}$) at infinite *Z*-**1** concentration and 32 M^{-1} as a Stern-Volmer constant (K_{SV}). The latter value is in satisfactory agreement with that obtained from the fluorescence quenching, 27 M^{-1}. Similarly the $E \rightarrow Z$ isomerization gives 0.015 as $\phi_{E \rightarrow Z}^{lim}$ and 122 M^{-1} as K_{SV}. This value agrees fairly well with K_{SV} from the fluorescence quenching, 94 M^{-1}. In acetonitrile the isomerization proceeded with much lower efficiencies as estimated from irradiation times needed for accomplishment of the photostationary state.

Triplet Energies of Oxime Ethers. An attempt was done to determine the triplet energies of *E*-**1** and *Z*-**1** by the procedure of Hammond and Saltiel,[10] since *E*-**1** and *Z*-**1** did not emit phosphorescence in rigid glasses. Thus, the photostationary state isomer ratios of **1** were measured in the presence of various sensitizers with triplet energies covering 42—74 kcal mol^{-1} in benzene (Table 3). Figure 3 plots the ratio against the triplet energy of the sensitizer. This plot allows us to estimate the triplet energies of *E*-**1** and *Z*-**1** as ca. 52 and ca. 60 kcal mol^{-1}, respectively.[10]

Laser Flash Photolysis. On laser flash photolysis (LFP) of DCA (1×10^{-4} M) with 406-nm laser pulses from excimer laser (XeCl, 308 nm)-pumped dye laser (DPS) in deaerated benzene in the presence of *Z*-**1** (0.1 M) a transient absorption spectrum was observed in the 400—600 nm region (λ_{max} 442 nm), the lifetime being 9.5 μs as observed at 455 nm (Fig. 4). This spectrum can be attributed to DCA triplets.[11] In the absence of *Z*-**1** the intensity of the absorption was

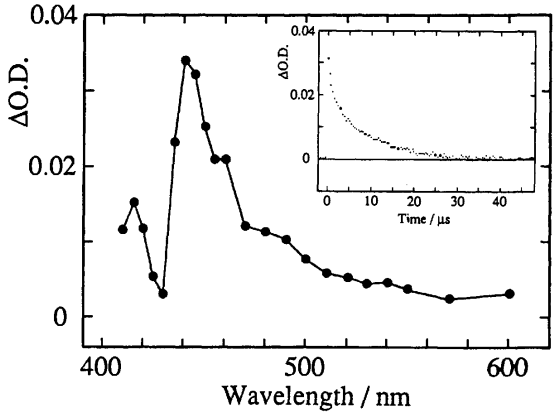

Fig. 4. Transient absorption spectrum in benzene with a decay curve.

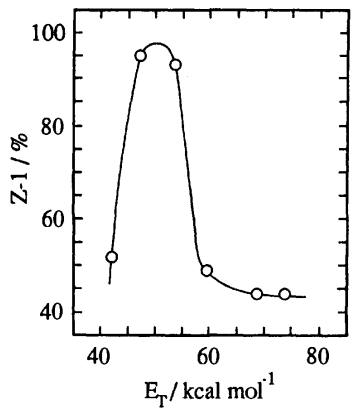

Fig. 3. Hammond-Saltiel plot of triplet sensitized isomerization of **1**.

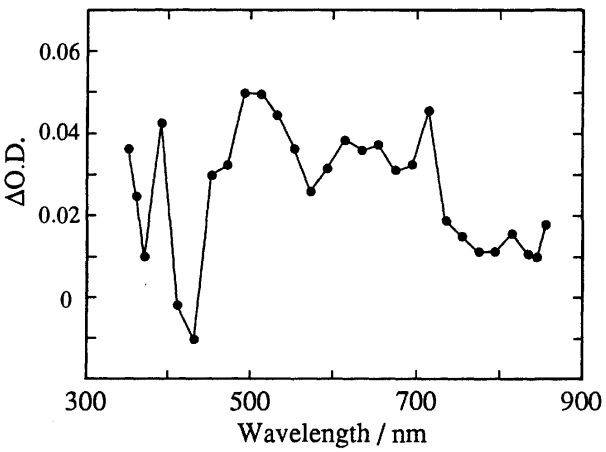

Fig. 5. Transient absorption spectrum in acetonitrile.

Table 3. Photostationary State Isomer Ratios in Triplet Sensitized Irradiation of Oxime Ether **1**

Sensitizer	Triplet energy[a]/kcal mol^{-1}	Isomer ratio	
		Z	*E*
Anthracene	42.0	52	48
Benz[*a*]anthracene	47.2	95	5
Benzil	53.4	93	7
2-Acetylnaphthalene	59.4	49	51
Benzophenone	68.6	44	56
Acetophenone	73.7	44	56

a) S. L. Murov, "Handbook of Photochemistry," Marcel Dekker, New York (1973), pp. 3—11.

several times weaker than that observed in its presence.

LEP of DCA with *Z*-**1** in acetonitrile gave a transient absorption spectrum different from that in benzene (Fig. 5). The absorption bands in the 440—750 nm region can be mainly attributed to DCA anion radicals,[12] and the bands in longer wavelengths than 750 nm might be attributed to *Z*-**1** cation radicals since γ-radiolysis of *Z*-**1** in Freon matrix gave absorption bands due to *Z*-**1** cation radicals in the 500—1000 nm region with λ_{max}'s at 650, 810, and 930 nm.[13]

Singlet oxygen luminescence was monitored at 1.27 μm using a germanium photodiode by exciting benzene solutions of DCA (1×10^{-4} M) with 406-nm laser pulses under air in the absence and presence of *Z*-**1**. In the absence of *Z*-**1** the emission was too weak to determine its lifetime; however, in the presence of *Z*-**1** (0.1 M) was exhibited a strong emission with a lifetime of 30 μs.[14]

Discussion

The quenching interaction of singlet excited DCA and the oxime ethers is considered to be accompanied by exciplex formation in benzene as evidenced by the long wavelength emission, and by electron transfer in acetonitrile as shown by transient absorption ascribed to DCA anion radicals and oxime ether cation radicals in laser plash photolysis. The changes of Gibbs' free energy ($\Delta G°$) associated with electron transfer from the DCA excited singlet to the oxime ethers in acetonitrile were estimated as −3.8 and −5.0 kcal mol^{-1} for *E*-**1** and *Z*-**1**, respectively, by Weller's equation (Eq. 1),[15]

$$\Delta G°/\text{kcal mol}^{-1} = 23.06(E_{ox} - E_{red} - e_0^2/a\varepsilon - E_{0,0}) \quad (1)$$

where E_{ox} and E_{red} indicate the oxidation potential of an oxime ether (1.81 V for *E*-**1** and 1.76 V for *Z*-**1** vs. SCE) and the reduction potential of DCA (−0.95 V), respectively, as determined in acetonitrile, $E_{0,0}$ is the singlet excitation energy of DCA (2.87 eV, estimated from its fluorescence spectrum), and $e_0^2/a\varepsilon$ is a Coulombic term (0.06 eV). These values show that the electron transfer can take place as an exothermic process in acetonitrile.

The $([E]/[Z])_{pss}$ ratio in DCA-sensitized irradiation is 1.4 in benzene from Table 1. The ratio is expressed by Eq. 2,

$$([E]/[Z])_{pss} = (k_q^Z/k_q^E)(\phi_{Z\to E}^{lim}/\phi_{E\to Z}^{lim}) \quad (2)$$

where k_q^Z and k_q^E are the rate constants for quenching of DCA excited singlets by *Z*-**1** and *E*-**1**, respectively, and the limiting quantum yields, $\phi_{Z\to E}^{lim}$ and $\phi_{E\to Z}^{lim}$, mean the quantum efficiencies with which the exciplexes give the isomerized derivatives. Combination of the observed ratios of k_q^Z/k_q^E, 0.28, and $\phi_{Z\to E}^{lim}/\phi_{E\to Z}^{lim}$, 4.2, gives $([E]/[Z])_{pss}$ as 1.2, which agrees well with the observed value, 1.4. This fact supports the sensitization with DCA of **1** isomerization.

Similarity in the photostationary isomer ratio between DCA and benzophenone sensitization in benzene (Table 2) suggests that the DCA-sensitization generates the triplet state of **1** as the intermediate for isomerization in benzene, as seen in the isomerization of olefins in the presence of electron donors[16] or acceptors[8b,17] in nonpolar solvents where the triplet state of olefins results from the exciplexes.

It is reasonably concluded from energetic considerations and laser flash photolysis study that the triplet state of **1** is the intermediate of isomerization. The Hammond–Saltiel plot (Fig. 3) gave the triplet energies of *E*-**1** and *Z*-**1** as ca. 52 and ca. 60 kcal mol^{-1}, respectively. It is noteworthy that the triplet energy of *Z*-**1** is close to that of naphthalene itself, 61 kcal mol^{-1},[18] indicating that the triplet excitation in *Z*-**1** is nearly localized in the naphthalene moiety which may be twisted around the C–C single bond from the C=N molecular plane. Also, the energies of the exciplexes of DCA with *E*-**1** and *Z*-**1** are estimated around 55 and 56 kcal mol^{-1}, respectively, from their emission maxima.

The energy diagram for DCA-sensitized isomerization of **1** in benzene is depicted in Scheme 1. On excitation of DCA in the presence of *E*-**1**, the resulting singlet excited DCA (66.2 kcal mol^{-1}) interacts with *E*-**1** to give an exciplex, which subsequently either is deactivated to the ground state through nonradiative pathways or exciplex emission, or produces the triplet state of *E*-**1** or DCA (41.5 kcal mol^{-1})[16b] in an exothermic way. In the case of *Z*-**1**, the formation of *Z*-**1** triplets from the exciplex of DCA and *Z*-**1** is nearly 3 kcal mol^{-1} endothermic. However, if the exciplex does not produce directly *Z*-**1** triplets (^{3}Z*) but produces the perpendicular triplet of **1** (^{3}P*) through a nonvertical pathway, it is certainly at least 5 kcal mol^{-1} exothermic, since in the triplet state of stilbene ^{3}P* is nearly the same as, or slightly lower than, ^{3}E* in energy.[1] In any case, ^{3}P* produced either from ^{3}E*, ^{3}Z*, or directly from the exciplexes undergoes deactivation to the ground state *E*-**1** and *Z*-**1** with a certain ratio.

Laser excitation of DCA in deaerated benzene exhibited only a weak transient absorption band due to DCA triplets because of low efficiency of intersystem crossing of DCA excited singlets.[19] It is remarkable that in the presence of *Z*-**1**, laser excitation of DCA afforded the absorption bands of the DCA triplets (λ_{max} 442 nm) with several times stronger intensity than in the absence of *Z*-**1**; however, any transient absorption bands assignable to the triplet states of **1** were not detected. This may be owing to their very short lifetimes, since, even on benzophenone-sensitized laser excitation, only the benzophenone triplet was observed with no detection of **1** triplets.

Likewise, laser excitation of DCA in aerated benzene

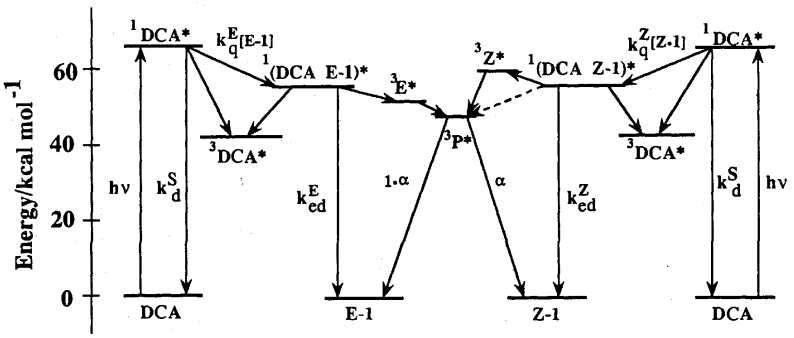

Scheme 1.

gave only a very low yield of singlet oxygen, as determined by singlet oxygen luminescene technique. This may be also due to the low quantum yield for intersystem crossing of the DCA excited singlets. However, in the presence of *Z*-**1**, a strong emission from singlet oxygen was detected. This is reasonably attributed to a more efficient production of the DCA triplets under these conditions.

The fact that the DCA triplet is produced from the excitation of DCA in the presence of *Z*-**1** but not in the absence of *Z*-**1** clearly shows that the quenching of DCA singlets by *Z*-**1** gives the DCA triplet and probably also the triplet state of **1**. Therefore, it is reasonable to propose such a mechanism for the isomerization as shown in Scheme 1, where *k*'s are the rate constants for the corresponding processes.

According to this mechanism, the quantum yields for the isomerization can be expressed as follows:

$$\phi_{E\to Z} = \frac{k_q^{E}[E\text{-}\mathbf{1}]}{\tau_s^{-1} + k_q^{E}[E\text{-}\mathbf{1}]} \cdot \phi_T^{E} \cdot (1-\alpha) \quad (3)$$

$$\phi_{Z\to E} = \frac{k_q^{Z}[Z\text{-}\mathbf{1}]}{\tau_s^{-1} + k_q^{Z}[Z\text{-}\mathbf{1}]} \cdot \phi_T^{Z} \cdot \alpha \quad (4)$$

where ϕ_T^E and ϕ_T^Z denote the efficiencies for the production of the triplet state of **1** from the exciplexes. Therefore, the Stern–Volmer equation can be reduced as follows:

$$\frac{1}{\phi_{E\to Z}} = \frac{1}{(1-\alpha)\phi_T^{E}}\left(1 + \frac{1}{k_q^{E}\tau_S[E\text{-}\mathbf{1}]}\right) \quad (5)$$

$$\frac{1}{\phi_{Z\to E}} = \frac{1}{\alpha\phi_T^{Z}}\left(1 + \frac{1}{k_q^{Z}\tau_S[Z\text{-}\mathbf{1}]}\right) \quad (6)$$

The limiting quantum yields at the infinite concentration of *E*-**1** and *Z*-**1**, $\phi_{E\to Z}^{lim}$ and $\phi_{Z\to E}^{lim}$, are written as follows:

$$\phi_{E\to Z}^{lim} = (1-\alpha)\phi_T^{E} \quad (7)$$

$$\phi_{Z\to E}^{lim} = \alpha\phi_T^{Z} \quad (8)$$

The values for α and $1-\alpha$, the ratios of giving *E* and *Z* from the common twisted triplet state of **1**, ^{3}P*, are seen as 0.56 and 0.44, respectively, from the photostationary state isomer ratio arising from sensitizers with sufficiently high triplet energies like acetophenone and benzophenone (Table 1). Substitution of the observed $\phi_{E\to Z}^{lim}$ and $\phi_{Z\to E}^{lim}$ values in Eqs. 7 and 8 affords ϕ_T^Z and ϕ_T^E as 0.14 and 0.027, respectively.

The above values ϕ_T's are nearly comparable or lower than the values for the triplet olefin production from the quenching of the singlet excited state of 2-NaphthylCH=CHBu^t with 1,4-dicyanobenzene in benzene, 0.26[8b] and for the quenching of the singlet excited stilbene with various amines in benzene, 0.09—0.51.[16a] The lower efficiency for the production of triplet **1** in the present reaction can be attributed to the dual courses which the exciplex can take, that is, giving either triplet **1** or triplet DCA; the latter is energetically preferable. Also, the present exciplexes might have higher probability to undergo deactivation than those between the olefins and electron donors or acceptors.

The isomerization efficiency was lower in acetonitrile than in benzene, indicating that the isomerization does not proceed efficiently through cation radicals of **1**. On LFP of DCA with *Z*-**1** in acetonitrile only the ionic species were observed but no triplets were detected. However, the photostationary state isomer ratio of DCA-sensitized isomerization was close to that of benzophenone sensitization in the same solvent (Table 1).

The ion radical pairs *E*-**1**$^+$/DCA$^-$ and *Z*-**1**$^+$/DCA$^-$ are estimated to be 63.5 and 62.4 kcal mol^{-1}, respectively, higher in energy than the neutral species in the ground state from their electrochemical potentials. Back electron transfer in the radical ion pairs can generate the triplet states of DCA and **1**; however, the major role in isomerization of **1** may be played by the **1** triplet thus formed.

References

1) a) J. Saltiel, J. D'Agostino, E. D. Megarity, L. Metts, K. R. Neuberger, M. Wrighton, and O. C. Zafiriou, *Org. Photochem.*, **3**, 1 (1973); b) J. Saltiel and J. L. Charlton,

"Rearrangement in Ground and Excited States," Vol. 3, ed by P. de Mayo, Academic Press, New York (1980), pp. 25—89; c) T. Arai, T. Karatsu, H. Misawa, Y. Kuriyama, H. Okamoto, T. Hiresaki, H. Furuuchi, H. Zeng, H. Sakuragi, and K. Tokumaru, *Pure Appl. Chem.*, **60**, 989 (1988), and references cited therein.

2) a) R. J. Drewer, "The Chemistry of the Hydrazo, Azo and Azoxy Groups," Part 2, ed by S. Patai, Wiley, New York (1975), pp. 935—1015; b) J. Ronayette, R. Arnaud, P. Lebourgeois, and J. Lemaire, *Can. J. Chem.*, **52**, 1848 (1974); J. Ronayette, R. Arnaud, and J. Lemaire, *ibid.*, **52**, 1858 (1974); R. Arnaud and J. Lemaire, *ibid.*, **52**, 1868 (1974).

3) a) G. Wettermark, "The Chemistry of the Carbon-Nitrogen Double Bond," ed by S. Patai, Wiley, New York (1970), pp. 565—596; b) A. Padwa, *Chem. Rev.*, **77**, 37 (1977).

4) C. G. McCarty, "The Chemistry of the Carbon-Nitrogen Double Bond," ed by S. Patai, Wiley, New York (1970), pp. 363—464.

5) a) A. Padwa and F. Albrecht, *J. Am. Chem. Soc.*, **94**, 1000 (1972); b) A. Padwa and F. Albrecht, *ibid.*, **96**, 4849 (1974); c) A. Padwa and F. Albrecht, *J. Org. Chem.*, **39**, 2361 (1974); d) T. Sato, T. Inoue, and K. Yamamoto, *Bull. Chem. Soc. Jpn.*, **45**, 1176 (1972).

6) a) R. S. Davidson, *Adv. Phys. Org. Chem.*, **19**, 1 (1983); b) S. L. Mattes and S. Farid, *Org. Photochem.*, **6**, 233 (1983); c) D. Creed and R. A. Caldwell, *Photochem. Photobiol.*, **41**, 715 (1985); d) M. A. Fox, *Adv. Photochem.*, **13**, 237 (1986); e) G. J. Kavarnos and N. J. Turro, *Chem. Rev.*, **86**, 401 (1986); f) J. Mattay, *Angew. Chem., Int. Ed. Engl.*, **26**, 825 (1987).

7) A. Okami, T. Arai, H. Sakuragi, and K. Tokumaru, *Chem. Lett.*, **1984**, 289; K. Ikoma, A. Okami, T. Arai, H. Sakuragi, and K. Tokumaru, *Tetrahedron Lett.*, **25**, 5161 (1984).

8) a) H. Sakuragi, R. Nakagaki, T. Oguchi, T. Arai, K. Tokumaru, and S. Nagakura, *Chem. Phys. Lett.*, **135**, 325 (1987); b) T. Oguchi, T. Arai, H. Sakuragi, and K. Tokumaru, *Bull. Chem. Soc. Jpn.*, **60**, 2395 (1987); c) Y. Kuriyama, T. Arai, H. Sakuragi, and K. Tokumaru, *Chem. Lett.*, **1988**, 1193.

9) S. L. Murov, "Handbook of Photochemistry," Marcel Dekker, New York (1973), p. 55.

10) G. S. Hammond and J. Saltiel, *J. Am. Chem. Soc.*, **85**, 2516 (1963); G. S. Hammond, J. Saltiel, A. A. Lamola, N. J. Turro, J. S. Bradshaw, D. O. Cowan, R. C. Counsell, V. Vogt, and C. Dalton, *ibid.*, **86**, 3197 (1964).

11) A. P. Darmanyan, *Chem. Phys. Lett.*, **110**, 89 (1984).

12) H. F. Davis, B. B. Lohray, K. R. Gopidas, C. V. Kumar, P. K. Das, and M. V. George, *J. Org. Chem.*, **50**, 3685 (1985).

13) We thank Professor T. Shida, Kyoto University, for measuring a spectrum of *Z*-**I** cation radicals generated by γ-radiolysis.

14) D. R. Kearns, "Singlet Oxygen," ed by H. H. Wasserman and R. W. Murray, Academic Press, New York (1979), pp. 115—137.

15) D. Rehm and A. Weller, *Isr. J. Chem.*, **8**, 259 (1970).

16) a) W. Hub, S. Schneider, F. Dörr, J. D. Oxman, and F. D. Lewis, *J. Am. Chem. Soc.*, **106**, 701 (1984); b) W. Hub, U. Klueter, S. Schneider, F. Dörr, J. D. Oxman, and F. D. Lewis, *J. Phys. Chem.*, **88**, 2308 (1984).

17) a) F. D. Lewis, J. R. Petisce, J. D. Oxman, and M. J. Nepras, *J. Am. Chem. Soc.*, **107**, 203 (1985); b) J. L. Goodman and K. S. Peters, *ibid.*, **107**, 1441, 5459 (1985).

18) Ref. 9, p. 3.

19) K. Kikuchi and H. Kokubun, private communication.

Redox Behavior of Simple Vitamin B_{12} Model Complexes and Electrochemical Catalysis of Carbon-Skeleton Rearrangements†

Yukito MURAKAMI,* Yoshio HISAEDA, Sheng-Di FAN, and Yoshihisa MATSUDA
Department of Organic Synthesis, Faculty of Engineering, Kyushu University,
Hakozaki, Higashi-ku, Fukuoka 812
(Received February 2, 1989)

Various cobalt complexes of 4,10-dipropyl-5,9-diazatrideca-4,9-diene-3,10-dione dioxime, $(C_2C_3)(DOH)_2pn$, were prepared, and redox behavior of them was investigated by means of cyclic voltammetry; Co(II)/Co(I) redox potentials in the range of −0.69 through −0.7 V vs. Ag/AgCl. The monomethylated complex, which has a cobalt-carbon bond at one axial site of the nuclear cobalt, was disproportionated to the dimethylated complex, involving two cobalt-carbon bonds at both axial sites, and the Co^I species by one-electron reduction. The dimethylated complex was inactive for electrochemical reduction, but transformed into the monomethylated complex via cleavage of a cobalt-carbon bond upon electrochemical oxidation. The electrolyses of 1-bromo-2,2-bis(ethoxycarbonyl)propane, 1-bromo-2-cyano-2-ethoxycarbonylpropane, and 2-acetyl-1-bromo-2-ethoxycarbonylpropane in the presence of $[Co^{III}\{(C_2C_3)(DO)(DOH)pn\}Br_2]$ in *N,N*-dimethylformamide did not proceed in a divided cell at −2.0 V vs. Ag/AgCl, since the corresponding dialkylated complexes, inactive for electrochemical reduction, were formed in the course of reaction. When imidazole was added to solutions for the electrolysis, the reaction proceeded efficiently by the trans effect arising from the coordinated axial base and the corresponding carbon-skeleton rearrangement products were obtained. On the other hand, the carbon-skeleton rearrangement proceeded in an undivided cell even in the absence of imidazole; the dialkylated complex was decomposed to give the monoalkylated complex and the reduction and rearrangement products by electrochemical oxidation on the anode.

Vitamin B_{12}-dependent enzymes catalyze various isomerization reactions which result in carbon-skeleton rearrangements: methylmalonyl-SCoA⇌succinyl-SCoA, β-methylaspartate⇌glutamate, and methylitaconate ⇌α-methyleneglutarate.[1] Clarification of these reaction mechanisms is a current research target in bioinorganic chemistry.[2] In this regard, various cobalt complexes have been synthesized as model complexes,[3] and mechanistic studies of various enzyme-mimic reactions have been carried out. One of the most important aspects in designing model complexes is to pay much attention to the redox potentials of the nuclear cobalt in connection with their catalytic activities. The catalytic reactions as mediated by vitamin B_{12} and its model complexes have been carried out by electrochemical means[4,5] in the light of redox behavior of such complexes.[6–8]

We have been dealing with hydrophobic vitamin B_{12} derivatives, which have ester groups in place of the peripheral amide moieties of the naturally occurring vitamin B_{12},[9–14] and found that electrochemical carbon-skeleton rearrangements were catalyzed efficiently by these complexes.[13] In those cases, the reaction takes place with a catalytic cycle shown in Fig. 1: the Co^{II} complex is electrochemically reduced to the Co^I species, and the corresponding alkylated complex is generated by reaction of the supernucleophilic Co^I species with a substrate, a substituted alkyl bromide (RX); the alkylated complex is subsequently decomposed by photolysis or electrolysis to afford the corresponding products, and the cobalt complex acts as a mediator repeatedly. This finding prompted us to develop a simple model complex, which shows redox

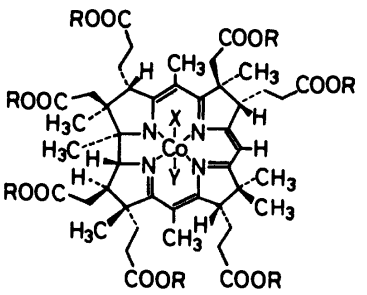

Hydrophobic Vitamin B_{12}

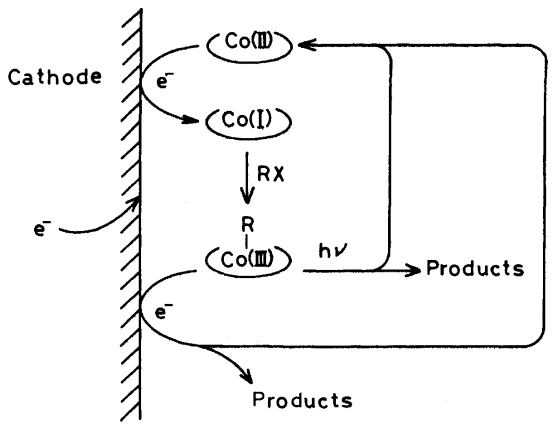

Fig. 1. Schematic representation of electrochemical catalysis.

† Contribution No. 897 from this Department. Preliminary communications; see Refs. 28 and 32.

behavior analogous to that of vitamin B_{12} with respect to the nuclear cobalt and catalyzes the isomerization reaction in a similar manner. We report here on the redox behavior of model complexes which are derived from the Costa's complex[15,16] by its modification. Furthermore, the electrochemical carbon-skeleton rearrangements catalyzed by these model complexes was compared with those catalyzed by the hydrophobic vitamin B_{12}.

Experimental

General Analyses and Measurements. Elemental analyses were performed at the Microanalysis Center of Kyushu University. IR spectra were taken on a JASCO IR-810 infrared spectrophotometer, while electronic absorption spectra were recorded on a Hitachi 220A or a Hitachi 340 spectrophotometer. ESR spectra were obtained on a JEOL JES-FElG X-band spectrometer equipped with an Advantest TR-5213 microwave counter and an Echo Electronics EFM-200 NMR field meter. ^1H and ^{13}C NMR spectra were taken on a Hitachi R-24B, a JEOL JNM-EX90, or a JEOL JNM-GSX400 spectrometer installed at the Center of Advanced Instrumental Analysis of Kyushu University. Assignments of NMR signals due to the cobalt complexes were carried out by means of the 2D-NMR technique (H-H and C-H COSY). Cyclic voltammograms were obtained on an apparatus composed of a Hokuto Denko HA-501 potentiostat/galvanostat and a Hokuto Denko HB-104 function generator. An applied potential between the working and reference electrodes in the electrolysis was maintained constant with a Hokuto Denko HA-305 potentiostat/galvanostat and an electrical quantity was recorded on a Hokuto Denko HF-201 coulomb/amperehour meter. GLC analyses were carried out on a Shimadzu GC-4C or a Shimadzu GC-9A apparatus equipped with a Shimadzu C-R3A-FFC chromatopac.

Materials. *N,N*-Dimethylformamide (DMF) was dried and purified just before use according to the standard procedure.[17] Tetrabutylammonium perchlorate (TBAP) was purchased from Nakarai Chemicals and used without further purification. Tetrabutylammonium tetrafluoroborate (TBAF) was prepared after a reported procedure.[18] The substrates such as 1-bromo-2,2-bis(ethoxycarbonyl)propane (**1**), 1-bromo-2-cyano-2-ethoxycarbonylpropane (**2**), and 2-acetyl-1-bromo-2-ethoxycarbonylpropane (**3**) and authentic samples of the corresponding products such as 2,2-bis(ethoxycarbonyl)propane (**A**), 1,2-bis(ethoxycarbonyl)-propane (**B**), 2-cyano-2-ethoxycarbonylpropane (**C**), 1-cyano-2-ethoxycarbonylpropane (**D**), 2-cyano-1-ethoxycarbonyl-propane (**E**), 2-acetyl-2-ethoxycarbonylpropane (**F**), 1-acetyl-2-ethoxycarbonylpropane (**G**), and 2-acetyl-1-ethoxycarbonyl-propane (**H**) were prepared according to the methods described in literature[13] and confirmed to be sufficiently pure by ^1H NMR and GLC. The chelating ligand, 4,10-dipropyl-5,9-diazatrideca-4,9-diene-3,11-dione dioxime, and its cobalt complexes with various axial ligands were prepared by referring to reported procedures[16,19–21] along with some modifications as shown in Scheme 1.

4,10-Dipropyl-5,9-diazatrideca-4,9-diene-3,11-dione Dioxime, $(C_2C_3)(DOH)_2pn$. This ligand was synthesized by the condensation of 3-hydroxyimino-4-heptanone (62.9 g, 0.44 mol), which was prepared from 4-heptanone and methyl nitrate,[22] and 1,3-propanediamine (16.35 g, 0.22 mol): yield 51.0 g (71.4%); IR (KBr) 3200 (OH), 1625 (C=N), 970 cm^{-1} (N–O); ^1H NMR ($CDCl_3$, TMS) δ=0.93 (6H, t, $CH_2CH_2C\underline{H}_3$), 1.03 (6H, t, $CH_2C\underline{H}_3$), 1.45 (4H, m, $CH_2C\underline{H}_2CH_3$), 2.03, (2H, m, $CH_2C\underline{H}_2CH_2$), 2.52 (4H, t, $C\underline{H}_2CH_2CH_3$), 2.91 (4H, q, $C\underline{H}_2CH_3$), 3.60 (4H, t, NCH_2), 6.0 (2H, bs, OH). Found: C, 63.02; H, 9.99; N, 17.08%. Calcd for $C_{17}H_{32}N_4O_2$: C, 62.91; H, 9.96; N, 17.27%.

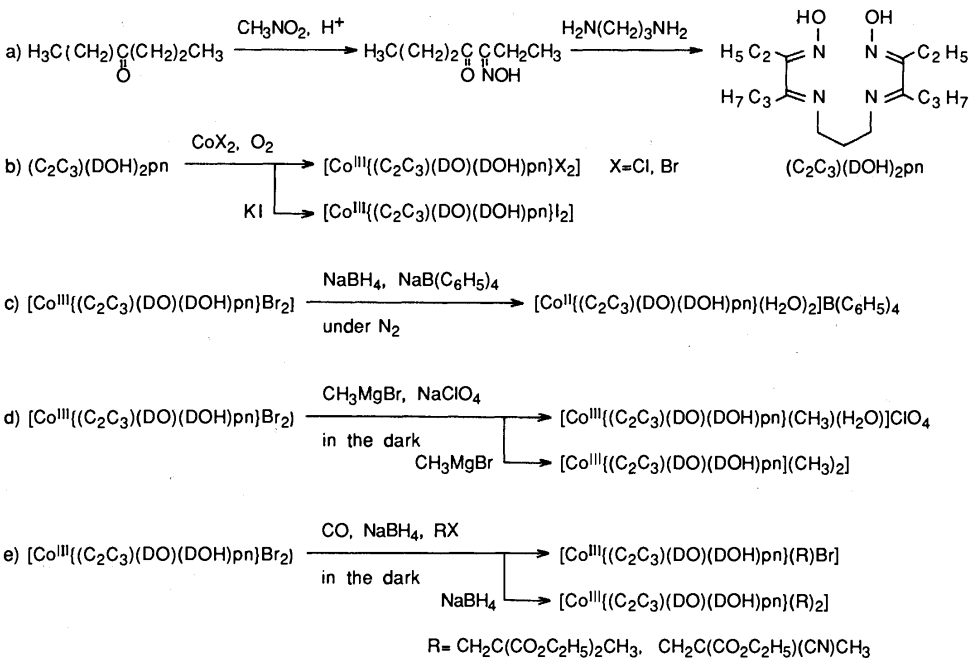

Scheme 1.

Dibromo(11-hydroxyimino-4,10-dipropyl-5,9-diazatrideca-4,9-dien-3-one oximato)cobalt(III), [Co^{III}\{(C_2C_3)(DO)(DOH)pn\}Br_2]. An acetone solution (10 mL) of (C_2C_3)$(DOH)_2$pn (1.6 g, 5.0×10^{-3} mol) was added dropwise to an aqueous solution (150 mL) of cobalt dibromide hexahydrate (2.0 g, 6.0×10^{-3} mol) while air was bubbled through the latter aqueous solution. After the reaction mixture was stirred for 4 h, precipitates were recovered by filtration and washed with water. The resulting cobalt complex was recrystallized from acetone-water (1:1 v/v) to afford dark green needles: yield 1.6 g (50%), mp 223—224 °C; IR (KBr) 700 cm^{-1} (Co-N); ^1H NMR ($CDCl_3$, TMS) δ=1.09 (6H, t, $CH_2CH_2C\underline{H}_3$), 1.23 (6H, t, $CH_2C\underline{H}_3$), 1.67 (4H, m, $CH_2C\underline{H}_2CH_3$), 2.61 (2H, m, $CH_2C\underline{H}_2CH_3$), 2.91 (4H, t, $C\underline{H}_2CH_2CH_3$), 2.98 (4H, q, $C\underline{H}_2CH_3$), 4.16 (4H, t, NCH_2), 19.37 (1H, s, OH); ^{13}C NMR ($CDCl_3$, TMS) δ=10.2 ($CH_2\underline{C}H_3$), 13.9 ($CH_2CH_2\underline{C}H_3$), 19.9 ($CH_2\underline{C}H_2CH_3$), 21.0 ($\underline{C}H_2CH_3$), 27.9 ($CH_2\underline{C}H_2CH_2$), 32.1 ($\underline{C}H_2CH_2CH_3$), 50.0 (NCH_2), 161.3 (ON=C), 177.7 (C-N=$\underline{C}$). Found: C, 37.72; H, 5.72; N, 10.33%. Calcd for $C_{17}H_{31}Br_2CoN_4O_2$: C, 37.66; H, 5.76; N, 10.33%.

Dichloro(11-hydroxyimino-4,10-dipropyl-5,9-diazatrideca-4,9-dien-3-one oximato)cobalt(III), [Co^{III}\{(C_2C_3)(DO)(DOH)pn\}Cl_2]. This complex was prepared from cobalt dichloride hexahydrate after the method employed for the preparation of [Co^{III}\{(C_2C_3)(DO)(DOH)pn\}Br_2], and obtained as dark green needles: yield 53%, mp 236—237 °C. Found: 44.99; H, 6.82; N, 12.32%. Calcd for $C_{17}H_{31}Cl_2CoN_4O_2$: C, 45.04; H, 6.89; N, 12.36%.

Diiodo(11-hydroxyimino-4,10-dipropyl-5,9-diazatrideca-4,9-dien-3-one oximato)cobalt(III), [Co^{III}\{(C_2C_3)(DO)(DOH)pn\}I_2]. This complex was prepared in the presence of a large excess of potassium iodide by the method employed for the preparation of [Co^{III}\{(C_2C_3)(DO)(DOH)pn\}Br_2], and obtained as dark purple prisms: yield 60%, mp 225—226 °C; λ_{max} (CH_2Cl_2) 338 (ε 1.99×10^4), 468 nm (1.02×10^4). Found: 32.12; H, 4.92; N, 8.78%. Calcd for $C_{17}H_{31}I_2CoN_4O_2$: C, 32.09; H, 4.91, N, 8.81%.

Diaqua(11-hydroxyimino-4,10-dipropyl-5,9-diazatrideca-4,9-dien-3-one oximato)cobalt(II) Tetraphenylborate, [Co^{II}\{(C_2C_3)(DO)(DOH)pn\}(H_2O)$_2$]B(C_6H_5)$_4$. This complex was prepared in Schlenk tubes under nitrogen atmosphere. [Co^{III}\{(C_2C_3)(DO)(DOH)pn\}Br_2] (0.30 g, 5.53×10^{-4} mol) in methanol-water (10:1 v/v, 50 mL) was treated with a slight excess of sodium tetrahydroborate. The solution turned blue initially, and then purple. After an aqueous solution (20 mL) of sodium tetraphenylborate (0.19 g, 5.53×10^{-4} mol) was added to it, the resulting reddish purple precipitates were recovered by filtration and washed with deaerated water. This product was recrystallized from methanol-water (10:1 v/v) to afford pale brown powder: yield 0.20 g (48%), decomp 86—87 °C. Found: C, 66.63; H, 7.51; N, 7.79%. Calcd for $C_{41}H_{55}BCoN_4O_4$: C, 66.76; H, 7.51; N, 7.60%.

Methylaqua(11-hydroxyimino-4,10-dipropyl-5,9-diazatrideca-4,9-dien-3-one oximato)cobalt(III) Perchlorate, [Co^{III}\{(C_2C_3)(DO)(DOH)pn\}(CH_3)(H_2O)]ClO_4. [Co^{III}\{(C_2C_3)(DO)(DOH)pn\}Br_2] (2.8 g, 5.2×10^{-3} mol) suspended in dry tetrahydrofuran (40 mL) was treated with methylmagnesium bromide (1.0×10^{-2} mol) at −60 °C under nitrogen atmosphere. After the resulting orange red solution was stirred for 2 h, cold water (10 mL) was added to it. The solution was neutralized with aqueous hydrochloric acid (2 mol dm^{-3}), tetrahydrofuran was removed completely in vacuo, and an excess amount of sodium perchlorate was added to the residue. After the solution was allowed to stand overnight in a refrigerator, a dark red solid was recovered and recrystallized from acetone-water (1:1 v/v) to afford fine red crystals: yield 0.73 g (31%), decomp 121—122 °C; IR (KBr) 1120, 630 cm^{-1} (ClO_4^-); ^1H NMR ($CDCl_3$, TMS) δ=0.61 (3H, s, Co-CH_3), 1.07 (6H, t, $CH_2C\underline{H}_3$), 1.18 (6H, t, $CH_2CH_2C\underline{H}_3$), 1.59 (4H, m, $CH_2C\underline{H}_2CH_3$), 2.23 (2H, m, $CH_2C\underline{H}_2CH_2$), 2.72 (8H, m, $C\underline{H}_2CH_2CH_3$ and $C\underline{H}_2CH_3$), 4.01 (4H, t, N-CH_2), 18.88 (1H, s, OH); λ_{max} (CH_2Cl_2) 468 nm (ε 3.32×10^4). Found: C, 41.96; H, 6.98; N, 10.84%. Calcd for $C_{18}H_{36}ClCoN_4O_7$: C, 41.99; H, 7.05; N, 10.88%.

Dimethyl(11-hydroxyimino-4,10-dipropyl-5,9-diazatrideca-4,9-dien-3-one oximato)cobalt(III), [Co^{III}\{(C_2C_3)(DO)(DOH)pn\}(CH_3)$_2$]. This compound was prepared in the presence of a large excess of methylmagnesium bromide after the method employed for the preparation of [Co^{III}\{(C_2C_3)(DO)(DOH)pn\}(CH_3)(H_2O)]ClO_4, and obtained as fine red crystals: yield 62%, decomp 118—119 °C; ^1H NMR ($CDCl_3$, TMS) δ=0.05 [6H, s, Co-$(CH_3)_2$], 1.00 (6H, t, $CH_2C\underline{H}_3$), 1.08 (6H, t, $CH_2CH_2C\underline{H}_3$), 1.47 (4H, m, $CH_2C\underline{H}_2CH_3$), 2.10 (2H, m, $CH_2C\underline{H}_2CH_2$), 2.55 (4H, t, $C\underline{H}_2CH_2CH_3$), 2.65 (4H, q, $C\underline{H}_2CH_3$), 3.73 (4H, t, N-CH_2), 19.59 (1H, s, OH); λ_{max} (CH_2Cl_2) 411 nm (ε 4.80×10^4). Found: C, 55.53; H, 9.10; N, 13.44%. Calcd for $C_{19}H_{37}CoN_4O_2$: C, 55.33; H, 9.04; N, 13.58%.

Bromo{2,2-bis(ethoxycarbonyl)propyl}(11-hydroxyimino-4,10-dipropyl-5,9-diazatrideca-4,9-dien-3-one oximato)cobalt(III), [Co^{III}\{(C_2C_3)(DO)(DOH)pn\}\{$CH_2C(CO_2C_2H_5)_2CH_3$\}Br]. A methanol solution (200 mL) containing [Co^{III}\{(C_2C_3)(DO)(DOH)pn\}Br_2] (500 mg, 9.2×10^{-4} mol) and 1-bromo-2,2-bis(ethoxycarbonyl)propane (1.0 g, 3.7×10^{-3} mol) was stirred while carbon monoxide was introduced into it until saturation was attained. After being stirred for 2 h, the solution turned reddish yellow, indicating formation of the Co^{II} complex. Sodium tetrahydroborate in methanol was added dropwise to the resulting solution until the solution turned deep blue under carbon monoxide atmosphere. The solution changed its color to orange after it was refluxed for 6 h in the dark. The solution was evaporated to dryness, a material insoluble in dichloromethane was removed by filtration, and then the dichloromethane solution was evaporated to dryness. The product was recrystallized from diethyl ether-tetrahydrofuran (1:20 v/v) to afford orange prisms: yield 450 mg (75%); IR (KBr) 1730 cm^{-1} (C=O); λ_{max} (CH_3OH) 474 nm. Found: C, 47.87; H, 7.00; N, 8.53%. Calcd for $C_{26}H_{46}BrCoN_4O_6$: C, 48.08; H, 7.14; N, 8.63%.

Bromo(2-cyano-2-ethoxycarbonylpropyl)(11-hydroxyimino-4,10-dipropyl-5,9-diazatrideca-4,9-dien-3-one oximato)cobalt(III), [Co^{III}\{(C_2C_3)(DO)(DOH)pn\}\{$CH_2C(CO_2C_2H_5)(CN)CH_3$\}Br]. This compound was prepared in the presence of 1-bromo-2-cyano-2-ethoxycarbonylpropane after the method for the preparation of [Co^{III}\{(C_2C_3)(DO)(DOH)pn\}\{$CH_2C(CO_2C_2H_5)_2CH_3$\}Br], and obtained as orange prisms: yield 63%; λ_{max} (CH_3OH) 465 nm. Found: C, 47.55; H, 6.80; N, 11.83%. Calcd for $C_{24}H_{41}BrCoN_5O_4$: C, 47.85; H, 6.86; N, 11.62%.

Bis{2,2-bis(ethoxycarbonyl)propyl}(11-hydroxyimino-4,10-dipropyl-5,9-diazatrideca-4,9-dien-3-one oximato)cobalt(III), [Co^{III}\{(C_2C_3)(DO)(DOH)pn\}\{$CH_2C(CO_2C_2H_5)_2CH_3$\}$_2$]. A methanol solution (200 mL) containing [Co^{III}\{(C_2C_3)(DO)(DOH)pn\}Br_2] (100 mg, 1.8×10^{-4} mol) and 1-bromo-2,2-bis(ethoxycarbonyl)propane (1.0 g, 3.7×10^{-3} mol), and sodium hydroxide (10 mg, 2.5×10^{-4} mol) was saturated with carbon monoxide by bubbling for 2 h. Sodium tetrahydroborate in

methanol was added dropwise to the resulting solution until the solution turned deep blue. The reaction mixture was then refluxed for 6 h in the dark and turned orange gradually. The mixture was evaporated to dryness, and a material insoluble in dichloromethane was removed by filtration. The dichloromethane solution was evaporated to afford an orange red solid. The product was purified by gel-filtration chromatography on columns of Sephadex LH-20 with methanol and silica gel (Wakogel C-100) with hexane–chloroform (1 : 1 v/v) in this sequence. The solution was evaporated to dryness to afford red powder: yield 74 mg (53%); IR (KBr) 1730 cm^{-1} (C=O); λ_{max} (CH_3OH) 405 nm. Found: C, 55.38; H, 7.96; N, 7.17%. Calcd for $C_{35}H_{61}CoN_4O_{10}$: C, 55.55; H, 8.12; N, 7.40%.

Bis(2-cyano-2-ethoxycarbonylpropyl)(11-hydroxyimino-4,10-dipropyl-5,9-diazatrideca-4,9-dien-3-one oximato)cobalt(III), [Co^{III}{(C_2C_3)(DO)(DOH)pn}{$CH_2C(CO_2C_2H_5)(CN)CH_3$}$_2$]. This compound was prepared in the presence of 1-bromo-2-cyano-2-ethoxycarbonylpropane after the method for the preparation of [Co^{III}{(C_2C_3)(DO)(DOH)pn}{$CH_2C(CO_2C_2H_5)_2$-CH_3}$_2$], and obtained as red powder: yield 59%; λ_{max} (CH_3OH) 402 nm. Found: C, 56.07; H, 7.75; N, 12.61%. Calcd for $C_{31}H_{51}CoN_6O_6$: C, 56.18; H, 7.76; N, 12.68%.

Cyclic Voltammetry. An electrochemical cell similar to that reported in literature[23] was used and equipped with platinum wire of 0.5-mm diameter as working and auxiliary electrodes. A saturated calomel electrode (SCE) or an Ag/AgCl electrode was served as reference which was separated from a bulk electrolyte solution by a salt bridge prepared with 1,2:4,5-*O*-dibenzylidene-D-glucitol[24] and a DMF solution of TBAP (5.0×10^{-2} mol dm^{-3}); potentials vs. SCE are more cathodic by 30 mV relative to those vs. Ag/AgCl. DMF solutions containing the cobalt complex and TBAP were deaerated prior to each measurement, and the inside of the cell was maintained under argon atmosphere throughout each measurement. All the measurements were carried out at 20±2 °C, and the scan rate was varied in a range from 10 through 200 mV s^{-1}. Half-wave potentials ($E_{1/2}$) and anodic and cathodic currents were evaluated according to the method described previously.[25]

In order to identify the species formed at respective potentials, controlled-potential electrolyses were carried out under various conditions in a three-electrode cell modified for electronic and ESR spectral measurements, as described previously.[25] An applied potential between the working and reference electrodes was maintained constant with a potentiostat.

Catalytic Reactions. The electrolyses of various substrates were carried out upon addition of the cobalt complex in a cylindrical three-electrode cell which was divided into two internal compartments with a single sheet of microporous polypropylene membrane and equipped with platinum meshes as working and auxiliary electrodes.[13] On the other hand, an undivided cell was utilized to perform effective catalytic reactions without additives. A DMF solution of the cobalt complex, a substrate, an additive (if necessary), and TBAF was subjected to electrolysis at an appropriate controlled-potential under argon atmosphere. Then, the reaction mixture was distilled in vacuo and analyzed for products by means of GLC. Identification of the reaction products was performed by coinjection of the distilled sample and the corresponding authentic samples into columns of Silicone DC-550 and Silicone SE-30. A capillary column of Polyethylene Glycol-20M was used for identification of isomers having similar structures. Each product separated by preparative GLC on Silicone DC-550 was identified by means of ^1H NMR spectroscopy.

Results and Discussion

ESR spectra of [Co^{II}{(C_2C_3)(DO)(DOH)pn}$(H_2O)_2$]-$B(C_6H_5)_4$ in base-off and base-on forms are shown in Fig. 2 at 77 K. A typical ESR spectrum of low spin cobalt(II) was observed for the complex in chloroform without a base (A in Fig. 2). When pyridine was added in a two- to ten-fold molar excess over a quantity of the cobalt complex, only one pyridine molecule underwent coordination to the central cobalt at its axial site (B in Fig. 2): a superhyperfine structure due to the interaction between the nitrogen nucleus (I=1) and the cobalt nucleus (I=7/2) was observed in the $g_{\parallel}$ region. In the presence of a large excess of pyridine (ca. 600-fold),

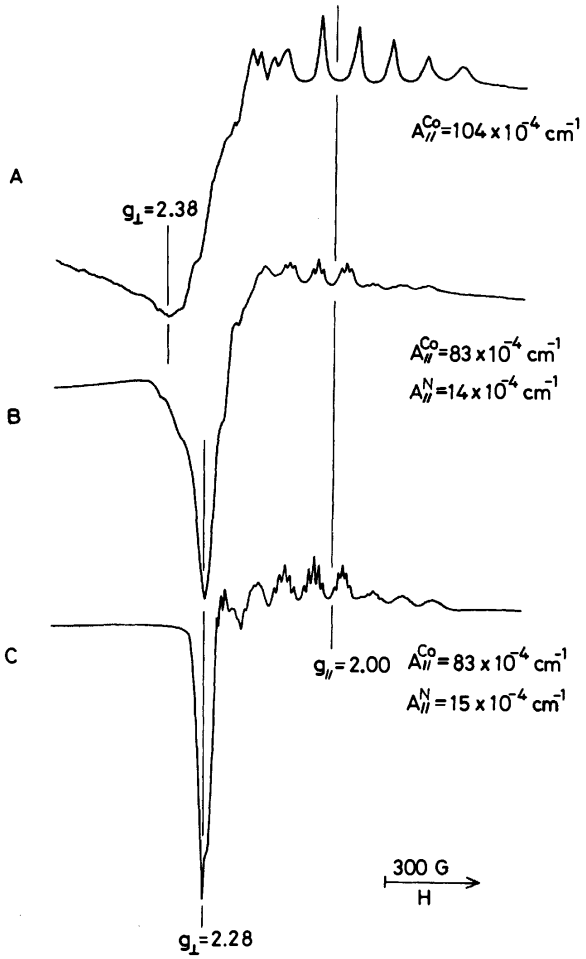

Fig. 2. ESR spectra of divalent cobalt complexes in chloroform at 77 K: A, [Co^{II}{(C_2C_3)(DO)(DOH)pn}-$(H_2O)_2$]$B(C_6H_5)_4$ (1.5×10^{-3} mol dm^{-3}); B, [Co^{II}{(C_2C_3)-(DO)(DOH)pn}$(H_2O)_2$]$B(C_6H_5)_4$ (1.7×10^{-2} mol dm^{-3}) and pyridine (1.8×10^{-1} mol dm^{-3}); C, [Co^{II}-{(C_2C_3)(DO)(DOH)pn}$(H_2O)_2$]$B(C_6H_5)_4$ (1.7×10^{-2} mol dm^{-3}) and pyridine (10 mol dm^{-3}).

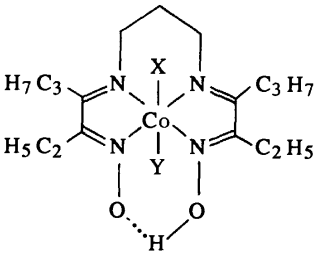

$[Co^{III}\{(C_2C_3)(DO)(DOH)pn\}Cl_2]$: X=Y=Cl

$[Co^{III}\{(C_2C_3)(DO)(DOH)pn\}Br_2]$: X=Y=Br

$[Co^{III}\{(C_2C_3)(DO)(DOH)pn\}I_2]$: X=Y=I

$[Co^{III}\{(C_2C_3)(DO)(DOH)pn\}(H_2O)_2]B(C_6H_5)_4$: X=Y=$H_2O$

$[Co^{III}\{(C_2C_3)(DO)(DOH)pn\}(CH_3)(H_2O)]ClO_4$: X=$CH_3$, Y=$H_2O$

$[Co^{III}\{(C_2C_3)(DO)(DOH)pn\}(CH_3)_2]$: X=Y=$CH_3$

$[Co^{III}\{(C_2C_3)(DO)(DOH)pn\}\{CH_2C(CO_2C_2H_5)_2CH_3\}Br]$:
X=$CH_2C(CO_2C_2H_5)_2CH_3$, Y=Br

$[Co^{III}\{(C_2C_3)(DO)(DOH)pn\}\{CH_2C(CO_2C_2H_5)(CN)CH_3\}Br]$:
X=$CH_2C(CO_2C_2H_5)(CN)CH_3$, Y=Br

$[Co^{III}\{(C_2C_3)(DO)(DOH)pn\}\{CH_2C(CO_2C_2H_5)_2CH_3\}_2]$:
X=Y=$CH_2C(CO_2C_2H_5)_2CH_3$

$[Co^{III}\{(C_2C_3)(DO)(DOH)pn\}\{CH_2C(CO_2C_2H_5)(CN)CH_3\}_2]$:
X=Y=$CH_2C(CO_2C_2H_5)(CN)CH_3$

both axial sites of the central cobalt were occupied by pyridine molecules as confirmed by ESR spectroscopy (C in Fig. 2). The present ESR behavior and the corresponding spin Hamiltonian parameters are comparable to those observed for the hydrophobic vitamin B_{12r} bearing a corrinoid ligand.[9]

Redox Behavior of Simple Vitamin B_{12} Model and Alkylated Derivatives. The redox behavior of the present complexes was investigated in DMF by means of cyclic voltammetry. A cyclic voltammogram of $[Co^{III}\{(C_2C_3)(DO)(DOH)pn\}I_2]$ is shown in Fig. 3. Three redox pairs were observed at −0.13, −0.70, and −1.45 V vs. Ag/AgCl in the range of 0 through −2.0 V vs. Ag/AgCl. The complex species responsible for these redox potentials were indentified by spectroscopic methods under controlled-potential electrolysis conditions as follows. The species present at +0.3 V vs. Ag/AgCl was ESR-silent, while ESR signals characteristic of Co(II) species were observed at −0.5 V vs. Ag/AgCl. Therefore, the redox potential at −0.13 V vs. Ag/AgCl is assigned to the Co(III)/Co(II) redox couple. The electrochemical reduction at −1.0 vs. Ag/AgCl was followed by electronic spectroscopy. An absorption maximum characteristic of the monomethylated complex was observed at 465 nm in the presence of methyl iodide; formation of the Co(I) species became evident at this potential. Consequently, the potential at −0.70 V vs. Ag/AgCl is assigned to the Co(II)/Co(I) redox couple. The potential at −1.45 V vs. Ag/AgCl is presumably concerned with the redox

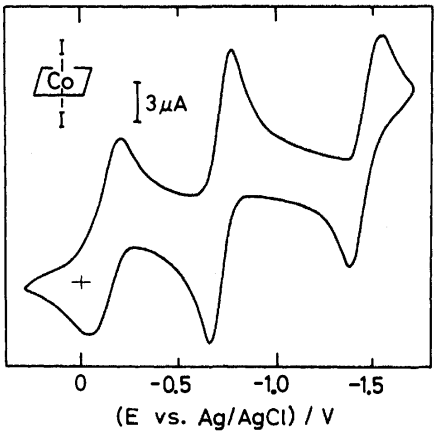

Fig. 3. Cyclic voltammogram of $[Co^{III}\{(C_2C_3)(DO)(DOH)pn\}I_2]$ (4.5×10^{-3} mol dm^{-3}) containing 0.10 mol dm^{-3} TBAP in DMF at 20±2 °C; scan rate, 100 mV s^{-1}.

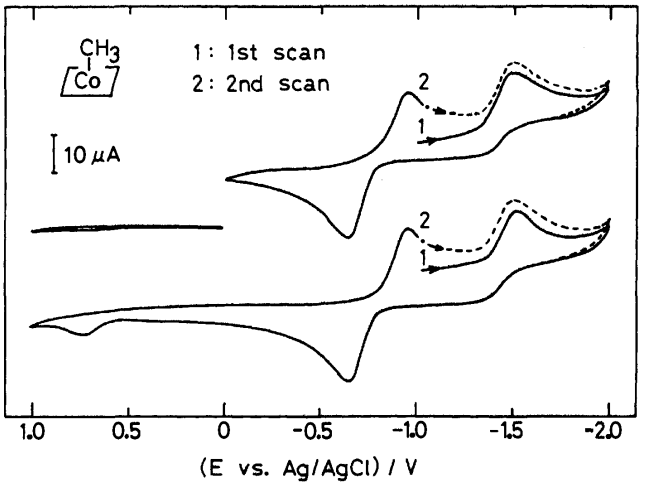

Fig. 4. Cyclic voltammogram of $[Co^{III}\{(C_2C_3)(DO)(DOH)pn\}(CH_3)(H_2O)]ClO_4$ (4.5×10^{-3} mol dm^{-3}) containing 0.10 mol dm^{-3} TBAP in DMF at 20±2 °C in the dark; scan rate, 100 mV s^{-1}.

reaction of the equatorial ligand. The complexes with the other halogen ligands, comparable redox potentials were observed: −0.16, −0.70, and −1.43 V vs. Ag/AgCl for $[Co^{III}\{(C_2C_3)(DO)(DOH)pn\}Br_2]$; −0.27, −0.69, and −1.46 V vs. Ag/AgCl for $[Co^{III}\{(C_2C_3)(DO)(DOH)pn\}Cl_2]$. As for $[Co^{II}\{(C_2C_3)(DO)(DOH)pn\}(H_2O)_2]B(C_6H_5)_4$, the reversible Co(II)/Co(I) redox couple was also observed at −0.69 V vs. Ag/AgCl. The above redox behavior is identical with that for the Costa's complex.[26,27] These Co(II)/Co(I) redox potentials are close to that observed for the hydrophobic vitamin B_{12};[10] −0.61 V vs. SCE in DMF. The Co(II)/Co(I) redox potential for cobaloxime, a vitamin B_{12} model frequently used, is observed by far in a more cathodic range relative to these values; −1.11 V vs. SCE in acetonitrile.[16]

The redox behavior of the mono- and dimethylated

cobalt complexes, $[Co^{III}\{(C_2C_3)(DO)(DOH)pn\}(CH_3)(H_2O)]ClO_4$ and $[Co^{III}\{(C_2C_3)(DO)(DOH)pn\}(CH_3)_2]$, respectively, was investigated in DMF.[28] The redox behavior of the Costa's complexes with the cobalt–carbon bond was studied in acetonitrile rather extensively.[16,29] As shown in Fig. 4 for $[Co^{III}\{(C_2C_3)(DO)(DOH)pn\}(CH_3)(H_2O)]ClO_4$, a single and irreversible one-electron reduction peak was observed at −1.50 V vs. Ag/AgCl during scanning for the potential range from −1.0 through −2.0 V vs. Ag/AgCl. In the course of scanning for the potential range from −1.0 V vs. Ag/AgCl toward the anodic side, there were observed two oxidation peaks; a reversible Co(I)/Co(II) oxidation peak at −0.65 V vs. Ag/AgCl and another irreversible and small oxidation peak at +0.73 V vs. Ag/AgCl, the latter originating from the one-electron oxidation of the dimethylated complex, $[Co^{III}\{(C_2C_3)(DO)(DOH)pn\}(CH_3)_2]$. The latter oxidation peak was not observed when the potential was scanned for the range from 0 through +1.0 V vs. Ag/AgCl.

After the controlled-potential electrolysis of $[Co^{III}\{(C_2C_3)(DO)(DOH)pn\}(CH_3)(H_2O)]ClO_4$ was completed at −2.0 V vs. Ag/AgCl under anaerobic conditions, the absorption maximum originally observed for $[Co^{III}\{(C_2C_3)(DO)(DOH)pn\}(CH_3)(H_2O)]ClO_4$ at 465 nm was shifted to 410 nm when the sample was exposed to air for elimination of the Co^{I} species; the latter band being due to $[Co^{III}\{(C_2C_3)(DO)(DOH)pn\}(CH_3)_2]$. This apparently indicates that the monomethylated complex is disproportionated to the dimethylated complex and the Co^{I} species by the electrochemical reduction (Eq. 1). When a large excess of imidazole was added, the

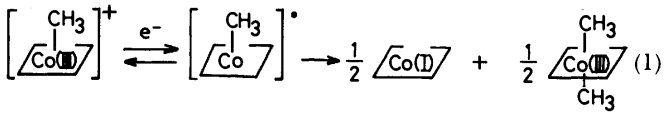

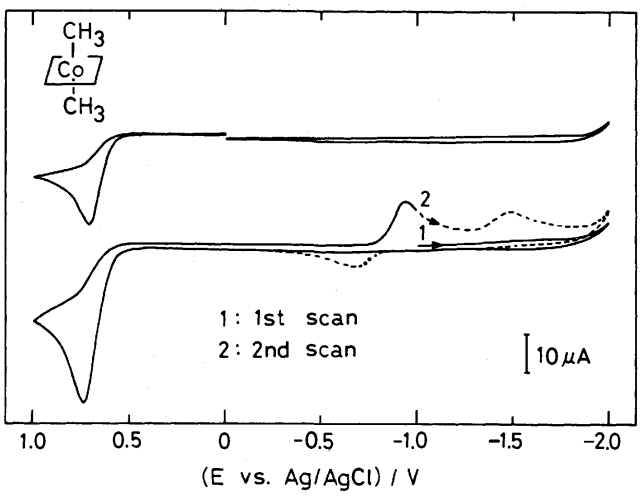

Fig. 5. Cyclic voltammogram of $[Co^{III}\{(C_2C_3)(DO)(DOH)pn\}(CH_3)_2]$ (4.5×10^{-3} mol dm^{-3}) containing 0.10 mol dm^{-3} TBAP in DMF at 20±2 °C in the dark; scan rate, 100 mV s^{-1}.

disproportionation reaction did not take place. This behavior is quite different from that observed for the corresponding hydrophobic vitamin B_{12}.[30] The one-electron reduction potential for the present monomethylated complex is close to those for the methylated hydrophobic vitamin B_{12} and methylcobinamide; −1.32 V vs. SCE in DMF[30] and −1.46 V vs. SCE in DMF–1-propanol (1:1 v/v),[31] respectively. On the other hand, the corresponding potential for methylcobaloxime is −2.2 V vs. SCE in acetonitrile at −26 °C,[16] which is by far in a more cathodic range relative to the value for vitamin B_{12} and must arise from the difference in ligand nature; the present and corrinoid ligands are monoanionic, while the cobaloxime ligand is dianionic.

The dimethylated complex is inactive for electrochemical reduction; no peak was observed in the potential range from 0 through −2.0 V vs. Ag/AgCl as shown in Fig. 5. An irreversible oxidation peak was observed at +0.73 V vs. Ag/AgCl. When the potential was sweeped repeatedly in the range of +1.0 through −2.0 V vs. Ag/AgCl, the redox behavior became similar to that of $[Co^{III}\{(C_2C_3)(DO)(DOH)pn\}(CH_3)(H_2O)]ClO_4$. These facts indicate that the dimethylated complex is cleaved to afford the monomethylated complex and the methyl radical by the electrochemical oxidation (Eq. 2).[29]

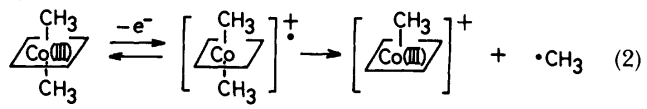

Catalytic Reactions under Electrochemical Conditions. On the basis of the above redox behavior, the catalytic function of $[Co^{III}\{(C_2C_3)(DO)(DOH)pn\}Br_2]$ was investigated by using 1-bromo-2,2-bis(ethoxycarbonyl)propane (**1**) as a substrate under electrochemical conditions (refer to Eq. 3).[32] The electrolysis was carried out in a

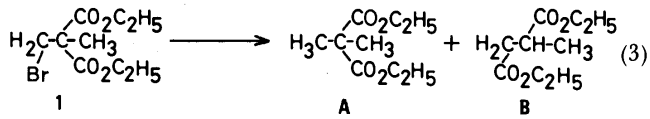

three-electrode cell, which was divided into two internal compartments with a diaphragm. The following findings were obtained on the basis of the product analyses under various conditions indicated in Table 1. (i) Products **A** and **B** were scarcely detected without imidazole at every potential in the range of −1.0 through −2.0 V vs. Ag/AgCl. (ii) The rearrangement product (**B**) was largely obtained at −1.5, −1.8, and −2.0 V vs. Ag/AgCl in the presence of imidazole. (iii) The rearrangement reaction proceeded more favorably under stronger reduction conditions. When other complexes, such as $[Co^{III}\{(C_2C_3)(DO)(DOH)pn\}Cl_2]$, $[Co^{III}\{(C_2C_3)(DO)(DOH)pn\}I_2]$, and

Table 1. Product Analyses for Controlled-Potential Electrolysis of **1** as Catalyzed by a Simple Vitamin B_{12} Model in the Divided Cell[a)]

Entry	Electrolysis conditions					Yield/%[e)]	
	Potential	Irradiation[b)]	Additive[c)]	Charge[d)]	Period	A	B
	V vs. Ag/AgCl			F mol^{-1}	h		
1	−1.0	Irradiation	Imidazole	0.6	26	ca. 2	Trace
2	−1.5	In the dark	None	0.5	24	Trace	Trace
3	−1.5	In the dark	Imidazole	2.0	14	16—20	18—26
4	−1.8	In the dark	None	0.5	24	1—2	Trace
5	−1.8	In the dark	Imidazole	2.0	10	35—40	40—47
6	−2.0	In the dark	None	2.0	7	7—11	1—2
7	−2.0	In the dark	Imidazole	2.0	6	20—25	55—61

a) Electrolysis was carried out in a two-compartment cell equipped with Pt electrodes at 20±2 °C under argon atmosphere. Starting solutions composed of: [Co^{III}\{(C_2C_3)(DO)(DOH)pn\}Br_2], 30 mg (5.5×10^{-5} mol); **1**, 1.0 g (3.8×10^{-3} mol); 30 mL of DMF containing 0.5 mol dm^{-3} TBAF. b) Irradiation with a 300-W tungsten lamp at a distance of 50 cm. c) Imidazole, 100 mg (1.5×10^{-3} mol). d) Electrical charge passed per mol of the substrate. e) Based on an initial amount of the substrate; the rest was the unreacted substrate; analyzed by GLC; refer to Eq. 3.

Table 2. Product Analyses for Controlled-Potential Electrolysis Catalyzed by a Simple Vitamin B_{12} Model in the Divided Cell[a)]

Substrate[b)]	Electrolysis conditions			Yield/%[d)]	
	Potential	Charge[c)]	Period	Unrearranged Product[e)]	Rearranged Product[f)]
	V vs. Ag/AgCl	F mol^{-1}	h		
2	−1.5	1.0	14	8—10	20—22
2	−2.0	2.1	8	12—14	74—76
3	−1.5	2.0	21	14—15	60—61
3	−2.0	2.0	6	3—4	85—90

a) Electrolysis was carried out in a two-compartment cell equipped with Pt electrodes at 20±2 °C under argon atmosphere. Starting solutions composed of: [Co^{III}\{(C_2C_3)(DO)(DOH)pn\}Br_2], 30 mg (5.5×10^{-5} mol); **2**, 1.0 g (4.5×10^{-3} mol) or **3**, 1.0 g (4.2×10^{-3} mol); imidazole, 100 mg (1.5×10^{-3} mol); 30 mL of DMF containing 0.5 mol dm^{-3} TBAF. b) Refer to Eqs. 4 and 5. c) Electrical charge passed per mol of the substrate. d) Based on an initial amount of the substrate; the rest was the unreacted substrate; analyzed by GLC; refer to Eqs. 4 and 5. e) Unrearranged products were **C** and **F** for substrates **2** and **3**, respectively. f) Rearrangement products were **D** and **E** for **2**, and **G** and **H** for **3**, respectively.

[Co^{II}\{(C_2C_3)(DO)(DOH)pn\}$(H_2O)_2$]$B(C_6H_5)_4$, were used as the catalysts, similar results were obtained.

In order to make further qualification of the simple vitamin B_{12} model as the isomerization catalyst, other substrates, such as 1-bromo-2-cyano-2-ethoxycarbonylpropane (**2**) and 2-acetyl-1-bromo-2-ethoxycarbonylpropane (**3**), were also used here. These substrates and the corresponding products are shown in Eqs. 4 and 5, and the product analysis data are shown in Table 2. The 1,2-migration of carboxylic ester, acetyl, and cyano groups proceeds efficiently under these experimental conditions.

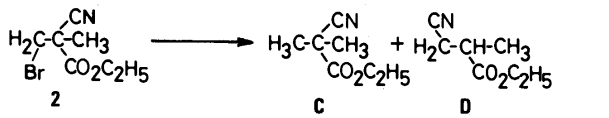

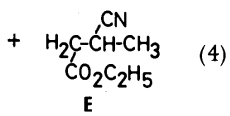

(4)

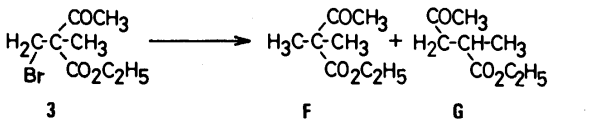

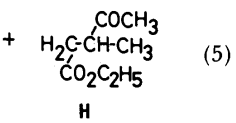

(5)

On careful comparison between the electrochemical carbon-skeleton rearrangement reactions catalyzed by the present simple vitamin B_{12} model and the hydrophobic vitamin B_{12},[33)] some differences are noted between these complexes in their catalytic performance. (i) The hydrophobic vitamin B_{12} does not require an organic base for the catalytic reaction, while a base such as imidazole is essential to the reaction catalyzed by the present complex. Imidazole must be bound to the nuclear cobalt of the alkylated vitamin B_{12} model, so that the cobalt-carbon bond is effectively activated by the trans effect arising from the coordinated axial base. The axial ligation constant (K) of imidazole to the monomethylated cobalt complex is fairly large; $\log K=2.67$ in DMF by means of the spectroscopic

method.[9] When imidazole is not present, the corresponding dialkylated complex, that is inactive for electrochemical reduction, is formed in the course of reaction, and consequently the catalytic reaction does not take place to a detectable extent. (ii) The hydrophobic vitamin B_{12} requires a proton source for the formation of product **B** during the electolysis at −1.5 V vs. Ag/AgCl, while the present model complex affords the products in a significant yield without such an additive under the comparable conditions. The reaction scheme in the divided cell is schematically illustrated in Fig. 6.

In the light of the redox behavior of the dimethylated complex, $[Co^{III}\{(C_2C_3)(DO)(DOH)pn\}(CH_3)_2]$, the dialkylated complex is expected to give products, plausibly involving the corresponding isomerization product, by electrochemical oxidation. Therefore, we removed the diaphragm from the divided cell and the electrolysis was carried out in a single-compartment cell under argon atmosphere. Substrates **1**, **2**, and **3** were subjected to electrolysis at −2.0 V vs. Ag/AgCl of the cathode in presence of the cobalt complex in the dark. The products were analyzed by means of GLC, as summarized in Table 3. These results indicate that the rearrangement reactions proceed efficiently in the undivided cell. Under such reaction conditions, the monoalkylated complex and the corresponding dialkylated complexes were formed in a stepwise manner as the intermediates. Reduction of the former complex and oxidation of the latter species must proceed at the cathode and the anode, respectively. In order to clarify the reaction process, the electrolyses of the monoalkylated and dialkylated complexes were carried out at −2.0 V and +1.0 V vs. Ag/AgCl, respectively, in the divided cell.

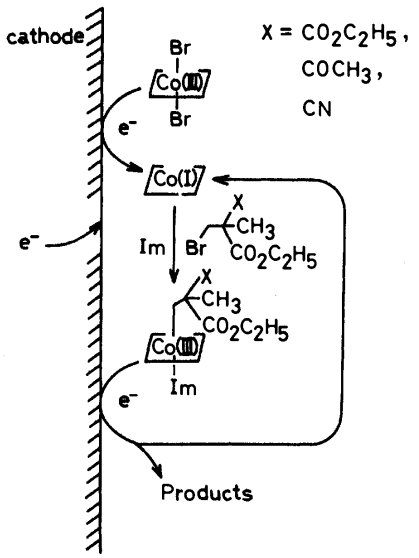

Fig. 6. Schematic representation of electrochemical catalysis in the divided cell.

A DMF solution (15 mL) of $[Co^{III}\{(C_2C_3)(DO)(DOH)pn\}\{CH_2C(CO_2C_2H_5)_2CH_3\}Br]$ (200 mg, 3.1×10^{-4} mol) and TBAF (2.0 g) was subjected to electrolysis at −2.0 V vs. SCE in the dark for 8 h. The monoalkylated complex was largely converted into the corresponding dialkylated complex as identified by electronic spectroscopy (Eq. 6), even though trace

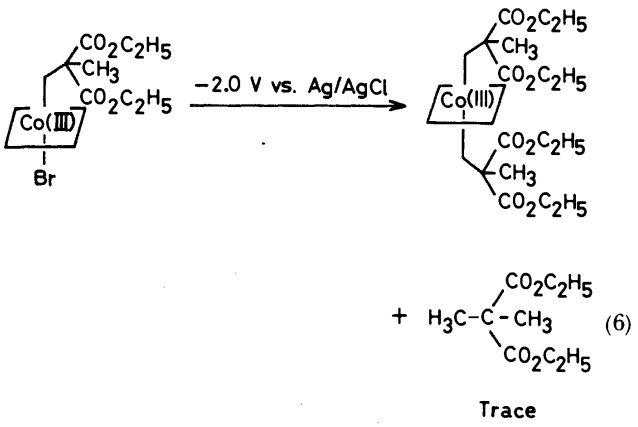

(6)

amounts of the reduction and rearrangement products were detected by GLC. When $[Co^{III}\{(C_2C_3)(DO)(DOH)pn\}\{CH_2C(CO_2C_2H_5)_2CH_3\}Br]$ was electrolyzed at +1.0 V vs. SCE, the reaction did not proceed to a

Table 3. Product Analyses for Controlled-Potential Electrolysis at −2.0 V vs. Ag/AgCl Catalyzed by a Simple Vitamin B_{12} Model in the Undivided Cell[a]

Substrate[b]	Electrolysis conditions		Yield/%[d]	
	Charge[c]	Period	Unrearranged product[e]	Rearranged product(s)[f]
	F mol^{-1}	h		
1	1.7	10	18—20	53—55
2	1.9	8	10—12	58—60
3	1.9	7	3—4	83—85

a) Electrolysis was carried out in the undivided cell equipped with Pt electrodes at 20±2 °C under argon atmosphere. Starting solutions composed of: $[Co^{III}\{(C_2C_3)(DO)(DOH)pn\}Br_2]$, 14 mg ($2.6\times10^{-5}$ mol); **1**, 1.0 g (3.8×10^{-3} mol), **2**, 1.0 g (4.5×10^{-3} mol), or **3**, 1.0 g (4.2×10^{-3} mol); 30 mL of DMF containing 0.5 mol dm^{-3} TBAF. b) Refer to Eqs. 3, 4, and 5. c) Electrical charge passed per mol of the substrate. d) Based on an initial amount of the substrate; the rest was the unreacted substrate; analyzed by GLC; refer to Eqs. 3, 4, and 5. e) Unrearranged products were **A**, **C**, and **F** for substrates **1**, **2**, and **3**, respectively. f) Rearrangement products: **B** for **1**, **D** and **E** for **2**, and **G** and **H** for **3**.

detectable extent as confirmed by electronic spectroscopy and GLC (Eq. 7). A small amount of the product

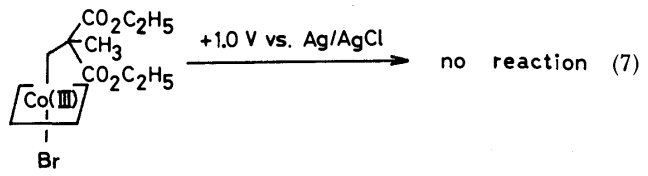

(7)

derived from the cleavage of the cobalt–carbon bond was detected in the electrolysis of $[Co^{III}\{(C_2C_3)(DO)(DOH)pn\}\{CH_2C(CO_2C_2H_5)_2CH_3\}_2]$ (200 mg, 2.6×10^{-4} mol) at −2.0 V vs. Ag/AgCl under the identical conditions. However, the rearrangement product was little obtained under such conditions (Eq. 8). On the

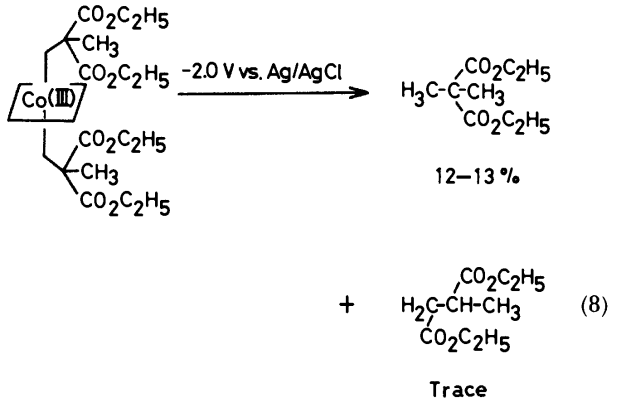

(8)

other hand, when the electrolysis was carried out at +1.0 V vs. Ag/AgCl for 6 h, the dialkylated complex was transformed into the monoalkylated one, and the rearrangement product was detected as the major one (Eq. 9).

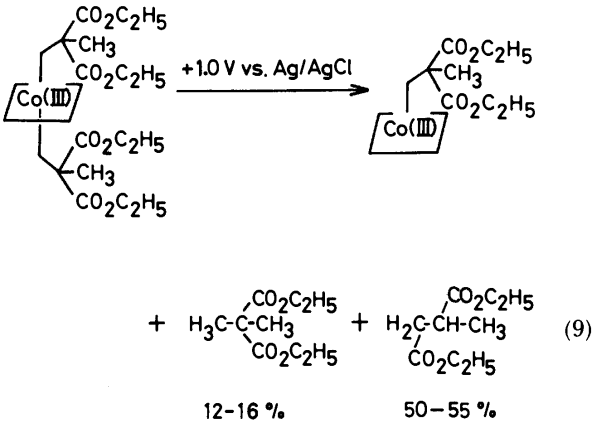

(9)

In the light of the above results, the electrolysis in the undivided cell plausibly proceeds via the reaction cycle shown in Fig. 7. The tervalent cobalt complex is first converted into the univalent cobalt complex by the electrochemical reduction, and the resulting species is subjected to the electrophilic attack by an alkyl bromide to afford the corresponding monoalkylated complex as the intermediate. This species is subsequently reduced to the one-electron reduction intermediate, which is then disproportionated to the dialkylated complex and the univalent cobalt species. The dialkylated complex is decomposed to give the monoalkylated complex and the products by the electrochemical oxidation on the anode.

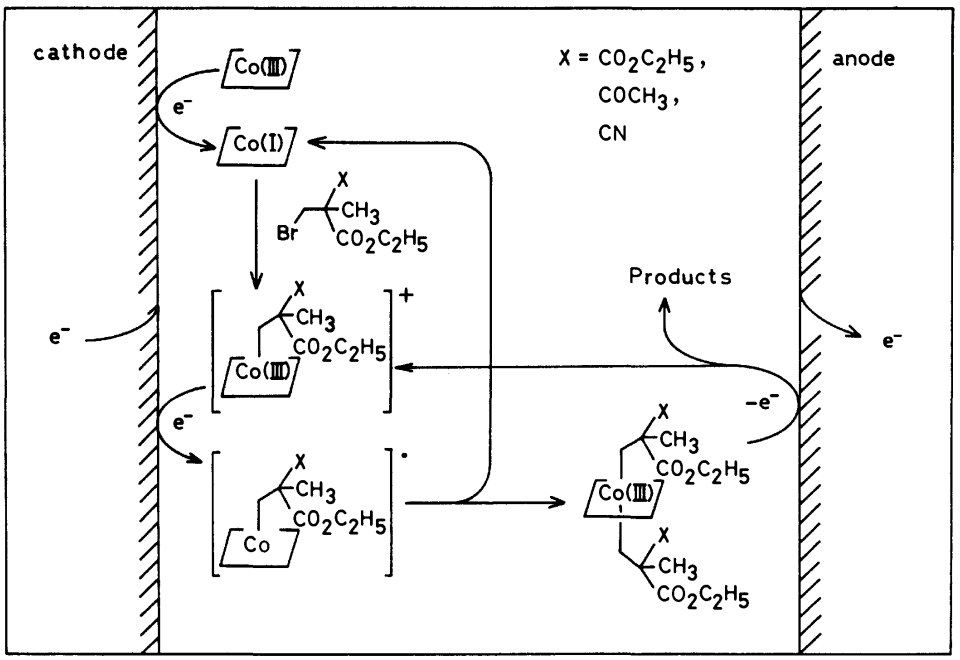

Fig. 7. Schematic representation of electrochemical catalysis in the undivided cell.

Conclusion

We clarified in the present work redox behavior of the simple vitamin B_{12} model as well as that of its alkylated derivatives in connection with the catalytic reactions of the vitamin B_{12} model under electrochemical conditions. A major difference between the simple vitamin B_{12} model complex and the hydrophobic vitamin B_{12} is in alkylation behavior; a dialkylated complex is obtained with the former species. The hydrophobic vitamin B_{12} does not form its dialkylated complex, since the steric hindrance is exercised by the methyl moiety at C(19) position of the corrin ring when an alkyl moiety attacks the nuclear cobalt from the α-face. The simple vitamin B_{12} model does not form its dialkylated complex when an axial base such as imidazole is added to the reaction media, and the electrochemical catalysis proceeds via a mechanism similar to that for the hydrophobic vitamin B_{12}. It became apparent that the coupled electrochemical redox processes facilitate the carbon-skeleton rearrangement via formation of the dialkylated complex as the oxidizable intermediate in the absence of an axial base.

The present work was supported by a Grant-in-Aid for Scientific Research on Priority Area of "Dynamic Interactions and Electronic Processes of Macromolecular Complexes" from the Ministry of Education, Science, and Culture (No. 63612004).

References

1) J. M. Pratt, "Coordination Chemistry of the B_{12} Dependent Isomerase Reactions," in "B_{12}," ed by D. Dolphin, John Wiley, New York (1982), Vol. 1, pp. 325—392.

2) B. T. Golding and D. N. Rao, "Adenosylcobalamin-dependent Enzymic Reactions," in "Enzyme Mechanisms," ed by M. I. Page and A. Williams, The Royal Society of Chemistry, London (1987), pp. 404—428.

3) J. Halpern, "Chemistry and Significance of Vitamin B_{12} Model Systems," in "B_{12}," ed by D. Dolphin, John Wiley, New York (1982), Vol. 1, pp. 501—542.

4) R. Scheffold, G. Rytz, and L. Walder, "Vitamin B_{12} and Related Co-Complexes as Catalysts in Organic Synthesis," in "Modern Synthetic Methods," ed by R. Scheffold, John Wiley, New York (1983), Vol. 1, pp. 355—440.

5) C. B. Zieglar, Jr. and A. Fischli, *Helv. Chim. Acta*, **68**, 181 (1985).

6) D. Lexa and J. M. Savéant, *Acc. Chem. Res.*, **16**, 235 (1983).

7) K. A. Rubinson, H. V. Parekh, E. Itabashi, and H. B. Mark, Jr., *Inorg. Chem.*, **22**, 458 (1983).

8) G. Costa, A. Puxeddu, and C. Tavagnacco, *J. Organomet. Chem.*, **296**, 161 (1985).

9) Y. Murakami, Y. Hisaeda, and A. Kajihara, *Bull. Chem. Soc. Jpn.*, **56**, 3642 (1983).

10) Y. Murakami, Y. Hisaeda, A. Kajihara, and T. Ohno, *Bull. Chem. Soc. Jpn.*, **57**, 405 (1984).

11) Y. Murakami, Y. Hisaeda, and T. Ohno, *Bull. Chem. Soc. Jpn.*, **57**, 2091 (1984).

12) Y. Murakami and Y. Hisaeda, *Bull. Chem. Soc. Jpn.*, **58**, 2652 (1985).

13) Y. Murakami, Y. Hisaeda, T. Ozaki, T. Tashiro, T. Ohno, Y. Tani, and Y. Matsuda, *Bull. Chem. Soc. Jpn.*, **60**, 311 (1987).

14) Y. Murakami, Y. Hisaeda, J. Kikuchi, T. Ohno, M. Suzuki, Y. Matsuda, and T. Matsuura, *J. Chem. Soc., Perkin Trans. 2*, **1988**, 1237.

15) G. Costa, *Coord. Chem. Rev.*, **8**, 63 (1972).

16) C. M. Elliott, H. Hershenhart, R. G. Finke, and B. L. Smith, *J. Am. Chem. Soc.*, **103**, 5558 (1981).

17) J. A. Riddick and W. B. Bunger, "Organic Solvents," Wiley-Interscience, New York (1970), p. 836.

18) H. O. House, E. Feng, and N. P. Peet, *J. Org. Chem.*, **36**, 2371 (1971).

19) G. Costa, G. Mestroni, and E. de Savorgnani, *Inorg. Chim. Acta*, **3**, 323 (1969).

20) G. Costa, G. Mestroni, G. Pellizer, G. Tauzher, and T. Licari, *Inorg. Nucl. Chem. Lett.*, **5**, 515 (1969).

21) G. Costa, G. Mestroni, and G. Tauzher, *J. Chem. Soc., Dalton Trans.*, **1972**, 450.

22) A. F. Ferris, *J. Org. Chem.*, **24**, 1726 (1959).

23) R. P. V. Duyne and C. N. Reilley, *Anal. Chem.*, **44**, 142 (1972).

24) F. Endo, *Yakugaku Zasshi*, **79**, 595 (1959).

25) Y. Matsuda, S. Yamada, and Y. Murakami, *Inorg. Chem.*, **20**, 2239 (1981).

26) G. Costa, A. Puxeddu, and E. Reisenhofer, *J. Chem. Soc., Dalton Trans.*, **1972**, 1519.

27) R. G. Finke, B. L. Smith, and M. W. Droege, C. M. Elliott, and E. Hershenhart, *J. Organomet. Chem.*, **202**, C25 (1980).

28) Y. Murakami, Y. Hisaeda, S.-D Fan, and Y. Matsuda, *Chem. Lett.*, **1988**, 835.

29) W. H. Tamblyn, R. J. Klingler, W. S. Hwang, and J. K. Kochi, *J. Am. Chem. Soc.*, **103**, 3161 (1981).

30) Y. Murakami, Y. Hisaeda, T. Tashiro, and Y. Matsuda, *Chem. Lett.*, **1985**, 1813.

31) D. Lexa and J. M. Savéant, *J. Am. Chem. Soc.*, **100**, 3220 (1978).

32) Y. Murakami, Y. Hisaeda, and S.-D Fan, *Chem. Lett.*, **1987**, 655.

33) Y. Murakami, Y. Hisaeda, T. Tashiro, and Y. Matsuda, *Chem. Lett.*, **1986**, 555.

Substituent Effect on the Enantiomer-Differentiating Reaction of Lithiomethyl *p*-Tolyl Sulfoxide with Meta- or Para-Substituted (*R*)-(−)-Menthyl Benzoates

Norio KUNIEDA,* Takeshi NAKANISHI, and Masayoshi KINOSHITA
Department of Applied Chemistry, Faculty of Engineering, Osaka City University, Sumiyoshi-ku, Osaka 558
(Received February 18, 1989)

Treatment of (*R*)-(−)-menthyl benzoates, which have a variety of meta- or para-substituents, with 2 equivalents of racemic lithiomethyl *p*-tolyl sulfoxide displays the feature of an enantiomer-differentiating reaction, affording the corresponding optically active β-keto sulfoxides. The degree and the direction of enantioselectivity were affected by the nature of the substituent on benzene ring. The electron-releasing substituents trend to increase the %e.e. value. The reversal in the configuration with the variation in the substituent which has a high electron-withdrawing *p*-CN group was also observed. The *R*/*S* values thus obtained gave a good correlation with Hammett's σ values (r=0.975), affording a negative straight line. Based on these observations, a plausible stereochemical course of this reaction has been discussed.

Electronic effects, in addition to steric bulk, have been evaluated experimentally and theoretically as one of the important factor which controls the direction and the extent of the asymmetric induction in certain asymmetric reactions.[1] On the basis of this concept, the investigation of the substituent effect in asymmetric reactions is considered to afford considerably quantitative informations which may help to clarify the stereochemical course of asymmetric reactions. However, up to now, only a few attentions have been focused on this problem.[2]

During the course of our research concerned with the asymmetric induction by chiral sulfinyl group,[3] we have now found that the reaction of lithiomethyl *p*-tolyl sulfoxide, derived from racemic methyl *p*-tolyl sulfoxide and lithium diethylamide, with a limited amount of substituted (*R*)-(−)-menthyl benzoates displays the feature of an enantiomer-differentiating reaction, affording the corresponding optically active β-keto sulfoxides, and the degree of enantioselectivity of this reaction is markedly affected by the nature of the substituent on benzene ring of the chiral benzoates. In this report, we compile substantial amounts of stereochemical data of the enantiomer-differentiating reaction of racemic α-lithiomethyl *p*-tolyl sulfoxide with (*R*)-(−)-menthyl benzoates possessing a variety of meta- or para-substituents and hence would like to discuss the role of the polar effect of the substituents on the enantioselectivity, as an effort to obtain detailed knowledge for the stereochemistry of this reaction.

Results and Discussion

The reaction of racemic lithiomethyl *p*-tolyl sulfoxide (**1**) with meta- or para-substituted (*R*)-(−)-menthyl benzoates (**2**) was carried out according to a procedure similar to that devised for the reaction of α-lithio sulfoxides with chiral sulfinates or chiral carboxylates described in our previous papers.[3c,f,g] When 2 equivalents of **1**, derived from racemic methyl *p*-tolyl sulfoxide and lithium diethylamide, was allowed to react with **2** in tetrahydrofuran (THF) at −78 °C, the corresponding optically active β-keto sulfoxide (**3**) was produced in a good yield (>92%), together with optically active methyl *p*-tolyl sulfoxide which has the opposite configuration to **3** (Eq. 1). The degree of

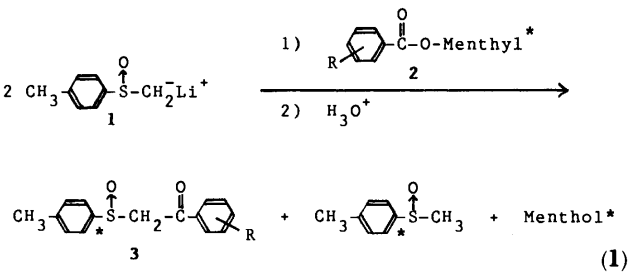

(1)

(The star indicates chiral center.)

2 and **3**
a: R=*p*-CH_3O, **b**: R=*p*-*t*-C_4H_9, **c**: R=*p*-CH_3,
d: R=*p*-*i*-C_3H_7, **e**: R=*m*-CH_3, **f**: R=H,
g: R=*p*-Cl, **h**: R=*m*-Cl, **i**: R=*p*-CN.

enantioselectivity of the reaction was estimated by determining the per cent enantiomeric excess (%e.e.) of **3** obtained. That is, the resulting **3** was isolated by a preparative thin-layer chromatography on silica gel and their predominant configuration and the %e.e. value were assigned by direct comparison with the specific rotation of the corresponding authentic (*R*)-(+)-**3**. The authentic (*R*)-(+)-**3** used here was synthesized by the reaction of lithiomethyl *p*-tolyl sulfoxide, derived from optically pure (*R*)-(+)-methyl *p*-tolyl sulfoxide, with the corresponding ethyl benzoates.[3g] Table 1 summarizes the results for the reactions of **1** with nine (*R*)-(−)-menthyl benzoates (**2a—i**) possessing a variety of meta- or para-substituents.

The enantioselectivity of this reaction was sensitive to reaction temperature. The decrease in temperature favored the formation of the predominant enantiomer. The diagram correlating log *R*/*S* against 1/*T* showed

Table 1. Results of the Enantiomer-Differentiating Reaction of α-Lithiomethyl *p*-Tolyl Sulfoxide (**1**) with Chiral Benzoates (**2**)[a]

Benzoates (**2**) R	β-Keto sulfoxides (**3**) $[\alpha]_D^{25}$[b]	$[\alpha]_D^{25}$[c]	%e.e.	*R*/*S*	ΔΔG* J mol^{-1}	ΔΔ*H** kJ mol^{-1}	ΔΔ*S** J K^{-1} mol^{-1}
p-CH_3O (**2a**)	**3a** +62.2±2.2°(3)[d]	+253°	24.6	1.65	815		
p-*t*-C_4H_9 (**2b**)	**3b** +53.0±2.2°(2)	+240°	22.1	1.57	729		
p-CH_3 (**2c**)	**3c** +43.8±0.9°(4)	+259°	16.9	1.41	553	−0.70	−0.78
p-*i*-C_3H_7 (**2d**)	**3d** +45.2±3.6°(3)	+248°	18.2	1.45	597		
m-CH_3 (**2e**)	**3e** +37.1±2.1°(3)	+253°	14.7	1.35	480		
H (**2f**)	**3f** +35.5±2.3°(7)	+265.5°	13.4	1.31	438	−0.58	−0.75
p-Cl (**2g**)	**3g** +24.7±3.9°(4)	+269°	9.2	1.20	300	−0.40	−0.43
m-Cl (**2h**)	**3h** +9.7±2.3°(4)	+260°	3.7	1.08	120		
p-CN (**2i**)	**3i** −5.0±0.5°(3)	+315°	1.6	1.03[e]	52		

a) In THF, at −78°C. b) In acetone. c) Specific rotations of the authentic (*R*)-(+)-β-keto sulfoxides (in acetone). d) Average values of 2—7 experiments. The number of experiments is shown in parentheses. e) *S*/*R*.

a linear positive slope over 103° temperature range (from 25 °C to −78 °C). The $\Delta\Delta H^*$ and $\Delta\Delta S^*$ values obtained in the reactions for **2c**, **2f**, and **2g** are listed in Table 1. These exhibited small negative values.

Table 1 clearly reveals that the %e.e. value for **3** obtained markedly affected by the nature of the substituent R. The degree of enantioselectivity varies from 1.6% to 24.6%. As gererally observed, the electron-releasing substituents trend to increase the %e.e. value. The best result has been obtained from the reaction of **1** with **2a** (R=*p*-CH_3O), affording (*R*)-(−)-**3a** of a 24.6% optical purity. Furthermore, the reversal in the configuration with the variation in the substituent R is also observed. Namely, the (*R*)-(−)-menthyl benzoates **2a**, **2b**, **2c**, **2d**, **2e**, **2f**, **2g**, and **2h** preferentially reacted with (*R*)-**1** to yield an excess of (*R*)-**3a—h**, while the ester **2i** which has a high electron-withdrawing *p*-CN group preferentially reacted with (*S*)-**1**, affording (*S*)-**3i** in excess.

When the logarithms of the *R*/*S* values thus obtained were plotted against Hammett's σ values,[4] as shown in Fig. 1, a negative straight line was obtained with the correlation coefficient r=0.975. In our previous paper,[3g] we have reported that the reaction of aryl lithiomethyl sulfoxides with (*R*)-(−)-menthyl carboxylates (R'-CO-O-Menthyl) is affected drastically by a steric bulk of the ester moiety R'. However, in the present reaction the demand for the steric effect owing to the substituent R on benzene ring was found to be negligibly small, even where R was bulky *t*-butyl group. Therefore, it can be recognized that the enantioselectivity on the reaction of **1** with **2** should be dependent on the polar effect of the substituent R.

Next the kinetic experiment was conducted on the rate of the reactions using **2a** (R=*p*-CH_3O), **2c** (R=*p*-CH_3), **2f** (R=H), and **2g** (R=*p*-Cl) in THF at −78 °C. The rate was measured by checking the consumption of the starting **1** by means of ^{1}H NMR (see Experimental). The resulting second order rate constants are listed in Table 2, and are found to be in a good correlation with Hammett's σ values[4] with a large positive σ value of +3.40 (r=0.999). The electron-withdrawing substituent on benzene ring of **2** increases the rate of the reaction. It reveals that the degree of enantioselectivity of the reaction decreases with increasing the reaction rate. This σ correlation and the magnitude of the ρ value of the kinetic data also suggest well that the reaction of **1** with **2** takes place through the B_{AC}-2 type mechanism[5] like in the case of the saponification of (−)-menthyl benzoates (ρ=2.628, at 30 °C).[6]

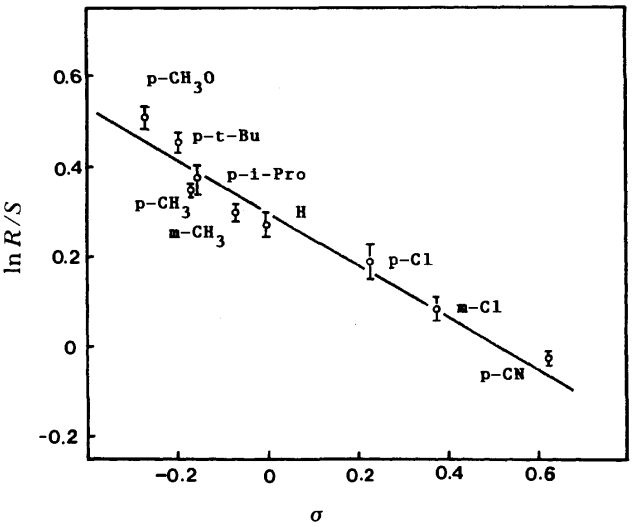

Fig. 1. ln *R*/*S* values of **3** obtained plotted against σ-values.

Table 2. Rate Constants of the Reaction of **1** with Chiral Benzoates (**2**)[a]

Benzoates (**2**) R	k_2 l mol^{-1} s^{-1}
p-CH_3O (**2a**)	4.75±0.55×10^{-4}
p-CH_3 (**2c**)	1.19±0.03×10^{-3}
H (**2f**)	3.67±0.19×10^{-3}
p-Cl (**2g**)	2.45±0.13×10^{-2}

a) In THF, at −78°C (see Experimental).

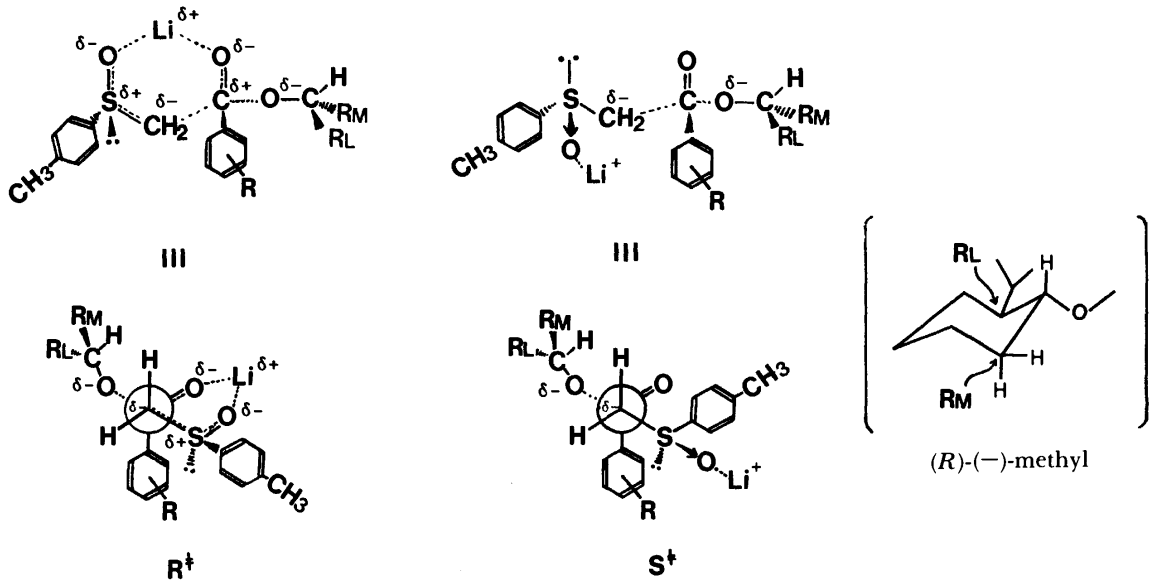

(The symbols R_M and R_L indicate medium and large groups respectively.)

Scheme 1.

As one of the current of stereochemical studies on the electrophilic substitutions of α-lithio sulfoxides, Marquet et al.[7] and Biellmann et al.[8] have proposed that an electrophilic assistance (a chelation) by the lithium cation on the α-lithio sulfoxides towards the electrophiles plays an important role. On the basis of this evidence together with the B_{AC}-2 mechanism and the prefered configuration for the (*R*)-(−)-menthyl carboxylates,[9] we have proposed[3g] that the reaction of aryl lithiomethyl sulfoxides with (*R*)-(−)-menthyl carboxylates proceeds via a six-membered cyclic transition state.[3b,10] Acoording to this prediction, as well as the steric requirements,[12] the reaction of (*R*)-(−)-menthyl benzoates (**2**) with (*R*)-**1** affording (*R*)-**3** takes a transition state **R*** in Scheme 1 preferentially. Most of the results for the direction of enantioselectivity of this reaction agree fairly well with this prediction. However contrary to our expections, the reaction **2i** with **1** afforded (*S*)-**3i** as described above. The change of the degree of enantioselectivity owing to the substituent R on benzene ring and the reversal in configuration from (*R*) to (*S*) in going from **3h** to **3i** may be attributed to the conformational change of the transition state. The two alternative transition states **R*** and **S*** in Scheme 1 may be postulated according to the polar character of the substituent R. There are differences between the two routes in the degree of bonding of both entering and leaving groups on carbonyl carbon atom at the transition state. Actually, it has been reported that the transition-state geometry is affected by the change of substituents.[13]

The reaction of **1** with (*R*)-(−)-menthyl benzoates which have the electron-releasing substituent proceed through the transition state **R*** which exhibits the formation of tight chelation by lithium cation, since the electron-releasing substituent on benzene ring of **2** should contribute to the formation of a rigid transition state. While (*R*)-(−)-menthyl benzoates which have the electron-withdrawing substituent such as *p*-CN show high reactivity toward **1**, and proceed preferentially through the formation of a loose transition state **S*** which does not participate in the chelate formation by lithium cation. This transition state is less sterically hindered than **R***. Incidentally, the lithium cation in the transition state **S*** is perhaps located at the sulfinyl oxigen, since it has been known that the lithiomethyl phenyl sulfoxide is stabilized by an internal chelation between the metalated carbon and the sulfinyl oxygen.[7]

Table 3. Results of the Reactions of **1** with **2f** and **2i** in the Presence of a Lithium Cation Trapping Agent[a]

Benzoates (**2**)		%e.e. of **3f** and **3i**	
		None	Kryptofix 211[b]
2f	**3f**	13.4(R)[c]	3.8(R)
2i	**3i**	1.6(S)	4.3(S)

a) In THF, at −78°C. b) 1.1 Equivalents based on **1**. c) Predominant configuration.

That is, a gradual change of the transition state from **R*** to **S*** with the increase of the electron-withdrawing character of the substituent R is posturated. In order to get a clue of this, the reactions of **1** with **2f** and **2i** were carried out in the presence of 4,7,13,18-tetraoxa-1,10-diazabicyclo[8.5.5]eicosane (Kryptofix 211)[14] as a trapping agent of the lithium cation. The results are listed in Table 3. To cite the result, the addition of 1.1 equivalents of Kryptofix 211 to the reaction of **1** with **2f** decreases the %e.e. value of (*R*)-**3f** about 3.5 times.

While the addition of 1.1 equivalents of Kryptofix 211 to the reaction of **1** with **2i** increases the %e.e. value of (*S*)-**3i** about 2.7 times.

Inspection of these data indicates that the transition state of the reaction of **1** with (*R*)-(−)-menthyl benzoates (**2**) markedly affected by the nature of the substituent R on benzene ring. We have now considered that the apparent difference in the mode of the transition states between **R*** and **S*** arises from the polar effect exerted by the substituent R.

Experimental

General. The optical rotations were measured with a Jasco DIP-360 type polarimeter. The ^{1}H NMR spectra were determined by using Jeol PS-100 spectrometer; the chemical shifts are reported in δ units, using tetramethylsilane as the internal reference. All the melting points were obtained with a Yanaco MP apparatus and are uncorrected. The IR spectra were taken on a Jasco A-202 type spectrometer.

Starting Materials. Racemic methyl *p*-tolyl sulfoxide was prepared by the periodate oxidation of methyl *p*-tolyl sulfide;[15] bp 99—100 °C/1.5 Torr (1 Torr=133.322 Pa), mp 43 °C (lit,[16] 42—43 °C). (*R*)-(+)-Methyl *p*-tolyl sulfoxide was prepared from (−)-menthyl (*S*)-*p*-toluenesulfinate, mp 107—107.5 °C, $[\alpha]_D^{25}$ −200° (*c* 0.520, acetone), and methylmagnesium iodide according to the method developed by Andersen;[17] mp 74.5 °C, $[\alpha]_D^{20}$ +146° (*c* 0.460, acetone)[lit,[18] mp 73—74.5 °C, $[\alpha]_D$ +145.5° (acetone)]. (−)-Menthol of commercial grade (Hoei Chemicals, Osaka) was used without further purification. (*R*)-(−)-Menthyl benzoates (**2**) were prepared by treating (−)-menthol with the corresponding substituted benzoic acid chlorides in dry ether in the presence of pyridine. $C_{10}H_{19}$-O-CO-C_6H_4-R; [R, mp or bp, specific rotation (*c*, solvent)], *p*-CH_3O (**2a**); 160—161 °C/1 Torr (lit,[19] 229—230 °C/15 Torr), $[\alpha]_D^{20}$ −79.2° (0.671, C_2H_5OH) (lit,[19] $[\alpha]_D^{20}$ −86.5° (neat)), *p*-*t*-C_4H_9 (**2b**); 171—172 °C/1 Torr, $[\alpha]_D^{20}$ −71.1° (1.56, C_2H_5OH), *p*-CH_3 (**2c**); 138—139 °C/1 Torr (lit,[19] 196—198 °C/11 Torr), $[\alpha]_D^{22}$ −85.3° (1.26, C_2H_5OH) (lit,[19] $[\alpha]_D^{20}$ −89.9° (neat)), *p*-*i*-C_3H_7 (**2d**), 166 °C/1—2 Torr, $[\alpha]_D^{20}$ −75.7° (1.37, C_2H_5OH), *m*-CH_3 (**2e**); 140 °C/2 Torr (lit,[6] 109—110 °C/0.1—0.2 Torr), $[\alpha]_D^{20}$ −85.9° (1.18, C_2H_5OH), $[\alpha]_D^{20}$ −89.6° (1.28, C_6H_5) (lit,[20] $[\alpha]_D$ −88.5° (C_6H_5)), H (**2f**); 54.5 °C (lit,[21] 55 °C), $[\alpha]_D^{20}$ −90.5° (1.53, C_2H_5OH) (lit,[21] $[\alpha]_D^{20}$ −83.5° (C_2H_5OH)), *p*-Cl (**2g**); 146 °C/0.5 Torr (lit,[6] 156 °C/1 Torr), $[\alpha]_D^{20}$ −78.3° (1.09, C_2H_5OH) (lit,[22] −80.6° (neat)), *m*-Cl (**2h**); 146—147 °C/1 Torr (lit,[6] 137 °C/0.5 Torr), $[\alpha]_D^{20}$ −80.0° (1.36, C_2H_5OH) (lit,[22] $[\alpha]_D$ −80.45° (neat)), *p*-CN (**2i**); ca. 150 °C/0.5 Torr (lit,[6] ca. 185 °C/1 Torr), $[\alpha]_D^{20}$ −81.0° (2.10, C_2H_5OH). Tetrahydrofuran (THF) was purified by fresh distillation from a solution of sodium benzophenone ketyl before use in all reactions. Butyllithium was obtained as a 1.56 mol dm^{-3} solution in hexane from Mitsuwa Chemical Co., Ltd. (Osaka). Kryptofix 211 was purchased from MERCK and used without further purification.

Reaction of Racemic α-Lithiomethyl *p*-Tolyl Sulfoxide (1) with Substituted (*R*)-(−)-Menthyl Benzoates (2). Into a 50 cm^3 two-necked, round-bottomed flask equipped with a rubber septum, a magnetic stirring bar, and a nitrogen-inlet tube was placed 15 cm^3 of dry THF, 5 mmol of butyllithium in hexane, and 370 mg (5 mmol) of diethylamine through the septum via a syringe at 0 °C under nitrogen. The flask was cooled to −78 °C, a solution of 5 mmol of racemic methyl *p*-tolyl sulfoxide in 2.5 cm^3 of dry THF was added, and the solution was stirred vigorously for 30 min at 0 °C. A solution of a (*R*)-(−)-menthyl benzoate (2.5 mmol) in 2.5 cm^3 of dry THF was then injected via a syringe, drop by drop, into the solution at −78 °C. After being stirred for an adequate time at −78 °C (the progresses of the reaction was monitored by TLC), the mixture was treated with water (10 cm^3), acidified (ca. pH 3) with 10% hydrochloric acid, and extraced with chloroform (3×10 cm^3). The combined chloroform layers were washed with brine, dried (Na_2SO_4), and evaporated in vacuo. Preparative thin-layer chromatography of the residue on silica gel (MERCK 60PF$_{245}$), using ether as the eluent, gave the analytically pure β-keto sulfoxide (**3**) which was subjected to optical rotation measurement.

Preparation of Authentic (*R*)-(+)-β-Keto Sulfoxides (3). The authentic optically pure meta- or para-substituted (*R*)-(+)-α-(*p*-tolylsulfinyl)acetophenones (**3**) were prepared by the same procedure as described in our previous paper.[3g] The treatment of α-lithiomethyl *p*-tolyl sulfoxide, derived from 1.54 g (10 mmol) of (*R*)-(+)-methyl *p*-tolyl sulfoxide and 11 mol of lithium diethylamide, was treated with 5 mmol of an ethyl benzoate in 25 cm^3 of dry THF at 0 °C. By a work-up similar to that used for the reaction of **1** and **2** described above, the corresponding dextrorotatory β-keto sulfoxide was produced. Recrystallization from ether or ethyl acetate yielded the analytically pure β-keto sulfoxide in satisfactory yield (78—93%). The authentic β-keto sulfoxides (**3**) obtained by this procedure exhibited the following properties. (*R*)-(−)-**3a**: mp 78.5—79 °C. $[\alpha]_D^{25}$ +253° (*c* 0.485, acetone). ^{1}H NMR ($CDCl_3$): δ=2.39 (s, 3H, -CH_3), 3.87 (s, 3H, -O-CH_3), 4.23, 4.49 (dd, *J*=14 Hz, 2H, -CH_2-), 6.85—8.00 (m, 8H, aromatic). IR (KBr): 2900, 1657, 1600, 1570, 1310, 1260, 1175, 1037, 1026, 986, 825 cm^{-1}.

Found: C, 66.38; H, 5.35%. Calcd for $C_{16}H_{16}SO_3$: C, 66.64; H, 5.59%.

(*R*)-(+)-**3b**; mp 88—88.5 °C. $[\alpha]_D^{25}$ +240° (*c* 0.335, acetone). ^{1}H NMR ($CDCl_3$): δ=1.30 (s, 9H, -C(CH_3)$_3$), 2.35 (s, 3H, -CH_3), 4.26, 4.46 (dd, *J*=14 Hz, 2H, -CH_2-), 7.15—7.85 (m, 8H, aromatic). IR (KBr): 2900, 1670, 1602, 1297, 1090, 1043, 1034, 995 cm^{-1}.

Found: C, 72.58; H, 7.15%. Calcd for $C_{19}H_{22}SO_2$: C, 72.57; H, 7.05%.

(*R*)-(+)-**3d**; mp 81.5 °C. $[\alpha]_D^{25}$ +248° (*c* 0.385, acetone). ^{1}H NMR ($CDCl_3$): δ=1.23 (d, *J*=7 Hz, 6H, -CH(C$\underline{H}_3$)$_2$), 2.35 (s, 3H, -CH_3), 2.87 (sept, 1H, -C$\underline{H}$(CH_3)$_2$), 4.25, 4.48 (dd, *J*=14 Hz, 2H, -CH_2-), 7.15—7.85 (m, 8H, aromatic). IR (KBr): 2900, 1675, 1600, 1300, 1040, 1032, 1015, 995, 830 cm^{-1}.

Found: C, 71.33; H, 6.77%. Calcd for $C_{18}H_{20}SO_2$: C, 71.97; H, 6.71%.

(*R*)-(+)-**3e**; mp 92.5 °C. $[\alpha]_D^{25}$ +253° (*c* 0.269, acetone). ^{1}H NMR ($CDCl_3$): δ=2.38 (s, 6H, 2×-CH_3), 4.25, 4.49 (dd, *J*=14 Hz, 2H, -CH_2-), 7.17—7.63 (m, 8H, aromatic). IR (KBr): 2590, 1670, 1603, 1300, 1150, 1050, 1033, 805 cm^{-1}.

Found: C, 70.32; H, 5.99%. Calcd for $C_{16}H_{16}SO_2$: C, 70.56; H, 5.90%.

(*R*)-(+)-**3g**; mp 168—169 °C. $[\alpha]_D^{25}$ +269° (*c* 0.541, acetone). ^{1}H NMR ($CDCl_3$): δ=2.39 (s, 3H, -CH_3), 4.27, 4.44 (dd, *J*=14 Hz, 2H, -CH_2-), 7.18—7.93 (m, 8H, aromatic). IR (KBr): 1674, 1585, 1290, 1085, 1035, 1017, 993, 825 cm^{-1}.

Found: C, 61.26; H, 4.38%. Calcd for $C_{15}H_{13}SO_2Cl$: C, 61.54; H, 4.47%.

(*R*)-(+)-**3h**; mp 105.5 °C. $[\alpha]_D^{25}$ +260° (*c* 0.226, acetone). ^{1}H NMR ($CDCl_3$): δ=2.39 (s, 3H, $-CH_3$), 4.27, 4.47 (dd, *J*=14 Hz, 2H, $-CH_2-$), 7.24—7.86 (m, 8H, aromatic). IR (KBr): 2920, 1675, 1592, 1425, 1300, 1200, 1085, 1039, 1028, 1015, 810 cm^{-1}.

Found: C, 61.54; H, 4.41%. Calcd for $C_{15}H_{13}SO_2Cl$: C, 61.54; H, 4.47%.

(*R*)-(+)-**3i**; mp 171—172 °C. $[\alpha]_D^{25}$ +315° (*c* 0.263, acetone). ^{1}H NMR ($CDCl_3$): δ=2.40 (s, 3H, $-CH_3$), 4.36, 4.43 (dd, *J*=14 Hz, 2H, $-CH_2-$), 7.31, 7.51 (dd, 4H, aromatic), 7.75, 7.96 (dd, 4H, aromatic). IR (KBr): 2900, 1686, 1405, 1356, 1295, 1086, 1034, 1016, 994, 835, 805 cm^{-1}.

Found: C, 67.43; H, 4.60%. Calcd for $C_{16}H_{13}SO_2N$: C, 67.82; H, 4.62%.

The authentic (*R*)-(+)-**3c** and (*R*)-(+)-**3f** have already been prepared in our previous paper.[3g]

Measurement of Enantiomeric Purity. The polarimetric analysis for the mixture of (*R*)- and (*S*)-β-keto sulfoxides (**3**) in acetone indicated that the specific rotation was nicely correlated with the composition of the enantiomeric mixture.[23] A typical experiment using the mixture of optically pure (*R*)-(+)-**3f** and racemic **3f** of various proportions is shown in Fig. 2. Therefore, the per cent enantiomeric excess (%e.e.) for the β-keto sulfoxides (**3**) obtained from the enantiomer-differentiating reaction of **1** and **2** was assigned by direct comparison with the specific rotation of the corresponding authentic **3**, i.e., %e.e.=optical purity=$[\alpha]_{obs}/[\alpha]_{max}\times 100$.[25]

Measurement of the Rate Constant for the Reaction of 1 and 2. The same experimental setup as has been described above was used. A solution of racemic **1** (2 mmol) in 7 cm^3 of dry THF was mixed rapidly with a solution of **2** (1 mmol) in 1 cm^3 of dry THF at −78 °C under nitrogen. From time to time the solution was quenched with water (10 cm^3) to stop the reaction, acidified, and extracted with chloroform (3×30 cm^3). The chloroform layer was washed with brine (3×20 cm^3) and dried (Na_2SO_4). The residue from the organic layer was subjected to the ^{1}H NMR measurement, and the consumption of **1** was measured by checking the methyl proton signal (δ=2.57, $CDCl_3$) of the resulting methyl *p*-tolyl sulfoxide. The second-order rate constant was determined according to the following equation; $kt=1/(C_1-C_2)\cdot\ln C_2(C_1-x)/C_1(C_2-x)$, where C_1 and C_2 represent the molar concentrations of **1** and **2** at time 0, respectively, and x represents the molar concentration that has reacted at time t.

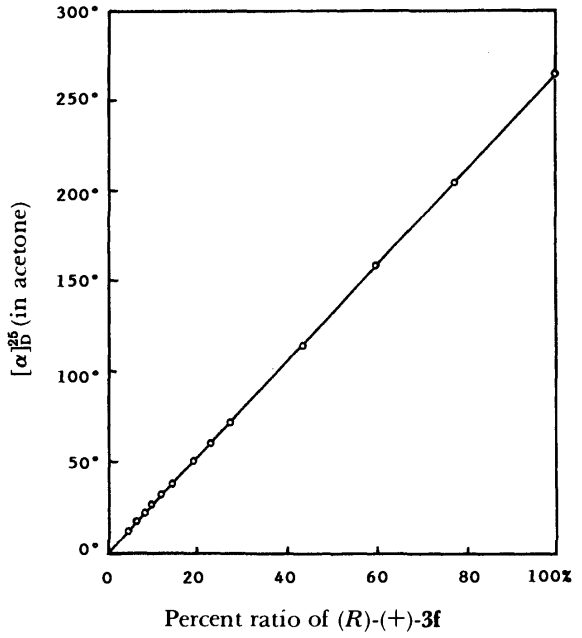

Fig. 2. Relationship between the per cent ratio of (*R*)-(+)-**3f** and the specific rotation.

References

1) H. B. Kagan and J. C. Fiaud, "New Approaches in Asymmetric Synthesis," in "Topics in Stereochemistry," ed by E. L. Eliel and N. Allinger, Interscience Pub., New York, N. Y. (1978), Vol. 10, p. 175; and references cited therein.

2) W. H. Pirkle, M. S. Hockstra, and W. H. Miller, *Tetrahedron Lett.*, **1976**, 2109; J. P. Guetté, J. Capillon, M. Perlet, and M. Guetté, *ibid.*, **1974**, 2409; S. Takenaka and M. Koden, *J. Chem. Soc., Chem. Commun.*, **1978**, 830; J. Capillon and J. P. Guetté, *Tetrahedron*, **35**, 1807, 1817 (1979); L. Duhamel and J. C. Plaquevent, *Bull. Soc. Chim. Fr.*, **1982**, II-75; H. Tomioka, N. Hayashi, Y. Izawa, and M. T. H. Lin, *J. Chem. Soc., Chem. Commun.*, **1984**, 476: B. Alcaide, C. L. Mardomingo, R. Perez-Ossorio, J. Plumet, R. Phan-Tan-Luu, and M. Sargent, *Can. J. Chem.*, **63**, 2241 (1985); F. A. Bottino and P. Finocchiaro, *Polyhedron*, **4**, 1507 (1985); C. K. Cheung, L. T. Tseng, M.-H. Lin, S. Srivastava, and W. J. leNoble, *J. Am. Chem. Soc.*, **108**, 1598 (1986); D. L. Hughes, U. H. Dolling, K. M. Ryan, E. F. Schoenewaldt, and E. J. J. Graboski, *J. Org. Chem.*, **52**, 4745 (1987).

3) a) N. Kunieda, J. Nokami, and M. Kinoshita, *Chem. Lett.*, **1973**, 871; b) N. Kunieda, J. Nokami, and M. Kinoshita, *ibid.*, **1974**, 369; c) N. Kunieda, J. Nokami, and M. Kinoshita, *Bull. Chem. Soc. Jpn.*, **49**, 256 (1976); d) N. Kunieda, J. Nokami, and M. Kinoshita, *Chem. Lett.*, **1977**, 289; e) J. Nokami, N. Kunieda, and M. Kinoshita, *ibid.*, **1977**, 249; f) N. Kunieda, H. Motaki, and M. Kinoshita, *ibid.*, **1978**, 713; g) N. Kunieda, A. Suzuki, and M. Kinoshita, *Bull. Chem. Soc. Jpn.*, **54**, 1143 (1981); h) N. Kunieda and M. Kinoshita, *Phosphorus and Sulfur*, **10**, 383 (1981); i) J. Nokami, T. Mandai, A. Nishimura, T. Takeda, S. Wakabayashi, and N. Kunieda, *Tetrahedron Lett.*, **27**, 5109 (1986); j) N. Kunieda and M. Kinoshita, *Chem. Express*, **3**, 121 (1988).

4) The σ value used here is that reported by Jaffe; H. H. Jaffe, *Chem. Rev.*, **53**, 191 (1953).

5) C. K. Ingold, "Structure and Mechanism in Organic Chemistry," Cornell University Press, Ithaca and London (1969), p. 1170.

6) R. W. Taft, Jr., M. S. Newman, and F. H. Verhoek, *J. Am. Chem. Soc.*, **72**, 4511 (1950).

7) G. Chassaing, R. Lett, and A. Marquet, *Tetrahedron Lett.*, **1978**, 471; G. Chassaing and A. Marquet, *Tetrahedron*, **34**, 1399 (1978).

8) J. F. Biellmann and J. J. Vicens, *Tetrahedron Lett.*, **1978**, 467.

9) A. McL. Mathieson, *Tetrahedron Lett.*, **1965**, 4137; R. J. B. Marsden and L. E. Sutton, *J. Chem. Soc.*, **1936**, 1383; M. Legrand and M. J. Rougier, "Application of the Optical Activity to Stereochemical Determination," in "Stereochem-

istry Fundamentals and Methods," ed by H. B. Kagan, Georg Thieme Publishers, Stuttgart (1977), Vol. 2, p. 130.

10) Many six-membered cyclic transition states have been proposed in the asymmetric induction by chiral sulfinyl compounds using organo metallic compounds.[3b,11]

11) For example; R. Annunziata, M. Cinquini, F. Cozzi, F. Montanari, and A. Restelli, *J. Chem. Soc., Chem. Commun.*, **1983**, 1138; M. Cinquini, A. Manfredi, H. Molinari, and A. Restelli, *Tetrahedron*, **41**, 4929 (1985); A. Annunziata, M. Cinquini, F. Cozzi, and A. Restelli, *J. Chem. Soc., Perkin Trans. 1*, **1985**, 2289, 2293; G. Solladie, C. Greck, G. Demailly, and A. Solladié-Cavallo, *Tetrahedron Lett.*, **23**, 5047 (1982); G. H. Posner and E. Asirvatham, *J. Org. Chem.*, **50**, 2589 (1985).

12) V. Prelog, *Helv. Chim. Acta*, **36**, 708 (1953); D. J. Cram and F. A. Abd Elhafez, *J. Am. Chem. Soc.*,**74**, 5828 (1952); T. J. Leitereg and D. J. Cram, *ibid.*, **90**, 4019 (1968).

13) E. R. Thornton, *J. Am. Chem. Soc.*, **89**, 2915 (1967); G. S. Hammond, *ibid.*, **77**, 334 (1955); R. A. More O'Ferrall, *J. Chem. Soc. B*, **1970**, 268, 274.

14) J. M. Lehn and J. P. Sauvage, *J. Chem. Soc., Chem. Commun.*, **1971**, 440.

15) N. J. Leonard and C. R. Johnson, *J. Org. Chem.*, **27**, 282 (1962).

16) A. Cerniani and G. Modena, *Gazz. Chim. Ital.*, **89**, 834 (1959).

17) K. K. Andersen, *Tetrahedron Lett.*, **1962**, 93.

18) K. Mislow, M. M. Green, P. Laur, J. T. Melillo, T. Simmons, and A. L. Ternay, Jr., *J. Am. Chem. Soc.*, **87**, 1958 (1965).

19) J. B. Cohen and H. W. Dudley, *J. Chem. Soc.*, **97**, 1732 (1910).

20) J. Kenyon and B. H. Pickard, *J. Chem. Soc.*, **107**, 35 (1915).

21) H. Rupe, *Justus Liebigs Ann. Chem.*, **327**, 157 (1903).

22) J. B. Cohen and S. H. C. Briggs, *J. Chem. Soc.*, **83**, 1213 (1903).

23) Horeau[24] has been reported that the per cent enantiomeric purity is not always same as the per cent optical purity.

24) A. Horeau, *Tetrahedron Lett.*, **1969**, 3121.

25) M. Raban and K. Mislow, "Topics in Stereochemistry," ed by E. L. Eliel and N. Allinger, Interscience Pub., New York, N. Y. (1967), Vol. 2, pp. 199—230.

Mercury-Photosensitized Decomposition of β-Butyrolactone

Shunzo YAMAMOTO,* Rinko GOHDA, Yoshimi SUEISHI, and Norio NISHIMURA
Department of Chemistry, Faculty of Science, Okayama University, 3-1-1, Tsushima-naka, Okayama 700
(Received November 24, 1988)

The mercury-photosensitized decomposition of β-butyrolactone has been investigated at temperatures between 353 and 393 K and pressures from 450 to 13600 Pa. The products were carbon dioxide, propylene, carbon monoxide, propylene oxide, acetone, and acetaldehyde. The yields of these products increased linearly with reaction time and light internsity, while they were independent of the lactone pressure. Three decomposition processes were proposed to explain the formation of the products. The decrease in the quantum yields of carbon dioxide, carbon monoxide, and acetaldehyde observed in the presence of *cis*-2-butene can be explained by the competitive quenching of the triplet mercury atom by the lactone and *cis*-2-butene (the quenching efficiency of lactone relative to that of *cis*-2-butene was estimated to be 0.61). The decrease in the quantum yields of carbon dioxide, propylene, and acetaldehyde by the addition of oxygen can again be explained only by the competitive quenching of the triplet mercury atoms by lactone and oxygen (k_Q(lactone)/k_Q(oxygen)=1.36). The quantum yields of propylene oxide and acetone, however, decrease more rapidly than predicted for competitive quenching. This indicates the existence of a reaction between oxygen and a biradical, which is a precursor of propylene oxide and acetone.

Recently, we have studied the mercury- and cadmium-photosensitized decompositions of γ-butyrolactone (γ-BL)[1] and β-propiolactone (PL)[2] and found the different kinetic behavior in the two photosensitized reactions. We have concluded that the mercury-photosensitized reaction proceeds through a lactone triplet state, while the cadmium-photosensitized reaction proceeds through an excited complex between an excited cadmium atom and a lactone molecule.

Recently, Frey and Watts[3,4] studied the thermal decomposition of β-butyrolactone (β-BL) and PL and pointed out that the introduction of a methyl group into the 4 position on the lactone ring accelerates the thermal decomposition rate, and that the rate acceleration can be attributed to the stabilization of a positive-charge center (by the methyl group) which develops on C_4 in the compex. We have investigated the mercury-photosensitized decomposition of β-BL in order to compare the results with those of the mercury-photosensitized reaction of PL and to test some of the mechanistic ideas developed for PL.

Experimental

The apparatus and techniques are similar to those used previously.[1,2]

An analysis of the products was performed using simple fractionation at 77 and 190 K, measurements with a gas burette, and gas chromatography. The light intensity absorbed by the mercury atoms at 253.7 nm was determined by *cis*-2-butene actinometry.

β-BL (Tokyo Kasei Ind., GR grade) was used after drying using a Molecular Sieve 5A and several trap-to-trap distillations. Known amounts of liquid lactone were injected into the reaction cell with a microsyringe and were fully degassed after many careful freeze-pump cycles. The pressure of β-BL in the cell was calculated by the perfect-gas equation. *cis*-2-Butene (NihonTokushu Gasu K.K., pure grade), O_2 (Takachiho Shoji, pure grade) were used as supplied.

Results and Discussion

Since the vapor pressure of β-BL is low at room temperature, it is necessary to elevate the reaction temperature in order to obtain sufficient vapor pressure. The mercury-photosensitized reaction was studied at 353, 373, and 393 K. The thermal decomposition at these temperatures and the direct photolysis at 253.7 nm were found to be negligible.

The major products of the mercury-photosensitized decomposition of β-BL were carbon dioxide, propylene, carbon monoxide, propylene oxide, acetone, and acetaldehyde. Yields of these products increased linearly with reaction time and light intensity, showing that they are primary products.

The yields of the products are shown in Fig. 1 as a function of lactone pressure. As Fig. 1 shows, the yields of all products are independent of the lactone pressure. The relative product yields to that of carbon dioxide at 353, 373, and 393 K are shown in Table 1. The ratios of the product yields are independent of temperature. The quantum yields (Φ) of products

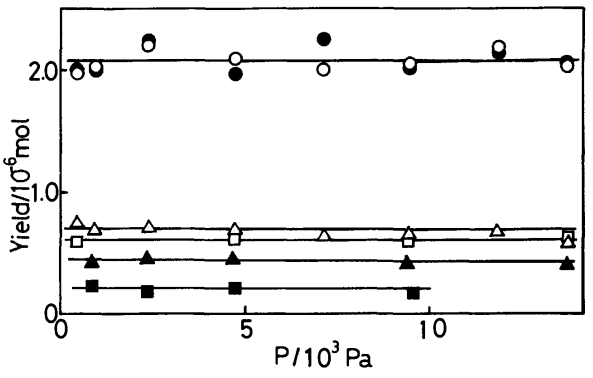

Fig. 1. Pressure dependence of product yields. CO_2 (○), propylene (●), acetaldehyde (□), CO (△), propylene oxide (▲), and acetone (■).

Table 1. Temperature Dependence of Yields of Products Relative to That of CO_2

T/K	C_3H_6	CH_3CHO	CO	C_3H_6O	$(CH_3)_2CO$
353	1.01	0.084	0.086	0.054	0.017
373	1.04	0.078	0.096	0.056	0.013
393	1.04	0.087	0.091	0.051	0.012

Table 2. Quantum Yields of Products in the Mercury-Photosensitized Decomposition of β-BL at 373 K

Products	CO_2	C_3H_6	CH_3CHO	CO	C_3H_6O	$(CH_3)_2CO$
	0.89±0.05	0.90±0.05	0.07±0.01	0.08±0.01	0.05±0.01	0.02±0.01

obtained at 373 K are listed in Table 2. The fact that the prodcut yields are independent of lactone pressure shows that the decomposition of β-BL may occur from the triplet state of the lactone. If the decomposition occurs from the vibrationally excited-electronic ground state which is produced by intersystem crossing, the product yields are expected to be largely pressure-dependent.

In order to explain the experimental results, the following set of reactions is proposed:

$$Hg(^1S_0) + h\nu(253.7\,nm) \rightarrow Hg(^3P_1) \quad (1)$$

$$Hg(^3P_1) \rightarrow Hg(^1S_0) + h\nu(253.7\,nm) \quad (2)$$

$$Hg(^3P_1) + L \rightarrow Hg(^1S_0) + {}^3L \quad (3)$$

$${}^3L \rightarrow CO_2 + CH_3CH{=}CH_2 \quad (4)$$

$${}^3L \rightarrow CO + \alpha CH_3\underline{CHCH_2}O + (1-\alpha)CH_3COCH_3 \quad (5)$$

$${}^3L \rightarrow CH_3CHO + CH_2CO \quad (6)$$

Here, ^3L denotes a triplet lactone.

As Table 2 shows, $\Phi(CO_2)+\Phi(CO)+\Phi(CH_3CHO)=1.05\pm0.05$. This shows that the decomposition from the excited triplet state leads to processes (4), (5), and (6).

Recently, Frey and Watts[3,4] investigated the thermal unimolecular decompositions of β-BL and PL and found relatively small energies of activation (163.4 and 180.5 kJ mol^{-1}). They pointed out that a biradical mechanism can be ruled out and a concerted pathway must be involved. Unlike the thermal decomposition, excitation in the mercury-photosensitized reaction undoubtedly provides sufficient energy to produce biradicals, which could then decompose.

If β-BL undergoes Norrish type I cleavage which is common in carbonyl compounds, the following biradicals are formed:

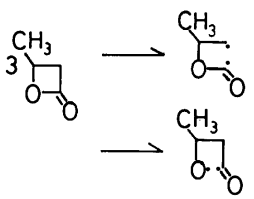

(7)

(8)

Reaction (7) is followed by elimination of carbon dioxide by breakage of the C_4–O bond and produces propylene. The biradical produced by Reaction (8) can either produce carbon monoxide and a biradical, $\cdot CH_2CH(CH_3)O\cdot$, by breakage of the O=C–C_3 bond or produce acetaldehyde and ketene by breakage of the C_3–C_4 bond.

The biradical, $\cdot CH_2CH(CH_3)O\cdot$, can either close to form propylene oxide or isomerize by hydrogen transfer to acetone, as shown by the following scheme:

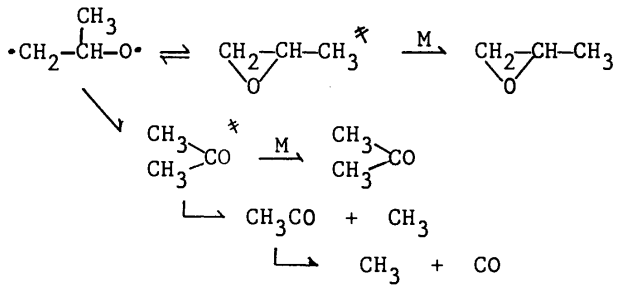

Scheme 1.

From the large exothermicity of the reactions, β-BL+Hg($^3P_1$)→CO+propylene oxide+Hg($^1S_1$) and β-BL+Hg($^2P_1$)→CO+acetone+Hg($^1S_0$), propylene oxide and acetone will be formed with large excess energy and may dissociate to CO and CH_3 radicals.

As described previously,[2] for the mercury-photosensitized reaction of PL yields of ethylene oxide and acetaldehyde, which are correspond to propylene oxide and acetone in the present case, show pressure dependence at lower pressures. From the pressure dependence of yields of ethylene oxide and acetaldehyde, we have estimated the excess energy of energized ethylene oxide and obtained the value of 272 kJ mol^{-1} which corresponds to about 78% of the enthalpy change for the reaction, PL+Hg(^3P)→ethylene oxide+CO+Hg($^1S_0$).

Here, we assume that almost the same fraction (75—80%) of the enthalpy changes of the following reactions are partitioned to propylene oxide and acetone:

$$Hg(^3P_1) + \beta\text{-BL} \rightarrow Hg(^1S_0) + CO + \underset{\diagdown\,/\,\diagdown}{CH_2CHCH_3\ \ \ \

system suppressed the formation of products. Figure 3 shows the effect of oxygen on the yields of products. As Fig. 3 shows, yields of all products decrease with increasing oxygen pressure. The solid line shows the relative quantum yields calculated using the following relative quenching efficiencies for β-BL and oxygen:

$k_Q(\beta\text{-BL})/k_Q(O_2)=1.36$ (obtained from $k_Q(\beta\text{-BL})/k_Q(cis\text{-2-butene})=0.61$ and $k_Q(O_2)/k_Q(cis\text{-2-butene})=0.45$[8])

The decrease in the quantum yields of carbon dioxide, propylene, and acetaldehyde can be explained by the competitive quenching of the triplet mercury atom by the lactone and oxygen. The decreases in the yields of propylene oxide and acetone, however, are steeper than those of other products. This shows that oxygen has additional effects on the formation of propylene oxide and acetone. As mentioned above, the biradical, $\cdot COCH_2(CH_3)O\cdot$, is a common intermediate for the formation of acetaldehyde and propylene oxide (and acetone). The difference in the effect of oxygen on the formation of acetaldehyde and that of propylene oxide and acetone shows that oxygen does not scavenge this biradical, but may scavenge another intermediate which locates between the biradical and propylene oxide and acetone (the final products).

The effect of oxygen on product yields can be discussed in terms of reactions schematically depicted in Scheme 2.

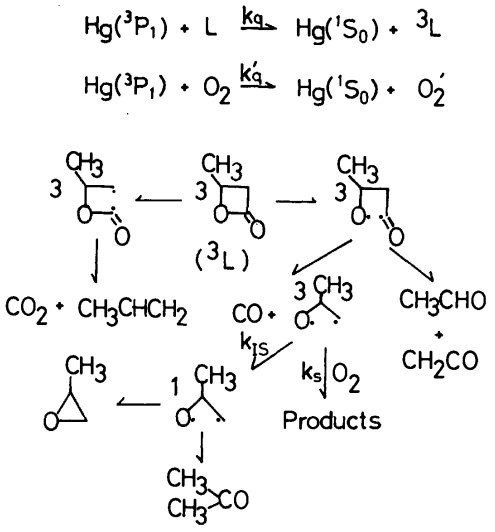

Scheme 2.

From this mechanism, the following equations can be derived:

$$\frac{\Phi_{CO_2}}{\Phi^\circ_{CO_2}}=\frac{\Phi_{CH_3CHCH_2}}{\Phi^\circ_{CH_3CHCH_2}}=\frac{\Phi_{CH_3CHO}}{\Phi^\circ_{CH_3CHO}}=\frac{k_q[L]}{k_q[L]+k'_q[O_2]} \quad (12)$$

$$\frac{\Phi_{CH_3\underline{CHCH_2O}}}{\Phi^\circ_{CH_3\underline{CHCH_2O}}}=\frac{\Phi_{(CH_3)_2CO}}{\Phi^\circ_{(CH_3)_2CO}}=\frac{k_q[L]}{k_q[L]+k'_q[O_2]}\frac{k_{IS}}{k_{IS}+k_s[O_2]} \quad (13)$$

The relationship between $\Phi_{CO2}/\Phi^\circ_{CO_2}$, $\Phi_{CH_3CH=CH_2}/\Phi^\circ_{CH_3CH=CH_2}$, and $\Phi_{CH_3CHO}/\Phi^\circ_{CH_3CHO}$ vs. oxygen pressure has been already discussed above. The additional effect of oxygen on the yields of propylene oxide and acetone mentioned above is expressed by the term $k_{IS}/(k_{IS}+k_s[O_2])$. The ratio of the rate constants, k_s/k_{IS}, was evaluated by fitting Eq. 13 to the experimental measurements ($k_s/k_{IS}=7.5\times10^{-1}$ Pa). The dashed curve in Fig. 3 shows the calculated values of Φ/Φ° for propylene oxide and acetone. If k_s has a typical value of 1.0×10^{13} cm^3 molecule^{-1} s^{-1} similar to that suggested for the analogous reaction of alkyl monoradicals,[9] then k_{IS} can be calculated to be 3.2×10^6 s^{-1}. This value is in reasonable agreement with that proposed by Montague for intersystem crossing of alkyl biradicals ($3\times10^6<k_{IS}<4.5\times10^8$ s^{-1}).[10]

According to recent kinetic studies[11-14] of the reaction of ethylene with the ground-state oxygen atom(O(^{3}P)), the reaction proceeds via two main channels: one yielding CH_2=CHO·+H (a) and the other, CH_3+HCO (b). The primary process is the addition of the oxygen atom to the C=C double bond to form a triplet biradical, $\cdot CH_2CH_2O\cdot$. Hunziker et al.[11] proposed a schematic potential energy diagram for the O + ethylene reaction and pointed out that the shift of a hydrogen atom in the triplet biradical to give triplet acetaldehyde requires a high activation energy. They also suggested that by collision it can be converted into an isoenergetic singlet biradical which would have low activation energy pathways available to give hot ground state oxide and aldehyde. Koda et al.,[15] however, pointed out that this mechanism cannot explain the pressure independence of the branching ratio over a wide range. They proposed a rapid collision-free intersystem crossing to interpret their experimental results. They assumed that the branching ratio of (b)/(a) is determined by the unimolecular dissociation rate of the triplet intermediate yielding CH_2=CHO·+H compared with the rate of the intersystem crossing to the singlet surface and can interpret the enhancement of the branching ratio by the deuterium substitution of ethylene.

The biradical produced in the mercury-photosensitized reaction of β-BL seems to be a triplet as shown above and to behave similarly to the triplet biradical formed in the oxygen-ethylene reaction and is converted into a singlet biradical by a collision-free intersystem crossing. The fate of the singlet biradical has already been discussed above.

References

1) S. Yamamoto, S. Matsuda, C. Ozaki, H. Takahoso, and N. Nishimura, *Bull. Chem. Soc. Jpn.*, **57**, 3408 (1984).

2) S. Yamamoto, R. Gohda, R. Morikawa, H. Takahoso, Y. Sueishi, and N. Nishimura, *Bull. Chem. Soc. Jpn.*, **59**, 2559 (1986).

3) H. M. Frey and H. P. Watts, *J. Chem. Soc., Faraday Trans. 1*, **79**, 1659 (1983).

4) H. M. Frey and I. M. Pidgeon, *J. Chem. Soc., Faraday Trans. 1*, **81**, 1087 (1985).

5) L. S. Kassel, *J. Phys. Chem.*, **32**, 225, 1065 (1928).

6) T. J. Hardwick, *Can. J. Chem.*, **46**, 2454 (1968).

7) S. W. Benson and H. E. O'Neal, "Kinetic Data on Gas Phase Unimolecular Reactions," NSRDS-NBS 21, U.S. 1970.

8) R. J. Cvetanovic, "Mercury Photosensitized Reactions," Progress in Reaction Kinetics, Vol. 2, ed. by G. Porter, The Macmillan Co., New York (1964), p. 39.

9) For example, R. P. Ruiz and K. D. Bayes, *J. Phys. Chem.*, **88**, 2592 (1984).

10) D. C. Montague, *J. Chem. Soc., Faraday Trans. 1*, **74**, 277 (1978).

11) H. E. Hunziker, H. Kneppe, and H. R. Wendt, *J. Photochem.*, **17**, 377 (1981).

12) J. F. Smalley, F. L. Nesbitt, and R. B. Klemm, *J. Phys. Chem.*, **90**, 491 (1986).

13) K. Mahmud, P. Marshall, and A. Fontijn, *J. Phys. Chem.*, **91**, 1568 (1987).

14) Y. Endo, S. Tsuchiya, C. Yamada, E. Hirota, and S. Koda, *J. Chem. Phys.*, **85**, 4446 (1986).

15) S. Koda, Y. Endo, E. Hirota, and S. Tsuchiya, *J. Chem. Phys.*, **91**, 5840 (1987).

An Oxygen Exchange of Arsenate and Alkylarsonate Ions with Water

Nobuko NIWA, Midori FUSHIMI, Masayasu IIDA, Yuko HORIE, Shinichi YAMABE,† and Akiko OKUMURA*
Department of Chemistry, Faculty of Science, Nara Women's University, Kita-uoya-nishi-machi, Nara 630
†Department of Chemistry, Nara University of Education, Takabatake-cho, Nara 630
(Received December 19, 1988)

The oxygen exchange rates, R's, between the alkylarsonates (methyl- and butyl-) and water were measured over the pH range greater than 9 and at 30 °C. The rates were analyzed in terms of the rate law, $R=k_1[R'\text{-}AsO_3H^-]+k_2[R'\text{-}AsO_3^{2-}]$ (R'-; alkyl-) to obtain k_1 to be 6.64×10^{-4} s^{-1} for methyl- and 4.38×10^{-4} s^{-1} for butylarsonate ions, respectively. The first-order oxygen exchange rate constants, k_1's, on the alkylarsonate univalent anions (methyl and butyl) are almost the same values, which indicates that the steric effect on the rate is absent. The rate constants, k_1's, correlate well with energy levels of the lowest unoccupied molecular orbitals (E_{LUMO}'s) of univalent anions of arsenic, arsenious, and alkylarsonic acids.

The important role of phosphoric acid and its derivatives in biochemical processes is known-well. There are many studies of the hydrolysis of organic phosphates[1] and the oxygen exchange of phosphoric acid with water.[2] The As and P atoms belong to the nonmetal Va group and consequently arsenic and phosphoric acids have similarity in structures and physical properties in solution. On the other hand, the difference of reactivity between them is enormous; the oxoanions of arsenic are reactive, while those of phosphorus are stable and unreactive. Many biochemical effects seem to be due to the ability of arsenic(V) to mimic the analogous phosphates; arsenate may substitute for phosphate as a substrate in certain phosphorylation[3] and some enzymatic arsenolyses.[4] The investigation of the behavior of arsenic(V) is important and is expected to shed light on the reaction mechanism of phosphoric(V) in biological systems.

While the oxygen exchange reactions between the oxoanions of phosphorus and water have been extensively studied, those of oxoanions of arsenic are rather few.[5–7]

The difficulty of the latter measurement by ^{18}O tracer method was mainly in the separation process of the oxoanions from the solution for isotopic oxygen analyses. As stated in a previous paper,[6] on the precipitation of the oxoanions by metal ions, the oxygen exchange of the oxoanions of arsenic is induced. In the case of some alkylarsonates, any precipitant could not separate oxoanions from the solution. NMR instrumentation recently available has alleviated these problems, but there still remains a difficulty in the preparation of ^{17}O-enriched compounds for ^{17}O NMR technique.

However, it is important to study kinetics of the oxygen exchange on As, because it provides information of the microscopic interaction between oxoanion and solvent water and between oxoanions in the solution.[6–10] Furthermore, the detailed kinetic data of the oxygen exchange of arsenate ions may explore the possibility of the use of ^{18}O-labelled arsenate in biochemical tracer work.

Here, we present new rate constants of R'-As(OH)O_2^- ions, where R' is the alkyl group (R'=methyl or butyl). It is of mechanistic interest to know how the alkyl substituent affects the oxygen-exchange rate. The long chain of the butyl would block the nucleophilic attack of a water molecule. After the first-order rate constants are measured, those substituent effects are investigated with the aid of the ab initio molecular orbital (MO) calculation. The relation between the electronic property and the reactivity of arsenate and alkylarsonate ions is sought. In particular, it should be carefully checked what kind of the isomer of the substrate is involved in the oxygen exchange reaction. As atom may have 3, 5, or 7 chemical bonds, and this freedom might be related to the intervention of unexpected isomers and subsequently to the anomalous rate constants. This is a pioneer work which deals with the S_N2 reaction of the As atom systematically.

Experimental and Computational

Materials. Methyl- and butylarsonates were prepared according to Quick.[11] Methylarsonate was recrystallized several times from aqueous ethanol solution (50 vol%). The methylarsonic acid derived from the purified salt has a melting point of 161 °C (161 °C[11]). The C and H contents by elemental analyses are: Found: C, 8.66; H, 3.62%. Calcd for $CH_3AsO_3H_2$: C, 8.58; H, 3.60%. A crude product of butylarsonate was acidified to form arsonic acid, which was purified by the crystallization from water and ethanol. The melting point of the acid are 161 °C (159—160 °C[11]), and elemental analyses gave: Found: C, 26.53; H, 6.12%. Calcd for $C_4H_9AsO_3H_2$: C, 26.40; H, 6.10%.

Rate Measurements. The oxygen-exchange rate of methylarsonate was followed by measuring the decrease in the ^{18}O contents of arsonate upon diluting an isotopically equilibrated solution of $CH_3AsO_3Na_2$ in [^{18}O]water with a large amount of isotopically normal water. A portion of the solution was drawn periodically and the arsonate was recovered by freeze-dry method, its oxygen being converted into carbon dioxide by the guanidinium chloride method.[12] The isotopic analysis of carbon dioxide was made on a Hitachi RMS-I-type mass spectrometer.

The rates of oxygen exchange of butylarsonate were obtained by ^{17}O NMR method. A weighed amount of butylarsonate enriched in ^{17}O was dissolved into 3 ml of water in an ice bath. After pH adjustment, the solution was transferred to a sample tube for running the NMR spectra. In the measurements, both the decrease in the intensity of ^{17}O-signal of the arsonate and the increase in that of water were followed. The rates on both the signals are satisfactorily agreed. ^{17}O NMR spectra were recorded at 36.6 MHz on a FT-NMR spectrometer, JEOL-GX270. The ^{17}O-chemical shift for n-$C_4H_9AsO_3Na_2$ is downfield from water by 130 ppm.

The rate of oxygen exchange, R, was calculated by means of the formulas:

$$R = -\frac{1}{t}\frac{[\text{arsonate}][H_2O]}{3[\text{arsonate}]+[H_2O]}\ln\frac{*O_t - *O_\infty}{*O_0 - *O_\infty}$$

where $*O_0$, $*O_t$, and $*O_\infty$ are ^{18}O (for methylarsonate) or ^{17}O (for butylarsonate) contents at the times 0, t, and infinity, respectively. [arsonate] and [H_2O] are the molar concentrations (mol dm^{-3}) of the arsonates and water, respectively.

The Dissociation Constants of Arsonic Acids. These were determined by the potentiometric titration at 30 °C and I=0.55 mol dm^{-3}. The values of pK_2 are 8.50 for methylarsonic acid and 8.88 for butylarsonic acid.

Ab Initio Molecular-Orbital (MO) Calculation. To compare the reactivity of arsonates for the oxygen exchange with each other, we performed an MO calculation on five substrates with the STO-3G* basis set (STO-3G plus six d orbitals on arsenic). All the electrons are explicitly considered, and the geometries are fully optimized using the GAUSSIAN 82 program.[13]

Results of Kinetics

The exchange rates for the two reactions were measured at 30 °C and over the pH range between 9 and 12 where the dominating ionic species of arsonates are R'-AsO_3^{2-} and R'-AsO_3H^- (R'=CH_3 or n-C_4H_9). The results are shown in Table 1.

The dependence of the rate on the concentration of arsonates was studied at pH 10.6 for methylarsonate (**A**) and pH 10.9 for butylarsonate (**B**). The plots of $\log_{10} R$ against $\log_{10}$[arsonate] give the straight lines with slopes of 0.92 for **A** and 1.07 for **B**, respectively (Fig. 1). The first-order dependence observed in Fig. 1 suggests that the oxygen exchange of arsonates proceeds through two parallel paths:

$$R'\text{-}AsO_3H^- + H_2{*}O \overset{k_1}{\rightleftharpoons} R'\text{-}AsO_2{*}OH^- + H_2O$$

$$R'\text{-}AsO_3^{2-} + H_2{*}O \overset{k_2}{\rightleftharpoons} R'\text{-}AsO_2{*}O^{2-} + H_2O$$

and the exchange rate law may be written as:

$$R = k_1[R'\text{-}AsO_3H^-] + k_2[R'\text{-}AsO_3^{2-}]$$

By the use of this relation, the exchange rates shown in Table 1 were analyzed and the values of k_1 and k_2 are obtained to be 6.64×10^{-4} s^{-1} and 2.69×10^{-4} s^{-1} for methylarsonate and 4.38×10^{-4} s^{-1} and 9.33×10^{-5} s^{-1} for butylarsonate, respectively. Noteworthy is the result that the four rate constants are of the same order, and a noticeable steric or hydrophobic effect of the butyl substituent is not observed.

Table 1. The pH Dependence of the Oxygen Exchange Rates of Methyl- and Butylarsonates (30 °C and I=0.55 mol dm^{-3}. [methylarsonate]=0.1 mol dm^{-3}, [butylarsonate]=0.2 mol dm^{-3})

R'-	pH	$R/10^{-5}$ mol dm^{-3} s^{-1}
CH_3-	9.17	5.07
	9.57	3.41
	10.02	2.91
	10.10	3.03
	10.13	2.36
	10.52	2.50
	10.60	2.89
n-C_4H_9-	9.01	4.68
	9.50	3.33
	9.71	2.71
	10.56	2.11
	11.11	1.69
	12.31	1.90

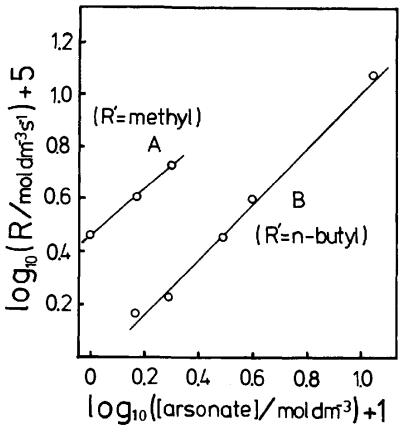

Fig. 1. The dependence of the exchange rate, R, on the concentration of arsonates.

The rate constants of the oxygen exchange between univalent anoin of arsonate and water, k_1's, thus obtained were used in the following discussion.

Computational Results and Discussion

First, measured exchange-rate constants [$k_1^{(A)}$, $k_1^{(B)}$, $k_1^{(C)}$, $k_1^{(D)}$] are compared with each other. $k_1^{(A)}$ and $k_1^{(B)}$ are presented in the previous section, and $k_1^{(C)}$ [6] and $k_1^{(D)}$ [7] are taken from literatures.

$$CH_3AsO_3H^- + H_2{*}O \longrightarrow CH_3AsO_2{*}OH^- + H_2O \quad \text{(A)}$$
$$k_1^{(A)} = 6.6\times10^{-4}\ \text{s}^{-1}$$

$$n\text{-}C_4H_9AsO_3H^- + H_2{*}O \longrightarrow n\text{-}C_4H_9AsO_2{*}OH^- + H_2O \quad \text{(B)}$$
$$k_1^{(B)} = 4.4\times10^{-4}\ \text{s}^{-1}$$

$$H_2AsO_4^- + H_2{}^*O \longrightarrow H_2AsO_3{}^*O^- + H_2O \quad (C)$$
$$k_1^{(C)} = 1.0\times10^{-4}\ s^{-1}$$

$$H_2AsO_3^- + H_2{}^*O \longrightarrow H_2AsO_2{}^*O^- + H_2O \quad (D)$$
$$k_1^{(D)} = 167\ s^{-1}$$

The relation of $k_1^{(D)} \gg k_1^{(A)} \simeq k_1^{(B)} > k_1^{(C)}$ is recognized. It seems to be curious that the $k_1^{(D)}$ (R′=H) is much larger than $k_1^{(A)}$ (R′=methyl) and $k_1^{(B)}$ (R′=butyl). Some anomalies for the large reactivity of H-AsO_3H^- must be present. To analyze this trend, an MO calculation is made for the following substrates.

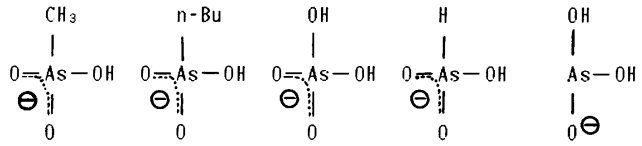

For $H_2AsO_3^-$, **D**, **Db** is an isomer of **Da**. The anomalous value of $k_1^{(D)}$ may be related to the isomer. Optimized geometries of **A**, **B**, **C**, **Da**, and **Db** are

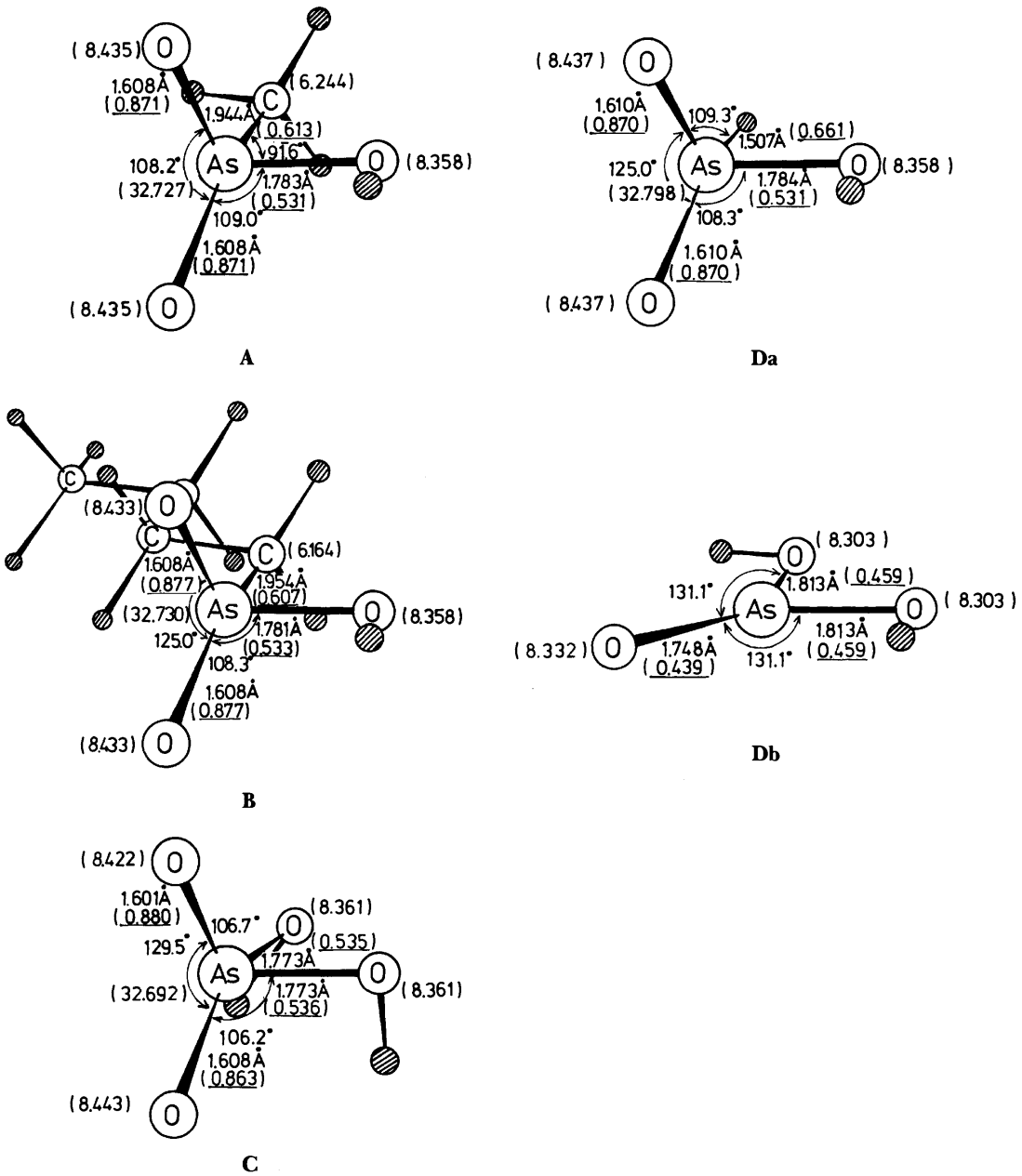

Fig. 2. Geometries of arsenate and alkylarsonate ions optimized with the STO-3G* basis set. Shaded circles denote hydrogen atoms. Values in parentheses stand for the atomic electronic density, and underlined ones do the atom-atom bonding populations.

exhibited in Fig. 2. The As-O bond length 1.78 Å of **A** and **B** is comparable to 1.71 Å of the crystal data of propylarsonic acid.[14] Likewise, the As-O 1.61 Å and As-C 1.94 (and 1.95) Å are comparable to 1.65 Å and 1.92 Å, respectively.[14]

First, the presence or the absence of the steric or hydrophobic effect by the butyl group is examind in Fig. 3. The figure shows the lowest unoccupied molecular orbital (LUMO) which undergoes the charge transfer from the nucleophile, water. The orbital extention of LUMO clearly demonstrates that H_2O attacks the back side of the As-OH bond. The butyl chain is distant from the channel of the nucleophilic attack, and the result that the path is not blocked by the alkyl chain is related to $k_1^{(A)} \simeq k_1^{(B)}$ (no steric effect).

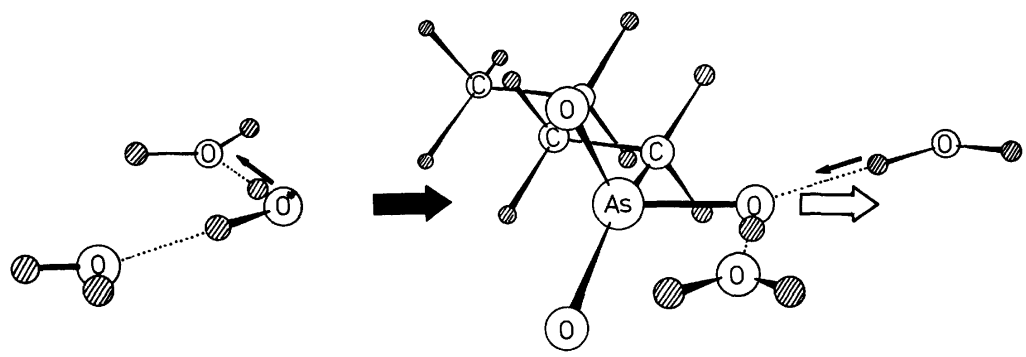

Second, the anomalously large value of $k_1^{(D)}$ is interpreted in terms of the computed data, i.e. the energy level of LUMO (E_{LUMO}). E_{LUMO}'s of **A**, **B**, **C**, **Da**, and **Db** vs. rate constants are plotted in Fig. 4. It is found that not E_{LUMO}(**Da**) but E_{LUMO}(**Db**) is in the line. Thus, $H_2AsO_3^-$ is present in the form of $(HO)_2AsO^-$, **Db**, which is consistent with the data of Raman spectra in aqueous solution.[15]

This finding of arsenious acid is the first case in which the structure of the oxoanion in the solution is identified on the basis of the kinetic results of the oxygen exchange. The combined treatment of the kinetic results and MO calculation used in this work seems to be applicable to S_N2 reaction on the heavy atoms other than As.

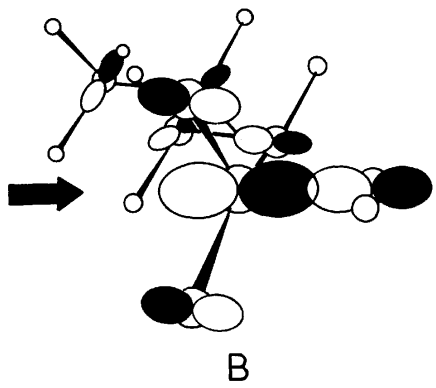

Fig. 3. The sketch of the orbital extension of the frontier orbital, LUMO, of the butylarsonate ion. The bold arrow indicates the direction of the nucleophilic attack of a water molecule.

Concluding Remarks

In this study, rate constants of oxygen exchange of alkylarsonate ions were measured. It is found that the steric effect does not dominate the rates. In the theoretical side, it is confirmed that the alkyl group is apart from the S_N2 path and therefore the rate is insensitive to the size of the alkyl chain. The remarkably large rate constant of the $H_2AsO_3^-$ is ascribed to the low-lying E_{LUMO} of [not $H\text{-}As(OH)O_2^-$] but $(OH)_2AsO^-$.

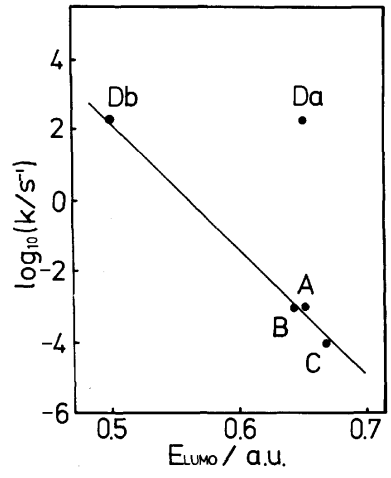

Fig. 4. The correlation between the energy of the lowest unoccupied molecular orbital (E_{LUMO}) and the logarithm of the rate constant at 30 °C for substrates **A**, **B**, **C**, and **D**. 1 a.u.=1 hartree=2.626×10^6 J mol^{-1}.

The authors thank the Institute for Molecular Science for the allotment of the computer time of the HITAC M-680H computer.

References

1) C. A. Bunton, D. R. Llewellyn, K. G. Oldham, and C. A. Vernon, *J. Chem. Soc.*, **1958**, 3574, 3588; C. A. Bunton, M. M. Mhala, K. G. Oldham, and C. A. Vernon, *ibid.*, **1960**, 3293.

2) B. Keisch, J. W. Kennedy, and A. C. Wahl, *J. Am. Chem. Soc.*, **80**, 4778 (1958); C. A. Bunton, D. R. Llewellyn, C. A. Vernon, and V. A. Welch, *J. Chem. Soc.*, **1961**, 1636.

3) N. Itada and M. Cohn, *J. Biol. Chem.*, **238**, 4026 (1963).

4) D. H. Slocum and J. E. Varner, *J. Biol. Chem.*, **235**, 492 (1960).

5) R. F. Kouba and J. E. Varner, *Biochem. Biophys. Res. Commun.*, **1**, 129 (1959).

6) A. Okumura and N. Okazaki, *Bull. Chem. Soc. Jpn.*, **46**, 2937 (1973).

7) W. C. Copenhafer and P. H. Rieger, *J. Am. Chem. Soc.*, **100**, 3776 (1978).

8) A. Okumura, N. Yamamoto, and N. Okazaki, *Bull. Chem. Soc. Jpn.*, **46**, 3633 (1973).

9) A. Okumura, S. Watanabe, M. Sakaue, and N. Okazaki, *Bull. Chem. Soc. Jpn.*, **52**, 2783 (1979).

10) A. Okumura, M. Somiya, S. Asai, and N. Okazaki, *Inorg. Chim. Acta*, **87**, 53 (1984).

11) A. J. Quick and R. Adams, *J. Am. Chem. Soc.*, **44**, 805 (1922).

12) P. D. Boyer, D. J. Graves, C. H. Suelter, and M. E. Dempsey, *Anal. Chem.*, **33**, 1906 (1961).

13) J. S. Binkley, R. A. Whiteside, K. Raghavachari, R. Seeger, D. J. DeFrees, H. B. Schlegel, M. J. Frisch, J. A. Pople, and L. R. Kahn, "GAUSSIAN 82 Release A," Carnegie-Mellon University, Pittsburg, U.S.A. (1982).

14) M. R. Smith, R. A. Zingaro, and E. A. Meyers, *J. Organomet. Chem.*, **27**, 341 (1971).

15) T. M. Loehr and R. A. Plane, *Inorg. Chem.*, **7**, 1708 (1968).

 © 1989 The Chemical Society of Japan Bull. Chem. Soc. Jpn., 62, 2245—2251 (1989)

Structure and Optical Properties of a Thermochromic Schiff Base. Low-Temperature Structural Studies of the *N,N'*-Disalicylidene-*p*-phenylenediamine and *N,N'*-Disalicylidene-1,6-pyrenediamine Crystals

Tamotsu INABE,* Naomi HOSHINO,† Tadaoki MITANI, and Yusei MARUYAMA*
Institute for Molecular Science, Myodaiji, Okazaki 444
(Received October 24, 1988)

The crystal structure of *N,N'*-disalicylidene-*p*-phenylenediamine (BSP[1]) has been determined at 108 K. This compound shows a thermochromic-type behavior in the crystalline state; this chromism has been interpreted in terms of an intramolecular proton transfer from the hydroxyl oxygen to the imine nitrogen through the O-H···N hydrogen bond. In comparison with the room-temperature structure, no significant differences in the molecular structure and the molecular packing in the lattice have been observed. The room-temperature and low-termperature structures of another *N*-salicylideneaniline derivative, *N,N'*-disalicylidene-1,6-pyrenediamine (DSPY), have also been determined. In contrast to BSP, the absence of a thermal proton-transfer process in DSPY is suggested by optical measurements. Comparative studies of these two compounds indicate that a conjugation system which is not included in a π-electron configurational change by the proton transfer must be coplanar with the hydrogen-bonded chelate ring for the thermal proton transfer.

The room-temperature structure and optical properties of a thermochromic derivative of *N*-salicylideneaniline, BSP, have been reported recently.[2] The thermochromism of *N*-salicylideneanilines in the crystalline state was established to be due to the self-isomerization of a molecule by proton transfer from the hydroxyl oxygen to the imine nitrogen.[3] The temperature dependences of the visible absorption and emission spectra of BSP are consistent with this interpretation. The OH and/or NH vibrational modes in the infrared spectra are supposed to be sensitive to such an isomerization process. The OH stretching mode actually showed a significant change in the peak profile with varying the temperature.[2] However, the change has not completely been interpreted due to its complicated feature.

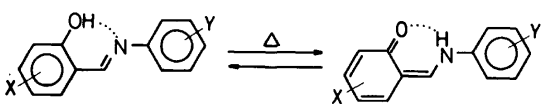

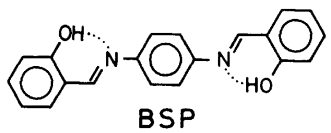

BSP

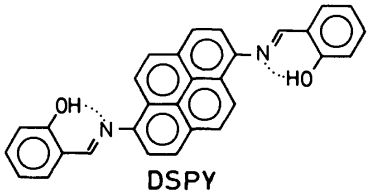

DSPY

† Present address: Department of Chemistry, Faculty of Science, Hokkaido University, Sapporo 060.

Among the other *N*-salicylideneaniline derivatives, DSPY has been found to show no thermochromic behavior, although it has a similar framework to BSP. Thus, a comparison of BSP and DSPY is expected to provide some information about the conditions of the structure and the electronic state required for the proton transfer in *N*-salicylideneanilines. In order to make a clear comparison, it is desirable to employ the structures determined at low temperatures, since the temperature influences not only the thermal motion of atoms but also the thermochromic effects in the case of BSP. In this paper, the room-temperature structure and the optical properties of DSPY as well as the low-temperature structure and that of BSP are presented.

Experimental

Materials. DSPY was prepared by condensation of 1,6-pyrenediamine and salicylaldehyde in the same manner as BSP,[2] and was recrystallized from benzene. 1,6-Pyrenediamine was synthesized following the method reported by Vollman et al.[5]

Optical Measurements. Single-crystal measurements (infrared absorption and visible absorption and emission spectra) were performed by the same methods reported before.[2]

X-Ray Structure Analyses. An automated RIGAKU AFC-5R diffractometer with graphite monochromatized Mo $K\alpha$ radiation was used for data collection of DSPY at room temperature. Thirty-one reflections with $20°<2\theta<30°$ were used to determine the lattice parameters. The crystal data are listed in Table 1. The intensity data were collected in the region $2\theta>50°$ ($-25\leqq h\leqq 25$, $-15\leqq k\leqq 15$, $0\leqq l\leqq 4$) in the θ-2θ mode (scan width, $(1.2+0.5\tan\theta)°$) at a scan rate of $6°\ \mathrm{min}^{-1}$. Background counts at each end were 4—10.5 s. The intensities of the three standards, monitored every 100 data measurements, showed no significant variation. 4360 unique reflections were measured. After reducing the symmetry, 851 independent reflections with $|F_o|>3\sigma(F_o)$ were used for a structure analysis.

Table 1. Crystal Data

	BSP (108 K)	DSPY (R.T.)	DSPY (108 K)
Chemical formula	$C_{20}H_{16}N_2O_2$	$C_{30}N_{20}N_2O_2$	$C_{30}N_{20}N_2O_2$
Molecular weight	316.35	440.49	440.49
Crystal color	Light yellow	Orange	Orange
Crystal size/mm	0.55×0.25×0.08	0.45×0.13×0.08	0.45×0.13×0.08
Crystal system	Monoclinic	Monoclinic	Monoclinic
Space group	$P2_1/c$	$P2_1/a$	$P2_1/a$
a/Å	14.605(4)	12.902(3)	12.837(3)
b/Å	4.551(1)	21.326(6)	21.396(7)
c/Å	12.092(4)	3.874(1)	3.795(1)
β/deg	112.87(2)	95.79(2)	95.53(3)
V/Å^3	740.5(4)	1060.6(5)	1037.4(5)
Z	2	2	2
D_c/g cm^{-3}	1.419	1.380	1.411
μ(Mo $K\alpha$)/cm^{-1}	0.867	0.811	0.830
R	0.048	0.046	0.047
R_w	0.059	0.050	0.048

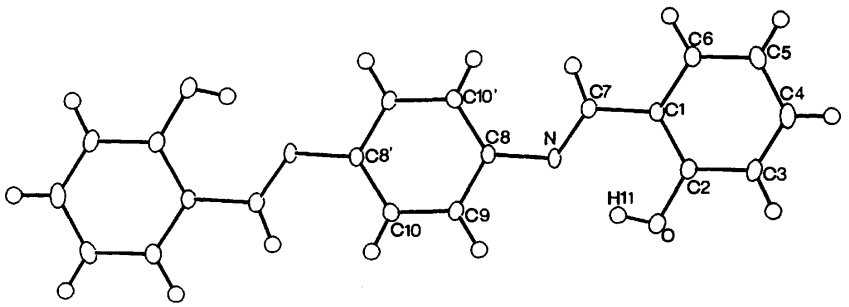

Fig. 1. ORTEP drawing[9] of BSP at 108 K showing the atom numbering scheme.

An automated RIGAKU AFC-5 diffractometer with a cold nitrogen gas flow equipment was used for the low-temperature data collection of BSP and DSPY. Twenty-five reflections for BSP and twenty-one reflections for BSDAP with $20°<2\theta<30°$ were used to determine the lattice parameters. The crystal data are shown in Table 1. The intensity data were collected in the region $2\theta<60°$ for both compounds ($-20\leqq h\leqq 18$, $0\leqq k\leqq 6$, $0\leqq l\leqq 17$ for BSP; $-17\leqq h\leqq 17$, $0\leqq k\leqq 30$, $0\leqq l\leqq 5$ for DSPY) in θ-2θ mode (scan width, $(1.2+0.5\tan\theta)°$) at a scan rate of 3° min^{-1}. Background counts at each end were 8—21.5 s. The intensities of the three standards, monitored every 100 data measurements, remained constant within 1% for both compounds. 2525 unique reflections for BSP and 3529 unique reflections for DSPY were measured. 1050 independent reflections (BSP) and 1160 reflections (DSPY) with $|F_o|>3\sigma(F_o)$ were used for structure analyses.

Crystal structures were solved by a direct method and all hydrogen atoms were determined from difference synthesis maps. A block-diagonal least-squares technique (UNICS III[6]) with anisotropic thermal parameters for nonhydrogen atoms and isotropic for hydrogen atoms (weighting scheme, $1/w=\sigma^2+(0.015|F_o|)^2$) was employed for the structure refinement.

Results and Discussion

BSP. The molecular structure derived at 108 K is shown in Fig. 1; the atomic parameters are listed in Table 2.[7] As can be seen from the thermal parameters, a reduction of the thermal motion by lowering the

Table 2. Atomic Parameters for BSP at 108 K

	x	y	z	B_{eq}/Å^2
		(×10^4)		
O	7922(1)	−2627(4)	1390(2)	1.5
N	8634(1)	−5698(4)	95(2)	0.9
C1	7338(2)	−2138(5)	−753(2)	0.9
C2	7293(2)	−1408(5)	355(2)	1.1
C3	6591(2)	652(5)	398(2)	1.4
C4	5948(2)	1950(5)	−645(2)	1.4
C5	5995(2)	1298(5)	−1753(2)	1.3
C6	6687(2)	−746(5)	−1797(2)	1.1
C7	8037(2)	−4308(5)	−845(2)	1.0
C8	9307(2)	−7841(5)	−4(2)	0.9
C9	9962(2)	−9076(5)	1072(2)	1.0
C10	10648(2)	−11206(5)	1083(2)	1.0
	x	y	z	B/Å^2
		(×10^3)		
H3	658(2)	101(6)	118(2)	2.0(0.6)
H4	543(2)	320(7)	−63(2)	2.2(0.6)
H5	553(2)	213(6)	−249(2)	1.5(0.6)
H6	673(2)	−127(6)	−259(2)	1.5(0.6)
H7	802(2)	−456(6)	−166(2)	1.7(0.6)
H9	995(2)	−841(6)	184(2)	1.4(0.6)
H10	1112(2)	−1181(6)	184(2)	0.9(0.5)
H11	837(3)	−357(9)	122(3)	7.0(1.1)

temperature was observed in all atoms except for the hydroxyl hydrogen H11. The interatomic distances and bond angles are listed in Table 3 for 108 K and room temperature. At room temperature, an alternation of bond lengths, which is expected when there exists a resonance contribution from the *o*-quinonoid structure, was recognized.[2] This tendency is less pronounced at 108 K. However, an alternation of the bond lengths still remains. From optical measurements, the energy difference between the enol and keto species was evaluated as being ca. 0.1 eV.[2] The thermal energy at 108 K is, thus, low enough to settle more than 99.99% of the molecules into the enol from. Therefore, the partial keto-like contribution seems to already exist in BSP before the color change becomes noticeable. This may be a common feature of thermochromic *N*-salicylideneanilines, since a similar partial contribution from the keto-like structure was observed in *N*-(5-chlorosalicylidene)aniline at 90 K.[4] The largest change in the bond length as a result of temperature appears in the N–C8 bond. The distance is shorter by 0.026 Å at 108 K than at room temperature. The conjugation system is not completely continuous in the limited structure of the proton-transferred species. Thus, the shorter N–C8 distance may indicate that the conjugation system is more extended at low temperatures.

Table 3. Interatomic Diastances and Bond Lengths of BSP

	Room temperature	108 K
Distance	*l*/Å	*l*/Å
C1–C2	1.404(3)	1.406(4)
C2–O	1.349(2)	1.350(3)
C2–C3	1.396(3)	1.405(4)
C3–C4	1.376(3)	1.378(3)
C4–C5	1.386(4)	1.399(4)
C5–C6	1.379(3)	1.390(4)
C1–C6	1.401(2)	1.402(3)
C1–C7	1.448(3)	1.456(4)
C7–N	1.284(2)	1.297(3)
N–C8	1.448(3)	1.422(3)
C8–C9	1.391(2)	1.398(3)
C9–C10	1.382(3)	1.391(4)
C8–C10′	1.395(3)	1.401(4)
O···N	2.607(2)	2.599(3)
Angle	*θ*/°	*θ*/°
C2–C1–C7	121.9(2)	121.8(2)
C6–C1–C2	118.5(2)	119.0(2)
C1–C2–O	121.2(2)	121.3(2)
C1–C2–C3	119.8(2)	119.8(2)
C2–C3–C4	120.1(2)	120.0(3)
C3–C4–C5	121.0(2)	121.0(3)
C4–C5–C6	119.2(2)	119.0(2)
C5–C6–C1	121.4(2)	121.1(3)
C6–C1–C7	119.6(2)	119.2(2)
C1–C7–N	121.9(2)	121.1(2)
C7–N–C8	121.6(2)	120.8(2)
N–C8–C9	116.8(2)	116.3(2)
C8–C9–C10	121.5(2)	121.3(3)
C9–C8–C10′	118.2(2)	118.6(2)
N–C8–C10′	125.0(2)	125.1(2)
C8′–C10–C9	120.4(2)	121.3(2)

The molecular packing in the lattice is practically the same as that observed at room temperature.[2] The temperature dependence of the lattice parameters are shown in Fig. 2(a). The thermal contraction is most noticeable in the *c** direction, which corresponds to the direction of side-by-side molecular arrangement. The interplanar distance between the mean molecular planes becomes shorter at 108 K (3.26 Å) than at room temperature (3.29 Å). The molecular overlap is shown in Fig. 3. This overlapping mode is convenient for the charge-transfer interaction to operate between the molecules. The azomethine (–CH=N–) groups act as an acceptor relative to the benzene rings in the OH species, and all –CH=N– groups effectively overlap with the benzene rings. When the temperature is

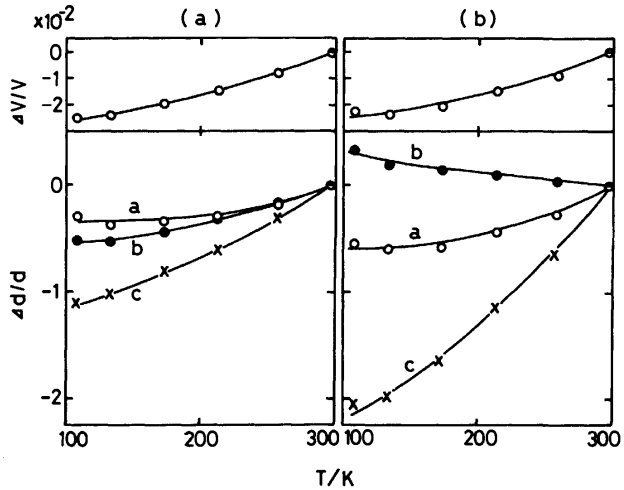

Fig. 2. Temperature dependence of lattice parameters (d and V are the room temperature parameters and volume, respectively, $\Delta d=d(T)-d$, and $\Delta V=V(T)-V$); BSP (a) and DSPY (b).

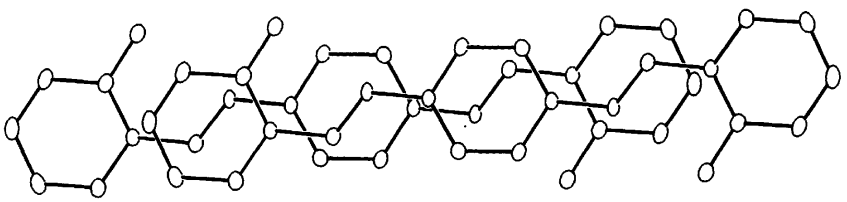

Fig. 3. Molecular overlapping between the BSP molecules.

increased, namely the content of the NH species is increased, the newly formed *p*-phenylenediamine moiety becomes a donor part and the *o*-quinonoid moiety becomes an acceptor part. The thermochromic band is, thus, assigned to the charge-transfer transition between these donor and acceptor portions.[2] Intermolecular charge-transfer interactions between such donor and acceptor portions may operate at higher temperatures.

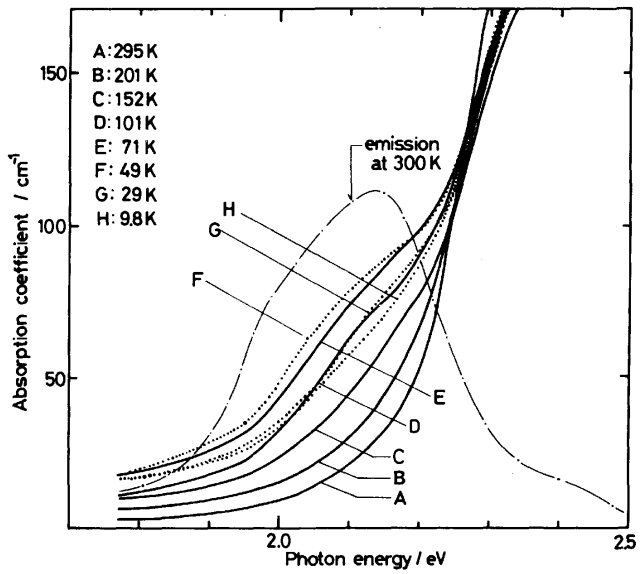

Fig. 4. Single crystal absorption spectral changes with temperature for DSPY.

DSPY. Although the molecule has a common framework with BSP, the optical properties observed for DSPY are significantly different from those observed for BSP. Figure 4 shows the single-crystal visible absorption spectra over a wide temperature range. The spectra change slightly at low temperatures. However, when the temperature is increased, noticeable growth of a new absorption observed in BSP does not occur in DSPY. The emission spectrum obtained at 300 K are also shown in Fig. 4, which corresponds well to the absorption spectra. In BSP the emission spectra show a large Stokes shift, which is a characteristic of the proton-transfer reaction. Judging from the absorption spectra, it can be concluded that the thermal proton-transfer reaction does not occur in the DSPY system.

The existence of a weak absorption band in the lower-energy region at low temperatures is interesting from a different point of view. Since this band diminishes at higher temperatures, it is obviously not related to the thermal proton transfer. In general, such growth of absorption at the lower-energy side by lowering the temperature is unusual, and the origin and mechanism of this growth in DSPY are unknown at the present stage.

The infrared spectra of DSPY were recorded at room temperature and at 6.3 K (Fig. 5). The position of the OH stretching mode shifts slightly with temperature; ca. 2800 cm^{-1} at 6.3 K, ca. 2850 cm^{-1} at room temperature. However, the peak profile does not change essentially. Thus, the results of the infrared spectra also suggests that the thermal proton-transfer process

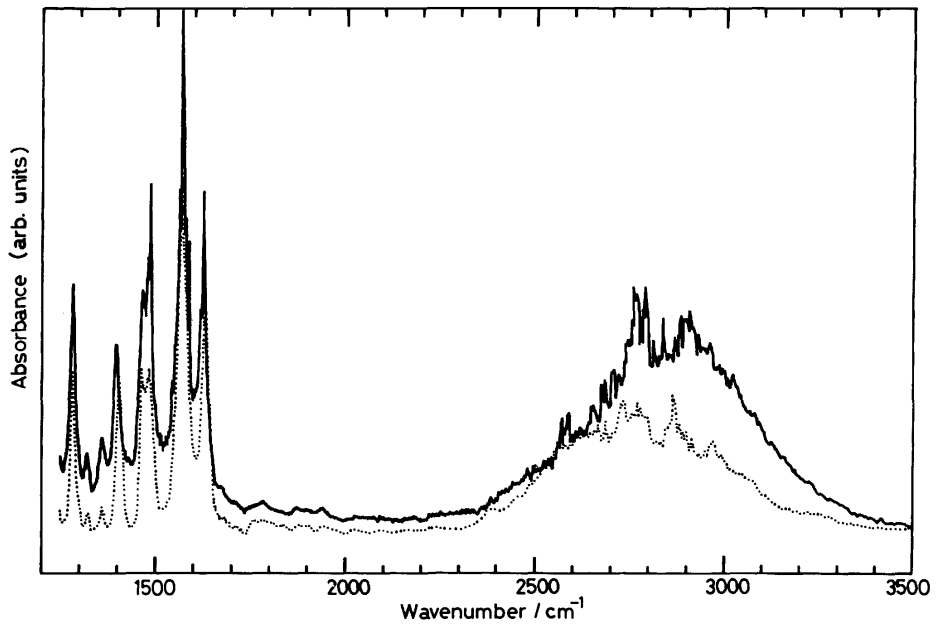

Fig. 5. Single crystal infrared spectra for DSPY at room temperature (solid line) and at 6.3 K (dotted line). The full scale does not coincide with each other because of the difference in the experimental conditions.

is absent in the DSPY system.

As shown in Fig. 6, a significant difference of the molecular structure was found by X-ray analysis. The atomic parameters are listed in Table 4;[7] the bond lengths and angles for both temperatures are listed in Table 5. Two terminal benzene rings are tilted with respect to the central pyrene plane, and the molecule is largely deformed from the planar structure. This tilting angle does not change with temperature: 42.0° at room temperature and 42.4° at 108 K, and no significant changes of the molecular dimensions by temperature have been observed. In DSPY there is no contribution from the quinonoid structure.

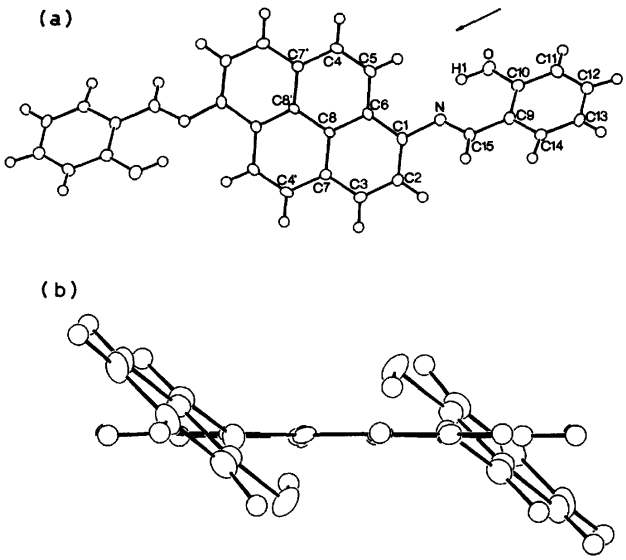

Fig. 6. ORTEP drawing of DSPY at 108 K showing the atom numbering scheme (a) and side view along the arrow indicated (b).

The observed O···N distance is slightly longer than that of BSP. However, the difference is small and it is not likely that the difference in the optical properties arises from it. The observed frequency of the OH stretching mode of DSPY is in good agreement with the value predicted from the Novak's relationship between the position of ν_{OH} and the O···N distance.[8]

The temperature dependence of the lattice parameters are shown in Fig. 2(b), and the crystal structure at 108 K is shown in Fig. 7. By lowering temperature, the length of the *b*-axis is slightly increased, while that of the *c*-axis is decreased. Consequently, the interplanar distance between the pyrene rings is shortened, i.e., 3.43 Å at room temperature and 3.39 Å at 108 K. However, all interatomic distances between the mole-

Table 4. Atomic Parameters for DSPY

	<108 K>					<300 K>			
	x	*y*	*z*	B_{eq}/Å^2		*x*	*y*	*z*	B_{eq}/Å^2
		(×10^4)					(×10^4)		
O	6262(2)	2575(1)	7075(6)	1.8	O	6289(2)	2568(1)	7003(8)	5.3
N	4791(2)	1875(1)	3902(7)	1.3	N	4811(2)	1870(1)	3900(8)	3.5
C1	4381(2)	1276(1)	2973(8)	1.1	C1	4402(3)	1271(2)	2983(10)	3.1
C2	3362(2)	1103(1)	3603(8)	1.1	C2	3393(3)	1097(2)	3605(10)	3.4
C3	3000(2)	504(1)	2823(8)	1.2	C3	3031(3)	501(2)	2834(10)	3.2
C4	6724(2)	568(1)	−580(8)	1.1	C4	6712(3)	567(2)	−576(10)	3.3
C5	6101(3)	996(1)	821(8)	1.1	C5	6102(3)	990(2)	839(10)	3.2
C6	5051(2)	839(1)	1554(8)	0.9	C6	5060(3)	836(2)	1550(10)	2.8
C7	3631(2)	56(1)	1384(8)	1.0	C7	3648(3)	55(2)	1377(10)	2.9
C8	4671(2)	226(1)	735(8)	0.9	C8	4677(3)	225(2)	733(10)	2.7
C9	4578(3)	2973(1)	4671(8)	1.2	C9	4610(3)	2969(2)	4740(11)	3.6
C10	5588(3)	3062(2)	6455(8)	1.3	C10	5618(3)	3056(2)	6500(11)	3.9
C11	5911(3)	3656(2)	7635(9)	1.6	C11	5939(3)	3644(2)	7635(11)	4.5
C12	5242(3)	4164(2)	6998(9)	1.7	C12	5270(4)	4151(2)	7109(12)	4.9
C13	4246(3)	4088(1)	5211(9)	1.6	C13	4280(3)	4080(2)	5384(13)	4.9
C14	3924(3)	3498(1)	4071(9)	1.4	C14	3954(3)	3491(2)	4258(12)	4.5
C15	4204(3)	2361(1)	3479(8)	1.3	C15	4235(3)	2361(2)	3569(10)	3.6
	x	*y*	*z*	*B*/Å^2		*x*	*y*	*z*	*B*/Å^2
		(×10^3)					(×10^3)		
H1	595(4)	219(2)	570(15)	10.5(1.7)	H1	604(5)	218(3)	557(16)	14.8(2.0)
H2	290(2)	141(1)	474(8)	1.1(0.7)	H2	294(3)	142(2)	459(9)	5.4(1.0)
H3	226(2)	40(1)	334(8)	1.7(0.7)	H3	228(3)	34(2)	330(9)	4.7(0.9)
H4	746(3)	69(1)	−106(9)	2.0(0.9)	H4	744(3)	72(1)	−114(9)	4.5(0.9)
H5	636(2)	143(1)	136(9)	2.0(0.8)	H5	633(3)	143(2)	123(9)	5.2(1.0)
H11	660(3)	369(2)	910(12)	4.6(1.2)	H11	664(4)	371(2)	912(12)	9.1(1.4)
H12	547(4)	459(2)	827(14)	6.0(1.5)	H12	550(4)	454(2)	826(12)	8.6(1.4)
H13	377(3)	445(2)	474(10)	2.7(0.9)	H13	376(3)	448(2)	527(10)	6.0(1.0)
H14	320(3)	340(2)	276(10)	3.2(0.9)	H14	322(4)	341(2)	359(14)	11.3(1.6)
H15	345(3)	233(2)	214(9)	2.3(0.8)	H15	350(3)	231(1)	233(9)	4.3(0.9)

Table 5. Interatomic Distances and Bond Angles of DSPY

	Room temperature	108 K		Room temperature	108 K
Distance	l/Å	l/Å	N-C1-C2	121.8(3)	121.8(3)
C1-C2	1.398(6)	1.403(5)	C1-C2-C3	120.6(4)	120.4(3)
C1-C6	1.409(5)	1.412(4)	C2-C3-C7	121.5(4)	121.5(3)
C1-N	1.413(5)	1.417(4)	C5-C4-C7′	121.3(4)	121.6(3)
C2-C3	1.376(5)	1.386(4)	C4-C5-C6	121.3(3)	121.0(3)
C3-C7	1.395(5)	1.399(5)	C1-C6-C5	122.5(3)	122.3(3)
C4-C5	1.349(6)	1.358(5)	C1-C6-C8	118.9(3)	119.1(3)
C4-C7′	1.430(5)	1.435(4)	C5-C6-C8	118.6(3)	118.7(3)
C5-C6	1.437(5)	1.442(5)	C3-C7-C4′	122.4(4)	122.4(3)
C6-C8	1.418(5)	1.423(4)	C3-C7-C8	118.5(3)	118.6(3)
C7-C8	1.423(5)	1.427(4)	C4′-C7-C8	119.1(3)	119.0(3)
C8-C8′	1.426(5)	1.433(4)	C6-C8-C7	120.3(3)	120.2(3)
C9-C10	1.419(6)	1.417(5)	C6-C8-C8′	120.2(3)	120.4(3)
C9-C14	1.400(5)	1.406(5)	C7-C8-C8′	119.5(3)	119.7(3)
C9-C15	1.442(6)	1.452(5)	C10-C9-C14	118.2(4)	118.3(3)
C10-C11	1.380(6)	1.396(5)	C10-C9-C15	122.0(4)	122.0(3)
C10-O	1.356(5)	1.361(4)	C14-C9-C15	119.7(4)	119.7(3)
C11-C12	1.385(6)	1.393(5)	C9-C10-O	120.7(4)	121.2(3)
C12-C13	1.388(6)	1.398(5)	C9-C10-C11	120.2(4)	120.3(3)
C13-C14	1.381(6)	1.386(5)	O-C10-C11	119.0(4)	118.5(3)
C15-N	1.283(5)	1.285(4)	C10-C11-C12	120.0(4)	119.7(3)
O···N	2.614(4)	2.612(3)	C11-C12-C13	121.1(4)	120.9(3)
			C12-C13-C14	119.1(4)	119.2(3)
Angle	γ/°	γ/°	C9-C14-C13	121.4(4)	121.5(3)
C2-C1-C6	120.1(3)	120.1(3)	C9-C15-N	122.0(4)	121.3(3)
N-C1-C6	118.0(3)	118.0(3)	C1-N-C15	120.9(3)	120.1(3)

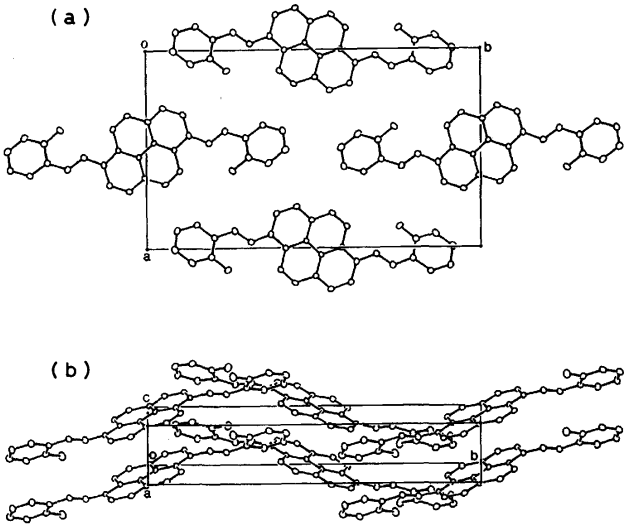

Fig. 7. Crystal structure of DSPY at 108 K; projection onto the (001) plane (a) and stacking structure (b).

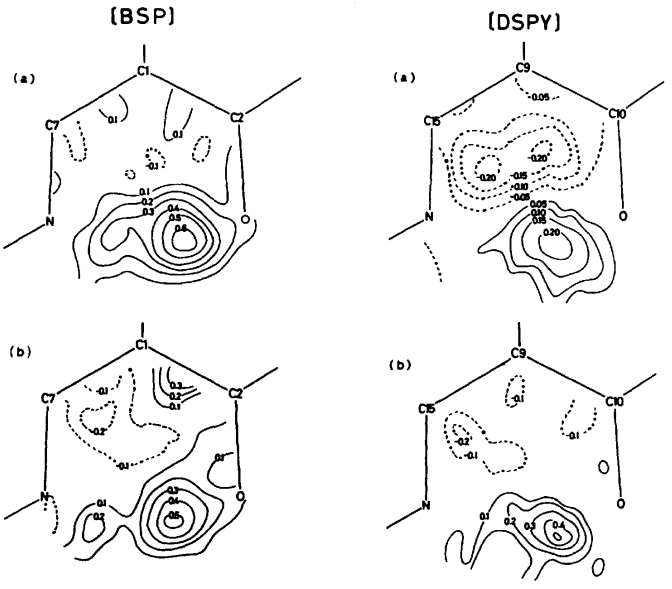

Fig. 8. Difference syntheses of the hydrogen bonded chelate ring of BSP and DSPY (e Å^{-3}); room temperature (a) and 108 K (b).

cules are larger than 3.4 Å, and there is no effective intermolecular interactions.

The results of the optical and structural studies of DSPY and BSP provide important information about the mechanism of the thermal proton transfer in *N*-salicylideneanilines. The geometrical circumstances of the hydroxyl hydrogen in DSPY are the same that in BSP. However, all data indicate no occurrence of thermal proton transfer in DSPY. In the case of BSP, the conjugation system is extended in the whole molecule, since the molecule is planar. Thus, the conjugation system in the central aromatic ring can participate in the stabilization of the partial contribution from the keto-like π-electron distribution. On the other hand, DSPY is not planar; thus, the conjugation system of the central aromatic ring is isolated from the terminal ones. In such a structure, the conjugation

system of the central aromatic group is not able to participate in the stabilization of the keto-like contribution. This seems to be important, since the partial contribution from the keto-like π-electron distribution in BSP is recognized even before the color change has become noticeable. It can therefore be concluded that one of the conditions required for the thermal proton transfer in *N*-salicylideneanilines is that the molecule is planar so that the conjugation system is sufficiently extended to be capable of the corresponding π-electron configuration of the isomer.

Another interesting feature observed in both BSP and DSPY is the large thermal parameters of the hydroxyl hydrogens, even at 108 K. Then, the difference syntheses were calculated by taking the parameters of the hydroxyl hydrogen out of the refined structures; the maps with regard to the hydrogen-bonded chelate rings are shown in Fig. 8. In DSPY, it is clearly seen that there exists only the OH proton at both temperatures. On the other hand, in addition to the OH proton, a contribution from the NH proton in BSP can be seen from the map. Thus, the differences in the optical properties between BSP and DSPY seem to be reflected in these maps. At low temperature, there still remains the contribution from the NH proton in BSP. In general, it is difficult to discuss quantitatively such a hydrogen distribution merely from the X-ray results. The microscopic aspect of the proton behavior in BSP will be clarified by more suitable techniques such as neutron diffractions or nuclear magnetic resonances.

We are grateful to Dr. Koshiro Toriumi of IMS for his helpful discussions about X-ray analysis.

References

1) The abbreviation is adopted from *N,N'*-bis(salicylidene)-*p*-phenylenediamine in Ref. 2.

2) N. Hoshino, T. Inabe, T. Mitani, and Y. Maruyama, *Bull. Chem. Soc. Jpn.*, **61**, 4207 (1988).

3) M. D. Cohen, G. M. J. Schmidt, and S. Flavian, *J. Chem. Soc.*, **1964**, 2041. E. Hadjoudis, *J. Photochem.*, **17**, 355 (1981).

4) J. Bregman, L. Leiserowitz, and G. M. Schmidt, *J. Chem. Soc.*, **1964**, 2068.

5) H. Vollman, H. Becker, M. Corell, H. Streek, and G. Langbein, *Justus Liebigs Ann. Chem.*, **531**, 1 (1937).

6) T. Sakurai and K. Kobayashi, *Rep. Inst. Phys. Chem. Res.*, **55**, 69 (1979).

7) The lists of structure factors and anisotropic thermal parameters for nonhydrogen atoms are deposited at the Office of the Editor of Bull. Chem. Soc. Jpn. (Document No. 8886).

8) A. Novak, *Struct. Bonding*, **18**, 177 (1974).

9) C. K. Johnson, ORTEP, Report ORNL-3794, Oak Ridge National Laboratory, Tennessee (1976).

Crystal Structures and Electrical Properties of Tetrakis(methylseleno)-tetrathiafulvalene ($TSeC_1$-TTF) and Two Phases of ($TSeC_1$-TTF)I_3

Ping WANG,* Tamotsu INABE, Chikako NAKANO, Yusei MARUYAMA,*
Hiroo INOKUCHI,* Naoko IWASAWA,† and Gunzi SAITO†
Institute for Molecular Science, Myodaiji, Okazaki 444
†The Institute for Solid State Physics, The University of Tokyo, Roppongi, Tokyo 106
(Received November 28, 1988)

The crystal structure and the electrical property of $TSeC_1$-TTF as well as those of the new complex ($TSeC_1$-TTF)I_3 with two kinds of phases are reported. The crystal structure of $TSeC_1$-TTF was determined to be monoclinic, space group $P2_1/a$, a=7.728(1), b=20.952(4), c=5.315(1) Å, and β=90.57(2)° having a unit cell volume of 860.6(3) Å^3. By an electrochemical method and a diffusion method, $TSeC_1$-TTF gave two forms of single crystals of ($TSeC_1$-TTF)I_3. The crystal data of one form; monoclinic, space group $P2_1/n$, a=24.359(1), b=11.831(3), c=7.842(6) Å, β=96.71(4)°, V=2244(1) Å^3 and those of the other; monoclinic, space group $P2_1/a$, a=23.174(5), b=11.727(3), c=8.960(5) Å, β=110.54(2)°, V=2280(1) Å^3. The former complex has lower resistivity, 4.1×10^4 Ω cm, compared with the latter one 1.1×10^8 Ω cm. The dimerization is more noticeable in the latter complex than in the former one.

For the purpose of developing organic molecules directed toward organic conductors, a family of TYC_n-TTF (Y=S, Se, and Te, n=1—18), shown in Fig. 1, has been prepared and the crystal structures and properties have been widely investigated.[1-3] As a part of the investigation, a variety of the charge-transfer complexes based on the TYC_n-TTF family have also been obtained,[4] and some of them show relatively high conductivities. In this paper the crystal structures and electrical properties of the donor $TSeC_1$-TTF and the new complex ($TSeC_1$-TTF)I_3 with two kinds of phases are presented.

Experimental

The synthesis of $TSeC_1$-TTF compound was reported in the preceding paper.[5] Two kinds of single crystals of $TSeC_1$-TTF were prepared by slow cooling method using different solvents after several days. Dark-red block-like single crystals of ($TSeC_1$-TTF) were grown in hexane solution with higher resistivity 8.5×10^7 Ω cm and higher melting point 106.3 °C, ($TSeC_1$-TTF)(H). On the other hand, red needle-like single crystals ($TSeC_1$-TTF) were grown in a mixed solvent of hexane and benzene with lower resistivity 1.0×10^6 Ω cm and lower melting point 92.5 °C, ($TSeC_1$-TTF)(L). Needle-like single crystals of ($TSeC_1$-TTF)I_3 were obtained by a diffusion method using iodine as an acceptor in a benzene solution after several days, which were black-colored needle-like crystals and the typical size was $0.01\times0.6\times0.01$ mm^3, ($TSeC_1$-TTF)I_3(N). On the other hand,

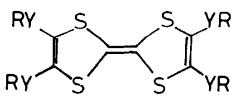

$R=-C_nH_{2n+1}$

Fig. 1. The molecular structure of TYC_n-TTF (Y= Selenium for $TSeC_n$-TTF, Y=sulfur for TTC_n-TTF and Y=tellurium for $TTeC_n$-TTF).

block-like single crystals of ($TSeC_1$-TTF)I_3 were obtained by an electrochemical method, ($TSeC_1$-TTF)I_3(B). In this method, tetrabutylammonium triiodide ($TBAI_3$) (50 mg) and $TSeC_1$-TTF (14.7 mg) were dissolved in a mixed solvent of THF and acetonitrile with a ratio of 1:10 with gentle heating under an argon atmosphere. Electrochemical oxidation was carried out with a constant current of 1 μA at a constant temperature (25 °C) on a vibration-free table. After 20 days, the anode was covered with a black-colored block-like microcrystalline material. The typical size of the crystals is $0.01\times0.02\times0.02$ mm^3, which is too small for a conductivity measurement.

The X-ray diffraction data collection was carried out with a Rigaku automated four-circle X-ray diffractometer AFC-5R and AFC-5 for the donor molecule ($TSeC_1$-TTF)(H) and the complexes of ($TSeC_1$-TTF)I_3(N) and ($TSeC_1$-TTF)I_3(B), respectively. For the compound of ($TSeC_1$-TTF)(H) the crystal data is: $Se_4S_4C_{10}H_{12}$, F.W. 575.84, monoclinic, space group $P2_1/a$, a=7.728(1), b=20.952(4), c=5.315(1) Å, β=90.57(2)°, V=860.6(3) Å^3, Z=2, D_{calc}=2.22 g cm^{-3} and μ(Mo $K\alpha$) =95.97 cm^{-1}. Intensity data was measured by the θ-2θ scan technique on the diffractometer with graphite monochromatized Mo $K\alpha$ radiation ($2\theta<60°$). 2830 unique reflections were measured. The structure was solved by the direct method using MULTAN 78 program system[6] and refined by the block-diagonal least-squares procedure using 1391 independent reflections with $|F_o|>3\sigma(|F_o|)$. After absorption correction the refinement was converged to a final R value of 0.063. For the complex ($TSeC_1$-TTF)I_3(N) the crystal data is: $Se_4S_4C_{10}H_{12}I_3$, F.W. 956.54, monoclinic, space group $P2_1/a$, a=23.174(5), b=11.727(3), c=8.960(5) Å, β=110.54(2)°, V=2280(1) Å^3, Z=4, D_{calc}=2.788 g cm^{-3} and μ(Mo $K\alpha$)=107.38 cm^{-1}. Intensity data were measured by the θ-2θ scan technique on the diffractometer with graphite monochromatized Mo $K\alpha$ radiation ($2\theta<60°$). 5928 unique reflections were measured. The structure was solved by the direct method using MULTAN 78 program system[6] and refined by the block-diagonal least-squares procedure using 1440 independent reflections with $|F_o|>3\sigma(|F_o|)$. After absorption correction the refinement was converged to a final R value of 0.069. For the complex ($TSeC_1$-TTF)I_3(B), the crystal data is: $Se_4S_4C_{10}H_{12}I_3$, F.W. 956.54, monoclinic, space group $P2_1/n$, a=24.359(7), b=11.831(3), c=7.842(6) Å, β=96.71(4)°, V=

2245(2) Å^3, Z=4, D_{calc}=2.83 g cm^{-3}, and μ(Mo $K\alpha$)=109.09 cm^{-1}. Intensity data was measured by the θ-2θ scan technique on the diffractometer with graphite monochromatized Mo $K\alpha$ radiation ($2\theta<60°$). 6904 unique reflections were measured. The structure was solved according to the Patterson method and refined by the block-diagonal least-squared procedure using 1857 independent reflections ($|F_o|>3\sigma(|F_o|)$). After absorption correction the refinement was converged to a final R value of 0.063. For all these analyses, anisotropic thermal parameters were adopted for all nonhydrogen atoms, and the hydrogen atoms were refined isotropically.[7]

The electrical resistivities were measured by a two probe method. The electrical contacts to the specimen crystals were made with gold paint. Only for ($TSeC_1$-TTF)I_3(B) polycrystalline samples were used, because the single crystal size was too small to measure the resistivity.

Results and Discussion

$TSeC_1$-TTF. The atomic coordinates for ($TSeC_1$-TTF)(H) are listed in Table 1. The molecular and crystal structures are shown in Figs. 2 and 3. Along the c-axis, the $TSeC_1$-TTF molecules are stacked with overlapping as shown in Fig. 3(c), where the distance between the two C_2S_4 molecular planes is 3.481(3) Å. The shortest intermolecular Se-Se contact is 3.670(1) Å which is much shorter than the sum of the van der Waals radii (4.00 Å). The shortest intermolecular S-S contact is 3.663(3) Å, which is still shorter than the sum of the van der Waals radii (3.70 Å). The shortest intermolecular S-Se contact is 3.890(2) Å, which is a little longer than the sum of the van der Waals radii (3.85 Å). The molecule has a special structure which is neither of the chair nor boat form and is of similar to that of $TSeC_4$-TTF's.[2] The four terminal Se-C bonds of a molecule are almost perpendicular to each other. Such kind of molecular shape leads to the electrical resistivities of $7.3\times10^8/4.1\times10^9/8.5\times10^7$ (Ω cm), which is slightly anisotropic.

Table 1. Positional Parameters ($\times10^4$) and Equivalent (Isotropic Thermal Parameters of ($TSeC_1$-TTF)(H)

	X	Y	Z	B_{eq}/Å^2
Se1	2470 (1)	1366 (0)	−1950 (2)	3.4
Se2	−1282 (1)	2035 (0)	232 (2)	3.7
S1	1785 (2)	277 (1)	2012 (4)	3.0
S2	−1445 (3)	858 (1)	3855 (4)	3.2
C1	67 (9)	233 (4)	4162 (13)	2.5
C2	1146 (9)	1011 (3)	676 (13)	2.4
C3	−297 (9)	1268 (4)	1498 (13)	2.6
C4	4535 (13)	868 (6)	−1748 (22)	6.4
C5	−911 (14)	2572 (5)	3212 (17)	4.8

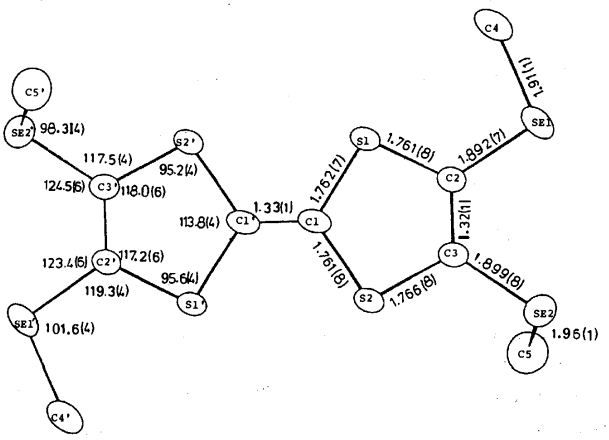

Fig. 2. ORTEP[8] drawing of $TSeC_1$-TTF(H) showing bond lengths and bond angles.

It should be noted here that $TSeC_1$-TTF, by using different solvent, gives two kinds of single crystal with the same chemical composition and the same density but displaying very different physical properties. One is block-like dark red single crystal with higher melting point and higher resistivity [($TSeC_1$-TTF)(H)]; and the other one is needle-like red single crystal with lower melting point and lower resistivity [($TSeC_1$-TTF)(L)]. The difference in resistivity is about 2 orders. The crystal data are still quite different. However, the structure analysis for the single crystal with lower melting point [($TSeC_1$-

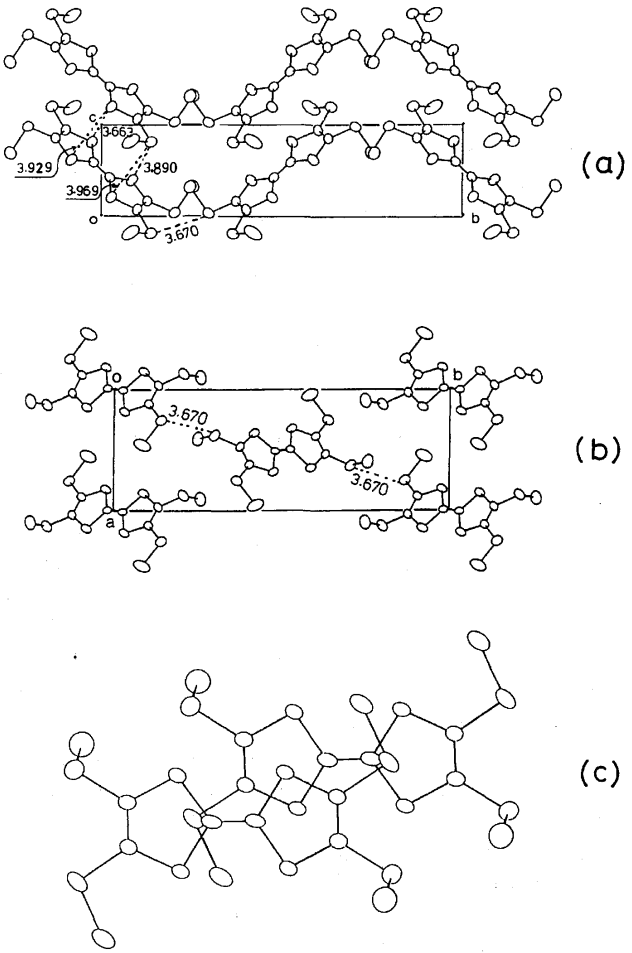

Fig. 3. The crystal structure of $TSeC_1$-TTF(H) projected along the a-axis (a), projected along the c*-axis (b), and the mode of overlapping of $TSeC_1$-TTF (c).

Table 2. Crystal Data and Resistivities

	$TSeC_1$-TTF(L)	$TSeC_1$-TTF(H)	$(TSeC_1$-TTF$)I_3$(B)	$(TSeC_1$-TTF$)I_3$(N)
T_m/°C	92.5	106.3		
ρ_{RT}/Ω cm	1.03×10^6	8.5×10^7	$4.1\times10^{4a)}$	1.1×10^8
	Red needle-like	Dark red block-like	Black block-like	Black needle-like

a) The resistivity was measured by using polycrystalline samples.

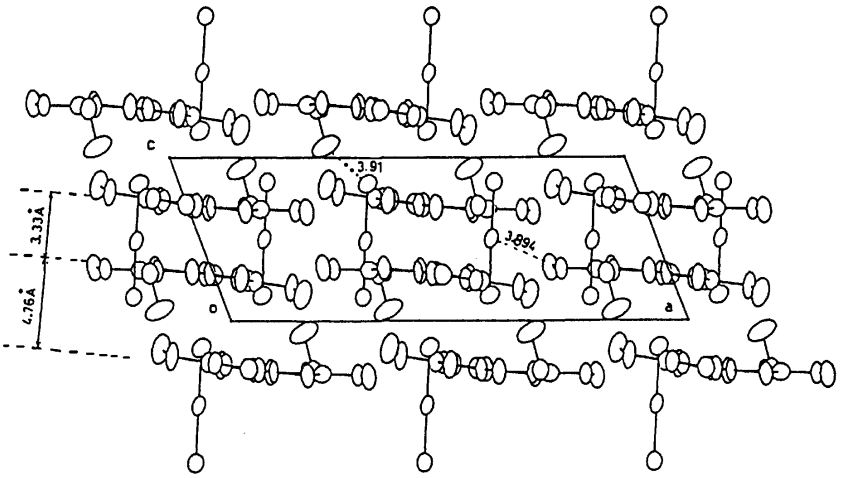

Fig. 4. Crystal structure of $(TSeC_1$-TTF$)I_3$(N) projected along the b-axis.

TTF)(L)] is somehow difficult. To elucidate the interesting problem of the donor molecule itself, some more detailed works are going on.

Comparing with TTC_1-TTF and $TTeC_1$-TTF,[9] the magnitude of resistivity of $TSeC_1$-TTF(H) is just in between of them. In TTC_1-TTF the central C_6S_8 moiety is nonplanar and the molecular structure has a boat form. Because of the weak intermolecular interactions between adjacent C_6S_8 moieties and the absence of discernible intermolecular overlaps between adjacent π systems, the resistivity is as high as 2.9×10^{10} Ω cm, which is much higher than that of $TSeC_1$-TTF in high or low phase. For $TTeC_1$-TTF[10] the magnitude of the resistivity, 8.1×10^4 Ω cm, is the lowest in the TYC_1-TTF group (Y=S, Se, and Te). The central $C_6S_4Te_4$ moiety of $TTeC_1$-TTF is planar unlike TTC_1-TTF and $TSeC_1$-TTF. $TTeC_1$-TTF molecules are stacked to form a column structure with the interplanar distance of 3.76 Å. Tellurium atoms between neighboring columns form zigzag chains along the stacking axis of $TTeC_1$-TTF molecules. The distance between those two Te atoms is 3.644(2) Å, which is significantly shorter than the van der Waals distance (4.12 Å).

$(TSeC_1$-TTF$)I_3$(N). The atomic coordinates for the crystal of $(TSeC_1$-TTF$)I_3$(N) are listed in Table 3. The crystal structure is shown in Figs. 4 and 5. Along the c-axis, $TSeC_1$-TTF molecules are stacked in the dimerized form with overlapping as shown in Fig. 5(b). The distances between the two optimal planes of the central C_2S_4 parts of a dimer and between those of two dimers are 3.33 and 4.76 Å, respectively. The shortest intermolecular Se–Se contact within the dimer is 3.845(6) Å (Fig. 4(b)), which is much shorter than the sum of the van der Waals radii (4.00 Å). The shortest

Table 3. Positional Parameters (×10⁴) and Equivalent Isotropic Thermal Parameters of $(TSeC_1$-TTF$)I_3$(N)

	X	Y	Z	B_{eq}/Å²
I1	1397 (1)	6944 (2)	5064 (3)	5.9
I2	1928 (1)	7074 (2)	8511 (3)	6.6
I3	871 (1)	6803 (2)	1576 (3)	8.0
Se4	693 (1)	13639 (3)	2486 (5)	6.8
Se5	−2326 (1)	8428 (3)	3210 (5)	7.2
Se6	−1382 (2)	6171 (3)	2944 (5)	7.0
Se7	1584 (2)	11394 (3)	2085 (6)	8.4
S8	−439 (4)	8078 (8)	3051 (13)	8.2
S9	−197 (3)	11750 (8)	2908 (12)	7.6
S10	−1219 (3)	9983 (8)	3267 (12)	7.4
S11	566 (4)	9856 (8)	2625 (14)	8.6
C12	−507 (12)	9550 (32)	3007 (40)	8.4
C13	836 (12)	11255 (22)	2440 (36)	5.3
C14	−1558 (13)	8615 (27)	3149 (37)	6.5
C15	−1200 (12)	7764 (27)	3089 (40)	6.9
C16	−82 (12)	10318 (28)	2915 (42)	7.5
C17	14 (14)	14320 (31)	2845 (43)	8.3
C18	475 (12)	12045 (24)	2602 (39)	6.4
C19	−1481 (20)	6011 (30)	691 (47)	10.7
C20	−2550 (14)	9937 (27)	3303 (47)	8.5
C21	1770 (17)	9835 (32)	1643 (54)	10.9

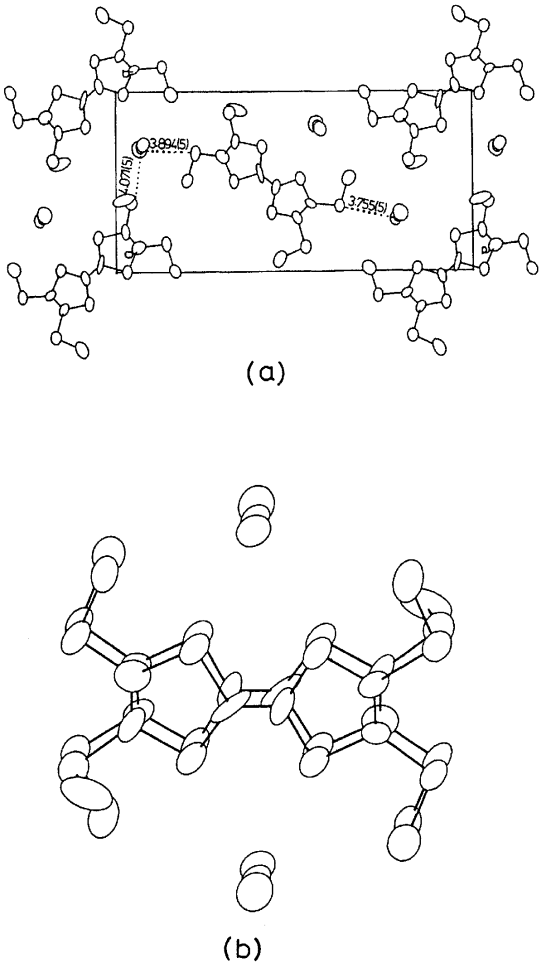

Fig. 5. Crystal structure of (TSeC1-TTF)I3(N) projected along the c*-axis (a) (only half of the molecules in a cell are shown here) and the mode of overlapping of TSeC1-TTF (b).

intermolecular S–S contact within the dimer is 3.4(1) Å, which is still much shorter than the sum of the van der Waals radii (3.70 Å). The shortest distance between the donor molecule and the acceptor molecule I_3, that is the Se–I contact, is 3.755(5) Å (Fig. 5(a)), which is still much shorter than the sum of the van der Waals radii (4.15 Å). The donor molecule TSeC1-TTF in the complex has a slightly bent structure (Fig. 6), the dihedral angles between the optimal plane of the central C_2S_4 part and the planes of the two C_2Se_2 parts are 6.51(9) and 1.8(4)°, respectively, and only one Se–C bond is obviously perpendicular to the connected C_2Se_2 part. Although the distances between Se and Se, and S and S are 3.845(6) and 3.40(1) Å within the dimer, which are much shorter than the respective sum

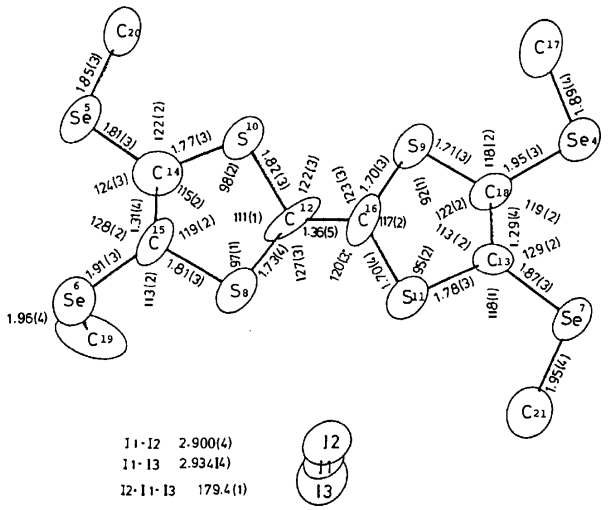

Fig. 6. ORTEP drawing of (TSeC1-TTF)I3 in the complex (TSeC1-TTF)I3(N) showing bond lengths and bond angles.

Table 4. Positional Parameters (×10⁴) and Equivalent Isotropic Thermal Parameters of (TSeC1–TTF)I3(B)

	X	Y	Z	B_{eq}/Å²
I1	1530 (1)	2050 (1)	983 (2)	3.8
I2	873 (1)	1593 (2)	3832 (3)	5.1
I3	2191 (1)	2397 (2)	−1798 (3)	5.3
Se4	−1283 (1)	−8998 (2)	5 (4)	3.9
Se5	488 (1)	−1517 (2)	3566 (4)	3.7
Se6	−2196 (1)	−6783 (2)	−1105 (4)	3.9
Se7	1368 (1)	−3641 (2)	4960 (4)	3.8
S8	−311 (3)	−3450 (5)	2057 (8)	3.3
S9	448 (3)	−5285 (5)	3181 (8)	3.2
S10	−469 (3)	−7091 (5)	1359 (8)	3.3
S11	−1210 (3)	−5215 (5)	408 (8)	3.1
C12	657 (10)	−3918 (18)	3729 (28)	3.0
C13	−1118 (11)	−7439 (20)	378 (31)	3.8
C14	−568 (9)	−5651 (18)	1388 (26)	2.2
C15	302 (11)	−3087 (19)	3191 (28)	3.6
C16	−166 (11)	−4887 (20)	2109 (28)	3.4
C17	−1513 (13)	−6595 (19)	−43 (30)	4.6
C18	−111 (11)	−894 (23)	2075 (40)	5.6
C19	−1557 (14)	−9281 (24)	2248 (37)	6.4
C20	1715 (11)	−5076 (26)	4891 (37)	5.3
C21	−2524 (13)	−5299 (24)	−696 (41)	6.1

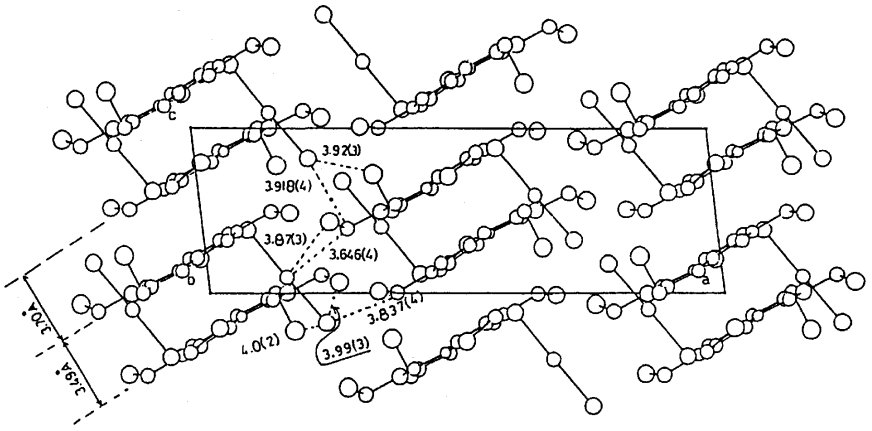

Fig. 7. Crystal structure of $(TSeC_1\text{-}TTF)I_3$(B) projected along the b-axis.

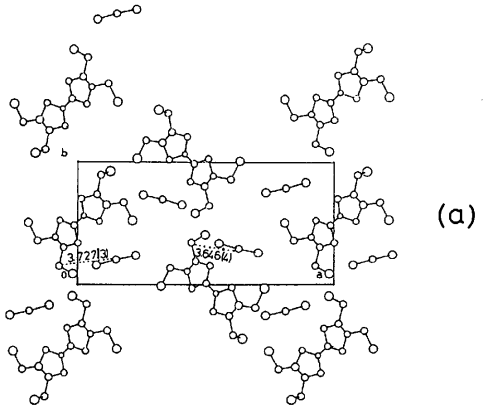

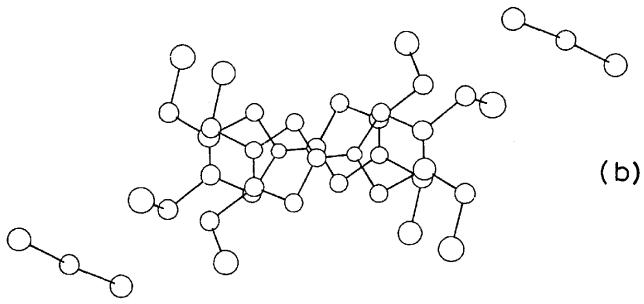

Fig. 8. Crystal structure of $(TSeC_1\text{-}TTF)I_3$(B) projected along the c*-axis (a) (only half of the molecules in a cell are shown here) and the mode of overlapping of $TSeC_1$-TTF (b).

of the van der Waals radii, the electrical conductivity is mainly dominated by the dimerized structure. Therefore, the resistivity appeared as high as $1.1\times10^8\ \Omega$ cm, which is in the same order as that of the donor $TSeC_1$-TTF(H) ($8.5\times10^7\ \Omega$ cm) and higher than that of the donor in another phase (TSeC$_1$-TTF)(L) ($1.0\times10^6\ \Omega$ cm).

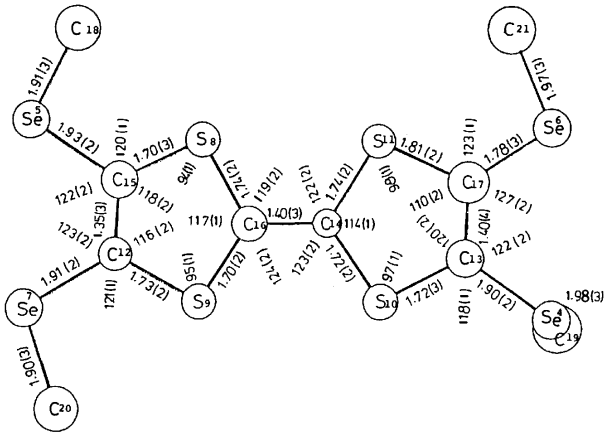

Fig. 9. ORTEP drawing of $TSeC_1$-TTF in the complex $(TSeC_1\text{-}TTF)I_3$(B) showing bond lengths and bond angles.

$(TSeC_1\text{-}TTF)I_3$(B). The atomic coordinates for the single crystal $(TSeC_1\text{-}TTF)I_3$(B) are listed in Table 4. The crystal and molecular structures are shown in Figs. 7, 8, and 9. The donor molecule has a bent structure, and the planes of the two C_2Se_2 parts are slightly bent towards the same direction from the optimal plane of central C_2S_4 part, where the dihedral angles between the optimal plane of the central C_2S_4 part and the planes of the two C_2Se_2 part are 2.0(2) and 4.2(2)°, respectively; and only one Se–C bond is obviously perpendicular to the connected C_2Se_2 part. Along the c-axis, the $TSeC_1$-TTF molecules are stacked in one-dimensional way with overlapping as shown in Figs. 7 and 8, and the distances between the two molecular planes are 3.49(1) and 3.70(2) Å, respectively. The difference between them is not so large as comparing with that of $(TSeC_1\text{-}TTF)I_3$(N). Thus, the degree of dimerization is relatively small. The shortest intermolecular Se–Se contact is 3.637(5) Å which is much shorter than the sum of the van der Waals radii. The shortest intermolecular S–S contact is 3.52(1) Å

which is still much shorter than the sum of the van der Waals radii. Although the shortest interplane distance, 3.49(1) Å, is longer than that of ($TSeC_1$-TTF)I_3(N) (3.33 Å) and the overlapped area (Fig. 8(b)) is smaller than that of ($TSeC_1$-TTF)I_3(N), the resistivity is as low as $4.1\times10^3\,\Omega$ cm even for the polycrystalline samples, because the degree of dimerization of this complex is much smaller than that of the complex ($TSeC_1$-TTF)I_3(N).

Comparing with the iodine complex of TTC_1-TTF, (TTM-TTF)$I_{2.47}$,[11] the resistivities of ($TSeC_1$-TTF)I_3(N) and ($TSeC_1$-TTF)I_3(B) are much higher than that of (TTM-TTF)$I_{2.47}$, $7-10\times10^{-3}\,\Omega$ cm. Anyhow, the relatively high resistivities of ($TSeC_1$-TTF)I_3(N) and ($TSeC_1$-TTF)I_3(B) should also be originated in the simple salt formation.

In summary, we have obtained two kinds single crystals for the donor molecules $TSeC_1$-TTF, ($TSeC_1$-TTF)(H), and ($TSeC_1$-TTF)(L). For the single crystal ($TSeC_1$-TTF)(H), the crystal structure has been analyzed. We have also obtained two kinds of single crystals of a 1:1 triiodide of $TSeC_1$-TTF, ($TSeC_1$-TTF)I_3(N), and ($TSeC_1$-TTF)I_3(B), depending on the preparation methods. Both of the crystal structures have been solved, and we found out some specific factors to understand their properties. We have measured the electrical properties for the complexes of a 1:1 triiodide of $TSeC_1$-TTF in the two different phases. Although the relatively high resistivities of these materials should be originated in the simple salt formation, the degree of dimerization still play a very important role to determine the electrical properties.

References

1) P. Wang, T. Enoki, K. Imaeda, H. Inokuchi, N. Iwasawa, H. Yamochi, H. Urayama, and G. Saito, *J. Phys. Chem.*, in press.

2) P. Wang, T. Mori, C. Nakano, Y. Maruyama, H. Inokuchi, N. Iwasawa, and G. Saito, *Bull. Chem. Soc. Jpn.*, **61**, 3455 (1988).

3) H. Inokuchi, G. Saito, P. Wu, K. Seki, T. B. Tang, T. Mori, K. Imaeda, T. Enoki, Y. Higuchi, K. Inaka, and N. Yasuoka, *Chem. Lett.*, **1986**, 1263.

4) N. Iwasawa, F. Shinozaki, G. Saito, K. Oshima, T. Mori, and H. Inokuchi, *Chem. Lett.*, **1988**, 215.

5) H. Yamochi, N. Iwasawa, H. Urayama, and G. Saito, *Chem. Lett.*, **1987**, 2265.

6) P. Main, S. E. Hull, L. Lessinger, G. Germain, J. P. Declercq, and M. M. Woolfson, MULTAN 78 (1987), Univs. of York, England and Louvain, belgium.

7) Tables of equations of the planes, anisotropic thermal parameters, F_o-F_c, coordinates of hydrogen atoms for the compounds of $TSeC_1$-TTF, ($TSeC_1$-TTF)I_3(N), and ($TSeC_1$-TTF)I_3(B), respectively, are deposited as Document No. 8884 at the office of the Editor of Bull. Chem. Soc. Jpn.

8) C. K. Johnson, ORTEP, Report ORNL-3794, Oak Ridge National Laboratory, Tennessee (1976).

9) K. Imaeda, T. Enoki, Z. Shi, P. Wu, N. Okada, H. Yamochi, G. Saito, and H. Inokuchi, *Bull. Chem. Soc. Jpn.*, **60**, 3136 (1987).

10) H. Inokuchi, K. Imaeda, T. Enoki, T. Mori, Y. Maruyama, G. Saito, N. Okada, H. Yamochi, K. Seki, Y. Higuchi, and N. Yasuoka, *Nature (London)*, **329**, 39 (1987).

11) P. Wu, T. Mori, T. Enoki, K. Imaeda, G. Saito, and H. Inokuchi, *Bull. Chem. Soc. Jpn.*, **59**, 127 (1986).

Dielectric Relaxation and Intermolecular Association for 1-Decanol. Temperature and Dilution Dependences of Monomer and Three Hydrogen-Bonded Species

Toshiomi SHINOMIYA†
School of Pharmaceutical Sciences, Kitasato University, Shirokane, Minato-ku, Tokyo 108
(Received December 8, 1988)

The dielectric constants and losses have been measured at frequencies from 1.35 to 4500 MHz for pure 1-decanol at 15—40 °C and for cyclohexane and heptane solutions of 1-decanol at 25°C. The absorption has been resolved into three different Debye-like dispersion regions. The assignments of the three regions were made as follows: the first region being due to a linear hydrogen-bonded chain polymer (C_1), the second one to a chain dimer and trimer (C_2), and the third one to a free monomer (C_3). Four concentrations of these species (C_{1-3}) and a nonpolar cyclic polymer (C_R) were evaluated by applying a modified Kirkwood-Fröhlich equation to each dispersion region. Each of the four concentrations indicates a reasonable behavior regarding the temperature and dilution dependences. The C_1 decreases and, mainly, the C_3 increases as the temperature increases. For cyclohexane and heptane solutions, the C_1 decreases rapidly and the C_R increases correspondingly with decreasing alcohol concentration. The free energies of activation are 23.2 for the first region, 17.3 for the second region, and 11.9 kJ mol^{-1} for the third region.

Many studies[1-3] have reported the co-existence of the alcohol monomer and various hydrogen-bonded species. There is now a general agreement that the alcohol molecule has a tendency to form aggregates in a dilute solution and in the pure liquid state. Wide-range measurements of complex dielectric constants also indicated two or three different dispersion regions. At low temperatures, Cole and Davidson[4] obtained three dispersion regions for 1-propanol. Dannhauser[5] also obtained three dispersion regions for 5-methyl-3-heptanol and 6-methyl-3-heptanol. He assigned the three dispersion regions to a free monomer, OR group in the linear chain structure, and the linear hydrogen-bonded chain species. At room temperatures, Lebrun[6] measured the dielectric constants and losses for higher normal alcohols at a frequency range of 1—9.5×10^3 MHz, obtaining two relaxation times. Garg and Smyth[7] obtained three relaxation times for the ten normal alcohols from propyl through undecyl at 16 wavelengths. They attributed the long relaxation time to the breaking of hydrogen bonds in molecular aggregates followed by ROH rotation, the intermediate relaxation time to a reorientation of a free monomer, and the short relaxation time to a relaxation of the hydroxyl group by rotation around its C–O bond. Glasser et al.[8] obtained two or three relaxation times for heptane solutions of some normal alcohols. In addition to the results of Garg and Smyth, they reported that the intermediate process is related to the reorientation of a free monomer and, possibly, a small multimer or a polymer chain segment.

We are studying hydrogen bonding and intermolecular structures in liquid alcohols. In a previous paper,[9] we proposed a modified Kirkwood-Fröhlich equation for obtaining the concentration of the first dispersion region for 28 linear alcohols. Now we have extended the investigations by performing the assignment of the three dispersion regions and by obtaining the four concentrations of monomer and three hydrogen-bonded species. The concentrations are discussed in terms of changes in the temperature and dilution.

Experimental

Purification of Materials. Commercial heptane was washed with mixed acid, concentrated sulfuric acid, water, 10% potassium hydroxide solution, 1 M potassium permanganate solution (1 M=1 mol dm^{-3}), and again with water. After standing over calcium chloride for 24 hours, it was fractionally distilled. The distillate was dried over calcium hydride and distilled before use. Cyclohexane was purified by the same method as heptane. 1-Decanol was fractionally distilled twice as described before[9] and finally distilled in a grease-free apparatus before use.

Apparatus. The dielectric constants and losses were measured using the following three apparatus over frequencies from 1.35 to 4500 MHz. A Boonton Radio RX meter (Type 250A) was used for measurements at frequencies of 1.35, 6.3, 17, 30, and 45 MHz. Measurements at frequencies 60, 80, 100, 150, 200, 250, 300, 400, and 480 MHz were made with a Hewlett-Packard VHF Bridge (Model 803A). A General Radio Precision Slotted Line (Type 900-LB) was used for measurements at frequencies of 600, 750, 1000, 1400, 2000, 3000, and 4500 MHz. In the measurements of low and high frequency regions, two cells were carefully made of a GR Precision Inner-Conductor Rod, an Outer-Conductor Tube, and a GR 900-BT connector. This equipment was described in detail in a previous paper.[9]

Results and Discussion

Dielectric Relaxation. The Cole–Cole plots are

† Present address: 207-52, Shirahata kami-cho, Kanagawa-ku, Yokohama 221.

shown for pure 1-decanol at 15, 20, 25, 35, and 40 °C in Fig. 1 and for cyclohexane solutions of 1-decanol at 25 °C in Fig. 2. The first dispersion region can be described by a Debye-like semicircular arc, though it is evident that the experimental data can not be satisfactorily fitted by the arc in the high-frequency region of the dispersion. At first glance it looks as if the Cole–Cole plots can be grouped into three dispersion types as pointed out for isomeric decanols in a previous paper.[9] The first type is best described by several overlapping Debye-like semicircular arcs, such as pure 1-decanol at 15 °C in Fig. 1. The second one by a Davidson–Cole skewed arc, such as pure 1-decanol at 40 °C in Fig. 1 and 60 mol% in Fig. 2. The third one by a Cole–Cole depressed-center semicircular arc, such as 30 mol% in Fig. 2. It has usually been considered that the dispersion type was determined by a difference in the measured compounds. However, the shape of the locus of the dispersion is dependent of the temperature and dilution. The shape of the locus for one compound changes from a Debye type to a Davidson–Cole type, as shown in Fig. 1 and from a Davidson–Cole type to a Cole–Cole type, as shown in Fig. 2. This fact indicates that the difference in these dispersion types is determined by a ratio of the magnitudes between the first and other regions calculated. It was, therefore, assumed that dielectric absorption was the sum of several overlapping Debye-like dispersion regions. In this study, the experimental data were analyzed by separation into three different dispersion regions. The dielectric parameters of the three regions were calculated using a least-squares method, as described in a previous paper.[9] The limiting high-frequency dielectric constant, ε_3, of the third region contains experimental errors because of lack of the higher frequencies of the region. Therefore, the ε_3 was assumed to be an average value in all measurements, whose value was calculated using $(\varepsilon_3-1)/(\varepsilon_3+2)=(n_D^2-1)(1+0.19)/(n_D^2+2)$. The calculated dielectric parameters are given in Table 1, together with the refractive indices n_D (measured by the use of a Pulfrich refractometer), densities d, and with viscosities η. The calculated results of the three dispersion regions are also shown by the solid lines in Figs. 1 and 2.

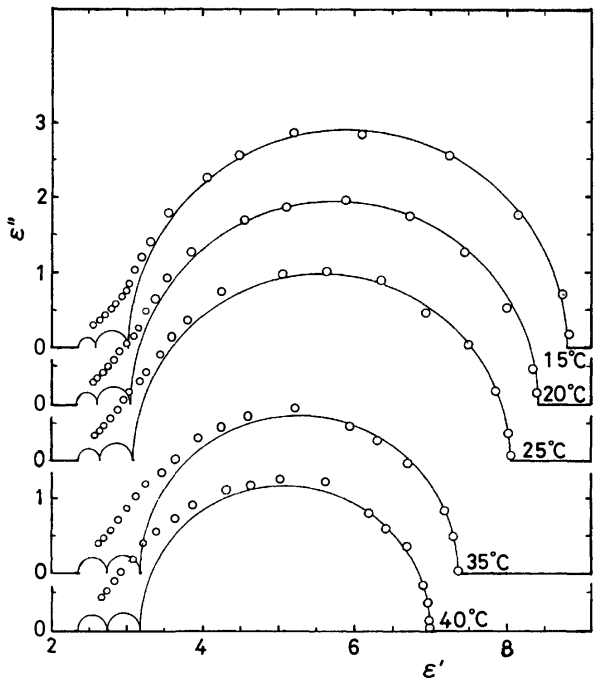

Fig. 1. Cole–Cole plots for pure 1-decanol at 15—40 °C. For clarity, curves have been displaced along the ordinate. Three dispersion regions calculated are shown by solid lines.

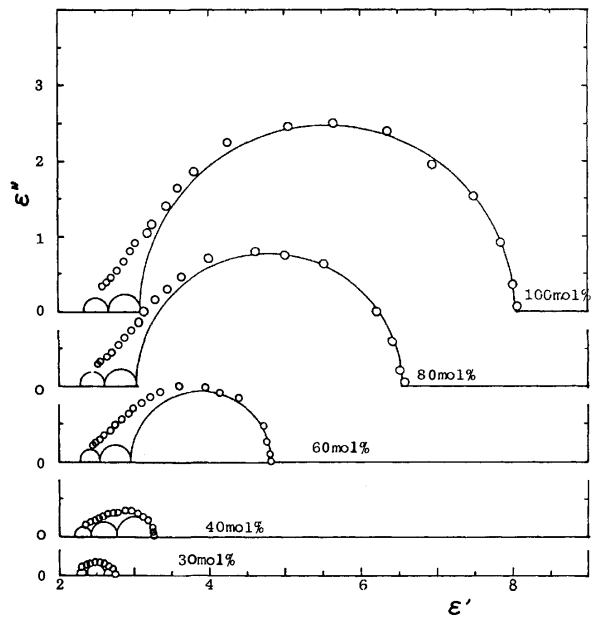

Fig. 2. Cole–Cole plots for cyclohexane solutions of 1-decanol at 25 °C. For clarity, curves have been displaced along the ordinate. Three dispersion regions calculated are shown by solid lines.

The thermodynamic parameters, the free energy of activation ΔF^*, the heat of activation ΔH^*, and the entropy of activation ΔS^*, were obtained by applying the Eyring's equation[9,10] to the three dispersion regions in Table 2.

Assignment of the Three Dispersion Regions. For very dilute cyclohexane solutions (less than 1 mol%) of ethanol, Ibbitson and Moore[11] reported that the near-infrared spectra contained a broad absorption band at 3350 cm^{-1} in addition to two bands at 3520—3540 and 3644—3650 cm^{-1}. From measurements of the dielectric constant and the solute polarization, they attributed the three bands to the presences of a nonpolar cyclic polymer, a linear dimer and trimer, and a free monomer. Meantime, the first dispersion region vanished in the vicinity of 15 mol% of 1-decanol, as shown in Table 1. This observation was in agreement with the results for cyclohexane solutions of 1-hexanol

Table 1. Dielectric Parameters, Refractive Indices, Densities, and Viscosities

	Dielectric constants				Relaxation times					
	ε_0	ε_1	ε_2	ε_3	τ_1	τ_2	τ_3	n_D	d	$\eta\times10^3$
					ps	ps	ps		g cm^{-3}	N s m^{-2}
t/°C					1-Decanol					
15	8.78	3.03	2.60	2.37	3302	178	20	1.4392	0.8328	17.84
20	8.38	3.07	2.63	2.36	2490	179	21	1.4374	0.8295	—
25	8.03	3.10	2.66	2.35	1888	176	20	1.4354	0.8261	11.74
35	7.33	3.20	2.75	2.33	1103	168	19	1.4317	0.8195	8.11
40	6.97	3.18	2.77	2.33	800	160	18	1.4299	0.8160	—
mol%					1-Decanol in cyclohexane at 25 °C					
80.01	6.54	3.04	2.62	2.30	1696	206	23	1.4336	0.8186	8.13
59.93	4.82	2.97	2.55	2.28	1438	246	28	1.4313	0.8096	5.15
39.92	3.28	2.78	2.43	2.22	1210	235	25	1.4287	0.7991	3.06
29.89	2.76	2.61	2.37	2.18	1115	266	27	1.4273	0.7934	2.26
mol%					1-Decanol in heptane at 25 °C					
79.93	6.11	3.02	2.61	2.31	1494	218	27	1.4285	0.8038	5.96
60.08	4.27	2.95	2.52	2.26	1207	282	32	1.4202	0.7781	2.97
39.98	2.90	2.64	2.36	2.17	878	265	31	1.4102	0.7491	1.47
30.02	2.51	2.45	2.26	2.11	901	243	34	1.4048	0.7333	1.05

Table 2. Thermodynamic Parameters, ΔF^*, ΔH^*, and ΔS^*, for Three Dispersion Regions of 1-Decanol

	ΔF^*[a]	ΔH^*	ΔS^*
	kJ mol^{-1}	kJ mol^{-1}	J K^{-1} mol^{-1}
First region	23.2	39.6	55.1
Second region	17.3	0.72	−55
Third region	11.9	2.2	−33

a) The values of ΔF^* was calculated at 298 K.

measured by Komooka[12] and of ethanol measured by Sagal.[13] From the above consideration, therefore, there are at least a free monomer, a linear dimer and trimer, and a nonpolar cyclic polymer in addition to a higher polar polymer which the first dispersion region originates. These species should correspond to the dielectric dispersion regions observed.

The relaxation times of unassociated liquids were collected from the literature for room-temperature values. Chlorobenzene[14,15] has a relaxation time of 11—14 ps, bromobenzene[14,15] 17—18 ps, 1-bromo-3-methylbutane[15,17] 13—22 ps, 1-chlorooctane[16] 17 ps, 1-bromooctane[15,16] 22—43 ps, 1-iodooctane[16,18] 39—45 ps. In view of these relaxation times, it is considered that the third relaxation time shown in Table 1 is attributed to the reorientation of a free monomer. The free energy of activation ΔF^* is 10.4 kJ mol^{-1} for chlorobenzene and 10.9 kJ mol^{-1} for 1-bromo-3-methylbutane, also corresponding to that of the third region, as shown in Table 2.

The first dispersion region is large, strongly dependent on the temperature (in comparison with the other), and decreases rapidly with dilution. This process is apparently associated with a linear hydrogen-bonded species. It has been reported that this process could be ascribed to the breaking of the hydrogen bonds in molecular aggregates followed by ROH rotation,[7] to a single highly polymer,[1] and to the switching mechanism of the OH moment as one hydrogen bond is broken and another formed.[13] In addition to these models, it may be considered to be due to the existence of an alcohol molecule which forms two hydrogen bonds between an oxygen atom in the molecule and two hydrogen atoms of neighboring molecules, since the magnitude of this region is much greater than the other. Such an alcohol molecule has three hydrogen bonds instead of the four hydrogen bonds of a water molecule in the "flickering cluster model"[19] proposed by Frank and Wen. If such a molecule exists, a more complex polymer can be formed disorderly by joining two linear and cyclic polymers in a three-dimensional spread. The existence of such a molecule, however, has still not been confirmed by experiments. Studies of the X-ray diffraction[20] interpreted this aggregate as a linear hydrogen-bonded chain polymer. It is, therefore, considered that the first dispersion region is attributed to the linear hydrogen-bonded chain polymer. This polymer has various chain lengths which may be dependent on the temperature, dilution, and amount of shielding of the hydroxyl group.

Since the second dispersion region is always small in magnitude, it may be considered to be formed as an intermediate. It becomes difficult to separate the first and second regions as the temperature increases. When the magnitude of the first region decreases, there are some cases in which there is no distinction between the first and second regions. From the above consideration, the second process is due to a short linear chain polymer, such as a chain dimer and trimer.

It is concluded that the first region can be attributed to a linear hydrogen-bonded chain polymer (probably $n \geqq 4$), the second region to a chain dimer and trimer ($n=2$ and 3), and the third region to a free monomer ($n=1$).

The experimental data, inclusive of the three values measured by Garg and Smyth[7] at wavelengths of 3.22, 1.25, and 0.22 cm, have been resolved into four different Debye-like dispersion regions. The four relaxation times obtained are 2490, 179, 27.9, and 3.06 ps at 20 °C and 800, 160, 23.7, and 2.91 ps at 40 °C for pure 1-decanol. The second region could not be found in the Garg and Smyth's analysis because of experimental errors[8] in their measurements at the highest band of the RX meter. The band of the RX meter was not used in our measurements. Meantime, Glasser et al.[8] resolved the dielectric absorption into three dispersion regions at higher concentrations for heptane solutions of some normal alcohols. It is considered that the three regions measured by Glasser et al. correspond to the three higher-frequency regions, except for the lowest-frequency region. The free energies of activation for the four dispersion regions are about 23.2, 17.3, 12.7, and 7.3 kJ mol^{-1}, respectively.

In this study, the highest-frequency region could not be obtained because of the narrow range of the measuring frequencies. This region is attributed to a relaxation of the hydroxyl group by rotation around its C–O bond, as described by Garg and Smyth.[7]

Concentrations of Monomer and Three Hydrogen-Bonded Species. In a previous paper,[9] we proposed a modified Kirkwood-Fröhlich equation as follows:

$$\varepsilon_{i-1} - \varepsilon_i = \frac{3\varepsilon_{i-1}}{2\varepsilon_{i-1} + \varepsilon_i}\left(\frac{\varepsilon_i + 2}{3}\right)^2 \frac{4\pi N_A \mu_0^2}{3 \times 10^3 kT} C_i g_i, \quad (1)$$

$$C_0 = \sum_{i=1}^{k} C_i + C_R, \quad (2)$$

$$g = 1, \text{ if } n = 1 \text{ and } g = 1 + Z\sum_{m=2}^{n} f\left(\cos^2\frac{\theta}{2}\right)^{m-1}, \text{ if } n \geqq 2, \quad (3)$$

$$f = \frac{(\mu_H + \mu_R)(\mu_H + \mu_R \cos\theta)}{\mu_H^2 + \mu_R^2 + 2\mu_H\mu_R \cos\theta}.$$

In this equations, ε_{i-1} and ε_i are the limiting low- and high-frequency dielectric constants of the i-th dispersion, N_A is Avogadro's number, μ_0 the dipole moment of the molecule in vacuum, kT the thermal energy, g_i the Kirwood correlation factor of the i-th dispersion, C_0 the gross stoichiometric concentration in mol dm^{-3} of all alcohol molecules, C_i the alcohol concentration at which the i-th dispersion originates, C_R that of nonpolar cyclic polymer, and Z the coordination number. Additionally, μ_H and μ_R are the components of the dipole moment of alcohol molecule ROH along the O–H and O–R bonds, respectively, θ is the angle between the O–H and O–R bonds, m represents m-th molecule, and n is the number of alcohol molecule in the linear hydrogen-bonded chain polymer. It was assumed in Eqs. 1—3 that $Z=2$, $\mu_H=1.53$ D, $\mu_R=1.20$ D, $\mu_0=1.68$ D, and $\theta=105°$ for linear alcohols such as 1-decanol.

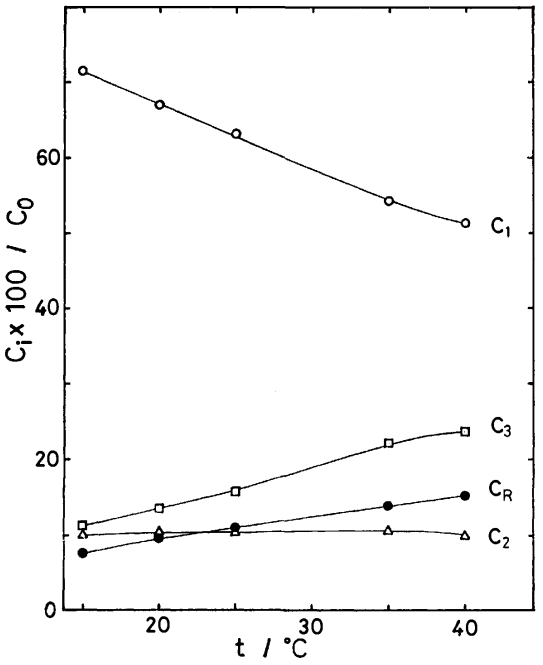

Fig. 3. Percentages of C_i for pure 1-decanol as a function of temperature.

The g factor can be calculated from Eq. 3. The value of the g factor is 1 if $n=1$, 1.87 if $n=2$, 2.19 if $n=3$, 2.31 if $n=4$, 2.36 if $n=5$, and 2.38 if $n \geqq 6$, respectively. According to our assignments, it is assumed that the g_1 is 2.38 for the first region, the g_2 is 2.03 as an average value for the second region, and the g_3 is unity for the third region. The concentrations C_i can be calculated from Eq. 1 by making use of these g_i factors and of the experimental values of ε_{i-1} and ε_i listed in Table 1. The percentages of C_1, C_2, C_3, and C_R against the gross stoichiometric concentration C_0, $C_i \times 100/C_0$, are shown for change of temperature (Fig. 3) and for change of dilution (Fig. 4). For example, the respective percentages of C_1, C_2, C_3, and C_R are 71, 10, 11, and 8% at 15 °C and 52, 10, 24, and 16% at 40 °C for pure 1-decanol. Those for cyclohexane solutions of 1-decanol are 54, 11, 19, and 16% at 80 mol% and 16, 17, 21, and 46% at 40 mol% at 25 °C. Figure 3 shows that the C_1 decreases and both C_3 and C_R increase, as the temperature increases. C_2 does not change in the temperature range 15—40 °C. It is considered that depolymerization occurs for the linear hydrogen-bonded chain polymer. For cyclohexane and heptane solutions of 1-decanol, it is shown in Fig. 4 that the C_1 decreases rapidly and that C_R increases correspondingly, as the concentration of 1-decanol decreases. Both

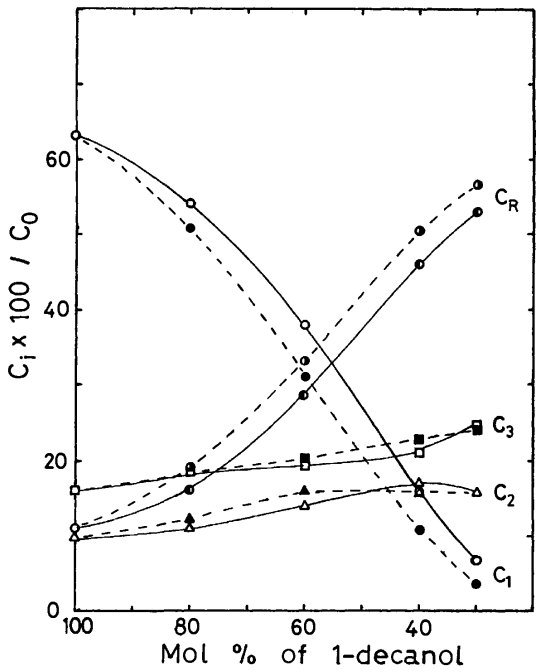

Fig. 4. Percentages of C_i for cyclohexane and heptane solutions of 1-decanol as a function of mol% of 1-decanol. Cyclohexane solutions are shown by solid lines and heptane solutions are shown by dotted lines.

C_2 and C_3 also increase slightly. The length of the linear hydrogen-bonded chain polymer probably becomes short by breaking the hydrogen bonds due to a hindrance of the nonpolar solvent. It is considered from Fig. 4 that the nonpolar cyclic polymer becomes a most stable structure in dilute solutions, although the linear hydrogen-bonded chain polymer is favorable in pure 1-decanol. We can understand the behavior of the four concentrations regarding the changes in temperature and dilution.

References

1) A. N. Fletcher and C. A. Heller, *J. Phys. Chem.*, **71**, 3742 (1967).
2) D. Hadzi, "Hydrogen Bonding," Pergamon Press, New York, N. Y. (1959).
3) W. Dannhauser, *J. Chem. Phys.*, **48**, 1911 (1968).
4) R. H. Cole and D. W. Davidson, *J. Chem. Phys.*, **20**, 1389 (1952).
5) W. Dannhauser, *J. Chem. Phys.*, **48**, 1918 (1968).
6) A. Lebrun, *Ann. Phys.*, **10**, 16 (1955).
7) S. K. Garg and C. P. Smyth, *J. Phys. Chem.*, **69**, 1294 (1965).
8) L. Glasser, J. Crossley, and C. P. Smyth, *J. Chem. Phys.*, **57**, 3977 (1972).
9) T. Shinomiya, *Bull. Chem. Soc. Jpn.*, **62**, 908 (1989).
10) S. Glasstone, K. J. Laidler, and H. Eyring, "The Theory of Rate Processes," McGraw-Hill Book Company, Inc., New York, N. Y. (1941).
11) D. A. Ibbitson and L. F. Moore, *J. Chem. Soc. B*, **1967**, 76.
12) H. Komooka, *Bull. Chem. Soc. Jpn.*, **45**, 1696 (1972).
13) M. W. Sagal, *J. Chem. Phys.*, **36**, 2437 (1962).
14) S. K. Garg and C. P. Smyth, *J. Chem. Phys.*, **42**, 1397 (1965).
15) K. Baba and K. Kamiyoshi, *J. Phys. Chem.*, **81**, 1872 (1977).
16) E. J. Hennelly, W. M. Heston, Jr., and C. P. Smyth, *J. Am. Chem. Soc.*, **70**, 4102 (1948).
17) S. H. Glarum, *J. Chem. Phys.*, **33**, 639 (1960).
18) F. I. Mopsik and R. H. Cole, *J. Chem. Phys.*, **44**, 1015 (1966).
19) G. Nemethy and H. A. Scheraga, *J. Chem. Phys.*, **36**, 3382 (1962).
20) W. C. Pierce and D. P. MacMillon, *J. Am. Chem. Soc.*, **60**, 779 (1938).

^{35}Cl NQR in $SnCl_4 \cdot 2Me_2O$ and $SnCl_4 \cdot 2Et_2O$

Mitsuo MISHIMA* and Tsutomu OKUDA†
Department of Chemistry, Shimane Medical University, Izumo 693
†Department of Chemistry, Faculty of Science, Hiroshima University, Naka-ku, Hiroshima 730
(Received January 21, 1989)

^{35}Cl NQR spectra in $SnCl_4 \cdot 2Me_2O$ and $SnCl_4 \cdot 2Et_2O$ have been observed. Three crystal modifications of $SnCl_4 \cdot 2Me_2O$ have been found. A cis geometry is suggested for one of them, and a trans geometry for the remainder. A transformation between the cis and trans isomers in the solid state is indicated. The Zeeman effect on single crystals of *cis*-$SnCl_4 \cdot 2Me_2O$ and $SnCl_4 \cdot 2Et_2O$ has provided detailed information on bond angles and bond character. It is confirmed that the molecular geometry of *cis*-$SnCl_4 \cdot 2Me_2O$ belongs to the C_2 group and that $SnCl_4 \cdot 2Et_2O$ has a trans geometry. The η values of the Cl atoms in *cis*-$SnCl_4 \cdot 2Me_2O$ are negligibly small and those of the Cl atoms in $SnCl_4 \cdot 2Et_2O$ are 0.11. The relatively small η values for the latter are ascribed to π bonding between the Sn and Cl atoms.

Raman and Mössbauer spectroscopies revealed that several octahedral complexes of $SnX_4 \cdot 2L$ (X=Cl, Br; L=Lewis bases) exist in a cis or trans form in the solid state, depending on the conditions of preparation and purification.[1,2] It was demonstrated by Raman[1] and NMR[3-5] measurements that a number of SnX_4 complexes are at cis-trans equilibrium in solution. On the other hand, Davanzo and Gushikem[6] obtained evidence for the cis-trans transformation in the solid state through studies of vibrational spectroscopy, thermal analysis, and X-ray powder diffraction, and reported the transition temperature. For the solid $SnCl_4 \cdot 2Me_2O$, however, the cis geometry was proposed on the basis of Raman spectra.[1]

NQR is a useful method for examining configurations of $SnCl_4$ complexes.[7-9] We examined $SnCl_4 \cdot 2Me_2O$ and $SnCl_4 \cdot 2Et_2O$ by means of NQR in order to determine their molecular geometries. Furthermore, the Zeeman effect of ^{35}Cl on single crystals of *cis*-$SnCl_4 \cdot 2Me_2O$ and $SnCl_4 \cdot 2Et_2O$ was examined to obtain information on bond angles and bond characters.

Experimental

The complex $SnCl_4 \cdot 2Me_2O$ was prepared by bubbling a gas of dimethyl ether into a dichloromethane solution of tin(IV) chloride. The crystalline solid was filtered and purified by recrystallization from dichloromethane or chloroform and sublimation. The contents of tin and chlorine were determined gravimetrically.[10] (Found: Sn, 33.8; Cl, 40.4. Calcd: Sn, 33.7; Cl, 40.2%). The complex $SnCl_4 \cdot 2Et_2O$ was prepared by the method described in the literature[11] and identified by measuring its melting point[10,12] and NQR frequencies.[13] Single crystals of the complexes were grown in evacuated sealed tubes by sublimation.

The NQR spectrometer used was a Dean-type superregenerative spectrometer with frequency modulation. The Zeeman effect was examined by means of the zero-splitting cone method. A magnetic field was supplied by means of a Helmholtz coil. Temperature was determined by the use of a copper-constantan thermocouple. Temperature below room temperature in the Zeeman study was controlled by varying the flow of the nitrogen gas from liquid nitrogen.

Results and Discussion

The NQR spectrum for $SnCl_4 \cdot 2Me_2O$ obtained by recrystallization differed from that for the sample obtained by sublimation above 50 °C. The ^{35}Cl resonance frequencies are shown as a function of temperature in Fig. 1. The recrystallized sample gave two NQR lines and the sublimed one only one line. The former is tentatively termed Form-1 and the latter Form-2. The NQR spectrum of Form-2 suggests that the four Sn-Cl bonds of the complex are equivalent. Therefore, the molecule in Form-2 has a trans configuration.[7] Form-1 is assumed to be a cis isomer, judging from the magnitude of the splitting between adjacent NQR lines. This was confirmed by the Zeeman study on a single crystal. In Form-1 the

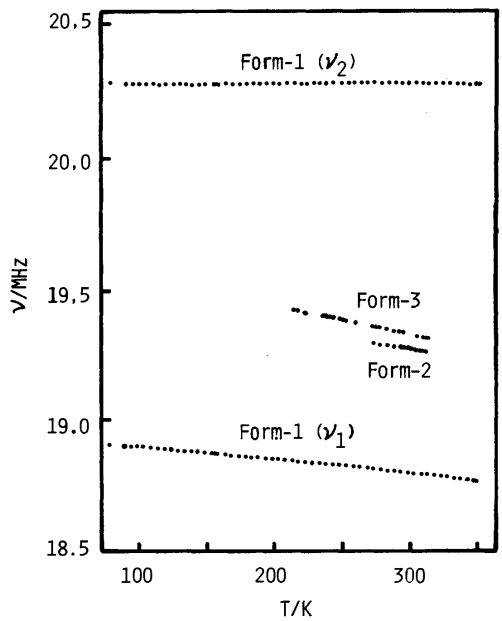

Fig. 1. Temperature dependence of ^{35}Cl resonance frequencies of $SnCl_4 \cdot 2Me_2O$.

frequency of the lower resonance line, ν_1, decreased monotonously with a rise in temperature, whereas the higher resonance line, ν_2, had a very small temperature coefficient and the minimum frequency was 20.278 MHz near 140 K and the maximum one 20.287 MHz near 285 K, suggesting the existence of intermolecular interaction.

Form-2 was unstable at room temperature and, in one night at the longest, changed to another modification (Form-3) which yielded also only one resonance line. When Form-2 was cooled to near 270 K, it changed immediately to Form-3. This transformation became rapid with lowering temperature. When Form-2 was cooled to 77 K, the absorption lines for Form-1 appeared immediately. Form-3 was also unstable and was transformed to Form-1 at room temperature in a day. This transformation also became rapid with lowering temperature, and this change took place immediately at temperature below less than ca. 210 K. The resonance frequencies for Form-2 and Form-3 decreased with a rise in temperature and faded out at 311 K and 314 K, respectively. Both the ν_1 and ν_2 lines in Form-1 disappeared at 350 K without broadening. When the sample was cooled rapidly to room temperature, it gave the same NQR line as did Form-2. Accordingly, this suggests a transition from the cis isomer to the trans one. Although the transition point was reproducible within ±1.5 K, the sample maintained at ca. 340 K for a day gave the same spectrum as did Form-2 at room temperature. Accordingly, the observed transition point seems not to be intrinsic.

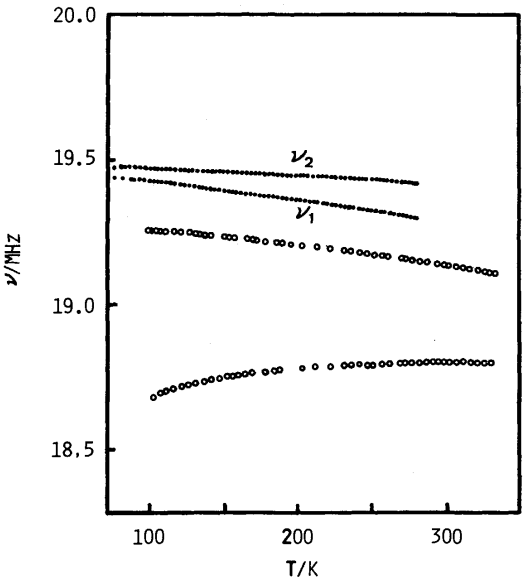

Fig. 2. Temperature dependence of ^{35}Cl resonance frequencies of $SnCl_4 \cdot 2Et_2O$ (●) and $SnCl_4 \cdot 2THF$ (○).

The temperature dependence of the NQR frequencies of $SnCl_4 \cdot 2Et_2O$ is shown in Fig. 2. The resonance lines decreased in frequency with a rise in temperature and disappeared near 280 K. For this complex, a trans geometry was proposed on the basis of the NQR[7] and the vibrational spectra.[11,14] In the trans complex with tetrahydrothiophen $SnCl_4 \cdot 2THT$, the geometry of which was determined by X-ray analysis,[15] no resonance lines were detected at room temperature, although two resonance lines were observed below ca. 210 K.[8,9] The resonance lines of $SnCl_4 \cdot 2THF$, which has a trans geometry in solid,[11] disappeared at 330 K as shown in Fig. 2. The temperature variations of the NQR frequencies of $SnCl_4 \cdot 2THF$ in the range of 100 to 300 K were in good agreement with those of $SnCl_4 \cdot 2THF$ reported by Rupp-Bensadon and Lucken.[9] In some cis-complexes such as $SnCl_4 \cdot 2POCl_3$,[16] $SnCl_4 \cdot 2SeOCl_2$,[16] $SnCl_4 \cdot 2MeCN$, and $SnCl_4 \cdot 2Me_3CCN$ the NQR lines could be detected up to the melting point. It is of interest that in the octahedral complexes of $SnCl_4$ the fade-out phenomenon of the NQR lines is characteristic of the trans geometry.

The Zeeman effect on the ^{35}Cl lines in Form-1 of

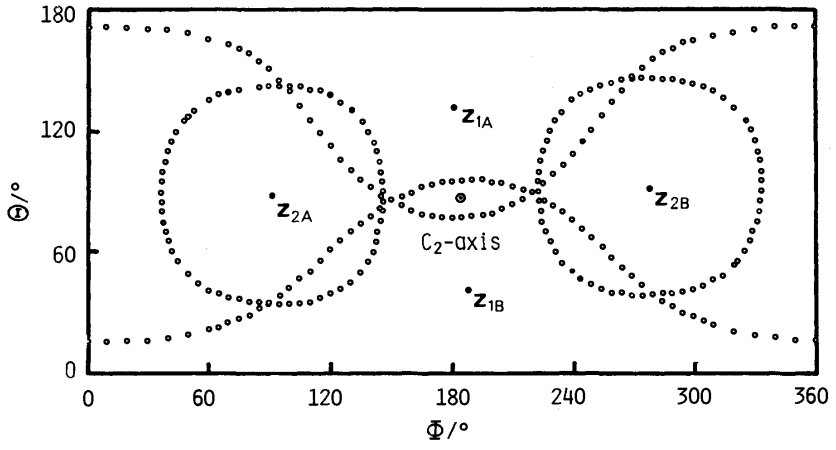

Fig. 3. Zero-splitting patterns of ^{35}Cl NQR lines in Form-1 of $SnCl_4 \cdot 2Me_2O$.

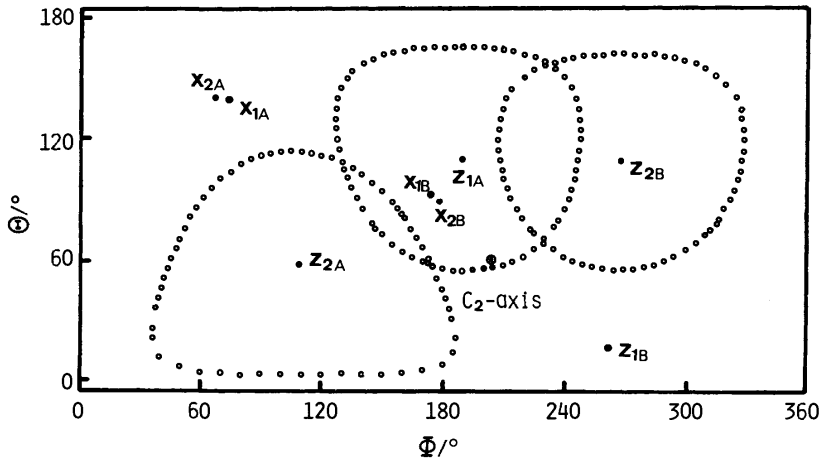

Fig. 4. Zero-splitting patterns of ^{35}Cl NQR lines in $SnCl_4 \cdot 2Et_2O$.

Table 1. ^{35}Cl NQR Parameters for $SnCl_4 \cdot 2Me_2O$ and $SnCl_4 \cdot 2Et_2O$

Compound		Frequency/MHz		η/%	e^2Qqh^{-1}/MHz
$SnCl_4 \cdot 2Me_2O$		77 K	293 K		
Form-1	ν_1	18.906	18.807	4.9	37.600
	ν_2	20.281	20.287	2.7	40.569
Form-2		—	19.279		
Form-3		—	19.340		
$SnCl_4 \cdot 2Et_2O$		77 K	235 K		
	ν_1	19.435	19.341	11.4	38.601
	ν_2	19.474	19.440	11.6	38.793

$SnCl_4 \cdot 2Me_2O$ and $SnCl_4 \cdot 2Et_2O$ was observed at room temperature and at 235 K, respectively. The zero-splitting patterns are shown in Figs. 3 and 4, where z_i indicates the direction of the z axis of the efg tensor at the Cl atom which yields a ν_i resonance line. The observed loci were analyzed by the least squares method to obtain the direction of the efg tensor and the asymmetry parameter (η). The locus is expressed for ^{35}Cl nucleus as follows;

$$\sin^2\theta_0 = 2/(3 - \eta\cos 2\phi_0), \quad (1)$$

where θ_0 and ϕ_0 are the polar and azimuthal angles, respectively. The NQR parameters are listed in Table 1. In $SnCl_4 \cdot 2Me_2O$ a pair of zero-splitting loci were obtained for each resonance line and a twofold axis was determined from the distribution of the Zeeman patterns. The resonance lines of $SnCl_4 \cdot 2Me_2O$ were comparatively weak and each NQR line gave partly overlapped Zeeman patterns. Consequently, the directions of the z axes of the efg tensors and the values of the asymmetry parameters were not so accurate. In $SnCl_4 \cdot 2Et_2O$ the lower resonance line, ν_1, gave only one locus although the two loci were obtained from the higher resonance line, ν_2, as shown in Fig. 4. The reason is because the efg axis of the partner locus is nearly parallel to the rf field. A twofold axis can be determined from the loci for the ν_2 line and the predicted direction of the missing z axis (z_{1B}) is shown in Fig. 4. Therefore, the crystals of these complexes belong to the monoclinic system.

Table 2. Angles between the efg z Axes in $SnCl_4 \cdot 2Me_2O$[a)]

	z_{1A}	z_{1B}	z_{2A}
z_{1B}	92.2°		
z_{2A}	93.5°	91.1°	
z_{2B}	91.1°	93.5°	173.4°

a) Estimated error ±0.3°.

The angles between the Sn–Cl bonds have been deduced, assuming that the principal z axis of the efg tensor is parallel to the Sn–Cl bond. The results for $SnCl_4 \cdot 2Me_2O$ are listed in Table 2. These angles reveal that Form-1 of $SnCl_4 \cdot 2Me_2O$ has a cis geometry. The ν_1 and ν_2 lines can be assigned to the equatorial and the axial chlorine atoms, respectively. The molecular geometry of Form-1 is shown in Fig. 5(a). The molecule possesses a twofold axis, parallel to that of the crystal. The bond angles in this complex are very similar to those of the other cis isomers of the octahedral $SnCl_4$ complexes found by X-ray studies.[17–19] In the monomeric cis-complexes, the angles of $\angle Cl_1SnCl_1$ are greater than 100° and those of $\angle Cl_2$-$SnCl_2$ range from 161.9° to 166.6°. Therefore the molecule in Form-1 of $SnCl_4 \cdot 2Me_2O$ is less distorted.

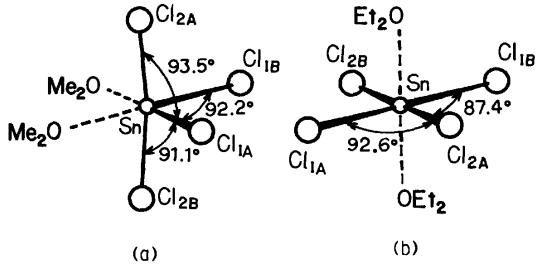

Fig. 5. Molecular shapes of Form-1 of $SnCl_4 \cdot 2Me_2O$ (a) and $SnCl_4 \cdot 2Et_2O$ (b).

Table 3. Angles between the efg Axes and the Crystal Axis in $SnCl_4 \cdot 2Et_2O$[a]

	z_1	x_1	x_2	C_2-axis
z_1				52.34°
z_2	92.58°			78.64°
Plane z_1z_2		86.59°	86.52°	40.59°

a) Estimated error ±0.05°.

It is concluded from the Zeeman analysis that the complex of Et_2O has a trans configuration. This is in agreement with the geometry proposed on the basis of the infrared and Raman spectra.[10,13] As shown in Fig. 4, two of the zero-splitting cones, one from each of the resonance lines, were assigned to each crystal site on the basis of the orientations of the efg axes. The z axes of these cones are nearly at right angles to each other, as can be seen from Table 3. This requires that there are two pairs of chemically equivalent chlorine atoms in a molecule and that the z axes at the chlorine atoms in each pair are collinear. Accordingly, the molecule of $SnCl_4 \cdot 2Et_2O$ has an inversion center at the tin atom and the four Sn–Cl bonds are coplanar. The bond angle $\angle Cl_1SnCl_2$ is close to those in $SnCl_4 \cdot 2Et_3P$ (89.9° and 90.1°).[20] The Sn–Cl_1 and Sn–Cl_2 bonds make angles of 52.3° and 78.6°, respectively, to the twofold axis of the crystal, as is shown in Table 3. The molecule has neither symmetrical plane nor symmetrical axis. The atomic arrangement around the tin atom is very similar to that in $SnCl_4 \cdot 2Et_3P$.[20]

In the Et_2O complex, the Cl_1 atom has almost the same η-value as the Cl_2 atom. These values are somewhat greater than those found in the cis complexes.[16] The x axes of these chlorine atoms are nearly at right angles to the equatorial plane, as can be seen from Table 3. This suggests π interaction between the tin and chlorine atoms. The energy level of the oxygen $2p\pi$ orbital is about 3 eV lower than that of the chlorine $3p\pi$ orbital.[21,22] It is therefore predicted that the chlorine atom donates more charges to the vacant $d\pi$ orbital on the tin atom than the oxygen atom. On the other hand, the oxygen p orbitals do not take part in the π-bonding lying in the equatorial plane. If this is the case, the populations of the p_x orbital on the chlorine atom are more decreased. The difference in population between the p_x and p_y orbitals is estimated to be 0.027 by using the Bersohn's relation.[23] The ionic character of the Sn–Cl bond is calculated to be 57 per cent, assuming that the s character of the bonding orbital of the Cl atom is 0.15.[24]

In the cis isomer of the Me_2O complexes, the η-values are very small. Therefore, the Sn–Cl bonds are almost cylindrically symmetrical. The equatorial Cl atoms are 3 per cent more ionic than the axial ones. This trend is consistent with that in other cis complexes.[16] Since the trans isomers of the Me_2O complex have only one absorption line and the symmetry of the Me_2O moelcule is C_{2v}, the complexes are required to possess at least a twofold axis and a mirror plane. It is therefore considered that the trans complexes have C_{2h}, C_{2v}, or D_{2h} symmetry.

References

1) S. J. Ruzicka and A. E. Merbach, *Inorg. Chim. Acta*, **20**, 221 (1976).
2) D. Tudela and V. Fernadez, *J. Chem. Soc., Dalton Trans.*, **1985**, 1281.
3) S. J. Ruzicka and A. E. Merbach, *Inorg. Chim. Acta*, **22**, 191 (1977).
4) C. T. G. Knight and A. E. Merbach, *Inorg. Chem.*, **24**, 576 (1985).
5) C. T. G. Knight and A. E. Merbach, *J. Am. Chem. Soc.*, **106**, 804 (1984).
6) C. U. Davanzo and Y. Gushikem, *J. Chem. Soc., Dalton Trans.*, **1981**, 843.
7) Yu. K. Maksyutin, E. N. Gruyanova, E. A. Kravchenko, and G. K. Semin, *J. Chem. Soc., Chem. Commun.*, **1973**, 429.
8) P. J. Huggett, R. J. Lynch, T. C. Waddington, and K. Wade, *J. Chem. Soc., Dalton Trans.*, **1980**, 1164.
9) J. Rupp-Bensadon and E. A. C. Lucken, *J. Chem. Soc., Dalton Trans.*, **1983**, 495.
10) E. T. Hitchcock and P. J. Edving, *Anal. Chim. Acta*, **28**, 417 (1963).
11) I. R. Beattie and L. Rule, *J. Chem. Soc.*, **1965**, 2995.
12) D. C. Bradley, E. V. Caldwell, and W. Wardlaw, *J. Chem. Soc.*, **1957**, 3039.
13) D. Biedenkapp and A. Weiss, *Z. Naturforsch.*, **19a**, 1518 (1964).
14) I. R. Beattie and L. Rule, *J. Chem. Soc.*, **1964**, 3267.
15) I. R. Beattie, R. Hulme, and L. Rule, *J. Chem. Soc.*, **1965**, 1581.
16) M. Mishima, *J. Sci. Hiroshima Univ.*, **A46**, 41 (1982).
17) Y. Hermodsson, *Acta Crystallogr.*, **13**, 656 (1960).
18) C.-I. Bränden, *Acta Chem. Scand.*, **17**, 759 (1963).
19) M. Webster and E. A. Bränden, *J. Chem. Soc. A*, **1969**, 2443.
20) G. G. Mather, G. M. McLaughlin, and A. Pidcock, *J. Chem. Soc., Dalton Trans.*, **1973**, 1823.
21) H. A. Skinner and H. O. Pritchard, *Trans. Faraday Soc.*, **49**, 1254 (1953).
22) J. Hinze and H. H. Jaffe, *J. Am. Chem. Soc.*, **84**, 540 (1962).
23) R. Bersohn, *J. Chem. Phys.*, **22**, 2078 (1954).
24) C. H. Townes and B. P. Dailey, *J. Chem. Phys.*, **17**, 782 (1949).

Preparation, Crystal Structure, and Solid State Properties of Highly Conductive (Phthalocyaninato)platinum Radical Salts: $PtPc(ClO_4)_{0.5}$ and $PtPc(AsF_6)_x$

Hideo YAMAKADO, Kyuya YAKUSHI,*,† Nobuhiro KOSUGI, Haruo KURODA, Atsushi KAWAMOTO,†† Jiro TANAKA,†† Tadashi SUGANO,††† Minoru KINOSHITA,††† and Shojun HINO††††
Department of Chemistry, Faculty of Science, The University of Tokyo, Hongo, Tokyo 113
††Department of Chemistry, Faculty of Science, Nagoya University, Furo-cho, Chikusa-ku, Nagoya 464
†††Institute for Solid State Physics, The University of Tokyo, Roppongi, Tokyo 106
††††Department of Image Science and Technology, Faculty of Engineering, Chiba University, Yayoi-cho, Chiba 260
(Received January 20, 1989)

New conducting salts of (phthalocyaninato)platinum (PtPc), $PtPc(ClO_4)_{0.5}$ and $PtPc(AsF_6)_x$, were prepared by electrochemical oxidation. A crystal of $PtPc(ClO_4)_{0.5}$ belongs to a tetragonal system with a space group of $P4/mcc$, the lattice constants being a=14.062(1) Å, c=6.510(1) Å, and Z=2. They are metallic at least down to 120 K, the room-temperature conductivity being $\sigma=10^2$—10^3 S cm^{-1}. XPS indicates that the conduction pathway is located mainly at the ligand chain due to a partial oxidation of the ligand-centered HOMO. ESR experiments have also strongly supported this conclusion. The bandwidth of the ligand-centered conduction band has been estimated to be 1.2 eV from the plasma frequency, $\hbar\omega_p$=0.87 eV, which is obtained by the polarized reflectance spectrum.

Highly conductive iodine salts of metallo-macrocyclic compounds have been extensively studied by groups at Northwestern University.[1-10] These partially oxidized phthalocyanine salts have a stable metallic ground state against Peierls distortion at low temperature, although they have a one-dimensional column structure with a metal-over-metal overlapping mode. On the other hand, the mixed-valent platinum complex, $K_2Pt(CN)_4Br_{1/3}\cdot 3H_2O$ (KCP), has been reported to have a mixed-valent groud state between Pt^{2+} and Pt^{4+},[11,12] which might give rise to a movement of paired electrons.[13] However, it shows a semiconductive behavior at low temperature,[14] because it suffers the Peierls distortion.[15] Therefore it may be interesting to make a partially oxidized platinum chain which is stable against this type distortion, Such materials might possibly be found by searching for the conductive platinum macrocyclic compounds. This was the motivation of the present research. In this paper we report on the preparation and solid-state properties of the partially oxidized salts of (phthalocyaninato)-platinum (PtPc), $PtPc(ClO_4)_{0.5}$ and $PtPc(AsF_6)_x$, which were prepared for the first time in the research described here.

Experimental

PtPc was synthesized from phthalonitrile and $PtCl_2$,[16] and purified several times by a vacuum sublimation. The partially oxidized salts, $PtPc(ClO_4)_{0.5}$ and $PtPc(AsF_6)_x$, were obtained by the electrochemical method in a 1-chloronaphthalene solution using supporting electrolytes of (n-Bu)$_4$NX, (X=ClO_4 and AsF_6). The electrochemical reaction was carried out for about 2 weeks in a galvanostatic mode (1—5 μA) at 120 °C in an Ar or N_2 atmosphere. The concentration of PtPc was ca. 3×10^{-4} mol l^{-1}, and those of the supporting electrolytes were (2×10^{-3}—2×10^{-2}) mol l^{-1}. The crystals were grown along the c-axis, the typical dimensions being $0.01\times0.01\times2$ mm^3. The chemical composition of $PtPc(ClO_4)_{0.5}$ was determined from an X-ray crystal structure analysis.

The intensities of X-ray diffraction were measured at room temperature with a Rigaku AFC-5 automated diffractometer combined with a Rotaflex RU-200, using Cu $K\alpha$ radiation monochromated with a graphite plate. The dimensions of the crystal used in this experiment were $0.03\times0.03\times0.6$ mm^3. The crystal belongs to a tetragonal system with a space group of $P4/mcc$, the cell constants being a=14.062(1) Å, c=6.510(1) Å, and Z=2. We obtained 554 unique reflections, in which 405 reflections with $F_o>3\sigma(F_o)$ were used for the analysis. An absorption correction was made with a program (ACACA) written by C. T. Prewitt. The structure was solved by a heavy-atom method and was refined by a block-diagonal least-squares method with anisotropic temperature factors. The hydrogen atoms were neglected in this analysis. The final R-value was 0.055. The anisotropic temperature factors and F_o-F_c data are deposited as Document No. 8883 at the office of the Editor of Bull. Chem. Soc. Jpn. The computer program used in this analysis was UNICS III system.[17]

The electrical conductivity of a single crystal was measured along the needle axis from 290 K down to 10 K by the use of a four-probe ac method with a frequency of 70 Hz, the constant current being 10 μA. The voltage drop between the inner probes was detected by a lock-in-amplifier (EG & G 5205) which was controlled by a microcomputer. The phase change of the voltage was automatically checked at each temperature. Needle-like crystals were mounted on 10 μm gold wires with carbon paint to obtain electrical contact. The unnested voltage was tolerably small.

XPS was measured by a Kratos XSAM 800 ultrahigh vacuum photoelectron spectrometer using the Mg $K\alpha$ line as

† Present address: Institute for Molecular Science, Myodaiji-cho, Okazaki, Aichi 444.

the excitation source. PtPc was deposited on the copper sample holder through vacuum sublimation. Powdered samples of $PtPc(ClO_4)_{0.5}$ and $PtPc(AsF_6)_x$ were pressed onto the copper holder. No surface treatment was conducted so as to avoid any damage to the sample. Calibration of the spectrometer was performed by Au4f lines and the Au Fermi edge.

The ESR spectra were measured with a JEOL JES-FE1XG and a Varian E-112 using an X-band at temperatures between 290 and 4.2 K. About 80 slim crystals were aligned with silicone grease on a teflon sample holder so that the needle axes were parallel to each other. The crystals were so small that the ambiguity of the alignment was about 10°. The *g*-value was determined by a comparison of the ESR signal of solid Li-TCNQ. The spin susceptibility was calibrated by the integrated intensity of violanthrone, the static magnetic susceptibility of which had been measured. The intensity was obtained from a double integration of the ESR signal.

Polarized reflectance spectra were measured in the spectral range from 4200 to 25000 cm^{-1} with the polarization directions parallel and perpendicular to the *c*-axis at room temperature. The reflectance spectra were measured with a microspectrophotometer. The absolute reflectivity was obtained by comparing with the reflected light from a Si single crystal.

Results and Discussion

Crystal Structure. The atomic parameters of $PtPc(ClO_4)_{0.5}$ are compiled in Table 1. Figure 1 shows side and top views of the molecular column of PtPc in the crystal of $PtPc(ClO_4)_{0.5}$. The space group is the same as those of NiPcI,[1] $NiPc(BF_4)_{0.33}$,[7] $NiPc(ClO_4)_{0.42}$,[9] H_2PcI,[8] CoPcI,[6] and CuPcI.[10] The crystal is composed of molecular columns piled up along the *c*-axis. In this column the phthalocyanine molecules are stacked with a staggered angle of 40.7°. At the same time, the phthalocyanine molecules make molecular layers on the (001) plane. ClO_4^- is located at the interlayer position, as shown in the side view. The site occupancy of ClO_4^- is 0.5, so that the anions are positionally disordered. Since the diameter of ClO_4^- (ca. 5.6 Å)[19] is larger than half the *c*-axis, the anions and voids should be located alternately along the *c*-axis, and these one-dimensionally ordered anions are probably arranged randomly along the *a*- and *b*-axes. Furthermore, the large temperature factors of ClO_4^- indicate that the anion is also rotationally disordered. Table 2 shows a comparison of the average bond distances of PtPc. Since the atomic scattering factor of a platinum atom is much larger than those of carbon and nitrogen atoms, the standard deviations of the bond distances are large: 0.02 Å for Pt–N distance and 0.03—0.04 Å for N–C and C–C bond. In addition, the molecular geometry of the Pc ring is insensitive to the valency.[20] Therefore it is not possible to judge from the molecular geometry whether the ring is oxidized or not. Since the oscillation and Weissenberg photographs of $PtPc(AsF_6)_x$ are essentially the same as those of $PtPc(ClO_4)_{0.5}$, we consider that the former is isostructural to the latter.

Table 1. Fractional Atomic Coordinates (×10⁴) and Equivalent Temperature Factors ($B_{eq}=(4/3)\sum_{ij}\beta_{ij}(a_i\cdot a_j)$)

Atom	*x*	*y*	*z*	B_{eq}
Pt	0	0	0	2.9
N(1)	1296(16)	577(13)	0	4.2
N(2)	809(14)	2257(13)	0	3.7
C(1)	1475(22)	1530(22)	0	3.9
C(2)	2453(18)	1728(19)	0	4.1
C(3)	3028(18)	2569(17)	0	4.6
C(4)	4016(21)	2407(22)	0	6.3
C(5)	4445(20)	1507(23)	0	6.6
C(6)	3899(20)	675(23)	0	6.0
C(7)	2874(16)	807(18)	0	3.8
C(8)	2129(15)	131(22)	0	3.1
Cl	5000	5000	2500	17.2
O	4279(69)	4537(66)	1835(241)	18.2

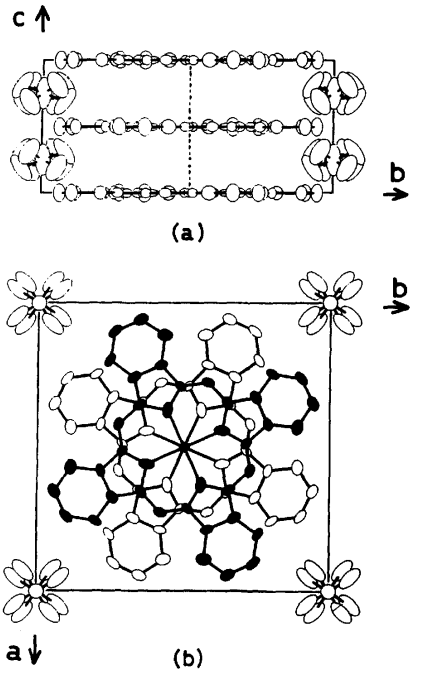

Fig. 1. (a) Side view and (b) top view of the crystal structure of $PtPc(ClO_4)_{0.5}$. The occupancy of ClO_4^- is 0.5.

Table 2. Average Bond Distances of PtPc

	$PtPc(ClO_4)_{0.5}$[a]	α-PtPc[b]	γ-PtPc[b]
$Pt-N_p$	1.99(2)	1.98	1.99
N_p-C_a	1.35(4)	1.38	1.40
N_m-C_a	1.36(4)	1.33	1.34
C_a-C_b	1.41(4)	1.49	1.44
C_b-C_b	1.42(4)	1.37	1.47
C_d-C_d	1.40(4)	1.40	1.38
C_b-C_c	1.44(4)	1.41	1.42
C_c-C_d	1.41(4)	1.41	1.42

a) This work. b) C. J. Brown.[18]

Electrical Resistivity. The electrical resistivity of $PtPc(ClO_4)_{0.5}$ along the *c*-axis is 10^{-2}—$10^{-3}\,\Omega$ cm at room temperature. The temperature dependence of the resistivity shown in Fig. 2 is one of the examples in which the cooling and warming rate is 0.5 K min^{-1}. The resistivity decreases at least down to 120 K upon cooling the sample. Below 100 K resistivity jumps take place at various temperatures which are not reproducible; the resistivity gradually increases up to 10^3 times the room-temperature value at 10 K. However, the resistivity recovers the starting value again upon warming the sample to room temperature. This temperature dependence of the resistivity is not reproducible against the heat cycles. The resistivity curve below 50 K cannot be described by a simple exponential function, $\rho(T)/\rho_{RT} \propto \exp(E_a/kT)$, but is well reproduced by the fluctuation-induced tunneling conduction model[21] which is applied to the analysis of the resistivity curves of doped polyacetylene and other inhomogeneous materials. We surmise that the metallic domains still remains at low temperature in $PtPc(ClO_4)_{0.5}$. A more elaborate investigation is necessary for an elucidation of the resistivity in the low-temperature region. Similar electrical properties have also been observed for $PtPc(AsF_6)_x$.

X-Ray Photoelectron Spectra. The X-ray photoelectron spectrum (XPS) has been used to determine the valency of atoms and molecules. For example, XPS played a crucial role in elucidating the mixed-valent state between Pt^{2+} and Pt^{4+} in the KCP crystal.[12] In the present case, however, no difference has been observed among PtPc, $PtPc(ClO_4)_{0.5}$, and $PtPc(AsF_6)_x$ as concerns the line shapes of $Pt4f_{7/2}$ and $Pt4f_{5/2}$, except for a slight increase (0.2 eV) in the linewidth for the oxidized salts. Their binding energies are the same as each other, the values being 73.2 and 76.6 eV for $Pt4f_{7/2}$ and $Pt4f_{5/2}$, respectively. As for the phthalocyanine ring, the line shape of the N1s spectrum is almost exactly the same as each other, and its binding energy is 398.9 eV. In contrast, the line shape of the C1s photoelectron spectra of $PtPc(ClO_4)_{0.5}$ and $PtPc(AsF_6)_x$ is slightly different from that of PtPc. Figure 3 shows a comparison of the line shapes of $PtPc(ClO_4)_{0.5}$ and PtPc. According to the theoretical work of NiPc by Kutzler and Ellis,[22] the highest occupied molecular orbital (HOMO) of NiPc is composed of the $2p_z$ orbitals of carbon atoms and has nodes at the nitrogen atoms and the nickel atom. Since this character of HOMO is also expected in PtPc, the observed result indicates that a partial oxidization occurs mainly in the phthalocyanine ring. The slight chemical shift of the binding energy of C1s is consistent with the ligand-centered oxidation. These XPS results mean that the conduction pathway is not on the Pt chain but, rather, on the Pc rings in contrast to KCP.

Electron Spin Resonance. Figure 4 shows the

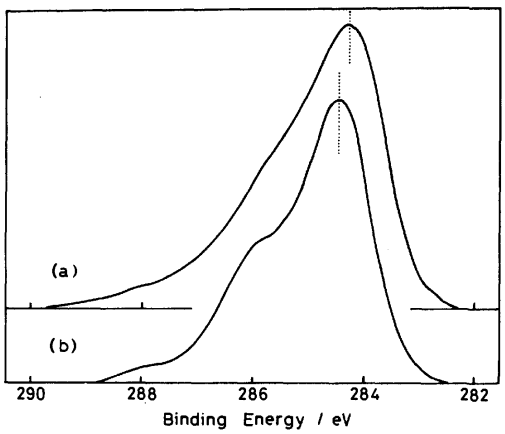

Fig. 3. XPS spectra of the C 1s region of (a) $PtPc(ClO_4)_{0.5}$ and (b) PtPc.

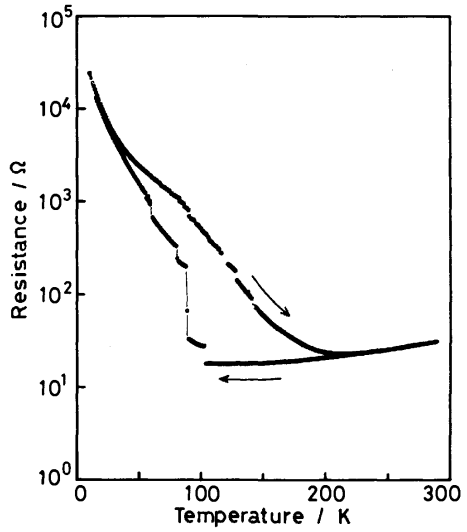

Fig. 2. The first heat cycle of the electrical resistivity of $PtPc(ClO_4)_{0.5}$.

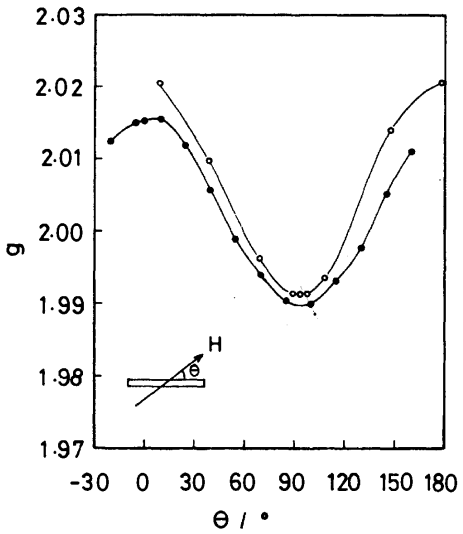

Fig. 4. Angular dependence of the ESR signal of $PtPc(ClO_4)_{0.5}$. The solid and open circles correspond to the room temperature and 4.2 K, respectively.

angular dependence of the g-value of $PtPc(ClO_4)_{0.5}$ at room temperature and 4.2 K. From the tetragonal symmetry of the crystal and molecule, the principal values of the PtPc molecule can be directly determined from this angular dependence. The principal values are given in Table 3, together with the corresponding values of the other related molecules. The symbols, // and ⊥, denote the directions parallel and perpendicular to the normal of the molecular plane. Since the principal values of $PtPc(ClO_4)_{0.5}$ are completely different from the corresponding values of KCP,[23] the unpaired electrons are not in the $5d_{z^2}$ band located at the platinum chain. On the other hand, the g-values are also slightly different from those of the ligand-oxidized cation radical, e.g. $Ni^{2+}Pc^{1-}$.[26] Therefore, the oxidation is mainly ligand-centered, though the unpaired electron also has a slight d-character. This result is similar to that of $NiPc(SbF_6)_{0.5}$.[24,25] However, the relation, $g_{//} > g_{\perp}$, is reverse to that of $NiPc(SbF_6)_{0.5}$,[24,25] in which the d-character of the unpaired electron is interpreted based on the exchange interaction between the conduction electrons on the ligand and the small amount of the localized spins on the $3d_{z^2}$ orbital of nickel atoms. This anisotropy indicates that the $5d_{z^2}$ orbital of Pt is not responsible for the d-character of the unpaired electron, but that the orbital of the unpaired electron has a character of d_{xz} and d_{yz}.[27] It is not reasonable to simply replace the role of $5d_{z^2}$ by $5d_{xz}$ and $5d_{yz}$, because the latters are expected to be strongly hybridized with the π-orbital (e_g) of the ligand in contrast to the former.[22] We thus consider that this molecular orbital with e_g symmetry is mixed to some extent with the ligand-centered HOMO (a_{1u}) in the solid state because the symmetry restriction is released in the general point of the Brillouin zone. However, the contribution of the e_g orbital seems to be very small, because the observed g-value is close to that of the ligand-centered unpaired spin, even at low temperature (as described in the next section). This conjecture is supported by the experimental result of XPS that the oxidation occurs mainly at the ligand part. The different anisotropy of the g-value between PtPc and NiPc is attributed to the electronic structures of their molecules. Unfortunately, details of the electronic structure of PtPc are not known, as compared with that of NiPc.

Figure 5 shows the temperature dependences of the spin susceptibilities, linewidths, and g-values. Upon cooling, $g_{//}$ and $g_{\perp}$ slightly increase from 2.016 and 1.989 to 2.023 and 1.992 at 4.2 K, respectively. This temperature dependence is much weaker than that of $NiPc(SbF_6)_{0.5}$.[25] This slight increase probably sug-

Table 3. Principal g-Values of $PtPc(ClO_4)_{0.5}$ and Other Complexes at Room Temperature

Compound	$g_{//}$	$g_{\perp}$	Reference
$PtPc(ClO_4)_{0.5}$	2.016	1.989	This work
$PtPc(AsF_6)_x$	2.016	1.990	This work
$Pt(CN)_4Br_{1/3}\ 3H_2O$	1.946	2.336	Mehran and Scott[23]
$NiPc(SbF_6)_{0.5}$	1.994	2.030	Yakushi et al.[24,25]
$Ni^{2+}Pc^{1-}$	2.003	2.003	Bobrovskii and Sidorov[26]

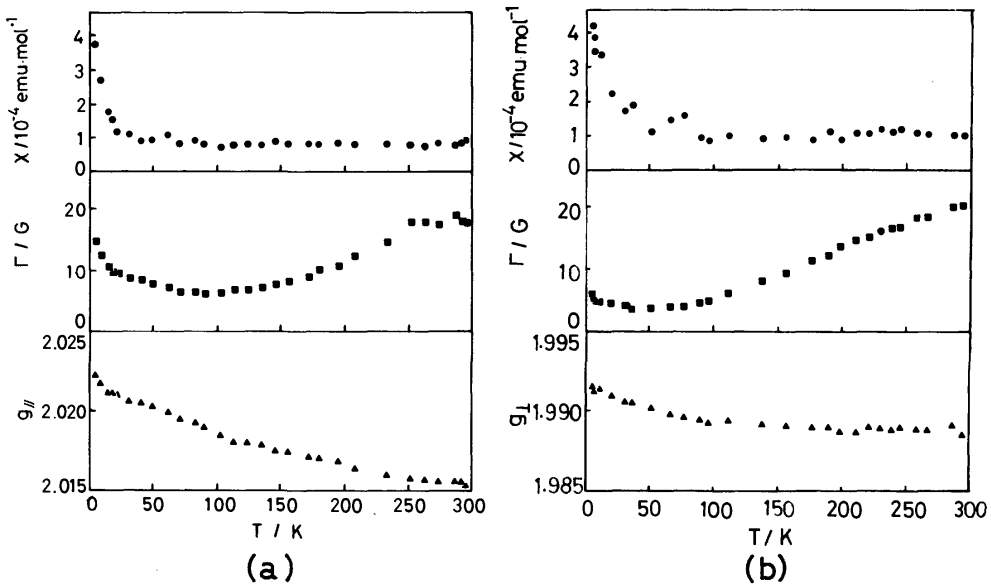

Fig. 5. Temperature dependence of the spin susceptibilities (χ), linewidths (Γ), and g-values (g). (a) $H//c$ and (b) $H \perp c$.

gests a change in the degree of mixing between the e_g and a_{1u} bands. The line shape of the ESR signal is Lorentzian over the whole temperature range. The spin susceptibility, which is obtained by the double integration of the observed signal, remains almost constant down to ca. 20 K. Combining this result with the metallic behavior of the electrical resistivity, the temperature-independent spin susceptibility is attributable to Pauli paramagnetism. The linewidths of organic metals usually decrease upon lowering the temperature, since they are determined mainly by the spin relaxation through the so-called Elliot mechanism.[28] Thus the gradual decrease of the linewidth also supports the view that the origin of the unpaired electrons is conduction electrons. This magnetic result suggests that $PtPc(ClO_4)_{0.5}$ is metallic, at least down to 20 K. Assuming the one-dimensional tight-binding model, we estimated the bandwidth, $4t$, using

$$4t = 4N_A\mu_B^2/(\pi \sin(k_f c)\chi), \quad (1)$$

where N_A is the Avogadro constant, μ_B the Bohr mageton, k_f the Fermi wave vector, c the inter-planar distance between the adjacent PtPc molecules, and χ the spin susceptibility (measured with a unit of emu mol^{-1}). The bandwidth of the ligand-centered band has been estimated to be 0.6—0.8 eV using $\chi=(1.0—0.7)\times10^{-4}$ emu mol^{-1} and $k_fc=(3/4)\pi$. The rise-up of χ in the region of $T<20$ K is attributable to the localized spins, the concentration of which is 4×10^{-3} spins per one $PtPc(ClO_4)_{0.5}$. Since the angular dependence of the g-value of the localized spins is almost the same as that of the conduction electrons (as shown in Fig. 4), the origin of the localized spins is not the magnetic impurity but, rather, a crystal defect. Incidentally, the ESR spectrum of $PtPc(AsF_6)_x$ is essentially the same as that of $PtPc(ClO_4)_{0.5}$, including the temperature dependence.

Polarized Reflectance Spectra. Figure 6 shows the reflectance spectra of $PtPc(ClO_4)_{0.5}$ polarized parallel and perpendicular to the c-axis. The plasma-edge like dispersion is observed only in the $//c$ polarization. This strong anisotropy clearly indicates the presence of a one-dimensional conduction band along the c-axis. We analyzed the $//c$ spectrum based on the Drude model, and obtained the plasma frequency, $\omega_p=7010$ cm^{-1}, the relaxation time of the conduction electrons, $\tau=0.8\times10^{-14}$ s, and the dielectric constant contributed from the electronic excitations in the higher wave number region, $\varepsilon(\text{core})=2.31$. The reflection spectrum calculated from these parameters is drawn by solid lines in Fig. 6. The bandwidth, $4t$, was calculated on the assumption of the one-dimensional tight-binding model using

$$4t = \{V_m(\hbar\omega_p)^2\}/\{4e^2c^2\sin(k_f c)\}, \quad (2)$$

where V_m is the volume of $PtPc(ClO_4)_{0.5}$, e the unit charge of an electron, and k_f and c are the same as those defined in Eq. 1. The bandwidth was estimated to be 1.2 eV, using $V_m=6.437\times10^{-22}$ cm^3, $\hbar\omega_p=0.87$ eV, and $k_fc=(3/4)\pi$. This bandwidth is 1.5—2.0 times larger than that estimated from the spin susceptibility. The difference between them is attributable to the effect of the electron-electron Coulomb interaction.[29] Since the optical spectrum of $PtPc(AsF_6)_x$ is the same as $PtPc(ClO_4)_{0.5}$, we surmise $x\approx0.5$ in $PtPc(AsF_6)_x$, because the position of the plasma edge in the reflection spectrum reflects the concentration of the conduction electrons, which is related to the chemical ratio.

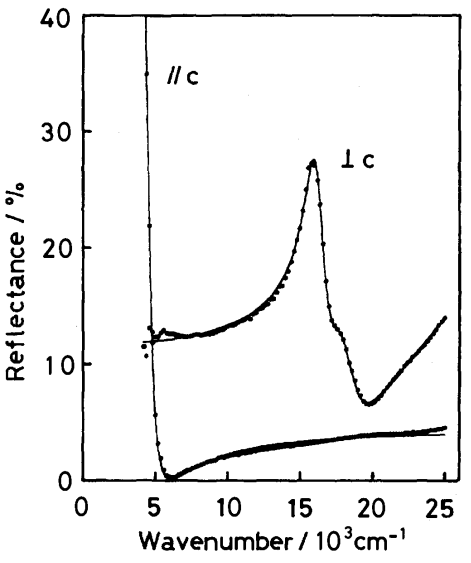

Fig. 6. Polarized reflectance spectrum of the $PtPc(ClO_4)_{0.5}$ single crystal. The circles and the solid lines are respectively the experimental data and the simulated curves based on the Drude model for the $//c$ spectrum and the Lorentz model for the $\perp c$ spectrum.

The $\perp c$ spectrum was simulated by three Lorentz oscillators so as to reproduce the experimental curve. The simulated curve is represented by the solid line in Fig. 6. The resonance frequencies of the Lorentz oscillators in the visible region are 16000 and 17900 cm^{-1}. The 16000 cm^{-1} electronic transition is assigned to the interband transition which corresponds to the Q-band in the free molecule of phthalocyanine. Probably, the shoulder at 17900 cm^{-1} cannot be assigned to the vibrational structure of the Q-band, since the intensity ratio to the main peak at 16000 cm^{-1} and the separation of the excitation energies depend significantly upon the central metals of such salts as $NiPc(SbF_6)_{0.5}$[25] and $CoPc(AsF_6)_x$.[30] The origin of this shoulder is not clear at present. However, it is possibly related to the mixed-valent nature of the phthalocyanine ring, since the monoclinic PbPc crystal[31] exhibits a strong Q-band, the shape of which is a single Lorentzian with a width of 1000 cm^{-1} (FWHM).[32]

We prepared $PtPc(ClO_4)_{0.5}$ and $PtPc(AsF_6)_x$, which were the first oxidized salts of PtPc, in the process of searching for a stable metallic platinum chain with a mixed-valent state. Both PtPc salts are isostructural and have one-dimensional column structures like the iodine complex of NiPc. They are metallic at least down to 120 K and probably to 20 K, or possibly to a temperature lower than that. Contrary to our expectation, however, the conducting pathway is not located on the platinum spine, but mainly on the ligand chain. The solid state properties are almost the same as those of $NiPc(SbF_6)_{0.5}$,[25] but the ESR properties are remarkably different.

References

1) C. J. Schramm, R. P. Scaringe, D. R. Stojakovic, B. M. Hoffman, J. A. Ibers, and T. J. Marks, *J. Am. Chem. Soc.*, **102**, 6702 (1980).

2) T. E. Phillips, R. D. Scaringe, B. M. Hoffman, and J. A. Ibers, *J. Am. Chem. Soc.*, **102**, 3435 (1980).

3) J. Martinsen, L. J. Pace, T. E. Phillips, B. M. Hoffman, and J. A. Ibers, *J. Am. Chem. Soc.*, **104**, 83 (1982).

4) J. Martinsen, S. M. Palmer, J. Tanaka, R. C. Greene, and B. M. Hoffman, *Phys. Rev. B*, **30**, 6269 (1984).

5) S. M. Palmer, J. L. Stanton, N. K. Jaggi, B. M. Hoffman, J. A. Ibers, and L. H. Schwartz, *Inorg. Chem.*, **24**, 2040 (1985).

6) J. Martinsen, J. L. Stanton, R. L. Greene, J. Tanaka, B. M. Hoffman, and J. A. Ibers, *J. Am. Chem. Soc.*, **107**, 6915 (1985).

7) T. Inabe, S. Nakamura, W. B. Liang, T. J. Marks, R. L. Burton, C. R. Kannewurf, and K. Imaeda, *J. Am. Chem. Soc.*, **107**, 7224 (1985).

8) T. Inabe, T. J. Marks, R. L. Burton, J. W. Lyding, W. J. McCarthy, C. R. Kannewurf, G. M. Reisner, and F. H. Herbstein, *Solid State Commun.*, **54**, 501 (1985).

9) M. Almeida, M. G. Kanatzidis, L. M. Tonge, T. J. Marks, H. O. Maracy, W. J. McCarthy, and C. R. Kannewurf, *Solid State Commun.*, **63**, 457 (1987).

10) M. Y. Ogawa, J. Martinsen, S. M. Palmer, J. L. Stanton, J. Tanaka, R. L. Greene, B. M. Hoffman, and J. A. Ibers, *J. Am. Chem. Soc.*, **109**, 1115 (1987).

11) K. B. Efetov and A. I. Larkin, *Sov. Phys. JETP*, **42**, 390 (1976).

12) G. A. Sawatzky and E. Antonides, *J. Phys.*, **37**, C4-117 (1976).

13) H. Nagasawa, *Phys. Status Solidi B*, **109**, 749 (1982).

14) A. S. Berenblyum, L. I. Buravov, M. D. Khidekel', I. F. Shchegolev, and E. B. Yakimov, *JETP Lett.*, **13**, 440 (1971).

15) J. Bernasconi, P. Bruesch, and H. R. Zeller, *J. Phys. Chem. Solids*, **35**, 145 (1974).

16) P. A. Barett, C. E. Dent, and R. P. Linstead, *J. Chem. Soc.*, **1936**, 1719.

17) T. Sakurai and K. Kobayashi, *Rep. Inst. Phys. Chem. Res.*, **55**, 69 (1979).

18) C. J. Brown, *J. Chem. Soc. A*, **1968**, 2494.

19) R. D. Shannon, *Acta Crystallogr., Sect. A*, **32**, 751 (1976).

20) K. Yakushi, M. Sakuda, H. Kuroda, A. Kawamoto, and J. Tanaka, *Chem. Lett.*, **1986**, 1161.

21) P. Sheng, *Phys. Rev. B*, **6**, 2180 (1980). This model explains well the resistivity curve from 50 K to 4.2 K which was measured on the different sample shown in Fig. 2.

22) F. W. Kutzler and D. E. Ellis, *J. Chem. Phys.*, **84**, 1033 (1986).

23) F. Mehran and B. A. Scott, *Phys. Rev. Lett.*, **31**, 1347 (1973).

24) K. Yakushi, H. Yamakado, M. Yoshitake, N. Kosugi, H. Kuroda, A. Kawamoto, J. Tanaka, T. Sugano, M. Kinoshita, and S. Hino, *Synth. Met.*, **28**, F95 (1989).

25) K. Yakushi, H. Yamakado, M. Yoshitake, N. Kosugi, H. Kuroda, T. Sugano, M. Kinoshita, A. Kawamoto, and J. Tanaka, *Bull. Chem. Soc. Jpn.*, **62**, 687 (1989).

26) A. P. Bobrovskii and A. N. Sidorov, *J. Struct. Chem. (Engl. Transl.)*, **17**, 50 (1976).

27) J. S. Griffith, *Discuss. Faraday Soc.*, **26**, 81 (1958).

28) R. J. Elliot, *Phys. Rev.*, **96**, 266 (1954).

29) C. S. Jacobsen, *J. Phys. C*, **19**, 5463 (1986).

30) H. Yamakado and K. Yakushi, unpublished data.

31) Since the first singlet excited state of metallo-phthalocyanine is degenerate, the Q-band is split into 4 absorption bands in almost all metallo-phthalocyanine crystals because of the low site symmetry and the exciton effect. However, the exceptional case is found in the monoclinic form of PbPc, in which the arrangement of PbPc is nearly tetragonal like the partially oxidized salts of metallo-phthalocyanine.

32) Y. Iyechika, K. Yakushi, and H. Kuroda, *Chem. Phys.*, **87**, 101 (1984).

Magnetic and Electric Properties of a Cation Radical Salt Tris(decacyclene) Bis(hexafluorophosphate), $(Dc)_3(PF_6)_2$

Tadashi SUGANO and Minoru KINOSHITA*
The Institute for Solid State Physics, The University of Tokyo, Roppongi, Minato-ku, Tokyo 106
(Received January 26, 1989)

A cation radical salt between a π-electron donor decacyclene and hexafluorophosphate, $(Dc)_3(PF_6)_2$, was prepared by electrochemical synthesis, and conductivity (90—350 K), electron paramagnetic resonance (4—400 K) and static susceptibility (2—300 K) were measured. The salt was found to be semiconductive with the conductivity of ca. 4×10^{-2} S cm^{-1} at room tempertature and the activation energy of 66±3 meV. The magnetic measurements show that this salt is paramagnetic and spin susceptibility is thermally activated with the activation energy of 17 meV resulting from antiferromagnetic intermolecular interaction, although the dication of electron donor might be expected to have triplet spin multiplicity to stabilize ferromagnetic spin alignment in the ground state. The magnetism of $(Dc)_3(PF_6)_2$ is discussed in terms of charge-transfer interaction among donors.

Since McConnell proposed a model for ferromagnetic (FM) spin alignment in purely organic compounds using ionic charge-transfer (CT) complexes in 1967,[1] some its modifications have been suggested for ionic CT complexes and ion radical salts[2-5] and the model has thoroughly been generalized including organometallic complexes.[6] In these models, it is essential that an ionic CT complex or ion radical salt is consisting of molecules which exhibit high spin multiplicity in the CT excited states and/or in the ground state.[1-6]

For the ion radical salts, virtual disproportionation, where an electron on one molecule which has doubly degenerate orbital (d) occupied by one (d^1) or three (d^3) electrons is transferred to an adjacent molecule with the same electronic configuration, could stabilize FM coupling between the molecules.[2,6] This mechanism may further be extended to the case of a crystal consisting of molecules having higher degeneracy.[6] Similarly, one electron transfer between molecular sites with doubly (or multiply) degenerate orbitals with heterospin configurations (e.g., d^1 and d^2; d^2 and d^3) could result in FM or ferrimagnetic (FIM) coupling.[4,6] In contrast to the situations mentioned above, for the CT complexes, antiferromagnetic (AFM) coupling is predicted for virtual backward CT from a d^1 site to a non-degenerate site (s) with single occupancy (s^1) and also for virtual backward CT from d^3 to s^1,[6] whereas the inverse (forward CT) processes could result in FM coupling.[1-3,6] In other words, whether ion radical salts are in a uni or mixed valence state, they would be more appropriate candidates than ionic CT complexes to realize FM spin alignment, since the FM intermolecular coupling could be stabilized regardless of the direction of CT. Such prescription therefore leads us to study an ion radical salt based on an organic molecule with symmetry higher than C_3. Such a molecule is known to possess degeneracy in the highest occupied molecular orbital (HOMO) and the lowest unoccupied molecular orbital (LUMO), when it is free.

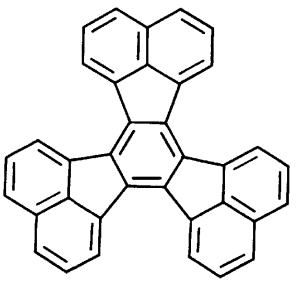

Fig. 1. Molecular structure of decacyclene.

Some aromatic molecules with a three- or six-fold axis of rotation such as decacyclene (diacenaphtho[1,2-*j*:1′,2′-*l*]fluoranthene),[7] 1,3,5-triphenylbenzene,[7,8] hexamethoxytriphenylene,[9] hexachlorobenzene,[10] and hexaazaoctadecahydrocoronene[11] have in fact been shown to have triplet ground state when they were in the dication or dianion state. Therefore, ion radical salts of these aromatic molecules may be a good candidate to establish FM intermolecular coupling in a solid. Cation radical salts of polycyclic aromatic hydrocarbons have been prepared by galvanostatic electrochemical oxidation with an appropriate supporting electrolyte,[12] although some aromatic hydrocarbons such as naphthalene are unstable in atmosphere.[13] We have prepared the cation radical salts of decacyclene (Fig. 1) by the electrochemical oxidation. In this paper, we describe the characterization and investigation of electric and magnetic properties of the cation radical salt with hexafluorophosphate.[14]

Experimental

Decacyclene (Aldrich Chemical Co. Inc.) was recrystallized from a nitrobenzene solution and sublimed twice at 320 °C under 1 Pa. Black single crystals shaped like long needle were prepared by electrochemical oxidation of decacyclene in a dichloromethane solution on a platinum anode under a constant current of 2 μA at 0 °C for 160 hours. Tetrabutyl-

ammonium hexafluorophosphate was used as a supporting electrolyte. The crystals are stable in a dry atmosphere but mechanically unstable and readily decomposed to yield decacyclene when they are ground in an agate mortar.

A preliminary X-ray diffraction analysis shows that this cation radical salt has 3:2 stoichiometry, i.e., tris(decacyclene) bis(hexafluorophosphate), $(Dc)_3(PF_6)_2$. The salt crystallizes in the hexagonal system, space group $P6_322$, with the following cell constants: a=27.896(4) Å, c=10.422(1) Å, V=7024(2) Å^3, Z=4, D_x=1.55 Mg m^{-3} and D_{obs}=1.55 Mg m^{-3}.[15] The crystals were elongated along the crystallographic c-axis with dimensions 2—5 mm in length and 0.05—0.1 mm in width.

Direct current electrical conductivity was measured on a single crystal by means of the four probe technique with silver paste (du Pont No. 4929). Electron paramagnetic resonance (EPR) spectra of a single crystal were recorded on a JEOL JES-FE1X spectrometer at 9 GHz with a cylindrical cavity in the TE_{011} mode. Sample temperature was varied and controlled by using an Oxford ESR900 cryostat of continuous flow type and a DTC-2 temperature controller in the range from 4 to 300 K. A JEOL EXDVT-1 temperature controller was also used in the range from 300 to 400 K. The g factor was determined by comparing the resonance position with that of Li^+TCNQ^- (g=2.0026). The modulation width was always kept much less than one-tenth of the linewidth to prevent line shape from distortion due to overmodulation.

Magnetic susceptibility was measured with a Faraday-type susceptometer over the temperature range from 2 to 300 K on a bundle (1 mg) of the single crystals in a small quartz bucket (ca. 20 mg) at 5 T and on the polycrystalline sample (12 mg) in a quartz bucket (ca. 100 mg) at 3 T. The details of the apparatus were described previously.[16]

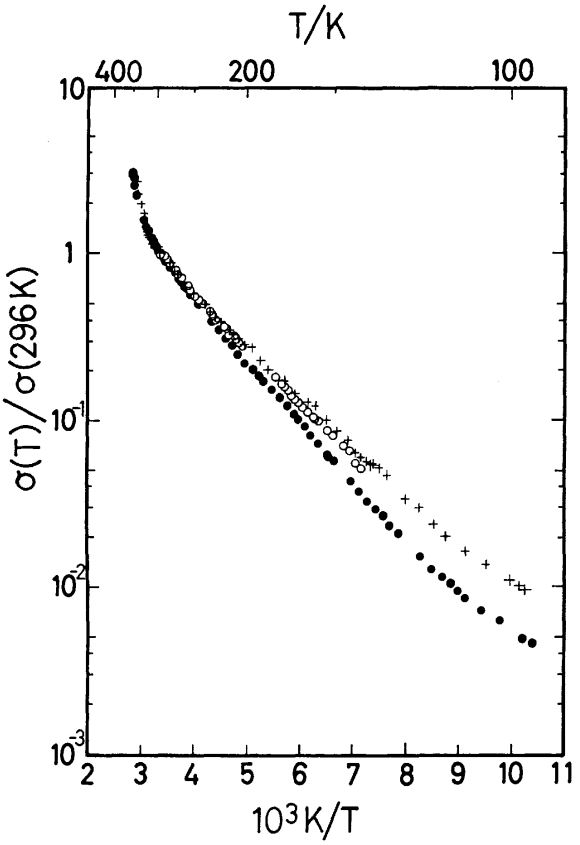

Fig. 2. Temperature dependence of conductivity σ of $(Dc)_3(PF_6)_2$. The conductivities observed for different crystals are normalized at 296 K and represented by crosses, open and closed circles. The conductivity σ follows $\sigma=\sigma_0\exp(-E_c/kT)$ with (2—6)×10^{-2} S cm^{-1} at 296 K and the activation energy E_c=66±3 meV.

Results

Semiconductive behavior with the conductivity (2—6)×10^{-2} S cm^{-1} at 296 K and the activation energy E_c=66±3 meV (1 eV=1.602×10^{-19} J) is observed for $(Dc)_3(PF_6)_2$ in the range from 90 to 300 K as shown in Fig. 2. Three different crystals gave very similar temperature dependence, although the conductivity values varied from sample to sample in the range indicated, probably due to inaccuracy of sample dimensions used in the conductivity calculation. As the temperature increases from room temperature, the conductivity increases more steeply than that in the low temperature region. This phenomenon was reproducible but no indication for phase transitions in the vicinity of room temperature was observed in the magnetic measurements as described below.

The EPR spectra of the single crystal of $(Dc)_3(PF_6)_2$ exhibit a Lorentzian shaped line over the whole temperature range between 4 and 403 K examined here as shown in Fig. 3. The g factor is found to be 2.0025(2) and independent of temperature. This indicates that the unpaired electrons in $(Dc)_3(PF_6)_2$ reside only on the decacyclene molecules. The g factors of aromatic hydrocarbons are given by g=2.00257—(19×10^{-5})λ, where λ is the coefficient of the Hückel MO energy level, $\alpha+\lambda\beta$, occupied by an odd electron.[17] We have calculated MO of decacyclene in the Hückel approximation and found that λ=0.4807 for HOMO which are doubly degenerate and occupied by an odd number of electrons when decacyclene is in the monocation radical state. The g factor is then calculated to be 2.00248 with λ=0.4807. This value is in good agreement with the observed value. It is worth noting that the g factor of PF_5^- radical observed under various conditions is known to be 1.9985(6), 2.00174(2), and 2.0039(2).[18]

The EPR absorption intensity is thermally activated except for the low temperature region below about 40 K where the susceptibility follows the Curie law as shown in Fig. 4. Such activation behavior is reminiscent of the moderately conducting ion radical salts.[19]

The peak-to-peak linewidth B_{pp} observed for the decacyclene cation radical salt is sharp, but not very sharp in comparison with that observed for the following cation radical salts of polycyclic aromatic hydrocarbons having metallic conductivity. The line-

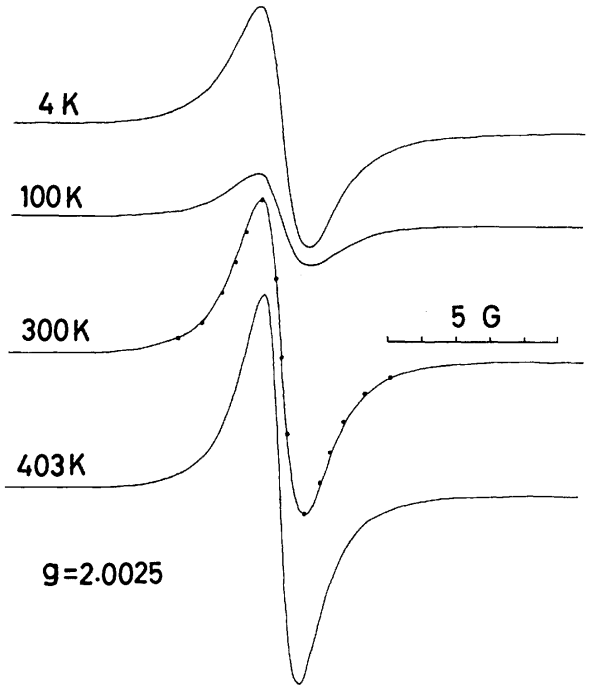

Fig. 3. First derivative curves of EPR spectra of the single crystal of $(Dc)_3(PF_6)_2$ at several temperatures. Closed circles on the 300 K spectrum represent the Lorentzian fit.

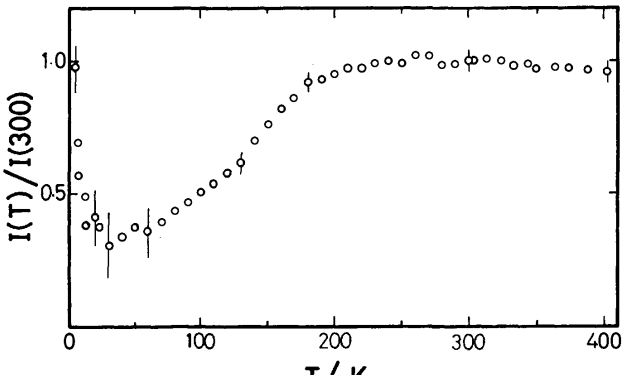

Fig. 4. Temperature dependence of the relative intensity of EPR of $(Dc)_3(PF_6)_2$ normalized at 300 K. Estimated errors are indicated by thin lines. The intensity is thermally activated above 40 K.

width of $(Dc)_3(PF_6)_2$ varies from 155 μT below 60 K down to 117 μT at 403 K as shown in Fig. 5, while the linewidths of the cation radical salts of other hydrocarbons are reported to be 60—80 μT for $(perylene)_2(XF_6)_{1.1}(CH_2Cl_2)_{0.85}$ (X=As or Sb) at 100—300 K,[20] 1.5 μT for $(fluoranthene)_2PF_6$ at 300 K,[21] and 0.25 μT for $(naphthalene)_2AsF_6$ at 300 K.[22] The linewidth of these salts would be ascribed qualitatively to the motional narrowing effect. The conductivity at room temperature is about 0.04 S cm^{-1} for $(Dc)_3(PF_6)_2$ examined here, 160 S cm^{-1} for $(perylene)_2(XF_6)_{1.1}(CH_2Cl_2)_{0.85}$,[20] 1000 S cm^{-1} for $(fluoranthene)_2PF_6$.[23] Since the motional narrowing becomes effective in highly-conducting solid, the linewidth is expected to decrease in the order of $(Dc)_3(PF_6)_2$, the perylene salt, and the fluoranthene salt, as actually observed. The fact that the linewidth of $(Dc)_3(PF_6)_2$ decreases monotonically upon increasing the temperature also supports the motional narrowing effect because the conductivity increases with the increase of temperature. The linewidth is temperature independent below ca. 60 K. Simultaneously, the Curie contribution becomes dominant in the susceptibility. Therefore, the constant linewidth at low temperatures is ascribed to extrinsic origin such as lattice defects.

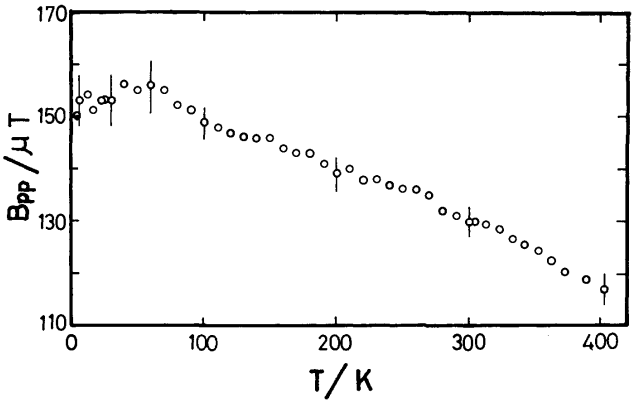

Fig. 5. Temperature dependence of peak-to-peak linewidth of EPR of $(Dc)_3(PF_6)_2$. Estimated errors are indicated by thin lines.

The static susceptibility observed for the bundle of the single crystals of $(Dc)_3(PF_6)_2$ exhibits the temperature dependence similar to that of the EPR absorption intensity obtained for the single crystal as shown in Fig. 6. That is, the paramagnetic susceptibility, which is determined by subtracting the diamagnetic contribution $\chi_d=-8.9\times10^{-4}$ emu mol^{-1} (1 emu mol$^{-1}=4\pi$ cm^3 mol^{-1}) estimated by Pascal's law, is thermally activated except for the low temperature region where the susceptibility follows the Curie law with the Curie constant $C=5.5\times10^{-3}$ emu K mol^{-1} (1 emu K mol$^{-1}=4\pi$ cm^3 K mol^{-1}) corresponding to 0.7% spins with $S=1/2$.

On the contrary, as shown in Fig. 7, the static susceptibility of the polycrystalline sample is very different from that of the single crystals. Substantial increase in the paramagnetism following the Curie-Weiss law is observed. The Curie constant is $C=0.130$ emu K mol^{-1} (17% spins with $S=1/2$) and the Weiss constant is $\theta=-5$ K. The finite Weiss constant of the polycrystalline sample results from the interaction between the Curie spins of high concentration. Since $(Dc)_3(PF_6)_2$ is mechanically unstable, the polycrystalline sample seems to include greater number of defects than the single crystals. Therefore, the large Curie paramagnetism in the polycrystalline sample is

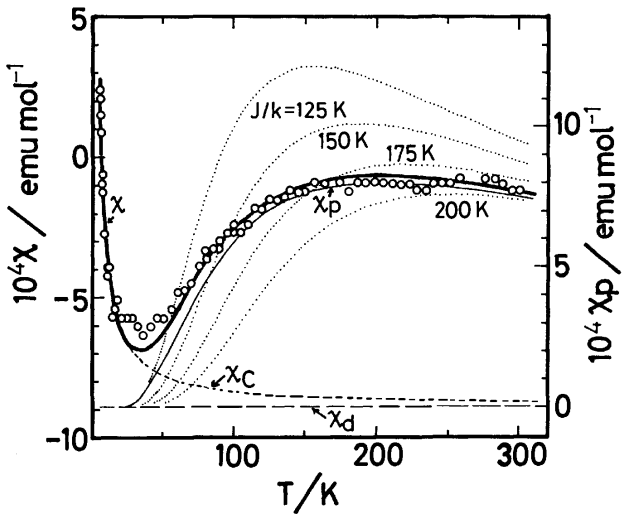

Fig. 6. Temperature dependence of static susceptibility of the bundle of single crystals of $(Dc)_3(PF_6)_2$ is shown by open circles. The diamagnetic (χ_d) and Curie (χ_C) contributions are represented by broken and dashed lines, respectively. The thin line indicates the intrinsic paramagnetic susceptibility (χ_P) calculated by the equation $\chi_P=(C/T)\exp(-E_m/kT)$ with $E_m/k=202$ K. The total susceptibility $\chi=\chi_P+\chi_C+\chi_d$ is shown by the thick line. The dotted lines show the theoretical curves calculated in terms of the single-triplet model with J/k=125, 150, 175, and 200 K.

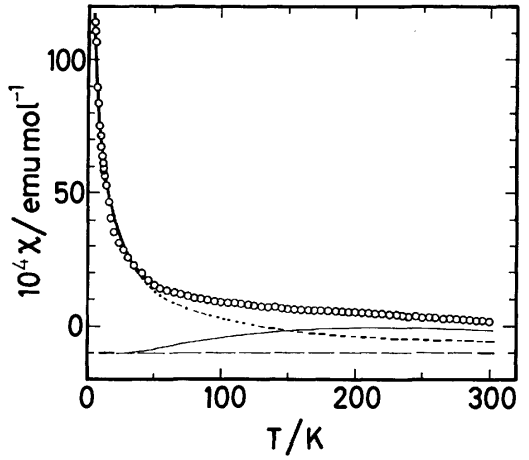

Fig. 7. Temperature dependence of static susceptibility of a polycrystalline sample of $(Dc)_3(PF_6)_2$. The lines represent the same meanings as shown in Fig. 7. It is to be noted that χ_C is about 25 times as large as that of the single crystals, while χ_P and χ_d alter a little.

ascribed to the increase of defects or paramagnetic centers produced by the crystal deterioration. Now it is clear that the Curie contribution observed in the single crystals of $(Dc)_3(PF_6)_2$ is extrinsic in origin and we analyze the paramagnetic susceptibility by subtracting the contribution.

The intrinsic paramagnetic susceptibility χ_P shown by the thin solid line in Fig. 6 is well described by the equation $\chi_P=(C/T)\exp(-E_m/kT)$ with E_m=17.4 meV or E_m/k=202 K. The diamagnetic (χ_d) and Curie (χ_C) contributions are represented by broken and dashed lines, respectively. The total susceptibility χ calculated by summing χ_P, χ_C, and χ_d is shown by the thick solid line in Fig. 6 and it agrees well, as a matter of course, with the observed susceptibility. The magnetic activation energy E_m obtained is about four times as small as the electric activation energy E_c. Such discrepancy is commonly observed for semiconducting organic ion radical solids and interpreted in terms of on-site Coulomb repulsion between itinerant electrons with AFM coupling.[19] The singlet-triplet model $\chi_P=(4C/T)[3+\exp(2J/kT)]^{-1}$ based on AFM coupling between two doublet sites fails to explain the intrinsic paramagnetism of $(Dc)_3(PF_6)_2$. In this case, the exchange coupling constant J/k should vary from 125 K below 50 K to 200 K above room temperature as shown by dotted lines in Fig. 6. Therefore, the AFM interaction among the spin centers residing on the decacyclene molecules seems to be not restricted within the nearest-neighbor spin centers but extended to second- and third-neighbors.

Discussion

The EPR and static susceptibility investigations demonstrate that $(Dc)_3(PF_6)_2$ is paramagnetic over the whole temperature range between 2 and 400 K. The activation behavior of susceptibility suggests the AFM coupling between unpaired electrons on the decacyclene molecules in spite of its capability to cause FM intermolecular interactions.

The decacyclene molecules seem to be stacked face-to-face taking into account their largely planar molecular structure, although the crystal structure of $(Dc)_3(PF_6)_2$ has not yet been solved. Namely, the decacyclene molecules are expected to form a segregated column structure. The 3:2 stoichiometry of the decacyclene salt with the monovalent anion PF_6^- indicates that two of three decacyclene molecules are formally ionized to monocation radicals and one of them remains neutral. The moderate conductivity observed for the salt supports such a mixed valence state. Therefore, $(Dc)_3(PF_6)_2$ can be regarded as a heterospin system consisting of the d^3 (Dc^+) and d^4 (Dc) configurations.

The models proposed by McConnell[1] and other authors[2-6] are based on the CT interaction within molecular dyads. Such a molecular dyad approach, however, could not be applicable to $(Dc)_3(PF_6)_2$ in the mixed valence state, because two different pairs of electronic configurations, i.e., d^3d^4 and d^4d^4, must be considered simultaneously. For the semiconducting cation or anion radical salts with 3:2 or 2:3 stoichiometry such as $(TTF)_3(BF_4)_2$,[24] $Cs_2(TCNQ)_3$,[25] and $Rb_2(TCNQ)_3$,[26] where the number of unpaired

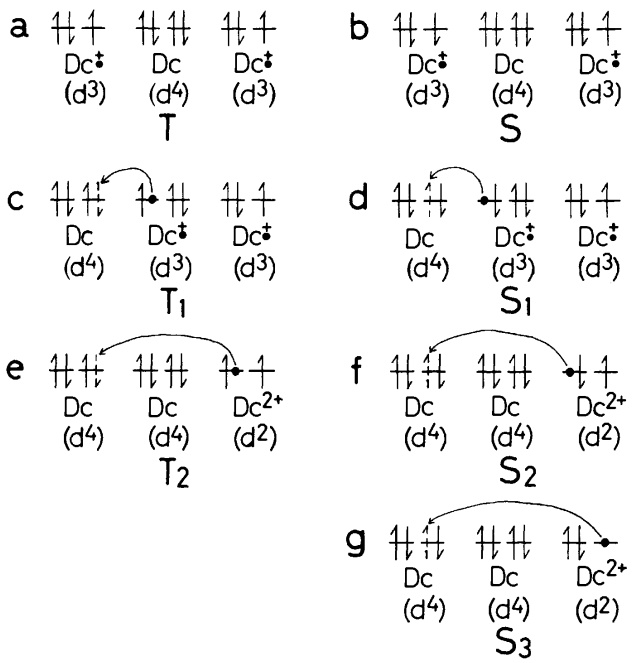

Fig. 8. Ground configurations T and S and excited charge-transfer configurations T_1, T_2, S_1, S_2, and S_3, for an electron transfer among monocation radicals and neutral molecule of decacyclene forming a triad.

electrons per molecule is 2/3 on an average, it is known that molecular triads consisting of the ionized molecules at each terminal and the neutral molecule at the center form an infinite stacking column in the solid. We assume therefore that $(Dc)_3(PF_6)_2$ crystallizes in this type of structure, since it is a semiconductive cation radical salt with 3:2 stoichiometry like $(TTF)_3(BF_4)_2$.

If this is the case, the ground electronic configuration of $(Dc)_3(PF_6)_2$, in the zero-th order approximation, can be described as a heterospin system composed of two d^3 and one d^4 states ($d^3d^4d^3$) as depicted schematically in Fig. 8a for the triplet state (T) and Fig. 8b for the singlet state (S). In terms of this configuration, the interaction is restricted within a triad. However, the discussion on the triad could be generalized to a system of an extended array of triads. Configurations T and S are the no-bond structures and they are nearly degenerate. Strictly speaking, T is slightly more stable than S by the direct exchange interaction represented by the exchange integral. However, such stabilization should be small in the case of intermolecular interaction.

There is a low-lying CT excited configuration ($d^4d^3d^3$ or $d^3d^3d^4$) in each of the triplet (T_1) and singlet (S_1) manifold as shown in Figs. 8c and 8d.[27] These excited configurations T_1 and S_1 admix with the ground configurations, thereby stabilizing T and S, respectively. The magnitude of stabilization is a function of the energy separation (diagonal term) and the magnitudes of the transfer integrals (off-diagonal terms) between the configurations concerned as discussed previously.[28] The diagonal terms in the triplet and singlet manifold would not be very different from each other because the excited configurations consist of two d^3 and one d^4 states as in the ground configurations; only the molecular sites on which the unpaired electrons reside are different. The off-diagonal terms for both manifolds would also not be very different from each other, although numerical calculations of the off-diagonal terms has not been carried out since the crystal structure is not determined yet. Therefore, the ground configurations T and S would be stabilized down to a similar amount by the admixture with the low-lying excited CT configurations T_1 and S_1.

Therefore, we have to consider other excited CT configurations of higher energy. Of these, the configurations T_2, S_2, and S_3 shown in Figs. 8e, 8f, and 8g[29] would contribute considerably to stabilization of the ground configurations T and S. The CT absorption band corresponding to the excitation to the state mainly consisting of S_2 or S_3, as well as that to the state based on S_1, is usually observed in the near-infrared region for most ion radical salts.[30] The diagonal terms for these configurations are, therefore, not too large in spite of on-site Coulomb repulsion on the dication of d^2 configuration. Further, the diagonal term for T_2 must be smaller than that for S_2 and S_3 by the amount of the intramolecular exchange energy. The transfer integral (off-diagonal term) of the salt is expected not to be small, because the transfer integral is known to be large for the cation radical salts of polycyclic hydrocarbons.[31] Therefore, the stabilizations of T and S by admixture of the configurations T_2, S_2, and S_3 are not negligibly small. Since there are two singlet configurations of nearly the same energy, the stabilization of S by admixture of S_2 and S_3 would surpass the stabilization of T, even though the diagonal term for T_2 is more favorable than that for S_2 and S_3. This is a possible reason why $(Dc)_3(PF_6)_2$ does not exhibit FM coupling. There are, of course, many other excited configurations of higher energy and these would also stabilize T and S. However, these would contribute to a similar amount in both manifolds.

Finally, it may be pointed out that there still remain other possibilities of destabilizing ferromagnetically coupled state. For example, there would be Jahn-Teller distortion[32] of a decacyclene molecule removing the orbital degeneracy to increase the diagonal term for the triplet configurations. Although it is known that the dianion of decacyclene has the triplet state as the lowest state in a solution,[7] the electronic structure of its dication is not known. It is therefore of great interest to investigate the molecular and crystal structure of $(Dc)_3(PF_6)_2$ to acquire further insight into the magnetic interaction in this salt.

Conclusion

We have synthesized the cation radical salt between decacyclene and hexafluorophosphate anion with 3:2 stoichiometry. The magnetic and electric properties of the salt were investigated by means of the conductivity, EPR, and static susceptibility measurements. The spin susceptibility of the semiconductive salt is thermally activated with the activation energy of 17 meV, being smaller than that of electrical conduction 66 meV. These results indicate that the unpaired electrons are coupled antiferromagnetically, although the salt apparently meets the requirements of the models for organic ferromagnetism. A possible reason why $(Dc)_3(PF_6)_2$ does not exhibit ferromagnetic intermolecular interaction has been discussed on the basis of the mixed valence state. It is worth noting that magnetic and structural investigations of the salt consisting solely of monovalent decacyclene ions and free from neutral molecules are inevitable to examine the simple and familiar models for ferromagnetic spin alignment based on charge-transfer interaction in organic compounds.

This work was in part supported by a Grant-in-Aid for the Scientific Research from the Ministry of Education, Science and Culture.

References

1) H. M. McConnell, *Proc. Robert A. Welch Found. Conf. Chem. Res.*, **11**, 144 (1967).
2) Y. Sato, Thesis of the University of Tokyo (1970).
3) R. Breslow, *Pure Appl. Chem.*, **54**, 927 (1982).
4) K. A. Williams, M. J. Nowak, E. Dormann, and F. Wudl, *Synth. Met.*, **14**, 233 (1986).
5) J. B. Torrance, S. Oostra, and A. Nazzal, *Synth. Met.*, **19**, 708 (1987).
6) J. S. Miller, A. J. Epstein, and W. M. Reiff, *Chem. Rev.*, **88**, 201 (1988) and references cited therein.
7) R. E. Jesse, P. Biloen, R. Prins, J. D. W. van Voorst, and G. J. Hoijtink, *Mol. Phys.*, **6**, 633 (1963).
8) J. A. M. van Broekhoven, J. C. Sommerdijk, and E. de Boer, *Mol. Phys.*, **20**, 993 (1971).
9) K. Bechgaard and V. D. Parker, *J. Am. Chem. Soc.*, **94**, 4749 (1972).
10) E. Wasserman, R. S. Hutton, V. J. Kuck, and E. A. Chandross, *J. Am. Chem. Soc.*, **96**, 1965 (1974).
11) R. Breslow, P. Maslak, and J. S. Thomaides, *J. Am. Chem. Soc.*, **106**, 6453 (1984).
12) V. Enkelmann, *J. Phys. (Paris)*, **44**, C3-1147 (1983) and references cited therein.
13) H. P. Fritz, H. Gebauer, P. Friedrich, P. Ecker, R. Artes, and U. Schubert, *Z. Naturforsch., B*, **33**, 498 (1978).
14) This work was partly reported in the paper presented in the Abstracts of the Symposium on Molecular Structure, Nagoya, Japan (1984), p. 342. V. Enkelmann reported preparation of $(Dc)_3(AsF_6)_2$ in Ref. 12 without describing its physical properties. After completed our work, we have learned that decacyclene cation radical salts with 3:2 stoichiometry with eight monovalent inorganic anions including PF_6^- and AsF_6^- were synthesized by J. B. Torrance et al. and reported in *J. Appl. Phys.*, **63**, 2962 (1988). Temperature dependence of the static susceptibilities of $(Dc)_3(PF_6)_2$ and $(Dc)_3(SbF_6)_2$ reported by them exhibits activating behavior similar to that shown by us.
15) T. Sugano, S. Sato, and M. Kinoshita, unpublished.
16) M. Takahashi, T. Sugano, and M. Kinoshita, *Bull. Chem. Soc. Jpn.*, **57**, 26 (1984).
17) A. J. Stone, *Mol. Phys.*, **6**, 509 (1963).
18) Landolt-Börnstein, "New Series," Vol. 9, Part a, 155 (1977); Vol. 17, Subvol. a, 95 (1987).
19) Z. G. Soos and D. J. Klein, "Molecular Association," Vol. 1, ed by R. Foster, Academic Press, New York (1975), p. 1.
20) J. S. Schilling, M. Weger, K. Bender, D. Schweitzer, and H. J. Keller, *Solid State Commun.*, **48**, 281 (1983).
21) E. Dormann, W. Stocklein, G. Sachs, B. Bail, and M. Schwoerer, *J. Phys. (Paris)*, **44**, C3-1413 (1983).
22) E. Muller, J. U. von Schutz, and H. C. Wolf, *Mol. Cryst. Liq. Cryst.*, **93**, 407 (1983).
23) G. G. Maresch, A. Grupp, M. Mehring, J. U. von Schutz, and H. C. Wolf, *J. Phys. (Paris)*, **46**, 461 (1985).
24) J.-P. Legros, M. Bousseau, L. Valade, and P. Cassoux, *Mol. Cryst. Liq. Cryst.*, **100**, 181 (1983).
25) C. J. Fritchie, Jr. and P. Arthur, Jr., *Acta Crystallogr.*, **21**, 139 (1966).
26) R. J. van der Wal and B. van Bodegom, *Acta Crystallogr., Sect. B*, **34**, 1700 (1978).
27) Strictly speaking, $2^{-1/2}(d^4d^3d^3 \pm d^3d^3d^4)$ should be taken to satisfy the symmetry requirement.
28) K. Awaga, T. Sugano, and M. Kinoshita, *Chem. Phys. Lett.*, **141**, 540 (1987).
29) Strictly speaking, $2^{-1/2}(d^4d^4d^2 \pm d^2d^4d^4)$ should be taken to satisfy the symmetry requirement.
30) J. Tanaka, M. Tanaka, T. Kawai, T. Takabe, and O. Maki, *Bull. Chem. Soc. Jpn.*, **49**, 2358 (1976).
31) H. P. Geserich, R. Wilckens, W. Ruppel, V. Enkelmann, G. Wegner, G. Wieners, D. Schweitzer, and H. J. Keller, *Mol. Cryst. Liq. Cryst.*, **93**, 385 (1983).
32) The recent report, J. S. Miller, D. A. Dixon, J. C. Calabrese, *Science*, **240**, 1185 (1988), shows experimentally that hexaazaoctadecahydrocoronene dication in its tetraflouroborate and hexafluorophosphate salts is distorted by the Jahn-Teller effect to stabilize the singlet ground state in the solids.

Pyranyl Radicals and Their Dimers

Hiroki KAWATA and Shigeya NIIZUMA*
College of Humanities and Social Sciences, Iwate University, Ueda, Morioka 020
(Received February 6, 1989)

Photochemical and chemical reduction of pyrylium salts in THF solution gave their corresponding radicals which were in equilibrium with dimers. The quantum yields for raidcal formation and the standard enthalpy change ΔH_0 for dimerization decrease with increasing the electron-donating character of the substituting groups in the pyrylium ring. Specially, ΔH_0 for pentaphenylpyranyl and pentaphenylthiopyranyl radicals, in which all carbons in the ring are substituted by phenyl groups, become possitive. The absorption maxima and their molar extinction coefficients of pyranyl radicals, and concurrently the equilibrium constants for the dimerization were determined spectrophotometrically.

Pyranyl radicals are formed by one-electron reduction of the parent pyrylium salts with chemical (organic reducing agent,[1] zinc or other metals,[2] and Grignard reagent[3]), electrochemical[4] and photochemical[5] reactions in the degassed aprotic solvents. They are in equilibrium with their diamagnetic dimers (Scheme 1). This equilibrium lies in favor of the radical at room temperature except the compounds which have a methyl group[1] or a hydrogen atom[2f,6a,c] at 4-position carbon in the pyrylium ring. In such compounds, no equilibrium is observed and the dimer is formed directly at room temperature, so that no ESR signal can be detected. The NMR spectra of the dimers obtained by zinc metal reduction or the reduction with disodiocyclooctatetraene reflected the configuration of the σ bonding between the 4-position carbons of each pyranyl moiety.[1,6c] The equilibrium between pyranyl radicals and their dimers is similar to the case of the dimerization of pyridinyl radicals,[7] where the dimeric intermediate, radical pair, was involved in the dimerization of the radical.

Photoirradiation of 2,4,6-triphenyl-, 2-*t*-butyl-4,6-diphenylpyrylium and 2,4,6-triphenylthiopyrylium tetrafluoroborates in degassed tetrahydrofuran (THF) gave the corresponding radicals by electron transfer from the solvent, THF, itself with relatively high quantum yields.[5] 2,4,6-Triphenylpyranyl radical has a light red color in THF solution and shows the ESR signal with well-resolved hyperfine structure (hfs) at room temperature. With decreasing the temperature, the color fades and at the same time the intensity of the ESR signal decreases because of its dimer formation. In this paper, the investigation of the chemical properties of various kinds of pyranyl radicals formed by the photoreduction or by the zinc metal reduction of pyrylium salts is reported. The dimerization of 2,3,4,5,6-pentaphenylpyranyl and 2,3,4,5,6-pentaphenylthiopyranyl radicals was found to be an endothermic reaction, it being remarkable in comparison with that of other pyranyl radicals.

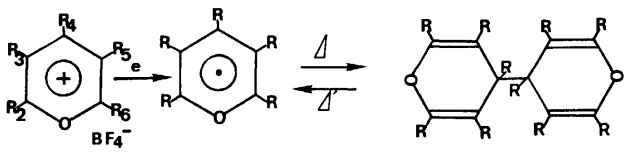

Scheme 1.

Experimental

The pyrylium salts used are all tetrafluoroborates and were supplied by Prof. Suzuki in this University. They decompose gradually in solution if the solvent contains a small amount of water. The solvents THF and 2-methyl-THF (G.R. of Wako Junyaku) were distilled over calcium hydride and stocked on a sodium-potassium alloy in an ampoule connected to a vacuum line. Triphenylphosphine (G.R. of Kanto Kagaku) was recrystallized twice from ethanol. The degassed sample solution was exposed to a continuous irradiation in a 1×1×4 cm quartz cell. The light source was a Toshiba SHL-100 UV mercury lamp with Toshiba filter system (UVD-35 and L-1A for the 365 nm, P-39B and L-39 for the 406 nm, and V-40 and Y-43 for the 436 nm irradiation). The quantum yield of the photoreaction was determined at 25 °C using potassium tris-oxalatoferrate(III) as an actinometer. The absorption and the ESR spectra were measured with a Hitachi ERI-G3 spectrophotometer and a JEOL PE-1 or RE-2 ESR spectrometer, respectively. The ESR intensity was calculated by a double integration of the first derivative curve with a Graphtec KD-4030 degitizer on-line with a NEC PC-9801 personal computer. The absorption spectra at low tem-

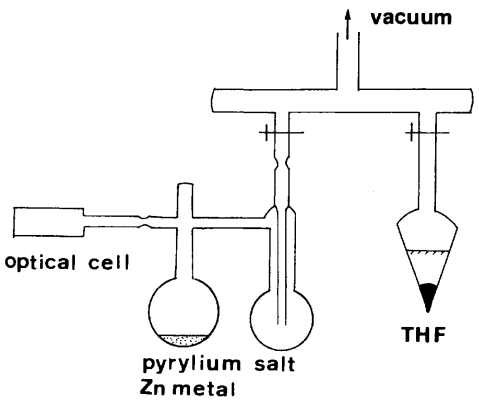

Fig. 1. Apparatus for the preparation of pyranyl radicals and the measurement of the absorption spectra.

perature were measured using a quartz Dewar vessel. The temperature was controlled with Dry Ice-methanol and liquid nitrogen.

The procedure of the preparation of the radical with zinc metal is as follows: Known amounts of pyrylium salt and an excess mole of zinc granular were put together into the reaction vessel connected to the vacuum line (see Fig. 1). After degassing the system, we introduced known amounts of solvent THF to it by distillation. The system was sealed and disconnected from the vacuum line. The solution was stirred with a Teflon-coated magnetic bar until the absorption of the starting material disappeared completely. All the sample solutions were degassed by means of the distillation method. The method of least squares was applied when a straight line was drawn in the analysis of the data.

Results and Discussion

Steady Light Irradiation. Photoirradiation of the degassed THF solution of 3-methyl-2,4,6-triphenyl-, (**1**), 2,3,4,6-tetraphenyl-, (**2**), 2,3,4,5,6-pentaphenyl-, (**3**), 2,4,6-tris(*p*-methoxyphenyl)pyrylium tetrafluoroborate (**4**), and 2,3,4,5,6-pentaphenylthiopyrylium tetrafluoroborate (**5**) gives the corresponding radicals when a reducing agent is added to the solution such as triphenylphosphine or hexamethylbenzene. Without these reductants, the radicals are not formed by the irradiation. Even with the reductants, they are not formed by dark reaction (i.e. by thermal reaction). The photoproducts for **2**, **3**, **4**, and **5** exhibited the strong but broad structureless ESR signals, while that for **1** had a well-resolved hfs. All of those photoproducts are considered to be neutral radicals produced by one-electron reduction. In the case of the photoreduction of 2,4,6-triphenylpyrylium salt, the solvent (THF) itself behaves as a reducing agent.

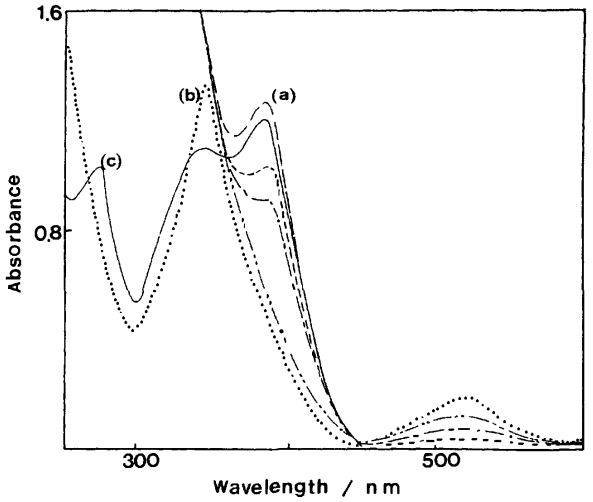

Fig. 2. (a) Spectral change of a solution of **1** containing 1.5×10^{-2} mol dm^{-3} triphenylphosphine on irradiation of 365 nm light with time: ——, 0 min; – – – –, 15 min; — — —, 45 min. (b) ------, Absorption spectrum of the radical for **1** (ca. 1.4×10^{-4} mol dm^{-3}) produced by the zinc metal reduction. (c) —, Absorption spectrum of **1** (1.4×10^{-4} mol dm^{-3}). All the spectra for (a), (b), and (c) were measured using the degassed THF solution and at 25°C.

On the photoirradiation, the concentration of pyrylium salts and triphenylphosphine were fixed to be 1.2×10^{-4} and 1.5×10^{-2} mol dm^{-3}, respectively. The irradiation wavelength was chosen to be 365 nm for **1** and **2**, 406 nm for **3** and **5**, and 436 nm for **4**. The spectral change observed on irradiating of **1** at 365 nm is shown in Fig. 2(a). The absorption of the product at 520 nm increases with the irradiation time at the expense of that of **1** at 385 nm. An isosbestic point appeares at 448 nm. The absorption band shorter than 330 nm could not be measured due to that of triphenylphosphine overlapping there. All the photoproducts have a very weak absorption extending beyond 900 nm. Molar extinction coefficient, ε, is 50—200 dm^3 mol^{-1} cm^{-1} at the wavelength region 600—900 nm. Since both pyrylium salts and the corresponding dimers have no absorption band at the wavelength 480—570 nm, the quantum yields for the formation of radical can be determined photometrically using the second main peak of radicals located in this region (discussed later) if only the extinction coefficient of the radical and the equilibrium constant K_d for the dimer formation are known. On the other hand, the same radicals as those produced by photoreaction were obtained chemically by the reduction with granules of zinc metal in degassed THF solution. The absorption spectrum of the radical produced from **1** obtained in this way is shown in Fig. 2(b). It has the absorption maxima at 342 and 520 nm. Making a comparison between the absorption spectrum of **1** (Fig. 2(c)) and that of the zinc reduction product, we found that **1** was quantitatively converted into the radical by zinc metal reduction. Other pyrylium salts are also reduced completely to the corresponding radicals by zinc metal. The radicals obtained in this way are stable in the degassed THF solution. But they all decompose on introducing air to the solution except for the radical from **4**, which reverts to the starting substance.

In order to know the exact molar extinction coefficients of these radicals, we must refer to the reaction the radical is concerned with. Consider the equilibrium between the radical and its dimer as

$$2\,\text{Radical} \rightleftarrows \text{Dimer}. \qquad (1)$$

The equilibrium constant K_d for the dimer formation is

$$K_d = [D]/[R]^2 = \{C_0 - [R]\}/2[R]^2, \qquad (2)$$

where [D] and [R] are the concentration of the dimer and the radical, respectively, and C_0 is the initial concentration of the pyrylium salt and equals [R]+2[D]. If α is the ratio of [R] to C_0,[8] then K_d is

$$K_d = (1 - \alpha)/2C_0\alpha^2. \qquad (3)$$

Table 1. Absorption Maxima of Radicals, Quantum Yield of Radical Formation, Standard Enthalpy Variation for Dimer Formation, and Equilibrium Constant of Dimer Formation

Compound	Absorption maxima (nm) and ε of radicals[a]	Quantum yield of radicals[b]	ΔH_0/kcal mol^{-1} for 2R ⟶ D	K_d (25 °C)
1	342(10800), 520(1780)	0.022	−14.5[c], −14.2[d]	1690
2	345(13800), 515(3180)	0.029	−12.3[c]	875
3	355(11200), 376(11000) 490(3760)	0.017	+2.36[d]	18700
4	358(34600), 562(3770)	0.014	−15.4[c]	505
5	363(10900), 470(1690)	—	+3.72[d]	1770

a) Obtained by the use of the Eq. 5 in degassed THF solution and ε is in 10^{-3} mol^{-1} cm^2. b) Quantum yield for the radical formation irradiated with the 365 nm for **1** and **2**, the 405 nm for **3** and the 436 nm for **4** at 25 °C. The value for **5** could not be determined since the absorption of the starting **5** was overlapping to that of the radical around 470 nm because of the conjugation of *p*-methoxyphenyl group with pyrylium ring. c) Determined photometrically. d) Determined by the ESR method.

We define the apparent molar extinction coefficient ε at a given wavelength by the following equation.

$$\varepsilon = \alpha\varepsilon_R + (1 - \alpha)\varepsilon_D/2. \quad (4)$$

Here, ε_R and ε_D are the molar extinction coefficients for the radical and its dimer. As the dimer has no absorption at an observing wavelength, we put ε_D as zero. Then, Eq. 3 becomes Eq. 5.

$$\varepsilon = \varepsilon_R - (2K_d/\varepsilon_R)\, C_0\varepsilon^2. \quad (5)$$

We derive respectively ε_R and K_d from the intercept and the slope of the straight line obtained by plotting ε vs. $C_0\varepsilon^2$. The absorption maxima and their molar extinction coefficients for the several kinds of radicals generated by the reduction with the zinc metal are summarized in Table 1 together with the equilibrium constants for the dimerization. The K_d value for **2** was determined to be 875 (at 515 nm) and 915 dm^3 mol^{-1} (at 345 nm) by the method mentioned above. The former is more reliable than the latter in view of the absorption band purity.

The quantum yields listed in Table 1 were calculated as follows: the initial concentration of the radical, $[R]_0$, formed by the irradiation is expressed as $[R]_0=[R]+2[D]$. [R] can be obtained directly from the absorption of the radical and [D] can be calculated from the relation $[D]=K_d[R]^2$. Thus, we can know the true concentration of the radical immediately after irradiation. The quantum yields listed in Table 1 indicate that the compound containing the pyrylium ring substituted by the stronger electron-donating groups has a lower quantum yield. The quantum yields of 2,4,6-triphenylpyranyl and 2,4,6-tris(*p*-methoxyphenyl)pyranyl radical formation are respectively 0.21[5] and 0.014, the latter containing three additional methoxyl groups to the former. The same tendency is seen in the data for **1**, **2**, and **3**. This is explained by the fact that the electron-donating group destabilizes the lowest unoccupied molecular orbital (LUMO) of the pyrylium cation and, as a consequence, destabilizes the highest occupied molecular orbital (HOMO) of the radical. The pyrylium salt substituted by electron-donating group has a higher absolute value of the reduction potential,[2f,9] which is related to the LUMO with the equation of $E_{red}{}^{1/2}= E(\mathrm{LUMO})+C$.[10] Here $E_{red}{}^{1/2}$ is the reversible polarographic half-wave reduction potential and C is a constant including the potential of the reference electrode. All the pyranyl and thiopyranyl radicals prepared so far have the absorption maxima at the wavelength region from 340 to 360 nm, 470 to 560 nm and near IR (weaker compared with the other two bands). These characteristic absorption bands are very useful in identifying the pyranyl or thiopyranyl radicals.

Dimerization of Pyranyl Radicals. Generally the pyranyl radicals are in equilibrium with their corresponding dimers as described above. It is confirmed by measuring the change of the intensity of the ESR signals and/or of the absorbance of the pyranyl radicals with various temperature range. Figure 3 depicts the temperature dependence of the absorption spectra of the radical for **1** in THF. The 520 nm band decreases in intensity with lowering the temperature and almost disappears at −50 °C. It recovers, however, the original intensity through warming back to the room temperature. The equilibrium is favorable for dimer at low temperature. While 2,2′,4,4′,6,6′-hexamethyl-4,4′-bi-4*H*-pyran has a tail of the absorption band at 220 nm in ethanol,[1] 2,2′,3,3′,5,5′,6,6′-octaphenyl-4,4′-bi-4*H*-pyran shows the absorption maxima at 248 nm and the shoulder at 290 nm in degassed THF solution.[6c] 2,2′,4,4′,6,6′-Hexaphenyl-4,4′-bi-4*H*-pyran has an absorption band at 248 nm in degassed cyclohexane.[2a] Thus, we can infer from their structure that the σ-bonding dimers of other radicals may have no absorption band at longer wavelength region.

We can know the concentration of the radicals which come to equilibrium with their dimers by observing the absorbance at 520 nm for the radical from **1**, 515 nm for that from **2**, 490 nm for that from **3**, 562 nm for that from **4**, and 470 nm for that from **5** at a

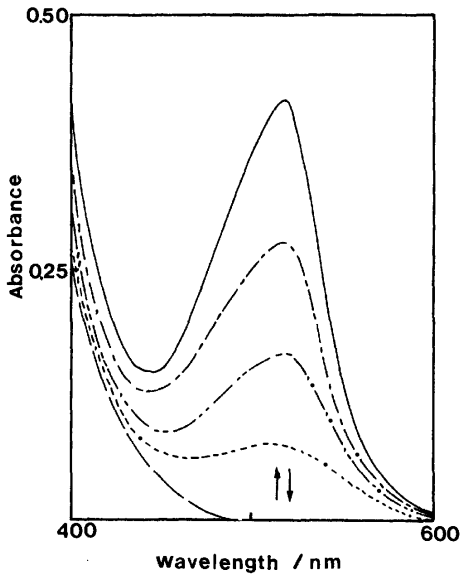

Fig. 3. Temperature effect on the absorption spectrum of the radical for **1**. The concentration of the radical is 2.4×10^{-4} mol dm^{-3}. (a) —, 25 °C; (b) – –, 10 °C; (c) – · –, −5 °C; (d) ·····, −20 °C; (e) – – –, −50 °C. These changes are reversible.

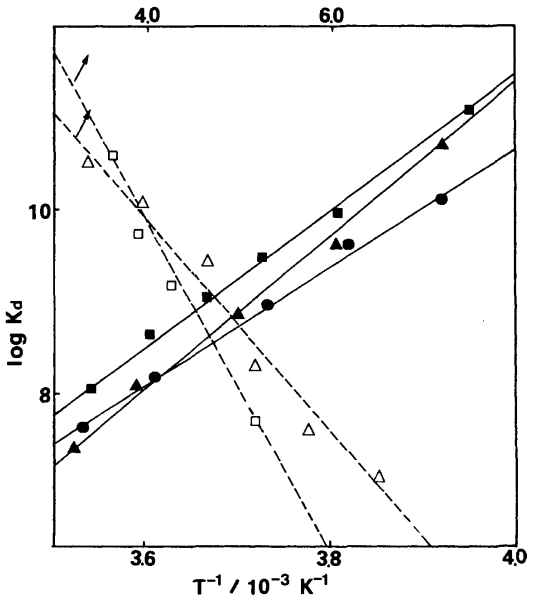

Fig. 4. The plot of $\log K_d$ for the various dimer formations vs. T^{-1}; (■) for **1**, (●) for **2**, (▲) for **4**, (△) for **3**, and (□) for **5**.

given temperature. The plot of $\log K_d$ (from Eq. 2) against T^{-1} gave a good linear correlation for various radicals as shown in Fig. 4. From the possitive slope of these lines, the standard enthalpy change ΔH_0 involved in the dimer formation are calculated to be −14.5, −12.3, and −15.4 kcal mol^{-1} for **1**, **2**, and **4**, respectively, as listed in Table 1. On the contrary to the above cases, the intensity of the absorbance of the radical from **3** at 490 nm increases with lowering the

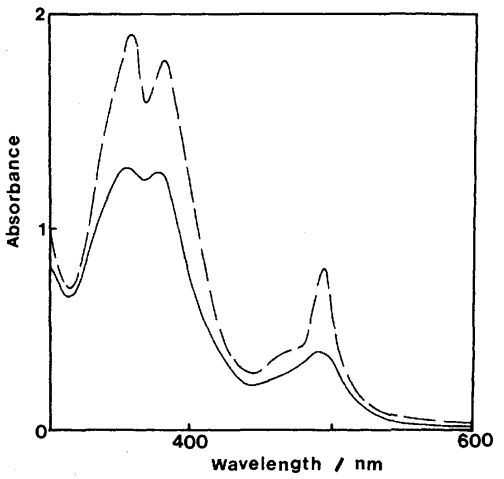

Fig. 5. The absorption spectra of the radical for **3** in the degassed 2-methyl-THF solution: (a) —, 25 °C; (b) – –, 77 K. The concentration of the radical is 1.0×10^{-4} mol dm^{-3}.

temperature and vice versa. Similarly the absorption of the radical from **5** behaves the same temperature dependence as that from **3**.

Figure 5 shows the absorption spectra of the 2-methyl-THF solution of the radical from **3** at room temperature and 77 K, respectively. Indeed the 355, 376 and 490 nm absorbances for the radical increase at 77 K.

The amount of the absorbance change within the temperature range of −40—+30 °C is so small and not enough to determine ΔH_0 for the radicals from **3** and **5**. We took advantage of their ESR signals, which were easily measurable over a wide range of temperature. The equilibrium constant K_d can be calculated by Eq. 6, provided we estimate the signal intensity at an infinite (either plus or minus) temperature, I_∞, by the extraporation.

$$K_d = (I_\infty - I)/I^2. \quad (6)$$

The standard enthalpy change for the dimerization of the radical for **1** obtained by the ESR method is −14.2 kcal mol^{-1}, which is in good agreement with that determined photometrically, −14.5 kcal mol^{-1}. ΔH_0 for **3** and **5** determined by the ESR method are possitive, being 2.36 and 3.72 kcal mol^{-1}, respectively. ΔH_0 of the latter is larger than that of the former. This should be attributed to the difference in the electronegativities between oxygen and sulfur atom in the heterocycles: the oxygen atom enhances the electron-donating charactor of the phenyl groups more than the sulfur atom does. Consequently, the oxygen destabilizes the radical more than the sulfur does. This argument is applicable for the difference in K_d between **3** and **5**. The K_d for the former is larger about one order of magnitude than that for the latter, as similar to the results for 2,4,6-triphenylpyranyl radical and

2,4,6-triphenylthiopyranyl radical.[20] The order of the electron-donating power of the substituents is *p*-methoxyphenyl>methyl>phenyl group. ΔH_0 values for the compounds containing these three groups increases in this order (see Table 1). This may be due to the radical destabilizing character of the electron-donating groups. On the other hand, as the number of phenyl group increases, the values of ΔH_0 of the radicals for **3** and **5** become large, and turn to positive, the equilibrium between radical and its dimer being favorable for radical at low temperature. This abnormality can be explained by the steric hindrance of the phenyl groups with respect to the dimerization (see below).

Configuration of Dimer. All dimers mentioned above may be expected to be formed through the σ bonding between the carbons at 4-position of each radical in the light of the configuration of the dimers of 2,4,6-trimethyl- and 2,3,5,6-tetraphenylpyranyl radicals. In practice, it is possible to assemble the dimers of σ-bonding configuration for **1**, **2**, and **4** with a Corey-Pauling-Kolton (CPK) space filling molecular models, though the dimer for **1** or **2** which has a substituent larger than a hydrogen atom at 3-position carbon is highly strained. As to the dimer for **3** and **5**, however, it is absolutely impossible to construct them with the CPK molecular model because of the large steric hindrance of phenyl groups both 3- and 5-position in the pyrylium or thiopyrylium ring. The apparent temperature effects on the intensity of the radical absorbances at 490 (for **3**) and 470 nm (for **5**) are similar to that for 1-alkyl-4-carbomethoxy pyridinyl radical,[11] where the intensity of the absorbance at ca. 640 nm increases with decreasing the temperature, due to a charge-transfer complex formation between two pyridinyl radicals.

In our case, however, the amounts of these pyranyl and thiopyranyl radicals are confirmed to increase with lowering the temperature by the ESR measurement. The absorption in visible region is not the charge-transfer band but the monomer radical band in comparison with those of radicals for **1**, **2**, **4**, and other pyrylium salts.[5] Thus, a potential energy of a radical and a dimer vs. the reaction coordinate diagram is considered to be different between the equilibrium for ordinary pyrylium salts and that for **3** and **5**. Taking into account the large steric hindrance of phenyl groups, it is reasonable that the potential energies of the radicals of **3** and **5** are lower than that of the dimers. Moreover, the dimers for **3** and **5** may not have the tight σ bonding at 4-position carbon of the radical. Then, two possible structures of the dimer are considered. One is **6** in which one radical attacks a benzene ring of another radical in 4-position carbon, analogous to the case of the dimerization of triphenylmethyl radical.[12] It is possible to make the molecule of **6** with CPK model. The other is the ordinary dimer configuration with a σ bonding at 4-position carbon, not tight but very loose bonding taking into account the flexibility of the pyrylium or thiopyrylium ring.

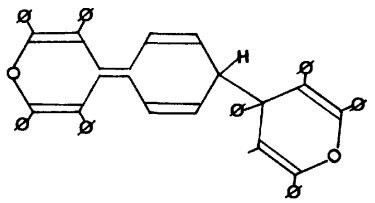

6

The authors wish to thank Prof. Yoshizo Suzuki for supplying the pyrylium salts. We are also indebted to Dr. Kazuaki Shimada for his help in taking NMR spectra.

References

1) K. Conrow and P. C. Radlick, *J. Org. Chem.*, **26**, 2260 (1961).

2) a) A. T. Balaban, C. Bratu, and C. N. Rentea, *Tetrahedron*, **10**, 265 (1964). b) V. A. Palchkov, Yu. A. Zhdanov, and G. N. Dorofeenko, *Zh. Org. Khim.*, **1**, 1171 (1965). c) I. Degani and C. Vincenz, *Bull. Sci., Fac. Chim. Ind. Bologna.*, **25**, 77 (1967). d) L. A. Polyakova, K. A. Bilevich, N. N. Bubnov, G. N. Dorofeenko, and O. Yu. Okhlobystin, *Dokl. Akad. Nauk SSSR.*, **212**, 370 (1973). e) V. B. Panov, M. V. Nekhoroshev, and O. Yu. Okhlobystin, *Dokl. Akad. Nauk SSSR.*, **242**, 372 (1978). f) V. Wintgens, J. Pouliquen, J. Kossanyi, and M. Heintz, *Nouveau J. Chim.*, **10**, 345 (1986).

3) A. Safieddine, J. Royer, and J. Dreux, *Bull. Soc. Chim. Fr.*, **2**, 703 (1972).

4) a) E. Gard and A. T. Balaban, *J. Electroanal. Chem.*, **4**, 48 (1962). b) M. Feldman and S. Winstein, *Tetrahedron Lett.*, **1962**, 853. c) F. Pragst, *Electrochim. Acta*, **21**, 407 (1976). d) F. Pragst and U. Seydewitz, *J. Prakt. Chem.*, **319**, 952 (1977). e) F. Pragst, R. Ziedig, U. Seydewitz, and D. Driesel, *Electrochim. Acta*, **25**, 341 (1980).

5) S. Niizuma, N. Sato, H. Kawata, Y. Suzuki, T.Toda, and H. Kokubun, *Bull. Chem. Soc. Jpn.*, **58**, 2599 (1985).

6) a) H. Kawata, Y. Suzuki, and S. Niizuma, *Tetrahedron Lett.*, **27**, 4489 (1986). b) J. Alizon, J. Gallice, H. Robert, G. Delplanque, C. Weyl, C. Fabre, and H. Strzelecka, *Mol. Cryst.*, **33**, 91 (1976). c) Spectroscopic data for the dimer of 2,2′,3,3′,5,5′,6,6′-octaphenyl-4,4′-bi-4*H*-pyran: Precise mass. Calcd for $C_{58}H_{42}O_2$: 770.3185. Found: 770.3185. ^{1}H NMR ($CDCl_3$) δ 4.39 (s, 2H), 6.80—7.24 (m, 40H).

7) a) H. Watanabe, Y. Ikegami, and S. Seto, *Chem. Lett.*, **1972**, 1107. b) S. Tero-Kubota, Y. Sano, and Y. Ikegami, *J. Am. Chem. Soc.*, **104**, 3711 (1982). c) E. M. Kosower, "Topics in Current Chemistry," (1983), p. 112.

8) P. de Mayo and H. Y. Ng, *Can. J. Chem.*, **55**, 3767 (1977).

9) V. Wintgens, J. Pouliquen, M. Simalty, and J. Kossanyi, *J. Photochem.*, **26**, 131 (1984).

10) F. D. Saeva and G. R. Olin, *J. Am. Chem. Soc.*, **102**, 299 (1980).

11) M. Itoh and S. Nagakura, *J. Am. Chem. Soc.*, **89**, 3959 (1967).

12) C. Wentrup, "Reactive molecules," John Wiley & Sons, Inc. (1984), Chap. 2.

 © 1989 The Chemical Society of Japan Bull. Chem. Soc. Jpn., 62, 2284—2295 (1989) [Vol. 62, No. 7

The Hypervirial Condition in the Hückel Model

Makoto ISIHARA
Department of General Education, Shotoku-Gakuen Women's Junior College, Nakauzura 1-38, Gifu 500
(Received March 1, 1989)

This paper analyzes a fundamental aspect of the Hückel model through the hyperviral theorem. The analysis leads to the condition to be satisfied by bond orders and site electron densities as a set of linear equations. The condition, named the hypervirial condition, is common to all the eigenstates of the Hückel model Hamiltonian and brings information on a sort of detailed balance in electron distribution. The hypervirial and the symmetry conditions are related to each other, being consistent but not fully equivalent. Examination of the relation between the two conditions results in the concept of the "intrinsic" hypervirial condition that remains nontrivial with the symmetry condition fulfilled. Several examples provide various expressions obtainable from the hypervirial condition to facilitate understanding the nature of the condition. A few features of the hypervirial condition for alternant systems are mentioned.

The Hückel medel[1,2] is one of the simplest independent-particle models in the electronic structure theory of molecules and has been extensively used and investigated since the dawn of quantum chemistry.[3] The model will never lose its value in studies on molecular electronic structures particularly of conjugated systems, at least as a qualitative guide. We should regard the Hückel model as a tool of sketching out some essentials of the behavior of electrons in molecules rather than a crude approximation to real systems.

Nowadays we have no practical difficulty at all in "solving" the Hückel model numerically for individual systems except for extreme cases. With the Hückel matrix given, or usually with a pertinent set of geometrical parameters inputted, the computer immediately prints out molecular orbitals, their energies, electron densities, bond orders, and so on. This does not mean, however, that nothing remains to be explored in the world of the Hückel model. Above all, significant is to investigate the general characteristics of the model itself which might be hardly revealed through individual numerical calculations. In fact, for example, various graph-theoretical approaches[4] and the propagator formalism[5] as well as Coulson and Longuet-Higgins' formalism[6] have enriched our recognition on the Hückel model soundly.

What is intended in this paper is not to propose a novel far-reaching methodology but only to analyze a certain fundamental aspect of the Hückel model through the hypervirial theorem.[7] Still, the author believes that this must advance our understanding of the Hückel model.

We have the six sections below: the first is the preliminary section where basic definitions are introduced on the Hamiltonian, bond orders, and so on. In the second section the hypervirial condition upon bond orders and site electron densities are derived from the hypervirial theorem. The third section describes the symmetry condition in the language of permutation group theory, outlining the relation between the hypervirial and the symmetry conditions. The fourth section concerns the intrinsic hypervirial condition that remains nontrivial with the symmetry condition fulfilled. Several illustrative examples follow in the subsequent section. The last section touches upon the hypervirial condition for alternant systems.

Preliminaries

Suppose an electronic system of m sites. Denote the set $\{1,\cdots,m\}$ of the sites by M and the set $\{\uparrow,\downarrow\}$ of the one-electron spin states by Ω. The Hückel model assumes that the system has the $2m$ one-electron quantum states $\{r\mu\}$ specified by the site $r\in M$ and the spin $\mu\in\Omega$[8] and that the creators $\{a^\dagger_{r\mu}\}$ and the annihilators $\{a_{r\mu}\}$ for the one-electron quantum states $\{r\mu\}$ fulfil the canonical anticommutation relation. The Hückel model Hamiltonian H is defined with the creators and the annihilators as

$$H=\sum_{r,s\in M} b_{rs}\,(a^\dagger_{r\uparrow}a_{s\uparrow}+a^\dagger_{r\downarrow}a_{s\downarrow}), \tag{1}$$

where $\{b_{rs}\}$ are the components of what is called the Hückel matrix. Assume that the Hückel matrix B is real symmetric, which makes the model transparent without serious loss of physical contents. The matrix is almost always simplified further.

Designate the two ordered pairs of different sites $r,s\in M$ as rs and sr. Let L denote the set of all the pairs composed of different sites of M. Call the pair rs the connected pair if the sites r and s are bonded, noting that the word "bonded" is used here with regard to the site framework but not to the electronic structure considered. Denote the subset of L that consists of all the connected pairs by Y and the complementary subset by $\overline{Y}$. Let us refer to the model with the simplification

$$b_{rs}=\begin{cases}\beta_{rs} & (rs\in Y)\\ 0 & (rs\in\overline{Y})\end{cases} \tag{2}$$

as the semisimple Hückel model[9] and to the model with the more popular simplification

$$b_{rs} = \begin{cases} \alpha & (r=s) \\ \beta & (rs\in Y) \\ 0 & (rs\in\overline{Y}) \end{cases} \tag{3}$$

as the simple Hückel model.

The most informative quantities of definite physical meaning in the Hückel model are electron densities $\{q_r\}$ on sites and bond orders $\{p_{rs}\}$ between sites.[10] Let us call them p-densities generically for convenience' sake, often designating q_r as p_{rr}. Although p-densities are defined originally in terms of Hückel orbital coefficients, we can generalize the definition quite naturally. Put

$$\begin{cases} \rho_{\mu rs} = (a^\dagger_{r\mu}a_{s\mu} + a^\dagger_{s\mu}a_{r\mu})/2 \\ \zeta_{\mu rs} = -\,\mathrm{i}\,(a^\dagger_{r\mu}a_{s\mu} - a^\dagger_{s\mu}a_{r\mu})/2 \end{cases} \quad (r,s\in M;\ \mu\in\Omega) \tag{4}$$

and define

$$\begin{cases} p_{\mu rs} = \langle|\rho_{\mu rs}|\rangle \\ z_{\mu rs} = \langle|\zeta_{\mu rs}|\rangle \end{cases} \quad (r,s\in M;\ \mu\in\Omega) \tag{5}$$

for each eigenstate $|\rangle$ of H. We can define p-densities by

$$p_{rs} = \langle|(\rho_{\uparrow rs} + \rho_{\downarrow rs})|\rangle = p_{\uparrow rs} + p_{\downarrow rs} \qquad (r,s\in M). \tag{6}$$

The matrix P of the component $\{p_{rs}\}$ is real symmetric necessarily. Let us call the matrix the p-density matrix.[11]

Hypervirial Condition

The hypervirial theorem affirms that any eigenstate $|E\rangle$ of the Hamiltonian $\hat{H}$ of a system fulfils

$$\langle E|[\hat{H}, \hat{A}]|E\rangle = 0 \tag{7}$$

for any linear operator $\hat{A}$ of the system. Since the Hückel model has the one-body Hamiltonian conserving the spin, essential is the one-body hypervirial theorem[12]

$$\langle|[H, a^\dagger_{r\mu}a_{s\mu}]|\rangle = 0 \qquad (r,s\in M;\ \mu\in\Omega), \tag{8}$$

which is rewritten by calculating the commutator as

$$\sum_{t\in M}(b_{rt}\langle|a^\dagger_{t\mu}a_{s\mu}|\rangle - \langle|a^\dagger_{r\mu}a_{t\mu}|\rangle\, b_{ts}) = 0 \qquad (r,s\in M;\ \mu\in\Omega). \tag{9}$$

Thus, we find that the combination corresponding to

$$\langle|[H, \mathrm{i}\zeta_{\mu rs}]|\rangle = 0 \qquad (r<s\in M;\ \mu\in\Omega) \tag{10}$$

suffices to give the linear equations for $\{p_{\mu rs}\}$

$$\sum_{t\in M}(b_{rt}p_{\mu ts} - p_{\mu rt}b_{ts}) = 0 \qquad (r<s\in M;\ \mu\in\Omega). \tag{11}$$

Here, the case of $r>s$ is excluded because the equation for rs is essentially identical with that for sr; the case of $r=s$, giving nothing, is also excluded. By virtue of the linearity the same equations hold for $\{p_{rs}\}$. Let us refer to the equations the hypervirial relationships and shorten "hypervirial relationship" to "HVR" from now on.

We can take the other combination independent of the above one. The combination corresponding to

$$\langle|[H, \mathrm{i}\rho_{\mu rs}]|\rangle = 0 \qquad (r\leqq s\in M;\ \mu\in\Omega) \tag{12}$$

leads to the linear equations for $\{z_{\mu rs}\}$

$$\sum_{t\in M}(b_{rt}z_{\mu ts} - z_{\mu rt}b_{ts}) = 0 \qquad (r\leqq s\in M;\ \mu\in\Omega). \tag{13}$$

However, after all, these equations do not give more than the reality condition

$$z_{\mu rs} = 0 \qquad (r,s\in M;\ \mu\in\Omega), \tag{14}$$

which is a natural consequence of the reality assumption of the Hückel matrix.

To return, regarding the HVRs for p-densities as a condition imposed upon p-densities, call it the hypervirial condition, which is abbreviated as the HVC in the following. The HVC can be expressed compactly in the matrix form as[13,14]

$$[B, P] = 0. \tag{15}$$

In particular, for the simple Hückel model, we have

$$[J, P] = 0 \tag{16}$$

with the adjacency matrix J.[15,16] Bear it in mind that the HVC is common to all the eigenstates of H without regard to the number of electrons contained. Say, by supposing the one-electron eigenstate, p-densities in the HVC are read as the p-densities due to one Hückel orbital. With the number n of electrons fixed, we have the number condition

$$n = \sum_{r\in M} p_{rr} \tag{17}$$

as a condition independent of the HVC. Then, the HVC plus the number condition is common to all the n-electron eigenstates of H.

Now let n_μ denote the number of μ-spin electrons in a system. When $n_\uparrow$ and $n_\downarrow$ differ, each of the HVCs upon $\{p_{\uparrow rs}\}$ and upon $\{p_{\downarrow rs}\}$ becomes meaningful under the number conditions for n_μ's.[17] However, as long as we do not substitute numbers for n_μ's, the condition upon $\{p_{\mu rs}\}$ is identical with that upon p-densities in the form of equations. In what follows, the condition upon p-densities is treated representatively; it is enough to affix the subscript "$\uparrow$" or "$\downarrow$" (or "μ") to "p"

and "n" for the others.

A little arrangement of terms in HVRs is preferable, particulary for practical purposes. Putting

$$d_{rs} = b_{rs}(q_r - q_s), \tag{18}$$

$$e_{rs} = (b_{rr} - b_{ss})\, p_{rs}, \tag{19}$$

and

$$f_r^s = \sum_{t \neq r,s} b_{rt} p_{ts}, \tag{20}$$

we write the HVR for rs as

$$e_{rs} + f_r^s - f_s^r = d_{rs}. \tag{21}$$

The left side concerns only bond orders, while the right does site electron densities. Note that d_{rs} and e_{rs} are antisymmetric for the interchange of r and s, but that f_r^s and f_s^r differ in general. We can leave d_{rs} and e_{rs} out of account, respectively, for $b_{rs}=0$ and for $b_{rr}=b_{ss}$. Let C_r^s be the set of sites adjacent to r other than s. Note that C_s^r differs from C_r^s in general. For the semisimple Hückel model, the summation in f_r^s runs over C_r^s and the term d_{rs} vanishes unless rs is a connected pair. In particular, the simple Hückel model has the exquisitely simple HVRs independent of values of α and β;

$$\tilde{f}_r^s - \tilde{f}_s^r = \tilde{d}_{rs} \tag{22}$$

with

$$\tilde{f}_r^s = \sum_{t \in C_r^s} p_{ts} \tag{23}$$

and

$$\tilde{d}_{rs} = \begin{cases} q_r - q_s & (rs \in Y) \\ 0 & (rs \in \overline{Y}). \end{cases} \tag{24}$$

Table 1 is an adequate dictionary for a diagrammatic representation of HVRs for the semisimple Hückel model, which can be used for the simple Hückel model with trivial translation. The diagrammatic representation will be found quite useful for writing out HVRs for individual systems. It may help us conceive the physical meaning of HVRs.

It is obvious that the HVC brings information on a sort of detailed balance in electron distribution in a system. Some portion of the balance is, however, often ascribable to the symmetry of the system. The number N_h of independent HVRs is given by

$$N_h \leqq m(m-1)/2. \tag{25}$$

Table 1. Diagrammatic Representation of HVRs for the Semisimple Hückel Model[a]

Term	Diagram	
	For adjacent rs	For nonadjacent rs
f_r^s	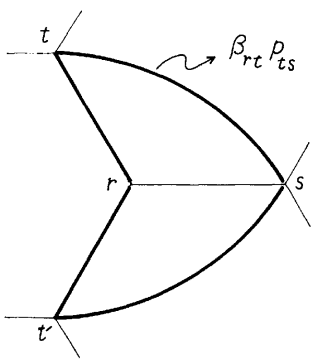	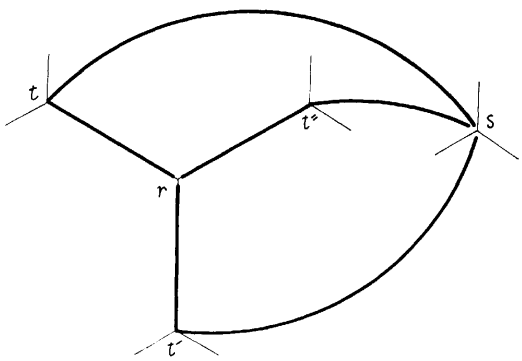
e_{rs}	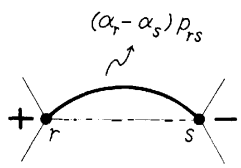	
d_{rs}	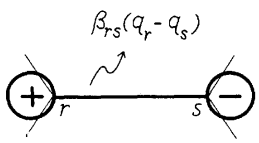	

a) Read f_r^s as $\tilde{f}_r^s$ and d_{rs} as $\tilde{d}_{rs}$ with all β's unity for the simple Hückel model, which has no term corresponding to e_{rs}.

The equality holds only for systems of no "spatial" symmetry at all. The symmetry condition often makes some HVRs trivial, while the HVC often contains some part of the symmetry condition. Let us proceed with this problem.

Symmetry Condition

The symmetry of molecular systems is to be treated generally through the point group.[18] However, it is pertinent and rather essential for the present purpose to consider the symmetry of the Hückel matrix with permutation groups.[19] Let S_m be the symmetric group on M and designate the element consequent on the action of $x \in S_m$ on $r \in M$ simply as xr. Let G, a subgroup of S_m, be the permutation group consisting of all the permutations $\{x\}$ that keep the Hückel matrix B invariant in the sense that

$$b_{xrxs} = b_{rs} \qquad (r,s \in M). \tag{26}$$

The permutation group G carries the characteristics of the symmetry of B which fully reflects the symmetry of a system in the Hückel model.

Here, tentatively, the state $|\rangle$ is said to be faithful if it fulfils

$$\langle|\rho_{\mu xrxs}|\rangle = \langle|\rho_{\mu rs}|\rangle \quad (r,s \in M;\ \mu \in \Omega)\ (x \in G). \tag{27}$$

Any nondegenerate eigenstate of H is easily proved to be faithful. For degenerate eigenstates, however, relevant choice is required for the eigenstates to be faithful. Arbitrary configurations composed of Hückel orbitals cannot necessarily lead us to faithful states, even if they are eigenstates of H. Only faithful eigenstates are natural and satisfactory as stationary states of an entire system.[10,20] Let us confine ourselves to faithful eigenstates when the permutational symmetry is considered.

Two elements $r,s \in M$ are said to be transitive if there exists $x \in G$ satisfying $s = xr$. The transitivity is an equivalence relation and gives the classification of M

$$M = \Gamma_1 + \cdots + \Gamma_v \tag{28}$$

with $\{\Gamma_i\}$ the equivalence classes, which are called the orbits on M.[21] Let V denote the set $\{1,\cdots,v\}$ of the subscripts of the orbits. Likewise, two elements $rs,tu \in L$ are said to be transitive if there exists $x \in G$ satisfying $tu = xrxs$. We have the classification of L

$$L = \Lambda_1 + \cdots + \Lambda_w \tag{29}$$

with $\{\Lambda_i\}$ the orbits on L. Denote the set $\{1,\cdots,w\}$ of the subscripts by W. The orbit on M and that on L are often called the site orbit and the pair orbit, respectively. The number of elements contained in an orbit is conventionally called the length of the orbit. Using the concept of orbits, we can write the permutational symmetry condition as

$$\begin{cases} q_r = q_s & (r,s \in \Gamma_i) \qquad (\text{each } i \in V) \\ p_{rs} = p_{tu} & (rs,tu \in \Lambda_i) \qquad (\text{each } i \in W). \end{cases} \tag{30}$$

Note that this does not always reproduce the transpositional symmetry inherent in bond orders completely.[22] The modifier "permutational" stands for this fact. The symmetry condition is abbreviated as the SC in the following.

Let us define the subset Δ_i of L, which is said to be dual with Λ_i, as

$$\Delta_i = \{rs \mid sr \in \Lambda_i\} \qquad (i \in W). \tag{31}$$

Evidently, the subset Δ_i is a pair orbit, identical or disjoint with Λ_i. The pair orbit Λ_i is said to be selfdual if identical with Δ_i, and nonselfdual otherwise. Let w° be the number of selfdual orbits plus half the number of nonselfdual ones. Arranging the subscripts of pair orbits relevantly, we can make the w° "pseudorbits"[23]

$$\Theta_i = \Lambda_i \cup \Delta_i \qquad (i \in W^\circ = \{1,\cdots,w^\circ\}). \tag{32}$$

constitute L. The pseudorbits enable us to incorporate the transpositional symmetry into the SC;

$$\begin{cases} q_r = q_s & (r,s \in \Gamma_i) \qquad (\text{each } i \in V) \\ p_{rs} = p_{tu} & (rs,tu \in \Theta_i) \qquad (\text{each } i \in W^\circ). \end{cases} \tag{33}$$

For the number N_p of symmetry-independent p-densities, we have

$$N_p = v + w^\circ \tag{34}$$

immediately from this.

To see the general relation between the HVC and the SC, let us use the matrix notation, denoting the permutation matrix corresponding to $x \in G$ by X. The transpositional symmetry is always presupposed here; we can identify the SC with the permutational SC. What serves the purpose is the Lie–Jacobi identity

$$[[B, P], X] + [[P, X], B] + [[X, B], P] = 0 \quad (x \in G), \tag{35}$$

which is reduced by the invariance of B to

$$[[B, P], X] = [[X, P], B] \qquad (x \in G), \tag{36}$$

showing the consistency of the HVC and the SC immediately. If the HVC is presupposed, we have

$$[[X, P], B] = 0 \qquad (x \in G). \tag{37}$$

Clearly, this cannot make all $[X, P]$'s for $x \in G$ vanish in general. On the other hand, with the SC presupposed, we have

$$[[B, P], X] = 0 \qquad (x \in G). \tag{38}$$

This assures that $[B, P]$ has the same permutational symmetry as B and P, but does not suffice to reproduce the HVC in general. The next section will clarify what follows upon the HVC from the presupposed SC in some detail.

Group theory is ready to provide some interesting results about the number of site orbits, that of pair orbits, lengths of them, and so on. However, let us skip the subject now, which is of rather mathematical interest. Actually, it is not difficult to check site orbits and pair orbits for a given system, usually much easier than to find the permutation group itself.

Intrinsic Hypervirial Condition

Because the SC is quite simple and much more accessible than the HVC, we suppose that the SC is fulfilled prior to the HVC in taking account of both. Let us refer to the HVR left nontrivial with the SC fulfilled as the intrinsic HVR and name the condition consisting of intrinsic HVRs the intrinsic HVC. The reason why we treat the SC using the concept of orbits is that the concept is advantageous for describing the intrinsic HVC.

For two arbitrary elements rs and $r's'$ of a pair orbit, we always have the permutation $x \in G$ that fulfils $r'=xr$ and $s'=xs$. Hence, noting

$$\sum_{t \in M} b_{rt} p_{ts} = \sum_{t \in M} b_{r'xt} p_{xts'} = \sum_{t \in M} b_{r't} p_{ts'}, \tag{39}$$

we find that the HVR for $r's'$ is identical with that for rs. Since the HVRs for rs and for sr are essentially identical, we can conclude that each pseudorbit corresponds to its HVR, whether the HVR is intrinsic or not. This neat result, mentioned in the preceding section already, is not all that follow from the presupposed SC.

Let rs be an arbitrary element of a selfdual orbit. Then, there exists the permutation $x \in G$ that fulfils $x(rs)=sr$. Since this means $xr=s$ and $xs=r$, we have

$$\sum_{t \in M} b_{rt} p_{ts} = \sum_{t \in M} b_{sxt} p_{xtr} = \sum_{t \in M} b_{st} p_{tr}, \tag{40}$$

which makes the HVR for rs trivial. Thus, the intrinsic HVC contains no HVRs for selfdual orbits. This is the most crucial result that is also fundamental for writing out intrinsic HVRs for individual systems.

To outline locations of selfdual and nonselfdual orbits in L, it is suitable to define the region L_{ij} as

$$L_{ij} = \{rs \in L \mid r \in \Gamma_i;\ s \in \Gamma_j\} \qquad (i,j \in V). \tag{41}$$

Let us refer to L_{ij} as the diagonal region if $i=j$ and as the off-diagonal region otherwise. Diagonal regions are defined for site orbits of length more than unity. We readily find that no orbit spreads over separate regions and that no orbit in off-diagonal regions is selfdual. Hence, orbits in off-diagonal regions are to correspond to intrinsic HVRs. Since orbits in the off-diagonal region L_{ji} are dual with orbits in L_{ij}, we have only to consider off-diagonal regions for $i<j$. On the other hand, orbits in diagonal regions are almost exclusively selfdual and scarcely lead to intrinsic HVRs. Roughly speaking, as the symmetry of a system becomes lower, we have more intrinsic HVRs.

Actually, it is never laborious to check whether a site pair belongs to a selfdual orbit or not; yet, as to orbits in diagonal regions, the following cases are worth noting.

(1) If the length of an orbit Γ_i is two, then L_{ii} is a selfdual orbit in itself.

(2) Let Γ_i be an orbit of length $|\Gamma_i|$ more than two. If there exists no other site orbit of the same length as $|\Gamma_i|$, then all the orbits in L_{ii} are selfdual.

(3) As a corollary of the above, if we have only one orbit on M, that is, if M itself is an orbit, then all the pair orbits are selfdual.

The proofs of these are omitted, but it will be easy to comprehend them by supposing relevant configurations of sites.

Now assume that we have more than one orbits Γ_i's of the same length more than two. Of course, it is probable for orbits in L_{ii}'s to be selfdual. However, if G is a cyclic group of order more than two, it is possible for orbits in L_{ii}'s to be nonselfdual. Then, HVRs for orbits in different L_{ii}'s are, moreover, not all independent of each other. Such a case is very exceptional and not discussed here in further detail. Instead, a typical example is shown in Fig. 1, which will be enough to understand when exceptional cases occur.

Consider the number N_p° of p-densities left independent with both of the SC and the HVC fulfilled. Put exceptional cases aside for brevity. The number of intrinsic HVRs is equal to that of pseudorbits in off-diagonal regions, so that, using the number N' of pseudorbits in diagonal regions, we have

$$N_p^\circ = v + N'. \tag{42}$$

Let N_i' denote the number of pseudorbits in the

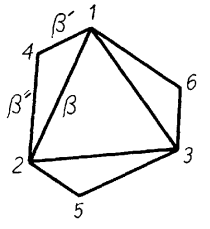

Fig. 1. Nonselfdual orbits in diagonal regions: $\Gamma_1=\{1,2,3\}$, $\Gamma_2=\{4,5,6\}$, $\Delta_1=\{12,23,31\}$, $L_{11}=\Delta_1+\Delta_1$, and so on.

diagonal region for an orbit Γ_i of length $|\Gamma_i|$. The obvious, rough estimate

$$N_i' \leqq |\Gamma_i| - 1 \qquad (i \in V) \tag{43}$$

leads to

$$N' = \sum_{i \in V} N_i' \leqq m - v \tag{44}$$

and gives

$$N_p^\circ \leqq m. \tag{45}$$

If $|\Gamma_1|$ is more than two and if G contains a cyclic group of order $|\Gamma_1|$, then we have the better estimate

$$N_1' \leqq [|\Gamma_1|/2], \tag{46}$$

where $[\cdots]$ is Gauß' symbol. This can improve the estimate for N_p° considerably for systems of high symmetry.

The discussion in this section may be too crude from a mathematical point of view; there is plenty of room for refinement. Nevertheless, the results obtained here is adequate to work with the intrinsic HVC practically.

Illustrative Examples

What the HVC implies will be understood well through working on several examples. Some hints as to when and how to utilize the HVC may also be obtained. The best way for writing out HVRs for individual systems (without computers) is probably to use the diagrammatic repesentation over so-called structure formulas. Although the diagrammatic method needs neither the Hückel matrix nor the p-density matrix written explicitly, most of the following examples have expressions of the matrices for the sake of clarity, half of the off-diagonal components being often omitted to avoid useless complexity.

Simple Systems. The simplest example that has the intrinsic HVC is the asymmetric two-site system shown in Fig. 2 (a). Put

$$B = \begin{pmatrix} \alpha & \beta \\ \beta & \alpha' \end{pmatrix} \tag{47}$$

and

$$P = \begin{pmatrix} q & p \\ p & q' \end{pmatrix}. \tag{48}$$

The nonselfdual orbit {12} corresponds to the intrinsic HVR

$$(\alpha - \alpha')\,p = \beta\,(q - q'), \tag{49}$$

which means that the bond order is proportional to the difference between the electron densities on the two sites with the proportionality constant $\beta/(\alpha-\alpha')$. If $\beta=0$, then we have $p=0$ for $\alpha' \neq \alpha$. If we put $\alpha'=\alpha$, the HVR becomes $q'=q$ for nonvanishing β. Then, the HVR is not intrinsic, contained in the SC.

The three-site chain system is another instructive simple example. Let the middle site be the third one, as shown in Fig. 2 (b). The semisimple Hückel model for the system has

$$B = \begin{pmatrix} \alpha & 0 & \beta \\ 0 & \alpha'' & \beta'' \\ \beta & \beta'' & \alpha' \end{pmatrix} \tag{50}$$

and

$$P = \begin{pmatrix} q & p' & p \\ p' & q'' & p'' \\ p & p'' & q' \end{pmatrix}. \tag{51}$$

The three HVRs for the pairs 12, 13, and 23 are

$$\begin{cases} (\alpha - \alpha'')\,p' + \beta p'' - \beta'' p = 0 \\ (\alpha - \alpha')\,p - \beta'' p' = \beta\,(q - q') \\ (\alpha'' - \alpha')\,p'' - \beta p' = \beta''\,(q'' - q'). \end{cases} \tag{52}$$

The case of $\alpha''=\alpha$ lets the first HVR mean

$$p/\beta = p''/\beta'', \tag{53}$$

which is ready to give $p''=p$ for $\beta''=\beta$. Really, assume that $\beta''=\beta$ besides $\alpha''=\alpha$. Then, the two site orbits $\Gamma_1=\{1,2\}$ and $\Gamma_2=\{3\}$ follow immediately. The diagonal region L_{11} contains only one selfdual orbit $\Lambda_1=\{12,21\}$; the off-diagonal region L_{12} does only one nonselfdual orbit $\Lambda_2=\{13,23\}$. We have the SC that

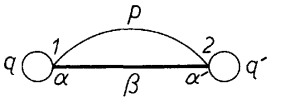

(a)

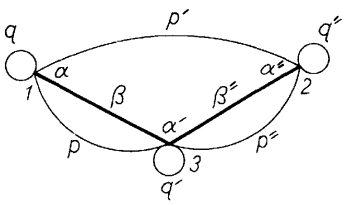

(b)

Fig. 2. Simple systems.

$q''=q$ and $p''=p$. Intrinsic is only the HVR for Λ_2

$$q - ((\alpha - \alpha')/\beta)p = q' - p', \tag{54}$$

which is reduced further to

$$q = q' - p' \tag{55}$$

in the simple Hückel model.

A Theorem on Invariants in Chains. It will be suitable to mention here a general theorem for chains in the simple Hückel model. Only bifurcation sites being aside, the theorem is valid for any chain part of arbitrary systems. The term "chain part" should be taken here in a broad sense; a chain part is able to have no end site or to be a part of a ring. The theorem is explained in Figs. 3 and 4.

Let K be the set of nonterminal sites $\{1,\cdots,k\}$ in a chain and q_r be the electron density on the site $r\in K$. Each site of K has two adjacent sites; let p_r denote the bond order between the two sites adjacent to r. Define the modified electron density $\tilde{q}_r$ on the site r as

$$\tilde{q}_r = q_r - p_r \qquad (r\in K). \tag{56}$$

Then, the HVC leads us to the invariance of the modified site electron density in the chain;

$$\tilde{q}_r = \tilde{q}_s \qquad (r,s\in K). \tag{57}$$

Moreover, if the chain has an end site, we have

$$\tilde{q}_r = q_0 \qquad (r\in K), \tag{58}$$

where q_0 is the electron density on the end site. Of course, this can be paraphrased into the invariance of the modified site electron density in the chain by the natural definition $\tilde{q}_0=q_0$. Thus, we can assign a unique modified site electron density to a chain.

This theorem holds for any eigenstate of H, whether faithful or not, without regard to the number of electrons or the alternant symmetry. Hence, we may regard the theorem as a generalization of Coulson-Rushbrooke's theorem,[24] as far as chain parts are concerned. Unfortunately, the bifurcation site prevents us from defining the modified electron density on the site uniquely. If we intend to sustain the invariance of the modified site electron density including bifurcation sites, it seems to be inevitable to assign a few direction-dependent modified electron densities to bifurcation sites.

We can generalize the theorem into "the invariance of the modified p-density in a chain" directly. The modified bond order between adjacent sites is definable for chains containing more than one sites apart from bifurcation sites. Here, use single letters $\{1,\cdots,\tau\}$ for nonterminal connected pairs in a chain. Denote the set by T, each pair of which has two adjacent sites. Let p_ξ be the bond order for the pair $\xi\in T$ and p'_ξ be that between the two sites adjacent to ξ. Then, it follows from the HVC that the modified bond order

$$\tilde{p}_\xi = p_\xi - p'_\xi \qquad (\xi\in T) \tag{59}$$

is invariant in the chain;

$$\tilde{p}_\xi = \tilde{p}_\eta \qquad (\xi,\eta\in T). \tag{60}$$

If the chain has an end connected pair, we have

$$\tilde{p}_\xi = p_0 \qquad (\xi\in T) \tag{61}$$

with the bond order p_0 for the end connected pair. It is

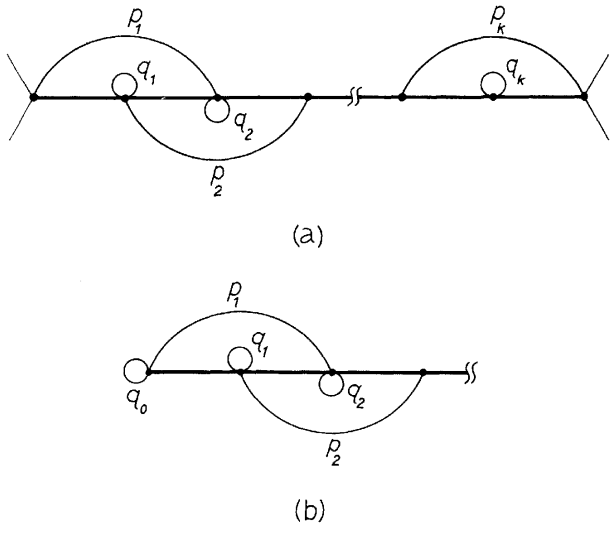

Fig. 3. The invariance of the modified site electron density in a chain: (a) $\tilde{q}_1=\tilde{q}_2=\cdots=\tilde{q}_k$ with $\tilde{q}_r=q_r-p_r$, (b) $\tilde{q}_0=\tilde{q}_1=\tilde{q}_2=\cdots$ with $\tilde{q}_0=q_0$.

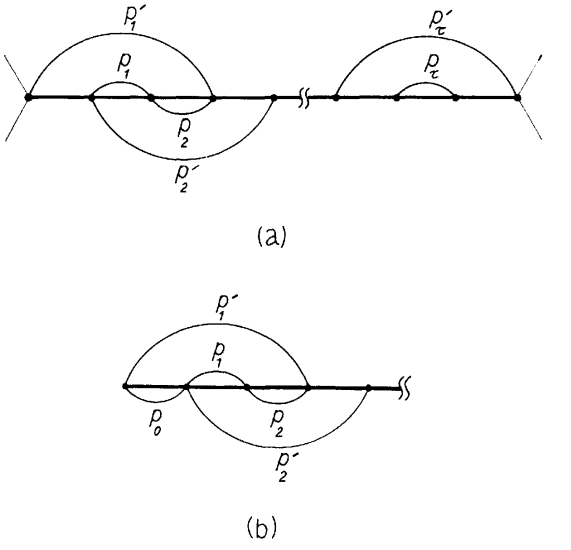

Fig. 4. The invariance of the modified bond order between adjacent sites in a chain: (a) $\tilde{p}_1=\tilde{p}_2=\cdots=\tilde{p}_\tau$ with $\tilde{p}_\xi=p_\xi-p'_\xi$, (b) $\tilde{p}_0=\tilde{p}_1=\tilde{p}_2=\cdots$ with $\tilde{p}_0=p_0$.

easy to apply the above treatment to bond orders between sites distant in a chain, with defining modified bond orders relevantly.

Consider the bond order p_e between the two end sites of a chain. Successive applications of the above theorem for modified p-densities enable us to connect p_e with other two p-densities in a simple way as follows. For even-membered chains, use the bond order p for the central connected pair and the bond order p' for the connected pair adjacent to it; for odd-membered chains, use the electron density q on the central site and the electron density q' on the site adjacent to it. Then, we have

$$\begin{cases} p_e = p - p' & \text{(even-membered)} \\ p_e = q - q' & \text{(odd-membered).} \end{cases} \tag{62}$$

Figure 5 shows a few representatives with the notation.

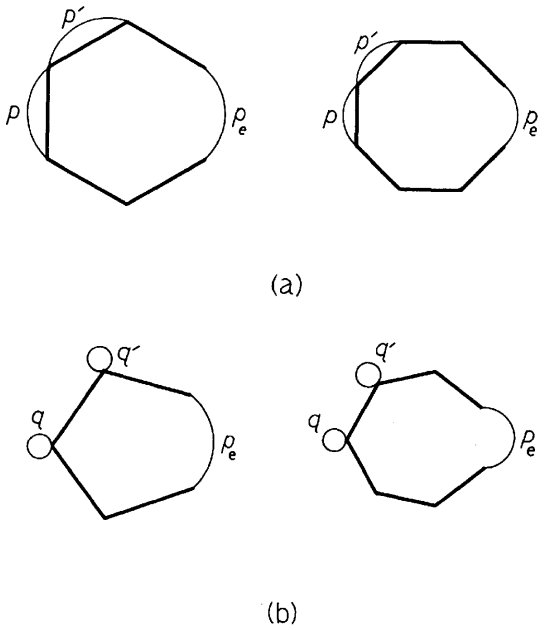

Fig. 5. The bond order between the two ends of a chain: (a) $p_e=p-p'$, (b) $p_e=q-q'$.

Systems of a Ring with a Site Attached. Let us take the simple Hückel model for the system shown in Fig. 6 (a), which is appropriate for practice-minded readers to master handling HVRs. Putting

$$B = \begin{pmatrix} \alpha & \beta & \beta & 0 \\ & \alpha & \beta & 0 \\ & & \alpha & \beta \\ & & & \alpha \end{pmatrix} \tag{63}$$

and

$$P = \begin{pmatrix} q & p & p' & p'' \\ & q & p' & p'' \\ & & q' & p^\circ \\ & & & q^\circ \end{pmatrix}, \tag{64}$$

we have the three site orbits $\Gamma_1=\{1,2\}$, $\Gamma_2=\{3\}$, and $\Gamma_3=\{4\}$. Each of the three off-diagonal regions L_{12}, L_{13}, and L_{23} is a nonselfdual orbit in itself, so that the intrinsic HVRs are

$$\begin{cases} p' - p - p'' = q - q' \\ p^\circ + p'' - p' = 0 \\ 2p'' = q' - q^\circ. \end{cases} \tag{65}$$

Now let us express p', p°, and p'' in terms of the other p-densities q, q', q°, and p. Then, we have

$$p' = p + q - (q' + q^\circ)/2, \tag{66}$$

$$p^\circ = p + q - q', \tag{67}$$

and

$$p'' = (q' - q^\circ)/2. \tag{68}$$

Further, the number condition

$$n = 2q + q' + q^\circ \tag{69}$$

can eliminate, say, q', from these. Using the "excess electron densities on sites"

$$\begin{cases} \underline{q} = q - n/4 \\ \underline{q}^\circ = q^\circ - n/4, \end{cases} \tag{70}$$

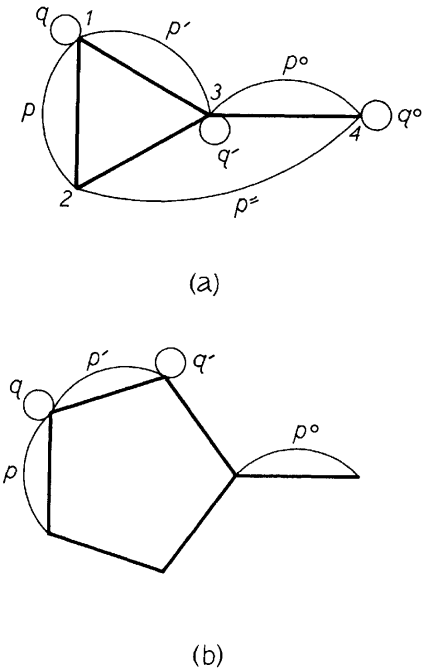

Fig. 6. Systms of a ring with a site attached.

we obtain

$$p' = p + 2\underline{q}, \tag{71}$$

$$p^\circ = p + 3\underline{q} + \underline{q}^\circ, \tag{72}$$

and

$$p'' = -\underline{q} - \underline{q}^\circ. \tag{73}$$

When we take account of the number condition, the concept of excess electron densities on sites is useful in general.

Another system similar to this is shown in Fig. 6 (b) together with the notation used below. Treating the system within the simple Hückel model, we have the four site orbits $\Gamma_1=\{1,2\}$, $\Gamma_2=\{3,4\}$, $\Gamma_3=\{5\}$, and $\Gamma_4=\{6\}$. The off-diagonal region L_{12} contains two nonselfdual orbits, while each of L_{13}, L_{14}, L_{23}, L_{24}, and L_{34} is a nonselfdual orbit in itself. Thus the intrinsic HVC consists of seven HVRs expressed in terms of thirteen p-densities. Here, let us only show a few expressions for p°, without writing the HVRs explicitly. It is easy to derive

$$p^\circ = p' + q - q' \tag{74}$$

from the HVRs. As another expression, say, we have

$$p^\circ = p + 2\underline{q} + \underline{q}', \tag{75}$$

using the number condition.

Systems of a Site over a Ring. Consider the six-site system composed of a pentagonal ring and an additional site over the ring. See Fig. 7. Assuming the five-fold axis, put

$$B = \begin{vmatrix} \alpha^\circ & \beta^\circ & 0 & 0 & \beta^\circ & \beta \\ & \alpha^\circ & \beta^\circ & 0 & 0 & \beta \\ & & \alpha^\circ & \beta^\circ & 0 & \beta \\ & & & \alpha^\circ & \beta^\circ & \beta \\ & & & & \alpha^\circ & \beta \\ & & & & & \alpha' \end{vmatrix} \tag{76}$$

and

$$P = \begin{vmatrix} q^\circ & p_1^\circ & p_2^\circ & p_2^\circ & p_1^\circ & p \\ & q^\circ & p_1^\circ & p_2^\circ & p_2^\circ & p \\ & & q^\circ & p_1^\circ & p_2^\circ & p \\ & & & q^\circ & p_1^\circ & p \\ & & & & q^\circ & p \\ & & & & & q' \end{vmatrix}. \tag{77}$$

Since the site orbits are $\Gamma_1=\{1,\cdots,5\}$ and $\Gamma_2=\{6\}$, we have only one off-diagonal region L_{12}, which is a nonselfdual orbit in itself and gives one HVR. If we define α and q for the ring by

$$\alpha = \alpha^\circ + 2\beta^\circ \tag{78}$$

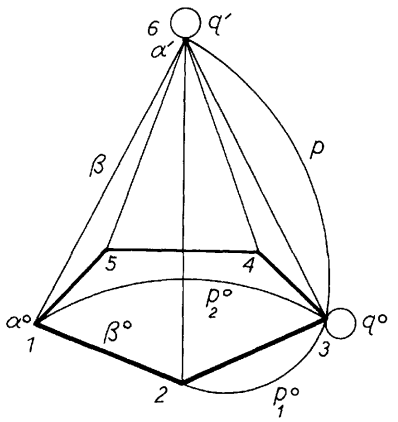

Fig. 7. A site over a pentagonal ring.

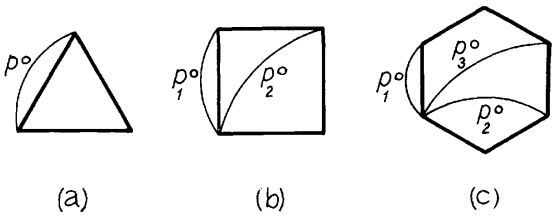

Fig. 8. Ξ's for polygonal rings: (a) $\Xi=2p^\circ$, (b) $\Xi=2p_1^\circ+p_2^\circ$, (c) $\Xi=2p_1^\circ+2p_2^\circ+p_3^\circ$.

and

$$q = q^\circ + \Xi \tag{79}$$

with

$$\Xi = 2p_1^\circ + 2p_2^\circ, \tag{80}$$

we can write the HVR in the same form as that for the asymmetric two-site system as

$$(\alpha - \alpha')p = \beta(q - q'). \tag{81}$$

However, there exists the qualitative difference between them that arises from the contents of α and q. Only when either $(\alpha-\alpha')$ or $(q-q')$ is negative, we have positive p under negative β. Further, for $|p|$ not to be negligible, it is necessary that $|\alpha-\alpha'|$ is comparable with or smaller than $|\beta|$. The contents of α and q are thus significant.

Even if a pentagonal ring is replaced with another polygonal ring of m° sites, we have a HVR of the same form as the above by reading Ξ as the sum of $m^\circ-1$ bond orders between one site and the others of the polygonal ring. A few Ξ's are given in Fig. 8.

Interacting Subsystems. Suppose the six-site system composed of the four- and the two-site chain subsystems interacting with each other. See Fig. 9. The system provides a simple example suggesting some applicability of the HVC to problems on reactivity. Adopting the simple Hückel model in the subsystems and assuming the reflection symmetry, we have

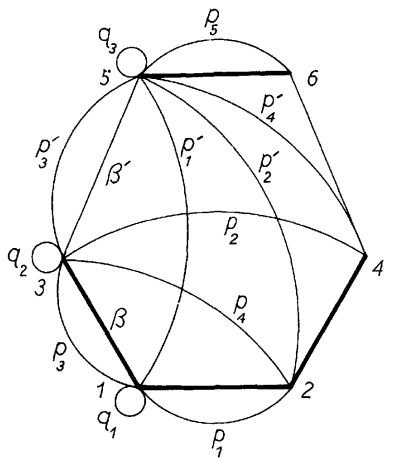

Fig. 9. Interacting four- and two-site subsystems.

$$B = \begin{vmatrix} \alpha & \beta & \beta & 0 & 0 & 0 \\ & \alpha & 0 & \beta & 0 & 0 \\ & & \alpha & 0 & \beta' & 0 \\ & & & \alpha & 0 & \beta' \\ & & & & \alpha & \beta \\ & & & & & \alpha \end{vmatrix} \tag{82}$$

and

$$P = \begin{vmatrix} q_1 & p_1 & p_3 & p_4 & p_1' & p_2' \\ & q_1 & p_4 & p_3 & p_2' & p_1' \\ & & q_2 & p_2 & p_3' & p_4' \\ & & & q_2 & p_4' & p_3' \\ & & & & q_3 & p_5 \\ & & & & & q_3 \end{vmatrix}. \tag{83}$$

The site orbits are $\Gamma_1=\{1,2\}$, $\Gamma_2=\{3,4\}$, and $\Gamma_3=\{5,6\}$; each of L_{12}, L_{13}, and L_{23} contains two nonselfdual orbits. Thus, we have the six HVRs

$$\begin{cases} p_4 - \lambda p_1' = q_1 - q_2 \\ p_2 + p_3 - p_1 - \lambda p_2' = 0 \\ p_3' - \lambda p_3 = 0 \\ p_4' - \lambda p_4 = 0 \\ p_1' - p_4' = \lambda (q_2 - q_3) \\ p_2' - p_3' + \lambda (p_5 - p_2) = 0, \end{cases} \tag{84}$$

where

$$\lambda = \beta'/\beta \tag{85}$$

is regarded as standing for the strength of the interaction between the subsystems. The HVRs allow us to express the four intersubsystem bond orders p_1', p_2', p_3', and p_4' in terms of six relevant intrasubsystem p-densities.

If we use the electron densities q_1, q_2, and q_3 and the intrasubsystem bond orders p_1, p_3, and p_5 between adjacent sites, then we have

$$p_1' = \lambda (1 - \lambda^2)^{-1}(q_1 - q_3), \tag{86}$$

$$p_2' = \lambda (1 - \lambda^2)^{-1}(p_1 - p_5), \tag{87}$$

$$p_3' = \lambda p_3, \tag{88}$$

and

$$p_4' = \lambda (1 - \lambda^2)^{-1} q_1 - \lambda q_2 - \lambda^3 (1 - \lambda^2)^{-1} q_3. \tag{89}$$

The third equation for p_3' is crucial. Let β be negative and p_3 be positive. If $|\beta'|$ is small, then $|p_3'|$ will be small necessarily. The sign of p_3' is, however, opposite to that of β'. This means that $|p_3'|$ can be enlarged in "positive feedback" with $|\beta'|$. Another remarkable point is that p_1' and p_4' are, respectively, closely related to the inter- and intra-subsystem differences between the electron densities. This stands out in the approximate expressions

$$p_1' \simeq \lambda (q_1 - q_3) \tag{90}$$

and

$$p_4' \simeq \lambda (q_1 - q_2) \tag{91}$$

for the weak interaction $|\lambda| \ll 1$.

It is, of course, possible to use other intrasubsystem p-densities than the above. Say, we can rewrite p_3' as

$$p_3' = \lambda (1 - \lambda^2)^{-1} p_1 - \lambda p_2 - \lambda^3 (1 - \lambda^2)^{-1} p_5$$

$$\simeq \lambda (p_1 - p_2) \tag{92}$$

using p_1, p_2, and p_5.

Generally speaking, we should derive the most advisable expression from HVRs to our purpose. As far as the expression is reasonably simple, we will find its physical meaning, aside from whether or not our intuition is able to draw some image about the meaning.

The Hypervirial Condition for Alternant Systems

Many conjugated systems have the alternant symmetry, which leads to the outstanding consequences for the m-electron ground state of an m-site system, Coulson-Rushbrooke's theorem and others.[24,25] It is never futile to mention the HVC for alternant systems specially. For the assignment of starred and unstrarred sites, follow the convention.

Let $M^\star$ and $M^\odot$ be the subsets of M that consist of all the starred sites and all the unstarred sites, respectively. The Hückel matrix of the alternant symmetry has the components

$$b_{rs}=\begin{cases}\delta_{rs}\alpha & (r,s\in M^{\star}\text{ or }r,s\in M^{\odot})\\ \begin{cases}\beta_{rs} & (rs\in Y)\\ 0 & (rs\in\overline{Y})\end{cases} & \begin{pmatrix}r\in M^{\star},\ s\in M^{\odot}\\ \text{or}\\ r\in M^{\odot},\ s\in M^{\star}\end{pmatrix}\end{cases}. \tag{93}$$

Let us use the symbols

$$p_{rs}=\begin{cases}p^{\star}_{rs} & (r,s\in M^{\star})\\ p^{\odot}_{rs} & (r,s\in M^{\odot})\\ p^{\times}_{rs} & (r\in M^{\star},s\in M^{\odot}\text{ or }r\in M^{\odot},s\in M^{\star})\end{cases} \tag{94}$$

distinctively. The set C^s_r contains only either starred or unstarred sites. Let us affix "$\star$" or "$\odot$" to C^s_r to show the attribute of the sites contained therein. It is readily found that the HVC includes the following three classes of HVRs.

$$\sum_{t\in C^s_r\odot}(\beta_{rt}p^{\times}_{ts}-p^{\times}_{rt}\beta_{ts})=0 \qquad (r<s\in M^{\star}), \tag{95}$$

$$\sum_{t\in C^s_r\star}(\beta_{rt}p^{\times}_{ts}-p^{\times}_{rt}\beta_{ts})=0 \qquad (r<s\in M^{\odot}), \tag{96}$$

and

$$\sum_{t\in C^s_r\odot}\beta_{rt}p^{\odot}_{ts}-\sum_{t\in C^s_r\star}p^{\star}_{rt}\beta_{ts}=d_{rs} \qquad (r\in M^{\star},\ s\in M^{\odot}) \tag{97}$$

with

$$d_{rs}=\begin{cases}\beta_{rs}(p^{\star}_{rr}-p^{\odot}_{ss}) & (rs\in Y)\\ 0 & (rs\in\overline{Y}).\end{cases} \tag{98}$$

The primary feature is that $\{p^{\star}_{rs},\ p^{\odot}_{rs}\}$ and $\{p^{\times}_{rs}\}$ enter the HVRs separately. In particular, the first and the second classes concern only the bond orders $\{p^{\times}_{rs}\}$ without regard to any site electron density. Note that, so far, the state is not specified.

Now let us confine ourselves to the m-electron ground state. The well-known two consequences of the alternant symmetry[24,26]

$$\begin{cases}p^{\star}_{rr}=1 & (r\in M^{\star})\\ p^{\odot}_{rr}=1 & (r\in M^{\odot})\end{cases} \tag{99}$$

and

$$\begin{cases}p^{\star}_{rs}=0 & (r\neq s\in M^{\star})\\ p^{\odot}_{rs}=0 & (r\neq s\in M^{\odot})\end{cases} \tag{100}$$

are related to each other through the third class of HVRs, forming an "admissible solution" of the HVRs. Since the rest is only $\{p^{\times}_{rs}\}$, the first and the second classes of HVRs can be utilized for determining them directly with some auxiliary conditions. As a matter of fact, the main condition used by Hall in his method of determining bond orders in alternant systems is really the HVRs.[27] Although he said nothing about the hypervirial theorem there, his method is an interesting application of the HVC.[28]

References

1) E. Hückel, *Z. Phys.*, **70**, 204 (1931); **72**, 310 (1931); **76**, 628 (1932). It is surprising that the scope of this inceptive work ranges over fairly wide subjects, though the papers may be of only historical value now.

2) As a readable monograph, for example, K. Yates, "Hückel Molecular Orbital Theory," Academic Press, New York (1978). There are so many books having a pertinent description of the Hückel model that no particular recommendation is intended.

3) The Hückel orbital theory has been established gradually through a number of contribution following Hückel's work. Among others, the successive studies by Lennard-Jones, Coulson, Longuet-Higgins, Hall, and their coworkers played a leading role in analyzing the nature of the Hückel orbital and in refining Hückel's work, though only a few of their many papers are cited explicitly in this paper.

4) N. Trinajstić, "Hückel Theory and Topology," in "Semiempirical Method of Electronic Structure Calculation Part A: Techniques" ed by H. F. Schaefer III, Plenum, New York (1977), which contains a key bibliography up to 1976. In recent years, chemical applications of graph theory have developed divergingly; for example, "Mathematics and Computational Concepts in Chemistry," ed by N. Trinajstić, Ellis Horwood Ltd., Chichester, (1986) contains several reviews and topics on chemical graph theory. There are too many papers to cite separately, even if we confine ourselves to the characteristic polynomial which is a central bridge between the Hückel model and graph theory. See the review article H. Hosoya, Discrete Applied Mathematics, **19**, 239 (1988) and the references cited therein.

5) S. Aono and K. Nishikawa, *Bull. Chem. Soc. Jpn.*, **53**, 3418 (1980); S. Aono, T. Ohmae, and K. Nishikawa, *ibid.*, **54**, 1645 (1981); K. Nishikawa, M. Yamamoto, and S. Aono, *J. Chem. Phys.*, **78**, 5031 (1983). Aono and his coworkers applied their method to various problems; for example, S. Aono and K. Nishikawa, *Bull. Chem. Soc. Jpn.*, **58**, 288 (1985); T. Ohmae, K. Nishikawa, and S. Aono, *ibid.*, **58**, 294 (1985); M. Yamamoto, K. Nishikawa, and S. Aono, *ibid.*, **58**, 3176 (1985). See also J. Linderberg and Y. Öhrn, "Propagators in Quantum Chemistry," Academic Press, New York (1973), Chap. 3.

6) C. A. Coulson and H. C. Longuet-Higgins, *Proc. R. Soc. London, Ser. A*, **191**, 39 (1947); **192**, 16 (1947).

7) J. O. Hirschfelder, *J. Chem. Phys.*, **33**, 1462 (1961), in which the hypervirial theorem originated. Recently an excellent monograph on this theorem was published: F. M. Fernández and E. A. Castro, "Hypervirial Theorems," Springer-Verlag, Berlin (1987), which has a useful bibliography every chaper. S. T. Epstein, "The Variation Method in Quantum Chemistry," Academic Press, New York (1974) includes a neat description of the hypervirial theorem and several theorems related to it.

8) The word "spin" is used in place of "one-electron spin state" for brevity, which will cause no confusion.

9) Do not take the word "bonded" too literally in defining the connected pair. Then, the semisimple Hückel model is, actually, the most general Hückel model.

10) C. A. Coulson, *Proc. R. Soc. London, Ser. A,* **169**, 413 (1939) and the references cited therein.

11) Without the diagonal components, it would be proper to call this matrix the bond order matrix. Really, this matrix is a kind of density matrices, but the term "density matrix" is so variously used that it is preferable to prefix "*p*" the prevalent symbol for the bond order. Hence the generic name "*p*-density."

12) M. Isihara, *Bull. Chem. Soc. Jpn.*, **54**, 3312 (1981).

13) We can also state that the product *BP* is real symmetric, since both of *B* and *P* are real symmetric.

14) Hückel orbitals do not appear at all throughout the present treatment. Derivation via the orbitals is, of course, possible. However, the derivation seems to be inevitably less general in the specification of the state and to leave the physical ground of the HVC obscure.

15) The adjacency matrix is what Ruedenberg named the topological matrix; K. Ruedenberg, *J. Chem. Phys.*, **22**, 1878 (1954).

16) In some sense, we may say that the HVC in the simple Hückel model depends only on the adjacency, but this should be never misunderstood to mean that bond orders between nonadjacent sites are superfluous.

17) M. Isihara, *Bull. Chem. Soc. Jpn.*, **58**, 2472 (1985); **59**, 3963 (1986).

18) The point group is described in many books on molecular orbital theory. As a standard monograph, F. A. Cotton, "Chemical Applications of Group Theory," John Wiley & Sons, New York (1963).

19) The use of permutation groups is prevalent in constructing spin eigenfunctions for many-electron systems. As another interesting application of permutation groups in quantum chemistry, H. C. Longuet-Higgins, *Mol. Phys.*, **6**, 445 (1963).

20) G. W. Wheland, *Proc. R. Soc. London, Ser. A*, **164**, 397 (1938).

21) For the transitivity, the orbit, and other concepts related to them, consult the literature on group theory, particularly on permutation groups.

22) Say, suppose *G* to be the group consisting of only the identity or a cyclic group of order more than two.

23) A pseudorbit corresponds to an orbit obtained by ignoring the order in site pairs. If only the SC were considered, the nonordered pair would be used from the outset.

24) C. A. Coulson and G. S. Rushbrooke, *Proc. Camb. Phil. Soc.*, **36**, 193 (1940); H. C. Longuet-Higgins, *J. Chem. Phys.*, **18**, 265 (1950).

25) The classical studies cited in Ref. 24 were followed by various developments; for example, A. D. McLachlan, *Mol. Phys.*, **2**, 271 (1959); J. Koutecký, *J. Chem. Phys.*, **44**, 3702 (1966). See also Ref. 4.

26) Note that the state is assumed to be faithful.

27) G. G. Hall, *Proc. R. Soc. London, Ser. A*, **229**, 254 (1955); K. Ruedenberg, *J. Chem. Phys.*, **29**, 1232 (1958).

28) The HVC in the Hückel model seems to have drawn no attention somewhy, at least explicitly. The reason may include the confusion of the HVC with the reality condition or, paradoxically, the tractability of the Hückel orbital theory.

Chelate Stability Constants of *N*-(*o*-Hydroxybenzyl)iminodiacetic Acid (HBIDA) with Yttrium and Lanthanoid Ions

Isao YOSHIDA,* Fumio SAGARA, and Keihei UENO
Department of Industrial Chemistry, Kumamoto Institute of Technology,
Ikeda 4-22-1, Kumamoto 860
(Received September 16, 1988)

Chelate stability constants of *N*-(*o*-hydroxybenzyl)iminodiacetic acid with yttrium and some lanthanoid ions (M^{3+}) were determined by the potentiometric method at 25 °C and at an ionic strength of 0.1 with potassium nitrate. The computation of the titration data indicated that four kinds of complexes, ML, ML_2^{3-}, $M(HL)^+$, and $M(HL)_2^-$ (except for thulium and lutetium) were formed on each metal ion and the values of the stability constants increased with the increase of atomic number of the element. The values found for the stability constants of yttrium complexes are between those for gadolinium and terbium ions.

It has been reported that *N*-(*o*-hydroxybenzyl)-iminodiacetic acid (HBIDA, H_3L) is a tetradentate chelating ligand in which the phenolic oxygen, in addition to the iminodiacetate group, can coordinate to metal ions such as iron(III), copper(II), nickel(II), zinc(II), and cobalt(II), and their stability constants have also been reported.[1] However, no stability constants have been reported on the HBIDA complexes with lanthanoid and yttrium ions. The chelate stability constants of many amine-*N*-polycarboxylic acids[2] including iminodiacetic acid (IDA)[3] with trivalent lanthanoid ions including yttrium have now been measured to understand the factors which influence the formation and stability of the lanthanoid ion complexes.[4]

It is interesting to study the complexes formation of the ligands which have phenolic oxygen as an additional coordination site such as HBIDA with lanthanoid ions. Accordingly, complex formation of HBIDA with lanthanoid ions has been investigated and their stability constants discussed in comparison with those for IDA and other amine-*N*-polycarboxylic acids.

Experimental

The HBIDA employed was synthesized according to Harris et al.[1] The crude product was recrystallized more than five times from water, and the purity of the final product was checked by elemental analyses, NMR spectrum and molecular weight determination by alkalimetry. The stock solutions of the metal ions were prepared from analytical grade metal nitrates or oxides and were standardized by direct EDTA titration using the appropriate indicator.[5] The 35 cm^3 of the solution containing 0.1 mmol of HBIDA and 0.05 mmol of metal ion was titrated with 0.1 M (1 M=1 mol dm^{-3}) carbonate-free potassium hydroxide solution, and the free hydrogen ion concentration was measured with a Denkikagaku Keiki IOC-10 pH meter by a procedure similar to that described in a previous report.[6] During the titrations, the solutions were kept under a nitrogen atmosphere, at 25±0.5 °C and at an ionic strength of 0.1 with potassium nitrate.

The ultraviolet absorption spectra of the 2×10^{-4} M of ligand solutions were measured at $p[H^+]=11-12.5$ in 1 cm-length quartz cell using a Shimadzu UV-180 spectrophotometer. During the measurements, the sample solutions were kept at 25±0.5 °C and at an ionic strength of 0.1 with potassium nitrate.

Results and Discussion

From the titration data of the ligand in the absence of metal ion, the two final protonation constants were calculated directly using a computer program SUPERQUAD.[7] The first protonation constant was determined by the spectrophotometric method. The following values; $\log K^H_1=11.94$, $\log K^H_2=8.15$, and $\log K^H_3=2.34$, were obtained, respectively. These values were in good agreements with those reported by Harris et al.[1] and were used in the calculations of the stability constants of the metal complexes

The titration data for the 1:2 metal to ligand systems were also analyzed by the use of the same program. The computer calculations indicated the formation of the following complexes, ML, ML_2^{3-}, MLH^+, and $ML_2H_2^-$ (except for thulium and lutetium) and evaluated the values of their stability constants. The results are summarized in Table 1, in which β functions are defined as follows.

$$\beta_1 = [ML]/[M^{3+}][L^{3-}], \quad \beta_2 = [ML_2^{3-}]/[M^{3+}][L^{3-}]^2,$$
$$\beta_{M(LH)} = [M(LH)^+]/[M^{3+}][LH^{2-}] \quad \text{and}$$
$$\beta_{M(LH)_2} = [M(LH)_2^-]/[M^{3+}][LH^{2-}]^2.$$

The value of the stability constant of the 1:1 HBIDA complexes, $\log \beta_1$, increases with an increase in the atomic number of the lanthanoid ions, starting from the first element (11.65 for lanthanum) to the last element (14.87 for lutetium) as shown in Table 1. This stability trend suggests that the HBIDA belongs to the ligand of the first group according to Moeller et al.[4] who have pointed out that the ligand such as IDA and nitrilotriacetic acid (NTA) belonged to the first group. NTA is a well known tetradentate ligand which coordinates to a metal ion with three carboxylate-oxygen atoms and an amino-nitrogen atom, and its stability constants with lanthanoid ions have been reported.[8] The stability constants for the 1:1 HBIDA

Table 1. The Stability Constants, β_n and $\beta_{M(LH)_n}$ (n=1, 2), of HBIDA Complexes of Lanthanoid and Yttrium Ions (25 °C, I=0.1 with KNO_3)

Metal ions	log β_1[a]	log β_2	log $\beta_{M(LH)}$	log $\beta_{M(LH)_2}$
Y	13.63(0.01)	24.17(0.01)	5.85(0.02)	12.32(0.03)
La	11.65(0.02)	19.67(0.01)	4.95(0.03)	10.87(0.03)
Ce	12.01(0.05)	20.76(0.01)	5.45(0.05)	11.48(0.04)
Pr	12.21(0.04)	21.20(0.01)	5.63(0.03)	11.76(0.04)
Nd	12.46(0.04)	21.98(0.01)	5.80(0.03)	11.86(0.04)
Sm	13.08(0.06)	23.16(0.01)	5.77(0.04)	12.32(0.06)
Eu	13.42(0.02)	23.93(0.01)	5.95(0.03)	12.40(0.04)
Gd	13.55(0.01)	24.13(0.01)	5.82(0.03)	12.23(0.04)
Tb	13.88(0.01)	24.73(0.01)	5.87(0.04)	12.45(0.06)
Dy	14.07(0.01)	25.18(0.01)	5.91(0.03)	12.51(0.04)
Ho	14.14(0.02)	25.30(0.01)	5.97(0.04)	12.48(0.10)
Er	14.30(0.01)	25.93(0.01)	6.22(0.02)	12.20(0.12)
Tm	14.48(0.01)	26.48(0.04)	6.40(0.02)	
Yb	14.54(0.01)	26.67(0.03)	6.44(0.02)	12.59(0.09)
Lu	14.87(0.01)	27.76(0.01)	6.71(0.02)	

a) Values in parentheses are standard deviations.

complexes are higher than those for the NTA complexes, the increments being 1.29 with the lanthanum- and 2.38 with the lutetium complex, in log unit.

On the other hand, the values for the stability constants of the 1:1 HBIDA complexes are about twice as large as those of the 1:1 IDA complexes, in log unit.[3] Since IDA binds to a metal ion as a tridentate ligand in the 1:1 normal complexes, the increase in the stability constants of the HBIDA is likely to be due to the tetradentate nature of the ligand. Such a coordination has been reported on some divalent metal complexes, such as with nickel(II) and zinc(II).[1]

As to the overall stability constants of the 1:2 metal to ligand complexes of HBIDA, log β_2, the value also increases with an increase in the atomic number of the elements, starting from lanthanum (19.67) to lutetium (27.76). It was found from these values that the second stepwise stability constants $K_{ML_2}=[ML_2^{3-}]/[ML][L^{3-}]$ were in a range of 8.02 (lanthanum) to 12.89 (lutetium) in log unit. Such an increase in the values of the second stepwise constants of the 1:2 complexes with an increase in atomic number of lanthanoid ions is common to the complexes by complexane-type or related ligands. Such a trend has been also found in the values of the second stepwise stability constants of the 1:2 metal to IDA complexes in which no steric hindrance due to the coordinated ligands has been found.[3] This suggests that no steric hindrance occurs between the two ligands in the 1:2 HBIDA complexes as in the case of the IDA complexes.[3] The corresponding value for the 1:2 yttrium complex is found in between those for gadolinium and terbium as in the case of the 1:1 complex.

The stability constant of the protonated 1:1 HBIDA complex, log $\beta_{M(LH)}$, also increases with the increase in the atomic number of the element. The value for the yttrium complex is again found in lie between the values for the gadolinium and terbium complexes as in the case of the nonprotonated complexes. These values are smaller than those of the 1:1 IDA complexes, indicating that, in the protonated 1:1 metal to HBIDA complex, the phenolate oxygen is not involved in the coordination, but is protonated to form a free phenol group. Eventually, HBIDA is likely to behave as tridentate ligand.

Concerning the overall stability constant of the protonated 1:2 HBIDA complex, the values for log $\beta_{M(LH)_2}$ are higher than those of the 1:2 IDA complexes for the lighter lanthanoid group.[3] However, the increments decrease with an increase in the atomic number of the elements; both values become almost same at holmium, then, the values for the IDA complex becoming higher than those for the HBIDA only after the erbium complex. These results suggest that the diprotonated 1:2 HBIDA complexes of the lighter lanthanoid ions are unusually stable, if one remembers that the stabilities of the protonated 1:1 HBIDA complexes are lower than those of the 1:1 IDA complexes. The second stepwise stability constant of the diprotonated 1:2 HBIDA complex ($K_{M(LH)_2}=[M(LH)_2^-]/[M(LH)^+][LH^{2-}]$) was found to be 5.92 in log units at lanthanum from Table 1. This value is higher by 0.97 log units than the value for the first constant. The value for the second stepwise constant becomes smaller with the increasing atomic number of the lanthanoid elements, but it is still in a similar level of the first ones at erbium and at ytterbium. These rather high values for the overall stability constants of the diprotonated 1:2 HBIDA complex seem to be exceptional, if one remembers that the second stepwise stability constant does not generally exceed that of the first one. In the case of the transition metal complexes of HBIDA, the values for the second stepwise stability constants are 65.0 and 63.1 per cent of the first ones, for cobalt(II) and zinc(II), respectively. Thus,

the unusually high values for the diprotonated 1:2 HBIDA complex are peculiar to the lanthanoid ions, and may be partly due to hydrogen bonding between two free phenol groups of the coordinated HBIDA. In the case of the transition metal complexes, the ionic radii are too small to allow the formation of such hydrogen bonding.

References

1) W. R. Harris, R. J. Motekaitis, and A. E. Martell, *Inorg. Chem.*, **14**, 974 (1975).
2) A. E. Martell and R. M. Smith, "Critical Stability Constants," Plenum Press, New York (1982), Vols. 1 and 5.
3) L. C. Thompson, *Inorg. Chem.*, **1**, 490 (1962).
4) T. Moeller, D. F. Martin, L. C. Thompson, R. Ferrus, G. R. Feistel, and W. J. Randall, *Chem. Rev.*, **65**, 1 (1965).
5) K. Ueno, "Kire-to tekitei hou", Nankodo, Tokyo (1972), p. 410.
6) I. Yoshida, F. Sagara, and K. Ueno, *Anal. Sci.*, **4**, 69 (1988).
7) P. Gans, A. Sabatini, and A. Vacca, *J. Chem. Soc., Dalton Trans.*, **1985**, 1195.
8) T. Moeller and R. Ferrus, *Inorg. Chem.*, **1**, 49 (1962).

 © 1989 The Chemical Society of Japan Bull. Chem. Soc. Jpn., 62, 2299—2306 (1989)

Thermotropic Behavior of Proteins and Acylated Proteins in Monolayers

Tomoyoshi MITA
Department of Natural Science, Osaka Women's University,
Daisen-cho, Sakai, Osaka 590
(Received December 19, 1988)

In order to obtain information concerning the effect of proteins on the thermotropic properties of biological membranes, the temperature-dependences of monolayers of different proteins and some acyl derivatives of bovine serum albumin (BSA) have been investigated. The hydrophobic proteins such as hemoglobin, β-lactoglobulin, and β-casein formed dilute monolayers, whereas the hydrophilic proteins such as cytochrome C and lysozyme formed concentrated monolayers. BSA showed an intermediate isotherm between those of dilute and concentrated films. The monolayers of BSA, cytochrome C, and lysozyme were gradually expanded with increasing temperatures. However, the temperature-dependences of the monolayers of hemoglobin, β-lactoglobulin, β-casein, and acyl derivatives were significantly different from those of the monolayers of hydrophilic proteins. In detail, the monolayers of hemoglobin and β-lactoglobulin formed the most compact structures around 20 °C and 30 °C, respectively, while the monolayers of β-casein formed the most expanded structure around 30 °C. In addition, the monolayers of acetyl and propionyl derivatives formed the most compact structures around 30 °C. These results suggest that the hydrophobicity of protein is an important factor relating to thermal stability of proteins in monolayers.

Lipids and proteins are the main constituents of biological membranes. One of the major concerns in membrane biology is to understand how lipids and proteins interact with each other and how such interaction affects the properties of both lipids and proteins in membranes.

Membrane properties are sensitive to environmental influences such as temperature. From this viewpoint, the protozoan *Tetrahymena pyriformis* has been used as the model system for investigating molecular mechanisms involved in cellular acclimation to environmental temperature extremes.[1-3] Furthermore, the effects of lipids on the thermotropic properties of biological membranes have been investigated extensively.[4-11] However, the interpretation of such studies may be complicated by the present lack of detailed information concerning the effect of proteins on the thermotropic properties of biological membranes. One way to gain detailed insight into the molecular aspects of such interactions may be to investigate the thermotropic properties of proteins in membranes.

Because of the strongly amphipathic nature of protein, the change to an extended conformation in which the protein molecule lowers the Gibbs energy of the system by maximizing contact of nonpolar side chains with the nonpolar phase, within steric limitations, is understandable.[12] In biological membranes, integral proteins penetrate the hydrocarbon region (hydrophobic), while peripheral proteins are located adjacent the outer or inner surface (hydrophilic) of the membranes. The integral proteins are arranged in such a manner that their polar groups are either exposed to the aqueous environment or associated electrostatically with the hydrophilic groups of membrane, while nonpolar parts of the protein maintain contact with the inner hydrophobic region.[13] From this viewpoint, Jähnig[14] has analyzed the factors that effect the thermodynamics of the partitioning of proteins between aqueous and membrane phases, and demonstrated that the hydrophobic effect provides the main driving force for insertion into the membrane.

In order to model the physical properties of biological membranes, artificial bilayers such as vesicle, planar bilayers such as black lipid membrane, and monolayers are often used. Although the monolayer does not completely mimic the specific environments of cell membrane surfaces, the study of spread monolayers offers useful insights into the surface conformational behavior of proteins.[15] Another advantage of using a monolayer technique is that the orientation of the protein molecules at the interface is understood precisely and the area occupied by each molecule can be determined over wide limits by careful compression of the film.

With this in mind, the author started the current work to estimate the thermotropic behavior of different native proteins in monolayers. Although the proteins used were not membrane bound but water soluble, they were chosen because of their well-known amino acid sequences and three dimensional structures. On the other hand, the hydrophobicity of proteins can be converted by the technique of selective chemical modification. For example, acylation of lysine side chains in proteins is not only the modification leading to loss of charge, but the reaction leading to significant increase of hydrophobicity. Therefore some acyl derivatives of protein have been used as a model for investigating the hydrophobic effect.[16] The present work also intends to investigate the contributions of hydrophobic effects of proteins in membranes through measurements of the temperature-dependence of monolayers of some acylated proteins.

Experimental

Chemicals. All chemicals were of the highest purity available, used without further purification. Water was distilled once, passed through a mixed ion bed exchanger, and redistilled.

Proteins. The following proteins of high purity were used in this study as obtained from the suppliers: Bovine serum albumin (BSA), bovine hemoglobin (2×crystallized), horse cytochrome C (Type III), β-casein, and β-lactoglobulin (contain variant A and B) were from Sigma Chemical Co., lysozyme (6×crystallized) was a product of Seikagaku Kogyo Co. (Japan).

Acylation of the Proteins. For this study the acetyl, propionyl, butyryl, and palmitoyl derivatives of BSA were prepared by the method of Fraenkel-Conrat.[17] Satisfactory compounds were obtained by reacting with appropriate anhydride in 50% saturated sodium acetate solution at 0 °C. Acetylation required 1 h, whereas propionylation and butyrylation required 2 h. The palmitoyl derivative was prepared by reacting BSA in 50% saturated sodium acetate solution with palmitic anhydride dissolved in ethanol, at 50 °C.[18] Palmitoylation required 10 min. The reaction mixtures were exhaustively dialyzed against water to remove excess reagent. The palmitoyl derivative was then washed with diethyl ether to remove unreactive palmitic anhydride. These derivatives were isolated by lyophilization.

Extent of Acylation. The extent of acylation of BSA was measured by the loss of ninhydrin-positive color in the derivatives compared to BSA.[19]

Apparatus. A Kyowa's surface pressure apparatus (Kyowa Surface Science Co.) was used. The film balance is fully automated and provide with continuous recording of surface pressure versus film area. The inside dimensions of the Teflon-coated trough were 70×14×0.5 cm.

Spreading Solvents. A 50% 1-propanol containing 0.5 mol dm^{-3} sodium acetate was employed as a spreading solvent for BSA, hemoglobin, β-casein, cytochrome C, and lysozyme. Acidic chloroform-methanol (2:1 v:v with 1 cm^3 concd HCl/250 cm^3 solvent)[20] was used for β-lactoglobulin, acetyl-BSA, and propionyl-BSA. A 50% 1-propanol containing 0.05 mol·dm^{-3} sodium carbonate was used for butyryl-BSA and palmitoyl-BSA. These solutions were stored in the refrigerator and used after about 24 h. Comparison of spreading solvents was made by spreading BSA from a 50% 1-propanol containing 0.5 mol·dm^{-3} sodium acetate. No difference was found in the surface pressure-area isotherm.

Surface Pressure. Surface pessure was measured by the Wilhelmy method, using a roughened glass plate. The films were compressed by the moveable Teflon barrier. In the experiments reported below, no buffer was used, in order to provide a very simple subphase. The water was poured into the trough to a height of 1—2 mm above the rim. The surface of the substrate was cleaned by moving the Teflon barrier from one side of the trough to the other. The cleaning of the surface was repeated until the surface pressure of the substrate did not exceed 0.2 mN·m^{-1}. Constant temperature were controlled by running water in the trough surrounded by a water jacket and regulated by a Cool Mate (TE-105 M, Toyo Seisakusho Co.) circulation bath. The temperature was monitored below and as close as possible to the surface of the water phase. The monolayers were made on the surface by using a microsyringe (Hamilton Co.). For the surface pressure-area (π-A) isotherms, exactly 0.05 mg of protein was spread from a 0.05% solution onto an area of 897 cm^2. Monolayer spreading was made by the direct application of numerous small drops (≈0.0006 cm^3) of spreading solution to the surface of the substrate. A time interval of 30 min was allowed for the equilibration of the monolayer before it was compressed. The π-A isotherms for proteins were made by using a compression velocity of 0.0567 $m^2 \cdot mg^{-1} \cdot min^{-1}$. Each part of the experiment was replicated at least three times and then averaged.

Results

Unlike the common substances studied as insoluble monolayers, quantitative spreading of water soluble proteins requires that none is able to dissolve into the bulk solution and diffuse away. For this purpose, two techniques are developed.[21] One is achieved by allowing a very thin layer of the solution to flow down a glass rod before reaching the water surface, this was just introduced by Trurnit.[22] Another satisfactory quantitative spreading technique is also achieved by the direct application of small drops of protein solution which is prepared with 50% 1-propanol containing 0.5 mol·dm^{-3} sodium acetate, as introduced by Ställberg and Teorell.[23] A comparison of the two spreading techniques was made using lysozyme. No difference was found between the two techniques, and the latter was used in this study.

Characteristics of Protein Monolayers at an Air-Water Interface. The wide variety of surface behavior exhibited by proteins at the air-water interface is illustrated by the properties of β-casein, hemoglobin, β-lactoglobulin, BSA, cytochrome C, and lysozyme. Figure 1 shows the π-A isotherms obtained at 25 °C for monolayers of the six proteins spread on water. β-

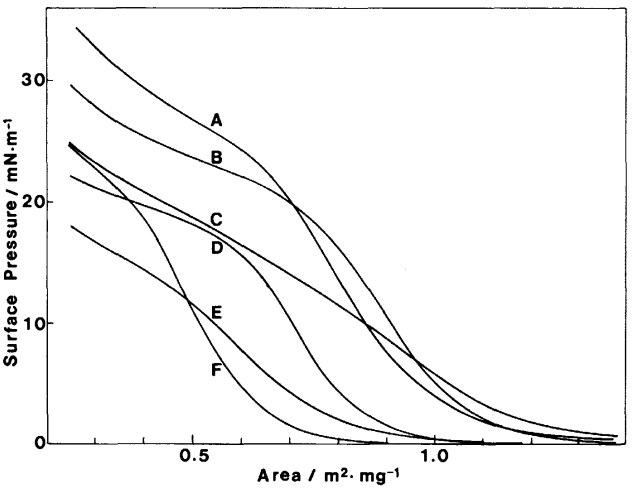

Fig. 1. π-A isotherms for monolayers of different proteins spread on water at 25 °C. A) β-Lactoglobulin, B) hemoglobin, C) β-casein, D) BSA, E) cytochrome C, F) lysozyme.

Table 1. Some Structural Parameters, Ratio of Polar to Apolar Amino Acid Residues, and Hydrophobicity Parameters for Various Proteins

Protein	Polar-apolar ratio	Hydrophobicity parameter, $H\phi_{ave}$ /kJ·res.$^{-1}$	Helix content (%)	SS bond content per molecule	Molecular weight
β-Casein	0.86	5.57	10	0	23000
Hemoglobin	1.09	4.65	75	0	64500
β-Lactoglobulin	1.28	4.98	55	2	18400
BSA	1.63	4.35	55	17	66300
Cytochrome C	2.04	4.23	45	0	11700
Lysozyme	2.26	4.06	35	4	14300

Casein, hemoglobin, and β-lactoglobulin formed dilute monolayers, whereas cytochrome C and lysozyme formed concentrated films. BSA showed an isotherm intermediate between those of the dilute and concentrated films. Dilute protein monolayers are supposed to be completely unfolded molecules, whereas concentrated films are considered to contain incompletely unfolded molecules.[24]

Some structural parameters of these proteins are summarized in Table 1, together with the ratio of polar to apolar amino acid residues and the hydrophobicity parameter. The values of the ratio of polar to apolar amino acids were estimated by Hatch's theory.[25] Proteins with a large proportion of apolar residues exhibit the lower values of the ratio of polar to apolar amino acids (below 1.5). The hydrophobicity parameter, the average hydrophobicity ($H\phi_{ave}$), is based on Tanford's Gibbs energies to transfer the amino acid side chains from an organic environment to an aqueous environment.[26] This was calculated by Bigelow's theory.[27] Proteins with high hydrophobicity exhibit the higher values of $H\phi_{ave}$ (over 4.6 kJ·res.$^{-1}$). It is clear from Fig. 1 and Table 1 that proteins such as β-casein, hemoglobin, and β-lactoglobulin, with either a high content of apolar residues or high hydrophobicity, unfold more easily than proteins such as cytochrome C and lysozyme, with either a low content of apolar amino acids or low hydrophobicity.

Effect of Temperature on Various Protein Monolayers at an Air-Water Interface. The π-A isotherms for various protein monolayers over a range of temperature 10—40 °C are shown in Figs. 2—7. Figures 2—4 show the isotherms for the monolayers of BSA, cytochrome C, and lysozyme spread on water at different temperatures, respectively. These monolayers gradually expanded with increasing temperature. Figures 5—7 show the isotherms for the monolayers of hemoglobin, β-lactoglobulin, and β-casein spread on water at different temperatures, respectively. The temperature-dependences of the monolayers of these proteins were considerably smaller than those of the monolayers of hydrophilic proteins such as BSA, cytochrome C, and lysozyme over the whole temperature range measured. Figure 8 shows the plots of area as a function of temperatures for various protein monolayers at (a)

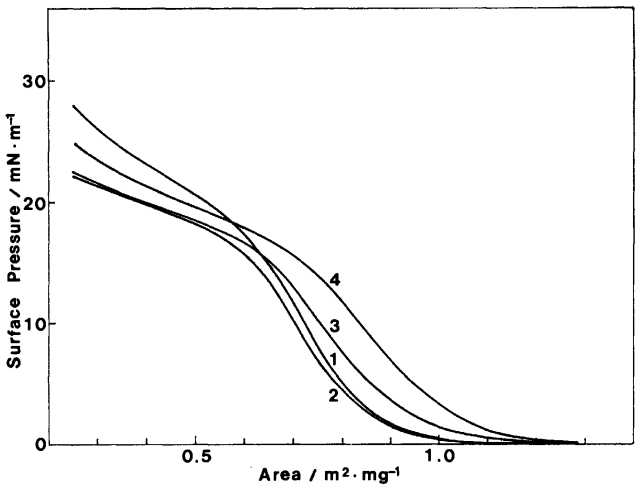

Fig. 2. π-A isotherms for BSA monolayer at different temperatures. Isotherm temperatures are numbered with increasing temperatures: 1) 12.9 °C, 2) 23.1 °C, 3) 33.5 °C, 4) 43.0 °C.

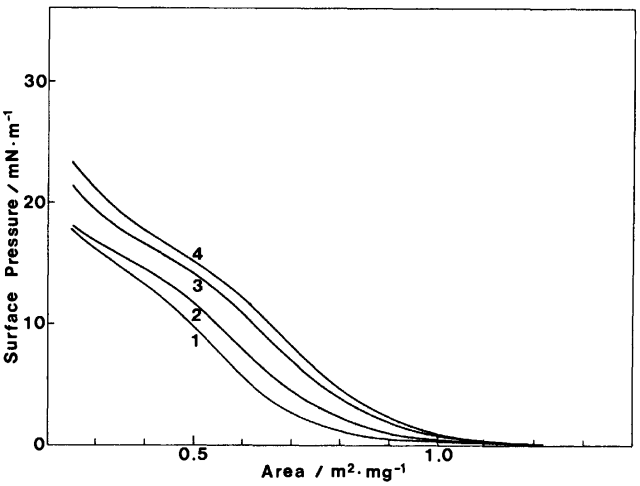

Fig. 3. π-A isotherms for cytochrome C monolayer at different temperatures. 1) 11.9 °C, 2) 24.1 °C, 3) 32.8 °C, 4) 41.0 °C.

π=5 mN·m^{-1} and (b) π=15 mN·m^{-1}, derived from Figs. 2—7. The result indicates that BSA, cytochrome C, and lysozyme at the interface exhibit the extended conformations with increasing temperatures, while

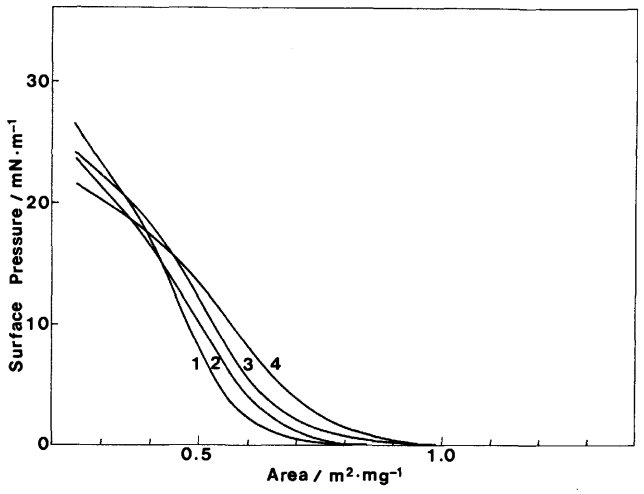

Fig. 4. π-A isotherms for lysozyme monolayer at different temperatures. 1) 10.6°C, 2) 15.4°C, 3) 25.1°C, 4) 34.5°C.

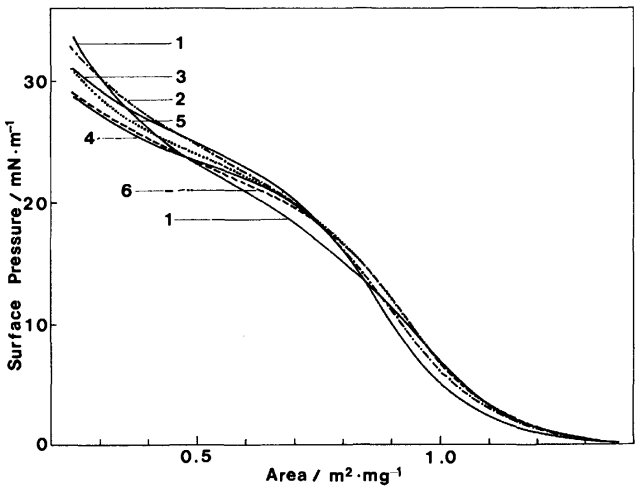

Fig. 5. π-A isotherms for hemoglobin monolayer at different temperatures. 1) 7.2°C, 2) 11.2°C, 3) 19.8°C, 4) 24.4°C, 5) 32.7°C, 6) 41.8°C.

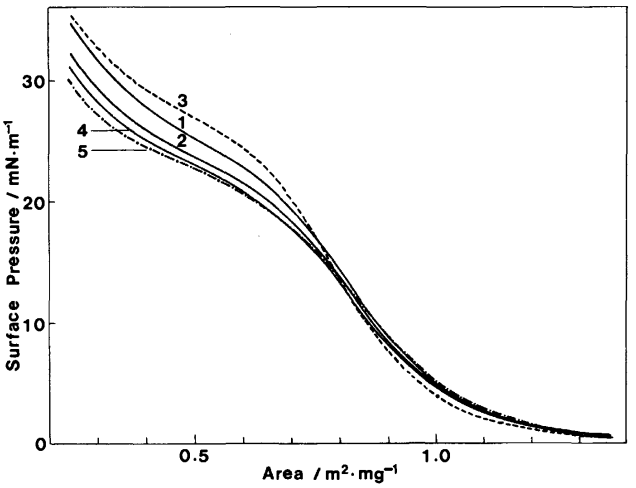

Fig. 6. π-A isotherms for β-lactoglobulin monolayer at different temperatures. 1) 11.6°C, 2) 16.3°C, 3) 26.7°C, 4) 39.8°C, 5) 45.9°C.

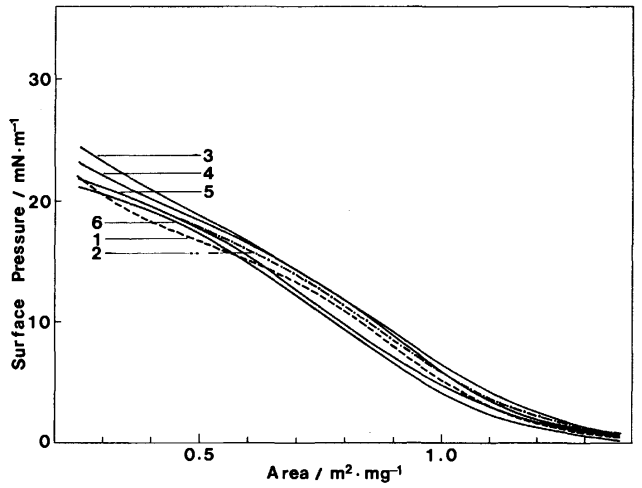

Fig. 7. π-A isotherms for β-casein monolayer at different temperatures. 1) 9.5°C, 2) 16.6°C, 3) 24.5°C, 4) 29.4°C, 5) 36.8°C, 6) 39.5°C.

hemoglobin and β-lactoglobulin at the interface exhibit the most compact conformations around 20 °C and 30 °C, respectively, and β-casein exhibits the most extended conformation around 30 °C.

Characteristics of Monolayers of BSA and Its Derivatives at an Air-Water Interface. On acylation the amino groups involved were principally the ε-NH_2 of the lysines and the terminal amino group of the protein.[16] Tanford[26] has shown that the Gibbs energy change to be expected when methylene or methyl groups are transferred from organic solvent to water is +3.06 kJ·mol^{-1} at 25 °C. By using this value, acylated lysines, i.e., acetyl, propionyl, butyryl, and palmitoyl lysines were assigned hydrophobicities of 15.3, 18.4, 21.4, and 64.1 kJ·mol^{-1}, respectively. $H\phi_{ave}$ is the total hydrophobicity divided by the number of residues.[27] $H\phi_{ave}$ of acyl derivatives of BSA in this way could be calculated. Table 2 shows the extent of substitution of amino acid residues and $H\phi_{ave}$ of BSA and its derivatives.

Figure 9 shows the isotherms obtained at 25 °C for monolayers of BSA and its derivatives spread on water. An interesting feature of these isotherms is the expansion as the length of alkyl side chain on the modifying acyl group was increased up to n=2 (propionyl) but the condensation as it was further increased up to n=15 (palmitoyl), compared to the isotherm of BSA.

Effect of Temperature on Monolayers of Acyl Derivatives of BSA at an Air-Water Interface. The π-A isotherms for the monolayers of acyl derivatives of BSA over a range of temperature 10—40 °C are shown

Table 2. Degree of Substitution of Amino Acid Residues and Hydrophobicity Parameters for BSA and Its Derivatives

BSA and its derivative	Degree of substitution of amino acid residue (%)	Hydrophobicity parameter, $H\phi_{ave}$/kJ·res.$^{-1}$
BSA	—	4.35
Acetyl-BSA	66.9	4.98
Propionyl-BSA	67.4	5.19
Butyryl-BSA	63.9	5.36
Palmitoyl-BSA	98.5	10.17

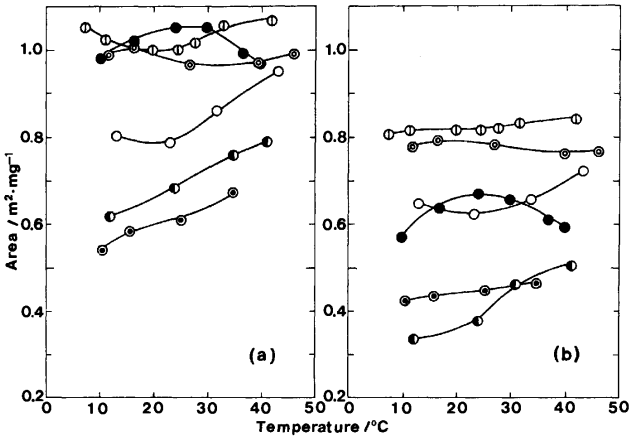

Fig. 8. Plots of area as a function of temperature for various monolayers at (a) π=5 mN·m^{-1} and (b) π=15 mN·m^{-1}, derived from Figs. 2—7. The symbols indicate ⓓ, hemoglobin; ◎, β-lactoglobulin; ●, β-casein; ○, BSA; ◐, cytochrome C; ⊙, lysozyme.

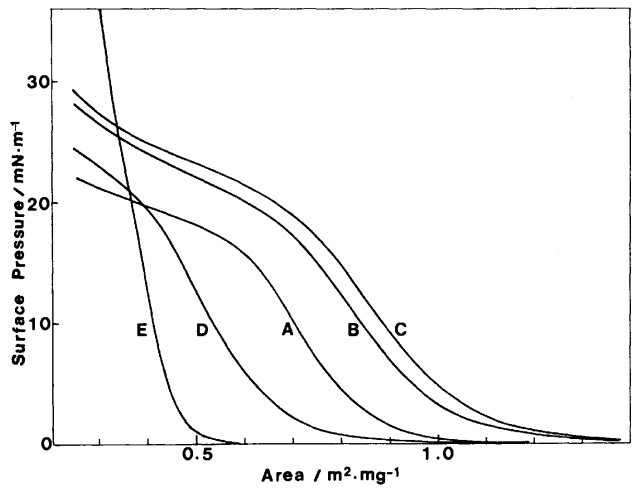

Fig. 9. π-A isotherms for monolayers of BSA and its derivatives spread on water at 25°C. A) BSA, B) acetyl-BSA, C) propionyl-BSA, D) butyryl-BSA, E) palmitoyl-BSA.

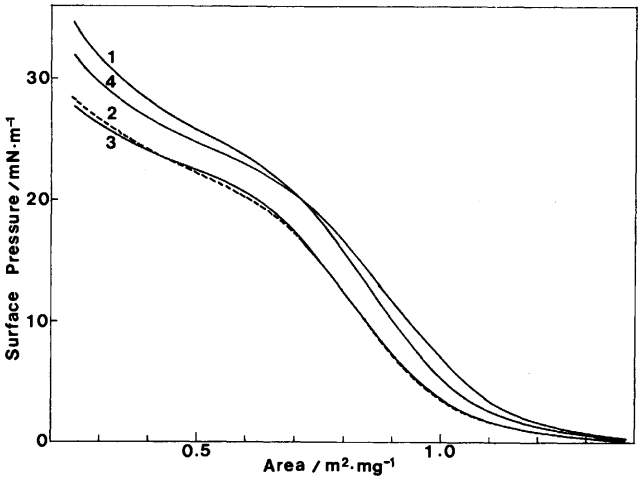

Fig. 10. π-A isotherms for acetyl-BSA monolayer at different temperatures. 1) 9.8°C, 2) 23.5°C, 3) 31.7°C, 4) 41.2°C.

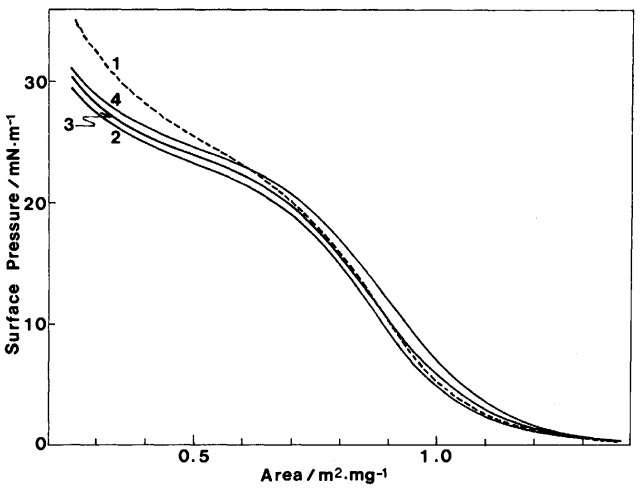

Fig. 11. π-A isotherms for propionyl-BSA monolayer at different temperatures. 1) 11.1°C, 2) 24.0 °C, 3) 35.1°C, 4) 41.3°C.

in Figs. 10—13. Figures 10 and 11 show the isotherms for acetyl-BSA and propionyl-BSA monolayers spread on water at different temperatures, respectively. The isotherms of their derivatives showed a decremental shift with increasing temperatures up to 30 °C but an incremental one with increasing temperatures above 30 °C, indicating that the temperature-dependences of their derivatives were essentially different from that of BSA in Fig. 5. Figures 12 and 13 show the isotherms for butyryl-BSA and palmitoyl-BSA monolayers spread

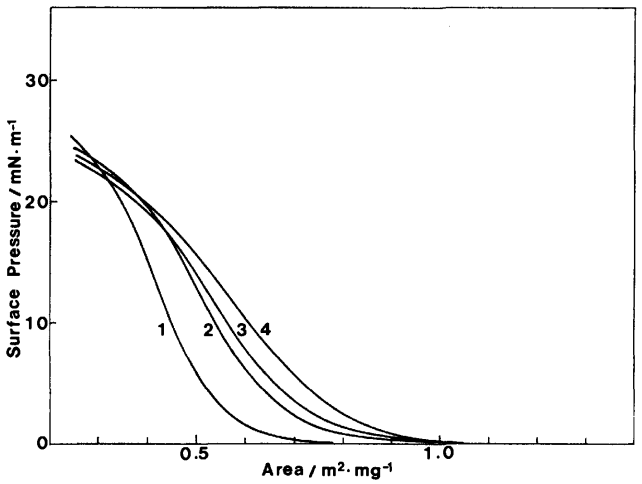

Fig. 12. π-A isotherms for butyryl-BSA monolayer at different temperatures. 1) 8.6°C, 2) 23.6°C, 3) 30.9°C, 4) 42.9°C.

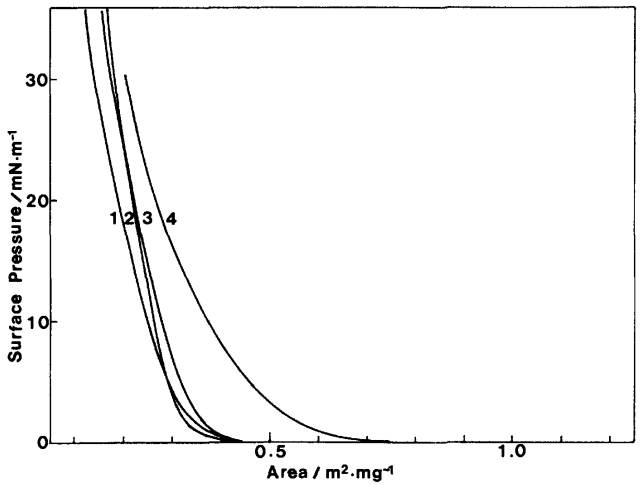

Fig. 13. π-A isotherms for palmitoyl-BSA monolayer at different temperatures. 1) 12.5°C, 2) 23.0°C, 3) 32.5°C, 4) 42.2°C.

on water at different temperatures. These monolayers were gradually expanded with increasing temperatures, although the hydrophobicities of their derivatives were higher than those of acetyl and propionyl derivatives. Figure 14 shows the plots of area as a function of temperature for the monolayers of BSA and its derivatives at (a) π=5 mN·m^{-1} and (b) π=15 mN·m^{-1}, derived from Figs. 2 and 10—13. The result indicates that acetyl and propionyl derivatives at the interface exhibit the most compact conformations around 30°C, while that butyryl and palmitoyl derivatives exhibit the extended conformations with increasing temperatures.

Discussion

It is assumed that proteins at an air-water interface lose their tertiary structure. They exist in extended

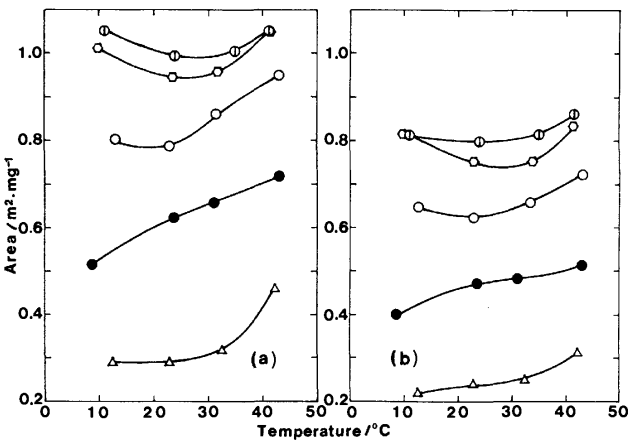

Fig. 14. Plots of area as a function of temperature for monolayers of BSA and its derivatives at (a) π=5 mN·m^{-1} and (b) π=15 mN·m^{-1}, derived from Figs. 2 and 10—13. ○, BSA; ○, acetyl-BSA; ⊕, propionyl-BSA; ●, butyryl-BSA; △, palmitoyl-BSA.

conformations with hydrophobic domains oriented at the interface and hydrophilic domains directed toward the aqueous phase. However, the unfolding of a protein molecule at the interface is not infinite but within steric limitations such as intramolecular disulfide bonding. Accordingly, the unfolding of proteins at the interface is considered as follows. The hydrophobic proteins such as β-casein, hemoglobin, and β-lactoglobulin unfold more easily than the hydrophilic proteins such as cytochrome C and lysozyme. Particularly, β-casein is a flexible more or less random coil molecule without any disulfide bond and with a low helix content, while lysozyme is a rigid globular molecule, the peptide chain being crosslinked by four disulfide bonds (Table 1). In this way, the degree of unfolding may be influenced not only by the hydrophobicity but by the flexibility of the molecule. Similar results have been obtained by Evans et al.,[16] Birdi,[28] and Graham and Phillips.[29]

Privalov et al.[30-33] has extensively studied the stability of the native conformation of proteins in an aqueous phase. The stability of the protein is usually described in terms of the denaturation Gibbs energy for the unfolded and native conformations. That is, the Gibbs energy of protein unfolding, $\Delta G^u(T)$, can be expressed as

$$\Delta G^u(T) = \Delta H^u(T) - T\,\Delta S^u(T) \qquad (1)$$

where $\Delta H^u(T)$ and $\Delta S^u(T)$ are the net change of enthalpy and entropy of protein unfolding, respectively. $\Delta G^u(T)$ is generally shown as a function of temperature. According to Privalov and Khechinashvili,[30] $\Delta G^u(T)$~T curves for lysozyme and ribonuclease decrease steeply with increasing temperatures, respectively. However, $\Delta G^u(T)$~T curves for myoglobin and trypsin

inhibitor have the maximum values at about 30 °C and decrease again with decreasing temperatures, indicating so-called cold denaturation.[34] A similar result has been obtained by Ooi and Oobatake.[35] The extent of protein unfolding may be correlated to the Gibbs function as follows. The native protein progressively unfolds with diminishing the Gibbs energy. In this way, the hydrophilic proteins such as lysozyme (see Table 1) and ribonuclease (polar–apolar ratio of 2.64, average hydrophobicity of 3.68 kJ·res.$^{-1}$) tends to unfold with increasing temperatures, while the hydrophobic proteins such as myoglobin (polar–apolar ratio of 1.26, average hydrophobicity of 4.84 kJ·res.$^{-1}$) and trypsin inhibitor (polar–apolar ratio of 1.57, average hydrophobicity of 4.94 kJ·res.$^{-1}$) aquire the most compact structures around 30 °C.

The thermodynamics of protein adsorption at an interface has been noted by MacRitchie,[36] indicating that the entropy gain due to hydrophobic domains is the dominant factor governing protein adsorption at an interface. Therefore, the above phenomenon in the aqueous phase would apply to protein unfolding at the interface, i.e., the temperature-dependence of unfolding of protein in membranes would be dependent on the degree of hydrophobicity of the protein. The hydrophilic proteins such as BSA, cytochrome C, and lysozyme at the interface exhibited the extended conformations with increasing temperatures (Figs. 2—4 and 8). In addition, the hydrophobic proteins such as hemoglobin and β-lactoglobulin at the interface exhibited the most compact conformations around 20 °C and 30 °C, respectively (Figs. 5, 6, and 8). It is particularly interesting that hemoglobin which is similar to myoglobin in structure and function exhibits the behavior of cold denaturation at the interface. These results suggest that Privalov's thermodynamics may be applied to the mechanisms of protein unfolding not only in the aqueous phase but also at an interface.

However, the thermotropic behavior of β-casein monolayer is in conflict with the above consideration. This may be explained as follows. The decrease in the Gibbs energy is attributed to a hydration effect due to hydrated water around the protein molecule.[35] In this sense, the hydration effect of the protein at the interface will be diminished compared to that of the protein in the aqueous phase. β-Casein, a flexible more or less random coil molecule, may exist in a completely extended conformation with its hydrophobic domains oriented at the interface and its hydrophilic domains directed toward the aqueous phase. Accordingly the thermotropic behavior of β-casein at the interface may be significantly different from that of β-casein in the aqueous phase.

The above speculation was confirmed by investigating the thermotropic behavior of monolayers of acyl derivatives of BSA. The monolayers of acetyl-BSA and propionyl-BSA, where the hydrophobic domains were introduced by acylation of the lysine side chains, were more expanded than that of unmodified BSA (Fig. 9). Furthermore, the isotherms for the acetyl and propionyl derivatives showed distinct decremental shifts with increasing temperatures up to 30 °C, but an incremental one with further increasing temperatures, i.e., these derivatives exhibited the most compact conformations at the interface around 30 °C (Figs. 10, 11, and 14).

On the other hand, the monolayers of butyryl and palmitoyl derivatives, where the hydrophobicities were higher than those of acetyl and propionyl derivatives, were more condensed than that of unmodified BSA. In addition, the monolayers of the butyryl and palmitoyl derivatives were simply expanded with increasing temperatures, despite their significantly high hydrophobicities (Figs. 12—14, Table 2). Particularly, both the shape of the isotherm and the temperature-dependence of the monolayer of the palmitoyl derivative were similar to those of dipalmitoylphosphatidylcholine (DPPC). Phillips[4] has discussed the temperature-dependence of lipid monolayers in the following terms. When the hydrocarbon chains are sufficiently long, condensed monolayers are formed, whereas with shorter chains, liquid-expanded films occur. When the temperature is greater than the phase transition temperature T_c (41 °C in the case of DPPC), the monolayer is completely expanded and the π–A isotherm does not show an intermediate region. When the temperature is considerably lower than T_c, the monolayer will be fully condensed. At intermediate temperatures, the π–A isotherms show the well-pronounced change of slope due to the onset of two-dimensional crystallization. It is seen from Fig. 12 and Table 2 that the apparent area occupied per palmitoyl side chain in the monolayer of palmitoyl-BSA is 7.0×10^{-19} m^2 at 23 °C. When DPPC is spread on water, the area per molecule in the monolayer is about 4.8×10^{-19} m^2 below T_c.[4] Since palmitoyl side chains therefore comprise about 34% of the total area at the air–water interface, the thermotropic behavior of the palmitoyl side chains will become pronounced rather than that of hydrophobic domains in protein.

In conclusion, the results obtained in this study suggest that the hydrophobicity of the protein is the dominant factor determining the thermal stability of proteins in monolayers. This study is being continued to obtain further information about the hydrophobic effect of proteins in membranes through the measurements of the temperature-dependence on mixed monolayers constituted of proteins and lipids.

The skillful technical assistance of Misses Junko Hata, Kyoko Morikawa, Sizuko Nomura, and Kana Tabata is gratefully acknowledged.

References

1) G. A. Thompson, Jr., and Y. Nozawa, *Biochim. Biophys. Acta*, **472**, 55 (1977).
2) B. F. Dickens, C. E. Martin, G. P. King, J. S. Truner, and G. A. Thompson, Jr., *Biochim. Biophys. Acta*, **598**, 217 (1980).
3) B. F. Dickens and G. A. Thompson, Jr., *Biochemistry*, **19**, 5029 (1980).
4) M. C. Phillips, *Prog. Surf. Memb. Sci.*, **5**, 139 (1972).
5) C. D. Linden, K. L. Wright, H. M. McConnell, and C. F. Fox, *Proc. Natl. Acad. Sci. U.S.A.*, **70**, 2271 (1973).
6) S. Razin, *Prog. Surf. Memb. Sci.*, **9**, 257 (1975).
7) D. L. Malchior and J. M. Steim, *Ann. Rev. Biophys. Bioeng.*, **5**, 205 (1976).
8) A. G. Lee, *Biochim. Biophys. Acta*, **472**, 237 (1977).
9) A. G. Lee, *Biochim. Biophys. Acta*, **472**, 285 (1977).
10) A. Csordas and K. Schauenstein, *Biochim. Biophys. Acta*, **856**, 212 (1986).
11) H. G. L. Coster and D. R. Laver, *Biochim. Biophys. Acta*, **857**, 95 (1986).
12) F. MacRitchie, *J. Colloid Interface Sci.*, **105**, 119 (1985).
13) H. Hanssens, J. C. Van Ceunebroek, H. Pottel, G. Preaux, and F. Van Cauwelaert, *Biochim. Biophys. Acta*, **817**, 154 (1985).
14) F. Jähnig, *Proc. Natl. Acad. Sci. U.S.A.*, **80**, 3691 (1983).
15) N. F. Zhou and B. A. Pethica, *Langmuir*, **2**, 47 (1986).
16) M. T. A. Evans, J. Mitchell, P. R. Mussellwhite, and L. Irons, "Advances in Experimental Medicine and Biology," ed. by M. Blank, Plenum Press, New York (1970),Vol. 6, pp. 1—22.
17) J. Fraenkel-Conrat, *Arch. Biochem. Biophys.*, **27**, 109 (1950).
18) Z. Haque and M. Kito, *Agric. Biol. Chem.*, **48**, 1099 (1984).
19) E. W. Yemm and E. C. Cocking, *Analyst*, **80**, 209 (1955).
20) D. G. Cornell and R. H. Carroll, *J. Colloid Interface Sci.*, **108**, 226 (1985).
21) T. Yamashita, *Tampakushitsu Kakusan Koso*, **20**, 1048 (1975).
22) H. J. Trurnit, *J. Colloid Sci.*, **15**, 1 (1960).
23) S. Ställberg and T. Teorell, *Trans. Faraday Soc.*, **35**, 1413 (1939).
24) H. B. Bull, *Adv. Protein Chem.*, **3**, 95 (1947).
25) F. T. Hatch, *Nature*, **206**, 777 (1965).
26) C. Tanford, *J. Am. Chem. Soc.*, **84**, 4240 (1962).
27) H. F. Bigelow, *J. Theoret. Biol.*, **61**, 187 (1967).
28) K. S. Birdi, *J. Colloid Interface Sci.*, **43**, 544 (1973).
29) D. E. Graham and M. C. Phillips, "Foams," ed. by R. J. Akers, Academic Press, London (1976), pp. 237—255.
30) P. L. Privalov and N. N. Khechinashvili, *J. Mol. Biol.*, **86**, 665 (1974).
31) P. L. Privalov and N. N. Khechinashvili, *Biofizika*, **19**, 14 (1974).
32) P. L. Privalov, *Adv. Protein Chem.*, **33**, 167 (1980).
33) P. L. Privalov, *Adv. Protein Chem.*, **35**, 1 (1982).
34) P. L. Privalov, Y. V. Griko, S. Y. Venyaminov, and V. P. Kutyshenko, *J. Mol. Biol.*, **190**, 487 (1986).
35) T. Ooi and M. Oobatake, *J. Biochem.*, **103**, 114 (1988).
36) F. MacRitchie, *Adv. Protein Chem.*, **32**, 283 (1976).

 © 1989 The Chemical Society of Japan Bull. Chem. Soc. Jpn., 62, 2307—2314 (1989)

Cyclohepta[*b*][1,4]benzoxazines 3.[1] The Reaction of 6-Bromocyclohepta-[*b*][1,4]benzoxazine with *o*-Aminophenol[2]

Tetsuo Nozoe,* Harue Okai, Hidetsugu Wakabayashi,*,† and Sumio Ishikawa†
Tokyo Research Laboratories, Kao Corporation, Bunka-2, Sumida-ku, Tokyo 131
†Department of Chemistry, Faculty of Science, Josai University, Sakado-shi, Saitama-ken 350-02
(Received January 5, 1989)

The reaction of 6-bromocyclohepta[*b*][1,4]benzoxazine (**19**) and *o*-aminophenol (**3**) was studied and compared with that of 3-bromo-2-methoxytropone (**2**) with **3**. 14H-[1,4]Benzoxazino[3′,2′:3,4]cyclohepta[1,2-*b*]-[1,4]benzoxazine, 10-(*o*-hydroxyanilino)cyclohepta[*b*][1,4]benzoxazine (**D**), 1- and 4-formylphenoxazines and their Schiff bases (**C** and **X**) were obtained in very good yields by modifying the conditions of the reaction of **19** with **3**. Structures of **D**, **C**, and their isomers were determined and the possible reaction pathways for the formation of various products are discussed.

We have reported that the reaction of 2-bromo-7-methoxytropone (**1**) and 3-bromo-2-methoxytropone (**2**) with *o*-aminophenol (**3**) in refluxing acetic acid gave quite different results: while **1** afforded mainly 2-bromo-7-(*o*-hydroxyanilino)tropone (**4**) besides small amounts of two by-products (compounds **A** and **B**, vide infra),[3] the reaction of **2** turned out to be very

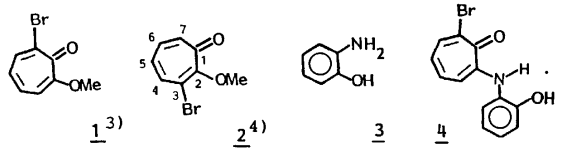

1[3] 2[4] 3 4

complex, giving various colorful products, which were easily separated by preparative silica-gel TLC and conveniently named compounds **A**—**L** according to their decreasing R_f-values.[4] The structures of most of these compounds (**A**, **B**, **F**, **G**, **J**, and **L**) were determined by spectroscopy, as shown in Chart 1. Among them, compounds **5** (**G**) and **6** (**J**) were 1:1 condensation products, whereas compounds **10** (**A**), **7** (**B**), **C**, **D**, **9** (**F**), and **8** (**L**) were 1:2 condensation products; compound **B** was a secondary product from compound **C** (see below). Compound **D** (**15**, Scheme 1) changed to compound **A** (**10**) by autoxidation, while compound **C** (**18**, Scheme 1) gradually decomposed to compound **B** (**7**) on heating in methanol.[4] However, since **C** and **D** were not isolated as pure materials, we could not determine their exact structures at that time.

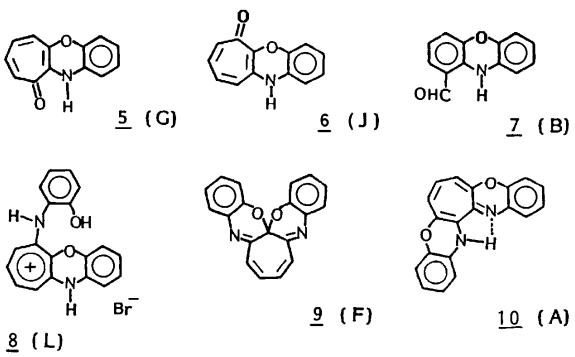

5 (G) 6 (J) 7 (B)

8 (L) 9 (F) 10 (A)

Chart 1.

Meanwhile, we were able to resolve the chiral acetal **9** (**F**) and its derivatives into their optical antipodes and to determine their absolute configurations by an X-ray method[5] and by theoretical calculations of their CD spectral data.[6]

It has generally been recognized that the course of various reactions of troponoids are often extremely sensitive towards a slight structural difference of both substrates and reagents, as well as the reaction conditions employed (solvent and concentration, temperature, and with or without catalyst, etc.).[2,5] However, the considerable difference between the reactions of two isomers (**1** and **2**) with **3** under the same conditions was far beyond our expectation.

At that time, we considered that the methoxyl group at C-2 of **2** would be very inactive to the nucleophilic replacement due to steric interferences (between carbonyl and bromine atom), and we believed that 1:1 condensation products (**J** and **G**) had been produced via **11** (normal substitution at C-3) and **12** (cine substitution at C-7). On the other hand, compounds **D**, **A** (**10**), **C**, and **B** (**7**) were thought to be formed through a common intermediate, **15**, via 2,3-disubstituted product **13** followed by an oxidative ring closure to **10**, and a rearrangement to **18** and **7** via spirooxazole **17**. The possible pathways proposed then are summarized in Scheme 1; however, we did not have any positive proof of the intermediates for each products.

Takase and his coworkers found[8] that the treatment of **2** and morpholine or pyrrolidine first afforded two monosubstitution products (normal and cine at C-3 and C-7, respectively), and then the 2,3- and 2,7-disubstituted products. However, differing from the above-mentioned case, the most preferable site of substitution of **2** with arylamine has recently been found by us to be the C-2 and then C-7 positions.[9] We have also found that the bromine atoms on a cyclohepta[*b*][1,4]benzoxazine ring are easily saponified by warm acetic acid to give cyclohepta[*b*][1,4]-

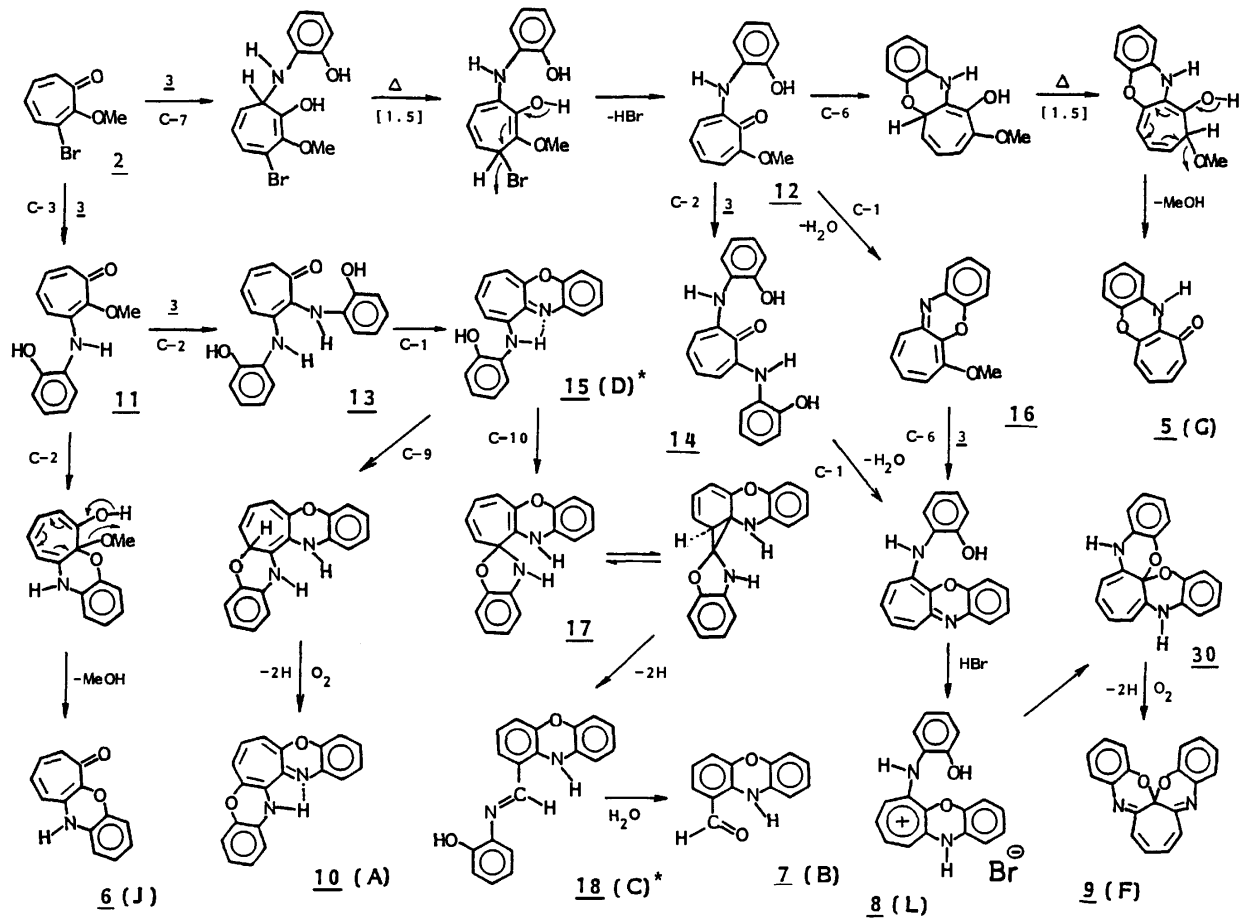

Scheme 1.[4] * Structure of these compounds were determined in this paper.

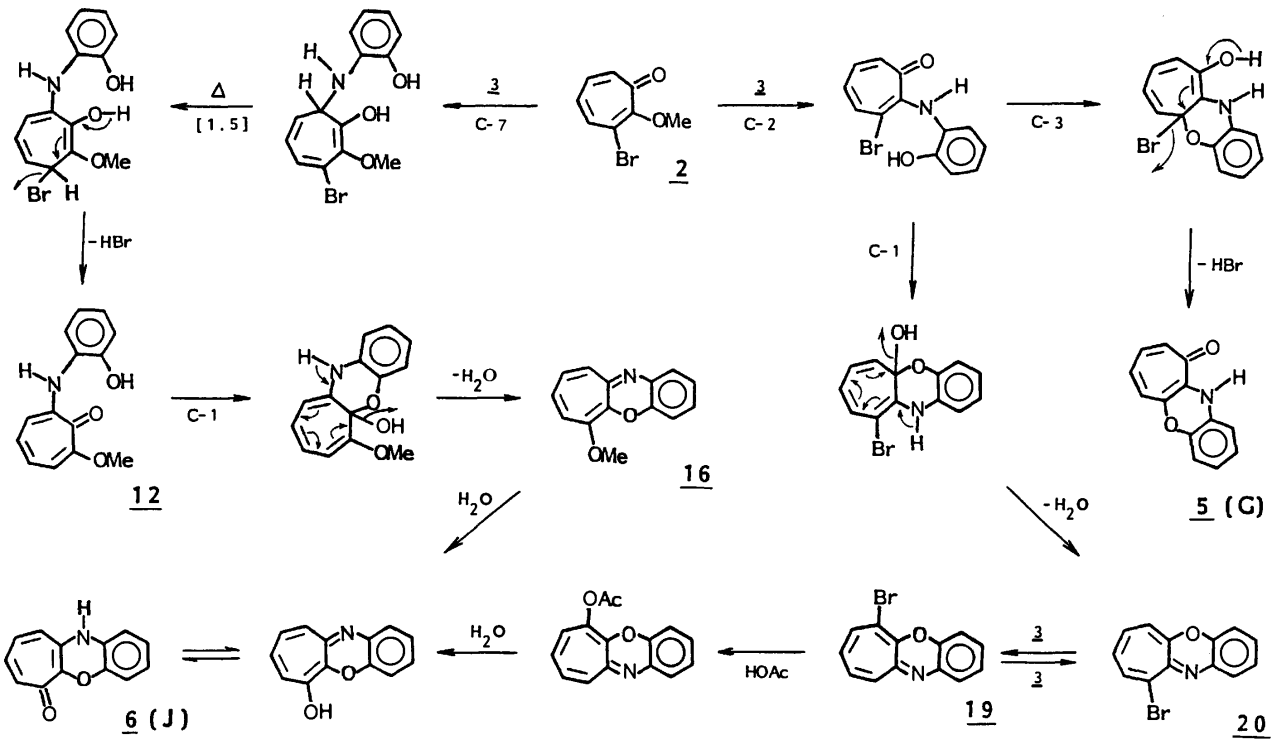

Scheme 2.

benzoxazines.[10] Therefore, the formation of 1:1 condensation products should now be formulated, as in Scheme 2.

In this paper, we would like to describe the reaction of 6-bromocyclohepta [*b*][1,4]benzoxazine (**19**) with **3** and *p*-anisidine along with a reexamination of the reactions of **2** with **3**, to obtain useful information about these very complex reactions of the special heterocyclic tropylium system.

Results and Discussion

Reaction of 2 with 3. To obtain uselful information about the formation sequence of various products from **2** and **3** and to confirm the structures of intermediates for these compounds, we first reexamined the reaction in refluxing acetic acid by periodically checking the reactant with the reversed-phase high-pressured liquid chromatography (HPLC) equipped with a stopped-flow UV-spectrometer. An example of the chromatograph of the reaction mixture heated at 120 °C for 30 min is shown in Fig. 1a. Each peak was characterized by the stopped-flow UV-visible spectra as well as MS after separation and the assignment of the main peaks was made as follows: peaks 1 (**L**), 3(**3**), 5(**J**), 8 (**2** and **H**[1]), and 10 (**G**). When the heating was continued for several hours, peaks 11 — 16 began to appear at a retention time (RT) of 20—50 min, as seen in their amplified figures in Fig. 1b. Peaks 12, 13, and 14 were identified by TLC and UV to be compounds **C**, **D**, and **B** (**7**), respectively.

After heating **2** and **3** in acetic acid for 60 min, the reaction mixture was separated by HPLC (Fig. 1b) and we obtained small amounts of compounds **C** and **D**. Compound **D** ($C_{19}H_{14}N_2O_2$, reddish-brown needles, mp 135—138 °C decomp) was quantitatively converted into **10** (**A**, $C_{19}H_{12}N_2O_2$) by silica-gel TLC eluted with benzene. Orange-colored compound **C** (mp 158—160 °C, $C_{19}H_{14}N_2O_2$), which gradually degraded to **7** (**B**) on heating or standing in methanol, was therefore thougth to be a Schiff base (**18**) of **7**. Upon the addition of a trace of dil sulfuric acid the methanolic solution of **C** instantly became deep purple red and then discolored after 10—20 seconds, giving HPLC peaks due to **7** and oxidative dimer **H**[1] (**22**),[7] but only a trace amount of **3**; we found that **22** was, however, not produced when the experiment was conducted under nitrogen.

Since the quantity of pure compounds **C** and **D** were not sufficient for their structural studies, we then studied the reaction of **3** with **19** as an analogue of the possible reaction intermediates, **16** and **20**, under various conditions.

Reaction of 19 and 3. Under Acidic Conditions. On heating **19** with **3** in acetic acid at 120 °C for 1.5 h and after careful separation of the reaction mixture, compounds **L** (**8**, 55%), **D** (25%), the rearranged product **B** (**7**, ca. 10%), and a trace amount of compound **A** were isolated. Compound **D** was assigned to have the structure of 10-(*o*-hydroxyanilino)-cyclohepta[*b*][1,4]benzoxazine (**15**), based on the evidence of the spectral data; the AA'BB' singal pattern of the four protons on the seven-membered ring in the ^{1}H NMR spectrum should be noted (see Experimental part). Pure **15** is stable as crystals, but its methanolic solution was autoxidized rapidly in the presence of a weak base or an acid to give a quantitative yield of **10** (**A**, Scheme 3). Hydroperoxyl radical (HOO·), which is expected to be liberated when **15** (**D**) is autoxidized to **10** (**A**) [and **8** (**L**) to **9** (**F**)], would induce oxidation of **3** to the dehydro dimer **22**. As a consequence, **22** always accompanies, as one of the products, in the reaction of this series. **10** exists as a symmetrical and almost planar hydrogen bonded form, as shown by X-ray crystallography,[11] and does not open its benzoxazine ring, even upon heating with methanolic

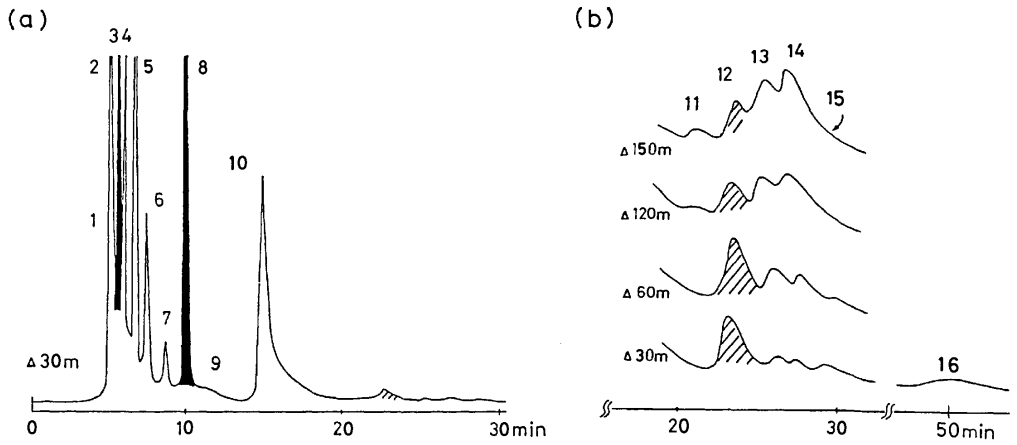

Fig. 1. Time-dependent HPLC chromatograms of the reaction of **2** and **3** in AcOH at 120 °C for 30 minutes.

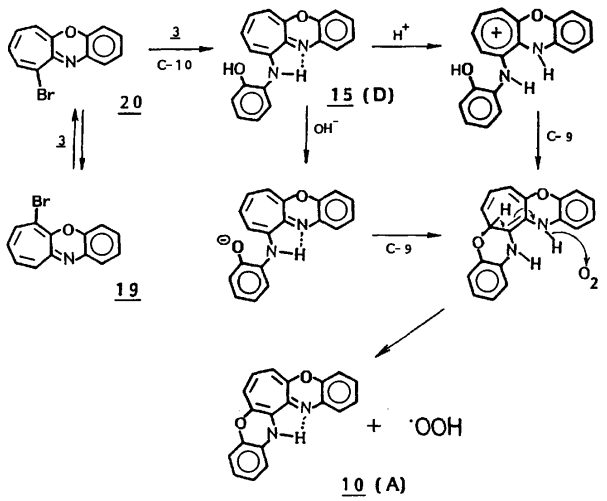

Scheme 3.

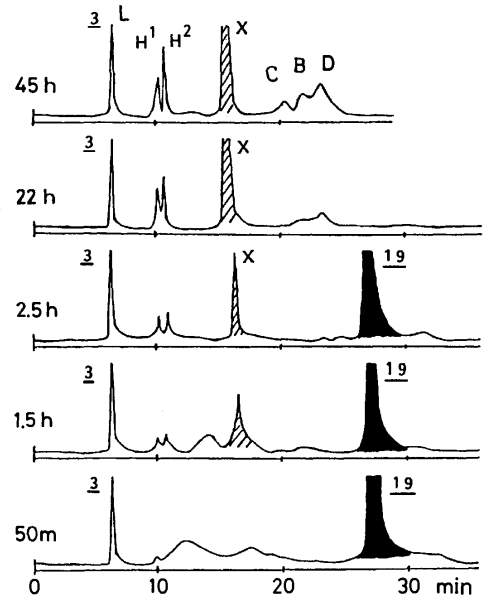

Fig. 2. Time-dependent HPLC chromatograms of the reaction of **19** and **3** in MeOH at room temp in the presence of DABCO.

alkali. We could not obtain its *N*-methyl or *N*-acetyl derivative by ordinary method, presumably because of the strong intramolecular hydrogen bonding.

Under Basic Conditions. Since compound **C** was extremely unstable in dil mineral acid, we then examined the reaction of **19** with **3** at room temperature in methanol containing an equivalent of 1,4-diazabicyclo[2.2.2]octane (DABCO) in order to neutralize HBr produced during the reaction; the time-dependent HPLC chromatograms are shown in Fig. 2. Many initially observed peaks became simplified after a few hours. Then, peaks of **3** (RT, 6 min), **22** (H^1, RT, 10.5 min), H^2 (RT, 11 min), and **X** (RT, 16 min) as well as weak peaks of **8** (**L**), **C**, **7** (**B**), and **15** (**D**)

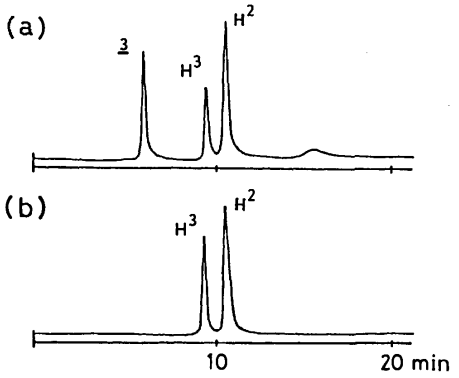

Fig. 3. (a) HPLC chromatograms of compound **X** in MeOH containing a trace amount of dil sulfuric acid. (b) HPLC chromatograms of compound H^2 in MeOH containing a trace amount of dil sulfuric acid.

remained unchanged; unknown peak **X** corresponding to the main peak gradually crystallized out. Compound **X** (yellow needles, mp 210—211 °C) showed IR absorbance maxima at 3350 and 1618 cm^{-1} due to NH and C=N, respectively, exhibited ^1H NMR (DMSO-d_6) signals at δ 8.85, 8.75, and 8.27 due to OH, NH, and HC=N, respectively, and was identified to be an isomer of compound **C** by MS. The addition of a small amount of dil sulfuric acid to compound **X** dissolved in methanol, resulting in the production of a deep purple color, quickly followed by a complete bleaching of the solution. This solution was found to consist of three components: **3**, H^2 (RT, 11 min), and H^3 (RT, 9.8 min) by HPLC (Fig. 3a). Compound H^2 (yellow needles, mp 186—187 °C) isolated by TLC, showed IR absorbance maxima at 3250 (NH) and at 2840, 2780, and 1675 cm^{-1} (CHO), and exhibited ^1H NMR (acetone-d_6) signals at δ 10.36 (CHO), 7.61 (NH), and 7.02 (1 benzene ring proton adjacent to CHO). These data and the results of the X-ray analysis[12] indicate that compound H^2 is 4-formylphenoxazine (**24**), an isomer of **7** (**B**). Compound H^3 [UV λ_{max} (MeOH) 236 and 318 nm] was partly produced from **24** [UV λ_{max} (MeOH) 228, 276, 313, and 416 nm, (MeOH+6 M HCl) 236 and 318 nm] in MeOH by the addition of a small amount of dil sulfuric aicd (Fig. 3b). The compound isolated from peak H^3 showed the same HPLC retention time (11 min) and MS of **24**, suggesting that H^3 would be the hemiacetal **24a**, which is stabilized somewhat by hydrogen bonding with the *O*-atom of heterocyclic ring.

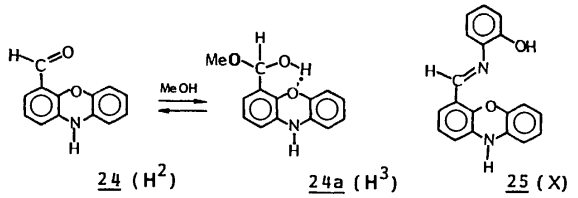

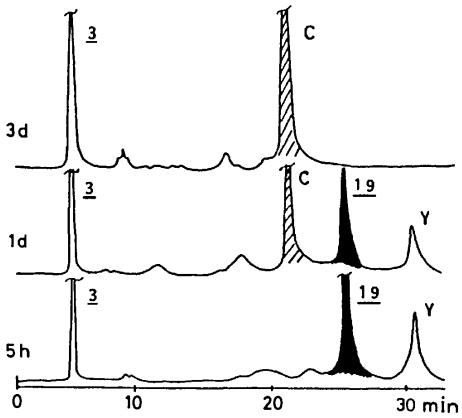

Fig. 4. Time-dependent HPLC chromatograms of the reaction of **19** and **3** in MeOH at 5 °C.

Under Neutral Conditions. Since we unexpectedly obtained the Schiff base **25** instead of the Schiff base of **7**(**B**) in the presence of DABCO, reactions of **19** and **3** in MeOH at 5 °C were performed without the base and were periodically monitored by HPLC. As shown in Fig. 4, a peak of compound **Y** (see later) appears first, and compound **C** increased as **Y** and **19** decreased among the reaction mixture. Almost no other products [e.g. **7** (**B**), **10** (**A**), **15** (**D**)] were observed in this case, even upon standing for 3 days. The product corresponding to the main peak of compound **C** gradually crystallized out in high yield. The IR spectrum of compound **C** showed OH and NH absorptions at 3470 and 3200 cm^{-1}, respectively. The ^1H NMR spectrum consisted of a proton signal of the benzene ring adjacent to the C=N group (δ 6.88, dd, J=8 and 2 Hz) and the signals at δ 9.78, 8.50, and 6.05 due to OH, HC=N, and NH groups, respectively. Taken together with the results of high-resolution MS, compound **C** was unambiguously identified as being the Schiff base **18** of 1-formylphenoxazine (**7**). A complete assignment for the ^1H NMR signals was made by using a decoupling technique; the result is described in the Experimental section.

When this reaction of **19** with **3** is studied using greater amounts for preparative purposes, we obtained about 70% yield of **18** (**C**), besides a 20% yield of **15** (**D**) and a trace amount of the ring-opened product **4**.[3] It is noted that the yields of **15** and **18** highyl depend on the reaction conditions employed; for example, at 50 °C a 30% yield of **18** and 50% of **15** were produced along with 10% of **4**. The temporary deep-violet color observed when trace acid was added to the soltion of **18** is considered to be due to the formation of a cyanine dye-type iminium salt of the Schiff base **18**, (or its 4-isomer in the case of **24**). This was followed by facile hydrolysis to produce **7** (or **24**) and **3** (Scheme 4). As for **Y**, we later identified it[13] to be a 10-bromo compound **20** produced by an unpercedented inter-

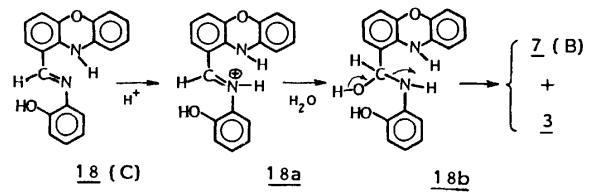

Scheme 4.

molecular heterocyclic exchange reaction between **19** and **3**. Isomers **19** and **20** are shown in the presence of **3** to exist in solution at equilibrium, as shown in Scheme 2.

From its structure, we first considered[2] that **15** was formed from 6-bromo compound **19** by cine substitution at C-10 followed by [1,5]hydrogen-shift. However, this assumption became doubtful because **15** was produced from **19** and **3**, even at low temperature (described before). Indeed, a recent study of the reaction of 10-bromo compound **20** with arylamine has confirmed that **15** is the normal substitution product of **20** with **3** (Scheme 3).[14]

To clarify the reason why two different Schiff bases, **18** and **25**, are produced from **19** and **3**, in the absence or presence of base (DABCO), we examined the reaction of **19** with the *p*-anisidine (**26**) having no OH group at the *o*-position. Upon standing a methanolic

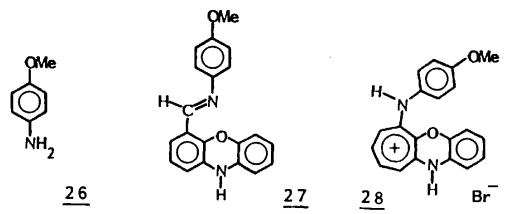

solution of **19** and **26**, we obtained, besides some ring-opened compound **4**, mainly rearranged 4-formylphenoxazine (**24**, 65%) which was produced by the hydrolysis of Schiff base **27**. Upon heating at 50 °C, a 57% yield of 6-substituted cations **28**, 38% fo **24** and some anilinotropone **4** were obtained. The addition of DABCO or acetic acid to the methanolic solution of **19** and **26** did not change the result, and no C-10 substituted compound (**D**-type) and 1-formylphenoxazine (**7**) were formed. However, an almost quantitative yield of **28** was obtained upon refluxing **19** and **26** in acetic acid. Compound **28** (reddish-brown needles, mp >300 °C), which exhibited a UV spectrum very similar to that of **8** (**L**), was assigned to have a structure of 6-(*p*-methoxyanilino)cyclohepta[*b*][1,4]benzoxazine hydrobromide on the basis of spectral data (see Experimental part). From this evidence, and also from the structure of **9** (**F**), **8** (**L**) is obviously the normal substitution product derived from **3** and **19** and stabilized as the HBr salt. 6-(*o*-Hydroxyanilino)cyclohepta-[*b*][1,4]benzoxazine (**29**) was obtained as a yellowish-

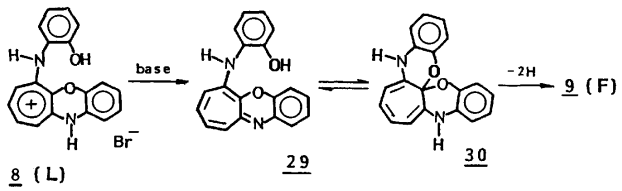

Scheme 5.

brown solid by neutralizing the salt **8**. However, it was very unstable in open air and was easily dehydrogenated to give stable dehydro acetal **9** (**F**) via acetal **30** (Scheme 5).

These results indicate that the presence of an OH group at ortho to the anilino nitrogen is essential to produce **7**, **10**, **15**, and **18**. Since the rearranged product **18** was produced by the reaction of **19** and **3** in neutral or even weakly acidic conditions, and also from its structure, we first speculated[4] that the spiroxazole intermediate **17** produced from **15** by ring closue at C-10 rearranged to Schiff base **18** via norcaradiene form (in Scheme 1).

However, we later confirmed that **15** (**D**) did not yield the rearranged product under various conditions. Therefore, the formation of Schiff base **27** (**X**-type) from **19** and *p*-anisidine (**26**) must have proceeded by the attack of the arylamine at C-7 (to give **31**), followed by rearrangement via norcaradiene **31a** shown in Scheme 6. The production of **25** (and **24**) from **19** and **3** in the presence of a base can be similarly interpreted, since the heterocycle exchange reaction[13] of **19** to **20** is significantly retarded by a base. These pieces of evidence indicate that **15** (**D**) and **18** (**C**) are not derived directly from 6-bromo compound **19** by a cine

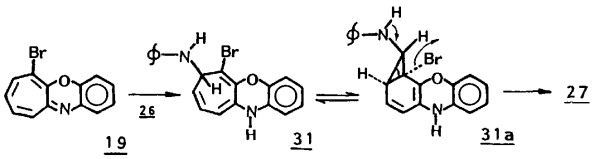

Scheme 6.

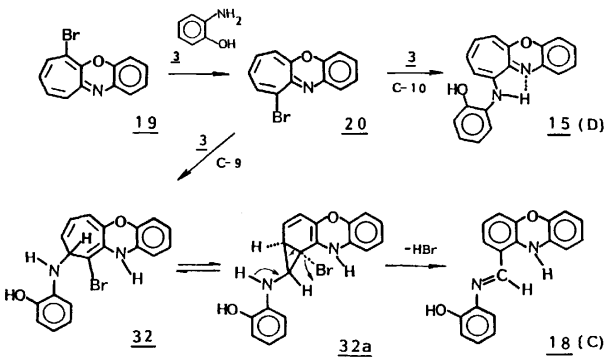

Scheme 7.

substitution at C-10, but instead, are produced from the exchanged 10-bromo compound **20** by normal substitution at C-10 (for **15**) and by an attack at C-9 (for **18**), as illustrated in Scheme 7.

Thus, the unusually complex nature of the reaction of **19** and **3** was finally unveiled by the discovery of the novel and facile heterocycle-exchange reaction between the substrate and the reagent,[13] details of which will be reported elsewhere.

Experimental

Melting points were determined with a Yanagimoto MP-3S and are uncorrected. The IR and electronic spectra were measured by using a Shimadzu IR-450 and a Shimadzu UV-202 spectrometer, respectively; the UV spectra in acid or alkali solutions were taken after adding a few drops of 6 M HCl or 6 M NaOH (1 M=1 mol dm^{-3}) to the sample solution. The ^{1}H NMR spectra were measured in $CDCl_3$ (unless otherwise specified) with a JEOL JNM-PS/PFT (100 MHz) or a JEOL JNM-GX270 (270 MHz) spectrometer using TMS as the internal standard. The assignments of all signals were made by empoloying a first-order analysis with the aid of a decoupling technique. The mass spectra were taken on a JEOL JMS-DX300 mass spectrometer and a Shimadzu LKB 9000 GC-mass spectrometer at 70 eV. The HPLC was carried out with Hitachi gel #3011 with MeOH–hexane (9:1) as the solvent. The centrifugal chromatography was performed with a Hitachi CLC-5 instrument in a Fuji silica gel layer (KT-2151, 3 mm thickness) using benzene as an eluent. TLC analyses were carried out with Merck Kieselgel 60F-254 plate.

Reaction of 3-Bromo-2-methoxytropone (2) with *o*-Aminophenol (3). a) At 120 °C: A solution of 167 mg (0.78 mmol) of **2** and 127 mg (1.17 mmol) of **3** in 5 cm^3 of acetic acid was heated at 120 °C for 1 h and then evaporated in vacuo. The residue was preliminarily separated into four fractions by means of silica-gel column with benzene–MeOH (20:1) as the eluent. Each fraction was carefully separated by preparative HPLC with Hitachi gel #3019 using MeOH–hexane (9:1) or TLC with silica gel 60F-254 (0.25 mm, Merck) using benzene–MeOH (10:1) as the eluent, giving compounds **A**[4] (10 mg, 4% yield), **B**[4] (7 mg, 4% yield), **C** (see below, 3 mg, 1% yield), **D** (see below, 2 mg, 1% yield), **G**[4] (35 mg, 21% yield), **J**[4] (16 mg, 10% yield), and **L**[4] (82 mg, 28% yield), besides the recovered **2** (30 mg, 20%).

b) At 60 °C: A solution of 30 mg (0.14 mol) of **2** and 30 mg (0.28 mmol) of **3** in 3 cm^3 of methanol was heated at 60 °C for 5 h, followed by the same work-up procedures mentioned above, giving 2 mg (5%) of **G**, besides the recovered **2** (25 mg, 85%).

c) At 80 °C: Procedures similar to the those at 60 °C were employed. Thus, a solution of 20 mg (0.1 mol) of **2** and 20 mg (0.2 mmol) of **3** was heated in 2 cm^3 of 1-butanol at 80 °C for 3 h, giving 4 mg (20%) of **G** and a small amount of **J**, besides the recovered **2** (15 mg, 75%).

Reaction of 6-Bromocyclohepta[*b*][1,4]benzoxazine (19) and *o*-Aminophenol (3). A. Under Acidic Conditions: A solution of 50 mg (0.2 mmol) of **19** and 30 mg (0.3 mmol) of **3** in 2 cm^3 of acetic acid was heated at 120 °C for 1 h. The solvent was evaporated in vacuo and the residue was chromatographed in a column of silica gel with benzene,

giving 40 mg (55%) of compounds **L**, 15 mg (25%) of **D**, 4 mg (10%) of **B**, and a trace amount of **A**.

B. Under Basic Conditions: A solution of 20 mg (0.07 mmol) of **19**, 12 mg (0.11 mmol) of **3**, and 14 mg (0.11 mmol) of DABCO in 2 cm^3 of methanol was allowed to stand for 1 d at room temp. After cooling, the ppt was filtered off and recrystallized from methanol to give 14 mg (64%) of compound **X** (see below). The above filtrate was a mixture of compounds **A, B, C, D, H¹, H²** (see below), **4**[3] and **L** (by TLC, HPLC, and UV).

C. Under Neutral Conditions: a) Similar procedures for acidic conditions were followed. Thus, 30 mg (0.11 mmol) of **19** with 22 mg (0.22 mmol) of **3** in 2 cm^3 of methanol was heated at 50 °C for 3 h, giving 18 mg (50%) of compounds **D**, 10 mg (30%) of **C**, and 3 mg (10%) of **4**.

b) Similar procedures for basic conditions were followed. Thus, a soluion of 22 mg (0.08 mmol) of **19** and 13 mg (0.12 mmol) of **3** in 1 cm^3 of methanol was kept at 5 °C (refrigerator) for 3 d, giving 17 mg (70%) of **C**, 4 mg (15%) of **D**, and a small amount of **4**.

Compound C, Schiff Base of 1-Formylphenoxazine (18): Orange needles; mp 158 — 160 °C (from benzene); UV λ_{max} (MeOH) 227 (log ε 4.56), 279 (4.07), 327 (4.03), 344[sh] (3.98), 363[sh] (3.82), and 430 nm (3.88), (MeOH+6 M NaOH) 226 (log ε 4.63), 275 (4.17), 315 (3.84), and 407 nm (4.00); IR (KBr) 3470 (NH) and 1615 cm^{-1} (C=N); ^{1}H NMR (270 MHz) δ=9.78 (1H, br, OH), 8.50 (1H, s, HC=N), 7.20 (1H, td, J=8.0 and 1.7 Hz, H-4′), 7.07 (1H, dd, J=8.0 and 1.7 Hz, H-6′), 7.03 (1H, dd, J=8.0 and 1.7 Hz, H-3′), 6.95 (1H, td, J=8.0 and 1.7 Hz, H-5′), 6.88 (1H, dd, J=7.5 and 2.1 Hz, H-2), 6.72 (1H, td, J=7.5 and 2.0 Hz, H-8), 6.64 (4H, m, H-3,4,7,9), 6.40 (1H, dd, J=7.5 and 2.0 Hz, H-6), and 6.05 (1H, br, NH); ^{13}C NMR (67.8 MHz) δ (off resonance)=162.7 (d, HC=N), 150.1 (s), 144.1 (s), 143.8 (s), 137.4 (s), 134.5 (s) 130.0 (s), 128.2 (d), 127.9 (d), 123.9 (d), 122.4 (d), 120.9 (d), 119.5 (d), 117.6 (d), 117.2 (d), 117.1 (s), 115.6 (d), 115.2 (d), and 114.3 (d).

Found: m/z 302.1090. Calcd for $C_{19}H_{14}N_2O_2$: M, 302.1054.

Hydrolysis of C: To a solution of **C** (20 mg, 0.07 mmol) in methanol (2 cm^3) was added a trace of dil sulfuric acid. Then, the mixture, which instantly became deep purple red and then discolored after 10 — 20 seconds, was evaporated in vacuo. The residue was neutralized with aq $NaHCO_3$ and extrated with benzene.

The extracts were combined, dried (Na_2SO_4) and evaporated in vacuo. The residue was chromatogrphed on silica gel thin-layer plates with benzene as the eluent, followed by recrystallization from benzene, giving **B** and **3** in almost quantitative yields.

Compound D, 10-(*o*-Hydroxyanilino)cyclohepata[*b*][1,4]-benzoxazine (15): Reddish brown needles (from MeOH); mp 135 — 138 °C (decomp); UVλ_{max} (MeOH) 233 (log ε 4.30), 265 (4.34), 311[sh] (3.99), and 467 nm (4.08), (MeOH+6 M HCl) 220 (log ε 4.34), 265 (4.35), 273 (4.36), 303 (4.08), 451[sh] (3.91), and 499 nm (3.91); IR (KBr) 3350 (OH), 3250 (NH), and 1600 cm^{-1} (C=N); ^{1}H NMR (270 MHz) δ=9.86 (1H, br, OH), 8.58 (1H, br, NH), 7.24 (1H, dd, J=7.5 and 1.6 Hz, H-6′), 7.06 (1H, td, J=8 and 2 Hz, H-3′), 6.86 (1H, td, J=8 and 2 Hz, H-5′), 6.79 (3H, m, H-1,2,3), 6.53 (1H, m, J=8 and 2 Hz, H-4), 6.34 (2H, m, H-6,9), and 6.14 (2H, m, H-7,8).

Found: m/z 302.1080. Calcd for $C_{19}H_{14}N_2O_2$: M, 302.1054.

Conversion of D into A: a) A solution of 2 mg of **D** in 2 cm^3 of methanol was allowed to stand for 2 d at room temp. After removing the solvent in vacuo, the residue was recrystallized from hexane, giving **A** in an almost quantitative yield.

b) A solution of 1 mg of **D** in 2 cm^3 of methanol containing a drop of 6 M NaOH was allowed to stand for 3 h at room temp. After removal of the solvent in vacuo, the residue was chromatographed in a column of silica gel with benzene as the eluent, giving **A**.

Compound H², 4-Formylphenoxazine (24): Yellow needles (from MeOH); mp 186 — 187 °C (decomp); UV λ_{max} (MeOH) 228 (log ε 4.53), 236[sh] (4.44), 276 (3.90), 313 (3.81), and 416 nm (3.43), (MeOH+6 M HCl) 236 (log ε 4.57), and 318 nm (3.94); IR (KBr) 3260 (NH), 2840, 2780, and 1675 cm^{-1} (CHO); ^{1}H NMR (270 MHz, acetone-d_6) δ=10.36 (1H, s, CHO), 7.61 (1H, br, NH), 7.02 (1H, dd, J=8 and 2 Hz, H-3), 6.81 (1H, t, J=8 Hz, H-2), 6.76 (2H, m, H-7,9), 6.71 (1H, dd, J=8 and 2 Hz, H-1), 6.27 (1H, td, J=8 and 2 Hz, H-8), and 6.54 (1H, dd, J=8 and 2 Hz, H-6); ^{13}C NMR (67.8 MHz, acetone-d_6) δ (off resonance)=188.2 (d, CHO), 147.6 (s), 143.3 (s), 134.3 (s), 132.7 (s), 125.4 (d), 124.3 (d), 121.9 (d), 118.8 (d), 118.7 (d), 116.4 (d), and 114.5 (d).

Found: m/z 211.0658. Calcd for $C_{13}H_9NO_2$: M, 211.0633.

Compound H³, 4-Formylphenoxazine Hemiacetal (24a): To a solution of compound **X** (1 mg) in methanol (0.5 cm^3) was added a trace of dil sulfuric acid. After 10 min at room temp, the solution was found to be a mixture of **3** (RT, 6 min), **H²** (RT, 11 min), and **H³** (RT, 9.8 min) by means of reversed-phase HPLC and UV absorptions. The compound isolated from peak **H³** showed the same RT (11 min by repeated HPLC) and MS (M^+, 211) as those of **24**.

Compound X, Schiff Base of 4-Formylphenoxazine (25): Yellow needles; mp 210 — 211 °C decomp (from MeOH); UV λ_{max} (MeOH) 230 (log ε 4.73), 285 (4.14), 324 (4.11), 353[sh] (4.05), and 425 nm (3.44), (MeOH+6 M NaOH) 230 (log ε 4.76), 271 (4.23), 315[sh] (3.98), and 399 nm (3.88); IR (KBr) 3350 (NH) and 1618 cm^{-1} (C=N); ^{1}H NMR (270 MHz) δ=9.05 (1H, s, HC=N), 7.48 (1H, dd, J=8 and 2 Hz, H-3), 7.34 (1H, dd, J=8 and 2 Hz, H-6′), 7.21 (1H, td, J=8 and 2 Hz, H-4′), 7.01 (1H, dd, J=8 and 2 Hz, H-3′), 6.93 (1H, td, J=8 and 2 Hz, H-5′), 6.82 (1H, t, J=8 Hz, H-2), 6.74 — 6.82 (2H, m, H-7,9), 6.71 (1H, td, J=8 and 2 Hz, H-8), 6.48 (1H, dd, J=8 and 2 Hz, H-1), 6.43 (1H, dd, J=8 and 2 Hz, H-6), and 5.26 (1H, br, NH); (100 MHz, DMSO-d_6) δ=8.85, 8.75, and 8.27 (3H, s, NH, OH, and HC=N, respectively), 7.37 (1H, dd, J=8.0 and 2.0 Hz, H-3), 6.4 — 7.4 (10H, m, others).

Found: m/z 302.1041. Calcd for $C_{19}H_{14}N_2O_2$: M, 302.1054.

Hydrolysis of X: Similar procedures for compound **C** were followed. Thus, 50 mg (0.17 mmol) of compound **X** in 5 cm^3 of methanol gave **3** and 33 mg (94%) of **H²**.

Reaction of 19 with *p*-Anisidine (26). a) At Room Temperature: A solution of 50 mg (0.18 mmol) of **19** and 30 mg (0.28 mmol) of **26** in 2 cm^3 of methanol was stirred for 1 d at room temp. After removal of the solvent, the residue was chromatographed in a column of silica gel with benzene–methanol (50:1) as the eluent, giving 11 mg (20%) of **28** and 25 mg (65%) of **H²**, along with a small amount of ring-opened compound **4**.

b) At 50 °C: A solution of 42 mg (0.15 mmol) of **19** and 28 mg (0.23 mmol) of **26** in 2 cm^3 of methanol was heated at 50 °C for 3 h, followed by the same work-up procedures as above, giving 35 mg (57%) of **28**, 12 mg (38%) of **H²**, and a small amount of **4**.

c) **At 120 °C:** The procedures similar to those at 50 °C were employed. Thus, 30 mg (0.11 mmol) of **19** and 20 mg (0.18 mmol) of **26** were heated in 2 cm^3 of methanol at 120 °C for 1 h, giving 26 mg (75%) of **28**, 4 mg (15%) of **H²**, and a small amount of **4**.

6-(*p*-Methoxyanilino)cyclohepta[*b*][1,4]benzoxazine (28): Reddish brown needles (from methanol); mp >300 °C (decomp); UV λ_{max}(MeOH) 234, 268, 300, and 428 nm, (MeOH+6 M NaOH) 238, 304, 451, 480^{sh}, and 630 nm; ^{1}H NMR (270 MHz, CD_3OD) δ=7.23 (2H, m, H-2′,6′), 7.08 (2H, m, H-3′, 5′), 6.98—7.20 (3H, m, H-8,9,10), 6.85—6.95 (3H, m, H-1,2,3), 6.38 (1H, m, H-7), 6.61 (1H, m, H-4), and 3.85 (3H, s, OCH_3).

Found: *m/z* 316.1217. Calcd for $C_{20}H_{16}N_2O_2$: M, 316.1211.

We thank Professor Hiroshi Yamamoto (Okayama Univ.) for helpful discussions. We also thank Professor Yoichi Iitaka and Mrs. Hikaru Nakamura (Tokyo Univ.) for their kindly performing X-ray analyses for Compounds **10** and **24**.

References

1) Part 2: H. Wakabayashi, S. Ishikawa, H. Okai, and T. Nozoe, *Bull. Chem. Soc. Jpn.*, **58**, 2840 (1985).

2) A part of the results were presented: T. Nozoe, H. Okai, H. Wakabayashi, K. Shindo and S. Ishikawa, 41th National Meeting of the Chemical Society of Japan, Higashi Osaka, April 1980, Abstr., No. 2K33. and Tokyo, March 1981, Abstr., No. 1H39; 14th Japanese Symposium on the Chemistry of Nonbenzenoid Aromatic Compounds, Okayama, October 1981, Abstr., No. 1X11. For reviews, see T. Nozoe, *Pure Appl. Chem.*, **54**, 957 (1982); T. Nozoe, *Chemistry (Chinese Chem. Soc., Taiwan)*, **41**, A43 (1983).

3) T. Nozoe, T. Someya, and H. Okai, *Bull. Chem. Soc. Jpn.*, **52**, 1156 (1979).

4) T. Someya, H. Okai, H. Wakabayashi, and T. Nozoe, *Bull. Chem. Soc. Jpn.*, **56**, 2756 (1983).

5) T. Nozoe, H. Okai, H. Wakabayashi, and S. Ishikawa, *Chem. Lett.*, **1984**, 1145; Y. Okamoto, S. Honda, H. Yuki, H. Nakayama, Y. Iitaka, and T. Nozoe, *ibid.*, **1984**, 1149.

6) N. Harada, H. Uda, T. Nozoe, Y. Okaomoto, H. Wakabayashi, and S. Ishikawa, *J. Am. Chem. Soc.*, **109**, 1662 (1987).

7) P. V. Subbarao and C. S. Vaidyanathan, *Arch. Biochem. Biophys.*, **118**, 388 (1967).

8) Y. Sasakawa, M. Yasunami, and K. Takase, 37th National Meeting of the Chemical Society of Japan, Kanagawa, April 1978, Abstr., II, p. 805.

9) H. Wakabayashi, S. Ishikawa, H. Okai, and T. Nozoe, 47th National Meeting of the Chemical Society of Japan, Kyoto, April 1983, Abstr., II, 4F33; to be published.

10) H. Wakabayashi, S. Ishikawa, and T. Nozoe, 50th National Meeting of the Chemical Society of Japan, Tokyo, April 1985, Abstr., II, 1T17; to be published.

11) Recently, structure **10** for Comound **A** was confirmed by X-ray crystallographic analysis and the results will be reported elsewhere by Prof. Y. Iitaka and Mrs. H. Nakamura, Department of Pharmaceutical Sciences, Tokyo University.

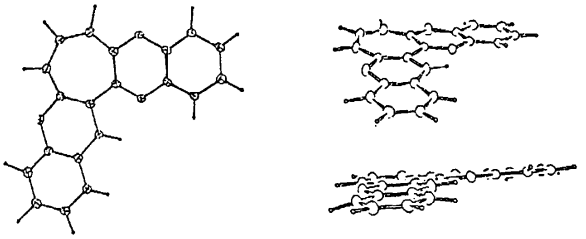

12) The X-ray crystallographic analysis of Compound **24** by Prof. Y. Iitaka and Mrs. H. Nakamura (to be published):

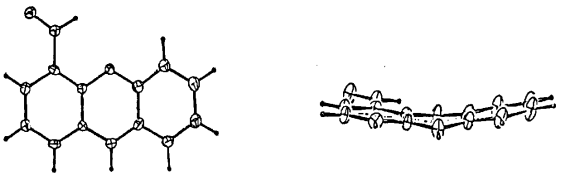

13) T. Nozoe, H. Okai, H. Wakabayashi, and S. Ishikawa, *Chem. Lett.*, **1988**, 1589.

14) T. Nozoe, H. Okai, H. Wakabayashi, K. Shindo, and S. Ishikawa, 15th Japanese Symposium on the Chemistry of Nonbenzenoid Aromatic Compounds, Kyoto, October 1982, Abstr., No. C1-17.

Stereoselective Synthesis of 2,4-Diamino Acids by Asymmetric Hydrogenation

Nam Gyu PARK, Sannamu LEE,* Hiroshi MAEDA,† Haruhiko AOYAGI, and Tetsuo KATO††
Laboratory of Biochemistry, Faculty of Science, Kyushu University 33, Higashi-ku, Fukuoka 812
(Received February 4, 1989)

A stereoselective synthesis of unusual basic amino acids, ornithine, 2,4-diaminopentanoic acid, and 2,4-diamino-6-methylheptanoic acid, was achieved by the hydrogenation of cyclic α,β-dehydro dipeptides obtained by the condensation of cyclo(-Gly-L(or D)-aminoacyl-) and protected linear or chiral amino aldehydes. The degree of chiral induction greatly depended on the bulkiness of the side chains of α,β-dehydro amino acids. The R_f values on paper chromatography of (2*S*,4*S* or 2*R*,4*S*)-diaminopentanoic acid prepared by the present method were different from the reported values of a compound which had been obtained from metabolic products of *Clostridium sticklandii* and estimated to be 2,4-diaminopentanoic acid.

In any study on the design, synthesis and structure-function of bioactive peptides, the use of unusual amino acids as starting materials is often important. We have established a synthetic method of optically active α-amino acids by asymmetric hydrogenation of cyclic α,β-dehydro dipeptides and successfully prepared lots of α-amino acids.[1-4] However, the method was applied only for the preparation of neutral amino acids. It seems interesting how the chiral induction in hydrogenation would be influenced by a functional and/or chiral side chain in cyclic α,β-dehydro dipeptides. We selected in the present study ornithine (**3**) with a functional side chain, and 2,4-diaminopentanoic acid (**1**) and 2,4-diamino-6-methylheptanoic acid (**2**) with a chiral side chain as target materials (Fig. 1).

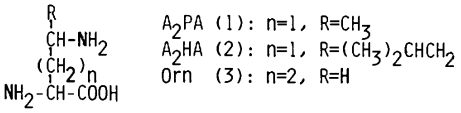

Fig. 1. Structure of synthetic amino acids.

Among compounds **1**—**3**, **1** was reported to be a metabolic intermediate in the an aerobic oxidation of ornithine in *Clostridium sticklandii*.[5] The structure was estimated merely from the behavior on paper chromatography and the metabolic pathway because of the scarce presence of the intermediate in the cells. Since the isolation and identification of the intermediate have not yet been carried out, its chemical and optical identification is attractive. Compound **2** was previously synthesized as a diastereoisomer by catalytic hydrogenation of ethyl 3-propyl-5-pyrazolinecarboxylate, but not obtained as an optically active one.[6] Hence, the stereoselective synthesis of the optically active diastereoisomer is also of interest.

Results and Discussion

The synthetic route for **1** and **2** is shown in Fig. 2. We previously reported that when L-amino acid[7] was used in cyclic α,β-dehydro dipeptide as a chiral source,

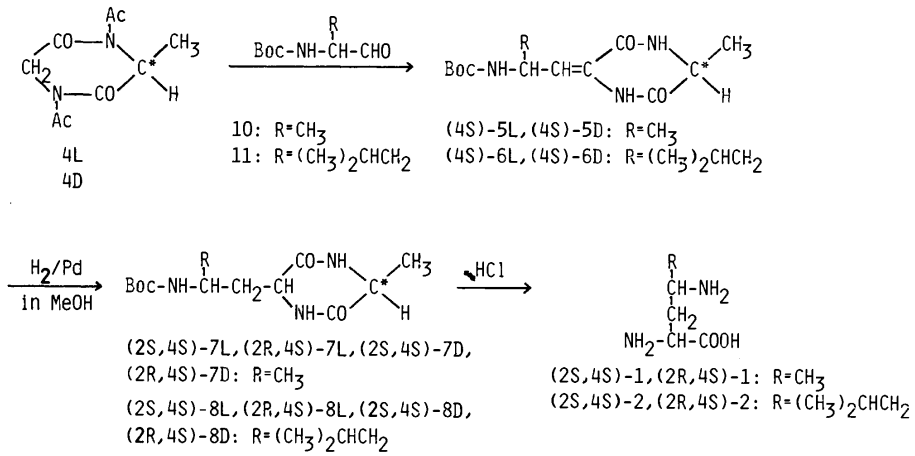

Fig. 2. Synthetic route for 2,4-diamino acids (**1** and **2**).

† Present address: Nippon Mining Co., Ltd., Toda 355.
†† Present address: Kumamoto Institute of Technology, Kumamoto 860.

asymmetric hydrogenation exclusively gave L-amino acid.[1] If the asymmetric hydrogenation of cyclic α,β-dehydro dipeptides (**5** and **6**) proceeds stereospecifically, it is able to synthesize stereoselectively two optical isomers of **1** and those of **2**, respectively, via the condensation of **4L** and **4D** with the protected (2*S*)-2-amino aldehyde (**10** or **11**) followed by hydrogenation. As an asymmetric source, we chose neutral L- or D-alanine because of the easy separation of alanine from basic amino acids, i.e., final products.

In the synthesis of **1**, the condensation of **4L** with Boc-(2*S*)-alaninal (**10**)[8] in the presence of *t*-BuOK[9] gave cyclic acetyl-α,β-dehydro dipeptide, which was then deacetylated by the action of 1-(2-aminoethyl)-piperazine to afford cyclic α,β-dehydro dipeptide, (4*S*)-**5L**. A mixture of (2*S*,4*S*)-**7L** and (2*R*,4*S*)-**7L** was obtained by hydrogenation of (4*S*)-**5L** in the presence of Pd-black. In order to determine the formation ratio of (2*S*,4*S*)-**1** and (2*R*,4*S*)-**1**, the hydrogenated mixture was subjected to acid hydrolysis and then amino acid analysis. The elution pattern of the hydrolysate is shown in Fig. 3. The stereochemistry in this amino acid was deduced as follows: the main product should be (2*S*,4*S*)-**1**, based on the previously proposed mechanism for the asymmetric hydrogenation of cyclic α,β-dehydro dipeptides.[1] The peak ratio of (2*S*,4*S*)-**1** and (2*R*,4*S*)-**1** in the hydrolysate was 3:2. The color yield of the purified optical isomers, (2*S*,4*S*)-**1** and (2*R*,4*S*)-**1**, for ninhydrin was determined to be ca.1:1. Thus, the chiral induction of (2*S*,4*S*)-**1** and (2*R*,4*S*)-**1** in hydrogenation was calculated to be 3:2, as shown in Table 1. After the isomers were separated with AG 50WX8 using a sodium citrate buffer (pH 5.28) as an eluent, the final products were purified by recrystallization. Their purity was confirmed by thin-layer chromatography and elemental analysis. The preparation of **1** from (4*S*)-**5D** was also carried out similarly (Fig. 2). The use of **4D** instead of **4L** gave highly stereoselectively (2*R*,4*S*)-**1** (Table 1). Compound **2** was obtained from **4L** or **4D** and Boc-(2*S*)-leucinal (**11**)[8] in the same manner as described above. The ^{1}H NMR spectra of (4*S*)-**6L** and (4*S*)-**6D** obtained (Fig. 4) showed that the signal peaks corresponding to each functional group were observed. It is suggested that the *Z*- or *E*-isomer was formed stereoselectively without racemization in the condensation reaction. To determine the geometric isomers of *Z*- or *E*-isomer, we measured the NOESY spectrum by 2D NMR spectroscopy. The correlation between the amide proton of piperazinedione (–C=C–NH–) and proton of asymmetric carbon (–N–CH–C=) in the NOESY spectrum indicates that these proton are closely located. Consequently, (4*S*)-**6L** and (4*S*)-**6D** are not *E*-isomer but *Z*-isomer. Compounds (4*S*)-**5L** and (4*S*)-**5D** also showed NMR spectra similar to those of (4*S*)-**6L** and (4*S*)-**6D**, respectively (data not shown). Compounds (4*S*)-**6L** and (4*S*)-**6D** were not obtained in good yields. The low yields can probably be attributable to slow reaction, because the TLC of the reaction mixture showed main spots of the product and the starting materials, including some minor spots. The condensation of **4L** with **11** gave selectively (2*S*,4*S*)-2,4-diamino-6-methylheptanoic acid (**2**). In the case of **4D**, the product was a mixture of (2*S*,4*S*)-**2** and (2*R*,4*S*)-**2**, although the formation of (2*R*,4*S*)-**2** was fairly preferential. In the case of **3**, Boc-3-aminopropionaldehyde was obtained from Boc-3-amino-1-propanol by oxidation with pyridium dichromate,[10] and diethylamine was used instead of 1-(2-aminoethyl)piperazine in the step of deacetylation. Compound **3** was obtained in good optical yield from cyclo(-ΔOrn(Boc)-L-Ala-) (**9**), which was derived from **4L** and Boc-3-aminopropionaldehyde.

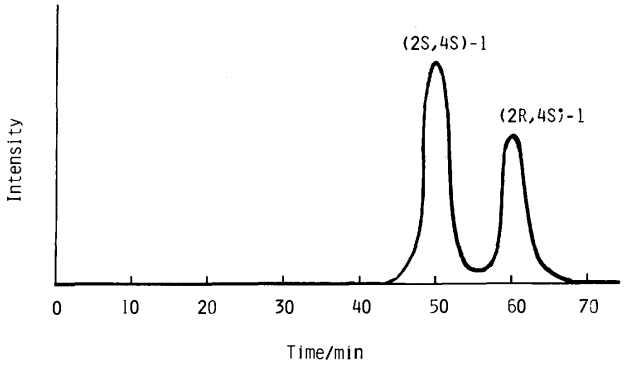

Fig. 3. Elution pattern of A_2PA.

We previously presented a presumptive mechanism on the asymmetric hydrogenation of cyclic α,β-dehydro dipeptide; the rigid planar structure of cyclic α,β-dehydro dipeptide, which is induced when the peptide is absorbed on the catalyst, has an important effect on asymmetric hydrogenation.[11] However, if there is a group which makes adsorption of the ring structure on the catalyst disadvantageous, the chiral induction in hydrogenation will decrease. The fact that L-ornithine (**3**) was obtained in good optical yield indicates that, when L-alanine was used as a chiral source, the

Table 1. Chiral Induction in Hydrogenation of Cyclic Dehydrodipeptides

Cyclic dehydrodipeptide	Amino acid	Chiral induction
(4*S*)-**5L**	A_2PA	3:2 (2*S*,4*S*:2*R*,4*S*)
(4*S*)-**5D**	A_2PA	1:5 (2*S*,4*S*:2*R*,4*S*)
(4*S*)-**6L**	A_2HA	95:5 (2*S*,4*S*:2*R*,4*S*)
(4*S*)-**6D**	A_2HA	2:3 (2*S*,4*S*:2*R*,4*S*)

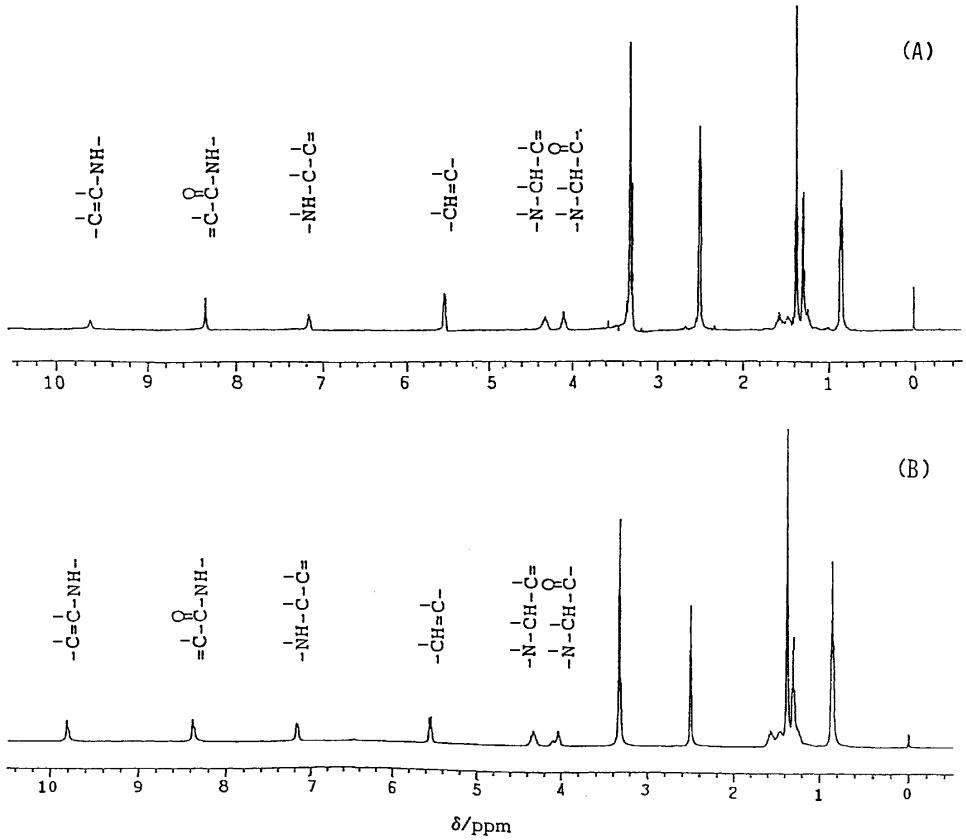

Fig. 4. ^{1}H NMR spectra of dehydro compounds (4*S*)-**6L** (A) and (4*S*)-**6D** (B).

Table 2. Comparison of the Chromatographic Property of Synthetic Compounds **1**, L-Ornithine, and Reported Compound[a)]

Solvent	(2*S*,4*S*)-**1**	(2*R*,4*S*)-**1**	L-Orn	Reported compound	L-Orn
MeOH:H_2O:pyridine (20:5:1)	0.08	0.12	0.13	0.46[b)]	0.16[b)]
1-Propanol:pyridine:H_2O (1:1:1)	0.10	0.22	0.23	0.42[b)]	0.22[b)]

a) Paper chromatography was carried out on Whatmann 3MM paper. b) Cited from Ref. 5.

adsorption of the urethane group on a catalytic surface had no effect on the optical yield. In the case of (4*S*)-**5L**, (4*S*)-**5D**, and (4*S*)-**6D**, the optical yields were relatively low. It is considered from the CPK model that free rotation between β- and γ-carbon atoms in the dehydro moiety is hindered because of collision of urethane NH and α-NH in the dehydroamino acid residue. Consequently, the side chain (CH_3 or $(CH_3)_2CHCH_2$) and the Boc group project to the upper and lower side, respectively, of the piperazinedione ring or vice versa. This indicates that the extent of chiral induction is not necessarily determined only by the methyl side chain in the Ala residue, i.e., chiral source. Interestingly, (4*S*)-**6L** could be highly selectively hydrogenated, although we can not now explain the reason.

The R_f values on paper chromatography of synthetic (2*S*,4*S*)-**1** and (2*S*,4*R*)-**1** were quite different from those of the reported compound which was estimated previously as 2,4-diaminopentanoic acid (see Table 2). Therefore, the structure of the metabolic intermediate should be reexamined. To date, the intermediates in the similar reactions in the lysine fermentation have been identified as 3,6-diaminohexanoic acid (β-lysine),[12] 3,5-diaminohexanoic acid,[13,14] and 5-amino-3-oxohexanoic acid.[15] Another amino acid has been tentatively identified as 2,5-diaminohexanoic acid.[16]

We tried to develop our asymmetric synthesis for the preparation of unusual basic amino acids. Further work along this line is in progress in order to obtain stereoselectively complicated amino acid, such as ones containing two or more asymmetric centers.

Experimental

Thin-layer chromatography was performed on silica gel G (Merck) with the following solvent systems: R_f^1 *n*-BuOH–AcOH–pyridine–H_2O (4:1:1:2, v/v); R_f^2, $CHCl_3$–MeOH (5:1, v/v); R_f^3, $CHCl_3$–EtOAc (1:1, v/v); R_f^4, *n*-BuOH–AcOH–H_2O (1:1:2, v/v). Optical rotations were measured on a Union high-sensitivity polarimeter PM-71. Amino acid analyses were performed with a Hitachi KLA-5 amino acid analyzer after the hydrolysis in 6 M HCl (1 M=1 mol dm^{-3}) in sealed tubes at 110 °C for 24 h. ^1H NMR spectra were determined at 25 °C with JEOL JNN-GX-400 spectrometer (400 MHz) using Me_4Si as the internal standard in DMSO-d_6.

Cyclo(-Ac-Gly-Ac-L-Ala-) (4L) and Cyclo(-Ac-Gly-Ac-D-Ala-) (4D). Compound **4L** and **4D** were synthesized by the same procedure as that described in the literature.[1]

Cyclo(-ΔA$_2$PA(Boc)-L-Ala-) ((4S)-5L). To a chilled solution of **4L** (2.2 g, 10.5 mmol) in DMF (15 ml) were added a solution of *t*-BuOK (1.2 g, 10.5 mmol) in *t*-BuOH (20 ml) and **10** (1.82 g, 10.5 mmol)[8] at 0 °C. The mixture was stirred at 0 °C for 2 h and at 25 °C for 3 h. After evaporation in vacuo, the residue was dissolved in EtOAc, washed with water, dried over Na_2SO_4 and evaporated. Oily cyclo(-ΔA$_2$PA-N-Ac-L-Ala-) was dissolved in DMF (5 ml), and to the solution was added 1-(2-aminoethyl)piperazine (2.6 ml) at 0 °C. The solution was stirred at 0 °C for 1 h and at 25 °C for 2 h and evaporated in vacuo. The residue was dissolved in EtOAc, washed with 10% citric acid and aq. NaCl, dried over Na_2SO_4 and evaporated. The residual oil was crystallized by the addition of MeOH–ether. Yield, 600 mg (28%); mp 215—220 °C; $[\alpha]_D^{20}$ +106° (*c* 1.0, MeOH); R_f^2 0.73. Found: C, 54.81; H, 7.34; N, 14.70%. Calcd for $C_{13}H_{21}O_4N_3$: C, 55.11; H, 7.47; N, 14.83%. Compound (4*S*)-**5D** was prepared similarly from **4D** and **10**. Yield, 59%; mp 210—214 °C; $[\alpha]_D^{20}$ +104° (*c* 1.0, MeOH); R_f^2 0.68. Found: C, 55.22; H, 7.47; N, 14.55%.

Cyclo(-ΔA$_2$HA(Boc)-L-Ala-) ((4S)-6L). Compound (4*S*)-**6L** was synthesized by the same procedure as that described above using **4L** (1.7 g, 7.9 mmol) and **11** (2.36 g, 10.5 mmol).[8] Yield, 475 mg (19%); mp 187—191 °C; $[\alpha]_D^{20}$ +106° (*c* 1.0, MeOH); R_f^3 0.34. Found: C, 58.66; H, 8.39; N, 12.65%. Calcd for $C_{16}H_{27}O_4N_3$: C, 59.06; H, 8.39; N, 12.91%. Compound (4*S*)-**6D** was prepared similarly from **4D** and **11**. Yield 19%; mp 179—185 °C; $[\alpha]_D^{20}$ +108° (*c* 1.0, MeOH); R_f^3 0.33. Found: C, 58.78; H, 8.39; N, 12.76%.

Cyclo(-A$_2$PA(Boc)-L-Ala-). Compound (4*S*)-**5L** (567 mg, 2 mmol) was dissolved in MeOH (20 ml) and hydrogenated at 1 atm pressure of H_2 in the presence of Pd black (20 mg) for 5 h at 25 °C. The filtrate was evaporated and the residue was crystallized by the addition of ether–petroleum ether. The hydrogenated compound was observed to show two spots by R_f^3, owing to the presence of diastereomers ((2*S*, 4*S*)-**7L** and (2*R*,4*S*)-**7L**). Yield of the diastereomers, 525 mg (92%), R_f^3 0.27 and 0.15. Cyclo(-A$_2$PA(Boc)-D-Ala-) was prepared similarly. Yield of the diastereomers ((2*S*,4*S*)-**7D** plus (2*R*,4*S*)-**7D**), 90%; R_f^3 0.25 and 0.15.

Cyclo(-A$_2$HA(Boc)-L-Ala-). This compound was synthesized by the same procedure as described above using (4*S*)-**6L** (423 mg, 1.3 mmol). The yield of the diastereomers ((2*S*, 4*S*)-**8L** plus (2*R*,4*S*)-**8L**), 362 mg (85%); R_f^3 0.38 and 0.36. Cyclo(-A$_2$HA(Boc)-D-Ala-) was prepared similarly. The yield of the diastereomers ((2*S*,4*S*)-**8D** plus (2*R*,4*S*)-**8D**) was 93%; R_f^3 0.37 and 0.34.

2,4-Diaminopentanoic Acid ((2*S*,4*S*)-1 and (2*R*,4*S*)-1). Cyclo(-A$_2$PA(Boc)-L-Ala-) (428 mg, 1.5 mmol) was hydrolyzed with 6 M HCl at 110 °C for 24 h. The solution was evaporated several times by the addition of water. The residue dissolved in water was put on a column of Dowex 50WX8 (200—400 mesh, H^+ form). The column was washed with water, 1 M pyridine, and eluted with 2 M aq. ammonia. The eluate was evaporated several times by the addition of water. The enantiomeric ratio of (2*S*,4*S*)-**1** and (2*R*,4*S*)-**1** was determined using a portion of the residue as 3:2 with an amino acid analyzer. The yield of (2*S*,4*S*)-**1** plus (2*R*,4*S*)-**1** was 172 mg (87%); R_f^1 0.33 and 0.25. The ratio of (2*S*,4*S*)-**1** and (2*R*,4*S*)-**1** from cyclo(-A$_2$PA(Boc)-D-Ala-) was 1:5. The yield of (2*S*,4*S*)-**1** plus (2*R*,4*S*)-**1** in a 1.5 mmol scale was 163 mg (82%); R_f^1 0.33 and 0.25. The residue was solidified from H_2O–acetone as its monohydrochloride by the addition of an equivalent hydrochloric acid.

2,4-Diamino-6-methylheptanoic Acid ((2*S*,4*S*)-2 and (2*R*, 4*S*)-2). Hydrolysis of cyclo(-A$_2$HA(Boc)-L-Ala-) and cyclo(-A$_2$HA(Boc)-D-Ala-) (327 mg, 1 mmol each) was performed by the same procedure as that described above. The ratios of (2*S*,4*S*)-**2** and (2*R*,4*S*)-**2** were determined as 95:5 from cyclo(-A$_2$HA(Boc)-L-Ala-) and 2:3 from cyclo(-A$_2$HA(Boc)-D-Ala-), respectively. Yields of (2*S*,4*S*)-**2** plus (2*R*,4*S*)-**2** from cyclo(-A$_2$HA(Boc)-L-Ala-) and from cyclo(-A$_2$HA(Boc)-D-Ala-) were 194 mg (92%) and 169 mg (80%), respectively; R_f^1 0.64 and 0.25.

Separation of (2*S*,4*S*)-1 and (2*R*,4*S*)-1. Diastereomeric 2,4-diaminopentanoic acid (**1**) from cyclo(-A$_2$PA(Boc)-L-Ala-) (68 mg 0.4 mmol) was separated into its diastereoisomers by chromatography using a colum (1.8×150 cm) of AG 50WX8 (200—400 mesh, H^+ from). Diastereomers were eluted with a 0.35 M sodium citrate buffer of pH 5.28. The component of the fraction from 1850 to 2000 ml was confirmed to be (2*S*,4*S*)-**1** and that of the fraction from 2300 to 2450 ml to be (2*R*,4*S*)-**1**, using an amino acid analyzer. Each of the fractions containing (2*S*,4*S*)-**1** and (2*R*,4*S*)-**1** was concentrated. The concentrated solution was desalted using Dowex 50WX8 (200—400 mesh, H^+ form). After washing with water, the basic amino acid was eluted with 2 M aq. ammonia. The eluate was evaporated several times in order to remove excess ammonia by the addition of water. The residue was recrystallized from H_2O–acetone as its monohydrochloride. Recoveries of (2*S*,4*S*)-**1** and (2*R*,4*S*)-**1** were 32 mg (77%) and 16 mg (59%), respectively. (2*S*,4*S*)-**1**; mp 185—191 °C (decomp); $[\alpha]_D^{20}$ +7.2° (*c* 0.3, H_2O); R_f^1 0.33. Found: C, 35.90; H, 7.65; N, 16.21%. Calcd for $C_6H_{12}O_2N_2 \cdot HCl$: C, 35.61; H, 7.77; N, 16.61%. (2*R*,4*S*)-**1**; mp 198—202 °C (decomp); $[\alpha]_D^{20}$ −5.0° (*c* 1.0, H_2O); R_f^1 0.25. Found: C, 35.77; H, 7.78; N, 16.03%. Diastereomeric **1** (68 mg, 0.4 mmol) from cyclo(-A$_2$PA(Boc)-D-Ala-) was also treated similarly. Recoveries of (2*S*,4*S*)-**1** and (2*R*,4*S*)-**1**, 6 mg (45%) and 40 mg (72%).

Separation of (2*S*,4*S*)-2 and (2*R*,4*S*)-2. Diastereoisomeric 2,4-diamino-6-methylheptanoic acid from cyclo(-A$_2$HA(Boc)-L-Ala-) (105 mg, 0.5 mmol) was separated into its diastereoisomers by chromatography using a column (1×30 cm) of AG 50WX8 (200—400 mesh, H^+ form). Diastereoisomers were eluted with a 0.35 M sodium citrate buffer of pH 5.28. The component of the fraction from 350 to 500 ml was

confirmed to be (2*S*,4*S*)-**2**, and that of the fraction from 650 ml to 800 ml to be (2*R*,4*S*)-**2**, and worked up as described above. Recoveries of (2*S*,4*S*)-**2** and (2*R*,4*S*)-**2** were 82 mg (82%) and 4 mg (74%), respectively. (2*S*,4*S*)-**2**; mp 235—240 °C (decomp); $[\alpha]_D^{20}$ +7.6° (*c* 0.5, H_2O); R_f^1 0.63. Found: C, 45.28; H, 9.02; N, 13.30%. Calcd for $C_8H_{18}O_2N_2 \cdot HCl$: C, 45.60; H, 9.09; N, 13.30%. (2*R*,4*S*)-**2**; mp 245—248 °C (decomp); $[\alpha]_D^{20}$ −5.3° (*c* 0.5, H_2O); R_f^1 0.55. Found: C, 45.35; H, 9.25; N, 13.15%. Diastereomeric **2** (105 mg) from cyclo(-A_2HA(Boc)-D-Ala-) was also treated similarly. Recoveries of (2*S*,4*S*)-**2** and (2*R*,4*S*)-**2** were 32 mg (76%) and 53 mg (83%), respectively.

Cyclo(-ΔOrn(Boc)-L-Ala-) (9). To a solution of Boc-$NH(CH_2)_3OH$ (9.58 g, 54.7 mmol) in CH_2Cl_2 (200 ml) was added pyridium dichromate (43.76 g, 109 mmol). The mixture was stirred at room temperature for 24 h. After evaporation in vacuo, the residue dissolved in EtOAc was put on a column of silica gel and the portion containing aldehyde was collected. After evaporation in vacuo, crude aldehyde (6.31 g, 12.2 mmol) was obtained. To a solution of crude aldehyde in DMF (40 ml) were added a solution of *t*-BuOK (1.64 g, 12.2 mmol) in *t*-BuOH (30 ml) and **4L** (2.63 g, 12.2 mmol) at 0 °C. The mixture was stirred at 0 °C for 2 h, at 25 °C for 24 h and evaporated in vacuo. The residue was dissolved in EtOAc, washed with water, dried over Na_2SO_4 and evaporated. The residue was dissolved in DMF (6 ml) and was added to $NH_2NH_2 \cdot H_2O$ (0.97 ml, 12.2 mmol). The mixture was stirred at 25 °C for 2 h and evaporated. The residue was crystallized by the addition of ether. Yield, 1.85 g (54%); mp 233—235 °C; $[\alpha]_D^{20}$ −12.4° (*c* 1.0, DMF); R_f^2 0.69. Found: C, 55.03; H, 7.56; N, 14.78%. Calcd for $C_{13}H_{21}O_4N_3$: C, 55.11; H, 7.47; N, 14.83%.

Cyclo(-Orn(Boc)-L-Ala-). This compound was synthesized from **9** (220 mg, 0.78 mmol) by the same procedure as described for the preparation of cyclo(-A_2PA(Boc)-L-Ala-). The yield was 208 mg (94%).

L-Ornithine (3). The hydrolysis of cyclo(-Orn(Boc)-L-Ala-) (460 mg, 1.6 mmol) was performed by the same procedure described for the preparation of **1**. This compound was confirmed to be L-Orn, as compared with authentic L-Orn by thin-layer chromatography and polarimetry. The yield was 130 mg (62%); R_f^1 0.03, R_f^4 0.54; $[\alpha]_D^{20}$ +17.1° (*c* 1.0, H_2O) (lit,[17] $[\alpha]_D^{20}$ +16.8° (*c* 1, H_2O)).

References

1) S. Lee, T. Kanmera, H. Aoyagi, and N. Izumiya, *Int. J. Peptide Protein Res.*, **13**, 207 (1979).

2) T. Kanmera, S. Lee, H. Aoyagi, and N. Izumiya, *Int. J. Peptide Protein Res.*, **16**, 280 (1980).

3) Y. Hashimoto, H. Aoyagi, M. Waki, T. Kato, and N. Izumiya, *Int. J. Peptide Protein Res.*, **21**, 11 (1983).

4) H. Aoyagi, F. Horike, A. Nakagawa, S. Yokote, N. Park, Y. Hashimoto, T. Kato, and N. Izumiya, *Bull. Chem. Soc. Jpn.*, **59**, 323 (1986).

5) J. K. Dyer and R. N. Costilow, *J. Bacteriol.*, **101**, 77 (1970).

6) H. E. Carter, F. R. Van Abeele, and J. W. Rothrock, *J. Biol. Chem.*, **178**, 325 (1949).

7) The symbols of L and D have been used for amino acids of chiral source because of simple and familiar expression.

8) H. Tobe, H. Morishima, H. Naganawa, T. Takita, T. Aoyagi, and H. Umezawa, *Agric. Biol. Chem.*, **43**, 591 (1979).

9) The abbreviations recommended by the IUPAC-IUB commission of Biochemical Nomenclature (*J. Biol. Chem.*, **247**, 977 (1972)) have been used. Additional abbreviations: DMF, *N*,*N*-dimethylformamide; Δ, α,β-dehydro; A_2PA, 2,4-diaminopentanoic acid; A_2HA, 2,4-diamino-6-methylheptanoic acid; *t*-BuOK, potassium *t*-butoxide.

10) C. F. Stanfield, J. E. Parker, and P. Kanellis, *J. Org. Chem.*, **46**, 4797 (1981).

11) N. Izumiya, S. Lee, T. Kanmera, and H. Aoyagi, *J. Am. Chem. Soc.*, **99**, 8346 (1977).

12) R. N. Costilow, O. M. Rochovansky, and H. A. Barker, *J. Biol. Chem.*, **241**, 1573 (1966).

13) E. E. Dekker and H. A. Barker, *J. Biol. Chem.*, **243**, 3232 (1968).

14) L. Tsai and T. C. Stadtman, *Arch. Biochem. Biophys.*, **125**, 210 (1968).

15) E. A. Rimerman and H. A. Barker, *J. Biol. Chem.*, **243**, 6151 (1968).

16) T. C. Stadtman and L. Tsai, *Biochem. Biophys. Res. Commun.*, **28**, 920 (1967).

17) P. Karrer, K. Escher, and R. Widmer, *Helv. Chim. Acta*, **9**, 301 (1926).

 © 1989 The Chemical Society of Japan Bull. Chem. Soc. Jpn., 62, 2320—2327 (1989) [Vol. 62, No. 7

Synthesis and Structural Analysis of 4-Deoxy-4-(hydroxyphosphinyl and phenylphosphinyl)-D-ribofuranoses

Tadashi HANAYA and Hiroshi YAMAMOTO*
Department of Chemistry, Faculty of Science, Okayama University,
Tsushima, Okayama 700
(Received February 13, 1989)

Methyl 2,3-*O*-isopropylidene-β-D-ribopyranoside gave efficiently (in 4 steps) methyl 4-deoxy-4-[dimethoxyphosphinyl and (methoxy)phenylphosphinyl]-2,3-*O*-isopropylidene-β-D-ribopyranosides (ca. 30% overall yield). These were led (in 2—3 steps) to the title compounds and then converted into 1,2,3,5-tetra-*O*-acetyl-4-deoxy-4-(methoxyphosphinyl and phenylphosphinyl)-D-ribofuranoses, whose structures and $^3T_2$ (and $^2T_3$) conformations were established by spectroscopy.

Various sugar analogues possessing a phosphorus atom in place of oxygen in the hemiacetal ring have been prepared in recent years;[1-6] e.g., 5-deoxy-5-phosphinyl-D-glucopyranoses (**1**).[4,7] These compounds are of interest in view of their physicochemical properties as well as potential biological activity.[1] As for analogues of D-ribose type, 4,5-dideoxy-4-(phenylphosphinyl)- (**2**)[8] and 4-deoxy-4-(ethylphosphinyl)-D-ribofuranoses (**3**)[3] have been synthesized in lengthy steps as a mixture with their L-lyxofuranose analogues (particularly in the case of **2**). We wish to report herein our detailed studies on synthesis and structural analysis of D-ribofuranose analogues having a hydroxyphosphinyl group in the ring,[9] as well as of those having PO(Ph) as a representative arylphosphinyl group in the ring. Although PO(OH)-in-ring sugar analogues were usually found more difficult to prepare than those having an alkyl- or arylphosphinyl group in the ring,[1,3,10] both 4-deoxy-4-(hydroxyphosphinyl and phenylphosphinyl)-D-ribofuranoses have become available in almost comparably good yield. The present synthesis also clarifies the ambiguity that existed in the previous synthetic schemes concerning the epimerization caused by hydride reduction of some intermediates.[4,7]

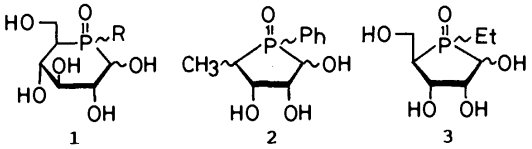

Results and Discussion

For synthesis of the D-ribofuranose analogues **3**,[3] methyl 2,3-*O*-isopropylidene-α-L-lyxopyranoside (**5**, prepared,[3,11] with some difficulty, from D-galacturonic acid **4** in 4 steps) was used as the precursor of the preparation of the starting material, (methyl 2,3-*O*-isopropylidene-β-D-*erythro*-pentopyranosid)-4-ulose (**6**)[3] (Scheme 1). However, we have now found it more convenient to utilize instead methyl 2,3-*O*-isopropylidene-β-D-ribopyranoside (**7**) for preparation of **6**, because **7** is readily available in quantities, though along with the chromatographically separable 3,4-*O*-isopropylidene isomer, from D-ribose in 2 steps.[12] Oxidation of **7** with pyridinium chlorochromate (PCC) in dichloromethane in the presence of Molecular Sieves (3A) now furnished **6** more effectively than the previous oxidation procedure for **5** (see Scheme 1).

Compound **6** was then converted into the tosylhydrazones **8a,b**[3] (as a 4:1 mixture of *Z* and *E* isomers) in 95% yield. This in turn was treated with an excess of dimethyl phosphonate in the presence of trifluoromethanesulfonic acid at 25 °C for 5 h, giving the (4*S*)-phosphonate **9** (56% isolated yield) and the (4*R*)-epimer **10** (10%), together with minor proportions of by-products **11** (10%), **12** (4%), and **13** (1.5%). These compounds were chromatographically separable, and their structural and conformational assignments (see Scheme 2) were made on the basis of spectral data (in particular by ^{1}H NMR, see the complete assignments given in the Experimental section). For distinction between the two major products **9** and **10**, the following characteristic δ, ^3J, and ^4J values of their ^{1}H NMR data were taken into consideration: δ 4.85 (H-1), $J_{1,2}$=4.7 Hz, and $J_{2,P}$=1.2 Hz for **9** (predominantly in $^1C_4$ form) and δ 4.17 (H-1), $J_{1,2}$=7.2 Hz, and $J_{3,5e}$=1.5 Hz for **10** ($^4C_1$). Among the minor products, **11** was readily protected again with 2,2-dimethoxypropane to

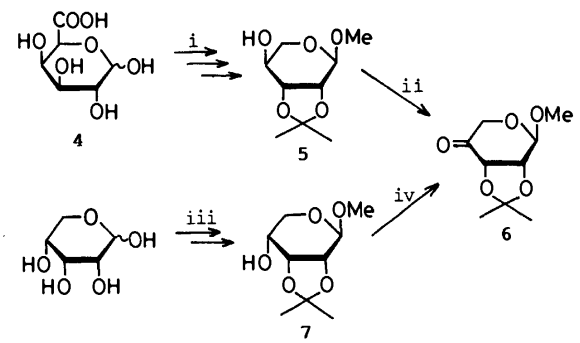

Scheme 1. Preparation of **6**. i, Refs. 3 and 11, 38%. ii, DMSO-$(COCl)_2$-TEA, 74% (Ref. 3). iii, Ref. 12, 15%. iv, PCC/CH_2Cl_2, 94%.

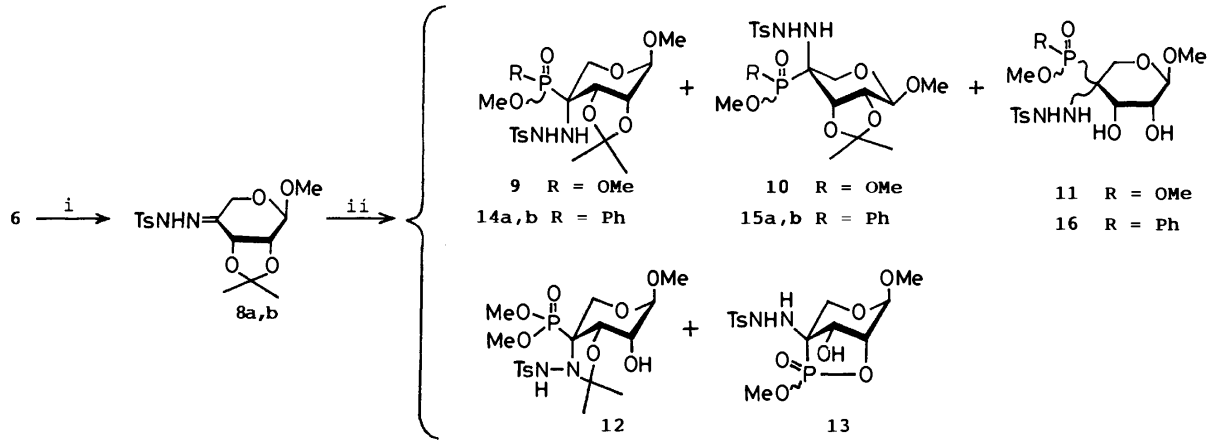

Scheme 2. Preparation and Conformations of **9**—**16**. i, $TsNHNH_2$, 95%. ii, $HP(O)(OMe)_2$ or $PhP(O)H(OMe)/CF_3SO_3H$.

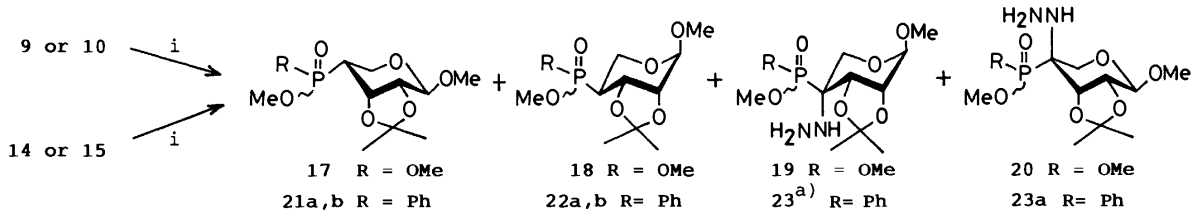

Scheme 3. Preparation of **17**—**23**. i, $NaBH_4$/THF. a) A 7:1 mixture of (4*S*)- and (4*R*)-epimers.

reproduce the above 2,3-*O*-isopropylidene compounds **9** and **10**.

Similarly, the addition of methyl phenylphosphinate to **8a,b** took place smoothly, affording (4*S*)-phosphinates **14a,b** (60% yield) and (4*R*)-epimers **15a,b** (6%), together with the deprotected products **16** (9%), each being a mixture of inseparable, two diastereomers due to asymmetry of the phosphorus atom. Their structures and the preferred conformations shown in Scheme 2 were established as described above (for **9**—**11**); note that no minor products corresponding to **12** and **13** were obtained in this case. This is the first time that both epimers of the phosphonate or phosphinate addition products have been isolated and characterized in this type of synthetic scheme for the sugar ring-C–P bond formation.[1]

Reductive removal of the tosylhydrazino group from these addition products were then studied in detail. Thus, upon treatment of the major (4*S*)-epimer **9** with sodium borohydride in THF at 25 °C for 12 h, it was found that methyl 4-deoxyl-4-(dimethoxyphosphinyl)-2,3-*O*-isopropylidene-β-D-ribopyranoside (**17**) and α-L-lyxopyranoside (**18**) were produced in a ratio of 85:15, respectively (Scheme 3). When the minor (4*R*)-epimer **10** was subjected to the same reduction, **17** and **18** were obtained notably in almost the same ratio as above. The structural assignments of these C-4 epimers were based on their spectral data (see the Experimental section); the following characteristic ^1H NMR data in particular served for clear distinction between them, δ 4.37 (H-1), $J_{3,4}$=3.0 Hz, and $J_{3,5e}$=0.8 Hz for **17** ($^4C_1$) vs. δ 4.79 (H-1), $J_{1,5e}$=2.0 Hz, $J_{2,P}$=1.6 Hz, and $J_{3,4}$=8.4 Hz for **18** ($^1C_4$). Besides **17** and **18**, a minor proportion of detosylated hydrazino compounds **19** (12%) and **20** (7%) were produced from **9** and **10**, respectively. By the analysis of the NMR data, all of these compounds (**17**—**20**) are most likely to have conformations (in $CDCl_3$) in which the phosphonate group is predominantly linked equatorially (see Scheme 3).

Similar results were obtained for the reductive cleavage of 4-deoxy-4-[(methoxy)phenylphosphinyl] compounds **14** and **15**, thus either of these compounds providing the D-ribopyranosides **21a,b** and L-lyxopyranosides **22a,b** in a ratio of 88:12, besides a minor amount (7% yield) of hydrazino compounds **23** consisting of a ca. 1:7 mixture of (4*R*)- and (4*S*)-epimers (Scheme 3). Furthermore, the borohydride reduction of a pure epimer **15a**, which was the only crystalline compound among the four diastereomers **14a,b** and **15a,b**, was found to give the same ratio (88:12) of two pure diastereomers **21a** and **22a**, together with a minor proportion of a pure (4*R*)-4-hydrazino-epimer **23a**; note that no other isomers **21b** and **22b** were produced from **15a**. These results therefore indicated that an epimerization took place at C-4 (but not at the P atom) during the borohydride

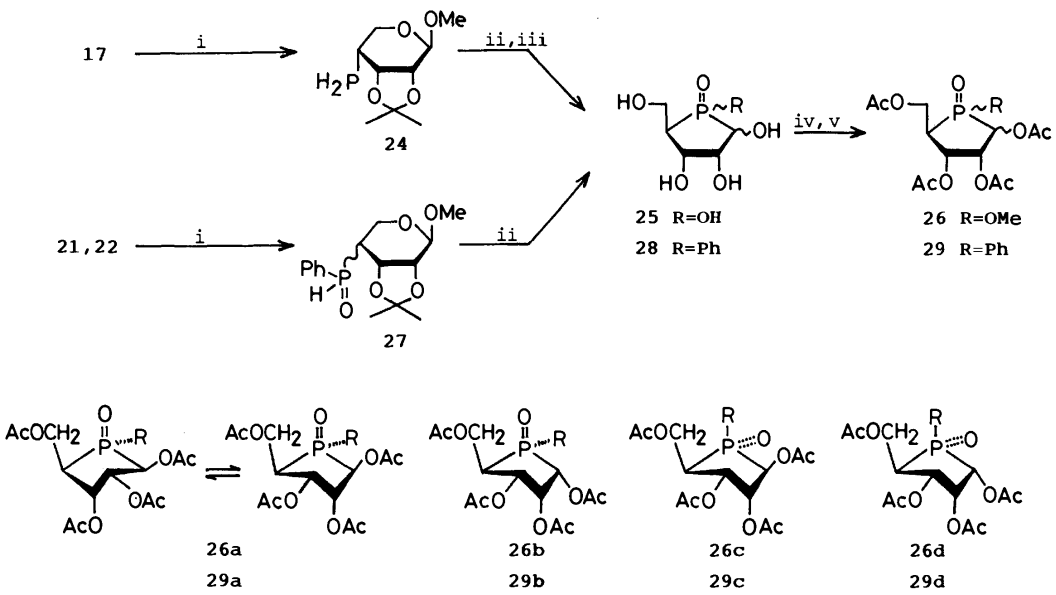

Scheme 4. Synthesis and Conformations of **26** and **29**. i, SDMA/benzene. ii, 0.5 M HCl-*i*PrOH. iii, aq H_2O_2. iv, CH_2N_2/MeOH–DMSO. v, Ac_2O–Pyridine.

reduction of all of these hydrazino compounds **9**, **10**, **14**, and **15**, resulting in the formation of the major products **17** and **21a,b** presumably through a thermodynamically controlled process.

The D-ribose type precursor **17** was then reduced with an excess (3 equiv) of sodium dihydrobis(2-methoxyethoxy)aluminate (SDMA)[13] in benzene at 5 °C for 1 h, giving solely methyl 4-deoxy-2,3-*O*-isopropylidene-4-phosphino-β-D-ribopyranoside **24** (Scheme 4); it should be noticed that no epimerization occurred at C-4 of **17** with SDMA (see below), in contrast to the equilibration (at C-5) observed in the case of 5-deoxy-5-[ethyl(methoxy)phosphinyl]-α-D-*xylo*-hexofuranoses to give predominantly 5-deoxy-5-(ethylphosphinyl)-L-idopyranoses.[5c]

The extremely air-sensitive compound **24** was promptly hydrolyzed under argon with mineral acid at 90 °C for 1 h to effect deprotection and the subsequent ring transposition. Oxidation of the resulting air-sensitive[10] phosphinediyl-in-ring compound with hydrogen peroxide at 25 °C for 1 d afforded 4-deoxy-4-(hydroxyphosphinyl)-D-ribofuranoses (**25**). For isolation and characterization, **25** were converted into its 4-(methoxyphosphinyl) tetraacetates **26** by the usual method (in 17% overall yield from **17**) (see Scheme 4). Rechromatography of **26** in a column of silica gel with 19:1 ethyl acetate–ethanol as the eluant afforded pure 1,2,3,5-tetra-*O*-acetyl-4-deoxy-4-[(*R*)-methoxyphosphinyl]-β-D-ribofuranose (**26a**, 6.3% yield from **17**), its α-anomer **26b** (3.3% yield), and the 4-[(*S*)-*P*]-β-isomer **26c** (2.8%), and its α-anomer **26d** (1.7%). Structures of **26a—d** were established by the analysis of their spectral data (Experimental section) and the approximate conformations of these isomers shown in Scheme 4 were derived from the analysis of 500 MHz ^{1}H NMR spectra (see below). The fact that the products **26a—d** were all D-ribofuranose configuration proved that no epimerization actually took place at C-4 of **26** during the SDMA reduction to yield **24**.

The conversion of 4-[(methoxy)phenylphosphinyl] compounds **21** and **22** into the corresponding PO(Ph)-in-ring D-ribofuranose analogues **28** was conducted by the same procedures described above. Namely, the SDMA reduction of **21** (or **22**) gave the 4-(phenylphosphinyl)-β-D-*erythro*-pentopyranoside **27**, which was then treated with dilute acid to provide predominantly 4-deoxy-4-(phenylphosphinyl)-D-ribofuranoses (**28**). Characterization of **28** was made as the 4-deoxy-4-(phenylphosphinyl) tetraacetates **29a—d** (see Scheme 4) as described above for **26a—d**.

^{1}H NMR Spectral Analysis of Tetra-*O*-acetyl-4-deoxy-4-(methoxy- and phenylphosphinyl)-D-ribofuranoses (26a—d and 29a—d). For the structural assignments of these new products, the chemical shift of each proton signal and the dependence of $^2J_{H,P}$, $^3J_{H,P}$, $^3J_{H,H}$, and $^4J_{H,H}$ values on their dihedral angles were carefully taken into consideration; the precise parameters obtained at 500 MHz for these compounds are summarized in Table 1. Some characteristic features of **26** and **29** are discussed here in detail, although in many cases they closely resemble those of the previously obtained **2** and **3**.

(1) The orientation of the ring P=O group can be established by the δ values of H-4 in combination with

Table 1. ^{1}H NMR (500 MHz) Parameters for **26** and **29** in $CDCl_3$

Compd	Chemical shift (δ)										
	H-1	H-2	H-3	H-4	H-5	H′-5	Ac-1,2,3,5[a]	POMe	Ph(o)	Ph(m)	Ph(p)
26a	4.94	5.58	5.42	2.66	4.43	4.28	2.19, 2.10, 2.10, 2.09	3.92			
26b	5.20	5.72	5.24	2.76	4.36	4.36	2.14, 2.09, 2.09, 2.06	3.90			
26c	5.03	5.43	5.27	2.84	4.33	4.22	2.15, 2.13, 2.11, 2.08	3.80			
26d	4.81	5.75	5.07	2.96	4.37	4.23	2.19, 2.16, 2.07, 2.06	3.89			
29a	5.09	5.75	5.64	3.02	4.52	4.44	2.20, 2.12, 2.10, 1.90		7.87	7.56	7.62
29b	5.48	5.94	5.56	3.10	4.51	4.44	2.21, 2.10, 1.78, 1.77		7.89	7.52	7.69
29c	5.32	5.64	5.49	3.23	4.18	4.03	2.21, 2.13, 1.85, 1.77		7.76	7.55	7.62
29d	5.28	5.95	5.20	3.32	4.14	3.86	2.26, 2.11, 2.09, 1.83		7.77	7.56	7.62

	Coupling constant (Hz)												
	$J_{1,2}$	$J_{1,4}$	$J_{1,P}$	$J_{2,3}$	$J_{2,P}$	$J_{3,4}$	$J_{3,P}$	$J_{4,5}$	$J_{4,5'}$	$J_{4,P}$	$J_{5,5'}$	$J_{5,P}$	$J_{5',P}$	J_{POMe}
26a	6.4	0.5	6.6	3.9	11.1	5.7	18.0	6.7	7.2	16.7	11.8	12.8	13.2	11.5
26b	4.7	0	7.7	3.3	31.0	11.1	2.5	6.8	6.8	17.7	—	15.8	15.8	11.2
26c	3.8	0.5	5.5	3.7	21.3	8.3	8.7	7.0	8.0	18.8	11.3	10.1	9.8	10.7
26d	4.9	0	6.4	3.2	32.5	11.2	0.8	6.7	7.9	19.0	11.3	17.5	10.1	11.2
29a	4.6	0.5	2.2	3.8	14.8	8.2	9.7	8.0	7.0	7.8	11.5	9.4	15.0	b)
29b	5.1	0	11.7	3.3	27.5	11.6	1.7	6.0	8.7	8.4	11.4	18.7	10.0	
29c	3.2	0.8	7.8	3.9	16.9	10.2	5.1	6.8	8.3	22.2	11.6	17.5	10.7	
29d	4.7	0	1.4	3.2	27.4	11.6	0.8	6.1	8.3	23.0	11.6	17.8	12.2	

a) The assignments of acetoxyl groups may have to be interchanged. b) J Values for P-Ph: $J_{P,o}$=12.5, $J_{P,m}$=3.5, $J_{P,p}$=1.5, $J_{o,p}$=7.8, $J_{m,p}$=7.5, and $J_{o,p}$=1.5 Hz. Compounds **29b—d** show similar J values.

the $J_{4,P}$ values. In the present study, a slightly upfield shift of these signals with a smaller $J_{4,P}$ value† is observed for **26a,b** and **29a,b**, thus showing an almost trans relationship between H-4 and the ring P=O for these compounds. The cis or gauche relationship for **26c,d** and **29c,d** was confirmed by the large $J_{4,P}$ values.† The anomeric orientation of C-1 is similarly derived from the magnitudes of δ values of H-1 and the $J_{1,P}$ values as well as the presence of $J_{1,4}$. Namely, a relatively large values of δ and $J_{1,P}$† for H-1 of **26b,c** and **29b,c** indicate the cis (or gauche) relationship of the H-1 and P=O groups, whereas the small $J_{1,P}$ values† point out an almost trans relationship for **26a,d** and **29a,d**. The presence of a small long-range W-coupling ($J_{1,4}$) observed for **26a,c** and **29a,c** indicates the β-configuration of H-1. Therefore, combination of these data readily permits unambiguous establishment of the configurations of H-1 as well as ring-phosphorus atom of aldopentofuranoses.

(2) Compounds **26b—d** and **29b—d** have a large $J_{2,P}$ values and small $J_{3,P}$ and thus are considered to exist preponderantly in the E_2 (or readily variable $^3T_2$) conformation. The concurrent differences in the δ values of H-2 (larger) and H-3 (smaller) further support their respective quasi-equatorial and quasi-axial orientation. Compounds **26a** and **29a** have rather close magnitudes of $J_{2,P}$ and $J_{3,P}$ and the δ values of H-2 and H-3. This suggests an averaging between the interconverting $^3T_2$ and $^2T_3$ conformations with a slight tendency towards $^3T_2$ and $^2T_3$ form (respectively for **26a** and **29a**), judging from the magnitudes of the corresponding δ and J values. The conformations of these P-in-ring D-ribofuranoses are of interest in view of the reported monocyclic furanoid derivatives including many nucleosides and nucleotides which are regarded as existing as rapidly interconverting conformation in solution, favoring puckering the C-2–C-3 region of the furanoid ring.[14]

The present findings are believed to have clearly proved the equilibrated epimerization caused by the hydride reagents in favor of the formation of the key intermediate methyl 4-deoxy-4-phosphinyl-β-D-ribopyranosides, as well as to have established an efficient synthetic scheme for preparation of D-ribofuranose analogues having various kinds of phosphinyl or phosphino group in the hemiacetal ring. The extension of this work including improvement of the yields of the ring-transposition steps and preparation of D-ribofuranose analogues having various other kinds of *P*-substituents, as well as biological evaluation of the compounds, is in progress.

Experimental

Melting points were determined with a Yanagimoto MP-S3 instrument and were uncorrected. All reactions were monitored by TLC (Merck silica gel 60F, 0.25 mm) with (*A*) AcOEt, (*B*) 1:1 AcOEt-hexane, (*C*) 19:1 AcOEt-EtOH, and (*D*) 5:3:1 2-propanol-AcOEt-water as the eluant; components were detected by exposing the plates to UV light and/or by spraying them with 20% sulfuric acid-ethanol, with subsequent heating. Column chromatography was

† For these features, an exception lies in the parameters for the methoxyphosphinyl compounds **26a—d**, having intermediate, close magnitudes of $J_{1,P}$ and $J_{4,P}$. These unusual parameters have also been observed for per-*O*-acetyl-5-deoxy-5-(methoxyphosphinyl)-D-xylo-[10] and D-gluco-pyranoses.[4]

performed by Wako C-200 silica gel. The ^{1}H NMR spectra were measured in $CDCl_3$ (unless otherwise specified) with a Hitachi R-600 (60 MHz) or Varian VXR-500 instrument (500 MHz, the CS-NMR Lab., Okayama Univ.) at 27 °C. Chemical shifts (at 500 MHz unless otherwise stated) were recorded as δ values relative to tetramethylsilane as the internal standard. The assignments of all signals were made by employing a first-order analysis with the aid of decoupling technique and, when necessary, the parameters were confirmed by a computer-assisted simulation analysis. The mass spectra (EI, unless otherwise specified) were taken on a Shimadzu LKB-9000 low-resolution or a JEOL JMX-HX100 high-resolution instrument and were given in terms of *m/z* (rel intensity) compared with the base peak.

(Methyl 2,3-*O*-Isopropylidene-β-D-*erythro*-pentopyranosid)-4-ulose[3] (6). To a stirred suspension of finely powdered Molecular Sieves 3A (20 g) and PCC (10.0 g, 46.4 mmol) in dry CH_2Cl_2 (150 cm^3) was added a soln of **7**[12] (4.29 g, 21.0 mmol) in dry CH_2Cl_2 (50 cm^3) at 0 °C. The mixture was stirred at 20 °C for 4 h and then 2-propanol (5 cm^3) was added at 0 °C. The mixture was stirred at 20 °C for 2 h, triturated with ether (500 cm^3) for 2 h, and the ppt was filtered off through activated carbon. The filtrate was evaporated in vacuo and the residue was purified by short-pass chromatography with 2:1 AcOEt–hexane as an eluant, giving **6** as a colorless syrup (3.98 g, 94%, lit,[3] 74% from **5**): R_f=0.60 (*B*); ^{1}H NMR[15] δ=1.37, 1.51 (3H each, 2s, CMe_2), 3.47 (3H, s, MeO-1), 4.13, 4.18 (1H each, 2d, $J_{5,5'}$=16.8 Hz, H-5,5′), 4.41 (1H, d, $J_{2,3}$=6.8 Hz, H-3), 4.42 (1H, dd, $J_{1,2}$=0.8 Hz, H-2), and 4.78 (1H, br s, H-1).

(Methyl 2,3-*O*-Isopropylidene-β-D-*erythro*-pentopyranosid)-4-ulose (*Z*)- and (*E*)-4-Tosylhydrazones[3] (8a,b). A slightly modified procedure was employed to give a better yield of the product. Thus, to a soln of **6** (3.94 g, 19.5 mmol) in absolute methanol (100 cm^3) was added tosylhydrazine (4.00 g, 21.5 mmol) under stirring at room temp. After 6 h, the mixture was evaporated in vacuo. The residue was diluted with CH_2Cl_2, washed with dil HCl, aq $NaHCO_3$, and then with water. The organic layer was dried (Na_2SO_4) and evaporated in vacuo. The residue was purified by column chromatography with 1:1 AcOEt–hexane, giving **8** as a colorless amorphous solid (6.84 g, 95%): R_f=0.50 (**8a**), 0.42 (**8b**) (*B*) (4:1, lit,[3] 91% yield, 1:1); ^{1}H NMR[15] for **8a** (*Z*) δ=1.05, 1.33 (3H each, 2s, CMe_2), 2.41 (3H, s, MeC_6-S), 3.41 (3H, s, MeO-1), 4.06, 4.20 (1H each, 2d, $J_{5,5'}$=14.8 Hz, H-5,5′), 4.13 (1H, dd, $J_{2,3}$=5.8, $J_{1,2}$=0.8 Hz, H-2), 4.83 (1H, d, H-3), 4.87 (1H, br s, H-1), 7.28, 7.80 (2H each, 2br d, J=8.4 Hz, C_6H_4-S), and 9.69 (1H, br s, NH); for **8b** (*E*) δ=1.32, 1.45 (3H each, 2s, CMe_2), 2.43 (3H, s, MeC_6-S), 3.34 (3H, s, MeO-1), 4.16 (1H, br d, $J_{2,3}$=7.4 Hz, H-2), 4.26 (2H, s, H-5,5′), 4.55 (1H, br s, H-1), 4.67 (1H, d, H-3), 7.31, 7.83 (2H each, 2br d, J=8.3 Hz, C_6H_4-S), and 7.61 (1H, br s, NH), for the reasoning behind the respective assignments of *Z* and *E* isomers to **8a** and **8b**, see Ref. 16.

Methyl (4*R* and 4*S*)-4-Deoxy-4-(dimethoxyphosphinyl)-4-(2-tosylhydrazino)-β-D-*erythro*-pentopyranosides (9—13). To a mixture of **8** (1.28 g, 3.76 mmol) and dimethyl phosphinate (3.30 g, 30.0 mmol) was added trifluoromethanesulfonic acid (0.100 cm^3, 1.13 mmol) at 0 °C under argon, followed by stirring at 25 °C for 5 h. The mixture was diluted with CH_2Cl_2, washed with saturated aq $NaHCO_3$ and then with water, dried (Na_2SO_4), and evaporated in vacuo. The residue was chromatographed on a silica-gel column with 2:1 AcOEt–hexane (which was gradually changed to AcOEt), giving **9—13**.

9 [(4*S*)-2,3-*O*-Isopropylidene-epimer]: Colorless syrup (1.01 g, 56%); R_f=0.33 (*A*); ^{1}H NMR δ=1.32, 1.35 (3H each, 2s, CMe_2), 2.42 (3H, s, MeC_6-S), 3.47 (3H, s, MeO-1), 3.77, 3.84 [3H each, 2d, J_{POMe}=10.7, 10.5 Hz, P(OMe)$_2$], 3.88 (1H, dd, $J_{5e,5a}$=12.6, $J_{5a,P}$=7.0 Hz, H-5a), 4.03 (1H, ddd, $J_{2,3}$=6.7, $J_{1,2}$=4.7, $J_{2,P}$=1.2 Hz, H-2), 4.14 (1H, dd, $J_{5e,P}$=11.4 Hz, H-5e), 4.30 (1H, br s, NH-4), 4.59 (1H, dd, $J_{3,P}$=8.5 Hz, H-3), 4.85 (1H, d, H-1), 6.40 (1H, br s, TsNH), and 7.30, 7.80 (2H each, 2br d, J=8.1 Hz, C_6H_4-S); MS *m/z* 480 (M^+; 0.7), 465 (7), 325 (7), 293 (10), 221 (30), 207 (29), 193 (100), 178 (30), 165 (51), 137 (27), 109 (46), and 91 (55).

Found: *m/z* 480.1341. Calcd for $C_{18}H_{29}N_2O_9PS$: M, 480.1331.

10 [(4*R*)-2,3-*O*-Isopropylidene-epimer]: Colorless needles (178 mg, 10%); R_f=0.23 (*A*); mp 156—157 °C (from AcOEt–hexane); ^{1}H NMR δ=1.33, 1.51 (3H each, 2s, CMe_2), 2.42 (3H, s, MeC_6-S), 3.47 (3H, s, MeO-1), 3.70 (1H, dt, $J_{5e,5a}$=12.9, $J_{5e,P}$=1.6, $J_{3,5e}$=1.5 Hz, H-5e), 3.76, 3.83 [3H each, 2d, J_{POMe}=10.8, 10.9 Hz, P(OMe)$_2$], 3.88 (1H, dd, $J_{1,2}$=7.2, $J_{2,3}$=5.1 Hz, H-2), 3.92 (1H, dd, $J_{5a,P}$=1.9 Hz, H-5a), 3.95 (1H, br s, NH-4), 4.17 (1H, d, H-1), 4.36 (1H, ddd, $J_{3,P}$=3.5 Hz, H-3), 6.58 (1H, br s, TsNH), and 7.32, 7.79 (2H each, 2br d, J=8.2 Hz, C_6H_4-S); MS *m/z* 465 ($M-CH_3$; 0.8), 325 (1.5), 293 (14), 281 (30), 221 (59), 207 (39), 178 (72), 165 (40), 149 (58), 109 (90), and 91 (100).

11: Pale yellow syrup (165 mg, 10%); R_f=0.15—0.08 (*A*); ^{1}H NMR (60 MHz) δ=2.40 (3H, s, MeC_6-S), 3.47 (3H, s, MeO-1), 3.0—3.6 (2H, m, HO-2,3), 3.77, 3.82 [3H each, 2d, J_{POMe}=11.0 Hz, P(OMe)$_2$], 3.7—4.6 (5H, m, H-2,3,5,5′, NH-4), 4.70 (1H, br d, $J_{1,2}$=3.0 Hz, H-1), 6.9—7.2 (1H, m, TsNH), and 7.30, 7.84 (2H each, 2d, J=8.1 Hz, C_6H_4-S).

12 [(4*S*)-3-*O*:4-*N*-Isopropylidene-isomer]: Colorless prisms (68 mg, 4%); R_f=0.28 (*A*); mp 153—154 °C (from AcOEt); ^{1}H NMR δ=0.62, 1.33 (3H each, 2s, CMe_2), 2.33 (1H, br s, HO-2), 2.42 (3H, s, MeC_6-S), 3.46 (3H, s, MeO-1), 3.68 (1H, dd, $J_{1,2}$=6.5, $J_{2,3}$=3.0 Hz, H-2), 3.78, 3.97 [3H each, 2d, J_{POMe}=10.9, 11.0 Hz, P(OMe)$_2$], 3.80 (1H, dd, $J_{5e,5a}$=12.5, $J_{5a,P}$=3.5 Hz, H-5a), 4.06 (1H, dd, $J_{5e,P}$=4.2 Hz, H-5e), 4.52 (1H, d, H-1), 4.61 (1H, dd, $J_{3,P}$=15.6 Hz, H-3), 7.23 (1H, br s, TsNH), and 7.30, 7.82 (2H each, 2br d, J=8.3 Hz, C_6H_4-S); MS *m/z* 465 ($M-CH_3$; 2.5), 433 (2), 325 (2), 295 (3), 207 (32), 189 (55), 178 (55), 149 (58), 109 (60), and 91 (100).

Found: *m/z* 465.1120. Calcd for $C_{17}H_{26}N_2O_9PS$: $M-CH_3$, 465.1097.

13 [(4*R*)-4-(2-*O*-*Cyclo*-methoxyphosphinyl)-isomer]: Colorless prisms (23 mg, 1.5%); mp 202—204 °C decomp (from AcOEt); R_f=0.10 (*A*); ^{1}H NMR (in 9:1 $CDCl_3$–DMSO-d_6) δ=2.35 (3H, s, MeC_6-S), 2.50 (1H, br s, HO-3), 3.31 (3H, s, MeO-1), 3.71 (3H, d, J_{POMe}=11.1 Hz, POMe), 3.81 (1H, dd, $J_{5a,P}$=22.6, $J_{5e,5a}$=11.6 Hz, H-5a), 3.84 (1H, dd, $J_{5e,P}$=5.0 Hz, H-5e), 4.25 (1H, br s, NH-4), 4.34 (1H, dd, $J_{2,P}$=20.0, $J_{1,2}$=2.5, $J_{2,3}\simeq$0 Hz, H-2), 4.41 (1H, d, $J_{3,P}$=28.3 Hz, H-3), 4.71 (1H, d, $J_{1,2}$=2.5 Hz, H-1), 7.23, 7.69 (2H each, 2br d, J=8.2 Hz, C_6H_4-S), and 7.88 (1H, br s, TsNH).

Compound **11** (165 mg) was stirred at 25 °C for 8 h in 2,2-dimethoxypropane (5 cm^3) containing 4 M hydrochloric acid (1 M=1 mol dm^{-3}) in 1,4-dioxane (0.1 cm^3). The soln was neutralized with anhyd $NaHCO_3$, filtered, and evaporated in vacuo. The residue was purified by column chromatog-

raphy, giving **9** and **10** (153 mg in total, 85%).

Methyl (4*R* and 4*S*)-4-Deoxy-4-[(*R* and *S*)-(methoxy)-phenylphosphinyl]-4-(2-tosylhydrazino)-β-D-*erythro*-pentopyranosides (14—16). By the use of the same procedures as those for preparation of **9** and **10**, compound **8** (820 mg, 2.21 mmol) was treated with methyl phenylphosphinate (2.70 g, 17.3 mmol) and trifluoromethanesulfonic acid (0.060 cm^3, 0.68 mmol) at 20 °C for 10 h. Purification by column chromatography gave **14—16**.

14a,b {(4*S*)-2,3-*O*-Isopropylidene-4-[(*R* and *S*)-*P*]-diastereomers}: Colorless syrup (698 mg, 60%, a 2:1 mixture of **14a** and **14b**); R_f=0.50—0.46 (*A*); ^{1}H NMR for **14a** δ=1.23, 1.37 (3H each, 2s, CMe_2), 2.39 (3H, s, MeC_6-S), 3.43 (3H, s, MeO-1), 3.69 (3H, d, J_{POMe}=10.8 Hz, POMe), 3.79 (1H, dd, $J_{5c,5a}$=12.8, $J_{5a,P}$=7.5 Hz, H-5a), 3.86 (1H, dd, $J_{2,3}$=6.8, $J_{1,2}$=4.9 Hz, H-2), 3.94 (1H, dd, $J_{5c,P}$=10.7 Hz, H-5e), 4.35 (1H, dd, $J_{3,P}$=9.2 Hz, H-3), 4.58 (1H, br s, NH-4), 4.87 (1H, d, H-1), 6.62 (1H, br s, TsNH), 7.22, 7.71 (2H each, 2br d, *J*=8.3 Hz, C_6H_4-S), 7.49 [2H, m, $J_{o,m}$=7.6, $J_{m,p}$=7.3, $J_{P,m}$=3.6 Hz, Ph(*m*)], 7.63 [1H, m, $J_{o,p}$=$J_{P,p}$=1.5 Hz, Ph(*p*)], and 7.76 [2H, m, $J_{P,o}$=11.4 Hz, Ph(*o*)], for **14b** δ=1.36, 1.42 (3H each, 2s, CMe_2), 2.39 (3H, s, MeC_6-S), 3.47 (3H, s, MeO-1), 3.52 (1H, dd, $J_{5c,5a}$=12.8, $J_{5a,P}$=9.0 Hz, H-5a), 3.67 (3H, d, J_{POMe}=10.9 Hz, POMe), 3.74 (1H, dd, $J_{5c,P}$=14.9 Hz, H-5e), 4.06 (1H, dd, $J_{2,3}$=6.4, $J_{1,2}$=5.3 Hz, H-2), 4.58 (1H, br s, NH-4), 4.59 (1H, d, H-1), 4.75 (1H, dd, $J_{3,P}$=7.5 Hz, H-3), 6.52 (1H, br s, TsNH), 7.20, 7.61 (2H each, 2br d, *J*=8.3 Hz, C_6H_4-S), 7.53 [2H, m, Ph(*m*)], 7.65 [1H, m, Ph(*p*)], and 7.76 [2H, m, Ph(*o*)].

15a,b {(4*R*)-2,3-*O*-Isopropylidene-4-[(*R* and *S*)-*P*]-diastereomers}: Colorless syrup (70.3 mg, 6.3%), recrystallization of the syrup from AcOEt–hexane yielded **15a** (50.3 mg) as colorless needles, mp 172—173 °C; R_f=0.30 (*A*); ^{1}H NMR for **15a** δ=1.20, 1.43 (3H each, 2s, CMe_2), 2.40 (3H, s, MeC_6-S), 3.41 (3H, s, MeO-1), 3.59 (1H, dd, $J_{5c,5a}$=12.8, $J_{5a,P}$=2.2 Hz, H-5a), 3.65 (1H, dt, $J_{5c,P}$=1.0, $J_{3,5c}$=0.8 Hz, H-5e), 3.74 (3H, d, J_{POMe}=11.1 Hz, POMe), 3.99 (1H, dd, $J_{1,2}$=7.3, $J_{2,3}$=5.0 Hz, H-2), 4.03 (1H, d, H-1), 4.19 (1H, ddd, $J_{3,P}$=1.3, $J_{3,5e}$=0.8 Hz, H-3), 4.27 (1H, br s, NH-4), 6.83 (1H, br s, TsNH), 7.27, 7.75 (2H each, 2d, *J*=8.3 Hz, C_6H_4-S), 7.48 [2H, m, Ph(*m*)], 7.60 [1H, m, Ph(*p*)], and 7.84 [2H, m, Ph(*o*)]; MS *m/z* 511 ($M-CH_3$; 0.8), 371 (2.2), 327 (13), 263 (13), 224 (56), 195 (32), 183 (48), 155 (100), 141 (32), and 91 (47).

16: Pale yellow syrup (96 mg, 9%); R_f=0.22—0.10 (*A*); ^{1}H NMR (60 MHz) δ=2.40 (3H, s, MeC_6-S), 3.30, 3.33 (3H each, 2s, MeO-1), 3.3—3.6 (2H, m, HO-2,3), 3.58, 3.68 (3H each, 2d, J_{POMe}=11.1 Hz, POMe), 3.7—4.65 (5H, m, H-2,3,5,5′, NH-4), 4.65—4.80 (1H, m, H-1) 6.8—7.1 (1H, m, TsNH), and 7.20—8.05 (9H, m, C_6H_4-S, C_6H_5-P).

Compound **16** (96 mg) was converted into **14** and **15** (84 mg in total, 80%) by the same procedures for **11**.

Methyl 4-Deoxy-4-(dimethoxyphosphinyl)-2,3-*O*-isopropylidene-β-D-ribo- (17), α-L-Lyxo- (18), (4*S*)-4-Hydrazino-β-D-*erythro*-pentopyranoside (19), and (4*R*)-Epimer (20). A. From 9. Sodium borohydride (140 mg, 3.70 mmol) was added to a soln of **9** (514 mg, 1.07 mmol) in dry THF (15 cm^3) at 0 °C. The mixture was stirred at 25 °C for 12 h. After evaporation of the solvent in vacuo, the residue was diluted with $CHCl_3$, and the ppt was filtered off through activated carbon. The filtrate was washed twice with water, dried (Na_2SO_4), and evapotated in vacuo. The residue was chromatographed on a silica-gel column with AcOEt as an eluant, giving **17—19**.

17: Colorless syrup (153 mg, 48%); R_f=0.35 (*A*); ^{1}H NMR δ=1.36, 1.51 (3H each, 2s, CMe_2), 2.72 (1H, dddd, $J_{4,P}$=23.8, $J_{4,5a}$=11.8, $J_{4,5e}$=5.5, $J_{3,4}$=3.0 Hz, H-4), 3.44 (1H, s, MeO-1), 3.72, 3.75 [3H each, 2d, J_{POMe}=11.1, 10.8 Hz, $P(OMe)_2$], 3.81 (1H, ddd, $J_{5c,5a}$=11.3, $J_{5a,P}$=4.3 Hz, H-5a), 3.90 (1H, dddd, $J_{5c,P}$=2.2, $J_{3,5e}$=0.8 Hz, H-5e), 3.90 (1H, dd, $J_{2,3}$=6.1, $J_{1,2}$=4.8 Hz, H-2), 4.37 (1H, d, H-1), and 4.60 (1H, ddd, $J_{3,P}$=3.0 Hz, H-3); MS *m/z* 281 ($M-CH_3$; 72), 265 (9), 238 (27), 221 (91), 207 (30), 179 (25), 149 (22), 137 (97), 127 (24), 110 (43), 100 (100), and 85 (39).

Found: *m/z* 281.0764. Calcd for $C_{10}H_{18}O_7P$: $M-CH_3$, 281.0790.

18: Colorless syrup (26.0 mg, 8.2%); R_f=0.38 (*A*); ^{1}H NMR δ=1.35, 1.53 (3H each, 2s, CMe_2), 2.35 (1H, br dtd, $J_{4,P}$=19.3, $J_{4,5a}$=8.9, $J_{3,4}$=8.4, $J_{4,5e}$=5.1 Hz, H-4), 3.40 (1H, s, MeO-1), 3.775, 3.78 [3H each, 2d, J_{POMe}=10.9, 10.8 Hz, $P(OMe)_2$], 3.79, 3.81 (1H each,§ H-5a,5e), 3.97 (1H, dt, $J_{2,3}$=5.0, $J_{1,2}$=1.9, $J_{2,P}$=1.6 Hz, H-2), 4.51 (1H, ddd, $J_{3,P}$=11.4 Hz, H-3), and 4.79 (1H, t, $J_{1,5e}$=2.0 Hz, H-1); MS *m/z* 296 (M^+; 0.5), 281 ($M-CH_3$; 12), 221 (39), 177 (41), 149 (25), 109 (57), 100 (100), and 85 (3).

Found: *m/z* 281.0760. Calcd for $C_{10}H_{18}O_7P$: $M-CH_3$, 281.0790.

19: Colorless needles (42.0 mg, 12%); mp 133—134 °C (from AcOEt–hexane); R_f=0.59 (*A*); ^{1}H NMR δ=1.37, 1.61 (3H each, 2s, Me_2C), 3.41 (3H, s, MeO-1), 3.87, 3.875 [3H each, 2d, J_{POMe}=10.5 Hz, $P(OMe)_2$], 3.65 (1H, dd, $J_{5a,5e}$=12.9, $J_{5a,P}$=12.3 Hz, H-5a), 3.92 (1H, ddd, $J_{5e,P}$=4.5, $J_{1,5e}$=1.0 Hz, H-5e), 3.95 (1H, m, HN-4), 4.05 (1H, ddd, $J_{2,3}$=6.3, $J_{1,2}$=3.0, $J_{2,P}$=1.0 Hz, H-2), 4.63 (1H, dd, $J_{3,P}$=9.3 Hz, H-3), 4.70 (1H, dd, H-1), and 5.98, 6.03 (1H each, 2m, H_2NN-4); MS *m/z* 326 (M^+; 59), 311 (11), 307 (11), 294 (27), 279 (12), 259 (10), 247 (17), 229 (35), 217 (79), 205 (21), 194 (31), 177 (51), 166 (100), 156 (23), 141 (29), 136 (34), 127 (61), 109 (71), 99 (68), and 80 (67).

Found: *m/z* 326.1235. Calcd for $C_{11}H_{23}N_2O_7P$: M, 326.1243.

B. From 10. The same procedures described above for the conversion of **9** were followed. Thus, **10** (160 mg) gave **17** (48.6 mg, 49%), **18** (8.7 mg, 9%), and **20** (7.5 mg, 7%) after purification by column chromatography.

20: Colorless syrup; R_f=0.57 (*A*); ^{1}H NMR δ=1.39, 1.55 (3H each, 2s, CMe_2), 3.52 (3H, s, MeO-1), 3.82, 3.93 [3H each, 2d, J_{POMe}=10.7 Hz, $P(OMe)_2$], 3.97 (1H, ddd, $J_{5a,5e}$=13.3, $J_{5e,P}$=2.2, $J_{3,5e}$=1.6 Hz, H-5e), 3.98 (1H, m, HN-4), 4.03 (1H, dd, $J_{2,3}$=5.5, $J_{1,2}$=4.7 Hz, H-2), 4.15 (1H, ddd, $J_{3,P}$=3.0 Hz, H-3), 4.48 (1H, d, H-1), and 5.47, 6.48 (1H each, 2m, H_2NN-4).

Methyl 4-Deoxy-2,3-*O*-isopropylidene-4-[(*R* and *S*)-(methoxy)phenylphosphinyl]-β-D-ribo- (21a,b), α-L-Lyxo- (22a,b), (4*R* and 4*S*)-4-Hydrazino-β-D-*erythro*-pentopyranosides (23), and (4*R*)-Epimer (23a). A. From 14 and 15. By the use of the same procedures as those for **9**, a 9:1 mixture of **14** and **15** (450 mg, 0.855 mmol) was treated with sodium borohydride (100 mg, 2.64 mmol) at 20 °C for 20 h, giving **21a**, **21b**, **22a,b**, and **23**, after separation by column chromatography.

21a: Colorless prisms (98.2 mg, 34%); R_f=0.34 (*A*); mp

§ Their splitting patterns uncertain because of overlapping with other signals.

126—127 °C (from AcOEt–hexane); ^{1}H NMR δ=1.30, 1.48 (3H each, 2s, CMe_2), 2.73 (1H, dddd, $J_{4,P}$=18.5, $J_{4,5a}$=11.7, $J_{4,5e}$=5.5, $J_{3,4}$=3.0 Hz, H-4), 3.44 (3H, s, MeO-1), 3.73 (3H, d, J_{POMe}=11.1 Hz, POMe), 3.80 (1H, t, $J_{2,3}$=5.9, $J_{1,2}$=5.2 Hz, H-2), 3.91 (1H, ddd, $J_{5e,5a}$=11.3, $J_{5a,P}$=3.8 Hz, H-5a), 3.98 (1H, ddt, $J_{5e,P}$=1.3, $J_{3,5e}$=1.2 Hz, H-5e), 4.30 (1H, dddd, $J_{2,3}$=5.9, $J_{3,P}$=3.9 Hz, H-3), 4.33 (1H, d, H-1), 7.48 [2H, m, Ph(*m*)], 7.57 [1H, m, Ph(*p*)], and 7.79 [2H, m, Ph(*o*)]; MS *m/z* 343 (M+1; 1.2), 327 (42), 311 (11), 284 (29), 225 (17), 195 (27), 183 (98), 173 (42), 155 (100), 141 (30), 128 (31), and 100 (95).

Found: *m/z* 327.0983. Calcd for $C_{15}H_{20}O_6P$: M−CH_3, 327.0997.

21b: Colorless syrup (57.2 mg, 20%); R_f=0.30 (*A*); ^{1}H NMR δ=1.31 (6H, s, CMe_2), 2.80 (1H, dddd, $J_{4,P}$=21.3, $J_{4,5a}$=12.0, $J_{4,5e}$=5.3, $J_{3,4}$=3.0 Hz, H-4), 3.43 (3H, s, MeO-1), 3.71 (3H, d, J_{POMe}=11.2 Hz, POMe), 3.75 (1H, ddd, $J_{5e,5a}$=10.9, $J_{5a,P}$=3.7 Hz, H-5a), 4.00 (1H, ddt, $J_{5e,P}$=1.3, $J_{3,5e}$=1.2 Hz, H-5e), 4.31 (1H, d, H-1), 4.55 (1H, dt, $J_{3,P}$=3.2 Hz, H-3), 7.48 [2H, m, Ph(*m*)], 7.57 [1H, m, Ph(*p*)], and 7.77 [1H, m, Ph(*o*)].

22a,b: Colorless syrup (21.0 mg, 7.2%, an inseparable 2:1 mixture of **22a** and **22b**); R_f=0.40 (*A*); ^{1}H NMR for **22a** δ=1.31, 1.39 (3H each, 2s, CMe_2), 2.43 (1H, dddd, $J_{4,P}$=13.0, $J_{4,5a}$=10.5, $J_{3,4}$=8.6, $J_{4,5e}$=4.4 Hz, H-4), 3.36 (3H, s, MeO-1), 3.61 (1H, dddd, $J_{5e,5a}$=12.1, $J_{5e,P}$=7.9, $J_{1,5e}$=1.5 Hz, H-5e), 3.71 (3H, d, J_{POMe}=11.2 Hz, POMe), 3.77 (1H, ddd, $J_{5a,P}$=3.5 Hz, H-5a), 3.93 (1H, dt, $J_{2,3}$=5.2, $J_{1,2}$=1.9, $J_{2,P}$=1.5 Hz, H-2), 4.65 (1H, ddd, $J_{3,P}$=10.7 Hz, H-3), 4.77 (1H, t, H-1), 7.49 [2H, m, $J_{o,m}$=7.5, $J_{m,p}$=7.3, $J_{P,m}$=3.5 Hz, Ph(*m*)], 7.57 [1H, m, $J_{o,p}$=$J_{P,p}$=1.5 Hz, Ph(*p*)], and 7.79 [2H, m, $J_{P,o}$=11.8 Hz, Ph(*o*)], for **22b** δ=1.23, 1.32 (3H each, 2s, CMe_2), 2.47 (1H, dddd, $J_{4,P}$=13.5, $J_{4,5a}$=10.5, $J_{3,4}$=9.1, $J_{4,5e}$=4.5 Hz, H-4), 3.54 (3H, s, MeO-1), 3.66 (3H, s, J_{POMe}=11.2 Hz, POMe), 3.70, 3.78 (1H each,§ H-5a,5e), 3.85 (1H, dt, $J_{2,3}$=5.2, $J_{1,2}$=1.8, $J_{2,P}$=1.5 Hz, H-2), 4.52 (1H, ddd, $J_{3,P}$=11.6 Hz, H-3), 4.79 (1H, t, $J_{1,5e}$=1.5 Hz, H-1), 7.49 [2H, m, Ph(*m*)], 7.57 [1H, m, Ph(*p*)], and 7.79 [2H, m, Ph(*o*)]; MS *m/z* 342 (M^+; 0.5), 327 (31), 311 (10), 267 (33), 225 (23), 209 (35), 195 (11), 183 (44), 173 (21), 155 (100), 128 (63), and 77 (41).

Found: *m/z* 327.0972. Calcd for $C_{15}H_{20}O_6P$: M−CH_3, 327.0997.

23: Colorless syrup (22.2 mg, 7.0%, a ca. 7:1 mixture of (4*S*) and (4*R*) epimers); R_f=0.55—0.50 (*A*); ^{1}H NMR (60 MHz) δ=1.26, 1.37, 1.43, 1.58 (6H, 4s, CMe_2), 3.35, 3.45, 3.48 (3H, 3s, MeO-3), 3.76, 3.81 (3H, d, J_{POMe}=10.8 Hz, POMe), 3.60—4.20 (3H, m, H-5,5′, NH-4), 4.20—4.95 (3H, m, H-1,2,3), 5.6—6.2 (2H, m, H_2NN-4), and 7.45—8.00 (5H, m, PPh).

B. From 15a. By the same procedures described above, **15a** (60.0 mg) was converted into **21a** (22.2 mg, 57%), **22a** (3.0 mg, 7.7%), and **23a** (2.5 mg, 5.9%).

23a: Colorless prisms, mp 169—170 °C (from AcOEt–hexane); R_f=0.50 (*A*); ^{1}H NMR δ=1.26, 1.28 (3H each, 2s, CMe_2), 3.48 (3H, s, MeO-3), 3.87 (1H, br d, $J_{5e,5a}$=13.3, $J_{5a,P}$=0.5 Hz, H-5a), 3.90 (3H, d, J_{POMe}=10.7 Hz, POMe), 3.93 (1H, ddd, $J_{2,3}$=5.5, $J_{3,P}$=2.9, $J_{3,5e}$=2.0 Hz, H-3), 4.02 (1H, t, $J_{1,2}$=5.8 Hz, H-2), 4.06 (1H, m, NH-4), 4.16 (1H, dt, $J_{5e,P}$=2.0 Hz, H-5e), 4.30 (1H, d, H-1), 5.32 (2H, br s, H_2NN-4), 7.49 [2H, m, $J_{o,m}$=7.8, $J_{m,p}$=7.6, $J_{P,m}$=3.6 Hz, Ph(*m*)], 7.61 [1H, m, $J_{m,p}$=1.5, $J_{P,p}$=1.3 Hz, Ph(*p*)], and 7.82 [2H, m, $J_{P,o}$=11.7 Hz, Ph(*o*)].

Methyl 4-Deoxy-2,3-*O*-isopropylidene-4-phosphino-β-D-ribopyranoside (24). To a soln of **17** (220 mg) in dry benzene (4 cm^3) was added, with stirring, a soln of SDMA[13] (70% in toluene, 0.65 cm^3, 3 equiv) in dry benzene (1 cm^3) in small portions at 5 °C under argon. The stirring was continued at this temp for 1 h. Then, water (0.5 cm^3) was added at 0 °C and the mixture was stirred for 30 min. The ppt was centrifuged and washed with several portions of benzene. The organic layers were combined and evaporated in vacuo, giving **24** as a colorless syrup: R_f=0.68 (*A*); MS *m/z* 221 (M+1; 59), 205 (15), 189 (12), 155 (38), 129 (26), 112 (45), 100 (55), and 43 (100); the specimen was not stable enough for ^{1}H NMR and other spectral measurements.

1,2,3,5-Tetra-*O*-acetyl-4-deoxy-4-[(*R* and *S*)-methoxyphosphinyl]-α,β-D-ribopyranoses (26a—d). The above syrup **24** was immediately dissolved in 2-propanol (2 cm^3) and 0.5 M hydrochloric acid (2 cm^3). The mixture was degassed with argon and then stirred at 90 °C for 1 h. After cooling, the reactant was neutralized by adding enough Amberlite IRA-45. The resin was filtered off and washed with water, and the filtrate was evaporated in vacuo. The residue was dissolved in water (2 cm^3), treated with 30% aq hydrogen peroxide (0.2 cm^3) at room temp for 1 d, and concentrated in vacuo to give crude 4-deoxy-4-(hydroxyphosphinyl)-D-ribofuranoses (**25**) as a colorless syrup: R_f=0.10 (*D*).

Compound **25** was methylated with ethereal diazomethane in 1:1 DMSO–MeOH (4 cm^3) at 0 °C. When the reaction mixture became turbid, it was concentrated in vacuo and repeatedly treated with ethereal diazomethane in the same mixed solvent. The solvent was evaporated in vacuo to give the 4-(methoxyphosphinyl) derivative [R_f=0.73 (*D*)]. This was acetylated with acetic anhydride (1.5 cm^3) in dry pyridine (3 cm^3), giving a mixture of tetraacetates **26a—d**, which were separated by column chromatography with a gradient eluant of 3:1 AcOEt–hexane→AcOEt→19:1 AcOEt–EtOH.

26a (4-[(*R*)-Methoxyphosphinyl]-β-isomer): Colorless syrup (17.8 mg, 6.3% yield from **17**); R_f=0.47 (*A*); ^{1}H NMR, see Table 1; MS *m/z* 380 (M^+; ≃0), 354 (0.6), 338 (2.1), 320 (0.8), 296 (32), 278 (19), 236 (24), 218 (15), 193 (16), 177 (42), 149 (31), 123 (21), and 43 (100).

Found: *m/z* 338.0748. Calcd for $C_{12}H_{19}O_9P$: M−CH_2CO, 338.0767.

26b (4-[(*R*)-*P*]-α-Isomer): Colorless syrup (9.3 mg, 3.3% yield from **17**); R_f=0.42 (*A*); ^{1}H NMR, see Table 1; MS *m/z* 381 (M+1; 3.8), 353 (1.8), 338 (4.3), 321 (1.9), 296 (90), 278 (41), 250 (40), 236 (74), 218 (35), 207 (40), 193 (52), 177 (100), 165 (50), 147 (47), 123 (68), and 43 (100).

Found: *m/z* 381.0952. Calcd for $C_{14}H_{22}O_{10}P$: M+1, 381.0951.

26c (4-[(*S*)-*P*]-β-Isomer): Colorless syrup (7.8 mg, 2.8% yield from **17**); R_f=0.40 (*A*); ^{1}H NMR, see Table 1.

26d (4-[(*S*)-*P*]-α-Isomer): Colorless syrup (4.8 mg, 1.7% yield from **17**); R_f=0.34 (*A*); ^{1}H NMR, see Table 1.

1,2,3,5-Tetra-*O*-acetyl-4-deoxy-4-[(*R* and *S*)-phenylphosphinyl]-α,β-D-ribopyranoses (29a—d). The procedures similar to those for **26** from **17** were employed. Thus, **21** (140 mg, 0.41 mmol) was treated with SDMA (0.25 cm^3, 0.85 mmol) at 5 °C for 1 h, giving phosphine oxide **27** as a colorless syrup: R_f=0.70 (*A*). This was refluxed with 1:1 ethanol–0.5 M HCl (4 cm^3, oxygen-free) for 3 h to afford **28** as colorless syrup: R_f=0.48 (*D*). This was acetylated with

Ac_2O–pyridine to give a mixture of **29a—d**, which were separated by column chromatography.

29a (4-[(*S*)-Phenylphosphinyl]-β-isomer): Colorless syrup (20.3 mg, 12% yield from **21**); R_f=0.41 (*A*); ^{1}H NMR, see Table 1; MS *m/z* 426 (M^+; ≃0), 342 (13), 324 (13), 256 (15), 185 (15), and 81 (100); FAB-MS (thioglycerol matrix, with xenon gas) *m/z* 427 (M+1; 100), 385 (21), 369 (53), 343 (13), 327 (10), 309 (16), 267 (11), 223 (14), and 207 (13).

Found: *m/z* 427.1187. Calcd for $C_{19}H_{24}O_9P$: M+1, 427.1158.

29b (4-[(*S*)-*P*]-α-Isomer): Colorless syrup (7.7 mg, 4.4% yield); R_f=0.36 (*A*); ^{1}H NMR, see Table 1.

29c (4-[(*R*)-*P*]-β-Isomer): Colorless syrup (10.9 mg, 6.3% yield); R_f=0.33 (*A*); ^{1}H NMR, see Table 1; MS, *m/z* 426 (M^+; ≃0), 368 (28), 341 (10), 282 (10), 256 (45), 236 (82), 185 (35), and 81 (100); FAB-MS (thioglycerol matrix, with xenon gas), 427 (M+1; 100), 385 (12), 367 (21), 343 (8), 325 (12), 309 (12), 282 (10), 265 (12), 230 (12), 223 (25), 205 (18), and 185 (46).

Found: *m/z* 427.1158. Calcd for $C_{19}H_{24}O_9P$: M+1, 427.1158.

29d (4-[(*R*)-*P*]-α-Isomer): Colorless syrup (5.0 mg, 2.9% yield); R_f=0.27 (*A*); ^{1}H NMR, see Table 1.

Besides these separated products, an inseparable mixture of unidentified products [R_f=0.35—0.20 (*A*), ca. 2% yield from **21**] was obtained, although they were speculated to be the L-lyxofuranose derivatives.

When a 9:1 mixture of **21** and **22** was subjected to the same procedures described above, **29a—d** were also obtained predominantly in similar yields to those described above.

We are grateful to Mr. Shin-ichi Takekuma (Kinki Univ., Osaka) for the measurement of mass spectra. The present work was partially supported by Grant-in-Aid for Scientific Research No. 63540500 from the Ministry of Education, Science and Culture.

References

1) For a review, see H. Yamamoto and S. Inokawa, *Adv. Carbohydr. Chem. Biochem.*, **42**, 135 (1984).

2) Z. J. Witczak and R. L. Whistler, *J. Carbohydr. Chem.*, **2**, 351 (1983).

3) H. Yamamoto, Y. Nakamura, S. Inokawa, M. Yamashita, M.-A. Armour, and T. T. Nakashima, *J. Org. Chem.*, **49**, 1364 (1984); P. Luger, E. Müller, H. Yamamoto, and S. Inokawa, *Carbohydr. Res.*, **145**, 25 (1985).

4) H. Yamamoto, T. Hanaya, H. Kawamoto, S. Inokawa, M. Yamashita, M.-A. Armour, and T. T. Nakashima, *J. Org. Chem.*, **50**, 3516 (1985).

5) a) H. Yamamoto, T. Hanaya, N. Shigetoh, H. Kawamoto, and S. Inokawa, *Chem. Lett.*, **1987**, 2081; b) T. Hanaya, N. Shigetoh, and H. Yamamoto, *Bull. Chem. Soc. Jpn.*, **61**, 2499 (1988); c) H. Yamamoto, T. Hanaya, H. Kawamoto, and S. Inokawa, *J. Org. Chem.*, **53**, 4790 (1988); d) H. Yamamoto, T. Hanaya, N. Shigetoh, H. Kawamoto, and S. Inokawa, *Chem. Lett.*, **1989**, 351.

6) M. Yamashita, M. Yamada, M. Sugiura, H. Nomoto, and T. Oshikawa, *Nippon Kagaku Kaishi*, **1987**, 1207.

7) H. Yamamoto, K. Yamamoto, S. Inokawa, M. Yamashita, M.-A. Armour, and T. T. Nakashima, *J. Org. Chem.*, **48**, 435 (1983).

8) H. Yamamoto, Y. Nakamura, S. Inokawa, M. Yamashita, M.-A. Armour, and T. T. Nakashima, *Carbohydr. Res.*, **102**, 185 (1982).

9) A part of the results have been reported as a communication: H. Yamamoto, T. Hanaya, H. Kawamoto, and S. Inokawa, *Chem. Lett.*, **1989**, 121.

10) H. Yamamoto, T. Hanaya, S. Inokawa, K. Seo, M.-A. Armour, and T. T. Nakashima, *Carbohydr. Res.*, **114**, 83 (1983); H. Yamamoto, T. Hanaya, S. Inokawa, and M.-A. Armour, *ibid.*, **124**, 195 (1983); H. Yamamoto, T. Hanaya, S. Inokawa, M. Yamashita, M.-A. Armour, and T. T. Nakashima, *ibid.*, **128**, C5 (1984).

11) M. Bobek and R. L. Whistler, *Methods Carbohydr. Chem.*, **6**, 292 (1972).

12) N. A. Hughes and C. D. Maycock, *Carbohydr. Res.*, **35**, 247 (1974); S. Inokawa, T. Mitsuyoshi, H. Kawamoto, and H. Yamamoto, *ibid.*, **142**, 321 (1985).

13) V. Bažant, M. Čapka, M. Černy, V. Chvalovský, K. Kochloefl, M. Kraus, and J. Málek, *Tetrahedron Lett.*, **1968**, 3303; SDMA is commercially purchased from Aldrich Chemical Co., Inc. as Red-Al®.

14) M. Sundaralingam, *J. Am. Chem. Soc.*, **87**, 599 (1965); J. F. Stoddart, "Stereochemistry of Carbohydrates," Wiley, New York (1971); S. J. Angyal, *Carbohydr. Res.*, **77**, 37 (1979).

15) Although insufficiently resolved ^{1}H NMR data at 60 MHz were reported for these compound in lit,[3] the complete parameters obtained at 500 MHz in the present study are shown here to unambiguously confirm the structural assignments.

16) H. Yamamoto, C. Hosoyamada, H. Kawamoto, S. Inokawa, M. Yamashita, M.-A. Armour, and T. T. Nakashima, *Carbohydr. Res.*, **102**, 159 (1982).

Total Syntheses of (+)-Altholactone [(+)-Goniothalenol] and Three Stereocongeners and Their Cytotoxicity against Several Tumor Cell Lines[1)]

Yoshihide UENO, Kin-ichi TADANO,* Seiichiro OGAWA,*
Jerry L. MCLAUGHLIN,† and Ahmad ALKOFAHI†
Department of Applied Chemistry, Faculty of Science and Technology, Keio University, Hiyoshi, Kohoku-ku, Yokohama 223
†Department of Medicinal Chemistry and Pharmacognosy, School of Pharmacy and Pharmacal Science, Purdue Unviversity, West Lafayette, Indiana 47907, U. S. A.
(Received March 4, 1989)

Enantiospecific total synthesis of (+)-altholactone [(+)-goniothalenol] (**1**), a novel tetrahydrofuropyran-5-one possessing significant cytotoxicity against several tumor cell lines, has been achieved by using L-arabinose as the redundant starting material. The pivotal tetrahydrofuran formation was realized by treatment of the diastereomeric mixture of (2*S*,3*R*)-4,5-epoxy-5-phenyl-1,2,3-pentanetriol 1,3-benzylidene acetals **8** and **8'** with silica gel. Simultaneous stereochemical inversion at C-4 and C-5 of the major cyclization product, *O*,*O'*-benzylidene derivative of (2*S*,3*R*,4*S*,5*S*)-2-(hydroxymethyl)-5-phenyltetrahydrofuran-3,4-diol (**11**), to the 2*S*,3*R*,4*R*,5*R* diastereomer **10** was achieved by hydroboration of (2*S*,3*S*)-3-hydroxy-2-(hydroxymethyl)-5-phenyl-2,3-dihydrofuran *O*,*O'*-benzylidene derivative (**18**) which derived from **11**. Pfitzner-Moffatt oxidation of **10** followed by $NaBH_4$ reduction gave the 2*S*,3*R*,4*S*,5*R* diastereomer **20** exclusively. Displacement of the triflate group in (2*S*,3*R*,4*S*,5*S*)-2-(hydroxymethyl)-5-phenyl-4-[(trifluoromethylsulfonyl)oxy]tetrahydrofuran-3-ol *O*,*O'*-benzylidene derivative (**21**) by acetate, which was prepared from **11**, furnished the 2*S*,3*R*,4*R*,5*S* diastereomer **22**. The total synthesis of **1** was completed by Collins oxidation of (2*S*,3*R*,4*R*,5*R*)-2-(hydroxymethyl)-3,4-bis(methoxymethoxy)-5-phenyltetrahydrofuran (**34**), which was prepared from **10**, and subsequent Witting olefination with (ethoxycarbonylmethylene)triphenylphosphorane followed by hydrolysis. By employing the analogous reaction sequence, compounds **11**, **20**, and **22** were efficiently converted into (+)-7,8-di-*epi*- (**2**), (+)-7-*epi*- (**3**), and (+)-8-*epi*-altholactone (**4**), respectively. The cytotoxicity of **1**—**4** against several tumor cell lines was examined.

In 1977, Loder and Nearn reported the isolation of a novel tetrahydro-5*H*-furo[3,2-*b*]pyran-5-one derivative from the extracts of the bark of an unnamed *Polyathia* species (Annonaceae) and they named this natural product "altholactone".[2)] The relative configuration of altholactone was determined by means of spectral analyses of it and some derivatives, and the absolute configuration of natural (+)-enantiomer was tentatively assigned to be **1** based on correlation of the CD spectrum of it with those of the structurally defined natural α,β-unsaturated δ-lactones.[2)] Compound **1** was later isolated from the ethanolic extract of the stem bark of *Goniothalamus giganteus* (Annonaceae) by one of us (J. L. M.),[3)] and the proposed relative configuration was confirmed by the X-ray crystallographic analysis. This tetrahydrofuropyran-5-one **1** is known to possess bioactivities such as an antitumor activity against murine P388 leukemia in vivo at 45 mg/kg and shows lethality to brine shrimp (LC_{50} 234 μg ml^{-1}).[3)] As the structurally similar natural products to **1**, goniothalamin,[4)] goniodiol,[5)] goniotriol,[5)] dihydrokawain-5-ol,[6)] olguine,[7)] anamarine,[8)] and asperlin[9)] were isolated from some plants and a fungus. Some of them (goniothalamin, goniodiol, and goniotriol) were reported to have an asymmetric carbon atom with *S* configuration as δ-carbon of the α,β-unsaturated δ-lactone moiety. On the other hand, the same position of the other natural products was *R* configuration. These facts provoke much interest in the biosynthetic correlation of **1** to the other natural products. This structural uniqueness and biological importance of **1** prompted us to undertake the total synthesis of **1**. Very recently, two total syntheses of **1** and its (−)-enantiomer have been reported by Gesson and coworkers[10)] and by Gillhouley and Shing.[11)] In this article, we describe in detail our independent total syntheses of **1** and three stereocongeners, namely, (+)-7,8-di-*epi*- (**2**), (+)-7-*epi*- (**3**), and (+)-8-*epi*-altholactone (**4**).[12)] The cytotoxicity of **1**—**4** against several tumor cell lines was examined and the results are also described herein.

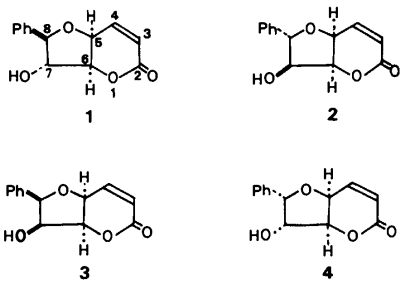

Results and Discussion

Syntheses of (+)-Altholactone (1) and Three Stereocongeners (2—4). As a starting material for the enantiospecific total synthesis of **1**, we chose the known 1,3-*O*-benzylidene-L-arabinitol (**5**) which was readily prepared from L-arabinose by a two-step reaction sequence.[13)] The C-2 and C-3 of **5** correspond to C-5 and C-6 (altholactone numbering) of **1**. Oxidative cleavage of the glycol in **5** with $NaIO_4$ in

aqueous MeOH and subsequent Wittig olefination with benzylidenetriphenylphosphorane, prepared by BuLi treatment of benzyltriphenylphosphonium chloride,[14] furnished a 1:3 mixture of **6Z** and **6E** in a combined yield of 84%. These geometrical isomers were cleanly separated by silica-gel chromatography. The *Z* isomer **6Z** was isomerized to **6E** in 81% yield by treatment wth thiophenol (PhSH) in refluxing benzene in the presence of 2,2′-azobis(2-methylpropanenitrile) (AIBN).[15] Epoxidation of **6E** with *m*-chloroperbenzoic acid (mCPBA) in refluxing CH_2Cl_2 provided an inseparable mixture of (*R*,*R*)- (**8**) and (*S*,*S*)-epoxides (**8′**). The ratio of **8** to **8′** could not be determined by its ^1H NMR spectral analysis. It was found that tetrahydrofuran formation took place partly during purification of the mixture of **8** and **8′** by silica-gel chromatography. Therefore, the mixture of **8** and **8′** in CH_2Cl_2 was kept standing with silica gel (30 to 40 multiple weight of **6E**) at room temperature for 25—35 h. As a result, the cyclization products **10** and **11** were obtained in 19% and 73% yields, respectively, after chromatographic separation on silica gel. From these results, the ratio of **8** to **8′** was estimated to be 1 to 3.8. The effect of the C-2 substituent on the epoxidation was next pursued. The benzoate **7** was prepared by the standard benzoylation of **6E**. Treatment of **7** with mCPBA in refluxing CH_2Cl_2 gave an inseparable mixture of **9** and **9′**. The benzoyl groups of this mixture were removed with sodium methoxide, and the resulting mixture of **8** and **8′** was treated with silica gel as described above. Compound **11** was obtained by crystallization of the reaction mixture in 83% yield. The other cyclization product **10** was obtained in 6% yield after silica-gel chromatography of the mother liquor. In consideration of the yields of **10** and **11**, the ratio of the epoxides **9** and **9′** was estimated to be 1 to 13.8.[16] By reason that the combined yield of **10** and **11** was sufficiently high, the silica-gel-promoted cyclization found in the present work is worthy to note.[17,18] The structures of **10** and **11** could not be determined unambiguously from their ^1H NMR spectra. However, these were established as follows. Hydrolysis of **10** and **11** with 1 M† HCl gave the debenzylidene derivatives **12** and **13**. The primary hydroxyl groups in **12** and **13** were silylated to give **14** and **15**. Treatment of **14** with 2,2-dimethoxypropane in the presence of 10-camphorsulfonic acid (CSA) resulted in a quantitative recovery of **14**. On the other hand, compound **15** was converted into the isopropylidene derivative **16** in 87% yield under the same reaction conditions. These results

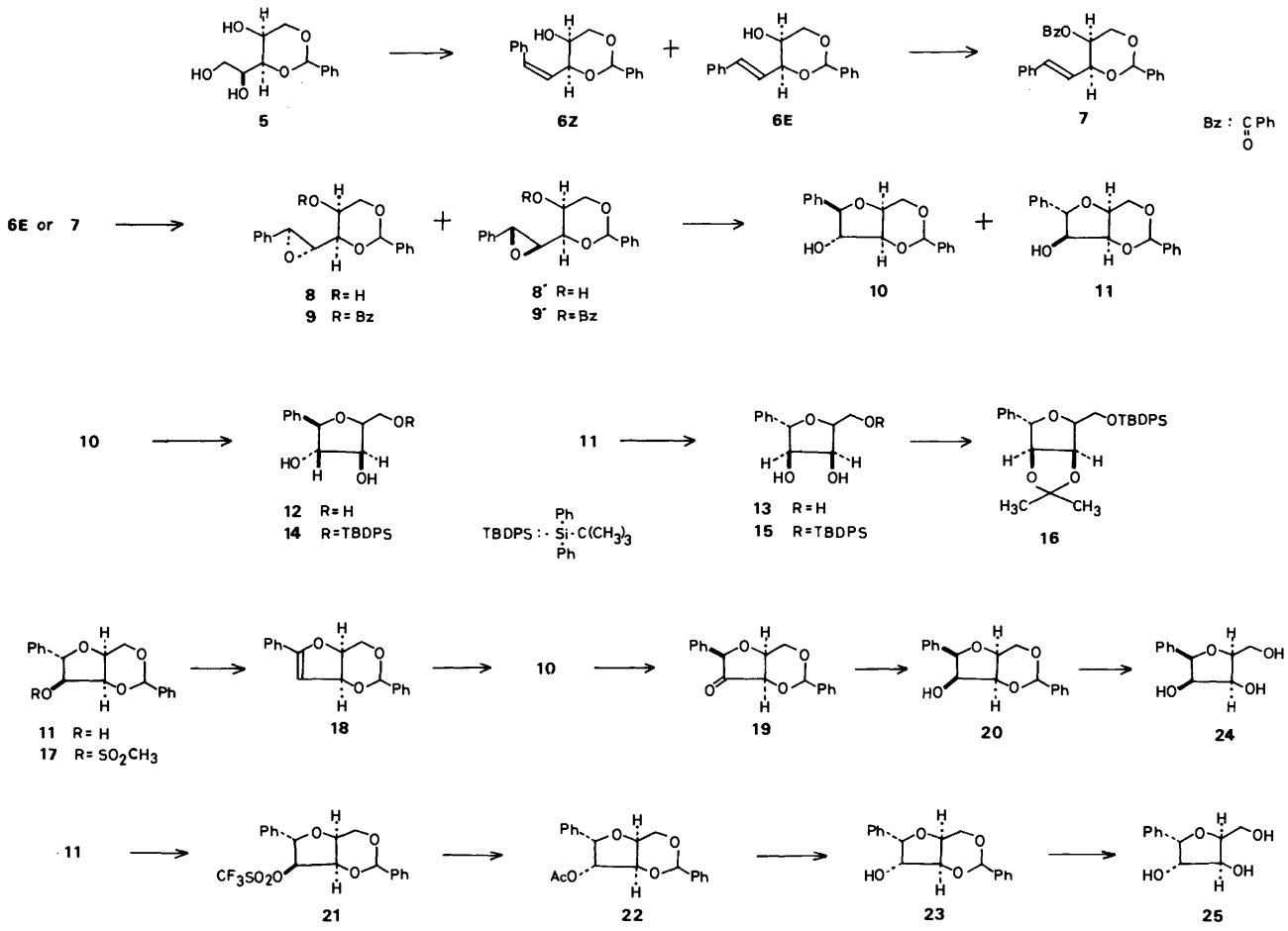

† 1 M=1 mol dm^{-3}.

reveal that relationship of the vicinal diols are trans for **14** and cis for **15**. The structures of **10** and **11** were established as depicted.

Unfortunately, the minor cyclization product **10** possesses all of the required asymmetric carbons. Therefore, the conversion of **11** into **10** was investigated. For this purpose, an introduction of a hydroxyl group at C-3 of a model such as **18** by hydroboration protocol was examined. The attack of borane to **18** was expected to proceed from the less hindered convex face. The dihydrofuran **18** was prepared as follows. Methanesulfonylation of **11** gave the mesylate **17**. Brief exposure of **17** to *t*-BuOK in refluxing THF resluted in the formation of **18** through elimination of methanesulfonic acid. As anticipated, the hydroboration of **18** with BH_3–THF complex in THF followed by oxidative work-up with H_2O_2 furnished **10** as a single product in 65% yield from **17**. Two other diastereomers **20** and **23**, the proper synthetic precursors for **3** and **4**, were prepared as follows. Pfitzner–Moffatt oxidation[19] of **10** gave **19** smoothly,[20] and $NaBH_4$ reduction of **19** gave **20** in 83% yield from **10**. The attack of the hydride occurred exclusively from the convex face of **19**. Trifluoromethanesulfonylation of **11** gave the triflate **21**. Displacement of the triflate group by acetate group in S_N2 fashion took place by heating of **21** in DMF with AcOK at 135 °C. The acetate **22** was obtained in 79% yield.[21] Deacetylation of **22** with sodium methoxide gave **23**. Direct displacement of the triflate group by hydroxyl group was achieved by treatment of **21** in DMF–DMSO with KO_2.[22] Compound **23** was obtained in 58% yield.

The remaining elaboration for the total synthesis of **1** from **12** was an introduction of 2-pyrone unit, and this was accomplished as follows. Selective tritylation of **12** gave the mono trityl ether **26** in 75% yield. The remaining hydroxyl groups were protected as methoxymethyl (MOM) ethers to provide **30** in 89% yield. Hydrolysis of **30** with *p*-TsOH provided the detritylated product **34**. Collins oxidation[23] of **34** followed by Wittig olefination of thus formed aldehyde[24] with (ethoxycarbonylmethylene)triphenylphosphorane in MeOH gave *Z* and *E* isomers of α,β-unsaturated esters **38Z** and **38E** in 62% and 9% yields, respectively. Finally, hydrolysis of **38Z** with 1 M HCl provided (+)-altholactone **1** as needles in 96% yield in consequence of deprotection of the MOM ethers followed by δ-lactonization. The ^1H (400 MHz) and ^{13}C (100 MHz) NMR spectra of synthetic **1** were identical with those of natural product. Mixed melting point of synthetic **1** (mp 113—114 °C) with natural **1** (mp 110 °C[3]) showed no depression (mmp 112—113 °C). Furthermore, the

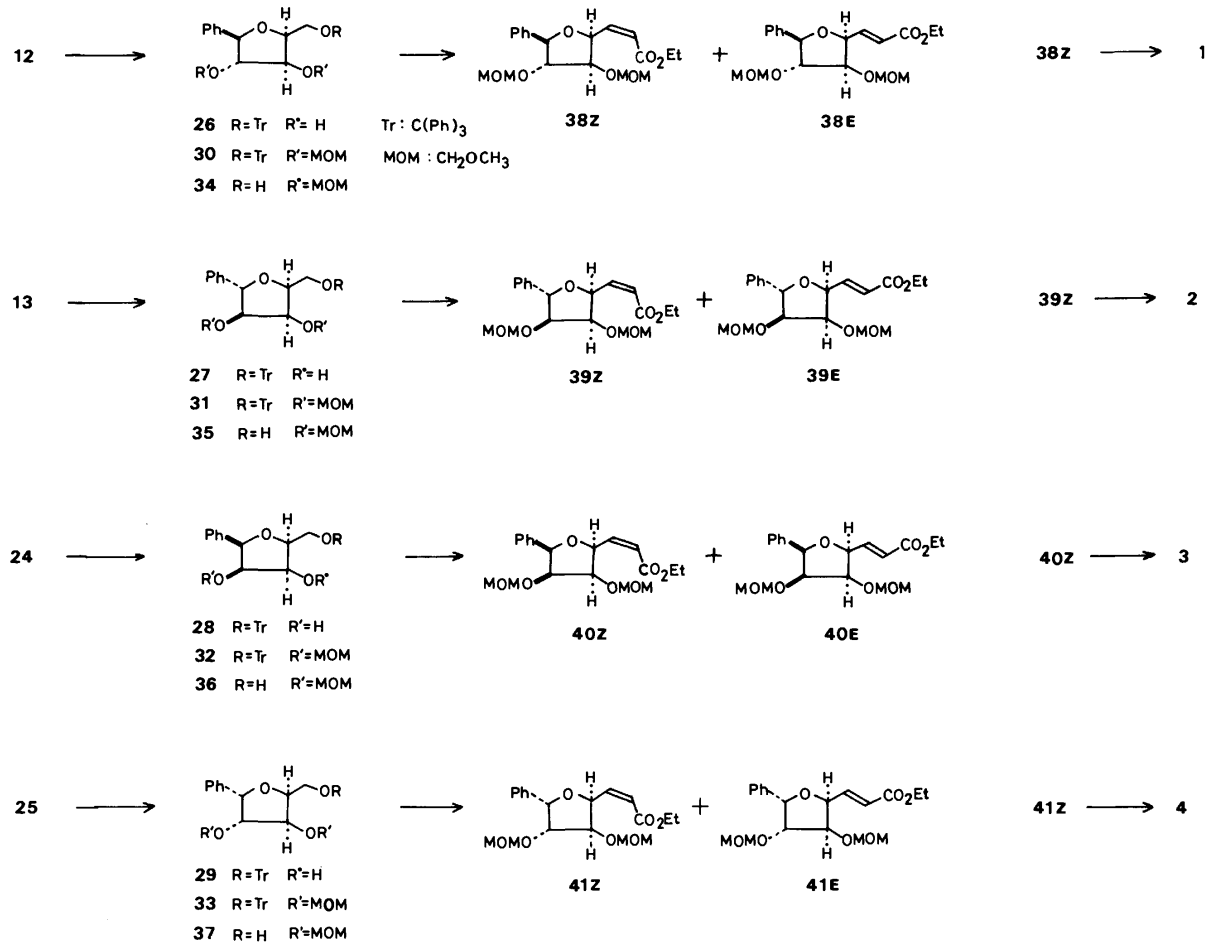

specific rotation of synthetic **1** [$[\alpha]_D^{33}$ +180.8° (*c* 0.52, EtOH)] revealed that the absolute configuration of natural **1** [$[\alpha]_D^{20}$ +188°[2] and $[\alpha]_D^{25}$ +184.7°[3]] is 5*S*,6*R*, 7*R*,8*R*.

The syntheses of three stereocongeners **2**—**4** were accomplished by the virtually same reaction sequence described above. Debenzylidenation of **20** and **23** gave the triols **24** and **25**. By the sequence of tritylation, methoxymethylation, and detritylation, the triol **13** was converted into **35** in an overall yield of 51% via **27** (72%) and **31** (91%). Similarly, compound **24** was converted into **36** in an overall yield of 51% via **28** (79%) and **32** (90%). Also, compound **37** was obtained from **25** in an overall yield of 82% via **29** (93%) and **33** (94%). By the Collins oxidation followed by Wittig olefination, compounds **35**, **36**, and **37** were transformed to *Z* and *E* isomers of the α,β-unsaturated esters, **39Z** (58%) and **39E** (5%), **40Z** (72%) and **40E** (5%), and **41Z** (53%) and **41E** (4%). Hydrolysis of **39Z**, **40Z**, and **41Z** with 1 M HCl gave (+)-7,8-di-*epi*- (**2**), (+)-7-*epi*- (**3**), and (+)-8-*epi*-altholactone (**4**), in 78%, 79%, and 82% yields, respectively. The stereocongeners **2**—**4** were fully characterized by the spectral means. In addition, the synthesis of **3** has been reported very recently by Gillhouley and Shing.[11] The physical data of our synthetic **3** [mp 117—117.5 °C, $[\alpha]_D^{30}$ +23.0° (*c* 0.50, EtOH)] coincides well with those of the reported data [mp 121—123 °C, $[\alpha]_D^{22}$ +23.5° (*c* 0.4, EtOH)].

Cytotoxicity of (+)-Altholactone (1) and Three Stereocongeners (2—4). The cytotoxicity assays of **1**—**4** were carried out by using the following tumor cells: 9PS, a methylcholanthrene induced murine leukemia; 9KB, a human nasopharyngeal carcinoma; A-549, a human lung-cell cancer; MCF-7, a human breast cancer; HT-29, a human colon cancer. The ED_{50} values ($\mu g\ ml^{-1}$) of **1**—**4** are as follows. **1**: 9PS (2.01×10^{-1}), 9KB (3.03), A-549 (>10), MCF-7 (>10), HT-29 (2.49); **2**: 9PS (9.4×10^{-1}), 9KB (>10), A-549 (5.85), MCF-7 (4.7), HT-29 (4.7×10^{-1}); **3**: 9PS (1), 9KB (2.6), A-549 (4.6), MCF-7 (4.8), HT-29 (2.1); **4**: 9PS (9.5×10^{-1}), 9KB (>10), A-549 (>10), MCF-7 (>10), HT-29 (4.5). From these results, the level of cytotoxicity of **2**—**4** seems to be marginal. It appears that the 8-*epi* isomer **4** is less active than the other isomers, but **4** may be selectively active in the colon tumor. Meanwhile, the cytotoxicity of natural **1** was examined in detail at the National Cancer Institute. The cytotoxicity of **1** is quite potent (10^{-5} to 10^{-7} molar for IC_{50} values), and the results are listed in Table 1.

Table 1. The NCI Human Tumor Panel Cytotoxicity Results for **1**

Disease cell	log (IC_{50})
Fibroblast	
CCD-19Lu	−4.6
Leukemia	
MOLT-4	−6.1
K-562	−5.4
P388/ADR	−5.6
P388	−5.6
Non-small cell lung cancer	
H522	−5.8
H23	−5.6
H125	−6.0
H358	−5.5
H460	−5.5
A549(ATCC)	−5.1
H322	−5.2
EKVX	−5.0
Small cell lung cancer	
DMS114	−5.5
Colon cancer	
LoVo	−5.5
WIDR	−5.6
SW620	−5.5
DLD-1	−5.4
HT29	−5.3
Breast cancer	
MCF7	−5.5
MCF7/ADR	−5.6
CNS cancer	
TE671	−5.5
U251	−5.5
Melanoma	
SK-MEL-5	−5.9
LOX	−5.5
RPMI-7951	−5.5
Malme-3M	−5.3
SK-MEL-2	−5.6
Ave. log (IC_{50})	−5.5
Delta	0.6
Range	1.6

Experimental

General Procedures. Reactions were carried out at room temperature unless otherwise described. Melting points were determined with a Mitamura Riken micro melting points apparatus and are uncorrected. Specific rotations were measured with a Jasco DIP-4 polarimeter in a 10 mm cell. Column chromatography was performed on Silicagel 60 (Katayama Chemicals), flash column chromatography was performed on Wako C-300 (Wako Pure Chemicals), and thin-layer chromatography (TLC) was performed on a glass plate coated with Kieselgel 60 GF_{254} (Merck) followed by detection using UV light and/or charring with H_2SO_4. Preparative TLC (PTLC) was performed on a glass plate (20×20 cm) coated with Kieselgel PF_{254} (Merck), and compounds were extracted with CH_2Cl_2 or AcOEt. IR spectra were recorded with a Hitachi Model 225 (KBr) or with a Jasco Model A-202 (neat) spectrometer. ^1H NMR spectra at 90 MHz were recorded with a Varian EM-390 spectrometer, and ^1H NMR at 400 MHz and ^{13}C NMR at 100 MHz were recorded with a JEOL JNM-GX 400 FT NMR spectrometer with internal standard of Me_4Si. High-resolution mass spectra were obtained with a Hitachi Model M-80 spectrometer.

Benzene, dichloromethane (CH_2Cl_2), and *N*,*N*-dimethylformamide (DMF) were dried over CaH_2 and then distilled. Acetone was dried over $CaSO_4$ and then distilled. Pyridine was distilled over NaOH. Tetrahydrofuran (THF) was

distilled over $LiAlH_4$ and then over Na/benzophenone.

Glycol Cleavage of 5 and Successive Wittig Olefination with Benzylidenetriphenylphosphorane. (2*S*,3*S*,4*Z*)- and (2*S*,3*S*,4*E*)-1,3-*O*-Benzylidene-5-phenyl-4-pentene-1,2,3-triol (6Z and 6E). To a solution of **5** (15.0 g, 62.4 mmol) in methanol (350 ml) was added an aqueous solution (150 ml) of $NaIO_4$ (14.7 g, 68.6 mmol). This mixture was stirred for 30 min, and the resulting white solids were removed by filtration. The filtrate was concentrated in vacuo. The residue was partitioned between AcOEt (600 ml) and H_2O (150 ml). The aqueous phase was extracted with AcOEt (2×300 ml). The combined organic phases were dried (Na_2SO_4) and concentrated in vacuo to give an aldehyde, which was subjected to Wittig reaction directly. The Wittig reaction was carried out under an argon atmosphere. To a suspension of benzyltriphenylphosphonium chloride (48.2 g, 124 mmol) in THF (250 ml) was injected BuLi (1.60 M solution in hexane, 77.5 ml, 124 mmol). After being stirred for 1 h, a THF solution (50 ml) of the aldehyde above was added to the ylide solution. After being stirred for 1 h, 1% aqueous NH_4Cl solution (90 ml) and H_2O (300 ml) were added to the mixture. This aqueous mixture was extracted with AcOEt (3×450 ml). The organic phases were combined, dried (Na_2SO_4), and concentrated in vacuo. The residue was treated with a small amount of AcOEt, and insoluble materials were removed. The filtrate was concentrated in vacuo. Column chromatography of the residue (AcOEt/hexane 1:10) provided **6Z** (3.60 g, 21%) and **6E** (11.1 g, 63%). **6Z** as white crystals, mp 106—107 °C: R_f 0.73 (AcOEt/hexane 1:1): $[\alpha]_D^{23}$ −340° (*c* 1.05, $CHCl_3$); IR ν_{max}^{KBr} 3320, 1445, 1390, 1330, 1130, 1075 cm^{-1}; ^1H NMR (90 MHz, $CDCl_3$) δ=2.70—3.10 (br s, 1H), 3.37—3.67 (m, 1H), 4.12 (dq, 2H, *J*=1 and 11 Hz), 4.72 (d, 1H, *J*=9 Hz), 5.63 (s, 1H), 6.07 (dd, 1H, *J*=9 and 12 Hz), 6.79 (d, 1H, *J*=12 Hz), 7.25—7.65 (m, 10H). Found: C, 76.48; H, 6.56%. Calcd for $C_{18}H_{18}O_3$: C. 76.57; H, 6.43%. **6E** as white crystals, mp 109.5—110 °C: TLC R_f 0.65 (AcOEt/hexane 1:1); $[\alpha]_D^{22}$ +61.0° (*c* 1.51, $CHCl_3$); IR ν_{max}^{KBr} 3570, 2980, 1490, 1450, 1395, 1370, 1350, 1215, 1145, 1115, 1070 cm^{-1}; ^1H NMR (90 MHz, $CDCl_3$) δ=2.60—3.00 (br s, 1H), 3.43—3.73 (br s, 1H), 4.05, 4.19 (each dd, each 1H, *J*=1 and 12 Hz), 4.55 (d, 1H, *J*=6 Hz), 5.67 (s, 1H), 6.32 (dd, 1H, *J*=6 and 16.5 Hz), 6.75 (d, *J*=16.5 Hz, 1H), 7.17—7.67 (m, 10H). Found: C, 76.64; H, 6.42%. Calcd for $C_{18}H_{18}O_3$: C, 76.57; H, 6.43%.

Isomerization of 6Z to 6E. A mixture of **6Z** (3.60 g, 12.8 mmol), PhSH (0.66 ml, 6.4 mmol), and AIBN (420 mg, 2.56 mmol) in benzene (120 ml) was refluxed for 30 min. The mixture was then concentrated in vacuo. Pure **6E** (2.92 g, 81%) was obtained by flash column chromatography (AcOEt/hexane 1:10) of the residue.

Epoxidaion of 6E Followed by Treatment with Silica Gel. (2*S*,3*R*,4*R*,5*R*)- and (2*S*,3*R*,4*S*,5*S*)-2-(Hydroxymethyl)-5-phenyltetrahydrofuran-3,4-diol *O*,*O*′-Benzylidene Derivatives (10 and 11). A mixture of **6E** (1.62 g 5.74 mmol) and mCPBA (2.49 g, 14.4 mmol) in CH_2Cl_2 (30 ml) was refluxed for 30 min. The mixture was diluted with CH_2Cl_2 (120 ml) and washed with 20 wt% aqueous $Na_2S_2O_3$ (2×80 ml) and saturated aqueous $NaHCO_3$ (2×80 ml). The organic phase was dried (Na_2SO_4) and concentrated in vacuo to give an inseparable mixture of **8** and **8′** as amorphous solids, which was used in the next step without further purification. The mixture of **8** and **8′** was dissolved in CH_2Cl_2 (120 ml) and silica gel (60 g) was added. The mixture was kept standing for 36 h. Then the silica gel was removed by filtration, washed with CH_2Cl_2 (500 ml), AcOEt (500 ml), and EtOH (250 ml). The combined filtrate and washings were concentrated in vacuo. The residue was purified by flash column chromatography (AcOEt/$PhCH_3$ 1:40, 1:20, and 1:5 successively). From the fractions corresponding to R_f 0.46 (AcOEt/$PhCH_3$ 1:3), compound **11** (1.25 g, 73%) was obtained as crystals, mp 127—128 °C. From the fractions corresponding to R_f 0.21, compound **10** (124 mg) was obtained as crystals, mp 131—132 °C. The fractions corresponding to R_f 0.31 was also concentrated in vacuo to give uncyclized **8**. Thus obtained **8** was treated with silica gel (10 g) in CH_2Cl_2 (20 ml) for 6 days. Filtration and chromatographic purification as described above gave an additional **10** (208 mg, total 332 mg, 19%). **10**: $[\alpha]_D^{25}$ +28.4° (*c* 0.90, $CHCl_3$) IR ν_{max}^{KBr} 3430, 2910, 2880, 1450, 1390, 1335, 1245, 1210, 1125, 1080, 1055 cm^{-1}; ^1H NMR (90 MHz, $CDCl_3$) δ=2.30 (br s, 1H), 3.97—4.30 (m, 4H), 4.50 (d, 1H, *J*=12 Hz), 4.80 (d, 1H, *J*=2 Hz), 5.46 (s, 1H), 7.17—7.60 (m, 10H). Found: C, 72.62; H, 6.12%. Calcd for $C_{18}H_{18}O_4$: C, 72.47; H, 6.08%. **11**: $[\alpha]_D^{23}$ −11.3° (*c* 1.00, $CHCl_3$); IR ν_{max}^{KBr} 3420, 1450, 1390, 1360, 1215, 1150, 1095, 1050 cm^{-1}; ^1H NMR (90 MHz, $CDCl_3$) δ=2.50—2.75 (m, 1H), 3.97—4.60 (m, 5H), 5.01 (d, 1H, *J*=8 Hz), 5.59 (s, 1H), 7.23—7.67 (m, 10H). Found: C, 72.56; H, 6.11%. Calcd for $C_{18}H_{18}O_4$: C, 72.47; H, 6.08%.

(2*S*,3*S*,4*E*)-1,3-*O*-Benzylidene-2-*O*-benzoyl-5-phenyl-4-pentene-1,2,3-triol (7). To a stirred solution of **6E** (6.88 g, 24.4 mmol) in pyridine (180 ml) was added benzoyl chloride (9.26 ml, 78.1 mmol) at 0 °C. After being stirred for 20 h, the resulting crystals were removed by filtration. The filtrate was concentrated in vacuo. The residue was partitioned between CH_2Cl_2 (1500 ml) and saturated aqueous $NaHCO_3$ (500 ml). The organic phase was washed with saturated aqueous $NaHCO_3$ (500 ml) and H_2O (500 ml) successively. The organic phase was dried (Na_2SO_4) and concentrated in vacuo. The resulting crystals were recrystallized from AcOEt to give **7** (7.73 g). The mother liquor was concentrated and recrystallization of the residue gave an additional **7** (1.02 g, total 8.75 g, 93%), mp 164.5—165.5 °C: TLC R_f 0.69 (AcOEt/toluene 1:5), $[\alpha]_D^{22}$ +161° (*c* 1.19, $CHCl_3$); IR ν_{max}^{KBr} 2850, 1715, 1445, 1350, 1265, 1085 cm^{-1}; ^1H NMR (90 MHz, $CDCl_3$) δ=4.22, 4.51 (each d, each 1H, *J*=15 Hz), 4.75—4.90 (m, 1H), 5.07—5.20 (m, 1H), 5.75 (s, 1H), 6.26 (dd, 1H, *J*=6 and 16.5 Hz), 6.69 (d, 1H, *J*=16.5 Hz), 7.17—7.73, 8.07—8.30 (m, 15H). Found: C, 77.90; H, 5.86%. Calcd for $C_{25}H_{22}O_4$: C, 77.70; H, 5.74%.

Conversion of 7 into 10 and 11. Compound **7** (16.4 g, 42.2 mmol) in CH_2Cl_2 (200 ml) was oxidized with mCPBA (18.3 g, 106 mmol) under reflux for 2.5 h. After extractive workup as described in the case of **8** and **8′**, the mixture of **9** and **9′** was obtained. The mixture of **9** and **9′** was dissolved in MeOH (750 ml), and MeONa (1 M in MeOH, 63.6 ml, 63.6 mmol) was added. After being stirred for 2.5 h, the solution was neutralized with 1 M HCl and concentrated in vacuo. Extractive workup (AcOEt/H_2O) of the residue gave a mixture of **8** and **8′**, which was treated with silica gel (600 g, 32 h). Recrystallization of the concentrate of the reaction mixture from MeOH provided **11** (8.37 g). From the mother liquor, an additional **11** (2.13 g, total 10.5 g, 83%) and **10** (759 mg, 6%) were obtained by the similar chromatographic purification and retreatment with silica gel as described above. Compounds **10** and **11** from **6E** and those from **7** were identical in all respects.

Debenzylidenation of 10 and 11. (2*S*,3*R*,4*R*,5*R*)- and (2*S*,3*R*,4*S*,5*S*)-2-(Hydroxymethyl)-5-phenyltetrahydrofuran-3,4-diol (12 and 13). A solution of **10** (845 mg, 2.8 mmol) in a mixture of 1,4-dioxane (20 ml) and 1 M HCl (20 ml) was refluxed for 30 min. The mixture was neutralized with 4 M NaOH, then concentrated in vacuo. The residue was partitioned between AcOEt (40 ml) and water (50 ml). The organic phase was dried (Na_2SO_4) and concentrated. The residue was purified by silica-gel chromatography (AcOEt/hexane 2:3) to give **12** (529 mg, 89%) as a colorless oil: TLC R_f 0.41 (EtOH/$PhCH_3$ 1:4); $[\alpha]_D^{25}$ +24.4° (*c* 0.76, MeOH); IR ν_{max}^{neat} 3380, 2880, 1495, 1455, 1100, 1085 cm^{-1}; ^1H NMR (90 MHz, CD_3OD) δ=3.81—4.41 (m, 5H), 4.52 (d, 1H, *J*=6 Hz), 7.15—7.51 (m, 5H).

Compound **11** (850 mg) was converted into **13** (489 mg, 82%) as described in the preparation of **12** after chromatographic purification, mp 81.5—82.5 °C: TLC R_f 0.17 (EtOH/$PhCH_3$ 1:10); $[\alpha]_D^{29}$ −41.3° (*c* 1.15, MeOH); IR ν_{max}^{KBr} 3400, 2885, 1450, 1340, 1280, 1150 cm^{-1}; ^1H NMR (90 MHz, CD_3OD) δ=3.80—4.12 (m, 3H), 4.19—4.48 (m, 2H), 4.80 (d, 1H, *J*=7.5 Hz), 7.25—7.59 (m, 5H). Found: C, 62.88; H, 6.69%. Calcd for $C_{11}H_{14}O_4$: C, 62.84; H, 6.71%.

***t*-Butyldiphenylsilylation of 12 and 13. (2*S*,3*R*,4*R*,5*R*)- and (2*S*,3*R*,4*S*,5*S*)-2-[(*t*-Butyldiphenylsilyloxy)methyl]-5-phenyltetrahydrofuran-3,4-diol (14 and 15).** To a solution of **12** (10 mg, 0.05 mmol) in DMF (0.5 ml) were added *t*-butylchlorodiphenylsilane (0.015 ml, 0.06 mmol) and imidazole (8 mg, 0.12 mmol). After being stirred for 3.5 h, the silylating reagent (0.03 ml) and imidazole (16 mg) were added, and the mixture was stirred more 2 h. The mixture was concentrated in vacuo, and AcOEt (4 ml) was added to the residue. The insoluble materials were removed by filtration, and the filtrate was concentrated. The residue was purified by PTLC (EtOH/$PhCH_3$ 1:10) to give **14** (17 mg, 79%) as a colorless oil: TLC R_f 0.73 (EtOH/$PhCH_3$ 1:5); ^1H NMR (90 MHz, $CDCl_3$) δ=1.02 (s, 9H), 1.52—1.80, 2.39—2.72 (m, each 1H), 3.55—4.45 (m, 5H), 4.57 (d, 1H, *J*=6 Hz), 7.15—7.85 (m, 15H).

Analogously as described above, compound **13** (20 mg) was converted into **15** (37 mg, 85%). **15** as a colorless oil: TLC R_f 0.66 (AcOEt/hexane 1:2); $[\alpha]_D^{29}$ −31.5° (*c* 1.56, $CHCl_3$); IR ν_{max}^{neat} 3400, 2940, 2860, 1430, 1110 cm^{-1}; ^1H NMR (90 MHz, $CDCl_3$) δ=1.10 (s, 9H), 3.40—3.85 (m, 2H), 3.90—4.53 (m, 5H), 4.92 (d, 1H, *J*=6 Hz), 7.30—7.55, 7.65—7.89 (m, 15H).

Isopropylidenation of 15. A mixture of **15** (21 mg, 0.05 mmol), 2,2-dimethoxypropane (0.008 ml), and CSA (3 mg) in acetone (0.5 ml) was stirred for 2 h, and neutralized with saturated aqueous $NaHCO_3$, then concentrated. The residue was purified by PTLC (AcOEt/hexane 1:10) to give **16** (20 mg, 87%) as a pale yellow oil. **16**: TLC R_f 0.85 (AcOEt/hexane 1:4); $[\alpha]_D^{28}$ −4.3° (*c* 1.00, $CHCl_3$); IR ν_{max}^{neat} 2940, 1430, 1385, 1375, 1215, 1120 cm^{-1}; ^1H NMR (90 MHz, $CDCl_3$) δ=1.08 (s, 9H), 1.32, 1.45 (each s, 3H×2), 4.05 (s, 3H), 4.62—4.98 (m, 2H), 5.12 (s, 1H), 7.30—7.52, 7.62—7.82 (m, 15H).

(2*S*,3*R*,4*S*,5*S*)-2-(Hydroxymethyl)-4-[(methylsulfonyl)oxy]-5-phenyltetrahydrofuran-3-ol *O*,*O*′-Benzylidene Derivative (17). To a stirred solution of **11** (1.67 g, 5.6 mmol) in pyridine (35 ml) were added methanesulfonyl chloride (0.65 ml, 8.4 mmol) and DMAP (137 mg, 1.12 mmol). After being stirred for 2.5 h, the mixture was concentrated in vacuo. The residue was partitioned between CH_2Cl_2 (600 ml) and H_2O (200 ml). The organic phase was dried (Na_2SO_4) and concentrated in vacuo. The resulting crystals were recrystallized from AcOEt to give **17** (1.35 g). The mother liquor was concentrated, and the residue was purified by a silica-gel column chromatography (AcOEt/$PhCH_3$ 1:5) to give an additional **17** (0.58 g, total 1.93 g, 93%), mp 186—186.5 °C. **17**: TLC R_f 0.48 (AcOEt/$PhCH_3$ 1:3); $[\alpha]_D^{22}$ −75.2° (*c* 1.24, $CHCl_3$);IR ν_{max}^{KBr} 2920, 1410, 1350, 1175 cm^{-1}; ^1H NMR (90 MHz, $CDCl_3$) δ=2.83 (s, 3H), 4.00—4.57 (m, 3H), 4.75—5.03 (m, 2H), 5.37 (d, 1H, *J*=6 Hz), 5.58 (s, 1H), 7.30—7.68 (m, 10H). Found: C, 60.75; H, 5.51%. Calcd for $C_{19}H_{20}O_6S$: C, 60.62; H, 5.36%.

Elimination of the Mesyloxy Group in 17, Successive Hydroboration of the Dihydrofuran Derivative 18 Followed by Oxidative Work-up. Conversion of 17 into 10. A mixture of **17** (1.96 g, 5.21 mmol) and *t*-BuOK (2.04 g, 18.2 mmol) in THF (140 ml) was refluxed for 20 min under argon atmosphere. The reaction mixture was mainly consisted of the dihydrofuran **18**, and used directly without purification [**18**: ^1H NMR (90 MHz, $CDCl_3$) δ=4.05—4.45 (m, 2H), 4.70 (d, 1H, *J*=12.5 Hz), 5.00 (t, 1H, *J*=3 Hz), 5.47 (s, 1H), 5.66 (d, 1H, *J*=2.5 Hz), 7.22—7.80 (m, 5H)]. The mixture in THF obtained above was cooled to 0 °C, and BH_3–THF complex (1 M in THF, 31.3 ml, 31.3 mmol) was added. After being stirred for 1.5 h, 2 M aqueous NaOH (26 ml) and H_2O (30 ml) were added successively to the mixture. After being warmed to room temperature, H_2O_2 (35 wt% in H_2O, 28 ml) was added to the mixture which was stirred more 1.5 h. To the mixture was added saturated aqueous Na_2SO_3 (30 ml), and the mixture was stirred for 1 h. This was diluted with AcOEt (500 ml), washed with 0.1 M HCl (100 ml) and saturated aqueous $NaHCO_3$ (100 ml). The organic phase was dried (Na_2SO_4) and concentrated in vacuo. The residue was purified by repeated flash column chromatography (AcOEt/$PhCH_3$ 1:5) to give **10** (1.09 g 65%), which was identical with an authentic sample described above in all respects.

Pfitzner-Moffatt Oxidation of 10 and Successive $NaBH_4$ Reduction. (2*S*,3*R*,4*S*,5*R*)-2-(Hydroxymethyl)-5-phenyltetrahydrofuran-3,4-diol *O*,*O*′-Benzylidene Derivative (20). To a stirred solution of **10** (913 mg, 3.06 mmol) in benzene (85 ml) were added DMSO (1.31 ml, 18.4 mmol), pyridine (0.37 ml, 4.6 mmol), CF_3COOH (0.35 ml, 4.6 mmol), and dicyclohexylcarbodiimide (1.89 g, 9.2 mmol). After being stirred for 30 min, the resulting white solids were filtered off. The filtrate was diluted with AcOEt (500 ml), and this was washed with H_2O (100 ml). The organic phase was dried (Na_2SO_4) and concentrated in vacuo. To the residue was added a small amount of AcOEt, and the precipitates were filtered off. The filtrate was concentrated in vacuo to give crude tetrahydrofuranone **19**, which was reduced directly. The residue was dissolved in MeOH (20 ml), and $NaBH_4$ (174 mg, 4.6 mmol) was added. After being stirred for 1 h, the mixture was neutralized with Amberlite IR-120 (H^+). The resin was removed by filtration and washed with MeOH. The combined filtrate and washings were concentrated in vacuo. The residue was purified by flash column chromatography (AcOEt/$PhCH_3$ 1:20) to give **20** (758 mg, 83%) as white crystals, mp 121—122 °C. **20**: TLC R_f 0.43 (AcOEt/$PhCH_3$ 1:2); $[\alpha]_D^{27}$ +12.7° (*c* 1.42, $CHCl_3$); IR ν_{max}^{KBr} 3560, 2915, 1400, 1225, 1210, 1150, 1095, 1080, 1065 cm^{-1}; ^1H NMR (90 MHz, $CDCl_3$) δ=2.00 (br s, 1H), 3.92—4.01 (m, 1H), 4.18 (dd, 1H, *J*=2 and 13.5 Hz), 4.38 (dd, 1H, *J*=2 and

6 Hz), 4.55 (d, 1H, J=13.5 Hz), 4.54—4.96 (m, 1H), 5.20 (d, 1H, J=9 Hz), 5.53 (s, 1H), 7.25—7.77 (m, 10H). Found: C, 72.34; H, 6.06%. Calcd for $C_{18}H_{18}O_4$: C, 72.47; H, 6.08%.

Inversion of the Hydroxyl Group at C-4 in 11 via Triflate 21. (2*S*,3*R*,4*R*,5*S*)-4-Acetoxy-2-(hydroxymethyl)-5-phenyltetrahydrofuran-3-ol *O,O'*-Benzylidene Derivative (22). To a stirred solution of **11** (1.00 g, 3.35 mmol) in pyridine (20 ml) were added triethylamine (1.87 ml, 13.4 mmol) and trifluoromethanesulfonic anhydride (1.70 ml, 10.1 mmol) at −15 °C. After being stirred at −15 °C for 2 h, the mixture was concentrated in vacuo. The residue was partitioned between AcOEt (200 ml) and H_2O (100 ml). The organic phase was washed with saturated aqueous NaCl (2×100 ml), dried (Na_2SO_4), and concentrated in vacuo to give crude triflate **21**, which was rapidly passed through a silica-gel column by flash chromatography (AcOEt/hexane 1:10 then 1:5). The fractions having R_f 0.55 (AcOEt/hexane 1:2) were concentrated in vacuo to give **21** as a yellow solid (1.31 g). A mixture of **21** (1.31 g) and potassium acetate (1.49 g, 15.2 mmol) in DMF (26 ml) was heated at 135 °C for 1 h with stirring. After being cooled to room temperature, insoluble materials were removed by filtration. The filtrate was concentrated in vacuo. The residue was partitioned between AcOEt (200 ml) and H_2O (50 ml). The organic phase was washed with saturated aqueous NaCl (50 ml), dried (Na_2SO_4), and concentrated. The residue was purified by flash column chromatography (AcOEt/hexane 1:10 then 1:5) to give **22** (902 mg, 79%) as white crystals, mp 123—124 °C. **22**: TLC R_f 0.69 (AcOEt/hexane 1:2); $[\alpha]_D^{21}$ +16.9° (c 1.57, $CHCl_3$); IR ν_{max}^{KBr} 3060, 2920, 2900, 1740, 1370, 1240, 1140 cm^{-1}; ^1H NMR (90 MHz, $CDCl_3$) δ=1.72 (s, 3H), 4.05—4.35, 4.49—4.70 (each m, each 2H), 5.55 (s, 1H), 5.57—5.77 (m, 2H), 7.30—7.69 (m, 10H). Found: C, 70.29; H, 5.94%. Calcd for $C_{20}H_{20}O_5$: C, 70.57; H, 5.92%.

(2*S*,3*R*,4*R*,5*S*)-2-(Hydroxymethyl)-5-phenyltetrahydrofuran-3,4-diol *O,O*-Benzylidene Deriative (23). A mixture of **22** (1.97 g, 5.79 mmol) and MeONa (1 M in MeOH, 8.7 ml, 8.7 mmol) in MeOH (40 ml) was stirred for 30 min. The mixture was neutralized with Amberlite IR-120 (H^+), the resin was removed by filtration, washed with MeOH. The combined filtrate and washings were concentrated in vacuo. The residual crystals were recrystallized from toluene to give **23** (1.53 g). By silica-gel column chromatography of the concentrate of the mother liquor (AcOEt/hexane 1:10 then 1:4), an additional **23** (0.10 g, total 1.63 g, 94%) was obtained. **23** as white crystals, mp 154—155 °C: TLC R_f 0.49 (AcOEt/hexane 1:2); $[\alpha]_D^{23}$ +76.1° (c 1.43, $CHCl_3$); IR ν_{max}^{KBr} 3330, 2920, 1490, 1445, 1390, 1300, 1210, 1125, 1110, 1080, 1065 cm^{-1}; ^1H NMR (90 MHz, $CDCl_3$) δ=1.85 (br s, 1H), 4.02—4.69 (m, 5H), 5.54 (s, 1H), 5.61 (d, 1H, J=3 Hz), 7.30—7.67 (m, 10H). Found: C, 72.22; H, 6.08%. Calcd for $C_{18}H_{18}O_4$: C, 72.47; H, 6.08%.

Direct Preparation of 23 from 21 with KO_2. Compound **21** (20.0 mg), which was prepared from 17.8 mg of **11** as described above, was dissolved in DMSO-DMF (v/v 1/1, 1 ml). To the solution were added a solution of 18-crown-6 (55 mg) and KO_2 (13 mg) in DMSO-DMF (v/v 1/1, 1 ml). After being stirred for 30 min, the mixture was quenched with 5% aqueous $Na_2S_2O_3$ (5 ml). This aqueous solution was extracted with CH_2Cl_2 (4×10 ml). The combined extracts were dried (Na_2SO_4), and concentrated in vacuo. The residue was purified by PTLC (AcOEt/hexane 2:3) to give **23** (10.2 mg, 58% from **11**), which was identical with an authentic sample in all respects.

Debenzylidenation of 20 and 23. (2*S*,3*R*,4*S*,5*R*)- and (2*S*,3*R*,4*R*,5*S*)-2-(Hydroxymethyl)-5-phenyltetrahydrofuran-3,4-diol (24 and 25). By the analogous reaction conditions and work-up as described in the preparation of **12**, 836 mg of **20** was converted into debenzylidene derivative **24** (503 mg, 85%) as white crystals, mp 100.5—101 °C. **24**: TLC R_f 0.22 (EtOH/$PhCH_3$ 1:4); $[\alpha]_D^{28}$ −89.4° (c 1.50, MeOH); IR ν_{max}^{KBr} 3280, 1450, 1315, 1280, 1200, 1145, 1125, 1100, 1050 cm^{-1}; ^1H NMR (90 MHz, CD_3OD) δ=3.77—3.92 (m, 2H), 4.00—4.22 (m, 2H), 4.58 (dd, 1H, J=4.5 and 7.5 Hz), 4.85 (d, 1H, J=3 Hz), 7.25—7.55 (m, 5H). Found: C, 62.68; H, 6.63%. Calcd for $C_{11}H_{14}O_4$: C, 62.84; H, 6.71%.

Analogously, compound **23** (1.57 g) was debenzylidenated to give **25** (1.02 g, 92%) as white crystals, mp 100—101 °C. **25**: TLC R_f 0.31 (EtOH/$PhCH_3$ 1:5); $[\alpha]_D^{23}$ +94.0° (c 2.13, MeOH); IR ν_{max}^{KBr} 3440, 2930, 2880, 1480, 1450, 1285, 1260, 1200, 1070 cm^{-1}; ^1H NMR (90 MHz, CD_3OD) δ=3.80—4.00 (m, 2H), 4.08—4.54 (m, 3H), 5.23 (d, 1H, J=3 Hz), 7.21—7.56 (m, 5H). Found: C, 62.83; H, 6.67%. Calcd for $C_{11}H_{14}O_4$: C, 62.84; H, 6.71%.

Selective Tritylation of the Primary Hydroxyl Groups in 12, 13, 24, and 25. (2*S*,3*R*,4*R*,5*R*)-, (2*S*,3*R*,4*S*,5*S*)-, (2*S*,3*R*,4*S*,5*R*)-, and (2*S*,3*R*,4*R*,5*S*)-5-Phenyl-2-[(triphenylmethoxy)methyl]tetrahydrofuran-3,4-diol (26, 27, 28, and 29). To a solution of **12** (507 mg, 2.41 mmol) in pyridine (15 ml) were added triphenylmethyl chloride (1.01 g, 3.62 mmol) and DMAP (59 mg, 0.48 mmol). After being stirred at 90 °C for 8 h, the mixture was concentrated in vacuo. The residue was dissolved in AcOEt (400 ml) and washed with H_2O (2×100 ml). The organic phase was dried (Na_2SO_4) and concentrated in vacuo. The residue was purified by silica-gel column chromatography (AcOEt/hexane 1:2 containing 1% Et_3N, then EtOH/$PhCH_3$ 1:40) to give **26** (823 mg, 75%) as a pale yellow oil: TLC R_f 0.62 (EtOH/$PhCH_3$ 1:5 containing 1% Et_3N); $[\alpha]_D^{28}$ −26.9° (c 1.16, $CHCl_3$); IR ν_{max}^{neat} 3430, 3060, 3040, 2940, 2880, 1600, 1490, 1450, 1320, 1220, 1150, 1100 cm^{-1}; ^1H NMR (90 MHz, $CDCl_3$) δ=2.80—3.70 (m, 4H), 3.87—4.33 (m, 3H), 4.56 (d, 1H, J=6 Hz), 7.10—7.67 (m, 20H).

Analogously as described above, **13** (440 mg), **24** (500 mg), and **25** (967 mg) were converted into **27** (686 mg, 72%), **28** (851 mg, 79%), and **29** (1.94 g, 93%). **27** as a pale yellow oil: TLC R_f 0.70 (AcOEt/hexane 1:2); $[\alpha]_D^{29}$ −19.1° (c 1.10, $CHCl_3$); IR ν_{max}^{neat} 3410, 3100, 3070, 3045, 2870, 1600, 1495, 1450, 1400, 1325, 1220, 1155, 1080, 1045 cm^{-1}; ^1H NMR (90 MHz, $CDCl_3$) δ=2.57—3.29 (br s, 1H), 3.31—3.71 (m, 2H), 3.99 (dd, 1H, J=4.5 Hz and 7.5 Hz), 4.23—4.52 (m, 2H), 4.85 (d, 1H, J=7.5 Hz), 7.25—7.62 (m, 20H). **28** as a pale yellow oil: TLC R_f 0.37 (AcOEt/hexane 1:2 containing 1% Et_3N); $[\alpha]_D^{27}$ −71.1° (c 1.45, $CHCl_3$); IR ν_{max}^{neat} 3400, 3050, 3025, 2925, 2875, 1600, 1485, 1445, 1215, 1070 cm^{-1}; ^1H NMR (90 MHz, $CDCl_3$) δ=2.41—3.22 (br, 2H), 3.40, 3.72 (each dd, each 1H, J=4.5 and 10.5 Hz), 4.06—4.52 (m, 3H), 4.93 (d, 1H, J=4.5 Hz), 7.25—7.65 (m, 20H). **29** as a colorless foam: TLC R_f 0.66 (EtOH/$PhCH_3$ 1:5 containing 1% Et_3N); $[\alpha]_D^{23}$ +43.6° (c 2.05, $CHCl_3$); IR ν_{max}^{neat} 3450, 3055, 3025, 2930, 2875, 1600, 1490, 1445, 1220, 1180, 1150 cm^{-1}; ^1H NMR (90 MHz, $CDCl_3$) δ=1.45 (br s, 1H), 3.54 (d, 2H, J=6 Hz), 4.12—4.22 (m, 1H), 4.36—4.66 (m, 2H), 5.40 (d, 1H, J=3 Hz), 7.25—7.63 (m, 20H).

Methoxymethylation of Compounds 26, 27, 28, and 29. (2*S*,3*R*,4*R*,5*R*)-, (2*S*,3*R*,4*S*,5*S*)-, (2*S*,3*R*,4*S*,5*R*)-, and (2*S*,3*R*,4*R*,5*S*)-3,4-Bis(methoxymethoxy)-5-phenyl-2-[(triphenyl-

methoxy)methyl]tetrahydrofuran (30, 31, 32, and 33). To a solution of **26** (823 mg, 1.82 mmol) in THF (20 ml) were added *N,N*-diisopropylethylamine (19.0 ml, 109 mmol) and freshly distilled chloromethyl methyl ether (7.47 ml, 98.3 mmol). After being refluxed for 2 h under argon atmosphere, the mixture was diluted with AcOEt (500 ml). The solution was washed with H_2O (100 ml), saturated aqueous NaCl (100 ml), and then dried (Na_2SO_4), and concentrated in vacuo. The residue was purified by siliica-gel chromatography (AcOEt/hexane 1:40 containing 1% Et_3N) to give **30** (875 mg, 89%) as a pale yellow oil: TLC R_f 0.72 (AcOEt/$PhCH_3$ 1:5 containing 1% Et_3N); $[\alpha]_D^{28}$ +48.4° (*c* 1.21,$CHCl_3$); IR ν_{max}^{neat} 3060, 3040, 2950, 2900, 1600, 1495, 1450, 1215, 1150, 1100, 1080 cm^{-1}; ^1H NMR (90 MHz, $CDCl_3$) δ=3.02, 3.33 (each s, each 3H), 3.14—3.43 (m, 1H), 3.68 (dd, 1H, *J*=6 and 9 Hz), 3.88—4.93 (m, 6H), 4.13 (dd, 1H, *J*=3 and 9 Hz), 4.85 (d, 1H, *J*=3 Hz), 7.01—7.86 (m, 20H). Found: C, 75.86; H, 6.90%. Calcd for $C_{34}H_{36}O_6$: C, 75.53; H, 6.71%.

By the analogous procedure for the preparation of **30**, **27** (667 mg), **28** (822 mg), and **29** (1.88 g) were converted into **31** (726 mg, 91%), **32** (888 mg, 90%), and **33** (2.12 g, 94%). **31** as a pale yellow oil: TLC R_f 0.52 (AcOEt/hexane 1:5 containing 1% Et_3N); $[\alpha]_D^{29}$ −12.4° (*c* 1.58, $CHCl_3$); IR ν_{max}^{neat} 3075, 3050, 2960, 2910, 1600, 1500, 1460, 1225, 1160, 1080, 1060, 1035 cm^{-1}; ^1H NMR (90 MHz. $CDCl_3$) δ=3.06, 3.22 (each s, each 3H), 3.12—3.42, 3.50—3.72 (each m, 2H), 4.12 (dd, 1H, *J*=4.5 and 9 Hz, 1H), 4.30—4.78 (m, 6H), 4.83 (d, 1H. *J*=9 Hz), 7.15—7.69 (m, 20H). **32** as a pale yellow oil: TLC R_f 0.44 (AcOEt/hexane 1:3 containing 1% Et_3N); $[\alpha]_D^{26}$ + 11.6° (*c* 2.17, $CHCl_3$); IR ν_{max}^{neat} 3055, 3025, 2950, 2895, 1600, 1490, 1445, 1210, 1145, 1070, 1025 cm^{-1}; ^1H NMR (90 MHz, $CDCl_3$) δ=2.89, 3.20 (each s, each 3H), 3.30—3.85 (m, 2H), 4.02—4.60 (m, 6H), 5.00 (d, 1H, *J*=4.5 Hz), 7.18—7.70 (m, 20H). Found: C, 75.91; H, 6.74%. Calcd for $C_{34}H_{36}O_6$: C, 75.53; H, 6.71%. **33** as a pale yellow oil: TLC R_f 0.68 (AcOEt/$PhCH_3$ 1:4 containing 1% Et_3N); $[\alpha]_D^{24}$ +82.8° (*c* 2.42, $CHCl_3$); IR ν_{max}^{neat} 3060, 3040, 2950, 2900, 1600, 1490, 1445, 1220, 1150, 1110, 1070, 1035 cm^{-1}; ^1H NMR (90 MHz, $CDCl_3$) δ=2.94, 3.25 (each s, each 3H), 3.60 (dd, 1H, *J*=6 and 9 Hz), 4.10—4.80 (m, 8H), 5.15 (d, 1H, *J*=3 Hz), 7.20—7.68 (m, 20H).

Detritylation of 30, 31, 32, and 33. (2*S*,3*R*,4*R*,5*R*)-, (2*S*,3*R*,4*S*,5*S*)-, (2*S*,3*R*,4*S*,5*R*)-, and (2*S*,3*R*,4*R*,5*S*)-2-(Hydroxymethyl)-3,4-bis(methoxymethoxy)-5-phenyltetrahydrofuran (34, 35, 36, and 37). A solution of **30** (853 mg, 1.58 mmol) in a mixture of AcOEt (30 ml) and MeOH (30 ml) containing *p*-TsOH (monohydrate, 601 mg, 3.16 mmol) was stirred for 45 min. The mixture was neutralized with Et_3N and concentrated in vacuo. The residue was purified by silica-gel chromatography (AcOEt/$PhCH_3$ 1:3) to give **34** (440 mg, 94%) as a colorless oil. **34**: TLC R_f 0.30 (EtOH/$PhCH_3$ 1:10); $[\alpha]_D^{27}$ +66.3° (*c* 1.13, $CHCl_3$); IR ν_{max}^{neat} 3460, 2950, 2900, 1600, 1500, 1450, 1400, 1365, 1210, 1150, 1100, 1040, 1030 cm^{-1}; ^1H NMR (90 MHz) δ=2.45 (br s, 1H), 3.24 (s, 6H), 3.66—4.39 (m, 5H), 4.39—4.85 (m, 5H), 7.07—7.49 (m, 5H); MS *m/z* calcd for $C_{15}H_{21}O_6$ (M^+−H) 297.1336, observed 297.1329.

Analogously as described above, **31** (712 mg), **32** (839 mg), and **33** (2.12 g) were converted into **35** (306 mg, 78%), **36** (332 mg, 72%), and **37** (1.10 g, 94%). **35** as a colorless oil: TLC R_f 0.20 (AcOEt/hexane 1:2) $[\alpha]_D^{28}$ +5.2° (*c* 1.63, $CHCl_3$); IR ν_{max}^{neat} 3450, 2950, 2900, 1600, 1490, 1450, 1400, 1360, 1300, 1220, 1150, 1080, 1050, 1020 cm^{-1}; ^1H NMR (90 MHz, $CDCl_3$) δ=2.85 (br s, 1H), 3.15, 3.42 (each s, each 3H), 3.82 (d, 2H, *J*=6 Hz), 4.05 (dd, 1H, *J*=4.5 and 7.5 Hz), 4.24—4.78 (m, 6H), 4.93 (d, 1H, *J*=7.5 Hz), 7.18—7.46 (m, 5H) MS *m/z* calcd for $C_{15}H_{23}O_6$ (M^++H), 299.1493, observed 299.1497. **36** as a colorless oil: TLC R_f 0.12 (AcOEt/hexane 1:2); $[\alpha]_D^{26}$ +2.4° (*c* 1.52, $CHCl_3$); IR ν_{max}^{neat} 3470, 2950, 2900, 1600, 1500, 1460, 1370, 1260, 1220, 1155, 1030 cm^{-1}; ^1H NMR (90 MHz, $CDCl_3$) δ=2.90, 3.45 (each s, each 3H), 3.92 (d, 2H, *J*=4.5 Hz), 4.05—4.50, 4.61—4.85 (m, 7H), 5.00 (d, 1H, *J*=3 Hz), 7.58—7.86 (m, 5H). Found: C, 60.63; H, 7.51%. Calcd for $C_{15}H_{22}O_6$: C, 60.39; H, 7.43%. **37** as a colorless oil: TLC R_f 0.18 (AcOEt/hexane 1:2); $[\alpha]_D^{24}$ +89.3° (*c* 1.24, $CHCl_3$); IR ν_{max}^{neat} 3450, 2950, 2890, 1600, 1495, 1455, 1400, 1360, 1215, 1150, 1105, 1045 cm^{-1}; ^1H NMR (90 MHz, $CDCl_3$) δ=2.40 (br s, 1H), 2.98, 3.48 (each s, each 3H), 3.90 (dd, 2H,*J*=3 and 6 Hz), 4.1—4.59 (m, 5H), 4.75 (s, 2H), 5.25 (d, 1H, *J*=3.5 Hz), 7.22—7.52 (m, 5H).

Collins Oxidation of 34, 35, 36, and 37, and Successive Wittig Olefination with (Ethoxycarbonylmethylene)triphenylphosphorane. (2*S*,3*R*,4*R*,5*R*)-, (2*S*,3*R*,4*S*,5*S*)-, (2*S*,3*R*,4*S*,5*R*)-, and (2*S*,3*R*,4*R*,5*S*)-2-[(*Z*)- and (*E*)-2-(Ethoxycarbonyl)-ethenyl]-3,4-bis(methoxymethoxy)-5-phenyltetrahydrofuran (38Z and 38E, 39Z and 39E, and 40Z and 40E, and 41Z and 41E). The oxidation was carried out under argon atmosphere. To a mixture of pyridine (3.40 ml, 42.0 mmol) and CH_2Cl_2 (30 ml) was added CrO_3 (2.10 g, 21.0 mmol) at 0 °C. After being stirred for 13 h, a solution of **34** (418 mg, 1.40 mmol) in CH_2Cl_2 (5 ml) was added to the mixture. The mixture was stirred for 15 min, and applied on a short silica-gel column (12 g). The column was eluted with ether to give an aldehyde [R_f 0.46 (AcOEt/$PhCH_3$ 1:2)], which was subjected to the Wittig reaction. A mixture of the aldehyde obtained and (ethoxycarbonylmethylene)triphenylphosphorane (975 mg, 2.80 mmol) in MeOH (10 ml) was stirred for 30 min, and concentrated in vacuo. The residue was purified by flash chromatography (AcOEt/hexane 1:10 then 1:5) to give **38Z** (320 mg, 62%) and **38E** (47 mg, 9%). **38Z** as a colorless oil: TLC R_f 0.71 (AcOEt/$PhCH_3$ 1:2); $[\alpha]_D^{29}$ +176° (*c* 1.13, $CHCl_3$); IR ν_{max}^{neat} 3000, 2950, 2900, 1720, 1655, 1600, 1500, 1450, 1200, 1155, 1110 cm^{-1}; ^1H NMR (90 MHz, $CDCl_3$) δ=1.30 (t, 3H, *J*=7.5 Hz), 3.18, 3.35 (each s, each 3H), 4.06—4.21 (m, 1H), 4.18 (q, 2H, *J*=7.5 Hz), 4.42—4.85 (m, 6H), 5.43—5.61 (m, 1H), 5.92 (dd, 1H, *J*=1.5 and 12 Hz), 6.53 (dd, 1H, *J*=7.5 and 12 Hz), 7.23—7.55 (m, 5H). Found: C, 62.47; H, 7.10%. Calcd for $C_{19}H_{26}O_7$: C, 62.28; H, 7.15%. **38E** as a colorless oil: TLC R_f 0.62 (AcOEt/$PhCH_3$ 1:2); $[\alpha]_D^{30}$ +15.7° (*c* 0.96, $CHCl_3$); IR ν_{max}^{neat} 3000, 2950, 2900, 1720, 1665, 1600, 1500, 1470, 1455, 1370, 1305, 1265, 1220, 1180, 1155, 1105 cm^{-1}; ^1H NMR (90 MHz, $CDCl_3$) δ=1.30 (t, 3H, *J*=7.5 Hz), 3.22, 3.34 (each s, each 3H), 4.06—4.22 (m, 2H), 4.21 (q, 2H, *J*=7.5 Hz), 4.44—4.79 (m, 5H), 4.82 (d, 1H, *J*=4.5 Hz), 6.23 (dd, 1H, *J*=1.5 and 16.5 Hz), 7.08 (dd, 1H, *J*=6 and 16.5 Hz), 7.22—7.51 (m, 5H). Found: C, 61.99; H, 6.99%. Calcd for $C_{19}H_{26}O_7$: C, 62.28; H, 7.15%.

By the analogous reaction conditions and work-up described for preparation of 38Z and **38E**, **35** (264 mg), **36** (345 mg), and **37** (944 mg) were converted into **39Z** (188 mg, 58%) and **39E** (16 mg, 5%), **40Z** (305 mg, 72%) and **40E** (23 mg, 5%), and **41Z** (614 mg, 53%) and **41E** (46 mg, 4%). **39Z** as a colorless oil: TLC R_f 0.46 (AcOEt/hexane 1:4); $[\alpha]_D^{29}$ +34.5° (*c* 1.56, $CHCl_3$); IR ν_{max}^{neat} 3000, 2960, 2950, 2900, 2850, 1720, 1655, 1600 1500, 1470, 1460, 1420, 1400, 1310, 1200, 1160 cm^{-1}; ^1H NMR (90 MHz, $CDCl_3$) δ=1.30 (t, 3H, *J*=7.5 Hz), 3.11, 3.39 (each s, each 3H), 4.10—4.30 (m, 1H),

4.20 (q, 2H, J=7.5 Hz), 4.40—4.82 (m, 5H), 5.08 (d, 1H, J=7.5 Hz), 5.78—5.98 (m, 1H), 5.95 (dd, 1H, J=1 and 12 Hz), 6.50 (dd, 1H, J=7.5 and 12 Hz), 7.20—7.55 (m, 5H). Found: C, 62.18; H, 7.06%. Calcd for $C_{19}H_{26}O_7$: C, 62.28; H, 7.15%. **39E** as a colorless oil: TLC R_f 0.28 (AcOEt/hexane 1:4); $[\alpha]_D^{29}$ −17.6° (*c* 1.48, $CHCl_3$); IR ν_{max}^{neat} 3000, 2950, 2900, 2835, 1720, 1660, 1600, 1500, 1470, 1460, 1400, 1370, 1300, 1270, 1220, 1180, 1155, 1130 cm^{-1}; ^1H NMR (90 MHz, $CDCl_3$) δ=1.28 (t, 3H, J=7.5 Hz), 3.15, 3.40 (each s, each 3H), 4.17 (q, 2H, J=7.5 Hz), 4.10—4.82 (m, 6H), 4.82—5.05 (m, 1H), 5.00 (d, 1H, J=7.5 Hz), 6.11 (dd, 1H, J=1 and 16.5 Hz), 7.03 (dd, 1H, J=6 and 16.5 Hz), 7.30—7.57 (m, 5H). Found: C, 61.96; H, 7.02%. Calcd for $C_{19}H_{26}O_7$: C, 62.28; H, 7.15%. **40Z** as a colorless oil: TLC R_f 0.49 (AcOEt/hexane 1:3); $[\alpha]_D^{25}$ +6.8° (*c* 1.33, $CHCl_3$); IR ν_{max}^{neat} 2950, 2900, 1710, 1645, 1600, 1500, 1450, 1410, 1380, 1360, 1260, 1185, 1150 cm^{-1}; ^1H NMR (90 MHz, $CDCl_3$) δ=1.31 (t, 3H, J=7.5 Hz), 2.90, 3.39 (each s, each 3H), 4.20 (q, 2H, J=7.5 Hz), 4.30—4.82 (m, 6H), 5.05 (d, 1H, J=3 Hz), 5.82 (t, 1H, J=4.5 HZ), 5.98 (d, 1H, J=12 Hz), 6.66 (dd, 1H, J=4.5 and 12 Hz), 7.26—7.58 (m, 5H); MS *m/z* calcd for $C_{19}H_{26}O_7$ (M^+), 366.1676, observed, 366.1662. **40E** as a colorless oil: TLC R_f 0.30 (AcOEt/hexane 1:3); $[\alpha]_D^{25}$ −79.8° (*c* 1.42, $CHCl_3$); IR ν_{max}^{neat} 3000, 2950, 2900, 1720, 1660, 1600, 1500, 1450, 1370, 1300, 1270, 1250, 1215, 1150 cm^{-1}; ^1H NMR (90 MHz, $CDCl_3$) δ=1.32 (t, 3H, J=7.5 Hz), 2.90, 3.40 (each s, each 3H), 4.22 (q, 2H, J=7.5 Hz), 4.21—4.86 (m, 7H), 5.05 (d, 1H, J=3 Hz), 6.09 (d, 1H, J=15 Hz), 7.25 (dd, 1H, J=6 and 15 Hz), 7.32—7.56 (m, 5H); MS *m/z* calcd for $C_{19}H_{26}O_7$ (M^+) 366.1676, observed 366.1669. **41Z** as a colorless oil: TLC R_f 0.60 (AcOEt/hexane 1:2); $[\alpha]_D^{23}$ +161.8° (*c* 1.66, $CHCl_3$); IR ν_{max}^{neat} 2980, 2950, 2890, 1715, 1640, 1600, 1490, 1450, 1410, 1380, 1360, 1300, 1190, 1150 cm^{-1}; ^1H NMR (90 MHz, $CDCl_3$) δ= 1.31 (t, 3H, J=7.5 Hz), 2.97, 3.40 (each s, each 3H), 4.22 (q, 2H, J=7.5 Hz), 4.18—4.73 (m, 6H), 5.40 (d, 1H, J=3.5 Hz), 5.80—6.00 (m, 1H), 5.95 (dd, 1H, J=1.5 and 12 Hz), 6.50 (dd, 1H, J=7.5 and 12 Hz), 7.27—7.58 (m, 5H); MS *m/z* calcd for $C_{19}H_{26}O_7$ (M^+) 366.1677, observed 366.1688. **41E** as a colorless oil: TLC R_f 0.51 (AcOEt/hexane 1:2); $[\alpha]_D^{23}$ +116.2° (*c* 1.79, $CHCl_3$); IR ν_{max}^{neat} 2980, 2950, 1720, 1660, 1600, 1500, 1455, 1370, 1300, 1260, 1215, 1180, 1150 cm^{-1}; ^1H NMR (90 MHz, $CDCl_3$) δ=1.30 (t, 3H, J=7.5 Hz), 2.95, 3.43 (each s, each 3H), 4.22 (q, 2H, J=7.5 Hz), 4.11—4.52 (m, 4H), 4.71 (d, 2H, J=3 Hz), 4.98—5.18 (m, 1H), 5.31 (d, 1H, J=3 Hz), 6.23 (dd, 1H, J=2.5 and 16.5 Hz), 7.11 (dd, 1H, J=5.5 and 16.5 Hz), 7.29—7.55 (m, 5H); MS *m/z* calcd for $C_{19}H_{26}O_7$,(M^+) 366.1677, observed 366.1667.

Demethoxymethylation of 38Z, 39Z, 40Z, and 41Z Accompanied by γ-Lactonization. (+)-Altholactone (1), (+)-7,8-Di-*epi*- (2), (+)-7-*epi*- (3), and (+)-8-*epi*-Altholactone (4). A solution of **38Z** (320 mg, 0.87 mmol) in a mixture of 1 M HCl (8 ml) and 1,4-dioxane (8 ml) was refluxed for 1 h and concentrated in vacuo. The residue was partitioned between AcOEt (100 ml) and saturated aqueous $NaHCO_3$ (30 ml). The organic phase was dried (Na_2SO_4) and concentrated in vacuo. The residue was purified by flash chromatography (AcOEt/hexane 1:2) to give **1** (195 mg, 96%) as needles, mp 113—114 °C: TLC R_f 0.40 (AcOEt/hexane 1:1); $[\alpha]_D^{33}$ +180.8° (*c* 0.52 EtOH); IR ν_{max}^{KBr} 3430, 3070, 3040, 2950, 2930, 2900, 1730, 1640, 1600, 1490, 1365, 1245, 1150, 1100, 1090 cm^{-1}; ^1H NMR (400 MHz, $CDCl_3$) δ=2.66 (d, 1H, J=4.4 Hz), 4.45 (dd, 1H, J=2.4 and 5.9 Hz, after irradiation of the doublet at δ=2.66), 4.65 (1H, t, J=5.4 Hz), 4.74 (d, 1H, J=5.9 Hz), 4.95 (dd, 1H, J=2.4 and 5.4 Hz), 6.22 (d, 1H, J=10.2 Hz), 6.99 (dd, 1H, J=5.4 and 10.2 Hz), 7.29—7.36 (m, 5H) ^{13}C NMR (100 MHz, $CDCl_3$) δ=68.15 (d), 83.56 (d), 86.03 (d), 86.63 (d), 123.59 (d), 126.12 (d), 128.34 (d), 128.63 (d), 138.12 (s), 140.56 (d), 161.70 (s). Found: C, 67.24; H, 5.18%. Calcd for $C_{13}H_{12}O_4$: C, 67.23; H, 5.21%.

By the analogous procedure described for the preparation of **1**, **39Z** (164 mg), **40Z** (305 mg), and **41Z** (271 mg) were converted into **2** (81.5 mg, 78%), **3** (153 mg, 79%), and **4** (140 mg, 82%), respectively. **2** as a needles, mp 99—100 °C; TLC R_f 0.52 (AcOEt/hexane 1:1); $[\alpha]_D^{30}$ +74.1° (*c* 0.54, EtOH); IR ν_{max}^{KBr} 3430, 3080, 3050, 2945, 1730, 1645, 1610, 1500, 1460, 1400, 1255, 1170, 1130 cm^{-1}; ^1H NMR (400 MHz, $CDCl_3$) δ=3.30 (d, 1H, J=6.4 Hz), 4.26 (dd, 1H, J=5.4 and 7.3 Hz, after irradiation of the doublet at δ=3.30), 4.78 (d, 1H, J=7.3 Hz), 4.88 (dd, 1H, J=4.4 and 5.9 Hz), 5.04 (dd, 1H, J=5.4 and 5.9 Hz), 6.20 (d, 1H, J=9.3 Hz), 6.87 (dd, 1H, J=4.4 and 9.3 Hz), 7.30—7.38 (m, 5H); ^{13}C NMR (100 MHz, $CDCl_3$) δ=67.73 (d), 78.32 (d), 78.51 (d), 83.30 (d), 122.95 (d), 125.69 (d), 128.27 (d), 128.62 (d), 138.47 (s), 141.77 (d), 161.23 (s). Found: C, 67.21; H, 5.20%. Calcd for $C_{13}H_{12}O_4$; C, 67.23; H, 5.21%. **3** as needles, mp 117—117.5 °C: TLC R_f 0.43 (AcOEt/hexane 1:1); $[\alpha]_D^{30}$ +23.0° (*c* 0.50, EtOH); IR ν_{max}^{KBr} 3380, 3050, 2940, 2880, 1710, 1635, 1600, 1480, 1400, 1345, 1280, 1245, 1200, 1155 cm^{-1}; ^1H NMR (400 MHz, $CDCl_3$) δ=2.24 (d, 1H, J=5.9 Hz), 4.52 (t, 1H, J=4.4 Hz, after irradiation of the doublet at δ=2.24), 4.78 (ddd, 1H, J=1.0, 3.4, and 7.8 Hz), 5.06 (d, 1H, J=4.4 Hz), 5.22 (dd, 1H, J=4.4 and 7.8 Hz), 6.11 (dd, 1H, J=1.0 and 10.3 Hz), 6.85 (dd, 1H, J=3.4 and 10.3 Hz), 7.29—7.39 (m, 5H). ^{13}C NMR (100 MHz, $CDCl_3$) δ=67.23 (d), 73.70 (d), 79.69 (d), 80.72 (d), 121.56 (d), 126.90 (d), 128.32 (d), 128.44 (d), 135.28 (s), 141.70 (d), 161.21 (s). Found: C, 67.23; H, 5.40%. Calcd for $C_{13}H_{12}O_4$: C, 67.23; H, 5.21%. **4** as needles, mp 193.5—194 °C: TLC R_f 0.46 (AcOEt/hexane 1:1); $[\alpha]_D^{26}$ +224° (*c* 0.5, EtOH); IR ν_{max}^{KBr} 3440, 3060, 2940, 2920, 2860, 1700, 1635, 1600, 1490, 1450, 1385, 1355, 1325, 1260, 1255, 1195, 1160 cm^{-1}; ^1H NMR (400 MHz, $CDCl_3$) δ=1.66 (d, 1H, J=2.4 Hz), 4.50 (d, 1H, J=2.0 Hz, after irradiation of the doublet at δ 1.16), 4.88 (t 1H, J=4.9 Hz), 5.08 (dd, 1H, J=2.0 and 4.9 Hz), 5.35 (d, 1H, J=2.0 Hz), 6.20 (d, 1H, J=9.8 Hz), 7.00 (dd, 1H, J=4.9 and 9.8 Hz), 7.33—7.43 (m, 5H); ^{13}C NMR (100 MHz, $CDCl_3$) δ=68.13 (d), 77.89 (d), 83.54 (d), 84.25 (d), 123.08 (d), 126.62 (d), 128.62 (d), 128.89 (d), 134.72 (s), 140.59 (d), 161.01 (s). Found: C, 67.09; H, 5.43%. Calcd for $C_{13}H_{12}O_4$: C, 67.23; H, 5.21%.

We are grateful to Mr. Hisao Arita of Keio University for performing elemental analyses. Support for the biological assays was obtained from grant No. 30909 from the National Cancer Institute, and cytotoxicities were determined through the cooperation of the Cell Culture Laboratories, Purdue Cancer Research Center.

References

1) The synthetic part of this work was presented at the 56th National Meeting of the Chemical Society of Japan, Tokyo, April 1—4 1988. Abstract 4IXB 31.

2) J. W. Loder and R. H. Nearn, *Heterocycles*, **7**, 113 (1977).

3) A. A. E. El-Zayat, N. R. Ferrigni, T. G. McCloud, A. T. McKenzie, S. R. Byrn, J. M. Cassady, C.-j. Chang, and J.

L. McLaughlin, *Tetrahedron Lett.*, **26**, 955 (1985). In this communication, compound **1** was named "goniothalenol," however, the name "altholactone" used in Ref. 2 has a precedence.

4) Isolation and structure determination of (+)-(*S*)-goniothalamin: J. R. Hlubucek and A. V. Robertson, *Aust. J. Chem.*, **20**, 2199 (1967). K. Jewers, J. B. Davis, J. Dougan, A. H. Manchanda, G. Blunden, A. Kyi, and S. Wetchapinan, *Phytochemistry*, **11**, 2025 (1972). The absolute configuration of natural (+)-goniothalamin is still a confusing problem. The following enantiospecific syntheses of (*S*)- and/or (*R*)-goniothalamin reveal that natural (+)-enantiomer should have *R* configuration: H. H. Meyer, *Liebigs Ann. Chem.*, **1979**, 484; B. O'Connor and G. Just, *Tetrahedron Lett.*, **27**, 5201 (1986); F. Gillard, D. Heissler, and J.-J. Riehl, *J. Chem. Soc., Perkin Trans. 1*, **1988**, 2291. (+)-Goniothalamin and its (+)-oxide were isolated from the other plant recently: T. W. Sam, C. Sew-Yew, S. Matsjeh, E. K. Gan, D. Razak, and A. L. Mohamed, *Tetrahedron Lett.*, **28**, 2541 (1987).

5) (+)-Goniodiol and (+)-goniotriol: S. K. Talapatra, D. Basu, T. Deb, S. Goswami, and B. Talapatra, *Indian J. Chem. Sect. A*, **24**, 29 (1985).

6) H. Achenbach and G. Wittmann, *Tetrahedron Lett.*, **1970**, 3259.

7) A. Alemany, C. Márquez, C. Pascual, S. Valverde, A. Perales, J. Fayos, and M. Martínez-Ripoll, *Tetrahedron Lett.*, **1979**, 3579.

8) Isolation and structure determination of (+)-anamarine: A. Alemany, C. Márquez, C. Pascual, S. Valverde, M. Martínez-Ripoll, J. Fayos, and A. Perales, *Tetrahedron Lett.*, **1979**, 3583. Total synthesis of unnatural (−)-anamarine: F. W. Lichtenthaler, K. Lorenz, and W.-y. Ma, *ibid.*, **28**, 47 (1987); S. Valverde, A. Hernandez, B. Herradon, R. M. Rabanal, and M. Martin-Lomas, *Tetrahedron*, **43**, 3499 (1987). Total synthesis of natural (+)-anamarine: K. Lorenz and F. W. Lichtenthaler, *Tetrahedron Lett.*, **28**, 6437 (1987).

9) Isolation: A. D. Argoudelis, J. H. Coats, and R. R. Herr, *Antimicrob. Agents Chemother.*, **1965**, 801. Structure determination: A. D. Argoudelis and J. F. Zieserl, *Tetrahedron Lett.*, **1966**, 1969; K. Fukuyama, Y. Katsube, A. Noda, T. Hamasaki, and Y. Hatsuda, *Bull. Chem. Soc. Jpn.*, **51**, 3175 (1978). Total synthesis of (+)-asperlin: H. Hiraoka, K. Furuta, N. Ikeda, and H. Yamamoto, *ibid.*, **57**, 2777 (1984). Total synthesis of natural (+)-asperlin: T. Murayama, T. Sugiyama, and K. Yamashita, *Agric. Biol. Chem.*, **50**, 1923 (1986); **51**, 2055 (1987).

10) J.-P. Gesson, J.-C. Jacquesy, and M. Mondon, *Tetrahedron Lett.*, **28**, 3945, 3949 (1987).

11) J. G. Gillhouley and T. K. M. Shing, *J. Chem. Soc., Chem. Commun.*, **1988**, 976.

12) Total synthesis of **1** was reported preliminarily as a communication: K. Tadano, Y. Ueno, and S. Ogawa, *Chem. Lett.*, **1988**, 111.

13) A. B. Foster, A. H. Haines, J. Homer, J. Lehmann, and L. F. Thomas, *J. Chem. Soc.*, **1961**, 5005.

14) L. D. Bergelson, L. I. Barsukov, and M. M. Shemyakin, *Tetrahedron*, **23**, 2709 (1967).

15) M. Schwarz, G. F. Graminski, and R. M. Waters, *J. Org. Chem.*, **51**, 260 (1986).

16) The *t*-butyldiphenylsilyl ether of **6E** was prepared by the standard procedure. Epoxidation of this silyl ether with mCPBA gave the (*S,S*)-epoxide and (*R,R*)-epoxide in 88% and 9% yields, respectively. The major epoxide was converted into **11** in 86% yield by desilylation followed by silica-gel-promoted cyclization.

17) For reviews on silica-gel promoted organic synthesis: A. McKillop and D. W. Young, *Synthesis*, **1979**, 401; M. Hojo and R. Masuda, *Yuki Gosei Kagaku Kyokai Shi*, **37**, 557 (1979).

18) Recently, a report concerning glycosides formation via intramolecular ring closure of hydroxy-enol ethers derived from carbohydrates is published: F. Nicotra, L. Panza, F. Ronchetti, G. Russo, and L. Toma, *J. Chem. Soc., Perkin Trans. 1*, **1987**, 1319.

19) G. H. Jones and J. G. Moffatt, "Methods in Carbohydrate Chemistry," ed by R. L. Whistler and J. N. BeMiller, Academic Press, New York (1972), Vol. VI, p. 315.

20) The oxidation of **10** was examined with PCC and under the Swern conditions. Both cases resulted in the formation of complex mixture.

21) The transformation of **11** to **23** was investigated under the following conditions. a) PCC or Swern oxidation of **11** gave a complex mixture. b) The Mitsunobu inversion of **11** with benzoic acid resulted in a recovery of **11**. c) S_N2 reaction of the mesylate **17** with AcONa, AcOK, or BzONa in hot DMF did not proceed and **17** was recovered intact.

22) E. J. Corey, K. C. Nicolaou, M. Shibasaki, Y. Machida, and C. S. Shiner, *Tetrahedron Lett.*, **1975**, 3183.

23) J. C. Collins and W. W. Hess, *Org. Synth.*, **52**, 5 (1972).

24) $NaBH_4$ reduction of the aldehydes derived from **34—37** regenerated **34—37** as a sole product. These results indicate that no epimerization occurred under the Collins oxidation conditions.

 © 1989 The Chemical Society of Japan Bull. Chem. Soc. Jpn., 62, 2338—2341 (1989) [Vol. 62, No. 7

Synthesis and Reaction of 2,2′-Biquinolyl

Shoji WAKABAYASHI,* Yukihiro KUBO, Takashi TAKEDA, Jun-ichi UENISHI, and Shigeru OAE*
Department of Chemistry, Faculty of Science, Okayama University of Science, Ridai-cho, Okayama 700
(Received January 9, 1989)

A title compound is readily prepared from methyl 2-quinolyl sulfoxide (**3**) with methylmagnesium bromide in excellent yield and an ipso addition of alkylmagnesium halides to 2,2′-biquinolyl (**4**) is also described.

Ligand coupling reaction of aryl sulfoxides with Grignard reagents has been developed by S. Oae and co-workers.[1] This reaction is interesting in not only mechanistic aspects[2] but also synthetic applicabilities for various types of benzyl-, allyl-, or aryl-substituted aromatic compounds.[3] Recently a formation of

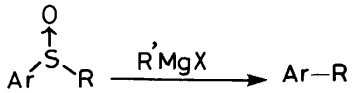

Ar:Heteroaryl, Aryl
R :Benzyl, Allyl, Aryl
R':Alkyl

bi(heteroaryl) compounds has been reported in the reaction of alkyl pyridyl sulfoxides with alkyl Grignard reagents.[4] This homolytic coupling reaction was found by treating of methyl 2-pyridyl sulfoxide (**1**) with a primary alkyl Grignard reagent in ether or THF and resulted 2,2′-bipyridyl (**2**) in moderate yields.

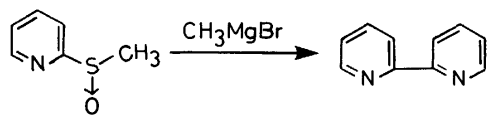

1 2

In an extension of this study to obtain bi(heteroaryl) compounds, we would like to describe herein a facile preparation of 2,2′-biquinolyl (**4**) under very mild conditions and also the first example of an alkyl Grignard addition to **4**.

When methyl 2-quinolyl sulfoxide (**3**)[5] was treated with one equivalent of methylmagnesium bromide at room temperature in THF, the reaction completed instantaneously giving **4** exclusively in 90 to 98% yields. This reaction takes place even at lower temperatures. The reaction appears to complete in less than 20 s at −78 °C affording **4** in more than 90% yield. This remarkably high reaction rate is in contrast to that of the formation of **2**, which required about 10 hours to complete the reaction of **1** with methylmagnesium bromide at −78 °C. Approximately the formation of **4** is at least 10^3 faster than that of **2**. The compound **4** is currently used for a wide poupose of coating materials, chelating reagents and catalysts as a copper complex in the modern technological fields.[6]

Among the recent reports for the preparation of **4**, i.e., palladium-catalyzed coupling reaction,[7] nickel-catalyzed coupling reaction[8] or electrochemical reaction,[9] this preparative method offers several advantages such as the mildest reaction conditions, the shortest reaction time, the simple operation and also the high yield.

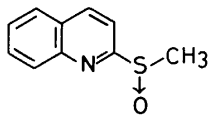

3

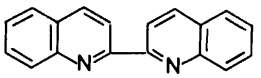

4

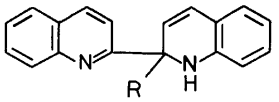

5a-g

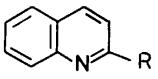

6a-g

R; a, CH_3-
b, CH_3CH_2-
c, $(CH_3)_3CHCH_2$-
d, $(CH_3)_2CH$-
e, Ph-
f, $CH_2=CHCH_2$-
g, $CH_2=CH(CH_3)CH$-

Another interesting aspect is that the reaction of the same substrate **3** with two equivalents of methylmagnesium bromide did not stop at the same stage of **4** but proceeded further. Eventualy 2-methyl-1,2-dihydro-2,2′-biquinolyl (**5a**) was isolated in 79% yield. This compound was identified by spectroscopic analysis. A mass spectrum has shown the molecular ion peak at 272 (*m/z*), which has lost a methyl group to give a base peak appearing at 257 (*m/z*). In a ^{1}H NMR spectrum a singlet peak at δ 1.83 for 3 protons indicates quaternary methyl group and a broad singlet of secondary amine proton appears at δ 5.01. A ^{13}C NMR spectrum has also supported this structure. Thus the spectrum shows the C-2 substituted methyl carbon at δ 30.84 and C-2 methine carbon at δ 59.15. These carbons appear as a quartet and a singlet

Table 1. Reaction of **3** with Grignard Reagents

Grignard reagent	(equiv)	Products (yield/%)
CH_3MgBr	1.1	**4** (98)
	2.1	**5a** (79)
CH_3CH_2MgBr	2.1	**5b** (61)
$(CH_3)_2CHCH_2MgCl$	2.1	**5c** (77)
$(CH_3)_2CHMgCl$	2.1	**5d** (26)[a]
PhMgBr	2.1	**6e** (20) **4** (50)
$CH_2=CHCH_2MgCl$	2.1	**6f** (80)
$CH_2=CH(CH_3)CHMgCl$	2.1	**6g** (74)

a) The major product was isopropyl 2-quinolyl sulfoxide in 61% yield.

respectively by a off-resonance experiment. In a IR spectrum an absorption of the secondary amine is observed at 3390 cm^{-1}.

Table 1 lists the results in the reactions with several Grignard reagents. Ethyl-, isobutyl-, and isopropylmagnesium halides provided the corresponding C-2 alkyl-substituted products **5b**, **5c**, and **5d** in 61%, 77%, and 26% yields, respectively. In the case of isopropylmagnesium chloride the ligand-exchange product, isopropyl 2-quinolyl sulfoxide was obtained in 61% yield along with the desired product. The reaction of phenylmagnesium bromide gave none of **5e** but **4** as a major product and 2-phenylquinoline (**6e**)[10] as a minor product. Normal ligand-coupling reaction is predominant in the reaction of allyl- and (1-methyl-2-propenyl)magnesium chloride affording 2-allyl- and 2-(1-methyl-2-propenyl)quinolines **6f** and **6g**[11] along with unseparable isomeric α,β-unsaturated compounds in 80% and 74% yields.

The compound **5** have been confirmed to be formed from 2,2′-biquinolyl intermediate. In fact the reaction of **4** with one equivalent of alkylmagnesium halides such as methyl-, ethyl-, isobutyl-, and isopropylmagnesium halides, afforded exclusively the corresponding C-2 alkyl-substituted products, **5a**, **5b**, **5c**, and **5d** in 59%, 68%, 90%, and 39% yields, respectively. However the reaction with phenylmagnesium bromide and allylmagnesium chloride have shown to be totally unreacted. The products **5a—d** are considerably stable in frozen benzene at −20 °C for a month but are oxidized spontaneously at room temperature to **4** within a couple of days. Particularly, in the case of **5d** the transformation to **4** takes within a half day in $CDCl_3$ which is much faster than the others. Meanwhile, oxidation of **5a** with DDQ in benzene afforded **4** instantaneously at 0 °C. The half life time of **5a** in acidic ethanol containing 5% of *dl*-10-camphorsulfonic acid was 4 hours and that under the sunlight or ultraviolet irradiation was about a half hour in the same solvent. But no transformation was observed in a day in basic ethanol containing 5% of triethylamine.

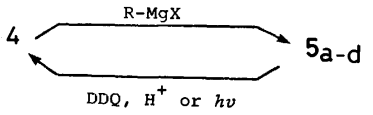

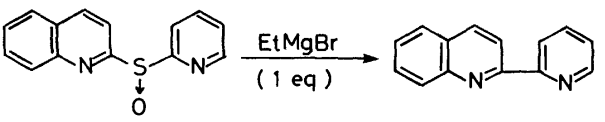

7 8

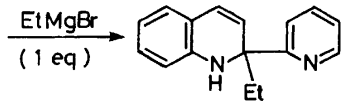

9

Investigations of this addition[12] were carried out in other substrates. None of the corresponding C-2 alkyl-substituted pyridine and/or 1,2-dihydro-2,2′-bipyridyl has been detected in the reaction of **1** with methyl- or ethylmagnesium bromide even when the Grignard reagent has been used in a large excess. Meanwhile treatment of one equivalent of ethylmagnesium bromide with 2-pyridyl 2-quinolyl sulfoxide (**7**) has been found to give ligand-coupling product, 2-(2-pyridyl)quinoline (**8**) in 54% yield as a sole product, which upon treatment with another equivalent of ethylmagnesium bromide gave successively 2-ethyl-2-(2-pyridyl)-1,2-dihydroquinoline (**9**) in 35% yield. In the addition of ethylmagnesium bromide to 2-substituted quinolines **6e** or **6f**, only the starting materials were recovered quantitatively. All these observations reveal clearly that this Grignard addition is a substrate specific reaction to 2-(2-pyridyl and/or 2-quinolyl)-quinolines. The produced compound **9** as well as **5a—d** are structurally unique and are fairly stable at low temperature under inert atmosphere, but oxidized easily in certain conditions to give back to **8** and/or **4** quantitatively.

Experimental

Melting points were taken on Yanaco melting point apparatus and were uncorrected. Spectra were measured with the following instruments; ^1H and ^{13}C NMR: JEOL-GX400 (400 MHz and 100 MHz), low- and high-resolution MS: JEOL-JMS-303HF and IR: JASCO IRA-1. NMR spectra were obtained in $CDCl_3$ with tetramethylsilane as an internal standard. Mass spectra were obtained with a direct

inlet method at 70 eV by the Analytical Center of Okayama University of Science. Only strong and/or structurally important peaks are reported here for MS and IR. All reactions were carried out under Argon atmosphere. Solvents (THF and ether) for the reactions were freshly distilled over sodium benzophenone ketyl before the use. Methyl- and ethylmagnesium bromide were purchased from the Kanto Chemical Co. Other Grignard reagents were freshly prepared in dry ether or THF by the procedure in literatures.[13] Thin-layer chromatography (TLC) was carried out on 0.25 mm E. Merck precoated silica-gel plates (60F-254) and for silica-gel column chromatography Wako gel (C-200) was used.

Reactions of 3 with Grignard Reagents. To a stirred THF (3 ml) solution of **3** (1 mmol) was added Grignard reagent (1.1 mmol or 2.1 mmol) in THF or ether solution dropwise at room temperature. After 30 min reaction mixture was quenched with a saturated ammonium chloride solution (3 ml) and extracted with ether (50 ml). The ethereal layer was washed with water (2 ml) and brine (2 ml) and dried over $MgSO_4$. The solvent was removed and the residue was purified by column chromatography on silica gel.

5a: Colorless oil, R_f=0.22 (10% ether in hexane); ^{1}H NMR δ=1.83 (3H, s), 5.01 (1H, bs), 5.89 (1H, d, J=9.9 Hz), 6.47 (1H, d, J=9.9 Hz), 6.56 (1H, d, J=8.1 Hz), 6.58 (1H, td, J=7.4, 0.3 Hz), 6.90 (1H, dd, J=7.5, 1.7 Hz), 6.99 (1H, td, J=7.7, 1.7 Hz), 7.49 (1H, td, J=7.2, 1.1 Hz), 7.68 (1H, d, J=8.6 Hz), 7.69 (1H, td, J=7.2, 2.3 Hz), 7.76 (1H, dd, J=8.2, 2.3 Hz), 8.07 (1H, d, J=9.8 Hz), 8.09 (1H, d, J=8.6 Hz); ^{13}C NMR δ=30.84 (q), 59.15 (s), 113.18 (d), 117.41 (d), 118.77 (d), 119.53 (s), 125.27 (d), 126.19 (d), 126.84 (d), 126.87 (d), 127.40 (d), 127.95 (s), 128.99 (d), 129.38 (d), 129.42 (d), 136.62 (d), 143.06 (s), 147.25 (s), 165.74 (s); MS m/z (rel intensity, %) 272 (M^+, 17), 257 (base), 128 (30); IR ($CHCl_3$) 1460, 1600, 2960, 3390 cm^{-1}. HRMS Found: m/z 272.1307. Calcd for $C_{19}H_{16}N_2$: M, 272.1313.

5b: Colorless oil, R_f=0.29 (10% ether in hexane); ^{1}H NMR δ=0.96 (3H, t, J=7.6 Hz), 2.02 (1H, dq, J=14.1, 7.6 Hz), 2.12 (1H, dq, J=14.1, 7.6 Hz), 5.08 (1H, bs), 5.88 (1H, d, J=9.9 Hz), 6.52 (1H, d, J=9.9 Hz), 6.55 (1H, td, J=7.8, 0.8 Hz), 6.61 (1H, d, J=7.9 Hz), 6.88 (1H, dd, J=7.4, 1.6 Hz), 6.99 (1H, td, J=7.8, 1.9 Hz), 7.49 (1H, td, J=7.5, 1.5 Hz), 7.61 (1H, d, J=8.8 Hz), 7.68 (1H, td, J=7.7, 2.1 Hz), 7.76 (1H, dd, J=8.3, 1.5 Hz), 8.06 (1H, d, J=9.2 Hz), 8.09 (1H, d, J=8.8 Hz); ^{13}C NMR δ=8.48 (q), 36.13 (t), 62.36 (s), 113.05 (d), 117.02 (d), 118.71 (d), 119.46 (s), 126.07 (d), 126.26 (d), 126.29 (d), 126.78 (s), 127.37 (d), 128.29 (d), 128.93 (d), 129.29 (d), 129.40 (d), 136.46 (d), 143.64 (s), 147.29 (s), 165.48 (s); MS m/z (rel intensity, %) 286 (M^+, 3), 257 (base), 158 (15), 128 (22); IR ($CHCl_3$) 1460, 1600, 2950, 3400 cm^{-1}. HRMS Found: m/z 286.1478. Calcd for $C_{20}H_{18}N_2$: M, 286.1469.

5c: Colorless oil, R_f=0.31 (10% ether in hexane); ^{1}H NMR δ=0.87 (3H, d, J=6.6 Hz), 0.94 (3H, d, J=6.2 Hz), 1.90 (1H, dd, J=13.2, 6.6 Hz), 1.99 (1H, m), 2.04 (1H, dd, J=13.2, 6.2 Hz), 5.07 (1H, bs), 5.91 (1H, d, J=9.6 Hz), 6.46 (1H, d, J=9.6 Hz), 6.54 (1H, td, J=7.3, 1.1 Hz), 6.58 (1H, d, J=8.1 Hz), 6.86 (1H, dd, J=7.3, 1.7 Hz), 6.89 (1H, td, J=7.7, 1.5 Hz), 7.46 (1H, td, J=7.0, 1.1 Hz), 7.59 (1H, d, J=9.2 Hz), 7.66 (1H, td, J=7.0, 1.5 Hz), 7.73 (1H, dd, J=8.1, 1.8 Hz), 8.06 (1H, d, J=8.8 Hz), 8.06 (1H, d, J=9.2 Hz); ^{13}C NMR δ=24.41 (t), 24.44 (q), 24.52 (q), 51.74 (d), 62.38 (s), 113.05 (d), 116.98 (d), 118.54 (d), 119.36 (d), 125.69 (d), 126.06 (d), 126.74 (s), 126.80 (d), 127.27 (d), 127.35 (d), 128.94 (d), 129.29 (d), 129.38 (d), 136.51 (d), 143.42 (s), 147.72 (s), 165.88 (s); MS m/z (rel intensity, %) 314 (M^+, 8), 258 (base), 186 (57), 143 (18), 128 (58); IR ($CHCl_3$) 1480, 1600, 2940, 3380 cm^{-1}. HRMS Found: m/z 314.1782. Calcd for $C_{22}H_{22}N_2$: M, 314.1795.

5d: Colorless oil, R_f=0.37 (10% ether in hexane); ^{1}H NMR δ=0.85 (1H, d, J=6.6 Hz), 0.98 (1H, d, J=6.6 Hz), 2.48 (1H, m), 5.16 (1H, bs), 5.91 (1H, d, J=9.8 Hz), 6.50 (1H, d, J=9.8 Hz), 6.51 (1H, td, J=7.5, 0.7 Hz), 6.61 (1H, d, J=7.7 Hz), 6.83 (1H, dd, J=7.3, 1.5 Hz), 6.97 (1H, td, J=7.3, 1.7 Hz), 7.48 (1H, td, J=7.0, 1.1 Hz), 7.53 (1H, d, J=8.6 Hz), 7.67 (1H, td, J=7.3, 2.0 Hz), 7.75 (1H, dd, J=8.1, 1.7 Hz), 8.05 (1H, d, J=9.5 Hz), 8.07 (1H, d, J=8.6 Hz); ^{13}C NMR δ=17.64 (q), 39.04 (d), 65.05 (s), 112.92 (d), 116.77 (d), 118.95 (d), 119.95 (s), 126.70 (d), 126.78 (d), 126.93 (d), 127.38 (d), 127.63 (d), 128.42 (s), 128.93 (d), 129.54 (d), 136.74 (d), 144.02 (s), 147.89 (s), 165.70 (s); MS m/z (rel intensity, %) 300 (M^+, 2), 257 (base), 128 (20); IR ($CHCl_3$) 1465, 1600, 2960, 3360 cm^{-1}. HRMS Found: m/z 300.1658. Calcd for $C_{21}H_{20}N_2$: M, 300.1625.

6e:[10] Mp 80 °C (from hexane); R_f=0.25 (10% ether in hexane); ^{1}H NMR δ=7.47—7.56 (5H, m), 7.73 (1H, td, J=6.8, 1.4 Hz), 7.84 (1H, dd, J=7.5, 0.4 Hz), 7.89 (1H, d, J=8.6 Hz), 8.17 (1H, d, J=7.2 Hz), 8.18 (1H, td, J=5.1, 0.8 Hz), 8.23 (1H, d, J=8.6 Hz).

6f:[11] Colorless oil, R_f=0.25 (10% ether in hexane); ^{1}H NMR δ=3.77 (2H, d, J=7.0 Hz), 5.18 (1H, d, J=10.9 Hz), 5.22 (1H, d, J=17.8 Hz), 6.14 (1H, ddt, J=17.8, 10.9, 7.0 Hz), 7.31 (1H, d, J=8.2 Hz), 7.49 (1H, td, J=7.9, 1.5 Hz), 7.68 (1H, td, J=7.7, 1.8 Hz), 7.77 (1H, dd, J=8.5, 1.5 Hz), 8.05 (1H, d, J=8.4 Hz), 8.06 (1H, d, J=8.4 Hz).

6g:[11] Colorless oil, R_f=0.38 (10% ether in hexane); ^{1}H NMR δ=1.54 (3H, d, J=7.2 Hz), 3.85 (1H, m), 5.14 (1H, ddd, J=10.3, 1.6, 1.3 Hz), 5.19 (1H, ddd, J=17.4, 1.6, 1.3 Hz), 6.18 (1H, ddd, J=17.4, 10.3, 6.5 Hz), 7.32 (1H, d, J=8.5 Hz), 7.49 (1H, td, J=7.8, 1.0 Hz), 7.69 (1H, td, J=7.7, 1.8 Hz), 7.78 (1H, dd, J=7.9, 1.1 Hz), 8.07 (1H, d, J=8.0 Hz), 8.08 (1H, d, J=8.0 Hz).

2-Pyridyl 2-Quinolyl Sulfoxide (7). To a mixture of 2-chloroquinoline (2.945 g, 18 mmol) and 2-pyridinethiol (2.0 g, 18 mmol) in hexamethylphosphoric triamide (HMPA, 20 ml) was added pieced of sodium metal (414 mg, 18 mmol) by several portions and the mixture was heated at 80 °C with stirring. After 2 days it was quenched with water (20 ml) and extracted with ether (200 ml). The ethereal layer was washed with water (3 ml×5) and brine (3 ml) and dried over $MgSO_4$. The solvent was removed and the crude sulfide, R_f=0.23 (20% ether in hexane), was used for the next reaction without any purification. To a chloroform solution (15 ml) of the crude sulfide was added carefully m-chloroperbenzoic acid portionwise at room temperature and the reaction was monitored by TLC to check the starting material consumed. It was diluted with chloroform (100 ml) and washed with aq. sodium thiosulfate (6 ml×2), aq. sodium hydrogencarbonate (6 ml×2), water (6 ml), and brine (6 ml) and dried over $MgSO_4$. After removal of the solvent under reduced pressure the residue was purified by column chromatography on silica gel eluted with 60% ethyl acetate in hexane to give **7** (1.5 g) in 35% yield. Mp 86—87 °C (from benzene); ^{1}H NMR δ=7.30 (1H, m), 7.59 (1H, td, J=8.3, 1.6 Hz), 7.76 (1H, td, J=7.9, 0.7 Hz), 7.83 (1H, d, J=8.5 Hz), 7.86 (1H, td, J=7.7, 1.4 Hz), 8.04 (1H, dd, J=8.6, 1.1 Hz), 8.11 (1H, d, J=8.1 Hz), 8.21 (1H,

d, J=8.8 Hz), 8.30 (1H, d, J=8.8 Hz), 8.58 (1H, d, J=5.3 Hz); ^{13}C NMR δ=115.53 (d), 119.52 (d), 124.96 (d), 127.85 (d), 128.04 (d), 128.43 (s), 129.78 (d), 130.59 (d), 137.98 (d), 138.45 (d), 147.57 (s), 150.06 (d), 163.68 (s), 163.87 (s); IR ($CHCl_3$) 1060, 1580, 1590, 2960 cm^{-1}. Found: C, 66.18; H, 3.80; N, 11.00; S, 12.59%. Calcd for $C_{14}H_{10}N_2OS$: C, 66.12; H, 3.96; N, 11.02; S, 12.61%.

2-(2-Pyridyl)quinoline (8).[14] Methylmagnesium bromide (0.8 ml, 0.5 M solution in THF; 1 M=1 mol dm^{-3}) was dropped into **7** (94 mg, 0.36 mmol) in THF (4 ml) at room temperature. The mixture was stirred for 15 min at the same temperature. Then it was quenched with a saturated ammonium chloride solution (8 ml) and extracted with chloroform (40 ml). The organic layer was washed with water (2 ml×2) and brine (2 ml) and dried over $MgSO_4$. The solvent was removed and the residual oil was chromatographed on silica gel eluted with 25% ether in hexane to afford **8** (40 mg) in 54% yield. Mp 98 °C (from ethanol); R_f=0.20 (30% ether in hexane); ^{1}H NMR δ=7.36 (1H, td, J=6.4, 1.4 Hz), 7.56 (1H, td, J=7.1, 1.5 Hz), 7.74 (1H, dt, J=7.9, 1.5 Hz), 7.85 (1H, d, J=8.5 Hz), 7.88 (1H, td, J=7.3, 1.9 Hz), 8.19 (1H, d, J=8.7 Hz), 8.29 (1H, d, J=8.2 Hz), 8.56 (1H, d, J=8.2 Hz), 8.66 (1H, dd, J=8.1, 1.1 Hz), 8.75 (1H, ddd, J=4.7, 1.9, 1.1 Hz).

2-Ethyl-2-(2-pyridyl)-1,2-dihydroquinoline (9). To a stirred THF solution (3 ml) of **8** (58 mg, 0.28 mmol) was dropped ethylmagnesium bromide (0.34 ml, 1 M solution in THF) at room temperature. After 3 min it was quenched with a saturated ammonium chloride solution (3 ml) and extracted with chloroform (20 ml). The organic layer was washed with water (5 ml) and brine (5 ml) and dried over $MgSO_4$. The solvent was removed under reduced pressure and the residue was purified by silica-gel column chromatography eluted with 15% ether in hexane to give **9** as colorless oil (23 mg) in 35% yield. R_f=0.32 (30% ether in hexane); ^{1}H NMR δ=0.91 (3H, t, J=7.3 Hz), 1.98 (2H, qd, J=7.3, 0.7 Hz), 4.77 (1H, bs), 5.82 (1H, dd, J=9.9, 1.4 Hz), 6.50 (1H, d, J=9.9 Hz), 6.53 (1H, d, J=8.4 Hz), 6.55 (1H, td, J=7.3, 1.1 Hz), 6.87 (1H, dd, J=7.3, 1.1 Hz), 6.97 (1H, td, J=7.7, 1.5 Hz), 7.09 (1H, ddd, J=7.3, 4.8, 1.1 Hz), 7.42 (1H, ddd, J=7.0, 1.1, 0.7 Hz), 7.61 (1H, td, J=7.8, 1.8 Hz), 8.56 (1H, ddd, J=4.8, 1.8, 1.1 Hz); ^{13}C NMR δ=8.56 (q), 35.99 (t), 61.70 (s), 112.82 (d), 117.06 (d), 119.54 (s), 120.61 (d), 121.44 (d), 126.10 (d), 126.36 (d), 126.81 (d), 128.86 (d), 136.46 (d), 143.44 (s), 149.01 (d), 165.83 (s); MS m/z (rel intensity, %) 236 (M^+, 45), 208 (base), 158 (70), 143 (30), 128 (33), 104 (40), 77 (20); IR ($CHCl_3$) 1450, 1580, 1630, 2950, 3400 cm^{-1}. HRMS Found: m/z 236.1313. Calcd for $C_{16}H_{16}N_2$: M, 236.1313.

References

1) S. Oae, T. Kawai, and N. Furukawa, *Tetrahedron Lett.*, **25**, 69 (1984); S. Oae, *Croat. Chem. Acta*, **59**, 129 (1986); S. Oae, *Phosphorus and Sulfur*, **27**, 13 (1986); S. Oae, "Reviews on Heteroatom Chem.," ed by S. Oae, MYU, Tokyo (1988).

2) S. Oae, T. Kawai, N. Furukawa, and F. Iwasaki, *J. Chem. Soc., Perkin Trans. 2*, **1987**, 405; S. Oae , T. Takeda, T. Kawai, and N. Furukawa, *Phosphorus and Sulfur*, **34**, 133 (1987).

3) S. Oae, T. Takeda, and S. Wakabayashi, *Tetrahedron Lett.*, **29**, 4445 (1988); S. Wakabayashi, M. Ishida, T. Takeda, and S. Oae, *ibid.*, **29**, 4441 (1988).

4) T. Kawai, N. Furukawa, and S. Oae, *Tetrahedron Lett.*, **25**, 2549 (1984); S. Oae, T. Kawai, and N. Furukawa, *Phosphorus and Sulfur*, **34**, 123 (1987).

5) G. B. Barlin and W. V. Brown, *J. Chem. Soc. B*, **1968**, 1435.

6) Hitachi, Co. Ltd., Jpn. Patent 59190353 (1984); H. Monien, U. Gerlach, and P. Jacob, *Fresenius' Z. Anal. Chem.*, **306**, 136 (1981); F. J. Waller, EP 195515 (1986).

7) M. Ishikura, I. Oda, and M. Terashima, *Heterocycles*, **23**, 2375 (1985).

8) R. Vanderesse, M. Lourak, Y. Fort, and P. Caubere, *Tetrahedron Lett.*, **27**, 5483 (1986); M. Tiecco, L. Testaferri, M. Tingoli, D. Chianelli, and M. Montanucci, *Synthesis*, **1984**, 736.

9) Y. Rollin, M. Troupel, D. G. Tuck, and J. Perichon, *J. Organomet. Chem.*, **303**, 131 (1986).

10) L. S. Povarov, V. I. Grigos, and B. M. Mikhailov, *Izv. Acad. Nauk SSSR, Ser. Khim.*, **1963**, 2039.

11) D. Pini, R. Lazzaroni, S. Bertozzi, and P. Saluadori, *Gazz. Chem. Ital.*, **113**, 227 (1983).

12) It is well-known that some organometallic reagents nucleophilically attack C-2 position on pyridine ring as well as on quinoline ring. Examples in the cases of quinoline see, J. J. Eisch and D. R. Comfort, *J. Org. Chem.*, **40**, 2288 (1975).

13) "Preparative Polar Organometallic Chemistry," ed by L. Brandsma and H. D. Verkruijsse, Springer Verlag, Berlin (1987).

14) D. H. Hey and J. M. Williams, *J. Chem. Soc.*, **1950**, 1678.

Electronic Control of Stereoselectivity in the Metal Hydride Reductions of a Series of Substituted 3,4-Dihydro-1,4-ethanonaphthalen-2(1*H*)-ones

Keiji OKADA,* Seiji TOMITA, and Masaji ODA*
Department of Chemistry, Faculty of Science, Osaka University, Toyonaka, Osaka 560
(Received February 20, 1989)

The anti/syn stereoselectivity in the metal hydride reductions of a series of substituted 3,4-dihydro-1,4-ethanonaphthalen-2(1*H*)-ones was studied. The observed steroselectivity sequence was found to be parallel with the homoconjugation sequence except for the case of 5,8-dimethoxy-substituted derivative: the portion of anti attack increases as the benzene ring becomes electron-rich. The results were rationalized by Cieplak's transition state model or by the nonclassical carboncation model. A special coordinated transition state was considered to explain the results for 5,8-dimethoxy-substituted compound.

Because of the homoconjugation interaction between the carbonyl group and the endocyclic double bond, bicyclo[2.2.2]oct-5-en-2-one has attracted considerable attention. This interaction has been investigated in terms of ^{13}C NMR,[1] PES,[2] and CD[3] studies. The homoconjugation interaction may also be revealed by chemical reactions especially by the stereoselectivity in nucleophilic additions. Hitherto, several experimental data in the nucleophilic additions toward this substrate have been reported. Metal hydrides such as sodium borohydride[4] or lithium aluminum hydride[5] are known to attack the carbonyl group predominantly from the anti side of the double bond, whereas Grignard reagents such as alkyl- or vinylmagnesium halides[6,7] mainly attack from the syn side. The origin of the stereoselectivity has not been considered in most cases. However, Snowden and co-workers speculated a steric factor in the Grignard reactions.[6] Brown and Muzzio considered a steric effect between attacking hydride and the π-electrons of C_5–C_6 double bond.[4] We have recently reported the anti/syn stereoselectivity of metal hydride reductions of a series of substituted 1,2,3,4-tetrahydro-1,4-methanonaphthalen-9-ones and have found that the electron-donating substituents on the benzene ring increase the portion of anti attack.[8] In order to know whether this substituent effect in bicyclic systems is general or not, we have extended our study to bicyclo[2.2.2]oct-5-en-2-one. In this paper, the metal hydride reductions of a series of substituted 3,4-dihydro-1,4-ethanonaphthalen-2(1*H*)-ones (**1a—e**) are investigated.

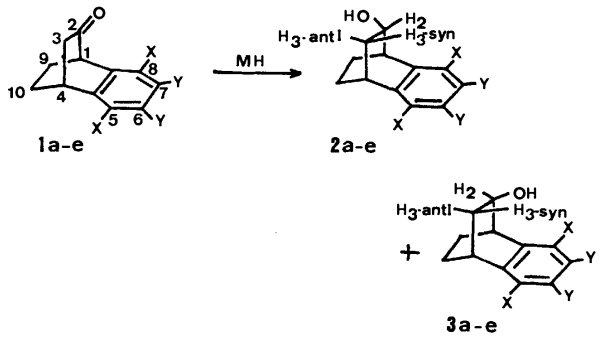

a: X=Y=F, b: X=Y=Cl, c: X=Y=H,
d: X=OMe; Y=H, e: X=H; Y=OMe

Results and Discussion

Stereochemistry of Anti- (2a—e) and Syn-Alcohols (3a—e). The reduction of substituted 3,4-dihydro-1,4-ethanonaphthalen-2(1*H*)-ones (**1a—e**) with various metal hydrides gave the corresponding anti- (**2a—e**) and syn-alcohols (**3a—e**) in high yields (>78%). The produced alcohols can be separated by preparative TLC or gas chromatography. In Table 1, the ^1H NMR data of the alcohols are listed. Among the methylene protons, the H_3-anti proton appears in the range of δ 2.2—2.4 as a d-d-d like multiplet for the anti-alcohols (**2a—e**) or a d-d-d pattern (typically, J=14, 9, and 3 Hz) for the syn-alcohols (**3a—e**). The H_3-syn proton and other four methylene protons appear in the higher field (δ 1.0—2.2) as multiplets. By addition of a NMR shift reagent, Eu(fod)$_3$, the H_3-syn proton of the syn-alcohols (**3a—e**) becomes separable as a multiplet having a geminal coupling of J=ca. 14 Hz from other methylene protons. The lower chemical shift of the H_3-syn proton compared with that of the H_3-anti proton is probably due to the anisotropic effect of the benzene ring.

Table 1 also summarizes the relative shift values (1.00 for H_1 proton in both alcohols) induced by Eu(fod)$_3$ for the H_3 and other protons. It is clear from the table that the H_3-anti proton of the anti-alcohols has a larger relative shift (1.0—1.2) than that of the syn-alcohols (0.5—0.6). The relative shifts for other protons are reasonable except for the large induced shifts of the aromatic and methoxyl protons of **2e** and **3e**, the large shifts being ascribed to the partial coordination of Eu(fod)$_3$ onto the methoxyl groups. However,this coordination would not much affect the shift of H_3-anti proton because of the relatively long distance between the H_3-anti proton and the coordinated metal center. The assigned stereochemistry is

Table 1. Chemical Shift (δ)[a] and Relative Shift Values[b] Induced by Eu(fod)$_3$ for Protons of **2a**—e and **3a**—e

	H_2	H_1 and H_4	H_3-anti	H_3-syn and $H_{9,10}$	Aromatic protons	Methoxyl protons
X=Y=F	3.93	3.44[c]	ca. 2.40	1.05—2.15	—	—
2a	(1.78)	(1.00, 0.37)[d]	(1.11)			
X=Y=Cl	3.93	3.64[c]	ca. 2.40	1.05—2.15	—	—
2b	(1.83)	(1.00, 0.37)[d]	(1.10)			
X=Y=H	3.92	3.00[c]	ca. 2.29	1.10—2.15	7.15[c]	—
2c	(1.71)	(1.00, 0.41)[d]	(1.22)		(0.18)[c]	
X=OMe, Y=H	3.89	3.47[c]	ca. 2.28	0.98—2.10	6.67[c]	3.75, 3.76
2d	(2.00)	(1.00, 0.40)[d]	(1.13)		(0.13)[c]	(0.06, 0.09)
X=H, Y=OMe	3.92	2.92[c]	ca. 2.30	1.05—2.15	6.70, 6.74	3.87[c]
2e	(1.42)	(1.00, 0.66)[d]	(0.97)		(1.29, 1.24)[d]	(1.00)[c]
X=Y=F	4.21	3.50[c]	2.25	1.05—1.90	—	—
3a	(1.39)	(1.00, 0.36)[d]	(0.56)	(1.26)[e]		
X=Y=Cl	4.23	3.71[c]	2.25	1.05—1.90	—	—
3b	(1.38)	(1.00, 0.35)[d]	(0.49)	(1.07)[e]		
X=Y=H	4.08	3.06[c]	2.25	1.05—1.80	7.18[c]	—
3c	(1.56)	(1.00, 0.39)[d]	(0.57)	(1.44)[e]	(0.51,[f] 0.23[c])	
X=OMe, Y=H	4.10	3.61, 3.50	2.17	1.00—1.80	6.70[c]	3.76, 3.77
3d	(1.38)	(1.00, 0.41)[d]	(0.57)	(1.01)[e]	(0.20)[c]	(0.11, 0.19)
X=H, Y=OMe	4.08	3.01[c]	2.22	1.05—1.80	6.75, 6.80	3.88[c]
3e	(1.55)	(1.00, 0.49)[d]	(0.61)	(1.12)[e]	(0.57, 0.76)[d]	(0.34, 0.38)

a) Measured in $CDCl_3$ (ca. 25—30 mg/0.3 cm^3). b) In parenthesis; determined by successive addition of ca. 5 mg of Eu(fod)$_3$ up to ca. 20 mg. c) An averaged value. d) Respective values. e) For H_3-syn proton. f) For one of the aromatic protons.

Table 2. Product Ratios (**2a**—e : **3a**—e) in the Metal Hydride Reductions of **1a**—e[a]

Reagent	Solvent	**1a**	**1b**	**1c**	**1d**	**1e**
LAH	THF	43 : 57	35 : 65	14 : 86	13 : 87	15 : 85
LAH	Ether	40 : 60	36 : 64	27 : 73	38 : 62	30 : 70
DIBAL-H	Ether	54 : 46	53 : 47	28 : 72	29 : 71	21 : 79
LTBA[b]	Ether	53 : 47	52 : 48	54 : 46	55 : 45	59 : 41
$NaBH_4$	EtOH	63 : 37	61 : 39	27 : 73	38 : 62	27 : 73
$(BH_3)_2$	THF	84 : 16	90 : 10	52 : 48	65 : 35	45 : 55
Sia_2BH[c]	Diglyme	73 : 27	69 : 31	37 : 63	40 : 60	27 : 73

a) All reactions were performed at 0 °C. b) Lithium tri-*t*-butoxyaluminum hydride. c) Bis(1,2-dimethylpropyl)borane (disiamylborane).

also in good accordance with the fact that the H_2-methine proton of the anti-alcohols has a lower chemical shift (δ ca. 3.9) than that (δ 4.1—4.2) of the syn-alcohols owing to the expectable anisotropy effect of the benzene ring. In our previous study,[8] we have observed that the syn-alcohols derived from a series of the related methanonaphthalen-9-ones have shorter GC retention time (OV-17) than the corresponding anti-alcohols. The GC retention time for these isomeric alcohols probably relates to their vapor pressure at the GC conditions. The higher vapor pressure of the syn alcohols can be expected from the possible intramolecular hydrogen bond between the hydroxyl group and the benzene π-bond. In the present system (**2a**—**e** and **3a**—**e**), the stereochemical assignment by this qualitative GC method resulted in a complete agreement with that from the NMR shift reagent study.

Stereoselective Metal Hydride Reductions of 1a—e. Table 2 shows the ratios of anti/syn-alcohols in the reductions using typical metal hydrides. Although some of these values differ only slightly and are nearly equal within the experimental error (±2%), there is apparently an overall trend that the portion of syn-alcohol (anti attack) increases in the sequence of **1a**⇄**b**→**d**⇄**c**→**e** in most cases despite of considerably different sizes and reactivities of the reagents. In particular, the reductions with sodium borohydride, diisobutylaluminum hydride, and bis(1,2-dimethylpropyl)borane (common name "disiamylborane" is used hereafter) follow this sequence. A small change in the sequence is observed with lithium aluminum hydride and diborane reductions. The anti/syn selectivity varies most widely in the reduction with disiamylborane. In this case, the main product is switched from the anti- to the syn-alcohol when the benzene ring becomes electron rich (**2a**/**3a**=73/27→**2e**/**3e**=27/73). Similar trends are observed for the reduction with diisobutylaluminum hydride, sodium borohydride, and diborane. With a very bulky

hydride, tri-*t*-butoxyaluminum hydride, the anti/syn ratio is almost constant (ca. 1:1) for **1a—e**; this result suggests that the electronic perturbation of the substituents is minimized for this bulky reagent and probably also suggests that the steric congestion in both the anti and syn sides would not be much different for **1a—e**.

Several comments on the results of Table 2 can be given. The selectivity is considerably dependent on the reagents for the each substrate; the anti/syn ratio varies from 40/60 (LAH in ether) to 84/16 (diborane in THF) for reduction of **1a**, from 35/65 (LAH in THF) to 90/10 (diborane in THF) for **1b**, from 13/87—15/85 (LAH in THF) to 54/46—65/35 (lithium tri-*t*-butoxyaluminum hydride in ether or diborane in THF) for **1c—e**. Among the reducing reagents used, the reductions with lithium aluminum hydride give the highest portion of anti attack for all the substrates. On the other hand, the reductions with borane reagents tend to produce the high portion of syn attack for **1a,b**. Although the reason for these selectivity change is not clear at present, it may relate with several factors such as the structure of reactive species,[9] the mode and degree of solvation,[9] Lewis acidity of the reagents,[10] and the ability of reagents for electron transfer.[11]

Obviously, the observed sequence of **1a≒b→d≒c→e** cannot be rationalized by steric effect of the substituents on the benzene ring. On the contrary, this sequence seems to be explicable by the electron-donating ability of the substituents on the benzene ring with the exception of **1d**. The electronic perturbation of the substituents to the reactive center would increase in the sequence of **1a→b→c→d→e**, in which methoxyl groups at C_6 and C_7 positions would have a larger electronic effect than those at C_5 and C_8 positions from the consideration of molecular orbitals of the benzo moieties. We have previously shown that the IR carbonyl stretching frequencies of a series of the related methanonaphthalenones are lined parallel with the electron donating ability of the benzene rings as well as the homoconjugation interaction.[8] The observed frequencies of the starting ketones (**1a—e**) follow the expected sequence [IR, ν_{CO} (cm^{-1}) in CCl_4; 1736 for **1a**, 1733 ($CDCl_3$) for **1b**, 1733 for **1c**, 1728 for **1d**, 1725 for **1e**]. Presumably, the deviation for **1d** in the sequence of stereoselectivity is due to the special coordination of the metal hydrides on the neighboring methoxyl group in the transition state as shown in structure **A** which would increase the portion of syn attack. As recognized from inspection of the molecular model, this type of coordination is much weak for **1e** and for the corresponding 1,2,3,4-tetrahydro-1,4-methano naphthalen-9-one derivatives in which such an anomalous effect was not observed in the metal hydride reductions,[8] because of the long distance between n-orbital of the carbonyl oxygen and the lone-pair electrons of the methoxyl group and because of the poor overlapping direction of these orbitals, respectively. Considering the above coordination factor for **1d**, we conclude that the variation of anti/syn stereoselectivity in the metal hydride reductions of **1a—e** is electronic in origin.

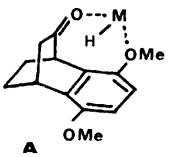

A

Several electronic factors in nucleophilic additions to cyclic ketones have been previously reported.[12,13] Among them, as we have pointed out in our previous report,[8] a qualitative transition state model developed by Cieplak seems to be attractive. Cieplak assumed that a newly formed bond between nucleophiles and carbonyl carbons is weak and intrinsically electron deficient in the transition state and therefore characterized as a low-lying antibonding σ^*-orbital.[10] In his model, the transition state can be stabilized by the interaction between the σ^*-orbital and electron-donating orbitals neighboring the carbonyl group, so that the favorable transition state is such that the nucleophiles approach to the carbonyl carbon from the anti side of donor orbital. More recently, le Noble and co-workers have reportd that the model developed by Cieplak reasonably explains the stereoselectivity in the reduction of a series of 5-substituted adamantanones.[14]

Application of Cieplak's model to our system gives satisfactory explanation. We show qualitative sketches of the transition states for the anti attack (**B**) and the syn attack (**C**). In the transition state **B**, the elec-

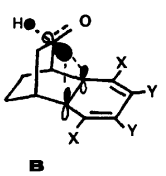

B

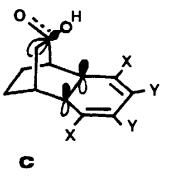

C

tron-deficient σ^*-orbital can be much stabilized by the bonding interaction with π-orbital of the benzene ring with a larger overlap of back side lobe of the σ^*-orbital. Electron donating substituents on the benzene ring would increase the stabilization gain in the transition state **B** and hence the anti attack. However, a similar explanation is afforded by the consideration of contribution of the nonclassical carbocation. As Cieplak pointed out, the incipient C-H bond is electron-deficient in nature, some positive charge remains on the carbonyl carbon with the greater extent than the ground state. When the benzene ring becomes electron-rich, the transition state for the anti attack would be stabilized as shown in **D**. Both the explanations are related to the stabilization

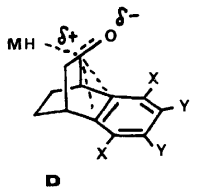

D

gain obtained by the HOMO-LUMO interaction between the benzene π-orbital and the p-orbital of the carbonyl carbon in the transition state. The interaction in the transition state must be parallel with that in the ground state (homoconjugation interaction).

Apart from the above explanations, it may be interesting to consider the role of secondary orbital interaction in the metal hydride reductions. As shown in **E**, incoming hydride would experience the antibonding repulsive secondary orbital interaction with

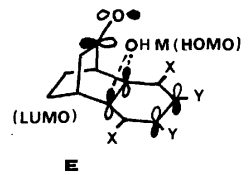

E

the benzene π-orbital. Although kinetic treatment was not investigated in this paper, this interaction predicts that the lower reactivity in the syn side should be observed as the benzene ring becomes electron-rich. In this context, Brown and Muzzio reported the rate study of sodium borohydride reduction of bicyclo[2.2.2]oct-5-en-2-one and its saturated analogue.[4] According to their study, the predominant anti attack is mainly due to the enhanced rate in the anti side. From this result, the antibonding secondary orbital interaction is not likely to be an origin of the stereoselectivity.

In summary, we have observed that the anti/syn stereoselectivity of a series of substituted 3,4-dihydro-1,4-ethano-naphthalen-2(1*H*)-ones is parallel with the homoconjugation interaction except for **1d**: the portion of anti attack increases as the benzene ring becomes electron-rich. A special coordinated transition state was considered to rationalize the results for **1d**. It should be noted that the variation of anti/syn stereoselectivity in the present system is considerably small when compared to the corresponding 1,2,3,4-tetrahydro-1,4-methanonaphthalen-9-one derivatives.[8] The reason would be simply due to the weaker interaction between the benzene π-orbital and the reactive center in **1a—e** in the transition state.

Experimental

General. Melting points were measured on a Mettler FP2 apparatus and are uncorrected. IR spectra were recorded with a Hitachi EPI-G3 grating spectrophotometer and wavenumbers were corrected with use of polystyrene film. The wavenumbers of the carbonyl stretching for **1a—e** were directly read from the spectrophotometer at their maximum absorptions. ^{1}H NMR spectra were obtained at 90 MHz on a JEOL FX-90Q or 100 MHz on a Varian XL-100. ^{13}C NMR spectra were taken with a JEOL FX-90Q (22.5 MHz). Mass spectra were measured on a JEOL JMS-01SG-2 mass spectrometer. GLC analysis were performed on a Hitachi 063 gas chromatography with a glass column packed with Silicone OV-17 (3%) on Chromosorb W AW DMCS (1 m). Column chromatography was carried out with Merck Kieselgel 60 and preparative TLC with Merck Kieselgel GF_{254} (Type 60). Lithium aluminum hydroide, sodium borohydride, lithium tri-*t*-butoxyaluminum hydride, and diisobutylaluminum hydride were commercial products. Diborane and disiamyborane were generated in situ prior to use.[15] Compounds **1a—d** were prepared according to the reported methods.[16] All the solvents were distilled before use.

Synthesis of 3,4-Dihydro-6,7-dimethoxy-1,4-ethanonaphthalen-2(1*H*)-one (1e). To a stirred solution of 280 mg (1.28 mmol) of 1,2,3,4-tetrahydro-6,7-dimethoxy-1,4-methanonaphthalen-9-one[8] in dichloromethane (6 cm^3) cooled at 0 °C under nitrogen, was sucessively added over 1 min boron trifluoride etherate (0.02 cm^3) and ethyl diazoacetate (217 mg, 1.90 mmol). After 4 h stirring at room temperature, the reaction mixture was treated with saturated aqueous sodium hydrogencarbonate (5 cm^3) and dichloromethane (20 cm^3). The separated organic layer was washed with brine (5 cm^3) and dried over magnesium sulfate. Purification with preparative TLC (hexane:ethyl acetate=3:1 (v/v)) gave 221 mg (57%) of a mixture of the syn and anti isomer (ca. 1:1 ratio) of the α-keto ester. The solution of 221 mg (0.727 mmol) of the α-keto ester in a mixture of dioxane (6 cm^3) and hydrochloric acid (2 mol dm^{-3}, 6 cm^3) was refluxed for 2 h. After cooling to room temperature, water (20 cm^3) was added and the mixture was extracted with ethyl acetate (20 cm^3) twice. The organic layer was dried over magnesium sulfate and evaporated under reduced pressure. The resulting crude α-keto carboxylic acid was dissolved in 4 cm^3 of *o*-dichlorobenzene and the solution was refluxed for 1 h under nitrogen atmosphere. The solvent was evaporated under reduced pressure. Purification with preparative TLC (hexane:ethyl acetate=3:1 (v/v)) gave 93 mg (53%) of **1e**: colorless prisms from hexane; mp 100—101 °C; IR (CCl_4) 2925, 2850, 1725, 1504, 1466, 1348, 1290, 1260, 1233, 1011 cm^{-1}; ^{1}H NMR (100 MHz, $CDCl_3$) δ=1.50—2.50 (m, 6H), 3.35 (m, 1H), 3.52 (m, 1H), 3.84 (s, 3H), 3.86 (s, 3H), 6.75 (s, 1H), 6.80 (s, 1H); ^{13}C NMR ($CDCl_3$) δ=23.55, 25.34, 36.25, 42.13, 52.02, 56.11, 108.22, 109.55, 128.29, 135.23, 148.01, 148.37, 211.51; MS (75 eV) *m/z* (%) 232 (M^+; 100), 204 (30), 190 (55), 189 (57). Found: C, 72.35; H, 7.01%. Calcd for $C_{14}H_{16}O_3$: C, 72.39; H, 6.94%.

Prototypical Procedure for Reductions with Lithium Aluminum Hydride. To a suspension of 20 mg (0.53 mmol) of lithium aluminum hydride in 5 cm^3 of dry ether under nitrogen at 0 °C was added dropwise over 2 min a solution of 100 mg (0.410 mmol) of **1a** in 5 cm^3 of dry ether. After 30 min, the reaction was quenched by addition of 0.08 cm^3 of water. The ether layer was dried over magnesium sulfate. Separation with preparative TLC (hexane:ethyl acetate=5:1 (v/v)) gave 38 mg of **2a** and 56 mg of **3a** in overall yield of 93% (**2a**:**3a**=40:60). The yields and product ratios for other derivatives were as follows, in ether: 93% (**2b**:**3b**=36:64) for **1b**, 81% (27:73) for **1c**, 90% (38:62) for **1d**,

and 99% (30:70) for **1e**, in THF: 79% (43:57) for **1a**, 87% (35:65) for **1b**, 85% (14:86) for **1c**, 95% (13:87) for **1d**, 85% (15:85) for **1e**. **2a**: colorless needles from hexane; mp 81—82 °C, IR (KBr) 3270, 2955, 1507, 1401, 1343, 1062, 1048, 1022, 1012, 1003, 952, 870, 819 cm^{-1}; ^1H NMR (100 MHz, $CDCl_3$) δ=1.05—2.15 (m, 6H), ca. 2.40 (m, 1H), 3.44 (m, 2H), 3.93 (m, 1H). Found: C, 58.43; H, 4.03%. Calcd for $C_{12}H_{10}OF_4$: C, 58.54; H, 4.09%. **3a**: colorless needles from hexane; mp 96—99 °C, IR (KBr) 3250, 1950, 1502, 1408, 1351, 1118, 1078, 1043, 1028, 935, 862, 832 cm^{-1}; ^1H NMR (100 MHz, $CDCl_3$) δ=1.05—1.90 (m, 6H), 2.25 (ddd, 1H, J=14.0, 9.0, and 3.0 Hz), 3.50 (m, 2H), 4.21 (m, 1H). Found: C, 58.72; H, 3.99%. Calcd for $C_{12}H_{10}F_4$: C, 58.58; H, 4.09%. **2b**: colorless needles from benzene-hexane; mp 138—141 °C, IR (KBr) 3300, 2950, 1394, 1380, 1340, 1279, 1224, 1172, 1078, 1050, 1010 cm^{-1}; ^1H NMR (100 MHz, $CDCl_3$) δ=1.05—2.15 (m, 6H), ca. 2.40 (m, 1H), 3.64 (m, 2H), 3.93 (m, 1H). Found: C, 46.58; H, 3.23%. Calcd for $C_{12}H_{10}OCl_4$: C, 46.19; H, 3.23%. **3b**: colorless prisms from benzene-hexane; mp 143—144 °C; IR (KBr) 3305, 2955, 2865, 1472, 1386, 1359, 1348, 1290, 1226, 1179, 1090, 1039 cm^{-1}; ^1H NMR (100 MHz, $CDCl_3$) δ=1.05—1.90 (m, 6H), 2.25 (ddd, 1H, J=14.0, 9.0, and 3.0 Hz), 3.71 (m, 2H), 4.23 (m, 1H). Found: C, 46.41; H, 3.28%. Calcd for $C_{12}H_{10}OCl_4$: C, 46.19; H, 3.23%. **2c**: colorles needles from hexane; mp 70—71 °C; IR (KBr) 3325, 2925, 1488, 1463, 1075, 1048, 1006, 754 cm^{-1}; ^1H NMR (100 MHz, $CDCl_3$) δ=1.10—2.15 (m, 6H), ca. 2.29 (m, 1H), 3.00 (m, 2H), 3.92 (m, 1H), 7.15 (s, 4H). Found: C, 82.68; H, 8.12%. Calcd for $C_{12}H_{14}O$: C, 82.72; H, 8.10%. **3c**: colorless needles from hexane; mp 102—104 °C; IR (KBr) 3265, 2930, 2855, 1488, 1460, 1349, 1332, 1081, 1033, 988, 750 cm^{-1}; ^1H NMR (100 MHz, $CDCl_3$) δ=1.05—1.80 (m, 6H), 2.25 (ddd, 1H, J=14.0, 9.0, and 3.0 Hz), 3.06 (m, 2H), 4.08 (m, 1H), 7.18 (s, 4H). Found: C, 82.61; H, 8.08%, Calcd for $C_{12}H_{14}O$: C, 82.72; H, 8.10%. **2d**: colorless prisms from benzene-hexane; mp 115—116 °C; IR (KBr) 3275, 2940, 2825, 1499, 1464, 1453, 1340, 1323, 1280, 1261, 1239, 1112, 1088, 1071, 1054, 1010, 792, 712 cm^{-1}; ^1H NMR (100 MHz, $CDCl_3$) δ=0.98—2.10 (m, 6H), ca. 2.28 (m, 1H), 3.47 (m, 2H), 3.75 (s, 3H), 3.76 (s, 3H), 3.89 (m, 1H), 6.67 (s, 2H). Found: C, 71.69; H, 7.80%. Calcd for $C_{14}H_{18}C_3$: C, 71.77; H, 7.74%. **3d**: colorless prisms from benzene-hexane; mp 92—93 °C; IR (KBr) 3465, 2935, 2860, 1499, 1439, 1339, 1261, 1243, 1115, 1087, 1052, 1035, 958, 800, 711 cm^{-1}; ^1H NMR (100 MHz, $CDCl_3$) δ=1.00—1.80 (m, 6H), 2.17 (ddd, 1H, J=14.0, 9.0, and 3.0 Hz), 3.50 (m, 1H), 3.61 (m, 1H), 3.76 (s, 3H), 3.77 (s, 3H), 4.10 (m, 1H), 6.70 (s, 2H). Found: C, 71.67; H, 7.75%. Calcd for $C_{14}H_{18}O_3$: C, 71.77; H, 7.74%. **2e**: colorless plates from benzene-hexane; mp 105—106 °C; IR (KBr) 3520, 3305, 2925, 2850, 1508, 1470, 1458, 1449, 1340, 1288, 1261, 1228, 1184, 1113, 1051, 1008, 992 cm^{-1}; ^1H NMR (100 MHz, $CDCl_3$) δ=1.05—2.15 (m, 6H), ca. 2.30 (m, 1H), 2.92 (m, 2H), 3.87 (s, 6H), 3.92 (m, 1H), 6.70 (s, 1H), 6.74 (s, 1H). Found: C, 71.54; H, 7.77%. Calcd for $C_{14}H_{18}O_3$: C, 71.77; H, 7.74%. **3e**: colorless prisms from benzene-hexane; mp 122—123 °C; IR (KBr) 3980, 3400, 2915, 2840, 1510, 1461, 1364, 1280, 1232, 1208, 1075, 1030, 1009, 803 cm^{-1}; ^1H NMR (100 MHz, $CDCl_3$) δ=1.05—1.80 (m, 6H), 2.22 (ddd, 1H, J=14.0, 9.0, and 3.0 Hz), 3.01 (m, 2H), 3.88 (s, 6H), 4.08 (m, 1H), 6.75 (s, 1H), 6.80 (s, 1H). Found: C, 71.81; C, 7.85%. Calcd for $C_{14}H_{18}O_3$: C, 71.77; H, 7.74%.

Prototypical Procedure for Reduction with Diisobutylaluminum Hydride. To a solution of 100 mg (0.410 mmol) of **1a** in 10 cm^3 dry ether under nitrogen at 0 °C was dropwise a hexane solution (1.32 cm^3) of diisobutylaluminum hydride (2.30 mmol). After being stirred for 30 min at 0 °C, the mixture was treated with 2 cm^3 of ethanol, 8 cm^3 of aqueous hydrochloric acid (2 mol dm^{-3}), and 10 cm^3 of ether. The separated ether layer was washed with brine and dried over magnesium sulfate. The products were separated with preparative TLC (hexane:ethyl acetate=5:1 (v/v)) to give 50 mg of **2a** and 43 mg of **3a** in overall yield of 92% (**2a**:**3a**=54:46). The yields and the ratios of anti- and syn-alcohols were as follows; 93% (**2b**:**3b**=53:47) for **1b**, 93% (28:72) for **1c**, 89% (29:71) for **1d**, 89% (21:79) for **1e**.

Prototypical Procedure for Reductions with Lithium Tri-*t*-butoxyaluminum Hydride. To a suspension of 420 mg (1.65 mmol) of lithium tri-*t*-butoxyaluminum hydride in 5 cm^3 of dry ether under nitrogen at 0 °C was added a solution of 100 mg (0.410 mmol) of **1a** in dry ether (5 cm^3). After stirring overnight at 0 °C, the mixture was treated with 3 cm^3 of ethanol, 8 cm^3 of aqueous hydrochloric acid (2 mol dm^{-3}), and 10 cm^3 of ether. The separated ether layer was washed with brine, dried over magnesium sulfate. The products were purified with preparative TLC to give 47 mg of **2a** and 42 mg of **3a** in overall yield of 88% (**2a**:**3a**=53:47). The yields and rations of anti- and syn-alcohols were as follows, 91% (**2b**:**3b**=52:48) for **1b**, 94% (54:46) for **1c**, 98% (55:45) for **1d**, 93% (59:41) for **1e**.

Prototypical Procedure for Reductions with Diborane. To a suspension of 31 mg (0.82 mmol) of sodium borohydride in dry THF(10 cm^3) under nitrogen at 15—18 °C was added dropwise 0.13 cm^3 (1.0 mmol) of boron trifluoride etherate. After 30 min stirring, a solution of 100 mg (0.410 mmol) of **1a** in 5 cm^3 dry THF was added to the mixture and stirred for 30 min at 0 °C. The mixture was treated with 3 cm^3 of ethanol and 8 cm^3 of aqueous hydrochloric acid (2 mol dm^{-3}), and extracted with 15 cm^3 of ether twice. The ether layer was washed with brine and dried over magnesium sulfate. Separation with preparative TLC gave 62 mg of **2a** and 12 mg of **3a** in overall yield of 73% (**2a**:**3a**=84:16). The yields and ratios of anti- and syn-alcohols were as follows; 94% (**2b**:**3b**=90:10) for **1b**, 80% (52:48) for **1c**, 84% (65:35) for **1d**, 83% (45:55) for **1e**.

Prototypical Procedure for Reductions with Disiamylborane. To a suspension of 31 mg (0.82 mmol) of sodium borohydride and 0.21 cm^3 (2.0 mmol) of 2-methyl-2-butene in 10 cm^3 of dry diglyme under nitrogen at 0 °C was added 0.13 cm^3 (1.0 mmol) of boron trifluoride etherate. The mixture was stirred for 30 min at 0 °C. To this suspension was added over 2 min a solution of 100 mg (0.410 mmol) of **1a** in diglyme (5 cm^3) at 0 °C. After being stirred for 3 h, aqueous sodium hydroxide (3 mol dm^{-3}, 10 cm^3) and 30% aqueous hydrogen peroxide (8 cm^3) was added and the mixture was stirred overnight at room temperature. The mixture was treated with ice-water and extracted with 40 cm^3 of eter twice. The ether layer was washed with brine and dried over magnesium sulfate. Separation with preparative TLC gave 59 mg of **2a** and 22 mg of **3a** in overall yield of 80% (**2a**:**3a**=73:27). The yields and ratios of anti- and syn-alcohols were as follows; 78% (**2b**:**2b**=69:31) with 7% recovery of **1b**, 95% (37:63) for **1c**, 81% (40:60)for **1d**, 86% (27:73) for **1e**.

NMR Shift Reagent Study. The alcohols (**2a—e**, **3a—e**) were each dissolved in $CDCl_3$ (25—30 mg/ ca. 0.3 cm^3) in a NMR tube. The shift reagent, Eu(fod)$_3$, was weighed out and added into the solution four times in about 5 mg portions, and the ^1H NMR spectrum was measured each

time. The plots of the observed relative shift of each proton vs. the amount of added $Eu(fod)_3$ gave good straight lines. From the slope of each proton, the relative shift value was calculated.

References

1) Gurudate and J. B. Stothers, *Can. J. Chem.*, **47**, 3601 (1969); J. B. Stothers, J. R. Swenson, and C. T. Tan, *ibid.*, **53**, 581 (1975).

2) G. Hentrich, E. Gunkel, and M. Klessinger, *J. Mol. Struct.*, **21**, 231 (1974).

3) P.-A. Carrupt and P. Vogel, *Tetrahedron Lett.*, **22**, 4721 (1981).

4) H. C. Brown and J. Muzzio, *J. Am. Chem. Soc.*, **88**, 2811 (1966).

5) R. R. Fraser and S. O'Farrell, *Tetrahedron Lett.*, **1962**, 1143.

6) R. L. Snowden and K. H. Schulte-Elte, *Helv. Chim. Acta*, **64**, 2193 (1981).

7) A. P. Kozikowski and R. J. Schmiesing, *J. Org. Chem.*, **48**, 1000 (1983).

8) K. Okada, S. Tomita, and M. Oda, *Bull. Chem. Soc. Jpn.*, **62**, 459 (1989).

9) G. H. Heinsohn and E. C. Ashby, *J. Org. Chem.*, **38**, 4232 (1973); E. C. Ashby, F. R. Dobbs, and H. P. Hopkins, Jr., *J. Am. Chem. Soc.*, **97**, 3158 (1975); E. C. Ashby and J. R. Boone, *ibid.*, **98**, 5524 (1976); E. C. Ashby and J. R. Boone, *J. Org. Chem.*, **41**, 2890 (1976); E. C. Ashby and S. A. Noding, *ibid.*, **44**, 4371 (1979); J. Klein and E. Dunkelblum, *Tetrahedron*, **23**, 205 (1967); D. C. Wigfield and F. W. Gowland, *J. Org. Chem.*, **45**, 653 (1980).

10) A. S. Cieplak, *J. Am. Chem. Soc.*, **103**, 4540 (1981).

11) E. C. Ashby, A. B. Goel, and R. N. DePriest, *J. Am. Chem. Soc.*, **102**, 7779 (1980).

12) D. C. Wigfield, *Tetrahedron*, **35**, 449 (1979) and references cited therein.

13) M. R. Giddings and J. Hudec, *Can. J. Chem.*, **59**, 459 (1981).

14) C. K. Cheung, L. T. Tseng, M.-H. Lin, S. Srivastava, and W. J. le Noble, *J. Am. Chem. Soc.*, **108**, 1598 (1986).

15) H. C. Brown and A. W. Moerikofer, *J. Am. Chem. Soc.*, **84**, 1478 (1962).

16) P. C. Buxton, N. J. Hales, B. Hankinson, H. Heaney, S. V. Ley, and R. P. Sharma, *J. Chem. Soc., Perkin Trans. 1*, **1974**, 2681; N. J. Hales, H. Heaney, and S. V. Ley, *ibid.*, **1974**, 2702; K. Kitahonoki and Y. Takano, *Tetrahedron Lett.*, **1963**, 1597; G. A. Russell, G. W. Holland, and K.-Y. Chang, *J. Am. Chem. Soc.*, **89**, 6629 (1967).

Lanthanoid(III) Trichloride-Tin(II) Chloride Mediated Cycloaddition Reaction of α,α′-Dibromo Ketones with 1,3-Dienes or Enamines

Shin-ichi FUKUZAWA,* Masakazu FUKUSHIMA, Tatsuo FUJINAMI, and Shizuyoshi SAKAI
Department of Materials Science, Faculty of Engineering,
Shizuoka University, Hamamatsu, Shizuoka 432
(Received February 25, 1989)

The reaction of α,α′-dibromo ketones with 1,3-dienes in the presence of $CeCl_3$–$SnCl_2$ in tetrahydrofuran is found to give the corresponding [3+4] cycloadduct in fair to good yields under mild conditions. Furan and cyclopentadiene serve as highly efficient receptors of the oxyallyl intermediate to give bicyclic cycloadducts. The reaction of 2,4-dibromo-3-pentanone with isoprene gives both [3+4] and [3+2] cycloadducts. [3+2] Cycloaddition proceeds similarly with enamines to afford 2-cyclopenten-1-ones after treatment with 3% ethanolic NaOH solution.

Organic synthesis using lanthanoid compounds has been of current interest.[1] Lanthanoid(III) trichloride ($LnCl_3$) has appeared to be one of the attractive reagent for organic synthesis. The combination with $NaBH_4$[2] or $LiAlH_4$[3] is efficient for 1,2-regioselective reduction of α,β-unsaturated carbonyl compounds, organic halides, and phosphine oxide. They can also be employed together with Grignard reagents or organolithium reagents for regio- and stereoselective alkylation of carbonyl compounds.[4] The characteristic of these reactions may be explained by the lanthanoid ion being a weak Lewis acid and having a high affinity for oxygen.[5] These combined reagents have recently been accepted into the repertoire of standard synthetic methodology. Lanthanoid(III) trichloride has been used as a Lewis acid catalyst for Friedel–Crafts reaction,[6] aldol reaction of silyl enol ether,[7] and ring opening reaction of oxirane.[8] Other trivalent lanthanoid reagents than $LnCl_3$ are also found to be useful for organic synthesis. For example, lanthanoid perchlorate and triflate are good catalyst for preparation of 4-substituted 2,6-dimethylpyrimidines from amines and nitriles.[9] Lanthanoid triflate can also be used with alkyllithium for the conversion of tertiary amines to ketones.[10] Lanthanoid tris[bis(trimethylsilyl)amide] has been developed for regioselective alkylation of epoxides with alkyllithium, where $LnCl_3$ poorly works.[11]

On the other hand, we previously reported a facile aldol synthesis from α-halo ketones and carbonyl compounds by using the combined reagent of $CeCl_3$–$SnCl_2$; a cerium enolate was assumed to be an intermediate.[12] The success of this reaction is due to activation of carbonyl group by cerium(III) ion promoting the reduction of the halogen group by $SnCl_2$. When we applied this combined reagent to a reaction of α,α′-dibromo ketone with furan and cyclopentadiene, the bicyclooctenones, i.e., [3+4] cycloadducts were produced in high yields. As α,α′-dibromo ketone has been recognized as a suitable building block for preparation of five- and seven-membered carbocycles by reaction with alkenes and 1,3-dienes, respectively,[13] the following reagents so far been developed for the reaction: Cu/NaI,[14] Zn/Cu,[15] Fe/graphite,[16] and $Fe_2(CO)_9$.[17] The former three reagents requires some activations and reaction system is heterogeneous. $Fe_2(CO)_9$ is toxic and expensive, and it requires long reaction time and high reaction temperature, although it appears to be an excellent reagent for both [3+4] and [3+2] cycloadditions. $CeCl_3$–$SnCl_2$ reagent can be more conveniently used for the cycloaddition reaction of some α,α′-dibromo ketones, and the reaction procedure is quite simple. The reaction is homogeneous, needs no activation, and is carried out at room temperature in the air. Both $CeCl_3$ and $SnCl_2$ are easily kept with a little care of moisture, non toxic, and inexpensive.

We would like to report here a facile [3+4] and [3+2] cycloaddition reaction of α,α′-dibromo ketones with 1,3-dienes and enamines by $CeCl_3$–$SnCl_2$, respectively.

Results and Discussion

Reaction of α,α′-Dibromo Ketones with Furans in the Presence of the Combined Reagent of $LnCl_3$–$SnCl_2$: The reaction of 2,4-dibromo-3-pentanone (**1**) with furan in tetrahydrofuran (THF) proceeded smoothly at 0 °C to room temperature to afford the cycloadduct (**4**) in good yield when the combined reagent of $CeCl_3$–$SnCl_2$ was employed. The results are shown in Table 1. One equivalent of $SnCl_2$ to **1** was sufficient for the reaction (Run 1), but an excess of $SnCl_2$ gave a more satisfactory yield of **4**; a three-fold excess of $SnCl_2$ was enough to obtain a reasonable

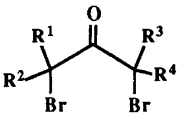

1; $R^1=R^3=Me$, $R^2=R^4=H$

2; $R^1=R^2=R^3=R^4=Me$

3; $R^1=R^2=Me$, $R^3=R^4=H$

Table 1. Cycloadduct Synthesis from **1** and Furan by $LnCl_3$-$SnCl_2$[a]

Run	Ln in $LnCl_3$	Isolated yield (%) of **4**[b]
1	Ce[c]	76
2	Ce[d]	81
3	Ce	90
4	Ce[e]	90
5	Ce[f]	0
6	Ce[g]	0
7	Ce[h]	0
8	—[i]	0
9	La	74
10	Sm	90
11	Eu	69
12	Er	72

a) **1** (4 mmol), furan (40 mmol), $LnCl_3$ (4 mmol), $SnCl_2$ (12 mmol), THF (15 cm^3); 0 °C, 2 h then rt, 3 h. b) A mixture of **4a**, **4b**, and **4c**. c) $SnCl_2$ (4 mmol). d) $SnCl_2$ (8 mmol). e) 0 °C, 2 h then rt, 22 h. f) Without $SnCl_2$. g) SnF_2 (12 mmol) was used. h) $PbCl_2$ (12 mmol) was used. i) Without $CeCl_3$.

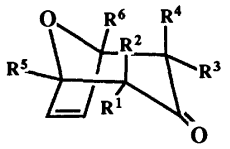

4a;R^1=R^3=Me, R^2=R^4=R^5=R^6=H
4b;R^2=R^4=Me, R^1=R^3=R^5=R^6=H
4c;R^1=R^4=Me, R^2=R^3=R^5=R^6=H
5a;R^1=R^3=R^5=Me,R^2=R^4=R^6=H
5b;R^1=R^3=R^6=H, R^2=R^4=R^5=Me
6a;R^1=R^3=R^5=R^6=Me, R^2=R^4=H
6b;R^1=R^3=H, R^2=R^4=R^5=R^6=Me
7;R^1=R^2=Me, R^3=R^4=R^5=R^6=H
8;R^1=R^2=R^3=R^4=Me, R^5=R^6=H

result (Run 3). No reaction took place in the absence of either $CeCl_3$ or $SnCl_2$ (Run 5,8). The use of SnF_2 or $PbCl_2$ (lead and tin are both 4B element) instead of $SnCl_2$ results in no reaction with the recovery of starting **1**. It may be concluded that the combination of $CeCl_3$ and $SnCl_2$ is essential to the reaction. Cycloadduct **4** was a mixture of three stereoisomers with respect to the two methyl groups (**4a**, **4b**, and **4c**).[18] The isomer ratio was determined by ^1H NMR integration of the bridgehead protons and olefinic protons after addition of the shift reagent [Eu(dpm)$_3$] according to the literature.[17b] The isomer ratio did not change when the reaction was carried out for a longer time (Run 4), indicating that the isomerization in **4** was not involved in the system and the configuration must be determined at a cycloaddition step.

Other lanthanoid trichloride such as $LaCl_3$, $SmCl_3$, $EuCl_3$, and $ErCl_3$ can be used for the reaction; the yields and isomer ratios were virtually the same despite variation of the lanthanoid metal. For reasons of economy $CeCl_3$ was chosen for investigation.

The cycloadducts of **1** with the substituted furans such as 2-methylfuran and 2,5-dimethylfuran were also obtained as mixtures of two types of cis adducts in good yields, no trans isomers being produced. The reaction of the other dibromide (**2** and **3**) with furan similarly gave 1:1 adduct (**7** and **8**, respectively) in high yields. The results are summarized in Table 2 (Runs 2, 3, 7, and 10).

Reaction with Cyclopentadiene: The reaction of the dibromides with 1,3-dienes including furans are also shown in Table 2. The $CeCl_3$-$SnCl_2$ promoted the reaction of the dibromides (**1**—**3**) and cyclopentadiene gave the bicyclic ketones (**9**—**11**) in high yields (Runs 4, 8, 11). The cycloadduct derived from **1** was two types of cis adducts (**9a** and **9b**) in a ratio of **9a**:**9b**=72:28. No trans isomer was discernible in this reaction. The structural determination of the adduct was carried out by ^1H NMR by reference to the literature.

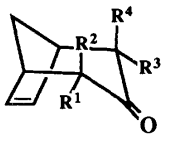

9a;R^1=R^3=Me, R^2=R^4=H
9b;R^1=R^3=H, R^2=R^4=Me
10;R^1=R^2=Me, R^3=R^4=H
11;R^1=R^2=R^3=R^4=Me

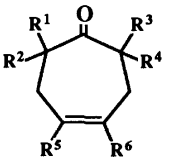

12;R^1=R^3=R^5=R^6=Me, R^2=R^4=H
13;R^1=R^3=R^5=Me, R^2=R^4=R^6=H
15;R^1=R^2=R^5=R^6=Me, R^3=R^4=H
16;R^1=R^2=R^3=R^4=R^5=R^6=Me

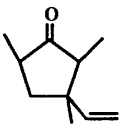

14

Reaction with Open-Chain 1,3-Dienes: Reaction of **1**—**3** with open-chain 1,3-dienes were examined by using 1,3-butadiene, isoprene, and 2,3-dimethyl-1,3-butadiene. With 2,3-dimethyl-1,3-butadiene the corresponding 4-cycloheptenones (**12**, **13**, **15**, and **16**) were obtained in moderate yields, but less than that with cyclic dienes (Table 2, Runs 5, 9, and 12). It is interesting that the reaction of **1** with isoprene gave **14** as [3+2] cycloadduct in addition to the expected [3+4] cycloadduct **13** (Run 6). A similar result is reported in the reaction of α-bromo silyl enol ether with isoprene.[18] Unfortunately, the cycloadduct with 1,3-butadiene could not be isolated and many products were formed. As a [3+2] cycloadduct with isoprene was obtained, we tried the reaction of **1** with monoalkenes such as styrene and α-methylstyrene, but results was no reaction.

Reaction with Enamines: Although the reaction of an α,α′-dibromo ketone with alkenes did not produce

Table 2. Cycloadducts Synthesis from **1**—**3** and 1,3-Dienes by $CeCl_3$–$SnCl_2$[a]

Run	α,α′-Dibromo ketone	1,3-Diene	Product and isolated yield (%)
1	**1**	Furan	**4a**, **4b**, **4c**, 90 (**4a**:**4b**:**4c**=62:28:10)[b]
2	**1**	2-Methylfuran	**5a**, **5b** 78 (**5a**:**5b**=70:30)[b]
3	**1**	2,5-Dimethylfuran	**6a**, **6b** 91 (**6a**:**6b**=63:37)[b]
4	**1**	Cyclopentadiene	**9a**, **9b** 88 (**9a**:**9b**=72:28)[b]
5	**1**	2,3-Dimethyl-1,3-butadiene[c]	**12**, 48
6	**1**	Isoprene	**13**, 37; **14**, 33
7	**2**	Furan	**7**, 77
8	**2**	Cyclopentadiene	**10**, 70
9	**2**	2,3-Dimethyl-1,3-butadiene	**15**, 30
10	**3**	Furan	**8**, 78
11	**3**	Cyclopentadiene	**11**, 71
12	**3**	2,3-Dimethyl-1,3-butadiene	**16**, 37

a) **1**—**3** (4 mmol), 1,3-diene (40 mmol), $CeCl_3$ (4 mmol), $SnCl_2$ (12 mmol), THF (15 cm^3); 0 °C, 2h then rt, 3 h. b) Determined by ^1H NMR with Eu(dpm)$_3$. c) 1,3-Diene (12 mmol).

Table 3. Cycloadducts Synthesis from **1**—**2** and Enamines by $CeCl_3$–$SnCl_2$[a]

Run	α,α′-Dibromo ketone	Enamine	Product isolated yield (%)	Isomer ratio[b] (trans:cis)
1	**1**	**17**	**21**, 54	95:5
2	**1**	**18**	**22**, 55	94:6
3	**1**	**19**	**23**, 55	93:7
4	**1**	**20**	**24**, 48	—
5	**2**	**18**	**25**, 28[20]	—

a) **1**, **2** (4 mmol), enamine (12 mmol), $CeCl_3$ (4 mmol), $SnCl_2$ (12 mmol), THF (15 cm^3); rt, 5 h then treated with 3% NaOH/EtOH (3 cm^3) for 30 min. b) Determined by GLC.

[3+2] cycloadducts, the cycloadducts with activated alkenes such as enamines could be obtained. For example, when a mixture of **1** and 1-morpholinocyclopentane (**17**) were reacted in the presence of $CeCl_3$–$SnCl_2$ in THF at 0 °C and subsequently treated with 3% ethanolic NaOH, 2-cyclopenten-1-one (**21**) was produced in a moderate yield as a mixture of cis and trans isomers in a ratio of cis:trans=6:94. The other examples are given in Table 3.[20]

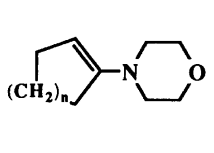

17;n=1
18;n=2
19;n=3

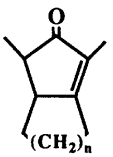

21;n=1
22;n=2
23;n=3

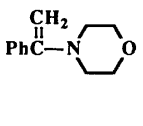

20

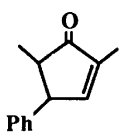

24

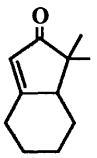

25

Reaction Mechanism: Treatment of **1** with 1 equiv of $CeCl_3$–$SnCl_2$ (1:1) followed by with D_2O in THF gave 2-bromo-4-deuterio-3-pentanone (**26**). This result may suggest that the first step of the reaction of α,α′-dibromo ketone with $CeCl_3$–$SnCl_2$ involves a single debromination just like a Reformatsky reaction to afford a corresponding cerium α-bromo enolate (**27a**).[12] The enolate **27a** suffers further elimination of bromide ion by way of S_N1 like reaction to give the oxyallyl cation (**28a**) which undergoes [3+4] and [3+2] cycloadditions with 1,3-dienes and enamines, respectively.[15b,17a] α-Halo silyl enol ether (**27b**) is an isolated metal α-halo enolate and has been designed for the synthetic equivalent of an oxyallyl cation.[19] Then the

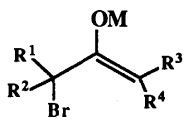

27a;M=$CeCl_2$
27b;M=$SiMe_3$

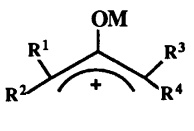

28a; M=$CeCl_2$
28b;M=$SiMe_3$

plausible key intermediate of the oxyallyl cation seems to be the ceruim α-bromo enolate.

Experimental

^{1}H NMR spectra were recorded with Hitachi R-24 (60 MHz) and Hitachi R-600 (60 MHz) instrument in $CDCl_3$ solutions with $SiMe_4$ as an internal standard. IR spectra were taken with Shimadzu IR 410. GLC analyses were carried out by using a Shimadzu 8A apparatus on EGSS-X(3%)-Chromosorb-W(2 m) and Silicone DC QF-1(5%)-Chromosorb-W(2 m) columns (N_2 as carrier gas).

Frash column chromatography was performed by EYELA EF-10 apparatus by using Merck Kieselgel 60 (230—400 mesh) or Wako C-300. Preparative TLC separation was conducted using 20×20 cm glass plates coated with a 2.0 mm thick layer of Merck Kieselgel PF_{254} gipsphaltig.

Tetrahydrofuran was distilled from sodium benzophenone ketyl under nitrogen. Anhydrous $LaCl_3$, $CeCl_3$, $SmCl_3$, $EuCl_3$, and $ErCl_3$ were obtained by drying the commercial hydrate with $SOCl_2$.[13] Anhydrous tin(II) chloride was purchased from Wako Pure Chemicals Co. and further dried at 200 °C in vacuo before use.

α,α'-Dibromo ketones (**1**, **2**, and **3**) were prepared by a dibromination of the corresponding ketones with bromine in diethyl ether catalyzed by phosphorus tribromide.[15a] Furan, 2-methylfuran, and 2,5-dimethylfuran were distilled over potassium hydroxide. Cyclopentadiene was distilled by thermolysis of commercial dicyclopentadiene at 200 °C just prior to use. Enamines were prepared from the corresponding ketones and morpholine in the presence of a catalytic amount of *p*-toluenesulfonyl chloride in refluxing benzene.

Reaction of α,α'-Dibromo Ketones with 1,3-Dienes in the Presence of $CeCl_3$-$SnCl_2$. General Procedure: Anhydrous $CeCl_3$ (1.00 g, 4 mmol) and $SnCl_2$ (2.27 g, 12 mmol) were placed in a 50 cm^3 two-neck round bottom flask containing a magnetic stirrer bar. To this THF (10 cm^3) was introduced followed by addition of a mixture of α,α'-dibromo ketone (4 mmol) and 1,3-diene (12—40 mmol) in 5 cm^3 of THF at 0 °C with stirring. The mixture was stirred at 0 °C for 2 h and then at room temperature for additional 3 h. The solution was poured into diluted HCl, extracted with chloroform (20 cm^3×3), dried ($MgSO_4$), and evaporated under reduced pressure. The residue was passed through a short alumina column (2 cm×3 cm) eluted with chloroform to remove a polymeric product. Removal of the solvent by a rotary evaporator left the almost pure adduct by ^{1}H NMR analysis, which was further subjected to preparative TLC or flash column chromatography on silica gel (hexane–ethyl ehter=10:1 as eluent). All the cycloadducts were known compounds, then the identification and isomer ratio of the products were carried out by ^{1}H NMR and IR by reference to the literature.[15,17b] The spectra data of all the products were satisfied with the structure of the reported ones. The isomer ratio of the products, **4a**:**4b**:**4c**, **5a**:**5b**, and **6a**:**6b** were determined by ^{1}H NMR integration of the bridge head protons and olefinic protons with the shift reagent, Eu(dpm)$_3$.

Reaction of α,α'-Dibromo Ketone with Enamine by $CeCl_3$-$SnCl_2$: Anhydrous $CeCl_3$ (1.00 g, 4 mmol) and $SnCl_2$ (2.27 g, 12 mmol) were placed in a 50 cm^3 two-neck round bottom flask containing a magnetic stirrer bar. THF (10 cm^3) was introduced to the flask followed by addition of THF (5 cm^3) solution of α,α'-dibromo ketone (4 mmol) and enamine (12 mmol) at room temperature with stirring. The mixture was stirred at room temperature for 5 h, then diluted with ethyl acetate (50 cm^3), treated with saturated $NaHCO_3$ (30 cm^3), and filtered. The filtrate was washed with brine (30 cm^3×2), and dried ($MaSO_4$), After evaporation of the solvent the residue (the undeaminated adduct) was treated with 3% ethanolic NaOH solution (3 cm^3) at room temperature for 30 min. The solution was diluted with ethyl acetate (50 cm^3), neutralized with dilute HCl (20 cm^3), washed with brine (30 cm^3×2), then dried over $MgSO_4$. Evaporation of the solvent left a yellow oil which was passed through a short alumina column (2 cm×3 cm) with chloroform. The adduct (cyclopentenone derivative) was isolated by flash column chromatography on silica gel (hexane–ethyl acetate =10:1 as eluent). The cyclopentenone was obtained as a mixture of cis and trans (except for **24** and **25**). The stereoisomers was separated by preparative TLC (hexane–ethyl acetate=10:1). ^{1}H NMR and IR spectra of the products were identical with those of the reported ones.[17c] The isomer ratio was determined by GLC.

References

1) For reviews, a) H. B. Kagan, "Fundamental and Technologycal Aspects of Organo-f-Element Chemistry," ed by T. J. Marks and I. L. Fragara, NATO ASI, Dordrecht (1985), pp. 49—76. b) H. B. Kagan and J. L. Namy, *Tetrahedron*, **42**, 6573 (1986). c) T. Imamoto, *Yuki Gosei Kagaku Kyokai Shi*, **46**, 540 (1988).

2) a) J.-L. Luche, *J. Am. Chem. Soc.*, **100**, 2226 (1978). b) J.-L. Luche, J. R. Hahn, and P. Crabbe, *J. Chem. Soc., Chem. Commun.*, **1978**, 601. c) A. L. Gemal and J.-L. Luche, *J. Am. Chem. Soc.*, **103**, 5454 (1981).

3) a) S. Fukuzawa, T. Fujinami, S. Yamauchi, and S. Sakai, *J. Chem. Soc., Perkin Trans. 1*, **1986**, 1929. b) T. Imamoto, T. Takeyama, and T. Kusumoto, *Chem. Lett.*, **1985**, 1491.

4) For recent examples, a) T. Imamoto, T. Kusumoto, Y. Tawarayama, Y. Sugiura, T. Mita, Y. Hatanaka, and M. Yokoyama, *J. Org. Chem.*, **49**, 3904 (1984). b) T. Imamoto, N. Takiyama, and N. Nakamura, *Tetrahedron Lett.*, **26**, 4763 (1985). c) L. A. Paquett and K. S. Learn, *J. Am. Chem. Soc.*, **108**, 7873 (1986). d) S. E. Denmark, T. Weber, and D. W. Piotrowski, *ibid.*, **109**, 2224 (1987). e) C. R. Johnson and B. D. Tait, *J. Org. Chem.*, **52**, 281 (1987). f) B. A. Narayanan and W. H. Bunnelle, *Tetrahedron Lett.*, **28**, 6261 (1987). g) M. B. Anderson and Fuchs, *Synth. Commun.*, **1987**, 621.

5) G. Klopman, *J. Am. Chem. Soc.*, **90**, 223 (1968).

6) N. Mine, Y. Fujiwara, and H. Taniguchi, *Chem. Lett.*, **1986**, 357.

7) A. E. Vougioukas and H. B. Kagan, *Tetrahedron Lett.*, **28**, 5513 (1987).

8) A. E. Vougioukas and H. B. Kagan, *Tetrahedron Lett.*, **28**, 6065 (1987).

9) a) J. H. Forsberg, T. M. Balasubramanian, and V. T. Spaziano, *J. Chem. Soc., Chem. Commun.*, **1976**, 1060. b) J. Forsberg, V. T. Spaziano, T. M. Balasubramanian, G. K. Liu, S. A. Kinsley, C. A. Duckworth, J. J. Poteruca, P. S. Brown, and J. L. Miller, *J. Org. Chem.*, **52**, 1017 (1987).

10) S. Collins and Y. Hong, *Tetrahedron Lett.*, **28**, 4391 (1987).

11) I. Mukerji, A. Wayda, G. Dabbagh, and S. H. Berts, *Angew. Chem., Int. Ed. Engl.*, **25**, 760 (1986).

12) S. Fukuzawa, T. Tsuruta, T. Fujinami, and S. Sakai, *J. Chem. Soc., Perkin Trans. 1*, **1987**, 1473.

13) H. M. R. Hoffmann, *Angew. Chem.*, **20**, 877 (1973).

14) M. R. Aschcroft and H. M. R. Hoffmann, *Org. Synth.*, **58**, 17 (1978).

15) a) H. M. R. Hoffmann, K. E. Clemens, E. A. Schmidt, and R. H. Smithers, *J. Am. Chem. Soc.*, **94**, 3201 (1972). b) H. M. R. Hoffmann, K. E. Clemens, and R. H. Smithers, *ibid.*, **94**, 3940 (1972). c) N. N. Joshi and H. M. R. Hoffmann, *Tetrahedron Lett.*, **27**, 687 (1986).

16) D. Savia, E. Tagliavini, C. Trombini, and A. Umani-Ronchi, *J. Org. Chem.*, **47**, 876 (1982).

17) a) R. Noyori and Y. Hayakawa, *Org. React.*, **29**, 163 (1983). b) R. Noyori and Y. Hayakawa, H. Tanaka, S. Murai, R. Kobayashi, and N. Sonoda, *J. Am. Chem. Soc.*, **100**, 1759 (1978). c) T. Takaya, S. Makino, Y. Hayakawa, and R. Noyori, *ibid.*, **100**, 1765 (1978). d) Y. Hayakawa, K. Yokoyama, and R. Noyori, *ibid.*, **100**, 1791 and 1799 (1978).

18) The cycloaddition with furan by zinc also gives the three stereo isomers and explanation for the preferential formation of **4a** is discussed.[15b]

19) a) H. Sakurai, A. Shirahata, and A. Hosomi, *Angew. Chem., Int. Ed. Engl.*, **18**, 163 (1979). b) N. Shimizu and Y. Tsuno, *Chem. Lett.*, **1979**, 103. c) N. Shimizu, M. Tanaka, and Y. Tsuno, *J. Am. Chem. Soc.*, **104**, 1330 (1982).

20) The reaction of **2** with **18** should give two regio-isomers, **29** and **30**, but only **29** could be suffered from deamination to form **25**; **30** does not have an α-proton from the carbonyl group. We did not isolate the products as undeaminated forms.

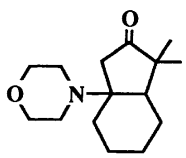

29

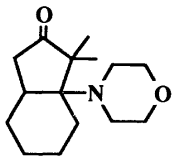

30

The Esterification of Carboxylic Acid with Alcohol over Hydrous Zirconium Oxide

Kyoko TAKAHASHI,* Makoto SHIBAGAKI, and Hajime MATSUSHITA
Life Science Research Laboratory, Japan Tobacco, Inc., 6-2 Umegaoka, Midori-ku, Yokohama, Kanagawa 227
(Received February 13, 1989)

The esterification of carboxylic acids with alcohols proceeded efficiently with hydrous zirconium oxide to give the corresponding esters in the vapor phase, in the liquid phase, and in an autoclave. The steric hindrance of carboxylic acids and alcohols affected the esterification by lowering the reactivity. With a rise in the reaction temperature, the conversion of the carboxylic acid increased. The dehydration of alcohols was prevented by using hydrous zirconium oxide in spite of the high reaction temperature. The reaction rate is first-order with respect to the concentration of the catalyst and an alcohol and is inversely proportional to that of the carboxylic acid. Transesterification also proceeded efficiently.

In our previous papers,[1-5] we reported that hydrous zirconium oxide has the catalytic activity for the reduction of aldehydes and ketones with 2-propanol and the amidation of carboxylic acid with amine. Since the hydrous zirconium oxide was expected to have affinities for both carboxylic acids and alcohols, the esterification of carboxylic acids with alcohols was carried out by the catalysis of the oxide.

In the esterification of carboxylic acids with alcohols, homogeneous catalysts, such as sulfulic acid and hydrochloric acid, are usually used. These methods, however, need tedious work-up procedures in the isolation of the products. Recently, heterogeneous catalysts, such as Nafion-H,[6] the zirconium oxide–sulfate ion,[7] the titanium oxide–sulfate ion,[8] heteropoly acids supported on carbon,[9] silica–alumina, zeolite HY,[10] cation-exchange resin, and niobic acid,[11] have been reported to be effective catalysts for the esterification. These are all solid acid or solid superacid catalysts, however, there is a fear of unfavorable side reactions such as dehydration because of the strong acidity of the catalyst. As heterogeneous catalysts for the esterification, titanium alkoxide and zirconium alkoxide supported on silica, alumina, or silica–alumina have also been reported.[12] The preparation of these catalysts is, however, troublesome.

The hydrous zirconium oxide consists of hard and translucent granules. According to the X-ray diffraction analysis, the oxide was shown to be amorphous. Esterification over hydrous zirconium oxide has the following advantages: 1) the hydrous zirconium oxide is easily prepared by the neutralization of an aqueous zirconium dichloride oxide solution; 2) the products can easily be isolated by filtering-off the catalyst and subsequently evaporating the solvent, because the catalyst is insoluble in any solvent; 3) the oxide is stable at room temperature in air, and 4) the oxide is not sensitive to air or water, and the esterification does not require water-free conditions.

In this paper, we wish to report that the hydrous zirconium oxide catalyzes the esterification of carboxylic acid with alcohol efficiently and that it also catalyzes the transesterification. These reactions were carried out in the vapor phase, in the liquid phase, and in an autoclave. The hydrous zirconium oxide does not have a strong acid strength on the surface, and such undesirable side reactions as dehydration can be avoided, unlike as in the cases of acid catalysts. The mechanism of esterification over hydrous zirconium oxide was also studied in vapor-phase reactions.

Experimental

Materials. Commercial reagents were used for the reaction without any further purification.

Hydrous Zirconium Oxide. To a solution of zirconium dichloride oxide ($ZrOCl_2 \cdot 8H_2O$)(200 g of a solid in 10 dm^3 of deionized water) we slowly added an aqueous solution of sodium hydroxide (1 mol dm^{-3}) at room temperature. Constant, gentle stirring was maintained, and the addition was continued until the pH of the resulting solution reached 6.80. The resulting product was filtered and washed free from chloride ions. The gel was spread on a glass plate and dried in air at room temperature for 10 h and then at 80 °C for 2 h. Fifty-four grams of hydrous zirconium oxide were obtained in the form of granules, which were subsequently heated at 300 °C for 5 h.

General Procedures for Vapor-Phase Reactions. The catalytic esterification was carried out in a glass-flow reactor (6.5 mm in diameter) with a fixed-bed catalyst: flow rate of nitrogen gas=60 cm^3 min^{-1}; catalyst=2.0 g, 24—60 mesh; reaction temperature=135—280 °C. A mixture of a carboxylic acid, an alcohol, and a hydrocarbon as an internal standard was fed into the reactor (5 or 10 cm^3 h^{-1}) by means of a microfeeder. In some cases, benzene was also added to dilute the reaction mixture. The activity and selectivity of the reaction were determined after the steady states has been reached. The products were then analyzed by gas chromatography (a capillary column PEG 20M 30 m). The products were identified by a comparison of their retention times with those of authentic samples.

General Procedures for Liquid-Phase Reaction. In a 25 cm^3 round-bottomed flask equipped with a reflux condenser we placed the catalyst (2.0 g), a carboxylic acid, an alcohol, and a hydrocarbon as an internal standard. The contents were then heated under a gentle reflux. In some reactions, toluene was added to the solution in order to raise the reaction temperature. In some cases, the reaction

mixture was placed in an oil bath kept at 77.0±0.1 °C. The reaction mixture was collected after 5 hours, and the products were analyzed by means of gas chromatography.

General Reaction Procedures in an Autoclave. In a 100-cm^3 autoclave were placed the catalyst (2.0 g), a carboxylic acid, an alcohol, and a hydrocarbon as an internal standard. The autoclave was then heated to the reaction temperature (130—240 °C) and kept there for 2 h. The analysis of the products was performed in a manner similar to described above.

Surface Acidity. The quantity of surface acidic sites was measured by the butylamine-titration method using various Hammett indicators.

Results and Discussion

Esterification in the Vapor Phase. The results of vapor-phase esterification of carboxylic acids with alcohols over hydrous zirconium oxide are listed in Table 1. The esterification of carboxylic acids, except for adamantanecarboxylic acid, with primary alcohols gave the corresponding esters in high yields (Entries 1—7). In the case of the reaction with secondary alcohols, the conversion of the carboxylic acid increased in this order: tertiary<secondary<primary. These results can be explained by the steric hindrance of the carboxylic acid (Entries 9—14). The esterification with tertiary alcohol gave the ester in a low yield (Entry 16). The esterification of cyclohexanecarboxylic acid with primary alcohol gave the ester in a higher yield than that with secondary alcohol (Entries 3 and 11). As has been described above, the steric hindrance of alcohols also affected the esterification. The higher the reaction temperature, the more carboxylic acid was consumed. The selectivity for the ester, however, was lowered, and the reaction gave the alcohol as a by-product of the reduction of the carboxylic acid (Entries 4 and 5). The selectivity for the ester was 100% in the esterification with benzyl alcohol at 150 °C (Entry 8).

Table 1. Esterification in the Vapor Phase over Hydrous Zirconium Oxide[a)]

Entry	Reactant		Temperature/°C	Conversion/%	Selectivity/%
1		C_2H_5OH	200	100	100
2		C_2H_5OH	200	100	100
3		C_2H_5OH	215	100	91
4		C_2H_5OH	200	99	98
5		C_2H_5OH	250	100	60
6		C_2H_5OH	200	100	100
7		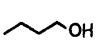	250	100	78
8[b)]	CH_3COOH		150	37	100
9			215	100	87
10			200	96	97
11			215	80	94
12			200	31	100
13[c)]	CH_3COOH		200	100	100
14[c)]			200	34	98
15[c)]			280	22	83
16	C_2H_5COOH		200	7	98

a) Catalyst: 2.0 g; carboxylic acid: 0.1 mol dm^{-3} in alcohol; sample feed: 10 $cm^3 h^{-1}$. b) Acetic acid: benzyl alcohol=2.5:1; sample feed: 5 $cm^3 h^{-1}$. c) Carboxylic acid: 0.1 mol dm^{-3}; alcohol: 0.5 mol dm^{-3} in benzene.

Table 2. Transesterification of Ethyl Acetate in the Vapor Phase

Entry	Reactant	Temperature/°C	Conversion/%	Selectivity/%
1		200	100	100
2	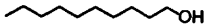	200	99	99
3		200	98	98
4		190	97	96
5	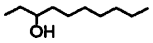	200	93	99
6		200	43	100
7		200	14	—
8		200	27	84
9	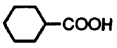	200	1	95

Catalyst: 2.0 g; sample feed: 10 $cm^3 h^{-1}$; carboxylic acid or alcohol: 0.10 mol dm^{-3} in ethyl acetate.

Table 3. Esterification in the Liquid Phase over Hydrous Zirconium Oxide (**1**)[a]

Entry	Reactant(mmol)				Catalyst/g	Conv./%	Select./%
1	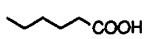	(2)	C_2H_5OH	(100)	2	100	100
2[b]	CH_3COOH	(2)	C_2H_5OH	(20)	2	98	100
3	C_2H_5COOH	(25)		(63)	2	91	100
4[c]	CH_3COOH	(2)		(32)	4	100	100
5[d]	CH_3COOH	(1)		(10)	1	100	100
6	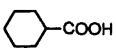	(2)	C_2H_5OH	(100)	2	87	100
7	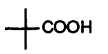	(2)	C_2H_5OH	(100)	2	50	100
8	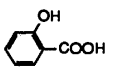	(2)	CH_3OH	(100)	2	13[e]	—
9	CH_3COOH	(31)		(13)	1	65	100
10	CH_3COOH	(31)		(13)	1	10	100
11[b]	CH_3COOH	(31)		(13)	1	42	100
12	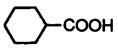	(31)		(13)	1	28	100

a) Reflux for 5 h. b) Toluene (4 cm^3) was added. c) Reflux for 2 h. d) Toluene (2 cm^3) was added and reflux for 1 h. e) Yield of methyl salicylate.

Since the reaction with benzyl alcohol at 150 °C over Nafion H caused undesirable polymerization,[6] the hydrous zirconium oxide is superior to the superacid catalyst. Moreover, the hydrous zirconium oxide caused scarcely any dehydration of alcohols.

Transesterification in the Vapor Phase. The reactions of alcohols or carboxylic acids with ethyl acetate—that is, transesterification—were investigated by means of the catalysis of the hydrous zirconium oxide in the vapor phase. The transesterification, an useful method for the preparation of esters, needs water-free conditions; and it is used for the preparation of polyesters. The results of the reaction catalyzed by the hydrous zirconium oxide are listed in Table 2.

Generally, most of the alcohols were converted to the corresponding acetates in the transesterification with ethyl acetate; the selectivity of the reaction was very high in each case. Primary alcohols were more reactive than secondary ones, while tertiary ones were not efficiently reacted. In the case of menthol, the reactivity was lowered by its steric hindrance. The transesterification of carboxylic acids gave the esters in low yields.

Esterification in the Liquid Phase. The esterifications of carboxylic acids with alcohols over the hydrous zirconium oxide were investigated in the liquid phase; the results are listed in Table 3. The reactions were carried out at the reflux temperature of the solution. Most of the carboxylic acids were converted to the corresponding esters in high yields. In the esterification with primary alcohol, the reactivities increased in this order: tertiary carboxylic acid< secondary one<primary one, the same as in the vapor-phase reactions (Entries 1—7). The yields of the ester in the reactions with primary alcohols were higher than in those with secondary alcohol. The esterification of acetic acid with menthol gave the ester in a lower yield than that with cyclohexanol (Entries 9 and 10). The yield was, however, increased by adding toluene to the reaction mixture. This suggests that raising the reaction temperature enhanced the reactivity, even in the reaction of menthol (Entry 11). In the case of the reaction of salicylic acid with methanol, the corresponding methyl ester was obtained in a 13% yield (Entry 8). The low conversion of salicylic acid was explained by its strong adsorption, since the pK_a value of salicylic acid (2.98) was lower than that of the other carboxylic acid (ca. 4.8) shown in Table 3. This suggests that the reactivity was inhibited by the adsorption of carboxylic acid. In order to clarify the

Table 4. Esterification in the Liquid Phase over Hydrous Zirconium Oxide (2)[a]

Entry	Reactant		Temp./°C	Conv./%	Select./%
1	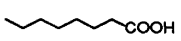	C_2H_5OH	77	94	100
2	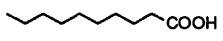	C_2H_5OH	77	84	100
3[b]	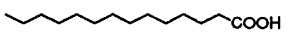	C_2H_5OH	77	30	100
4	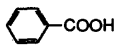	C_2H_5OH	77	29	100
5			77	59	100
6	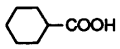	C_2H_5OH	77	72	100
7	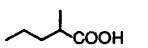	C_2H_5OH	77	46	100
8	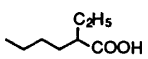	C_2H_5OH	77	5	100
9		C_2H_5OH	77	16	100
10[b]	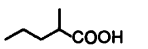	C_2H_5OH	77	35	100
11	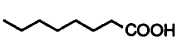		77	15	100
12	CH_3COOH		77	Trace	—

a) Catalyst: 1.0 g; carboxylic acid: 5 mmol; alcohol: 50 mmol; reaction for 5 h. b) Catalyst: 0.5 g; carboxylic acid: 2.5 mmol; alcohol: 50 mmol; reaction for 5 h.

difference in reactivity between carboxylic acids and between alcohols, the esterification was carried out at the same temperature (77 °C) in the liquid phase. The results are shown in Table 4. In the reaction of primary carboxylic acid with primary alcohol, the reactivity of the esterification was lowered according to the length of the carbon chain (Entries 1—3, and 5). In the reaction of secondary carboxylic acid with primary alcohol, the reaction of the carboxylic acid which possesed a methyl group at a α-position was lower than that of cyclohexane carboxylic acid. Further, the carboxylic acid which possesed a ethyl group in the α-position gave the ester in a lower yield. These results suggest that the steric hindrance of carboxylic acid affects the reaction. The esterification of tertiary carboxylic acid with primary alcohol gave the ester in a low yield because of the steric hindrance. In the case of benzoic acid, the reactivity was relatively low. This result was caused by the relatively low pK_a value (4.20) of benzoic acid, much as in the case of salicylic acid. The reactivities of alcohol increased in this order: tertiary alcohol<secondary one<primary one. The esterification in the liquid phase over hydrous zirconium oxide was affected by the steric hindrace of carboxylic acids and alcohols. Though the conversion in the liquid-phase esterification was lower than the vapor-phase reaction because of the lower reaction temperature, the selectivity was always 100%.

Table 5. Transesterification of Ethyl Acetate in the Liquid Phase over Hydrous Zirconium Oxide[a)]

Entry	Reactant	Conversion /%	Selectivity /%
1	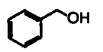	32	100
2		44	100
3	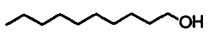	22	100
4		12	100
5	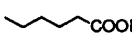	—	0
6	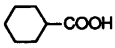	—	0

a) Catalyst: 2.0 g; carboxylic acid or alcohol: 2 mmol; ethyl acetate: 60 mmol; reaction for 5 h.

Transesterification in the Liquid Phase. The results of the transesterification of alcohols and carboxylic acids with ethyl acetate in the liquid phase are shown in Table 5. The tendency of the reactivities of several alcohols was similar to that in the vapor phase. The yield of the ester in the transesterification of primary alcohol was higher than that of the secondary one, and the reaction of carboxylic acid did not proceed. The selectivities of the esters were usually 100%.

Dependence on the Molar Ratio of Carboxylic Acid to Alcohol in Liquid-Phase Esterification. Table 6 shows the dependence on the molar ratio of acetic acid to ethyl alcohol in liquid-phase esterification. When either carboxylic acid or alcohol was used in excess, the ester was given efficiently. The reaction in even an equimolecular quantity of acetic acid and ethyl alcohol gave the ester in a 77% yield. The selectivity of the ester was always 100%.

Esterification in an Autoclave. It has been described that the reaction temperature affects the esterification over hydrous zirconium oxide. In order to obtain the ester in a higher yield, the esterification was carried out in an autoclave at a high temperature. The results are shown in Tables 7 and 8. The esterification in an autoclave gave the ester in a higher yield than that in a vapor-phase or liquid-phase reaction. The decarboxylation of salicylic acid and the dehydration of secondary and tertiary alcohol occurred slightly. It was learned that *t*-butyl alcohol could easily be dehydrated by using an acid catalyst at a high temperature. However, it was interesting that the esterification proceeded preferentially over hydrous zirconium oxide. The reaction of acetic acid with ethylene glycol and glycerol gave, selectively, the diacetate and triacetin respectively. Although the reaction of terephtalic acid gave both diacetate and monoacetate, the reactions of other dibasic acids and acid anhydrides gave the diesters selectively. By using an autoclave, the esterification of the polyhydric alcohol or dibasic acid over hydrous zirconium oxide proceeded effectively.

Transesterification in an Autoclave. Table 9 shows the results of the transesterification over hydrous zirconium oxide in an autoclave. The yields were higher than those in a vapor-phase or liquid-phase reaction. The conversion of carboxylic acid increased,

Table 6. Dependence on the Molar Ratio of Acid to Ethyl Alcohol in the Liquid Phase over Hydrous Zirconium Oxide[a)]

Entry	Acetic acid/mmol	Ethyl alcohol/mmol	Conversion[b)]/%	Selectivity/%
1	25	125	96	100
2	25	62.5	86	100
3	25	25	77	100
4	62.5	25	94[c)]	100

a) Catalyst: 2.0 g; reflux for 5 h. b) Based on acetic acid. c) Based on ethyl alcohol.

Table 7. Esterification in an Autoclave over Hydrous Zirconium Oxide (1)[a]

Entry	Reactant (mmol)				Temp./°C	Conv./%	Select./%
1	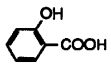	(10)	CH_3OH	(740)	180	69	99.6[c]
2	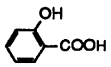	(10)	CH_3OH	(740)	210	100	95[c]
3	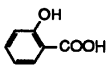	(10)	CH_3OH	(740)	240	100	91[c]
4[b]	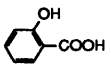	(30)	CH_3OH	(740)	210	100	91[c]
5[b]	CH_3COOH	(520)		(10)	210	99	99
6	CH_3COOH	(520)		(30)	180	98	95
7	CH_3COOH	(520)		(30)	210	81	70
8	CH_3COOH	(30)		(315)	180	25	100
9	CH_3COOH	(30)		(315)	210	50	100
10	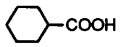	(10)		(288)	210	100	100
11		(10)		(390)	210	54	100

a) Catalyst: 2.0 g; reaction for 2 h. b) Reaction for 1.5 h. c) Product was methyl salicylate.

Table 8. Esterification in an Autoclave over Hydrous Zirconium Oxide (2)[a]

Entry	Reactant (mmol)				Temp./°C	Conv./%	Select./%
1	CH_3COOH	(350)	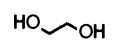	(10)	180	100	100
2	CH_3COOH	(350)	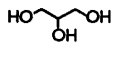	(20)	180	80	99[b]
3	CH_3COOH	(350)	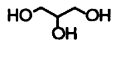	(10)	200	96	100[b]
4	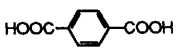	(10)	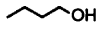	(220)	180	86	48[c]
5		(10)		(220)	180	69	100
6		(10)	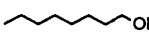	(127)	200	99	100
7	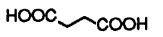	(10)		(220)	180	98	100

a) Catalyst: 2.0 g; reaction for 2 h; product was diester. b) Product was triacetin. c) The other product was a monoester.

Table 9. Transesterification in an Autoclave over Hydrous Zirconium Oxide

Entry	Reactant	Temperature/°C	Conversion/%	Selectivity/%
1	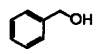	150	100	66
2	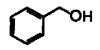	130	96	98
3	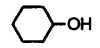	150	68	68
4	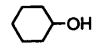	130	18	100
5	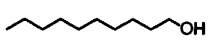	150	98	100
6	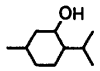	160	4	62
7	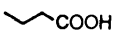	180	84	85
8	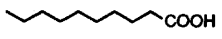	200	33	100
9	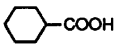	200	75	100

a) Catalyst: 2.0 g; carboxylic acid or alcohol: 10 mmol; ethyl acetate: 20 cm^3; reaction for 2 h.

Table 10. Acid Amounts on The Hydrous Zirconium Oxide

Acidity	$H_0 \leq -8.2$	$H_0 \leq -5.6$	$H_0 \leq -3.0$	$H_0 \leq 1.5$
Amount/mol g^{-1}	0	8×10^{-6}	5×10^{-4}	1.4×10^{-3}

and the selectivity decreased, with the rise in the reaction temperature. The reaction with menthol gave the ester in a low yield because of its steric hindrance. Although the transesterification with carboxylic acid gave the ester in neither a vapor nor a liquid phase, it could proceed efficiently in an autoclave.

Durability of Hydrous Zirconium Oxide in Vapor-Phase Esterification. In order to estimate the durability of the hydrous zirconium oxide, the esterification of acetic acid with ethyl alcohol was carried out at 250 °C in the vapor phase. As a result, the catalytic activity of the hydrous zirconium oxide was kept for at least 170 h. This showed that the hydrous zirconium oxide is a durable heat-stable catalyst.

Surface Acidity. The findings on the surface acidity of the hydrous zirconium oxide are shown in Table 10. The acid amounts at $H_0 \leq -8.2$ and $H_0 \leq -5.6$ are 0 and 8×10^{-3} mmol·g^{-1} respectively. This shows that the hydrous zirconium oxide does not have as strong acid sites as the other solid acid catalysts. From the point of view of avoiding such side reactions as the dehydration of alcohols, low acidity is an advantage in an esterification catalyst. The hydrous zirconim oxide has the same activity for esterification as a superacid catalyst such as Nafion H. This suggests that the hydrous zirconium oxide is different from an acid catalyst. Most solid acids decrease in acidity upon the adsorption of water; however, it has been reported[13] that the niobic acid is not deactivated by the adsorption of water. Judging from the result of keeping its activity under an atmosphere of water vapor, the hydrous zirconium oxide might have a character similar to that of the niobic acid. However, the surface acidity of the hydrous zirconium oxide is lower than that of niobic acid.[11]

Dependence on the Catalyst Amount in a Vapor-Phase Reaction. For determining the order of catalyst amounts, the esterification rates of acetic acids with ethyl alcohol were measured over the range from 1.0 to 6.0 g of the catalyst. As a result, the esterification rates, r, were directly proportional to the amounts of the catalysts. Hence the rate, r, should be introduced as:

$$r = k\cdot[\text{cat.}], \quad (1)$$

where [cat.] and k are the concentration of the catalyst and the first-order rate constant respectively. Therefore, the specific rate, r_0, is:

$$r_0 = r/[\text{cat.}]. \quad (2)$$

Dependence on the Reaction Temperature in a Vapor-Phase Reaction. In order to investigate the

dependence on the reaction temperature, the esterifications of acetic acid with ethyl alcohol were carried out under the following two kinds of conditions: 1) the concentration of acetic acid, that of ethyl alcohol, the sample feed, and the temperature range were 2.77 mmol·cm^{-3}, 13.9 mmol·cm^{-3}, 10 cm^3·h^{-1}, and 120—220 °C respectively; 2) they were 6.66 mmol·cm^{-3}, 9.88 mmol·cm^{-3}, 5 cm^3·h^{-1}, and 135—250 °C respectively. Linear relationships between the natural logarithm of the specific rate vs. the reciprocal the absolute temperature, that is, the Arrhenius plot, were obtained in both cases. From the inclination of the lines, the activation energies were estimated to be, on the average, 12.4 kcal·mol^{-1}.

Dependence on the Alcohol Concentration in a Vapor-Phase Reaction. For determining the order of alcohol concentrations, the esterification rates of acetic acid with ethyl alcohol were measured under the following conditions: the concentration of acetic acid was constant at 1.53 mmol·cm^{-3}, the concentration of ethyl alcohol was changed in the range from 1.53 to 15.3 mmol·cm^{-3}, and benzene was added as a diluent to keep the volume of the reaction mixture constant. The correlation between the natural logarithm of the concentration of ethyl alcohol and that of the specific rate indicated that the order in alcohol concentrations was estimated to be first-order.

Dependence on the Carboxylic Acid Concentration in a Vapor-Phase Reaction. In order to investigate the dependence on the carboxylic acid concentration, the esterification of acetic acid with ethyl alcohol was carried out under the following conditions: the concentration of ethyl alcohol was constant at 7.65 mmol·cm^{-3}, the concentration of acetic acid was changed in the range from 0.918 to 2.55 mmol·cm^{-3}, and benzene was used as a diluent. The correlation between the natural logarithm of the concentration of acetic acid and that of the specific rate indicated that the reaction rate could be estimated to be of a minus first-order dependence on the concentration of acetic acid.

Kinetic Discussion in a Vapor-Phase Reaction. As has been described above, the reaction rate of the esterification over hydrous zirconium oxide in the vapor phase, r, is:

$$r = k' \cdot [\text{cat.}]^1 \cdot [\text{A}]^1 \cdot [\text{C}]^{-1}, \tag{3}$$

where k', [cat.], [A], and [C] are the rate constant, the concentration of the catalyst, that of ethanol, and that of acetic acid respectively. These results suggest that the rate-determining step is the step subsequent to the adsorption of the carboxylic acid and alcohol on the catalyst.

The result of the minus first-order dependence on the concentration of acetic acid suggests that acetic acid inhibits the reaction by adsorption on the surface of the hydrous zirconium oxide. We assume that the

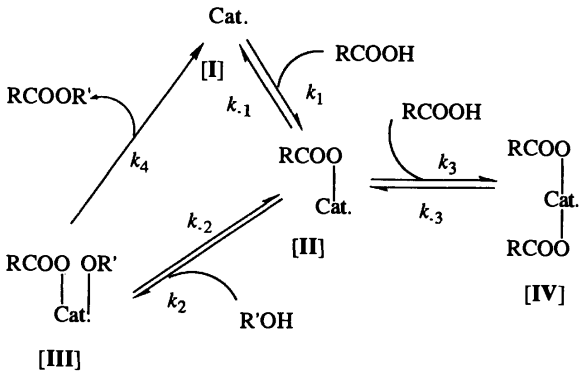

Scheme 1.

mechanism of the esterification of carboxylic acid with alcohol over the hydrous zirconium oxide in the vapor phase is as is shown in the Scheme 1.

Based on the proposed scheme, the following equation was obtained by the use of the stationary-state method, while the esterification rate is expressed by:

$$r = \frac{k_1 \cdot k_2 \cdot k_4 \cdot [\text{A}] \cdot [\text{C}] \cdot [\text{cat.}]}{k_{-1} \cdot k_{-2} + k_1 \cdot k_2 \cdot [\text{C}] + k_1 \cdot k_2 \cdot [\text{A}] \cdot [\text{C}] + k_{-1} \cdot k_{-2} \cdot K_3 \cdot [\text{C}]^2 + k_4 \cdot B}$$

$$= \frac{k \cdot K_1 \cdot K_2 \cdot [\text{A}] \cdot [\text{C}] \cdot [\text{cat.}]}{1 + K_1 \cdot [\text{C}] + K_1 \cdot K_2 \cdot [\text{A}] \cdot [\text{C}] + K_1 \cdot K_3 \cdot [\text{C}]^2 + k \cdot B/(k_{-1} \cdot k_{-2})}, \tag{4}$$

$$(B = k_{-1} + k_2 \cdot [\text{A}] + k_1 \cdot [\text{C}] + k_{-1} \cdot k \cdot K_3 \cdot [\text{C}]^2)$$

where K_1, K_2, and k are k_1/k_{-1}, k_2/k_{-2}, and k_4 respectively. The kinetic results show that the last step constitutes the rate-determining step. Therefore, k is far less than k_n, and the rate equation can be rewritten as:

$$r \fallingdotseq \frac{k \cdot K_1 \cdot K_2 \cdot [\text{A}] \cdot [\text{C}] \cdot [\text{cat.}]}{1 + K_1 \cdot [\text{C}] + K_1 \cdot K_2 \cdot [\text{A}] \cdot [\text{C}] + K_1 \cdot K_3 \cdot [\text{C}]^2}. \tag{5}$$

Furthermore, the inhibition of the carboxylic acid suggests that k_3 is larger than k_{-3}— that is, $K_3 > K_n$; hence, the rate equation becomes:

$$r \fallingdotseq \frac{k \cdot K_1 \cdot K_2 \cdot [\text{A}] \cdot [\text{C}] \cdot [\text{cat.}]}{K_1 \cdot K_3 \cdot [\text{C}]^2} = \frac{k \cdot K_2 \cdot [\text{A}] \cdot [\text{cat.}]}{K_3 \cdot [\text{C}]}. \tag{6}$$

This equation apparently corresponds to Eq. 3, and the proposed scheme may be concluded to be reasonable.

References

1) H. Matsushita, S. Ishiguro, H. Ichinose, A. Izumi, and S. Mizusaki, *Chem. Lett.*, **1985**, 731.

2) M. Shibagaki, K. Takahashi, and H. Matsushita, *Bull.*

Chem. Soc. Jpn., **61**, 3283 (1988).
3) M. Shibagaki, H. Kuno, K. Takahashi, and H. Matsushita, *Bull. Chem. Soc. Jpn.*, **61**, 4153 (1988).
4) M. Shibagaki, K. Takahashi, H. Kuno, H. Kawakami, and H. Matsushita, *Chem. Lett.*, **1988**, 1633.
5) K. Takahashi, M. Shibagaki, H. Kuno, H. Kawakami, and H. Matsushita, *Bull. Chem. Soc. Jpn.*, **62**, 1333 (1989).
6) G. A. Olah, T. Keumi, and D. Meidar, *Synthesis*, **1978**, 929.
7) M. Hino and K. Arata, *Chem. Lett.*, **1981**, 1671.
8) K. Tanabe, H. Hattori, Y. Ban'i, and A. Mitsutani, Jpn. Patent Appl., No. 55-115570 (1980).
9) Y. Izumi and K. Urabe, *Chem. Lett.*, **1981**, 663.
10) E. Santacesaria, D. Gelosa, P. Danise, and S. Carra, *J. Catal.*, **80**, 427 (1983).
11) Z. Chen, T. Iizuka, and K. Tanabe, *Chem. Lett.*, **1984**, 1085.
12) J. F. White, *Jpn. Kokai Tokkyo Koho*, Jp 52-75684.
13) T. Iizuka, K. Ogasawara, and K. Tanabe, *Bull. Chem. Soc. Jpn.*, **56**, 2927 (1983).

 © 1989 The Chemical Society of Japan Bull. Chem. Soc. Jpn., 62, 2362—2368 (1989) [Vol. 62, No. 7

Multi-Ionic Potential and Membrane Permeability Matrix. III. Diffusion and Concentration of Ions within Membrane Phase as a Controlling Factor to Ion Permselectivity

Kozue KAIBARA,* Hiroyoshi INOUE, and Toshio ARITOMI
Department of Chemistry, Faculty of Science, Kyushu University,
Hakozaki, Higashi-ku, Fukuoka 812
(Received February 15, 1989)

Membrane concentrations of cations in the NaCl-CsCl and NaCl-$CaCl_2$ systems with a highly selective cation-exchange membrane were measured under the extensive external electrolyte conditions. The modes of membrane/solution distribution and diffusion of cations, as a controlling factor to the membrane permselectivity, were correlated consistently with the electrochemical and cation flux data, as well as with the estimated membrane permselectivity parameters. The NaCl-CsCl uni-uni valent cation system was characterized well by the Na^+/Cs^+ concentration ratio of external solution, since the Na^+/Cs^+ concentration ratio in the membrane phase was related directly to the external ratio. Na^+/Cs^+ diffusion coefficient ratio varied from 0.5 to 3 with increasing external Na^+/Cs^+ concentration ratio from 1/100 to 100. While in the NaCl-$CaCl_2$ uni-bi valent cation system, the high and constant membrane concentration of Ca^{2+} regulated the transport process. The Na^+/Ca^{2+} diffusion coefficient ratio ranged from 0.5 to 500 with external Na^+/Ca^{2+} ratio from 1/100 to 100. Analyses on the phenomenological coefficients, describing the inter-cationic correlations within the membrane phase, as a function of the external cation concentration ratio were also carried out.

Selective ion transport processes across a charged-membrane are controlled, in general, by the modes of ionic migration within the membrane phase and by the profiles of ionic distribution between the membrane and external phases (see e.g., Refs. 1—3). Therefore, the phenomenological studies of the membrane transport process, such as the measurements of transmembrane potential, conductance, and ion flux, as well as the estimations of membrane transport parameters describing the permeability and selectivity to permeant ions, must be consistent with the results on the estimations of ionic behaviors within the membrane phase. The aim of the present experiments is to examine the conditions of permeant ions within the membrane phase and to correlate these results systematically with the results based on the linear phenomenological analyses in the multi-ionic transport systems with a cation-exchange membrane.[4,5] The substantial ion permselectivity of an ion-exchange membrane should be evaluated in the multiple counterion systems and the practical ion-exchange membrane related techniques are operated usually in a multi-ionic system as in the sea water condensation process (see e.g., Refs. 6—9). The present experiments are designed not only for the detailed phenomenological descriptions of the multi-ionic membrane transport process but also for the survey of a more efficient operating condition in the ion-exchange membrane-related processes.

Experimental

A typical highly selective cation-exchange membrane, CK-1,1.0t (Asahi Chemical Industry Co., Ltd.), was used throughout the present experiments. The basic physicochemical properties of the CK-1, 1.0t membrane were noted in earlier papers.[4,5,10] Electrolyte solutions were prepared from extra pure salts with twice-distilled water. All the measurements were carried out at regulated room temperature, 25±1 °C.

In the present experiments, the membrane properties were examined in NaCl-CsCl and NaCl-$CaCl_2$ systems, where the concentration of one of the electrolytes is varied from 10^{-1} to 10^{-3} mol dm^{-3} and that of the other electrolyte is kept constant at 10^{-1}, 10^{-2}, or 10^{-3} mol dm^{-3}. Then, the concentration ratios of the two kinds of external electrolytes ranged at 100—1/100. In case of the CK-1, 1.0t membrane, the previous experimental results on the single electrolyte systems indicated that the cation concentrations within the membrane phase are almost constant at below the external electrolyte concentration of around 5×10^{-1} mol dm^{-3} and, above this external concentration, rapid increases in the membrane cation concentration due to a drastic intrusion of Donnan adsorbed cations are observed.[10] Accordingly in the present experimental conditions, it is expected that the total cation concentrations in the membrane phase are kept at a constant level and that the effects of relative occupancy of respective cations for available membrane sites upon the membrane transport process can be examined systematically.

Membrane concentrations of the respective cations were measured by the following procedures. A piece of the CK-1, 1.0t membrane sample (0.1—0.2 g, ca.1 cm^2), preweighed at the reference conditions in which all the membrane samples were equilibrated sufficiently with 10^{-1} mol dm^{-3} NaCl solution, was immersed in the test aqueous solution with an appropriate electrolyte composition for 96 h to establish sufficiently an equilibrium condition of ions within the membrane phase. Then the test membrane sample, being wiped off the adhering electrolyte solution, was washed with distilled water for 72 h to extract Donnan adsorbed ions. It was required at least 50 h to elute stiffly adsorbed Donnan ions in the CK-1, 1.0t membrane. In the next step, remaining cations which are thought to be bound to ion-exchange sites were extracted perfectly by means of soaking the membrane sample into 1 mol dm^{-3} HCl solution for 24 h. Cation concentrations in the respective aqueous eluents were measured with an atomic absorption spectrophotometer (Hitachi 180-50) after the suitable dilution

steps and/or, in case of the bi-cationic systems, the appropriate treatments to prevent from the interference due to the coexisting cations. The Cs^+ concentrations were measured with addition of $CaCl_2$ into the eluent sample solutions to inhibit the ionizations of Cs and to increase the spectral intensities.

Electrochemical measurements to estimate the transmembrane potential and conductance data as well as intercompartmental cation flux measurements were described in earlier papers.[4,5] The experimental systems consisted of aqueous solution phases I and II separated by the membrane, one of which contains NaCl as electrolyte and the other, CsCl or $CaCl_2$. The concentration of one of the electrolytes in phase I was varied from 10^{-1} to 10^{-3} mol·dm^{-3} and that of the other electrolyte in phase II was kept constant at 10^{-1}, 10^{-2}, or 10^{-3} mol dm^{-3}. The respective electrolyte concentrations in phases I and II correspond to those in the systems for the membrane ion concentration measurements described above. As will be discussed in the later section, the membrane-electrolyte solution systems in the present study are close fairly to the cationic equilibrium condition, so the experimental data obtained from the two types of the systems, the binary (two counterion) systems equilibrated or separated with a cation-exchange membrane, are correlated well to each other.

Results and Discussion

Thermodynamic background for the analyses of the present membrane transport process can be summarized as follows. When Z_1-valent metal, M_1, and Z_2-valent metal M_2 in chloride form are dissolved in the aqueous phases I and II separated by the membrane phase, respectively, the fundamental linear phenomenological equation employing the membrane permeability matrix as a principal transport parameter is expressed as:[4,5]

$$\begin{bmatrix} J_{M_1} \\ J_{M_2} \\ J_{Cl} \end{bmatrix} = - \begin{bmatrix} P_{M_1\cdot M_1} & P_{M_1\cdot M_2} & P_{M\cdot Cl} \\ P_{M_2\cdot M_1} & P_{M_2\cdot M_2} & P_{M_2\cdot Cl} \\ P_{Cl\cdot M_1} & P_{Cl\cdot M_2} & P_{Cl\cdot Cl} \end{bmatrix} \begin{bmatrix} -a^{I}_{M_1}\exp(-Z_1FV/2RT) \\ a^{II}_{M_2}\exp(Z_2FV/2RT) \\ a^{II}_{Cl}\exp(-FV/2RT) - a^{I}_{Cl}\exp(FV/2RT) \end{bmatrix} \quad (1)$$

where J is the ionic flux, a is the activity, V is the membrane potential, F is the Faraday constant, R is the gas constant, and T is the absolute temperature; the subscripts M_1, M_2, and Cl refer to metal cations, M_1 and M_2, and chloride ion; the superscripts I and II indicate the solution phase. The 3×3 matrix in the right hand side of Eq. 1 is the membrane permeability matrix, of which elements represent the partial contributions of the inter-ionic correlations indicated by the subscript indices on the membrane transport processes. The respective matrix elements can be estimated based on the membrane potential, conductane, and ion flux data.[4,5] Since the electroconductive membrane permeabilities to metal cations M_1 and M_2 and to Cl^-, P_{M_1}, P_{M_2}, and P_{Cl}, are defined as a function of the membrane permeability matrix elements:

$$\begin{aligned} P_{M_1} &= P_{M_1\cdot M_2} + (Z_2P_{M_2\cdot M_1} - P_{Cl\cdot M_1})/Z_1 \\ P_{M_2} &= P_{M_2\cdot M_2} + (Z_1P_{M_1\cdot M_2} - P_{Cl\cdot M_2})/Z_2 \\ P_{Cl} &= P_{Cl\cdot Cl} - (Z_1P_{M_1\cdot Cl} + Z_2P_{M_2\cdot Cl}) \end{aligned} \quad (2)$$

the membrane electric current, I, is expressed as:

$$\begin{aligned} I &= F(Z_1J_{M_1} + Z_2J_{M_2} - J_{Cl}) \\ &= [FZ_1P_{M_1}a^{I}_{M_1}\exp(-Z_1FV/2RT) \\ &\quad - FZ_2P_{M_2}a^{II}_{M_2}\exp(Z_2FV/2RT)] \\ &\quad + FP_{Cl}[a^{II}_{Cl}\exp(-FV/2RT) - a^{I}_{Cl}\exp(FV/2RT)] \end{aligned} \quad (3)$$

The electroconductive membrane permeabilities to respective ions can be estimated directly from the electrochemical data such as the membrane potentials and conductances.[4,5,11]

Introducing the membrane permeability to whole cations, $P_{M_1\text{-}M_2}$, defined as:

$$P_{M_1\text{-}M_2} = (Z_1P_{M_1}Z_2P_{M_2})^{1/2}\exp[-(Z_1 - Z_2)FV/4RT] \quad (4)$$

the cationic component of membrane electric current, the term in the first brackets in Eq. 3, can be modified and the expression for the membrane electric current is reduced to:

$$\begin{aligned} I &= -2FP_{M_1\text{-}M_2}(a^{I}_{M_1}a^{II}_{M_2})^{1/2}\sinh[(Z_1 + Z_2)F(V - V_{M_1\text{-}M_2})/4RT] \\ &\quad + 2FP_{Cl}(a^{I}_{Cl}a^{II}_{Cl})^{1/2}\sinh[-F(V - V_{Cl})/2RT] \end{aligned} \quad (5)$$

where $V_{M_1\text{-}M_2}$ is the cationic equilibrium membrane potential, which corresponds to the Nernstian equilibrium potential for a single cationic system, and V_{Cl} is the Nernstian equilibrium membrane potential for Cl^-. The expression for $V_{M_1\text{-}M_2}$ is derived from Eq. 3 by introducing the conditions, I=0 and P_{Cl}=0 as:

$$V_{M_1\text{-}M_2} = -[2RT/(Z_1 + Z_2)F]\ln(Z_2P_{M_2}a^{II}_{M_2}/Z_1P_{M_1}a^{I}_{M_1}) \quad (6)$$

Equation 6 deduces that the linear relationships of $V_{M_1\text{-}M_2}$ with logarithmic $a^{I}_{M_1}$ correspond to the constant P_{M_1}/P_{M_2}. The transmembrane potential in the absence of electric current, V_0, is related to $V_{M_1\text{-}M_2}$ and V_{Cl} as:

$$V_0 = t_{M_1\text{-}M_2}V_{M_1\text{-}M_2} + t_{Cl}V_{Cl} \quad (7)$$

where $t_{M_1\text{-}M_2}$ and t_{Cl} are the transport numbers to the whole metal cations and Cl^-, respectively.

The membrane permselectivity to ions depends, in general, upon the membrane/solution distribution and migration speed of permeating ions.[1-3] The membrane permeability ratio of cations, P_{M_1}/P_{M_2}, can be expressed as:[4,12,13]

$$\frac{P_{M_1}}{P_{M_2}} = \frac{D^m_{M_1}}{D^m_{M_2}} \frac{C^m_{M_1,Total}/C^m_{M_2,Total}}{C^s_{M_1}/C^s_{M_2}} \quad (8)$$

where D^m is the diffusion coefficient of metal cation within the membrane phase and, C^m and C^s are the cation concentrations in the membrane phase and in the external solution, respectively. The total membrane concentration of metal cation M, $C^m_{M,Total}$, is the sum of two components of cation concentration within the membrane phase as:

$$C^m_{M,Total} = C^m_{M,H_2O} + C^m_{M,HCl} \quad (9)$$

where C^m_{M,H_2O} is the Donnan adsorbed component of metal cation M eluted with distilled water and $C^m_{M,HCl}$ is the site-bound component of metal cation M eluted with HCl solution as described in the experimental section. In the present study, changes in $C^m_{M,Total}$, C^m_{M,H_2O}, and $C^m_{M,HCl}$ for Na^+, Cs^+, and Ca^{2+} were measured as a function of the concentration and composition of external electrolyte solution. The respective components of the membrane cation concentrations are expressed in the unit of mol per kg of wet membrane sample in the reference conditions. Correlations of the membrane cation concentration with the membrane transport phenomena, such as the transmembrane potentials and ion fluxes, were examined systematically in the following part of this section.

C^m_{M,H_2O} and $C^m_{M,HCl}$ as a Function of the External Electrolyte Concentration. Figure 1 illustrates the Na^+ and Cs^+ concentrations within the CK-1, 1.0t membrane phase as a function of the external electrolyte concentration for the NaCl-CsCl systems, in which the concentration of NaCl or CsCl was varied from 10^{-1} to 10^{-3} mol dm^{-3} and that of the other electrolyte was kept constant at 10^{-2} mol dm^{-3}. As a result of the fact that 85—99% of Na^+ and more than 99% of Cs^+ were bound to the ion-exchange sites, the total site-bound cations, which should be constant and equivalent to the exchange capacity, came up to 98—99% of the total cations in the membrane phase, and accordingly Cl^- ions were almost perfectly excluded from the membrane phase. When the external NaCl and CsCl concentrations were the same, i.e., $C^s_{NaCl} = C^s_{CsCl} = 10^{-2}$ mol dm^{-3}, the concentration of the site-bound Cs^+ was as twice as that of the site-bound Na^+, so that $C^m_{Na,HCl}/C^m_{Cs,HCl} \cong 1/2$. Under the external condition, $C^s_{NaCl}/C^s_{CsCl} \cong 2.5$, the equivalent amounts of Na^+ and Cs^+ were bound to the ion-exchange sites, i.e., $C^m_{Na,HCl} = C^m_{Cs,HCl}$. The Donnan adsorbed cation component contained more Na^+ than Cs^+ in the external concentration range studied, for example, $C^m_{Na,H_2O}/C^m_{Cs,H_2O} \cong 1.4$ when $C^m_{NaCl} = C^s_{CsCl} = 10^{-2}$ mol dm^{-3} and $C^m_{Na,H_2O}/C^m_{Cs,H_2O} \cong 2$, when $C^s_{NaCl}/C^s_{CsCl} \cong 2.5$.

In case of the systems where Ca^{2+} permeates across the CK-1, 1.0t cation-exchange membrane, the membrane/solution distributions of Na^+ and Ca^+ were entirely different from those of Na^+ and Cs^+. Figure 2 summarizes the Donnan adsorbed and site-bound cation concentrations of Na^+ and Ca^{2+} for the

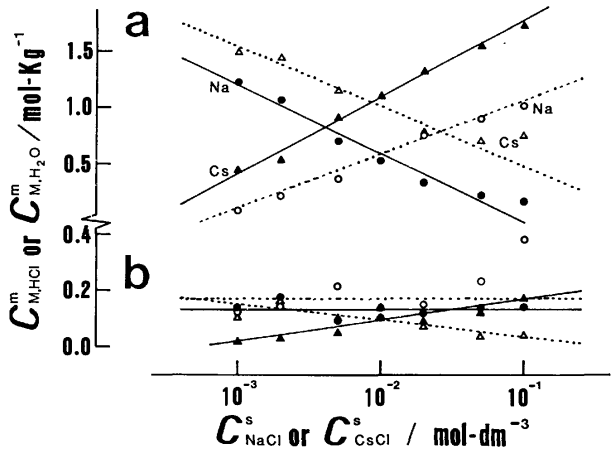

Fig. 1. Concentrations of the site-bound and Donnan adsorbed fractions of cations, Na^+ and Cs^+, in NaCl-CsCl systems. Concentrations within the membrane phase, $C^m_{M,HCl}$ and C^m_{M,H_2O}, as a function of the external electrolyte concentration, C^s_{NaCl} or C^s_{CsCl} equilibrated with the membrane phase. Upper frame a indicates $C^m_{M,HCl}$ and lower frame b indicates C^m_{M,H_2O}. ●: Na^+, ▲: Cs^+ in 10^{-2} mol dm^{-3} C^s_{NaCl} system. ○: Na^+, △: Cs^+ in 10^{-2} mol dm^{-3} C^s_{CsCl} system.

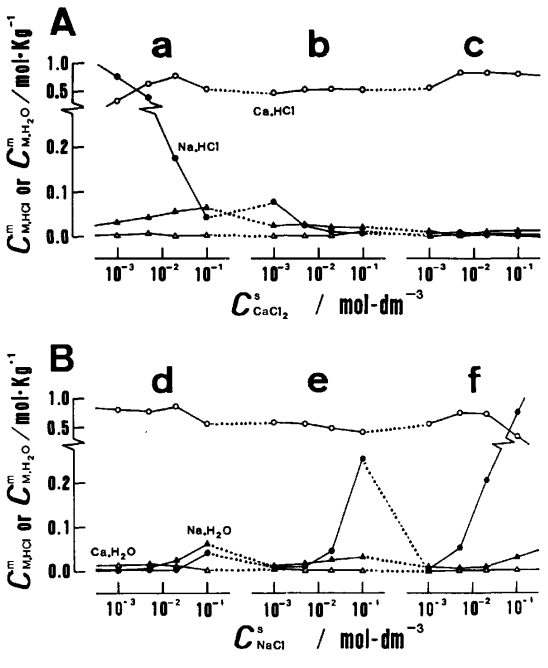

Fig. 2. Concentrations of the site-bound and Donnan adsorbed fractions of cations, Na^+ and Ca^{2+}, in NaCl-$CaCl_2$ systems. Concentrations within the membrane phase, $C^m_{M,HCl}$ and C^m_{M,H_2O}, as a function of the external electrolyte concentration, C^s_{NaCl} or $C^s_{CaCl_2}$. Constant C^s_{NaCl} system (A) and constant $C^s_{CaCl_2}$ system (B). C^s_{NaCl}, a: 10^{-1}; b: 10^{-2}; c: 10^{-3} mol dm^{-3}. $C^s_{CaCl_2}$, d: 10^{-1}; e: 10^{-2}; f: 10^{-3} mol dm^{-3}. ●: C^m_{NaHCl}, ○: $C^m_{Ca,HCl}$, ▲: C^m_{Na,H_2O}, △: C^m_{Ca,H_2O}.

NaCl–$CaCl_2$ systems, in which the external concentration of NaCl or $CaCl_2$ was varied from 10^{-1} to 10^{-3} mol dm^{-3} and that of the other electrolyte was kept constant at 10^{-1}, 10^{-2}, or 10^{-3} mol dm^{-3}. As can be seen in Fig. 2, the site-bound Ca^{2+} amounted to 97—99% of the total Ca^{2+} within the membrane phase keeps almost constant level. On the other hand, the site-bound Na^+ is varied from 15 to 96% of the total Na^+ in the membrane phase. In the external condition, $C^s_{NaCl}/C^s_{CaCl_2}<10$, the site-bound Ca^{2+} amounted to 80—98% of the total membrane cations. The concentrations of Donnan adsorbed Na^+ were 10 times larger than those of Ca^{2+}, when the external NaCl and $CaCl_2$ concentrations are the same, $C^s_{NaCl}=C^s_{CaCl_2}=$ 10^{-1}, 10^{-2}, or 10^{-3} mol dm^{-3}.

Membrane/Solution Distribution of Cations and Membrane Transport Phenomena. Quantitative and qualitative differences in the membrane/solution distribution of cations between the NaCl–CsCl and the NaCl–$CaCl_2$ systems cause characteristic and distinctive membrane transport phenomena in these systems. Figure 3 shows the correlations of the total cation concentration in the CK-1, 1.0t membrane (Fig. 3-C) with the membrane potential (Fig. 3-A) and inter-compartmental ion flux (Fig. 3-B) data for the NaCl–CsCl systems as a function of the external NaCl/CsCl concentration ratio. The total membrane concentrations of Na^+ and Cs^+, $C^m_{Na,Total}$ and $C^m_{Cs,Total}$, changed as the external Na^+ and Cs^+ concentrations, C^s_{NaCl} and C^s_{CsCl}, changed. $C^m_{Na,Total}$, was almost equal to $C^m_{Cs,Total}$ when $C^s_{NaCl}/C^s_{CsCl}=2.5$. These results indicate that the membrane affinities to Cs^+ are higher than those to Na^+. It is suggested that the higher membrane affinities to Cs^+ arise partly from accessibilities of Cs^+ to the fixed cation-exchange sites due to smaller hydrated radius of Cs^+ than that of Na^+. Under the external conditions where C^s_{NaCl}/C^s_{CsCl} ratios are lower than 1/10 or higher than 100, available exchange-sites were occupied by a large amount of Cs^+ or Na^+, respectively (see also Fig. 7-B).

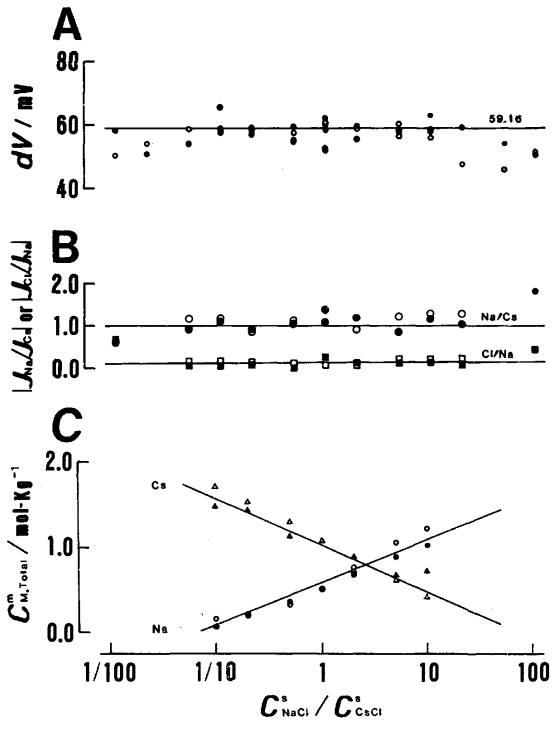

Fig. 3. Membrane potential gradient (for details see text), dV, inter-compartmental ionic flux ratio, $|J_{Na}/J_{Cs}|$ or $|J_{Cl}/J_{Na}|$, and total metal cation concentration within the membrane phase, $C^m_{Na,Total}$ or $C^m_{Cs,Total}$, as a function of external NaCl/CsCl concentration ratio, C^s_{NaCl}/C^s_{CsCl}. Closed and open marks indicate the constant C^s_{NaCl} and C^s_{CsCl} systems, respectively. These constant external electrolyte concentrations correspond to the constant electrolyte concentration in phase II separated from phase I by the membrane. In B, ● and ○: $|J_{Na}/J_{Cs}|$, ■ and □: $|J_{Cl}/J_{Na}|$. In C, ● and ○: $C^m_{Cs,Total}$, ▲ and △: $C^m_{Na,Total}$.

The transmembrane potential data are plotted as the gradient of the potential vs. logarithm of the mean electrolyte activity of phase I curve, dV ($=\Delta V/\Delta \log a^I_{M_1}$), in Fig. 3-A. It was suggested, on the basis of experimental results showing the almost perfect exclusion of Cl^- from the membrane phase, that the membrane process in the NaCl–CsCl system is controlled only by cations, Na^+ and Cs^+. In that case, the transmembrane potentials for the NaCl–CsCl systems are expected to be nearly equal to $V_{Na\text{-}Cs}$ and, accordingly, the estimated dV values should be close to 59.16 mV at 25 °C with the constant cationic permeability ratio, P_{Na}/P_{Cs}, as seen in Fig. 3-A (refer to Eq. 6). The inter-compartmental ion flux data also support these situations. As can be seen in Fig. 3-B, the Cl^- flux is suppressed at an extremely low level and the membrane transport process can be characterized by the Na^+ and Cs^+ fluxes in opposite directions with each other.

For the NaCl–$CaCl_2$ systems, the ideal uni- and bivalent cationic equilibrium potential, $V_{Na\text{-}Ca}$, is 39.44 mV at 25 °C as calculated from Eq. 6 with the constant P_{Na}/P_{Ca}. As can be seen in Fig. 4-A, the potential gradient dV values correspond to the ideal $V_{Na\text{-}Ca}$ values within the external electrolyte concentration range, $1/10<C^s_{NaCl}/C^s_{CaCl_2}<10$. However, the estimated dV values deviate positively or negatively in the external conditions where $C^s_{NaCl}/C^s_{CaCl_2}$ is higher than 10 or lower than 1/10, respectively. Corresponding to these transmembrane potential responses, the inter-compartmental ion fluxes varied in multiple modes. It is shown in Fig. 4-B that Cl^- flux is negligible in the range of $1/10<C^s_{NaCl}/C^s_{CaCl_2}<10$, so the Na^+ and Ca^{2+} fluxes flowing in opposite directions from each other control the transport processes across the CK-1, 1.0t cation-exchage membrane in the same manner as the above NaCl–CsCl systems are controlled only by Na^+ and Cs^+ fluxes. Out of this concentration range, the Na^+ and Cl^- fluxes increased with increasing relative concentration of external Na^+, whereas the Ca^{2+} and

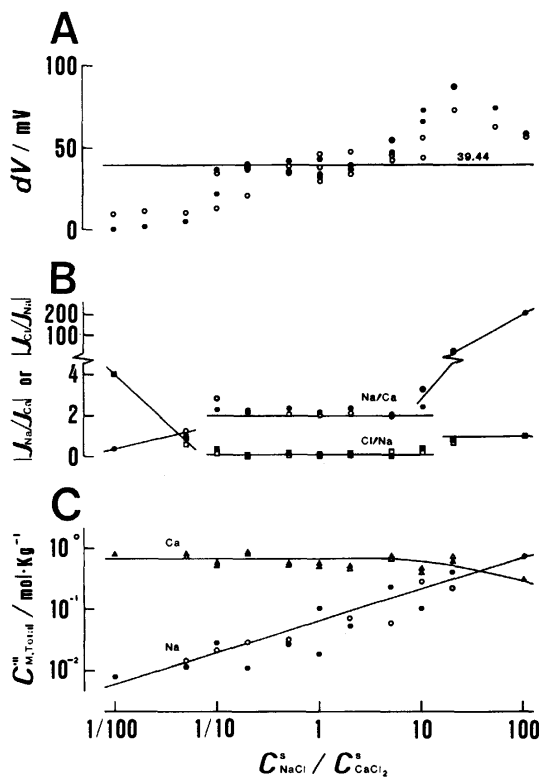

Fig. 4. Membrane potential gradient, dV, ionic flux ratio, $|J_{Na}/J_{Ca}|$ or $|J_{Cl}/J_{Na}|$, and total metal cation concentration within the membrane phase, $C^{m}_{Na,Total}$ or $C^{m}_{Ca,Total}$, as a function of the external NaCl/$CaCl_2$ concentration ratio, $C^{s}_{NaCl}/C^{s}_{CaCl_2}$. Closed and open marks indicate the constant C^{s}_{NaCl} and $C^{s}_{CaCl_2}$ systems, respectively. In B, ● and ○: $|J_{Na}/J_{Ca}|$, ■ and □: $|J_{Cl}/J_{Na}|$. In C, ● and ○: $C^{m}_{Na,Total}$, ▲ and △: $C^{m}_{Ca,Total}$.

Cl^- fluxes increased with decreasing Na^+ concentrations. It can be recognized that the ion transport processes of the NaCl-$CaCl_2$ system with a highly permselective cation-exchange membrane shift from the $CaCl_2$ transporting process ($J_{Ca}=(1/2)J_{Cl}$, $J_{Na}=0$), through the Na-Ca transporting process ($J_{Na}=-2J_{Ca}$, $J_{Cl}=0$), and finally to the NaCl transporting process ($J_{Na}=J_{Cl}$, $J_{Ca}=0$), as an increase in the relative Na^+ concentration of the external phase.

These membrane transport characteristics should be a reflex of the Na^+ and Ca^+ concentration profiles within the membrane phase plotted in Fig. 4-C. The total Ca^{2+} concentration in membrane, $C^{m}_{Ca,Total}$, was kept at high and constant level throughout the external concentration range studied, while the total Na^+ concentration within membrane, $C^{m}_{Na,Total}$, varied from a low level at 1/100 of $C^{m}_{Ca,Total}$ to high level comparable with $C^{m}_{Ca,Total}$, with the external Na^+ concentration change. In the limits of the $C^{m}_{Na,Total}/C^{m}_{Ca,Total}$ values from 1/20 ($C^{s}_{NaCl}/C^{s}_{CaCl_2}=1/10$) to 1/2 ($C^{s}_{NaCl}/C^{s}_{CaCl_2}=10$), the membrane process was controlled only by cations, Na^+ and Ca^{2+}. The Na^+ concentrations within the membrane phase increased with increasing external Na^+ concentrations, and finally reached at the same level as the membrane Ca^{2+} concentration when the external solution contained Na^+ in 30 times of Ca^{2+} concentration. The results given in Figs. 4-B and C suggest that, in the membrane utilizing techniques where the permeations of bivalent cation have to be avoided as far as possible, such as in the desalination process of sea water, the membrane concentration of bivalent cation should be kept, at least, not exceeding ca. 75% of the total membrane cations. Such a condition can be realized, in case of the CK-1, 1.0t cation-exchange membrane, by keeping the external bivalent cation concentrations at below 1/20 of the univalent cation concentrations.

Membrane/Solution Distribution of Cations and Membrane Transport Parameters. The ion concentration profiles within charged membrane phase, as an origin of the generation of a variety of the membrane transport phenomena, were discussed further in terms of the membrane transport parameters. As pointed out already, the NaCl-CsCl system with the CK-1, 1.0t membrane can be characterized as a cationic equilibrium system, in which the oppositely running Na^+ and Cs^+ fluxes with almost the same magnitudes were observed. And, accordingly the membrane potential responses are recognized as an ideal equilibrium potential for Na^+ and Cs^+ showing the linear relationships against the logarithmic external activity, $\log a^{I}_{M_I}$, with the slope of 59.16 mV predicted from Eq. 6. In these situations, the P_{Na}/P_{Cs} values calculated based on the electrochemical data are almost constant at 0.72 corresponding with the ideal value calculated based on Eq. 6 as shown in Fig. 5-A. A slight deviation of P_{Na}/P_{Cs} values from the ideal value was observed: the substantial negative and positive deviations were recognized in the higher and lower $C^{s}_{NaCl}/C^{s}_{CsCl}$ regions, respectively, where the gradient of the membrane potential vs. logarithmic activity curves decreases similarly as illustrated in Fig. 3-A. These results were caused partly from the Cl^- transport across the membrane at quite low levels.

On the other hand, the Cl^- transport process was involved considerably in the ion transport phenomena across the CK-1, 1.0t membrane for the NaCl-$CaCl_2$ system as discussed above. In Fig. 5-B1, the P_{Na}/P_{Ca} values estimated from the electrochemical data are plotted and compared with those, indicated by the solid curve, evaluated from Eq. 6 providing that the observed transmembrane potentials correspond to the cationic equilibrium potential $V_{Na\text{-}Ca}$. For the potential responses illustrated in Fig. 4-A, the P_{Na}/P_{Ca} values, calculated from Eq. 6 with the condition of $P_{Cl}=0$, no longer give a constant value for the whole concentration ranges studied. When the system was characterized by only the cation transport process, the constant P_{Na}/P_{Ca} values were obtained as in the NaCl-CsCl system. As can be seen in Fig. 5-B1, a large positive deviation of the P_{Na}/P_{Ca} values from those evaluated by Eq. 6 are observed in the system with high $C^{s}_{NaCl}/C^{s}_{CaCl_2}$ ratio,

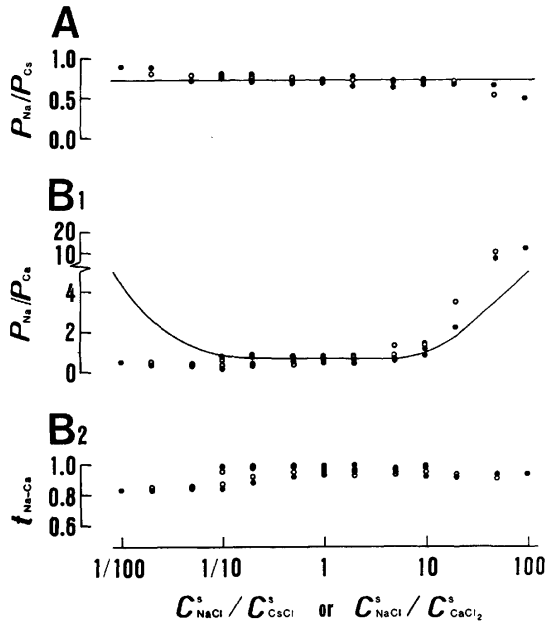

Fig. 5. Membrane permeability ratios, P_{Na}/P_{Cs} (A) and P_{Na}/P_{Ca} (B1), and transport number to whole cation, $t_{Na\text{-}Ca}$ (B2), as a function of the external NaCl/CsCl or NaCl/$CaCl_2$ concentration ratio, C^s_{NaCl}/C^s_{CsCl} or $C^s_{NaCl}/C^s_{CaCl_2}$. Closed marks indicate the constant C^s_{NaCl} system and open marks indicates the constant C^s_{CsCl} (A) or constant $C^s_{CaCl_2}$ (B1 and 2) systems.

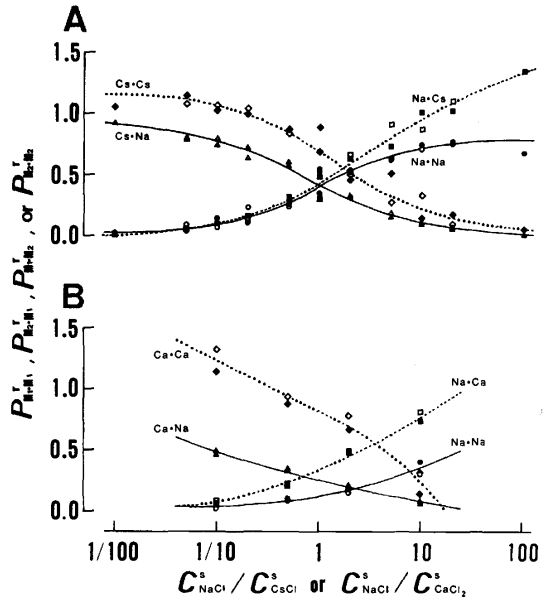

Fig. 6. Membrane permeability matrix elements as a function of the external electrolyte concentration ratio, C^s_{NaCl}/C^s_{CsCl} or $C^s_{NaCl}/C^s_{CaCl_2}$. Closed marks indicate the constant C^s_{NaCl} system and open marks indicate the constant C^s_{CsCl} (A) or constant $C^s_{CaCl_2}$ (B) systems. ● and ○: $P^r_{M_1\cdot M_1}$ ▲ and △: $P^r_{M_2\cdot M_1}$, and ■: and □ $P^r_{M_1\cdot M_2}$, ◆ and ◇: $P^r_{M_2\cdot M_2}$.

where the transport process can be characterized by the NaCl transport with small Ca^{2+} flux. On the other hand, in the low $C^s_{NaCl}/C^s_{CaCl_2}$ systems where the transport process can be characterized by the $CaCl_2$ transport with small Na^+ flux, the P_{Na}/P_{Ca} values kept at relatively constant level and a large negative deviation from the values based on Eq. 6 was observed. To examine further the influence of Cl^- permeation on the transport process across a cation-exchange membrane, the transport number to whole cation, Na^+ and Ca^+, $t_{Na\text{-}Ca}$, relative to t_{Cl} was evaluated in the NaCl-$CaCl_2$ systems. As shown in Fig. 5-B2, the $t_{Na\text{-}Ca}$ values decrease in these systems and there is a substantial effect of Cl^- transport on the cation transport.

When the membrane transport processes are controlled only by two cationic species, M_1 and M_2, the 3×3 membrane permeability matrix in Eq. 1 can be reduced to the 2×2 matrix describing the partial contributions of the inter-cationic correlations on the membrane process.[4,5] Figure 6 summarizes the elements of the 2×2 membrane permeability matrix for the NaCl-CsCl and NaCl-$CaCl_2$ systems estimated from the electrochemical and inter-compartmental ion flux data with the nonequilibrium thermodynamic relations discussed earlier. For the NaCl-$CaCl_2$ system, the permeability matrix element calculations were available only for the system in which Cl^- flux is negligible. In Fig. 6, the permeability matrix elements are plotted as a relative value against the membrane permeability to whole cation, $P_{M_1\text{-}M_2}$, as:

$$P^r_{M_1\cdot M_1} = P_{M_1\cdot M_1}/P_{M_1\text{-}M_2},\quad P^r_{M_1\cdot M_2} = P_{M_1\cdot M_2}/P_{M_1\text{-}M_2} \qquad (10)$$
$$P^r_{M_2\cdot M_1} = P_{M_2\cdot M_1}/P_{M_1\text{-}M_2},\quad P^r_{M_2\cdot M_2} = P_{M_2\cdot M_2}/P_{M_1\text{-}M_2}$$

Magnitudes of the membrane permeability matrix element driven by the electrochemical activity difference of some cations (see Eq. 1) increased with increasing relative concentration of those cations. The membrane permeability matrix representations including the Cl^- relating components were discussed in earlier papers of this series for the NaCl-$CaCl_2$ systems.[5]

Membrane/Solution Distribution and Diffusion of Cations within Membrane Phase. It has been an established concept based on the theoretical and experimental investigations of the membrane transport phenomena that the ion permselectivity of a charged membrane can be determined as a function of the migration speed of ions within the membrane phase and of the membrane/solution distribution coefficient of permeating ions. As a conclusion of the present experiments, the diffusion coefficient ratio of cations, $D^m_{M_1}/D^m_{M_2}$, and the cation concentration ratio, $C^m_{M_1,Total}/C^m_{M_2,Total}$, in the CK-1, 1.0t membrane phase are examined as a function of the external electrolyte concentration ratio, $C^s_{M_1Cl_1}/C^s_{M_2Cl_2}$. The results are summarized in Fig. 7. These two quantities are

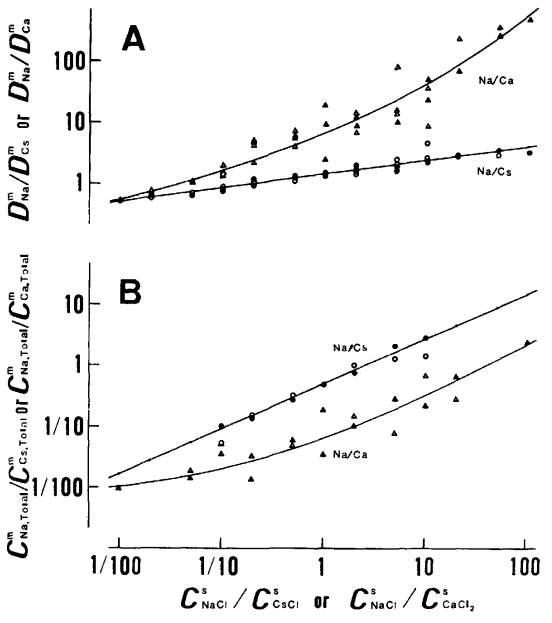

Fig. 7. Diffusivity ratio (A), D^m_{Na}/D^m_{Cs} or D^m_{Na}/D^m_{Ca}, and total cation concentration ratio (B), $C^m_{Na,Total}/C^m_{Cs,Total}$ or $C^m_{Na,Total}/C^m_{Ca,Total}$, within the membrane phase as a function of the external concentration ratio, C^s_{NaCl}/C^s_{CsCl} or $C^s_{NaCl}/C^s_{CaCl_2}$. Closed marks indicate the constant C^s_{NaCl} system and open marks indicate the constant C^s_{CsCl} or C^s_{CaCl} systems. ● and ○ refer to Na/Cs ratios, and, ▲ and △ refer to Na/Ca ratios.

important as a controlling factor to the membrane permselectivity in the multi-ionic systems. In case of the NaCl-CsCl system, in which all the permeating cations are univalent, the Na/Cs diffusivity ratio within the membrane phase was kept at an almost constant level, whereas the Na/Cs concentration ratio changed considerably corresponding with the changes in external Na/Cs concentration ratio. When bivalent cations were introduced as permeating species as in the NaCl-$CaCl_2$ system, the Na/Ca diffusivity ratio varied considerably, from 0.5 to 500, as compared with that of the NaCl-CsCl system. As mentioned before, at the upper or lower limilts of the Na/Ca diffusivity ratios, the systems were characterized by the NaCl or $CaCl_2$ transport process. Changes in the Na/Ca membrane concentration ratio within the membrane phase, on the other hand, were depressed to the limits not exceeding 100 times against the 10000 times changes in the external Na/Ca concentration ratio, from 1/100 to 100.

In the multi-ionic system with a highly permselective ion exchange membrane, the membrane transport process can be characterized as a function of the external electrolyte composition when the charges of counterions are the same. When the system contains the counterions with different charges, the membrane transport process tends to be controlled by the counterions with higher charges based on the monopolistic occupation of the available ion-exchange sites of membrane with multivalent counterions.

The authors wish to thank Asahi Chemical Industry Co., Ltd. for providing the ion-exchange membrane, CK-1, 1.0t, used in the present investigation. One of the authors (K. K.) is grateful to the Ministry of Education, Science and Culture for a Grant-in-Aid for Scientific Research on Priority Areas and to the Kurata Foundation for the research grant support.

References

1) F. Helfferich, "In Exchange," McGraw-Hill, New York (1962).
2) N. Lakshminarayanaiah, "Transport Phenomena in Membranes," Academic Press, New York (1969).
3) M. E. Starzak, "The Physical Chemistry of Membranes," Academic Press, Orlando, Florida (1984).
4) K. Kaibara and H. Kimizuka, *Bull. Chem. Soc. Jpn.*, **55**, 1743 (1982).
5) K. Kaibara, H. Inoue, and H. Kimizuka, *Bull. Chem. Soc. Jpn.*, **60**, 3175 (1987).
6) V. S. Soldano and V. A. Bychkova, *Russ. J. Phys. Chem.*, **44**, 1297 (1970).
7) M. A. Lake and S. S. Melsheimer, *AIChE J.*, **24**, 130 (1978).
8) R. Smith and E. Woodburn, *AIChE J.*, **24**, 577 (1978).
9) M. J. Manning and S. S. Melsheimer, *Ind. Eng. Chem., Fundam.*, **22**, 311 (1983).
10) K. Kaibara, K. Saito, and H. Kimizuka, *Bull. Chem. Soc. Jpn.*, **46**, 3712 (1973).
11) K. Kaibara, H. Inoue, S. Tsuruyama, and H. Kimizuka, *Bull. Chem. Soc. Jpn.*, **61**, 1517 (1988).
12) H. Kimizuka and K. Kaibara, *J. Colloid Interface Sci.*, **52**, 516 (1975).
13) H. Kimizuka, K. Kaibara, E. Kumamoto, and M. Shirozu, *J. Membrane Sci.*, **4**, 81 (1978).

Substituent-Group Effects on the Fluorescence of Aluminum-Schiff Base Complexes and Their Application to the Determination of Aluminum

Izuo AOKI,* Toshiaki MATSUNAGA,† and Kunihiro WATANABE†
R. & D. Laboratory for Speciality Chemicals, Nippon Soda Co., Ltd., Goi-minamikaigan, Ichihara-shi, Chiba 290
†Faculty of Science and Technology, Science University of Tokyo, 2641, Yamazaki, Noda-shi, Chiba 278
(Received December 21, 1988)

The effects of the substituents in the Schiff-base *N*-salicylidene-*o*-aminophenol (SOAP) on the fluorescence of its aluminum complexes were investigated. *N,N'*-Disalicylideneethylenediamine (DSED) derivatives were used as aldehyde reagents for the condensation to prepare 25 different SOAP compounds, for these reagents can be conveniently hydrolyzed to yield salicylaldehyde derivatives. *o*-Aminophenol (OAP) derivatives were used as amine reagents for the SOAP compounds. A methoxyl group at the 4-position of the benzylidene group in the Schiff base and a sulfo group at the 5-position in the amine component increased the fluorescence intensity of the complex. The relationship between the fluorescence intensity and the structure of the complex was investigated by the Free-Wilson method of estimation, and good agreements were obtained between the experimental and the calculated values of the fluorescence intensities. The fluorometric determination procedure of aluminum was established by using 4,4'-dimethyl DSED and 4-sulfo OAP. Aluminum can be accurately determined in the range from 0.001 to 3 μg/25 ml under optimum conditions.

N-Salicylidene-*o*-aminophenol (SOAP) is an excellent fluorometric reagent for aluminum, gallium, and beryllium.[1-6] Derivatives of SOAP may have even better sensitivities than the parent compound. Several substituted SOAP have been examined in connection with the fluorometric determination of aluminum. Some SOAP derivatives, which have only one substituent group in the aldehyde or amine component, have been described in previous studies.[2-4] Only a few studies involving SOAP with two or more substituent groups have been performed,[7] however, except with alkyl derivatives.[5]

In the case of 2,2'-dihydroxyazobenzene, which has a structure analogous to the SOAP structure, some derivatives with two or three substituents have been synthesized, and several derivatives, such as Superchrome Garnet Y and Lumogallion, have been found to be excellent fluorometric reagents.[8-11] In the present paper, the fluorescence properties of aluminum complexes with 25 SOAP derivatives including several combinations of various substituent groups were systematically examined in order to establish the lower detection limits for the fluorometric determination of aluminum. The relationship between the fluorescence intensities and the structures of the aluminum complexes has been explained by means of the Free-Wilson method of estimation.[12] Furthermore, the fluorometric determination of aluminum has been established by using the most sensitive reagent, which is superior to the conventional one, *N*-salicylidene-2-aminophenol-4-sulfonic acid.[2]

Experimental

Apparatus. The fluorescence spectra and the intensity were measured with a Hitachi Model 204 fluorescence spectrophotometer fitted with a 150 W Xenon lamp. The absorption spectra were measured with a Shimadzu Model UV-200S double-beam spectrophotometer. A Toa pH Meter, Model HM-20E, was used for the pH measurements.

Reagents. Standard Solution of Aluminum: A stock solution of aluminum was prepared by dissolving 0.5038 g of aluminum (99.99%) with 20 ml of concentrated hydrochloric acid and then diluting the solution to 500 ml with water. The standard solution was prepared by suitable dilution with 0.1 M hydrochloric acid (1 M=1 mol dm^{-3}) from the stock solution.

***N,N'*-Disalicylideneethylenediamine (DSED) and Its Derivatives:** DSED and its derivatives were synthesized by the condensation of salicylaldehyde and its derivatives with ethylenediamine[8] and then characterized by means of elemental analysis, their melting points, and their IR spectra. These compounds were dissolved in *N,N*-dimethylformamide (DMF). The aldehydes, which were not commercially available, were prepared by the Duff reaction.[13]

***o*-Aminophenol (OAP) and Its Derivatives:** OAP (Wako Pure Chemical Industries, Ltd.) and its derivatives (Tokyo Kasei Kogyo Co., Ltd.) were purified by the method of Charles and Freiser.[14] These compounds were then dissolved in 0.1 M ammonia or DMF, containing ascorbic acid (6.0×10^{-2} M). These solutions are subject to oxidation, but were sufficiently stable for use over a period of 8 hours.

***N*-(2-Hydroxy-4-methylbenzylidene)-2-aminophenol-4-sulfonic Acid:** This compound was synthesized by the condensation of 2-hydroxy-4-methylbenzaldehyde with 2-aminophenol-4-sulfonic acid by the method of Freeman and White.[8] The product thus obtained was purified by repeated recrystallizations from ethanol containing activated charcoal.

Uranine Standard Solution: 0.1 g of uranine (Wako Pure Chemical Industries, Ltd.) was dissolved in 100 ml of water, after which the solution was diluted appropriately with

water to give solutions containing (5.0×10^{-2}—1.0) μg ml^{-1}. These solutions were employed as reference standards of the fluorescence in adjusting the sensitivity of the instrument.

All the other reagents used were special-grade or equivalent.

General Procedure. To a sample solution containing an appropriate amount of aluminum ions, add 1 ml of a DSED-derivatives solution, 1 ml of an OAP-derivatives solution, and 1 ml of a 20% ammonium acetate solution. Adjust the pH to the required value with a diluted hydrochloric acid or an ammonia solution; then dilute the solution to 25 ml with water. After mixing thoroughly, warm the solution at 50 °C for 10 min and then cool to room temperature. Measure the fluorescence intensity at the optimum excitation and emission wavelengths, using an uranine solution as the reference standard.

As has been described by Yamamoto et al.,[15] the correction of the experimental fluorescence intensity for variations in photomultiplier response and the source intensity with the wavelength were not performed because the maximum excitation and emission wavelengths of this series of the complexes lay within a narrow region. The excitation and emission spectra and the maximum wavelengths of the complexes were the corrected values in the present paper.[16]

Results and Discussion

Formation of an Aluminum-Schiff Base Complex. According to the general procedure, DSED was hydrolyzed in an aqueous solution to liberate salicylaldehyde (SAL), which then reacted with aluminum and OAP to form a fluorescent Schiff-base complex (Scheme 1). Such a reaction had previously been utilized for the fluorometric determination of beryllium,[17] zinc,[18] aluminum,[19] and magnesium.[20] Although the same complex is formed when SOAP is used instead of DSED and OAP, the procedure in this study has the advantage that the most suitable concentrations of SAL and OAP can be selected in order to obtain the optimum fluorescence conditions, and so the fluorescence intensity of the reagent blank can be decreased.

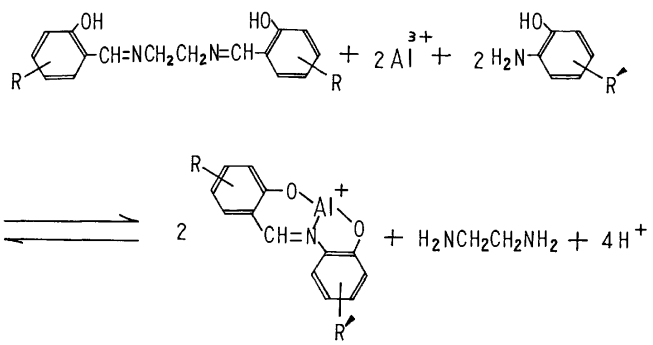

Scheme 1.

In all cases, the fluorescence intensity of the aluminum complex required 80 min to reach its maximum at 20 °C, but readily reached its maximum intensity at 50 °C within 5 min. The fluorescence intensity is stable for at least 2 h.

The absorption spectra of the reagents alone indicated that a free Schiff base was not formed under the optimum conditions for the formation of the aluminum complex. This suggests a mechanism for this formation of the aluminum-Schiff base complex in which SAL and OAP first coordinate to the aluminum ion, thus forming a ternary chelate compound, this compound is then transformed into a Schiff-base complex by the kinetic template mechanism.[19-22]

The molar ratio of aluminum to ligand in the complex was determined fluorometrically by the continuous-variation method. The results indicate that the metal-ligand ratio is 1:1.

Fluorescence Properties of Aluminum-Schiff Base Complexes. The fluorescence properties of aluminum complexes with 25 SOAP derivatives were examined. Their fluorescence characteristics, as obtained under the optimum conditions, are summarized in Table 1.

Aluminum formed fluorescent complexes with a Schiff base in a weakly acidic solution. The optimum pH's for the fluorescence intensity were near pH 5. The optimum concentrations of DSED derivatives and OAP derivatives were about 1.5×10^{-4} M and ($2-5)\times10^{-4}$ M respectively in the final solution. The excitation and emission maxima of aluminum complexes occur at wavelengths of 395—420 nm and 485—535 nm respectively. Some typical excitation and emission spectra of aluminum complexes are shown in Fig. 2.

The fluorescence intensities of the aluminum complexes were markedly changed by the substituent groups on the Schiff base. A methoxyl group at the 4-position of the benzylidene group in the Schiff base (No. **3** in Table 1) and a sulfo group at the 5-position in the amine component (No. **9**) increased the fluorescence intensity of the complexes. These results were consistent with those reported by Morishige.[5] However, the combination of a methyl or a methoxyl group at the 4-position in the aldehyde component and a sulfo group at the 5-position in the amine component (No. **16** or **19**) further increased the fluorescence intensity. The fluorescence enhancement upon the introduction of these substituent groups was due to the increase in the molar absorptivity and the fluorescence quantum yield of its aluminum complex, as will be described below.

The relationship between the fluorescence intensity and the structure of the complex was investigated by means of the Free-Wilson method of estimation, which has been known as a mathematical technique describing the structure-biological activity relationships of a series of chemical analogs.[12] The mathematical model used is based upon the assump-

Table 1. Optimum Fluorescence Conditions for Aluminum-Schiff-Base Complexes

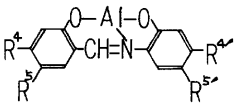

No.	Substituent				DSED Derivative concn. (10^{-4} M)	OAP Derivative concn. (10^{-4} M)	pH	Relative fluorescence intensity[b]		Wavelength[c] (nm)	
	R^4	R^5	$R^{4'}$	$R^{5'}$				Net intensity[a]	Blank	Ex.	Em.
1	H	H	H	H	1.5	6.9	5.0	38.8	4.0	405	520
2	CH_3	H	H	H	1.4	6.9	5.3	51.5	6.5	400	505
3	OCH_3	H	H	H	1.3	6.9	5.3	70.0	10.0	400	500
4	OH	H	H	H	1.3	8.3	5.1	49.0	7.5	400	500
5	H	CH_3	H	H	1.0	6.2	5.3	49.0	7.0	405	510
6	H	OH	H	H	1.4	6.9	5.3	7.5	6.7	415	520
7	H	H	CH_3	H	1.5	4.4	5.1	52.5	6.0	405	520
8	H	H	OH	H	1.5	3.0	4.6	65.0	12.0	400	500
9	H	H	H	SO_3H	1.1	2.4	5.3	93.0	6.5	400	490
10	H	H	H	COOH	1.5	4.3	5.1	67.0	11.5	400	500
11	H	H	H	Cl	1.5	4.2	5.3	23.5	3.5	415	535
12	CH_3	H	OH	H	1.4	2.4	4.6	59.5	11.5	400	500
13	OCH_3	H	OH	H	1.3	1.8	5.0	38.5	10.0	400	495
14	OCH_3	H	CH_3	H	1.3	4.4	5.3	68.5	10.0	400	500
15	OH	H	OH	H	1.3	1.8	4.8	31.5	9.0	395	490
16	CH_3	H	H	SO_3H	1.4	3.2	5.3	110.5	6.5	400	490
17	CH_3	H	H	COOH	1.4	6.4	5.0	91.5	20.5	400	500
18	CH_3	H	H	Cl	1.1	6.3	5.3	49.0	5.0	420	530
19	OCH_3	H	H	SO_3H	1.3	4.8	5.5	113.5	12.5	400	490
20	OCH_3	H	H	COOH	1.3	6.4	5.0	111.0	26.5	395	485
21	OH	H	H	SO_3H	1.0	4.0	5.5	92.5	6.5	400	485
22	OH	H	H	COOH	1.0	6.4	5.0	81.5	21.5	395	485
23	OH	H	H	Cl	1.3	5.3	5.5	50.2	4.8	410	520
24	H	CH_3	H	SO_3H	1.4	2.4	5.5	83.7	6.8	420	490
25	H	CH_3	H	Cl	1.1	6.3	5.3	49.0	7.0	420	530

a) Al(III): 0.25 μg/25 ml (3.7×10^{-7} M). b) 70 div. vs. 0.5 μg ml^{-1} uranine (setting 405 nm/500 nm). c) Corrected value.

tion that the fluorescence intensity [I] in a series of analogs can be given as the sum of the "overall average" values (μ) and the contribution of each substituent [R]; i.e.,

$$\mu + \Sigma[R] = [I] \quad (1)$$

where [R] is the specific value determined by a substituent group at a certain position. Furthermore, the sum of [R] at each position is restricted to zero in this model; i.e.,

$$\Sigma[R] = 0 \quad \text{(at each position)}. \quad (2)$$

The application of this method of estimation to the fluorescence intensities of aluminum complexes of 9 SOAP derivatives, which have substituent groups at the 5-position on the benzylidene group in each component of the Schiff base, has been investigated by Yamamoto et al.[15] They reported that this method could be applied to that series of Schiff bases.

This method was applied to the experimental fluorescence intensities of a total of 25 aluminum complexes in our study. The μ and [R] values were calculated by means of multiple regression analysis using a computer. Then the calculated values were substituted into Eq. 1; the fluorescence intensity of each complex was thus obtained. The results are presented as the correlation of the calculated values with the experimental values of the fluorescence intensities in Fig. 1 (Key, O). Good agreements were obtained between these two values, with the relation of $y=1.00x+0.021$ and a correlation coefficient of 0.940. These results indicated that this method could also be applied to the series of Schiff bases which have substituent groups at the 4- and 5-positions in each component.

Moreover, the μ and [R] values were calculated by using the experimental values of 11 kinds of complexes which have only one substituent group in either the aldehyde or amine component of the Schiff base (μ;50.2, $[H]_{R^4}$;−5.4, $[CH_3]_{R^4}$;7.3, $[OCH_3]_{R^4}$;25.8, $[OH]_{R^4}$;4.8, $[H]_{R^5}$;2.1, $[CH_3]_{R^5}$;12.3, $[OH]_{R^5}$;−29.2, $[H]_{R^{4'}}$;−1.4, $[CH_3]_{R^{4'}}$;12.3, $[H]_{R^{5'}}$;−6.8, $[SO_3H]_{R^{5'}}$;47.9, $[COOH]_{R^{5'}}$;21.4, $[Cl]_{R^{5'}}$;−22.1). The fluorescence intensities of the complexes which have a combination of two substit-

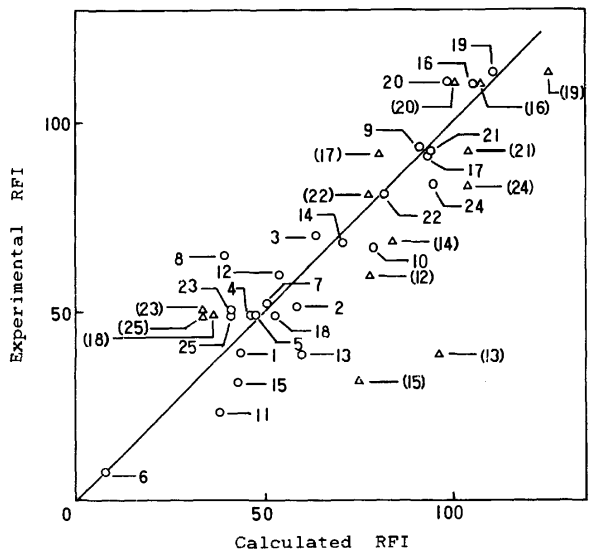

Fig. 1. Relationship between experimental and calculated values of fluorescence intensities of aluminum complexes (for key to substituents, see Table 1). O; calculated from all of 25 aluminum complexes. Δ: calculated from 11 aluminum complexes, which have only one substituent.

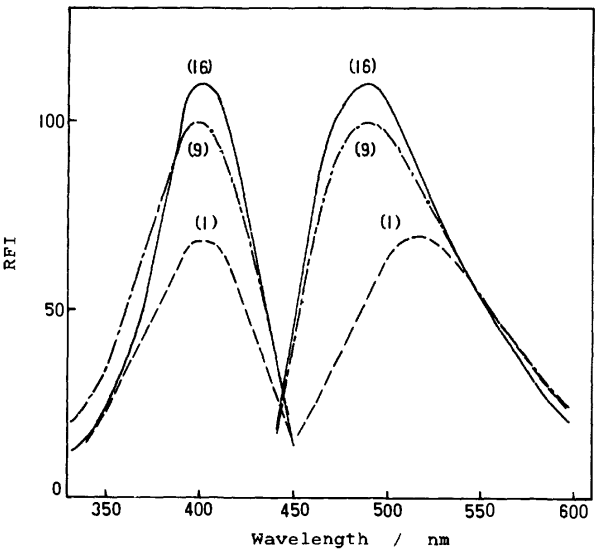

Fig. 2. Corrected excitation and emission spectra of aluminum complexes with Schiff bases; (1) SOAP (*N*-salicylidene-*o*-aminophenol), (9) *N*-salicylidene-2-aminophenol-4-sulfonic acid, (16) *N*-(2-hydroxy-4-methylbenzylidene)-2-aminophenol-4-sulfonic acid. Conditions for (1), (9), and (16); reference to Table 1.

uent groups were estimated by the use of the μ and [R] values obtained. As is shown in Fig. 1 (Key, Δ), a linear relationship was observed between the estimated and the experimental values, with the relation of $y=0.771x+20.1$ and a correlation coefficient of 0.917, except for the complexes which have a hydroxyl group at the 4-position in the amine component of the Schiff base (Nos. **12**, **13**, and **15**). These results suggest that, if the fluorescence intensities of several compounds among these series of Schiff base are experimentally measured, a better structure for the fluorometric reagent can be predicted by means of this method of estimation. In general, the combination of two substituent groups, both of which increase the fluorescence intensity, will provide a much stronger fluorescence. On the other hand, the combination of substituent groups, one of which increases the fluorescence intensity, while the other decreases it, will cause their properties to cancel each other out. The exception of the hydroxyl group at the 4-position in the amine component suggests that this group interacts with a substituent group in the aldehyde component to contribute to the fluorescence intensity.

The molar absorptivity (ε), the fluorescence quantum yield (ϕ_f), and the fluorescence sensitivity index (FSI) of the aluminum-SOAP complex (No. **1**) have been reported by Morishige (ε=20400, ϕ_f=0.205, and FSI=0.309).[4] The substitution of a sulfo group at the 5-position in the amine component (No. **9**) caused a remarkable increment in ϕ_f (0.802) and a slight decrement of ε (14100), so that FSI was raised to 0.653.[4] In this study a much higher FSI (0.766) was achieved by the combination of a methyl group and a sulfo group (No. **16**), where ϕ_f and ε were 0.810 and 18100 respectively.

Fluorometric Determination of Aluminum

Procedure I. The combination of *N,N'*-bis(4-methylsalicylidene)ethylenediamine [4,4'-dimethyl DSED] and 2-aminophenol-4-sulfonic acid [4-sulfo OAP], which form Complex No. **16** (in Table 1), was the most suitable reagent for the fluorometric determination of aluminum because of its high sensitivity and its reproducibility, with a low blank value. The analytical conditions were, therefore, investigated further.

The excitation and emission spectra of the aluminum complexes of these reagents are shown in Fig. 2. The optimum excitation and emission wavelengths are 400 (uncorrected value: 410) nm and 490 (480) nm respectively.

The effect of the pH on the fluorescence intensity is indicated in Fig. 3. The aluminum complex showed maximum fluorescence in the pH region of 5.1—5.5.

Figure 4 shows the effect of the concentration of the reagent at the optimum pH. The maximum fluorescence intensity was achieved with 1.4×10^{-4} M of 4,4'-dimethyl DSED and 3.2×10^{-4} M of 4-sulfo OAP in the final solution. These concentrations correspond to the addition of 1 ml of 0.1% 4,4'-dimethyl DSED and 1 ml of 0.15% 4-sulfo OAP in a 25-ml solution for the determination of aluminum.

0.1% 4,4'-dimethyl DSED dissolved in DMF was stable for over one month. 0.15% 4-sulfo OAP in a

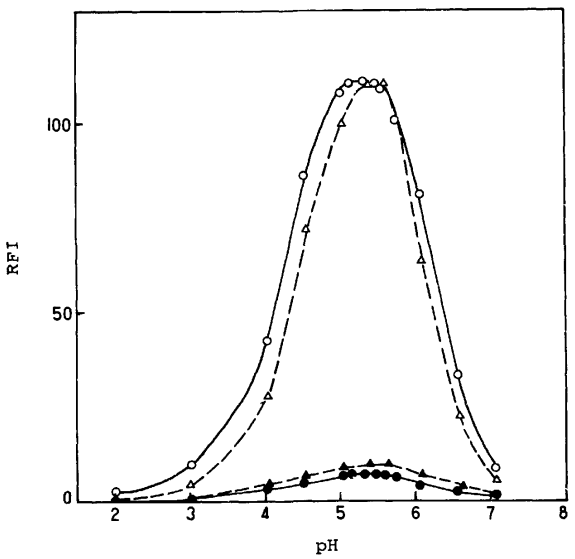

Fig. 3. Effect of pH on fluorescence intensity. Al(III): 0.25 μg/25 ml (3.7×10^{-7} M), Wavelength: 400 nm/490 nm, 70 div. vs. 0.5 μg ml^{-1} uranine (setting 405 nm/500 nm), Reagent: O; 4,4′-dimethyl DSED (1.4×10^{-4} M)+4-sulfo OAP (3.2×10^{-4} M): Δ; *N*-(2-hydroxy-4-methylbenzylidene)-2-aminophenol-4-sulfonic acid (4.8×10^{-4} M): ●; reagent blank of O: ▲; reagent blank of Δ.

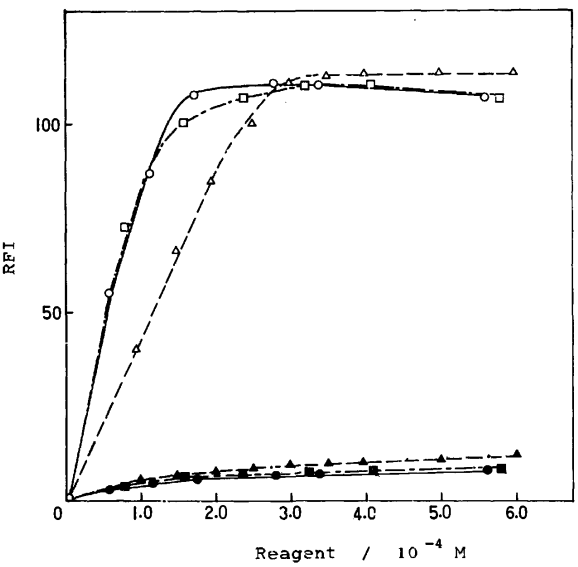

Fig. 4. Effect of concentration of 4,4′-dimethyl DSED (O), 4-sulfo OAP (□) and *N*-(2-hydroxy-4-methylbenzylidene)-2-aminophenol-4-sulfonic acid (Δ) on fluorescence intensity. Al(III): 0.25 μg/25 ml (3.7×10^{-7} M), pH: 5.3, Wavelength: 400 nm/490 nm, 70 div. vs. 0.5 μg ml^{-1} uranine (setting 405 nm/500 nm), O: containing 4-sulfo OAP (3.2×10^{-4} M): □: containing 4,4′-dimethyl DSED (1.4×10^{-4} M), ●: reagent blank of O: ■: reagent blank of □, ▲: reagent blank of Δ.

0.1 M ammonia solution containing ascorbic acid (6.0×10^{-2} M) was stable for use over a period of 24 h, while this solution without ascorbic acid was subject to oxidation and exhibited a brown color. This solution should, therefore, be made up daily.

According to the general procedure, aluminum can be determined in the range from 0.001 to 3 μg/25 ml with a relative error of 3% under optimum conditions, as has been described above.

The effects of diverse ions were also studied. The following cations in 100-fold excesses did not interfere with the determination of aluminum: silver(I), arsenic(III), barium(II), boron(III), cadmium(II), calcium(II), magnesium(II), manganese(II), mercury(II), molybdenum(VI), thallium(I), and zinc(II). Cobalt(II), chromium(VI), copper(II), indium(III), iron(II), iron(III), and nickel(II) caused negative errors in 10-fold excesses. Beryllium(II) and gallium(III) in 10-fold excesses did not interfere at all.

Procedure II. As has been mentioned, the same complex is formed by using only the Schiff base [i.e., *N*-(2-hydroxy-4-methylbenzylidene)-2-aminophenol-4-sulfonic acid] instead of those two components. Another procedure was also investigated by using the Schiff base as a fluorometric reagent, because the Schiff base in a DMF solution is more stable than 4-sulfo OAP.

The excitation and emission spectra, and the optimum wavelengths of the aluminum complex with this reagent, were just the same as those obtained by Procedure I.

The effect of the pH on the fluorescence intensity is indicated in Fig. 3. The aluminum complex showed its maximum fluorescence at pH 5.3—5.5.

Various amounts of a 0.075% (2.4×10^{-3} M) Schiff-base solution were added to a solution containing 0.25 μg of aluminum, after which the fluorescence intensity was measured at the optimum pH. As is shown in Fig. 4, 4.8×10^{-4} M is adequate. This concentration is equivalent to the addition of 5 ml of a 0.075% reagent solution in 25 ml for the procedure of determining aluminum. The 0.075% reagent solution is stable for over one month.

Aluminum can be determined in the same range as in Procedure I, i.e., from 0.001 to 3 μg/25 ml.

The authors are very grateful to Dr. Yoshimoto Abe, Faculty of Science and Technology, Science University of Tokyo, for his helpful discussions.

References

1) R. M. Dagnall, R. Smith, and T. S. West, *Talanta*, **13**, 609 (1966).
2) K. Morishige, *Anal. Chim. Acta*, **72**, 295 (1974).
3) K. Morishige, *Anal. Chim. Acta*, **73**, 245 (1974).
4) K. Morishige, *J. Inorg. Nucl. Chem.*, **40**, 843 (1978).
5) K. Morishige, *Anal. Chim. Acta*, **121**, 301 (1980).
6) K. Watanabe and I. Aoki, *Bunseki Kagaku*, **34**, 16 (1985).
7) R. J. Argauer and C. E. White, *Anal. Chem.*, **36**, 2141 (1964).

8) D. C. Freeman, Jr., and C. E. White, *J. Am. Chem. Soc.*, **78**, 2678 (1956).
9) K. Hiraki, *Bull. Chem. Soc. Jpn.*, **46**, 2438 (1973).
10) K. Hiraki, *Bull. Chem. Soc. Jpn.*, **45**, 1395 (1972).
11) K. Hiraki, *Bull. Chem. Soc. Jpn.*, **45**, 789 (1972).
12) S. M. Free and J. M. Wilson, *J. Med. Chem.*, **7**, 398 (1964).
13) J. C. Duff, *J. Chem. Soc. (London)*, **1941**, 547.
14) R. G. Charles and H. Freiser, *J. Am. Chem. Soc.*, **74**, 1385 (1952).
15) K. Yamamoto, H. Sunada, N. Yonezawa, and A. Otsuka, *Bunseki Kagaku*, **28**, 205 (1979).
16) M. Watanabe, "Keikou Bunseki (Fluorometry)," Hirokawa (1970), p. 68.
17) K. Watanabe and I. Aoki, *Bunseki Kagaku*, **34**, 497 (1985).
18) K. Watanabe and I. Aoki, *Bunseki Kagaku*, **35**, 1 (1986).
19) K. Watanabe and I. Aoki, *Bunseki Kagaku*, **35**, 487 (1986).
20) K. Watanabe and I. Aoki, *Bunseki Kagaku*, **35**, 795 (1986).
21) D. Hopgood and D. L. Leussing, *J. Am. Chem. Soc.*, **91**, 3740 (1969).
22) B. E. Leach and D. L. Leussing, *J. Am. Chem. Soc.*, **93**, 3377 (1971).
23) T. Fujita, "Yakubutu no kouzou-kassei soukan (Structure-Activity Relationships—Quantitative Approaches)," Kouzou-soukan Konwakai, Nankoudou (1979), p. 299.

 © 1989 The Chemical Society of Japan Bull. Chem. Soc. Jpn., 62, 2375—2378 (1989)

A Resonance Raman Study of Polymeric Thiolato Cobalt(III) Complexes: Possible Bridging Modes

Kan KANAMORI,* Sonomi INO, Yumiko MIZUNO, Isao KANESAKA, Kiyoyasu KAWAI, and Jinsai HIDAKA†
Department of Chemistry, Faculty of Science, Toyama University, Gofuku, Toyama 930
†Department of Chemistry, University of Tsukuba, Tsukuba, Ibaraki 305
(Received January 13, 1989)

The resonance Raman spectra of polymeric $Co^{III}\{SCH_2CH(NH_2)COOH\text{-}S\}_3$ and $Na_3Co^{III}(SCH_2COO\text{-}S)_3$ complexes were investigated. The complexes gave two totally symmetric Co–S stretchings, indicating the presence of two different Co–S–Co bridging modes in the complexes. Possible bridging modes are discussed in relation to their structures.

Schubert[1] first obtained the red H_3Co(cysteinato)$_3$ complex, which is insoluble in acids and water, but soluble in alkali to give cherry-red solutions. Neville and Gorin[2] and Gorin and Spessard[3] proposed that, in this complex, both thiolato and carboxylato groups are coordinated to cobalt(III). However, when the complex was reinvestigated by McCormick and Gorin,[4] they concluded, on the basis of the infrared spectra, that the complex is polymeric and consists only of thiolate bridges. Similar polymeric complexes have been prepared with hexanethiol,[4] 3-mercaptopropionate,[4] 2-mercaptoethanol,[5] mercaptoacetate,[6] and ethyl mercaptoacetate.[6] However, no difinitive data have been reported so far concerning the bridging mode in the polymeric thiolato complexes. We here wish to present the first report on the bridging mode of the polymeric thiolato cobalt(III) complexes, as studied by means of the resonance Raman spectra.

Experimental

Preparation. The polymeric complexes, $Co\{SCH_2CH(NH_2)COOH\text{-}S\}_3$[1] and $Na_3Co(SCH_2COO\text{-}S)_3$,[6] and the trinuclear complex, $K_3[Co\{Co(SCH_2CH(NH_2)COO\text{-}N,S)_3\}_2]$,[7] were prepared according to the methods in the literature and were identified by means of their electronic-absorption spectra.

Measurements. The samples used for Raman measurements were in the form of aqueous solutions or disks. The disks were spun to avoid thermal decomposition induced by laser illumination. The Raman spectra were recorded on a JASCO R-800 laser Raman spectrophotometer. Excitation profiles were obtained by using the laser lines of a Spectra Physics 164 Ar^+ laser (514.5, 501.7, 496.5, 488.0, 476.5, 465.8, and 457.9 nm) and of a Coherent Radiation model CR599 dye laser employing Rhodamine 6G dye (610.0, 588.0, and 567.8 nm). The laser power was below 100 mW for solid samples. The spectral band width was set at 5 cm^{-1}. The Raman intensities were measured relative to the totally symmetric S–O stretching mode of the potassium sulfate incorporated in the sample. Corrections of the observed intensity were applied to the fourth power of the wavenumber of scattered radiation and the instrumental response. The intensities were averaged over more than three measurements.

Results and Discussion

Raman Spectra. A polymeric complex, $Co(SCH_2CH(NH_2)COOH\text{-}S)_3$, gives very intense Raman bands in the 200—500 cm^{-1} region and some very weak bands in the 600—1000 cm^{-1} region in the solid state with 488.0-nm excitation. An alkaline solution of the complex gives essentially the same spectrum as that obtained in the solid state, indicating that the polymeric structure is retained also in the solution. Figure 1 shows the polarized resonance Raman spectra in the 200—500 cm^{-1} region of the complex in a 0.1 mol dm^{-3} NaOH solution. The depolarization ratios of the 406-, 341-, 280-, and 220-cm^{-1} bands are all near to 1/3; ρ=0.34, 0.33, 0.31, and 0.32 respectively. Thus, all these bands can reasonably be assigned to totally symmetric

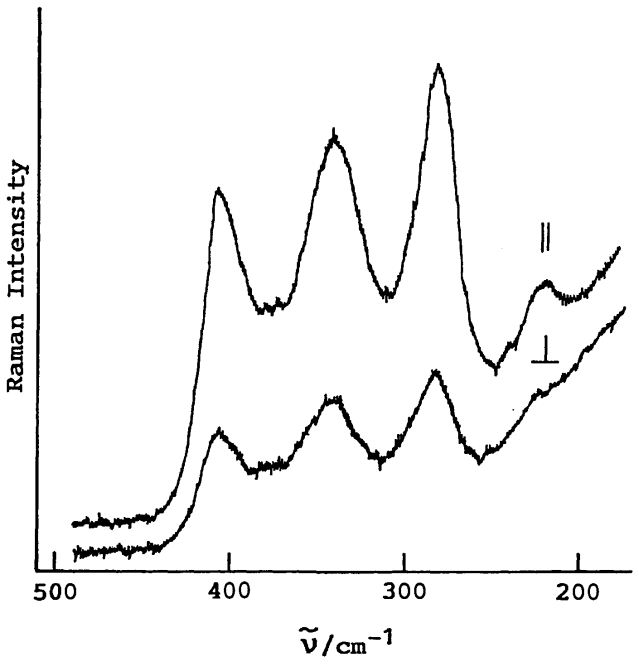

Fig. 1. Polarized resonance Raman spectra of polymeric tris(cysteinato-*S*)cobalt(III) in 0.1 mol dm^{-3} NaOH solution with 488.0-nm excitation (500 mW).

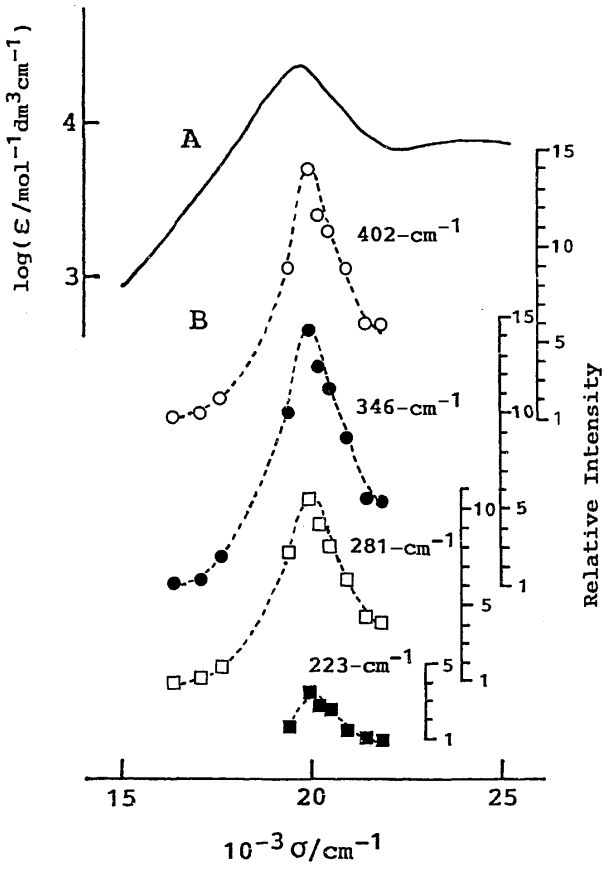

Fig. 2. Electronic absorption spectrum of polymeric tris(cysteinato-*S*)cobalt(III) in 0.1 mol dm^{-3} NaOH solution and the excitation profiles of the 402-, 346-, 281-, and 223-cm^{-1} bands in the solid state.

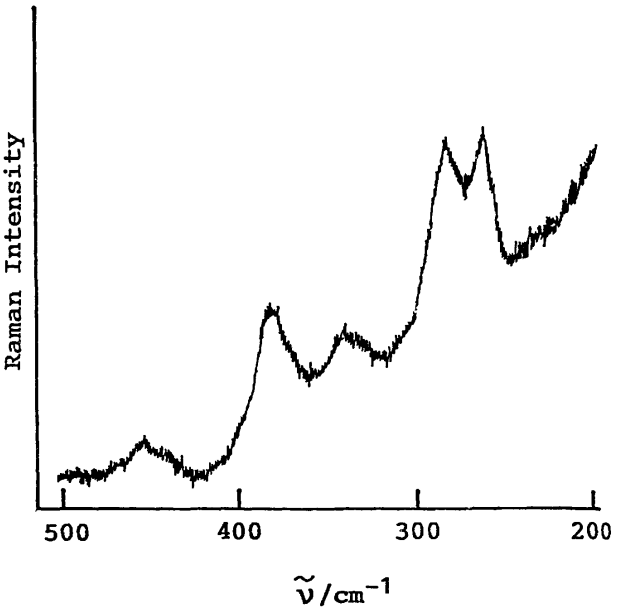

Fig. 3. Resonance Raman spectra of polymeric $Na_3Co(SCH_2COO\text{-}S)_3$ in aqueous solution with 514.5-nm excitation (150 mW).

modes. The depolarization ratios, 1/3, under these resonance condition correspond well with those expected for an electronic transition between the nondegenerate states of symmetries lower than cubic, but still not very low.[8]

Figure 2-A shows the electronic absorption spectrum of the $Co(SCH_2CH(NH_2)COOH\text{-}S)_3$ complex in an alkaline solution. The electronic absorption band at 19600 cm^{-1} has been assigned to the charge-transfer transition between the cobalt(III) and bridging sulfur because of its high intensity.[6] This charge-transfer-band position corresponds well with those of the charge-transfer bands of the trinuclear complexes containing sulfur bridges, such as $[Co\{Co(SCH_2CH_2NH_2)_3\}_2]^{3+}$[9] and $[Co\{Co(SCH_2CH(NH_2)COO\text{-}N,S)_3\}_2]^{3-}$.[10,11]

The excitation profiles of the four bands (402, 346, 281, and 223 cm^{-1}) of the polymeric $Co(SCH_2CH(NH_2)\text{-}COOH\text{-}S)_3$ complex were obtained for the solid sample, because the solid sample gives more intense Raman bands than does the solution; the results are shown in Fig. 2-B. The excitation profiles of the four bands reach their maxima at 20500 cm^{-1}, close to the electronic absorption maximum at 19600 cm^{-1}, indicating that the resonant transition is a charge-transfer one between the cobalt(III) and bridging sulfur.

When the electron giving rise to a resonant transition is localized on the coordinating atom, an intense resonance enhancement can not be expected for intraligand vibrational modes. The resonant transition of the present polymeric thiolato complexes is just such a case. Therefore, all the four resonance-enhanced Raman bands observed for each polymeric thiolato complex should be assigned to the vibrational modes of the Co–S moiety and not to the intraligand modes—that is, they should be assigned to the Co–S stretchings and Co–S–Co or S–Co–S bendings.

Figure 3 illustrates the resonance Raman spectrum in an aqueous solution of the polymeric $Co(SCH_2\text{-}COO\text{-}S)_3^{3-}$. $Na_3Co(SCH_2COO\text{-}S)_3$ and $Co(SCH_2COOH\text{-}S)_3$ in the solid state give practically the same spectra. The four bands in the 200—400 cm^{-1} region can be assigned to modes similar to those observed for the polymeric $Co(SCH_2CH(NH_2)COOH\text{-}S)_3$ in the corresponding region, since all the bands are polarized and since the excitation profiles of the bands reach their maxima at ca. 20000 cm^{-1}.

Bands characteristic of metal-sulfur stretchings have been observed in the region of 300—400 cm^{-1}.[12] For the trinuclear μ-S complex, $[Co\{Co(SCH_2CH_2NH_2)_3\}_2]^{3+}$, the Co–S stretchings have been assigned to the 358- and 345-cm^{-1} bands, and the bendings, to the 278- and 262-cm^{-1} bands.[9] We observed the Co–S stretching at 370 cm^{-1} and the bendings at 301 and 258 cm^{-1} for $K_3[Co\{Co(SCH_2CH(NH_2)COO\text{-}N,S)_3\}_2]$. On the basis of the assignment for the trinuclear complexes and the measurement of the depolarization ratios, the bands at

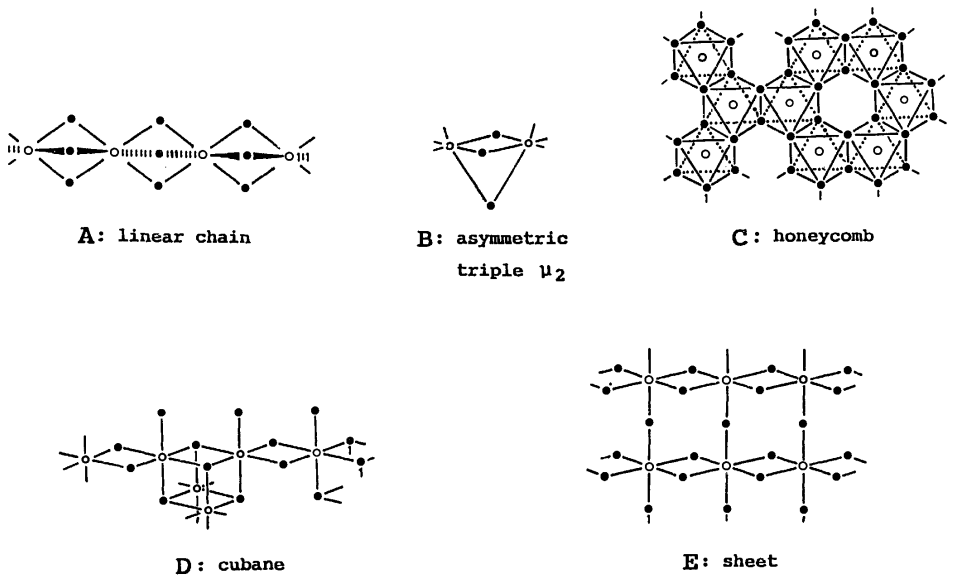

Fig. 4. Possible bridging modes of polymeric Co(S-R)$_3$ complex (● and O denote sulfur and cobalt atom, respectively).

402 and 346 cm^{-1} of the polymeric Co(SCH$_2$CH(NH$_2$)-COOH-*S*)$_3$ complex can be assigned to the totally symmetric Co–S stretchings, and the bands at 281 and 223 cm^{-1}, to the totally symmetric bending modes. Similarly, the bands at 379 and 339 cm^{-1} of the polymeric Na$_3$Co(SCH$_2$COO-*S*)$_3$ complex can be assigned to the totally symmetric Co–S stretchings, and those at 281 and 262 cm^{-1}, to the totally symmetric bendings.

It is noted that, on going from the polymeric Co(SCH$_2$CH(NH$_2$)COOH-*S*)$_3$ to the polymeric Na$_3$Co-(SCH$_2$COO-*S*)$_3$, the band at 402 cm^{-1} shifts to lower wavenumbers, and the band at 223 cm^{-1}, to higher wavenumbers, while the other two bands remain at almost the same position. This spectral behavior may suggest that, in these complexes, there are two types of bridging modes and that the bridging geometry (Co–S bond length and/or Co–S–Co angle) of one of them is affected by the nature (probably the bulkiness) of pendant group, while the other is not. A change in the bridging geometry would result in the frequency shift of the Co–S stretching and the Co–S–Co bending.

The weak band at 453 cm^{-1} of the polymeric Na$_3$Co(SCH$_2$COO-*S*)$_3$ complex can not be assigned at present. The position is, however, somewhat higher for a Co–S stretching band.

Possible Bridging Modes. Figure 4 shows possible bridging modes for the present polymeric thiolato complexes, Co(S-R)$_3$. It is well-known that thiolates can take a variety of bridging modes because of the flexibility of the sulfur bridging. For example, the M–S–M angles are ca. 60° in [(Me$_2$S)Cl$_2$W(SEt)$_3$WCl$_2$-(SMe$_2$)][13] while they are ca. 140° in [Fe$_3$(SPh)$_3$Cl$_6$]$^{3-}$.[14] Though these facts allow us to apply a variety of bridging modes to the present polymeric thiolato complex, the present results of the totally symmetric Co–S stretchings restrict the possibility of the bridging mode as follows!

(A) The linear chain structure with two triple μ_2-bridges proposed by McCormick and Gorin[4] has been found in the trinuclear complexes, [Co{Co(SCH$_2$CH$_2$-NH$_2$-*N*,*S*)$_3$}$_2$]$^{3+}$ [15] and [Co{Co(SCH$_2$CH(NH$_2$)COO-*N*,*S*)$_3$}$_2$]$^{3-}$.[10] This structure is, however, inconsistent with the present Raman results, because the structure gives only one totally symmetric Co–S stretching band if the triple μ_2-bridge is symmetric.

(B) An asymmetric triple μ_2-bridge caused by the elongation of an M–S–M moiety has been found in low-symmetry mixed-ligand complexes such as [Re$_2$-(SC$_6$H$_4$Me)$_7$(NO)$_2$]$^-$.[16] A lowering of the symmetry of the triple μ_2-bridge caused by this kind of distortion gives two totally symmetric Co–S stretchings. This distortion, however, seems to be unlikely in the present polymeric complexes, with only one kind of ligand, as in [Co{Co(SCH$_2$CH$_2$NH$_2$-*N*,*S*)$_3$}$_2$]$^{3+}$ [15] and [Co{Co-(SCH$_2$CH(NH$_2$)COO-*N*,*S*)$_3$}$_2$]$^{3-}$.[10]

(C) A honeycomb structure with three double μ_2-bridges such as [Co{(OH)$_2$Co(en)$_2$}$_3$]$^{6+}$ [17] is also inconsistent with the Raman results for the same reason as has been mentioned in (A).

(D) Structure **D** containing a cubane structure has three μ_3-bridging thiolates, one double μ_2-bridging thiolate, and one nonbridging thiolate. A cubane structure with thiolato-bridges has also been found in [Re$_4$(CO)$_{12}$(SMe)$_4$].[18] For Structure **D**, the three Co–S(μ_3) bonds are not equivalent; that is, two of them are trans to the Co–S(μ_2) bond, while one is trans to the Co–S (nonbridging) bond. Thus, this structure should give three totally symmetric Co–S(bridging)

stretchings (two Co-S(μ_3) stretchings and one Co-S(μ_2) stretching).

(E) The sheet structure proposed by McCormick and Gorin[4] consists of two different μ_2-bridging modes—namely, two double μ_2-bridges and two single μ_2-bridges. Structure **E** gives two totally symmetric Co-S stretchings. Such greatly different Co-S-Co bridging modes are probable causes of the appreciable difference in the wavenumbers of the two Co-S stretchings of the present polymeric thiolato complexes. In conclusion, the present polymeric thiolato cobalt(III) complexes are highly likely to have the sheet structure **E**.

References

1) M. P. Schubert, *J. Am. Chem. Soc.*, **53**, 3851 (1931).
2) R. G. Neville and G. Gorin, *J. Am. Chem. Soc.*, **78**, 4893 (1956).
3) G. Gorin, J. E. Spessard, G. A. Wessler, and J. P. Oliver, *J. Am. Chem. Soc.*, **81**, 3193 (1959).
4) B. J. McCormick and G. Gorin, *Inorg. Chem.*, **2**, 928 (1963).
5) K. Hori, *Nippon Kagaku Zasshi*, **91**, 547 (1970).
6) K. Hori, *Nippon Kagaku Zasshi*, **92**, 322 (1971).
7) T. Konno, S. Aizawa, K. Okamoto, and J. Hidaka, *Chem. Lett.*, **1985**, 1017.
8) R. J. H. Clark and B. Stewart, *Struct. Bonding (Berlin)*, **36**, 1 (1979).
9) D. P. Strommen, K. Bajdor, R. S. Czernuszewicz, E. L. Blinn, and K. Nakamoto, *Inorg. Chim. Acta*, **63**, 151 (1982).
10) K. Okamoto, S. Aizawa, T. Konno, H. Einaga, and J. Hidaka, *Bull. Chem. Soc. Jpn.*, **59**, 3859 (1986).
11) S. Aizawa, K. Okamoto, H. Einaga, and J. Hidaka, *Bull. Chem. Soc. Jpn.*, **61**, 1601 (1988).
12) K. Nakamoto, "Infrared and Raman Spectra of Inorganic and Coordination Compounds," 3rd ed, John Wiley and Sons, New York (1977), Part III-19.
13) P. M. Boorman, V. D. Patel, K. A. Kerr, P. W. Codding, and R. V. Roey, *Inorg. Chem.*, **19**, 3508 (1980).
14) K. S. Hagen and R. H. Holm, *J. Am. Chem. Soc.*, **104**, 5496 (1982).
15) M. J. Heeg, E. L. Blinn, and E. Deutsch, *Inorg. Chem.*, **24**, 1118 (1985).
16) P. J. Blower, J. R. Dilworth, J. P. Hutchinson, and J. A. Zubieta, *Transition Met. Chem.*, **7**, 354 (1982).
17) U. Thewalt, *Chem. Ber.*, **104**, 2657 (1971); U. Thewalt and J. Ernst, *Z. Naturforsch., Teil B*, **30**, 818 (1975); D. A. Dixon, R. E. Marsh, and W. P. Schaeffer, *Acta Crystallogr., Sect. B*, **34**, 807 (1978).
18) W. Harrison, W. C. Marsh, and J. Trotter, *J. Chem. Soc., Dalton Trans.*, **1972**, 1009.

Solvent Extraction of Thallium(I) Picrate into Benzene with Mixtures of Crown Ethers and Tributyl Phosphate

Yasuyuki TAKEDA
Department of Chemistry, Faculty of Science, Chiba University, Yayoi-cho, Chiba 260
(Received December 27, 1988)

Synopsis. Thallium(I) picrate was extracted into benzene at 25 °C with crown ether (15-crown-5 (15C5) and benzo-15-crown-5 (B15C5)) and/or tributyl phosphate (TBP). The crown ether complex with thallium picrate (1:1:1) accepts one TBP molecule. The thallium picrate complex with B15C5 and TBP is more stable than the corresponding 15C5 complex in benzene.

Solvent extraction of metal ions by crown compounds is widely studied in various fields.[1] Numerous basic data about extraction process have been reported to date, and furthermore, crown compounds have been used as extraction reagents for separation and determination of metal ions, particularly alkali and alkaline earth metal ions.

There are many factors which influence extractability and extraction-selectivity of crown compounds for metal ions; namely, (1) distribution of a crown compound itself, (2) stability of a crown compound complex with a metal ion in an aqueous solution, (3) extraction of a crown compound complex with a metal ion, (4) a counter anion which forms an ion pair with a cationic crown compound complex, (5) diluent, (6) coexisting species in an aqueous phase, (7) coexisting another ligand in an organic phase, and (8) structure of a crown compound. As for the factor (7), extractability of crown ethers for alkali and alkaline earth metal ions is enhanced by the addition of donor solvents such as tributyl phosphate (TBP), trioctylphosphine oxide, and bis(2-ethylhexyl)hydrogenphosphate.[1,2] This synergistic increase is due to the fact that crown ether–metal ion complexes form adducts with the donor solvents. The stoichiometry of the adduct complex with an alkali metal ion is metal ion:crown ether:donor solvent=1:1:1.[1,2]

In the present work, since scarcely any data on synergistic extractions of crown ether–Tl^+ complexes with donor solvents have been reported, extraction of thallium(I) picrate was conducted in the presence of crown ether and/or TBP at 25 °C between benzene and water. Compositions of the extracted complexes and adduct-formation constants in benzene have been determined. The synergistic extraction-behavior of Tl^+ was compared with that of Rb^+, which is a s-block element and nearly equal to Tl^+ in size. The crown ethers used in this study were 15-crown-5 (15C5) and benzo-15-crown-5 (B15C5). Their cavities (0.85—1.1 Å[1] (radius)) are smaller than Tl^+.

Experimental

Materials. 15-Crown-5 (Nisso Co., Ltd.) and analytical-grade TBP (Wako Pure Chemicals, Ltd.) were used without further purification. Benzo-15-crown-5 (Merck Japan Ltd.) was dissolved in heptane, and filtered while hot. It was recrystallized from heptane twice and, prior to use, dried at 40 °C in vacuo. The purity of $TlNO_3$ and concentrations of picric acid solutions were determined by EDTA and alkaline titrations, respectively. Analytical-grade benzene was washed twice with distilled water.

Procedure. All the experiments were conducted at 25±0.2 °C. The experimental procedures were similar to those in the previous paper.[2] Concentrations of $TlNO_3$, picric acid, TBP, 15C5, and B15C5 were 4.2×10^{-5}—4.2×10^{-3}, 4.4×10^{-4}—4.9×10^{-3}, 8.0×10^{-2}—9.7×10^{-1}, $(1.4—2.9)\times10^{-2}$, and 6.5×10^{-4}—1.6×10^{-1} mol dm^{-3}, respectively. All the extractions were carried out in the pH range of 1.9—5.7. Concentrations of thallium(I) extracted into benzene phase were determined by atomic absorption spectrometry.

Results and Discussion

Equilibrium constants can be defined by the following equations:

$$K_{ex}(MLL'A) = [MLL'A]_o[H^+]/[M^+][L]_o[L']_o[HA]_o, \quad (1)$$

$$K_{D,L} = [L]_o/[L], \quad (2)$$

$$K_{ex}(HA) = [HA]_o/[H^+][A^-], \quad (3)$$

$$K_{MLL'A,o} = [MLL'A]_o/[MLA]_o[L']_o, \quad (4)$$

where the subscript "o" and the lack of a subscript refer to the organic and the aqueous phase, respectively; M^+, A^-, L, and L′ denote a monovalent metal ion, a picrate ion, crown ether, and another neutral ligand, respectively. All the activity coefficients of chemical species have been assumed as unity. The $K_{ex}(HA)$

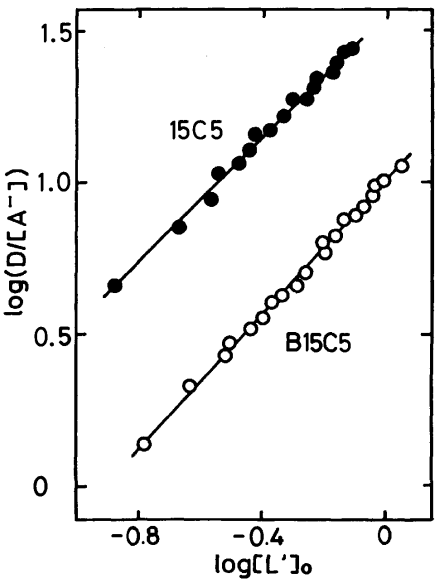

Fig. 1. Plots of $\log(D/[A^-])$ vs. $\log[L']_o$ for 15C5- and B15C5-TBP systems.

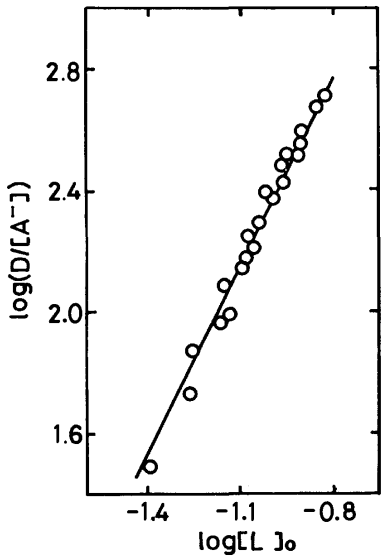

Fig. 2. Plots of $\log(D/[A^-])$ vs. $\log[L]_o$ for the B15C5 system.

value was spectrophotometrically determined to be 247.

When both L and L′ is in the benzene phase, the distribution ratio (D) is represented by

$$D = [MLL'A]_o/[M^+]. \quad (5)$$

Substitution of Eqs. 1 and 3 into Eq. 5 gives

$$D = K_{ex}(MLL'A)K_{ex}(HA)[L]_o[L']_o[A^-]. \quad (6)$$

$\log(D/[A^-])$ vs. $\log[L']_o$ plots for 15C5- and B15C5-TBP systems are shown in Fig. 1. The plots for 15C5 and B15C5 in Fig. 1 have a slope of 1. $\log(D/[A^-])$ vs. $\log[L]_o$ plots for the 15C5- and B15C5-TBP systems were similar (a straight line with a slope of 1), and so have been omitted. $\log(D/[A^-])$ vs. $\log[L]_o$ plots for the B15C5 system in Fig. 2 show a straight line with a slope of 2, where L=L′=B15C5. This indicates that B15C5 forms a 2:1 complex with Tl^+. Thus, K_{ex}(MLL′A) can be described by Eq. 1. When L′=TBP, the value of $[L']_o$ in Eq. 6 was supposed to be nearly equal to that of $[L']_t$, and those of $[L]_o$ and $[A^-]$ were calculated from Eqs. 7 and 8 respectively:

$$[L]_o = ([L]_t - [MLL'A]_o - [MLA]_o)/(1 + K_{D,L}^{-1}), \quad (7)$$

$$[A^-] = ([HA]_t - [M]_{o,t})/\{1 + (K_{HA} + K_{ex}(HA))[H^+]\}, \quad (8)$$

where the subscript "t", $[M]_{o,t}$, and K_{HA} denote the total concentration, the total concentration of thallium in the organic phase, and the association constant of picric acid (K_{HA}=1.9[5][3]). When both L and L′ are B15C5, values of $[B15C5]_o$ and $[A^-]$ in Eq. 6 were calculated from Eqs. 9 and 8, respectively:

$$[L]_o = ([L]_t - 2[M]_{o,t})/\{1 + K_{D,L}^{-1} - K_{ex}(HA)K_{ex}(MLA)[M^+][A^-]\}, \quad (9)$$

where $K_{ex}(MLA) = [MLA]_o[H^+]/[M^+][L]_o[HA]_o$ (K_{ex}(MLA)=6.9[4]) and $[M^+] = [M]_t - [M]_{o,t}$. The equilibrium constants obtained from these data are summarized in Table 1.

Table 1. Equilibrium Constants at 25 °C

$K_{D,L}$		15C5 0.15[6][5]		B15C5 20[6]	
		L	L′	Tl^+	Rb^+
$\log K_{ex}$(MLL′A)	15C5	TBP		1.58	0.56[7]
	B15C5	TBP		1.17	0.37[6]
	B15C5	B15C5		1.95	1.22[6]
$\log K_{MLL'A,o}$[a]	15C5	TBP		0.17	0.81[7]
	B15C5	TBP		0.33	1.32[6]
	B15C5	B15C5		1.11	2.17[6]

a) $K_{MLL'A,o} = [MLL'A]_o/[MLA]_o[L']_o$.

By way of example, for the crown ether-TBP mixed system, D values of Tl(I) are 4.6×10^{-3} ($[15C5]_t = 2.9\times10^{-2}$ M (1 M=1 mol dm^{-3}), $[Tl]_t = 2.0\times10^{-3}$ M, $[HA]_t = 5.6\times10^{-4}$ M, $[TBP]_t = 3.2\times10^{-1}$ M) and 2.1×10^{-3} ($[B15C5]_t = 4.0\times10^{-3}$ M, $[Tl]_t = 2.0\times10^{-3}$ M, $[HA]_t = 4.5\times10^{-4}$ M, $[TBP]_t = 3.3\times10^{-1}$ M). This shows that only a slight amount of Tl(I) ((0.2—0.5)%) is extracted into a benzene phase.

Ionic radius of Tl^+ (1.50 Å[8]) is nearly equal to that of Rb^+ (1.49 Å[8]). Thallium(I), however, is much more extracted into benzene than Rb^+ with mixtures of crown ether and TBP. Mixtures of 15C5 and TBP are more effective for extraction of Tl^+ than those of B15C5 and TBP.

The crown ether complex with thallium picrate (1:1:1) accepts one TBP molecule. From the structure of the crown ether complex with Tl^+ held in the cavity, a picrate anion- and a TBP molecule-contact are possible in respective directions perpendicular to the plane of the ring.

$K_{MLL'A,o}$ designates adduct-formation constant of a MLA complex with L′ in a benzene solution. It is seen from $\log K_{MLL'A,o}$ values in Table 1 that extractability of Tl^+ is slightly enhanced by the addition of TBP. Since Tl^+ and Rb^+ have nearly equal sizes, 15C5 and B15C5 complexes with Tl^+ are expected to be similar in size and shape to those with Rb^+, respectively; in addition, free energy of hydration of Tl^+ (343 kJ mol^{-1} [9]) is much the same as that of Rb^+ (320 kJ mol^{-1} [9]); however, $\log K_{MLL'A,o}$ values of Tl^+ are relatively smaller than those of Rb^+. This cannot clearly be explained at the present time.

When L′=TBP, $\log K_{MLL'A,o}$ value of Tl^+ for B15C5 is larger than that for 15C5. The same tendency was observed for Rb^+ and Cs^+.[6] Benzo-15-crown-5 has two aromatic ether oxygen atoms. It thus appears that electron density in the B15C5 cavity is lower than that in the 15C5 cavity. Consequently, surface charge density of an exposed part of the metal ion trapped in the cavity may be lower for 15C5 than for B15C5. This is responsible for the larger $\log K_{MLL'A,o}$ value of B15C5 than that of 15C5. A Tl(B15C5)$_2$A complex is more stable than a Tl(B15C5)(TBP)A complex in a benzene solution. This may be attributed to the fact that B15C5 has more donor oxygen atoms than TBP.

References

1) Y. Takeda, "The Solvent Extraction of Metal Ions by Crown Compounds, Host Guest Complex Chemistry III," Springer-Verlag, Topics in Current Chemistry, Vol. 121, Heidelberg, (1984), Chap. 1.

2) Y. Takeda, *Bull. Chem. Soc. Jpn.*, **56**, 2589 (1983).

3) "Dissociation Constants of Organic Acids in Aqueous Solution," ed by G. Kortün, W. Vogel, and K. Andrussov, Butterworths, London (1961).

4) Y. Takeda, M. Nemoto, and S. Fugiwara, *Bull. Chem. Soc. Jpn.*, **55**, 3438 (1982).

5) Y. Takeda and H. Kato, *Bull. Chem. Soc. Jpn.*, **52**, 1027 (1979).

6) Y. Takeda, Y. Wada, and S. Fujiwara, *Bull. Chem. Soc. Jpn.*, **54**, 3727 (1981).

7) Y. Takeda, *Bull. Chem. Soc. Jpn.*, **54**, 526 (1981).

8) R. D. Shannon and C. T. Prewitt, *Acta Crystallogr., Sect. B*, **25**, 925 (1969).

9) H. L. Friedman and C. V. Krishnan, "Water," ed by F. Franks, Plenum, New York (1973), Vol. 3, p. 55.

The Crystal and Molecular Structures of Bis[1,2-bis(methylthio)vinylenedithio]-tetrathiafulvalene (TMTVT)

Hideyuki NAKANO, Takashi NOGAMI,* Yasuhiko SHIROTA, Shigeharu HARADA, and Nobutami KASAI

Department of Applied Chemistry, Faculty of Engineering, Osaka University, Yamadaoka, Suita, Osaka 565

(Received January 5, 1989)

Synopsis. An X-ray crystal structure analysis of the title molecule (TMTVT) was made. The central portion of tetrathio-TTF was shown to be almost planar, and the outer portions of the two bis(methylthio)vinylenes are bent toward opposite directions each other. TMTVT molecules form a columnar stack toward the *c*-axis with equal intermolecular spacings.

Bis(ethylenedithio)tetrathiafulvalene (BEDT-TTF) is known to give several ambient presssure organic superconductors.[1] The most characteristic feature of BEDT-TTF salts is their two-dimensional electrical properties, which arise from S····S contacts that are shorter than the van der Waals distance between adjacent donor molecules in the crystal.[2] This crystal structure results in a suppression of a Peierls transition inherent in a one-dimensional system. TTF derivatives possessing multi-chalcogen atoms are attractive donor molecules, because they are expected to give complexes which are highly conductive down to low temperatures; this is a prerequisite for realizing organic superconductors. We have synthesized several TTF derivatives possessing eight or twelve chalcogen atoms.[3-7] This paper reports on an X-ray crystal structure analysis of bis[1,2-bis(methylthio)vinylenedithio]-tetrathiafulvalene (TMTVT) which has the largest number of sulfur atoms (twelve)[5] in the TTF-derivatives ever known.

Experimental

$C_{14}H_{12}S_{12}$, M 565.04, monoclinic, space group $P2_1/n$, a=7.939(1), b=28.302(2), c=5.067(1) Å, β=95.74(1)°, V=1132.8(2) Å^3, D_c=1.657 g cm^{-3} for Z=2. The crystal used had a needle shape with 0.04×0.16×0.46 mm^3. Reflection intensities were measured by the θ-2θ scan technique up to 2θ=120° on a Rigaku rotating anode four-circle diffractometer using nickel-filtered Cu $K\alpha$ radiation. The scan rate was 4° min^{-1} and the scan width $\Delta\theta$=(1.4+0.15 tan θ)°. Backgrounds were counted for 3 s at both ends of each scan. No significant intensity decay of the standard reflections, which were measured after every 100 reflections, was detected. Of the 1997 reflections measured, 1564 were observed ($|F_o|>2\sigma(F_o)$). The usual Lorentz and polarization corrections were applied, but no absorption correction was made [μ(Cu $K\alpha$)=102.8 cm^{-1}].

Structure Solution and Refinement

The structure was solved by a direct method (*MULTAN* 78),[8] and was refined anisotropically by a block-diagonal least-squares procedure (*HBLS* V).[9] The function minimized was $\sum\omega(\Delta F)^2$. The weighting function used in the final stage of the refinement was $\omega=[\sigma^2(F_o)-0.0826|F_o|+0.0166|F_o|^2]^{-1}$. The hydrogen atoms could not be found on a D-map, which is probably due to either the rotation or the large amplitude of vibration of the methyl group. Therefore, the hydrogen atoms were not included in the final refinement. Atomic scattering factors were taken from those of International Tables for X-Ray Crystallography.[10] The final R index was 0.091. The atomic coordinates and equivalent isotropic temperature factors[11] are given in Table 1.† Bond lengths and bond angles are shown in Fig. 1, and the crystal structures in Figs. 2 and 3.

Table 1. Atomic Parameters of Nonhydrogen Atoms with Equivalent Isotropic Temperature Factors[11]

Atom	x	y	z	B_{eq}/Å^2
C(1)	0.9558(5)	0.0132(1)	0.0785(9)	3.77
C(2)	0.7200(5)	0.0521(1)	0.320(1)	3.84
C(3)	0.8654(5)	0.0710(1)	0.429(1)	4.09
C(4)	0.5610(6)	0.1337(2)	0.388(1)	4.42
C(5)	0.7065(6)	0.1530(2)	0.494(1)	4.30
C(6)	0.3231(9)	0.1415(3)	−0.051(1)	7.01
C(7)	0.9400(8)	0.2188(3)	0.350(2)	7.6
S(1)	0.7329(1)	0.01139(4)	0.0630(3)	4.14
S(2)	1.0537(1)	0.05421(4)	0.3074(3)	4.31
S(3)	0.5240(1)	0.07249(4)	0.3995(3)	4.29
S(4)	0.8665(2)	0.11692(5)	0.6626(3)	4.61
S(5)	0.3871(2)	0.16848(6)	0.2647(4)	5.99
S(6)	0.7490(2)	0.21363(5)	0.5121(4)	6.10

Results and Discussion

The TMTVT molecules are on the centers of symmetry. The central tetrathio-TTF portion of the TMTVT molecule is approximately planar; this plane is almost perpendicular to the b-c plane. Two bis(methylthio)vinylene portions at both ends of the molecule are bent toward opposite directions from each other (Fig. 1(b)). Both BEDT-TTF[14] and bis(vinylenedithio)tetrathiafulvalene (VT)[15] possess planar structures only at the central tetrathioethylene portion. Comparing the molecular structure of TMTVT with those of BEDT-TTF and VT, the central planar portion is extended more widely in the former molecule. The crystal structure is characterized by a face-to-face stack of TMTVT molecules toward the c-axis with equal intermolecular spacings (Fig. 2(a)). The interplanar distance between adjacent molecules is 3.53 Å. S····S contacts [3.700(3) Å] almost equal to the van der Waals radius (3.7 Å) are found between methylthio groups of TMTVT molecules belonging to the adjacent stacks [S(5)(x,y,z)····S(6)

† Tables of anisotropic thermal parameters and observed and calculated structure factors are kept at the Chemical Society of Japan, Document No. 8880.

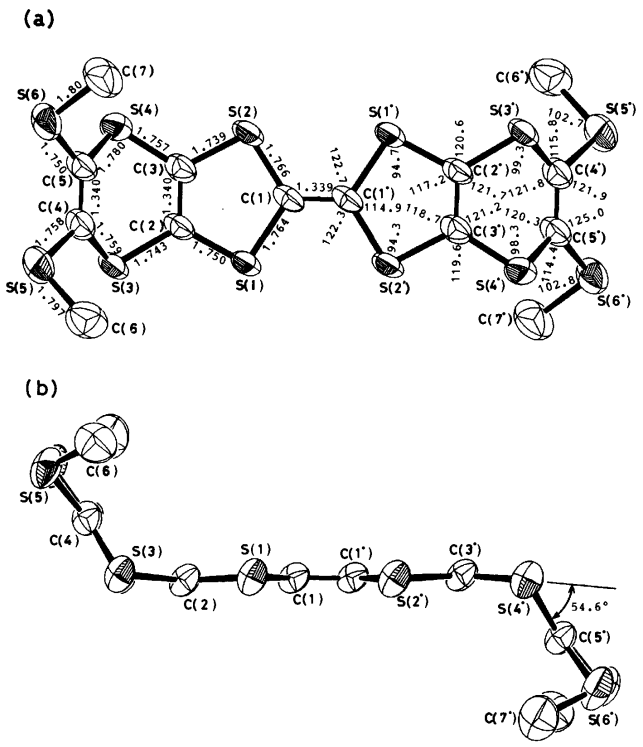

Fig. 1. Molecular structure of TMTVT.[12] (a) Over view, (b) side view. Nonhydrogen atoms are drawn as thermal ellipsoids with 50% probability level. Estimated standard deviations of the bond lengths and angles are 0.005—0.01 Å and 0.3—0.4°, respectively.

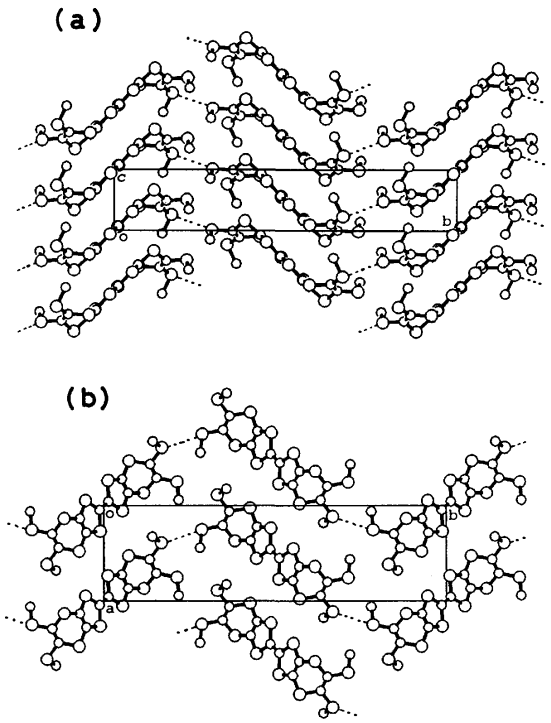

Fig. 2. Crystal structure of TMTVT[13] projected along the *a* axis (a) and the *c* axis (b). Dotted line indicates intermolecular S····S contact almost equal to the van der Waals distance (3.7 Å).

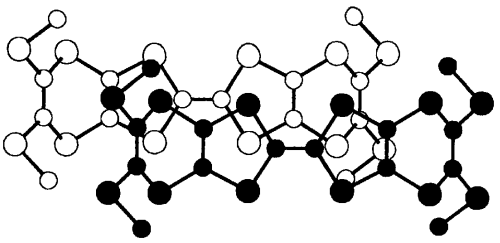

Fig. 3. Overlap of two TMTVT molecules.[13]

$(-0.5+x,0.5-y,-0.5+z)$], and are shown by dotted lines in Fig. 2. All of the other S····S distances are longer than the van der Waals radius. Figure 2(b) shows a side-by-side arrangement of molecules of equal height. All of the side-by-side S····S distances are longer than the van der Waals radius, unlike the cases of BEDT-TTF salts.[2] Figure 3 shows the overlap of two TMTVT molecules projected normal to the molecular plane. The two molecules shift with each other in order to avoid direct overlap of carbon and sulfur atoms between them.

We are grateful for Protein Engineering Center, Institute for Protein Research, Osaka University, for the use of the diffractometer and ACOS S850 computer.

References

1) H. Urayama, H. Yamochi, G. Saito, K. Nozawa, T. Sugano, M. Kinoshita, S. Sato, K. Oshima, A. Kawamoto, and J. Tanaka, *Chem. Lett.*, **1988**, 55.

2) J. M. Williams and K. Carneiro, *Adv. Inorg. Chem. Radiochem.*, **29**, 249 (1985).

3) K. Inoue, Y. Tasaka, O. Yamazaki, T. Nogami, and H. Mikawa, *Chem. Lett.*, **1986**, 781.

4) T. Nakamura, S. Iwasaka, H. Nakano, K. Inoue, T. Nogami, and H. Mikawa, *Bull. Chem. Soc. Jpn.*, **60**, 365 (1987).

5) H. Nakano, T. Nakamura, T. Nogami, and Y. Shirota, *Chem. Lett.*, **1987**, 1317.

6) T. Nogami, *Jpn. J. Appl. Phys., Series 1, Superconducting Materials*, **1988**, 197.

7) H. Nakano, T. Nogami, and Y. Shirota, *Bull. Chem. Soc. Jpn.*, **61**, 2973 (1988).

8) P. Main, S. E. Hull, L. Lessinger, G. Germain, J.-P. Declercq, and M. M. Woolfson, *MULTAN* 78, "A System of Computer Programs for the Automatic Solution of Crystal Structures from X-Ray Diffraction Data," Univ. of York, England and Louvain, Belgium, 1978.

9) T. Ashida, *HBLS* V, The Universal Crystallographic Computing System-Osaka, The Computation Center, Osaka University, 1979, p. 53.

10) "International Tables for X-Ray Crystallography," Kynoch Press, Birmingham, England, Vol. IV, (1974), p. 71.

11) W. C. Hamilton, *Acta Crystallogr.*, **12**, 609 (1959).

12) C. K. Johnson, *ORTEP II*, Report ORNL-5138, Oak Ridge National Laboratory, Tennessee, 1976.

13) W. D. S. Motherwell and W. Clegg, *PLUTO* 78, Program for Plotting Crystal and Molecular Structures, University of Cambridge, England, 1978.

14) H. Kobayashi, A. Kobayashi, Y. Sasaki, G. Saito, and H. Inokuchi, *Bull. Chem. Soc. Jpn.*, **59**, 301 (1986).

15) H. Kobayashi, A. Kobayashi, T. Nakamura, T. Nogami, and Y. Shirota, *Chem. Lett.*, **1987**, 559.

The Molecular Structure of a Schiff Base Complex, [*N,N'*-Ethylenebis-(1-phenyl-2-imino-1-butanonato)](acetonitrile)-manganese(III) Perchlorate

Duanjun Xu,* Banglin Chen, Ke Chen, Chaorong Chen,
Kunio Miki,*,† and Nobutami Kasai†
Department of Chemistry, Zhejiang University, Hangzhou, China
†Department of Applied Chemistry, Faculty of Engineering, Osaka University, Yamadaoka, Suita, Osaka 565
(Received February 15, 1989)

Synopsis. The molecular structure of a novel Schiff base complex, [*N,N'*-ethylenebis(1-phenyl-2-imino-1-butanonato)]-(acetonitrile)manganese(III) perchlorate has been determined by X-ray diffraction method. The molecule has an elongated octahedral geometry around the metal atom.

A number of studies have been reported on the crystal structures of *N,N'*-bis(1-methyl-3-oxobutylidene)ethylenediamine type Schiff base complexes of transition metals such as Cu(II), Co(II), and V(II).[1] The chemical behavior of the Schiff base complexes of Mn(III) has also been paid attention because of important roles in some biochemical processes, e.g. in manganesesuperoxide dismutase[2,3] and pseudocatalase[4] which are known to contain Mn(III) ions. The structure of Mn(III) complex, [Mn(acen)Cl] containing a tetradentate *N,N'*-ethylenebis(4-imino-2-pentanonato) ligand (abbreviated to acen and formerly called *N,N'*-ethylenebis(acetylacetone iminato)), has been determined by X-ray analysis.[5] In this paper we describe the preparation and molecular structure of a novel Mn(III) Schiff base complex, [Mn(bzacen)(CH_3CN)(ClO_4)] containing a similar tetradentate *N,N'*-ethylenebis(1-phenyl-2-imino-1-butanonato) ligand (abbreviated to bzacen and formerly called *N,N'*-ethylenebis(benzoylacetone iminato)).

Experimental

The Schiff base, H_2bzacen and $Mn(C_2H_3O_2)_3\cdot 2H_2O$ were prepared as described previously.[6,7] A mixture of H_2bzacen and $Mn(C_2H_3O_2)_3\cdot 2H_2O$ was refluxed in 2-propanol for 3 h. The resulting precipitate was washed with 2-propanol and dissolved in methanol, to which aqueous solution of sodium perchlorate was added. Red thin-plate crystals were obtained by recrystallization from a mixed solution of benzene and acetonitrile.

Crystal Data. [$Mn(C_{22}H_{22}O_2N_2)(CH_3CN)(ClO_4)$], M=541.44, orthorhombic, space group *Pnma*, a=9.077(1), b=15.563(1), c=17.205(2)Å, U=2430.5 Å^3, Z=4, D_c=1.48 g cm^{-3}, D_m=1.49 g cm^{-3}, μ(Mo $K\alpha$)=7.3 cm^{-1}.

A well-shaped crystal was mounted on an Enraf-Nonius CAD4 diffractometer. Accurate unit-cell parameters were determined by the least-squares fit of 2θ values of 25 strong reflections. Integrated intensities were collected by the θ-2θ scan technique with the scan rate of 5.5° min^{-1} and the scan width of $\Delta 2\theta=(1.2+0.7\tan\theta)°$. The scan was repeated with a slower rate for weak reflections. A total of 2552 independent reflections was obtained within $2°<2\theta<52°$. Intensity data were corrected for usual Lp effects but absorption and extinction corretions were ignored.

The structure was solved by the heavy atom method. The systematic absences suggested that the possible space group is either *Pnma* or $Pn2_1a$. When the space group is assumed as

Table 1. Fractional Atomic Coordinates and Equivalent Isotropic Thermal Parameters of Non-H Atoms with e.s.d.'s in Parentheses

Atom	x	y	z	B_{eq}[a]/Å^2
Mn	0.1787(3)	0.25	0.0350(2)	3.2
O	0.0903(9)	0.1641(5)	0.0969(5)	4.1
N	0.2759(9)	0.1659(6)	−0.0321(5)	3.2
C(1)	0.269(1)	0.0815(8)	−0.0248(6)	3.4
C(2)	0.185(1)	0.0414(7)	0.0340(6)	3.4
C(3)	0.102(1)	0.0816(7)	0.0888(6)	2.8
C(4)	0.021(1)	0.0324(7)	0.1502(6)	2.6
C(5)	0.013(1)	−0.0579(7)	0.1508(7)	3.7
C(6)	−0.058(1)	−0.0983(7)	0.2106(7)	4.4
C(7)	−0.123(1)	−0.0537(9)	0.2699(7)	5.2
C(8)	−0.119(1)	0.0330(9)	0.2696(7)	5.2
C(9)	−0.049(1)	0.0775(8)	0.2086(6)	3.6
C(10)	0.356(1)	0.0236(9)	−0.0786(7)	4.7
C(11)	0.367(2)	0.2040(9)	−0.0910(9)	6.3
Cl	−0.1898(6)	0.25	−0.0495(4)	5.3
O(1A)	−0.030(1)	0.25	−0.0533(8)	5.9
O(2A)	−0.241(2)	0.25	−0.1295(10)	10.1
O(3A)	−0.237(1)	0.1765(6)	−0.0092(7)	7.7
C(1S)	0.667(3)	0.25	0.1727(17)	10.3
C(2S)	0.520(3)	0.25	0.1415(14)	7.0
N(1S)	0.399(2)	0.25	0.1194(9)	5.5

a) As defined by Hamilton.[10]

Pnma considering the molecular symmetry of the present complex, the structure was reasonably solved. All the nonhydrogen atoms were refined anisotropically and the hydrogen atoms except for those of the methyl group were included in the structure factor calculation. The refinement of structure was carried out by the block-diagonal least-squares procedures using the *HBLS*-V program.[8] The final refinement converged the R and R_w factors to 0.084 and 0.106 for 999 observed reflections ($|F_o|>3\,\sigma(|F_o|)$), respectively. The weighting scheme used is $w=(\sigma^2+a|F_o|+b|F_o|^2)^{-1}$ where a and b used in the final refinement cycles are 0.2237 and 0.0003, respectively. The atomic scattering factors were taken from the International Tables for X-ray Crystallography.[9] The final atomic parameters are listed in Table 1.†

Results and Discussion

The molecular structure of the title complex is shown in Fig. 1 together with atomic numbering system. Bond distances and angles are listed in Table 2. During the course of the structure analysis, both ClO_4 anion and the CH_3CN solvent molecule were found to be coordinated to the Mn(III) atom. The molecule has crystallographic C_s symmetry, in which the Mn(III) atom is located onto a mirror plane together with atoms of two axial ligands, Cl, O(1A), O(2A), C(1S), C(2S), and N(1S).

The coordination geometry around the Mn(III) atom is elongated octahedral as expected for a high spin d^4 metal ion due to the Jahn-Teller effet. In the equatorial plane, the tetradentate bzacen ligand is coordinated to the metal atom with bond distances of Mn–O=1.889(9) and Mn–N=1.955(10) Å, which agree with the average values of the similar complex.[5] The bond distances between the Mn(III) atom and the axial ligands, Mn–O(1A)[2.44(2) Å] and Mn–N(1S)[2.47(2) Å] are about 0.5 Å longer than the corresponding distances between the metal and the bzacen ligand in the equatorial plane. The ClO_4 anion and CH_3CN molecule are semi-coordinated to the metal atom from

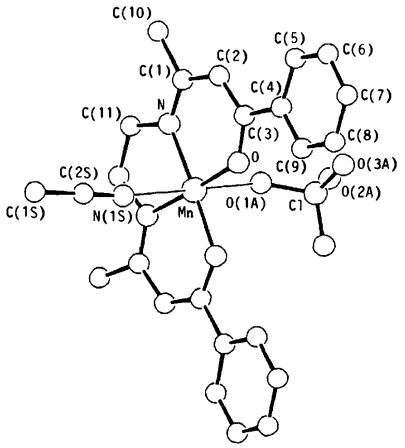

Fig. 1. The molecular structure of [Mn(bzacen)-(CH_3CN)(ClO_4)] together with atomic numbering system.

Table 2. Bond Distances and Angles for Non-H Atoms with e.s.d.'s in Parentheses

(a) Bond distance/Å			
Mn–O	1.889(9)	Mn–N	1.955(10)
Mn–O(1A)	2.43(2)	Mn–N(1S)	2.47(2)
N–C(1)	1.32(2)	N–C(11)	1.44(2)
C(1)–C(2)	1.41(2)	C(1)–C(10)	1.51(2)
C(2)–C(3)	1.36(2)	C(3)–O	1.30(2)
C(3)–C(4)	1.50(2)	C(4)–C(5)	1.41(2)
C(4)–C(9)	1.38(2)	C(5)–C(6)	1.37(2)
C(6)–C(7)	1.37(2)	C(7)–C(8)	1.35(2)
C(8)–C(9)	1.41(2)	C(11)–C(11′)	1.43(4)
C(1S)–C(2S)	1.44(4)	C(2S)–N(1S)	1.16(3)
Cl–O(1A)	1.46(2)	Cl–O(2A)	1.45(2)
Cl–O(3A)	1.40(1)		
(b) Bond angle/°			
O–Mn–N	92.9(4)	O–Mn–N′	177.0(4)
O–Mn–O′	90.1(4)	N–Mn–N′	84.1(4)
O–Mn–O(1A)	91.3(5)	N–Mn–O(1A)	89.0(5)
O–Mn–N(1S)	90.7(5)	N–Mn–N(1S)	89.0(5)
O(1A)–Mn–N(1S)	177.3(6)	Mn–O–C(3)	127.3(8)
Mn–N–C(1)	126.2(9)	Mn–N–C(11)	113.5(9)
C(1)–N–C(11)	120(1)	N–C(1)–C(2)	122(1)
N–C(1)–C(10)	121(1)	C(2)–C(1)–C(10)	117(1)
C(1)–C(2)–C(3)	127(1)	C(2)–C(3)–C(4)	122(1)
O–C(3)–C(2)	125(1)	O–C(3)–C(4)	113(1)
N–C(11)–C(11′)	114(1)	C(1S)–C(2S)–N(1S)	177(3)
O(1A)–Cl–O(2A)	106(1)	O(1A)–Cl–O(3A)	109(1)
O(2A)–Cl–O(3A)	112(1)	O(3A)–Cl–O(3A′)	109(1)

† The tables for anisotropic temperature factors of nonhydrogen atoms, for atomic coordinates of hydrogen atoms, and for observed and calculated structure factors are deposited as Document No. 8882 at the Office of the Editor of Bull. Chem. Soc. Jpn.

both apical sites. This six-coordinate octahedral geometry in the present complex is in contrast with the five-coordinate square-pyramidal structure in [Mn(acen)Cl].[5] The coordination ability of the solvent molecule may affect the resulted structure of the present complex.

Bond distances and angles in the chelate ligand agree within experimental errors, with the values reported hitherto in the similar complexes.[1,5] As observed in the tetradentate acen ligand in Schiff base complexes, the delocalization of double bonds within the N–C(1)–C(2)–C(3)–O chelate ring is also observed in this bzacen ligand. The bridging CH_2–CH_2 bond distance in this ligand, C(11)–C(11′)=1.43(4) Å is somewhat shorter than the expected value. Similar shortened CH_2–CH_2 distances observed in the acen ligand were reported in the Mn(III)[5] and V(IV)[11] complexes [1.40(1) and 1.42(3) Å, respectively].

All the atoms except for two phenyl groups in the bzacen ligand are coplanar with the Mn(III) atom, the maximum atomic deviation from the least-squares plane being 0.03 Å. The plane of the phenyl group is also almost included in the co-plane of the chelate atoms of the bzacen ligand. The dihedral angle between these two planes is only 6.8°.

References

1) M. Calligaris, G. Nardin, and L. Randaccio, *Coord. Chem. Rev.*, **7**, 385 (1972).
2) B. B. Keele, Jr., J. M. McCord, and I. Fridovich, *J. Biol. Chem.*, **245**, 6176 (1970).
3) J. J. Villafranca, F. J. Yost, Jr., and I. Fridovich, *J. Biol. Chem.*, **249**, 3532 (1974).
4) Y. Kono and I. Fridovich, *J. Biol. Chem.*, **258**, 6015 (1983).
5) L. J. Boucher and V. E. Day, *Inorg. Chem.*, **16**, 1360 (1977).
6) P. J. McCarthy, R. J. Hovey, K. Uno, and A. E. Martell, *J. Am. Chem. Soc.*, **77**, 5829 (1955).
7) E. I. Heiba. R. M. Dessau, and W. J. Koehl, Jr., *J. Am. Chem. Soc.*, **91**, 138 (1969).
8) T. Ashida, *HBLS*-V, The Universal Crystallographic Computing System-Osaka, The Computation Center, Osaka Univ., (1979), p. 53.
9) International Tables for X-ray Crystallography, Vol. IV, p. 71 (1974).
10) W. C. Hamilton, *Acta Crystallogr.*, **12**, 609 (1959).
11) D. Bruins and D. L. Weaver, *Inorg. Chem.*, **9** 130 (1970).

Adsorption-Assisted Desorption and Cross Desorption of CO and H_2 on Nickel Polycrystalline Surfaces

Taro YAMADA,*,† Runsheng ZHAI,†† Yasuhiro IWASAWA, and Kenzi TAMARU†††
Department of Chemistry, Faculty of Science, The University of Tokyo, 7-3-1 Hongo, Bunkyo-ku, Tokyo 113
†The Institute for Solid State Physics, The University of Tokyo, 7-22-1 Roppongi, Minato-ku, Tokyo 106
††Dalian Institute of Chemical Physics, Chinese Academy of Sciences, 129 Street, Dalian, Liaoning Province, People's Republic of China
†††Science University of Tokyo, 1-3 Kagurazaka, Shinjuku-ku, Tokyo 162
(Received February 18, 1989)

Synopsis. The rates of adsorption and desorption during co-adsorption process of CO and H_2 on the Ni polycrystalline surface were measured. The desorption rate of CO(a) was enhanced by the presence of CO(g) or H_2(g) in the gas phase. The desorption rate of adsorbed hydrogen was accelerated by CO(g) but not by H_2(g).

A series of our previous works on the adsorption process of CO

$$\mathrm{CO(g)} \underset{v_-}{\overset{v_+}{\rightleftarrows}} \mathrm{CO(a)} \qquad (1)$$

on several group-VIII metal surfaces has shown that the absolute desorption rate v_- is almost proportional to the ambient CO pressure while the adsorption is actually proceeding.[1-6] There is a great enhancing contribution by gas-phase molecules to the desorption rate process—"adsorption-assisted desorption"(AAD)—besides the thermal desorption.

This time we took the same approach for co-adsorption of CO and H_2 on nickel polycrystalline surfaces. Adsorption of CO and H_2 on group-VIII metal surfaces was investigated in relation with the mechanism of methanation etc.[7-14] However there are few cases in which the dynamics of adsorption and desorption were mesured while the adsorption process is actually going on. We studied adsorption-desorption kinetics of the co-adsorption of CO and H_2 on Ni polycrystalline surfaces during the adsorption process.

The adsorption rate v_+ and the desorption rate v_- of CO and H_2 are mathematically divided into 16 components as functions of the surface concentration of CO(a) and H(a), N_{CO} and N_H, and the gas-phase pressures P_{CO} and P_{H_2}. For example, the important components of the desorption rate of CO are:

$$\begin{aligned} v^{CO}_- = {} & v^{CO}_-(N_{CO}) && \text{: thermal desorption} \\ & + v^{CO}_-(N_{CO}, P_{CO}) && \text{: AAD} \\ & + v^{CO}_-(N_{CO}, P_{H_2}) && \text{: cross desorption by } H_2\text{(g)} \\ & + v^{CO}_-(N_{CO}, N_H) && \text{: surface effect by H(a)} \\ & + (12 \text{ other components}) && \end{aligned} \qquad (2)$$

where each $v^{CO}_-(*,*)$ falls zero when any one of the variables inside parentheses is zero.

The values of those components are obtained by measuring the amounts of the surface species as functions of time. Each component is distinguished by gas-switching technique between corresponding molecules. This technique is the extended version of the "isotope-jump method".[1] The rates are calculated from the change of the surface concentrations of the adsorbates measured by the flash desorption at each point of time. We expected changes in the rate of desorption of H(a) by CO(g), and vice versa, as well as ADD of CO and H_2. We call these phenomena the "cross desorption". It is distinguished from ADD, in which the desorption of the surface species is enhanced by the same species in the gas phase. In this paper we mainly mention about the desorption processes. The adsorption rates were difficult to measures precisely enough in some cases.

Experimental

Experiments were performed in an ultrahigh vacuum apparatus equipped with a mass spectrometer (MS), a sample temperature programmer, an Auger electron spectrometer, etc.[1] Several pieces of Ni foil (0.03 mm thickness, 1.4 cm^2 total area) were used as the samples. The surfaces were cleaned by Ar ion bombardment and annealing. The gas samples were $^{12}C^{16}O$, $^{12}C^{18}O$, H_2 and D_2 obtained from commercial vessels. The procedures of gas-switching experiments were as follows. Details in calibration and calculation procedures are describe elsewhere.[1]

(1) Clean up the surface by flashing up to 800 K.
(2) Keep the sample at the desired temperature/K.
(3) At time $t=0$, start introducing Gas 1 (the species to leave on the surface) at the desired pressure P_1/Pa.
(4) At time $t=t_1$, stop introducing Gas 1, and, at the same time, start introducing Gas 2 (The gas-phase species) at pressure P_2/Pa.
(5) At time $t=t_1+t_2$, flash the sample and record the flash-desorption trace of the desired species by MS.

For each pair of Gases 1 and 2, measurements were done at various T, P_1, P_2, t_1, and t_2, and the surface concentrations of Gases 1 and 2 (N_{CO} and N_H/N_D/molecules·cm^{-2}) were obtained from the peak ares of flash desorption in (5).

The obtained surface concentrations N's were plotted as functions of t_2 with fixed T, P, and t_1. These t_2–N curves were numerically curve-fitted to exponential functions, and the differerential conefficients at $t=t_1+0$ were calculated. These differential coefficients i.e. the slopes of the tangents at the right side of t_1 are the rates of adsorption of the "Gas 2" species, and the rates of desorption (negatively signed) of the "Gas 1" species. In some cases precise determination of adsorption rate was not possible because of the background gas pressure. We mainly focussed on the desorption rates.

Results and Discussion

1. Gas 1=$^{12}C^{18}O$, Gas 2=$^{12}C^{16}O$ {$v^{CO}_\pm(N_{CO}, P_{CO})$}. The kinetics of absorption of CO without H_2(g) were

examined. We can measure the absolute rates of adsorption and desorption of CO by distinguishing Gases 1 and 2 using isotope-labelled molcules. The absolute rates of adsorption and desorption are dependent on the surface concentration N_{CO} and the gas-phase pressure P_{CO}.[4] The absolute adsorption rate $v^{CO}{}_+$ is a nonlinear function of N_{CO} and proportional to P_{CO}. The initial adsorption rate ($v^{CO}{}_+$ when $N_{CO}=0$) is independent of the temperature T between 329 K and 394 K. The desorption rate $v^{CO}{}_-$ is greatly affected by the gas-phase pressure of CO:

$$v^{CO}{}_- = \mu_{CO} N_{CO} = (\mu_{CO}{}^0 + k_{CO} P_{CO}) N_{CO}. \quad (3)$$

Figure 1 shows the rate constant μ_{CO} as a function of P_{CO} and T. The rate constant at $P_{CO}=0$, $\mu_{CO}{}^0$, corresponds to the thermal desorption process, the pressure-dependent part of the rate constant is proportional to P_{CO}. We call this kind of kinetics "adsorption-assisted desorption (AAD)".[1-6] So far we have proposed several models to elucidate the mechanism of acceleration of the desorption by the effect of the gas phase.[14]

2. Gas 1=D_2, Gas 2=H_2{$v^{H_2}{}_\pm(N_H, P_{H_2})$}. Whether AAD is applicable for gases other than CO is an attractive question.[15,16] The absolute rates of adsorption and desorption of H_2 only were measured in the same manner as CO by using H_2 and D_2. The species desorbed by flash desorption procedure are H_2, HD, and D_2. The amounts of H(a) and D(a) were calculated by summing the areas of those three peaks. The absolute adsorption rate $v^{H_2}{}_+$ was a nonlinear function of N_D and proportional to P_{H_2}. It decreased with increasing temperature T. Figure 2 shows the absolute desorption rate $v^D{}_-$ as a function of N_D and P_{H_2}. It is approximately proporitional to $(N_D)^2$ in the high coverage region. $v^D{}_-$ did not change when the pressure P_{H_2} changed. Namely, AAD did not occur in the case of H_2 on Ni.

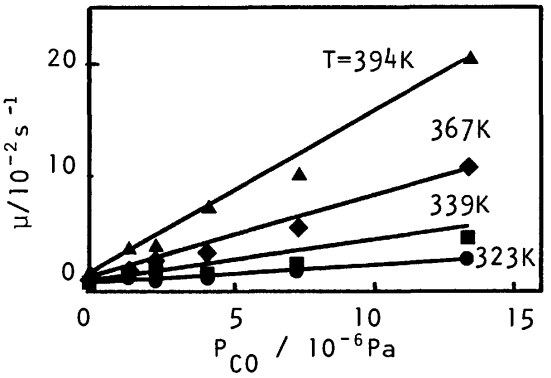

Fig. 1. The absolute desorption rate constant of CO, μ, as a function of pressure P_{CO} and temperature T.

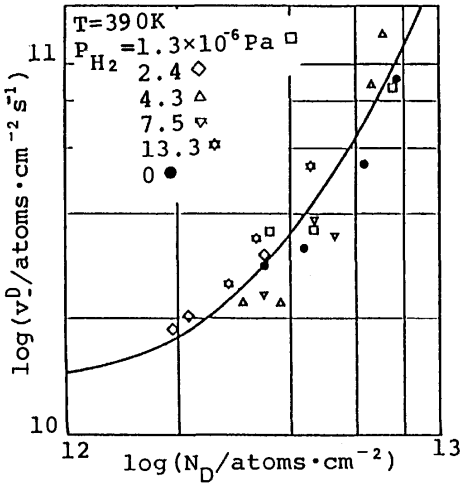

Fig. 2. The absolute desorption rate of D(a), $v^D{}_-$, as a function of the surface concentration N_D and pressure P_{H_2}.

3. Gas 1=CO, Gas 2=H_2{$v^{H_2}{}_+(N_{CO}, P_{H_2})$ and $v^{CO}{}_-(N_{CO}, P_{H_2})$}. If Gas 2 is a different chemical species from Gas 1, we see the effects of the adlayer of Gas 1 on the adsorption of Gas 2, and the effects of Gas 2 in the gas phase on the desorption from the adlayer of Gas 1. Replacement of the adsorbates in the equilibrium condition is trivial and well recognized. We observe the effects of the gas phase molecules on the desorption kinetics. In the present case the gas-phase species is H_2, and the adlayer species is CO. It was difficult to calculate $v^{H_2}{}_+$ precisely, as the amount of H(a) was suppressed by coexistence fo CO. The adsorption step of H_2(g) ($v^{H_2}{}_+$) was strongly poisoned by CO(a).

The desorption of CO(a) was weakly enhanced by H_2(g). Figure 3 shows CO(a) (N_{CO}) decreasing after the gas phase was switched to H_2. It decreased a little bit faster at $P_{H_2}=1.3\times10^{-4}$ Pa than a $P_{H_2}=0$, i.e. $v^{CO}{}_-(N_{CO}, P_{H_2})>0$. The "cross desorption" of CO(a) by H_2(g) was demonstrated in this experiment.

4. Gas 1=D_2, Gas 2=CO{$v^{CO}{}_+(N_D, P_{CO})$ and $v_-(N_D, P_{CO})$}. The reverse case of 3. was examined. The adsorption rate of CO was almost indifferent of the surface concentration of D(a) at temperatures higher than 329 K. The result was almost the same as the data of the absolute adsorption rate.[5]

Figure 4 shows the desorption rate of D, $v^D{}_-$, as a function of N_D and P_{CO}. In Fig. 4, $v^D{}_-$ is fitted to second-order functions of N_D, that is,

$$v^D{}_- = \mu_D (N_D)^2 \quad (4)$$

Cross desorption of D(a) by CO(g) is obvious in this

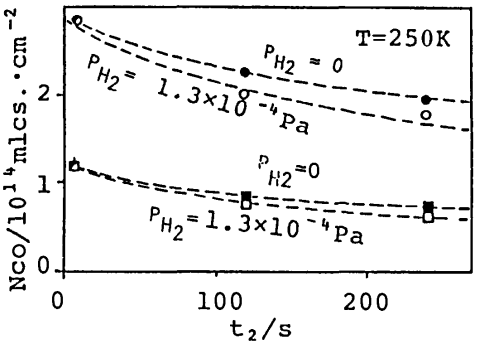

Fig. 3. The surface concentration of CO(a), N_{CO}, as a function of time t_2 with ambient H_2 molecules at pressure P_{H_2} for two initial N_{CO}'s.

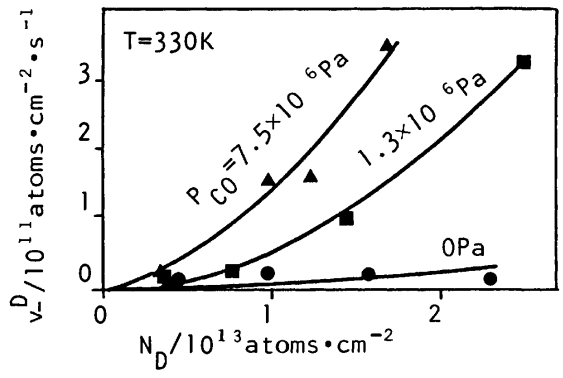

Fig. 4. The desorption rate of D(a), v^D_-, as a function of the surface concentration of D(a), N_D, and pressure of CO, P_{CO}.

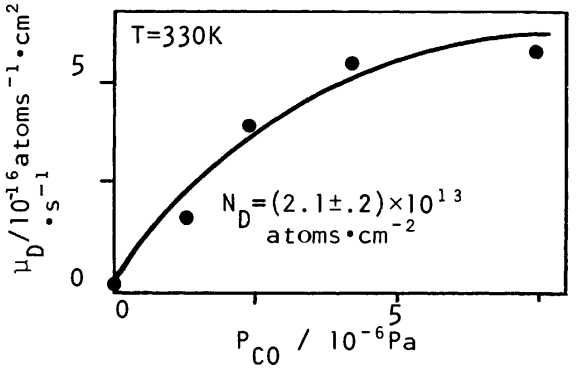

Fig. 5. The 2nd-order rate constant of D(a), μ_D, as a function of CO pressure P_{CO}.

case. Figure 5 shows P_{CO}-dependence of the second-order rate constant μ_D of v^D_-. It is curve fitted to

$$\mu_D = \mu_D^0 + k_{D,CO}P_{CO}^{0.74}. \quad (5)$$

The heat of adsorption of CO is larger than that of H_2.[17] If there is a direct energy-transfer process between adsorbates upon adsorption of CO, desorption of H(a) can be accelerated by CO, but not by H_2.

5. Gas 1=D_2 and CO, Gas 2=Vacuum {$v^D_-(N_D, N_{CO})$ and $v^{CO}_-(N_D, N_{CO})$}. This experiment was done to distinguish the effect of the gas-phase molecules from that of the adsorbed molecules. The desorption of molecules into vacuum indicates the effects of one adsorbed species to the other adsorbed species. Figure 6 shows the second-order rate constant μ_D of D(a) when N_D was constant and N_{CO} was varied. μ_D was not significantly changed by N_{CO}, namely, the desorption of CO did not depend on the surface concentration of D(a) at the same temperature.

To summarize, we observed the acceleration of desorption of a surface species by the same species in the gas phase—adsorption-assited desorption— of CO

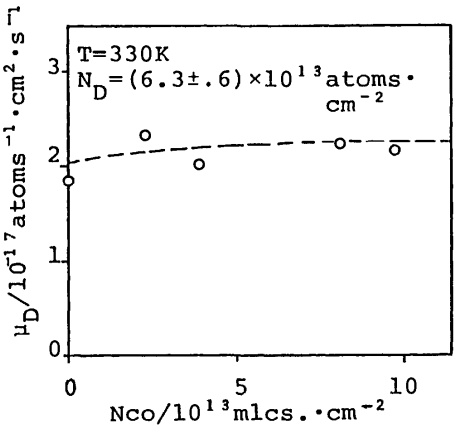

Fig. 6. The 2nd-order desorption rate constant of D(a), μ_D, as a function of the surface concentration of CO(a), N_{CO}. This measurement was done without ambient gas molecules.

but not of H_2. The adsorption of CO(g) is indifferent of the presence of H_2(g) or H(a), and desorption of CO(a) is weakly promoted by H_2(g). Adsorption of H_2 is poisoned by CO(a), and desorption of H(a) is accelerated by CO(g). The acceleration of desorption of H(a) is not due to the surface interaction with CO(a), but to the interaction between CO(g) and H(a) when CO reaches the surface.

References

1) T. Yamada, T. Onishi, and K. Tamaru, *Surf. Sci.*, **133**, 533 (1983).
2) T. Yamada and K. Tamaru, *Surf. Sci.*, **138**, L155 (1984).
3) T. Yamada and K. Tamaru, *Surf. Sci.*, **146**, 341 (1984).
4) T. Yamada, T. Onishi, and K. Tamaru, *Surf. Sci.*, **157**, L389 (1985).
5) T. Yamada and K. Tamaru, *Z. Phys. Chem. NF*, **144**, 195 (1985).
6) T. Yamada, R. -S. Zhai, Y. Iwasawa, and K. Tamaru, *Surf. Sci.*, **205**, 82 (1988).
7) H. H. Madden, J. Küppers, and G. Ertl, *J. Chem. Phys.*, **58**, 3401 (1973).
8) K. Christmann, O. Shober, and G. Ertl, *J. Chem. Phys.*, **60**, 4719 (1974).
9) C. R. Helms and R. J. Madix, *Surf. Sci.*, **52**, 677 (1975).
10) H. Conrad, G. Ertl, J. Küppers, and E. E. Latta, *Surf. Sci.*, **57**, 475 (1976).
11) W. Erley and H. Wagner, *Surf. Sci.*, **74**, (1978) 333.
12) H. Ibach, W. Erley, and H. Wagner, *Surf. Sci.*, **92**, 29 (1980).
13) D. W. Goodman and M. Kiskinova, *Surf. Sci.*, **105**, L265 (1981).
14) K. Tamaru and T. Yamada, *Shokubai*, **27**, 350 (1985).
15) P. W. Tamm and L. D. Schmidt, *J. Chem. Phys.*, **51**, 5352 (1969).
16) P. W. Tamm and L. D. Schmidt, *J. Chem. Phys.*, **52**, 1150 (1970).
17) J. B. Benziger and R. J. Madix, *Surf. Sci.*, **79**, 394 (1979).

A Flow-Through Detector Based on the Photoelectrochemical Reaction of an Anthraquinone-2,6-disulfonate Dianion/ Cationic Perfluoro Polymer Complex

Naoyoshi EGASHIRA,* Toshirou FUJISAWA, and Kazuya OHGA*
Department of Environmental Chemistry and Engineering, Faculty of Engineering, Oita University, 700 Dannoharu, Oita 870-11
(Received December 22, 1988)

Synopsis. A glassy carbon electrode modified with an anthraquinone-2,6-disulfonate dianion/cationic perfluoro polymer complex was used as the working electrode of a flow-through detector based on a photoelectrochemical reaction. Several α-amino acids gave anodic photocurrents. The photocurrent-peak area of proline increased linearly with the concentration in the range of 0.5—10 mmol dm^{-3} and the detection limit (S/N=2) was 5×10^{-5} mol dm^{-3}.

In a previous paper,[1] we reported a new electrochemical flow-through detector which was equipped with a working electrode modified with polystyrene having pendant anthraquinone groups. The principle of detection proposed involves photochemical reduction of the anthraquinone moiety by analytes and electrochemical oxidation of the resulting reduced form of the anthraquinone on the electrode to give an anodic current. The detector has the advantage of permitting direct analyses of α-amino acids and amines which are undetectable by conventional electrochemical detectors without pretreatment.[2,3] However, a dimethyl sulfoxide solution that is rarely used for HPLC analysis of amino acids was required as the mobile phase because of the hydrophobicity of the polymer used. In the present paper, we described a modified electrode favorable for an aqueous mobile phase using a hydrophilic polymer, a complex (Fig. 1) formed from a cationic perfluoro polymer (CPF) and disodium anthraquinone-2,6-disulfonate (ADS).

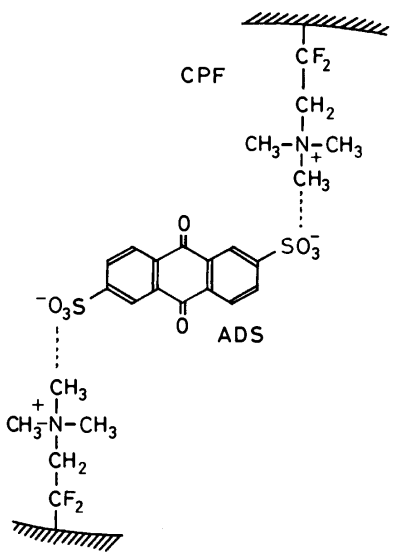

Fig. 1. CPF/ADS complex.

Experimental

A CPF film (Toyo Soda Co.) was finely cut and mixed with H_2O/CH_3OH/2-propanol (volume ratio, 1:1:1).[4] The mixture was refluxed with stirring at 70 °C for 36 h and filtered. The concentration of CPF in the filtrate was estimated to be 0.84 mg cm^{-3} on evaporating the solvent and weighing the remaining CPF. A given amount of ADS was added to 1 cm^3 of the CPF solution to yield a complex solution.

A glassy carbon disk (Tokai Carbon GC-30S) of 0.6 cm in diameter was coated with 0.1 cm^3 of the complex solution and dried under reduced pressure. The polymer-film thickness of the modified electrode obtained was evaluated to be about 3 μm with an Ono Sokki DG-215 digital dial gauge having a spindle. The flow-through cell used was the same as reported previously[1] and was equipped with a glass window (Corning) to cut off light of wavelengths shorter than 310 nm. The light source was a 500-W xenon lamp (Shimadzu). The light intensity was estimated to be 3.2 μW cm^{-2} with a Tokyo Kougaku Kikai UVR-365 exposure meter which responds to light from 310 to 400 nm. The modified electrode, a platinum plate (0.15 cm^2), and a Ag/AgCl electrode were employed as the working, counter, and reference electrodes, respectively. A potential of 0.2 V was imposed on the working electrode in order to reoxidize the reduced form of ADS. A N_2-bubbled phosphate buffer solution (0.1 mol dm^{-3}, pH 11) was allowed to flow through the cell at a rate of 1.0 cm^3 min^{-1}

Results and Discussion

The cyclic voltammogram of the modified electrode showed reversible redox peaks around −0.6 V as shown in Fig. 2, indicating that the electrode can be used effectively to detect the reduced form of ADS. A potential difference between the redox peaks of about 0.2 V was larger than those for electroactive species immobilized on electrodes in the form of monolayers,[5] probably because of an uncompensated ohmic resistance of the polymer film.[6] A maximum anodic peak current was obtained with a film prepared from 1.2 mg of ADS and 1 cm^3 of the CPF solution; further addition of ADS to the CPF solution did not significantly increase the photocurrent, as is described below.

Figure 3 shows the anodic photocurrents resulting from the intermittent injection (20 mm^3) of a buffer solution of proline (1 mmol dm^{-3}) into the cell. The peak area of the current was found to be reproducible at about ±3% and to increase linearly with the concentration of proline in the range of 0.5—10 mmol dm^{-3} (Fig. 4). The detection limit was 5×10^{-5} mol dm^{-3} (S/N=2) comparable to that of a differential refractive index detector.[7]

Other α-amino acids also gave photocurrent peaks,

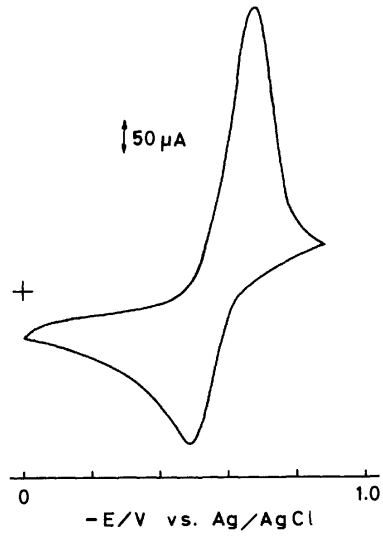

Fig. 2. Cyclic voltammogram of a modified electrode (area: 0.283 cm^2) with a CPF/ADS complex in 0.1 mol dm^{-3} phosphate buffer (pH 11). The sweep rate was 0.1 V s^{-1} and the weight ratio of ADS to CPF was 1.4.

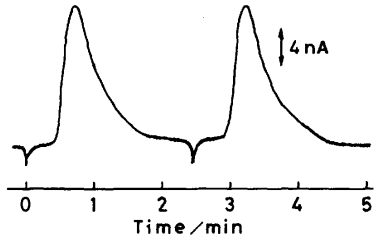

Fig. 3. Photocurrent response of the modified electrode (ADS/CPF weight ratio=1.4) induced by intermittent injection of proline (10 mmol dm^{-3}, 20 mm^3).

though the currents were lower than that of proline: The peak areas of methionine, lysine, histidine, and valine were 0.14, 0.14, 0.10, and 0.04 μC, respectively, when the same molar quantities as that of proline (0.2 μmol, 0.33 μC) were injected. In addition, it is important to note here that dark currents were not observed for these amino acids. These results suggest

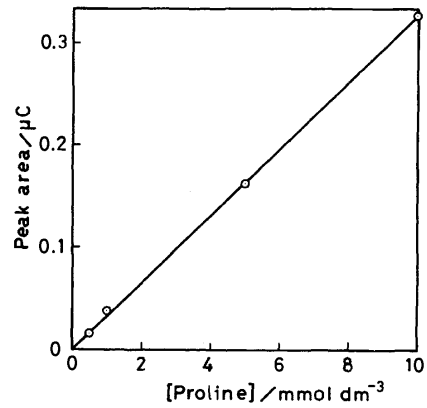

Fig. 4. A calibration curve of the peak area vs. the concentration of proline. Injection volume was 20 mm^3.

that the CPF/ADS-modified electrode is applicable to HPLC analysis of such electroinactive amino acids with aqueous mobile phases.

The proline peak area was unchanged for about 7 h after an initial unstable period (2 h), but subsequently, decreased gradually, probably owing to loss of ADS from the complex. Thus, the development of a more stable photoresponsive polymer would be required for this type of detector to have long life.

The present work was partially supported by a Grant-in-Aid for Scientific Research No. 62750768 from the Ministry of Education, Science and Culture.

References

1) N. Egashira, T. Fujisawa, and K. Ohga, *Denki Kagaku*, **57**, 65 (1989).
2) K. Shimada, M. Tanaka, and T. Nambara, *J. Chromatogr.*, **227**, 445 (1982).
3) W. A. Jacobs and P. T. Kissinger, *J. Liq. Chromatogr.*, **5**, 881 (1982).
4) N. Oyama, T. Ohsaka, and T. Okajima, *Anal. Chem.*, **58**, 979 (1986).
5) A. J. Bard and L. R. Faulkner, "Electrochemical Methods," John Wiley & Sons, New York (1980), p. 204.
6) P. Daum and R. W. Murray, *J. Phys. Chem.*, **85**, 389 (1981).
7) M. M. Munk, *J. Chromatogr. Sci.*, **8**, 491 (1970).

Effect of 2,2′-Bipyridine on Nickel(II)-Halide Interactions within Their Ternary Complexes in *N,N*-Dimethylformamide

Shin-ichi ISHIGURO* and Kazuhiko OZUTSUMI†
Department of Electronic Chemistry, Tokyo Institute of Technology at Nagatsuta, Midori-ku, Yokohama 227
(Received February 20, 1989)

Synopsis. The formation of ternary (2,2′-bipyridine)-bromonickel(II) complexes has been studied by calorimetry in *N,N*-dimethylformamide containing 0.16 mol dm^{-3} $(C_2H_5)_4NClO_4$ as a constant ionic medium at 25 °C. The data are well explained in terms of the formation of $[NiBr(bpy)]^+$ and $[NiBr(bpy)_2]^+$ (bpy=2,2′-bipyridine), and their formation constants, enthalpies and entropies were determined. It is elucidated that the affinities of Br^- as well as Cl^- ions to $[Ni(bpy)]^{2+}$ and $[Ni(bpy)_2]^{2+}$ are enhanced almost to the same extent over Ni^{2+}. The enhancement is ascribed mainly to an increase in entropies upon complexation in both Ni^{II}–Cl^-–bpy and Ni^{II}–Br^-–bpy systems.

Affinities of halide ions to a metal ion change depending on the solvent.[1] Ligating anions or molecules to a metal ion in ternary systems also influence the affinities of halide ions.[2] In the ternary Ni^{II}–Cl^-–bpy (bpy=2,2′-bipyridine) system the formation of $[NiCl(bpy)]^+$, $[NiCl_2(bpy)]$, $[NiCl(bpy)_2]^+$, and $[NiCl_2(bpy)_2]$ has been proposed in DMF.[3] It is found that the log K_1 value for the formation of $[MCl]^+$ is appreciably larger for M=$[Ni(bpy)]^{2+}$ or $[Ni(bpy)_2]^{2+}$ than for Ni^{2+}. Furthermore, the enhanced complexation is essentially due to the increased entropies and the corresponding enthalpies remain rather constant. Relative affinities among halide ions to nickel(II) ion may be of interest in view of hard and soft acids and bases. Therefore, we examined the complexation equilibria in the Ni^{II}–Br^-–bpy system in DMF by calorimetry at 25 °C, and the result was compared with that in the Ni^{II}–Cl^-–bpy system.

Results and Discussion

Calorimetric titration curves obtained in the ternary Ni^{II}–Br^-–bpy system are depicted in Fig. 1. The heat of reaction q measured at each titration point is normalized with the volume of the titrant added δv and the concentration of the ligand ions in the titrant $C_{X,tit}$, and the term $-q/(\delta v C_{X,tit})$ is plotted against C_X/C_M, where C_X and C_M denote the total concentrations of the bromide and metal ions, respectively, in solution. As seen in Table 1 the formation of various sets of ternary $[NiBr_p(bpy)_q]^{(2-p)+}$ complexes was assumed along with the relevant binary complexes. Analyzed on the basis of the known thermodynamic parameters for the binary 2,2′-bipyridine[3] and bromo[4] complexes of nickel(II), the titration curves in Fig. 1 are finally explained in terms of the formation of $[NiBr(bpy)]^+$ and $[NiBr(bpy)_2]^+$ (case A in Table 1). The solid lines in Fig. 1, calculated using the constants for case A in Table 1, well reproduce the experimental points. It is elucidated that the formation of $[NiBr_2(bpy)]$ and $[NiBr_2(bpy)_2]$ is practically negligible in contrast to that of the corresponding $[NiCl_2(bpy)]$ and $[NiCl_2(bpy)_2]$ complexes.[3] It is also noted that the formation of $[NiBr_2]$ is virtually negligible in DMF.[4]

In Table 2 are compared the thermodynamic parameters for the formation of $[MX]^+$ (X=Cl, Br and M=Ni^{2+}, $[Ni(bpy)]^{2+}$, $[Ni(bpy)_2]^{2+}$). We see from Table 2 that for $[Ni(bpy)]^{2+}$ as well as $[Ni(bpy)_2]^{2+}$ the log K_1(Br) value is smaller than the log K_1(Cl) value, and the decrement is to an almost similar extent to that for Ni^{2+}. The ΔH_1°(Br) value is larger than the ΔH_1°(Cl) value for $[Ni(bpy)]^{2+}$ as well as $[Ni(bpy)_2]^{2+}$, and the increment is also to an almost similar extent to the value for Ni^{2+}. On the othen hand, practically the

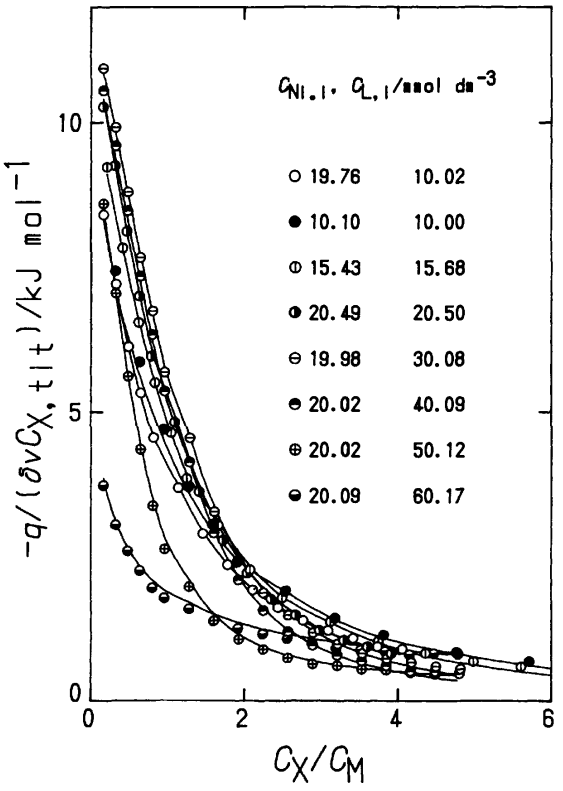

Fig. 1. Calorimetric titration curves obtained for the Ni^{II}–Br^-–bpy system in *N,N*-dimethylformamide containing 0.16 mol dm^{-3} $(C_2H_5)_4NClO_4$ at 25 °C. The concentrations of Ni^{2+} ion and 2,2′-bipyridine in initial test solutions, $C_{Ni,i}$ and $C_{L,i}$/mmol dm^{-3}, are given.

† Presesnt address: Department of Chemistry, University of Tsukuba, Ibaraki 305.

Table 1. Least-Squares Refinement of Overall Formation Constants, $\log(\beta_{1pq}/\mathrm{mol}^{-(p+q)}\,\mathrm{dm}^{3(p+q)})$ and Enthalpies, $\Delta H^\circ_{\beta 1pq}/\mathrm{kJ\ mol}^{-1}$, of $[NiBr_p(bpy)_q]^{(2-p)+}$ (bpy=2,2′-bipyridine) in *N,N*-Dimethylformamide Containing 0.16 mol dm^{-3} $(C_2H_5)_4NClO_4$ at 25 °C[a]

	Case A	Case B	Case C
$\log\beta_{111}$	7.80(0.04)	8.00(0.09)	7.8(0.14)
$\log\beta_{112}$	13.39(0.03)	13.38(0.03)	13.39(0.03)
$\log\beta_{121}$	—	2.65(0.24)	7.1[b]
$\log\beta_{122}$	—	—	5.3(0.5)
$\Delta H^\circ_{\beta 111}$	−11.6(0.9)	−15.7(1.4)	−12.2(3.4)
$\Delta H^\circ_{\beta 112}$	−48.1(0.4)	−47.9(0.4)	−47.9(0.6)
$\Delta H^\circ_{\beta 121}$	—	very large	40.5[b]
$\Delta H^\circ_{\beta 122}$	—	—	very large
U[c]	0.0717	0.0535	0.0647
R[d]	0.0305	0.0264	0.0290

a) Values in parentheses refer to 3σ. The total number of calorimetric data points is 132. The assumed complexes are [111] and [112] in case A, [111], [112], and [121] in case B, and [111], [112], [121], and [122] in case C. The overall formation constant and enthalpies of formation of the relevant binary complexes, $[NiBr]^+$ ($\log\beta$=1.20, ΔH°=17.5 kJ mol^{-1}), $[Ni(bpy)]^{2+}$ (5.90, −31.1), $[Ni(bpy)_2]^{2+}$ (11.18, −63.8), $[Ni(bpy)_3]^{2+}$ (15.43, −92.2) were fixed as known parameters. b) Very large standard deviation. c) Error-square sum. d) The Hamilton R factor.

Table 2. Stepwise Formation Constants, $\log(K_1/\mathrm{mol}^{-1}\,\mathrm{dm}^3)$, Enthalpies, $\Delta H^\circ_1/\mathrm{kJ\ mol}^{-1}$, and Entropies, $\Delta S^\circ_1/\mathrm{J\ K}^{-1}\,\mathrm{mol}^{-1}$, for the reaction, $M^{2+}+X^-=[MX]^+$, where X=Cl or Br, and M=Ni, [Ni(bpy)], or $[Ni(bpy)_2]$ (bpy=2,2′-bipyridine), in *N,N*-Dimethylformamide at 25 °C

	X	Ni^{2+}	$[Ni(bpy)]^{2+}$	$[Ni(bpy)_2]^{2+}$
$\log K_1$	Cl	2.85[a]	3.68[b]	3.77[b]
	Br	1.20[c]	1.90	2.21
ΔH°_1	Cl	8.6[a]	8.4[b]	7.9[b]
	Br	17.5[c]	19.5	15.7
ΔS°_1	Cl	83[a]	99[b]	99[b]
	Br	82[c]	102	95

a) Ref. 6. b) Ref. 3. c) Ref. 4.

same ΔS°_1 values for Cl and Br are found for all the M ions. These results imply that the Ni^{II}–X^- (X=Cl, Br) interactions are not appreciably influenced by the coordination of 2,2′-bipyridine molecules to the nickel(II) ion, in other words, the coordination of 2,2′-bipyridine molecules to nickel(II) ion does not change virtually the hard and soft nature of the nickel(II) ion.

With regard to the bromo complexes the $\log K_1$ value for $[Ni(bpy)]^{2+}$ is larger than that for Ni^{2+}. The value for $[Ni(bpy)_2]^{2+}$ is also larger than that for Ni^{2+}. The larger $\log K_1$ values are ascribed mainly to the increased entropies upon complexation, and the change in the corresponding enthalpies is rather small. The same conclusion has been obtained for X=Cl. Consequently, the entropy increase seems to be independent of the kind and nature of halide ions. Nickel(II) ion and its binary 2,2′-bipyridine complexes are solvated to form six-coordinated $[Ni(dmf)_6]^{2+}$, $[Ni(bpy)(dmf)_4]^{2+}$ and $[Ni(bpy)_2(dmf)_2]^{2+}$ in DMF. Therefore, a specific or steric intermolecular bpy–dmf interaction might occur in $[Ni(bpy)(dmf)_4]^{2+}$ and $[Ni(bpy)_2(dmf)_2]^{2+}$, which is expected to lead to the entropy increase for $[Ni(bpy)]^{2+}$ and $[Ni(bpy)_2]^{2+}$.

Experimental

Reagents. Chemicals used were prepared or purified as described elsewhere.[3]

Measurements. Calorimetric measurements were carried out using an on-line controlled calorimetry system.[5] Varying concentrations of nickel(II) perchlorate 2,2′-bipyridine solutions (40 cm^3) containing 0.16 mol dm^{-3} $(C_2H_5)_4NClO_4$ as a constant ionic medium were titrated with a 0.16 mol dm^{-3} $(C_2H_5)_4NBr$ solution. The detailed procedure of the measurements is described elsewhere.[3]

References

1) S. Ahrland, *Pure Appl. Chem.*, **51**, 2019 (1979).
2) H. Sigel, "Metal Ions in Biological Systems," Marcel Dekker, Inc., New York (1973), Vol. 2.
3) S. Ishiguro, K. Ozutsumi, and H. Ohtaki, *J. Chem. Soc., Dalton Trans.*, **1989**, 655.
4) K. Ozutsumi and S. Ishiguro, to be published.
5) H. Suzuki and S. Ishiguro, *Netsu Sokutei*, **15**, 152 (1988).
6) S. Ishiguro, K. Ozutsumi, and H. Ohtaki, *Bull. Chem. Soc. Jpn.*, **60**, 531 (1987).

Photoreaction of (*E*)-1-Mesityl-2-(2,4,6-tri-*t*-butylphenyl)diphosphene

Masaaki YOSHIFUJI,*,† Takahiro SATO, and Naoki INAMOTO
Department of Chemistry, Faculty of Science, The University of Tokyo, Hongo, Tokyo 113
(Received September 20, 1988)

Synopsis. Photoirradiation of (*E*)-1-mesityl-2-(2,4,6-tri-*t*-butylphenyl)diphosphene gave 1,2-bis(2,4,6-tri-*t*-butylphenyl)diphosphene via a cyclotetraphosphane.

In connection with our study on the photolysis of such organophosphorus compounds in low coordination states as listed below (**1**—**4**),[1,2a,3,4] an unsymmetrical diphosphene was prepared[5] and was irradiated with a mercury lamp.[6] In order to observe *E*/*Z* isomerization around the P=P double bond (**5**⇄**6**) which had been observed for a symmetrical diphosphene **2** (**2**⇄**7**),[2a,7] or the ligand **5** on the metal carbonyls (**1**),[1] (*E*)-1-mesityl-2-(2,4,6-tri-*t*-butylphenyl)diphosphene (**5**) was dissolved in tetrahydrofuran (THF) and was irradiated at −40 °C, monitoring by the ^{31}P NMR at −56 °C at an appropriate time interval. Figure 1 shows some selected ^{31}P NMR spectra during the photolysis through a Pyrex filter. The starting diphosphene **5**, which gives an AB quartet[5] at low field, however, afforded the symmetrical (*E*)-diphosphene **2**,[2b] on irradiation, together with the *Z*-isomer **7**,[2a,7] giving their signals at δ_P 488.3 and δ_P 367.7, respectively. The peaks due to **2** and **7** increased on long irradiation while the complicated but symmetrical signals appeared at around δ_P 0 to −50 which did not correspond to **6**. The spectrum was simulated by the parameters of AA'BB' spin system given in Table 1 as cyclotetraphosphane (**8**), a head-to-head dimer of the starting diphosphene **5**. Figure 2 shows the simulated spectrum by LAOCOON 3.

The photolysis of 1-(pentamethylcyclopentadienyl)-

Table 1. ^{31}P NMR Parameters of **8**

Chemical shift[a]/Hz		Coupling constant/Hz	
P_1	−360	$J_{12}=J_{34}$	−160
P_2	−1529	$J_{13}=J_{24}$	25
P_3	−1529	J_{14}	−105
P_4	−360	J_{23}	−95

a) In arbitrary unit.

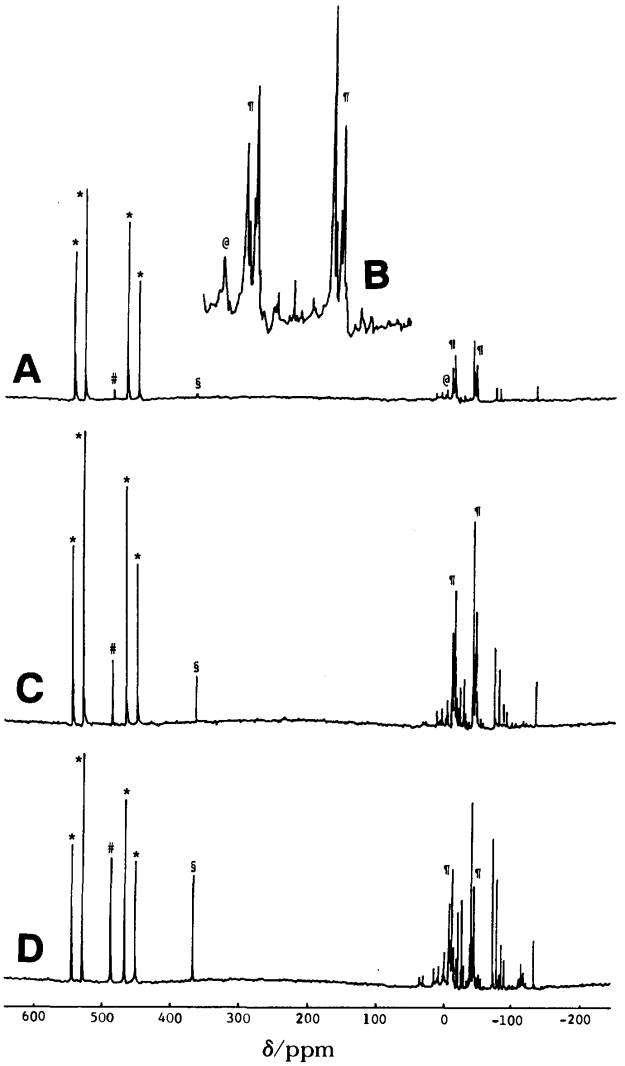

Fig. 1. ^{31}P NMR Spectra (−56 °C) during the photolysis of **5**. A) After 20-min irradiation. @: 85% H_3PO_4; *: **5**; #: **2**; §: **7**; ¶: **8** (expanded spectrum: B). C) After 52-min irradiation. D) After 121-min irradiation.

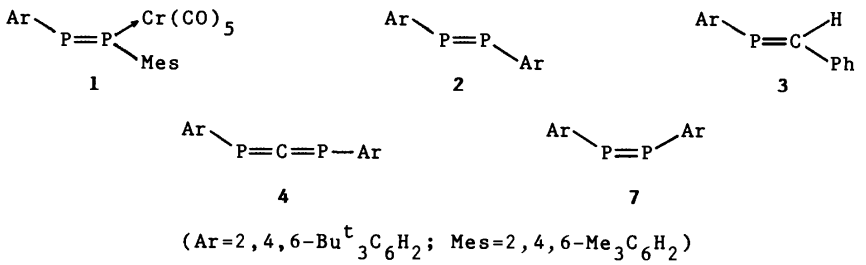

Scheme 1.

† Present address: Department of Chemistry, Faculty of Science, Tohoku University, Aoba, Sendai 980.

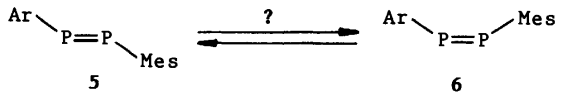

Scheme 2.

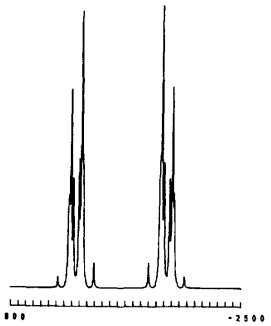

Fig. 2. Simulated spectrum of **8** with parameters listed in Table 1.

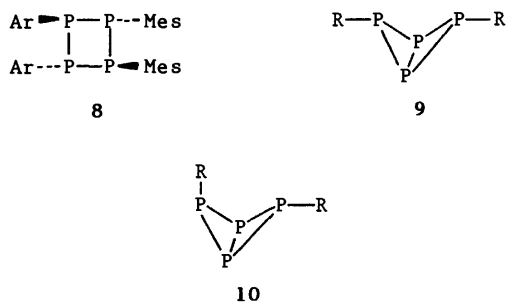

Scheme 3.

2-(2,4,6-tri-*t*-butylphenyl)diphosphene was recently reported by Jutzi and Meyer indicating the intermediacy of cyclotetraphosphanes for the formation of the symmetrical diphosphene **2** and/or bicyclo[1.1.0]tetraphosphanes like **9** or **10**.[8] Our results also suggested that an intermediate **8** decomposed to **2** followed by photo-equilibrium of **2** to **7**.

The whole process apparently resembles to a metathesis of olefins,[9] but in the present case, the other part of dimesityldiphosphene was not observed, probably because of its instability. At higher field there were observed some unknown peaks, however, it should be noted that we were not able to detect either **6**, **9**, or **10**.

In conclusion, it seems likely that photolysis of diphosphenes, depending upon the substituents and irradiation conditions, gives dimerization, cleavage, and *E*/*Z* isomerization.

Experimental

Preparation of (*E*)-1-Mesityl-2-(2,4,6-tri-*t*-butylphenyl)diphosphene (5). The diphosphene **5** was prepared according to the method described before.[5]

Photolysis of the Diphosphene 5. The diphosphene **5** (183.7 mg, 0.431 mmol) was dissolved in 1 ml of THF in an NMR sample tube of 10 mmϕ under argon and the sample was irradiated through a 2 mm thick Pyrex filter with a Riko 100-W medium-pressure mercury lamp at −40 °C. The irradiated sample was monitored by ^{31}P NMR at −56 °C at a certain time interval. Some ^{31}P NMR spectra taken at 36.3 MHz were shown in Fig. 1. The similar results were obtained after irradiation over a period of 1 h without the Pyrex filter at −75 °C. Attempts to isolate **8** failed.

Simulation of ^{31}P NMR Spectrum. The signals were analyzed as the AA'BB' spin system by a modified version of LAOCOON 3 program. The parameters were listed in Table 1 and the simulated spectrum was shown in Fig. 2.

This work was supported in part by the Grant-in-Aid for Scientific Research No. 62540371 from the Ministry of Education, Science and Culture. The author thank Toyo-Stauffer Chemical Company, Ltd., for the donation of organolithium reagents throughout this work.

References

1) M. Yoshifuji, T. Hashida, N. Inamoto, K. Hirotsu, T. Horiuchi, T. Higuchi, K. Ito, and S. Nagase, *Angew. Chem., Int. Ed. Engl.*, **24**, 211 (1985).

2) a) M. Yoshifuji, T. Sato, and N. Inamoto, *Chem. Lett.*, **1988**, 1735; b) M. Yoshifuji, I. Shima, N. Inamoto, K. Hirotsu, and T. Higuchi, *J. Am. Chem. Soc.*, **103**, 4587 (1981); **104**, 6167 (1982).

3) M. Yoshifuji, K. Toyota, and N. Inamoto, *Tetrahedron Lett.*, **26**, 1727 (1985).

4) M. Yoshifuji, K. Toyota, T. Niitsu, N. Inamoto, Y. Okamoto, and R. Aburatani, *J. Chem. Soc., Chem. Commun.*, **1986**, 1550.

5) M. Yoshifuji, K. Shibayama, N. Inamoto, T. Matsushita, and K. Nishimoto, *J. Am. Chem. Soc.*, **105**, 2495 (1983).

6) M. Yoshifuji, T. Sato, and N. Inamoto: this work was presented in part at the 53rd National Meeting of the Chemical Society of Japan, Nagoya, October 1986, Abstr., No. 3E30, and at the 1st International Conference of Heteroatom Chemistry, Kobe, July 1987, Abstr., No. PS1006.

7) A.-M. Caminade, M. Verrier, C. Ades, N. Paillous, and M. Koenig, *J. Chem. Soc., Chem. Commun.*, **1984**, 875.

8) P. Jutzi and U. Meyer, *J. Organomet. Chem.*, **326**, C6 (1987); **333**, C18 (1987).

9) S. G. Davies, "Organotransition Metal Chemistry. Application to Organic Synthesis, "Pergamon Press, Oxford (1982), Vol. 2, p. 251.

Convenient Syntheses of Condensed Phenalenones. The Synthesis of Indeno[1,2-*a*]phenalene-6,8-dione and Its Dication

Shigeyasu KURODA,* Syuzi HIROOKA, Eishi TANAKA, Yuriko FUKUYAMA
Tomohiko TSUCHIDA, and Koichi NAKAGAWA
Department of Industrial Chemistry, Faculty of Engineering, Toyama University, Gofuku 3190, Toyama 930
(Received October 15, 1988)

Synopsis. Convenient and general syntheses of condensed phenalenones with various ring systems fused at the 7 and 8-positions are described together with the synthesis of indeno[1,2-*a*]phenalene-6,8-dione (quinone) and the formation of its di-cationic species in strong acidic media.

Although many types of condensed phenalenones have been actively studied,[1] there have been few general methods for their synthesis. Other condensed phenalenones such as those having fused rings at 7- and 8-positions have remained to be investigated.[2] In the course of our synthetic study of such new systems we devised a new convenient and general method for the synthesis of condensed phenalenones (**1**). Further the title cationic species (**3**) generated from quinone (**2**) is of interest regarding its tropicity, since the structurally related dication (**5**) generated from cyclohepta[*a*]phenalene-6,12-dione (**4**) was found to show diatropicity[3] in spite of the 16-π epectron system.

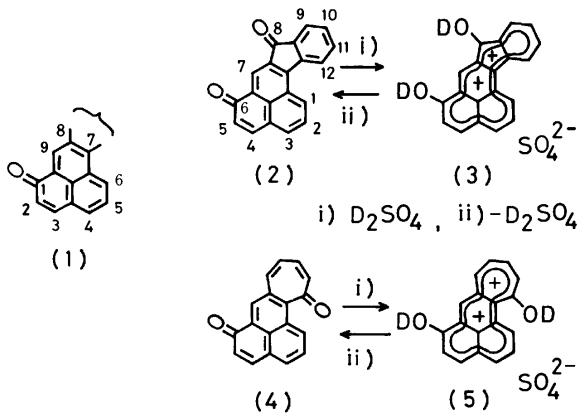

(1) (2) (3) (4) (5)

The reaction of cycloheptanone (**7a**) with one equivalent of 1-formyl-2-methoxynaphthalene (**6**) in the presence of sodium methoxide in dry tetrahydrofuran (THF) under reflux for 3.5 h gave an α,β-unsaturated ketone (**8a**) as pale yellow needles in 90% yield. The direct cyclodehydration of **8a** by 90% sulfuric acid (H_2SO_4) at 45 °C for 25 min provided an expected phenalenone derivative (**12a**) as yellow needles, but in very low yield. The alternative method was next employed. The catalytic hydrogenation of **8a** with H_2/PtO_2 at 2.7 atm for 3 h gave a saturated ketone (**9a**) as pale yellow oil almost quantitatively. This was subjected cyclodehydration under similar conditions without further pruification to give **12a** in 60% yield. This cyclization might have proceeded through the cationic species **11** generated by oxidation of cyclodehydrated product **10** with H_2SO_4.[4] For the synthesis of systems fused with five and six membered ring, the enamines **7b** and **7c** were used instead of ketones to avoid double condensation of **6** with cyclic ketones. The compounds **8b** and **8c** were obtained in 75% and 76% yield, respectively, by the reaction of **7**, and **7c** with **6** in toluene under reflux for 5 h follwed by hydrolysis. Then similar treatment as above furnished phenalenone derivatives **12b** and **12c** in 60% and 35% yield, respectively, via saturated ketones **9b** and **9c**, and cationic intermediates **11**.

The IR spectra showed that the absorption band of a carbonyl group shifted to larger wavenumber in the order of **12a**, **12b**, and **12c**. This suggests that the contribution of the dipolar structure decreases in this order. The same tendency was observed in the ^1H NMR spectra; the ^1H NMR singals of the phenalenone moiety slightly shifted up-field in the same order. In the UV spectra also, the bathochromic shifts (hexane to ethanol) of longest absorption maxima of these compounds decreases as the fused ring size decreases. These indicate that the increased strain in the fused ring diminishes the contribution of the dipolar structure. These compounds generated the cationic species **13a**, **13b**, and **13c** in a strong acid such as trifluoroacetic acid, as confirmed by the spectral evidences especially from the ^1H NMR and UV spectroscopy. The ^1H NMR signals of these cationic species showed the down field shifts by ca. 1 ppm. However, the electronic state of the cationic species does not seem to be greatly affected by the size of the fused ring, as is deduced from the similarity of their chemical shift values. In the UV spectra, the longest absorption maxima of these compounds shifted to longer wavelength by 30—50 nm as compared with those of phenalenones.

The syntheses of **12d** and the title new quinone **2** were similarly achieved as shown in the scheme. The structures of these compounds, including the synthetic intermediates, were determined spectroscopically and by elemental analysis. It is noted that the IR spectrum of **2** showed the characteristic absorption band of a carbonyl group in a five-membered ring at 1708 cm^{-1}. The dicationic species **3** generated by dissolving **2** in strong acid was confirmed by the UV and ^1H NMR spectra. In the UV spectrum, the larger shift of the longest wavelength absorption band of **3** (about 100 nm) compared to the above-mentioned condensed penalenones (about 50 nm) suggests the generation of a dicationic species. Unfortunately, because of its low solubility in various solvents such as DMSO, DMF, and $CDCl_3$, the ^{13}C NMR spectrum of **2** could not be obtained. However, the ^1H chemical shifts of **2** in D_2SO_4 showed that all protons of both the phenalenone moiety and the indenone moiety were shifted to low field by 0.70 ppm and 0.38 ppm, respectively, (av. 0.57 ppm) compared to those of **2** in $CDCl_3$. The down field shifts of the

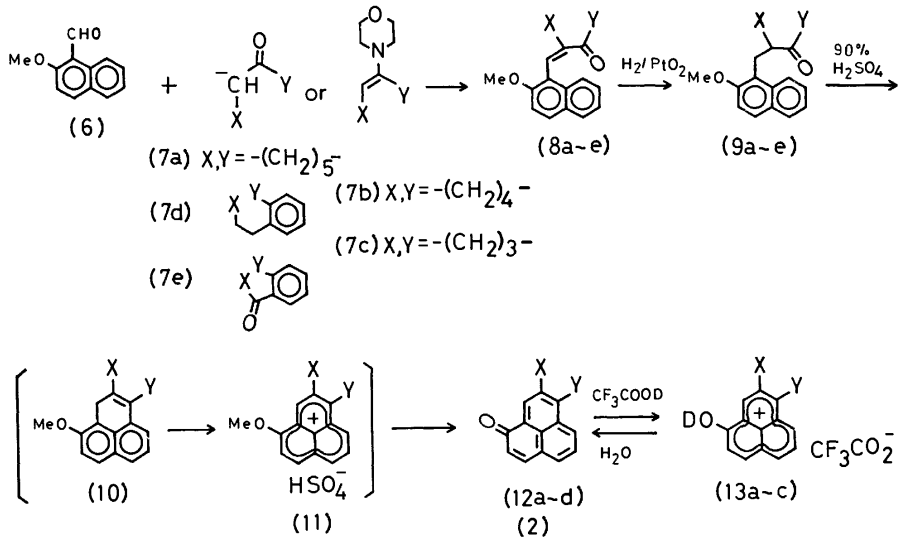

indenone moiety could not be interpreted only by the deshielding effect of the monocation generated in the phenalenone moiety, but it should be considered as due to the generation of the dicationic species. Then, it is to be noted that the protons of the phenalenone moiety of **3** (av. 8.70 ppm) in D_2SO_4 resonated at higher field than those of the dicationic species **5** (av. 9.15 ppm) by 0.45 ppm. This might be interpreted by some contribution of a paratropic rather than the diatropic character expected for 18-π electrons, in accord with the case of the dicationic species of cyclohepta[*a*]-phenalene-6,12-dione **5**[2] in which the diatropic character was observed in spite of its 16-π electronic system.[3]

Experimental

All melting points are uncorrected. The ^1H NMR spectra were taken on a Hitachi R-24 (60 MHz) and on a JEOL-FX 90 (90 MHz) spectrometers, in chloroform-*d* (TMS as internal standard) trifluoroacetic acid-*d* (TMS), and deuteriosulfuric acid (dichloromethane as internal standard). The ^{13}C NMR spectra were taken on a JEOL-FX 90 (23 MHz) spectrometer, in chloroform-*d* (TMS as internal standard) and trifluoroacetic acid-*d* (TMS). The mass spectra were taken on a JEOL-OISG-2 mass spectrometer. The UV and IR spectra were taken on a Hitachi EPS-3T spectrometer and on a IR-810 spectrometer, respectively.

The Following Procedures a) and b) Are Representative for the Preparation of Condensed Compounds 8a, 8b, 8c, 8d, and 8e. a) Condensation of Cyclic Ketones with 1-Formyl-2-methoxynaphthalene 6. To a solution of 3.00 g (16 mmol) of **6** and 1.80 g (16 mmol) of **7a** in 30 mL of anhydrous THF 0.90 g (16 mmol) of sodium methoxide was added and refluxed for 3 h. After cooling the solution was poured onto dil. hydrochloric acid (HCl) and extracted three times with 20 mL of ether. The combined organic layer was washed with water and brine, and dried over anhydrous $MgSO_4$. After removal of the solvent in vacuo, the residue was chromatographed on silica gel to give 4.32 g (90%) of **8a**, from benzene elution.

8a; pale yellow oil; IR (film) 3027w, 1665vs, 1250s, 926m, 788m, 730m cm^{-1}; ^1H NMR ($CDCl_3$) δ=7.70—7.50 (m, 4H), 7.40—7.10 (m, 4H), 3.78 (s, 3H, -OMe), 2.60 (m, 2H), 2.30 (m, 2H), 1.60 (m, 6H); MS *m/z* 280 (M^+, 100%), and HRMS Found: 280.1461, Calcd for $C_{19}H_{20}O_2$: 280.1461.

8d; pale yellow needles (recrystallized from hexane); mp 72—74 °C; IR (KBr) 3060w, 1670vs, 1610m, 1258vs, 740m, 706m cm^{-1}; ^1H NMR ($CDCl_3$) δ=8.70 (m, 1H), 8.75—7.10 (m, 6H), 3.81 (s, 3H, -OMe), 2.70 (m, 2H), 2.58 (m, 2H); MS *m/z* 314 (M^+, 100%); Anal. ($C_{22}H_{18}O_2$) C, H.

8e; (56%); orange needles (recrystallized from hexane and dichloromethane); mp 218—219 °C; IR (KBr) 3055w, 2925w, 1680vs, 1615s, 1248vs, 725m cm^{-1}; ^1H NMR ($CDCl_3$) δ=8.18 (s, 1H), 7.90—7.00 (m, 10H), 3.75 (s, 3H, -OMe), MS *m/z* 294 (M^+, 100%); Anal. ($C_{21}H_{14}O_3$) C, H.

b) **Condensation Reaction of Enamines with 6.** The mixture of 2.30 g (13.5 mmol) of **6** and 2.35 g (13.5 mmol) of *N*-cyclohexenylmorpholine **7b** in 15 mL of dry toluene was refluxed for 12 h. The cooled reaction mixture was added to 10 mL of 3 M-HCl solution and refluxed for 30 min. The resulting mixture was extracted with ether (15 mL×3). The combined organic layer was washed with water and brine three times each, and dried over anhydrous $MgSO_4$. After removal of the solvent, the residue was chromatographed on silica gel to give 4.45 g (76%) of pale yellow solid of **8b** from benzene elution, and recrystallized from hexane.

8b; pale yellow needles; mp 107—109 °C; IR (KBr) 3045w, 2850w, 1680vs, 1615s, 1245vs, 800m, 740m cm^{-1}; ^1H NMR ($CDCl_3$) δ=7.70 (m, 7H), 3.26 (s, 3H, -OMe), 2.50—2.00 (m, 4H), 1.95—1.40 (m, 4H), MS *m/z* 266 (M^+, 28%), 236 (100%); Anal. ($C_{18}H_{18}O_2$) C, H.

Similarly **8c** was obtained in 74% yield; pale yellow needles hexane); mp 97—98.5 °C; IR (KBr) 3050w, 1710vs, 1610m, 780m cm^{-1}; ^1H NMR ($CDCl_3$) δ=7.80—7.60 (m, 4H), 7.50—7.15 (m, 3H), 3.84 (s, 3H, -OMe), 2.42 (t, *J*=7.2 Hz, 2H), 2.40 (t, *J*=7.2 Hz, 2H), MS *m/z* 252 (M^+, 20%), 221 (100%); Anal. ($C_{17}H_{16}O_2$) C, H.

General Procedure for the Catalytic Hydrogenation of α,β-Unsaturated Ketones and the Following Cyclodehydration Reaction. To a solution of ca. 15 mmol of the unsaturated ketone in excess of ten times its weight of ethyl acetate (ca. 50—60 mL) a catalytic amount of platinum dioxide (ca. 1 mg) was added and hydrogenated under medium pressure (2.7—3.0 atm) of hydrogen at room temperature for 3.5 h. The resulting mixture was filtered and concentrated under reduced pressure to give the hydrogenated product. The resulting residue was added to about ten times its weight of 90% sulfuric acid and stirred at 45 °C for 25 min in an oil bath. The mixture was poured onto a large excess (ca. ten times of weights) of ice-water, and extracted with dichloromethane (50 mL×3). The combined organic layer was washed three times with water and brine, and dried over anhydr. $MgSO_4$.

After removal of the solvent, the residure was chromatographed on silica gel to give phenalenone derivatives from dichloromethane eluent; These were recrystallized from hexane.

9a; pale yellow oil; IR (film) 3050w, 2930w, 1730vs, 1690s, 1250s, 938m, 800m, 745m cm^{-1}; ^1H NMR ($CDCl_3$) δ=7.60—6.90 (m, 6H), 3.75 (s, 3H, -OMe), 3.40—3.15 (m, 3H), 2.80—2.35 (m, 4H), 1.80—1.40 (m, 6H); MS *m/z* 282 (M^+, 100%), 141 (98%), HRMS Found: 282.1635, Calcd for $C_{19}H_{22}O_2$: 282.1620.

9b; pale yellow oil; IR (film) 3050w, 3000w, 1700vs, 1620m, 1590s, 1150m, 802m, 749m cm^{-1}; ^1H NMR ($CDCl_3$) δ=8.05—7.00 (m, 6H), 3.80 (s, 3H), 3.50 (m, 1H), 2.50—1.50 (m, 10H), MS *m/z* 270 (M^+, 100%); HRMS Found: 268.1421, Calcd for $C_{18}H_{20}O_2$: 268.1460.

9c; pale yellow oil; IR (film) 3060w, 2940w, 1736vs, 1625s, 1255vs, 1160s, 810m, 750m cm^{-1}; ^1H NMR ($CDCl_3$) δ=7.95 (d, *J*=8.8 Hz, 1H), 7.70 (m, 2H), 7.55—7.18 (m, 3H), 3.88 (s, 3H, -OMe), 3.52 (dd, *J*=4.8 and 14.0 Hz, 1H), 3.10 (dd, *J*=12.0 and 14.0 Hz, 1H), 2.60—2.10 (m, 3H), 2.0—1.50 (m, 4H); MS *m/z* 252 (M^+, 35%), 171 (100%); HRMS Found: 252.1296, Calcd for $C_{17}H_{18}O_2$: 252.13404.

9d; pale yellow needles (hexane); mp 110—111 °C; IR (KBr) 3025w, 1662vs, 1608s, 1240vs, 796m, 732m cm^{-1}; ^1H NMR ($CDCl_3$) δ=8.02 (m, 2H), 7.70 (m, 2H), 7.25 (m, 6H), 3.85 (m, 1H), 3.83 (s, 3H, -OMe), 3.22 (dd, *J*=12.0 and 16.0 Hz, 1H), 2.80 (m, 3H), 1.94 (m, 2H), MS *m/z* 316 (M^+, 100%); Anal. ($C_{22}H_{20}O_2$) C, H.

9e; pale yellow needles (hexane); mp 169—172 °C; IR (KBr) 3040w, 2920vs, 1721s, 1685vs, 1238vs, 1066s, 786m, 720 cm^{-1}; ^1H NMR ($CDCl_3$) δ=8.02—7.63 (m, 6H), 7.55—7.10 (m, 4H), 3.77 (s, 3H, -OMe), 3.61 (d, *J*=6.2 Hz, 2H), 3.33 (dd, *J*=6.2 and 8.6 Hz, 1H), MS *m/z* 316 (M^+, 100%); Anal. ($C_{21}H_{16}O_3$) C, H.

12a; pale yellow needles (hexane); mp 122—123 °C; IR (KBr) 3055w, 3030w, 1625vs, 1575s, 1200vs, 828m, 733m cm^{-1}; ^1H NMR ($CDCl_3$) δ=8.37 (s, H-9), 8.22 (dd, *J*=2.0 and 7.0 Hz, H-6), 7.63 (d, *J*=10 Hz, H-3), 7.50 (dd, *J*=2.0 and 7.0 Hz, H-4), 7.47 (t, *J*=7.0 Hz, H-5), 6.62 (d, *J*=10 Hz, H-2); ^{13}C NMR ($CDCl_3$) δ=185.6 (s), 148.3 (s), 142.6 (d), 141.6 (d), 132.1 (d), 130.5 (s), 130.4 (d), 128.8 (d), 128.5 (s), 128.1 (d), 127.8 (s), 127.3 (s), 126.1 (d), 36.4 (t), 32.0 (t), 29.0 (t), 27.3 (t), 26.8 (t); UV (hexane) λ_{max} 390 (log ε=4.14), 325 (3.57), 255 nm (4.42); UV (EtOH) λ_{max} 405 (log ε=4.04), 330 (3.70), 255 nm (4.35); MS *m/z* (M^+, 100%); 219 (20%); Anal. ($C_{18}H_{16}O_2$) C, H.

12b; (35%); pale yellow needles (hexane); mp 81.5—82.5 °C; IR (KBr) 3040w, 1637vs, 1585m, 1402m, 1185s, 833m, 750m, 707m cm^{-1}; ^1H NMR ($CDCl_3$) δ=8.36 (s, H-9), 8.18 (dd, *J*=2.0 and 7.0 Hz, H-6), 7.60 (d, *J*=10.0 Hz, H-3), 7.58 (dd, *J*=2.0 and 7.0 Hz, H-4), 7.46 (t, *J*=7.0 Hz, H-5), 6.61 (d, *J*=10.0 Hz, H-2); ^{13}C NMR ($CDCl_3$) δ=185.8 (s), 142.0 (d), 141.2 (s), 136.2 (s), 132.6 (d), 131.3 (s), 130.3 (s), 128.8 (d), 128.0 (s), 127.9 (s), 127.1 (d), 126.2 (d), 126.1 (d), 30.3 (t), 26.4 (t), 22.7 (t), 22.5 (t); UV (hexane) λ_{max} 375 (log ε=4.08), 325 (3.53), 260 nm (4.40); UV (EtOH) λ_{max} 385 (log ε=4.10), 330 (3.40), 260 nm (4.35); MS *m/z* 234 (M^+, 100%); Anal. ($C_{17}H_{14}O$) C, H.

12c; (25%) pale yellow needles (hexane); mp 88—89 °C; IR (KBr) 3055w, 1645vs, 1580s, 1372s, 855m, 772m cm^{-1}; ^1H NMR ($CDCl_3$) δ=8.35 (s, H-9), 7.83 (dd, *J*=2.0 and 7.0 Hz, H-6), 7.45 (t, *J*=7.0 Hz, H-5), 7.55 (d, *J*=10.0 Hz, H-3), 7.54 (dd, *J*=2.0 and 7.0 Hz, H-4), 6.60 (d, *J*=10.0 Hz, H-2); ^{13}C NMR ($CDCl_3$) δ=185.7 (s), 148.9 (s), 142.7 (s), 141.4 (d), 130.4 (d), 128.9 (s), 128.7 (d), 128.5 (d), 128.3 (s), 128.1 (s), 127.2 (d), 126.4 (s), 126.2 (d), 33.3 (t), 31.6 (t), 24.3 (t); UV (hexane) λ_{max} 385 (log ε=4.10), 330 (3.40), 255 nm (4.40); UV (EtOH) λ_{max} 390 (log ε=4.09), 330 sh (3.30), 260 nm (4.41); MS *m/z* 220 (M^+, 100%); 159 (20%); Anal. ($C_{16}H_{12}O$) C, H.

12d; (78%); yellow needles (hexane); mp 185—186.5 °C; IR (KBr) 3025w, 1625vs, 1342s, 1118s, 778m, cm^{-1}; ^1H NMR ($CDCl_3$) δ=8.61 (dd, *J*=1.5 and 8.2 Hz, H-6), 8.56 (s, H-9), 7.77 (d, *J*=9.8 Hz, H-3), 7.56 (m, 6H), 6.75 (d, *J*=9.8 Hz, H-2); 3.08 (t, *J*=8.3 Hz, 2H), 2.84 (t, *J*=8.3 Hz, 2H); MS *m/z* 282 (M^+, 100%); Anal. ($C_{21}H_{14}O$) C, H.

2; (61% from **7e**); red needles (*N,N*-dimethylformamide); mp 330—332 °C; IR (KBr) 1708s, 1637vs, 1615s, 830m, 725m cm^{-1}; ^1H NMR ($CDCl_3$) δ=8.87 (s, H-7), 8.73 (dd, *J*=0.8 and 8.06 Hz, H-1), 8.18 (d, *J*=8.06 Hz, H-3), 7.83 (d, *J*=6.80 Hz, H-12), 7.81 (d, *J*=6.85 Hz, H-9), 7.72 (d, *J*=9.67 Hz, H-4); 7.71 (dd, *J*=8.06 and 8.46 Hz, H-2), 7.64 (dd, *J*=1.4 and 6.80 Hz, H-11), 7.44 (ddd, *J*=0.8, 6.80, and 6.85 Hz, H-10), 6.75 (d, *J*=9.67 Hz, H-5), MS *m/z* 282 (M^+, 100%); UV (CH_2Cl_2) λ_{max} 480 sh (log ε=3.35), 455 (3.50), 425 (3.50), 407 (3.85), 380 (3.75), 345 (3.82), 335 (3.90), 265sh nm (4.30); Anal. ($C_{20}H_{10}O_2$) C, H.

3; ^1H NMR (D_2SO_4-CH_2Cl_2) δ=9.44 (s, H-7), 9.40 (d, *J*=5.89 Hz, H-1), 8.89 (d, *J*=7.23 Hz, H-3), 8.84 (d, *J*=9.20 Hz, H-4), 8.40 (bd, *J*=7.90 Hz, H-12), 8.30 (bd, *J*=8.10 Hz, H-9), 8.06 (dd, *J*=5.89 and 7.23 Hz, H-2), 7.85 (dd, *J*=7.76 and 7.90 Hz, H-11), 7.69 (dd, *J*=7.76 and 8.10 Hz, H-10), 7.64 (d, *J*=9.20 Hz, H-5); ^{13}C NMR (D_2SO_4) δ=199.20 178.05, 160.28, 155.81, 150.67, 142.81, 141.84, 141.59, 135.06, 134.79, 134.68, 132.92, 132.21, 130.40, 129.21, 128.05, 126.99, 122.63, 120.49; UV (H_2SO_4) λ_{max} 600 sh (log ε=2.90), 520sh (3.85), 495 (3.92), 465 (3.96), 390 (4.25), 330 (3.95), 270 nm (3.23).

13a; ^1H NMR (CF_3COOD-TMS) δ=9.19 (s, H-9), 9.18 (dd, *J*=8.0 and 1.0 Hz, H-6), 8.73 (d, *J*=9.0 Hz, H-3), 8.70 (dd, *J*=7.0 and 1.0 Hz, H-4), 8.15 (dd, *J*=8.0 and 7.0 Hz, 5-H), 7.66 (d, *J*=9.0 Hz, H-2); ^{13}C NMR (CF_3COOD) δ=179.7 (s), 167.7 (s), 153.5 (d), 148.5 (s), 145.6 (s), 142.4 (d), 140.7 (d), 131.6 (s), 130.2 (d), 128.7 (d), 125.4 (s), 122.3 (s), 121.5 (s), 37.3 (t), 32.5 (t), 32.1 (t), 28.0 (t), 27.9 (t); UV (H_2SO_4) λ_{max} 445 (log ε=4.10), 435 (4.12), 370 (4.25), 260sh nm (4.15).

13b; ^1H NMR (CF_3COOD) δ=9.11 (s, H-9), 9.06 (d, *J*=8.0 Hz, H-6), 8.67 (d, *J*=9.0 Hz, H-3), 8.59 (d, *J*=8.0 Hz, H-4), 8.08 (t, *J*=8.0 Hz, H-5), 7.59 (d, *J*=9.0 Hz, H-2); ^{13}C NMR (CF_3COOD) δ=179.7 (s), 159.4 (s), 153.6 (d), 143.6 (s), 143.2 (d), 141.6 (s), 138.6 (d), 131.7 (s), 129.4 (d), 127.7 (s), 124.2 (d), 121.5 (s), 120.7 (d), 30.3 (t), 28.1 (t), 21.9 (t), 21.8 (t); UV (H_2SO_4) λ_{max} 476sh (log ε=3.20), 435 (4.18), 390 (3.95), 297 (4.21), 250 nm (4.15).

13c; ^1H NMR (CF_3COOD) δ=9.24 (s, H-9), 8.89 (dd, *J*=8.1 and 1.0 Hz, H-6), 8.71 (d, *J*=9.2 Hz, H-3), 8.67 (dd, *J*=8.1 and 1.0 Hz, H-4), 8.14 (t, *J*=8.1 Hz, H-5), 7.65 (d, *J*=9.2 Hz, H-2); ^{13}C NMR (CF_3COOD) δ=179.5 (s), 168.0 (s), 152.7 (d), 148.4 (s), 144.9 (d), 140.7 (d), 137.2 (d), 129.6 (s), 129.2 (d), 128.1 (s), 124.9 (d), 122.7 (s), 121.0 (d), 33.5 (t), 33.0 (t), 24.6 (t); UV (H_2SO_4) λ_{max} 440 (log ε=4.20), 435sh (4.18), 390sh (3.95), 375 (4.15), 297 (4.21), 250 nm (4.15).

We are grateful for the financial support from the science and technical foundation of Asahi Glass Co. Ltd., (1987—1988).

References

1) I. Murata, K. Yamamoto, T. Hirotsu, and M. Morioka, *Tetrahedron Lett.*, **1972**, 331; I. Murata, K. Yamamoto, and T. Hirotsu, *ibid.*, **1972**, 3389; I. Murata, K. Yamamoto, and Y. Kayane, *Angew. Chem., Int. Ed. Engl.*, **13**, 807 (1974); I. Murata and K. Yamamoto, *Chem. Lett.*, **1973**, 413.
1973, 413.

2) L. Birkpfer, S. M. Kim, and H. D. Engels, *Ber.*, **95**, 1495 (1962); D. H. Reid, *Quart. Rev.*, **19**, 274 (1965).

3) S. Kuroda, Y. Fukuyama, T. Tsuchida, E. Tanaka, and S. Hirooka, *Angew. Chem.*, **97**, 770 (1985).

4) J. W. Larsen, P. A. Bouis, C. R. Watson, Jr., and R. M. Pagni, *J. Am. Chem. Soc.*, **96**, 2284 (1974).

Oxovanadium(V)-Induced Ring-Opening Oxygenation of Cyclic Ketones in Alcohol

Toshikazu HIRAO,* Makoto MORI, and Yoshiki OHSHIRO*
Department of Applied Chemistry, Faculty of Engineering, Osaka University, Yamadaoka, Suita, Osaka 565
(Received November 7, 1988)

Synopsis. Cyclic ketones underwent ring-opening oxygenation on treatment with $VO(OEt)Cl_2$ in alcohol under oxygen to give the corresponding keto ester or diesters depending on the substituent at 2-position. This system was applicable to a catalytic reaction.

Higher oxidation state species of transition metals induce effective oxidative transformations. Vanadium compounds including oxovanadium ones have been known to be useful in oxidation. Their utilization is, however, limited mostly in acidic water,[1] which reduces the synthetic versatility. We herein describe that oxovanadium(V) ethoxides are sufficiently used in the ring-opening oxygenation reactions of cyclic ketones in alcohol.

2-Methylcyclohexanone (**1a**) was oxidized to ethyl 6-oxoheptanoate (**2a**) on treatment with the solution of $VO(OEt)_3$ or $VO(OEt)Cl_2$ in ethanol under oxygen. The regioselective bond cleavage between carbonyl carbon and 2-carbon was observed without formation of the regioisomer (Eq. 1). Molecular oxygen was introduced effectively in this system to form the carbonyl function since only a trace amount of the keto ester **2a** was obtained under nitrogen. Reaction in methanol led to the predominant formation of the corresponding

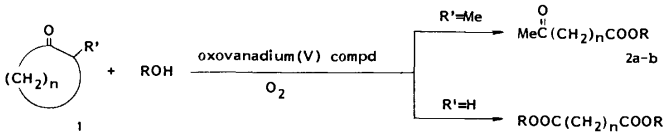

(1)

methyl ester **2b** with a small amount of **2a**, suggesting that the alkoxyl group is derived from the solvent. The reactivities of vanadium compounds were found to depend on their substituents; $VO(acac)_2$ and $V(acac)_3$ were less active than $VO(OEt)Cl_2$. $VO(OEt)Cl_2$ worked well with cyclohexanone (**1c**) as listed in Table 1, but use of $VO(OEt)_3$ gave a poor yield of diethyl adipate (**2c**) under the same conditions. The similar difference in reactivities was also observed in oxygenation of unsubstituted cyclic ketones such as cycloheptanone (**1d**) and cyclooctanone (**1e**). It is assumed to be due to the high Lewis acidity of $VO(OEt)Cl_2$.

In contrast, substitution with chloro group at 2-position of cyclohexanone resulted in the facile oxidation with either $VO(OEt)_3$ or $VO(OEt)Cl_2$ giving the same diester **2c** as obtained from cyclohexanone (Eq. 2, Table 1).

Table 1. Vanadium-Induced Oxygenation Reactions

1	Vanadium Compd[a]	ROH, R	Time/h	2	Yield/%
(**1a**)	$VO(OEt)Cl_2$	Et	3	$MeC(=O)(CH_2)_4COOEt$ (**2a**)	52
1a	$VO(OEt)Cl_2$	Et	3[b]	**2a**	3
1a	$VO(OEt)_3$	Et	22	**2a**	50
1a	$VO(OEt)_3$	Me	30	$MeC(=O)(CH_2)_4COOMe$ (**2b**)	60[c]
1a	$VO(acac)_2$	Et	30	**2a**	30
1a	$V(acac)_3$	Et	30	**2a**	19
(**1c**)	$VO(OEt)Cl_2$[d]	Et	30	$EtOOC(CH_2)_4COOEt$ (**2c**)	64
1c	$VO(OEt)_3$	Et	30	**2c**	3
(**1d**)	$VO(OEt)Cl_2$	Et	30	$EtOOC(CH_2)_5COOEt$ (**2d**)	40
1d	$VO(OEt)_3$	Et	30	**2d**	Trace
(**1e**)	$VO(OEt)Cl_2$	Et	20	$EtOOC(CH_2)_6COOEt$ (**2e**)	35
1e	$VO(OEt)_3$	Et	11	**2e**	0
(**1f**)	$VO(OEt)Cl_2$	Et	3	**2a**	46
1f	$VO(OEt)_3$	Et	11	**2a**	57

a) Vanadium compound (1.0 equiv) was used unless otherwise stated. b) Reaction was carried out under nitrogen. c) The keto ester **2a** was obtained in 7% yield. d) $VO(OEt)Cl_2$ (1.25 equiv) was used.

Table 2. Oxovanadium(V)-Catalyzed Oxygenation Reactions[a)]

1	Oxovanadium Compd/equiv		Time/h	2	Yield/%
1a	$VO(OEt)Cl_2$	0.2	10	**2a**	50
1a	$VO(OEt)Cl_2$	0.05	30	**2a**	53
1a	$VO(OEt)_3$	0.2	11	**2a**	3
1c	$VO(OEt)Cl_2$	0.2	60	**2c**	30
1f	$VO(OEt)Cl_2$	0.2	10	**2c**	52

a) Reactions were carried out in ethanol.

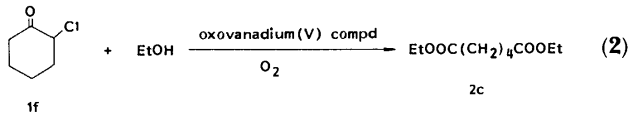

(2)

Another interesting feature should be noted that a catalytic system was achieved by use of $VO(OEt)Cl_2$ under oxygen (Eq. 3). Some results are summarized in Table 2, showing that 0.05 mol equiv of $VO(OEt)Cl_2$ were enough for the oxygenation reaction. An active oxovanadium species seems to be regenerated in situ. With $VO(OEt)_3$ employed, however, such a catalytic cycle was not observed under the similar conditions.

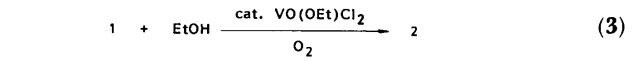

(3)

Although the reaction mechanism has not been elucidated yet, one of the plausible paths is figured out as follows. Oxovanadium(V) ethoxide is assumed to work as a Lewis acid to generate the thermodynamically stable enolate, which is considerd to undergo the similar oxygenation reaction as reported.[1,2)]

The chemistry of transition metal enolates recently draws much attention because it has been scarcely explored despite valuable intermediates in organic syntheses.[3)] Considering oxovanadium(V) ethoxides as Lewis acids with oxidation ability, the above-mentioned ring-opening oxygenation reaction is considered to present such an example.

Experimental

^1H NMR spectra were measured on JEOL JNM-FX90Q spectrometer; IR spectra were measured using Hitachi 270-30 spectrometer. Mass spectra were determined by the electron impact method on Hitachi RMV-6E. $VO(OEt)Cl_2$ was prepared from $VOCl_3$ and an equimolar amount of ethanol with bubbling nitrogen into the hexane solution at room temperature and distilled under the reduced pressure (bp 36—38 °C/1 mmHg†). $VO(OEt)_3$ was supplied from Shinko Chemical Co., Ltd. Ketones and alcohols were purified according to usual methods.

† 1 mm Hg=133.322 Pa.

The Representative Procedure for the Oxovanadium(V)-Induced Oxygenation Reaction of 1. To a solution of 2-methylcyclohexanone (**1a**, 0.224 g, 2.0 mmol) in ethanol (2 mL) was added $VO(OEt)Cl_2$ (0.366 g, 2.0 mmol) at room temperature. The mixture was stirred at reflux under oxygen (1 atm, gasbag) for 3 h. Saturated aqueous $NaHCO_3$ solution (30 mL) was added to the resultant mixture, which was extracted with ether (5×30 mL). The combined ethereal solution was washed with saturated aqueous NH_4Cl solution (10 mL) and then water (10 mL), dried over Na_2SO_4, and concentrated. The yield of ethyl 6-oxoheptanoate (**2a**) was determined by GLC (52% yield, PEG 20M 10%, 2.1 m column, 200 °C). If necessary, the residue was chromatographed on silica-gel column to give **2a**. The reactions of other cyclic ketones and 2-chlorocyclohexanone (**1f**) were carried out in the similar way as mentioned above. The reaction conditions are listed in Table 1. These products were identified by comparison of spectral data with those of the authentic samples.[4)]

The Oxovanadium(V)-Catalyzed Oxygenation Reaction of 1. The amount of $VO(OEt)Cl_2$ was reduced in the catalytic reactions as shown in Table 2. The procedure is similar as described in the stoichiometric reactions.

This study was partly supported with Grant-in-Aid for Special Project Research from the Ministry of Education, Science and Culture.

References

1) W. A. Waters and L. S. Littler, "Oxidation in Organic Chemistry," ed by K. B. Wiberg, Academic Press, New York (1965), Part A, p. 186; F. Freeman, "Organic Syntheses by Oxidation with Metal Compounds," ed by W. J. Mijs and C. R. H. I. de Jonge, Plenum Press, New York (1986), p. 1.

2) S. Ito and M. Matsumoto, *J. Org. Chem.*, **48**, 1133 (1984) and references cited therein.

3) T. Hirao, S. Nagata, and T. Agawa, *Tetrahedron Lett.*, **26**, 5795 (1985) and references cited therein.

4) H. Mckennis, Jr. and V. du Vigneaud, *J. Am. Chem. Soc.*, **68**, 832 (1946); A. Müller, *Org. Synth.*, Coll. Vol. II, 535 (1943).

On the Reaction of *N*-Vinyliminophosphoranes with 2,4,6-Cyclooctatrienone. Intermediate Formation of 8-Azabicyclo-[5.3.1]undeca-2,4,7,9-tetraene Ring System[1)]

Makoto NITTA* and Nobuhiro KANOMATA
Department of Chemistry, School of Science and Engineering, Waseda University, Shinjuku-ku, Tokyo 169
(Received November 12, 1988)

Synopsis. The reaction of *N*-(1-phenylvinyl)iminotriphenylphosphorane and of *N*-(1,3,5-cycloheptatrienyl)iminotributylphosphorane with 2,4,6-cyclooctatrienone gave an intermediacy of 8-azabicyclo[5.3.1]undeca-2,4,7,9-tetraene derivatives, which underwent an intramolecular Diels–Alder reaction to construct a tetracyclic ring system.

The 1,6-methano[10]annulenes[2,3)] and their nitrogen analogues[4,5)] have been widely investigated by Vogel et al. and have been recognized as aromatic compounds in terms of their chemical and spectroscopic properties. The synthesis of 1,5-methano[10]-annulene (**1**)[6,7)] was accomplished via two different routes, and the ^{1}H NMR clarified that the diamagnetic ring current is induced in this system, despite the expected differences in the pi-bond torsion between the two isomeric annulenes. However, no synthetic entry into 8-azabicyclo[5.3.1]undeca-1,3,5,7,9-pentaene (**2**), which is an analogue of **1**, has appeared. Thus, we attempted the synthesis of the 8-azabicyclo[5.3.1]undeca-2,4,7,9-tetraene skeleton, the dehydrogenation of which was expected to give the ring system, **2**.

Our synthetic strategy is based upon utilizing *N*-vinyliminophosphoranes, which are very convenient synthones for constructing various heterocyclic ring systems.[8–13)] Among these synthetic reactions, *N*-(1-phenylvinyl)iminotriphenylphosphorane (**4**) reacted with a series of cyclic α,β-unsaturated ketones **3** to give [*n*](2,4)pyridinophane derivatives (**6**, n=6—9), as shown in Scheme 1.[12)] Therefore, the preparation of an 8-azabicyclo[5.3.1]undeca-2,4,7,9-tetraene ring system by using *N*-vinyliminophosphoranes, **4** and *N*-(1,3,5-cycloheptatrienyl)iminotributylphosphorane (**15**), with 2,4,6-cyclooctatrienone seemed to be promising.

The reaction of **7**[14)] and **4**[9,11)] in anhydrous 1,2-dimethylbenzene under reflux for 15 h gave 9-phenyl-10-azatetracyclo[5.3.1.0.^{1,5}0^{6,8}]undeca-3,9-diene (**11**) in 47% yield (Scheme 2). The formation of **11** can be reasonably explained as follows.[12)] The Michael addition of **4** to the β-carbon atom of **7** gives **8**, the hydrogen transfer of which gives **9**. The intramolecular aza-Wittig reaction of **9** is expected to give **10**. However, compound **10** seems to be labile under reaction conditions and underwent an intramolecular Diels–Alder reaction to give **11**. The thermal lability of **10** to give **11** is reminiscent of the thermal reactivity of bicyclo[5.3.1]undeca-2,4,7,9-tetraene, the C_2=C_3 double bond and diene system in which are located appropriate for the Diels–Alder reaction.[6a)] The assignments of ^{1}H and ^{13}C resonances of **11** are accomplished by 2D ^{1}H NMR and 2D ^{1}H–^{13}C NMR analysis. Considering the ^{1}H NMR spectrum, a pair of methylene protons (11-H_2) appears at δ 1.93 and δ 0.85, which is shielded by the C=N double bond. The remaining signals appear at δ 1.93—1.99 (5-H, 6-H, and 7-H), δ 2.56 (8-H), δ 2.66 and 2.85 (a pair of methylene protons, 2-H_2) δ 5.76 and 5.79 (a pair of vinyl protons, 3-H and 4-H), and δ 7.39 and 7.38 (phenyl group). The ^{1}H NMR and ^{13}C NMR (see Experimental) characteristics are in good accordance with the proposed structure of **11**. Since we could not succeed in isolating the intermediate **10**, we tried a retro Diels–Alder reaction of **11** to **10**. However, the flash pyrolysis of **11** at 400 °C afforded 6,7-dihydro-2-phenyl-4-vinyl-5*H*-cyclopenta[*b*]pyridine (**13**) and 2-phenyl-4-vinyl-7*H*-cyclopenta[*b*]pyridine (**14**) in 22 and 4% yield, respectively. The spectral data of **13** and **14** supported the structures (see Experimental). The formation of **13** and **14** is explained by retro Diels–Alder reaction including methylene bridge, a typical Cope rearrangement of tricyclo[3.2.1.0^{2,7}]oct-3-ene system,[15)] to result in the formation of an intermediate **12** followed by hydrogen transfer or dehydrogenation (Scheme 2).

Similarly, the reaction of **9** with *N*-(1,3,5-cycloheptatrienyl)iminotributylphosphorane (**15**)[13)] in anhydrous bromobenzene under reflux afforded a mixture of 2-

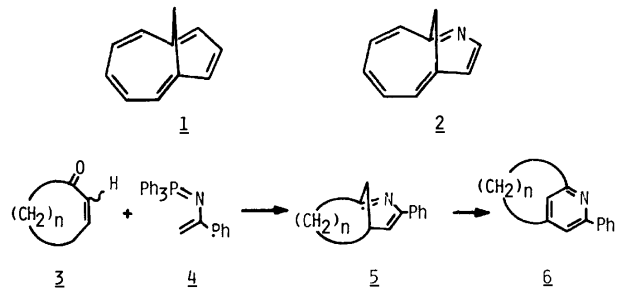

Scheme 1.

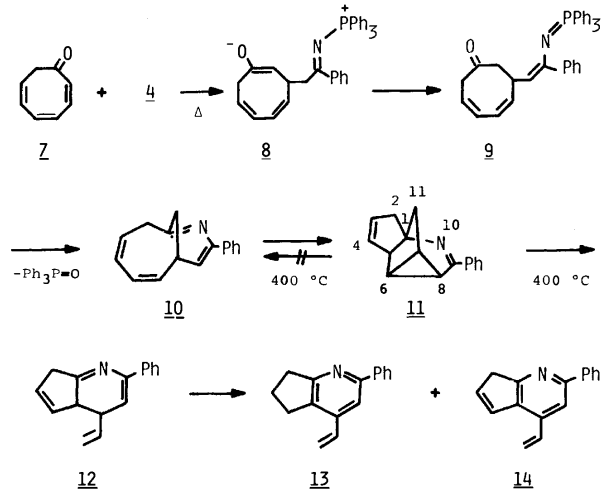

Scheme 2.

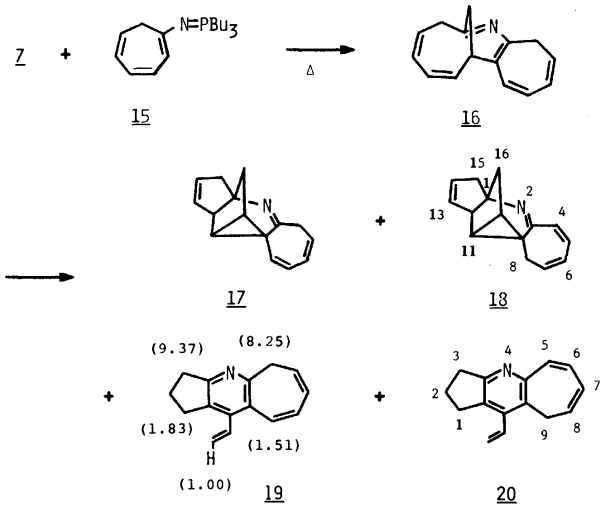

Scheme 3.

azapentacyclo[8.5.1.0.^{1,12}0.^{3,9}0^{9,11}]hexadeca-2,5,7,13-tetraene (**17**) (35%), 2-azapentacyclo[8.5.1.0.^{1,12}0.^{3,9}0^{9,11}]-hexadeca-2,4,6,13-tetraene (**18**) (35%), 1,2,3,5-tetrahydro-10-vinylcyclohepta[*b*]cyclopenta[*e*]pyridine (**19**) (5%), and 1,2,3,9-tetrahydro-10-vinylcyclohepta[*b*]cyclopenta-[*e*]pyridine (**20**) (1.4%), via the possible intermediate **16** (Scheme 3). Although the isolation of both **17** and **18** was unsuccessful, compound **18** was isolated in pure form in the thermal reaction of a mixture of **17** and **18** (vide infra). The ^{1}H NMR spectrum of **18** exhibited signals of a shielded methylene proton (16-H) at δ 0.65, which is located over the C=N double bond, a pair of methylene protons (15-H$_2$) at δ 2.55 and 2.70, two vinyl protons (13-H and 14-H) at δ 5.69, and four protons (10-H, 11-H, 12-H, and 16-H) at δ 1.50—1.90. The chemical shifts and the coupling patterns of these signals are similar to the corresponding signals of **11**. The remaining signals on the cycloheptadiene moiety for **18** appear at δ 6.48 (4-H), δ 6.20 (5-H), and δ 5.99 (6-H and 7-H), in addition to the signals of a pair of methylene protons at δ 2.23 and 2.29 (8-H$_2$). The assigned ^{1}H NMR and ^{13}C NMR (see Experimental) characteristics are in good accordance with the proposed structure **18**. On the other hand, the ^{1}H NMR signals corresponding to **17** were read from the spectrum of a mixture of **17** and **18**. The signals of a shielded methylene proton (16-H) appearing at δ 0.73, three methine protons (10-H, 11-H, and 12-H) and a methylene proton (16-H) at δ 1.47—2.07, a pair of methylene protons (15-H$_2$) at δ 2.37—2.77, and a pair of vinyl protons (13-H and 14-H) appearing at around δ 5.71 are suggestive of a skeleton similar to **18**. Furthermore, two methylene protons appearing at δ 3.00—3.20 and four vinyl protons (5-H, 6-H, 7-H, and 8-H) appearing at δ 5.30—6.55 are suggestive of the cycloheptadiene moiety. A characteristic difference between **17** and **18** is the chemical shifts of methylene protons in their cycloheptadiene rings. The fact that the methylene signals (4-H$_2$) of **17** appear at lower field than those (8-H$_2$) of **18** is ascribed to a deshielding effect of the nitrogen atom which is close to 4-H$_2$ in **17**. The ^{1}H NMR and ^{13}C NMR (assigned in Experimental) spectra of **19** and **20** revealed that they have a cycloheptatriene ring fused on the pyridine ring. The methylene protons in the cycloheptatriene rings of **19** (δ 3.19) and **20** (δ 2.97), and the pseudo-contact ^{1}H NMR spectra of **19** obtained by using Eu(fod)$_3$ unequivocally supported the structures. The relative down-field shifts of the δ's of typical protons are given in parentheses in the structural formula **19**. Compound **18** could be derived from 1,5-hydrogen shift of **17**. The independent thermal reaction of a 1/1 mixture of **17** and **18** in bromobenzene under reflux gave **19** and **20**, in addition to **18**. The pathways for the formation of **19** and **20** can be expalined by a Cope rearrangement of **17** and **18**, as in the case of **11**. The thermal isomerization reaction of **19** in refluxing bromobenzene also occurred to give **20**, thus suggesting the interconversion between **19** and **20**.

The smallest cyclic α,β-unsaturated ketone which reacted with *N*-vinyliminophosphoranes is cyclononenone, giving [6](2,4)pyridinophane (Scheme 1).[12] We have clarified here that the *N*-vinyliminophosphoranes, **4** and **15**, actually react with 8-membered ketone **7** to form constrained intermediates, 8-azabicyclo[5.3.1]undeca-2,4,7,9-tetraene derivatives **10** and **16**.

Experimental

The IR spectra were recorded on a Shimadzu IR-400 spectrometer. The ^{1}H NMR spectra were recorded on a Hitachi R-24 or on a Hitachi R-90H spectrometer. The ^{13}C NMR spectra were recorded on a Hitachi R-90H or on a JEOL GSX400 spectrometer. The 2D ^{1}H NMR and 2D ^{1}H–^{13}C NMR experiments were performed on a JEOL GSX400 spectrometer. The chemical shifts are given in ppm (δ) relative to the internal SiMe$_4$ standard. The mass and high-resolution mass spectral studies were conducted using Shimadzu GCMS QP-1000 and JEOL JMS-DX300 spectrometers. The desired 2,4,6-cyclooctatrienone (**7**),[14] *N*-(1-phenylvinyl)iminotriphenylphosphorane (**4**)[9,11] and *N*-(1,3,5-cycloheptatrienyl)iminotributylphosphorane (**15**)[13] were prepared by the methods described in the literature. All the reactions were carried out under a dry nitrogen atmosphere.

Reaction of 7 with 4. A solution of **7** (60 mg, 0.50 mmol) and **4** (284 mg, 0.75 mmol) in anhydrous 1,2-dimethylbenzene (5 cm^3) was refluxed for 15 h. After the solvent was evaporated, the residue was separated by TLC on silica gel using benzene–ethyl acetate (10/1) as a developer to give **11** (52 mg, 47%), triphenylphosphine oxide (120 mg, 58%) and acetophenone (12 mg, 13%) which arise from the hydrolysis of **4**. For **11**: Mp 44—47 °C; IR (CCl_4), 3059, 2930, 2860, 1592, 1562, 1494, 1446, 1383, 1351, 1292, 1256, 1196, 1182, 1156, 1122, 1106, 1096, 1070, 1022, 992, 936, 842 cm^{-1}; ^{1}H NMR ($CDCl_3$), δ=0.85 (1H, dd, J=11.0, 1.0 Hz), 1.93 (1H, dd, J=11.0, 2.0 Hz), 1.93—1.99 (3H, m), 2.56 (1H, t, J=7.5 Hz), 2.66 (1H, ddd, J=16.0, 2.5, 1.2 Hz), 2.85 (1H, ddd, J=16.0, 2.5, 1.6 Hz), 5.76 (1H, dtd, J=6.1, 2.5, 1.6 Hz), 5.79 (1H, ddt, J=6.1, 2.5, 1.2 Hz), 7.39 (3H, m), 7.83 (2H, m); ^{13}C NMR ($CDCl_3$), δ=18.9 (d, 6-C or 7-C), 19.3 (d, 7-C or 6-C), 20.9 (d, 8-C), 31.4 (t, 11-C), 40.3 (t, 2-C), 50.9 (d, 5-C), 71.1 (s, 1-C), 126.1 (2C, d, Ph), 128.1 (2C, d, Ph), 129.2 (d, Ph), 129.8 (d, 3-C or 4-C), 131.5 (d, 4-C or 3-C), 139.2 (s, Ph), 167.0 (s, 9-C); MS, *m/z* (rel intensity), 221 (M^+, 68), 220 (100). Found: *m/z* 221.1219. Calcd for $C_{16}H_{15}N$: M, 221.1204.

Thermal Reaction of 11. A solution of **11** (100 mg, 0.45 mmol) in anhydrous benzene (20 cm^3) was passed through a Pyrex column (15 mm×120 mm) containing glass beads (ϕ=2 mm) preheated at 400 °C under a nitrogen stream (flow rate=20 cm^3 min^{-1}). After concentration of the

collected pyrolysate, the resulting residue was separated by TLC on alumina using hexane–ether (4/1) to give **13** (22 mg, 22%) and **14** (4 mg, 4%). For **13**: Yellow oil; IR (CCl_4), 3067, 2960, 2848, 1593, 1581, 1565, 1500, 1461, 1443, 1430, 1388, 1337, 1224, 1031, 990, 924, 877, 694 cm^{-1}; ^1H NMR ($CDCl_3$), δ=2.14 (2H, tt, J=8.1, 7.9 Hz), 2.99 (2H, t, J=7.9 Hz), 3.08 (2H, t, J=8.1 Hz), 5.50 (1H, dd, J=11.0, 1.1 Hz), 5.90 (1H, dd, J=17.6, 1.1 Hz), 6.76 (1H, dd, J=17.6, 11.0 Hz), 7.29—7.49 (4H, m), 7.89—8.00 (2H, m); ^{13}C NMR ($CDCl_3$), δ=22.8 (t, 6-C), 29.5 (t, 5-C), 34.4 (t, 7-C), 114.4 (d, 3-C), 118.9 (t, $=CH_2$), 126.8 (2C, d, Ph), 128.2 (d, Ph), 128.4 (2C, d, Ph), 132.6 (s, 4a-C), 133.6 (d, -CH=), 139.9 (s, Ph), 141.0 (s, 4-C), 156.2 (s, 2-C), 166.4 (s, 7a-C); MS, m/z (rel intensity), 221 (M^+, 75), 220 (100). Found: m/z 221.1199. Calcd for $C_{16}H_{15}N$: M, 221.1204. For **14**: Yellow oil; IR (CCl_4), 3071, 2930, 1593, 1502, 1461, 1433, 1378, 1226, 1027, 988, 922, 874, 693 cm^{-1}; ^1H NMR (CCl_4), δ=3.48 (2H, m), 5.50 (1H, dd, J=11.0, 1.2 Hz), 5.94 (1H, dd, J=16.8, 1.2 Hz), 6.85 (1H, dd, J=16.8, 11.0 Hz), 6.93—7.67 (6H, m), 7.85—8.08 (2H, m); MS, m/z (rel intensity), 219 (M^+, 100). Found: m/z 219.1050. Calcd for $C_{16}H_{13}N$: M, 219.1048.

Reaction of 7 with 15. A solution of **7** (600 mg, 5.00 mmol) and **15** (2.30 g, 7.50 mmol) in anhydrous bromobenzene (20 cm^3) was heated under reflux for 3 h. After the solvent was evaporated, the resulting residue was separated by column chromatography on silica gel. The fractions eluted with benzene–ethyl acetate (9/1) afforded a mixture of **19** and **20** (98 mg, 9%). The fractions eluted with benzene–ethyl acetate (8/2) afforded a mixture of **17** and **18** (741 mg, 71%) in a ratio of 1/1. The mixture of **19** and **20** was separated by TLC on alumina using hexane–ether (4/1) as developer. The first band from the TLC plates contained **19** (53 mg, 5%). The second band contained **20** (15 mg, 1.4%). For **18**: Oil; IR (CCl_4), 3035, 2931, 2855, 1600, 1551, 1442, 1427, 1345, 1294, 1180, 1114, 940, 894, 880 cm^{-1}; ^1H NMR ($CDCl_3$), δ=0.65 (1H, d, J=11.4 Hz), 1.50—1.90 (4H, m), 2.23 (1H, dd, J=14.9, 5.9 Hz), 2.29 (1H, dd, J=14.9, 5.7 Hz), 2.55 (1H, d, J=16.3 Hz), 2.70 (1H, dd, J=16.3, 3.1 Hz), 5.69 (2H, m), 5.99 (2H, m), 6.20 (1H, dd, J=11.6, 4.8 Hz); ^{13}C NMR ($CDCl_3$), δ=25.4 (d, 10-C or 11-C), 25.7 (d, 11-C or 10-C), 30.2 (t, 8-C), 31.1 (t, 16-C) 37.3 (s, 9-C), 39.9 (t, 15-C), 50.4 (d, 12-C), 72.0 (s, 1-C), 127.7 (d, 7-C), 129.6 (d, 14-C), 130.8 (d, 6-C) 131.4 (d, 13-C), 132.0 (d, 5-C), 133.5 (d, 4-C), 170.0 (s, 3-C); MS, m/z (rel intensity), 209 (M^+, 48), 208 (100). Found: m/z 209.1195. Calcd for $C_{15}H_{15}N$: M, 209.1204. The ^1H NMR signals for **17** was read from the spectrum of a mixture of **17** and **18** as follows: δ=0.73 (1H, d, J=11.0 Hz), 1.47—2.07 (4H, m), 2.37—2.77 (2H, m), 3.00—3.20 (2H, m), 5.71 (2H, m), 5.30—6.55 (4H, m). For **19**: Oil; IR (CCl_4), 3083, 3031, 2882, 2856, 2847, 1622, 1584, 1559, 1542, 1427, 1402, 1384, 1366, 1242, 1212, 1162, 998, 933, 850 cm^{-1}; ^1H NMR ($CDCl_3$), δ=2.06 (2H, tt, J=7.9, 7.7 Hz), 2.90 (2H, t, J=7.7 Hz), 3.00 (2H, t, J=7.9 Hz), 3.19 (2H, d, J=6.6 Hz), 5.52 (1H, dd, J=17.6, 1.7 Hz), 5.64 (1H, dd, J=11.6, 1.7 Hz), 5.84 (1H, dt, J=9.7, 6.6 Hz), 6.11 (1H, dd, J=9.7, 4.8 Hz), 6.53 (1H, dd, J=11.7, 4.8 Hz), 6.80 (1H, dd, J=17.6, 11.6 Hz), 7.11 (1H, d, J=11.7 Hz); ^{13}C NMR ($CDCl_3$), δ=23.2 (t, 2-C), 30.5 (t, 1-C), 34.4 (t, 3-C), 37.5 (t, 5-C), 121.9 (t, $=CH_2$), 125.0 (s, 9a-C), 125.7 (d, 6-C), 126.9 (d, 7-C), 128.4 (d, 8-C), 128.7 (d, 9-C), 131.8 (s, 10a-C), 132.7 (d, -CH=), 139.8 (s, 10-C), 153.8 (s, 4a-C), 165.7 (s, 3a-C); MS, m/z (rel intensity), 209 (M^+, 100). Found: m/z 209.1211. Calcd for $C_{15}H_{15}N$: M, 209.1204. For **20**: Oil; IR (CCl_4), 3083, 3031, 2891, 2858, 2846, 1622, 1581, 1542, 1432, 1381, 1182, 992, 930 cm^{-1}; ^1H NMR ($CDCl_3$), δ=2.08 (2H, quint, J=7.3 Hz), 2.95 (2H, t, J=7.3 Hz), 2.97 (2H, d, J=6.7 Hz), 3.01 (2H, t, J=7.3 Hz), 5.51 (1H, dd, J=17.6, 1.5 Hz), 5.65 (1H, dd, J=11.6, 1.5 Hz), 5.81 (1H, dt, J=9.7, 6.7 Hz), 6.16 (1H, dd, J=9.7, 5.3 Hz), 6.65 (1H, dd, J=11.6, 5.3 Hz), 6.88 (1H, dd, J=17.6, 11.6 Hz), 7.30 (1H, d, J=11.6 Hz); ^{13}C NMR ($CDCl_3$), δ=23.4 (2-C), 27.8 (9-C), 30.9 (1-C), 34.2 (3-C), 121.3 ($=CH_2$), 124.5 (9a-C), 126.4 (8-C), 126.8 (7-C), 129.9 (6-C), 132.7 (-CH=), 134.5 (5-C), 134.8 (10a-C), 139.4 (10-C), 153.0 (4a-C), 162.4 (3a-C); MS, m/z (rel intensity), 209 (M^+, 100). Found: m/z 209.1189. Calcd for $C_{15}H_{15}N$: M, 209.1204.

Thermal Reaction of 17 and 18. A 1/1 mixture of **17** and **18** (209 mg, 1.00 mmol) in anhydrous bromobenzene (10 cm^3) was heated under reflux for 3 h. The reaction mixture was then concentrated and separated by column chromatography on silica gel using benzene–ethyl acetate (10/1) as eluent to give a mixture of **19** and **20** (8 mg, 4%), in addition to **18** (39 mg, 19%).

Thermal Reaction of 19. A solution of **19** (35 mg, 0.167 mmol) in anhydrous bromobenzene (3 cm^3) was heated under reflux for 3 h. After solvent removal in vacuo, the resulting residue was separated by TLC on alumina using hexane–ether (8/1) as a developer to give **19** (21 mg, 60%) and **20** (7 mg, 20%).

References

1) On the reaction of *N*-vinyliminophosphoranes. Part 10. Part 9: Ref. 13.

2) E. Vogel and H. D. Roth, *Angew. Chem.*, **76**, 145 (1964).

3) D. Cremer and B. Dick, *Angew. Chem., Int. Ed. Engl.*, **21**, 865 (1982).

4) M. Schäfer-Ridder, A. Wagner, M. Schwamborn, H. Schreiner, E. Devrout, and E. Vogel, *Angew. Chem., Int. Ed. Engl.*, **17**, 853 (1978); R. J. Hunadi and G. K. Helmkamp, *J. Org. Chem.*, **46**, 2880 (1981); G. Hiken, T. Kinkel, M. Schwamborn, J. Lex, H. Schmickler, and E. Vogel, *Angew. Chem., Int. Ed. Engl.*, **21**, 784 (1982).

5) H. J. Gölz, J. M. Muchowski, and M. L. Maddox, *Angew. Chem., Int. Ed. Engl.*, **17**, 855 (1978); W. J. Lipa, H. T. Crawford, P. C. Radlick, and G. K. Helmkamp, *J. Org. Chem.*, **43**, 3813 (1978); M. L. Maddox, J. C. Martin, and J. M. Muchowski, *Tetrahedron Lett.*, **21**, 7 (1980); J. C. Martin and J. M. Muchowski, *J. Org. Chem.*, **49**, 1040 (1984); W. Tückmantel, G. Andree, A. Seidel, H. Schmickler, J. Lex, E. Kraka, M. Haug, D. Cremer, and E. Vogel, *Angew. Chem., Int. Ed. Engl.*, **24**, 592 (1985).

6) a) S. Masamune, D. W. Brooks, K. Morio, and R. L. Sobczak, *J. Am. Chem. Soc.*, **98**, 8277 (1976). b) S. Masamune and D. W. Brooks, *Tetrahedron Lett.*, **1977**, 3239.

7) L. T. Scott, W. R. Brunsvold, M. A. Kirms, and I. Erden, *J. Am. Chem. Soc.*, **103**, 5216 (1981).

8) T. Kobayashi and M. Nitta, *Chem. Lett.*, **1985**, 1459.

9) T. Kobayashi, Y. Iino, and M. Nitta, *Nippon Kagaku Kaishi*, **1987**, 1237; Y. Iino, T. Kobayashi, and M. Nitta, *Heterocycles*, **24**, 2437 (1986); T. Kobayashi and M. Nitta, *Chem. Lett.*, **1986**, 1549.

10) Y. Iino and M. Nitta, *Bull. Chem. Soc. Jpn.*, **61**, 2235 (1988).

11) M. Nitta, Y. Iino, E. Hara, and T. Kobayashi, *J. Chem. Soc., Perkin Trans. 1*, **1989**, 51; M. Nitta and T. Kobayashi, *Chem. Lett.*, **1986**, 463.

12) N. Kanomata and M. Nitta, *Tetrahedron Lett.*, **29**, 5957 (1988).

13) Y. Iino, E. Hara, and M. Nitta, *Bull. Chem. Soc. Jpn.*, **62**, 1913 (1989).

14) A. C. Cope and B. D. Teffany, *J. Am. Chem. Soc.*, **73**, 4158 (1951).

15) P. Gilgenm, J. Zsindely, and H. Schmid, *Helv. Chim. Acta*, **56**, 681 (1973); J. P-Katalinic, J. Zsindely, and H. Schmid, *Helv. Chim. Acta*, **56**, 2796 (1973); M. Nitta, A. Sekiguchi, and H. Koba, *Chem. Lett.*, **1981**, 933.

Enhanced Cyclization of *N*-Benzyloxycarbonyl-*N*-substituted Dipeptide Methyl Esters with Ammonia

Katsuhiro KAWASHIRO,* Kazuhisa NISHIGUCHI, and Ikuo KUROSAKA
Department of Chemical Science and Technology, Faculty of Engineering, The University of Tokushima, Minamijosanjima, Tokushima 770
(Received November 18, 1988)

Synopsis. Cyclization of *N,N'*-[*N*-(benzyloxycarbonyl)(Z)-iminobis(methylenecarbonyl)]bis[glycine] dimethyl ester to the hydantoin derivative took place easily under mild ammonolysis conditions. Replacement of Z by *p*-methoxybenzyloxycarbonyl also led to the cyclization. Influence of different substituent groups on the cyclization was studied with some *N*-Z-dipeptide methyl esters.

The benzyloxycarbonyl (Z) has been used frequently in peptide synthesis as an amino-protecting group. However, elimination of Z has been reported in some instances. For example, some *N*-Z-peptide esters give hydantoins or urea derivatives with the loss of benzyl alcohol by alkaline saponification, where glycine is next to N-terminal residue.[1-3] In addition, *N*-Z-dipeptide esters carrying glycine as C-terminus were converted to 3-(carbamoylmethyl)hydantoins, when the side chain of the N-terminal amino acid is rather large such as benzyl, 2-(methylthio)ethyl, or isobutyl group.[4,5] The present study concerns enhanced cyclization of *N*-Z- and *N*-*p*-methoxybenzyloxycarbonyl (Z(OMe))-*N*-substituted glycylglycine methyl esters with ammonia.

Results and Discussion

In an attempt to obtain *N,N'*-[*N*-Z-iminobis(methylenecarbonyl)]bis[glycinamide] (**2**), the corresponding dimethyl ester (**1**) was subjected to ammonolysis in methanol (MeOH) containing dry ammonia (ca. 6 M) (1 M=1 mol dm^{-3}) at room temperature for 24 h. Contrary to expectation, the product was soluble in water, ^{1}H and ^{13}C NMR spectra of which no longer showed signals characteristic of phenyl group. The amino acid analysis of the acid hydrolyzate revealed the presence of glycine and ammonia in a molar ratio of 1:2, and the absence of iminodiacetic acid (IDAA). The findings suggested that cyclization with a loss of Z group took place during the ammonolysis. The ^{1}H NMR spectrum was well consistent with a cyclic structure, 3-(carbamoylmethyl)-1-(carbamoylmethylaminocarbonylmethyl)hydantoin (**3**). The signals could be assigned as follows: A doublet at δ=3.66 is ascribed to NHCH_2 protons; three singlets at 3.94, 4.02, and 4.07 to the three CH_2, respectively; a pair of singlet at 7.08 and 7.35 to $CONH_2$; a pair of singlet at 7.22 and 7.56 to $CONH_2$; a triplet at 8.32 to NH.

For further identification of the product, the acid hydrolyzate was trimethylsilylated with *N,O*-bis(trimethylsilyl)(TMS)-trifluoroacetamide (BSTFA) and then analyzed by the gas chromatography-mass spectrometry (GC-MS). On GC, two peaks eluted: The first peak was identified as an *N,N,O*-tri-TMS derivative of glycine. In the mass spectrum of the second peak, the molecular (M^+) and M−15 (CH_3) ions were observed at *m/z* 360 and 345, respectively, indicating that this compound is the *O,O'*-di-TMS derivative of 1,3-bis(carboxymethyl)hydantoin (mol. wt.=360). Thus the ammonolysis product was confirmed not to be the linear diamide (**2**), but the cyclic amide (hydantoin derivative, **3**).

As shown in Scheme 1, ring closure to **3** involves proton abstraction from nitrogen of the peptide bonds of **2**. Then, the resulting anion (**4**) attacks the carbonyl carbon of the Z group, giving **3** along with the benzyloxyde anion. The ring closure is completed when the benzyloxyde anion abstracts a proton from the conjugate acid BH^+ forming benzyl alcohol. The hydantoin ring is not opened by the excess of ammonia because of its weak basicity.[6] The time course of the ammonolysis at room temperature was followed by HPLC. Benzyl alcohol and **3** were the final products. In contrast, **2** was found to be an intermediate product, which disappeared completely in 8 h.

When Z(OMe) was used as an *N*-protecting group (**5**) instead of Z, the cyclization also took place, but that was not the case for *t*-butoxycarbonyl (Boc) group (**6**); in the latter instance, the *N*-protected linear diamide (**7**) was obtained. This difference can be explained in terms of the nature of the *N*-protecting groups. The phenyl group of Z and Z(OMe) stabilizes the benzyloxyde-type anion by electron-withdrawing, leading to the cyclization. In contrast, the *t*-butyl group of Boc makes the corresponding anion very unstable by electron-repelling, and it consequently prevents the cyclization.

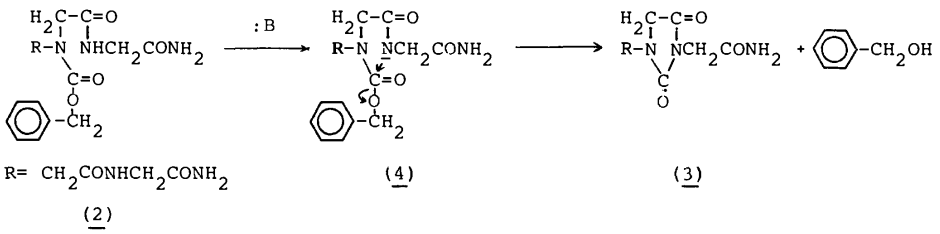

Scheme 1. A possible mechanism for cyclization.

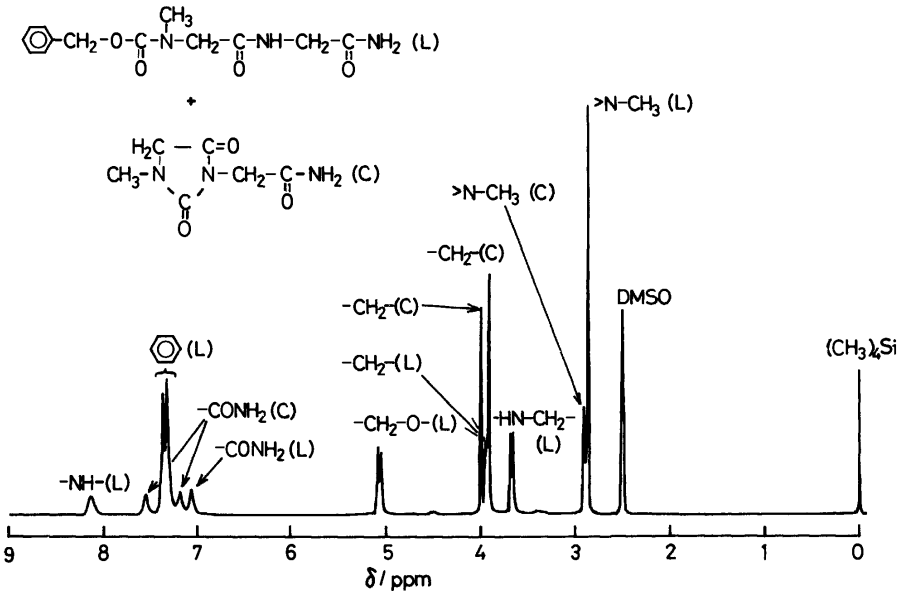

Fig. 1. ^{1}H NMR spectrum for the ammonolysis product of **9**.

Table 1. Results of the Ammonolysis of *N*-Z-dipeptide Methyl Esters

Parent ester	Ratio of the product	
	Linear amide	Cyclic amide
Z-DL-Ala-Gly-OMe (**8**)	100	—
Z-Sar-Gly-OMe (**9**)	54	46
Z-CEGly-Gly-OMe (**10**)	40	60
Z-CEAla-Gly-OMe (**11**)	8	92
Z-CEGly-DL-Ala-OMe (**12**)	100	—
Z(OMe)-CEGly-Gly-OMe (**13**)[a)]	60	40

a) *N*-Z(OMe) derivative.

In order to investigate the influence of different substituent groups, some *N*-Z-dipeptide methyl esters were subjected to ammonolysis at room temperature for 24 h (Table 1). The NH of peptide bond was allowed to be free, because this NH plays an important role in the cyclization (Scheme 1). The ratio between linear and cyclic amides in the products was determined by the ^{1}H NMR spectroscopy.

Figure 1 shows the ^{1}H NMR spectrum for the ammonolysis product of Z-Sar-Gly-OMe (**9**). The absence of singlet at δ=3.6 indicated that ammonolysis of the ester was completed under these conditions. From the comparison of the spectrum (Fig. 1) with that of authentic Z-Sar-Gly-NH_2, the signals marked as L were assigned to the linear amide. But one of the two signals of $CONH_2$ overlaps with phenyl protons of Z. The remaining signals marked as C were well consistent with the cyclic amide, 3-(carbamoylmethyl)-1-methylhydantoin (**14**) as follows: A singlet at δ=2.91 was ascribed to NCH_3 protons; a singlet at 3.91 to CH_2; a singlet at 3.99 to CH_2; a pair of singlets at 7.19 and 7.55 to $CONH_2$. In this instance, the ratio of the two amides was determined by comparing the integrated value of CH_2O protons at δ=5.04 and 5.08 (linear amide) with that of NCH_3 at δ=2.87 and 2.91 (both amides). The formation of **14** was also confirmed by GC-MS after trimethylsilylation of the hydrolyzate of the reaction mixture.

As can be seen in Fig. 1, the absorption of the phenyl and CH_2O protons appeared like a doublet, respectively, thouth they must be singlets normally. For example, these two appeared as singlets for Z-Gly-Gly-NH_2. However, we found that **9** also exhibited such a signal splitting in the 200 MHz spectrum. Therefore, it seems plausible to consider that the signal splitting is due to the presence of the two conformational isomers in a DMSO solution of *N*-Z-*N*-substituted glycylglycine methyl esters and amides. In the 60 MHz spectra, such a signal splitting was not observed because of low resolution.

Table 1 presents the results of the ammonolysis. As we expected, the cyclization was not observed for Z-Gly-Gly-OMe and Z-DL-Ala-Gly-OMe (**8**), which carry no *N*-substituent groups. On the other hand, *N*-Z-*N*-substituted dipeptide esters having glycine residue as C-terminus were generally prone to ring closure. For example, **9** gave a mixture of the linear and cyclic amides in a ratio of 54:46, while its isomer **8** yielded only the normal linear amide. This difference could be explained in terms of the resonance effect. The contribution of resonance structure B increases the electron density on the carbonyl carbon of Z, so

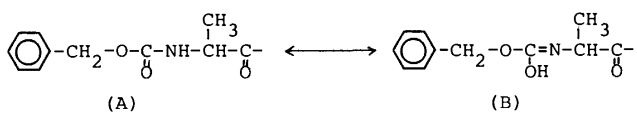

(A) (B)

that the amide anion cannot attack it (Scheme 1). In contrast, such resonance is no longer possible with *N*-Z-*N*-substituted dipeptide esters, the carbonyl carbons of which remain electron-lacking.

The cyclization seems to depend on the nature of the *N*-substituent groups. For example, the extent of the cyclization of Z-CEGly-Gly-OMe[7] (**10**) was higher than that of **9**. This finding could be explained in terms of the difference in electron-repelling ability of the two substituent groups, CH_2CH_2CN and CH_3; the latter repels electron more strongly than the former, increasing electron density of the carbonyl carbon of Z of **9**. The substitution on α-carbon of the N-terminal glycine enhanced the cyclization significantly, as shown for Z-CEAla-Gly-OMe[7] (**11**). In contrast, the substitution on α-carbon of the C-terminal glycine prevented the cyclization completely, as shown for Z-CEGly-DL-Ala-OMe (**12**). This finding indicates that glycine residue carrying a reactive amino group must be present as C-terminus for the cyclization, because the hydantoin is a secondary amide, the diacyl derivative of C-terminal amino acid.

As we can expect, the corresponding *N*-Z(OMe)-dipeptides were also found to cyclize under the ammonolysis conditions. In the instance of Z(OMe)-CEGly-Gly-OMe (**13**), the extent of the cyclization was comparable with that of the corresponding *N*-Z derivative (**10**).

In conclusion, a special care in ammonolysis of *N*-Z- and *N*-Z(OMe)-*N*-substituted dipeptide esters was suggested. Such cyclization, however, will provide a convenient method for the synthesis of 1,3-disubstituted hydantoins.

Experimental

All the melting points determined by a Yanagimoto micro-melting point apparatus were not corrected. ^1H NMR spectra were obtained by a JEOL FX-200 (FT 200 MHz) spectrometer using tetramethylsilane as an internal reference. GC-MS was carried out as previously reported[8] to give 20 eV spectra. HPLC was carried out by a JASCO 880 pump connected with a JASCO 875 UV monitor (column, Finepak SIL C_{18}).

***N*-Protected IDAAs.** Introduction of Z, Z(OMe), and *t*-Boc to IDAA was carried out using Z-Cl,[9] MZ-SDP,[9] and Boc-SDP,[9] respectively, according to the conventional methods.

Z-IDAA: Yield 73%; mp 82—84 °C. Anal. ($C_{12}H_{13}NO_6$) C, H, N.

Z(OMe)-IDAA: Yield 85%; mp 121—122 °C. Anal. ($C_{13}H_{15}NO_7$) H, C, N.

***t*-Boc-IDAA:** Yield 65%; mp 117—120 °C. Anal. ($C_9H_{15}NO_6$) C, H, N.

***N*-Protected IDAA Disuccinimido Esters.** These were prepared by the dicyclohexylcarbodiimide method.

Z-IDAA Disuccinimido Ester: Yield 93%; mp 178—181 °C. Anal. ($C_{20}H_{19}N_3O_{10}$) C, H, N.

Z(OMe)-IDAA Disuccinimido Ester: Yield 64%; mp 201—203 °C. Found: C, 51.03; H, 4.44; N, 8.96%. Calcd for $C_{21}H_{21}N_3O_{11}$: C, 51.33; H, 4.31; N, 8.55%.

***t*-Boc-IDAA Disuccinimido Ester:** Yield 96%; mp 171—174 °C. Anal. ($C_{17}H_{21}N_3O_{10}$) C, H, N.

***N,N'*-[*N*-Protected Iminobis(methylenecarbonyl)]bis[glycine] Dimethyl Esters.** These were prepared by coupling of the *N*-protected IDAA disuccinimido ester with glycine methyl ester.

Z-N($CH_2CONHCH_2COOCH_3$)$_2$ (1): Yield 51%; mp 89—92 °C. Anal. ($C_{18}H_{23}N_3O_8$) C, H, N.

Z(OMe)-N($CH_2CONHCH_2COOCH_3$)$_2$ (5): Yield 53%; mp 82—84 °C. Anal. ($C_{19}H_{25}N_3O_9$) C, H, N.

***t*-Boc-N($CH_2CONHCH_2COOCH_3$)$_2$ (6):** Yield 50%; mp 120—123 °C. Anal. ($C_{15}H_{25}N_3O_8$) C, H, N.

Ammonolysis of 1, 5, and 6. The *N*-protected ester (1 g) was dissolved in MeOH (5 ml) and then 50 ml of MeOH containing dry NH_3 (ca. 6 M) was added. After standing at room temperature for 24 h, the solution was evaporated to dryness and then the residue was recrystallized. The time course of **1** was followed with HPLC by analyzing the aliquots of the reaction mixture at appropriate intervals.

Ammonolysis of 1: Yield 56%; mp 209—211 °C. Anal. ($C_9H_{13}N_5O_5$ (cyclic amide)) C, H, N.

Ammonolysis of 5: Yield 65%; mp 207—209 °C. Found: C, 39.98; H, 4.80; N, 25.34%. Calcd for $C_9H_{13}N_5O_5$ (cyclic amide): C, 39.86; H, 4.83; N, 25.82%.

Ammonolysis of 6: Yield 90%; mp 87—90 °C. Anal. ($C_{13}H_{23}N_5O_6$ (linear amide)) C, H, N. The amino acid analysis of the hydrolyzate revealed the presence of glycine and IDAA in a molar ratio of 2:1.

***N*-Z- and *N*-Z(OMe)-dipeptide Methyl Esters.** Compounds **8**—**13** were prepared by the conventional method of peptide synthesis. The elemental analyses were well agreed with the calculated values except **12**. Melting points were as follows: Z-DL-Ala-Gly-OMe (**8**), 74—76 °C; Z-Sar-Gly-OMe (**9**), 74—77 °C; Z-CEGly-Gly-OMe (**10**), 60—63 °C; Z-CEAla-Gly-OMe (**11**), 103—105 °C; Z-CEGly-DL-Ala-OMe (**12**), oil; Z(OMe)-CEGly-Gly-OMe (**13**), 83—85 °C.

Ammonolysis of *N*-Z- and *N*-Z(OMe)-dipeptide Methyl Esters. The ester (1 g) was dissolved in MeOH (6 ml) and then 50 ml of MeOH containing dry NH_3 (ca. 6 M) was added. After ammonolysis at room temperature for 24 h, the solution was evaporated to dryness with a rotary evaporator. The residue was dried in vacuum. A part of the residue was dissolved in DMSO-d_6 and ^1H NMR spectra were obtained.

References

1) K. Schlögl, F. Wessely, and H. Woidich, *Monatsch. Chem.*, **87**, 425 (1956).

2) J. A. Maclaren, *Aust. J. Chem.*, **11**, 360 (1958).

3) M. Bodanszky, J. T. Sheehan, M. A. Ondetti, and S. Lande, *J. Am. Chem. Soc.*, **85**, 991 (1963).

4) J. S. Fruton and M. Bergmann, *J. Biol. Chem.*, **145**, 253 (1942).

5) C. A. Dekker, S. P. Taylor, and J. S. Fruton, *J. Biol. Chem.*, **180**, 155 (1949).

6) M. Bodanszky and J. Martinez, *Synthesis*, **1981**, 333.

7) *N*-(2-Cyanoethyl)glycine and *N*-(2-cyanoethyl)-DL-alanine were abbreviated as H-CEGly-OH and H-CEAla-OH, respectively.

8) K. Kawashiro, S. Morimoto, and H. Yoshida, *Bull. Chem. Soc. Jpn.*, **57**, 2871 (1984).

9) The reagents were obtained from Peptide Institute, Inc.

Decomposition Reaction of 3-Aryl-6-disubstituted Amino-1,4,2,5-dithiadiazines in the Solid State

Katsumi YONEMOTO* and Isao SHIBUYA
National Chemical Laboratory for Industry, Tsukuba, Ibaraki 305
(Received December 3, 1988)

Synopsis. 3-Diethylamino-6-phenyl-1,4,2,5-dithiadiazine, on standing in air at room temperature, decomposed to afford 5-diethylamino-3-phenyl- and 3,5-bis(diethylamino)-1,2,4-thiadiazoles, whereas in the melt and in solution it was remarkably stable. With increasing bulkiness of substituents (Ar and/or NR_2) in 1,4,2,5-dithiadiazines, their stability in the solid state clearly enhanced. Some interstack interactions in the crystal seem to favor the decomposition.

The chemistry of 1,4-dithiins[1] and their aza analogues, 1,4,2-dithiazines,[2] interesting 8π-electron ring systems, has been extensively studied. Higher aza-analogous ring systems, 1,4,2,5-[3] and 1,4,2,6-dithiadiazine isomers,[4] were prepared as diaryl derivatives for the first time in 1984 by two independent groups. Thermal and photochemical decompositions of 3,5-diphenyl-1,4,2,6-dithiadiazine were reported.[4] We have recently prepared unsymmetrically substituted 1,4,2,5-dithiadiazines through a ring expansion of the corresponding 1,4,2-dithiazolium salts by incorporating one nitrogen atom using *N*-unsubstituted sulfenamides[5] or an I_2–NH_3 system.[6] We now report on the stability and decomposition of 3-aryl-6-(disubstituted amino)-1,4,2,5-dithiadiazines (**1**) in the solid state.

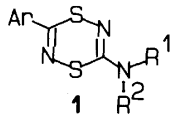

1

Results and Discussion

Some of 3-aryl-6-(disubstituted amino)-1,4,2,5-dithiadiazines, when allowed to stand in air at room temperature, gradually decomposed to give a colorless oil, in contrast to the high stability of 3,6-diaryl-1,4,2,5-dithiadiazines under similar conditions.[3] The decomposition was monitored by following the color fading of yellow crystal and by TLC. Decomposition times, as required for crystalline compounds to be completely decomposed, are listed in Table 1. In the melt and in solution, on the contrary, dithiadiazines **1** were all remarkably stable. For example, compound **1c** was completely recovered after a week in the melt at 76 °C (>mp 71.5 °C) and after a few months in CH_2Cl_2, MeCN, or EtOH. Thus the stability of **1** depends markedly on the phases.

1,4,2,5-Dithiadiazines, which, if planar, would show the 8π-antiaromatic character, actually assume a boat-like conformation[3b,5] common to 1,4-dithiins,[1] which accounts for the thermal stability of the electron rich π-system. The authors speculate that the boat-shaped structure (characterized especially by the fold angle of hetero-ring and the bulkiness of substituents) will have an effect on the mode of stacking with varying intermolecular interactions which either favors or disfavors the observed decomposition, and that the close intermolecular contact in crystal will result in an increase in the fold angle to instabilize the dithiadiazine ring system itself.

Based on the above speculation, the stability of **1** is expected to be dependent on the electron-donating nature of disubstituted amino groups, which seems to be related to the fold angle. The stability of **1a—f** bearing different disubstituted amino groups and the same phenyl group at the C-3 and C-6 positions, respectively, was examined (Entries 1—6). The electron-donating ability of disubstituted amino groups can be estimated from the basicity of the corresponding secondary amines, and accordingly the data are arranged in the decreasing order of pK_a values.[7] However, there is no correlation between the stability of **1** and the electron-donating ability of substituents.

In order to obtain additional information concerning the electron density on the ring carbons C-3 and C-6, ^{13}C NMR spectra were measured. The chemical shifts for ring carbon bearing Ph and that bearing NR_2 are clearly dependent on the nature of disubstituted amino groups, but bear no correlation to the stability of **1**.

We turn our attention to the steric effect of substituents. It can be seen from Entries 1—6 that **1b, e,** and **f** bearing rather bulky substituents, diisopropylamino, morpholino, and *N*-methylphenylamino groups, respectively, are stable, whereas **1c** and **1d** bearing the smaller diethylamino and dimethylamino groups, respectively, have lower stability. The introduction of methoxyl or chloro group on the para-position of the phenyl group in **1a** enhanced the stability of crystal (Entries 7 and 8). Furthermore, the substitution of bulky aryl groups for the phenyl group in **1c**, with the small diethylamino group at the other position kept intact, also tends to retard the decomposition (Entries 10—14).

From the above results, the difference in stability among **1** in the solid state proved to be ascribable to the steric effect of substituents at the C-3 and C-6 positions rather than to their electronic effect.

In order to obtain further information on the decomposition, we examined products attributable to decomposition fragments; the results are presented in Table 2. Compound **1c** decomposed in the solid state to afford 5-diethylamino-3-phenyl-1,2,4-thiadiazole (**2a**) and 3,5-bis(diethylamino)-1,2,4-thiadiazole (**3a**), together with considerable amounts of benzonitrile and elemental sulfur. The formation of **2a** is rationalized by thermal elimination of sulfur (position 1 in **1c**) from the unstable 8π-electron ring system to

Table 1. Stability of 1,4,2,5-Dithiadiazines **1** in the Solid State

Entry	1,4,2,5-Dithiadiazines **1**				Dec. time[b]	^{13}C NMR[c]	
	No.	Ar	NR^1R^2	(pK_a)[a]	d	Ar–C	R^1R^2N–C
1	**1a**	Ph		(11.12)	10		
2	**1b**	Ph	N^iPr_2	(11.05)	Stable	177.5	161.6
3	**1c**	Ph	NEt_2	(10.94)	0.5	177.0	162.5
4	**1d**	Ph	NMe_2	(10.73)	0.5	176.0	163.6
5	**1e**	Ph		(8.33)	Stable	176.0	163.2
6	**1f**	Ph	NMePh	(4.85)	Stable	173.4	161.1
7	**1g**				Stable[d]		
8	**1h**				Stable[d]	175.5	163.5
9	**1i**				Stable	175.0	163.4
10	**1j**		NEt_2		6		
11	**1k**		NEt_2		0.5	176.7	162.6
12	**1l**		NEt_2		0.5		
13	**1m**	[e]	NEt_2		3		
14	**1n**		NEt_2		3		

a) The pK_a value of secondary amine HNR^1R^2 in aqueous solution at 25 °C. b) The time in which crystals have been completely decomposed. c) The assignment of the two quaternary carbons was based on results of 2D COLOC.[13] d) Decomposition was observed after several months. e) Phenylene form.

Table 2. Decomposition Reaction of 1,4,2,5-Dithiadiazines **1** in the Solid State and in the Melt

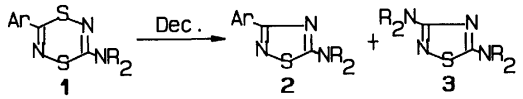

1 **2** **3**

Compd	Conditions	Product yield/%[a]	
		2	**3**[b]
1c	Solid/r.t./0.5 d	15	72
1c	Melt/200 °C/0.5 h	21	28
1c	+Ph_3P/r.t./20 d[c]	44	3
1d	Solid/r.t./0.5 d	5	54
1j	Solid/r.t./6 d	18	69
1n	Solid/r.t./3 d	—	92
1f	Melt/200 °C/2 h	25	11

a) ArCN and S_8 were also formed in considerable amounts. b) Conversion yield based on **1**. c) A 1:1 solid mixture of **1c** and Ph_3P.

afford the more stable 6π-electron one. Such a sulfur extrusion is common to 6-membered 8π-electron ring systems such as 1,4-dithiins[1b,c] and 1,4,2-dithiazines.[2] On the other hand, the formation of **3a** is unique and requires a more complex pathway, because two diethylamino groups are introduced on the 1,2,4-thiadiazole ring. Although 3,5-diphenyl-1,2,4-thiadiazole was not formed, one other product was separated by TLC in a trace amount. It seems to be 3-diethylamino-5-phenyl-1,2,4-thiadiazole, an isomer of **2a**, merely because of the presence of the molecular ion peak at *m/z* 233 (100%) in mass spectrum. The selectivity of the sulfur extrusion can be interpreted in terms of considerable contribution of valence isomer **A** leading to **2a**, compared with **B**, owing to the higher electron-donating ability of diethylamino group than that of phenyl group. Other unstable dithiadiazines **1d**, **j**, and n also decomposed to afford **3** as a main product.

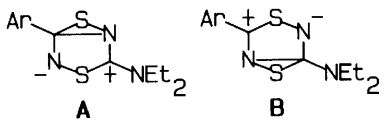

A **B**

Compound **1c**, which is stable in the melt, decomposed at higher temperature. When heated at 200 °C for 30 min, **1c** was completely decomposed to afford a black oil comprised of **2a** (21%) and **3a** (28%). A 1:1 solid mixture of **1c** and Ph_3P, which was prepared by evaporation of their CH_2Cl_2 solution and allowed to stand in air, slowly decomposed to afford **2a** in 44% yield as a main product and a small amount of **3a**, with triphenylphosphine sulfide formed as expected. It was further found that the stable derivative **1f** also decomposed when heated at 200 °C for 2 h to give the corresponding two 1,2,4-thiadiazole deriva-

tives **2c** and **3c** in low yields.

Information concerning the solid state structure of unstable derivatives has been difficult to obtain. However, an X-ray analysis of stable 3-(*p*-chlorophenyl)-6-morpholino-1,4,2,5-dithiadiazine was successfully performed in our previous work.[5] Direct overlapping occurs between the dithiadiazine rings (head to head with an S···S′ separation of 4.06 Å), but the formation of **3** cannot be directly predicted by the molecular orientation. At present, we believe that this decomposition proceeds much faster in the geometrically fixed crystal in which some interstack interactions favor unimolecular and bimolecular decompositions leading to **2** and **3**, respectively. For detailed interpretation of the mechanism for the formation of **3**, further investigations are needed. This decomposition is also attractive as an alternative synthetic method for 3,5-bis(disubstituted amino)-1,2,4-thiadiazoles, which are limitedly accessible by other methods.[8] Further studies on the decomposition in solution, including photolysis, are in progress.

Experimental

^{1}H and ^{13}C NMR spectra were recorded on a Hitachi R-40 and a JEOL FX-90A spectrometer, respectively, in $CDCl_3$, using TMS as an internal standard. Two-dimensional $^1J_{CH}$ shift-correlation spectra and long-range ($^nJ_{CH}$) shift-correlation spectra (COLOC) were recorded on a Bruker AC 200P spectrometer at 50.13 MHz for ^{13}C. Mass spectra were taken on a Hewlett Packard 5995A spectrometer by the electron impact ionizing technique at 70 eV.

3-Aryl-6-(disubstituted amino)-1,4,2,5-dithiadiazines **1** were prepared from the corresponding 1,4,2-dithiazolium salts using our reported procedures, and recrystallized from appropriate solvents (MeCN–ether, CH_2Cl_2–hexane, etc.).[5,6]

Decomposition Reaction of 1. Decomposition reactions of **1** (1 mmol) were carried out in the solid state at room temperature or in the melt at 200 °C. Decomposition times are listed in Tables 1 and 2. Crude products were purified by preparative TLC on silica gel. Their yields are presented in Table 2.

5-Diethylamino-3-phenyl-1,2,4-thiadiazole 2a:[9] ^{1}H NMR δ=1.28 (6H, t, J=7.2 Hz), 3.53 (4H, q, J=7.2 Hz), 7.4—7.6 (3H, m), and 8.2—8.3 (2H, m); MS *m/z* (rel intensity) 233 (M^+; 43), 149 (100), 135 ($PhCNS^+$; 72), and 130 (Et_2NCNS^+; 37).

5-Dimethylamino-3-phenyl-1,2,4-thiadiazole 2b:[10] ^{1}H NMR δ=3.19 (6H, s), 7.4—7.6 (3H, m), and 8.2—8.3 (2H, m); MS *m/z* (rel intensity) 205 (M^+; 47), 149 (100), 135 ($PhCNS^+$; 64), and 102 (Me_2NCNS^+; 62).

5-(*N*-Methylphenylamino)-3-phenyl-1,2,4-thiadiazole 2c:[10] ^{1}H NMR δ=3.64 (3H, s), 7.0—7.7 (8H, m), and 8.2—8.3 (2H, m); MS *m/z* (rel intensity) 267 (M^+; 85), 164 ($MePhNCNS^+$; 49), and 135 ($PhCNS^+$; 100).

3-(*p*-*t*-Butylphenyl)-5-diethylamino-1,2,4-thiadiazole 2d: Mp 45.5—47.0 °C; ^{1}H NMR δ=1.28 (6H, t, J=7.2 Hz), 1.34 (9H, s), 3.53 (4H, q, J=7.2 Hz), 7.45 and 8.16 (2H×2, d, J=8.5 Hz); MS *m/z* (rel intensity) 289 (M^+; 86), 274 (94), and 130 (Et_2NCNS^+; 100).

3,5-Bis(diethylamino)-1,2,4-thiadiazole 3a: oil; ^{1}H NMR δ=1.17 and 1.23 (6H×2, t, J=7.2 Hz), 3.41 and 3.53 (4H×2, q, J=7.2 Hz); ^{13}C NMR δ=12.68 (q), 13.60 (q), 43.12 (t), 45.70 (t), 167.72 (s), and 181.67 (s); MS *m/z* (rel intensity) 228 (M^+; 67) and 72 (Et_2N^+; 74).

3,5-Bis(dimethylamino)-1,2,4-thiadiazole 3b:[11] ^{1}H NMR δ=3.06 and 3.08 (6H×2, s); ^{13}C NMR δ=38.65 (q), 39.87 (q), 169.19 (s), and 183.38 (s); MS *m/z* (rel intensity) 172 (M^+; 100), 129 (62), and 102 (Me_2NCNS^+; 98).

3,5-Bis(*N*-methylphenylamino)-1,2,4-thiadiazole 3c:[12] ^{1}H NMR δ=3.50 and 3.54 (3H×2, s), and 7.0—7.6 (10H, m); ^{13}C NMR δ=39.03 (q), 40.47 (q), 124.00 (d), 124.09 (d), 127.01 (d), 128.47 (d), 129.83 (d), 144.92 (s), 146.05 (s), 166.32 (s), and 182.95 (s); MS *m/z* (rel intensity) 296 (M^+; 79), 190 (M^+—MePhN; 59), 164 ($MePhNCNS^+$; 16), 132 ($MePhNCN^+$; 22), and 82 (100).

We are grateful to Dr. Hiroshi Moriyama for the 2D NMR experiments.

References

1) a) K. Kobayashi, *Yuki Gosei Kagaku Kyokai Shi*, **40**, 642 (1982). b) K. Kobayashi, K. Mutai, and H, Kobayashi, *Tetrahedron Lett.*, **1979**, 5003. c) J. Nakayama, M. Kashiwagi, R. Yomoda, and M. Hoshino, *Nippon Kagaku Kaishi*, **1987**, 1424.

2) J. Nakayama, A. Sakai, A. Tokiyama, and M. Hoshino, *Tetrahedron Lett.*, **24**, 3729 (1983); E. Fanghänel, *J. Prakt. Chem.*, **318**, 127 (1976).

3) a) B. G. Lenz and B. Zwanenburg, *J. Chem. Soc., Chem. Commun.*, **1984**, 1386. b) J. M. M. Smits, P. T. Beurskens, B. G. Lenz, and B. Zwanenburg, *Acta Crystallogr., Sect. C*, **41**, 1086 (1985).

4) S. T. A. K. Daley, C. W. Rees, and D. J. Williams, *J. Chem. Soc., Chem. Commun.*, **1984**, 57; S. T. A. K. Daley and C. W. Rees, *J. Chem. Soc., Perkin Trans. 1*, **1987**, 207.

5) K. Yonemoto, I. Shibuya, and K. Honda, *Bull. Chem. Soc. Jpn.*, **61**, 2232 (1988).

6) K. Yonemoto and I. Shibuya, *Chem. Lett.*, **1989**, 89.

7) J. W. Smith, "Basicity and Complex Formation" in "The Chemistry of the Amino Group," John Wiley & Sons, London (1968), Chap. 4, pp. 161—204; "Dissociation Constants of Organic Bases in Aqueous Solution" in "CRC Handbook of Chemistry and Physics," 67th ed, ed by R. C. Weast, CRC Press, Inc., Florida (1986), P. D-159.

8) F. Kurzer, *Adv. Heterocycl. Chem.*, **32**, 285 (1982).

9) H. Grube and H. Suhr, *Chem. Ber.*, **102**, 1570 (1969).

10) J. Goerdeler and K. H. Heller, *Chem. Ber.*, **97**, 225 (1964).

11) J. E. Oliver, *J. Org. Chem.*, **36**, 3465 (1971).

12) A. R. Butler, C. Glidewell, I. Hussain, and P. R. Maw, *J. Chem. Res. (M)*, **1980**, 1843.

13) H. Kessler, C. Griesinger, J. Zarbock, and H. R. Loosli, *J. Magn. Reson.*, **57**, 331 (1984).

Insolubilizing Studies of Water-Soluble Poly(Lys Tyr) by Tyrosinase[1)]

Akira NAGAI and Hiroyuki YAMAMOTO*
Institute of High Polymer Research, Faculty of Textile Science and Technology, Shinshu University, Ueda 386
(Received December 8, 1988)

Synopsis. Insolubilization of water-soluble synthetic poly(Lys Tyr) was examined using tyrosinase in water and simulated seawater systems. Tyrosinase oxidized tyrosine aromatic nuclei, causing intermolecular crosslinking reactions. The salinity, system pH and α-chymotrypsin are considered to play roles in the insolubilizing reaction.

It has been widely observed in both sea and fresh water that water-soluble proteins normally remain insoluble or surface adhesive in biological systems. Lindner et al.[2)] proposed a mechanism called auto-crosslinking to explain the adhesive properties of proteins secreted by barnacles and mussels. Auto-crosslinking occurs between tyrosyl residues of protein side-chains and the free amino or other reactive groups of other protein molecules with a phenolase enzyme forming an intermolecular crosslink. In this mechanism an oxidase enzyme secreted from byssus and enzyme glands of *Mytilus edulis* plays an initial primary role in protein insolubilization, followed by adhesion.[3,4)] Oxidase also participates in arthropods and chicken-egg shell hardening on land.[5)] These adhesive and hardening phenomena, however, consist of many complex factors, and the auto-crosslinking mechanism described above has not yet been confirmed in a simple protein model.

We have investigated the polymer chemistry of some polypeptide models of *Mytilus edulis*, barnacle, silkworm and caddisworm.[6–9)] This report describes insolubilizing experiments on synthetic poly(Lys Tyr) using tyrosinase in the presence of activator α-chymotrypsin.

Experimental

Poly(Lys[1] Tyr[1]) (hydrobromide, molecular weight 90000), tyrosinase and α-chymotrypsin were purchased from Sigma. Simulated sea water was produced according to the analytical values of six major inorganic salts (NaCl, $MgCl_2$, Na_2SO_4, $CaCl_2$, KCl, and $NaHCO_3$).[10)] The viscosity of poly(Lys Tyr) with and without an enzyme was measured using an Ubbelohde viscometer at 25 °C in both fresh water and seawater. The absorption spectra was measured using a spectrophotometer (Jasco UVIDEC-1).

Results and Discussion

Poly(Lys Tyr) is soluble in fresh water but not in real and simulated seawater. It can, however, be solubilized when the salt concentration is less than 20% of real seawater, with a pH of less than 9. The viscometric characteristics of poly(Lys Tyr) in water and simulated seawater (20% concentration) with and without tyrosinase are depicted in Fig. 1. A slight decrease in the specific viscosity of the polypeptide was found in water. In 20% seawater poly(Lys Tyr), with and without tyrosinase, increases its viscosity to similar levels within 20 h to a 4-fold maximum after 2 days. This increase is attributable to a hydrophobic stacking of tyrosine aromatic nuclei in the polypeptide side chains. After 20 h the poly(Lys Tyr) solution with tyrosinase exhibited a pale brownish purple color. In the tyrosinase free system, however, a white precipitate developed after 70 h. When α-chymotrypsin is added to a poly(Lys Tyr) solution containing tyrosinase, the

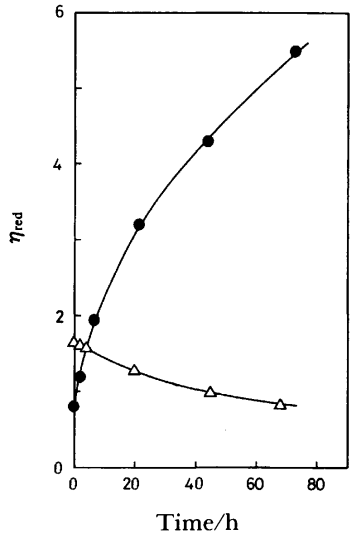

Fig. 1. Apparent viscosity change of poly(Lys Tyr) in aqueous media at pH 6.5 and 25 °C: △ with and without tyrosinase in water; ● with and without tyrosinase in 20% simulated seawater. Concentrations: poly(Lys Tyr) 0.25%; tyrosinase 1200 units.

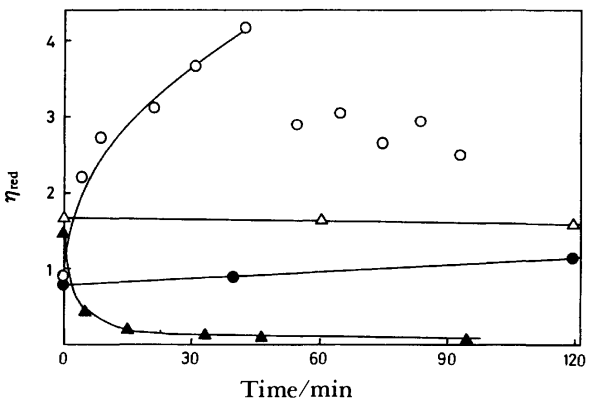

Fig. 2. Viscosity change of poly(Lys Tyr) in aqueous media at pH 6.5 and 25 °C: ○ tyrosinase and α-chymotrypsin in simulated seawater; ▲ tyrosinase and α-chymotrypsin in water; ● both with and without tyrosinase in simulated seawater; △ both with and without tyrosinase in water. Concentrations: poly(Lys Tyr) and tyrosinase, see caption for Fig. 1; α-chymotrypsin 3.6 units; 20% simulated seawater.

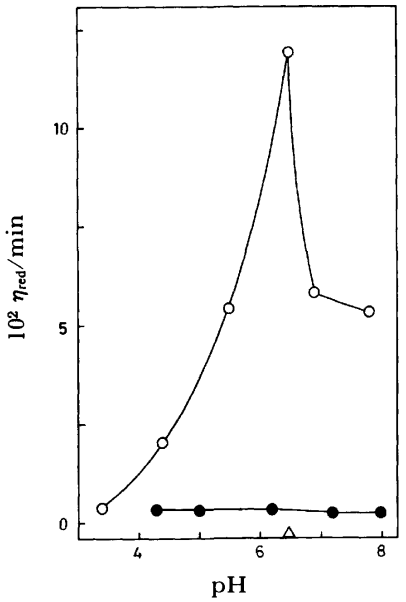

Fig. 3. pH dependence of viscosity change of poly(Lys Tyr) in aqueous media at 25 °C: O tyrosinase and α-chymotrypsin in simulated seawater; ● tyrosinase in simulated seawater; Δ tyrosinase in water. Concentrations, see captions for Figs. 1 and 2.

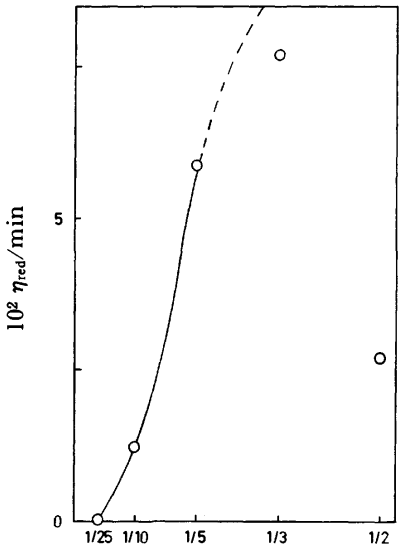

Fig. 4. Effect of salinity on viscosity change of poly(Lys Tyr) in simulated seawater. --- Turbidity observed in freshly prepared solution.

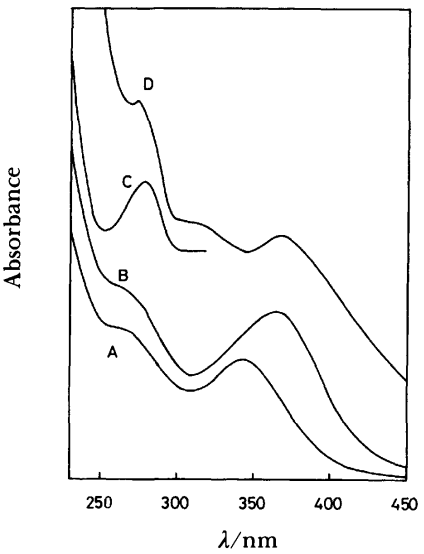

Fig. 5. Absorption spectra of products of poly(Lys Tyr) and model compounds. (A) Boc-L-Dopa quinone and (B) crosslinked Boc-L-Dopa quinone-α-Boc-L-lysine in water-alcohol (1:1 v/v);(C) poly(Lys Tyr) in simulated seawater; (D) 8 mol dm^{-3} HCl solution of partially hydrolyzates from the reaction of poly(Lys, Tyr), tyrosinase and α-chymotrypsin.

viscosity increases rapidly for up to 45 min and a precipitate may be observed by naked eye after 50 min in 20% sea water; the viscosity thereafter gradually decreases to 100 min (Fig. 2). The complex results shown in Figs. 1 and 2 suggest that a system containing poly(Lys Tyr), tyrosinase, and α-chymotrypsin in seawater acts as an auto-crosslinking model. α-Chymotrypsin is believed to cleave the polypeptide at its Tyr sites and to accelerate oxidation at the polypeptide terminals by tyrosinase, followed by the formation of intermolecular crosslinks.

The effects of pH on the viscosity change are depicted in Fig. 3. The viscosity of poly(Lys Tyr) in the presence of tyrosinase slowly decreased in water (pH 6.5) over 4 days. Tyrosinase in seawater induces a minor pH independent of the increase in the viscosity. The presence of both tyrosinase and α-chymotrypsin in seawater is associated with maximum pH-dependent viscosity changes, at around pH 6.5. The effect of salinity levels in this system at pH 6.5 is depicted in Fig. 4. No change in the viscosity was observed in 4% simulated seawater; increasing the salinity accelerated the viscosity change to a maximum level at 20% simulated seawater. At above 33% seawater concentration the hydrophobic stacking effect between Tyr residues predominates, causing a rapid visible precipitation, as described in the explanation of results in Fig. 1.

Absorption spectroscopy was selected to monitor the reaction in the investigation of the auto-crosslink mechanism. A low molecular weight *t*-butoxycarbonyl (Boc)-L-β-3,4-dihydroxyphenyl-α-alanine (Dopa) quinone-α-Boc-L-lysine model system was prepared to confirm the explanation given for the results of Figs. 2—4 (the synthesis will be described elsewhere). The absorption spectra of Boc-Dopa quinone, Boc-L-Dopa quinone-α-Boc-L-lysine, poly(Lys Tyr) and crosslinked poly(Lys Tyr) containing tyrosinase and α-chymotrypsin in aqueous media are depicted in Fig. 5. The absorption spectra of Boc-L-Dopa quinone (curve A) exhibited an absorption band at 340 nm and a shoulder at around 270 nm. To this solution was added α-Boc-L-lysine (no absorption in the 230—450 nm wavelength range). The development rate of the new absorption band at 360—365 nm due to the

crosslink reaction was gradual and slowed down after overnight (curve B). Poly(Lys Tyr) exhibits an absorption peak at 275 nm (curve C). The addition of tyrosinase and α-chymotrypsin to the poly(Lys Tyr) solution caused a rapid 275-nm spectroscopic change (decrease) in seawater and turbidity after about 4 min, while the same system in water exhibited a much slower change. The precipitated materials were collected by centrifugation and partially hydrolyzed by an 8 mol dm^{-3} HCl solution for 3 days at 50 °C, while becoming a clear solution. Curve D in Fig. 5 exhibits an absorption band at 360—365 nm which agreed with the absorption result of curve B of the crosslinked model compound.

From the above-mentioned results, the oxidase enzyme tyrosinase was found to catalyze a succesive reaction from phenol to catechol and, finally, to *o*-quinone in both fresh water and seawater. The oxidation reaction is much faster toward tyrosine than toward tyrosine copolymer. α-Chymotrypsin, thought to exist in the integument and to act as a kind of activator of prephenoloxidase, randomly digests the tyrosine copolymer at aromatic residues and accelerates oxidation by tyrosinase, followed by rapid precipitate formation due to intermolecular crosslinking. This may be a possible insolubilizing mechanism of adhesive proteins in water systems.

The present work was partly supported by a Grant-in-Aid for Scientific Research (No. 61490014) from the Ministry of Education, Science and Culture.

References

1) Orally reported in the 37th Symposium of Polymer Society Japan, Fukuoka, October 1988; *Polymer Preprints Jpn.*, **37**, 1917 (1988).
2) E. Lindner, "Marine Biodeterioration: An Interdisciplinary Study," ed. by J. D. Costlow and R. C. Tipper, Naval Institute Press (1984), p. 183.
3) C. H. Brown, *Quarterly Journal of Microscopical Science*, **93**, 487 (1952).
4) J. H. Waite, *Int. J. Adhesion and Adhesives*, **7**, 9 (1987).
5) D. J. Crisp, Proc. 3rd Inter. Congress on Marine Corrosion and Fouling, p. 691 (1973).
6) H. Yamamoto, *Nippon Kagaku Kaishi*, **1986**, 90.
7) H. Yamamoto, *J. Chem. Soc., Perkin Trans. 1*, **1987**, 613.
8) H. Yamamoto, *J. Adhesion Sci. Tech.*, **1**, 177 (1987).
9) H. Yamamoto, T. Okada, A. Nagai, and A. Nishida, *Nippon Kagaku Kaishi*, **1988**, 1771.
10) K. Wadachi, "Encyclopedia of Oceans (Kaiyo no Jiten)," Tokyo-do Press (1976), p. 75.

Solubilization of Hemin in Neutral and Acidic Aqueous Solutions by Forming Complexes with Water-Soluble Macromolecules

Isamu INAMURA,* Masayuki ISSHIKI, and Takeo ARAKI
Department of Chemistry, Faculty of Science, Shimane University, Matsue 690
(Received December 13, 1988)

Synopsis. Hemin was solubilized in neutral and acidic aqueous solutions by complexing with poly(*N*-vinylpyrrolidone) (PVP), polyethylene glycol (PEG), poly(vinyl alcohol) (PVA) and dextran. In neutral aqueous solutions, hemin in the PVP, PEG, and PVA complexes was monomeric and that in the dextran complex was dimeric. The effects of pH and ultraviolet (UV) irradiation on the spectroscopic properties of the complexes were examined.

It is well-known that hemin is soluble in organic solvents, alkaline aqueous solutions, and aqueous detergent micelles, but insoluble in neutral and acidic aqueous solutions.[1-3] Nishida et al.[4] reported that in alkaline aqueous solutions the aggregated ferroheme (ferroprotoporphyrin IX) and ferroheme·pyridine complex dissociated into the monomers upon the addition of water-soluble macromolecules.

We have recently succeeded in solubilizing hemin in neutral and acidic aqueous solutions by means of water-soluble linear polymers of PVP, PEG, PVA, and dextran. The properties of hemin in aqueous macromolecular solutions were investigated by comparing its absorption spectra with those of hemin in dimethyl sulfoxide (DMSO), an aqueous NaOH solution, and an aqueous Triton X-100 solution.

Experimental

Materials. Hemin (chlorohemin) manufactured by Eastman Kodak Co. was used without further purification. PVP (molecular weight (mol wt), 40000) and PEG (mol wt, 20000) were purchased from Kishida Chemical Co., Ltd. PVA (PVA-117: mol wt, 77000, degree of saponification, 98.5 mol%) was kindly donated by Kuraray Co., Ltd. Dextran (mol wt, 75000) was purchased from Wako Pure Chemical Industries, Ltd. PVP, PEG, PVA, and dextran were purified by reprecipitation of them in solvent-nonsolvent, namely in water-acetone, benzene-petroleum ether, water-methanol, and water-ethanol, respectively.

Method for Solubilization of Hemin in Neutral and Acidic Aqueous Solutions. Solid hemin (0.5 mg) was added to an aqueous macromolecular paste (PVP, PEG, and dextran, 33%; PVA, 15%) containing 1.0 g polymer and gently stirred. The mixture was added by 0.3 ml of 28% aqueous ammonia and stirred gently, resulting in hemin being dissolved. It was then evaporated to a hemin-polymer film under reduced pressure at room temperature. A small amount of water was added onto the film, and stirred gently at room temperature (PVP, PEG, and dextran films) or 100 °C (PVA film) until a paste was formed. The paste was diluted with water to a given concentration, resulting in a neutral aqueous macromolecular solution of hemin.

Acidic aqueous macromolecular solutions of hemin were obtained by the addition of concentrated hydrochloric acid to the neutral aqueous solutions.

Hemin was also dissolved in an aqueous Triton X-100 solution in a similar way by using aqueous ammonia.

Analytical Methods. The absorption spectra at room temperature were measured with a double-beam spectrophotometer, UVIDEC-510 (Japan Spectroscopic Co., Ltd.).

Photobleaching of Hemin. Photobleaching experiments were carried out under ultraviolet (UV) light. UV irradiation was performed with a fluorescence lamp (Mitsubishi GL-15) placed 10 cm from a quartz cuvette containing the hemin solution. The photodegradation (%) of hemin was calculated by dividing the absorbance after UV irradiation by that before irradiation. The wavelengths used to monitor the photodegradation were those of the absorption maxima of Soret bands.

Results and Discussion

There have been several suggestions that a sharp

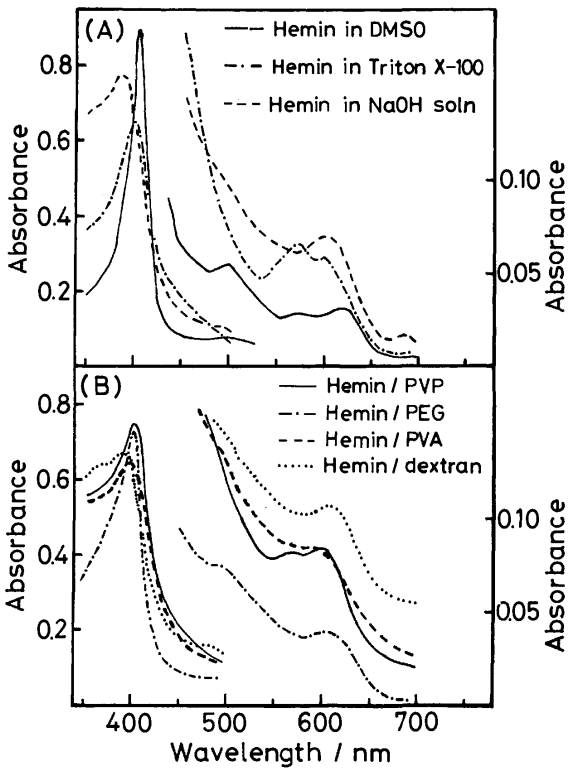

Fig. 1. Absorption spectra of hemin in different states. (A) hemin dissolved in various solvents: ——, hemin in DMSO (hemin, 5.1×10^{-6} mol dm^{-3}); —·—·—, hemin in an aqueous Triton X-100 solution (hemin, 1.0×10^{-5} mol dm^{-3}; Triton X-100, 1.0%, pH 5.7); ---, hemin in an aqueous NaOH solution (hemin, 1.5×10^{-5} mol dm^{-3}; pH 10.4). (B) hemin-macromolecular complexes in water: ——, hemin-PVP complex (hemin, 1.53×10^{-5} mol dm^{-3}; pH 7.5); —·—·—, hemin-PEG complex (hemin, 1.0×10^{-5} mol dm^{-3}; pH 7.1); ---, hemin-PVA complex (hemin, 1.6×10^{-5} mol dm^{-3}; pH 6.3); ·····, hemin-dextran complex (hemin, 1.3×10^{-5} mol dm^{-3}; pH 7.5).

single Soret band corresponds to monomeric ferriheme (ferriprotoporphyrin IX), whereas a doublet shows the presence of dimers.[1,5] Further, the absorption spectra of ferriheme are considered to depend on the species bound to iron at the fifth and sixth positions.[1]

Figure 1-(A) shows the absorption spectra of hemin dissolved in various solvents. The absorption maxima were as follows: 405, 498, 575, and 623 nm for hemin in DMSO; 401, 573, and 600 nm for hemin in an aqueous Triton X-100 solution; 360, 388, 500, and 603 nm for hemin in an aqueous NaOH solution. It is generally considered that hemin is monomeric in DMSO[1] and aqueous Triton X-100 solutions,[2,3] and dimeric[6] in aqueous NaOH solutions.[2]

Hemin was dissolved in neutral aqueous solutions by means of water-soluble linear polymers of PVP, PEG, PVA, and dextran. The resulting solutions gave the absorption spectra of hemin shown in Fig. 1-(B). Since hemin itself is insoluble in neutral aqueous solutions,[1-3] it can be inferred that the linear polymers complexed with hemin, resulting in the solubilization of hemin in neutral aqueous solutions. The polymers probably bound hemin within a random coil of the chain.

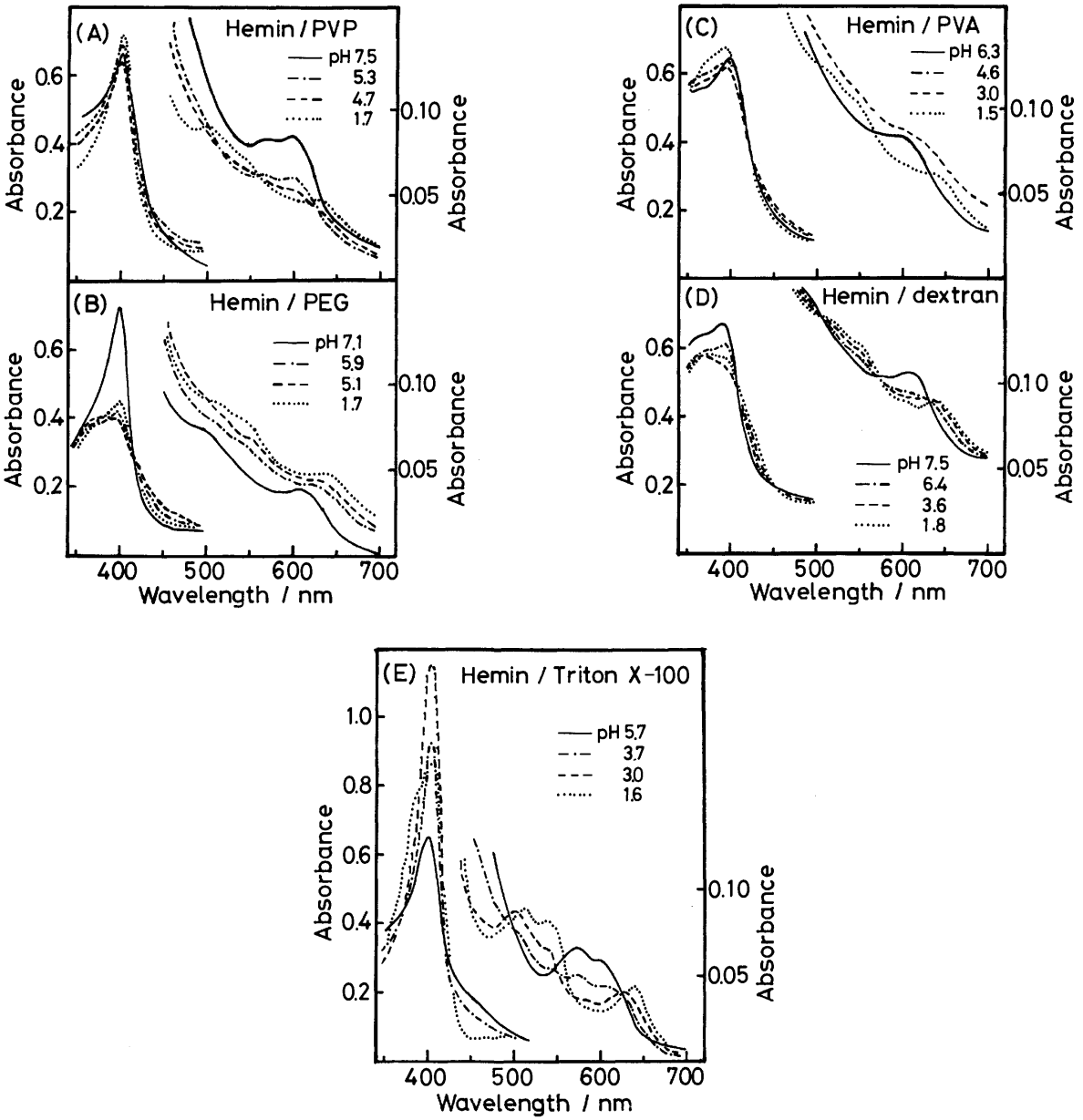

Fig. 2. Dependence on pH of absorption spectra for hemin in different states. The concentrations of hemin were the same as in Fig. 1. (A) hemin-PVP complex in water, (B) hemin-PEG complex in water, (C) hemin-PVA complex in water, (D) hemin-dextran complex in water, (E) hemin in an aqueous Triton X-100 (1.0%) solution.

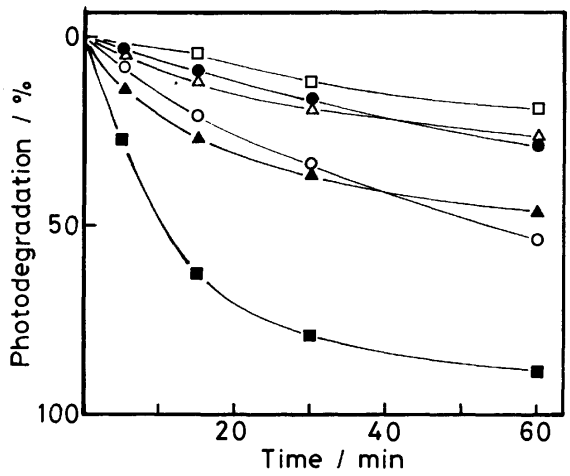

Fig. 3. Photodegradation of hemin in different states by irradiation of UV light. The wavelengths monitoring the photodegradation were those of absorption maxima of Soret bands. The concentrations of hemin were the same as in Fig. 1. ○, hemin-PVP complex in water (pH 7.5); ▲, hemin-PEG complex in water (pH 6.9); ●, hemin-PVA complex in water (pH 7.1); △, hemin-dextran complex in water (pH 7.5); □, hemin in aqueous Triton X-100 (1.3%) solution (pH 6.5); ■, hemin in DMSO.

The absorption maxima for the hemin-macromolecular complexes in neutral aqueous solutions (Fig. 1-(B)) were as follows: 401, 568, and 600 nm for PVP complex; 400, 490, and 608 nm for PEG complex; 398 and 600 nm for PVA complex; 365, 389, and 608 nm for dextran complex. The PVP, PEG, and PVA complexes have a sharp single Soret band which resembled, in both shape and position, that of hemin in DMSO and the aqueous Triton X-100 solution. However, the dextran complex had a double Soret band similar to that of hemin in an aqueous NaOH solution. On the other hand, the Q-bands of the PVP and PEG complexes resembled those of hemin in the aqueous Triton X-100 solution and DMSO, respectively. The Q-bands of the dextran complex were similar to those of hemin in the aqueous NaOH solution. From these results, it can be inferred that hemin in the PVP, PEG, and PVA complexes is monomeric and that in the dextran complex it is dimeric.

Figure 2 shows the dependence on pH of the absorption spectra of hemin in different states. The pH-dependence of the Soret bands of the hemin-macromolecular complexes markedly depended on the polymer species. The Soret bands of the PVP complex became narrower as the pH decreased, as well as those of hemin in the aqueous Triton X-100 solution. The Soret band of the PEG and PVA complexes became broader with decreasing pH, and the Soret band of the PEG complex was largely decreased in intensity, even at pH 5.9. In the case of the dextran complex, as the pH decreased the intensity of the Soret band at 365 nm became larger than that at 389 nm. From these results it is considered that the monomeric hemin in the PVP complex was stable even in acidic aqueous solutions, but that in the PEG and PVA complexes was unstable and probably changed into a dimer or aggregates under acidic conditions.

The pH-dependence of the Q-bands for the hemin-macromolecular complexes hardly depended on the polymer species, as shown in Fig. 2. At the lowest pH, three new peaks were observed at similar positions for each complex: that is, at 500, 540, and 628 nm for PVP complex; at 500, 548, and 640 nm for PEG complex; at 510, 545, and 640 nm for PVA complex; at 515, 550, and 638 nm for dextran complex. For hemin in the aqueous Triton X-100 solution, the pH-dependence of the Q-bands were clearly observed, showing it to be similar to that for the hemin-macromolecular complexes. That is, at the lowest pH (1.6), three new peaks appeared at 510, 541, and 640 nm. The appearance of three new peaks for all of the samples implies that upon adding hydrochloric acid to neutral aqueous solutions of hemin to lower the pH (see Experimental section), the chloro ligand bound to iron gradually increases in the presence of excess of Cl^- ions.[1)]

Figure 3 shows the photodegradation of hemin in different states upon irradiation of UV light. It was found that hemin in macromolecular complexes in neutral aqueous solutions was more stable against UV irradiation than that in DMSO. The rates of photodegradation of hemin in macromolecular complexes depended on the polymer species. That is, hemin in the PVA and dextran complexes was photodegraded more slowly than that in the PVP and PEG complexes. Hemin in the aqueous Triton X-100 solution was more stable against UV irradiation than that in macromolecular complexes.

From the above results it can be inferred that in neutral aqueous solutions the carbonyl group of PVP and ether oxygen of PEG have a stronger coordinating power to iron of hemin than the hydroxyl group of PVA and dextran. Ether oxygen of PEG, however, probably loses its strong coordinating power in acidic aqueous solutions.

References

1) S. B. Brown and I. R. Lantzke, *Biochem. J.*, **115**, 279 (1969).
2) J. Simplicio, *Biochemistry*, **11**, 2525 (1972).
3) J.-H. Fuhrhop and K. M. Smith, "Porphyrins and Metalloporphyrins," ed by K. M. Smith, Elsevier, Amsterdam (1975), p. 757.
4) H. Nishide, K. Mihayashi, and E. Tsuchida, *Biochim. Biophys. Acta*, **498**, 208 (1977).
5) D. W. Urry, *J. Am. Chem. Soc.*, **89**, 4190 (1967).
6) S. B. Brown, T. C. Dean, and P. Jones, *Biochem. J.*, **117**, 733 (1970).

Nucleophilic Displacement of Bis(perfluoroalkanoyl) Peroxides with Perfluoroalkanoate

Masato YOSHIDA,* Shyuichi SASAGE, Nobumasa KAMIGATA, Hideo SAWADA,† and Masaharu NAKAYAMA†

Department of Chemistry, Faculty of Science, Tokyo Metropolitan University, Fukazawa, Setagaya-ku, Tokyo 158
†Tsukuba Research Laboratory, Nippon Oil & Fats Co., Ltd., Tokodai, Tsukuba-city, Ibaraki 300-26

(Received January 11, 1989)

Synopsis. Bis(perfluoroalkanoyl) peroxide ($(R_FCO_2)_2$) suffered a nucleophilic displacement with perfluoroalkanoate ($R_F'CO_2^-$) to give new mixed peroxide ($R_F(CO)OO(CO)R_F'$). When thiophene was reacted with bis(perfluoroalkanoyl) peroxide in the presence of pyridinium perfluoroalkanoate, not only the perfluoroalkyl group (R_F) of the peroxide, but also perfluoroalkyl group (R_F') of perfluoroalkanoate, was introduced into thiophene.

The O–O bonds of diacyl peroxides are usually weak and homolytic cleavages take place easily. On the other hand, diacyl peroxides, especially which have strong electron-withdrawing groups, also react as electrophiles in the presence of nucleophiles such as amines, sulfides, or electron-rich benzenes.[1] We have been studying the reactions of bis(perfluoroalkanoyl) peroxides (**1**) and found three types of reactions: (1) a homolytic cleavage of the O–O bond, (2) electron transfer from substrate to the peroxide, and (3) a nucleophilic reaction on the O–O bond of the peroxide.[2] Due to the strong electron-withdrawing fluoroalkyl groups peroxide **1** easily suffered electron transfers or nucleophilic attacks. In the course of the study we found that perfluoroalkanoate ($R_F'COO^-$) attacked bis(perfluoroalkanoyl) peroxide ($(R_FCOO)_2$) to give new mixed peroxide ($R_F(CO)OO(CO)R_F'$); the results will be described herein.

$C_nF_{2n+1}\overset{\overset{O}{\|}}{C}OO\overset{\overset{O}{\|}}{C}C_nF_{2n+1}$

n = 1 (1a), n = 3 (1b), n = 7 (1c)

In the reaction of pyridinium perfluorobutyrate with **1c**, not only perfluoroheptylpyridines but also perfluoropropylpyridines were formed. Both perfluorodecane ($C_{10}F_{22}$) and perfluorotetradecane ($C_{14}F_{30}$) were also detected as coupling products of perfluoroalkyl radicals by GC-MS.

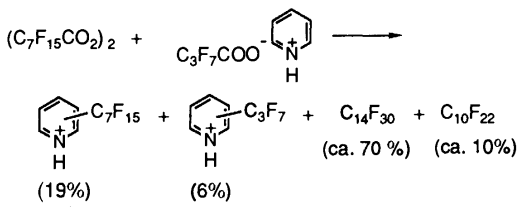

In order to explain these results, we propose the exchange of the perfluoroheptanoyloxy group in **1c** with perfluorobutyrate to give mixed diacyl peroxide and perfluoroheptanoate, as shown in Scheme 1 (Eq. 1). Peroxide **1c** decomposes homolytically to give perfluorotetradecane via a perfluoroheptyl radical (Eq. 2 in Scheme 1). The mixed peroxide also decomposes to perfluoroheptyl and perfluoropropyl radicals and perfluorododecane is produced as a coupling product (Eq. 3 in Scheme 1). The cage escaped perfluoroheptyl or perfluoropropyl radical attacks the pyridinium salt to give perfluoroheptyl- or perfluorpropylpyridine (Eqs. 4 and 5 in Scheme 1).[3] This is the first example of a nucleophilic displacement of the carboxy group in diacyl peroxide with another carboxylate to give new mixed peroxide (as far as we know,[4]), whereas a nucleophilic displacement with carbanions[5,6] or halide anions[7] has in general been well-investigated.

We have reported that peroxide **1** reacts with an electron-rich substrate to give a perfluoroalkylated compound via electron transfer from the substrate to **1**.[2,3] Thus, if a nucleophilic displacement of peroxide **1** with perfluoroalkanoate while affording mixed peroxide occurs, the perfluoroalkyl group of the pyridinium perfluoralkanoate should be introduced into the substrate when **1** reacts with an electron-rich substrate in the presence of pyridinium perfluoroalkanoate. Since we have thoroughly studied the perfluoroalkylation of thiophene,[3,8] we chose thiophene

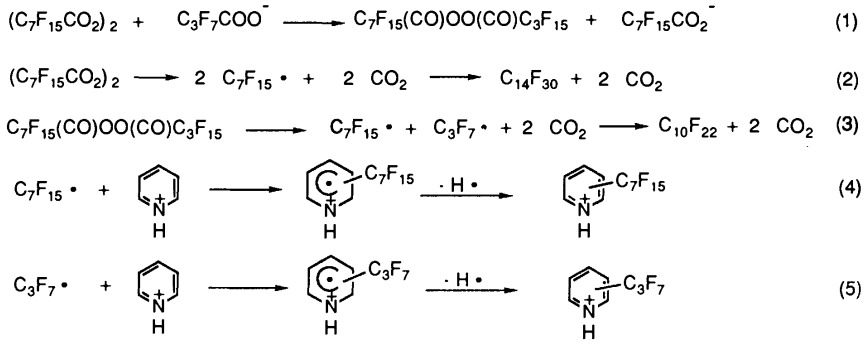

Scheme 1.

Table 1. Perfluoroalkylation of Thiophene with **1** in the Presence of Pyridinium Perfluoroalkanoate[a)]

Run	R_F of **1**	R_F' of pyridinium salt/mmol		Yields of products/%		Total yield
1	C_3F_7	C_7F_{15}	1.0	18	23	41
2	C_7F_{15}	C_3F_7	1.0	20	17	37
3	C_3F_7	C_7F_{15}	0.5	32	22	54
4	C_3F_7	C_7F_{15}	1.5	11	23	34
5[b)]	C_3F_7	None		98	—	98
6	C_7F_{15}	None		97	—	97
7	CF_3	C_7F_{15}	1.0	19	48	67
8	C_3F_7	C_9F_{19}	1.0	32	20	52

a) 0.5 mmol of peroxide was used. The yield was determined by GC based on peroxide. b) From Ref. 3.

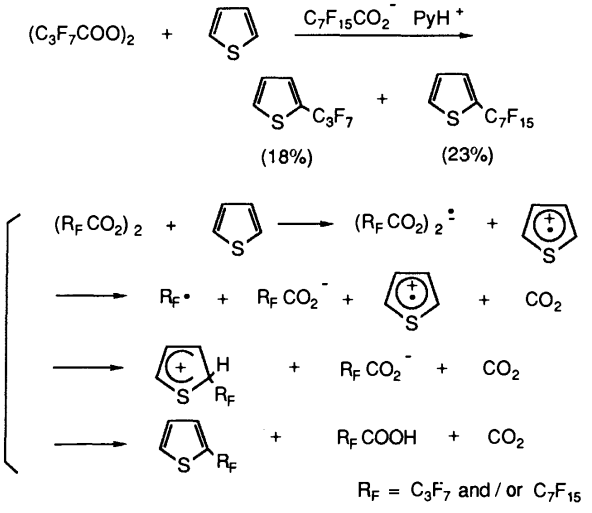

Scheme 2.

as the substrate for an examination of perfluoroalkylation using this method.

Peroxide **1b** was reacted with pyridinium perfluorooctanoate at 0°C for 1 h and then thiophene was added. The resulting solution was further kept at 40 °C for an additional 3 h under vacuum conditions. As expected, 2-(perfluoroheptyl)thiophene was obtained in a yield of 23% in addition to 2-(perfluoropropyl)thiophene in 18% yield, as shown in Scheme 2. The ratio of perfluoropropylthiophene and perfluoroheptylthiophene remained unaltered, even when **1b** and pyridinium perfluorooctanoate was reacted for more than 1 h; then, thiophene was added. Similarly, reactions of **1** with thiophene in the presence of some pyridinium perfluoroalkanoate were performed under various conditions; the results are summarized in Table 1.

In the reaction of thiophene with **1c** in the presence of pyridinium perfluorobutyrate, the perfluoropropyl group was introduced into thiophene. The ratio of perfluoroheptylthiophene and perfluoropropylthiophene was almost the same as that obtained from a reaction system of **1b** and pyridinium perfluorooctanoate (Table 1, Runs **1** and **2**). This means that in the reaction systems of peroxide **1** and pyridinium perfluoroalkanoate, equilibrium as shown below must be attained:

$$(C_3F_7CO_2)_2 + C_7F_{15}CO_2^- \rightleftharpoons C_3F_7(CO)OO(CO)C_7F_{15} + C_3F_7CO_2^-$$

$$C_3F_7(CO)OO(CO)C_7F_{15} + C_7F_{15}CO_2^- \rightleftharpoons (C_7F_{15}CO_2)_2 + C_3F_7CO_2^-$$

Thus, perfluoroheptylthiophene is expected to be obtained selectively when a large excess of pyridinium perfluorooctanoate per **1b** is used. However, the total yield of perfluoroalkylated thiophenes decreased upon increasing the amounts of the pyridinium salt, whereas the ratio of perfluoroheptylthiophene per perfluoropropylthiophene increased (Table 1, Runs **1**, **3**, and **4**). Perfluoroalkylations of thiophene with **1b** or **1c** proceeded almost quantitatively (Table 1, Runs **5** and **6**); however, in the reaction of thiophene with **1** in the presence of pyridinium salt, the total yield of perfluoroalkylthiophenes was about 40%, as shown in Table 1, Runs **1** and **2**. The low yields of perfluoroalkylthiophenes in these reaction systems may not be attributed to the homolytic decomposition of **1** during the exchange reaction of **1** with perfluoroalkanoate, because the homolytic decomposition of **1b** or **1c** does not occur at 0 °C for 1 h. However, it was reported that a N-lone pair of amine attacked nucleophilically the O–O bond of **1b** to decompose the peroxide rapidly, even at 0 °C.[3)] Probably, peroxide **1** reacted with free pyridine which was liberated from the pyridinium salt during the exchange reaction; thus, the yield of perfluoroalkylated thiophene in the presence of pyridinium salt might have been decreased, especially when the amount of pyridinium salt was increased.

By choosing the peroxide, the ratio of perfluoroheptylthiophene per total yield of perfluoroalkylated thiophenes could be increased; the ratio of perfluoroheptylthiophene per total yield was larger in a reaction using **1a** as the peroxide than in one using **1b** (Table 1, Runs **1** and **7**). Peroxide **1a** might suffer a nucleophilic displacement with perfluoroalkanoate more easily than **1b**.

It is very interesting from the view of synthetic chemistry that the perfluoroalkyl group of pyridinium

perfluoralkanoate is introduced into thiophene. We have been studying the synthesis of the diacyl peroxides which contain perfluoroalkyl groups. However, we have not succeeded in the synthesis of the diacyl peroxides which contain perfluoroalkyl chains longer than perfluoroheptyl. We therefore tried to prepare perfluorononylthiophene in a reaction of thiophene with pyridinium perfluorododecanoate in the presence of **1b** (Table 1, Run **8**). Although the yield of the perfluorononylthiophene was not sufficient, the perfluorononyl group could be introduced into thiophene without the synthesis of bis(perfluorododecanoyl) peroxide.

Perfluoroalkylation with peroxide **1** was shown to be a useful and effective method in our previous papers.[2,3,8] In this paper we show that the perfluoroalkyl group can be introduced into thiophene, even if the corresponding peroxide can not be synthesized.

Experimental

^{1}H NMR spectra were taken with a JEOL JNM PMX 60si (60MHz) spectrometer. ^{13}C NMR spectra were taken with a JEOL JNM Fx90Q FTNMR spectrometer. IR spectra were recorded on a Hitachi 260-10 spectrometer. Gas chromatography was performed by a Hitachi 163 or 263-30 gas chromatograph with a SE-30 (10%) 1 m stainless-steel column. Gel-permeation chromatography was performed by means of a JAI Model LC-08 liquid chromatograph equipped with JAIGEL-1H columns (20 ϕ×600 mm×2) and using chloroform as an eluent. Mass spectra were obtained with JEOL JMS DX-300 spectrometer by an electron-impact (EI) ionization technique at 70 eV.

Materials. The syntheses of bis(perfluoroalkanoyl) peroxides were described in the literature.[3,9] These peroxides were used as solutions of Freon 113 without isolation. Pyridinium perfluoroalkanoates were prepared from pyridine with the corresponding perfluoroalkanoic acids. Pyridinium perfluorobutyrate (mp 56—58 °C (from ether)), pyridinium perfluorooctanoate (mp 69—70 °C (from ether)), and pyridinium perfluorododencanoate (mp 101—103 °C (from ether)).

Reaction of Pyridinium Perfluorobutyrate with Bis(perfluorooctanoyl) Peroxide. A solution containing 2 mmol of bis(perfluorooctanoyl) peroxide and 1 mmol of pyridinium perfluorobutyrate in 25 ml of Freon 113 in a degassed sealed tube was kept at 40 °C for 5 h. The solution was then washed with 20 ml of 5% NaOH and 20ml of water. The organic layer was analyzed by GC-MS.

Reaction of Thiophene with Pyridinium Perfluoroalkanoate in the Presence of Peroxide. The reaction was typically performed as follows. A solution containing 0.5 mmol of **1b** and 1.0 mmol of pyridinium perfluorooctanoate in 5 ml of Freon 113 was stirred for 1 h in an ice bath, and then 1.0 mmol of thiophene was added. The resulting mixture was degassed and kept at 40 °C for 3 h in a sealed tube. The reaction mixture was chromatographed over silica gel (Wakogel C-60) using ether as an eluent in order to remove the pyridinium salt and acid. The yields of the perfluoroalkylated thiophene were determined by GC using chlorobenzene as an internal standard. Perfluoropropylthiophene and perfluoroheptylthiophene were isolated using gel-permeation chromatography.

Reaction of Thiophene with 1c without Pyridinium Salt. A solution containing 2 mmol of **1c** and 4 mmol of thiophene in 25 ml Freon 113 was degassed and kept at 40 °C for 3 h in a sealed tube. The solution was washed with 20 ml of water and the organic layer was analyzed by GC-MS. The yield of perfluoroheptylthiophene was determined by GC using chlorobenzene as an internal standard.

2-Pentadecafluoroheptylthiophene; ^{1}H NMR($CDCl_3$) δ= 7.17 (1H), 7.4—7.6 (2H); ^{13}C NMR ($CDCl_3$) δ=127.5(C5), 130.3 (C4), 130.8 (C3); IR 1360 (CF_3), 1220 (CF_2) cm^{-1}; MS *m/z* 452 (M^+); Exact MS: *m/z* 451.9765, Calcd for $C_{11}H_3F_{15}S$: 451.9717.

2-(Nonadecafluorononyl)thiophene; ^{1}H NMR ($CDCl_3$) δ=7.00 (1H), 7.2—7.5 (2H); ^{13}C NMR ($CDCl_3$) δ=127.4 (C5), 130.2 (C4), 130.6 (C3); IR 1360 (CF_3), 1200 (CF_2) cm^{-1}; MS *m/z* 552 (M^+); Exact MS: *m/z* 551.9664, Calcd for $C_{13}H_3F_{19}S$: 551.9652.

The spectral data for 2-(heptafluoropropyl)thiophene was reported in the literature.[3]

References

1) W. A. Pryor and W. H. Hendrickson, Jr., *J. Am. Chem. Soc.*, **105**, 7114 (1983); W. A. Pryor and H. T. Bickly, *J. Org. Chem.*, **37**, 2885 (1972); C. Walling and C. Zhao, *Tetrahedron*, **38**, 1105 (1982), and the references cited therein.

2) M. Yoshida, H. Amemiya, M. Kobayashi, H. Sawada, H. Hagii, and K. Aoshima, *J. Chem. Soc., Chem. Commun.*, **1985**, 234; M. Yoshida, K. Moriya, H. Sawada, and M. Kobayashi, *Chem. Lett.*, **1985**, 755; M. Yoshida, M. Kobayashi, H. Sawada, H. Hagii, and K. Aoshima, *Nippon Kagaku Kaishi*, **1985**, 1958.

3) Perfluoropropylation of pyridinium salt by perfluoropropyl radical produced from **1b** was reported; H. Sawada, M. Yoshida, H. Hagii, K. Aoshima, and M. Kobayashi, *Bull. Chem. Soc. Jpn.*, **59**, 215 (1986).

4) The decomposition of acetyl peroxide in the presence of acetate salts was studied, but the nucleophilic displacement with another carboxylate has not been reported; T. Koenig and R. Wielesek, *J. Am. Chem. Soc.*, **91**, 2551 (1969).

5) S. -O. Lawesson, C. Frisell, D. Z. Denney, and D. B. Denney, *Tetrahedron*, **19**, 1229 (1963).

6) M. Yoshida, K. Shimokoshi, and M. Kobayashi, *Chem. Lett.*, **1987**, 433.

7) N. J. Bunce and D. D. Tanner, *J. Am. Chem. Soc.*, **91**, 6097 (1969); J. K. Kochi, B. M. Graybill, and M. Kurz, *ibid.*, **86**, 5257 (1964).

8) M. Yoshida, T. Yoshida, N. Kamigata, and M. Kobayashi, *Bull. Chem. Soc. Jpn.*, **61**, 3549 (1988).

9) M. Yoshida, T. Yoshida, M. Kobayashi, and N. Kamigata, *J. Chem. Soc., Perkin Trans. 1*, **1989**, 909.

Synthesis of Novel 10-Se-3 Type Selenatetraazapentalene Derivatives with a Hypervalent Selenium

Noboru MATSUMURA,* Masaaki TOMURA, and (the late) Shigeo YONEDA
Department of Applied Chemistry, College of Engineering, University of Osaka Prefecture, Sakai, Osaka 591
(Received February 4, 1989)

Synopsis. Novel selenatetraazapentalene derivatives, 2,3-disubstituted 6,7-dihydro-5*H*-2a-selena(2*a*-Se^{IV})-2,3,4a,7a-tetraazacyclopent[*cd*]indene-1,4(2*H*,3*H*)-dithione, were synthesized by a convenient one-pot reaction using the lithium selenoureide/phenacyl chloride/alkyl isothiocyanate system in good yields.

Chemistry of 1,6,6a-trithia(6*a*-S^{IV})pentalene and analogous compounds has attracted much attention because of their unusual electronic structure, and many 6a-thia(S^{IV})pentalene derivatives containing 10π-electrons in the framework were synthesized.[1] We have recently reported that 12π-thiatetraazapentalene derivatives having π-hypervalent sulfur and two thiocarbonyl groups in the frameworks are synthesized by a convenient one-pot reaction using the lithium thioureide/phenacyl chloride/alkyl isothiocyanate system.[2] However, compounds of this type have not been so well-investigated to date.[3] For a detailed study of the physical and chemical properties of this 12π-tetraazapentalene derivatives, we have tried a synthesis of 12π-selenatetraazapentalenes having a hypervalent selenium (10-Se-3 type).

In this paper, we report the synthesis of 2,3-disubstituted 6,7-dihydro-5*H*-2a-selena(2*a*-Se^{IV})-2,3,4a,7a-tetraazacyclopent[*cd*]indene-1,4(2*H*,3*H*)-dithione (**4**) and its spectral characterization.

Results and Discussion

The 6-membered-ring selenourea (**2**) was prepared by the reaction of *S*,*S*′-dimethyl dithioselenocarbonate (**1**)[4] with 1,3-propanediamine. The reaction was carried out in tetrahydrofuran (THF) at room temperature for 1 h under argon, and further purification with flash-chromatography afforded cyclic selenourea **2** in 35% yield. Selenourea **2** was slightly unstable and colored to red gradually under the atmosphere.

Synthetic reaction of selenatetraazapentalene derivatives **4** was carried out under the same conditions which were used in the synthesis of 10-S-3 type thiatetraazapentalenes.[2] Selenourea **2** was treated with two molar equivalents of butyllithium in THF at 0 °C for 1 h under argon. The resulting dianion (**3**) was allowed to react with a molar equivalent of phenacyl chloride under reflux for 1 h. After cooling to room temperature, a solution of alkyl isothiocyanate (R=CH_3, CH_3CH_2, or CH_2=$CHCH_2$; three times molar quantity of **2**) in THF was added, and the reaction mixture was stirred at room temperature for 20 h. Usual workup and purification gave selenatetraazapentalene derivatives **4a—c** in poor yields (7—12%). It is considered that the poor yields of **4** are due to the thermolability of the dianion **3**. Therefore, the reaction of the dianion **3** with phenacyl chloride was carried out at room temperature. Consequently, the yields of 10-Se-3 type selenatetraazapentalene derivatives **4** have risen remarkably. Scheme 1 shows the reaction pathway for the formation of **4** and the yields of products.

Compounds **4** are considerably stable in air. UV spectra of **4a—c** in acetonitrile show a strong absorption band near 260 nm, and there is no absorption band in the visible region. The structure of **4** was determined by IR, ^{1}H NMR, ^{13}C NMR, mass spectra, and elemental analyses.

Experimental

General. Melting points were determined on a Yanagimoto MP-S3 melting point apparatus and were uncorrected. ^{1}H and ^{13}C NMR spectra were obtained using a JEOL JNM-GX270 spectrometer. Chemical shifts are reported in ppm from TMS as an internal standard and are given in δ units. The IR and UV spectra were determined on a Hitachi 215 Grating infrared spectrometer and Shimadzu UV-265 spectrometer, respectively. Mass spectra were obtained with a Shimadzu LKB-9000 instrument equipped with a solid injector; the ionizing voltage was 70 eV. Purifications of products were conducted by column chromatography on silica gel (Wakogel C-300).

3,4,5,6-Tetrahydro-2(1*H*)-pyrimidineselenone (2). 1,3-Propanediamine (2.87 mmol) was added dropwise to a solution of *S*,*S*′-dimethyl dithioselenocarbonate (**1**) (1.89 mmol) in 30 ml of tetrahydrofuran (THF) at room temperature

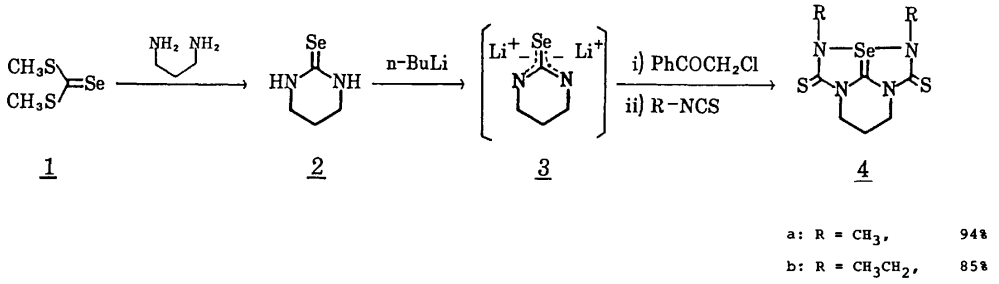

Scheme 1.

under argon. The reaction mixture was stirred under the same conditions for 1 h. After THF was evaporated, the residue was flash-chromatographed on silica gel (chloroform:ethyl acetate=3:1 as an eluent) to give 108 mg of **2** in 35% yield. Reprecipitation from hexane and then recrystallization from methanol afforded pure **2** as a colorless solid: mp 198—201 °C (decomp); IR (KBr) 3180 (NH), 2940, 1560, 1315, and 1205 cm^{-1}; ^1H NMR ($CDCl_3$) δ=1.99 (m, 2H, $NCH_2\underline{CH_2}CH_2N$), 3.31 (d of t, 4H, J=2.0 and 6.0 Hz, $NC\underline{H_2}CH_2C\underline{H_2}N$), and 7.06 (br, 2H, NH); MS m/z (rel intensity) 166 (M^++2; 18), 164 (M^+, based on ^{80}Se isotope peak; 100), 162 (M^+−2; 48), 149 (8), 116 (26), 84 (24), and 83 (25). The microanalysis (C, H, N) was in satisfactory agreement with the calculated value within ±0.5%.

Typical Procedure for the Synthesis of 4. To a cooled THF solution (0 °C, 25 ml) of **2** (94 mg, 0.58 mmol) was added a hexane solution of butyllithium (1.25 mmol) with stirring at 0 °C under argon, and the mixture was stirred for 1 h under the same conditions. To the resulting dianion **3** was added dropwise a THF solution (5 ml) of phenacyl chloride (0.58 mmol). After stirring at room temperature for 1 h under argon, a solution of methyl isothiocyanate (1.74 mmol) in THF (5 ml) was added, and the reaction mixture was stirred under the same conditions for 20 h. After THF was evaporatd, the residue was poured into an aqueous ammonium chloride. The solution was extracted with chloroform, and the extract was washed with water, dried over anhydrous Na_2SO_4, and condensed under reduced pressure. Flash-chromatography of the residue on silica gel using chloroform as an eluent gave 167 mg (94%) of **4a** as a colorless solid. Recrystalization from hexane–chloroform afforded a pure sample.

2,3-Dimethyl-6,7-dihydro-5*H*-2a-selena(2*a*-*Se*^{IV})-2,3,4a,7a-tetraazacyclopent[*cd*]indene-1,4(2*H*,3*H*)-dithoine (4a). Mp 213—216 °C (decomp); IR (KBr) 2930, 1575, 1535, 1500, 1185, and 1110 cm^{-1}; ^1H NMR ($CDCl_3$) δ=2.36 (m, 2H, $NCH_2\underline{CH_2}CH_2N$), 3.32 (s, 6H, 2×$CH_3$), and 4.49 (t, 4H, J=6.0 Hz, $N\underline{CH_2}CH_2C\underline{H_2}N$); ^{13}C NMR ($CDCl_3$) δ=20.28, 33.52, 46.48, 159.21, and 171.13; UV (CH_3CN) 213 (log ε 4.23), 259 (4.41), ca. 290 (sh, 3.85), and 325 nm (3.56); MS m/z (rel intensity) 237 (3), 235 (M^+-CH_3NCS, based on ^{80}Se isotope peak; 10), 233 (4), 193 (3), 122 (4), 97 (8), 73 (100), 72 (55), and 69 (29). Found: C, 31.23; H, 4.06; N, 18.33%. Calcd for $C_8H_{12}N_4S_2Se$: C, 31.27; H, 3.94; N, 18.23%.

2,3-Diethyl-6,7-dihydro-5*H*-2a-selena(2*a*-*Se*^{IV})-2,3,4a,7a-tetraazacyclopent[*cd*]indene-1,4(2*H*,3*H*)-dithione (4b). Mp 195—198 °C (decomp); IR (KBr) 2960, 2920, 1570, 1535, 1480, 1305, 1180, and 1115 cm^{-1}; ^1H NMR ($CDCl_3$) δ=1.35 (t, 6H, J=7.0 Hz, 2×$CH_2\underline{CH_3}$), 2.36 (m, 2H, $NCH_2\underline{CH_2}CH_2N$), 3.87 (q, 4H, J=7.0 Hz, 2×$\underline{CH_2}CH_3$), and 4.50 (t, 4H, J=6.0 Hz, $N\underline{CH_2}CH_2C\underline{H_2}N$); ^{13}C NMR ($CDCl_3$) δ=14.23, 20.23, 42.58, 46.21, 159.41, and 169.91; UV (CH_3CN) 215 (log ε 4.28), 261 (4.48), ca. 292 (sh, 3.90), and 325 nm (3.65); MS m/z (rel intensity) 251 (6), 249 ($M^+-CH_3CH_2NCS$, based on ^{80}Se isotope peak; 31), 247 (16), 111 (10), 87 (100), 83 (36), and 72 (36). Found: C, 35.76; H, 4.96; N, 16,70%. Calcd for $C_{10}H_{16}N_4S_2Se$: C, 35.82; H, 4.81; N, 16.71%.

2,3-Diallyl-6,7-dihydro-5*H*-2a-selena(2*a*-*Se*^{IV})-2,3,4a,7a-tetraazacyclopent[*cd*]indene-1,4(2*H*,3*H*)-dithione (4c). Mp 164—167 °C (decomp); IR (KBr) 2950, 1565, 1515, 1460, 1305, 1160, 1130 and 930 cm^{-1}; ^1H NMR ($CDCl_3$) δ=2.37 (m, 2H, J=6.0 Hz, $NCH_2\underline{CH_2}CH_2N$), 4.44 (m, 4H, 2×$CH_2$=$CH\underline{CH_2}N$), 4.51 (t, 4H, J=6.0 Hz, $N\underline{CH_2}CH_2C\underline{H_2}N$), 5.25—5.34 (m, 4H, 2×$\underline{CH_2}$=$CHCH_2N$), and 5.92—6.07 (m, 2H, 2×CH_2=$\underline{CH}CH_2$-N); ^{13}C NMR ($CDCl_3$) δ=20.19, 46.33, 50.53, 118.79, 132.69, 160.13, and 170.64; UV (CH_3CN) 215 (log ε 4.32), ca. 242 (sh, 4.19), 261 (4.45), ca. 290 (sh, 3.90), and 328 nm (3.67); MS m/z (rel intensity) 263 (7), 261 (M^+-CH_2=$CHCH_2NCS$, based on ^{80}Se isotope peak; 10), 259 (5), 99 (100), 72 (29), and 67 (16). Found: C, 40.46; H, 4.54; N, 15.36%. Calcd for $C_{12}H_{16}N_4S_2Se$: C, 40.11; H, 4.49; N, 15.59%.

References

1) N. Lozac'h, *Adv. Heterocycl. Chem.*, **13**, 161 (1971); K. Akiba and N. Inamoto, *Kagaku No Ryoiki, Zokan*, **124**, 93 (1980); K. Akiba, *Nippon Kagaku Kaishi*, **1987**, 1130; A. S. Ingram, D. H. Reid, and J. D. Symon, *J. Chem. Soc., Perkin Trans. 1*, **1974**, 242; Y. Yamamoto and K. Akiba, *Heterocycles*, **13**, 297 (1979); M. Yokoyama, T. Shiraishi, H. Hatanaka, and K. Ogata, *J. Chem. Soc., Chem. Commun.*, **1985**, 1704.

2) N. Matsumura, M. Tomura, Y. Tsuchiya, S. Yoneda, and M. Nakamura, *Chem. Express*, **1**, 487 (1986); N. Matsumura, M. Tomura, O. Mori, Y. Tsuchiya, S. Yoneda, and K. Toriumi, *Bull. Chem. Soc. Jpn.*, **61**, 2419 (1988).

3) R. J. S. Beer, N. H. Holmes, and A. Naylor, *J. Chem. Soc., Perkin Trans. 1*, **1979**, 2909; N. Matsumura, M. Tomura, O. Mori, and S. Yoneda, *Chem. Lett.*, **1987**, 1065; N. Matsumura, M. Tomura, O. Mori, M. Ukawa, and S. Yoneda, *Heterocycles*, **1987**, 3070; N. Matsumura, O. Mori, M. Tomura, and S. Yoneda, *Chem. Lett.*, **1989**, 39.

4) M. Yokoyama and H. Hatanaka, *Synthesis*, **1985**, 891.

Reactions of Tetrasulfur Tetranitride with Tropolone and Its Several Halogeno Derivatives. Preparations of 4*H*-Cyclohepta[*c*][1,2,5]thiadiazol-4-ones, 6*H*-Cyclohepta[*c*][1,2,5]thiadiazol-6-one, and 7*H*-Cyclohepta-[1,2-*c*:3,4-*c'*]bis[1,2,5]thiadiazol-7-ones

Akira MORI, Hisataka NAKASHIMA,† Shuntaro MATAKA, Masashi TASHIRO, and Hitoshi TAKESHITA*
Institute of Advanced Material Study, 86, Kyushu University, Kasuga-koen, Kasuga, Fukuoka 816
†Graduate School of Engineering Sciences, 39, Kyushu University, Kasuga-koen, Kasuga, Fukuoka 816
(Received February 6, 1989)

Synopsis. The reactions of tropolones with tetrasulfur tetranitride gave 4*H*-cyclohepta[*c*][1,2,5]thiadiazol-4-ones, 6*H*-cyclohepta[*c*][1,2,5]thiadiazol-6-one, and 7*H*-cyclohepta[1,2-*c*:3,4-*c'*]bis[1,2,5]thiadiazol-7-ones (9—56% yields) in one step. The yields of the products were not improved so much under high pressure and by the addition of a radical initiator.

Recently, we reported the reactions of tetrasulfur tetranitride (**1**) with alkyl- and alkylhalogeno phenols to give 2,1,3-benzothiadiazoles in a one-step procedure.[1] From the reactions of **1** with bromocatechols and bromoresorcinols, benzobis- and benzotris[1,2,5]thiadiazoles were prepared.[2] Dihydroxynaphthalene derivatives also gave the corresponding naphtho[1,2,5]thiadiazoles.[3] The 1,2,5-thiadiazole ring system was converted by reduction to 1,2-diamino-, 1,2,3,4-tetraamino-, and hexaaminobenzenes[2] and also used as a building unit for preparation of electron acceptors and electron donors.[4,5] In these regards, since the reaction of **1** was limited to benzenoids, we extended the reaction of **1** to troponoids to prepare new heterocyclic troponoids.

When a toluene solution of tropolone (**2**) and **1** was refluxed for 9 h, a single product (**3**) was obtained after silica-gel chromatography. The ^{1}H NMR spectrum of **3** showed three olefinic proton signals, a singlet at δ=7.76 and an *AB* quartet with a large magnitude of vicinal spin–spin coupling constant (J=12.5 Hz) at δ=7.29 and 8.10, confirming that the seven-membered ring is maintained. Therefore, the structure of **3** can be identified to be 5-hydroxy-6*H*-cyclohepta[*c*][1,2,5]-thiadiazol-6-one. Since we had previously experienced that the yields of thiadiazoles are frequently improved by the use of halogeno derivatives,[1] we then turned our attention to reactions with halogeno tropolones. In contrary to **2**, the reaction with 3-bromotropolone (**4**) was somewhat complicated and gave three products (**5**—**7**), of which **5** was a 1:1-condensation product and the others were 2:1-condensates. The NMR spectrum of **5** showed two doublet signals at δ=8.14 (J=9.5 Hz)

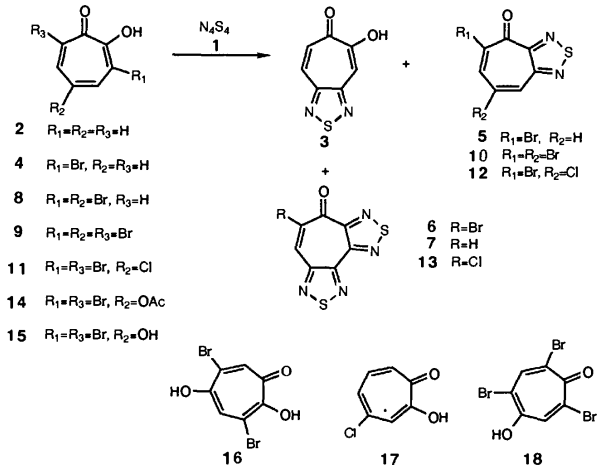

Scheme 1.

Table 1. Reaction Conditions and Product Yields of Tropolones with **1**

Substrate (Ratio)	Temp/°C	Press/bar	Time/h	Additive	Products/% 5	6	7	10
4 (1:1)	110	1	14	—	4	2	26	
4 (1:2)	110	1	10	—	8	7	25	
4 (1:2.6)	110	1	10	—	11	9	18	
4 (1:3)	110	1	14	V-40		15	28	
4 (1:3)	110	1	48	—		14	26	
4 (1:5)	110	1	21	V-40	10	6	16	
4 (1:5)	110	1	21	—	2	2	10	
4 (1:5)	110	1	48	—		16	31	
9 (1:2)	110	1	9	—		21		35
9 (1:3)	110	1	21	—		36		
9 (1:3)	100	3000	10	—		47		
9 (1:3)	110	1	12	V-40		36		12
9 (1:3)	100	3000	10	V-40		41		12
9 (1:3.5)	110	1	16	V-40		40		8
9 (1:3)	110	1	48	—		44		

and 7.78 (J=11.7 Hz) and a doublet of doublets signal at 6.81. For the bromine-containing minor product, **6**, a singlet signal appeared at δ=8.84, while the bromine-free product, **7**, showed an AB quartet (J=13.0 Hz). The yields of **6** and **7** were improved to some extent when **1** was used in excess. The results are summarized in Table 1. Compounds **6** and **7** were also obtained from the reactions of 3,5-dibromotropolone (**8**) with **1** in 24 and 22% yields, respectively. From 3,5,7-tribromotropolone (**9**), another bromine-containing 1:1-condensate (**10**) was obtained in 21% yield together with **6** in 35% yield. Similarly, 3,7-dibromo-5-chlorotropolone (**11**) gave a dihalogeno 1:1-condensate (**12**) and an unseparable mixture of **6** and a chlorine-containing product (**13**). The results concerning the reaction of **9** with **1** under various conditions are tabulated in Table 1.

As shown in Table 1, the yields of products did not show much improvement, either under a high pressure of 3000 bar or by the addition of V-40, a radical initiator.

Furthermore, reactions with five halotroponoids (**14**—**18**) were carried out. No identified product has, however, been detected.

As an extention, the preparation of the tris[1,2,5]-thiadiazole derivative was investigated. No expected product was obtained from the reactions of **6** and **7** with **1** under similar conditions.

To check the reactivity of the carbonyl group of **7**, a couple of reactions with carbonyl reagents were attempted: Treatment with hydroxylamine hydrochloride and malononitrile afforded condensates (**19** and **20**) in 76 and 3% yields, respectively. The reaction of the carbonyl group in **7** with a bulky dicyanomethylene group was sterically unfavorable.

In order to introduce oxygen functions into the seven-membered conjugated system, the hydrogen peroxide-oxidation of **7** was carried out, and the epoxide (**21**) was obtained in 57% yield. However, an attempt to convert the epoxide to a hydroxy ketone, corresponding "tropolone", has so far been unsuccessful.

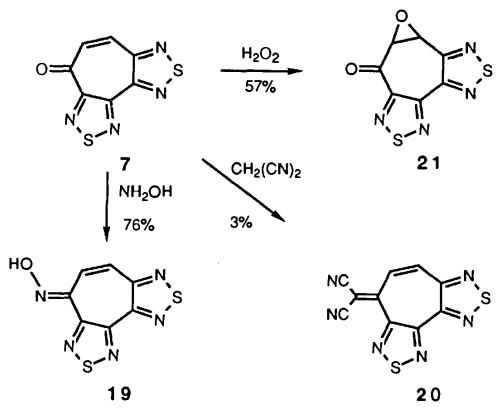

Scheme 2.

Although the yields of condensates between tropolones and tetrasulfur tetranitride were not high, the present method was valuable with respect to a one-step procedure for new heterocyclic troponoids.

Experimental

Reaction of Tropolone (2) with 1. A toluene solution (10 cm³) of **2** (174 mg) and **1** (287 mg) was stirred at room temperature for 1 h and refluxed for 9 h. The mixture was cooled and the solvent was evaporated. The residue was chromatographed on a silica-gel column to give 17.1 mg (9%) of **3** and 43.8 mg (25%) of **2**.

3: Brownish crystals (benzene), mp 146—148 °C (decomp); ^{1}H NMR[6] δ=7.29 (1H, d, J=12.5 Hz), 7.76 (1H, s), 8.10 (1H, d, J=12.5 Hz), and 8.10 (1H, s): ^{13}C NMR δ=108.2, 129.9, 132.7, 154.7, 155.0, 157.1, and 181.0; IR (KBr) 3290, 1632, 1592, 927, 883, 875, and 857 cm^{-1}; MS m/z (%) 180 (M^+, 41), 152 (base), 124 (40), 97 (17), 80 (21), 71 (15), and 52 (33).

Found: m/z 179.9992. Calcd for $C_7H_4N_2O_2S$: M, 179.9993.

Reaction of 3-Bromotropolone (4) with 1. a) A toluene solution (8 cm³) of **4** (150 mg) and **1** (166 mg) was refluxed for 14 h. The mixture was purified by silica-gel chromatography to give 7.8 mg (4%) of **5**, 4.3 mg (2%) of **6**, and 43.3 mg (26%) of **7**.

5: Pale yellow crystals (methanol), mp 160—161 °C (decomp); ^{1}H NMR δ=6.81 (1H, dd, J=11.7, 9.5 Hz), 7.78 (1H, d, J=11.7 Hz), and 8.14 (1H, d, J=9.5 Hz); ^{13}C NMR δ=126.5, 128.8, 135.9, 138.8, 155.7, 157.5, and 172.3; IR (KBr) 1637, 1615, 880, 845 and 815 cm^{-1}; UV (MeOH) 222 (ε 11900, sh), 231.6 (12800), 266.8 (11000), 301 (2200, sh), and 370.8 nm (6300); MS m/z (%) 244 (M^++2, 89), 242 (M^+, 87), 216 (61), 214 (57), 163 (23), 135 (base), 108 (24), 76 (24), and 50 (19).

Found: C, 34.82; H, 1.33; N, 11.68%. Calcd for $C_7H_3N_2OSBr$: C, 34.59; H, 1.24; N, 11.52%.

6: Yellow crystals (chloroform–hexane), mp 236—238 °C (decomp); ^{1}H NMR δ=8.84 (1H, s); ^{13}C NMR δ=131.9, 133.6, 149.9, 150.0, 153.0, 153.6, and 172.1; IR (KBr) 1645, 1390, 1265, 1105, 895, 880, and 860 cm^{-1}; UV (MeOH) 207 (ε 19200, sh), 220 (18500, sh), 231.6 (19400), 266.4 (16000), 300 (4000, sh), and 369.6 nm (9000); MS m/z (%) 302 (M^++2, base), 300 (M^+, 92), 274 (63), 272 (59), 221 (30), 193 (71), 161 (20), 83 (48), and 64 (39).

Found: C, 28.02; H, 0.40; N, 18.55%. Calcd for $C_7H_4N_4OS_2Br$: C, 27.92; H, 0.33; N, 18.61%.

7: Yellow crystals (chloroform–hexane), mp 168—170 °C (decomp); ^{1}H NMR δ=7.10 (1H, d, J=13.0 Hz) and 7.96 (1H, d, J=13.0 Hz); ^{13}C NMR δ=131.2, 132.6, 150.8, 151.1, 154.4, 155.9, and 178.1; IR (KBr) 1635, 1420, 1095, 875, 870, and 855 cm^{-1}; UV (MeOH) 205.6 (ε 18500), 243.2 (9700), 254 (8100, sh), 286.4 (15500), and 314.0 nm (15400); MS m/z (%) 222 (M^+, 8), 194 (53), 142 (33). 116 (26), 84 (49), 58 (73), 52 (80), and 46 (base).

Found: C, 37.63; H, 0.71; N, 25.01%. Calcd for $C_7H_2N_4OS_2$: C, 37.83; H, 0.91; N, 25.21%.

b) A toluene solution (150 cm³) of **4** (1.04 g) and **1** (4.76 g) was refluxed for 48 h. Silica-gel chromatography gave 248 mg (16%) of **6** and 356 mg (31%) of **7**.

Reaction of 3,5-Dibromotropolone (8) with 1. A toluene solution (15 cm³) of **8** (68.8 mg) and **1** (136 mg) was refluxed for 12 h to give 18.2 mg (24%) of **6** and 12 mg (22%) of **7**.

Reaction of 3,5,7-Tribromotropolone (9) with 1. a) A toluene solution (7 cm³) of **9** (193 mg) and **1** (219 mg) was refluxed for 7.5 h. Silica-gel chromatography gave 37.2 mg (21%) of **10** and 57.9 mg (35%) of **6**.

10: Yellow crystals (benzene), mp 194—196 °C (decomp); ^{1}H NMR δ=8.20 (1H, d, J=1.8 Hz) and 8.37 (1H, d, J=1.8 Hz); ^{13}C NMR δ=122.6, 130.3, 134.7, 142.5, 144.0, 156.0, and 171.5; IR (KBr) 1639, 920, 880, and 850 cm^{-1}; UV (MeOH) 212.0 (ε 15100), 232.4 (17000), 268.0 (16000), 308 (2500, sh), and 375.2 nm (7500); MS m/z (%) 324 (M^++4, 53), 322 (M^++2, base), 320 (M^+, 50), 296 (32), 294 (63), 292 (31), 215 (45), 213 (44), 150 (58), 134 (34), 76 (26), 57 (30), and 50 (25).

Found: C, 26.39; H, 0.72; N, 8.51%. Calcd for $C_7H_2N_2OSBr_2$: C, 26.11; H, 0.63; N, 8.70%.

b) A toluene solution (8 cm^3) of **9** (50.1 mg) and **1** (79 mg) was heated at 100 °C for 10 h under 3000 bar. Silica-gel chromatography gave 20 mg (47%) of **6**.

Reaction of 3,7-Dibromo-5-chlorotropolone (11) with 1. A toluene solution (10 cm^3) of **11** (203 mg) and **1** (264 mg) was refluxed for 9 h. Silica-gel chromatography of the mixture gave 41.8 mg (23%) of **12** and 46.2 mg of a mixture of **6** (21%) and **13** (9%).

12: Brown needles (benzene), mp 134—136 °C (decomp); ^1H NMR δ=7.97 (1H, d, J=1.8 Hz) and 8.23 (1H, d, J=1.8 Hz); IR (KBr) 1640, 1600, 1360, 930, 880, and 855 cm^{-1}; MS m/z (%) 280 (M^++4, 28), 278 (M^++2, base), 276 (M^+, 72), 252 (19), 250 (61), 248 (46), 234 (11), 232 (15), 171 (23), 169 (63), and 50 (21).

Found: m/z 275.8781 (M^+), 277.8772 (M^++2), and 279.8710 (M^++4). Calcd for $C_7H_2N_2OClBr$: 275.8760 (M), 277.8740 (M+2), and 279.8710 (M+4).

Attempted Reactions of Halotroponoids (14+18) with 1. A toluene solution of a halotroponoid and **1** was refluxed for 9 h. No expected product was detected.

Reaction of 6 with 1. A toluene solution (4 cm^3) of **6** (10 mg) and **1** (9.2 mg) was refluxed for 11 h. Compound **6** (10 mg) was recovered unchanged.

Reaction of 7 with 1. A toluene solution (8 cm^3) of **7** (13.6 mg) and **1** (13.5 mg) was refluxed for 13 h. Compound **7** (13.4 mg) was recovered unchanged.

Reaction of 7 with Hydroxylamine Hydrochloride. To an ethanol solution (3 cm^3) of **7** (20.2 mg) was added an aqueous solution (3 cm^3) of hydroxylamine hydrochloride (6.9 mg) in the presence of AcONa (12.7 mg) and the mixture was refluxed for 5.5 h. The solvent was evaporated and the residue was washed with water to give 16.4 mg (76%) of **19**.

19: Yellow crystals (diethyl ether), mp 194-197 °C (decomp); IR (KBr) 3342, 3246, 1627, 1032, and 953 cm^{-1}; MS m/z (%) 237 (M^+, base) and 207 (61).

Found: m/z 236.9782. Calcd for $C_7H_3N_5OS_2$: M, 236.9779.

Reaction of 7 with Malononitrile. To an anhydrous dichloromethane solution (7 cm^3) of **7** (78.3 mg) and malononitrile (34.9 mg) were added $TiCl_4$ (0.2 cm^3) and then anhydrous pyridine (0.3 cm^3) at 0 °C. The mixture was stirred at room temperature for 5 h. The mixture was diluted with a 10% aqueous HCl solution and extracted with AcOEt. After evaporating the solvent, the residue was purified by silica-gel chromatography to give 2.6 mg (3%) of **20**.

20: Yellow crystals (benzene), mp 188—190 °C (decomp); ^1H NMR δ=7.51 (1H, d, J=12.8 Hz) and 7.70 (1H, d, J=12.8 Hz); IR (KBr) 2216, 1615, and 1526 cm^{-1}; UV (MeOH) 208.8 (ε13400), 265 (6200, sh), 271.2 (6700), 308.0 (9400), 351 (8400, sh), 366 (9300, sh), and 387.2 nm (10300); MS m/z (%) 270 (M^+, base), 244 (12), 218 (9), 85 (11), 83 (24), and 63 (10).

Found: m/z 269.9786. Calcd for $C_{10}H_2N_6S_2$: M, 269.9782.

Epoxidation of 7. To an anhydrous DMSO solution (5 cm^3) of **7** (50.6 mg) were added 35% H_2O_2 (2 cm^3) and (n-Bu)$_4$NF (115 mg) and the mixture was stirred at room temperature for 13 h. The mixture was poured into water and extracted with AcOEt. Silica-gel chromatography of the residue gave 30.9 mg (57%) of **21**.

21: Colorless crystals (chloroform-hexane), mp 177—178 °C; ^1H NMR δ=4.44 (1H, d, J=4.4 Hz) and 5.02 (1H, d, J=4.4 Hz); ^{13}C NMR δ=55.2, 64.5, 149.1, 150.5, 154.7, 155.0, and 188.7; IR (KBr) 1703, 1030, 885, 842, and 819 cm^{-1}; MS m/z (%) 238 (M^+, 11), 210 (10), 138 (10), 86 (34), 71 (30), 58 (47), and 46 (base).

Found: C, 35.28; H, 0.76; N, 23.46%. Calcd for $C_7H_2N_4O_2S_2$: C, 35.29; H, 0.85; N, 23.52%.

References

1) S. Mataka, K. Takahashi, S. Shiwaku, and M. Tashiro, *J. Chem. Res. (S)*, **1985**, 246; *J. Chem. Res. (M)*, **1985**, 3649.

2) S. Mataka, K. Takahashi, H. Eguchi, and M. Tashiro, 56th National Meeting of the Chemical Society of Japan, Tokyo, April 1988, Abstr., No. 3XIC18.

3) K. Takahashi, M. Tashiro, S. Mataka, T. Hatta, and O. Tsuge, 58th National Meeting of the Chemical Society of Japan, Kyoto, April 1989, Abstr., No. 2IIIG38.

4) Y. Yamashita, T. Suzuki, T. Mukai, and G. Saito, *J. Chem. Soc., Chem. Commun.*, **1985**, 1044.

5) Y. Yamashita and T. Miyashi, *Chem. Lett.*, **1988**, 661.

6) All NMR spectra were measured in $CDCl_3$ with a GSX 270 H and an FX 100 Spectrometers, JEOL.

Electroorganic Synthesis Using Organometals. 2. Reductive Dehalogenation of Halides with Carbonylferrates Derived from Pentacarbonyliron(0) and Cathodically-Generated Methoxide Ion

Shigeto HASHIBA, Toshio FUCHIGAMI,* and Tsutomu NONAKA*
Department of Electronic Chemistry, Tokyo Institute of Technology,
4259 Nagatsuta, Midori-ku, Yokohama 227
(Received March 9, 1989)

Synopsis. A stoichiometry for the reductive dehalogenation of an organic halide with carbonylferrates was established: One mol of the halide was quantitatively reduced with the carbonylferrates derived from 0.2 mol of pentacarbonyliron(0) and 2 mol of cathodically-generated tetramethylammonium methoxide. The dehalogenation was also examined using a variety of halides under the stoichiometric reaction conditions.

Organic synthetic chemistry using transition metal carbonyls has been extensively developed.[1] Particularly, pentacarbonyliron(0) [$Fe(CO)_5$] has been favorably used because of its relatively low toxicity and price.[2] Pentacarbonyliron(0) itself has a reducing power and can be used as a unique reducing reagent. For instance, it reduces selectively vinyl chlorides, enol acetates and α,β-unsaturated aldehydes to the corresponding olefins, but the reduction requires undesirable reaction conditions such as high temperature, long reaction time and the use of large excess amounts of $Fe(CO)_5$, and product yields are not high.[3] On the other hand, alkali metal tetracarbonylferrates [$M_2Fe(CO)_4$ and $MHFe(CO)_4$; M=K, Na], which can be conveniently prepared, mostly in situ, from $Fe(CO)_5$ and alkali metal hydroxides (NaOH, KOH), have stronger reducing powers and can be used for the selective hydrogenation of α,β-unsaturated compounds[1-6] and for the selective dehalogenation of α-halo ketones at room temperature.[7] However, in all the reactions, more than one mol of $Fe(CO)_5$ (or the tetracarbonylferrates) to one mol of the substrates must be used to obtain reasonable or high product yields. Exceptionally, Takegami et al.[8] reported that one mol of allyl chloride could be reductively dechlorinated with 0.33 mol of $K_2Fe(CO)_4$ to give 0.63 mol of propylene and 0.06 mol of 1,5-hexadiene. If the reaction were completed, this fact would suggest that 0.5 mol of $K_2Fe(CO)_4$ is stoichiometrically consumed to dechlorinate 1 mol of the chloride. However, there was no evidence for the completion of the reaction. Collman et al.[9] made a kinetic and mechanistic study on oxidative addition of alkyl halides to $Na_2Fe(CO)_4$ and proposed a two-electron S_N2-type mechanism with no detectable competing one-electron halogen atom abstraction and/or radical chain mechanism,[10] but did not mention stoichiometry of the reductive dehalogenation reaction which occurs successively to the oxidative addition. Moreover, although the stoichiometry of formation reaction of the ferrates has been established,[11-13] in the in situ preparation of the ferrates used actually as reducing reagents, 0.5 mol of NaOH to 1 mol of $Fe(CO)_5$ was used in a case[4] while 3 mol of KOH in another one.[7]

In this work, an overall stoichiometry for the reductive debromination of an organic bromide was established, and then the dehalogenation of a variety of halides was examined under the stoichiometric reaction conditions.

Results and Discussion

Establishment of Stoichiometry. For a stoichiometric study it is desired that a reaction completes under given reaction conditions within an experimental time scale used. However, the reductive dehalogenation with sodium and potassium ferrates does not seem to proceed at reaction rates enoughly high to perform successfully the stoichiometric study because of low product yields and/or long reaction times.[7,8] For instance, 1 mol of 2-bromocamphor,[7] which was selected as a substrate in this work, reacted with $KHFe(CO)_4$ prepared from 1 mol of $Fe(CO)_5$ and 3 mol of KOH, in a 1,2-dimethoxyethane–ethanol mixture for a few days at room temperature to give camphor in only 59%. Generally, the reactivity of anion reagents is enhanced by weakening interaction with their counter cations. In fact, the oxidative addition of alkyl halides to $Na_2Fe(CO)_4$ is accelerated by using crown ethers, cryptands and highly nucleophilic solvents, or by replacing the counter cation (Na^+) by quaternary ammonium cations.[9] Ferrates and their analogues can be also prepared using alkali metal alkoxides instead of NaOH and KOH.[14,15] In this work, a quanternary ammonium alkoxide was used.

Preparation of anion reagents with onium counter cations from the corresponding alkali metal salts is mostly troublesome and not practical, since the use of expensive crown ethers and onium fluorides is required in an ordinary method. Phase-transfer catalysts also are not always applicable owing to the impossibility of realizing anhydrous reaction conditions. On the other hand, cathodic reduction of a certain kind of organic compounds can easily generate anionic species with onium counter cations, when onium salts are used as supporting electrolytes. Previously,[16-19] it was confirmed that anionic species generated cathodically from alcohols, carboxylic acids, carbon acids and amides in nonaqueous cathodic solutions containing quaternary ammonium salt supporting electrolytes are much more reactive bases than those generated using alkali metal salt electrolytes. In this work, methanol solutions of tetramethylammonium methoxide ($Me_4N^{+\cdot\cdot-}OMe$) in various concentrations could be prepared by electrolyzing a methanol solution of Me_4NCl at various amounts of charge passed in a divided cell. One mol of the methoxide is formed by passing 1 F (1 F=96484.56 C) of charge, according to the following equation:

Table 1. Reductive Dehalogenation of Halides under the Stoichiometric Conditions[a]

Run	Halide	Yield[b]/%	By-product (Yield/%)
1	Octyl iodide	68	
2	Cyclohexyl iodide	58	
3	1-Bromo-2-phenylethane	5	Styrene (90)
4	1-Bromo-1-phenylethane	30	2,3-Diphenylbutane (15)
5	*meso*-1,2-Dibromo-1,2-diphenylethane	0	*trans*-Stilbene (86)
6	Tripenylmethyl bromide	50	Methyl triphenylmethyl ether (33)
7	Phenacyl bromide	82	Methyl phenacyl ether (trace)
8	*p*-Bromophenacyl bromide	78	
9	3-Bromocamphor	91	

a) See the text. b) For the corresponding normal dehalogenation products.

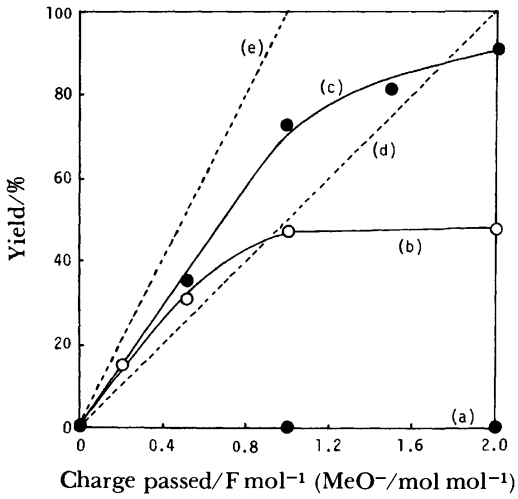

Fig. 1. Relationship between camphor yield and amount of charge passed (methoxide) in the reductive debromination of 3-bromocamphor. (a) 0, (b) 0.1, and (c) 0.2 mol of $Fe(CO)_5$ to 1 mol of 3-bromocamphor, and theoretical lines for (d) two-electron and (e) one-electron reduction.

$$MeOH + e \xrightarrow{Me_4NCl} Me_4N^+ \cdot^- OMe + \frac{1}{2}H_2$$

To the cathodic solution electrolyzed at a prescribed amount of charge between 0 to 2.0 F mol^{-1} of 3-bromocamphor, which correspond to 0 to 2.0 mol of methoxide/mol of 3-bromocamphor, was added a prescribed amount of $Fe(CO)_5$ (0 to 0.2 mol/mol of 3-bromocamphor) and then α-bromocamphor itself. The reaction mixture was stirred for 3 h at room temperature. A longer reaction time did not result in any detectable increase in the yield of camphor.

As shown in Fig. 1, the debromination of 3-bromocamphor did not occur with neither $Fe(CO)_5$ nor methoxide [see (a)]. When 0.1 mol of $Fe(CO)_5$ to 1 mol of 3-bromocamphor was used, the yield of camphor reached to ca. 50% at 1.0 F of charge (corresponding to 1.0 mol of cathodically-generated methoxide) per 1 mol of 3-bromocamphor and no increase was observed at a larger amount (2.0 F) of charge [see (b)]. On the other hand, the yield approximated to 100% at 2.0 F using 0.2 mol of $Fe(CO)_5$ [see (c)]. These facts suggest that 3-bromocamphor is debrominated to camphor by overall two-electron reduction which consumes stoichiometrically 0.2 mol of $Fe(CO)_5$ and 2 mol of methoxide, and consequently a stoichiometry for the reactants and camphor formed can be formulated as follows:

$$R\text{-}Br + \frac{1}{5}Fe(CO)_5 + 2\,MeO^- \xrightarrow{H^+} R\text{-}H + [X]$$

R-Br and R-H: 3-bromocamphor and camphor, respectively
H^+: Proton from water added in work-up procedure
[X]: A mixture of unknown products

Composition of [X], which should consist of iron and bromine compounds and probably CO_2,[20] has remained unknown, because products other than camphor were not analyzed. Therefore, at present it is difficult to discuss reaction mechanism in detail.

It is interesting that curves (b) and (c) at amounts of charge smaller than 1.0 and 2.0 F, respectively, lie in an area between straight lines (d) and (e) which indicate theoretical yields in the two- and one-electron reductions, respectively (see Fig. 1), though the overall reaction is the two-electron reduction as descrived above. This fact suggests that the one-electron reduction occurs concurrently with the two-electron reduction under conditions where amounts smaller than 10 mol of methoxide to 1 mol of $Fe(CO)_5$, or that an iron complex with more reducing capacity is formed under such conditions. Concerning the latter, it should be noted that contribution of the reduction with the zero-valent iron of $Fe(CO)_5$ is negligibly small to explain reasonably increases in the capacity.

Reductive Dehalogenation of a Variety of Halides under the Stoichiometric Conditions. The establishment of stoichiometry for the starting compounds is practically useful for performing efficiently the reductive dehalogenation from a synthetic aspect, though the reaction mechamism has not been clarified. Table 1 shows results of the dehalogenation of a variety of halides under the stoichiometric conditions where 1 mol of halides, 0.2 mol of $Fe(CO)_5$ and 2 mol of methoxide were used.

As shown in Table 1, most of iodides and bromides used could be dehalogenated using a much smaller amount of $Fe(CO)_5$ than that reported in previous papers[4-8] to give the corresponding products in good or high yields. Alkyl chlorides were hardly dechlorinated.[9] Bromobenzene also could not be debrominated.

Some types of side reactions occurred. The normal debromination of 1-bromo-2-phenylethane was almost completely suppressed due to predominant occurrence

of hydrogen bromide elimination with base, and consequently the main product was styrene (Run 3). The side reaction of a benzyl bromide seems to proceed mainly by a one-electron reduction process via the corresponding benzyl radical intermediate (Run 4). Although *meso*-1,2-dibromo-1,2-diphenylethane has two bromine atoms at the benzyl position and also gave exclusively *trans*-stilbene which is apparently a one-electron reduction product, the reaction mechanism is not necessarily rationalized by the one electron-transfer process (Run 5).[21] The formation of methyl ethers as by-products may be owing to direct nucleophilic reaction of methoxide with bromides (Runs 6, 7).

Instead of methanol, ethanol, ethanethiol, 2-propanol, phenol, and acetic acid were also used as sources of cathodically-generated bases, but they did not give any satisfactory results except for ethanol.

Experimental

Chemicals used were commercially available.

A typical experimental procedure was as follows: A methanol solution (10 cm^3 as either a catholyte or an anolyte) containing Me_4NCl (0.4 mol dm^{-3}) as a supporting electrolyte was galvanostatically electrolyzed at 1 A dm^{-2} of cathodic current density under a nitrogen atmosphere at room temperature in a divided cell. The cathode and anode were platinum plates. After a prescribed amount of charge was passed, a prescribed amount of $Fe(CO)_5$ was added to the catholyte. After allowed to stand for 15 min, a halide (1 mmol) was added. The reaction mixture was stirred for 3 h at room temperature under a nitrogen atmosphere, and then poured into a 1% hydrochloric acid solution. The resulting mixture was repeatedly extracted with ether and the combined ethereal extract was washed with a 1% sodium hydrogencarbonate solution and water, and then was dried over anhydrous sodium sulfate. The ethereal solution obtained thus was subjected to gas chromatography (PEG 20M column, 60—170 °C) for product analysis. The products were also separated by thin layer chromatography (Silica gel, hexane).

References

1) For a review: R. Noyori, "Kagaku Sosetsu, No. 19," ed by T. Shiba, Gakkai Shuppan Center, Tokyo (1978), Chap. 6.
2) For a review: H. Takaya and R. Noyori, *Yuki Gosei Kagaku Kyokai Shi*, **35**, 615 (1977).
3) S. J. Nelson, G. Detre, and M. Tanabe, *Tetrahedron Lett.*, **1973**, 447.
4) R. Noyori, I. Umeda, and T. Ishigami, *J. Org. Chem.*, **37**, 1542 (1972).
5) M. Yamashita, Y. Watanabe, T. Mitsudo, and Y. Takegami, *Tetrahedron Lett.*, **1975**, 1867.
6) J. P. Collman, R. G. Finke, P. L. Matlock, R. Wahren, and J. I. Brauman, *J. Am. Chem. Soc.*, **98**, 4685 (1976).
7) H. Alper, *Tetrahedron Lett.*, **1975**, 2257.
8) Y. Takegami, Y. Watanabe, T. Mitsudo, and T. Okajima, *Bull. Chem. Soc. Jpn.*, **42**, 1992 (1969).
9) J. P. Collman, R. G. Finke, J. N. Cawse, and J. I. Brauman, *J. Am. Chem. Soc.*, **99**, 2515 (1977).
10) The two-electron S_N2 mechanism can be also supported from a stereochemical result of the reductive debromination of 3-bromocamphor with $KDFe(CO)_4$.[7]
11) W. Hieber and G. Brendel, *Z. Anorg. Allgem. Chem.*, **289**, 338 (1957).
12) H. W. Sternberg, R. Markby, and I. Wender, *J. Am. Chem. Soc.*, **78**, 5704 (1956).
13) H. W. Sternberg, R. Markby, and I. Wender, *J. Am. Chem. Soc.*, **79**, 6116 (1957).
14) H. Hock and H. Stuhlman, *Chem. Z.*, **55**, 874 (1931); *Chem. Abstr.*, **25**, 935 (1932).
15) E. J. Corey and L. S. Hegedus, *J. Am. Chem. Soc.*, **91**, 1233 (1969).
16) T. Fuchigami, T. Awata, T. Nonaka, and M. M. Baizer, *Bull. Chem. Soc. Jpn.*, **59**, 2873 (1986).
17) T. Komori, T. Nonaka, T. Fuchigami, and K. Zhang, *Bull. Chem. Soc. Jpn.*, **60**, 2315 (1987).
18) M. Minato, T. Nonaka, and T. Fuchigami, *Chem. Lett.*, **1986**, 1071.
19) S. Hashiba, T. Fuchigami, and T. Nonaka, *J. Org. Chem.*, **54**, 2475 (1989).
20) Considerable amounts of CO_2 were evolved in the dechlorination of allyl chloride.[8]
21) J. Casanova and H. R. Rogers, *J. Org. Chem.*, **39**, 2408 (1974)

Synthesis of 2-Methylsulfonylmethyl-3,4,5-trimethoxybenzyl Methyl Ether. Confirmation of the Structure of Two Pyrogallols Isolated from Red Alga

Susumu OHIRA,* Fukue SHIRANE,† Hiroshi NOZAKI,* Shigeru YAHIRO, and Mitsuru NAKAYAMA*,††
Department of Biological Chemistry, Faculty of Science, Okayama University of Science, Ridai-cho, Okayama 700
†Department of Chemistry, Faculty of School Education, Hiroshima University, Shinonome, Hiroshima 734
††Department of Agricultural Chemistry, College of Agriculture, University of Osaka Prefecture, Sakai 591
(Received February 7, 1989)

Synopsis. 2-Methylsulfonylmethyl-3,4,5-trimethoxybenzyl methyl ether was synthesized in 4 steps from methyl 3,4,5-trimethoxybenzoate, confirming the structure of the natural phenol.

We recently reported the isolation of 3,4,5-trihydroxybenzyl methyl ether (**1**) and 2-methylsulfonylmethyl-3,4,5-trihydroxybenzyl methyl ether (**2**) from the red alga *Grateloupia filicina* (Wulfen) J. Agardh.[1] Both of the compounds showed moderate antibacterial activity against *Bacillus substilis*. Described here is our attempted approach to the unique sulfone (**2**), resulting in the synthesis of its trimethyl derivative (**11**). The complete identity of synthetic **11** and the derivative from the natural product denied the possibility of another structure (**3**) for the sulfone.

3,4,5-Trimethoxybenzyl alcohol was treated with sodium hydride and methyl iodide to give a methyl ether (**4**), whose spectral and physical properties were identical with those of the derivative from the natural phenol (**1**). Compound **4** was exposed to chloromethyl methyl sulfide and tin(IV) chloride,[2] giving not the desired sulfide (**9**) but the chloride (**5**) as a major product. Under the same conditions, however, methyl 3,4,5-trimethoxybenzoate (**6**) could be converted smoothly to sulfide (**7**) in 70% yield. **7** was reduced with lithium aluminum hydride to alcohol (**8**). In contrast to the preparation of **4**, treatment of **8** with methyl iodide and sodium hydride produced many compounds containing low yield of the desired methyl ether (**9**). When **8** was heated in refluxing methanol in the presence of *p*-toluenesulfonic acid,[3] **9** was obtained in 53% yield,[4] accompanied by the pentamethoxy compound (**10**). Oxidation of the sulfide (**9**) proceeded cleanly with excess *m*-chloroperbenzoic acid, affording the sulfone (**11**).

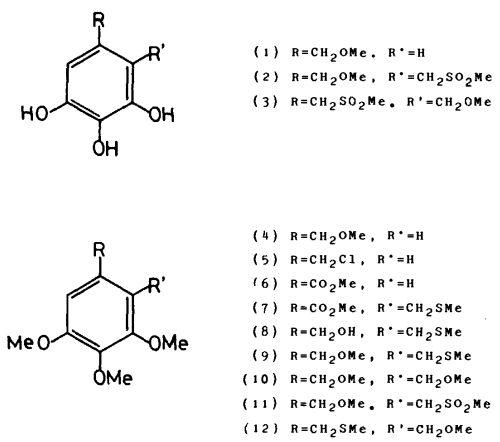

Fig 1.

The last stage toward **2** in our plan was the cleavage of all of the methyl ether on **11** and selective methylation of the benzylic hydroxyl group. Unfortunately, all trials for demethylation of **11** were unsuccessful despite use of various conditions using boron tribromide,[5] aluminum chloride–ethanethiol[6] and sodium iodide–chlorotrimethylsilane.[7]

To confirm the structure of **2**, then, natural phenol was converted to **11** with methyl iodide and sodium hydride. The spectral and physical properties of synthetic **11** and the derivative from the natural product were identical in all respects.

Experimental

3,4,5-Trimethoxybenzyl Methyl Ether (4). To a solution of 3,4,5-trimethoxybenzyl alcohol (973 mg, 4.91 mmol) in dry THF (80 ml), was added sodium hydride (60% suspension, 245 mg, 6.13 mmol) and methyl iodide (3.49 ml, 56.1 mmol) at room temperature. After stirring for 12 h, aqueous ammonium chloride was added to the mixture and THF was evaporated. The aqueous residue was extracted with ether and the organic layer was dried (Na_2SO_4) and evaporated. Column chromatography on silica gel using ethyl acetate–hexane (1:1) gave **4** (885 mg, 93%) as an oil. IR ($CHCl_3$) ν 1593, 1503, 1035 cm^{-1}; ^1H NMR ($CDCl_3$) δ=3.41 (3H, s, $CH_2O\underline{CH_3}$), 3.85 (3H, s, OCH_3, 4 position), 3.87 (6H, s, OCH_3, 3 and 5 position), 4.40 (2H, s, $\underline{CH_2}OCH_3$), 6.60 (2H, s, aromatic). Found: *m/z* 212.1048. Calcd for $C_{11}H_{16}O_4$: M, 212.1048.

Methylation of the Natural Phenol (1). To a solution of the phenol (**1**) (18.3 mg, 0.107 mmol) in THF (2 ml), was added sodium hydride (60% suspension, 40 mg, 1.0 mmol), methyl iodide (0.5 ml, 8 mmol), and dimethyl sulfoxide (1 ml) as a cosolvent. After refluxing overnight, water and ethyl acetate was added to the mixture. The organic layer was dried ($MgSO_4$) and evaporated to give the crude product. Purification by preparative TLC using ethyl acetate–benzene (1:2) gave **4** (15.0 mg, 66%) as an oil. The IR, ^1H NMR, mass spectrum and the R_f value of TLC in various solvent system were identical with those of the synthetic sample.

Methyl 2-Methylthiomethyl-3,4,5-trimethoxybenzoate (7). To a solution of methyl 3,4,5-trimethoxybenzoate (**6**) (1.152 g, 5.10 mmol) and chloromethyl methyl sulfide (0.55 ml, 6.6 mmol) in dry dichloromethane (15 ml), was added tin(IV) chloride (0.19 ml, 1.6 mmol) at 0°C. Another portions of tin(IV) chloride (0.19 ml and 0.10 ml, 2.5 mmol totally) was added to the mixture, while the reaction was carried out at room temperature for 7 h. After addition of aqueous sodium hydogencarbonate, the organic layer was dried (Na_2SO_4) and evaporated. The crude product was purified by column chro-

matography on silica gel using ethyl acetate–hexane (1:3—1:1) as eluent to give **7** (1.098 g, 70%) as an oil. IR ($CHCl_3$) ν 1717 cm^{-1} (ester CO); ^1H NMR ($CDCl_3$), δ=2.03 (3H, s, SCH_3), 3.85 (3H, s, OCH_3), 3.88 (9H, s, OCH_3), 4.09 (2H, s, SCH_2–), 7.20 (1H, s, aromatic); MS *m/z* (rel intensity) 286 (26, M^+), 255 (6), 239 (100), 224 (15), 179 (7). Found: *m/z* 286.0888 Calcd for $C_{13}H_{18}O_5$: M, 286.0876.

2-Methylthiomethyl-3,4,5-trimethoxybenzyl Alcohol (8). To a suspension of lithium aluminum hydride (233 mg, 6.14 mmol) in dry ehter (30 ml), was added a solution of **7** (1.057 g, 3.70 mmol) in ehter (5 ml) at 0°C. After stirring at room temperature for 2 h and destroying the excess hydride with ethyl acetate, 10% aqueous sodium hydroxide was added until white aluminum oxide separates. The organic layer was dried (Na_2SO_4) and evaporated. Purification by column chromatography on silica gel using ethyl acetate–hexane (1:1) as eluent gave **8** (835 mg, 87%) as an oil. IR ($CHCl_3$) ν 3426 cm^{-1} (alcohol); ^1H NMR ($CDCl_3$) δ=2.07 (3H, s, SCH_3), 3.78—3.88 (9H, OCH_3), 4.63 (2H, bd, J=3.5 Hz, CH_2OH), 6.74 (1H, s, aromatic); MS *m/z* (rel intensity) 258 (3, M^+), 211 (100), 196 (22), 181 (14), 152 (16), 61 (7). Found: *m/z* 258.0976 (M^+). Calcd for $C_{12}H_{18}O_4S$: M, 258.0926.

2-Methylthiomethyl-3,4,5-trimethoxybenzyl Methyl Ether (9). A solution of **8** (90.2 mg, 0.35 mmol) and *p*-toluenesulfonic acid (7 mg, 0.04 mmol) in methanol (5 ml) was refluxed for 6 h. After addition of aqueous sodium hydrogencarbonate, methanol was evaporated and the aqueous residue was extracted with ether. The organic layer was dried (Na_2SO_4) and evaporated. The crude product was chromatographed on silica gel using ethyl acetate–hexane (1:3) as eluent to give **9** (50.1 mg, 53%) as an oil. IR ($CHCl_3$) ν 1124 cm^{-1}; ^1H NMR ($CDCl_3$) δ=2.05 (3H, s, SCH_3), 3.38 (3H, s, $CH_2O\underline{CH_3}$), 3.74—3.87 (11H, $\underline{CH_2}S$ and three OCH_3), 4.48 (2H, s, $\underline{CH_2}OCH_3$), 6.64 (1H, s, aromatic); MS *m/z* (rel intensity) 272 (1, M^+), 224 (100), 209 (20), 195 (99), 180 (14). Found: *m/z* 272.1079. Calcd for $C_{13}H_{20}O_4S$: M, 272.1081.

2-Methylsulfonylmethyl-3,4,5-trimethoxybenzyl Methyl Ether (11). To a solution of **9** (282 mg, 1.04 mmol) in dry dichloromethane (10 ml), was added sodium hydrogencarbonate (342 mg, 4.07 mmol) and then *m*-chloroperbenzoic acid (710 mg, 4.10 mmol) at room temperature. After stirring for 2 h, aqueous sodium sulfite, aqueous sodium hydrogencarbonate and dichloromethan was added to the mixture. The organic layer was dried (Na_2SO_4) and evaporated. Purification by column chromatography on silica gel using ethyl acetate–hexane (1:1) as eluent gave **11** (207 mg, 66%) as solid, which was recrystallized from ether. Mp 94.5—96.5°C; IR ($CHCl_3$) ν 1600, 1499, 1461, 1412, 1310, 1197, 1127 cm^{-1}; ^1H NMR ($CDCl_3$) δ=2.80 (3H, s, SO_2CH_3), 3.40 (3H, s, $CH_2O\underline{CH_3}$), 3.83, 3.87, 3.93 (each 3H, s, OCH_3), 4.44, 4.57 (each 2H, s, CH_2S and CH_2O) 6.77 (1H, s, aromatic); MS *m/z* (rel intensity) 304 (2, M^+), 225 (48), 195 (100), 180 (13). Found: *m/z* 304.1017. Calcd for $C_{13}H_{20}O_6S$: M, 304.0980.

Methylation of 2-Methylsulfonylmethyl-3,4,5-trihydroxybenzyl Methyl Ether (2). A solution of **2** (2.5 mg, 0.0095 mmol) in THF (0.5 ml) was treated with sodium hydride (60% suspension in mineral oil, 2 mg, 0.05 mmol) and methyl iodide (0.2 ml, 5 mmol) for 24 h at room temperature, and refluxed overnight. Aqueous ammonium chloride was added to the mixture, which was extracted with dichloromethane and the organic layer was dried (Na_2SO_4) and evaporated. Preparative TLC on silica gel using ethyl acetate–hexane (1:1) as solvent gave **11** (0.7 mg, 24%). The IR, ^1H NMR, mass spectra, the GC retention time, and the R_f value of TLC in various solvent system were identical with those of the synthetic sample.

References

1) H. Nozaki, K. Minohara, I. Miyazaki, H. Kondo, F. Shirane, and M. Nakayama, *Agric. Biol. Chem.*, **52**, 3229 (1988).

2) I. Fleming and J. Iqbal, *Synthesis*, **1982**, 937.

3) The facility of the benzyl cation formation in the reaction **4**→**5** stimulated us to use these conditions.

4) We carried out the NOE experiment for the compound, because formation of the isomer (**12**) is also possible by neighbouring participation of the sulfur atom. The NOEs obtained by each irradiations of the related protons (aromatic and $\underline{CH_2}OCH_3$) were predictable only from the structure (**9**). We thank Dr. Kazunobu Noumi, Pharmaceuticals Research Center, Kanebo, Ltd. for the experiment.

5) K. Hayashi, K. Tokura, K. Okabe, K. Yamamoto, and K. Tawara, *Chem. Pharm. Bull.*, **30**, 2860 (1982).

6) M. Node, K. Nishide, K. Fuji, and E. Fujita, *J. Org. Chem.*, **45**, 4275 (1980).

7) T. Morita, Y. Okamoto, and H. Sakurai, *J. Chem. Soc., Chem. Commun.*, **1978**, 875.

Shift References in High-Resolution Solid-State NMR

Shigenobu HAYASHI* and Kikuko HAYAMIZU
National Chemical Laboratory for Industry, Tsukuba, Ibaraki 305
(Received February 7, 1989)

Synopsis. The high-resolution solid-state ^{13}C, ^{29}Si, ^{31}P, ^{23}Na, ^{27}Al, and ^{11}B NMR spectra of several compounds have been measured using magic-angle sample spinning. Their isotropic chemical-shift values have been determined accurately to use as shift references in solid-state NMR; this makes comparison between literature shift data possible.

High-resolution solid-state NMR has been widely used for such lighter nuclides as ^{13}C, ^{29}Si, and ^{3}P in the solid state.[1] By using this technique, chemical shifts in solids can be determined accurately, and nonequivalent sites can sometimes be distinguished.

The chemical shift can be expressed as the deviation of the resonance frequency with respect to reference materials. For example, tetramethylsilane (TMS) is universally used as an internal shift reference in liquid-state ^{13}C, ^{1}H, and ^{29}Si NMR. On the other hand, in solid-state NMR, an external reference is used instead of an internal reference. A correction of the bulk magnetic susceptibility is, however, necessary in the case of an external reference, though it is not discussed in the present work.

For the reference materials in solid-state NMR, the following properties are desirable:

(1) The central peak is very sharp under magic-angle sample spinning (MAS).

(2) The material contains a large amount of the observed nuclei, thus making the detection easy.

(3) For the $I \geqq 1$ spins, the crystal symmetry is very high, and so the spins have no electric-field gradient. This means that the center transition ($m=1/2 \leftrightarrow -1/2$) has neither broadening nor a shift caused by the second-order quadrupole effect.

(4) The compounds are available commercially.

(5) The spin-lattice relaxation time of the observed nucleus (or of the proton when the cross-polarization technique is used) is short enough.

(6) The materials are stable in air.

(7) The materials can be used for the set-up of the spectrometer. This means that solid materials are preferable.

Various second-reference materials have been used,[2] but their bases are sometimes ambiguous or have not been described explicitly. While the magnetic field was relatively low, any difference in the second-reference materials was little trouble since the resolution in high-resolution solid-state NMR was not so good as in liquid-state NMR. However, in the high-field NMR instruments recently developed the resolution is sometimes comparable to that in liquid-state NMR, and the chemical shift can be determined very accurately. The use of different second-reference materials might, therefore, now cause some deviation in shift values.

The aim of this paper is to present data on several materials which can be used as second references. This would enable us to compare literature data. We have measured the high-resolution solid-state ^{13}C, ^{29}Si, ^{31}P, ^{23}Na, ^{27}Al, and ^{11}B NMR spectra of several compounds and have determined the isotropic chemical shift accurately.

Experimental

The compounds were available commercially. High-resolution solid-state NMR spectra were measured by the use of a Bruker MSL400 pulsed spectrometer at room temperature. The probe was doubly tuned to the observed nucleus and proton, being capable of proton-dipolar decoupling and cross-polarization if necessary. The magic-angle sample-spinning technique[3] was used to determine the isotropic chemical shift accurately. The spinning rate of the rotor was changed between 2 and 4 kHz; typically, 4 kHz was used. A JEOL FX200 pulsed spectrometer was also used, and the values obtained by the two spectrometers agreed within the limits of experimental error. The static magnetic fields were 9.40 and 4.69 T for MSL400 and FX200 respectively. Since the precision and reproducibility were somewhat better in MSL400, the results obtained by the use of MSL400 will be described here. The higher-frequency shift is expressed as positive.

Results and Discussion

Table 1 summarizes the chemical-shift values of the compounds studied in this work, including the first-reference materials. For practical purposes, materials widely used in liquid-state NMR were selected as the first-reference materials and no correction of the bulk magnetic susceptibility was performed. The experimental errors in Table 1 reflect the reproducibility of the measurements carried out in this work.

^{13}C. The first-reference compound is tetramethylsilane (TMS). It is difficult to deal with neat TMS because of its low boiling point, and the TMS solution might include the solvent effect on the shift. Experimentally, no sharp resonance line of neat TMS was observed in this work. Adamantane, glycine, and hexamethylbenzene have been used as the second-reference compounds. Especially for adamantane, Earl and VanderHart,[4] have measured the chemical shift precisely, getting the value of 29.50±0.10 ppm with respect to TMS. This value is adapted in the present paper, since to our knowledge, this is the most reliable value available at present. VanderHart[5] has also reported field-dependent ^{13}C chemical shifts in solids, among which adamantane shows a field-independent chemical shift. The chemical shifts of glycine and hexamethylbenzene obtained in the present work are given in Table 1.

^{29}Si. The first-reference compound is, again, TMS; TMS is not adequate for routine use for the same reasons as in the case of ^{13}C. The second-reference compounds used are 3-(trimethylsilyl)propionic-d_4 acid sodium salt (TSPA: $(CH_3)_3Si(CD_2)_2COONa$), hexa-

Table 1. Chemical Shifts

Nuclei	Compounds	Chemical shifts (ppm)	
^{13}C	Tetramethylsilane	(0)[a]	
	Adamantane	38.55±0.02	29.50[b]
	Glycine	176.50±0.03	43.70±0.05
	Hexamethylbenzene	132.15±0.03	17.21±0.05
^{29}Si	Tetramethylsilane	(0)[a]	
	3-(trimethylsilyl)propionic-d_4 acid Na salt (TSPA)	1.50[b]	
	Hexamethylcyclotrisiloxane	−9.68±0.05	
	Silicone rubber (Poly(dimethylsiloxane))	−22.42±0.05	
	Hexamethyldisiloxane	6.56±0.05	
^{31}P	85% H_3PO_4	0[b]	
	$(NH_4)_2HPO_4$	1.33±0.02	
	$NH_4H_2PO_4$	1.00±0.03	
^{23}Na	1M NaCl aqueous solution	0[b]	
	NaCl	7.21±0.03	
	NaBr	5.04±0.02	
	NaI	−3.25±0.06	
^{27}Al	1M $AlCl_3$ aqueous solution	0[b]	
	$NaAlO_2$	79.33±0.15	
^{11}B	$(C_2H_5)_2O \cdot BF_3$	0[b]	
	BPO_4	−3.60±0.03	
	$NaBH_4$	−42.06±0.02	

a) This value was not checked in the present work. b) This value is assumed in the present work; therefore, it has no experimental error.

methylcyclotrisiloxane (HMCTS), silicone rubber (poly(dimethylsiloxane)), and hexamethyldisiloxane (HMDS). Among these, TSPA is assumed to have a chemical shift of 1.50 ppm in this work, though there is no clear basis for this assumption. The chemical shifts of $(CH_3)_3Si(CH_2)_3COOH$ (1.54 ppm) and $(CH_3)_3Si(CH_2)_4COOH$ (1.53 ppm)[6] might form a basis. However, the obtained values of HMCTS (−9.68 ppm), silicone rubber (−22.42 ppm), and HMDS (6.56 ppm) are reasonable considering the values in the literature.[6] The error in the value of TSPA is considered to be less than 0.10 ppm, although the shift of TSPA should be related to TMS experimentally.

^{31}P. The first-reference material is 85% H_3PO_4. $(NH_4)_2HPO_4$ (1.33 ppm) and $NH_4H_2PO_4$ (1.00 ppm), which have no crystalline waters, can be used as the second-reference compounds. Some inorganic phosphates contain crystalline waters and/or they are hygroscopic, which influence the chemical shift.

^{23}Na. The first-reference material is a 1M NaCl aqueous solution (1M=1 mol dm^{-3}). NaCl (7.21 ppm), NaBr (5.04 ppm), and NaI (−3.25 ppm) can be the second-reference compounds.

^{27}Al. The first-reference material is a 1 M $AlCl_3$ aqueous solution. $NaAlO_2$ (79.33 ppm) can be the second-reference compound.

^{11}B. The first-reference compound is $(C_2H_5)_2O \cdot BF_3$ (diethyl ether-boron trifluoride (1/1)). This compound is a strong Lewis acid, and it is very reactive. The use of second-reference compounds, such as anhydrous BPO_4 (−3.60 ppm) and $NaBH_4$ (−42.06 ppm), is preferable.

When chemical shifts in solid and liquid states are compared, some problems are left unsolved, as has been pointed above and as will be described below. In the cases of ^{13}C and ^{29}Si, conversions to the TMS reference could not be checked in the present paper, although the ^{13}C reference has previously been checked by Earl and VanderHart.[3] The effect of the bulk magnetic susceptibility should always be taken into consideration when the chemical shifts are discussed in detail.

However, for practical purposes, the determination of a chemical shift by using the external reference described above is sufficient. The shift value can easily be corrected when more reliable reference data are obtained. In order to make this later correction possible, though, it is strongly recommended that the reference materials actually used should be explicitly described in the paper.

References

1) C. A. Fyfe, "Solid State NMR for Chemists," C. F. C. Press, Guelph (1983).

2) In this paper, the first-reference materials are assumed to have a chemical shift of 0 ppm, while the chemical shifts of the second-reference materials are given with respect to that of the first-reference materials.

3) E. R. Andrew, *Prog. Nucl. Magn. Reson, Spectrosc.*, **8**, 1 (1972).

4) W. L. Earl and D. L. VanderHart, *J. Magn. Reson.*, **48**, 35 (1982).

5) D. L. VanderHart, *J. Chem. Phys.*, **84**, 1196 (1986).

6) H. Marsmann, *NMR, Basic Principles and Progress*, **17**, 65 (1981)

The Crystal and Molecular Structures of Tetraethylammonium [Tetraaquatetrakis(isothiocyanato)neodymate(III) and europate(III)], $[(C_2H_5)_4N][M(NCS)_4(H_2O)_4]$, (M=Nd, Eu)

Akira OUCHI
Department of Chemistry, College of Arts and Sciences, The University of Tokyo, Komaba, Meguro-ku, Tokyo 153
(Received December 1, 1988)

Synopsis. The crystal and molecular structures of the title new complexes were determined by means of a single-crystal X-ray diffraction method. The crystals of the neodymium(III) complex, $NdC_{12}H_{28}N_5O_4S_4$, F. W. 578.87, are triclinic, space group $P\bar{1}$, a=14.13(2), b=15.39(1), c=12.92(1) Å, α=106.81(8), β=114.70(9), γ=90.09(10)°, U=2418(5) Å^3, Z=4, D_m=1.57(3), D_x=1.59 g cm^{-3}, μ(Mo $K\alpha$)=25.22 cm^{-1}. The isomorphous europium(III) complex was also obtained: a=14.069(9), b=15.328(9), c=12.865(9) Å, α=106.98(5), β=114.57(5), γ=90.07(6)°, U=2390(3) Å^3, D_m=1.60(3), D_x=1.63 g cm^{-3}, μ(Mo $K\alpha$)=30.04 cm^{-1}. Two crystallographically independent neodymium(III) atoms in a unit cell have approximately the same coordination geometry: square antiprism 4*O*,4*N*-octa-coodination. A pair of the O atoms as well as N atoms are in cis positions on the top square and in trans positions on the bottom square of each polyhedron, where the lines connecting both pairs of the N atoms on both squares are approximately parallel.

The structures of metal thiocyanato complexes have already been actively investigated.[1,2] Among them, the lanthanoid complexes are interesting because of their specific coordination number (for example, six in tetrabutylammonium salts, $[(C_4H_9)_4N]_3[M(SCN)_6]$[3]), and of their coordination geometry (for example, cubic in $[(C_2H_5)_4N]_4[M(SCN)_7(H_2O)]$ (**1**)[4]).

In this line of the study, we obtained another types of lanthanoid thiocyanato complexes (shown in the title), $[(C_2H_5)_4N][Nd(SCN)_4(H_2O)_4]$ (**2**), and the isomorphous europium(III) complex (**3**). It is very interesting that when using almost the same starting solution, crystals of **2** were obtained when this solution was kept in benzene vapor, while crystals of **1** were obtained when it was kept over silica gel. Although the structures of the complexes $K_4[M(SCN)_4(H_2O)_4]\cdot(SCN)_3\cdot nH_2O$ (M=Nd) (**4**), Eu (**5**)) have already been reported,[5] they are double salts in which, moreover, the counter cation is K^+: the coordination geometry of the anionic complexes is much affected by the kinds of counter cations.[6-8] We therefore examinted the structures of **2** and **3** by the single-crystal X-ray diffraction technique.

Experimental

Synthesis of Tetraethylammonium [Tetraaquatetrakis(isothiocyanato)neodymate(III)] (2). Neodymiun and tetraethylammonium thiocyanates were obtained as reported previously.[4] Into a methanolic solution (15 cm^3) containing 1.0 mmol of $Nd(SCN)_3$ and 0.2 cm^3 of water, 0.80 g (4.3 mmol) of $[(C_2H_5)_4N](SCN)$ was dissolved and left standing in a desiccator over benzene for several weeks: crystals of **2** were deposited. Yield: 0.46 g (0.80 mmol, 80%). The europium complex (**3**) was also obtained by the same technique and almost in the same yield. Attempts to synthesize types of La and the Pr complexes by this technique failed. Calcd for $MC_{12}H_{28}N_5S_4O_4$: M=Nd, Nd, 24.92; C, 24.90; H, 4.88; N, 12.10%; M=Eu, Eu, 25.91; C, 24.57; H, 4.81; N, 11.94%. Found: M=Nd, Nd, 24.98; C, 25.15; H, 5.05; N, 12.12%; M=Eu, Eu, 25.85; C, 24.57; H, 4.75; N, 11.78%.

Single Crystal X-Ray Structure Analysis. The crystal of **2** used for a structure analysis was pale violet in color, and parallelepiped in shape (0.30×0.30×0.28 mm^3); that of **3** was colorless and in a similar shape (0.29×0.29×0.29 mm^3). The intensities in the range $3<2\theta<50°$ (2θ) were collected on a Rigaku AFC-6A automated four-circle X-ray diffractometer using graphite monochromated Mo $K\alpha$ radiation (λ= 0.71073 Å) by means of a ω-2θ scan technique (scan speed, 4° min^{-1} (ω); scan width (ω), 1.07+0.35tanθ° for **2**, and 1.15+0.35tanθ° for **3**). The intensities were corrected for Lorentz and polarization factors, but not for absorption or extinction. Of 8576 independent intensities collected, 6453 reflections with $|F_o|>3\sigma(|F_o|)$ were used for the structure determination of **2**, and 6438 in 8465 reflections for that of **3**.

All calculations were carried out on a HITAC M-682H computer at the Computer Center of the University of Tokyo using a local version of the UNICS program.[9] The scattering factors were taken from Ref. 10.

The structure of **2** was solved by the heavy-atom method, and the positional and thermal parameters were refined by a block-diagonal least-squares method. No hydrogen atom was included in the structure factor calculations. The structure of **3** was refined in the same way, starting from the final values of **2**. At the final stage of the refinement, the shifts of the parameters were less than one third of the corresponding standard deviations. The final R values applying anisotropic temperature factors were 0.040 (R_w=0.052) for **2**, and 0.055 (R_w=0.061) for **3**.[11]

If only complex anions were considered, the centers of symmetry of the crystal exist at the middle points of both pairs of the respective kinds of complex metal atoms, Nd(1) and Nd(2). The tetraethylammonium ions centered by the N(3) atoms are also distributed so as to take the same positions as the centers of symmetry. On the other hand, the central nitrogen atoms, N(4) and N(5), of the other two kinds of tetraethylammonium ions exist just at the centers of symmetry. As these cations were found not to be cetrosymmetric, we had to assume that the respective eight ethyl carbon atoms around each central nitrogen atom were disordered at two positions with equal occupancy factors. On the calculation, the positions of the N(4) and N(5) atoms were fixed at 0.5, 0.5, 0.5 and 0.5, 0, 0.5, respectively.

Results and Disccusion

Selected bond lenghts of **2** and **3** are shown in Table 1. A perspective drawing of a complex centered by the Nd(1) atom is shown Fig. 1, and a projection of the unit cell of the neodymium complex along the c-axis is shown in Fig. 2.[1]

There are two kinds of crystallographically independent complexes; however, they are approximately in the same form. All the complexes are in a square-

Table 1. Selected Bond Lengths (l/Å) of the Complexes, with the Standard Deviations in Parentheses

M=	Nd	Eu	M=	Nd	Eu
M(1)-N(11)	2.504(8)	2.453(11)	M(1)-O(11)	2.457(7)	2.403(9)
M(1)-N(12)	2.504(7)	2.455(10)	M(1)-O(12)	2.470(9)	2.424(12)
M(1)-N(13)	2.493(7)	2.445(10)	M(1)-O(13)	2.492(8)	2.442(11)
M(1)-N(14)	2.505(8)	2.470(10)	M(1)-O(14)	2.465(8)	2.420(11)
M(2)-N(21)	2.486(11)	2.46(2)	M(2)-O(21)	2.454(7)	2.392(9)
M(2)-N(22)	2.503(7)	2.455(9)	M(2)-O(22)	2.468(7)	2.418(10)
M(2)-N(23)	2.498(8)	2.450(10)	M(2)-O(23)	2.485(6)	2.428(7)
M(2)-N(24)	2.503(9)	2.459(13)	M(2)-O(24)	2.493(9)	2.444(12)

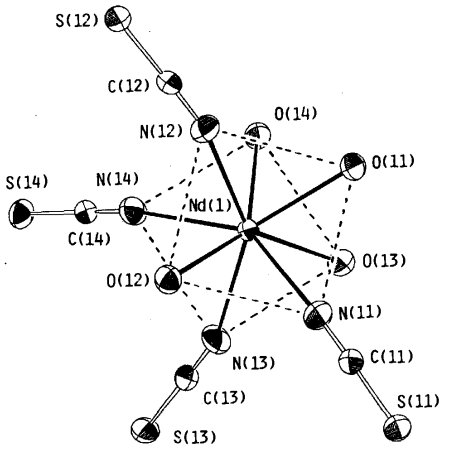

Fig. 1. Perspective drawing of the neodymium(III) complex anion centered by Nd(1) atom, with the numbering scheme of the atoms: 30% probability ellipsoids are shown for the atoms in the figure.

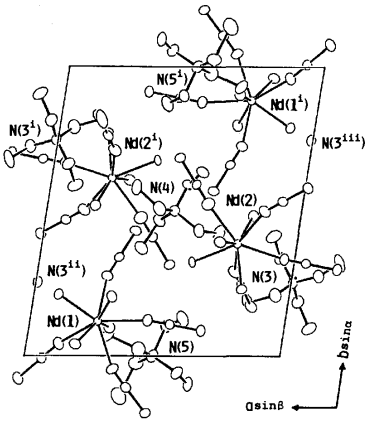

Fig. 2. A projection of the unit-cell of the neodymium(III) complex along c-axis. The numbering of the metal and the tetraethylammonium nitrogen atoms are also shown. Only one in possible two arrangements are shown for the tetraethylammonium carbon atoms around the N(4) and N(5) atoms, respectively. The carbon atoms around the N(3ⁱⁱ) and N(3ⁱⁱⁱ) atoms are not shown. Key to the symmetry operations: i, 1−x, 1−y, 1−z; ii, 1+x, y, z; iii, −x, 1−y, 1−z.

antiprism 4*N*,4*O*-octa-coordination. On a top square of each coordination polyhedron, the two N atoms as well as the two O atoms take a cis configuration, respectively, while on the bottom square they take a trans configuration: the lines through two N atoms on the respective faces are approximately parallel. The mean squares planes of the respective four atoms at the apexes of the top and the bottom squares of each coordination polyhedron are nearly parallel (dihedral angles are: 3.5, 3.2° for **2**, and 2.7, 3.1° for **3**). As shown in Table 1, the M-N and the M-O bond lengths of **2** and **3** are distributed over a relatively wide range, and the longest or shortest members are not always the same in both complexes.

The average of the eight bond lengths are: **2**, Nd-N, 2.500 (2.486(11)—2.504(8)); Nd-O, 2.473 (2.454(7)—2.493(9)) Å; **3**, Eu-N, 2.456 (2.445(9)—2.470(10)); Eu-O, 2.421 (2.392(9)—2.444 (12)) Å. These M-N(SCN) and M-O(H_2O) bond lengths are not much different from the corresponding ones of the related compounds.[4,5,13] However, as mentioned above, in **2** and **3** the average M-O bond length is a little shorter than the average M-N length in each complex. This tendency is also found in the tetramethylammonium salts, $[(CH_3)_4N]_3[M(SCN)_6(CH_3OH)(H_2O)]$, (M=La through Er), which are also in the square antiprism coordination geometry.[13] On the other hand, in **4** and **5**, although the anionic complexes have the same chemical composition and the coordination geometry, their M-O(H_2O) is reported to be longer than M-N(SCN) in each complex.[5] Probably this fact is caused by the types of counter cations. Since the tetramethyl- and tetraethylammonium ions are surrounded by hydrocarbon groups, they are less polar than the potassium ions.

The average M-N-C and N-C-S angles are: **2**, 163.4 (158.4(9)—170.5(5)) and 178.8 (177.3(6)—179.5(7))°; **3**, 164.3 (157.6(14)—171.6(8)) and 178.2 (176.8(10)—178.8(11))°, respectively.

In the crystals of **2** and **3** the metal atoms are arranged approximately on lines parallel to the b-axis (intersecting the ac-plane at about 0.25, 0, 0, and 0.75, 0, 0). The dihedral angles between the top or the bottom square planes of the coordination polyhedrons and the ab-plane are small (**2**, 10.4—14.2; **3**, 10.9—14.0°). The N atoms of the counter cations are also arranged approximately on lines parallel to the b-axis, intersecting the ac-plane at about 0, 0, 0.5 and 0.5, 0, 0.5). Thus, in the crystal, the layers of the anions and the cations are piled alternately along the a-axis as well as c-axis.

References

1) A. F. Wells, "Structural Inorganic Chemistry," 5th ed, Clarendon Press, Oxford, U. K. (1984), p. 935.

2) K. Vrieze and G. van Koten, "Comprehensive Coordination Chemistry," ed by Sir G. Wilkinson, R. D. Gillard, and J. A. McCleverty, Pergamon Press, U. K. (1987), Vol. 2, p. 225.

3) J. L. Martin, L. C. Thompson, L. J. Radonovich, and M. D. Glick, *J. Am. Chem. Soc.*, **90**, 4493 (1968).

4) Y. Tateyama, Y. Kuniyasu, Y. Suzuki, and A. Ouchi, *Bull. Chem. Soc. Jpn.*, **61**, 2805 (1988).

5) P. I. Lazarev, L. A. Aslanov, V. M. Ionov, and M. A. Porai-Koshits, *Koord. Khim.*, **1**, 710 (1975), also *Struct. Report*, **41A**, 210 (1975).

6) G. Thiele and D. Messer, *Z. Anorg. Allg. Chem.*, **464**, 255 (1980).

7) Y. Kuniyasu, Y. Suzuki, M. Taniguchi, and A. Ouchi, *Bull. Chem. Soc. Jpn.*, **60**, 179 (1987).

8) M. Taniguchi and A. Ouchi, *Bull. Chem. Soc. Jpn.*, **62**, 424 (1989).

9) "Universal Crystallographic Computation Program System (UNICS)," ed by T. Sakurai, Crystallographic Society of Japan, Tokyo (1967).

10) "International Tables for X-Ray Crystallography," Kynoch Press, Birmingham (1974), Vol. IV, pp, 72, 150.

11) $R=\sum||F_o|-|F_c||/\sum|F_o|$; $R_w=[\sum w(|F_o|-|F_c|)^2/\sum wF_o^2]^{1/2}$, where $w=1/[\{\sigma(|F_o|)\}^2+(F_w\times F_o)^2]$, $F_w=0.02$ for **2**, and 0.025 for **3**. (F_w values were tried to move between 0.015 and 0.04, and the used values were found to be the best ones, respectively).

12) The final atomic positional, equivalent isotropic and anisotropic thermal parameters, final F_o-F_c tables of the complex, the perspective drawings of the complex around the Nd(2) atom and of the unit cell, and some bond lengths and bond angles data are deposited as Document No. 8885 at the Office of the Editors of *Bull. Chem. Soc. Jpn.*

13) F. Matsumoto, N. Matsumura, and A. Ouchi, *Bull. Chem. Soc. Jpn.*, **62**, 1809 (1989).

 © 1989 The Chemical Society of Japan Bull. Chem. Soc. Jpn., 62, 2435—2440 (1989)

CIDEP Study of the Photoreduction of Aromatic Ketones with Alkoxides in Alcohols

Keishi OHARA, Hisao MURAI, and Keiji KUWATA*
Department of Chemistry, Faculty of Science, Osaka University, Toyonaka, Osaka 560
(Received November 9, 1988)

The photoreductions of xanthone and benzophenone with alkoxides in several alcohols were studied by observing CIDEP. The total emission spectra, observed after the photoexcitation, were assigned to the ketone anion radicals having TM spin polarization. The dependence of the spectral line width upon alkoxides indicates the existence of a hyperfine interaction between the ketone anion radical and the alkali metal cation, even in the early stage of the photochemical reaction in an alcoholic media. A careful analysis of the spectral pattern leads to the conclusion that the counter radical of the ketone anion interacting as a geminate pair which is responsible for the RPM polarization, is other than a methoxyl radical in these systems.

ESR studies on the aromatic ketone anions formed by the reduction with alkali metals in ethereal solvents proved the properties of ion pairs between the ketone anion radicals and the alkali metal cations.[1-4] The phenomenon of an 'atom transfer' in the electron-transfer process has also been shown.[5] On the other hand, the photoreduction of aromatic ketones has been investigated in several systems extensively.[6,7] Alkoxides are known to be one of the good reducing agents used in the photoreaction of aromatic ketones in alcoholic media. The primary steps in this photochemical reaction, especially concerning the behavior of the alkali metal cation and the alkoxyl radical, are of great interest, but few studies on this problem has been reported.[1]

The studies on CIDEP (chemically induced dynamic electron polarization) provide information about the primary steps of photochemical reactions, and are powerful tools for studying the reaction dynamics. The time-resolved study of the CIDEP spectra provides information about the chemical exchange and/or electron spin exchange reactions which induce the relaxation processes.[8]

In the present paper, the CIDEP investigation of the photoreduction of aromatic ketones, xanthone (9-xanthenone), and benzophenone (diphenylmethanone), with alkoxides in several alcohols is presented. New information concerning the presence of a weak interaction between the ketone anions and the alkali metal cations in alcoholic media in the early stage of the photochemical reaction is given. To our knowledge, this paper represents the first CIDEP investigation on the ion pairs formed in the photochemical reaction of aromatic ketones and alkoxides in alcoholic solvents.

Experimental

Xanthone and benzophenone were recrystallized repeatedly from acetone. A sodium methoxide ($NaOCH_3$), 28% methanol solution provided by Wako Pure Chemical Industries, Ltd., was used as received. Potassium methoxide ($KOCH_3$) as ca. 10% methanol solution was prepared by the reaction of potassium metal and methanol. The solvents used in this experiment were ethanol, 2-propanol, cyclohexanol, and a 1 : 1 (v/v) mixture of cyclohexanol and isobutyl alcohol (2-methyl-1-propanol). Commercially available special-grade alcohols provided by Wako Pure Chemical Industries, Ltd. were used as received. Throughout most of the present experiment, the concentrations of xanthone and benzophenone were 0.01 and 0.1 mol dm^{-3}, respectively, unless otherwise noted. The mixing ratio of a methanol solution of alkoxide and the other alcoholic solvents was 1 : 9 in volume in most cases. The concentrations of $NaOCH_3$ and $KOCH_3$ in the solution used in the experiment were ca. 0.5 and 0.1 mol dm^{-3}, respectively. The solutions were deoxygenated by bubbling with pure nitrogen gas prior to the CIDEP measurements.

A nitrogen gas laser (λ=337.1 nm, 5 mJ/pulse) was used for the photoexcitation with a repetition rate of 7.5 Hz. Steady-state ESR was observed by an X-band ESR spectrometer using 100-kHz field modulation during the pulsed laser excitation. The CIDEP spectra were measured by a modified X-band ESR spectrometer (time resolution of 60 ns) for the time-resolved measurement using no field modulation. A boxcar integrator was used to record the time-resolved ESR spectra at several fixed gate times after the laser pulse. The gate width of the boxcar integrator was 0.2 or 0.5 μs. The steady-state ESR and CIDEP measurements were carried out at room temperature. The solutions were flowed at a constant rate of ca. 25 ml h^{-1} through a flat quartz cell of 0.3-mm depth in an ESR cavity of TE_{011} mode. The details were similar to those reported before.[9,10]

Results and Discussion

(I) Xanthone. Figure 1 shows typical results of the steady-state ESR spectra observed during the in situ laser photolysis in the systems of xanthone/$NaOCH_3$ and xanthone/$KOCH_3$ in the mixture of cyclohexanol and isobutyl alcohol (HB). These spectra were assigned to xanthone anion radical from their hyperfine structure (hfs). Other radical species could not be detected. The hyperfine coupling constants (hfc) were in good agreement with those reported in the literature.[11] The line width of the spectra observed using $NaOCH_3$ was much broader than those observed using $KOCH_3$. The change in the concentration of

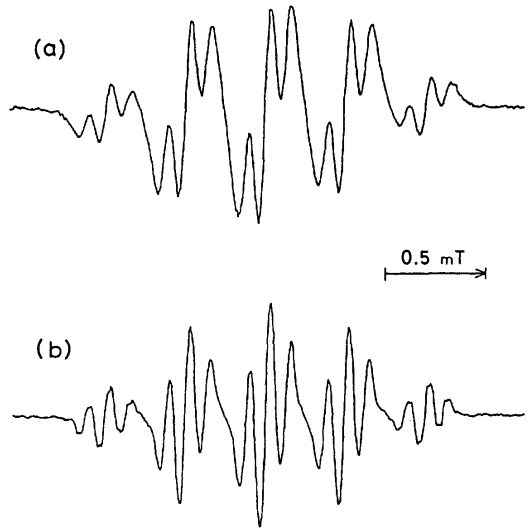

Fig. 1. Steady state ESR spectra observed during the in situ laser photolysis of (a) xanthone/$NaOCH_3$ and (b) xanthone/$KOCH_3$ in HB.

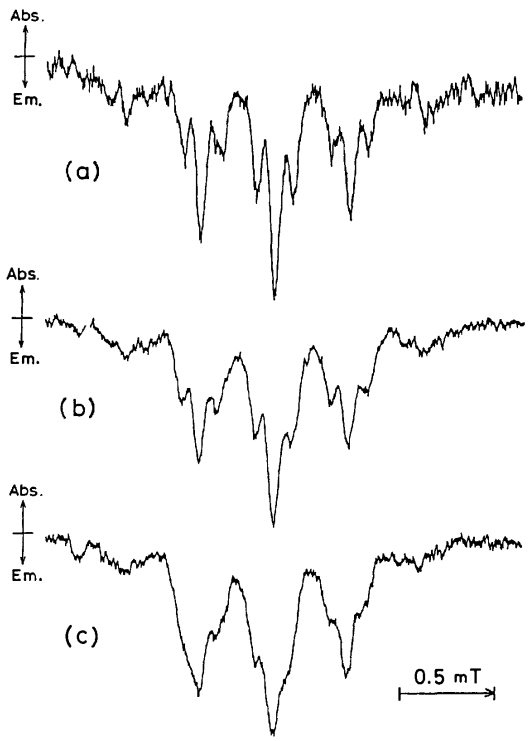

Fig. 2. Time resolved ESR spectra observed in the systems of xanthone and $NaOCH_3$ (a) in ethanol, (b) in 2-propanol and (c) in HB with the gate opening time from 1.0 to 1.2 μs after the laser pulse.

xanthone and alkoxides did not affect the respective spectral patterns and the line width, though it did affect the signal intensities. These results imply the existence of a certain interaction which affects the line width of the ESR spectra between the alkali metal cation and the radical anion in alcoholic media. The line width of the spectra observed using $NaOCH_3$ drastically varied with the solvent alcohol. This effect also appeared weakly in a system containing $KOCH_3$.

Figure 2 shows the time-resolved ESR spectra observed in a system of xanthone and $NaOCH_3$ in various alcohols with the gate opening time from 1.0 to 1.2 μs after the laser pulse. In all the time-resolved ESR spectra shown in the present paper, the downward signals show the microwave emission. These spectra were assigned to the xanthone anion radical; other radical species could not be detected. The spectral hfs were the same as those observed in the steady-state ESR.

The total emission pattern of these spectra clearly shows the feature of the triplet mechanism (TM) of CIDEP; namely, the photochemical reaction is much faster than the spin-lattice relaxation process of the spin polarized triplet state of precursor xanthone. The intensity of hyperfine (hf) lines in the lower field was slightly stronger than that of the corresponding $|M_I|$ lines in the higher field. This fact suggests a slight superposition of emission on the lower-field side and absorption on the higher-field side (E/A pattern), which is due to the radical pair mechanism (RPM) between the geminately produced radicals. The CIDEP signals decayed in some tens of microseconds, depending upon the experimental conditions. This signal decay does not reflect the chemical reaction but, rather, CIDEP relaxation, since the steady state ESR measurement provides the equilibrated spectrum of the anion radical. The line width of the CIDEP spectra varied with the solvent. It became broader with an increase in the molecular weight of the alcohols used in this experiment.

Figure 3 shows the CIDEP spectra observed using

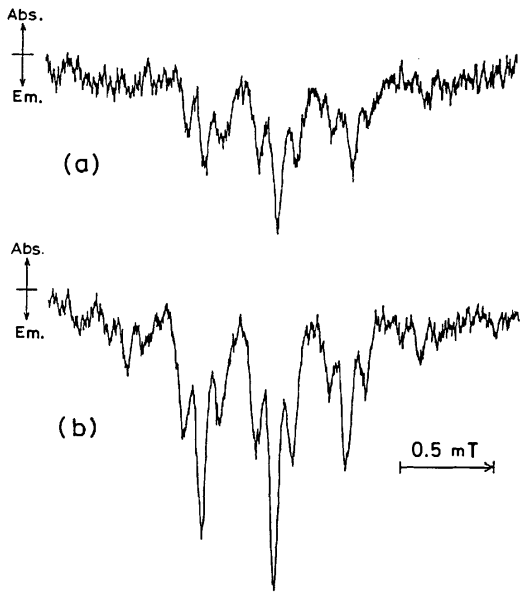

Fig. 3. Time resolved ESR spectra observed in the systems of xanthone and $KOCH_3$ (a) in 2-propanol and (b) in HB with the gate opening time from 1.0 to 1.2 μs after the laser pulse.

$KOCH_3$ in 2-propanol and HB. The spectral hfs and the total emission pattern are almost the same as those observed using $NaOCH_3$. The line width observed in this system is much sharper than that observed in the system containing $NaOCH_3$, as it is clearly demonstrated by comparing Figs. 2 and 3. The solvent effect on the line width, similar to the system of $NaOCH_3$, also appeared weakly. The dependence of the line width upon the solvents and alkoxides observed in the CIDEP study is similar to the result of the steady-state ESR observation described above. Even immediately (0.1 μs) after the photoexcitation, the CIDEP spectra were essentially identical to those observed in the later region, except for the line width. This line-broadening in the early period usually occurs in CIDEP measurements.[12,13] These results clearly demonstrate that the same interaction as that observed in the steady-state ESR takes place even in the period earlier than 10^{-7}s after the photoexcitation.

The photoreduction of xanthone with alkoxides can be represented as follows:

$$Xn+h\nu \longrightarrow Xn(S_1)^* \xrightarrow{ISC} Xn(T_1)^* \quad (1)$$

$$Xn(T_1)^* + MOCH_3 \longrightarrow Xn^{\cdot-} + M^+ + {}^{\cdot}OCH_3, \quad (2)$$

where M denotes alkali metal and the asterisks represent the electronic excited states. Xanthone is excited by a laser pulse to the excited singlet state (S_1), and the spin-selective intersystem crossing (ISC) induces spin polarization in the triplet state (T_1): namely, the uppermost spin-sublevel is exclusively populated.[14,15] This excited triplet state reacts with alkoxides very quickly while the spin polarization is conserved. Therefore, the product anion radical, preserving the spin polarization, shows the total emission spectra. This xanthone anion radical and the alkali metal cation form the ion pair soon after the photochemical reaction in the alcoholic solvents. This ion-pair formation is considered to be analogous to that reported in the system of alkali metal reduction of aromatic ketones in ethereal solvents.[1-3] Although the methoxyl radical carrying TM spin polarization may be produced by this photoreduction, we could not detect this particular radical. Alcohol radicals which may be produced by a secondary reaction of this radical were not observed either. The failure to detect these radical species may be explained by the rapid relaxation of the spin polarization of the methoxyl radical.

The line width of these CIDEP spectra is considered to be caused by a hyperfine interaction between the alkali metal cation and the radical anion; therefore, the hfc of sodium nuclei is larger than that of potassium. This is analogous to the results in an ethereal solution, reported in the literature.[1,2,11] However, this hyperfine interaction in alcoholic solvents is much weaker than that in ethereal solvents. Thus, the solvent effect on the line width may also be explained by a variation of the hyperfine interaction, possibly due to the polarity of the solvent. This means that the hyperfine interaction between the radical anion and the alkali metal cation becomes stronger with a decrease in the polarity of the solvent.

The existence of the paramagnetic dimer of ketone anion radicals was reported,[16] which might obscure the hfs of the ESR spectrum. In the present experiment, however, this contribution to the line width may be negligible since the concentration of radicals in our observing systems, probably less than 10^{-4} mol dm^{-3}, was scarce enough not to form the dimer.

In ordinary steady-state ESR, the variation of spin-spin relaxation time by electron transfer between radical species and its parent molecule is one of the causes of line-broadening. In the time-resolved ESR studies, however, it is known that such an exchange reaction sensitively affects the time evolution of the CIDEP spectrum.[8,13,17] In the presence of the electron-transfer process, the effective relaxation time of CIDEP signals is dependent upon the line degeneracy D_i, microwave field strength ω_1, and the concentration of parent molecule $[A]$. The apparent spin-spin and spin-lattice relaxation times (T_{2i}^{ET} and T_{1i}^{ET}) for a line i at low ω_1 are as follows:

$$\frac{1}{T_{2i}^{ET}} = \frac{1}{T_2} + \frac{(D - D_i)}{D} k_{ET}[A] \quad (3)$$

and

$$\frac{1}{T_{1i}^{ET}} = \frac{1}{T_1} + \omega_1^2 \left(\frac{1}{T_{2i}^{ET}} - \frac{1}{T_1}\right)^{-1} \quad (4)$$

where D is the total line degeneracy and k_{ET} is the rate constant of the electron-transfer reaction.

The CIDEP spectra observed in systems of $NaOCH_3$ with xanthone of different concentrations and by shifting the gate opening time of the boxcar integrator are shown in Fig. 4. The hfs of spectra, its total emission pattern and the line width were not seriously affected by the concentration of xanthone and the gate-opening time. On the other hand, the observable spin-lattice relaxation time of the spin polarization on each hf line was different. The center line of the respective triplet ones of the spectra decayed faster than its neighboring lines. This result can be considered to demonstrate the dependence of the effective relaxation times upon the line degeneracy.

The concentration dependence of the signal decay is clearly demonstrated by a comparison of Figs. 4a and 4b. The observed decay rate of the CIDEP signals increases with a decrease in the concentration of xanthone. This may be explained by the term $k_{ET}[A]$, which affects the observed values of the relaxation time in Eqs. 3 and 4. A system using potassium methoxide provided similar results.

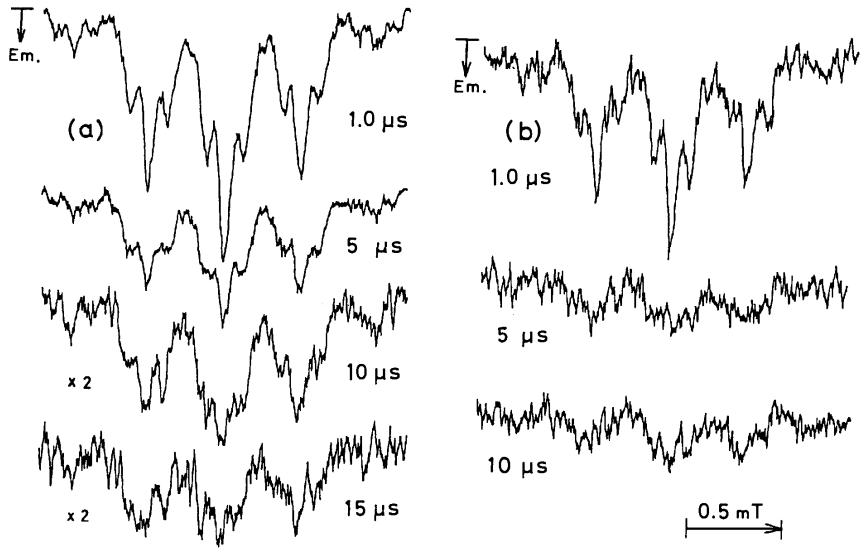

Fig. 4. Time evolution of CIDEP spectra observed by shifting gate opening time (fixed gate width of 0.5 μs) of the boxcar integrator in the system of xanthone/$NaOCH_3$ in 2-propanol. The concentration of xanthone is (a) 6.9×10^{-3} mol dm^{-3} and (b) 1.9×10^{-3} mol dm^{-3}.

These results seem to suggest that the electron-transfer reaction from a xanthone anion radical to its parent molecule takes place. The rate of the electron-transfer reaction is reported to be slow (k_{ET} is ca. 10^7 $mol^{-1}\,dm^3\,s^{-1}$) in the case of fluorenone anion radical in alcoholic media.[18] If this value is adopted in the present system, the contribution of the electron-transfer reaction to the result shown in Fig. 4 is thought not to be very significant. On the other hand, the excitation by the attenuated laser light provided data concerning a fast decay, compared with the one excited by intense light. This result suggests that the concentration of radicals also affects the apparent decay rate of the spin polarization: that is, the relaxation mechanism such as the electron spin-exchange reaction must also be taken into account in this particular system. In this case, the apparent relaxation rate of hf line i may also be expressed in an identical form to that used in Eqs. 3, where the spin-exchange rate and the radical concentration must be used, instead of k_{ET} and $[A]$,[13] respectively.

After all, it was suggested that the spin-exchange reaction between anion radicals and the electron transfer from the xanthone anion radical to its parent molecule takes place in the early period after photoreduction, and the interaction of the ion pair continues

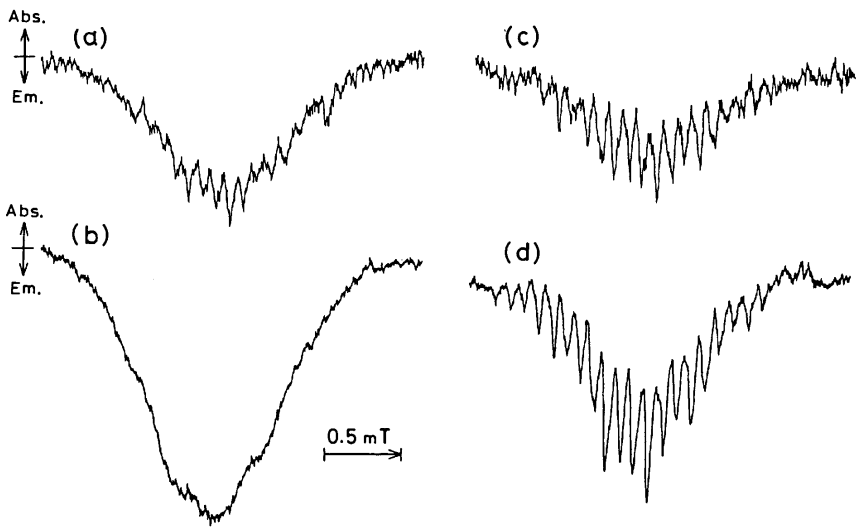

Fig. 5. Time resolved ESR spectra observed by the photoreduction of benzophenone with alkoxides in various alcohols with gate opening time from 1.0 to 1.2 μs. (a) $NaOCH_3$/2-propanol, (b) $NaOCH_3$/HB, (c) $KOCH_3$/2-propanol, and (d) $KOCH_3$/HB.

during these processes. The transfer of the alkali metal cation takes place along with the electron-transfer reaction, which is known as an 'atom transfer'.[5]

(II) Benzophenone. Figure 5 shows the CIDEP spectra observed in the photolysis of benzophenone instead of xanthone in alcoholic solvents containing $NaOCH_3$ or $KOCH_3$. These spectra, having a total emission pattern of TM, are assigned to benzophenone anion radical by an analysis of the hfs,[1,2] which clearly appeared in the system of potassium methoxide. No other species, such as the alcohol radical, was detected. The spectral change with the solvent and the alkoxide showed a similar tendency to that observed using xanthone. The change in the concentration of benzophenone did not affect the spectral pattern or line width seriously, though the decay of the signal became fast upon diluting the concentration. This situation was also the same as that observed using xanthone. Steady-state ESR measurements also provided an ordinary ESR spectrum of the anion radical during the laser photolysis. Consequently, the photochemical primary reaction and successive processes in the system of benzophenone are very similar to those of xanthone: namely, there exists a hyperfine interaction between the benzophenone anion and the alkali metal cation; solvation also affects the interaction.

Concerning the contribution of RPM to the total emission spectra observed in both xanthone and benzophenone systems, a unique and important feature of this reaction is obtained. Usually, RPM provides the E/A character by S-T_0 mixing of the two geminately produced radicals having nearly the same g-value. In the present experimental systems, the counter radical of the ketone anion is predicted to be a methoxyl radical which must be produced in the early stage of this reaction. The methoxyl radical is known to have a larger g-value,[19,20] g_{iso}=2.029,[21] while the ketone anion radicals have a g-value of 2.0036,[22] which is close to that of a free electron. This larger difference of the g-values almost gives a symmetrical total absorption spectrum of the ketone anion through S-T_0 mixing.[23-25]

The simulated CIDEP spectra of the ketone anion radical of pure TM polarization and of pure RPM regarding the above-mentioned assumption in the case of benzophenone, are shown in Figs. 6a and 6b, respectively. The hfc of A(o)=0.280 mT, A(m)=0.100 mT, A(p)=0.354 mT and the line width of 0.030 mT (FWHM) are employed for the anion radical. These hfc values, which are obtained from the observed CIDEP spectrum, are in good agreement with those reported before.[1,2] In order to reproduce the observed spectra of the distorted total emission pattern, the contribution of TM must be slightly stronger than that of RPM. This situation hardly takes place due to the following two reasons. The signal intensity might be very weak owing to a cancellation of the emission and absorption components under the condition assumed above, though the observed signal intensity was almost comparable with the ordinary TM spectrum observed in several systems. Secondly, since the spin-lattice relaxation of triplet ketones competes with its chemical reactions, the spectral pattern could be sensitively influenced by such experimental

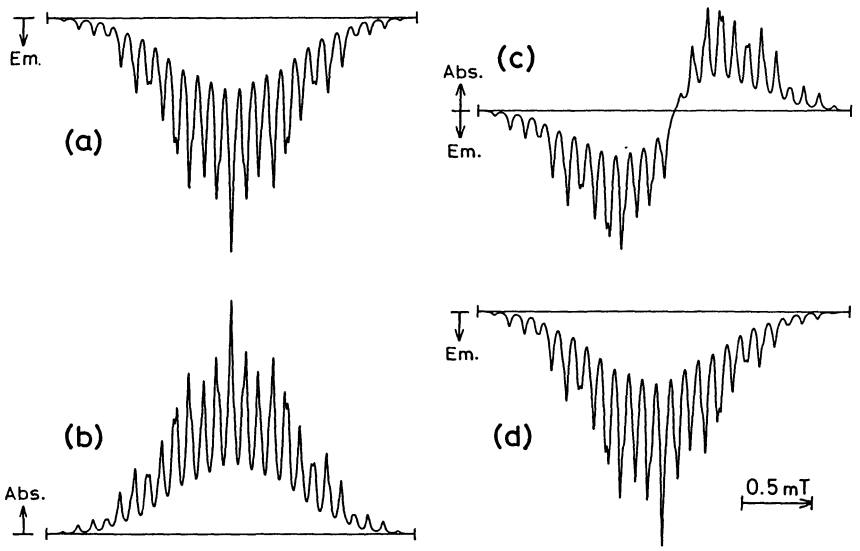

Fig. 6. Simulated CIDEP spectra of benzophenone anion radical in the cases of (a) pure TM, (b) pure RPM assuming the counter radical is methoxyl radical having a hfc of 5.2 mT,[19] and (c) pure RPM assuming the counter radical is methanol radical having a g-factor of 2.0032 and hfc's of A_{CH}=1.75 mT and A_{OH}=0.100 mT.[26] (d) Mixed spectrum of 80% of (a) and 20% of (c), whose intensities are normalized previously.

conditions as the viscosity of the solution or the concentration of solutes, though no such effect has been observed.

Figure 6c shows the simulated CIDEP spectrum of pure RPM obtained by assuming an alcohol radical (hydroxymethyl radical) as the counter one. Figure 6d shows the hybrid spectrum of Figs. 6a and 6c, where the predominant contribution of TM is assumed. In the system of xanthone, similar results were obtained by simulation. Therefore, it was tentatively concluded that the counter radical interacting as a geminate pair is not methoxyl but, perhaps an alcohol radical such as the hydroxymethyl radical produced by a secondary reaction with the solvent or by a fast isomerization of the methoxyl radical.[20] The lifetime of the methoxyl radical would be shorter than the time required for S-T_0 mixing (10^{-9}—10^{-7} s).[23-25]

In conclusion, the photoreduction of xanthone and benzophenone in alcoholic solvents was investigated by CIDEP. The product anion radical and the alkali metal cation form the ion pair soon after the photochemical reaction. The time-resolved ESR study demonstrated that the hyperfine interaction of the ion pair exists, even in the early stage of the photoreaction. It was also suggested that the electron spin-exchange process between the ketone anion radicals possibly occurs along with an electron-transfer reaction. The E/A distortion component of the total emission spectrum could be explained by the contribution of the geminate pair RPM; also, the counter radical of the anion radical of ketones in the geminate cage was shown to be other than the alkoxyl radical.

References

1) P. B. Ayscough and R. Wilson, *J. Chem. Soc.*, **1963**, 5412.
2) N. Hirota and S. I. Weissman, *J. Am. Chem. Soc.*, **86**, 2537 (1964).
3) N. Hirota, *J. Phys. Chem.*, **71**, 127 (1967).
4) E. Wahrhurst and M. Wilde, *Trans. Faraday Soc.*, **67**, 605 (1971).
5) F. C. Adam and S. I. Weissman, *J. Am. Chem. Soc.*, **80**, 1518 (1958).
6) S. G. Cohen, A. Parola, and G. H. Parsons Jr., *Chem. Rev.*, **73**, 141 (1973).
7) J. G. Calvert and J. N. Pitts, "Photochemistry," John Wiley & Son, Inc. New York (1966).
8) S. Basu, K. A. McLauchlan, and A. J. D. Ritchie, *Chem. Phys. Lett.*, **105**, 447 (1984).
9) Y. Sakaguchi, H. Hayashi, H. Murai, and Y. J. I'Haya, *Chem. Phys. Lett.*, **110**, 275 (1984).
10) H. Hayashi, Y. Sakaguchi, H. Murai, and Y. J. I'Haya, *J. Phys. Chem.*, **90**, 4403 (1986).
11) B. J. Tabner and J. R. Zdysiewicz, *J. Chem. Soc. B*, **1971**, 1659.
12) P. J. Hore and K. A. McLauchlan, *J. Magn. Reson.*, **36**, 129 (1979).
13) P. J. Hore and K. A. McLauchlan, *Mol. Phys.*, **42**, 533 (1981).
14) A. Chakrabarti and N. Hirota, *J. Phys. Chem.*, **80**, 2966 (1976).
15) H. Murai, M. Minami, and Y. J. I'Haya, *J. Phys. Chem.*, **92**, 2120 (1988).
16) N. Hirota and S. I. Weissman, *J. Am. Chem. Soc.*, **86**, 2538 (1964).
17) P. J. Hore and K. A. McLauchlan, *Mol. Phys.*, **42**, 1009 (1981).
18) B. F. Wong and N. Hirota, *J. Am. Chem. Soc.*, **94**, 4419 (1972).
19) M. Iwasaki and K. Toriyama, *J. Am. Chem. Soc.*, **101**, 1964 (1979).
20) M. Iwasaki and K. Toriyama, *J. Am. Chem. Soc.*, **101**, 2516 (1979).
21) Calculated value using the reported g_{max} and g_{min} in Refs. 19 and 20, and assuming g_{int} almost equals g_{min}.
22) C. C. Felix and B. S. Prabhananda, *J. Magn. Reson.*, **57**, 146 (1984).
23) L. Monchick and F. J. Adrian, *J. Chem. Phys.*, **68**, 4376 (1978).
24) C. D. Buckley, A. I. Grant, K. A. McLauchlan, and A. J. D. Ritchie, *Faraday Discuss. Chem. Soc.*, **78**, 257 (1984).
25) C. D. Buckley and K. A. McLauchlan, *Mol. Phys.*, **54**, 1 (1985).
26) G. P. Laroff and R. W. Fessenden, *J. Phys. Chem.*, **77**, 1283 (1973).

Solvent Effect on the Hydrogen Bonds between Guanine and Cytosine and between Hypoxanthine and Cytosine

Yoshihisa OHTA, Kichisuke NISHIMOTO,* Hidetsugu TANAKA,†† Yoshihiro BABA,† and Akihiro KAGEMOTO†
Department of Chemistry, Faculty of Science, Osaka City University, Sumiyoshi-ku, Osaka 558
†Department of General Education, Laboratory of Chemistry, Osaka Institute of Technology, Asahi-ku, Osaka 535
(Received November 9, 1988)

The solvent effect on the hydrogen bonds between guanine and cytosine and between hypoxanthine and cytosine was studied by means of solution calorimetry and ab initio MO calculations. The experimental enthalpy changes for guanine-cytosine and hypoxanthine-cytosine systems in aqueous solution were estimated to be about −10 and −14 kJ mol^{-1}, respectively. In order to explain these experimental results, the electronic structures of hydrated bases and hydrated base pairs were calculated, assuming two types of hydration schemes. In the first type, it was expected that the complementary base pairs were destabilized in aqueous solution. In the second type, the stabilization energies in aqueous solution were calculated to be −11.9 kJ mol^{-1} for the hydrated guanine-cytosine system and −18.5 kJ mol^{-1} for hypoxanthine-cytosine one, respectively, which agreed with the experimental results. This suggests that water molecules bound to base pairs contribute to the stabilization/destabilization of hydrogen bonds between bases. The present calculation showed the possibility of C-H$^{\delta+}$···O hydrogen-bond formation between the complementary base pair and H_2O.

It is well-known that deoxyribonucleic acid (DNA) is a macromolecule with a double-stranded helical structure formed by a complementary interaction between purine and pyrimidine bases,[1] bringing about a helix-coil transition by a change in the environmental conditions, such as pH, ionic strength, or temperature.[2]

In previous papers,[3,4] in order to clarify the stabilization scheme of DNA molecule in aqueous solution, the enthalpy changes of duplex formations by an equimolar mixture of poly(riboguanylic acid)-(poly(G)) with poly(ribocytidylic acid) (poly(C)), and of poly(riboinosinic acid)(poly(I)) with poly(C) solutions with a 0.1 mol dm^{-3} Tris-HCl buffer solution at pH 7.60 were measured using LKB batch-type microcalorimeter at 298.15 K. Poly(I) contains hypoxanthine, which is a deamino analogue of guanine. We reported that the enthalpy changes accompanying duplex formation were about −9 kJ (mol of base pair)$^{-1}$ for the poly(G)·poly(C) duplex, and about −21 kJ (mol of base pair)$^{-1}$ for the poly(I)·poly(C) duplex, respectively. The estimated enthalpy changes between polynucleotides may correspond to the total energy containing various types of interactions such as the hydrogen bonding between bases, the solvent effect of water, the stacking effect, conformational change, and the dissociation of self-associated poly(G) and poly(I).[3-19] Especially, the hydrogen bonds between bases may mainly contribute to both the stability and conformation of polynucleotides.

Recently,[20] we reported on theoretical and experimental studies concerning the Watson-Crick and the Hoogsteen pairs of adenine-uracil hydrogen-bonded systems, and pointed out that not only the hydrogen bonding between bases, but also the solvent effect of water played an important role in the stability of base pairs in aqueous solution.

Clementi and Corongiu[19] investigated theoretically the hydration schemes of guanine, cytosine, and the guanine-cytosine pair by means of isoenergy contour map analysis and Monte Carlo simulations.

In the present study, in order to elucidate the solvent effect of water on the stability of a base pair, the energies of nonhydrated and hydrated complementary base pairs (Watson-Crick pairing) of guanine with cytosine and of hypoxanthine with cytosine were calculated by an ab initio MO method, by assuming two types of hydration schemes. These results were compared with the results of solution calorimetric experiments.

Experimental

9-Methylguanine, cytosine (Cyt), and hypoxanthine (Hyp) were purchased from Tokyo Kasei Kogyo Co., Ltd., Japan, and used without further purification. 9-Methylguanine, instead of guanine (Gua), was used because of the requirement of higher solubility in aqueous solution.

Water was purified by an ordinary method,[21] and finally distilled by the use of a long column.

A 0.1 mol dm^{-3} Tris-HCl (tris(hydroxymethyl)aminomethane-hydrochloric acid) solution was used as the buffer solution (pH 7.0).

In this study, an LKB batch-type microcalorimeter was used (described in a previous paper[22]). The measured temperature was 298.15±0.005 K. For measurements of the heat of mixing, equal volumes (about 2 ml) of 5×10^{-4} mol dm^{-3} Gua or Hyp and Cyt solutions were mixed.

Calculations

Ab initio MO calculations were carried out with IMSPACK[23] and GAUSSIAN 80[24] programs using STO-3G minimal basis set.[25] The geometry of Hyp was optimized (see Fig. 1). The geometries of Gua and Cyt were taken from Del Bene[26] and Matsushita et al.[27] respectively.

†† Present address: Mitsui Petrochemical Industries, Ltd., Iwakuni, Yamaguchi 740.

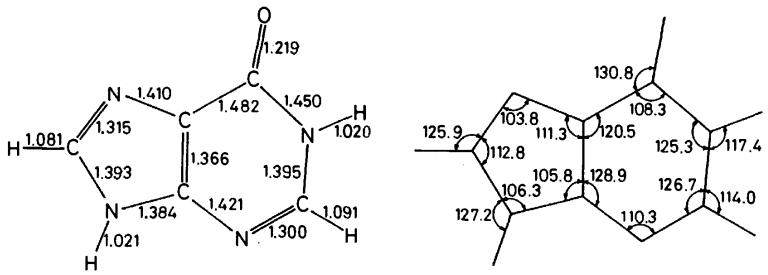

Fig. 1. The optimized structure of Hyp. Units are angstroms and degrees.

Since the hydrogen bond is much weaker than the usual covalent bond, it is expected that the geometries of bases might be almost unchanged by hydrogen-bond formation. Therefore, we optimized only the hydrogen-bonding regions of the nonhydrated base pairs, and the hydrated bases and base pairs.

For the calculation of intermolecular interaction energy, an extended basis set, such as 4-31G or 6-31G*, is recommended. However, since the number of basis sets for hydrogen-bonded systems in the present work was very large, the STO-3G minimal basis set was used. The purpose of this work was to perform both comparative and qualitative studies of the effects of hydrogen bonding and hydration on the physicochemical properties of DNA. For this purpose, the STO-3G minimal basis set proved to be useful.

Results and Discussion

Hydrogen-Bonding Interactions of Gua with Cyt and of Hyp with Cyt. Since it is well-known experimentally that Watson-Crick pairing is the most stable structure in possible hydrogen-bonding schemes of Gua with Cyt,[28] we calculated this type of base pair. The Watson-Crick pairing of Hyp with Cyt was also calculated. The optimized geometric parameters for the hydrogen-bonding region of Gua-Cyt and Hyp-Cyt pairs are shown in Fig. 2, together with the experimental values of the 9-ethylguanine-1-methylcytosine pair determined by X-ray diffraction crystallography (in parenthesis[28]). As can be seen in Fig. 2a, the calculated intermolecular distances are somewhat underestimated. This is a general tendency as long as one uses STO-3G minimal basis set.

The calculated results of the hydrogen-bonding energies (E_{HB}), the magnitude of the charge transfer from pyrimidine to purine bases (Δq), and dipole moments (μ) for Gua-Cyt and Hyp-Cyt pairs are summarized in Table 1, together with the vector sum of the dipole moments of monomers (μ_{SUM}). As can be seen in Table 1, E_{HB} was estimated to be −111.3

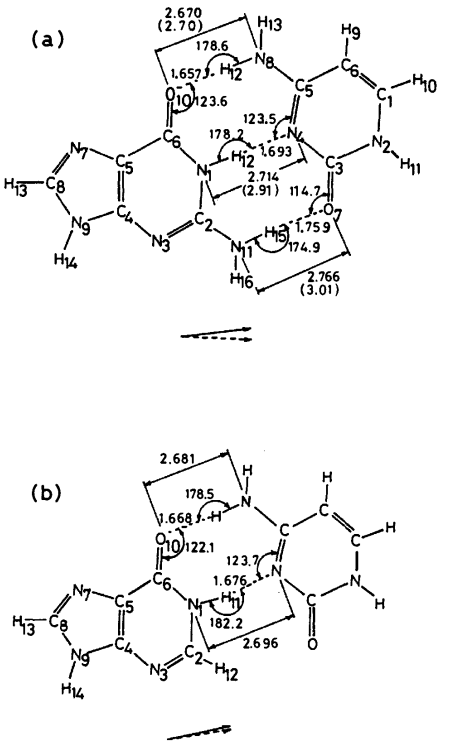

Fig. 2. The optimized geometric parameters of (a) Gua-Cyt and (b) Hyp-Cyt pairs. Units are angstroms and degrees. The solid and broken arrows show the direction of dipole moments for base pairs and of the vector sum of dipole moments for monomers, respectively.

Table 1. The Calculated Results of the Hydrogen-Bonding Energies, E_{HB}, the Magnitude of the Charge Transfer from Pyrimidine to Purine Bases, Δq, Dipole Moments of Base Pairs, μ, and the Vector Sum of Dipole Moments of Monomers, μ_{SUM}, for Gua-Cyt and Hyp-Cyt Pairs

	E_{HB}/kJ mol^{-1}	Δq/e[a]	μ[b]/Debye	μ_{SUM}[b]/Debye
Gua-Cyt pair	−111.3	0.06	6.53	4.78
Hyp-Cyt pair	−82.4	0.02	4.13	3.11

a) e=−1.6×10^{-19} C. b) The direction refers to Fig. 2.

kJ mol^{-1} for Gua-Cyt pair and −82.4 kJ mol^{-1} for Hyp-Cyt one, respectively. Hereafter, we call the hydrogen bonds between the complementary bases the internal hydrogen bonds. Therefore, E_{HB} is the energy of the internal hydrogen bonds. The calculated result for the Gua-Cyt pair is comparable with the experimental one reported by Yanson et al. ($\Delta H°$=−87.9 kJ mol^{-1})[6,7] and with the calculated one by Forner et al. (E_{HB}=−124.1 kJ mol^{-1}).[8] Since the calculated dipole moment of the Gua-Cyt pair is larger than that of the Hyp-Cyt one, it is expected that in a polar solvent, the Gua-Cyt pair may be more stable than that of Hyp-Cyt due to a dipole-dipole interaction between solute and solvent molecules.

In order to obtain informations concerning the nature of the internal hydrogen bonds of Gua-Cyt and Hyp-Cyt pairs, the calculated hydrogen-bonding energies were decomposed into physically meaningful energy components such as the electrostatic (E_{ES}), the exchange repulsion (E_{EX}), the polarization (E_{PL}), and the charge-transfer (E_{CT}) energies, according to the Kitaura-Morokuma method.[29] The results are summarized in Table 2, where $E_{CT(X\to Y)}$ and $E_{CT(Y\to X)}$ refer to the charge-transfer interaction energies from Gua and Hyp to Cyt, respectively. As can be seen in Table 2, the dominant energy components for both Gua-Cyt and Hyp-Cyt pairs are the electrostatic and the charge-transfer interactions, as in the usual hydrogen-bonded systems.[30]

It should be noted that for the Hyp-Cyt pair, $E_{CT(Y\to X)}$ (−50.6 kJ mol^{-1}) is almost the same as $E_{CT(X\to Y)}$ (−49.8 kJ mol^{-1}), though the Gua-Cyt pair, $E_{CT(Y\to X)}$ (−88.3 kJ mol^{-1}), is much larger than $E_{CT(X\to Y)}$ (−51.5 kJ mol^{-1}). This result is because in the Gua-Cyt pair, two hydrogen bonds (N_1-H_{12}···N_4 and N_{11}-H_{15}···O_7) contribute to $E_{CT(Y\to X)}$, while only one hydrogen bond (O_{10}···H_{12}-N_8) contributes to $E_{CT(X\to Y)}$. On the other hand, in the Hyp-Cyt pair, one hydrogen bond (O_{10}···H_{12}-N_8) contributes to $E_{CT(X\to Y)}$ and one hydrogen bond (N_1-H_{11}···N_4) to $E_{CT(Y\to X)}$.

Table 2. Hydrogen-Bonding Energies and Their Components for the Gua-Cyt and Hyp-Cyt Pairs

		Gua-Cyt pair /kJ mol^{-1}	Hyp-Cyt pair /kJ mol^{-1}
E_{HB}		−111.3	−82.4
E_{ES}		−141.0	−112.1
E_{EX}		212.5	166.5
E_{PL}		−13.0	−9.2
E_{CT}		−140.2	−101.3
E_{CT}	$E_{CT(X\to Y)}$[a]	−51.5	−49.8
	$E_{CT(Y\to X)}$[a]	−88.3	−50.6

a) X refers to Gua for Gua-Cyt pair and to Hyp for Hyp-Cyt one. Y refers to Cyt.

The Results of Calorimetric Measurements

The heats of mixing of Gua and Cyt solutions and Hyp and Cyt solutions were measured using an LKB batch-type microcalorimeter at 298.15±0.005 K. The experimental results were exothermic, suggesting that the mixed systems were stabilized by complementary base-pair formation, if we assumed that the heat of dilution of each base was negligible.

The obtained results are summarized in Table 3, together with the $\Delta H°$-values reported by other investigators.[5-7] As can be seen in Table 3, it is of interest to note that the stability ($\Delta H°=H°$(base pair A-B)−$H°$(base A)−$H°$(base B)) of the Gua-Cyt system decreases with an increase in the polarity of solvents. From the point of view of a dipole-dipole interaction,

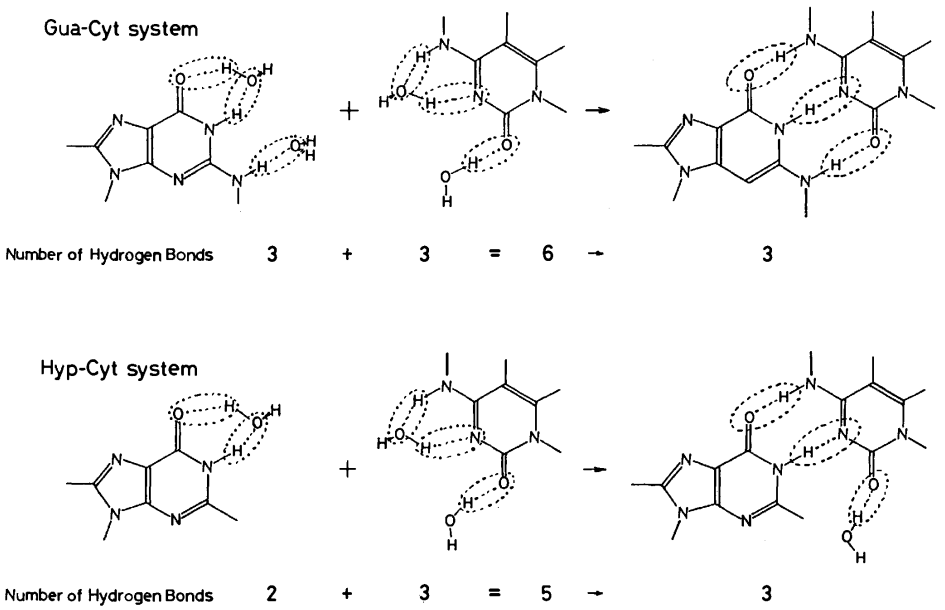

Table 3. Experimental Enthalpy Changes of the Hydrogen-Bond Formation between Gua and Cyt and between Hyp and Cyt

Solvent	Enthalpy change, ΔH° /kJ (mol base pair)$^{-1}$		Ref.
	Gua-Cyt pair	Hyp-Cyt pair	
H_2O[a]	−10	−14	This work
$CHCl_3$[b]	−42—−48	−38	5
Gas phase	−87.9		6,7

a) The concentration of 5×10^{-4} mol dm^{-3}. b) Guanosine and Cytisine for Gua-Cyt pair, and 2′,3′-*O*-benzylidine-5′-*O*-tritylinosine and cytisine for Hyp-Cyt pair.

the stability of complementary base pairs is expected to increase with an increase in the polarity of solvents, and also with an increase in the dipole moment of the base pair. Actually, in $CHCl_3$ solutions, the Gua-Cyt system (calculated dipole moment μ=6.53 Debye) is more stable than the Hyp-Cyt system (μ=4.13 Debye) (see Table 3). Therefore, the decrease of stability in the aqueous solution comes from destabilization due to the dehydration of a hydrated base in the process forming a base pair. That is, in the Gua-Cyt system, the number of hydrogen bonds decreases from six to three(hydrated four H_2O molecules are removed and three internal hydrogen bonds are formed in Gua-Cyt pair), while in the Hyp-Cyt system, the number of hydrogen bonds decreases from five to three (see figure given below). As a result, the stability of the base pair in aqueous solution is reversed; that is, the order of stability is Hyp-Cyt pair>Gua-Cyt pair.

Hydration Effect on the Internal Hydrogen Bonds of Gua-Cyt and Hyp-Cyt Pairs. In order to elucidate the hydration effect on the stability of internal hydrogen bonds of the complementary base pair, hydrated bases and base pairs were calculated by ab initio MO methods, by assuming various degrees of hydration.

To consider possible hydration schemes for Gua, Hyp, and Cyt, the net charges (Mulliken population of atoms) were calculated. The results are shown in Fig. 3. As can be seen, there are eight hydrogen-bonding sites (proton donating or accepting site) in Gua and six sites in Hyp and Cyt, respectively, at which hydration is possible. We distinguish the hydrogen-bonding site and the hydration region. The possible hydration regions of bases are shown in Fig. 3. There are five hydration regions ((A)—(E)) in Gua, four regions ((F)—(I)) in Hyp, and four regions ((J)—(M)) in Cyt.

At the hydration regions, two types of hydration schemes are possible. The first type is as follows. Since each proton-donating or -accepting site in a base can bind with one H_2O molecule, two H_2O molecules can be coordinated at each bay-like region (A), (C), (D), (H), (I), (J), or (L) shown in Fig. 3. In this case,

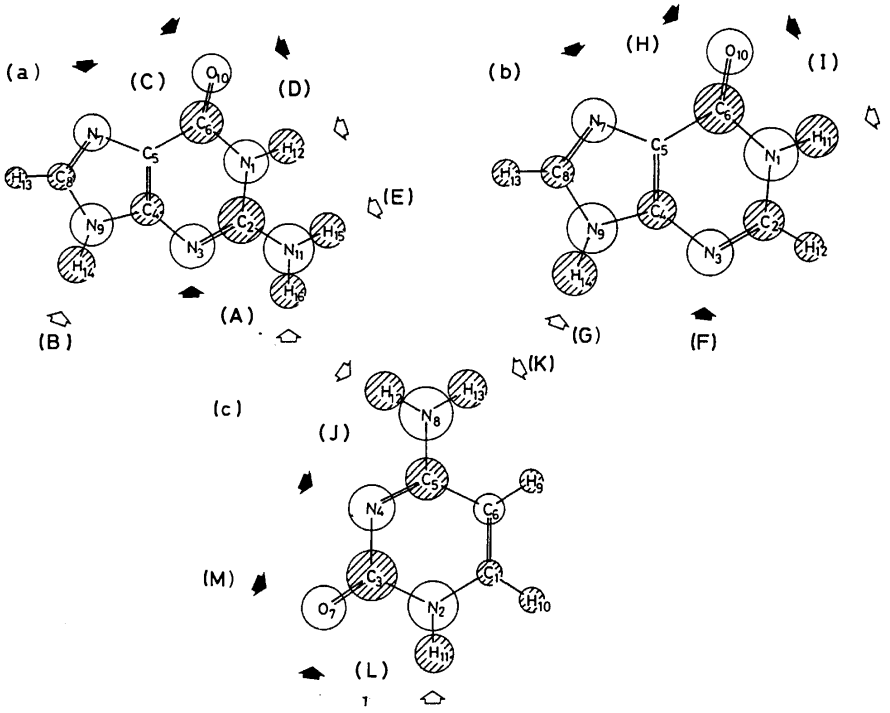

Fig. 3. The net charges of (a) Gua, (b) Hyp, and (c) Cyt. The open and shaded circles represent the negative and positive net charges, respectively. The area of the circle shows the relative magnitude of the net charge. The open and shaded arrows indicate the location of proton donating and accepting sites. The uppercase alphabetical letters represent the hydration regions.

there are some interactions between hydrated H_2O's in these regions, such as hydrogen bonding, dipole-dipole interactions and steric hindrance. Therefore, we optimized each hydrogen-bonding moiety of hydrated bases. At other regions ((B), (E), (F), (G), (K), and (M)), one H_2O molecule is coordinated. Furthermore, there are some direct interactions between hydration regions (A) and (B), between (D) and (E), between (F) and (G), and between (J) and (M). Thus, geometry optimization was performed at these regions simultaneously. The calculated results are shown in Figs. 4a, b, and c.

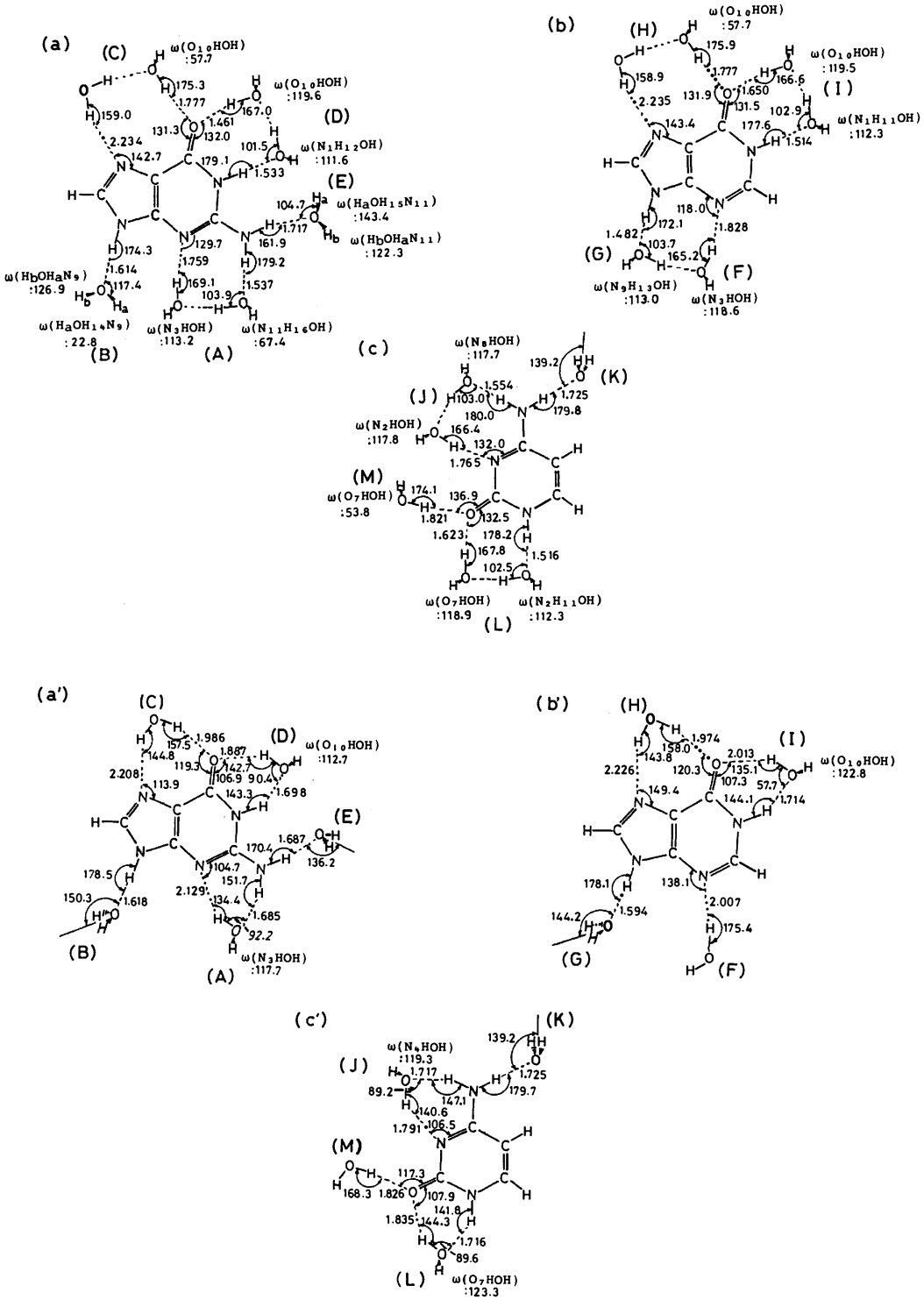

Fig. 4. The optimized geometric parameters of (a) and (a′) hydrated Gua, (b) and (b′) hydrated Hyp, and (c) and (c′) hydrated Cyt. Units are angstroms and degrees. Dihedral angles are given as follows; for an example, the dihedral angle between N_3-H-O and H-O-H planes at region (A) in the hydrated Gua(figure a′) is given by $\omega(N_3HOH)$: 117.7.

In the second type of hydration scheme, one H_2O molecule is bound between proton-donating and -accepting sites in each bay- like region shown in Figs. 4a′, b′, and c′. Optimized geometric parameters are shown n Figs. 4a′, b′, and c′.

The hydration scheme of Gua shown in Fig. 4a′ is rather similar to that of Pullman et al.[12] and that of Clementi and Corongiu.[19] The hydration scheme of Cyt, shown in Fig. 4c′, is similar to that of Clementi and Corongiu calculated by Monte Calro simulations.[19] However, it is somewhat different from that of Pullman et al.[12]

The electron density changes due to internal hydrogen-bond formation of Gua-Cyt and Hyp-Cyt pairs were calculated (Fig. 5). As can be seen in Fig. 5, it is of interest to note that the charge densities on the H_9 and H_{10} atoms of the C-H bonds of Cyt in the Gua-Cyt pair and those on the H_{12} atom of the C-H bond of Hyp, and H_9 and H_{10} atoms of Cyt in the Hyp-Cyt pair considerably decreased by the formation

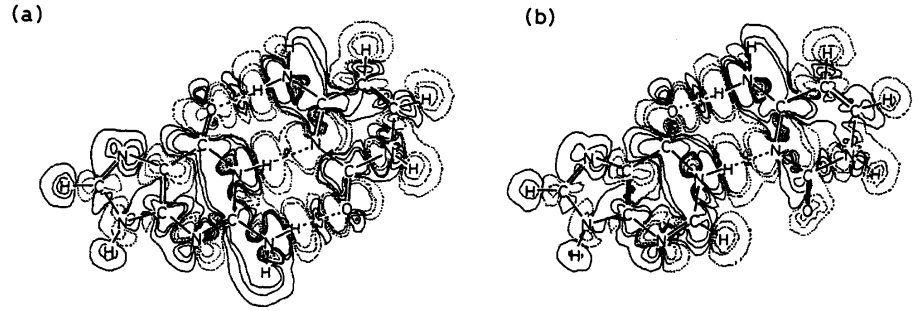

Fig. 5. The electron density changes due to the hydrogen-bond formation of (a) Gua-Cyt and (b) Hyp-Cyt pairs. Full and dotted lines indicate the density increase and decrease, respectively. The values of these lines are ±0.0001, ±0.0005, and ±0.001 (Bohr)$^{-3}$, successively.

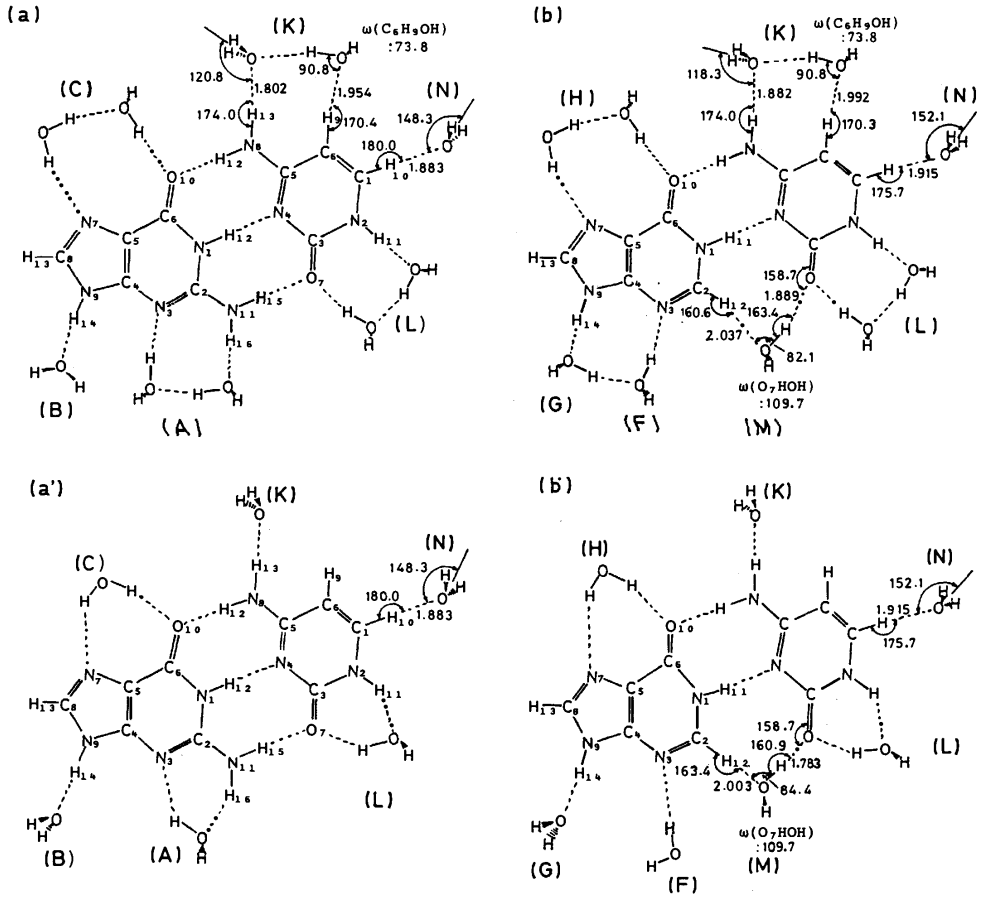

Fig. 6. The hydration schemes and optimized geometric parameters between base pair and water molecule of (a) and (a′) Gua-Cyt and (b) and (b′) Hyp-Cyt pairs. Units are angstroms and degrees.

of internal hydrogen bonds. Therefore, these hydrogen atoms come to have unusual, positive net charges. This result expects an unusual C-$H^{\delta+}$···O hydrogen-bond formation with H_2O at H_{12} of Hyp in the Hyp-Cyt pair. Also, there is a possibility of a similar type hydrogen bonding between H_2O and C_6-H_9 or C_1-H_{10} of Cyt in both Gua-Cyt and Hyp-Cyt pairs.

In order to investigate this type of interesting C-$H^{\delta+}$···O hydrogen bonding, we carried out ab initio MO calculations, while assuming various possible hydration schemes (Figs. 6a, b, a′, and b′). The optimized geometrical parameters are shown in these figures. Our result shows that C-$H^{\delta+}$···O hydrogen bonds are possible in both Gua-Cyt and Hyp-Cyt pairs.

Goldblum et al. investigated the hydration scheme of the Gua-Cyt pair using an overlap multipole procedure.[11] However, their scheme is somewhat different from ours. On the other hand, the hydration scheme of the Gua-Cyt pair shown in Fig. 6a is rather similar to that of Clementi and Corongiu studied by Monte Carlo simulations.[19]

In order to estimate the effect of hydration on the internal hydrogen bonds of complementary base pairs, Gua-Cyt and Hyp-Cyt pairs with various degrees of hydration were calculated. The calculated results are summarized in Table 4. For the Gua-Cyt pair, the internal hydrogen bonds are stabilized by hydration at regions (C), (K), and (N), but destabilized by that at regions (A), (B), and (L) in both hydration schemes (Figs. 6a and 6a′). Especially, H_2O molecules which arehydrated to an amino group (region (A)) brought about a significant destabilization of internal hydrogen bonds of the Gua-Cyt pair. It is of interest to note that the same result was also found in the hydration to the amino group of the adenine-uracil pair.[20] On the other hand, for the Hyp-Cyt pair, hydration at regions (H), (K), (N), and (M) causes a stabilization of the internal hydrogen bonds, while that at region (L) brings about destabilization in both hydration schemes (Figs. 6b and 6b′).

When all of the possible donating and accepting sites are hydrated, the Hyp-Cyt pair is considerably stabilized, while the Gua-Cyt pair is slightly destabilized (see Table 4). This result can be explained as follows: The charge-transfer interaction at the internal hydrogen bonds of the Gua-Cyt pair is weakened, while that of the Hyp-Cyt pair is strengthened, due to a change in the HOMO and LUMO energies by hydration. Both the Gua-Cyt and Hyp-Cyt pairs are stabilized by C-$H^{\delta+}$···O hydrogen-bond formation.

The experimental results show that the enthalpy changes due to complementary base-pair formation in aqueous solution were rather small compared with those in $CHCl_3$ or the gas phase. As mentioned in the previous section, this is due to destabilization by the dehydration of hydrated bases in the process of complementary base-pair formation.

In order to explain the experimental results quantitatively, the energy differences between the hydrated bases and base pairs were evaluated by the following energy cycles. For the first type of hydration scheme

Table 4. The Calculated Hydrogen-Bonding Energies between Hydrated Gua and Cyt, and between Hydrated Hyp and Cyt for Various Hydration

Gua-Cyt pair			Hyp-Cyt pair		
Region[a]	E_{HB} / kJ mol^{-1}	ΔE_{HB}[b] / kJ mol^{-1}	Region[a]	E_{HB} / kJ mol^{-1}	ΔE_{HB}[c] / kJ mol^{-1}
Nonhydrated	−111.3		Nonhydrated	−82.4	
(Hydration schemes shown in Figs. 6a and b)					
A	−100.0	+11.3	F+G	−86.0	−3.6
B	−108.8	+2.5			
C	−112.0	−0.7	H	−82.7	−0.3
K	−118.5	−7.2	K	−86.8	−4.4
L	−108.0	+3.3	L	−81.1	+1.3
N	−115.0[d]	−3.7	N	−84.2[d]	−1.8
			M	−84.9[d]	−2.5
A+B+C+K+L+N	−109.8[d]	+1.5	F+G+H+K+L+N+M	−102.8[d]	−20.4
(Hydration schemes shown in Figs. 6a′ and b′)					
A	−103.5	+7.8	F	−84.1	−1.7
B	−107.9	+3.4	G	−79.1	+2.7
C	−114.3	−3.0	H	−84.6	−2.2
K	−112.7	−1.4	K	−82.7	−0.3
L	−110.3	+1.0	L	−81.8	+0.6
N	−115.0[d]	−3.7	N	−84.2[d]	−1.8
			M	−88.1[d]	−5.7
A+B+C+K+L+N	110.1[d]	+1.2	F+G+H+K+L+N+M	−93.3[d]	−10.9

a) Refer to Fig. 6. b) $\Delta E_{HB}=E_{HB}-(-111.3)$. c) $\Delta E_{HB}=E_{HB}-(-82.4)$. d) The values contain the C-$H^{\delta+}$···O hydrogen-bonding energies.

of the Gua-Cyt system (Fig. 6a), the energy cycle (Cycle 1) can be expressed as follows:

$$\begin{array}{ccc} (\text{Gua} + 8\text{H}_2\text{O}) & \xrightarrow[\Delta E_1]{} & (\text{Gua-8H}_2\text{O}) \\ + & & + \\ (\text{Cyt} + 6\text{H}_2\text{O}) & \xrightarrow[\Delta E_2]{} & (\text{Cyt-6H}_2\text{O}) \\ \downarrow \Delta E_5 & & \downarrow \Delta E_3 \\ (\text{Gua-Cyt} + 14\text{H}_2\text{O}) & \xrightarrow[\Delta E_4]{} & (5\text{H}_2\text{O-Gua-Cyt-5H}_2\text{O}) + 2(\text{H}_2\text{O})_2 \end{array}$$

For the second type hydration scheme (Fig. 6a'), it (Cycle II) can be expressed as follows:

$$\begin{array}{ccc} (\text{Gua} + 5\text{H}_2\text{O}) & \xrightarrow[\Delta E_1]{} & (\text{Gua-5H}_2\text{O}) \\ + & & + \\ (\text{Cyt} + 4\text{H}_2\text{O}) & \xrightarrow[\Delta E_2]{} & (\text{Cyt-4H}_2\text{O}) \\ \downarrow \Delta E_5 & & \downarrow \Delta E_3 \\ (\text{Gua-Cyt} + 9\text{H}_2\text{O}) & \xrightarrow[\Delta E_4]{} & (3\text{H}_2\text{O-Gua-Cyt-3H}_2\text{O}) + \frac{3}{2}(\text{H}_2\text{O})_2 \end{array}$$

Similarly, for the first type hydration scheme of the Hyp-Cyt system (Fig. 6b), it (Cycle III) is represented as follows:

$$\begin{array}{ccc} (\text{Hyp} + 6\text{H}_2\text{O}) & \xrightarrow[\Delta E_1]{} & (\text{Hyp-6H}_2\text{O}) \\ + & & + \\ (\text{Cyt} + 6\text{H}_2\text{O}) & \xrightarrow[\Delta E_2]{} & (\text{Cyt-6H}_2\text{O}) \\ \downarrow \Delta E_5 & & \downarrow \Delta E_3 \\ (\text{Hyp-Cyt} + 12\text{H}_2\text{O}) & \xrightarrow[\Delta E_4]{} & (4\text{H}_2\text{O-Hyp-Cyt-5H}_2\text{O}) + (\text{H}_2\text{O})_2 \\ & & \quad \diagdown \text{H}_2\text{O} \diagup \end{array}$$

For the second type of hydration scheme (Fig. 6b'), it (Cycle IV) is given by

$$\begin{array}{ccc} (\text{Hyp} + 4\text{H}_2\text{O}) & \xrightarrow[\Delta E_1]{} & (\text{Hyp-4H}_2\text{O}) \\ + & & + \\ (\text{Cyt} + 4\text{H}_2\text{O}) & \xrightarrow[\Delta E_2]{} & (\text{Cyt-4H}_2\text{O}) \\ \downarrow \Delta E_5 & & \downarrow \Delta E_3 \\ (\text{Hyp-Cyt} + 8\text{H}_2\text{O}) & \xrightarrow[\Delta E_4]{} & (3\text{H}_2\text{O-Hyp-Cyt-3H}_2\text{O}) + \frac{1}{2}(\text{H}_2\text{O})_2 \\ & & \quad \diagdown \text{H}_2\text{O} \diagup \end{array}$$

where, it was assumed that the removed H_2O molecules formed the dimer. The dimerization energy was calculated to be -21.3 kJ mol^{-1}.

The calculated values are summarized follows:

Cycle I: $\Delta E_1 = -373.8$ kJ mol^{-1}
$\Delta E_2 = -287.4$ kJ mol^{-1}
$\Delta E_4 = -445.2$ kJ mol^{-1}
$\Delta E_5 = -111.3$ kJ mol^{-1}

Table 5. The Calculated Energy Differences by Hydrogen-Bond Formation between Hydrated Gua and Cyt and between Hydrated Hyp and Cyt, and the Experimental Enthalpy Changes in Aqueous Solution

	ΔE_3[a]	ΔE_3[b]	$\Delta H°$[c]
	kJ mol^{-1}	kJ mol^{-1}	kJ mol^{-1}
Gua-Cyt pair	+104.7(Cycle I)	−11.9(Cycle II)	−10
Hyp-Cyt pair	+97.5(Cycle III)	−18.5(Cycle IV)	−14

a) The first type of hydration schemes. b) The second type of hydration schemes. c) Data from calorimetric experiment (see Table 3).

Cycle II: $\Delta E_1 = -191.1$ kJ mol^{-1}
$\Delta E_2 = -144.4$ kJ mol^{-1}
$\Delta E_4 = -236.1$ kJ mol^{-1}
$\Delta E_5 = -111.3$ kJ mol^{-1}

Cycle III: $\Delta E_1 = -305.9$ kJ mol^{-1}
$\Delta E_2 = -287.4$ kJ mol^{-1}
$\Delta E_4 = -413.4$ kJ mol^{-1}
$\Delta E_5 = -82.4$ kJ mol^{-1}

Cycle IV: $\Delta E_1 = -138.7$ kJ mol^{-1}
$\Delta E_2 = -144.4$ kJ mol^{-1}
$\Delta E_4 = -219.2$ kJ mol^{-1}
$\Delta E_5 = -82.4$ kJ mol^{-1}

ΔE_5 is equal to E_{HB} (the internal hydrogen-bonding energy of complementary base pair in vacuo). The values are given in Table 1. Comparing the hydration energy of Gua with that of Hyp in both Cycles (ΔE_1), we can see that the hydrated Gua is more stable than the hydrated Hyp. This is due to the existance of an amino group at which stable hydration occurs.

ΔE_3 is the energy difference, which may correspond to the mixing process in the calorimetric experiment. It can be estimated by using the energies in the energy cycles mentioned above. The obtained results are summarized in Table 5, together with the $\Delta H°$-values determined from calorimetric experiments. The magnitudes of the calculated energy differences (ΔE_3), based on Cycles II and IV, are in good agreement with the experimental enthalpy change, while those based on Cycles I and III disagree with the experiment. It is of interest to note that the order of the ΔE_3-values of hydrated Gua-Cyt and Hyp-Cyt pairs in both energy cycles agrees with that of the experimental $\Delta H°$-values.

Conclusions

Stabilization due to the formation of hydrogen bonds between Gua and Cyt and between Hyp and Cyt in vacuo and in aqueous solution was investigated by means of ab initio MO calculations and solution calorimetry.

The calculated hydrogen-bonding energies in vacuo were -111.3 kJ mol^{-1} for the Gua-Cyt pair and -82.4 kJ mol^{-1} for Hyp-Cyt, respectively. Thus, the Gua-Cyt pair was more stable than the Hyp-Cyt pair in vacuo. The main contributions to the internal hydrogen bonds of Gua-Cyt and Hyp-Cyt pairs were both electrostatic and charge-transfer interactions. For the Gua-Cyt pair, the charge transfer from Cyt to Gua through the hydrogen bonds was larger than that from Gua to Cyt. Since the dipole moment of the Gua-Cyt pair was larger than that of Hyp-Cyt, the Gua-Cyt pair was expected to be more stable than the Hyp-Cyt pair in a polar solvent because of the stabilization due to the dipole-dipole interaction between solute and solvent. This expectation agreed with the experiments concerning $CHCl_3$ solutions. However, the calorimetric measurement showed that in aqueous solution, the Hyp-Cyt pair was more stable than Gua-Cyt. That is, the enthalpy changes of the association of Gua with Cyt and of Hyp with Cyt in aqueous solution were estimated to be -10 kJ mol^{-1} for the Gua-Cyt system and -14 kJ mol^{-1} for the Hyp-Cyt system by using a solution microcalorimeter.

In order to explain this result, we carried out ab initio MO calculations of hydrated bases and base pairs, by assuming two types of hydration schemes. Using the energy cycles, we estimated the energies corresponding to the experimental heats of mixing (ΔE_3). The calculated ΔE_3's based on the second type hydration scheme agreed with the experiments. Thus, the expermental results for aqueous solutions could be explained by dehydration in the course of complementary base-pair formation.

From the calculated results, it was shown that there was a possibility of C-H$^{\delta+}$···O hydrogen-bond formation between a H_2O molecule and a base pair. Furthermore, it was indicated that a H_2O molecule bound to an amino group of Gua destabilized the internal hydrogen bonds of complementary base pairs, however, that to the amino group of Cyt stabilized the internal hydrogen bonds.

In conclusion, the present work showed that hydration/dehydration had an important effect on the stability of the complementary base pair.

We are grateful to the Computer Center of the Institute for Molecular Science for the use of HITAC M-680H and S-820/80 computers. This work was partly supported by the Grant-in-Aid for Scientific Research (No. 62470013) from the Ministry of Education, Science and Culture.

References

1) J. D. Watson and F. H. C. Crick, *Nature(London)*, **171**, 737 (1953).

2) W. Saenger, "Principles of Nucleic Acid Structure," Springer-Verlag, New York (1984), Chap. 8.

3) Y. Baba, K. Fujioka, and A. Kagemoto, *Polym. J.*, **10**, 241 (1978).

4) K. Fujioka, Y. Baba, and A. Kagemoto, *Polym. J.*, **12**, 843 (1980).

5) Y. Kyogoku, R. C. Lord, and A. Rich, *Biochim. Biophys. Acta*, **179**, 10 (1969).

6) L. F. Sukhodub and I. K. Yanson, *Nature(London)*, **264**, 245 (1976).

7) I. K. Yanson, A. B. Tepletsky, and L. F. Sukhodub, *Biopolymers*, **18**, 1149 (1979).

8) W. Förner, P. Otto, and J. Ladik, *Chem Phys.*, **86**, 49 (1984).

9) A. Pohorille, S. K. Burt, and R. D. MacElroy, *J. Am. Chem. Soc.*, **106**, 402 (1984).

10) A. Sarai and M. Saito, *Int. J. Quantum Chem.*, **28**, 399 (1985).

11) A. Gordblum, D. Perahia, and A. Pullman, *FEBS Lett.*, **91**, 213 (1978).

12) B. Pullman, S. Miertus, and D. Perahia, *Theor. Chim. Acta*, **50**, 317 (1979).

13) J. T. Powell, E. G. Richards, and W. B. Gratzer, *Biopolymers*, **11**, 235 (1972).

14) J. Langlet, P. Claverie, F. Caron, and J. C. Boeuve, *Int. J. Quantum Chem.*, **19**, 299 (1981).

15) M. Aida and C. Nagata, *Int. J. Quantum Chem*, **29**, 1253 (1986).

16) P. Hobza and C. Sandorfy, *J. Am. Chem. Soc.*, **109**, 1302 (1987).

17) E. Clementi, J. Mehl, and W. Von Niessen, *J. Chem. Phys.*, **54**, 508 (1971).

18) R. Scordamaglia, F. Carallone, and E. Clementi, *J. Am. Chem. Soc.*, **99**, 5545 (1977).

19) E. Clement and G. Corongiu, *J. Chem. Phys.*, **72**, 3979 (1980).

20) Y. Ohta, H. Tanaka, Y. Baba, A. Kagemoto, and K. Nishimoto, *J. Phys. Chem.*, **90**, 4438 (1986).

21) A. Weissberger and E. S. Proskauer, "Organic Solvents," Interscience, New York (1955).

22) Y. Baba, S. Tanaka, and A. Kagemoto, *Makromol. Chem.*, **178**, 2117 (1977).

23) K. Morokuma, S. Kato, K. Kitaura, I. Ohmine, S. Sakai, and S. Obara, IMS Computer Center Program Library, The Institute for Molecular Science, Program No. 372 (1980).

24) J. S. Binkley, R. A. Whiteside, R. Krishnan, R. Seeger P. J. DeFrees, H. B. Schlegel, S. Topiol, L. R. Kahn, and J. A. Pople, *Quantum Chemistry Program Exchange*, **13**, 406 (1981).

25) W. J. Hehre, R. F. Stewart, and J. A. Pople, *J. Chem. Phys.*, **51**, 2657 (1969).

26) J. E Del Bene, *J. Phys. Chem.*, **87**, 367 (1983).

27) T. Matsushita, Y. Baba, and A. Kagemoto, unpublished work.

28) S. Arnott and D. W. L. Hukins, *J. Mol. Biol.*, **81**, 93 (1973).

29) K. Kitaura and K. Morokuma, *Int. J. Quantum Chem.*, **10**, 325 (1976).

30) K. Morokuma and K. Kitaura, "Chemical Applications of Atomic and Molecular Electrostatic Potentials," Plenum, New York (1981), pp. 215—242.

On the Relationship between the Chemical Structure and the Cyclic AMP Phosphodiesterase Inhibitory Activity of Flavonoids as Studied by ^{13}C NMR

Yohko SAKAMOTO,* Taichi OHMOTO, Tamotsu NIKAIDO, Kazuo KOIKE, Tsuyoshi TOMIMORI,†
Yukinori MIYAICHI,† Yoshiaki SHIRATAKI,† F. D. MONACHE,††
B. BOTTA,†† Ichiro YOKOE,††† Manki KOMATSU,†††
Shosuke WATANABE,†††† and Isao ANDO†††††
School of Pharmaceutical Sciences, Toho University, Funabashi, Chiba 274
†School of Pharmacy, Hokuriku University, Kanazawa 920-11
††Centro Chimica dei Recettori del C. N. R., Universita Cattolica, del, S. Cuore, Roma, Italy
†††Faculty of Pharmaceutical Sciences, Josai University, Saitama 350-02
††††Nihon Junior College of Economics, Sakai, Musashino, Tokyo 180
†††††Department of Polymer Chemistry, Tokyo Institute of Technology, Ookayama, Meguro-ku, Tokyo 152
(Received November 19, 1988)

The relationship between the chemical structure and the cyclic adenosine monophosphate phosphodiesterase inhibitory activity was studied regarding forty-eight flavones, thirty-five flavanones, and six isoflavones by using the ^{13}C NMR chemical shift averaged over all aromatic carbons in a compound. The average value of potent ^{13}C chemical shifts over the aromatic carbons active flavonoids (IC_{50} 0.6—20.0 $\times 10^{-5}$ M/L) are within the range from δ 133.5 to δ 135.7, but those of the inactive flavonoids and the weak active flavonoids are not within this range. This means that the averaged ^{13}C chemical shift becomes an "index" for testing the inhibitory activity. Further, the above relationship was proposed as a means for conveniently determining the inhibitory activity.

3′,5′-Cyclic adenosine monophosphate (cAMP) phosphodiesterase (PDE) inhibition can be used as a screening agent to detect physiologically active compounds.[1] It is known that there is a close relationship between the inhibition of PDE in vitro among 158 therapeutic agents tested for PDE inhibition and the physiological activity in vivo.[2-6] Moreover, many flavonoids have been identified as having a potent inhibitory activity on cAMP PDE.[7-10] These results indicate that the PDE inhibitors might have a variety of physiological activities. However, it takes a long time to determine such physiological activities using the conventional method. Thus, it has been important to develop a simple method.

We studied the relationship between the inhibitory activity on cAMP PDE of flavonoids and the averaged ^{13}C NMR chemical shifts (δ_{av}) for all carbons in the ring structures of these compounds. We also clarified whether or not the averaged ^{13}C NMR chemical shift is useful for studying the cAMP PDE inhibitory activity and using its relationship as a simple method for determining physiological activities. The averaged ^{13}C NMR chemical shifts employed in this work reflect the electronic structure and electronic states of the molecules[11,12] which may govern the mechanism of the inhibitory activity. As shown in the theory of ^{13}C shielding in aromatic hydrocarbons,[13] the chemical shift δ of each carbon can be expressed as $\delta \propto 1/\Delta E \cdot Q$, where ΔE is the averaged excitation energy, and Q is a function of the electron density and bond order of a molecule.

The averaged excitation energy is assumed to be a constant for the aromatic compounds considered here.[11]

Thus, we expect that the averaged ^{13}C NMR chemical shift is a measure of the inhibitory activity.

Experimental

Authentic samples were used in the tests for the evaluation of the inhibitory activity on cAMP phosphodiesterase which had been isolated or prepared during structural studies.[1,8,14] (Tables 1, 2, and 3), (Fig. 1 (a), (b), and (c)). Cyclic AMP PDE inhibitory activity was assayed by the method described in a previous paper.[14]

The ^{13}C NMR spectra were recorded with Fourier transform spectrometers (JEOL JNM FX-90 Q, JEOL JNM GX-270 and JEOL JNM GX-400) operating at 22.5, 67.5, and 100.4 MHz, respectively, at room temperature. Dimethyl-d_6 sulfoxide was used as a solvent. The concentration of the samples was 2—10% (w/v). The chemical shifts were expressed in ppm relative to tetramethylsilane (TMS).

Results and Discussion

The averaged ^{13}C NMR chemical shifts (δ_{av}) over all the ring carbons of flavonoids and 50% inhibitory concentrations (IC_{50})cAMP PDE inhibitory activities of these samples are shown in Tables 1, 2, and 3. The compounds listed in these tables can be divided into three groups: potent inhibitory groups (IC_{50}=0.6—20.0$\times 10^{-5}$ M/L and δ_{av}=133.5—135.7), weak inhibitory groups (IC_{50}=20.1—35.3$\times 10^{-5}$M/L and $\delta_{av} \leqq$ 133.5), and inactive groups ($IC_{50} \geqq 35.3 \times 10^{-5}$ M/L$\geqq$135.7). The relationship between the δ_{av} of the individual compound and the IC_{50} value in the cAMP PDE inhibition is shown in Fig. 2. As can be seen from this figure, it is found that there is a correlation between IC_{50} and δ_{av} in the range from 133.5 to 135.7 . This means that δ_{av} can be used to discern whether the

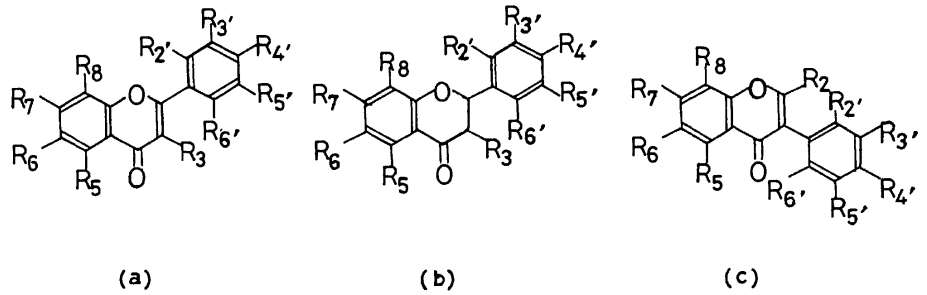

(a) (b) (c)

Fig. 1. (a) Flavone compounds. (b) Flavanone compounds. (c) Isoflavone compounds.

Table 1. cAMP PDE Inhibitory Activity and Averaged ^{13}C NMR Chemical Shifts ($\bar{\delta}$) of Flavones

No.	Substituents										IC_{50} ($\times 10^{-5}$M/L)	Averaged ^{13}C ($\bar{\delta}$)
	R_3	R_5	R_6	R_7	R_8	$R_{2'}$	$R_{3'}$	$R_{4'}$	$R_{5'}$	$R_{6'}$		
1	H	H	H	H	H	H	H	H	H	H	13.2	133.7
2	H	OH	H	OMe	H	H	H	H	H	H	150.0	132.6
3	H	OH	OH	OH	H	H	H	H	H	H	7.6	133.5
4	H	OH	OMe	OH	H	H	H	H	H	H	5.7	134.6
5	H	OH	OH	Oglu	H	H	H	H	H	H	24.2	133.7
6	H	OH	H	OH	OH	H	H	H	H	H	7.2	133.7
7	H	OH	H	OH	OMe	H	H	H	H	H	15.0	134.7
8	H	OH	H	OMe	OMe	H	H	H	H	H	5.3	134.5
9	H	OMe	H	OH	OMe	H	H	H	H	H	7.2	134.2
10	H	OH	H	OAc	OMe	H	H	H	H	H	16.9	135.3
11	H	OAc	H	OAc	OMe	H	H	H	H	H	31.0	135.4
12	H	OMe	H	OAc	OMe	H	H	H	H	H	7.8	134.8
13	H	OH	H	OH	H	OH	H	H	H	H	14.2	133.7
14	H	OH	H	OH	H	H	H	OH	H	H	26.9	133.4
15	H	OH	H	OMe	H	H	H	OH	H	H	61.6	132.6
16	H	OH	H	OH	H	H	H	OMe	H	H	57.4	132.7
17	OH	OH	H	OH	H	H	H	OH	H	H	22.5	133.0
18	H	OH	OH	OH	H	H	H	OH	H	H	21.2	133.2
19	H	OH	OMe	OH	H	H	H	OH	H	H	4.2	134.2
20	H	OH	OMe	OMe	H	H	H	OH	H	H	11.8	134.3
21	H	OH	OMe	OMe	H	H	H	OMe	H	H	31.6	134.2
22	H	OH	H	OH	OMe	H	H	OH	H	H	6.5	134.4
23	H	OH	OMe	OMe	OH	H	H	H	H	H	8.3	135.7
24	H	OH	H	OH	H	H	OH	OH	H	H	20.8	133.3
25	H	OH	H	OH	H	H	OMe	OH	H	H	35.3	133.0
26	H	Oglu	H	OH	H	H	OH	OH	H	H	62.5	133.2
27	H	OH	H	Oglu	H	H	OH	OH	H	H	32.3	133.1
28	H	OH	H	OH	OMe	OH	H	H	H	H	0.6	134.6
29	H	OH	H	OH	OMe	OMe	H	H	H	H	6.7	134.7
30	H	OMe	H	OH	OMe	OMe	H	H	H	H	7.2	134.3
31	H	OH	H	OMe	OMe	OAc	H	H	H	H	5.5	135.7
32	H	OAc	H	OMe	OMe	OAc	H	H	H	H	>500.0	135.8
33	H	OH	H	OH	OMe	OH	H	H	OH	OMe	2.5	135.7
34	H	OH	OMe	OH	H	H	OH	OH	H	H	5.3	133.9
35	H	OH	OMe	OMe	H	H	OMe	OH	H	H	3.2	134.0
36	H	OH	H	OH	OMe	OH	H	H	H	OMe	16.9	134.7
37	H	OH	H	OMe	OMe	OH	H	H	H	OH	6.7	134.6
38	H	OH	H	OH	OMe	OMe	H	H	H	OMe	7.4	134.6
39	H	OH	H	OMe	OMe	OH	H	H	H	OMe	6.3	134.7
40	H	OH	H	OMe	OMe	OMe	H	H	H	OMe	16.5	134.6
41	H	OMe	OMe	OMe	OMe	H	H	OMe	H	H	28.2	136.7
42	OH	OH	H	OH	H	OH	H	H	H	OH	9.6	134.1
43	OH	OH	H	OH	H	OH	H	OH	H	H	16.3	133.1
44	OH	OH,	H	OH	H	H	OH	OH	H	H	31.7	132.6
45	OMe	OMe	H	OMe	H	H	OMe	OMe	H	H	12.9	133.9
46	Orha	OH	H	OH	H	H	OH	OH	H	H	17.6	134.6
47	OH	OH	H	Oglu	H	H	OH	OH	H	H	13.9	133.5
48	OH	OH	H	OH	H	H	OH	Oglu	H	H	10.0	134.0

Table 2. cAMP PDE Inhibitory Activity and Averaged ^{13}C NMR Chemical Shifts (δ) of Flavanones

No.	Substituents										IC_{50} ($\times 10^{-5}$M/L)	Average $^{13}C(\delta)$ (a)	(b)
	R_3	R_5	R_6	R_7	R_8	$R_{2'}$	$R_{3'}$	$R_{4'}$	$R_{5'}$	$R_{6'}$			
49	H_2	H	H	OH		H	H	H	H	H	1.1	134.6	133.6
50	H_2	H	H	OMe		H	H	H	H	H	16.4	134.1	133.5
51	H_2	H			H	H	H	OH	H	H	4.5	135.9	134.6
52	H_2	H			H	H	H	OH	H	H	18.4	134.3	
53	H_2	H	H	OMe	Me	H	H	OMe	H	H	11.7	133.6	
54	H_2	OH	H	OMe		H	H	H	H	H	16.9	135.1	133.9
55	H_2	OH	H	OH	H	H	H	OH	H	H	109.0	136.1	
56	H_2	OH		OH	H	H	H	OH	H	H	6.0	136.5	135.3
57	H_2	OH	H	OH		H	H	OH	H	H	2.8	136.4	134.7
58	H_2	OH	H	OH		H		OH	H	H	2.4	136.5	134.4
59	H_2	OH	H	OH		H	H	OH	H	H	2.7	136.4	134.7
60	H_2	OH	OH	OH	H	H	H	H	H	H	5.3	135.4	
61	H_2	OH	OMe	OH	H	H	H	H	H	H	>500.0	136.1	
62	H_2	OH	Me	OMe	H	H	H	OMe	H	H	6.2	134.3	
63	H_2	OH	OH	OgluAOMe	H	H	H	OH	H	H	3.8	135.1	
64	H_2	OH	H	OgluAOMe	OH	H	H	OH	H	H	3.4	135.2	
65	H_2	OH	H	OMe	Me	H	H	OMe	H	H	8.1	133.9	
66	H_2	OH	H	OH	OMe	OH	H	H	H	H	14.1	135.7	
67	H_2	OH	H	OH	OMe	H	H	OH	H	H	32.4	136.2	
68	H_2	OH	H	OH	OMe	OMe	H	H	H	H	6.2	136.0	
69	H_2	OMe	H	OH	OMe	OMe	H	H	H	H	20.5	135.2	
70	H_2	OH	H	OMe	OMe	OH	H	H	OH	H	9.2	135.6	
71	H_2	OH	H	OMe	OMe	OH	H	H	H	OMe	9.8	135.7	
72	H_2	OH	OMe	OMe	H	OH	H	H	H	OMe	13.4	135.7	
73	H_2	OH	H	OH		OH	H	H	H	H	1.4	136.3	134.6
74	H_2	OH	H	OH	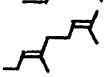	OH	H	OH	H	H	4.6	136.0	134.3
75	H_2	OH	H	OH		OH	H	OH	H	H	3.9	135.9	134.3
76	H_2	OH	H	OH		OMe	H	OH	H	H	5.7	135.2	133.7
77	H_2	OMe	H	OH		OH	H	OH	H	H	2.5	135.4	133.9
78	H_2	OMe	H	OH	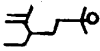	OH	H	OH	H	H	6.3	135.4	134.7
79	H_2	OH		OH		OH	H	OH	H	H	4.0	136.4	134.4
80	H_2	OH		OH		OH	H	OH	H	H	3.1	136.5	134.8
81	OH	OMe	H	OH	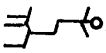	OH	H	OH	H	H	17.2	135.6	134.9
82	H_2	OH	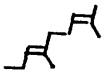	OH	H	OH	H	OH	H	H	3.1	136.0	134.3
83	H_2	OH	H	OH	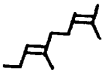	OH	H	OH	H	OH	5.0	136.1	134.3

compounds being considered are potent inhibitors or not. Thirty flavones compounds **1**, **3**, **4**, **6**, **7**, **8**, **10**, **12**, **13**, **19**, **20**, **22**, **23**, **28**, **29**, **30**, **31**, **33**, **34**, **35**, **36**, **37**, **38**, **39**, **40**, **42**, **45**, **46**, **47**, and **48** have potent cAMP PDE inhibitory activity,[8] and their averaged chemical shifts are within the range δ 133.5 to 135.7. The δ_{av} values for the remaining eleven compounds **2**, **14**, **15**, **16**, **17**, **18**, **24**, **25**, **26**, **27**, and **44** are smaller than 133.5, while those for compounds **32** and **41** are larger than 135.7. The thirteen compounds, except for **32**

Table 3. cAMP PDE Inhibitory Activity and Averaged ^{13}C NMR Chemical Shifts ($\bar{\delta}$) of Isoflavones

No.	Substituents R_5	R_6	R_7	R_8	$R_{2'}$	$R_{3'}$	$R_{4'}$	$R_{5'}$	$R_{6'}$	IC_{50} ($\times10^{-5}$M/L)	Averaged ^{13}C ($\bar{\delta}$) (a)	(b)
84	H	H	OH	H	H	H	OH	H	H	28.3	133.0	
85	H	H	OH	H	H	H	OMe	H	H	49.6	132.8	
86	H	H	OH	H	H	OH	OMe	H	H	17.3	133.5	
87	OH	H	OH	H	H	H	OH	H	H	12.1	133.8	
88	OH		OH		H	H	OH	H	H	20.3	134.8	133.1
89	OH	OMe	OH	H	H	OH	OMe	OMe	H	1.1	134.7	

a) The δ_{av} of the individual compounds having no prenyl groups. b) The δ_{av} of the individual compounds having prenyl groups or having no prenyl groups and isoflavones.

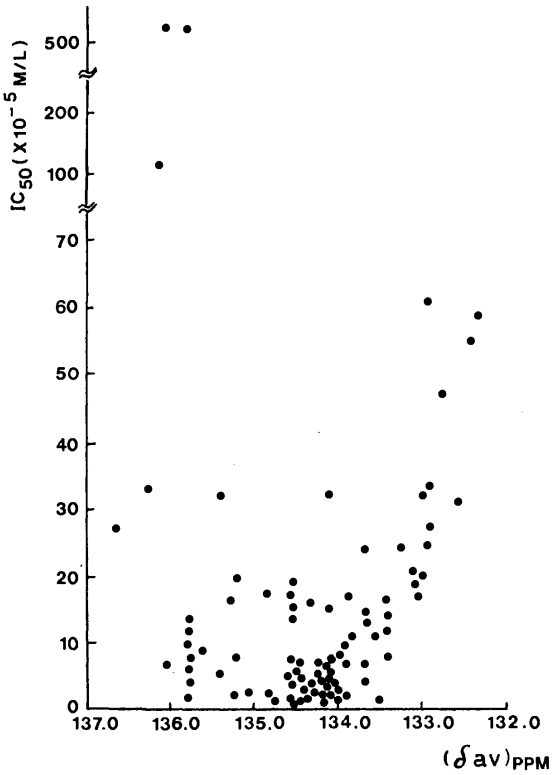

Fig. 2. The relationship between the averaged ^{13}C NMR chemical shifts (δ_{av}) of flavones and their cAMP PDE inhibitory activity IC_{50}.

and **41**, have a large IC_{50} value (>20.1) and, thus, inactive property. The δ_{av} value of **43** is slightly lower than 133.5, suggesting that this compound has a strong cAMP PDE inhibitory activity.

The values of δ_{av} for **5**, **11**, and **21** are within the range 133.5—135.7; thus, these compounds can be expected to be in the potent inhibitory group. However, the values of IC_{50} for **5**, **11**, and **21** are not contained in the potent inhibitory group. This means that it is not easy to exactly determine the borderline region.

Next, we consider the effect of the substituent group of the compounds on the relationship between the cAMP PDE inhibitory activity and δ_{av}. When the hydroxyl group or methoxyl group is substituted at the C-5, 7 or 4′-positions on an aromatic ring of compounds **14**, **15**, and **16**, their cAMP PDE inhibitory activity is detected slightly or not and the values of δ_{av} are smaller than 133.5. When the methoxyl group is substituted at the C-6 position on an aromatic ring in compounds **4**, **19**, **20**, **23**, **34**, and **35**, the increase in cAMP PDE inhibitory activity can be recognized[8] and the δ_{av} values are within the range 133.5—135.7. When the hydroxyl group, methoxyl group or *o*-glucosyl group is substituted at the C-5, 7, 3′ or 4′-positions on an aromatic ring of compounds **24**, **25**, **26**, and **27**, the cAMP PDE inhibitory activity is detected slightly or not and the values of δ_{av} are smaller than 133.5. However, when the methoxyl group or *o*-rhamnosyl group is substituted at the C-3 position on the aromatic ring of compounds **45** and **46**, the increase in cAMP PDE inhibitory activity can be recognized and the δ_{av} values are within the range 133.5—135.7. Eleven flavanones compounds **51**, **56**, **57**, **58**, **59**, **73**, **74**, **75**, **79**, **82**, and **83** have potent cAMP PDE inhibitory activity.[9] However, as can be seen from Table 2, the δ_{av} value of compounds having no prenyl, geranyl and lavandulyl group **51**, **56**, **57**, **58**, **59**, **79**, and **80**, are within the range 135.9—136.5, beyond the range 133.5—135.7.

On the other hand, in the case of having a prenyl group, it has been found that the value of δ_{av} for compounds **49**, **50**, **54**, **76**, **77**, **78**, and **81** are within the range 133.5—135.7, having a prenyl group.

It is considered that the prenyl group is a factor for having the cAMP PDE inhibitory activity, from the result of using the averaged value of the ^{13}C NMR chemical shift.

Flavanones derivatives[9] having no prenyl groups **52**, **53**, **60**, **62**, **63**, **64**, **65**, **66**, **69**, **70**, **71**, and **72** have a potent cAMP PDE inhibitory activity, and the δ_{av} values are within the range 133.5 to 135.7, as well as flavones. Compounds **55**, **61**, and **67** can be expected to be inactive groups or weak inhibitory group; the values of δ_{av} are larger than 135.7. Similary, concerning isoflavone derivatives, compounds **86**, **87**, **88**, and **89** showed potent cAMP PDE inhibitory activity.

The δ_{av} values of compounds **84** and **85** are smaller than 133.5. Therefore, these can be expected to be a weak inhibitory group or an inactive group.

Finally, we conclude the following. The cAMP PDE inhibitory activity for flavonoids can be examined from the averaged ^{13}C NMR chemical shift over all ring carbons. Further, it can be suggested that it is very useful to use this approach for drug design.

References

1) T. Nikaido, Y.-I. Sung, T. Ohmoto, and U. Sankawa, *Chem. Pharm. Bull.*, **32**, 578 (1984).

2) I. Weinryb, M. Chasin, C. A. Free, D. N. Harris, H. Goldenbery, I. M. Michel, V. S. Paik, M. Phillips, S. Samaniego, and S. M. Hess, *J. Pharm. Sci.*, **61**, 1556 (1972).

3) M. Samir and W. E. Kreighbaum, *J. Pharm. Sci.*, **64**, 1 (1975).

4) Y. Furutani, M. Shimada, M. Hamada, T. Takeuchi, and H. Umezawa, *J. Antibiot.*, **28**, 558 (1975).

5) Y. Kumada, H. Naganawa, H. Iinuma, M. Matsuzaki, T. Takeuchi, and H. Umezawa, *J. Antibiot.*, **29**, 882 (1976).

6) A. Beretz, M. Joly, J. C. Stoclet, and R. Anton., *Planta Medica.*, **36**, 193 (1979).

7) T. Nikaido, T. Ohmoto, U. Sankawa, T. Hamanaka, and K. Totsuka, *Planta Medica*, **46**, 162 (1982).

8) T. Nikaido, T. Ohmoto, U. Sankawa, T. Tomimori, Y. Miyaichi, and Y. Imoto, *Chem. Pharm. Bull.*, **36**, 654 (1988).

9) T. Ohmoto, R. Aikawa, T. Nikaido, U. Sankawa, Wu Li Jun, A. Ueno, and S. Fukushima, *Chem. Pharm. Bull.*, **34**, 2094 (1986).

10) T. Nikaido, T. Ohmoto, T. Kinoshita, U. Sankawa, F. D. Monache, B. Botta, T. Tomimori, Y. Miyaichi, Y. Shirataki, I. Yokoe, and M. Komatsu, *Chem. Pharm. Bull.*, **37**, (5), 1392 (1989).

11) Y. Sakamoto and S. Watanabe, *Bull. Chem. Soc. Jpn.*, **59**, 3033 (1986).

12) Y. Sakamoto and Y. Sakamoto, *Bull. Chem. Soc. Jpn.*, **62**, 330 (1989).

13) "Theory of NMR Parameters," ed by I. Ando and G. A. Webb, Academic Press (1983).

14) T. Nikaido, T. Ohmoto, N. Noguchi, T. Kinoshita, H. Saitoh, and U. Sankawa, *Planta Medica*, **43**, 18 (1981).

 © 1989 The Chemical Society of Japan Bull. Chem. Soc. Jpn., 62, 2455—2460 (1989)

Nitrogen-15 NMR Chemical Shifts in Metal-Ammine Complexes. II.[1] Cobalt(III) Ammine and Amine Complexes

Yoshiaki NAKASHIMA,* Masayuki MUTO,† Keiichi KAWANO,††
Yoshimasa KYOGOKU,††† and Yuzo YOSHIKAWA††††
Faculty of Education, Wakayama University, Wakayama 640
†††Institute for Protein Research, Osaka University, Suita 565
††††Department of Chemistry, Faculty of Science, Okayama University, Okayama 700
(Received December 5, 1988)

^{15}N nuclear magnetic resonance spectra were measured for $[CoX(^{15}NH_3]^{n+}$ ($X=CN^-$, $^{15}NH_3$, H_2O, and Br^-) and *cis*-$[CoX_2(en\text{-}^{15}N,^{15}N)_2]^{n+}$ ($X_2=(CN^-)_2$, $(NO_2^-)_2$, en-^{15}N,^{15}N, ox^{2-}, and $(H_2O)_2$; en-^{15}N,^{15}N and ox^{2-} represent the ^{15}N-enriched ethylenediamine and oxalate ion, respectively). Two sharp signals of ^{15}N NMR were observed for $[CoX(^{15}NH_3)_5]^{n+}$ except for the cases of $X=^{15}NH_3$ and NO_2^-. The signals of ^{15}N NMR in *cis*-$[CoX_2(en\text{-}^{15}N,^{15}N)_2]^{n+}$, were assigned on the basis of the selectively proton irradiated spectra at frequencies which had been already assigned to each amino proton. The chemical shifts of ^{15}N NMR are correlated to the Co-N bond strength; it is expected that the stronger is the Co-N bond, the greater is the shift of the ^{15}N NMR signal to a higher field. When we express $[CoX(^{15}NH_3)_5]^{n+}$ and *cis*-$[CoX_2(en\text{-}^{15}N,^{15}N)_2]^{n+}$ as $[CoXN_5]^{n+}$ and *cis*-$[CoX_2N_4]^{n+}$, the effect on the ^{15}N NMR chemical shifts by the substituent X is roughly additive.

One of the authors (Y.N.) has been able to semi-quantitatively explain the behaviors of the ^1H NMR chemical shifts in $[CoX(NH_3)_5]^{n+}$ by assuming that the induced ^1H NMR chemical shifts by changing X are mainly due to a change in the magnetic anisotropy of the Co(III) ion.[2-4] However, there were some descrepancies between the calculated and observed values. They were significantly large for the protons of NH_3 trans to X in complexes with $X=CN^-$ and NO_2^-. The chemical shift of the observed signals to higher fields than the calculated ones might be caused by increased electron densities on the trans ammine protons induced by the large inductive effects of X. The H-D exchange rates of the ammine protons were related to their acidity.[5] The trans ammine protons exchange more slowly than the cis ones with $X=CN^-$ and NO_2^-.[5] On the other hand, though the trans ammine protons exchange faster than the cis ones with $X=H_2O$, Cl^-, and Br^-, there has been no evidence of decreased electron densities of the trans ammine protons in the ^1H NMR chemical shifts.[4] ^1H NMR chemical shifts of ammine protons are easily affected by the solvent; in contrast, though, it has been reported that the chemical shifts of the NMR signals of ^{15}N directly bound to cobalt(III) are hardly affected by the solvent.[6] It is, therefore, expected that information concerning the Co-N bond strength and the acidity of ammine protons can be obtained from ^{15}N NMR chemical shifts with no solvent effect.

Lehman and Fung measured the ^{15}N NMR for $[CoX(^{15}NH_3)_5]^{n+}$ by the use of the INDOR technique, and then erroneously assigned the ^1H NMR chemical shift signals.[7] Thus, we doubted the shift directions of the ^{15}N NMR signals since their assignments of the ^{15}N NMR signals depended upon those of the proton signals.[7] The ^{14}N NMR signals of the same samples were also measured by Herbison-Evans and Richards.[8] The signals of $[Co(H_2O)(NH_3)_5]^{3+}$ and $[CoCl(NH_3)_5]^{2+}$ were single and the shift values were lower than that of $[Co(NH_3)_6]^{3+}$. It was one aim of the present work to determine the correct ^{15}N shift values of $[CoX(^{15}NH_3)_5]^{n+}$ relative to that of $[Co(^{15}NH_3)_6]^{3+}$ by directly observing the ^{15}N NMR signals. Furthermore, it would be interesting to find out whether the effect of substituent X_2 on the chemical shifts of ^{15}N NMR signals in *cis*-$[CoX_2(en\text{-}^{15}N,^{15}N)_2]^{n+}$ is additive or not.

Experimental

Materials. The $[CoX(^{15}NH_3)_5](NO_3^-)_n$ ($X=NO_2^-$, $^{15}NH_3$, H_2O, and Br^-) and the *cis*-$[CoX_2(en\text{-}^{15}N,^{15}N)_2]^{n+}$ ($X_2=(CN^-)_2$, $(NO_2^-)_2$, en-^{15}N,^{15}N, ox^{2-}, and $(H_2O)_2$) were synthesized according to the well-established methods.[9] The $[Co(CN)(NH_3)_5](ClO_4)_2$ containing $^{15}NH_3$ was synthesized by the method of Sibert.[10] The en-^{15}N,$^{15}N\cdot 2HCl$ and $^{15}NH_3$ were obtained from British Oxygen Co., Ltd., and their ^{15}N contents were 98 and 99.5%, respectively. Ligands diluted 30 to 40% of ^{15}N were used in all preparations of the complexes.

Equipments and Measurements. About 200 mg of each complex was dissolved in 1.5 ml of DMSO-d_6 in a 10-mmϕ tube and 1000—10000 transients were accumulated for $[CoX(^{15}NH_3)_5]^{n+}$. About 100 mg was dissolved in 1.5 ml of a DCl-D_2O solution (pD=2) in a 10-mmϕ tube and 1000—10000 transients were accumulated for *cis*-$[CoX_2(en\text{-}^{15}N,^{15}N)_2]^{n+}$. *cis*-$[Co(H_2O)_2(en\text{-}^{15}N,^{15}N)_2]^{3+}$ was dissolved in CF_3COOD. ^{15}N NMR spectra were recorded on a JEOL PFT-100 pulsed Fourier transform NMR spectrometer operated at 10.1 MHz. Only that of $[Co(en\text{-}^{15}N,^{15}N)_3]^{3+}$ (Fig. 2) was measured for a 0.1 M aqueous solution (1M=1 mol dm^{-3}) on a JEOL JNM-FX60 spectrometer at 6.06 MHz (204000 repetitions). $Na^{15}NO_2$ or $Na^{15}NO_3$ was used as an external reference of ^{15}N NMR signals.

† Present address: Seiwa Technological Laboratories Ltd., Tokyo 174.
†† Present address: Faculty of Dentistry, Kyusyu University, Fukuoka 812.

Results

Hexaammine- and Pentaamminecobalt(III) Complexes. The ^{15}N resonance spectra of $[CoX(^{15}NH_3)_5]^{n+}$ (X=CN^-, NO_2^-, $^{15}NH_3$, H_2O, and Br^-) are shown in Fig. 1. The ^{59}Co resonance spectra have already been measured for several Co(III) complexes.[11] By comparing ^{15}N and ^{59}Co NMR spectra, it was found that the broader is the line of the ^{59}Co NMR signal, the sharper is the line of ^{15}N NMR signal of $^{15}NH_3$ group directly bound to Co(III) ion. The ^{15}N NMR signal of $[Co(^{15}NH_3)_6]^{3+}$ is broad and complicated. This is due to coupling between the ^{15}N and ^{59}Co nuclei, resulting in the slow quadrupolar relaxation rate of the nuclear magnetic moment of ^{59}Co under high symmetry around the ^{59}Co nucleous.[12] In $[CoX(^{15}NH_3)_5]^{n+}$ the resonance signal of ^{15}N trans to X was distinguished from that of the cis on the basis of their intensities. The chemical shift values are given in Table 1. We erroneously reported the shift value of $[Co(^{15}NH_3)_6]^{3+}$ in a previous report,[1] taking the signal position of the impurity. In the present study, the central position of the broad signal was adopted as the correct shift value.[12] It can be seen from Table 1 that the ^{15}N NMR signal of the trans $^{15}NH_3$ of $[CoX(^{15}NH_3)_5]^{n+}$ appears at a higher field from that of $[Co(^{15}NH_3)_6]^{3+}$ and the cis one at a lower field with X=H_2O, Cl^-, and Br^-. In contrast, the trans $^{15}NH_3$ with X=CN^- gives an ^{15}N signal at a lower field and a cis one at a higher field. The ^{15}N NMR signals of $[Co(NO_2)(^{15}NH_3)_5]^{2+}$ were broad and not clearly separated.

Table 1. ^{15}N NMR Shift Values in $[CoX(^{15}NH_3)_5]^{n+}$ Relative to That of $[Co(^{15}NH_3)_6]^{3+}$

X	Trans	Cis
CN^-	−23.9	1.7
NO_2^- [b]	−11	−16
NH_3	0.0[a]	0.0[a]
H_2O	20.7	−5.5
Cl^- [c]	8.6	−6.2
Br^-	2.8	−3.0

a) The shift value (418.2 ppm) of $[Co(^{15}NH_3)_6]^{3+}$ as a standard of $^{15}NO_3^-$ was calculated from that as a standard of $^{15}NO_2^-$. b) The ^{15}N resonance signals of $[Co(NO_2)(^{15}NH_3)_5]^{2+}$ were not as sharp as that of the other $[CoX(^{15}NH_3)_5]^{n+}$ complexes as shown in Fig. 1. Therefore, the appropriate shift positions were given, which differ to some extent from those in Part I.[1] c) The values are from Ref. 7. The chemical shift values were recalculated considering the difference of 6.5 ppm between the present and the literature values of $[Co(^{15}NH_3)_6]^{3+}$.

Table 2. ^{15}N NMR Shift Values in *cis*-$[CoX_2(en\text{-}^{15}N, ^{15}N)_2]^{n+}$ Relative to That of $[Co(en\text{-}^{15}N,^{15}N)_3]^{3+}$

X_2	Trans	Cis
$(CN^-)_2$	−16.6	4.0
$(NO_2^-)_2$	−2.8	−2.8
en	0.0[a]	0.0[a]
ox^{2-}	8.1	−8.9
$(H_2O)_2$	9.4	−8.0

a) The shift value (392.0 ppm) of $[Co(en\text{-}^{15}N,^{15}N)_3]^{3+}$ was calculated from that as a standard of $^{15}NO_2^-$.

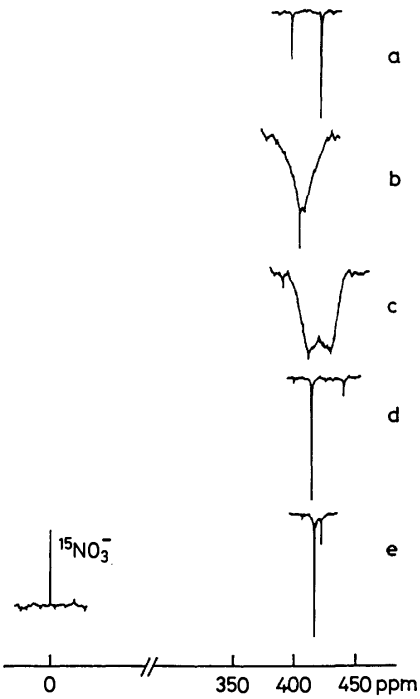

Fig. 1. ^{15}N NMR spectra of (a) $[Co(CN)(^{15}NH_3)_5]^{2+}$, (b) $[Co(NO_2)(^{15}NH_3)_5]^{2+}$, (c) $[Co(^{15}NH_3)_6]^{3+}$, (d) $[Co(H_2O)(^{15}NH_3)_5]^{3+}$, and (e) $[CoBr(^{15}NH_3)_5]^{2+}$.

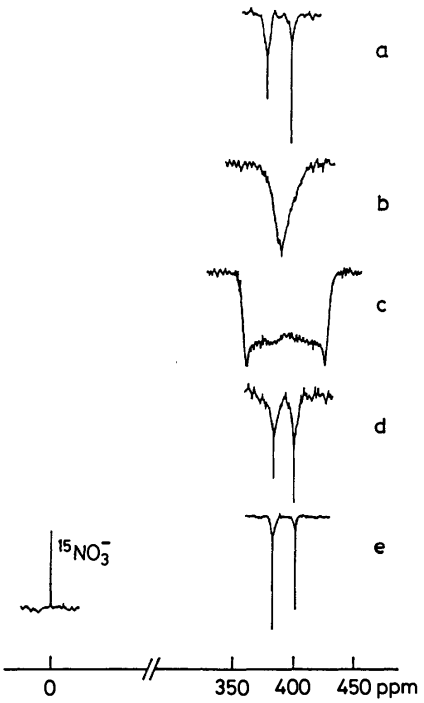

Fig. 2. ^{15}N NMR spectra of (a) *cis*-$[Co(CN)_2(en\text{-}^{15}N, ^{15}N)_2]^+$, (b) *cis*-$[Co(NO_2)_2(en\text{-}^{15}N,^{15}N)_2]^+$, (c) $[Co(en\text{-}^{15}N,^{15}N)_3]^{3+}$, (d) $[Co(ox)(en\text{-}^{15}N,^{15}N)_2]^+$, and (e) *cis*-$[Co(H_2O)_2(en\text{-}^{15}N,^{15}N)_2]^{3+}$.

Tris- and *cis*-Bis(ethylenediamine)cobalt(III) Complexes. The ^{15}N NMR spectra of the *cis*-$[CoX_2(en\text{-}^{15}N,^{15}N)_2]^{n+}$ ($X_2=(CN^-)_2$, $(NO_2^-)_2$, en-^{15}N,^{15}N, ox^{2-}, and $(H_2O)_2$) are shown in Fig. 2. The observed shift values are given in Table 2. The ^{15}N NMR signal of $[Co(en\text{-}^{15}N,^{15}N)_3]^{3+}$ was very broad for the same reason as that of $[Co(^{15}NH_3)_6]^{3+}$.[12] The central position of the signal was adopted as its chemical shift value. Each of the two ^{15}N NMR signals of $[Co(ox)(en\text{-}^{15}N,^{15}N)_2]^+$ could be assigned on the basis of the spectra selectively irradiated at the resonance frequency of amino protons,[5,13] as shown in Fig. 3. The intensity of the ^{15}N NMR signal in a lower field was more strongly enhanced when the amino proton signal at −5.1 ppm (-NH_2 cis to X) was irradiated, as shown in Fig. 3c. Thus, the ^{15}N NMR signal in the lower field corresponds to that of the amino group cis to O^- in $X_2=ox^{2-}$. Accordingly, the ^{15}N NMR signal in the higher field should correspond to that of the amino group trans to O^-; this was ascertained from selective irradiation, as shown in Fig. 3d. In contrast, the selectively proton-decoupled ^{15}N NMR spectra of *cis*-$[Co(CN)_2(en\text{-}^{15}N,^{15}N)_2]^+$ revealed that the lower-field signal corresponds to that of the amino group trans to CN^-, and the higher-field signal to the cis one. These findings were also confirmed regarding the proton spectra selectively irradiated at ^{15}N NMR signal frequencies, based on the fact that the ^{1}H NMR signal in a higher field was that of the amino group cis to CN^- in $X_2=(CN^-)_2$.[5,13-15] The ^{15}N NMR signal for *cis*-$[Co(NO_2)_2(en\text{-}^{15}N,^{15}N)_2]^+$ was not clearly separated, being broader than that in $[Co(NO_2)(^{15}NH_3)_5]^{2+}$, as shown in Fig. 2b.

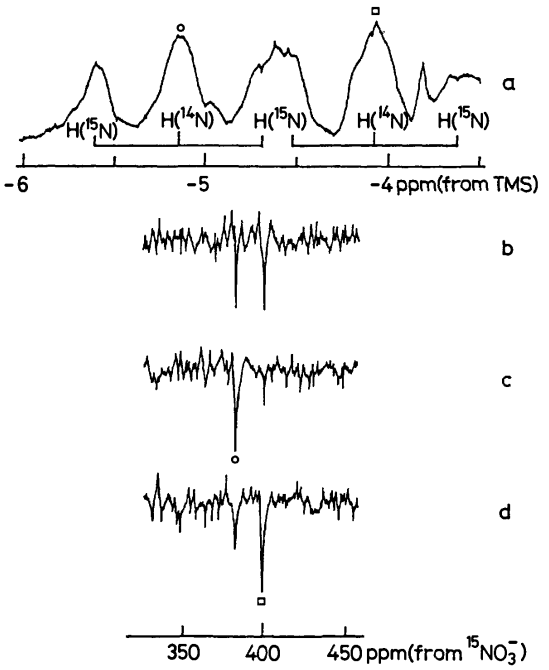

Fig. 3. (a) ^{1}H NMR spectrum of the amino group in $[Co(ox)(en\text{-}^{15}N,^{15}N)_2]^+$ at 99.5 MHz, (b) Proton noise decoupled ^{15}N NMR spectrum at 10.1 MHz, (c) ^{15}N NMR spectrum selectively irradiated at the frequency of the amino proton cis to O^- (at −5.1 ppm), (d) ^{15}N NMR spectrum selectively irradiated at the frequency of the amino proton trans to O^- (at −4.2 ppm).

Discussion

Generally, the magnetic shielding constant consists of three terms, as follows:

$$\sigma=\sigma_D+\sigma_P+\sigma_L, \quad (1)$$

where σ_D and σ_P are diamagnetic and paramagnetic terms, respectively, due to the electron of the observed atom; σ_L is the long-range magnetic term due to the other atoms in the molecule.[16] Solvent effects are not considered in this equation.

Hexaammine- and Pentaamminecobalt(III) Complexes. In the present case, the chemical shift induced by the magnetic anisotropy of the Co(III) ion may be the dominant part in σ_L. As shown in Eqs. 7 and 8 of Ref. 4, the ^{15}N NMR chemical shift induced by the Co(III) ion of $^{15}NH_3$ in $[CoX(^{15}NH_3)_5]^{n+}$ can be expressed relative to that of $[Co(^{15}NH_3)_6]^{3+}$, as follows:

$$\sigma_L=[\sigma(NH_3)-\sigma(X)]/3R^3\langle r^{-3}\rangle \text{ for trans } (\theta=0)$$

and

$$\sigma_L=-[\sigma(NH_3)-\sigma(X)]/6R^3\langle r^{-3}\rangle \text{ for cis } (\theta'=0),$$

where parameters $\sigma(NH_3)$ and $\sigma(X)$ are the paramagnetic shielding constants of ^{59}Co contributed by ligands NH_3 and X, respectively.[3,4] The relevant quantities used in the present study, except for R (adopted 2 Å as Co-N bond length[17]), have already been presented in Refs. 3 and 4. Subtracting the calculated σ_L from the observed σ, $\sigma_D+\sigma_P$ are obtained from Eq. 1. These values are given in Table 3. The contributions of σ_L are less than about 2 ppm and $\sigma_D+\sigma_P$ plays a main role in the ^{15}N NMR chemical shifts for $[CoX(^{15}NH_3)_5]^{n+}$, whereas σ_L does the same in the ^{1}H NMR chemical shifts. The ^{14}N NMR spectra of free NH_3 and $[Co(NH_3)_6]^{3+}$ were measured in liquid by Herbison-Evans and Richards and later by Bramley et al.[8,18] The chemical shift due to complex formation was to a higher field (about 50 ppm in Ref. 8 and a bout 130 ppm in Ref. 18). In their reports, the ^{14}N NMR chemical shift was mainly caused by the

Table 3. ^{15}N NMR Shift Values, σ_L and $(\sigma_D+\sigma_P)$ in $[CoX(^{15}NH_3)_5]^{n+}$ Relative to That of $[Co(^{15}NH_3)_6]^{3+}$

	σ_L		$(\sigma_D+\sigma_P)$	
X	Trans	Cis	Trans	Cis
CN^-	−2.3	1.1	−21.6	0.6
NH_3	0.0	0.0	0.0	0.0
H_2O	1.5	−0.8	19.2	−4.7
Cl^-	1.2	−0.6	7.4	−5.6
Br^-	1.0	−0.5	1.8	−2.5

magnetically-susceptible nonbonding paired electrons of NH_3 (σ_P). Regarding complex formation, these are constrained largely between the metal and nitrogen atoms as a bonding electron pair, and are considerably less susceptible to the magnetic field; thus, they contribute less to the nitrogen σ_P part in Ramsay's formula.[16] We calculated a higher shift value (70 ppm), based on the same ideas presented in Refs. 8 and 18.[19]

The contribution of NH_3 makes the hydrogens acidic; therefore, the protons can possibly be exchanged with those (deuterons) in the solution. For $[CoX(NH_3)_5]^{n+}$ complexes with X=H_2O, Cl^-, Br^-, or other weaker ligands than NH_3 in the spectrochemical series, it has been considered that the H-D exchange rates of the protons of NH_3 trans to X are faster than that of the cis ones.[5,21,25] With X=CN^-, the case is inverse.[5,21] With X=NO_2^-, the ^1H NMR signal did not split to each of the trans and cis signals of NH_3. Sakaguchi et al. have speculated from plots of the an H-D exchange rates that the protons of the trans NH_3 undergo an H-D exchange more slowly than that of the cis group (with X=CN^- and NO_2^-).[5] It could be said that the protons of NH_3 (trans or cis to X), whose ^{15}N NMR signal shifts to a higher field than another, undergo an H-D exchange faster than those of another NH_3 in $[CoX(NH_3)_5]^{n+}$. With X=Cl^-, the higher-field shift of the ^{15}N NMR signal of NH_3 trans to Cl^- corresponds to a faster H-D exchange rate of the protons. It can be seen from Table 3 that if X is a weaker ligand than $^{15}NH_3$ in the spectrochemical series, the ^{15}N NMR signal of $^{15}NH_3$ trans to X shifts to a higher field from that in X=NH_3 and cis signal to a lower field. Provided that the higher the magnetic field of ^{15}N NMR signal, the faster the H-D exchange rate of ammine protons and the stronger the Co-N bond, the shift directions are consistent with the findings of the H-D exchange rate of NH_3.[5,21] The lower-field shift of the ^{15}N NMR signal of the trans $^{15}NH_3$ in $[Co(CN)(^{15}NH_3)]^{2+}$ corresponds to a decrease in the H-D exchange rate of ammine protons trans to CN^-.[5,21,25] In the process of the synthesis of $[Co(CN)(NH_3)_5]^{2+}$, ^{15}N was introduced in the last step, as shown below:

$$[Co(CN)(NH_3)_4(H_2O)]^{2+} + {}^{15}NH_3 + {}^{15}NH_4Cl \rightarrow [Co(CN)(^{15}NH_3)_n(NH_3)_{5-n}]^{2+} + HCl.$$

The ^1H NMR signal of the last product is shown in Fig. 4. It can be seen from Fig. 4 that the NH_3 trans to CN^- was much more substituted by $^{15}NH_3$ than the cis. It may be considered that the lower-field shift of the ^{15}N NMR signal, the decrease in the H-D exchange rate, and the weakened Co-N bond strength for the NH_3 trans to CN^- are caused by the same origin, i.e., an inductive trans effect of CN^-. Similar phenomena have been observed by Halpern et al. in the synthesis of *trans*-$[Co(^{15}NH_3)(SO_3)(NH_3)_4]^+$, where the NH_3 trans to SO_3^{2-} was mostly substituted by

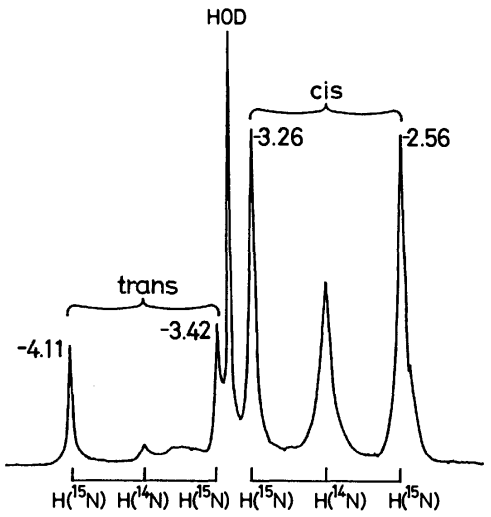

Fig. 4. ^1H NMR spectrum of $[Co(CN)(^{15}NH_3)_n(NH_3)_{5-n}]^{2+}$ in DMSO-d_6. Shift values are ppm from an external reference (TMS). Coupling constants, $^1J_{NH}$ are 68 and 70 Hz for trans and cis NH_3 respectively (measured at 99.5 MHz).

$^{15}NH_3$, though the cis NH_3 was not. It was caused by a marked trans-labilizing influence of the S bonded sulfito ligand.[22]

As mentioned above, the shift direction of ^{15}N NMR signals of trans and cis $^{15}NH_3$ in $[CoX(NH_3)_5]^{n+}$ are correlated to the H-D exchange rates and the Co-N bond strengths, though the relation can not be quantitatively interpreted at present.

The ^{14}N NMR signals are broad owing to a quadrupolar relaxation of ^{14}N nucleous; the ^{14}N NMR signals were inseparable from each of the trans and cis signals. The ^{15}N NMR signals were separated into two sharp signals without problems related to the quadrupolar relaxation of ^{15}N nucleous (Fig. 1), except for X=NO_2^- and $^{15}NH_3$. These exceptions are due to coupling between the ^{15}N and ^{59}Co nuclei. The lower-field shifts of ^{14}N NMR signals for X=H_2O and Cl^- from $[Co(^{14}NH_3)_6]^{3+}$ in Ref. 8. represent the weighted mean values of one trans and four cis shifts of the corresponding ^{15}N signals.

Tris- and *cis*-Bis(ethylenediamine)cobalt(III) Complexes. The ^{15}N NMR shift value of $[Co(en\text{-}^{15}N,{}^{15}N)_3]^{3+}$ was obtained from the central position of the broad signal. In *cis*-$[CoX_2(en\text{-}^{15}N,{}^{15}N)_2]^{n+}$ with X_2=ox^{2-}, CO_3^{2-} (weaker ligands than en), the higher-field shifts of the ^1H NMR signals of the trans amino protons are consistent with the theory of anisotropy of Co(III) ion.[3,13] The assignment of the NMR signals and the H-D exchange in *cis*-$[CoX_2(en\text{-}^{15}N,{}^{15}N)_2]^{n+}$ have been studied in more detail by Nakazawa et al.,[14] where one half of the trans aminoproton signals undergoes a large counterion-dependent shift in DMSO-d_6; it is therefore assigned to the trans hydrogens directed approximately parallel to the molecular two-fold axis of the complexes with X_2=$(CN^-)_2$,

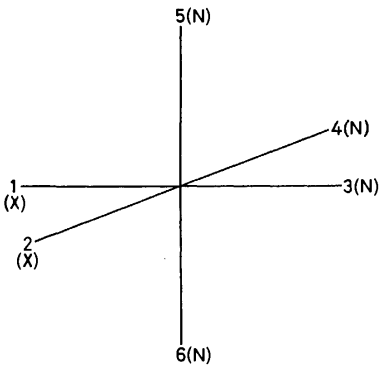

Fig. 5. Framework of *cis*-$[CoX_2N_4]^{n+}$ with numbering of ligating atoms.

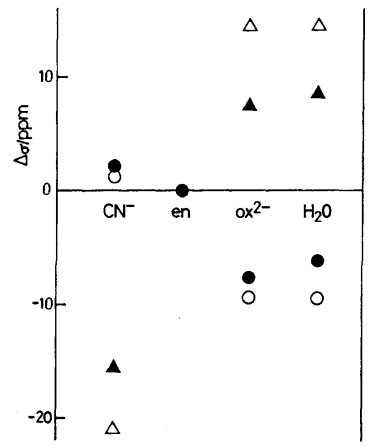

Fig. 6. Plots of ^{15}N NMR shift values $(\sigma_D+\sigma_P)$ of $-^{15}NH_2$ in *cis*-$[CoX_2(en\text{-}^{15}N,^{15}N)_2]^{n+}$. Circles and triangles are for cis and trans to X, respectively (open for calculated; solid for observed (Table 4)). The calculated values are $\{(\sigma_D+\sigma_P)(trans)+(\sigma_D+\sigma_P)(cis)\}$ and $\{(\sigma_D+\sigma_P)(cis)\times 2\}$ (Table 3), for trans and cis ^{15}N to X, respectively (see text). The calculated value for the aqua complex was also used for the oxalato one.

$(NO_2^-)_2$, $acac^-$, ox^{2-}, and mal^{2-}. On the other hand, we found that upon deuteration of amino protons, the noise-decoupled NMR signal of the ^{13}C adjacent to the deuterated amino nitrogen shifted by about 0.15 ppm per substituted deuteron to a higher field.[15] The lower-field signal of the $^{13}C\{^1H\}$NMR spectrum in *cis*-$[Co(CN)_2(en)_2]^+$ splits at first; this has already been assigned to that of the ^{13}C adjacent to the $-NH_2$ cis to CN^-.[23] Thus, the amino protons cis to CN^- were deuterated first, and the adjacent ^{13}C NMR signal shifted to a higher field in acidified D_2O. This result is different from that found by Nakazawa et al.

Assignments of ^{15}N NMR signals were confirmed by the selective irradiation of the ^{1}H NMR signals of $-^{15}NH_2$. Accordingly, the assignments of the ^{1}H NMR signals of $-NH_2$ are very important for the assignment of the ^{15}N NMR signals. The results for $X_2=(NO_2^-)_2$ and ox^{2-} were the same as those by Nakazawa et al. and might also be similar for $X_2=acac^-$ and mal^{2-}.

Table 4. ^{15}N NMR Shift Values, σ_L and $(\sigma_D+\sigma_P)$ in *cis*-$[CoX_2(en\text{-}^{15}N,^{15}N)_2]^{n+}$ Relative to That of $[Co(en\text{-}^{15}N,^{15}N)_3]^{3+}$

	σ_L		$(\sigma_D+\sigma_P)$	
X_2	Trans	Cis	Trans	Cis
$(CN^-)_2$	−1.0	1.9	−15.6	2.1
en	0.0	0.0	0.0	0.0
ox^{2-}	0.6	−1.2	7.5	−7.7
$(H_2O)_2$	0.9	−1.8	8.5	−6.2

The additivity of the effect of the substituent X on the ^{15}N NMR chemical shifts was examined in the aforementioned $[CoXN_5]^{n+}$- and *cis*-$[CoX_2N_4]^{n+}$-type complexes, as shown below. The effect is separated into two parts: trans and cis. Each can be easily obtained from experimental data for $[CoXN_5]^{n+}$ complexes. On the basis of this data, the ^{15}N MMR shift values for *cis*-$[CoX_2N_4]^{n+}$ complexes can be estimated. The framework of *cis*-$[CoX_2N_4]^{n+}$ is shown with numbering of ligating atoms in Fig. 5. The trans nitrogen atoms located at positions 3 and 4 are subject to a trans effect from one X and a cis effect from another X. The cis nitrogen atoms at positions 5 and 6 are subject to only a cis effect from X at positions 1 and 2. The calculated values are shown along with the observed ones (Table 4) in Fig. 6. It seems to be roughly additive between the trans and the cis effects, thus postulated to be separately caused by ligand X on the ^{15}N NMR chemical shifts.

References

1) Part I: Y. Nakashima, M. Muto, I. Takagi, and K. Kawano, *Chem. Lett.*, **1975**, 1075.
2) H. Yoneda and Y. Nakashima, *Bull. Chem. Soc. Jpn.*, **47**, 669 (1974).
3) Y. Nakashima, U. Sakaguchi, and H. Yoneda, *Bull. Chem. Soc. Jpn.*, **48**, 762 (1975).
4) Y. Nakashima, *Bull. Chem. Soc. Jpn.*, **48**, 766 (1975).
5) U. Sakaguchi, K. Maeda, and H. Yoneda, *Bull. Chem. Soc. Jpn.*, **49**, 397 (1976).
6) B. M. Fung, S. C. Wei, T. H. Martin, and I-Yuan Wei, *Inorg. Chem.*, **12**, 1203 (1973).
7) J. W. Lehman and B. M. Fung, *Inorg. Chem.*, **11**, 214 (1972).
8) D. Herbison-Evans and R. E. Richards, *Mol. Phys.*, **8**, 19 (1964).
9) See for example, a) F. Basolo and R. K. Murman, "Inorganic Synthesis," Vol. 4, p. 171 (1953); b) "Shin Jikken Kagaku Koza," Maruzen, Tokyo (1977), Vol. 8, pp. 1249, 1252, 1251, and 1264.
10) H. Sibert, *Z. Anorg. Allg. Chem.*, **327**, 63 (1964).
11) F. Yajima, Y. Koike, A. Yamasaki, and S. Fujiwara, *Bull. Chem. Soc. Jpn.*, **47**, 1442 (1974).
12) A. Yamasaki, Y. Miyakoshi, M. Fujita, Y. Yoshikawa, and H. Yamatera, *J. Inorg. Nucl. Chem.*, **41**, 473 (1979).
13) U. Sakaguchi, S. Yamazaki, and H. Yoneda, *Bull.*

Chem. Soc. Jpn., **49**, 402 (1976).
14) H. Nakazawa, U. Sakaguchi, H. Yoneda, and Y. Morimoto, *Inorg. Chem.*, **20**, 973 (1981).
15) Y. Nakashima, Y. Yoshikawa, F. Mitani, and K. Sasaki, *J. Magn. Reson.*, **69**, 162 (1986).
16) N. F. Ramsay, *Phys. Rev.*, **78**, 699 (1950).
17) a) M. Iwata and Y. Saito, *Acta Crystallogr., Sect. B*, **29**, 822 (1973); b) "International Tables for X-Ray Crystallography," Kynoch Press, Birmingham (1968), Vol. III, p. 270.
18) R. Bramley, B. N. Figgis, and R. S. Nyholm, *J. Chem. Soc. A*, **1967**, 861.
19) T. Hara and Y. Nakashima, presented at the 27th Symposium on Coordination Chemistry of the Chemical Society of Japan, Matsumoto, Oct., 1977, p. 207.
20) D. A. Buckingham, B. M. Foxman, and A. M. Sargeson, *Inorg. Chem.*, **9**, 1790 (1970).
21) R. Bramley, I. I. Creaser, D. J. Mackey, and A. M. Sargeson, *Inorg. Chem.*, **17**, 244 (1978).
22) J. Halpern, R. A. Palmer, and L. M. Blakley, *J. Am. Chem. Soc.*, **88**, 2877 (1966).
23) Y. Yoshikawa, Y. Masuda, H. Yamatera, S. Utsuno, and Y. Nakashima, *J. Magn. Reson.*, **58**, 473 (1984).
24) M. Witanowski, *J. Am. Chem. Soc.*, **90**, 5683 (1968).
25) D. A. Buckingham, I. I. Olsen, and A. M. Sargeson, *Aust. J. Chem.*, **20**, 597 (1967).

A Complex Generated in a Cationic Surfactant-Aromatic Additive System

Hirotaka HIRATA,* Yumi KANDA, and Yuko SAKAIGUCHI
Niigata College of Pharmacy, Department of Physical Chemistry, 2-13-5, Kamishin'eicho, Niigata 950-21
(Received December 23, 1988)

Aqueous binary solutions of hexadecyltrimethylammonium bromide (HTAB) and *o*-iodophenol (OIPh) exhibit remarkable viscoelasticity. From the centrifuged sediment of such a solution a *crystalline* product was isolated on long standing. Elementary analysis of the *crystals* for C, H, and N gave an estimated composition consistent with a one-to-one molar ratio of the two substances. Comparisons with DSC and IR measurements on the *crystal* and equimolar mechanical mixtures suggested that a *crystalline* complex was formed characterized by low thermal stability.

By electron microscopy we have recently identified elongated rod like micelles in several cationic surfactants such as HTAB or *N*-hexadecylpyridinium bromide on treatment with some aromatic derivatives.[1-3] These solutions often exhibit high viscoelasticity and spinnability. We have established that the viscoelasticity in solution arises from a cobweb-like entanglement of the elongated rod shaped micelles.[3]

Other investigators accumulated informations about the cause of the solution behaviors over the extensive areas,[4,5] but little is yet known about the condition suitable for the generation of such gigantic micelles in solution containing quaternary ammonium cationic surfactants and aromatic compounds, though there has been speculation about the interactions taking place in such systems.[6]

In the sediment centrifuged from HTAB/OIPh aqueous solutions after long standing we have isolated a *crystalline* product. This material exhibits strong viscoelasticity and spinnability when dissolved in water and appeared to be a complex of HTAB and OIPh. Elementary analysis, differential scanning calorimetry (DSC) and infrared spectroscopy (IR) of the *crystals* have been carried out.

Results and Discussion

The *crystals* are prismatic with average size about 1 mm×3mm. They exhibt lateral cleavage streaks and a granular structure.

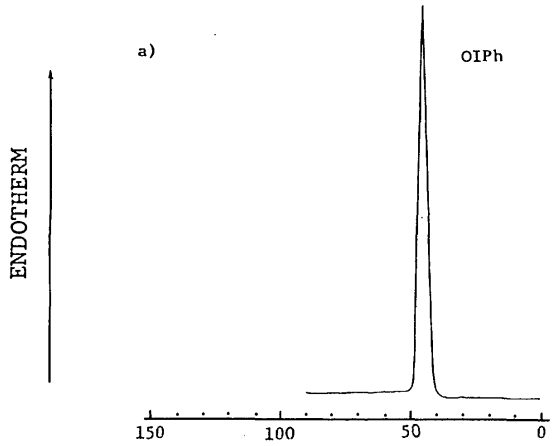

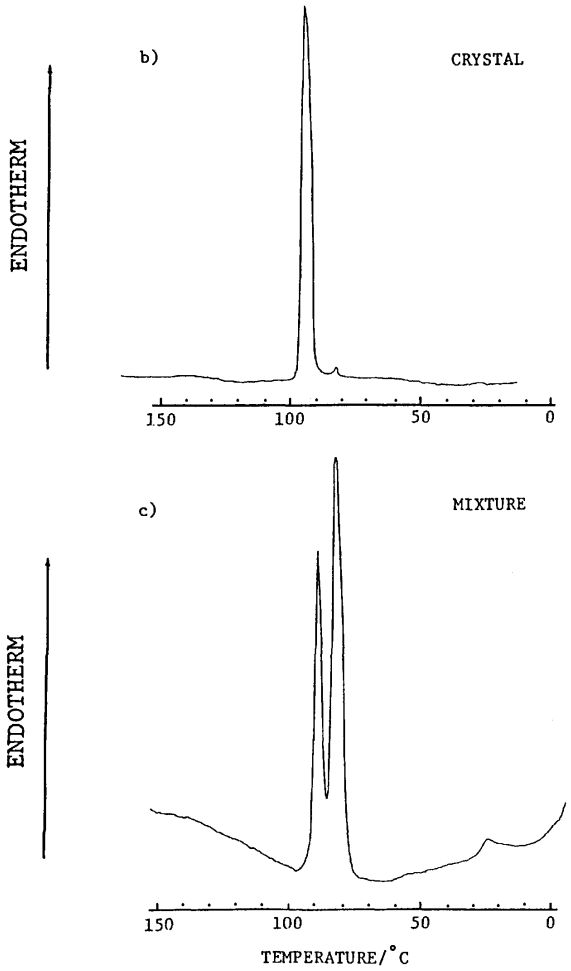

Fig. 1. The thermogram in DSC of a) OIPh, b) *crystal*, and c) the mechanical mixture of one-to-one molar ratio of HTAB and OIPh.

Table 1. The Results of the Elementary Analysis of the *Crystal* Obtained from the Sediment Solution of the HTAB/OIPh System

	Content	
	Observed	Calculated[a]
C (%)	51.28	51.37
H (%)	8.10	8.05
N (%)	2.48	2.40

a) The values are those which supposed to be composed of HTAB and OIPh in the molar ratio of unity.

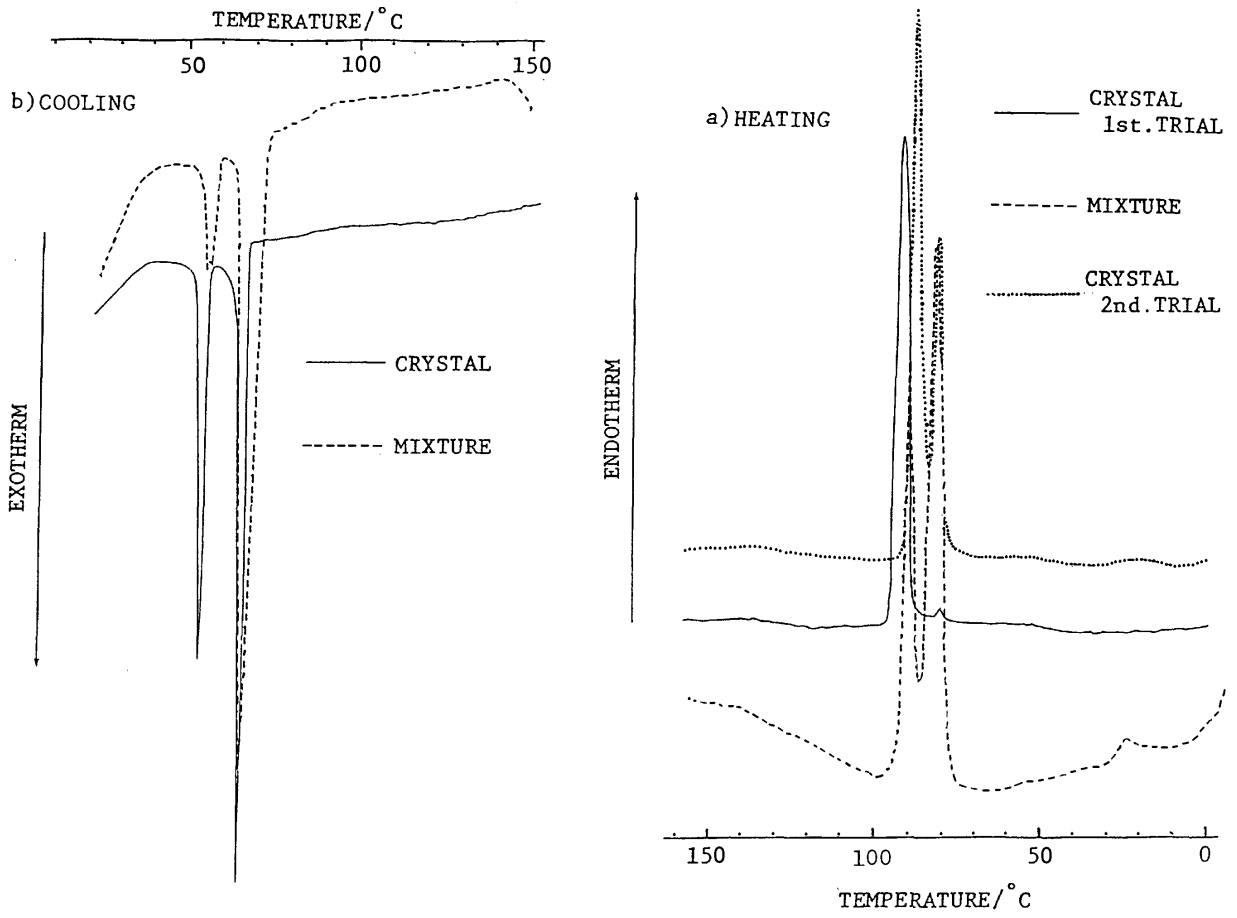

Fig. 2. The thermograms in DSC of the *crystal* and the mechanical mixture in one-to-one molar ratio, a) a comparison of the profiles in the repeated trial upon the first heating of the *crystal* with the second one and with the profile of the mixture. In the mixture the profile was not changed depending on the repetition, b) a comparison of the cooling profile of the *crystal* with that of the mechanical mixture.

Elementary analyses of the washed and dried material for C, H, and N are given in Table 1. These are in good accord with the values expected for each component and suggest a one-to-one molar complex formation. From the elementary analysis some anticipation of containing water hydrated was denied after a treatment of a one overnight drying before analysis. But it appeared for the *crystals* to occlude some water in the initial stage of having just been taken out of the sediment solution, because the *crystals* decreased their weight by about 20% during a one ovenight evacuation at room temperature. The fact was also supported in the thermal analyses (see below).

Microscopic examination at ×40 of a small *crystal* immersed in water showed a swollen profile domain surrounding the *crystal*. On touching the swollen region with a needle tip the region changed abruptly to a heavy viscoelastic solution. This observation seems to be very important to deduce the molecular weight of the *crystalline* species and the relation of the solution behaviors to the gigantic micellar figures observed in the electron micrographs.

In Fig. 1 the DSC's of the *crystals* and the equimolar simple mechanical mixtures of the single component constituents are compared. In this respect the behavior of the *crystal* and the equimolar mixture both differ from each other, i.e. OIPh only shows a characteristic endotherm at 42.3 °C corresponding to its solid to liquid phase transition. HTAB was assumed to have a very high temperature transition near 235—237 °C.[7]

All thermal behaviors can be compared with the observations under a polarizing microscope. The single endotherm of the *crystal* at 94.5 °C corresponds to a solid-smectic phase change observed as the disappearance of the sharp crystal edge seen under the microscope. The as yet uncharacterized smectic phase persists to considerably higher temperatures in accord with that no other peaks are observed in the DSC above 94.5 °C. Microscope image changes are also observed at temperatures consistent with the endothermal peaks in the DSC diagrams. Judged from their fluidity the phase transitions would appear to be due to smectic changes.

On subsequent cyclic thermal changes the endothermal peak profile of the *crystal* separated into a doublet at 83.0 °C and 88.0 °C (Fig. 2a) after the first cycle, but subsequent cycles produced no further change. In

the cooling stage the exothermal profile for the *crystal* was identical with that of the equimolar mixture. (Fig. 2b) This would suggest that there is a thermally induced dissociation of the complex. On the contrary, on a second heating cycle of the mixture changes occur in the thermogram which approaches that of the *crystal*. No restoration of the initial peak profile of the *crystal* DSC may also be explained by the fact that the *crystal* is a high molecular weight entity which would be difficult to restore the original crystal lattice during such a rapid cooling. From this we infer that the HTAB/OIPh *crystalline* complex has an equilibrium point towards the components. In reversal a system of components readily deviates to the complex side.

Some effects of moisture are observed in the thermogram of the *crystal*. After several DSC cycles a specimen left overnight in moist air exhibited other peaks in the low temperature region (Fig. 3). These can be attributed to water retained in the crystal lattice. Exposure to moisture increased the *crystal* weight by about 1% and restored the initial state after several DSC cycles with decrease of those peaks of the moisture origin. This suggests that the HTAB/OIPh complex can accomodate some water of hydration.

Figure 4 shows the IR spectra of the *crystal* and the equimolar mixture. There are significant differences between 1400 and 700 cm^{-1} due to additional bands in

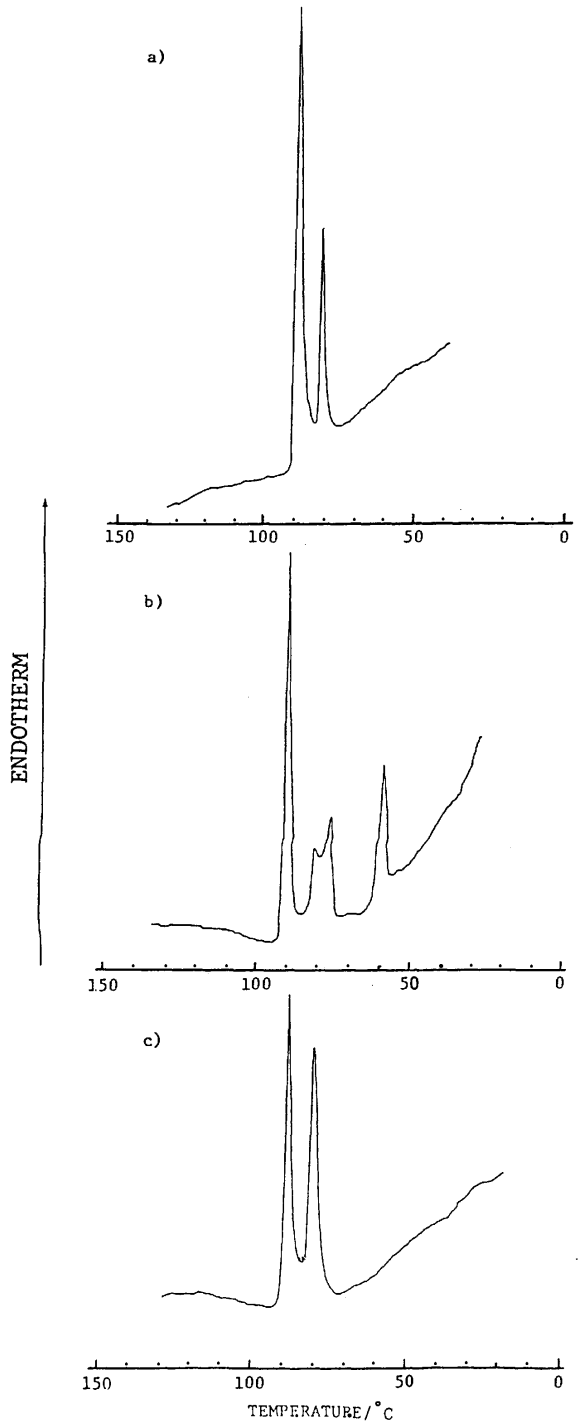

Fig. 3. The effect of the water hydrated on the *crystal* DSC, a) before moistened after several repeated trials, b) one-over-night moistened specimen, and c) after the second trial of the moistened specimen. In the succesive trials the profiles were almost not changed any more.

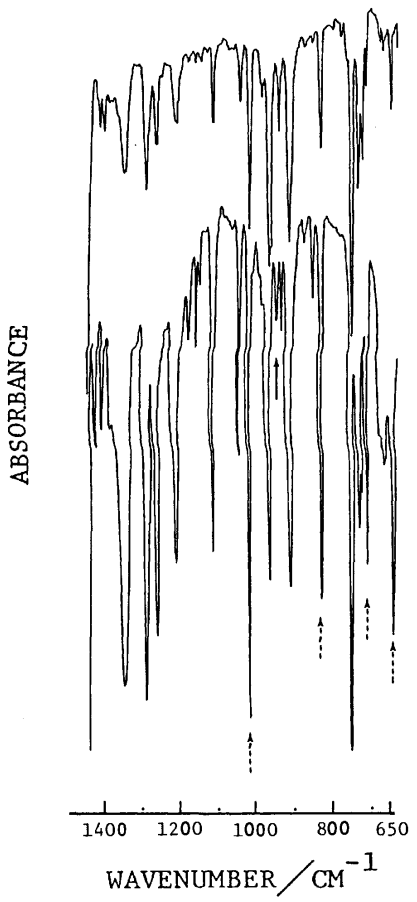

Fig. 4. The IR absorption spectra of the *crystal* (below) and the mechanical mixture in one-to-one molar ratio (above). ↑ shows a newly splitted doublet band, observed in the *crystal*, from a singlet band of the mechanical mixture. ↕ shows the remarkably increased bands in the *crystal* compared with those of the mechanical mixture.

the spectrum of the *crystal*. There are also some notable intensity reversals. New bands occur at 931 cm^{-1} and 938 cm^{-1}; these would appear to result from a splitting of the 938 cm^{-1} band. Intensity reversals are noted in four regions (Fig. 4). These would appear to involve a nearly 4-fold enhancement in the intensity for the *crystal*. From these we infer that there are changes on the skeletal motions of the benzene nucleus of OIPh. This may be associated with a difference of the surrounding field in the *crystal* and the equimolar mixture.

From these differences in the DSC's and IR spectra of the *crystal* and the equimolar mixture we may deduce that the interactions between the aromatic and quaternary ammonium groups is not very great and that the complex formation and dissociation can easily be induced by heat.

X-Ray analysis of the *crystalline* species is currently in progress revealing the crystal structure is *Pnn*2 orthorhombic with lattice constants a=8.722 Å, b=39.954 Å, c=8.404 Å, $\alpha=\beta=\gamma=90°$ with a unit cell volume of V=2928.6 $Å^3$. Some structural aspects of the *crystal* have also been known.[8] Further work is under way to refine these data to ascertain the exact structure of the complex *crystal* with particular consideration to the interaction of the materials, the large elongated micelle structure and the behavior of the solutions.

We are indebted for the elementary analysis to the members of the Assay Laboratory of the Protein Research Institute of Osaka University.

Experimental

HTAB was used after one recrystallization of commercially available material from an acetone-methanol mixture. OIPh was of pure reagent grade, used as purchased. The sediment solutions of HTAB/OIPh were obtained by centrifugal separation at 60000 rpm for 1 h. using a Hitachi SPC85H centrifuge. The DSC measurements were carried out using a Rigaku Denki Co. Low Temperature Differential Scanning Calorimeter. Since the profile shift of the thermogram was considerable in repeated runs, especially following the initial heating, the cycles were always repeated on a way of a heating-after-cooling cycle. The rate of temperature scan was maintained at 10 K m^{-1} in both directions. IR measurements were made on a Hitachi 260-10 Infrared Spectrometer. The spectra were measured as KBr disks.

References

1) T. Shikata, Y. Sakaiguchi, H. Urakami, A. Tamura, and H. Hirata, *J. Colloid Interface Sci.*, **119**, 291 (1986).
2) Y. Sakaiguchi, T. Shikata, H. Urakami, A. Tamura, and H. Hirata, *Colloid Polym. Sci.*, **265**, 750 (1987).
3) Y. Sakaiguchi, T. Shikata, H. Urakami, A. Tamura, and H. Hirata, *J. Electron Microsc.*, **36**, 168 (1987).
4) J. Ulmius, H. Wennerstrom, L. B. Johansson, G. Lindblom, and S. Gravsholt, *J. Phys. Chem.*, **83**, 2232 (1979).
5) H. Hoffmann, G. Platz, H. Rehage, W. Schorr, and W. Ulbricht, *Ber. Bunsenges. Phys. Chem.*, **85**, 255 (1981).
6) C. A. Bunton and M. J. Minch, *J. Phys. Chem.*, **78** 1490 (1974).
7) W. Gledhill, *Pharm. J.*, **151**, 184 (1943).
8) H. Hirata, Y. Kanda, and M. Kimura, in contribution.

 © 1989 The Chemical Society of Japan Bull. Chem. Soc. Jpn., 62, 2465—2473 (1989)

Physicochemical Properties of Polyacrylates Containing Tetraphenylporphinatocobalt(II) and Chloro(tetraphenylporphinato)iron(III) as Side Chains

Mikiharu KAMACHI,* Mahito SHIBASAKA, Atushi KAJIWARA, Wasuke MORI,† and Michihiko KISHITA†
Department of Macromolecular Science, Faculty of Science, Osaka University, Toyonaka, Osaka 560
†Department of Chemistry, College of General Education, Osaka University, Toyonaka, Osaka 560
(Received January 10, 1989)

Polyacrylates containing tetraphenylporphinatocobalt(II) (TPP-Co(II)) and chloro(tetraphenylporphinato)iron(III) (TPP-Fe(III)Cl) as side chains were prepared. Their physicochemical properties were investigated by UV-visible spectroscopy, ESR spectroscopy, and magnetic susceptibility (χ_M) measurement. In comparison of the visible spectra of polymers with those of the corresponding monomers, hypochromism of the Soret band and some of Q bands was observed in both polymers. In the measurements of ESR spectra, hyperfine splitting constants and anisotropic g-values of TPP-Co(II) or -Fe(III)Cl moieties bound to the polymers were somewhat different from those of TPP-Co(II) and -Fe(III)Cl, respectively. These differences in spectroscopic behavior suggest that there are some interactions between porphinatometal ion moieties in the polymers. The values of χ_M for the polymers containing TPP-Co(II) were found to obey the Curie-Weiss law with θ=190 K, which was explained in terms not only of spin-orbit interaction of the Co(II) ion but also antiferromagnetic interaction among the Co(II) ions. The magnetic moment of the TPP-Co(II) moiety bound to the polymer is smaller than that of TPP-Co(II), indicating occurrence of an antiferromagnetic interaction between Co(II) ions in the polymer. The values of χ_M for polymers containing TPP-Fe(III)Cl were found to obey the Curie-Weiss law with θ=20 K. This can be explained in terms of the presence of antiferromagnetically-interacting sites. From the experimental results, it is concluded that the antiferromagnetic interaction between TPP-metal ions bound to the polymer is larger than that of the corresponding TPP-metal ions. Molecular oxygen is adsorbed to polyAOTPP-Co(II) and 5-(4-propanoyloxyphenyl)-10,15,20-triphenylporphinatocobalt(II) (POTPP-Co(II)) below 180 K. Magnetic susceptibility measurement and ESR study show that molecular oxygen is bound to the Co(II) ion by chemisorption whose binding energy is 24 kJ M^{-1}.

Many studies of physicochemical properties of tetraphenylporphinatometal ions have been reported.[1-5] However, there have been few studies of polymers containing metalloporphins in the side chain, although the polymers seem to have interesting and unusual properties caused by an aggregate of porphin moieties.[6,7] To our knowledge, no homoplymerization of vinyl compounds containing porphin moieties in the side chains has been reported except for our papers.[8] Recently, we succeeded in the preparation of this type of polymer by radical polymerization of 5-(4-acryloyloxyphenyl)-10,15,20-triphenylporphine (AOTPP).[8]

In the course of our study of the magnetic properties of polymers containing paramagnetic species in the side chain,[9-12] we found that polyacrylates containing tetraphenylporphinatosilver(II) (TPP-Ag(II)) have strong antiferromagnetic interactions.[9] Since cobalt(II) and iron(III) which are composed of electronic configurations of d^7 and d^5, respectively, have a possibility of multiplet state, and hence have the potential of leading to ferromagnetic substances,[13,14] polyacrylates containing tetraphenylporphinato-Co(II) or -Fe(III)Cl (TPP-Co(II) or -Fe(III)Cl) as side chains were prepared and their magnetic properties were investigated. They showed antiferromagnetic behavior, contrary to expectation.

In this paper, we present the results of the preparation and the spectroscopy of the polymers (polyAOTPP-Co(II) and -Fe(III)Cl), as well as their magnetic properties. The antiferromagnetic behavior observed in the polymers is ascribable to the electronic interaction between the TPP-metal moieties bound to the polymers, which was found by UV-visible and ESR spectroscopy. In addition, adsorption of molecular oxygen on polyAOTPP-Co(II) is considered.

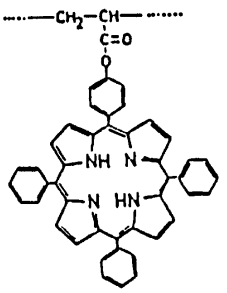

PolyAOTPP

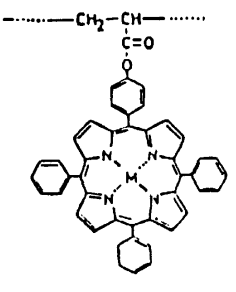

PolyAOTPP-M
M: Co(II) or Fe(III)Cl

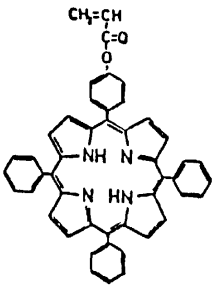

AOTPP

Experimental

Materials. Solvents were purified by distillation under nitrogen atmosphere. 5-(4-Acryloyloxyphenyl)-10,15,20-triphenylporphine (AOTPP) and its polymer (poly(AOTPP)) were prepared as described previously.[8] The molecular weight of the polymer was determined to be 80000—100000 by GPC measurements.[8] 5,10,15,20-Tetraphenylporphine (TPP) was synthesized according to Alder et al.[15] Tetraphenylporphinatocobalt(II) was prepared according to Bucher et al.[16] in 96% yield. Chlorotetraphenylporphinatoiron(III) was prepared according to Maricondi et al.[17] in 64.8%. 5-(4-Hydroxyphenyl)-10,15,20-triphenylporphine (HOTPP) was prepared by the method described previously.[8]

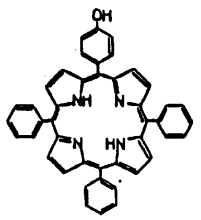

HOTPP

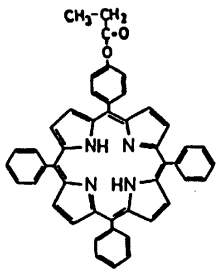

POTPP

5-(4-Propanoyloxyphenyl)-10,15,20-triphenylporphine (POTPP) was prepared by adding propanoyl chloride to a THF solution of HOTPP and triethylamine. The crude product was purified by column chromatography, followed by repeated recrystallization from chloroform-methanol. Yield 90%.

Found: C, 82.07; H, 5.04; N, 8.13%

Calcd for $C_{47}H_{35}N_4O_2$: C, 82.07; H, 5.13; N, 8.15%

5-(4-Propyloyloxyphenyl)-10,15,20-triphenylporphinatocobalt(II) [POTPP-Co(II)] was prepared as follows: POTPP (0.61g) and cobalt(II) (0.30 g) acetylacetonate were dissolved in 100 ml chloroform. The solution was refluxed for 1 h and chloroform was removed by a rotatory evaporator. The product was purified by repeated precipitation from chloroform-methanol. The content of Co(II) was determined by flame spectrometric analysis.

Found: C, 76.22; H, 4.47; N, 7.64; Co, 7.6%

Calcd for $C_{47}H_{33}N_4O_2Co$: C, 75.80; H, 4.47; N, 7.52; Co; 7.91%.

Poly[5-(4-acryloyloxyphenyl)-10,15,20-triphenylporphinatocobalt(II): Poly(AOTPP) (0.40 g) and cobalt(II) acetylacetonate (0.40 g) were dissolved in 100 ml THF. The solution was refluxed for 24 h and THF was removed by a rotatory evaporator. During the reflux, the reaction was followed by taking visible spectra of the solution at different times. Chloroform was added to the residue to dissolve the polymer, and the polymer was isolated by precipitation with methanol and purified by repeated precipitations from chloroform-methanol. The precipitated polymer was isolated by centrifugation and dried in vacuo overnight. The content of Co(II) was determined to be 74 mol% of the TPP-moiety by flame spectrometric analysis.

Poly[chloro-5-(4-acryloyloxyphenyl)-10,15,20-triphenylporphinatoiron(III)Cl]: poly(AOTPP) (0.25 g) and iron(III) chloride (0.14 g) was mixed in 100 ml of toluene containing 5 ml of methanol. The mixture was refluxed for 24 h and filtered to remove unreacted iron(III) chloride. The filtrate was washed with water. The polymer was isolated from the organic layer by evaporation, dried in vacuo, dissolved in benzene, and reprecipitated with ethanol. The polymer was purified by repeated precipitation from benzene-ethanol. The precipitated polymer was isolated by filtration, and dried in vacuo overnight. Yield 0.27 g.

The content of Fe(III) ions was determined to be 92 mol% of the TPP-moiety by flame spectrometric analysis.

Measurements. UV-visible spectra were recorded on a Hitachi 124 spectrophotometer. IR spectra were recorded on a JASC DS-402G spectrophotometer.

ESR spectra were measured with a JEOL Model JES FE 1X ESR spectrometer with 100 kHz modulation. A TE_{011} mode cylindrical cavity with a variable temperature adaptor (ES-UCT-2AX) was used. The temperature was controlled by a variable temperature control unit (ES-VT-3A). ESR measurements at 77 K were carried out using an insertion-type liquid nitrogen Dewar, a tip of which is made of doublefold Suprasil tubes. The *g*-values were estimated using MnO as a standard sample which was provided by JEOL.

Gram magnetic susceptibility (χ_g) was determined by the Gouy method at room temperature. Water was used as a standard sample for χ_g. The value of χ_g for water was found to be -0.727×10^{-6} cgs emu, being in agreement with the established value. The temperature dependence of χ_g was determined by the Faraday method, using a Cahn RH electric balance in a temperature range from 4 K to 300 K. The molar magnetic susceptibilities (χ_M) were corrected by the following equation to remove diamagnetic contributions from the ligand

$$\chi_M=\chi_g\times M-\chi_{dia}$$

where M is molecular weight of TPP-metal or monomer unit of the polymer, and χ_{dia} for TPP-Co(II), TPP-Fe(III)Cl, polyAOTPP-Co(II), and polyAOTPP-Fe(III)Cl were calculated to be -521×10^{-6}, -542×10^{-6}, -498×10^{-6}, and -418×10^{-6} cgs emu, respectively. The effective magnetic moment (μ_{eff}) was calculated from the following equation:

$$\mu_{eff}=2.33\sqrt{\chi_M\cdot T}$$

The amount of molecular oxygen absorped was determined from the difference in the weight of samples before and after O_2 gas was introduced into the system.

Results and Discussion

UV-Visible Spectra. UV-visible spectra of TPP-Co(II) and polyAOTPP-Co(II) are shown in Fig. 1. Both compounds have the Soret band at 411 nm and Q bands in the region from 500 to 700 nm, as shown in the spectra of metalloporphins.[8] The wavelength of the Soret band of polyAOTPP-Co(II) is similar to that of TPP-Co(II), but the molecular extinction coefficient (ε) of polyAOTPP-Co(II) is smaller than that of TPP-Co(II). Q bands of polyAOTPP-Co(II) are broader than those of TPP-Co(II). Close examination of the spectra shows that at 530 nm the value of ε

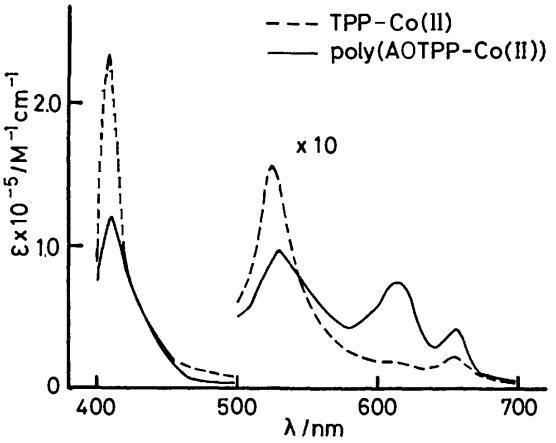

Fig. 1. Visible spectra of TPP-Co(II) and polyAOTPP-Co(II) in chloroform at room temperature. (----) TPP-Co(II), and (——) polyAOTPP-Co(II).

of polyAOTPP-Co(II) is smaller than that of TPP-Co(II), and that at 670 nm the former is larger than the latter. In addition, at 610 nm a stronger and broader absorption band is more clearly observed in spectrum of polyAOTPP-Co(II). The UV-visible spectrum of 5-(4-propanoyloxyphenyl)-10,15,20-triphenylporphinatocobalt(II) (POTPP-Co(II)) was measured to study the influence of the ethoxycarbonyl group bound to the TPP on the spectrum. Since the spectrum of POTPP is almost the same as that of TPP except for the slight change in λ_{max} and ε, the presence of the ethoxycarbonyl group is not considered to be an important factor for the difference in molecular extinction coefficients of the absorption bands between TPP-Co(II) and polyAOTPP-Co(II). The case where all the metal ions incorporated into the polymer are not bound to the TPP moieties might be considered as the origin of this difference. However, IR absorption bands due to TPP-Co(II) moieties of the polymer was almost the same as those of TPP-Co(II). Moreover, the local structure around a Co(II) ion in TPP-Co(II) and polyAOTPP-Co(II) was investigated by the EXAFS method. A Co(II)-N distance was determined to be 2.1 Å in polyAOTPP-Co(II), being consistent with 2.1 Å in TPP-Co(II).[18] This result shows that Co(II) ions incorporated into the polymer are mostly bound to the TPP moieties as TPP-Co(II). Therefore, the difference in the absorption bands between polyAOTPP-Co(II) and AOTPP-Co(II) is reasonably ascribed to the hypochromism and the hyperchromism, which suggests that there are some interactions between TPP-Co(II) moieties in the polymer.[19] It has been usually considered that there is no stacking between TPP rings because of steric repulsion by the phenyl groups.[20] Recently, however, the presence of interaction due to close approach of the two porphin rings has been found in porphin dimers in organic solvents[21] and in aqueous solution of tetrakis(4-sulfophenyl)porphin,[22] and the change in the values of ε has been explained in terms of an exciton coupling model.[7] Bulky TPP moieties bound to a polymer chain are possibly forced into some interactions due to their close approach.

UV-visible spectra of TPP-Fe(III)Cl and polyAOTPPFe(III)Cl are shown in Fig. 2. The values of ε of the Soret band (416 nm) and the absorption band at 515 nm are smaller in polyAOTPP-Fe(III)Cl than in TPP-Fe(III)Cl. The absorption band at 653 nm of polyAOTPP-Fe(III)Cl is stronger and is shifted 3 nm to longer wavelength than the corresponding band of TPP-Fe(III)Cl. In addition, an absorption near 558 nm is observed in polyAOTPPFe(III)Cl. The observed spectroscopic absorption feature of polyAOTPP-Fe(III)Cl is similar to that of polyAOTPP-Co(II), suggesting the presence of exciton coupling between porphin moieties in a polymer chain.

ESR Spectra of Polycrystalline State. Figure 3 shows the ESR spectra of the powdered samples of

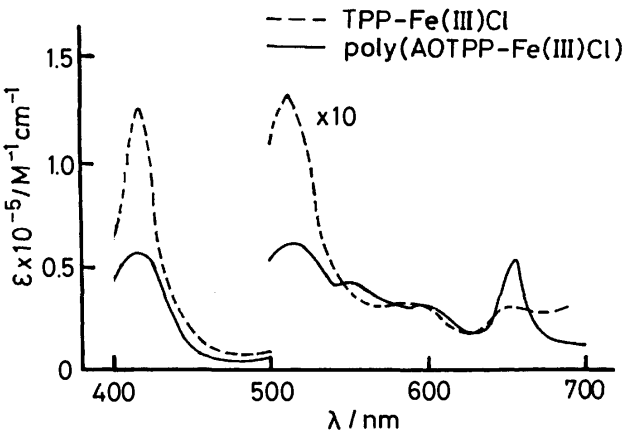

Fig. 2. Visible spectra of TPP-Fe(III)Cl and polyAOTPP-Fe(III)Cl in chloroform at room temperature. (----) TPP-Fe(III)Cl and (——) polyAOTPP-Fe(III)Cl.

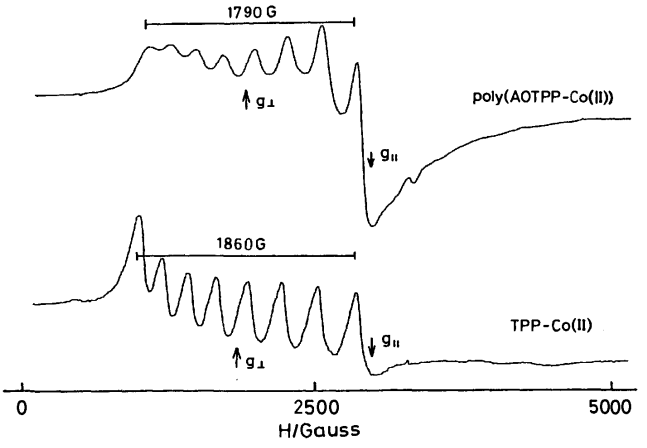

Fig. 3. ESR spectra of TPP-Co(II) and polyAOTPP-Co(II) powders in vacuo at 77 K.

TPP-Co(II) and polyAOTPP-Co(II) in vacuo at 77 K. The spectrum of TPP-Co(II) is similar to those of cobalt(II) phthalocyanine[23] 5,10,15,20-tetrakis(*p*-methylphenyl)porphinatocobalt(II).[24] These spectra are composed of two anisotropic resonance lines ($g_{//}$ and $g_{\perp}$) with an anisotropic magnetic interaction between an unpaired electron and a cobalt nucleus of spin $I=7/2$. The spectrum can be interpreted by the following spin Hamiltonian reflecting the axial symmetry:[23]

$$H=\beta[g_{//}H_zS_z+g_{\perp}(H_xS_x+H_yS_y)]+AS_zI_z+B(S_xI_x+S_yI_y) \quad (1)$$

where A and B are the cobalt nuclear hyperfine interaction constants.

The low-field set of 8 intense lines shows that the resonance lines are not equally spaced and their hyperfine splitting constants increase from 194 to 310 (1G=10^{-4} T) with increasing magnetic field. The progressive hyperfine splitting can be explained in terms of the anisotropic resonance condition with substantial second-order interactions as follow:[23]
For the direction pararell to the magnetic field,

$$H_{//}=(H_0/g_{//})-(AM_I/g_{//})-B^2[I(I+1)-M_I^2](2g_{//}H_0)^{-1}. \quad (2)$$

For the direction perpendicular to the magnetic field,

$$H_{\perp}=(H_0/g_{\perp})-(BM_I/g_{\perp})-(A^2+B^2)[I(I+1)-M_I^2](4g_{\perp}H_0)^{-1}. \quad (3)$$

The high-field set of lines that belong to $g_{//}$ also should be theoretically composed of eight lines. However, the signals of this set were much weaker, being detected as five lines by increasing the amplification of the spectrometer. The remaining three lines are hidden by the strong $g_{\perp}$ resonances. The four hyperfine splitting constants estimated from the five lines are unequal and larger than 300 G. This spectrum is almost the same as that of 5,10,15,20-tetrakis(*p*-methylphenyl)porphinatocobalt(II).[24] The spin Hamiltonian parameters were determined to be $g_{//}=1.80$, $g_{\perp}=3.59$, $A=197\times10^{-4}$ cm^{-1}, and $B=395\times10^{-4}$ cm^{-1} by the same method as Refs. 22 and 23. The deviation from the free electron value of $g=2.0023$ implies that spin-orbit interactions are operative in the Co(II)-TPP molecule.

The ESR spectrum of polyAOTPP-Co(II) shows the superposition of anisotropic resonance lines about $g=2.0$ on the spectrum similar to that of TPP-Co(II). Although accurate g-values of the former are not clear because of the low resolution of the spectrum, the values of $g_{//}$ and $g_{\perp}$ estimated approximately from the maximum and minimum of the spectrum seems to be 2.2 and 2.0, respectively. This anisotropic spectrum is similar to that of reduced vitamin B_{12} which is five-coordinated owing to the attachment of 5,6-dimethylbenzimidazole.[25] The presence of the five-coordinated TPP-Co(II) moieties in polyAOTPP-Co(II) seems to be in accord with the finding of UV-visible spectroscopy that TPP-moieties bound to a polymer chain are forced to make some interaction. The spectrum similar to that of TPP-Co(II) is composed of the low-field set of 8 intense lines whose hyperfine splitting constants increase from 178 to 306 G with increasing magnetic field, and the weaker high-field set which could be observed as 5 peaks, whose hyperfine splitting constants changes from 303 to 430 G, by increasing the amplification. The remaining three lines are hidden by the low field set of $g_{//}$ with stronger intensities. The respective 8 lines in the lower-field set of polyAOTPP-Co(II) are broader than the corresponding lines of TPP-Co(II), and hyperfine splitting constants of the former are smaller than those of the latter. The comparison of these spectra shows that there is an exchange interaction between TPP-Co(II) moieties in polyAOTPP-Co(II),[26] which explains the difference in the temperature dependence of χ_M and μ_{eff} between polyAOTPP-Co(II) and TPP-Co(II) in the section of magnetic properties.

Figure 4 shows the ESR spectra of the powdered samples of TPP-Fe(III)Cl and PolyAOTPP-Fe(III)Cl in vacuo at 77 K. The resonance lines of TPP-Fe(III)Cl were observed at $g=6.4$ and $g=2.0$, being typical of d^5-high spin Fe(III)Cl complexes.[27] The ESR spectrum of polyAOTPP-Fe(III)Cl is similar to that of TPP-Fe(III)Cl except for the broadening of the signal at $g=6.0$ and the increase in the intensity of the resonance line at $g=2.0$. The difference in the line width and the signal intensity between polyAOTPP-Fe(III)Cl and Fe(III)Cl seems to be consistent with the presence of an exchange interaction between TPP-Fe(III)Cl moieties in the polymer, which was observed by measurement of the temperature dependence of χ_M and μ_{eff} in the next section.

Magnetic Properties. The temperature dependence of χ_M^{-1} and μ_{eff} is shown in Fig. 5. The straight line for the χ_M^{-1}-temperature relationship intersects

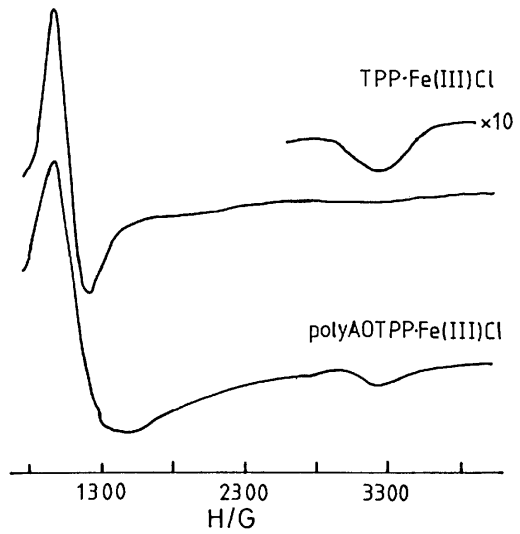

Fig. 4. ESR spectra of TPP-Fe(III)Cl and polyAOTPP-Fe(III)Cl powders in vacuo at 77 K.

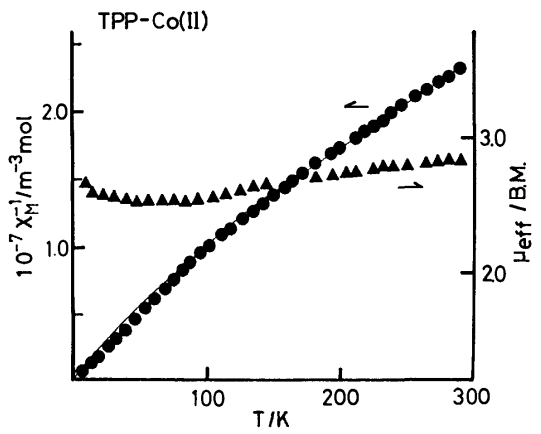

Fig. 5. Temperature dependence of χ_M^{-1} and of TPP-CO(II). (——) Calculated line.

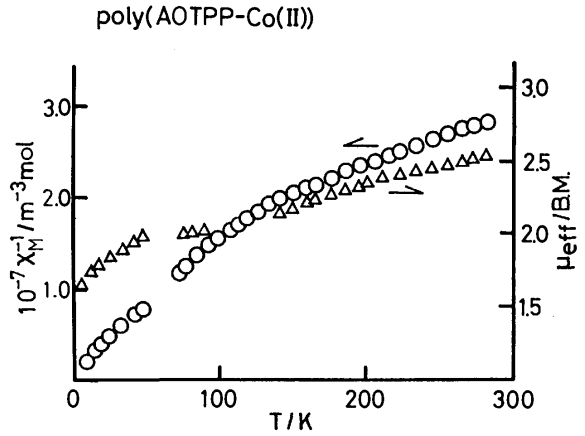

Fig. 6. Temperature dependence of χ_M^{-1} and of polyAOTPP-Co(II).

the ordinate above the origin, indicating that χ_M obeys the Curie-Weise law ($\chi_M=C/(T-\theta)$) with $\theta=-45$ K. This result suggests an antiferromagnetic interaction between TPP-Co(II) molecules each of which has an unpaired electron because of low spin d^7 configuration.[28] If the deviation from the Curie law ($\chi_M=C/T$) is due to the antiferromagnetic interaction the magnetic moment estimated from χ_M should be lower than the spin-only value of 1.73 B.M.[29] The magnetic moment observed at room temperature is 2.83 B.M., being larger than the spin-only value. This rather large value of the magnetic moment leads to the supposition that incomplete quenching of the orbital moment takes place in TPP-Co(II) because of low spin d^7 configuration and results in an anisotropic magnetic susceptibility ($g_{//}$ and $g_\perp$) due to the spin-orbit interaction.[30] Accordingly, the deviation of the temperature dependence of χ_M^{-1} from the Curie law is probably caused by the anisotropic magnetic susceptibility. Anisotropic susceptibilities are estimated by Eqs. 4 and 5:[30,31]

$$\chi_{//} = \frac{N\beta^2}{kT} \tag{4}$$

$$\chi_\perp = \frac{N\beta^2}{4kT}\left(2+\frac{6\lambda}{\Delta E}\right)^2 + \frac{3N\beta^2}{\Delta E+\lambda/2} + \frac{3N\beta^2}{\Delta E+\lambda/2} \tag{5}$$

where λ is a spin-orbit coupling constant, ΔE transition energy, N Avogadro's number, B Bohr magneton, k Boltzmann constant, and T temperature.

The value of ΔE is determined by Eq. 6 on the assumption[32] that λ is 400 cm^{-1}, which is 75% of that for the free Co(II) ion.

$$\Delta E = \frac{6\lambda}{g_\perp - g_e} \tag{6}$$

where the $g_\perp$ value was determined to be 3.32 from ESR spectra. From Eq. 6, ΔE was estimated to be 1800 cm^{-1}. Anisotropic magnetic susceptibilities at various temperatures were calculated from Eqs. 5 and 6 by using these ΔE and λ various.[31] Average magnetic susceptibilities χ at various temperature were calculated from Eq. 7 using $\chi_{//}$ and $\chi_\perp$.

$$\chi = \frac{1}{3}\chi_{//} + \frac{2}{3}\chi_\perp \tag{7}$$

The temperature dependence of the average magnetic susceptibility is in agreement with the experimental data shown Fig. 5. Therefore, the temperature dependence of χ_M is mainly ascribed to the spin-orbit coupling of Co(II) itself rather than the antiferromagnetic interaction between TPP-Co(II) molecules.

PolyAOTPP-Co(II): The temperature dependences of χ_M^{-1} and μ_{eff} of polyAOTPP-Co(II) are shown in Fig. 6. The straight line covering the high temperature range of the χ_M^{-1}-temperature relation intersects above the origin, indicating that χ_M obeys the Curie-Weiss law with $\theta=-190$ K. The magnetic moment of polyAOTPP-Co(II) was 2.58 BM, being smaller than that of TPP-Co(II)(2.83 BM). Moreover, the former decreased more markedly with lowering the temperature than the latter. This result shows that the antiferromagnetic interaction as well as anisotropic susceptibilities caused by the spin-orbital coupling should be involved in the magnetic behavior of polyAOTPP-Co(II). Accordingly, the temperature-dependence of magnetic susceptibility involving both factors was estimated. The theoretical temperature dependence χ_M^{-1} was found to be in better agreement with the experimental data by using the spin-spin interaction between three Co(II) ions rather than two Co(II) ions. Equations 4 and 5 were corrected by taking into account an antiferromagnetic interaction between three Co(II) ions as in Eqs. 8 and 9:[33]

$$\chi_{//} = \frac{N\beta^2}{3kT}\frac{\exp(3x)+5}{\exp(3x)+1} \tag{8}$$

$$\chi_\perp = \frac{1}{3}\frac{N\beta^2}{3kT}\left(2+\frac{6\lambda}{\Delta E}\right)\frac{\exp(3x)+5}{\exp(3x)+1} + \frac{3N\beta^2}{\Delta E+\lambda/2} + \frac{3N\beta^2}{\Delta E-\lambda/2} \tag{9}$$

where $x=-J/kT$.

In this calculation, λ and ΔE were assumed to be the same as those used in Eqs. 4 and 5, because the remarkable wavelength changes in these values between TPP and poly AOTPP was not found in UV-visible absorption and g values in ESR, respectively. The temperature dependence of the average $\bar{\chi}$ was estimated by using various coupling constants for antiferromagnetic interaction. Results are shown in Fig. 7. The best fit between theoretical and experimental curves was obtained with $J=-45$ cm^{-1}. Since polyAOTPP-Co(II) is considered to have various sites of different J values, this $J=-45$ cm^{-1} is an average of various J values.

TPP-Fe(III)Cl and PolyAOTPP-Fe(III)Cl: The temperature dependences of χ_M^{-1} and μ_{eff} of TPP-Fe(III)Cl are shown in Fig. 8. The straight line for the χ_m^{-1}-temperature relationship intersects the ordinate above the origin, indicating that χ_M obeys the Curie-Weiss law with $\theta=-11$ K. Since the ESR spectrum of TPP-Fe(III)Cl shows the high-spin d^5 config-

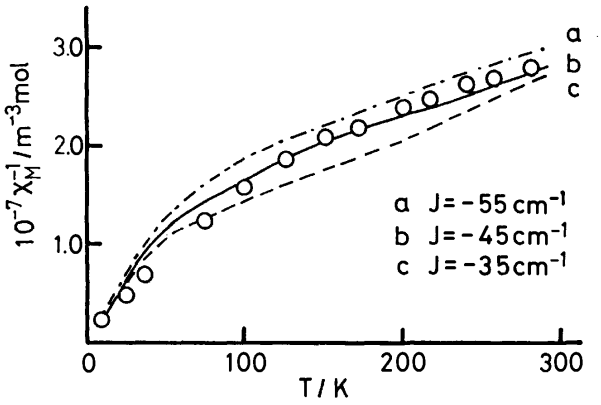

Fig. 7. Theoretical curves for the temperature dependence of the magnetic susceptibility of polyAOTPP-Co(II) with various antiferromagnetic interaction. $J=-55$ cm^{-1}, (b) $J=-45$ cm^{-1}, (c) $J=-35$ cm^{-1}.

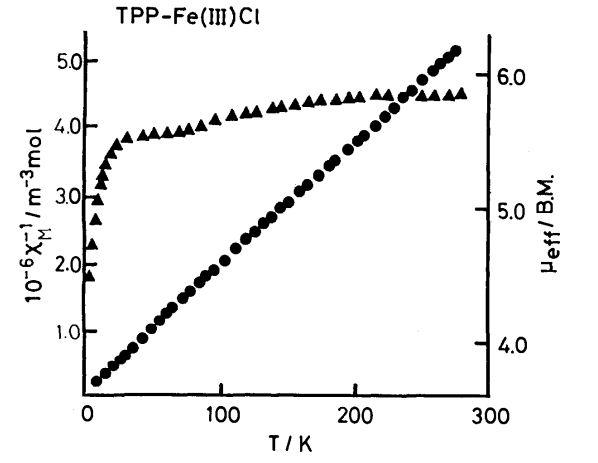

Fig. 8. Temperature dependence of χ_M^{-1} and μ_{eff} of TPP-Fe(III)Cl.

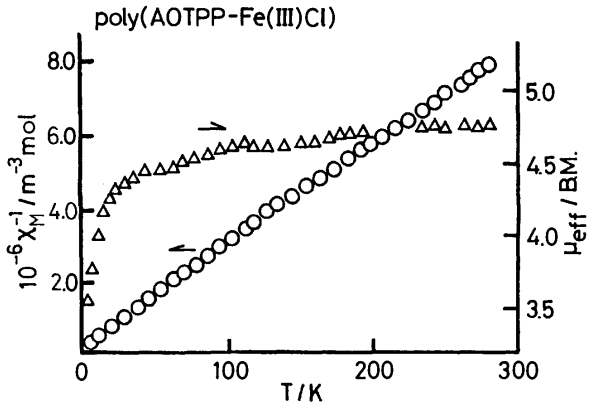

Fig. 9. Temperature dependence of χ_M^{-1} and μ_{eff} of polyAOTPP-Fe(III)Cl.

uration, anisotropic magnetic susceptibility due to the spin-orbit coupling interaction might be reasonably removed from the origin of deviation of the temperature dependence of χ_M^{-1} from the Curie law. Accordingly, the deviation is ascribed to the antiferromagnetic interaction. The magnetic moment of 5.82 B.M. is smaller than 5.92 B.M. of the spin-only value of d^5-high spin configuratic,[33] supporting that there are weak antiferromagnetic interaction.

The temperature dependences of χ_M^{-1} and μ_{eff} of polyAOTPP-Fe(III)Cl are shown in Fig. 9. The straight line for χ_M^{-1}-temperature relation intersects above the origin, indicating that χ_M^{-1} obeys the Curie-Weiss law with $\theta=-20$ K. The magnetic moment of polyAOTPP-Fe(III)Cl was 4.90 B.M. at room temperature, being smaller than that of TPP-Fe(III)Cl. Since TPP-Fe(III)Cl moieties bound to a polymer chain are considered to have various antiferromagnetically interacting sites, the temperature dependence of χ_M was apparently simulated by Eq. 10 derived for paramagnetic compound with exchange interaction of J on the assumption of the two paramagnetic sites with J_1 and J_2 as primary approximation.[34]

$$\chi_M=\sum_i\left(\frac{P_iNg^2\beta^2}{kT}\right)\frac{55+30x^{10}+14x^{18}+5x^{14}+x^{18}}{11+9x^{10}+7x^{18}+5x^{14}+3x^{18}+x^{30}} \quad (10)$$

where $x=\exp(-J_i/kT)$ and P_i indicates molar fraction of site occupancy with J_i.

The temperature dependence of χ_M^{-1} for polyAOTPP-FeCl(III)Cl was best simulated using the ratio of $P_1:P_2=42:58$ for the sites with $J_1=-50$ cm^{-1} and $J_2=0$ cm^{-1}, respectively. The reason why polyAOTPP-Fe(III)Cl has larger antiferromagnetic interaction than TPP-Fe(III)Cl might be ascribed to the fact that the porphin moieties are forced to collect near the chain.

Oxygen Adsorption of PolyAOTPPCo(II). The temperature dependences of χ_M^{-1} and μ_{eff} of TPP-Co(II) and polyAOTPP-Co(II) under 20 mmHg (1 mmHg≈133.322 Pa) of O_2 are shown in Figs. 10

and 11, respectively. These temperature dependences of χ_M^{-1} and μ_{eff} of TPP-Co(II) were not different from those in the absence of O_2, indicating that there is no special interaction between O_2 and the Co(II) ion.

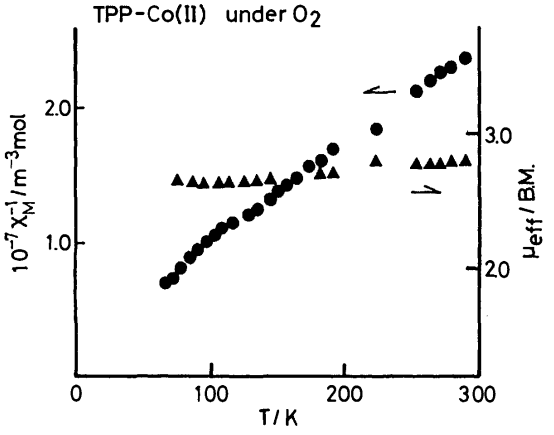

Fig. 10. Temperature dependence of χ_M^{-1} and μ_{eff} of TPP-Co(II) in the presence of molecular oxygen.

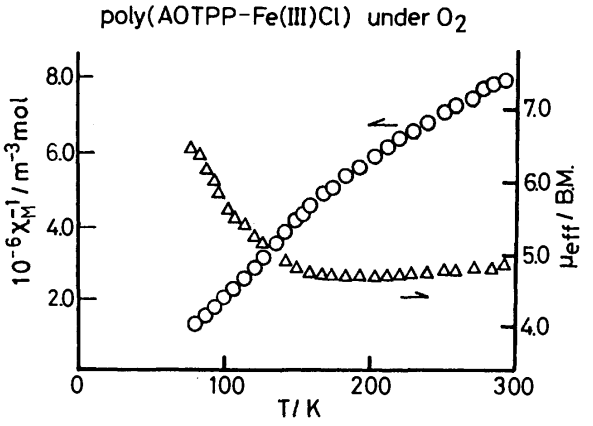

Fig. 11. Temperature dependence of χ_M^{-1} and μ_{eff} of polyAOTPP-Co(II) in the presence of molecular oxygen.

The temperature dependences of χ_M^{-1} and μ_{eff} of polyAOTPP-Co(II) under 20 mmHg O_2 was not different from those in the absence of O_2 at temperatures higher than 250 K, but they were markedly different from that in the absence of O_2 below 200 K (Fig. 6). Magnetic moment μ_{eff} increased from 2.5 BM to 3.3 BM with lowering the temperature from 180 K to 70 K. In order to make clear the origin of the abnormal behavior of the magnetic susceptibility under O_2 at low temperature, the O_2 pressure dependence of weight at 77 K was measured at various pressures of O_2 using a magnetic balance. The weight increased on increasing the pressure of O_2, and became a limiting value at pressures higher than 70 mmHg, in which the ratio of O_2 to Co(II) ion is almost 1.0. The pressure dependence of the adsorbed O_2 shows a Langmuir type isotherm curve. This result shows that there is special interaction between Co(II) and O_2. The ESR spectrum of polyAOTPP-Co(II) was measured in the presence of O_2 and compared with that in vacuum, as shown in Fig. 12. The ESR spectrum of polyAOTPP-Co(II) under O_2 shows the appearence of a new absorption band at 3350 G (g=2.01) in addition to that in the absence of O_2. The intensity of the new resonance line increased on lowering the temperature. Similar ESR spectra have been observed in oxygen-containing samples of tetrakis(*p*-methylphenyl)-porphine and tetrakis(*p*-methoxyphenyl)porphine in toluene-glass with *N*-substituted imidazole and amine,[24] and have been ascribed to the O_2 adduct prepared by chemical adsorption of O_2 on five-coordinated amine-Co(II) complex.[24,35] Since the ESR spectrum of polyAOTPP-Co(II) in vacuo showed the presence of the five-coordinated TPP-Co(II) moieties, the new resonance line at 3350 gauss in the presence of O_2 can reasonably be ascribed to the O_2 adduct of the TPP-Co(II) moiety. For an understanding of the strength of the adsorption of O_2,

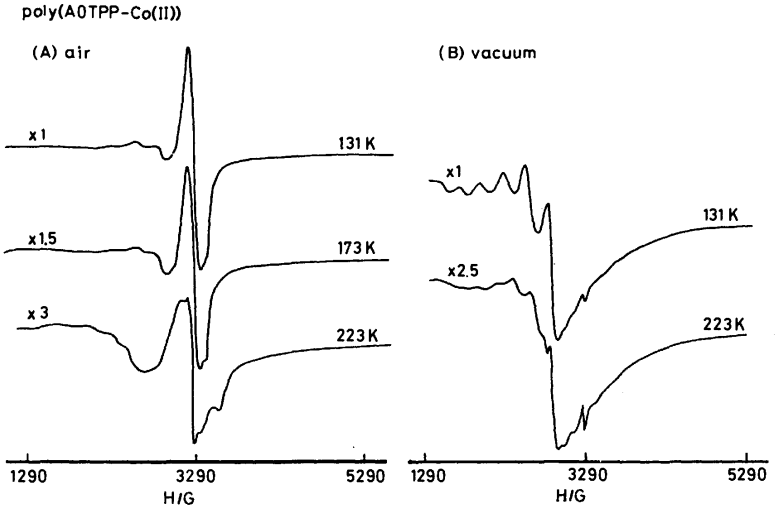

Fig. 12. ESR spectrum of polyAOTPP-Co(II) under molecular oxygen at 77 K.

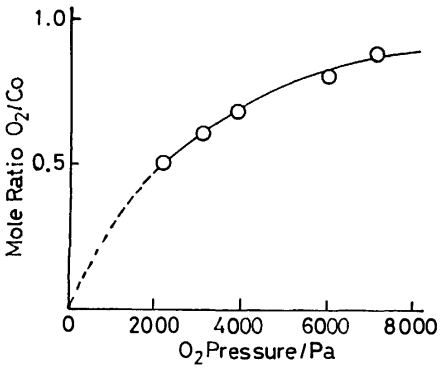

Fig. 13 Oxygen adsorption of polyAOTPP-Co(II) as a function of oxgen pressure at 77 K. (——) Eye-guided line.

the oxygen-pressure dependence of weight of polyAOTPP-Co(II) was measured at various temperatures under 20 mmHg of O_2. The weight of O_2 adsorbed depended on the temperature and reversibly changed on varying the temperature. Therefore, the following relation is considered on the adsorption.

$$\mathrm{Co(II)\cdots O_2} \underset{k_{-1}}{\overset{k_1}{\rightleftharpoons}} \mathrm{Co(II)} + \mathrm{O_2} \tag{11}$$

$$k = \frac{k_1}{k_{-1}} = \frac{[\mathrm{Co(II)}][\mathrm{O_2}]}{[\mathrm{Co(II)}\cdots\mathrm{O_2}]} = \frac{[\mathrm{Co(II)}]\,P_{\mathrm{O_2}}}{[\mathrm{Co(II)}\cdots\mathrm{O_2}]} \tag{12}$$

Since the amount of oxygen adsorbed is estimated to be less than 3% of total O_2 of the measuring system even if the TPP-Co(II) moieties adsorb completely O_2, P_{O_2} can resonably be regarded as constant in all experiments. The temperature dependence of K/P_{O_2} is regarded as that of K. Thus, the binding energy for O_2-adsorption was estimated to be 24 kJ mol^{-1} from the temperature dependence of K/P_{O_2}, which corresponds to the chemical adsorption.

Similarly, POTPP-Co(II) adsorbs O_2. Since TPP-Co(II) does not adsorb O_2, it is assumed that the ester group plays an important role for the chemical adsorption of O_2.

The authors would like to express their sincere appreciation to professor Shun-ichi Nozakura, Osaka University, for his encouragement. This work was partly supported by a Grant-in-Aid for Scientific Research on Priority Area "Macromolecule-Complexes (No. 62612001)" from the Ministry of Education, Science and Culture.

References

1) "Porphyrins and Metalloporphyrins," ed by K. M. Smith, Elsevier, New York (1975).
2) B. D. Berezin, "Coordination Compounds of Porphyrins and Phthalocyanines," John-Wiley, New York.
3) "The Porphyrins," ed by D. Dolphin, Academic Press, New York (1978), Vol. IV.
4) E. Tsuchida, E. Hasegawa, and T. Kanayama, *Macromolecules*, **11**, 947 (1978).
5) E. Tsuchida, H. Nishide, M. Yuasa, E. Hasegawa, and Y. Matsushita, *J. Chem. Soc., Dalton Trans.*, **1984**, 1147.
6) J. J. Katz, L. L. Shipman, J. M. Cotton, and T. R. Janson, "The Porphyrins," ed by D. Dolphin, Academic Press, New York (1987), Vol. V, pp. 401—458.
7) M. Gouterman, D. Halten, and A. Lieberman, *Chem. Phys.*, **25**, 139 (1977).
8) M. Kamachi, X. S. Cheng, T. Kida, A. Kajiwara, and S. Nozakura, *Macromolecules*, **20**, 2665 (1987). M. Kamachi, H. Akimoto, S. Nozakura, *J. Polym. Sci., Polym. Lett. Ed.*, **21**, 693 (1983).
9) M. Kamachi, H. Akimoto, W. Mori, and M. Kishita, *Polym. J.*, **16**, 23 (1984).
10) M. Kamachi, M. Tamaki, Y. Morishima, and S. Nozakura, W. Mori, and M. Kishita, *Polym. J.*, **14**, 363 (1982).
11) M. Kamachi, H, Enomoto, M. Shibasaka, W. Mori, and M. Kishita, *Polym. J.*, **18**, 439 (1986).
12) M. Kamachi, X. S. Cheng, H. Aota, W. Mori, and M. Kishita, *Chem. Lett.*, **1987**, 2331.
13) P. E. Selwood, "Magnetochemistry," Interscience, New York (1975).
14) O. Kahn, J. Glay, Y. Journaux, J. Jaud, and I. Morgenstern-Badarau, *J. Am. Chem. Soc.*, **104**, 2165 (1982).
15) A. D. Alder, F. Longo, J. Finarelli, J. Goldmacher, J. Assour, and L. Korshakoff, *J. Org. Chem.*, **32**, 476 (1967).
16) J. W. Bucher, G. Eikelmann, L. Puppe, K. Rhobock, H. H. Schreehage, and D. Week, *Ann. Chem.*, **745**, 135 (1971).
17) C. Maricodi, W. Swift, and D. K. Straub, *J. Am. Chem. Soc.*, **91**, 5205 (1969).
18) M. Kamachi, A. Kajiwara, and H. Maeda, to be published. The X-ray absorption measurements were made with synchrotron radiation by use of the EXAFS facilities in the National Laboratory of High Energy Physics.
19) W. I. White, "The Porphyrins" IV. ed by D. Dorphin, Academic Press, New York (1978), pp. 306—314.
20) K. A. Zacharrasse and D. G. Whitten, *Chem. Phys. Lett.*, **22**, 527 (1973).
21) R. L. Brookfield, H. Ellul, A. Harriman, and G. Porter, *J. Chem. Soc., Faraday Trans. 2*, **1986**, 82, 219.
22) M. Krishnamurthy, J. R. Sutter, and P. Hambright, *J. Chem. Soc., Chem. Commun.*, **1975**, 13.
23) J. M. Assour and W. K. Kahn, *J. Am. Chem. Soc.*, **87**, 207 (1965).
24) F. A. Walker, *J. Mag. Res.*, **15**, 201 (1978).
25) G. N. Schrauzer and L. Lee, *J. Am. Chem. Soc.*, **90**, 6541 (1968).
26) J. E. Wertz and J. Bolton, "Electron Spin Resonance," McGraw-Hill, New York (1972), p. 201.
27) M. Momenteaw, *Biochim. Biophys. Acta*, **304**, 814 (1973).
28) J. L. Hoard, "Porphyrins and Metalloporphyrins," ed by K. M. Smith, Elsevier, New York (1978), p. 359. F. A. Walker, *J. Am. Chem. Soc.*, **92**, 4235 (1970).
29) C. J. O'Conner, "Progress in Inorganic Chemistry," John-Wiley, New York (1980), Vol. 28, p. 246.
30) E. A. Boudreaux and L. N. Mulay, "Theory and Application of Molecular Paramagnetism," John-Wiley, New York (1976).

31) R. L. Martin and L. N. Mitra, *Chem. Phys. Lett.*, **3**, 183 (1969).
32) A. K. Gregson, R. L. Martin, and S. Mitra, *Chem. Phys. Lett.*, **5**, 310 (1970).
33) S. Emori, M. Inoue, M. Kishita, and R. Kubo, *Inorg. Chem.*, **7**, 2419 (1968).
34) A. Earnshaw, "Introduction to Magnetochemistry," Academic Press, New York (1968), p. 77.
35) H. Sakurai and K. Ishizu, *J. Am. Chem. Soc.*, **104**, 4960 (1982).

ESR Studies on Chain Transfer Reactions: Rate Constants for the Reactions of Model Radicals of Polystyrene Growing Chain Ends with Tetrahalomethanes and Thiophenols

Yoko KUWAE and Mikiharu KAMACHI*
Department of Macromolecular Science, Faculty of Science, Osaka University, Toyonaka, Osaka 560
(Received January 28, 1989)

The absolute rate constants for reactions of the model radicals of the growing chain ends of styrene and methacrylonitrile with tetrahalomethanes and thiophenols were determined by spin-trapping methods using ESR spectroscopy. The model radicals were produced by the photodecomposition of 1,1′-diphenylazoethane and 2,2′-azobisisobutyronitrile. In the case of the styrene model radical, the rate constants for the halogen abstraction reaction from CBr_4, $CBrCl_3$, and CCl_4 were 1.1×10^7, 2.0×10^6, and 1.1×10^5 $M^{-1}s^{-1}$, respectively, and increased with increasing electron affinity of tetrahalomethanes. The rate constants for the hydrogen abstraction reaction from thiophenols were of the order 10^6 $M^{-1}s^{-1}$, independent of the electron-donating and -accepting properties of the para substituents. In the case of the methacrylonitrile model radical, the rate constants for the halogen abstraction reaction from CBr_4 and $CBrCl_3$ were 1.1×10^5 and 4.5×10^3 $M^{-1}s^{-1}$, respectively. The rate constants for the hydrogen abstraction reaction from thiophenols with $-CH_3$, -H, and -Cl substituent in the para position were 4.5×10^4, 2.7×10^4, and 1.7×10^4 $M^{-1}s^{-1}$, respectively. The rate constants decreased with increasing the electron-withdrawing power of the substituent.

It has been well-known that tetrahalomethanes and thiol derivatives are strong chain-transfer reagents for the radical polymerization of styrene.[1,2] Although the chain-transfer constants (C_s) have been determined by the Mayo equation,[1] the values of C_s reported for strong chain-transfer reagents, such as CBr_4 and $CBrCl_3$, have varied over two orders of magnitude.[3-6] From a study of the dependence of C_s on the extent of polymerization, Thomson and Walter[6] pointed out the fact that this deviation is mainly due to the effect of a rapid removal of the transfer reagents on the degree of polymerization, since most of the strong transfer reagents are considered to be consumed at 0.5—0.7% conversion and the subsequent reaction probably similar to bulk polymerization. Since it is difficult to accurately estimate C_s for strong chain-transfer reagents by the Mayo equation, the value of C_s should be evaluated under the conditions where it is not influenced by the extent of polymerization.

Recently, we reported on a method for determining the absolute rate constants of model radicals of the propagating chain ends with tetrahalomethane using a spin-trapping ESR method.[12] In the present work, we applied this method to the halogen- and hydrogen-abstraction of the α-methylbenzyl radical (CH_3-$\dot{C}HC_6H_5$), which is a model radical for the polystyrene end, from tetrahalomethanes and thiophenols.

The absolute rate constant, k_{trs}, provides more direct information concerning the mechanism of the chain-transfer reaction than C_s. An understanding of the mechanism of the chain-transfer reaction to strong transfer reagents possibly provides important information concerning the chemical properties of the propagating radical and the radical reaction control, such as the transformation of a radical reaction to an ionic reaction through the complex formation or electron transfer of the propagating radical to additives. In this paper, therefore, we determined the absolute rate constants for hydrogen abstraction of the 1-cyano-1-methylethyl radical (an electropositive radical) from thiophenols and reevaluated k_x for halogen-abstraction reactions of this radical from halomethanes. Additionally, these rate constants were compared with the corresponding ones of the α-methylbenzyl radical.

Experimental

Materials. 1,1′-Diphenylazoethane was prepared according to the oxidation of the corresponding hydrazine derivatives. 2-(*t*-Butylthio)acrylonitrile was prepared by Viehe's method.[14] Thiophenols, commercially available, were purified by distillation or recrystallization. Azobisisobutyronitrile (AIBN) and tetrahalomethanes were purified as described previously.[12]

The ESR spectra were recorded on a Japan Electron Optics Laboratory Model JES-FE 1X ESR spectrometer under irradiation with a 500-W high-pressure mercury lamp (Ushio 500) at 80 °C. The temperature in the cavity of the ESR spectrometer was controlled with a variable temperature accessory (ES-VT-3A). The simulation for the overlap of two adducts was carried out using a JEOL ESR simulation program (0398) operating on a EC 6 computer.

A solution of an azocompound (2.0×10^{-2}—1.0×10^{-1} M; 1M=1 mol dm^{-3}), a trapping reagent (6.4×10^{-1}—6.4×10^{-3} M), and a transfer reagent (0.9—7.8×10^{-2}M) in toluene was put into a sample tube equipped with an ESR cell (spectrocil 3 mm) in the side arm, degassed by repeated melting and freezing under vacuum, and then sealed. The UV spectra were measured on a Hitachi 124 UV-visible spectrometer. Ionization potentials were measured by photoelectron spectroscopy with calibration by xenon as an internal standard (IP 12.130 eV).

An estimation of the kinetic parameter was carried out by a computer calculation using a nonlinear least-square method, whose program was Sals II written by Nakagawa et al. (Tokyo University).

Results

Addition Reaction of α-Methylbenzyl Radical to 2-(*t*-Butylthio)acrylonitrile. Figure 1 shows the ESR spectrum observed under irradiation of a mixture of 1,1′-diphenylazoethane and 2-(*t*-butylthio)acrylonitrile, a spin-trapping reagent (T). The ESR spectrum of a triplet of triplets of doublets with hyperfine splitting constants of 1.1, 0.28, and 0.08 mT, respectively, was reasonably assigned to the adduct of the model radical of the polystyrene propagating end to T.[12,14] The change in the ESR spectrum with the reaction time showed that the concentration of the adduct became stationary within several minutes after irradiation. The signal due to the α-methylbenzyl radicals (M·) could not be detected, indicating that the stationary concentration of M· was negligibly small, as compared with that of the adduct (MT·). Therefore, the bimolecular self-termination of M· was not taken into account in the kinetic treatment. Thus, the reactions are shown in Eqs. 1 to 4:

$$\text{M-N=N-M} \xrightarrow{I} \text{M}\cdot \qquad I\text{: Rate} \qquad (1)$$

$$\text{M}\cdot + \text{T} \xrightarrow{k_1} \text{MT}\cdot \qquad (2)$$

$$\text{MT}\cdot + \text{M}\cdot \xrightarrow{k_2} \text{product} \qquad (3)$$

$$\text{MT}\cdot + \text{MT}\cdot \xrightarrow{k_3} \text{product} \qquad (4)$$

The assumption of the steady state for the concentrations of M· and MT· leads to

$$[\text{T}] = \frac{k_2}{k_2} \frac{[\text{MT}\cdot](1+k_3/I[\text{MT}\cdot]^2)}{(1-k_3/I[\text{MT}\cdot]^2)}. \qquad (5)$$

The relation between the stationary concentration of MT· and T is shown in Fig 2. Ratios k_2/k_1 and k_3/I were determined from Eq. 5 by a computation using the data shown in Fig. 2: results are shown in Table 1,

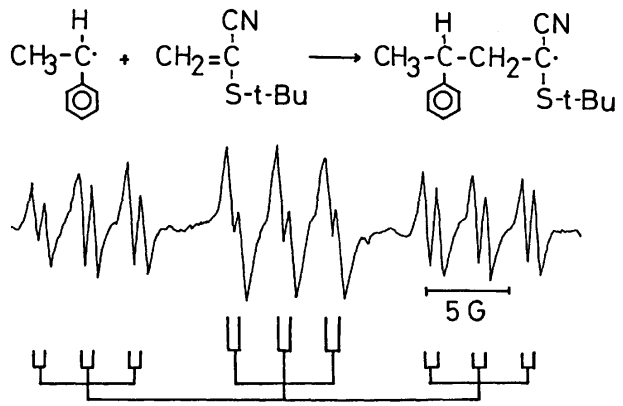

Fig. 1. ESR spectrum observed on irradiation of a mixture of 1,1′-diphenylazoethane and 2-(*t*-butylthio)acrylonitrile (T) in toluene at 80 °C. [1,1′-diphenylazoethane]=5×10⁻² M and [T]=0.64 M.

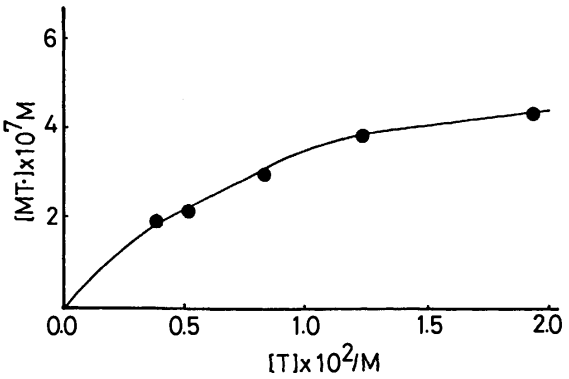

Fig. 2. Relation between MT· and T concentrations at 80 °C. [1,1′-diphenylazoethane]=5.0×10⁻² M.

Table 1. Kinetic Data in Addition Reaction of Model Radicals to 2-(*t*-Butylthio)acrylonitrile[a,b]

	k_2/k_1	k_3/I
	10^{-4}	$10^{10}M^{-2}$
$(CH_3)_2\dot{C}CN$	0.10±0.014	39
$CH_3\dot{C}HC_6H_5$	0.54±0.21	58

a) 80 °C in toluene. [M-N=N-M]=5×10⁻²M. b) Run number 3.

along with data for AIBN. The value of k_3/I for the reaction of 1,1′-diphenylazoethane is larger than that of AIBN. The difference is probably due to the difference in *I*.

Halogen- and Hydrogen-Abstraction Reaction of the Model Radical from Tetrahalomethanes and Thiophenols. The intensity of the ESR spectra of the adducts (MT· and RT·) was much lower in the absence of UV light irradiation at 80 °C than that under UV irradiation. Accordingly, the adducts obtained thermally were neglected in the kinetic study under UV light irradiation. Figure 3 shows a typical example

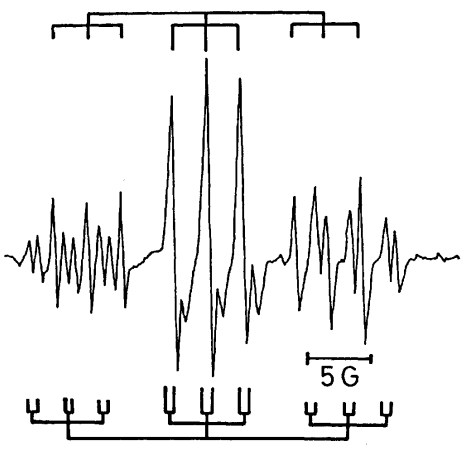

Fig. 3. ESR spectrum observed on the UV irradiation of a mixture of azo compound, thiophenol, and T in toluene at 80 °C. [1,1′-diphenylazoethane]=8.0×10⁻² M, [thiophenol]=8.0×10⁻² M, and [T]=0.32 M.

of the ESR spectra observed upon irradiating a mixture of thiophenol, 1,1′-diphenylazoethane, and T. The spectrum (Fig. 3) showed an overlap of a triplet of triplets of doublets and a triplet of triplets, which were reasonably assigned to the adducts of the α-methylbenzyl radical and the sulfur-centered radical produced from thiophenol,[12,14] respectively. An overlap of two kinds of a triplet of triplets was observed in a mixture of thiophenol, AIBN, and T, which was assigned to the adducts of the 1-cyano-1-methylethyl radical and the sulfur-centered radical. Similar spectra were observed in mixtures of azo compounds, tetrahalomethane and T.[12] The hyperfine splitting constants of the adducts are shown in Table 2. The reactions are shown in the following schemes:

$$M\text{-}N{=}N\text{-}M \xrightarrow{I} M\cdot \quad (1)$$

$$M\cdot + T \xrightarrow{k_1} MT\cdot \quad (2)$$

$$M\cdot + RX \xrightarrow{k_x} MX + R\cdot \quad (6)$$

$$R\cdot + T \xrightarrow{k_{1x}} RT\cdot \quad (7)$$

$$RT\cdot + RT\cdot \xrightarrow{k_3} RTTR \quad (8)$$

$$RT\cdot + MT\cdot \xrightarrow{k_3} RTTM \quad (9)$$

$$MT\cdot + MT\cdot \xrightarrow{k_3} MTTM \quad (10)$$

Since M· and R· were not observed in the ESR spectra, the self-coupling reactions of these radicals were not taken into account. The stationary state treatment on R·, RT·, and MT· yields

$$\frac{[RT\cdot]}{[MT\cdot]} = \frac{k_{1x}[R\cdot][T]}{k_1[M\cdot][T]} = \frac{k_x[RX]}{k_1[T]}. \quad (11)$$

A typical example of a plot of [RT·]/[MT·] vs. the concentrations of transfer reagents is shown in Fig. 4. A linear relation was observed, the ratio, k_x/k_1, being calculated from the slope. Results are shown in Tables 3 and 4. Since the kinetic parameters obtained so far were k_x/k_1, k_2/k_1, and k_3/I, the absolute rate constants of each elementary process could not be directly estimated. If k_2 can be evaluated, k_1 could be estimated from k_2/k_1, and then k_x from k_x/k_1 using the obtained k_1. However, it is hard to directly measure the cross-coupling rate constant (k_2). If self-coupling reactions of M· and MT· are determined, the rate constants of a cross-coupling reaction can generally be estimated as the geometrical mean of the self coupling constants:

$$k_2 = (k_3 k_M)^{1/2}, \quad (12)$$

where k_M and k_3 are the rate constants for the self-coupling reactions of M· and MT·, respectively.

The k_M's for $CH_3\dot{C}HC_6H_5$ and $(CH_3)_2\dot{C}CN$ have already been reported to be 4.7×10^9 $M^{-1}s^{-1}$ [15] and 8×10^9 $M^{-1}s^{-1}$,[16] respectively. We determined k_3 to be $6.5\pm3\times10^8$ $M^{-1}s^{-1}$ as an average of data for 5 radicals estimated in a previous paper.[12] Accordingly, k_2's for these reactions were estimated from Eq. 12, being

Table 2. Hyperfine Splitting Constants for Adducts Obtained by Reaction of Carbon Radicals with 2-(*t*-Butylthio)acrylonitrile[a]

radical	a_H(mT)	a_{CN}(mT)	a_H(mT)
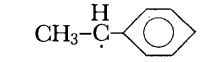	11.0	2.8	0.8
$(CH_3)_2\dot{C}$-CN	8.8	2.8	—
·CBr_3	7.7	2.6	—
·CCl_3	8.0	2.6	—
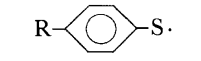	9.6	2.6	—

a) 80 °C in toluene.

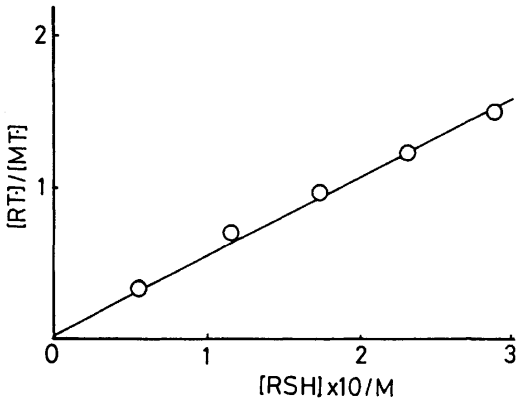

Fig. 4. Plot of [RT·]/[MT·] vs. [RSH] in the stationary concentration of RT· and MT·. [1,1′-diphenylazoethane]=5.0×10^{-2} M and T=0.32 M.

Table 3. Relative Rate Constants for Radicals $CH_3\dot{C}R_1R_2$ in Halogen Abstraction[a,b]

R_1	R_2	k_x/k_1		
		CBr_4	$CBrCl_3$	CCl_4
$-CH_3$	-CN	5.0±0.4	0.20±0.019	—
-H	-Ph	37 ±0.15	6.6 ±0.64	0.38±0.029

a) 80 °C in toluene, [M-N=N-M]=5×10^{-2} M. b) Run number 3.

Table 4. Relative Rate Constants for Radicals $CH_3\dot{C}R_1R_2$ in Hydrogen Abstraction from Thiophenol ($HS\text{-}C_6H_4\text{-}Z(p)$)[a,b]

R_1	R_2	k_x/k_1			
	Z=	-Cl	-H	$-CH_3$	
$-CH_3$	-CN	0.76±0.020	1.2±0.14	2.1±0.12	
-H	-Ph	23 ±1.5	25 ±1.1	23 ±1.5	

a) 80 °C in toluene, [M-N=N-M]=5×10^{-2} M. b) Run number 3.

Table 5. Rate Constants for Halogen Abstraction of $CH_3\dot{C}R_1R_2$ from Tetrahalomethanes[a)]

R_1	R_2	k_x / $10^5 M^{-1}s^{-1}$		
		CBr_4	$CBrCl_3$	CCl_4
$-CH_3$	-CN	2.1	0.084	—
-H	-Ph	110	20	1.1

a) 80 °C in toluene.

Table 6. Rate Constants for Hydrogen Abstraction of $CH_3\dot{C}R_1R_2$ from Thiophenols ($HS-C_6H_4-Z(p)$)[a)]

R_1	R_2	k_x / $10^7 M^{-1}s^{-1}$		
	Z=	-Cl	-H	$-CH_3$
$-CH_3$	-CN	3.1×10^{-2}	5.0×10^{-2}	8.8×10^{-2}
-H	-Ph	0.68	0.74	0.68

a) 80 °C in toluene.

Table 7. Ionization Potential of Thiophenols (eV)

-Cl	-H	$-CH_3$
8.54	8.44	8.26

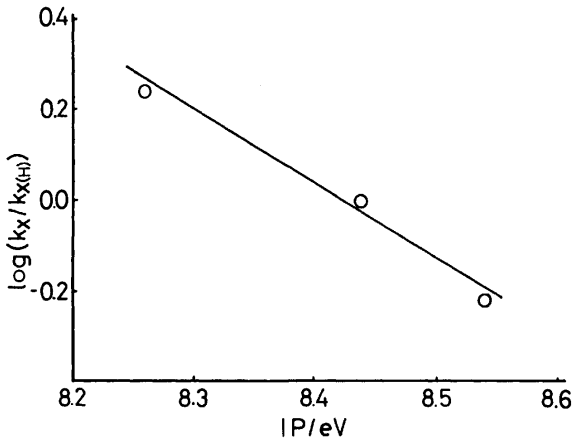

Fig. 5. Relation between rate constants and ionization potentials of thiophenols in the hydrogen abstraction reactions of $(CH_3)_2\dot{C}CN$ from the S-H bonds.

5.5×10^9 M^{-1} s^{-1} and 4.2×10^9 M^{-1} s^{-1} for $CH_3\dot{C}HC_6H_5$ and $(CH_3)_2\dot{C}CN$, respectively. Then, the k_1's were estimated from k_1/k_2 and the k_x's from k_x/k_1 (Table 5). It can be seen that the k_x's for reactions between $CH_3\dot{C}HC_6H_5$ and tetrahalomethanes decreased in the order $CBr_4>CBrCl_3>CCl_4$: k_x of $CH_3\dot{C}HC_6H_5$ with CBr_4 was 6 and 10^2 times as large as those with $CBrCl_3$ and CCl_4, respectively. A similar trend in k_x for the halogen-abstraction reaction of $(CH_3)_2\dot{C}CN$ from tetrahalomethanes was observed (Table 5). The k_x's for the reaction of $CH_3\dot{C}HC_6H_5$ with CBr_4 and $CBrCl_3$ were about 50 and 200 times as large as those of $(CH_3)_2\dot{C}CN$ with the corresponding tetrahalomethanes, respectively.

In the case of thiophenols, k_x's of $CH_3\dot{C}HC_6H_5$ were in order of 10^7, being independent of the nature of para substituents (Table 6), while k_x's of $(CH_3)_2\dot{C}CN$ were in the order of 10^5 and decreased with electron-accepting substituents. The value of $\ln k_x$ for $(CH_3)_2\dot{C}CN$ was linearly correlated with the ionization potential of thiophenols (Fig. 5).

Discussion

To our knowledge, the absolute rate constants for the halogen-abstraction reaction of carbon radicals from tetrahalomethanes have been reported for only a few radicals, such as the methyl, *t*-butyl,[17] and phenyl radicals.[18,19] Therefore, we could not check the reliability of our data by comparison with other data. The k_x's for the halogen-abstraction reaction of the phenyl radical from CBr_4 and CCl_4 have been reported to be 5×10^9 [19] and 5.8×10^6 M^{-1} s^{-1},[18] respectively, two orders of magnitude larger than the corresponding k_x of $CH_3\dot{C}HC_6H_5$, (Table 5). This difference can reasonably be explained by the lower reactivity of $CH_3\dot{C}HC_6H_5$ due to resonance stabilization than that of the phenyl radical. The k_x's for the halogen abstraction reactions of $CH_3\cdot$, $(CH_3)_3C\cdot$, and $(CH_3)_2\dot{C}OCH_2CH_3$ from CCl_4 have been reported to be 3.35×10^2 (80 °C),[7] 4.9×10^4 (30 °C),[17] and 1.0×10^8 M^{-1} s^{-1},[20] respectively. The k_x of $CH_3\dot{C}HC_6H_5$ from CCl_4 is larger than that of $\cdot CH_3$, and less than that of $(CH_3)_2\dot{C}OCH_2CH_3$. The k_x of $CH_3\dot{C}HC_6H_5$ at 80 °C is twice as large as that for $(CH_3)_3\dot{C}$ at 30 °C. When the k_x of the latter radical at 80 °C is calculated on the assumption that its activation energy is 13.8 kJ mol^{-1},[17] it is estimated to be 1.06×10^5 M^{-1} s^{-1}, being of the same order as the k_x for the former. The k_x for the halogen abstraction reaction of carbon radicals has been found to be of the following order:

$$(CH_3)_2\dot{C}OCH_2CH_3>\dot{C}(CH_3)_3=CH_3\dot{C}HC_6H_5>\dot{C}H_3.$$

This order seems to be correlated with the electron-donating property of the α-substituents. These results show that our method for the determination of the rate constant of the halogen-abstraction reaction leads to reasonable rate constants. However, when the k_x's of $(CH_3)\dot{C}HC_6H_5$ were compared with the corresponding k_{trs}'s which were calculated from k_p and C_s's for the radical polymerization of styrene, a remarkable difference between k_x and k_{trs} was found (Table 5).

The determination of C_s has usually been carried out using the Mayo equation:[21]

$$1/P_n = 1/P_{n0} + C_s[S]/[M], \quad (13)$$

where P_n and P_{n0} are the number degree of polymerization of the polymer produced in the presence and absence of transfer reagents[S], respectively; [S]/[M] is

the molar ratio of the transfer reagent to the monomer. Thomas et al.[6] pointed out the fact that C_s in a CBr_4-styrene system was dependent on the extent of polymerization: C_s was 420 in the extent of polymerization to 0.5%, and 2.1 when the reaction was performed to 5% conversion. In addition, an accurate determination of the number average degree of polymerization is necessary for an accurate determination of C_s. Since a significant loss of low-molecular-weight polymer obtained in the low extent of polymerization leads to an overestimation of P_n, the C_s obtained by the Mayo equation seems to be smaller than the true value.

When thiophenols were used as chain-transfer reagents, the k_x's for the hydrogen-abstraction reactions of the styrene model radical from thiophenols was of the 10^6 order of magnitude, being consistent regarding the order of magnitude with the rate constant for the hydrogen abstraction of benzyl radical from thiophenol at 80 °C, which was estimated from the rate constant at 25 °C and the activation energy.[22,23] In addition, our results show that the k_x's is one order smaller than its halogen abstraction rate constant from CBr_4.[24] Since the C_s's of thiophenol derivatives have been reported to be one or two orders smaller than that of CBr_4[24] in the radical polymerization of styrene, the k_x for the hydrogen abstraction of α-methylbenzyl radical from thiophenol seems to be reasonable. To our knowledge, only a few absolute rate constants for the hydrogen abstraction of carbon radicals from thiophenol have been reported: The k_x's of the hydrogen-abstraction of phenyl, butyl, octyl, isopropyl, and *t*-butyl radicals from thiophenol are 1.9×10^9,[18] 1.36×10^8,[23] 9.2×10^7,[23] 1.05×10^8,[23] and $8.0\times10^7=1.47\times10^8$ [23] $M^{-1}s^{-1}$, respectively. These values are one or two orders of magnitude larger than the k_x of $CH_3\dot{C}HC_6H_5$. This styrene model radical is considered to be less reactive than phenyl radical and alkyl radicals, since the former radical is more stabilized through a delocalization of unpaired electron than the latter radicals. Accordingly, the difference in the rate constants between the model radicals and the others can be reasonably explained on the basis of the stabilization of the radical.

The k_x of $(CH_3)_2\dot{C}CN$ with thiophenols were an order of magnitude of 10^2 smaller than that of $CH_3\dot{C}HC_6H_5$, being dependent on the nature of the substituent binding to the benzene ring of thiophenol: the larger the electron-donating property of the substituent, the larger the k_x. The values of $\ln k_x$ were linearly correlated with the ionization potential of thiophenols. This result suggests the possibility that the hydrogen abstraction of $(CH_3)_2\dot{C}CN$ from thiophenol takes place through electron transfer or the charge-transfer complex of the radical. The k_x for the halogen abstraction of the styrene model radical from thiophenols might be too large for the substituent effect to be observed.

In conclusion, the rate constants for the halogen-abstraction reaction of the model radicals from tetrahalomethanes decreased in the order

$$CBr_4 > CBrCl_3 > CCl_4.$$

The rate constants (k_x) obtained by this method were larger than the corresponding chain-transfer rate constants (k_{trs}) calculated from the largest C_s and propagation rate constants of styrene (k_p).[12] This difference between k_x and k_{trs} can possibly be ascribed to an underestimation of C_s due to the removal of a fraction of a lower molecular weight polymer in the determination of the C_s values. In benzenethiols, the hydrogen-abstraction rate constants of the styrene model radical were an order of magnitude of 10^7, being independent of the substituents which were introduced in the para-positions of the aromatic ring; however, the rate constants of the methacrylonitrile model radical were an order of magnitude of 10^4, and decreased with increasing the electron-accepting power of the substituent.

References

1) G. Ordian, "Principle of Polymerization," 2nd ed., Wiley-Interscience, New York (1970), p. 235.
2) "Polymer Handbook," ed. by J. Brandrup and E. H. Immergut, Wiley-Interscience, New York (1970).
3) N. Fuhrman and R. B. Mesrobian, *J. Am. Chem. Soc.*, **76**, 3281 (1954).
4) J. W. Breitenbach, O. F. Olaj, and A. Schwindler, *Monatsh*, **91**, 205 (1960).
5) R. A. Gregg and F. R. Mayo, *J. Am. Chem. Soc.*, **75**, 3530 (1953).
6) R. A. M. Thomson and I. R. Walters, *Trans. Faraday Soc.*, **67**, 3046 (1971).
7) K. V. Macken and H. W. Sidebottom, *Int. J. Chem. Kinet.*, **11**, 511 (1979).
8) H. Paul, *Int. J. Chem. Kinet.*, **11**, 495 (1979).
9) A. B. Ross and P. Neta, "Rate Constants for Reactions of Aliphatic Carbon-centered Reactions in Aqueous Solution," National Bureau of Standard, (1982).
10) "Landholt-Bernstein New Series," ed. by H. Fischer, Group II, Vol. 13a, Springer Verlag, Berlin.
11) A. F. Trotman-Dickenson, "Advance in Free-Radical Chemistry," ed. by G. H. Williams, Logos Press, London (1965), Vol. 1, pp. 1—38.
12) Y. Kuwae, M. Kamachi, K. Hayashi, and H. G. Viehe, *Bull. Chem. Soc. Jpn.*, **59**, 2325 (1986).
13) G. Henrici-Olive and S. Olive, *Makromol. Chem.*, **37**, 71 (1960).
14) V. H. C. Viehe, R. Merenyl, L. Stella, and M. Janousek, *Angew. Chem.*, **91**, 982 (1979).
15) O. von Brede, W. Helmstreit, and R. Mehnert, *J. Prakt. Chem.*, **316**, 402 (1974).
16) S. A. Weiner and G. S. Hammond, *J. Am. Chem. Soc.*, **91**, 986 (1969).
17) "Landolt-Bernstein New Series," ed. by H. Fischer, Group II, Vol. 13a, p. 10.
18) Ref. 17, pp. 25—26.
19) Ref. 17, p. 26.
20) R. Koester and K. D. Asmus, *Z. Naturforsch., B*, **26**,

1104 (1971).
21) G. Odian, "Principles of Polymerization," 2nd ed., McGraw-Hill, New York (1970), p. 237.
22) J. A. Franz, N. K. Suleman, and M. S. Alnajjar, *J. Org. Chem.*, **51**, 19 (1986).
23) J. A. Franz, B. A. Bushaw, and M. S. Alnajjar, *J. Am. Chem. Soc.*, **111**, 268 (1989).
24) L. J. Young, "Polymer Handbook," ed. by J. Brandrup and E. H. Immergut, John-Wiley & Sons, New York, N. Y. II-82 and II-95.

Shock Tube Studies of the H_2-O_2 Reaction by Atomic Resonance Absorption Spectroscopy

Tohru KOIKE
Department of Chemistry, National Defense Academy, Hashirimizu, Yokosuka 239
(Received January 24, 1989)

The increases of O-atoms and of H-atoms in the reaction between H_2 and O_2 in shock waves were measured over the temperature range of 1000—1400 K by atomic resonance absorption spectroscopy. The induction times of the absorptions by these two species were evaluated and computer modeling was carried out to reproduce these values. As one of the initiations of the H_2-O_2 reaction, $H_2+O_2=H+HO_2$ was found to play an important role in the progress of the reaction. The rate constant of this reaction was evaluated as: $k=4.1\times10^{16}$ exp(−285 kJ/RT) $cm^3 \cdot mol^{-1} \cdot s^{-1}$.

The reaction of H_2-O_2 in shock waves has been studied in a wide temperature range by many researchers and is well-known to proceed through chain initiations, chain branchings, and chain terminations. Although reliable rate constants are proposed for most of the important elementary reactions of each step,[1] some of them are still controversial.

Atomic resonance absorption spectroscopy (ARAS) is very sensitive and concentrations of O-atoms and H-atoms of about 10^{-12} mol·cm^{-3} can be detected. Most of the studies by ARAS have been made to clarify the reaction of reactants highly diluted in Ar, e.g., ppm order. Two points could be given for the advantage in using the ARAS under such experimental conditions. One is that the reactions intended to measure should not be affected by secondary reactions. The other is that temperature variation by the progress of the reaction could be almost avoided. Detailed reviews of shock tube studies using this technique have recently been given by Just.[2]

ARAS has also been applied to the kinetic study of the H_2-O_2 reaction by Pamidimukkala and Skinner in the temperature range of 1919—2781 K[3] and by Frank and Just in the temperature range of 1700—2500 K.[4] They measured the test gas mixtures of $H_2/N_2O/Ar$ with or without O_2. Since the reaction mechanisms are specifically devised to explain the experimental result thus obtained, some of the elementraty reactions which are important under ordinary conditions are excluded from the reaction mechanisms.

We also applied ARAS to the H_2-O_2 reaction at lower temperatures than those of these two studies. Due to the slowness of growth rates of O- and H-atoms under such conditions at lower temperatures, these atoms are produced only in small amounts. We had to use test gas mixtures of rather higher concentrations of reactants than those previously used for ARAS. Thus, we could study the early stages of the reaction and could obtain the rate constant of $H_2+O_2=HO_2+H$.

Experimental

The test section of the rectangular shock tube used in a former study[5] on incident shock waves was reconstructed so as to be applicable to the ARAS measurements as follows.

Observation windows were located 3.3 m down-stream from the diaphragm section. Two of the 4 observation windows, made of MgF_2, had two vacuum tight flanges for the ARAS. A quartz tube was connected perpendicularly to one of the windows. A rotary pump was used to let gas mixtures of H_2 or O_2 diluted in He by 1% flow at 2 Torr (1 Torr ≈ 133.322 Pa) through the quartz tube. A microwave generator (Raytheon, PGM10×1) was used to discharge the gas mixture and the emissions were used as the light source of the ARAS. For the other window, a vacuum-UV-monochromator (Minuteman, 302-VM, dispersion=40 nm mm^{-1}) was located to isolate the desired emission lines centered at 121.6 nm for the Lyman-α line of H-atoms and at 130.5 nm for the O-triplet line of O-atoms. The VUV monochromator having entrance and exit slits of 1 mm width was evacuated to about 5×10^{-4} Torr using a rotary pump combined with a liquid-N_2 trap. A solar blind photomultiplier (Hamamatu, R-1459) was used as a detector. The signals from the detector were fed into an operational amplifier, and then, recorded on a digital oscilloscope (Iwatsu, DS-6121) combined with an XY-recorder.

The test section of the shock tube was evacuated to less than 10^{-5} Torr before each run. Gases for the test gas were 99.999% pure H_2, 99.999% pure O_2, and 99.999% pure Ar and were used without further purification. The compositions of the two test gases prepared are shown in the footnote of Fig. 3.

A trial run with a test gas of pure Ar was carried out and it was confirmed that no appreciable absorption was observed under the present experimental conditions. With regard to the absorptions of test gas mixtures of O_2/Ar and H_2O/Ar in the present temperature range, only small absorptions at the shock front attributable to O_2 and H_2O were observed.

Results and Discussion

Figure 1 is a sample oscillogram exhibiting the time profile of the absorption at 130.5 nm. The absorption occurs immediately after the shock arrival to the observation window; it holds a plateau value and then increases exponentially to a high value. From the oscillograms, the absorption at the shock front and the induction times, τ, defined as the time interval between the shock arrival to the observation window

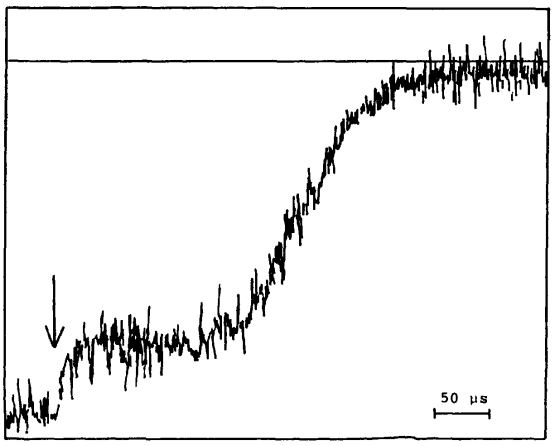

Fig. 1. A sample oscillogram of the absorption profile at 130.5 nm.
Test gas: $H_2/O_2/Ar=1.1/5.8/93.1$.
$P_1=20$ Torr, $T_2=1080$ K.
The upper line shows the zero-level of the incident light intensity. The arrow shows the shock front.

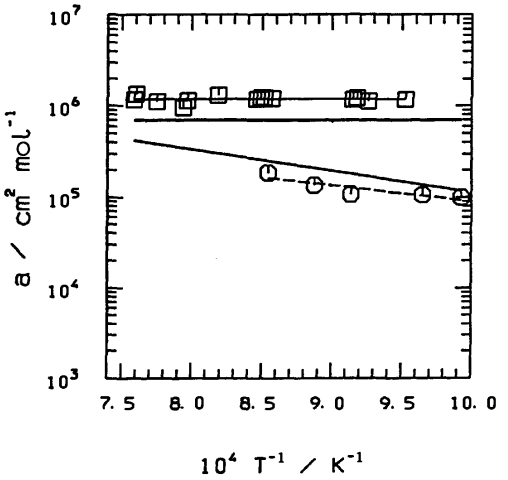

Fig. 2. Absorptivities, a, vs. $10^4/T$.
Squares; at 130.5 nm, Octagonals; at 121.6 nm.
Lines through each data point show least squares fit. Thick lines are extrapolated values:[4] Upper; at 130.5 nm, Lower; at 121.6 nm.

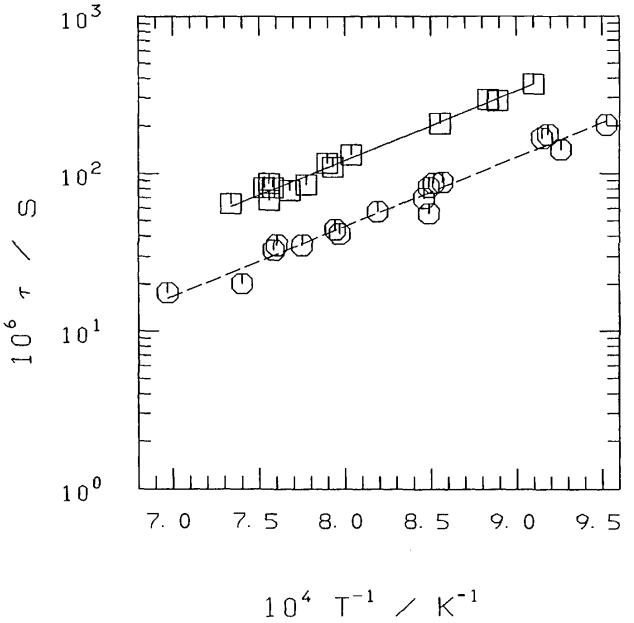

Fig. 3. Induction times, τ, obtained at 130.5 nm vs. $10^4/T$.
Squares: $H_2/O_2/Ar=4.8/1/94.2$.
Octagonals: $H_2/O_2/Ar=1.1/5.8/93.1$.
Lines through each data point show least squares fit. Computer modeling was done to reproduce these lines.

and the foot of the exponential absorption rise, were evaluated.

The absorption at the shock front can be attributed to the absorption by O_2, since the absorption by H_2 is reported to be negligible.[4] Figure 2 shows the absorptivity, a, evaluated from the absorption as: $a=\ln(I_0/I)/(d[O_2])$, where I_0=incident light intensity. I=transmitted light intensity at the shock front, and d=optical path length. There seems to be no temperature dependence for the a values at 130.5 nm. The a values of O_2 for the Lyman-α line at 121.6 nm are also shown in the figure. These a values are smaller than those at 130.5 nm and are seen to increase with temperature. The thick lines are extrapolated values from the reported ones[4] obtained at much higher temperatures than the present. It is seen that the present values and the extrapolated values are close to each other. Thus, the present optical system can be considered to be working well.

Figure 3 shows the temperature dependence of τ evaluated from the absorption time profile at 130.5 nm. It is seen that the temperature dependence of τ is almost the same for the two mixtures investigated. As for the absolute value of τ, it gets smaller with larger concentration of O_2. The lines are the least-squares fit for the data points.

The results shown in Fig. 3 were subjected to interpretation by computer modeling. The induction times by modeling were evaluated from the time profile of the modeled O-atom concentration, i.e., the reaction time when the concentration value reaches 1.66×10^{-12} mol·cm^{-3} for the O-atom was assumed to correspond to the induction time.[4]

The computer program used in modeling is the same one as was used in the former study.[5] In the modeling, numerical integration is carried out by taking into account both the forward and reverse rates of each elementary reaction, and the reverse rate constants are calculated from the forward rate constants combined with equilibrium constants based on appropriate thermochemical data.[6]

Warnatz et al.[1,7] has recently reviewed the reaction mechanism of H_2-O_2 and recommended the rate constants of Reactions 2—11 which are valid over the temperature range of 1000—2500 K as shown in Table

Table 1. Reaction Mechanism and Rate Constant
$k=A\,T^n \exp(-E/RT)$
(mol, cm, s, and J units)

Reaction	A	n	E	W[a]	PS	FJ
1) $H_2+O_2=H+HO_2$	4.1 +16[b]	0	2.85+5	*		
2) $H_2+AR=H+H+Ar$	2.2 +14	0	4.0 +5	*	*	*
3) $O_2+AR=O+O+Ar$	1.2 +14	0	4.5 +5	*	*	*
4) $H+O_2=OH+O$	1.22+17	−0.91	6.91+4	*	*	*
5) $O+H_2=OH+H$	1.5 + 7	2.0	3.16+4	*	*	*
6) $OH+H_2=H_2O+H$	1. + 8	1.6	1.38+4	*	*	*
7) $H+O_2+AR=HO_2+Ar$	7. +17	−0.8	0	*	*	
8) $OH+OH=H_2O+O$	1.5 + 9	1.14	0	*	*	
9) $H+HO_2=OH+OH$	1.5 +14	0	4.2 +3	*		
10) $OH+HO_2=H_2O+O_2$	2. +13	0	0	*		
11) $O+HO_2=OH+O_2$	2. +13	0	0	*		

a) The reactions designated by * in the last three columns are those adopted by Warnatz (W), Pamidimukkala and Skinner (PS), and Frank and Just (FJ). b) The number after + exhibits an index for 10.

1. We tried to reproduce the τ values in Fig. 3 by computer modeling adopting his mechanism. As for the rate constant of Reaction 1, we adopted the value of the reverse direction, k_{-1}, recommended also by Warnatz.[1] It was found that the τ values by modeling thus carried out are larger than those measured. The present τ values could not also be reproduced using the two reaction mechanisms which are in accordance with the results by ARAS,[3,4] as described above. It can be pointed out that the two reaction mechanisms are for much higher temperatures than the present. Any of the reactions, which are important in the present lower temperature range, are expected to be ignored or treated to have a small role in their reaction mechanisms. As for the test gas mixtures measured by ARAS, N_2O was used as oxidizer with or without O_2. Since the concentration of O_2 seems to be small in the mixtures without O_2, chain termination, Reaction 7, was not taken into account in the reaction mechanism by Frank and Just.[4] With regard to the initiation reactions, $H_2+O_2=OH+OH$ was taken into account by Frank and Just.[4] In the reaction mechanism proposed by Warnatz, the reverse reaction of $H+HO_2=H_2+O_2$, Reaction 1, can also be a chain initiation. He did not, however, specify the kind of product of Reaction 1. Among the three reaction mechanisms considered, the mechanism giving the closest τ values in Fig. 3 is that of Frank and Just.[4] Since rate constants of important reactions are not so different from each other over the present temperature range, such a discrepancy between the values by experiment and those by modeling could be attributed to whether appropriate initiation reactions were taken into account in the reaction mechanism.

We accepted the rate constants by Warnatz[1] and assumed Reaction 1 to be one of the chain initiations in the H_2-O_2 reaction. The rate of the reaction having a four-center path, $H_2+O_2=OH+OH$, can be considered to be small,[8] since this reaction has much higher activation energy than Reaction 1 does. Then, we only changed the k value of Reaction 1 so as to be in accord with the least squares lines in Fig. 3 and finally we succeeded in modeling them with the following value for k_1.

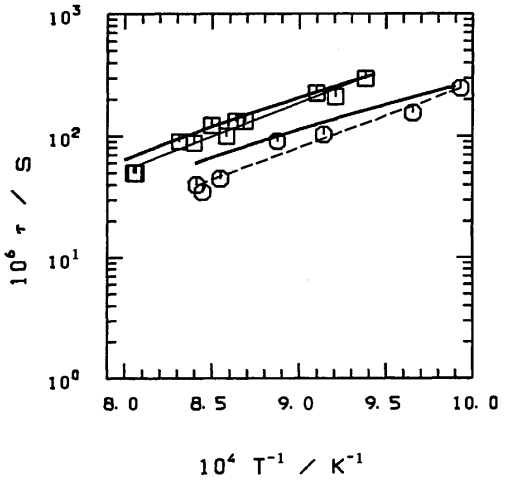

Fig. 4. τ obtained at 121.6 nm vs. $10^4/T$.
Symbols are the same as those in Fig. 3.
Lines through each data point show least squares fit. Thick lines show the values by computer modeling using the reaction mechanism in Table 1.

$$k_1=4.1\times10^{16}\exp(-285\ \mathrm{kJ}/RT)\ \mathrm{cm^3\cdot mol^{-1}\cdot s^{-1}}$$

The reaction mechanism of the 11 elementary reactions shown in Table 1 is the conclusion of this study and the lines in Fig. 3 are the results of modeling, which agree well with the experiment.

Figure 4 shows the relation between the τ values of the absorption by H-atoms and $10^4/T$. Since the absorption by H-atoms is larger than that by O-atoms, the temperatures of the data points are seen to be shifted to a lower region than those by O-atoms shown in Fig. 3. The two thin lines are least-squares fits to the data points. The thick lines are obtained by computer modeling using the reaction mechanism in

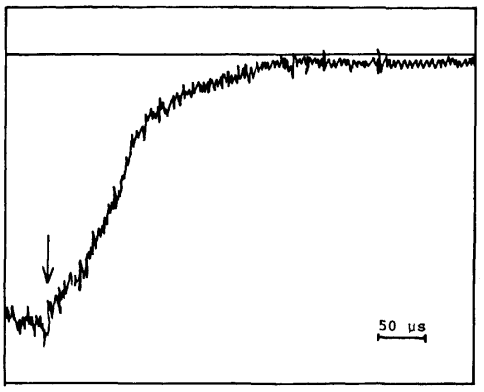

Fig. 5. A sample oscillogram showing the absorption at 121.6 nm by H-atoms.
Test gas: $H_2/O_2/Ar=4.8/1/94.2$
$P_1=20$ Torr, $T_2=1288$ K
The upper line shows the zero-level of the incident light intensity. The arrow shows the shock front.

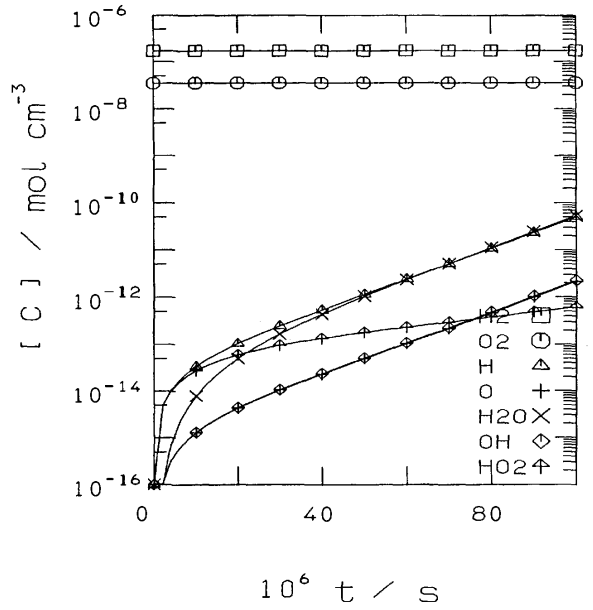

Fig. 6. Computer modeling for the absorption profile shown in Fig. 5.
It is seen that the concentration of H-atoms at 50 μs is above the threshold value of 8.3×10^{-13} mol·cm^{-3}.

Table 1. The threshold value of the H-atoms was assumed to be 8.3×10^{-13} mol·cm^{-3}.[4] Although the relation between experiment and modeling is seen to be good for most the cases, a complete agreement between them was not established.

We could obtain an agreement of the τ values between experiment and modeling for O-atoms and H-atoms as above. Therefore, it can be concluded that the threshold values of concentrations of these two species[4] assumed for modeling are appropriate in the present case.

Figure 5 is an oscillogram showing the absorption of the Lyman-α line obtained at much higher temperatures than that of Fig. 1. The absorption at 50 μs (lab. time) is seen to occur and can be attributed to H-atoms. We compared this with the result by computer modeling using the reaction mechanism in Table 1 under the same experimental conditions of Fig. 5. The concentration profiles of each species thus obtained are shown in Fig. 6. It is seen that the concentration of H-atoms at 50 μs is larger than the threshold value of 8.3×10^{-13} mol·cm^{-3}. If a smaller value was assigned for the k_1, the concentration at 50 μs obtained by modeling fell below the value of the detection limit. The absorption by H-atoms at 50 μs must be unobservable in this case. Therefore, it is confirmable also on the basis of such a degree of absorption that Reaction 1 plays an important role as a chain initiation in the reaction mechanism of H_2-O_2.

It should be pointed out that the present k_1 does not agree with literature values.[1,9] Baulch et al.[9] recommended the k_1 value. The present k_1 is larger than their value extrapolated to the temperature range of this study by almost one order. With regard to the extrapolated k_1 value derived from the k_{-1} by Warnatz,[1] it does not accord with the value in Table 1 either. These literature values are considered to be valid below 1000 K, though not in the present temperature range.

It is also seen from Fig. 6 that the concentrations of reactants, H_2 and O_2, do virtually remain constant even if the reaction passes through the time τ. In accordance with this figure, modeling also indicates that the reaction temperature does not change at all and equals that of the shock front. Such experimental conditions of a constant temperature above 1000 K with very small concentrations of H- and O-atoms continuing a few hundred μs may give a reaction environment to study reactions between such atoms and any interesting species. Therefore, it can be inferred that this study might have introduced a new way of shock tube research using ARAS.

The author wishes to thank Prof. Kihei Morinaga, National Defense Academy, for his useful discussions and continuous encouragement throughout this work. The author wishes also to thank important comments of reviewers concerning the initiation step of the H_2-O_2 reaction.

References

1) J. Warnatz, "Combustion Chemistry," ed. by W. C. Gardiner, Jr., Springer-Verlag (1984).
2) Th. Just, "Shock Waves in Chemistry," ed. by A. Lifshitz, Marcel Dekker (1981).
3) K. M. Pamidimukkala and G. B. Skinner, *J. Chem. Phys.*, **76**, 311 (1982).
4) P. Frank and Th. Just, *Ber. Bunsenges. Phys. Chem.*, **89**, 181 (1985).
5) T. Koike and K. Morinaga, *Bull. Chem. Soc. Jpn.*, **49**, 1457 (1976).

6) D. R. Stull and H. Prophet, "JANAF Thermochemical Tables," 2nd ed., NBS NSRDS 37 (1971).
7) S. M. Hwang, W. C. Gardiner, Jr., M. Frenklach, and Y. Hidaka, *Combust. Flame*, **67**, 65 (1987).
8) S. W. Benson, "Thermochemical Kinetics," 2nd ed., Wiley (1976).
9) D. L. Baulch, D. D. Drysdale, D. G. Horne, and A. C. Lloyd, "Evaluated Kinetic Data for High Temperature Reactions," Vol. 1, Butterworths (1973).

 © 1989 The Chemical Society of Japan Bull. Chem. Soc. Jpn., 62, 2485—2491 (1989)

Gel Filtration Chromatographic Study of Micellar Growth of Polyethylene Glycol Dodecyl Ethers

Noriaki FUNASAKI,* Sakae HADA, and Saburo NEYA
Kyoto Pharmaceutical University, Yamashina-ku, Kyoto 607
(Received February 4, 1989)

The aggregation properties of polyethylene glycol dodecyl ethers ($C_{12}E_n$; n=4, 5, and 8) are investigated with frontal gel (Sephadex G-200 and Sephacryl S-500) filtration chromatography (GFC) at 25 °C. At the trailing boundary of derivative GFC patterns for $C_{12}E_5$, unusual two peaks of micelles appear together with a peak of monomer. These micellar peaks are assigned to two types of micelle, viz., large (R_h=30 nm) and small (R_h=5 nm) micelles. As the $C_{12}E_5$ concentration is increased, the peak height for the large micelle increases more rapidly than that for the small micelle. Analysis of the centroid elution volume data by asymptotic theory reveals that the large micelle is the hexamer of the small micelle. This conclusion is supported by computer simulations of the GFC patterns, based on plate theory. In the derivative pattern of the trailing boundary for $C_{12}E_8$, the micellar peak becomes sharper and shifts to larger elution volume side, with increasing concentration. This pattern is well simulated with the assumption of linear concentration dependence of the micellar elution volume. Micelle size of $C_{12}E_8$ appears to remain constant. For $C_{12}E_4$, which is hydrophobically adsorbed on the gels, huge micelles coexist with a small amount of large micelles (R_h=33 nm).

In spite of the large amount of research that has been carried out by using a number of experimental techniques, it is still a matter of controversy if the aggregation number of nonionic surfactant micelles increases or not with increasing surfactant concentration.[1-17] For polyethylene glycol dodecyl ethers ($C_{12}E_n$) at 25 °C, Tanford et al. reported that micellar growth occurs only at $n \leqq 6$.[1] Hexaethylene glycol dodecyl ether ($C_{12}E_6$) has therefore become one of the most extensively investigated nonionic surfactants.[2] Experimental techniques applied for investigations of pentaethylene glycol ($C_{12}E_5$) and octaethylene glycol ($C_{12}E_8$) dodecyl ethers include static (SLS)[3-8] and dynamic (DLS)[7-9] light scattering, nuclear magnetic resonance (NMR),[8-10] static (SNS)[11,12] and dynamic (DNS)[11] neutron scattering, fluorescence decay (FD),[13] fluorescence quenching (FQ),[13] sedimentation velocity (SV), viscosity (VIS),[1,6] gel filtration chromatography (GFC),[1] electron paramagnetic resonance (EPR),[14,15] vapor pressure osmometry (VPO),[16] and electric birefringence.[17] There is general agreement that the $C_{12}E_8$ micelle little grows at 25 °C, but the contradiction remains unsolved for $C_{12}E_5$. For $C_{12}E_5$, EPR[14] and VPO[16] data were interpreted as showing that the $C_{12}E_5$ micelle remains small independently of concentration, whereas SLS[4,5,8,9] and NMR[8] data suggested that $C_{12}E_5$ micelles are polydisperse and increase with increasing concentration.

Two models for micellar growth have been proposed. One is multiple equilibrium model, which assumes that size of large micelles are highly polydisperse and increases with increasing concentration.[18] The second is secondary aggregation model, which assumes that size of large micelles is almost monodisperse and remains constant independently of concentration.[1,2,8,19] The former model denies the presence of the second critical micelle concentration, whereas the latter predicts it.[19]

The advantage of GFC as well as SV over other techniques is to separate mixtures different in size. For the quantitative analysis of GFC patterns for self-associating systems, the large sample size (frontal) method is generally used.[2,20] The small sample size (zonal) method showed that the $C_{12}E_8$ micelle does not grow with increasing concentration at 25 °C.[1] The $C_{12}E_6$ micelle was investigated by both the zonal and frontal methods. The zonal method showed that this micelle grows.[1] The frontal method showed that small and large micelles coexist in equilibrium with each other.[2]

In this work, we investigate aggregation behavior of $C_{12}E_5$, $C_{12}E_8$, and tetraethylene glycol dodecyl ether ($C_{12}E_4$) by the frontal GFC method at 25 °C. In the derivative elution pattern, only one micellar peak is observed for $C_{12}E_8$, whereas two separate micellar peaks are present for $C_{12}E_5$ and $C_{12}E_4$. These results will be analyzed by the asymptotic and plate theories that we have already developed.[2,20]

Theoretical Basis

Secondary Aggregation Model for Micellar Growth. Multiple equilibrium model, which takes into consideration all aggregated species, will be formally the most comprehensive theory for micelle formation.[18] Secondary aggregation model,[19] which will be described below, may be regarded as a special case of this theory.

A small micelle may be formed from m_1 monomers as follows:

$$\underset{C_1}{m_1 \text{ monomers}} \overset{K_1}{\rightleftarrows} \underset{C_2}{\text{small micelle}} \tag{1}$$

and

$$K_1 = C_2/C_1^{m_1}. \tag{2}$$

A large micelle may be formed by the aggregation of m_2 small micelles:

$$m_2 \text{ small micelles} \underset{C_2}{\overset{K_2}{\rightleftarrows}} \underset{C_3}{\text{large micelle}} \quad (3)$$

and

$$K_2=C_3/C_2^{m_2}. \quad (4)$$

The total concentration C_0 of surfactant may be written as

$$C_0=C_1+C_2+C_3, \quad (5)$$

where all concentrations are expressed on a monomer basis. When m_1 is very large, we can use the approximation of C_1=cmc.

GFC Patterns for Micellar Systems. According to asymptotic theory,[2,20] the centroid volume V_c is defined as

$$V_c=\int_0^{C_0} V\mathrm{d}C/C_0, \quad (6)$$

where V represents the volume flow through the column since introduction of the sample's leading edge. For the above system, V_c can be written as

$$V_c=(C_1V_1+C_2V_2+C_3V_3)/C_0, \quad (7)$$

where V_1, V_2, and V_3 denote the elution volumes of the monomer, the small micelle, and the large micelle, respectively. By using the approximation of C_1=cmc, one can obtain

$$C_2=[C_0(V_c-V_3)+\mathrm{cmc}(V_3-V_1)]/(V_2-V_3) \quad (8)$$

and

$$C_3=[C_0(V_2-V_c)+\mathrm{cmc}(V_1-V_2)]/(V_2-V_3). \quad (9)$$

By using Eqs. 4, 8, and 9, we can determine m_2 and K_2 from GFC elution volume data.

A gel column may be regarded to consist of n successive plates, and each plate is composed of the stationary gel phase and the mobile aqueous phase. This plate theory has been reported for micellar systems in detail.[20] The void volume V_0 and the number n of plates are required for computer-simulation based on this theory. The derivative elution curve provides more detailed information than the original curve.[2,20] For the above micellar system, the plate theory can simulate the derivative pattern.[2,20]

Experimental

Materials. Homogeneous samples of $C_{12}E_8$, $C_{12}E_5$, and $C_{12}E_4$ were obtained from Nikko Chemicals. The purities of these samples were determined to be 99% or more by a Shimadzu GC-8A gas chromatograph. Sephadex G-200 and Sephacryl S-500 were purchased from Pharmacia Fine Chemicals. Blue dextran used for the determination of the void volume was obtained from Pharmacia. Proteins (Sigma) and beads (Dow Chemical Co.) whose hydrodynamic radii R_h (nm) are known were used for the determination of R_h's of micelles; R_h=1.9 (whale myoglobin type II), R_h=3.5 (bovine serum albumin), R_h=4.6 (yeast alcohol dehydrogenase), R_h=8.5 (thyroglobulin), R_h=10.7 (fibrinogen), and R_h=19 (polystyrene carboxylate modified beads). The ion-exchanged water was twice distilled and degassed before use.

Methods. The four columns shown in Table 1 were used, and the flow rate (cm^3h^{-1}) for each column is 6 (A), 8 (B), 24 (C), and 2.3 (D). The temperature of all columns was controlled at 25±0.2 °C. A sample or eluent was charged with a mini-pump. A large volume of sample over the total gel volume V_t was charged so that a plateau region might appear on the elution curve. Elution was monitored continuously with a refractive index monitor and recorded with a Shimadzu Chromatopac C-R1B data processor, except for column D. For the column D experiments the eluate was collected with a fraction collector and the concentration of $C_{12}E_4$ in each fraction was determined by gas chromatography. The refractive index of surfactant solution showed an approximately linear relationship with concentration. When necessary, a correction was made by using the calibration relationship. The derivative of an elution curve was obtained from slopes at appropriate intervals of V. The experimental procedure of GFC has already been reported in detail.[2]

Computer Simulation. Plate theory was used for simulation of the elution curve and its derivative. The equilibria of micellization and partition of a surfactant between the mobile and stationary phases were assumed to be established instantaneously. The simulation procedure has been reported elsewhere.[2,20]

Results and Discussion

$C_{12}E_5$. The dashed line in Fig. 1a shows a typical elution curve in the trailing boundary region for $C_{12}E_5$ (C_0=1.531 mmol dm^{-3}). Since a large amount of a sample was charged, the concentration of $C_{12}E_5$ in the first plateau region was equal to that of the charged sample. The concentration of $C_{12}E_5$ in the second plateau region is close to the cmc values (mmol dm^{-3}), 0.06[21] and 0.064,[22] as we have already predicted theoretically for micellar systems.[20] The derivative of this elution curve (solid line) shows three maxima and two minima. This pattern is unusual, since all GFC derivative patterns reported up to now have only two maxima due to the monomer and the micelle. The first largest peak (V_{3p}) has an elution volume close to the void volume, and therefore, this may be assigned to a large micelle. The last peak (V_{1p}) has a normal elution volume close to the total volume V_t of column A (Table 1). The second peak (V_{2p}) may be due to a small micelle.

To confirm this unusual result, we carried out a similar experiment on column B. As Fig. 1b shows, a very similar derivative pattern was obtained on column B. The first peak appeared near the void volume of column B (Table 1), and the size and shape of the second peak due to a small micelle are close to those on column A, when the difference in V_t between columns A and B is taken into consideration.

Figure 2 shows the derivative pattern for $C_{12}E_5$ as a function of C_0, obtained on column A. The positions of the three peaks little changed with C_0. The

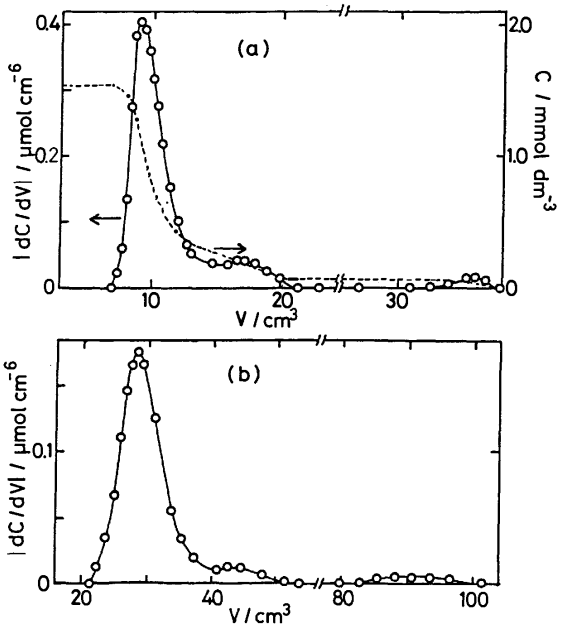

Fig. 1. Elution curve (dashed line) and its derivative (solid line) for $C_{12}E_5$ under two experimental conditions: on column A at C_0=1.5313 mmol dm^{-3} (a) and on column B at C_0=1.530 mmol dm^{-3} (b).

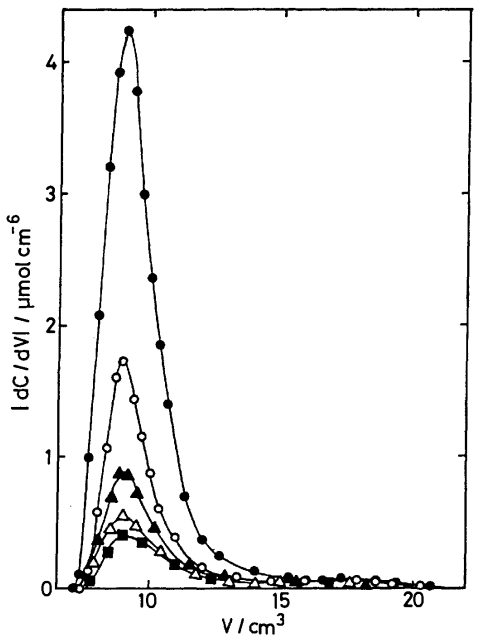

Fig. 2. Derivative elution curves for $C_{12}E_5$ on column A at five charged concentrations (C_0/ mmol dm^{-3}): 1.5313 (■); 1.8829 (△); 2.5676 (▲); 4.2537 (○); 10.6343 (●). The monomer region is omitted.

Table 1. Characteristics of the Columns Used

Column	Gel	Total volume	Void volume	Surfactant
		cm^3	cm^3	
A	G-200	30.2	9.5	$C_{12}E_5$
B	G-200	84.4	30.2	$C_{12}E_5$, $C_{12}E_8$
C	S-500	28.9	9.2[a]	$C_{12}E_4$, $C_{12}E_5$
D	G-200	31.2	9.8	$C_{12}E_4$

a) Estimated as the total volume multiplied by 0.32.

Table 2. Aggregation Numbers and Hydrodynamic Radii of $C_{12}E_5$ Micelles in Dilute Solution at 25 °C

C	m	R_h	Method	Reference
mmol dm^{-3}		nm		
cmc	3270		SLS	4
3.4	3600		SLS	5
cmc	2850	25.2	SLS, NMR	8
7.38		16.2	NMR	9
24.6		28	NMR	10
20%		2.3	EPR	14
cmc	112		VPO	16
		4.9[a]	GFC	This work
9.82		30[b]	GFC	This work

a) Estimated from V_2 for the small micelle. b) Estimated from the micellar peak for the large micelle by using column C.

height of the monomer peak remained unchanged with C_0, whereas those of the small and large micelles increased with increasing C_0 little and markedly, respectively.

Table 2 summarizes the literature values of m and R_h in dilute solution at 25 °C. These m values are very large, and consequently we can use the phase separation approximation, C_1=cmc. The simplest model which may apply to the results shown in Fig. 2 is the secondary aggregation model described in the Theoretical Basis section. Substitution of Eqs. 8 and 9 into Eq. 4 yields

$$\log[C_0(V_2-V_c)+\mathrm{cmc}(V_1-V_2)]=m_2\log[C_0(V_c-V_3)+\mathrm{cmc}(V_3-V_1)]+\log K-(m_2-1)\log(V_2-V_3) \quad (10)$$

The V_c value can be determined from both the leading and trailing boundaries of a frontal elution curve. Since these V_c values were close, we used the average of them. The centroid volumes, V_2 and V_3, of the small and large micelles are expected to be close to the corresponding peak volumes, V_{2p} and V_{3p}. The difference in V between the centroid and the peak stems from both asymmetry of the peak and the concentration dependence of the peak position. Furthermore V_1 should be close to V_c at infinite dilution, whereas V_3 should be close to V_c at infinite concentration. By employing values of V_1=35.5 cm^3, V_2=17.0 cm^3, V_3=9.5 cm^3, and cmc=0.06 mmol dm^{-3}, we plotted the V_c data on column A according to Eq. 10 in Fig. 3. By the least-squares method, we obtained values of m_2=6.04 and K_2=6.25 (mmol dm^{-3})$^{-5.04}$. From this m_2 value we can suggest that the large micelle of $C_{12}E_5$ is the hexamer of the small micelle.

Computer Simulation of GFC Patterns for $C_{12}E_5$. The computer simulation of GFC patterns based on plate theory has become a useful tool for investigating

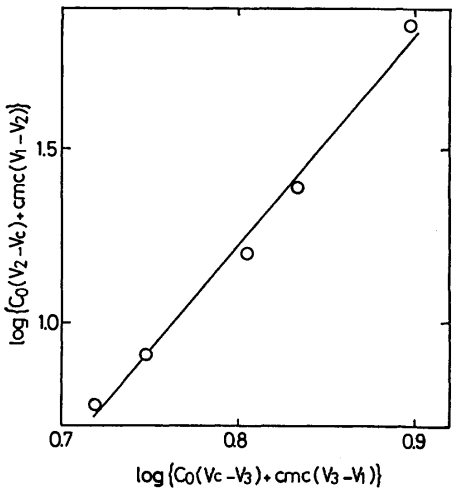

Fig. 3. Centroid volume data plotted according to Eq. 10 for $C_{12}E_5$ by using values of V_1=35.5 cm^3, V_2=17.0 cm^3, V_3=9.5 cm^3, and cmc=0.06 mmol dm^{-3}.

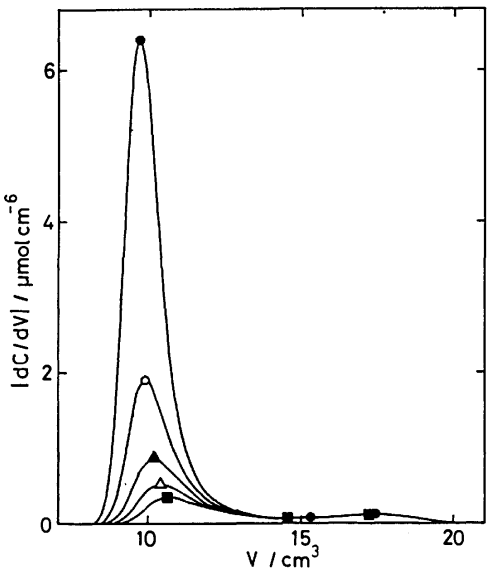

Fig. 4. Computer-simulated derivative patterns for $C_{12}E_5$ at the concentrations corresponding to Fig. 2. Input data used for the simulation: n=100, V_0=7.0 cm^3, V_1=35.5 cm^3, V_2=17.0 cm^3, V_3=9.5 cm^3, m_2=6, K_2=6.25 (mmol dm^{-3})$^{-5}$, and cmc=0.06 mmol dm^{-3}.

the aggregation properties of surfactants.[2,20,23] Taking into the literature m values (Table 2), we used values of m_1=500 and m_2=6. The elution volumes estimated above, V_1=35.5 cm^3, V_2=17.0 cm^3, and V_3=9.5 cm^3 were also used below. A K_1 value of 5×10^{606} (mmol dm^{-3})$^{-499}$ were estimated from the equation,[20] K_1=cmc$^{1-m_1}$/($2m_1$), by using cmc=0.06 mmol dm^{-3} and m_1=500. A K_2 values of 6.25 (mmol dm^{-3})$^{-5}$ were used. As fitting parameters, we used V_0=7.0 cm^3 and n=100. Figure 4 shows the computer simulated GFC patterns of $C_{12}E_5$, corresponding to the experimental ones (Fig. 2). Very close patterns were obtained by using cmc=0.06 mmol dm^{-3} (phase separation model), without using the m_1 and K_1 values, though they are not shown.

In Fig. 4 two peaks for small and large micelles are reproduced. This result differs from that of $C_{12}E_6$; the GFC derivative patterns for $C_{12}E_6$ had only one peak for the micelle, and the micellar elution volume decreased markedly with increasing C_0.[2] These different patterns can be ascribed to the difference in m_2; m_2=6 for $C_{12}E_5$ and m_2=2 for $C_{12}E_6$. The computer simulations based on plate theory correspond to the experimental GFC patterns for these surfactants. Furthermore we recall that asymptotic theory predicts only one peak at m=2 and two peaks at $m\geqq3$ for the monomer-m-mer system.[20] For the small micelle, both the observed and simulated values of V_{2p} slightly increased with increasing C_0, but the height simulated is larger than the observed one. For the large micelle, the simulated V_{3p} value decreased with increasing C_0 more rapidly than the observed one. Considering the inaccuracies in both experiment and theory, we did not attempt further improvements of fitting.

The hydrodynamic radius R_h of a species can be estimated from its elution volume V_e by using a calibration relationship between R_h and V_e for the proteins described in the Experimental section. For the small micelle of $C_{12}E_5$, we obtained values of R_h=5.0 nm (C_0=1.531 mmol dm^{-3}, on column A) and R_h=5.3 nm (C_0=1.530 mmol dm^{-3}, on column B) from their V_{2p} values, and a value of R_h=4.9 nm from V_2=17.0 cm^3. For the large micelle of $C_{12}E_5$, we could not determine the R_h value from the Sephadex G-200 data,since V_{3p} and V_3 were close to the exclusion limit of R_h for this gel. By using column C (Sephacryl S-500), we estimated a value of R_h=30 nm (C_0=9.816 mmol dm^{-3}).

$C_{12}E_8$. For $C_{12}E_8$ at 25 °C, there is general agreement that the micelle size little changes with C_0.[1,3,6-13,16]

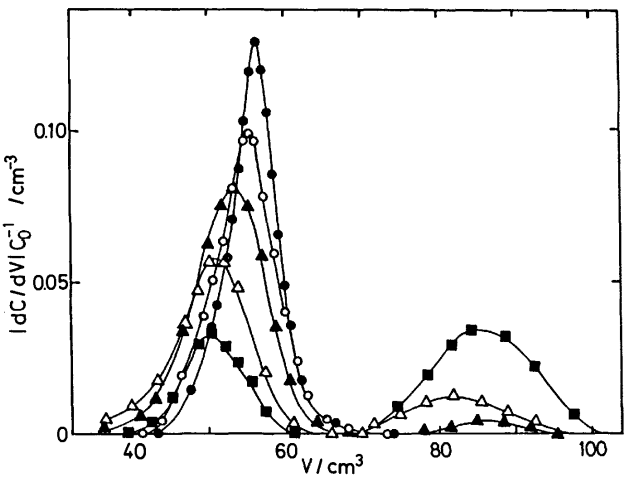

Fig. 5. Reduced derivative patterns for $C_{12}E_8$ at five charged concentrations (C_0/mmol dm^{-3}): 0.164 (■); 0.329 (△); 0.986 (▲); 21.655 (○); 42.336 (●).

Table 3 summarizes the literature values of m and R_h in dilute solution at 25 °C. The derivative patterns for $C_{12}E_8$ at the trailing boundary are shown in Fig. 5, where the ordinate is divided by C_0 for representing the GFC data in a wide range of C_0. As expected, there appeared a single peak of the micelle. As we have shown theoretically, the concentration dependence of the micellar peak V_{mp} is rather complicated;[24] when m is large enough, like $C_{12}E_5$, V_{mp} increases slightly with increasing C_0. The increase of V_{mp} shown in Fig. 5 is much larger than that predicted by plate theory. Furthermore the peak height of the micelle should be roughly proportional to C_0 at high concentrations, and consequently the peak divided by C_0 should have a constant height. As Fig. 5 shows, the micellar peak at C_0=42.336 mmol dm^{-3} is higher than that at C_0=21.655 mmol dm^{-3}. Though the reason has not yet been clarified, the peak position V_p sometimes increases with increasing C_0.[25] Then, as C_0 increases, the leading peak becomes broader, whereas the trailing peak becomes sharper.[20,26] These tendencies have been explained on the basis of plate theory for a nonassociable protein.[26] Values of cmc were reported to be 0.11[22] and 0.07 mmol dm^{-3}.[27]

Taking into consideration the above-mentioned results, we computer-simulated the derivative curve by using the following values; V_0=5.0 cm^3, V_1=83.8 cm^3, V_2=0.0822C_0+51.93 cm^3, and cmc=0.10 mmol dm^{-3}. The derivative patterns thus computed are shown by dashed lines. The solid lines were computed by using the mass action model; values of m=100 and K=4.9×10^{96} (mmol dm^{-3})$^{-99}$ were used instead of the cmc value (phase separation model). Though the difference between the solid and dashed lines is minor, the solid line is closer to the observed value than the dashed line. These computed patterns well reproduce the observed results (Fig. 5). Therefore, the increase of the micellar elution volume does not reflect true changes in micelle size.

The R_h value for the $C_{12}E_8$ micelle might be estimated to be 3.8 nm from the V_{2p} value at C_0=42.336 mmol dm^{-3}. For the monomer-m-mer system we have shown that the elution volume at infinite concentration corresponds to the true R_h value for the m-mer.[24] Therefore "true" R_h value for the $C_{12}E_8$ micelle may be smaller than 3.8 nm, as have been reported by other workers (Table 3).

$C_{12}E_4$. For $C_{12}E_4$ at 25 °C, values of cmc=0.04,[28] 0.046,[16] and 0.064[22] mmol dm^{-3} and R_h=180 nm (SLS)[29] have been reported. On two columns, columns C and D, we investigated the GFC patterns of $C_{12}E_4$. In the elution pattern of this surfactant, the concentration at the first plateau region was smaller than the initially charged concentration C_0, as shown in Figs. 7a (Sephadex G-200) and 7b (Sephacryl S-500). For the both columns the concentration at the second plateau region was close to the cmc and the V_1 value was much larger than the V_t value (Table 1). The

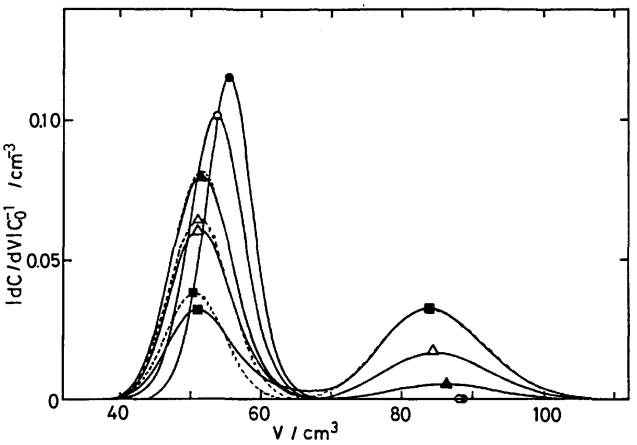

Fig. 6. Computer-simulated reduced derivative patterns for $C_{12}E_8$ at the five concentrations corresponding to Fig. 5. Input data used for the simulation according to two models: for mass action model (solid lines), n=120, V_0=5.0 cm^3, V_1=83.8 cm^3, V_2=0.0822C_0+51.93 cm^3, m=100, and K=4.9×10^{96} (mmol dm^{-3})$^{-99}$; for phase separation model (dashed lines), cmc=0.10 mmol dm^{-3} and the same values of n, V_0, V_1, and V_2.

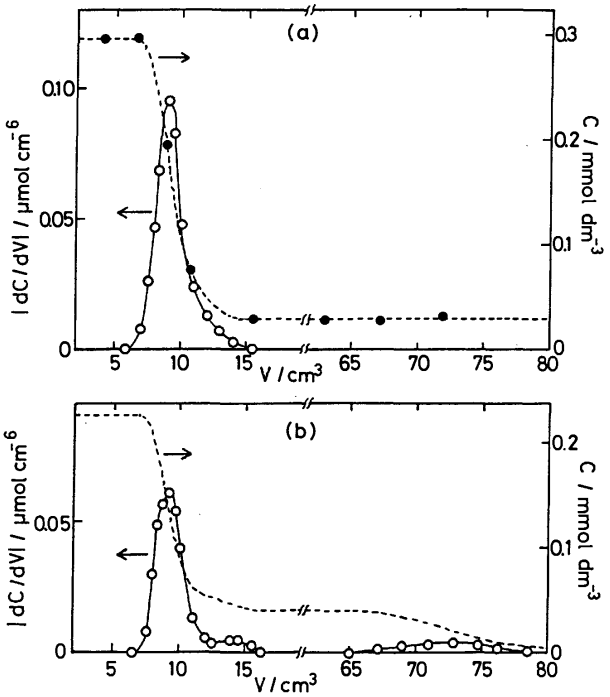

Fig. 7. Elution curves (dashed lines) and their derivatives (solid lines) for $C_{12}E_4$ under two experimental conditions: column D and C_0=0.508 mmol dm^{-3} (a); column C and C_0=0.276 mmol dm^{-3} (b).

latter fact indicates that the $C_{12}E_4$ monomer is adsorbed on the gels. This adsorption is ascribed to the hydrophobicity of $C_{12}E_4$. The reason for the reduction of concentration in eluate below C_0 may be ascribed to the adsorption or the clogging of huge micelles of $C_{12}E_4$ to the gel network. On Sephacryl S-500, the large peak appeared near the void volume

Table 3. Aggregation Numbers and Hydrodynamic Radii of $C_{12}E_8$ Micelles in Dilute Solution at 25 °C

C / mmol dm^{-3}	m	R_h / nm	Method	Reference
cmc	120	3.6	SV	1
cmc		3.5	GFC, VIS	1
8.2	97		GFC, SLS	3
cmc	62	2.8	SLS, VIS	6
cmc	120	3.4	SLS, DLS	7
cmc	90	3.0	SLS, NMR	8
9.3		3.3	NMR	9
cmc		3.1	NMR	10
2.5%	90	3.1	SNS, DNS	11
28	82	3.0	SNS	12
7	92		FD	13
3%	105		FQ	13
cmc	39		VPO	16
42.34		3.8[a)]	GFC	This work

a) Estimated from the micellar peak shown in Fig. 5. The "true" value is expected to be smaller.

(Table 1) and the small peak has a value of R_h=33 nm. On Sephadex G-200, a single peak appeared near the void volume of this column, since all micelles of $C_{12}E_4$ are too large as compared with the gel pores.

Micellar Growth of Polyethylene Glycol Dodecyl Ethers at 25 °C. As Table 2 shows, VPO and EPR data on $C_{12}E_5$ have been interpreted as showing that small micelles form independently of C_0 above the cmc.[14,16] On the other hand, the NMR and SLS data (Table 2) suggested that large micelles form and grow with increasing C_0.[4,5,8-10] A similar controversy continues for $C_{12}E_6$.[2]

Our present and previous researches clearly showed that micellar size of $C_{12}E_4$, $C_{12}E_5$, $C_{12}E_6$, and $C_{12}E_8$ increases with a decrease of the polyoxyethylene chain length and with increasing C_0 except for $C_{12}E_8$ this result is consistent with others.[1,3,6-13,16] However our result on $C_{12}E_8$ does not show that smaller micelles do not form at very low concentrations, especially near the cmc. Very small m values have been reported, as shown in Table 3.[6,16] This discrepancy in m may stem from the difference in the extrapolation procedure of low concentration data to the cmc.

Our GFC data on $C_{12}E_5$ clearly indicate that small micelles coexist with large micelles. This result was analyzed in terms of the secondary aggregation model, viz., by assuming that sizes of these micelles are independent of C_0. This assumption may be valid in the concentration range which we investigated (C_0= 1.53—10.4 mmol dm^{-3}). Outside this range, smaller or larger micelles may form.

The molecular lengths of $C_{12}E_4$, $C_{12}E_5$, and $C_{12}E_8$ in the most stretched conformation are 3.2 nm, 3.5 nm, and 4.4 nm, respectively. From comparison between these values and R_h's, the $C_{12}E_8$ micelle is almost spherical and all the $C_{12}E_4$ and $C_{12}E_5$ micelles are nonspherical (probably rodlike).

The most important conclusion in this work is that the small and large micelles coexist for $C_{12}E_4$ and $C_{12}E_5$.

List of Symbols.

C_0; Total concentration of surfactant on a monomer basis
C_1; Monomer concentration of surfactant
C_2; Concentration of small micelles on a monomer basis
C_3; Concentration of large micelles on a monomer basis
K_1; Equilibrium constant of formation of small micelles from monomers
K_2; Equilibrium constant of formation of large micelles from small micelles
m; Number of monomers in a micelle
m_1; Number of monomers in a small micelle
m_2; Number of small micelles in a large micelle
n; Number of plates or number of oxyethylene units
V_0; Void volume
V_1; Centroid elution volume of monomers
V_2; Centroid elution volume of small micelles
V_3; Centroid elution volume of large micelles
V_c; Overall centroid elution volume
V_t; Total volume of gel bed
V_{1p}; Peak position of monomers in the derivative pattern
V_{2p}; Peak position of small micelles in the derivative pattern
V_{3p}; Peak position of large micelles in the derivative pattern

Thanks are due to Ms. M. Abe for technical assistance.

References

1) C. Tanford, Y. Nozaki, and M. F. Rohde, *J. Phys. Chem.*, **81**, 1550 (1977).
2) N. Funasaki, S. Hada, and S. Neya, *J. Phys. Chem.*, **92**, 3488 (1988) and references cited therein.
3) S. Maezawa, Y. Hayashi, J. Ishii, K. Kameyama, and T. Takagi, *Biochim. Biophys. Acta*, **747**, 291 (1983).
4) N. Nishikido, M. Shinozaki, G. Sugihara, and M. Tanaka, *J. Colloid Interface Sci.*, **82**, 352 (1981).
5) M. Okawauchi, M. Shinozaki, Y. Ikawa, and M. Tanaka, *J. Phys. Chem.*, **91**, 109 (1987).
6) T. Sato, Y. Saito, and I. Anzai, *J. Chem. Soc., Faraday Trans. 1*, **84**, 275 (1988).
7) M. Corti, C. Minero, and V. Degiorgio, *J. Phys. Chem.*, **88**, 309 (1984).
8) W. Brown, Z. Pu, and R. Ryahen, *J. Phys. Chem.*, **92**, 6086 (1988).
9) T. Kato, S. Anzai, S. Takano, and T. Seimiya, Proceedings of the 39th Sympsium on Colloid and Interface Chemistry, the Chemical Society of Japan (1986), p. 160.
10) P. G. Nilsson, H. Wennerström, and B. Lindman, *J. Phys. Chem.*, **87**, 1377 (1983).
11) M. Zulauf, K. Weckström, J. B. Hayter, V. Degiorgio, and M. Corti, *J. Phys. Chem.*, **89**, 3411 (1985).
12) L. Magid, R. Triolo, and J. S. Johnson, Jr., *J. Phys. Chem.*, **88**, 5730 (1984).
13) W. Binana-Limbele and R. Zana, *J. Colloid Interface Sci.*, **121**, 81 (1988).
14) J. M. DiMeglio, L. Paz, M. Dvolaitzky, and C. Taupin, *J. Phys. Chem.*, **88**, 6036 (1984).
15) D. O. Lasic, *J. Colloid Interface Sci.*, **113**, 188 (1986).
16) T. M. Herrington and S. S. Sahi, *J. Colloid Interface Sci.*, **121**, 107 (1988).

17) P. G. Nesson and R. Jennings, *Faraday Discuss. Chem. Soc.*, **76**, 353 (1983).
18) J. M. Corkill, J. F. Goodman, T. Walker, and J. Wyer, *Proc. R. Soc. London, Ser.* A, **312**, 243 (1969). P. Mukerjee, *J. Phys. Chem.*, **76**, 565 (1972). R. J. M. Tausk and J. Th. G. Overbeek, *Biophys. Chem.*, **2**, 175 (1974). P. J. Missel, N. A. Mazer, G. B. Benedek, C. Y. Young, and M. C. Carey, *J. Phys. Chem.*, **84**, 1044 (1980). E. Y. Sheu, S.-H. Chen, and J. S. Huang, *J. Phys. Chem.*, **91**, 3306 (1987).
19) P. H. Elworthy and C. B. MacFarlane, *J. Chem. Soc.*, **1963**, 907. S. Ikeda, "Surfactants in Solution," ed by K. L. Mittal and B. Lindman, Vol. 2, Plenum, New York (1984), p. 825. T. Imae, R. Kamiya, and S. Ikeda, *J. Colloid Interface Sci.*, **108**, 215 (1985). S. Ikeda, S. Ozeki, and K. Kakiuchi, *J. Phys. Chem.*, **92**, 3465 (1988). G. Porte, Y. Poggi, J. Appell, and G. Maret, *ibid.*, **88**, 5713 (1984). W. H. Richtering, W. Burchard, E. Jahns, and H. Finkelmann, *ibid.*, **92**, 6032 (1988).
20) N. Funasaki, S. Hada, and S. Neya, *Bull. Chem. Soc. Jpn.*, **62**, 380 (1989).
21) H. Lange, *Kolloid Z.*, **201**, 131 (1965).
22) M. J. Rosen, A. W. Cohen, M. Dahanayake, and X. Hua, *J. Phys. Chem.*, **86**, 541 (1982).
23) T. Nakagawa, *Yukagaku*, **20**, 277 (1971).
24) N. Funasaki, S. Hada, and S. Neya, *Bull. Chem. Soc. Jpn.*, **61**, 2961 (1988).
25) G. K. Ackers, *Adv. Protein Chem.*, **24**, 343 (1970).
26) D. J. Winzor and L. W. Nichol, *Biochim. Biophys. Acta*, **104**, 1 (1965).
27) K. Meguro, Y. Takasawa, N. Kawahashi, Y. Tabata, and M. Ueno, *J. Colloid Interface Sci.*, **83**, 50 (1981).
28) M. J. Schick, *J. Colloid Sci.*, **17**, 801 (1962).
29) H. Hoffmann, H. S. Kielman, D. Pavlovic, and G. Platz, *J. Colloid Interface Sci.*, **80**, 237 (1981).

Studies on the Area-Temperature Isobars of Insoluble Monolayers at the Air/Water Interface. I. Development of a Microcomputer-Controlled Instrument for Measuring Precise Area-Temperature Isobars[1)]

Teiji KATO,* Tatsushi WAKANA, Katsunori OHSHIMA, and Katsuhiro SUZUKI
Department of Applied Chemistry, Faculty of Engineering, Utsunomiya University, 2753, Ishii-machi, Utsunomiya 321
(Received February 25, 1989)

A microcomputer-controlled instrument for measuring precise area-temperature (A-T) isobars of insoluble monolayers at the air/water interface was developed. To obtain precise A-T isobars, leakage or dissolution of film material must be checked. Before starting A-T isobar measurements, area or structural relaxations must be completed. A-T isobars of monolayers of cadmium eicosanoate, L-α-dipalmitoyl phosphatidylcholine (DPPC), trioctadecanoyl glyceride (TOG), and *cis*-9-octadecen-1-ol were measured. Precise A-T isobars can afford two-dimensional isobaric thermal expansivities of insoluble monolayers by differentiation with respect to temperature. The thermal expansivities were evaluated as around 9.0×10^{-4} K^{-1} for condensed monolayers and around 30×10^{-4} K^{-1} for liquid-expanded monolayers.

According to Crisp or Gaines,[2)] the number of degrees of freedom of a system of an insoluble monolayer on the water surface is given by the following equation,

$$F=C^{B}+C^{S}-P^{B}-q+3, \quad (1)$$

where F=number of degrees of freedom, C^{B}=number of components in bulk and equilibrated throughout the system, C^{S}=number of components confined to the surface, P^{B}=number of bulk phases, and q=number of surface phases in equilibrium with one another. In the derivation of the phase rule, it was assumed that film material should be confined completely to the surface phase and neither dissolution nor vaporization of film material should occur.

In the case of a single component monolayer, as $C^{S}=1$, $C^{B}=2$ (water and gas) and $P^{B}=2$ (a liquid and a gas phase), the number of degrees of freedom of the system is given as follows:

$$F=2+1-2-q+3=4-q. \quad (2)$$

There are three degrees of freedom when the monolayer consists of one surface phase. They are external pressure (three-dimensional), temperature and surface pressure (two-dimensional). Since experiments on insoluble monolayers are usually performed under atmospheric pressure, external pressure is dealt with not as a variable but rather as a constant (fixed to the atmospheric pressure). There is another experimental variable used usually, i.e., molecular area which can be changed by moving barriers confining the insoluble monolayer. There are three ways to take two variables from three, and there are three types of experiments on insoluble monolayers. The first is the surface pressure-area (π-A) isotherm where surface pressure is measured as a function of the molecular area, keeping temperature constant. The second is the area-temperature (A-T) isobar where the molecular area is measured as a function of temperature, keeping surface pressure constant. The third is the surface pressure-temperature (π-T) isochore or isoarea where surface pressure is measured as a function of temperature, keeping molecular area constant. π-A isotherms are the most popular and the most widely used thermodynamic measurements of insoluble monolayers. But it is very difficult to measure precise A-T isobars or π-T isochores because dissolution of film material into the subphase water or leakage of the film material through corners of barriers, even in a very small amount, will introduce fatal errors to the results. There are only a few papers reporting A-T isobars,[3,4)] and no reports on π-T isochores.

This paper reports development of a micromputer-controlled instrument for measuring A-T isobars of insoluble monolayers at the air/water interface and discusses procedures to obtain precise A-T isobars using this instrument. A-T isobars of some amphiphilic materials were measured with this instrument and two-dimensional isobaric thermal expansivities calculated from the isobars are also reported.

Experimental

Materials. L-α-Dipalmitoylphosphatidylcholine (DPPC, synthetic, 99+%), trioctadecanoyl glyceride (TOG, 99%) eicosanoic acid (99%), and *cis*-9-octadecen-1-ol (99%) were purchased from Sigma Chemicals and were used as film materials without further purification. Spectro-grade benzene, hexane, chloroform, ethanol, and methanol were used as spreading solvents. They were purchased from Wako Chemicals and were used without further rectification. Water for subphase was distilled using an all Pyrex distillation apparatus. Guaranteed grade sulfuric acid (Wako Chemicals) was used to adjust pH of the subphase water. Guaranteed grade cadmium acetate (Wako Chemicals) was used to prepare 10^{-3} M (1M=1 mol dm^{-3}) subphase for monolayers of eicosanoic acid.

Instrumentation. Figure 1 shows a block diagram of the instrument developed. Signals from two Wilhelmy-type surface balances and sheath platinum wire resistance thermometers were A/D converted and inputed into a 16-bit microcomputer (PC-286V, Epson). The microcomputer

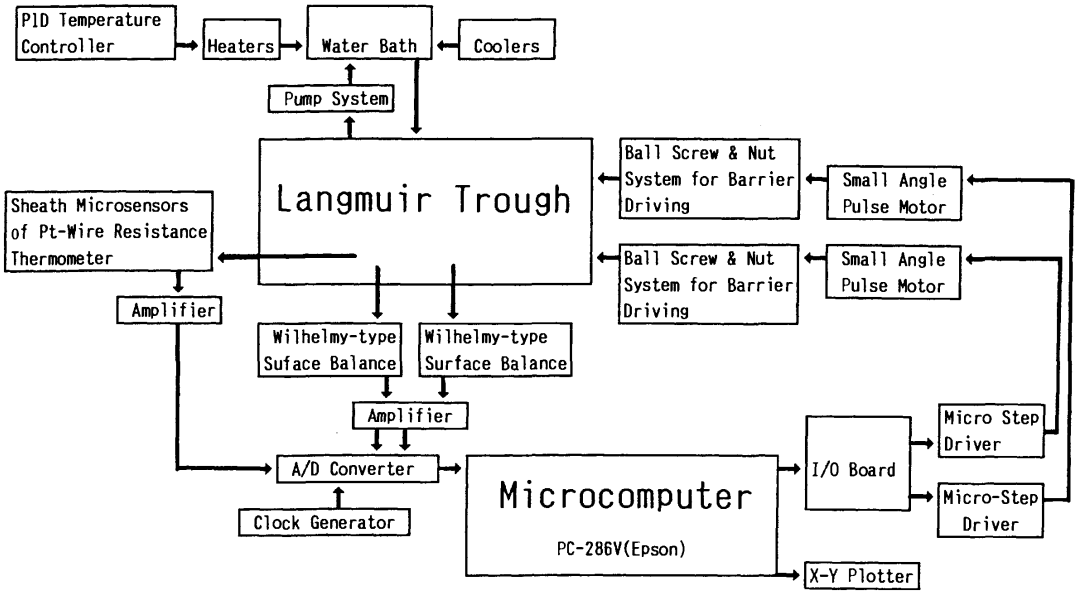

Fig. 1. Block diagram of the instrument.

feedback-controlled the monolayer surface pressure and maintained it strictly constant, based on the signals from the two surface balances by the method stated below. Temperature of subphase water was changed by circulating temperature controlled water from a water bath, which was equipped with control-heaters and coolers, through in a double-bottomed Langmuir trough. The monolayer temperature was measured with thin sheath microsensors of platinum wire resistance thermometers (sheath diameter=0.5 mm, element wire diameter=50 μm, 100 ohm), whose vertical position could be finely adjusted using a rack-and-pinion device.

The surface pressure of a monolayer must be strictly constant during an A-T isobar measurement. But it is difficult to keep it constant, based on signals from a single Wilhelmy-type surface balance because the zero-point of the balance itself changes with changing temperature of the subphase water. There are three reasons for drift of the zero point of the surface balance with changing temperature, i.e., changes of surface tension and density of subphase water, change of position of water surface by evaporation, and change of the dimensions of the Langmuir trough itself by thermal expansion. To overcome these difficulties, this instrument was equipped with two Wilhelmy-type surface balances; one was located in the monolayer-covered water area and another was in the clean water area. The microcomputer feedback-controlled positions of two barriers confining the monolayer through an I/O and a control boards (SMBMP, San-ei Electric Co., Ltd.), micro-step drivers (FD-5500WS, San-ei Electric Co., Ltd.), small-angle pulse motors (Vexta, Oriental Motors Co., Ltd.) and ball-screw and nut systems, to maintain the difference of outputs of the two surface balances constant. By this means, all causes of the zero-point drift of the surface balances with changing temperature could be cancelled completely and the pressure could be kept strictly constant during A-T isobar measurements. Four control parameters (the trigger interval, the real-time smoothing number, the surface compressibility of a monolayer and the feedback gain) were also used to control the surface pressure precisely.[5] Pressure fluctuation during the A-T isobar measurements was controlled within ± 0.15 mN m^{-1} in general. The spreading technique of monolayers restricted reproducibility in the molecular area of the A-T isobars and it was $\pm 1.0\%$ but the fluctuation in area during measurements was ± 0.001 nm^2 molecule^{-1} at most. These fluctuations were much less than those reported in previous A-T isobar measurements.[3]

A very shallow-type Langmuir trough was constructed using long rectangular rods of Teflon on a double-bottomed brass base which was coated with a thin pressure-sensitive Teflon adhesive sheet (inside dimensions of the trough, 80×16×0.4 cm). Only 600 ml of subphase water was required for the reason that the heat capacity of the system should be as small as possible to effect temperature change of the system rapidly.

Leakage and/or dissolution of the monolayers introduces serious errors into the A-T isobar. It is difficult to prevent leakage of monolayers at higher surface pressures and at higher temperatures by conventional rectangular barriers. The barriers used for this instrument were made from Teflon and have recesses of 1.5 mm depth in both ends to fit the inside width of the rims of the Langmuir trough (Fig. 2 (a)). Moreover, the barriers were equipped with flexible Teflon sheet-made skirts at the four corners of the recesses which slided smoothly without leakage of film molecules even when the temperature of the system changed widely (Fig. 2 (b) and (c)).

Dissolution of film material must be also avoided. Since film dissolution is a rate process and is accelerated by increasing temperature, the time that the film material is at high temperature must be short. Thus, the rates of temperature rising and lowering should be as high as possible to minimize the effect of dissolution. In this instrument, the maximum rate of temperature change was about 2 °C min^{-1} on average. Dissolution of film material can be checked by comparing an A-T isobar obtained at temperature rising with one at temperature lowering. If the two isobars coincide well with one other, we can confirm that there was no leakage or dissolution of the film material during measurement.

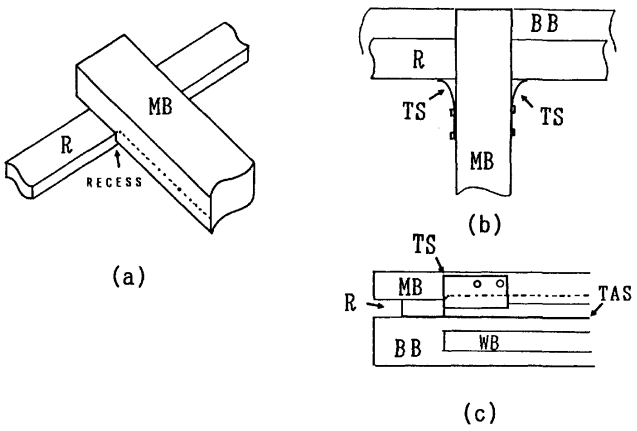

Fig. 2. Structure of the barriers used. (a) Fitness of the recesses of the barriers with rims of the Langmuir trough. (b) Top view of the barrier with flexible Teflon sheet-made skirts which slide smoothly against rims of the Langmuir trough. (c) Side view of the barrier and the trough. MB: moving barrier, R: rim of the Langmuir trough, TS: Teflon-made skirt, TAS: Teflon adhesive sheet, BB: brass base, WB: water bath, ----: water level.

Precise A-T isobars can afford two-dimensional isobaric thermal expansivities by differentiation with respect to temperature. If there is no phase transition of the film material in the temperature range measured, the isobar will appear as a straight line as a whole, and hence it is easy to calculate the thermal expansivity by numerical differentiation with respect to temperature using linear regression analysis. If there are some phase transitions, the A-T isobar has some kinks. Correlation factors of the linear regression analysis are also calculated. All results are finally sent to an X-Y plotter for drawing normalized figures.

Results and Discussion

Dissolution. Figure 3 shows A-T isobars of DPPC at 40 mN m^{-1} exhibiting the effect of partial dissolution at higher temperature. The monolayer of DPPC was spread from a mixed solvent solution of hexane and ethanol (9:1 in volume) on pH 2 water. A Cloehn microsyringe of a gas-tight type which was connected to a synchronous motor-driven micrometer was used to administer the desired quantity of the spreading solution. The temperature was raised up to 45 °C at a rate of 2 °C min^{-1} and was kept constant there for 40 min, then lowered to 10 °C at the same rate. A phase transition begins at 42 °C. Dissolution of DPPC molecules occurred at the higher temperature and the A-T isobar measured under temperature lowering shifted downward about 4% in molecular area. The two isobars, however, were almost parallel below 42 °C, and this means that dissolution may be neglected in this temperature span.

Many of the A-T isobars of film materials forming stable insoluble monolayers could be measured up to about 45 °C without taking into account the dissolution under the conditions of this high rate of temperature change.

Area or Structural Relaxation. Figure 4 shows A-T isobars of an eicosanoic acid monolayer at 10 mN m^{-1} on water containing 10^{-3} M cadmium acetate. The monolayer was spread from a benzene solution. There are two isobars shown in the figure. Curves (a) and (b) are isobars measured with the temperature rising and lowering, respectively. The discrepancy between isobars (a) and (b) shows an area-relaxation effect of the monolayer.

An insoluble monolayer after just being compressed to a certain high pressure at low temperatures is in some unstable state and exhibits a tendency to relax to a more stable closed-packed state with time. The relaxation time depends on many factors, such as temperature, surface pressure, pH or ion types in the subphase etc. In general, the relaxation time is very long at low temperatures and at high pressures. Moreover, the relaxation takes longer time in a solid state than in a liquid state. Cadmium eicosanoate

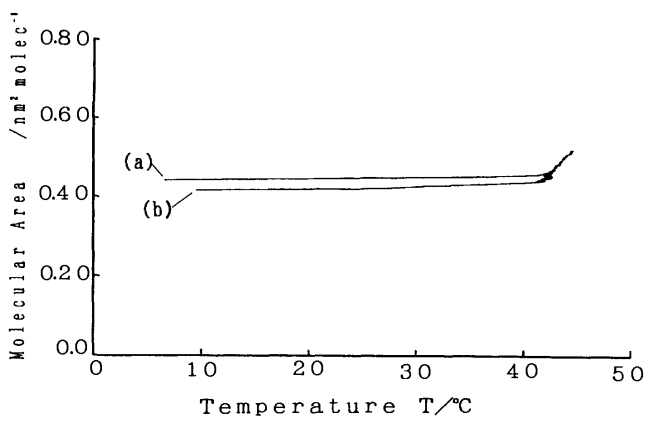

Fig. 3. A-T isobars of DPPC at 40 mN m^{-1} showing partial dissolution of the film material. (a) A-T isobar of DPPC measured at temperature rising. (b) A-T isobar of DPPC measured at temperature lowering, after keeping at 45 °C for 40 min.

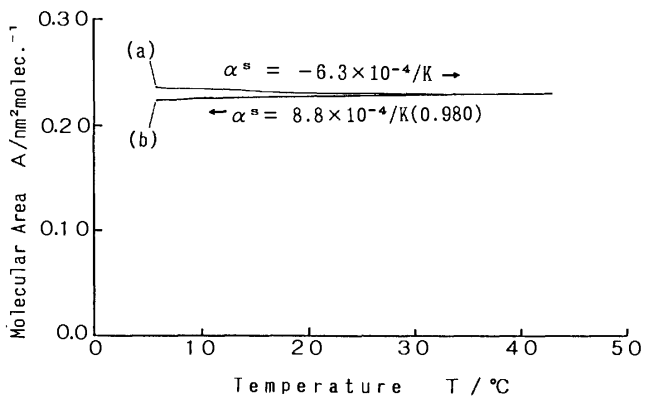

Fig. 4. A-T isobars of an eicosanoic acid monolayer at 10 mN m^{-1} on 10^{-3} M cadmium acetate showing the "thermally stimulated area relaxation" effect. (a) A-T isobar measured with the first rising of temperature without "isobaric thermal treatment." (b) A-T isobar measured with the temperature lowering. (See text.)

(see Fig. 4) is in a solid state in monolayers at 10 mN m^{-1}, and it takes very long time to relax especially at the starting low temperature of the A-T isobar measurement. The relaxation time becomes shorter as the temperature increases, and curve (a) gradually approaches curve (b) which exhibits no relaxation effect. It can be considered that curve (b) shows the true isobar of a cadmium eicosanoate monolayer under these conditions. The thermal expansivity calculated from isobar (a) was negative as shown in Fig 4. Curve (a) shows a "temperature accelerated" or "thermally stimulated" area relaxation process of the insoluble monolayer.

It is very interesting to point out that the discrepancy of the isobars (a) and (b) at 6 °C, about 5% in molecular area, corresponds well to the "hole" area detected by electron microscopic observation of monolayers of long-chain acids and their barium salts.[6] From the results shown in Fig. 4, it can be inferred that such "holes" in monolayers will disappear by "isobaric thermal treatment" up to a certain high temperature.

To eliminate the relaxation effect from A-T isobar measurements, we adopted the following experimental procedures: A monolayer is spread and is compressed to some constant pressure at room temperature. Then, the temperature of the system is raised to a certain high value where the relaxation time is very short, followed by lowering of the temperature to the starting point of the A-T isobar measurement, keeping pressure constant through out the whole time. The maximum temperature of the "isobaric thermal treatment" depends on the film material, the constant pressure and other experimental conditions. A-T isobars shown hereafter were measured with the procedures stated above, and it was checked that there was no significant leakage or dissolution of film material during measurement.

A-T Isobars of Some Typical Insoluble Monolayers. Figure 5 shows A-T isobars of a cadmium eicosanoate monolayer under the same conditions as those shown in Fig. 4. The relaxation effect disappeared and the two isobars, (a) and (b), coincided well with each other, except the part above 20 °C where isobar (b) showed a small undulation. The minimum surface compressibility of the monolayer at 9.8 °C was 1.0×10^{-3} m mN^{-1} which was a very small value corresponding to that of a solid state. The two-dimensional isobaric thermal expansivities and the correlation factors for the two isobars were calculated as 9.0×10^{-4} K^{-1} (0.998) and 9.9×10^{-4} K^{-1} (0.974) respectively.

Figure 6 shows an A-T isobar of a trioctadecanoyl glyceride monolayer which was spread from a benzene solution on pH 3 subphase (20 mN m^{-1}). The material has three hydrophobic long chains and forms very stable insoluble monolayers. The minimum surface compressibility at 6.4 °C was as small as 1.5×10^{-3} m mN^{-1}, corresponding to a value of a solid state. The monolayer exhibits no phase transition at 20 mN m^{-1} in the temperature span measured and the curve looks like a straight line. The two-dimensional thermal expansivity and the correlation factor calculated from the isobar were 9.0×10^{-4} K^{-1}

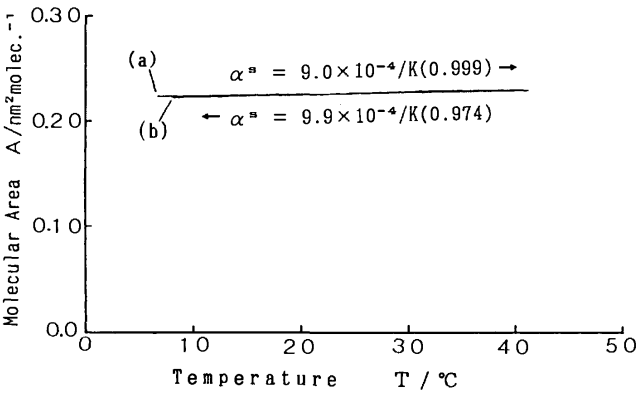

Fig. 5. A-T isobars of an eicosanoic acid monolayer which was measured following the procedures described in the text to eliminate the relaxation effect. Other experimental conditions are the same as those shown in Fig. 4. (a) An A-T isobar measured at temperature rising. (b) An A-T isobar measured at temperature lowering.

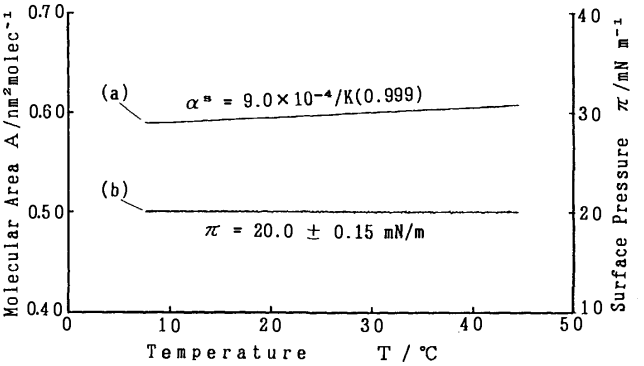

Fig. 6. (a) An A-T isobar of a TOG monolayer on pH 3 subphase at 20 mN m^{-1} measured at temperature rising, and (b) surface pressure fluctuation.

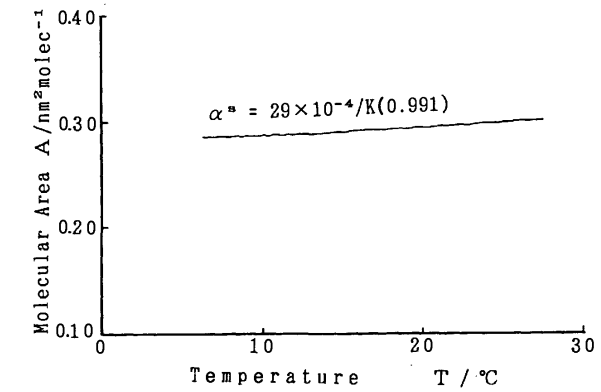

Fig. 7. An A-T isobar of an *cis*-9-octadecen-1-ol monolayer on distilled water at 15 mN m^{-1}.

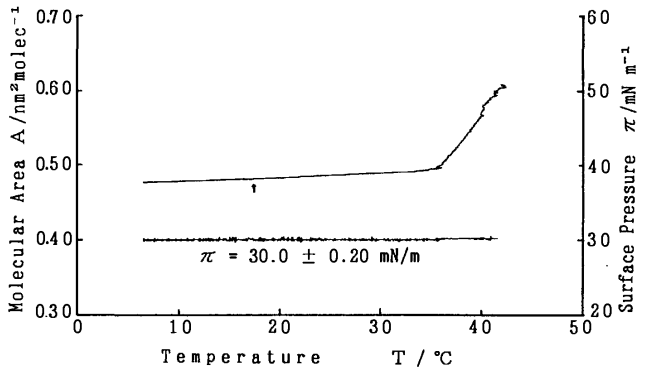

Fig. 8. An A-T isobar of a DPPC monolayer on pH 3 subphase at 30 mN m^{-1}. The isobar shows two phase transitions. The second-order one is detected at 18 °C and the "first-order" one at above 36 °C. The pressure was controlled strictly at 30.0±0.20 mN m^{-1} in spite of the existence of phase transitions.

and 0.999, respectively. The surface pressure fluctuation is also shown in the figure. In spite of the wide range of temperature change, it can be seen that pressure was controlled at 20.0±0.15 mN m^{-1} during the A-T isobar measurements.

Figure 7 shows an A-T isobar of a *cis*-9-octadecen-1-ol monolayer at 15 mN m^{-1} spread from a benzene solution on distilled water. This material has a cis-unsaturation in the middle of the hydrophobic chain and forms a typical liquid-expanded monolayer. As the solubility of this material in water is much larger than that of the corresponding saturated material, measurement was stopped at about 27 °C to reduce dissolution. A small relaxation effect was observed in the low temperature region of the isobar. The two-dimensional thermal expansivity of the liquid-expanded monolayer was calculated from the isobar data except at the low temperature region as 29×10^{-4} K^{-1} (0.991) which is much larger than those obtained for monolayers in a condensed state.

Figure 8 shows an A-T isobar of a DPPC monolayer at 30 mN m^{-1} on pH 3 subphase as well as the pressure fluctuation during the measurement. This material also forms stable insoluble monolayers but exhibits two phase transitions, one appears as a slight inflection at 18 °C (pointed by an upward arrow) and the other appears at 35 °C as a large stepwise change in molecular area as seen from the figure. In spite of the fact that the monolayer exhibits a phase transition with accompanying large area change, it can be seen that the surface pressure was kept constant at 30.0±0.20 mN m^{-1}. It can be considered that the phase transition detected at 18 °C corresponds to the second-order from phase IV (crystalline, non tilted) to phase III (crystalline, tilted) of DPPC.[3] Two-dimensional thermal expansivities of the condensed state below and above this transition were 9.0×10^{-4} K^{-1} (0.980) and 1.3×10^{-3} K^{-1} (0.995), respectively. The transition at the higher temperature corresponds to the first-order one from phase III to phase II (anisotropic fluid). Thermodynamics predicts that a first-order phase transition should appear as a vertical line in an A-T isobar. In practice, however, the A-T isobar in the transition region is not vertical but slanted. This may be because the molecular processes involved in the transition require some time to complete or the transition has a second-order character by approaching a critical point of the coexisting region of phase II and III as pointed out by Albrecht.[3]

Conclusion

A computer-controlled instrument for measuring A-T isobars of insoluble monolayers at the air/water interface was developed. By adopting a double surface balance system, the pressure could be controlled within ±0.15 mN m^{-1} using four control parameters. To obtain precise A-T isobars, it must be checked that there is no significant dissolution of film material into the subphase or no leakage of the material as shown by the agreement of two isobars measured at temperature rising and lowering. Before starting measurements, structural or area relaxations after compression must also be completed at a certain high temperature. In relation to the relaxation processes, the "isobaric thermal treatment" technique was proposed to densify insoluble monolayers, and this treatment will be a powerful tool to obtain dense and "defect-free" LB films.

Precise A-T isobars can afford two-dimensional isobaric thermal expansivities of insoluble monolayers that have never been reported. The thermal expansivities are about 30×10^{-4} K^{-1} for monolayers in the liquid-expanded state and about 10×10^{-4} K^{-1} for monolayers in the condensed states. A-T isobars will play important roles, together with the π-A isotherms, in considering physical properties or polymorphism of insoluble monolayers at the air/water interface.

References

1) This work has been presented in part at the 41st Annual Meeting of Colloid and Interfacial Chemistry, Sendai, September, 1988(Abstr. No.2F503)

2) G. L. Gaines, Jr., "Insoluble Monolayers at Liquid-Gas Interface," Interscience Publishers, New York (1966), Chap. 6, p. 283.

3) O. Albrecht, H. Gruler, and E. Sackman, *J. Phys. (Paris)*, **39**, 301 (1978).

4) O. Albrecht, *Thin Solid Films*, **99**, 227 (1983).

5) T. Kato and T. Watanabe, *Nippon Kagaku Kaishi*, **1987**, 954.

6) N. Uyeda, T. Takenaka, K. Aoyama, M. Matsumoto, and Y. Fujiyoshi, *Nature (London)*, **327** (6120), 319 (1987).

 © 1989 The Chemical Society of Japan Bull. Chem. Soc. Jpn., 62, 2497—2501 (1989)

Solution Properties of Sodium Perfluoroalkanoates. Heats of Solution, Viscosity *B* Coefficients, and Surface Tensions

Kunio TAMAKI,* Yoko ŌHARA, and Sumiko WATANABE
Department of Chemistry, Yokohama City University, Kanazawa-ku, Yokohama 236
(Received March 13, 1989)

The heats of solution, the viscosity *B* coefficients, and the surface activities of sodium perfluoroalkanoates, $F(CF_2)_nCOONa$, n=1—4, 6, 7), in water were measured. The changes in the heat capacity for dissolution in water, ΔC_p^∞, calculated from the heats of solution at 15, 25, and 35 °C, were positive for the salts, and the ΔC_p^∞ values increased with an increase in n. The increment in the ΔC_p^∞ values per CF_2 group was 93 J K^{-1} mol^{-1}. The viscosity *B* coefficients increased with the chain length at a definite temperature, and the increment in the viscosity *B* coefficients per CF_2 group was 0.119 dm^3 mol^{-1} at 25 °C. Further, the viscosity *B* coefficients for all the salts decreased with the increase in the temperature between 15 and 35 °C. Traube factors, as obtained from the surface tensions, were found to be 3.0 for the homologs from C_2 salt to C_7 salt. The results are discussed in comparison with those of sodium alkanoates, $H(CH_2)_nCOONa$.

The behavior of homologous organic monovalent anions, such as alkyl sulfates,[1,2] alkanesulfonates,[3] and dialkyl phosphates,[4] in water were discussed in previous papers. Perfluoroalkanoates are other organic monovalent anions. It is well-known that perfluoroalkanoic acids are considerably more hydrophobic than alkanoic acids. This stronger hydrophobicity of perfluorocarbon compounds leads to a greater lowering of the surface tensions[5] and to lower critical micelle concentration values[6] when compared to hydrocarbon compounds of the same chain length. In the present paper, experimental results will be reported on the temperature dependence of the heats of solution and the viscosity *B* coefficients, and on the surface active properties in water at 25 °C for the homologs of sodium perfluoroalkanoates ($F(CF_2)_nCOONa$, which will be abbreviated as f-C_n). The results will be discussed in comparison with those for homologs of sodium alkanoates ($H(CH_2)_nCOONa$, which will be abbreviated as C_n).

Experimental

Homologs of f-C_n were prepared by the neutralization of the corresponding perfluoroalkanoic acids (97—99%) with a solution of sodium hydroxide, after which the water was evaporated to dryness; the salts were purified several times by recrystallization from benzene-ethanol solutions. The salts of f-C_1 and f-C_2 were hygroscopic; all the salts were dried in vacuo at room temperature for several days, and the molecular weights were checked by means of volumetric analysis. A known amount of a sample was dissolved in water and passed through an ion-exchange resin in the hydrogen form; the eluent was titrated with a standard NaOH solution. It was found that the obtained samples have no water of crystallization. The homologs of C_n were commercial samples. The salts of C_1 and C_2 were used as received. The other C_n samples were purified by recrystallization from ethanol. All the salts were dried in vacuo at 100 °C for several days. The water was triply distilled.

The heats of solution were measured at 15, 25, and 35 °C using a twin isoperibol calorimeter, TIC-2C, of the Tokyo Riko Co., Ltd., by a method similar to that described in a previous paper.[3]

The viscosities were measured at 15, 25, and 35 °C using an automatic viscometer of the Shibayama Scientific Co., Ltd. The densities were measured using a vibrating-tube densimeter, twin-type SS-D-200, of the Shibayama Scientific Co., Ltd. The details of the procedure were described in a previous paper.[3] The electric conductivities were measured with an LCR meter, AG-4301B, of the Ando Electric Co., Ltd., using a frequency of 1000 Hz.

The surface tensions were measured at 25°C by means of the Wilhelmy method using a CBVP-A3 tensiometer of the Kyowa Kaimenkagaku Co., Ltd.

Results and Discussion

Heats of Solution. Heat-of-solution measurements were carried out in the concentration range of $(1.8—3.6)\times10^{-3}$ mol dm^{-3} (below the critical micelle concentrations). In this concentration range, any dependence of the heat of solution on the concentration is within the limit of experimental error, so the average of three or more measurements has been taken as the heat of solution at an infinite dilution ΔH_s^∞. The ΔH_s^∞ values of f-C_n salts in water are listed in Table 1. The results from the ΔH_s^∞ values were then used to calculate the change in the heat capacity for dissolution at an infinite dilution, ΔC_p^∞:

$$\Delta C_p^\infty = d\Delta H_s^\infty/dT, \quad (1)$$

where T is the temperature. The ΔC_p^∞ values obtained at 25 °C are also listed in Table 1.

The sign and magnitude of ΔC_p^∞ can be taken as a relative measure of the structural effect upon the solvent water.[7,8] The ΔC_p^∞ values of common salts indicate negative values, whereas the ΔC_p^∞ values of hydrophobic solutes indicate positive values. As may be seen in Table 1, the ΔC_p^∞ signs of the f-C_n salts are all positive, indicating that these salts behave as structure-makers in water. Figure 1 shows an approximate linear relation between the ΔC_p^∞ values and the number of carbon atoms in the perfluoroalkyl chain, n; the average increment in the ΔC_p^∞ values per

Table 1. Heats of Solution and Heat-Capacity Changes of $F(CF_2)_nCOONa$

n	ΔH_s^∞/kJ mol^{-1}			ΔC_p^∞/J K^{-1} mol^{-1}
	15 °C	25 °C	35 °C	25 °C
1	−9.18±0.10	−8.70±0.02	−7.98±0.02	60±13
2	−12.43±0.10	−11.35±0.04	−9.71±0.03	136±16
3	−9.74±0.02	−7.32±0.03	−5.05±0.02	235±7
4	−6.17±0.10	−3.09±0.10	0.10±0.01	314±24
6	1.89±0.02	7.16±0.02	12.02±0.02	507±6
7	6.61±0.02	12.80±0.02	18.92±0.04	616±7

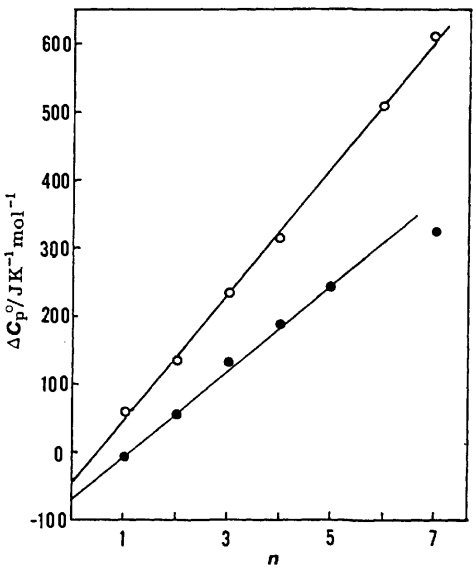

Fig. 1. Plots of ΔC_p^∞ against n.
○, $F(CF_2)_nCOONa$; ●, $H(CH_2)_nCOONa$.[9]

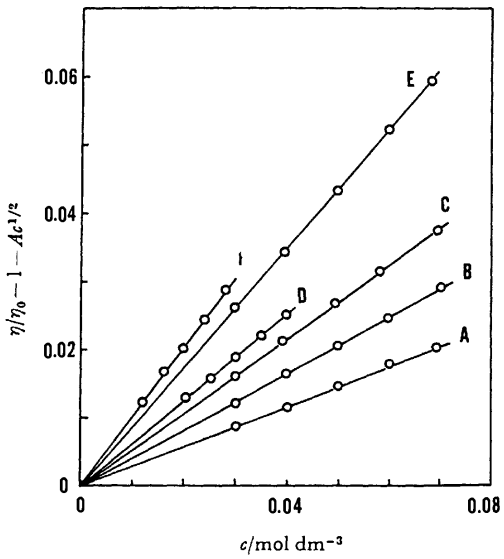

Fig. 2. Plots of $\eta/\eta_0-1-Ac^{1/2}$ against c for $F(CF_2)_n$-COONa at 25 °C.
A, CF_3COONa; B, C_2F_5COONa; C, C_3F_7COONa; D, C_4F_9COONa; E, $C_6F_{13}COONa$; F, $C_7F_{15}COONa$.

CF_2 group is 93 J K^{-1} mol^{-1}. The ΔC_p^∞ values for C_n salts in the temperature range of 25—35 °C, reported by Chaula and Ahluwalia,[9] are also included in Fig. 1. The average increment in ΔC_p^∞ per CH_2 group was reported as 59 J K^{-1} mol^{-1}. Therefore, the increment in the ΔC_p^∞ value per CF_2 group is about 1.6 times that of the CH_2 group.

The Viscosity *B* Coefficients. The viscosity of an aqueous solution of an electrolyte, η, for concentrations up to about 0.1 mol dm^{-3} can be represented by the Jones-Dole equation:[10]

$$\eta/\eta_0 = 1 + Ac^{1/2} + Bc, \quad (2)$$

where η_0 is the viscosity of water, c is the molar concentration, A is a constant related to ion-ion interaction, and B is the viscosity B coefficient. The A constant was interpreted theoretically by Falkenhagen and Vernon;[11] it can be calculated using the data of the limiting equivalent conductivities of the salt, the cation, and the anion. Equation 2 may be converted to:

$$\eta/\eta_0 - 1 - Ac^{1/2} = Bc. \quad (3)$$

When the left-hand side of Eq. 3, using the calculated values of A is plotted against c, the viscosity B coefficient is obtained as the slope of a straight line. The limiting molar conductivities required for the calculation of the A values in Eq. 3 for f-C_n salts were obtained from the measurements of the electric conductivities for aqueous solutions of these salts. The $Ac^{1/2}$ factor in Eq. 3 is relatively small, and the A values are insensitive to the variation in the temperature in the range of 15—35 °C, therefore, the values of A calculated using the limiting molar conductivities at 25 °C were also used for the A values at 15 and 35 °C. The A values for C_n salts were calculated from the limiting molar conductivities in the literature.[12] For example, Fig. 2 shows the results of the plotting of Eq. 3 for the f-C_n series at 25 °C. For each salt, the measurements were carried out in the concentration range below the critical micelle concentration. The values of A and B are listed in Table 2. The viscosities of the C_n salts at 25 °C were reported in a previous paper.[13] In this work, the temperature dependence of the viscosity B coefficients for the C_n series (n=1—7) were reinvestigated by means of a more elaborate method; the B values thus obtained are also included in Table 2. The viscosity B coefficient is related to the ion-solvent interaction and to the size and shape

Table 2. The Values of A, B, and dB/dT

n	A	B			dB/dT
	$dm^{3/2}mol^{-1/2}$	dm^3mol^{-1}			$dm^3mol^{-1}K^{-1}$
		15 °C	25 °C	35 °C	25 °C
		$F(CF_2)_nCOONa$			
1	0.0082	0.300	0.296	0.279	−0.0011
2	0.00865	0.424	0.418	0.373	−0.0026
3	0.0093	0.586	0.544	0.507	−0.0040
4	0.0096	0.688	0.635	0.589	−0.0050
6	0.0099	0.962	0.875	0.797	−0.0083
7	0.0101	1.141	1.027	0.945	−0.0098
		$H(CH_2)_nCOONa$			
1	0.0082	0.320	0.317	0.307	−0.00065
2	0.0088	0.423	0.406	0.381	−0.0021
3	0.0092	0.517	0.498	0.463	−0.0027
4	0.0097	0.596	0.555	0.512	−0.0042
5	0.0099	0.687	0.631	0.581	−0.0053
6	0.0104	0.763	0.700	0.645	−0.0059
7	(0.0107)	0.860	0,768	0.724	−0.0068

of the ion, and it is highly specific for the electrolyte and the temperature.[14]

The B values of both homologous series of salts are found to increase with the chain length at a definite temperature. The average increment in the B values per CF_2 group for the f-C_n series is larger than the increment in the B values per CH_2 group for C_n; the values are 0.119 dm^3mol^{-1} per CF_2 group and 0.074 dm^3mol^{-1} per CH_2 group at 25 °C.

The temperature dependence of the B values may be regarded as an index of the solute-solvent interaction; the B values increase with the temperature for a solvent-structure-breaking salt, while they decrease with the temperature for a solvent-structure-making solute.[15] For both the homologous organic salts, it may be seen in Table 2 that the B values decrease as the temperature is raised from 15 to 35 °C; these salts behave as structure-making salts in the water phase. The B values of electrolytes are determined by adding the individual contributions of the ions. Fortunately, the B value of sodium ion is insensitive to the temperature.[16] Therefore, the temperature dependences of the viscosity B coefficients of the sodium salts of both series of organic acids discussed above conveniently reflect the nature of the organic anions, and both $F(CF_2)_nCOO^-$ and $H(CH_2)_nCOO^-$ anions are structure-making ions. The temperature dependence of the viscosity B coefficients at 25 °C, dB/dT, are also listed in Table 2. Previous experimental results of dB/dT are available for C_1(−0.0022 $dm^3mol^{-1}K^{-1}$), C_2(−0.0025 $dm^3mol^{-1}K^{-1}$), and C_3(−0.0028 $dm^3mol^{-1}K^{-1}$).[17] As is evident in Table 2, the dB/dT values for the f-C_n series are smaller than those for the C_n series with the same number of carbon atoms. In Fig. 3 the dB/dT values are plotted against n; the dB/dT values decrease with the number of carbon atoms in the perfluoroalkyl or alkyl chains of both series of salts; this means that the hydrophobic hydration

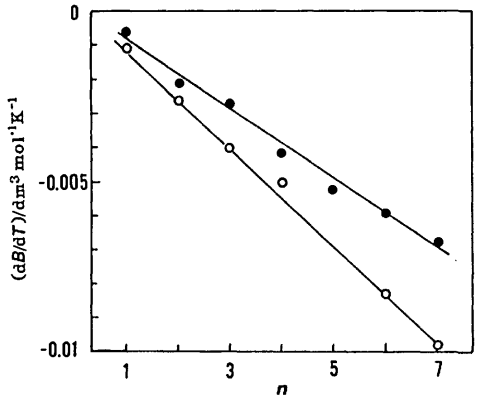

Fig. 3. Plots of dB/dT against n at 25 °C. ○, $F(CF_2)_nCOONa$; ●, $H(CH_2)_nCOONa$.

increase with the length of the chains. The average value of dB/dT per CF_2 group is −0.00144 $dm^3mol^{-1}K^{-1}$, while the value per CH_2 group is −0.00102 $dm^3mol^{-1}K^{-1}$. These values reflect the stronger hydrophobic nature of the f-C_n series than that of the C_n series.

Surface Tensions. Figure 4 shows the surface tensions, γ, of aqueous solutions of the f-C_n series as a function of the logarithmus of the molar concentration at 25 °C. It may be seen that all the salts reduce the surface tension of pure water. The shape of the surface tension-versus-concentration curve for an organic salt in aqueous solutions is considered to give a rough criterion of the behavior of the salt in water; common salt raises the surface tension of water, whereas hydrophobic salt reduces it.[18] Thus, f-C_n salts are excellent hydrophobic structure-makers in water. On the other hand, the surface tensions of aqeous solutions of the C_n series have been reported in the literature;[19] C_1 salt raises the surface tensions of pure water, whereas C_2 and higher homologous salts reduce

Table 3. Traube Factors, K, for $F(CF_2)_nCOONa$

n	γ=60 mN m^{-1}		γ=50 mN m^{-1}		γ=40 mN m^{-1}	
	c/mol dm^{-3}	K	c/mol dm^{-3}	K	c/mol dm^{-3}	K
2	0.52		1.45			
		3.0		2.8		
3	0.185		0.52		1.15	
		3.0		3.1		3.0
4	0.062		0.17		0.39	
		3.2		3.1		3.1
6	0.0060		0.0175		0.040	
		3.0		3.1		3.3
7	0.0020		0.0056		0.0122	

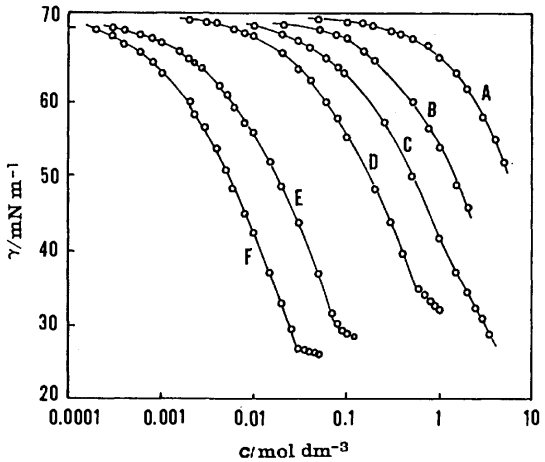

Fig. 4. Plots of surface tensions against c for $F(CF_2)_nCOONa$ at 25 °C.
A, CF_3COONa; B, C_2F_5COONa; C, C_3F_7COONa; D, C_4F_9COONa; E, $C_6F_{13}COONa$; F, $C_7F_{15}COONa$.

the surface tension of water. Therefore, the surface-active properties of the f-C_n series are much more higher than those of the C_n series.

In addition, the critical micelle concentrations can be estimated from the surface-tension-versus-concentration curves in Fig. 4; the values are 0.030 mol dm^{-3} for f-C_7 salt, 0.080 mol dm^{-3} for f-C_6 salt, and 0.55 mol dm^{-3} for f-C_4 salt. However, the critical micelle concentration becomes obscure for f-C_3 salt.

It may be found in Fig. 4 that the concentrations required for an equal lowering of the surface tension diminish by a constant factor for an additional CF_2 group in the perfluorocarbon chain. This is in accord with Traube's rule, which is expressed as;

$$C_n/C_{n+1}=K, \tag{4}$$

where C_n and C_{n+1} are, respectively, the concentrations for successive members of the series with n and $n+1$ CF_2 groups at an equal lowering of the surface tension; K is termed the Traube factor. The values of K obtained from Fig. 4 are summarized in Table 3. It may be seen in Table 3 that the Traube factors are about 3.0 for the homologs from f-C_2 salt to f-C_7 salt. In a previous paper,[20] for homologous strong electrolytes K was derived as:

$$K=\exp(-\Delta G/2RT), \tag{5}$$

where ΔG is the free energy of the adsorption of the CF_2 or CH_2 group from water to the surface, R is the gas constant, and T is the temperature. By the substitution of K=3.0 at 25 °C into Eq. 5, ΔG becomes −5.4 kJ mol^{-1}. This value is comparable to those in the literature: −5.4 kJ mol^{-1} reported by Phillips[21] and −5.9 kJ mol^{-1} reported by Davies and Rideal.[22]

The authors wish to thank Dr. Yujin Tabata, Nihon Surfactant Ind. Co., Ltd., for generous donation of the perfluoroalkanoic acids.

References

1) K. Tamaki, Y. Isomura, and Y. Ōhara, *Bull. Chem. Soc. Jpn.*, **45**, 2939 (1972).
2) K. Tamaki, Y. Ōhara, and Y. Isomura, *Bull. Chem. Soc. Jpn.*, **46**, 1551 (1973).
3) K. Tamaki, Y. Ōhara, M. Inabe, T. Mori, and F. Numata, *Bull. Chem. Soc. Jpn.*, **56**, 1930 (1983).
4) K. Tamaki, K. Suga, and E. Tanihara, *Bull. Chem. Soc. Jpn.*, **60**, 1225 (1987).
5) K. Shinoda, M. Hato, and T. Hayashi, *J. Phys. Chem.*, **76**, 909 (1972).
6) P. Mukerjee and K. J. Mysels, "Critical Micelle Concentrations of Aqueous Surfactants Systems," Natl. Stand. Ref. Data Ser. (U. S.) Natl. Bur. Stand. 1971, NSRDS-NBS 36.
7) E. M. Arnett and J. J. Campion, *J. Am. Chem. Soc.*, **92**, 7097 (1970).
8) T. S. Sarma and J. C. Ahluwalia, *Chem. Soc. Rev.*, **2**, 203 (1973).
9) B. Chawla and J. C. Ahluwalia, *J. Solution Chem.*, **4**, 383 (1975).
10) G. Jones and M. Dole, *J. Am. Chem. Soc.*, **51**, 2950 (1929).
11) H. Falkenhagen and E. L. Vernon, *Z. Physik.*, **33**, 140 (1932).
12) P. Franzosini and M. Sanesi, "Thermodynamic and Transport Properties of Organic Salts," Pergamon Press, Oxford (1980), pp. 275—278.
13) K. Tamaki, Y. Ōhara, H. Kurachi, M. Akiyama, and H. Odaki, *Bull. Chem. Soc. Jpn.*, **47**, 384 (1974).
14) R. H. Stokes and R. Mills, "Viscosity of Electrolytes

and Related Properties," Pergamon, Oxford (1965).
15) R. L. Kay, T. Vituccio, C. Zawoyski, and D. F. Evans, *J. Phys. Chem.*, **70**, 2336 (1966).
16) D. J. P. Out and L. M. Los, *J. Solution Chem.*, **9**, 19 (1980).
17) K. Miyajima, M. Sawada, and M. Nakagaki, *Bull. Chem. Soc. Jpn.*, **55**, 3101 (1982).
18) K. Tamaki, *Bull. Chem. Soc. Jpn.*, **47**, 2764 (1974).
19) Landolt-Bornstein, "Zahlenwerte and Funktionen," 2 Band, 3 Teil, Springer-Verlag (1956), p. 454.
20) K. Tamaki, *Bull. Chem. Soc. Jpn.*, **38**, 1987 (1965).
21) J. N. Phillips, *Trans. Faraday Soc.*, **51**, 561 (1955).
22) J. T. Davies and E. K. Rideal, "Interfacial Phenomena," Academic Press (1961), p. 160.

Adsolubilization Behavior of Dyes Caused by Mixed Surfactant Bilayers Formed on Alumina

Kunio Esumi,* Yuichi Sakamoto, Tetsuya Nagahama, and Kenjiro Meguro
Department of Applied Chemistry and Institute of Colloid and Interface Science, Science University of Tokyo, Kagurazaka, Shinjuku-ku, Tokyo 162
(Received March 24, 1989)

The adsolubilization of dyes (yellow OB and azobenzene) was performed on mixed bilayers consisting of anionic and nonionic surfactants formed on α-alumina. The adsolubilization capacity of the two dyes increased with the increase in the concentration of the dyes solubilized in the supernatant. The mixed bilayer consisting of anionic hydrocarbon (lithium dodecyl sulfate) and nonionic hydrocarbon surfactants (polyoxyethylene nonylphenyl ether) showed a greater adsolubilization capacity than that consisting of anionic fluorocarbon (lithium perfluorooctanesulfonate) and nonionic hydrocarbon surfactants. Further, the adsolubilization capacity of the dyes was affected by the oxyethylene chain length of the nonionic hydrocarbon surfactant in the mixed bilayer.

The solubilized amounts of solubilizates depend on the kinds of surfactants. Generally, the order of solubilization capacity, i.e., the moles of hydrocarbons and polar compounds solubilized per mole of surfactant, appears to be as follows: nonionics>cationics>anionics for surfactants with the same hydrophobic chain length.[1-3] The solubilization behavior by mixed micelles of anionic and nonionic surfactants has also been investigated;[4-7] Muto et al.[8] reported, from their comparisons of ideal and observed solubilized amounts, that the ratio of observed solubilized amounts to ideal amounts of yellow OB and azobenzene decreases when two surfactants are mixed, while it decreases with an increase in the difference of the moles of solubilizates per mole of surfactant between two surfactants in the mixed systems.

On the other hand, the structure of a surfactant adsorbed layer on particles has been characterized by using a fluorescence technique, ESR, and Raman spectroscopy.[9-11] Chandar et al.[9] demonstrated that the adsorbed layer of sodium dodecyl sulfate at the alumina-water interface is similar to that in hemimicellization. Esumi et al.[12,13] reported on mixed surfactant bilayers consisting of hydrocarbon and fluorocarbon surfactants formed on ferric hydrosol and alumina. The microenvironmental properties of these mixed bilayers were studied on the alumina by means of the fluorescence-probing method. However, this fluorescence-probing method could not be used for ferric hydrosol because of the large scattering by the sol alone. Such adsorbed surfactants of micelle-like surfactant aggregates are called admicelles.[14] When micelles incorporate other molecules into their structure, it is called solubilization: here, incorporation by admicelles will be referred to as adsolubilization.[15]

Recently, we found[16] that some alcohols are adsolubilized more efficiently into anionic surfactant bilayers formed on alumina than they are solubilized into the micelles. Thus, it is interesting to compare the solubilization behavior into a micelle system to the adsolubilization into the surfactant bilayer on particles, since they seem to have similar properties.

In this work, the adsolubilization of yellow OB and azobenzene into single and mixed surfactant bilayers formed on α-alumina is investigated by measuring the amounts of the dyes adsolubilized.

Experimental

Materials. Lithium perfluorooctanesulfonate (LiFOS) and lithium dodecyl sulfate (LiDS) were synthesized.[17] LiFOS was purified by repeated crystallizations from dioxane after extraction with ethanol, and LiDS with ethanol together, and with a mixture of hexane and 2-propanol. The purity of these samples was confirmed by elemental analyses and by the lack of a minimum in the surface tension. The polyoxyethylene nonylphenyl ethers (NP7.5 and NP20) were supplied by the Nikko Chemicals Co., Ltd.; each number of the NP indicates the average oxyethylene chain length in the molecule. These NPs were used without further purification. The yellow OB and azobenzene were obtained from the Tokyo Kasei Co. and were used as received.

The alumina used was α-alumina of a 99.995% purity, supplied by Showa Denko K. K. The specific surface area, determined from the nitrogen-gas adsorption at −196 °C, was 10.1 $m^2 g^{-1}$ The average particle diameter was 500 nm, as determined by means of a particle analyzer based on photon correlation spectroscopy (Autosizer Model 700, Malvern Co., Ltd.).

Methods and Measurements. An aqueous surfactant solution required to form a bilayer was placed in contact with 0.3 g of alumina. A series of solutions was prepared, containing various concentrations of yellow OB or azobenzene solubilized in surfactant solutions. Then, these solutions containing solubilizates were added to the suspensions. After attaining the equilibrium of adsolubilization, the suspension was centrifuged. The concentration of dyes solubilized in the supernatant was determined using a UV spectrophotometer (200 A, Hitachi Co.).

The amount of solubilizates adsolubilized was determined from the difference between the concentrations before and

after the adsolubilization. Similarly, the amounts of solubilizates solubilized in micelles in the absence of alumina were determined. The amounts of anionic surfactants adsorbed were determined by means of an isotachophoretic analyzer (IP-3A, Shimadzu Ltd.), while those of nonionic surfactants, which have an absorption band at 275 nm, were determined by means of a UV spectrophotometer.

All the experiments were performed at 25 °C and at pH 3.5, which was adjusted by the use of nitric acid. In order to keep the ionic strength constant, 10 mmol dm^{-3} of lithium nitrate was used.

Calorimetric measurements were made with a Multi micro calorimeter MMC-5111 (Tokyo Rico Co., Ltd.), in which the reaction vessel was immersed in a thermostatted bath maintained at 25±0.05 °C. The enthalpies of the formation of surfactant bilayers on the alumina were determined by breaking glass ampoules containing flocculated alumina in an LiDS or LiFOS aqueous solution into NP aqueous solutions. Correction was made for the heat change associated with the breaking of the ampoules and with mixing of the surfactant aqueous solutions.

Results and Discussion

When LiFOS or LiDS is adsorbed on positively charged alumina, the alumina flocculates. In this study, it is found that the optimum flocculation concentration for alumina is 1 mmol dm^{-3} for both LiFOS and LiDS. On the addition more than 0.6 mmol dm^{-3} of NPs to the optimum flocculated alumina, the alumina becomes redispersed. This redispersion process has been interpreted as being caused by the formation of a mixed bilayer[12,18,19] on the alumina in such a manner that the NP molecule is adsorbed on the LiFOS or LiDS-covered alumina, with its hydrophilic groups oriented towards the liquid phase. Thus, the mixed bilayer of LiFOS and NP is formed by the interaction between the hydrocarbon chains of NP and the fluorocarbon chains of LiFOS, while that of LiDS and NP is formed by the interaction between the hydrocarbon chains of NP and of LiDS. The redispersion state was confirmed by measuring the particle size of alumina; it was found to be about 500 nm. The interior environment in the mixed bilayer thus formed appears to have properties similar to those in mixed micelles.

Figure 1 shows the adsolubilization capacity for yellow OB in the mixed bilayers on the alumina. Here, the additive concentration of NPs was 1 mmol dm^{-3}. The adsolubilization capacity for yellow OB is expressed by dividing the amount of the yellow OB adsolubilized per unit of weight of the alumina by the total amounts of surfactants adsorbed per unit of weight of the alumina. Table 1 tabulates the amounts of surfactants adsorbed in the mixed bilayers. It can be seen that the amount of NP decreases with an increase in the oxyethylene chain lengths of NP for both LiDS-NP and LiFOS-NP

Table 1. Amounts of Surfactants Adsorbed in Mixed Bilayers

System	Amount adsorbed ($\times 10^{-5}$ mol g^{-1})			
	LiFOS	LiDS	NP	Total
LiFOS-NP7.5	1.62	—	2.30	3.92
LiDS-NP7.5	—	1.98	3.20	5.18
LiFOS-NP20	1.62	—	1.80	3.42
LiDS-NP20	—	1.98	2.20	4.18

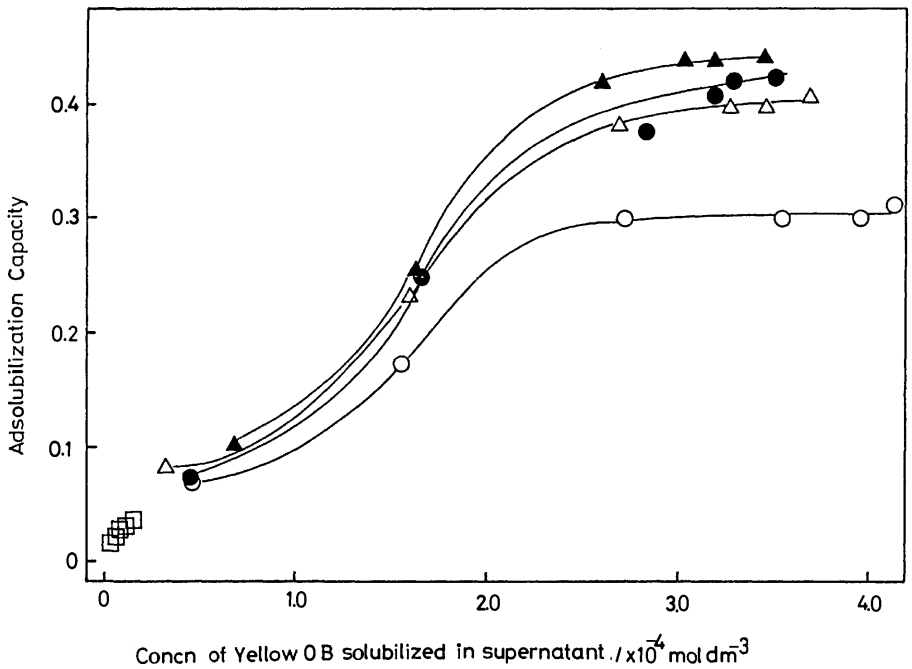

Fig. 1. Adsolubilization capacity for yellow OB in bilayers on alumina as a concentration of yellow OB solubilized in supernatant: (△) LiDS-NP7.5; (○) LiFOS-NP7.5; (▲) LiDS-NP20; (●) LiFOS-NP20; (□) LiDS-LiDS.

systems, and that the total amount of surfactant is greater for the LiDS-NP system than for the LiFOS-NP system with the same oxyethylene chain length of NP. The adsolubilization capacities for yellow OB in the mixed bilayers increase with an increase in the concentration of yellow OB solubilized in the supernatant; they appear to approach 0.5 except for the LiFOS-NP7.5 system. This indicates that the incorporation of yellow OB occurs systematically with the mixed bilayer (ratio of yellow OB : NP : LiDS or LiFOS=1 : 1 :1). These results also show that the systems containing NP20 have a higher adsolubilization capacity than those containing NP7.5, and that the LiDS-NP systems also have a higher adsolubilization than do the LiFOS-NP systems with the same ethylene oxide chain length of NP.

These differences may be attributed to the location of the adsolubilization site of yellow OB and to the magnitude of the hydrocarbon chain-hydrocarbon chain interaction and the hydrocarbon chain-fluorocarbon chain interaction of the surfactants. That is, generally it may be said that yellow OB is soluble in the poly(oxyethylene) shell of nonionic surfactant micelles and in the hydrocarbon core of anionic surfactant micelles.[20] In the mixed bilayers, since yellow OB is considered to be adsolubilized mainly in the poly(oxyethylene) chains of NP, the adsolubilization capacity of a system containing NP20 is greater than that of a system containing NP7.5. The difference in the adsolubilization capacity between the LiFOS-NP20 and LiDS-NP20 systems is small, however, probaly because of the less significant contributions from the hydrocarbon chain-hydrocarbon chain and hydrocarbon chain-fluorocarbon chain interactions. On the other hand, in the systems containing NP7.5, the adsolubilization capacity for yellow OB in the LiDS-NP7.5 system is greater than that in the LiFOS-NP7.5 system. This is presumably caused by the difference in the magnitudes of the hydrocarbon chain-hydrocarbon chain interaction and the hydrocarbon chain-fluorocarbon chain interaction of the surfactants.

Actually, from the measurement of the enthalpy of formation of a mixed bilayer, the enthalpy of the LiDS-NP7.5 system (-17.3 kJ mol^{-1}) was found to be greater than that of the LiFOS-NP7.5 system (-14.1 kJ mol^{-1}). This result supports the view that the hydrocarbon chain-hydrocarbon chain interaction of the LiDS-NP7.5 system is much stronger than the hydrocarbon chain-fluorocarbon chain interaction of the LiFOS-NP7.5 system. Mukerjee[21] has also pointed out that the hydrocarbon-hydrocarbon interaction is more favorable than the hydrocarbon-fluorocarbon interaction.

Further, the adsolubilization capacities for yellow OB in the single bilayers of LiDS and of LiFOS were measured in order to compare them with those in the mixed bilayers. However, the adsolubilization capacity for yellow OB in the LiFOS bilayer was too small to detect, as was to be expected from the amount of yellow OB solubilized in the LiFOS micelle.[8] The adsolubilization capacity for yellow OB in the LiDS bilayer (Fig. 1) is considerably smaller than that in the

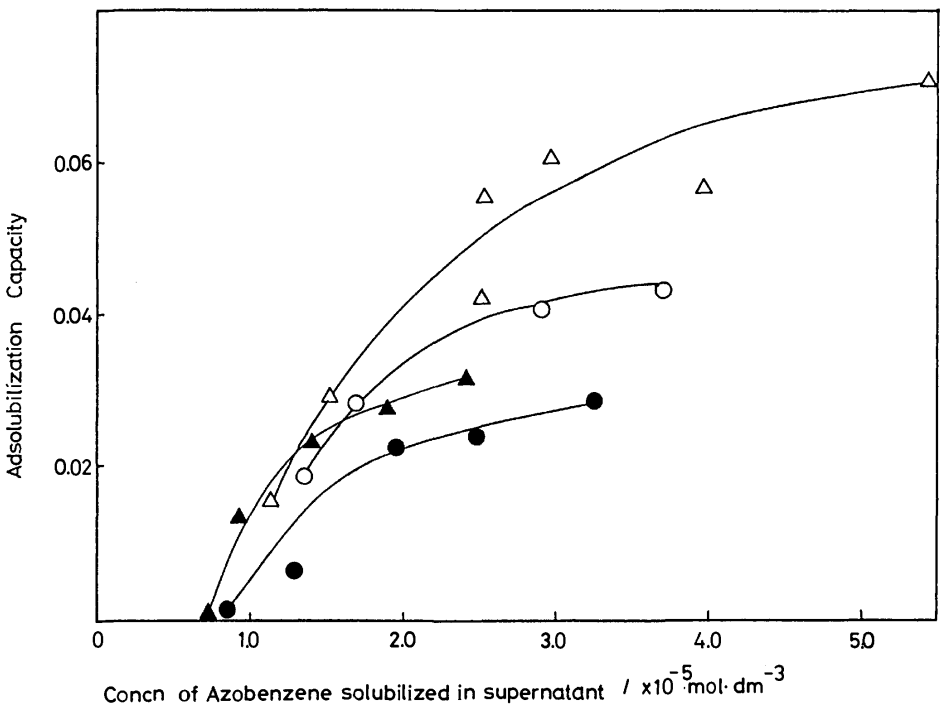

Fig. 2. Adsolubilization capacity for azobenzene in bilayers on alumina as a concentration of azobenzene solubilized in supernatant: (△) LiDS-NP7.5; (○) LiFOS-NP7.5; (▲) LiDS-NP20; (●) LiFOS-NP20.

mixed bilayers, suggesting that the hydrocarbon core in the LiDS bilayer has a very low adsolubilization capacity for yellow OB. This result corresponds with the low solubilization capacity for yellow OB in SDS micelles.[8] It is noteworthy that the adsolubilization capacities for yellow OB in the mixed bilayers are large compared to the solubilization capacity for yellow OB in the micelles; the solubilization capacities of NP7.5 and NP20 for yellow OB are 0.20 and 0.12 respectively.

The adsolubilization of azobenzene, which is soluble in the deep region of the poly(oxyethylene) shell for nonionic surfactant micelles, in the hydrocarbon core for the anionic surfactant micelles, and in both regions for mixed micelles,[22] was undertaken. Figure 2 shows the adsolubilization capacity for azobenzene in the LiDS-NP and LiFOS-NP systems. The adsolubilization capacity for azobenzene in the respective bilayers of LiDS and LiFOS was not large enough to measure. It is apparent, however, that the adsolubilization capacity for azobenzene in the LiDS-NP system is greater than that for the LiFOS-NP system, indicating that the adsolubilization of azobenzene is less favorable in the hydrocarbon chain-fluorocarbon chain layer for the LiFOS-NP system than in the hydrocarbon chain-hydrocarbon chain layer for the LiDS-NP system. This result emphasizes the aversion of aromatic compounds for fluorocarbon chains previously noted by the present authors.[17,23,24] The adsolubilization capacity for azobenzene decreased with the increase in the oxyethylene chain length of NP, contrary to the case of yellow OB. This result is presumably associated with the hydrophobic interactions in the bilayers; these interactions will increase with a decrease in the oxyethylene chain length of NP. This difference is also supported by the fact that the solubilization capacity for azobenzene in NP7.5 is greater than that for azobenzene in NP20. As well as yellow OB, the adsolubilization capacity for azobenzene in the mixed bilayers is greater than the solubilization capacity for azobenzene in NP7.5 and NP20; their capacities are 3.79×10^{-3} in NP7.5 and 3.44×10^{-3} in NP20 respectively.

In order to describe adsolubilization behavior using two solubilizates, we employed a partition coefficient K of the solubilizate between the bilayer and the

Table 2. Partition Coefficients of Yellow OB and Azobenzene in Bilayers

	Yellow OB		Azobenzene	
	Concn. in supernatant (μmol dm^{-3})	Partition coefficient (mol^{-1})	Concn. in supernatant (μmol dm^{-3})	Partition coefficient (mol^{-1})
LiDS-LiDS	3.3	4800		
	6.1	3400		
	8.1	3300		
	11.3	2600		
	14.7	2400		
	15.5	2500		
LiDS-NP7.5	33	2600	11.5	1400
	160	1400	15.2	2000
	270	1400	25.3	2200
	327	1200	28.4	2200
	338	1200	54.4	1300
	343	1200		
LiFOS-NP7.5	49	1500	13.6	1400
	156	1100	17.6	1600
	273	1100	28.2	1500
	356	800	37.3	1400
	391	800		
	413	800		
LiDS-NP20	68	1500	9.2	1500
	163	1600	14.0	1700
	260	1600	18.8	1500
	306	1400	23.8	1300
	317	1400		
	344	1300		
LiFOS-NP20	45	1600	14.0	400
	166	1500	19.5	1200
	282	1300	24.0	1000
	318	1300	33.3	900
	327	1300		
	351	1200		

aqueous phases. The partition coefficient K is defined by Eq. 1:

$$K = \frac{S_{AC}}{S_W} \quad (1)$$

where S_{AC} is the adsolubilization capacity for dyes in the bilayer phase, and S_W, the concentration of dyes solubilized in the supernatant. These K values are tabulated in Table 2. The order in the magnitude of K for yellow OB is roughly as follows: LiDS-LiDS> LiDS-NP7.5, LiDS-NP20, and LiFOS-NP20> LiFOS-NP7.5. On the other hand, the K values for azobenzene are almost the same in all the systems except for the LiFOS-NP20 system. Wu et al.[15] reported that the partition coefficient of styrene into an SDS bilayer on alumina is around 300. This value is low compared with that for the dyes used here because they used ethanol to increase the solubility of styrene in an aqueous solution. For the adsolubilization of 1-hexanol and heptafluoro-1-butanol into the respective bilayers of LiDS and LiFOS,[16] the partition coefficient was obtained in the range between 100 and 500. The present data show that water-insoluble dyes, such as yellow OB and azobenzene, are adsolubilized more efficiently in the bilayers than are styrene and the two alcohols. Furthermore, it is noteworthy that, compared to the K values between micelles and bilayers, the efficiency of incorporation for water-insoluble compounds in the bilayers is significantly greater than that in micelles.[8]

The above results lead to the conclusion that water-insoluble dyes are adsolubilized into surfactant bilayers formed on the alumina, where the adsolubilization capacity of the mixed bilayer is greater for the LiDS-NP system than for the LiFOS-NP system. Further, in the mixed bilayers of the LiDS-NP and LiFOS-NP systems, the adsolubilization capacity for yellow OB increases with an increase in the oxyethylene chain length of NP, whereas that for azobenzene decrease with an increase in the oxyethylene chain length of NP. These phenomena are presumably associated with the different locations of the dyes in the mixed bilayers. The adsolubilization capacity for yellow OB and azobenzene in the bilayers is considerably greater than the solubilization capacity in the corresponding micelles.

References

1) J. W. McBain and P. H. Richards, *Ind. Eng. Chem.*, **38**, 642 (1946).
2) S. Saito, *J. Colloid Interface Sci.*, **24**, 227 (1967).
3) F. Tokiwa, *J. Phys. Chem.*, **72**, 1214 (1968).
4) F. Tokiwa and K. Tsuji, *Bull. Chem. Soc. Jpn.*, **46**, 1338 (1973).
5) N. Nishikido, *J. Colloid Interface Sci.*, **60**, 242 (1977).
6) C. M. Nguyen, J. F. Scamehorn, and S. D. Christian, *Colloids Surf.*, **30**, 335 (1988).
7) M. Abe, N. Suzuki, and K. Ogino, *J. Colloid Interface Sci.*, **99** 226 (1984).
8) Y. Muto, M. Asada, A. Takasawa, K. Esumi, and K. Meguro, *J. Colloid Interface Sci.*, **124**, 632 (1988).
9) P. Chandar, P. Somasundaran, and N. J. Turro, *J. Colloid Interface Sci.*, **117**, 31 (1987).
10) P. Chandar, P. Somasundaran, K. C. Waterman, and N. J. Turro, *J. Phys. Chem.*, **91**, 148 (1987).
11) P. Somasundaran, J. T. Kunjappu, C. V. Kumar, N. J. Turro, and J. K. Barton, *Langmuir*, **5**, 215 (1989).
12) K. Esumi, Y. Sakamoto, and K. Meguro, *Colloid Polym. Sci.*, **267**, 525 (1989).
13) K. Esumi, Y. Sakamoto, K. Yoshikawa, and K. Meguro, *Colloid Surf.*, **36**, 1 (1989).
14) J. H. Harwell, Ph. D. Dissertation, The University of Texas at Austin, 1983.
15) J. Wu, J. H. Harwell, and E. A. O'Rear, *Langmuir*, **3**, 531 (1987).
16) K. Esumi and K. Meguro, unpublished work.
17) K. Meguro, M. Ueno, and T. Suzuki, *J. Jpn. Oil Chem. Soc.*, **31**, 909 (1982).
18) K. Esumi, Y. Ono, M. Ishizuka, and K. Meguro, *Colloids Surf.*, **32**, 139 (1988).
19) K. Esumi, Y. Sakamoto, K. Yoshikawa, and K. Meguro, *Bull. Chem. Soc. Jpn.*, **61**, 1475 (1988).
20) F. Tokiwa and K. Tsuji, *Bull. Chem. Soc. Jpn.*, **46**, 2684 (1973).
21) P. Mukerjee, *J. Am. Oil Chem. Soc.*, **59**, 573 (1982).
22) Y. Nemoto and H. Funahashi, *Hyomen*, **15**, 625 (1977).
23) K. Meguro, Y. Muto, F. Sakurai, and K. Esumi, "Phenomena in Mixed Surfactant Systems," ACS Symposium Series, No.311 (1986), p. 61.
24) T. Suzuki, K. Esumi, and K. Meguro, *J. Colloid Interface Sci.*, **93**, 205 (1983).

 © 1989 The Chemical Society of Japan Bull. Chem. Soc. Jpn., 62, 2507—2511 (1989)

Adsorption at Water/Air Interface and Micelle Formation of Decylammonium Bromide and Decylammonium Chloride Mixture

Hitoshi MATSUKI,* Naoko ANDO, Makoto ARATONO, and Kinsi MOTOMURA
Department of Chemistry, Faculty of Science, Kyushu University 33, Fukuoka 812
(Received April 12, 1989)

The surface tension of the aqueous solution of decylammonium bromide (DeAB) and decylammonium chloride (DeAC) mixture was measured as a function of the total molality and composition of surfactants at 298.15 K under atmospheric pressure. By applying the thermodynamic equations derived previously to the experimental results, the compositions in the mixed adsorbed film and mixed micelle were evaluated. It was found that the adsorbed film and micelle are rich in DeAB, which is more surface active than DeAC, compared with the aqueous solution. Further, the DeAB and DeAC molecules were concluded to mix ideally in the states of the adsorbed film and micelle. On the other hand, the compositions were compared with those of dodecylammonium chloride (DAC)-DeAC mixture at the critical micelle concentration (cmc). The discrepancy between the compositions was proved to be related closely to the differences between the cmc's and between the surface tension values at the cmc of pure surfactants.

The miscibility of surfactants in adsorbed films and micelles has been clarified thermodynamically by use of the excess thermodynamic quantities defined with reference to dividing planes and the two-dimensional phase diagrams representing the relation between the compositions of surfactants in the aqueous solution, adsorbed film, and micelle.[1-5] In the previous paper, the adsorbed film and micelle of dodecylammonium chloride (DAC)-decylammonium chloride (DeAC) mixture have been investigated by measuring the surface tension of the aqueous solution;[1,4] the difference of the surfactant ions has been shown to produce a considerable effect on the adsorption and micelle formation.

It is now important to examine the miscibility of surfactants having different counter ions in the adsorbed films and micelles, because the densities of aqueous solutions,[6-9] the micelle aggregation numbers,[10] and the surface activities[11,12] of surfactants are greatly dependent on the counter ion. In the present study, we adopt the decylammonium bromide (DeAB)-DeAC mixture. The surface tension of the aqueous solution is measured as a function of the total concentration and composition of the surfactants in the neighborhood of the critical micelle concentration (cmc) at constant temperature under atmospheric pressure. The results are compared with those of the DAC-DeAC system at the cmc.

Experimental

Decylammonium bromide was prepared from decylamine (Tokyo Kasei's guaranteed reagent) and hydrobromic acid (Nacalai Tesque's guaranteed reagent) and recrystallized five times from ethanol. Decylammonium chloride was prepared and purified by the method described previously.[1] The purity of the surfactants was checked by observing the absence of a minimum on the surface tension vs. concentration curves. Water was triply distilled from dilute alkaline permanganate solution.

The surface tension of aqueous solutions was measured by the drop volume technique described previously.[13] The error estimated for the value of surface tension was less than 0.05 mN m^{-1}. The measurements were carried out at the temperature kept constant at 298.15 K by immersing the cell in a thermostat under atmospheric pressure.

Results and Discussion

It has been shown that the total molality and composition of a surfactant mixture in the aqueous solution are appropriate for the variables to provide information concerning the adsorption behavior and micelle formation of the mixture at constant temperature T and pressure p.[1-5] Here the total molality and composition are defined respectively by

$$m = m_1 + m_2 \quad (1)$$

and

$$X_2 = m_2/m, \quad (2)$$

where m_i is the molality of surfactant i and the component 2 refers to DeAC. The surface tension γ was measured as a function of m at several X_2 values at 298.15 K under atmospheric pressure.

Figure 1 shows the variation in γ with m. It is seen

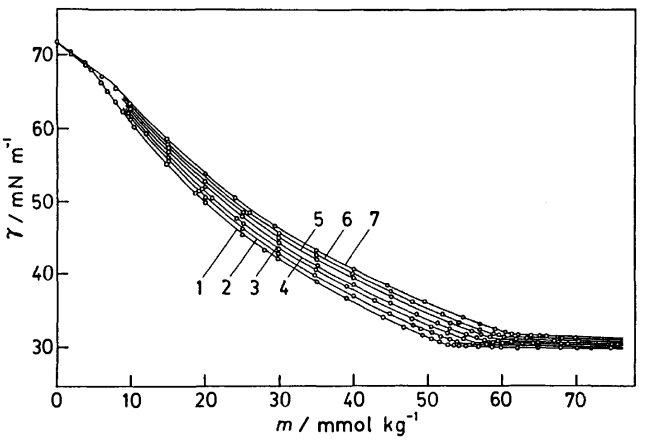

Fig. 1. Surface tension vs. total molality curves at constant composition: (1) X_2=0; (2) 0.299; (3) 0.500; (4) 0.650; (5) 0.800; (6) 0.900; (7) 1.

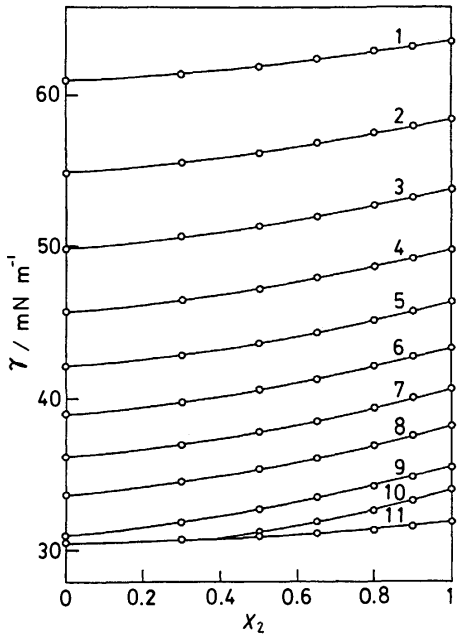

Fig. 2. Surface tension vs. composition curves at constant total molality: (1) m=10 mmol kg^{-1}; (2) 15; (3) 20; (4) 25; (5) 30; (6) 35; (7) 40; (8) 45; (9) 51; (10) 55; (11) γ^{cmc} vs. X_2.

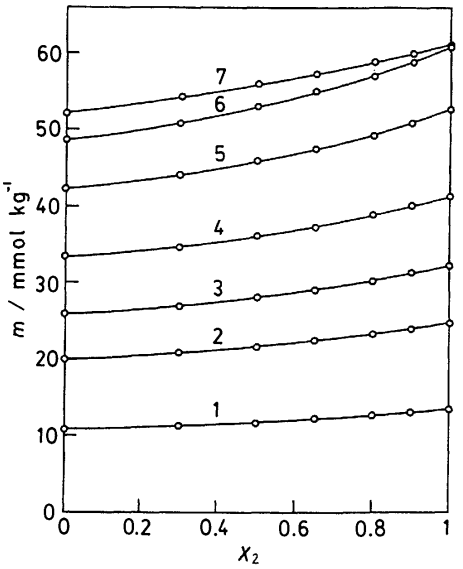

Fig. 3. Total molality vs. composition curves at constant surface tension: (1) γ=60 mN m^{-1}; (2) 50; (3) 45; (4) 40; (5) 35; (6) 32; (7) cmc vs. X_2.

that the value of γ decreases with increasing m and in the range of concentration above the cmc it does slightly and linearly. Further, the curve seems to have a distinct break point at the concentration corresponding to the cmc. By picking up the γ values at a concentration below the cmc from Fig. 1, the γ vs. X_2 curve is obtained and depicted together with the surface tension at the cmc γ^{cmc} vs. X_2 curve in Fig. 2. It is seen that the curves deviate slightly downward from the straight line connecting the γ values of pure DeAB and DeAC. Further, the m vs. X_2 curve at constant γ can also be obtained from Fig. 1; it is shown together with the cmc vs. X_2 curve in Fig. 3. We can find that the shape of the curve is convex downward at a low surface tension value though linear at a high one.

Let us first deal with the adsorption behavior of the surfactant mixture. According to the thermodynamics of adsorption of ionic surfactant mixtures developed previously,[1,2] the surface tension can be written as a function of m and X_2 at a concentration below the cmc at constant T and p:

$$d\gamma = -2(RT\Gamma^{H}/m)dm - [RT\Gamma^{H}(X_2^{H}-X_2)/X_1X_2]dX_2, \quad (3)$$

where the total surface density of surfactants Γ^{H} and the composition of DeAC in the mixed adsorbed film X_2^{H} are defined respectively by

$$\Gamma^{H} = \Gamma_1^{H} + \Gamma_2^{H} \quad (4)$$

and

$$X_2^{H} = \Gamma_2^{H}/\Gamma^{H} \quad (5)$$

Here Γ_i^{H} is the surface excess number of moles of surfactant i with reference to the two dividing planes making the surface excess numbers of moles of air and water zero.[14,15]

The value of Γ^{H} is evaluated by applying the following equation derived from Eq. 3 to the γ vs. m curve given in Fig. 1:

$$\Gamma^{H} = -(m/2RT)(\partial\gamma/\partial m)_{T,p,X_2}. \quad (6)$$

The Γ^{H} value is plotted against m at constant X_2 in Fig. 4; it is observed to increase with increasing m and approach the saturated value at a concentration near the cmc. It should be noted that the discontinuous change in Γ^{H} at a low concentration corresponds to the phase transition in the adsorbed film.[16]

It is apparent from Eq. 3 that there are two approaches to the evaluation of the composition in

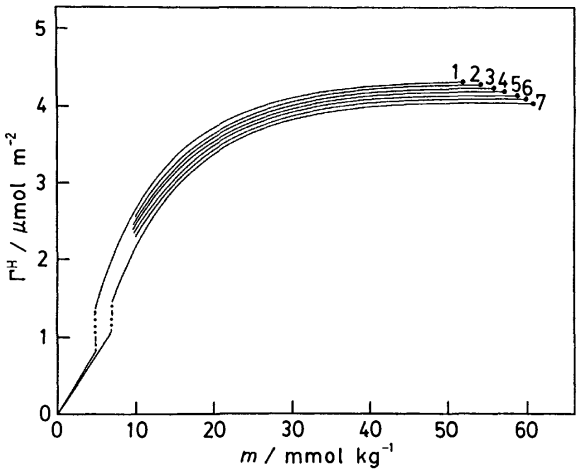

Fig. 4. Total surface density vs. total molality curves at constant composition: (1) X_2=0; (2) 0.299; (3) 0.500; (4) 0.650; (5) 0.800; (6) 0.900; (7) 1; (●) total surface density at the cmc $\Gamma^{H,cmc}$.

the mixed adsorbed film; one is the application of the equation

$$X_2^H = X_2 - (X_1X_2/RT\Gamma^H)(\partial\gamma/\partial X_2)_{T,p,m} \quad (7)$$

to the γ vs. X_2 curve at constant T, p, and m shown in Fig. 2 and the other is the application of the equation

$$X_2^H = X_2 - 2(X_1X_2/m)(\partial m/\partial X_2)_{T,p,\gamma} \quad (8)$$

to the m vs. X_2 curve at constant T, p, and γ shown in Fig. 3. The X_2^H values are presented in the forms of γ vs. X_2^H and m vs. X_2^H curves respectively in Figs. 5 and 6, where the corresponding γ vs. X_2 and m vs. X_2 curves are also depicted. It is seen that the value of X_2^H is smaller than that of X_2; that is, the mixed adsorbed film is enriched with DeAB, which has a smaller γ value than DeAC, over the whole range of composition. Taking account of the difference in chemical structure between DeAB and DeAC, the counter ion is said to have some effect on the adsorption behavior of surfactant ion. However, it is found that the composition difference $X_2-X_2^H$ is small compared with that of the DAC-DeAC system which is characterized by the different surfactant ion and the same counter ion.[1,4] Furthermore, the m vs. X_2^H curve seems not to deviate appreciably from the line connecting the m values of the pure surfactants. These findings indicate that the DeAB and DeAC molecules mix almost ideally in the adsorbed film.

Now let us consider the mixed micelle formation of surfactants. The thermodynamic equation describing the behavior of the mixed micelle at the cmc at constant T and p is[3]

$$-2(RT/\mathrm{cmc})\mathrm{dcmc} - [RT(X_2^M - X_2)/X_1X_2]\mathrm{d}X_2 = 0, \quad (9)$$

where X_2^M is the composition of DeAC in the mixed micelle defined by

$$X_2^M = N_2^M/(N_1^M + N_2^M), \quad (10)$$

where N_i^M is the number of molecules of surfactant i in one mixed micelle particle defined with regard to the spherical dividing surface which makes the excess number of moles of water zero. From Eq. 9, we can derive the relation between X_2^M and the derivative of the cmc with respect to X_2:

$$X_2^M = X_2 - 2(X_1X_2/\mathrm{cmc})(\partial\mathrm{cmc}/\partial X_2)_{T,p}. \quad (11)$$

The X_2^M value obtained from the cmc vs. X_2 curve shown in Fig. 3 is expressed in the form of the cmc vs. X_2^M curve in Fig. 7, where the cmc vs. X_2 curve is also drawn. It is seen that the population of DeAC in the mixed micelle is smaller than that in the solution although the difference between them is small. Sim-

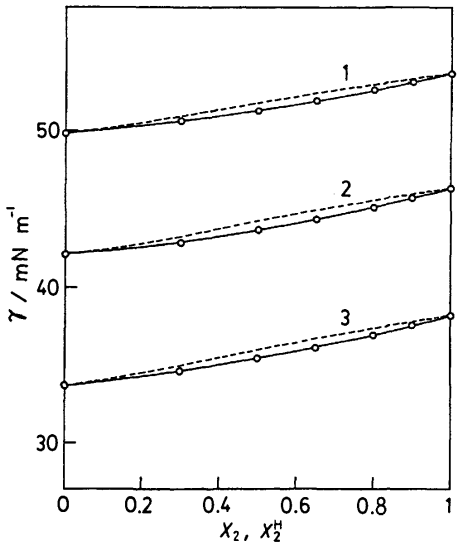

Fig. 5. Surface tension vs. composition curves at constant total molality: (1) m=20 mmol kg^{-1}; (2) 30; (3) 45; (——) X_2; (----) X_2^H.

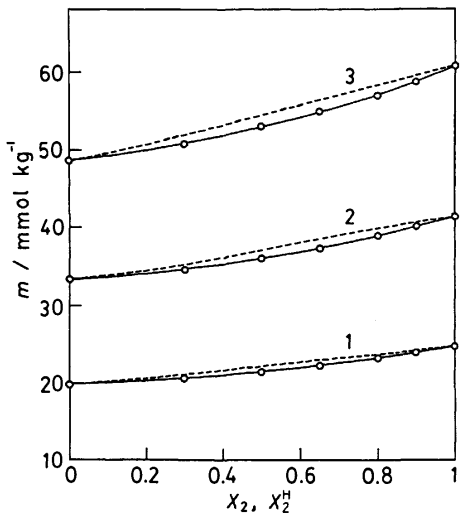

Fig. 6. Total molality vs. composition curves at constant surface tension: (1) γ=50 mN m^{-1}; (2) 40; (3) 32; (——) X_2; (----) X_2^H.

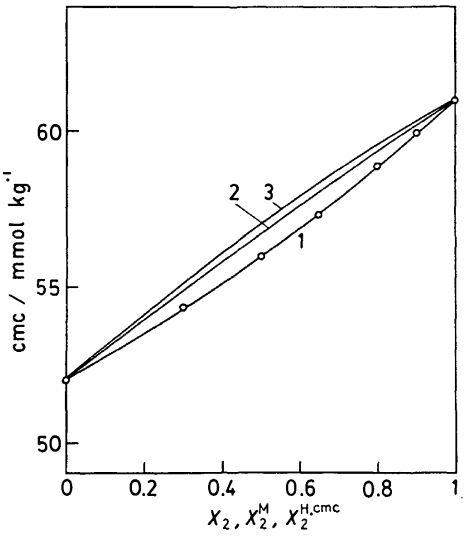

Fig. 7. Critical micelle concentration vs. composition curves: (1) cmc vs. X_2; (2) cmc vs. X_2^M; (3) cmc vs. $X_2^{H,cmc}$.

ilar behavior was observed in the case of the potassium dodecyl sulfate-sodium dodecyl sulfate system.[3] Therefore, we may say that the DeAB and DeAC molecules mix ideally in the micelle as those in the adsorbed film.

Further, the X_2^H value at the cmc $X_2^{H,cmc}$ can be calculated by use of the composition dependence of the γ^{cmc} shown in Fig. 2 and the relation

$$X_2^{H,cmc} = X_2^M - (X_1X_2/RT\Gamma^{H,cmc})(\partial\gamma^{cmc}/\partial X_2)_{T,p}, \quad (12)$$

which is derived by combining Eq. 3 at the cmc with Eq. 9. Here $\Gamma^{H,cmc}$ is the total surface density of surfactants at the cmc represented by the closed circle in Fig. 4. The value of $X_2^{H,cmc}$ is shown in the form of the γ^{cmc} vs. $X_2^{H,cmc}$ plot in Fig. 8 and also in the form of the cmc vs. $X_2^{H,cmc}$ plot in Fig. 7. Comparing the values of $X_2^{H,cmc}$ and X_2^M, we notice that the micelle is slightly rich in DeAC compared with the adsorbed film. Since the difference between the values are small, however, it may be concluded that the miscibility of surfactants in the micelle is similar to that in the adsorbed film. This fact gives support to our view that the behavior of surfactants in the micelle resembles thermodynamically that in the adsorbed film.[4,17]

Finally, it is useful to compare the relation between the compositions in the aqueous solution, adsorbed film, and micelle of the DeAB-DeAC mixture with that of the DAC-DeAC mixture at the cmc. The cmc vs. composition curves are drawn in Fig. 9. It is clearly seen that the diagram of the DeAB-DeAC system is extremely thin compared with that of the DAC-DeAC system. To visualize the difference between the two systems quantitatively, the $X_2-X_2^M$, $X_2-X_2^{H,cmc}$, and $X_2^{H,cmc}-X_2^M$ values are plotted against X_2 in Fig. 10. Both the adsorbed film and the micelle are seen to be enriched with the surfactant which has the lower γ^{cmc} and cmc values. However, the $X_2-X_2^M$ and $X_2-X_2^{H,cmc}$ values of the DeAB-DeAC mixture are much smaller than those of the DAC-DeAC mixture; this may be attributable to a small difference in cmc between the constituents of the former mixture. On the other hand, the $X_2^{H,cmc}-X_2^M$ values of both the mixtures seem not to be different from each other, which arises from the fact that their differences in γ^{cmc}

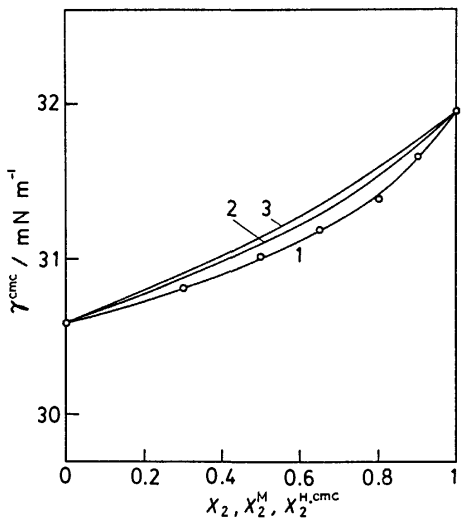

Fig. 8. Surface tension at the cmc vs. composition curves: (1) γ^{cmc} vs. X_2; (2) γ^{cmc} vs. X_2^M; (3) γ^{cmc} vs. $X_2^{H,cmc}$.

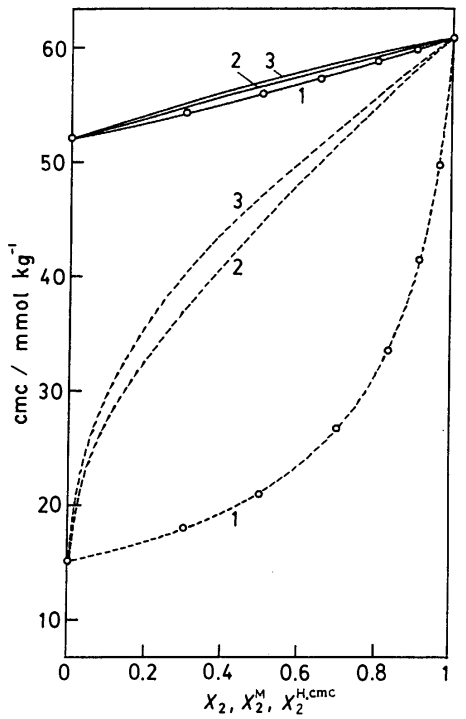

Fig. 9. Critical micelle concentration vs. composition curves: (1) cmc vs. X_2; (2) cmc vs. X_2^M; (3) cmc vs. $X_2^{H,cmc}$; (——) DeAB-DeAC system; (----) DAC-DeAC system.

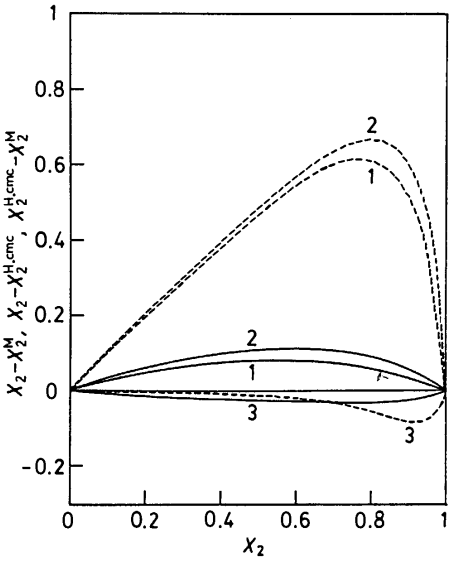

Fig. 10. Difference in composition vs. composition curves at the cmc: (1) $X_2-X_2^M$ vs. X_2; (2) $X_2-X_2^{H,cmc}$ vs. X_2; (3) $X_2^{H,cmc}-X_2^M$ vs. X_2; (——) DeAB-DeAC system; (----) DAC-DeAC system.

between the constituents are comparable.

Further information about the miscibility of surfactants in the adsorbed film and micelle will be provided by examining the mixture of surfactants without a common ion.

References

1) M. Aratono, S. Uryu, Y. Hayami, K. Motomura, and R. Matuura, *J. Colloid Interface Sci.*, **93**, 162 (1983).

2) S. Uryu, M. Aratono, M. Yamanaka, K. Motomura, and R. Matuura, *Bull. Chem. Soc. Jpn.*, **56**, 3219 (1983).

3) K. Motomura, M. Yamanaka, and M. Aratono, *Colloid Polym. Sci.*, **262**, 948 (1984).

4) K. Motomura, H. Matsukiyo, and M. Aratono, *ACS Symp. Ser.*, **311**, 163 (1986).

5) N. Ikeda, E. Shiota, M. Aratono, and K. Motomura, *Bull. Chem. Soc. Jpn.*, **62**, 410 (1989).

6) J. E. Desnoyers and M. Arel, *Can. J. Chem.*, **45**, 359 (1967).

7) M. Sakurai, T. Komatsu, and T. Nakagawa, *Bull. Chem. Soc. Jpn.*, **48**, 3491 (1975).

8) G. M. Musbally, G. Perron, and J. E. Desnoyers, *J. Colloid Interface Sci.*, **48**, 494 (1974).

9) L. M. Kushner, W. D. Hubbard, and R. A. Parker, *J. Research NBS*, **59**, 113 (1957).

10) A. Malliaris, J. L. Moigne, J. Sturm, and R. Zana, *J. Phys. Chem.*, **89**, 2709 (1985).

11) K. Tamaki, *Bull. Chem. Soc. Jpn.*, **40**, 38 (1967).

12) K. Tamaki, *Colloid Polym. Sci.*, **252**, 547 (1974).

13) K. Motomura, S. Iwanaga, Y. Hayami, S. Uryu, and R. Matuura, *J. Colloid Interface Sci.*, **80**, 32 (1981).

14) K. Motomura, *J. Colloid Interface Sci.*, **64**, 348 (1978).

15) K. Motomura and M. Aratono, *Langmuir*, **3**, 304 (1987).

16) M. Aratono, S. Uryu, Y. Hayami, K. Motomura, and R. Matuura, *J. Colloid Interface Sci.*, **98**, 33 (1984).

17) K. Motomura, S. Iwanaga, M. Yamanaka, M. Aratono, and R. Matuura, *J. Colloid Interface Sci.*, **86**, 151 (1981).

Effects of Temperature on the Solvent Extraction of Zinc and Cadmium Complexes with 8-Quinolinol and 2-Methyl-8-quinolinol into 1,1,2,2-Tetrachloroethane, 1-Octanol, and *p*-Xylene

Eiichiro NAKAYAMA,* Yoshiki SOHRIN,† Kenji ISSHIKI,†† Hajime KARATANI,††† and Etsu YAMADA††††
Research Center for Instrumental Analysis, Faculty of Science, Kyoto University, Sakyo-ku, Kyoto 606
†Institute for Chemical Research, Kyoto University, Uji, Kyoto 611
††Faculty of Home Economics, Kouchi Women's University, Eikokuji, Kouchi 780
†††Faculty of Textile Science, Kyoto Institute of Technology, Sakyo-ku, Kyoto 606
††††Center for Waste Water Treatment, Kyoto Institute of Technology, Sakyo-ku, Kyoto 606
(Received September 26, 1988)

The effects of temperature on the extraction of zinc(II) and cadmium(II) complexes with 8-quinolinol (HQ) and 2-methyl-8-quinolinol (HR) into three different types of organic solvents whose boiling points are relatively high were studied. 1) In the case of 1,1,2,2-tetrachloroethane (TCE), the extraction equilibrium can be written as follows (except for that of zinc with 2-methyl-8-quinolinol):

$$2M^{2+} + 6HQ_{(o)} + X^- \rightleftarrows M_2Q_3(HQ)_3^+{}_{(o)} + X^-{}_{(o)} + 3H^+,$$

where X^- refers to various inorganic anions. An ion-pair of the binuclear complex (complex ion pair) dissociates into a complex cation and an inorganic anion in the organic phase. The distribution ratios decrease remarkably with an increase in temperature. 2) In the 1-octanol (S) extraction system, zinc and cadmium are extracted as solvent-adducts, such as $MQ_2 \cdot S_2$. The distribution ratios are almost constant with a change in temperature. 3) In the *p*-xylene extraction system, a hydrated metal complex, $MQ_2 \cdot 2H_2O$, may precipitate and be deposited at the interface of both phases, except for the extraction of zinc with 2-methyl-8-quinolinol. 4) The zinc complexes of 2-methyl-8-quinolinol are extracted into TCE and *p*-xylene as anhydrous complexes, such as MR_2. The distribution ratios increase with an increase in temperature. Moreover, zinc can be separated from cadmium at high temperatures using 2-methyl-8-quinolinol and TCE.

Numerous studies have been conducted regarding the various factors affecting the solvent extraction of metal chelate. A few thermodynamic studies have been carried out. In these studies, however, measurements were conducted in the low-temperature region, below 50 °C, since volatile organic solvents, such as chloroform and benzene, were used.[1-5] As previously reported,[6-8] we studied the temperature effects on the extraction of 8-quinolinol, itself, and its divalent metal chelates into several organic solvents whose boiling points are relatively high over the temperature range 10 to 90 °C.

In this study the effects of temperature on the extraction behavior of zinc and cadmium with 8-quinolinol and 2-methyl-8-quinolinol between water and three different organic solvents were investigated with regard to the extraction mechanism. The organic solvents used were 1,1,2,2-tetrachloroethane, 1-octanol, and *p*-xylene, which were chosen as homologues of chloroform, 1-butanol, and benzene, respectively. The results for 2-methyl-8-quinolinol were compared with those for 8-quinolinol. Moreover, in order to corroborate the dissociation of the binuclear complex in TCE, the conductivities of the extract into TCE were measured.

Experimental

Reagents. Commercially available 8-quinolinol was purified by recrystallization from ethanol after steam distillation. A ^{65}Zn solution (1 mCi) was obtained from the Japan Radioisotope Association. Sodium salts of perchlorate, nitrate and chloride and other chemicals were all of analytical grade.

Apparatus. Extraction was carried out in a cylindrical glass tube with a magnetic stirrer in a water bath. The temperature was controlled by a thermoregulator to ±0.1 °C. A JASCO Ubest-30 spectrophotometer was used for the determination of 2-methyl-8-quinolinol. The concentration of zinc was determined by measuring the γ-radioactivity of aliquots of both aqueous and organic phases with a Packard Auto-Gamma 5100 single-channel pulse-height analyzer. Cadmium in both the phases was determined by a Nippon Jarrel Ash 8200 atomic absorption spectrophotometer equipped with a Nippon Jarrel Ash FLA 100 graphite furnace atomizer. For pH measurements, a Hitachi-Horiba M-5 pH meter equipped with a glass-calomel electrode pair for high-temperature work was used.

The conductivity measurements were carried out at 25.00±0.01 °C with a Yokogawa Hewlett Packard bridge, Type BV-Z-13B and a Yanagimoto conductivity cell, Type C.

Procedures. Partition of 2-Methyl-8-quinolinol: Equal (25 ml) volumes of the TCE solution containing a known concentration of 2-methyl-8-quinolinol and an aqueous solution pre-saturated with TCE were shaken in a constant-temperature bath for 3 h. The aqueous phase was adjusted to pH 8 with a borate buffer solution, and to an ionic strength of 0.1 with sodium perchlorate. After equilibration, the phases were immediately separated and cooled to room temperature. An aliquot of the aqueous phase was extracted into chloroform, while an aliquot of the organic phase was dissolved into chloroform. Then, the concentrations of 2-methyl-8-quinolinol were determined by measuring its UV absorbance at 312 nm.

Extraction Procedure: A 30 ml portion of a buffered zinc or cadmium solution was stirred with a 10 ml portion of 8-

quinolinol or 2-methyl-8-quinolinol solution of organic solvents standing in a constant-temperature bath for 30 min, which was found to be adequate for the attainment of distribution equilibrium. The pH of the initial aqueous solution was adjusted to the desired value with a small amount of an acetic acid-acetate buffer solution. Also, the ionic strength of the aqueous solution was adjusted to 0.1 with sodium salts.

The pH value of the aqueous phase, measured in situ after stirring, was taken as the equilibrium pH value. After phase separation, the concentration of zinc was determined by measuring the γ-radioactivity of aliquots of both phases with a single-channel pulse-height analyzer. In the case of cadmium, the concentration of cadmium in the aqueos phase was immediately determined with an atomic absorption spectrophotometer; the organic phase was analyzed after back extracting into a nitric acid solution. In each case, the volume of the aqueous phase was corrected for temperature with the values of the water density given in the Smithsonian tables; the volumes of the organic phases were corrected for temperature with experimentally determined density functions. Thus, the density at any temperature employed could be calculated using the following formulae: $1.597-1.562\times10^{-3}$ ($t-20$) for 1,1,2,2-tetrachloroethane, $0.8610-8.783\times10^{-4}$($t-20$) for *p*-xylene, and $0.8256-7.415\times10^{-4}$ ($t-20$) for 1-octanol, where temperature is in degrees centigrade.

All the extraction experiments were carried out below pH 5.5, since metal ions could be adsorbed on the wall of a glass container or the interface of both phases at higher pH.

Results and Discussion

Extraction of Zinc and Cadmium Complexes of 8-Quinolinol into TCE in the Presence of Several Inorganic Anions. The extraction of the zinc 8-quinolinol complex has been reported by several investigators.[9-14] A number of different species thought to have been extracted into the chloroform have been proposed: for example, $ZnQ_2HQ\cdot H_2O$,[9] $ZnQ_2(HQ)_2$,[10,11] and $ZnQ_2HQ\cdot S$,[12] where S represents the organic solvent. Furthermore, Oki et al.[13] and Sekido et al.,[14,15] have reported that an ionic association complex having the composition $Zn_2Q_3(HQ)_3{}^+ClO_4{}^-$ is extracted into chloroform from a zinc solution containing perchlorate ion.

Four types of plots were analyzed in order to determine the composition of zinc chelate under various conditions: $\log D$ vs. $\log[HQ]_0$, $\log D$ vs. pH, $\log D$ vs. $\log[X^-]$, and $\log D$ vs. $\log[Zn]_T$ at constant conditions for all the other factors, respectively. Herer, D is the distribution ratio of zinc; $[HQ]_o$, the concentration of 8-quinolinol in the organic phase; $[X^-]$, the concentration of inorganic anions in the aqueous phase; and $[Zn]_T$, the total concentration of zinc, respectively. Plots of $\log D$ vs. $\log[HQ]_0$ at 20 °C in the presence of perchlorate and chloride ions are shown in Fig. 1. It seems that three 8-quinolinol molecules combine with one zinc ion in these extraction systems, since all curves have solpes of 3. The curves in Fig. 2 show the relationship between $\log D$ and the pH at various

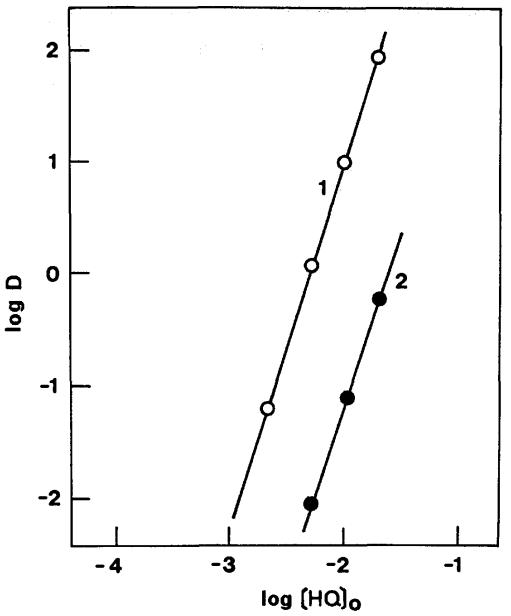

Fig. 1. Effects of 8-quinolinol concentration on the distribution ratio of zinc between TCE and water in the presence of perchlorate and chloride at 20 °C. $[Zn]_T=10^{-6}$ M, 0.09 M salts+0.01 M (AcOH-AcONa buffer) pH 5.0, 1; $NaClO_4$, 2; NaCl.

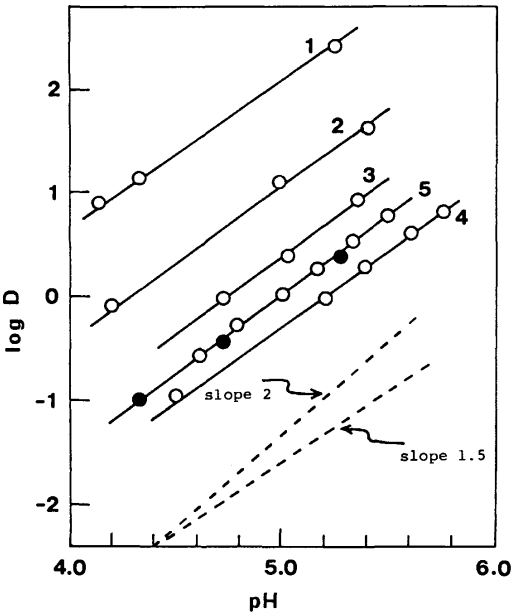

Fig. 2. Effects of pH on the distribution ratio of zinc between TCE and water.
1—5; $NaClO_4$ system, $[HQ]_o=2\times10^{-2}$ M, 1; 20 °C, 2; 40 °C, 3; 60 °C, 4; 80 °C, 5; $[HQ]_o=5\times10^{-3}$ M, 25 °C, ●; NaCl system, $[HQ]_o=2\times10^{-2}$ M, 20 °C.

temperatures. The curves have slopes of 1.5 for the perchlorate system in the temperature range 20 to 80 °C and for the chloride system at 20 °C, as indicated by solid circles. In these systems it is supposed that one and a half hydrogen ions dissociate from three molecules of 8-quinolinol to form a chelate in the aqueous phase. In other words, three molecules of 8-

quinolinol and one and half molecules of hydrogen ions apparently combine with one zinc ion. In Fig. 3 values of log D are plotted against log[X^-]. In the perchlorate and chloride systems, the slopes of curves (1) and (2) both equal 0.5 at pH 5.0. This phenomenon is not accidental at pH 5.0, but also holds at different pH. It seems that half a molecule of anion apparently attaches itself to one zinc molecule in these systems. The curves in Fig. 4 show the relationship between log D and log$[Zn]_T$ in the perchlorate and chloride systems. The curves have slopes of nearly 0, though log D values increase only slightly as the concentration of zinc increases. The fact that log D is independent of the concentration of zinc has been considered to indicate that a mononuclear complex is the predominant zinc species in the organic phase.[13] However, if a mononuclear complex were the predominant species, unusual ionic dissociation of the binuclear complex in the organic phase must be assumed as follows, since the apparent composition of this complex is $ZnQ_3H_{3/2}X_{1/2}$ from above results:

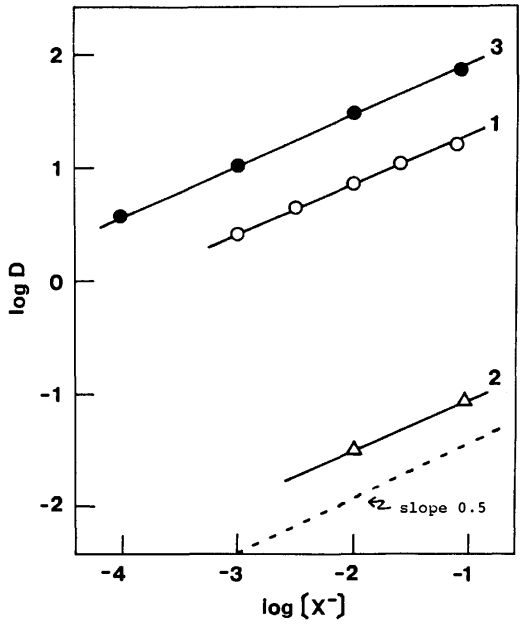

Fig. 3. Effects of concentration of inorganic anions on the distribution ratio of zinc between TCE and water at 20 °C.
$[HQ]_o=10^{-2}$ M, pH 5.0, 1; $NaClO_4$ system, 2; NaCl system, 3; $[HQ]_o=10^{-1}$ M, pH 3.8, $NaClO_4$ system.

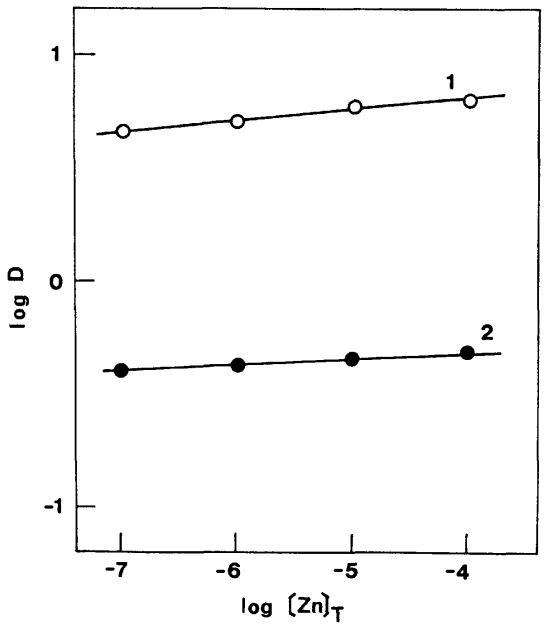

Fig. 4. Effects of metal concentration on the distribution ratio of zinc between TCE and water at 20 °C.
$[HQ]_o=2\times10^{-2}$ M, 1; $NaClO_4$ system, pH 4.0, 2; NaCl system, pH 4.8.

$$Zn_2Q_6H_3X_{(o)} \rightleftarrows ZnQ_3H_2^+{}_{(o)} + ZnQ_3HX^-{}_{(o)}, \quad (1)$$

where subscript o refers to the species in the organic phase.

Then, if the binuclear complex almost dissociates in the organic phase,

$$Zn_2Q_6H_3X_{(o)} \rightleftarrows Zn_2Q_6H_3^+{}_{(o)} + X^-{}_{(o)}, \quad (2)$$

the distribution ratio of zinc between the organic and aqueous phases in the acidic media would be given by following equation, since the simple zinc ion is the predominant zinc species in the aqueous phase:

$$D = \frac{2[Zn_2Q_6H_3^+]_o}{[Zn^{2+}]} \quad (3)$$

The extraction equation can be written as

$$2Zn^{2+} + 6HQ_{(o)} + X^- \rightleftarrows Zn_2Q_3(HQ)_3^+{}_{(o)} + X^-{}_{(o)} + 3H^+. \quad (4)$$

The extraction constant is

$$K_{ex} = \frac{[Zn_2Q_3(HQ)_3^+]_o[X^-]_o[H^+]^3}{[Zn^{2+}]^2[HQ]_o^6[X^-]} \quad (5)$$

In order to keep the electrical neutrality in the organic phase, $[Zn_2Q_3(HQ)_3^+]_o=[X^-]_o$, Eq. 5 can be transformed into

$$K_{ex} = \frac{[Zn_2Q_3(HQ)_3^+]_o^2[H^+]^3}{[Zn^{2+}]^2[HQ]_o^6[X^-]} \quad (6)$$

The distribution ratio, D can be given as

$$D = 2K_{ex}^{1/2}[HQ]_o^3[H^+]^{-3/2}[X^-]^{1/2}. \quad (7)$$

This equation means that plots of log D vs. log$[HQ]_o$ show a slope of 3, plots of log D vs. pH a slope of 1.5 and plots of log D vs. log[X^-] a slope of 0.5. Thus, the assumption that the ion pair of the binuclear complex would dissociate in the organic phase agrees well with the experimental results.

The dissociation of ion-associated complexes in an organic solvent with a dielectric constant that is relatively high, such as nitrobenzene (34.8), has already been reported. However, the dielectric constant of

TCE is 8.2 (at 20 °C). In order to corroborate the dissociation of the binuclear complex in TCE, the conductivities (Λ) of the extract into TCE in the presence of perchlorate or chloride were measured at 25 °C. The zinc concentration was varied from 10^{-5} to 10^{-3} M (1 M=1 mol dm^{-3}). Plots of Λ vs. $\sqrt{C}$ of zinc chelate of 8-quinolinol extracted into TCE are shown in Fig. 5. The limiting equivalent conductivities (Λ_0) can be calculated from the equation as follows:

$$\Lambda_0 = \frac{0.820|Z_i|}{\eta r_s}, \quad (8)$$

where η is the viscosity of the organic solvent and r_s is the Stokes radius. η of TCE at 25 °C is 1.60. The ionic radii of perchlorate and chloride are 2.4 Å[16] and 1.67 Å.[17] The ionic radius of the complex cation, $Zn_2Q_6H_3^+$, was estimated to be 8.7 Å by assuming it is 1.5-times larger than that of the simple chelate, ZnQ_2 (5.8 Å).[18] The dissociation constants were calculated to be 5.04×10^{-6} and 2.67×10^{-6}, respectively, from the degrees of dissociation ($\alpha=\Lambda/\Lambda_0$). Therefore, at a zinc concentration of 10^{-6} M, where the extraction experiment was carried out, it is considered that 98 and 77% of the ion pair of the binuclear zinc complexes could dissociate in TCE when in the presence of perchlorate and chloride, respectively. The results of conductivity measurements endorse the assumption that the ion pair of the binuclear complex dissociates into a complex cation and an inorganic anion in TCE.

The extraction behavior of cadmium chelate of 8-quinolinol into TCE is similar to that of the zinc chelate. The binuclear complex also dissociates in the organic phase as

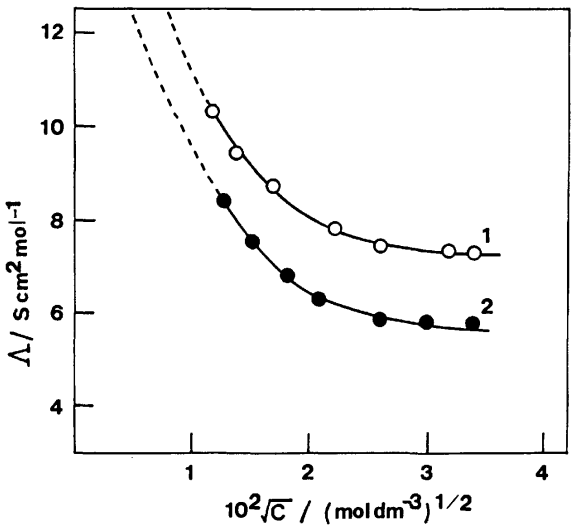

Fig. 5. Λ vs. $\sqrt{C}$ plots of zinc chelate of 8-quinolinol extracted into TCE at 25 °C.
1; $NaClO_4$ system, 2; NaCl system.

$$2Cd^{2+}+6HQ_{(o)}+X^- \rightleftarrows Cd_2Q_3(HQ)_3^+{}_{(o)}+X^-{}_{(o)}+3H^+. \quad (9)$$

The slopes of the plots of log D vs. log $[HQ]_o$, log D vs. pH and log D vs. log $[X^-]$ are 3, 1.5, and 0.5, respectively.

Plots of log D vs. $1/T$ for zinc and cadmium in the presence of perchlorate and chloride ions are shown in Fig. 6. The distribution ratios decrease remarkably with an increase in temperature for both zinc and cadmium. The curves for cadmium are linear up to fairly high temperatures, even for the chloride system, when compared to that of zinc. The changes of the slope of log D vs. $1/T$ suggest that the extracted species at high-temperature ranges are different from those at low-temperature ranges. This is supported by the fact that the slopes of the plots of log D vs. log $[HQ]_o$ in the zinc extraction system become smaller than 3 at high temperatures, especially for smaller anions, such as chloride and sulfate.[7] At high temperatures, the extraction of anhydrous chelate ZnQ_2 may occur in a manner similar to the 2-methyl-8-quinolinol system (as stated below). In the case of cadmium, a stable ion-associated compound is formed even in the chloride system at high temperatures because the ionic radius of the complex cation for cadmium is larger than that for zinc.

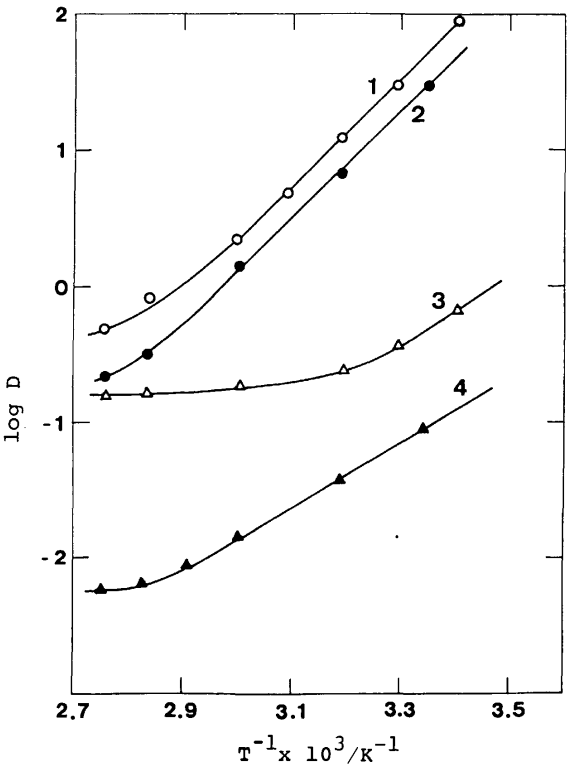

Fig. 6. Effects of temperature on the distribution ratio of zinc and cadmium with 8-quinolinol between TCE and water.
pH 5.0, 1; Zn, $NaClO_4$ system, $[HQ]_o=2\times10^{-2}$ M, 2; Cd, $NaClO_4$ system, $[HQ]_o=10^{-1}$ M, 3; Zn, NaCl system, $[HQ]_o=2\times10^{-2}$ M, 4; Cd, NaCl system, $[HQ]_o=10^{-1}$ M.

Extraction of Zinc and Cadmium with 2-Methyl-8-quinolinol into TCE in the Presence of Several Inorganic Anions. Since the chemical nature of 2-methyl-8-quinolinol is similar to that of 8-quinolinol, a large difference in the extraction behaviors of metal ions between both the ligands is not observed in most cases. In some cases, however, the structures of complexes with 2-methyl-8-quinolinol are quite different from those with 8-quinolinol, probably due to a steric hindrance effect of the methyl group, although this is debatable.[19]

The extraction of zinc and cadmium with 2-methyl-8-quinolinol into TCE in the presence of perchlorate and chloride ions was studied at various temperatures for a comparison with that with 8-quinolinol.

Plots of log D vs. variables such as pH, the concentrations of 2-methyl-8-quinolinol and concentrations of inorganic anions were obtained in order to determine the stoichiometry of the extracted species. The slopes of log D vs. pH, log D vs. log$[HR]_o$ and log D vs. log$[X^-]$ are 1.5, 3, and 0.5, respectively. Additionally, plots of log D vs. log$[Cd]_T$ are constant in the cadmium concentration range 10^{-6} M to 10^{-4} M. Therefore, the extraction behavior of the cadmium chelate of 2-methyl-8-quinolinol into TCE is similar to those of zinc and cadmium chelates of 8-quinolinol into TCE.

Hence, the extraction equation can be given as

$$2Cd^{2+} + 6HR_{(o)} + X^- \rightleftarrows Cd_2R_3(HR)_3^+{}_{(o)} + X^-{}_{(o)} + 3H^+. \quad (10)$$

The extraction behavior of zinc-2-methyl-8-quinolinol chelate into TCE is unlike the case of cadmium. The slopes of log D vs. pH are 2 at each temperature. The plots of log D vs. log$[HR]_o$ at a constant pH are linear with a slope of 2. The distribution ration of zinc are uneffected by the kind of inorganic anion involved. Thus, it can be concluded that only a single species, the simple 1 : 2 chelate, ZnR_2, is present in TCE. The overall raction can be represented by

$$Zn^{2+} + 2HR \rightleftarrows ZnR_2 + 2H^+. \quad (11)$$

In Fig. 7, the values of log D at pH 5.5 are plotted against the reciprocal of temperature for zinc and cadmium. In the case of cadmium, the distribution ratios decrease remarkably with an increase in temperature for perchlorate and chloride. The trend is similar to those of zinc and cadmium chelates of 8-quinolinol into TCE. However, in the case of zinc, the distribution ratios increase with an increase in temperature. The opposite effect is noted in the cases of cadmium and zinc with 8-quinolinol. These results indicate that the difference in distribution ratios of zinc and cadmium can be enhanced at high temperatures. Hence, solvent extraction with 2-methyl-8-quinolinol at high temperatures can be applied to the separation of zinc and cadmium in aqueous samples.

The principal difference between 8-quinolinol and

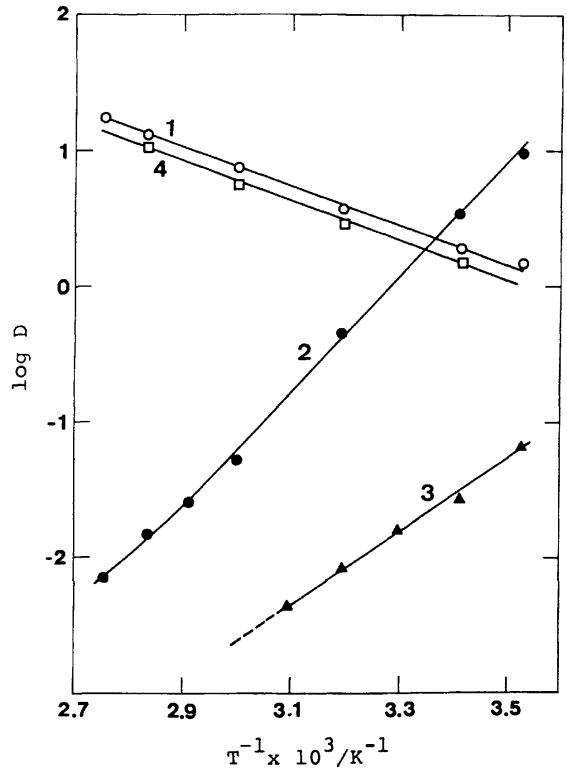

Fig. 7. Effects of temperature on the distribution ratio of zinc and cadmium with 2-methyl-8-quinolinol between TCE (or p-xylene) and water. pH 5.5, solvent=TCE, 1; Zn , $[HR]_o=5\times10^{-2}$ M, 2; Cd, $NaClO_4$ system, $[HR]_o=10^{-1}$ M, 3; Cd, NaCl system 4; solvent=p-xylene, Zn, $[HR]_o=2\times10^{-1}$ M.

2-methyl-8-quinolinol in the extraction of zinc into TCE is that the former forms a self-adduct complex whereas the latter forms a simple 1 : 2 complex. In the case of cadmium, both the ligands form self-adduct complexes, probably because the ionic radius of cadmium (0.97 Å) is larger than that of zinc (0.74 Å).

Extraction of Zinc and Cadmium with 8-Quinolinol and 2-Methyl-8-quinolinol into p-Xylene. In the 8-quinolinol extraction system, the precipitation of zinc and cadmium chelates occur even in the low-pH range. Therefore, a detailed investigation concerning the temperature effects was omitted. The total γ-activities of ^{65}Zn in both the aqueous and organic phases suddenly decrease above pH 4.5 after 10 min of shaking. At pH 5.0, about 20% of zinc disappears after 1 min of shaking, and almost all zinc in both phases disappears after 20 min of shaking. These phenomena indicate that the hydrated chelate $ZnQ_2{\cdot}2H_2O$ may precipitate and be deposited at the interface of both phases.

In the 2-methyl-8-quinolinol extraction system, no zinc in either phase disappears. This indicates that the 2-position methyl group not only interrupts the formation of a self-adduct complex of zinc, but also makes the dehydration of the zinc chelate easy. The extraction of zinc with 2-methyl-8-quinolinol into p-

xylene was evaluated by a slope analysis. The results showed that the zinc chelate of 2-methyl-8-quinolinol is extracted into *p*-xylene as a simple 1:2 complex, ZnQ_2, similar to the case of the extraction of the zinc chelate of 2-methyl-8-quinolinol into TCE. The distribution ratios increase with an increase in temperature, as shown in Fig. 7. Similar effects are noted in zinc extraction with 2-methyl-8-quinolinol into TCE.

Extraction of Zinc and Cadmium with 8-Quinolinol or 2-Methyl-8-quinolinol into 1-Octanol. According to the report of Schweitzer et al.,[1] when 1-butanol is used as an extracting solvent, the zinc chelate of 8-quinolinol is extracted as a solvent-adduct compound, $ZnQ_2 \cdot S_2$ (S is an alcohol molecule). In the case of a 1-octanol extraction system, the extraction mechanism of zinc and cadmium with 8-quinolinol or 2-methyl-8-quinolinol is similar to the case of 1-butanol. The slopes of log *D* vs. log[HQ(or HR)]$_o$ exhibit a linear range with a slope of 2. Additionally, the plots of log *D* vs. log[S]$_o$, when 1-octanol is dissolved in hexane, give a straight line of slope 2. These results suggest that the extracted species in octanol is a solvent-adduct compound, $MQ_2 \cdot S_2$ or $MR_2 \cdot S_2$. Temperature effects on the distribution ratios of zinc and cadmium with 8-quinolinol and 2-methyl-8-quinolinol are shown in Fig. 8. The distribution ratios are almost constant with a change in temperature.

Thermodynamic Parameters. The thermodynamic parameters for the distribution of 8-quinolinol[6] and 2-methyl-8-quinolinol between organic solvents and water are listed in Table 1. The values of log K_{DR} (K_{DR} is the distribution constant of reagent) for TCE, which have not been reported, are of a similar order to those for chloroform.[20,21] In all cases the ΔH values are negative and the ΔS values are positive. Hence, the fact that 8-quinolinol and 2-methyl-8-quinolinol are more soluble in organic solvents such as TCE, *p*-xylene, and 1-octanol than in water is due to the favorable contributions of both enthalpy and entropy. All the values of ΔH for the distribution processes of 8-quinolinol and 2-methyl-8-quinolinol are smaller than the values of the hydrogen-bond energy (10 to 25

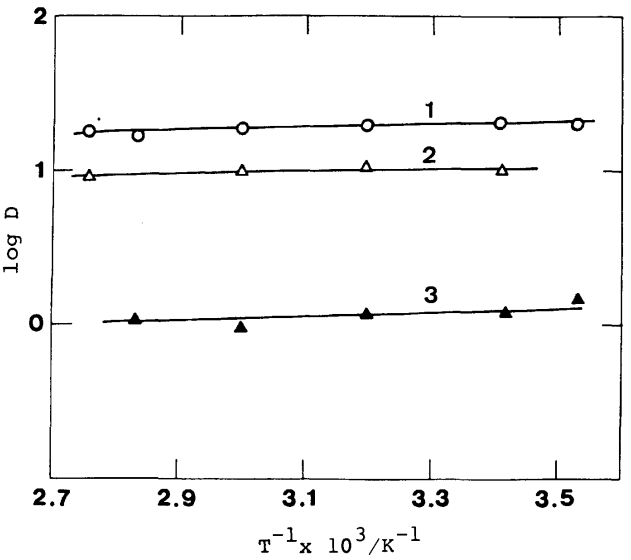

Fig. 8. Effects of temperature on the distribution ratio of zinc and cadmium between 1-octanol and water.
1; Zn, 8-quinolinol, [HQ]$_o$=10^{-2} M, 2; Zn, 2-methyl-8-quinolinol, [HR]$_o$=5×10^{-2} M, 3; Cd, 2-methyl-8-quinolinol, [HR]$_o$=5×10^{-2} M.

Table 1. Thermodynamic Values for the Distribution of 8-Quinolinol and 2-Methyl-8-quinolinol between Organic Solvents and Water at 20 °C

Ligand	Solvent	log K_{DR}	ΔG	ΔH	ΔS
			kJ mol^{-1}	kJ mol^{-1}	J K^{-1} mol^{-1}
8-Quinolinol	TCE	2.64	−14.8	−5.02	33.5
	p-Xylene	2.09	−11.7	−4.18	25.5
	1-Octanol	1.94	−10.9	−3.35	25.9
2-Methyl-8-quinolinol	TCE	3.15	−17.7	−9.10	29.4

Table 2. Thermodynamic Values for Extraction of Zn(II) with 8-Quinolinol and 2-Methyl-8-quinolinol into TCE, *p*-Xylene, and 1-Octanol at 20 °C

Ligand	Solvent	Species	log K_{ex}	ΔG	ΔH	ΔS
				kJ mol^{-1}	kJ mol^{-1}	J K^{-1} mol^{-1}
8-Quinolinol	TCE	$Zn_2Q_3(HQ)_3{}^+ClO_4{}^-$	−0.66	3.70	−153	−535
	TCE	$Zn_2Q_3(HQ)_3{}^+Cl^-$	−4.70	26.4	−95.4	−416
	p-Xylene	Precipitated	—	—	—	—
	1-Octanol	$ZnQ_2 \cdot S_2$	—	—	≃0	—
2-Methyl-8-quinolinol	TCE	ZnR_2	−8.10	45.4	33.5	−40.6
	p-Xylene	ZnR_2	−9.42	52.8	33.5	−65.9
	1-Octanol	$ZnR_2 \cdot S_2$	—	—	≃0	—

Table 3. Thermodynamic Values for Extraction of Cd(II) with 8-Quinolinol and 2-Methyl-8-quinolinol into TCE, *p*-Xylene, and 1-Octanol at 20 °C

Ligand	Solvent	Species	$\log K_{ex}$	ΔG	ΔH	ΔS
				kJ mol^{-1}	kJ mol^{-1}	J K^{-1} mol^{-1}
8-Quinolinol	TCE	$Cd_2Q_3(HQ)_3^+ClO_4^-$	−5.57	31.2	−169	−683
	TCE	$Cd_2Q_3(HQ)_3^+Cl^-$	−10.33	58.0	−108	−567
	p-Xylene	Precipitated	—	—	—	—
	1-Octanol	$CdQ_2 \cdot S_2$	—	—	≃0	—
2-Methyl-8-quinolinol	TCE	$Cd_2R_3(HR)_3^+ClO_4^-$	−8.92	50.0	−163	−727
	TCE	$Cd_2R_3(HR)_3^+Cl^-$	−13.27	74.4	−106	−616
	p-Xylene	precipitated	—	—	—	—
	1-Octanol	$CdR_2 \cdot S_2$	—	—	≃0	—

kJ mol^{-1}).

The thermodynamic parameters for the extraction of zinc and cadmium with 8-quinolinol and 2-methyl-8-quinolinol into TCE, *p*-xylene, and 1-octanol are summarized in Tables 2 and 3.

In a series of the ion-associated complexes of zinc and cadmium, the values of ΔH are largely negative, which shows that the extraction of the complex ion pair is an exothermic reaction. The order of their ΔH values correlates with their extractability. Thus, the larger is the size of an inorganic anion or metal ion, the larger is the absolute values of ΔH. The values ΔS are also largely negative and proportional to those of ΔH in the ion-associated complex series of metals and inorganic anions. This is generally the trend observed in the thermodynamics of ion-pair extraction, indicating that the exothermic property is partly compensated with the term of ΔS. The values of ΔH for the extraction of cadmium with 2-methyl-8-quinolinol are similar to those of cadmium with 8-quinolinol in the presence of perchlorate and chloride. The extraction mechanism of cadmium with 2-methyl-8-quinolinol is similar to that of cadmium with 8-quinolinol.

The extraction of zinc with 2-methyl-8-quinolinol into TCE and *p*-xylene is an endothermic reaction, unlike the extraction of zinc with 8-quinolinol into TCE. It has been reported that this behavior is characteristic of chelating reactions in which the water molecules of the inner-coordination sphere of the metal ion are displaced by the chelating reagent.[22] The extraction constant (K_{ex}) of zinc with 2-methyl-8-quinolinol into TCE and *p*-xylene is a composite of the chelate formation constant, β_2, and its distribution constant, K_{DC}, as well as of the reagent acid-dissociation constant, K_a, and its distribution constant, K_{DR}: $K_{ex}=\beta_2 K_{DC} K_a^2 / K_{DR}^2$. β_2 and K_a are independent of the organic solvent. Therefore, the difference in the extraction constant between TCE and *p*-xylene can be related to the difference in the product, $K_{DC}K_{DR}^{-2}$. The values of ΔH for extraction constants are both 33.5 kJ mol^{-1} for TCE and *p*-xylene. It is conceivable that the difference in the ΔH values for the distribution coefficients of 2-methyl-8-quinolinol between TCE and *p*-xylene would be small, since the difference in the ΔH values for those of 8-quinolinol between both the solvents is also small (Table 1). Therefore, it is considered that the value of ΔH for the distribution constant of the zinc chelate with 2-methyl-8-quinolinol into TCE is almost the same as that into *p*-xylene. This means that the distribution of ZnR_2 into the organic phase is controlled by its own dehydration. The minute difference in the ΔG values between the TCE and *p*-xylene system is attributed to the ΔS term, probably due to the solvent-adduct ability of TCE with zinc chelates. The ΔH values for solvent-adduct systems are quite small, being close to zero.

References

1) F. F. Dyer and G. K. Schweizer, *Anal. Chim. Acta*, **23**, 1 (1960).
2) G. K. Schweizer and G. R. Coe, *Anal. Chim. Acta*, **24**, 311 (1961).
3) H. E. Hellwege and G. K. Schweizer, *Anal. Chim. Acta*, **28**, 236 (1963).
4) J. G. Mason and I. Lipshitz, *Talanta*, **18**, 1111 (1971).
5) G. R. Choppin, A. T. Kandil, H. F. Aly, and M. Raieh, *J. Inorg. Nucl. Chem.*, **37**, 229 (1975).
6) E. Nakayama, *Memoirs of the Faculty of Science, Kyoto University, Series A of Physics, Astrophysics, Geophysics and Chemistry*, **35**, 203 (1977).
7) E. Nakayama, *Memoirs of the Faculty of Science, Kyoto University, Series A of Physics, Astrophysics, Geophysics and Chemistry*, **35**, 210 (1977).
8) E. Yamada, E. Nakayama, and M. Sato, *Bull. Chem. Soc. Jpn.*, **62**, 1047 (1989).
9) Fa-Chun Chou, Q. Fernando, and H. Freiser, *Anal. Chem.*, **37**, 361 (1965).
10) J. Stary, *Anal. Chim. Acta*, **28**, 132 (1963).
11) S. Ôki, *Bunseki Kagaku*, **18**, 822 (1969).
12) G. K. Schweitzer, R. B. Neel, and F. R. Clifford, *Anal. Chim. Acta*, **33**, 514 (1965).
13) S. Ôki and I. Terada, *Anal. Chim. Acta*, **61**, 49 (1972).
14) E. Sekido, Y. Yoshimura, and Y. Masuda, *J. Inorg. Nucl. Chem.*, **38**, 1183 (1976).
15) E. Sekido and Y. Yoshimura, *J. Inorg. Nucl. Chem.*, **38**, 1187 (1976).
16) H. D. B. Jenkins and K. P. Thakur, *J. Chem. Educ.*, **56**, 576 (1979).

17) R. D. Shannon, *Acta Crystallogr., Sect. A*, **32**, 751 (1976).
18) L. L. Merritt, Jr. R. I. Cady, and B. W. Mundy, *Acta Crystallogr.*, **7**, 473 (1959).
19) R. L. Stevenson and H. Freiser, *Anal. Chem.*, **39**, 1354 (1967).
20) J. Fresco and H. Freiser, *Anal. Chem.*, **36**, 631 (1964).
21) J. Stary and H. Freiser, "Equilibrium Constants of Liquid-Liquid Distribution Reactions Part IV: Chelating Extractants," Pergamon Press (1978), p. 66.
22) G. R. Choppin and H. G. Friedman, *Inorg. Chem.*, **5**, 1599 (1966).

Solvent Effect on the Liquid-Liquid Partition of 21*H*,23*H*-Porphine between Various Organic Solvents and Acidic Aqueous Solutions

Yoshito WAKUI,† Hisanori IMURA, and Nobuo SUZUKI*
Department of Chemistry, Faculty of Science, Tohoku University, Sendai 980
(Received December 16, 1988)

The liquid-liquid partition equilibrium of 21*H*,23*H*-porphine has been investigated at 25 °C. Organic phases were heptane, dodecane, carbon tetrachloride, benzene, toluene, chloroform, dichloromethane, and 1-octanol. The acidic aqueous phases were 5×10^{-2}—5×10^{-1} M hydrochloric acid. Porphine is present in such acidic solutions as a diprotonated form and no dimerization was found in any of the systems. The organic solvent effect on the partition coefficient of porphine is discussed with the aid of regular solution theory, and the solubility parameter of porphine is estimated as 10.7±0.6 $cal^{1/2}$ $cm^{-3/2}$.

Porphyrin and related derivatives are important compounds in biochemistry and geochemistry. In relation with chemical separation and natural migration of these porphyrin compounds, a systematic study on the solution behavior of porphyrins and their metal chelates is desirable. However, little is known about the solubility and the liquid-liquid partition of these porphyrin compounds. The solution behavior of a solute is governed by the physicochemical nature of the solute and solvents. The liquid-liquid partition of various organic solutes including metal β-diketonate complexes has been systematically studied and elucidated with the aid of regular solution theory and the scaled particle theory.[1-6]

In the present study, we have prepared high purity 21*H*,23*H*-porphine, which is the simplest porphyrin compound, having no substituent group. We have investigated its partition equilibria between various organic solvents and acidic aqueous solutions. The solvent effect is quantitatively discussed with the aid of regular solution theory.

Experimental

Materials. 2-Pyrrolecarbaldehyde (99% purity, Aldrich) was used as purchased. Carbon tetrachloride, chloroform, and dichloromethane were of spectroscopic grade (Spectrosol, Dojindo Lab.), and chloroform was used after washing several times with redistilled water. Other organic solvents were of guaranteed reagent grade and purified by ordinary methods.[7]

Hydrochloric acid was of analytical reagent grade (Wako Co.). The acid solutions were standardized with sodium carbonate (primary standard, Asahi glass Co.).

Unless otherwise stated, reagents used were of guaranteed reagent grade.

Preparation and Purification of 21*H*,23*H*-Porphine. 21*H*,23*H*-Porphine was synthesized by the method of Longo et al.,[8] and purified by a method modified somewhat from those of Rothemund[9] and Krol.[10] 2-(Hydroxymethyl)pyrrole, a starting material for synthesis of porphine, was prepared by reduction of 2-pyrrolecarbaldehyde with sodium borohydride according to the literature.[11] A crude product of porphine was obtained by keeping the dilute solution of 2-(hydroxymethyl)pyrrole in ethylbenzene at 100±2 °C with stirring. The ethylbenzene solution after reaction was fed into a silica-gel column (Kicselgel 60 HR, Merck) and eluted with benzene. The benzene solution obtained was washed with 50% (v/v) acetic acid and then 0.35% (w/v) hydrochloric acid. Porphine was extracted from benzene to 5% (w/v) hydrochloric acid. The aqueous solution was neutralized with a saturated sodium acetate solution and shaken with benzene to extract porphine. After washing with water, the benzene solution was concentrated with a rotary evaporator, and methanol was added to crystallize the porphine. A dark auburn crystalline product was filtered and dried over phosphorus pentaoxide in vacuo at 120 °C. Identification of the product was accomplished by C, H, N analysis, mass spectroscopy, proton magnetic resonance spectroscopy, and electronic absorption spectroscopy. The purity was also checked with high-performance liquid chromatography (column, LiChrosorb RP-18; mobile phase, acetone:acetonitrile:water=25:200:11.3; detection wavelength, 395 nm) and found to be more than 99%.

Apparatus. Absorbance of a solution was measured with a spectrophotometer (UVIDEC-2, JASCO). To prevent adsorption of porphine onto the wall of the glassware including volumetric flasks, and the quartz cell in the absorbance measurement, they were treated with dimethyldichlorosilane before use.

The extraction vial was shaken with a mechanical shaker at about 350 strokes per min. The density of the porphine solution was measured with a digital precision density meter (Anton Paar DMA-50). All experiments were carried out in a thermostated room at 25±0.5 °C.

Partition Experiments. An organic solvent and an acidic aqueous solution were preequilibrated to each other. A certain volume of the organic solution of porphine in 10^{-7}—10^{-4} M (1 M=1 mol dm^{-3}) was shaken with the acidic aqueous solution for 5—60 min and centrifuged. The ionic strength of an acidic aqueous solution was kept at 0.50 M with sodium chloride. The distribution ratio (D) of porphine which was the ratio of the total concentration of porphine in the organic phase to that in the aqueous phase was determined from the absorbance of the organic phases before (A_i) and after (A) shaking; $D=(V_a/V_0)A/(A_i-A)$, where V_a and V_0 are volume of the aqueous and the organic phase respectively. To ascertain achievement of the partition equilibrium, porphine was dissolved in an acidic aqueous solution and shaken with the organic solvent. The distribution ratio determined from the absorbance of the

† Present address: Government Industrial Research Institute, Tohoku, Nigatake, Sendai 983.

Table 1. Wavelengths Used for the Absorbance Measurement of Porphine in Various Solvents

Solvent	Wavelength[a]/ nm	Wavelength[b]/ nm
Heptane	391.6	
Dodecane	393.5	
Carbon tetrachloride	396.8	490.1
Benzene	396.4	489.5
Toluene	396.4	
Chloroform	394.8	489.7
Dichloromethane	393.4	488.9
1-Octanol	393.7	
Water[c]	393.9	542.1

a) Soret band. b) Q Band was also used for the partition measurement. c) 0.5 M hydrochloric acid.

equilibrated aqueous phases is in good agreement with that obtained above. The wavelengths used for the absorbance measurement in different organic solvents are shown in Table 1. Lambert-Beer's rule was confirmed in the absorbance range of 0.13—0.67 in benzene and the acidic aqueous solution.

Density Measurement. The partial molar volume of porphine was calculated from the densities of porphine solutions in varying concentrations. The solubility of porphine in various organic solvents was remarkably low. A sufficient solubility of porphine to measure the difference in the density of the solution was obtained using only pyridine as a solvent. The concentration range of porphine was 4×10^{-4}—2×10^{-3} M. The uncertainty in the density measurement was within $\pm1\times10^{-5}$ g cm^{-3}.

Results and Discussion

Partition Equilibrium. Porphine (denoted as H_2A) is a nitrogen base and its partition between an organic phase and an acidic aqueous phase can be represented by the following equilibria.

$$H_2A + nH^+ \rightleftarrows H_{n+2}A^{n+} \qquad K_n = \frac{[H_{n+2}A^{n+}]}{[H_2A][H^+]^n}, \quad (1)$$

$$H_2A \rightleftarrows H_2A_o \qquad P = \frac{[H_2A]_o}{[H_2A]}, \quad (2)$$

where K_n and P are the overall protonation constant and the partition coefficient, respectively. The subscript o refers to the organic phase. Dimerization of porphine in the organic and aqueous phases is negligible under the present experimental conditions of sufficiently low concentration of porphine (vide infra). The distribution ratio of porphine is given by

$$D = \frac{[H_2A]_o}{[H_2A] + [H_3A^+] + [H_4A^{2+}] + \cdots + [H_{n+2}A^{n+}]}. \quad (3)$$

If a single species of protonated porphine is present in the aqueous phase, the distribution ratio can be written as

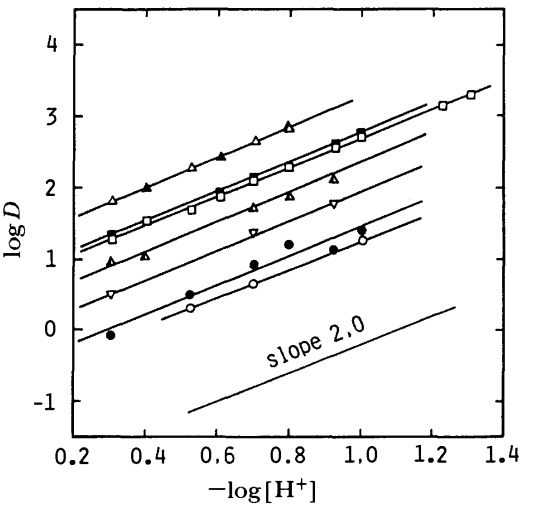

Fig. 1. Distribution ratio of porphine as a function of hydrogen ion concentration in the aqueous phase.
○, Heptane; ●, dodecane; ▲, carbon tetrachloride; □, benzene; ■, toluene; △, chloroform; ▲, dichloromethane; ▽, 1-octanol.

Table 2. Effect of the Porphine Concentration on the Partition Equilibrium of Porphine at 25 °C

$[H^+]$/M	$[\text{Porphine}]_{org}$[a]/ M	$[\text{Porphine}]_{aq}$[b]/ M	$\log P \cdot K_2^{-1}$
4.98×10^{-1}	3.80×10^{-7}	1.96×10^{-8}	0.68
3.98×10^{-1}	1.52×10^{-6}	4.40×10^{-8}	0.74
2.99×10^{-1}	3.90×10^{-6}	7.82×10^{-8}	0.64
2.49×10^{-1}	7.15×10^{-6}	9.50×10^{-8}	0.67
1.99×10^{-1}	6.62×10^{-6}	5.25×10^{-8}	0.70
1.59×10^{-1}	1.56×10^{-5}	7.84×10^{-8}	0.70
1.19×10^{-1}	1.69×10^{-4}	4.62×10^{-7}	0.72
9.96×10^{-2}	1.68×10^{-4}	3.31×10^{-7}	0.70
5.97×10^{-2}	1.64×10^{-4}	1.19×10^{-7}	0.69
4.98×10^{-2}	1.64×10^{-4}	8.50×10^{-8}	0.68

a) Equilibrium concentration in benzene phase. b) Equilibrium concentration in aqueous phase.

$$D = \frac{P}{K_n[H^+]^n}. \quad (4)$$

The dependence of the distribution ratio of porphine on the hydrogen ion concentration and the solute concentration was investigated in detail in the benzene system. The plots of $\log D$ as a function of $\log[H^+]$ are shown in Fig. 1, together with those for other solvents. The plots for benzene give a straight line with a slope of 2.0 which is determined by the least squares method, and those for other solvents also give the slope of 2.0±0.1. These demonstrate that only a single species of diprotonated porphine, H_4A^{2+}, is present in the acidic aqueous solution of 5×10^{-2}—5×10^{-1} M H^+. The effect of the porphine concentration on the partition equilibrium was investigated, that is, the distribution ratios of porphine with various initial concentrations were determined at different hydrogen ion concentrations. In Table 2, the

results are expressed as the product of two constants of P and K_2^{-1} calculated from Eq. 4 by knowing n=2. A constant value of 0.69±0.03 is obtained over a wide range of porphine concentration, and this supports no dimerization of porphine in either phase.

The values of $\log P \cdot K_2^{-1}$ for different solvents are listed in Table 3. The value increases in the following order; heptane<dodecane<1-octanol<carbon tetrachloride<benzene≈toluene<chloroform≈dichloromethane. As the protonation constant K_2 is not influenced by the organic solvents, the difference in these values is directly proportional to those in the partition coefficients P for the organic solvents.

Partial Molar Volume of Porphine. The partial molar volume is one of the important physical measures in solution chemistry, but no data for porphine and related compounds have yet been reported. In this paper, the partial molar volume of porphine is measured and used in the calculation based on regular solution theory. The partial molar volume of porphine is calculated from the relation between the mean molar volume obtained from the density measurement, V_m, and the molar fraction of porphine, X_2,

$$V_m = \overline{V}_1 + (\overline{V}_2 - \overline{V}_1)X_2 \quad (5)$$

where $\overline{V}_1$ and $\overline{V}_2$ refer to the partial molar volumes of solvent and solute. The plots for Eq. 5 are shown in Fig. 2. The equation, $\overline{V}_m$=(80.4±0.002)+(155.3±15.3)X_2, was obtained by the least squares method, and the partial molar volume of porphine, $\overline{V}_2$=236±15 cm^3 mol^{-1} (95% confidence limit), was determined.

Solvent Effect on Partition Coefficient. The activity coefficient of a nonelectrolyte solute, γ_s, can be expressed on the basis of regular solution theory.[12]

$$\ln \gamma_s = \frac{V_s}{RT}(\delta_1^2 + \delta_s^2 - 2\delta_1\delta_s), \quad (6)$$

where V and δ are the molar volume and solubility parameters respectively, and the subscripts 1 and s denote solvent and solute, respectively. Since the activily of a solute in the organic phase is equal to that in the aqueous phase in partition equilibrium, the partition coefficient of a solute expressed as a molar fraction, P^X, is related to the activity coefficient;

$$P^X = \frac{X_{s,o}}{X_{s,a}} = \frac{\gamma_{s,a}}{\gamma_{s,o}}, \quad (7)$$

where X is the molar fraction and the subscript a denotes the aqueous phase. From Eqs. 6 and 7, the following equation can be derived,

$$\frac{RT}{V_s}\ln P^X + \delta_o^2 = 2\delta_s\delta_o + \frac{RT}{V_s}\ln \gamma_{s,a} - \delta_s^2. \quad (8)$$

Substituting Eq. 4 (as n=2) into Eq. 8, we obtain.

$$\frac{RT}{V_s}(\ln D^X + 2\ln[H^+]) + \delta_o^2 = 2\delta_s\delta_o + \frac{RT}{V_s}\left(\ln \gamma_{s,a} - \ln K_2 - \frac{V_s\delta_s^2}{RT}\right), \quad (9)$$

where D^X is the distribution ratio expressed as a molar fraction. Since the second term of the right hand side of Eq. 9 is independent of the organic solvent, the plots of the left hand side against the solubility

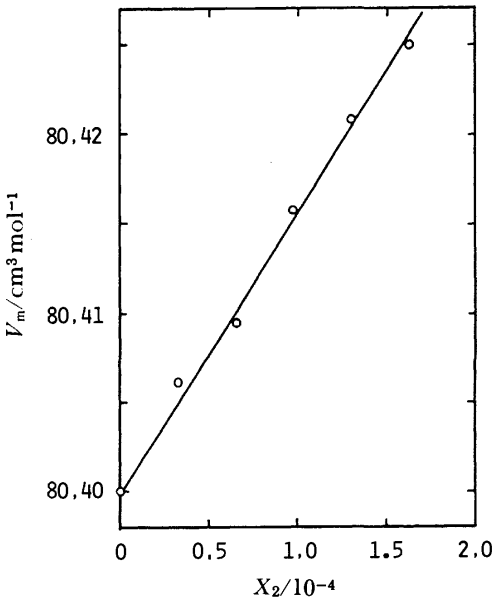

Fig. 2. Linear relationship between the mean molar volume of porphine solution in pyridine (V_m) and the molar fraction of porphine (X_2).

Table 3. Equilibrium Constants in the Partition of Porphine at 25 °C

No.	Solvent	δ_0[a]	$\log P \cdot K_2^{-1}$	$\log P^X \cdot K_2^{-1}$[c] (experimental)	$\log P^X \cdot K_2^{-1}$[c] (calculated)[d]
1	Heptane	7.431	−0.75±0.01	−3.32±0.01	−3.36
2	Dodecane	7.841	−0.55±0.12	−2.94±0.12	−2.92
3	Carbon tetrachloride	8.584	0.33±0.06	−2.43±0.06	−2.28
4	Benzene	9.158	0.69±0.03	−2.10±0.03	−1.91
5	Toluene	8.913	0.77±0.02	−1.95±0.02	−2.05
6	Chloroform	9.300[b]	1.24±0.03	−1.60±0.03	−1.84
7	Dichloromethane	9.830	1.23±0.02	−1.70±0.02	−1.63
8	1-Octanol	10.239	−0.06±0.03	−2.61±0.03	−1.53

a) Calculated from the heat of vaporization of the solvent.[7] b) From the literature.[15] c) From Eq. 4, expressed in molar fraction. d) From Eq. 9 (see text).

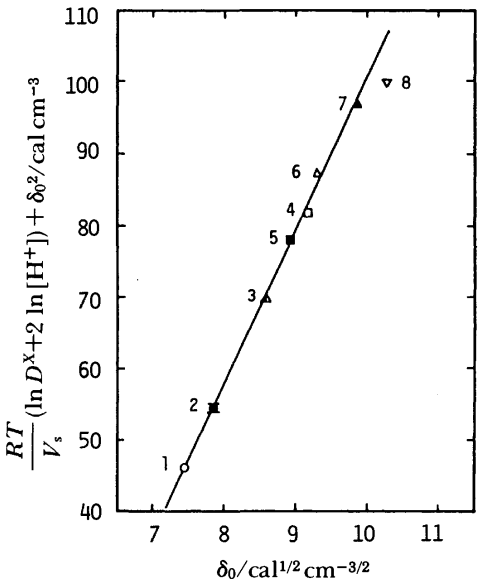

Fig. 3. Evaluation of the solvent effect of partition coefficient of porphine based on the regular solution theory. The numbers refer to those in Table 3.

parameter of the organic solvent, δ_0, should give a straight line, and the solubility parameter of porphine, δ_s, can be calculated from the slope. The $V_s$is replaced by the partial molar volume of porphine determined above. Even if the V_s value changes by 10% to larger or smaller values, it has an influence on the δ_s value of less than 3%. The solubility parameter of the organic solvent is calculated from the heat of vaporization of solvent at 25 °C.[7]

As shown in Fig. 3, the plots give a good linear relationship for heptane, dodecane, benzene, toluene, carbon tetrachloride, chloroform, and dichloromethane. Hence, these organic solutions of porphine may be designated regular solutions. The solubility parameter of porphine is calculated to be 10.7±0.6 cal$^{1/2}$ cm$^{-3/2}$ (95% confidence limit, 1 cal$^{1/2}$ cm$^{-3/2}$= 2.0455 J$^{1/2}$ cm$^{-3/2}$) by the least squares method of the plots for seven nonpolar solvents. This value is close to those of heterocyclic amines such as pyridine (10.7 cal$^{1/2}$ cm$^{-3/2}$) and quinoline (10.8 cal$^{1/2}$ cm$^{-3/2}$) which are calculated from the heat of vaporization of the pure liquid.[13]

The plot for 1-octanol is lower than the straight line drawn here. Considering that a direct solvation of 1-octanol to porphine possibly accompany a positive deviation, this negative deviation may be attributed to a peculiar behavior of a self-associated solvent such as 1-octanol which is refer to a larger δ_0 of 1-octanol (δ_0=10.2 cal$^{1/2}$ cm$^{-3/2}$). In other words it is unreasonable to treat the 1-octanol system strictly as a regular solution. It is interesting to note that chloroform does not cause any deviation in Fig. 3. This must be compared with a previous research of the solvent effect on the partition coefficient of heterocyclic amine such as 1,10-phenanthroline,[14] where a linear relationship expressed as Eq. 8 was again clear for heptane, cyclohexane, carbon tetrachloride, and benzene, but a large positive deviation was observed for chloroform. This was attributed to a specific interaction such as hydrogen bonding, between phenanthroline and chloroform. These results suggest that the nitrogen atoms in porphine hardly hydrogen bond with proton donors such as chloroform and 1-octanol.

The log $P^X \cdot K_2^{-1}$ for each solvent was calculated from Eq. 9 by knowing the second term of the right hand side from the intercept in Fig. 3. Table 3 shows that the calculated values are in good agreement, except for 1-octanol, with those obtained experimentally from D^X and [H$^+$] by Eq. 4. The log $P^X \cdot K_2^{-1}$ value for other nonpolar solvents can be calculated in this manner.

At present, P^X and/or K_2 can not be determined independently due to their high partition coefficient and the low solubility of porphine in the aqueous solvent. However the solvent effect on the liquid-liquid partition of the mother compound porphine can be quantitatively evaluated. This may be valuable information in understanding the solution behavior of porphyrin compounds.

References

1) H. M. N. H. Irving, "Application of the Solubility Concept in Liquid-Liquid Extraction, In Ion Exchange and Solvent Extraction," ed by J. A. Marinsky and Y. Marcus, Marcel Dekker, New York (1974), Vol. 6, p. 139.

2) N. Suzuki, T. Yoshida, and H. Watarai, *Bull. Chem. Soc. Jpn.*, **55**, 121 (1982).

3) H. Watarai, M. Tanaka, and N. Suzuki, *Anal. Chem.*, **54**, 702 (1982).

4) H. Watarai, H. Oshima, and N. Suzuki, *Quant. Stract. -Act. Relat.*, **3**, 17 (1984).

5) H. Imura and N. Suzuki, *Talanta*, **32**, 785 (1985).

6) H. Imura, S. Matsumora, and N. Suzuki, *Bull. Chem. Soc. Jpn.*, **59**, 621 (1986).

7) J. A. Riddick and W. B. Bunger, "Techniques of Chemistry, Vol. II, Organic Solvents," 3rd ed, Wiley Interscience, London (1970).

8) F. R. Longo, E. J. Thorne, A. D. Adler, and S. Dym, *J. Heterocycl. Chem.*, **12**, 1305 (1975).

9) P. Rothemund, *J. Am. Chem. Soc.*, **58**, 625 (1936).

10) S. Krol, *J. Org. Chem.*, **24**, 2065 (1959).

11) R. M. Silverstein, E. E. Ryskiewicz, and S. W. Chaikin, *J. Am. Chem. Soc.*, **76**, 4485 (1954).

12) J. H. Hildebrand and R. L. Scott, "Solubility of Nonelectrolytes," Dover, New York (1964).

13) A. F. M. Barton, *Chem. Rev.*, **75**, 731 (1975).

14) S. Nakamura, H. Imura, and N. Suzuki, *Inorg. Chim. Acta*, **109**, 157 (1985).

15) H. M. N. H. Irving and J. S. Smith, *J. Inorg. Nucl. Chem.*, **30**, 1873 (1968).

Structures and Spectral Properties of Some Bis(β-diketonato)copper(II)–Diazole Complexes. I. The 1:4 and 1:1 Adducts of Bis-(1,1,1,5,5,5-hexafluoro-2,4-pentanedionato)copper(II) and 3-Methyl-1*H*-pyrazole

Tamizo KOGANE,* Minoru ISHII,†,†† Kazumasa HARADA,† Reiko HIROTA,† and Masayoshi NAKAHARA†
Industrial Research Institute of Kanagawa Prefecture, Showa-machi, Kanazawa-ku, Yokohama 236
†Department of Chemistry, Faculty of Science, Rikkyo University, Nishi-ikebukuro, Toshima-ku, Tokyo 171
(Received January 5, 1989)

$Cu(hfac)_2(5\text{-}Hmpz)_4$ (**1**) and $Cu(hfac)_2(5\text{-}Hmpz)$ (**2**) (Hhfac=1,1,1,5,5,5-hexafluoro-2,4-pentanedione; 5-Hmpz=5-methyl-1*H*-pyrazole) have been prepared by the stoichiometric reactions of $Cu(hfac)_2$ with 3-methyl-1*H*-pyrazole in petroleum ether. The structures of **1** and **2** have been determined by X-ray analyses. Crystal data for **1**: triclinic, $P\bar{1}$, a=9.531(1), b=10.286(2), c=8.891(2) Å, α=95.85(2), β=95.52(2), γ=85.41(1)°, V=860.9(3) Å^3, Z=1, and R=0.061. Crystal data for **2**: triclinic, $P\bar{1}$, a=9.647(6), b=12.075(9), c=9.130(5) Å, α=107.43(5), β=99.30(5), γ=87.20(6)°, V=1001.3(12) Å^3, Z=2, and R=0.064. In **1**, the geometry about each copper atom is approximately that of a tetragonal bipyramid, with four nitrogen atoms from 5-Hmpz molecules in the equatorial plane and two oxygen atoms from each hfac ligand in the axial positions. Each of the uncoordinated oxygen atoms of hfac ligands is intramolecularly hydrogen-bonded with two imino groups of adjacent 5-Hmpz molecules. In IR spectra, the split bands of ν_{C-O} were observed at 1648 and 1659 cm^{-1}. In **2**, each copper atom is approximately in an environment of a tetragonal pyramid, with an oxygen atom from a hfac ligand at the apex and a nitrogen atom from a 5-Hmpz molecule in the basal plane. The copper atom is located slightly above the plane. The split bands of ν_{C-O} were observed at 1644, 1662, 1669 cm^{-1}. An interpretation of the observed IR spectral bands is proposed.

Diazoles have both a pyridine-type nitrogen and a pyrrole-type nitrogen (imino group) in the same molecule, and they can react bifunctionally with many metal ions or Lewis acids giving a variety of products.[1,2] We have reported that the reaction of bis(nonfluorinated β-diketonato)copper(II) with diazoles gave diazole adducts and/or μ-diazolato complexes.[3] However, the reactions of diazoles with bis-(fluorinated β-diketonato)copper(II) have scarcely been investigated. It is well known that bis(fluorinated β-diketonato)copper(II) is a strong Lewis acid and reacts with unidentate nitrogen heterocycles, e.g., pyridine, substituted pyridines, quinoline, etc., producing 1:1 and/or 1:2 adducts.[4] However, the structures of these adducts have not been fully elucidated. For several adducts of $Cu(hfac)_2$ with bidentate ligands having nitrogen donors, X-ray analyses have been made. For example, adducts with 2,2′-bipyridine (bpy),[5] 1,4-diazabicyclo[2.2.2]octane (ted),[6] pyrazine (pyz),[7] 1,8-bis(dimethylamino)naphthalene,[8] and *N*,*N*-dimethylethylenediamine (dmed)[9] have been isolated and their structures determined. It has been observed that, of these adducts, only the last one cited above, $Cu(hfac)_2(dmed)_2$, contains unidentate hfac ligands. We have prepared the 1:4 and 1:1 adducts of $Cu(hfac)_2$ with 3-methyl-1*H*-pyrazole and here we discuss their structures in relation to the hydrogen bonds and spectral properties.

Experimental

Materials. Bis(1,1,1,5,5,5-hexafluoro-2,4-pentanedionato)-copper(II) was prepared by the reported method.[10] 3-Methyl-1*H*-pyrazole (Tokyo Kasei) was used without further purification.

Preparation of the Complexes. $Cu(hfac)_2(5\text{-}Hmpz)_4$: $Cu(hfac)_2$ was warmed with four times molar quantities of 3-methyl-1*H*-pyrazole in petroleum ether under reflux for 1 h. After standing for several days, violet crystals were formed and dried in vacuo. Found: C, 38.56; H, 3.19; N, 13.93; Cu, 7.84%. Calcd for $C_{26}H_{26}N_8O_4F_{12}Cu$: C, 38.74; H, 3.25; N, 13.90; Cu, 7.88%.

$Cu(hfac)_2(5\text{-}Hmpz)$: $Cu(hfac)_2$ was warmed with an equimolar quantity of 3-methyl-1*H*-pyrazole in petroleum ether under reflux for 1 h. After cooling, a green precipitate was formed. It was filtered and recrystallized from petroleum ether. Found: C, 30.14; H, 1.46; N, 4.86%. Calcd for $C_{14}H_8N_2O_4F_{12}Cu$: C, 30.04; H, 1.44; N, 5.00%.

Spectral Measurement. IR spectra were recorded on a Hitachi Model 225 grating infrared spectrophotometer.

Crystal Structure Analysis. Lattice constants were first approximately determined from Weissenberg photographs obtained with Cu$K\alpha$ radiation. Crystallographic data of both adducts are listed in Table 1. The X-ray diffraction data were collected by use of an automated four-circle diffractometer, Rigaku AFC-5, with a graphite-monochromated Mo$K\alpha$ radiation (λ=0.71073 Å) up to 2θ=60°, the θ-2θ scan technique being employed. The diffraction intensities were monitored by five standard reflections for every 50 reflections recorded. No signs of decomposition of the crystals were observed. The usual corrections for Lorentz and polarization effects were made with both crystals, but no absorption correction was applied. Independent reflections with $|F_o| > 3\sigma(|F_o|)$, 2173 and 2915 reflections for **1** and **2**, respectively, were used for the structure determinations. Calculations were carried out on a FACOM M-360 computer at the Rikkyo University Computer Center using the UNICS-III[11] and ORTEP Programs.[12] The atomic-scattering factors including the

†† Present address: Chemistry Laboratory, Faculty of Education, Yamagata University, Koshirakawa, Yamagata 990.

Table 1. Crystallographic Data and Experimental Details

	1	2
Formula	$CuC_{26}H_{26}F_{12}N_8O_4$	$CuC_{14}H_8F_{12}N_2O_4$
M	806.07	559.76
Crystal system	Triclinic	Triclinic
Space group	$P\bar{1}$	$P\bar{1}$
a/Å	9.531(1)	9.647(6)
b/Å	10.286(2)	12.075(9)
c/Å	8.891(2)	9.130(5)
α/°	95.85(2)	107.43(5)
β/°	95.52(2)	99.30(5)
γ/°	85.41(1)	87.20(6)
U/Å^3	860.9(3)	1001.3(12)
Z	1	2
D_m/Mg m^{-3}	1.55	1.84
D_c/Mg m^{-3}	1.554	1.856
Crystal size/mm	0.5×0.3×0.25	0.5×0.45×0.4
$F(000)$	407	550
μ(Mo $K\alpha$)/cm^{-1}	7.4	12.2
Scan rate/° min^{-1}	6	6
Scan range (2θ)/°	2—60	2—60
No. of reflection measured	4471	6226
No. of unique data used for calc. $\lvert F_o\rvert > 3\sigma(\lvert F_o\rvert)$	2173	2915
R[a)]	0.061	0.064

a) $R=\sum\lvert\lvert F_o\rvert-\lvert F_c\rvert\rvert/\sum\lvert F_o\rvert$ (unit weight).

Table 2. Final Atomic Coordinates (×10^4 Except for H and ×10^3 for H), with Estimated Standard Deviations in Parentheses, and Their Equivalent Isotropic Temperature Factors, for **1**

Atom	x	y	z	B_{eq}/Å^2
Cu	0	0	0	4.1
O(1)	−1198(5)	−2199(4)	6(5)	6.2
O(2)	−2666(5)	−2012(4)	2691(5)	7.2
N(1)	431(5)	−1408(4)	2783(5)	5.0
N(2)	598(5)	−301(4)	2173(5)	4.6
N(3)	−2744(5)	329(4)	1318(5)	4.5
N(4)	−1830(4)	870(4)	548(5)	4.4
C(1)	−1479(7)	−4092(6)	−1622(7)	6.1
C(2)	−1756(6)	−3228(5)	−168(6)	4.6
C(3)	−2648(6)	−3734(5)	748(7)	5.2
C(4)	−3028(6)	−3073(6)	2101(7)	5.3
C(5)	−4021(9)	−3726(8)	2996(9)	8.5
C(6)	1460(6)	359(6)	3162(7)	5.3
C(7)	1860(7)	−316(7)	4399(7)	5.9
C(8)	1189(7)	−1459(6)	4134(6)	5.2
C(9)	1208(10)	−2592(7)	5046(8)	8.8
C(10)	−2448(7)	2016(6)	280(8)	6.4
C(11)	−3712(7)	2224(7)	882(9)	7.0
C(12)	−3899(6)	1123(6)	1542(7)	5.2
C(13)	−5060(7)	724(9)	2389(9)	8.2
F(1)	−1568(7)	−5317(4)	−1608(6)	12.5
F(2)	−2274(7)	−3725(6)	−2758(5)	13.7
F(3)	−213(6)	−3990(6)	−2019(7)	13.0
F(4)	−4743(10)	−2985(6)	3791(11)	22.9
F(5)	−4857(7)	−4469(7)	2201(7)	16.1
F(6)	−3362(9)	−4544(9)	3800(10)	21.3
H(N1)	−19(6)	−190(5)	238(6)	7(2)[a)]
H(N3)	−261(5)	−46(4)	151(5)	4(1)[a)]

a) Isotropic temperature factor.

anomalous scattering factors were taken from Ref. 13 for nonhydrogen atoms and from Ref. 14 for hydrogen atom. The structures were solved by the heavy atom method, and refined by standard Patterson, Fourier, and block-diagonal least-squares techniques. The CF_3 groups are rotationally disordered about the C-C bonds. The greater uncertainty is reflected in the higher standard deviations for F(4) and F(6) in **1** and for F(2) and F(3) in **2**. The final R values were 0.061 for **1** and 0.064 for 2, respectively. The positions of all hydrogen atoms were determined from the difference Fourier map. The final atomic coordinates of both complexes are given in Tables 2 and 3, and the geometries of the metal coordination spheres in Tables 4 and 5.[15]

Results and Discussion

ORTEP projections of **1** are shown in Figs. 1a and 1b with the atomic numbering. The molecule has a center of symmetry. A copper atom lies in the center of a tetragonally distorted octahedron and is coordinated with the four nitrogen atoms from 5-Hmpz molecules in the equatorial plane and by two oxygen atoms from different hfac ligands in the axial positions.

Table 3. Final Atomic Coordinates (×10^4), with Estimated Standard Deviations in Parentheses, and Their Equivalent Isotropic Temperature Factors, for **2**

Atom	x	y	z	B_{eq}/Å^2
Cu	−8(1)	1617(1)	1409(1)	4.6
O(1)	1819(4)	1408(4)	2543(5)	5.4
O(2)	755(4)	2794(4)	683(5)	5.6
O(3)	−1742(4)	1619(4)	−26(4)	5.3
O(4)	−897(4)	3015(4)	3158(4)	5.4
N(1)	159(5)	−396(4)	2613(6)	4.9
N(2)	−670(5)	259(4)	1884(6)	4.9
C(1)	4100(7)	1737(7)	3846(10)	7.5
C(2)	2875(6)	2037(5)	2760(7)	4.6
C(3)	3020(6)	2928(6)	2165(8)	5.3
C(4)	1943(6)	3226(5)	1156(7)	5.0
C(5)	2189(8)	4231(7)	527(9)	6.8
C(6)	−3793(7)	2176(7)	−1301(9)	7.5
C(7)	−2685(6)	2386(5)	144(7)	4.7
C(8)	−2857(6)	3306(5)	1384(7)	5.2
C(9)	−1956(6)	3543(5)	2822(7)	4.9
C(10)	−2354(8)	4573(6)	4112(8)	6.8
C(11)	−1956(7)	−79(7)	1876(9)	6.5
C(12)	−1925(8)	−925(7)	2596(9)	7.1
C(13)	−545(7)	−1126(5)	3044(7)	5.2
C(14)	145(9)	−1965(7)	3826(9)	7.2
F(1)	3940(6)	924(6)	4326(9)	14.6
F(2)	5160(6)	1466(10)	3258(11)	21.3
F(3)	4493(10)	2540(6)	4946(10)	25.3
F(4)	1460(6)	5134(4)	1116(7)	10.8
F(5)	3481(5)	4587(5)	877(8)	12.4
F(6)	1870(8)	3969(5)	−941(6)	13.9
F(7)	−3307(5)	1783(6)	−2560(5)	12.4
F(8)	−4634(6)	3014(5)	−1342(6)	13.2
F(9)	−4629(6)	1341(6)	−1301(7)	13.6
F(10)	−1800(8)	5505(5)	4125(8)	14.7
F(11)	−3636(6)	4792(6)	4062(8)	16.2
F(12)	−1918(10)	4498(6)	5433(6)	17.9

Table 4. Selected Bond Lengths and Bond Angles around the Copper Atom, with Estimated Standard Deviations in Parentheses, for **1**

Bond length (l/Å)		Bond angle (ϕ/°)			
Cu-O(1)	2.615(4)	Cu-O(1)-C(2)	172.6(4)	O(1)-Cu-N(2)	83.0(2)
Cu-N(2)	2.008(5)	O(1)-Cu-N(4)	85.9(2)	N(2)-Cu-N(4)	91.6(2)
Cu-N(4)	1.976(4)	Cu-N(2)-N(1)	124.0(4)	Cu-N(2)-C(6)	128.9(4)
		Cu-N(4)-N(3)	124.2(3)	Cu-N(4)-C(10)	131.4(4)

Table 5. Selected Bond Lengths and Bond Angles around the Copper Atom, with Estimated Standard Deviations in Parentheses, for **2**

Bond length (l/Å)		Bond angle (ϕ/°)			
Cu-O(1)	1.941(5)	O(1)-Cu-O(2)	90.9(2)	O(1)-Cu-O(3)	170.2(2)
Cu-O(2)	1.956(5)	O(1)-Cu-O(4)	101.4(2)	O(2)-Cu-O(3)	89.1(2)
Cu-O(3)	1.951(4)	O(2)-Cu-O(4)	88.9(2)	O(3)-Cu-O(4)	88.4(2)
Cu-O(4)	2.196(5)	N(2)-Cu-O(1)	88.1(2)	N(2)-Cu-O(2)	171.5(2)
Cu-N(2)	1.975(5)	N(2)-Cu-O(3)	90.5(2)	N(2)-Cu-O(4)	99.6(2)
		Cu-N(2)-N(1)	124.0(4)	Cu-N(2)-C(11)	130.8(5)

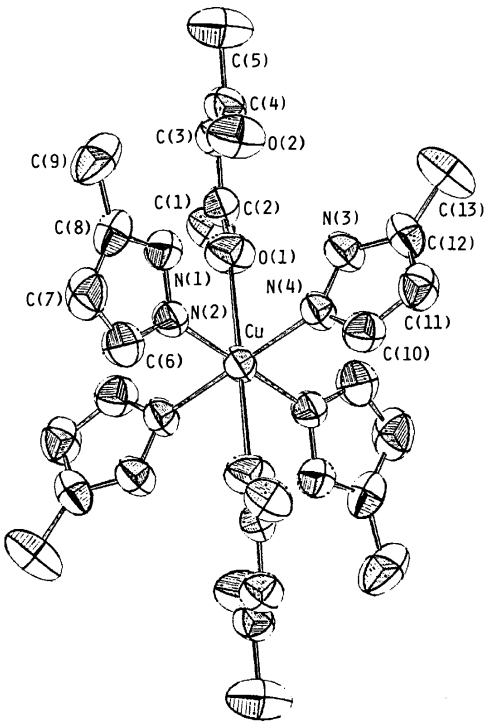

Fig. 1a. A perspective drawing of the structure of **1**, showing the numbering scheme of the atoms (50% probability thermal ellipsoids). Unlabeled atoms are related to labeled atoms by the inversion center. Fluorine atoms attached to C(1) and C(5) are omitted for clarity.

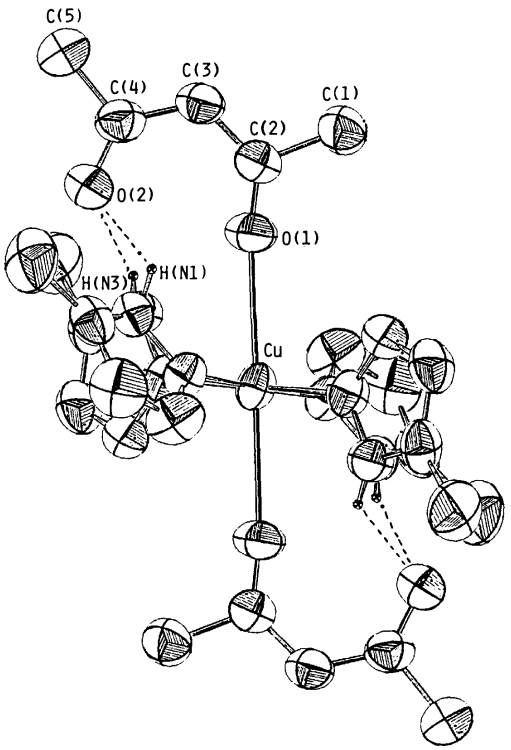

Fig. 1b. A perspective drawing of the molecular structure of **1**, showing the intramolecular hydrogen bonds. Only the H(N1) and H(N3) hydrogen atoms are shown.

The basic structure of **1** is rather similar to that of $Cu(hfac)_2(dmed)_2$, which also has a coordination of a tetragonal pyramid, with four nitrogen atoms in the equatorial plane and two oxygen atoms from unidentate hfac ligands at the apexes.

Another well-defined adduct with unidentate hfac ligand is Cu(acac)(hfac)(phen) (Hacac=2,4-pentanedione, phen=1,10-phenanthroline), which is five-coordinated, however, and an oxygen atom of hfac ligand is in the apical position of a tetragonal pyramid, the basal positions being occupied with two nitrogen atoms from a phen molecule and two oxygen atoms from an acac ligand.[16]

The 3-methyl-1*H*-pyrazole used as a starting material is found in the form of 5-Hmpz in the adduct, which is also the case with $[Cu_2F_2(3,5\text{-Hdmpz})_4(5\text{-Hmpz})_2](BF_4)_2$[17] (3,5-Hdmpz=3,5-dimethyl-1*H*-pyrazole). The 5-substituted form may be more favorable than the other tautomer, probably because

Table 6. Selected Bond Lengths of hfac's Ligands and around the Copper Atom in Nitrogen Base Adducts

Complex	C(2)-C(3) (C(7)-C(8))	C(3)-C(4) C(8)-C(9)	C(2)-O(1) C(7)-O(3)	C(4)-O(2) C(9)-O(4))	Bond length (l/Å) Cu-O(1) (Zn-O(1))	Cu-O(2) (Zn-O(2))	Cu-O(3)	Cu-O(4)	Cu-N(1) (Zn-N(1))	Cu-N(2)
Six coordinated										
Cu(hfac)$_2$(ted)[6]	1.378(9)	1.382(9)	1.247(8)	1.262(7)	1.958(5)	1.954(5)			2.566(7)	
Cu(hfac)$_2$(py)$_2$[18]	1.386(14)	1.378(13)	1.24(1)	1.257(11)	2.266(6)	2.002(6)			2.003(6)	2.021(7)
	1.418(13)	1.353(15)	1.238(10)	1.263(10)			2.300(6)	1.994(5)		
Zn(hfac)$_2$(py)$_2$[18]	1.407(19)	1.359(17)	1.249(15)	1.288(14)	2.159(7)	2.069(8)			2.116(7)	
Cu(hfac)$_2$(pyz)[7]	1.38(1)	1.37(1)	1.25(1)	1.27(1)	2.004(7)	1.924(7)			2.529(9)	
Unidentate hfac's										
Adduct **1**	1.395(8)	1.385(9)	1.212(7)	1.222(8)	2.615(4)				2.008(5)	1.976(4)
Cu(hfac)$_2$(dmed)$_2$[9]	1.385(5)	1.395(4)	1.235(4)	1.233(4)	2.793(2)				1.989(3)	2.064(3)
Five coordinated										
Adduct **2** ring 1	1.364(9)	1.383(9)	1.254(8)	1.239(8)	1.941(5)	1.956(5)			1.975(5)	
ring 2	1.354(9)	1.412(9)	1.259(8)	1.223(8)			1.951(4)	2.196(5)		
[Cu(hfac)$_2$]$_2$(pyz)[7]	1.39(3)	1.37(3)	1.24(2)	1.26(2)	1.96(1)	1.93(1)			2.25(2)	
	1.39(2)	1.36(2)	1.26(2)	1.22(2)						
Unidentate hfac's										
Cu(acac)(hfac)(phen)[16]										
	1.395(11)	1.410(12)	1.235(9)	1.224(10)	1.901(5)	1.912(5)	2.341(5)		2.014(5)	2.015(6)

of the less steric crowding around the coordinating site.

Table 4 contains the selected bond lengths and bond angles in **1**. Also in Table 6, the bond lengths and bond angles of several adducts of bis(β-diketonato)-copper(II) in the literatures are summarized for comparison.

The Cu-O(1) distance (2.615(4) Å) is considerably longer than the corresponding Cu-O distances found in bis(2,4-pentanedionato)copper(II) or its adducts. For example, the average Cu-O bond lengths in planar Cu(hfac)$_2$ and cis-octahedral Cu(hfac)$_2$(py)$_2$[18] are 1.989(14) and 2.283(12) Å, respectively. In the case of the adducts containing unidentate hfac ligands, a comparably long Cu-O distance of 2.793(2) Å, and a some shorter Cu-O distance of 2.341(5) Å have been observed in Cu(hfac)$_2$(dmed)$_2$ and Cu(acac)(hfac)-(phen), respectively.

The hfac ligand is planar and has an approximate C_2 symmetry axis. The C(2)-O(1) and C(4)-O(2) distances are similar, i.e., 1.212(7) and 1.222(8) Å, respectively, and the C(2)-C(3) and C(3)-C(4) distances have nearly the same values of 1.395(8) and 1.385(9) Å, respectively.

These data suggest the complete delocalization of π-electrons in the hfac chelate ring. The C-O and C-C distances agree with the corresponding bond lengths in Cu(hfac)$_2$(dmed)$_2$ and Cu(acac)(hfac)(phen), and it has been discussed that these two adducts also have delocalized hfac rings.

As shown in Figs. 1a and 1b, the geometry of the unidentate hfac ligand in the molecule is unique in that Cu-O(1)-C(2) bond angle is exceptionally large (172.6(4)°), which is only comparable with the corresponding angle of 166.7(2)° in Cu(hfac)$_2$(dmed)$_2$. It is also of interest that the C_2 symmetry axis of hfac ligand is not perpendicular to the CuN_4 plane but is rather slanted against it, so that the coordinated O(1) atom lies nearer to the plane than the uncoordinated O(2) atom. The distances from the CuN_4 plane to O(1) and O(2) are 2.588(5) and 3.050(7) Å, respectively, while the Cu-O(2) distance is 4.414(5) Å. It may be reasonable that both in **1** and Cu(hfac)$_2$(dmed)$_2$, the geometry of the hfac ligands is stabilized by intramolecular hydrogen bonding. In Cu(hfac)$_2$(dmed)$_2$, the distances of the uncoordinated oxygen atom from the copper atom and from a NH_2-nitrogen atom of a dmed ligand are 4.226 Å and 2.995(3) Å, respectively. These values suggest that the uncoordinated oxygen atoms have no interaction with the copper atom and are intramolecularly hydrogen-bonded to the N atoms of the chelated dmed molecules.

Table 7. Distances O···N (l/Å) and Angles (ϕ/°) O···H-N of Hydrogen Bonds for **1**

O···N		O···H-N	
O(1)···N(3)	3.065(6)	O(1)···H(N3)-N(3)	125(4)
O(1)···N(1)	2.867(6)	O(1)···H(N1)-N(1)	132(5)
O(2)···N(3)	2.802(7)	O(2)···H(N3)-N(3)	157(4)
O(2)···N(1)	3.056(7)	O(2)···H(N1)-N(1)	133(5)

The data of several interactions between oxygen atoms and imino groups in **1** are summarized in Table 7. In Fig. 1b a perspective drawing of the structure of **1** is shown, indicating the hydrogen bonds. The uncoordinated oxygen atom forms intramolecular hydrogen bonds with adjacent two imino groups of the 5-Hmpz molecules. One bond is O(2)···H(N3)-N(3) and the other, probably a weaker one, is O(2)···H(N1)-N(1). In addition, it may be possible that a very weak hydrogen bond O(1)···H(N1)-N(1) is formed between the coordinated hfac oxygen atom and an imino group. The rather short distance of O(1)-H(N1) may favor the bond formation.

The Cu-N bond lengths have usual values, but it is interesting that the distances of adjacent Cu-N are not equal. Thus for Cu-N(2) and Cu-N(4), the bond lengths are 2.008(5) and 1.976(4) Å, respectively.

The planes of the coordinated 5-Hmpz molecules are slanted against the equatorial plane, so that the two imino groups are favorably located to form hydrogen bonds with an adjacent oxygen atom. The dihedral angle between the planes of the two adjacent 5-Hmpz molecules is 78.4°.

An ORTEP projection of adduct **2** is shown in Fig. 2. The molecule contains a five-coordinated copper ion, coordinated with two bidentate hfac ligands and a 5-Hmpz molecule.

The geometry is that of a tetragonal pyramid with an oxygen atom from a hfac ligand at the apex and nitrogen atom from a 5-Hmpz molecule in the basal plane. The copper atom is above the basal plane by 0.157(2) Å. This structure is similar to that of $Cu(acac)_2(4\text{-ampy})$ (4-ampy=4-aminopyridine), which is the only 1 : 1 adduct of bis(β-diketonato)copper(II) so far investigated by X-ray analysis.[19]

Table 5 contains the selected bond lengths and bond angles of **2**. The apical Cu-O(4) distance (2.196(5) Å) is greater than the basal Cu-O distances, the mean value of which is 1.950(12) Å. These values are comparable with the corresponding values of $Cu(acac)_2(4\text{-ampy})$.

Of the two hfac chelate rings, the one almost in the basal plane (ring 1) is different from the other (ring 2). In the ring 1, C(2)-C(3) and C(3)-C(4) distances as well as C(2)-O(1) and C(4)-O(2) distances are similar to each other. On the other hand, the other hfac chelate ring (ring 2) is distorted. The C(7)-C(8) and C(8)-C(9) distances are different from each other and so are the C(7)-O(3) and C(9)-O(4) distances. The alternation of long and short bond lengths in the

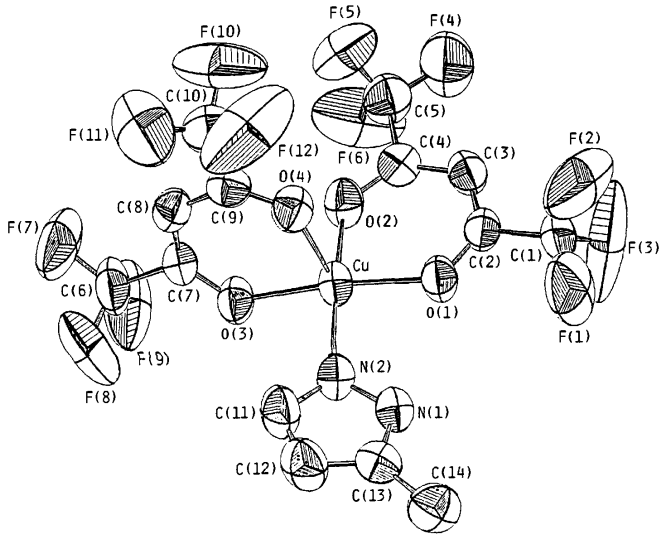

Fig. 2. A perspective drawing of the structure of **2**, showing the numbering scheme of the atoms (50% probability thermal ellipsoids).

β-diketonato chelate rings has been observed in the cis-octahedral adducts of $Cu(hfac)_2(py)_2$ and $Cu(hfac)_2(bpy)$. It has not been fully established that these facts may suggest the presence of a partially localized structure of hfac ligands.

The hfac rings are planar and dihedral angle of each hfac plane against O_3N plane is 1.53° and 78.2°. The angle between the two hfac planes is 76.8°.

Although the adducts **1** and **2** were prepared by stoichiometric reactions of $Cu(hfac)_2$ and 3-methyl-1*H*-pyrazole, the 1 : 2 adduct was not obtained by the similar method. The adduct **1** loses three molecules of 3-methyl-1*H*-pyrazole on standing for several weeks in the atmosphere, yielding **2**. This change may correspond to the bond formation by the uncoordinated carbonyls in **1**, displacing the 5-Hmpz molecules.

In Table 8, IR spectral data of **1** and **2** are listed. In general, the adduct formation of $Cu(hfac)_2$ and $Cu(tfac)_2$ (Htfac=1,1,1-trifluoro-2,4-pentanedione) weakens the Cu-O bonds, as evidenced by the shifts of the carbonyl stretching bands to the higher-frequency side from those observed for the parent complexes.[6,16,18,20]

Attempts have also been made to correlate the C-O bond lengths of the adducts to the ν_{C-O} frequencies at about 1650 cm^{-1} of IR spectra.[18] However, the approach to the bond types of the adducts by this way has not been fully attained.

The sharp band at 3424 cm^{-1} of **2** is definitely assignable to ν_{N-H} vibration of a free imino group. There is no interaction of hydrogen bonding, as it has been reported that, on making a hydrogen bond, the ν_{N-H} band shifts to lower-frequency side and line broadening occurs.[21] The O(1)-N(1) distance of 2.788(7) Å and O(1)···H(N1)-N(1) angle of 118(5)° may not be favorable for formation of a hydrogen bond. On the other hand, the spectrum of **1** has two broad bands in this region at 3270 cm^{-1} and at about 3200 cm^{-1}. Therefore these bands of **1** are assigned to the ν_{N-H} vibration of hydrogen-bonded imino groups.

The split ν_{N-H} bands may be indicative of the two different N-H···O hydrogen bonds described above.

Two separate bands with approximately equal intensities are observed in the IR spectrum of **1** at 1648 and 1659 cm^{-1}, which may be assigned to the ν_{C-O} vibrations of the coordinated and uncoordinated carbonyl groups, respectively.

Table 8. IR Spectral Data

Assignment	Adduct **1**	Adduct **2**	$Cu(hfac)_2$[22]
ν_{N-H}/cm^{-1}	3270(m)	3424(m)	
	ca. 3200(m, br)		
ν_{C-O}/cm^{-1}		1669(m)	
	1659(s)	1662(m)	
	1648(s)	1644(s)	1644(s)
		1615(w)	1614(w)
		1607(w)	

On the other hand, the spectra of **2** have three bands in carbonyl region at 1644, 1662, and 1669 cm^{-1} with approximate intensities of 2 : 1 : 1, respectively. For the adducts of bis(β-diketonato)metal(II) complexes, the splitting of a ν_{C-O} band in IR spectra has been reported only in the case of cis-octahedral Zn(hfac)$_2$(py)$_2$ observed at 1645 and 1660 cm^{-1},[18] which have been assigned to the stretching vibrations of carbonyls in the chelated hfac ligands with long and short C-O distances, respectively.

Thus far no information on the splitting of ν_{C-O} bands in the spectra of bis(β-diketonato)copper(II) adducts has been given. However, if the precise data are accumulated, the IR spectra may be of diagnostic help in predicting these structures of the adducts.

The authors are grateful to Ms. Michiko Umehara of Rikkyo University for the Weissenberg photograph techniques and Mr. Takayoshi Ozawa of this Institute for the elemental analysis.

References

1) S. Trofimenko, *Chem. Rev.*, **72**, 497 (1972).
2) R. J. Sundberg and R. B. Martin, *Chem. Rev.*, **74**, 471 (1974).
3) T. Kogane and R. Hirota, *Bull. Chem. Soc. Jpn.*, **53**, 91 (1980).
4) a) D. P. Graddon, *Coord. Chem. Rev.*, **4**, 1 (1969). b) R. C. Mehrotra, R. Bohra, and D. P. Gaur, "Metal β-Diketonates and Allied Derivatives," Academic Press, London (1978), Chap. 2.
5) M. V. Veidis, G. H. Schreiber, T. E. Gough, and G. J. Palenik, *J. Am. Chem. Soc.*, **91**, 1859 (1969).
6) R. C. E. Belford, D. E. Fenton, and M. R. Truter, *J. Chem. Soc., Dalton Trans.*, **1972**, 2208.
7) R. C. E. Belford, D. E. Fenton, and M. R. Truter, *J. Chem. Soc., Dalton Trans.*, **1974**, 17.
8) M. R. Truter and B. L. Vickery, *J. Chem. Soc., Dalton Trans.*, **1972**, 395.
9) M. A. Bush, D. E. Fenton, R. S. Nyholm, and M. R. Truter, *Chem. Commun.*, **1970**, 1335; M. A. Bush and D. E. Fenton, *J. Chem. Soc. A*, **1971**, 2446.
10) J. A. Bertrand and R. I. Kaplan, *Inorg. Chem.*, **5**, 489 (1966).
11) T. Sakurai and K. Kobayashi, *Rikagaku Kenkyusho Hokoku*, **55**, 69 (1978).
12) C. K. Johnson, ORTEP, (1965). Report ORNL-3794, Oak Ridge National Laboratory, Tennessee.
13) "International Tables for X-Ray Crystallography," Kynoch Press, Birmingham (1974), Vol. IV, pp. 73, 79.
14) R. F. Stewart, E. R. Davidson, and W. T. Simpson, *J. Chem. Phys.*, **42**, 3175 (1965).
15) The remaining bond lengths and angles, the coordinates and isotropic temperature factors of hydrogen atoms, the anisotropic thermal parameters of the nonhydrogen atoms, and the F_o-F_c tables have been deposited as Document No. 8888 at the Office of the Editor of Bull. Chem. Soc. Jpn.
16) N. A. Bailey, D. E. Fenton, M. V. Franklin, and M. Hall, *J. Chem. Soc., Dalton Trans.*, **1980**, 984.
17) F. J. Rietmeijer, R. A. G. De Graaff, and J. Reedijk, *Inorg. Chem.*, **23**, 151 (1984).
18) J. Pradilla-Sorzano and J. P. Fackler, Jr., *Inorg. Chem.*, **12**, 1174 (1973).
19) G. W. Bushnell, *Can. J. Chem.*, **49**, 555 (1971).
20) D. E. Fenton, R. S. Nyholm, and M. R. Truter, *J. Chem. Soc. A*, **1971**, 1577.
21) D. B. Powell and N. Sheppard, *Spectrochim. Acta*, **17**, 68 (1961).
22) K. Nakamoto, "Infrared and Raman Spectra of Inorganic and Coordination Compounds," 4th ed, John Wiley & Sons, New York (1986), p. 263.

 © 1989 The Chemical Society of Japan Bull. Chem. Soc. Jpn., 62, 2530—2535 (1989) [Vol. 62, No. 8

Syntheses, and Crystal and Molecular Structures of Tetraethylammonium [Hexakis(isothiocyanato)lanthanoidates(III)] Including Aromatic Hydrocarbon or Halohydrocarbon: $[(C_2H_5)_4N]_3[M(NCS)_6]\cdot G$ (M=Er, or Yb; G=Benzene, Fluorobenzene, Toluene, or Chlorobenzene)

Hisanori Arai,† Yasuo Suzuki,† Naomi Matsumura,†† Toshio Takeuchi,††† and Akira Ouchi*
Department of Chemistry, College of Arts and Sciences, The University of Tokyo, Komaba, Meguro-ku, Tokyo 153
†Department of Industrial Chemistry, Faculty of Engineering, Meiji University, Higashi-Mita, Tama-ku, Kawasaki-shi, Kanagawa 214
††Department of Chemistry, School of Hygienic Sciences, Kitasato University, Kitasato, Sagamihara-shi, Kanagawa 228
†††Department of Natural Sciences, Faculty of Science and Technology, Sophia University, Kioi, Chiyoda-ku, Tokyo 102
(Received January 25, 1989)

The title new complexes were synthesized and their crystal and molecular structures were determined by the single-crystal X-ray diffraction method. The crystal form of $[(C_2H_5)_4N]_3[Yb(NCS)_6]\cdot(C_6H_6)$, for example, is monoclinic, space group $P2_1/c$, a=19.458(12), b=14.046(6), c=18.288(7) Å, β=91.28(4)°, Z=4, and the final R value obtained was 0.064. The other seven crystals are isomorphous with each other. The central metal atom is in an octahedral hexa-coordination geometry: six nitrogen atoms of isothiocyanate ions are ligated to each metal atom. Each solvent molecule is arranged betweeen each pair of neighboring metal atoms along the [1 $\bar{1}$ 0] axis in each crystal. The cations are arranged approximately between each pair of metal atoms along the [0 1 1], [0 $\bar{1}$ 1], and [1 1 0] axes, respectively. They were stable for more than a few weeks at room temperature; however, when heated at about 80—90 °C, their guest molecules were lost.

Although lanthanoids are hard elements[1] and they prefer to be coordinated to oxygen donor ligands,[2] the nitrogen atom of a thiocyanate ion (SCN) can be ligated to the metal atom. The M-N(NCS) bond is relatively weak in aqueous solution;[3] however, it is more stable in some organic solvents used for the solvent extraction of the metals.[4]

The crystal and molecular structures of the tetrabutylammonium hexakis(isothiocyanato)lanthanoidates (III) (M=Pr—Yb) have already been elucidated: six nitrogen atoms of NCS are ligated to the central metal atom in an octahedral geometry.[5] However its coordination number (6) is rather abnormal, since the preferred coordination number of lanthanoid complexes is eight or nine, although seven, ten, and to a less extent, the other numbers are also found in the other complexes. Coordination numbers of six or lower are found only in the complexes when the ligand is too massive to take higher coordination numbers; however, the SCN ion is not large.

In cases of some aqua-isothiocyanato mixed complexes, the coordination number of the central lanthanoid atoms is eight: $K_4[M(NCS)_4(H_2O)_4](SCN)_3\cdot nH_2O$ (M=Nd, Eu),[6] $[(C_2H_5)_4N]_4[M(NCS)_7(H_2O)]$ (M=La, Ce, Pr; Nd, Dy, Er),[7] and $[(CH_3)_4N]_3[M(NCS)_6(CH_3OH)(H_2O)]$ (M=La—Er)[8] are examples. Recently, we obtained some anhydrous isothiocyanato complexes of lanthanoids in which the metal atom is hepta-coordinated, such as $[(CH_3)_4N]_4[M(SCN)_7]$ (M=Dy, Er, Yb),[8] and $[(C_2H_5)_4N]_4[M(SCN)_7]\cdot C_6H_6$ (M=La, Pr).[9] The last example is regarded as being a kind of inclusion compound, since it has one benzene molecule per one metal atom in a crystal, and no bonding has been recognized between the molecule and the cations or anions. Therefore, it seemed to be interesting to find some other such type adducts of complexes of lanthanoids. We were able to synthesize the title new complexes, and have investigated their properties by the thermoanalytical technique as well as by infrared spectra. Moreover, their crystal and molecular structures were determined by the single-crystal X-ray diffraction technique.

Experimental

Synthesis of Tetraethylammonium [Hexakis(isothiocyanato)erbate(III)]·Benzene (1), the Isomorphous Benzene Adduct of Ytterbate(III) (2), and the Isomorphous Complexes Including Fluorobenzene (3,4), Toluene (5,6), or Chlorobenzene (7,8).§ The starting erbium(III) thiocyanate (in methanolic solution) and solid tetraethylammonium thiocyanate were obtained (as mentioned in a previous paper).[7] Into a methanolic solution (10 cm³) of erbium thiocyanate (1.0 mmol) tetraethylammonium thiocyanate (0.61 g, 3.2 mmol) was added and dissolved. To the solution, the ethanol-benzene mixture (1 : 1=v/v, 20 cm³) was added and the mixture was dried up using a rotary evaporator at about 80 °C. The dehydration process was repeated twice, and the residue was dissolved into 10 cm³ of methanol (GR grade reagent of Wako Pure Chemical Ind. Ltd.: it contains at most 0.2% of water). After a trace of insoluble matter was filtered off, the solution was left standing in the benzene-vapor moiety for several days. The precipitate was

§ Odd number ones are erbate, and even number ones are ytterbate.

separated, washed with a small portion of ethanol, and dried in a silica-gel desiccator overnight. Yield: 0.72 g (0.73 mmol, 73%). The isomorphous ytterbium complex (**2**) was obtained by almost the same technique.

The other six isomorphous adducts, the respective erbium (odd number ones) and ytterbium complexes (even number ones) including fluorobenzene, toluene, or chlorobenzene, were also synthesized by the same technique: keeping the starting solution in a desiccator over respective solvents.

In Table 1, are shown their elemental analyses and the numbering of the complexes. The yields of complexes **2**—**8**, starting from 1.0 mmol of the respective metal thiocyanates, are: **2**, 0.65 g, 66%; **3**, 0.83 g, 83%; **4**, 0.76 g, 75%; **5**, 0.55 g, 55%; **6**, 0.60 g, 60%; **7**, 0.50 g, 49%; and **8**, 0.45 g, 44%.

All of them are pale orange in color and are relatively stable: their crystals could be kept at room temperature for at least a few weeks without decomposition, although they lost their guests and became pulverized after a longer time. When they were kept in a stoppered bottle at about 6 °C or lower, they were stable for more than six months.

Attempts to synthesize the isomorphous complexes of dysprosium or of lighter lanthanoids, including any of the above-mentioned guests have not yet been successful.

X-Ray Structure Analysis. Crystallographic data of **1**—**8**, the size of the used crystal (approximately parallelepiped), and some experimental conditions for the X-ray structure analyses of **1**—**6** are listed in Table 2.

Reflections were collected on a Rigaku AFC-6A automated four-circle X-ray diffractometer, with graphite monochromated Mo$K\alpha$ radiation (λ=0.71073 Å), an ω-2θ scan technique being employed (scan speed 4° min^{-1}). The used crystals were coated with a cyanoacrylate resin to

Table 1. Elemental Analyses (Calculated Values in Parentheses) (n/%) and the Numbering of the Complexes, $[(C_2H_5)_4N]_3[M(NCS)_6]\cdot G$

No.	G	M	Formula	M	C	H	N
1	C_6H_6	Er	$ErC_{36}H_{66}N_9S_6$	16.89	43.61	6.71	12.70
				(16.99)	(43.92)	(6.76)	(12.80)
2	C_6H_6	Yb	$YbC_{36}H_{66}N_9S_6$	17.59	43.26	6.59	12.61
				(17.47)	(43.66)	(6.72)	(12.73)
3	C_6H_5F	Er	$ErC_{36}H_{65}N_9S_6F$	16.81	42.76	6.53	12.73
				(16.68)	(43.13)	(6.54)	(12.57)
4	C_6H_5F	Yb	$YbC_{36}H_{65}N_9S_6F$	17.12	42.55	6.43	12.43
				(17.16)	(42.88)	(6.50)	(12.50)
5	C_7H_8	Er	$ErC_{37}H_{68}N_9S_6$	16.65	44.24	6.79	12.88
				(16.75)	(44.50)	(6.86)	(12.62)
6	C_7H_8	Yb	$YbC_{37}H_{68}N_9S_6$	17.10	43.93	6.72	12.56
				(17.23)	(44.25)	(6.82)	(12.55)
7	C_6H_5Cl	Er	$ErC_{36}H_{65}N_9S_6Cl$	16.48	42.08	6.44	12.56
				(16.41)	(42.43)	(6.43)	(12.37)
8	C_6H_5Cl	Yb	$YbC_{36}H_{65}N_9S_6Cl$	16.81	42.16	6.42	12.39
				(16.88)	(42.19)	(6.39)	(12.30)

Table 2. Crystallographic Data and Various Experimental Conditions for the Complexes, $[(C_2H_5)_4N]_3[M(NCS)_6]\cdot G$, Space Group, $P2_1/c$, Z=4

No.	**1**	**2**	**3**	**4**	**5**	**6**	**7**[13]	**8**[13]
M=	Er	Yb	Er	Yb	Er	Yb	Er	Yb
G=	C_6H_6	C_6H_6	C_6H_5F	C_6H_5F	C_7H_8	C_7H_8	C_6H_5Cl	C_6H_5Cl
F. W.	984.64	990.42	1002.60	1008.38	998.63	1004.41	1019.05	1024.83
a(l/Å)	19.516(5)	19.458(12)	19.489(17)	19.466(10)	19.769(9)	19.763(8)	19.662(19)	19.644(14)
b(l/Å)	14.091(4)	14.046(6)	14.030(15)	14.036(14)	14.111(4)	14.115(7)	14.067(14)	14.064(6)
c(l/Å)	18.647(6)	18.288(7)	18.471(19)	18.42(3)	18.398(6)	18.360(9)	18.555(14)	18.548(8)
β(ϕ/°)	91.20(2)	91.28(4)	90.86(8)	90.95(8)	92.04(3)	92.22(4)	91.70(7)	91.85(5)
U(v/Å^3)	5046(2)	4998(4)	5050(9)	5032(9)	5129(3)	5118(4)	5130(7)	5121(5)
D_m(d/g cm^{-3})	1.30(3)	1.31(3)	1.32(3)	1.32(3)	1.29(3)	1.29(3)	1.31(3)	1.34(3)
D_x(d/g cm^{-3})	1.30	1.32	1.32	1.33	1.29	1.30	1.32	1.33
μ(Mo$K\alpha$) (n/cm^{-1})	20.00	22.43	20.03	22.33	19.69	21.92	20.20	22.42
N_m[a]	9266	6889	6957	6939	9484	7079		
N_c[b]	3066	2814	2510	2311	2314	2353		
R[c]	0.068	0.064	0.074	0.069	0.091	0.079		
V_c[d](v/mm^3)	0.33×0.32 ×0.20	0.35×0.33 ×0.30	0.30×0.25 ×0.20	0.32×30 ×0.30	0.31×0.31 ×0.31	0.32×0.31 ×0.31		
S_w[e](ω/°)	1.16+ 0.5 tanθ	1.07+ 0.5 tanθ	1.08+ 0.35 tanθ	1.15+ 0.35 tanθ	1.27+ 0.5 tanθ	1.21+ 0.5 tanθ		
S_R[f](2θ/°)	3—50	3—45	3—45	3—45	3—50	3—45		

a) Number of reflections measured. b) Number of reflections used for the calculation (reflections of $|F_o|>3\sigma(|F_o|)$ were used). c) $R=\sum||F_o|-|F_c||/\sum|F_o|$ d) The size of the crystal used (approximately in parallelepiped in shape). e) Scan width (ω). f) Scanned range (2θ).

prevent the escape of the guest; however, it was not necessary to seal the crystal in a glass capillary. During the intensity collection (about 5—7 days) a decrease in the standard reflection intensities was not recognized in the cases of complexes **1**—**4**, and less than 8% in the cases of the complexes **5** and **6**. The intensities were corrected for Lorentz and polarization factors, though no corrections were made for absorption.

Structure Determination. The structure of **2** was solved by the heavy-atom method. The positions of the metal and some sulfur atoms were deduced from the three-dimensional Patterson map, and the other atoms were located by successive Fourier syntheses. Their positional and thermal parameters were refined by a block-diagonal least-squares method. No hydrogen atom was included in the structure factor calculations.

It was found that several atoms have relatively large temperature factors, although this phenomenon had already been found for atoms loosely packed in the crystal in some other lanthanoid complexes.[10] Although the intensity measurement process was repeated for **2** using another crystal, the result was not improved: the temperature factors of some atoms were still very large. The occupancy factors of the atoms of the guest molecule were examined by a full-matrix least squares method; they converged to approximately 1.0.

After repeated refinement steps, some parameters were still moving over 3 times of their respective standard deviations, though their values almost converged. Therefore, at the final refinement steps, such parameters were fixed in the structure calculations.[13]

The structure of **1** was determined starting from the final parameters of **2**, and refined in a similar way.

The structures of **3** and **5** were obtained starting from the final parameters of **2**, and refined in a similar way. The positions of the fluorine atom of **3** and the methyl carbon atom of **5** were obtained from their difference synthesis maps. The structures of **4** and **6** were obtained starting from the final parameters of **3** and **5**, respectively, and their parameters were refined in the same way.

In **3** and **4**, from their difference synthesis map, the position of the fluorine atom was divided into two, F(1A) and F(1B), which were bonded to C(63) and C(66), respectively, with an equal occupancy factor.

In **5**, or **6**, from their difference synthesis maps, the position of the methyl carbon atom of toluene molecule was found to be not disordered, which is bonded to C(66).

All calculations were carried out on a HITAC M-682H computer at the Computer Center of the University of Tokyo, using a local version of the UNICS program.[11] The atomic scattering factors were taken from Ref. 12.

Other Measurements. Their infrared absorption spectra

Table 3. Final Atomic Coordinates ($\times 10^4$) and Isotropic or Equivalent Isotropic Temperature Factors (B_{eq}/Å^2) of Tetraethylammonium [Hexakis(isothiocyanato)ytterbate(III)]·Benzene with Estimated Standard Deviations in Parentheses

Atom[c]	x	y	z	B_{eq}/Å^2[a]	Atom[c]	x	y	z	B_{eq}/Å^2[a]
Yb(1)	0.0	0.0	0.0	8.0	C(35)	2571(12)	891(15)	−231(13)	10.3
Yb(2)	5000.0	5000.0	0.0	5.0	C(36)	3144(13)	272(13)	−559(14)	10.7
S(11)	1839(4)	873(7)	1807(4)	13.3	C(37)	2898(12)	2265(17)	−1135(11)	10.4
S(12)	−1695(4)	554(6)	1967(4)	11.7	C(38)	2251(12)	2138(16)	−1575(11)	10.4
S(13)	386(5)	3336(7)	−639(7)	19.3	C(41)	5384(10)	3874(13)	2782(10)	7.2
S(21)	6918(3)	5316(4)	1848(3)	8.0	C(42)	4949(13)	4183(18)	3413(12)	10.9
S(22)	3390(4)	4297(5)	2032(3)	10.5	C(43)	6225(11)	2976(16)	3593(10)	9.1
S(23)	5380(4)	1516(4)	432(3)	8.9	C(44)	6773(12)	3743(19)	3520(12)	11.7
N(11)	845(9)	259(14)	813(8)	9.9	C(45)	6170(10)	2755(14)	2200(9)	7.4
N(12)	−764(9)	306(14)	872(9)	10.3	C(46)	6584(13)	1864(18)	2234(12)	11.8
N(13)	68(10)	1572(15)	−316(11)	12.4	C(47)	5273(12)	2117(14)	3115(11)	8.8
N(21)	5893(7)	5294(10)	813(8)	7.2	C(48)	4723(12)	1979(16)	2483(13)	10.9
N(22)	4253(8)	4798(9)	956(8)	6.7	C(61)	7254(14)	3749(19)	−246(15)	13.4
N(23)	5199(7)	3399(10)	85(8)	6.7	C(62)	7708(12)	3794(17)	−780(14)	11.4
N(31)	2790(7)	1971(11)	−288(8)	7.2	C(63)	8263(14)	3085(22)	−767(14)	14.2
N(41)	5777(7)	2925(10)	2909(7)	6.4	C(64)	8257(11)	2419(17)	−232(15)	11.5
N(51)	−340(10)	3604(13)	1857(9)	10.8	C(65)	7741(13)	2322(17)	286(14)	12.1
C(11)	1259(10)	551(16)	1240(11)	8.4	C(66)	7221(13)	3019(18)	205(13)	11.4
C(12)	−1143(11)	398(15)	1345(11)	8.3	C(51)[b]	−110(13)	2502(17)	1821(13)	11.3
C(13)	174(11)	2234(15)	−472(13)	9.3	C(52)[b]	422(13)	2688(17)	2565(13)	11.3
C(21)	6305(9)	5268(11)	1240(9)	5.6	C(53)[b]	140(13)	4298(18)	2012(13)	11.3
C(22)	3897(10)	4571(13)	1417(10)	6.6	C(54)[b]	684(13)	4106(18)	1298(13)	11.3
C(23)	5285(9)	2610(13)	245(9)	5.7	C(55)[b]	−672(13)	3801(18)	2603(13)	11.3
C(31)	3492(11)	2175(17)	83(13)	10.8	C(56)[b]	−1395(13)	3294(17)	2502(13)	11.3
C(32)	3468(11)	1885(16)	913(11)	9.5	C(57)[b]	−685(12)	3556(18)	1181(13)	11.3
C(33)	2182(11)	2501(16)	43(13)	10.2	C(58)[b]	−1191(13)	4459(19)	1129(13)	11.3
C(34)	2330(12)	3616(15)	42(13)	10.6					

a) The equivalent isotropic temperature factors were computed using the following expression: $B_{eq}=4/3(B_{11}a^2+B_{22}b^2+B_{33}c^2+B_{13}ac\cos\beta)$. The B_{ij}'s are defined by: $T=\exp[-(h^2B_{11}+k^2B_{22}+l^2B_{33}+2hkB_{12}+2hlB_{13}+2klB_{23})]$. b) Their B_{iso} was all fixed at the value, 11.3 Å^2. c) The numbering of the tetraethylammonium atoms are as follows: the ethyl carbon atoms, C(n1), C(n3), C(n5), and C(n7), which are bonded to the carbon atoms C(n2), C(n4), C(n6), and C(n8) respectively, are located around the central nitrogen atom N(n1) tetrahedrally (n=3—5). The benzene carbon atoms are numbered from C(61) to C(66) succesively.

Table 4. Selected Bond Lengths (l/Å) and Bond Angles (ϕ/°) of the Adducts of Tetraethylammonium Hexakis(isothiocyanato)erbate(III) and -ytterbate(III), (**1**—**6**), $[(C_2H_5)_4N]_3[M(NCS)_6]\cdot G$ (M=Er, Yb; G=Benzene, Fluorobenzene, or Toluene), with the Standard Deviations in Parentheses

No.[a]	**1**	**2**	**3**	**4**	**5**	**6**
M=	Er	Yb	Er	Yb	Er	Yb
G=	C_6H_6	C_6H_6	C_6H_5F	C_6H_5F	C_7H_8	C_7H_8
M(1)-N(11)	2.27(2)	2.22(2)	2.27(3)	2.23(3)	2.27(4)	2.25(3)
M(1)-N(12)	2.29(2)	2.25(3)	2.31(3)	2.28(3)	2.26(4)	2.32(3)
M(1)-N(13)	2.32(2)	2.29(2)	2.22(4)	2.19(3)	2.34(3)	2.32(3)
M(2)-N(21)	2.31(2)	2.30(2)	2.33(3)	2.37(3)	2.28(3)	2.23(3)
M(2)-N(22)	2.33(2)	2.32(2)	2.32(3)	2.25(3)	2.35(4)	2.24(3)
M(2)-N(23)	2.32(1)	2.29(1)	2.29(2)	2.28(2)	2.35(2)	2.28(2)
M-N (av.)[b]	2.31	2.28	2.29	2.27	2.31	2.27
N(n)-C(n) (av.)[b]	1.09	1.13	1.12	1.12	1.11	1.11
	(0.91—	(1.00—	(1.06—	(1.03—	(1.02—	(1.03—
	1.15)	1.16)	1.18)	1.21)	1.22)	1.23)
C(n)-S(n) (av.)[b]	1.61	1.60	1.62	1.61	1.59	1.60
	(1.57—	(1.56—	(1.54—	(1.54—	(1.49—	(1.48—
	1.65)	1.64)	1.70)	1.69)	1.67)	1.69)
N(11)-M(1)-N(12)	88.1(8)	89.1(9)	88.0(11)	89.8(11)	89.1(13)	90.8(11)
N(11)-M(1)-N(13)	88.6(8)	88.0(8)	87.2(13)	85.6(12)	85.6(12)	86.2(11)
N(12)-M(1)-N(13)	92.0(9)	92.1(8)	92.0(13)	90.8(12)	91.3(12)	91.7(10)
N(21)-M(2)-N(22)	90.4(7)	90.7(7)	92.1(10)	90.8(10)	89.2(12)	88.9(12)
N(21)-M(2)-N(23)	90.0(6)	90.5(6)	90.1(8)	90.5(8)	89.5(10)	89.2(10)
N(22)-M(2)-N(23)	86.3(6)	86.4(6)	85.1(8)	85.0(9)	86.4(11)	87.0(10)
M(1, 2)-N(n)-C(n) (av.)[b]	170	170	170	170	168	169
	(167—	(167—	(165—	(166—	(164—	(166—
	176)	175)	174)	178)	172)	174)
N(n)-C(n)-S(n) (av.)[b]	177	176	175	175	173	176
	(175—	(174—	(172—	(171—	(171—	(168—
	178)	178)	177)	179)	176)	179)

a) Numbers of the complexes (see Table 1). b) Average of the six values of the all SCN ions.

were obtained by means of a JASCO A-202 grating infrared spectrophotometer, using paraffin oil and hexachloro-1,3-butadiene mull. Simultaneous thermogravimetric (TG) and differential thermal analysis (DTA) were carried out with a Rigaku "Thermoflex" M-8075 using samples weighing about 10 mg, at a heating rate of 10 °C min^{-1} in air, with α-alumina used as a reference.

Results and Discussion

The final atomic coordinates and isotropic or equivalent isotropic temperature factors (B_{eq}/Å^2) of **2** are tabulated in Table 3; some selected bond lengths and bond angles of **1**—**6** are listed in Table 4. Perspective drawings of complex **2** around atoms Yb(1) and Yb(2) are shown in Figs. 1 and 2, and a projection of its unit cell along the b-axis in Fig. 3.[13]

In **2**, both of the crystallographically independent metal atoms, Yb(1) and Yb(2), are at the centers of symmetry, and are hexa-coordinated in an octahedral geometry: six nitrogen atoms of SCN ions are in coordination. The average M-N bond length is 2.28 Å (2.22—2.32 Å), which is a little shorter than the sum of the Shannon's crystal radii, 2.33Å.[14] The average bond angles, Yb-N-C and N-C-S, are 170 (167—175) and 176 (174—178)°, respectively.

Among the six coordinated SCN ions, four ions are situated approximately on a plane parallel to the ac-plane and are arranged approximately to [1 0 1] and [$\bar{1}$ 0 1]; the other two SCN ions are arranged approximately along the b-axis.

The tetraethylammonium ions around the N(41) and N(51) atoms are arranged approximately between each pair of neighboring metal atoms along [0 1 1] and [0 $\bar{1}$ 1]: the N(41) atoms are between the Yb(2)

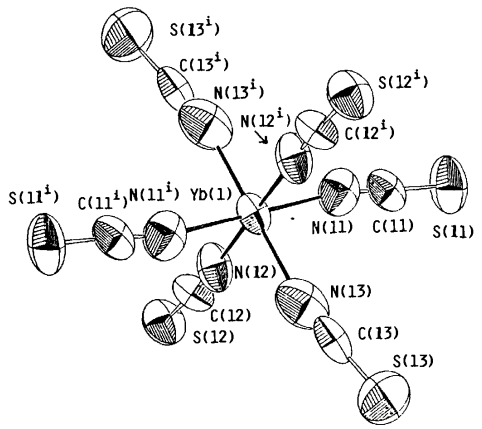

Fig. 1. Perspective drawing of tetraethylammonium [hexakis(isothiocyanato)ytterbate(III)]·benzene (**2**) around Yb(1) atom together with the numbering scheme of the atoms. Key to the symmetry operation: i, $-x$, $-y$, $-z$.

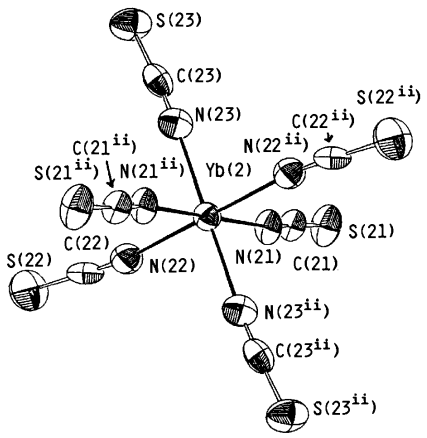

Fig. 2. Perspective drawing of tetraethylammonium [(hexakis(isothiocyanato)ytterbate(III)]·benzene (**2**) around Yb(2) atom together with the numbering scheme of the atoms. Key to the symmetry operation: i, 1−x, 1−y, −z.

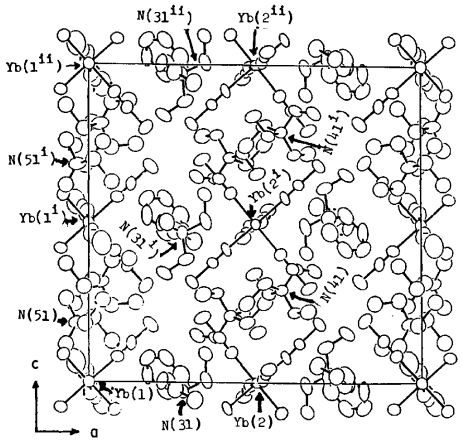

Fig. 3. Projection of the unit cell of tetraethylammonium [hexakis(isothiocyanato)ytterbate(III)]·benzene (**2**) along b-axis. The numbering scheme of some metal and ammonium nitrogen atoms are also shown. Key to the symmetry operations: i, *x*, 0.5−*y*, 0.5+*z*; ii, *x*, *y*, 1+*z*.

atoms, while the N(51) atoms are between the Yb(1) atoms. Another tetraethylammonium ion around the N(31) atom and the benzene molecule are arranged between each pair of Yb(1) and Yb(2) atoms along [1 1 0] and [$\bar{1}$ 1 0], respectively.

The structure of the isomorphous erbium complex (**1**) has essentially the same structure as **2**, although the average Er-N bond length is 2.31 Å (2.27(2)—2.33(2) Å) which is longer than the corresponding length of **2**, due to the longer metal crystal radii (the sum of the Shannon's crystal radii of Er-N is 2.35 Å). The reported Er-N(SCN) bond length of $[Er(SCN)_6]^{3-}$ ion in its tetrabutylammonium salt is 2.34(2) Å, which is a little longer than that of **1**.[5] Other than the metal ionic size and, consequently, the M-N bond lengths and the unit-cell volume, the structures of **1** and **2** are approximately the same.

We can compare with each other the relative volumes (where the organic molecules are included) from their unit-cell volumes of the same metal complexes, ytterbium ones: the unit-cell volumes of **2**, **4**, **6**, and **8** are 4998(4), 5032(9), 5118(4), and 5121(5) Å^3, respectively. Therefore, the space for the guest is expanded a little, depending on the increase in the volume of the guest molecule.

Although the unit cell of each erbium complex is a little larger than that of the corresponding ytterbium complex, almost no difference could be recognized between the thermal properties of the corresponding adducts of both metals (as shown in the later part of this paper). However, the same type inclusion compounds of dysprosium or smaller atomic number lanthanoids were not obtained. The formation of this kind of adduct is likely only for a limited range of sizes of the complex: the distance between the cations and anions should be kept to an appropriate value.

Qualitatively, we guess that, in cases of the isothiocyanato complexes of lanthanoids, when the organic groups of the cations are sufficiently large to supply enough non-polar moiety in the crystal, the coordinated SCN ions, which also contain a non-polar part (sulfur and carbon atoms), are capable of moving around their regular positions. As a result, the SCN ions are sufficiently bulky to be in hexa-coordination to lanthanoid metals. The structure of $[(C_4H_9)_4N]_3[M(NCS)_6]$ can be explained in terms this hypothesis. In cases of the present complexes, although the ethyl group of the cation is not sufficiently large, the central metal atom is relatively small (Er or Yb); moreover, some non-polar hydrocarbon or halohydrocarbon molecules are included. As a result, the SCN ions assume an octahedral geometry.

In infrared absorption spectra of the complexes **1**—**8**, the bands due to the N-bonded SCN ion appear in the same region as the other metal complexes:[15] ν(CN), 2050(s); ν(CS), 730(shoulder, partly overlapped with the peak of the cation); δ(SCN), 480 cm^{-1}. The bands due to the tetraethylammonium ion are commonly found in the specta of **1**—**8**, at about 1490(s), 1440(s), 1395(s), 1364(m), 1170(s), 1052(m), 997(s), 780(s), and 720(m) cm^{-1}. The peak of the mode of the out-of-plane deformation of the benzene ring is characteristic to complexes **1**—**8**, and is useful for identifying whether the complex really includes a guest or not. The peaks of **1** and **2** appear at 687 cm^{-1}, which is a liitle blue shifted from that of the free benzene (673 cm^{-1}). Such a shift in the peak of a guest molecules around 680—690 cm^{-1} was not observed in the spectra of **3**—**8**. The peaks of the guests in the infrared spectra are as follows: **3** and **4**, 683, 750, 805, 899, 1220, 1500, and 1598 cm^{-1}; **5** and **6**, 460, 693, 722, 1030, and 1080 cm^{-1}; and **7** and **8**, 682, 701, 1022, 1085, 1450, 1481, and 1584 cm^{-1} peaks, respectively. None of them shift much from the peak wavenumbers of the respective free guests.

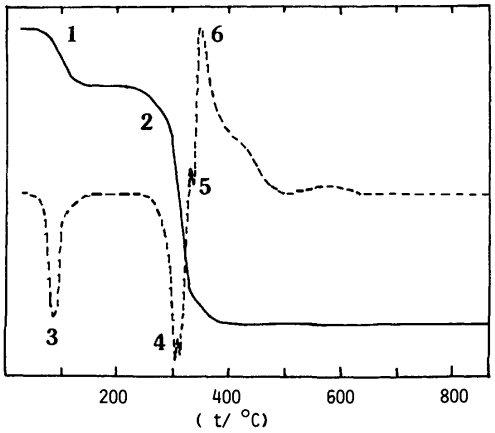

Fig. 4. TG(——) and DTA(----) curves of tetraethylammonium [hexakis(isothiocyanato)ytterbate(III)]·benzene (**2**). Mass loss of TG was taken downward and the exothermic change of DTA was taken upward. The temperature corresponding with the points numbered from **1** to **6** of the runs with the complexes **1**, **2**, **4**, **6**, and **8** are shown in Table 5.

Table 5. Thermal Analytical Data of the Complexes

Complex	1[b]	2[b]	3[b]	4[b]	5[b]	6[b]	R[c]
1[a]	81	297	93	303, 312	333	351	22
2[a]	88	285	99	304, 315	330	353	22
4[a]	82	288	94	305		330	24
6[a]	81	288	91	311	335	351	20
8[a]	83	285	95	302		343	23

a) Complexes shown in Table 1. b) The points shown in Fig. 4 (the temperatures in the table are shown in the unit of (t/°C)). c) The weight of residue after heating the samples up to 1000 °C (shown in weight %).

The simultaneous TG-DTA curves of complex **2** is shown in Fig. 4. The general feature of the curves of the other complexes are almost the same. The corresponding temperatures at points **1**—**6** shown in Fig. 4 (of the complexes **1**, **2**, **4**, **6**, and **8**) are listed in Table 5.

From these results, it was shown that when the temperature was increased, all kinds of guest molecules in them were removed at about 80—90 °C: no serious difference was found between their degradation temperatures. The change was found to be endothermic from their DTA curves, and the mass loss of this step of each complex approximately coincided with the molecular weight of each guest.

Between the first and second mass-loss steps, the vacant cage structure, $[(C_2H_5)_4N]_3[M(NCS)_6]$ (M=Er, Yb), was thought to be stable. In the respective infrared spectra of the residues after heating complexes **1**—**8**, about 2—5 h at 110 °C, the peaks of the guests completely disappeared, while the peaks of the SCN^- and $[(C_2H_5)_4N]^+$ ions were retained almost in the same wavenumber region. Each mass loss by this heating process also corresponded approximately with the weight of the included guest calculated from its formula.

At about 280—290 °C the complexes decomposed by one-step degradation, as shown by the TG curve; however, it consists of several complicated endo- and exothermic steps, judging from their DTA curves.

After the second step of decomposition, no specific changes were observed on the TG and DTA curves, and the residues after being heated to 1000 °C were mainly the respective metal oxides.

The authors wish to thank Shin-Etsu Chemical Ind. Co., Ltd., for presenting us with highly pure lanthanoid oxides.

References

1) R. G. Pearson, *J. Chem. Educ.*, **45**, 581 (1968).
2) T. Moeller, "Comprehensive Inorganic Chemistry," ed by J. C. Bailar, Jr., H. J. Emeléus, Sir R. Nyholm, and A. F. Trotman-Dickenson, Pergamon Press, Oxford (1973), Vol. 4, p. 22.
3) "Gmelin Handbook of Inorganic Chemistry," 8th ed, Springer Verl. Berlin (1986), Syst. No. 39, Part D4, p. 340.
4) H. Yoshida, *J. Inorg. Nucl. Chem.*, **24**, 4257 (1962).
5) J. L. Martin, L. C. Thompson, L. J. Radonovich, and M. D. Glick, *J. Am. Chem. Soc.*, **90**, 4493 (1968).
6) P. I. Lazarev, L. A. Aslanov, V. M. Ionov, and M. A. Porai-Koshits, *Koord. Khim.*, **1**, 710 (1975); also in *Struct. Report*, **41A**, 210 (1975).
7) Y. Tateyama, Y. Kuniyasu, Y. Suzuki, and A. Ouchi, *Bull. Chem. Soc. Jpn.*, **61**, 2805 (1988).
8) F. Matsumoto, N. Matsumura, and A. Ouchi, *Bull. Chem Soc. Jpn.*, **62**, 1809 (1989).
9) F. Matsumoto, T. Takeuchi, and A. Ouchi, *Bull. Chem. Soc. Jpn.*, **62**, 2078 (1989).
10) T. Imai, M. Nakamura, K. Nagai, Y. Ohki, Y. Suzuki, M. Shimoi, and A. Ouchi, *Bull. Chem. Soc. Jpn.*, **59**, 2115 (1986).
11) "The Universal Crystallographic Computation Program System (UNICS)," ed by T. Sakurai, Crystallographic Society of Japan, Tokyo (1967).
12) "International Tables for X-Ray Crystallography," Kynoch Press, Birmingham (1974), Vol. IV, pp. 72, 150.
13) The final atomic positional and thermal parameters, some comments about the structure calculations of the **1**—**8**, and the final F_o—F_c tables of **1**—**6**, as well as some additional data of their bond lengths and bond angles are deposited as Document No.8889 at the Office of the Editor of Bull. Chem. Soc. Jpn.
14) R. D. Shannon, *Acta Crystallogr., Sect. A*, **32**, 751 (1976). According to this paper, the crystal radii are: Er(III) (Coordination Number=6), 1.030; Yb(III) (Coordination Number=6) 1.008, and N(−3) (Coordination Number=4), 1.32 Å. From these data, the Er-N and Yb-N distances are calculated to be 2.35 and 2.33 Å, respectively.
15) K. Nakamoto, "Infrared and Raman Spectra of Inorganic and Coordination Compounds," 4th ed, Wiley, New York (1986), p. 283.

Selective Fluorimetric Determination of Trace Amounts of Cobalt(II) with the System of Fluorescein-Hydrogen Peroxide-Tiron†

Itsuo MORI,* Yoshikazu FUJITA, Yoshihiro NAKAHASHI, Kinuko IKUTA, and Keiji KATO
Osaka University of Pharmaceutical Sciences, Matsubara-shi, Osaka 580
(Received February 27, 1989)

The decomposition reactions of fluorescein (Fl) or its halo derivatives in the basic region were systematically investigated in the presence of an oxidizing agent such as hydrogen peroxide and/or a metal ion such as cobalt(II) and/or catalytic agent such as tiron as an activator. Moreover, a highly selective spectrophotofluorimetric method for the determination of trace amounts of cobalt(II) was established by measuring the difference in relative fluorescence intensities (ΔF) between Fl-tiron-hydrogen peroxide and Fl-tiron-hydrogen peroxide-cobalt(II) solutions at an emission wavelength of 510 nm, with an excitation wavelength of 490 nm (the calibration graph was linear in the range of 0—6 ng cobalt(II) per 25 cm^3). The applications to the assay of cobalt in cyanocobalamine (vitamin B_{12}) preparations and its eye drops were also investigated, the results were relatively good.

For the spectrophotometric determination of trace amounts of cobalt(II), various kinetic and catalytic reactions between diphenol compounds, such as Pyrogallol Red (PR), phenylfluorone (Phfl), *o*-hydroxyhydroquinonephthalein (Qnph), and cobalt(II), in the presence of an oxidizing agent such as hydrogen peroxide have been investigated.[1-5] In this paper, we investigated the use of fluorescein (Fl) as a fluorescence reagent for the spectrofluorometric determination of trace metal ions; firstly, the fluorescence reactions among Fl or its halo derivatives and an oxidizing agent, such as hydrogen peroxide and/or metal ions such as cobalt(II) were systematically investigated; secondly, a fluorimetric method for the determination of trace amounts of cobalt(II) using the fluorescence reaction (fluorescence-quenching) among trace amounts of cobalt(II), Fl, tiron and hydrogen peroxide in the basic region was proposed and applied to the assay of cyanocobalamine (vitamin B_{12}) preparations.

Experimental

Apparatus and Reagents. Fluorescence-intensity measurements were made on a Shimadzu Model RF-540 spectrofluorophometer using 10-mm silica cells and a xenon arc source. A Hitachi-Horiba model F-8 pH meter, equipped with glass and a calomel combined electrode, was used for all the pH measurements.

Deionized water was used throughout. All reagents were of an analytical reagent grade. A stock solution of cobalt(II) (1.0×10^{-2} mol dm^3) was prepared by dissolving cobalt chloride in water, correcting by chelatometry,[6] and a 5.0×10^{-4} mol dm^{-3} cobalt(II) working solution was prepared by the suitable dilution of the stock solution just before use. Fl, its halo-derivative solution (1.0×10^{-3} mol dm^{-3}), and a 0.3% tiron solution were prepared by dissolving, respectively, Fl, its halo-derivatives[7,8] (highly purified Fl derivatives by recrystallization), and tiron in methanol. A 1.0% hydrogen peroxide solution was prepared by the dilution of a 30% hydrogen peroxide solution (Mitsubishi-Edogawa Chemical Co., Ltd.).

Standard Procedure. To each series of 30-cm^3 Erlenmyer flask, add an aliquot of a solution containing between 0 and 6.0 ng of cobalt(II). Add 2.0 cm^3 of a 1 M sodium hydroxide solution (1M=1 mol dm^{-3}), 1.0 cm^3 of a 1.0% hydrogen peroxide solution, 1.0 cm^3 of a 3.0% tiron solution, and 1.0 cm^3 of a 1.0×10^{-3} mol dm^{-3} Fl solution, and dilute to 10.0 cm^3 volume with water. A reflux condenser is attached, and the mixed solution (Solution A, Fl/cobalt(II)/tiron/hydrogen peroxide solution) is heated for 45 min together with Solution B (Fl/tiron/hydrogen peroxide solution), after with Solutions A and B are diluted to a 25-cm^3 volume with water. Measure the difference in fluorescence intensities (ΔF) between Solutions A and B at the emission wavelength of 510 nm with the excitation wavelength of 490 nm.

Results and Discussion

Fluorescence-Quenching Reaction between Fluorescein or Its Derivatives and Hydrogen Peroxide, and the Effects of Metal Ions and Oxidizing Agents. Firstly, the decomposition reactions of Fl and its halo derivatives, such as 2,7-dichlorofluorescein (2,7-Cl_2Fl), 3′,4′,5′,6′-tetrachlorofluorescein (3′,4′,5′,6′-Cl_4Fl), 2,4,5,7-tetrachloro-, 2,4,5,7-tetrabromo-, or 2,4,5,7-tetraiodofluorescein (2,4,5,7-Cl_4Fl, 2,4,5,7-Br_4Fl, 2,4,5,7-I_4Fl), in the presence of hydrogen peroxide as an oxidizing agent were systematically investigated by heating at 60 °C under various pH areas. As is shown in Table 1, the decomposition reactions (fluorescence-quenching) were obvious in basic media; all these halo-Fl derivatives except Fl and 3,4,5,6-Cl_4 Fl were easily decomposed[7,8] and then converted to non-fluorescence substances, but these fluorescence intensities were relatively small, unstable and varied widely in value (93%—108%). On the other hand, the fluorescence intensity of 3,4,5,6-Cl_4Fl was very stable, and it was not entirely decomposed by hydrogen peroxide. Fl was slightly decomposed by an oxidation reaction in the presence of hydrogen

† Application of Xanthene Derivatives to Analytical Chemistry. Part LXXVI. Presented at the 37th Annual Meeting of Analytical Chemistry of Japan, Sapporo, October 1988. Part LXXV: I. Mori, Y. Fujita, K. Ikuta, Y. Nakahashi, and M. Ohji, *Fresenius Z. Anal. Chem.*, **334**, 49 (1989).

Table 1. Decomposition Reactions of Fl and Halo-Fl Derivatives at 0.4 M Sodium Hydroxide in the Presence or Absence of 0.025% Hydrogen Peroxide

Fl deriv.	Em max nm	Absence of H_2O_2 R.fl. Int./% 0 min	Absence of H_2O_2 R.fl. Int./% 100 min	Presence of H_2O_2 R.fl. Int./% 0 min	Presence of H_2O_2 R.fl. Int./% 100 min	ΔF %
Fl	510	100.0	99.5	100.0	96.4	3.6
3,4,5,6-Cl_4Fl	530	57.7	57.7	57.7	57.6	0.2
2′,7′-Cl_2Fl	525	45.3	43.8	45.3	24.6	45.7
2′,4′,5′,7′-Cl_4Fl	535	30.1	15.1	30.1	2.5	91.7
2′,4′,5′,7′-Br_4Fl	535	28.3	16.8	28.3	4.8	83.0
2′,4′,5′,7′-I_4Fl	550	22.1	20.9	22.1	12.0	45.7

Fl and halo-Fl: 1.0×10^{-5} mol dm^{-3}; heating at 60 °C; Ex: 365 nm.

Table 2. Inhibition of Fluorescence-Quenching Reactions of Fl-Hydrogen Peroxide Solutions in the Presence of Various Metal Ions in the Presence or Absence of Tiron

Metal ions	Tiron absence R.fl. Int./% mol dm^{-3}	Tiron absence R.fl. Int./% at 510 nm	Tiron absence Ratio of R.fl. Int. at 510 nm	Tiron presence R.fl. Int./% mol dm^{-3}	Tiron presence R.fl. Int./% at 510 nm	Tiron presence Ratio of R.fl. Int. at 510 nm
—	—	31.9	—	—	19.6	—
Co(II)	2.0×10^{-8}	64.5	1.021[a] (20.042[b])	0.2×10^{-8}	99.0	4.051[a] (810.2[b])
Fe(III)	40.0×10^{-8}	119.9	2.760[a] (2.760[b])	8.0×10^{-8}	31.8	0.622 (3.11[b])
Cu(II)	40.0×10^{-8}	117.5	2.682[a] (2.682[b])	40.0×10^{-8}	103.8	4.490 (4.49[b])
Mn(II)	40.0×10^{-8}	73.6	1.307[a] (1.307[b])	20.0×10^{-8}	79.9	3.077 (6.15[b])
Ni(II)	400.0×10^{-8}	145.2	3.533[a] (0.355[b])	20.0×10^{-8}	162.4	7.286 (15.57[b])

Tiron absence—Fl: 4.0×10^{-5} mol dm^{-3}; H_2O_2: 0.025%; NaOH: 0.08 M;
Tiron presence—Fl: 4.0×10^{-5} mol dm^{-3}; H_2O_2: 0.04%; NaOH: 0.08 M; Tiron: 0.14%; Ex: 490 nm; at heating for 45 min on a reflux.
a) Rate of R. fl. Int. of {(Fl-H_2O_2-metal ion)−(Fl-H_2O_2)}/(Fl-H_2O_2). b) Rate of inhibition on fluorescence quenching under correction of coexisting metal-ion concentration—40.0×10^{-8} mol dm^{-3}.

peroxide, and its fluorescence reaction could easily be reproduced (97.5%—102.4%). Thus, because Fl has an appropriate stability and decomposed property for an oxidation-destruction reaction using hydrogen peroxide, and because the subsequent purification of Fl[7,8] was very easy, Fl was used as a fluorescence reagent for further investigations.

Secondly, the enhancement effect of such metal-ions as cobalt(II), iron(III), manganese(II), and copper(II) by the fluorescence-quenching reaction on the Fl used was systematically investigated. As is shown in Table 2, the difference in fluorescence intensity (ΔF) between Solution A (Fl/hydrogen peroxide/metal ions solution) and Solution B (Fl/hydrogen peroxide solution) was largest and showes most clearly in the presence of trace amounts of cobalt(II). That is, the amounts of ΔF in the presence of cobalt(II) was about 60-times that of ΔF in the presence of nickel(II) (ratio of inhibition of fluorescence-quenching; rates of relative fluorescence intensity on {(Fl-hydrogen peroxide-metal ion)−(Fl-hydrogen peroxide)}/(Fl-hydrogen peroxide), using a correction of the coexisting metal-ion concentration (ratio of fl.Int.), 20.042 for cobalt(II) vs. 0.355 for nickel(II)), the fluorescence-decomposition reaction of Fl was inhibited in proportion to the coexisting cobalt(II) concentrations.

Thirdly, the effect of the oxidizing agent was investigated in the oxidation and decomposition reactions of Fl; sodium hypochlorite, hydrogen peroxide, sodium nitrite, potassium iodate, chloramine B, potassium peroxodisulfate, etc. were used as oxidizing agents. The use of 1.0—2.0 cm^3 of a 1.0% hydrogen peroxide solution as an oxidating agent gave a large and reproducible ΔF. Although the quenching reaction was influenced by the amounts of hydrogen peroxide, further investigation was carried by using Fl and, finally, 0.04% hydrogen peroxide.

Effect of Activator. In this decomposition reaction of Fl, the fluorescence intensity of Fl-hydrogen peroxide-cobalt(II) system remained in the basic medium was significantly enhanced by the coexistence of a biphenol organic reagent, such as tiron, pyrocatechol, or gallic acid, as is shown in Table 3. In measuring the difference in fluorescence intensities the best results were produced using tiron as an activator; the optimum tiron concentration was 0.1—0.3% in the final solution. The inhibition phenomena of fluorescence-quenching (=difference in fluorescence intensities between Solution A (Fl/hydrogen peroxide/tiron/cobalt(II) solution) and Solution B (Fl/hydrogen peroxide/tiron solution)) were larger and more obvious than in the absence of a tiron-quenching ratio (difference in relative fluorescence intensities between Solutions A and B against the

Table 3. Effects of Activators on Fluorescence-Quenching Reaction

Activators	Procedure A R.fl. Int./% 510 nm		Procedure A Ratio of R.fl. Int.[a] at 510 nm	Procedure B Ratio of R.fl. Int.[a] at 510 nm
	Fl-H_2O_2	Fl-H_2O_2-Co(II)		
—	16.8	34.8	1.071	0.102
Tiron	17.1	61.8	2.614	4.051
Pyrogallol	16.0	49.5	2.094	0.25
Pyrocatechol	25.4	50.9	1.004	0.10
2,3-dihydroxy benzoic acid	23.7	49.6	1.093	0.10
Luminol	17.4	35.3	1.029	0.10
Resorcinol	17.9	34.7	0.939	0.10
Phenol	16.3	38.2	1.344	0.10
Glycerol	19.4	32.9	0.696	0.10
Gallic acid	30.0	65.4	1.180	0.10
Phenylalanine	22.1	39.8	0.801	0.10
Norepinephrine	23.0	64.5	1.804	0.10

Procedure A—Co(II) taken: 8.0×10^{-9} mol dm^{-3}; activator: 4.0×10^{-4} mol dm^{-3}; hydrogen peroxide: 0.03%; NaOH: 0.08 M; Fl: 4.0×10^{-5} mol dm^{-3}. Procedure B—Co(II) taken: 2.0×10^{-9} mol dm^{-3}; activator: 0.14%; hydrogen peroxide: 0.04%; NaOH: 0.08 M; Fl: 4.0×10^{-5} mol dm^{-3}; Ex: 490 nm; at heating on reflux for 45 min.

a) Rate of R.fl. Int. on {(Fl-H_2O_2-Co(II)-activator)—(Fl-H_2O_2-activator)}/(Fl-H_2O_2-activator).

relative fluorescence intensity of Solution B); they were 4.051 (in the presence of tiron) and 1.021 (without tiron), while the rates of fl.Int. were 810.2 (in the presence of tiron) and 20.042 (without tiron) for 40.0×10^{-8} mol dm^{-3} cobalt(II)). Thus, the fluorescence-quenching among Fl, hydrogen peroxide, and cobalt(II) in the presence of tiron gave the largest value. That is, the apparent fluorescence-quenching reaction in the presence of cobalt(II) and tiron was about 40-times that in the absence of tiron, and about 300-times that with copper(II) alone; rates of fl.Int.: 810.2 for cobalt(II), 4.490 for copper(II). The maximum and almost costant value was obtained by using a final tiron concentration of 0.2%—0.1%; for the analytical procedure, a final tiron concentration of 0.14% was used.

Fluorometry of Cobalt(II). Fluorescence Spectra. Figure 1 shows the excitation spectrum of the Fl solution and the emission spectra of Fl-hydrogen peroxide and Fl-hydrogen peroxide-cobalt(II) solutions after heating reactions at reflux for 45 min on basic media. The excitation spectrum of the Fl-hydrogen peroxide solution showed an excitation band with a maximum at 490 nm when an emission wavelength at 510 nm was used and an emission band at 510 nm when an excitation wavelength at 490 nm was used. Also, ΔF at 510 nm was proportional to the concentration of trace cobalt(II).

Effect of Concentration of Alkali. The quenching phenomena were recognized over a wide basical range; a maximum and almost constant ΔF value was obtained in a basic medium of a 0.02—0.5 M NaOH final solution under the optima excitation and emission wavelengths (Ex 490 nm, Em 510 nm). Although the elution of metal-ions from the glassware

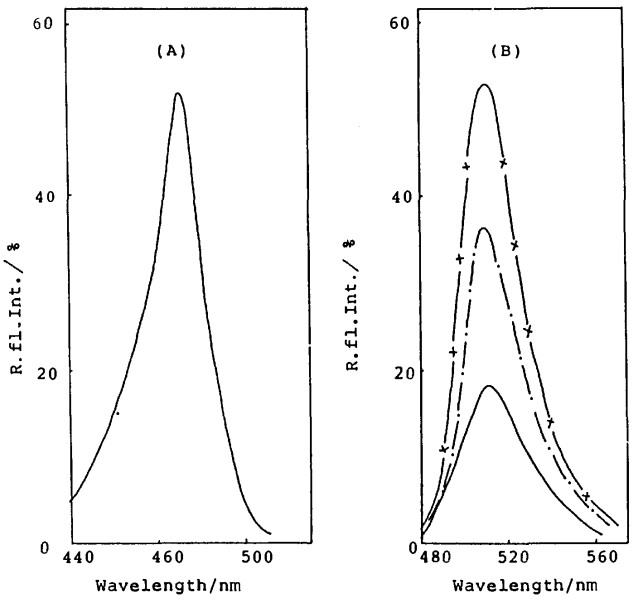

Fig. 1. Excitation spectrum of Fl solution, and emission spectra of Fl-hydrogen peroxide solution in the presence or absence of cobalt(II) at basical media in the presence of tiron.
(A) Excitation spectrum; NaOH: 0.08 M; Fl: 4.0×10^{-5} M; Em 510 nm. (B) Emission spectra; NaOH: 0.08 M; Fl: 4.0×10^{-5} M; hydrogen peroxide: 0.04%; at reflux heating for 45 min; Ex 490 nm;
———: {Fl-H_2O_2-tiron}soln;
— - —: {Fl-H_2O_2-Co(II)-tiron} soln (Co(II) 5.0×10^{-10} M);
—×—: {Fl-H_2O_2-Co(II)-tiron} soln (Co(II) 1.0×10^{-9}M.

was presumed, a final concentration of 0.08 M NaOH was selected for the recommended procedure for the assay of cobalt(II).

Effect of Fl Concentration. As the fluorescence-quenching is influenced by the purity of Fl, previously highly purified Fl was used. The effect of the Fl concentration was then considered. The best result was produced by using 1.0—1.5 cm^3 of a 1.0×10^{-3} mol dm^{-3} Fl (highly purified by recrystallization from Fl acetyl compound) methanol solution per 25 cm^3; a final solution of 4.0×10^{-5} mol dm^{-3} Fl was used for further investigations.

Effects of Temperature and Time. The effect of the temperature was studied at 50 °C, 60 °C, 80 °C, and 100 °C. An inhibition of the fluorescence-quenching was observed when the temperature was increased; the maximum quenching was obtained at reflux on a hotplate. The maximum quenching phenomenon was obtained by heating at reflux for 30 min or less, the fluorescence intensity was thereafter kept constant for longer than 60 min. Therefore, a standing time of 45 min using reflux heating was selected for the standard procedure. Although the coexistence effect of surfactants (nonionic, anionic, and cationic) was investigated, no enhancement effect at all was observed.

Calibration Graph. The calibration graph of cobalt(II) was linear over the range from 0 to 6 ng cobalt(II)/25 cm^3. For 3 ng of cobalt(II) in 25 cm^3, the coefficient of variation, as estimated from 5 replicates, was 2.5%.

Effect of Diverse Ions. The influences of diverse ions on the determination of 2.9 ng of cobalt(II) upon the use of the fluorescence reaction of a Fl-hydrogen peroxide-tiron-cobalt(II) system were also examined. The tolerance limit was taken as the amount that caused about a ±3% error in the fluorescence intensity. The coexistence of numerous metal-ions besides iron(III), manganese(II), copper(II), and nickel(II) did not interfere at all. That is, the coexistence of iron(III) gave a positive error when present in a 400-fold excess over cobalt(II), and the coexistence of copper(II), manganese(II), or nickel(II) also gave a positive error when present in a 50-fold excess over cobalt(II). On the other hand, the coexistence of almost any anion did not interfere, though the cyanide ion gave a negative error when present in a 40-fold excess over cobalt(II). The results are given in Table 4.

Mechanism of Fluorescence-Quenching Reaction. Although further investigation is necessary, the fluorescence-quenching reaction among Fl, hydrogen peroxide, cobalt(II), and tiron was estimated. Firstly, the oxidation and decompostion reaction of Fl by hydrogen peroxide was catalytically enhanced by the presence of small amounts of cobalt(II). Secondly, by the coexistence of tiron as an activator, the total amounts of hydrogen peroxide as an oxidation agent decreased following a reaction between tiron and hydrogen peroxide, or one of tiron, hydrogen peroxide, and cobalt(II). Then the R.fl.Int. of the Fl-hydrogen peroxide-tiron-cobalt(II) solution was found to be proportional to the amounts of cobalt(II); the total hydrogen peroxide concentration was less than the reference solution (Fl/hydrogen peroxide/tiron solution). Thus, the fluorescence-quenching reaction was recognized.

Table 4. Effects of Foreign Ions

Foreign ion	Added			Rate of R.fl. Int.[a)]	Recovery /%
	as	μg/25 cm^3	Mole ratio		
—	—	—	—	4.051	—
Sn(IV)	Sulphate	1.19	200	4.059	100.2
V(V)	Vanadate	2.55	1000	4.060	100.2
Mo(VI)	Molybdate	4.80	1000	4.052	100.0
Ti(IV)	Sulfate	2.38	1000	4.058	100.2
Al(III)	Nitrate	1.35	1000	4.080	100.7
Th(IV)	Nitrate	11.60	1000	4.063	100.3
Bi(III)	Nitrate	10.45	1000	4.072	100.5
Fe(III)	Sulfate	2.33	800	5.192	128.2
		1.17	400	4.059	100.2
Mn(II)	Chloride	0.27	100	5.224	129.0
		0.14	50	4.082	100.7
Cu(II)	Nitrate	0.32	100	4.581	113.1
Ni(II)	Nitrate	0.29	100	5.807	143.3
NO_3^-	Sodium	3.10	1000	4.050	100.0
CN^-	Potassium	0.13	100	3.621	89.4
S^{2-}	Sodium	1.60	1000	4.031	99.5
F^-	Sodium	0.94	1000	4.043	99.8
Citrate	Sodium	7.40	1000	4.042	99.8
Tartrate	Sodium	9.35	1000	4.044	99.8

Co(II) taken: 2.0×10^{-9} mol dm^{-3} (2.9 ng/25 cm^3); hydrogen peroxide: 0.04%; NaOH: 0.08 M; tiron: 0.14%; Fl: 4.0×10^{-5} mol dm^{-3}; Ex 490 nm; Em: 510 nm;
a) Rate of R.fl. Int. on {(Fl-H_2O_2-tiron-Co(II))−(Fl-H_2O_2-tiron)}/(Fl-H_2O_2-tiron).

Table 5. Results of Determinations of Cobalt in Pharmaceutical Preparations

Sample	Calculated /%	Cobalt found/%			Recovery[a] of proposed
		Proposed	ICP-AES	JP-XI[b]	
Cyanocobalamine No. 1	4.34	4.29	4.37	—	96.8
No. 2	4.34	4.34		4.27	—
Drop eye	0.000043	0.000042	0.000042	0.000054	95.2
Sample[c]	0.0043	0.0043	0.0042		97.5

a) Average recoveries from five determinations; cobalt(II) taken—2.9 ng/25 cm^3. b) Japanese Pharmacopoeia XI. c) Prepared sample.

Application. To verify the usefulness of the recommended procedure, the proposed method was applied to the determination of cobalt in cyanocobalamine (vitamin B_{12}) and also in some eye-drop and synthetic pharmaceutical preparations containing vitamin B_{12}. As is shown in Table 5, which gives the recovery data for 3—4 replicates of each sample, the results were relatively good. By using a reflux heating procedure on a hotplate, the proposed method does not require a preliminary decomposition procedure, and it is very simple, rapid, and selective.

In conclusion, the proposed method for the spectrophotometric determination of cobalt(II) based on the fluorescence-quenching of Fl by coexisting hydrogen peroxide, tiron, and cobalt(II) is simpler, more sensitive, and more reproducible than previous reported methods.[2,4,5,9-11] It works by means of a reaction between such organic reagents as Pyrogallol Red, Pyrocatechol Violet, and tiron and an oxidizing agent. The proposed method is very selective and excellent in its effect on foreign ions. Moreover, for the assay of cobalt containing organo compounds such as cyanocobalamine, the proposed method does not require any particular preparatory procedures; organo compounds are decomposed by standard procedures and their fluorescence is quenched well.

References

1) B. E. Rpzink, V. T. Chuiko, and V. I. Vershinin, *Zh. Anal. Khim.*, **27**, 395 (1972).
2) M. Liobat-Estelles, A. Sevillano-Cabeza, and J. Medina-Escriche, *Analyst(London)*, **111**, 193 (1986).
3) I. Mori, Y. Fujita, K. Fujita, Y. Nakahashi, T. Tanaka, and S. Ishihara, *Fresenius Z. Anal. Chem.*, **330**, 619 (1988).
4) M. Otto, J. Rentsch, and G. Werner, *Anal. Chim. Acta*, **147**, 267 (1983).
5) T.Yamano, *Mikrochim. Acta*, **1984**, 425.
6) K. Ueno, "Chelatometry," Nankodo Pub. Co., Tokyo (in Japanese) (1972), p.230.
7) I. Mori, *Yakugaku Zasshi*, **85**, 486 (1965).
8) T. Ohno and I. Mori, *Yakugaku Zasshi*, **84**, 1134 (1964).
9) V. I. Verninin, V. T. Chuiko, and B. E. Reznik, *Zh. Anal. Khim.*, **27**, 395 (1972).
10) T. Deguchi, A. Higashi, and I. Sonemasa, *Bull. Chem. Soc. Jpn.*, **59**, 295 (1986).
11) A. I. Merkulov and R. I. Skvortsova, *Zh. Anal. Khim.*, **36**, 1778 (1981).

 © 1989 The Chemical Society of Japan Bull. Chem. Soc. Jpn., 62, 2541—2546 (1989)

Solvent Influence on the Circular Dichroism Spectrum of Potassium Ethylenediaminetetraacetatocobaltate(III)

Toshiaki TAURA
Department of Chemistry, University of Aichi Prefecture,
Takadacho 3-28, Mizuho-ku, Nagoya 467
(Received February 2, 1989)

The circular dichroism (CD) spectrum of optically active potassium ethylenediaminetetraacetatocobaltate(III), (+)-K[Co(edta)]·$2H_2O$, was measured in water and a variety of organic solvents: ethylene glycol, methanol, formamide, ethanol, 2-propanol, chloroform, nitromethane, dichloromethane, dimethyl sulfoxide, acetonitrile, *N*,*N*-dimethylformamide, benzonitrile, *N*,*N*-dimethylacetamide, and acetone. The spectra in organic solvents were obtained for the solutions of the complex anion, which were prepared by the addition of a macrobicyclic polyether, cryptand 222. It was found that the peak positions and intensities of the CD bands are markedly influenced by the solvent molecules and this solvent influence on the peak position is linearly correlated to the influence on the corresponding first d-d absorption spectrum. Therefore, the solvent influence on the CD spectrum of this complex is suggested to be caused by the change in the d-d transition energy of this Co(III) complex anion. Furthermore, the positions and intensities of the CD peaks were also correlated with the electrophilic ability (the acceptor number: *AN*) and the bulk polarity (the dielectric constant) of the solvent, respectively. It is proposed that the inherent CD spectrum of $[Co(edta)]^-$ that is not solvated could be estimated on the basis of this correlation.

In the field of coordination chemistry, the circular dichroism (CD) spectra of metal complexes, especially cobalt(III) complexes, have been utilized to determine their absolute configuration around the central metal ions.[1] This is because the CD spectra in the d-d transition region are mainly dependent on the configuration of the metal complex, though these are affected to some extent by the conformation of the chelating ligand or the so-called vicinal effect from the ligand asymmetry. However, the CD spectra are sometimes influenced drastically by the outersphere interaction with the counter ion and the solvent molecule. Therefore, one can not obtain any decisive conclusion about the absolute configuration of the complex ion if the influence of the outersphere interaction is not made clear. The influence of the counter ion has so far been investigated for many cobalt(III) complexes:[2] $[Co(en)_3]^{3+}$ (en=ethylenediamine) and other cationic Co(III) complexes; the counter ions are oxoacid anions (PO_4^{3-}, SO_4^{2-}, etc.) and some dicarboxylates. As for the influence of the solvent, only a few systematic studies would appear to have been made on the circular dichroism of optically active metal complexes. Concerning the solvent influence on the CD spectra two reasons have so far been proposed. Bosnich and Harrowfield[3] reported that the CD spectra of cobalt(III) complexes of *trans*-$[Co(N)_4(X)_2]^+$ are markedly solvent-dependent, where $(N)_4$ refers to chiral quadridentate amines. In their first paper, they suggested that *trans*-(*R*,*R*)-[Co(3,2,3-tet)$(N_3)_2$]ClO_4(3,2,3-tet=$NH_2(CH_2)_3NH(CH_2)_2NH(CH_2)_3NH_2$) changed the sign of the CD peak in the longest wavelength region and this is due to the change of the chelate-ring conformation. By contrast, Hawkins et al.[4] investigated the CD and proton NMR spectra of some *trans*-$[Co(R\text{-pn})_2(X)_2]^{n+}$ and related complexes in a variety of solvents (*R*-pn=(*R*)-1,2-propanediamine). They ascribed the solvent dependence of the CD spectra to the stereoselective hydrogen bonding that is formed between the equatorial amino hydrogens of the complex cation and the solvent molecules, leading to the induction of the new asymmetry on the coordinated nitrogens. Thus, in both these two investigations it was proposed that the main factors of this solvent influence on the CD are the change of the chelate-ring conformation and the vicinal effect caused by the asymmetry induction on the coordinated nitrogens.

On the other hand, it has been found that the peak position of the first d-d absorption band is considerably influenced by solvent molecules when the absorption spectrum of K[Co(edta)]·$2H_2O$ was obtained in several organic solvents;[5] the complex is solubilized by the addition of a macrocyclic polyether, 18-crown-6 ether and cryptand 222.[6] This phenomenon makes us expect that the CD spectrum of this complex shows a fairly intensive solvent dependence. This complex anion, $[Co(edta)]^-$, has no amino hydrogens in the ligand and seems to have no flexible chelate rings leading to the drastic conformational change. Therefore, this should be a type of complex different from those considered in the above literature.

From this viewpoint, we have observed the CD spectra of optically active potassium ethylenediaminetetraacetatocobaltate(III) in a variety of solvents in order to elucidate how the CD of this complex is influenced by the solvent. The peak positions and intensities in each solvent are examined on the basis of the corresponding peak positions in the d-d absorption spectra, the dielectric constants and the acceptor numbers of solvents; the last parameter was proposed by Mayer et al. as a means of estimating the electrophilic ability of the solvents.[7] Thereafter, we have tried to obtain the inherent CD spectrum of

$[Co(edta)]^-$ without the contribution of the outersphere interactions.

Experimental

Materials. $K[Co(edta)]\cdot 2H_2O$ was prepared and resolved into two enantiomers $(+)_{546}$- and $(-)_{546}$-$K[Co(edta)]\cdot 2H_2O$[8] by using $(-)$-$[Co(NO_2)_2(en)_2]Br$[9] which was resolved by potassium antimony (*R,R*)-tartrate. The purity of these complexes was checked by spectroscopic methods: 580 nm (−1.72) and 500 nm (+0.77) for (+)-isomer from the less soluble diastereomeric salt [lit,[10] 578 nm (+1.50) and 504 nm (−0.76) for (−)-isomer]. Cryptand 222 was purchased from Merck Co. The organic solvents were of the purest grade commercially available and were used without further purification. The solvents used here are as follows: water, ethylene glycol, methanol, formamide, ethanol, 2-propanol, chloroform, nitromethane, dichloromethane, dimethyl sulfoxide, acetonitrile, *N,N*-dimethylformamide, benzonitrile, *N,N*-dimethylacetamide, and acetone.

Measurements. The circular dichroism (CD) spectra were recorded at ambient temperature[11] on the solutions of $(+)$-$K[Co(edta)]\cdot 2H_2O$ ($(1.00—1.50)\times 10^{-3}$ mol dm^{-3}) for water, and for organic solvents containing cryptand 222 (the 1.5 times concentration). A JASCO J-40CS recording spectropolarimeter with a 1-cm cell was used for the CD measurements. The CD spectra are not influenced by the addition of various amounts of cryptand 222 or by a change of the concentration of the cobalt(III) complex.[12] Furthermore, the slight amount of hydrate water ($(2.00—3.00)\times 10^{-3}$ mol dm^{-3}) were not a problem because the CD spectrum of the anhydrous salt of this complex shows only a minor change (within experimental error) in the solvents of acetonitrile and chloroform.

Results and Discussion

The CD spectra of $(+)_{546}$-$K[Co(edta)]\cdot 2H_2O$ (edta= $^-OOCCH_2(^-OOCCH_2)NCH_2CH_2N(CH_2COO^-)$-$CH_2COO^-$) in water and in chloroform are shown in Fig. 1. It is obvious that these CD spectra are very different from one another in the position and intensity of the peak. In both solvents, the CD spectra of this complex apparently have two components in the first d-d transition region (440—700 nm): a A_2 component of minus sign in the longer wavelength region and a B_2 or B_1 component (overlapped) of plus sign in the shorter wavelength region. (The assignment of the CD peaks has been made for the complex of C_2 symmetry near to the C_{2v} limit by McCaffery et al.[13] and the assignment of $[Co(edta)]^-$ has been carried out by Douglas et al.[10]) The peak positions of both components appear in a longer wavelength region in chloroform than in water. The intensity of the A_2 component is greater in water but that of the B_2 or B_1 component is slightly smaller in water than in chloroform. As the $[Co(edta)]^-$ anion is inert and stable in these solvents, this difference in CD is due to the outersphere interaction between the complex anion and solvent molecules.[14,15]

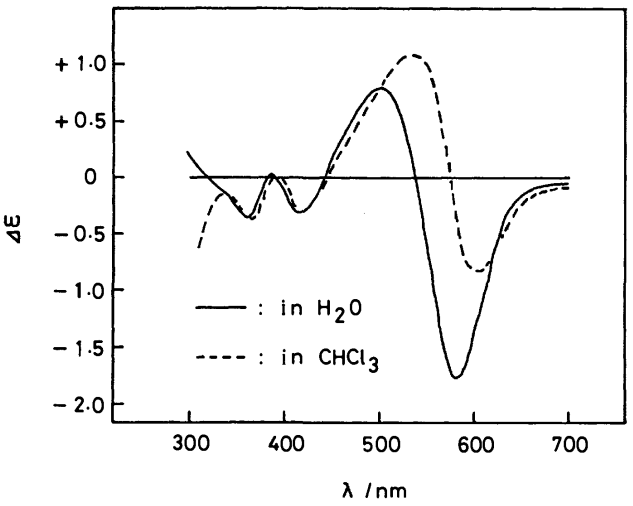

Fig. 1. The CD spectra of $(+)$-$K[Co(edta)]\cdot 2H_2O$ in water (H_2O) and chloroform ($CHCl_3$).

Table 1. The Peak Positions and Intensities of the First d-d Circular Dichroism (CD) Bands of $(+)_{546}$-$K[Co(edta)]\cdot 2H_2O$ in a Variety of Solvents

Solvent	*AN*[a]	Dielectric constant	λ_1/nm	λ_2/nm	$\Delta\varepsilon_1$	$\Delta\varepsilon_2$
H_2O	54.8	78.5	580	500	−1.72	+0.77
EG		37.7	589	514	−1.57	+1.13
CH_3OH	41.3	32.6	591	517	−1.45	+1.00
FA	39.8	109.5	584	504	−1.91	+0.75
C_2H_5OH	37.1	24.3	593	521	−1.27	+1.14
i-C_3H_7OH	33.5	18.3	598	525	−1.17	+1.33
$CHCl_3$	23.1	4.8	606	535	−0.81	+1.12
CH_3NO_2	20.5	36.7	594	518	−1.44	+0.86
CH_2Cl_2	20.4	8.9	603	528	−0.98	+0.84
Me_2SO	19.3	46.7	596	523	−1.60	+0.99
CH_3CN	18.9	36.0	595	519	−1.43	+0.75
DMF	16.0	36.7	599	528	−1.45	+1.08
C_6H_5CN	15.5	25.2	600	528	−1.32	+0.95
DMA	13.6	37.8	602	532	−1.32	+1.18
Me_2CO	12.5	20.7	602	531	−1.12	+1.00

a) *AN* refers to the acceptor number of the solvent.

All data of the peak positions and intensities of the CD obtained are presented in Table 1 for a variety of solvents: H_2O, ethylene glycol (EG), methanol (CH_3OH), formamide (FA), ethanol (C_2H_5OH), 2-propanol (i-C_3H_7OH), chloroform ($CHCl_3$), nitromethane (CH_3NO_2), dichloromethane (CH_2Cl_2), dimethyl sulfoxide (Me_2SO), acetonitrile (CH_3CN), *N,N*-dimethylformamide (DMF), benzonitrile (C_6H_5CN), *N,N*-dimethylacetamide (DMA), and acetone (Me_2CO). This table also includes the acceptor numbers (*AN*) and the dielectric constants of solvents.

Correlation between the Peak Positions in CD and Absorption Spectra. At first we consider the correlation between the peak positions (λ_{max}(CD)) in the CD spectra and the peak positions (λ_{max}(ABS)) in the first d-d absorption spectra.[16] In Fig. 2, are plotted the λ_{max}(CD) values of the A_2 component against the λ_{max}(ABS) values[5] of the first d-d transition band in the corresponding solvents: H_2O, EG, CH_3OH, FA, C_2H_5OH, i-C_3H_7OH, $CHCl_3$, CH_3NO_2, CH_2Cl_2, Me_2SO, CH_3CN, DMF, C_6H_5CN, DMA, and Me_2CO. This figure indicates a linear correlation between these two values. Figure 3, in which the same plot for the B_2 or B_1 component is shown, suggests that the λ_{max}(CD) values are also linearly correlated to the λ_{max}(ABS) values. Therefore, the solvent dependence of the peak position of the CD in the first d-d transition region is completely due to the change in the d-d transition energy of this complex anion.

In the works of Bosnich and Hawkins, it seems that there is no such correlation between the peak positions in CD and absorption spectra. This is because the newly induced ligand asymmetry and the change

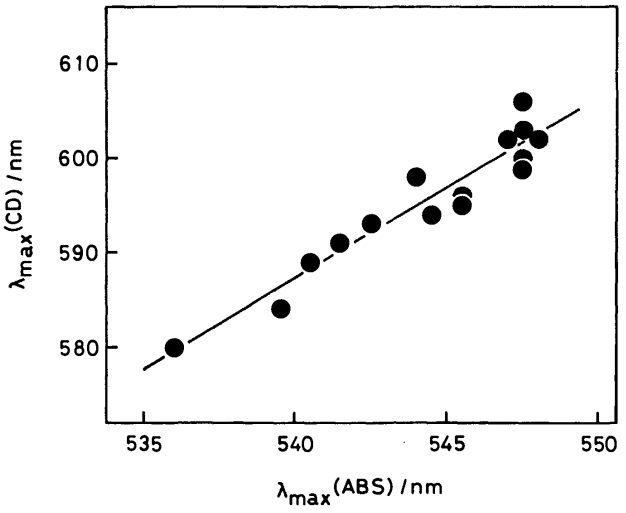

Fig. 2. The correlation between the peak positions (λ_{max}(CD): λ_1 in Table 1) of the A_2 component in the CD spectrum and the peak positions (λ_{max}(ABS)) of the first d-d absorption band in a variety of solvents. The data are plotted for the solvents presented in Table 1; the slope is 1.916 and the correlation coefficient is 0.955. The values of the peak positions of absorption bands are taken from Ref. 5.

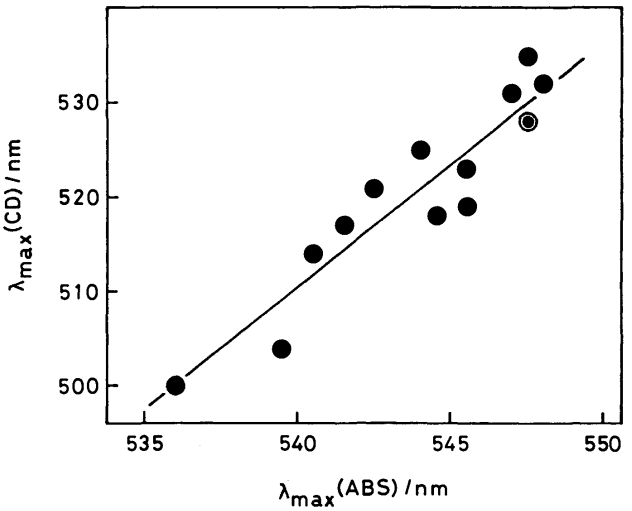

Fig. 3. The correlation between the peak positions (λ_{max}(CD): λ_2 in Table 1) of the B_2 or B_1 component in the CD spectrum and the peak positions (λ_{max}(ABS)) of the first d-d absorption band in a variety of solvents. The data are plotted for the solvents presented in Table 1; the slope is 2.586 and the correlation coefficient is 0.937. The values for absorption bands are from Ref. 5.

of the ligand conformation do not influence the absorption spectra in this way. Therefore, this suggests that the solvent influence is not generated from these two factors.

Correlation between the Peak Positions in CD and the Acceptor Numbers of Solvents. Furthermore, in order to elucidate the origin of this CD change more clearly, this solvent dependence is examined on the basis of the acceptor numbers (*AN*) that are proposed as a measure of estimating the electrophilic ability of solvents. In Table 1, it is apparent that λ_{max}(CD) (in later sections λ_{max} is used in place of λ_{max}(CD)) values are shifted to the shorter wavelength region as the acceptor number (*AN*) increases. The acceptor number indicates that the solvent bearing the large *AN* value is a strong electron acceptor. Therefore, solvent molecules interact strongly with the anion like $[Co(edta)]^-$ if the solvent bears a large value of the acceptor number. This interaction has already been investigated by the carbon-13 NMR studies.[15] It was reported in this NMR study that protic solvents bearing large *AN* values interact with negatively charged carboxyl groups of $[Co(edta)]^-$ through the hydrogen bonding between solvent hydrogens and carboxyl oxygens of the complex anion. Further, the solvent influence on the carbon-13 NMR chemical shift is rationalized by the electron-withdrawing effect caused by the hydrogen-bond formation. Accordingly, the CD change, which is due to the change of the d-d transition energy, is also supposed to be attributed to this hydrogen-bond formation between solvent molecules and $[Co(edta)]^-$ and to the electron-withdrawing effect. The correlation between this hydrogen bond-

ing and the change in the electronic state of the complex has now been studied by MO calculation.[5b] Then, the contribution of the solvent interaction to the peak positions of CD will be estimated quantitatively.

In Figs. 4 and 5, are plotted the λ_{max} values of the A_2 and B_2 or B_1 (abbreviated as B later on) components against the acceptor numbers of solvents. These figures indicate that the plots of λ_{max} give straight lines (the correlation coefficients are 0.821 and 0.801, respectively). The linearities of the lines suggest that the λ_{max} values in some solvent can be approximately estimated by using the acceptor number of the solvent. If the complex anion is hypothetically free from the solvation in hexane that bears the *AN* value of zero, the peak positions of the $[Co(edta)]^-$ anion that is not solvated could then be obtained by the extrapolations of these lines. The λ_{max} values of A_2 and B components in the solvent are calculated by the following equations (error bars are for one standard deviation):

$$\lambda_{max}(A_2) = \lambda_{max}^{\circ}(A_2) - (0.47 \pm 0.09) \times AN$$

$$\lambda_{max}(B) = \lambda_{max}^{\circ}(B) - (0.63 \pm 0.14) \times AN$$

where $\lambda_{max}^{\circ}(A_2)$, $\lambda_{max}^{\circ}(B)$, and *AN* refer to the peak positions ($\lambda_{max}^{\circ}(A_2)=608\pm3$ nm and $\lambda_{max}^{\circ}(B)=539\pm4$ nm determined by a linear least-squares analysis) in hexane as a standard solvent (*AN*=0) and the acceptor number of the solvent, respectively. The first terms in these equations could correspond to the inherent peak positions of the A_2 and B components for $[Co(edta)]^-$ that is not solvated and the second terms to the electron-withdrawing effect that is attributed to solvating molecules. Therefore, we could separate the inherent peak positions from the contributions of the solvent molecules.

The second terms in these equations are slightly different from each other (the coefficients are −0.47 for λ_{max} (A_2) and −0.63 λ_{max} (B), respectively). Though the origin of this slight difference is not clear, these terms should be in principle the same because stereoselective solvation does not exist in this system, as has been shown in the carbon-13 NMR study.[15] The solvent molecules interact equivalently with the four (axial and equatorial) carboxyl oxygens.

Correlation between the Intensities in CD and the Dielectric Constants of Solvents. One of the most interesting results in this work is the correlation between the intensities in CD and the dielectric constants of the solvents. The intensities of the CD peaks are varied from one solvent to another in Table

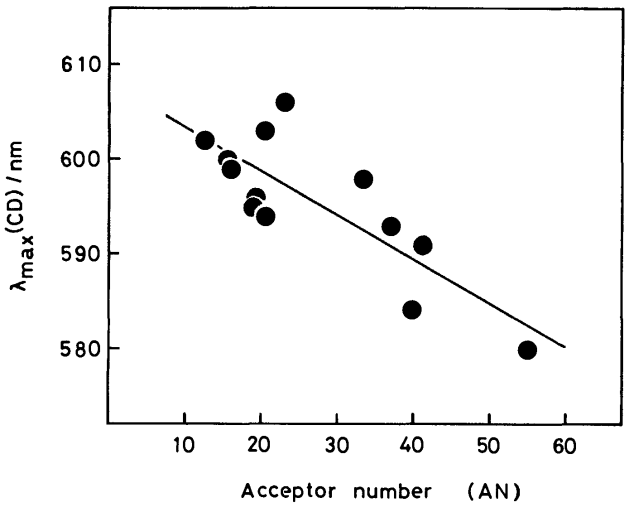

Fig. 4. The correlation between the peak positions (λ_{max}(CD): λ_1 in Table 1) of the A_2 component and the acceptor numbers (*AN*) of the solvents. The data are plotted for the solvents except for ethylene glycol (EG) presented in Table 1.

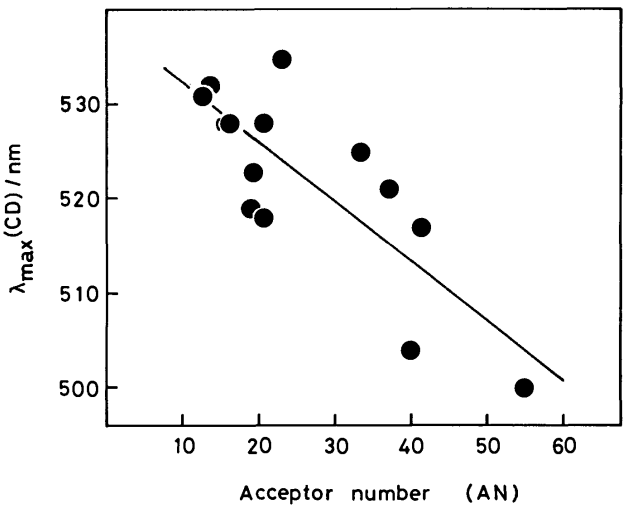

Fig. 5. The correlation between the peak positions (λ_{max}(CD): λ_2 in Table 1) of the B_2 or B_1 component and the acceptor numbers (*AN*) of the solvents. The data are plotted for the solvents except for ethylene glycol (EG) presented in Table 1.

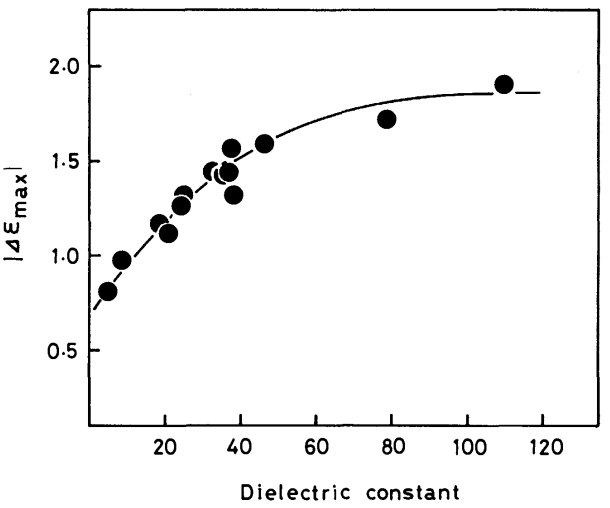

Fig. 6. The correlation between the intensities ($|\Delta\varepsilon_{max}|$: the absolute values of $\Delta\varepsilon_1$ in Table 1) of the A_2 component and the dielectric constants of the solvents.

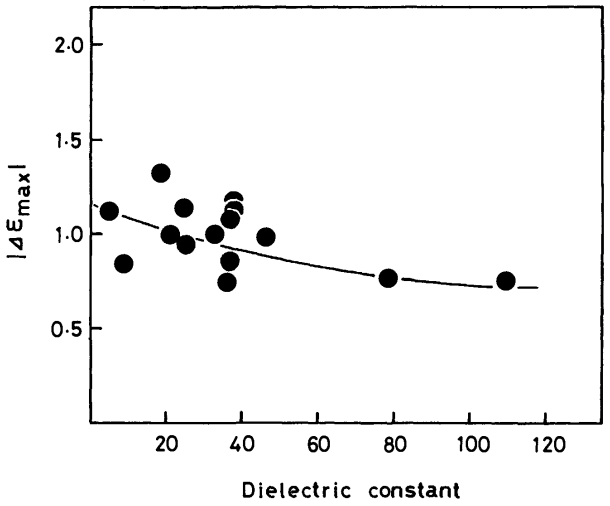

Fig. 7. The correlation between the intensities ($|\Delta\varepsilon_{max}|$: the absolute values of $\Delta\varepsilon_2$ in Table 1) of the B_2 or B_1 component and the dielectric constants of the solvents.

1. This variation is found to be correlated to the polarities of solvents, indicated by the dielectric constant. In Figs. 6 and 7, the intensities of the A_2 and B components are plotted against the dielectric constants of the solvents. The intensity of the B component does not drastically vary in this series of solvents. (The larger deviation of the plot in Fig. 7 is probably because this CD band contains two components B_2 and B_1.) In contrast to this component, the CD intensity of the A_2 component increases markedly and continuously as the dielectric constant of the solvent increases (Fig. 6). This A_2 component of the CD of $[Co(edta)]^-$ is assigned by McCaffery et al. and Douglas et al. The transition for the A_2 component is polarized along the C_2 axis of the complex, which is illustrated in Fig. 8. The electric dipole moment of this complex also extends along the C_2 direction, and so the polarization of the complex along this direction could increase more because of the polar environment of a large dielectric constant around the complex anion. Though a theoretical interpretation for the change of the rotational strength according to the dielectric constant of the solvent could not be suggested, it is probable that the rotational strength of the transition component A_2 polarized along the direction

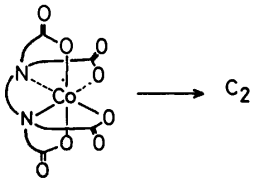

Fig. 8. The direction of the polarization for the A_2 transition and of the electric dipole moment of $[Co(edta)]^-$. The absolute configuration corresponds to the $(+)_{546}$-isomer that is used in this work.

of the dipole increases as the polarization of the complex along this direction increases.

We can confirm this result by considering the datum for formamide. This is one of the solvents bearing a dielectric constant larger than that of water. The dielectric constant of formamide (109.5) is much greater than that of water (78.5). In Fig. 6 one can clearly observe that the intensity of the A_2 component in formamide is much greater than the intensity in water.

It can be concluded that the intensity of the A_2 component which appears in the longest wavelength region increases as the dielectric constant corresponding to the bulk polarity of the solvent increases though the correlation is not linear.

From this correlation, we can tentatively estimate the intensities of the A_2 and B_2 or B_1(B) components in the hypothetical environment of the dielectric constant zero. These values are −0.70 (±10% error) for the A_2 and +1.15 (±20% error) for the B, which are evaluated by the extrapolation of the plots in Figs. 6 and 7. It is certain that, generally speaking, the solvent influence on the CD intensity depends not only on the dielectric constant but also on other solvent properties, ex. refractive indices. In this case the CD-intensity variation seems to depend mainly on the dielectric constants of the solvents.

Conclusion

The solvent influence on the circular dichroism spectrum of $[Co(edta)]^-$ has been rationalized by examining the correlation between the peak positions of the CD spectra and the acceptor numbers, and the correlation between the intensities of the CD bands and the dielectric constants of the solvents. Based on this rationalization, the CD spectrum was divided into the inherent CD and the contribution of the solvent influence. Eventually, the inherent CD spectrum of optically active $[Co(edta)]^-$ that is not solvated could be proposed. The peak positions and intensities for $(+)_{546}$-isomer are 608±3 nm (−0.70) and 539±4 nm (+1.15) [obsd.: 580 nm (−1.72) and 500 nm (+0.77) in water].

The author wishes to thank Prof. J. Fujita for the use of a JASCO J-40CS recording spectropolarimeter at Nagoya University.

References

1) C. J. Hawkins, "Absolute Configuration of Metal Complexes," Wiley Interscience, New York (1971), Chap. 5.
2) S. F. Mason and B. J. Norman, *J. Chem. Soc. A*, **1966**, 307; H. L. Smith and B. E. Douglas, *Inorg. Chem.*, **5**, 784 (1966); A. M. Sargeson, *Transition Metal Chem.*, **3**, 303 (1966); J. E. Sarneski and F. L. Urbach, *J. Am. Chem. Soc.*, **93**, 884 (1971); T. Taura and H. Yoneda, *Inorg. Chem.*, **17**, 1495 (1978); T. Taura, *J. Am. Chem. Soc.*, **101**, 4221 (1979).

3) B. Bosnich and J. M. Harrowfield, *J. Am. Chem. Soc.*, **94**, 989 (1972); B. Bosnich and J. M. Harrowfield, *Inorg. Chem.*, **14**, 828, 847, 861 (1975).

4) C. J. Hawkins, G. A. Lawrance, and R. M. Peachey, *Aust. J. Chem.*, **30**, 2115 (1977); C. J. Hawkins and M. L. McEniery, *Aust. J. Chem.*, **32**, 1433 (1979); C. J. Hawkins and J. Martin, *Inorg. Chem.*, **21**, 1074 (1982).

5) a) T. Taura, *Chem. Lett.*, **1984**, 2011; b) T. Taura, unpublished results.

6) T. Taura, *Inorg. Chim. Acta*, **98**, L15 (1985); T. Taura, presented at the 50th Annual Meeting of the Chemical Society of Japan, April 1985 (Abstract I, 1K18).

7) U. Mayer, V. Gutmann, and W. Gerger, *Monatsh. Chem.*, **106**, 1235 (1975).

8) F. P. Dwyer, E. C. Gyarfas, and D. P. Mellor, *J. Phys. Chem.*, **59**, 296 (1955); F. P. Dwyer and F. L. Garvan, *Inorg. Synth.*, **6**, 192 (1960).

9) F. P. Dwyer and F. L. Garvan, *Inorg. Synth.*, **6**, 195 (1960).

10) B. E. Douglas, R. A. Haines, and J. G. Brushmiller, *Inorg. Chem.*, **2**, 1194 (1963).

11) The temperature for the measurement is 23—25 °C. The CD spectrum was measured more than twice. The peak position was the same within experimental error (±1 nm) and the intensity was reproduced within ±3% of random errors. Therefore, the CD spectrum is not dependent on the temperature under the conditions used here.

12) It seems that there is no influence of the ion association with K^+ or the $K^+ \cdot$ C222 complex on the CD spectra of the $[Co(edta)]^-$ anion, where C222 refers to cryptand 222.

13) A. J. McCaffery, S. F. Mason, and B. J. Norman, *J. Chem. Soc.*, **1965**, 5094.

14) The absorption and CD spectra in the solvents did not show the time dependence during the measurements.

15) T. Taura, *Inorg. Chem.*, **27**, 2845 (1988).

16) The plot of the wavenumbers (cm^{-1}) of the peak positions against the acceptor number also gives the straight line. The intercepts and correlation coefficients are quite similar to those obtained from the plots of the wavelengths (nm). The intercept and correlation coefficient are 16440±80 cm^{-1} (608 nm) and 0.820 for the A_2 component and 18550±150 cm^{-1} (539 nm) and 0.801 for the B component, respectively.

Substituent Group Electronic Effects on Inversion and Proton-Exchange Rates at Chiral Nitrogen Centers for a Series of Bis(β-diketonato)-(*N*-methylethylenediamine)cobalt(III) Complexes

Guilin MA, Masaaki KOJIMA, and Junnosuke FUJITA*
Department of Chemistry, Faculty of Science, Nagoya University, Chikusa-ku, Nagoya 464-01
(Received April 3, 1989)

The rates of the base-catalyzed proton exchange (deuteration, k_D) and inversion (epimerization, k_{ep}) at chiral nitrogen centers of $[Co(Xacac)_2(Me\text{-}en)]^+$ (Xacac: NO_2acac=3-nitro-2,4-pentanedionate, Clacac=3-chloro-2,4-pentanedionate, CH_3acac=3-methyl-2,4-pentanedionate; Me-en=*N*-methylethylenediamine) in aqueous solutions have been measured at 34.0 °C, and the results were compared with one another and with those of the corresponding acac complex (acac=2,4-pentanedionate) in order to investigate the substituent influence on the rates. The k_D and k_{ep} values of the NO_2acac complex are ca. 10^4 and ca. 10^6 times, respectively, larger than those of the CH_3acac complex. The effect of substituents is electronic and the Hammett relationship was found to hold for both deuteration and epimerization rates. The reduction (Co^{3+}/Co^{2+}) half-wave potential, $E_{1/2}$ obtained by rotating glassy carbon electrode voltammetry increases from −0.59 V (vs. SCE) for the CH_3acac complex to −0.08 V for the NO_2acac complex. A linear dependence was observed between $E_{1/2}$ and the Hammett parameter.

The kinetics of inversion and proton exchange at chiral secondary amine nitrogen centers of metal complexes have been studied extensively.[1] However, factors influencing the rates are not clear yet. In a previous paper,[2] we measured the rates of base-catalyzed epimerization and deuteration of $[Co(acac \text{ or } ox)_2(Me\text{-}en)]^{+or-}$ (ox=oxalate ion), and found that the rates of the uninegative ox complex are greater than those of the unipositive acac complex. The results indicate that the rates are largely affected by the electronic effect of coexisting ligands rather than the number of positive charges on the complex.[3]

In order to investigate the electronic effect on the rates of proton exchange and inversion in more detail, we have prepared a series of $[Co(Xacac)_2(Me\text{-}en)]^+$, in which the hydrogen atom at the 3-position of the acac ligand is replaced by a methyl, chloro, or nitro group.

Experimental

The $[Co(acac)_2(Me\text{-}en)]^+$ complex was prepared and separated into the two racemic pairs of diastereomers, *Λ*(*R*)*Δ*(*S*) and *Λ*(*S*)*Δ*(*R*), as described previously.[4]

[Co(CH_3acac)$_3$]. To a solution of $CoCl_2 \cdot 6H_2O$ (5 g, 21 mmol) in water (5 cm^3) was added 30% H_2O_2 (7.5 cm^3). This solution was added to an ice-cold slurry of $KHCO_3$ (15 g) in water (15 cm^3) with stirring. The resulting green solution of $[Co(CO_3)_3]^{3-}$[5] was filtered. To the filtrate was added 3-methyl-2,4-pentanedione[6] (7.2 g, 63 mmol) and the mixture was heated at 40 °C for 1.5 h to yield a green solid. The product was collected by filtration, washed with water, and recrystallized from chloroform by adding petroleum ether. Yield: 4.0 g. The ^{1}H NMR spectrum in $CDCl_3$ was identical with that reported by Brown et al.[7]

***Λ*(*R*)*Δ*(*S*)- and *Λ*(*S*)*Δ*(*R*)-[Co(CH_3acac)$_2$(Me-en)]ClO_4.** Active charcoal (0.2 g) and a solution of Me-en (0.244 g, 3.3 mmol) in methanol (20 cm^3) were added to a solution of [Co(CH_3acac)$_3$] (1.2 g, 3.0 mmol) in methanol (80 cm^3). The mixture was stirred for 45 min and then filtered. The purple filtrate was diluted with water (1 dm^3), and applied on a column (φ3 cm×20 cm) of SP-Sephadex C-25. By elution with 0.05 mol dm^{-3} NaCl, a purple and a red (probably $[Co(CH_3acac)(Me\text{-}en)_2]^{2+}$) band developed in this order. The eluate containing the purple band was collected and evaporated to a small volume under reduced pressure. To the concentrate sodium perchlorate was added to yield purple crystals, which were recrystallized from water (60 °C). Yield: 0.4 g. The crystals were a mixture of the two isomers, and they were separated by a column chromatographic method. About 0.15 g of the mixture was dissolved in water and the solution was applied on a column (φ2.2 cm×50 cm) of SE-Toyopearl HW-40[8] (fine). A recycling chromatographic technique with an eluent of 0.05 mol dm^{-3} NaCl was employed. After two times of recycling, two isomers, *Λ*(*R*)*Δ*(*S*) and *Λ*(*S*)*Δ*(*R*) were eluted separately in this order. From each eluate the perchlorate of the isomer was obtained by the same method as that described above. Found for the *Λ*(*R*)*Δ*(*S*)-isomer: C, 39.22; H, 6.12; N, 6.09%. Found for the *Λ*(*S*)*Δ*(*R*)-isomer: C, 39.36; H, 6.14; N, 6.18%. Calcd for $C_{15}H_{28}N_2O_8ClCo$: C, 39.27; H, 6.15; N, 6.11%.

***Λ*(*R*)*Δ*(*S*)- and *Λ*(*S*)*Δ*(*R*)-[Co(Clacac)$_2$(Me-en)]ClO_4.** These complexes were prepared by chlorination of the corresponding isomers of $[Co(acac)_2(Me\text{-}en)]ClO_4$ with *N*-chlorosuccinimide by a method similar to that for [Co(Clacac)-(en)$_2$]$(ClO_4)_2$[9] (en=ethylenediamine). To a suspension of *Λ*(*R*)*Δ*(*S*)-$[Co(acac)_2(Me\text{-}en)]ClO_4 \cdot 0.5H_2O$ (0.66 g, 1.54 mmol) in 0.01 mol dm^{-3} $HClO_4$ (8 cm^3) was added *N*-chlorosuccinimide (0.49 g, 3.67 mmol) little by little, and the mixture was stirred for 30 min at 50 °C. After cooling, the purple product was collected by filtration, and recrystallized from 0.01 mol dm^{-3}$HClO_4$. Yield: 0.26 g. The *Λ*(*S*)*Δ*(*R*)-isomer was obtained from *Λ*(*S*)*Δ*(*R*)-$[Co(acac)_2(Me\text{-}en)]ClO_4$ by the same method. Found for the *Λ*(*R*)*Δ*(*S*)-isomer: C, 31.14; H, 4.43; N, 5.57%. Found for the *Λ*(*S*)*Δ*(*R*)-isomer: C, 31.10; H, 4.40; N, 5.59%. Calcd for $C_{13}H_{22}N_2Cl_3CoO_8$: C, 31.25; H, 4.44; N, 5.61%.

***Λ*(*R*)*Δ*(*S*)- and *Λ*(*S*)*Δ*(*R*)-[Co(NO_2acac)$_2$(Me-en)]ClO_4.** These complexes were prepared by nitration of the corresponding isomers of $[Co(acac)_2(Me\text{-}en)]ClO_4$ in a manner similar to that for [Co(NO_2acac)$_3$].[10] A mixture of finely ground $Cu(NO_3)_2 \cdot 3H_2O$ (1.93 g, 8.0 mmol) and acetic anhydride (60 cm^3) was stirred for 15 min at 0 °C. To the slurry was added *Λ*(*R*)*Δ*(*S*)-$[Co(acac)_2(Me\text{-}en)]ClO_4 \cdot 0.5H_2O$ (0.6 g, 1.4 mmol).

The mixture was stirred for 3 h at 0 °C, and then for 1 h at room temperature. The blue solution was mixed with water (90 g) and ice (90 g), and the mixture was evaporated to a small volume under reduced pressure. To the concentrate was added sodium perchlorate to yield purple crystals. They were collected by filtration and recrystallized from 0.01 mol dm^{-3} $HClO_4$. Yield: 0.4 g. The $\Lambda(S)\Delta(R)$-isomer was obtained from $\Lambda(S)\Delta(R)$-[Co(acac)$_2$(Me-en)]ClO_4 by the same method. Found for the $\Lambda(R)\Delta(S)$-isomer: C, 30.29; H, 4.22; N, 10.76%. Found for the $\Lambda(S)\Delta(R)$-isomer: C, 29.86; H, 4.25; N, 10.83%. Calcd for $C_{13}H_{22}N_4ClCoO_{12}$: C, 29.99; H, 4.26; N, 10.76%.

Measurements. Absorption and ^{1}H NMR spectra were measured on a Hitachi 323 spectrophotometer and a Hitachi R-90H spectrometer, respectively. Electrochemical measurements were performed at 24 °C by using a Fuso HECS 321B potential sweep unit. Rotating disk experiments were carried out on a three-electrode system composed of glassy carbon rotating disk (2000 rev min^{-1}), platinum wire, and saturated calomel electrodes as the working, auxiliary, and reference electrodes, respectively. KCl was used as the supporting electrolyte at 0.1 mol dm^{-3} concentration.

Deuteration Studies. The rates of deuteration at the chiral amine nitrogen centers of the Clacac and CH_3acac complexes were measured in a phosphate buffer, pD 4.8—6.2 and pD 7.7—9.2, respectively at 34.0 °C, while those of the NO_2acac complex in a phthalate buffer (pD 2.4—3.1) at 34.0 °C. The empirical formula, pD=pH meter reading +0.4, was used to calculate [OD$^-$].[11] The complex perchlorates were converted into the more soluble chlorides with a Dowex 1X8 anion exchanger in the chloride form. The deuteration rates were followed by monitoring signal changes in the ^{1}H NMR spectra. The N-CH_3 doublet signal becomes a singlet by deuteration. All rates were followed for at least two half-lives. From the spectral changes, pseudo-first-order rate constants for deuteration, $k_{D(obsd)}$ were obtained as described previously.[12] For each complex, the $k_{D(obsd)}/[OD^-](=k_D)$ values are constant at 34.0 °C in the pD range measured, indicating that the reaction is first order in [OD$^-$]. Thus, the rate law was the same as that obtained previously for other amine complexes, $R=k_D$[complex][OD$^-$].[1]

Epimerization Studies. The rates of epimerization of the NO_2acac and the Clacac complexes were measured in a phosphate buffer (pH 6.4—7.2) and a borate buffer (pH 9.1—10.2), respectively, while that of the CH_3acac complex in 0.1 mol dm^{-3} NaOH (pH 12.6 at 34.0 °C) and a saturated aqueous solution of $Ca(OH)_2$ (pH 12.1 at 34.0 °C). The rates were followed by the same method as described previously.[12-14] It involves separation of two isomers of the complexes by a high-performance liquid chromatographic method. Analysis of chromatograms changed with reaction time gives the pseudo-first-order rate constant, $k_{ep(obsd)}$. The rate law for the epimerization reaction was the same as that for racemization (epimerization) of other chiral amine complexes, $R=k_{ep}$[complex][OH$^-$].[1] The runs starting from either of the isomers gave the same result within the experimental error. From these observations, the reaction can be expressed as

$$\Lambda(S)\Delta(R) \underset{k_{-1}}{\overset{k_1}{\rightleftharpoons}} \Lambda(R)\Delta(S).$$

The forward and reverse second-order rate constants, k_1 and k_{-1} were obtained from k_{ep} ($k_{ep}=k_1+k_{-1}$) and the equilibrium constant ($K_{eq}=k_1/k_{-1}$).

Results and Discussion

Preparation and Characterization of the Complexes. The [Co(CH_3acac)$_2$(Me-en)]$^+$ complex was prepared by the reaction of [Co(CH_3acac)$_3$] with Me-en in the presence of active charcoal. Four stereoisomers, $\Lambda(R)$, $\Lambda(S)$, $\Delta(R)$, and $\Delta(S)$ are possible for the complex (Fig. 1). The isomers were separated into two racemic pairs of the diastereomers, $\Lambda(R)\Delta(S)$ and $\Lambda(S)\Delta(R)$ by column chromatography on SE-Toyopearl. The structures of the isomers were assigned from the chemical shift of the *N*-methyl group in ^{1}H NMR spectra taking a shielding effect by the CH_3acac chelate ring into consideration; an isomer which shows a doublet attributable to the *N*-methyl group at a higher magnetic field is assigned to the $\Lambda(S)\Delta(R)$ isomer (Fig. 1 and Table 1). The isomers ($\Lambda(R)\Delta(S)$ and $\Lambda(S)\Delta(R)$) of [Co(Clacac)$_2$(Me-en)]$^+$ and [Co(NO_2acac)$_2$(Me-en)]$^+$ were prepared by chlorination and nitration, respectively of the corresponding isomers of [Co(acac)$_2$(Me-en)]$^+$. The configurations of the parent complexes remained unchanged as verified by the ^{1}H NMR spectra.

The distributions of the isomers at equilibrium (34 °C) were analyzed by the reversed-phase high-performance liquid chromatographic technique, and the results are given in Table 1. The difference in stability is very small between the isomers for each complex. Table 1 also gives the absorption spectral data for the [Co(Xacac)$_2$(Me-en)]$^+$ complexes, and the spectra are shown in Fig. 2. The $\Lambda(S)\Delta(R)$ isomers, in which the *N*-methyl group is situated over one of the Xacac chelate rings exhibit the first d-d absorption

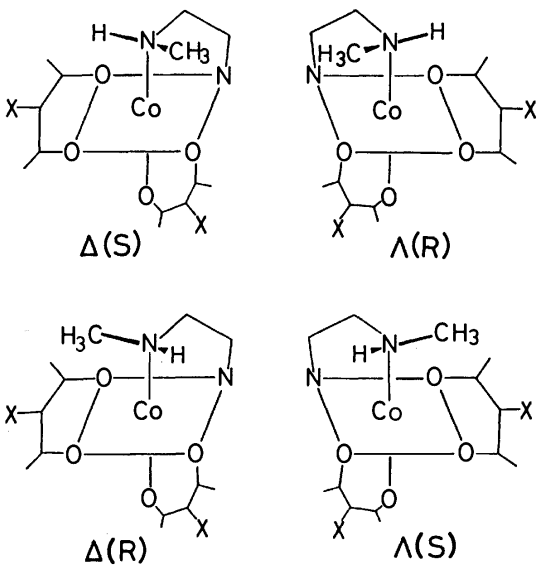

Fig. 1. The four stereoisomers of [Co(Xacac)$_2$(Me-en)]$^+$.

Table 1. ^{1}H NMR and Absorption Spectral Data for [Co(Xacac)$_2$(Me-en)]$^+$ and the Distributions of the Isomers at Equilibrium (34 °C)

Xacac	Isomer	^{1}H NMR (δ)		Absorption[c]			Relative
		NCH_3	$\underline{N}H$ (CH_3)	$\tilde{\nu}_{max}/10^3$ cm^{-1} (log ε)			abundance/%
NO_2acac	$\Lambda(S)\Delta(R)$	2.03d	7.50[a]	18.79(2.19)	30.77(3.81)	40.49(3.03)	44
	$\Lambda(R)\Delta(S)$	2.43d	6.50[a]	18.87(2.20)	30.86(3.82)	40.82(3.05)	56
Clacac	$\Lambda(S)\Delta(R)$	2.00d	6.65[a]	18.32(2.20)	28.99(3.75)	40.00(4.45)	40
	$\Lambda(R)\Delta(S)$	2.15d	5.45[a]	18.38(2.25)	28.99(3.83)	40.00(4.45)	60
acac	$\Lambda(S)\Delta(R)$	1.80d	5.70[b]	18.32(2.16)	30.77(3.80)	40.65(4.41)	45
	$\Lambda(R)\Delta(S)$	2.10d	5.25[b]	18.38(2.17)	30.77(3.80)	40.65(4.43)	55
CH_3acac	$\Lambda(S)\Delta(R)$	1.77d	5.55[b]	18.12(2.25)	28.99(3.83)	40.16(4.40)	45
	$\Lambda(R)\Delta(S)$	1.92d	5.00[b]	18.21(2.30)	29.07(3.87)	40.32(4.43)	55

a) In D_2O-DCl. b) In D_2O. c) In 0.01 mol dm^{-3} $HClO_4$.

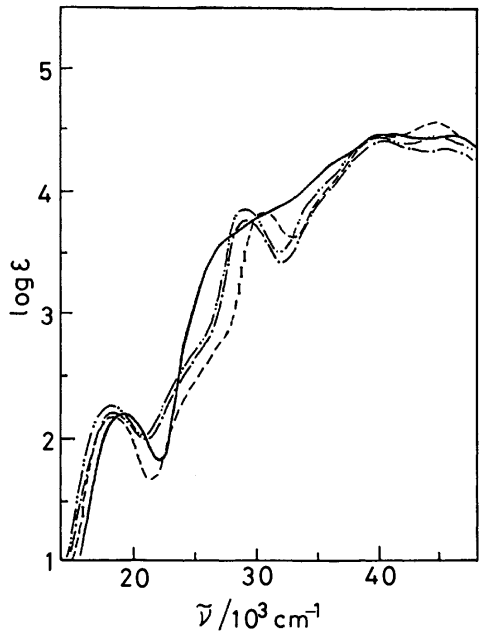

Fig. 2. Absorption spectra of $\Lambda(S)\Delta(R)$-[Co(Xacac)$_2$-(Me-en)]$^+$ in 0.01 mol dm^{-3} HCl, Xacac=NO_2acac (——), Clacac (—·—), acac (----), and CH_3acac (—··—).

band at lower energy than that of the $\Lambda(R)\Delta(S)$ isomers. The first absorption band shifts to lower energy as Xacac is changed from NO_2acac through Clacac and acac to CH_3acac. The shift will be related with the electronic effect of the X substituent on acac, since no steric interaction seems to occur among the X substituent and other ligands.

Electrochemistry and ^{1}H NMR Spectra. Electrochemistry is very useful for measuring electronic effects of substituents on the ligand in metal complexes. Rotating glassy carbon electrode voltammograms of the [Co(Xacac)$_2$(Me-en)]$^+$ complexes were measured in 0.1 mol dm^{-3} KCl vs. a saturated calomel electrode (SCE), and the results are summarized in Table 2. The complexes show a quasi-reversible reduction wave assignable to the Co^{3+}/Co^{2+} couple. The half-wave potentials ($E_{1/2}$ values) range from −0.08 V to −0.59 V. The difference in $E_{1/2}$ between the isomers is small in each complex. The $E_{1/2}$'s are plotted as a function of the Hammett σ_p parameter for the X substituent in [Co(Xacac)$_2$(Me-en)]$^+$ (Fig.3). A linear relationship between them indicates that the electronic effect of a substituent at the 3-position of the acac ligand is transmitted through the ligand to the metal ion in these complexes. It has been demonstrated that polarographic reduction potentials of Cr(III) and Ru(III) β-diketonates correlate well with the substituent electronic effects as measured by Hammett substituent effects.[15,16]

If the electronic effect is transmitted further to the amine nitrogen atoms, it should be reflected on the properties of the amine group. This is especially true for ^{1}H NMR spectroscopy, where an increase

Table 2. Electrochemical Data for the Reduction of [Co(Xacac)$_2$(Me-en)]$^+$ (vs. SCE) at 24 °C[a]

Xacac	Substituent parameter/σ_p	Isomer	$E_{1/2}$/V	$\lvert E_{3/4}-E_{1/4}\rvert$/V[b]
NO_2acac[c]	+0.78	$\Lambda(S)\Delta(R)$	−0.08	0.095
		$\Lambda(R)\Delta(S)$	−0.08	0.095
Clacac	+0.23	$\Lambda(S)\Delta(R)$	−0.28	0.095
		$\Lambda(R)\Delta(S)$	−0.27	0.095
acac	0	$\Lambda(S)\Delta(R)$	−0.47	0.100
		$\Lambda(R)\Delta(S)$	−0.47	0.105
CH_3acac	−0.17	$\Lambda(S)\Delta(R)$	−0.59	0.090
		$\Lambda(R)\Delta(S)$	−0.56	0.100

a) By glassy carbon rotating disk experiments (in water containing 0.1 mol dm^{-3} KCl with a 0.01 V s^{-1} scan rate; 2000 rev min^{-1}). b) $E_{3/4}$ and $E_{1/4}$ are potentials at three-fourth and one-fourth of the limiting current value, respectively. c) Adjusted to pH 4 with dil $HClO_4$.

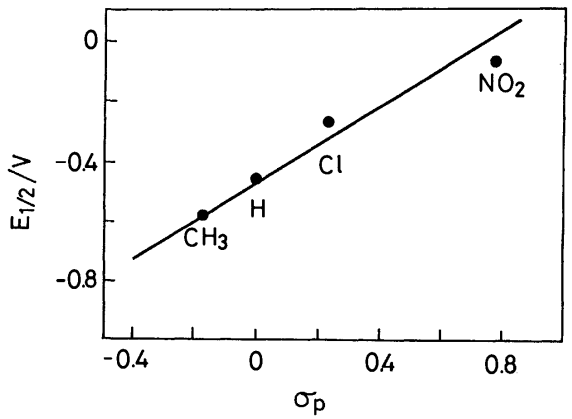

Fig. 3. Plot of the reduction half-wave potentials ($E_{1/2}$) vs. the Hammett parameter σ_p for $[Co(Xacac)_2(Me\text{-}en)]^+$ (Xacac=NO_2acac, Clacac, acac, and CH_3acac).

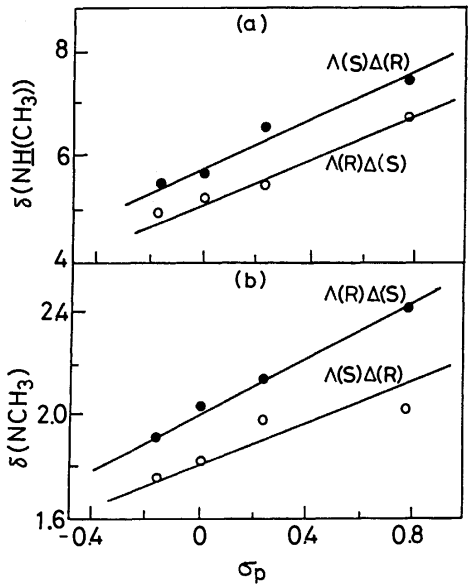

Fig. 4. Correlation of the ^1H NMR chemical shifts with the Hammett parameter, σ_p: $\delta(N\underline{H}(CH_3))$ vs. σ_p (a) and $\delta(NCH_3)$ vs. σ_p (b).

(decrease) in electron density on a particular proton will lead to a high (low) field shift for that proton. The chemical shift data of the $N\underline{H}(CH_3)$ and NCH_3 indicate this electronic effect (Table 1). For example, the $N\underline{H}(CH_3)$ signal of $\Lambda(S)\Delta(R)$-$[Co(NO_2acac)_2(Me\text{-}en)]^+$ is shifted 1.95 ppm downfield from its position in the spectrum of the corresponding CH_3acac complex. The nitro group withdraws electron density from the *N*-methyl nitrogen atom to cause the downfield shift of the amine proton signal. Plots of the chemical shifts of the $N\underline{H}(CH_3)$ and NCH_3 protons vs. the Hammett substituent constants (σ_p) were linear (Fig. 4).

Deuteration and Eqimerization Reactions. Table 3 gives the rate constants for deuteration, k_D at chiral nitrogen centers of the $[Co(Xacac)_2(Me\text{-}en)]^+$ complexes. The k_D value of the NO_2acac complex is ca. 10^4 times as large as that of the CH_3acac complex. A decrease in electron density on the amine nitrogen should labilize the hydrogen to promote H-D exchange. A linear relationship holds as shown in Fig. 5, where the logarithms of the deuteration rate constants for the Xacac complexes relative to that for the acac complex are plotted against the Hammett σ_p values. Although such a Hammett relationship has been reported to hold for deuteration of $[Co(Xacac)_2(en)]^+$ (Xacac=NO_2acac, Bracac, acac) in a D_2O-DMSO-d_6 mixture (weight ratio 1 : 3.9), the NO_2acac complex was deuterated faster than the acac complex only by a factor of 12.[16] The factor of the present Me-en complex in D_2O is 1600.

The rate constants for epimerization, k_{ep} of the $[Co(Xacac)_2(Me\text{-}en)]^+$ complexes are given in Table 3. Electronic contributions of the X substituents induce pronounced effect on the rates. For example, the epimerization rate of the NO_2acac complex is ca. 10^6 times greater than that of the CH_3acac complex. There also exists a linear Hammett relationship as

Table 3. A Comparison of Data for the Deuteration and Inversion at Chiral Nitrogen Centers of $[Co(Xacac)_2(Me\text{-}en)]^+$ at 34.0 °C

Xacac	Isomer	$k_D/M^{-1}s^{-1}$ [b]	$k_{ep}/M^{-1}s^{-1}$	(k_1 or k_{-1})/$M^{-1}s^{-1}$	r=(k_1 or k_{-1})/k_D
NO_2acac	$\Lambda(S)\Delta(R)$	1.4×10^7		k_1: 3.7×10^3	2.6×10^{-4}
			6.6×10^3		
	$\Lambda(R)\Delta(S)$	2.1×10^6		k_{-1}: 2.9×10^3	1.4×10^{-3}
Clacac	$\Lambda(S)\Delta(R)$	9.1×10^4		k_1: 2.5	2.8×10^{-5}
			4.2		
	$\Lambda(R)\Delta(S)$	1.7×10^4		k_{-1}: 1.7	1.0×10^{-4}
acac[a]	$\Lambda(S)\Delta(R)$	8.9×10^3		k_1: 7.1×10^{-2}	7.7×10^{-6}
			1.3×10^{-1}		
	$\Lambda(R)\Delta(S)$	c)		k_{-1}: 5.9×10^{-2}	
CH_3acac	$\Lambda(S)\Delta(R)$	7.9×10^2		k_1: 1.6×10^{-3}	2.0×10^{-6}
			2.9×10^{-3}		
	$\Lambda(R)\Delta(S)$	1.5×10^2		k_{-1}: 1.3×10^{-3}	8.3×10^{-6}

a) From Ref. 12. b) 1 M=1 mol dm^{-3}. c) The data could not be obtained because of the overlapping of the N-CH_3 and C-CH_3 signals.

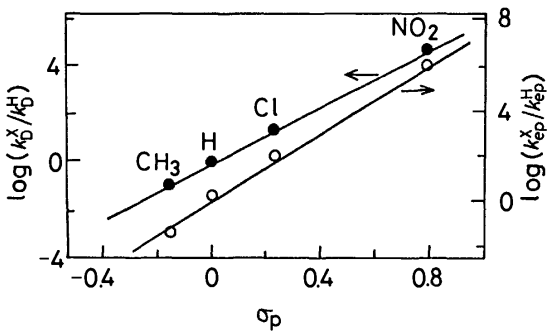

Fig. 5. Plot of $\log(k_D^X/k_D^H)$ vs. the Hammett σ_p for $\Lambda(S)\Delta(R)$-$[Co(Xacac)_2(Me\text{-}en)]^+$ (●) and plot of $\log(k_{ep}^X/k_{ep}^H)$ vs. the Hammett σ_p for $[Co(Xacac)_2(Me\text{-}en)]^+$ (○).

shown in Fig. 5. We assume here that the proton-exchange and epimerization reactions proceed by Eqs. 1—3.[1,18]

$$\Lambda(S)\text{-}[Co(Xacac)_2(NH(CH_3)CH_2CH_2NH_2)]^+ + OH^- \underset{k+H^+}{\overset{k-H^+}{\rightleftharpoons}} \Lambda(S)\text{-}[Co(Xacac)_2(^-N(CH_3)CH_2CH_2NH_2)] + H_2O \quad (1)$$

$$\Lambda(S)\text{-}[Co(Xacac)_2(^-N(CH_3)CH_2CH_2NH_2)] \underset{k'_i}{\overset{k_i}{\rightleftharpoons}} \Lambda(R)\text{-}[Co(Xacac)_2(^-N(CH_3)CH_2CH_2NH_2)] \quad (2)$$

$$\Lambda(R)\text{-}[Co(Xacac)_2(^-N(CH_3)CH_2CH_2NH_2)] + H_2O \underset{k'-H^+}{\overset{k'+H^+}{\rightleftharpoons}} \Lambda(R)\text{-}[Co(Xacac)_2(NH(CH_3)CH_2CH_2NH_2)]^+ + OH^- \quad (3)$$

The actual rate of inversion of the amido complex is k_i (k'_i) and is pH independent.[19] The measured rate constant for epimerization (k_{ep}) is pH dependent since the rate depends on the amount of amido complex present. The ratio, $r=(k_1$ or $k_{-1})/k_D$, which is determined by partitioning the deprotonated intermediate between inversion and reprotonation, becomes a direct measure of the actual rate of inversion if the reprotonation rate is constant (diffusion controlled). This is the case when the pK_a values of $[Co(Xacac)_2(Me\text{-}en)]^+$ exceed 14, as has been estimated for other cobalt(III)-amine complexes.[1,20] A plot of $\log(r^X/r^H)$ against σ_p is found to be linear (reaction constant $\rho=+2.2$), where r^X and r^H denote the r values of the Xacac and acac complexes, respectively (Fig. 6).

The selenium atom of a selenide (RSeR′) ligand becomes chiral on coordination to a metal ion. We have studied the inversion at the selenium atom in $[Co(Xacac)_2(CH_3SeCH_2CH_2NH_2)]^+$ and found that the Hammett relationship holds for the rates of the Clacac, acac, and CH_3acac complexes, where the reaction constant ρ is -2.9, a negative value.[21] The first step of inversion at a chiral nitrogen center will be the abstraction of the coordinated secondary amine proton by OH^- to yield a pyramidal center (Eq. 1).

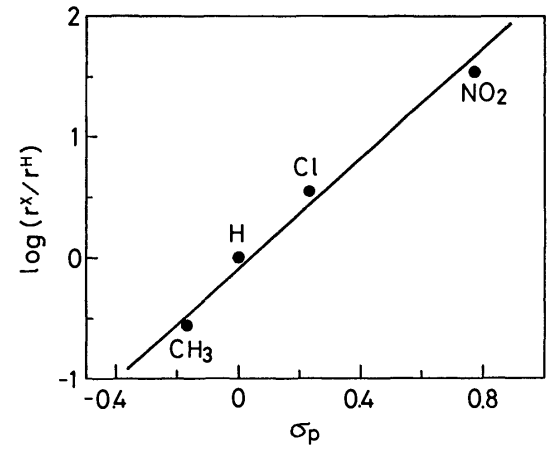

Fig. 6. Plot of $\log(r^X/r^H)$ vs. the Hammett σ_p for $[Co(Xacac)_2(Me\text{-}en)]^+$.

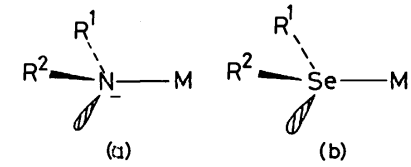

Fig. 7. Structures of the pyramidal amide intermediate (a) and the coordinated selenide (b).

The structure of the pyramidal amide intermediate will be similar to that of the coordinated selenide (Fig. 7), but inverse electronic effect was found. For a pyramidal atomic inversion, it is usually observed that an electronegative substituent on the central atom decreases the rate of inversion.[22] The Se inversion of the cobalt-selenides is the case.

The reason for the inverse electronic effect of the N inversion of $[Co(Xacac)_2(Me\text{-}en)]^+$ is difficult to explain. The cobalt-amide intermediates possess a formal negative charge on nitrogen, and the electronic effect of the charge might play an important role in controlling the stereochemistry to affect the inversion rate. The importance of electrostatic effect (electron repulsion effect) as a rate-controlling factor for an atomic inversion was pointed out by Anet et al.[23] They studied the rates of the N inversion of $(CH_2)_2NX$ and those of the C inversion of R_2C^-X. The effect of the group X on the negatively charged carbanion system was found to differ from that on the neutral aziridine system. The lack of correlation between the two systems was ascribed to the difference in electrostatic effect between them. A similar discussion might be made for the cobalt-amide intermediates, since they are isoelectronic with cobalt-selenides as carbanions are with amines.

The present work was supported by a Grant-in-Aid for Scientific Research No. 61430013 from the Ministry of Education, Science and Culture.

References

1) W. G. Jackson and A. M. Sargeson, "Rearrangement in Coordination Complexes," in "Rearrangements in Ground and Excited States," ed by P. de Mayo, Academic Press, New York (1980), Vol. 2, p. 273, and references therein.

2) G. Ma, T. Hibino, M. Kojima, and J. Fujita, *Bull. Chem. Soc. Jpn.*, **62**, 1053 (1989).

3) J. W. Palmer and F. Basolo, *J. Phys. Chem.*, **64**, 778 (1960); F. Basolo, J. W. Palmer, and R. G. Pearson, *J. Am. Chem. Soc.*, **82**, 1073 (1960).

4) Y. Ouyang, M. Kojima, and J. Fujita, *Bull. Chem. Soc. Jpn.*, **57**, 3574 (1984).

5) M. Shibata, *Nippon Kagaku Zasshi*, **87**, 771 (1966).

6) A. W. Johnson, E. Markham, and R. Price, *Org. Synth.*, Coll. Vol. V, 785 (1973).

7) A. J. Brown, O. W. Howarth, and P. Moore, *J. Am. Chem. Soc.*, **100**, 713 (1978).

8) M. Fujita, Y. Yoshikawa, and H. Yamatera, *Chem. Lett.*, **1982**, 437.

9) K. Kuroda, K. Yoshitani, K. Kunigita, Y. Kamiiba, and K. Watanabe, *Bull. Chem. Soc. Jpn.*, **49**, 2445 (1976).

10) J. P. Collman and W. L. Young, III, *Inorg. Synth.*, VII, 205 (1963).

11) P. K. Glasoe and F. A. Long, *J. Phys. Chem.*, **64**, 188 (1964).

12) M. Kojima, T. Hibino, Y. Ouyang, and J. Fujita, *Inorg. Chim. Acta*, **117**, 1 (1986).

13) K. Nakajima, M. Kojima, M. Fujita, and J. Fujita, *J. Chromatogr.*, **301**, 241 (1984); K. Nakajima, M. Kojima, and J. Fujita, *ibid.*, **362**, 281 (1986).

14) K. Nakajima, M. Kojima, and J. Fujita, *Bull. Chem. Soc. Jpn.*, **59**, 3505 (1986).

15) G. S. Patterson and R. H. Holm, *Inorg. Chem.*, **11**, 2285 (1972).

16) R. F. Handy and R. L. Lintvedt, *Inorg. Chem.*, **13**, 893 (1974).

17) K. Ito, H. Isono, E. Iwamoto, and Y. Yamamoto, *Inorg. Chem.*, **23**, 850 (1984).

18) J. B. Goddard and F. Basolo, *Inorg. Chem.*, **8**, 2223 (1969).

19) T. P. Pitner and R. B. Martin, *J. Am. Chem. Soc.*, **93**, 4400 (1971).

20) R. G. Pearson and F. Basolo, *J. Am. Chem. Soc.*, **78**, 4878 (1956).

21) K. Nakajima, M. Kojima, and J. Fujita, *Bull. Chem. Soc. Jpn.*, **59**, 3505 (1986).

22) J. B. Lambert, *Top. Stereochem.*, **6**, 19 (1971) and references therein.

23) F. A. L. Anet, R. D. Trepka, and D. J. Cram, *J. Am. Chem. Soc.*, **89**, 357 (1967).

Use of Polyoxetane Resin-Supported Quaternary Onium Salts as a Polymeric Phase-Transfer Catalyst for Preparing Ethers from Hydroxy Compounds and Alkyl Halides

Masatoshi MOTOI,* Katsuhiko SHIMAMURA, Chikako SHIMAMURA, Satoru MURAMOTO, Shigeyoshi KANOH, and Hiroshi SUDA
Department of Chemistry and Chemical Engineering, Faculty of Technology, Kanazawa University, Kodatsuno, Kanazawa-shi 920
(Received December 23, 1988)

As a polymer support for preparing polymeric phase-transfer catalysts (PTC), soft, moderately polar polyoxetane resins were employed which were synthesized by a cationic ring-opening copolymerization of oxetanes $Br(CH_2)_nOCH_2$-X with bisoxetanes X-$CH_2O(CH_2)_nOCH_2$-X, where X=3-methyl-3-oxetanyl and n=4 or 6. In a few cases of those polymerizations, 3-(2-oxadecyl)-3-methyloxetane was used as a comonomer with a lipophilic pendant. The terminal bromine of the pendant groups of such polyoxetane resins was quaternized with tributylamine or tributylphosphine in DMF in order to examine the phase-transfer catalyzing ability of the resultant quaternary onium bromides in the etherification reaction between alkyl halides and alcohols or phenols. These reactions gave the desired products in fairly good yields within reaction periods of 1—3 h, indicating that the catalytic activities of those PTCs are comparable to that of tetrabutylammonium bromide. A fairly high catalytic activity of the polymeric PTC was observed at each of ten stages in a process using the polymeric PTC repeatedly for the etherification reaction of 3-hydroxymethyl-3-methyloxetane with 1,4-dibromobutane.

It has recently been increasingly recognized that synthetic polymers can be conveniently used in organic syntheses as reagents, catalysts, membranes, and substances with other various functionalities.[1,2] The polymeric phase-transfer catalyst (PTC) has attracted the attention of investigators who have hoped to readily obtain novel and important organic compounds by a simple work-up of a reaction mixture and to use the catalyst repeatedly after easily recovering it. Hereby, the use of various polymeric PTCs in organic syntheses has been reviewed.[1-6]

In the preparation of the polymeric PTCs, insoluble cross-linked polystyrenes have been widely used as polymeric supports for anchoring a catalytic group to the support. These polymeric supports have not always been used advantageously in organic syntheses using polar or ionic reagents and solvents, due to the low polarity of the polystyrene support. Furthermore, the movability of the catalytic group, which is anchored to hard (or unflexible) polymer matrices of the polystyrene support, would be more or less restricted, exerting an entropically unfavorable influence on the catalytic behavior. The catalytic activity of PTC was enhanced upon introducing a moderately long spacer between the catalytic group and the polymer matrix;[7] owing to the existence of such a long spacer, the catalytic group was kept apart from sterically crowded polymer matrices. In order to improve such undesirable qualities of the polymeric support as hardness (or unflexibility), low polarity, and low hydrophilicity, polyoxiranes have also been chosen as soft, polar, or hydrophilic segments in block and graft polymers.[8-12] Particularly, poly(oxyethylene) (POE) has often been successfully applied not only to the segments mentioned above, but also to catalysts and ionophors, which realize their functions via a cooperative action of the ether oxygen.[13-16]

In our previous papers, we reported facile syntheses of oxetanes **3a** and **3b** carrying ω-bromo-2-oxapolymethylene side chains at the C-3 position of an oxetane ring, of bisoxetanes **4a** and **4b** being as a cross-linking agent, and of soft, moderately polar polyoxetane resins **5** by a cationic ring-opening copolymerization of those oxetanes.[17] We also briefly reported a fairly high catalytic activity of a polymeric PTC, which was prepared by quaternizing the pendant bromide of a polyoxetane resin with tributylamine (**6**), on the etherification reaction between the alcohol **1** and the dibromide **2a**.[18]

Thus, polyoxetane resins are thought to be very promising as a polymeric support. So far, there has been no investigation concerning the phase-transfer

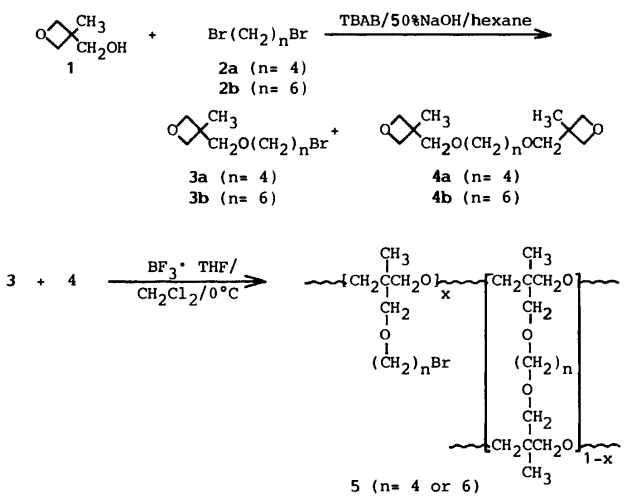

Scheme 1.

catalysis using such polyoxetane resin-supported onium salts as a PTC, although polystyrene resin-supported PTCs have often been employed in various reactions of organic synthesis.[1-5] In this article, our investigation results are described in more detail concerning the application of polyoxetane resins to the polymeric support of PTCs for readily preparing several ethers from hydroxy compounds and alkyl halides.

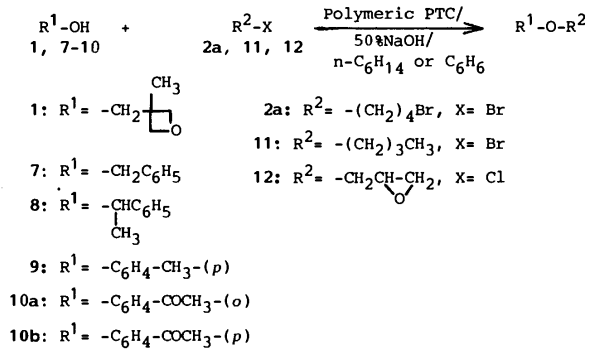

Scheme 2.

Experimental

Materials. Oxetanes **3a** and **3b**, bisoxetanes **4a** and **4b**, and 3-(2-oxadecyl)-3-methyloxetane (**13**) were prepared by the phase-transfer catalytic reaction according to a method reported by us previously.[17] The hydroxy compounds **7**—**10**, the alkyl halides, **2a**, **2b**, **11**, and **12**, and tetrabutylammonium bromide (TBAB) were used without further purification of commercially available reagents. 1-Benzyloxy-4-bromobutane (**24**), 1-benzyloxybutane (**25**),[19] 1-(1-phenylethoxy)butane (**26**), benzyl 2,3-epoxypropyl ether (**27**),[20] 2,3-epoxypropyl 1-phenylethyl ether (**28**),[20] 1-(*p*-methylphenoxy)butane (**29**),[21] 1-(*o*- and *p*-acetylphenoxy)-4-bromobutanes (**30a** and **30b**), and 1,4-bis(*o*- and *p*-acetylphenoxy)butanes (**31a** and **31b**) were prepared by a phase-transfer catalytic reaction of the appropriate alcohol or phenol with the halide in the presence of TBAB, and were employed to draw calibration curves of the gas chromatography (GC) determination. IR and ^{1}H NMR spectra confirmed structures of these compounds.

24: bp 79—80 °C (14.7 Pa); IR(neat) 3075, 3040, 1600, 1580, 735, and 695 (monosubstituted benzene), and 1100 cm^{-1} (aliphatic ether); ^{1}H NMR($CDCl_3$) δ=1.6—2.2 [4H, m, $OCH_2(C\underline{H}_2)_2CH_2Br$], 3.42, 3.48 [each 2H, each bt, $C\underline{H}_2(CH_2)_2C\underline{H}_2Br$], 4.48 (2H, s, OCH_2Ar), and 7.33 (5H, m, ArH).

Found: C, 54.23; H, 6.19; Br, 32.83%. Calcd for $C_{11}H_{15}BrO$: C, 54.33; H, 6.23; Br, 32.86%.

26: bp 93—94 °C (0.31 kPa); IR(neat) 3075, 3040, 1600, 1500, 760, and 700 (monosubstituted benzene), and 1100 cm^{-1} (aliphatic ether).

30a: bp 132.5 °C (26.7 Pa); IR(neat) 3075, 3040, 1595, 1575, 1480, and 750 (1,2-disubstituted benzene), 1670 (C=O), and 1240 cm^{-1} (aromatic ether); ^{1}H NMR($CDCl_3$) δ=1.7—2.3 [4H, m, $OCH_2(C\underline{H}_2)_2CH_2Br$], 2.58 (3H, s, $COCH_3$), 3.2—3.7 (2H, bt, CH_2Br), 3.8—4.3 (2H, bt, CH_2OAr), 6.7—7.9 (4H, m, ArH).

Found: C, 52.97; H, 5.54; Br, 29.62%. Calcd for $C_{12}H_{15}BrO_2$: C, 53.15; H, 5.59; Br, 29.47%.

30b: bp 147 °C (20.0 Pa); IR(neat) 3060, 3000, 1600, 1575, 1510, and 830 (1,4-disubstituted benzene), 1685 (C=O), and 1250 cm^{-1} (aromatic ether); ^{1}H NMR($CDCl_3$) δ=1.8—2.3 [4H, m, $OCH_2(C\underline{H}_2)_2CH_2Br$], 2.54 (3H, s, $COCH_3$), 3.3—3.7 (2H, bt, CH_2Br), 3.9—4.3 (2H, bt, CH_2Ar), and 6.7—8.1 (4H, quartet-like, ArH).

Found: C, 53.02; H, 5.51; Br, 29.24%. Calcd for $C_{12}H_{15}BrO_2$: C, 53.15; H, 5.59; Br, 29.47%.

31a: mp 151.5—152.5 °C (acetone); IR(KBr) 1595, 1570, 1500, 1465, and 779 (1,2-disubstituted benzene), 1665 (C=O), and 1235 cm^{-1} (aryl ether); ^{1}H NMR($CDCl_3$) δ=1.8—2.3 [4H, m, $(C\underline{H}_2)_2CH_2OAr$], 2.61 (6H, s, $COCH_3$), 3.9—4.4 (4H, m, CH_2OAr), and 6.8—7.9 (8H, m, ArH).

Found: C, 73.29; H, 6.77%. Calcd for $C_{20}H_{22}O_4$: C, 73.59; H, 6.81%.

31b: mp 146.0—147.5 °C (acetone); IR(KBr) 1595, 1579, 1500, and 1465 (1,4-disubstituted benzene), 1670 (C=O), and 1240 cm^{-1} (aryl ether); ^{1}H NMR($CDCl_3$) δ=1.8—2.3 [4H, m, $(C\underline{H}_2)_2CH_2OAr$)], 2.56 (6H, s, $COCH_3$), 3.9—4.3 (4H, m, CH_2OAr), and 6.8—8.2 (8H, quartet-like, ArH).

Found: C, 73.60; H, 6.76%. Calcd for $C_{20}H_{22}O_4$: C, 73.59; H, 6.81%.

The polyoxetane resins with the pendant bromide were made by the copolymerization of **3a** or **3b** with **4a** or **4b**, and, if necessary, **13** in dichloromethane (DCM) at 0 °C with boron trifluoride (BF_3)-tetrahydrofuran (THF) complex (0.5% to total mole of the oxetane ring) as an initiator, as described by us previously.[17] The seven polymeric PTCs were prepared by heating a polyoxetane-supported bromide with a threefold molar excess of tributylamine (**6**) or -phosphine (**14**) in DMF at 100 °C for 10 h. The polymeric catalyst was filtered, washed successively with methanol and ether, and dried at 80 °C under reduced pressure of 27 Pa for 6 h.

Phase-Transfer Catalytic Reaction between Hydroxy Compounds and Alkyl Halides. In a round-bottomed flask there were placed a polymeric PTC, a hydroxy compound, an alkyl halide, and an internal standard of GC analysis. A 50% aqueous sodium hydroxide (NaOH) solution and hexane as a solvent were added into the mixture of reactants with ice-cooling. This was heated under reflux with efficiently stirring by means of a magnetic or mechanical stirrer. At every desired time, the mixture was cooled below 5 °C and an aliquot of the organic layer was withdrawn into a microsyringe to determine the product yield by GC. In a reaction on a preparative scale using 10 g of **1**, water (300 cm^3) was added into the resulting mixture below 5 °C after an appropriate reaction time. This was transferred to a separatory funnel to extract the product with ether. An aqueous layer was discarded as thoroughly as possible and the remainder was filtered to separate the polymeric catalyst. The polymer was washed successively with water, ether, and methanol. Here, methanol was successfully used to rinse the funnel. The organic layer of the filtrate was dried over Na_2SO_4 and distilled to give the products. In the examination of the repeated use of the polymeric PTC, the polymer collected by filtration was employed during the next stage of the process, using it repeatedly in the reaction between **1** and **2a** after or without drying the polymeric PTC.

Measurement. GC analysis of the products was performed in a Shimadzu GC 8A apparatus: glass column (3.2ϕ×1 m) packed with Silicone High Vacuum Grease

(30%)/Celite (80—100 mesh); carrier gas, He (66 cm^3 min^{-1}); temp, 140 or 210 °C. The IR spectra were recorded on a JASCO A-202 spectrometer, and on a ^1H NMR 60 (Hitachi R-24B) or 100 MHz instrument (JEOL FX-100S) using $CDCl_3$ as a solvent and TMS as an internal standard. A differential scanning calorimetry (DSC) measurement was carried out in a DSC/560 (Daini Seikohsha) at a heating rate of 20 °C min^{-1} for a sample in air.

Results and Discussion

Preparation of Polyoxetane Resin-Supported PTCs. The polyoxetane supports **15-I**, **16-I**, **17-I**, **18-I**, **19-I**, and **20-I** carrying a bromide at the pendant spacer end were prepared by cationic ring-opening copolymerization of **3** with **4**. All cross-linked polyoxetanes, thus obtained, were white elastic polymers insoluble in the ordinary organic solvents used, although the homopolymers from **3a** and **3b** were viscous materials with number-average molecular weight ($\bar{M}_n$) 3300—5500 and soluble in the ordinary solvents.[17] In a few cases of the above polymerization, **13** was used as a comonomer with a lipophilic pendant group. Those oxetane derivatives showed IR absorption bands due to a cyclic ether linkage at 980 and 835 cm^{-1}; however, these bands disappeared in the IR spectra of the polymers.[17] The pendant bromide of the supports was quaternized by heating with **6** or **14** in DMF at 100 °C to obtain the polymeric PTCs **15-II** to **20-II** carrying an onium bromide at the pendant spacer end. The polymeric PTCs, so obtained, are listed in Table 1. The mole fractions of the monomeric units (x, y, and z) in a starting polymer are assumed to be identical, respectively, with those in monomers charged in the copolymerization. The content of the onium bromide was calculated on the basis of nitrogen or phosphorus content determined by elemental analysis. IR spectra of the quaternized polymers indicated a considerably strong, broad band around 3400 cm^{-1}, even after drying the polymer at 60 °C for 8 h in vacuo, suggesting that the onium salt may adsorb molecules of water rigidly. For the present, to roughly estimate the mole fraction k of the monomeric unit with the pendant onium salt in a PTC, the k value was calculated on the basis of the nitrogen or phosphorus content and mole fractions x, y, and z in the dried PTC.

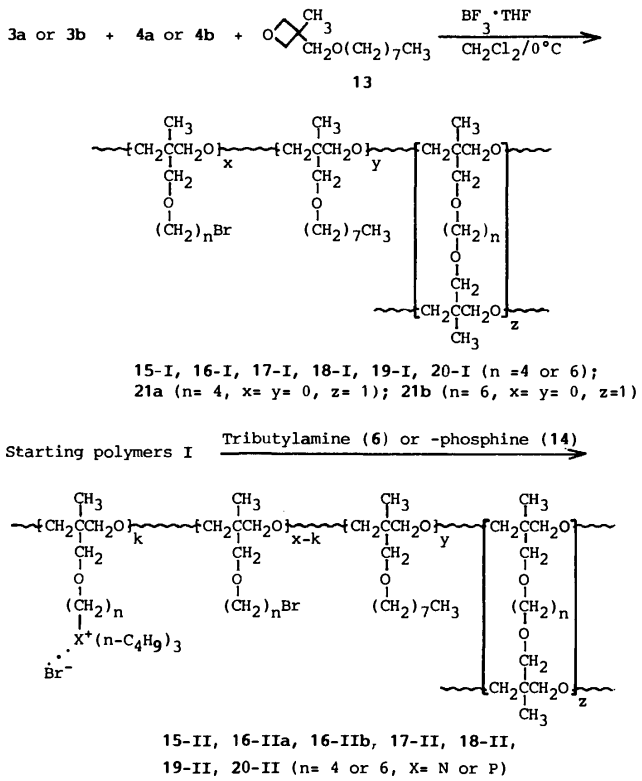

Scheme 3.

Table 1. Polymeric Catalysts Used for the Phase-Transfer Catalytic Reaction

PTC No.	Anal. (%) for N or P	k[c]	Onium bromide[a]	Starting polymer[b]			
					Mole fractions		
			mequiv g^{-1}	n	x	y	z
15-II	N, 2.48	0.63	1.77	4	0.90	0.00	0.10
16-IIa	N, 1.50	0.33	1.07	4	0.70	0.00	0.30
16-IIb	P, 5.32	0.64	1.72	4	0.70	0.00	0.30
17-II	N, 1.04	0.21	0.74	4	0.50	0.00	0.50
18-II	N, 2.08	0.48	1.48	4	0.74	0.17	0.09
19-II	N, 0.94	0.18	0.67	4	0.36	0.50	0.14
20-II	N, 1.70	0.42	1.21	6	0.79	0.00	0.21

a) Milliequivalent of the onium per g of a dry polymer. b) These polymers were used as polymer supports with a pendant bromide for preparing the polymeric PTCs. The letters n, x, y, and z are presented in Scheme 3. c) A mole fraction of the unit with an onium group, as shown in Scheme 3.

Phase-Transfer Catalysis Using the Polymeric PTC. The phase-transfer catalyzing abilities of the polymeric PTCs were examined in an etherification reaction between the hydroxy compounds and the halides. Figure 1 and Table 2 show the results of a phase-

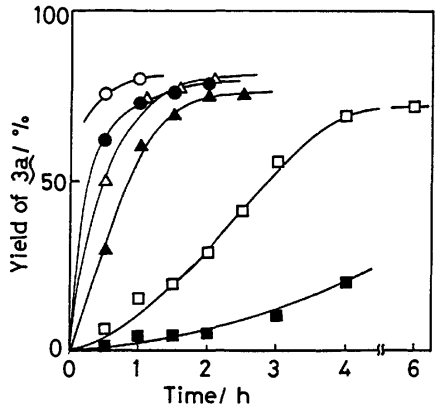

Fig. 1. Time-yield curves for the phase-transfer catalytic reaction of **1** with **2a** at 70 °C in the presence of **16-IIa**: **1**, 1.99 mmol; **2a**, 5.98 mmol; n-$C_{16}H_{34}$, 1.07 mmol; 50% NaOH, 2.8 g; hexane, 2.0 cm^3. Mol% of an ammonium group to **1**: (●) 2.7; (△) 1.1; (▲) 0.3; (□) 0.1; (○) 1.7 mol% of TBAB; (■) without PTC.

Table 2. Ether Synthesis from **1** and **2a** by Phase-Transfer Catalysis Using the Polymeric PTC[a]

PTC (Mol% to **1**)[b]	Product	Yields of **3a** and **4a** by GC/% Reaction time/h 0.5	1.0	1.5	2.0	3.0	4.0
15-II (3.0)	**3a:**	50.4	66.7	72.1	77.1		
	4a:	2.9	7.0	8.7	8.7		
16-IIb (4.3)	**3a:**	77.5	83.2	84.0	85.8	87.6	
	4a:	8.5	8.1	8.6	9.1	9.6	
15-II (2.7)[c]	**3a:**	57.2	69.0	73.7	80.9	86.2	
	4a:	3.1	4.5	5.2	5.7	6.5	
TBAB (5.0)	**3a:**	83.0	81.1				
	4a:	14.6	14.6				
16-IIa (2.7)[d]	**3a:**	35.4	19.7	6.6	1.9	0.0	
	4a:	19.4	35.7	46.8	51.3	52.0	
TBAB (5.0)[d]	**3a:**	5.8	0.2	0.0			
	4a:	56.8	62.0	63.1			
21a[e]	**3a:**	1.3	2.1	4.4	6.2	24.3	27.3
21b[e]	**3a:**	1.3	2.5	4.0	5.3	8.3	13.4
POE 400[e]	**3a:**	35.4	48.4	66.7	71.6	77.8	
None	**3a:**	1.2	2.9	4.1	4.8	11.1	20.9

a) **1**, 1.99 mmol; **2a**, 5.98 mmol; *n*-$C_{16}H_{34}$ (internal standard of GC determination), 1.07 mmol; 50% NaOH, 2.8 g; hexane, 2.0 cm^3; at reflux temperature. b) Mol% of the onium bromide to **1**. c) Benzene was used as a solvent. d) **1** and **2a** were charged at a molar ratio of 1 : 1. e) 0.5 mol of ether oxygen of **21a**, **21b**, or POE 400 was used per one mole of **1**.

transfer catalytic reaction of **1** with **2a** using each of the several polymeric PTCs in 50% NaOH and an organic solvent at 70 °C. As shown in Fig. 1, a rate of the formation of **3a** decreased with an decrease in the amount of **16-IIa** from 2.7 to 0.1 mol% to **1**. A fairly good yield of 67% for **3a** was reached, even in the presence of only 0.1 mol% of the ammonium salt of polymeric PTC, although a prolonged reaction time of 4 h was required. When 1.1 to 2.7 mol% of the pendant ammonium salt was used, the formation rates of **3a** are almost comparable to the reaction rate in the presence of 1.7 mol% of TBAB. However, **3a** was formed very slowly in the absence of the catalyst. Similarly, in the presence of each polymeric PTC other than **16-IIa**, a sufficient yield of **3a** or **4a** as a main product was achieved within a few hours (Table 2). The formation of the main product depended on a **2a**/**1** molar ratio of 3.0 or 1.0. The catalytic activity of the phosphonium bromide of **16-IIb** was somewhat higher than that of the corresponding ammonium bromide of **16-IIa** and seemed to be comparable to the catalytic activity of TBAB. It is generally known that quaternary phosphonium salts act as PTC more effectively than the ammonium analogues (vide infra).

Effect of the Polyether Network: Regarding the reaction using a polymeric PTC at a **2a**/**1** mole ratio of 3.0, **4a** was formed in lower yields than that with TBAB, suggesting that it is somewhat difficult to form **4a** from substrate **3a**, which has a bulkier substituent than **2a**, and the nucleophile **1** at the S_N2 reaction stage crowded with polymer matrices. In our previous investigation of the preparation of oxetane derivatives under the phase-transfer catalytic conditions using TBAB in 50% NaOH and an organic solvent, it was found that hexane and ether were suitable solvents for such synthesis, while the catalysis of TBAB in benzene gave **3a** in a lower yield by about 13% than in hexane.[17] However, the yield of **3a** with **15-II**, in spite of using benzene as a solvent, was comparable to the yield of **3a** formed by the reaction in a hexane solvent, indicating that an aliphatic ether structure of the polyoxetane backbone of polymeric PTC plays an important role upon the above catalysis as the so-called "solid phase cosolvent" for the production of **3a** in higher yield.[22] The polyoxetane resin with a pendant onium salt spread in the form of oily or gelatinous particles over the interface between organic and aqueous layers; this aspect was clearly observed when the reaction mixture was permitted to stand in a reactor. On the other hand, the ether network of such polyoxetanes as **21a** and **21b** was hardly swellable in water and somewhat swellable in such organic solvents as ether, chloroform, and benzene, although the level of swellability of the polyether network itself in such solvents was not quite so remarkable as that of the polymeric PTC. The remarkable swelling of the polyoxetane support in the phase-transfer catalysis is attributable to the hydrophilicity of the pendant onium salt as well as to an expanding ability of the soft or elastic cross-linked network containing the ether linkage abundantly. Such a formation of the oily or gelatinous particles due to the swelling of the polymeric PTC has been not observed in the case of using the hard or rigid network of the cross-linked polystyrene support with the pendant onium salt. The ether network of **21a** and **21b** could hardly conduct the phase-transfer catalytic reaction of **1** with **2a**, since the relationships between the reaction time and the product yield are almost similar to that for the reaction in the absence of a PTC (Table 2). POE with a molecular weight of 400 showed a fairly high catalytic activity in the above-mentioned reaction, owing to a cooperative action of ether oxygens of POE. The ether network itself of the polyoxetane support can probably not efficiently solvate the sodium alkoxide **22** (which is generated from **1** and concentrated NaOH) via cooperative action analogous to that of POE, although an ether network of **21a** seems to have the slight ability to transfer the

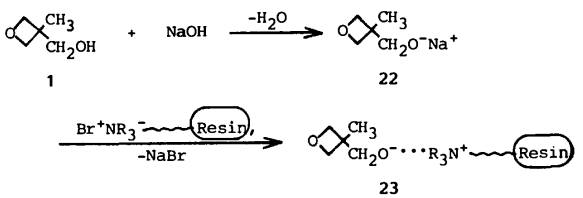

Scheme 4.

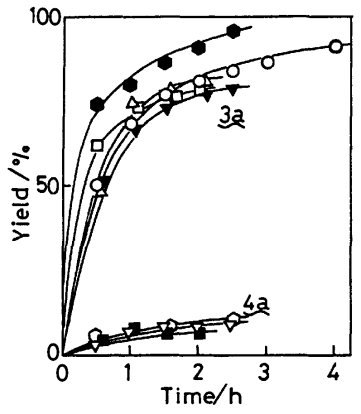

Fig. 2. Influence of the cross-linking agent and of the spacer length on yields of **3a** (▼, △, □, ○, ●) and **4a** (▽, ■, ○) in the phase-transfer catalytic reaction at a **1**/**2a** mole ratio of 1:3. PTC, mole fraction of **4a** or **4b** in a polymeric support, and mol% of an ammonium group to **1**: (▼, ▽) **15-II**, 0.10, 3.0; (△) **16-IIa**, 0.30, 1.1; (□, ■) **16-IIa**, 0.30, 2.7; (○) **17-II**, 0.50, 1.1; (●, ○) **20-II**, 0.21, 3.0.

ionic species **22** from an aqueous layer to an organic one.

Effects of the Cross-Linking Level and the Spacer: In Fig. 2, in comparisons of the PTCs used in a similar amount of the ammonium group between **16-IIa** and **17-II** (each 1.1 mol% to **1**), and **15-II** and **16-IIa** (each about 3 mol% to **1**), their apparent catalytic activities are taken to be comparable to each other, in spite of the order **15-II**>**16-IIa**>**17-II** for the *k* value and the inverted order for the *z* value. These results are interesting since, in general, the catalytic activity of a polymeric catalyst is considered to be lowered by decreasing the loading of a catalytic group and by increasing the mole fraction of the cross-linking agent in a polymeric support. Furthermore, the formation rate of **3a** is also hardly influenced by varying the amount of the ammonium group from 1.1 to 3.0% molar respect to **1**, as shown in the use of **16-IIa**, suggesting that an optimum amount of the catalytic group lies in a range 1 to 3 mol% to **1** (also see Figs. 1 and 4). When the pendant ammonium group of a PTC acts as a countercation accompanying an alkoxide anion of **22** into an organic layer, access of the accompanied alkoxide anion to each other, due to a local assembly of the ammonium group in the PTC, is undesired because of an electrostatic and/or a steric repulsion between the counteranions. Such a locally increased concentration of the ammonium group is realized by increasing the *k* value and/or the amount of the PTC used. A limited amount of the assembling ammonium group acts effectively as the countercation accompanying the alkoxide anion, particularly when using PTCs with high loading (or high *k* values).

It is concluded, therefore, that the *k* and *z* values have little influence on the catalytic activity of the PTC based on a polyoxetane support. Thus, the yield of **3a** reached a range of 76—80% within 2 h in every case of using the polymeric PTCs with cross-linking levels of 10, 30, and 50 mol%. Even the polymeric PTC with a 50 mol% cross-linking level swelled sufficiently under applied phase-transfer catalytic conditions. These results suggest that polyether networks with cross-linking levels of up to 50 mol% are soft (or elastic) and swellable enough for their use as a polymeric support of the PTC, being a contrast to the widely employed polystyrene supports containing only a few mol% of divinylbenzene as a cross-linking agent; use of PTCs with higher divinylbenzene contents frequently leads to remarkably lower product yields or requires hard reaction conditions to obtain a fairly good product yield.

The somewhat improved yields of **3a** were obtained by lengthening the spacer by an ethylene unit in both the side chain and cross-linking agent of a polymeric PTC, as shown in each comparison between **15-II** and **20-II**, and between **16-IIa** and **20-II** (each about 3 mol% to **1**). **20-II** gave a slightly higher yield of **3a** than **15-II** and **16-IIa** within the same reaction time, although **20-II** has a lower *k* and higher *z* values than **15-II**, and a higher *k* and lower *z* values than **16-IIa**. However, the loading and cross-linking levels of these PTCs are taken to be unimportant here (as mentioned above). Presumably, a longer spacer of the cross-linking agent causes the network to expand more sufficiently, and a longer spacer of the side chain causes the catalytic group to be located more apart from the crowded polymer matrices. It has also been reported that lengthening an alkyl chain between polymer matrices and a terminal onium group of the side chain significantly improves the yield of *O*-alkylated product in a phase-transfer catalytic reaction of 2-naphthol with benzyl bromide.[1,7]

Effect of the Lipophilic Pendant Group: Furthermore, in designing a polymer which is effective for a phase-transfer catalysis, it is important to find an optimum with respect to the relative content of the hydrophilic and lipophilic groups in a polymer. At the S_N2 reaction stage of the phase-transfer catalysis, it is required to create lipophilic domains dissolving the organic substrate to be allowed to react with the nucleophile which is transferred in the form of **23** from the aqueous phase to the organic phase. On the other hand, hydrophilic domains are required to stabilize ionic species of **23** transferred into the polymer matrices. The interesting behavior of water was also reported with respect to the mechanism of phase-transfer catalysis.[23,24] Thus, the polymeric PTCs **18-II** and **19-II** were employed to examine an effect of the lipophilic octyl group on the catalytic activity (Fig. 3). Use of the polymeric PTC **18-II** with 17 mol% of the monomeric unit **13** did not indicate the appreciable improvement of the catalytic activity, as compared with that of **16-IIa** with no octyl group, assuming use

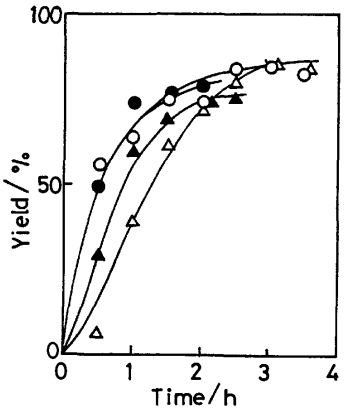

Fig. 3. Influence of a lipophilic unit **13** on a yield of **3a** in the phase-transfer catalytic reaction at a **1**/**2a** molar ratio of 1 : 3. PTC, mole fraction of **13**, and mol% of an ammonium group to **1**: (●) **16-IIa**, 0, 1.1; (▲) **16-IIa**, 0, 0.3; (○) **18-II**, 0.17, 0.7; (△) **19-II**, 0.50, 0.3.

of the similar amount of the ammonium group to each other for these PTCs (0.7 and 1.1 mol% to **1**, respectively). However, as shown obviously in a comparison between phase-transfer catalytic reactions using quaternary ammonium salts of **16-IIa** and **19-II** in 0.3% molar respect to **1**, a lower rate was observed in the formation of **3a** in the presence of **19-II**, which is considered to have an almost comparable content of lipophilic domains relative to **16-IIa** since the lipophilic character of a PTC support is realized not only by the pendant octyl group but also by hydrocarbon chains in the spacers of the monomeric units **3a** and **3b**, some bromine atoms of which are converted into the terminal quaternary onium bromide to act as a catalytic group, and of the cross-linking agent units **4a** and **4b**. When a PTC support has considerably high content of the monomeric unit **13**, the polymeric PTC must consequently contain the catalytic group in its low content. Such a catalytic group is apt to be surrounded with lipophilic hydrocarbon chains which are abundantly present in the pendants and cross-linkages of the PTC support. Probably, the octyl pendant of polymeric PTCs with considerably high contents of the monomeric **13** behaved as a somewhat sterically hindering group and/or as a lipophilic group, which is undesirable for the hydrophilic alcohol **1** (or its alkoxide ion **23**). The high contents of monomeric units having such long alkyl groups are not required virtually for preparing polymeric PTCs of the reaction using hydrophilic reactants. At this time, however, it is difficult to describe whether the existence of a lower content of the monomeric unit **13** in a polymeric PTC is required to design a polymeric PTC having an optimum relative content of the hydrophilic and lipophilic domains. This problem should be clarified by further investigations of the design of various functional polymers.

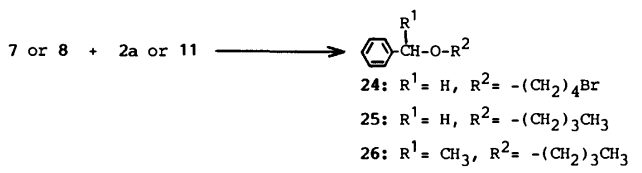

Scheme 5.

Preparation of the Other Ether Compounds by the Phase-Transfer Catalysis Using a Polymeric PTC: The onium salts attached to the polyoxetane resins were effective for the phase-transfer catalysis between aralkyl alcohols **7** or **8**, and alkyl bromide **2a** or **11** (Figs. 4—6). The catalytic activities of **16-IIa** and **16-IIb** were comparable to that of TBAB in producing **25** under the same reaction conditions (Fig. 4). When 1-phenylethanol (**8**) was used in place of **7**, the considerably prolonged reaction time was required to obtain a

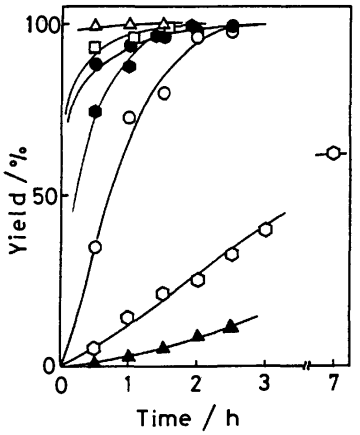

Fig. 4. Time-yield curves in the phase-transfer catalytic reaction at a **7**/**11** molar ratio of 1 : 3 in hexane-50% NaOH. PTC and mol% of ammonium group to **1**: (●) **16-IIa**, 2.9; (◐) **16-IIa**, 1.3; (○) **16-IIa**, 0.8; (◯) **16-IIa**, 0.1; (□) **16-IIb**, 4.3; (△) TBAB, 4.3; (▲) without PTC.

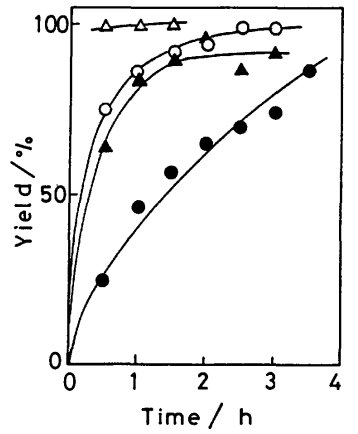

Fig. 5. Time-yield curves for **25** (△, ○) and **26** (▲, ●) in the phase-transfer catalytic reaction at a **7** or **8**/**11** molar ratio of 1 : 3 in hexane-50% NaOH. PTC and mol% of an ammonium group to **1**: (○, ●) **15-II**, 5.4; (△, ▲) TBAB, 5.0.

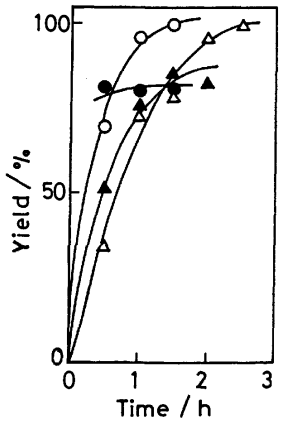

Fig. 6. Time-yield curves for **24** (●, ▲) and **25** (○, △) in the phase-transfer catalytic reaction at a **7**/**2a** or **11** molar ratio of 1:3 in hexane-50% NaOH. PTC and mol% of an ammonium group to **1**: (▲, △) **16-IIa**, 0.8; (●, ○) **20-II**, 3.3.

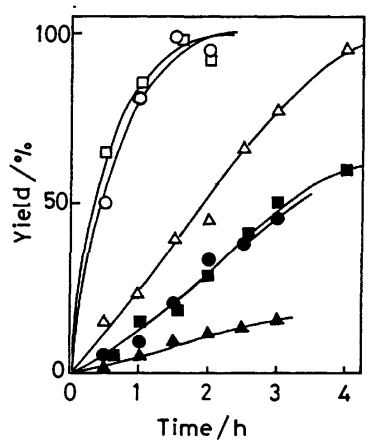

Fig. 7. Time-yield curves for **27** (○, △, □) and **28** (●, ▲, ■) at a **7** or **8**/**17** molar ratio of 1:3 in hexane-50% NaOH. PTC, mol% of an ammonium group to **1**, and reaction temperature: (○, ●) **16-IIa**, 3.5, reflux; (△, ▲) **16-IIb**, 3.4, 25 °C; (□, ■) **16-IIb**, 3.3, reflux.

satisfactory yield of **26** in every case using the polymeric PTC or TBAB, probably due to the steric hindrance of methyl group toward the nucleophilic reaction of **8** (Fig. 5). The glycidyl ethers **27** and **28** were also produced by the phase-transfer catalytic reaction of **7** or **8** with epichlorohydrin (**17**) in ether at 25 °C or reflux temperature in the presence of the polymeric PTC (Fig. 7). The phase-transfer catalysis of **7** with **17** at reflux temperature gave **27** in satisfactory yield, while **28** was given in much lower yield by a reaction of **8** with **17** under the influence of a steric hindrance of the benzylic methyl group. Mouzin et al. have prepared various glycidyl ethers by the phase-transfer catalytic reaction of alcohols with **17** in the presence of tetrabutylammonium hydrogensulfate without a solvent, and have recommended a reaction temperature of up to 25 °C for the reaction conditions.[20] In our results, the yields of **28** by a 2 h-reaction in the presence of **16-IIb** were lower by 40—60% than those of **27** under the same reaction conditions, while at the most 20% for the difference of yield between **27** and **28** was reported by Mouzin and his coworkers. The lower yield of **28** obtained by using the polymeric PTC seems to be ascribable to the formation of a sterically hindered reaction stage involving a benzylic methyl group of **8** and the bulky polymer matrices.

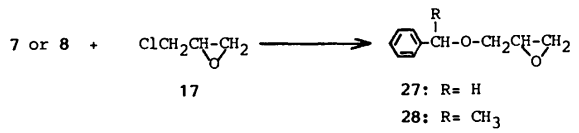

Scheme 6.

An *O*-alkylation of phenols was also examined by reactions of phenols with alkyl bromides using the polymeric PTC under the phase-transfer catalytic conditions (Table 3). The catalytic activity of the polymeric PTC was fairly high, as compared to that of TBAB with respect to the formation of those *O*-alkylated products. The reaction of **10a** with **2a** in the presence of **15-II** gave the monosubstituted product **30a** almost exclusively, although in the other

Table 3. Etherifications of Phenols with Bromides under Phase-Transfer Catalytic Conditions[a]

		PTC		Product		
Phenol	Bromide	(mol%)[b]	Time/h	No.	Yield/%	Molar ratio, **30**:**31**
9	**11**	**16a-II** (1.9)	5	**29**	91.6	—
9	**11**	**15-II** (3.9)	2.5	**29**	98.9	—
9	**11**	TBAB (5.0)	2	**29**	90.1	—
10a	**2a**	**15-II** (5.0)	4	**30a**	94.1	ca.100:0
				31a	0.6	
10a	**2a**	TBAB (5.0)	2	**30a**	73.7	94:6
				31a	8.7	
10b	**2a**	**15-II** (5.0)	6.5	**30b**	80.7	94:6
				31b	10.3	
10b	**2a**	TBAB (5.0)	4.5	**30b**	81.2	95:5
				31b	8.2	

a) Phenol, 36.7 mmol; bromide, 0.11 mol; benzene, 20 cm^3; 50% NaOH, 48 g; under reflux.
b) Mole percent of phase-transfer catalyst (PTC) to the phenol.

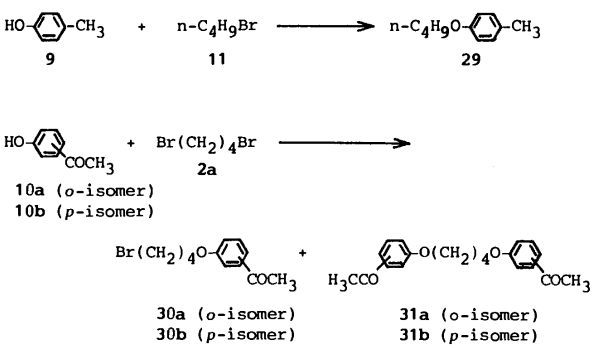

Scheme 7.

reactions in the presence of the polymeric PTC or TBAB the mono-, **30a** or **30b**, and the disubstituted products, **31a** or **31b**, were formed in a ratio of about 95 : 5, regardless of using either an ortho- or para-isomer. It is also thought that the acetyl substituent at the ortho position appreciably influenced the formation of **31a** via the further reaction of **30a** with **10a** in the sterically crowded matrices of the polymeric PTC.

Repeated Use of the Polymeric PTC: The catalytic activity of polymeric PTC **15-II** was examined in a process using the PTC repeatedly in the reaction between **1** and **2a** at the mole ratio of 3.0 in 50% NaOH and hexane. The considerably high phase-transfer catalyzing ability of **15-II** was obviously shown at each of ten stages in the process (Table 4). The reaction rate was enhanced by increasing the concentrations of the reactants (or by decreasing a volume of hexane). When a dried PTC was used, a somewhat longer reaction period was required to obtain a satisfactory yield (75—85%) of **3a**, as compared with that in the use of a wet PTC. This indicates the requirement of a certain period for swelling the dried matrices with the organic and aqueous mediums used in the present catalysis.

Table 4. Examination of Repeated Use of a Polymeric PTC in Ether Formation from **1** and **2a**[a]

Stage No.	Hexane cm³	Product	Yields of **3a** and **4a**/% Reaction time/h 0.5	1.0	1.5	2.0	2.5	3.0
1	20	**3a:**	50.4	66.7	72.1	77.1	78.4	
		4a:	2.9	7.0	8.7	8.7	8.9	
2	20	**3a:**	57.7	69.1	74.4	77.2	81.3	
		4a:	4.7	7.0	8.8	9.8	10.5	
3	50	**3a:**	20.8	39.4	62.7	65.7	75.3	74.7
		4a:	0.5	2.3	5.2	6.8	7.5	6.9
4[b]	20	**3a:**	66.0	76.9	77.0	81.3		
		4a:	5.8	6.9	7.5	8.0		
5	5	**3a:**	76.2	78.2	88.9			
		4a:	6.9	7.6	8.8			
6	5	**3a:**	74.1	81.1	86.9			
		4a:	8.2	8.4	8.7			
7	5	**3a:**	79.5	86.6	87.1			
		4a:	7.3	8.4	6.6			
8	5	**3a:**	74.0	79.0	81.5	82.1		
		4a:	5.8	6.5	7.3	8.6		
9[c]	20	**3a:**	55.3	72.9	82.0	91.0	94.2	
		4a:	3.1	7.3	8.4	9.4	9.2	
10[b]	20	**3a:**	61.3	79.3	88.6	89.2		
		4a:	3.6	7.3	8.5	9.4		

a) **1**, 19.9 mmol; **2a**, 58.7 mmol; polymeric PTC used on the reaction at the 1st stage, 0.33 g by dry weight of **15-II** (3.0 mol% to **1**); *n*-$C_{16}H_{34}$, 1.35 mmol; 50% NaOH, 26 g; at reflux temperature. b) A wet polymeric PTC was used. c) 0.27 g of dried **15-II** was recovered after the reaction at the 8th stage and, subsequently, was reused at this stage.

The unchanged pendant bromide of the polymeric PTC may be converted into the corresponding ether linkage by a phase-transfer catalytic reaction with the hydroxy compound used as the reactant, although the structural change of the pendant group was not confirmed in the present study. This problem is taken to be unimportant since the high catalytic activity was maintained during the experiment of the repeated use of polymeric PTC. The polymeric PTC was easily separated from a reaction mixture by filtration and reused at the next stage of the phase-transfer reaction after or without drying the PTC. A loss of 18% by weight of the dry catalytic PTC initially used was observed before reusing the PTC at the 9th stage, corresponding to an about 97% recovery of PTC per each stage.

The present polymeric PTCs were also proved to be useful for the ether synthesis on a preparative scale. The reaction of 10 g of **1** with three equivalents of **2a** in hexane in the presence of **17-II** in only 0.1% molar respect to **1** gave pure **3a** in a 74% isolated yield. **27** was isolated in a 85% yield by a reaction of 10 g of **7** with **17** in ether in the presence of **16-IIb** in 0.4 mol% of phosphonium salt to **7**.

Influence of the Reaction Temperature: The reaction temperature should be kept in a range of 70 to

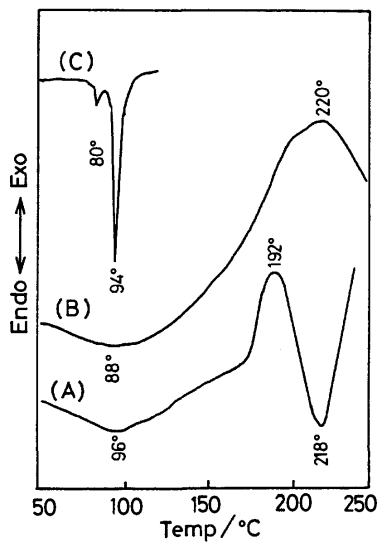

Fig. 8. DSC curves for polymeric PTCs **16-IIa** (A) and **16-IIb** (B), and TBAB (C).

80 °C in using the present polymeric PTCs. At lower temperatures the ether product was formed slowly, presumably requiring a prolonged reaction time to obtain a satisfactory yield. When those PTCs were used at temperatures above 100 °C, their catalytic activities decreased with the reaction time and, consequently, the reuse of the polymer as PTC became virtually impossible. Figure 8 shows the results of DSC measurements for the polymeric PTCs **16-IIa** and **16-IIb**, and TBAB. Probably due to a thermal decomposition, the quaternary ammonium-containing **16-IIa** begins to behave exothermally around 100 °C after indicating an endothermal peak at about 96 °C, which corresponds to a melting point of 94 °C for TBAB. The quaternary phosphonium-containing **16-IIb**, which has an exothermal peak at 220 °C, is taken to be somewhat more thermally stable than **16-IIa** with an exothermal peak at 192 °C. These results are compatible with those obtained for quaternary onium salts with low molecular weights.[25]

In this paper we have demonstrated one of the applications of polyoxetane resins to a polymeric support for preparing functionalized polyethers. It is thus concluded that quaternary onium salts based on a soft, moderately polar polyoxetane support are useful polymeric PTCs for the facile synthesis of ethers.

References

1) S. L. Regen, *Angew. Chem., Int. Ed. Engl.*, **18**, 421 (1979).

2) A. Akelah and D. C. Sherrington, *Chem. Rev.*, **81**, 557 (1981).

3) A. Akelah, *Synthesis*, **1981**, 413.

4) W. T. Ford and M. Tomoi, *Adv. Polym. Sci.*, **55**, 49 (1984).

5) S. Kondo, K. Ohta, Y. Inagaki, M. Minafuji, H. Yasui, N. Nakashima, M. Iwasaki, K. Furukawa, and K. Tsuda, *Pure Appl. Chem.*, **60**, 387 (1988).

6) "Phase-Transfer Catalysis, New Chemistry, Catalysts, and Applications," ACS Symposium Series 326, ed by C. M. Starks, Am. Chem. Soc., Washington (1987).

7) J. M. Brown and J. A. Jenkins, *J. Chem. Soc., Chem. Commun.*, **1976**, 458; M. Tomoi, Shiiki, and H. Kakiuchi, *Makromol. Chem.*, **187**, 357 (1986).

8) Y. Imai, M.Kajiyama, S. Ogata, and M. Kakimoto, *Polym. J.*, **16**, 267 (1984).

9) N. Yui, K. Nojima, K. Sanui, and N. Ogata, *Polym. J.*, **17**, 968 (1985).

10) D. J. Bannister, M. Doyle, and D. R. Macfarland, *J. Polym. Sci., Polym. Lett. Ed.*, **23**, 465 (1985).

11) H. Becker, H.-W. Lucas, J. Maul, V. R. R. Pillai, H. Anzinger, and M. Mutter, *Makromol. Chem., Rapid Commun.*, **3**, 217 (1982).

12) M. Mutter, K.-H. Altmann, and J. Schmit, *Makromol. Chem., Rapid Commun.*, **6**, 785 (1985).

13) Y. Kimura, P. Kirszensztejn, and S. L. Regen, *J. Org. Chem.*, **48**, 385 (1983).

14) R. Neumann and Y. Sasson, *J. Org. Chem.*, **49**, 1282 (1984).

15) S. Iwabuchi, T. Nakahara, A. Tsuchida, and K. Kojima, *Makromol. Chem.*, **184**, 535 (1983).

16) T. Higashimura, T. Nakamura, and S. Aoshima, *Polym. Bull.*, **17**, 389 (1987).

17) M. Motoi, H. Suda, K. Shimamura, S. Nagahara, M. Takei, and S. Kanoh, *Bull. Chem. Soc. Jpn.*, **61**, 1653 (1988).

18) M. Motoi, S. Nagahara, M. Yokoyama, S. Kanoh, and H. Suda, *Kobunshi Ronbunshu*, **46**, 59 (1989).

19) E. M. Van Duzee and H. Adkins, *J. Am. Chem. Soc.*, **57**, 147 (1935).

20) G. Mouzin, H. Couss, J.-P. Riew, and A. Duflos, *Synthesis*, **1983**, 117.

21) *Beilstein Handbuch der Org. Chem.*, **6**, 393 (1923).

22) S. L. Regen and L. Dulak, *J. Am. Chem. Soc.*, **99**, 623 (1977).

23) M. E. Childs and W. P. Weber, *J. Org. Chem.*, **41**, 3486 (1976).

24) J. W. Zubrick, B. I. Dunber, and H. D. Durst, *Tetrahedron Lett.*, **1975**, 71.

25) J. Ugelstadt, T. Ellingsen, and A. Berge, *Acta Chem. Scand.*, **20**, 1593 (1966).

Nucleophilic Substitution Reactions of Alkyl Halides by Using New Polymer-Supported Reagents Containing Hemin

Kiyoshi SAITO and Kaoru HARADA*
Department of Chemistry, University of Tsukuba, Tsukuba, Ibaraki 305
(Received January 5, 1989)

A new polymer reagent consisting of hemin, divinylbenzene, and 2-methyl-5-vinylpyridine was synthesized by suspension copolymerization. Substitution reactions of primary, secondary, and tertiary alkyl halides with the hemin copolymer combined with cyanide, azide, and thiocyanate ions were given satisfactory yields. This reaction mechanism was revealed to be a S_Ni type on the basis of stereochemical study. The hemin copolymer was not only a polymer-supported reagent with functional capabilities, but also served to separate the product from the reaction mixture.

Ferri-protoporphyrin IX chloride (hemin) is a kind of tetrapyrrole derivative containing a large π-electron system and shows aromatic property. The axial coordination site of porphyrin is an interesting reaction field for various organic reactions. Recently, catalytic oxidation and epoxidation using metalloporphyrin complexs have revealed that the reactions take place on the coordination site of the metalloporphyrin.[1] However, studies on the reaction using ligands other than oxygen have not been reported to the best of our knowledge. Methemoglobin or ferrihemoglobin, in which the heme-ion carries an extra positive charge, has been found to have high affinity for cyanide ion.[2] We have synthesized beads shape hemin containing copolymer by suspension copolymerization[3] in order to prevent the stacking of hemin. It has been shown that the copolymer functions as a cyanide ion exchanger.[3] In this study we would like to describe the application of the hemin copolymer combined with various ligands as a polymer-supported reagent, for nucleophilic substitution in nonaqueous solvents. The use of crown ether as a phase transfer catalyst and of commercial anion-exchange resin as a polymer reagent for nucleophilic substitution in nonaqueous system has been reported.[4-7] In these systems, the mechanism of the reaction is of the S_N2 type. The nucleophilic substitution using Amberlyst A26 (**2**), was reported previously in a nonaqueous system.[5] The polymer investigated in this study is a copolymer consisting of hemin, divinylbenzene (DVB), and 2-methyl-5-vinylpyridine (MVP) (**1**). Figure 1 shows the difference in the binding of the nucleophile at the ion exchange site of **1** and **2**. In **2**, the nucleophile is combined with electrostatic interaction. On the other hand, in **1**, the chemical bonding of the nucleophile with the central iron has both electrostatic and also coordination properties.

Hemin-copolymer (1)

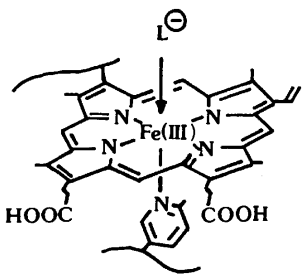

Amberlyst A26 (2)

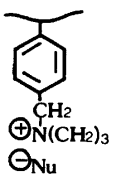

Fig. 1. The difference in the binding of the nucleophile at the ion exchange site of **1** and **2**.

Experimental

Synthesis of Hemin Copolymer (1) by Suspension Polymerization:[3] All the monomers used were as described previously.[3] The suspension polymerization was carried out with a standard apparatus for suspension polymerization.

Adsorption Experiment with Cyanide Ion: Copolymer **1** (chloride form, 0.155—0.189 g) was stirred in 50 ml $Na_2B_4O_5$-KH_2PO_4 buffer solution (pH 9; ionic strength 0.1) containing different amounts of KCN (2.14×10^{-4}—2.14×10^{-2} mol dm^{-3}). Detailed procedures of the experiments have been described previously.[3] **Azide Ion:** Copolymer **1** (chloride form, 0.155—0.189 g) was stirred for 12 h in water (50 ml) containing different amounts of NaN_3 (2.14×10^{-4}—2.14×10^{-2} mol dm^{-3}). The azide ion concentration of the supernatant was measured by the method of Labruto and Randisi.[8] **Thiocyanate Ion:** Copolymer **1** (chloride form, 0.155—0.189 g) was stirred for 12 h in water (50 ml) containing different amounts of KSCN (2.14×10^{-4}—2.14×10^{-2} mol dm^{-3}). The thiocyanate ion concentration

of the supernatant was measured by the method of Kruse and Mellon.[9]

Polymer-Supported Reagents (CN, N_3, SCN-Modified Hemin Copolymer): Copolymer **1** (chloride form, 10.0 g) was stirred for 12 h with potassium cyanide (7.0 g) or sodium azide (7.0 g) or potassium thiocyanate (10.0 g) in water (100 ml). The treated resin was filtered off and washed successively with water, methanol, and acetone before drying under reduced pressure at 60 °C.

To estimate the molar quantity of the nucleophile combined with the hemin copolymer, the prepared polymer-supported reagent was packed in a column (40 cm×10 mm diameter) and the nucleophile was eluted with 0.5 M NaOH.

CN, N_3, SCN-Bound Amberlyst A26:[5] Amberlyst A26 (chloride form, 100 g) was stirred for 6 h with potassium cyanide (42 g) or sodium azide (42 g) or potassium thiocyanate (60 g) in water (400 ml). The resin was filtered off and washed successively with water, tetrahydrofuran, and ether before drying under reduced pressure at 40 °C.

Substitution Reactions. The typical procedure of the substitution reaction is as follows: a mixture of halide (1 mmol), **1**-supported anion or **2**-supported anion (1 mmol), and benzene (30 ml) was stirred and heated at 60 °C or 80 °C for 10 h. The resin was filtered off and washed successively with benzene (10 ml×2) and ether (10 ml×2) (the ether was used for washing to elute the substitution product completely). The chemical yields were determined by GC analysis in comparison with authentic samples. The product was confirmed by IR and ^{1}H NMR spectrometry.

Synthesis of Optically Active α-Bromo Acid Methyl Ester. Optically active α-bromo acids were prepared from (*R*)- or (*S*)-amino acids in the usual way as follows: (*S*)-(−)-leucine (10 g, 76 mmol) in cold 3 M H_2SO_4 (300 ml; 1M=1 mol dm^{-3}), containing potassium bromide (55 g, 6 mol equiv) was treated with sodium nitrite (15 g, 2.7 mol equiv) at 0 °C for 0.5 h. The solution was kept at 0 °C for 1 h and then stirred for 1 h with ether (150 ml). The layers were separated and the aqueous solution was extracted with ether. The combined organic solution was dried ($MgSO_4$) and evaporated. After distillation of the crude product, 9.2 g (62%) of purified (*S*)-2-bromo-4-methylpentanoic acid was obtained, bp 97—98 °C (33.33 Pa); $[\alpha]_D^{20}$−33.4° (*c* 2, methanol), lit, $[\alpha]_D^{27}$−34° (methanol).[10] Esterification of the acid with diazomethane gave (−)-methyl-(*S*)-2-bromo-4-methylpentanoate, bp 50 °C (267 Pa). All optical purities of (*R*)- or (*S*)-α-bromo acids were determined by polarimeter before esterification with diazomethane.

(*R*)-2-Bromo propanoic acid, $[\alpha]_D^{22}$+27.3° (*c* 2, methanol), 84% e.e., lit, $[\alpha]_D^{23}$+32.4±3.6° (*c* 0.49, methanol);[16] (*S*)-2-bromo propanoic acid $[\alpha]_D^{22}$−24.5° (*c* 2, methanol), 89% e.e., lit, $[\alpha]_D^{27}$−27.6° (methanol);[10] (*R*)-2-bromo-3-phenylpropanoic acid, $[\alpha]_D^{22}$+10.4° (*c* 2, methanol), 100% e.e., lit, $[\alpha]_D^{20}$+9.0°;[17] (*S*)-2-bromo-3-phenylpropanoic acid, $[\alpha]_D^{22}$ −10.7° (*c* 2, methanol), 100% e.e., lit, $[\alpha]_D^{25}$−10.0° (*c* 2, methanol);[18] (*R*)-2-bromo-4-methylpentanoic acid, $[\alpha]_D^{22}$ +37.8° (*c* 2, methanol), 99% e.e., lit, $[\alpha]_D^{22}$+38.2±1.8° (*c* 2, methanol);[19] (*R*)-2-bromo-3-methylbutanoic acid, $[\alpha]_D^{22}$ +16.1° (*c* 2, methanol), 100% e.e., lit, $[\alpha]_D^{25}$+15.5 (methanol);[20] (*S*)-2-bromo-3-methylbutanoic acid, $[\alpha]_D^{22}$ −17.2° (*c* 2, methanol), 100% e.e., lit, $[\alpha]_D^{27}$−16.8° (methanol).[10]

Characterization of the Substituted Product. After substitution of the optically active α-bromo acid methyl ester with N_3-modified **1**, the resulting α-azido acid methyl ester was hydrogenated over 5% or 20%-Pd/C in the usual manner to form the α-amino acid methyl ester. A 5 mg sample of the α-amino acid methyl ester in 20 ml of 3 M HCl in *i*-PrOH was heated at 100 °C (30 min). The reaction mixture was evaporated under vacuum and the residue was dissolved in 20 ml of dichloromethane. The solution was cooled by using a Dry Ice-acetone bath and 4 ml of trifluoroacetic anhydride (TFAA) was added. The solution was warmed to room temprature, and allowed to stand for 1 h. The reaction mixture was evaporated under vacuum, the residue was dissolved in dichloromethane, and the enantiomeric excess (e.e.) was determined by GC analysis using a chiral stationary phase (Chirasil-Val III).[11]

ESR Spectra. The interaction between the substituted product (R-CN, R-N_3, R-SCN) and the hemin group in copolymer **1** was characterized by electron spin resonance (ESR) spectroscopy which was made at liquid nitrogen temperature with a JEOL-8 JES-FELX spectrometer.

Separation Experiment. The substitution reaction using hemin copolymer **1** was stopped at 65% yield and the reaction mixture containing **1** was packed in a column. After unreacted substrate was compleatly removed by elution with benzene, the reaction product was eluted with ether.

Results and Discussion

Adsorption Experiment. The coordination sphere around the central iron of the hemin in the copolymer was characterized by ESR spectroscopy.[3] The spectrum indicated the five-coordinated high spin type of ferri-porphyrin characterized by ESR signal with g=6.[3] On the other hand, the axial coordination number of N_3^- and SCN^- ions was close to one, as estimated from the results of adsorption experiments similar to those described previously.[3] These results could indicate that the hemin copolymer **1** contains hemin in which the fifth coordination site of the iron(III) is occupied with the MVP residue, and N_3^- and SCN^- ions bind to the sixth coodination position.

Table 1. Nucleophilic Substitution of R-X with CN^-, N_3^-, or SCN^- Ions Adsorbed onto **1**[a]

R-X	Reaction temp	Yield of substituted products/%		
	°C	R-CN[b]	R-N_3[c]	R-SCN[d]
$CH_3(CH_2)_7Br$	80	78	89	87
$CH3(CH_2)_3Br$	60	86	92	98
$CH_3CH_2CH(CH_3)Br$	60	76	83	90
$(CH_3)_3CBr$	60	70	74	83
$CH_3CH_2C(CH_3)_2Br$	60	70	73	81
$PhCH_2Br$	60	75	92	94
$PhCH(CH_3)Br$	80	78	80	86
$(Ph)_2CHBr$	80	76	80	83
$(Ph)_2C(CH_3)Br$	80	73	75	78
$(Ph)_3CBr$	80	80	80	82
Me_3Si-Cl	60	91	91	97

a) 6 h, [R-X]=[**1**-Nu]=1 mmol/30 ml benzene. b) Reaction with CN^- ion adsorbed onto **1**. c) Reaction with N_3^- ion adsorbed onto **1**. d) Reaction with SCN^- ion adsorbed onto **1**.

Table 2. Nucleophilic Substitution of R-X with CN^- Ion Adsorbed onto Commercial Anion Exchange Resins or KCN

Substrate	X	Reaction condition				Yield of nitrile	Ref.
		Reagent[a]	Solv.	Temp °C	Time h	%	
$CH_3(CH_2)_2X$	Br	a	—	80	1	70	1
$CH_3(CH_2)_3X$	Br	a	—	80	1	65	1
$CH_3CH_2CH(CH_3)X$	Cl	a	—	110	1	24	1
$(CH_3)_3CX$	Cl	a	—	110	1	0	1
	Br	KCN	DMSO			Elimination product	13
$CH_3(CH_2)_7X$	Br	b	Benzene	80	6	90	2
$PhCH_2X$	Br	a	EtOH	65	1.5	53	3
		b	Benzene	79	6	87	2

a) Abbreviations used : a, CN-bound Amberlite IRA400; b, CN-bound Amberlyst A26.

Substitution Reactions. The results are summarized in Table 1. The yields of the resulting nitrile, azide, or thiocyanate from halides are high, and by-products were not detected in the reaction mixture, even though the results described here were obtained by using equimolar reagents. Commercial anion-exchange resins have also been used as the polymer-reagent in substitution reactions involving cyanide ion.[4-6] However these commercial resins were not very active in the substitution reaction. Secondary halides gave the corresponding nitriles in low yields, and tertiary halides did not give any substitution products (Table 2). Previously, trimethylacetnitrile has been prepared by dehydration of trimethylacetamide[12] or by addition reaction of HCN to isobutene.[13] The substitution reaction of *t*-butyl bromide with KCN in DMSO did not give the corresponding nitrile but yielded the elimination product (Table 2).[14]

After the substitution reaction, it was found that most of the products were adsorbed onto the hemin site in the resin. The adsorbed products could easily be desorbed with ether or hexane.

The polymer reagent described in this paper is much more effective than the commercial anion-exchange resins, probably because the cyanide ion is adsorbed at the hemin site in **1** with ionic as well as with coordination bond. Taking this point into account, the substitution reaction of cinnamyl bromide with thiocyanate ion was investigated (Table 3). Harrison and Hodge have described this reaction using **2**-supported thiocyanate[5] (Table 3). They reported that the initial product of the reaction between **2**-supported thiocyanate and cinnamyl bromide was cinnamyl thiocyanate, but after prolonged reaction time the product rearranged to isothiocyanate.[5] In our reaction, however the only product obtained by the substitution reaction was cinnamyl thiocyanate under the same reaction conditions as Ref. 5). Therefore, the rearrangement of the initial product was prevented by the coordination of the product on the hemin site.

Table 3. Nucleophilic Substitution of Cinnamyl Bromide[a] with SCN^- Ion Adsorbed onto **1** or **2**

Substrate	Product group	Yield of product/%			
		1		**2**[2]	
		Benzene	Toluene	Benzene	Toluene
PhCH=CHBr	-SCN	99	98	67	11
	-NCS	0	0	31	82

a) 80 °C, 6 h.

ESR Spectra. From the results described above, it can be assumed that some interaction exist between the product and the hemin residue under the reaction conditions. This interaction could be confirmed by ESR spectrometry (Fig. 2). Figure 2 shows the change of spectral pattern of butyl thiocyanate with **1**. In Fig. 2, (a) and (b) were measured before and after adsorption of the thiocyanate using a 1 : 2 mixture of the thiocyanate and benzene, and these are in accord with those of high- and low-spin Fe(III)-porphyrins, respectively. Spectrum (c) was obtained after desorp-

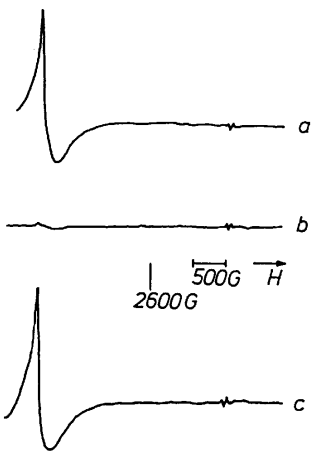

Fig. 2. ESR spectra of **1** at liquid nitrogen temperature. a, **1**; b, after adsorption of the thiocyanate for a 1 : 2 mixture of butyl thiocyanate and benzene; c, after desorption of the thiocyanate with hexane.

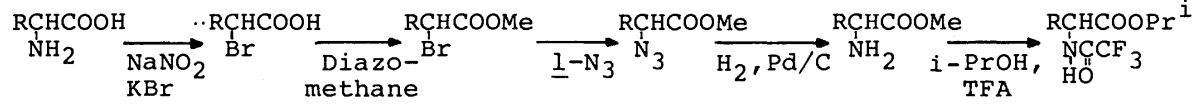

Scheme 1.

Table 4. Nucleophilic Substitution of Optically Active α-Bromo Acid Methyl Ester [R-C*H(Br)COOMe] with N_3^- Ion Adsorbed onto **1**[a]

R		Reagent	O.P.[b] %	C.Y.[c] %	e.e.[d] %		e.e./O.P. %	Ref.
CH_3-	(*R*)	**1**-N_3^-	84	98	(*R*)	74	88	—
	(*S*)	**1**-N_3^-	89	96	(*S*)	80	90	—
$PhCH_2$-	(*R*)	**1**-N_3^-	100	93	(*R*)	97	97	—
	(*S*)	**1**-N_3^-	100	95	(*S*)	91	91	—
$(CH_3)_2CHCH_2$-	(*R*)	**1**-N_3^-	99	97	(*R*)	96	97	—
		2-N_3^-	99	10	(*S*)	80	—	—
	(*S*)	**1**-N_3^-	98	95	(*S*)	91	93	—
		2-N_3^-	100	13	(*R*)	76	—	—
		NaN_3[e]	76	38	(*R*)	79	—	15
$(CH_3)_2CH$-	(*R*)	**1**-N_3^-	100	98	(*R*)	92	92	—
	(*S*)	**1**-N_3^-	100	98	(*S*)	98	98	—

a) 6 h, 60 °C, [RCHBrCOOMe]=[N_3^-]=1 mmol/30 ml benzene. b) Optical purity of α-bromo acid. c) Chemical yield of α-azido acid methyl ester. d) Enantiomeric excess of amino acid was determined by GC analysis e) 22 h, 60 °C, presence of 18-crown-6.

tion of the thiocyanate with hexane, and the pattern agrees with that of high-spin as it was before. The same spectral changes were observed in all of the substitution products. These results indicate that the interaction of the substitution product to the hemin site is coordination bond.

Reaction Mechanism. Taking into account the results mentioned above, it could be contemplated that these reactions proceed in the vicinity of the sixth coordination site of hemin residue in **1**. And the hemin site in the polymer reagent could not only be an ion exchange site, but also an excellent reaction field in the nucleophilic substitution. In order to further investigate this point, we have carried out stereochemical studies under the same conditions in which various optically active α-bromo acid methyl esters were used. The chemical pathway from the preparation of the substrate to the final product is shown in Scheme 1. Table 4 shows the optical purity (O.P.) of the α-bromo acid, the chemical yield (C.Y.) of α-azido acid methyl ester, the enantiomeric excess (e.e.) of the derivatized amino acid, and real retention of configuration in the substitution reaction (e.e./O.P.). As is evident from Table 4, this substitution reaction proceeded almost quantitatively, and the results of the substitution reaction agreed with these of the reaction proceed with S_Ni mechanism, with e.e./O.P. of approximately 100%.[21] In contrast with our results, the yields of the substitution products using azide bound **2**, and NaN_3 in the presence of crown ethers[13] (Table 4) were both low and the configurations of the products were inverted under the same conditions we used.

The interaction between substitution product, α-azido acid methyl ester, and the hemin residue in copolymer **1** was confirmed by ESR spectrometry.

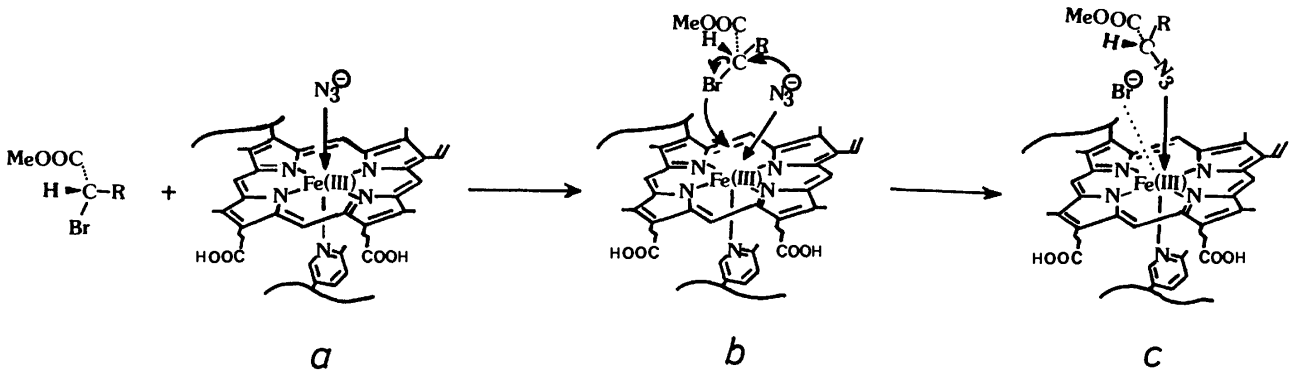

Scheme 2. A possible reaction pathway of the nucleophilic substitution of optically active α-bromo acid methyl ester with N_3^- ion combined with **1** in benzene at 60 °C.

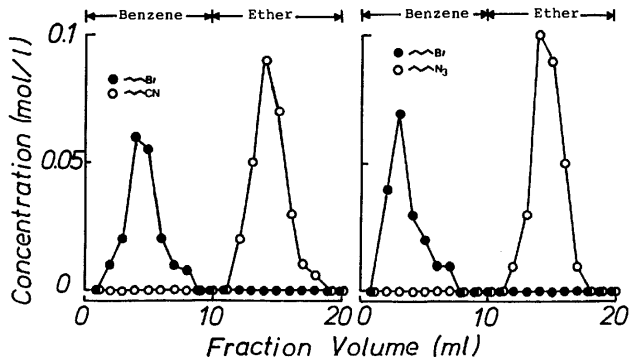

Fig. 3. Column separations of substitution reaction mixtures with **1**.

The same spectral changes were observed as shown in Fig. 2.

The mechanism of nucleophilic substitution reaction in this study could be explained as shown in Scheme 2. The nucleophile is adsorbed onto 6th coodination site of hemin in resin **1** on the basis of the coordination number of CN^-, N_3^-, and SCN^- (n=1)[3] and ESR spectra[3] (Scheme 2, *a*). It can be concluded from the results of ESR spectroscopic analysis (Fig. 2) (Scheme 2, *c*), that most of the reaction products are coordinated to the hemin site after substitution reaction. Taking into consideration the facts that (i) the substituted products were obtained from tertiary alkyl bromide in benzene; (ii) cinnamyl thiocyanate was produced in high yield; (iii) the reactions using optically active substrates proceeded with complete retention of configuration; it could be interpreted that the reaction is a S_Ni type substitution reaction (Scheme 2, *b*).

Column Separation. Copolymer **1** is not only a polymer-supported reagent with functional capability, but also serves to separate the product from the reaction mixture. The products were coordinated to hemin sites in the reaction solvent and could be desorbed easily with hexane or ether. Therefore, the separation characteristics of **1** were further investigated by using the column. The substitution reaction was stopped at 65% yield and the reaction mixture adsorbed in **1** was packed in a column. Figure 4 shows a typical column separation of the substrate (●) and the reaction product (○). When the reaction mixture was packed and eluted through a column with benzene (●), only the substrate(1-bromobutane) was in the eluent. The adsorbed reaction product (valeronitrile or butyl azide) was eluted almost completely with ether (recovery ca. 99 %).

References

1) J. T. Groves and T. E. Nemo, *J. Am. Chem. Soc.*, **105**, 5786 (1983).
2) J. M. Rifkind, *Inorg. Biochem.*, **2**, 832 (1973).
3) E. Kokufuta and K. Saito, *J. Appl. Polym. Sci.*, **34**, 517 (1987).
4) N. Urata, *Nippon Kagaku Kaishi*, **83**, 1105 (1962).
5) C. R. Harrison and P. Hodge, *Synthesis*, **1980**, 299.
6) M. Gordon and C. E. Griffin, *Chem. Ind.*, **1962**, 1019.
7) F. Manescalchi, M. Orena, and D. Savoia, *Synthesis*, **1979**, 445.
8) G. Labruto and D. Randisi, *Ann. Chem. Applic.*, **22**, 319 (1932).
9) J. M. Kruse and M. G. Mellon, *Anal. Chem.*, **25**, 446 (1953).
10) W. Gaffield and W. G. Galetto, *Tetrahedron*, **27**, 915 (1971).
11) H. Frank, G. J. Nicolson, and E. Bayer, *J. Chromatogr.*, **146**, 197 (1978).
12) W. Lehnert, *Tetrahedron Lett.*, **1971**, 1501.
13) B. S. Hendrik, *Neth. Appl.*, **69**, 495 (1971).
14) L. Friedman and H. Shechter, *J. Org. Chem.*, **25**, 877 (1960).
15) Y. Nakajima, *Tetrahedron Lett.*, **1978**, 3107.
16) H. Hashimoto and H. Simon, *Angew. Chem.*, **87**, 111 (1975).
17) E. Fischer and W. Schoeller, *Ann. Chem.*, **357**, 1 (1907).
18) A. F. Spatola and A. L. Bettag, *J. Org. Chem.*, **46**, 2393 (1981).
19) J. A. Yankeelov, Jr., K. F. Fok, and D. J. Carothers, *J. Org. Chem.*, **43**, 1623 (1978).
20) R. J. Anderson, K. G. Adams, and C. A. Henrick, *J. Agric. Food Chem.* **33**, 508 (1985).
21) P. A. Levene and A. Rothen, *J. Biol. Chem.*, **127**, 237 (1939).

 © 1989 The Chemical Society of Japan Bull. Chem. Soc. Jpn., 62, 2567—2574 (1989)

Mass Spectrum and Thermal Behavior in Solid State of *N,N*-Di(1-hydroxyalkyl)-2-imidazolidinone

Choichiro SHIMASAKI,* Kyoko NAKAJIMA, Yuka SUGIMORI, Eiichi TSUKURIMICHI, and Toshiaki YOSHIMURA
Faculty of Engineering, Toyama University, Gofuku, Toyama 930
(Received January 12, 1989)

1,3-Bis(1-hydroxyalkyl)-2-imidazolidinones (**1**) were prepared by the reaction of imidazolidinone with propyl-, butyl-, isobutylaldehyde. They were unstable and moisture-sensitive substances, except for 1,3-bis(1-hydroxybutyl)-2-imidazolidinone (**1c**). In the decomposition by the electron impact of **1** and the dimer of **1c**, the molecular ion peak of **1** was not detected. The fragmentation of the imidazolidinone ring was considered to take place after a successive cleavage of the two side chains of **1**. The pyrolysis reaction of **1** was found to be a thermal decomposition via a molten state after a condensation reaction. The order of the pyrolysis was calculated on the basis of DSC curves. The condensation stage for **1c** apparently obeyed 1/2-order kinetics. From the dependence of the velocity on the temperature in DTA and the thermogravimetric analysis, the activation energy of decomposition was calculated; the value for the former was 67 and the latter 73 kJ mol^{-1}. The mechanism of pyrolysis was supported by the results of the IR spectrum and chemical analysis.

The derivatives of 2-imidazolidinone (**2**) have many advantages over any other substituted ureas. Furthermore, **2** has two active imino groups similar to the amino groups of urea. Compound **2** cannot produce compounds which have an intermolecular ether formation, such as tetrahydro-4*H*-1,3,5-oxadiazin-4-one. If **1** is cured at a certain temperature, the curing process must be similar to those of the main chain formation for the urea resin. The thermal decomposition of 1-hydroxyalkyl-2-imidazolidinone was previously reported by the present authors.[1] In this work, the decomposition study was extended to 1,3-bis(1-hydroxyalkyl)-2-imidazolidinone. The present authors investigated the condensation reaction of **1c** under no alkaline and acid catalyst conditions by IR, ^{1}H and ^{13}C NMR measurements. DSC and DTA are useful tools for measuring the thermally induced conformation transition of macromolecules as well as the polymerization process. An application of DSC and DTA to the study of polymerization provides information for kinetic data, such as the activation parameter.

Experimental

Materials. Compound **2**, ethanol, and methanol were of reagent grade and were used without further purification. The propionaldehyde, butyraldehyde, and isobutyraldehyde were distilled before use.

Preparation of Sample. 1,3-Bis(1-hydroxypropyl)-2-imidazolidinone (**1a**) was prepared according to the reported method for methylolurea.[2] The general procedure was as follows. *N*-(Hydroxymethyl)urea (**2** 21.5g (0.25 mol)) was suspended in 10 ml of ethanol under a nitrogen atmosphere. The ethanol solution was kept at pH 11 with a 8 M-NaOH aqueous solution (1 M=1 mol dm^{-3}) as the catalyst. After being stirred for 15 min, 35 ml of propionaldehyde was added dropwise to this suspension, which was kept under 15 °C by ice. White crude crystals were filtered with suction and dried in a desiccator. Recrystallization from chloroform gave white needle crystals of **1a**. 1,3-Bis(1-hydroxybutyl)-2-imidazolidinone (**1b**), and 1,3-di(1-hydroxy-2-methylpropyl)-2-imidazolidinone (**1c**) were prepared in a manner similar to **1a** by using 45 ml of butyr- or isobutyraldehyde and 10 ml of methanol.

Measurements. Elemental analyses of samples were carried out by using a Hitachi C,H,N-analyzer-026 at the Toyama Medical and Pharmacy University. IR spectra of samples were recorded on a Nipponbunko IR-810 using the KBr-disc method. The ^{1}H and ^{13}C NMR spectra of each solution was taken on a JNM-FX-90-FT-NMR instrument. A TMS was used as a reference. **1c** was dissolved in a deuterated dimethyl sulfoxide solution, and **1a**, **1b**, and **2** in a deuterated chloroform solution. A mass spectrum of each sample was taken with an ionization potential of 20 eV using a JEOL-JMS-D300 by EI method. Samples were heated in air using α-Al_2O_3 as reference by a Rigakudenki TG-DSC apparatus and Rigakudenki CN8078B2 (High Temperature Type) TG-DTA apparatus. DSC measurements were performed without using a reference by a Dupont 1090 DSC instrument.

Results and Discussion

Synthesis of 1. The physical properties of **1** are summarized in Table 1; the results from elemental analyses give the same values as those calculated. Most characteristic absorption in the IR spectra of **1** were identical. Only the absorption of **1** due to ν_{OH} (chelation) at about 3200 cm^{-1} was different among the three substrates. This absorption peak appears in the spectra of **1a**, **1b**, but not in **1c**. This result shows that only **1a** and **1b** have intramolecular hydrogen bonds. Figure 1 shows the possible schema A and B for the hydrogen bonding. From the fact that **1a** and **1b** decompose at lower temperatures than **1c**, it is suggested that *N*-(1-hydroxyalkyl)-2-imidazolidinone was formed by an elimination of aldehyde, provided that **1** has a structure of B. The absorption in the area 1680 cm^{-1} is sharp and shown in a single peak due to $\nu_{C=O}$. The absorption intensity of $\nu_{C=O}$ increases with increasing length of the side chain in **1**. In the mass spectra of **1**, the parent peak is not detected, but the peak of

Table 1. Physical Properties of **1a**, **1b**, and **1c**

		1a	**1b**	**1c**
	C	52.52(53.45)[a]	56.79(57.37)	57.52(57.37)
Elemental analysis/%	H	8.77(8.97)	9.67(9.63)	9.58(9.63)
	N	14.12(13.85)	12.29(12.16)	12.19(12.16)
Melting point/ °C		101.9	96.5	131.8
Yield/%		62.0	94.0	98.0
IR spectra/cm^{-1}	ν_{OH}	3370	3350	3350
	ν_{OH} (chelation)	3200	3200	—
	ν_{CH}	2880, 2970	2870, 2970	2870, 2970
	$\nu_{C=O}$	1680	1685	1665
	ν_{C-O}	1080	1100	1040
^1H NMR position/ppm	In ring			
(Relative intensity: multiplicity)[b]	$-(CH_2)_2-$	3.387(4H : m)	3.339(4H : m)	3.234(4H : m)
	In substituent group			
	$-CH_3$	0.917(6H : t)	0.960(6H : d)	0.769, 0.947(6H : d)
	$-CH_2-$	1.627(4H : m)	1.459(8H : m)	—
	-CH-	5.191(2H : m)	5.388(2H : m)	1.722, 4.676(2H : m)
	-OH	4.557(2H : d)	4.894(2H : d)	5.482(2H : d)
^{13}C NMR	In ring			
	$-(CH_2)_2-$	36.730	36.795	35.958
	C=O	161.277	159.752	159.923
	In substituent group			
	CH_3	9.832	13.773	18.503, 19.234
	$-CH_2-$	26.708	18.491	—
	-CH-	77.632	82.740	80.375, 31.155

a) Calculated values in parentheses. b) d: doublet, t: triplet, m: multiplet.

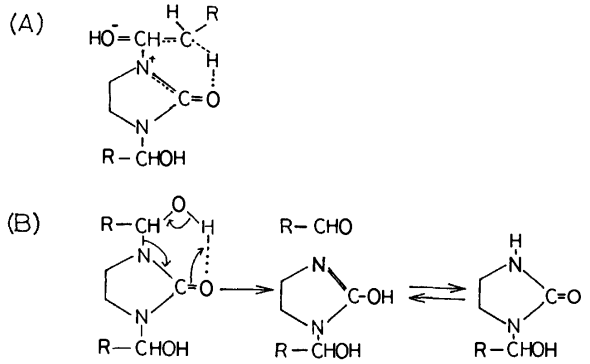

Fig. 1. Structure of A and B for **1**.

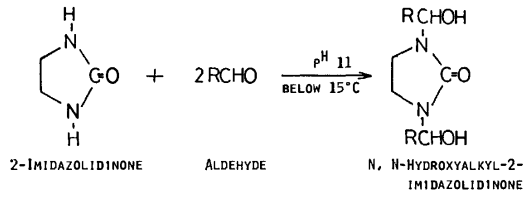

Scheme 1.

$(M-2H_2O)^+$ is detected as a base peak. The analytical and spectroscopic data in Table 1 indicate that the structure of **1** is the same as that proposed in Scheme 1.

The Fragmentation Mechanism for 1. The main cleavage mechanism for **1a** and **1b** is shown in Figs. 2 and 3, respectively. The molecular ion peak for both samples could not be detected. A very characteristic peak in both samples is the $(M-2H_2O)^+$ peak, which is the base peak. The elimination of the methyl group arises from one substituent group which is

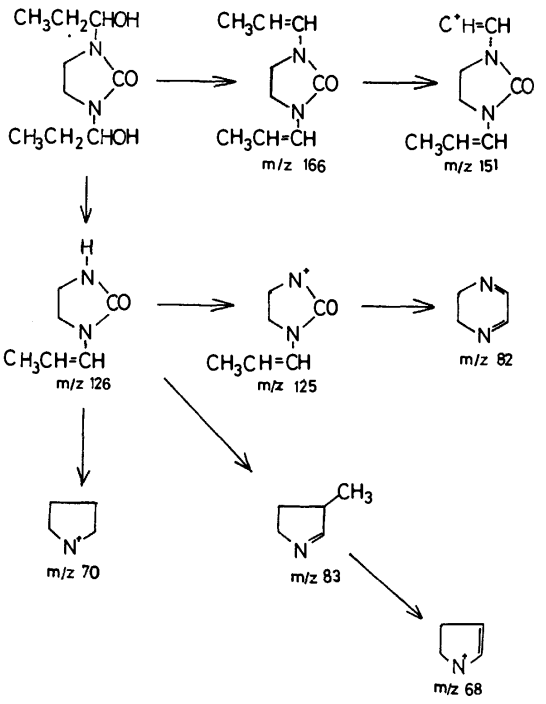

Fig. 2. The main cleavage mechanism for **1a**.

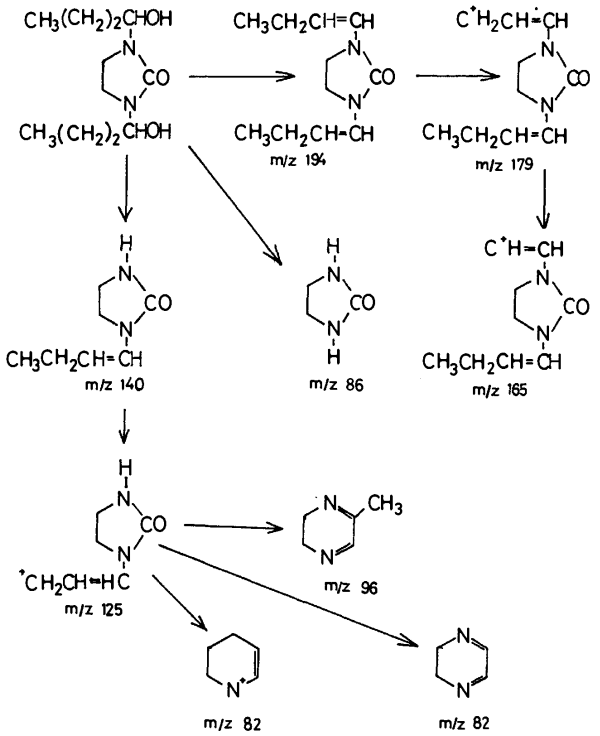

Fig. 3. The main cleavage mechanism for **1b**.

present in the base peak. The peaks at m/z 151 and 179 for **1a** and **1b** are the results of the ions from those base peaks. Although small in size, the peaks at m/z 126 and 140 for **1a** and **1b**, respectively, are due to a fragment ion resulting from the loss of aldehyde and water from the two substituent groups. The peak at m/z 125 appeared in both samples. In **1a**, this peak is due to the fragment ion resulting from the loss of the 1-hydroxypropyl group and water from the two substituent groups. In **1b**, this peak is due to the fragment ion resulting from the loss of propionaldehyde, water, and ethyl group from the two substituent groups. The peak due to the formyl group (m/z 58 or 72) and that due to the hydroxyl group (m/z 59) have been detected. From the fragment ion peaks at m/z 126 and 125, the functional group such as a carbonyl group, cyanic acid, and methyl group seems to be eliminated easily. In addition, the peak due to the elimination of two formyl groups (m/z 86) for both samples is also detected.

Figure 4 shows the detailed cleavage mechanism from the starting fragment ion at m/z 125 of **1b**. There are three cleavage patterns: I, II, and III. Considering the high resolution for the identification of the atomic content of the ions, it was concluded that fragmentation in I and II occurred through the loss of the carbonyl group, while III followed from the loss of HNCO (cyanic acid); the former fragmentation ion is

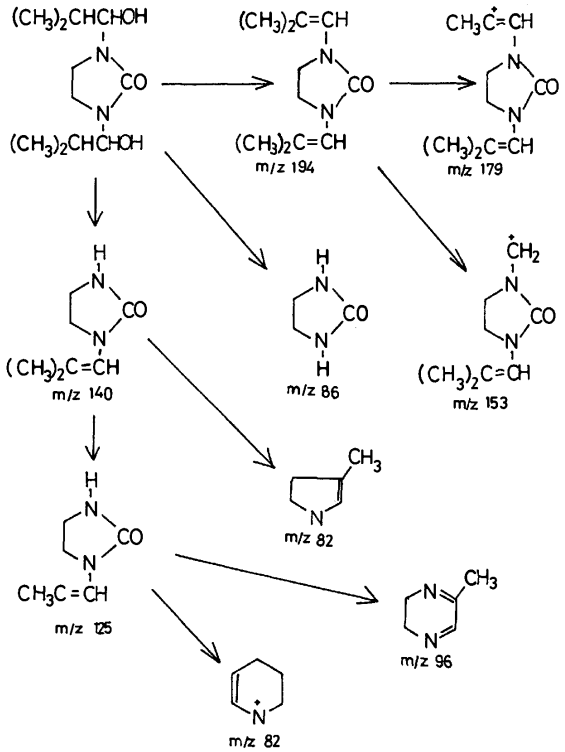

Fig. 5. The main cleavage mechanism for **1c**.

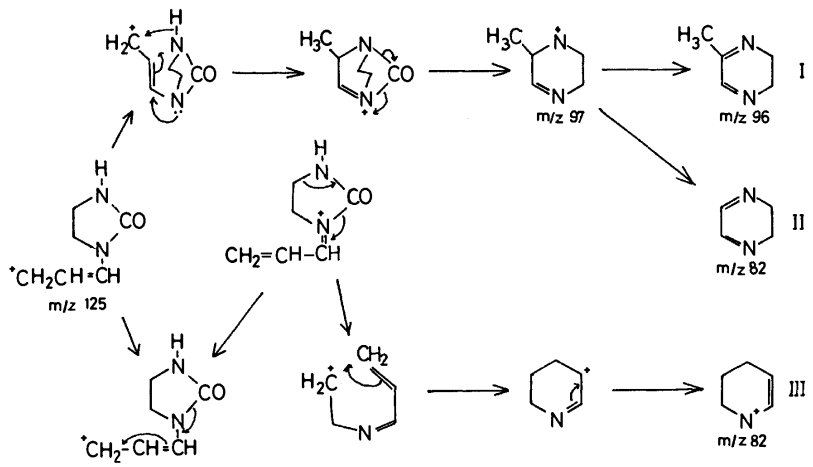

Fig. 4. The detailed cleavage mechanism for **1b**.

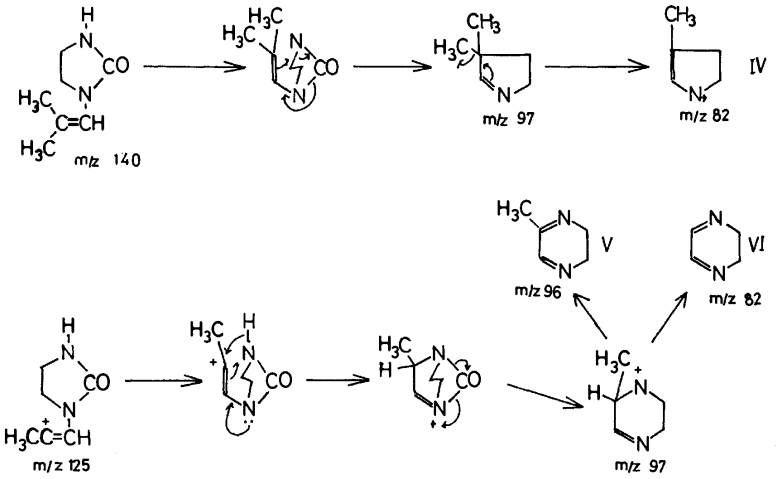

Fig. 6. The detailed cleavage mechanism for **1c**.

due to $C_5H_9N_2$ at m/z 97, the latter is C_5H_8N at m/z 82. The difference of cleavage patterns in I and II was confirmed by evidence from the high-resolution mass spectrum at m/z 96 and 82, which corresponds to fragment ions $C_5H_8N_2$ and $C_4H_6N_2$, respectively. These fragment ions are formed by the loss of proton and methyl groups from the ion at m/z 97.

The main cleavage mechanism for **1c** is shown in Fig. 5. The fragment ion detecting in **1c** is similar to that obtained for **1b**. Figure 6 shows the detailed cleavage mechanism from the starting fragment ions at m/z 140 and 125. Also, there are three cleavage patterns, such as IV, V, and VI. The IV cleavage pattern is confirmed from the fact that the fragment ions, $C_6H_{11}N$ (m/z 97) and HCNO (m/z 43) were detected, and, furthermore, the ion resulting from the loss of methyl group in the former fragment ion at m/z 97 was identified. The V and VI cleavage patterns are similar to I and II in Fig. 4, respectively.

Thermal Analysis. Figure 7 shows TG-DSC curves for **1**. These DSC curves exhibited an endothermic and an exothermic peak. The endothermic peak is attributed to both molten and condensation for **1**. However, the exothermic peaks for **1** are not always clear over a wide temperature range. The TG curve shows that the pyrolysis process for **1** takes place in two stages. In Fig. 7, the first plateau of the TG curve is probably due to a condensation of **1** to a dimer compound. The other plateau corresponds to a thermal degradation and a decomposition reaction. The TG-DSC measurement for **1c** was carried out at five heating rates from 0.625 to 20 °C min^{-1}. Figure 8 shows the DSC curves of **1c**. As shown in Fig. 8, both, the primary and secondary peak of the DSC curves shifted to higher temperature as the heating rate increased. At a heating rate of less than 10 °C min^{-1}, a new sharp peak appears in the area of 130 °C between the primary and secondary peak. **1c** melts rapidly at 132 °C. According to this fact, this sharp peak may be due to a molten stage. However, the

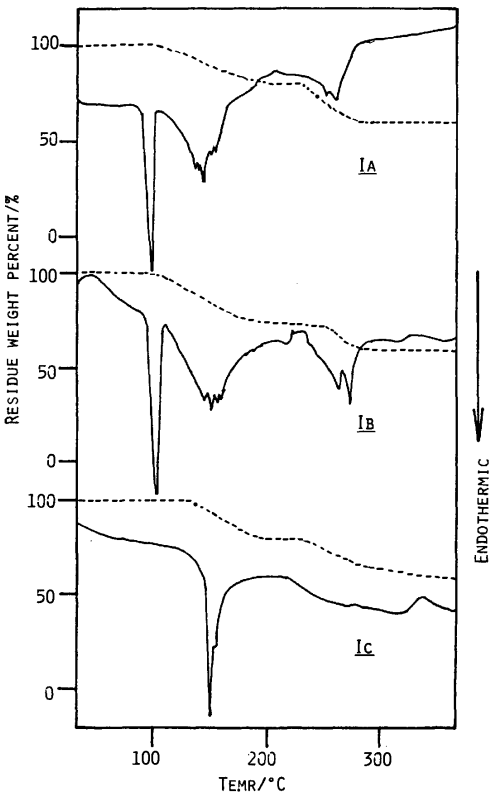

Fig. 7. TG-DSC curves for **1**.

fraction of the residual weight around 130 °C has a value approximated to that of the (molecular weight of **2**)/(molecular weight of **1c**) ratios. Since the melting point of **2** is 131 °C, this molten stage may not be due to the melting point for the eutectic mixture, but for **2**. Furthermore, TG-DTA measurement for **1c** was carried out at the heating rate from 2 to 10 °C min^{-1}. Both the primary and secondary peaks of the DTA curves shifted to higher temperatures with an increase in the heating rate, similarly to the DSC curves.

Kinetic Discussion for 1c. The kinetic discussion

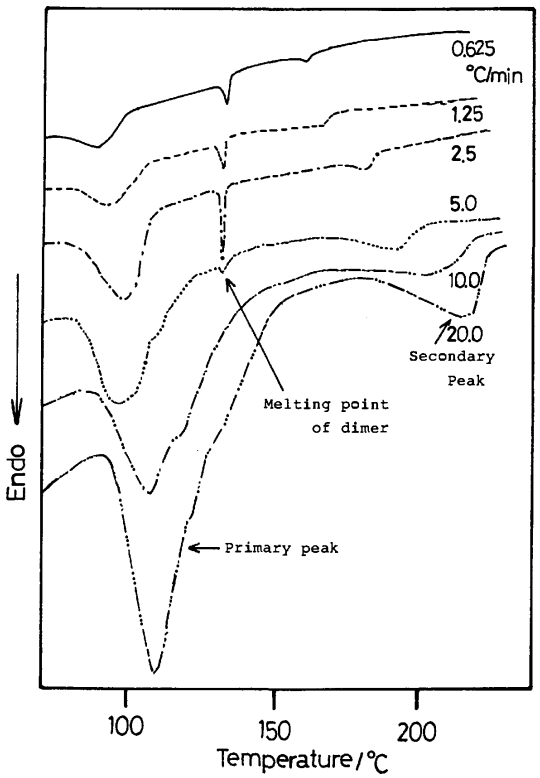

Fig. 8. DSC curves for **1c** at various heating rates.

is carried out in terms of the thermal analysis. Two methods for obtaining kinetic parameters from TG-DTA curves were applied. These methods are based on the general form of kinetic formulae and are applicable to general types of relation governed by a single activation energy. One method by Ozawa[3] utilizes the linear relation between the reciprocal of the absolute temperature and a definite fraction of the weight loss and the heating rate in TG curves in order to estimate the activation energy. The other method by Kissinger[4] requires information concerning both the temperature of the maximum peak and the heating rate in DTA curves; the Kissinger's plot is made for an apparent activation energy. According to Ozawa's method in thermal analysis, we carried out observations of the change in TG curves by different heating rates (ϕ). In each definite fraction of weight loss (θ), this method utilizes a linear relation between the reciprocal of the absolute temperature and the ordinal logarithm of the heating rate. The structural quantity is assumed to change the following ordinary reaction kinetics:

$$\theta = \Delta E/\phi R \cdot \rho(\Delta E/RT), \tag{1}$$

where ΔE and R are the activation energy and the gas constant, respectively. Also,

$$\log \rho(y) \simeq -2.315 - 0.4567y \quad (20<y<60). \tag{2}$$

Thus,

$$\log\phi_1 + 0.4567\Delta E/RT_1 = \log\phi_2 + 0.4567\Delta E/RT_2 = \cdots\cdots . \tag{3}$$

When an ordinary logarithm for a heating rate in Eq. 1 as the abscissa and the reciprocal of the absolute temperature as the ordinate is plotted, we obtained a straight line. From the gradient of this straight line, corresponding to $-0.4567\Delta E/R$, the activation energy was obtained.

It is evident, therefore, that the variation of the peak maximum for DTA curve can be expressed by means of an equation of the form

$$-\Delta E/R = \Delta \log(\phi/T_m^2)/\Delta(1/T_m), \tag{4}$$

where ϕ stands for the heating rate; ΔE, for the activation energy; T_m, for the temperature of the DTA-maximum; and R, for the gas constant. This method utilizes the linear relation between the $\Delta(1/T_m)$ and

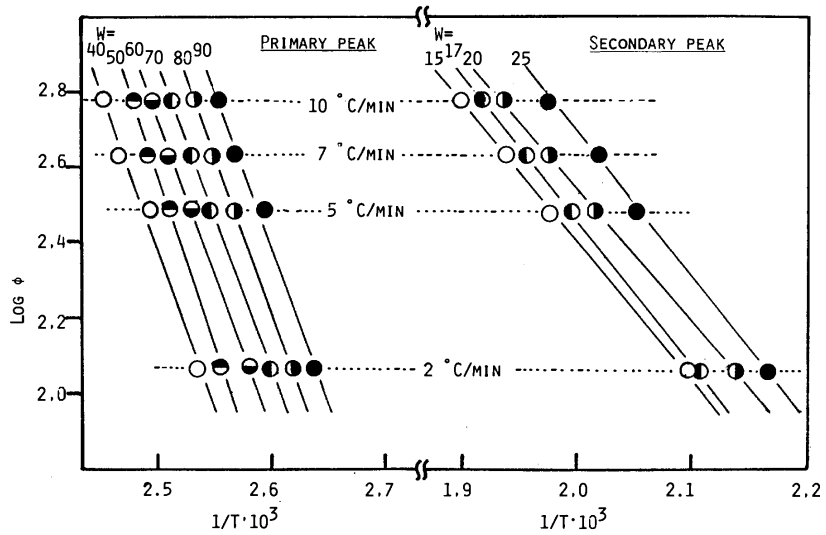

Fig. 9. Plots of logarithms of heating rate versus the reciprocal of absolute temperature for given conversation of pyrolysis of **1c**.

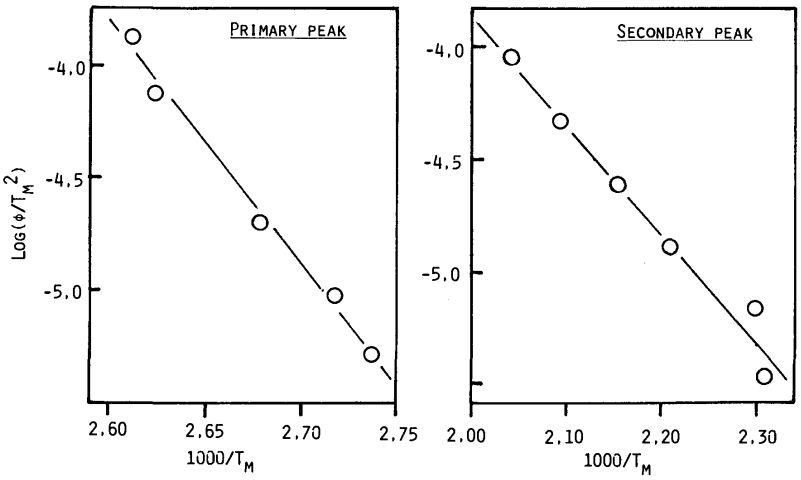

Fig. 10. Kissinger's plots for **1c**.

Table 2. The Apparent Activation Energy by TG and DTA Method of **1c**

Reaction process	Activation energy/kJ mol^{-1}	
	TG method	DTA method
Polycondensation	67	73
Pyrolysis	150	145

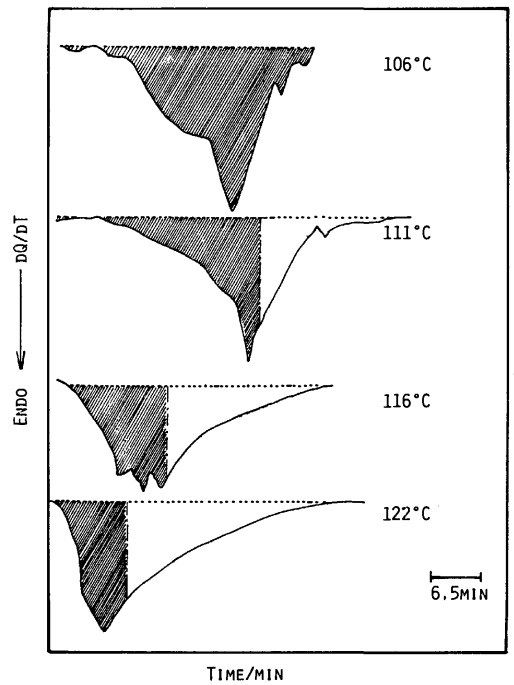

Fig. 11. Isothermal pyrolysis curves of **1c** at various temperatures.

$\Delta\log(\phi/T_m^2)$. For these TG and DTA curves, Ozawa's or Kissinger's plots of **1c** were linear. Figures 9 and 10 show the results of these plots. Table 2 shows the values of the activation energy which was calculated from these plots.

Next, a kinetic study was carried out in terms of McGhie method.[5] DSC measurements were carried out over the temperature range 105—120 °C by a method in which the sample was hermetically sealed in an aluminum pan and in a DSC cell using an isothermal mode. Figure 11 shows typical isothermal condensation curves for **1c**. This kinetic study of the pyrolysis process of **1c** was carried out for the shaded parts with the same heat quantity. The 1/2-order kinetics plot of $2\times[a^{1/2}-(a-x)^{1/2}]$ vs. $t-t_0$ for each curve is linear, where a is the area under a given isothermal curve, and x is the fractional area up to time t. Figure 12 shows these plots for isothermal reactions of four samples at 106, 111, 116, 122 °C. The data have been normalized with respect to time by plotting the time after an induction period of t_0. Thus, each isothermal curve yielded two important quantities, t_0 and k. The kinetic data for the condensation of **1c** are summarized in Table 3.

Table 3. Rate Constants and Kinetic Data for the Polycondensation Process of **1c**

a) Rate constants

T/K	Rate constant, k/mol$^{1/2}\cdot$l$^{-1/2}\cdot$s^{-1}
379	0.978×10^{-2}
384	1.372×10^{-2}
389	1.661×10^{-2}
395	2.367×10^{-2}

b) Kinetic data

A/mol$^{1/2}\cdot$l$^{-1/2}\cdot$s^{-1}	E_a/kJ$\cdot$mol^{-1}	ΔH/kJ$\cdot$mol^{-1}	ΔS/e. u.
1.62×10^{7}	68	64	28

Thermal Condensation of 1c. The thermal condensation of **1c** was considered from the results of IR spectra, ^{1}H and ^{13}C NMR spectra, mass spectra, and elemental analysis. **1c** was heated for various times under isothermal, or at various temperatures, under a nitrogen atmosphere in a thermostat. The IR spectra of the condensation product for **1c** show that the absorption due to ν_{C-O} at about 1100 cm^{-1} decreases in intensity. When the heating time was changed, the

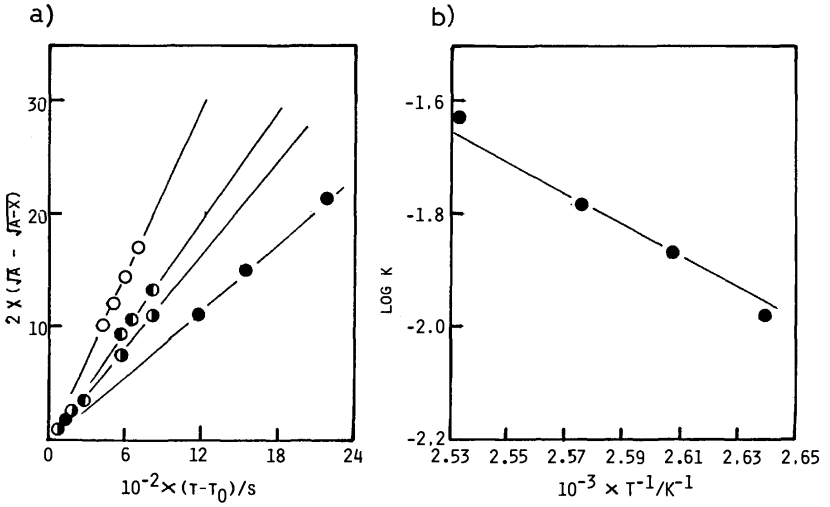

Fig. 12. a) 1/2 order kinetic plots of $2\times[a^{1/2}-(a-x)^{1/2}]$ vs. $t-t_0$ for the isothermal polycondensation of **1c**. b) Arrehenius plots of the 1/2 order kinetic constant for the polycondensation of **1c**.

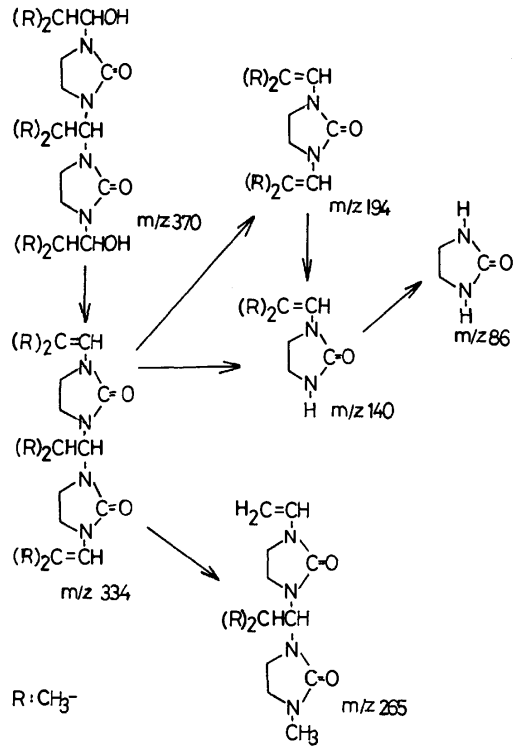

Fig. 13. Main fragmentation for dimer of **1c**.

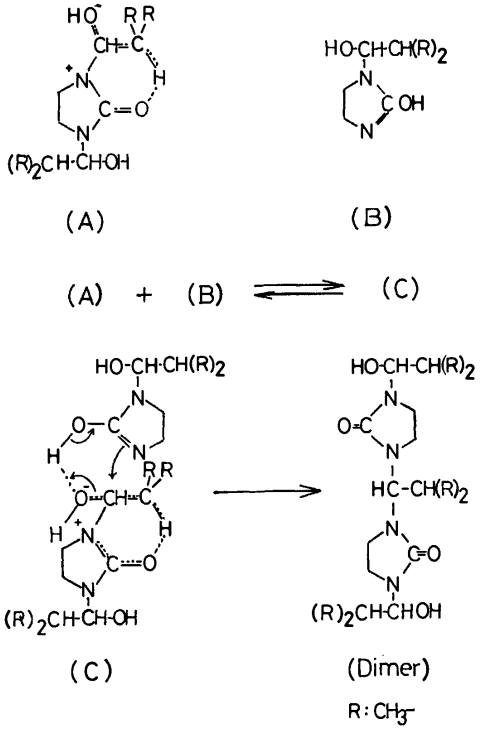

Fig. 14. The dimerization process for **1c**.

absorption peak due to $\nu_{C=O}$ at about 1680 cm^{-1} shifted to larger wavenumber with increasing time. The peak due to $\nu_{C=O}$ shifted at 1700 cm^{-1} after heating it for 5 h. The absorption peak due to ν_{OH} decreased in intensity with increasing heating time. On the other hand, when the temperature was changed, the heating product at 110 °C showed similar changes after 5 h. Also, the absorption peak due to ν_{NH} in the neighborhood of 3400 cm^{-1} appears at 145 °C. From these results it seems that both dehydration and condensation occur simultaneously for the thermal reaction of **1c**. The ^{13}C NMR spectra of **1c** shows that the signal at δ 159.923, due to the carbonyl group, separates into two signals, and that the signal due to the α-carbon atom attached to the hydroxyl group splits into three parts after condensation. These results show that the formation process of the dimer seemed to be dehydration after intermolecular hydrogen bonding. In the ^1H NMR spectra of **1c** and its condensation product, it was observed that the signal due to the hydroxyl group disappeared after condensation. The mass spectra of the condensation products also support this dimer

formation. There are no peaks due to trimer or oligomer in these mass spectra. The observed fragment ions in the mass spectra of the condensation products support the main fragmentation mechanism of the dimer in the case of **1c**. In the mass spectra after heating for 5 h, a peak at m/z 334 was detected. This peak is due to the fragmentation ion peak which is formed by the loss of two moles of water from molecular ion (M^+). The peak due to a molecular ion which is a dimer of **1c** was not detected. The maximum mass number ion peak obtained for these mass spectra, was the peak at m/z 265. The obtained fragment ion peak was cleared by considering the high-resolution mass spectra for an identification of the atomic content of the ions. Figure 13 shows the main cleavage mechanism of the dimer in the case of **1c**.

Reaction Mechanism for Thermal Condensation of 1c in Solid State. The possible structure of intermediates formed during the activated state in the course of the dimerization process for **1c** is the activated complex (A) and the enol type (B), like lactim in Fig. 14. The presence of (A) was confirmed by ESR measurements[1] in the case of 1-mono(1-hydroxyalkyl)-2-imidazolidinone; (B) gave no direct evidence concerning its existence in the solid state. In the molten state, however, the (B) had likewise been formed in the case of cyanuric acid. By a comparison of structures (A) and (B), the hydroxyl group of (A) was easier to eliminate than that of (B). In the next step, the activated complex (C) (Fig. 14) was formed from (A) and (B). It is expected for **1c** that the DSC measurement was taken in order to obtain information regarding the formation of (C) to the dimer. From these results, it is clear that (A), (B), and (C) are formed during the induction period.

We wish to thank Miss Misao Shinoda for the Mass spectra and Mr. Yoshiharu Yoneyama for NMR measurements. We thank Prof. Shigeya Takeuchi for good advice regarding DSC measurements.

References

1) C. Shimasaki, R. Kanayama, H. Yoshida, and M. Yugamidani, *Bull. Chem. Soc. Jpn.*, **60**, 193 (1987).
2) S. Takeuchi, "Yukikagobutsugoseiho," ed by Yukigosei Kagakukyokai, Gihodo (1969), pp. 27, 61.
3) T. Ozawa, *Bull. Chem. Soc. Jpn.*, **38**, 1881 (1965).
4) H. E. Kissinger, *Anal. Chem.*, **29**, 1702 (1957).
5) A. R. McGhie, P. S. Kalyanaraman, and A. F. Garito, *J. Polym. Sci., Polym. Lett. Ed.*, **16**, 335 (1978).

Copper(I) Salt Catalyzed Reaction of 1,1,1-Trichloro-2,2,2-trifluoroethane with Trimethylsilyl Enol Ethers. A Convenient Synthesis of β-Chloro-β-(trifluoromethyl) α,β-Unsaturated Carbonyl Compounds

Takashi Okano, Toru Uekawa, and Shoji Eguchi*
Institute of Applied Organic Chemistry, Faculty of Engineering,
Nagoya University, Chikusa-ku, Nagoya 464-01
(Received January 23, 1989)

β-Chloro-β-(trifluoromethyl) α,β-unsaturated carbonyl compounds were obtained by the reaction of trimethylsilyl enol ethers with CF_3CCl_3 and CuCl, followed by dehydrochlorination with triethylamine or DBN. Aromatic enol ethers gave moderate to good yields of the chloro(trifluoromethyl)methylene ketone derivatives but aliphatic enol ethers and silyl ketene acetal gave only lower yields.

Synthetic methods for the preparation of trifluoromethyl-substituted organic compounds have drawn considerable interest recently because of their remarkable biological activity.[1] As one of versatile and economical reagents, 1,1,1-trichloro-2,2,2-trifluoroethane (**1**) has been utilized extensively to effect polyhaloalkylmetal addition to carbonyl compounds.[2,3] On the other hand, the addition of polyhalocarbons to carbon-carbon double bonds is known to be catalyzed effectively by copper chloride-2-aminoethanol redox system.[4] The successful addition of polyhalocarbons to trimethylsilyl enol ethers catalyzed by copper(I) chloride to afford β-halo α,β-unsaturated ketones has been reported also by Murai et al.[5] In spite of these pioneering works, the scope and limit of the Cu(I) catalyzed addition reaction of polyfluorinated **1** with silyl enol ethers seem to be yet unclarified. We report here the Cu(I) catalyzed addition reaction of **1** with various types of trimethylsilyl enol ethers, that provides a convenient regiospecific route to β-chloro-β-(trifluoromethyl) α,β-unsaturated ketones.[6] These compounds seem to be difficult to prepare regiospecifically by enol chlorination route of 1-trifluoromethyl-1,3-diketones. The reaction of 1-trifluoromethyl-3-aryl- or -3-alkyl-1,3-diketones with thionyl chloride has been reported to afford a regioisomeric mixture of the corresponding enol chlorides or only undesired α-chloromethylene ketone derivatives.[7]

Results and Discussion

Since dichloromethylenation of acetophenone trimethylsilyl enol ether (**2a**) with CCl_4 in the presence of CuCl was reported by Murai et al.,[5] we examined first the reaction of **2a** with two equivalent of CF_3CCl_3 (**1**). In the presence of a catalytic amount of CuCl (0.1 equivalent), the reaction in DMF (*N*,*N*-dimethylformamide) at 80 °C afforded a mixture of saturated ketone **3** and dehydrochlorinated ketone **4a** (*E* : *Z* ratio was 10 : 90). Since **3** and **4a** were not readily separable, the mixture was treated with triethylamine at room temperature to complete the dehydrochlorination, affording **4a** in 23% yield. The *E* : *Z* ratio of **4a** was 10 : 90 as determined ^{19}F NMR data. A strong anisotropic effect for the carbonyl bond to CF_3 group was observed for *E*-isomer **4a**-*E* (δ 13.56 for **4a**-*E* and 8.65 for **4a**-*Z*, CF_3COOH as an external standard).[8,9]

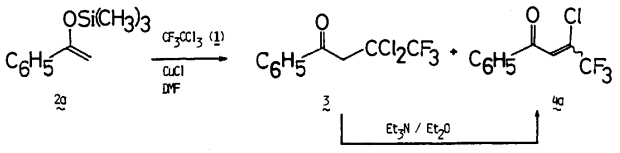

Scheme 1.

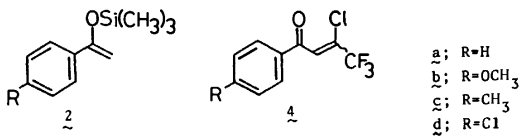

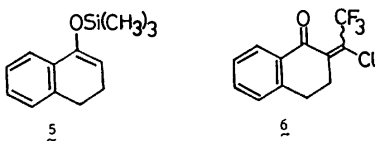

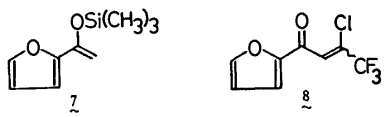

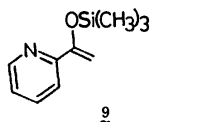

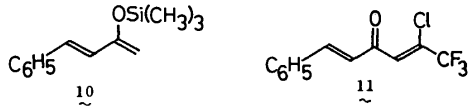

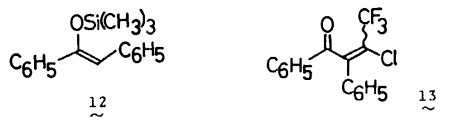

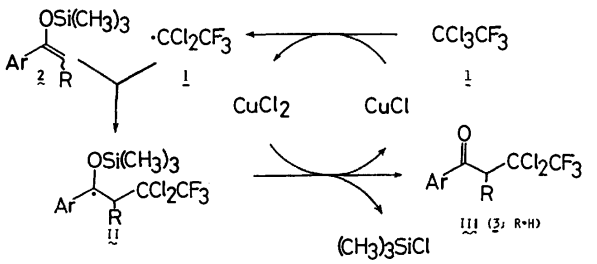

Scheme 2.

As outlined in Scheme 2, the reaction mechanism may involve one-electron transfer from CuCl to CF_3CCl_3 to afford a radical intermediate, $CF_3CCl_2\cdot$ (**I**). Following the addition of the β-position of the electron-rich silyl enol ether **2** to form benzyl radical **II**, oxidative desilylation with Cu(II) cation yields saturated ketone **3**. A partial dehydrochlorination of the primary product **3** under the reaction conditions gives unsaturated ketone **4**.

The use of large excess of **1** (20-fold equivalent) as well as equimolar CuCl along with addition of 4A Molecular Sieves to trap liberated HCl[10] raised the yield upon dehydrochlorination with triethylamine to 52%. DMF has been predicted as the most favorable solvent for electron transfer reactions,[11] in fact, no other solvent such as acetonitrile, dioxane, ethanol, nor pyridine gave better results.

Under the reaction conditions mentioned above, various silyl enol ethers were converted into unsaturated ketones with a β-trifluoromethyl group (Table 1).[12]

Table 1. β-Chloro-β-(trifluoromethyl) α,β-Unsaturated Carbonyl Compounds from Trimethylsilyl Enol Ethers and CF_3CCl_3

Entry	Silyl enol ether	Product	Reaction time/h	Yield (%)[a]	*Z*:*E*
1	**2a** R=H	**4a**	3	52	90:10
2	**2b** R=OCH_3	**4b**	2	44	92: 8
3	**2c** R=CH_3	**4c**	2	49	93: 7
4	**2d** R=Cl	**4d**	1	55	93: 7
5	**5**	**6**	12	49	30:70
6	**7**	**8**	1	70	97: 3
7	**9**	—	2	0[b]	—
8	**10**	**11**	3	59	>99: 1
9	**12**	**13**	15	14[c]	12:88
10	**14**	**15**	5	12(15)[d]	88:12
11	**16**	**17**	5	21(39)[d]	88:12
12	**18**	—	36	0[e]	—
13	**19**	**20**	7.5	32[c]	58:42
14	**21**	**22**	3	15	79:21

a) Isolated yield. b) A complex mixture was obtained. c) 1,5-Diazabicyclo[4. 3. 0]non-5-ene was used in dehydrochlorination. d) GLC yield determined by addition of adamantane as an internal standard; see Experimental. e) Cyclohexanone was a major product.

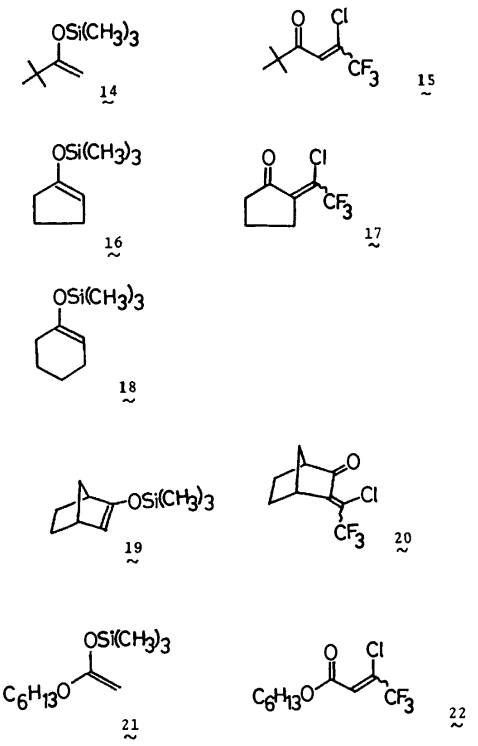

Aromatic ketone derivatives **4b—d** and **6** were obtained in moderate yields from the corresponding silyl enol ethers **2b—d** and **5**. Among heterocyclic enol ethers **7** and **9**, **7** gave furyl ketone **8** in 70 % yield, but pyridyl enol ether **9** afforded only a complex mixture due to the side reactions between CuCl and the pyridine moiety. Even in the case of conjugated silyl enol ether **10** which can generate a stable allyl radical intermediate, dienone **11** was obtained in 59% yield. Since $CF_3CCl_2\cdot$ radical is a bulky intermediate, sterically hindered substrates such as the diphenyl derivative **12** are unfortunately less reactive, affording the corresponding enones only in lower yields.

In contrast to aromatic enol ethers, alkyl or alicyclic enol ethers **18** and **21**, except sterically favorable methylene derivative **14** or strained cyclic enol ethers **16** and **19**, were not suitable substrates for this reaction because of the relative instability of the radical intermediates involved. Pinacolone silyl enol ether (**14**) gave *t*-butyl ketone **15** in 15% yield based on GLC. Silyloxycyclopentene (**16**) and silyloxynorbornene (**19**) gave α-[chloro(trifluoromethyl)methylene] ketones **17**

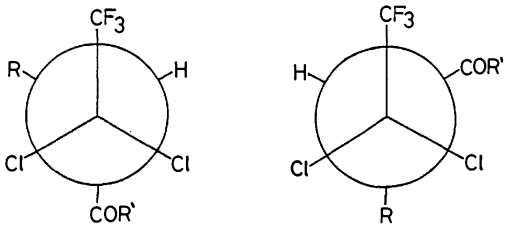

IV V

and **20** in lower yields. However, less strained silyloxycyclohexene (**18**) was unreactive under the reaction conditions except by slow hydrolysis to form cyclohexanone.[13] It is notable that benzo-fused derivative **5** is a suitable substrate in which a cyclohexadiene subunit is involved. Ketene silyl acetal **21** also gave unsaturated ester **22** in a low yield.

In the elimination step, triethylamine was effective in the most cases, but the more basic 1,5-diazabicyclo-[4.3.0]non-5-ene (DBN) was needed to obtain sterically hindered ketones **13** and **20**. The stereoselectivity of the elimination depends on the structure of the saturated intermediate **III** (Scheme 2). The *E*:*Z* isomer ratio was not changed before and after the triethylacetyl compounds, **2a—d**, **7**, **10**, **14**, and **21**, and cyclopentene **16** and **19** gave *Z*-isomers as major products via anti-elimination of HCl from the more stable via anti-elimination of HCl from the more stable conformers **IV** (R=H- or $-CH_2-$) where R'CO- group and CF_3- group are antiperiplanar. However, **5** and **12** gave *E*-isomers as major products. The increased repulsion between α-R group (R=$-CH_2-$ or Ph-) and CF_3 group destabilizes **IV** relative to conformer **V** affording *E*-isomers via anti-dehydrochlorination.[14]

In conclusion, CF_3CCl_3 (**1**) was found to be a convenient trifluoromethyl-containing synthon for methylenation of various silyl enol ethers, with some limitations in the applicable substrates. The resulting chlorinated unsaturated carbonyl compounds have synthetic potential for other transformations to trifluoromethyl-containing organic compounds.[15]

Experimental

All the melting points were taken on a Yanagimoto micromelting point hot stage apparatus and are uncorrected. ^1H NMR spectra were recorded on a JEOL JNM-FX-60 FT NMR spectrometer at 60 MHz and on A JEOL JNM-GX-500 FT NMR spectrometer at 500 MHz in $CDCl_3$. ^{19}F NMR spectra were recorded on a Hitachi R-20 instrument at 56.45 MHz in $CDCl_3$. Chemical shifts were reported in parts per million (δ) relative to Me_4Si as an internal standard for ^1H and to CF_3COOH as an external standard for ^{19}F. IR spectra were obtained on a JASCO IRA-1 spectrometer. Mass spectra (MS) were obtained on a ESCO EMD-05B mass spectrometer at 70 eV. Microanalyses were performed with a Perkin-Elmer 240B elemental analyzer. GLC analyses were carried out by using a Shimadzu GC-14A gas chromatograph on a 2 m packed column with OV-17 as stationary phase. Silyl enol ethers were prepared by ordinary methods; trimethylsilylation of lithium enolate prepared from a ketone or an ester with LDA, or by the reactions of ketones with chlorotrimethylsilane and triethylamine in DMF.

Preparation of β-Chloro-β-(trifluoromethyl) α,β-Unsaturated Ketones. A Typical Method: 3-Chloro-4,4,4-trifluoro-1-phenyl-2-buten-1-one (4a): A mixture of **2a** (192 mg, 1.00 mmol), **1** (3.82 g, 20.0 mmol), CuCl (49 mg, 1.0 mmol), and 4A Molecular Sieves (1.00 g) in anhydrous DMF (2 ml) was refluxed under nitrogen atmosphere for 3 h, and then Molecular Sieves were removed by filtration. To the filtrate was added Et_2O (50 ml) and saturated aqueous NaCl (50 ml). After separation of organic layer, the aqueous layer was extracted with Et_2O. The extracts were combined and dried (Na_2SO_4). After removal of the solvent by distillation, the residue was purified on a short silica gel (Fuji-Davison BW-300) column (1:1 hexane-CH_2Cl_2). The resultant mixture of **3** and **4a** (153 mg) was dissolved in Et_2O (2 ml) and triethylamine (110 mg, 1.00 mmol) was added. The mixture was stirred at room temperature overnight. The solvent was evaporated and the residue was chromatographed on a silica gel column (1:1 hexane-CH_2Cl_2) to give **4a** as pale yellow oil; 120 mg (52%); ^1H NMR ($CDCl_3$) δ=8.0—7.3 (m, 5H) and 7.44 (m, 1H); ^{19}F NMR ($CDCl_3$) δ=13.56 (s, 0.10F) and 8.65 (s, 0.90F); IR(neat) 3060, 1680, 1624, 1602, 1580, 1450, 1276, 1224, 1190, and 1150 cm^{-1}; MS *m/z* (rel intensity) 236(M^++2, 5), 234(M^+, 16), 206(8), 105(100), 77(94), 51(68), and 50(20). Found: C, 51.30; H, 2.48%. Calcd for $C_{10}H_6ClF_3O$: C, 51.20; H, 2.58%.

3-Chloro-4,4,4-trifluoro-1-(4-methoxyphenyl)-2-buten-1-one (4b). As described above, a mixture of **2b** (455 mg, 2.05 mmol), **1** (7.67 g, 40.9 mmol), CuCl (203 mg, 2.05 mmol), 4A Molecular Sieves (2.0 g) in DMF (3 ml) was treated and workup gave **4b** as pale yellow oil; 232 mg (44%); ^1H NMR($CDCl_3$) δ=7.91 (d, 2H, *J*=9.0 Hz), 7.39 (m, 1H), 6.98 (d, 2H, *J*=9.0 Hz), and 3.90 (s,3H); ^{19}F NMR($CDCl_3$) δ=13.70 (s, 0.08F) and 8.88 (s, 0.92F); IR(neat) 3045, 3020, 2970, 2945, 2840, 1678, 1600, 1576, 1514, 1460, 1444, 1422, 1260, 1236, 1184, 1168, and 1150 cm^{-1}; MS *m/z* 266(M^++2, 9), 264(M^+, 27), 236(19), 135(100), 107(19), 92(31), 77(40), 64(25), 63(31), 51(11), and 50(20). Found: C, 50.01; H, 2.96%. Calcd for $C_{11}H_8ClF_3O_2$: C, 49.92; H, 3.05%.

3-Chloro-4,4,4-trifluoro-1-(4-methylphenyl)-2-buten-1-one (4c). As described above, a mixture of **2c** (491 mg, 2.38 mmol), **1** (8.92 g, 47.6 mmol), CuCl (236 mg, 2.38 mmol), and 4A Molecular Sieves (2.38 g) in DMF (2 ml) was treated and workup gave **4c** as pale yellow oil; 237 mg (49%); ^1H NMR($CDCl_3$) δ=7.83 (d, 2H, *J*=8.2 Hz), 7.41 (m, 1H), 7.31 (d, 2H, *J*=8.2 Hz), and 2.44 (s, 3H); ^{19}F NMR($CDCl_3$) δ=14.30 (s, 0.07F) and 8.94 (s, 0.93F); IR(neat) 3050, 1678, 1602, 1576, 1408, 1280, 1270, 1230, 1180, and 1150 cm^{-1}; MS *m/z* 250(M^++2, 7), 248(M^+, 21), 220(10), 119(100), 91(64), 89 (12), 65(39), 63(21), 51(17), and 50(12). Found: C, 53.07; H, 3.26%. Calcd for $C_{11}H_8ClF_3O$: C, 53.14; H, 3.24%.

3-Chloro-4,4,4-trifluoro-1-(4-chlorophenyl)-2-buten-1-one (4d). As described above, a mixture of **2d** (548 mg, 2.41 mmol), **1** (9.02 g, 48.1 mmol), CuCl (238 mg, 2.40 mmol), and 4A Molecular Sieves (2.40 g) in DMF (3 ml) was treated and workup gave **4d** as pale yellow oil; 353 mg (55%); ^1H NMR($CDCl_3$) δ=7.88 (d, 2H, *J*=9.0 Hz), 7.53 (d, 2H, *J*=9.0 Hz), and 7.41 (m, 1H); ^{19}F NMR($CDCl_3$) δ=13.78 (s, 0.07F) and 8.94 (s, 0.93F); IR(neat) 3110, 3080, 1682, 1624, 1596, 1576, 1494, 1402, 1280, 1224, 1190, and 1156 cm^{-1}; MS *m/z* 272(M^++4, 3), 270(M^++2, 20), 268(M^+, 27), 242(12), 240 (19), 157(14), 141(30), 139(100), 113(13), 111(54), 86(35), 84(52), 76(17), 75(70), 74(17), 51(26), and 50(52). Found: C, 44.75; H, 1.76%. Calcd for $C_{10}H_5ClF_3O$: C, 44.64; H, 1.87%.

3,4-Dihydro-2-(1-chloro-2,2,2-trifluoroethylidene)-1(2*H*)-naphthalenone (6). As described above, a mixture of **5** (531 mg, 2.43 mmol), **1** (9.11 g, 48.6 mmol), CuCl (241 mg, 2.43 mmol), and 4A Molecular Sieves (2.40 g) in DMF (3 ml) was treated and workup gave **6** as pale yellow oil; 309 mg (49 %); ^1H NMR (500 MHz)($CDCl_3$) δ=8.096 (dd, 0.70H, *J*=7.9 and

1.2 Hz), 8.036 (dd, 0.30H, J=7.5 and 1.2 Hz), 7.533 (td, 1H, J=7.5 and 1.2 Hz), 7.377 (t, 1H, J=7.5 Hz), and 7.269 (d, J=7.5 Hz); ^{19}F NMR($CDCl_3$) δ=19.09 (s, 0.30F) and 17.83 (s, 0.70F); IR(neat) 3070, 3030, 2980, 2910, 1684, 1600, 1480, 1454, 1432, 1370, 1300, 1268, 1240, 1222, 1206, 1180, 1162, and 1132 cm^{-1}; MS m/z 262(M^++2, 17), 260(M^+, 53), 234(21), 232 (60), 225(20), 197(42), 187(54), 146(16), 128(52), 127(17), 118(37), 91(19), 90(100), 99(78), 88(12), 78(12), 77(32), 76(20), 75(28), 74(15), 73(25), 65(12), 64(37), 63(81), 62(28), 57(12), 51(89), and 50(58). Found: C, 55.24; H, 3.13%. Calcd for $C_{12}H_8ClF_3O$: C, 55.30; H, 3.09%.

3-Chloro-4,4,4-trifluoro-1-(2-furyl)-2-buten-1-one (8). As described above, a mixture of **7** (557 mg, 3.06 mmol), **1** (11.45 g, 61.1 mmol), CuCl (303 mg, 3.06 mmol), and 4A Molecular Sieves (3.01 g) in DMF (2 ml) was treated and workup gave **8** as a pale yellow solid; 447 mg (70%); mp 54—56 °C; ^{1}H NMR($CDCl_3$) δ=7.66 (m, 1H), 7.51 (s, 1H), 7.32 (d, 1H, J=3.7Hz), and 6.61 (dd, 1H, J=3.7 and 1.5 Hz); ^{19}F NMR($CDCl_3$) δ=12.58 (s, 0.03F) and 7.25 (s, 0.97F); IR(KBr) 3280, 3140, 3070, 1672, 1626, 1562, 1466, 1395, 1342, 1290, 1275, 1244, 1206, 1164, and 1150 cm^{-1}; MS m/z 226(M^++2, 10), 224(M^+, 27), 198(10), 196(30), 157(11), 95(100), and 69(25). Found: C, 42.76; H, 1.83%. Calcd for $C_8H_4ClF_3O_2$: C, 42.79; H, 1.80%.

(1*E*,4*Z*)-5-Chloro-6,6,6-trifluoro-1-phenyl-1,4-hexadien-3-one (11). As described above, a mixture of **10** (446 mg, 2.04 mmol), **1** (3.75 g, 20.0 mmol), CuCl (198 mg, 2.00 mmol), and 4A Molecular Sieves (2.00 g) in DMF (3 ml) was treated and workup gave **11** as a pale yellow solid; 314 mg (59%); Mp<30 °C; ^{1}H NMR($CDCl_3$) δ=7.65 (d, 1H, J=16.4 Hz), 7.3—7.9 (m, 5H), 7.17 (m, 1H), and 6.88 (d, 1H, J=16.4Hz); ^{19}F NMR($CDCl_3$) δ=8.79(s); IR(KBr) 3070, 3060, 1660, 1640, 1630, 1600, 1580, 1500, 1456, 1336, 1300, 1274, 1200, 1174, and 1140 cm^{-1}; MS m/z 262(M^++2, 18), 260(M^+, 49), 259(76), 197 (14), 157(10), 131(35), 128(15), 103(74), 102(22), 78(13), 77(100), 76(13), 75(18), 63(32), 51(38), and 50(38). Found: C, 55.20; H, 3.09%. Calcd for $C_{12}H_8ClF_3O$: C, 55.30; H, 3.09%.

3-Chloro-4,4,4-trifluoro-1,2-diphenyl-2-buten-1-one (13). As described above, a mixture of **12** (329 mg, 1.23 mmol), **1** (4.61 g, 24.6 mmol), CuCl (122 mg, 1.23 mmol), and 4A Molecular Sieves (1.23 g) in DMF (2 ml) was treated and after treatment with DBN (153 mg, 1.23 mmol) in Et_2O (3 ml), workup gave **13** as a colorless solid; 55 mg (14%); Mp 43—45 °C; ^{1}H NMR (500 MHz) ($CDCl_3$) δ=8.008 (d, 0.88H, J=7.9 Hz), 7.944 (d, 0.12H, J=7.3 Hz), 7.624 (t, 0.88H, J=7.3 Hz), 7.577 (t, 0.12H, J=7.3 Hz), and 7.45—7.33(m, 5H); ^{19}F NMR($CDCl_3$) δ=16.83 (s, 0.88F) and 14.05 (s, 0.12F); IR(KBr) 3060, 1678, 1598, 1580, 1492, 1450, 1300, 1250, 1184, and 1140 cm^{-1}; MS m/z 312(M^++2, 2), 310(M^+, 5), 106(14), 105(100), 77(50), 51(33), and 50(20). Found: C, 62.10; H, 3.52%. Calcd for $C_{16}H_{10}ClF_3O$: C, 61.85; H, 3.24%.

5-Chloro-6,6,6-trifluoro-2,2-dimethyl-4-hexen-3-one (15). As described above, a mixture of **14** (437 mg, 2.54 mmol), **1** (9.52 g, 50.8 mmol), CuCl (251 mg, 2.54 mmol), and 4A Molecular Sieves (2.5 g) in DMF (3 ml) was treated and workup gave **15** as colorless oil; 65 mg (12%); ^{1}H NMR($CDCl_3$) δ=7.21 (d, 1H, J=0.9 Hz) and 1.20 (s, 9H); ^{19}F NMR($CDCl_3$) δ=12.61 (s, 0.12F) and 7.43 (s, 0.88F); IR(neat) 2970, 2940, 2910, 2860, 1704, 1622, 1474, 1464, 1390, 1364, 1280, 1246, 1180, and 1150 cm^{-1}; MS m/z 157($M^+-C_4H_9$, 3),[16] 101(25), 59(100), 57(63), and 56(50). Found: C, 44.49; H, 4.96%. Calcd for $C_8H_{10}ClF_3O$: C, 44.78; H, 4.70%.

2-(1-Chloro-2,2,2-trifluoroethylidene)cyclopentanone (17). As described above, a mixture of **16** (160 mg, 1.02 mmol), **1** (3.77 g, 20.1 mmol), CuCl (101 mg, 1.02 mmol), and 4A Molecular Sieves (1.03 g) in DMF (2 ml) was treated and workup gave **17** as pale yellow oil; 41 mg (21%); ^{1}H NMR (500 MHz)($CDCl_3$) δ=3.100 (tq, 0.88H, J=7.1 and 3.3 Hz), 2.915 (tq, 0.12H, J=7.5 and 2.8 Hz), 2.551 (t, 0.12H, J=7.8 Hz), 2.479 (t, 0.88H, J=8.0 Hz), and 2.08—1.96 (m, 1H); ^{19}F NMR($CDCl_3$) δ=18.09 (t, 0.12F, J=3 Hz) and 14.19 (t, 0.88F, J=3 Hz); IR(neat) 2960, 2890, 1750, 1636, 1476, 1456, 1296, 1280, 1220, 1200, 1184, 1176, and 1150 cm^{-1}; MS m/z 200(M^++2, 2), 198(M^+, 6), 149(31), 97(10), 85(14), 83(15), 81(11), 73 (18), 71(25), 70(12), 69(25), 67(11), 65(11), 57(67), 56(24), 55(51), 53(11), 51(12), and 41(100). Found: C, 42.27; H, 2.98%. Calcd for $C_7H_6ClF_3O$: C, 42.34; H, 3.05%.

3-(1-Chloro-2,2,2-trifluoroethylidene)bicyclo[2.2.1]-heptan-2-one (20). As described above, a mixture of **19** (435 mg, 2.39 mmol), **1** (8.94 g, 47.7 mmol), CuCl (236 mg, 2.38 mmol), and 4A Molecular Sieves (2.40 g) in DMF (3 ml) was treated and after treatment with DBN (297 mg, 2.39 mmol) in THF (2 ml), workup gave **20** as pale yellow oil; 170 mg (32%); ^{1}H NMR($CDCl_3$) δ=3.5—4.0 (m, 2H), 2.7—3.0 (m, 2H), and 1.3—2.3 (m, 6H); ^{19}F NMR($CDCl_3$) δ=14.32 (s, 0.42F) and 11.99 (s, 0.58F); IR(neat) 2960, 2890, 1750, 1636, 1476, 1456, 1296, 1280, 1220, 1184, 1176, and 1150 cm^{-1}; MS m/z 226(M^++2, 9), 224(M^+, 25), 196(35), 161(79), 141(54), 91(46), 85(13), 79(40), 77(18), 75(25), 69(18), 68 (70), 67(100), 66(79), 63(27), 55(63), 54(13), 53(20), and 51(38). Found: C, 48.12; H, 3.58%. Calcd for $C_9H_8ClF_3O$: C, 48.13; H, 3.59%.

Hexyl 3-Chloro-4,4,4-trifluoro-2-butenoate (22). As described above, a mixture of **21** (131 mg, 0.61 mmol), **1** (2.27 g, 12.1 mmol), CuCl (60 mg, 0.61 mmol), and 4A Molecular Sieves (0.6 g) in DMF (3 ml) was treated and workup gave **22** as pale yellow oil; 24 mg (15%); ^{1}H NMR($CDCl_3$) δ=6.67 (d, 1H, J=0.7 Hz), 4.16 (t, 2H, J=7 Hz), and 1.1—0.7 (m, 11H); ^{19}F NMR ($CDCl_3$) δ=7.48 (s, 0.21F) and 7.13 (s, 0.79F); IR(neat) 3070, 2960, 2930, 2860, 1740, 1658, 1464, 1380, 1320, 1280, 1254, 1186, and 1140 cm^{-1}; MS m/z 223(M^+—Cl, 0.5),[16] 215(0.6), 201(1), 159(25), 157(78), 84(52), 83(18), 69(43), 55(100), and 54(48). Found: C, 46.25; H, 5.61%. Calcd for $C_{10}H_{14}ClF_3O_2$: C, 46.43; H, 5.46%.

Determination of GLC Yields: After the elimination reaction, a comparable amount of adamantane was added to the ethereal solution as an internal standard before the final workup, and then the mixture was analyzed on a GLC by comparison of relative sensitivity with an authentic sample of an *E*- and *Z*-mixture.

References

1) For recent reviews, see J. Mann, *Chem. Soc. Rev.*, **16**, 381 (1987); J. T. Welch, *Tetrahedron*, **43**, 3213 (1987) and references cited therein.

2) a) M. Fujita and T. Hiyama, *Tetrahedron Lett.*, **27**, 3665 (1986). b) H. Tanaka, S. Yamashita, Y. Katayama, and S. Torii, *Chem. Lett.*, **1986**, 2043. c) M. Fujita and T. Hiyama, *Bull. Chem. Soc. Jpn.*, **60**, 4377 (1987) and references cited therein. d) M. Fujita, K. Kondo, and T. Hiyama, *ibid.*, **60**, 4385 (1987). e) M. Fujita and T. Hiyama, *ibid.*, **61**, 3321 (1988).

3) For trifluoromethylation of carbonyl compounds with trifluoromethyltrimethylsilane. See G. K. S. Prakash, R. Krishnamurti, and G. A, Olah, *J. Am. Chem. Soc.*, **111**,

393 (1989) and references cited therein.

4) D. J. Burton and L. J. Kehoe, *J. Org. Chem.*, **35**, 1339 (1970).

5) S. Murai, Y. Kuroki, T. Aya, N. Sonoda, and S. Tsutsumi, *J. Chem. Soc., Chem. Commun.*, **1972**, 741.

6) For reported syntheses of β-trifluoromethyl α,β-unsaturated ketones and -esters, see a) D. Cantacuzene and R. Dorme, *Tetrahedron Lett.*, **1975**, 2031. b) A. Yu. Volkonskii, E. I. Mysov, and E. M. Rokhlin, *Izv. Akad. Nauk, SSSR, Ser. Khim.*, **6**, 1356 (1984); *Chem. Abstr.*, **102**, 24711f (1985). c) C. Portella and M. Iznaden, *Tetrahedron Lett.*, **28**, 1655 (1987).

7) K. I. Pashkevichi, M. B. Bobrov, A. Ya. Aizikovich, and M. N. Rudyay, *Izv. Akad. Nauk, SSSR, Ser. Khim.*, **9**, 2125 (1986); *Chem. Abstr.*, **107**, 77277f (1987).

8) These enones should take the shown s-cis like conformations because of severe steric repulsion between chloro(trifluoromethyl)methylene group and another substituent on C=O for the s-trans like conformations based on molecular model studies.

9) For ^{1}H and ^{19}F NMR data of some *E*- and *Z*-β-chloro-β-trifluoromethyl substituted alkenes, see Refs. 2c, 2d, and T. Hiyama, K. Sato, and M. Fujita, *Bull. Chem. Soc. Jpn.*, **62**, 1352 (1989).

10) L. M. Weinstock, S. Karady, F. E. Roberts, A. M. Hoinwski, G. S. Brenner, T. B. K. Lee, W. C. Lumma, and M. S. Sletzinger, *Tetrahedron Lett.*, **1975**, 3975.

11) B. H. Lipshutz, R. S. Wilhelm, S. T. Nugent, R. D. Little, and M. M. Baizar, *J. Org. Chem.*, **43**, 3306 (1984).

12) The *E*:*Z* ratio was determined by ^{19}F and ^{1}H NMR spectra, and GLC analyses.

13) Trimethylsilyl enol ether **18** decomposes to cyclohexanone and 2-chlorocyclohexanone by $CuCl_2$; Y. Ito, M. Nakatsuka, and T. Saegusa, *J. Org. Chem.*, **45**, 2022 (1980).

14) Molecular model studies indicate clearly a larger steric repulsion between CF_3 group and C-3 methylene group in the conformer **IV** of intermediate **III** derived from **5** than in the conformer **V** assuming a half-chair cyclohexenone ring with C-2 equatorial CCl_2CF_3 substituent. Similarly, the steric repulsion between α-phenyl group and CF_3 group is larger in the conformer **IV** than in the conformer **V** for **III** derived from **12**.

15) For example, see P. A. Wender and A. M. White, *J. Am. Chem. Soc.*, **110**, 2218 (1988).

16) M^+ was not observed.

 © 1989 The Chemical Society of Japan Bull. Chem. Soc. Jpn., 62, 2580—2584 (1989) [Vol. 62, No. 8

Addition of 9-Diazofluorene to Unsubstituted and Chloro-Substituted 1,4-Benzoquinones. A Comparison with the Addition of Diphenyldiazomethane

Takumi OSHIMA* and Toshikazu NAGAI
Institute of Chemistry, College of General Education, Osaka University, Toyonaka, Osaka 560
(Received February 4, 1989)

Unsubstituted 1,4-benzoquinone (**1a**) reacted at the C=C double bond with 9-diazofluorene (9-DF) to give norcarene dione **2a** and 4,7-dihydroxy-3*H*-indazole **4a**. Similarly, the reaction of 2-chloro-1,4-benzoquinone (**1b**) with 9-DF yielded norcarene dione **2b** and 4,7-dihydroxy-3*H*-indazole **4b**, together with tricyclic dione **3b**. 2,3-dichloro-1,4-benzoquinone (**1c**) and 9-DF produced norcarene dione **2c**, 4,7-dihydroxy-3*H*-indazole **4c**, and its fluorenyl ether **5c**. Reactions of 2,5- and 2,6-dichloro- and trichloro-1,4-benzoquinones (**1d**, **1e**, and **1f**) with 9-DF provided norcarene diones **2d**, **2e**, and **2f** and tricyclic diones **3d** and **3e**, respectively. On the other hand, tetrachloro-1,4-benzoquinone (**1g**) converted 9-DF into 9,9′-bifluorenylidene possibly via a 1 : 1 betaine intermediate arising from the C=O double bond addition. These results were markedly different from those of the previous diphenyldiazomethane reactions and are discussed in terms of structural changes of these diazoalkanes.

Since the early pioneering work by Pechmann for the addition of diazomethane to 1,4-benzoquinone,[1] the addition chemistry of diazoalkanes to quinones has received the continuing interest of several workers from synthetic and mechanistic points of view.[2] The products of these reactions are strongly dependent on the electronic and structural natures of these substrates. We previously reported that the reactions of diphenyldiazomethane (DDM) with unsubstituted and variously chloro-substituted 1,4-benzoquinones proceed through the addition to the quinonoid C=C or C=O double bonds, giving 4,7-dihydroxy-3*H*-indazoles, cyclopropane derivatives, or 1 : 1 betaine intermediates.[3] The addition modes varied with the numbers and with the substitution patterns of the chloro substituents. The unsubstituted quinone reacted only at the C=C double bond,[4] while the chlorinated quinones successively raised the proportion of the C=O addition with the increasing Cl substituents.[3] An extreme example is tetrachloro-1,4-benzoquinone, which reacted only at the C=O double bond.[5] We now report on an extended investigation of the reaction of planar 9-diazofluorene (9-DF) with a series of chloro-substituted 1,4-benzoquinones, especially focusing attention on the effects of the structural change of the diazoalkanes on the modes of additions.

Results and Discussion

In 1955, Horner and Lingnau reported that the reaction of 9-DF with 1,4-benzoquinone (**1a**) gives 90% 4,7-dihydroxy-3*H*-indazole **4a** on standing for a long time, together with a small amount of nitrogen-free norcarene dione **2a** (2%).[6] About twenty years later, Shechter et al. attained a high yield (73%) of **2a** when the reaction was carried out in refluxing benzene.[7] These products appear to be given by way of dipolar addition, followed by two competitive processes; dienolization and nitrogen release of the primary adduct pyrazoline **I** (Scheme 1.)

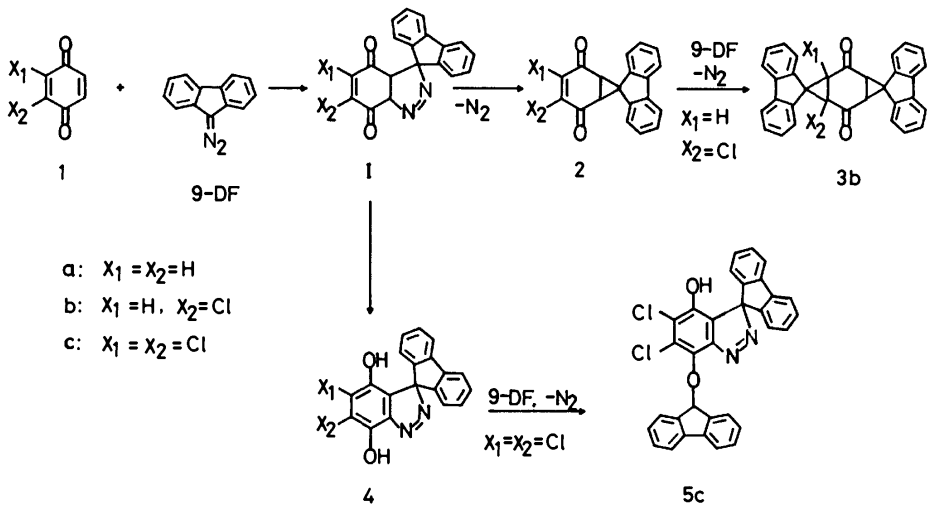

Scheme 1.

In contrast to Horner's result, but close to that of Shechter, the present equimolar reaction of 9-DF and **1a** yielded **2a** (61%) as a major product, even at 25 °C along with a moderate amount of **4a** (34%). An elevation of the reaction temperature to 60 °C moved the competing processes to the nitrogen release, as found in the yields of **2a** (77%) and **4a** (20%). A similar trend of accerelating the nitrogen release has been noticed for the previous reaction of diphenyldiazomethane (DDM) with **1a**.[3] The DDM reaction, which exclusively produced several dienolization products at 25 °C, gave rise to the corresponding norcarene dione in 12% yield at 80 °C.

The reaction of 2-chloro-1,4-benzoquinone (**1b**) with 9-DF at 25 °C gave tricyclic dione **3b** (13%), together with norcarene dione **2b** (50%) and 4,7-dihydroxy-3*H*-indazole **4b** (22%). The diadduct **3b** is the secondary product arising from a further additon of 9-DF to the resulting **2b**, as confirmed by a treatment of 9-DF with **2b**. The stereochemistry of **3b** is unknown, partly because of the very low solubility in common solvents. However, **3b** was shown to be not a mixture of stereoisomers by a careful HPLC measurement. We tentatively assign the stereochemically pure **3b** to be the anti-form since the syn-configuration suffers a considerable steric repulsion between the fluorenylidene ring protons, as estimated from its molecular model.[8] The monoadduct **2b** offered coupled NMR peaks with a narrow range of δ 3.4—3.5 assignable to the two nonequivalent bridgehead protons in bicyclo[4.1.0]hept-3-ene-2,5-dione system, indicating that the addition took place at the unchlorinated C=C bond of **1b**. Evidently, this site selectivity may be ascribed to the steric repulsive effects exerted by the Cl substituent, because the MNDO calculation[9] rather predicts an opposite addition to the chlorinated C=C bond, as previously described in the case of DDM reactions.[3]

2,3-Dichloro-1,4-benzoquinone (**1c**) also reacted at the unchlorinated C=C bond and brought about a significant increase in dienolization products, **4c** (56%) and **5c** (10%), relative to norcarene dione **2c** (18%). This appears to be performed by the two meta- and para-directing Cl (electron-withdrawing) substituents, cooperatively capable of activating the migrating protons. The formation of fluorenyl ether **5c** of **4c** only for this case is also attributable to the two chloro substituents which increse the acidity of phenolic OH of **4c** to react with 9-DF. Such etherification was quite usual in the DDM reactions, where considerable amounts of benzhydryl ethers of the corresponding 4,7-dihydroxy-3*H*-indazoles were provided not only for **1c** but also for unchlorinated **1a** and monochlorinated **1b**.[3] Primarily, the lower nucleophilicity of 9-DF compared to DDM may be due to the conjugation between the diazo and planar dibenzocyclopentadienylidene moieties.[10]

Escaping dienolization owing to the lack of the unsubstituted C=C bonds, 2,5- and 2,6-dichloro-1,4-benzoquinones (**1d** and **1e**), and trichloro-1,4-benzoquinone (**1f**) gave norcarene diones, **2d** (80%), **2e** (10%), and **2f** (97%) and tricyclic diones, **3d**(8%) and **3e** (42%), respectively (Scheme 2). Compounds **3d** and **3e** seem to have a stable anti-form in analogy with **3b**. Rather surprising is the abnormally high yield of secondary product **3e** for the case of *m*-dichlorinated **1e**. This implies that the resulting **2e** tends to react with 9-DF much faster than does the parent quinone **1e**. Indeed, the second-order rate constant (k= 7.00×10^{-3}/s^{-1} mol^{-1}, 30 °C, in benzene) of the addition of 9-DF to **2e** was about 5-times larger than that of the addition to **1e** (1.31×10^{-3}). The intriguing behavior of **1e** was also noted for the DDM reactions, where only this quinone yielded a small amount of tricyclic dione in the ordinary conditions.[3] No explanation for these unusual results can be offered at the present

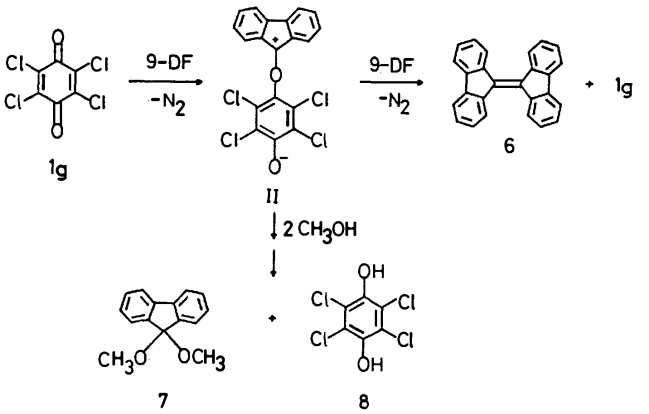

Scheme 3.

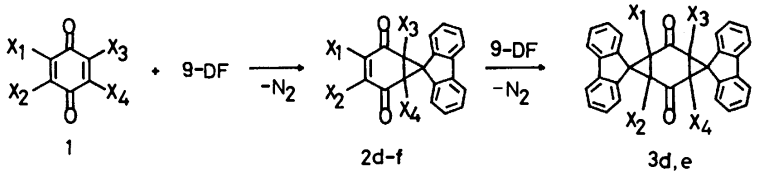

d: $X_1=X_4=Cl$, $X_2=X_3=H$
e: $X_1=X_3=Cl$, $X_2=X_4=H$
f: $X_1=X_2=X_3=Cl$, $X_4=H$

Scheme 2.

time.

As expected from the complete blocking of both of the C=C double bonds with the Cl substituents, tetrachloro-1,4-benzoquinone (**1g**) gave no norcarene dione with 9-DF as well as the reaction with DDM[5] but, rather, very slowly converted it into 9,9′-bifluorenylidene (**6**) at 25 °C.[10] However, refluxing an equimolar solution of 9-DF and **1g** in benzene (1.30×10^{-2} mol dm^{-3}) for ten hours provided an almost quantitative yield of **6** with a substantial recovery of **1g** (Scheme 3). This observation, combined with the fact that only 16% 9-DF underwent spontaneous decomposition to give **6** in an identical refluxing time (by HPLC), substantiates some certain participation of quinone **1g**, even in this accelerated condition. The formation of the dimeric olefin is suggestive of a carbenic process involving fluorenylidene (Fl).[11] An attempt was made to capture the possible carbene intermediate by adding 10 equiv excess of methanol. This trapping experiment at 80 °C still provided **6** in 90% yield, together with a small amount of fluorenone dimethyl acetal (**7**, 7%) and tetrachlorohydroquinone (**8**, 5%). The **7** and **8** can be regarded as arising from a redoxical acetalization of a 1 : 1 betaine intermediate II by considering that the reaction of DDM with **1g**[5] and 2,3-dichloro-5,6-dicyanobenzoquinone (DDQ)[12] proceeds through similar intermediates and affords benzophenone dimethyl acetal in high yield when methanol is introduced. However, the absence of fluorenyl methyl ether, a well-known methanol adduct with Fl,[13] does not bear out the carbene mechanism for the formation of a large amount of **6**. Here, it should be remembered that **1g** converted phenyldiazomethane into stilbene by way of a 1 : 1 betaine intermediate, like II.[14] Moreover, a very recent investigation of the reaction of 9-DF with DDQ revealed that this system also provides a small amount of **6** along with the norcarene dione at ordinary temperature.[15] The mechanistic interpretation for the formation of **6** rests on the 1 : 1 betaine intermediate. Accordingly, we believe that the most plausible pathway providing **6** likewise involves the betaine **II** as a key intermediate, as formulated in Scheme 3. Incidentally, a marked difference in the chemical behavior between DDM and 9-DF betaines is noticiable. The DDM betaines derived from **1g** and DDQ tended to polymerize to poly(hydroquinone benzhydryl ether)s and were well-collapsed by the addition of methanol to benzophenone dimethyl acetal and hydroquinones.[5,12] On the other hand, the possible 9-DF betaines did not polymerize but, rather, underwent a further attack of another molecule of 9-DF to produce dimeric olefin **6**.

Thus, the present 9-DF reactions were apparently different from the previous DDM reactions in that the former diazoalkane exhibited only C=C additions, with one exception of the C=O addition for tetrachlorinated **1g**. However, the latter one significantly increased the C=O additions with increasing the Cl substituents of quinones as follows: **1a**, 0%; **1b**, 9%; **1c**, 12%; **1d**, 51%; **1e**, 50%; **1f**, 60%; **1g**, 100%.[3] To explain the outstanding difference, we suggest that the most important effect of replacing the twisted diphenyl groups with the planar biphenyl-2,2′-diyl one at the diazo-carbon is to change the structural properties of the diazoalkanes so that the 9-DF can more easily approach the intrinsically reactive C=C double bonds than DDM. That 9-DF reactions furnished diadducts in fair yields for quinones **1b**, **1d**, and **1e** also attributable to such structural framework of 9-DF by which the less-repulsive access to the C=C double bonds of the monoadducts will be achieved. The gradual variation of the DDM reactions to the C=O additions in going from **1a** to **1g**, therefore, may be rationalized as a result of avoiding the increasing steric repulsion caused when the nonplanar DDM approaches the C=C double bonds with increasing Cl substituents. These steric considerations may also well explain the change of the addition modes of 9-DF and DDM toward DDQ. 9-DF preponderantly added to the C=C double bond having the CN substituents to give norcarene dione,[15] while DDM provided no such cycloadduct but instead afforded the product due to the C=O addition[12] in a manner similar to the reaction with **1g**.[5] The present 9-DF reactions are also characterized by providing large amounts of nitrogen-released cycloadducts for quinones **1a—c** in contrast to the DDM reactions. This is partly because the fluorenylidene structure, which resonates with the cleaving C(3)-N(2) bond much better than the diphenylmethylene one, would facilitate the loss of nitrogen from the pyrazoline adducts (**I**).

Experimental

The IR, NMR, and mass spectra were taken with a Perkin Elmer 983G, a Varian EM 390, a JEOL GSX 400, and a Hitachi RMU 6E spectrometers, respectively.

Materials. The 9-diazofluorene (9-DF) was prepared by the oxidation of 9-fluorenone hydrazone with yellow mercury oxide[16] in ether and purified by recrystallization from ether; mp 94—95 °C. All quinones were provided and purified as described elsewhere.[3] Benzene was refluxed over lithium aluminium hydride and fractionated.

Spiro[fluorene-9,7′-[3′]norcarene]-2′,5′-dione (2a) and Spiro[3*H*-indazole-3,9′-fluorene]-4,7-diol (4a). A solution of **1a** (250 mg, 2.31 mmol) and 9-DF (444 mg, 2.31 mmol) in benzene (5 ml) was stored for 6 h at 25 °C. The precipitate was filtered, washed with ether (10 ml×2), and then with acetone (10 ml×2) to give analytically pure **2a** (305 mg, 48.5%). Recrystallization from a large volume of benzene yielded yellow needles: mp 256—257 °C, (lit,[6] 256 °C; lit,[7] 263—264 °C); IR(KBr) 1666, 1447, 734 cm^{-1}; ^{1}H NMR($CDCl_3$) δ=3.33 (s, 2H, cyclopropyl H), 6.8—7.9 (m, 10H, vinyl H+aromatic H); MS, *m/z* 272(M^+). Anal. ($C_{19}H_{12}O_2$) C, H. The filtrate and the washing were combined and concentrated to dryness. The solid residue was chromatographed on silica gel to provide a second crop of **2a** (75 mg, 12%) with benzene as an eluent. Further elution

with benzene-ether (1 : 1) gave **4a** (235 mg, 34%); yellow crystals (from acetone), mp 250 °C (decomp) (lit,[6] 252 °C); IR(KBr) 3416, 3238, 1447, 1275, 748 cm^{-1}; ^1H NMR (acetone-d_6) δ=6.5—8.0 (m, 10H, aromatic H), 7.65 (s, 1H, OH, exchangeable with CD_3OD), 9.17 (s, 1H, OH, exchangeable with CD_3OD); MS, m/z 300(M^+). Anal. ($C_{19}H_{12}O_2N_2$) C, H, N.

In a separated experiment, equimolar **1a** (2.31 mmol) and 9-DF in benzene (5 ml) were allowed to react for 3 h at 60 °C. The **2a** (485 mg, 77%) and **4a** (140 mg, 20%) were obtained on the same work-up treatment as above.

3′-Chlorospiro[fluorene-9,7′-[3′]norcarene]-2′,5′-dione (2b), 1′-Chlorodispiro[fluorene-9,4′-tricyclo[5.1.0.0^{3,5}]octane-8′,9″-fluorene]-2′,6′-dione (3b), and 5-Chlorospiro[3*H*-indazole-3,9′-fluorene]-4,7-diol (4b). A solution of **1b** (740 mg, 5.19 mmol) and 9-DF (1.00 g, 5.21 mmol) in benzene (15 ml) was allowed to stand for 6 h at 25 °C. The white solid formed was filtered and washed with acetone (10 ml×2) to give analytically pure **3b** (320 mg, 13%): mp 218—220 °C; IR(KBr) 1691, 1447, 1229, 734 cm^{-1}. The NMR of **3b** could not be determined because of its insolubility in common solvents. MS, m/z 470 (M^+). Anal.($C_{32}H_{19}O_2Cl$) C, H. The filtrate and the washing were combined and evaporated to dryness. The solid residue was chromatographed on silica gel. Elution with hexane-benzene (1 : 3) yielded the recovered **1b** (90 mg). Further elution produced **2b** (795 mg, 50%) with benzene and **4b** (88 mg, 5%) with benzene-ether (1 : 1). Recrystallization of **2b** from benzene gave yellow prisms: mp 210—220 °C; IR(KBr) 1685, 1665, 736 cm^{-1}; ^1H NMR($CDCl_3$) δ=3.43 (d×d, J=7.3 and 1.5 Hz, 1H, cyclopropyl H), 3.49 (d, J=7.3 Hz, 1H, cyclopropyl H), 6.9—7.9 (m, 9H, vinyl H+aromatic H); MS, m/z 306 (M^+). Anal.($C_{19}H_{11}O_2Cl$) C, H. Recrystallization of **4b** from benzene-ether mixture provided yellow plates: mp 210 °C (decomp); IR(KBr) 3264, 1446, 1226, 750 cm^{-1}; ^1H NMR($CDCl_3$) δ=4.83 (s, 1H, OH, exchangeable with CD_3OD), 6.6—7.9 (m, 9H, aromatic H), 8.00 (s, 1H, OH, exchangeable with CD_3OD); MS, m/z 334 (M^+). Anal.($C_{19}H_{11}O_2N_2Cl$) C, H, N.

In a separate experiment, monoadduct **2b** (31 mg, 0.1 mmol) in benzene (1 ml) was allowed to react with excess 9-DF (96 mg, 0.5 mmol) for 1 d at 25 °C. Diadduct **3b** was obtained in 90% yield.

3′,4′-Dichlorospiro[fluorene-9,7′-[3′]norcarene]-2′,5′-dione (2c), 5,6-Dichlorospiro[3*H*-indazole-3,9′-fluorene]-4,7-diol (4c), and 5,6-Dichloro-7-(9-fluorenyloxy)spiro[3*H*-indazole-3,9′-fluoren]-4-ol (5c). A solution of **1c** (330 mg, 1.86 mmol) and 9-DF (360 mg, 1.88 mmol) in benzene (5 ml) was stored for 3 h at 25 °C. The solvent was evaporated and the solid residue was chromatographed on silica gel. Elution with hexane-benzene (2 : 1) provided the recovered **1c** (30 mg) and **2c** (111 mg, 18%): mp 209—210 °C, yellow plates (from benzene); IR(KBr) 1687, 1555, 1079, 739 cm^{-1}; ^1H NMR($CDCl_3$) δ=3.55 (s, 2H, cyclopropyl H), 6.8—7.8 (m, 8H, aromatic H); MS, m/z 340 (M^+). Anal. ($C_{19}H_{10}O_2Cl_2$) C, H. Further elution with benzene gave **5c** (103 mg, 10%): mp 200 °C (decomp), pale yellow prisms (from chloroform); IR(KBr) 3437, 1435, 1197, 739 cm^{-1}; ^1H NMR($CDCl_3$) δ=5.13 (s, 1H, OH, exchangeable with CD_3OD), 6.7—8.0 (m, 17H, methine+aromatic H); MS, m/z 532 (M^+). Anal. ($C_{32}H_{18}O_2N_2Cl_2$) C, H, N. Finally, **4c** (386 mg, 56%) was eluted with benzene-ether (3 : 1). Recrystallization of **4c** from hexane-ether mixture yielded yellow needles: mp 215 °C (decomp); IR(KBr) 3424, 1449, 1083, 750 cm^{-1}; ^1H NMR(acetone-d_6) δ=6.6—8.0 (m, 8H, aromatic H), 7.87 (s, 1H, OH, exchangeable with CD_3OD), 10.1 (s, 1H, OH, exchangeable with CD_3OD); MS, m/z 368 (M^+). Anal. ($C_{19}H_{10}O_2N_2Cl_2$) C, H, N.

1′,4′-Dichlorospiro[fluorene-9,7′-[3′]norcarene]-2′,5′-dione (2d) and 1′,4′-Dichlorodispiro[fluorene-9,4′-tricyclo-[5.1.0.0^{3,5}]octane-8′,9″-fluorene]-2′,6′-dione (3d). A solution of **1d** (660 mg, 3.73 mmol) and 9-DF (720 mg, 3.75 mmol) in benzene (20 ml) was stored for 1 d at 25 °C. The solid formed was filtered and washed with benzene (5 ml×2) to leave analytically pure **3d** (154 mg, 8%): mp>350 °C; IR(KBr) 1698, 1443, 1286, 736 cm^{-1}. The NMR of **3d** could not be taken because of its insolubitity. MS, m/z 504 (M^+). Anal. ($C_{32}H_{18}O_2Cl_2$) C, H. The filtrate and the washing were combined and concentrated to give yellow crystals of **2d** (990 mg, 78%): mp 126—127 °C, pale yellow prisms (from benzene); IR(KBr) 1681, 1579, 989, 729 cm^{-1}; ^1H NMR($CDCl_3$) δ=3.77 (s, 1H, cyclopropyl H), 7.19 (s, 1H, vinyl H), 7.1—7.9 (m, 8H, aromatic H); MS, m/z 340 (M^+). Anal. ($C_{19}H_{10}O_2Cl_2$) C, H.

1′,3′-Dichlorospiro[fluorene-9,7′-[3′]norcarene]-2′,5′-dione (2e) and 1′,3′-Dichlorospiro[fluorene-9,4′-tricyclo-[5.1.0.0^{3,5}]octane-8′,9″-fluorene]-2′,6′-dione (3e). A solution of **1e** (1.00 g, 5.65 mmol) and 9-DF (1.08 g, 5.62 mmol) in benzene (20 ml) was stored for 6 h at 25 °C. The solid formed was filtered and washed with benzene (5 ml×2) and acetone (5 ml×2) to leave analytically pure **3e** (1.20 g, 42%) as a pale-yellow powder: mp>350 °C; IR(KBr) 1711, 1448, 1216, 741 cm^{-1}. The NMR of **3e** could not be taken because of its insolubility. MS, m/z 504(M^+). Anal. ($C_{32}H_{18}O_2Cl_2$) C, H. The filtrate and the washing were concentrated and chromatographed on silica gel. After elution of the recovered **1d** (0.39 g) with hexane-benzene (2 : 1), the **2e** (245 mg, 13%) was obtained with benzene. Recrystallization with hexane-benzene mixture produced yellow prisms: mp 127—129 °C IR(KBr) 1699, 1666, 1589, 1263, 1058, 721 cm^{-1}; ^1H NMR($CDCl_3$) δ=3.67(d, J=1.50 Hz, 1H, cyclopropyl H), 7.0—7.8 (m, 9H, vinyl H+aromatic H); MS, m/z 340 (M^+). Anal. ($C_{19}H_{10}O_2Cl_2$) C, H.

In separate experiments, solutions of **1e** (300 mg, 1.69 mmol) and 9-DF (650 mg, 3.38 mmol) in benzene (5ml) and of **2e**(100 mg, 0.294 mmol) and 9-DF (57 mg, 0.297 mmol) in benzene (3ml) were allowed to react as above. Both reactions provided 1 : 2 adduct **3e** in more than 96% yield.

The kinetic reactions were carried out in the presence of 30- (for **1e**) and 12-fold (for **2e**) molar excess of 9-DF ($3.6—7.7\times10^{-2}$ mol dm^{-3}) to permit a pseudo-first-order kinetic treatment. The rates were determined by following the relative decrease of **1e** and **2e** with respect to *p*-cyanobenzaldehyde and solvent benzene as internal standards, respectively, with a Hitachi 655A-12 HPLC instrument equipped with a Hitachi D-2000 chromato-integrator. The HPLC conditions using a Radial Pak cartridge C18(Waters Associates, Inc.) are as follows; 1 ml min^{-1}, eluents: 30% (for **1e**) and 20% aqueous methanol (v/v) (for **2e**), UV-detector wavelength: 254 and 273 nm for **1e** and **2e**, respectively.

1′,3′,4′-Trichlorospiro[fluorene-9,7′-[3′]norcarene]-2′,5′-dione (2f). A solution of **1f** (600 mg, 2.84 mmol) and 9-DF (545 mg, 2.84 mmol) in benzene (10 ml) was stored at 25 °C for 3 d. The solid formed was filtered and washed with benzene (5 ml×3) to give **2f** (980 mg, 92%): mp 210 °C (decomp), orange granulates (from acetone); IR(KBr) 1692,

1225, 1088, 729 cm^{-1}; ^1H NMR(acetone-d_6) δ=4.18 (s, 1H, cyclopropyl H), 6.7—7.8(m, 8H, aromatic H); MS, *m/z* 374 (M^+). Anal. ($C_{19}H_9O_2Cl_3$) C, H. The filtrate was chromatographed on silica gel to yield a second crop of **2f** (53 mg, 5%) with benzene as an eluent.

Reaction of 9-DF with Tetrachloro-1,4-benzoquione (1g) with or without Added Methanol. A solution of 9-DF (0.50 g, 2.6 mmol) and **1g** (0.64 g, 2.6 mmol) in benzene (20 ml) was refluxed for 10 h. The solvent was evaporated and the dark-red residue was washed with ether (10 ml×3) to give recovered **1g** (0.45 g, 70%). The ether solution was concentrated to dryness and subjected to silica-gel chromatography. Elution with hexane-benzene (1 : 4 v/v) yielded 9,9′-bifluorenylidene (**6**, 415 mg, 97%) and the second crop of **1g** (0.18 g, 28%).

As a trapping experiment, a solution of 9-DF (0.50 g), **1g** (0.64 g), and 10 equiv of methanol (0.83 g) in benzene (20 ml) was refluxed for 10 h. The same work-up as above recovered **1g** (0.40 g, 62.5%). The washing ether was evaporated and the dark-red residue was immediately submitted for NMR measurement. The singlet at δ 3.30 ($CDCl_3$), which was only one signal detectable in a field higher than δ 7.0 was assigned to the CH_3O groups of fluorenone dimethyl acetal (**7**) by comparison with spectrum of authentic sample[17] as well as chemical proof being hydrolyzed to fluorenone upon treatment with dilute hydrochloric acid. The absolute yield of acetal **7** (7%) was determined by the integral ratio with 1,1,1,2-tetrachloroethane (δ=4.20) as an internal standard. After a complete hydrolysis of acetal, the reaction product on chromatography over silica gel gave **6** (385 mg, 90%), the second crop of recovered **1g** (175 mg, 27%), and fluorenone (30 mg, 6%) with 5—30% benzene in hexane and tetrachlorohydroquinone (**8**, 30 mg, 5%) with 5% ether in benzene.

References

1) H. Pechmann and E. Seel, *Ber.*, **32**, 2292 (1899).

2) a) C. D. Gutsche, *Org. React.*, **8**, 364 (1954); b) K. T. Finley, "The Chemistry of the Quinonoid Compounds," ed by S. Patai, John Wiley & Sons (1974), Chap. 17; c) D. S. Wulfmann, G. Linstrumell, and C. F. Cooper, "The Chemistry of Diazonium and Dizao Groups," ed by S. Patai, John Wiley & Sons (1978), Chap. 18; d) M. Regitz and H. Heydt, "1,3-Dipolar Cycloaddition Chemistry," ed by A. Padwa, John Wiley & Sons (1984), Chap. 4; e) B. Eistert, J. Riedinger, G. Kuffner, and W. Lazik, *Chem. Ber.*, **106**, 727 (1973), and other papers in this series; f) F. M. Dean, L. E. Houghton, R. Nayyir-Mashir, and C. Thebtaranonth, *J. Chem. Soc., Perkin Trans. 2*, **1980**, 1994, and other papers in this series.

3) T. Oshima and T. Nagai, *Bull. Chem. Soc. Jpn.*, **61**, 2507 (1988).

4) L. F. Fieser and M. A. Peters, *J. Am. Chem. Soc.*, **53**, 4080 (1931).

5) T. Oshima and T. Nagai, *Bull. Chem. Soc. Jpn.*, **53**, 3284 (1980).

6) L. Horner and E. Lingnau, *Justus Liebigs Ann. Chem.*, **591**, 21 (1955).

7) G. W. Jones, D. R. Kerur, T. Yamazaki, and H. Shechter, *J. Org. Chem.*, **39**, 492 (1974).

8) Estimated by a HGS molecular structure model(type B, Marzen Co., Inc.).

9) a) W. Thiel, *QCPE*, **11**, 353 (1978); b) Y. Beppu and I. Ninomiya, *QCPE*, **14**, 409 (1981); c) Y. Sasaki, T. Takagi, A. Tanaka, and R. Tokura, *Bulletin of Computation Center Osaka University*, **14**, 103 (1985).

10) The lower reactivity of 9-DF as a 1,3-dipole or a nucleophile can be predictable from the smaller HOMO coefficient and the unfavorable net atomic charge (−0.135) at the diazo-carbon compared to DDM; the corresponding values for DDM are 0.66 and −0.157, respectively; see Ref. 3.

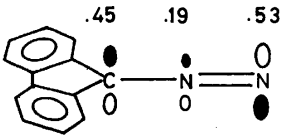

HOMO (-8.09 ev)
9-DF

11) L. S. Singer and I. C. Lewis, *J. Am. Chem. Soc.*, **90**, 4212 (1968).

12) T. Oshima and T. Nagai, *Bull. Chem. Soc. Jpn.*, **54**, 2039 (1981).

13) a) P. B. Grasse, B.-E. Brauer, J. J. Zupancic, K. J. Kaufmann, and G. B. Schuster, *J. Am. Chem. Soc.*, **105**, 6833 (1983); b) G. B. Schuster, *Adv. Phys. Org. Chem.*, **22**, 311 (1986).

14) T. Oshima and T. Nagai, *Tetrahedron Lett.*, **1979**, 2789; *Bull. Chem. Soc. Jpn.*, **53**, 726 (1980).

15) T. Shingaki, H. Kuma, Y. Kushi, and T. Nagai, *Bull. Chem. Soc. Jpn.*, **62**, 444 (1989).

16) H. Staudinger and O. Kupfer, *Ber.*, **44**, 2197 (1911).

17) T. Oshima and T. Nagai, *J. Org. Chem.*, **54**, 1465 (1989).

Oxidation Using Quaternary Ammonium Polyhalides. III.[1] An Effective Oxidation of Alcohols and Ethers by the Use of Benzyltrimethylammonium Tribromide

Shoji KAJIGAESHI,* Hiroshi KAWAMUKAI, and Shizuo FUJISAKI
Department of Industrial Chemistry, Faculty of Engineering, Yamaguchi University, Tokiwadai, Ube 755
(Received February 10, 1989)

The reaction of primary alcohols or simple ethers and α,ω-diols or cyclic ethers with a stoichiometric amount of benzyltrimethylammonium tribromide (BTMA Br_3) in carbon tetrachloride in the presence of Na_2HPO_4 aq or in acetic acid in the presence of CH_3CO_2Na aq at 60—70 °C gave dimeric esters and lactones respectively in good yields. The reaction of secondary alcohols with 1 equiv of BTMA Br_3 in the presence of a buffer at 60 °C gave ketones.

The dimeric esterification of primary alcohols **1** has been presented in several reports. For example, bromine-potassium bromate in water,[2] sodium dichromate-sulfuric acid,[3] sodium hypochlorite in acetic acid,[4] calcium hypochlorite in acetonitrile-acetic acid,[5] and sodium bromite ($NaBrO_2$) in acetic acid[6] have been used for the dimeric esterification of **1**. Dimeric esters **3** can be obtained by bubbling oxygen into a solution of **1** in acetic acid in the presence of cobalt acetate bromide.[7] Reduced copper-[8] and ruthenium-[9] catalyzed transformation of **1** to **3** have also been reported. The treatment of tributylstannyl alkoxides by NBS in carbon tetrachloride affords **3**.[10] We have recently reported that **1** can be converted into **3** by the use of sodium bromate in the presence of a catalytic amount of hadrobromic acid.[11]

Methods for the oxidative esterification of simple ethers **2** have also been described in the literature (Refs. 5 and 11).

Silver carbonate on Celite[12] and the ruthenium catalyst[9] has been used for the intramolecular oxidative lactonization of α,ω-diols **4**. Compounds **4** have also been oxidized to lactones **6** by sodium bromite in aqueous acetic acid[6] and by sodium bromate in 47% hydrobromic acid.[11] Bromine in an aqueous acetate buffer at pH 5 acts as an oxidant for the cleavage of THF to afford γ-butyrolactone.[13]

There are a number of methods concerning the oxidation of secondary alcohols **7** to ketones **8**. Several methods have been shown in the literature (Refs. 4, 10, and 11).

During the course of our investigation of the utility of benzyltrimethylammonium tribromide (BTMA Br_3) as a brominating agent,[14] we have now found that BTMA Br_3 is also an effective oxidizing agent.[15] In this paper, we wish to report on the oxidation of alcohols and ethers using BTMA Br_3 in the presence of such buffer as aqueous Na_2HPO_4 or CH_3CO_2Na.

Results and Discussion

The reaction of **1** or **2** with a calculated amount of BTMA Br_3 in carbon tetrachloride-water in the presence of Na_2HPO_4 at 60 °C gave **3** in good yields. In

Table 1. Oxidation of Primary Alcohols **1** and Simple Ethers **2** with BTMA Br_3 in the Presence of aq Na_2HPO_4[a] (in CCl_4 at 60 °C)

Run	Substrate 1 or 2	BTMA Br_3/ Substrate	Reaction time/h	Product 3	Yield[b]/ %
1	CH_3CH_2OH	1.1	7	$CH_3CO_2CH_2CH_3$	11[c]
2	$CH_3(CH_2)_2OH$	1.1	5.5	$CH_3CH_2CO_2(CH_2)_2CH_3$	52[c]
3	$CH_3(CH_2)_3OH$	1.1	4.5	$CH_3(CH_2)_2CO_2(CH_2)_3CH_3$	55[c]
4	$(CH_3)_2CHCH_2OH$	1.1	12	$(CH_3)_2CHCO_2CH_2CH(CH_3)_2$	80
5	$CH_3(CH_2)_4OH$	1.1	3.5	$CH_3(CH_2)_3CO_2(CH_2)_4CH_3$	84
6	$(CH_3)_2CH(CH_2)_2OH$	1.1	5	$(CH_3)_2CHCH_2CO_2(CH_2)_2CH(CH_3)_2$	77
7	$CH_3(CH_2)_5OH$	1.1	5	$CH_3(CH_2)_4CO_2(CH_2)_5CH_3$	96
8	$(C_2H_5)_2CHCH_2OH$	1.1	24	$(C_2H_5)_2CHCO_2CH_2CH(C_2H_5)_2$	69
9	$CH_3(CH_2)_7OH$	1.1	8.5	$CH_3(CH_2)_6CO_2(CH_2)_7CH_3$	99
10	$CH_3(CH_2)_{11}OH$	1.1	4	$CH_3(CH_2)_{10}CO_2(CH_2)_{11}CH_3$	91
11	Ph-CH_2OH	1.1	5	Ph-CHO	89
12	Ph-CH_2CH_2OH	1.1	4	Ph-$CH_2CO_2CH_2CH_2$-Ph	23[d]
13	$[CH_3(CH_2)_2]_2O$	2.2	3	$CH_3(CH_2)_2CO_2(CH_2)_3CH_3$	33
14	$[CH_3(CH_2)_5]_2O$	2.2	5	$CH_3(CH_2)_4CO_2(CH_2)_5CH_3$	78
15		4.4	14	$CH_3(CH_2)_4CO_2(CH_2)_5CH_3$	90
16	$(Ph\text{-}CH_2)_2O$	2.2	10.5	Ph-CHO	63

a) About a 2 equiv of Na_2HPO_4 to BTMA Br_3 was used. b) Yield of isolated product. c) The exact yield was not calculated due to the volatility of the product, but a significant conversion was indicated by the IR and ^1H NMR analyses. d) Yield was based on ^1H NMR.

Table 2. Lactonization of α,ω-Diols **4** and Cyclic Ethers **5** with BTMA Br_3 in the Preesence of a Buffer

Run	Substrate **4** or **5**	BTMA Br_3/ Substrate	Reaction conditions			Product **6**	Yield[a]/ %
			Temp/°C	Time/h	Buffer (Solvent)		
1	$HO-(CH_2)_4-OH$	2.1	70	5.5	Na_2HPO_4[b] (CCl_4)		60
2	$HO-(CH_2)_5-OH$	2.1	70	2.5	CH_3CO_2Na[c] (CH_3CO_2H)		49
3	$HO-(CH_2)_6-OH$	2.1	70	2.5	Na_2HPO_4[b] (CCl_4)	Mixture[d]	—
4		2.1	70	4	CH_3CO_2Na[c] (CH_3CO_2H)	Mixture[d]	—
5		2.1	60	4.5	Na_2HPO_4[b] (CCl_4)		55
6		2.1	60	10	Na_2HPO_4[b] (THF)		67[e]
7		2.1	70	8.5	CH_3CO_2Na[c] (CH_3CO_2H)		13

a) Yield of isolated product. b) About a 2 equiv of Na_2HPO_4 to BTMA Br_3 was used. c) About a 4 equiv of CH_3CO_2Na to BTMA Br_3 was used. d) The mixture of ε-caprolactone, a linear ester from 2 molecules of $HO-(CH_2)_6-OH$, and a polyester was confirmed by its ^1H NMR spectrum. e) The yield was obtained on the basis of the BTMA Br_3 used.

the absence of Na_2HPO_4, however, the reaction proceeded slowly and gave **3** in low yields. In the case of benzyl alcohol, the only oxidation product was benzaldehyde. The results are summarized in Table 1.

It is reasonable to assume that BTMA Br_3 can be dissociated by water as is shown in Eq. 1;[16]

$$\text{BTMA } Br_3 + H_2O \rightleftarrows \text{BTMA Br} + \text{HOBr} + \text{HBr}. \quad (1)$$

The hypobromous acid thus produced may act as the major active oxidizing species and may convert alcohols into esters as follows;

$$\underset{\mathbf{1}}{2\,R\text{-}CH_2OH} + 2\,\text{HOBr} \longrightarrow \underset{\mathbf{3}}{R\text{-}CO_2CH_2R} + 2\,H_2O + 2\,\text{HBr}. \quad (2)$$

Overall:

$$\underset{\mathbf{1}}{2\,R\text{-}CH_2OH} + 2\,\text{BTMA } Br_3 \longrightarrow \underset{\mathbf{3}}{RCO_2CH_2R} + 2\,\text{BTMA Br} + 4\,\text{HBr}. \quad (3)$$

In the case of ethers:

$$\underset{\mathbf{2}}{R\text{-}CH_2OCH_2R} + 2\,\text{BTMA } Br_3 + H_2O \longrightarrow \underset{\mathbf{3}}{R\text{-}CO_2CH_2R} + 2\,\text{BTMA Br} + 4\,\text{HBr}. \quad (4)$$

Generated hydrobromic acid can be removed by the Na_2HPO_4 which has been added previously:

$$HBr + Na_2HPO_4 \longrightarrow NaH_2PO_4 + NaBr \quad (5)$$

Thus, the equilibrium in Eq. 1 lies to the right, and the reaction (Eqs. 3 and 4) should proceed smoothly. In practice, a 2 equiv of Na_2HPO_4 to BTMA Br_3 was used.[17] Our experimental results agreed stoichiometrically with these equations, 3 and 4.

The reaction of **4** or cyclic ethers **5** with a stoichiometric amount of BTMA Br_3 in carbon tetrachloride or in acetic acid in the presence of aqueous Na_2HPO_4 or CH_3CO_2Na respectively at 60—70 °C gave **6**. The results are summarized in Table 2. The reactions can be presented in the following equations:

$$\underset{\mathbf{4}}{HO\text{-}(CH_2)_n\text{-}OH} + 2\,\text{BTMA } Br_3 \longrightarrow \underset{\mathbf{6}}{\text{ 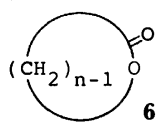 }} + 2\,\text{BTMA Br} + 4\,\text{HBr}. \quad (6)$$

$$\underset{\mathbf{5}}{\text{ 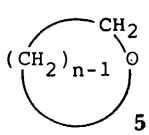 }} + 2\,\text{BTMA } Br_3 + H_2O \longrightarrow \mathbf{6} + 2\,\text{BTMA Br} + 4\,\text{HBr}. \quad (7)$$

The ring cleavage of **5** should occur first in the case of the reaction of **5** with BTMA Br_3.

The oxidation of **7** with an equimolar amount of BTMA Br_3 in the presence of a buffer (CH_3CO_2Na aq in acetic acid or Na_2HPO_4 aq in carbon tetrachloride) at 60 °C afforded the corresponding **8** in good yields. The results are summarized in Table 3.

Table 3. Oxidation of Secondary Alcohols **7** with BTMA Br_3 in the Presence of a Buffer (at 60 °C)

Run	Substrate **7**	BTMA Br_3/ Substrate	Reaction conditions: Temp/ °C	Time/ h	Buffer (Solvent)	Product **8**	Yield[a]/ %
1	CH_3CH_2-CH-$(CH_2)_2CH_3$ (OH)	1.1	60	2	CH_3CO_2Na[b] (CH_3CO_2H)	CH_3CH_2-C-$(CH_2)_2CH_3$ (O)	80
2		1.1	60	3	Na_2HPO_4[c] (CCl_4)	Mixture	—
3	$CH_3(CH_2)_5$-CH-CH_3 (OH)	1.1	60	2	CH_3CO_2Na[b] (CH_3CO_2H)	$CH_3(CH_2)_5$-C-CH_3 (O)	98
4	Ph-CH-CH_3 (OH)	1.1	50	2	CH_3CO_2Na[b] (CH_3CO_2H)	Ph-C-CH_3 (O)	87
5		1.1	50	1	— (CH_3CO_2H)	Mixture[d]	—
6	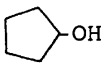	1.1	60	1	CH_3CO_2Na[b] (CH_3CO_2H)	Mixture[e]	—
7	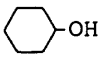	1.1	60	1	CH_3CO_2Na[b] (CH_3CO_2H)	Mixture[f]	—
8	Ph-CH-Ph (OH)	1.1	60	12	CH_3CO_2Na[b] (CH_3CO_2H)	Ph-C-Ph (O)	100
9		1.1	60	15	Na_2HPO_4[c] (CCl_4)	Ph-C-Ph (O)	100
10	Ph-C(=O)-CH(OH)-Ph	1.1	60	10.5	CH_3CO_2Na[b] (CH_3CO_2H)	Ph-C(=O)-C(=O)-Ph	83
11		1.1	60	11	Na_2HPO_4[c] (CCl_4)	Ph-C(=O)-C(=O)-Ph	64
12	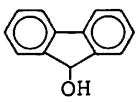	1.1	60	15	CH_3CO_2Na[b] (CH_3CO_2H)	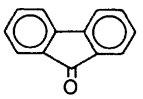	23
13		2.1	60	24	Na_2HPO_4[c] (CCl_4)	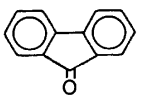	100
14		1.1	60	15	Na_2HPO_4[c] (CCl_4)	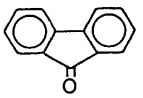	73
15		1.1	60	12	Na_2HPO_4[c] ($CHCl_3$)	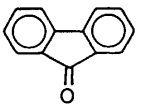	89

a) Yield of isolated product. b) About a 4 equiv of CH_3CO_2Na to BTMA Br_3 was used. c) About a 2 equiv of Na_2HPO_4 to BTMA Br_3 was used. d) A mixture of acetophenone, α-bromoacetophenone, and the starting material, e) a mixture of cyclopentanone, 2-bromocyclopentanone, and the starting material, and f) a mixture of cyclohexanone, 2-bromocyclohexanone, and the starting material, were confirmed by mean of their respective ^1H NMR spectra.

$$\underset{\text{OH}}{\text{R-CH-R}^1} + \text{BTMA Br}_3 \quad \textbf{7}$$

$$\longrightarrow \underset{\text{O}}{\text{R-C-R}^1} + \text{BTMA Br} + 2\,\text{HBr} \quad (8)$$

$$\textbf{8}$$

We believe that, although other procedures for the esterification of primary alcohols and ethers, the lactonization of α,ω-diols and cyclic ethers, and the oxidation of secondary alcohols have been reported, our methods are more effective because of their ease, simplicity, mildness of conditions, and good product yields.

Experimental

Preparation of Ester from Alcohol. Typical Procedure (Run 9 in Table 1): To a solution of 1-octanol (1.30 g, 10 mmol) in carbon tetrachloride (10 ml) we added BTMA Br_3 (4.29 g, 11 mmol) and a solution of $Na_2HPO_4 \cdot 12\ H_2O$ (9.31 g, 26 mmol) in water (10 ml). The reaction mixture was stirred for 8.5 h at 60 °C until the initial orange color faded. The solution was then cooled to room temperature and treated with a 20% aqueous solution of $NaHSO_3$ (10 ml). The organic layer was separated and washed with water (100 ml), dried over $MgSO_4$, and evaporated in vacuo to give octyl octanoate as a colorless oil; yield: 1.27 g (99%), bp 153.5 °C/7 mmHg (lit,[18] bp 305.9 °C/760 mmHg; 1 mmHg≈133.322 Pa).

Preparation of Ester from Simple Ether. Typical Procedure (Run 14 in Table 1): To a solution of dihexyl ether (0.94 g, 5 mmol) in carbon tetrachloride (10 ml) we added BTMA Br_3 (4.29 g, 11 mmol) and a solution of $Na_2HPO_4 \cdot 12H_2O$ (8.60 g, 24 mmol) in water (10 ml). The reaction mixture was then stirred for 5 h at 60 °C until the initial orange color faded. The solution was cooled to room temperature and was worked up as has been described above for the preparation of octyl octanoate to give hexyl hexanoate as a colorless oil; yield: 0.78 g (78%), bp 238—240 °C/760 mmHg (lit,[19] bp 245.6 °C/760 mmHg).

Praparation of Lactone from α,ω-Diol. Typical Procedure (Run 1 in Table 2): To a solution of 1,4-butanediol (0.90 g, 10 mmol) in carbon tetrachloride (10 ml) we added BTMA Br_3 (8.19 g, 21 mmol) and a solution of $Na_2HPO_4 \cdot 12\ H_2O$ (16.41 g, 46 mmol) in water (20 ml). The reaction mixture was stirred for 5.5 h at 70 °C until the initial orange color faded, and then cooled to room temperature. To the mixture we added 20% $NaHSO_3$ aq (10 ml) and then a saturated Na_2CO_3 solution was added until the solution had been made alkaline enough. The reaction mixture was extracted with CH_2Cl_2 (10 ml×4), and ether (50 ml) was added to the CH_2Cl_2 solution in order to precipitate BTMA Br, which was insoluble in ether. The mixture was then filtered, and the filtrate was dried over $MgSO_4$ and evaporated in vacuo to give γ-butyrolactone as a colorless oil; yield: 0.52 g (60%), bp 205 °C/760 mmHg (lit,[20] bp 50—55 °C/3 mmHg).

Preparation of Lactone from Cyclic Ether. Typical Procedure (Run 5 in Table 2): To a solution of THF (0.72 g, 10 mmol) in carbon tetrachloride (10 ml) we added BTMA Br_3 (8.19 g, 21 mmol) and a solution of $Na_2HPO_4 \cdot 12\ H_2O$ (15.04 g, 42 mmol) in water (20 ml). The reaction mixture was stirred for 4.5 h at 60 °C until the initial orange color faded and was then worked up as has been described above to give γ-butyrolactone as a colorless oil; yield: 0.47 g (55%), bp 199 °C/760 mmHg (lit, [20] bp 50—55 °C/3 mmHg).

Preparation of Ketone from Secondary Alcohol. Typical Procedure (Run 3 in Table 3): To a solution of 2-octanol (1.31 g, 10 mmol) in acetic acid (2 ml) we added BTMA Br_3 (3.90 g, 10 mmol) and a solution of $CH_3CO_2Na \cdot 3\ H_2O$ (5.72 g, 42 mmol) in water (20 ml). The reaction mixture was stirred for 2 h at 60 °C until the initial orange color had faded and then cooled to room temperature. To the mixture we added 20% $NaHSO_3$ aq (10 ml); a saturated Na_2CO_3 solution was then added until the solution had been made alkaline enough. The organic layer was separated and washed with water (100 ml), dried over $MgSO_4$, and evaporated in vacuo to give 2-octanone as a colorless oil; yield: 1.25 g (98%), bp 175 °C/760 mmHg (lit,[21] 172 °C/760 mmHg).

References

1) Part II of this series: S. Kajigaeshi, T. Kakinami, T. Yamaguchi, T. Uesugi, and T. Okamoto, *Chem. Express*, **4**, 177 (1989).

2) L. Farkas and O. Schächter, *J. Am. Chem. Soc.*, **71**, 2827 (1949).

3) G. R. Robertson, *Org. Synth.*, **I**, 138 (1948).

4) R. V. Stevens, K. T. Chapman, and H. N. Weller, *J. Org. Chem.*, **45**, 2030 (1980).

5) S. O. Nwaukwa and P. M. Keehn, *Tetrahedron Lett.*, **23**, 35 (1982).

6) T. Kageyama, S. Kawahara, K. Kitamura, Y. Ueno, and M. Okawara, *Chem. Lett.*, **1983**, 1097.

7) A. S. Hay and H. S. Blanchard, *Can. J. Chem.*, **43**, 1306 (1965).

8) K. Takeshita, S. Nakamura, and K. Kawamoto, *Bull. Chem. Soc. Jpn.*, **51**, 2622 (1978).

9) S. Murahashi, K. Ito, T. Naota, and Y. Maeda, *Tetrahedron Lett.*, **22**, 5327 (1981).

10) T. Ogawa and M. Matsui, *J. Am. Chem. Soc.*, **98**, 1629 (1976).

11) S. Kajigaeshi, T. Nakagawa, N. Nagasaki, H. Yamasaki, and S. Fujisaki, *Bull. Chem. Soc. Jpn.*, **59**, 747 (1986).

12) M. Fetizon, M. Golfier, and J-M. Louis, *Tetrahedron*, **31**, 171 (1975).

13) N. C. Deno and N. H. Potter, *J. Am. Chem. Soc.*, **89**, 3550 (1967).

14) S. Kajigaeshi and T. Kakinami, *Yuki Gosei Kagaku Kyokaishi*, **46**, 986 (1988); and the references cited therein.

15) a) S. Kajigaeshi, K. Asano, S. Fujisaki, T. Kakinami, and T. Okamoto, *Chem. Lett.*, **1989**, 463. b) S. Kajigaeshi, T. Kakinami, T. Yamaguchi, T. Uesugi, and T. Okamoto, *Chem. Express*, **4**, 177 (1989).

16) Actually, BTMA Br_3 was slightly dissolved in water, and the aqueous solution, which had been stirred for 5 min at 60 °C, dyed a potassium iodide starch paper a deep blue; the pH of the solution was obtained as 3.1.

17) For example, in the case of the reaction of butyl alcohol with BTMA Br_3 (1 equiv) and aqueous Na_2HPO_4 (2 equiv) in CCl_4, the pH values of the solution were obtained as follows; 8.1 (at initial time), 7.0 (at 2.5 h after), and 3.12 (at 24 h after).

18) "Beilsteins Handbuch der Organischen Chemie," ed by B. Prager and P. Jacobson, Verlag ver Julius Springer, Berlin, **2**, 348 (1920).

19) "Beilsteins Handbuch der Organischen Chemie," ed by B. Prager and P. Jacobson, Verlag ver Julius Springer, Berlin, **2**, 323 (1920).

20) Y. Kamiya and S. Takemura, *Chem. Pharm. Bull.*, **21**, 1401 (1973).

21) "The Merck Index: An Encyclopedia of Chemicals and Drugs," 10th ed, ed by M. Windoholz, Merck & Co., N. J., 681 (1983).

 © 1989 The Chemical Society of Japan Bull. Chem. Soc. Jpn., 62, 2589—2593 (1989)

A Model Study of Rhodopsin Regeneration in Visual Cell. Photoisomerization of all-trans Retinal in Phosphatidylcholine Vesicles

Hiroshi TANIE, Katsunori OHBA, Minoru SAKURAI,*
Yoshio INOUE, and Riichiro CHÛJÔ
Department of Biomolecular Engineering, Tokyo Institute of Technology, O-okayama 2-chome, Meguroku, Tokyo 152
(Received January 31, 1989)

The photochemical behavior has been investigated for all-trans retinal in egg york phosphatidylcholine(EPC) vesicles and dipalmitoylphosphatidylcholine (DPPC) vesicles. In EPC vesicles, 10% of all-trans isomer is isomerized to 11-cis one upon direct irradiation of 15 W-fluorescence light for 180 min. In organic solvents the photoisomerization of all-trans isomer is induced depending on the dielectric constant of solvent. The distributions of retinal isomers in EPC vesicles is similar to those obtained in less polar solvents, such as diethyl ether. Significant difference is not recognized between the distributions of retinal isomers in DPPC vesicles at the above and below T_c. These results indicate that photoisomerization of retinal in PC vesicles is dominated by the electric properties of enviroment of retinal rather than the packing effect of PC membrane.

The vertebrate rhodopsin is embedded in the disk membrane of the rod outer segment (ROS) of a photoreceptor cell. Rhodopsin consists of an apoprotein opsin and a chromophore 11-cis retinal bound to opsin via protonated Schiff base linkage with a side chain of a lysine residue (e.g. Lys^{296} in bovine rhodopsin[1]). The illumination of rhodopsin leads to the isomerization of the 11-cis to all-trans form and finally to the release of the all-trans isomer from opsin.[2-5] Owing to poor solubility of retinal to water the released retinal possibly remains in the disk membrane, which is mainly composed of phosphatidylcholine (PC) and phosphatidylethanolamine (PE). Since PE has an amino group, retinal can form Schiff base with PE in the disk membrane. It has been reported that in the final stage of rhodopsin bleaching (metarhodopsin III) the populations of free, lipid-bound and protein-bound retinal are 34, 15, and 51%, respectively.[6] Although the metabolic pathway of the released retinal remains unclear, a possible one is that it is utilized for the rhodopsin regeneration. In order for rhodopsin regeneration to proceed all-trans retinal should be reisomerized to 11-cis form. When rhodopsin is partially bleached, photochemical reisomerization of the released retinal occurs in the disk membrane.[7] A mechanism for the above process has been proposed by Shichi and Somers[8,9] that the released all-trans retinal is reisomerized photochemically to 11-cis form as protonated retinal-PE Schiff base. This mechasnism is based on the following experimental data: (a) the bleached ROS complex shows an absorption maximum at 458 nm that is similar to the absorption maximum of protonated retinal-PE Schiff base, (b) 450—460 nm light covering the absorption maximum of 458 nm is the most effective on the formation of rhodopsin and (c) the formation of rhodopsin is markedly reduced by partial delipidation and restored by the addition of PE. According to an another report[7] the reisomerization probably occurs photochemically as free retinal, too.

On the other hand it has been reported that retinal-incorporated egg york PC vesicles are damaged by the singlet oxygen produced by the light absorption of retianl.[10-12] In acetonitrile retinal is also damaged by singlet oxygen.[13] Hence, in the disk membrane retinal may be damaged together with membrane by photochemically produced singlet oxygen.

In order to clarify the mechanisms of these reactions in which the released all-trans retinal participates, the photochemical behavior must be investigated for retinal in membrane. Many studies have been reported on photochemical isomerization of all-trans retinal in organic solvents using HPLC (high-performance liquid chromatography) the formation of 11-cis isomer increases with an increases of the polarity of solvents, and the formation of 11-cis isomer increases with an increase of the polarity of solvents, and the formation of 11-cis isomer seems to be reduced by the viscosity of solvents. The data obtained in solution are insufficient to understand the photochemical behavior in the disk membrane since membrane has some characteristics different from solvents i.e., (a) the microscopic inhomogeneity in electric properties arising from the water-hydrocarbon interface and (b) the packing effect of alkyl chains of phospholipids. There have been some reports on the photoisomerization of retinal in organized systems such as micells and membrane.[15,16] However, these reports disconcerned the regeneration process of rhodopsin.

In this report the experiments are designed in order to extract and clarify the effect of the above two factors, namely the inhomogeneity in environment and the packing effect on the photoisomerization of

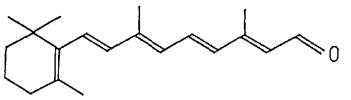

all-trans retinal

retinal. Sonicated PC vesicle is used as a model of the disk membrane, and all-trans retinal is photoisomerized in it. We shall indicate that the significant amount of 11-cis retinal is photochemically produced in the model membrane system.

Experimental

Materials. Vitamin A was purchased from Riken Vitamin Co. Ltd. All-trans retinal was crystallized by oxidation of vitamin A with manganese dioxide in petroleum ether. Egg york phosphatidylcholine (EPC) and dipalmitoyl phosphatidylcholine (DPPC) were purchased from Sigma Chemical Co. All solvents used in the experiments were guaranteed grade.

Preparation of Vesicles. Chloroform solution of retinal and phospholipids, EPC, or DPPC were evaporated, giving a dry thin film. Molar ratio of retinal and PC was 1:5. Phospholipid dispersions were prepared by the addition of 50 mM KCl aqueous solution (1 M=1 mol dm^{-3}) to the dry film and subsequent shaking. The dispersions were then sonicated for 20 min under cooling by ice/water with Ultrasonic Disruptor Model UR-200P (Tomy Seiko Co., Ltd., frequency 20 kHz, output power 200 W). The resultant vesicle solutions were centrifuged at 15000 rpm for 40 min to remove multilayer vesicles and metallic titanium fragments from sonicator's microtip.

Photoisomerization of Retinal in Phospholipids. Irradiation was carried out under 15 W-fluorescence light for an appropriate duration. A 15 W-fluorescence lamp is used as a light source, due to relatively close distribution of wave length compared with that of sun light. 5 cm^3 methanol and 5 cm^3 1,2-dichloroethane were added to the sample and the suspensions were centrifuged at 10000 rpm for 2 min. The lower layer was collected and the organic solvent was removed by evaporation, followed by dissolving to solvent for HPLC. The samples were filtrated through the membrane milipore filters. The HPLC analysis were performed using Waters Model-590 HPLC, with a μ-porasil column (3.9 mm×30cm) under the conditions of flow rate 2.0 cm^3 min^{-1}, 6% diethyl ether/hexane (v/v) as a eluent, and 365 nm UV detection. The eluent and samples used were filtrated through membrane milipore filters before use.

The Photoisomerization of Retinal in Organic Solvents. Retinal was dissolved into the organic solvent used until the absorbance of the solution reached about 2. Irradiation is carried out under 15 W-fluorescence light for 90 min. After irradiation the solvents were removed by evaporation, followed by redissolved to solvent for HPLC. The HPLC analyses were similarly performed to the above procedure.

DSC Experiments. Retinal incorporated vesicles were prepared as mentioned above. Sample was injected into a small volume pan and the characteristics were recorded on DSC 10 (Seiko I&E) with heating rate of 0.5 °C min^{-1}.

All manipulations were performed under red dim light except the photoisomerization procedures.

Results

Estimation of Retinal Photo-Damage in EPC Vesicles. In Fig. 1 is shown the HPLC chromatogram of extract from retinal/EPC vesicles irradiated for 40 h. The peakes appearing in the retention time range of 4 to 10 min correspond to configurational isomers of retinal. Additional three broad peakes were found in the retention time range of 15 to 40 min. One of the three peaks found just before 20 min increases with the duration of irradiation. The identification of this peak has not been performed in particular. The hemiacetal isomer of 5,8-peroxyretinal is one of possible candidates, because 5,8-peroxyretinal is produced by the photoisomerization of all-trans retinal in aerated solution,[13] and easily isomerized to the hemiacetal isomer.[17] An absorption coefficient was reported for hemiacetal isomer of 5,8-peroxyretinal ($\varepsilon_{320\ nm}$=33000 in hexane[17]). This value was used in order to estimate the extent of oxidation.[16] According to the estimation, only 3% of retinal is damaged (converted to other compounds) during irradiation for 3 h. During irradiation for 40 h the damaging of retinal increased up to 13%.

Determination of Optimum Irradiation Time. In Fig. 2 the fractional populations of retinal isomers were plotted against a function of photo-irradiation

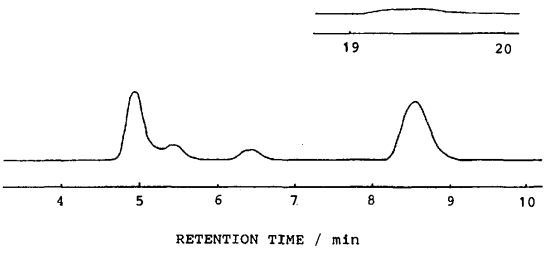

Fig. 1. HPLC chromatogram of extract from retinal/EPC vesicles after irradiated for 40 h.

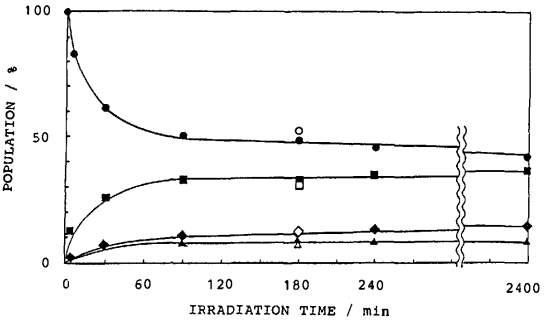

Fig. 2. The plots of the populations of retinal isomers formed in EPC vesicles vs. the duration of irradiation (at room temperature); ●○ all-trans, ■□ 13-cis, ◆◇ 11-cis, ▲△ 9-cis. The solid and open simbols correspond to the composition obtained in the absence and the presence of α-tocopherol, respectively. [retinal]:[EPC]=1:5.

Table 1. Populations of Retinal Isomers Formed in EPC Vesicles

Isomerization conditions	Isomer formed/%				
	13-cis	11-cis	9-cis	7-cis	All-trans
Irradiation	32.6	10.2	9.0	Trace	48.3
Dark incubation	2.4	Trace	Trace	Trace	97.6

Table 2. Populations of Retinal Isomers Formed by Irradiation in Organic Solvents

Organic solvent	Dielectric constant	Isomer formed/%					Distribution type[a]
		13-cis	11-cis	9-cis	7-cis	All-trans	
Hexane	1.88	25.7	Trace	3.4	Trace	70.9	A
Diethyl ether	4.34	37.3	6.9	6.2	Trace	49.5	B
Chloroform	4.81	29.0	28.2	10.3	1.1	31.4	B
Ethyl acetate	6.02	34.5	14.9	12.4	Trace	38.2	B
Methanol	32.70	14.7	35.7	11.5	Trace	38.1	C
Acetonitrile[b]	37.50	18.7	43.4	11.7	5.8	20.4	C

a) See text. b) Ref. 12.

time. Fig. 2 indicates that the populations of retinal isomers approaches gradually to those at 40 h. In order to minimize the retinal damaging and to approach populations close to those in the photoequilibrium state, we determined the best irradiation time to be 180 min.

α-Tocopherol is well-known as a scavenger of singlet oxygen in biomembranes.[18-20] Retinal was photoisomerized in α-tocopherol/EPC vesicles. In Fig. 2 are shown the results for 180 min irradiation. The similarity of these two distributions of isomers obtained in the absence and in the presence of α-tocopherol indicates that the oxidation of retinal inaffects the isomerization behavior of retinyl polyene during irradiation for 180 min.

Photoisomerization of Retinal in EPC Vesicles. In Table 1 are summerized the populations of retinal isomers formed during direct irradiation (upper) and dark incubation (lower) in EPC vesicles. The isomerization time is 180 min in each case. Upon irradiation for 180 min in EPC vesicles 13-cis, 11-cis, and 9-cis isomers are formed with the populations of 33, 10, and 9%, respectively. 11-cis Isomer (important in rhodopsin regeneration) is formed less than 13-cis isomer. On the other hand, upon dark incubation for 180 min 11-cis and 9-cis isomers are not formed but only 13-cis isomer is formed with the population of 2.4%. No formation of 11-cis isomer is consistent with an earlier report.[21] It is noted that only under the irradiation conditions, 11-cis isomer can be formed.

Photoisomerization of Retinal in Organic Solvents. In Table 2 are summerized the populations of retinal isomers in the photostationary state in various organic solvents. By monitoring the change of the UV absorbance, it is confirmed that the photostationary state is attained by irradiation of 90 min. In order to investigate the dependence of isomer populations on the polarity of solvent, various types of solvents were selected so as to cover the wide range of the dielectric constants. In hexane 13-cis and 9-cis isomers were formed with the populations of 26 and 3%, repectively. 11-cis Isomer was not formed upon irradiation in hexane. In the solvents with relatively low dielectric constants, 4 to 6, 11-cis isomer is less formed than 13-cis isomer. In diehtyl ether, for example, 13-cis, 11-cis, and 9-cis isomers are formed with the populations of 37, 7, and 6%, respectively. In the solvents with relatively high dielectric constants, 30 to 40, 11-cis isomer is more formed than other cis isomers. In methanol, for example, 13-cis, 11-cis, and 9-cis isomers are formed with the populations of 15, 36, and 12%, respectively. On the basis of the relative population of 11-cis isomer against other cis isomers, we can classify the isomer distributions in those solvents into three types, named type A, type B, and type C (see the last column of Table 2). Type A is characterized as no formation of 11-cis isomer. Type B is characterized as the cis isomer formtions in the order of 13-cis>11-cis>9-cis. And type C is characterized as the preferencial formation of 11-cis isomer among cis ones. According to this classification, the formation of 11-cis isomer increases in the order of type A<type B<type C. We, therefore, found a good correlation between the distributions and the polarity (dielectric constant) of the solvents. That is to say, the relative

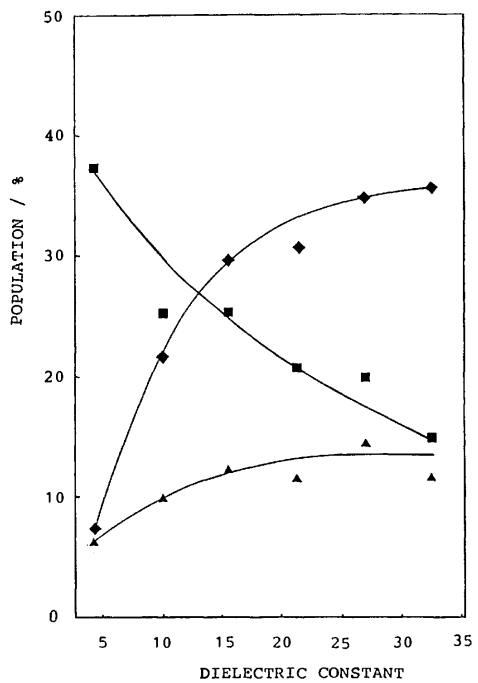

Fig. 3. The dielectric-constant dependence of the populations of retinal isomers formed in diethyl ether/methanol mixture (at room temperature); ■ 13-cis, ◆ 11-cis, ▲ 9-cis.

population of 11-cis retianl increases with an increase of the polarity of the environments.

Photoisomerization of Retinal in Diethyl Ether-Methanol Mixture. In order to confirm the polarity dependence of distributions of cis isomers, we used diethyl ether-methanol mixtures as the solvents for the isomerization reaction. In Fig. 3 the populations of cis isomers are plotted against the dielectric constants of solvents. The dielectric constans are calculated on the basis of linear combination of those of two components. In Fig. 3 is shown that with an increase in the dielectric constant the population of the 11-cis isomer increases while that of 13-cis isomer decreases. Irrespective of solvent composition, the 9-cis isomer is smaller than both 11-cis and 13-cis isomers. At low dielectric constants, 4 to 10, the population of 11-cis isomer is smaller than that of 13-cis isomer, and thus the isomer distributions is classified into the type B. At relatively higher dielectric constants, 15 to 33, the order of the formation of 11-cis and 13-cis isomers is altered and the isomer distributions is classified into the type C. These findings are confirmations for the correlation between the polarity of solvent and the distributions of retianl isomers.

We attempt to apply the above classification to the isomer distributions resulting from the photoisomerization of retinal in EPC vesicles (Table 1, upper). The isomer distribution in EPC vesicles can be assigned to one of these three types defined the above, namely, type B. Since the isomer distribution in EPC vesicles is comparable to those obtained in solutions of less polar solvents, especially in diethyl ether, we can suppose that the photoisomerization of retinal in EPC vesicles is also dominated by the polarity of its surrounding environment, and that retinal receives photon in an apolar region, such as hydrocarbon core of the vesicles.

Photoisomerization of Retinal in DPPC Vesicles. The gel-liquid crystal phase transition temperature T_c was measured for retinal-containing DPPC vesicles. From DSC (differencial scanning calorimetry) chromatogram, T_c of retinal/DPPC vesicles (molar ratio 1 : 5) was determined to be 37.7 °C. The T_c obtained here is lower by ca. 4.5 °C than that of pure DPPC vesicles, 41.2 °C. The lowering of T_c induced by incorporation of retinal is consistent with a previous report.[22]

In Table 3 are summerized the populations of retinal isomers formed during irradiation for 180 min in DPPC vesicles. In order to investigate the effect of mobility of lipids on isomerization process, irradiation were carried out at the temperatures above and below T_c, 51 °C and 24 °C, respectively. In the liquid crystal state (above T_c), 13-cis, 11-cis, and 9-cis isomers are formed with the populations of 36, 5, and 10%, respectively. In the gel state (below T_c), 13-cis, 11-cis, and 9-cis isomers are formed with the populations of 32, 5, and 10%, respectively. Both distributions at these two temperatures correspond to the medium type between A and B. No significant difference is recognized between the distributions formed at these two different temperatures. These findings indicate that the photoisomerization of retinal is inaffected by the change in the packing effect depending on the state of alkyl chain.

Table 3. Populations of Retinal Isomers Formed by Irradiation in DPPC Vesicles

Temperature /°C	Isomer formed/%				
	13-cis	11-cis	9-cis	7-cis	All-trans
51 (above T_c)	36.4	4.6	10.2	Trace	48.8
24 (below T_c)	32.4	5.3	11.9	Trace	50.3

Discussion

In the final stage of the rhodopsin bleaching, the major fraction of the retinal molecules released from opsin dissociates into free form in the disk membrane.[6] Thus, if these retinals are isomerized to 11-cis form and subsequently bind to opsin, the significant amount of rhodopsin is expected to be regenerated. It has been reported that second step (binding to opsin) in the regeneration process proceeds efficiently in the disk membrane.[9] The efficiency of rhodopsin regeneration, therefore, depends on that of the first step (isomerization to 11-cis isomer), which can be estimated from the present data. Irradiation experiments were carried out using the usual light source (15 W-fluorescence light), which does not contain the light of ultraviolet region (<400 nm). The present results indicate that under the irradiation of visible rays all-trans isomer (λ_{max}=387 nm) is efficiently isomerized to cis isomers in lipid membrane. Consequently, 10% of the all-trans is isomerized to 11-cis and simultaneously the comparable amount of 9-cis is produced. 9-cis Isomer can also bind with opsin, giving isorhodopsin. On the other hand, during dark incubation, 9- and 11-cis isomers are not produced in the lipid membrane. These results suggest that the significant amount of natural pigments can be regenerated through the light adaption of the disk membrane containing the bleached rhodopsin.

The population of 11-cis (10%) obtained here are inconsistent with that (0.3%) appearing elsewhere.[14] The origin of this discrepancy may be attributable to the difference in irradiation intensity. 400 W-mercury lamp was used in Ref.13. Stronger irradiation may induce various side reactions involving the formation of epoxyretinal.

The isomer distribution in EPC vesicles is similar to those in the medium of relatively lower dielectric constant. This finding suggests that the photoisomerization behavior of retinal in EPC vesicles is mainly controlled by electric properties of its environment. And the principal moiety of the retinal molecule should be located in a hydrophobic region of

EPC vesicles. In nonpolar solvent such as hexane 11-cis isomer is, however, not formed. Thus in EPC vesicles the retinyl polyene must be partially exposed to the polar region of EPC vesicles. Probably the -C=O group of retinal is in contact with the polar head groups of lipids. Such a location and orientation of retinal are consistent with the results of ESR[23] and NMR[15,24] studies on retinal-vesicles and -micelles systems. However, on the basis of the present results, the inhomogeneity of polarity in EPC vesicles is not necessarily important for the control of the photoisomerization pathway of retinal. Rather, the idea of the average polarity of the environment is sufficient to explain the observed isomer distribution.

No significant difference appearing in the isomer distributions in DPPC vesicles at above and below T_c. This finding suggests directly that the change in the packing effect induced by the phase transition of lipid inaffects the photoisomerization behavior of retinal. This is consistent with the fact that the trend of the isomer distribution is not largely different from that observed in solution. The incorporation of retinal into vesicles causes to increase lipid-lipid distance, leading to the decrease in the cooperativity of lipid molecules. This is supported by the facts that the incorporation of retinal leads to increasing the proton permiation,[25] broadening of the DSC transition[22] and lowering of the Tc of DPPC vesicles.[22] The weakening of the packing facilitates the isomerization of retinal, which may inaffects in lipid packing.

The isomer distribution attained in EPC vesicles is compared with that in DPPC vesicles. The formation of 11-cis in DPPC vesicles are smaller than in EPC vesicles, and the formation of 9-cis and 13-cis isomers in DPPC are larger than those in EPC vesicles. As indicated in Fig. 3 in the medium of lower dielectric constant (ca. 10), the populations of these isomers dramatically changes in the region of dielectric constant. In other words, the slight variation of the environment causes the largely different isomer populations in a lower dielectric medium. EPC and DPPC are different in the spiecies of fatty acid chains, indicating variation of the dielectric properties of hydrophobic core of membrane, and in the extent of retinal penetration. This is the main origin of the observed difference in the isomer distribution between EPC and DPPC vesicles.

In summary, we used the PC vesicles as a model of disk membrane. In EPC vesicles 10% of 11-cis retinal are formed by irradiation of 15 W-fluorescence light. Since 11-cis isomer is not formed during dark incubation, photoisomerization process is effective to form 11-cis isomer. On the other hand, the photoisomerization data in organic solvents are useful to explain the photoisomerization in EPC vesicles, and to estimate the environment of retinal in PC vesicles.

References

1) N. G. Abdulaev, I. D. Artamonov, A. S. Bogachuk, M. Y. Feigina, M. B. Kostina, A. B. Kudelin, V. I. Martynov, A. I. Miroshnikov, A. S. Zolotarevand, and Y. A. Ovchinikov, *Biochem. Int.*, **5**, 693 (1982).

2) G. Wald, *Science*, **162**, 230 (1968).

3) R. R. Birge, *Ann. Rev. Bioeng.*, **10**, 315 (1981).

4) T. Yoshizawa, *Adv. Biophys.*, **17**, 5 (1984).

5) R. S. H. Liu and T. Mirzadegan, *J. Am. Chem. Soc.*, **110**, 8617 (1988).

6) P. J. G. M. van Breugel, P. H. M. Geurts, S. L. Bonting, and F. J. M. Daemen, *Biochim. Biophys. Acta*, **509**, 136 (1978).

7) W. F. Zimmerman, M. T. Yost, and F. J. M. Daemen, *Nature, (London)*, **250**, 66 (1974).

8) H. Shich and R. L. Somers, *J. Biol. Chem.*, **249**, 6570 (1974).

9) H. Shich and R. L. Somers, *Photochem. Photobiol.*, **22**, 187 (1975).

10) M. Delmelle, *Photochem. Photobiol.*, **27**, 731 (1978).

11) M. Delmelle, *Photochem. Photobiol.*, **28**, 357 (1978).

12) M. Delmelle, *Photochem. Photobiol.*, **29**, 713 (1979).

13) K. Tsujimoto, H. Hozoji, M. Ohashi, M. Watanabe, and H. Hattori, *Chem. Lett.*, **1984**, 1673.

14) K. Tsukida, A. Kodama, and M. Ito, *J. Chromatogr.*, **134**, 331 (1977),

15) J. Lauterwein and C. Pattaroni, *Biochem. Biophys. Res. Commun.*, **108**, 1300 (1982).

16) P. Deval and A. K. Singh, *J. Photochem. Photobiol. A: Chem.*, **42**, 329 (1988).

17) D. -A. Lerner, J.-C. Mani, and M. Mousseron-Canet, *Bull. Soc. Chim. Fr.*, **1970**, 1968.

18) M. Fragata and F. Bellemere, *Chem. Phys. Lipids*, **27**, 93 (1980).

19) R. A. Dilley and D. G. McConnell, *J. Membr. Biol.*, **2**, 317 (1970).

20) A. T. Diplock and J. A. Lucy, *FEBS Lett.*, **29**, 205 (1973).

21) G. W. T. Groenendijk, C. W. M. Jacobs, S. L. Bonting, and F. J. M. Daemen, *Eur. J. Biochem.*, **106**, 119 (1980).

22) D. Clausse, I. Sifrini, and J. P. Dumas, *Thermochim. Acta*, **122**, 123 (1987).

23) S. R. Wassall, T. M. Phelps, M. R. Aldrecht, C. A. Laugsford, and W. Stillwell, *Biochim. Biophys. Acta*, **939**, 393 (1988).

24) Y. Inoue, Y. Hanafusa, M. Toda, and R. Chûjô, *Bull. Chem. Soc. Jpn.*, **55**, 540 (1982).

25) W. Stillwell, K. Doram, and S. Karimi, *J. Memb. Sci.*, **8**, 3 (1981).

Mechanism of the Reaction of (Arylthio)trimethylgermanes with 1-Aryl-1-bromoethanes—Kinetic and Stereochemical Studies—

Seizi KOZUKA,* Takemi NITTA, Shoji TAMURA, and Waichiro TAGAKI
Department of Applied Chemistry, Faculty of Engineering, Osaka City University, Sugimoto 3-chome, Sumiyoshi, Osaka 558
(Received February 22, 1989)

Kinetic and stereochemical studies have been conducted on the reaction of (arylthio)trimethylgermanes with 1-aryl-1-bromoethanes. The reaction has been found to obey a first-order kinetic equation. The rates of the reaction of the substituted arylethanes were well-correlated with σ^+ constants. Optically active 1-bromo-1-phenylethane gave racemic phenyl 1-phenylethyl sulfide by the reaction with trimethyl(phenylthio)germane. An S_N1 ionization of 1-aryl-1-bromoethanes has been suggested as the reaction mechanism.

We have reported a kinetic study on the reaction of (arylthio)trimethylgermanes with benzyl bromides giving aryl benzyl sulfides and bromotrimethylgermane.[1] The reaction obeyed a second-order kinetic equation and gave apparently negative ρ value due to the substituents on the arylthio group. Accordingly, a nucleophilic attack of the sulfur atom on the benzylic carbon atom has been suggested as the reaction mechanism (Scheme 1).

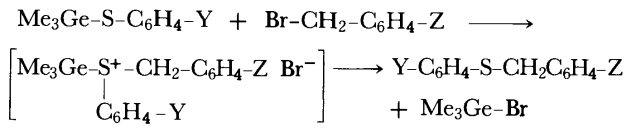

Scheme 1.

A quite different kinetic aspect was observed for the reaction of (arylthio)trimethylgermanes with aroyl chlorides.[2] The reaction also obeyed a second-order kinetic equation, however, quite different in the substituent effects. Namely, positive ρ values were observed for both due to the substituents on the arylthio moiety and to the substituents on the aroyl group. These substituent effects together with the observed large solvent effects on the rate of the reaction were well-rationalized in terms of 5-coordinated process involving unfavorable equilibrium formation of the intermediate **2** which was followed by rate-determining attack of the arenethiolate ion on the carbonyl carbon atom (Scheme 2).[2]

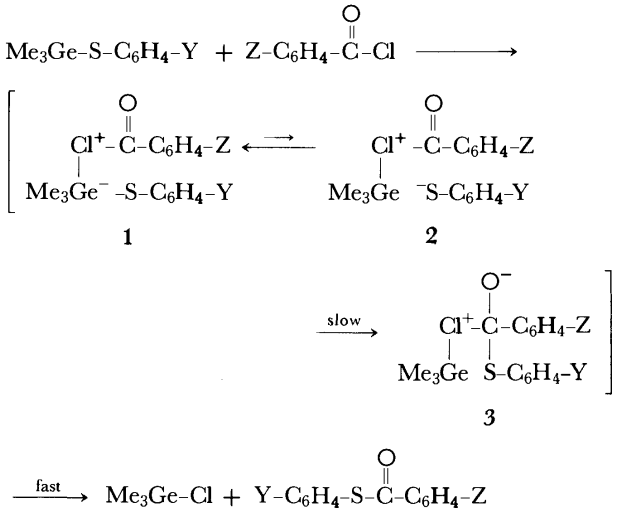

Scheme 2.

The difference in their mechanisms of those two reactions was explained in terms of different steric requirements of the reactants. Benzyl bromide can accept a bimolecular nucleophilic attack even by such bulky nucleophiles as (arylthio)trimethylgermanes. On the other hand, aroyl halides involve addition intermediates during the course of a nucleophilic addition-elimination process and hence hardly accept attack of a bulky nucleophile like the arylthiogermanes. Thus, the reaction with aroyl chlorides proceeds by another process, i.e., 5-coordination of the metal atom.[1]

The same concept can be applied to rationalizing mechanistic difference in the analogous reactions. It is quite natural that the reaction of (arylthio)trimethylstannanes, a compound bearing longer metal-sulfur bond than that of germanium-sulfur, with benzyl halides proceeds by a nucleophilic attack.[3] The longer stannyl-sulfur bond provides a room for a bimolecular nucleophilic process in the reaction even with aroyl chlorides which demands more space for the nucleophilic attack forming an intermediate **4**,

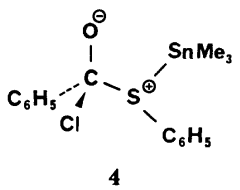

4

than that required for benzylic substrate.[4] On the contrary, (arylthio)trimethylsilanes can only undergo the 5-coordination process in the reaction even with phenacyl bromide which has been known as one of the most reactive substrates for S_N2 reactions.[5]

Based on these considerations, the length of germanium-sulfur bond in (arylthio)trimethylgermanes is critical which allows to proceed a bimolecular nucleophilic process in the reaction with benzyl halides.

An increment of some steric hindrance on benzyl halides may cause the change of the reaction mechanism from the bimolecular nucleophilic process to another, i.e., 5-coordination process. Thus, we have tried the reaction of (arylthio)trimethylgermanes with benzyl bromides bearing a methyl group at the α-position, that is 1-aryl-1-bromoethanes. Another possible mechanism would be the S_N1 process since the bromoalkane undergoes a facile unimolecular ionization.

Results and Discussion

Trimethyl(phenylthio)germane (247 mg, 1.27 mmol) was allowed to react with an equimolar amount of 1-bromo-1-phenylethane (235 mg, 1.27 mmol) at 100 °C for 41 h. The ^{1}H NMR spectrum of the reaction mixture showed signals only corresponding to the products although prolonged heating after completion of the reaction resulted in formation of some amount of unidentified side-product which might form from thermolysis of the product. Bromotrimethylgermane and phenyl 1-phenylethyl sulfide were isolated from the reaction mixture and characterized. Thus, the present reaction appeared to be a quite similar reaction in the type of the products with those of the reaction with benzyl halides[3] as shown in Scheme 3.

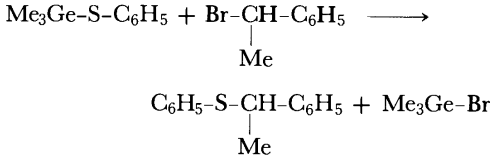

Scheme 3.

The reaction was carried out in a solvent with a small excess amount of the bromide. This is typical kinetic conditions for second-order reactions. The reaction was monitored by observing ^{1}H NMR trimethyl signals of the starting germane (δ=0.47) and the product, bromotrimethylgermane (δ=0.85). The rate constant was obtained by least-squares calculation of relative intensity of the trimethyl signals at time intervals. The second-order kinetic equation, each first-order in respective to the two reactants, failed to reveal linear kinetic plot. On the other hand, the first-order equation in respective to the concentration of the bromoethane gave a satisfactory result up to more than 90% completion. The result suggests the first-order reaction dependent only on the concentration of the bromoethane. The first-order dependency was also confirmed by the kinetic experiments with various concentrations of the phenylthiogermane. The rate constants thus obtained were nearly identical regardless of the different concentrations of the phenylthiogermane. Thus, the reaction was found to be of a first-order dependent only on the concentration of 1-bromo-1-phenylethane even under typical second-order reaction conditions. Accordingly, it is quite natural that the effect of the substituents (Y) of the arylthio group on the rate of the reaction appeared insignificant. These results are shown in Table 1.

Table 1. First-Order Rate Constants for the Reaction of $Me_3GeSC_6H_4$-Y with $C_6H_5CH(Me)Br$

[GeS][a]	[RBr][a]	[GeS]/[RBr]	Y	Solvent	Temp /°C	$k_1\times10^5$ /s^{-1}	γ[b]
0.131	0.318	0.4	H	C_6H_5CN	110	6.39±0.18	0.999
0.262	0.318	0.8	H	C_6H_5CN	110	7.00±0.31	0.999
0.380	0.318	1.2	H	C_6H_5CN	110	7.22±0.70	0.998
0.262	0.318	0.8	H	C_6H_5CN	100	2.99±0.03	0.999
0.262	0.318	0.8	H	C_6H_5CN	120	15.6 ±0.64	0.999
0.262	0.318	0.8	*m*-Cl	C_6H_5CN	110	4.57±0.16	0.998
0.262	0.318	0.8	*p*-Cl	C_6H_5CN	110	5.89±0.16	0.999
0.262	0.318	0.8	*p*-Me	C_6H_5CN	110	6.14±0.25	0.999
0.262	0.318	0.8	*p*-OMe	C_6H_5CN	110	5.18±0.13	0.999
0.262	0.318	0.8	*m*-Cl	C_6H_5OMe	120	0.77±0.14	0.993
0.262	0.318	0.8	*p*-Cl	C_6H_5OMe	120	0.73±0.10	0.996
0.262	0.318	0.8	H	C_6H_5OMe	120	0.91±0.05	0.999
0.262	0.318	0.8	*p*-Me	C_6H_5OMe	120	0.83±0.05	0.998
0.262	0.318	0.8	*p*-OMe	C_6H_5OMe	120	0.75±0.02	0.999
0.262	0.318	0.8	H	C_6H_5OMe	110	0.39±0.07	0.994
0.262	0.318	0.8	H	C_6H_5OMe	130	2.06±0.18	0.997
0.262	0.318	0.8	H	C_6H_5Me	130	0.27±0.03	0.986
0.262	0.318	0.8	H	C_6H_5Me	140	0.68±0.04	0.988
0.262	0.318	0.8	H	C_6H_5Me	150	1.23±0.14	0.986

$\Delta H^{\neq}_{400}$=101.0 kJ mol^{-1}, $\Delta S^{\neq}_{400}$=−63.2 J K^{-1} mol^{-1}, in C_6H_5CN 0.999.[b]
$\Delta H^{\neq}_{400}$=106.4 kJ mol^{-1}, $\Delta S^{\neq}_{400}$=−73.1 J K^{-1} mol^{-1}, in C_6H_5OMe 0.999.
$\Delta H^{\neq}_{400}$=107.0 kJ mol^{-1}, $\Delta S^{\neq}_{400}$=−87.8 J K^{-1} mol^{-1}, in C_6H_5Me 0.999.
k_{rel} in C_6H_5Me : C_6H_5OMe : C_6H_5CN=1 : 7.6 : 125 at 130 °C.

a) Concentrations: mol dm^{-3}. b) Correlation coefficient.

Table 1 also contains activation parameters and the solvent effects on the rates of the reaction. The observed entropy of activation values are negative but these results do not contradict with the unimolecular ionization mechanism. The values observed for the analogous reactions of this type involving bimolecular nucleophilic or 5-coordination process as their mechanisms have been known much more negative than those observed for the present study in various solvents.[6] The values presently observed suggest looser transition state for the reaction than those proceeding bimolecular mechanisms. The smaller negative entropy of activations in absolute values in more polar solvents, shown in Table 1, are in accordance with the unimolecular ionization although it is difficult to explain why they are still negative. Substantially smaller enthalpy values observed in polar solvents suggest an ionic process for the present reaction and is in line with the large solvent effect.

Contrary to insignificant substituent effect of the arylthio group (Y), the substituents on 1-aryl-1-bromoethanes (Z) affect largely the rates of the reaction. The results are given in Table 2. Linear Hammett plots were obtained with σ^+ constants giving large negative ρ values for both the reactions in benzonitrile and anisole, although they are slightly curved upward as shown in Fig. 1. The effects of Z in both the solvents are nearly comparable with those of the unimolecular ionization of benzylic substrate.[7] The small upward deviations of the plots for the electron-withdrawing substituents may be explained by the minor contribution of a bimolecular nucleophilic substitution. The unimolecular ionization would become more unfavorable with the electron-withdrawing substituents and the bimolecular nucleophilic process would contribute more.

Table 2. First-Order Rate Constants for the Reaction of $Me_3GeSC_6H_5$ (0.262 mol dm^{-3}) with Z-$C_6H_4CH(Me)Br$ (0.318 mol dm^{-3})

Solvent	Temp/°C	Z	$k_1\times10^5$/s^{-1}	γ[a]
C_6H_5CN	70	*p*-Me	5.27±0.49	0.998
C_6H_5CN	80	*p*-Me	13.64±0.47	0.999
C_6H_5CN	110	H	7.00±0.31	0.999
C_6H_5CN	110	*p*-Cl	3.36±0.27	0.999
C_6H_5CN	110	*n*-Cl	0.47±0.06	0.998
C_6H_5OMe	80	*p*-Me	1.30±0.34	0.979
C_6H_5OMe	90	*p*-Me	2.96±0.21	0.998
C_6H_5OMe	130	H	2.06±0.18	0.997
C_6H_5OMe	130	*p*-Cl	1.52±0.02	0.999
C_6H_5OMe	130	*m*-Cl	0.30±0.03	0.992

a) Correlation coefficient of the kinetic plot.

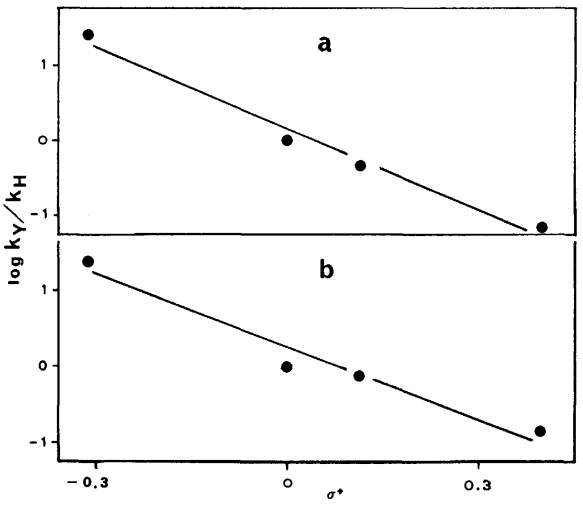

Fig. 1. Plots of the rate constants of the reactions of $Me_3GeSC_6H_5$ with Z-$C_6H_4CH(Me)Br$ against σ^+ constants, (a) in benzonitrile, (b) in anisole.

In a control experiment, 1-bromo-1-phenylethane was heated in the presence of 2,6-lutidine, instead of the thiogermane, in benzonitrile under the same reaction conditions used for the kinetic experiments. Styrene was obtained in about 70% yield which is quite comparable with the conversion of the reaction with the thiogermane under the same reaction conditions (65%) as shown in Scheme 4. The unimolecular ionization of the bromoethane has been confirmed under the kinetic conditions.

$$C_6H_5CH(Me)Br \ (318\ mmol\ dm^{-3}) \xrightarrow[110°C,\ 3.75\ h,\ in\ benzonitrile]{2,6\text{-lutidine (382 mmol dm}^{-3})} C_6H_5CH{=}CH_2 \quad (70\%\ yield)$$

Scheme 4.

Optically active (+)-1-bromo-1-phenylethane was allowed to react with an equimolar amount of trimethyl(phenylthio)germane. Phenyl 1-phenylethyl sulfide thus obtained was found to be racemized nearly completely (Scheme 5). This is conclusive evidence supporting a unimolecular ionization of the bromoethane.

$$Me_3GeSC_6H_5 + (+)\text{-}C_6H_5C^*H(Me)Br\ (40\%\ ee) \xrightarrow[100°C,\ 41\ h]{} C_6H_5C^*H(Me)SC_6H_5 \quad (51\%\ yield,\ 1.2\%\ ee)$$

Scheme 5.

All the results obtained in the present study suggest a mechanism involving unimolecular ionization of 1-aryl-1-bromoethanes at the rate-determining step (rds) for the reaction (Scheme 6). The present study, however, does not rule out minor contribution of a bimolecular nucleophilic process especially for the reaction with the 1-aryl-1-bromoethanes bearing electron-withdrawing substituents.

Among the three possible mechanisms mentioned earlier, the unimolecular ionization of 1-bromo-1-phenylethane has been confirmed in the present reaction. Although our hypothesis of the steric control

Table 3. Mechanism of the Reactions: Me_3≡IVb-VIb-R′+R-X⟶Me_3≡IVb-X+R-VIb-R′

IVb-VIb	R′	R-X	Mechanism	Ref.
Ge-S	Aryl	Aryl-$CH(CH_3)$-Br	S_N1	This work
Ge-S	Aryl	Aryl-CH_2-Br	S_N2	1
Ge-S	Aryl	Aryl-C(O)-Cl	5-Coordination	2
Si-S	Aryl	Aryl-C(O)CH_2-Br	5-Coordination	5
Si-S	Aryl	Aryl-C(O)-Cl	5-Coordination	12
Si-O	Alkyl, Aryl	Alkyl, Aryl-S(O)-Cl	S_N2[a]	13
Sn-S	Alkyl, Aryl	Alkyl, Aryl-CH_2-Cl, Br, I	S_N2	1, 3
Sn-S	Aryl	Aryl-C(O)-Cl	S_N2[a]	4
Sn-O	Aryl	Aryl-CH_2-Br	S_N2	14
Sn-O	Aryl	Alkyl-$S(O_2)$-Cl	4-Center	15

a) Bimolecular nucleophilic addition-elimination.

$$C_6H_5CH(Me)Br \xrightarrow{rds} [C_6H_5C^+H(Me)\ Br^-] \xrightarrow{Me_3GeSC_6H_5} C_6H_5CH(Me)SC_6H_5 + Me_3GeBr$$

Scheme 6.

on the reaction mechanism could not be clarified by the present study, this study revealed a first example of an S_N1 reaction for the reaction of the compounds bearing IVb atom-VIb atom bonds as summarized in Table 3. The particular mechanism is undoubtedly due to the nature of the substrate, 1-aryl-1-bromoethanes which easily undergoes unimolecular ionization. The present reaction is also an example of S_N1 reaction under unusual reaction conditions for the process. Most of the S_N1 reactions have been known to proceed with large excess of nucleophiles in polar media, or nucleophiles as the solvents.

It is interesting to note here, the halogen-exchange reaction of 1-bromo-1-phenylethane with mercury(II) thiocyanate in dibutyl ether at 0 °C giving thiocyanate. The mechanism has been suggested as the unimolecular ionization standing on the racemization of optically active 1-phenylethyl moiety during the reaction.[8] This is another unimolecular nucleophilic reaction under abnormal reaction conditions for the process. The reaction, however, may better be explained by initial association of 1-bromo-1-phenylethane with the salt followed by ionization of the formed complex or mercury(II) salt-assisted ionization of the reactant. 1-Bromo-1-phenylethane is fairly stable in nonpolar media below room temperatures in the absence of the salt. Kinetic study on the halogen-exchange reaction is desired to clarify the possible complexation of the bromoethane with mercury(II) salts. However, it is difficult to determine kinetic order of the salts because of their limited solubility in the solvent. On the other hand, no dependency of concentration of the nucleophile on the rate of the reaction has been confirmed in the present study. In this connection, the present reaction is not only a first example of S_N1 reaction of the compounds bearing IVb atom-VIb atom bonds with haloalkanes but also a unique unimolecular nucleophilic substitution proceeding with a small amount of nucleophile in nonpolar media.

Experimental

Materials. Solvents were dried and distilled. Substituted 1-bromo-1-phenylethanes were prepared by reduction of the corresponding acetophenones.[9] Commercially available optically active (−)-1-phenylethanol was brominated with PBr_3 obtaining (+)-1-bromo-1-phenylethane.[10] Preparation of (arylthio)trimethylgermanes was reported previously.[2]

Product Analysis. Trimethyl(phenythio)germane (0.25 g, 1.3×10^{-3} mol) was heated with an equimolar amount of 1-bromo-1-phenylethane (0.24 g, 1.3×10^{-3} mol) in a sealed tube at 100 °C for 41 h. ^{1}H NMR analysis of the reaction mixture showed only signals due to bromotrimethylgermane (δ 0.85, s, 9H) and phenyl 1-phenylethyl sulfide (δ 1.60, d, 3H; 4.30, q, 1H; 7.20, broad, 10H) and small amounts of the remaining reactants. The conversion was 85%. Bromotrimethylgermane was isolated by distillation (bp 113—114 °C, 84.2% yield). Phenyl 1-phenylethyl sulfide was isolated from the residue by column chromatography on silica gel with hexane as the eluent (0.14 g, 51.4% yield). The reaction of optically active compound was carried out similarly. Rotations ($[\alpha]_D$) of the starting 1-bromo-1-phenylethane and obtained phenyl 1-phenylethyl sulfide were, +69.0 ° (ethanol, c 2.35, 40.3% ee) and −9.04 ° (ethanol, c 0.55), respectively. Optical purity of the sulfide was determined by converting to the corresponding sulfone,[11] −1.14 ° (methanol, c 0.39, 1.2% ee).

Kinetics. The kinetic procedure was essentially the same to that previously reported.[1] Initial concentrations were 0.262 and 0.318 mol dm^{-3} for the thiogermane and the bromoethane, respectively.

The Reaction of 1-Bromo-1-phenylethane in the Absence of the Thiogermane. A mixture of 1-bromo-1-phenylethane (0.294 g, 0.318 mol dm^{-3}) and 2,6-lutidine (0.204 g, 0.382 mol dm^{-3}) in benzonitrile (0.50 cm^3) was sealed in a glass tube and heated at 110±0.1 °C for 3.75 h. After heating, the precipitated salt was filtered off. Styrene was identified by the pattern of its olefinic protons in the ^{1}H NMR spectrum of the filtrate and the yield was estimated by intensity of the signals relative to that of the remaining 1-bromo-1-phenylethane.

References

1) S. Kozuka, S. Tamura, S. Ishibashi, S. Ohya, and W.

Tagaki, *Bull. Chem. Soc. Jpn.*, **60**, 4061 (1987).

2) S. Kozuka, S. Tamura, T. Yamazaki, S. Yamaguchi, and W. Tagaki, *Bull. Chem. Soc. Jpn.*, **58**, 3277 (1985).

3) S. Kozuka and S. Ohya, *J. Organomet. Chem.*, **149**, 161 (1978); *Bull. Chem. Soc. Jpn.*, **51**, 2651 (1978).

4) S. Kozuka and I. Naribayashi, *Bull. Chem. Soc. Jpn.*, **52**, 3638 (1979).

5) S. Kozuka, T. Higashino, and T. Kitamura, *Bull. Chem. Soc. Jpn.*, **54**, 1420 (1981).

6) See Refs. 1—5 and references cited therein.

7) H. C. Brown and Y. Okamoto, *J. Am. Chem. Soc.*, **79**, 1913 (1957).

8) N. Watanabe, M. Okamoto, and S. Uemura, *Bull. Chem. Soc. Jpn.*, **47**, 2745 (1974).

9) M. Kuchar, B. Brunova, V. Rejholec, Z. Roubal and O. Nemecek, *Collect. Czech. Chem. Commun.*, **41**, 633 (1976).

10) R. O. Hutchins, D. Maasilamani, and C. A. Maryanoff, *J. Org. Chem.*, **41**, 1071 (1976).

11) E. J. Corey and T. H. Lowry, *Tetrahedron Lett.*, **1965**, 803.

12) S. Kozuka and I. Naribayashi, *Mem. Fac. Engin. Osaka City Univ.*, **22**, 115 (1981).

13) S. Kozuka and T. Higashino, *Tetrahedron Lett.*, **21**, 2067 (1980); *Bull. Chem. Soc. Jpn.*, **54**, 1183 (1981).

14) S. Kozuka, A. Kikuchi, and S. Yamaguchi, *Bull. Chem. Soc. Jpn.*, **54**, 307 (1981), S. Kozuka, O. Natori, and W. Tagaki, *Mem. Fac. Engin. Osaka City Univ.*, **23**, 73 (1982).

15) S. Kozuka, S. Yamaguchi, and W. Tagaki, *Chem. Lett.*, **1981**, 1299; *Bull. Chem. Soc. Jpn.*, **56**, 573 (1983).

Syntheses of Cholesta-5,7-diene-3β,25-diol and Cholesta-5,7-diene-1α,3β,25-triol

Yoji TACHIBANA,* Shinji YOKOYAMA, and Masahiro TSUJI
Central Research Laboratory, Nisshin Flour Milling Co., Ltd.,
Tsurugaoka, Ooimachi, Irumagun, Saitama 354
(Received February 25, 1989)

Adducts of 3β-acetoxy- and 1α,3β-diacetoxy-23,24-dinorchola-5,7-dien-22-al (**7** and **14**) with 4-phenyl-3*H*-1,2,4-triazole-3,5-dione prepared by the ozonolysis of the corresponding adducts of ergosteryl acetate and 1α-acetoxyergosteryl acetate were transformed into 22-bromo-3β-tetrahydropyranyloxy- and 22-iodo-1α,3β-bis-(tetrahydropyranyloxy)-23,24-dinorchola-5,7-diene (**11** and **26**). The halide derivatives (**11** and **26**) were coupled with 2-methyl-4-phenylsulfonyl-2-(tetrahydropyranyloxy)butane (**6**) to afford 23-phenylsulfonyl-3β,25-bis(tetrahydropyranyloxy)- and 23-phenylsulfonyl-1α,3β,25-tris(tetrahydropyranyloxy)cholesta-5,7-diene (**12** and **27**). The reductive desulfonylation and deprotection of the tetrahydropyranyl group of **12** and **27** provided the title compounds, cholesta-5,7-diene-3β,25-diol (**1**) and cholesta-5,7-diene-1α,3β,25-triol (**2**).

It has been reported that vitamin D_3 must be metabolized to 25-hydroxyvitamin D_3 (25-OH-D_3) in the liver, and subsequently to 1α,25-dihydroxyvitamin D_3 (25-$(OH)_2$-D_3) in the kidney, before eliciting its hormonal activity.[1] Many workers have reported the syntheses of cholesta-5,7-diene-3β,25-diol (**1**)[2] and cholesta-5,7-diene-1α,3β,25-triol (**2**),[3-5] the precursors of 25-(OH)-D_3 and 1α,25-$(OH)_2$-D_3. Concerning the syntheses of **1** and **2**, any process of preparing them utilizing cholest-5-ene-3β,25-diol[6] and cholest-5-ene-1α,3β,25-triol[7] as key intermediates generally gives poor yields of **1** and **2** due to the side reactions involving the formation of a considerable amount of undesired 4,6-diene isomers.

We previously reported the synthesis of 1α-acetoxyergosteryl acetate (**3**) and 1α-hydroxyergosterol (**4**).[8] The C-22 aldehyde or alcohol readily obtainable from **3** and **4** seemed to be a good synthon for the preparation of 1α-hydroxylated steroidal 5,7-diene derivatives. In the present paper, the alternative syntheses of **1** and **2**, by the coupling of the corresponding steroidal 5,7-diene part and the side chain moiety, is described.

We first examined the synthesis of **1**. The C 5 synthon to constitute C (23)—C (27) side chain part was prepared as shown in Scheme 1. Methyl phenyl sulfone was treated with 2,2-dimethyloxirane in the presence of sodium hydride to give phenylsulfonyl alcohol (**5**). The hydroxyl group of **5** was protected as a tetrahydropyranyl ether (**6**) in the usual manner.

Ergosterol was converted into the known C-22 aldehyde (**7**) via route involving the protection of the 5,7-diene with 4-phenyl-3*H*-1,2,4-triazole-3,5-dione (PTAD) and ozonolysis according to the procedure described by Barton et al.[9] The aldehyde (**7**) was reduced with $LiAlH_4$ to afford the diol (**8**), which was treated with an equimolar amount of *p*-toluenesulfonyl chloride to give C-22 tosylate (**9**) selectively. After the hydroxyl group of **9** was protected as a tetrahydropyranyl ether, the resulting **10** was converted to C-22 bromide (**11**) by treatment with lithium bromide.[10] The bromide (**11**) was condensed with

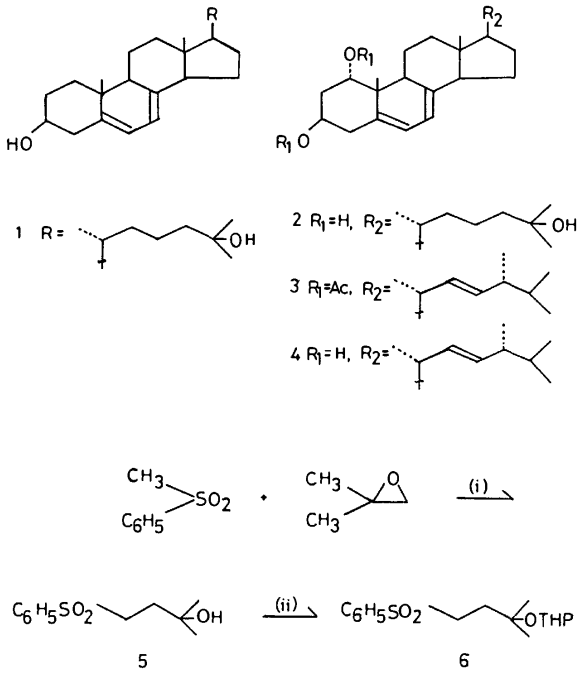

Scheme 1. (i) NaH, (ii) DHP-PPTS.

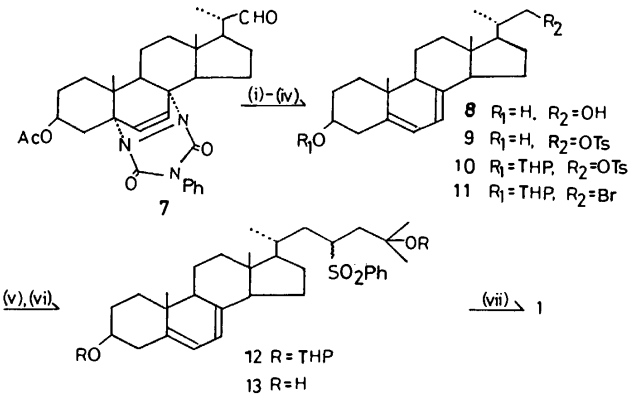

Scheme 2. (i) $LiAlH_4$, (ii) TsCl-Py, (iii) DHP-PPTS, (iv) LiBr-Li_2CO_3, (v) BuLi/**6**, (vi) PPTS/EtOH, (vii) Na-Hg.

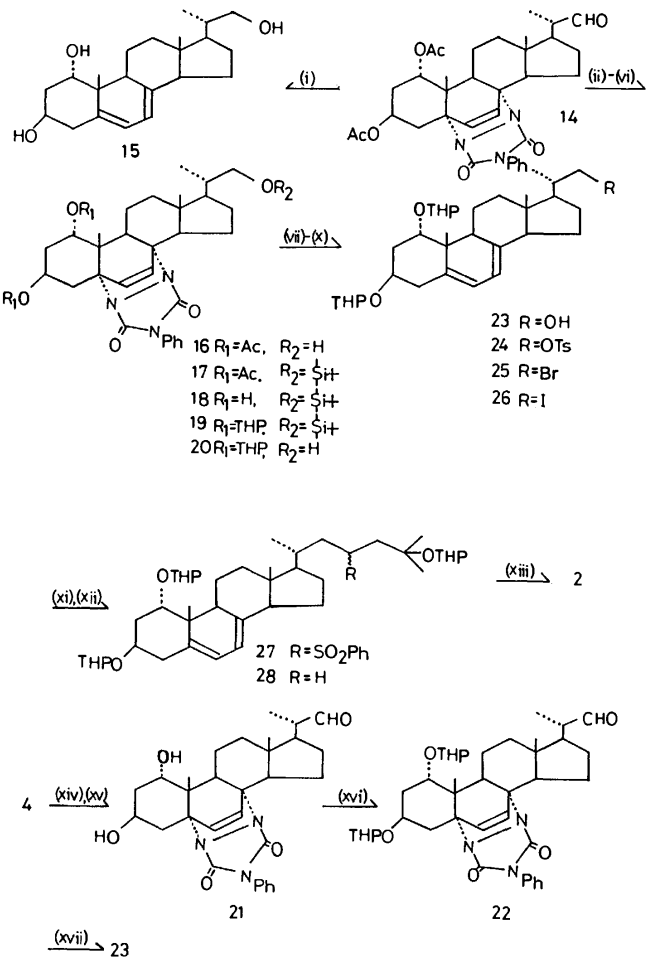

Scheme 3. (i) $LiAlH_4$, (ii) $NaBH_4$, (iii) *t*-$BuMe_2SiCl$-imidazole, (iv) KOH/EtOH, (v) DHP-PPTS, (vi) Bu_4NF/THF, (vii) $LiAlH_4$, (viii) TsCl-Py, (ix) LiBr-Li_2CO_3, (x) NaI, (xi) BuLi/**6**, (xii) Na-Hg, (xiii) PPTS/EtOH, (xiv) 4-Phenyl-3*H*-1,2,4-triazole-3,5-dione (xv) O_3-Me_2S, (xvi) DHP-PPTS, (xvii) $LiAlH_4$.

the C 5 alcohol derivative (**6**) in the presence of BuLi to provide the 23-phenylsulfonyl derivative (**12**). The deprotection of the tetrahydropyranyl group of **12** under acidic conditions, followed by the reductive desulfonylation[11] of the diol (**13**) with sodium amalgum led to the target compound (**1**) (Scheme 2).

In a manner similar to that described above, the synthesis of **2** was achieved as outlined in Scheme 3. The C-22 aldehyde (**14**) was synthesized by the ozonolysis of the adduct of **3** with PTAD.[12] As described in the synthesis of **1**, we attempted the selective tosylation for the hydroxyl group (at C-22) of the triol (**15**) prepared by the reduction of the aldehyde (**14**) with $LiAlH_4$. However, in contrast to the tosylation of **8**, the reaction of **15** with *p*-toluenesulfonyl chloride gave mixtures. Thus, the aldehyde (**14**) was subjected to reduction with $NaBH_4$ to produce the C-22 alcohol (**16**). The acetyl groups of **16** seemed to be unstable under the basic conditions employed here, and therefore, they were converted to tetrahydropyranyl groups as follows.[13] The protection of the hydroxyl group at C-22 as *t*-butyldimethylsilyl ether and the successive hydrolysis of the acetyl groups afforded the 1,3-diol (**18**). The protection of the hydroxyl groups of **18** as tetrahydropyranyl ether followed by the removal of the *t*-butyldimethylsilyl group with Bu_4NF provided the C-22 alcohol (**20**). The alcohol (**20**) was then treated with $LiAlH_4$ to give bis(tetrahydropyranyloxy) C-22 alcohol (**23**).

Alternatively, the alcohol (**23**) was obtained from 1α-hydroxyergosterol (**4**). The Diels-Alder adduct of **4** with PTAD was ozonized to yield the C-22 aldehyde (**21**). No epimerization of **21** (at C-20) was observed at this stage.[9] The protection of the 1,3-diol of **21** as tetrahydropyranyl ether and the subsequent reduction with $LiAlH_4$ produced the 5,7-diene (**23**). Subsequently, the alcohol (**23**) was reacted with *p*-toluenesulfonyl chloride to afford C-22 tosylate (**24**). The bromide (**25**) derived from **24** proved to be rather unreactive toward **6**. Accordingly, the tosylate (**24**) was converted to the corresponding iodide (**26**) by means of reaction with sodium iodide in boiling acetone.[13]

The iodide (**26**) was condensed with the sulfone (**6**) under the same conditions described above to yield the 23-phenylsulfonyl derivative (**27**). The reductive elimination of the phenylsulfonyl group with Na-Hg and the subsequent cleavage of the tetrahydropyranyl groups furnished the desired compound, cholesta-5,7-diene-1α,3β,25-triol (**2**).

Since 1α-hydroxylated C-22 alcohol (**23**) is obtainable from 1α-acetoxyergosteryl acetate or 1α-hydroxyergosterol, the procedure described here will provide a convenient synthetic method for the preparation of 1α-hydroxylated provitamin D derivatives.

Experimental

Melting points are uncorrected. UV spectra were taken on a Hitachi 320 spectrometer. ^1H NMR spectra were recorded in $CDCl_3$ on a JEOL JNF-FX200 spectrometer with TMS as an internal standard. Mass spectra were measured on a Hitachi M-80 mass spectrometer. Solvents were removed under reduced pressure.

2-Methyl-4-phenylsulfonyl-2-(tetrahydropyranyloxy)-butane (6). A dimethyl sulfoxide solution (70 ml) containing methyl phenyl sulfone (21.8 g) and sodium hydride (3.4 g) was heated at 70 °C for 1.5 h and then the solution was diluted with tetrahydrofuran (THF) (70 ml). To the solution, isobutylene oxide (14.0 g) in 35 ml of THF was added dropwise at 0 °C. The mixture was allowed to react for 3 h at 0 °C. After THF was removed, the residue was extracted with benzene. The benzene solution was washed with brine, dried over sodium sulfate and concentrated to dryness. The residue was purified by silica-gel chromatography. Elution with ethyl acetate/hexane (1/4, v/v) gave 2-methyl-4-phenylsulfonyl-2-butanol (**5**).[11] 20.7 g (65%).

A dichloromethane solution (250 ml) of **5** (8.0 g), dihydropyran (4.4 g), and pyridinium *p*-toluenesulfonate

(PPTS) (0.9 g) was reacted at room temperature for 6 h. The solution was washed with brine, dried (sodium sulfate) and evaporated. The residue was crystallized from ethyl acetate to afford **6**. 8.3 g (76%); mp 80—82 °C (lit,[11] 84—85 °C).

23,24-Dinorchola-5,7-diene-3β,22-diol (8). To a THF (60 ml) solution of $LiAlH_4$ (3.0 g) was added dropwise the solution of **7** (2.9 g in 50 ml of THF). The mixture was refluxed for 3 h. After decomposition of the excess $LiAlH_4$ with water, the solution was filtered on Celite. The residue after the evaporation of THF was crystallized from chloroform-methanol to yield **8**. 1.3 g (73%); mp 195—197 °C; *m/z* 330 (M^+); ^1H NMR δ=5.40, 5.58 (2H, m, H-6, H-7), 3.65 (2H, m, H-22), 3.40 (1H, m, H-3). Found: C, 79.65; H, 10.40%. Calcd for $C_{22}H_{34}O_2$; C, 79.95; H, 10.37%.

23,24-Dinorchola-5,7-diene-3β,22-diol 22-*p*-Toluenesulfonate (9). **8** (740 mg) and *p*-toluenesulfonyl chloride (635 mg) in a pyridine solution (10 ml) were reacted at room temperature for 6 h. The solution was then extracted with chloroform, washed with 10% hydrochloric acid, brine, and saturated sodium bicarbonate, dried (sodium sulfate), and evaporated. The residue was purified by means of chromatography on silica gel. Elution with chloroform/hexane (3/2, v/v) and crystallization of the crude product from ethyl acetate-hexane afforded **9**. 650 mg (60%); mp 163—165 °C; *m/z* 484 (M^+), 466 (M^+-H_2O); ^1H NMR δ=7.79 (2H d, *J*=8.4 Hz, aryl), 7.34 (2H, d, *J*=8.4 Hz, aryl), 5.56, 5.38 (2H, m, H-6, H-7), 3.97 (1H, m, H-22), 3.81 (1H, m, H-22), 3.64 (1H, m, H-3), 2.45 (3H, s, CH_3 (tosyl)). Found: C, 71.56; H, 8.49%. Calcd for $C_{29}H_{40}O_4S$: C, 71.70; H, 8.52%.

3β-Tetrahydropyranyloxy-23,24-dinorchola-5,7-dien-22-ol *p*-Toluenesulfonate (10). The tosylate (**9**) (600 mg) was dissolved in dichloromethane (10 ml). Dihydropyran (155 mg) and PPTS (30 mg) were added to the solution and the mixture was stirred at room temperature for 4 h. The solution was washed with brine and dried (sodium sulfate). The residue after the evaporation of solvent was crystallized from methanol to afford **10**. 470 mg (67%); mp 148—149 °C; *m/z* 568 (M^+), 484 (M^+—DHP); ^1H NMR δ=7.79 (2H, d, *J*=8.4 Hz, aryl), 7.34 (2H, d, *J*=8.4 Hz, aryl), 5.35, 5.55 (2H, m, H-6, H-7), 4.70 (1H, m, CH(THP)), 3.90 (1H, m, CH_2(THP)), 3.82, 3.70 (2H, m, H-22), 3.50 (1H, m, CH_2(THP)), 2.45 (3H, s, CH_3 (tosyl)). Found: C, 71.49; H, 8.48%. Calcd for $C_{34}H_{48}O_5S$: C, 71.79; H, 8.48%.

22-Bromo-3β-tetrahydropyranyloxy-23,24-dinorchola-5,7-diene (11). A *N,N*-dimethylformamide solution (5 ml) of the tosylate (**10**) (470 mg), lithium carbonate (58 mg) and lithium bromide (330 mg) was heated at 70 °C for 1 h. The mixture was extracted with chloroform, washed with brine, dried (sodium sulfate) and concentrated to dryness. The residue was chromatographed on silica gel (eluted with 5% ethyl acetate in hexane) to yield, **11**. 305 mg (77%); mp 146—149 °C (crystallized from ethyl acetate). ^1H NMR δ=5.37, 5.55 (2H, m, H-6, H-7), 4.75 (1H, m, CH(THP)), 3.81 (1H, m, CH_2 (THP)), 3.63 (1H, m, H-3), 3.52 (2H, m, H-22, CH_2(THP)), 3.36 (1H, m, H-22). Found: C, 67.67; H, 8.63%. Calcd for $C_{27}H_{41}O_2Br$: C, 67.91; H, 8.65%.

23-(Phenylsulfonyl)cholesta-5,7-diene-3β,25-diol (13). The sulfone derivative (**6**) (213 mg) was dissolved in THF (5 ml) and cooled to −20 °C. To the solution, was added dropwise 10% BuLi hexane solution (0.4 ml) and then the mixture was reacted with stirring at −20 °C for 1 h. To the solution was added the 22-bromide (**11**) (65 mg) in a mixture solution of HMPA (0.1 ml) and THF (0.5 ml). The mixture solution was stirred at −20 °C for 3 h. After the addition of sat ammonium chloride, the mixture was extracted with chloroform, washed with brine, dried (sodium sulfate) and evaporated. The residue was purified by chromatography on silica gel. Elution with 10% ethyl acetate in hexane afforded (**12**) (100 mg). The crude product was dissolved in ethanol (5 ml) and PPTS (16 mg) was added. The mixture solution was reacted at 50 °C for 3 h and extracted with chloroform. The solution was washed with brine, dried (sodium sulfate) and concentrated to dryness. The residue was chromatographed on silica gel (eluted with 20% ethyl acetate in hexane) to give **13**. 38 mg (51%) (amorphous powder); *m/z* 540 (M^+); ^1H NMR δ=7.91—7.95 (2H, m, aryl), 7.54—7.70 (2H, m, aryl), 5.57, 5.35 (2H, m, H-6, H-7), 3.70 (1H, m, H-3), 3.45 (1H, m, H-23).

Cholesta-5,7-diene-3β,25-diol (1). A solution of the sulfone derivative (**13**) (38 mg) in methanol (15 ml) saturated with Na_2HPO_4 was treated with 5% Na-Hg (2.5 g) at 35 °C for 4 h. After the separation of Hg by filtration, the solution was extracted with chloroform, washed with brine, and dried (sodium sulfate). Evaporation of the solvent left solid, which was crystallized from chloroform-hexane to provide **1**. 14 mg (50%); mp 182—183 °C. (lit,[2] 185—187 °C). UV λ_{max} 282 nm (ε=11900, ethanol).

22-Hydroxy-5α,8α-(4-phenyl-3,5-dioxo-1,2,4-triazolidine-1,2-diyl)-23,24-dinorchol-6-ene-1α,3β-diol 1,3-Diacetate (16). To a ethanol solution (10 ml) of sodium borohydride (0.6 g) was added a solution of **14** (2.0 g) in chloroform (50 ml) and the mixture was reacted with stirring at 0 °C for 30 min. The solution was washed with 50% acetic acid, sat sodium hydrogencarbonate and brine, dried (sodium sulfate) and evaporated. Crystallization of the residue from chloroform-hexane afforded **16**. 1.8 g, (90%); mp 196—198 °C; *m/z* 370 (M^+—triazolidine—CH_3COOH); ^1H NMR δ=7.26—7.52 (5H, m, aryl), 6.45, 6.34 (2H, ABq, *J*=8.0 Hz, H-6, H-7), 5.91 (1H, m, H-3), 5.11 (1H, brs, H-1), 3.21—3.38 (2H, m, H-22), 2.01, 2.03 (6H, s, $COCH_3$). Found: C, 66.94; H, 7.15; N, 6.82%. Calcd for $C_{34}H_{43}O_7N_3$: C, 67.42; H, 7.15; N, 6.94%.

22-(*t*-Butyldimethylsilyloxy)-5α,8α-(4-phenyl-3,5-dioxo-1,2,4-triazolidine-1,2-diyl)-23,24-dinorchol-6-ene-1α,3β-diol 1,3-Diacetate (17). To a solution of **16** (1.8 g) in *N,N*-dimethylformamide (5 ml) was added *t*-butyldimethylsilyl chloride (0.9 g) and imidazole (0.9 g). The mixture was warmed at 40 °C for 30 min and extracted with ether, washed with brine and evaporated. Purification on silica gel (eluted with ethyl acetate/hexane (3/7, v/v)) afforded **17**. 1.8 g (amorphous powder) (84%); *m/z* 484 (M^+—triazolidine—CH_3COOH); ^1H NMR δ=7.25—7.52 (5H, m, aryl), 6.45, 6.32 (2H, ABq, *J*=8.0 Hz, H-6, H-7), 5.88 (1H, m, H-3), 5.12 (1H, brs, H-1), 3.58 (1H, m, H-9), 3.28 (2H, m, H-22), 2.01, 2.03 (6H, s, $COCH_3$).

22-(*t*-Butyldimethylsilyloxy)-5α,8α-(4-phenyl-3,5-dioxo-1,2,4-triazoline-1,2-diyl)-23,24-dinorchol-6-ene-1α,3β-diol (18). A methanol solution (50 ml) of **17** (1.7 g) and potassium carbonate (0.4 g) was heated at 60 °C for 1 h. After methanol was removed, the residue was extracted with chloroform, washed with brine and concentrated. The residue was crystallized from methanol-benzene to provide **18**. 1.3 g (85%); mp 222—224 °C; *m/z* 460 (M^+—triazolidine); ^1H NMR δ=7.23—7.39 (5H, m, aryl), 6.35, 6.18 (2H, ABq,

J=8.0 Hz, H-6, H-7), 4.80 (1H, m, H-3), 3.69 (1H, brs, H-1), 3.61 (1H, m, H-9), 3.05—3.29 (2H, m, H-22). Found: C, 67.50; H, 8.50; N, 6.36%. Calcd for $C_{36}H_{53}N_3O_5Si$: C, 67.97; H, 8.41; N, 6.61%.

22-(*t*-Butyldimethylsilyloxy)-5α,8α-(4-phenyl-3,5-dioxo-1,2,4-triazoline-1,2-diyl)-1α,3β-bis(tetrahydropyranyloxy)-23,24-dinorchol-6-ene (19). The bis(silyl ether) (**18**) (1.2 g) was dissolved in dichloromethane (20 ml). To the solution, dihydropyran (350 mg) and PPTS (70 mg) were added. The mixture solution was reacted under reflux for 4 h. The solution was washed with brine, dried (sodium sulfate) and evaporated. The residue was purified by silica-gel chromatography. Elution with ethyl acetate/hexane (1/4, v/v) gave **19** as an amorphous powder. 1.1 g (75%); m/z 442 (M^+−triazolidine−2DHP−H_2O); ^{1}H NMR δ=7.20—7.50 (5H, m, aryl), 6.35, 6.49 (2H, ABq, J=8.0 Hz, H-6, H-7), 4.85 (2H, s, CH(THP)), 4.95 (1H, m, H-3), 3.40—3.92 (7H, m, CH_2(THP), H-1, H-9, H-22), 3.15—3.28 (1H, m, H-22). Found: C, 68.47; H, 8.65; N, 5.16%. Calcd for $C_{46}H_{70}N_3O_7$: C, 68.60; H, 8.78; N, 5.22%.

5α,8α-(4-Phenyl-3,5-dioxo-1,2,4-triazolidine-1,2-diyl)-1α,3β-bis(tetrahydropyranyloxy)-23,24-dinorchol-6-en-22-ol (20). To a THF solution (50 ml) of **19** (1.0 g) was added 2.5 ml of 1 M (1 mol dm^{-3}) tetrabutylammonium fluoride THF solution. The solution was stirred at room temp for 2 h and then extracted with ethyl acetate, washed with brine and evaporated. The residue was chromatographed on silica gel. Elution with ethyl acetate/hexane (3/7, v/v) afforded **20** (amorphous solid). 0.8 g (95%); m/z 514 (M^+−triazolidine); ^{1}H NMR δ=7.21—7.49 (5H, m, aryl), 6.29, 6.43 (2H, ABq, J=8.0 Hz, H-6, H-7), 4.79—4.86 (2H, m, CH(THP)), 3.90 (2H, m, CH_2(THP)), 3.30—3.76 (6H, m, H-1, H-9, H-22, CH_2(THP)).

1α,3β-Dihydroxy-5α,8α-(4-phenyl-3,5-dioxo-1,2,4-triazolidine-1,2-diyl)-23,24-dinorchol-6-en-22-al (21). 1α-Hydroxyergosterol (**4**) (270 mg) was dissolved in acetone (50 ml). To the solution was added PTAD by portion until the red color of the solution persisted. Removal of solvent and crystallization from acetone afforded 1α-hydroxy-5α,8α-(4-phenyl-3,5-dioxo-1,2,4-triazolidine-1,2-diyl) ergosterol. 270 mg (87%); mp 237—238 °C; m/z 412 (M^+−triazolidine); ^{1}H NMR δ=7.28—7.41 (5H, m, aryl), 6.23, 6.39 (2H, m, H-6, H-7), 5.20 (2H, m, H-22, H-23), 4.84 (1H, m, H-3), 3.80 (1H, m, H-1). Found: C, 73.42; H, 8.38; N, 6.93%. Calcd for $C_{36}H_{49}O_4N_3$: C, 73.56; H, 8.40; N, 7.15%.

A 1% pyridine-dichloromethane solution (150 ml) of the adduct (200 mg) was ozonized at −60 °C (ozonizer E0-301, Okano Works Ltd.) until almost all the starting material was consumed (monitored by thin-layer chromatography). After argon gas was passed through the vessel, dimethyl sulfide (1 ml) was added. The solution was warmed slowly to room temperature, washed with brine, dried (sodium sulfate) and evaporated. The residue was chromatographed on silica gel. Elution with ethyl acetate/chloroform (1/4, v/v) gave **21** (amorphous powder) 140 mg (79%); m/z 344 (M^+−triazolidine); ^{1}H NMR δ=9.57 (1H, d, J=3.4 Hz, H-22), 7.29—7.40 (5H, m, aryl), 6.24, 6.36 (2H, ABq, J=8.1 Hz, H-6, H-7), 4.76 (1H, m, H-3), 3.76 (1H, m, H-1).

5α,8α-(4-Phenyl-3,5-dioxo-1,2,4-triazolidine-1,2-diyl)-1α,3β-bis(tetrahydropyranyloxy)-23,24-dinorchol-6-en-22-al (22). To a solution of the 22-aldehyde (**21**) (135 mg) in dichloromethane (10 ml) were added dihydropyran (108 mg) and PPTS (20 mg). The mixture was allowed to react at room temperature for 12 h. The solution was washed with brine, dried (sodium sulfate) and evaporated. The residue was purified by silica-gel chromatography (eluted with ethyl acetate/hexane (1/9, v/v)) to provide **22** ((108 mg (61%)) along with 5α,8α-(4-phenyl-3,5-dioxo-1,2,4-triazolidine-1,2-diyl)-3β-tetrahydropyranyloxy-23,24-dinorchol-6-en-22-al (42 mg (20%)). m/z 326 (M^+−triazolidine−2DHP−H_2O); ^{1}H NMR δ=9.56 (1H, d, J=3.4 Hz, H-22), 7.30—7.45 (5H, m, aryl), 6.36 (2H, m, H-6, H-7), 4.92 (1H, m, H-3), 4.80—4.85 (2H, m, CH(THP)), 3.89 (2H, m, CH_2(THP)), 3.70 (1H, brs, H-1), 3.50 (2H, m, CH_2(THP)).

1α,3β-Bis(tetrahydropyranyloxy)-23,24-dinorchola-5,7-dien-22-ol (23). (a) (from **20**). A THF solution containing $LiAlH_4$ (0.7 g) was added dropwise the THF solution (50 ml) of **20** (0.7 g). The mixture was reacted under reflux for 1 h. After decomposition of excess $LiAlH_4$, the solution was filtered on Celite. The solution was concentrated and the residue was extracted with ethyl acetate. The solution was washed with brine and evaporated. The residue was purified by silica-gel chromatography. Elution with ethyl acetate/hexane (1/3, v/v) gave **23** (amorphous powder). 0.5 g (95%); ^{1}H NMR δ=5.37, 5.64 (2H, m, H-6, H-7), 4.65—4.80 (2H, m, CH(THP)), 4.13 (1H, m, H-3), 3.89 (2H, m, CH_2(THP)), 3.75 (1H, brs, H-1), 3.65 (1H, m, H-22), 3.52—3.88 (3H, m, CH_2(THP), H-22).

(b) (from **22**). To a THF solution (20 ml) of $LiAlH_4$ (300 mg) was added **22** (100 mg) in THF (20 ml). The mixture was refluxed with stirring for 1 h. After the decomposition of the excess $LiAlH_4$, the solution was filtered on Celite. After the removal of the solvent, the residue was extracted with ethyl acetate. The solution was washed with brine, dried (sodium sulfate) and evaporated. The residue was chromatographed on silica gel. Elution with ethyl acetate/chloroform (1/9, v/v) yielded **23**. 48 mg (63%); the ^{1}H NMR spectrum agreed with that of **23** obtained from **20**.

22-Iodo-1α,3β-bis(tetrahydropyranyloxy)-23,24-dinorchola-5,7-diene (26). To a pyridine solution (5 ml) of **23** (400 mg) was added *p*-toluenesulfonyl chloride (600 mg). The mixture was reacted with stirring at room temperature for 1 h. The solution was extracted with ether, washed with 10% hydrochloric acid, sodium hydrogencarbonate and brine and dried (sodium sulfate). After evaporation of ether, the residue was purified on silica gel. Elution with ethyl acetate/hexane (1/9, v/v) provided 1α,3β-bis(tetrahydropyranyloxy)-23,24-dinorchola-5,7-dien-22-ol *p*-toluenesulfonate (**24**). 450 mg (89%); ^{1}H NMR δ=7.29 (2H, d, J=8.0 Hz, aryl), 7.24 (2H, d, J=8.0 Hz, aryl), 5.35, 5.63 (2H, m, H-6, H-7), 4.68—4.80 (2H, m, CH(THP)), 4.15 (1H, m, H-3), 3.75—4.05 (7H, m, H-1, H-22, CH_2(THP)), 2.25 (3H, s, CH_3(tosyl)).

An acetone solution (5 ml) of the tosylate (**24**) (400 mg) and sodium iodide (540 mg) was heated under reflux for 1 h. The residue after evaporation of acetone was chromatographed on silica gel (eluted ethyl acetate/hexane (1/9, v/v) to give **26** (amorphous powder). 324 mg (85%); m/z 624 (M^+), 540 (M^+−DHP); ^{1}H NMR δ=5.36, 5.64 (2H, m, H-6, H-7), 4.67—4.78 (2H, m, CH(THP)), 4.12 (1H, m, H-3), 3.80—3.98 (2H, m, CH_2(THP)), 3.75 (1H, brs, H-1), 2.45—2.67 (2H, m, CH_2(THP)), 2.20—2.40 (2H, m, H-22). Found: C, 60.99; H, 7.62%; Calcd for $C_{32}H_{49}IO_4$; C, 61.52; H, 7.92%.

23-Phenylsulfonyl-1α,3β,25-tris(tetrahydropyranyloxy)-cholesta-5,7-diene (27). A THF solution (10 ml) of **6** (910

mg) was cooled −20 °C. To the solution was added dropwise a 10% BuLi hexane solution (1.8 ml). The mixture was stirred at −20 °C for 30 min. To the mixture solution was added dropwise a solution of **26** (570 mg in 5 ml of THF and 0.5 ml of HMPA). The mixture was allowed to react for 30 min at −20 °C and for 1 h at 0 °C. After the reaction was stopped by adding sat. ammonium chloride, the mixture was extracted with ethyl acetate, washed with brine, dried (sodium sulfate) and evaporated. The residue was purified by chromatography on silica gel. Elution with ethyl acetate/hexane (1/4, v/v) yielded **27**. 700 mg (95%); *m/z* 706 (M^+−DHP−H_2O; ^{1}H NMR δ=7.50—7.97 (5H, m, aryl), 5.35, 5.62 (2H, m, H-6, H-7), 4.81 (3H, brs, CH(THP)), 4.14 (1H, m, H-3), 3.80—4.00 (3H, m, CH_2(THP)), 3.76 (1H, brs, H-1), 3.35—3.50 (3H, m, CH_2(THP)).

1α,3β,25-Tris(tetrahydropyranyloxy)cholesta-5,7-diene (28). A methanol solution (60 ml) (saturated with Na_2HPO_4) of **27** (700 mg) was treated with 5% Na-Hg (8.0 g) at room temperature for 6 h. After Hg was removed by filtration on Celite, the mixture was extracted with ether and washed with brine. The residue after evaporation of ether was chromatographed on silica gel. Elution with ethyl acetate/hexane (1/9, v/v) afforded **28**. 520 mg (90%); *m/z* 584 (M^+−DHP); ^{1}H NMR δ=5.36, 5.64 (2H, m, H-6 H-7), 4.69 (3H, m, CH(THP)), 4.12 (1H, m, H-3) 3.91 (3H, m, CH_2(THP)), 3.74 (1H, brs, H-1), 3.46 (3H, m, CH_2(THP)).

Cholesta-5,7-diene-1α,3β,25-triol (2). A mixture of **28** (400 mg) and PPTS (24 mg) in ethanol (6 ml) was heated at 55 °C for 4 h. The solution was extracted with ether, washed with brine and dried (sodium sulfate). The residue after evaporation of ether was purified by chromatography on silica gel. Elution with ethyl acetate/chloroform (1/3, v/v) gave the crude **2**, which was crystallized from ether-hexane to provide **2** as colorless needles. 205 mg (82%); mp 207—208 °C (lit,[3] 211—213 °C); UV λ_{max} 282 nm (ε=11800, ethanol).

References

1) H. F. DeLuca, H. E. Paaren, and H. K. Schnoes, *Top. Curr. Chem.*, **83**, 1 (1979); H. F. DeLuca and H. K. Schnoes, *Ann. Rep. Med. Chem.*, **19**, 179 (1984).

2) J. A. Campbell, D. M. Squires, and J. C. Babcock, *Steroids*, **13**, 567 (1969).

3) T. Sato, H. Yamauchi, Y. Ogata, T. Kunii, K. Kagei, S. Toyoshima, and T. Kobayashi, *Chem. Pharm. Bull.*, **26**, 2933 (1978).

4) K. Ochi, I. Matsunaga, H. Nagano, M. Fukushima, M. Shindo, C. Kaneko, M. Ishikawa, and H. F. DeLuca, *J. Chem. Soc., Perkin Trans. 1*, **1979**, 165.

5) T. Kametani and H. Furuyama, *Med. Res. Rev.*, **7**, 147 (1987).

6) J. M. Blunt and H. F. DeLuca, *Biochemistry*, **8**, 671 (1969); W. G. Salmond and M. C. Sobala, *Tetrahedron Lett.*, **1977**, 1695; F. J. Sardina, A. Mourino, and L. Castedo, *ibid.*, **24**, 4477 (1983); K. Miyamoto, N. Kubodera, E. Maruyama, K. Ochi, T. Mori, and I. Matsunaga, *Synth. Commun.*, **16**, 513 (1986).

7) D. H. R. Barton, R. H. Hesse, M. Pechet, and E. Rizzardo, *J. Chem. Soc., Chem. Commun.*, **1974**, 103; M. Morisaki, K. Bannai, and N. Ikekawa, *Chem. Pharm. Bull.*, **21**, 1853 (1973); E. J. Semmler, M. F. Holick, H. K. Schnoes, and H. F. DeLuca, *Tetrahedron Lett.*, **1972**, 4147; J. A. Iacobelli and M. R. Uskokovic, *Helv. Chim. Acta*, **57**, 781 (1974).

8) Y. Tachibana, *Bull. Chem. Soc. Jpn.*, **61**, 3915 (1988).

9) D. H. R. Barton, T. Shioiri, and D. A. Widdowson, *J. Chem. Soc. C*, **1971**, 1968; J. W. Morzycki, H. K. Schnoes, and H. F. DeLuca, *J. Org. Chem.*, **49**, 2148 (1984).

10) H. Takayama, M. Ohmori, and S. Yamada, *Tetrahedron Lett.*, **21**, 5027 (1980); S. Yamada, M. Shiraishi, M. Ohmori, and H. Takayama, *ibid.*, **25**, 3347 (1984).

11) A. Fürst, L. Labler, and W. Meier, *Helv. Chim. Acta*, **65**, 1499 (1982).

12) M. Tsuji, Doctral Thesis, University of Tokyo, Tokyo, Japan, 1988.

13) S. K. Dasgupta, K. R. Crump, and M. Gut, *J. Org. Chem.*, **39**, 1658 (1974); Y. Kobayashi, T. Taguchi, S. Mitsuhashi, T. Eguchi, E. Oshima, and N. Ikekawa, *Chem. Pharm. Bull.*, **30**, 4297 (1982); R. R. Sicinski, H. F. DeLuca, H. K. Schnoes, Y. Tanaka, and C. M. Smith. *Bioorg. Chem.*, **15**, 152 (1987); T. Taguchi, R. Namba, M. Nakazawa, M. Nakajima, Y. Nakama, Y. Kobayashi, N. Hara, and N. Ikekawa, *Tetrahedron Lett.*, **29**, 227 (1988).

The Synthesis of 4,5-Ethylenedithio-4′,5′-vinylenedithiotetrathiafulvalene (EVT) and Its Methyl and Dimethyl Derivatives (EMVT, EDMVT), and the Molecular and Crystal Structures of EVT

Hideyuki NAKANO, Kenji MIYAWAKI, Takashi NOGAMI,* Yasuhiko SHIROTA, Shigeharu HARADA, and Nobutami KASAI
Department of Applied Chemistry, Faculty of Engineering, Osaka University, Yamadaoka, Suita, Osaka 565
(Received March 8, 1989)

New donor molecules, 4,5-ethylenedithio-4′,5′-vinylenedithiotetrathiafulvalene (EVT) and its methyl and dimethyl derivatives (EMVT and EDMVT), were synthesized for the study of conducting organic salts. They are unsymmetrical TTF derivatives possessing moieties of both BEDT-TTF and bis(vinylenedithio)tetrathiafulvalene (VT) or its methyl and dimethyl derivatives. Their oxidation potentials were measured and then compared with those of the related donor molecules. The X-ray crystal structure analysis of EVT revealed that its molecular and crystal structures are very close to that of BEDT-TTF.

BEDT-TTF salts have given a variety of organic superconductors, and the superconducting transition temperature has now been raised to 10.4 K or 11.1 K in $(BEDT\text{-}TTF)_2Cu(SCN)_2$.[1] The crystal structures of the BEDT-TTF salts exhibit sulfur-sulfur networks shorter than the van der Waals distance among donor sites.[2] This crystal structure is believed to be effective for suppressing the Peierls transition inherent in a one-dimensional system. The donor molecules possessing molecular structures similar to BEDT-TTF are interesting, because they can be expected to give highly conducting organic complexes even at low temperatures. The replacement of the ethylene group of BEDT-TTF with vinylene group is one of the most attractive strategies in this regard. Thus, we synthesized bis(vinylenedithio)tetrathiafulvalene (VT) and its dimethyl and tetramethyl derivatives (DMVT and TMVT respectively).[3] Detailed electrical and structural studies of VT_2PF_6 revealed that this salt exhibits a quasi-one-dimensional electrical property and that a metal-insulator (M-I) transition occurs around 180 K.[4] Several VT-salts also showed an M-I transition,[5] probably due to the one-dimensional nature. Therefore, we have synthesized new unsymmetrical TTF-derivatives, EVT, EMVT, and EDMVT, which possess moieties of both BEDT-TTF and VT or its methyl and dimethyl derivatives, in the hope that they might give two-dimensional conducting salts. Here, EVT, EMVT, and EDMVT stand for 4,5-ethylenedithio-4′,5′-vinylenedithiotetrathiafulvalene, 4,5-ethylenedithio-4′,5′-(methylvinylenedithio)tetrathiafulvalene, and 4,5-ethylenedithio-4′,5′-(dimethylvinylenedithio)tetrathiafulvalene respectively.[6] The molecular and crystal structures of EVT are also reported.

Experimental

4,5-Ethylenedithio-4′,5′-vinylenedithiotetrathiafulvalene (EVT). To a mixture of 4,5-ethylenedithio-1,3-dithiole-2-thione (1.0 g, 4.45 mmol)[7] and 4,5-vinylenedithio-1,3-dithiol-2-one (0.92 g, 4.45 mmol),[3] we added triethyl phosphite (20 ml), which had been distilled freshly. The temperature of the solution was gradually elevated to 110 °C with stirring under a nitrogen atmosphere; thereafter, it was stirred for another 2 h at 110 °C. After cooling to room temperature, the precipitate was collected, washed with methyl alcohol, and dried under a vacuum. The crude product was chromatographed on a silica-gel column, using carbon disulflde as an eluent; the second main fraction gave almost pure EVT (0.75 g, 44%). Recrystallization from benzene gave reddish orange needle crystals. Mp 218°C (decomp). MS m/z 382 (M^+). Calcd for $C_{10}H_6S_8$: C, 31.39; H, 1.58; S, 67.03%. Found: C, 31.74; H, 1.57; S, 66.74%. ^1H NMR (CS_2) δ=3.25 (4H, s), 6.47 (2H, s). UV λ_{max}^{THF} ($\log\varepsilon$) 318.4 nm (4.33), 344.4 nm (4.24).

4,5-Ethylenedithio-4′,5′-(methylvinylenedithio)tetrathiafulvalene (EMVT) and 4,5-Ethylenedithio-4′,5′-(dimethylvinylenedithio)tetrathiafulvalene (EDMVT). EMVT and EDMVT were synthesized under reaction conditions similar as those described for EVT. 4,5-Methylvinylenedithio-1,3-dithiol-2-one[3] and 4,5-dimethylvinylenedithio-1,3-dithiol-2-one[3] were, therefore, used instead of 4,5-vinylenedithio-1,3-dithiol-2-one for the synthesis of EMVT and EDMVT respectively. EMVT: yield, 61%. orange needles. Mp 210 °C (decomp). MS m/z 396 (M^+). Calcd for $C_{11}H_8S_8$: C, 33.30; H, 2.03; S, 64.66%. Found: C, 33.40; H, 1.89; S, 64.39%. ^1H NMR (CS_2) δ=2.12 (3H, s), 3.26 (4H, s), 6.02 (1H, s). UV λ_{max}^{THF} ($\log\varepsilon$) 318.0 nm (4.12), 346.0 nm (4.02).

EDMVT: yield, 49%. yellow needles. Mp 217 °C (decomp). MS m/z 410 (M^+). Calcd for $C_{12}H_{10}S_8$: C, 35.09; H, 2.45; S, 62.45%. Found: C, 35.08; H, 2.30; S, 62.35%. ^1H NMR (CS_2) δ=2.30 (6H, s), 3.28 (4H, s). UV λ_{max}^{THF} ($\log\varepsilon$) 318.4 nm (4.15), 346.8 nm (4.06).

Determination of Molecular and Crystal Structures of EVT. $C_{10}H_6S_8$, M=382.68, monoclinic, space group $P2_1/n$, a=6.563(1), b=13.507(8), c=15.866(8) Å, β=93.47(2)°, V=1404(1) Å^3, D_c=1.80 g cm^{-3} for Z=4. The crystal used had a needle shape with approximate dimensions of 0.19×0.60×0.18 mm^3. The reflection intensities were measured by the θ-2θ scan technique up to 2θ=55° on a Rigaku AFC-4 four-circle diffractometer, using Mo $K\alpha$ radiation (λ=0.70926 Å). The scan rate was 4° min^{-1}, and the scan width, $\Delta\theta$=(1.20+0.5 tanθ)°. Backgrounds were counted for 3 s at both ends of a scan. No significant intensity decay of the standard reflections, which were measured after every 100 reflections, was detected. Of the 3513 reflections mea-

Table 1. Atomic Parameters of Nonhydrogen Atoms of EVT Molecule, with Equivalent Isotropic Temperature Factors[11]

Atom	x	y	z	B_{eq}/Å^2
C(1)	0.1049(8)	0.0455(5)	0.3656(4)	2.4
C(2)	0.0823(9)	−0.0236(5)	0.2143(4)	3.2
C(3)	0.278(1)	−0.0347(6)	0.2432(4)	3.6
C(4)	0.168(1)	−0.1268(7)	0.0728(5)	5.7
C(5)	0.375(1)	−0.0816(8)	0.0835(6)	6.1
C(6)	0.0677(8)	0.0970(5)	0.4362(4)	2.5
C(7)	−0.0831(9)	0.2199(5)	0.5374(4)	2.9
C(8)	0.1120(9)	0.2114(5)	0.5652(4)	2.6
C(9)	−0.175(1)	0.2847(6)	0.6917(5)	4.6
C(10)	0.024(1)	0.2773(6)	0.7200(5)	4.4
S(1)	−0.0877(3)	0.0184(1)	0.2877(1)	3.2
S(2)	0.3430(3)	−0.0045(1)	0.3478(1)	3.3
S(3)	−0.0278(3)	−0.0524(2)	0.1143(1)	4.3
S(4)	0.4806(3)	−0.0800(3)	0.1877(1)	6.3
S(5)	−0.1765(3)	0.1414(1)	0.4571(1)	3.0
S(6)	0.2558(3)	0.1195(1)	0.5175(9)	2.9
S(7)	−0.2554(3)	0.2992(1)	0.5839(1)	3.9
S(8)	0.2262(3)	0.2771(1)	0.6501(1)	3.9

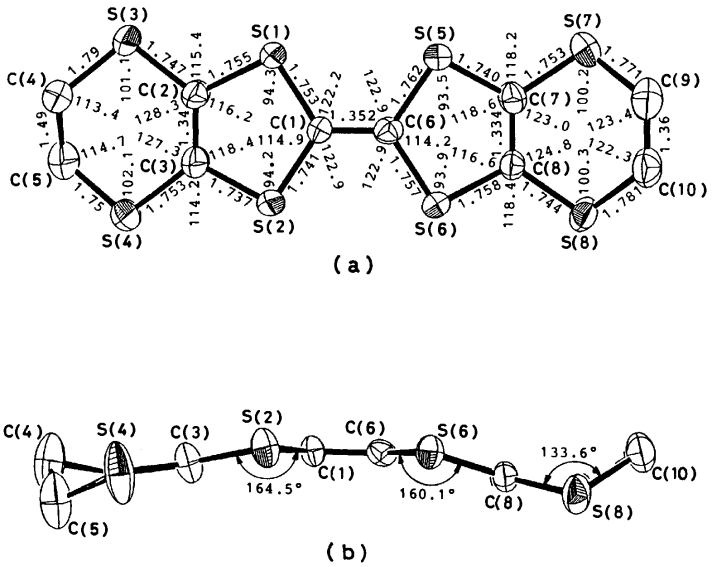

Fig. 1. Molecular structure of EVT.[14] (a) Over view, (b) side view. Nonhydrogen atoms are drawn as thermal ellipsoids with 50% probability level. Estimated standard deviations of the bond lengths and angles are 0.006—0.02 Å and 0.3—0.7° respectively.

sured, the number of reflections observed was 2517 ($|F_o|>2\sigma(F_o)$). The usual Lorentz and polarization corrections were applied, but no absorption correction was made [μ(Mo$K\alpha$)=11.9 cm^{-1}].

The structure was solved by the direct method (*MULTAN* 78)[8] and was refined anisotropically by a block-diagonal least-squares procedure (*HBLS* V).[9] The hydrogen atoms could not be found on a D-map, probably because of their large thermal motion. Therefore, the hydrogen atoms were omitted in the final refinement. The function minimized was $\sum\omega(\Delta F)^2$. The weighting function used in the final stage of the refinement was $\omega=[\sigma^2(F_o)+0.0654|F_o|+0.0005|F_o|^2]^{-1}$. The atomic scattering factors were taken from those of the International Tables for X-Ray Crystallography.[10] The final R index was 0.070. The atomic coordinates of nonhydrogen atoms with equivalent isotropic temperature factors[11] are given in Table 1.[12] The bond lengths and bond angles are shown in Fig. 1.

Results and Discussion

Synthesis and Oxidation Potentials of EVT, EMVT, and EDMVT. The cross-coupling reaction of 4,5-ethylenedithio-1,3-dithiole-2-thione (**1**)[7] and 4,5-vinylenedithio-1,3-dithiol-2-one (**2**)[3] or its methyl (**3**) or dimethyl derivatives (**4**)[3] gave EVT, EMVT, or

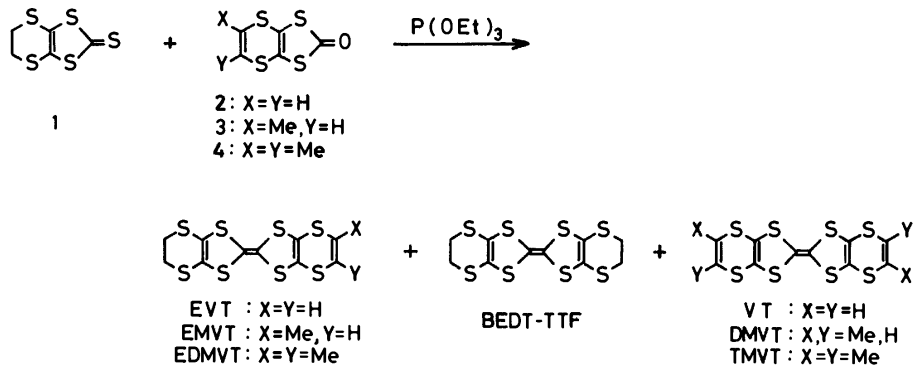

Scheme 1.

Table 2. Half-Wave Oxidation Potentials of Donor Molecules in a THF Solution

Donor	$E_{1/2}(1)$ V vs. SCE	$E_{1/2}(2)$ V vs. SCE
EVT	0.75	
EMVT	0.76	
EDMVT	0.76	
BEDT-TTF[a)]	0.69	0.82
VT[a)]	0.83	
DMVT[a)]	0.80	
TMVT[a)]	0.80	

a) Ref 3.

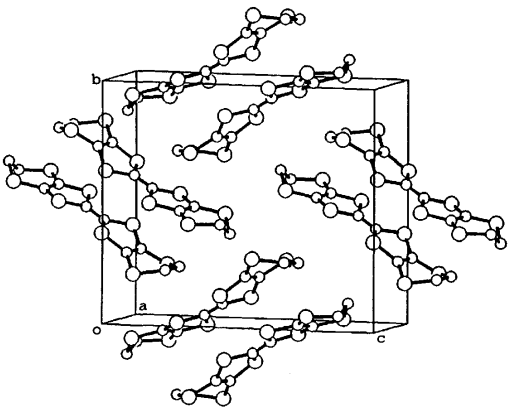

Fig. 2. Crystal structure of EVT.[15)]

EDMVT as the main product (Scheme 1). Self-coupling products (BEDT-TTF and VT or DMVT or TMVT) were always found as minor products. The amount of the cross-coupling product was usually more than 70% of the total coupling products. It is fortunate that, although the reaction products have similar molecular structures, the cross-coupling product can easily be separated from the self-coupling products by means of silica-gel chromatography, using carbon disulfide as the eluent. The absence of the self-coupling products in the purified EVT, EMVT, and EDMVT was confirmed by a study of the mass spectra. The coupling reaction of a mixture of **1** and 4,5-vinylenedithio-1,3-dithiole-2-thione[3)] in triethyl phosphite gave BEDT-TTF as the main product. Thus, **2** should be used instead of its thiocarbonyl derivative in order to obtain EVT.

The cyclic voltammetries of EVT, EMVT, and EDMVT were measured for THF solutions by using tetrabutylammonium perchlorate as the electrolyte and platinum plates as electrodes. Table 2 summarizes their half-wave oxidation potentials (vs. SCE), together with those of BEDT-TTF, VT, DMVT, and TMVT for the sake of comparison.[3)] EVT, EMVT, and EDMVT gave only one redox wave. Since the oxidation potentials of BEDT-TTF, VT, DMVT, and TMVT have been found to be in the order of BEDT-TTF<DMVT≈TMVT<VT,[3)] the following order of the oxidation potentials is predicted: BEDT-TTF< EVT<VT, BEDT-TTF<EMVT<DMVT, BEDT-TTF<EDMVT<TMVT. Table 2 shows that the prediction is satisfied for these new donor molecules.

The electrochemical crystallization of EVT was made for I_3-, PF_6-, AsF_6-, and IBr_2-salts. Their electrical conductivities at 0 °C were 184 $S\,cm^{-1}$ (I_3-salt), 0.76 $S\,cm^{-1}$ (PF_6-salt), 0.17 $S\,cm^{-1}$ (AsF_6-salt), and 4.2 $S\,cm^{-1}$ (IBr_2-salt). The temperature dependence of their electrical conductivities showed semiconducting behavior.

Molecular and Crystal Structures of EVT. The EVT molecule is not planar (Fig. 1(b)). The central portion of tetrathio-substituted ethylene is almost planar, but the outer parts are all bent in the same direction. This molecular structure is much closer to that of BEDT-TTF[13)] than to that of VT; the outer parts of VT are bent in the opposite directions.[4)] The pair-by-pair arrangement of EVT molecules, related by a center of symmetry, is shown in Fig. 2. The molecular arrangement is very close to that found in the BEDT-TTF crystal.[13)] The mode of overlapping of the paired molecules is shown in Fig. 3. The mode of the overlapping of the two molecules is also very close to that of BEDT-TTF.[13)] Several intermolecular S···S distances [S(5)(x,y,z)···S(6)($-x,-y,1-z$) (=3.588(3) Å), S(1)(x,y,z)···S(4)($-1+x,y,z$)(=3.431(4) Å), S(3)(x,y,z)···S(4)($-1+x,y,z$)(=3.516(4) Å), and S(7)

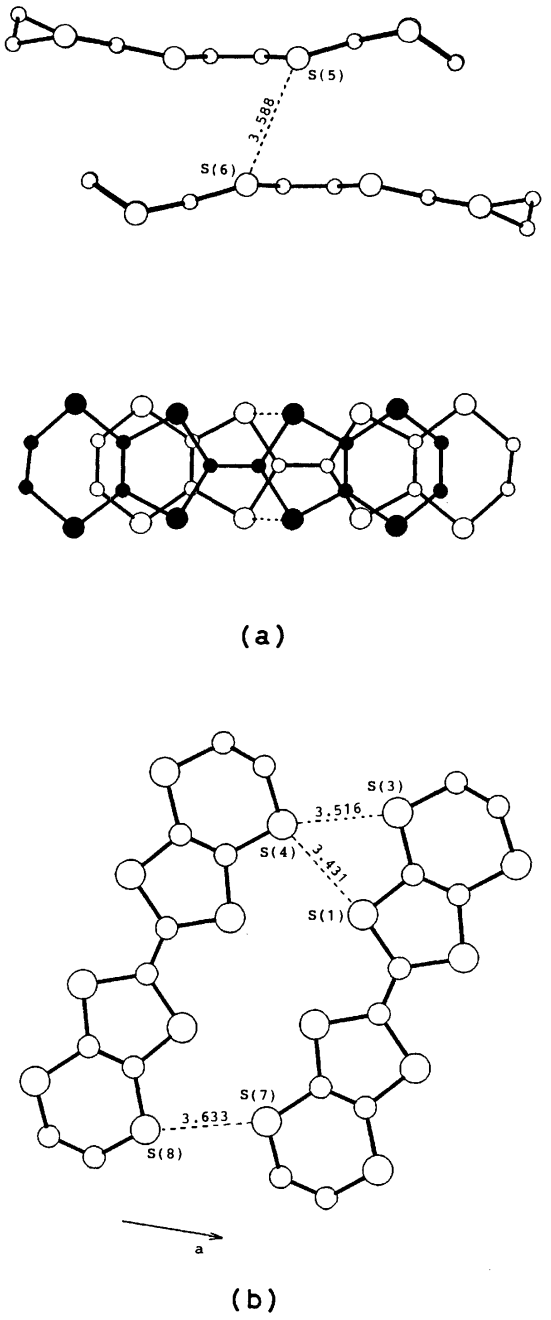

Fig. 3. (a) The mode of overlapping of the paired EVT molecules.[15] The dotted lines indicate the S···S contacts shorter than van der Waals distance (3.7 Å). (b) Molecular arrangememt along the *a* axis.[15]

(x,y,z)····S(8) $(-1+x,y,z)$(=3.633(3) Å)] are shorter than the van der Waals distance (3.7 Å) (Figs. 3(a) and 3(b)).

We are grateful to the Protein Engineering Center, Institute for Protein Research, Osaka University, for the use of the ACOS S850 computer.

References

1) H. Urayama, H. Yamochi, G. Saito, K. Nozawa, T. Sugano, M. Kinoshita, S. Sato, K. Oshima, and K. Kawamoto, *Chem. Lett.*, **1988**, 55; D. Schweitzer, K. Polychroniadis, T. Klutz, H. J. Keller, I. Hennig, I. Heinen, U. Haeberlen, E. Gogu, and S. Gaertner, *Synth. Met.*, **27**, A465 (1988). See also *Synth. Met.*, **27**, Nos. 1, 2, 3, and 4 (1988), Proceedings of the International Conference on Science and Technology of Synthetic Metals (ICSM '88), Santa Fe, NM, USA.

2) J. M. Williams, M. A. Beno, H. H. Wang, P. C. W. Leung, T. J. Emge, U. Geiser, and K. D. Carlson, *Acc. Chem. Res.*, **18**, 261 (1985); J. M. Williams and K. Carneiro, *Adv. Inorg. Chem. Radiochem.*, **29**, 249 (1985).

3) K. Inoue, Y. Tasaka, O. Yamazaki, T. Nogami, and H. Mikawa, *Chem. Lett.*, **1986**, 781; T. Nogami, K. Inoue, T. Nakamura, S. Iwasaka, H. Nakano, and H. Mikawa, *Synth. Met.*, **19**, 539 (1987); T. Nakamura, S. Iwasaka, H. Nakano, K. Inoue, T. Nogami, and H. Mikawa, *Bull. Chem. Soc. Jpn.*, **60**, 365 (1987); T. Nakamura, T. Nogami, and Y. Shirota, *ibid.*, **60**, 3447 (1987); H. Nakano, T. Nogami, and Y. Shirota, *ibid.*, **61**, 2973 (1988).

4) H. Kobayashi, A. Kobayashi, T. Nakamura, T. Nogami, and Y. Shirota, *Chem. Lett.*, **1987**, 559.

5) Unpublished data.

6) G. C. Papavassiliou et al. have recently reported the synthesis of these new donor molecules by different routes from ours, but without any detailed descriptions of the synthetic procedures and the characterizations of the products. G. C. Papavassiliou, G. A. Mousdis, S. Y. Yiannopoulos, V. C. Kakoussis, and J. S. Zambounis, *Synth. Met.*, **27**, B373 (1988).

7) G. Steimecke, H-J. Sieler, R. Kirmse, and E. Hoyer, *Phosphorus and Sulfur*, **7**, 49 (1979); J. M. Williams, M. A. Beno, H. H. Wang, P. E. Reed, L. J. Azevedo, and J. E. Schirber, *Inorg. Chem.*, **23**, 1790 (1984).

8) P. Main, S. E. Hull, L. Lessinger, G. Germain, J-P. Declercq, and M. M. Woolfson, *MULTAN* 78, "A System of Computer Programs for the Automatic Solution of Crystal Structures from X-Ray Diffraction Data," Univ. of York, England and Louvain, Belgium, 1978.

9) T. Ashida, *HBLS* V, The Universal Crystallographic Computing System-Osaka, The Computation Center, Osaka University (1979), p. 53.

10) "International Tables for X-Ray Crystallography," Kynoch Press, Birmingham, England (1974), Vol. IV, p. 71.

11) W. C. Hamilton, *Acta Crystallogr.*, **12**, 609 (1959).

12) Tables of the anisotropic thermal parameters of non-hydrogen atoms and the observed and calculated structure factors are kept at the Chemical Society of Japan, Document No. 8887.

13) H. Kobayashi, A. Kobayashi, Y. Sasaki, G. Saito, and H. Inokuchi, *Bull. Chem. Soc. Jpn.*, **59**, 301 (1986).

14) C. K. Johnson, *ORTEP II*, Report ORNL-5138, Oak Ridge National Laboratory, Tennessee, 1976.

15) W. D. S. Motherwell and W. Clegg, *PLUTO* 78, Program for Plotting Crystal and Molecular Structures, University of Cambridge, England, 1978.

Preparation of 3,6-Disubstituted Pyridazines from 3-Thiapentane-1,5-diones via 2,7-Dihydro-1,4,5-thiadiazepines

Juzo NAKAYAMA,* Toru KONISHI, Akihiko ISHII, and Masamatsu HOSHINO
Department of Chemistry, Faculty of Science, Saitama University, Urawa, Saitama 338
(Received March 18, 1989)

A series of 3-thiapentane-1,5-diones condense with hydrazine in the presence of a catalytic amount of *p*-toluenesulfonic acid in refluxing ethanol to give 2,7-dihydro-1,4,5-thiadiazepines in excellent yields. Thermal decomposition of the latter compounds in refluxing diethylene glycol affords the corresponding pyridazines in high yields with evolution of hydrogen sulfide. The above procedure is generally applicable to the preparation of a wide variety of 3,6-disubstituted pyridazines which are of structural interest and otherwise difficult to prepare.

In recent years we have been investigating the synthesis using 3-thia- and 3-selenapentane-1,5-diones as the starting materials.[1,2] In this connection, we were interested in the reports by Loudon and Young[3] and by Ajello.[4] The former group reports that the thermolysis of 2,7-dihydro-3,6-diphenyl-1,4,5-thiadiazepine (**2a**), obtainable by condensation of 1,5-diphenyl-3-thiapentane-1,5-dione (**1a**) with hydrazine, affords 3,6-diphenylpyridazine (**3a**) with evolution of hydrogen sulfide. The latter author also describes the formation of **3a** by thermolysis of 2,7-dihydro-3,6-diphenyl-1,4,5-selenadiazepine (**5a**) obtainable from 1,5-diphenyl-3-selenapentane-1,5-dione (**4a**). These reactions apparently seem to provide promising routes to substituted pyridazines. Their synthetic utility, however, has not been fully explored. We therefore planned to establish the generality of the above synthesis. We have chosen 3-thiapentane-1,5-diones (**1**) as the starting material since a wide variety of **1** are readily obtainable. Although 3-selenapentane-1,5-diones had become readily obtainable,[2a] the use of these compounds was abandoned because thermolysis of 2,7-dihydro-1,4,5-selenadiazepines might evolve highly toxic hydrogen selenide. Thus, herein we report the general synthesis of 3,6-disubstituted pyridazines (**3**) from **1** via 2,7-dihydro-1,4,5-thiadiazepines (**2**).

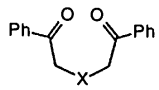

1a : X = S
4a : X = Se

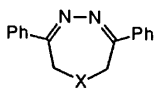

2a : X = S
5a : X = Se

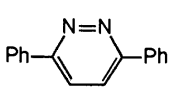

3a

Results and Discussion

3-Thiapentane-1,5-diones (**1**) are easily prepared in good yields by adding an aqueous solution of sodium sulfide to a stirred and ice-cooled solution of an α-halo ketone in acetone.[5] Some α-halo ketones are commercial sources and were used as purchased and the others were prepared by bromination of the corresponding methyl ketones.[6] The yields of **1** thus obtained are summarized in the Scheme 1.

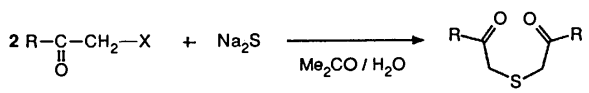

1

2,7-Dihydro-1,4,5-thiadiazepines (**2**) were obtained by condensation of **1** with hydrazine. The best results are generally attained by heating **1** with 1.6 equiv of hydrazine monohydrate in refluxing ethanol in the presence of a catalytic amount of *p*-toluenesulfonic acid (TsOH). Only **2g** was prepared by condensation in hot acetic acid. Reaction conditions and the yields of **2** are also summarized in the Scheme 1.

Sataty has shown that some 2,7-dihydro-1,4,5-thiadiazepines exist in a skew-boat conformation in solutions.[7] Actually, in the ^{1}H NMR spectra determined in deuteriochloroform as the solvent at 27 °C, the methylene protons of every **2** appear as AB quartet with J=12—13 Hz. These observations show that all of **2** exist in the skew-boat conformation **2'**, which results in the chemical shift non-equivalence of the methylene protons H^1 and H^2, in solutions around room temperature. The doublets of compounds **2h**—**j** appear as rather broad signals. This suggests that the ring inversion of these compounds occurs to some extent, while that of the other compounds are slow enough on the ^{1}H NMR time scale at room temperature.

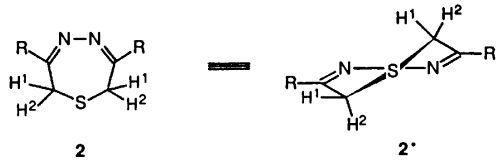

2 **2'**

Conversion of **2** to the corresponding 3,6-disubstituted pyridazines **3** was cleanly attained by heating **2** in refluxing diethylene glycol. The evolution of hydrogen sulfide was observed in every case during the reaction. Reaction conditions and the yields of **3**

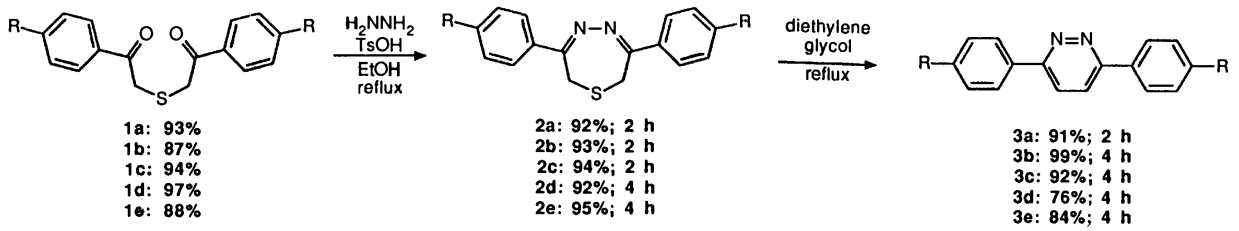

1a: 93%
1b: 87%
1c: 94%
1d: 97%
1e: 88%

2a: 92%; 2 h
2b: 93%; 2 h
2c: 94%; 2 h
2d: 92%; 4 h
2e: 95%; 4 h

3a: 91%; 2 h
3b: 99%; 4 h
3c: 92%; 4 h
3d: 76%; 4 h
3e: 84%; 4 h

a: R=H, b: R=Me, c: R=OMe, d: R=Cl, e: R=Br

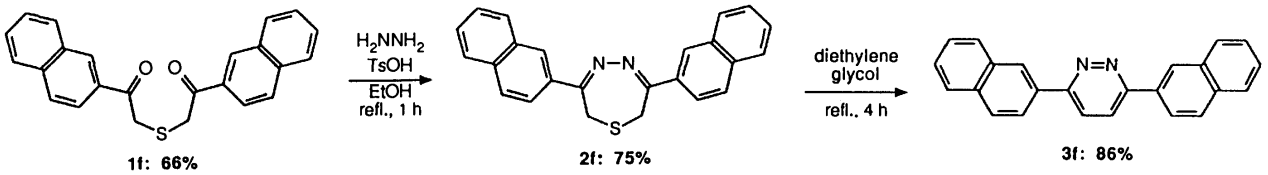

1f: 66%

2f: 75%

3f: 86%

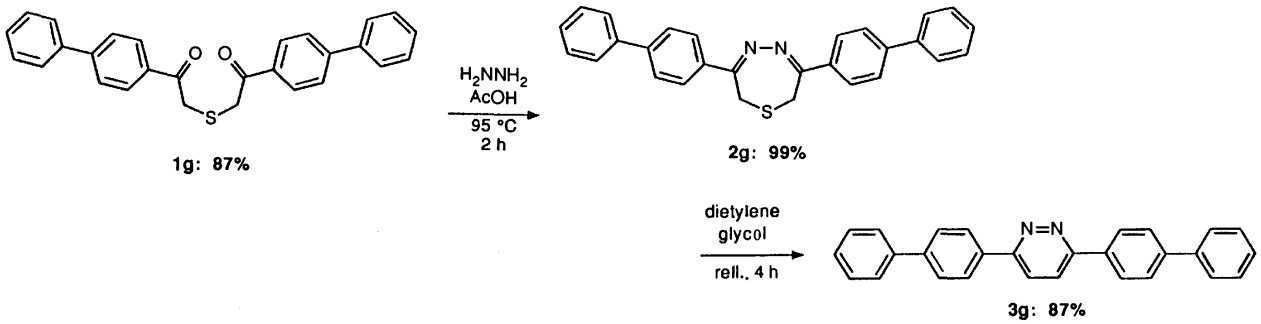

1g: 87%

2g: 99%

3g: 87%

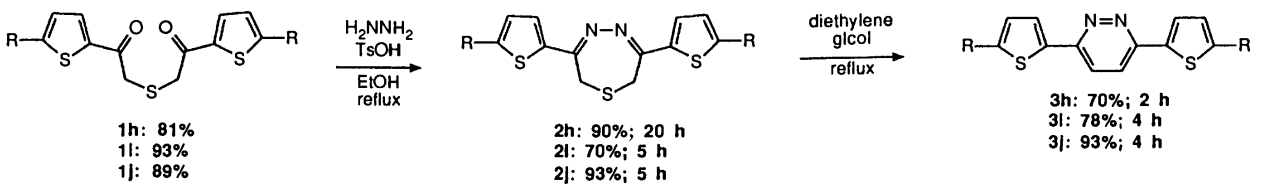

1h: 81%
1i: 93%
1j: 89%

2h: 90%; 20 h
2i: 70%; 5 h
2j: 93%; 5 h

3h: 70%; 2 h
3i: 78%; 4 h
3j: 93%; 4 h

h: R=H, i: R=Cl, j: R=Br

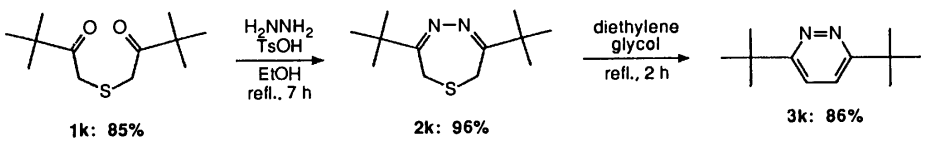

1k: 85%

2k: 96%

3k: 86%

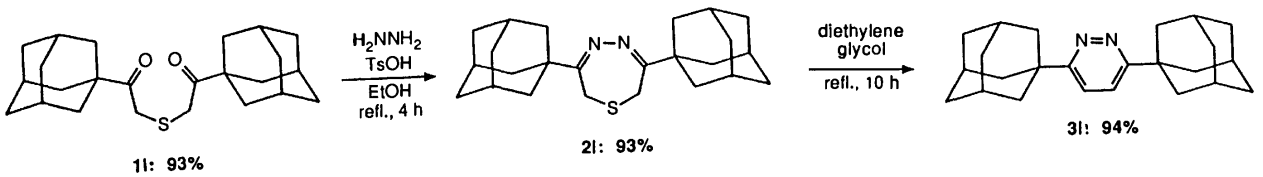

1l: 93%

2l: 93%

3l: 94%

Scheme 1.

thus prepared are summarized in the Scheme 1.

As to the mechanism of the above thermolysis, the followings seem plausible. When **2** were heated in a highly polar solvent diethylene glycol, they probably partly tautomerize to the amino forms **6**, although we could not obtain the evidence for the existence of **6** by ^{1}H NMR and IR spectra determined in deuteriochloroform and carbon tetrachloride, respectively, at room temperature. Then **6** should undergo the carbon (sp^3)-sulfur bond cleavage to lead to the heterotrienes **7**, which in turn undergo electrocyclic ring closure to afford the heterocycles **8**. Finally **8** aromatize to give the final products **3** with loss of hydrogen sulfide.[8]

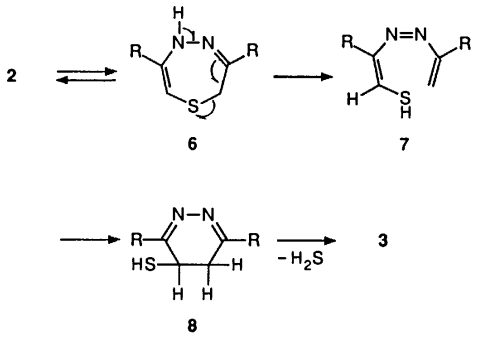

The synthetic method of **3** described above is convenient from the following points of view.

a) The standard method of synthesis of the pyridazine ring involves the action of hydrazine on 1,4-dicarbonyl compounds or their equivalent.[9] The preparation of 1,4-dicarbonyl compounds, however, often requires tedious or sophisticated procedures. In the present case, the starting **1** are readily obtainable.

b) None of the steps in the present synthesis requires any expensive reagents or special techniques. Work-up procedure is also simple and good overall yields are attained.

c) The method provides the synthesis of pyridazines which are of interest as the starting compounds for the preparation of conducting materials (**3g—j**).

d) The method allows the preparation of pyridazines having highly bulky groups such as *t*-butyl and 1-adamantyl (**3k** and **31**).

Experimental

General. Melting points were determined on a MEL-TEMP capillary tube apparatus and are uncorrected. ^{1}H NMR spectra were recorded on a JEOL PMX-60, a JEOL FX-90Q, or a Bruker AM-400 spectrometer and ^{13}C NMR spectra on a JEOL FX-90Q or on a Bruker AM-400 spectrometer. Chemical shifts are expressed in parts per million from tetramethylsilane as an internal standard. Mass spectra were measured on a Shimadzu QP-1000 spectrometer with ionization energy of 70 or 20 eV. High resolution mass spectra were determined on a JEOL DX-303 spectrometer. IR spectra were taken on a Hitachi 270-50 spectrometer. UV spectra were recorded on a Hitachi 340 spectrometer. Column chromatography was conducted using E. Merck silica gel 60 (70—230 mesh). Sodium sulfide enneahydrate, hydrazine monohydrate, and diethylene glycol are commercial sources and were used as purchased.

Elemental analyses were performed by Analytical Center of Saitama University, for which we thank Professor M. Sato and his staff.

General Procedure for the Preparation of 3-Thiapentane-1,5-diones (1). A solution of sodium sulfide enneahydrate (5 mmol) in 10 ml of water was added to a stirred and ice-cooled solution of an α-halo ketone (10 mmol) in an appropriate amount of acetone (20—60 ml). After completion of the addition, the mixture was warmed to room temperature and stirred for a few hours. The resulting crystalline precipitate was collected by filtration, washed with water and then with a small amount of cold methanol or ethanol, and recrystallized from an appropriate solvent. In the case of the crystalline precipitate being not separated or separated only in a small amount, the mixture was concentrated and the resulting precipitate was treated as described above.

2-Bromo-, 2-bromo-4′-methyl-, 2-bromo-4′-methoxy-, 2-bromo- 4′-chloro-, 2,4′-dibromo-, and 2-bromo-4′-phenylacetophenones, 2-bromo-2′-acetonaphthone (bromomethyl 2-naphthyl ketone), and 1-adamantyl bromomethyl ketone are commercial sources and were used as purchased. 2-(Bromoacetyl)thiophene, 2-(bromoacetyl)-5-chlorothiophene, and bromomethyl *t*-butyl ketone were obtained by bromination of commercially available 2-acetylthiophene, 2-acetyl-5-chlorothiophene, and *t*-butyl methyl ketone, respectively.[6] 2-(Bromoacetyl)-5-bromothiophene was synthesized by bromination of 2-acetyl-5-bromothiophene which is obtainable from 2-acetylthiophene.

1,5-Diphenyl-3-thiapentane-1,5-dione (**1a**),[5] 1,5-bis(4-methylphenyl)-3-thiapentane-1,5-dione (**1b**),[5] 1,5-bis(4-methoxyphenyl)-3-thiapentane-1,5-dione (**1c**),[5] 1,5-bis(4-chlorophenyl)-3-thiapentane-1,5-dione (**1d**),[5] 1,5-bis(4-bromophenyl)-3-thiapentane-1,5-dione (**1e**),[5] 1,5-di-2-naphthyl-3-thiapentane-1,5-dione (**1f**),[1a] 1,5-di-2-thienyl-3-thiapentane-1,5-dione (**1h**),[5] and 1,5-di-*t*-butyl-3-thiapentane-1,5-dione (**1k**)[5] are known compounds.

The following **1** are new compounds.

1,5-Di-4-biphenyl-3-thiapentane-1,5-dione (1g): mp 178—179 °C; white crystals from benzene; ^{1}H NMR ($CDCl_3$) δ=4.03 (4H, s, CH_2), 7.4—8.1 (18H, m); ^{13}C NMR ($CDCl_3$) δ=37.67, 127.27, 128.30, 128.95, 129.22, 134.21, 139.73, 146.24, 193.75; IR(KBr) 1678 cm^{-1} (C=O). Anal. ($C_{28}H_{22}O_2S$) C, H.

1,5-Bis(5-chloro-2-thienyl)-3-thiapentane-1,5-dione (1i): mp 96—97 °C; pale yellow crystals from ethanol; ^{1}H NMR ($CDCl_3$) δ=3.82 (4H, s, CH_2), 6.97 (2H, d, *J*=4 Hz), 7.57 (2H, d, *J*=4 Hz); ^{13}C NMR ($CDCl_3$) δ=36.97, 127.71, 132.69, 140.44, 140.87, 186.27. Anal. ($C_{12}H_8Cl_2O_2S_3$) C, H.

1,5-Bis(5-bromo-2-thienyl)-3-thiapentane-1,5-dione (1j): mp 113—114 °C; pale yellow crystals from carbon tetrachloride; ^{1}H NMR ($CDCl_3$) δ=3.82 (4H, s, CH_2), 7.11 (2H, d, *J*=4 Hz), 7.50 (2H, d, *J*=4 Hz); ^{13}C NMR ($CDCl_3$) δ=37.13, 123.59, 131.28, 133.12, 143.74, 186.05. Anal. ($C_{12}H_8Br_2O_2S_3$) C, H.

1,5-Di-1-adamantyl-3-thiapentane-1,5-dione (1l): mp 81—82 °C; white crystals from methanol; ^{1}H NMR ($CDCl_3$) δ=1.62—2.05 (30H, m), 3.49 (4H, broad s, CH_2); IR (KBr)

1704, 1678 cm^{-1} (C=O). Anal. ($C_{24}H_{34}O_2S$) C, H.

General Procedure for the Preparation of 2,7-Dihydro-1,4,5-thiadiazepines (2). A mixture of a 3-thiapentane-1,5-dione (**1**; 10 mmol) and hydrazine monohydrate (16 mmol) in ethanol (50—100 ml) containing *p*-toluenesulfonic acid monohydrate (ca. 10 mg) was heated under reflux until the starting sulfide had disappeared. The mixture was cooled to room temperature and the resulting crystalline precipitate was collected by filtration, washed with a small amount of cold ethanol, and recrystallized from an appropriate solvent.

Only compound **2g** was prepared by heating **1g** (5 mmol) and hydrazine monohydrate (8 mmol) in acetic acid (150 ml) at 95 °C for 2 h.

3,6-Diphenyl-2,7-dihydro-1,4,5-thiadiazepine (2a): mp 181—182 °C (lit,[3] mp 174—175 °C); white fine needles from ethanol; ^1H NMR ($CDCl_3$) δ=3.22 (2H, d, J=12 Hz), 3.54 (2H, d, J=12 Hz), 7.21—7.43 (6H, m), 7.69—7.81 (4H, m); ^{13}C NMR ($CDCl_3$) δ=26.46, 127.17, 128.79, 130.15, 135.18, 151.65.

3,6-Bis(4-methylphenyl)-2,7-dihydro-1,4,5-thiadiazepine (2b): mp 206—207 °C (lit,[3] mp 215 °C); white crystals from carbon tetrachloride; ^1H NMR ($CDCl_3$) δ=2.41 (6H, s), 3.33 (2H, d, J=13 Hz), 3.64 (2H, d, J=13 Hz), 7.27 (4H, d, J=8 Hz), 7.79 (4H, d, J=8 Hz); ^{13}C NMR ($CDCl_3$) δ=21.31, 26.35, 127.06, 129.50, 132.42, 140.33, 151.54.

3,6-Bis(4-methoxyphenyl)-2,7-dihydro-1,4,5-thiadiazepine (2c): mp 214—215 °C; white needles from benzene; ^1H NMR ($CDCl_3$) δ=3.31 (2H, d, J=13 Hz), 3.61 (2H, d, J=13 Hz), 3.87 (6H, s), 6.97 (4H, d, J=9 Hz), 7.84 (4H, d, J=9 Hz); ^{13}C NMR ($CDCl_3$) δ=26.29, 55.44, 114.27, 127.76, 128.63, 151.27, 161.30; IR (Nujol) 1600, 1546, 1506, 1302, 1254, 1176, 1018, 842 cm^{-1}; UV/Vis (CH_2Cl_2) 282 (ε=18000), 316 nm (sh, 15000). Anal. ($C_{18}H_{18}N_2O_2S$) C, H, N.

3,6-Bis(4-chlorophenyl)-2,7-dihydro-1,4,5-thiadiazepine (2d): mp 195—196 °C; white needles from carbon tetrachloride; ^1H NMR ($CDCl_3$)δ=3.20 (2H, d, J=13 Hz), 3.68 (2H, d, J=13 Hz), 7.43 (4H, d, J=9 Hz), 7.83 (4H, d J=9 Hz); ^{13}C NMR ($CDCl_3$) δ=26.29, 128.41, 129.06, 133.40, 136.38, 150.62; IR (Nujol) 1650, 1592, 1492, 1318, 1090, 1008, 896, 832 cm^{-1}; UV/Vis (CH_2Cl_2) 276 (ε=17000), 316 nm (9200). Anal. ($C_{16}H_{12}Cl_2N_2S$) C, H, N.

3,6-Bis(4-bromophenyl)-2,7-dihydro-1,4,5-thiadiazepine (2e): mp 208—209 °C (lit,[3] mp 202 °C); white fine needles from ethanol; ^1H NMR ($CDCl_3$) δ=3.29 (2H, d, J=13 Hz), 3.62 (2H, d, J=13 Hz), 7.58 (4H, d, J=8.5 Hz), 7.76 (4H, d, J=8.5 Hz); ^{13}C NMR ($CDCl_3$) δ=26.29, 128.57, 132.04, 133.83, 143.37, 150.68.

3,6-Di-2-naphthyl-2,7-dihydro-1,4,5-thiadiazepine (2f): mp 223—224 °C; white needles from carbon tetrachloride; ^1H NMR ($CDCl_3$) δ=3.57 (2H, d, J=13 Hz), 3.80 (2H, d, J=13 Hz), 7.52—7.57 (4H, m), 7.87—7.95 (6H, m), 8.14—8.17 (2H, m), 8.28 (2H, s); IR (Nujol) 1598, 1550, 1316, 1150, 858, 822, 748 cm^{-1}; UV/Vis (CH_2Cl_2) 264 (ε=33000), 316 nm (sh, 16000). HRMS Found: m/z 366.1193. Calcd for $C_{24}H_{18}N_2S$: M, 366.1191.

3,6-Di-4-biphenylyl-2,7-dihydro-1,4,5-thiadiazepine (2g): mp 267 °C (decomp); white crystals from chloroform ^1H NMR ($CDCl_3$) δ=3.51 (2H, d, J=13 Hz), 3.65 (2H, d, J=13 Hz), 7.40—8.05 (18H, m); IR (KBr) 1604, 1572, 1488, 1438, 1326, 844, 762, 734, 688 cm^{-1}; UV/Vis (CH_2Cl_2) 296 (ε=36000), 322 nm (sh, 34000). HRMS Found: m/z 418.1501. Calcd for $C_{28}H_{22}N_2S$: M, 418.1503.

3,6-Di-2-thienyl-2,7-dihydro-1,4,5-thiadiazepine (2h): mp 198—199 °C; pale yellow crystals from benzene/hexane; ^1H NMR ($CDCl_3$) δ=3.47 (2H, d, J=13 Hz), 3.62 (2H, d, J=13 Hz), 7.04—7.14 (2H, m), 7.36—7.50 (4H, m); ^{13}C NMR ($CDCl_3$) δ=26.83, 127.54, 129.71, 139.79, 148.13; IR (KBr) 3072, 1556, 1438, 1310, 1148, 1058, 1016, 856 cm^{-1}; UV/Vis (CH_2Cl_2) 276 (ε=15000), 318 nm (14000); MS m/z 278 (M^+). Anal. ($C_{12}H_{10}N_2S_3$) C, H, N.

3,6-Bis(5-chloro-2-thienyl)-2,7-dihydro-1,4,5-thiadiazepine (2i): mp 209—210 °C; pale yellow crystals from ethanol; ^1H NMR ($CDCl_3$) δ=3.41 (2H, d, J=12.5 Hz), 3.55 (2H, d, J=12.5 Hz), 6.91 (2H, d, J=4 Hz), 7.14 (2H, d, J=4 Hz); IR (Nujol) 1558, 1528, 1324, 1214, 1008, 816, 726, 698 cm^{-1}. UV/Vis (CH_2Cl_2) 294 (ε=14000), 348 nm (19000); MS m/z, M^+ (relative intensity) 346 (100), 347 (15), 348 (70), 349 (11), 350 (21). Anal. ($C_{12}H_8Cl_2N_2S_3$) C, H, N.

3,6-Bis(5-bromo-2-thienyl)-2,7-dihydro-1,4,5-thiadiazepine (2j): mp 180 °C (decomp); pale yellow crystals from benzene; ^1H NMR ($CDCl_3$) δ=3.24 (2H, d, J=13 Hz), 3.78 (2H, d, J=13 Hz), 7.05 (2H, d, J=4 Hz), 7.11 (2H, d, J=4 Hz); IR (Nujol) 3092, 1558, 1436, 1320, 1214, 1070, 1018, 982, 818 cm^{-1} UV/Vis (CH_2Cl_2) 296 (ε=19000), 345 nm (25000). HRMS Found: m/z 435.8229. Calcd for $C_{12}H_8{}^{79}Br^{81}BrN_2S_3$: M, 435.8196.

3,6-Di-*t*-butyl-2,7-dihydro-1,4,5-thiadiazepine (2k): mp 144—145 °C; white flakes from ethanol; ^1H NMR ($CDCl_3$) δ=1.26 (18H, s), 2.86 (2H, d, J=12 Hz), 3.02 (2H, d, J=12 Hz); ^{13}C NMR ($CDCl_3$) δ=23.75, 28.03, 37.83, 160.54; IR (KBr) 2976, 2924, 1590, 1462, 1422, 1360, 1176, 1070, 904, 720 cm^{-1}. Anal. ($C_{12}H_{22}N_2S$) C, H, N.

3,6-Di-1-adamantyl-2,7-dihydro-1,4,5-thiadiazepine (2l): mp 271—272 °C; white prisms from benzene/hexane; ^1H NMR ($CDCl_3$) δ=1.60—2.05 (30H, m), 2.88 (2H, d, J=12 Hz), 3.02 (2H, d, J=12Hz); ^{13}C NMR ($CDCl_3$) δ=22.95, 29.19, 36.71, 39.80, 40.09, 160.79; IR (KBr) 2904, 2848, 1582, 1450, 1342, 1280, 1250, 1100, 1028, 838 cm^{-1}; UV/Vis (CH_2Cl_2) 268 nm (ε=20000); MS m/z 382 (M^+). Anal. ($C_{24}H_{34}N_2S$) C, H, N.

General Procedure for the Preparation of 3,6-Disubstituted Pyridazines (3) from 2,7-Dihydro-1,4,5-thiadiazepines (2). A suspension of a 2,7-dihydro-1,4,5-thiadiazepine (**2**, 1 mmol) in diethylene glycol (10 ml) was heated under reflux until the starting **1** had been completely consumed (for the time of refluxing, see the Scheme 1). The evolution of hydrogen sulfide during the reaction was observed in every case. The mixture was cooled to room temperature and the resulting crystalline precipitate of **3** was collected by filtration, washed with a small amount of cold methanol or ethanol, and recrystallized from an appropriate solvent. The original filtrate and washings were combined, diluted with water, and extracted with dichloromethane. The extract was purified by column chromatography on silica gel to give an additional amount of **3**.

3,6-Diphenylpyridazine (3a): mp 222—223 °C (lit,[3] mp 222 °C; ^1H NMR ($CDCl_3$) δ=7.40—8.20 (10H, m), 7.87 (2H, s); ^{13}C NMR ($CDCl_3$) δ=126.62, 128.30, 129.01, 136.21, 138.54, 157.67.

3,6-Bis(4-methylphenyl)pyridazine (3b): mp 231—232 °C (lit,[3] mp 236 °C); ^1H NMR ($CDCl_3$) δ=2.43 (6H, s), 7.33 (4H, d, J=8 Hz), 7.86 (2H, s), 8.04 (4H, d, J=8 Hz) ^{13}C NMR ($CDCl_3$) δ=21.25, 123.75, 126.73, 129.71, 133.45, 140.06, 157.34.

3,6-Bis(4-methoxyphenyl)pyridazine (3c): mp 238—240 °C (lit,[10] mp 235 °C); ^1H NMR ($CDCl_3$) δ=3.89 (6H, s),

7.06 (4H, d, J=9 Hz), 7.83 (2H, s), 8.11 (4H, d, J=9 Hz).

3,6-Bis(4-chlorophenyl)pyridazine (3d): mp 265—267 °C (lit,[11] mp 264 °C; ^{1}H NMR ($CDCl_3$) δ=7.52 (4H, d, J=9 Hz), 7.91 (2H, s), 8.11 (4H, d, J=9 Hz).

3,6-Bis(4-bromophenyl)pyridazine (3e): mp 285—286 °C (lit,[3] mp 288 °C); ^{1}H NMR ($CDCl_3$) δ=7.68 (4H, d, J=9 Hz), 7.91 (2H, s), 8.04 (4H, d, J=9 Hz).

3,6-Di-2-naphthylpyridazine (3f): mp 280—281 °C; pale yellow crystals from 1,2-dichloroethane; ^{1}H NMR ($CDCl_3$) δ=7.56—7.58 (4H, m), 7.92—7.94 (2H, m), 7.99—8.05 (4H, m), 8.15 (2H, s), 8.36—8.39 (2H, m), 8.67 (2H, s). HRMS Found: m/z 332.1311. Calcd for $C_{24}H_{16}N_2$: M, 332.1314.

3,6-Di-4-biphenylylpyridazine (3g): mp 357—359 °C; white powder (purified by sublimation at 345—350 °C/0.01 Torr); ^{1}H NMR ($CDCl_3$) δ=7.38—8.26 (18H, m), 8.01 (2H, s); IR (KBr) 1584, 1486, 1418, 1166, 1040, 1002, 828, 758, 718, 682, 582, 472 cm^{-1}. Anal. ($C_{28}H_{20}N_2$) C, H, N.

3,6-Di-2-thienylpyridazine (3h): mp 181—182 °C (lit,[12] mp 175—176 °C); ^{1}H NMR ($CDCl_3$) δ=7.13 (2H, dd, J=5, 4 Hz), 7.47 (2H, dd, J=5, 1 Hz), 7.63 (2H, dd, J=4, 1 Hz), 7.71 (2H, s).

3,6-Bis(5-chloro-2-thienyl)pyridazine (3i): mp>300 °C (decomp); yellow crystals from benzene; IR (KBr) 1554, 1444, 1122, 1014, 838, 788, 530, 456 cm^{-1}; MS m/z, M^+ (relative intensity) 312 (100), 314 (85), 316 (25). Anal. ($C_{12}H_6Cl_2N_2S_2$) C, H, N.

3,6-Bis(5-bromo-2-thienyl)pyridazine (3j): mp>300 °C (decomp): yelllow crystals from benzene; IR (KBr) 1552, 1436, 1122, 838, 790, 746, 586 cm^{-1}. HRMS Found: m/z 401.8309. Calcd for $C_{12}H_6{}^{79}Br^{81}BrN_2S_2$: M, 401.8318.

3,6-Di-*t*-butylpyridazine (3k): mp 179—180 °C; white crystals from pentane; ^{1}H NMR ($CDCl_3$) δ=1.44 (18H, s), 7.44 (2H, s); ^{13}C NMR ($CDCl_3$) δ=30.00, 36.53, 123.10, 167.58; IR (KBr) 2972, 1588, 1538, 1482, 1366, 1152, 1038, 872 cm^{-1}. Anal. ($C_{12}H_{20}N_2$) C, H.

3,6-Di-1-adamantylpyridazine (3l): mp 278—280 °C; white crystals from methanol; ^{1}H NMR ($CDCl_3$) δ=1.61—2.08 (30H, m), 7.37 (2H, s); ^{13}C NMR ($CDCl_3$) δ=28.68, 36.70, 38.16, 41.73, 122.72, 167.25; IR (KBr) 2904, 2848, 1582, 1452, 1422, 1312, 1056, 810 cm^{-1}. Anal. ($C_{24}H_{32}N_2$) C, H, N.

References

1) For synthesis with 3-thiapentane-1,5-diones, see a) J. Nakayama, H. Motoyama, H. Machida, M. Shimomura, and M. Hoshino, *Heterocycles*, **22**, 1527 (1984); b) J. Nakayama, H. Machida, and M. Hoshino, *Tetrahedron Lett.*, **26**, 1981 (1985); c) J. Nakayama, H. Machida, R. Saito, and M. Hoshino, *ibid.*, **26**, 1983 (1985); d) J. Nakayama, M. Shimomura, M. Iwamoto, and M. Hoshino, *Heterocycles*, **23**, 1907 (1985); e) J. Nakayama, H. Machida, R. Saito, K. Akimoto, and M. Hoshino, *Chem. Lett.*, **1985**, 1173; f) J. Nakayama, Y. Nakamura, S. Murabayashi, and M. Hoshino, *Heterocycles*, **26**, 939 (1987); g) J. Nakayama, S. Yamaoka, and M. Hoshino, *Tetrahedron Lett.*, **28**, 1799 (1987); h) J. Nakayama, K. Hidaka, and M. Hoshino, *Heterocycles*, **26**, 1785 (1987); i) J. Nakayama, S. Murabayashi, and M. Hoshino, *ibid.*, **26**, 2599 (1987); j) J. Nakayama, S. Yamaoka, and M. Hoshino, *Tetrahedron Lett.*, **29**, 1161 (1988); k) J. Nakayama, A. Ishii, Y. Kobayashi, and M. Hoshino, *J. Chem. Soc., Chem. Commun.*, **1988**, 959; l) J. Nakayama, S. Yamaoka, T. Nakanishi, and M. Hoshino, *J. Am. Chem. Soc.*, **110**, 6598 (1988); m) J. Nakayama, Y. Kumano, and M. Hoshino, *Tetrahedron Lett.*, **30**, 847 (1989).

2) For synthesis with 3-selenapentane-1,5-diones, see a) J. Nakayama, M. Shibuya, and M. Hoshino, *Heterocycles*, **26**, 909 (1987); b) J. Nakayama, Y. Ikuina, F. Murai, and M. Hoshino, *J. Chem. Soc., Chem. Commun.*, **1987**, 1072; c) J. Nakayama, F.Murai, H. Hoshino, and A. Ishii, *Tetrahedron Lett.*, **29**, 1399 (1988); d) J. Nakayama and Y. Sugihara, *Chem. Lett.*, **1988**, 1317; e) J. Nakayama and Y. Sugihara, *J. Phys. Org. Chem.*, **1**, 59 (1988).

3) J. D. Loudon and L. B. Young, *J. Chem. Soc.*, **1963**, 5496.

4) E. Ajello, *J. Heterocycl. Chem.*, **9**, 1427 (1972).

5) Y. Miyahara, *J. Heterocycl. Chem.*, **16**, 1147 (1979).

6) R. M. Cowper and L. H. Davidson, *Org. Synth.*, Coll. Vol. II, 480 (1966).

7) I. Sataty, *J. Heterocycl. Chem.*, **7**, 431 (1970).

8) An alternative mechanism involves the thermal extrusion of sulfur from **2** to give the heterotrienes **9**, which cyclize to the dihydropyridazines **10**. Finally dehydrogenation of **10** by the sulfur affords **3** and hydrogen sulfide.

9) M. Tisler and B. Stanovnik, *Adv. Heterocycl. Chem.*, **9**, 211 (1968): **24**, 363 (1979); G. R. Newkome and W. W. Paudler, "Contemporary Heterocyclic Chemistry," John Wiley, New York (1982), p. 184; T. L. Gilchrist, "Heterocyclic Chemistry," Pitman, London, (1985), p. 322.

10) D. R. Borthankur, D. Prajapati, and J. S. Sandhu, *Heterocycles*, **26**, 337 (1987).

11) N. Campbell and N. M. Khanna, *J. Chem. Soc., Suppl. Issue*, **1949**, 33.

12) J.-P. Montheard and J.-C. Dubois, *J. Heterocycl. Chem.*, **22**, 719 (1985).

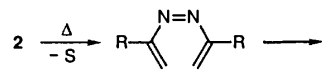

9

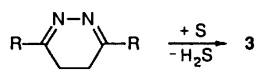

10

 © 1989 The Chemical Society of Japan Bull. Chem. Soc. Jpn., 62, 2613—2617 (1989)

Catalytic Oxygenation of Benzene. Catalyst Design and Its Performance

Atsutaka KUNAI,* Takayuki WANI, Yasushi UEHARA, Fumiaki IWASAKI, Yasushi KURODA, Sotaro ITO, and Kazuo SASAKI
Department of Applied Chemistry, Faculty of Engineering, Hiroshima University, Shitami, Saijo-cho, Higashi-Hiroshima 724
(Received March 18, 1989)

A catalyst system for oxygenation reaction of benzene has been discussed. The catalyst system is composed of Pd and Cu species and operates in neat benzene under ambient conditions by feeding hydrogen and oxygen to the system. By selecting the reaction conditions properly, either phenol or benzoquinone is obtained as the major product.

There is a strong demand in the chemical industry to produce phenol or phenolic compounds in much more efficient ways.[1] Undoubtedly, the most efficient process currently operating in the chemical industry is the "Cumene Process." This process, however, necessitates multi-step operations throughout the whole process and accompanies by-production of equimolar amount of acetone. If benzene is directly converted to phenols without any by-product under moderate conditions, a great benefit will be brought about.

Many reactions are known which lead to phenol from benzene.[1,2] They are, however, too much basic[3-6] to be used for the practical purpose or require severe reaction conditions[7,8] and/or expensive chemical reagents.[7,9] In this paper, we report the nature and the performance of some new solid catalysts developed for the one-step production of phenol.

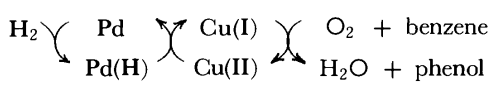

Scheme 1.

The catalyst system is basically composed of Pd and Cu species and operates in neat benzene under ambient conditions by feeding hydrogen and oxygen gases. The reaction sequence occurring in this system may be expressed as in Scheme 1, where palladium mediates electron transfer from hydrogen to copper(II) ions. The copper(I) ions thus produced activate dioxygen to produce phenol. Furthermore, the main product can be altered at will from phenol to *p*-benzoquinone if the reaction conditions are slightly modified. It should be noted that no effective catalyst has been known so far for the direct conversion of benzene to benzoquinone.

Experimental

Catalyst Preparation. The solid catalysts examined in this study were prepared in three different ways. **Catalyst A:** $PdCl_2$ (0.5 mmol), Cu(II) salt (10 mmol), and silica gel (10 g, Merck No. 9385, 230—400 mesh ASTM) were added to water (30 cm^3) altogether and exposed to ultrasonic wave for 90 min. The resultant mixture was heated to dryness on a steam bath under gentle agitation. **Catalyst B:** $PdCl_2$ was first dissolved in dil HCl (30 cm^3) and Cu(II) salt and silica gel were then added to the solution. The mixture was dried in the same way as described in the catalyst A. **Catalyst C:** A mixture of $PdCl_2$ and silica gel in water was stirred at 60 °C for 2 h to disperse the Pd salt on the silica surface. Copper(II) sulfate was then loaded on it. The mixture was dried in the same manner as described above.

Oxidation of Benzene. Experiments under atmospheric conditions were conducted in an Erlenmeyer flask (50 cm^3) equipped with two gas inlets and one outlet. A mixture of benzene (20 cm^3) and the catalyst (2 g) was taken in the flask and shaken in a thermostated bath at 25 °C at the rate of 140 times/min with 30 mm stroke under atmospheric pressure. The reacting gases were fed to the flask in two different modes. **(1) Simultaneous gas feeding:** During the whole reaction, both hydrogen and oxygen were passed through the flask simultaneously. **(2) Alternate gas feeding:** Gases in the flask were first replaced with hydrogen and shaken for a desired time. Hydrogen was then switched to either air or pure oxygen and the flask was again shaken. This alternate gas feeding was repeated several times in some experiments.

Experiments under pressurized conditions were carried out in a glass-made autoclave equipped with a mechanical stirrer by applying the alternate gas-feeding.

Product Analysis. During the reaction, a small amount of sample was taken up periodically for HPLC analysis. The products were analyzed by using Merck Lichrosorb RP-18 (10×250 mm) as the stationary phase and a solution of acetonitrile–phosphate buffer of pH 3.5 (1 : 3) as the eluent.

Results and Discussion

1. Catalyst Design. The solid catalyst designed in this study is basically composed of 2 mmol of copper(II) sulfate and a catalytic amount of palladium chloride (0.1 mmol) supported on 2 g of silica. By feeding hydrogen, $PdCl_2$ is reduced to metallic Pd.

As for the role of copper species in the oxidation of benzene, we have already demonstrated that, in aqueous acid solutions, low valent copper ions activate dioxygen to generate hydroxyl radicals (Eqs. 1 and 2), which react with benzene to yield phenolic compound (Eq. 3).[10-13]

$$O_2 + 2Cu^+ + 2H^+ \longrightarrow H_2O_2 + 2Cu^{2+} \quad (1)$$

Table 1. Catalytic Oxidation of Benzene by Simultaneous Feeding of Hydrogen and Oxygen[a)]

Reaction time/h	0.5	1	2	3	4	5	6	7	8	9
PhOH/μmol	4.7	15	48	77	114	141	167	183	205	229

a) The reaction was carried out using the catalyst C by simultaneous feeding of H_2 and O_2.

Table 2. Effect of Oxidation Time on the Phenol Yield[a)]

Oxidation time/min	5	10	15	20	25	30
PhOH/μmol	18.2	18.6	19.5	19.3	19.6	19.8

a) The reaction was carried out using the catalyst C by alternate feeding of H_2 and O_2. The oxidation started after the catalyst had been treated under H_2 for 90 min.

$$H_2O_2 + Cu^+ + H^+ \longrightarrow \cdot OH + Cu^{2+} + H_2O \quad (2)$$

$$\cdot OH + C_6H_6 + Cu^{2+} \longrightarrow C_6H_5OH + Cu^+ + H^+ \quad (3)$$

Since Cu(I) ions are consumed during the reaction, it is necessary to recycle Cu(I) ions by some suitable means in order to set up a continuous reaction system. This may be performed by using hydrogen as the reducing agent when certain metal catalyst is present in the system. Palladium seemed to be the best candidate among such catalysts (Eq. 4).[14)]

$$2\,Cu^{2+} + H_2 \xrightarrow{Pd} 2\,Cu^+ + 2\,H^+ \quad (4)$$

The overall stoichiometry of the reactions expressed by Eqs. 1—4 can simply be summarized as in Eq. 5 for phenol or in Eq. 6 for benzoquinone. It is interesting to see that the overall reaction of this system resembles in some sense the reactions catalyzed by oxygenase, where dioxygen is activated by some electron-transfer systems to be incorporated in organic substrates. The equations predict that either phenol or benzoquinone will be produced continuously by feeding both hydrogen and oxygen.

$$C_6H_6 + H_2 + O_2 \longrightarrow C_6H_5OH + H_2O \quad (5)$$

$$C_6H_6 + H_2 + 2\,O_2 \longrightarrow C_6H_4O_2 + 2\,H_2O \quad (6)$$

2. Reactions with Catalysts Made from $CuSO_4$. As will be described in the later section, counter ions of copper salts in the catalyst show a definite effect on the reaction pathways. In this section, the nature of the catalyst made from $CuSO_4$ is discussed.

At first, the catalytic oxidation of benzene was conducted by feeding hydrogen and oxygen simultaneously at 25 °C for 9 h. Table 1 shows results obtained with the catalyst C. As is seen in the table, phenol accumulates steadily with increasing reaction time except for the initial period of the reaction, indicating that the catalytic cycle supposed in Scheme 1 is effectively operating. The anomaly appearing in the initial stage may be due to the reduction of Pd(II) to Pd(0).

The simultaneous gas feeding has a definite risk of explosion. We accordingly examined the performance of the alternate gas feeding, where the catalyst may be activated to produce Cu(I) ions in the stage of hydrogen and benzene may be oxidized in the stage of oxygen. The latter method has an additional merit to present separately the behaviors of the catalyst during each stage of hydrogen and oxygen. The results shown in Table 2 were given by using the catalyst C, which was treated with hydrogen for 90 min. The yields of phenol were almost unchanged while the oxidation time was varied from 5 to 30 min,

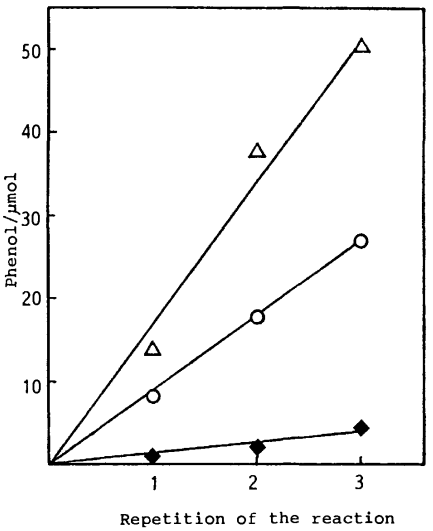

Fig. 1. Effect of reduction time on the phenol yield. The reactions were carried out using catalyst C by applying alternate feeding of H_2 and O_2. Symbols stand for the reduction time of 15 (◆), 30 (○), and 90 (△) min, respectively. Oxidation time was fixed at 5 min.

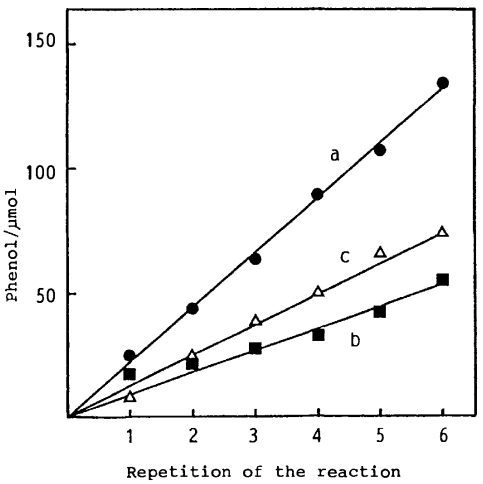

Fig. 2. Effect of preparation methods on the catalyst performance. The reactions were carried out in the same manner as described in Table 3 except that hydrogen reduction (30 min) and air-oxidation (30 min) were applied in each reaction cycle. Symbols stand for the catalysts of type A (●), B (■), and C (△), respectively.

Table 3. Effect of Catalyst Composition on the Phenol Yield[a)]

Run	Catalyst composition			Additive	Product
	SiO_2/g	$CuSO_4$/mmol	$PdCl_2$/mmol	CH_3COOH/g	Phenol/μmol
1	2	2	0.1	1	83
2	2	2	0.1	0	51
3	2	2	0.2	0	50
4	2	2	0	1	0
5	2	2	0	0	0
6	2	0	0.1	1	3
7	2	0	0.1	0	Trace
8	0	2	0.1	1	Trace
9	0	2	0.1	0	Trace
10	2	2	b)	0	4
11	c)	2	0.1	0	5

a) The reactions were performed using the catalysts corresponding to type A by applying alternate feeding of H_2 for 2 h and air for 1 h. In Runs 8 and 9, powdery mixture of $CuSO_4$ and $PdCl_2$ were used without support. b) H_2PtCl_6 (0.1 mmol) was used instead of $PdCl_2$. c) Alumina (2 g) was used instead of silica.

indicating that the time for 5 min must be enough to complete the oxidation.

In order to see the behavior of catalyst activation under hydrogen atmosphere, the time of hydrogen treatment was varied while the oxidation time was fixed at 5 min. The same process was repeated up to 3 times for each reaction. Results obtained were plotted in Fig. 1, which indicated that the catalyst activation with hydrogen was rather a slower step and the activation was still insufficient even after 90 min.

It should be noted that the preparation method of the catalysts affects the catalyst performance appreciably. This is shown in Fig. 2, where hydrogen and air were fed alternately by a period of every 30 min and the hydrogen/air cycle was repeated 6 times. Lines a, b, and c in the figure stand for results obtained with the catalysts A, B, and C, respectively. Undoubtedly, the catalyst A gave the best result among the three catalysts tested. The rate of phenol production with the catalyst A amounted to 22 μmol per cycle, compared with the corresponding rates of the catalysts B and C (9 μmol and 13 μmol, respectively).

The catalyst A was prepared by using ultrasonic wave for dispersing Pd salt on the silica surface instead of mechanical stirring which was employed for the catalyst C. The different performance appearing in the figure may be attributed to the size and distribution of the catalyst components, particularly of Pd. Superiority of using ultrasonic wave is doubtless.

In contrast, the performance of the catalyst B was the worst among the three. In order to ensure the complete dissolution of $PdCl_2$, this catalyst was prepared by dissolving $PdCl_2$ with a small amount of dil HCl. The worst performance is probably caused by excess chloride ions left in the catalyst.

Results in Table 3 prove that each catalyst component fills its own role in the catalytic cycle. In experiments for this table, the catalysts corresponding to type A were first activated with hydrogen for 2 h and then used for air-oxidation of benzene for 1 h. It is clearly indicated that, as far as the alternate gas feeding is concerned, the best performance is obtained only when Pd and Cu species are both loaded on the silica surface (Runs 1 to 3).[15)]

When $PdCl_2$ was replaced by H_2PtCl_6 (Run 10), phenol was certainly produced, but the yield was low. The catalyst composed of Pd alone produced only a trace amount of phenol (Runs 6 and 7). The absence of silica support seriously decreased the catalyst activity (Runs 8 and 9). When alumina was used instead of silica (Run 11), the yield of phenol decreased markedly, indicating that the supporting material should be hydrophilic and acid-resistant. Silica appears to satisfy these requirements. On the other hand, the inefficiency of alumina catalyst may be attributed to the degradation of alumina surface with sulfuric acid liberated during the reduction of Cu(II) salt.[16)]

3. Effect of Counter Ion in Cu Salts. Previous studies have shown that phenol and hydroquinone are formed competitively from the same intermediate, hydroxycyclohexadienyl radical (Eq. 7).[13)] The product selectivity was quite sensitive to the pH value of aqueous solution.[12)] Phenol predominated in solutions of lower pH, but the relative yield of hydroquinone to phenol (HQ/P) increased markedly with the increase in pH. At about pH=3.5, the HQ/P ratio became 2.5.

$$\cdot OH + C_6H_6 \longrightarrow \cdot C_6H_6OH \begin{cases} \longrightarrow \text{Phenol} \\ \longrightarrow \text{HQ} \end{cases} \quad (7)$$

In the present case, the solution phase is neat benzene and the acidity control in it seems difficult. There is, however, a possibility of controlling the acidity over the surface of the solid catalyst used here.

Table 4. Oxidation of Benzene with Catalysts Made from Various Cu Salts[a)]

Cu salt of	PhOH/μmol	BQ/μmol	Cu salt of	PhOH/μmol	BQ/μmol
SO_4^{2-}	51	5.2	PO_4^{3-}[b)]	40	0.1
Cl^-	0	0	AcO^-	0.4	0
NO_3^-	32	2.2	AcO^-[c)]	34	7.3
ClO_4^-	64	1.0			

a) The reaction was carried out in the same manner as Table 3. b) Phosphoric acid (0.85g) was also loaded onto the support. c) Acetic acid (2 g) was dissolved into benzene.

Table 5. Effect of Oxygen Pressure on the Product Selectivity[a)]

Cu salt	AcOH/vol%	Ratio of BQ/PhOH (Total products/μmol)			
		air, 1 atm	O_2, 1 atm	O_2, 3 atm[b)]	O_2, 6 atm[b)]
$Cu(OAc)_2$	2.5	—	0.79 (47.1)	1.50 (29.6)	—
	5.0	0.16 (24.6)	0.63 (44.2)	1.53 (57.6)	1.39 (29.6)
	10.0	0.20 (41.0)	0.61 (62.6)	0.84 (45.8)	—
	20.0	—	0.45 (43.4)	—	—
$CuSO_4$	0	0.10 (56.2)	0.11 (37.0)	0.12 (70.6)	—
	10.0	0.01 (31.2)	0.15 (39.0)	—	—

a) The reactions were carried out in the same manner as Table 3. b) Hydrogen reduction was also done under the same pressure.

During the stage of catalyst activation with hydrogen, copper(II) salt, CuX_2, is reduced to CuX and liberates free acid, HX (Eq. 8). Accordingly, we can expect that the acid strength of HX affects the fate of the intermediate species.

$$2\,CuX_2 + H_2 \longrightarrow 2\,CuX + 2\,HX \qquad (8)$$

This point was examined using several copper(II) salts as listed in Table 4. Reactions were conducted with the catalysts of type A in the same manner as noted on the margin of Table 3.

For salts of strong acid, sulfate, nitrate, and perchlorate, the reaction proceeded to produce 30—50 μmol of phenol. In contrast, no reaction was observed in the case of chloride. This is because initial activation of $PdCl_2$ to Pd(0) did not occur as was confirmed by visual observation.

In the case of acetate salt, when no particular treatment was applied, hydrogen reduction of Cu(II) to Cu(I) ions was extremely slow leading to a very low yield of phenol. For accelerating the reaction, addition of free acid was found to be effective. In fact when a small amount of acetic acid was added deliberately to benzene, the reaction proceeded at a reasonable rate. The yield of benzoquinone was still minor.

It is interesting to see that, however, the relative yield of *p*-benzoquinone vs. phenol (Q/P) increases in the following order: $ClO_4^- < NO_3^- < SO_4^{2-} < AcO^-$: the sequence being in accordance with the decreasing acid strength of their corresponding free acids.

In the case of phosphate salt, the yield of quinone is exceptionally low. In this case, phosphoric acid was used and impregnated onto the silica support during the process of catalyst preparation, because the phosphate salt was hardly soluble in water. Regarding this, it should be noted that the silica surface modified with phosphoric acid exhibits a strong acidity. In fact, the Hammett's H_0 function of the modified surface is said to be comparable with that of sulfuric acid.[17)]

4. Alteration of Product Selectivity. In the foregoing section, it has been indicated that the control of surface acidity permitted alteration of the product selectivity: Q/P varies from 0.02 in perchlorate case to 0.21 in acetate case. This tendency may be amplified by increasing oxygen concentration, since benzoquinone comes from the adduct of hydroxycyclohexadienyl radical with dioxygen.[11)] This point was investigated with the use of the acetate catalyst made by procedure A. Results are summarized in Table 5.

The data of the acetate catalyst indicate that the product ratio is sensitive to the oxygen pressure in the surrounding gas. As far as the oxygen source was ordinary air, the product ratio, Q/P, was only 0.21 even in the highest case. At 5% level of acetic acid added deliberately, the value increased from 0.16 to 1.53 corresponding to the change of oxygen pressure from 0.2 (air) to 3 atm, respectively. At 6 atm, the value tended to saturate. An addition of acetic acid was necessary for accelerating the reaction rate. As the data indicated, however, excess addition of it seemed to affect the Q/P ratio negatively.

In Table 5, are also shown the data for the sulfate catalyst for comparison. The Q/P ratio, in this case, never exceeded 0.15 even if pressurized oxygen was supplied. This clearly indicates that oxygen effect saturates below 1 atm when Cu salt is of a strong acid. In other words, the choice of counter ion is quite important for the effective performance of the diox-

ygenation reaction of benzene. The effect of counter ion is in agreement with our previous observation, where we have found that the pressure effect is pH dependent and saturates at low level at lower pH.[12]

Seemingly complicated effects of oxygen pressure, acid concentration, and counter ion in Cu salt are a reflection of multivariable nature of the reaction system. The highest value attained here, ca. Q/P=1.5, seems rather low, but we believe that the value will be improved by further modification of the reaction conditions.

The catalyst system described above has several advantages. Firstly, the reaction can be performed under very mild conditions and hence the total selectivity of oxygenated products, phenol and benzoquinone, is quite high. No other product is detected in the reaction mixture. Secondly, the catalyst preparation is simple and the catalysts having the same activity are always obtained. Thirdly, benzene can directly react with catalysts without any use of solvents. This fact leads to an additional advantage, i.e. the extremely simple isolation of the reaction products. Finally, either phenol or benzoquinone can be selectively obtained at will by a slight modification of the reaction conditions. With the use of the copper perchlorate catalyst, phenol is almost exclusively produced regardless of other conditions. Air is sufficient as the oxygen source. On the other hand, benzoquinone is obtained as the major product when the copper acetate system is employed in combination with the use of slightly pressurized oxygen.

References

1) S. Ito and K. Sasaki, *Yuki Gosei Kagaku Kyokaishi*, **41**, 839 (1983).

2) D. F. Sangster, "Free Radical and Electrophilic Hydroxylation," in "The Chemistry of Hydroxyl Group," ed by S. Patai, Interscience, London (1971), Part 1, Chap. 3, pp. 133—191.

3) L. M. Dorfman, I. A. Taub, and R. E. Bühler, *J. Chem. Phys.*, **36**, 3051 (1962).

4) C. Walling and R. A. Johnson, *J. Am. Chem. Soc.*, **97**, 363 (1975).

5) S. Udenfriend, C. T. Clark, J. Axelrod, and B. B. Brodie, *J. Biol. Chem.*, **208**, 731 (1954).

6) G. A. Hamilton, *J. Am. Chem. Soc.*, **86**, 3391 (1964).

7) M. Iwamoto, T. Takenaka, J. Hirata, H. Furukawa, and S. Kagawa, *Shokubai*, **24**, 103 (1982).

8) T. Jintoku, H. Taniguchi, and Y. Fujiwara, *Chem. Lett.*, **1987**, 1865.

9) S. Tamagaki, K. Hotta, and W. Tagaki, *Chem. Lett.*, **1982**, 651.

10) K. Sasaki, S. Ito. Y. Saheki, T. Kinoshita, T. Yamasaki, and J. Harada, *Chem. Lett.*, **1983**, 37,

11) A. Kunai, S. Hata, S. Ito, and K. Sasaki, *J. Org. Chem.*, **51**, 3471 (1986).

12) S. Ito, A. Kunai, H. Okada, and K. Sasaki, *J. Org. Chem.*, **53**, 296 (1988).

13) S. Ito, T. Yamasaki, H. Okada, S. Okino, and K. Sasaki, *J. Chem. Soc., Perkin Trans. 2*, **1988**, 285.

14) A. Kunai, K. Ishihata, S. Ito, and K. Sasaki, *Chem. Lett.*, **1988**, 1967.

15) Somewhat different aspect appears when the mode of gas feeding is simultaneous. This point will be discussed in the succeeding paper.

16) It is well known that the interaction between Pd and alumina is much stronger than that between Pd and silica. This may also be one of the reasons.

17) H. A. Benesi, *J. Am. Chem. Soc.*, **78**, 5494 (1956).

Total Synthesis of Erythronolide A[1)]

Masaya NAKATA,* Masayuki ARAI, Katsuhiko TOMOOKA,
Naoki OHSAWA, and Mitsuhiro KINOSHITA*
Department of Applied Chemistry, Faculty of Science and Technology, Keio University,
Hiyoshi, Kohoku-ku, Yokohama 223
(Received March 29, 1989)

The enantiospecific total synthesis of erythronolide A (**1**) through (9*S*)-9-deoxo-9-hydroxyerythronolide A (**2**) from the chiral C1—C6, C7—C9, and C10—C13 synthetic segments is described. The C10—C13 segment, (3*R*,4*R*,5*R*)-5-*O*-benzyl-2-iodo-3,4-*O*-isopropylidene-4-methyl-1-heptene-3,4,5-triol (**11**) was synthesized in 16 steps and an 8.3% overall yield from D-ribose. The C7—C9 segment, (*S*)-(+)-2-(2-bromo-1-methylethyl)-1,3-dioxolane (**47**) was prepared from methyl (*S*)-(+)-3-hydroxy-2-methylpropionate in 8 steps and a 49% overall yield. The coupling of the Grignard reagent, prepared from magnesium and **47**, and the C1—C6 segment, 3,5,7-tri-*O*-benzyl-1,4,6-trideoxy-4,6-di-*C*-methyl-*keto*-L-*ido*-2-heptulose (**13**), afforded 5,7,9-tri-*O*-benzyl-2,3,6,8-tetradeoxy-2,4,6,8-tetra-*C*-methyl-L-*threo*-L-*ido*-nonose ethylene acetal (**48**) and its C4-epimer in 79% and 8% yields, respectively. 5,7,9-Tri-*O*-benzyl-4-*O*-*t*-butyldimethylsilyl-2,3,6,8-tetradeoxy-2,4,6,8-tetra-*C*-methyl-L-*threo*-L-*ido*-nonose (**12**), derived from **48**, was subjected to coupling reaction with the lithium reagent prepared from **11** to afford about 5 : 1 excess of the "Cram" product **50**. The homogeneous hydrogenation of **50** with [ClRh(Ph$_3$P)$_3$] gave 1,3,5,13-tetra-*O*-benzyl-6-*O*-*t*-butyldimethylsilyl-2,4,7,8,10,14,15-heptadeoxy-11,12-*O*-isopropylidene-2,4,6,8,10,12-hexa-*C*-methyl-D-*arabino*-D-*gluco*-L-*ido*-pentadecitol (**54**) and its C10-epimer in 41% and 7% yields from **12**, respectively. The conversion of **54** to **2** was accomplished by a sequence of reactions including the Corey-Nicolaou lactonization method in a 17% overall yield. Selective 3,5-*O*-benzylidenation of **2** followed by PCC oxidation and debenzylidenation gave **1** in 52% yield.

During the last decade, the total syntheses of various types of macrolide antibiotics have been achieved and well documented.[2)] Of these macrolides, erythromycin A is an extremely important 14-membered macrolide antibiotic.

The only total synthesis of erythromycin A has been accomplished by Woodward and collaborators.[3)] After the first completion of the total synthesis of erythronolide A, aglycone of erythromycin A, by Corey et al. in 1979,[4)] several groups have succeeded in the synthesis of erythronolide A or the key intermediate carbamate in Woodward's total synthesis of erythromycin A.[5)] We wish to report in this full account[6)] the details of the total synthesis of erythronolide A.

Synthetic Strategy. We chose (9*S*)-9-deoxo-9-hydroxyerythronolide A (**2**) as a synthetic precursor of erythronolide A (**1**) by anticipating that the former could be converted into the latter through straightforward short steps (Scheme 1). Moreover, in the previous syntheses of erythronolide A,[4,5)] **2** has never been utilized as a practical synthetic precursor. The first crucial step for the synthesis of **2** should be the macrolactonization of the suitably protected seco-acid. In that sense, Woodward et al.[3)] had investigated extensively the structure-reactivity relationships of the lactonization. They concluded that *S*-configuration at C9 and cyclic protecting groups at C3/C5 and C9/C11 are required for efficient lactonization. Indeed, they realized good yield of lactonization of the naturally derived (9*S*)-9-hydroxy seco-acid 3,5 : 9,11-bis(cyclic acetal) derivative **3** by the Corey-Nicolaou method.[7)] By this fact, we thought the diacetonide **4** would be also a good precursor for the Corey-Nicolaou macrolactonization method, giving **2**.

The next crucial step should be the effectively stereocontrolled enantiospecific synthesis of the key intermediate **4**. This seemed to be solved by the synthetic plan which was guided by our "two-stage coupling process."

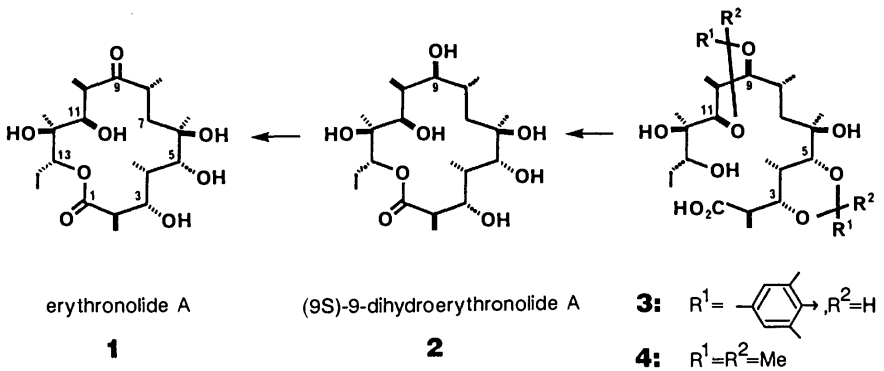

Scheme 1.

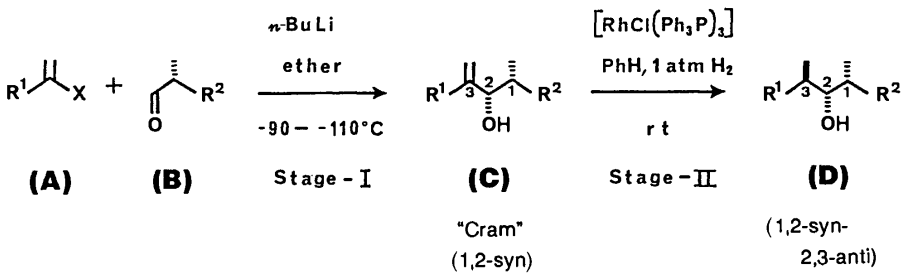

Scheme 2.

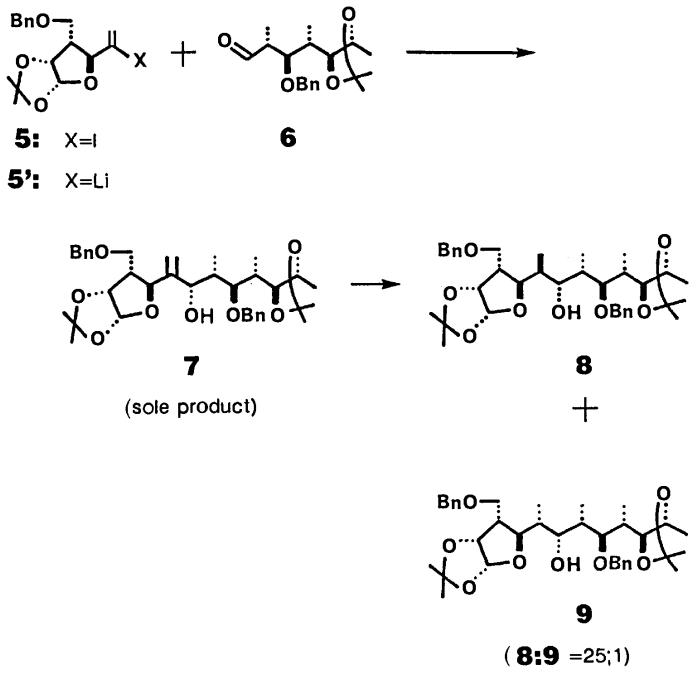

Scheme 3.

This new coupling process consists of two consecutive reaction stages (Scheme 2). The first stage is the "Cram (1,2-syn)" selective coupling reaction of a chiral vinyl halide (**A**) with a chiral α-methyl aldehyde (**B**) and the second one is the highly 2,3-anti-selective homogeneous hydrogenation of the major Cram type intermediary coupling product (**C**) with Wilkinson's catalyst. Consequently, the coupling of (**A**) and (**B**) by this process affords preferencially the final product (**D**) with 1,2-syn-2,3-anti configuration. In fact, this process was practicable in the enantiospecific synthesis of the ansa-chain portion of rifamycin W.[8] One example is showen in Scheme 3. The reaction of the chiral vinyllithium reagent **5'** prepared from the vinyl iodide **5** and the chiral (2*R*)-2-methyl aldehyde **6** gave a sole coupling product **7** (61% yield), which was subsequently hydrogenated homogeneously to give the anti-product **8** (95% yield) and the syn-product **9** (3.8% yield).

We can see in the polyol **10**, which is the hypothetical precursor of **4**, the three consecutive carbon chain (C8 to C10) having a 1,2-syn-2,3-anti configuration (Scheme 4). Therefore, a "two-stage coupling process" disconnection of the C9–C10 bond affords two subunits, **II** and **III**, through the vinylidene compound **I**. As the perspective view of the strategic vinyl iodide **11**, corresponding to the suitablly protected subunit **II**, seemed to be similar to that of **5** (Scheme 5), the reaction of the vinyllithium reagent **11'**, prepared from **11**, and (2*R*)-2-methyl aldehyde **12**, corresponding to the subunit **III**, would provide predominantly the "Cram" type of (9*S*)-8,9-syn-product, which could be homogeneously hydrogenated to produce selectively the (9*S*)-9,10-anti-product convertible into the desired polyol **10**. The aldehyde **12**, with the desired C6 chiral center, would be formed predominantly by the α-chelation controlled addition reaction,[9] of an appropriately protected chiral Grignard reagent to the chiral methyl ketone **13**,[10] which was previously synthesized in our laboratories as a versatile C1—C6 segment of **1**.

Preparation of Vinyl Iodide 11. The acetonide **14**[11] was obtained in 83% yield by treatment of D-ribose in acetone with 2,2-dimethoxypropane and a catalytic

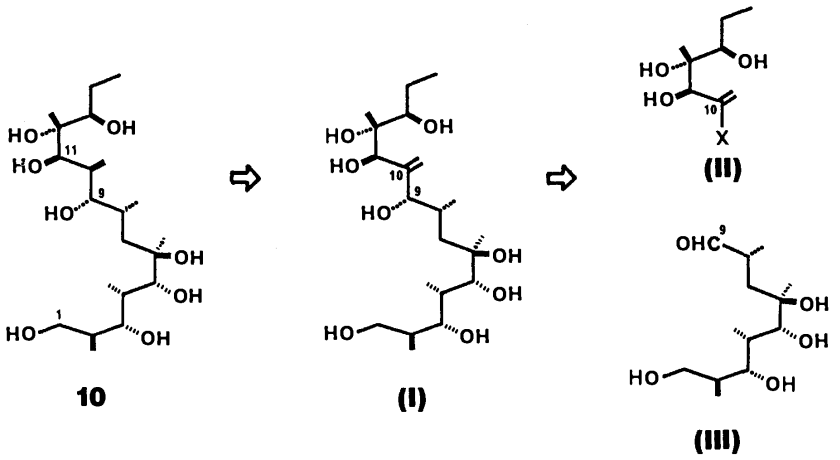

Scheme 4.

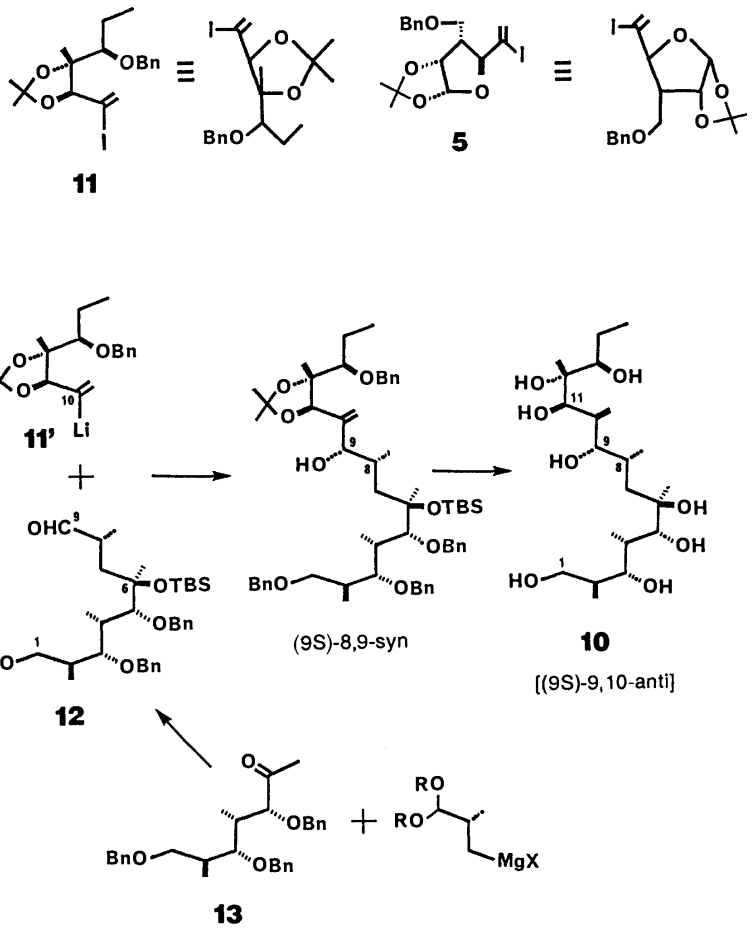

Scheme 5.

amount of H_2SO_4 (Scheme 6). The Grignard reaction of **14** with excess methylmagnesium iodide in diethyl ether afforded the alcohol **15** as a sole product in 73% yield. Regardless of the configuration at the newly formed Cl-stereocenter, the alcohol **15** can be used in the synthetic route since at a later stage this alcohol function is oxidized to a methyl ketone. We determined, however, its Cl-configuration (vide infra).

Oxidative cleavage of the glycol function in **15** with $NaIO_4$ followed by $LiAlH_4$ reduction of the resulting aldehyde afforded the alcohol **16** in 97.5% yield, whose primary alcohol was protected as its *t*-butyldiphenylsilyl (TBDPS) ether **17** (97%). Oxidation of **17** with PCC provided the methyl ketone **18** in a quantitative yield.

Since the attempts of 2-*O*-benzylation of **17** for the

purpose of straightforward determination of its (2*S*)-configuration was unsuccessful, the C2-epimer **19** was prepared (57%) along with **17** (28%) by $LiAlH_4$ reduction of **18** (Scheme 7). The 2-*O*-benzylation of **19** followed by removal of the silyl ether protecting group afforded the alcohol **20** in 91% yield. After treatment of **20** with aqueous acetic acid, the resulting triol was oxidized successively with $NaIO_4$ and CrO_3 to afford (*R*)-(+)-2-benzyloxypropionic acid **21**. The acid **21** was proved to be the enantiomer of the reported (*S*)-(−)-2-benzyloxypropionic acid[12] (see Experimental section).

The chelation controlled Grignard reaction of **18** with vinylmagnesium bromide in THF provided the products **22** and **23** in 94% yield as a 77:1 mixture of epimers (^1H NMR). Silica-gel chromatography separated **22** (85%) and **22**+**23** (8%; 5.7:1 mixture in favor of **22**) (Scheme 8). The (2*R*)-configuration of

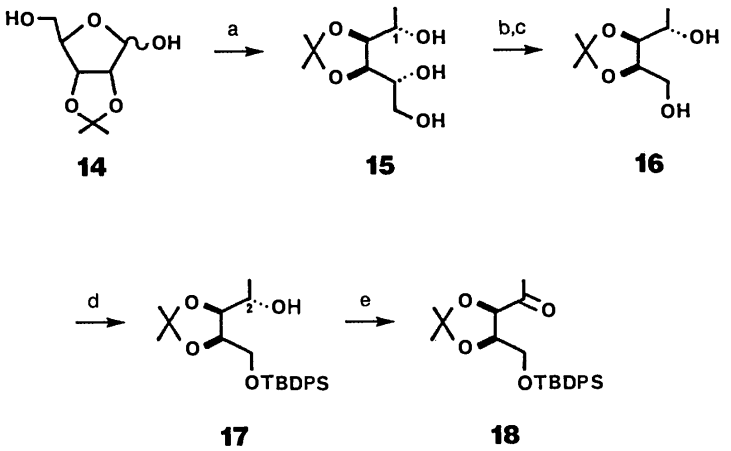

Scheme 6. (a) MeMgI, ether; (b) $NaIO_4$, aq acetone; (c) $LiAlH_4$, THF; (d) TBDPSCl, imidazole, DMF; (e) PCC, MS 3AP, CH_2Cl_2.

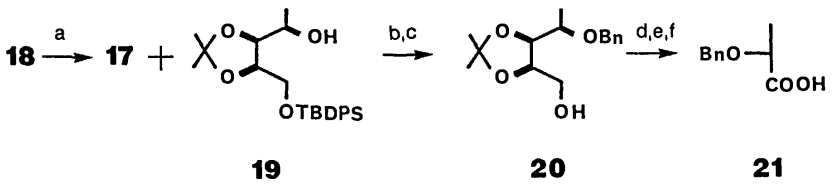

Scheme 7. (a) $LiAlH_4$, ether, −78 °C; (b) NaH, BnBr, THF; (c) TBAF, THF; (d) 75% AcOH, 80 °C; (e) $NaIO_4$, aq acetone: (f) CrO_3-AcOH-Py.

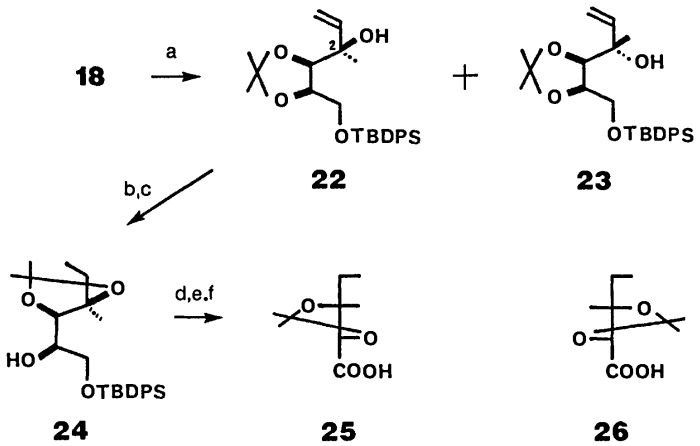

Scheme 8. (a) CH_2=CHMgBr, THF; (b) H_2/[ClRh-(Ph_3P)$_3$], benzene; (c) $ZnBr_2$, CH_2Cl_2; (d) TBAF, THF; (e) $NaIO_4$, aq acetone; (f) KIO.

22 was confirmed by the following manner. Reduction of double bond followed by $ZnBr_2$-promoted acetonide migration afforded **24**. After removal of the silyl ether protecting group, the diol was oxidized successively with $NaIO_4$ and KIO to give the carboxylic acid **25**, which was proved to be the epimer of **26**[13] by comparing optical rotation and ^1H NMR spectrum.

Ozonolysis of **22** followed by addition of ethylmagnesium bromide to the resulting aldehyde gave a ca. 1.6 : 1 mixture of the desired **27** and its epimer **28** in 63.5% combined yield. Since chromatographic separation of **27** and **28** was quite difficult, the isomeric

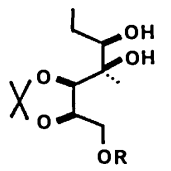

27: R=TBDPS

29: R=H

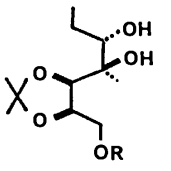

28: R=TBDPS

30: R=H

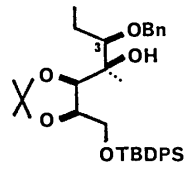

31

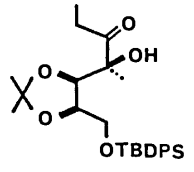

35

ratio was assumed based on the isolated yields of the chromatographycally separable products, **29** and **30**, obtained by desilylation of the epimeric mixture.

Direct *O*-benzylation of the mixture, **27** and **28**, with NaH and benzyl bromide in THF afforded fortunately only one isomeric *O*-benzyl derivative **31** (55%), and a 1 : 4.9 mixture of **27** and **28** was recovered (28%). The (3*R*)-configuration of **31** was confirmed by the following manner (Scheme 9). After desilylation of **31**,

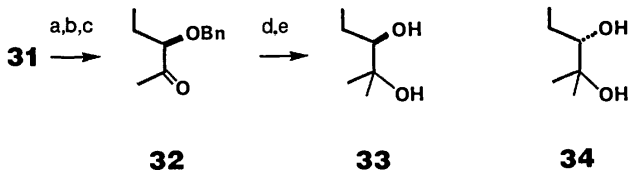

32 **33** **34**

Scheme 9. (a) TBAF, THF; (b) 50% AcOH, 115 °C; (c) $NaIO_4$, aq acetone; (d) MeMgI, ether; (e) H_2/Pd, *t*-BuOH.

acidic hydrolysis of acetonide protecting group followed by $NaIO_4$ oxidation gave methyl ketone **32**. The Grignard reaction of **32** with methylmagnesium iodide followed by debenzylation gave the diol **33**. This diol (*R*)-(+)-**33** was proved to be the enantiomer of the reported (*S*)-(−)-**34**.[14] From this result, the configurations of the compounds **27**—**31** were established as depicted.

The aforesaid unchanged epimeric mixture in favor of the (3*S*)-epimer **28** was converted into the ketone **35** by DMSO-oxidation in 90% yield. $LiAlH_4$ reduction of **35** in diethyl ether at −78 °C gave a 5 : 1 epimeric mixture in preponderance of **27**, which was again benzylated to afford **31** in 55% yield from **35**; the total yield of **31** from **22** amounted to 43.8%. Brief exposure of **31** to 0.5 equiv of $FeCl_3$ in acetone led to the isomeric acetonide **36** (95%), which was desilylated to give **37** in 92% yield. Oxidative cleavage of the glycol function in **37** with $NaIO_4$ followed by successive treatment of the resulting aldehyde with methylmagnesium iodide and PCC provided the methyl ketone **38** in a 92% overall yield, which was converted through its hydrazone into the vinyl iodide **11** according to the improved procedure of Barton et al.[15] (Scheme 10).

Preparation of Aldehyde 12. With the chiral vinyl iodide **11**, C10—C13 segment of **1**, in hand, we turned our attention to the synthesis of the second requisite **12**, C1—C9 segment of **1**. For the purpose of synthesizing **12** from the previously prepared C1—C6 segment **13**,[10] an adequate C7—C9 segment had first to be inquired. After many unsuccessful attempts, the

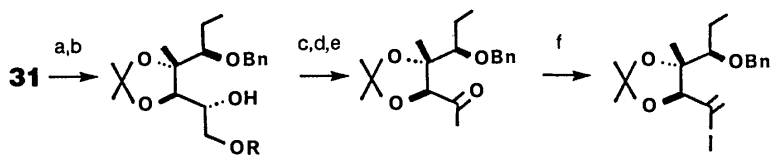

36: R=TBDPS

37: R=H

38 **11**

Scheme 10. (a) $FeCl_3$, acetone; (b) TBAF, THF; (c) $NaIO_4$, aq acetone; (d) MeMgI, ether; (e) PCC, MS 3AP, CH_2Cl_2; (f) 1) $NH_2NH_2 \cdot H_2O$, Et_3N, EtOH, 70 °C. 2) I_2, tetramethylguanidine, toluene, 0 °C.

most adequate synthetic segment was found to be (*S*)-(+)-2-(2-bromo-1-methylethyl)-1,3-dioxolane **47**.

As detailed below (Scheme 11), **47** was efficiently constructed from the known aldehyde **44**,[16] which in turn was prepared from the commercially available methyl (*S*)-(+)-3-hydroxy-2-methylpropionate **39**. Tritylation of **39** followed by $LiAlH_4$ reduction of the resulting unpurified **40** gave the alcohol **41**. Benzylation of **41** with NaH and benzyl bromide in THF gave **42**, which was hydrolyzed with Amberlyst 15 in methanol to afford the alcohol **43**. Swern oxidation of **43** gave the aldehyde **44**, which was directly acetalized with ethylene glycol and *p*-toluenesulfonic acid in acetonitrile to provide **45**. After hydrogenolysis of **45**, the resulting alcohol **46** was transformed into the desired bromide **47** by treating with ethyl bromid-triphenylphosphine and diethyl azodicarboxylate[17] in THF in a 49% overall yield from **39**.

The methyl ketone **13** was treated in diethyl ether with an excess Grignard reagent prepared from 13 equiv of magnesium and 4.3 equiv of **47** to afford the alcohol **48** and its C4-epimer in 79% and 8% isolated yield, respectively (Scheme 12). The configuration at the newly formed C4-stereocenter was assumed to be (*R*) by considering the α-chelation controlled Grignard addition reaction,[9] and established at a later stage. Thus obtained **48** was silylated with *t*-butyldimethylsilyl triflate (TBSOTf) and 2,6-lutidine in CH_2Cl_2 to give **49** in 89% yield. The last step in the synthesis of the aldehyde **12** was to remove the acetal protecting group in **49**. This transformation proved to be troublesome to some extent. Among a wide variety of conditions employed, tin(II) chloride-acetone combination gave satisfactory yield of **12** (72%).

Preparation of Polyol Derivative 56. The stage was now set for us to examine the feasibility of the stereocontrolled coupling between **11** and **12** (Scheme 13). A 1.9 M ethereal solution (1 M=1 mol dm^{-3}) of **11** (3 equiv) was lithiated with 3 equiv of butyllithium at −100 °C for 15 min under argon. To this solution was added a 0.3 M etherial solution of **12** (1 equiv) and stirred at −100 °C for 1 h. Quenching with saturated aqueous NH_4Cl followed by chromatographic isolation afforded the major coupling product **50** (ca. 50%

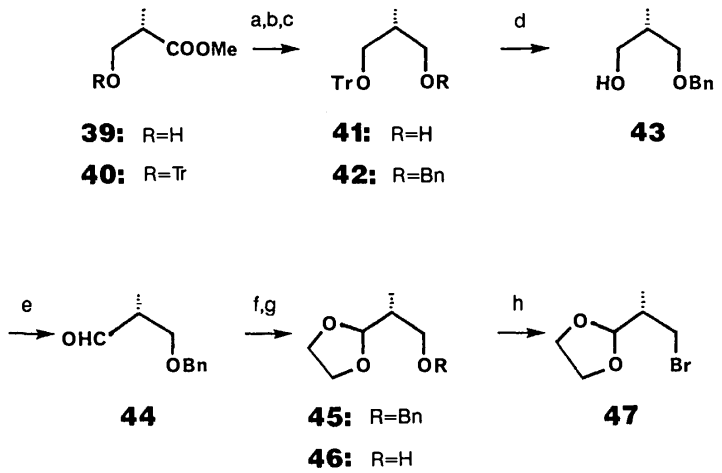

Scheme 11. (a) TrCl, Et_3N, DMAP, CH_2Cl_2; (b) $LiAlH_4$, THF; (c) NaH, BnBr, THF; (d) Amberlyst 15, MeOH, 50 °C; (e) $(COCl)_2$, DMSO, CH_2Cl_2, Et_3N, −78 °C; (f) $HOCH_2CH_2OH$, *p*-TSA, MeCN; (g) H_2/Pd, MeOH; (h) EtBr, Ph_3P, DEAD, THF.

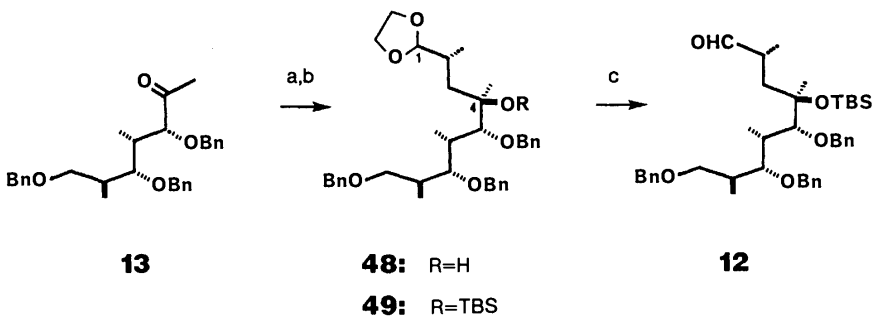

Scheme 12. (a) **47**, Mg, ether, then add **13**; (b) TBSOTf, 2,6-lutidine, CH_2Cl_2; (c) $SnCl_2$, acetone.

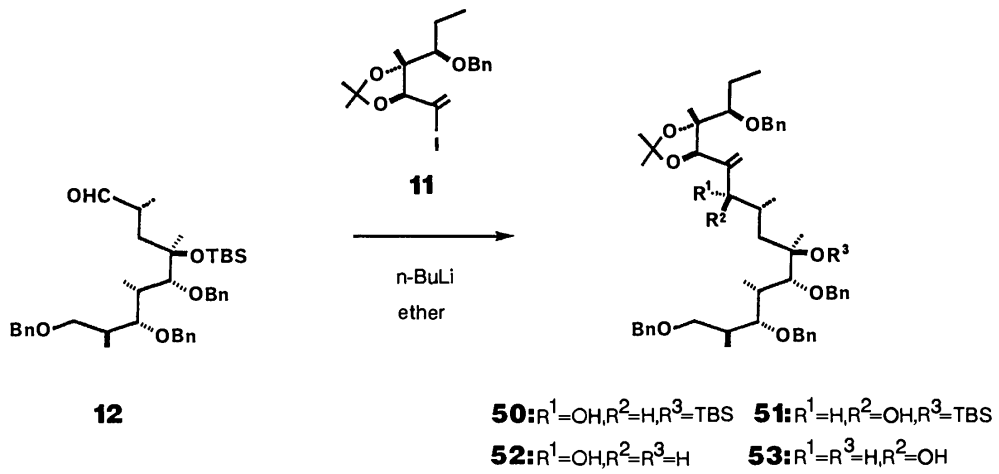

Scheme 13.

yield from **12**) contaminated with a by-product, probably one of the by-products originated from **11**, and the pure minor one **51** (10% yield from **12**). The yield of **50** was assumed based on the yield of **51** and on a ratio (5 : 1) of the corresponding separable desilylation products (**52** and **53**), derived from the crude mixture of **50** and **51**. The next step was homogeneous hydrogenation of the desired Cram type coupling product **50**. Usually this type of reaction is carried out smoothly at room temperature and 1 atm H_2 in benzene solution with 0.25 equiv of [ClRh(Ph_3P)$_3$] as catalyst for several hours.[8] However, hydrogenation of **50** under the usual conditions was very slow. After several experiments, we found that the crude **50** was homogeneously hydrogenated in benezene with 0.25 equiv of [ClRh(Ph_3P)$_3$] under 50 atm H_2 at 24 °C for 5 d to afford **54** 41% from **12**) and its C10-epimer **55** (7% from **12**). Hydrogenation of **50** was also carried out using [Rh(NBD(DIPHO-4)]BF_4[18] instead of the Wilkinson's catalyst, but no improvements in the reaction rate and the isomeric ratio were observed. The configuration of **54** was confirmed by the following manner. After desilylation and deacetonization of **54** with 46% aqueous HF-acetonitrile, the resulting alcohol was benzylated with 4 equiv of benzyl chloride and 8 equiv of KOH in DMF at 24 °C for 5 h to give **56** in 81% yield. Direct benzylation of **54** gave **57** in 84% yield. On the other hand, $LiAlH_4$ reduction of the naturally derived **2**[19,20] gave **10** in 72% yield, which was benzylated to afford **56** and **58**. The ratio of **56** and **58** depended on the reaction conditions used for benzylation (see Experimental section).

Acetonization of **58** followed by silylation provided **57**. The synthetic **56** and **57** were spectroscopically and chromatographycally identical with the corresponding materials obtained by the aforesaid transformations starting from naturally derived **2**. Consequently the structure showed for **48**, **49**, **12**, **50**, **54**, and **55** were determined and the anti-selectiveity in homo-

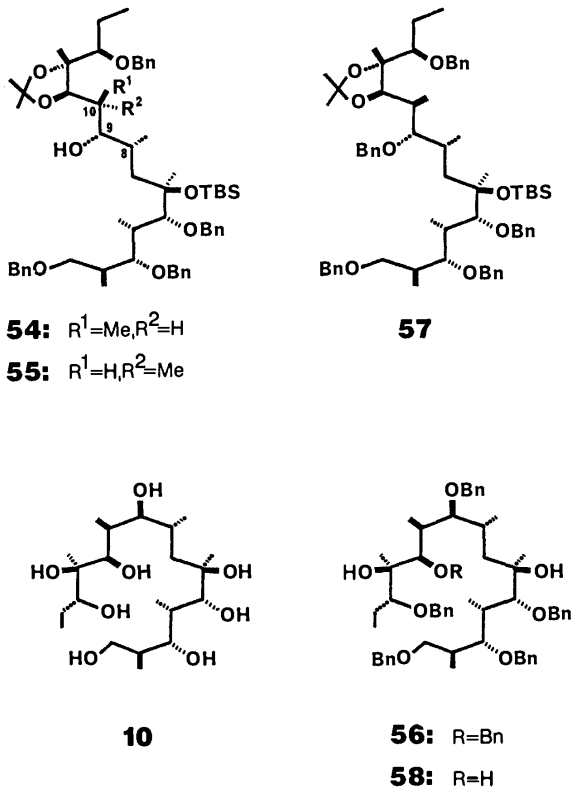

geneous hydrogenation of the "Cram" product **50** was also confirmed.

Preparation of Erythronolide A. Having thus prepared the polyol derivative **56**, which has the entire chiral sequence of (9*S*)-9-deoxo-9-hydroxyerythronolide A (**2**) in the proper absolute configuration, attention was directed toward the facile transformation of **56** into **2**. Protection of the tertiary alcohol function of **56** with triethylsilyl triflate and 2,6-lutidine provided all protected polyol **59** in 93% yield. Hydrogenolysis of **59** over palladium-black in ethanol furnished **60**. After the protection of the primary alcohol function of **60** with TBDPSCl and imidazole,

selective acetonization[4] of the resulting **61** with 2-methoxypropene and pyridinium *p*-toluenesulfonate (PPTS) in CH_2Cl_2 afforded the desired 3,5:9,11-

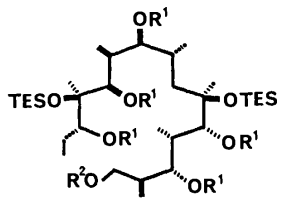

59: $R^1=R^2=Bn$
60: $R^1=R^2=H$
61: $R^1=H, R^2=TBDPS$

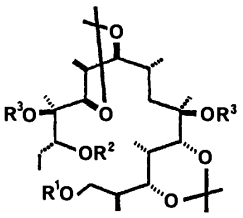

62: $R^1=TBDPS, R^2=H, R^3=TES$
63: $R^1=TBDPS, R^2=Ac, R^3=TES$
64: $R^1=R^3=H, R^2=Ac$

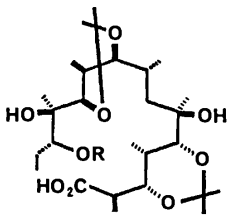

65: R=Ac
4: R=H

diacetonide **62** in 64% yield from **59**. The standard acetylation of **62** followed by desilylation of the acetate **63** with tetrabutylammonium fluoride (TBAF) in THF at 60 °C furnished **64** in 70% yield from **62**. Oxidation of **64** with 4 equiv of PDC in the presence of 3A Molecular Sieves in DMF afforded the acid **65**, which was deacetylated with 1-M NaOH-dioxane (1:1) to give the seco-acid 3,5:9,11-diacetonide **4** in 82% yield. Treatment of **4** with 1.5 equiv of triphenylphosphine and 1.5 equiv of di-(2-pyridyl) disulfide in THF yielded the 2-pyridinethiol ester, which was purified by silica-gel column chromatography (95% yield). This ester was subjected to lactonization by the modified Corey-Nicolaou method[7] using toluene instead of xylene to give the intramolecular cyclization product **66** in 65% yield. The protected lactone **66** was treated with 50% aqueous acetic acid to afford (9*S*)-9-deoxo-9-hydroxyerythronolide A (**2**) in quantitative yield. The synthetic sample of **2** was identical in all respects with a sample of the naturally derived **2**.[20] The overall yield of **2** from **56** was 21.1% in 11 steps.

The lactone **2** was led to **1** by the straightforward transformation. Selective 3,5-*O*-benzylidenation[3] of **2** with benzaldehyde dimethyl acetal and 10-camphorsulfonic acid (CSA) in CH_2Cl_2 gave **67** in 80% yield. Selective oxidation[21] of **67** followed by

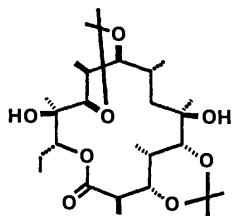

66

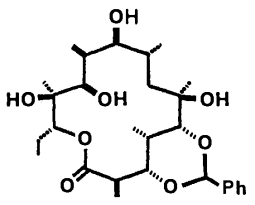

67

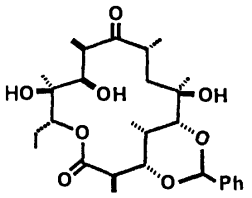

68

hydrogenolysis of the resulting ketone **68** with palladium-black in methanol furnished erythronolide A (**1**) in 66% yield. The synthetic sample of **1** was identical in all respects with naturally derived erythronolide A.[22]

Thus the new synthetic route to erythlonolide A through (9*S*)-9-deoxo-9-hydroxyerythronolide A from **13** was completed.

Experimental

Melting points were determined on a micro hot-stage Yanaco MP-S3 and were uncorrected. Optical rotations were measured on a JASCO DIP-360 photoelectric polarimeter in chloroform unless otherwise noted. IR spectra were recorded on a Hitachi Perkin-Elmer 225 spectrometer and ^1H NMR spectra on either a Varian EM-390 or a Bruker WM 250 spectrometer in $CDCl_3$ using TMS as internal standard. Mass spectra were recorded on Hitachi M-80 mass spectrometer. Silica-gel TLC and column chromatography were performed on Merck TLC 60F-254 and Merck Kieselgel 60, respectively. In general, organic solvents were purified and dried by the appropriate procedure, and evaporation and concentration were carried out under reduced pressure below 30 °C, unless otherwise noted.

2,3-*O*-Isopropylidene-D-ribofuranose (14).[11] To a stirred solution of D-ribose (25.0 g, 0.167 mol) and 2,2-dimethoxypropane (21.5 ml, 0.175 mol) in dry acetone (500 ml) at 0 °C was added concd H_2SO_4 (0.025 ml). After being stirred in a refrigerator (5 °C) for 20 h, the reaction mixture was neutralized with solid Na_2CO_3 and the insoluble materials were filtered off and washed with acetone. The combined filtrate and washings were concentrated. The residue was chromatographed on silica gel (1.6 kg) with 10:1 chloroform-methanol to afford **14** [26.2 g, 83%; R_f=0.39 (10:1 chloroform-methanol)] as a practically pure pale yellow syrup and 3,4-*O*-isopropylidene-D-ribopyranose [1.70 g, 5.5%; R_f=0.26 (10:1 chloroform-methanol)] as colorless needles.

2,3-*O*-Isopropylidene-1-*C*-methyl-D-allitol (15). To a stirred solution of methylmagnesium iodide [prepared from 33.5 g 1.38 mol) of magnesium powder and 94.3 ml (1.51 mol) of iodomethane] in dry diethyl ether (1050 ml) at 0 °C was added dropwise a solution of **14** (26.2 g, 0.138 mol) in dry diethyl ether (524 ml). The reaction mixture was stirred at 23 °C for 3.5 h. Saturated aqueous NH_4Cl (100 ml) was added to the ice-cooled reaction mixture. The phases were separated and the aqueous layer was thoroughly extracted with ethyl acetate. The combined organic layers were washed with saturated aqueous NaCl, dried, and concentrated. The residue was chromatographed on silica gel (1.7 kg) with 1 : 4 benzene-ethyl acetate to afford **15** (26.5 g, 73%) as colorless crystals and 2.20 g (7.9%) of **14** was recovered: R_f=0.28 (1 : 4 benzene-ethyl acetate); mp 72—73 °C (needles, ether-hexane); $[\alpha]_D^{15}$ +27.5° (*c* 1.00); ^{1}H NMR (90 MHz) δ=1.32 (3H, d, 1-Me, J=6.0 Hz), 1.35 and 1.39 (each 3H, each s, CMe_2), 3.3—4.9 (9H, m).

Found: C, 52.64; H, 8.59%. Calcd for $C_9H_{18}O_5$: C, 52.41; H, 8.80%.

1-Deoxy-3,4-*O*-isopropylidene-D-ribitol (16). To a stirred solution of **15** (19.0 g, 0.0921 mol) in acetone (380 ml) at 0 °C was added dropwise a solution of $NaIO_4$ (59.1 g, 0.276 mol) in water (590 ml). The reaction mixture was stirred at 24 °C for 1 h. Acetone was removed under reduced pressure and the aqueous layer was extracted with ethyl acetate. The combined organic layers were washed with saturated aqueous NaCl, dried, and concentrated. The residue (16.0 g) was dissolved in dry THF (640 ml) and then cooled to 0 °C. To this was added portionwise $LiAlH_4$ (3.83 g, 0.101 mol) and the reaction mixture was stirred at 20 °C for 20 min. Wet diethyl ether (300 ml) and water (200 ml) were added carefully to the ice-cooled reaction mixture and the insoluble materials were filtered through Celite and washed with ethyl acetate. The combined filtrate and washings were concentrated and the residue was chromatographed on silica gel (330 g) with 1 : 1 benzene-ethyl acetate to afford **16** (15.8 g, 97.5%) as colorless crystals: R_f=0.34 (1 : 1 benzene-ethyl acetate); mp 47—49 °C (cubes, ether-petroleum ether); ^{1}H NMR (90 MHz) δ=1.31 (3H, d, 3×H-1, J=6.0 Hz), 1.34 and 1.39 (each 3H, each s, CMe_2), 2.90—3.60 (2H, br, 2×OH), 4.26 (1H, dq, H-2, $J_{2,3}$=7.2 Hz).

Found: C, 54.64; H, 8.93%. Calcd for $C_8H_{16}O_4$: C, 54.53; H, 9.15%.

5-*O*-(*t*-Butyldimethylsilyl)-1-deoxy-3,4-*O*-isopropylidene-D-ribitol (17). To a stirred solution of **16** (15.7 g, 89.1 mmol) in dry DMF (157 ml) were added at 0 °C imidazole (7.87 g, 116 mmol) and *t*-butylchlorodiphenylsilane (27.8 ml, 107 mmol). The reaction mixture was stirred at 24 °C for 2 h 40 min. The reaction mixture was poured into cold water (150 ml) and the mixture was extracted with ethyl acetate. The extracts were washed with saturated aqueous NaCl, dried, and concentrated. The residue was chromatographed on silica gel (1.5 kg) with 25 : 1 benzene-ethyl acetate to afford **17** (35.6 g, 97%) as a colorless syrup: R_f=0.41 (25:1 benzene-ethyl acetate); $[\alpha]_D^{19}$ +8.0°, $[\alpha]_{365}^{19}$ +29° (*c* 1.12); ^{1}H NMR (90 MHz) δ=1.07 (9H, s, *t*-Bu), 1.28 and 1.30 (each 3H, each s, CMe_2), 1.34 (3H, d, 3×H-1, J=7.0 Hz), 3.58 (1H, dd, H-5, J_{gem}=10.2 and $J_{4,5}$=3.9 Hz), 3.81 (1H, d, H-5′, $J_{4,5'}$=0 Hz), 3.95—4.5 (4H, m), 7.3—7.8 (10H, m, 2×Ph).

Found: C, 69.24; H, 8.05%. Calcd for $C_{24}H_{34}O_4Si$: C, 69.52; H, 8.27%.

5-*O*-(*t*-Butyldiphenylsilyl)-1-deoxy-3,4-*O*-isopropylidene-*keto*-D-*erythro*-2-pentulose (18). To a stirred suspension of PCC (71.7 g, 332 mmol) and Molecular Sieves 3A powder (MS3AP) (83.1 g) in dry CH_2Cl_2 (208 ml) was added dropwise at 0 °C a solution of **17** (34.5 g, 83.2 mmol) in dry CH_2Cl_2 (138 ml). After 2 h at 22 °C, the reaction mixture was diluted with diethyl ether (200 ml) and the resulting suspension was transferred to a column filled with silica gel (930 g). The column was eluted with diethyl ether and the eluant was concentrated to give practically pure sample of **18** (34.3 g, 100%) as a pale yellow syrup. A portion of this was chromatographed on silica gel with 40 : 1 benzene-ethyl acetate to afford an analytically pure sample of **18**: R_f=0.55 (25 : 1 benzene-ethyl acetate); $[\alpha]_D^{22}$ +49.0° (*c* 0.97); IR ($CHCl_3$) 1712 cm^{-1}; ^{1}H NMR (90 MHz) δ=1.03 (9H, s, *t*-Bu), 1.37 and 1.57 (each 3H, each s, CMe_2), 2.27 (3H, s, 3×H-1), 3.72 (2H, d, 2×H-5, $J_{4,5}$=3.0 Hz), 4.30—4.60 (2H, m), 7.3—7.8 (10H, m, 2×Ph).

Found: C, 69.60; H, 7.63%. Calcd for $C_{24}H_{32}O_4Si$: C, 69.87; H, 7.82%.

$LiAlH_4$ Reduction of 18: To a stirred suspension of $LiAlH_4$ (50.0 mg, 1.32 mmol) in dry diethyl ether (1 ml) at −78 °C was added a solution of **18** (543 mg, 1.32 mmol) in dry diethyl ether (5.4 ml). After 2 h at −78 °C, wet diethyl ether was added to the reaction mixture. The insoluble materials were filtered through Celite and washed with ethyl acetate. The combined filtrate and washings were concentrated and the residue was chromatographed on silica gel (40 g) with 25 : 1 benzene-ethyl acetate to afford **17** (154 mg, 28%) and **19** (313 mg, 57%) as colorless syrups. **19**: R_f=0.27 (25 : 1 benzene-ethyl acetate); $[\alpha]_D^{20}$ 0°, $[\alpha]_{365}^{20}$ +15° (*c* 1.01); ^{1}H NMR (90 MHz) δ=1.08 (9H, s, *t*-Bu), 1.27 (3H, d, 3×H-1, J=4.5 Hz), 1.35 and 1.43 (each 3H, each s, CMe_2), 2.62 (1H, d, OH, J=3.0 Hz), 3.6—4.3 (5H, m), 7.3—7.8 (10H, m, 2×Ph).

Found: C, 69.80; H, 8.21%. Calcd for $C_{24}H_{34}O_4Si$: C, 69.52; H, 8.27%.

Transformation of 19 to (*R*)-2-Benzyloxypropinoic Acid (21). To a stirred solution of **19** (122 mg, 0.294 mmol) in dry THF (0.61 ml) at 0 °C was added NaH (19 mg, 0.44 mmol; 55% dispersion in mineral oil). After 0.5 h at room temperature, the mixture was cooled to 0 °C and benzyl bromide (0.052 ml, 0.44 mmol) was added. After being stirred at room temperature for 8 h, ice-water was added and the mixture was extracted with ethyl acetate. The extracts were washed with saturated aqueous NaCl, dried and concentrated. The crude residual syrup (148 mg) was dissolved in THF (1.5 ml) and cooled to 0 °C. 1M solution of TBAF in THF (0.585 ml) was added to the above solution. After 2 h at 0 °C, ice-water was added and the mixture was extracted with ethyl acetate. The extracts were washed with saturated aqueous NaCl, dried, and concentrated. The residue was chromatographed on silica gel (2.5 g) with 3 : 1 toluene-ethyl acetate to afford **20** (70.7 mg, 91% from **19**) as a colorless syrup, which was dissolved in 75% aqueous acetic acid (1.4 ml) and the mixture was heated at 80 °C for 10 h. The reaction mixture was concentrated and the residual triol (60.1 mg) was dissolved in acetone (1.4 ml) and cooled to 0 °C. A solution of $NaIO_4$ (125 mg, 0.584 mmol) in water (1.25 ml) was added and the mixture was stirred at 24 °C for 3 h. Acetone was removed under reduced pressure (50 mmHg; 1 mmHg≈133.322 Pa, 0 °C) and the aqueous phase was extracted with diethyl ether. The extracts were washed with saturated aqueous NaCl, dried, and concentrated. The residue was chromatographed on silica gel (0.5 g) with

6:1 hexane-ethyl acetate to afford (*R*)-2-benzyloxypropanal (43.6 mg, 100%) as a colorless syrup [^{1}H NMR (90 MHz) δ=1.31 (3H, d, 3×H-3, J=6.9 Hz), 3.88 (1H, dq, H-2, J=1.5 and 6.9 Hz) , 4.63 (2H, s, OC$\underline{H}_2$Ph), 7.37 (5H, s, Ph), and 9.69 (1H, d, CHO, J=1.5 Hz)]. This aldehyde (43.6 mg) was dissolved in a solution of CrO_3 in acetic acid and pyridine (3.5 ml; prepared from 1 g of CrO_3, 30 ml of acetic acid, and 1 ml of pyridine). After 3 h at 23 °C, ice-water was added and the mixture was extracted with diethyl ether. The etracts were washed with saturated aqueous $KHSO_4$, NaCl, dried, and concentrated (0 °C, 50 mmHg). The residue was chromatographed on silica gal (5 g) with 30:10:1 hexane-ethyl acetate-acetic acid to afford **21** (24.0 mg, 50% from **20**) as a colorless syrup: R_f=0.21 (30:10:1 hexane-ethyl acetate-acetic acid); $[\alpha]_D^{18}$ +54°, $[\alpha]_{546}^{18}$ +85° (*c* 2.30, benzene) [(*S*)-(−)-2-benzyloxypropionic acid: $[\alpha]_{546}$ −78.6° (*c* 2.3, benzene)[12]]; ^{1}H NMR (90 MHz) δ=1.47 (3H, d, 3×H-3, J=7.2 Hz), 4.12 (1H, q, H-2, J=7.2 Hz), 4.52 and 4.71 (each 1H, ABq, J=12.0 Hz), 7.37 (5H, s, Ph), and 8.0—8.4 (1H, br, COOH).

5-*O*-(*t*-Butyldiphenylsilyl)-1-deoxy-3,4-*O*-isopropylidene-2-*C*-vinyl-D-ribitol (22) and arabinitol (23). To a stirred solution of vinylmagnesium bromide [prepared from 343 mg (14.1 mmol) of magnesium powder and 0.99 ml (14.0 mmol) of vinyl bromide] in dry THF (36 ml) at 0 °C was added dropwise a solution of **18** (582 mg, 1.41 mmol) in dry THF (12 ml). After 3 h at room temperature, water was carefully added to the ice-cooled reaction mixture. The insoluble materials were filtered through Celite and washed with ethyl acetate. The combined filtrate and washings were washed with saturated aqueous NaCl, dried, and concentrated. The residue was chromatographed on silica gel (50 g) with 10:1 hexane-ethyl acetate to afford **22** (527 mg, 85%) and a mixture of **22** and **23** (50 mg, 8.0%) as colorless syrups. The ratio of **22** and **23** of this mixture by ^{1}H NMR was 5.7:1. Therefore, the ratio of **22** and **23** was 77:1. **22**: R_f=0.37 (10:1 hexane-ethyl acetate); $[\alpha]_D^{24}$ +32.5° (*c* 1.00); ^{1}H NMR (90 MHz) δ=1.06 (9H, s, *t*-Bu), 1.30, 1.35, and 1.37 (each 3H, each s, 3×Me), 3.54 (1H, dd, H-5, $J_{4,5}$=3.6 and J_{gem}=10.5 Hz), 3.95—4.4 (4H, m) , 5.12 (1H, dd, C=CH (cis) J=1.8 and 10.5 Hz), 5.52 (1H, dd, C=CH (trans), J=1.8 and 17.7 Hz), 6.36 (1H, dd, C$\underline{H}$=CH$_2$), and 7.3—7.75 (10H, m, 2×Ph) [^{1}H NMR (90 MHz) of the mixture of **22** and **23** showed the following additional peaks; 5.06 (dd, C=CH) (cis), J=1.8 and 10.5 Hz), 5.31 (dd, C=CH (trans), J=1.8 and 17.7 Hz), 5.98 (dd, C$\underline{H}$=CH$_2$), which were attributed to **23**].

Found: C, 70.27; H, 8.05%. Calcd for $C_{26}H_{36}O_4Si$: C, 70.55; H, 8.20%.

Transformation of 22 to (4*S*,5*R*)-(−)-5-Ethyl-2,2,5-trimethyl-1,3-dioxolane-4-carboxylic Acid (25). A mixture of **22** (147 mg, 0.334 mmol), [ClRh(Ph$_3$P)$_3$] (61.8 mg, 0.668 mmol), and benzene (7.4 ml) was stirred at 23 °C for 4 h under atmospheric pressure of H_2. The reaction mixture was concentrated and the residue was passed through Florisil (11 g) with diethyl ether. The eluant was concentrated to give a colorless syrup (137 mg, 93%) [R_f=0.47 (10:1 toluene-ethyl acetate); ^{1}H NMR (90 MHz) δ=0.96 (3H, t, J=7.5 Hz), 1.08 (9H, s, *t*-Bu), 1.28, 1.32, and 1.37 (each 3H, each s, 3×Me), 1.71 (2H, q), 3.33 (1H, s, OH), 3.59 (1H, dd, J=3.9 and 10.2 Hz), 3.9—4.35 (3H, m), and 7.3—7.8 (10H, m, 2×Ph)]. To a stirred solution of this syrup (130 mg, 0.294 mmol) in dry CH_2Cl_2 (1.3 ml) was added $ZnBr_2$ (66.4 mg, 0.295 mmol) at 0 °C and the mixture was stirred at 0 °C for 2 h. Saturated aqueous Na_2CO_3 solution was added and the mixture was extracted with ethyl acetate. The extracts were washed with saturated aqueous NaCl, dried, and concentrated. The residue was chromatographed on silica gel (15 g) with 20:1 toluene-ethyl acetate to afford **24** (108 mg, 83%) as a colorless syrup [R_f=0.44 (30:1 toluene-acetone); ^{1}H NMR (90 MHz) δ=1.00 (3H, t, J=7.5 Hz), 1.09 (9H, s, *t*-Bu), 1.24, 1.30, and 1.36 (each 3H, each s, 3×Me), 1.50—1.85 (2H, m), 2.48 (1H, d, OH, J=5.7 Hz), 3.6—3.95 (4H, m), and 7.3—7.8 (10H, m, 2×Ph)]. To a stirred solution of **24** (104 mg, 0.235 mmol) in dry THF (1.0 ml) was added at 0 °C TBAF (0.47 ml). After 1.5 h at 0 °C, ice-water was added and the mixture was extracted with ethyl acetate. The extracts were washed with saturated aqueous NaCl, dried, and concentrated. The residue was chromatagraphed on silica gel (5 g) with 3.5:1 chloroform-acetone to give a colorless syrup (47.8 mg, 99%) [R_f=0.48 (1:3 toluene-ethyl acetate); ^{1}H NMR (90 MHz) δ=0.98 (3H, t, J=7.5 Hz), 1.23, 1.33, and 1.40 (each 3H, each s, 3×Me), 1.5—1.85 (2H, m), 2.5—2.85 (2H, br, 2×OH), 3.6—4.0 (4H, m)]. To a stirred solution of this syrup (45.6 mg, 0.223 mmol) in acetone (1.4 ml) was added at 0 °C a solution of $NaIO_4$ (95.5 mg, 0.446 mmol) in water (1 ml). After 1 h at 26 °C, acetone was removed by evaporation and the residue was extracted with ethyl acetate. The extracts were washed with saturated aqueous NaCl, dried, and concentrated to afford an aldehyde (12.0 mg, 31%; the low yield might be attributed to the volatility of the sample.) as a colorless syrup [R_f=0.76 (3:1 chloroform-acetone); ^{1}H NMR (90 MHz) δ=0.98 (3H, t, J=7.5 Hz), 1.16, 1.38, and 1.54 (each 3H, each s, 3×Me), 1.5—1.85 (2H, m), 4.12 (1H, d, J=2.0 Hz), and 9.75 (1H, d, J=2.0 Hz)]. To a solution of this aldehyde (12.0 mg, 0.070 mmol) in dioxane (0.3 ml) were added at 27 °C water (0.1 ml), K_2CO_3 (60.9 mg, 0.44 mmol), a solution of $KHCO_3$ (44.2 mg, 0.44 mmol) in water (0.49 ml), iodine (52.0 mg, 0.200 mmol), and a solution of KI (68.6 mg, 0.41 mmol) in water (0.06 ml), successively. After 2 h at 27 °C, solid $Na_2S_2O_3$ (102 mg, 0.41 mmol) was added and the mixture was extracted with diethyl ether. The aqueous phase was acidified (pH 2—3) with 10% aqueous H_2SO_4 under ice-cooling and immediately extracted with chloroform. The extracts were washed with saturated aqueous NaCl, dried, and concentrated to afford almost pure sample of **25** (6.8 mg, 52%) as colorless crystals: R_f=0.30 (80:5:1 chloroform-ethanol-acetic acid); $[\alpha]_D^{18}$ −27°, (*c* 0.84), ^{1}H NMR 90 MHz) δ=1.02 (3H, t, J=7.5 Hz), 1.22, 1.39, and 1.54 (each 3H, each s, 3×Me), 1.6—2.0 (2H, m), 4.43 (1H, s), and 8.2—8.65 (1H, br, COOH). The ^{1}H NMR of the authentic (+)-**26**[13] [$[\alpha]_D^{20}$ +26°, (*c* 0.84)] was identical with the above one.

3-*O*-Benzyl-7-*O*-(*t*-butyldiphenylsilyl)-1,2-dideoxy-5,6-*O*-isopropylidene-4-*C*-methyl-D-*manno*-heptitol (31). A solution of **22** (0.850 g, 1.93 mmol) in dry CH_2Cl_2 (43 ml) was stirred at −78 °C under bubbling with ca. 2% O_3 in O_2 (4300 ml, ca. 3.8 mmol). Dimethyl sulfide (1.42 ml, 19.3 mmol) was added and the mixture was warmed gradually to room temperature. The mixture was washed with water and saturated aqueous NaCl, dried, and concentrated. The residue was chromatographed on silica gel (130 g) with 5:1 hexane-ethyl acetate to afford an aldehyde (0.620 g, 73%) as a colorless syrup [^{1}H NMR (90 MHz) δ=1.09 (9H, s), 1.29 (3H, s), 1.37 (3H, s), 1.40 (3H, s), 9.81 (1H, s)]. To a stirred solution of ethylmagnesium bromide [prepared from magnesium powder (0.27 g, 11 mmol) and ethyl bromide (0.84 ml, 11 mmol) in dry diethyl ether (19 ml) at 0 °C was added a

solution of the above aldehyde (0.620 g, 1.40 mmol) in dry diethyl ether (19 ml). After 1.5 h at room temperature, $Na_2SO_4 \cdot 10H_2O$ was added carefully to the ice-cooled reaction mixture. The insoluble materials were filtered through Celite and washed with ethyl acetate. The combined filtrate and washings were washed with saturated aqueous NaCl, dried, and concentrated. The residue was chromatographed on silica gel (35 g) with 4:1 hexane-ethyl acetate to afford an inseparable mixture of **27** and **28** (0.580 g, 88%) as a colorless syrup. To a solution of the above mixture in dry THF (2.9 ml) were added at 0 °C NaH (65 mg, 2.70 mmol) and benzyl bromide (0.22 ml, 1.84 mmol) and the mixture was stirred at 21 °C for 4 h. Ice-water was added and the mixture was extracted with ethyl acetate. The extracts were washed with saturated aqueous NaCl, dried, and concentrated. The residue was chromatographed on silica gel (28 g) with 20:1 hexane-ethyl acetate to afford **31** (380 mg, 55%) as a colorless syrup. The column was further eluted with 4:1 hexane-ethyl acetate to afford a mixture of **27** and **28** (162 mg, 28%). **31**: R_f=0.43 (6:1 hexane-ethyl acetate); $[\alpha]_D^{29}$ +7.5°, $[\alpha]_{365}^{29}$ +27.5° (*c* 1.00); ^{1}H NMR (90 MHz) δ=1.08 (12H, s, *t*-Bu involving 3×H-1), 1.29 and 1.39 (6H and 3H, each s, 4-Me and CMe_2), 1.5—2.1 (2H, m), 3.5—4.5 (6H, m), 4.72 (2H, s, $OC\underline{H}_2Ph$), and 7.2—8.0 (15H, m, 3×Ph).

Found: C, 72.27; H, 8.09%. Calcd for $C_{34}H_{46}O_5Si$: C, 72.56; H, 8.24%.

Desilylation of a Mixture of 27 and 28. (a) The mixture of **27** and **28** (12.4 mg, 0.0262 mmol) obtained from the Grignard reaction was dissolved in THF (0.124 ml) and solution of 1 M TBAF in THF (0.053 ml) was added under ice-cooling. After 1 h at 0 °C, ice-water was added and the mixture was extracted with ethyl acetate. The extracts were washed with saturated aqueous NaCl, dried, and concentrated. The residue was chromatographed on silica gel (0.75 g) with 25:1 chloroform-methanol to afford **29** (3.6 mg, 59%) and **30** (2.3 mg, 37%) as colorless syrups. **29**: R_f=0.45 (25:1 chloroform-methanol); ^{1}H NMR (90 MHz) δ=1.0—1.3 (6H, m), 1.26, 1.37, and 1.49 (each 3H, each s, 4-Me and CMe_2). **30**: R_f=0.36 (25:1 chloroform-methanol); ^{1}H NMR (90 MHz) δ=0.9—1.2 (6H, m), 1.22, 1.37, and 1.49 (each 3H, each s, 4-Me and CMe_2).

(b) The mixture of **27** and **28** recovered after the benzylation reaction was desilylated as in the case of (a) to afford **29** and **30** in a ratio of 1:4.9.

(c) The mixture of **27** and **28** prepared from ketone **35** by $LiAlH_4$ reduction (vide infra) was desilylated as in the case of (a) to afford **29** and **30** in a ratio of 5:1.

Transformation of 31 to (*R*)-2-Methylpentane-2,3-diol (33). 1 M TBAF in THF (0.314 ml) was added to a stirred, ice-cooled solution of **31** (88.5 mg, 0.157 mmol), in dry THF (0.89 ml). After 1 h at 0 °C, ice-water was added and the mixture was extracted with ethyl acetate. The extracts were washed with saturated aqueous NaCl, dried, and concentrated. The residue was chromatographed on silica gel (5 g) with 1:1 hexane-ethyl acetate to afford a diol (49.1 mg, 96%) as colorless needles [mp 94.5—100.5 °C; R_f=0.15 (3:1, hexane-ethyl acetate); ^{1}H NMR (90 MHz) δ=1.04 (3H, t, 3×H-1, *J*=7.2 Hz), 1.23 (3H, s, 4-Me), 1.35 and 1.52 (each 3H, each s, CMe_2), 1.5—2.0 (2H, m), 2.6—2.9 (2H, br, 2×OH), 3.47 (1H, dd, H-3, *J*=3.6 and 9.0 Hz), 3.7—3.85 (2H, m), 4.21 (1H, dt, H-6, $J_{6,7}$=6.0 Hz), 4.41 (1H, d, H-5, $J_{5,6}$=6.0 Hz), 4.68 (1H, s, $OC\underline{H}_2Ph$), and 7.35 (5H, s, Ph)]. A mixture of the above diol (45.0 mg, 0.139 mmol) and 50% aqueous acetic acid (0.9 ml) was heated at 115 °C for 2 h, then concentrated. The residue was chromatographed on silica gel (6 g) with 10:1 chloroform-methanol to afford a tetrol (37.5 mg, 95%) as colorless needles [mp 88—89.5 °C; R_f=0.19 (1:3 hexane-ethyl acetate); $[\alpha]_D^{24}$ +75° (*c* 1.00); ^{1}H NMR (90 MHz) δ=1.10 (3H, t, 3×H-1, *J*=7.0 Hz), 1.23 (3H, s, 4-Me), 1.5—1.9 (3H, m), 2.7—3.0 (2H, br, 2×OH), 3.4—3.9 (6H, m), 4.64 and 4.76 (each 1H, ABq, $OC\underline{H}_2Ph$, *J*=10.5 Hz), and 7.35 (5H, s, Ph)]. A solution of $NaIO_4$ (65.3 mg, 0.305 mmol) in water (0.65 ml) was added to a stirred, ice-cooled solution of the above tetrol (26.3 mg, 0.0925 mmol) in acetone (0.53 ml). After 1.5 h at room temperature, the reaction mixture was filtered and the filtrate was concentrated. The residue was chromatographed on silica gel (1 g) with 30:1 toluene-ethyl acetate to afford **32** (14.9 mg, 84%) as a colorless syrup [^{1}H NMR (90 MHz) δ=0.95 (3H, t, 3×H-5, *J*=7.0 Hz), 1.68 (2H, dq, 2×H-4, $J_{3,4}=J_{4,5}$=7.0 Hz), 2.17 (3H, s, 3×H-1), 3.71 (1H, t, H-3), 4.47 and 4.60 (each 1H, ABq, $OC\underline{H}_2Ph$, *J*=12.0 Hz), and 7.38 (5H, s, Ph)]. A solution of **32** (13.4 mg, 0.0697 mmol) in dry diethyl ether (0.27 ml) was added to a solution of methylmagnesium iodide [prepared from magnesium powder (20.3 mg, 0.836 mmol) and iodomethane (0.0564 ml, 0.906 mmol)] in dry diethyl ether (0.58 ml) under ice-cooling. After 2 h at 20 °C, saturated aqueous NH_4Cl was added and the mixture was extracted with ethyl acetate. The extracts were washed with saturated aqueous NaCl, dried, and concentrated. The residue was chromatographed on silica gel (1 g) with 10:1 benzene-ethyl acetate to afford (*R*)-3-benzyloxy-2-methyl-2-pentanol (13.1 mg, 90%) as a colorless syrup [R_f=0.19 (20:1 benzene-ethyl acetate); $[\alpha]_D^{19}$ −7.7°, $[\alpha]_{365}^{19}$ −25.5° (*c* 0.98); ^{1}H NMR (90 MHz) δ=1.04 (3H, t, 3×H-5, *J*=6.3 Hz), 1.15 and 1.20 (each s, each 3H, 2-Me and 3×H-1), 1.4—1.8 (2H, m), 2.18 (1H, s, OH), 3.12 (1H, dd, H-3, *J*=4.5 and 6. 0 Hz), 4.61 and 4.73 (each 1H, ABq, $OC\underline{H}_2Ph$, *J*=10.5 Hz), and 7.35 (5H, s, Ph); Found: C, 74.72; H, 9.45%. Calcd for $C_{13}H_{20}O_2$: C, 74.96; H, 9.68%]. A mixture of the above alcohol (13.0 mg, 0.0624 mmol), palladium black, and *t*-BuOH (0.3 ml) was stirred at 28 °C for 0.5 h under bubbling with H_2. Catalyst was filtered off and the filtrate was concentrated to afford **33** (7.4 mg, 100%) as a colorless syrup: R_f=0.40 (10:1 chloroform-methanol); $[\alpha]_D^{18.5}$ +27.3° (*c* 1.10, ether); ^{1}H NMR (90 MHz) δ=1.03 (3H, t, 3×H-5, *J*=6.0 Hz), 1.15 and 1.20 (each 3H, each s, 3×H-1 and 2-Me), 2.45—2.65 (2H, br, 2×OH), 3.28 (1H, dd, H-3, *J*=3.0 and 9.0 Hz). The product **33** was proved to be the enantiomer of **34** by comparing its optical rotation with that of **34** [$[\alpha]_D$ −32.6° (*c* 1.10, diethyl ether)].[14]

7-*O*-(*t*-Butyldiphenylsilyl)-1,2-dideoxy-5,6-*O*-isopropylidene-4-*C*-methyl-*keto*-D-*arabino*-3-heptulose (35). To a mixture of **27** and **28** (0.720 g, 1.52 mmol), dry benzene (5 ml), dry DMSO (1.17 ml, 16.4 mmol), and dry pyridine (0.117 ml, 1.45 mmol) at 0 °C were successively added trifluoroacetic acid (0.062 ml, 0.81 mmol) and a solution of DCC (952 mg, 4.61 mmol) in dry benzene (3.24 ml). After 5 h at room temperature, the reaction mixture was filtered and the filtrate was washed with saturated aqueous $KHSO_4$, $NaHCO_3$, and NaCl solutions, dried, and concentrated. The residue was chromatographed on silica gel (85 g) with 10:1 pet. ether-diethyl ether to afford **35** (650 mg, 90%) as a colorless syrup: R_f=0.53 (10:1 toluene-ethyl acetate); $[\alpha]_D^{29}$ 0°, $[\alpha]_{365}^{29}$ −17.5° (*c* 1.00); IR (0.15 M in $CHCl_3$) 1713 cm^{-1}; ^{1}H NMR (90 MHz) δ=1.06 (3H, t, 3×H-1, *J*=7.5 Hz), 1.08

(9H, s, *t*-Bu), 1.27 and 1.36 (3H and 6H, each s, 4-Me and CMe_2), 2.69 (2H, q, 2×H-2), 3.65—4.45 (5H, m), and 7.3—7.85 (10H, m, 2×Ph).

Found: C, 68.68; H, 8.06%. Calcd for $C_{27}H_{38}O_5Si$: C, 68.90; H, 8.14%.

$LiAlH_4$ Reduction of 35 and Benzylation of the Resulting Mixture of 27 and 28. To a stirred suspension of $LiAlH_4$ (104 mg, 2.74 mmol) in dry diethyl ether (2.0 ml) at −78 °C was added a solution of **35** (1.25 g, 2.66 mmol) in dry diethyl ether (12 ml). After 2 h at −78 °C, wet diethyl ether was added to the reaction mixture and the mixture was warmed to room temperature. The insoluble materials were filtered off through Celite and washed with ethyl acetate. The combined filtrate and washings were concentrated and the residue was chromatographed on silica gel (35 g) with 6:1 toluene-ethyl acetate to afford a mixture of **27** and **28** (1.05 g, 83.6%). To a solution of this mixture in dry THF (5.3 ml) at 0 °C was added NaH (213 mg, 4.89 mmol, 55% dispersion in mineral oil). The mixture was stirred at 21 °C for 0.5 h. Benzyl bromide (0.40 ml, 3.36 mmol) was added to the above ice-cooled suspension and the mixture was stirred at 21 °C for 4.5 h. Ice was added and the mixture was extracted with ethyl acetate and the extracts were washed with saturated aqueous NaCl, dried, and concentrated. The residue was chromatographed on silica gel (120 g) with 20:1 hexane-ethyl acetate to afford **31** (845 mg, 68%) as a colorless syrup.

3-*O*-Benzyl-7-*O*-(*t*-butyldiphenylsilyl)-1,2-dideoxy-4,5-*O*-isopropylidene-4-*C*-methyl-D-*manno*-heptitol (36). To a stirred solution of **31** (1.47 g, 2.61 mmol) in dry acetone (37 ml) at 0 °C was added a solution of $FeCl_3$ (212 mg, 1.31 mmol) in dry acetone (7.4 ml). After 1 h at 29 °C, saturated aqueous $NaHCO_3$ was added to the reaction mixture. The insoluble materials were filtered through Celite and washed with ethyl acetate. The filtrate and washings were washed with saturated aqueous NaCl, dried, and concentrated. The residue was chromatographed on silica gel (75 g) with 100:1 toluene-acetone to afford **36** (1.39 g, 95%) as a colorless syrup: R_f=0.49 (60:1 toluene-ethyl acetate); $[\alpha]_D^{26}$ −17.5° (*c* 1.00); ^{1}H NMR (90 MHz) δ=1.06 (3H, t, 3×H-1, *J*=7.4 Hz), 1.08 (9H, s, *t*-Bu), 1.25 (3H, s, 4-Me), 1.31 and 1.36 (each 3H, each s, CMe_2), 1.73 (2H, q, 2×H-2), 3.38 (1H, dd, H-3, *J*=6.3 and 5.7 Hz), 3.6—4.25 (5H, m), 4.67 (2H, s, $OC\underline{H}_2Ph$), and 7.25—7.85 (15H, m, 3×Ph).

Found: C, 72.84; H, 8.11%. Calcd for $C_{34}H_{46}O_5Si$: C, 72.56; H, 8.24%.

3-*O*-Benzyl-1,2-dideoxy-4,5-isopropylidene-4-methyl-D-*manno*-heptitol (37). To a stirred solution of **36** (1.30 g, 2.31 mmol) in THF (13 ml) at 0 °C was added 1 M TBAF in THF (4.6 ml). After 1 h at 0 °C, ice was added and the mixture was extracted with chloroform. The extracts were washed with saturated aqueous NaCl, dried, and concentrated. The residue was chromatographed on silica gel (50 g) with 2:1 hexane-ethyl acetate to afford **37** (691 mg, 92%) as a colorless syrup: R_f=0.23 (6:1 hexane-ethyl acetate); $[\alpha]_D^{22}$ −45.0° (*c* 1.00); ^{1}H NMR (90 MHz) δ=1.10 (3H, t, 3×H-1, *J*=7.5 Hz), 1.23, 1.30, and 1.40 (each 3H, each s, 4-Me and CMe_2), 1.6—2.1 (3H, m, 2×H-2 and OH), 3.34 (1H, dd, H-3, *J*=5.5 and 5.5 Hz), 3.55—4.30 (5H, m), 4.53 and 4.76 (each 1H, ABq, $OC\underline{H}_2Ph$, *J*=10.8 Hz), 7.39 (5H, s, Ph).

Found: C, 66.52; H, 8.60%. Calcd for $C_{18}H_{24}O_5$: C, 66.64; H, 8.70%.

5-*O*-Benzyl-1,6,7-trideoxy-3,4-*O*-isopropylidene-4-*C*-methyl-keto-D-*arabino*-2-heptulose (38). To a solution of **37** (723 mg, 2.23 mmol) in acetone (14.5 ml) at 0 °C was added a solution of $NaIO_4$ (524 mg, 2.45 mmol) in water (5.2 ml). After 3 h at 27 °C, acetone was removed by evaporation and the residue was extracted with $CHCl_3$. The extracts were washed with saturated aqueous NaCl, dried, and concentrated. The residual aldehyde [652 mg, 100%; ^{1}H NMR (90 MHz) δ=4.45 (1H, s, H-2), 9.63 (1H, s, CHO)] was dissolved in dry diethyl ether (13 ml) and added to a stirred solution of methylmagnesium iodide [prepared from magnesium powder (0.54 g, 22 mmol) and iodomethane (1.53 ml, 24.6 mmol)] in dry diethyl ether (28 ml) under ice-cooling. After 2 h at 27 °C, $Na_2SO_4 \cdot 10H_2O$ was added to the ice-cooled reaction mixture and the insoluble materials were filtered off through Celite and washed with $CHCl_3$. The filtrate and washings were washed with saturated aqueous NaCl, dried, and concentrated. The residue was chromatographed on silica gel (70 g) with 6:1 hexane-ethyl acetate to afford **fr.1** (91.7 mg, 13.3%) and **fr.2** (531 mg, 77.3%) as colorless syrups, both of which are the desired alcohol: R_f=0.58 (fr. 1), 0.40 (fr.2) (4:1 hexane-ethyl acetate). This epimeric mixture (623 mg, 2.02 mmol) was dissolved in dry CH_2Cl_2 (2.5 ml) and added to a stirred suspension of PCC (1.72 g, 8.07 mmol), MS 3AP (2.02 g) in dry CH_2Cl_2 (5.0 ml) at 0 °C. The reaction mixture was stirred at 25 °C for 1.5 h. Diethyl ether (5 ml) was added and the suspension was transferred to a column filled with silica gel (23 g). The column was eluted with diethyl ether and the eluant was concentrated to give **38** (607 mg, 98%) as a colorless syrup: R_f=0.61 (6:1 hexane-ethyl acetate); $[\alpha]_D^{21}$ 0°, $[\alpha]_{365}^{21}$ +25.0° (*c* 1.00); IR ($CHCl_3$) 1720 cm^{-1}; ^{1}H NMR (90 MHz) δ=1.00 (3H, t, 3×H-7, *J*=7.0 Hz), 1.14 (3H s, 4-Me), 1.35 and 1.53 (each 3H, each s, CMe_2), 1.4—1.85 (2H, m), 2.23 (3H, s, 3×H-1), 3.38 (1H, dd, H-5, *J*=4.8 and 8.4 Hz), 4.51 (1H, s, H-3), 4.63 and 4.78 (each 1H, ABq, $OC\underline{H}_2Ph$, *J*=11.4 Hz), and 7.33 (5H, s, Ph).

Found: C, 70.44; H, 8.42%. Calcd for $C_{18}H_{26}O_4$: C, 70.56; H, 8.55%.

5-*O*-Benzyl-1,2,6,7-tetradeoxy-2-iodo-3,4-*O*-isopropylidene-4-*C*-methyl-D-*arabino*-1-heptenitol (11). To a stirred solution of **38** (520 mg, 1.70 mmol) in ethanol (0.58 ml) were added triethylamine (2.01 ml, 14.4 mmol) and $NH_2NH_2 \cdot H_2O$ (0.33 ml, 6.8 mmol). After 1 h at 70 °C, the reaction mixture was cooled to room temperature and diluted with CH_2Cl_2. The mixture was washed with water, saturated aqueous NaCl, dried, and concentrated. The residual pale yellow syrup (544 mg, 100%) was dissolved in dry toluene (19 ml) and added at 0 °C to a mixture of iodine (946 mg, 3.73 mmol), 1,1,3,3-tetramethylguanidine (10.6 ml, 84.5 mmol), and dry toluene (5.5 ml). After 0.5 h at 0 °C, the reaction mixture was diluted with diethyl ether, washed with saturated aqueous $Na_2S_2O_3$, 10% aqueous citric acid, and saturated aqueous NaCl, dried, and concentrated. The residue was chromatographed on silica gel (26 g) with 50:50:1 hexane-toluene-ethyl acetate to afford **11** (389 mg, 55%) as a colorless syrup: R_f=0.74 (6:1 hexane-ethyl acetate); $[\alpha]_D^{18.5}$ 0°, $[\alpha]_{365}^{18.5}$ −11.2° (*c* 1.12); ^{1}H NMR (90 MHz) δ=1.04 (3H, t, 3×H-7, *J*=7.2 Hz), 1.29 (3H, s, 4-Me), 1.37 and 1.52 (each 3H, each s, CMe_2), 1.55—1.7 (2H, m), 3.56 (1H, t, H-5, *J*=6.0 Hz), 4.52 (1H, s, H-3), 4.70 (2H, s, $OC\underline{H}_2Ph$), 6.08 and 6.62 (each 1H, each d, 2×H-1, *J*<1.0 Hz), and 7.32 (5H, s, Ph).

Found: C, 51.65; H, 5.87; I, 30.75%. Calcd for $C_{18}H_{25}O_3I$: C, 51.93; H, 6.05; I, 30.48%.

Methyl (*S*)-(+)-2-Methyl-3-triphenylmethoxypropionate

(40). A mixture of methyl (*S*)-(+)-3-hydroxy-2-methylpropionate (**39**) (2.00 g, 16.9 mmol), triphenylmethyl chloride (4.96 g, 17.8 mmol), triethylamine (3.54 ml, 25.4 mmol), DMAP (103 mg, 0.85 mmol), and dry CH_2Cl_2 (20 ml) was stirred at 23 °C for 15 h. The reaction mixture was poured into 50% aqueous NH_4Cl (20 ml). The phases were separated, and the aqueous layer was extracted with CH_2Cl_2 (20 ml×2). The combined organic layers were washed with saturated aqueous NaCl (20 ml), dried, and concentrated to give crude crystals (6.49 g, 100% up) of **40**, which was used without any further purification. A portion of this was chromatographed on silica gel with toluene to afford an analytically pure sample of **40**: mp 100—101 °C; R_f=0.38 (toluene); $[\alpha]_D^{31}$ +19.6° (*c* 1.00); IR (KBr) 1726 cm^{-1}; ^1H NMR (90 MHz) δ=1.13 (3H, d, 2-Me, *J*=6.6 Hz), 2.5—2.9 (1H, m, H-2), 3.05—3.45 (2H, m, 2×H-3), 3.70 (3H, s, OMe), and 7.1—7.55 (15H, m, Tr).

Found: C, 80.05; H, 6.78%. Calcd for $C_{24}H_{24}O_3$: C, 79.97; H, 6.71%.

(*R*)-(+)-2-Methyl-3-triphenylmethoxypropanol (41). To a stirred solution of the crude **40** (6.19 g) in dry THF (62 ml) at 0 °C was added $LiAlH_4$ (0.65 g, 17 mmol). After 50 min at room temperature, water (0.65 ml), 15% aqueous NaOH (0.65 ml), and water (1.95 ml) were added successively to the cooled (0 °C) reaction mixture. The insoluble materials were filtered off with Celite and washed with diethyl ether. The filtrate and washings were concentrated and the residue was chromatographed on silica gel (220 g) with 9:1 toluene-ethyl acetate to give **41** (4.89 g, 86% from **39**) as a pale yellow syrup, which on standing crystallized. An analytical sample was obtained by recrystallization from ethyl acetate-hexane: mp 74—76 °C; R_f=0.13 (8:1 hexane-acetone); $[\alpha]_D^{29}$ +28.4° (*c* 1.00); ^1H NMR (90 MHz) δ=0.84 (3H, d, 2-Me, *J*=6.9 Hz), 1.8—2.3 (1H, m), 2.21 (1H, d, OH, *J*=5.7 Hz), 2.9—3.35 (2H, m), 3.58 (2H, dd, 2×H-1, *J*=5.7 Hz), and 7.15—7.55 (15H, m, Tr).

Found: C, 82.59; H, 7.38%. Calcd for $C_{23}H_{24}O_2$: C, 83.10; H, 7.28%.

(*R*)-(−)-2-(2-Benzyloxy-1-methylethyl)-1,3-dioxolane (45). To a stirred solution of **41** (1.50 g, 4.51 mmol) in dry THF (15 ml) at 0 °C was added NaH (0.394 g, 9.02 mmol, 55% dispersion in mineral oil). After 1 h at room temperature, benzyl bromide (1.07 ml. 9.02 mmol) was added to the mixture under ice-cooling. The new mixture was heated under reflux (70 °C) for 2 h. The reaction mixture was cooled to 0 °C and ethanol (0.53 ml) was added and the mixture was stirred for 1 h. Cold water (20 ml) was added and extracted with diethyl ether. The extracts were washed with saturated aqueous NaCl, dried, and concentrated. The residue was chromatographed on silica gel (100 g) with 50:1 hexane-acetone to give a practically pure sample of **42** (1.91 g, 100%) as a pale yellow syrup [R_f=0.32 (50:1 hexane-acetone); $[\alpha]_D^{33}$ +4.3°, $[\alpha]_{365}^{33}$ +14.8° (*c* 0.88)]. This sample (1.73 g, 4.09 mmol) was dissolved in methanol (17.3 ml) and Amberlyst 15 (123 mg) was added. The mixture was heated at 50 °C for 3.5 h under vigorous stirring. The reaction mixture was filtered off and washed with methanol. The filtrate and washings were concentrated and the residue was chromatographed on silica gel (21 g) with 3.5:1 benzene-ethyl acetate to give **43** (612 mg, 83% from **41**) as a colorless syrup [R_f=0.32 (3.5:1 benezene-ethyl acetate); $[\alpha]_D^{33}$ −15.6° (*c* 1.37) [lit,[16] $[\alpha]_D$ −11.3° (*c* 16.05)]]. A solution of DMSO (0.469 ml, 6.61 mmol) in dry CH_2Cl_2 (1.2 ml) was added to a solution of oxalyl chloride (0.434 ml, 4.97 mmol) in dry CH_2Cl_2 (12 ml) at −78 °C under argon. After 3 min, a solution of **43** (551 mg, 3.06 mmol) in dry CH_2Cl_2 (3.6 ml) was added dropwise and the resulting suspension was stirred at −78 °C for 15 min. After addition of triethylamine (2.31 ml, 16.6 mmol), the mixture was gradually warmed to 0 °C for a period of 20 min. A mixture of 4:1 benzene-ether and water was added to the reaction mixture and phases were separated. The aqueous phase was extracted with 4:1 benzene-ether and the combined organic layers were washed with saturated aqueous NaCl, dried, and concentrated. The residual colorless aldehyde **44** was used without any further purification [R_f=0.64 (5:1 toluene-ethyl acetate) $[\alpha]_D^{33}$ −28.0° (*c* 1.40), [lit, [16] $[\alpha]_D$ −28° (*c* 1.40)]]. To a stirred mixture of **44** (514 mg, 2.88 mmol), ethylene glycol (1.60 ml, 28.8 mmol), and dry acetonitrile (5.14 ml) at 0 °C was added *p*-toluenesulfonic acid (45.1 mg, 0.288 mmol). After 35 h at 21 °C, the reaction mixture was poured into saturated aqueous $NaHCO_3$. The mixture was extracted with CH_2Cl_2 and the extracts were washed with saturated aqueous NaCl, dried, and concentrated. The residue was chromatographed on silica gel (30 g) with 15:1 toluene-ethyl acetate to give **45** (630 mg, 98%) as a colorless syrup: R_f=0.52 (10:1 toluene-ethyl acetate) $[\alpha]_D^{17}$ −3°, $[\alpha]_{365}^{17}$ +9° (*c* 0.81); ^1H NMR (90 MHz) δ=1.00 (3H, d, 2-Me, *J*=6.5 Hz), 1.85—2.3 (1H, m), 3.3—3.7 (2H, m) 3.7—4.0 (4H, m, OCH_2CH_2O), 4.52 (2H, s, OCH_2Ph), 4.86 (1H, d, H-1, $J_{1,2}$=5.4 Hz), 7.33 (5H, s, Ph).

Found: C, 70.15; H, 8.35%. Calcd for $C_{13}H_{18}O_3$: C, 70.25; H, 8.16%.

(*R*)-(−)-2-(2-Hydroxy-1-methylethyl)-1,3-dioxolane (46). A mixture of **45** (8.60 g, 38.7 mmol), palladium black, and methanol (86 ml) was vigorously stirred at room temperature for 1 h under bubbling with H_2. The catalyst was filtered off and washed with methanol. The filtrate and washings were concentrated to afford **46** (5.11 g, 100%) which was distilled under reduced pressure to give pure **46** (4.51 g, 88%) as a colorless oil: bp 69—71 °C (4 mmHg); $[\alpha]_D^{18}$ −6°, $[\alpha]_{365}^{18}$ −16.5° (*c* 1.21); ^1H NMR (90 MHz) δ=0.96 (3H, d, 2-Me, *J*=7.5 Hz), 1.8—2.2 (1H, m), 2.6—2.85 (1H, br t, OH), 3.5—3.8 (2H, m), 3.8—4.15 (4H, m, OCH_2CH_2O), and 4.77 (1H, d, H-1, $J_{1,2}$=7.3 Hz).

Found: C, 54.76; H 9.06%. Calcd for $C_6H_{12}O_3$: C, 54.53; H, 9.15%.

(*S*)-(+)-2-(2-Bromo-1-methylethyl)-1,3-dioxolane (47). To a stirred solution of **46** (970 mg, 7.34 mmol) and triphenylphosphine (2.89 g, 11.0 mmol) in dry THF (9.7 ml) at −5 °C was added dropwise diethyl azodicarboxylate (1.70 ml, 11.0 mmol). After 5 min at −5 °C, ethyl bromide (0.822 ml, 11.0 mmol) was added and the mixture was stirred at 20 °C for 2 h. The reaction mixture was concentrated under reduced pressure (120 mmHg) and the residue was chromatographed on silica gel (100 g) with 10:1 hexane-ethyl acetate to afford an oil (1.10 g, 77%) which was distilled to give a pure **47** (903 mg, 63%) as a colorless oil: bp 54—56 °C (3 mmHg); $[\alpha]_D^{16}$ +3°, $[\alpha]_{365}^{16}$ +11° (*c* 1.15); ^1H NMR (90 MHz) δ=1.09 (3H, d, 2-Me, *J*=6.5 Hz), 1.9—2.2 (1H, m), 3.29—3.4 (each 1H, each dd, H-3 and 3′, $J_{3,3'}$=9.3, $J_{2,3}$=7.0, and $J_{2,3'}$=4.5 Hz), 3.93 (1H, br s, OCH_2CH_2O), and 4.71 (1H, d, H-1, $J_{1,2}$=5.5 Hz).

Found: C, 37.10; H, 5.49; Br, 40.68%. Calcd for $C_6H_{11}O_2Br$: C, 36.95; H, 5.68; Br, 40.96%.

5,7,9-Tri-*O*-benzyl-2,3,6,8-tetradeoxy-2,4,6,8-tetra-*C*-methyl-L-*threo*-L-*ido*-nonose Ethylene Acetal (48) and Its C-4 Epimer. To a stirred suspension of magnesium powder

(687 mg, 28.3 mmol) in dry diethyl ether (50.5 ml) was added at room temperature 1,2-dibromoethane (0.244 ml, 2.83 mmol). After 0.5 h at room temperature, **47** (1.84 g, 9.43 mmol) in dry diethyl ether (92 ml) was added and the new mixture was stirred at room temperature for 1 h. To this was added **13** (1.01 g, 2.19 mmol) in dry diethyl ether (5.05 ml) and the mixture was stirred at room temperature for 2 h. Ice was added and the insoluble materials were filtered off with Celite and washed with ethyl acetate. The filtrate and washings were separated and the aqueous phase was extracted with ethyl acetate. The combined organic layers were washed with saturated aqueous NaCl, dried, and concentrated. The residue was chromatographed on silica gel (200 g) with 7:1 hexane-acetone to afford **48** (999 mg, 79%) and its C4-epimer (101 mg, 8.0%) as colorless syrups.

48: R_f=0.41 (15:1 benzene-acetone); $[\alpha]_D^{16}$ +3°, $[\alpha]_{365}^{16}$ +20° (*c* 0.64); ^{1}H NMR (90 MHz) δ=0.9—1.3 (12H, m), 1.5—2.5 (5H, m), 3.3—3.8 (5H, m), 3.8—4.1 (4H, m, $OC\underline{H}_2C\underline{H}_2O$), 4.56 and 4.67 (each 2H, each s, 2×$OC\underline{H}_2Ph$), 4.5—4.95 (3H, m, H-1, $OC\underline{H}_2Ph$), and 7.3—7.6 (15H, m, 3×Ph).

Found: C, 74.71; H, 8.44%. Calcd for $C_{36}H_{48}O$: C, 74.97; H, 8.38%.

C4-epimer of **48**: R_f=0.34 (15:1 benzene-acetone); ^{1}H NMR (90 MHz) δ=0.9—1.3 (12H, m, 4×Me), 1.4—2.7 (6H, m), 3.35—4.15 (8H, m), 4.53 and 4.59 (each 2H, each s, 2×$OC\underline{H}_2Ph$), 4.4—5.15 (3H, m, H-1 and $OC\underline{H}_2Ph$), and 7.3—7.6 (15H, m, 3×Ph).

5,7,9-Tri-*O*-benzyl-4-*O*-*t*-butyldimethylsilyl-2,3,6,8-tetradeoxy-2,4,6,8-tetra-*C*-methyl-L-*threo*-L-*ido*-nonose Ethylene Acetal (49). To a solution of **48** (1.06 g, 1.84 mmol), 2,6-lutidine (0.852 ml, 7.31 mmol) in dry CH_2Cl_2 (10.6 ml) was added at 0 °C TBDMSOTf (1.27 ml, 5.53 mmol). After 2 h standing at 25 °C, ice was added and the mixture was extracted with CH_2Cl_2. The extracts were washed with saturated aqueous NaCl, dried, and concentrated. The residue was chromatographed on silica gel (50 g) with 8:1 hexane-ethyl acetate to give **49** (1.13 g, 89%) as a colorless syrup: R_f=0.67 (3:1 hexane-ethyl acetate); $[\alpha]_D^{16}$ +0°, $[\alpha]_{365}^{16}$ +8° (*c* 0.64); ^{1}H NMR (90 MHz) δ=(9H, s, *t*-Bu), 0.8—1.15 (9H, m, 2, 6, and 8-Me), 1.35 (3H, s, 4-Me), 1.5—2.5 (5H, m), 3.26 (1H, d, *J*=2. 1 Hz), 3.4—3.7 (3H, m), 3.8—4.1 (5H, m, $OC\underline{H}_2C\underline{H}_2O$+1H), 4.56 and 4.65 (each 2H, each s, 2×$OC\underline{H}_2Ph$), 4.4—4.95 (3H, m, H-1, and $OC\underline{H}_2Ph$), and 7.3—7.55 (15H, m, 3×Ph).

Found: C, 73.21; H, 8.92%. Calcd for $C_{42}H_{62}O_6Si$: C, 73.00; H, 9.04%.

1,3,5,13-Tetra-*O*-benzyl-6-*O*-*t*-butyldimethylsilyl-2,4,7,8,10,14,15-heptadeoxy-11,12-*O*-isopropylidene-2,4,6,8,12-penta-*C*-methyl-10-*C*-methylene-D-*erythro*-L-*ido*-L-*ido*-pentadecitol (50) and Its D-*erythro*-L-*ido*-L-*altro* Epimer 51. To a solution of **49** (406 mg, 0.588 mmol) in dry acetone (20 ml) was added $SnCl_2$ (112 mg, 0.588 mmol) and the mixture was stirred at 26 °C for 19 h. The reaction mixture was poured into a cold saturated aqueous $NaHCO_3$ and extracted with ethyl acetate. The extracts were washed with saturated aqueous NaCl, dried, and concentrated. The residue was chromatographed on silica gel (200 g) with 100:1 toluene-acetone to afford **12** (275 mg, 72%) as a colorless syrup [R_f=0.53 (8:1 hexane-ethyl acetate)]. To a cooled (−100 °C), stirred solution of **11** (531 mg, 1.28 mmol) in dry diethyl ether (0.667 ml) was added 1.38 M butyllithium in hexane (0.924 ml, 1.28 mmol) and the mixture was stirred at −100 °C for 15 min. To this was added the above aldehyde **12** (275 mg, 0.425 mmol) in dry diethyl ether (1.38 ml) and the mixture was stirred at −100 °C for 1 h. The reaction mixture was quenched with saturated aqueous NH_4Cl and extracted with ethyl acetate. The extracts were washed with saturated aqueous NaCl, dried, and concentrated. The residue was chromatographed on silica gel (80 g) with 25:1 toluene-ethyl acetate to afford **11** (32% recovered), and a mixture of **50**, **51**, and impurities (0.45 g). This mixture was re-chromatographed on silica gel (50 g) with 10:1 hexane-ethyl acetate to afford **50**+impurities (252 mg) and **51** (40.1 mg, 10%). This impure **50** was directly used to the next step. **50**: R_f=0.38 (25:1 toluene-acetone); ^{1}H NMR (250 MHz) δ=0.09 and 0.10 (each 3H, each s, $SiMe_2$), 0.88 (9H, s, *t*-Bu, containing one of the doublets of three methyls), 0.95—1.05 (9H, one t and two d, 3×Me), 1.14, 1.32, and 1.48 (3H, 6H, and 3H, each s, 4×Me), 1.55—1.8 (3H, m), 1.8—2.0 (1H, m), 2.01 (1H, br d, OH, *J*=3.8 Hz), 2.1—2.35 (2H, m), 3.19 (1H, d, *J*=1.8 Hz), 3.25—3.6 (4H, m), 3.92 (1H, br t, H-9, *J*=3.8 Hz), 4.3—4.75 (9H, m), 5.33 and 5.47 (each 1H, each s), and 7.1—7.35 (20H, m), and some impurities' peaks. **51**: R_f=0.36 (25:1 toluene-acetone); $[\alpha]_D^{34}$ −6.5°, $[\alpha]_{365}^{34}$ −17.1° (*c* 1.00); ^{1}H NMR (250 MHz) δ=0.11 and 0.13 (each 3H, each s, $SiMe_2$), 0.88 (9H, s, *t*-Bu), 0.93, 1.04, and 1.06 (each 3H, each d, 2, 4, and 8-Me, *J*=6.8, 6.8, and 6.8 Hz), 1.03 (3H, t, 14-Me, *J*=7.5 Hz), 1.13, 1.30, 1.36, and 1.44 (each 3H, each s, 4×Me), 1.6—2.35 (7H, m), 3.21 (1H, d, *J*=2.0 Hz), 3.35 (1H, dd, *J*=6.8 and 9.0 Hz), 3.4—3.55 (3H, m), 4.05 (1H, br, H-9), 4.34 and 4.73 (each 1H, ABq, $OC\underline{H}_2Ph$, *J*=12.5 Hz), 4.45 and 4.48 (each 1H, ABq, $OC\underline{H}_2Ph$, *J*=12.5 Hz), 4.53 and 4.58 (each 1H, ABq, $OC\underline{H}_2Ph$, *J*=11.3 Hz), 4.62 (2H, s, $OC\underline{H}_2Ph$), 4.71 (1H, s, H-11), 5.16 and 5.31 (each 1H, each s, $C{=}C\underline{H}_2$), and 7.1—7.35 (20H, m, 4×Ph).

Desilylation of the Coupling Products. The crude coupling products (220 mg) containing **50**, **51**, and impurities were dissolved in THF (4.4 ml) and to this was added 1 M solution of TBAF in THF (0.47 ml). After 2 h at 25 °C, ice-water was added and the mixture was extracted with ethyl acetate. The extracts were washed with saturated aqueous NaCl, dried and concentrated. The residue was chromatographed on silica gel (35 g) with 5:1 hexane-ethyl acetate to afford **52** (63.5 mg) and **53** (12.1 mg). **52**: R_f=0.36 (5:1 hexane-ethyl acetate); ^{1}H NMR (250 MHz) δ=0.82 (3H, d, *J*=7.0 Hz), 0.99 (3H, d, *J*=7.0 Hz), 1.01 (3H, t, *J*=7.0 Hz), 1.08 (3H, d, *J*=7.0 Hz), 1.11, 1.15, 1.36, and 1.50 (each 3H, each s, 4×Me), 1.55—2.3 (7H, m), 2.65—2.95 (2H, br), 3.15 (1H, d, *J*=2.3 Hz), 3.35—3.65 (4H, m), 4.25—4.75 (10H, m), 5.41 and 5.52 (each 1H, each s), and 7.2—7.35 (20H, m). **53**: R_f=0.31 (5:1 hexane-ethyl acetate); ^{1}H NMR (250 MHz) δ=0.86 (3H, d, *J*=6.3 Hz), 0.91 (3H, d, *J*=6.8 Hz), 0.98 (3H, t, *J*=74 Hz), 1.02 (3H, d, *J*=7.3 Hz), 1.06, 1.08, 1.28, and 1.41 (each 3H, each s, 4×Me), 1.5—2.25 (7H, m), 2.9—3.15 (2H, br), 3.25—3.45 (3H, m), 3.5—3.6 (2H, m), 4.3—4.7 (10H, m), 5.29 and 5.40 (each 1H, each s), and 7.15—7.35 (20H, m).

1,3,5,13-Tetra-*O*-benzyl-6-*O*-*t*-butyldimethylsilyl-2,4,7,8,10,14,15-heptadeoxy-11,12-*O*-isopropylidene-2,4,6,8,10,12-hexa-*C*-methyl-D-*arabino*-D-*gluco*-L-*ido*-pentadecitol (54) and Its D-*arabino*-L-*ido*-L-*ido* Epimer 55. A mixture of **50** (61.9 mg; contaminated with impurity), $[ClRh(PPh_3)_3]$, and degassed benzene (3.1 ml) was placed in autoclave and stirred under 50 kg cm^{-2} at 24 °C for 5 d. The reaction mixture was concentrated and the residue was passed through Florisil (100—200 mesh, 2 g) with ether and again concentrated. The residue was chromatographed on silica

gel (6 g) with 100:1 toluene-acetone to afford **54** (39.9 mg, 41% from **12**) and **55** (6.5 mg, 7% from **12**) as colorless syrups.

54: R_f=0.67 (6:1 hexane-ethyl acetate); ^{1}H NMR (250 MHz) δ=0.12 and 0.13 (each 3H, each s, $SiMe_2$), 0.86 (9H, s, *t*-Bu), 0.62, 0.89, 1.02, 1.03, and 1.06 (each 3H, each d, 5×Me, J=7.0, 7.0, 7.5, 7.3, and 6.8 Hz), 1.02 (3H, t, 14-Me, J=7.5 Hz), 1.22, 1.33, 1.34, and 1.42 (each 3H, each s, 4-Me), 1.5—2.35 (8H, m), 3.19 (1H, d, J=1.5 Hz), 3.32 (1H, dd, J=7.3 and 4.0 Hz), 3.34 (1H, dd, J=7.3 and 10.0 Hz), 3.4—3.55 (3H, m), 4.11 and 4.71 (each 1H, ABq, $OC\underline{H}_2Ph$, J=12.5 Hz), 4.45 and 4.48 (each 1H, ABq, $OC\underline{H}_2Ph$, J=12.5 Hz), 4.53 (1H, d, J=0.5 Hz), 4.53 and 4.60 (each 1H, ABq, $OC\underline{H}_2Ph$, J=11.3 Hz), 4.63 and 4.71 (each 1H, ABq, $OC\underline{H}_2Ph$, J=12.5 Hz), and 7.1—7.35 (20H, m, 4×Ph).

55: R_f=0.60 (6:1 hexane-ethyl acetate); ^{1}H NMR (250 MHz) δ=0.08 (6H, s, $SiMe_2$), 0.87 (9H, s, *t*-Bu), 0.85—1.10 (15H, m, 5×Me), 1.20, 1.31, 1.39, and 1.43 (each 3H, each 5, 4×Me), 1.5—2.35 (8H, m), 3.07(1H, dd, J=11.3 and 6.0 Hz), 3.2—3.55 (7H, m), 4.35—4.75 (8H, m), and 7.15—7.35 (20H, m, 4×Ph).

1,3,5,9,11,13-Hexa-*O*-benzyl-2,4,7,8,10,14,15-heptadeoxy-2,4,6,8,10,12-hexa-*C*-methyl-D-*arabino*-D-*gluco*-L-*ido*-pentadecitol (56) and Its 11-Debenzylated Product 58. (a) To a stirred solution of **10** (1.69 g, 3.98 mmol) in dry DMF (68 ml) at 0 °C was added freshly powdered KOH (7.11 g, 127 mmol) and the mixture was stirred at 22 °C for 1 h. To this was added benzyl chloride (7.32 ml, 63.7 mmol) at 0 °C and the mixture was stirred at 22 °C for 6.5 h. Ice-water was added and the mixture was extracted with ethyl acetate and the extracts were washed with saturated aqueous NaCl, dried, and concentrated. The residue was chromatographed on silica gel (299 g) with 5:1 hexane-acetone to afford **56** (2.24 g, 58%), **58** (74 mg, 2%), and a mixture of partially benzylated products (1.12 g) as colorless syrups.

56: R_f=0.44 (5:1 hexane-acetone); $[\alpha]_D^{29}$ +7.1°, $[\alpha]_{365}^{29}$ +22.2° (*c* 0.90); ^{1}H NMR (250 MHz) δ=0.93 (3H, d, J=7.5 Hz), 0.97 (3H, t, 14-Me, J=7.5 Hz), 1.01 (3H, d, J=7.3 Hz), 1.07 (3H, d, J=7.0 Hz), 1.11 (3H, d, J=7.0 Hz), 1.17 and 1.21 (each 3H, each s, 6- and 12-Me), 1.39 (1H, dd, H-7′, $J_{7',8}$=5.0, $J_{7,7'}$=13.8 Hz), 1.57 (1H, ddq, H-14, $J_{14,15}$=$J_{13,14}$=7.5, $J_{14,14'}$=15.0 Hz), 1.76 (1H, ddq, H-14′, $J_{14',15}$=7.5, $J_{13,14'}$=3.8 Hz), 1.88 (1H, dd, H-7, $J_{7,7'}$=13.8, $J_{7,8}$=5.0 Hz), 2.0—2.3 (4H, m), 2.55 and 2.65 (each 1H, each s, 2×OH), 3.18 (1H, d, H-11, $J_{10,11}$=1.5 Hz), 3.30 (1H, dd, H-13), 3.33 (1H, dd, H-1, $J_{1,1'}$=9.3 and $J_{1,2}$=5.3 Hz), 3.43 (1H, dd, H-1′, $J_{1',2}$=9.3 Hz), 3.5—3.6 (2H, m, H-3 and 9), 4.04 (1H, d, H-5, $J_{4,5}$=0.5 Hz), 4.35—4.8 (12H, m, 6×$OC\underline{H}_2Ph$), and 7.15—7.35 (30H, m, 6×Ph).

Found: C, 78.65; H, 8.30%. Calcd for $C_{63}H_{80}O_8$: C, 78.39; H, 8.35%.

58: R_f=0.39 (5:1 hexane-acetone) $[\alpha]_D^{23}$ +15.0°, $[\alpha]_{365}^{23}$ +45.6° (*c* 1.00); ^{1}H NMR (90 MHz, characteristic peaks only), δ=2.34, 3.07, and 3.70 (each br s, each 1H, 3×OH), 4.4—4.8 (10H, m, 5×$OC\underline{H}_2Ph$), and 7.15—7.4 (25H, m, 5×Ph).

Found: C, 76.60; H, 8.39%. Calcd for $C_{56}H_{74}O_8$: C, 76.85; H, 8.52%.

(b) Treatment of a mixture of **10** (667 mg, 1.57 mmol), benzyl chloride (2.89 ml, 25.1 mmol), powdered KOH (2.82 g, 50.3 mmol), and DMF (10 ml) in a sonicator (65 W, 48 kHz) at room temperature for 3.5 h yielded **58** (436 mg, 29%), **56** (346 mg, 23%), and a mixture of partially benzylated products (844 mg).

1,3,5,9,13-Penta-*O*-benzyl-6-*O*-*t*-butyldimethylsilyl-2,4,7,8,10,14,15-heptadeoxy-11,12-*O*-isopropylidene-2,4,6,8,10,12-hexa-*C*-methyl-D-*arabino*-D-*gluco*-L-*ido*-pentadecitol (57). (a) To a stirred solution of **58** (276 mg, 0.315 mmol) and 2,2-dimethoxypropane (0.194 ml, 1.57 mmol) in dry acetone (5.51 ml) was added at 0 °C a 1 v/v% solution of concd H_2SO_4 in dry acetone (0.0276 ml). After 2.5 h at 20 °C, the mixtuere was neutralized with solid Na_2CO_3 and insoluble materials were filtered off and the filtrate was concentrated and chromatographed on silica gel (9 g) with 50:1 CH_2Cl_2-ethyl acetate to afford the acetonide (271 mg, 94%) as a clorless syrup [R_f=0.44 (5:1 hexane-ethyl acetate); $[\alpha]_D^{25}$ −6.2°, $[\alpha]_{365}^{25}$ −24.6° (*c* 100); Found: C, 77.19; H, 8.41%. Calcd for $C_{59}H_{78}O_8$: C, 77.43; H, 8.59%.]. To a stirred solution of this (247 mg, 0.270 mmol) in dry CH_2Cl_2 (0.27 ml) was added 2,6-lutidine (0.126 ml, 1.08 mmol) and cooled to 0 °C. To this was added TBDMSOTf (0.186 ml, 0.809 mmol) and the mixture was stirred at 20 °C for 2.5 h. Ice-water was added and the mixture was extracted with CH_2Cl_2. The extracts were washed with saturated aqueous NaCl, dried, and concentrated. The residue was chromatographed on silica gel (30 g) with 30:1 hexane-acetone to afford **57** (264 mg, 95%) as a colorless syrup: R_f=0.69 (4:1 hexane-ethyl acetate); $[\alpha]_D^{28}$ +10.4°, $[\alpha]_{365}^{28}$ +37.4° (*c* 1.00); ^{1}H NMR (250 MHz) δ=0.07 and 0.09 (each s, each 3H, $SiMe_2$), 0.83 (3H, d, J=6.8 Hz), 0.88 (9H, s, *t*-Bu), 0.89 (3H, t, 3×H-15, J=7.5 Hz), 0.95 (3H, d, J=6.5 Hz), 1.01 (3H, d, J=7.3 Hz), 1.03 (3H, d, J=7.5 Hz), 1.21, 1.36, and 1.46 (3H, 6H, and 3H, each s), 1.5—2.4 (8H, m), 3. 13 (1H, dd, J=6.3 and 6.3 Hz), 3.19 (1H, d, J=2.0 Hz), 3.25—3.55 (4H, m), 4.3—4.75 (11H, m, 5×$OC\underline{H}_2Ph$ and 1H), and 7.15—7.35 (25H, m, 5×Ph).

Found: C, 75.66; H, 8.86%. Calcd for $C_{65}H_{92}O_8Si$; C, 75.83; H, 9.01%.

(b) To a solution of **54** (17.2 mg, 0.0183 mmol) in dry DMF (0.86 ml) was added at 0 °C powdered KOH (2.1 mg, 0.037 mmol) and the mixture was stirred at 24 °C for 1 h. To this was added benzyl chloride (0.0042 ml, 0.037 mmol) at 0 °C and the mixture was stirred at 24 °C for 4 h. After work-up, the residue was chromatographed on silica gel (1 g) with 5:1 hexane-acetone to afford **57** (15.9 mg, 84%) as a coloress syrup. This synthetic sample of **57** was identical with naturally derived **57** by ^{1}H NMR, $[\alpha]_D$, and TLC.

Transformation of 54 to 56. **54** (23.9 mg, 0.0254 mmol) was dissolved in 1:2 (v/v) mixture of 46% aqueous HF-acetonitrile (0.72 ml) and the solution was stirred at 24 °C for 1 h. Water was added and the mixture was extracted with CH_2Cl_2. The extracts were washed with saturated aqueous NaCl, dried, and concentrated. The residue was chromatographed on silica gel (1 g) with 4:1 toluene-ethyl acetate to give a diol (18.9 mg, 95%) as a colorless syrup. 17.0 mg (0.0216 mmol) of this was dissolved in dry DMF (0.85 ml) and cooled to 0 °C. To this was added powdered KOH (9.7 mg, 0.17 mmol) and the mixture was stirred at 24 °C for 1 h. This mixture was cooled to 0 °C and benzyl chloride (0.0099 ml, 0.086 mmol) was added. The new mixture was stirred at 24 °C for 5 h. After work-up, the residue was chromatographed on silica gel (1.5 g) with 5:1 hexane-ethyl acetate to give **56** (17.9 mg, 81% from **54**) as a colorless syrup. This synthetic sample of **56** was identical with naturally derived **56** by ^{1}H NMR (250 MHz), $[\alpha]_D$, and TLC.

1,3,5,9,11,13-Hexa-*O*-benzyl-2,4,7,8,10,14,15-heptadeoxy-2,4,6,8,10,12-hexa-*C*-methyl-6,12-di-*O*-triethylsilyl-D-*arabino*-

D-*gluco*-L-*ido*-pentadecitol (**59**). To a stirred mixture of **56** (669 mg, 0.693 mmol), 2,6-lutidine (0.305 ml, 2.77 mmol), and dry CH_2Cl_2 (13.4 ml) was added at 0 °C triethylsilyl trifluoromethanesulfonate (0.426 ml, 2.08 mmol). After 1.5 h at 23 °C, ice-water was added and the mixture was extracted with CH_2Cl_2. The extracts were washed with saturated aqueous NaCl, dried, and concentrated. The residue was chromatographed on silica gel (40 g) with 30 : 1 hexane-ethyl acetate to give **59** (766 mg, 93%) as a colorless syrup: R_f=0.64 (5 : 1 hexane-acetone); $[\alpha]_D^{30}$ +19.4° (*c* 1.00); ^{1}H NMR (250 MHz) δ=0.5—0.7 (12H, m, 6×SiC$\underline{H}_2$Me), 0.82 (3H, t, 3×H-15, *J*=7.5 Hz), 0.85—1.0 (24H, m, 6×SiCH$_2\underline{Me}$, 8- and 10-Me), 1.01 (3H, d, 4-Me, *J*=7.0 Hz), 1.02 (3H, d, 2-Me, *J*=7.0 Hz), 1.31 and 1.33 (each 3H, each s, 6- and 12-Me), 1.4—1.95 (5H, m), 1.95—2.15 (1H, m, H-8), 2.15—2.4 (2H, m, H-2 and 4), 3.15—3.25 (3H, m, H-9, 11, and 13), 3.33 (1H, dd, H-1, J_{gem}=9.5, and $J_{1,2}$=7.0 Hz), 3.47 (1H, dd, H-1′, $J_{1',2}$=7.3 Hz), 3.51 (1H, dd, H-3, *J*=3.8, and 5.5 Hz), 3.78 (1H, s, H-5, $J_{4,5}$=0 Hz), 4.3—4.95 (12H, m, 6×OC$\underline{H}_2$Ph), and 7.15—7.4 (30H, m, 6×Ph).

Found: C, 75.21; H, 9.01%. Calcd for $C_{75}H_{108}O_8Si_2$: C, 75.46; H, 9.12%.

1-*O*-*t*-Butyldiphenylsilyl-2,4,7,8,10,14,15-heptadeoxy-3,5:9,11-di-*O*-isopropylidene-2,4,6,8,10,12-hexa-*C*-methyl-6,12-di-*O*-triethylsilyl-D-*arabino*-D-*gluco*-L-*ido*-pentadecitol (62). A mixture of **59** (100 mg, 0.0839 mmol), palladium black, and ethanol (2.0 ml) was stirred at 20 °C for 0.5 h under bubbling with H_2, and the suspension was filtered. The filtrate was evaporated and the residue was chromatographed on silica gel (10 g) with 3 : 1 hexane-acetone to afford **60** (50.3 mg, 92%) as colorless foam. 46.6 mg (0.0714 mmol) of this sample was dissolved in dry DMF (4.66 ml) and imidazole (19.4 mg, 0.285 mmol) was added. This mixture was cooled to 0 °C and TBDPSCl (0.0742 ml, 0.285 mmol) was added and the new mixture was stirred at 25 °C for 3 h. The reaction mixture was poured into ice-water and extracted with ethyl acetate. The extracts were washed with saturated aqueous NaCl, dried, and concentrated. The residue was chromatographed on silica gel (10 g) with 4 : 1 toluene-ethyl acetate to give **61** (52.1 mg, 82%) as a colorless syrup [R_f=0.51 (3 : 1 hexane-acetone); ^{1}H NMR (90 MHz) δ=0.5—0.8 (12H, m, 6×SiC$\underline{H}_2$Me), 0.8—1.15 (33H, m, 11×Me), 1.05 (9H, s, *t*-Bu), 1.17 (6H, s), 1.25—2.1 (8H, m), 2.75 (1H, d, OH, *J*=8.3 Hz), 3.00 (1H, d, OH, *J*=6.8 Hz), 3.13 (1H, d, OH, *J*=6.5 Hz), 3.30 and 3.60 (each 1H, each s, 2×OH), 3.25—3.9 (6H, m), 4.15 (1H, d, *J*=11.3 Hz), and 7.25—7.75 (10H, m, 2×Ph)]. 42.3 mg (0.0474 mmol) of this sample was dissolved in dry CH_2Cl_2 (0.85 ml) and 2-methoxypropene (0.025 ml, 0.24 mmol) was added. The mixture was cooled to 0 °C and PPTS (1.2 mg, 0.0047 mmol) was added and the new mixture was stirred at 25 °C for 3 h. The reaction mixture was neutralized with solid Na_2CO_3 and insoluble materials were filtered off. The filtrate was concentrated and the residue was chromatographed on silica gel (5 g) with 50 : 1 toluene-ethyl acetate to afford **62** (39.2 mg, 85%) as colorless foam: R_f=0.78 (8 : 1 hexane-ethyl acetate); $[\alpha]_D^{29}$ +31.2°, (*c* 1.00); ^{1}H NMR (250 MHz) δ=0.45—0.7 (12H, m, 6×SiC$\underline{H}_2$Me), 0.8—1.1 (33H, m, 11×Me), 1.05 (9H, s, *t*-Bu), 1.17, 1.22, 1.27, 1.28, 1.40, and 1.41 (each 3H, each s, 6×Me), 1.50—2.0 (9H, m), 3.18 (1H, dd, *J*=1.5 and 7.0 Hz), 3.47 (1H, dd, *J*=10.3 and 6.0 Hz), 3.5—3.8 (5H, m), 7.1—7.25 and 7.35—7.55 (6H and 4H, m, 2×Ph).

Found: C, 67.80; H, 9.77%. Calcd for $C_{55}H_{98}O_8Si_3$: C, 67.99; H, 10.17%.

13-*O*-Acetyl-2,4,7,8,10,14,15-heptadeoxy-3,5;9,11-di-*O*-isopropylidene-2,4,6,8,10,12-hexa-*C*-methyl-D-*arabino*-D-*gluco*-L-*ido*-pentadecitol (64). A mixture of **62** (58.3 mg, 0.0600 mmol), acetic anhydride (0.0283 ml, 0.300 mmol), 4-dimethylaminopyridine (0.7 mg, 0.006 mmol), and dry pyridine (1.17 ml) was heated at 60 °C for 20 h. Ice-water was added and the mixture was extracted with ethyl acetate and the extracts were washed with saturated aqueous NaCl, dried, and concentrated. The residue was chromatographed on silica gel (6 g) with 50 : 1 hexane-acetone to afford **63** (52.3 mg, 86%) as a colorless syrup [R_f=0.55 (20 : 1 hexane-ethyl acetate); ^{1}H NMR (90 MHz, representatives only) δ=2.08 (3H, s, OAc), 4.93 (1H, dd, H-13, *J*=2.3 and 9.0 Hz)]. 48.0 mg (0.0474 mmol) of this sample was dissolved in dry THF (0.96 ml) and to this was added 1 M TBAF in THF (0.284 ml). After 8 h at 60 °C, ice-water was added and the mixture was extracted with ethyl acetate. The extracts were washed with saturated aqueous NaCl, dried, and concentrated. The residue was chromatographed on silica gel (5 g) with 2 : 1 hexane-ethyl acetate to afford **64** (21.0 mg, 81%) as colorless foam: R_f=0.07 (4 : 1 hexane-ethyl acetate); $[\alpha]_D^{30}$ +29.8°, (*c* 1.00); IR ($CHCl_3$) 1729 cm^{-1}; ^{1}H NMR (250 MHz) δ=0.91 (3H, 14-Me, *J*=7.5 Hz), 0.97 (3H, d, *J*=7.0 Hz), 1.03 (3H, d, *J*=7.0 Hz), 1.04 (3H, d, *J*=7.0 Hz), 1.07 (3H, d, *J*=7.0 Hz), 1.16, 1.17, 1.26, 1.35, 1.41, and 1.42 (each 3H, each s, 6×Me), 1.4—1.65 (1H, m, H-14), 1.6—1.95 (8H, m), 2.09 (3H, s, OAc), 2.31 and 2.40 (each 1H, each br s, 2×OH), 3.31 (1H, dd, *J*=2.5 and 6.5 Hz), 3.5—3.65 (5H, m), 4.90 (1H, dd, H-13, *J*=3.3 and 9.0 Hz).

Found: C, 63.34; H, 9.56%. Calcd for $C_{29}H_{54}O_9$: C, 63.71; H, 9.95%.

3,5:9,11-Di-*O*-isopropylidene-(9*S*)-9-deoxo-9-hydroxy-erythronolide A (66). To a stirred suspension of PDC (188 mg, 0.499 mmol) and MS 3AP (125 mg) in dry CH_2Cl_2 (0.55 ml) was added at 0 °C a solution of **64** (68.2 mg, 0.125 mmol) in dry CH_2Cl_2 (0.27 ml). After 4 h at 22 °C, the reaction mixture was diluted with diethyl ether (0.5 ml) and the suspension was transferred to a column filled with silica gel (1 g). The column was eluted with diethyl ether and the eluant was concentrated. The residue was chromatographed on silica gel (2 g) with 60 : 20 : 1 hexane-ethyl acetate-acetic acid to afford **65** (59.2 mg, 85%) as a colorless syrup [R_f=0.48 (50 : 50 : 1 hexane-ethyl acetate-acetic acid); ^{1}H NMR (90 MHz, representitatives only) δ=2.07 (3H, s, OAc), 2.60 (1H, m), 3.28 (1H, dd, *J*=2.4 and 6.0 Hz), 3.52 (1H, d, *J*=1.5 Hz), 3.63 (1H, d, *J*=3.8 Hz), 3.83 (1H, dd, *J*=2.3 and 9.8 Hz), and 4.90 (1H, dd, H-13, *J*=3.8 and 9.0 Hz)]. This was dissolved in 1,4-dioxane (0. 13 ml) and 1 M aqueous NaOH (0.126 ml) was added. After 2 h at 23 °C, the reaction mixture was neutralised with CG 50 and filtered. The filtrate was concentrated and the residue was chromatographed on silica gel (2 g) with 2 : 1 hexane-acetone to afford **4** (52.4 mg, 96%) as a colorless syrup [R_f=0.23 (30 : 10 : 1 hexane-acetone-acetic acid)]. This was dissolved in dry THF (1.04 ml) and triphenylphosphine (39.4 mg, 0.150 mmol) and di-(2-pyridyl) disulfide (33.1 mg, 0.150 mmol) were added and stirred at 22 °C for 8 h. After concentration, the residue was chromatographed on silica gel (6.5 g) with 1 : 1 hexane-ethyl acetate to afford pyridyl ester of **4** (58.3 mg, 95%) as a colorless syrup, which was dissolved in dry toluene (5.83 ml) and this solution was slowly added to a refluxing dry toluene (41.2 ml) with

syringe pump during a period of 10 h under argon. After further 14 h standing at 110 °C, the mixture was concentrated and the residue was chromatographed on silica gel (3 g) with 5 : 1 hexane-acetone to afford **66** (31.0 mg, 65%) as a clorless foam: R_f=0.61 (3 : 1 hexane-acetone); $[\alpha]_D^{33}$ +12.1°, $[\alpha]_{365}^{33}$ +40.0° (*c* 0.66); IR ($CHCl_3$) 1720 cm^{-1}; ^1H NMR (250 MHz) δ=0.84 (3H, t, 14-Me, *J*=7.5 Hz), 1.01 (3H, d, 4-Me, *J*=6.8 Hz), 1.14 and 1.23 (each 3H, each s, 6- and 12-Me), 1.18 (3H, d, 2-Me), 1.24 (3H, d, 10-Me), 1.28 (3H, d, 8-Me, *J*=6.0 Hz), 1.46, 1.48, and 1.49 (3H, 6H, and 3H, each s, 2×CMe_2), 1.5—1.65 (3H, m, H-4, 7′, and 14′), 1.82 (1H, dq, H-10, *J*=7.3, $J_{9,10}$=0, and $J_{10,11}$=1.8 Hz), 1.94 (1H, ddq, H-14, *J*=7.5, $J_{14,14'}$=14.8, and $J_{13,14}$=2.5 Hz), 2.05—2.25 (3H, m, H-7, 8, and OH), 2.75 (1H, dq, H-2, $J_{2,3}$=10.8, and $J_{2,Me}$=6.5 Hz), 2.96 (1H, s, OH), 3.12 (1H, d, H-9, $J_{8,9}$=11.0 Hz), 3.60 (1H, d, H-11), 3.78 (1H, dd, H-3, $J_{3,4}$=1.0 Hz), 3.97 (1H, d, H-5, $J_{4,5}$=1.5 Hz), and 5.06 (1H, dd, H-3, $J_{13,14'}$=11.3 Hz).

Found: *m/z*, 485.3110. Calcd for $C_{26}H_{45}O_8$: M^+−Me, 485.3111.

(9*S*)-9-Deoxo-9-hydroxyerythronolide A (2). A mixture of **66** (69.4 mg, 0.139 mmol) and 50% aqueous acetic acid (1.39 ml) was stirred at 24 °C for 4 h. After concentration, the residual sample of **2** (58.3 mg, 100%) was recrystallised from acetone-hexane to afford a pure sample of **2**. This sample was identical in all respects [mp, TLC, ^1H NMR (250 MHz), and $[\alpha]_D$], with a sample of **2** prepared by the literature procedure.[20]

Data of 2: R_f=0.15 (3 : 1 hexane-ethyl acetate); mp 203—206 °C (acetone-hexane) [lit,[20a] 185—187 °C, lit,[20b] 199—200°C, mp of **2** prepared by the method of lit,:[20b]: 202—205 °C (acetone-hexane)]; $[\alpha]_D^{27}$ +9.5°, $[\alpha]_{365}^{27}$ +24.7° (*c* 2.00, MeOH) lit,[20a] $[\alpha]_D^{27}$ +9.5° (*c* 2.00, MeOH), lit,[20b] $[\alpha]_D^{25}$ +9.5° (*c* 2.00, MeOH), $[\alpha]_D$ of **2** prepared by the method of lit,:[20b] $[\alpha]_D^{30}$ +9.5°, $[\alpha]_{365}^{30}$ +24.1° (*c* 200, MeOH)]; ^1H NMR (250 MHz) δ=0.90 (3H, t, 3×H-15, *J*=7.3 Hz), 1.04 (3H, d, 4-Me, *J*=7.5 Hz), 1.05 (3H, s), 1.24 (3H, s), 1.24 (3H, d, 10-Me, *J*=7.3 Hz), 1.29 (6H, d, 2- and 8-Me, *J*=7.0 Hz) 1.2—1.35 (1H, m, H-7), 1.42 (1H, dd, H-7′, $J_{7,7'}$=15.0 and $J_{7',8}$=2.5 Hz), 1.45—1.65 (3H, m, H-4, 8, and 14), 1.95 (1H, ddq, H-14′, $J_{13,14'}$=2.3, $J_{14,14'}$=14.5 and $J_{14',Me}$=7.3 Hz), 2.0—2.1 (1H, m, H-10), 2.07 (1H, br s, OH), 2.63 (1H, br s, OH), 2.79 (1H, dq, H-2, $J_{2,3}$=10.3 and $J_{2,Me}$=7.0 Hz), 2.97 (1H, ddd, H-9, *J*=2.3, 9.0, and $J_{9,OH}$=9.0 Hz), 3.13 (1H, br s, OH), 3.48 (1H, dd, H-11, $J_{10,11}$=1.0 and $J_{11,OH}$=4.3 Hz), 3.57 (1H, d, 9-OH, *J*=9.0 Hz), 3.63 (1H, br s, OH), 3.85 (1H, d, H-3, $J_{2,3}$=10.3 and $J_{3,4}$=0 Hz), 3.95 (1H, br s, H-5, $J_{4,5}$=0 Hz), 4.30 (1H, d, 11-OH, *J*=4.3 Hz), and 4.64 (1H, dd, H-13).

Found: C, 59.73; H, 9.30%. Calcd for $C_{21}H_{40}O_8$: C, 59.98; H, 9.59%.

Erythronolide A (1). To a stirred mixture of **2** (37.6 mg, 0.0894 mmol), benzaldehyde dimethyl acetal (0.067 ml, 0.45 mmol), and dry CH_2Cl_2 (1.88 ml) was added at 0 °C CSA (2.1 mg, 0.0089 mmol). After 24 h at 0 °C, solid Na_2CO_3 was added and the insoluble materials were filtered off. The filtrate was concentrated and the residue was chromatographed on silica gel (9 g) with 3 : 2 hexane-ethyl acetate to afford **67** (36.5 mg, 80%) as colorless needles [R_f=0.68 (2 : 1 hexane-acetone); $[\alpha]_D^{26}$ +5.4°, $[\alpha]_{365}^{26}$ +11.2° (*c* 1.00); mp 128—130 °C (acetone-hexane); IR ($CHCl_3$) 1728 cm^{-1}; ^1H NMR (250 MHz) δ=0.87 (3H, t, 14-Me, *J*=7.5 Hz), 1.13 and 1.31 (each 3H, each s, 6- and 12-Me), 1.15 (3H, d, 4-Me, *J*=7.0 Hz), 1.24 (3H, d, 10-Me, *J*=7.3 Hz), 1.27 (3H, d, 2-Me, *J*=7.7 Hz), 1.32 (3H, d, 8-Me, *J*=7.5 Hz), 1.4—2.1 (7H, m), 2.41 (1H, br, 12-OH), 2.81 (1H, d, 9-OH, *J*=4.5 Hz), 2.91 (1H, dq, H-2, $J_{2,3}$=10.8 Hz), 3.1—3.2 (1H, m, H-9) , 3.14 (1H, s, 6-OH), 3.73 (1H, br s, H-11, $J_{10,11}$<1.0 Hz), 3.79 (1H, dd, H-3, $J_{3,4}$=1.0 Hz), 3.96 (1H, d, H-5, $J_{4,5}$=1.0 Hz), 4.26 (1H, d, 11-OH, *J*=1.6 Hz), 5.13 (1H, dd, H-13, $J_{13,14}$=2.3 and $J_{13,14}$=11.0 Hz), 5.65 (1H, s, $OC\underline{H}_2Ph$), 7.35—7.45 and 7.45—7.55 (3H and 2H, each m, Ph)]. A solution of this sample **67** (19.5 mg, 0.0383 mmol) in dry CH_2Cl_2 (0.078 ml) was added to a stirred suspension of PCC (132 mg, 0.613 mmol), MS 3AP (153 mg), and dry CH_2Cl_2 (0.38 ml) at 0 °C. After 0.5 h at 0 °C, the reaction mixture was diluted with diethyl ether (0.5 ml) and the suspension was transferred to a column filled with silica gel (1 g). The column was eluted with diethyl ether and the eluant was concentrated. The residue was chromatogaphed on silica gel (1 g) with 1 : 1 hexane-ethyl acetate to afford **68** (15.6 mg, 80%) as a colorless syrup [R_f=0.60 (2 : 1 toluene-acetone); $[\alpha]_D^{22}$ −36.6°, (*c* 1.00, MeOH); IR ($CHCl_3$) 1705 cm^{-1}; ^1H NMR (250 MHz) δ=0.90 (3H, t, 3×H-15, *J*=7.5 Hz), 1.10 (3H, s), 1.18 (3H, d, 4-Me, *J*=7.5 Hz) , 1.21 (3H, d, 10-Me, *J*=7.5 Hz), 1.25 (3H, s), 1.28 (3H d, 2-Me, *J*=6.5 Hz), 1.34 (3H, d, 8-Me, *J*=6.0 Hz), 1.59 (1H, ddq, H-14, $J_{13,14}$=10.3 and $J_{14,14'}$=14.8 Hz), 1.71 (2H, d, 2×H-7, $J_{7,8}$=7.3 Hz), 1.78 (1H, ddq, H-4, $J_{3,4}$=1.0 and $J_{4,5}$=1.3 Hz), 1.97 (1H, ddq, H-14′, $J_{13,14'}$=2.0 Hz), 2.31 (1H, br, OH), 2.60 (1H, br s, OH), 2.85—3.1 (3H, m), 3.29 (1H, d, 11-OH, *J*=5.0 Hz), 3.76 (1H, dd, H-11, *J*=5.0 and 5.0 Hz), 3.83 (1 H, dd, H-3, $J_{2,3}$=10.3 Hz), 4.01 (1H, d, H-5), 4.88 (1H, dd, H-13, *J*=2.0 and 10.3 Hz), 5.68 (1H, s, $OC\underline{H}_2Ph$), 7.3—7.45 and 7.45—7.55 (3H and 2H, m, Ph)]. A mixture of this sample **68** (23.5 mg, 0.0464 mmol), palladium black, and MeOH (0.71 ml) was stirred at 25 °C for 0.5 h under bubbling with H_2, and the suspension was filtered. The filtrate was concentrated and the residue was chromatographed on silica gel (1 g) with 2 : 1 toluene-acetone to afford **1** (15.9 mg, 82%) as colorless needles. The synthetic sample of **1** proved to be identical with the naturally derived erythronolide A[22] by spectroscopic means and mixed mp measurement: R_f=0.23 (2 : 1 hexane-acetone); mp 170—172 °C (acetone-hexane) [lit,[22] mp 172—173 °C, lit,[4] 168—172 °C, mp of **1** prepared by the method of lit,[22] 170—172 °C]; mix. mp 170—172 °C; $[\alpha]_D^{28}$ −36.7° (*c* 0.90, MeOH) [lit,[4] $[\alpha]_D^{25}$ −37° (*c* 0.90, MeOH) $[\alpha]_D$ of **1** prepared by the method of lit,:[22] −37.3° (*c* 0.90, MeOH)]; IR ($CHCl_3$) 1743 cm^{-1}; ^1H NMR (250 MHz) δ=0.85 (3H, t, 3×H-15, *J*=7.5 Hz), 1.01 (3H, d, 4-Me, *J*=7.3 Hz), 1.16 (3H, d, 10-Me, *J*=7.3 Hz), 1.17 (3H, s), 1.19 (3H, d, *J*=6.5 Hz), 1.24 (3H, d, *J*=6.5 Hz), 1.36 (3H, s), 1.4—1.6 (2H, m), 1.8—2.05 (3H, m), 2.48 (1H, s, OH), 2.6—2.8 (2H, m), 2.84 (1H, d, OH, *J*=3.8 Hz), 3.07 (1H, br q, H-10, $J_{10,11}$=0 Hz), 3.13 (2H, br s, 2×OH), 3.55—3.7 (2H, m), 3.81 (1H, br s, H-11, $J_{11,OH}$=0 Hz), 3.93 (1H, d, OH, *J*=2.5 Hz), and 5.04 (1H, dd, H-13, $J_{13,14}$=2.3 and $J_{13,14'}$=10.8 Hz). After addition of D_2O, the signals of H-5, H-3, and H-11 changed to 3.56 (d, $J_{4,5}$=2.5 Hz), 3.62 (d, $J_{3,4}$=0 and $J_{2,3}$=10.5 Hz), and 3.81 (d, $J_{10,11}$=1.0 Hz), respectively.

Found: C, 60.20; H, 8.86%. Calcd for $C_{21}H_{38}O_8$: C, 60.27; H, 9.15%.

We are gratefull to Prof. Sumio Umezawa, Institute of Bioorganic Chemistry, and the late Prof. Hamao Umezawa, Institute of Microbial Chemistry for their generous support of our program. Financial support by the Ministry of Education, Science, and Culture (Grant-in-Aid for Special Research) and by the Japan

Antibiotics Research Association Research Grant are deeply acknowledged. We are also indebted to Mr. Saburo Nakada, Keio University, for elemental analyses, Miss Yoshiko Koyama, Institute of Bioorganic Chemistry, for 250 MHz ^{1}H NMR spectral analyses, and Mr. Koichi Inoshita for his technical assistance.

References

1) "Synthetic Studies of Erythromycins. IV." For Part II and III, see Ref. 6.

2) S. Masamune, G. S. Bates, and J. W. Corcoran, *Angew. Chem., Int. Ed. Engl.*, **16**, 585 (1977); K. C. Nicolaou, *Tetrahedron*, **33**, 683 (1977); T. G. Back, *ibid.*, **33**, 3041 (1977); I. Paterson and M. Mansuri, *ibid.*, **41**, 3569 (1985).

3) R. B. Woodward, E. Logusch, K. P. Nambiar, K. Sakan, D. E. Ward, B.-W. Au-Yeung, P. Balaram, L. J. Browne, P. J. Card, C. H. Chen, R. B. Chenevert, A. Fliri, K. Frobel, H.-J. Gais, D. G. Garratt, K. Hayakawa, W. Heggie, D. P. Hesson, D. Hoppe, I. Hoppe, J. A. Hyatt, D. Ikeda, P. A. Jacobi, K. S. Kim, Y. Kobuke, K. Kojima, K. Krowicki, V. J. Lee, T. Leutert, S. Malchenko, J. Martens, R. S. Matthews, B. S. Ong, J. B. Press, T. V. RajanBabu, G. Rousseau, H. M. Stauter, M. Suzuki, K. Tatsuta, L. M. Tolbert, E. A. Truesdale, I. Uchida, Y. Ueda, T. Uyehara. A. T. Vasella, W. C. Vladuchick, P. A. Wade., R. M. Williams, and H. N.-C. Wong, *J. Am. Chem. Soc.*, **103**, 3210, 3213, 3215 (1981).

4) E. J. Corey. P. B. Hopkins, S. Kim, S. Yoo, K. P. Nambiar, and J. R. Falck, *J. Am. Chem. Soc.*, **101**, 7131 (1979).

5) B. Bernet, P. M. Bishop, M. Caron, T. Kawamata, B. L. Roy, L. Ruest, G. Sauve, P. Soucy, and P. Deslongchamps, *Can. J. Chem.*, **63**, 2810, 2814, 2818 (1985); G. Stork and S. D. Rychnovsky, *J. Am. Chem. Soc.*, **109**, 1565 (1987); H. Tone, T. Nishi, Y. Oikawa, M. Hikota, and O. Yonemitsu, *Tetrahedron Lett.*, **28**, 4569 (1987); T. Nakata, M. Fukui, and T. Oishi, *ibid.*, **29**, 2219, 2223 (1988).

6) Preliminary accounts of this work have already appeared: M. Kinoshita, M. Arai, K. Tomooka, and M. Nakata, *Tetrahedron Lett.*, **27**, 1811 (1986); M. Kinoshita, M. Arai, N. Ohsawa, and M. Nakata, *ibid.*, **27**, 1815 (1986).

7) E. J. Corey and K. C. Nicolaou, *J. Am. Chem. Soc.*, **96**, 5614 (1974).

8) M. Nakata, K. Toshima, T. Kai, and M. Kinoshita, *Bull. Chem. Soc. Jpn.*, **58**, 3457 (1985).

9) W. C. Still and J. H. McDonald, III, *Tetrahedron Lett.*, **21**, 1031 (1980); D. J. Cram and K. R. Kopecky, *J. Am. Chem. Soc.*, **81**, 2748 (1959).

10) M. Kinoshita, N. Ohsawa, and S. Gomi, *Carbohydr. Res.*, **109**, 5 (1982).

11) P. A. Leven and R. S. Tipson, *J. Biol. Chem.*, **115**, 731 (1936); N. A. Hughes and P. R. H. Speakman, *Carbohydr. Res.*, **1**, 171 (1965); J. Gelas and D. Horton, *ibid.*, **45**, 181 (1975); M. Kiso and A. Hasegawa, *ibid.*, **52**, 95 (1976).

12) K. Steiner, U. Graf, and E. Hardegger, *Helv. Chim. Acta*, **54**, 845 (1971).

13) M. Kinoshita, H. Hamazaki, and M. Awamura, *Bull. Chem. Soc. Jpn.*, **51**, 3595 (1978).

14) D. G. Manwaring, R. W. Rikards, and R. M. Smith, *Tetrahedron Lett.*, **1970**, 1029.

15) D. H. R. Barton, G. Bashiardes, and J.-L. Fourrey, *Tetrahedron Lett.*, **24**, 1605 (1983); D. H. R. Barton, G. Bashiardes, and J.-L. Fourrey, *Tetrahedron*, **44**, 147 (1988).

16) A. I. Meyers, K. A. Babiak, A. L. Campbell, D. L. Comins, M. P. Fleming, R. Henning, M. Heuschmann, J. P. Hudspeth, J. M. Kane, P. J. Reider, D. M. Roland, K. Shimizu, K. Tomioka, and R. D. Walkup, *J. Am. Chem. Soc.*, **105**, 5015 (1983).

17) H. Loibner and E. Zbiral, *Helv. Chim. Acta*, **59**, 2100 (1976).

18) D. A. Evans and M. M. Morrissey, *J. Am. Chem. Soc.*, **6**, 3866 (1984) and references cited therein.

19) We wish to thank the Pfizer Taito Co., Ltd. (Japan) for the kind supply of natural erythromycin A.

20) a) M. V. Sigal, Jr., P. F. Wiley, K. Gerzon, E. H. Flynn, U. C. Quarck, and O. Weaver, *J. Am. Chem. Soc.*, **78**, 388 (1956); P. H. Jones and E. K. Rowley, *J. Org. Chem.*, **33**, 665 (1968).

21) E. J. Corey and L. S. Melvin, Jr., *Tetrahedron Lett.*, **1975**, 929.

22) R. A. LeMahieu, M. Carson, and R. W. Kierstead, *J. Med. Chem.*, **17**, 953 (1974).

Preparation of Perfluoroalkyl Ketones by the Reaction of Perfluoroalkyllithiums with Esters

Hidemitsu UNO,* Yasukazu SHIRAISHI, and Hitomi SUZUKI*,†
Advanced Instrumentation Center for Chemical Analysis, Department of Chemistry, Faculty of Science, Ehime University, Bunkyo-cho 2-5, Matuyama 790
(Received April 27, 1989)

A variety of esters react with perfluoroalkyllithiums in situ generated from perfluoroalkyl iodides and methyllithium to give perfluoroalkyl ketones in good yields. Perfluoroalkyllithiums add to α, β-unsaturated esters only in the 1,2-addition mode even in the presence of copper salt. Exception was observed in the reaction with maleates where perfluoroalkylated succinic esters and normal 1,2-addition products are obtained in comparable amounts.

In recent years increasing attention has been paid to perfluoroalkyl-containing substances because of their unique properties which are not observed for fluorine-free partners. Straight chain perfluoroalkylalkanes are reported to form two different kinds of micelles depending on solvents[1] and to crystallize as a smetic liquid crystal.[2] Methodology for the introduction of the perfluoroalkyl group into a molecule[3] is, however, as yet far from maturity which makes a target compound often difficult to access. One of the important problems involved therein is thermal instability of perfluoroalkyl Grignard and lithium reagents which easily suffer β-elimination.[4] Thus, most efforts have been placed on the activation of thermally more stable reagents such as perfluoroalkylzinc[5] and -copper.[6] Unfortunately, these reagents, can not be successfully used for the perfluoroalkylation of unactivated esters due to their low nucleophilicity. Gassman and his co-worker have reported that pentafluoroethyllithium was conveniently generated from a metal halogen exchange reaction of pentafluoroethyl iodide with methyllithium at −78 °C and it reacted smoothly with aldehydes and ketones to give alcohols.[7] Gassman and our group have recently shown that this methodology can be extended to the preparation of perfluoroalkyl ketones from non-activated

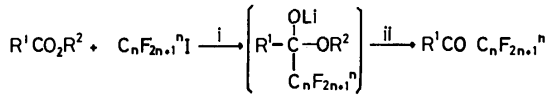

Scheme 1. Reagents and conditions: i, MeLi-LiBr, ether, −78 °C, 1 h. ii, H^+.

Table 1. Perfluoroalkylation of Esters

Entry	Ester **1**	Perfluoroalkyl iodide **2**	Product	Yield/%[a]
1	$PhCO_2CH_3$ (**1a**)	$C_8F_{17}{}^nI$ (**2a**)	$PhCOC_8F_{17}{}^n$ (**3**)	86
2	(*E*)-$PhCH{=}CHCO_2CH_3$ (**1b**)	**2a**	(*E*)-$PhCH{=}CHCOC_8F_{17}{}^n$ (**4a**)	93
3	**1b**	$C_6F_{13}{}^nI$ (**2b**)	(*E*)-$PhCH{=}CHCOC_6F_{13}{}^n$ (**4b**)	83
4	**1b**	$C_4F_9{}^nI$ (**2c**)	(*E*)-$PhCH{=}CHCOC_4F_9{}^n$ (**4c**)	85
5	**1b**	$C_3F_7{}^iI$ (**2d**)	—	—
6	**1b**	**2a**	$PhCH(CH_3)CH_2COC_8F_{17}{}^n$ (**5a**)[b]	75
7	**1b**	**2b**	$PhCH(CH_3)CH_2COC_6F_{13}{}^n$ (**5b**)[b]	52
8	**1b**	**2c**	$PhCH(CH_3)CH_2COC_4F_9{}^n$ (**5c**)[b]	37
9	(*E*)-$PhCH{=}CHCO_2C_2H_5$ (**1c**)	**2a**	**4a**	83
10	$PhC{\equiv}CCO_2CH_3$ (**1d**)	**2a**	$PhC{\equiv}CCOC_8F_{17}{}^n$ (**6**)	95
11	$PhCH_2CH_2CO_2CH_3$ (**1e**)	**2a**	$PhCH_2CH_2COC_8F_{17}{}^n$ (**7**)	86
12	$(CH_3)_2CHCO_2CH_3$ (**1f**)	**2a**	$(CH_3)_2CHCOC_8F_{17}{}^n$ (**8**)	72
13	$(CH_3)_3CCO_2CH_3$ (**1g**)	**2a**	$(CH_3)_3CCOC_8F_{17}{}^n$ (**9**)	60
14	$BrCH_2CO_2CH_3$ (**1h**)	**2a**	$BrCH_2COC_8F_{17}{}^n$ (**10**)	86
15	(*E*)-$CH_3CH{=}CHCO_2CH_3$ (**1i**)	**2a**	(*E*)-$CH_3CH{=}CHCOC_8F_{17}{}^n$ (**11**)	58
16	(*E*)-$CH_3CH{=}C(CH_3)CO_2CH_3$ (**1j**)	**2a**	(*E*)-$CH_3CH{=}C(CH_3)COC_8F_{17}{}^n$ (**12**)	74
17	$CH_2CH_2CH_2C{=}O$ (**1k**)	**2a**	$CH_2CH_2CH_2C(OH)C_8F_{17}{}^n$ (**13**)	99
18	$CH_2{=}CHCO_2CH_3$ (**1l**)	**2a**	$PhSCH_2CH_2COC_8F_{17}{}^n$ (**14**)[c]	58
19	$CH_2{=}C(CH_3)CO_2CH_3$ (**1m**)	**2a**	$PhSCH_2CH(CH_3)COC_8F_{17}{}^n$ (**15**)[c]	80

a) Isolated yield. b) The reaction was carried out by using 2 equiv of methyllithium-lithium bromide in the presence of MeCu (1 equiv). c) Thiophenol was added to the reaction mixture and the mixture was stirred for 1 h at the room temperature before quenching with aqueous NH_4Cl.

† Present address: Department of Chemistry, Faculty of Science, Kyoto University, Kyoto 606.

esters (Scheme 1).[8-10] During the course of examining the scope of preparative utility of perfluoroalkyllithiums, we have also found the reaction with maleic esters affords perfluoroalkylsuccinates, which may be considered as a potential building block for synthesis of perfluoroalkyl-bearing cyclic compounds. In this paper, we report the full results of our study on the reaction of perfluoroalkyllithiums with various esters.

Results and Discussion

In situ generation of perfluoroalkyllithiums (1.1 equiv) by the reaction of perfluoroalkyl iodides with methyllithium in the presence of esters at −78 °C led to the formation of perfluoroalkyl ketones in good yields (Table 1). Addition of perfluoroalkyllithiums occurred only at the ester carbonyl group in the reactions with α,β-unsaturated esters and an α-bromo ester. It is noteworthy that methyl acrylate (**1l**) and methacrylate (**1m**) were also subject to 1,2-addition of the perfluoroalkyllithium reagent to give vinyl ketones (or hemiacetals) which could be easily isolated as the thiophenol-trapped compounds **14** and **15**, respectively. In the presence of methylcopper (1 equiv) and excess amounts of methyllithium (2 equiv), methyl cinnamate (**1b**) first underwent 1,2-addition of perfluoroalkyllithiums to form unsaturated ketones **4a—4c**, which then suffer 1,4-addition of methyllithium to afford saturated ketones **5a—5c**. In neither case bis-perfluoroalkylated compounds could be isolated in detectable amounts, which forms a marked contrast to the results obtained by Gassman and his co-worker.[10] This discrepancy may be rationalized by taking into account of the difference in amount and concentration of the lithium reagent employed. In order to obtain a perfluoroalkyl ketone, the use of a slightly excess of perfluoroalkyllithium is essential. When a large excess of perfluoroalkyllithium is used, the heat evolved during the generation of the lithium reagent will destroy the hemiacetal intermediate derived from the reagent and the ester. From this point of view, lower concentration of the reagent appears to be desirable, but it is not crucial as far as the reagents are satisfactorily soluble at low temperatures employed. We carried out the reaction by using 1.1 equiv of perfluorooctyl iodide (**2a**) to esters at 0.1 mol dm^{-3} concentration so as to keep them good soluble in ether at −78 °C. Under these conditions, the amount of methyllithium should be only in a slightly excess to the ester in order to prevent further reactions with perfluoroalkyllithium or methyllithium.

To get further insight into the reactivity of the reagents and regioselectivity of perfluoroalkylation, we conducted the reaction of perfluorooctyllithium with α,β-unsaturated diesters and the results are summarized in Table 2. Under the conditions employed (1.1 molar ratio of perfluorooctyllithium to esters), neither two perfluoroalkyl groups nor a pair of perfluoroalkyl and methyl groups could be introduced into molecules. The reaction with diethyl acetylenedicarboxylate (**1n**) gave the α-amino α,β-unsaturated ester **16**, which was presumably derived from 1,2-addition of perfluorooctyllithium followed by conjugate addition of ammonia generated upon quenching from aqueous ammonium chloride. When the reaction with **1n** was quenched with dilute hydrochloric acid, an intractable mixture was obtained. Perfluoroalkylation of diethyl azodicarboxylate (**1o**) occurred at the nitrogen atom to give *N*-perfluorooctyl-*N,N'*-hydrazinedicarboxylate **17** in 65% yield. From the reaction mixture diethyl *N*-methylhydrazine-*N,N'*-dicarboxylate (**18**) was also isolated in 18% yield. It is interesting to note that the reaction with the fumarate **1p** gave the trans γ-keto ester **19a** as a single product in 61% yield, while a similar reaction with the maleate **1q** produced the perfluorooctylsuccinate **20a** and an isomeric mixture of **19a** (*E*/*Z*=ca. 10/1) in comparable yields. Such Michael-type addition of a perfluoroalkylmetallic reagent is very rare.[11] In order to find

Table 2. Perfluorooctylation of α,β-Unsaturated Diesters

Entry	Ester	Products (Yield/%)[a]
20	$MeO_2CC{\equiv}CCO_2Me$ **1n**	$MeO_2CC(NH_2)=CHCORf$ **16** (71)
21	$EtO_2CN=NCO_2Et$ **1o**	$EtO_2CN(Rf)NHCO_2Et$ **17** (65) + $EtO_2CN(Me)NHCO_2Et$ **18** (18)
22	(*E*)-$Bu^nO_2CCH=CHCO_2Bu^n$ **1p**	(*E*)-$Bu^nO_2CCH=CHCORf$ (*E*)-**19a** (61)
23	(*Z*)-$Bu^nO_2CCH=CHCO_2Bu^n$ **1q**	**19a**[b] (46) + $Bu^nO_2CC(Rf)HCH_2CO_2Bu^n$ **20a** (21)
24	(*E*)-$MeO_2CCH=CHCO_2Me$ **1r**	(*E*)-$MeO_2CCH=CHCORf$ (*E*)-**21** (63)

a) Rf denotes $C_8F_{17}{}^n$. The yields refer to isolated ones. b) *E*/*Z*=ca. 10/1 (determined by NMR).

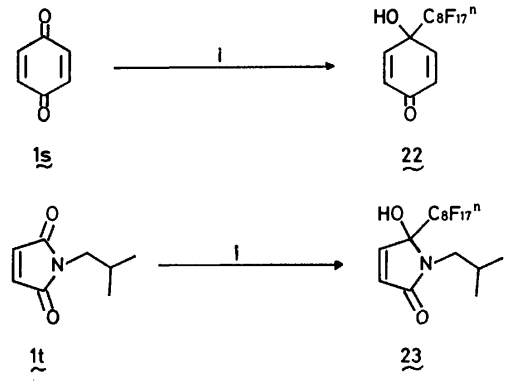

Scheme 2. Reagents and conditions: i, $C_8F_{17}{}^nI$, MeLi-LiBr, ether, −78 °C, 1 h.

additional examples, substrates with a cis-enedione structure similar to maleate were subjected to this perfluoroalkylation. The reactions of 1,4-benzoquinone (**1s**) and *N*-isobutylmaleimide (**1t**), however, resulted only in the expected formation of the quinol **22** and the lactam **23**, respectively (Scheme 2).

Since the formation of perfluoroalkylsuccinates appeared us to be quite interesting both from mechanistic and synthetic points of view, we examined the product selectivity for the reaction of dibutyl maleate under various conditions (Scheme 3 and Table 3). The important point is whether the perfluoroalkylsuccinate **20** will be formed by reactions with reagents other than perfluoroalkyllithium. Participation of perfluoroalkyl radical species could be ruled out because neither the formation of a radical addition product nor a marked change in the relative ratio of **19** and **20** was observed in the presence or absence of norbornene and styrene (Entries 30 and 31).[12] As the hypervalent iodine species such as Rf_2I^- were suggested to increase the stability of perfluoroalkyl anions,[13] we next examined whether such species play a role in determining the product distribution. The generation of perfluorobutyllithium from the metal-exchange reaction of the perfluorobutyl stannane **27** with methyllithium, in the presence of the maleate **1q**, led to the formation of both succinate **20c** and γ-keto ester **19c** in a ratio similar to that obtained from the reaction of the corresponding perfluoroalkyl iodide (Entry 32). In the reaction of **1q** using an excess of perfluorooctyl iodide (Entry 25), the ratio was also similar. Thus we may hold at present that the hypervalent perfluoroalkyl iodine species, even if they might exist, exsert little influence upon the partition between conjugate and 1,2-mode additions to maleates.

Perfluoroalkylation of the maleate **1q** in the presence of BF_3 is worthy to note (Entry 29). Proton and ^{13}C NMR analyses of the reaction mixture revealed the presence of three major products: **19b** (*Z*/*E*=>20/1), the succinate **20b**, and the hemiacetal[14] **24** (**19b** : **20b** : **24**=7 : 10 : 23). The hemiacetal structure of

Table 3. Perfluoroalkylation of Dibutyl Maleate (**1q**)

Entry	RfX	Additive (equiv)	Yield/%[a]	
			19	**20**
25	**2a**[b]	—	36	28
26	**2b**	—	63 (1.8 : 1)[c]	
27[d]	**2b**	—	39 (1.7 : 1)[c]	
28	**2c**	—	52 (1.7 : 1)[c]	
29	**2b**	$BF_3 \cdot OEt_2$ (1)	91 (3.0 : 1)[c]	
30	**2b**	Norbornene (1)	55 (1.8 : 1)[c]	
31	**2a**	Styrene (1)	76 (2.0 : 1)[c]	
32	$C_4F_9{}^nSnBu^n{}_3$ **27**	—	64 (2.1 : 1)[c]	

a) Isolated yield. b) Five equiv. to **1q**. c) Separation of **19** and **20** was not attempted. Numerals in parentheses refer to the ratios of 1,2- and 1,4-addition products in the crude reaction mixture estimated by NMR. d) Reaction temperature was −100 °C.

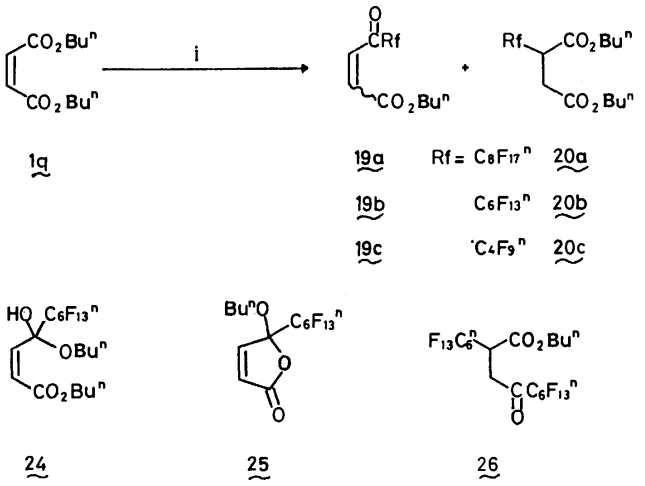

Scheme 3. Reagents and conditions: i, RfX, MeLi-LiBr, ether, −78 °C, 1 h.

24 was supported by the following observations: The NMR signals of **24** gradually disappeared as time passed. The signals of **19b** and 1-butanol became relatively stronger as compared with those of the succinate **20b** and new signals due to the lactone **25** appeared. After 3 days the reaction mixture was subjected to chromatographic separation to yield a mixture of **19b** (*Z*/*E*=6/5), **20b**, **25** (91%, **19b** : **20b** : **25**= 56 : 24 : 5), and a trace amount of the bisperfluorohexylated compound **26** (0.3%). Regiochemical assignment of **26** was based on the ^{13}C NMR absorptions of the ester carbonyl which appeared as double of doublets attributable to $^3J_{CF}$ coupling (6 and 3 Hz). The lactone **25** was isolated by GPC and its structure was confirmed by spectroscopic data. Thus in this reaction too, the 1,2-addition to one of the ester carbonyls was preferred to the conjugate addition. Coordination of BF_3 to the ester group would favor the 1,2-mode of addition of perfluoroalkyllithium[15] under these amphiphilic conditions.[16] The high yield and (*Z*)-stereoselectivity of **19b** may also reflect the stabilizing effect of BF_3 for the anion of the hemiacetal **24**.

Experimental

Melting points were measured with a Yanagimoto micro-melting point apparatus and are uncorrected. All distillation temperatures refer to the Kugelrohr bath temperature. Unless otherwise noted, all NMR spectra were observed with JEOL PMX-60 and GSX-270 spectrometers by using $CDCl_3$ as solvent, tetramethylsilane as an internal standard for ^1H and ^{13}C, and $CFCl_3$ for ^{19}F. Mass spectra were measured with a Hitachi M80LCAPI spectrometer under the following ionizing conditions: EI (20 eV) and CI (70 eV, methane as CI gas). IR spectra were recorded on a Hitachi 270-30 spectrophotometer. Column chromatography was carried out using Wakogel C-200. Preparative GPC was performed using JAI LC-08 with JAI-1H (20 mmID×60 cm) and JAI-2H (20 mmID×60 cm) columns. Diethyl ether was distilled from sodium benzophenone ketyl and stored over sodium wire. Dichloromethane was distilled from calcium hydride and stored over 4A Molecular Sieves. Esters and perfluoroalkyl iodides were purified by simple distillation. Methyllithium was titrated prior to use. Other commercially available materials were used without further purification. Perfluorobutyltributylstannane (**27**) was prepared according to a procedure similar to that used for pentafluoroethyltriallylstannane.[17]

Preparation of Perfluorobutyltributylstannane (27). To an ethereal solution (100 ml) of **2c** (5.19 g, 15 mmol) was added dropwise an ethereal solution of methyllithium-lithium bromide (10 mmol) at −90—−80 °C over 10 min. With an interval of 10 min tributylstannyl chloride (3.26 g, 10 mmol) in ether (10 ml) was added to the white suspension at −80 °C and the reaction mixture was allowed gradually to warm to room temperature with stirring. After 1 h the solvent was removed and the residual syrup was distilled under reduced pressure to give 2.05 g of **27** as a colorless oil (110—115 °C/0.15 mmHg††). The purity of **27** estimated by NMR was ca. 70%. Major contaminants were tributylmethylstannane (ca. 10%), tributylstannyl bromide (ca. 15%), and tributylstannyl chloride (ca. 5%). The product was used without further purification. **27**: ^1H NMR δ=0.92 (9H, t, J=7.3 Hz) and 1.15—1.70 (12H, m); ^{19}F NMR δ=−81.72 (3F, tt, J=9 and 4 Hz), −118.12 (2F, m, $J_{Sn\text{-}F}$=ca. 187 Hz), −119.22 (2F, m), and −126.53 (2F, br t, J=12 Hz); IR (neat) 2964s, 2924s, 1466m, 1348m, and 1300—1100vs cm^{-1}; MS (EI) m/z (rel intensity) 453 [M^+−Bu (^{120}Sn), 15%], 452 [M^+−Bu (^{119}Sn), 6], 451 [M^+−Bu (^{118}Sn), 12], 450 [M^+−Bu (^{117}Sn), 6], 449 [M^+−Bu (^{116}Sn), 6], 397 (4), 291 (100), 253 (71), and 235 (75).

General Procedure for Perfluoroalkylation of Esters. To an ethereal solution of **1** (1 mmol) and **2** (1.2 mmol) was added an ethereal solution of methyllithium-lithium bromide (1.1 mmol) at −78 °C during the course of 5 min and the mixture was stirred for 1 h at this temperature. The reaction was quenched by the addition of aqueous NH_4Cl and the product was extracted with ether. The organic phase was washed with brine, dried over Na_2SO_4, and evaporated. The residue was purified by column chromatography (hexane-CH_2Cl_2) and/or distillation.

Compound 3. Distillation temp 140 °C/22 mmHg; ^1H NMR (CCl_4) δ=7.44—7.62 (3H, m) and 8.01 (2H, m); ^{19}F NMR δ=−80.42 (3F, tt, J=10 and 2 Hz), −113.13 (2F, t, J=13 Hz), −121.32 (4F, m), −122.29 (4F, m), −123.19 (2F, m), and −126.62 (2F, m); IR (neat) 1714vs, 1600s, 1454s, 1328s, and 1300—1100vs cm^{-1}; MS (CI) m/z (rel intensity) 525 (M^++1, 99) and 105 (100) (Found: C, 34.21; H, 1.09%. Calcd for $C_{15}H_5OF_{17}$: C, 34.37; H, 0.96%).

Compound 4a. Mp 61—62 °C; ^1H NMR (CCl_4) δ=7.11 (1H, d, J=16 Hz), 7.41—7.75 (5 H, m), and 8.03 (1H, d, J=16 Hz); ^{19}F NMR δ=−81.25 (3F, tt, J=10 and 2 Hz), −121.38 (2F, t, J=13 Hz), −121.78 (2F, m), −122.34 (4F, m), −122.61 (2F, m), −123.18 (2F, m), and −126.58 (2F, m); IR (KBr) 1708vs, 1610vs, 1348s, 1330s, and 1300—1100vs cm^{-1}; MS (EI) m/z (rel intensity) 550 (M^+, 15%), 131 (100), and 77 (25) (Found: C, 37.02; H, 1.36%. Calcd for $C_{17}H_7OF_{17}$: C, 37.11; H, 1.28%).

Compound 4b. Mp 47—48 °C; ^1H NMR (CCl_4) δ=7.03 (1H, d, J=16 Hz), 7.74 (5H, m), and 7.92 (1H, d, J=16 Hz); ^{19}F NMR δ=−81.25 (3F, tt, J=10 and 2 Hz), −121.39 (2F, t, J=13 Hz), −122.68 (2F, m), −123.27 (2F, m), −126.60 (2F, m), and −121.97 (2F, m); IR (KBr) 1708vs, 1610vs, 1348s, and 1300—1100vs cm^{-1}; MS (EI) m/z (rel intensity) 450 (M^+, 18), 131 (100), 103 (59), and 77 (33) (Found: C, 39.94; H, 1.65%. Calcd for $C_{15}H_7OF_{13}$: C, 40.02; H, 1.57%).

Compound 4c. Mp 29 °C; ^1H NMR (CCl_4) δ=7.03 (1H, d, J=16 Hz), 7.44 (5H, m), and 7.90 (1H, d, J=6 Hz); ^{19}F NMR δ=−81.43 (3F, tt, J=10 and 2 Hz), −121.54 (2F, t, J=12 Hz), −123.61 (2F, m), and −126.16 (2F, m); IR (neat) 1710vs, 1610vs, 1340vs, and 1300—1100vs cm^{-1}; MS (EI) m/z (rel intensity) 350 (M^+, 24%), 131 (100), 103 (58), and 77 (30).

Compound 5a. Mp 37—38 °C; ^1H NMR δ=1.26 (3H, d, J=7 Hz), 2.96 (2H, d, J=7 Hz), 3.43 (1H, m), and 7.22 (5H, m); ^{19}F NMR δ=−81.24 (3F, tt, J=10 and 2 Hz), −120.96 (2F, m), −121.85 (2F, m), −122.43 (6F, m), −123.21 (2F, m), and −126.61 (2F, m); IR (neat) 2972m, 1760vs, 1456m, 1370s, and 1300—1100vs cm^{-1}; MS (EI) m/z (rel intensity) 566 (M^+, 37%), 147 (58), 131 (43), 119 (52), and 105 (100) (Found: C, 38.16; H, 2.10%. Calcd for $C_{18}H_{11}OF_{17}$: C, 38.18; H, 1.96%).

Compound 5b. Distillation temp 83—85 °C/0.7 mmHg; ^1H NMR δ=1.26 (3H, d, J=7 Hz), 2.96 (2H, d, J=7 Hz), 3.38 (1H, m), and 7.22 (5H, m); ^{19}F NMR δ=−81.33 (3F, tt, J=10 and 2 Hz), −120.91 (2F, m), −121.99 (2F, m), −122.65 (2F, m), −123.32 (2F, m), and −126.64 (2F, m); IR (neat) 2972m, 1760vs, 1498m, 1366m, 1316m, and 1300—1100vs cm^{-1}; MS (EI) m/z (rel intensity) 466 (M^+, 22%), 147 (49), and 105 (100) (Found: C, 41.12; H, 2.40%. Calcd for $C_{16}H_{11}OF_{13}$: C, 41.22; H, 2.40%).

Compound 5c. Distillation temp 68—71 °C/0.6 mmHg; ^1H NMR δ=1.25 (3H, d, J=7 Hz), 2.90 (2H, d, J=7 Hz), 3.28 (1H, m), and 7.14 (5H, m); ^{19}F NMR δ=−81.44 (3F, tt, J=10 and 2 Hz), −121.16 (2F, m), −123.65 (2F, m), and −126.25 (2F, m); IR (neat) 2972m, 1758vs, 1356vs, and 1300—1100vs cm^{-1}; MS (EI) m/z (rel intensity) 366 (M^+, 12%), 147 (10), and 105 (100) (Found: C, 45.80; H, 3.03%. Calcd for $C_{14}H_{11}OF_9$: C, 45.92; H, 3.03%).

Compound 6. Mp 25 °C; ^1H NMR (CCl_4) δ=7.40—7.85 (br m); ^{19}F NMR δ=−81.40 (3F, tt, J=10 and 2 Hz), −118.81 (2F, t, J=13 Hz), −121.70 (2F, m), −122.13 (2F, m), −122.33 (2F, m), −123.20 (2F, m), and −126.65 (2F, m); ^{13}C NMR δ=84.23, 101.41, 118.16, 100—125 (8 C), 128.96, 132.62, 134.00, and 168.96 (t, J=31 Hz); IR (neat) 2196vs, 1702vs, 1330s, and 1300—1100vs cm^{-1}; MS (EI) m/z (rel intensity) 548 (M^+, 7%), 129 (90), and 101 (100) (Found: C, 37.25; H, 0.92%. Calcd for $C_{17}H_5OF_{17}$: C, 37.25; H, 0.92%).

Compound 7. Mp 38—39 °C; ^1H NMR (CCl_4) δ=2.97

†† 1 mmHg≈133.322 Pa.

(4H, m) and 7.17 (5H, m); ^{19}F NMR δ=−81.27 (3F, tt, J=10 and 2 Hz), −120.77 (2F, t, J=13 Hz), −121.82 (2F, m), −122.36 (4F, m), −122.66 (2F, m), −123.18 (2F, m), and −126.60 (2F, m); IR (neat) 2924m, 2856m, 1758vs, and 1300—1100vs cm^{-1}; MS (EI) m/z (rel intensity) 552 (M^+, 3%), 132 (45), and 105 (100) (Found: C, 37.20; H, 1.52%. Calcd for $C_{17}H_9OF_{17}$: C, 36.97; H, 1.64%).

Compound 8. Distillation temp 125 °C; ^{1}H NMR (CCl_4) δ=1.23 (6H, d, J=7 Hz) and 3.16 (1H, m); ^{19}F NMR δ=−81.41 (3F, tt, J=10 and 2Hz), −119.93 (2F, t, J=12 Hz), −121.77 (2F, m), −122.44 (6F, m), −123.24 (2F, m), and −126.69 (2F, m); IR (neat) 2988s, 2948m, 1756vs, 1326s, and 1300—1100vs cm^{-1}; MS (CI) m/z (rel intensity) 491 (M^++1, 100%) and 71 (16) (Found: C, 29.01; H, 1.43%. Calcd for $C_{12}H_7OF_{17}$: C, 29.41; H, 1.44%).

Compound 9. Distillation temp 125 °C; ^{1}H NMR (CCl_4) δ=1.34 (s); ^{19}F NMR δ=−81.42 (3F, tt, J=10 and 2 Hz), −113.25 (2F, t, J=13 Hz), −121.40 (4F, m), −122.41 (4F, m), −123.28 (2F, m), and −126.72 (2F, m); IR (neat) 2984s, 1738vs, 1372s, and 1300—1100vs cm^{-1}; MS (CI) m/z (rel intensity) 505 (M^++1, 100%) and 101 (87) (Found: C, 30.68; H, 1.75%. Calcd for $C_{13}H_9OF_{17}$: C, 30.97; H, 1.80%).

Compound 10. Mp 39 °C; ^{1}H NMR δ=4.31 (s); ^{19}F NMR δ=−81.25 (3F, tt, J=10 and 2 Hz), −118.53 (2F, t, J=12 Hz), −121.70 (2F, m), −122.34 (6F, m), −123.19 (2F, m), and −126.62 (2F, m); IR (KBr) 1770vs, 1336vs, and 1300—1100vs cm^{-1}; MS (CI) m/z (rel intensity) 543 (M^++1 ^{81}Br, 100%), 541 (M^++1 ^{79}Br, 98), 123 (75), 121 (77), 95 (23), and 93 (28) (Found: C, 22.17; H, 0.37%. Calcd for $C_{10}H_2BrOF_{17}$: C, 22.20; H, 0.37%).

Compound. 11. Distillation temp 60—63 °C/0.8 mmHg; ^{1}H NMR δ=2.04 (3H, dd, J=7.0 and 1.7 Hz), 6.56 (1H, dm, J=15.4 Hz), and 7.37 (1H, dq, J=15.4 and 7.0 Hz); ^{19}F NMR δ=−81.32 (3F, tt, J=10 and 2 Hz), −121.71 (4F, m), −122.40 (4F, m), −122.78 (2F, m), −123.22 (2F, m), and −126.63 (2F, m); IR (neat) 1724s, 1634s, 1324s, and 1300—1100vs cm^{-1}; MS (EI) m/z (rel intensity) 488 (M^+, 3%), 468 (100), 441 (78), 219 (39), 169 (43) and 119 (57) (Found: C, 29.20; H, 1.08%. Calcd for $C_{12}H_5OF_{17}$: C, 29.53; H, 1.03%).

Compound 12. Distillation temp 80—81 °C/0.6 mmHg; ^{1}H NMR δ=1.89 (3H, s), 1.98 (3H, d, J=7.0 Hz), and 7.09 (1H, q, J=7.0 Hz); ^{19}F NMR δ=−81.37 (3F, tt, J=10 and 2 Hz), −111.05 (2F, m), −121.37 (4F, m), −122.35 (4F, m), −123.23 (4F, m), and −126.65 (2F, m); IR (neat) 2963m, 1694vs, 1638vs, 1328s, and 1300—1100vs cm^{-1}; MS (EI) m/z (rel intensity) 502 (M^+, 6%), 483 (100), 455 (33), 169 (16), and 119 (18) (Found: C, 31.05; H, 1.70%; Calcd for $C_{13}H_7OF_{17}$: C, 31.09; H, 1.40%).

Compound 13. Mp 80 °C; ^{1}H NMR δ=2.17 (2H, m), 2.25 (2H, m), 2.82 (1H, br s), 4.01 (1H, td, J=7.7 and 6.7 Hz), and 4.21 (1H, td, J=7.7 and 4.6 Hz); ^{19}F NMR δ=−81.26 (3F, tt, J=10 and 2 Hz), −120.67 (2F, m), −121.28 (1F, dm, J=284 Hz), −122.37 (6F, m), −123.23 (2F, m), −123.71 (1F, dm, J=284 Hz), and −126.64 (2F, m); IR (KBr) 3372s, 2996m, 1336s, and 1300—1100vs cm^{-1}; MS (CI) m/z (rel intensity) 505 (M^+−1, 1%) 489 (100), and 467 (9); MS (EI) m/z (rel intensity) 505 (M^+−1, 8%), 489 (14), 476 (26), 131 (76), 107 (45), and 87 (100) (Found: C, 28.19; H, 1.29%. Calcd for $C_{12}H_7O_2F_{17}$: C, 28.48; H, 1.39%).

Compound 14. Mp 66—67 °C; ^{1}H NMR δ=3.05 (2H, m), 3.19 (2H, m), and 7.31 (5H, m); ^{19}F NMR δ=−81.23 (3F, tt, J=10 and 2 Hz), −120.82 (2F, t, J=13 Hz), −121.76 (2F, m), −122.32 (4F, m), −122.63 (2F, m), −123.17 (2F, m), and −126.58 (2F, m); IR (KBr) 2920m, 1760vs, 1336s, and 1300—1100vs cm^{-1}; MS (EI) m/z (rel intensity) 584 (M^+, 84%), 137 (29), 123 (100), 110 (50), and 109 (30) (Found: C, 35.08; H, 1.44%. Calcd for $C_{17}H_9OSF_{17}$: C, 34.95; H, 1.55%).

Compound 15. Mp<20 °C; ^{1}H NMR (CCl_4) δ=1.23 (3H, m), 3.05 (3H, m), and 7.32 (5H, m); ^{19}F NMR δ=−81.37 (3F, tt, J=10 and 2 Hz), −118.65 (1F, dt, J=292 and 13 Hz), −120.98 (1F, dt, J=292 and 13 Hz), −121.65 (2F, m), −122.31 (6F, m), −123.19 (2H, m), and −126.63 (2F, m); IR (neat) 3080m, 2988m, 1754vs, 1328s, and 1300—1100vs cm^{-1}; MS (EI) m/z (rel intensity) 598 (M^+, 33%), 151 (11), 123 (100), and 110 (17) (Found: C, 36.21; H, 1.87%. Calcd for $C_{18}H_{11}OSF_{17}$: C, 36.13; H, 1.85%).

Compound 16. Mp 86—87 °C; ^{1}H NMR (acetone-d_6) δ=3.95 (3H, s), 6.14 (1H, m), 8.22 (1H, br s), and 9.63 (1H, br s); ^{19}F NMR (acetone-d_6) δ=−80.69 (3F, tt, J=10 and 2 Hz), −119.79 (2F, t, J=12 Hz), −121.10 (2F, m), −121.53 (4F, m), −122.09 (2F, m), −122.09 (2F, m), −122.36 (2F, m), and −125.83 (2F, m); ^{13}C NMR δ=54.55, 90.04 (t, J=1 Hz), 100—125 (8 C), 154.01, 163.36, and 181.26 (t J=24 Hz); IR (KBr) 3484s, 3340s, 1740vs, 1664s, 1612vs, 1436vs, 1336vs, and 1300—1100vs cm^{-1}; MS (EI) m/z (rel intensity) 547 (M^+, 8%), 528 (3), 488 (6), and 128 (100) (Found: C. 28.77; H, 0.99; N, 2.60%. Calcd for $C_{13}H_6NO_3F_{17}$: C, 28.54; H, 1.11; N, 2.56%).

Compound 17. Distillation temp 101—103 °C/0.1 mmHg; ^{1}H NMR δ=1.29 (3H, t, J=7.0 Hz), 1.30 (3H, t, J=7.0 Hz), 4.26 (2H, m), 4.31 (2H, m), and 7.23 (1H, br s); ^{19}F NMR (50 °C) δ=−81.42 (3F, t, J=10 Hz), −92.21 (1F, dm, J=222 Hz), −93.64 (1F, dm, J=222 Hz), −121.38 (2F, m), −122.20 (6F, m). −123.03 (2F, m), and −126.47 (2F, m); ^{19}F NMR (23 °C) δ=−81.39 (3F, t, J=10 Hz), −92.25 (1F, dm, J=222 Hz, major conformation isomer, ca. 70%), −92.57 (1F, dm, J=222 Hz, minor conformation isomer, ca. 30%), −93.84 (1F, dm, J=222 Hz), −121.73 (2F, m), −122.43 (6F, m), −123.23 (2F, m), and −126.68 (2F, m); ^{13}C NMR δ=13.72, 14.00, 62.88, 64.43, 100—125 (8 C), 152.09, and 155.82; IR (neat) 3308s, 2992s, 2890m, 1746vs, 1514s, 1380s, and 1300—1100vs cm^{-1}; MS (CI) m/z (rel intensity) 595 (M^++1, 12%), 551 (11), 531 (14), 503 (100), 475 (20), and 450 (15) (Found: C, 28.49; H, 1.75; N, 4.85%. Calcd for $C_{14}H_{11}N_2O_4F_{17}$: C, 28.30; H, 1.87; N, 4.71%).

Compound 19a. (*E*)-Isomer: mp 46 °C; ^{1}H NMR δ=0.96 (3H, t, J=7.3 Hz), 1.42 (2H, m), 1.70 (2H, m), 4.26 (2H, t, J=6.7 Hz), 7.05 (1H, d, J=15.6 Hz), and 7.43 (1H, d, J=17.6 Hz); ^{19}F NMR δ=−81.26 (3F, tt, J=10 and 2 Hz), −121.40 (2F, tm, J=12 Hz), −121.74 (2F, m), −122.41 (6F, m), −123.22 (2F, m), and −126.61 (2F, m); IR (KBr) 2968s, 2888s, 1722vs, 1316vs, and 1300—1100 vs cm^{-1}; MS (CI) m/z (rel intensity) 575 (M^++1, 80%), 547 (14), 520 (13), 519 (100), 501 (19), and 155 (70).

Compound 19b. (*E*)-Isomer: ^{1}H NMR δ=0.97 (3H, t, J=7.3 Hz), 1.42 (2H, m), 1.70 (2H, m), 4.27 (2H, t, J=6.7 Hz), 7.07 (1H, d, J=15.9 Hz), and 7.44 (1H, d, J=15.9 Hz); ^{19}F NMR δ=−81.35 (3 F, tt, J=10 and 3 Hz), −121.33 (2F, t, J=12 Hz), −122.52 (2F, m), −123.24 (2F, m), and −126.61 (2F, m); ^{13}C NMR δ=13.48, 19.03, 30.46, 65.95, 100—125 (6C), 130.66, 137.43, 163.99, and 182.29 (t, J=27 Hz); IR (neat) 2968s, 1728vs, 1626m, 1470m, 1386s, 1360s, 1308s, and 1300—1100vs cm^{-1}; MS (CI) m/z (rel intensity) 475 (M^++1, 28%) 447 (8), 433 (8), 419 (100), 403 (15), 401 (27), and 155 (94) (Found: C, 35.43; H, 2.42%. Calcd for $C_{14}H_{11}O_3F_{13}$: C, 35.46; H, 2.34%).

(*Z*)-Isomer: ^{1}H NMR δ=0.94 (3H, t, J=7.3 Hz), 1.38 (2H,

m), 1.65 (2H, m), 4.23 (2H, t, J=6.7 Hz), 6.47 (1H, d, J=11.6 Hz), and 6.60 (1H, d, J=11.6 Hz); ^{19}F NMR δ=−81.31 (3F, tt, J=10 and 2 Hz), −120.78 (2F, t, J=12 Hz), −122.05 (2F, m), −122.70 (2F, m), −123.28 (2F, m), and −126.62 (2F, m); ^{13}C NMR δ=13.28, 18.92, 30.22, 65.90, 100—125 (6 C), 130.37, 134.04, 164.69, and 184.58 (t, J=28 Hz); IR (neat) 2968s, 1730s, 1626m, 1470m, 1404s, 1366s, 1316s, and 1300—1100vs cm^{-1}.

Compound 19c. Distillation temp 70—80 °C/0.07 mmHg; ^{1}H NMR δ=0.96 (3H, t), 1.42 (2H, m), 1.70 (2H, m), 4.26 (2H, t, J=6.7 Hz), 7.05 (1H, d, J=15.6 Hz), and 7.43 (1H, d, J=15.6 Hz); ^{19}F NMR δ=−81.38 (3F, tt, J=10 and 2 Hz), −121.57 (2F, m), −123.53 (2F, m), and −126.13 (2F, m); IR (neat) 2968s, 2880s, 1726vs, 1314vs, and 1300—1100vs cm^{-1}; MS (CI) m/z (rel intensity) 375 (M^++1, 29%), 319 (100), 303 (82), 301 (29), 263 (38), 209 (26), 157 (26), and 155 (48) (Found: C, 38.12; H, 2.92%; Calcd for $C_{12}H_{11}O_3F_9$: C, 38.52; H, 2.96%).

Compound 20a. Distillation temp 95 °C/0.08 mmHg; ^{1}H NMR δ=0.93 (6 H, t, J=7.3 Hz), 1.38 (4H, m), 1.58 (4H, m), 2.78 (1H, dd, J=17.1 and 3.7 Hz), 3.10 (1H, dd, J=17.1 and 11.5 Hz), 3.70 (1H, m), 4.11 (2H, t, J=6.7 Hz), and 4.19 (2H, t, J=6.7 Hz); ^{19}F NMR δ=−81.30 (3F, tt, J=10 and 2 Hz), −112.9 (1F, dm, J=278 Hz), −114.1 (1F, dm, J=278 Hz), −121.28 (2F, m), −122.01 (2F, m), −122.33 (4F, m), −123.18 (2F, m), and −126.60 (2F, m); ^{13}C NMR δ=13.47, 13.58, 18.88, 19.01, 30.24, 30.34, 30.50, 44.60 (t, J=22 Hz), 65.36, 66.20, 100—125 (8 C), 166.55 (dd, J=6 and 3 Hz), and 170.04; IR (neat) 2969vs, 2880s, 1746vs, 1312s, and 1300—1100vs cm^{-1}; MS (CI) m/z (rel intensity) 649 (M^++1, 51%), 593 (16), 547 (7), 519 (100), 499 (16), and 473 (10) (Found: C, 36.74; H, 3.21%. Calcd for $C_{20}H_{21}O_4F_{17}$: C, 37.05; H, 3.26%).

Compound 20b. Distillation temp 104 °C/0.3 mmHg; ^{1}H NMR δ=0.91 (6H, t, J=7.3 Hz), 1.40 (4H, m), 1.63 (4H, m), 2.80 (1H, dd, J=17.1 and 3.3 Hz), 3.11 (1H, dd, J=17.1 and 11.3 Hz), 3.71 (1H, m), 4.13 (2H, t, J=6.7 Hz), 4.20 (2H, t, J=6.7 Hz); ^{19}F NMR δ=−81.30 (3F, tt, J=10 and 3 Hz), −112.9 (1F, dm, J=279 Hz), −114.1 (1F, dm, J=279 Hz), −121.40 (2F, m), −122.25 (2F, m), −123.30 (2F, m), −126.65 (2F, m); ^{13}C NMR δ=13.22, 13.33, 18.86, 18.96, 30.20 (br), 30.26, 30.52, 44.68 (t, J=22 Hz), 65.35, 66.18, 100—125 (6 C), 166.62 (dd, J=6 and 3 Hz), 170.13; IR (neat) 2964s, 2880m, 1746vs, 1470m, 1420m, 1400m, 1348s, 1318s, and 1300—1100vs cm^{-1}. MS (CI) m/z (rel intensity) 549 (M^++1, 7%), 493 (7), 447 (7), 419 (100), 399 (20), and 373 (6).

Compound 20c. Distillation temp 84—90 °C/0.1 mmHg; ^{1}H NMR δ=0.93 (6 H, t, J=7.0 Hz), 1.38 (4H, m), 1.62 (4H, m), 2.79 (1H, dd, J=17.4 and 3.4 Hz), 3.11 (1H, dd, J=17.4 and 11.3 Hz), 3.72 (1H, m), 4.11 (1H, t, J=6.7 Hz), and 4.19 (1H, t, J=6.7 Hz); ^{19}F NMR δ=−81.46 (3F, tt, J=10 and 2 Hz), −113.01 (1F, dm, J=277 Hz), −114.27 (1F, dm, J=277 Hz), −122.36 (2F, m), and −126.41 (2F, m); ^{13}C NMR δ=13.49, 13.58, 18.88, 19.00, 30.22, 30.23 (br m), 30.49, 44.48 (t, J=22 Hz), 65.34, 66.19, 108.60 (tqt, J=270, 39, and 33 Hz), 110.69 (ttt, J=266, 36, and 32 Hz), 115.97 (tt, J=261 and 33 Hz), 117.29 (qt, J=188 and 33 Hz), 166.54 (dd, J=6 and 3 Hz), and 170.02; IR (neat) 2964s, 2876s, 1748vs, 1344s, 1312s, and 1300—1100vs cm^{-1}; MS (CI) m/z (rel intensity) 449 (M^++1, 5%), 393 (8), 347 (8), 337 (9), 320 (10), 319 (100), and 299 (19) (Found: C, 42.68; H, 4.57%. Calcd for $C_{16}H_{21}O_4F_9$: C, 42.87; H, 4.72%).

Compound 21. (*E*)-Isomer: ^{1}H NMR δ=3.87 (3H, s), 7.05 (1H, d, J=15.6 Hz), and 7.45 (1H, d, J=15.6 Hz); ^{19}F NMR δ=81.32 (3F, tt, J=10 and 2 Hz), −121.48 (2F, t, J=12 Hz), −121.75 (2F, m), −122.40 (6F, m), −123.21 (2F, m), and −126.63 (2F, m); IR (neat) 2960m, 1730vs, 1316vs, and 1300—1100vs cm^{-1}; MS (CI) m/z (rel intensity) 533 (M^++1, 100%), 503 (7), 501 (8), 130 (9), 117 (9), and 113 (84).

(*Z*)-Isomer: ^{1}H NMR δ=3.82 (3H, s), 6.47 (1H, d, J=11.9 Hz), and 6.61 (1H, d J=11.9 Hz); ^{19}F NMR δ=−81.28 (3F, tt, J=10 and 2 Hz), −120.77 (2F, t, J=12 Hz), −121.48 (2F, m), −122.37 (4F, m), −122.68 (2F, m), −123.21 (2F, m), and −126.62 (2F, m); IR (KBr) 3090m, 1744vs, 1716vs, 1332vs, and 1300—1100vs cm^{-1}.

Reaction with 1,4-Benzoquinone. To a solution of **1s** (1.08 g, 10 mmol) and **2a** (5.46 g, 10 mmol) in ether (150 ml) was added an ethereal solution of methyllithium-lithium bromide (10 mmol) at −78 °C over 10 min. During the course of addition, the yellow solution gradually turned to a bluish purple suspension. After stirring for 1 h, the reaction was quenched with aqueous NH_4Cl. The organic phase was separated and the aqueous phase was extracted with ether. The combined extracts were washed with brine and dried over Na_2SO_4. The solvent was evaporated and the residue was chromatographed on silica gel ($CHCl_3$ as eluant). The fractions containing **22** was collected and concentrated to ca. 20 ml. Forced cooling of this concentrate followed by filtration gave 2.66 g (50%) of **22** as colorless crystals; mp 107—108 °C. ^{1}H NMR δ=1.59 (1H, br s), 6.43 (2H, d, J=10.1 Hz), and 6.91 (2H, d, J=10.1 Hz); ^{13}C NMR (acetone-d_6) δ=72.52 (tt, J=24 and 1 Hz), 100—125 (8 C), 132.28, 143.21 (m), and 184.99. ^{19}F NMR δ=−81.25 (3F, tt, J=10 and 2 Hz), −119.45 (4F, m), −122.0—−122.5 (6F, m), −123.17 (2F, m), and −126.58 (2F, m); IR (KBr) 3224m, 1674vs, 1628s, 1408s, 1392s, 1372s, 1330s, and 1300—1100vs cm^{-1}; MS (EI) m/z (rel intensity) 528 (M^+, 1%), 512 (1), 488 (3), 173 (8), 169 (2), 143 (9), and 109 (100) (Found: C, 31.87; 0.87%. Calcd for $C_{14}H_5O_2F_{17}$: C, 31.84; H, 0.95%).

Reaction with *N*-Isobutylmaleimide. To an ethereal solution (20 ml) of **1t** (153 mg, 1 mmol) and **2a** (546 mg, 1 mmol) was added an ethereal solution of methyllithium-lithium bromide (1 mmol) at −78 °C. After stirring for 30 min, the reaction was quenched with aqueous NH_4Cl. The reaction mixture was extracted with ethyl acetate. The organic extract was washed with brine and dried over Na_2SO_4. The solvent was evaporated and the residue was chromatographed on silica gel ($CHCl_3$ as eluant) to give 241 mg (42%) of **23** as colorless crystals; mp 122—123 °C; ^{1}H NMR δ=0.88 (6H, d, J=7.3 Hz), 2.21 (1H, m), 3.10 (1H, dd, J=14.3 and 8.2 Hz), 3.32 (1H, br s), 3.44 (1H, dd, J=14.3 and 7.0 Hz), 6.29 (1H, d, J=6.1 Hz), and 6.97 (1H, dt, J=6.1 and 2.7 Hz); ^{19}F NMR δ=−81.24 (3F, tt, J=10 and 2 Hz), −118.85 (1F, dm, J=280 Hz), −119.60 (1F, dm, J=285 Hz), −119.83 (1F, dm J=280 Hz), −121.29 (1 F, dm, J=285 Hz), −122.20 (6F, m), −123.18 (2F, m), and −126.58 (2F, m); IR (KBr) 3128s, 2964s, 1672vs, 1372s, and 1300—1100vs cm^{-1}; MS (EI) m/z (rel intensity) 573 (M^+, 7%), 530 (100), 518 (74), 501 (26), and 154 (53) (Found: C, 33.85; H, 2.16; N, 2.56%. Calcd for $C_{16}H_{12}NO_2F_{17}$: C, 33.52; H, 2.11; N, 2.44%).

Entry 29. To a solution of **1q** (1.14 g, 5 mmol), **2b** (2.68 g, 6 mmol), and $BF_3 \cdot OEt_2$ (0.65 ml, 5 mmol) was added an ethereal solution of methyllithium-lithium bromide (5.5 mmol) at −78 °C over 20 min. After stirring for 1 h, the reaction mixture was quenched by the addition of aqueous NH_4Cl. The ethereal layer was separated and the aqueous phase was extracted with ether. The combined organic

phase was washed with brine and dried over Na_2SO_4. Evaporation of the solvent gave 3.57 g of a reddish brown oil, of which NMR analysis showed the presence of **19b** ($Z/E \geqq 20/1$), **20b**, **24**, and a small amount of 1-butanol (**19b** : **20b** : **24**=7 : 10 : 23). Column chromatography of the crude oil on silica gel (hexane-CH_2Cl_2 as eluant) gave 0.013 g of **26** and 2.25 g of a mixture of **19b** (Z/E=6/5), **20b**, and **25** (**19b** : **20b** : **25**=56 : 24 : 5). Separation of these compounds was carried out by preparative GPC.

Compound 24. ^{1}H NMR (typical signals) δ=6.20 (1H, d, J=13.2 Hz), 6.30 (1H, br d, J=13.2 Hz), and 8.88 (1H, br s); ^{13}C NMR (typical signals) δ=97.62 (t, J=26 Hz), 125.59, 144.20, and 168.23.

Compound 25. ^{1}H NMR δ=0.91 (3H, t, J=7.3 Hz), 1.38 (2H, m), 1.60 (2H, m), 3.43 (1H, dt, J=8.9 and 6.3 Hz), 3.57 (1H, dt, J=8.9 and 6.3 Hz), 6.52 (1H, d, J=5.8 Hz), and 7.27 (1H, d, J=5.8 Hz); ^{19}F NMR δ=−81.35 (3F, tt, J=10 and 2 Hz), −118.75 (1F, dm, J=282 Hz), −120.77 (2F, m), −121.51 (1F, dm, J=282 Hz), −122.35 (2F, m), −123.18 (2F, m), and −126.62 (2F, m); ^{13}C NMR δ=13.41, 18.76, 31.07, 64.87, 106.86 (dd, J=30 and 28 Hz), 100—125 (6 C), 128.65, 147.36 (d, J=2 Hz), and 167.47; IR (neat) 2968m, 1816vs, 1620m, 1474m, 1366s, 1332s, and 1300—1100vs cm^{-1}; MS (CI) m/z (rel intensity) 475 (M^++1, 5%), 447 (11), 419 (100), 401 (64), and 383 (6).

Compound 26. ^{1}H NMR δ=0.94 (3H, t, J=7.3 Hz), 1.40 (2 H, m), 1.63 (2H, m), 3.20 (1H, dd, J=19.4 and 2.6 Hz), 3.60 (1H, dd, J=19.4 and 10.9 Hz), 3.79 (1H, m), and 4.20 (2H, m); ^{19}F NMR δ=−81.29 (6F, t, J=10 Hz), −112.0 (1F, dm, J=284 Hz), −113.3 (1F, dm, J=284 Hz), −120.49 (2F, t, J=12 Hz), −121.23 (2F, m), −121.98 (2F, m), −122.25 (2F, m), −122.60 (2F, m), −123.27 (4F, m), and −126.60 (4F, m); ^{13}C NMR δ=13.41, 18.81, 30.15, 34.67 (br), 43.11 (t, J=22 Hz), 66.77, 100—125 (12 C), 165.45 (dd, J=6 and 3 Hz), and 190.69 (t, J=27 Hz); IR (neat) 2968s, 1754vs, 1404m, 1348s, 1320s, and 1300—1100vs cm^{-1}; MS (CI) m/z (rel intensity) 796 (M^++2, 2%), 795 (M^++1, 3), 767 (9), 739 (30), 735 (69), 721 (100), 699 (40), 681 (23), 535 (18), and 479 (6).

Reaction of Perfluorobutyltributylstannane (27) with Dibutyl Maleate (1q). To an ethereal solution (10 ml) of **1q** (228 mg, 1 mmol) and **27** (815 mg, purity ca. 70%) was added an ethereal solution of methyllithium-lithium bromide (1.5 mmol) at −78 °C. After stirring for 1 h, the reaction mixture was quenched by the addition of aqueous NH_4Cl and extracted with ether. The extract was washed with brine and dried over Na_2SO_4. Evaporation of the solvent gave a pale yellow oil, of which NMR analysis revealed the presence of **19c** (E/Z=10/1), **20c** (**19c** : **20c**=2.1 : 1), and tributylmethylstannane. Chromatography of the crude oil on silica gel gave tributylmethylstannane (510 mg) and a mixture of **19c** and **20c** (**19c** : **20c**=33 : 10).

We thank Dr. Kazuhiro Shimokawa (Daikin Kogyo Co., Ltd.) for a gift of perfluoroalkyl iodides.

References

1) M. P. Turberg and J. E. Brady, *J. Am. Chem. Soc.*, **110**, 7797 (1988); C. Pugh, J. Hopken, and M. Moller, *Polym. Prepr., Am. Chem. Soc., Div. Polym. Chem.*, **29**, 460 (1988).

2) T. P. Russell, J. F. Rabolt, R. J. Twieg, R. L. Siemens, and B. L. Farmer, *Macromolecules*, **19**, 1135 (1986).

3) P. Tarrant, *J. Fluorine Chem.*, **25**, 69 (1984).

4) E. S. Loo, *J. Org. Chem.*, **36**, 364 (1971); N. Thoai, *J. Fluorine Chem.*, **5**, 115 (1975); P. Johncock, *J. Organomet. Chem.*, **19**, 257 (1968).

5) T. Kitazume and N. Ishikawa, *J. Am. Chem. Soc.*, **107**, 5186 (1985); S. Benefice, H. Blancow, and A. Commeyras, *Tetrahedron*, **40**, 1541 (1984); A. Commeyras, *Ann. Chim. Fr.*, **9**, 673 (1984).

6) Y. Kobayashi, K. Yamamoto, and I. Kumadaki, *Tetrahedron Lett.*, **1979**, 4071; V. C. R. McLouglin and J. Thrower, *Tetrahedron*, **25**, 592 (1969).

7) P. G. Gassman and N. J. O'Reilly, *Tetrahedron Lett.*, **26**, 5243 (1985).

8) H. Uno, Y. Shiraishi, K. Shimokawa, and H. Suzuki, *Chem. Lett.*, **1987**, 1153.

9) For perfluoroalkylation of esters, also see: A. L. Henne and W. C. Francis, *J. Am. Chem. Soc.*, **75**, 992 (1953); O. R. Pierce and M. Levine, *ibid.*, **75**, 1254 (1953); O. R. Pierce, E. T. McBee, and G. F. Judd, *ibid.*, **76**, 474 (1954); E. T. McBee, C. W. Roberts, and S. G. Curtis, *ibid.*, **77**, 6387 (1955); L. S. Chen, G. J. Chen, and C. Tamborski, *J. Fluorine Chem.*, **26**, 341 (1984).

10) P. G. Gassman and N. J. O'Reilly, *J. Org. Chem.*, **52**, 2481 (1987).

11) In the recent report concerned with the reaction of trifluoromethylide, derived from the reaction of trifluoromethyltrimethylsilane with tetrabutylammonium fluoride, the conjugate addition of trifluoromethylide to cyclohexenone was observed to occur only in a small amount (<10%). See: G. K. Surya Prakash, R. Krishnamurti, and G. A. Olah, *J. Am. Chem. Soc.*, **111**, 393 (1989).

12) A. E. Feiring, *J. Org. Chem.*, **50**, 3269 (1985).

13) W. B. Farnham and J. C. Calabrese, *J. Am. Chem. Soc.*, **108**, 2449 (1986).

14) X. Creary, *J. Org. Chem.*, **52**, 5026 (1987).

15) No "ate" complexation of boron trifluoride with perfluoroalkyllithium seems to occur, because dibutyl maleate was recovered intact when it was added to a mixture of perfluorohexyllithium and $BF_3 \cdot OEt_2$ at −78 °C.

16) K. Maruoka, T. Itoh, M. Sakurai, K. Nonoshita, and H. Yamamoto, *J. Am. Chem. Soc.*, **110**, 3588 (1988).

17) K. Kawakami and H. Kuivila, *J. Org. Chem.*, **34**, 1502 (1969).

The Mechanism of Seasonal Variation in the Size Distributions of Atmospheric Chloride and Nitrate Aerosol in Tokyo

Hiroshi HARA,* Tsuyoshi KATO,†,†† and Hidetsuru MATSUSHITA
The Institute of Public Health, Shirokanedai 4-chome, Minato-ku, Tokyo 108
†Science University of Tokyo, Kagurazaka 1-chome, Shinjuku-ku, Tokyo 162
(Received December 19, 1988)

The volatility of ammonium chloride and nitrate was demonstrated to be responsible for the seasonal variation in size distributions that is the atmospheric fine-mode (<2 μm) chloride and nitrate aerosol were predominant in winter, but the coarse mode (>2 μm) was more pronounced in summer. An ion-balance examination and heating of winter aerosol samples demonstrated that fine-mode chloride and nitrate species are ammonium salts which are volatile at summer atmospheric temperatures. Both volatilized and unvolatilized concentrations of these chloride and nitrate species were determined both in winter and in summer to prove that the gas-solid interconversion took place in the atmosphere. The log-normal distributions of the ionic-component concentrations and the seasonal changes in the ionic composition of fine-mode aerosol were also discussed.

Chloride, like sulfate and nitrate[1,2] is one of the major ionic components of atmospheric aerosol. As yet, however, sufficient attention has not been paid to this component compared with sulfate and nitrate. Chloride has been considered to be of natural origin, such as sea spray and volcanic emission, whereas sulfate and nitrate have been studied in connection with photochemical air pollution and acid precipitation problems. Recently, however, the direct emission of hydrochloric acid associated with the burning of fossil fuels and of municipal refuse was noted, along with chlorine loss during the breakdown of seasalt by photoxidation with nitrogen dioxide along with aldehydes and through acidic displacement reactions.[3] Some of the HCl emitted into the atmosphere is expected to be transformed into ammonium chloride, which has been directly identified by means of X-ray diffraction analysis[4,5] or the IR spectrometry[6] of atmospheric aerosol, and has been speculated to exist in atmospheric aerosol on the basis of the observed seasonal trends in the chloride concentration[7,8] and in ammonium and nitrate losses from high-volume glass-fiber filters stored at room temperature.[9]

In the study of atmospheric aerosol, size distribution is a fundamental physicochemical parameter, like component concentrations, for the particle size is closely related to the source and restricts its aerodynamic behavior.[2,10,11] The size distribution of an aerosol mass is generally composed of fine (< 2 μm) and coarse (>2 μm) modes, with a distribution minimum at about 1—2 μm. The coarse-mode aerosol is directly emitted into the atmosphere, as seasalt aerosol and soil dust, for instance, whereas the fine is formed through gas-to-particle conversion, as sulfuric acid mist and automobile exhaust particles, for example. The fine- and coarse-mode concentrations are, however, essentially independent of each other.

Size-fractionated sampling and subsequent analysis has recently become a common procedure in aerosol chemistry. While there is a value in short term monitoring exercises, a full picture can only be drawn from data collected over lengthy periods.

On the basis of our June 1979—July 1982 observations in Tokyo, using an 8-stage Andersen sampler, we have discovered a seasonal variation in the size distribution of chloride aerosol and that the variation is air-temperature dependent.[7] The fine mode is predominant in winter, whereas the coarse is predominant in summer, which was comparable with the seasonal variation in the nitrate size distribution.[12,13] Similar seasonal changes have been noted in the U.S.[14] and England.[15]

We interpreted this variation as being due to the temperature dependence of the volatility of the chloride under the assumption that it was present as ammonium chloride.[7,8] A general review of this observation was given in a previous publication.[7]

This paper will report a further analysis of the data and experiments with collected aerosols in order to understand the variation mechanism of the distribution of chloride aerosol and to evaluate its significance in aerosol chemistry.

Experimental

The procedures have been described in detail elsewhere.[7,16] Aerosol was collected onto Teflon filters (Sumitomo Denko, Fluoropore FP 065) using an 8-stage Andersen sampler (Koritsu, KA-200P) on the rooftop (24 m) of the Institute of Public Health, about 3 km west of Tokyo Bay (Fig. 1). The water soluble components were extracted with an ion-chromatography eluent (0.0030 mol dm^{-3} $NaHCO_3$-0.0024 mol dm^{-3} Na_2CO_3) in an ultrasonic bath and were analyzed by two procedures: ion chromatography for chloride, nitrate, and sulfate (Dionex, System 10), and indophenol blue spectrophotometry for ammonium (Jasco, UV-1).[17]

Hydrochloric and nitric acids and ammonia in the atmosphere were sampled over the period from July, 1981, to February, 1982, with cellulose filters impregnated with

†† Present address: NEC Aviation and Space System, Inc., Shiba 5-chome, Minato-ku, Tokyo 108.

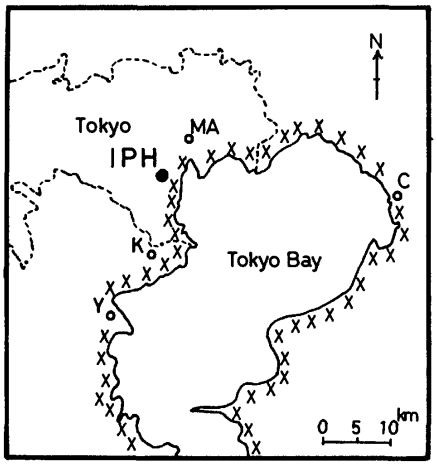

Fig. 1. Location of the sampling site: IPH, the Institute of Public Health; MA, Meteorological Agency; Y, Yokohama City; K, Kawasaki City; C, Chiba City. The coastal areas on Tokyo Bay are industrialized (x).

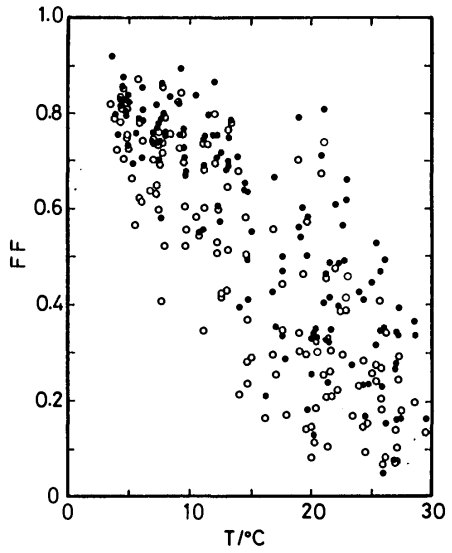

Fig. 2. Temperature dependence of FF's for chloride (O) and nitrate (●).

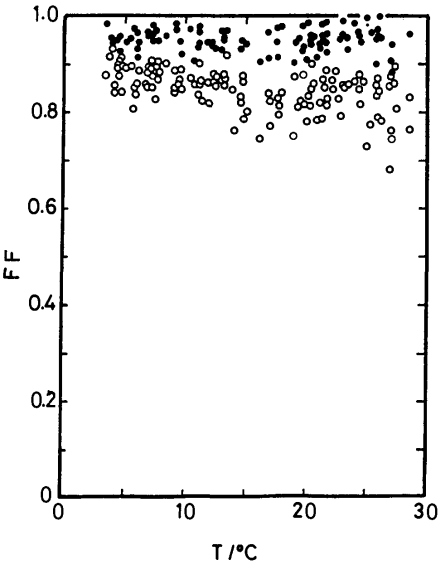

Fig. 3. Temperature dependence of FF's for sulfate (O) and ammonium (●).

sodium carbonate, sodium chloride, and oxalic acid respectively.[17] Each of the gases was extracted with doubly-distilled water and determined by means of spectrophotometry: the mercury(II)-thiocyanate, the hydrazine-reduction, and the indophenol-blue methods for hydrogen chloride, nitric acid, and ammonia respectively.[17]

Results and Discussion

Temperature Dependence of the Fine Fraction. The size-distribution data were quantitatively analyzed as a function of the temperature. The distribution pattern was quantified by defining an index, "Fine Fraction" (FF), as $F/(F+C)$, where C and F represent the concentration sums of Stages 0—4 (coarse mode) and Stage 5 to the backup filter (fine mode), because the 50% effective cutoff diameters (ECD) for Stages 4 and 5 are 2.1 and 1.1 μm respectively.

Each value of FF was plotted as a function of the temperature for chloride and nitrate (Fig. 2) and for sulfate and ammonium (Fig. 3). The mean temperature in the sampling period was calculated from the daily mean data determined by the Meteorological Agency in Chiyoda-ku, 6.5 km northeast of the sampling site (Fig. 1). As is shown in Fig. 2, the FF's for chloride and nitrate were evidently temperature-dependent; they increased drastically with a decrease in the temperature. In contrast, sulfate and ammonium exhibited fine-mode-dominant distribution irrespective of the temperature (Fig. 3).

Temperature Dependence of Fine- and Coarse-Mode Concentrations. A high FF value will be a result either of a high fine-mode concentration or of a low coarse-mode one. The fine- and coarse-mode concentrations were plotted against the temperatures for chloride and nitrate. The fine-mode chloride concentration was temperature-dependent, similar to the FF for chloride (Fig. 4 (a)). However, coarse-mode chloride seemed to demonstrate the opposite temperature dependence, but with a narrower variation range than that of the fine mode (Fig. 4 (b)). The concentration slightly increased with the temperature. Similar features appeared in nitrate (Fig. 5(a) and (b)), where the fine-mode concentrations also controlled the size distribution. We interpret these data for both anions as indicating that, schematically, the fine-mode concentration decreased profoundly with the temperature, while the coarse-mode concentration increased when the temperature rose within a limited variation range compared with those of the fine mode.

No attempts seem to have been made to discuss the concentrations of either chloride and nitrate in each

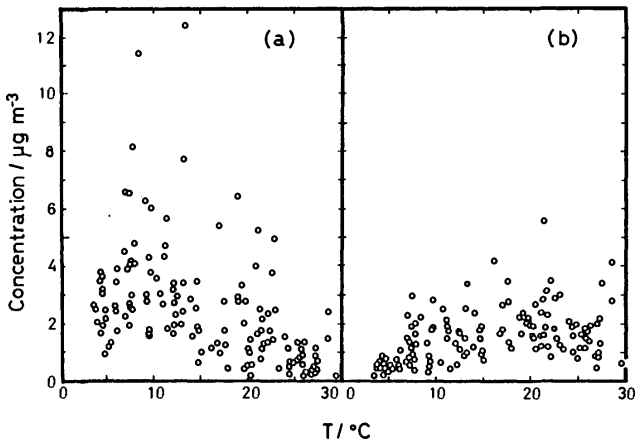

Fig. 4. Temperature dependence of (a) fine- and (b) coarse-mode chloride concentrations.

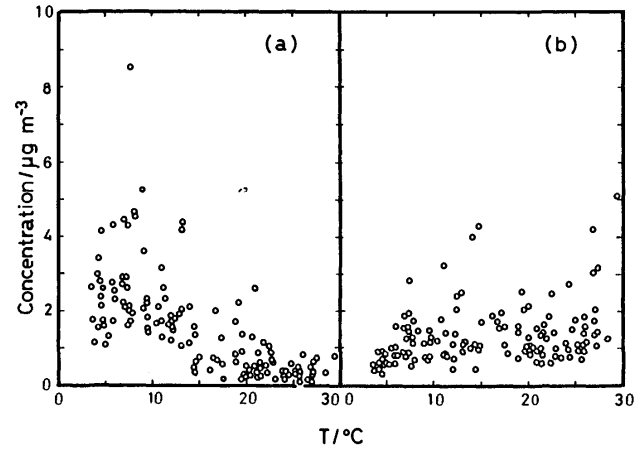

Fig. 5. Temperature dependence of (a) fine- and (b) coarse-mode nitrate concentrations.

mode in terms of the temperature, although it was pointed out nitrate aerosol shows a seasonal variation in its size distribution.

The temperature dependence of the coarse-mode chloride and nitrate will be explained in terms of both meteorology and chemistry on the assumption that those components originate from seasalt aerosol. The prevailing wind direction in Tokyo is northeast in winter and southwest in summer. Because of the location of Tokyo Bay relative to the sampling site (Fig. 1), the coarse-mode chloride is favored in the summer. Coarse-mode nitrate is attributed to the sodium nitrate[13,18] resulting from the chlorine-loss reaction:

$$NaCl + HNO_3 \longrightarrow NaNO_3 + HCl \quad (1)$$

Much more of the reactant, HNO_3, is photochemically formed in summer than in winter.

The temperature dependence of the fine mode will be discussed below.

Ion Balance. The next question is what is the chemical form of this fine-mode chloride responsible for the temperature dependence? In a previous paper,[7] we have speculated that this chloride is ammonium chloride, considering the reported identifications of this compound by means of IR spectrometry[6] and X-ray diffraction analysis.[5] Harrison and Pio[19] and Stevens et al.[20] also showed the ion-balance method, that ammonium chloride was one of the major compounds present in atmospheric aerosol. A similar analysis was applied to the present data.

Figure 6 is a plot of ammonium against the sum of the chloride, nitrate, and sulfate concentrations in the fine mode; the corresponding coarse-mode plot was not attempted because the sodium and calcium components, two major coarse-mode cations, were not determined in this study. The ion concentrations were expressed in units of μmol dm^{-3} to enable testing of the ion charge balance. Most of the points located on or slightly below the diagonal dotted 1 : 1 line were interpreted as corresponding to the condition in which all the anions cited were associated with ammonium ions.

The points falling below the line were attributable to the sulfuric acid and/or the ammoniumhydrogen sulfate, and possibly also to the sodium and calcium ions, which were not determined in this study. In some samples, a larger amount is obtained for ammonium than the three-anion sum. This may result from imprecision in analytical measurements, but in part it may also be due to the existence of organic salts of ammonium.

However, the data in Fig. 6 strongly suggest that the fine chloride and nitrate are in the form of the respective ammonium salts.

Simulation of Summer Temperatures. Another examination determined the chemical forms of fine-chloride and nitrate. Winter aerosol samples were subjected to heating in order to simulate summer

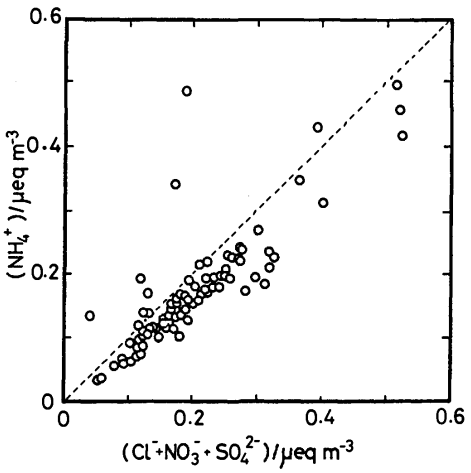

Fig. 6. Comparison of ammonium, and chloride, nitrate and sulfate concentrations in the fine mode on an equivalent basis.

temperature conditions. If the seasonal variation is derived from the temperature dependence of the gas-solid equilibria (Eqs. 2 and 3), the winter aerosol sample may be expected to exhibit a similar variation upon being heated to a summer temerature. Coarse- and fine-mode aerosol samples in winter were heated as follows. The filter at Stage 3 (50% ECD: 3.3 μm) and the backup filter were chosen to represent particles in the coarse- and fine-mode respectively. Filters with samples on were cut along a diagonal line into two equivalent parts. One part was directly subjected to the ion analysis as the reference. The other was heated, prior to the ion determination, in a temperature-controlled oven for 24 or 48 h at a typical summer temperature (between 25 and 30 °C).

Table 1 shows the ratio, C_a/C_b, of the concentrations after- (C_a) to before-heating (C_b), the subscripts a and b denote "after" and "before" respectively. For the coarse mode, the ratios were almost unity, which indicated that no vaporization took place at these temperatures. The coarse-mode ammonium was not determined because the concentration in this sample part was immeasurably small. In contrast, the fine-mode chloride, nitrate, and ammonium decreased in the C_a/C_b ratio, showing the vaporization losses of these ionic species. Nevertheless, the ratio of fine sulfate showed no appreciable change: $C_a/C_b=1.00\pm 0.06$.

For the fine mode, the ratio of the decreased amount of these anions to that of ammonium, $(\Delta Cl^- + \Delta NO_3^-)/\Delta NH_4^+$, was found to be 0.97 ± 0.12, essentially unity (Table 1). The fine-mode anionic species were concluded to form the respective ammonium salts: NH_4Cl, NH_4NO_3, $(NH_4)_2SO_4$, and their mixed salts, such as $(NH_4)_2SO_4\ nNH_4NO_3$ (n=1, 2).[5]

These findings show that fine-mode chloride, nitrate, and ammonium are highly volatile compared with the sulfate. Further, we interpret these results as indicating that the amount of species lost is in the form of NH_4Cl and NH_4NO_3 vapor. For the fine-mode ionic concentration of these winter samples, the averaged atmospheric concentration of ammonium (0.281 μequiv m^{-3}) agreed well with the averaged anion-sum (0.293 μequiv m^{-3}, where chloride: 0.090; nitrate: 0.077; sulfate: 0.126 μequiv m^{-3}).

Concentration Products of NH_3 and HCl, and NH_3 and HNO_3. Because both ammonium chloride and nitrate are volatile, hydrochloric and nitric acids volatalized from the fine-mode aerosol may be expected to exhibit complementary seasonal variations. However, the gaseous concentrations are restricted to the chemical equilibria, Eqs. 2 and 3:

$$NH_4Cl(s) \rightleftarrows NH_3(g) + HCl(g)\ K_2 \quad (2)$$

$$NH_4NO_3(s) \rightleftarrows NH_3(g) + HNO_3(g)\ K_3 \quad (3)$$

If these equilibria are attained in the atmosphere, the gas-concentration products, $P(NH_3)\cdot P(HCl)$ and $P(NH_3)\cdot P(HNO_3)$, should be equal to the equilibrium constants. The equilibrium constants for Eqs. 2 and 3 have been thermochemically calculated.[21-25]

In Fig. 7, the logarithm of the observed concentration products for NH_4Cl and NH_4NO_3 are plotted together with calculated and measured equilibrium constants, as a function of the reciprocal temperatures. The error bar corresponds to the assumed uncertainty of the gas concentration, 20% in either direction. The present plots agree very well with the predicted temperature dependences, K_2 and K_3, within the limits of experimental error. This agreement is encouraging.

The concentration product for NH_4Cl was found to be generally larger than that for NH_4NO_3; this was consistent with the fact that K_2 is larger than K_3, judging from both the calculated and measured vapor pressures.[21,24]

A number of groups have reported comparison of the observed NH_3-HCl[26-28] and NH_3-HNO_3[24,29-32] concentration products with calculations. For the NH_3-HNO_3 system, Hildermann et al.[31] have shown that measurements and theory are in good agreement for inland sites employing filter-based techniques without diffusion denuders. So far as we have sur-

Table 1. Concentration Ratios of after- to before Heating

No.	Sampling period	Coarse-mode			Fine-mode				$\Delta Cl^- + \Delta NO_3^-$
		Cl^-	NO_3^-	SO_4^{2-}	NH_4^+	Cl^-	NO_3^-	SO_4^{2-}	ΔNH_4^+
1	Feb. 5— 6, 1981	0.93	1.03	0.72	0.63	0.49	0.48	0.91	0.91
2	6— 7	0.94	0.98	0.95	0.76	0.62	0.68	1.03	1.11
3	13—14	0.78	0.86	1.13	0.56	0.39	0.65	0.91	0.95
4	16—17	1.00	0.96	1.00	0.69	0.53	0.56	1.01	0.80
5	18—19	1.07	0.97	0.93	0.84	0.71	0.78	0.99	1.08
6	20—21	0.91	0.97	1.25	0.82	0.83	0.69	1.02	0.89
7	26—28	0.82	0.83	1.04	0.71	0.54	0.61	1.05	1.01
8	Mar. 5— 7	0.98	1.04	1.01	0.80	0.36	0.76	1.09	0.90
9	5— 7	0.93	0.83	0.97	0.83	0.57	0.78	1.04	1.19
10	9—11	0.97	0.94	1.13	0.64	0.42	0.65	1.02	0.87
11	9—11	1.01	0.89	1.03	0.73	0.67	0.68	0.96	0.91
	Mean	0.94	0.94	1.01	0.73	0.56	0.67	1.00	0.97±0.12

Two Andersen samplers were simultaneously employed in March, 1981.

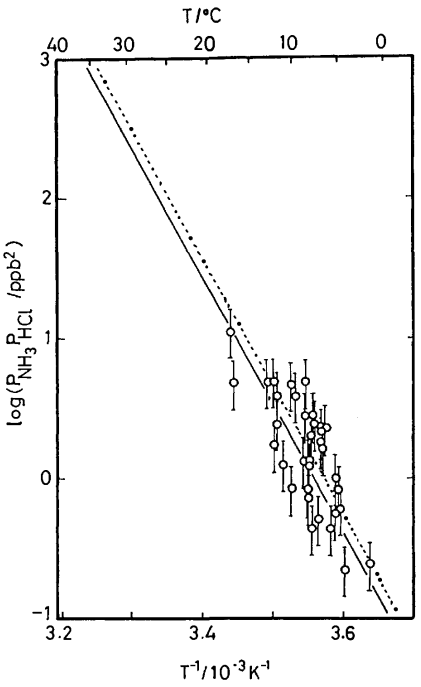

Fig. 7. Relationship between the measured NH_3–HCl products and ambient temperaute. The lines are calculated (——) and experimental (----) equilibrium constant, K_2.

veyed the literature, the other observational results exhibit considerable deviations in either direction from the predicted values even if the denuder method was applied to the nitric acid determinations. The magnitude of potential interference for the nitric acid measurement must be unequivocally determined in order to establish whether the equilibirum relationship, Eq. 3, holds in the atmosphere.

Theoretical models have been developed in consideration of several factors, such as the relative humidity[22,23,25] and such coexisting salts as $(NH_4)_2SO_4$.[25] Recently, however, Jaffe has pointed out potentially unwarranted confidence in the theoretical equilibrium constant.[35] If the free energy and enthalpy values are derived from the experimental equilibrium constants at temperatures well above the ambient conditions, as is the case for NH_4NO_3 (76—165 °C), the extrapolation of the calculated results on the basis of the thermodynamical vaules to ambient temperatures could lead to serious errors in the predicted concentration product.

The atmospheric concentration product in Eqs. 2 and 3 are still open to further discussion. Highly time-resolved observations and more sophisticated theoretical considerations based on reliable thermodynamical data are required to obtain quantitative explanations of these systems.[38–40]

***f*-Values.** In terms of the gas-particle distribution factor, defined as in Eq. 4, the involvement of the equilibria, Eqs. 2 and 3, in the seasonal-variation mechanism of the size-distribution was qualitatively examined. This factor was originally introduced by Grosjean and Friedlander[36] in examining carbonacious compounds, for the component, X, between the gas and aerosol phases as follows:

$$f(X)=P(X)/(G(X)+P(X)) \quad (4)$$

where $P(X)$ and $G(X)$ are the aerosol and gaseous concentrations, in $\mu g\,m^{-3}$ as X (Cl^- or NO_3^- in the fine mode or the corresponding gaseous form).

The temperature dependence of the values of this factor (the *f*-values) for chloride and nitrate species were examined over a wider range of temperature than that of the concentration products (Fig. 8). Over the range of 5—30 °C, the distribution factors decreased for both chloride and nitrate aerosol from near unity to zero with the temperature. This demonstrates that gaseous forms are favored in the summer period, while aerosol forms are favored in winter. These findings are in harmony with the above equilibria, Eqs. 2 and 3.

Tanaka et al.[28] undertook a similar investigation of gaseous and particulate chloride, nitrate, and ammonium species at a wooded park about 500 m from our institute in June, 1985, and February, 1986. The gas-particle distributions for chloride and nitrate were shown to be affected by the temperature in the same manner. Sasaki et al.[37] measured nitrate aerosol and nitric acid in four sites on the Kanto Plain from 28 to 30 July, 1983; they found that nitrate dominated over nitric acid as the temperature increased.

The restriction of the equilibria (Eqs. 2 and 3),

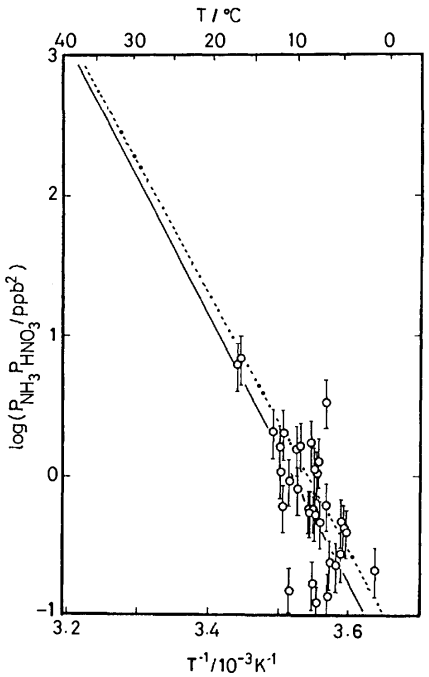

Fig. 8. Relationship between the measured NH_3–HNO_3 products and ambient temperaute. The lines are calculated (——) and experimental (----) equilibrium constant, K_3.

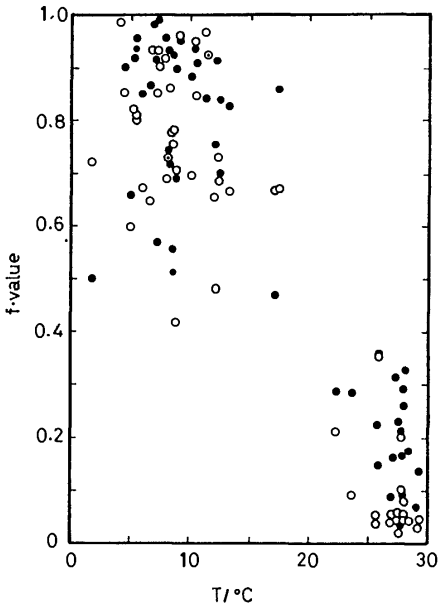

Fig. 9. Temperature dependence of *f*-values for chloride (O) and nitrate (●).

caused the seasonal variation over a wider range in the fine chloride and nitrate concentrations. In Tokyo, the range happens to be significantly both over and under the coase-mode concentrations; this results in our observed variation in the size distributions with the season.

Frequency Distributions. The cumulative distributions for the fine-, coarse-mode, and total concentrations of chloride, nitrate, sulfate, and ammonium aerosols are displayed in Fig. 9. The parameters approximated very closely to the log-normal distributions. Further, fine-mode chloride and nitrate showed bimodal distributions. This bimodal feature probably results from the temperature dependence of the equilibria, Eqs. 2 and 3.

Coarse nitrate and ammonium, as well as fine-mode chloride and nitrate, showed the bimodal distributions. A considerable change in the concentration level of fine chloride and nitrate (Figs. 4(a) and 5(a)) was observed at about 15 °C. At higher temperatures, the concentration level was rather lower than the level at lower temperatures. This change may be ascribed to the temperature dependence of the equilibria, Eqs. 2 and 3, which results in the bimodal distribution of the fine-chloride and nitrate concentrations. Although bimodal characteristics have also been observed for coarse nitrate and ammonium, no feasible explanation can as yet be offered for the distributional features of these species.

Anionic Composition of Coarse and Fine Aerosol. The relative molar-contributions of the three anions were obtained for fine and coarse modes respectively, classified with respect to the temperature (Fig. 10). In both modes, chloride was demonstrated to be a significant component.

For the fine mode, the relative composition depended dramatically upon the temperature. Chloride contributed 45% of the anions at temperatures below 5 °C. Nitrate exhibited a similar, but not so obvious, dependence. Sulfate contributed more as the temperature increased.

For the coarse mode, on the other hand, the composition was rather invariant with the temperature: chloride always constituted nearly half of the anions. Coarse chloride and nitrate are usually considered to be of seasalt origin and to result from the chlorine-loss reaction, Eq. 1, respectively. If the molar ratio of sulfate to chloride of the seawater (0.0517) is conserved throughout its transport as a seasalt particle, the seasalt sulfate was evaluated as contributing one-third of

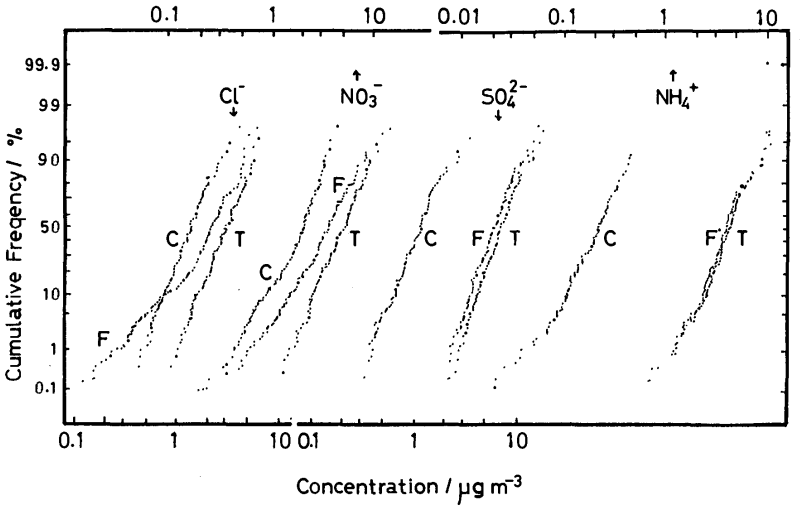

Fig. 10. Cumulative frequency distriubutions of concentrations for indicated species. F, fine-mode; C, coarse-mode; T, the sum of fine- and coarse-modes, F+C. The arrow near the name of a species indicates its concentration scale.

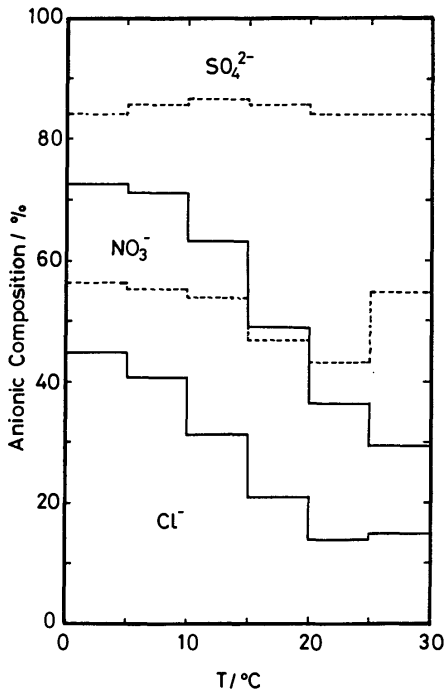

Fig. 11. Relative molar compositons of chloride, nitrate, and sulfate in the fine- (——) and coarse-mode (----) classified by temperature.

the coarse sulfate.

References

1) C. E. Junge, "Air Chemistry and Radioactivity," Academic Press, New York (1963), Chap. 2.

2) G. M. Hidy, "Aerosols," ed by S. D. Lee, T. Schneider, L. D. Grant, and P. J. Verkerk, Lewis Publishers, Chelsea, Michigan (1986), Chap. 2.

3) E. J. Kaplin, *Environ. Sci. Technol.*, **14**, 1149 (1980).

4) P. D. Biggins and R. M. Harrison, *Environ. Sci. Technol.*, **13**, 558 (1979).

5) R. M. Harrison and W. T. Sturges, *Atmos. Environ.*, **18**, 1829 (1984).

6) P. T. Cunningham, S. A. Johnson, and R. T. Yang, *Environ. Sci. Technol.*, **8**, 131 (1974).

7) H. Hara, K. Honda, K. Nagara, and A. Goto, *Nippon Kagaku Kaishi*, **1983**, 1221.

8) H. Hara, 1st Symposium on Aerosol Science and Technology, Tsukuba, August 1983, Abstr., No. B41.

9) K. Yoshizumi and T. Okita, *J. Air Pollut. Control Assoc.*, **33**, 224 (1983).

10) S. K. Friedlander, "Smoke, Dust, and Haze," John Wiley & Sons, New York (1977), p. 14.

11) J. L. Durham and J. R. Brock, "Aerosols," ed by S. D. Lee, T. Schneider, L. D. Grant, and P. J. Verkerk, Lewis Publishers, Chelsea, Michigan (1986), Chap. 17.

12) S. Kadowaki, *Atmos. Environ.*, **10**, 39 (1976).

13) S. Kadowaki, *Atmos. Environ.*, **11**, 671 (1977).

14) J. D. Spengler, and G. D. Thurstoni, *J. Air Pollut. Control Assoc.*, **33**, 1162 (1983).

15) M. Willson, A. G. Clarke, and E. M. Zeki, *Atmos. Environ*, **19**, 1081 (1985).

16) H. Hara, K. Nagara, K, Honda, and A. Goto, *Taiki Osen Gakkaishi*, **15**, 390 (1980).

17) S. Ohta, T. Okita, and H. Hara, *Taiki Osen Gakkaishi*, **13**, 239 (1978).

18) W. John, S. M. Wall, and J. L. Ondo, *Atmos. Environ.*, **22**, 1627 (1988).

19) R. M. Harrison and C. A. Pio, *Environ. Sci. Technol.*, **17**, 169 (1983).

20) R. K. Stevens, T. G. Dzubay, R. W. Shaw, Jr., W. A. McClenny, C. W. Lewis, and W. E. Willson, *Environ. Sci. Technol.*, **14**, 1491 (1980).

21) C. A. Pio and R. M. Harrison, *Atmos. Environ.*, **21**, 1243 (1987).

22) C. A. Pio and R. M. Harrison, *Atmos. Environ.*, **21**, 2711 (1987).

23) H. Hara, *Chem. Lett.*, **1988**, 713.

24) A. W. Stelson, S. K. Friedlander, and J. H. Seinfeld, *Atmos. Environ.*, **13**, 369 (1979).

25) A. W. Stelson, M. E. Bassett, and J. H. Seinfeld, "Chemistry of Particles, Fogs, and Rain," ed by J. L. Durham, Ann Arbor Science, Boston (1984), Chap. 1.

26) K. Inoue, K. Oka, K. Taguchi, and K. Yoshimura, *Osaka-fu Kogai Kanshi Center Shoho*, **6**, 93 (1983).

27) S. Ohta and M. Nakamura, 26th Annual Meeting of the Japan Society of Air Pollution, Tokyo, October 1985, Abstr., No. 647.

28) S. Tanaka, Y. Komazaki, K. Yamanaka, and Y. Hashimoto, *Nippon Kagaku Kaishi*, **1987**, 2338.

29) S. H. Cadle, R. J. Countess, and N. A. Kelly, *Atmos. Environ.*, **16**, 2501 (1982).

30) R. M. Harrison and C. A. Pio, *Tellus*, **35B**, 155 (1983).

31) L. M. Hildermann, A. R. Russell, and G. R. Cass, *Atmos. Environ.*, **18**, 1737 (1984).

32) E. K. Lewin, R. G. de Pena, and J. P. Shimshock, *Atmos. Environ.*, **20**, 59 (1986).

33) K. G. Anlauf, J. W. Bottenheim, K. A. Brice, P. Fellin, and H. A. Wiebe, *Atmos. Environ.*, **19**, 1859 (1986).

34) J. W. Erisman, A. W. M. Vermetten, and W. A. H. Asman, *Atmos. Environ.*, **22**, 1153 (1988).

35) D. A. Jaffe, *Atmos. Environ.*, **22**, 2329 (1988).

36) D. Grosjean and S. K. Friedlander, *J. Air Pollut. Control Assoc.*, **25**, 1038 (1975).

37) K. Sasaki, H. Kurita, G. R. Carmichael, Y. S. Chang, K, Murano, and H. Ueda, *Atmos. Environ.*, **22**, 1301 (1988).

38) A. G. Russel and G. R. Cass, *Atmos. Environ.*, **18**, 1815 (1984).

39) C. Pilinis and J. H. Seinfeld, *Atmos. Environ.*, **21**, 943, 2453 (1987).

40) R. L. Tanner, *Atmos. Environ.*, **16**, 2935 (1982).

Studies on the Electrochemical Behavior of Thiadiazole Derivatives. Electroreduction of 2-Benzoylamino-5-[cyanoaryl-hydrazonomethyl]-1,3,4-thiadiazoles

H. M. Fahmy,* M. Abdel Azzem,† M. Abdul Wahab, N. Abdel Fattah, and M. A. Aboutabl
Chemistry Department, Faculty of Science, Cairo University, Egypt
†El Monoufia University, Egypt
(Received June 13, 1988)

The electrochemical behavior of some 1,3,4-thiadiazole derivatives substituted at C_5 (carbon number five in thiadiazole ring) with a hydrazono group has been studied at a dropping mercury electrode (DME) in different pH values. Controlled potential electrolysis (CPE) in alkaline medium, cyclic voltammetry (CV), ultraviolet spectra (UV) and pK_a studies confirmed the proposed mechanism.

Literature scanning revealed that very little has been reported on the electroreduction of derivatives containing the thiadiazole ring structure. The results showed with no evidence or supports that the waves exhibited by these derivatives are due to the ring attack.[1-3] Furthermore, our laboratory investigated recently the electroreduction of a series of thiadiazole derivatives[4,5] substituted by an activated olefinic double bond where a Ziegler-Throp reaction[6] took place in which the hetero ring was unaffected. In a program aiming to study the electrochemical behavior of thiadiazole derivatives, it was found of interest to report the electroreduction of a series of 2-benzoylamino-5-[cyanoarylhydrazonomethyl]-1,3,4-thiadiazoles (**Ia—e**) together with a model compound namely 2-benzoylamino-5-cyanomethyl-1,3,4-thiadiazole (**II**) in order to increase data of such compounds to help in solving the conflicting results concerning the electroreactivity of this hetero ring which were proved to have pronounced medical and pharmaceutical activities.[7,8]

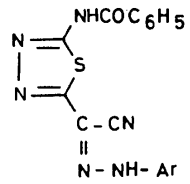

(I)

Ia Ar = C_6H_5
Ib Ar = p-Cl-C_6H_4
Ic Ar = p-OCH_3-C_6H_4
Id Ar = p-CH_3-C_6H_4
Ie Ar = m-NO_2-C_6H_4

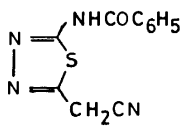

(II)

Experimental

(1) Organic Syntheses. (a) **2-Benzoylamino-5-cyanomethyl-1,3,4-thiadiazole (II)** was prepared according to literature[9] by refluxing a solution of 1-cyanoacetyl-4-benzoylthiosemicarbazide (1.0 g) in glacial acetic acid (30 ml) for five hours. The resulting solution was evaporated in vacuo and the remaining product was triturated with ethanol to give the solid product which was filtered off and recrystallized from acetic acid.

(b) 2-Benzoylamino-5-[cyanoarylhydrazonomethyl]-1,3,4-thiadiazoles (Ia—e) were prepared as follows: A solution of the appropriate aromatic diazonium salt (100 mmol) was added gradually to a cold solution of compound **II** (100 mmol) in ethanol (100 ml) and sodium acetate (13 g) with continuous stirring. The solid product thus formed was collected by filtration, washed with water, dried and finally crystallized from the appropriate solvent.

(2) Electrochemical Measurements. Polarograms were recorded with a Metrohm Polarecord E 506 with appropriate attachement E 505 using the Ag/10^{-2} M Ag^+ reference electrode and 10^{-4} M solutions in 50% by volume ethanolic Britton-Robinson buffers (1 M=1 mol dm^{-3}).[10] The capillary possessed the following characteristics in 0.1 M KNO_3 open circuit: t=3.9 s $drop^{-1}$, m=1.54 mg s^{-1} for h=52 cm. Cyclic voltammograms were recorded using a hanging drop mercury electrode (HDME) as working electrode with varying scan rates 50—800 mV s^{-1}. The pH-measurements were carried out with an Iskra Kranj pH-meter MA 5701.

(3) Spectrophotometric Measurements. Spectrophotometric measurements were carried out on a PYE Unicam 1800 spectrophotometer supplemented with a program controller automatic linear recording unit. The spectra were recorded on 4×10^{-5} M of the studied compound in 50% ethanolic Britton-Robinson buffer solutions. The pK_a were determined using the graphical correlation between pH and absorbance with their appropriate equations.[11]

(4) Preparative Electrolysis and Identification of the Resulting Products. The mercury pool electrolysis was carried out on 250 mg of the unsbstituted derivative in 200 ml 0.2 M NaOH due to the high insolubility of the compounds in acid media (BR acid mixture, dil HCl up to 2 M, H_2SO_4 up to 3.6 M and acetate buffer). By controlling the potential at −1.60 V vs. SCE, the current fell from 60 to 0.5 mA in ca. 4.5 hours of electrolysis. After complete electrolysis, the reaction mixture (pH=12.5) was acidified with concd HCl till pH≈1 at which the resulting compound began to precipitate. The product was filtered off and washed several times with hot ethanol (due to its insolubility in most solvents) to give a faint yellow compound of

mp=175 °C (yield ca. 60%) and identified as 2-benzoylamino-5-(α-aminocarboxymethyl)-1,3,4-thiadiazole. Azo dye test on the mother liquor gave a positive scarlet red color. IR of the resulting product (KBr) ν/cm^{-1}; 3460, 3240, 3030 (NH); 2900, 2760, 2700, 2640 (CH); 1660 (amide CO) (Fig. 1). ^1H NMR in DMSO: δ=4.08 (br., 1H, NH); 4.38 (1H, CH); 7.50 (6H, 3H aromatic protons and 3H, NH); 8.02 (2H, ortho-aromatic protons). ^1H NMR with D_2O: δ=4.38 (1H, CH); 7.50 (3H, aromatic protons); 8.02 (2H, ortho-aromatic protons). UV (in DMF) λ_{max} at 270, 372 nm respectively. Calcd: C, 47.4; H, 3.6; S, 11.5; N, 20.1; O, 17.2%. Found: C, 47.1; H, 5.0; S, 12.3; N, 18.8; O, 16.5%. MS m/z=278, 256, 212, 206, 195, 181, 151, and 110.

Results and Discussion

The polarograms of 10^{-4}M of **Ia**, taken as a typical example for the studied series **Ia—e**, are illustrated in Fig. 2. From the effect of mercury-height variation on i_l, cyclic voltammetry and routine analyses, it is found that each compound exhibits a four-electron diffusion-controlled irreversible wave A. This wave splits into two wavelets A_1 and A_2 of approximate

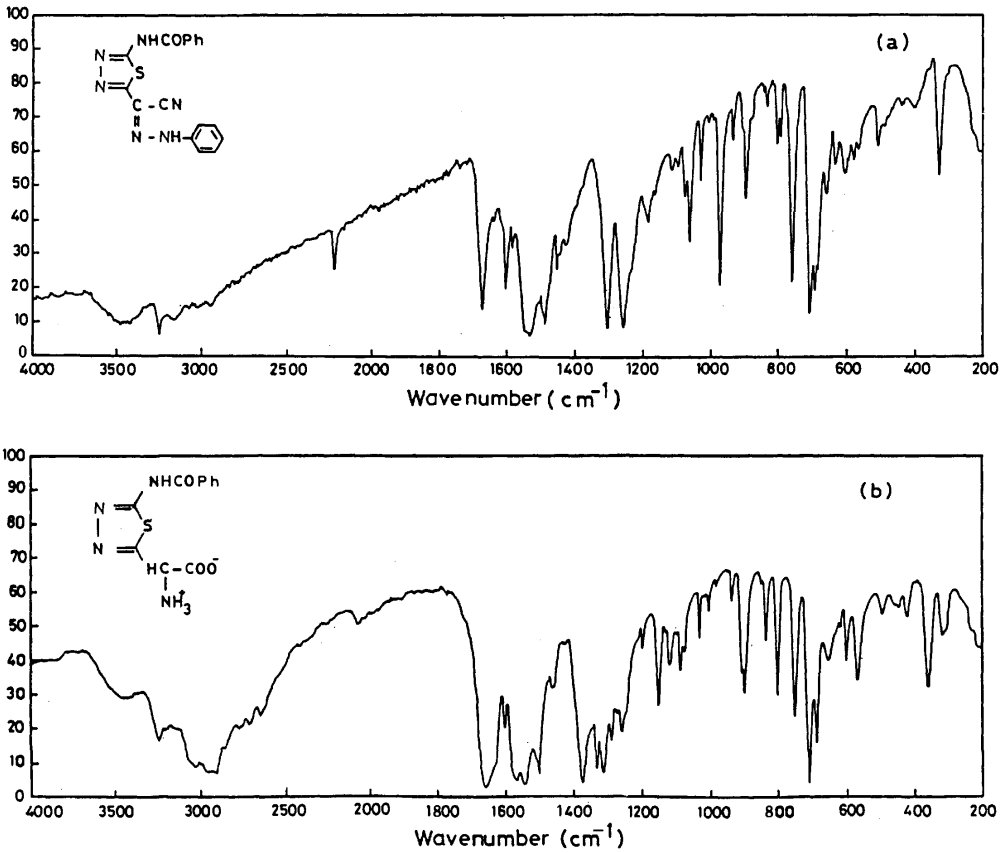

Fig. 1. (a) IR spectrum of starting compound **Ia** in KBr. (b) IR spectrum of product, obtained from CPE, in KBr.

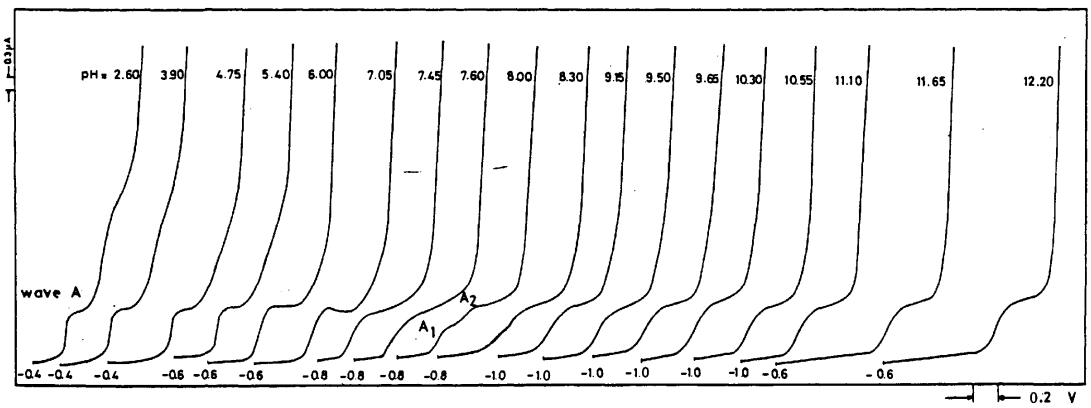

Fig. 2. Schematic representation of the polarograms of 10^{-4} M of compound **Ia** in 50% (v/v) ethanolic Britton-Robinson buffers.

Table 1. Linear Representation of $E_{1/2}$-pH Dependence for Wave A and Spectrophotometric Acid Dissociation Constants of 2-Benzoylamino-5-[cyanoaryl-hydrazonomethyl]-1,3,4-thiadiazole (**Ia—e**)

Compound	$E_{1/2}$-pH equation[a]	$E_{1/2}$-pH equation[b]	pK_{a1}	pK_{a2}
Ia	$E_{1/2}=-0.51-0.076$ pH	$E_{1/2}=-1.08-0.031$ pH	6.06	10.9
Ib	$E_{1/2}=-0.53-0.071$ pH	$E_{1/2}=-0.87-0.050$ pH	6.17	10.2
Ic	$E_{1/2}=-0.52-0.077$ pH	$E_{1/2}=-1.20-0.024$ pH	6.07	11.4
Id	$E_{1/2}=-0.52-0.077$ pH	$E_{1/2}=-1.20-0.023$ pH	6.17	11.2
Ie	$E_{1/2}=-0.47-0.076$ pH $E_{1/2}=-0.01-0.063$ pH[c]	$E_{1/2}=-1.02-0.035$ pH	6.02	9.03

a) Equation valid in the pH range 2—7.5. b) Equation valid at pH >9. c) Equation of the NO_2 group in the whole pH range.

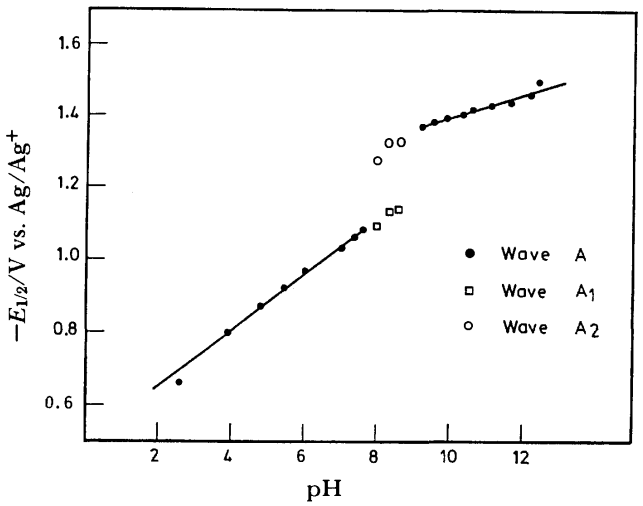

Fig. 3a. $E_{1/2}$-pH plots of the polarographic waves of 10^{-4} M compound **Ia** in 50% (v/v) ethanolic Britton-Robinson buffers.

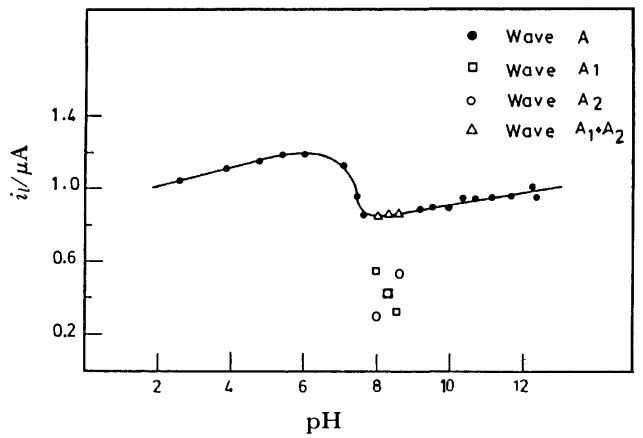

Fig. 3b. i_l-pH plots of the polarographic waves of 10^{-4} M compound **Ia** in 50% (v/v) ethanolic Britton-Robinson buffers.

equal heights in the narrow pH range 7.8—9.0, then A_1 and A_2 merge again to give A. The variation of $E_{1/2}$ and i_l with pH is given in Figs. 3a and 3b respectively. The shift of $E_{1/2}$ towards more negative potential with increase of pH for compounds **Ia—e** is compiled in Table 1.

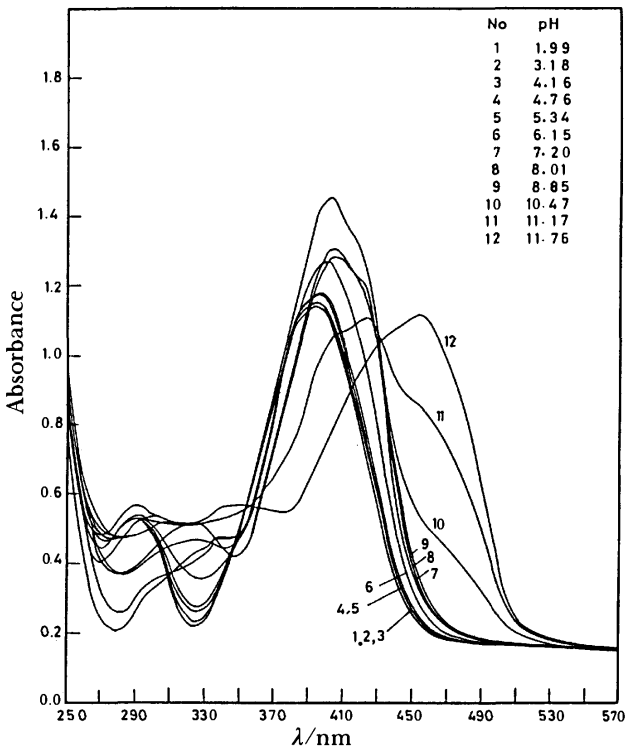

Fig. 4. Electronic absorption spectra of 4×10^{-5} M compound **Ia** in 50% (v/v) ethanolic Britton-Robinson buffers.

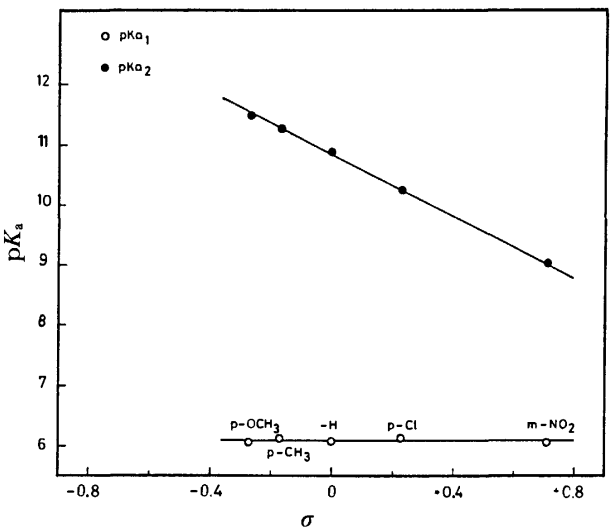

Fig. 5. pK_a-σ plots for compounds **Ia—e**.

Table 2. Polarographic Characteristics of 2-Benzoylamino-5-[cyanoarylhydrazonomethyl]-1,3,4-thiadiazole (**Ia**—e)

Compound No.	pH	$-E_{1/2}$/V vs. Ag/AgCl	$i_d/\mu A$	$RT/\alpha nF$	n	$D\times10^{-6}$/ $cm^2\,s^{-1}$
Ia	4.75	0.88	1.16	0.058	4	5.9895
	10.30	1.14	0.96	0.090	4	4.1022
Ib	4.75	0.88	0.95	0.050	4	4.0172
	10.30	1.37	0.89	0.079	4	3.5258
Ic	3.90	0.81	1.14	0.042	4	5.7847
	10.40	1.44	0.99	0.110	4	4.3626
Id	4.75	0.895	0.96	0.05	4	4.1022
	11.65	1.45	0.82	0.075	4	2.9930
Ie	4.75	0.835	0.99	0.070	4	4.3626
	11.65	1.41	0.93	0.060	4	3.8498

t=3.9 s. m=1.54 mg s^{-1}. c=0.1 mM(for D)=10^{-4} M for $E_{1/2}$ and i_l.

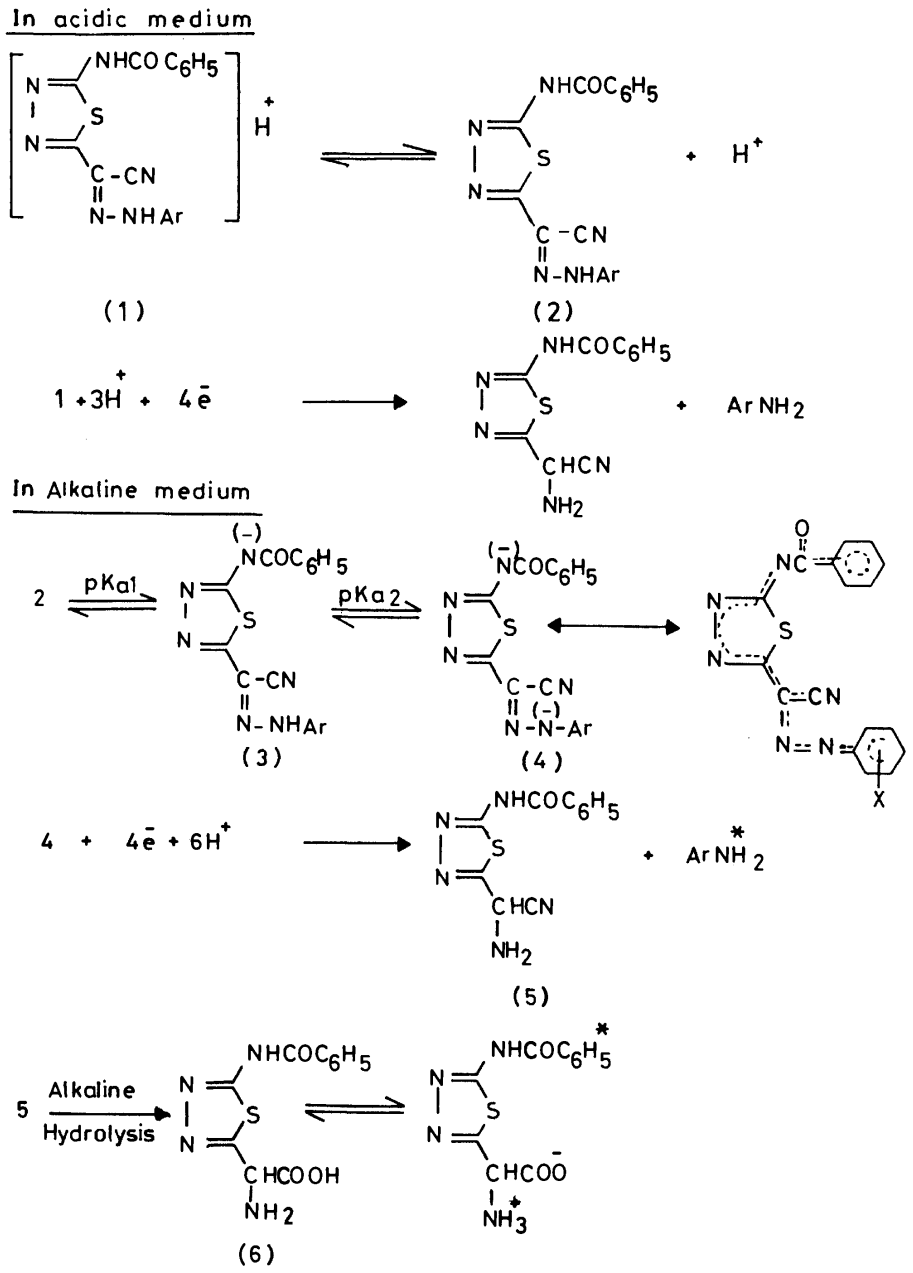

* Isolated and identified products

Scheme 1.

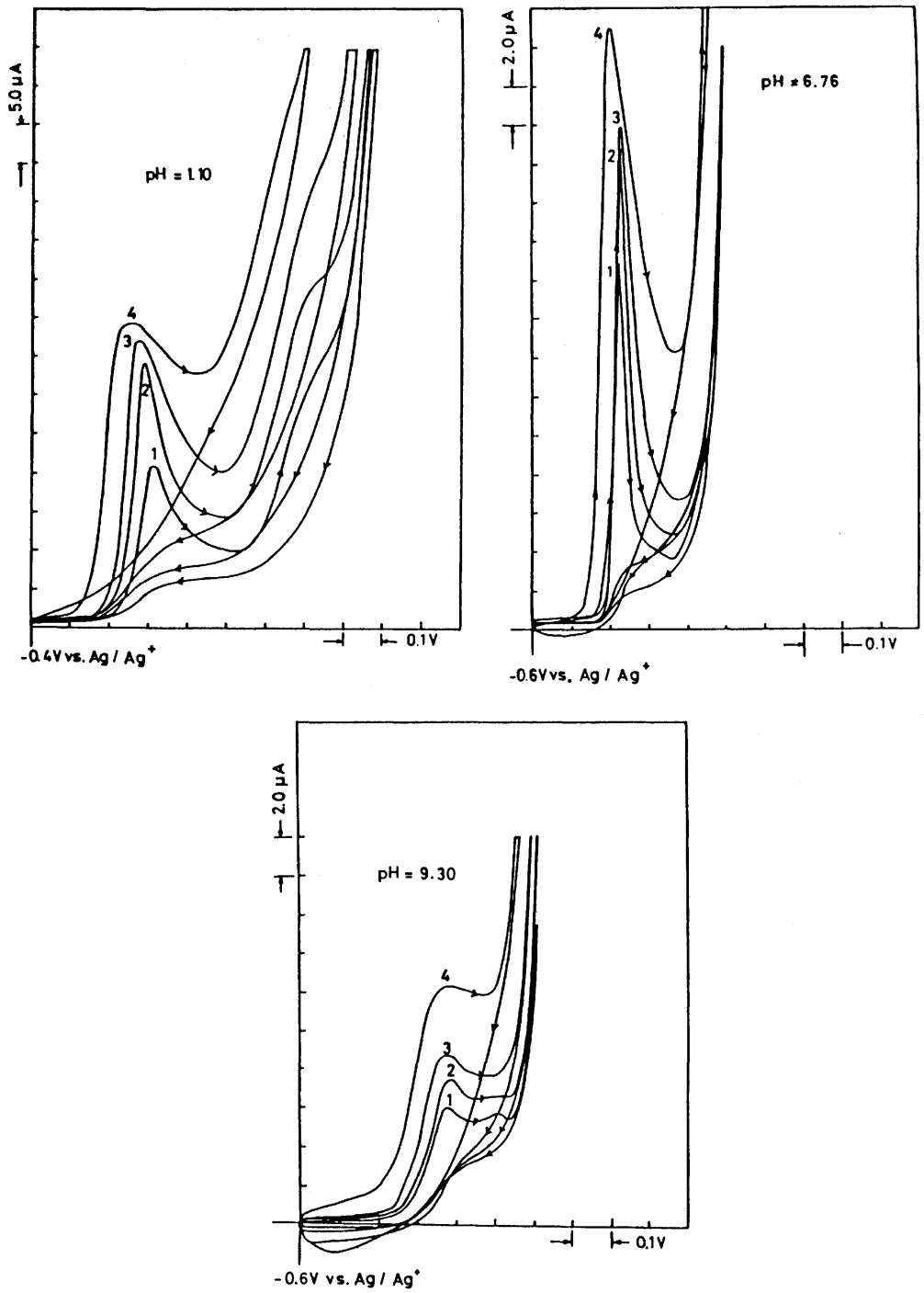

Fig. 6. Cyclic voltammograms of **Ia** at different pH values. 1; 50, 2; 100, 3; 200, 4; 500 mV s^{-1}.

The i_l-pH plot shows a moderate increase of i_l up to pH ca. 6 after which a weak dissociation curve appears in the pH range 6—8.5 followed again by a slight increase of i_l with increasing pH. In exception, compound **Ie** has revealed another four-electron wave. The less negative one was considered to correspond to the reduction of the NO_2 group into NHOH function. This assignment is based on the similar behavior of this wave with that reported for aromatic nitro compounds.[12]

Absorption Spectra of Compounds Ia—e and II. In solution of pH values 1.99—6.15 the absorption spectra of 4×10^{-5} M compound **Ia** are characterized by a strong band with λ_{max} at 396 and a weak one with λ_{max} at 290 nm. These are due to the absorption of the nonionized form liable to exist at low pH values. With increasing pH from 6.15 to 7.00 a red shift occurs giving rise to a band with λ_{max} at 404 nm and a shoulder at ca. 320 nm. As pH is further increased up to pH 8.85, the shoulder at 320 nm appears as a weak

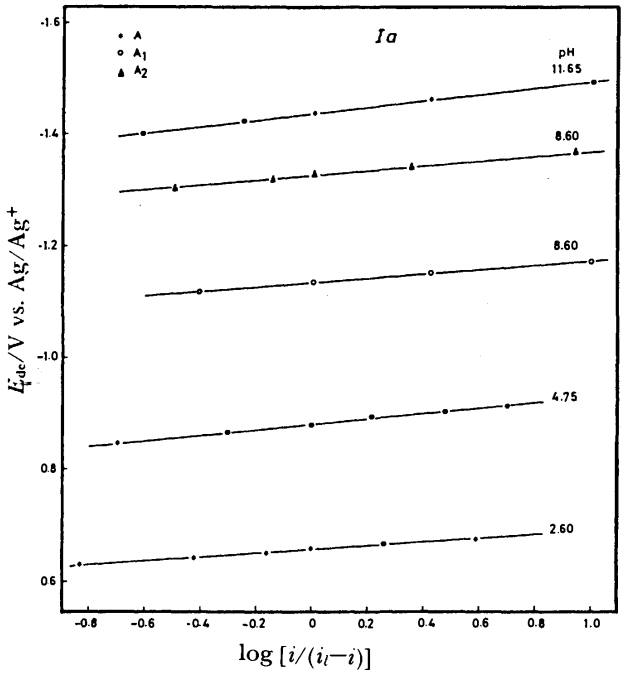

Fig. 7. Some representative logarithmic analysis plots for **Ia** at different pH values.

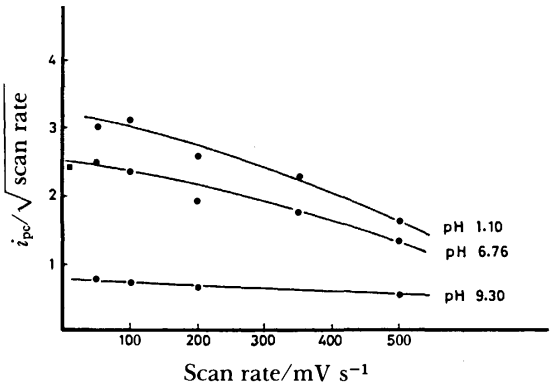

Fig. 8. Plots of the ratio of cathodic peak currents to the square roots of the scan rate as a function of the scan rate.

band at λ_{max}=322 nm. The shift of pH to the alkaline side is then accompanied by a red shift of the strong band as shown in Fig. 4. The absorption spectra are characterized by the presence of two isosbestic points at 304 and 346 nm in the pH range 1.99—8.85. The apparent ionization constant was calculated and the mean pK_a for each member is compiled in Table 1. The absorption spectra of model compound **II** showed one band at 270 nm in the pH range 1.99—6.15. At pH 6.15—11.76 the band is red-shifted acquiring λ_{max} at 310 nm. One isobestic point at 288 nm is observed throughout the whole pH range. Since all compounds **Ia—e** have practically constant pK_{a1} values ranging from 6.02 to 6.17 (cf. Table 1), it is clear that there is no dependence of ionization on the substituent effects. Hence, the ionizable center can be considered far from the aryl group, and this is confirmed by the fact that model compound **II** gave the same pK_a value (6.38). Therefore we can attribute the first pK_a to the ionization of the amide NH group (cf. Scheme 1). On the other hand, compounds **Ia—e** have another pK_{a2} depending mainly on the substituent effects as it is clear from the pK_a-σ correlation. Thus we can consider the pK_{a2} is due to hydrazono NH (cf. Scheme 1 and Fig. 5).

Mechanism of the Electrode Process. The behavior of wave A is in good agreement with the reported behavior of compounds containing the hydrazono linkage[13,14] and different from those containing the azo moiety.[15,16] This interpretation is confirmed by the fact that the wave corresponding to the reduction of the nitro moiety in compound **Ie** appeared before wave A.[17] Since the $E_{1/2}$ values of compounds **Ia—e** were pH-dependent and i_l-pH independent, it was concluded that both acidic and basic forms reach the electrode surface and are electroactive yielding the same product. Cyclic voltammograms at different pH values indicated that the processes are irreversible in nature (cf. Fig. 6) as confirmed by logarithmic analyses (cf. Table 2 and Fig. 7). It was shown that the relation between i_{pc} and $\sqrt{\nu}$ (where i_{pc} is the cathodic peak currents and ν is the scan rates) can be useful in deciding to which case in the Nicholson and Shain[18] classification a given process belongs. As is clear from Fig. 8 a CE mechanism takes place in acidic and neutral media which was confirmed by calculating $dE_{1/2}/d\,pH$ indicating that the protons are involved on the electrode reaction while it is an EC mechanism in alkaline medium. Based on the obtained results, one may propose Scheme 1 for the interpretation of these results. It is important to mention that it was difficult to carry out CPE in acidic medium due to the limited solubility of compounds **Ia—e**. Also, dianion **4** is stabilized through the spreading of the negative charge on the molecule. Finally we obtained compound **6** and not **5** due to the alkaline hydrolysis of the cyano group.[19]

The authors thanks Prof. M. R. H. Elmoghayar for providing the samples.

References

1) H. Lund, *Discuss. Faraday Soc.*, **45**, 193 (1968).
2) R. Zahradnik and J. Koutecky, *Collect. Czech. Chem. Commun.*, **26**, 156 (1961).
3) J. Goerdeler, J. Ohm, and O. Tegtmeyer, *Chem. Ber.*, **82**, 1534 (1955).
4) H. M. Fahmy, N. F. Abdel Fattah, M. R. H. Elmoghayar, and M. Abdel Azzem, *J. Chem. Soc., Perkin Trans. 2*, **1988**, 1.
5) M. Abdel Azzem, M. M. M. Ramiz, E. A. Ghali, H. M. Fahmy, and M. R. H. Elmoghayar, *Monatsh. Chem.*, **118**, 229 (1987).
6) S. Wawzonek, A. R. Zigman, and G. R. Tansen, *J. Electrochem. Soc.*, **117**, 1351 (1970).

7) D. Craciunescu, A. Doadrio Lopez, E. Gaston de Triarte, G. Tena, A. Gomez, R. Tena, and C. Chirvu, *An. R. Acad. Farm.*, **51**, 33 (1985).

8) R. Soliman, H. M. Mokhtar, and S. K. El Sadany, *J. Pharm. Sci.*, **73**, 403 (1984).

9) M. R. H. Elmoghayar, S. O. Abdalla, and M. Y. A. Nasr, *J. Heterocycl. Chem.*, **21**, 781 (1984).

10) H. T. S. Britton, "Hydrogen Ions," 4th ed, Chapman and Hall, London (1955), Vol. 1, p. 365.

11) R. M. Issa and A. H. Zwail, *J. Chem. U. A. R.*, **41**, 161 (1971).

12) H. Lund, "Cathodic Reduction of Nitro Compounds in Organic Electrochemistry," ed by M. M. Baizer, Dekker, New York (1973), Chap. VII, p. 315.

13) H. M. Fahmy, H. A. Daboun, K. Azziz, and M. Abdel Azzem, *J. Chem. Soc., Perkin Trans. 2*, **1983**, 425.

14) H. M. Fahmy, H. A. Ead, and M. Abdul Wahab, *J. Chem. Soc., Perkin Trans. 2*, **1985**, 45.

15) H. M. Fahmy, A. M. A. Helmy, and M. Abdel Azzem, *J. Electroanal. Chem.*, **201**, 101 (1986).

16) Yu. P. Kitaev, I. M. Skrebkova, and L. I. Maslova, *Izv. Akad. Nauk SSSR, Ser. Khim.*, **10**, 2194 (1970); *Chem. Abstr.*, **75**, 14233p (1971).

17) H. M. Fahmy, *Ann. Chim.*, **75**, 457 (1985).

18) R. S. Nicholson and I. Shain, *Anal. Chem.*, **36**, 106 (1964).

19) I. L. Finar, "Organic Chemistry," Vol. I, 6th ed, The English Language Book Society, (1973), p. 356.

 © 1989 The Chemical Society of Japan Bull. Chem. Soc. Jpn., 62, 2657—2661 (1989)

Alkylation of Toluene with 2-Propanol over Titania-Silica-Alumina Catalysts

K. V. C. Rao,* K. R. Sabu, and C. G. R. Nair†
Inter Disciplinary Research Group, Vikram Sarabhai Space Centre, Trivandrum-695022, India
†Department of Chemistry, University of Kerala, Trivandrum-695034, India
(Received July 11, 1988)

The alkylating activity of titania supported on silica-alumina has been reported earlier (V. G. Kumar, T. S. Shoba, and K. V. C. Rao, *Tetrahedron Lett.*, **26**, 3281 (1985)). Further investigations to synthesize such a catalyst with optimum alkylation activity resulted in the coprecipitation of the catalyst from a solution of pH 4—the test reaction selected being the alkylation of toluene with 2-propanol in a fixed bed tubular reactor. The product mixtures at different reaction times are analyzed to have a view on the variation of yields of different alkylated products with reaction time. The alkylated products are *o*-cymene, *p*-cymene, and diisopropyltoluenes (DIT). The presence of titania exerts a synergistic effect upon the alkylating activity of silica-alumina. Also the catalytic activity is governed by the physical characteristics of the catalyst like surface area and porosity. The trend of para-rich isomer distribution observed in the product mixture is attributed to the steric factors. It has been observed that *o*-cymene is formed at a constant rate whereas *p*-cymene formation decreased with reaction time. Increased formation of diisopropyltoluenes are observed with the passing of reaction time. Alkylation studies in the temperature range 165—240 °C have been done to find the effect of reaction temperature on the product distribution. Thus a decrease in the ortho to para molar ratio with increase in reaction temperature and increased formation of diisopropyltoluenes at lower temperatures are observed. No considerable reduction in the alkylation activity has been noticed up to five regeneration cycles.

Conventional catalysts like Lewis acids and mineral acids which are in use for the acid catalyzed alkylation reactions usually result in major corrosion problems due to large amounts of acid vapours.[1,2] Separation of the catalyst from the reaction products also poses difficulty in such homogeneous reactions. The introduction of solid acid catalysts like zeolites was a major breakthrough in alkylation chemistry.[2] Application of high-silica zeolites for alkylation process was realized commercially for the first time by Mobil/Badger[3] in 1980.[2] Crystalline aluminosilicate[4] and silica-alumina[5,6] were previously known to catalyze alkylation reactions. In addition, zeolites are modified by using alkaline earth metals[7] and Group IA,[8] Group IIIA,[9] and Group IVA[10] metals and are used for various alkylation reactions. The sulfates of metals like Zn, Al, Cd, Cu, and Ni supported on silica-alumina are used as catalysts in the alkylation of toluene with methanol of which zinc-sulfate supported on silica-alumina is the most active.[11] Silica-alumina,[12,13] reduced silica-alumina,[14] silica-alumina containing salts of Mn, Zn, Cr, Cu, Cd,[15] molecular sieves,[16] zeolites,[17,18] and rare-earth exchanged zeolites[19] are also used to alkylate benzene with ethylene.

Moreover, combinations of oxides of transition metals[20,21] alone or supported[22] on silica or silica-alumina are used for similar reactions. Certain supported systems like chromia/silica, molybdenum oxide on silica-alumina which are used for oligomerization and polymerization reactions respectively had indicated the utility of supported transition metal catalysts.[23–26] Incorporation of metal oxides may alter the catalytic activity and selectivity to different products.[27] A catalyst containing titanium oxide supported on silica-alumina was reported previously for the alkylation of different aromatic compounds.[28] A wide range of alkylating agents like alcohols, halides, and olefins have been used with this catalyst. The catalyst is reported to be regenerable also.

A systematic synthesis of Tisial catalysts and efficiency of these catalysts in the alkylation of toluene with 2-propanol has been reported in this paper. The catalytic activities of different Tisial catalysts are also compared with that of a synthetic silica-alumina sample. The effect of temperature on the catalytic activity of alkylation, the relative yields of different products and the regeneration studies of the catalyst have also been included.

Experimental

Sodium silicate (Scientific Chemicals), after dissolving in water, is filtered to remove any undissolved sediments. Aluminum sulfate used is of A.R. grade. Titanium tetrachloride is obtained from M/S Travancore Titanium Products, Chavara. Nitric acid and ammonia used are of chemically pure quality.

To an aqueous solution of sodium silicate (260 g dm^{-3} of distilled water) dilute nitric acid (1 : 1) is added at 90 °C under constant agitation, till the pH of the solution is reduced to one. The desired quantity of hot aluminum sulfate solution (333 g dm^{-3}) is added, followed by the addition of titanium tetrachloride (20 ml) under vigorous agitation. Ammonia solution is added slowly, till the required pH is attained. Precipitations are carried out at different pH's (2, 3, 4, 5, 6, 7, 8, and 9) and are designated as Tisial-2, Tisial-3, and so on. Silica-alumina catalyst is also synthesized at pH 4 without titania. The precipitates are washed with distilled water till free from sulfate ion and are extruded as pellets. These are dried at 120 °C for 12 h and sintered at 600 °C and used as catalysts for the

alkylation.

The silica to alumina molar ratio as well as titania contents of different catalysts determined by chemical analysis, and physical parameters such as pore volume, surface area etc., are included in Table 1.

The catalyst (25 g which corresponds to 60 ml in volume) is charged to a tubular glass reactor of 2.54 cm diameter. Provision is made to maintain the pre-catalyst, catalyst and post-catalyst zone temperatures at the desired levels. The reactor is fed under gravitational flow at a constant LHSV (liquid hourly space velocity) of 0.5 with a precalibrated capillary tube. The reaction products are collected by condensing the volatiles with chilled water. Samples are withdrawn from the bulk of the rection products at intervals of one hour and analyzed. The duration of each experiment is 7 h except for those done to study the effect of temperature on alkylation reaction, where it is 3 h. Toluene to 2-propanol molar ratio is kept at 3:1 in each experiment. To estimate the catalyst life for alkylation, the same catalyst (Tisial-5) is subjected to nine successive regenerations by passing air at the end of each experiment of 7 h at 600 °C.

Product mixtures are analyzed by gas chromatography in a Shimadzu GC-5A gas chromatograph. A stainless steel column (3 mm ϕ×2 m) packed with 5% SE 52 on Shimalite 60—80 mesh support is used under the experimental conditions of column temperature 120 °C, injection port temperature 220 °C, detector FID and carrier gas (Helium) flow rate of 60 cm^3 min^{-1}. A Shimadzu C-RIA data processor was used to calculate the peak areas. Products are found to be *p*-cymene (*p*-isopropyltoluene), *o*-cymene (*o*-isopropyltoluene), and three isomers of diisopropyltoluene (DIT). Percentage yields of alkylaromatics are calculated in the following way.

(i) For cymenes

$$\% \text{ Yield} = \frac{(\text{No of moles of cymene formed}) \times 100}{\text{No of moles of 2-propanol fed}}$$

(ii) For diisopropyltoluene (DIT):

$$\% \text{ Yield} = \frac{2 \times (\text{No of moles of DIT formed}) \times 100}{\text{No of moles of 2-propanol fed}}$$

Total Yield = (i) + (ii)

Products are also indentified by bp. Fractional distillation is done in a spinning band distillation column, B/R 36T; Option 3 (B. R. Instrument Coorporation, Maryland USA) at an rpm of 4000 and reflux ratio 20:1.

Results and Discussion

The extent of total conversion of 2-propanol to alkylaromatics over various Tisial and silica-alumina catalysts at 200 °C with reaction time is shown in Fig. 1. The conversion to *p*-cymene, *o*-cymene, and diisopropyltoluenes after the end of each hour of the experiment over Tisial-4 catalyst is given in Fig. 2.

Results of the study on regenerability and catalyst life is shown in Fig. 3.

Table 2 gives the mol% of 2-propanol converted to *o*-cymene and *p*-cymene over Tisial-4, Tisial-5, and silica-alumina catalysts.

The temperature dependence of alkylating activity

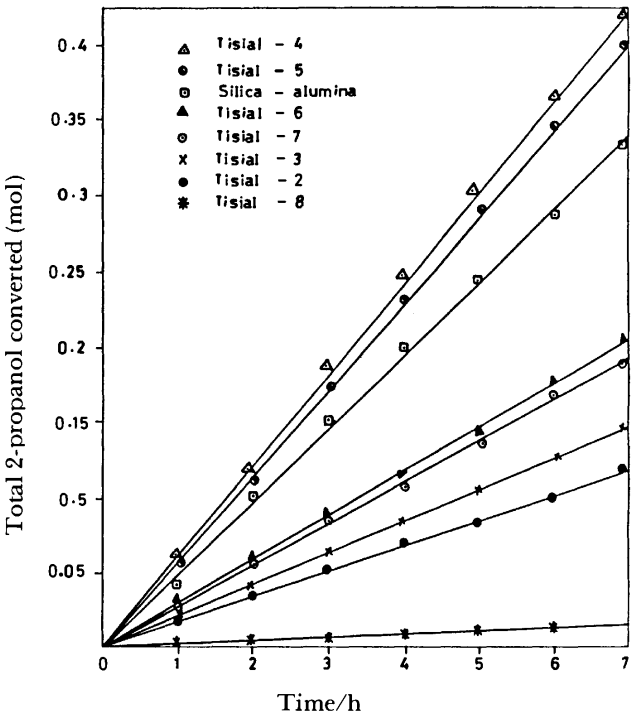

Fig. 1. Comparison of alkylating activity of different catalysts. (The cumulative number of moles of 2-propanol converted to alkylaromatics with reaction time is given.)
Reaction conditions; reaction temperature: 200 °C, LHSV: 0.5, 2-propanol/toluene (mole ratio)=1/3.

Table 1. Physicochemical Characteristics of Tisial Catalysts Precipitated at Different pH

Disignation	pH of co-pptn	SiO_2/Al_2O_3 (molar ratio)	$\%TiO_2$ (by wt)	Pore vol.	Surface area
				$cm^3 g^{-1}$	$m^2 g^{-1}$
Tisial-2	2	47.6	9.1	0.61	61.7
Tisial-3	3	39.2	10.0	0.68	67.5
Tisial-4	4	16.4	10.4	0.71	100.0
Tisial-5	5	9.0	12.3	0.60	65.5
Tisial-6	6	8.7	11.8	0.50	49.5
Tisial-7	7	8.3	11.1	0.35	46,0
Tisial-8	8	8.2	8.7	0.07	11.5
Tisial-9	9	7.8	8.6	0.03	—
SiO_2-Al_2O_3	4	16.3	—	1.20	135.0

is investigated over Tisial-4 catalyst at different temperatures viz. 165, 180, 200, 220, and 240 °C (Table 3).

The distribution of different components in the product mixture at different temperatures is given in Table 4.

The percentage of titania content varied only mariginally with the pH of coprecipitation, whereas silica to alumina molar ratio decreased drastically from 47.6 (pH=2) to 9 (pH=5) (Table 1) and further increase in pH does not have much effect. Lower pH may be maximizing the silica precipitation whereas precipitation of aluminum hydroxide is favored by higher pH. The surface area and pore volume of the catalyst also indicate an increase up to pH 4 and further a decrease as is evidenced from Table 1. These two physical parameters are considerably diminished by precipitation at higher pH. The conversion of 2-propanol to alkylaromatics over different Tisial catalysts also showed an identical trend, where

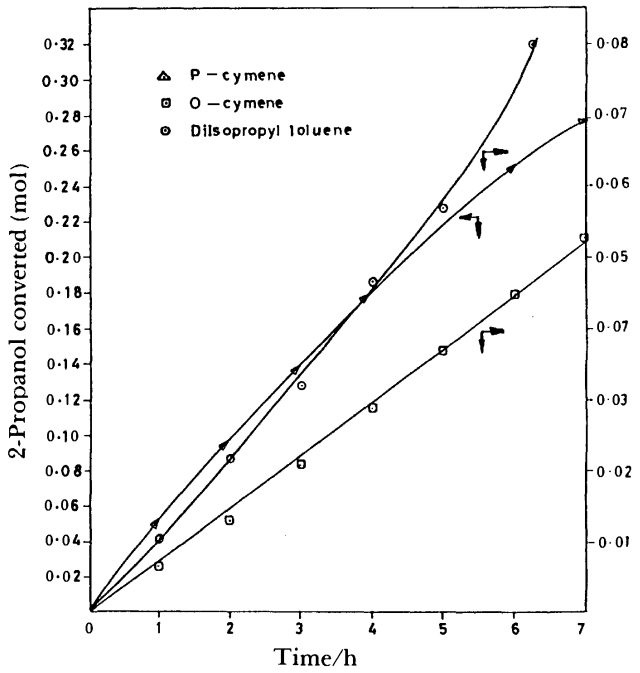

Fig. 2. Cumulative formation of *p*-cymene, *o*-cymene, and diisopropyltoluenes with reaction time over Tisial-4. (The number of moles of 2-propanol converted is given.)
Reaction conditions; reaction temperature: 200 °C, LHSV: 0.5, 2-propanol/toluene (mole ratio)=1/3.

Table 2. The Mole % of 2-Propanol Converted to *o*-Cymene and *p*-Cymene over Tisial-4, Tisial-5, and Silica-Alumina at 200 °C. Reaction Time: 7 h

Catalyst	% of 2-propanol converted;	
	to *o*-cymene	to *p*-cymene
Tisial-4	9.6	52.4
Tisial-5	10.0	46.4
$SiO-Al_2O_3$	9.3	37.3

Table 3. Effect of Temperature on the Alkylation Activity of Tisial-4. Reaction Time: 3 h

Temp	Yield/%				*o*/*p* ratio
°C	*o*-Cymene	*p*-Cymene	DIT	Total	
165	10.0	18.4	16.4	44.8	0.54
180	9.4	22.0	20.8	52.2	0.43
200	9.0	56.0	15.0	80.0	0.16
220	7.3	42.2	13.8	63.3	0.17
240	5.5	39.3	8.8	53.6	0.14

Table 4. Product Distribution (mol%) at Different Temperatures

Temp/°C	Toluene	*o*-Cymene	*p*-Cymene	DIT
165	88.3	3.2	5.9	2.6
180	86.0	3.1	7.2	3.5
200	72.8	2.9	21.5	2.6
220	81.0	2.4	14.4	2.3
240	84.0	1.7	12.6	1.6

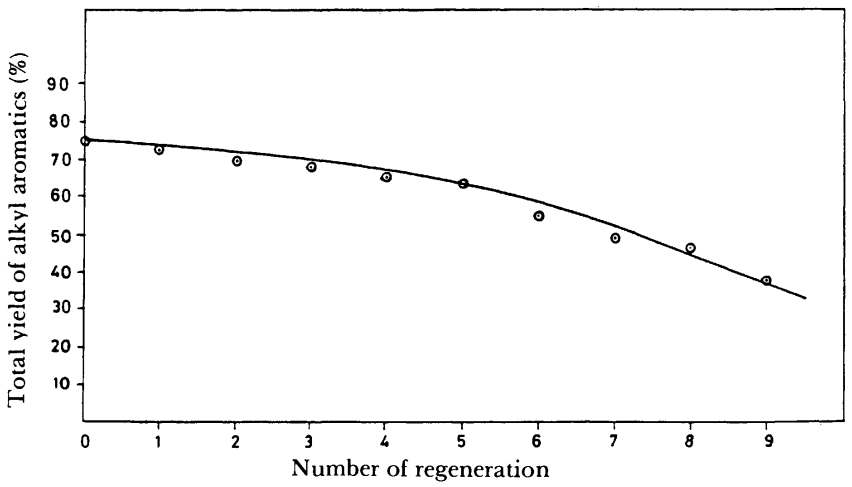

Fig. 3. Regeneration study over Tisial-5 catalyst. Reaction conditions; reaction temperature: 200 °C, LHSV: 0.5, 2-propanol/toluene (mole ratio)=1/3.

silica to alumina molar ratio of 16 (Tisial-4) appear to give optimum alkylation activity (Table 1 and Fig. 1). The comparison of the physicochemical characters as well as the activity for the alkylation of catalysts from Tisial-4 to Tisial-8 shows that the predominant factors governing the catalytic activity are the physical characteristics of the catalyst like surface area and pore volume, a higher value of which cause increased activity. However, the silica to alumina molar ratio also seems to be a controlling factor in the catalytic activity, which is evidenced by the lesser alkylating activity given by Tisial-2 and Tisial-3 with higher surface area and pore volume compared to Tisial-6 and Tisial-7 (Table 1 and Fig. 1).

The catalytic activity for the conversion of 2-propanol to alkylaromatics is much higher for Tisial-4 than for silica-alumina (Fig. 1). The surface area and pore volume for the latter are 135 $m^2 g^{-1}$ and 1.2 $cm^3 g^{-1}$ respectively and the corresponding values for Tisial-4 are 100 m^2 g^{-1} and 0.71 $cm^3 g^{-1}$ respectively. The silica to alumina molar ratio in both of these catalysts is 16. This reveals that the increased catalytic activity of Tisial-4 may be due to the presence of titania. When transition metal oxides are supported on silica-alumina, $\overset{+}{M}\cdots H$ species will be formed, where M is the transition metal.[28,29] These species initiate the alkylation reaction by the mechanism shown in Scheme 1.[28] The formation of the π-complex is possible because of the presence of low lying unoccupied d orbitals in the transition metal atom.[28,31] It may be presumed from the higher activity of the Tisial-4 catalyst that when titania is supported on silica-alumina, acid sites with suitable acid strength ($H_0 < +1.5$)[32] for the alkylation is increased. That is titania seems to exert a synergistic effect on silica-alumina.

Figure 1 also shows that the rate of formation of alkylaromatics remained constant with reaction time, for all the catalysts studied. In the product mixture the *p*-cymene content is more compared to *o*-cymene at a given time and the *o*-cymene concentration almost remained constant with reaction time. However, the rate of formation of *p*-cymene decreased with time and correspondingly the rate of formation of diisopropyltoluenes increased. This is illustrated in Fig. 2 by taking the case of Tisial-4. The trend of para-rich isomer may be due to the steric factors arising when the reacting species are adsorbed on adjoining sites.[33] Hence it can be assumed that the interaction between an adsorbed toluene molecule and the adsorbed alkylating moiety leads to the para isomer whereas the interaction of the latter with a free unadsorbed toluene in the gaseous state results in the ortho isomer. This also supports the observed lesser differences in the mol% of 2-propanol converted to *o*-cymene compared to that of *p*-cymene on Tisial-4, Tisial-5, and silica-alumina catalysts (Table 2). Also the simultaneous decrease of *p*-cymene and the increase of diisopropyltoluenes with time suggests that the *p*-cymene adsorbed is more prone to get further alkylated to produce diisopropyltoluenes. The results of the comparative study of Tisial-4 and silica-alumina show that the catalytic activity for the conversion of 2-propanol to alkylaromatics is increased by the presence of titania on silica-alumina.

Lesser amounts of alkyltoluenes are formed at temperatures lower than 200 °C. The optimum conversion of 2-propanol to alkylaromatics is observed at 200 °C (Table 3), above which it started decreasing. The increased conversion at 200 °C may be due to the effective diffusion of reactants into and the product molecules out from the pores of the catalyst.[34] The Lesser extent of formation of alkyltoluenes at temperatures 220 °C and 240 °C may be attributed to the possible formation of dealkylated product, namely toluene from the σ-complex (**2** of Scheme 1) by shifting the equilibrium. That is higher tempertures (>200 °C) favor the formation of toluene from the σ-complex, whereas lower temperatures give alkylated toluenes. This is inferred by the observation that the amount of unreacted toluene in the product mixture increased as the reaction temperature is increased

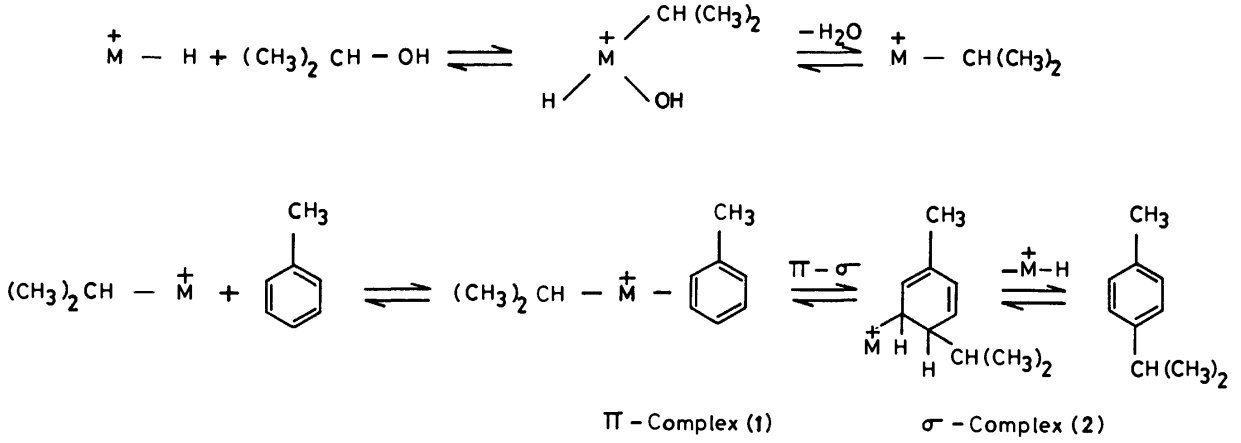

Scheme 1. The mechanism of alkylation catalyzed by transition metal oxide supported on silica-alumina.

beyond 200 °C (Table 4). Similarly, the dealkylation of formed cumene (isopropylbenzene) at temperatures >240 °C has also been observed by Baibuskii et al. over Y zeolite catalyst in the alkylation of benzene with propylene.[35]

In addition, the ortho isomer decreases marginally from 165 °C to 240 °C, while the para isomer shows an optimum at 200 °C (Table 3) and the ortho to para ratio decreases with increase of temperature. These observations are in line with those of alkylation reactions carried out on ion-exchanged zeolites.[32] Diisopropyltoluenes are formed in large amounts at lower temperatures (Table 3). This may be due to the high residence time of cymenes formed at lower temperatures resulting in further alkylation. In general, multialkylation may be favored at lower temperatures.[2]

Tisial-5 catalyst has been subjected to nine successive regenerations. The product pattern clearly indicate (Fig. 3) that alkylating activity of the catalyst is not appreciably affected by successive regenerations. This reveals that Tisial catalyst have sufficient active life for alkylation studies.

Conclusion

The silica-alumina supported titania catalysts are more active for the alkylation of toluene with 2-propanol than silica-alumina itself. Even in presence of titania, the physicochemical characteristics of the catalyst such as surface area, pore volume and silica to alumina molar ratio play a vital role in governing the catalytic activity. The Tisial catalyst co-precipitated from a solution of pH 4 has given the optimum conversion of 2-propanol to alkylaromatics. The para-rich isomer distribution can be attributed to steric factors. Multialkylation is found to be favoured at lower temperatures (<200 °C). The alkylating activity of the Tisial catalyst is not affected considerably by five successive regeneration cycles.

The authors gratefully acknowledge with thanks the support and encouragement given by Director, VSSC. They also acknowledge the help rendered by Dr. M. Rama Rao, Dr. V. G. Kumar, Mr. T. S. Radha Krishnan, Mr. S. Venkatachalam, and Mr. R. Natarajan for fruitful discussions. One of the authors (K. R. Sabu) acknowledges with gratitude the aid given to him by the U. G. C. in the form of a Junior Research Fellowship for carrying out this work.

References

1) H. Heinemann, *Catal. Rev.*, **8**, 312 (1974).
2) A. V. Deo, R. M. Cursetji, M. A. Purohit, V. G. Penkar, and V. V. Deshmukh, *Indian J. Technol.*, **21**, 363 (1983).
3) F. G. Devyer, P. J. Lewis, and F. H. Schineider, *Chem. Eng.*, **83**, 90 (1976).
4) E. F. Harper, D. Y. Ko, H. K. Lese, E. T. Sabourin, and R. C. Williamson, *ACS Symp. Ser.*, **55**, 371 (1977).
5) T. Saito, T. Tanno, Y. Iguchi, S. Shoji, (Hitachi Chem. Co., Ltd.) Ger. Offen. 2160465 (1972).
6) T. Saito, T. Tanno, T. Awano, and S. Shoji (Hitachi Ltd.) Ger. Offen 2239049 (1973).
7) C. C. Chiun (Mobil Oil Corp.) Eur. Patent Appl Ep 35836 16th Sep. 1981.
8) C. C. Chiun (mobil Oil Corp.) Eur. Patent Appl. Ep. 38116 21st Oct.1981.
9) C. C. Chiun (Mobil Oil Corp.) U. S. US 4302622 24th Nov.1981.
10) C. C. Chiun (Mobil Oil Corp.) U. S. US 4302620 24th Nov.1981.
11) K. Tarama, S. Yoshida, Y. Katayama, and T. Bitoh, *J. Jpn. Petroleum Inst.*, **11**, 771 (1968).
12) A. A. O. Kelly, *Ind. Eng. Chem.*, **39**, 154 (1947).
13) W. A. Schulze, U. S. Patent 2419796 April 29, 1947 to Phillips Petroleum.
14) E. F. Peter, U. S. Patent 2773108 Dec. 4,1956 to Standard Oil.
15) Y. Fukui, H. Takaoka, J. Ishii, and K. Hirai, *Bull. Chem. Soc. Jpn.*, **40**, 446 (1967).
16) Union carbide Bulletin F-2807(1966).
17) J. A. Rabo, U. S. Patent 3236721 Feb. 22, 1966 to Union Carbide.
18) R. N. Fleck, U. S. Patent 3298780 Jan. 17, 1967 to Union Oil Co.
19) J. J. Wise, U. S. Patent 3251897 May 17, 1966 to Socony Mobil Oil.
20) K. Tanabe, C. Ishiya, I. Matsuzaki, I. Ichikawa, and H. Hattori, *Bull. Chem. Soc. Jpn.*, **45**, 47 (1972).
21) Smith, W. Edward (General Electric Co.) Ger. Offen. 2716035 (1977).
22) I. Yusuke, H. Ress, and K. Vrabe, *J. Catal.*, **84**, 402 (1983).
23) V. G. Kumar, M. Rama Rao, P. V. Ravindran, and K. V. C. Rao, *J. Polym. Sci., Polym. Chem. Ed.*, **21**, 2133 (1983).
24) V. G. Kumar, S. Venkatachalam, and K. V. C. Rao, *J. Polym. Sci., Polym. Chem. Ed.*, **22**, 2317 (1984).
25) S. Venkatachalam, V. G. Kumar, and K. V. C. Rao, *J. Polym. Sci., Polym. Chem. Ed.*, **22**, 3805 (1984).
26) C. Groeneweld, P. P, M. M. Wittgen, H. R. M. Swinner, A. Wernsenn, and G. C. A. Schwitz, *J. Catal.*, **83**, 346 (1983).
27) I. M. Kolesnikov, L. M. Grinis, and Zh Prikl, *Khim (Leningrad)*, **55**, 340 (1982).
28) V. G. Kumar, T. S. Shoba, and K. V. C. Rao, *Tetrahedron Lett.*, **26**, 3281 (1985).
29) N. Calderon, J. P. Lawrence, and E. A. Ofstead, "Advances in Organometallic Chemistry," ed by F. G. A. Stone and R. West, Academic Press, New York (1977), p. 449
30) H. Werner and R. Feser, *Angew. Chem., Int. Ed. Engl.*, **18**, 157 (1979).
31) V. G. Kumar, T. S. Shoba, and K. V. C. Rao, *Tetrahedron Lett.*, **26**, 6245 (1985).
32) S. G. T. Bhat, *Indian J. Technol.*, **21**, 65 (1983).
33) S. G. T. Bhat, *J. Catal.*, **75**, 196 (1982).
34) T. Yashima, Y. Sakaguchi, and S. Namba, *Stud. Surf. Sci. Catal.*, **7**, 739 (1981).
35) V. L. Baibuskii, O. L. Knizhnikova, I. M. Gerzeliev, and S. N. Khadzhiev, *Khim. Tekhnol. Topl. Masel.*, **7**, 20 (1986).

Electrochemical Behavior of Azoxybenzene-4,4′-disulfonamide at Pyrolytic Graphite Electrode

R. N. GOYAL* and Sandhya BHARGAVA
Department of Chemistry, University of Roorkee, Roorkee-247667, India
(Received August 29, 1988)

The electrochemical reduction of azoxybenzene-4,4′-disulfonamide has been studied in the Britton Robinson buffers of pH range 3.0—10.6 at a pyrolytic graphite electrode. The electroreduction was found to occur in a single well defined 4e, $4H^+$ peak. The hydrazo compound has been identified as the main product of the electrode reaction.

The studies on the electrochemical behavior of azo compounds has attracted considerable attention[1,2] in the last decade due to their application in dyes and pharmacy. Azoxy compounds on the other hand have not attracted considerable attention in spite of the importance of azoxy group in enhancing the antibiotic as well as antifungal nature of an organic compound.[3,4] A well-known azoxy antibiotic Elaiomycin has been found very effective in vitro but not in vivo against Mycobacterium tubercuiosis.[5] The other antibiotic LL-BH 872a, having an azoxy group, has been reported as a new antifungal agent.[6] In view of the importance of azoxy compounds in medicine, it was considered interesting to study the redox behavior of azoxybenzene-4,4′-disulfonamide (**I**) claimed as peroxodisulfate oxidation product of sulfanilamide.[7] Since oxidation products of sulfonamides have been suggested[8] responsible for their bacteriostatic action, it is expected that the electrochemical behavior of this compound would throw light on the metabolic pathway of the bacteriostatic action of sulfanilamide.

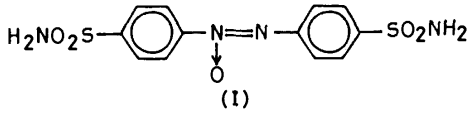

(I)

Experimental

Azoxybenzene-4,4′-disulfonamide was synthesized in the laboratory by the reported method[9] and its purity was ascertained by repeated crystallization, mp and TLC.

Equipments used for voltammetric and coulometric studies has been described elsewhere.[10] The UV spectral studies were carried out using Specord (C, Zeiss Zena) spectrophotometer. IR spectrum of the product was recorded on Beckmann IR-20 spectrophotometer. Thin-layer chromatography was carried out on silica Gel-G plates with benzene-methanol (80:20) as developer. The pyrolytic graphite electrode was prepared by the method reported earlier[11] and had an area ca. 2.0 mm^2. All potentials are referred to a saturated calomel electrode (SCE).

Chromatographic Procedure. For the identification of the product, about 8—10 mg of azoxybenzene-4,4′-disulfonamide was electroreduced at potentials more negative to peak 1c, in B. R. buffer of desired pH using a three compartment cell. A pyrolytic graphite plate (6×1 cm^2) was used as working electrode, cylinderical platinum gauze and SCE as the counter and reference electrodes respectively. The progress of electrolysis was monitored by recording cyclic voltammograms at different time intervals. The completely electrolyzed solution was transferred from the cell and lyophilized. The freeze-dried material was dissolved in 1—2 ml of distilled water and passed through a glass column packed with Sephadex G-10 (Sigma, bead size 40—120 μm) using doubly distilled water as eluant. This arrangement allowed separation of phosphate from the product. Fractions of 5 ml each were collected and their absorbance was monitored at 210 nm. The first peak to emerge out of the column (between volume 120—160 ml) was found to contain phosphate and rejected. The other peak between 200—230 ml was freeze-dried and analyzed by IR, melting point, and mass spectra.

The stock solution of compound **I** (2 mM; 1 M=1 mol dm^{-3}) was prepared in methanol (A. R.). The solutions for voltammetric studies were prepared by mixing 5.0 ml of azoxybenzene-4,4′-disulfonamide with 5.0 ml of B. R. buffers. The solutions were deaerated for 10—15 minutes and the curves were then recorded.

Results and Discussion

Linear sweep voltammetry of azoxybenzene-4,4′-disulfonamide at a scan rate of 10 mV s^{-1} exhibited a bump 1′c and a well defined reduction peak in B. R. buffers of pH range 3.0—10.6. The peak potential of the reduction peak was dependent on pH and shifted to more negative potential with increase in pH. The plot of E_p versus pH exhibited a break at around pH 6.8 (Fig. 1). The relationship between the peak potential and pH for the reduction peak (1c) is given by the equations:

$$E_p \text{ (pH 3.0—6.8)} = [-0.52-0.057 \text{ pH}] \text{ V vs. SCE}$$

$$E_p \text{ (pH 6.8—10.58)} = [-0.82-0.013 \text{ pH}] \text{ V vs. SCE}$$

Cyclic voltammetry of **I** at a scan rate of 100 mV s^{-1} exhibited a single reduction peak (1c) with a bump (1′c) in B. R. buffers of different pH when sweep was initiated in the negative direction. In the reverse sweep no peak was observed at pH<7.0. However, at pH>7.0 a bump closer to zero volt was occasionaly observed. Some of the typical cyclic voltammograms are presented in Fig. 2. The bump (1′c) was characterized as preadsorption peak due to strong adsorption

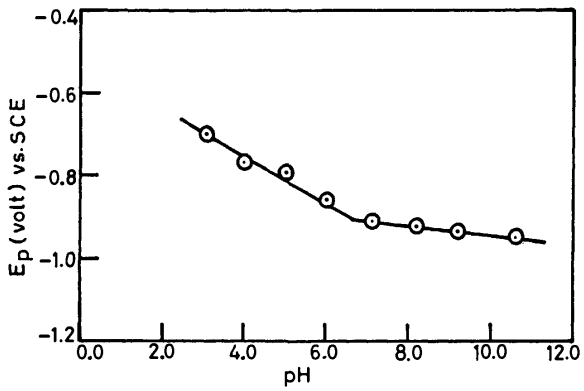

Fig. 1. Variation of E_p with pH for the voltammetric reduction peak 1c of azoxybenzene-4,4′-disulfonamide.

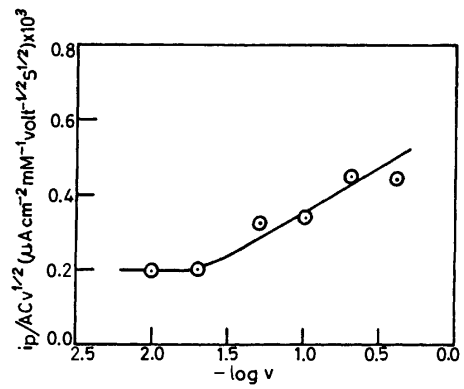

Fig. 3. Variation of peak current function with logarithm of sweep rate for peak 1′c.

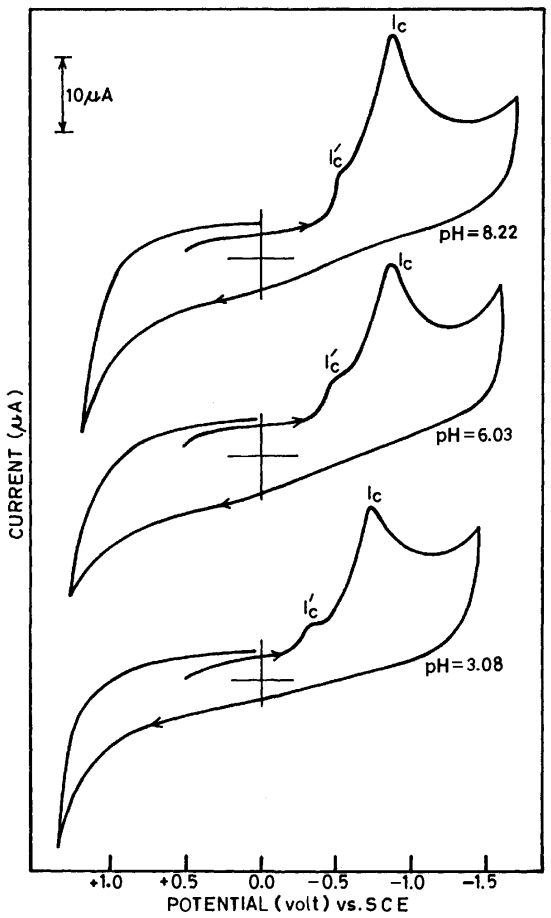

Fig. 2. Cyclic voltammograms of 1.0 mM azoxybenzene-4,4′-disulfonamide at the PGE in the phosphate buffers of different pH. Sweep rate 100 mV s^{-1}.

Table 1. Effect of Concentration of Azoxybenzene-4,4′-disulfonamide on the Ratio of Peak Currents for Peaks 1′c/1c

Concentration of I (mM)	1c′/1c
0.2	0.91
0.4	0.78
0.6	0.57
0.8	0.06
1.0	0.56
1.2	0.52
1.4	0.58
1.6	0.59
1.8	0.66
2.0	0.48
2.2	0.33

Table 2. Effect of Sweep Rate on the Relative Height of Peaks 1′c and 1c

Scan rate / mV s^{-1}	1′c/1c
20	0.30
50	0.45
100	0.45
200	0.62
500	0.69

of the product by monitoring the relative height of adsorption response (1′c) to diffusion response (1c) with increase in the concentration of compound **I**.[12] It was interesting to observe that the ratio of peak currents for peaks 1′c/1c decreases with increase in concentration of compound **I** (Table 1) and thus indicated that peak 1′c is preadsorption peak due to strong adsorption of the product.[12] A further confirmation was made by recording cyclic voltammograms of **I** at different sweep rates. It was found that the ratio of 1′c/1c increases with increase in sweep rate (Table 2). Hence it was believed that peak 1′c is due to the strong adsorption of the product. The peak current function ($i_p/ACV^{1/2}$) for peak 1′c was also plotted against the sweep rate. It was observed that the peak current function increases with increase in sweep rate in the range 20—500 mV s^{-1} (Fig. 3), thereby further indicating peak 1′c due to strong adsorption.

The peak 1c was found to be diffusion controlled at low concentrations whereas at higher concentrations an indication of weak adsorption of the reactant was noticed. The peak current values (i_p) for the reduc-

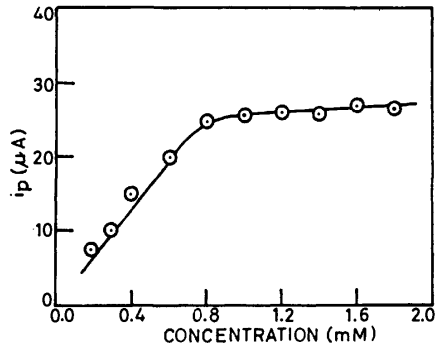

Fig. 4. Dependence of i_p on concentration for the reduction peak 1c at pH 7.26.

tion peak 1c increased linearly with increasing concentration of azoxybenzene-4,4′-disulfonamide upto a concentration of about 0.8 mM and at higher concentrations the peak current values had a tendency to become constant (Fig. 4). This behavior suggests complication due to the weak adsorption of the reactant.[13] Adsorption of the substrate at higher concentrations was further confirmed by the criteria proposed by Wopschall and Shain[14] for strong adsorption of product with weak adsorption of reactant. In such cases, at low scan rates (usually 10 to 500 mV s^{-1}) the adsorption peak current increases linearly with scan rate while diffusion peak current increases approximately as the square root of the sweep rate. A similar behavior was observed for peak 1′c and 1c in the case of azoxybenzene-4,4′-disulfonamide (Fig. 5). The strong adsorption of the product and the weak adsorption of reactant was further confirmed by plotting the ratio of adsorption (1′c) to diffusion (1c) peak current against $\sqrt{V}$. The dotted line shown in Fig. 6 indicates only adsorption of the product whereas the deviation of the observed behavior from straight line clearly pointed out that the reactant is weakly adsorbed and the product is strongly adsorbed in the present studies. This behavior is similar to that reported by Wopschall and Shain[15] for such systems.

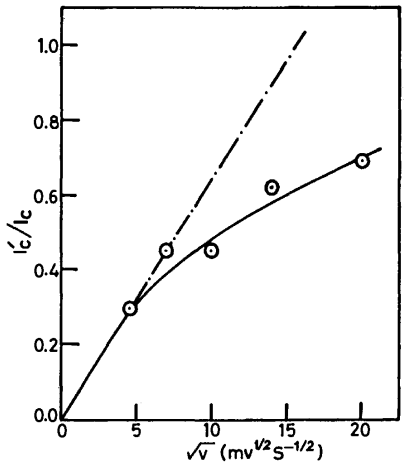

Fig. 6. Ratio of adsorption peak to diffusion peak (1′c/1c) as a function of square root of sweep rate. The dotted line indicates only adsorption of the product.

Table 3. Coulometric n-Values Observed for the Electroreduction of Azoxybenzene-4,4′-disulfonamide

pH	Potential V vs. SCE	Concn mM	Experimental n value[a]
3.08	0.9	0.5	4.12
	1.0	0.8	4.16
4.05	1.0	0.5	4.10
	1.0	0.8	3.88
5.06	1.1	0.5	3.92
6.03	1.1	0.5	4.16
	1.1	0.8	4.10
8.22	1.1	0.5	3.89
	1.1	0.8	3.90
10.58	1.1	0.5	4.04

a) Average of at least two replicate determination.

Controlled Potential Electrolysis. Controlled potential coulometry of azoxybenzene-4,4′-disulfonamide at pH values ranging from 3.0—10.58 at potentials more negative to peak 1c indicated that 4.0±0.1 electrons are transferred in the peak 1c process.

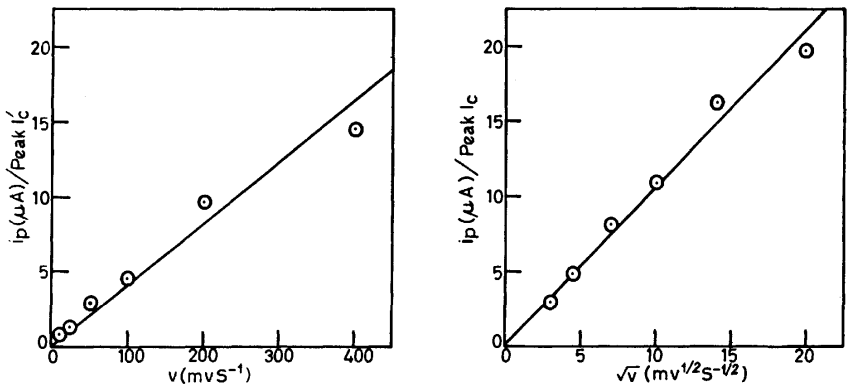

Fig. 5. Dependence of peak currents for peaks 1′c and 1c on V and $\sqrt{V}$ respectively.

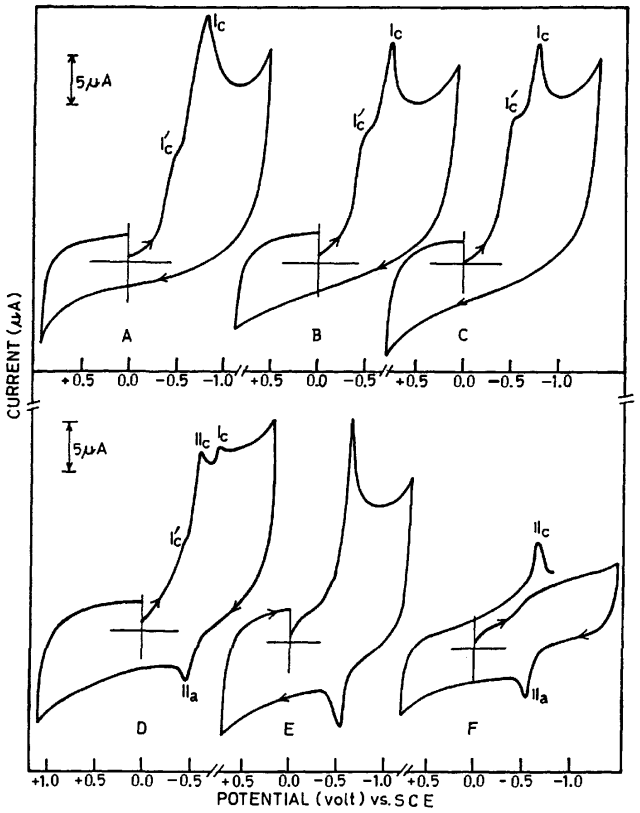

Fig. 7. Cyclic voltammograms of observed for 0.5 mM azoxybenzene-4,4′-disulfonamide undergoing electroreduction at −1.2 V. Curves were recorded at 0 (A), 10 (B), 30 (C), 60 (D), 90 (E), and 180 (F) min of electrolysis.

The values of n determined at various concentration of **I** and at different pH are presented in Table 3.

The progress of electrolysis was monitored by recording cyclic voltammograms at different time intervals. The cyclic voltammogram of azoxybenzene-4,4′-disulfonamide before electrolysis at pH 7.06 is presented by the curve A in Fig. 7. With progress of electrolysis reduction peak 1c decrease systematically whereas a new cathodic peak 11c starts appearing at a less negative potential after about 60 minutes of electrolysis. Peak 11c formed a quasi-reversible couple with peak 11a observed in subsequent sweep towards cathodic potentials. On further electrolysis, peak current for the redox couple 11c/11a increases. After about 3 h, peak 11c practically disappeared when sweep was initiated in negative direction. However, peak 11a was clearly observed and peak 11c was observed only in the second cycle (Fig. 5). The orange solution turned to colorless at the end of the electrolysis.

Spectral Studies. The UV/visible spectra of azoxybenzene-4,4′-disulfonamide were recorded in B. R. buffers in the pH range 3.08—10.58 to determine the pK_a. It was observed that compound **I** exhibits λ_{max} at 330 nm with a shoulder around 270 nm in the UV region and at 468 nm in the visible region below pH 6.03. In the pH range 6.03 to 7.07, the λ_{max} at longer wavelength shifted to 472 nm. At pH>7.07 the λ_{max} value was 480 nm. The absorbances at 350 and 472 nm were plotted against pH and gave an inflection point at around pH 6.8. Thus it is clear that below pH 6.8 compound **I** exists as a protonated species and at pH>6.8, it mainly exists as a neutral molecule. It is reported[16] that azoxy compounds are weak base and therefore protonation occurs on the oxygen atom. Hence the following species must exist in the solution.

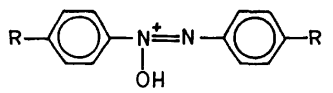

below pK_a

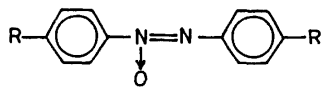

above pK_a

The observed value of pK_a for azoxybenzene-4,4′-disulfonamide is in the range observed for azoxybenzene and a large number of substituted azoxybenzene.[17]

The progress of the electrolysis of azoxybenzene-4,4′-disulfonamide was also monitored by recording the spectral changes during the electrolysis. The UV spectrum of 0.05 mM azoxybenzene-4,4′-disulfonamide at pH 7.26 before electrolysis exhibited λ_{max} at

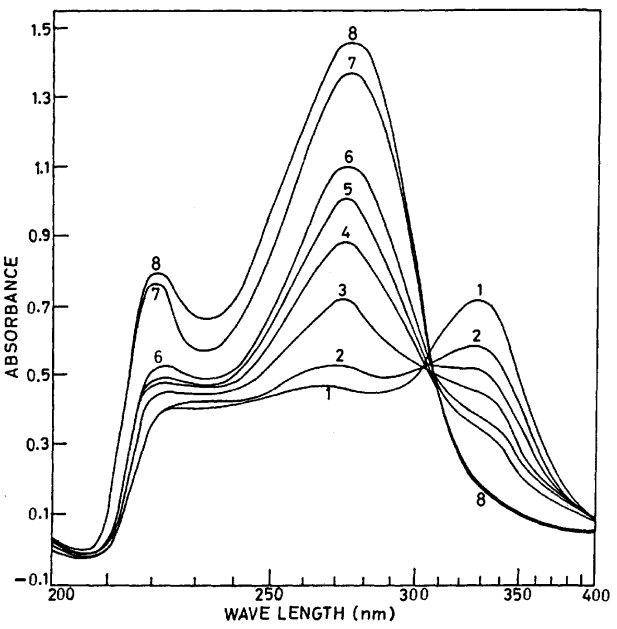

Fig. 8. Observed spectral changes for 0.5 mM azoxybenzene-4,4′-disulfonamide undergoing electroreduction at pH 7.26. Potential −1.2 V. Curves were recorded at 0 (1), 10 (2), 20 (3), 30 (4), 40 (5), 60 (6), 120 (7), and 180 (8) min of electrolysis.

330 nm (Fig. 8, Curve 1). Application of a potential more negative to peak 1c, leads to decrease in absorbance at 330 nm and a systematic increase in absorbance in the region 250—300 and 210—225 nm. At the end of electrolysis a maximum at 276 nm and 220 nm was observed with isosbestic point at 310 nm. This clearly indicates that products of electroreduction of **I** absorbs at shorter wavelength in comparison to the starting material and hence π-chromophore system has been decreased. An almost similar behavior was observed at pH 3.08 and 10.58.

Characterization of the Product. In order to characterize the end product of the electrode reaction, the electrolysis was carried out at pH 3.08 and 7.26. The exhaustively electrolyzed solution was lyophilized and passed through a Sephadex column. The volume collected between 200—230 ml on freeze drying gave light yellow product which was analyzed by TLC, mp, IR, and mass spectra. TLC of the product exhibited only one spot with R_f=0.04 indicating thereby the formation of a single product during electroreduction of compound **I**. The product had a melting point of 158 °C. IR spectrum of azoxybenzene-4,4′-disulfonamide exhibited a strong band at 1450 cm^{-1} (N→O) in addition to other strong bands at 1610, 1400, 1320, 1300, 1245, 1080, 1010, and 910 cm^{-1}. The band at 1450 cm^{-1} disappeared in the product thereby clearly indicating that oxidation is occuring at N→O linkage. The mass spectrum of the product exhibited a clear molecular ion peak at 342. Some other high mass peaks were at 326 (7.3%); 325 (3.4%); 324 (1.1%); 262 (11.8%); 261 (7.3%); 260 (4.3%); 171 (17.1%); 170 (13.3%); 169 (9.2%). However, no attempt was made to explain the fragmentation pattern.

Redox Behavior. The experimental results indicate that reduction of azoxybenzene-4,4′-disulfonamide involves a 4e, $4H^+$ reaction to give a product which absorbs at a shorter wavelength in comparison with the starting material.

As there is no separation of peaks, it appears that 4e, $4H^+$ electrode reaction occurs in a single step. However, the formation of a quasi-reversible couple at the end of the electrolysis corresponding to azo derivative indicates that electrode reaction involves two 2e, $2H^+$ steps and since their potential is close to one another a single 4e, $4H^+$ step was observed in cyclic voltammetry. The following tentative mechanism can be suggested:

The first step in the reaction appears to be 2e, $2H^+$ reduction of azoxybenzene-4,4′-disulfonamide (**I**) to give azobenzene-4,4′-disulfonamide (**II**). As reduction of **II** is easier than **I**, it further reduces by taking 2e, $2H^+$ to give hydrazobenzene-4,4′-disulfonamide (**III**). Since the cleavage of N→O bond of azoxybenzene requires more negative potentials than electroreduction of the -N=N- bond in azobenzene,[18] therefore, **II** can not be formed as a stable intermediatory product and **III** is directly obtained (Scheme 1).

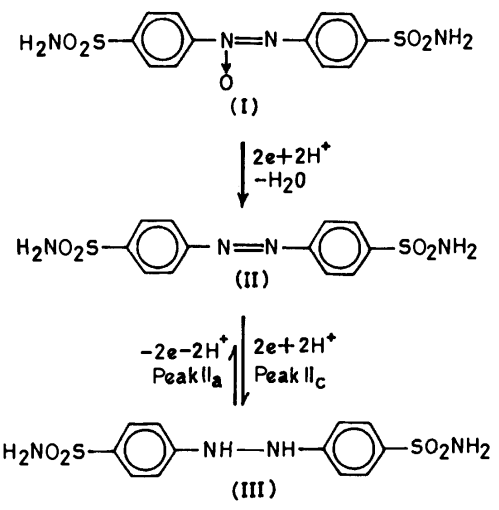

Scheme 1. Tentative mechanism proposed for the electroreduction of azoxybenzene-4,4′-disulfonamide.

To confirm whether the couple 11a/11c is due to the azohydrazobenzene-4,4′-disulfonamide system, cyclic voltammograms of azobenzene-4,4′-disulfonamide were recorded in buffers of different pH. The identical dE_p/dpH values clearly indicate that the redox couple 11a/11c is due to azobenzene-4,4′-disulfonamide. As hydrazobenzene-4,4′-disulfonamide (**III**) has less extensive π-conjugation system in comparison to **I**, the λ_{max} values in UV region shifted to shorter wavelengths.

Conclusion

It is apparent from the present studies that azoxybenzene-4,4′-disulfonamide is electroactive in nature and readily undergoes electroreduction in a 4e, $4H^+$ process to give hydrazo derivative as the final product. It has been suggested by Levitan et al.[19] that polarographic oxidation of sulfanilamide gives azoxybenzene-4,4′-disulfonamide together with other products. Since this compound is electroactive, it can undergo further reduction at higher negative potentials to give hydrazo compound as the ultimate product. Wawzonek[20] and others[21] have reported that electroreduction of azoxybenzene in acid media does not stop at hydrazo stage rather cleavage of NH-NH bond occurs to give aniline. However, in the present studies electroreduction of azoxybenzene-4,4′-disulfonamide gives hydrazo derivative as the final product. Thus it appears that the electron-withdrawing $-SO_2NH_2$ groups present in compound **I** inhibit the further reduction of -NH-NH- and only hydrazo product is formed. The nonreduction of -NH-NH- in presence of electron-withdrawing groups has been reported earlier by Florence[22] in azo/hydrazo benzene system. Azoxy compounds have also been reported to convert into azo compounds on prolonged electrolysis under controlled potential

conditions.[23] Hence it is possible that azoxy compound produced by polarographic oxidation of sulfanilamide converts to azo and then hydrazo product on prolonged electrolysis under controlled potential conditions.

Burton,[24] Mayer,[25] and others[26] have proposed that oxidation products of sulfonamides may partly be responsible for their antibacteria activity. Thus it is concluded that azoxybenzene-4,4′-disulfonamide, a suggested polarographic and chemical oxidation product of sulfanilamide is electroactive in nature and gives hydrazobenzene-4,4′-disulfonamide as the final product. Hence the redox behavior involved with compound **I** is most likely responsible for the bacteriostatic action of sulfanilamide.

The financal assistance for this work was provided by the Indian Council of Medical Research, New Delhi.

References

1) J. P. Stradins and V. T. Glezer, "Encyclopedia of the Electrochemistry of the Elements," ed by A. J. Bard and H. Lund, Vol. XIII, Marcel Dekker, N. Y. (1978), p. 163.
2) H. Lund, "Organic Electrochemistry," ed by M. Baizer, Marcel Dekker, N. Y. (1973).
3) A. Kobayashi, *Agric. Biol. Chem.*, **26**, 203 (1962).
4) T. H. Haskell, A. Ryder, and Q. R. Bartz, *Antibiot. Chemother.*, **4**, 141 (1954).
5) K. Okuma, G. Nakamura, and S. Yamashita, *J. Antibio. Ser. A.*, **10**, 224 (1957).
6) A. G. Karlson, *Antibiot. Chemother.*, **12**, 446 (1962).
7) S. P. Srivastava, A. Kumar, and A. K. Mittal, *Indian J. Chem.*, **17**, 593 (1979).
8) R. L. Mayer, *Bull. Acad. de Med.*, **117**, 727 (1937).
9) M. K. Seikel, *J. Am. Chem. Soc.*, **62**, 1214 (1940).
10) R. N. Goyal, R. Bhushan, and A. Agarwal, *J. Electroanal. Chem.*, **171**, 281 (1984).
11) R. N. Goyal, S. K. Srivastava, and R. Agarwal, *Bull. Soc. Chim. Fr.*, **4**, 656 (1985).
12) E. R. Brown and R. F. Large, "Physical Methods of Chemistry," ed by A. Weissberger and B. W. Rossiter, Wiley Interscience, N. Y. (1972).
13) R. S. Nicholson and I. Shain, *Anal. Chem.*, **36**, 706 (1964).
14) R. H. Wopschall and I. Shain, *Anal. Chem.*, **39**, 1514 (1967).
15) R. H. Wopschall and I. Shain, *Anal. Chem.*, **39**, 1535 (1967).
16) C. S. Hahn and H. H. Jaffe, *J. Am. Chem. Soc.*, **84**, 949 (1962).
17) P. J. Krueger, "The Chemistry of Hydrazo, Azo and Azoxy Groups," ed by S. Patai, John Wiley, N. Y. (1975), p. 173.
18) L. Chuang, I Fried, and P. J. Elving, *Anal. Chem.*, **37**, 1528 (1965).
19) N. I. Levitan, I. M. Kolthoff, W. G. Clark, and D. J. Tenenberg, *J. Am. Chem. Soc.*, **65**, 2265 (1943).
20) S. Wawzonek and J. D. Frederickson, *J. Am. Chem. Soc.*, **77**, 3988 (1955).
21) G. Costa, *Gazz. Chim. Ital.*, **83**, 875 (1953).
22) T. M. Florence, *J. Electroanal. Chem.*, **52**, 115 (1974).
23) F. G. Thomas and K. G. Boto, "The Chemistry of the Hydrazo, Azo, and Azoxy Groups," Part I, Wiley, London (1975), p. 443.
24) R. L. Mayer and C. Oechslin, *Compt. Rend.*, **205**, 181 (1937).
25) A. C. Burton, H. J. White, and E. K. Marshall, *Proc. Soc. Expt. Biol. Med.*, **42**, 847 (1939).
26) M. G. Sevag, M. Shelburne, and M. Ibsan, *J. Biol. Chem.*, **144**, 711 (1942).

Environmental Effects on the Absorption and Fluorescence Spectral Characteristics of Benzimidazole-2-carboxylic Acid and Its Ester

Hemant K. SINHA and Sneh K. DOGRA*
Department of Chemistry, Indian Institute of Technology, Kanpur-208016, India
(Received September 5, 1988)

The absorption and fluorescence spectra of benzimidazole-2-carboxylic acid (BIA) and 5-chlorobenzimidazole-2-carboxylic acid (CBIA) have clearly indicated that benzimidazole (BI) ring and -COOH group are coplanar to each other and are held together in a rigid frame by intramolecular hydrogen-bonding. Dual fluorescence in observed in polar and hydrogen bonding solvents. The short wavelength fluorescence band is assigned to a structure where the -COOH group is perpendicular to the BI moiety and the long wavelength fluorescence band to the planar configuration. This is further manifested from the spectral characteristics of the ester of 5-chlorobenzimidazole-2-carboxylic acid (CBIM). Various prototropic reactions taking place in S_0 and S_1 states for all the three molecules are studied in the H_0/pH/H_- range of −10 to 16. All the dissociation constants are determined, both in the S_0 and S_1 states and are discussed.

In the early 1950's, it was discovered that 5,6-dimethyl-1-(α-D-ribofuranosyl)benzimidazole is an integral part of the structure of vitamin B_{12}.[1,2] These findings stimulated great interest in the chemistry of benzimidazoles and related compounds. Though a detailed study of the physicochemical properties of benzimidazole molecule is available, the similar study on the derivatives of benzimidazole (BI) has received attention only recently.[3-17] We have started to look into the spectral (both absorption and fluorescence) aspects of the various derivatives of BI in detail.[6-17]

The present study on 2-substituted carboxylic acids of benzimidazole has been carried out from the following point of views: (i) The spectral characteristics of the aromatic moiety are changed by the interaction of basic substituents. It has been found in some cases that -COOH group is coplanar to the aromatic ring both in S_0 and S_1 states,[18-20] whereas in some cases, this group is coplaner in S_1 state and not in S_0 state.[21-25] In the present case, besides the transition moment vector which tries to bring the -COOH group in plane with the aromatic moiety, chances are that intramolecular hydrogen bonding will be present and thus will affect the spectral properties. (ii) Due to the competition between the inter- and intramolecular hydrogen bonding in polar and protic solvents, chances are that different conformers may be present in different solvents or there may be equilibrium distribution of conformers in the polar and protic solvents. (iii) The study on the bifunctional molecules containing both electron-withdrawing and electron-withdrawing groups are very rare.[26,27] In our molecules, the two electron-withdrawing chromophores are tertiary nitrogen atom and the carboxyl group. We would like to see the effect of one group over the other as well as overall effect of the two groups on benzimidazole moiety. Thus the absorption and fluorescence spectra of these molecules have been studied in different solvents. pH dependent study has also been carried out to identify the various prototropic species present in the ground and excited singlet states. pK_a values of the various equilibrium reactions have been calculated in the ground and excited singlet states and are discussed. Ester of the corresponding acid has been employed in the above study to supplement our results.

Methods and Materials

5-Chloro-2-(trichloromethyl)benzimidazole (CTMBI) was obtained from Aldrich Chemical Company. It was hydrolyzed to 5-chlorobenzimidazole-2-carboxylic acid (CBIA) by 2 M sodium hydroxide solution (1 M=1 mol dm^{-3}) as suggested in the literature.[28] Similarly for the preparation of benzimidazole-2-carboxylic acid (BIA), 2-(trichloromethyl)-benzimidazole (TMBI) was synthesised by a reaction of *o*-phenylenediamine with methyl trichloroacetimidate (obtained from Aldrich Chemical Company) in acetic acid medium. Several attempts to isolate only 2-(trichloromethyl)benzimidazole (as suggested in the literature)[28] failed. This method has always resulted in a mixture of two products i.e. 2-(trichloromethyl)benzimidazole and bi(benzimidazole). Later these two compounds were separated by preparative thick-layer chromatography using Merck Silicagel G for thin-layer chromatography. The eluting solvent was a mixture of ethyl acetate and benzene in 1:1 (v/v) ratio. TMBI was then hydrolyzed to give the corresponding acid (BIA) as mentioned in the case of CBIA. Methyl ester of CBIA (CBIM) was prepared by refluxing CTMBI in methanol for 20 hours.[28] The purity of all the compounds was checked by noting the sharp melting point as well as by spectroscopic methods. The purity was also checked by fluorescence techniques i.e. by getting same fluorescence maxima when excited with different wavelengths.

The procedure used for purification of the solvents, preparation of the solutions and carrying out the calculations is the same as described in our recent papers.[29-33]

Results and Discussion

Effect of Solvents. The absorption and fluorescence spectra of BI, BIA, CBIA, and CBIM are depicted in Figs. 1 and 2 respectively. The relevant spectral data of BIA, CBIA, and CBIM are compiled in Tables

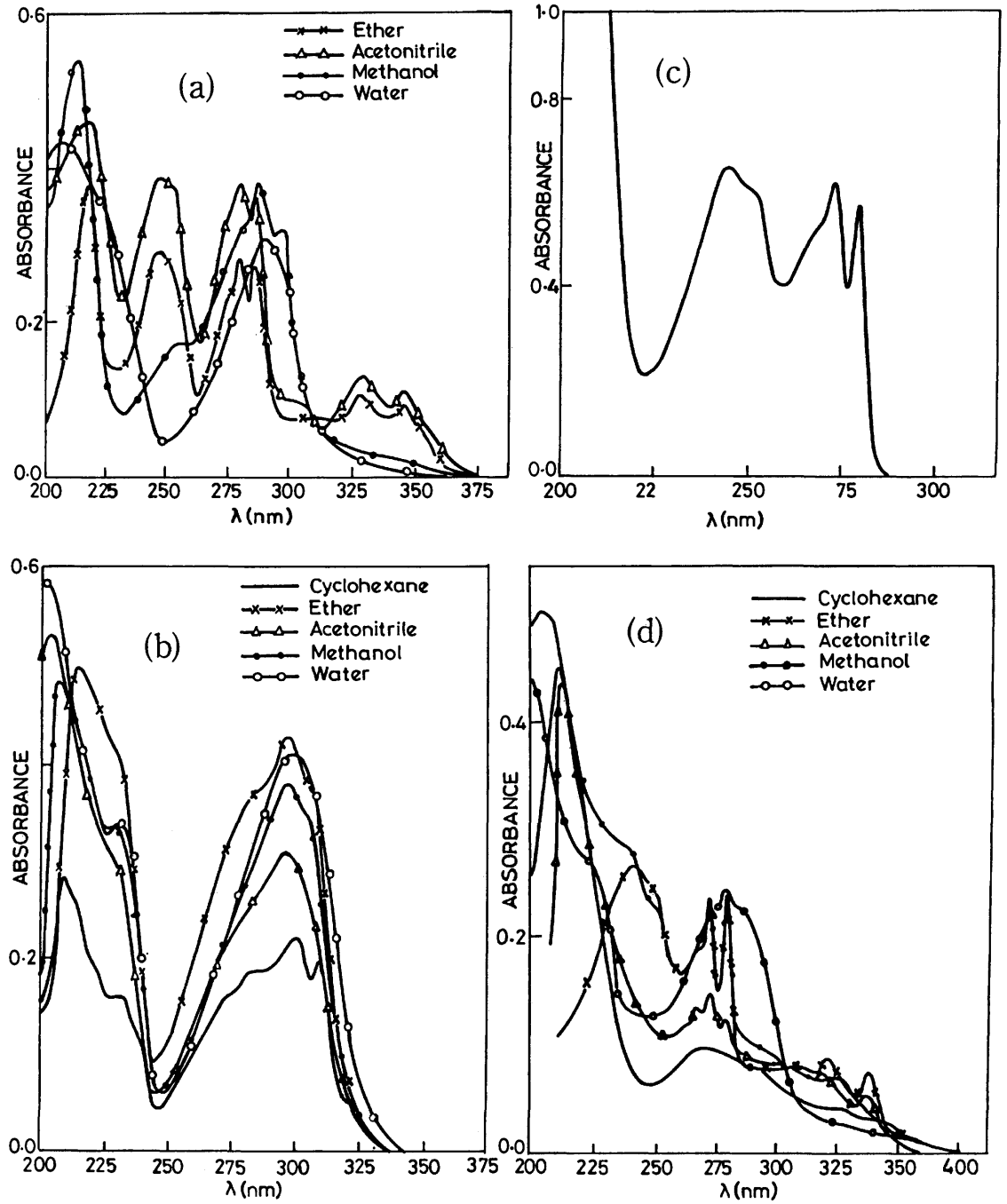

Fig. 1. Absorption spectra of (a) CBIA, (b) CBIM, (c) BI only in water and (d) BIA in different solvents at 298 K.

1 and 2. The absorption band maxima of all the three molecules are largely red-shifted as compared to BI.[34] Above 300 nm, the absorption band system of BIA and CBIA are nicely structured and weak with respect to other three band systems present below 300 nm, whereas in CBIM, this band system is broad and band maximum is close to 300 nm. The absorbance of this band system further decreases with the increase in polarity and hydrogen-bond-forming tendency of the solvents. The other band systems (ca. 280 nm, ca. 250 nm, and ca. 210 nm) are similar to BI. The absorption band maxima of all the band systems are nearly insensitive to the nature of the solvents.

Similar to the absorption spectra, the fluorescence spectra of BIA, CBIA, and CBIM are largely red-shifted as compared to BI.[34] The vibrational structure is observed in all the solvents with the exception of CBIM, where the vibrational structure is present only in cyclohexane. The vibrational frequencies observed in absorption and fluorescence spectra are the same i.e. 1100±50 cm^{-1} in CBIM and 1500±50 cm^{-1} in BIA and CBIA. Besides this, the fluorescence

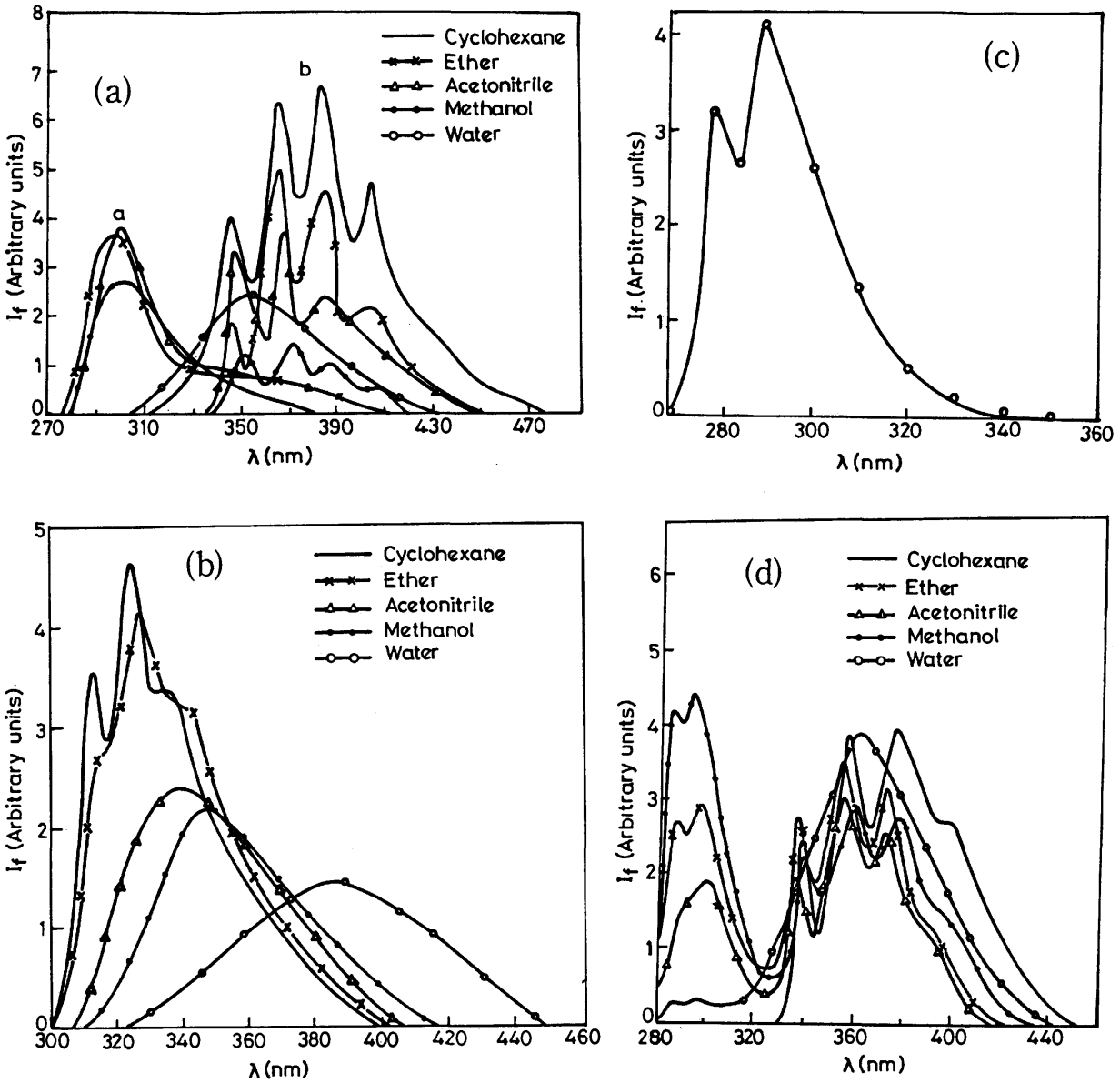

Fig. 2. Fluorescence spectra of (a) CBIA, (b) CBIM, (c) BI only in water and (d) BIA in different solvents at 298 K.

spectrum is not much separated from and makes mirror image with the absorption band.

Besides the structured long wavelength fluorescence (F_1), a second band system at ca. 300 nm is also observed in case of CBIA and BIA in all the solvents except cyclohexane. The excitation spectra recorded at 365 nm in all the solvents resemble the absorption spectra above 300 nm. However no useful information could be obtained from the excitation fluorescence spectra below 300 nm as the lamp intensity is very weak below 300 nm. Both the fluorescence band systems (F_1 and F_2) are hardly affected by varying the nature of solvents whereas that of CBIM shifts from 318 nm in cyclohexane to 390 nm in water.

Data of Tables 1 and 2 clearly indicate that the carboxyl group in these compounds is coplanar with the BI ring, both in the S_0 and S_1 states and hence extensive conjugation is observed. This behavior is similar to that observed in case of 4- and 5-indolecarboxylic acids[18,19] and different to many other carboxylic acids.[20,23,26,35] We suggest that the structured long wavelength absorption and fluorescence (F_1) from BIA and CBIA are due to the presence of intramolecularly hydrogen-bonded structure (**1**). This suggestion is based on the following facts. (i) The presence of intramolecular hydrogen bonding in BIA and CBIA leads to symmetrical structure. Presumably this will lead to the complete delocalization of π cloud

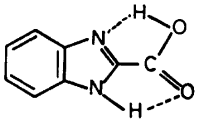

I

Table 1. Absorption Maxima (λ_a/nm) and log ε_{max} of CIBIA, BIA, and CBIM in Various Solvents and at Different Hydrogen Ion Concentration at 298 K

Solvent	λ_a/nm (log ε_{max})											
	CBIA				BIA				CBIM			
Cyclohexane									322 310 300	284 271	231	210
Ether	357 344 327 305	286 280 275	254 247	216	338 321	279 274 266	250 242	209 204	— 307 298	281 271	231	216
Acetonitrile	357 344 327 305	286 280 275	254 247		337 320	279 274 266	250 242	212	— 307 298	281 271	231	216
Methanol	362 (2.00) 345 (2.36)	287 (3.88) 280 (3.81)	254 (3.55)	211 (4.15)	340 (2.21) 322 (2.35)	279 (3.90) 273 (3.83) 266 (3.51)	250 (3.62) 241 (3.69)	211 (4.10)	— 305 (3.93) 297 (3.96)	281 (3.83)	231 (3.40)	205 (4.04)
H_0–5 (Dication)		311 (3.55)	237 (3.38)	207 (3.44)		304 (3.60)	235 (3.52)	230 (3.53)		307 (3.69)	237 (3.55)	207 (3.64)
H_0–1 (Monocation)		297 (3.52)	232 (3.40)	—		293 (3.71) 275 (3.55)	232 (3.70)	229 (3.51)		302 (3.71)	235 (3.62)	207 (3.62)
pH 2 (Neutral)	—	291 (3.61)	—	227 (3.60)		285 (3.70) 273 (3.52)	—	222 (3.69)		300	232	
pH 8 (Monoanion)		289 (3.69)	260 (3.41)	202 (3.78)		281 (3.65) 278 (3.62) 271 (3.59)	—	222 (3.55)		308 (3.77)	—	212[a] (3.84)
H_-16 (Dianion)		299 (3.69)	—	226 (3.89)		295 (3.75)	—	224 (3.80)			—	

a) pH=12.

over the BI moiety and the -COOH group. This may result in small dipole moment. Because of this the effect of solvents on the spectral characteristics will be minimum. This is reflected by the data of Table 1. A similar behavior is also observed in case of bibenzimidazole.[36] Further the presence of five-menbered intramolecularly hydrogen-bonded structure in case of ninhydrin has been proposed by Dewar.[37] The same argument does not hold for CBIM, where the intramolecular hydrogen-bonding interaction with tertiary nitrogen atom is removed. Due to this, though the red shift is observed in the absorption spectrum of BI, it is not to that extent as noticed in case of BIA and CBIA. This is further manifested by the loss in the vibrational structure as well as the blue shift observed in the absorption spectrum of CBIM in polar and hydrogen-bonding solvents. This is due to the interaction of intermolecular hydrogen-bonding of the solvents with tertiary nitrogen atom and thus rotation of the -$COOCH_3$ group out of the plane of BI. (ii) The presence of long wavelength band due to the dimer formation (as observed in case of benzoic acid[38]) is rejected on the ground that the increase in the concentration of these acids does not affect the ratio of the absorbances of the two band system. Secondly, the observation of vibrational sturcture in such a loosely formed dimer is difficult to explain. (iii) The decrease in the absorbance of long wavelength absorption maxima in BIA and CBIA with increase in the proton donor/acceptor capacity of the solvents is due to the competition between the intra- and intermolecular hydrogen bonding and thereby shifting the equilibrium toward the open structure. The similar band system is also observed in the absorption spectrum of 2-(2-aminophenyl)benzimidazole,[12] which was broad and the ring formed due to intramolecular hydrogen bonding is a six member one. Observation of similar vibrational frequency in absorption and fluorescence spectra and the mirror image symmetry suggest that the molecular conjugation and the geometry of BIA and CBIA in S_1 state differ very little from that in S_0 state. The similar vibrational fre-

Table 2. Fluorescence Maxima (λ_f/nm) and Quantum Yield (Φ_f) of CBIA, BIA, and CBIM in Various Solvents and at Different Hydrogen Ion Concentration at 298 K

Solvent	$\lambda_f(\phi_f)$				
	CBIA		BIA		CBIM
Cyclohexane	405		400		335
	384(0.01)	—	377(0.09)	—	326(0.10)
	366		355		318
	346		339		
Ether	405		393(sh)	297	343(0.11)
	385(0.01)	300(0.03)	372(0.13)	287(0.08)	328
	366		355		316
	346		336		
Acetonitrile	—		393	300(0.02)	342(0.07)
	385	300(0.03)	372(0.12)	288	
	367(0.02)		355		
	347		336		
Methanol	—		404(sh)	294(0.11)	348(0.03)
	386(0.03)	303(0.02)	377(0.14)	285	
	368		358		
	349		339		
H_0–1 (Monocation)	410		410		410
pH 2 (Neutral)	380		392		390
pH 8 (Monoanion)	345		360		360
H–16 (Dianion)	350		365		—

quency (ca. 1500 cm^{-1}) is also observed in the specturm of other 2-substituted benzimidazoles where the structure is rigid, for example, 2-(4-aminophenyl)-[11] and 2-(4-hydroxyphenyl)benzimidazoles.[15] The insensitivity of the fluorescence spectra of BIA and CBIA towards the nature of the solvents further extablishes the existence of rigid and symmetric structure (**1**) in the S_1 state. Since similar symmetric structure is not possible in CBIM, the vibrational structure is lost in more polar and protic solvents. Unlike absorption spectrum, the large red shift observed in the fluorescence spectrum of CBIA confirms the existence of manifold degeneracy of the excited singlet states of BI.[4,17,39] Both these molecules (CBIA and CBIM) contain electron-donating (Cl atom) in the benzene ring and electron-withdrawing group (-COOH or -COOMe) in the imidazole ring and thus will favor the charge transfer state to be of lowest energy. Whereas the effect of solvents on the fluorescence spectra has indicated that the π^* is the lowest energy state in CBIA and CT in CBIM. The presence of intramolecular hydrogen-bonding perturbations in CBIA may be responsible for inhibition of charge transfer from benzene to the carboxyl group. The migration of the charge density from the benzene ring towards the carboxylic acid group is further manifested from the low pK_a value of the protonation reaction of tertiary nitrogen atom (see later).

The fluorescence (F_2) spectrum closely resembles with that of parent BI molecule[34] or the monocation of the derivatives of BI where the CT transition is absent.[4,17] This fluorescence band can be assigned to the conformer where the -COOH group and BI ring are not coplanar (open strucure). Since only one fluorescence band (F_1) is observed in cyclohexane, it suggests that the open conformer is due to the competition between the intra- and intermolecular hydrogen bonding in polar and protic solvents. The following arguments can be given for rejecting the other possibility. (i) pK_a's of aromatic acids are close to 4,[40] whereas the pK_a for the protonation of tertiary nitrogen atom of BI is 5.53.[3] One can speculate the formation of zwitterion (**5**), with the carboxylato group perpendicular to the BI, both in S_0 and S_1 states. (ii) In our earlier paper,[39] it has been reported that the presence of strong electron-withdrawing groups (-CF_3, -CCl_3) at the 2-position decreases the pK_a value for the protonation reaction of the tertiary nitrogen atom to as low as ca. 1.0. In the present case, it is also expected that the pK_a for the same reaction of BIA and CBIA will also be low (ca. 0.5 see later). This is further confirmed by the similar value of pK_a (0.3) obtained for the prototropic reaction of CBIM, where the formation of zwitterion is not possible in this range of pH. (iii) The aromatic carboxylic acids are also stronger acids in nonpolar solvents as compared

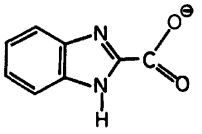

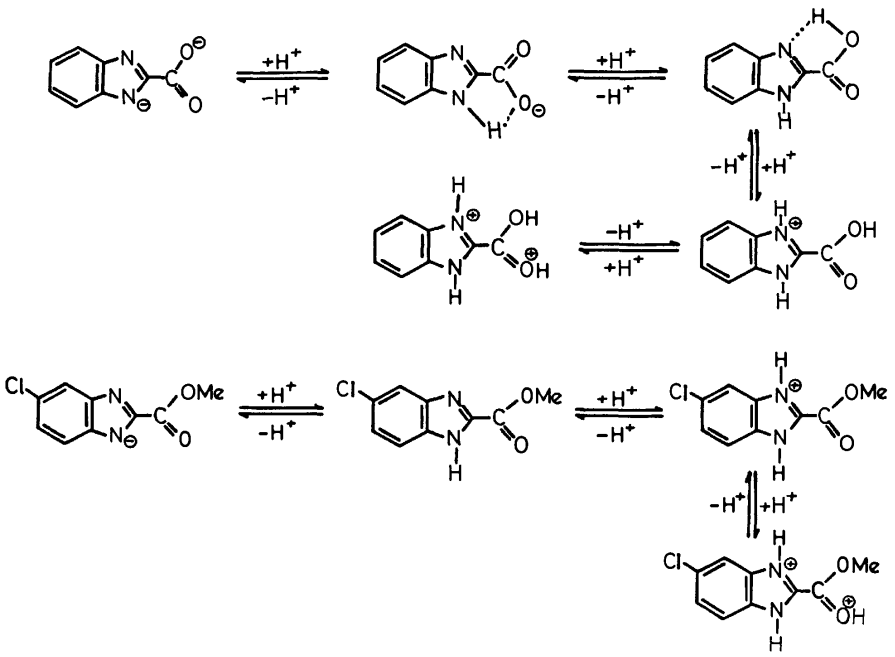

Scheme 1. Various prototropic reactions of CBIA and CBIM in the ground and excited singlet states.

to that in aqueous medium. Complete absence of F_2 in cyclohexane rejects the possibility of a zwitterion.

Effect of Acid Concentration. The absorption and fluorescence spectral data of BIA, CBIA, and CBIM at various acid concentrations are compiled in Tables 1 and 2 respectively. Scheme 1 represents the various prototropic species of BIA and CBIM identified in the H_0/pH/H_- range of −10 to 16.

CBIM. At the extreme acid conditions, the species is a dication formed by protonating the carbonyl group and tertiary nitrogen atom. With decrease of acid concentration a blue-shift, blue-shift and red-shift observed in the absorption spectra of the dication of CBIM is consistent with the deprotonation of $-C\overset{OMe}{\underset{OH^+}{<}}$, $>\overset{+}{N}-H$ and >N-H groups respectively. The species formed are monocation, neutral and monoanion and the changes observed in the absorption spectra are consistent with the deprotonation reactions of various groups. On the other hand, dication is non-fluorescent, but the fluorescence specturm of monocation is blue-shifted, followed by a further blue shift under the above environments. The latter one is unusual because the deprotonation of >N-H group leads to red shift in the fluorescence spectrum of neutral species, as noticed in the absorption spectrum. This can be explained as follows. As said earlier, the lowest energy first excited singlet state of neutral CBIM is CT in character, because of the flow of charge from benzene ring to carboxyl group. In monoanion the presence of negative charge on $>N^-$ will inhibit the flow of charge towards the electron-withdrawing group and thus CT state will be destabilized. Similar behavior is also observed when strong electron-withdrawing groups (-CF_3, -CCl_3) are present at position-2.[39]

Table 3. pK_a and pK_a* of Various Prototropic Reactions of BIA, CBIA, and CBIM at 298 K

Equilibrium			pK_a*		
			pK_a	Abs	Flu
BIA					
Dication	⇌	Monocation	−5.0	−2.4	—
Monocation	⇌	Neutral	0.4	2.4	2.8
Neutral	⇌	Monoanion	4.8	5.9	9.6
Monoanion	⇌	Dianion	13.1	9.6	12.3
CBIA					
Dication	⇌	Monocation	−4.9	−1.7	—
Monocation	⇌	Neutral	0.0	1.1	4.1
Neutral	⇌	Monoanion	4.3	4.8	9.8
Monoanion	⇌	Dianion	12.7	10.2	11.8
CBIM					
Dication	⇌	Monocation	−4.4	−3.2	—
Monocation	⇌	Neutral	0.3	0.8	2.9
Neutral	⇌	Monoanin	9.6	7.8	—

The pK_a values for the various prototropic reactions in S_0 state are calculated by using absorption spectral data and the values are listed in Table 3. The pK_a's for the monocation-neutral and neutral-monoanion equilibria are quite low as compared to those for BI (5.53[18] and 13.35).[41] This is because of the presence of electron-withdrawing -COOMe group, which decreases the charge densities at the tertiary nitrogen atom and the imino group. The pK_a values in the S_1 state are determined by using Forster cycle method[42] (whereever possible) and the fluorimetric titrations. The pK_a values for all the prototropic equilibria, determined from the fluorometric titrations agree

nicely with the pK_a values for the similar reactions in the ground state. This indicates that prototropic equilibria are not established in the S_1 state and could be due to the shorter lifetimes of the conjugate acid-base pairs. A similar behavior is observed in the protonation and deprotonation reactions of benzimidazoles.[17,39] Spectral changes do establish that the carbonyl group and tertiary nitrogen atom become stronger bases and >N-H becomes stronger acid on excitation to S_1 state.

BIA and CBIA. The nature of prototropic species formed in S_0 and S_1 states of BIA and CBIA in the H_0/pH/H_- range of −10 to 16 are the same i.e. in S_0 and S_1 states, dication, H_0 −2; monocation, H_0 −2 to pH 2; neutral, pH 2 to 4; monoanion, pH 4 to 11 and dianion, pH>11. This is also similar to the behavior of CBIM under the similar environments, with the following exceptions. (i) Monoanions in case of BIA and CBIA are formed by the deprotonation of -COOH group, as CBIM does not possess dissociated proton at pH≈4. pK_a for the neutal-monoanion equilibrium is consistent with the earlier results of carboxyl group.[43] (ii) A normal small red shift is observed in the absorption and fluorescence spectra when >NH group is deprotonated. This is because π^* state is the lowest excited singlet state in the monoanion and dianion of BIA and CBIA as compared to CBIM where CT is the lowest excited singlet state for the neutral and π^* is that for the monoanion. (iii) The pK_a value for the monoanion-dianion equilibrium (i.e. deprotonation of >N-H) of BIA (13.1) and CBIA (12.7) is higher than that for the CBIM (9.9). This could be due to the intramolecular hydrogen bond formed between the carboxylato group and the imino proton. A similar behavior is also observed in case of 2-(2-hydroxyphenyl)benzimidazole.[14]

Various prototropic reactions taking place in the complete range of −10 to 16 are depicted in the Scheme 1 and the pK_a values are compiled in Table 3.

Conclusion

The following conclusions can be arrived at from the above study: (i) The -COOH group in S_0 and S_1 states are coplanar with the BI moiety of CBIA and BIA. The -COOMe group of CBIM is better coplanar with the BI moiety in S_1 than S_0 state. (ii) Two conformers, one cyclic rigid and the other open structure, are present in case of BIA and CBIA. The latter is more favorable in the polar solvents. (iii) Charge transfer state is the emitting state in CBIM neutral species but π^* is the emitting state of monoanion of CBIM. In case of BIA and CBIA, the lowest excited state is of π^* character. (iv) The electron-withdrawing nature of -COOH/-COOMe group reduces the charge densities at the tertiary nitrogen atom and the imino group. This decreases the pK_a values for the protonation and deprotonation reactions.

The authors are thankful to the Department of Science and Technology, New Delhi, for the financial support to the project entitled "Proton Transfer Reactions in the Excited States".

References

1) R. Brnnet, *Chem. Rev.*, **63**, 573 (1963).
2) J. H. Lister, "Fused Pyrimidines," Part II, Wiley Interscience, New York (1971).
3) P. N. Preston, "Benzimidazoles and Congeneric Tricyclic Compounds," Wiley Interscience, New York (1981), p. 60.
4) P. C. Tway and L. J. Clinelove, *J. Phys. Chem.*, **86**, 5223, 5227 (1982).
5) M. Kondo and H. Kuwano, *Bull. Chem. Soc. Jpn.*, **42**, 1433, 5223 (1969).
6) M. Swaminathan and S. K. Dogra, *Indian J. Chem., Sect. A*, **22**, 407 (1983).
7) A. K. Mishra and S. K. Dogra, *Spectrochim. Acta, Part A*, **39**, 609 (1983).
8) A. K. Mishra and S. K. Dogra, *J. Photochem.*, **29**, 435 (1985).
9) A. K. Mishra and S. K. Dogra, *Indian J. Phys.*, **58B**, 480 (1984).
10) A. K. Mishra and S. K. Dogra, *Indian J. Chem., Sect. A*, **24**, 364, 815 (1985).
11) A. K. Mishra and S. K. Dogra, *Bull. Chem. Soc. Jpn.*, **58**, 3587 (1985).
12) A. K. Mishra and S. K. Dogra, *J. Photochem.*, **31**, 333 (1985).
13) H. K. Sinha and S. K. Dogra, *Spectrochim. Acta, Part A*, **41**, 961 (1985).
14) H. K. Sinha and S. K. Dogra, *Chem. Phys.*, **102**, 337 (1986).
15) H. K. Sinha and S. K. Dogra, *J. Photochem.*, **36**, 149 (1987).
16) H. K. Sinha and S. K. Dogra, *Indian J. Chem., Sect. A*, **25**, 1092 (1986).
17) M. Krishnamurthy, P. Phaniraj, and S. K. Dogra, *J. Chem. Soc., Perkin Trans. 2*, **1986**, 1971 and references listed therein.
18) M. Krishnamurthy, A. K. Mishra, and S. K. Dogra, *Photochem. Photobiol.*, **45**, 359 (1987).
19) M. Krishnamurthy, H. K. Sinha, and S. K. Dogra, *J. Lumin.*, **35**, 343 (1986).
20) P. J. Kovi and S. G. Schulman, *Anal. Chim. Acta*, **63**, 39 (1973).
21) J. J. Aaron, A. Tine, M. E. Wojciechowska, and C. Parkanyi, *J. Lumin.*, **33**, 33 (1985).
22) P. S. Song and W. E. Kurtin, *J. Am. Chem. Soc.*, **91**, 4982 (1969).
23) T. C. Werner and D. M. Hercules, *J. Phys. Chem.*, **73**, 2005 (1969).
24) T. C. Werner and D. M. Hercules, *J. Phys. Chem.*, **74**, 1030 (1970).
25) R. Manoharan and S. K. Dogra, *Spectrochim. Acta, Part A*, **43**, 91 (1987).
26) P. J. Kovi, C. L. Miller, and S. G. Schulman, *Anal. Chim. Acta*, **63**, 39 (1973).
27) P. J. Kovi, C. L. Miller, and S. G. Schulman, *Anal.*

Chim. Acta, **62**, 59 (1972).
28) C. Holan, E. L. Samlel, B. C. Ennis, and R. W. Hind, *J. Chem. Soc. C*, **1967**, 20.
29) M. Swaminathan and S. K. Dogra, *Indian J. Chem., Sect. A*, **22**, 853 (1983).
30) R. Manoharan and S. K. Dogra, *Can. J. Chem.*, **65**, 2013 (1987).
31) R. Manoharan and S. K. Dogra, *J. Photochem. Photobiol. A*, **43**, 81 (1988).
32) R. Manoharan and S. K. Dogra, *Bull. Chem. Soc. Jpn.*, **60**, 4409 (1987).
33) R. Manoharan and S. K. Dogra, *J. Phys. Chem.*, **92**, 5282 (1988).
34) H. C. Borresen, *Acta Chem. Scand.*, **17**, 921 (1963).
35) R. Manoharan and S. K. Dogra, *J. Photochem. Photobiol. A*, **43**, 119 (1988).
36) A. Kumar, H. K. Sinha, and S. K. Dogra, *Can. J. Chem.*, in press.
37) M. J. S. Dewar, *Nature (London)*, **155**, 50, 499 (1945).
38) J. C. Banm and D. S. McClure, *J. Am. Chem. Soc.*, **102**, 720 (1980).
39) H. K. Sinha and S. K. Dogra, *J. Chem. Soc., Perkin Trans. 2*, **1987** 1465.
40) J. F. Ireland and P. A. H. Wyatt, *Adv. Phys. Org. Chem.*, **12**, 159 (1976).
41) C. A. Bunton, L. S. Romsted, and L. Sepulveda, *J. Phys. Chem.*, **84**, 2611 (1980).
42) Th. Forster, *Z. Elektrochem.*, **54**, 50, 531 (1950).
43) J. March, "Advanced Organic Chemistry," Wiley Interscience, New York (1986), p. 230.

Solvent and Electrode Kinetic Effects on Cathodic Reduction of $I_3^- + 2e \rightarrow 3I^-$ in Some Pure and Mixed Dipolar Aprotic Solvents†

Swapan BHATTACHARYA and Kiron K. KUNDU*
Physical Chemistry Laboratories, Jadavpur University, Calcutta 700032, India
(Received September 14, 1988)

Exchange current densities (i_0) of the redox reaction $I_3^- + 2e^- = 3I^-$ have been determined at 25 °C on platinum (Pt) and graphite (C) electrodes in acetonitrile (ACN), propylene carbonate (PC), *N*,*N*-dimethylformamide (DMF), and their binary mixtures by potentiostatic polarization studies under near equilibrium conditions. The studies in pure solvents have also been extended to 15 and 35 °C and also on platinized graphite (C)Pt electrode. The kinetic solvent effect data at 25 °C have been analyzed in the light of relative solvation of I_2 and transition state (TS) as reflected from the previously reported transfer free energies (ΔG_t°) of I_2 and that of TS derived therein for the respective solvent systems. The electrocatalytic activities of (C)Pt electrode in different solvent systems are found to be of the same order as that of Pt electrode possibly because of its large roughness factor. But the observed energies of activation (E_a) being of the order C≫C(Pt) ≈Pt suggest that graphite is intrinsically a weaker electrocatalyst than both the (C)Pt and Pt electrodes, which are however equivalent to each other so far as electrocatalytic activity is concerned. Moreover, while the electrocatalytic activity of Pt and (C)Pt electrodes is found to be in the order ACN > PC > DMF, that of C is ACN > DMF > PC, which have been ascribed to result from the differential adsorption propensities of the solvent molecules with respect to Pt and C surfaces respectively.

The electrode kinetics of $I_3^- - I^-$ redox couple had received wide interests[1-12] long since. It is chiefly because of its fairly reversible character in both aqueous[7-9] and various nonaqueous[1-6,10-12] solvents especially on Pt surface. This makes it a suitable reference electrode for the use of different electrochemical studies and also as a galvanic element in some potential primary and secondary batteries.[12-19] In fact its fairly high exchange current densities (i_0) on Pt-surface in some nonaqueous solvents led Coetzee and Gardner[20] to recommend it as a useful reference electrode in those solvents.

Although it is well-known that the degree of reversibility of an electrode depends on the nature of the solvent, electrode surface, temperature etc., relatively few work[20,21] have yet been reported on these aspects of this redox couple. This should have been useful particularly to understand the relative electrode kinetic behavior of this galvanic element to be used either as cathodes in some high energy rechargeable nonaqueous batteries or as the redox couple in some potential nonaqueous photoelectrochemical (PEC) cells.

True, exchange current densities of the I_3^-/I^- redox couple on Pt, steel and glassy carbon electrodes in some pure nonaqueous solvents are available in the literature.[20,21] But they are referred to the different conditions and concentrations, and measured by different techniques. Consequently, these are not amenable to the direct comparison is respect of solvent kinetic effect and of the electrocatalytic activity of the different electrodes, which in fact are vital for the search of the proper solvent and electrode to be used as the potential galvanic elements with increased efficiency either in the nonaqueous batteries[22-24] or in nonaqueous PEC cells.[8,23]

In a recent study[24] from this laboratory it has been observed that the efficiency of charging-discharging behavior of a potential rechargeable cell comprising I_3^-/I^- as a galvanic element, in dipolar aprotic solvents like ACN, PC, and DMF and their binary mixtures is better in some of these mixtures than in pure solvents. So, it was considered highly interesting and useful to make systematic studies on the thermodynamic and kinetic aspects of the involved galvanic reactions not only on the widely used Pt electrode but also on some cheaper electrode substrates. With this end in view in a recent paper[25a] we have reported the solvent effect on the relative E° values of I_3^-/I^-, I_2/I_3^-, and I_2/I^- redox couples and the formation constant (K_f) of I_3^- as per $I_2 + I^- \rightleftarrows I_3^-$ equilibrium, in terms of the solvation behavior of I_2, I^-, and I_3^- species. In another paper[25b] we have also reported the rate constant (k_s) values of the galvanic reaction:

$$3I^- \rightleftarrows I_3^- + 2e\,;\; 2I_3^- \rightleftarrows 3I_2 + 2e$$

on Pt electrode as determined by use of cyclic voltammetric technique. Both these reactions however exhibited quasi-equilibrium type cyclic voltammograms (CVG) in each of these solvent systems, and as a result the evolution of k_s values posed to be an involved problem.

In the present paper we are therefore reporting the exchange current densities (i_0) of the galvanic reaction: $I_3^- + 2e \rightleftarrows I_3^-$ as determined by potentiostatic polarization technique under near equilibrium conditions using both the costly Pt and the cheaper graphite carbon (C) electrodes in each of the solvent systems. Moreover, the studies in pure solvents have also been extended to two other temperatures viz. 15 and 35 °C and also with platinized graphite (C)Pt

† Presented in the National Seminar on Electrodics held in Central Electrochemical Research Institute, Karaikundi, Tamilnadu, India during July, 23—25, 1988.

electrode. It is hoped that the activation energies (E_a) of the reaction on different electrode substrates and in different pure solvents will help reflect the intrinsic electrocatalytic activities of the three electrode substrates viz. Pt, C, and (C)Pt and also their relative electrocatalytic behavior in the three dipolar aprotic solvents. Moreover, with a view to have a preliminary reflection about the solvent effect on the reaction mechanism attempts have also been made to take CV's of the reaction in those pure solvents.

Experimental

The solvents ACN (AR, BDH), DMF (E. Merck), and PC (Koch Light) were purified by the methods described earlier.[26,27] KI (GR, E. Merck) was dried by keeping it in vacuum desiccator for a week. I_2 (E. Merck) was purified by sublimation twice under vacuo.

Solvent mixtures were prepared by weight. Solutions of I^- and I_3^- of known strengths in a given solvent were prepared by mixing the appropriate amounts of the standard stock solutions of KI and I_2 in that solvent, the concentrations of which being checked by potentiometric titration with standard $AgNO_3$ solution and volumetric titration with standard thiosulfate solution respectvely.

The cell used in the polarization studies under near equilibrium conditions consists of a three electrode assembly of which the counter electrode is a Pt-foil electrode of 4 cm^2. The test and reference electrodes are either two identical Pt-foils [geometric area A=0.5 cm^2] or of two graphite/platinized graphite electrodes [A=0.1 cm^2]. The advantage of taking the two identical electrodes is that the potential difference between them in any given solution is zero in absence of any external source.[20] The reference electrode immersed in the test solutions is separated from the remainder by a glass cage ending with a fibre-tip similar to that described earlier.[20] In the case of cyclic voltammetric measurements, however, instead of using Pt or C, aqueous saturated calomel electrode SCE(W) was used as the reference electrode. Potentiostatic polarization and linear sweep cyclic voltammetric measurements were carried out with a standard Wenking ST 72 potentiostat along with a Wenking model VSG 72 voltage scan generator. A Houston Omnigraphic X-Y(t) recorder (model 2000) recorded the current and potential which have also been checked by a Kiethley digital electrometer (model 616).

The Pt-foils were pretreated with aqua regia and activated by burning in ethanol flame. Graphite electrodes taken from Nippo dry battery were boiled alternatively in concentrated HCl and hot water, and then dried. They were then covered with a plastic sheet inert to the test solution and the open portion was then polished by rubbing it with a fine file. Some of the graphite electrodes were platinized from 2% hexachloroplatinic acid solution (prepared with 2 M HCl solution; 1 M=1 mol dm^{-3}) using a current of 5 mA from a DB 300 constant current source (Galvanostat) for 30 minutes. The roughness factors of these electrodes were being known from a similar study[28] from this laboratory. The solutions were static at the time of measurements but shaken with a magnetic stirrer at the end of a single measurement, when the drifted voltage of the test electrode reverts back to its original equilibrium value within a time period of maximum five minutes. The initial equilibrium values however reached by about 0.5 hour. The steady state current at a given overpotential η has however reached within 10 minutes. No significant transient effect was observed except immediately after the onset of the over potential, when the rate of rise of current was relatively high. IR-drop was also found to be negligibly small as verified by altering the distance between the test and the reference electrodes even at the relatively high current drain condition. All the solutions were deoxygenated by passing O_2-free pure N_2 for about 15—20 minutes.

Cyclic voltammograms (CVG's) of 0.001 M I_2 solution in presence of 0.1 M $NaClO_4$ supporting electrolyte in water, DMF, ACN, and PC were taken on Pt electrodes with a scan rate of 50 mV s^{-1}. In polarization studies the solution consisted of I_3^- and I^- with a concentration $C_{I_3^-}=C_{I^-}$=0.05 M in those pure organic solvents as well as 25, 50, 75 wt% of their binary mixtures.

Results

A set of typical current (i)-overpotential (η) plots for the I_3^-/I^- redox couples in these solvent systems are shown in Fig. 1. The linear portions in near equilibrium regions are shown, beyond which they are curved. The plots for both Pt and C electrodes in different solvent systems are exactly similar in nature but different only in the extent of linear portions which usually increased with increased exchange current densities for different electrode-solvent pairs, indicating greater reversibility. Since very much low current (ca. 10^{-6} A) passed in the experimental near equilibrium condition (10 mV>η>−10 mV), the mass transfer polarization has been taken to be negligibly small. Moreover, the fact that a few measurements

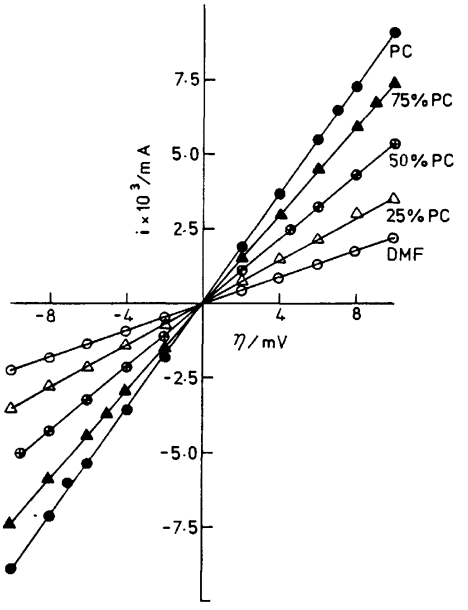

Fig. 1. Plots of $i\times10^3$/mA vs. η/mV for the cathodic solution of $I_3^-+2e^-\rightarrow3I^-$ on carbon electrodes in PC (●), 75% PC +25% DMF (▲), 50% PC +50% DMF (⊕), 25% PC +75% DMF (△), and DMF (○) solvents.

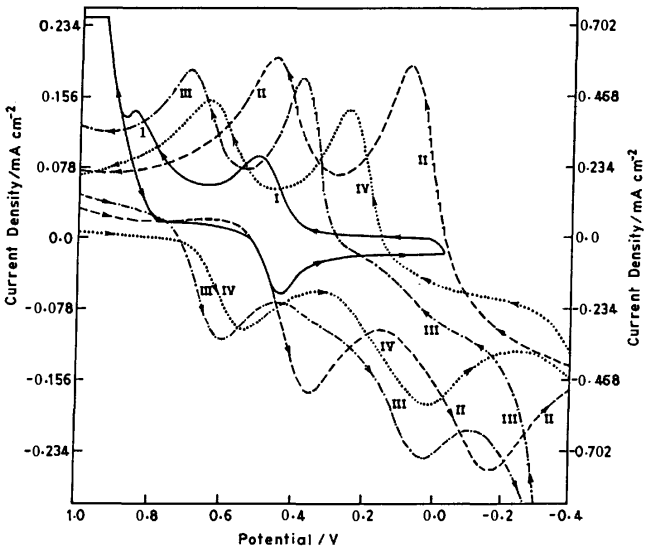

Fig. 2. Cyclic voltammograms of I_2 (10^{-3} M) solutions on platinum electrode. Reference electrode: saturated aqueous calomel. Solvents: H_2O (I) (current scale right hand side) (———), ACN (II) (---------), DMF (III) (—·—·—), PC (IV) (·····).

both at the static and stirring conditions of the solutions show no difference in the readings except some little fluctuations within tolerance limits, also appears to substantiate the above assumption.

The exchange current density (i_0) values for the reaction in different solvents have been determined by use of the Ohmic relation[29]

$$i_0 = \frac{RT\nu}{nF}(i/\eta)_{\eta\to 0} \qquad (1)$$

where i is the current, η is the overpotential, n is the number of electrons involved in the overall reaction, and ν is that in the rate-determining step (rds), which are taken to be 2 and 1 respectively.

In fact, although several mechanisms[20,21,29-33] have been proposed for the I_3^-/I^- system, none is without controversy. We therefore assumed, as Coetzee et al. did,[20] the widely accepted mechanism of Dane et al.[31]

$$I_3^- \rightleftarrows I_2 + I^-$$

$$I_2 + e^- \xrightarrow{\text{rds}} I_{ads} + I^-$$

$$I_{ads} + e^- \rightleftarrows I^-$$

Scheme 1.

for which $n=2$ and $\nu=1$. This is likely to be true in these solvent systems as well, as is evident from the similar behavior of CVG's in the solvents. As could be seen from Fig. 2, the observed CVG's exhibit two peaks in all the cosolvents including water, where the first peak is somewhat subdued. This kind of behavior has also been reported earlier in some of these cosolvents.[9,23] Thus the two peaks indicate that the reduction of I_2 takes place in two overall reactions

$$3I_2 + 2e = 2I_3^-$$

$$I_3^- + 2e = 3I^-$$

Scheme 2.

in all the cosolvent systems though at different potential regions because of the solvent effect on E° value.[26a] Notably, the peak currents (i_p) for both the reactions vary in the increasing order PC<DMF<ACN<H_2O whereas the peak potentials (E_p) vary in the order H_2O<DMF<PC<ACN. While the former order reflects relative kinetic solvent effect, the latter reveals the relative thermodynamic solvent effect of the reaction in the solvents concerned. Evidently, in H_2O the reactions are both thermodynamically and kinetically favorable, whereas in ACN although the reactions are not so much favorable thermodynamically, they are fairly so kinetically as compared to other cosolvents. Since the nature of CVG's for I_2-I_3^- and I_3^--I^-systems are nearly similar at least in all these organic solvents, their mechanisms are likely to be same in all the solvents concerned. This led us to believe, as Coetzee et al. did, that the widely accepted Dane et al.'s mechanism: Scheme 1 is also likely to be true in all these solvents.

Discussion

The values of the exchange current densities (i_0) in different solvent mixtures are presented in Table 1 and the variation of $RT \ln ({}_s i_0 / {}_r i_0)$ with cosolvent compo-

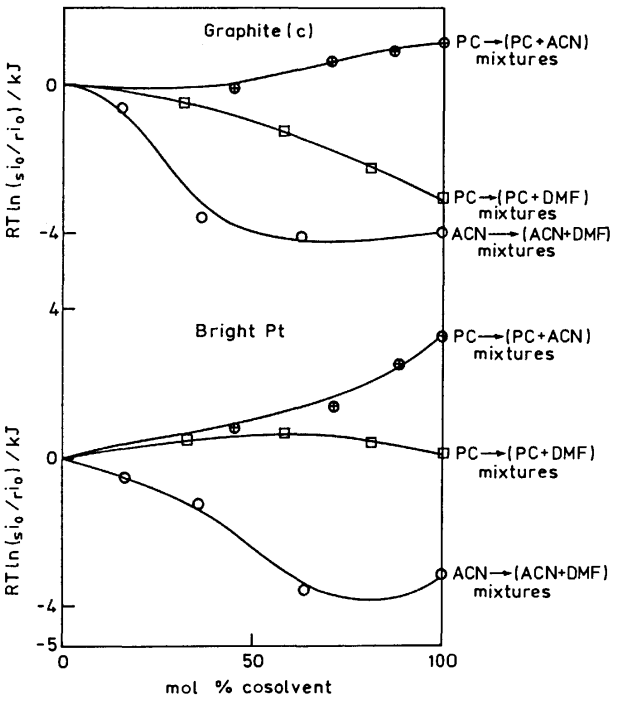

Fig. 3. Variation of $RT\ln({}_s i_0/{}_r i_0)$ against mol% cosolvent for the cathodic reduction of I_3^-+2e→3I^- on bright Pt and carbon C electrodes in PC→PC+ACN, PC→PC+DMF, and ACN→ ACN+DMF mixtures at 25 °C.

Table 1. Values of i_0 in A cm^{-2}, $RT\ln({}_si_0/{}_ri_0)$, $RT\ln({}_sk_s/{}_rk_s)$, $\Delta G_t^\circ(I_2)$, and $\Delta G_t^\circ(TS)$ in kJ mol^{-1} for the Cathodic Reduction of $I_3^-+2e\rightarrow 3I^-$ on Pretreated Bright Platinum (Pt) Electrode in Some Dipolar Aprotic Solvent Systems

Wt % cosolvent	Mole fraction cosolvent	$i_0\times10^5$	$RT\ln({}_si_0/{}_ri_0)$	$\Delta G_t^\circ(I_2)$	$-\delta(\Delta G^{\neq})=RT\ln\frac{{}_sK_s}{{}_rK_s}$	$\Delta G_t^\circ(TS)$
		PC → (PC+DMF) mixtures				
0	0	7.6	0	0	0	0
25	0.32	9.2	0.5	−6.8	−4.4	−2.5
50	0.58	10.1	0.7	−8.7	−4.6	−4.1
75	0.80	8.7	0.3	−9.3	−5.4	−3.9
100	1.00	8.1	0.2	(−9.5)	−5.6	−3.9
		PC → (PC+ACN) mixtures				
0	0	7.6	0	0	0	0
25	0.45	10.6	0.8	−0.4	−2.6	2.2
50	0.71	13.1	1.4	−0.2	−4.0	3.8
75	0.88	21.2	2.5	0.0	−3.7	3.7
100	1.00	28.0	3.2	0.0	−4.7	4.7
		ACN → (ACN+DMF) mixtures				
0	0	28.0	0	0	0	0
25	0.16	22.5	−0.5	−4.6	−3.1	−1.5
50	0.36	17.0	−1.2	−6.8	−2.4	−4.4
75	0.63	6.5	−3.6	−8.5	−2.8	−5.7
100	1.00	8.1	−3.1	(−9.5)	−1.2	−8.3

sition in Fig. 3, where subscripts s and r refer to the solvent and the assumed reference solvent respectively. In the cases of PC+ACN and ACN+DMF solvent systems, PC is the reference solvent and ACN and DMF are the cosolvents whereas in the case of ACN+DMF solvent system ACN is the reference solvent and DMF is the cosolvent. The results show a strong solvent dependence of i_0 values obtained for both types of electrodes: bright platinum (Pt) and graphite carbon (C), the highest value being almost 10 times greater than the lowest value. The order of the i_0 values of Pt electrode in different solvents follows the sequence: ACN≫DMF≈PC whereas that on C electrode is ACN>PC>DMF.

Moreover, from the data in Table 1 and in Fig. 3 it can be seen that in the case of Pt electrode while the i_0 values in PC-DMF solvent system remain more or less same with a slight maximum around 50 mol% DMF, those in PC-ACN solvent system increase almost monotonically with increase of cosolvent ACN and those in ACN-DMF system decrease monotonically upto 70 mol% of the cosolvent DMF beyond which there is an upward trend.

In the case of graphite electrode, although the behavior of $RT\ln({}_si_0/{}_ri_0)$-composition profiles in PC+ACN or ACN+DMF mixtures is nearly similar to those on Pt surface in the respective solvent systems, that for PC+DMF system takes a sharp downward trend right from zero percent DMF, instead of 50 mol% DMF observed in the case of Pt. Moreover, while the i_0 value in PC on C electrode remains nearly same as that on Pt electrode, this however gets increased with the addition of ACN and decreased with DMF. Evidently, rates of the electrode reaction are not only a function of the solvent properties but also on the electrode materials to some extent, as expected.

As the electrode reactions are multistep reactions, understanding of the solvent effect on electrode reactions, such as this, is an involved problem. This is because the reactions are not only guided by the solvated species involved in the different steps in Scheme 1 but also dependent on the coverage of the electrode by solvent molecules (θ_s). Besides, the solvent effect on the equilibrium potential $\Delta\phi_e$ involved in the expression for exchange current density (i_0):

$$i_0 = nF\vec{k}_s C_{I_2}\exp(-\beta\Delta\phi_e F/RT) \quad (2)$$

where $\vec{k}_s$ is the specific rate constant depending upon the solvent and the electrode surface, β the symmetry factor and other terms having usual significance, is also equally important. So, in order to see the true solvent effect let us examine the relative rates and solvation effect on the reactant I_2 in the rds and that of the transition state (TS) as obtained by use of the relation (3)

$$RT\ln({}_s\vec{k}_s/{}_r\vec{k}_s) = -\delta(\Delta G^{\neq}) = (-{}_s\Delta G^{\neq}) - (-{}_r\Delta G^{\neq}) = \Delta G_t^\circ(I_2) - \Delta G_t^\circ(TS) \quad (3)$$

which follows from the assumed rds as $I_2+e(M)\rightarrow$ TS→products and $RT\ln({}_s\vec{k}_s/{}_r\vec{k}_s)$ is related to $RT\ln({}_si_0/{}_ri_0)$ by Eq. A7 [vide appendix]. Here $\Delta G_t^\circ(i)$ stands for the transfer free energy of any species i from the standard state in the assumed reference solvent (r) to the standard state in the solvent (s) i.e. for the transfer process: i(r)→i(s). In Table 2 we present the values of transfer free energies of I_2 as obtained from a

Table 2. Values of i_0 in A cm^{-2}, $RT\ln({}_si_0/{}_ri_0)$, $RT\ln({}_sk_s/{}_rk_s)$, $\Delta G_t^\circ(I_2)$, and $\Delta G_t^\circ(TS)$ in kJ mol^{-1} for the Cathodic Reduction of $I_3^-+2e\rightarrow 3I^-$ on Pretreated Graphite (C) Electrode in Some Dipolar Aprotic Solvent Systems

Wt % cosolvent	Mole fraction cosolvent	$i_0\times10^5$	$RT\ln({}_si_0/{}_ri_0)$	$\Delta G_t^\circ(I_2)$	$-\delta(\Delta G^{\neq})=RT\ln\frac{{}_sK_s}{{}_rK_s}$	$\Delta G_t^\circ(TS)$
		PC → (PC+DMF) mixtures				
0	0	9.0	0	0	0	0
25	0.32	7.3	−0.5	−6.8	−5.3	−1.5
50	0.58	5.1	−1.4	−8.7	−6.7	−2.0
75	0.80	3.5	−2.3	−9.3	−8.1	−1.2
100	1.00	2.6	−3.1	(−9.5)	−8.8	−0.7
		PC → (PC+ACN) mixtures				
0	0	9.0	0	0	0	0
25	0.45	8.3	−0.2	−0.4	−3.6	3.2
50	0.71	11.5	0.6	−0.2	−4.7	4.5
75	0.88	12.5	0.8	0.0	−5.4	5.4
100	1.00	13.6	1.0	0.0	−6.9	6.9
		ACN→ (ACN+DMF) mixtures				
0	0	13.6	0	0	0	0
25	0.16	10.9	−0.6	−4.6	−3.2	−1.5
50	0.36	3.1	−3.7	−6.8	−4.8	−2.0
75	0.63	2.6	−4.1	−8.5	−3.3	−5.2
100	1.00	2.6	−4.1	(−9.5)	−2.1	−7.6

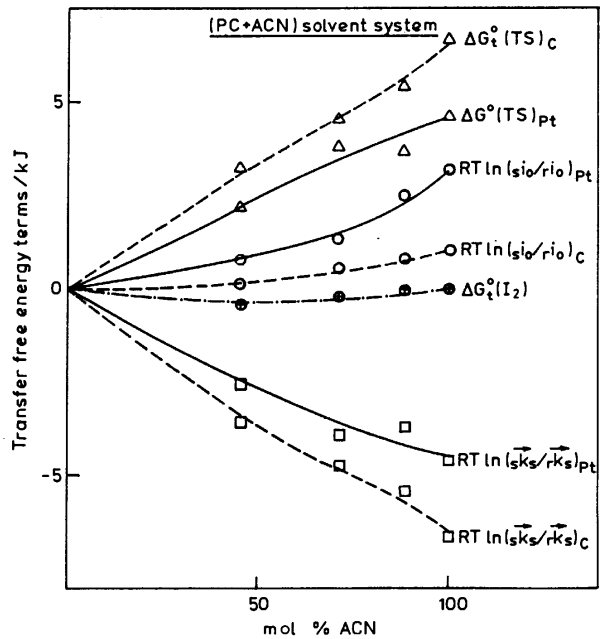

Fig. 4. Variation of $RT\ln({}_si_0/{}_ri_0)$ (○), $RT\ln({}_s\vec{k}_s/{}_r\vec{k}_s)$ (□), ΔG_t° (I_3) (—·—·—), and ΔG_t° (TS) (△) for the cathodic reduction of $I_3^-+2e^-\rightarrow 3I^-$ on Pt (solid lines) and graphite (C) (dotted lines) electrodes with mol% ACN in PC→PC+ACN solvent system.

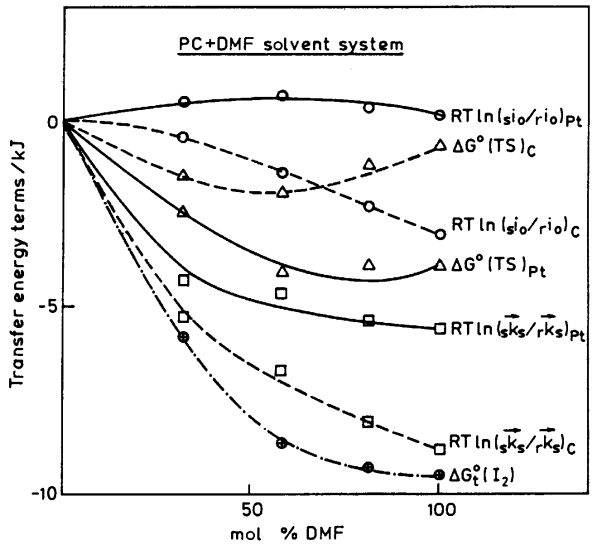

Fig. 5. Variation of $RT\ln({}_si_0/{}_ri_0)$ (○), $RT\ln({}_s\vec{k}_s/{}_r\vec{k}_s)$ (□), ΔG_t° (I_2) (—·—·—), and ΔG_t° (TS) (△) for the cathodic reduction of $I_3^-+2e^-\rightarrow 3I^-$ on Pt (solid lines) and graphite (C) (dotted lines) electrodes with mol% DMF in PC+DMF solvent system.

previous paper[25a] and those of $-\delta(\Delta G^{\neq})$ as well as ΔG_t°(TS) as computed by use of Eq. 3 for both Pt and C electrodes and for all the three solvent systems, taking PC as the reference solvent in the PC+DMF and PC+ACN solvent systems and ACN in the ACN+DMF solvent system. Figures 4—6 depict the plots of $\Delta G_t^\circ(I_2)$, $[-\delta(\Delta G^{\neq})=RT\ln({}_s\vec{k}_s/{}_r\vec{k}_s)]$, ΔG_t°(TS), and $RT\ln({}_si_0/{}_ri_0)$ values as a function of the composition of the added cosolvent for both Pt and C electrodes.

From the plots of $RT\ln({}_s\vec{k}_s/{}_r\vec{k}_s)$ it may be noted that the values of the rate constant $\vec{k}_s$ of the reaction decrease as DMF or ACN is added to PC in PC+DMF and PC+ACN solvent systems respectively, but the values pass through a distinct minima when DMF is added to ACN in ACN+DMF solvent system. Notably, the actual values on Pt and C electrodes though

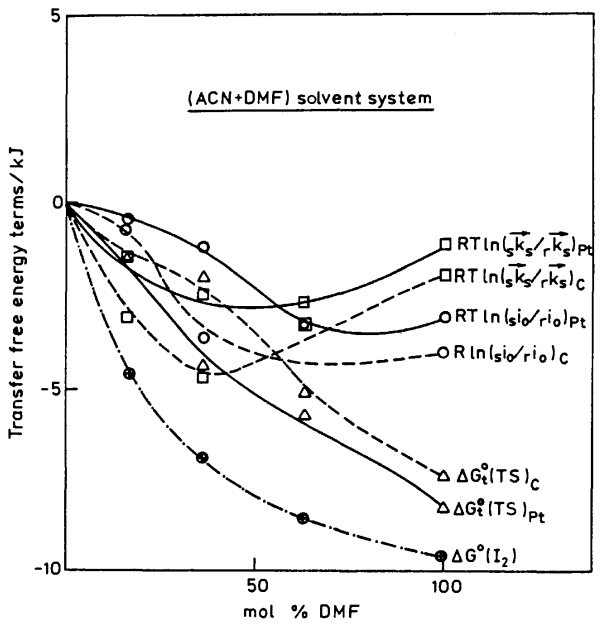

Fig. 6. Variation of $RT \ln ({}_s i_0/{}_r i_0)$ (○), $RT \ln ({}_s\vec{k}_s/{}_r\vec{k}_s)$ (□), ΔG_t° (I_2) (—·—·—), and ΔG_t° (TS) (△) for the cathodic reduction of $I_3^- + 2e^- \rightarrow 3I^-$ on Pt (solid lines) and graphite (C) (dotted lines) electrodes with mol% DMF in ACN→ACN+DMF solvent system.

differ appreciably, their overall behavior is more or less similar in nature in the respective solvents. Moreover, the relative behavior of $\vec{k}_s$ values is also fairly different from that of i_0 values in the respective solvents. Evidently, either the increasing solvation of the reactant I_2 in the rds or decreasing solvation of the transition state (TS) is responsible for the observed solvent effect on $\vec{k}_s$ values in these solvent systems.

Thus in PC+ACN solvent system as the cosolvent ACN is added to PC the solvation of I_2 hardly alters for $\Delta G_t^\circ(I_2)_{PC \rightarrow PC+ACN}$ remains nearly invariant, whereas the solvation of TS decreases to a large extent (see Fig. 4). And hence the decreased solvation of TS is responsible for the decreased rate constant values in the solvent system. The reason for decreased solvation of TS with increased ACN content may be attributed partly to the larger dipolar and dispersion interactions of TS with PC molecules compared to ACN molecules [μ_{PC}=4.98D, μ_{ACN}=3.92D; $\alpha_{PC}=8.56\times10^{-24}$ cm^3, $\alpha_{ACN}=4.41\times10^{-24}$ cm^3][25a] and partly to the smaller coverage θ_s and hence larger free surface $(1-\theta_s)$ in the case of PC molecules compared to the respective cases in the increased proportion of ACN molecules. This is because of the intrinsic structural and electronic configuration of the organic molecules. The decreased reaction rates on C surface compared to Pt surface seemingly result from the fact that a carbon atom with sp^2 electrons can usually be expected to undergo interaction with π-electron clouds of the donor -C≡N or >C=O groups of the solvent molecules. Moreover, as CH_3CN is smaller in size and bears greater thickness of the π-electron cloud than those of PC or DMF, it is expected to get adsorbed more on porous C electrode than bright Pt electrode.[34-36]

In PC+DMF solvent system, as DMF is added to PC the relative reaction rates get reduced on both the electrodes because of the pronounced solvation of I_2 molecules rather than the solvation of TS molecules which in fact get less solvated in the cases of both C and Pt electrodes at DMF rich compositions. Evidently, the effect of possible increased solvation of the TS by DMF molecules due to dispersion interactions[25a] is overcome by the superimposed effect of $(1-\theta_s)$ factors which seem to increase with DMF content and on C surface compared to Pt surface.

In ACN+DMF mixtures however, as DMF is added to ACN, the relative reaction rates, i.e. $RT \ln ({}_s\vec{k}_s/{}_r\vec{k}_s)$, are found to pass through a minimum in both the cases of Pt and C electrode surfaces. The observed variation of this is seemingly guided by the effect of pronounced solvation of I_2 molecules as opposed by the pronounced solvation of TS molecules which being larger in the case of Pt than on C surface, the relative profile for Pt lies above that for C. Since θ_{ACN} is likely to be greater than θ_{DMF}, solvation of TS through $(1-\theta_{org})$ is more in ACN-DMF mixtures than in ACN and this is again less on C surface than on Pt, thus resulting in the observed relative nature and positions of the profiles of relative rate constants on Pt and C surface in this solvent mixture. As the effect of temperature and the related energy of activation is expected to impart better reflection on the effect of electrode surfaces on the reaction rate, we may com-

Table 3. Logarithms of Exchange Current Densities at Different Temperatures and the Activation Energies (E_a)/kJ in the Different Solvents

$T^{-1}\times10^3$	$-\log i_0$								
	ACN			PC			DMF		
	PT	C/Pt	C	Pt	C/Pt	C	Pt	C/Pt	C
3.470	3.67	3.55	4.10	4.29	4.18	5.64	4.41	4.08	4.75
3.354	3.62	3.48	3.87	4.20	4.00	5.02	4.24	3.90	4.49
3.245	3.55	3.44	3.71	4.10	3.97	4.11	4.09	3.83	4.25
Activation energy (E_a)/kJ mol^{-1}	8.5	8.4	32.0	16.2	16.2	13.5	26.6	26.2	44.4

pare the i_0 values at different temperatures at least for three pure solvents as presented in Table 3. A plot of log i_0 vs. T^{-1} for the reaction at a particular concentration of the reacting species yielded straight lines. The slopes of the lines yielded the E_a values as

$$E_a = -[\delta \ln {}_s i/\delta(T)^{-1}]_{c=\text{const.}} \quad (4)$$

The E_a values so obtained are presented in Table 3. From the perusal of E_a values it may be noted that E_a values for both bright Pt and C(Pt) electrodes are nearly equal to each other in the respective solvents whereas that on bare C electrode is fairly larger than those of both bright Pt and (C)Pt electrodes. This implies that (C)Pt electrode is as good as bright Pt electrode as the electrocatalyst for this reaction, whereas the bare C electrode is a much weaker electrocatalyst than either of the other two types of electrodes. The catalytic effect of Pt surface compared to C surface may be attributed[20] to the fact that sp^2 hybridized electrons of graphite C atom interacts more strongly with the nonbonding and π electrons of the O and N centers of the solvent molecules rather than with 5s electrons of I atom. This again seemingly indicates that the relative values of θ_s play an important role in dictating the relative catalytic activity of the electrode surfaces.

It may also be noted that E_a values on Pt and (C)Pt electrodes in the three solvents lie in the order ACN< PC<DMF, while that on C electrode is ACN< DMF<PC. In fact while the E_a values on Pt and (C)Pt electrodes and in the ratio ACN:PC: DMF=1:2:3, that on bare C electrode is 1:4:1.5. The strikingly larger E_a values on C surface in PC compared to other solvents apparently indicates that the differential propensities for adsorption of cosolvent molecules (θ_s) on C compared to Pt surface is possibly the dictating factor. But as is clear from our earlier discussion, just as for i_0 values, the solvent effect on E_a values as well should be an involved problem, as the latter is afterall computed from the temperature coefficient of i_0 values rather than that of $\vec{k}_s$ values, which should give a better reflection of the solvent effect on the involved kinetics of the reaction. But the limited knowledge on the temperature coefficients of $\Delta G_t^\circ(i)$ terms and hence the $\vec{k}_s$ values does not permit us to further examine the solvent effect on E_a values at this stage.

Thanks are due to the CSIR, Govt. of India for the financial assistance.

Appendix I

Consider the reaction scheme (Scheme A) for the overall reaction $I_3^- + 2e^- \rightleftarrows 3I^-$:

$$I_3^- \rightleftarrows I_2 + I^-$$
$$I_2 + e^- \xrightarrow{\text{rds}} I^- + I \qquad \text{Scheme A.}$$
$$I + e^- \rightleftarrows I^-$$

The exchange current i_0 is given by

$$i_0 = nF\vec{k}_s C_{I_2} \exp(-\beta\Delta\phi_e F/RT) \quad (A1)$$

where the terms have usual significance. Replacing C_{I_2} by $K_f C_{I_3^-}/C_{I^-}$ where K_f stands for the formation constant of $I_3^- : I_2 + I^- \rightleftarrows I_3^-$, we have

$$i_0 = nF\vec{k}_s \frac{I}{K_f}\frac{C_{I_3^-}}{C_{I^-}} \exp(-\beta\Delta\phi_e F/RT) \quad (A2)$$

If we consider the equantities of $\ln i_0$ in the solvent (s) relative to the reference solvent (r) and multiply both sides by RT we have

$$RT\ln({}_s i_0/{}_r i_0) = RT\ln\frac{\vec{{}_s k_s}}{\vec{{}_r k_s}} + RT\ln\frac{{}_r K_f}{{}_s K_f} + RT[\Delta\ln\frac{C_{I_3^-}}{C_{I^-}}] - \beta F[{}_s\Delta\phi_e^\circ - {}_r\Delta\phi_e^\circ] + \beta F\frac{RT}{2F}[\Delta\ln\frac{C^3_{I^-}}{C_{I_3^-}}] \quad (A3)$$

where Δ's stand for the differences of the respective quantities in the solvent(s) and the reference solvent (r).

Since K_f values are fairly large and comparable,[25a] from the experimental condition we have $C_{I_3^-} = C_{I^-} = 0.05$ M for all the solvents.

and hence, $\Delta\ln(C_{I_3^-}/C_{I^-}) = 0$, and $\Delta\ln(C^3_{I^-}/C_{I_3^-}) = 0$

Thus we have $RT\ln({}_s i_0/{}_r i_0) = RT\ln(\vec{{}_s k_s}/\vec{{}_r k_s}) + RT\ln({}_r K_f/{}_s K_f) - \beta F({}_s\Delta\phi_e^\circ - {}_r\Delta\phi_e^\circ)$. (A4)

If we express the second and third terms of Eq. A4 in terms of the involved transfer free energies, ΔG_t° of the species involved

$$RT\ln({}_r K_f/{}_s K_f) = \Delta G_t^\circ(I_3^-) - \Delta G_t^\circ(I_2) - \Delta G_t^\circ(I^-) \quad (A5)$$

and $$-\beta F({}_s\Delta\phi_e^\circ - {}_r\Delta\phi_e^\circ) = \frac{3}{4}\Delta G_t^\circ(I^-) - \frac{1}{4}\Delta G_t^\circ(I_3^-) \quad (A6)$$

if β is taken equal to 1/2.

Replacing these terms by transfer free energy terms Eq. A4 can be written as

$$RT\ln({}_s i_0/{}_r i_0) = RT\ln(\vec{{}_s k_s}/\vec{{}_r k_s}) + \frac{3}{4}\Delta G_t^\circ(I_3^-) - \Delta G_t^\circ(I_2) - \frac{1}{4}\Delta G_t^\circ(I^-) \quad (A7)$$

As the transfer free energies of I_2, I_3^-, and I^- are already known for the concerned solvent systems,[25a] $RT\ln({}_s k_s/{}_r k_s)$ values for the systems can be computed by using Eq. A7.

References

1) M. C. Giordano, J. C. Bazan, and J. Arvia, *Electrochim. Acta*, **11**, 1553 (1966).

2) A. T. Hubbard, R. A. Osteryoung, and F. C. Anson, *Anal. Chem.*, **38**, 692 (1966).

3) I. E. Barbasheva, UYu M. Povarov, and D. D. Ludovlsev, *Elektrokhimiya*, **3**, 9, 1149 (1967)

4) I. M. Kolthoff and J. F. Coetzee, *J. Am. Chem. Soc.*, **75**, 1571 (1953).
5) Yu. M. Povàrov, I. E. Barbasheva, and D. D. Lukovlsev, *Elektrokhimiya*, **3**, 10, 1202 (1967); *Soviet Electochem.*, **3**, 1071 (1967).
6) A. I. Popov and D. H. Geske, *J. Am. Chem. Soc.*, **80**, 1340 (1958).
7) a) S. Mine, J. Sobkowski, and K. Kisowska, *Roezniki Chem.*, **40**, 9, 1575 (1966); b) G. Dryhurst and P. J. Elving, *Anal. Chem.*, **39**, 606 (1967).
8) a) H. Gerischer, *Advan. Electrochem., Electrochem. Eng.*, **1**, 1978 (1961); b) W. Kautek and F. Willing, *Electrochim. Acta*, **26**, 1702 (1981); c) O. Peraldo and L. Bicelli, *Trans SAEST*, **19**, 243 (1984).
9) R. Nakata, and S. Okazaki, and T. Fujinaga, *J. Electroanal. Chem.*, **125**, 413 (1981).
10) I. V. Nelson and R. T. Iwamoto, *J. Electroanal. Chem.*, **7**, 218 (1964).
11) M. C. Giordano, J. C. Bazan, and A. J. Arvia, *Electrochim. Acta*, **12**, 723 (1967)
12) G. Raspi, F. Pergola, and R. Guidelli, *Anal. Chem.*, **344**, 472 (1972).
13) V. A. Tyagai and G. Yu. Kolbasov, *Electrokhimiya*, **7**, 11, 1722 (1971).
14) H. S. Swofford and J. H. Propp, *Anal. Chem.*, **37**, 974 (1965).
15) a) S. Schuldiner and T. B. Warner, *Anal. Chem.*, **36**, 2510 (1964); b) F. C. Anson and R. A. Osteryoung, *Anal. Chem.*, **36**, 2511 (1964).
16) V. S. Bagotzky, Yu. B. Vassitiev, and I. I. Pyshnogracra, *Electrochim. Acta*, **16**, 12, 2141 (1971).
17) R. B. Fulton and H. S. Sworford, Jr., *Anal. Chem.*, **40**, 1373 (1968).
18) G. Piccardi and R. Guidelli, *J. Phys. Chem.*, **72**, 2782 (1968).
19) J. Jorne and P. G. Pai, *J. Electrochem. Soc.*, **132**, 1612 (1985).
20) J. F. Coetzee and C. W. Gardner, Jr., *Anal. Chem.*, **54**, 2530 (1982).
21) R. T. Iwamoto, *Anal. Chem.*, **31**, 955 (1959).
22) Y. Matsuda and H. Stake, *J. Electrochem. Soc.*, **127**, (1980).
23) S. Bhattacharya, U. Mondol, J. Dutta, K. Das, and K. K. Kundu, "Advances in Electrochemical Science and Technology," Oxford & IBH Publishing Co. Ltd., New Delhi (1988).
24) "Semiconductor Electrodes," ed by H. O. Finklaa, Elsevier (1988).
25) J. Dutta, A. Bhattacharya, and K. K. Kundu a) *Bull. Chem. Soc. Jpn.*, **61**, 1735 (1988); b) *Bull. Chem. Soc. Jpn.*, Communicated.
26) a) K. Das, A. K. Das, and K. K. Kundu, *Electrochim. Acta*, **26**, 471 (1981); b) K. Das, K. Bose, and K. K. Kundu, *Electrochim. Acta*, **26**, 479 (1981).
27) J. L. Murray and Y. L. Howard, *J. Phys. Chem.*, **77**, 26 (1973).
28) P. K. Guha, Ph. D. Thesis, Jadavpur University, Calcutta, India (1987).
29) J. O'M. Bockris, A. K. N. Reddy, "Modern Electrochemistry," Plenum Press, New York (1977), Vol. 2.
30) L. M. Dane, L. J. J. Janspen, and J. G. Hoogland, *Electrochim. Acta*, **13**, 507 (1968)
31) E. Gileadi, E. Kirowa-Eisner, J. Penciner, "Interfacial Electrochemistry," Addison, Wesley Publishing Company Inc, Massachusetts, U. S. A. (1975).
32) K. J. Velter, "Electrochemical Kinetics," Academic Press, New York (1967).
33) P. G. Desideri, L. Lepri, and D. Helmler, "Encyclopedia of Electrochemistry of the Elements," ed by A. Bard, Marcel Dekku, New York (1973), Vol. 1.
34) A. Wieedowski, *Electrochim. Acta*, **26**, 1121 (1981).
35) M. sSzklarezyk and J. Sobkowski, *Electrochim. Acta*, a) **26**, 345 (1981); b) **25**, 1597 (1980).
36) H. Yoshida and K. Kamegaua, Ext Abstr Program Bienn Conf Carbon 15th, 252 (1981).

Compensation Effect in the Electrical Conduction Process in Polyene Incorporated Lipid Films

D. SARKAR and T. N. MISRA*
Department of Spectroscopy, Indian Association for the Cultivation of Science, Jadavpur, Calcutta 700032, India
(Received September 26, 1988)

Phosphatidylcholine films doped with polyenes show compensation behavior at low polyene concentration and follow a three constant semiconduction equation $\sigma_T=\sigma_0' \exp(E/kT_0) \exp(-E/kT)$, σ_0' and T_0 being constants for the lipid and the other parameters having their usual meanings. Consistent values of the constants σ_0' and T_0 obtained from various methods of evaluation suggest that the compensation effect has a physical origin. Significant change in the semiconduction activation energy of lipid film on various polyene doping suggests strong lipid-polyene interaction in the doped films.

In our earlier communications we have demonstrated the validity of the compensation rule in the electrical conduction process in some polyenes[1,2] and nucleic acid bases.[3,4] In polyenes, the semiconduction activation energy was varied by chemical vapour adsorption whereas in nucleic acid bases such variation was attained by doping with acridine dyes at low concentrations.

It has been shown that these organic semiconductors satisfy the three constant equation

$$\sigma_T=\sigma_0' \exp(E/kT_0) \exp(-E/kT) \quad (1)$$

where the preexponential factor σ_0 in the conventional expression has been replaced by $\sigma_0' \exp(E/kT_0)$. Here T_0 and σ_0' are constants for a specific material. The dependence of T_0 and σ_0' on the number of chemical double bonds,[5,6] donor and/or acceptor concentration in complexes,[3,4] molecular substituent groups[2] and molecular geometry[7] has been demonstrated. In Eq. 1 we have not used a half energy as was originally done by Rosenberg as localized states generally dominate in wide band gap materials like organic semiconductors and consequently it is more realistic to write down the activation energy according to the convention of extrinsic semiconduction.

However, some reported experimental results on compensation effect have often been criticized as these cover a narrow temperature range. Also the demonstrated compensation effect cover the Ohmic conduction region only. In pure and polyene doped phosphatidylcholine films sandwiched between a conducting SnO_2-coated glass and a stainless steel electrode, the conduction is known to be due to Schottky mechanism.[8] Also, this being a stable system, we have been able to cover a wider temperature range making the $\log \sigma_T$ vs. $1/T$ plots more meaningful in the context of compensation behavior. The result presented in this paper is therefore thought to add further credence to the physical origin of compensation effect.

Electrical conduction of model lipid membrane has been studied extensively in bilayers[9,10] and in thin films.[11,12] Light mediated electrical properties of some polyene incorporated bilayer lipid membranes have been studied extensively by Tien and his coworkers.[13-16] Dark conductive properties of the films was, however, neglected by them. This study is thought worthwhile also because the semiconductive properties of pure and polyene doped phosphatidylcholine, which is a major constituent of many cell membranes, is of significant relevance to olfactory transduction mechanism[17] where carotenoids incorporated in the olfactory cell membranes are thought to be the receptors of olfactory signals.

Experimental

Highly purified (99%) hydrogenated L-α-phosphatidylcholine (Egg lecithin) in powder form was obtained from Sigma Chemicals Co. U. K. High quality β-carotene, astacin, and vitamin A alcohol were obtained as gift from Hoffman La Roche Co. Switzerland. These materials, after checking purity by absorption spectroscopy, were used without any further purification. Each polyene was mixed with phosphatidylcholine in ca. 10^{-2} wt/wt concentration and ground repeatedly in a mortar till a uniform mixture was obtained. This mixed sample in powder form was taken in a sandwich cell configuration between a stainless steel and a SnO_2-coated glass electrode separated by a 2 mil (1 mil=0.0254 mm) thick Teflon spacer and pressed moderately to get a uniform thin film. The cell was then placed in a suitably designed conductivity chamber.[1] A dc voltage of 25 V across the electrodes was supplied from a dry battery pack. Currents were measured by an electrometer amplifier (model EA 815) of ECIL, India. Temperature measurements were made by a copper-constantan thermocouple and a panel meter (model 100) of HIL, India.

Results and Discussion

The semiconduction activation energies of all the samples were measured several times under vacuum (10^{-3} Torr; 1 Torr≈133.322 Pa) as well as in dry nitrogen atmosphere. All measurements gave consistent values. Almost the same values were obtained in vacuum and in dry nitrogen. The current-voltage characteristics of all the samples show Schottky behavior in the experimental voltage regime. The room temperature conductivity of the pure lipid

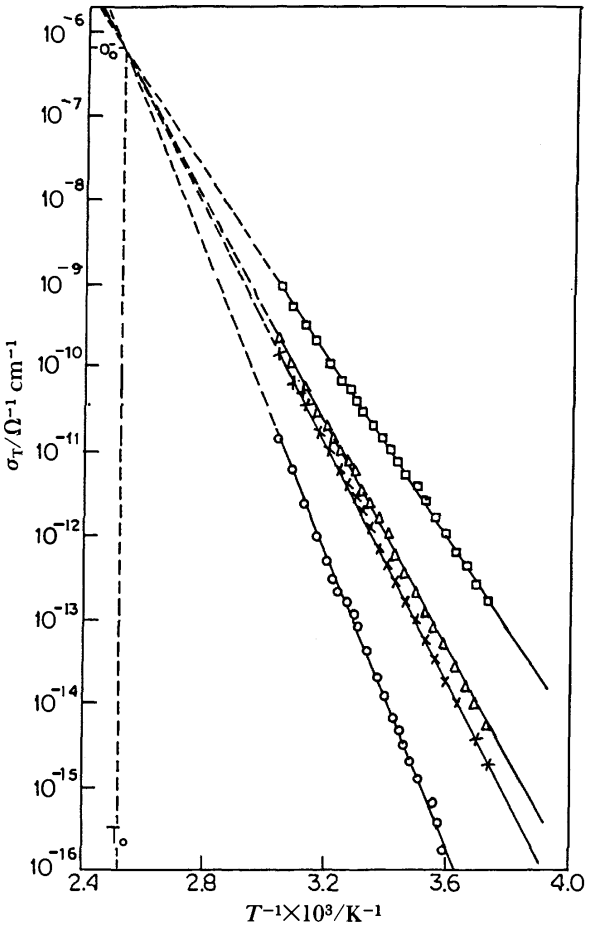

Fig. 1. The plot of $\log\sigma_T$ vs. $1/T$ for pure (—○—), β-carotene doped (—△—), vitamin A alcohol doped (—□—), and astacin doped (—×—) phosphatidylcholine films.

is ca. 10^{-13} $\Omega^{-1}cm^{-1}$. With polyene incorporation this value increases and the activation energy (which is 1.74 eV for the pure lipid) decreases. Such increase in conductivity of lipid films after polyene incorporation may be attributed to strong lipid-polyene interactions which may be of dipole-dipole,[18] hydrophobic or donor-acceptor[19] type. Donor-acceptor interactions increase the conductivity of lipid membrane on I_2 or water adsorption.[20]

In Fig. 1 we show $\log\sigma_T$ vs. $1/T$ plots for pure and β-carotene, astacin, and vitamin A alcohol doped lipid films. It is seen that the extrapolated lines in these plots intersect the ordinate at a wide variety of positions but they all pass approximately through a single point at a temperature T_0. This result is in conformity with Eq. 1. At the characteristic temperature T_0, the value of σ gives σ_0' value. For phosphatidylcholine, value of T_0 is 396.8 K and $\sigma_0'=7.5\times10^{-7}$ Ω^{-1} cm^{-1}. From Eq. 1 at any specific experimental temperature T_1, we get

$$\sigma(T_1)=\sigma_0' \exp(1/T_0-1/T_1)\,E/k \qquad (2)$$

$\sigma(T_1)$ will show different behavior with variation of E depending on whether $T_1>T_0$ or $T_1<T_0$. In our case $\sigma(T_1)$ increases with decreasing E as $T_1<T_0$.

Phosphatidycholine mixed with three different polyenes, β-carotene, astacin, and vitamin A alcohol has a distinct T_0 value. This result confirms our earlier observation[1,3] that T_0 is a molecular property of the semiconducting material.

Conpensation effect in the electrode limited conduction process has been discussed by Green.[21] He considered charge carrier injection at the semiconductor surface and showed that the preexponential factor in the standard semiconduction equation

$\sigma_T=\sigma_0 \exp(-E/kT)$ is given by

$$\sigma_0\approx n_0\left(\frac{kT}{h}\right)K \qquad (3)$$

where n_0 is the number of carriers available at the electrode and K is the transmission coefficient. If E is the energy obtained from the $\ln\sigma$ vs. $1/T$ plots and is small compared to the work-functions of the electrode and the semiconductor, then one gets

$$\ln K=A+BE+CE^2 \qquad (4)$$

where A; B, and C are some parameters. Neglecting the quadratic term

$$\log\sigma_0\approx C+C'E \qquad (5)$$

where C and C' are related to the parameters A and B. σ_0 represents the first two terms of Eq. 4. The compensation temperature T_0 of Eq. 4 is related to C' which in turn is related to the difference of the work functions of the electrode and the semiconductor and potential barrier width.

Roberts and Polanco[22] showed that for appropriate parameters, thermally assisted tunneling (TAT) yields the same shape of current voltage characteristics as in Schottky effect. It has been shown by Roberts[23] that for TAT, $\ln\sigma_{TAT}(max)$ vs. $1/T$ yields activation energy $E_{max}=\Phi-F_x$ where Φ is the potential barrier at the electrode-semiconductor interface and $F_x=(F/kT_x)^2$ $h^2/8m$ where F is the applied field and T_x is an arbitrary temperature. The curves at different F values pass through a focal point $T_0=(3/2)T_x$, where T_x is temperature corresponding to the average of the reciprocal temperatures through which experimental data points are collected. From Fig. 1, T_x=294 K and so the estimated T_0 value is 441 K. This is a value far beyond our experimental value which is ca. 400 K and is not within possible experimental error. Also for the TAT model proposed by Roberts,[23] the activation energy value should be temperature dependent and over an extended temperature range, the curves should deviate from the straight line. Our experimental results are at variance with this hypothesis. We therefore conclude that the thermally assisted tunneling model of Roberts cannot account for the obtained compensation effect in polyene doped lipid films.

True compensation effect is thought to arise from the existence of a linear relationship between the

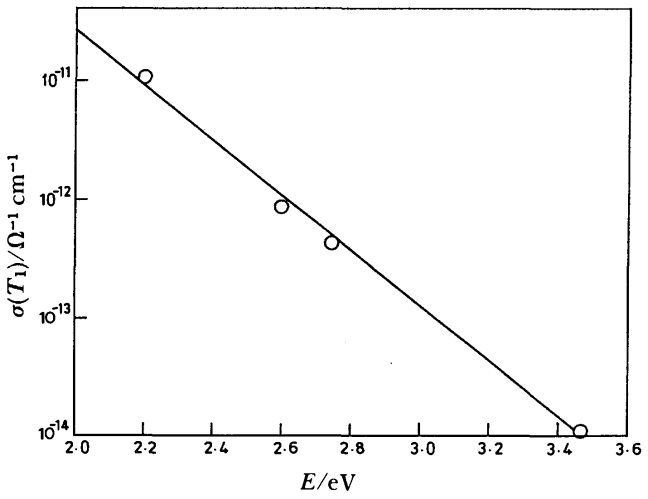

Fig. 2. The plot of $\log \sigma(T_1)$ vs. E at T_1=333.3 K for different polyene doped phosphatidylcholine films.

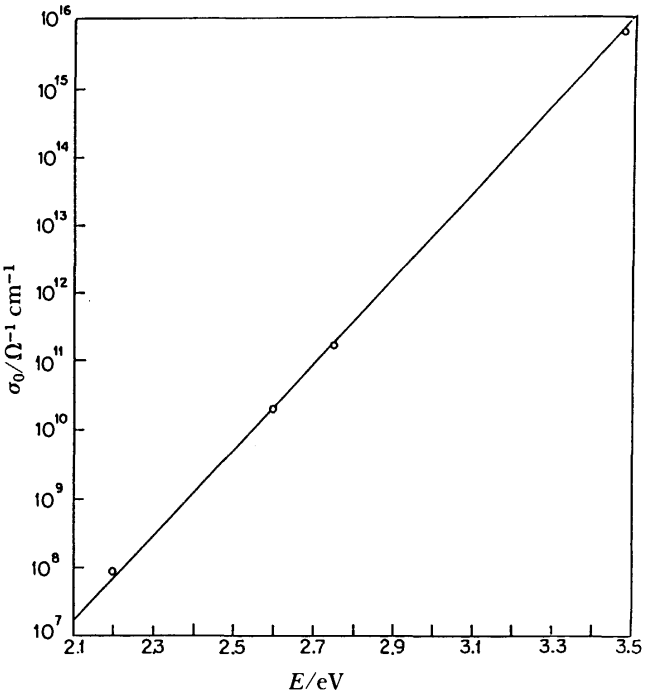

Fig. 3. The plot of $\log \sigma_0$ vs. E for different polyene doped phosphatidylcholine films.

activation energy and the activation entropy of the system. It has been pointed out by Johnston and Lyons[24] that if a true linear free energy relation (LFER) does hold for dark conduction. a physical relationship between σ_0 and E, $\log \sigma(T_1)$ vs. E must also be linear. In Fig. 2 we show such plot. T_0 and σ_0' are obtainable from the slopes and intercepts of these plots. These parameters can also be obtained from the plot of $\log \sigma_0$ vs. E as $\log \sigma_0 = \log \sigma_0' + E/kT_0$, σ_0 and E being experimentally measured. In Fig. 3 we show such plot. T_0 and σ_0' can be evaluated respectively from the slope and the intercept of this plot. In Table 1 we compare the values of T_0 and σ_0' obtained by various methods. The agreement is quite satisfactory. These results confirm that σ_0 and E are physically related and that T_0 has a physical origin. The meaning of T_0, however, remains unsettled. It has been established that T_0 is a molecular property of the semiconducting material.[25] In the theory based on rate process[26] T_0 has been attributed to the temperature at which the competing effects of energy and entropy balance each other.

Conclusion

The experimental results indicate that the compensation law is valid for electrical conduction process in various polyene doped phosphatidylcholine films where the conduction mechanism is electrode limited. Significant change in semiconduction activation energy of p lipid films on various polyene doping

Table 1. Comparison of T_0 and σ_0' Values of Pure and Various Polyene Doped Phosphatidylcholine Films

Different parameter	Phosphatidylcholine	Phosphatidylcholine+ β-carotene	Phosphatidylcholine+ astacin	Phosphatidylcholine+vitamin A alcohol
E/eV	1.74	1.30	1.38	1.10
$\sigma_T/\Omega^{-1}\,cm^{-1}$	1.20×10^{-13}	5.60×10^{-12}	3.00×10^{-12}	4.50×10^{-11}
$\sigma_0/\Omega^{-1}\,cm^{-1}$	6.46×10^{15}	1.88×10^{10}	1.70×10^{11}	8.50×10^{7}
$\sigma_0'/\Omega^{-1}\,cm^{-1}$ from Fig. 1.	←	7.50×10^{-7}	→	
$\sigma_0'/\Omega^{-1}\,cm^{-1}$ from Fig. 2.	←	1.20×10^{-6}	→	
$\sigma_0'/\Omega^{-1}\,cm^{-1}$ from Fig. 3.	←	8.90×10^{-7}	→	
T_0/K from Fig.1	←	396.8	→	
T_0/K from Fig.2	←	402.5	→	
T_0/K from Fig.3	←	399.8	→	

suggests strong lipid-polyene interaction as has been evidenced[13,14,27] from spectroscopic and other studies.

The authors express their thanks to M/s. Hoffman La Roche and Co., Ltd., Switzerland for generous gift of the polyenes.

References

1) B. Mallik, A. Ghosh, and T. N. Misra, *Bull. Chem. Soc. Jpn.*, **52**, 2091 (1979).
2) B. Mallik, A. Ghosh, and T. N. Misra, *Phys. Status Solidi (a)*, **62**, 267 (1980).
3) D. Sarkar, K. M. Jain, and T. N. Misra, *Bull. Chem. Soc. Jpn.*, **59**, 1561 (1986).
4) D. Sarkar and T. N. Misra, *Phys. Status Solidi (a)*, **99**, 251 (1987).
5) A. Sircar, B. Mallik, and T. N. Misra, *Phys. Status Solidi(a)*, **69**, 767 (1982).
6) A. Sircar, B. Mallik, and T. N. Misra, *Proc. Ind. Acad. Sci., Ser. A*, **93**, 99 (1984).
7) B. Mitra and T. N. Misra, *Jpn. J. Appl. Phys.*, **26**, 66, 695 (1987).
8) D. Sarkar and T. N. Misra, *Ind. J. Biochem. Biophys.*, **25**, 434 (1988).
9) P. S. O'Shea, G. Petone, R. P. Casey, and A. Azzi, *Biochem. J.*, **219**, 719 (1984).
10) E. Brynda, L. Nespurkova, and S. Nespurek, *Czech. J. Phys., B*, **35**, 873 (1985).
11) B. Rosenberg and G. L. Jendrasiak, *Chem. Phys. Lipids*, **2**, 47 (1968).
12) I. Szundi, *Chem. Phys. Lipids*, **34**, 323, 333, 343 (1984).
13) N. Kobamoto and H. Ti. Tien, *Biochim. Biophys. Acta*, **241**, 129 (1971).
14) N. Kobamoto and H. Ti. Tien, *Biochim. Biophys.*, **266**, 56 (1972).
15) H. Ti. Tien, *Bioelectrochem. Bioenergy.*, **9**, 559 (1982).
16) J. Kutnik and H. Ti. Tien, *Photobiochem. Photobiophys.*, **6**, 351 (1983).
17) B. Rosenberg, T. N. Misra, and R. Switzer, *Nature (London)*, **217**, 423 (1968).
18) V. D. Kolev, *J. Mol. Struct.*, **114**, 257 (1984).
19) A. Bertoluzza, S. Bonara, G. Fini, and M. A. Morelli, *Can. J. Chem.*, **63**, 1390 (1985).
20) B. Bhowmik, G. L. Jendrasiak, and B. Rosenberg, *Nature (London)*, **215**, 842 (1967)
21) M. E. Green, *J. Chem. Phys.*, **51**, 3279 (1969).
22) G. G. Roberts and J. I. Polanco, *Phys. Status Solidi (a)*, **1**, 409 (1970).
23) G. G. Roberts, *J. Phys. C*, **4**, 3167 (1971).
24) G. R. Johnston and L. E. Lyons, *Aust. J. Chem.*, **23**, 2187 (1970).
25) B. Rosenberg, B. Bhowmik, H. C. Harder, and E. Postow, *J. Chem. Phys.*, **49**, 4108 (1968).
26) B. Hartmann and R. W. Warfield, *J. Polym. Sci. B (Polym. Phys.)*, **24**, 877 (1986)
27) S. S. Broody, *Photobiochem. Photobiophys.*, **7**, 205 (1984).

 © 1989 The Chemical Society of Japan Bull. Chem. Soc. Jpn., 62, 2688—2692 (1989)

Electrochemical Generation and Properties of the *p*-Dinitrobenzene Radical Anion in *N,N*-Dimethylformamide

Alexandra SAUER, Fritz WASGESTIAN,* and Ulrich NICKEL†
Institute of Inorganic Chemistry, University of Cologne, 5000 Cologne 41, Federal Republic of Germany
†Institute of Physical and Theoretical Chemistry, University of Erlangen-Nuremberg, Federal Republic of Germany
(Received October 17, 1988)

Potentiostatic reduction of *p*-dinitrobenzene in *N,N*-dimethylformamide yielded the anion radical. By careful exclusion of water and oxygen it was obtained free from by-products. It was stable for several hours at room temperature. Its UV-visible absorbance was determined in combination with polarographic analysis. The behavior towards water and oxygen is reported.

The electrochemical reduction of *p*-dinitrobenzene (pDNB) has been extensively studied. Polarography showed two reversible reduction waves, corresponding to the formation of the singly and doubly charged anions $pDNB^{\cdot-}$ and $pDNB^{2-}$.[1-9] In aqueous solution *p*-nitrophenylhydroxylamine (Hy) was the first long-lived reduction product.[10] In aprotic solvents, however, $pDNB^{\cdot-}$ was found to be stable. In DMF (*N,N*-dimethylformamide) it was obtained by potentiostatic reduction and characterized by ESR spectroscopy.[5,6]

The reaction of *p*-dinitrobenzene with OH^- yielded *p*-nitrophenoxide (pNP^-).[11-13] In the absence of oxygen both pNP^- and $pDNP^{\cdot-}$ were observed spectrophotometrically in DMSO (dimethyl sulfoxide).[13]

Compared to the characterization by ESR and electrochemical methods the electronic absorption spectrum of $pDNB^-$ is not so well-known. In aqueous solution the radical spectrum was obtained after pulse radiolysis.[14,15] $pDNB^-$ decayed fast with a second order rate constant of 3.3×10^8 $M^{-1}s^{-1}$ (1 M=1 mol dm^{-3}). In glassy solution in 2-methyltetrahydrofuran (MTHF) the radical was stable.[16] Its spectrum showed a pronounced vibrational fine structure. Recently a matrix molecule reorientation effect has been observed in the same solvent that blurred out the vibrational fine structure and caused a time dependent blue shift.[17] In aprotic solvents the *p*-dinitrobenzene radical ($pDNB^{\cdot-}$) is sufficiently stable to be studied by conventional techniques at room temperature.

Preparation of the radical by reaction with OH^- in aqueous DMSO was associated with the formation of $pNP^{\cdot-}$.[13] In the absorption spectrum pNP^- superimposed the bands around 430 nm. The absorption coefficient which Abe and Ikegami[13] used in their kinetic treatment differed by more than one order of magnitude from that in glassy solution in MTHF. Brown et al.[18] obtained the radical by chemical reduction with sodium in 1,2-dimethoxyethane. They reported the absorption spectrum assuming quantitative conversion. However, the presence of pNP^- could not be convincingly excluded. In our opinion another determination of the spectral characteristics, that is not disturbed by by-products or secondary reactions, is necessary.

Experimental

N,N-Dimethylformamide (DMF), Fluka ppa or Merck, Uvasol, was dried with anhydrous $CuSO_4$ and distilled. Solutions were deoxygenated by purging with dry

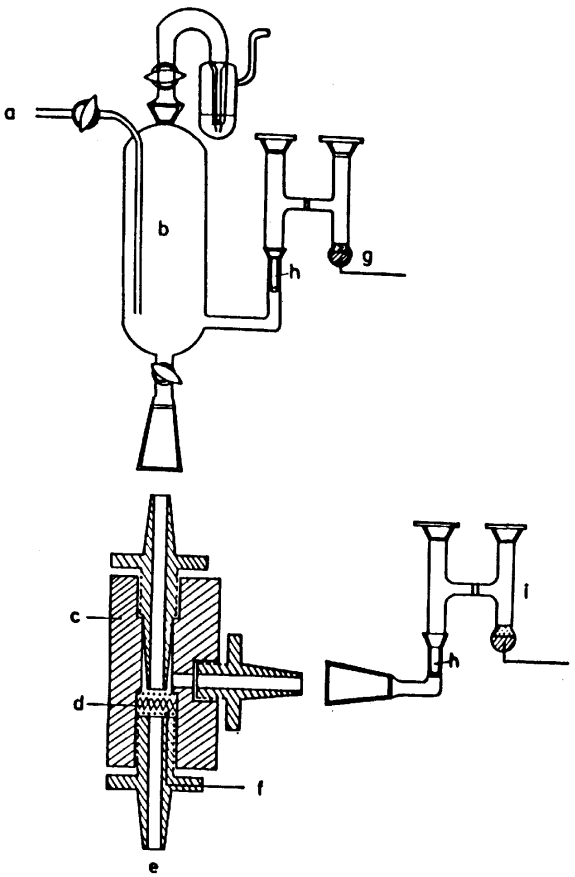

Fig. 1. Apparatus used for potentiostatic reduction of *p*-dinitrobenzene in DMF. a: argon entrance, b: vessel for stock solution, c: Teflon cell with working electrode, d: carbon fleece, e: exit to flow cell or ordinary spectrophotometric cell, f: Pt wire, g: counter electrode (SCE), h: agar-agar junction, i: reference electrode (SCE).

argon for 20 min. Supporting electrolytes were 0.1 M Bu_4NClO_4 (Fluka) or 0.1 M Et_4NClO_4 (Fluka). *p*-Dinitrobenzene (pDNB), Aldrich, was recrystallized from EtOH. For reasons of comparison the spectral data of *p*-nitrophenol (pNP) and *p*-nitrophenylhydroxylamine (Hy) were determined. pNP was obtained commercially (Merck), Hy was prepared according to literature.[19] Under our reaction conditions both were present in their base forms (pNP^- and Hy^-) with absorption maxima $\lambda(\varepsilon)$ [nm($l\,mol^{-1}\,cm^{-1}$)] at 432 (3.7×10^4) and 465; 485 (1.7×10^4); 520 sh, respectively. In the presence of pDNB the base form of the hydroxylamine formed an adduct with absorption at 500 (2×10^4). Absorption spectra were recorded on a Cary 2300 and a Uvikon 810 (Kontron). Polarograms were obtained by use of a potentiostat (HEKAelectronic PG 284) in combination with an xy-recorder (Servogor xy). The cathode was a dropping mercury electrode, the counter electrode a saturated calomel electrode (SCE), and the reference electrode was a Pt-electrode.

The apparatus used for the quantitative reduction is depicted in Fig. 1. The cathode was a carbon fleece contacted with a perfoliated gold foil. Counter and reference electrodes were SCEs separated from the solution by an agar-agar salt bridge. The use of a calomel electrode as counter electrode was advantageous, because its large mercury pool acted as reductant. By this means oxidation of the solvent was avoided. Voltage was supplied from a potentiostat (Wenking LB75 or 70TS1). The reductions were performed at flow rates of 0.5—0.8 ml min^{-1} and currents of 0.6—1 mA. After passing the fleece, the solution was directed either to a spectrophotometric flow cell or to the polarographic cell. After having recorded the polarogram, a sample of the solution was transferred to a spectrophotometric cell by use of a syringe and a hypodermic needle. During this operation the cell was standing in a flask that was flushed with argon. By the latter method polarographic as well as spectrophotometric analysis could be performed in the same solution.

Tandem cells were applied to study the effects of additives. These cells contained two separated compartments containing the reactants. By shaking the solutions could be mixed.

The spectral changes during oxidation were observed in ordinary spectrophotometer cells. Immediately after reduction the cells were transfered to the spectrophotometer. Recording was started approximately 1 min after reduction. The slowly penetrating air caused reaction.

The following absorptivity coefficients were used for the spectrophotometric analysis.

[nm]	[$M^{-1}\,cm^{-1}$]		
	$pDNB^{\cdot-}$	Hy	pNP^-
800	1.1×10^4	$\leqslant1.0\times10^2$	$\leqslant1.0\times10^2$
500	7.6×10^2	2.0×10^4	$\leqslant1.0\times10^2$
430	7.7×10^3	1.1×10^4	3.6×10^4

At first the radical concentration was determined from the absorbance at 800 nm. Then at 500 nm the concentration of *p*-nitrophenylhydroxylamine (pDNB-adduct) was obtained by subtracting the contribution by $pDNB^{\cdot-}$. Finally the concentration of pNP^- was obtained from the absorbance at 430 nm.

Results and Discussion

a) Potentiostatic Reduction and Quantitative Analysis. In DMF the polarographic reduction showed two reversible steps at −580 and −915 mV. SCE in reasonable agreement with literature.[1,4,5,8] The first reduction step led to the radical anion $pDNB^-$ and the second to $pDNB^{2-}$. Potentiostatic reduction at potentials between −600 and −900 mV only produced the single charged anion. Reduced solutions had the same ESR spectrum as previously reported for $pDNB^{\cdot-}$.[5,6]

Figure 2 shows polarograms of pDNB and its radical ion. If both species were present in solution, the oxidation current of the radical superimposed the reduction current of pDNB at the position of the first half wave potential. Their relative heights were a measure of the concentrations. In the absence of side reactions and assuming equal diffusion coefficients of pDNB and $pDNB^{\cdot-}$:

$$c(\text{pDNB}) = \frac{I_{red}}{I^0_{red}}\, c^0(\text{pDNB});$$

$$c(\text{pDNB}^{\cdot-}) = \frac{I_{ox}}{I^0_{red}}\, c^0(\text{pDNB}) \qquad (1)$$

where I^0_{red} and c^0(pDNB) are the reduction current and the pDNB concentration of the initial solution.

Table 1 presents a selection of our reduction experiments. The first set gives some preliminary results,

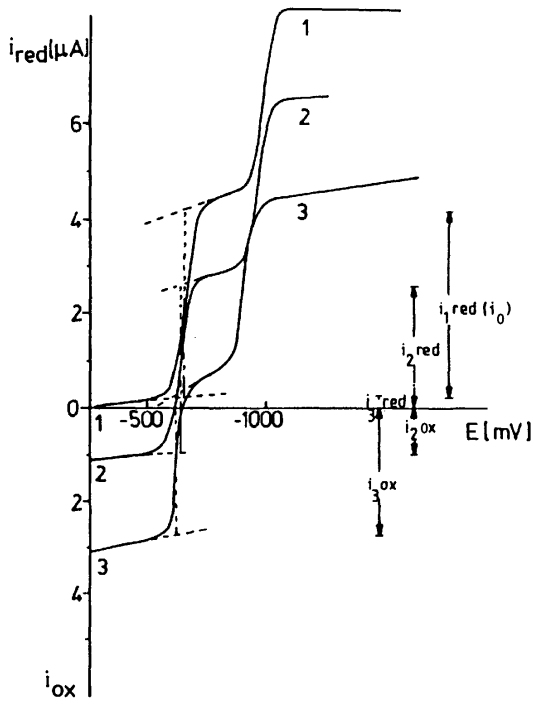

Fig. 2. Polarographic determination of pDNB and $pDNB^{\cdot-}$. 1: unreduced solution (1×10^{-3} M pDNB), 2: partly reduced solution (6×10^{-4} M pDNB. 3×10^{-4} M $pDNB^{\cdot-}$), 3: highly reduced solution (8×10^{-4} M $pDNB^{\cdot-}$).

Table 1. Survey on the Potentiostatic Reduction Experiments of *p*-Dinitrobenzene in DMF at Room Temperature by Means of the Apparatus Depicted in Fig. 1. Flow Rate 0.5—0.8 ml min^{-1}, Current 0.6—1 mA, Depending on the Potential E_{red}

$c_0 \times 10^4$ a) M		E_{red} mA	$c \times 10^4$/M pDNB^{-} a)		Hy	pNP^-
10.1	(8.7)	-800	0.55	(0.6)	0.31	0.09
9.7	(6.5)	-700	2.8	(2.4)	0.22	0.10
9.7	(5.9)	-950	2.9	(3.0)	0.12	0.18
4.9	(0.1)	-950	5.0	(4.9)	<0.02	<0.02
5.0	(0.1)	-950	4.8	(5.0)	<0.02	<0.02
2.4		-500	<0.02		<0.02	<0.02
		-600	<0.02		<0.02	<0.02
		-700	1.0		<0.02	0.08
		-800	2.5 b)		<0.02	0.02
		-1000	2.5 b)		0.01	0.05
		-1180	2.5 b)		0.09	0.08

a) In brackets concentrations determined polarographically after reduction. b) Radical concentrations determined at 750 nm.

where degassing was insufficient. The radical disappeared rather fast and pNP^- was formed. Whereas in well-degassed and carefully dried solutions the radical was stable for several hours. In those solutions the radical concentrations were determined polarographically. Set 2 compared the data with those obtained spectrophotometrically.

Solutions containing 5×10^{-4} M or less could be completely reduced potentiostatically. Immediately after reduction the solutions were practically free from by-products. The effect of the reduction potential is demonstrated in the last set. Potentials of −0.5 and −0.6 V did not cause reaction. At −0.7 V the pDNB was reduced but less than 50%. In this solution pNP^- was formed, whereas at −0.8 V the formation of pNP^- was negligible. At potentials sufficiently negative to produce the $pDNB^{2-}$ the hydroxylamine was found. In those solutions, where the pDNB was not completely reduced, the hydroxide ion, produced by electrolysis of traces of water or impurities of the electrolyte, led to substitution:[5]

$$RNO_2 + OH^- \longrightarrow ROH + NO_2^- \quad (2a)$$

$$ROH + OH^- \rightleftharpoons RO^- + H_2O \quad (2b)$$

$(R = O_2NC_6H_4)$

b) Spectral Characterization. From the electronic absorption spectrum recorded in combination with polarography (Fig. 3), the absorption coefficients were determined. By this procedure the spectrum was obtained without interference of pNP^- that overlaps the band at 400 nm.[13] Compared with the low-temperature spectrum in 2-methyltetrahydrofuran the bands are broadened and the vibrational fine structure has disappeared.

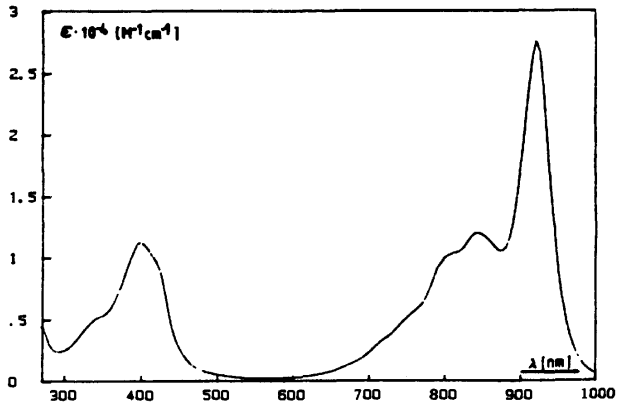

Fig. 3. UV-vis absorption spectrum of the *p*-dinitrobenzene radical anion. Avarage of 6 independent runs.

The absorbance is of the same order of magnitude as that in 2-methyltetrahydrofuran at low temperature. The spectral data estimated in Ref. 13 are obviously erroneous.

c) Reactivity of the Radical. The effect of additives was studied in the tandem cell. Dilution by DMF did not change the absorption spectrum. We regard this result as a proof that the system had no leakage. Addition of O_2 saturated DMF mainly reoxidized the radical. However, about 15% of the radical reacted to *p*-nitrophenoxide (pNP^-) probably with intermediate superoxide ions:

$$RNO_2^- + O_2 \longrightarrow RNO_2 + O_2^- \quad (3)$$

$$RNO_2^- + O_2^- \longrightarrow RO^- + NO_3^- \quad (4)$$

The reformed RNO_2 may also have reacted according to Eq. 2. The same percentage of pNP^- was also obtained after shaking in air.

The spectral changes during oxidation are shown in

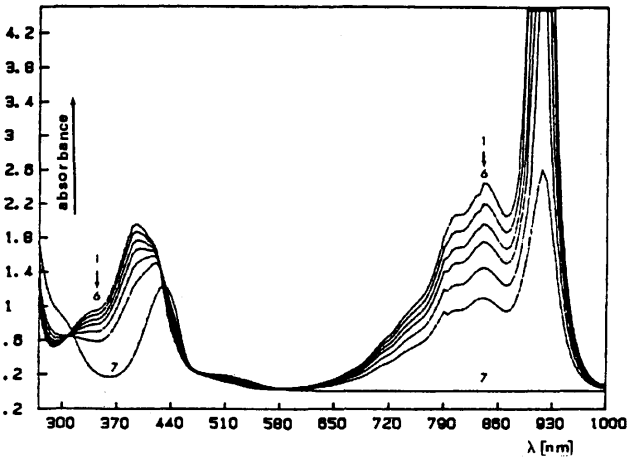

Fig. 4. Spectral changes during air oxidation of 1.7×10^{-4} M $pDNB^-$ 1: 0 min, 2: 5 min, 3: 15 min, 4: 26 min, 5: 47 min, 6: 83 min, 7: 18 h. Optical path length 1 cm, scan rate 5 nm s^{-1}, start at 1000 nm.

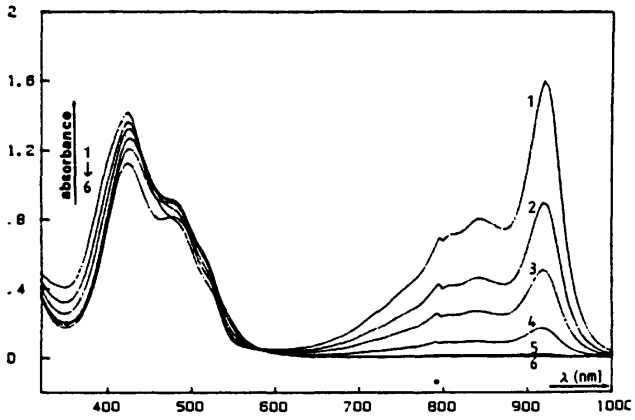

Fig. 5. Spectral changes during air oxidation of 1.2×10^{-4} M $pDNB^{\cdot-}$ in wet DMF (4 vol% H_2O). 1: 0 min, 2: 5 min, 3: 10 min, 4: 20 min, 5: 31 min, 6: 46 min. Pathlength 0.5 cm, other conditions as in Fig. 4.

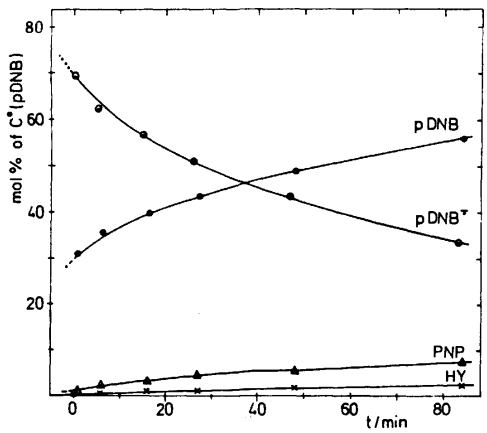

Fig. 6. Concentration changes during air oxidation of $pDNB^{\cdot-}$; analysis of data of Fig. 4; initial concentration of pDNB: 2.5×10^{-4} M.

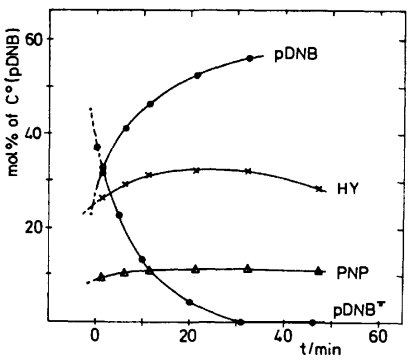

Fig. 7. Concentration changes during air oxidation of $pDNB^{\cdot-}$ in wet DMF; analysis of data of Fig. 5; initial concentration of pDNB 3.3×10^{-4} M.

Fig. 4. The disappearance of the radical caused the decrease of the band at 920 nm. In the 400 nm region the production of *p*-nitrophenoxide shifted the absorption maximum to 432 nm (absorption maximum of pNP^-). The curves pass through an isosbestic point at 310 nm although more than two components were present. However, the absorbance of pDNB, pNP^-, and $pDNB^{\cdot-}$ happens to be so similar at 310 nm that the minor contribution of pNP^- did not become evident. The reappearing pDNB produced the increase in absorbance at $\lambda<300$ nm. The weak absorbance at 510 nm was caused by traces of *p*-nitrophenylhydroxylamine which was present as an adduct of its base form with pDNB.

In wet DMF (4 vol% H_2O) the pattern was more complex (Fig. 5). The radical disappeared much faster; pNP^- and *p*-nitrophenylhydroxylamine (Hy) were produced in larger amounts. Initially, the hydroxylamine was formed as the base (absorption maximum at 480 nm), it reacted with pDNB forming the adduct with the absorption maximum at 500 nm.

Figures 6 and 7 show the kinetics in both systems. The remaining concentration of pDNB was determined from the sum of all the other known components. Figure 7 shows a decrease on hydroxylamine concentration that indicates the production of another compound. This could be *p*-nitronitrosobenzene which is formed by reaction of Hy with oxygen.[5] It does not absorb strongly in the visible region. Its intense absorption is found at 282 nm. For times longer than 30 min the sum analysis was not justified anymore. The radical decay was exponential in both solution.

We thank the "Deutsche Forschungsgemeinschaft" and the "Verband der Chemischen Industrie" for financial assistance.

References

1) A. H. Maki and D. H. Geske, *J. Am. Chem. Soc.*, **83**, 1852 (1961).
2) R. Koopmann and H. Gerischer, *Ber. Bunsenges. Phys. Chem.*, **70**, 127 (1966).
3) M. Svaan and V. D. Parker, *Acta Chem. Scand., Ser. B*, **40**, 36 (1986).
4) H. Bock and U. Lechner-Knoblauch, *Z. Naturforschung*, **40b**, 1463 (1985).
5) J. Q. Chambers III and R. N. Adams, *J. Electroanal. Chem.*, **9**, 400 (1965).
6) J. H. Freed and G. K. Fraenkel, *J. Chem. Phys.*, **40**, 1815 (1964).
7) E. Ahlberg, B. Svensmark, and V. D. Parker, *Acta Chem. Scand., Ser. B*, **34**, 53 (1980).
8) Z. V. Todres, A. A. Pozdeeva, V. A. Chernova, and S. I. Zhdanov, *Tetrahedron Lett.*, **1972**, 3835.
9) A. Darchen and C. Moinet, *J. Electroanal. Chem.*, **78**, 81 (1977).
10) L. Holleck and H. Schmidt, *Z. Elektrochem.*, **59**, 56 (1955).
11) K. Bowden and R. S. Cook, *J. Chem. Soc. B*, **1971**, 1765.
12) I. I. Bilkis and S. M. Shein, *Tetrahedron*, **31**, 969 (1975).

13) T. Abe and Y. Ikegami, *Bull. Chem. Soc. Jpn.*, **51**, 196 (1978).
14) P. Neta, M. G. Simic, and M. Z. Hoffman, *J. Phys. Chem.*, **80**, 2018 (1976).
15) V. Jagannadham and S. Steenken, *J. Am. Chem. Soc.*, **106**, 6542 (1984).
16) T. Shida and S. Iwata, *J. Phys. Chem.*, **75**, 2591 (1971).
17) R. K. Huddleston and J. R. Miller, *J. Phys. Chem.*, **86**, 2410 (1982).
18) R. G. Brown, A. Harriman, and L. Harris, *J. Chem. Soc., Faraday Trans. 2*, **74**, 1193 (1978).
19) R. Kuhn and F. Weygand, *Chem. Ber.*, **69**, 1969 (1936).

 © 1989 The Chemical Society of Japan Bull. Chem. Soc. Jpn., 62, 2693—2696 (1989)

Studies on Organomercury(II) Complexes of Maltol

Sangeeta BHATIA, Narender K. KAUSHIK,* and Gurvinder S. SODHI†
Department of Chemistry, University of Delhi, Delhi 110007, India
†Department of Chemistry, S. G. T. B. Khalsa College, University of Delhi, Delhi 110007, India
(Received May 24, 1988)

A number of organomercury(II) complexes involving maltol (**1**) of the type RHgL (**2**) [R=phenyl (C_6H_5), *o*-, *p*-hydroxyphenyl (*o*-, *p*-HOC_6H_4), *p*-acetoxyphenyl (*p*-$AcOC_6H_4$), 2-furyl (2-C_4H_3O); HL=maltol] have been synthesized and characterized. Conductance measurements indicate that the complexes are nonelectrolytes. From IR and UV studies, it is concluded that maltol acts as a bidentate ligand, coordinating to the mercury(II) ion through phenolic and carbonyl oxygen atoms. ^1H and ^{13}C NMR support the stoichiometry of the complexes. Fluorescence spectra have been recorded for *o*-, *p*-HOC_6H_4HgL complexes. For C_6H_4HgL, *p*-HOC_6H_4HgL, and *p*-$AcOC_6H_4HgL$ complexes, thermal studies (TG and DSC) have been carried out and relevant kinetic and thermodynamic parameters have been enumerated. In addition, the fragmentation pattern of the complexes has been analyzed on the basis of mass spectra.

During the course of our recent investigations on metal ion-biomolecule interactions, we have synthesized and characterized several organomercury(II) complexes and analyzed their biological activity.[1-6] The organomercury(II) purine complexes[3] were screened for C. N. S. activity; the isoniazid compounds[4] were tested for antitubercular activity; and the dithiocarbazate analogues[5] were examined for antifungal activity. To widen the scope of our investigations, we synthesized a few organomercury(II) complexes of maltol, an antibiotic substance and tested their antibacterial actvity.

Maltol (3-hydroxy-2-methyl-4*H*-pyran-4-one) (**1**) is found in the pine needles in the bark of larch. Since it is obtained as an alkaline degradation product of streptomycin salts,[7] its compounds exhibit considerable antibiotic activity. The interest in the metal complexes of maltol has arisen because of the following reasons. Firstly, since it is structurally related to flavones, the study of its complexes is expected to provide a model for the complexing properties of some naturally occurring keto-hydroxy systems. Secondly, the metal complexes of maltol possess relatively high stability owing to the formation of five membered chelate ring. Thirdly the metal complexes reveal a wide spectrum of antibacterial activity. It is expected that the antibiotic action of a drug is enhanced in the presence of metal ions, since the introduction of metal chelates in vivo prolongs the metabolism of the drug and leads to a more pronounced biological effect. In fact the present complexes have been found to be significantly active against *E. coli* and *P. pyocyanea* bacterial strains.

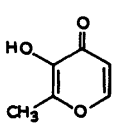

(1)

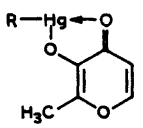

(2)

Experimental

The following instruments were used: Elico conductivity bridge, model CM-82 for conductivity measurements; Perkin-Elmer grating 621 spectrometer for IR spectra; Perkin-Elmer UV-visible spectrometer, model 554 for UV spectra; JEOL FX-200 spectrometer, for ^1H and ^{13}C NMR spectra; JASCO FP-550 spectrofluorometer for fluorescence studies; SETARAM G-70 thermoanalyzer for TG studies in air at a heating rate of 8° min^{-1}; Du Pont device for recording DSC curves up to 673 K at a heating rate of 8° min^{-1}. Mass spectra were recorded at Central Drug Research Institute, Lucknow (India).

Nitrobenzene was purified for conductance measurements by the method of Fay et al.[8] C_6H_5HgCl,[9] *o*-, *p*-HOC_6H_4HgCl,[10] *p*-$AcOC_6H_4HgCl$,[11] and 2-C_4H_3OHgCl[12] were prepared by standard methods. Maltol was purchased from Aldrich Chemical Co., Inc. USA.

Preparation of Complexes. A solution of RHgCl (0.05 mol) in 25 ml THF was added to a solution of maltol (0.05 mol) in 25 ml THF. The mixed solution was stirred for about 3 h at room temperature and filtered. The filtrate was evaporated under vacuum to one-fourth of its original volume and petroleum ether was added. The RHgL complexes separated out, which were filtered and dried. These were recrystallized from acetone solution by the addition of petroleum ether.

Results and Discussion

The complexes prepared are white in color and soluble in THF, DMSO, and acetone. The purity has been checked by elemental analyses, spectral studies and TLC. The conductance measured in 10^{-3} M (M=mol dm^{-3}) nitrobenzene solution (at 27 °C) was of the order of 0.5 Ω^{-1} cm^2 mol^{-1} for each of the complexes, indicating that they are nonelectrolytes. The results are summarised in Table 1.

Infrared Spectra. According to Katritzky and Jones[13] the absorption at 1660 cm^{-1} in maltol is assigned to ν(C=O) stretching frequency. This is lower than the conventional carbonyl stretching frequency partly because of the intramolecular hydrogen

Table 1. Analytical Data and Physical Characteristics

Complex	Decomp temp °C	$\Lambda/\Omega^{-1}cm^2mol^{-1}$	Found (Calcd)/% C	H	Hg
C_6H_5HgL	170	0.44	35.65 (35.73)	2.39 (2.43)	49.76 (49.80)
o-HOC_6H_4HgL	122	0.48	34.35 (34.37)	2.32 (2.39)	47.84 (47.97)
p-HOC_6H_4HgL	162	0.56	34.33 (34.37)	2.34 (2.39)	47.85 (47.97)
p-$AcOC_6H_4HgL$	116	0.50	36.57 (36.40)	2.49 (2.60)	43.51 (43.60)
2-C_4H_3OHgL	181	0.50	30.47 (30.53)	2.12 (2.04)	51.06 (51.15)

Table 2. ^{13}C NMR Data

Complex	R						Maltol					
	C_1	C_2	C_3	C_4	C_5	C_6	C'_2	C'_3	C'_4	C'_5	C'_6	CH_3
C_6H_5HgL	149.8	135.8	127.6	127.0	127.5	135.8	149.2	146.2	177.8	113.8	155.3	27.2
o-HOC_6H_4HgL	138.5	161.5	120.2	132.0	122.5	140.4	149.3	146.4	177.8	113.8	155.3	27.4
p-HOC_6H_4HgL	147.1	151.0	135.6	156.2	135.6	151.0	149.2	146.2	177.7	113.8	155.4	27.2
p-$AcOC_6H_4HgL$	148.6	138.1	122.2	150.7	122.2	138.1	149.1	146.2	177.8	113.9	155.2	27.2

bonding and partly due to the weakening of C=O bond by contributions from resonating structures. On complexation, this frequency is further lowered by ca. 45 cm^{-1}, indicating that C=O group is chelating. The ν(C=C) stretching frequency observed at 1580 cm^{-1} in case of the ligand is shifted to ca. 1560 cm^{-1} in complexes.[14]

In maltol, the band due to phenolic OH stretching occurs at 3200 cm^{-1} [15] and that due to δ(OH) at 1300 cm^{-1}.[14] These bands are absent in the spectra of the complexes, indicating the presence of metal-oxygen bond. A weak band at 450 cm^{-1} is attributed to ν(Hg-O) stretching vibrations.[16] The bands at 1290 and ca. 1220 cm^{-1} in case of ligand and complexes respectively are due to C-O-C stretching frequency.[15]

UV Spectra. The UV spectrum of maltol shows an intense band at 237 nm ($\log\varepsilon\approx6.7$) due to π-π^* absorption of chromophoric C=O group. This band is shifted to ca. 250 nm ($\log\varepsilon\approx6.1$) in case of the complexes. The shift in the absorption band due to carbonyl chromophore is attributed to the involvement of this group in complexation, thus supporting the conclusions drawn from IR studies.

^1H NMR Spectra. In ^1H NMR spectra, the following signals are attributed to the presence of maltol moiety in the complexes: δ 2.26 (s, 3H, CH_3 at C_2); δ 6.45 (d, 1H, H, J=6 Hz), 7.95 (d, 1H, H_6, J=6 Hz). The signal due to H_5 in free maltol absorbs at δ 6.30 (d, 1H, J=6 Hz). The downfield shift in case of metal complexes is due to involvement of carbonyl at C_4 in complexation. In the related kojic acid complexes,[6] the signals due to H_3 and H_6 absorb at ca. δ 6.93 and 8.05 respectively. In free kojic acid, the signal due to H_3 absorbs at δ 6.45 and that due to H_6 at δ 7.80. The downfield shift in these complexes is also attributed to the involvement of carbonyl at C_4 and hydroxyl at C_5 in complexation. The furyl group in the present complexes is identified by signals at δ 6.50 (d, 2H, J=10 Hz) and δ 7.52 (s, 1H).

^{13}C NMR Spectra. The C_4 carbonyl in pure maltol shows a resonance signal at δ 173.2 while the C_3 carbon absorbs at δ 143.2.[17] In metal complexes these signals appear at δ ca. 177.84 and 146.20 respectively. Thus, it is concluded that the complexes are formed by deprotonation of C_3 hydroxyl and chelation through C_4 carbonyl. In the ^{13}C NMR spectra of kojic acid the signals due to C_4 and C_5 appear at δ 174.61 and 145.82 respectively.[6] In the case of the complexes, the former signal is shifted to δ about 179.52 and the latter to δ about 148.71, indicating also that complexation involves C_4 carbonyl and deprotonated C_5 hydroxyl. In the present complexes, the C_2, C_5, and C_6 carbons absorb at δ ca. 149.25, 113.85, and 155.28 respectively. The methyl group at C_2 shows a resonance signal at δ ca. 27.20. The data are recorded in Table 2.

Fluorescence Studies. The o-, p-HOC_6H_4HgL complexes are fluorescent in nature. Hence their fluorescence spectra have been recorded. The absorption band is observed at 250 nm, while the emission band is at 500 nm. Thus in accordance with Franck-Condon principle and thermal relaxation of vibrational modes, the fluorescence spectra are observed on the red side of the absorption spectra in approximately mirror image relationship.[18] A slight distortion in the mirror image pattern arises due to the appearance of a weak band at 310 nm ($\log\varepsilon\approx1.5$), which is attributed to the forbidden transitions, $Hg6(^3P_1)\rightarrow Hg6(^1S_0)$

and $J=0\rightarrow J=0$.[17]

The spectra are free from antistokes effects. The pattern of the spectra follows Levschin's rule, indicating that the geometry of the excited state is similar to that of the ground state.[20] The quantum yield of fluorescence, ϕ_f, calculated by a relative method,[19] using anthracene as the reference are: *o*-HOC_6H_4HgL, 0.73; *p*-HOC_6H_4HgL, 0.72. Since the ϕ_f values show deviation from unity, it is inferred that fluorescence remains the dominant but not the exclusive mode of emission. The nonradiative modes are likely to be contributing to the emission process.

Thermal Studies. Thermogravimetric (TG) studies have been carried out for C_6H_5HgL, *p*-HOC_6H_4HgL, and *p*-$AcOC_6H_4HgL$ complexes. The weight loss in each case corresponds to the formation of HgO, which slowly volatilizes beyond 773 K. The order (n) and activation energy (E_a) for thermal decomposition reaction have been elucidated by the methods of Coats and Redfern.[21] The linearization curves are shown in Fig. 1.

The order of reaction in each case is one. A comparison of the activation energy data reveals that *p*-$AcOC_6H_4HgL$ complex has the lowest value of E_a. This may be explained on the basis of electron withdrawing effect of the acetoxyl group which weakens the R-Hg bond, making thermal degradation relatively easy. In case of *p*-HOC_6H_4HgL complex, the phenolic hydroxyl group is electron donating and the R-Hg bond is strengthened. Therefore the E_a value in this case is higher than in the unsubstituted C_6H_5HgL complex. That R-Hg bond cleavage is involved in the pyrolysis of the complexes is also indicated by the mass spectra, where peaks for $C_6H_5^+$, $HOC_6H_4^+$, and $AcOC_6H_4^+$ fragments have been observed.

The activation energy values of the present complexes are lower than those of the corresponding theophylline and theobromine analogues.[3] In the latter cases, the ligands are bound to the mercury(II) ion through nitrogen, which according to HSAB theory, is softer than oxygen. The soft mercury(II) ion thus forms a stronger bond with nitrogen than with oxygen. This makes thermal degradation of maltol complexes relatively easy and the reaction involves a lower value of E_a.

The apparent activation entropy,[22] $\Delta S^{\neq}$ has a positive value for all the complexes. The *p*-HOC_6H_4HgL complex has the highest value of $\Delta S^{\neq}$, while the *p*-$AcOC_6H_4HgL$ has the lowest. Hence, the former decomposes with greatest degree of randomness, while the latter with the least.

The TG data is supplemented by differential scanning calorimetry (DSC) studies. The thermal effects on DSC curves are endothermic in nature. The heat of reaction, ΔH has been enumerated from DSC curves. Thermal data are presented in Table 3.

Mass Spectra. The RHg^+, R^+, and Hg^+ ions dominate the mass spectra. The fragmentation pattern of

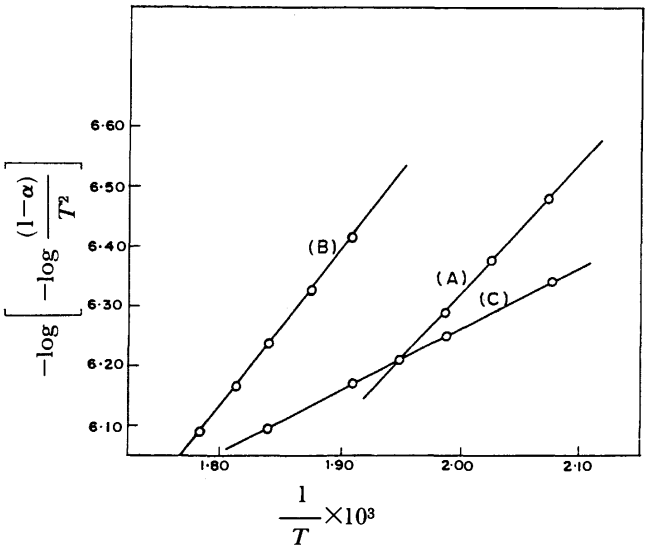

Fig. 1. Kinetic parameters from TG: (A) C_6H_5HgL, (B) *p*-HOC_6H_4HgL, (C) *p*-$AcOC_6H_4HgL$.

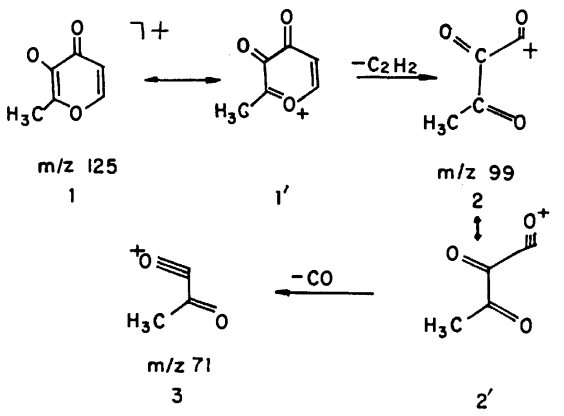

Scheme 1.

Table 3. Thermal Data

Complex	TG				DSC		
	Temp range / K	n	E_a / kJ mol^{-1}	$\Delta S^{\neq}$ / J deg^{-1} mol^{-1}	Thermal effect	T_{max} / K	ΔH / kJ mol^{-1}
C_6H_5HgL	453—523	1	42.46	29.59	Endothermic	495	108.92
p-HOC_6H_4HgL	453—573	1	50.99	38.99	Endothermic	518	128.92
p-$AcOC_6H_4HgL$	453—553	1	20.14	4.93	Endothermic	501	55.25

the RHg^+ portion is similar to that reported earlier.[4] The carbonium ion R^+ constitutes the base peak. The fragmentation of the ligand portion is shown in Scheme 1. The pattern is similar to that of 4-pyrone.[23] The molecular ion **1** (*m/z* 125) undergoes rearrangement to **1'** before losing C_2H_2. Fragment **2** (*m/z* 99) rearranges to **2'** and subsequently loses CO, resulting in fragment **3** (*m/z* 71).

Antibacterial Studies. The metal complexes have been tested against *E. coli* and *P. pyocyanea* bacterial strains using maltol as the standard for comparing the activity. The compounds were screened at two concentrations, 25 $\mu g\,ml^{-1}$ and 50 $\mu g\,ml^{-1}$. The inhibitory power of the complexes was greater than that of the control. The conpounds showed better inhibition at higher concentrations. At lower concentrations, the compounds were equally active against both bacterial strains. However, at higher concentrations, the order of activity against the two microorganisms was *P. pyocyanea*>*E. coli*. The C_6H_5HgL and *p*-$AcOC_6H_4HgL$ complexes were found to have higher activity than others.

One of the authors (G. S. S.) is thankful to the Indian National Science Academy, New Delhi for sanctioning bursary grant for a project of which the present work is a part.

References

1) G. S. Sodhi, R. K. Bajaj, and N. K. Kaushik, *Inorg. Chim. Acta*, **92**, L27 (1984).
2) S. Kamrah, G. S. Sodhi, and N. K. Kaushik, *Inorg. Chim. Acta*, **107**, 29 (1985).
3) S. Bhatia, N. K. Kaushik, and G. S. Sodhi, *J. Chem. Res. (S)*, **1987**, 186; (*M*) **1987**, 1519.
4) S. Bhatia, N. K. Kaushik, and G. S. Sodhi, *J. Inorg. Biochem.*, **29**, 181 (1987).
5) S. Bhatia, N. K. Kaushik, and G. S. Sodhi, *Inorg. Chim. Acta*, **127**, 141 (1987).
6) S. Bhatia, N. K. Kaushik, and G. S. Sodhi, *J. Coord. Chem.*, **16**, 311 (1987).
7) G. L. Jenkins, W. H. Hartung, K. E. Hamlin, and J. B. Data, "The Chemistry of Organic Medicinal Products," 4th ed, Chapman and Hall Ltd., London (1957), p. 314.
8) R. C. Fay and R. N. Lowry, *Inorg. Chem.*, **6**, 1512 (1967).
9) J. F. Kaplan and C. Mellick, U. S. Patent 2502222 (1950); *Chem. Abstr.*, **44**, 6882 (1950).
10) F. C. Whitmore and E. R. Hanson, *Org. Synth.*, Coll. Vol. I, 155 (1932).
11) F. C. Whitmore and E. B. Middleton, *J. Am. Chem. Soc.*, **43**, 2578 (1921).
12) H. Gilman and G. F. Wright, *J. Am. Chem. Soc.*, **55**, 3302 (1933).
13) A. R. Katritzky and R. A. Jones, *Spectrochim. Acta*, **17**, 64 (1961).
14) R. C. Agarwal, S. P. Gupta, and D. K. Rastogi, *J. Inorg. Nucl. Chem.*, **36**, 208 (1974).
15) N. K. Dutt and U. U. M. Sarma, *J. Inorg. Nucl. Chem.*, **37**, 1801 (1975).
16) C. Gerard, *Bull. Soc. Chim. Fr.*, **1979**, 451.
17) C. A. Kingsbury, M. Oliffton, and J. H. Looker, *J. Org. Chem.*, **41**, 2777 (1976).
18) E. J. Brown and F. Wokes, "The Fluorescence of Solution," Longmans Green, London (1953).
19) J. G. Calvert and J. N. Pitts, "Photochemistry," Wiley, New York (1966).
20) K. K. Rohtagi-Mukharjee, "Fundamentals of Photochemistry," Wiley-Eastern, New Delhi (1978).
21) A. W. Coats and J. P. Redfern, *Nature (London)*, **201**, 68 (1964).
22) J. Zsako', *J. Phys. Chem.*, **72**, 2406 (1968).
23) P. Beak, T. H. Kinstle, and G. A. Carls, *J. Am. Chem. Soc.*, **86**, 3833 (1964).

Ortho Effects in Organic Molecules on Electron Impact 17-Parallel Oxygen Transfers from Nitro Group to Olefinic Double Bond and Sulfur in α-(*o*-Nitrophenylthio)cinnamic Acids

D. V. RAMANA,* N. SUNDARAM, and M. GEORGE
Department of Chemistry, Indian Institute of Technology, Madras 600036, India
(Received October 3, 1988)

An oxygen transfer from the nitro group to the olefinic double bond followed by a simple cleavage affords intense fragment corresponding to *o*-nitrosophenylthio cation at *m/z* 138 during the mass spectral fragmentations of α-(*o*-nitrophenylthio)cinnamic acid. Single and double oxygen transfers from the nitro group to sulfur lead to concerted ejections of [SO+CO_2] and [SO_2+CO_2] from the molecular ion of this compound. The mechanisms proposed for these processes are supported by high-resolution data, CID linked scan spectra, D-labelling, and chemical evidence.

The nitro group is known to interact very effectively with the ortho substituent in aromatic systems by transfering oxygen atoms to multiple bonds[1-4] or heteroatoms[5,6] present in the side chain on electron impact. Sulfur in the form of a thiocarbonyl[7,8] and a sulfide[9,10] is known to interact with the nitro group by accepting one or more oxygen atoms with subsequent expulsions of neutral molecules.[11] The electron impact mass spectra of α-(*o*-nitrophenylthio)cinnamic acid derivatives **1**—**8** (Scheme 1) were undertaken in this work in order to study the ortho interaction of the nitro group with the side chain containing sulfur and an olefinic double bond with a carboxyl group.

Results and Discussion

The base peak in the mass spectrum of α-(*o*-nitrophenylthio)cinnamic acid (**1**) is at *m/z* 138, having an elemental composition of C_6H_4NOS (138.00095) (Scheme 2, Tables 1 and 4). Furthermore, examination of the B/E linked scan spectrum of the molecular ion of **1** (Table 2) revealed that the ion at *m/z* 138 is directly formed from the molecular ion. An *o*-nitrosophenylthio cation structure is assigned to the ion at *m/z* 138. This hypothesis is confirmed

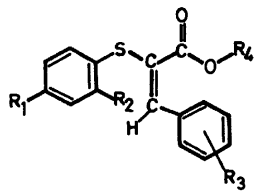

	R_1	R_2	R_3	R_4
1	H	NO_2	H	H
2	NO_2	H	H	H
3	H	NO_2	H	D
4	NO_2	H	H	D
5	H	NO_2	o-OCH_3	H
6	H	NO_2	p-OCH_3	H
7	H	NO_2	o-Cl	H
8	H	NO_2	p-Cl	H

Scheme 1.

Table 1. Partial Mass Spectra of Compounds **1**—**8**

Compoud No.	Relative abundance of								
	$M^{+\cdot}$	*m/z* 138	$[M-92]^{+\cdot}$	$[M-93]^+$	f	e	*m/z* 208	*m/z* 192	*m/z* 165
1	39 (301)	100	18 (209)	16 (208)	11 (193)	12 (192)	16	12	27
2	100 (301)	—	17 (209)	17 (208)	—	—	17	—	35
3	31 (302)	100	17 (210)	15 (209)	10 (194)	9 (193)	12	12	28
4	100 (302)	—	66 (210)	28 (209)	—	—	28	—	59
5	29 (331)	100	2 (239)	3 (238)	5 (223)	3 (222)	9	2	16
6	21 (331)	100	3 (239)	2 (238)	5 (223)	2 (222)	11	1	70
7	29 (335)	100	2 (243)	2 (242)	7 (227)	4 (226)	54	16	53
8	18 (335)	100	6 (243)	3 (242)	5 (227)	3 (224)	15	4	17

The figures in parentheses indicate *m/z* values the ions.

Table 2. B/E Linked Scan Spectrum of $M^{+\cdot}$ at m/z 301, m/z 209, 208, and 192 of Compound **1**

Parent ion (m/z)	m/z values of daughter ions							
301	237 (58)	236 (10)	209 (23)	208 (5)	193 (9)	192 (10)	191 (10)	138 (100)
209	208 (100)	192 (16)	181 (38)	180 (75)				
208	193 (7)	192 (7)	181 (100)	180 (80)	179 (36)	178 (14)		
192	191 (100)	165 (82)	164 (29)					

The figures in parentheses indicate relative abundances of the ions.

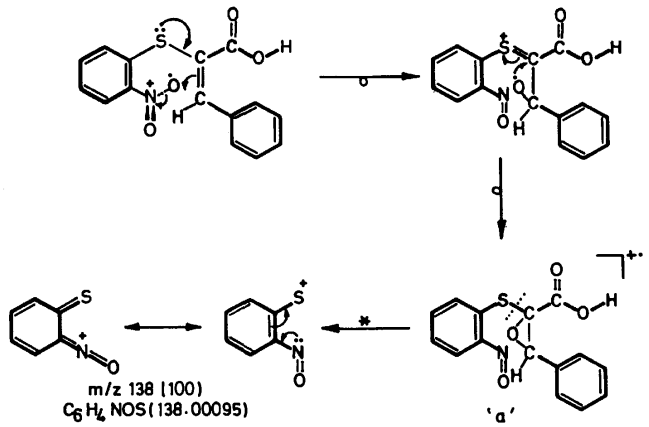

Scheme 2.

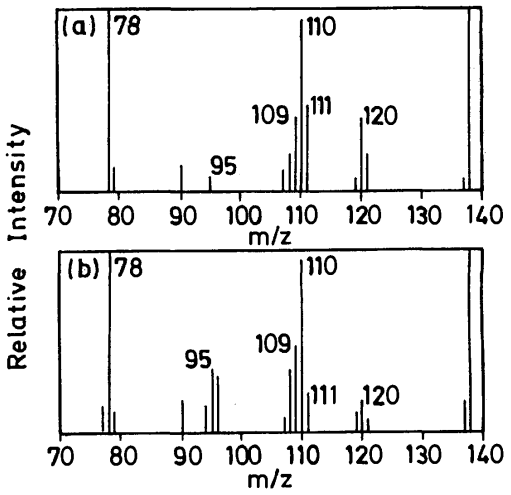

Fig. 1. CID B/E linked scan spectra of (a) m/z 138 of compound **1** and (b) m/z 138 of bis(*o*-nitrophenyl) disulfide.

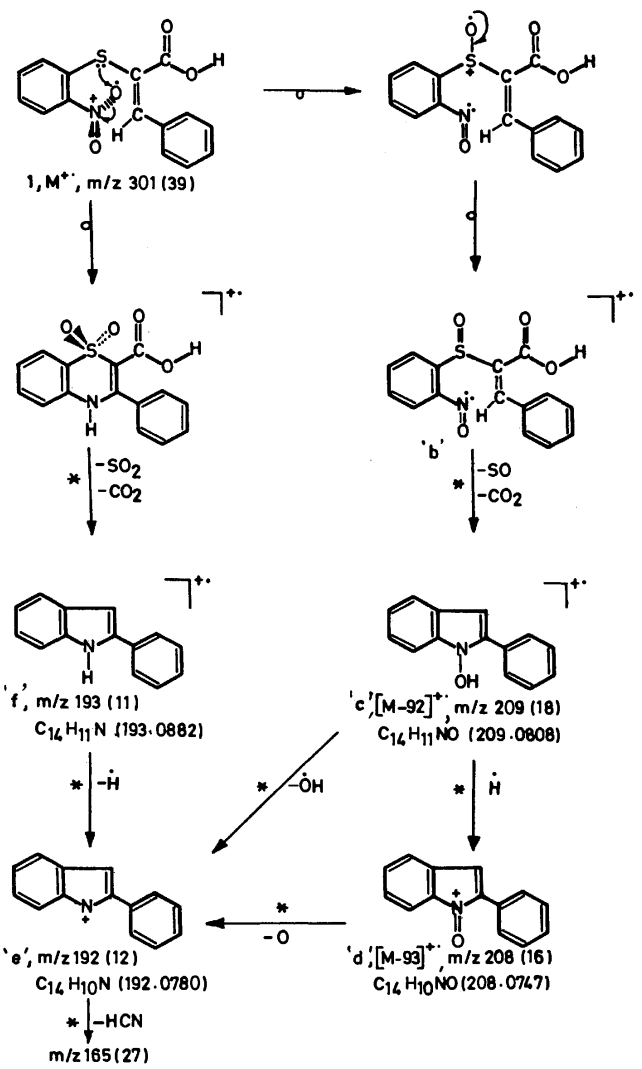

Scheme 3.

from the fact that the collision induced dissociation B/E linked scan spectrum of m/z 138 ion from compound **1** is identical with that of the ion at m/z 138 (Fig. 1) obtained from bis(*o*-nitrophenyl)disulfide, having *o*-nitrosophenylthio cation structure.[12]

Based on these observations, an oxygen transfer from the nitro group to the double bond in the side chain of compound **1** is envisaged for the formation of the rearranged molecular ion 'a' where a simple cleavage of the C-S bond affords the base peak in the spectrum at m/z 138 (Scheme 2). The proposed mechanism is further supported by the fact that the mass spectra of the substituted compounds **3** and **5**—**8** also have the base peaks at m/z 138 without any shifts (Table 1). Moreover, this ion is totally absent in the mass spectrum of the para isomer (**2**) (Table 1).

Single and double oxygen transfers from the nitro group to the sulfur in the side chain have also been

noticed in the mass specturm of compound **1** (Scheme 3). The single oxygen migration from the nitro group to sulfur leads to the rearranged molecular ion 'b'. Subsequent concerted ejection of SO and CO_2 from 'b' affords the ion 'c', $[M-92]^+$ at m/z 209 of 18% relative abundance. The extrusion of SO from 'b' can be visualized as the migration of the phenyl group from sulfur to the olefinic carbon followed by the expulsion of SO. Further loss of Ḣ from 'c' gives rise to an ion 'd' at m/z 208 (16) (Scheme 3). The elemental compositions $C_{14}H_{11}NO$ (209.0808) and $C_{14}H_{10}NO$ (208.0747) (Table 4) for 'c' and 'd' respectively obtained by high resolution technique, support the proposed elimination of SO and CO_2 from the molecular ion for the formation of 'c'. Both 'c' and 'd' lose ȮH and O respectively to give rise to a fragment 'e' at m/z 192.

The formation of 'e' at m/z 192 also takes place through another interesting parallel oxygen migration process. Initial double oxygen transfer from the nitro group to sulfur followed by concerted elimination of SO_2 and CO_2 directly from the molecular ion affords the interesting fragment ion 'f' at m/z 193 (11) (Scheme 3). An aryl migration from sulfur to the olefinic carbon after the initial double oxygen migration from the nitro group to sulfur can be proposed for the formation of 'f' $[M-SO_2]^{+\cdot}$. The expulsion of Ḣ from 'f' produces the ion 'e' at m/z 192. Also there is an evidence for the direct formation of 'e' from the molecular ion as seen in B/E linked scan spectrum of $M^{+\cdot}$ of **1** (Table 2). The elemental compositions $C_{14}H_{11}N$ (193.0882) and $C_{14}H_{10}N$ (192.0780) (Table 4) for 'f' and 'e' are in good agreement with the proposed elimination of SO_2 and CO_2 from the molecular ion for the formation of 'f'. The fragmentation pathways

Table 3. B/E Linked Scan Spectrum of $M^{+\cdot}$ at m/z 301 and m/z 210 of Compound **2**

Parent ion (m/z)	m/z values of daughter ions					
301	256	255	240	210	195	163
	(31)	(19)	(20)	(13)	(13)	(100)
210		209	178	166	165	
		(100)	(22)	(14)	(95)	

The figures in parentheses indicate relative abundances of the ions.

Table 4. High-Resolution Data

Compound	m/z	Formula	Observed	Calculated
1	138	C_6H_4NOS	138.0010	138.0030
	209	$C_{14}H_{11}NO$	209.0808	209.0841
	208	$C_{14}H_{10}NO$	208.0747	208.0762
	193	$C_{14}H_{11}N$	193.0882	193.0892
	192	$C_{14}H_{10}N$	192.0780	192.0813
2	210	$C_{14}H_{10}S$	210.0451	210.0520
	209	$C_{14}H_9S$	209.0409	209.0442
	208	$C_{14}H_8S$	208.0315	208.0364

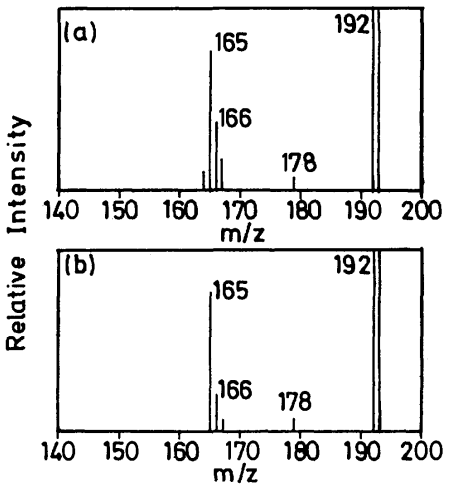

Fig. 2. CID B/E linked scan spectra of (a) ion 'f' and (b) m/z 193 from 2-phenylindole.

described in Scheme 2 are substantiated by linked scan B/E spectra of $M^{+\cdot}$, 'c', 'd', and 'e' (Table 2) of compound **1**. Similar single and double oxygen transfers from the nitro group to sulfur in the substituted compounds **5**—**8** lead to the formation of ions corresponding to 'c', 'd', 'f', and 'e' (Table 1). Also loss of substituent from 'e' in preference to loss of Ḣ leads to formation of the ion at m/z 208 and in turn to the formation of the fragment at m/z 192 in compounds **5**—**8** (Table 1).

A cyclic structure is proposed for 'c' from which the secondary fragmentations as observed in the mass spectrum of this compound are better explained. A 2-phenylindole structure is visualized for the ion 'f' at m/z 193 in compound **1**, instead of an open chain structure with an electron deficient nitrogen after the oxygen transfers. Evidence for the proposed structure for 'f' is obtained from the observation that the collision induced dissociation B/E linked scan spectrum of 'f' is identical with that of the molecular ion of 2-phenylindole (Fig. 2) taken as a reference compound. Furthermore the elemental compositions of

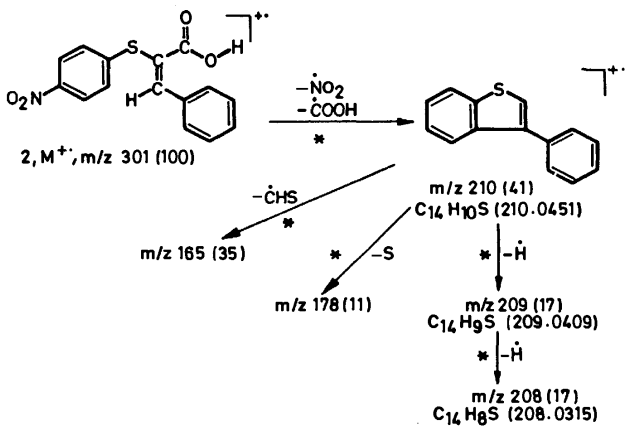

Scheme 4.

these ions as determined by the accurate mass measurements are also in agreement with those of the proposed structures.

However, the mass spectrum of the para isomer, **2**, also contains the peaks corresponding to $[M-92]^{+\cdot}$ and $[M-93]^{+}$ (Scheme 4) (Table 1). But the B/E linked scan spectra of $M^{+\cdot}$ and the abundant fragment ion at m/z 210 (Table 3) indicate that the mechanism of formation of the ions at m/z 209 and 208 in compound **2** is different from that noticed in compound **1**. A concerted elimination of $\dot{C}OOH$ and $\dot{N}O_2$ from the molecular ion affords the abundant ion at m/z 210. Two successive losses of $\dot{H}$ from the ion at m/z 210 produce the fragment ions at m/z 209 and m/z 208. The proposed mechanism is further supported by the elemental compositions $C_{14}H_{10}S$ (210.0451), $C_{14}H_9S$ (209.0409), and $C_{14}H_8S$ (208.0315) (Table 4) for the ions at m/z 210, 209, and 208 respectively.

Further evidence for the proposed ortho interactions are obtained from the mass spectra of deuterium analogues **3** and **4** (Scheme 4). The base peak in the mass spectrum of **3** is at m/z 138 since there is no involvement of the -COOH group in the formation of this ion. On the other hand, the concerted elimination of SO and CO_2 from the molecular ion affords the ion at m/z 210 which loses both $\dot{H}$ and $\dot{D}$ to give ions at m/z 209 and 208, respectively. Also the concerted ejection of SO_2 and CO_2 from the molecular ion of **3** produces an ion at m/z 194 (Scheme 5). These observations clearly indicate that the formation of 'c' and 'f' in compound **1** involves a decarboxylation process (elimination of SO and CO_2 or SO_2 and CO_2) and not an elimination of the $\dot{C}OOH$ as in the case of the para isomer, **2**. Moreover, the molecular ion of compound **4** undergoes, as expected, concerted expulsion of $\dot{N}O_2$ and $\dot{C}OOD$ giving rise to an abundant ion at m/z 210 as in compound **2** (Table 1).

It is evident from this study that the oxygen transfer to the olefinic double bond is more predominent, whereas the oxygen transfer to the sulfur is associated with the decarboxylation process.

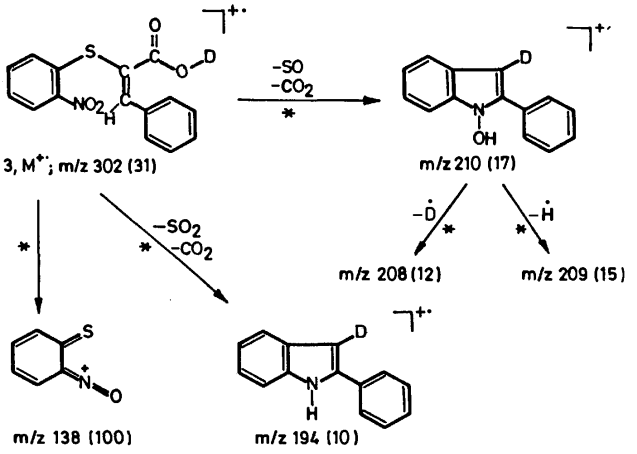

Scheme 5.

Experimental

Compounds **1**,**2**, and **5**—**8** were prepared[13,14] by condensation reactions of (2-nitrophenylthio)acetic acid or (4-nitrophenylthio)acetic acid with the appropriate substituted benzaldehyde, according to the procedure reported in literature for the preparation of these compounds. Compounds **3** and **4** were synthesized by refluxing 50 mg each of **1** or **2** with one ml of D_2O for 120 h followed by usual work-up. The D-incorporation is found to be 76% in **3** and 62% in **4**. The purity of the compounds was checked by TLC and was characterized by IR and NMR spectral data.

The low-resolution spectra were taken on a Varian MAT CH-7 mass spectrometer. The spectra were run at 70 eV with an emission current of 100 μA. All the compounds were introduced into the mass spectrometer through the direct probe insertion at a probe temperature varying between 70 and 110 °C. The high-resolution data (at a resolution of 5000, 10% valley) were recorded on a Finnigan MAT 8230 mass spectrometer at an ionization energy of 70 eV and an acceleration voltage of 3 kV. The linked scan spectra were run on a Finnigan MAT 90 mass spectrometer.

One of the authors (MG) thands CSIR (India) for a fellowship. The authors thank R. S. I. C., I. I. T., Madras for the high-resolution data and Finnigan MAT Ltd., England for the linked scan spectra.

References

1) J. Seibl and J. Völlmin, *Org. Mass Spectrom.*, **1**, 713 (1968).
2) D. Johnston and D. M. Smith, *Org. Mass Spectrom.*, **9**, 789 (1974).
3) D. V. Ramana and M. Vairamani, *Org. Mass Spectrom.*, **9**, 1158 (1974).
4) H. Schwarz, *Top. Curr. Chem.*, **73**, 232 (1978).
5) H. Schwarz and F. Bohlmann, *Org. Mass Spectrom.*, **9**, 283 (1974).
6) J. Martens, K. Praefcke, and H. Schwarz, *Org. Mass Spectrom.*, **8**, 317 (1974).
7) D. V. Ramana and H. F. Grutzmacher, *Org. Mass Spectrom.*, **16**, 227 (1981).
8) D. V. Ramana and S. K. Viswanadham, *Org. Mass Spectrom.*, **18**, 162 (1983).
9) J. Martens, K. Praefcke, and H. Schwarz, *Justus Liebigs Ann. Chem.*, **1975**, 62.
10) S. Pappalardo and M. Di Grazia, *Org. Mass Spectrom.*, **20**, 392 (1985).
11) D. V. Ramana, N. Sundaram, and M. George, *Org. Mass Spectrom.*, **22**, 140 (1987).
12) D. N. B. Mallen and J. M. Smith, *Org. Mass Spectrom.*, **14**, 171 (1979).
13) V. Baliah and T. Rangarajan, *J. Chem. Soc.*, **1960**, 4708.
14) V. Baliah and R. Varadachari, *J. Indian Chem. Soc.*, **31**, 666 (1955).

 © 1989 The Chemical Society of Japan Bull. Chem. Soc. Jpn., 62, 2701—2708 (1989)

The Synthesis of *C*-Nucleoside Precursors. II.[1] Synthesis and Conformational Analysis of 3-(Pentahydroxypentyl)-6-phenyl-1,2,4-triazolo[3,4-*a*]phthalazines[2]

Mohammed A. E. SHABAN* and Mamdouh A. M. TAHA
Department of Chemistry, Faculty of Science, Alexandria University, Alexandria, Egypt
(Received November 14, 1988)

Reaction of 1-hydrazino-4-phenylphthalazine with aldohexoses (D-galactose, D-glucose, D-mannose, and D-talose) and 6-deoxyaldohexoses (L-fucose and L-rhamnose) gave the colored *aldehydo*-sugar (4-phenyl-1-phthalazinyl)hydrazones or the colorless 3-(pentahydroxypentyl)-6-phenyl-1,2,4-triazolo[3,4-*a*]phthalazines. The former can be cyclized to the latter by catalytic dehydrogenation. Structure elucidation of the prepared compounds was made on the basis of their various spectral properties. The *C*-nucleoside precursors were further characterized as their *O*-acetyl derivatives and the configurational-conformational correlation of these acetates was studied. Some of the prepared compounds were screened for insectidicidal, nematicidal, and herbicidal activities and found to be inactive. They showed, however, good corrosion inhibition of aluminium in acid solutions.

Since the isolation[3,4] of the first *C*-nucleoside pseudouridine in 1957 from yeast RNA, extensive research efforts have been aimed at the isolation and synthesis of newer members as well as of analogs.[5-8] Such efforts are rationalized in terms of the multifarious biological activities exhibited by these compounds mainly as a result of their close structural relationship to nucleosides. *C*-Nucleosides may be synthesized[9] by the approach involving carbon-to-carbon bond formation between the anomeric center of the sugar moiety and a preformed heterocycle or by stepwise construction of the heterocyclic system onto a properly functionalized glycosyl derivative with a fixed anomeric configuration.[10] Albeit yielding mixture of anomers, dehydrative cyclization of the polyhydroxyalkyl chains of heterocyclic compounds carrying polyhydroxyalkyl groups (acyclic *C*-nucleosides) offers a relatively simple approach for the synthesis of *C*-nucleosides.[11]

Continuing our work on the synthesis of polyhydroxyalkyl derivatives of heterocycles[12] and fused heterocycles[13,14] uesful as *C*-nucleoside precursors, we describe in this paper the synthesis of the title compounds. Hydrazinophthalazines are among the most medicinally useful hypotensive agents[15,16] which exert their effect as vasodilators by acting on the arteriolar smooth muscles. Studies have shown that Schiff bases[16] of hydrazinophthalazines as well as their cyclization products: 3-substituted 1,2,4-triazolo-[3,4-*a*]phthalazines,[17,18] also retain the hypotensive activity. Thus, 3-alkyl-1,2,4-triazolo[3,4-*a*]phthalazines were found[17] to be as potent as theophylline in inhibiting cyclic adenosine monophosphate phosphodiesterase and possess smooth muscle relaxant activity. Hydrazinophthalazines, however, are not without adverse effects[15] and search for less toxic derivatives thereof is highly desirable. We anticipated that *aldehydo*-sugar 1-phthalazinylhydrazones or their cyclized products 3-(pentahydroxypentyl)-1,2,4-triazolo[3,4-*a*]phthalazines may possess more potent hypotensive activity and less adverse effects since sugar moieties are expected to increase penetration of drugs into and secretion out of biological systems as a result of increasing their hydrophilicity.

Results and Discussion

The reaction of monosaccharides with 1-hydrazinophthalazine was first reported as early as 1954 by Menziani;[19,20] the products were erroneously ascribed 1-(1-phthalazinyl)-2-(glycosyl)hydrazine structures. In a previous publication[13] from this laboratory, this reaction was reinvestigated and the products were found to be either the colored (yellow to orange) *aldehydo*-sugar 1-phthalazinylhydrazones or the colorless 3-(polyhydroxyalkyl)-1,2,4-triazolo[3,4-*a*]-phthalazines. Rosenthal and Lee[21] synthesized the *C*-nucleoside 3-(β-D-ribofuranosyl)-1,2,4-triazolo[3,4-*a*]phthalazine by condensation of 2,5-anhydro-3,4,6-tri-*O*-benzoyl-D-allonic acid with 1-hydrazinophthalazine followed by removal of the *O*-benzoyl groups.

In the present investigation the aldohexoses D-galactose (**2**), D-glucose (**4**), D-mannose (**5**), and D-

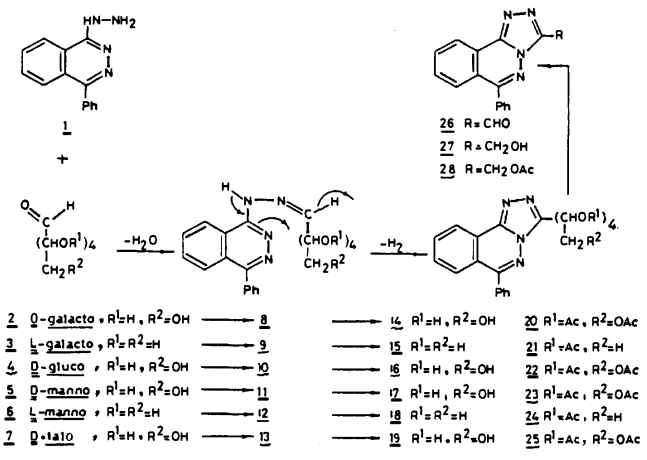

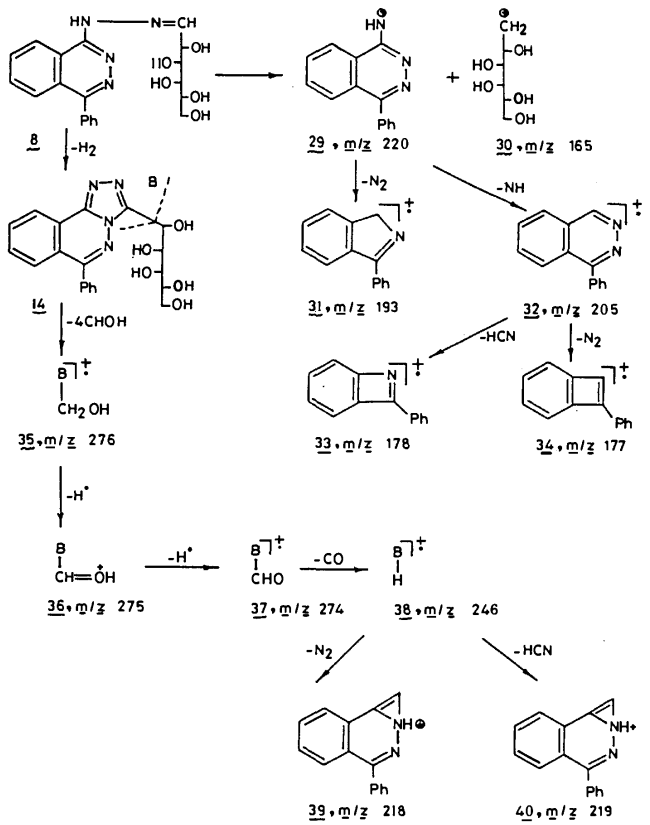

Scheme 1.

talose (**7**) as well as 6-deoxy-L-galactose (L-fucose, **3**) and 6-deoxy-L-mannose (L-rhamnose, **6**) were allowed to react with one molar equivalent of 1-hydrazino-4-phenylphthalazine[22,23] (**1**). The reaction products (**8** and **11**) of D-galactose and D-mannose were yellow and orange respectively while those (**16**, **19**, **15**, and **18**) of D-glucose, D-talose, L-fucose, and L-rhamnose were colorless.

The yellow product (**8**) of D-galactose had elemental analysis data agreeing with the monohydrate of the molecular formula $C_{20}H_{22}N_4O_5$. The IR spectrum of this product showed OH, NH, and C=N absorptions; its UV/visible spectrum revealed four maxima; and its ^{1}H NMR spectrum showed NH, CH=N, nine aromatic protons, and five OH signals. These data indicate that this product possesses the hydrazone structure: *aldehydo*-D-galactose (4-phenyl-1-phthalazinyl) hydrazone (**8**). The mass spectrum of **8** (see Scheme 1) did not show a molecular ion peak, yet revealed a fragmentation pattern consistent with the assigned structure. Cleavage of the hydrazono N-N bond gave the two fragments **29** (base peak, 100%) and **30** belonging to the phthalazine and sugar moieties respectively. Further cleavage of the heterocycle segment **29** gave fragments to which structures **31**—**34** were assigned on the basis of previous work[13,24-26] on similar systems.

The orange product obtained from the reaction of D-mannose (**5**) with 1-hydrazino-4-phenylphthalazine (**1**) gave analytical and spectral data similar to those obtained for hydrazone **8** and was, accordingly, assigned the structure of *aldehydo*-D-mannose (4-phenyl-1-phthalazinyl)hydrazone (**11**).

It was interesting to notice that repeated crystallization of the yellow hydrazone **8** gave a colorless product having different properties than those of the starting hydrazone. Thus, whereas **8** melted at 203—205 °C, the colorless product melted at 228—231 °C and the fingerprint region of their molecular spectra were substantially different. The UV/visible spectrum of the colorless product exhibited only two absorption maxima; the two other maxima which appeared in the spectrum of the hydrazone (**8**) were lacking. The ^{1}H NMR spectrum of the colorless product revealed the same number of aromatic and sugar chain protons as those of the parent hydrazone **8**, yet the azomethine and hydrazono protons (-CH=N-NH-) present in the spectrum of **8** were missing. In agreement with the ^{1}H NMR was the elemental analysis data which is compatible with the molecular formula $C_{20}H_{20}N_4O_5$; two hydrogens less than the starting hydrazone **8**. These data obviously indicated that repeated crystallization of **8** was accompanied by gradual thermal dehydrogenative cyclization until eventually transformed into the acyclic *C*-nucleoside 3-(D-*galacto*-pentahydroxypentyl)-6-phenyl-1,2,4-triazolo[3,4-*a*]-phthalazine (**14**). This cyclization was carried out more efficiently under catalysis conditions by heating aqueous methanolic solutions of **8** with 10% palladium-on-charcoal whereupon **14** was obtained in high purity and excellent yield. Similarly, catalytic dehydrogenative cyclization of the orange *aldehydo*-D-mannose (4-phenyl-1-phthalazinyl)hydrozone (**11**) by heating its solution in aqueous methanol with 10% palladium-on-charcoal also gave the colorless 3-(D-*manno*-pentahydroxypentyl)-6-phenyl-1,2,4-triazolo-[3,4-*a*]phthalazine (**17**).

Reaction of D-glucose (**4**) with 1-hydrazino-4-phenylphthalazine (**1**) under the same conditions which were used for the reaction with D-galactose (**2**) and D-mannose (**5**) gave, unexpectedly, and a colorless product; the anticipated yellow hydrazone **10** has never been obtained. The ^{1}H NMR of this colorless product showed signals of the nine aromatic protons as well as the alditol chain protons; no azomethine or hydrazono proton signals (-CH=N-NH-) were present. The elemental analysis data agreed with the molecular formula $C_{20}H_{20}N_4O_5$ with two hydrogens less than the expected hydrazone **10**. These data would reconcile with the structure 3-(D-*gluco*-pentahydroxypentyl)-6-phenyl-1,2,4-triazolo[3,4-*a*]-phthalazine (**16**). Thus, in contrast to D-galactose and D-mannose which gave the colored intermediate hydrazones, D-glucose directly gave the colorless cyclic triazolophthalazine. A plausible rationalization of this difference may be based upon the different solubilities of the intermediate hydrazones. The hydrazones (**8** and **11**) derived from D-galactose and D-

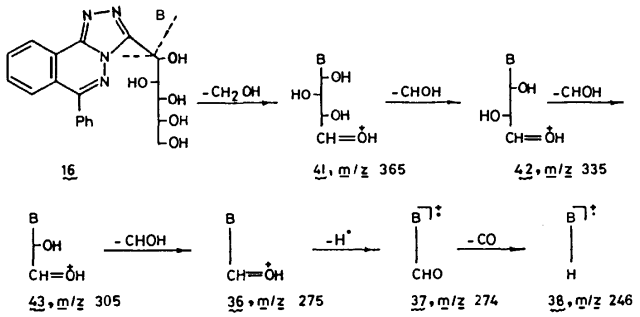

Scheme 2.

mannose were sparingly soluble enough to permit their separation while that (**10**) derived for D-glucose was soluble enough to remain in solution and, hence, undergoes thermal dehydrogenative cyclization to **16**. The mass spectrum of **16** did not reveal a molecular ion peak, yet showed the ($M-CH_2OH$) fragment (**41**, Scheme 2) which underwent sequential alditol chain fragmentation giving fragments **42**, **43**, and **36—38**. The B+30 fragment **36**, corresponding to the heterocyclic base carrying a protonated formyl group ($B-CHO^+H$), characteristic of [27] *C*-nucleosides appeared at *m/z* 275.

Similar to D-glucose (**4**), 1-hydrazino-4-phenylphthalazine (**1**) reacted with L-fucose (**3**), L-rhamnose (**6**), and D-talose (**7**) to give the corresponding colorless 3-(polyhydroxypentyl)-6-phenyl-1,2,4-triazolo[3,4-*a*]-phthalazine **15**, **18**, and **19** respectively.

Oxidative cleavage of the alditol chains of **14—19** with sodium periodate at room temperature gave 4-formyl-6-phenyl-1,2,4-triazolo[3,4-*a*]phthalazine (**26**). Reduction of **26** with sodium borohydride gave 3-hydroxymethyl-6-phenyl-1,2,4-triazolo[3,4-*a*]phthalazine (**27**). Acetylation of **27** gave 3-acetoxymethyl-6-phenyl-1,2,4-triazolo[3,4-*a*]phthalazine (**28**). In their study on the pathogenesis of 1-hydrazinophthalazine-induced systemic lupus erythematosus, Zimmer et al.[28] synthesized 3-hydroxymethyl-1,2,4-triazolo[3,4-*a*]phthalazine and proved, by direct comparison, that it is a major metabolite found in the urine of hypertensive patients on treatment with this drug. 3-Hydroxymethyl-6-phenyl-1,2,4-triazolo[3,4-*a*]phthalazine (**27**) may, therefore, be used for a imilar study.

For further characterization of the 3-polyhydroxypentyl-6-phenyl-1,2,4-triazolo[3,4-*a*]phthalazines (**14—19**) and in order to study the configurational-conformational correlations of their alditol chains, their per-*O*-acetyl derivatives were prepared by acetylation with acetic anhydride in the presence of pyridine. Out of the six prepared acetates, only three could be obtained in a crystalline form namely: 3-(D-*galacto*-1,2,3,4,5-pentaacetoxypentyl)- (**20**), 3-(D-*gluco*-1,2,3,4,5-pentaacetoxypentyl)- (**22**), and 3-(L-*galacto*-1,2,3,4-tetraacetoxypentyl)-6-phenyl-1,2,4-triazolo[3,4-*a*]phthalazine (**21**). The three other per-*O*-acetyl derivatives **23—25** having the D-*manno*-, 5-deoxy-L-*manno*-, and D-*talo*-pentitol configurations respectively were obtained as syrupy products. The IR spectra of the crystalline acetates (**20—22**) showed ester carbonyl absorptions and their ^{1}HNMR spectra revealed nine aromatic protons followed by the alditol chain protons signals (see Table 1). Among the alditol chain protons, H-1 resonated at the highest field due to electronic deshielding by the adjacent heterocyclic system.[29] Alditol H-2 resonated at the next lower field followed by H-3, H-4, H-5, and H-5′. These assignments were made on the basis of signal multiplicities and compared very well with those of acetylated alditol derivatives of 1,2,3-triazoles,[30] tetrazoles,[31] 1,3,4-oxadiazoles,[32] thiazoles,[33] and benzothiazoles.[34] Knowing[33,35–38] that the magnitude of vicinal proton-proton coupling constants of < 4 Hz correspond to protons having gauche orientation (dihedral angle ca. 60°) and that values of >7 Hz correspond to antiparallel orientation (dihedral angle

Table 1. Chemical Shifts[a] (δ) of the Alditol-Chain Protons of 3-(Polyacetoxypentyl)-6-phenyl-1,2,4-triazolo[3,4-*a*]phthalazines in $CDCl_3$ at 90 MHz

Compound	Configuration	H-1	H2	H-3		H-4	H-5	H-5′	H-5″
20	D-*galacto*-	6.55 d	—	5.68[b] m	—	5.36m	4.28 dd	3.92 dd	—
21	5-deoxy-L-*galcto*-	6.58 d	5.73 dd	5.48 dd		5.13m	—	1.16[b] d	—
22	D-*gluco*-	6.63 d	6.20 dd	—	5.13[b] m	—	4.15 dd	3.87 dd	—

a) Multiplicity of signals: d=doublet, dd=doublet of doublet, and m=multiplet.
b) Overlapping signals.

Table 2. Coupling Constants (Hz) of the Alditol-Chain Protons of 3-(Polyacetoxypentyl)-6-phenyl-1,2,4-triazolo[3,4-*a*]phthalazines

Compound	Configuration	$J_{1,2}$	$J_{2,3}$	$J_{3,4}$	$J_{4,5}$	$J_{4,5'}$	$J_{5,5''}$
20	D-*galacto*-	3	a)	a)	6	7.5	12
21	5-deoxy-L-*galacto*-	<3	9	4	7	—	—
22	D-*gluco*-	7.5	3	7.5	3	4.5	12

a) Unamenable to first order analysis due to overlapping of H-2 and H-3 signals.

ca. 180°), it is possible to predict the most favored conformations of compounds **20**, **21**, and **22** in terms of their observed coupling data (see Table 2).

The small $J_{1,2}$ value (≤3 Hz) of the two *galacto*-pentitol derivatives: 3-(D-*galacto*-1,2,3,4,5-pentaacetoxypentyl)-6-phenyl-1,2,4-triazolo[3,4-*a*]phthalazine (**20**) and 3-(L-*galacto*-1,2,3,4-tetraacetoxypentyl)-6-phenyl-1,2,4-triazolo[3,4-*a*]phthalazine (**21**) indicates a gauche arrangement of H-1 and H-2. Like 2-methyl- and 2-phenyl-(D-*galacto*-1,2,3,4,5-pentaacetoxypentyl)-1,3,4-oxadiazoles[32] and penta-*O*-acetyl-D-galactitol,[39] the H-2 and H-3 signals of the D-*galacto*- derivative **20** were unamenable for analysis due to their overlapping. Fortunately, however, the H-2 and H-3 signals of the 5-deoxy-L-*galacto*- derivative **21** were not overlapping and the first-order analysis of the coupling constants was possible. The $J_{2,3}$ value of this derivative is large enough (9 Hz) to indicate exclusive antiparallel disposition of H-2 and H-3. On the other hand, the $J_{3,4}$ value of 4 Hz points out to the gauche relation of H-3 and H-4. These data are very compatible with the expected extended, planar, zigzag conformations **44** and **45** of **20** and **21** respectively in which the bulky heterocycle extends away from the acetylated alditol chain. These conformations are free of any unfavorable eclipsed 1,3-interactions and conform with those assigned[31-34] for other heterocyclic compounds with *galacto*-pentitol side chain.

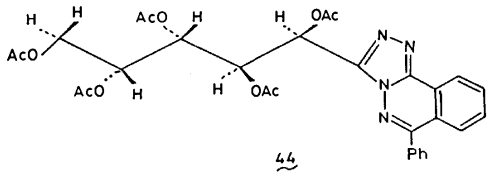

44

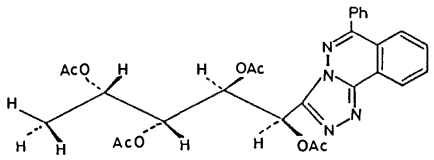

45

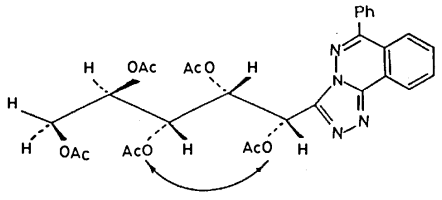

46

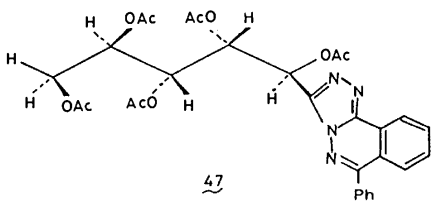

47

It would be expected that the extended, planar zigzag conformation **46** depicted for the 3-(D-*gluco*-1,2,3,4,5-pentaacetoxypentyl)-6-phenyl-1,2,4-triazolo-[3,4-*a*]phthalazine (**22**) represents a highly unfavorable situation owing to the dipolar eclipsed 1,3-interaction of the C-1 and C-3 acetoxyl groups. This expectation is, indeed, supported by the observed $J_{1,2}$ value (7.5 Hz); conformation **46** having H-1 and H-2 in a gauche arrangement would require a $J_{1,2}$ value of <4 Hz. Rotation about the C-1—heterocycle bond of **46** brings H-1 in the antiparallel orientation to H-2 and, therefore, mitigates the aforementioned 1,3-eclipsed interaction. This results in the formation of the "sickle" conformation **47** as a more favorable conformation of the D-*gluco*-derivative **22**. The observed $J_{2,3}$ and $J_{3,4}$ values (3 and 7.5 Hz respectively) are in congruence with the gauche and antiparallel dispositions of H-2–H-3 and H-3–H-4 respectively as depicted in the "sickle" conformation **47**.

Exploring some applications for the synthesized compounds, we have recently found[40,41] that 3-(D-*galacto*-pentahydroxypentyl)-6-phenyl-1,2,4-triazolo-[3,4-*a*]phthalazine (**16**) is a good inhibitor against the acid-corrosion of aluminium. Unfortunately however, compounds **8** and **11** showed no insecticidal activity when applied at the rate of 1000 ppm to the following insect species/host plant systems: mexican beet beetle (*Epilachna varivestis* Mulsant)/pinto bean (*Phaseolus vulgaris*); pea aphid (*Acyrthosiphon pisum* Harris)/fave bean (*Vicia faba*); southern armyworm (*Spodoptera eridania* Gramer)/pinto bean; and the two-spotted spider mite (*Tetranychus urticae*)/pinto bean.

Compounds **8** and **16** also showed no nematicidal activity at an application rate of 10 ppm against root-knot nematode (*Meloidogyne incognita*) hosted on cucumber (*Cucumis sativus*).

Compound **16** exhibited no herbicidal/plant growth regulation in the preemergence response and low activity (10—20%) in the post-emergence response screening when applied to the following test species: soybean (*Glycine max*, 20%); corn (*Zea mays*, 10%); wheat (*Triticum aestivum*, 10%); morningglory (*Ipomea spp*, 20%); velvetleaf (*Abutilon theophrasti*, 10%); barnyardgrass (*Echinochloa crus-galli*, 10%); and foxtail, green (*Setaria veridis*, 10%).

Experimental

General Methods. Melting points were determined with a Kofler block and are uncorrected. The infrared spectra (IR) were recorded for potassium bromide discs on a Unicam SP-1025 or Pye-Unicam SP-2000 spectrophotometers. Ultraviolet-visible spectra were recorded at ambient temper-

ature using a Unicam SP-1750 spectrophotometer. Proton magnetic resonance (^{1}H NMR) spectra were carried out at ambient temperature (ca. 25 °C) and at 90 MHz with a Varian EM-390 spectrometer for solutions in $CDCl_3$ or $(CD_3)_2SO$. Mass spectra were performed on an analytical system consisting of a Du Pont 21-419 mass spectrometer interfaced with a Du Pont 492-094 data-acquisition system. Follow up of the reactions and checking the homogeneity of the prepared compounds were made by performing thin-layer chromatography (TLC) on Silica gel G (Merck) precoated plates (layer thickness 0.25 mm) used without pretreatment. All the ratios of the solvent systems used were volume-to-volume (v/v); the distance of solvent travel was 5 cm, and the spots were detected by exposition to iodine vapour for a few minutes. All solvent evaporations were performed in a Buchi rotary evaporator under diminished pressure, with an outside bath temperature kept below 50 °C. Elemental microanalyses were performed in the Microanalysis Laboratory, Chemistry Department, Faculty of Science, Alexandria University using Perkin-Elmer Model PE-240 analyzer and in the Microanalysis Unit, Chemistry Department, Faculty of Science, Cairo Universtity.

***aldehydo*-D-Galactose(4-phenyl-1-phthalazinyl)hydrazone (8).** A solution of 1-hydrazino-4-phenylphthalazine (**1**, 1 g) in methanol (20 ml) was filtered through a fritted-glass funnel and added to a filtered solution of D-galactose (**2**, 0.8 g) in water (0.5 ml). The mixture was heated for 10 minutes on a boiling water bath and then kept for 24 hours at room temperature. The crystalline yellow product which separated, was filtered, washed several times with filtered methanol to give 1 g (59%) of **8** as yellow needles, mp 203—205 °C. All attempts to crystallize this hydrazone led to its transformation into the cyclic triazolophthalazine **14**. TLC in 1 : 1 chloroform-methanol, R_f: 0.52; $\lambda_{max}^{50\%EtOH}$ 338, 280, 240, and 212 nm, ($\log\varepsilon$: 4.61, 4.96, and 5.10); ν_{max}^{KBr} 3400 (broad, OH), 3300 (NH) and 1640 cm^{-1} (C=N); ^{1}H NMR $(CD_3)_2SO$: δ=12.15 (s, 1H, deuteratable, NH), 8.80 (d, 1H, CH=N), 8.75—7.40 (m, 9H, aromatic H), 4.82 (d, 1H, deuteratable, OH), 4.60 (m, 1H, alditol H), 4.40 (m, 2H, deuteratable, 2 OH) and 4.15 (m, 2H, deuteratable, 2 OH), the other protons together with the solvent absorption were congregated in a broad signal at δ 3.35.

Calcd for $C_{20}H_{22}N_4O_5 \cdot H_2O$: C, 57.69; H, 5.77; N, 13.46%. Found: C, 58.10; H, 5.60; N, 13.10%.

3-(D-*galacto*-Pentahydroxypentyl)-6-phenyl-1,2,4-triazolo[3,4-*a*]phthalazine (14). Method (A): Attempted crystallization of *aldehydo*-D-galactose (4-phenyl-1-phthalazinyl)hydrazone (**8**) from water-methanol gave a gelatinous product which showed two spots on TLC (1 : 1 chloroform-methanol). One spot migrated at a rate similar to that of the parent hydrazone **8** (R_f: 0.52) and the other was slightly less polar (R_f: 0.55) and corresponds to that of **14**. Repeated crystallization from the same solvent caused the gradual transformation of **8** into **14** which crystallized from water-methanol as colorless needles, mp 228—231 °C; TLC in 1 : 1 chloroform-methanol, R_f: 0.55; $\lambda_{max}^{50\%EtOH}$ 244 and 212 nm ($\log\varepsilon$: 4.81 and 4.63); ν_{max}^{KBr} 3420 (broad, OH) and 1630 cm^{-1} (broad C=N); ^{1}H NMR $(CD_3)_2SO$: δ=8.75—7.37 (m, 9H, aromatic H), 5.37 (m, 2H, alditol H), 4.75 (d, 1H, deuteratable, OH), 4.40 (m, 1H, deuteratable, OH), 4.22 (d, 3H, deuteratable, 3 OH), and 3.75 (m, 2H, alditol H), the other protons together with the solvent absorption were gathered in a broad signal at δ=3.53.

Calcd for $C_{20}H_{20}N_4O_5$: C, 60.60; H, 5.09; N, 14.13%. Found: C, 60.10; H, 5.05; N, 14.74%.

Method (B): A solution of *aldehydo*-D-galactose (4-phenyl-1-phthalazinyl)hydrazone (**8**, 1 g) in a mixture of water (5 ml) and methanol (20 ml) was treated with 10% palladium-on-charcoal (0.5 g) and refluxed for 4 hours. The catalyst was filtered off on a layer of Celite and the filtrate was evaporated to dryness. Crystallization of the residue from water-methanol gave 0.7 g (70%) of **14**, mp and mixed mp 228—231 °C, having the same spectral properties as that obtained according to method (A).

3-(D-*galacto*-1,2,3,4,5-Pentaacetoxypentyl)-6-phenyl-1,2,4-triazolo[3,4-*a*]phthalazine (20). 3-(D-*galacto*-Pentahydroxypentyl)-6-phenyl-1,2,4-triazolo[3,4-*a*]phthalazine (**14**, 1 g) was treated with pyridine (5 ml) and acetic anhydride (5 ml) for 24 hours at room temperature. The mixture was poured onto crushed ice and the product which separated was filtered, washed with water, and crystallized from methanol to give 0.9 g (59%) of **20**, mp 195—198 °C; TLC in 9 : 1 chloroform-methanol, R_f: 0.65; ν_{max}^{KBr} 1760 cm^{-1} (ester-carbonyl, *O*-acetyl groups); ^{1}H NMR ($CDCl_3$): δ=8.80—7.46 (m, 9H, aromatic H), 6.55 (d, 1H, alditol H-1), 5.68 (s, 2H, alditol H-2+H-3), 5.36 (m, 1H, alditol H-4), 4.28 (dd, 1H, alditol H-5), 3.92 (dd, 1H, alditol H-5′), 2.24, 2.13, 2.03 (3s, 3H each, 3 acetyl groups), and 1.98 (s, 6H, 2 acetyl groups).

Calcd for $C_{30}H_{30}N_4O_{10}$: C, 59.40, H, 4.99; N, 9.24%. Found: C, 59.85; H, 4.64; N, 9.67%.

3-(L-*galacto*-1,2,3,4-Tetrahydroxypentyl)-6-phenyl-1,2,4-triazolo[3,4-*a*]phthalazine (15). A solution of 1-hydrazino-4-phenylphthalazine (**1**, 1 g) in methanol (20 ml) was added to a solution of 6-*deoxy*-L-galactose (L-fucose, **3**, 0.69 g) in the least amount of water (ca. 0.2 ml), and the mixture was heated for 20 minutes on a boiling water bath. The product, which separated after cooling was filtered, washed with chloroform and ether, and crystallized from water-methanol to give 0.9 g (56%) of **15**, mp 243—245 °C, TLC in 1 : 1 chloroform-methanol, R_f: 0.52; ν_{max}^{KBr} 3400 (boroad, OH) and 1625 cm^{-1} (C=N); ^{1}H NMR $(CD_3)_2SO$: δ=8.60—7.35 (m, 9H, aromatic H), 5.35 (m, 2H, alditol H), 4.68 (s, 1H, deuteratable, OH) and 1.06 (d, 3H, pentitol CH_3), the other protons and hydroxyl protons together with the solvent absorption were congregated in a broad signal at δ=3.45.

Calcd for $C_{20}H_{20}N_4O_4$: C, 63.16; H, 5.26; N, 14.74%. Found: C, 63.51; H, 5.30; N, 14.79%.

3-(L-*galacto*-1,2,3,4-Tetraacetoxypentyl)-6-phenyl-1,2,4-triazolo[3,4-*a*]phthalazine (21). A solution of 3-(L-*galacto*-1,2,3,4-tetrahydroxypentyl)-6-phenyl-1,2,4-triazolo[3,4-*a*]-phthalazine (**15**, 1 g) in pyridine (4 ml) was treated with acetic anhydride (4 ml) and kept at room temperature for 24 hours. The mixture was poured onto crushed ice and the product which separated was filtered, washed with water, and crystallized from methanol to give 0.6 g (42%) of **21**, mp 252—255 °C; TLC in 9 : 1 chloroform-methanol, R_f: 0.62; ν_{max}^{KBr} 1760 and 1745 cm^{-1} (ester-carbonyl, *O*-acetyl groups); ^{1}H NMR ($CDCl_3$): δ=8.80—7.47 (m, 9H, aromatic H), 6.58 (d, 1H, alditol H-1), 5.73 (dd, 1H, alditol H-2), 5.48 (dd, 1H, alditol H-3), 5.13 (m, 1H, alditol H-4), 2.20, 2.11, 1.92, 1.88 (4s, 3H each, 4 acetyl groups), and 1.16 (d, 3H, pentitol CH_3).

Calcd for $C_{28}H_{28}N_4O_8$: C, 61.31; H, 5.11; N, 10.22%. Found: C, 61.35; H, 5.29; N, 10.16%.

3-(D-*gluco*-Pentaacetoxypentyl)-6-phenyl-1,2,4-triazolo-[3,4-*a*]phthalazine (16). A solution of 1-hydrazino-4-phenylphthalazine (**1**, 1 g) in methanol (30 ml) was treated with a solution of D-glucose (**4**, 0.8 g) in the least amount of water (ca. 0.3 ml) and the mixture was heated for 15 minutes on a boiling water bath. The mixture was left to attain ambient temperature and the product which separated was filtered, washed with chloroform and ether, and crystallized from water-methanol to give 1 g (59.5%) of **16**, mp 245—247 °C; TLC in 1:1 chloroform-methanol R_f: 0.52; ν_{max}^{KBr} 3500, 3380 (OH) and 1550 cm^{-1} (C=N); ^1H NMR $(CD_3)_2SO$: δ=8.70—8.45 (m, 9H, aromatic H), 5.58 (d, 1H, deuteratable, O<u>H</u>), 5.30 (m, 1H, alditol H), 4.60 (m, 2H, deuteratable proton, O<u>H</u>+ undeuteratable proton, alditol H), and 4.28 (m, 3H, deuteratable, 3O<u>H</u>), the other protons together with the solvent absorption were congregated in a broad signal at δ=3.30.

Calcd for $C_{20}H_{20}N_4O_5$: C, 60.60; H, 5.09; N, 14.13%. Found: C, 60.68; H, 5.24; N, 13.99%.

3-(D-*gluco*-1,2,3,4,5-Pentaacetoxypentyl)-6-phenyl-1,2,4-triazolo[3,4-*a*]phthalazine (22). 3-(D-*gluco*-Pentahydroxypentyl)-6-phenyl-1,2,4-triazolo[3,4-*a*]phthalazine (**16**, 1 g) was treated with pyridine (5 ml) and acetic anhydride (5 ml) and kept at room temperature for 24 hours. The mixture was poured onto crushed ice (150 ml) and the product which separated was filtered, washed with water, and crystallized from methanol to give 0.9 g (59%) of **22**, mp 140—142 °C. TLC in 9:1 chloroform-methanol; R_f: 0.52, ν_{max}^{KBr} 1760 and 1745 cm^{-1} (ester-carbonyl, *O*-acetyl groups); ^1H NMR ($CDCl_3$): δ=8.80—7.48 (m, 9H, aromatic H), 6.63 (d, 1H, alditol H-1), 6.20 (dd, 1H, alditol H-2), 5.13 (m, 1H, alditol H-3+H-4), 4.15 (dd, 1H, alditol H-5), 3.87 (dd, 1H, alditol H-5′), 2.07 (s, 6H, 2 acetyl groups), 2.02, 1.88, and 1.75 (3s, 3H each, 3 acetyl groups).

Calcd for $C_{30}H_{30}N_4O_{10}$: C, 59.40; H, 4.99; N, 9.24%. Found: C, 59.30; H, 5.09; N, 9.40%.

***aldehydo*-D-Mannose (4-Phenyl-1-phthalazinyl)hydrazone (11).** A solution of 1-hydrazino-4-phenylphthalazine (**1**, 1 g) in methanol (30 ml) was added to a solution of D-mannose (**5**, 0.8 g) in the least amount of water (ca. 0.2 ml) and the mixture was heated for 15 minutes on a boiling water bath. The mixture was kept at ambient temperature for an overnight and the orange crystalline product which separated was filtered, washed with chloroform and ether. Crystallization from water-methanol gave 1 g (59%) of **11**, as orange plates, mp 195—198 °C; TLC in 1:1 chloroform-methanol, R_f: 0.43; $\lambda_{max}^{50\%EtOH}$ 350 and 284 nm (log ε: 2.39 and 2.70); ν_{max}^{KBr} 3430, 3350 (OH), 3280 (NH), 1640, 1610, and 1595 cm^{-1} (C=N); ^1H NMR $(CD_3)_2SO$: δ=12.15 (s, 1H, deuteratable, N<u>H</u>), 8.37 (m, 1H, aromatic H), 5.05 (d, 1H, deuteratable, O<u>H</u>), and 4.60—4.10 (m, 5H, 4 deuteratable protons, 4O<u>H</u>+undeuteratable proton, alditol H), the other protons together with the solvent absorption were gathered in a broad signal at δ=3.35.

Calcd for $C_{20}H_{22}N_4O_5 \cdot H_2O$: C, 57.69; H, 5.77; N, 13.46%. Found: C, 58.01; H, 5.52; N, 13.20%.

3-(D-*manno*-Pentahydroxypentyl)-6-phenyl-1,2,4-triazolo-[3,4-*a*]phthalazine (17). To solution of *aldehydo*-D-mannose (4-phenyl-1-phthalazinyl)hydrazone (**11**, 1 g) in a mixture of water (10 ml) and methanol (30 ml) 10% palladium-on-charcoal (0.5 g) was added and the mixture was refluxed for 3 hours. The catalyst was filtered off on a bed of Celite and the filtrate was evaporated to dryness. Crystallization of the residue from water-methanol gave 0.8 g (81%) of **17**, mp 198—202 °C; TLC in 1:1 chloroform-methanol, R_f: 0.60; $\lambda_{max}^{50\%EtOH}$ 246 nm (log ε: 3.51); ν_{max}^{KBr} 3350 (broad, OH) and 1650 cm^{-1} (broad, C=N); ^1H NMR $(CD_3)_2SO$: δ=8.68—7.42 (m, 9H, aromatic H), 5.70 (d, 1H, deuteratable, O<u>H</u>), 5.27 (m, 1H, alditol H), 4.40 (m, 5H, 4 deuteratable protons, 4O<u>H</u>+undeuteratable proton, alditol H), and 3.75 (m, 4H, alditol H).

Calcd for: $C_{20}H_{20}N_4O_5 \cdot 0.5H_2O$: C, 59.26; H, 5.19; N, 13.83%. Found: C, 59.66; H, 5.16; N, 13.51%.

Attempted Preparation of 23. Acetylation of 3-(D-*manno*-(pentahydroxypentyl)-6-phenyl-1,2,4-triazolo[3,4-*a*]-phthalazine (**17**) with acetic anhydride in the presence of pyridine and processing of the reaction mixture as given for the preparation of **20** gave an uncrystallizable syrupy product.

3-(L-*manno*-1,2,3,4-Tetrahydroxypentyl)-6-phenyl-1,2,4-triazolo[3,4-*a*]phthalazine (18). A solution of 1-hydrazino-4-phenylphthalazine (**1**, 1 g) in methanol (20 ml) was added to a solution of 6-deoxy-L-mannose (L-rhamnose **6**, 0.69 g) in the least amount of water (ca. 0.2 ml) and the mixture was heated for 15 minutes on a boiling water bath. The mixture was kept for an overnight at room temperature and the product which separated was filtered, washed with chloroform and ether, and crystallized from water-methanol to give 0.8 g (50%) of **18**, mp 150—154 °C; TLC in chloroform-methanol, R_f: 0.70; ν_{max}^{KBr} 3300 (broad, OH) and 1640 cm^{-1} (broad, C=N); ^1H NMR $(CD_3)_2SO$: δ=8.68—7.41 (m, 9H, aromatic H), 5.66 (s, 1H, deuteratable, O<u>H</u>), 5.25 (m, 1H, alditol H), and 1.18 (d, 3H, pentitol C<u>H</u>$_3$), the other protons and hydroxyl protons together with the solvent absorption were gathered in a broad signal at δ=3.80.

Calcd for $C_{20}H_{20}N_4O_4 \cdot H_2O$: C, 60.30; H, 5.50; N, 14.07%. Found: C, 60.87; H, 5.51; N, 13.71%.

Attempted Preparation of 24. Acetylation of **18** with acetic anhydride and pyridine yielded uncystallizable syrupy product.

3-(D-*talo*-Pentahydroxypentyl)-6-phenyl-1,2,4-triazolo[3,4-*a*]phthalazine (19). A solution of 1-hydrazino-4-phenylphthalazine (**1**, 1 g) in methanol (20 ml) was treated with a solution of D-talose (**7**, 0.8 g) in the least amount of water (ca. 0.2 ml) and the mixture was heated for 15 minutes on a boiling water bath. The mixture was left to attain ambient temperature and the product which separated was filtered and washed with chloroform and ether. Crystallization from water-methanol gave 0.9 g (54%) of **19**, mp 238—240 °C; TLC in 1:1 chloroform-methanol, R_f: 0.54; ν_{max}^{KBr} 3580, 3260 (broad, OH), and 1620 cm^{-1} (C=N); ^1H NMR $(CD_3)_2SO$: δ=8.80—7.58 (m, 9H, aromatic H), 5.92 (m, 1H, deuteratable, O<u>H</u>), 5.45 (d, 1H, alditol H), 4.89 (d, 1H, deuteratable, O<u>H</u>), and 4.45 (m, 3H, 2 deuteratable protons, 2O<u>H</u>+undeuteratable proton, alditol H), the other protons and hydroxyl protons together with the solvent absorption were gathered in a broad siganl at δ=3.58

Calcd for $C_{20}H_{20}N_4O_5$: C, 60.60; H, 5.09; N, 14.13%. Found: C, 60. 32; H, 5.13; N, 14.01%.

Attempted Preparation of 25. Acetylation of **19** gave an uncrystallizable syrupy product.

3-Formyl-6-phenyl-1,2,4-triazolo[3,4-*a*]phthalazine (26). A suspension of any of the 3-(pentahydroxypentyl)-6-phenyl-1,2,4-triazolo[3,4-*a*]phthalazine (**14—19**, 1 g) in distilled water (15 ml) was treated with a solution of sodium periodate (2.4 g) in distilled water (15 ml) and stirred for one

hour at room temperature. The product was filtered, washed with water, 10% sodium thiosulfate solution and water, and crystallized from methanol to give 0.4 g (57%) of **26**, mp 223—225 °C; TLC in 1 : 1 chloroform–methanol, R_f: 0.76; ν_{max}^{KBr} 1740 (CHO) and 1620 cm^{-1} (C=N); ^1H NMR $(CD_3)_2SO$: δ=10.37 (s, 1H, CHO), and 8.85—7.50 (m, 9H, aromatic H).

Calcd for $C_{16}H_{10}N_4O \cdot 0.5H_2O$: C, 67.85; H, 3.89%. Found: C, 67.64; H, 4.31%.

3-Hydroxymethyl-6-phenyl-1,2,4-triazolo[3,4-*a*]phthalazine (27). A solution of sodium borohydride (0.1 g) in water (5 ml) was dropwisely added to a suspension of 3-formyl-6-phenyl-1,2,4-triazolo[3,4,-*a*]phthalazine (**26**, 1 g) in water (10 ml) while stirring. The mixture was kept at room temperature for an overnight and then treated with a few drops of acetic acid. The product which separated was filtered, washed with water and crystallized from methanol to give 0.7 g (70%) of **27**, mp 248—250 °C; TLC in 1 : 1 chloroform–methanol, R_f: 0.78; ν_{max}^{KBr} 3300 (broad, OH) and 1620 cm^{-1} (C=N); ^1H NMR ($CDCl_3$): δ=8.85—7.50 (m, 9H, aromatic H), 5.25 (s, 2H, CH_2), and 2.48 (s, 1H, deuteratable, OH).

Calcd for $C_{16}H_{12}N_4O$: C, 69.57; H, 4.35%. Found: C, 69.40; H, 4.49%.

3-Acetoxymethyl-6-phenyl-1,2,4-triazolo[3,4-*a*]phthalazine (28). 3-Hydroxymethyl-6-phenyl-1,2,4-triazolo[3,4-*a*]phthalazine (**27**, 1 g) was treated with pyridine (2 ml) and acetic anhydride (2 ml) at room temperature for 24 hours. The mixture was poured onto crushed ice and then extracted with chloroform. The extract was successively washed with aqueous solutions of potassium hydrogensulfate (10%), saturated sodium hydrogencarbonate and water, and dried (Na_2SO_4). Evaporation of the solvent gave a syrup which crystallized from methanol to give 0.7 g (61%) of **28**, mp 195 °C; TLC in 9 : 1 chloroform–methanol, R_f: 0.52; ν_{max}^{KBr} 1760 cm^{-1} (ester-carbonyl, *O*-acetyl group); ^1H NMR ($CDCl_3$): δ=8.85—7.52 (m, 9H, aromatic H), 5.74 (s, 2H, CH_2) and 2.18 (s, 3H, acetyl group).

Calcd for $C_{18}H_{14}N_4O_2 \cdot 0.5H_2O$: C, 66.06; H, 4.59; N, 17.13%. Found: C, 66.46; H, 4.60; N, 16.90%.

References

1) Reactions of Sugars with Amidrazones and Hydrazidines. Part II; for Part I, see Ref. 13.

2) In the preliminary reports on this work: M. A. E. Shaban, M. A. M. Nassr, and M. A. M. Taha, *Carbohydr. Res.*, **113**, C16 (1983); M. A. E. Shaban and M. A. M. Nassr, Am. Chem. Soc. 186th National Meeting, Washigton, D. C., (1983) CARB-23, the phenyl group position was erroneosly numbered 5.

3) W. E. Cohn, *Fed. Proc., Fed. Am. Soc. Exp. Biol.*, **16**, 166 (1957).

4) F. F. Davis and F. W. Allen, *J. Biol. Chem.*, **227**, 907 (1957).

5) R. J. Suhadolnik, "Nucleoside Antibiotics," Wiley-Interscience, New York, N. Y. (1970) pp. 354—404.

6) G. D. Daves, Jr., and C. C. Cheng, *Progr. Med. Chem.*, **13**, 303 (1976).

7) S. Hanessian and A. G. Pernet, *Adv. Carbohydr. Chem. Biochem.*, **33**, 111 (1976).

8) M. Slavik, "Antitumor Antibiotics," ed by S. K. Carter, H. Umezawa, J. Douros, and Y. Sukurai, Springer-Verlag, Berlin (1978).

9) See for example: M. P. Mertes, J. Zielinski, and C. Pillar, *J. Med. Chem.*, **10**, 320 (1967).

10) See for example: C. K. Chu, *Heterocycles*, **22**, 345 (1984); M. C. Clingerman and J. A. Secrist, III, *J. Org. Chem.*, **48**, 3141 (1983); W. J. Hennen, B. C. Hinshaw, T. A. Riley, S. G. Wood, and R. K. Robins, *J. Org. Chem.*, **50**, 1741 (1985).

11) See for example: J. G. Buchanan, S. J. Moorhouse, and R. H. Wightman, *J. Chem. Soc., Perkin Trans. 1*, **1981**, 2258; M. A. E. Sallam and S. M. E. Abdel Megid, *Carbohydr. Res.*, **125**, 85 (1984).

12) M. Shaban and M. Nassr, *Org. Prep. Proced. Int.*, **8**, 107 (1976), and previous references cited therein.

13) M. A. E. Shaban, R. S. Ali, and S. M. El-Badry, *Carbohydr. Res.*, **95**, 51 (1981).

14) M. A. E. Shaban, M. A. M. Taha, and A. Z. Nasr, Am. Chem. Soc. 190th National Metting, Chicago, Ill., CARB-28 (1985).

15) W. T. Comer and A. W. Gomoll, "Medicinal Chemistry," ed by A. Burger, Wiley-Interscience, New York (1970), pp. 1027—1064.

16) "Handbook of Experimental Pharmacology XXXIX: Antihypertensive Agents," ed by F. Gross, Springer-Verlag, Berlin (1977), p. 39.

17) A. Ishii, K. Kubo, T. Deguchi, and M. Tanaka, *Yakugaku Zasshi*, **99**, 533 (1979); *Chem. Abstr.*, **91**, 133826z (1979).

18) H. M. Faid Allah and R. Soliman, *J. Heterocycl. Chem.*, **24**, 667 (1987).

19) E. Menziani, *Bol. Sci. Fac. Chim. Ind. (Bologna)*, **12**, 162 (1954); *Chem. Abstr.*, **50**, 355i (1956).

20) E. Menziani, *Med. Sper.*, **25**, 277 (1954); *Chem. Abstr.*, **50**, 828g (1956).

21) A. Rosenthal and H. H. Lee, *J. Carbohydr. Nucleosides, Nucleotides*, **5**, 559 (1978).

22) J. Druey and B. H. Ringier, *Helv. Chim. Acta*, **34**, 195 (1951).

23) M. A. E. Shaban, unpublished results.

24) M. A. M. Nassr, S. M. El-Badry, and M. A. E. Shaban, *J. Chinese Chem. Soc.*, **32**, 65 (1985).

25) J. H. Bouri, R. G. Cooks, P. F. Donaghue, J. A. Halleday, and H. J. Rodda, *Aust. J. Chem.*, **20**, 2677 (1967).

26) Q. N. Porter and J. Baldas, "Mass Spectrometery of Heterocyclic Compounds," Wiley-Interscience, New York, N. Y. (1971), p. 463.

27) L. B. Townsend and R. K. Robins, *J. Heterocycl. Chem.*, **6**, 459 (1969).

28) H. Zimmer, R. Glaser, J. Kokosa, D. A. Garteiz, E. V. Hess, and A. Litwin, *J. Med. Chem.*, **18**, 1031 (1975).

29) H. S. El-Khadem, D. Horton, and T. F. Page, Jr., *J. Org. Chem.*, **33**, 347 (1968).

30) H. El-Khadem, D. Horton, and J. D. Wander, *J. Org. Chem.*, **37**, 1630 (1972).

31) A. M. Seldes, I. M. E. Thiel, and J. O. Deferrari, *Carbohydr. Res.*, **39**, 11 (1975).

32) A. M. Seldes, E. G. Gros, I. M. E. Thiel, and J. O. Deferrari, *Carbohydr. Res.*, **49**, 49 (1976).

33) J. B. Lee and B. F. Scanlon, *Tetrahedron*, **25**, 3413 (1969).

34) L. Szilagyi, R. Bognar, and I. Farkas, *Carbohydr. Res.*, **26**, 305 (1973).

35) L. D. Hall, *Advan. Carbohydr. Chem.*, **19**, 51 (1964).

36) R. U. Lemieux and J. D. Stevens, *Can. J. Chem.*, **43**,

2059 (1965).
37) B. Coxon, *Tetrahedron*, **21**, 3481 (1965).
38) J. M. Williams, *Carbohydr. Res.*, **11**, 347 (1969).
39) S. J. Angyal, R. Le Fur, and D. Gagnaire, *Carbohydr. Res.*, **23**, 121 (1972).
40) B. A. Abdel-Nabey, M. Shaban, and M. Essa, Proceedings, 6th Eur. Symp. on Corrosion Inhibitors, Ferrara, Italy, 1985, p. 295.
41) B. A. Abdel-Nabey, M. M. Essa, and M. A. E. Shaban, *Surface Technol.*, **26**, 165 (1985).

Cluster Chemistry. Catalytic Behavior of $[H_2Ru_4(CO)_{12}]^{2-}$ in Reduction of Benzaldehyde and Nitrobenzene

Fumio WADA,* Masanori SHIMUTA, and Tsutomu MATSUDA
Department of Organic Syntheses, Faculty of Engineering,
Kyushu University, Hakozaki, Fukuoka 812
(Received January 26, 1989)

Synopsis. The dianion, $[H_2Ru_4(CO)_{12}]^{2-}$, showed excellent catalytic activity for the reduction of nitrobenzene, but not of benzaldehyde. In the presence of benzaldehyde under H_2 pressure, the dianion was converted to a new species of good catalytic activity, which is closely similar to a complex obtained from the reaction of $[H_2Ru_6(CO)_{18}]$ with DBU (1,8-diazabicyclo[5.4.0]undec-7-ene).

We previously reported that the reaction of $[HRu_3(CO)_{11}]^-$ (**I**) with DBU under H_2 pressure gave $[H_2Ru_4(CO)_{12}]^{2-}$ (**II**), which can act as a catalyst for the water gas shift reaction.[1a] Although the catalytic behavior of **I** has been studied in various reactions,[2] very little is known about that of **II**. In this paper we report on the catalytic activity of the dianion **II** in the reduction of benzaldehyde and nitrobenzene, compared with those of monoanionic hydrido ruthenium clusters, such as **I** and $[H_3Ru_4(CO)_{12}]^-$ (**III**). We also describe the formation of a new active catalyst from **II** (or $[H_2Ru_6(CO)_{18}]$ with DBU) in the benzaldehyde reduction.

Results and Discussion

The hydrido clusters (**I**, **II**, and **III**) used in this study are interconvertible, depending upon both the ratio of CO/H_2 under pressure of 10—30 kg cm^{-2} and the type of base used.[1b] Thus, reduction using these clusters must be carried out under conditions where only a desired anionic cluster acts as the main catalyst, as shown in Table 1.

Moreover, the substrates were shown to affect the interconversion. In the presence of benzaldehyde (or nitrobenzene), **II** was transformed into species **IV**, which can be prepared by a reaction of $[H_2Ru_6(CO)_{18}]$ with DBU; however, **II** in the presence of nitrobenzene was converted to an insoluble higher unclear cluster(s) under pure hydrogen pressure (20 kg cm^{-2}). Runs 2, 6, and 7 in Table 1, therefore, were carried out under hydrogen containing 10% of CO in order to prevent any transformation of **II** during reduction.

The complex **III** prepared from $[H_4Ru_4(CO)_{12}]$ and NEt_3 was stable, even in the presence of benzaldehyde under pure H_2 pressure.

Table 1 shows the results of the reduction together with the anionic hydrido clusters existing in each reaction system before and after reaction. The structures of these clusters were confirmed by a comparison of their IR spectra with those of authentic samples.[1] As can be seen in Table 1, the catalytic activity of **I** for benzaldehyde reduction was low (comparable to the result reported by Laine[2]), whereas **II** and **III** showed moderate activity (Runs 2 and 3, respectively). When benzaldehyde reduction with **II** was carried out under pure H_2 pressure (Run 1), **II** was easily changed to another species **IV** during the reduction, and a much higher conversion of benzaldehyde was observed, suggesting the increased catalytic activity of **IV**. Figure 1a shows the IR spectra of **IV** and complex **V** prepared in situ from $[H_2Ru_6(CO)_{18}]$ and DBU in methanol. Complex **V** is not the same as the known complex $[HRu_6(CO)_{18}]^-$ prepared by protonation of $[Ru_6(CO)_{18}]^{2-}$.[4] The ^{1}H NMR spectrum of **V** in CD_3OD shows two kinds of proton resonances at τ=29.3 (H_a) and 29.5 (H_b), and the intensity ratio of H_a/H_b is almost 1 : 1. At present, it is not yet clear whether species **V** is a single species or a mixture of two complexes. In view of the close similarity of complexes **IV** to **V** regarding their IR spectra, the catalytic activity of **V** was examined for benzaldehyde reduction. As expected, the result was comparable

Table 1. Hydrogenation of Organic Compounds Catalyzed by Anionic Hydrido Ruthenium Clusters[a]

Run	Reactant	$P_{H_2}:P_{CO}$ (kg cm^{-2})	Convn. (%)	Prod.	Selectivity (%)	Anionic species[b] (by IR)
	C_6H_5CHO			$C_6H_5CH_2OH$		
1		20/0	91		89	IV[c]
2		18/2	37		80	$[H_2Ru_4(CO)_{12}]^{2-}$
3		0/20[d]	7		6	$[HRu_3(CO)_{11}]^-$
4		20/0[e]	27		75	$[H_3Ru_4(CO)_{12}]^-$
5		20/0[f]	100		89	V
	$C_6H_5NO_2$			$C_6H_5NH_2$		
6		19/1	93		100	$[H_2Ru_4(CO)_{12}]^{2-}$
7		18/2	92		94	$[H_2Ru_4(CO)_{12}]^{2-}$

a) Catalyst, 0.05 mmol; DBU, 0.5 ml; MeOH, 4.0 ml; substrate, 5.0 mmol; total pressure=20 kg cm^{-2}; 120±1 °C, 3 h. b) The existence of these anionic clusters was confirmed by IR except Run 1. c) The starting complex was **II**. d) NEt_3 and H_2O were used instead of DBU. e) NEt_3 instead of DBU was used. f) The starting complex was **V**.

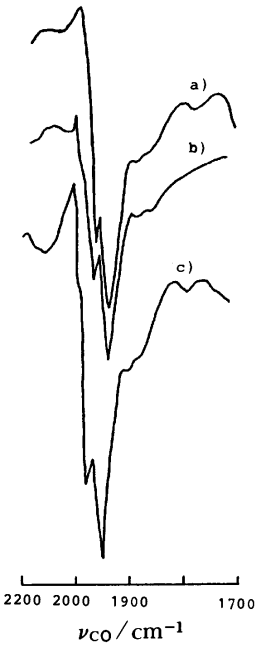

Fig. 1. IR spectrum in ν_{CO} region of the catalyst components after hydrogenation of benzaldehyde. a) **II** was used as a precursor under H_2 presure; b) the species **V** before reduction; c) after the reduction with **V**.

to that of **IV** (see Run 5), and the IR spectrum of the catalyst component in the ν_{CO} region shows that the starting complex **V** remains unchanged after reduction (see Fig. 1b and c). Unfortunately, many attempts to isolate **IV** have not yet been successful.

At present it is difficult to explain why species **IV** (or **V**) is so active for benzaldehyde reduction compared with other hydrido clusters, since the reactivity of the hydrogen atom in hydrido clusters does not always correspond to the hydridic character predicted from ^{1}H NMR.[5] A more detailed study is necessary in order to clarify the reactivity of **IV** (or **V**).

As mentioned above, the known anionic hydrido clusters (**I**, **II**, and **III**) are not good catalysts for benzaldehyde. The dianion **II**, however, acts as an excellent catalyst for nitrobenzene (Runs 6 and 7) under the same conditions (Run 2).[6] In the case of nitrobenzene reduction under pure H_2 pressure, **II** was readily converted not to **IV** but to higher nuclear cluster(s) which can be changed to **I** under CO pressure. This result suggests that the catalytic behavior of **II** in nitrobenzene reduction would be different from that of **II** in benzaldehyde reduction.

Experimental

The solvents and reagents used in this study were purified by distillation or recrystallization before use under N_2. All operations were carried out under a nitrogen atmosphere.

The typical reaction procedure was as follows. A catalyst solution (MeOH, 4 ml) containing only the desired anionic hydrido cluster (0.05 mmol) was previously prepared according to the methods described in the literature.[1] The catalyst solution (4 ml), benzaldehyde (or nitrobenzene) (5.0 mmol), and cyclohexanol (15 mmol) as an internal standard were placed in a 30 ml autoclave. Nitrogen in the autoclave was flushed three times with H_2, and then 20 kg cm^{-2} of H_2 (or a mixture of H_2 and CO) was charged. After the reaction at 120±1 °C for 3 h, the products were analyzed by GLC and the anionic clusters in the reaction mixture were identified by comparison of their IR spectra with those of authentic samples.[1]

References

1) a) F. Wada, M. Shimuta, and T. Matsuda, *Nippon Kagaku Kaishi*, **1985**, 503, and references cited therein; b) F. Wada, M. Shimuta, T. Goto, T. Ikeda, K. Kikukawa, and T. Matsuda, *Chem. Lett.*, **1983**, 1987; c) C. Ungerman, V. Landis, S. A. Moya, H. Cohen, M. Walker, R. G. Pearson, R. G. Rinker, and P. C. Ford, *J. Am. Chem. Soc.*, **101**, 5922 (1979) and references cited therein.

2) a) W. J. Thomson and R. M. Laine, "Catalytic Activation of Carbon Monoxide—ACS Symposium Series 152," ed by P. C. Ford, ACS, Washington (1981), p. 133. Turnover frequency moles of product/(mole of catalyst)(h) of $[HRu_3(CO)_{11}]^-$ is 9 at 125 °C for 1 h. b) R. A. Sheldon, "Chemicals from synthesis gas," D. Reidel Publishing Company, Holland (1983), p. 167.

3) C. C. Nagel and S. G. Shore, *J. Chem. Soc., Chem. Commun.*, **1980**, 530: ^{1}H NMR data for anionic hydrido ruthenium carbonyl clusters used here are as follows $[HRu_3(CO)_{11}]^-$, τ=25.8 ppm; $[H_3Ru_4(CO)_{12}]^-$, τ=27.0 ppm; $[H_2Ru_4(CO)_{12}]^{2-}$, τ=29.3 ppm.

4) C. R. Eady, B. F. G. Johnson, J. Leuies, M. C. Malatesta, P. Machis, and M. Mcpartlin, *J. Chem. Soc., Chem. Commun.*, **1976**, 945.

5) P. Chini, S. Martinengo, and G. Giordano, *Gazz. Chim. Ital.*, **102**, 330 (1972), For example, ^{1}H NMR of $[HRh_6(CO)_{15}]^-$ shows at τ=22.3 ppm, but the complex is active for benzaldehyde reduction (turnover frequency[2a]= 105±10 at 125 °C, for 1 h).

6) $[HRu_3(CO)_{11}]^-$ and $[H_3Ru_4(CO)_{12}]^-$ were less effective, compared with $[H_2Ru_4(CO)_{12}]^-$. $[HRu_3(CO)_{11}]^-$: conv. 94%, Select. 84%.; $[H_3Ru_4(CO)_{12}]^-$: conv. 89%, Select. 82%.

Fluorescence Polarization Spectra along the Rotational Contour of the $10a_0^1$ Absorption Band of Pyrazine Vapor

Nobuhiro OHTA,* Osamu SEKIGUCHI,† and Takeshi TAKEMURA
Division of Chemistry, Research Institute of Applied Electricity, Hokkaido University, Sapporo 060
†Faculty of General Studies, Gunma University, Aramakimati, Maebashi, Gunma 371
(Received March 11, 1989)

Synopsis. Fluorescence polarization spectra for the $10a_0^1$ perpendicular absorption band belonging to the $S_0 \rightarrow S_1$ transition of pyrazine vapor have been obtained at room temperature. The spectra are well reproduced theoretically by considering the resonance fluorescence from fully resolved rotational levels in S_1 and by employing a symmetric top approximation.

Fluorescence emission from free rotating molecules was demonstrated to be largely polarized even in such larger molecules as pyrazine, pyrimidine and 1,3,5-triazine.[1] The analysis of the degree of polarization of fluorescence along the rotational contour of the parallel vibronic absorption bands of these azaaromatic compounds was shown to give a clue to understand the mechanism of the intramolecular vibrational redistribution within the singlet manifold.[2] Similarly, the polarization of ensemble-averaged fluorescence was shown by Nathanson and McClelland to be important to determine the extent of intramolecular vibration-rotation energy transfer.[3]

Terazima and Lim[4] reported that excitation of the $10a_0^1$ band of S_1 pyrazine, which lies at 383 cm^{-1} above the $S_0 \rightarrow S_1$ origin and exhibits a rotational contour of typical perpendicular bands,[5] leads to the appearance of fluorescence which is nearly completely depolarized in a jet, in contrast with the 0-0 band. They suggested that these results come from a strong mixing between fluorescence emissions induced by the parallel and perpendicular transitions, respectively, since these two emissions are expected to show an opposite behavior on polarization. On the other hand, Pratt and co-workers[6] proposed a different interpretation of the fluorescence depolarization for the $10a_0^1$ band, based on the phosphorescence excitation spectrum in the $S_0 \rightarrow T_1$ absorption region. The S_1 surface is well known to be distorted along the coordinate of the ν_{10a} vibration because of strong vibronic coupling with higher lying singlet states,[7] whereas vibronic coupling is not important in T_1 according to the $S_0 \rightarrow T_1$ spectrum. Thus, the potential curve of the ν_{10a} vibration is different in S_1 and T_1. Because of enhanced Franck-Condon factor as well as differences in the admixed $\pi\,\pi^*$ character, therefore, the S_1-T_1 spin orbit matrix element might be significantly larger for the levels involving ν_{10a} vibration. Pratt and co-workers suggested that such a mode specificity in the S_1-T_1 spin orbit interaction may induce a mode specificity in the fluorescence polarization, i.e., fluorescence depolarization occurs following excitation into the S_1 vibronic levels effectively coupled to the triplet levels.

In the present study, excitation polarization (EP) spectra of pyrazine along the rotational contour of the $10a_0^1$ perpendicular absorption band were obtained in a bulk gas by monitoring the parallel and perpendicular fluorescence bands with out-of-plane and in-plane transition moments, respectively.

Experimental

All the optical measurements were carried out at room temperature. The experimental apparatus and procedures are the same as reported in previous papers.[2] Briefly, the output frequency of a pulsed dye laser (Molecron DL14), pumped by a nitrogen laser (Molectron UV22), was doubled by a KDP crystal. The generated UV light, which is linearly polarized and used for excitation, has a repetition rate of 20 pps, a linewidth of ca. 0.5 cm^{-1} and a duration of ca. 3 ns.

The fluorescence emitted at right angles to the direction of propagation of the laser light for excitation was passed through a polarization analyzer and then through a scrambler. The emission was dispersed by a grating monochromator and detected by a photomultiplier. The intensities of the fluorescence polarized parallel and perpendicular to the polarization direction of the exciting light are denoted by $I_{/\!/}$ and $I_\perp$, respectively and the degree of polarization (P) is defined as $P=(I_{/\!/}-I_\perp)/(I_{/\!/}+I_\perp)$. The EP spectra along the rotational contour were obtained by combining two fluorescence excitation spectra obtained by monitoring $I_{/\!/}$ and $I_\perp$, separately.

Results and Discussion

Figure 1 shows the EP spectra of pyrazine along the rotational contour of the $10a_0^1$ band, together with the absorption spectrum. The sample pressure is 0.25 and 1.23 Torr (1 Torr=133.322 Pa) for the EP and absorption spectra, respectively. The EP spectra shown in Figs. 1(a) and 1(b) were obtained, respectively, by monitoring the fluorescence of parallel band of $10a_1^1 6a_0^1$ at 336 nm, and the perpendicular band of $10a_2^1$ at 339.8 nm with a spectral resolution of 0.2 nm.[7] The absorption band located at ca. 20 cm^{-1} higher than the $10a_0^1$ exhibits a parallel-type rotational contour and assigned as the $6a_0^1 16b_0^1$ bands.[8] The absorption spectrum of the $10a_0^1$ band exhibits a perpendicular-type rotational contour, and the rotational analysis was completed by Thakur and Innes.[5] The EP spectra shown in Figs. 1(a) and 1(b) are very different from each other, e.g., the P value near the origin is ca. −0.15 for the parallel fluorescence band, whereas P near the origin is ca. 0.1 for the perpendicular fluorescence band.

The EP spectra were simulated with a symmetric top approximation in the same manner as reported in the previous papers.[2] By assuming that wavefunction can be separated into a rotational part and a vibronic part, the intensity of the resonance fluorescence emitted from the optically prepared level is

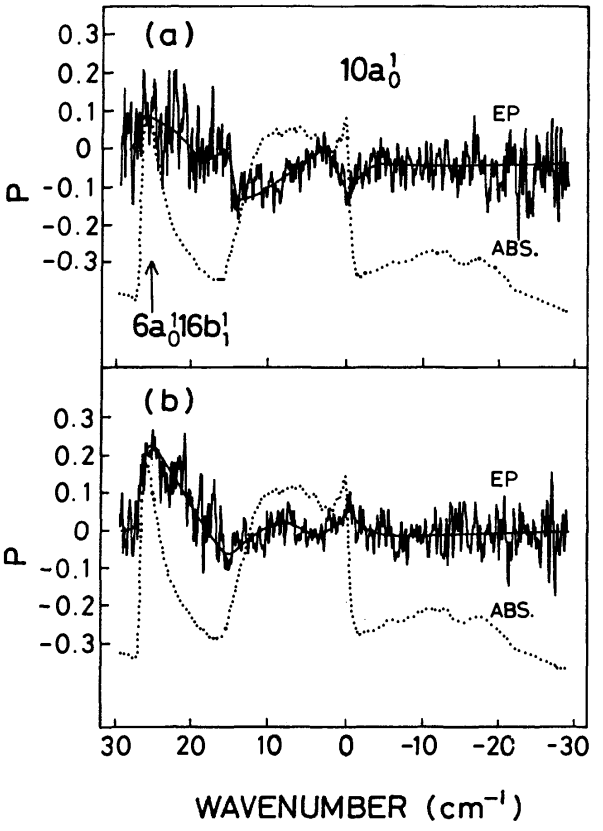

Fig. 1. Excitation polarization spectra of pyrazine vapor at 0.25 Torr along the rotational contour of the $10a_0^1$ band, obtained by monitoring the fluorescence at 336 nm (a) and at 339.8 nm (b). The dotted line represents the absorption spectrum. The band origin denoted by 0 is at 31258 cm^{-1}.[5] The absorption band lying at ~20 cm^{-1} above the $10a_0^1$ band is assigned as the $6a_0^1 16b_1^1$.[7]

given by

$$I \propto \nu_a \nu_e^4 \sum_{gg'} |M_g|^2 |M_{g'}|^2 f(JKJ'K'J''K'') \quad (1)$$

where

$$f(JKJ'K'J''K'') = (2J+1)^{-1} \times \sum_{MM'M''} |\langle J'K'M'|\Phi_{Fg}|JKM\rangle|^2 |\langle J''K''M''|\Phi_{Fg'}|J'K'M'\rangle|^2 \quad (2)$$

Here, ν_a, ν_e are the frequencies of the absorbed and emitted lights, respectively; M_g, $M_{g'}$ are the vibronic part of the dipole moment along the g and g' axes of the molecule-fixed Cartesian system, respectively; Φ_{Fg}, $\Phi_{F'g'}$ are the direction cosines between the F and g axes and between the F' and g' axes, respectively; $|JKM\rangle$, $|J'K'M'\rangle$ and $|J''K''M''\rangle$ represent the rotational wavefunctions of the initial, intermediate and final states, respectively. Note that F and F' represent the axes of the space-fixed Cartesian system in terms of which the radiation field is described. It is also noted that the polarization direction of the exciting light and the figure axis are regarded as X and z, respectively. Then, the fluorescence intensity at ν is given by

$$I(\nu) = \sum_{\nu_1 JKJ'K'J''K''} A(J'K') I g_{JK} P_{JK}(T) L(\nu - \nu_1) \quad (3)$$

where g_{JK}, $P_{JK}(T)$, $L(\nu-\nu_1)$ are the statistical weight, the Boltzman factor at a temperature of T, intensity of the exciting light at ν_a, respectively. ν_a is different from the excitation frequency ν of the maximum intensity by ν_1. A(J'K') is the factor to which fluorescence quantum yield is proportional.

With the relations M=M'=M'' and M=M'=M''±1 for the parallel and perpendicularly polarized fluorescence emissions, respectively,[9] the intensities of $I_{/\!/}(\nu)$ and $I_\perp(\nu)$ can be obtained from the above equations.

In the present experiments, the optical excitation was made for the perpendicular absorption band, i.e., g=x(y). The f values of Eq. 2 for F=F'=X and for F=X, F'=Y were evaluated for the individual rotational transitions of a symmetric top with the direction cosine matrix elements reported by Cross et al.[10] The EP spectra simulated for the parallel-type transition of emission, i.e., g'=z and for the perpendicular-type transition of emission, i.e., g'=x(y) are shown in Fig. 2, together with the simulated absorption spectrum. These spectra were obtained with the rotational constants: B''=0.20531 and C''=0.10249 in S_0 and B'=0.20322, and C'=0.10166 cm^{-1} in S_1.[5] Fluorescence emissions of pyrazine consist of fast and slow components.[11] In fact, the slow component occupies about 15% of the total fluorescence in intensity at 0.25 Torr for excitation into the $10a^1$. The quantum yield of the fast component is independent of the rotational level excited, whereas that of the slow component is nearly proportional to $(2J'+1)^{-1}$.[12] The simulated spectra shown in Figs. 2(a) and 2(b) were obtained by assuming that A(J'K') in Eq. 3 is constant, whereas the spectra in Figs. 2(c) and 2(d) were obtained by assuming that A(J'K') is $(2J'+1)^{-1}$.

Actually, the absorption spectrum is not well reproduced theoretically, as far as symmetric top approximation is employed. However, the EP spectra both for the parallel- and perpendicular-type fluorescence bands are reproduced very well by assuming a symmetric top approximation, as is seen in Figs. 1 and 2. In fact, Ray's parameter defined by $(2B-A-C)/(A-C)$ is 0.985 at the $10a^1$ level of S_1,[5] indicating that pyrazine is well regarded as an oblate symmetric top at this level. Accordingly, it is known that the EP spectra are not influenced by an asymmetry so severely as the absorption spectrum.

At several excitation positions along the rotational contour, the P value of each of the fast and slow components was evaluated by combining the total integrated intensity with the decays, both of which were obtained for each of $I_{/\!/}$ and $I_\perp$. However, a difference of P was not confirmed between the fast and slow components. These results are well understood from Fig. 2, i.e., the EP spectra simulated with the assumption that A(J'K') is constant are very similar to the spectra simulated with the assumption that A(J'K') is $(2J'+1)^{-1}$. It should be also noted that the EP spectrum for the $6a_0^1 16b_1^1$ band are very similar to those for the 0-0 band and that the observed spectra are similarly reproduced theoretically very well.[2]

Polarization property of fluorescence indicates that the emission whose intensity is proportional to $I_{/\!/}+2I_\perp$ must be monitored to obtain the true yield spectrum.

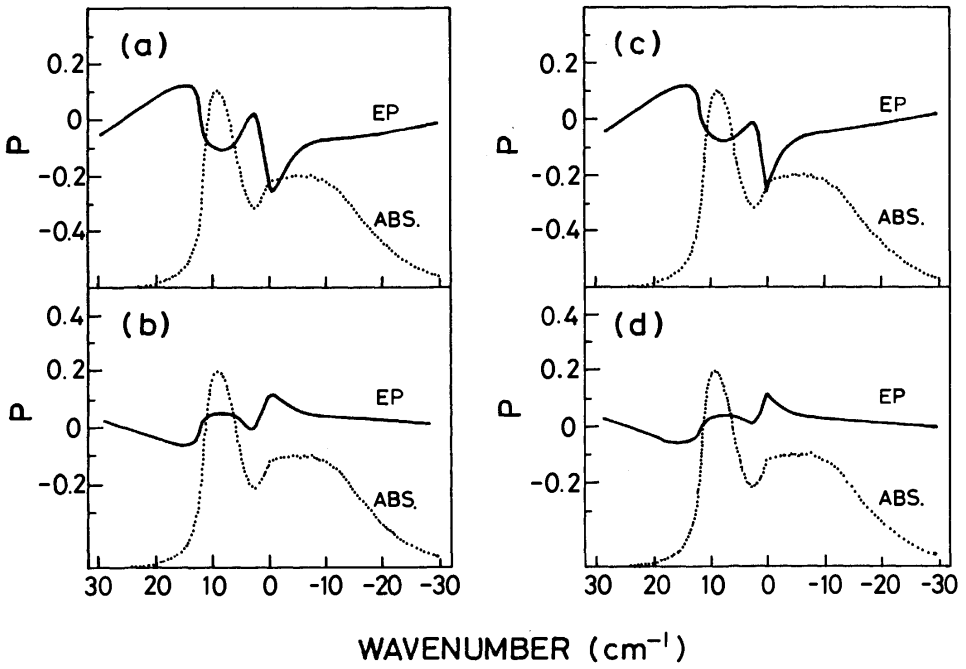

Fig. 2. Excitation polarization spectra at 298 K simulated for the $10a_0^1$ band of pyrazine according to Eqs. 1—3 with the following assumptions: (a) g=x(y), g'=z, and A(J'K') is constant; (b) g=x(y), g'=x(y), and A(J'K') is constant; (c) g=x(y), g'=z, and $A(J'K')=(2J'+1)^{-1}$; (d) g=x(y), g'=x(y), and $A(J'K')=(2J'+1)^{-1}$. The exciting light was assumed to have a triangle band-shape with a width (fwhm) of 0.5 cm^{-1}. Dotted line shows the simulated absorption spectra.

Previous conclusion for the $10a_0^1$ band that the fluorescence quantum yield of the fast component is nearly independent of the rotational level excited and that the yield of the slow fluorescence is proportional to $(2J'+1)^{-1}$ was derived from the yield spectra which were obtained without any polarization analyzer for emission.[12] The yield spectra obtained by setting the polarization analyzer for emission to the magic angle (54.7°), i.e., the observed fluorescence intensity corresponds to $I_{/\!/}+2I_{\perp}$, were confirmed to be very similar to the previous spectra. Fortunately, therefore, it is unnecessary to correct the previous conclusion concerning the excited rovibronic level dependence of the fluorescence quantum yield.

The EP spectra of pyrazine are well reproduced by considering the resonance fluorescence emitted from the individual rotational levels optically excited and by employing a symmetric top approximation, though the fluorescence consists of the fast and slow components which correspond to the dephasing decay and the population decay, respectively. Further, there is no evidence in the EP spectra that there is a mode specificity in the S_1-T_1 dynamics between the S_1 origin and the $10a^1$ level.

The authors thank Professor Emeritus Hiroaki Baba for his continuous encouragement. This work was partly supported by a Grant-in-Aid for Scientific Research on Priority Areas from the Ministry of Education, Science and Culture (No. 63606004).

References

1) N. Ohta, O. Sekiguchi, and H. Baba, *J. Chem. Phys.*, **82**, 1609 (1985).
2) N. Ohta, O. Sekiguchi, and H. Baba, *Chem. Phys. Lett.*, **126**, 124 (1986); *J. Chem. Phys.*, **88**, 68 (1988).
3) G. M. Nathanson and G. M. McClelland, *J. Chem. Phys.*, **81**, 629 (1984); **84**, 3170 (1986).
4) M. Terazima and E. C. Lim, *J. Chem. Phys.*, **86**, 4471 (1987).
5) S. N. Thakur and K. K. Innes. *J. Mol. Spectrosc.*, **52**, 130 (1974).
6) J. L. Tomer, K. W. Holtzclaw, D. W. Pratt, and L. H. Spangler, *J. Chem. Phys.*, **88**, 1528 (1988).
7) I. Suzuka, N. Mikami, and M. Ito, *J. Mol. Spectrosc.*, **52**, 21 (1974)
8) Y. Udagawa, M. Ito, and I. Suzuka, *Chem. Phys.*, **46**, 237 (1980).
9) R. N. Zare, *Acc. Chem. Res.*, **4**, 361 (1971), and references therein.
10) P. C. Cross, R. M. Hainer, and G. W. King, *J. Chem. Phys.*, **12**, 210 (1944).
11) A. Frad, F. Lahmani, A. Tramer, and C. Tric, *J. Chem. Phys.*, **60**, 4419 (1974).
12) O. Sekiguchi, Ph. D. Thesis, Hokkaido University, Sapporo (1985).

The Crystal and Molecular Structure of 2:2 Complex of 1,1,6,6-Tetraphenyl-2,4-hexadiyne-1,6-diol (DD) with 1-Methyl-2-(3-pyridyl)pyrrolidine (Nicotine)

Ken-ichi FUKAWA, Shigeharu HARADA, Nobutami KASAI,* Mari TODA (née SEGAWA),†
Koji MORI,† and Fumio TODA*,†
Department of Applied Chemistry, Faculty of Engineering, Osaka University, Suita, Osaka 565
†Department of Industrial Chemistry, Faculty of Engineering, Ehime University, Matsuyama 790
(Received March 22, 1989)

Synopsis. X-Ray crystal structure analysis of the title complex is described. $2(C_{30}H_{22}O_2),2(C_{10}H_{14}N_2)$, *F.W.* 1153.5, monoclinic, space group $P2_1$, a=28.913(2), b=12.353(1), c=9.340(1) Å, β=98.20(1)°, V=3301.7(6) Å^3, D_c=1.16 g cm^{-3} for Z=2. Two DD molceules are bound by two nicotine by four O-H···N hydrogen bonds to form a 2:2 complex. The crystal consists of these asymmetric 2:2 complexes.

Host-guest complexation method has been applied for the isolation of natural products.[1] Among them is the isolation of nicotine from tobacco leaves. In order to obtain structural informations on the complexation the crystal structure of the title 2:2 complex has been determined by means of X-ray diffraction.

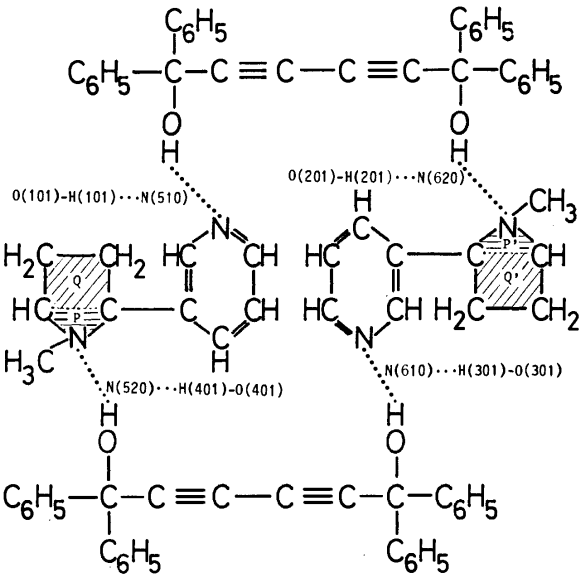

Experimental

A crystal with approximate dimensions of 0.5×0.3×0.2 mm was mounted on a goniometer head attached to a Rigaku rotating anode four-circle diffractometer at the Institute for Protein Research, Osaka University. Intensity data were collected using nickel filtered Cu $K\alpha$ radiation by the θ-2θ scan technique up to 2θ=120°. The scan rate was 12° min^{-1} and the scan width $\Delta\theta$=(1.2+0.15 tanθ)°. Backgrounds were counted for 3 s at both ends of a scan. Three standard reflections measured after every 100 reflections to monitor the stability and orientation of the crystal showed slight change through the experiment. Of the 5175 reflections measured, number of reflections observed is 4640 ($|F_o|>2\sigma(F_o)$), where σ is the standard deviation obtained from the counting statistics). Usual Lorentz and polarization corrections were applied but absorption effect was ignored [μ(Cu $K\alpha$)=5.64 cm^{-1}].

Structure Solution and Refinement

The structure was established by the direct method. First the *MULTAN* 78[2] program was used to solve the structure. It seemed that all the non-hydrogen atoms of DD molecules and several non-hydrogen atoms of

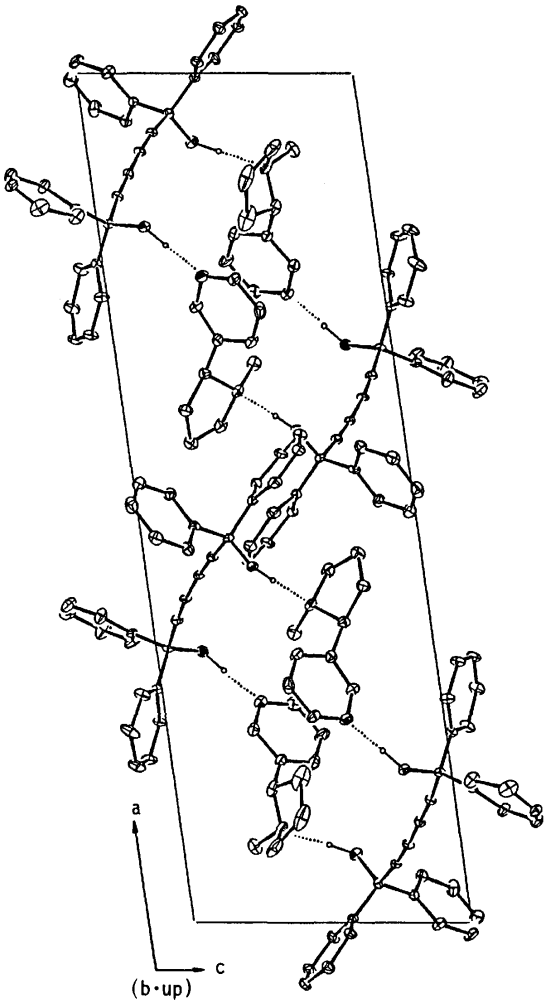

Fig. 1. Crystal structure projected along the b axis.[7] Non-hydrogen atoms are drawn as thermal ellipsoids with 10% probability level, and hydrogen atoms as spheres (B=1.0 Å). Hydrogen atoms not engaged in hydrogen bondings (shown by dotted lines) are omitted for clarity.

Table 1. Final Atomic Coordinates and Equivalent Isotropic Temperature Factors[5] for Non-Hydrogen Atoms with Estimated Standard Deviations in Parentheses

Atom	x	y	z	B_{eq}/Å^2	Atom	x	y	z	B_{eq}/Å^2
C(101)	0.8807(2)	0.1255(5)	0.1372(6)	4.3	C(313)	0.6360(3)	−0.4719(7)	1.3017(9)	7.8
C(102)	0.8551(2)	0.1982(4)	0.0881(6)	3.9	C(314)	0.6264(3)	−0.3659(9)	1.2939(10)	8.8
C(103)	0.8228(2)	0.2890(5)	0.0418(6)	4.1	C(315)	0.6397(3)	−0.3033(6)	1.1842(8)	7.0
C(104)	0.8412(2)	0.3619(5)	−0.0665(6)	4.2	O(301)	0.6809(2)	−0.3454(3)	0.8370(4)	5.1
C(105)	0.8668(3)	0.3197(6)	−0.1708(7)	6.3	C(401)	0.5910(2)	−0.0332(5)	0.8103(6)	4.2
C(106)	0.8787(3)	0.3865(7)	−0.2838(8)	7.1	C(402)	0.5696(2)	0.0414(4)	0.7536(6)	4.1
C(107)	0.8678(3)	0.4933(6)	−0.2861(7)	5.9	C(403)	0.5475(2)	0.1389(4)	0.6868(6)	3.8
C(108)	0.8420(4)	0.5299(7)	−0.1968(11)	10.4	C(404)	0.5340(2)	0.2137(5)	0.8026(6)	4.3
C(109)	0.8316(3)	0.4669(6)	−0.0696(9)	7.6	C(405)	0.4960(3)	0.1897(6)	0.8751(7)	6.1
C(110)	0.7754(2)	0.2438(5)	−0.0212(6)	4.1	C(406)	0.4839(3)	0.2526(9)	0.9802(8)	8.3
C(111)	0.7363(2)	0.3094(6)	−0.0211(8)	6.2	C(407)	0.5090(4)	0.3437(8)	1.0177(9)	8.5
C(112)	0.6926(2)	0.2716(7)	−0.0777(8)	6.4	C(408)	0.5473(3)	0.3751(7)	0.9462(8)	7.8
C(113)	0.6869(2)	0.1676(7)	−0.1365(8)	6.8	C(409)	0.5605(3)	0.3095(5)	0.8381(7)	6.2
C(114)	0.7240(3)	0.1079(6)	−0.1326(9)	7.0	C(410)	0.5034(2)	0.1120(5)	0.5790(6)	4.7
C(115)	0.7692(3)	0.1410(6)	−0.0796(8)	6.3	C(411)	0.4843(2)	0.0084(5)	0.5586(6)	5.0
O(101)	0.8193(2)	0.3555(3)	0.1671(4)	4.7	C(412)	0.4470(2)	−0.0088(7)	0.4523(8)	6.6
C(201)	0.9076(2)	0.0404(5)	0.1910(6)	4.2	C(413)	0.4250(3)	0.0644(9)	0.3758(8)	7.7
C(202)	0.9304(2)	−0.0345(5)	0.2442(6)	4.1	C(414)	0.4427(3)	0.1732(9)	0.3876(8)	8.5
C(203)	0.9530(2)	−0.1343(5)	0.3142(6)	4.5	C(415)	0.4823(3)	0.1975(6)	0.4905(8)	6.5
C(204)	0.9951(2)	−0.1045(5)	0.4272(5)	3.8	O(401)	0.5809(2)	0.1932(3)	0.6137(4)	4.3
C(205)	1.0169(2)	−0.1867(6)	0.5069(7)	5.6	C(510)	0.7254(3)	0.1999(6)	0.3148(8)	6.1
C(206)	1.0554(3)	−0.1666(6)	0.6087(7)	6.4	C(520)	0.6866(2)	0.1885(5)	0.3769(6)	5.2
C(207)	1.0720(2)	−0.0669(7)	0.6307(6)	6.4	C(530)	0.6846(3)	0.2539(7)	0.4978(8)	7.3
C(208)	1.0524(3)	0.0213(6)	0.5403(7)	6.2	C(540)	0.7205(4)	0.3168(8)	0.5433(8)	8.5
C(209)	1.0126(2)	−0.0040(5)	0.4430(6)	5.0	C(550)	0.7573(3)	0.3289(8)	0.4674(8)	7.5
C(210)	0.9666(2)	−0.2060(5)	0.1942(6)	4.7	C(560)	0.6466(3)	0.1137(6)	0.3123(7)	5.9
C(211)	0.9443(3)	−0.3022(5)	0.1568(7)	5.5	C(570)	0.6032(3)	0.1688(7)	0.2239(8)	7.1
C(212)	0.9589(4)	−0.3699(8)	0.0502(9)	8.4	C(580)	0.5654(3)	0.0832(8)	0.2272(8)	7.8
C(213)	0.9933(3)	−0.3423(8)	−0.0193(10)	8.6	C(590)	0.5855(3)	−0.0020(7)	0.3422(8)	7.4
C(214)	1.0137(3)	−0.2466(10)	0.0088(9)	8.8	C(500)	0.6582(3)	−0.0288(6)	0.4950(8)	7.0
C(215)	1.0014(3)	−0.1710(8)	0.1184(8)	7.4	N(510)	0.7606(2)	0.2670(6)	0.3514(7)	6.8
O(201)	0.9188(2)	−0.1897(3)	0.3840(4)	5.2	N(520)	0.6257(2)	0.0516(5)	0.4224(5)	5.3
C(301)	0.6190(2)	−0.1175(5)	0.8703(6)	4.0	C(610)	0.7733(3)	−0.1883(6)	0.6893(7)	6.3
C(302)	0.6441(2)	−0.1908(5)	0.9117(6)	4.8	C(620)	0.8088(3)	−0.1662(7)	0.6058(7)	6.3
C(303)	0.6768(2)	−0.2794(4)	0.9562(6)	3.7	C(630)	0.8109(3)	−0.2295(9)	0.4876(8)	8.3
C(304)	0.7259(2)	−0.2332(5)	1.0206(6)	4.2	C(640)	0.7794(3)	−0.3202(9)	0.4465(9)	9.2
C(305)	0.7318(3)	−0.1327(5)	1.0737(8)	6.3	C(650)	0.7424(3)	−0.3217(9)	0.5308(9)	8.9
C(306)	0.7753(3)	−0.0909(6)	1.1351(9)	9.2	C(660)	0.8415(3)	−0.0741(7)	0.6495(8)	7.5
C(307)	0.8152(3)	−0.1629(7)	1.1277(9)	8.3	C(670)	0.8294(6)	0.0257(8)	0.5429(13)	14.3
C(308)	0.8082(2)	−0.2635(9)	1.0802(9)	8.1	C(680)	0.8757(6)	0.0851(9)	0.5592(11)	14.8
C(309)	0.7639(2)	−0.2990(6)	1.0231(6)	5.5	C(690)	0.9112(4)	0.0135(10)	0.6712(11)	12.5
C(310)	0.6596(2)	−0.3473(4)	1.0783(6)	4.0	C(600)	0.9104(4)	−0.1713(10)	0.7434(9)	10.6
C(311)	0.6684(3)	−0.4593(6)	1.0811(9)	8.0	N(610)	0.7410(2)	−0.2663(6)	0.6513(6)	7.4
C(312)	0.6559(4)	−0.5212(6)	1.1826(9)	8.7	N(620)	0.8889(2)	−0.0944(6)	0.6370(6)	7.7

nicotine appeared on an E map, but the rest of non-hydrogen atoms of nicotine could not be located in spite of all possible efforts. The trial to solve the structure from the beginning by using the *SHELX-76*[3] program was successful. The structure was refined anisotropically by the least-squares procedure (*HBLS* V).[4] Hydrogen atoms except those of methyl groups were included in the refinements with isotropic temperature factors: R=0.063 for 4640 reflections ($|F_o|>2\sigma$). The function minimized in the refinement was $\sum w\Delta F^2$, and the weighting scheme used in the final stage of the refinement was $w=[\sigma^2(F_o)+0.01971|F_o|+0.00198|F_o|^2]^{-1}$. However, about one third of the hydrogen atoms could not be refined reasonably. All the hydrogen atoms refined were then relocated at the calculated positions, and the temperature factor of each hydrogen atom was assumed equal to the equivalent isotropic temperature factor of the non-hydrogen atom to which the hydrogen atom attached. Structure factor calculation gave the R value of 0.065. Atomic scattering factors used were taken from International Tables for X-Ray Crystallography.[6] Computations were done on an ACOS S930 computer at the Protein Engineering Center, Institute for Protein Research, Osaka University.

Final atomic parameters are given in Table 1.[††] Thermal parameters of atoms belong to the pyrrole ring of a nicotine molecule are fairly large. These might limit the accuracy of the result.

[††] Tables of anisotropic thermal parameters of non-hydrogen atoms, atomic parameters of hydrogen atoms, and observed and calculated structure factors are kept at the Chemical Society of Japan, Document No. 8890.

Results and Discussion

As seen in Fig. 1 the crystal is composed of a loose packing of 2:2 complex units of DD molecules with nicotine molecules. No close atomic contact less than 3.8 Å is observed between non-hydrogen atoms of adjacent complex units and also between those of pyridine rings of nicotine molecules in the complex unit.

The 2:2 complex has a sandwitch structure. The C-C≡C-C≡C-C backbone of each DD molecule bent inwardly in a small extent with the two hydroxyl groups inside and four phenyl groups outside. The two -C≡C- bond distances are 1.210(7) and 1.203(7) Å in one molecule and 1.190(7) and 1.191(7) Å in the other, whereas the central C-C distances in two molecules are 1.361(7) and 1.387(7) Å. All the bond angles on -C≡C-C≡C- linkages are slightly smaller than 180° [174.6(5), 177.2(6), 177.0(6), and 172.5(6)° in one molecule and 176.6(6), 174.9(6), 175.4(6), and 174.4(5)° in the other]. Two nicotine molecules are captured inside two DD molecules connected by four O-H···N hydrogen bonds. The nitrogen atom of the pyridine ring is bound to one of the hydroxyl groups of one DD by an approximately linear O-H···N hydrogen bond [O(101)···N(510)=2.806(7) and O(301)···N(610)=2.800 (8) Å]. The nitrogen atom of the pyrrole ring of the same nicotine molecule is also hydrogen bonded to the other hydroxyl group of the second DD [O(201)···N(620)=2.881(7) and O(401)···N(520)=2.930 (6) Å]. The pyrrole ring of nicotine takes an envelope form: the dihedral angle between planes defined by the nitrogen and two carbon atoms (Plane P or P′) and that made by the four carbon atoms(Plane Q or Q′) is 42.6(6) or 53.8(8)°. The pyridine ring and the Q plane (or Q′ plane) in the nicotine molecule makes approximately right angle [86.8(4) and 83.8(5)°]. Two pyridine rings of the different nicotine molecules are nearly parallel in the complex [dihedral angle: 7.9(3)°].

The present study was partially supported by a Grand-in-Aid for Scientific Research from the Ministry of Education, Science and Culture.

References

1) M. Segawa, K. Mori, and F. Toda, *Chem. Lett.*, **1988**, 1755.

2) P. Main, S. E. Hull, L. Lessinger, G. Germain, J. P. Declercq, and M. M. Woolfson, *MULTAN* 78, "A System Computer Programs for the Automatic Solution of Crystal Structures from X-Ray Diffraction Data," Univs. of York, England and Louvain, Belgium, 1978.

3) G. M. Sheldrick, *SHELX*-76, "Program for Crystal Structure Determination, Univ. of Cambridge, England, 1976.

4) T. Ashida, *HBLS* V, "The Universal Crystallographic Computing System-Osaka, The Computation Center, Osaka University, 1979.

5) W. C. Hamilton, *Acta Crystallogr.*, **12**, 609 (1959).

6) "International Tables for X-Ray Crystallography," Kynoch Press, Birmingham, England, 1974, Vol. IV, p. 71.

7) C. K. Johnson, *ORTEP* II, Report ORNL-5138, Oak Ridge National Laboratory, Tennessee, 1976.

Cobalt(III) Complexes with Quadridentate Ligands. IX.[1] High-Resolution Solid-State ^{13}C CP/MAS NMR Spectra of the Salicylato-, Carbonato-, Dichloro-, and Dinitro(quadridentate amine)-cobalt(III) Complexes

Yoshihisa YAMAMOTO,* Eiko TOYOTA, and Shigezo SHIMOKAWA†
Faculty of Pharmaceutical Sciences, Higashi Nippon Gakuen University, Ishikari-Tobetsu, Hokkaido 061-02
†NMR Laboratory, Faculty of Engineering, Hokkaido University, Sapporo 060
(Received November 2, 1988)

Synopsis. High-resolution solid-state ^{13}C CP/MAS NMR was applied to many cobalt(III) complexes, such as salicylato-, carbonato-, dichloro-, and dinitro(quadridentate amine)cobalt(III) complexes, $[CoL_2(\text{quadridentate amine})]^+$ (L: 1/2sal, $1/2CO_3$ Cl, NO_2; quadridentate amine: tren, trien, 2,3,2-tet, 3,2,3-tet, 3,3,3-tet). The signals of the methylene carbons of the coordinated quadridentate amine ligands in their complexes have been assigned to the center, NH_2- side, NH- side, and N- side methylene carbons. Also, the signals of the ring carbons of the coordinated salicylato ligand in their complexes have been assigned to the individual carbon atoms. It has been found that the signals of nonprotonated carbons (C-1, C-2, and C-7) of the coordinated salicylato ligand have been very high and that the ^{13}C CP/MAS NMR method is well-suited for studies of unstable compounds in solutions.

In the last decade, the high-resolution solid-state ^{13}C CP/MAS NMR method has been extensively applied to various organic materials.[2] This method has been proven to give very usuful information about the molecular structure and conformation of organic compounds,[3] the molecular motion of polymers,[4] and the rate processes in solids.[5] However, this method has not yet been adequately applied to the field of metal complexes. The present paper deals with the assignments of the ^{13}C NMR signals of the quadridentate amine and the ring carbons of the salicylato of $[CoL_2(\text{quadridentate amine})]^+$ (L: 1/2sal, $1/2CO_3$, Cl, NO_2; quadridentate amine: tren, trien, 2,3,2-tet, 3,2,3-tet, 3,3,3-tet) and deals with the application of the ^{13}C CP/MAS NMR method.

Experimental

Measurements. The ^{13}C CP/MAS NMR measurements were performed on a Bruker MSL high-power spectrometer operating at a field strength of 4.7 T, equipped with a double bearing (DB-MAS) and a variable-temperature probe unit. The resonance frequency was 50.323 MHz. A contact time of 2 ms was chosen, and the repetition time was 5 s. The 90° pulse width was typically 4 us for both ^{13}C and ^{1}H under cross-polarization conditions. The spectral width and data points were 30 kHz and 8 K points respectively. The spectra were usually obtained by the accumulation of from 300 to 500 FIDs, thus achieving a resonable signal-to-noise ratio for natural abundance samples. The ^{13}C chemical shifts were calibrated indirectly through external glycine-CO (δ=176.03; line width=15 Hz) relative to tetramethylsilane. The experimental errors of the ^{13}C chemical shift values were estimated to be within ±0.2 ppm. The alumina rotor with samples was spun at a rate of from 2500 to 3500 Hz with compressed dry air. Samples of ca. 150—250 mg were packed in the rotor. The ^{13}C NMR spectra in solutions were recorded with an FX-60 spectrometer (JEOL).

Preparation of Complexes. The $[Co(CO_3)(tren)]Cl \cdot 1.5H_2O$ (**1**), $[CoCl_2(tren)]Cl \cdot H_2O$ (**6**), $[Co(NO_2)_2(tren)]Cl$ (**11**), *cis*-α-$[Co(CO_3)(trien)]ClO_4 \cdot H_2O$ (**2**), *cis*-β-$[Co(CO_3)(trien)]Cl \cdot 1.5H_2O$ (**3**), *cis*-α-$[CoCl_2(trien)]Cl$ (**7**), *cis*-β-$[CoCl_2(trien)]Cl \cdot 0.5H_2O$ (**8**), *cis*-α-$[Co(NO_2)_2(trien)]Cl \cdot H_2O$ (**12**), *cis*-β-$[Co(NO_2)_2(trien)]NO_3$ (**13**), *cis*-β-$[Co(CO_3)(2,3,2\text{-tet})]Cl$ (**4**), *trans*-$[CoCl_2(2,3,2\text{-tet})]Cl \cdot 2.5H_2O$ (**9**), *cis*-β-$[Co(CO_3)(3,2,3\text{-tet})]Cl \cdot 3H_2O$ (**5**), and *trans*-$[CoCl_2(3,2,3\text{-tet})]Cl \cdot H_2O$ (**10**) were prepared according to previously published procedures.[6]

The *t*-$[Co(sal)(tren)]Cl \cdot H_2O$ (**14**), *p*-$[Co(sal)(tren)]Cl \cdot H_2O$ (**15**), *cis*-β_1-$[Co(sal)(trien)]Cl \cdot H_2O$ (**16**), *cis*-β_2-$[Co(sal)(trien)]Cl \cdot H_2O$ (**17**), *cis*-β_1-$[Co(sal)(2,3,2\text{-tet})]Cl \cdot H_2O$ (**18**), *cis*-β_2-$[Co(sal)(2,3,2\text{-tet})]Cl \cdot 2H_2O$ (**19**), *cis*-β_2-$[Co(sal)(3,2,3\text{-tet})]Cl \cdot 3H_2O$ (**20**), and *cis*-β_2-$[Co(sal)(3,3,3\text{-tet})]Cl \cdot H_2O$ (**21**) were also prepared according to previously published procedures.[7]

Abbreviations: tren: tris(2-aminoethyl)amine; trien: triethylenetetramine; 2,3,2-tet: 3,7-diazanonane-1,9-diamine; 3,2,3-tet: 4,7-diazadecane-1,10-diamine; 3,3,3-tet: 4,8-diazaundecane-1,11-diamine.

Results and Discussion

The coordinated quadridentate amine ligands of **1—3** exhibit the two ^{13}C CP/MAS NMR signals of the methylene carbons at δ=42—47 and 53—58, as is shown in Fig. 1. The signals at δ=42.2 and 56.3 of **1** have been assigned to the NH_2- side ($NH_2\mathbf{C}H_2\mathbf{C}H_2N$-) and N- side methylene carbons ($NH_2\mathbf{C}H_2\mathbf{C}H_2N$-) respectively of the coordinated tren ligand. The signals at δ=43—47 and 53—58 of **2** and **3** have been assigned to the NH_2- side and NH- side methylene carbons ($NH_2\mathbf{C}H_2\mathbf{C}H_2NH\mathbf{C}H_2$-) respectively. The signal of the NH_2- side methylene carbons of **2** is different from that of **3**; i.e., it is due to the configurations of cis-α and cis-β. The complexes **4** and **5** exhibit three signals of the methylene carbon at δ=22—29, 39—46, and 49—58. The signals at δ=39—46 and 49—58 were assigned to the NH_2- side and NH- side methylene carbons respectively by comparison with those of **1—3**. Accordingly, the signals at δ=22—29 are assigned to the center methylene carbons ($NH_n\mathbf{C}H_2\mathbf{C}H_2\mathbf{C}H_2NH$-, *n*: 1 or 2) of the coordinated quadridentate amine ligands. The signals of **3—5** are difficult to assign to the individual carbon atoms. However, the signals at δ=49.9 of **4** and at δ=49.8 of **5** are assigned to C-4 and C-6, and C-3 and C-7, methylene carbons[7c] respectively, because their methylene carbons are neighboring carbons of the center methylene carbons of C-2, C-5, or C-8. The signals at δ=

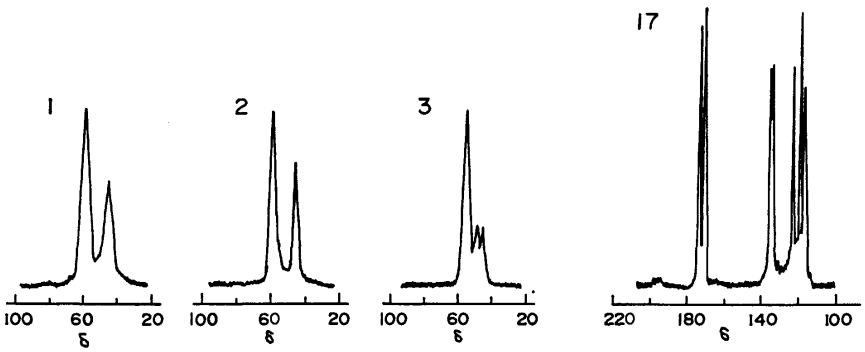

Fig. 1. The ^{13}C CP/MAS NMR spectra of complexes **1**—**3** and **17**.
1: $[Co(CO_3)tren]Cl \cdot H_2O$. **2**: *cis*-α-$[Co(Co(CO_3)trien]ClO_4 \cdot H_2O$.
3: *cis*-β-$[Co(CO_3)trien]Cl$. **17**: *cis*-β_2-$[Co(sal)trien]Cl \cdot H_2O$.

Table 1. ^{13}C CP/MAS NMR Spectra of **1**—**21**, and ^{13}C NMR Spectra of **1**, **3**—**6**, and **9**—**13** in D_2O

Complex No.	Center carbons δ	NH_2- side carbons δ	NH- (or N-) side carbons δ				CO_3 δ	Salicylato δ						
			C-3,	C-7	C-4,	C-6		C-1	C-2	C-3	C-4	C-5	C-6	C-7
1		42.2		(56.3)			170.4							
2		43.8		57.4			166.5							
3		44.1 46.7		53.7			167.1							
4	23.5	42.7	57.2		49.9		167.7							
5	22.9 28.9	39.8 45.1	49.8		53.8		166.7							
6		47.2		(64.1)										
7		45.7		55.9										
8		43.1 48.3		53.2										
9	29.3	45.5	55.4		49.9									
10	27.7	39.8	48.6		54.5									
11		46.2		(59.2 62.0)										
12		44.0		[54.5 58.2 59.2 60.5]										
13		43.7 48.5		[51.7 53.0]										
14		45.8		(60.9)				120.5	169.8	117.2	134.3	126.1	134.3	172.4
15		44.4		(60.1)				114.8	168.9	114.8	133.1	125.0	133.1	171.2
16		43.2[a]		51.6[a]				117.4	168.4	117.4	133.4	121.6	133.4	172.9
17		40.6[a]		52.2[a]				118.4	167.0	116.3	134.9	122.7	133.8	172.6
18	23.6	43.6[a]		50.5[a]				116.0	169.9	114.3	132.0	124.6	132.0	171.2
19	21.6	45.5[a]		52.1[a]				121.3	168.7	116.9	132.7	123.7	132.7	172.9
20	20.8 27.8	44.6[a]		47.6[a]				118.0	167.5	114.9	135.5	123.0	132.1	171.5
21	23.5	37.4[a]		48.2[a]				116.2	167.9	116.2	123.7	123.4	132.7	170.6
1		42.9		(53.5 55.8)			172.7							
3		42.4 47.4	[50.9 51.4		52.6 52.9]		167.4							
4	23.7	43.3 44.0	[47.2 50.4		50.9 56.0]		168.9							
5	22.2 27.0	39.7 40.1	[46.7 48.7		50.5 54.4]		168.0							
6		45.4 46.6		(61.2 63.0)										
9	28.8	43.3	55.6		49.1									
10	27.7	39.8	49.4		53.3									
11		45.2		(61.0 63.1)										
12		42.6		[55.5 57.5]										
13		42.9 47.0	[50.7 51.5		53.1 53.7]									

quadridentate amine

Standards: Glycine δ=42.9 and 43.8 for CH_2, δ=176.03 for ^{13}CO for solid-states; internal dioxane (δ=67.4) for solutions.
[ ]: The chemical shifts could not be assigned to the individual methylene carbon. a) Broad signal.

166—171 of **1**—**5** have been assigned to the coordinated carbonato carbons. The signals of the center, NH_2- side, NH- side, and N- side methylene carbons of the coordinated quadridentate amine ligands in **6**—**13** were assigned by comparison with those of **1**—**5**; these results are collected in Table 1. The signals at δ=20—28, ca. 37—46, ca. 47—53, and 60—61 of **14**—**21** were assigned to the center, NH_2- side, NH- side, and N- side methylene carbons of the coordinated quadridentate amine ligands respectively

by comparison with those of **1**—**13**. The salicylato carbon signals in the regions at δ=114—173 of the coordinated salicylato ligand have been assigned to the individual carbon atoms by comparison with those of **14**—**17**[7a,b] in solution; these results are collected in Table 1.

The chemical shifts of the center, NH_2- side, NH- side, and N- side methylene carbons of the coordinated quadridentate amine ligands of **1**—**13** are almost the same as those of **14**—**21**, and their chemical shifts are close to those in solutions, as is shown in Table 1 and Ref. 7. The methylene carbon signals can be affected by the electronic effect, the steric effect, the coordination number, or the configuration of the coordinated ligands in complexes; e.g., the NH_2- side and N- side methylene carbon signals of **1** appear at a higher field than those of **6** and **11**. The NH- side methylene carbon signals of **12** and **13** are very different from those of Complexes **2** and **3** and Complexes **7** and **8**. Also, the spectrum of **3** is different from that of **2**.

A difference between the ^{13}C CP/MAS NMR method and the ^{13}C NMR method was found in the signals of nonprotonated carbon and the measurements of unstable compounds in solutions: the signals of the C-1, C-2, and C-7 carbons (nonprotonated carbons) of the coordinated salicylato ligand have been very high, such as C-3, C-4, C-5, and C-6 carbons (protonated carbons), as is shown in Fig. 1. The ^{13}CNMR spectra of **2**, **7**, and **8** did not show the expected signals in solution, since they were changed to other species;[6b] e.g., the spectrum of **7** in solution is in agreement with that of $[Co(H_2O)_2(trien)]^{3+}$ (**22**). Also, the spectrum of **18**[7c] has not showed the expected signals, because **18** isomerizes to **19** in solution.

References

1) Part. VIII: Y. Yamamoto, K. Yoshii, E. Toyota, and K. Konno, *Bull. Chem. Soc. Jpn.*, **62**, 724 (1989).

2) M. Mehring, "Principles of High-resolution NMR in Solids," 2nd ed., Spinger-Verlag, Berlin (1983).

3) a) D. L. VanderHart, W. Earl, and A. N. Garroway, *J. Magn. Reson.*, **44**, 361 (1981); b) D. K. Dalling, K. W. Zilm, D. M. Grant, W. A. Heeschen, W. J. Horton, and R. J. Pugmire, *J. Am. Chem. Soc.*, **103**, 4817 (1981).

4) a) J. Schaefer, E. O. Stejskal, and R. Buchadahl, *Macromolecules*, **10**, 384 (1977); b) P. Caravatti, P. Neuenschwander, and R. R. Ernst, *Macromolecules*, **19**, 1889 (1986).

5) C. S. Yannoni, V. Macho, and P. C. Myhre, *J. Am. Chem. Soc.*, **104**, 907 (1982).

6) a) E. Kimura, S. Young, and J. P. Collman, *Inorg. Chem.*, **9**, 1183 (1970); b) A. M. Sargeson and G. H. Searle, *ibid.*, **6**, 787 (1967); c) B. Bosnich, R. D. Gillard, E. D. Mckenzie, and G. A. Webb, *J. Chem. Soc. A*, **1966**, 1331; d) B. Bosnich, J. M. Harrowfield, and H. Boucher, *Inorg. Chem.*, **14**, 815 (1975).

7) a) E. Toyota, Y. Yamamoto, and Y. Yamamoto, *Bull. Chem. Soc. Jpn.*, **61**, 3175 (1988); b) Y. Yamamoto and E. Toyota, *ibid.*, **52**, 2540 (1979); c) Y. Yamamoto, H. Kudo, and E. Toyota, *ibid.*, **56**, 1051 (1983).

The Resonance Raman Study on the Visible Absorption Spectrum of Tris(dithiooxalato-*S,S*)cobaltate(III)

Kan KANAMORI,* Akiko ONO, Sonomi INO, Isao KANESAKA, Kiyoyasu KAWAI, and Jinsai HIDAKA†
Faculty of Science, Department of Chemistry, Toyama University, Gofuku, Toyama 930
†Department of Chemistry, University of Tsukuba, Tsukuba, Ibaraki 305
(Received January 13, 1989)

Synopsis. The Raman bands due to the totally symmetric ν(C-C)+ν(C-S) and ν(Co-S) modes of tris(dithiooxalato-*S,S*)cobaltate(III) exhibit resonance enhancements with excitation lines in the visible region. The resonance Raman excitation profiles of the two modes reveal the presence of a charge-transfer transition in the visible absorption spectrum of the complex.

The electronic structure of a transition metal complex with dithiooxalate (dto^{2-}: $C_2S_2O_2^{2-}$) has been a subject of interest because of the considerably delocalized π-orbital system of the ligand. The electronic spectral properties of planar divalent metal complexes with dto^{2-} were studied in several ways. For example, Kida et al.[1] reported the electronic absorption spectra of $[M(dto)_2]^{2-}$ (M=Ni(II), Pd(II), and Pt(II)). Latham et al. assigned the electronic absorption bands of the above-mentioned complexes on the basis of a molecular orbital treatment.[2] The visible absorption feature of $[Ni^{II}(dto)_2]^{2-}$ was investigated in detail by the use of Raman excitation profiles.[3] For octahedral trivalent metal complexes with dto^{2-}, Carlin and Canziani[4] investigated the visible absorption spectra of $[M(dto)_3]^{3-}$ (M=Cr(III), Co(III), and Fe(III)) and Hidaka and Douglas[5] discussed the circular dichroism spectra of $[M(dto)_3]^{3-}$ (M=Cr(III), Co(III), and Rh(III)). Two shoulders at 17000 and 21800 cm^{-1} of $[Co^{III}(dto)_3]^{3-}$ were assigned to the d-d transitions.[4,5] However, the absorption coefficient ($\log\varepsilon$=3.5) of the 21800-cm^{-1} band seems to be large for a Laporte-forbidden d-d transition, even if the d-d transitions are allowed to occur, to some extent, by orbital mixing (covalency) between the sulfur donor and cobalt(III). Here, we report the resonance Raman excitation profiles of $[Co^{III}(dto\text{-}S,S)_3]^{3-}$ as well as the property of absorption bands in the visible region. The application of the resonance Raman effect to the electronic absorption spectral study of transition metal complexes has been reviewed.[6]

Experimental

Preparation of Complexes. $CaK[Co^{III}(dto\text{-}S,S)_3]\cdot 6H_2O$ was prepared according to a method described in the literature[7] and was identified by its electronic absorption spectrum.

Measurements. Samples for Raman measurements were provided as disks containing an appropriate amount of K_2SO_4 (8 to 12 times of the complex in weight) as an intensity standard. Disks were spun in order to avoid thermal decomposition. Raman spectra were recorded on a JASCO R-800 laser Raman spectrophotometer using a Spectra Physics 164 Ar^+ laser (514.5, 501.7, 496.5, 488.0, 476.5, 465.8, and 457.9 nm) and a Coherent Radiation model CR599 dye laser employing Rhodamine 6G dye (632.8, 610.0, 588.0, and 567.8 nm). The laser power was below 100 mW. The spectral band width was set to 5 cm^{-1}. Intensity measurements were made relative to the totally symmetric S-O stretching of the sulfate incorpolated in the sample. Corrections of the observed intensity were applied to the fourth power of the wavenumber of scattered radiation and the instrumental response. Intensities were averaged over more than three measurements.

Electronic absorption spectra were measured with a Hitachi 220 spectrophotometer.

Results and Discussion

Figure 1 shows the resonance Raman spectrum of $CaK[Co^{III}(dto\text{-}S,S)_3]$. The band at 1113 cm^{-1} can be assigned to the ν(C-C)+ν(C-S) mode and the band at 349 cm^{-1} to the ν(Co-S) mode in comparison with the

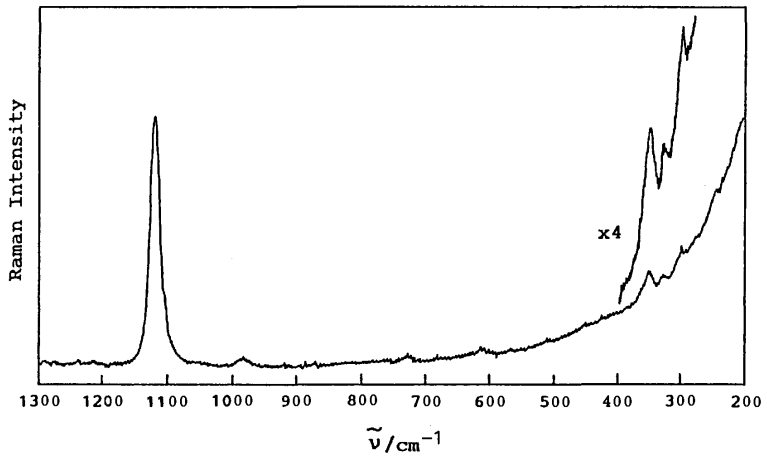

Fig. 1. Resonance Raman spectrum of $CaK[Co^{III}(dto\text{-}S,S)_3]$ (KBr disk, 488.0-nm excitation).

results of the normal coordinate analysis of $[Ni(dto\text{-}S,S)_2]^{2-}$,[3] where the ν(C-C)+ν(C-S) and ν_s(Ni-S) modes were assigned to the bands at 1085 and 317 cm^{-1}, respectively. The 1113-cm^{-1} band of $[Co^{III}(dto\text{-}S,S)_3]^{3-}$ is polarized in the solution Raman spectrum and can be assigned to the totally symmetric mode. The depolarization ratio of the 349-cm^{-1} band could not be determined precisely because of difficulty in observing the band of appropriate intensity in solution. This band, however, is the most intense band observed in the Co-S stretching region, and is reasonably assigned to the totally symmetric mode, since a totally symmetric metal-ligand stretching mode generally gives a far more intense Raman band than that of a non-totally symmetric mode as has been observed for the tris(chelate) complexes, $[Co^{III}(en)_3]^{3+}$ and $[Co^{III}(tn)_3]^{3+}$.[8]

Figure 2-A shows the visible absorption spectrum of $[Co^{III}(dto\text{-}S,S)_3]^{3-}$. The broad and unusually intense spectrum indicates that the d-d and charge-transfer transitions overlap each other. Low-energy metal-to-ligand charge-transfer transitions occur with high probability for complexes with dto^{2-} which have a low-energy π^*-orbital.[2]

Resonance Raman excitation profiles (that is, Raman intensities as a function of the excitation wavelength) have been successfully applied[3,9-13] to resolve overlapping absorption bands, especially those consisting of different types of transitions, such as d-d and charge-transfer transitions. This is because of the following features of resonance enhancements: (1) Excitation profiles are highly structured compared with electronic absorption spectra. (2) The extent of resonance enhancement greatly depends on the nature of resonant transitions. Resonance enhancement

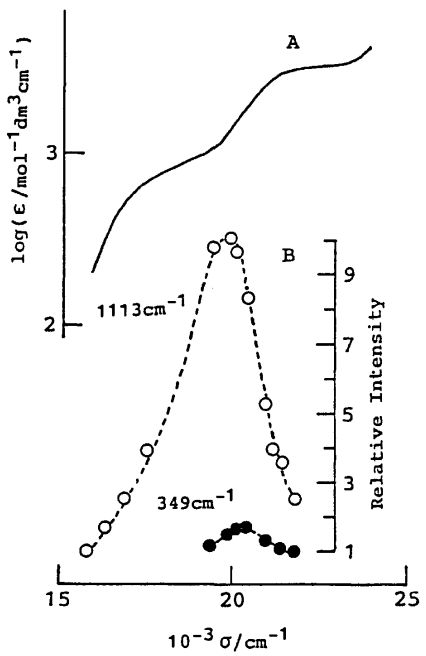

Fig. 2. A: Electronic absorption spectrum of $[Co^{III}(dto)_3]^{3-}$. B: Excitation profiles of the totally symmetric ν(C-C)+ν(C-S) and ν(Co-S). The weakest intensity was normalized to unity.

through an "A-type" interaction,[14] which concerns a single excited state, could hardly be expected within a Laporte-forbidden d-d transition.[15]

The strong resonance-enhancement was observed for the totally symmetric intra-ligand mode, ν(C-C)+ν(C-S), while the weak enhancement was observed for the totally symmetric metal-ligand mode, ν(Co-S).[16] The resonance-enhancement was not observed for the bands due to the non-totally symmetric modes. This observation indicates that the resonance-enhancement found in the present complex is the "A-type" which causes an intensity enhancement for the totally symmetric mode, but not for the non-totally symmetric mode. Therefore, the resonant transition must be a purely allowed transition, namely a charge-transfer transition. Figure 2-B illustrates the excitation profiles of the totally symmetric ν(C-C)+ν(C-S) and ν(Co-S) modes. The excitation profiles for both modes maximize at ca. 20000 cm^{-1}. This fact reveals that a charge-tansfer transition is situated at ca. 20000 cm^{-1} and overlaps with the two d-d transitions.

Coucouvanis and Piltingstrud[17] studied the absorption spectra of polynuclear complexes of the $[M(Ph_3P)_2]_3[M'(dto)_3]$-type (M=Cu(I), Ag(I); M'= Co(III), Al(III), Rh(III), and Cr(III)). They presumed that the band at ca. 20000 cm^{-1} of $[Co^{III}(dto)_3]^{3-}$ is due to a charge-transfer transition on the basis of the spectral change caused by the formation of an adduct with $[Cu^{I}(Ph_3P)_2]^{+}$. The present result is consistent with their suggestion.

References

1) S. Kida, K. Nakamoto, and R. Tsuchida, *Nippon Kagaku Zasshi*, **72**, 749 (1951).
2) A. R. Latham, C. V. Hascall, and H. B. Gray, *Inorg. Chem.*, **4**, 788 (1965).
3) R. S. Czernuszewicz, K. Nakamoto, and D. P. Strommen, *J. Am. Chem. Soc.*, **104**, 1515 (1982).
4) R. L. Carlin and F. Canzianni, *J. Chem. Phys.*, **40**, 371 (1964).
5) J. Hidaka and B. E. Douglas, *Inorg. Chem.*, **3**, 1724 (1964).
6) R. J. H. Clark, *Adv. Infrared Raman Spectrosc.*, **1**, 143 (1975).
7) F. P. Dwyer and A. M. Sargeson, *J. Am. Chem. Soc.*, **81**, 2335 (1959).
8) T. Kawamoto, H. Einaga, and J. Hidaka, *Bull. Chem. Soc. Jpn.*, **60**, 919 (1987).
9) B. P. Gaber, V. Miskowski, and T. G. Spiro, *J. Am. Chem. Soc.*, **96**, 6868 (1974).
10) R. J. H. Clark, P. C. Turtle, D. P. Strommen, B. Streusand, J. Kincaid, and K. Nakamoto, *Inorg. Chem.*, **16**, 84 (1977).
11) R. J. H. Clark and P. C. Turtle, *Inorg. Chem.*, **17**, 2526 (1978).
12) J. R. Campbell, R. J. H. Clark, and P. C. Turtle, *Inorg. Chem.*, **17**, 3622 (1978).
13) R. J. H. Clark, T. J. Dines, and M. Kurmoo, *Inorg. Chem.*, **22**, 2766 (1983).
14) A. C. Albrecht, *J. Phys. Chem.*, **34**, 1476 (1961).
15) Resonance enhancement of totally and non-totally symmetric modes was observed within the d-d absorption bands of nitrocobalt(III) complexes. This phenomenon was interpreted as a result of "B-type" interaction that concerns two excited states, namely the partly allowed d-d

and charge-transfer states. K. Kanamori, A. Shimizu, H. Sekino, S. Hayakawa, Y. Seki, and K. Kawai, *J. Chem. Soc., Dalton Trans.*, **1988**, 1827.

16) This is similar to the case of $[Fe^{II}(bpy)_3]^{2+}$ and $[Fe^{II}(phen)_3]^{2+}$ complexes of which the electronic configuration is same as that of the present complex (low spin d^6) and the visible absorption arises from a metal-to-ligand charge-transfer transition. Ref. 9.

17) D. Coucouvanis and D. Piltingstrud, *J. Am. Chem. Soc.*, **95**, 5556 (1973).

Amorphous and Crystalline Peroxopolytungstic Acids Formed from Tungsten and Hydrogen Peroxide

Hiroshi OKAMOTO,*,† Akira ISHIKAWA, and Tetsuichi KUDO††
Central Research Laboratory, Hitachi, Ltd., P. O. Box 2, Kokubunji, Tokyo 185
(Received March 15, 1989)

Synopsis. Peroxopolytungstic acids, $WO_3 \cdot xH_2O_2 \cdot yH_2O$ ($0 \leqq x \leqq 1$), formed directly from tungsten and hydrogen peroxide are found to be crystalline or amorphous depending on x.

A tungsten powder dissolves vigorously in a hydrogen peroxide (H_2O_2) aqueous solution.[1,2] A systematic study on the products obtained from the aqueous solution with various peroxide ion (O_2^{2-}) to W molar ratio showed that an amorphous or crystalline solid of peroxopolytungstic acids could be obtained depending on the molar ratio. This note presents the synthesis for and some characteristics of various peroxopolytungstic acids formed directly from W and H_2O_2.

After W was dissolved in an H_2O_2 solution, the H_2O_2 in the solution was catalytically decomposed stepwise with a platinized platinum net, then the solution was dried under blown air at room temperature to leave solids. The peroxo content in the solids obtained by this way was related to the H_2O_2 concentration in the solution just before drying, as shown in Fig. 1. Here, the H_2O_2 and W concentrations in the original solutions were varied as shown in the figure legend. The H_2O_2 concentration in solutions and peroxo content in solids were determined by a titration using a $KMnO_4$ solution.

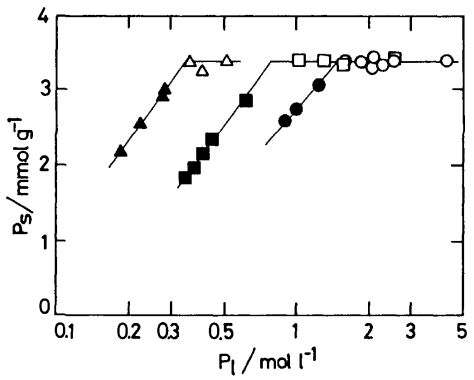

Fig. 1. Formation conditions for IPA and XW.
P_I: H_2O_2 concentration in the solution just before drying, P_s: Peroxo content in the obtained solids. Open symbols stand for XW and closed symbols for IPA. H_2O_2 and W concentrations in the starting solutions are 10 and 1.45 mol l^{-1} for circles, 5 and 0.79 mol l^{-1} for rectangles, and 1.7 and 0.35 mol l^{-1} for triangles.

† Present address: Advanced Research Laboratory, Hitachi, Ltd., P. O. Box 2, Kokubunji, Tokyo 185.
†† Present address: Institute of Industrial Science, University of Tokyo, 22-1 Roppongi 7 chome Minato-ku, Tokyo 106.

Despite decrease in the H_2O_2 concentration in the solution down to some value, the peroxo content for the solids remained constant at 3.39 ± 0.07 mmol g^{-1}. The solids were crystalline, which was confirmed by XRD. Some d-values are shown in Table 1. The crystal, XW, was insoluble in water or in an H_2O_2 solution. As H_2O_2 decomposition proceeded to pass through the point where a peroxide ion to tungsten molar ratio in the solution was approximately 1, an amorphous substance, IPA, was given instead of XW. A further decrease in H_2O_2 concentration in the solution allowed precipitation to take place, which is not shown in Fig. 1. The precipitate was amorphous. When the peroxo content in solid was decreased to 0, crystalline H_4WO_5 ($WO_3 \cdot 2H_2O$) was obtained.

To determine the composition for the solids, a thermal weight change was measured using TGA. The XW exhibited two discrete weight loss steps and finally changed to WO_3 at 398 °C. The first weight loss at approximately 110 °C caused XW to turn into another crystal, which we call XW′. Some d-values are shown in Table 1. The second weight loss at approximately 200 °C changed XW′ to an amorphous substance. On the the other hand, IPA showed indistinct weight loss steps and changed to WO_3 at 428 °C.

The peroxo content and the thermal weight change between rt and 500 °C gave the experimental formula as $WO_3 \cdot xH_2O_2 \cdot yH_2O$. It was found that XW had a maximum value of x, 0.97 ± 0.03, and a minimum value of y, 1.1 ± 0.1. Therefore, the formula for XW is thought to be basically $WO_3 \cdot H_2O_2 \cdot H_2O$. When $1 > x > 0$, $1.5 < y < 3.0$ and the peroxopolytungstic acids were amorphous IPA. The IPA with $1 > x \gtrsim 0.53$ was water-soluble, while the IPA with $0.53 \gtrsim x > 0$ was insoluble. For the extreme case of $x = 0$, the substance was $WO_3 \cdot 2H_2O$, as previously mentioned. Therefore, it follows that the substances formed directly from W and H_2O_2 are crystalline only for $x = 1$ or 0, while for $1 > x > 0$ they are amorphous, and phase sepa-

Table 1. Some XRD Lines for XW and XW′

XW		XW′	
d/pm	I/I_0	d/pm	I/I_0
902	27	682	16
610	82	588	46
548	18	559	100
472	27	381	13
448	3	467	18
393	8	340	50
365	41	315	28
359	28	309	31
322	100	294	4
307	55	279	10

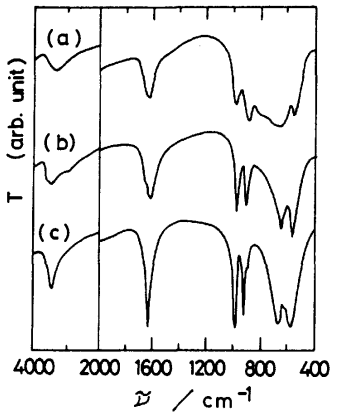

Fig. 2. Infrared spectra for IPA, XW, and XW'. (a) IPA, (b) XW, and (c) XW'.

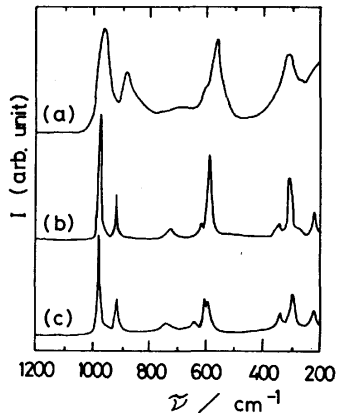

Fig. 3. Raman spectra for IPA, XW, and XW'. (a) IPA, (b) XW, and (c) XW'.

ration does not occur. The only water-soluble peroxopolytungstic acids are the IPA with $1>x\gtrsim0.53$.

A similar compositional analysis for XW', led to the formula for XW' being $WO_3 \cdot 0.94H_2O_2 \cdot 0.14H_2O$. However, the thermal changes from XW to XW' and from XW' to the amorphous substance were found to be time-dependent. Actually, the peroxo content for XW' decreased gradually with heating time and/or temperature increases. Therefore, an intermediate phase of XW' might have been mixed with some amorphous substance and XW fragments. Accordingly, the formula for XW' is supposed to be basically $WO_3 \cdot H_2O_2$.

Infrared and Raman spectra for IPA, XW, and XW' were very similar, as shown in Figs. 2 and 3, except for band sharpening and a small wavenumber shifting in the latter two. Although these small differences reflect differences in fine structures, the basic structure of IPA, XW, and XW' is concluded to be quite similar. Until now, all known coordination structures around W in peroxo containing polytungstic acid salts with a peroxo to W molar ratio=1, are octahedral with one corner of the octahedron at the center of the peroxo bond.[3,4] Therefore, IPA, XW, and XW' are supposed to have the same WO_7 pseudo-octahedral structure. By reference to the vibrational analyses[5,6] for $[Mo_6O_{19}]^{2-}$ and the Keggin structure such as $[SiW_{12}O_{40}]^{2-}$, IPA, XW, and XW' are considered to have both edge-shared and corner-shared pseudo-octahedral structures.

References

1) T. Kudo, H. Okamoto, K. Matsumoto, and Y. Sasaki, *Inorg. Chim. Acta*, **111**, L27 (1986).
2) A. Lottermoser, *Z. Elektrochem.*, **35**, 610 (1929).
3) Z. R.-Toros and B. K.-Prodic, *Acta Crystallogr., Sect. B*, **33**, 692 (1977).
4) R. Stomberg, *Acta Chem. Scand., Ser. A*, **39**, 507 (1985).
5) C. R.-Deltcheff, R. Thouvenot, and M. Fouassier, *Inorg. Chem.*, **21**, 30 (1982).
6) C. R.-Deltcheff, M. Fournier, R. Frank, and R. Thouvenot, *Inorg. Chem.*, **22**, 207 (1983).

The Regioselective Side-Chain Lithiation of 2-Methyl-3-thiophenecarboxylic Acid

Su HUI-WEN, Kazuo HIROSE, Kozo SHIRAI, and Takanobu KUMAMOTO*
Department of Chemistry, Faculty of Science, Tokai University,
Kitakaname, Hiratsuka, Kanagawa 259-12
(Received November 29, 1988)

Synopsis. It was found that the dilithium salt (**5**), which was lithiated at the side-chain of 2-methyl-3-thiophenecarboxylic acid (**4**), was produced regioselectively by the reaction of **4** with lithium diisopropylamide (LDA). The reactions of **5** with alkyl halides resulted in the formation of 2-alkyl-3-thiophenecarboxylic acids (**7**). Further, δ-lactone derivatives (**11**) were obtained by the cyclization of the adducts (**10**) which were produced from **5** with aldehydes and ketones.

The side-chain metalation of thiophene derivatives has attracted considerable attention[1a-c] in terms of its usefulness for the synthesis of many types of the thiophene derivatives. However, the selectivity of the side-chain metalation of the thiophene derivatives is reported to be unsatisfactory because of the metalation of the thiophene nuclei. For example, Lee et al.[1c] reported that lithiation of 3-methyl-2-thiophenecarboxylic acid (**1**) with two equivalents of lithium diisopropylamide (LDA) and subsequent treatment with methyl iodide gave a mixture of the products which were formed from the dilithium salts of **2** and **3** respectively, in the ratio of 35 : 65 (Scheme 1).

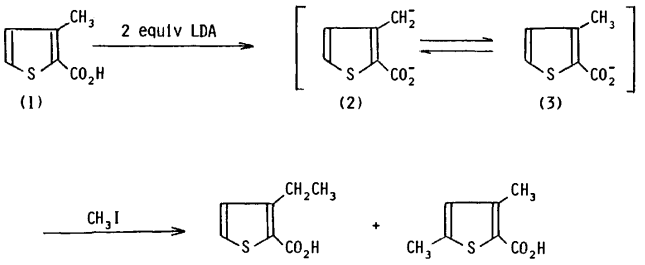

Scheme 1.

We report herein the selective side-chain lithiation of 2-methyl-3-thiophenecarboxylic acid (**4**) and some reactions of the resulting dilithium salt with electrophiles.

Results and Discussion

In the course of our studies on the Birch reduction of thiophene derivatvs,[2a,b] we examined the alkylation of 2-methyl-3-thiophenecarboxylic acid (**4**) and found the remarkably high regioselective side-chain lithiation of **4**. When the formation of a dilithium salt from **4** with two equivalents of lithium diisopropylamide (LDA) at −30 °C in THF was followed by alkylation with methyl iodide, 2-ethyl-3-thiophenecarboxylic acid (**7a**) was obtained in 80% yield without the formation of 2,5-dimethyl-3-thiophenecarboxylic acid (**8**). This result shows that the side-chain lithiation occurred selectively in sharp contrast to the reaction of 3-methyl-2-thiophenecarboxylic acid (**1**) with LDA. However, when butyllithium was used as the base instead of the LDA, regioselectivity was decreased and the mixture of **7a** and **8** was obtained in the ratio of 1 : 1. It is not clear at the present time why the selectivity of the lithiation is decreased by the use of the butyllithium.

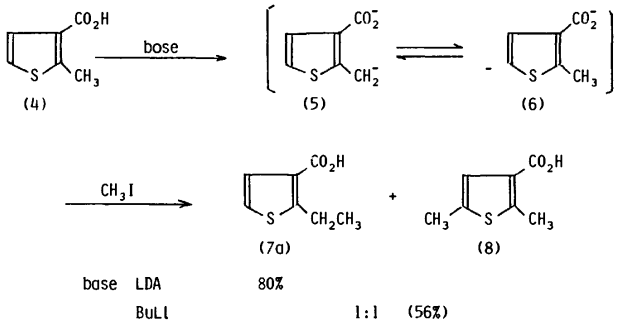

. The reactions of the dilithium salt **5** with several alkyl halides were carried out to yield 2-alkyl-3-thiophenecarboxylic acids (**7**). The results are summarized in Table 1. These reactions may be useful

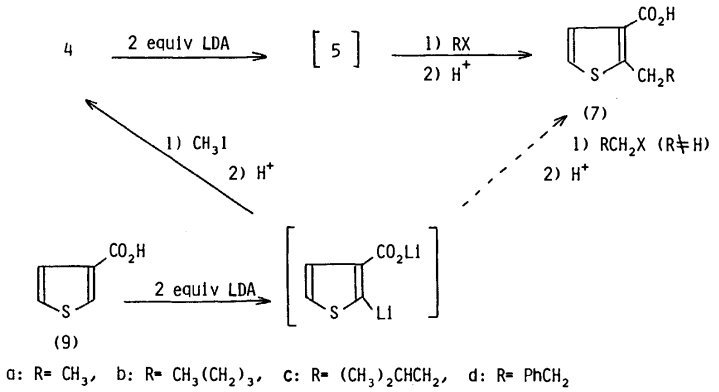

Scheme 2.

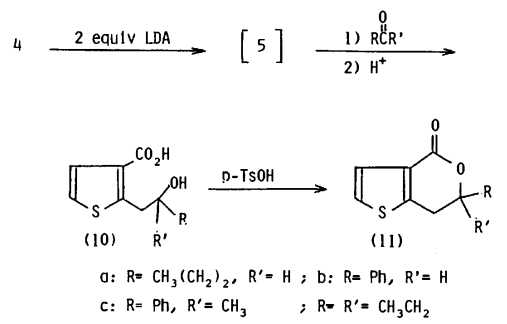

Table 1. Preparation of 2-Alkyl-3-thiophenecarboxylic Acid (**7**)

	R	Yields of **2**
7a	CH_3	80%
7b	$CH(CH_2)_3$	83%
7c	$(CH_3)_2CHCH_2$	70%
7d	$PhCH_2$	70%

Table 2. Preparation of 2-(2-Hydroxyalkyl)-3-thiophenecarboxylic Acid (**10**) and δ-Lactone Derivatives (**11**)

R	R'	Yields of **10** (%)		Yields of **11** (%)	
$CH_3(CH_2)_2$	H	**10a**	77	**11a**	86
Ph	H	**10b**	63	**11b**	87
Ph	CH_3	**10c**	61	**11c**	99
CH_3CH_2	CH_3CH_2	**10d**	81	**11d**	92

because the yields of the reaction of dilithium salt of 3-thiophenecarboxylic acid (**9**) with alkyl halides are not satisfactory for the practical synthesis of **7**, except for the case of the methyl iodide[1b] (Scheme 2).

Furthermore, the reactions of dilithium salt **5** with aldehydes or ketones produced the adducts (**10**) which were easily cyclized to δ-lactone derivatives **11** in refluxing benzene in the presence of *p*-toluenesulfonic acid. The results are summarized in Table 2.

Experimental

Preparation of 2-Ethyl-3-thiophenecarboxylic Acid (7a). Into a solution of LDA in 20 ml of THF, prepared from diisopropylamine (3.60 g, 35.6 mmol) and butyllithium (36.0 mmol), a solution of 2-methyl-3-thiophenecarboxylic acid (**4**) (2.53 g, 17.8 mmol) in 5 ml of THF was added at −30 °C under nitrogen. After the reaction mixture had been stirred for 1 h at −30 °C, a solution of methyl iodide (2.53 g, 17.8 mmol) in 5 ml of THF was added and stirring was continued for 2.5 h at −30 °C. The reaction mixture was quenched with 10% hydrochloric acid and extracted with ether. The ethereal layer was washed with small amounts of sodium sulfite solution and dried over magnesium sulfate. After removal of the ether, the resulting residue was chromatographed on a silica-gel column. From the elution with benzene-ether (5 : 1), 2.24 g (80%) of 2-ethyl-3-thiophenecarboxylic acid (**7a**) was obtained, mp 58—60 °C.[3] IR (KBr): 3300—2300 cm^{-1} (CO_2H), 1660 cm^{-1} (C=O); ^1H NMR ($CDCl_3$): δ=1.47 (3H, t), 3.46 (2H, q), 7.33 (1H, d), 7.73 (1H, d), 11.6 (1H, brs); MS: *m/z* 156 (M^+).

2-Pentyl-3-thiophenecarboxylic acid (**7b**), 2-(3-methylbutyl)-3-thiophenecarboxylic acid (**7c**), and 2-(2-phenylethyl)-3-thiophenecarboxylic acid (**7d**) were obtained by the similar procedure from **4** and the corresponding alkyl bromides. Yields and spectral data are as follows:

7b: Yield 83%; mp 62.5—63 °C; IR (KBr): 3500—2350 cm^{-1} (CO_2H), 1690 cm^{-1} (C=O); ^1H NMR($CDCl_3$): δ=0.89 (3H, t), 1.24—1.88 (6H, m), 3.22 (2H, t), 7.02 (1H, d), 7.46 (1H, d), 11.1 (1H, brs); MS: *m/z* 198 (M^+).

7c: Yield 70%; mp 64.5—65 °C; IR (KBr): 3500—2400 cm^{-1} (CO_2H), 1680 cm^{-1} (C=O); ^1H NMR ($CDCl_3$): δ=0.95 (6H, d), 1.60 (3H, t), 3.22 (2H, t), 7.02 (1H, d), 7.46 (1H, d), 11.1 (1H, brs); MS: *m/z* 198 (M^+).

7d: Yield 70%; mp 96—97 °C; IR (KBr): 3500—2400 cm^{-1} (CO_2H), 1700 cm^{-1} (C=O); ^1H NMR($CDCl_3$): δ=2.86—3.11 (2H, m), 3.38—3.62 (2H, m), 7.02 (1H, d), 7.12—7.33 (5H, m), 7.46 (1H, d), 11.1 (1H, brs); MS: *m/z* 236 (M^+).

Preparation of 2-(2-Hydroxypentyl)-3-thiophenecarboxylic Acid (10a). Into a solution of LDA in 20 ml of THF, prepared from diisopropylamine (1.78 g, 17.6 mmol) and butyllithium (17.0 mmol), a solution of **4** (1.14 g, 8.0 mmol) in 5 ml of THF was added at −30 °C under nitrogen. The reaction mixture was stirred for 1 h at −30 °C. A solution of butanal (0.58 g, 8.1 mmol) in 5 ml of THF was added to the reaction mixture and the resulting mixture was stirred for 2 h at −30 °C. The reaction mixture was acidified with 10% hydrochloric acid and extracted with ether. The ethereal layer was washed with saturated sodium chloride solution and dried over magnesium sulfate. After removal of the ether, the resulting residue was chromatographed on a silica-gel column. From the elution with benzene-ether (5 : 1), 1.32 g (77%) of the acid **10a** was obtained, mp 73—75 °C. IR (KBr): 3400 cm^{-1} (OH), 3100—2300 cm^{-1} (CO_2H), 1660 cm^{-1} (C=O); ^1H NMR ($CDCl_3$): δ=0.73—1.87 (7H, m), 3.39 (1H, dd), 3.48 (1H, dd), 3.79—4.21 (1H, m), 7.1 (1H, brs), 7.30 (1H, d), 7.69 (1H, d); MS: *m/z* 194 (M^+-H_2O, $-H_2$). Found: C, 56.24; H, 6.84%. Calcd for $C_{10}H_{14}O_3S$: C, 56.04; H, 6.59%.

By a similar procedure, 2-(2-hydroxy-2-phenylethyl)-3-thiophenecarboxylic acid (**10b**), 2-(2-hydroxy-2-phenylpropyl)-3-thiophenecarboxylic acid (**10c**) and 2-(2-ethyl-2-hydroxybutyl)-3-thiophenecarboxylic acid (**10d**) were obtained from **4** and corresponding aldehydes or ketones. The yields, spectral and analytical data are as follows:

10b: Yield 63%; mp 143—148 °C; IR (KBr): 3300 cm^{-1} (OH), 3100—2300 cm^{-1} (CO_2H), 1690 cm^{-1} (C=O); ^1H NMR ($CDCl_3$): δ=3.36—4.03 (2H, m), 5.12 (1H, q), 7.26 (1H, d), 7.65 (1H, d), 7.36—7.81 (5H, m); MS: *m/z* 248 (M^+). Found: C, 62.74; H, 4.66%. Calcd for $C_{13}H_{12}O_3S$: C, 62.90; H, 4.58%.

10c: Yield 61%; mp 115—117 °C; IR (KBr): 3400—2400 cm^{-1} (CO_2H), 1660 cm^{-1} (C=O); ^1H NMR ($CDCl_3$): δ=1.60 (3H, s), 3.50 (1H, d), 3.78 (1H, d), 7.01 (1H, d), 7.17—7.56 (6H, m); MS: *m/z* 244 (M^+-H_2O). Found: C, 63.99; H, 5.44%. Calcd for $C_{14}H_{14}O_3S$: C, 64.11; H, 5.38%.

10d: Yield 81%; mp 95—97 °C; IR (KBr): 3400—2200 cm^{-1} (CO_2H), 1660 cm^{-1} (C=O); ^1H NMR ($CDCl_3$): δ=0.91 (6H, t), 1.54 (4H, q), 3.31 (2H, s), 7.09 (1H, d), 7.37 (1H, d); MS: *m/z* 210 (M^+-H_2O). Found: C, 57.65; H, 7.11%. Calcd for $C_{11}H_{16}O_3S$: C, 57.88; H, 7.07%.

Preparation of 6,7-Dihydro-6-propyl-4*H*-thieno[3,2-*c*]-pyran-4-one (11a). A solution of **10a** (1.16 g, 54.2 mmol) and a catalytic amount of *p*-toluenesulfonic acid in 100 ml of benzene was refluxed for 3 h with a water separating apparatus. The mixture was evaporated and the resulting residue was chromatographed on a silica-gel column. From the elution with benzene, 0.91 g (86%) of the pyrane **11a** was obtained as an oil. IR (NaCl): 1700 cm^{-1} (C=O); ^1H NMR ($CDCl_3$): δ=0.96 (3H, t), 1.31—2.04 (4H, m), 2.92—3.10 (2H, m), 4.42—4.76 (1H, m), 7.14 (1H, d), 7.41 (1H, d); MS: *m/z* 196 (M^+). Found: C, 61.38; H, 6.35%. Calcd for

$C_{10}H_{12}O_2S$: C, 61.21; H, 6.17%.

By a similar procedure, 6,7-dihydro-6-phenyl-4*H*-thieno-[3,2-*c*]pyran-4-one (**11b**), 6,7-dihydro-6-methyl-6-phenyl-4*H*-thieno[3,2-*c*]pyran-4-one (**11c**), and 6,6-diethyl-6,7-dihydro-4*H*-thieno[3,2-*c*]pyran-4-one (**11d**) were formed from the corresponding acids **10**. The yields, spectral and analytical data are as follows:

11b: Yield 87%; mp 130 °C; IR (KBr): 1700 cm^{-1}(C=O); ^1H NMR ($CDCl_3$): δ=3.33 (2H, d), 5.64 (1H, t), 7.20 (1H, d), 7.36—7.60 (6H, m); MS: *m/z* 230 (M^+). Found: C, 67.72; H, 4.27%. Calcd for $C_{13}H_{10}O_2S$: C, 67.82; H, 4.38%.

11c: Yield 94%; oil; IR (NaCl): 1700 cm^{-1} (C=O); ^1H NMR ($CDCl_3$): δ=1.64 (3H, s), 3.41 (1H, d), 3.67 (1H, d), 7.05 (1H, d), 7.20—7.53 (6H, m); MS: *m/z* 244 (M^+). Found: C, 68.66; H, 5.04%. Calcd for $C_{14}H_{12}O_2S$: C, 68.84; H, 4.95%.

11d: Yield 92%; oil; IR (NaCl): 1700 cm^{-1} (C=O); ^1H NMR ($CDCl_3$): δ=0.93 (6H, t), 1.86 (4H, q), 3.06 (2H, s), 7.14 (1H, d), 7.44 (1H, d); MS: *m/z* 210 (M^+). Found: C, 62.93; H, 6.88%. Calcd for $C_{11}H_{14}O_2S$: C, 62.84; H, 6.71%.

References

1) a) A. J. Clarke, S. McNamara, and U. Metha-Cohen, *Tetrahedron Lett.*, **1974**, 2373. b) D. W. Knight and A. P. Nott, *J. Chem. Soc., Perkin Trans. 1*, **1983**, 791; c) N. P. Gould and T.-J. Lee, *J. Org. Chem.*, **45**, 4528 (1980).

2) a) M. Sado, H. Abe, N. Inuzuka, K. Shirai, and T. Kumamoto, *Bull. Chem. Soc. Jpn.*, **56**, 1665 (1983); b) T. Kumamoto, K. Hosoya, S. Kanzaki, K. Masuko, M. Watanabe, and K. Shirai, *ibid.*, **59**, 3097 (1986).

3) D. W. Knight and A. P. Nott, *Tetrahedron Lett.*, **21**, 5051 (1980).

Synthesis of Five-Membered Cyclic Ketones Using Potassium Tetracarbonylferrate(2−)

Masakazu YAMASHITA,* Masaya UCHIDA, Haruyoshi TASHIKA, and Rikisaku SUEMITSU
Department of Applied Chemistry, Doshisha University, Kamikyo-ku, Kyoto 602
(Received January 11, 1989)

Synopsis. Various five-membered cyclic ketones were prepared from 1,4-dihaloalkanes and potassium tetracarbonylferrate(2−) in moderate to high yields. However, the yields of six- or seven-membered cyclic ketones from the corresponding dihalides were rather low.

The alkali metal tetracarbonylferrate(2−) $M_2Fe(CO)_4$ (M=Na, K) (**1**) is one of the most characteristic reagents and is used as a stoichiometric reagent in the synthesis of carbonyl compounds including ketones, aldehydes, carboxylic esters and amides via acylcarbonylferrates.[1] On the other hand, saturated and unsaturated five-membered cyclic ketones are important compounds that are not only included in a large number of biologically active natural products as a structural feature, but also as a precursor of lactones by Baeyer-Villiger oxidation. Therefore, undiminished efforts have been devoted to the synthesis of this moiety.[2]

In this paper we wish to report on a facile synthetic method of the five-membered cyclic ketones from 1,4-dihaloalkanes using tetracarbonylferrate (**1**) as a carbonylating agent.

Experimental

The IR spectra were recorded on a Hitachi 260-10 Infrared Spectrophotometer. The NMR spectra were measured on a Hitachi R-600 FT-NMR spectrometer at 60 MHz, using tetramethylsilane (δ=0.00) as an internal standard; chemical shifts are given in ppm. The mass spectra (MS) were determined on a Hitachi RM-50 GC-MS spectrometer. Analytical gas chromatography was carried out on a Yanagimoto G-8 gas chromatograph with a column of 10% Silicone gum SE-30 on Chromosorb and a Shimadzu GC-14A instrument using a Shimadzu capillary column HiCap CBP1-W12-100. The column chromatography was performed on Nakarai silica gel 60 (230—400 mesh).

Materials. Tetrahydrofuran (THF) was dried and deoxygenated by distillation from potassium-benzophenone under argon just before use. *N*-Methyl-2-pyrrolidone (NMP) was dried by distillation at reduced pressure and stored over 3A molecular sieves. Pentacarbonyliron (Strem Chemical Co.) was used without further purification. Potassium tri-s-butylhydroborate was purchased from the Aldrich Chemical Co. as a 1.0 M (1 M=1 mol dm^{-3}) THF solution under the trade name K-Selectride. 1,4-Dibromobutane, 1,5-dibromopentane, and 1,6-dibromohexane were commercial products of the highest available purity. *cis*-1,2-Bis(bromomethyl)cyclohexane, 1,2-bis(bromomethyl)-4-methylcyclohexane, *endo-cis*-2,3-bis(bromomethyl)bicyclo-[2.2.1]heptane, 1,4-dibromo-2-phenylbutane, 1-bromo-3-(bromomethyl)pentadecane, and 1,5-dibromo-3-phenylpentane were prepared from *cis*-1,2-cyclohexanedicarboxylic anhydride,[3,4] 4-methyl-*cis*-1,2-cyclohexanedicarboxylic anhydride,[3,4] *cis*-5-bicyclo[2.2.1]heptene-*endo*-2,3-dicarboxylic anhydride,[5] diethyl 2-phenylsuccinate,[3,6,7] dodecylsuccinic anhydride,[3,7] and diethyl 3-phenylglutarate,[6,8] respectively, by usual hydrogenation and the following bromination. Potassium tetracarbonylferrate (**1**) was prepared by a method mentioned in the literature.[9]

Synthesis of *cis*-Bicyclo[4.3.0]nonan-8-one. General Procedure. Reactions were conducted under an argon atmosphere. To the THF solution (13 ml) of 1.0 M potassium tri-*s*-butylhydroborate, 0.79 ml of pentacarbonyliron (6 mmol) was added, and the reaction mixture was refluxed for 4 h. After cooling, a supernatant solution was removed, and the resultant white solid was washed several times with hexane and dried by blowing argon through the flask. Then, 30 ml of NMP was injected and 1,2-bis-(bromomethyl)cyolohexane (5 mmol) was added. After stirring the mixture for 24 h at room temperature, the solution was diluted with ether, washed three times with saturated brine, and the organic layer was dried over anhydrous magnesium sulfate, filtered and concentrated. The residue was separated by column chromatography (hexane : dichloromethane : diethyl ether=5 : 1 : 1) to afford bicyclo[4.3.0]nonan-8-one as oil in 61% isolated yield.[10] IR (cm^{-1}): 2935, 1743, 1163. ^{1}H NMR ($CDCl_3$) (δ): 1.18—1.78 (m, 8H), 2.03—2.58 (m, 6H). MS (*m/z*): 138 (M^+).

Other cyclic ketones were synthesized following the general procedure described above.[10]

***cis*-3-Methylbicyclo[4.3.0]nonan-8-one.** Yield 60%. Oil. IR (cm^{-1}): 2930, 1748, 1162. ^{1}H NMR δ=0.90 (d, 3H, J=4.0 Hz), 1.00—1.95 (m, 7H), 1.95—2.75 (m, 6H). MS (*m/z*): 152 (M^+).

***endo*-Tricyclo[3.2.1.0^{2,6}]decan-4-one.** Yield 52%. Oil. IR (cm^{-1}): 2960, 1742, 1175. ^{1}H NMR δ=1.25—1.70 (m, 6H), 2.17—2.88 (m, 8H). MS (*m/z*): 150 (M^+).

3-Phenylcyclopentanone. Yield 58%. Oil. IR (cm^{-1}): 2975, 1750, 1290, 760, 700. ^{1}H NMR δ=1.30 (m, 2H), 2.22—2.77 (m, 4H), 3.40 (m, 1H), 7.28 (s, 5H). MS (*m/z*): 160 (M^+).

3-Dodecylcyclopentanone. Yield 60%. Oil. IR (cm^{-1}): 2940, 1750, 1475, 1162. ^{1}H NMR δ=0.90 (t, 3H, J=4.0 Hz), 1.20—1.40 (m, 25H), 1.95—2.42 (m, 4H). MS (*m/z*): 252 (M^+).

4-Phenylcyclohexanone. Yield 15%. Mp 78—80 °C. IR (cm^{-1}): 2940, 1710, 759, 699. ^{1}H NMR δ=1.80—2.30 (m, 4H), 2.38—2.75 (m, 5H), 7.28 (s, 5H). MS (*m/z*): 174 (M^+).

Results and Discussion

The various 1,4-dibromoalkanes reacted with potassium tetracarbonylferrate (**1**) in NMP to give the five-membered cyclic ketones in good isolated yield. The results of these reactions are listed in Table 1. However, the yields of six- or seven-membered cyclic ketones were rather low. This shows that it is difficult to cyclize intramolecularly. In fact, ω-bromo aldehydes (**2**) were obtained as by-products in these reactions.

The mechanism of these reactions is considered to be as follows (Scheme 1). First, an dibromoalkane reacts with (**1**) to afford an alkylcarbonylferrate (**4**), which transforms into an acylcarbonylferrate (**4**) with the solvent assisted migratory insertion of carbon monoxide. Intramolecular cyclization of the acylcar-

Table 1. Reaction of Dibromoalkanes with $K_2Fe(CO)_4$

Run	Dibromoalkane	Product	Yiels(%)[a]
1	$Br(CH_2)Br$		(60)[b]
2	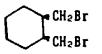	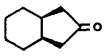	61
3	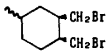	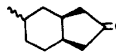	60
4	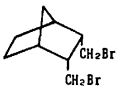	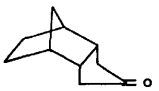	52
5	$CH_3(CH_2)_{11}CHCH_2CH_2Br$ CH_2Br	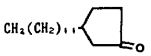	60
6	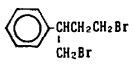	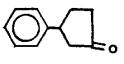	58
7	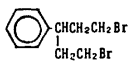	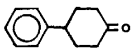	15
8	$Br(CH_2)_5Br$		(35)[b]
9	$Br(CH_2)_6Br$		(5)[b]

a) Isolated yields. b) Yields in parentheses are determined by GLC.

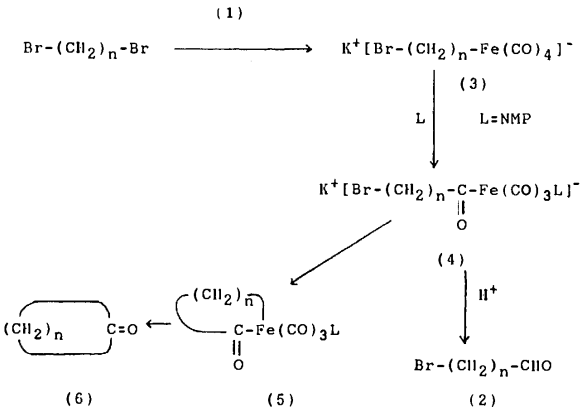

Scheme 1.

bonylferrate (**4**) leads to an acylalkyliron complex (**5**) which appears to collapse by reductive elimination to a cyclic ketone (**8**). In the reaction of (**1**) with 1,3-dibromopropane, the corresponding acylalkyliron complex (**5**) (n=3, L=triphenylphosphine) has been isolated as crystals.[11] The formation of ω-bromo aldehyde (**2**) is also considered to be derived from (**4**) by protonation in the work-up.[12]

By this method, five-membered cyclic ketones fused to the cyclohexane ring were prepared in good yields. The starting dibromoalkanes were easily prepared from the Diels-Alder adducts via hydrogenation and

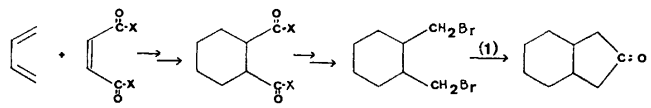

bromination. Therefore, this method is considered to be useful in the synthesis of these cyclic ketone skeletons which appear widely in naturally occurring organic compounds.

References

1) J. P. Collman, *Acc. Chem. Res.*, **1975**, 342; R. G. Finke and T. N. Sorrell, *Org. Synth.*, Coll. Vol. VI, 807 (1988); M. Yamashita, K. Miyoshi, Y. Nakazono, and R. Suemitsu, *Bull. Chem. Soc. Jpn.*, **55**, 1663 (1982); E. McMurry and A. Andrus, *Tetrahedron Lett.*, **21**, 4687 (1980); M. Yamashita, S. Yamamura, M. Kurimoto, and R. Suemitsu, *Chem. Lett.*, **1979**, 1067; M. P. Cooke, Jr. and R. M. Parlman, *J. Am. Chem. Soc.*, **99**, 5222 (1977); H. Alper, B. Marchand, and M. Tanaka, *Can. J. Chem.*, **57**, 598 (1979).

2) For example, C. H. Heathcock, S. L. Graham, M. C. Pirrung, F. Plavac, and C. T. White, "The Total Synthesis of Natural Products," ed by J. ApSimon, John Wiley & Sons, New York (1983), Vol. 5, p. 1.

3) J. M. Photis and L. A. Paquette, *Org. Synth.*, **57**, 53 (1977).

4) O. Kamm and C. S. Marrel, *Org. Synth.*, Coll. Vol. I, 25 (1944).

5) P. G. Gassman and K. T. Mansfield, *Org. Synth.*, Coll. Vol. V, 96 (1973).

6) L. J. Durham, D. J. McLeod, and J. Cason, *Org. Synth.*, Coll. Vol. IV, 635 (1962).

7) L. H. Smith, *Org. Synth.*, Coll. Vol. III, 793 (1955).

8) J. Cason, *Org. Synth.*, Coll. Vol. IV, 630 (1962).

9) J. A. Gladysz and W. Tam, *J. Org. Chem.*, **43**, 2279 (1978).

10) All the compounds gave satisfactory analytical data.

11) Y. Watanabe, T. Mitsudo, M. Yamashita, M. Tanaka, and Y. Takegami, *Chem. Lett.*, **1973**, 475.

12) M. P. Cooke, Jr., *J. Am. Chem. Soc.*, **92**, 6080 (1970).

Solubility and Coupling Reactivity of Protected Peptides in Highly Polar Solvents

Hisayuki MORII* and Kunihiro ICHIMURA
Research Institute for Polymers and Textiles, 1-1-4 Higashi, Tsukuba, Ibaraki 305
(Received January 20, 1989)

Synopsis. The solubility of protected peptides as well as the coupling rate was quantitatively examined in highly polar solvents. Symmetrical anhydrides in dimethyl sulfoxide (DMSO) containing *N,N*-dimethylformamide (DMF) or DMF solution of lithium chloride and diethyl phosphorocyanidate with triethylamine in DMSO-DMF were proved to be efficient coupling reagents for solid phase synthesis of hardly soluble peptides.

The demand for chemical synthesis of peptides is ever increasing in relation to peptides with non-natural sequences of amino acids. Kaiser et al. designed and synthesized non-natural amphiphilic peptides[1,2] possessing biological activities displayed by melittin and β-endorphin[3] whereas Ho et al. synthesized the 4-bundle helices[4] of peptides. However, syntheses of large peptides with regular sequences are often difficult probably because of the low solubility of the peptides. Narita et al. have investigated[5,6] the solubility and the conformation of the synthetic intermediates in organic solvents and suggested that the aggregation by the β-sheet formation causes the low solubility. In order to prevent the β-sheet formation, they recommended the use of *N*-substituted or α,α-disubstituted amino acid residues. However, when designed peptide sequence does not contain these residues destroying β-sheet structure, the use of highly polar solvents seems effective. Actually, DMF as well as DMF-DMSO[7] has been used in the fragment condensation to solubilize component peptides. DMF and NMP are also effective in the solid phase synthesis. Relatively high yields were obtained by using a DMF-DMSO mixed solvent.[4] The descriptions about the solubility of the protected peptides in highly polar solvents are qualitative in most papers and there are only few data available for the selection of coupling solvents.[8] During the course of our studies on non-natural long chain peptides, optimization of coupling conditions has been required. This paper deals with the more detailed examination of solubility of several types of peptides in highly polar solvents and the reactivity of several coupling reagents in these solvents.

Experimental

Materials[9] and Methods. The organic solvents were dried over Molecular Sieves 4A, and LiCl was dealt under dry conditions. TLC was performed on silica gel (Kieselgel $60F_{254}$, Merck). R_f values refer to the following solvent systems: R_f^1 ethyl acetate-MeOH (5:1 v/v), R_f^2 dioxane-MeOH (1:1), R_f^3 1-butanol-acetic acid-water (4:1:1), R_f^4 chloroform-MeOH (9:1). The optical rotations were determined with a Horiba SEPA-200 polarimeter at 24 °C. Elemental analyses were performed with a Yanaco MT-3 CHN Corder.

Synthesis. Boc-Asn-Asn-Phe-OBzl (Ia). This peptide was prepared stepwise by the standard solution technique.[10] R_f^2 0.86; R_f^3 0.80; R_f^4 0.10; $[\alpha]_D$ −11.3° (*c* 1.0, DMSO).

Boc-Asn-Asn-Phe-Ala-Asn-Asn-Phe-OBzl (Ib). This compound was prepared by the fragment condensation of Boc-Asn-Asn-Phe-OH with H-Ala-Asn-Asn-Phe-OBzl using WSC and HOBt. Mp 260—261 °C (decomp); $[\alpha]_D$ −20.6° (*c* 1.0, DMSO). Calcd for $C_{49}H_{63}N_{11}O_{14}\cdot H_2O$: C, 56.2; H, 6.3; N, 14.7%; Found: C, 56.0; H, 6.3; N, 15.1%.

Boc-Glu(OBzl)-Glu(OBzl)-Phe-Ala-Glu(OBzl)-Ala-Phe-Gly-OBzl (IIa). The peptide **IIa** was synthesized by a stepwise solid-phase procedure employing oxime resin described by Kaiser et al.[11] Mp 184—187 °C (decomp). Calcd for $C_{74}H_{86}N_8O_{17}\cdot H_2O$: C, 64.5; H, 6.4; N, 8.1%; Found: C, 64.5; H, 6.5; N, 8.1%.

Boc-Glu(OBzl)-Glu(OBzl)-Phe-Ala-Glu(OBzl)-Ala-Phe-Glu(OBzl)-Glu(OBzl)-Phe-Ala-Glu(OBzl)-Ala-Phe-Gly-OBzl (IIb). The fragment Boc-Glu(OBzl)-Glu(OBzl)-Phe-Ala-Glu(OBzl)-Ala-Phe-N_2H_3 was prepared by the cleavage of the heptapeptide resin with hydrazine according to the method of Kaiser et al.[11] Yield, 52%; R_f^1 0.78; R_f^2 0.86; R_f^4 0.58. Another fragment H-Glu(OBzl)-Glu(OBzl)-Phe-Ala-Glu(OBzl)-Ala-Phe-Gly-OBzl was obtained from compound **IIa** in 90% yield. The compound **IIb** was prepared with these two fragments according to the azide method. Mp 254—257 °C (decomp); $[\alpha]_D$ −5.0° (*c* 1.0, DMSO). Calcd for $C_{134}H_{153}N_{15}O_{30}\cdot 3H_2O$: C, 64.2; H, 6.4; N, 8.4%; Found: C, 64.4; H, 6.5; N, 8.8%.

Boc-Phe-Phe-Leu-Leu-Phe-Phe-Leu-Leu-Ala-OBzl (III). This compound was prepared in a similar manner as for the peptide **IIa**. Yield, 65%; mp 299—302 °C (decomp); $[\alpha]_D$ −23.2° (*c* 1.0, DMSO). Calcd for $C_{75}H_{101}N_9O_{12}\cdot H_2O$: C, 67.3; H, 7.8; N, 9.4%; Found: C, 67.6; H, 8.0; N, 9.5%.

To suppress racemization and side reactions in the fragment condensations, phenylalanine was chosen as C-terminus of carboxyl components. Little racemization was detected by ^1H NMR for compound **Ib**.

Solubility. The peptide was weighed precisely in a small tube and one or more drops of solvent was added to it. The suspension was stirred magnetically for one minute. By direct observation of the precipitant, it was judged whether an insoluble part was remained or not. The addition of the solvent and the judgement were repeated.

Determination of Coupling Rate. Five coupling reagents, i.e., DCC, HOBt-DCC, DEPC, DEPC-TEA, and symmetrical anhydride, were examined in the following way. Deprotected [4-(glycyloxymethyl)phenylacetamido]-methyl-resin (200 mg)[12] was placed in a test tube and suspended in a solvent. Boc-phenylalanine (2 equiv) was added subsequently. The coupling reaction was initiated with the addition of the coupling reagent such as DCC or DEPC. The reaction was pursued in 2.00 g of solvent. In the case of HOBt-DCC, HOBt (4 equiv) was added in advance. For DEPC-TEA, TEA was added one minute later after the addition of DEPC. Symmetrical anhydride was pre-formed with Boc-phenylalanine (4 equiv) and DCC (2 equiv) in dichloromethane and used as DMF solution. After specified times, the aliquots of the reaction mixture were removed and immediately washed with ethanol. The content of unreacted amino groups on the resin was deter-

mined by the method of Gisin,[13] which employs the salt formation with picric acid.

Results and Discussion

The amino acid residues in synthetic intermediates can be classified as follows: (i) unprotected residues which tend to form hydrogen bond, such as asparagine; (ii) hydrophilic residues with hydrophobic protecting groups; (iii) hydrophobic residues. The peptides **Ia** and **Ib** were designed to have an abundance of type-(i) residues. The peptides **IIa** and **IIb** were designed to be rich in type-(ii) residues and the peptide **III** was constructed with only type-(iii) residues. In common with the peptides **Ia—IIb** alanine and phenylalanine were used as the other residues.

The highly polar solvents such as HMPA, NMP, DMA, DMF, and DMSO are strong electron donors as well as strong electron acceptors on the basis of donor-acceptor concept.[14] HMPA is the strongest donor, and DMSO is the strongest acceptor among these solvents. Therefore, three representative solvents, i.e., HMPA, DMSO, and DMF, were examined in this study. DMF solution of LiCl was also examined because it is well-known as a good solvent for hydrogen-bonded compounds.

The characteristic solubility of the peptides in various solvent systems was obtained as shown in Fig. 1. The weights of peptide and solvent are represented as W_p and W_s, respectively. DMF has low solubilizing power for the peptides **Ia**, **Ib**, **IIb**, and **III**. These critical values of $\log(W_p/W_s)$ were in the range of -3 to -2. Only the peptide **IIa** was readily soluble in DMF. On the other hand, HMPA was a good solvent for the peptides **IIa**, **IIb**, and **III**. However, asparagine-rich peptides **Ia** and **Ib** had remarkably low solubility in HMPA. This result presumably relates to high donor character of HMPA. DMSO was quite a good solvent for the all peptides examined here. The critical values of $\log(W_p/W_s)$ were larger than -1.5. In comparison with the peptide **Ia** the peptide **Ib** had rather high solubility in DMSO in spite of the long chain length. This seems to be attributed to intramolecular hydrogen bonds.

DMF solution of LiCl was also a good solvent. The solubility of **Ib**, **IIa**, and **IIb** was comparable to that in DMSO. The peptides **Ia** and **III** were more soluble in DMF-LiCl than in DMSO. The solubility of these peptides was scarcely dependent on the content of LiCl in the range of 4% to 7%. In the mixed solvent systems, the solubility changes toward the mixing ratios were not simple. The peptide **III** had almost a constant solubility in DMF-HMPA system containing 0—80% of HMPA, though it had higher solubility in HMPA. It was also the case of DMF-DMSO system.

Further experiment suggested that the solubility in a mixed solvent depended on the order of mixing. For example, although the peptide **III** was insoluble in a mixture of DMF and DMSO at $W_p/W_s=10^{-2}$, the solubilization could be realized by dissolving it in pure DMSO at first and subsequently diluting with DMF to the same concentration. The procedure involving the devided addition of the solvents seems practically useful because mixed solvent systems give better coupling efficiency as described later.

For the solid-phase peptide synthesis, a rapid coupling reaction is desirable as a high efficiency can be achieved in a short time. Therefore, the coupling methods employing DCC, DCC-HOBt, DEPC, DEPC-TEA, and symmetrical anhydride were examined. The azide method and the pre-formed active ester methods were excluded because the former with diphenyl phosphorazidate was reported to be slower than DEPC method in DMF[15] and the latter reactions take place very slow in general.

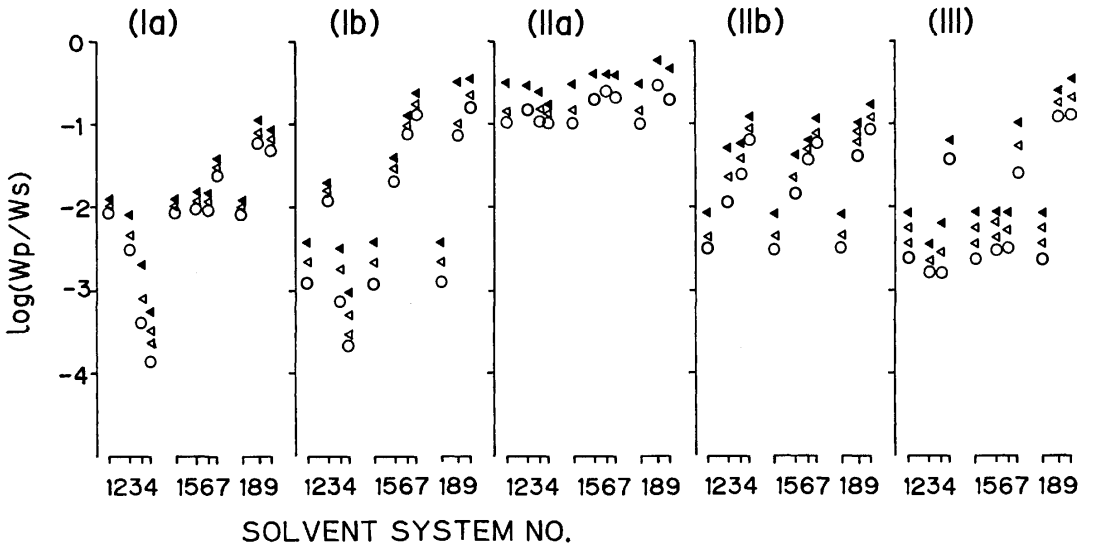

Fig. 1. Solubility of the peptides. The following solvent systems were used; 1: DMF, 2: HMPA-DMF (50 : 50 v/v), 3: HMPA-DMF (80 : 20), 4: HMPA, 5: DMSO-DMF (50 : 50), 6: DMSO-DMF (80 : 20), 7: DMSO, 8: DMF-LiCl (4%), 9: DMF-LiCl (7%). The open circles, the open triangles, and the closed triangles represent 'soluble', 'slightly insoluble', and 'apparantly insoluble', respectively.

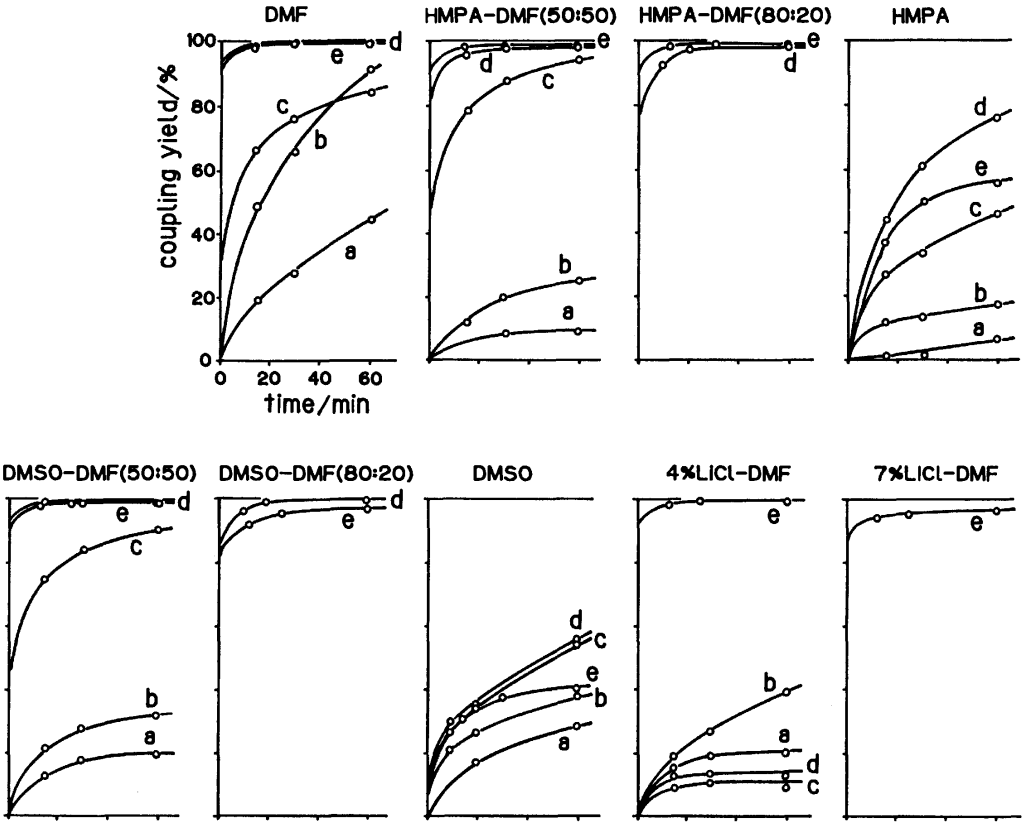

Fig. 2. Conversion curves of coupling reactions using DCC(a), DCC-HOBt(b), DEPC(c), DEPC-TEA(d) and symmetrical anhydride(e).

The conversion curves of those coupling reactions in various solvent systems are shown in Fig. 2. When DMF was used as a solvent, the coupling rate with DEPC-TEA and symmetrical anhydride were remarkably high. The result for DEPC-TEA is in line with the previous report.[15] On the other hand, DCC method is very slow. The coupling rates were considerably reduced for all the methods in HMPA as well as DMSO in comparison with those in DMF. This result means that the use of HMPA or DMSO alone is inadequete to realize both high solubilization and rapid coupling rate. Therefore, the coupling rates were examined in mixed solvent systems. In any mixed solvent containg DMF, the coupling reactions with DEPC-TEA and symmetrical anhydride method were as rapid as in DMF. The role of DMF seems to be essential for these rapid coupling reactions.

In conclusion, for the highly efficient synthesis of peptides the following methods can be recommended, i.e., symmetrical anhydride and DEPC-TEA in DMSO containing a small amount of DMF and the former method in DMF-LiCl.

References

1) E. T. Kaiser and F. J. Kezdy, *Science*, **223**, 249 (1984).
2) A. Khalil, N. Bramson, F. J. Kezdy, E. T. Kaiser, and A. M. Scanu, *Proteins*, **1**, 280 (1986).
3) J. W. Taylor, R. J. Miller, and E. T. Kaiser, *J. Biol. Chem.*, **258**, 4464 (1983).
4) S. P. Ho and W. F. DeGrado, *J. Am. Chem. Soc.*, **109**, 6751 (1987).
5) M. Narita, K. Ishikawa, J.-Y. Chen, and Y. Kim, *Int. J. Peptide Protein Res.*, **24**, 580 (1984).
6) M. Narita, T. Fukunaga, A. Wakabayashi, K. Ishikawa, and H. Nakano, *Int. J. Peptide Protein Res.*, **23**, 306 (1984).
7) N. Nishino, Y. Sugita, T. Yamamoto, and T. Fujimoto, *Rep. Asahi Glass Found. Ind. Technol.*, **48**, 149 (1986).
8) J. Kovacs, "The Peptides," Academic Press, New York (1979), Vol. 2, pp. 485—539.
9) The following abbreviations are used; Boc, *t*-butoxycarbonyl; OBzl, benzyl ester; DCC, dicyclohexylcarbodiimide; HOBt, 1-hydroxybenzotriazole; DEPC, diethyl phosphorocyanidate; TEA, triethylamine; MeOH, methanol; DMF, *N*,*N*-dimethylformamide; DMSO, dimethyl sulfoxide; HMPA, hexamethylphosphoric triamide; NMP, *N*-methylpyrrolidone; DMA, *N*,*N*-dimethylacetamide; WSC, 1-ethyl-3-(3-dimethylaminopropyl)carbodiimide hydrochloride.
10) O. Keller and J. Rudinger, *Helv. Chim. Acta*, **57**, 1253 (1974).
11) W. F. DeGrado and E. T. Kaiser, *J. Org. Chem.*, **45**, 1295 (1980).
12) A. R. Mitchell, S. B. H. Kent, M. Engelhard, and R. B. Merrifield, *J. Org. Chem.*, **43**, 2845 (1978).
13) B. F. Gisin, *Anal. Chim. Acta*, **58**, 248 (1972).
14) V. Gutmann, "The Donor-Acceptor Approach to Molecular Interactions," Plenum Press, New York (1978).
15) S. Yamada, N. Ikota, T. Shioiri, and S. Tachibana, *J. Am. Chem. Soc.*, **97**, 7174 (1975).

Organic Photochemical Reactions. XXXII.[1] Photochemical Ring-Cleavage Reactions of 2,2-Diaryloxetanes in the Presence of Electron Donor

Kenichi NAKABAYASHI,† Shin FUJIMURA, Masahide YASUDA, and Kensuke SHIMA*
Department of Industrial Chemistry, Faculty of Engineering, Miyazaki University, Gakuen-Kibanadai, Miyazaki 889-21
(Received February 20, 1989)

Synopsis. Photochemical ring-cleavage reactions of 2,2-diaryloxetanes in the presence of triethylamine gave 1,1-diarylethenes selectively.

The cleavage of the oxetane ring has been studied in reactions with Brønsted acid or metal ion as well as in pyrolysis[2] or infrared multiphoton induced photolysis.[3] In these studies, the regiochemical control of ring cleavage has been an interesting subject. We previously reported that regioselective ring-cleavage reactions of 2,2-diaryloxetanes (**1**) into substituted benzophenone and alkene pairs are achieved by a photochemical electron transfer from **1** to a typical electron acceptor, such as aromatic nitriles.[1] Thus, the photochemical electron transfer has proved to be a useful method for the ring cleavage of oxetanes. Therefore, our attention was focused on the photochemical reaction of **1** in the presence of electron donors (Scheme 1).

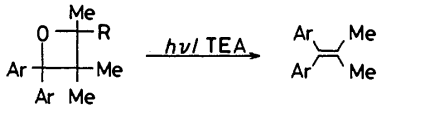

	Ar	R
1a	C_6H_5	H
1b	C_6H_5	Me
1c	p-MeC_6H_4	H
1d	p-MeC_6H_4	Me
1e	p-Cl C_6H_4	H
1f	p-Cl C_6H_4	Me
1g	p-MeOC_6H_4	H
1h	p-MeOC_6H_4	Me

	Ar
2a	C_6H_5
2b	p-MeC_6H_4
2c	p-ClC_6H_4

Scheme 1.

Results and Discussion

Reaction Products. Photoreactions of **1** were carried out by irradiation in the presence of an electron donor at 254 nm. In attempts to find the optimum reaction conditions, the photoreaction of **1b** was carried out under various conditions. Hexane, cyclohexane, dibutyl ether, and tetrahydrofuran (THF) were found to be better solvents, since the photoreaction was relatively efficient, while methanol and acetonitrile were poor solvents (Table 1). As an electron donor, triethylamine (TEA) was better than the other amines tested (e.g. aliphatic or aromatic amines). Therefore, photochemical ring-cleavage reactions were performed with TEA in hexane throughout the present investigation.

Photochemical ring-cleavage reactions of **1a—d** in the presence of TEA gave the corresponding 1,1-diarylethene (**2**), while acetaldehyde or acetone was not detected by careful GLC analysis, though these compounds were expected as other products of the ring cleavage of **1**. The reaction products were unambiguously identified by direct comparisons with authentic samples which were prepared by acid-catalyzed fragmentation of the corresponding oxe-

Table 1. Chemical and Quantum Yields in the Photochemical Ring Cleavage of **1b** in the Presence of TEA

Solvent	Yield of **2a**[a]	Conv. of **1b**	ϕ[b]
	%	%	
Hexane	48	70	0.046
Cyclohexane	50	68	—[c]
Dibutyl ether	64	67	0.020
THF	73	51	0.027
MeOH	24	66	—[c]
MeCN	28	57	0.013

a) GLC yields based on consumed **1**. b) Quantum yields at [TEA]=0.07 mol dm^{-3}. c) Not determined.

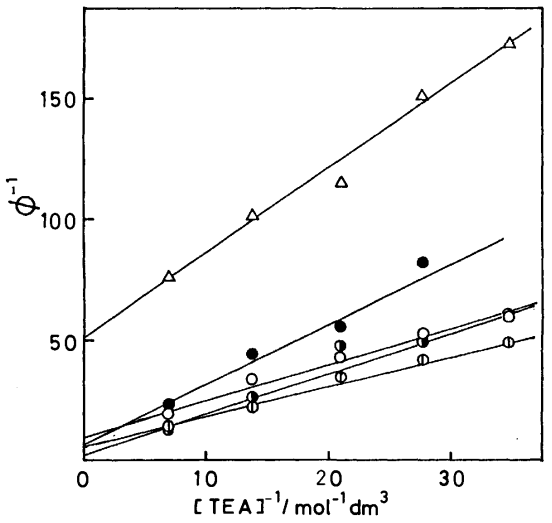

Fig. 1. Double-reciprocal plots of quantum yields vs. concentration of TEA for the photochemical ring-cleavage of **1a** (○), **1b** (◑), **1c** (◑), **1d** (●), and **1f** (△) in hexane.

† Present address: Department of Chemistry, Faculty of Education, Miyazaki University, Gakuen-Kibanadai, Miyazaki 889-21.

Table 2. Limiting Quantum Yields (ϕ^{∞}) in Photochemical Ring Cleavage of **1a—d, f** with TEA in Hexane

Oxetane	ϕ^{∞}
1a	0.09
1b	0.22
1c	0.31
1d	0.20
1f	0.02

tanes with *p*-toluenesulfonic acid. Substituted benzophenones and alkenes were not produced in the photoreaction. At low conversions (<5%), material balances were better than 90%, though other unreclaimed reactions increasingly occurred at higher conversions.

Quantum Yields. The formation of **2** increased linearly with the irradiation time up to 3% conversion. The formation of **2** increased with an increase in the concentration of TEA, but remarkably decreased at concentrations of TEA higher than 0.1 mol dm^{-3}. Since TEA has absorption at 254 nm in the UV spectrum, the absorption of incident light by TEA occurred to some extent. From the above-mentioned results, the photoexcitation of TEA would not bring about the ring-cleavage reactions of **1**. Therefore, the quantum yield (ϕ) for the formation of **2** at a given concentration of TEA was calculated on the basis of the light intensities absorbed by **1**. Thus, the quantum yields (ϕ) in various solvents were determined for the photochemical ring-cleavage reactions of **1b** (Table 1). Moreover, the limiting quantum yields (ϕ^{∞}) were determined by the usual double-reciprocal plots of ϕ vs. the concentration of TEA, for the photochemical ring-cleavage reactions of **1** in hexane (Fig. 1). The photochemical ring cleavage of **1a—d** proceeded in moderately high quantum yields, while those of **1f** occurred inefficiently. In the case of **1e, g, h**, no photochemical ring-cleavage occurred. The results are listed in Table 2.

Mechanism. No reaction occurred at all upon direct irradiation of **1** in the absence of TEA. The photochemical ring-cleavage of **1** occurred efficiently in nonpolar solvents, but proceeded inefficiently in polar solvents. Therefore, the exciplex formation between **1** and TEA can be assumed as being an initiation process, though no exciplex emission was observed in the cases of **1**-TEA pairs. An analogous 2,2,3,3-tetramethyl-4-(1-naphthyl)oxetane (**1i**) forms an emissive exciplex (λ_{max} 420 nm) with TEA in hexane; the photoreactions of **1i** with TEA gave 1-(1-naphthyl)-2-methylpropene (**2d**) (Scheme 2). Therefore, we assume a possible mechanism involving the exciplex formation followed by proton transfer from TEA to **1** in the exciplex or the ion pairs, as shown in Scheme 3. Similar mechanisms have been postulated for the photoreaction of aromatic hydrocarbons with TEA.[4] In a manner similar to that for acid-catalyzed fragmentation of oxetane ring, the protonated oxetane gives products (**2**) accompanying the formation of hydroxyalkyl radical which gives untractable materials. In polar solvents, the ion pair would dissociate into free ion radicals, and the inefficient photochemical ring-cleavage reactions would be attributed to the occurrence of unreclaimed reaction from free ion radicals.

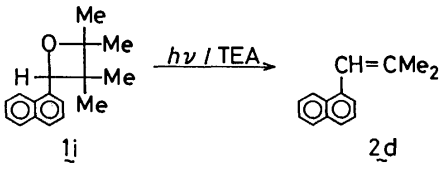

1i 2d

Scheme 2.

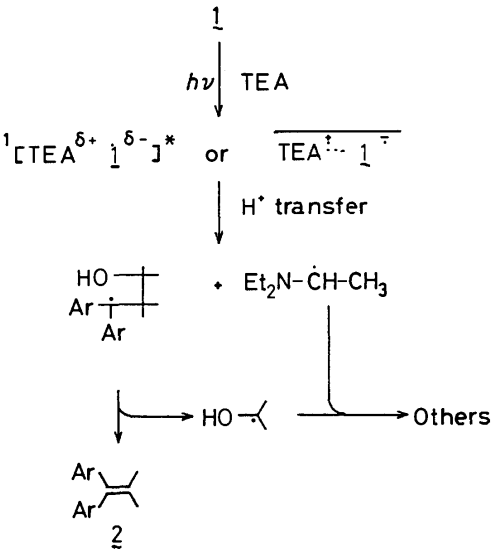

Scheme 3.

In conclusion, it was found that photochemical ring-cleavage reactions of **1** in the presence of electron donors give the corresponding 1,1-diarylethenes selectively, in contrast with the photoreaction in the presence of electron acceptors[1] which affords substituted benzophenones and alkenes.

Experimental

Gas chromatography was performed on a Shimadzu GC-8A gas chromatograph using a 50 cm column of 2% OV-1 or 2% OV-17 on Chromosorb W. UV spectra and fluorescence spectra were obtained on a Hitachi 150-20 spectrometer or a Hitachi MPF-4 spectrometer, respectively.

Materials. Solvents were purified by usual methods.[5] Triethylamine was distilled before use. Preparation of oxetanes (**1**) were carried out by irradiation of benzene solution containing the substituted benzophenone or 1-naphthaldehyde and the alkene by high-pressure Hg lamp according to the procedure described in the previous paper.[1]

Photoreactions and Determination of Quantum Yields. Concentration of **1** were set in 0.01 mol dm^{-3} and concentration of TEA was variable between 0.03 and 0.144 mol dm^{-3}. Aliquot portions (4 cm^3) of reactant solutions and actinometer solutions were introduced into quartz tubes (8 mm, i.d.) and degassed by four freeze-pump-thaw cycles under high vacuum. Irradiation was carried out with an Eikosha EL-A 10 low-pressure Hg lamp using a "merry-go-round" turntable. Incident light intensity (I^0) was determined by the use of photocleavage reaction of 1,2,3,4-tetraphenyl-

cyclobutane to stilbene as an actinometer.[6] Quantum yields were calculated using light intensities (I) corrected by Eq. 1:

$$I = I^0 \varepsilon^1[\mathbf{1}]/(\varepsilon^1[\mathbf{1}] + \varepsilon^{TEA}[TEA]) \quad (1)$$

where ε^1 and ε^{TEA} represent molar extinction coefficient of **1** and TEA at 254 nm, respectively.

This work was supported by a Grand-in-Aid for Scientific Research No. 62550616, from the Ministry of Education, Science and Culture.

References

1) Part XXXI: K. Nakabayashi, J. Kojima, K. Tanabe, M. Yasuda, and K. Shima, *Bull. Chem. Soc. Jpn.*, **62**, 96 (1989).

2) D. R. Arnold, "Advances in Photochemistry," ed by W. A. Noyes, Jr., G. S. Hammond, and J. N. Pitts, Jr., John Wiley and Sons, New York (1968), Vol. 6, p. 301; G. Jones, II, "Organic Photochemistry," ed by A. Padwa, Marcel Dekker, New York (1981), Vol. 5, p. 1; N. Shimizu, S. Yamaoka, and Y, Tsuno, *Bull. Chem. Soc. Jpn.*, **56**, 3853 (1983).

3) W. E. Farneth and D. G. Johnson, *J. Am. Chem. Soc.*, **106**, 1875 (1984); W. E. Farneth and D. G. Johnson, *ibid.*, **108**, 773 (1986).

4) D. Bryce-Smith and A. Gilbert, *Tetrahedron*, **33**, 2459 (1977).

5) D. D. Perrin, L. F. Armarego, and D. R. Perrin, "Purification of Laboratory Chemicals ," Pergamon Press, Oxford (1980).

6) S. Takamuku, K. Yonemoto, S. Toki, and H. Sakurai, *Nippon Kagaku Kaishi*, **1984**, 67.

A Synthetic Route of 1,4,8-Trimethoxy-2-naphthalenecarbaldehyde via Duff Formylation of 4,8-Dimethoxy-1-naphthol[1)]

Yasuhiro TANOUE, Akira TERADA,* and Yasuyuki MATSUMOTO
Department of Chemistry, Kyushu Institute of Technology, Tobata, Kitakyushu, Fukuoka 804
(Received March 3, 1989)

Synopsis. A convenient route for preparing 1,4,8-trimethoxy-2-naphthalenecarbaldehyde was accomplished by the following: The starting material, 4,8-dimethoxy-1-naphthol, was prepared from 1,5-dimethoxynaphthalene through 1-bromo-4,8-dimethoxynaphthalene. Formylation of this naphthol and subsequent methylation gave 1,4,8-trimethoxy-2-naphthalenecarbaldehyde.

During the course of our synthetic studies of bioactive naphthoquinone derivatives, the entitled aldehyde, 1,4,8-trimethoxy-2-naphthalenecarbaldehyde (**3**) became one of the important intermediates. This compound was also a key intermediate in the syntheses of anthracycline system compounds[2)] and of 2-azanaphthacenequinone.[3)] This aldehyde **3** was first prepared as follows: i) Friedel-Crafts acylation of 2,5-dimethoxytoluene (**1**) with succinic anhydride, ii) Clemmensen reduction, then iii) cyclization gave a tetralone (**2**).[4)] Oxidation of **2** with 2,3-dichloro-5,6-dicyano-1,4-benzoquinone and methylation by trimethyl orthoformate gave **3**[2,3)] (Scheme 1).

Rapoport et al.[5)] have obtained 4,8-dimethoxy-1-naphthol (**5**) by the following process (Scheme 2). The naphthol **5** was conveniently used in the syntheses of 2-bromojuglone[5)] and of pyranonaphthoquinone.[6)] We will report here a synthetic method of 1,4,8-trimethoxy-2-naphthalenecarbaldehyde **3** via this naphthol **5** starting from 1,5-dimethoxynaphthalene (**4**).

Results and Discussion

We easily prepared the naphthol **5** from **4**; the process was as follows: i) Bromination of **4** and ii) oxidation of the organolithium compound, 1-lithio-4,8-dimethoxynaphthalene (Scheme 3).

Although two-equimolar bromination of **4** gave 4,8-dibromo-1,5-dimethoxynaphthalene,[7)] one molar-equivalent of bromine conveniently afforded 1-bromo-4,8-dimethoxynaphthalene (**6**) in 98% yield. Such a process as the direct lithiation of **4** using *n*-BuLi, treatment with butylmagnesium bromide, and oxidation to obtain **5** was unsuccessful. We attempted a direct hydrolysis of **6** using caustic alkali in the presence of Cu and Cu_2O; however, we still obtained unsatisfactory results. Finally, we tried a one-pot procedure, such as the lithiation of **6** by *n*-BuLi, treatment with *n*-BuMgBr, and oxidation to **5**.

Regarding the preparation of the final product **3** from **5**, the following two procedures were desirable:

(A) Formylation of 1,4,5-Trimethoxynaphthalene Leading to 3. Since we found that a trial formylation of 1,4-dimethoxynaphthalene (**7**) by a Vilsmeier reaction afforded 1,4-dimethoxy-2-naphthalenecarbaldehyde (**8**) in almost quantitative yield, the same procedure was carried out for 1,4,5-trimethoxynaphthalene (**9**) which was obtained by methylation of **5** with dimethyl sulfate. However, the yield of our required

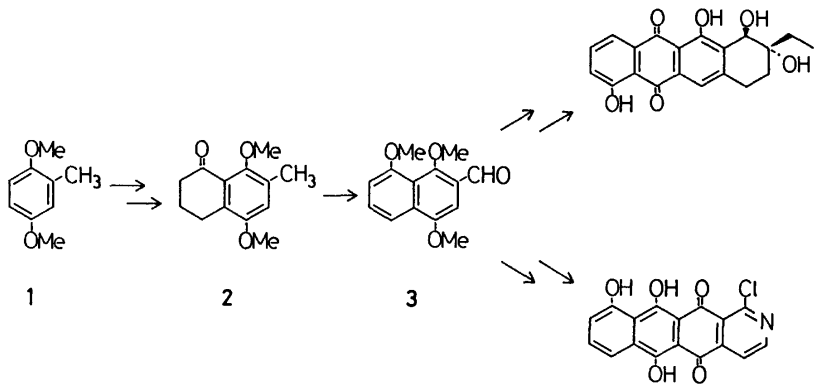

Scheme 1.

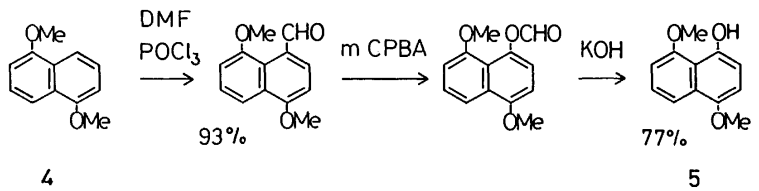

Scheme 2.

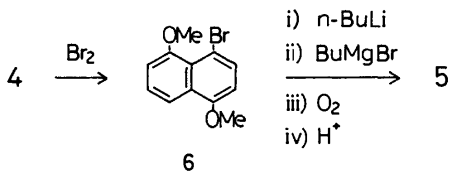

Scheme 3.

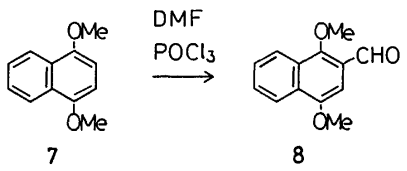

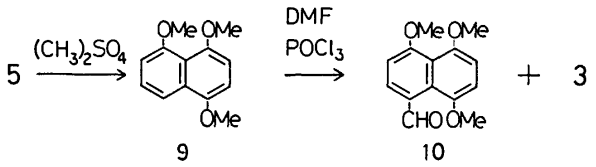

Scheme 4.

product (**3**) was slight (13%), and the main product was 4,5,8-trimethoxy-1-naphthalenecarbaldehyde (**10**) in 80% yield.

(B) Via Formylation of 5 to 1-Hydroxy-4,8-dimethoxy-2-naphthalenecarbaldehyde and Methylation to 3. Upon formylation the Vilsmeier reaction of **5** afforded mainly the formic ester (**11**) (62%) and the proposed 1-hydroxy-4,8-dimethoxy-2-naphthalenecarbaldehyde (**12**) was minor (24%). Another method, the Reimer-Tiemann reaction,[8] did not proceed. The Duff reaction[9] in acetic acid solvent resulted in 28% yield of **12**. The addition of an equimolar amount of *p*-toluenesulfonic acid monohydrate to this system resulted in a good yield of **12** (Scheme 5), though the reaction in trifluoro- and trichloroacetic acids gave only undesirable decomposition products (Table 1).

Methylation of **12** with methyl *p*-toluenesulfonate gave the final product **3** in 95% yield; with dimethyl sulfate the reaction was not satisfactory.

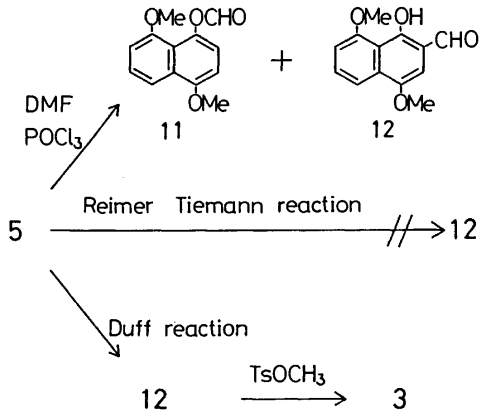

Scheme 5.

Experimental

Melting points were determined with a Yanagimoto micromelting point apparatus and were uncorrected. ^{1}H NMR spectra were taken on a JEOL JNM-60 in $CDCl_3$ using Me_4Si as an internal standard. Mass spectra and IR spectra were obtained with a JEOL DX-300 spectrometer, and a Hitachi 260-30 spectrometer, respectively. Column chromatography was carried out on silica gel (Wakogel C-200) or on alumina (Sumitomo, KCG-30) eluting with chloroform. Cu and Cu_2O powder of Wako Chemical Co. were used.

1-Bromo-4,8-dimethoxynaphthalene (6). Bromine (0.85 g, 5.3 mmol) in carbon tetrachloride (5 ml) was added dropwise to a solution of 1,5-dimethoxynaphthalene (**4**) (1.00 g, 5.3 mmol) in carbon tetrachloride (30 ml) at 70 °C. After stirring at 70 °C for 30 min, the solution was concentrated and the residue was chromatographed on silica gel to give 1.38 g (98%) of **6**. Recrystallization from hexane gave an analytical sample, mp 113—113.5 °C. IR (KBr) 1590, 1400, 1260, 1245, 1050, 800, and 740 cm^{-1}; ^{1}H NMR δ=3.94 (s, 6H, 2×OCH_3), 6.61 (d, J=8.4 Hz, 1H, ArH-2), 6.94 (dd, J=7.6 and 1.3 Hz, 1H, ArH-6), 7.32—7.46 (2d, J=8.4 and 7.6 Hz, 1H, ArH-7), 7.65 (d, J=8.4 Hz, 1H, ArH-3), 7.91 (dd, J=8.4 and 1.3 Hz, 1H, ArH-8); MS, m/z 268 (M^++2, 99.7%), 266 (M^+,100), 253 (48), 251 (49), 195 (26), 193 (28), and 115. Calcd for $C_{12}H_{11}O_2Br$: C, 53.96; H, 4.15%. Found: C, 53.07; H, 4.07%.

4,8-Dimethoxy-1-naphthol (5). A. Oxidation of the Lithium Compound of 6. A solution of **6** (0.20 g, 0.75 mmol) in tetrahydrofuran (10 ml) was cooled to −10 °C, and *n*-BuLi (1.20 ml, 1.87 mmol, 10 w/v % in hexane) was added and stirred at −10 °C for 1 h. To this system was added a solution of butylmagnesium bromide in tetrahydrofuran (Mg: 55 mg, 2.25 mmol; BuBr: 0.31 g, 2.25 mmol; THF: 10 ml) at −10 °C. After 40 min, dry oxygen was bubbled into the system for 1 h at such a rate as to keep the temperature

Table 1. Preparation of **12** from **5** by Duff Reaction

Entry	Solvent and catalyst	Condition		Yield/%
		Temp/ °C	Time/h	
1	CF_3COOH	85	3.5	0[a]
2	CCl_3COOH	95	1	0[a]
3	CH_3COOH	85	2	0[b]
4	CH_3COOH	Reflux	1	28
5	CH_3COOH, $TsOH\cdot H_2O$	Reflux	1	40
6	CH_3COOH, $TsOH\cdot H_2O$	Reflux	3	61
7	CH_3COOH, $TsOH\cdot H_2O$	Reflux	5	60
8	CH_3COOH, $TsOH\cdot H_2O$	Reflux	14	40

a) Decomposition product was obtained. b) Only starting material was recovered.

below 0 °C. The reaction mixture was decomposed by the addition of dil hydrochloric acid (50 ml), extracted with chloroform (50 ml×3), washed with brine, dried over anhydrous sodium sulfate, and concentrated. The residue was chromatographed on silica gel to give 33 mg (21%) of **5**, mp 154.5—156 °C (lit,[5] 155—156 °C) and 110 mg (78%) of 1,5-dimethoxynaphthalene. Here obtained **5** did not depress the melting point of an authentic sample[5] of **5** on admixture.

B. Hydrolysis of 6. A mixture of **6** (0.534 g, 2 mmol), Cu powder (20 mg), and Cu_2O powder (60 mg) in aqueous sodium hydroxide (2.5 M (1M=1 mol dm^{-3}), 100 ml) was stirred at 150 °C for 3 h in a stainless-steel autoclave. The reaction mixture was filtered, washed with chloroform, and the filtrate was acidified with hydrochloric acid and extracted with chloroform. The usual work-up and purification of the crude product by silica gel chromatography gave **5** (65 mg, 16%) (mp 155—156 °C) and 1,5-dimethoxynaphthalene (54 mg, 14%).

1,4-Dimethoxynaphthalene (**7**) and 1,4,5-trimethoxynaphthalene (**9**) (mp 120—121 °C, lit,[10] 119 °C) were prepared in 87 and 86% yield, respectively, by a similar method for synthesis of 1,5-dimethoxynaphthalene by Benthey et al.[11] **7**: mp 86.5—87.5 °C (hexane); IR (KBr) 1622, 1590, 1380, 1270, 1235, 1095, 1082, and 1020 cm^{-1}; ^1H NMR δ=3.85 (s, 6H, 2×OCH_3), 6.56 (s, 2H, ArH), 7.45 (m, 2H, ArH), and 8.21 (m, 2H, ArH); MS, *m/z* 188 (M^+), 173 (M^+-CH_3), and 145. Calcd for $C_{12}H_{12}O_2$: C, 76.57; H, 6.43%. Found: C, 76.97; H, 6.43%.

1,4-Dimethoxy-2-naphthalenecarbaldehyde (8). A solution of **7** (0.98 g, 5.21 mmol) in chloroform (19 ml) was added to a mixture of phosphoryl chloride (8.27 g, 53.9 mmol) and *N,N*-dimethylformamide (3.89 g, 53.2 mmol). The mixture was refluxed for 80 h and decomposed by the addition of ice water, and extracted with chloroform. After the usual work-up, the residue was chromatographed on silica gel to give 1.12 g (99.6%) of **8**. Recrystallization from hexane gave orange crystals, mp 119.5—120.0 °C. IR (KBr) 1675 (C=O), 1598, 1385, 1375, 1130, and 1100 cm^{-1}; ^1H NMR δ=3.98, 4.06 (each s, 3H, OCH_3), 7.09 (s, 1H, ArH-3), 7.38 (m, 2H, ArH), 8.18 (m, 2H, ArH), and 10.56 (s, 1H, CHO); MS, *m/z* 216 (M^+), 201 (M^+-CH_3), 173, and 145. Calcd for $C_{13}H_{12}O_3$: C, 72.21; H, 5.59%. Found: C, 71.89; H, 5.64%.

Formylation of 9 by a Vilsmeier Reaction. A mixture of **9** (961 mg, 4.41 mmol) in chloroform (20 ml) with $POCl_3$ (3.38 g, 22.0 mmol) and DMF (1.61 g, 22.0 mmol) was allowed to react for 10 h in the same manner as the formylation of **7** and gave 867 mg (80%) of 4,5,8-trimethoxy-1-naphthalenecarbaldehyde (**10**) and 140 mg (13%) of 1,4,8-trimethoxy-2-naphthalenecarbaldehyde (**3**).

10: Mp 186.5—187.5 °C (benzene-hexane (2:1)); IR (KBr) 1660 (C=O), 1610, 1590, 1065, and 1028 cm^{-1}; ^1H NMR δ=3.92, 3.93, 4.02 (each s, 3H, OCH_3), 6.90 (s, 2H, ArH-6,7), 6.91 (d, *J*=8.6 Hz, 1H, ArH-3), 7.93 (d, *J*=8.6 Hz, 1H, ArH-2), and 10.89 (s, 1H, CHO); MS, *m/z* 246 (M^+), 231 (M^+-CH_3), and 119. Calcd for $C_{14}H_{14}O_4$: C, 68.28; H, 5.73%. Found: C, 68.11; H, 5.78%.

3: Mp 90—91 °C (hexane) (lit,[2] 89—89 °C). IR (KBr) 1672 (C=O), 1620, 1607, 1583, 1382, and 1080 cm^{-1}; ^1H NMR δ=3.95, 4.01, 4.06 (each s, 3H, OCH_3), 6.99 (dd, *J*=7.9 and 1.2 Hz, 1H, ArH-7), 7.16 (s, 1H, ArH-3), 7.48—7.65 (2d, *J*=8.3 and 7.9 Hz, 1H, ArH-6), 7.92 (dd, *J*=8.3 and 1.2 Hz, 1H, ArH-5), and 10.57 (s, 1H, CHO); MS, *m/z* 246 (M^+), 231, 203, and 188. Calcd for $C_{14}H_{14}O_4$: C, 68.28; H, 5.73%. Found: C, 68.18; H, 5.78%.

Formylation of 5. The reaction of **5** (209 mg, 1.02 mmol) in chloroform (20 ml) with $POCl_3$ (800 mg, 5.1 mmol) and DMF (374 mg, 5.1 mmol) was carried out over 10 h using the same procedure mentioned above for the formylation of **7**, and gave 146 mg (62%) of 4,8-dimethoxy-1-naphthyl formate (**11**) and 56 mg (24%) of 1-hydroxy-4,8-dimethoxy-2-naphthalenecarbaldehyde (**12**).

11: Mp 137—138.5 °C (hexane); IR (KBr) 1730 (ester C=O), 1595, 1405, 1370, 1260, 1145, 1055, 845, 790, and 750 cm^{-1}; ^1H NMR δ=3.90, 3.98 (each s, 3H, OCH_3), 6.75 (d, *J*=8.3 Hz, 1H, ArH-3), 6.88 (dd, *J*=7.9 and 1.3 Hz, 1H, ArH-7), 7.06 (d, *J*=8.3 Hz, 1H, ArH-2), 7.33—7.47 (2d, *J*=9.3 and 7.9 Hz, 1H, ArH-6), 7.97 (dd, *J*=9.3 and 1.3 Hz, 1H, ArH-5), and 8.33 (s, 1H, HCO-); MS, *m/z* 232 (M^+), 204, 189, and 174. Calcd for $C_{13}H_{12}O_4$: C, 67.23; H, 5.21%. Found: C, 65.98; H, 5.12%.

12: Mp 117.5—118.5 °C (hexane); IR (KBr) 1655 (C=O), 1627, 1610, 1470, 1390, 1257, 1065 cm^{-1}; ^1H NMR δ=3.96, 4.10 (each s, 3H, OCH_3), 6.93 (dd, *J*=7.9 and 1.3 Hz, 1H, ArH-7), 7.07 (s, 1H, ArH-3), 7.44—7.57 (2d, *J*=8.3 and 7.9 Hz, 1H, ArH-6), 7.87 (dd, *J*=8.3 and 1.3 Hz, 1H, ArH-5), 10.23 (s, 1H, OH), and 10.52 (s, 1H, CHO); MS, *m/z* 232 (M^+), 217, 199, and 189. Calcd for $C_{13}H_{12}O_4$: C, 67.23; H, 5.21%. Found: C, 67.14; H, 5.24%.

Duff Reaction of 5. A mixture of **5** (204 mg, 1 mmol), hexamethylenetetramine (140 mg, 1 mmol), *p*-toluenesulfonic acid monohydrate (190 mg, 1 mmol), and acetic acid (5 ml) was refluxed for 3 h, decomposed by water and extracted with chloroform. The chloroform solution was washed with brine, dried over anhydrous sodium sulfate, and concentrated. The residue was chromatographed on silica gel to give 142 mg (61%) of **12**. Recrystallization from hexane gave an analytical sample, mp 117.5—118 °C, which did not depress the melting point of the above **12** on admixture.

Methylation of 12. A mixture of **12** (957 mg, 4.12 mmol), methyl *p*-toluenesulfonate (4.74 g, 6.18 mmol), sodium carbonate (3.30 g, 31 mmol) in *o*-dichlorobenzene (12 ml) was refluxed for 2 h. Water was added and the system was extracted with chloroform. After the usual work-up, the residue was purified by silica-gel chromatogaraphy and gave 960 mg (95%) of **3**. Recrystallization from hexane gave an analytical sample, mp 89—90 °C, which did not depress the melting point of **3** from the formylation of **9**.

References

1) Paper IX, on Synthesis of Naphthoquinone Derivatives. Paper VIII, Y. Tanoue, A. Terada, K. Torisu, and H. Taniguchi, *Bull. Chem. Soc. Jpn.*, **62**, 1211 (1989).

2) A. S. Kende, J. P. Gesson, and T. P. Demuth, *Tetrahedron Lett.*, **22**, 1667 (1981).

3) M. Croisy-Delcey and E. Bisagni, *J. Chem. Soc., Chem. Commun.*, **1984**, 897.

4) M. Asano and J. Hase, *J. Pharm. Soc. Jpn.*, **63**, 83 (1943); T. Momose, H. Oya, Y. Ohkura, and M. Iwasaki, *Chem. Pharm. Bull. (Tokyo)*, **2**, 119 (1954).

5) R. L. Hannan, R. B. Barker, and H. Rapoport, *J. Org. Chem.*, **44**, 2153 (1979).

6) H. Uno, *J. Org. Chem.*, **51**, 350 (1986).

7) A. Terada, Y. Tanoue, A. Hatada, and H. Sakamoto, *Bull. Chem. Soc. Jpn.*, **60**, 205 (1987).

8) H. Wynberg and E. W. Meijer, *Org. React.*, **28**, 1 (1982).

9) J. C. Duff, *J. Chem. Soc.*, **1941**, 547.

10) G. Malesani and M. G. Ferlin, *J. Heterocycl. Chem.*, **24**, 513 (1987).

11) W. H. Benthey, R. Robinson, and C. Weizmann, *J. Chem. Soc.*, **1907**, 104.

The Dehalogenation of *vic*-Dihaloalkanes to Alkenes with Sodium Trithiocarbonate or Sodium Dithiocarbonate in the Presence of Phase-Transfer Catalysts

Akira SUGAWARA,* Atsushi NAKAMURA, Akitoshi ARAKI, and Ryu SATO*,†
Department of Industrial Chemistry, Tsuruoka Technical College, Tsuruoka, Yamagata 997
†Departmernt of Resource Chemistry, Faculty of Engineering, Iwate University, Morioka 020
(Received March 6, 1989)

Synopsis. The reductive dehalogenation of *vic*-dihaloalkanes with aqueous sodium trithiocarbonate or sodium dithiocarbonate in the presence of a phase-transfer catalyst gave the corresponding alkenes in high yields under mild conditions.

There have been numerous reports on the methods of synthesizing various organic compounds using phase-transfer catalysts.[1] These phase-transfer systems have been effectively used to prepare many organosulfur compounds, such as sulfides[2] and dithiocarbonates.[3] Recently, we ourselves have also reported the synthesis of alkyl, aryl, alkanediyl, and cyclic trithiocarbonates in the presence of phase-transfer catalysts (PTC).[4] For the dehalogenations of *vic*-dihaloalkanes to alkenes, several procedures using a variety of reagents have been developed hitherto.[5] An interesting dehalogenation was provided by Nakayama and his co-workers.[6] They showed an effective dehalogenation of *vic*-dibromoalkanes to alkenes using aqueous sodium sulfide in the presence of a phase-transfer catalyst. The use of sodium hydrogensulfide has also been reported.[7] In the course of our investigations of the chemistry of various trithiocarbonates, we have now found that *vic*-dihaloalkanes such as 1,2-dibromo-1,2-diphenylethane (**1**) are reductively dehalogenated under mild conditions by treatment with sodium trithiocarbonate or sodium dithiocarbonate in the presence of PTC to give the corresponding alkenes in excellent yields (Scheme 1).

As shown in Table 1, the present reaction proceeded smoothly in the phase-transfer system when the mixture was stirred for a short period between 0 °C and room temperature. Consequently, we could obtain several alkenes from *vic*-dihaloalkanes in high yields. Trioctylmethylammonium chloride (TOMAC) was employed as a typical PTC and gave favorable results. It should be noted that the reaction of *meso*-1,2-dibromo-1,2-diphenylethane (**1a**) gave *trans*-stilbene (**2a**) exclusively (Entry 1, Table 1), whereas the *dl*-1,2-dibromo-1,2-diphenylethane (**1b**) afforded a mixture of *cis*- and *trans*-stilbene (Entry 7). No alkene was formed in the absence of PTC (Entry 4). In addition, the treatment of the *vic*-dihaloalkane (**1**) with aq. NaOH alone did not give any alkenes (Entry 6). When sodium trithiocarbonate was used as the reducing reagent, the reaction could be monitored by the decolorization of the orange color of the reaction mixture. The dehalogenation of **1a** was completely inhibited by the addition of a radical scavenger such as *N'*,*N'*-diphenyl-*N*-picrylhydrazyl to the reaction system. In the dark, we could also observe considerable retardation (Entries 1 and 2). Furthermore, the reaction of **1b** with sodium trithiocarbonate was greatly accelerated by the irradiation of a 300 W ref-lamp (Entry 8). Based on these results, the present reaction seems not to proceed through the E2-type mechanism proposed by Landini for the dehalogenation of *vic*-dihaloalkanes with sodium sulfide in the presence of PTC,[7] but through a radical mechanism involving one electron transfer which is similar to that proposed by Kormblum for the reductive elimi-

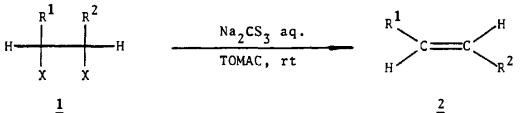

1 2

Scheme 1.

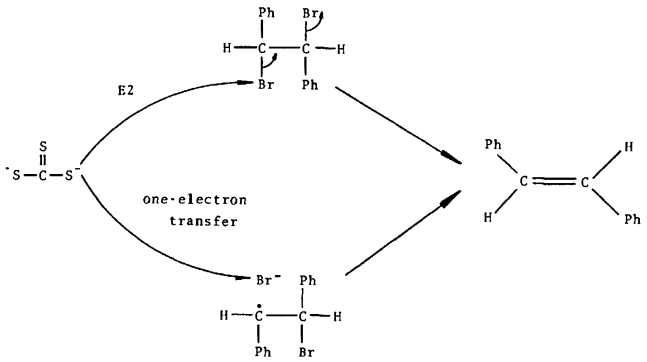

Scheme 2.

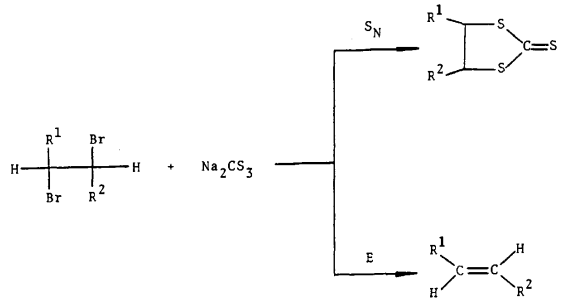

$R^1 = R^2$ = Alkyl	S_N
$R^1 = R^2$ = Phenyl	E
R^1 = Phenyl, R^2 = Carbonyl	E
R^1 = Phenyl, R^2 = H	E and S_N

Scheme 3.

Table 1. Reductive Dehalogenation of *vic*-Dihaloalkanes to Alkenes

Entry[a]	Substrates	Reducing Reagent	Reaction		Yield/%[b]	Products	Mp/°C
			Time/min	Temp/°C			
1[c]	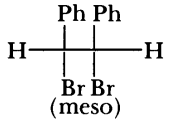	Na_2CS_3	10	rt	100	*trans*-Stilbene	118—120[9]
2[d]			10	rt	52		
3			60	0	100		
4[e]			3(h)	rt	0		
5[f]		CS_2+NaOH	60	rt	100		
6		NaOH	3(h)	rt	0		
7	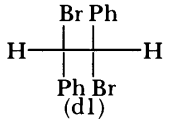	Na_2CS_3	5(h)	rt	95	Stilbene[9] (cis : trans=4 : 1)[g]	
8[h]			70	rt	98		
9[f]		CS_2+NaOH	3(h)	50	95		
10[i]	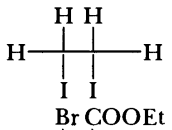	Na_2CS_3	10	rt	100	Ethene[10]	
11	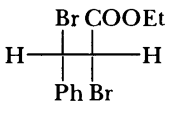	Na_2CS_3	60	rt	94	Ethyl cinnamate[11]	
12[f]		CS_2+NaOH	60	rt	97		
13	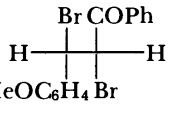	Na_2CS_3	60	rt	97	4-Methoxychalcone	72—74[12]
14[f]		CS_2+NaOH	60	rt	96		
15[j]	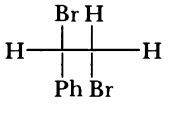	Na_2CS_3	60	50	78	Styrene[13]	
16[f]		CS_2+NaOH	4(h)	50	73		

a) *vic*-Dihaloalkanes, 2 mmol; Na_2CS_3, 6 mmol; TOMAC, 0.08 mmol. b) Isolated yields based on substrates. c) The reaction was inhibited by the addition of a radical scavenger such as *N'*,*N'*-diphenyl-*N*-picrylhydrazyl (0.1 mmol). d) The reaction was carried out in the dark. e) The reaction was carried out in the absence of PTC. f) A mixture of CS_2 (10 mmol) and NaOH (10 mmol) in water (10 ml) was stirred for 2 h at room temperature. g) By NMR analyses. h) The reaction was carried out under irradiation by a ref-lamp. i) The ethene liberated was collected in a gas buret. j) 4-Phenyl-1,3-dithiolane-2-thione was formed in a low yield (7%).

nation of *vic*-dinitro compounds to alkenes (Scheme 2).[8]

It is noteworthy that the elimination-type reaction (E) predominates over nucleophilic substitution (S_N) for the reaction of even *vic*-dihaloalkanes bearing an electron-withdrawing group, such as phenyl and carbonyl groups with sodium trithiocarbonate (Scheme 3).

As has been mentioned above, we succeeded in a new reductive dehalogenation of *vic*-dihaloalkanes to alkenes in the phase-transfer system. We wish to emphasize that the present procedure has several advantages, namely, efficiency of conversion, simplicity of operation, and mild conditions.

Experimental

The IR spectra were obtained on a Jasco IR-G spectrometer, while the NMR spectra were measured with a Varian Gemini-200 spectrometer (200 MHz) in $CDCl_3$, using TMS as the internal standard. The elemental analyses were determined with a Yanagimoto MT-3 apparatus. The ref-lamp used was a National REF-300W. All the melting points are uncorrected.

General Procedure. To a solution of *meso*-1,2-dibromo-1,2-diphenylethane (2 mmol) in benzene (5 ml) we added a 30% aqueous Na_2CS_3 solution (6 mmol) and trioctylmethylammonium chloride (0.08 mmol), the mixture was then stirred for 10 min at room temperature. After the completion of the reaction, the organic layer was washed with water and then dried over sodium sulfate. The residue obtained by the evaporation of the solvent was passed through a short silica gel column, using dichloromethane as the eluent, to give *trans*-stilbene in a 100% yield. The structure of the products was characterized by ^1H NMR, IR, and elemental analyses. The physical and spectral data of the alkenes were also compared with those authentic samples.[9-13]

4-Phenyl-1,3-dithiolane-2-thione: Mp 83—85 °C; IR (KBr) 1050 cm^{-1}; ^1H NMR ($CDCl_3$) δ=4.10 (m, 2H, CH_2), 5.65 (m, 1H, CH), and 7.40 (m, 5H, arom). Found: C, 50.61; H, 3.96%. Calcd for $C_9H_8S_3$: C, 50.87; H, 3.77%.

References

1) C. M. Straks, "Phese Transfer Catalysis," American Chemical Society (1986), p. 1.

2) I. Tabushi and T. Nishiya, "Sokanido Shokubai," Kagaku Dojin (1978), p. 253 and the referenced cited therein.

3) I. Degani and R. Fochi, *Synthesis*, **1978**, 365; I. Degani, R. Fochi, and V. Regondi, *ibid.*, **1980**, 375.

4) A. Sugawara, M. Shirahata, S. Sato, and R. Sato, *Bull. Chem. Soc. Jpn.*, **57**, 3353 (1984); A. Sugawara, K. Hasegawa, K. Suzuki, Y. Takahashi, and R. Sato, *ibid.*, **60**, 435 (1987); A. Sugawara, T. Sato, and R. Sato, *ibid.*, **62**, 339 (1989).

5) Nippon Kagakukai, "Shin Jikken Kagaku Koza 14-1," Maruzen (1977), p. 157; K. Fukunaga and H. Yamaguchi, *Synthesis*, **1981**, 879; F. Sato, T. Akiyama, K. Iida, and M. Sato, *ibid.*, **1982**, 1025; D. Savoia, E. Tagliavini, C. Trombini, and A. Umani-Ronchi, *J. Org. Chem.*, **47**, 876 (1982).

6) J. Nakayama, H. Machida, and M. Hoshino, *Tetrahedron Lett.*, **24**, 3001 (1983).

7) D. Landini, L. Milesi, M. L. Quadi, and F. Rolla, *J. Org. Chem.*, **49**, 152 (1984).

8) N. Kormblum, S. D. Boyd, H. W. Pinnick, and R. G. Smith, *J. Am. Chem. Soc.*, **93**, 4316 (1971).

9) W. C. Kray and C. E. Castro, *J. Am. Chem. Soc.*, **86**, 4603 (1964); D. Landini, S. Quici, and F. Rolla, *Synthesis*, **1975**, 397.

10) G. S. Reddy and J. H. Goldstein, *J. Am. Chem. Soc.*, **83**, 2045 (1961).

11) W. S. Wadsworth, Jr. and W. D. Emmons, *J. Am. Chem. Soc.*, **83**, 1733 (1961).

12) D. S. Noyce and W. A. Pryor, *J. Am. Chem. Soc.*, **81**, 618 (1959).

13) G. S. Reddy, C. E. Booyer, and J. H. Goldstein, *J. Chem. Phys.*, **34**, 700 (1961).

The Enantiomeric Purity of (*S*)- and (*R*)-4-Methylfarnesols Synthesized from Artificial Substrates by Means of a Farnesyl Diphosphate Synthase Reaction

Shin-ichi OHNUMA, Tanetoshi KOYAMA, and Kyozo OGURA*
Chemical Research Institute of Non-Aqueous Solutions, Tohoku University, Katahira, Sendai 980
(Received March 8, 1989)

Synopsis. Both (*S*)- and (*R*)-4-methylfarnesols, synthesized respectively from (*E*)- and (*Z*)-3-methyl-3-pentenyl diphosphates by means of farnesyl diphosphate synthase reactions, were demonstrated to be of almost 100% enantiomeric purity.

Although the utilization of enzymes to prepare chiral compounds of synthetic value is well documented,[1] only a limited number of studies have dealt with enzymes catalyzing carbon-to-carbon-bond formation. We have previously demonstrated the synthetic value of pig-liver farnesyl diphosphate synthase, showing that this enzyme can be used to prepare both (*S*)- and (*R*)-4-methylfarnesols and their homologues directly by the type of C-C bond-forming reactions[2] shown in Scheme 1. We have also synthesized insect metabolites and related compounds using some of these products as chiral synthons.[3-5] However, the enantiomeric purities of the 4-methylfarnesols synthesized by this enzymatic method remained to be determined accurately, though roughly opposite ORD spectra were previously observed for these alcohols.[2] We here wish to report evidence to show that the enantiomeric excesses of these alcohols are both almost 100%.

Results and Discussion

In order to determine the enantiomeric excess of the products derived from (*E*)- (**1**) and (*Z*)-3-methyl-3-pentenyl diphosphate (**2**), we first examined the conversion of racemic (2*E*,6*E*)-4-methylfarnesol (**3**) into diastereomeric derivatives that could be separated from each other. The racemic alcohol **3** was synthesized as follows: The Wittig reaction of 3-geranyl-2-butanone (**6**) with diethyl ethoxycarbonylmethylphosphonate gave a mixture of the *Z*,*E*- and *E*,*E*-isomers of ethyl 4-methylfarnesate, from which ethyl (*RS*)-(2*E*,6*E*)-4-methylfarnesate (**7**) was purified by silica-gel chromatography. Racemic **3** was then obtained by the $LiAlH_4$ reduction of **7**. The alcohol **3** was oxidized with MnO_2 to the aldehyde **4**, which was then oxidized with $NaClO_2$[6] to give (2*E*,6*E*)-4-methylfarnesic acid (**8**) in a quantitative yield. A chromatographic analysis of the methyl ester derived from **8** showed that no isomerization to the 2*Z* isomer had taken place during the oxidation. The oxidation of **4** was also carried out in D_2O so that epimerization could be monitored; it was confirmed by mass spectrometry that no deuterium was incorporated into the acid. The acid was then treated with (*S*)-1-(1-naphthyl)ethylamine in the presence of dicyclohexyl-

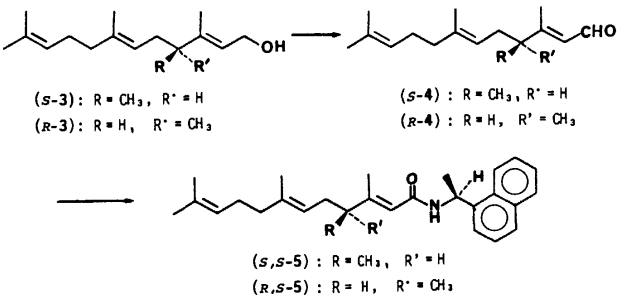

Scheme 2. Conversion of (*S*)- and (*R*)-4-methylfarnesols to the corresponding acid amides.
(1) MnO_2 (2) $NaClO_2$ (3) (*S*)-1-(1-Naphthyl)-ethylamine+DCC.

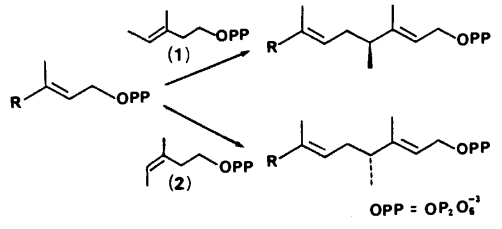

Scheme 1. Chiral synthesis by pig liver farnesyl diphosphate synthase.

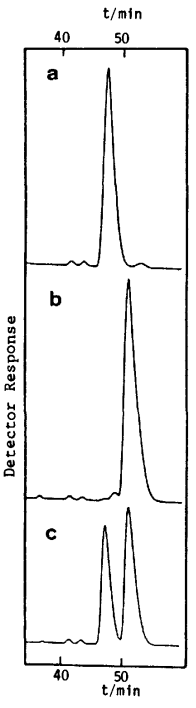

Fig. 1. HPLC of (a) (*R*,*S*)-**5**, (b) (*S*,*S*)-**5**, and (c) a mixture of (*R*,*S*)-**5** and (*S*,*S*)-**5**.

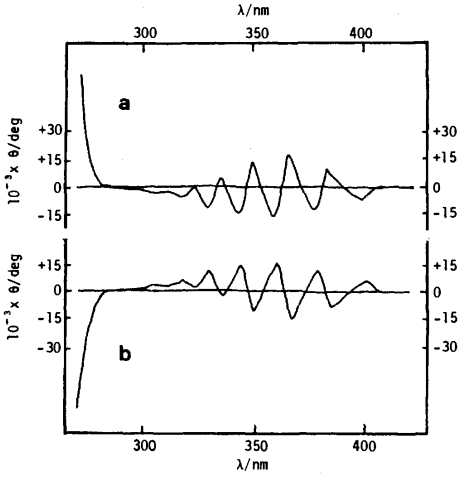

Fig. 2. CD spectra of (a) (*S*)-**4** (c=23.8 mol m^{-3}) and (b) (*R*)-**4** (c=19.8 mol m^{-3}).

carbodiimide to give a diastereomeric mixture of the corresponding amides, which could subsequently be well separated from each other by means of HPLC. Then, the (*S*)-4-methylfarnesol [(*S*)-**3**] and its *R* enantiomer [(*R*)-**3**], synthesized by the farnesyl diphosphate synthase method, were similarly converted into the corresponding amides, (*S,S*)-**5** and (*R,S*)-**5** respectively. As is shown in Fig. 1, the chromatography of the amides derived from the *S* and *R* isomers indicated that both (*S*)- and (*R*)-4-methylfarnesols had high enantiomeric purities. In other words, the introduction of a methyl group on either the *E* or the *Z* side of C-4 of isopentenyl diphosphate does not disturb the stereochemical course of the C-C bond formation.

The CD spectra of the (*S*)-4-methylfarnesal [(*S*)-**4**] and its *R* enantiomer [(*R*)-**4**], which are perfectly antipodal, also support the high optical purities of these compounds (Fig. 2).

Experimental

The (*S*)-1-(1-naphthyl)ethylamine was purchased from Aldrich. The alkaline phosphatase was obtained from Boehringer-Mannheim. The (*E*)-3-methyl-3-pentenyl diphosphate (**1**), its *Z* isomer (**2**), and geranyl diphosphate were prepared from the corresponding alcohols by diphosphorylation according to the method of Poulter et al.[7]

3-Geranyl-2-butanone (6). A solution of geranyl chloride (5.0 g, 28.9 mmol) in 30 ml of absolute ethanol was added, drop by drop, to a solution of the sodium compound of ethyl 2-methylacetoacetate (ethyl 2-methylacetoacetate, 4.59 g, 31.0 mmol; sodium ethoxide, 2.95 g, 43.4 mmol; and absolute ethanol, 170 ml) under a nitrogen atmosphere at 0 °C. After stirring has been continued at room temperature for 12 h, water was added and the mixture was extracted with hexane. The hexane extract was washed with saturated solutions of NH_4Cl and NaCl and dried over $MgSO_4$. The solvent was evaporated, and the residue was chromatographed on a column of silica gel. Elution with hexane/ethyl acetate (10/1) gave 6.75 g (83.4%) of ethyl 2-geranyl-2-methyl-3-oxobutanoate. A mixture of the ester (6.54 g, 23.2 mmol), 2 M KOH (150 ml; 1 M=1 mol dm^{-3}), and ethanol (25 ml) was stirred overnight at room temperature, after which the mixture was acidified and extracted with diethyl ether. The ether extract was worked up routinely to give **6** (4.82 g, 99%).

Ethyl (*RS*)-(2*E*,6*E*)-4-Methylfarnesate (7). To a suspension of NaH (1.06 g, 44 mmol) in dry benzene we added diethyl ethoxycarbonylmethylphosphonate (5.26 g, 23 mmol) and **6** (4.42 g, 21.3 mmol); the mixture was stirred at room temperature for 1 h and then at 65 °C overnight. Water and hexane were then added, and the mixture was shaken. The organic layer was treated as usual to give a mixture (22/3) of **7** and its 2*Z* isomer (1.50 g, 24%), from which the 2*E* isomer **7** was purified by HPLC on silica gel with hexane/ethyl acetate (200/1).

(*RS*)-4-Methylfarnesol (3). Ethyl 4-methylfarnesate (**7**, 194.2 mg, 0.7 mmol) was added under a nitrogen atmosphere to a suspension of $LiAlH_4$ (55.7 mg, 1.4 mmol) in diethyl ether (10 ml), after which the mixture was stirred at 0 °C. The reaction mixture was worked up routinely, and the product was purified by silica-gel chromatography with hexane/ethyl acetate (5/1). The yield of (*RS*)-**3** was 152.7 mg; 93%.

(*RS*)-4-Methylfarnesic Acid (8). A solution of $NaH_2PO_4 \cdot 2H_2O$ (107.0 mg, 0.68 mmol) and $NaClO_2$ (80.0 mg, 0.88 mmol) in water (0.81 ml) was added, drop by drop, to a stirred solution of (*RS*)-4-methylfarnesal (**4**, 21.3 mg), obtained by the MnO_2 oxidation of (*RS*)-**3** in *t*-butyl alcohol (1.9 ml) and 2-methyl-2-butene (0.5 ml). After being stirred at room temperature for 50 min, the mixture was diluted with water and extracted with hexane. The hexane extract was then purified by chromatography on silica gel with hexane/ethyl acetate (5/1) to give **8** in a quantitative yield.

For the reaction in D_2O, $NaD_2PO_4 \cdot 2D_2O$ and $(CH_3)_3COD$ were used instead of $NaH_2PO_4 \cdot 2H_2O$ and *t*-butyl alcohol.

***N*-[(*S*)-1-(1-Naphthyl)ethyl]-(*S*)-4-methylfarnesamide [(*S,S*)-5] and *N*-[(*S*)-1-(1-Naphthyl)ethyl]-(*R*)-4-methylfarnesamide [(*R,S*)-5].** (*S*)-1-(1-Naphthyl)ethylamine (7.5 mg, 0.044 mmol) was added to a solution of dicyclohexylcarbodiimide (9.9 mg, 0.048 mmol) and (*RS*)-4-methylfarnesic acid (**8**, 10.0 mg, 0.04 mmol) in dichloromethane, after which the mixture was stirred at room temperature overnight. The reaction mixture was then extracted with diethyl ether, and the extract was washed with saturated solutions of NH_4Cl, $NaHCO_3$, and NaCl. After the removal of the solvent, the residue was purified by silica-gel chromatography to give a diastereomeric mixture of the amides in a 23% yield.

Enzymatic Synthesis of (*S*)-4-Methylfarnesol [(*S*)-3] and Its *R* Enantiomer [(*R*)-3]. The enzymatic synthesis was carried out essentially by the same procedure as has been described previously,[2] except for the scale of incubation. The incubation volumes were 1.8 dm^3 and 7.2 dm^3 for the syntheses of (*S*)-**3** and (*R*)-**3** respectively. The yields of (*S*)-**3** and (*R*)-**3** were 24.8 mg and 47.0 mg respectively.

(*S*)-4-Methylfarnesal [(*S*)-4] and Its *R* Enantiomer [(*R*)-4]. Manganese dioxide (20 equiv) was added to a solution of (*S*)-**3** (24.8 mg) or (*R*)-**3** (47.0 mg) in dichloromethane, and the mixture was stirred at room temperature overnight. After the mixture had then been filtered, the filtrate was concentrated and the product was purified by silica-gel chromatography. The yields were both quantitative.

Conversion of (*S*)-4 and (*R*)-4 to Amides (*S,S*)-5 and (*R,S*)-5. (*S*)-4-Methylfarnesic acid [(*S*)-**8**, 15.4 mg] and its *R* enantiomer [(*R*)-**8**, 24.5 mg], which had been obtained respectively from (*S*)-**4** and (*R*)-**4** by $NaClO_2$ oxidation in D_2O, were treated with cyclohexylcarbodiimide as has been described for the reaction of (*RS*)-4-methylfarnesic acid (**8**).

HPLC Separation of (*S,S*)-5 and (*R,S*)-5. The separation of the diastereomeric amides, (*S,S*)-**5** and (*R,S*)-**5**, was performed by chromatography on a 4.6×250 mm column of Zorbax Sil with hexane/ethyl acetate saturated with water (30/1) at a flow rate of 2 ml min^{-1}. The enantiomeric

purities of (*S*,*S*)-**5** and (*R*,*S*)-**5** were both more than 98% ee.

This work was supported by the Asahi Glass Foundation for industrial technology, by special coordination funds of the Science and Technology Agency, and by a Grant-in-Aid for Scientific Research No. 63616502 from the Ministry of Education, Science and Culture. We wish to thank Dr. Nobuyuki Harada of this Institute for his help in the CD spectral measurements.

References

1) J. B. Jones, *Tetrahedron*, **42**, 3351 (1986).
2) T. Koyama, A. Saito, K. Ogura, and S. Seto, *J. Am. Chem. Soc.*, **102**, 3614 ((1980).
3) M. Kobayashi, T. Koyama, K. Ogura, S. Seto, F. J. Ritter, and I. E. M. Brüggemann-Rotgans, *J. Am. Chem. Soc.*, **102**, 6602 (1980).
4) T. Koyama, M. Matsubara, K. Ogura, I. E. M. Brüggemann, and A. Vrielink, *Naturwissenshaften*, **70**, 469 (1983).
5) T. Koyama, K. Ogura, F. C. Baker, G. C. Jamieson, and D. A. Schooley, *J. Am. Chem. Soc.*, **109**, 2853 (1987).
6) B. S. Bal, W. E. Childers, Jr., and H. W. Pinnick, *Tetrahedron*, **37**, 2091 (1981).
7) V. J. Davisson, A. B. Woodside, and C. D. Poulter, *Methods Enzymol.*, **110**, 130 (1985).

An Oxidative Dimerization of Anthrones by Oxygen-Metal Acetate System

Masahiko YAMAGUCHI,* Koichi HASEBE, Minoru UCHIDA,
Hirofumi HIGASHI, and Toru MINAMI
Department of Applied Chemistry, Kyushu Institute of Technology,
Sensui-cho, Tobata, Kitakyushu 804
(Received March 20, 1989)

Synopsis. Anthrones were oxidatively dimerized with oxygen in the presence of $Pb(OAc)_2$ giving 9,9′-bianthracene-10,10′(9*H*,9′*H*)-diones. The dimerization proceeds under mild reaction conditions, and gives products in good yields. Binaphthacenedione and bipentacenedione were also synthesized.

9′9-Bianthracene-10,10′(9*H*,9*H*)-diones and their derivatives possess interesting chemical, physical, or biological properties. For example, sennosides are natural purgatives,[1] and photochromism, thermochromism, or piezochromism of $\Delta^{10,10'}$-bianthrone, dehydro derivative of 9,9′-bianthracene-10,10′(9*H*, 9′*H*)-dione, has been known.[2] As for the synthesis of 9,9′-bianthracene-10,10′(9*H*,9′*H*)-diones, oxidative dimerization of anthrones has been conducted using several oxidants,[1-6] of which $FeCl_3$ was most frequently employed.[1a,2a,3] Although the dimerization can be carried out with oxygen more conveniently,[7] the reaction was sluggish, and relatively strong basic conditions were required for promotion. During our investigations on the synthesis of polycyclic aromatic compounds,[8] a novel oxygen-induced dimerization of anthrones, which proceeds under mild reaction conditions, was found.

When 2-methoxycarbonyl-3-methoxycarbonylmethyl-1,9-anthracenediol (**1a**)[8f] was treated with $Pb(OAc)_2$ in methanol at room temperature, oxidative dimerization reaction proceeded smoothly and 4,4′-dihydroxy-3,3′-bis(methoxycarbonyl)-2,2′-bis(methoxycarbonylmethyl)-9,9′-bianthracene-10,10′(9*H*,9′*H*)-dione (**2a**) was obtained in quantitative yield. The use of $Cd(OAc)_2$ gave **2a** in lower yield. Other metal acetates were less effective. Under oxygen atmosphere the reaction was accelerated. Although mass spectra of **2a** showed the parent peak corresponding to the monomer, the dimeric structure was determined by conversion to acetate **3a** or methyl ether **4a**, which gave parent peaks of dimers (Scheme 1). ^1H NMR spectra of **1a** showed the presence of two stereoisomers. Since **1a** exists in keto-form, they are *meso*- and *dl*-isomers concerning 9- and 9′-chiral centers.[9]

Several other anthrones were oxidatively dimerized in the presence of $Pb(OAc)_2$ in good yields (Table 1). Under the reaction conditions, 1,8-dihydroxyanthrone (**1c**) gave dimer **2c** of thermodynamically less stable *pseudoaxial-pseudoaxial*-type conformation rather than *pseudoequatorial-pseudoequatorial*-type.[7b] Two stereoisomers synthesized by the dimerization of anthrone **1d** or 12-naphthacenone **1e** were separable by silica gel chromatography. Equilibration between *meso*- and *dl*-isomer was not observed. The intercon-

Table 1. Oxidative Dimerization of Anthrones

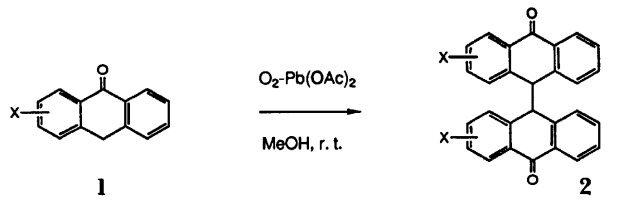

1 2

Entries	Anthrones		Yields/%
1	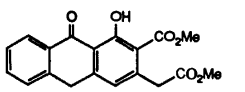	**1a**	92[a], 41[a,b]
2	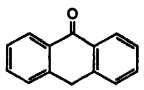	**1b**	84
3	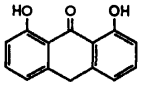	**1c**	41, 23[b]
4	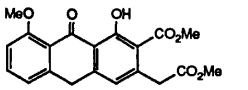	**1d**	73[a]
5	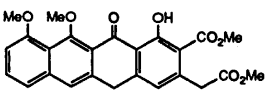	**1e**	59[a]

a) The products were a 1 : 1 mixture of two diastereomers.
b) Instead of $Pb(OAc)_2$, $Cd(OAc)_2$ was used.

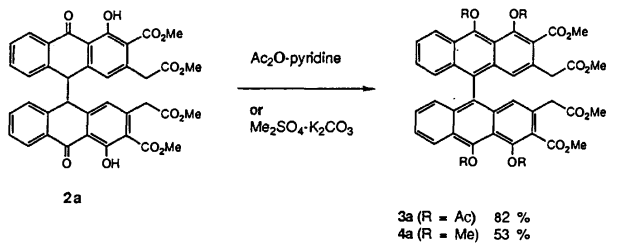

Scheme 1.

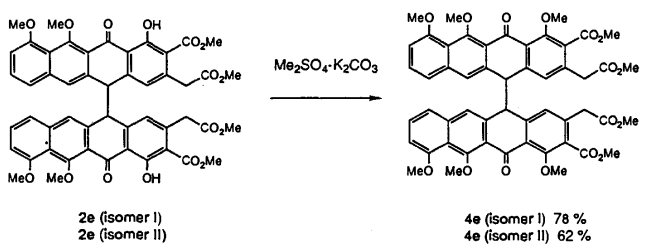

Scheme 2.

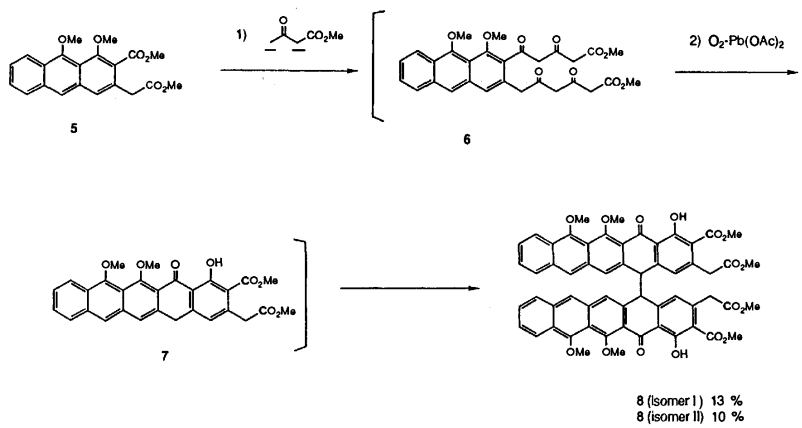

Scheme 3.

version did not proceed even under basic conditions. Each of the two isomers of **2e** gave distinct methylated product at 1-hydroxy group by treating with dimethyl sulfate and K_2CO_3 (Scheme 2). It is presumed that enolization is inhibited by severe steric repulsion between 12-hydroxyl group and substituents at 1- and 11-position in the planar structure of enol form. The behavior of **2e** is contrasted to that of **2a** lacking 8-substituent, which readily aromatized to **4a** (Cf. Scheme 1).

The dimerization reaction was applied to pentacenone **7** formed from dimethoxyanthracene **5** (Scheme 3). According to the reactions developed in our laboratory,[8] **5** was treated with methyl acetoacetate dianion followed by $Pb(OAc)_2$, and 5,5′-dipentacene-14,14′(5*H*,5′*H*)-dione (**8**) was obtained as a separable mixture of two stereoisomers. Here, $Pb(OAc)_2$ serves as the promoter of intramolecular condensation of polyketide intermediate **6** and oxidative dimerzation of **7**.

Experimental

Melting points were not corrected. NMR spectra were obtained on a JEOL JNM-FX-60. Chemical shift values are given in ppm relative to internal Me_4Si. IR spectra were recorded on a Shimadzu IR-408. High-resolution mass spectra were taken with JEOL JMS-DX-300. UV spectra were obtained on a Hitachi Model 150-20 double beam spectrophotometer.

1,1′-Dihydroxy-2,2′-bis(methoxycarbonyl)-3,3′-bis(methoxycarbonylmethyl)-10,10′,11,11′-tetramethoxy-5,5′-binaphthacene-12,12′(5*H*,5′*H*)-dione (2e). A mixture of (**1e**,[8f] 60 mg, 0.13 mmol) and $Pb(OAc)_2 \cdot 3H_2O$ (184 mg, 0.68 mmol) in methanol (4 mL) was stirred overnight vigorously. The mixture was filtered, and washed with dichloromethane. Solvents were removed in vacuo, and the residue was chromatographed on silica gel to give 16 mg (26%) of Isomer I (with higher R_f) and 19 mg (32%) of Isomer II (with lower R_f). Isomer I: Mp 222—225 °C ($CHCl_3$-hexane). ^1H NMR ($CDCl_3$) δ=3.57 (6H, s), 3.77 (6H, s), 3.90 (4H, s), 3.94 (6H, s), 3.98 (6H, s), 4.59 (2H, s), 6.36 (2H, s), 6.83 (2H, d, J=7 Hz), 7.04 (2H, s), 7.06 (2H, d, J=7 Hz), 7.50 (2H, t, J=7 Hz), 12.99 (2H, s). IR (KBr) 3400, 1740, 1720, 1630, 1605 cm^{-1}. HRMS Calcd for $C_{25}H_{22}O_8$: 450.1314. Found: 450.1282 (M/2+H). Isomer II: Mp 228—230 °C ($CHCl_3$-hexane). ^1H NMR ($CDCl_3$) δ=3.70 (16H, s), 3.92 (6H, s), 3.98 (6H, s), 4.66 (2H, s), 6.36 (2H, s), 6.85 (2H, d, J=8 Hz), 6.98 (2H, s), 7.09 (2H, d, J=8 Hz), 7.47 (2H, t, J=8 Hz), 12.94 (2H, s). IR (KBr) 3300, 1735, 1710, 1630, 1610 cm^{-1}. HRMS Calcd for $C_{25}H_{22}O_8$: 450.1314. Found: 450.1321 (M/2+H).

4,4′-Dihydroxy-3,3′-bis(methoxycarbonyl)-2,2′-bis(methoxycarbonylmethyl)-9,9′-bianthracene-10,10′(9*H*,9′*H*)-dione (2a). ^1H NMR ($CDCl_3$) δ=3.71 (5H, s), 3.74 (5 H, s), 3.93 (3H, s), 3.96 (3H, s), 4.61 (1H, s), 4.63 (1H, s), 6.33 (1H, s), 6.3—6.9 (2H, m), 6.68 (1H, s), 7.2—7.5 (4H, m), 7.7—8.0 (2H, m), 12.83 (1H, s), 12.88 (1H, s). IR (KBr) 3400, 1735, 1630, 1595 cm^{-1}. HRMS Calcd for $C_{19}H_{16}O_6$: 340.0947. Found: 340.0950 (M/2+H).

9,9′-Bianthracene-10,10′(9*H*,9′*H*)-dione (2b). Mp 270—272 °C decomp ($CHCl_3$). Lit, 264—266 °C decomp.[10] ^1H NMR spectra was identical to the reported data.[10]

4,4′,8,8′-Tetrahydroxy-9,9′-bianthracene-10,10′ (9*H*,9′*H*)-dione (2c). Mp 237 °C decomp (benzene). Lit, 230 °C decomp.[7b] ^1H NMR was identical to the reported data of *pseudoaxial-pseudoaxial*-type conformation.[7b]

4,4′-Dihydroxy-5,5′-dimethoxy-3,3′-bis(methoxycarbonyl)-2,2′-bis(methoxycarbonylmethyl)-9,9′-bianthracene-10,10′(9*H*,9′*H*)-dione (2d). Isomer I (with higher R_f): Mp 185—186 °C ($CHCl_3$-hexane). ^1H NMR ($CDCl_3$) δ=3.74 (6H, s), 3.81 (4H, s), 3.85 (6H, s), 3.95 (6H, s), 4.51 (2H, s), 5.88 (2H, d, J=7 Hz), 6.87 (2 H, s), 6.88 (2H, d, J=7 Hz), 7.26 (2H, t, J=7 Hz), 12.93 (2H, s). IR (KBr) 3500, 1735, 1620 cm^{-1}. UV ($CHCl_3$) λ_{max} 353 nm. HRMS Calcd for $C_{20}H_{18}O_7$: 370.1052. Found: 370.1079 (M/2+H). Isomer II (with lower R_f): Mp 192—194 °C ($CHCl_3$-hexane). ^1H NMR ($CDCl_3$) δ=3.65 (4H, s), 3.70 (6H, s), 3.92 (12H, s), 4.48 (2H, s), 6.25 (2H, s), 6.44 (2H, d, J=8 Hz), 6.93 (2H, s), 7.40 (2H, t, J=8 Hz), 12.87 (2H, s). IR (KBr) 3400, 1735, 1625 cm^{-1}. UV ($CHCl_3$) λ_{max} 353 nm. HRMS Calcd for $C_{20}H_{18}O_7$: 370.1052. Found: 370.1043 (M/2+H).

3,3′-Bis(methoxycarbonyl)-2,2′-bis(methoxycarbonylmethyl)-4,4′,10,10′-tetramethoxy-9,9′-bianthracene (4a). Under a nitrogen atmosphere, a mixture of **2a** (68 mg, 0.21 mmol), K_2CO_3 (119 mg, 0.86 mmol), dimethyl sulfate (0.5 mL), and acetone (5 mL) was stirred at reflux for 3 h. Then 2 M hydrochloric acid (1 M=1 mol dm^{-3}) was added, and organic materials were extracted twice with chloroform. Combined extracts were washed with water and brine, dried (Na_2SO_4), concentrated, and chromatographed on silica gel to give **4a** (41 mg, 53%). Mp 167—172 °C ($CHCl_3$-hexane). ^1H NMR ($CDCl_3$) δ=3.46 (10H, s), 3.96 (6H, s), 4.16 (6H, s), 4.22 (6H, s), 6.76 (2H, s), 6.7—7.6 (6H, m), 8.53 (2H, d, J=8 Hz). IR (KBr) 1740 cm^{-1}. UV ($CHCl_3$) λ_{max} 417, 395, 375, 269 nm. HRMS Calcd for $C_{42}H_{38}O_{12}$: 734.2364. Found: 734.2403.

1,1′,10,10′,11,11′-Hexamethoxy-2,2′-bis(methoxycarbon-

yl)-3,3′-bis(methoxycarbonylmethyl)-5,5′-binaphthacene-12,12′(5*H*,5′*H*)-dione (4e). Two isomers I and II of **2e** were methylated in 78 and 62% yields, respectively. **4e** (isomer I) synthesized from **2e** (isomer I): Mp 239—242 °C ($CHCl_3$-hexane). ^1H NMR ($CDCl_3$) δ=3.68 (6H, s), 3.70 (6H, s), 3.90 (6H, s), 3.91 (12H, s), 3.96 (4H, s), 4.53 (2H, s), 6.61 (2H, s), 6.7—7.1 (4H, m), 6.96 (2H, s), 7.36 (2H, t, J=8 Hz). IR (KBr) 1735, 1675, 1615, 1595, 1560 cm^{-1}. UV ($CHCl_3$) λ_{max} 383 nm. HRMS Calcd for $C_{26}H_{23}O_8$: 463.1392. Found: 463.1374 (M/2). **4e** (isomer II) synthesized from **2e** (isomer II): Mp 259—262 °C ($CHCl_3$-hexane). ^1H NMR ($CDCl_3$) δ=3.64 (10H, s), 3.73 (6H, s), 3.87 (6H, s), 3.89 (6H, s), 3.99 (6H, s), 4.57 (2H, s), 6.58 (2H, s), 6.7—7.2 (4H, m), 6.98 (2H, s), 7.42 (2H, t, J=7Hz). IR (KBr) 1740, 1685, 1620, 1600, 1565 cm^{-1}. UV ($CHCl_3$) λ_{max} 382 nm. HRMS Calcd for $C_{26}H_{24}O_8$: 464.1471. Found: 464.1494 (M/2+H).

3,3′-Bis(methoxycarbonyl)-2,2′-bis(methoxycarbonylmethyl)-4,4′,10,10′-tetraacetoxy-9,9′-bianthracene (3a). Under a nitrogen atmosphere, a mixture of **2a** (34 mg, 0.10 mmol), a catalytic amount of 4-dimethylaminopyridine, pyridine (2 mL), and acetic anhydride (0.5 mL) was stirred overnight at room temperature. Saturated aqueous $KHSO_4$ was added and organic materials were extracted twice with chloroform. Organic layer was washed with saturated aqueous $NaHCO_3$ and brine, dried (Na_2SO_4), concentrated, and chromatographed on silica gel to give **3a** (34 mg, 82%). Mp 140—144 °C (benzene-hexane). ^1H NMR ($CDCl_3$) δ=2.50 (6H, s), 2.65 (6H, s), 3.45 (6H, s), 3.60 (4H, s), 3.87 (6H, s), 6.8—7.7 (6H, m), 6.94 (2H, s), 8.08 (2H, d, J=8Hz). IR (KBr) 1770, 1730, 1615 cm^{-1}. MS 847 (M+H)

1,1′-Dihydroxy-2,2′-bis(methoxycarbonyl)-3,3′-bis(methoxycarbonylmethyl)-12,12′,13,13′-tetramethoxy-5,5′-bipentacene-14,14′(5*H*,5′*H*)-dione (8). Under a nitrogen atmosphere, a THF (4 mL) solution of methyl acetoacetate dianion[11] was prepared from methyl acetoacetate (132 mg, 1.7 mmol), sodium hydride (42 mg, 1.9 mmol), and hexane solution (1.1 mL) of butyllithium (1.7 mmol). Methyl 4,10-dimethoxy-3-methoxycarbonyl-2-anthraceneacetate (**5**,[8f] 78 mg, 0.21 mmol) in THF (2 mL) was added at 0 °C, and stirring was continued for 2 h at room temperature. The reaction mixture was poured on cooled 2 M hydrochloric acid, and organic materials were extracted twice with ethyl acetate. The combined organic layer was washed with water and brine, dried (Na_2SO_4), and concentrated. Methanol (2 mL) and $Pb(OAc)_2 \cdot 3H_2O$ (380 mg, 1.0 mmol) were added to the residue, and the mixture was stirred vigorously for 3 h at room temperature. Then, 2 M hydrochloric acid was added, and organic materials were extracted twice with ethyl acetate. Organic layer was washed with water and brine, dried (Na_2SO_4), concentrated, and chromatographed on silica gel giving isomer I (10 mg, 10%) and isomer II (13 mg, 13%) of **8**. Isomer I (with higher R_f): Mp 170—172 °C (AcOEt-hexane). ^1H NMR ($CDCl_3$) δ=3.67 (6H, s), 3.81 (6H, s), 3.93 (4H, s), 3.99 (12H, s), 4.62 (2H, s), 6.59 (2H, s), 7.09 (2H, s), 7.3—7.6 (4H, m), 7.87 (2H, s), 7.7—8.0 (2H, m), 8.1—8.4 (2H, m), 12.79 (2H, s). IR (KBr) 3400, 1735, 1630, 1600 cm^{-1}. UV ($CHCl_3$) λ_{max} 455, 339, 281, 258 nm. HRMS Calcd for $C_{29}H_{24}O_8$: 500.1470. Found: 500.1461 (M/2+H). Isomer II (with lower R_f): Mp 156—157 °C (AcOEt-hexane). ^1H NMR ($CDCl_3$) δ=3.72 (16H, s), 3.94 (6H, s), 4.01 (6H, s), 4.76 (2H, s), 6.40 (2H, s), 7.25 (2H, s), 7.4—7.7 (4H, m), 7.7—8.0 (2H, m), 7.88 (2H, s), 8.2—8.5 (2H, m), 12.90 (2H, s). IR(KBr) 3400, 1735, 1625, 1600 cm^{-1}. UV ($CHCl_3$) λ_{max} 454, 339, 264 nm. HRMS Calcd for $C_{29}H_{24}O_8$: 500.1470. Found: 500.1468 (M/2+H).

References

1) Examples: a) J. H. Zwaving, *Planta Med.*, **13**, 474 (1965). b) H. Oshio, S. Imai, S. Fujioka, T. Sugawara, M. Miyamoto, and M. Tsukui, *Chem. Pharm. Bull.*, **22**, 823 (1974).

2) Examples: a) I. Agranat and Y. Tapuhi, *J. Org. Chem.*, **44**, 1941 (1979). b) Y. Tapuhi, O. Kalisky, and I. Agranat, *J. Org. Chem.*, **44**, 1949 (1979).

3) Examples: a) W. Theilacker, G. Kortüm, H. Elliehausen, and H. Wilsik, *Chem. Ber.*, **89**, 1578 (1956). b) H. Auterhoff and F. C. Sherff, *Archiv Pharm.*, **293**, 918 (1960). c) E. D. Bergmann, H. Weiler-Feilchenfeld, A. Heller, C. Britzmann, and A. Hirschfeld, *Tetrahedron, Suppl.*, **7**, 349 (1966). d) R. Kinget, *Planta Med.*, **15**, 233 (1967).

4) Amine oxide: J. Haginiwa, Y. Higuchi, S. Ikeda, and M. Namba, *Yakugaku Zasshi*, **103**, 273 (1983).

5) NCS: H. D. Durst and M. P. Mack, *J. Org. Chem.*, **40**, 268 (1975).

6) Peroxide: H. H. Huang, *Aust. J. Chem.*, **29**, 2415 (1976).

7) a) A. Stoll, B. Becker, and A. Helfenstein, *Helv. Chim. Acta*, **33**, 313 (1950). b) W. Geiger, *Chem. Ber.*, **107**, 2976 (1974).

8) a) Review: M. Yamaguchi, *J. Synth. Org. Chem., Jpn*, **45**, 969 (1987). b) M. Yamaguchi, K. Shibato, and I. Hirao, *Chem. Lett.*, **1985**, 1145. c) M. Yamaguchi, K. Hasebe, and T. Minami, *Tetrahedron Lett.*, **27**, 2401 (1986). d) M. Yamaguchi, K. Hasebe, M. Uchida, A. Irie, and T. Minami, *Tetrahedron Lett.*, **28**, 2017 (1987). e) M. Yamaguchi, K. Shibato, H. Nakashima, and T. Minami, *Tetrahedron*, **44**, 4767 (1988). f) M. Yamaguchi, K. Hasebe, H. Higashi, M. Uchida, A. Irie, and T. Minami, submitted.

9) The stereochemistry of bianthrones was studied: a) D. W. Cameron, J. S. Edmonds, and W. D. Ravrety, *Aust. J. Chem.*, **29**, 1535 (1976). b) D. W. Cameron, J. S. Edmonds, G. I. Feutrill, and A. E. Hoy, *Aust. J. Chem.*, **29**, 2257 (1976).

10) The Aldrich Library of NMR Spectra, Vol. VI, 68A (1974).

11) S. N. Huckin and L. Weiler, *Tetrahedron Lett.*, **1972**, 2405; *Can. J. Chem.*, **52**, 1343 (1974).

Syntheses of Polypeptides by Hydrogenolysis of *N*-Benzyloxycarbonyl-Amino Acid Anhydrides

Toratane MUNEGUMI, Yan-Qing MENG, and Kaoru HARADA*
Department of Chemistry, University of Tsukuba, Tsukuba, Ibaraki 305
(Received March 27, 1989)

Synopsis. When anhydrides of *N*-benzyloxycarbonyl-DL-aspartic acid (Z-DL-Asp), Z-L-Asp, *N*-Z-DL-glutamic acid (Z-DL-Glu), Z-L-Glu, and *N*-Z-3-aminoglutaric acid (Z-β-Agl) were hydrogenolyzed in *N*,*N*-dimethylformamide (DMF), polypeptides were obtained in high yields. Hydrogenolyses of Z-DL-Glu and Z-L-Glu in dioxane gave pyroglutamic acid.

Although there are many investigations on the syntheses of polyamino acids, there have been few studies on the polymerization of amino acid anhydrides because of their instability and difficulty of isolation.[1] One way to overcome this difficulty would be to generate the amino acid anhydride in situ,[1-3] which would then react with each other to form polypeptides. The hydrogenation of 2-azidosuccinic anhydride in dioxane to afford polyaspartic acid has been reported.[2] However, the molecular weight and the structure of the product were not characterized in detail.[2] Aspartic acid anhydride was considered as the intermediate (actual monomer) in the polymerization.

In this paper, we wish to describe the polymerization reactions of amino acid anhydrides generated by the hydrogenolyses of anhydrides of *N*-benzyloxycarbonyl-DL-aspartic acid (Z-DL-Asp), Z-L-Asp, Z-DL-glutamic acid (Z-DL-Glu), Z-L-Glu, and Z-3-aminoglutaric acid (Z-β-Agl) in dioxane or *N*,*N*-dimethylformamide (DMF) over palladium on charcoal. Benzyloxycarbonyl (Z) group is a convenient protecting group and is easily removable by catalytic hydrogenolysis without any side reactions.[5] The Z-amino acid anhydrides (**4a—e**) were prepared and then hydrogenolyzed as shown in Scheme 1. The catalytic hydrogenolyses were carried out at room temperature in dioxane or DMF for 72 h. After hydrogenolysis, the solution obtained by filtration of the reaction mixture was evaporated and the residual product was purified by gel filtration.

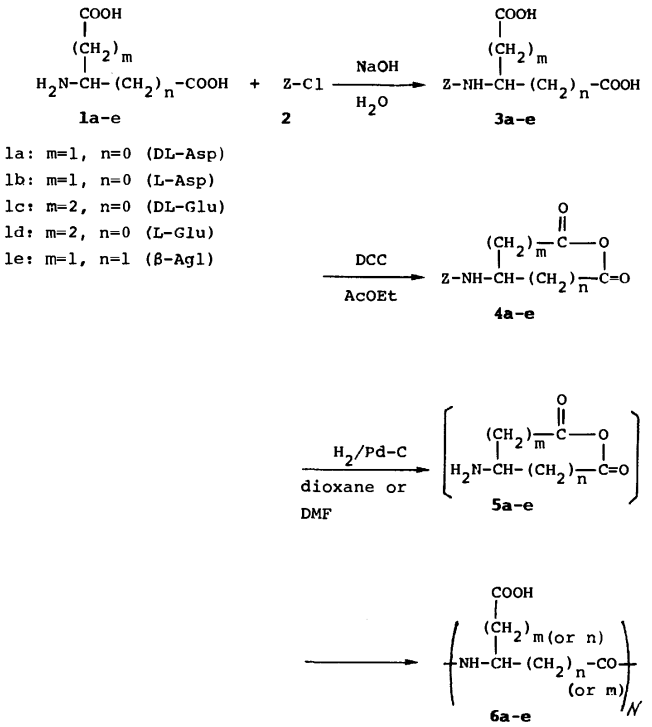

Scheme 1. Preparation of Z-amino acid anhydride and polymerization reaction by hydrogenolyses. Z: benzyloxycarbonyl-, β-Agl: 3-aminoglutaric acid, DCC: dicyclohexylcarbodiimide, AcOEt: ethyl acetate, DMF: *N*,*N*-dimethylformamide.

Results and Discussion

The yields of polypeptides, reaction conditions, amino acid recovery in acid-hydrolysates are listed in Table 1. Catalytic hydrogenolyses of Z-DL-Asp anhydride (**4a**) and Z-L-Asp anhydride (**4b**) in dioxane or DMF gave white powder whose molecular weights were estimated to be in the range of 3000 to 5000 by means of G-25 gel filtration. Amino acid recoveries after acid-hydrolysis were more than 90%. The IR spectrum of the white powder showed typical absorption bands of acidic polypeptides (1700 cm^{-1}: carboxylic acid; 1640 cm^{-1}: amide I; 1540 cm^{-1}: amide II).

Hydrogenolyses of anhydrides (**4c—e**) of Z-DL-Glu(**3c**), Z-L-Glu (**3d**), and Z-3-aminoglutaric acid (**3e**) in DMF gave peptides similar to those obtained after hydrogenolysis of Z-Asp anhydrides (**4a—b**). However, Z-DL-Glu anhydride (**4c**) and Z-L-Glu anhydride were hydrogenolyzed in dioxane to afford pyroglutamic acid in high yields (79, 80%). The hydrogenolysis of Z-L-Glu anhydride (**4d**) in glacial acetic acid or ethyl acetate also gave pyroglutamic acid.[4]

Although the polymerization reactions were carried out at room temperature, it is important to estimate the optical purity of Asp composing the poly-L-Asp, due to the possibility of racemization during the polymerization. If optically pure poly-L-Asp was obtained, it would be an interesting material for various studies. The actual ratio of D-Asp to L-Asp in the poly-L-Asp obtained from Z-L-Asp anhydride (**4b**) which was optically pure was determined by the gas chromatographic resolution of the derivatives of the enantiomers in the hydrolysate of the poly-L-Asp. Figure 1 shows the amino acid recovery and the D/L ratio of Asp against the hydrolysis time in 6 M HCl (1 M=1 mol dm^{-3}) at 110 °C. Free amino acid recovery reached 90% after 8 hours' hydrolysis. The D/L ratio of Asp increased proportionally with the hydrolysis time. After 8 hours' hydrolysis, the D/L ratio was 5%.

Table 1. Formation of Polypeptides by Hydrogenolyses of Z-Amino Acid Anhydrides (**4a—e**) in Dioxane or *N,N*-Dimethylformamide (DMF)

Substrate	Solvent	Product[a]	Yield/%[b]	AAA/%[c]	Elemental analysis/%	(C	H	N)
Z-DL-Asp Anhydride	Dioxane	Poly-Asp	71	101	Calcd for $C_4H_5NO_3 \cdot 0.81\ H_2O$	: 37.09	5.14	10.82
					Found	: 37.32	4.82	10.69
(**4a**)	DMF	Poly-Asp	87	95	Calcd for $C_4H_5NO_3 \cdot 0.41\ H_2O$	: 39.28	4.78	11.45
					Found	: 39.22	4.85	11.71
Z-L-Asp Anhydride	Dioxane	Poly-Asp	81		Calcd for $C_4H_5NO_3 \cdot 0.15\ H_2O$	: 40.78	4.54	11.89
					Found	: 40.79	4.73	11.64
(**4b**)	DMF	Poly-Asp	90	100	Calcd for $C_4H_5NO_3 \cdot 0.79\ H_2O$	: 37.09	5.14	10.82
					Found	: 37.17	4.93	10.64
Z-DL-Glu Anhydride	Dioxane	Pyro-Glu	80					
(**4c**)	DMF	Poly-Glu	55	88	Calcd for $C_5H_7NO_3 \cdot 0.51\ H_2O$	: 43.48	5.84	10.14
					Found	: 43.42	5.76	9.99
Z-L-Glu Anhydride	Dioxane	Pyro-Glu	79		Calcd for $C_5H_7NO_3$	: 46.51	5.46	10.85
					Found	: 46.04	5.51	10.65
(**4d**)	DMF	Poly-Glu	56	94	Calcd for $C_5H_7NO_3 \cdot 0.69\ H_2O$	: 42.43	5.96	9.89
					Found	: 42.42	5.63	9.78
Z-β-Agl Anhydride	Dioxane		—	—				
(**4e**)	DMF	Poly-β-Agl	91	78	Calcd for $C_5H_7NO_3 \cdot 0.32\ H_2O$	: 44.52	5.71	10.38
					Found	: 44.53	6.06	10.00

a) Molecular weights of polypeptides estimated by GPC were 3000—5000. b) Yield is expressed by the molar ratio of amino acid residue in product to substrate. c) Amino acid recovery in hydrolysate of polypeptide.

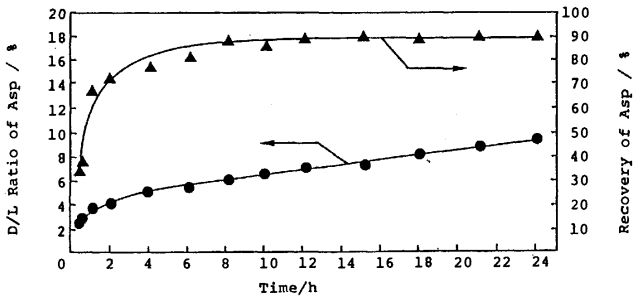

Fig. 1. Recovery and D/L ratio of Asp in acid-hydrolysate of the polypeptide which was obtained by the hydrogenolysis of Z-Asp anhydride (**4b**) in DMF.

The actual D/L ratio (3%) in poly-Asp before hydrolysis was estimated by extrapolating the value of D/L ratio to 0 hour. The existence of small amount of D-Asp(3%) would be due to the following three reasons: (1) racemization of L-Asp during the polymerization, (2) racemization during the hydrolysis of poly-Asp, and (3) existence of D-Asp in the starting material (Z-L-Asp anhydride). The third one would be negligible, because the optical purity of Z-L-Asp anhydride was almost 100% according to the gas chromatographic analysis of the derivative (*N*-trifluoroacetyl-Asp isopropyl ester) from Z-L-Asp anhydride. Similar experiments were carried out for the polypeptides derived from Z-L-Glu anhydride (**4d**) to show almost same racemization (3%).

In the present paper, we demonstrate a new synthetic method of polypeptides using catalytic hydrogenolysis. According to the best of our knowledge, this report would afford the first examples of the syntheses of poly-Glu and poly-β-Agl by hydrogenolysis of the corresponding amino acid anhydrides. Further characterizations such as determination of the ratios of β- or γ-carboxyl group to α-carboxyl group in the side chains are under investigation.

Experimental

All the melting points were not corrected. Optical rotations were measured with a JASCO DIP Polarimeter. All the gas chromatographic analyses were carried out with a Hitachi 163 gas chromatograph, and the peaks on the chromatograms were integrated with a Sic Chromatocoda 11. NMR spectra were measured on a JEOL FT-100 NMR spectrometer. IR spectra were measured with a Jasco Infrared spectrometer. Palladium on charcoal (5%) was purchased from Nippon Engelhald.

Materials. Amino Acids (1a—d). DL-Aspartic acid (**1a**), L-aspartic acid (**1b**), DL-glutamic acid (**1c**), and L-glutamic acid (**1d**) were purchased from Wako Pure Chemical Company. 3-Aminoglutaric acid (**1e**) was prepared by heating glutaconic acid monohydrate (Aldrich Chemical Company) and ammonia. Yield, 60%. Mp 274 °C (decomposed).

Preparation of Z-Amino Acids (3a—e). Z-Amino acids **3a—e** were prepared from benzyloxycarbonyl chloride (**2**) and amino acids (**1a—e**) by the manner in the literature.[5] **3a:** Yield, 63%, Mp 85—88 °C. **3b:** Yield, 89%, Mp 117—118 °C. $[\alpha]_D$ +8.8, *c* 1.0 (acetic acid). **3c:** Yield, 72%, Mp 117—119 °C. **3d:** Yield, 90%, Mp 112—113 °C. $[\alpha]_D^{25}$ −0.76 (*c* 10, acetic acid). **3e:** Yield, 73%, Mp 157—159 °C. ^{1}H NMR (CD_3OD): δ=2.59 (4H, d, *J*=6.4 Hz), 4.32 (1H, t, *J*=6.8 Hz), 5.06 (2H, s), 7.32 (5H, s). IR (KBr): 3350, 1720, 1540, 1430, 1240—1300 cm^{-1}. Calcd for $C_{13}H_{15}NO_6$: C, 55.51; H, 5.37; N, 4.99%. Found: C, 55.49; H, 5.01; N, 4.99%.

Preparation of Z-Amino Acid Anhydrides (4a—e).[5-7] **4a.**[5,6] To a cooled ethyl acetate solution (150 ml) of Z-DL-

Asp (**3a**) (13.3 g, 50 mmol), was added dicyclohexylcarbodiimide (DCC) (11.3 g, 55 mmol) dissolved in 50 ml ethyl acetate. The cyclization reaction was carried out for 1 h at 0 °C and for 24 h at room temperature. After usual work-up, Z-DL-Asp anhydride (**4a**) was obtained. Yield, 89%. Mp 120—122 °C. ^{1}H NMR ($CDCl_3$): δ=2.23 (2H, m), 4.36—4.64 (1H, m), 5.15 (2H,s), 7.36 (5H, s). IR (KBr): 3400, 1860, 1780, 1700, 1540, 1260 cm^{-1}. Calcd for $C_{12}H_{11}NO_5$: C, 57.83; H, 4.44; N, 5.62%; Found: C, 58.08; H, 4.68; N, 5.88%. **4b**, Yield, 98%. Mp 106—107 °C. $[\alpha]_D^{25}$ −29.1 (*c* 1.0, acetic acid). ^{1}H NMR ($CDCl_3$): δ=2.23 (2H, m), 4.36—4.64 (1H, m), 5.15 (2H, s), 7.36 (5H, s). IR (KBr): 3400, 1860, 1780, 1700, 1540, 1260 cm^{-1}. Calcd for $C_{12}H_{11}NO_5$: C, 57.83; H, 4.44; N, 5.62%; Found: C, 58.22; H, 4.50; N, 5.57%. **4c**, Yield, 96%. Mp 103—105 °C. ^{1}H NMR ($CDCl_3$) δ=1.8—2.2 (2H, m), 2.8—3.1 (2H, m), 4.3—4.6 (1H, m), 5.15 (2H, s), 5.6 (1H, br), 7.36 (1H, s). IR (KBr): 3400, 1820, 1770, 1730, 1540, 1260 cm^{-1}. Calcd for $C_{13}H_{13}NO_6$: C, 59.31; H, 4.97; N, 5.32%; Found: C, 59.04; H, 5.01; N, 5.27%. **4d**, Yield, 60%. Mp 76—77 °C. $[\alpha]_D^{20}$ −41.6 (*c* 9.98, acetic acid). ^{1}H NMR ($CDCl_3$): δ=1.8—2.2 (2H, m), 2.8—3.1 (2H, m), 4.3—4.6 (1H, m), 5.15 (2H, s), 5.6 (1H, br), 7.36 (1H, s). IR (KBr): 3400, 1820, 1770, 1730, 1540 cm^{-1}. Calcd for $C_{13}H_{13}NO_6$: C, 59.31; H, 4.98; N, 5.32%. Found: C, 59.19; H, 5.07; N, 5.35%. **4e**, Yield, 73%. Oil. ^{1}H NMR (DMSO-d_6): δ=2.64—3.20 (4H, m), 4.00—4.20 (1H, m), 5.04 (2H, s), 7.35 (5H, s), 7.90 (1H, br). IR (KBr): 3350, 1820, 1780, 1700, 1540, 1220—1280 cm^{-1}. Calcd for $C_{13}H_{13}NO_6$: C, 59.31; H, 5.98; N, 5.32%. Found: C, 59.71; H, 5.73; N, 5.64%.

Hydrogenolyses of Z-Amino Acid Anhydrides (4a—e) Followed by Polymerization. Z-DL-Asp anhydride (**4a**) (747 mg, 3.0 mmol) was dissolved in 5.0 ml dioxane or DMF, and was hydrogenolyzed over 5% palladium on charcoal (0.34 g) for 72 h under hydrogen atmosphere. After 3 hours' heating at 40 °C, the reaction mixture was filtered and the filtrate was evaporated in vacuo to give a residual product. The product was dissolved in water and was lyophilyzed to give white powder. The resulted white powder was dissolved in 5 ml of 0.5 M acetic acid and was loaded into a Sephadex column (G-10). Elution was carried out with 0.5 M acetic acid. The fractions which have the absorption at UV 230 nm and did not show ninhydrin color on TLC, were lyophilized to give white solid. Other Z-amino acid anhydrides (**4b**—e) were hydrogenolyzed by the similar manner to that described for **4a**.

Estimation of Molecular Weight of Polypeptides (6a—e). Molecular weights of all the purified polypeptides were estimated with Sephadex G-25 using 0.1 M sodium phosphate buffer (pH 6.8). The polypeptides were eluted earlier than oxidized Insulin (A and B chains, MW ca. 3000)[8] and later than the size exlusion limit (MW 5000) of this gel.

Determination of D/L Ratio of Asp in the Poly-L-Asp. The purified polypeptide **6b** (10 mg) was dissolved in 5 ml 6 M HCl and the solution in a sealed tube under vacuum was heated at 110 °C for 1 to 24 h. The D/L ratios of Asp were determined by the gas chromatographic resolution of enantiomeric *N*-trifluoroacetyl-Asp isopropyl esters using a chiral glass capillary column (Chirasil-Val[9] III).

References

1) A. Vegotsky, K. Harada, and S. W. Fox, *J. Am. Chem. Soc.*, **80**, 3361 (1958); J. Kovacs, H. Nagy Kovacs, I. Koneyves, J. Csaszar, T. Vajda, and H. Mix, *J. Org. Chem.*, **26**, 1084 (1961).

2) K. Freudenberg, G. Piazolo, and C. Knoevenagel, *Justus Liebigs Ann. Chem.*, **537**, 197 (1939).

3) T. Munegumi, Yan-Qing Meng, and K. Harada, *Chem. Lett.*, **1988**, 1643.

4) W. E. Hanby, S. G. Waley, and J. Watson, *J. Chem. Soc.*, **1950**, 3239.

5) M. Bergmann and L. Zervas, *Ber.*, **65**, 1192 (1932).

6) W. D. John and G. T. Young, *J. Chem. Soc.*, **1954**, 2870.

7) W. J. Le Quesne and G. T. Young, *J. Chem. Soc.*, **1950**, 1954.

8) K. S. Lee and D. G. Drescher, *J. Biol. Chem.*, **254**, 6248 (1979).

9) H. Frank, G. J. Nicholson, and E. Bayer, *J. Chromatogr. Sci.*, **15**, 174 (1977).

The Absolute Configuration of 4,6-Decadiyne-1,3,8-triol Isolated from *Gymnopilus spectabilis*

Masaru HASHIMOTO, Mitsutoshi YANAGIYA, Toshikatsu OKUNO,† and Haruhisa SHIRAHAMA*
Department of Chemistry, Faculty of Science, Hokkaido University, Sapporo 060
†Department of Agricultural Chemistry, Faculty of Agriculture, Hirosaki University, Aomori 036
(Received April 3, 1989)

Synopsis. The absolute configuration of 4,6-decadiyne-1,3,8-triol, isolated from *Gymnopilus spectabilis*, was established as (3*S*,8*S*) by the comparison of degradated compounds with synthetic ones.

A toxic mushroom *Gymnopilus spectabilis* has been widely known for unique and curious biological activity in Japan. It has been said if you would eat it erroneously, you should laugh out loudly and could not stop doing. Therefore, the mushroom was named "Big laughter mushroom" (Ohwaraitake in Japanese). Chemical constituents of this mushroom have been studied by two groups, Matsumoto's[1] and Nozoe's,[2,3] and they reported previously isolations and structural elucidations of bitter principles, gymnopilines, gymnoprenols[1,2] and 4,6-decadiyne-1,3,8-triol (**1**).[3] Now we wish to describe absolute configuration of compound **1**.

Decadiynetriol **1**, which was newly extracted from the mushroom, was converted to tribenzoate **2** in 78% yield and then ozonolysis of **2** was performed. After decomposition of the ozonide with hydrogen peroxide, the products were treated with diazomethane to give a mixture of two esters which was separated on silica-gel TLC plate developed by 20% ether-hexane to afford methyl 2-benzoyloxybutyrate (**3**) (R_f=0.45, $[\alpha]_D^{21}$ −1.7° (*c* 0.80, $CHCl_3$), $\Delta\varepsilon_{228}^{24}$ +5.0 (*c* 4.5×10^{-4} mol l^{-1}, MeOH)) and methyl 2,4-bis(benzoyloxy)butyrate (**4**) (R_f=0.30, $[\alpha]_D^{21}$ −20° (*c* 1.2, $CHCl_3$)) in 36 and 45% yield, respectively. On the other hand, they were also prepared from commercially available and optically active compounds. Through a known procedure,[4] (*S*)-(+)-2-aminobutyric acid was converted in 44% yield to hydroxy ester **5**, and it was benzoylated to give methyl (2*S*)-(−)-2-benzoyloxybutyrate (**3′**) ($[\alpha]_D^{22}$ −1.5° (*c* 1.6, $CHCl_3$), $\Delta\varepsilon_{228}^{24}$ +4.4 (3.4×10^{-4} mol l^{-1}, MeOH)) in 63% yield. Acetonide **6**, synthesized from (*S*)-(−)-malic acid in 47% yield by also known method,[5] was subjected to the following sequential reactions: i) reduction with borane dimethyl sulfide complex, ii) benzoylation of hydroxyl group, iii) removal of acetonide protective group under acidic conditions, iv) esterification with CH_2N_2, v) benzoylation of hydroxyl group, to yield methyl (2*S*)-2,4-bis(benzoyloxy)-butyrate (**4′**) ($[\alpha]_D^{23}$ −21° (*c* 1.0, $CHCl_3$)) was obtained in 65% over all yield. Both synthetic products **3′** and **4′** were identical with degradation products **3** and **4**, respectively, on spectral data (NMR, IR, and MS) including optical rotation and chromatographic behavior. Absolute configurations of both **3** and **4** were thus represented as *S*. Accordingly the stereochemistry of the natural product **1** should be assigned to 3*S* and 8*S* configurations.

Experimental

Melting point was uncorrected. All ^{1}H NMR spectra were measured on a Hitachi R-90H spectrometer in $CDCl_3$, and ^{13}C NMR spectrum was determined on a JEOL JNM-GX 270 spectrometer in CD_3OD. IR spectra were recorded

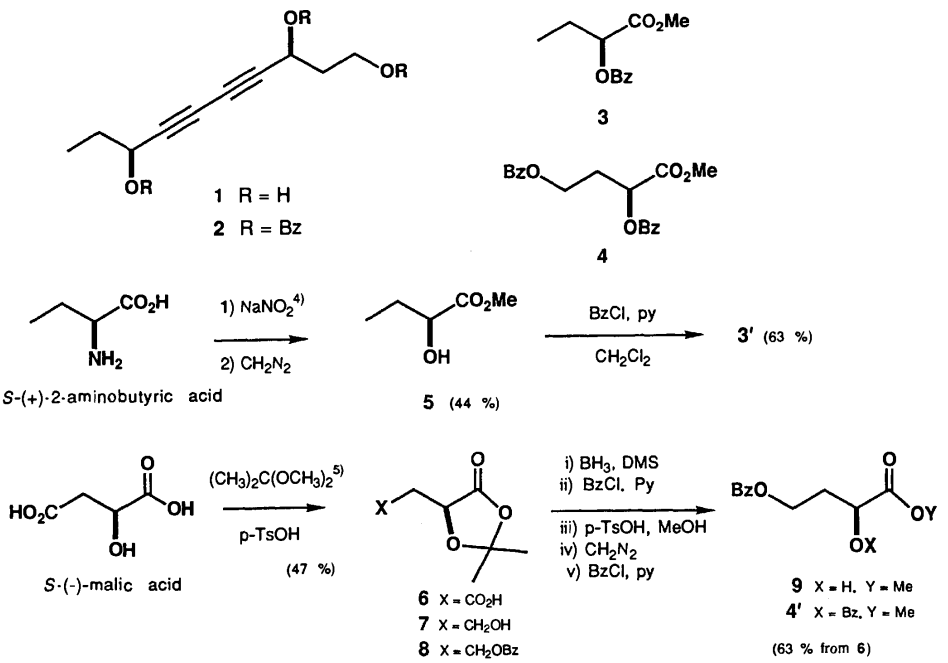

on a JASCO IR-S spectrophotometer. Optical rotations were obtained by JASCO DIP-360 digital polarimeter, and CD spectra by JASCO J-20A automatic recording spectropolarimeter. High and low mass spectra were recorded on a JEOL JMS-DX 303 spectrometer.

4,6-Decadiyne-1,3,8-triol (1).[3] The mushroom, Gymnopilus spectabilis, was collected in Aomori prefecture and **1** was isolated as colorless oil in 0.027% from fresh fruit bodies: $[\alpha]_D^{23}$ −5.8° (*c* 1.7, MeOH); ^{13}C NMR δ=9.76 (q), 31.72 (t), 41.30 (t), 59.05 (t), 60.20 (d), 64.31 (d), 68.93 (s), 69.09 (s), 81.25 (s), and 81.61 (s); FD-MS *m/z* 183 (M^++H) and 165 ((M^++H−H_2O), base peak).

(3*S*,8*S*)-1,3,8-Trisbenzoyloxy-4,6-decadiyne (2). 4,6-Decadiynetriol **1** (9.0 mg, 0.049 mmol) was treated with pyridine (0.20 ml) and benzoyl chloride (50 mg, 0.35 mmol) in dichloromethane (0.50 ml). After 6 h stirring, the mixture was poured into 0.5% citric acid solution and extracted with ether. The ethereal solution was washed with brine, dried (Na_2SO_4) and concentrated. Chromatography of the obtained oil on silica gel (2 g) with 50% hexane-ether gave tribenzoate **2** as amorphous solid (19 mg, 0.038 mmol, 78%): mp 97—102 °C; $[\alpha]_D^{21}$ +4.70° (*c* 1.7, $CHCl_3$); ^{1}H NMR δ=1.07 (3H, t, *J*=7 Hz), 1.94 (2H, quint, *J*=7 Hz), 2.38 (2H, q, *J*=6 Hz), 4.54 (2H, t, *J*=7 Hz), 5.59 (1H, t, *J*=7 Hz), 5.88 (1H, t, *J*=6 Hz), and 7—8 (15H); IR (Nujol) 1730, 1690, 1270, 1095, and 710 cm^{-1}; EI-MS *m/z* 494 (M^+) and 105 ($C_6H_5CO^+$, base peak); Found: *m/z* 494.1777, Calcd for $C_{31}H_{26}O_6$: M, 494.1730.

Oxidative Degradatioon of 1,3,8-Trisbenzoyloxy-4,6-decadiyne (2). To a dichloromethane solution (10 ml) of tribenzoate **2** (40 mg, 0.080 mmol), ozone gas was bubbled for 20 min at 0 °C. After removal of excess ozone by bubbling of oxygen, 30% hydrogen peroxide (0.10 ml) was added and the mixture was stirred for 20 min to decompose the ozonide product. Dimethyl sulfide (2.0 ml) was added to decompose excess peroxide. The solvent was removed and an obtained oil was diluted with methanol (10 ml). An ethereal solution of diazomethane was added until yellow color did not disappear. The mixture was diluted with ether, washed with water and brine, dried (Na_2SO_4) and concentrated. The purification of the oil by preparative TLC (silica gel) with 20% ether-hexane gave methyl 2-benzoyloxybutyrate (**3**) as a colorless oil (6.5 mg, 0.029 mmol, 36%) and methyl 2,4-bis(benzoyloxy)butyrate (**4**) as a colorless oil (13 mg, 0.036 mmol, 45%).

Methyl 2-Benzoyloxybutyrate (3): R_f=0.45 (silica gel, 20% ether-hexane); $[\alpha]_D^{21}$ −1.7° (*c* 0.80, $CHCl_3$) $\Delta\varepsilon_{228}^{24}$ +5.0 (*c* 4.5×10^{-4} mol l^{-1}, MeOH); ^{1}H NMR δ=1.09 (3H, t, *J*=7 Hz), 2.02 (2H, dq, *J*=6 and 7 Hz), 3.77 (3H, s), 5.21 (1H, t, *J*=6 Hz), 7.5 (3H, m), and 8.0 (2H, m); IR (film) 1760, 1730, 1115, and 715 cm^{-1}; EI-MS *m/z* 222 (M^+) and 105 ($C_6H_5CO^+$, base peak); Found: *m/z* 222.0887, Calcd for $C_{12}H_{14}O_4$: M, 222.0892.

Methyl 2,4-Bis(benzoyloxy)butyrate (4): R_f=0.30 (silica gel, 20% ether-haxane); $[\alpha]_D^{21}$ −21° (*c* 1.2, $CHCl_3$); ^{1}H NMR δ=2.48 (2H, q, *J*=7 Hz), 3.73 (3H, s), 4.54 (2H, t, *J*=6 Hz), 5.49 (1H, t, *J*=6 Hz), 7.5 (6H, m), and 8.0 (4H, m); IR (film) 1760, 1730, 1605, 765, and 715 cm^{-1}; EI-MS *m/z* 342 (M^+), 310 (M^+−MeOH), and 105 ($C_6H_5CO^+$, base peak); Found *m/z* 342.1102, Calcd for $C_{19}H_{18}O_6$: M, 342.1103.

Methyl (2*S*)-2-Benzoyloxybutyrate (3′). A solution of methyl (2*S*)-2-hydroxybutyrate (**5**) (43 mg, 0.41 mmol), pyridine (0.20 ml), and benzoyl chloride (60 mg, 0.43 mmol) in dichloromethane (1.0 ml) was stirred at room temperature for 10 h. The mixture was poured into water and extracted with ether. The organic layer was washed with brine, dried (Na_2SO_4), and concentrated. Chromatography of the residue on silica gel (3 g) with 15% ether-hexane gave benzoate **3′** as a colorless oil (68 mg, 63%); $[\alpha]_D^{22}$ −1.5° (*c* 1.6, $CHCl_3$), $\Delta\varepsilon_{228}^{24}$ +4.4 (3.4×10^{-4} mol l^{-1}, MeOH); Found: *m/z* 222.0905, Calcd for $C_{12}H_{14}O_4$: M, 222.0892.

Methyl (2*S*)-2,4-Bis(benzoyloxy)butyrate (4′). Borane dimethyl sulfide complex (2.0 ml, 21 mmol) was added to THF solution (50 ml) of (3S)-3,4-*O*-isopropyliden-4-oxobutyric acid (**6**) (1.0 g, 5.7 mmol) at 0 °C. After 5 h stirring, methanol was added slowly to decompose excess hydride. The mixture was poured into brine and extracted with chloroform. The organic solution was dried (Na_2SO_4), concentrated to afford an alcohol **7** (870 mg, 5.3 mmol, 93%): ^{1}H NMR δ=1.52, 1.65 (each 3H, s), 2.00 (2H, q, *J*=6 Hz), 2.31 (1H, brs), 3.81 (2H, s, *J*=6 Hz), and 4.55 (1H, dd, *J*=6 and 8 Hz).

To the dichloromethane solution (10 ml) of the alcohol **7** (870 mg, 5.3 mmol), pyridine (0.80 ml, 10 mmol) and benzoyl chloride (1.0 g, 7.1 mmol) were added at 0 °C. The mixture was allowed to warm to room temperature and was stirred for 12 h. The mixture was poured into water and extracted with ether. The ethereal solution was washed with brine, dried (Na_2SO_4), and concentrated to give a benzoyl ester **8** (1.3 g, 5.0 mmol, 94%): ^{1}H NMR δ=1.53, 1.57 (each 3H, s), 2.27 (2H, m), 4.50 (3H, m), 7.1—7.7 (3H), and 7.9—8.2 (2H).

The ester **8** (1.3 g, 5.0 mmol) was treated with *p*-TsOH (10 mg) in methanol (15 ml) for 10 h. To this solution, ethereal solution of diazomethane was added until yellow color did not disappear, and the solvent was removed to yield ester **9**: ^{1}H NMR δ=2.23 (2H, m), 2.92 (1H, brs), 3.24 (3H, s), 4.54 (2H, m), 7.2—7.6 (3H), and 7.9—8.2 (2H). The obtained ester **9** was stirred with benzoyl chloride (1.0 ml, 7.1 mmol) and pyridine (0.80 ml, 10 mmol) in dichloromethane (15 ml) at room temperature for 10 h. The mixture was poured into water and extracted with ether. The ethereal solution was washed with sat. $CuSO_4$ aqueous solution and brine, dried (Na_2SO_4), and concentrated. Chromatography of the residue on 40 g of silica gel with 25% ether-hexane gave 2,4-bis(benzoyloxy)butyrate **4′** as a colorless oil (1.3 g, 3.7 mmol, 74% through 2 steps): $[\alpha]_D^{23}$ −21° (*c* 1.0, $CHCl_3$); Found: *m/z* 342.1094, Calcd for $C_{12}H_{14}O_4$: M, 342.1103.

References

1) F. Aoyagi, S. Maeno, T. Okuno, H. Matsumoto, M. Ikura, K. Hikichi, and T. Matsumoto, *Tetrahedron Lett.*, **24**, 1991 (1983).

2) S. Nozoe, Y. Koike, E. Tsuji, G. Kusano, and H. Seto, *Tetrahedron Lett.*, **24**, 1731 (1983); S. Nozoe, Y. Koike, G. Kusano, and H. Seto, *ibid.*, **24**, 1735 (1983).

3) G. Kusano, Y. Koike, H. Inoue, and S. Nozoe, *Chem. Pharm. Bull.*, **34**, 3465 (1986).

4) K. Mori, M. Sasaki, S. Tamada, T. Suguro, and S. Masuda, *Tetrahedron*, **35**, 1601 (1979).

5) D. B. Collum, J. H. McDonald, III, and W. C. Still, *J. Am. Chem. Soc.*, **102**, 2120 (1980).

The Effect of Starting Source on the Concentration Distribution of Nickel Supported on Alumina

Tadahiro FUJITANI, Osamu UEKI, and Etsuro ECHIGOYA*
Department of Industrial Chemistry, Chiba Institute of Technology,
Tsudanuma, Narashino, Chiba 275
(Received March 2, 1989)

Synopsis. The concentration profile and particle size of nickel supported on alumina spheres were easily controlled by varying the starting source materials of the impregnation solution. Further, the reduction behavior of nickel oxide supported on alumina was influenced by the starting nickel source material.

The catalyst activity and selectivity of supported metal catalyst are strongly influenced by the amount of metal, the size of dispersed metal particles, the preparation method and the support composition. In particular, to improve the catalyst activity and durability it is necessary to control the distribution of metal particles in the catalyst. The control of a radial distribution of metal particles in the catalyst was easily achieved by changing factors as the impregnation period,[1] the pH of impregnation solution[2] and used additives.[3,4] However, only a few investigations have been reported about the effect of the source material on the physical properties and reactivity of the catalysts.[5,6]

In this paper, we wish to report on the effect of the starting source material on the metal particle distribution and physical properties of nickel supported on alumina sphere catalysts.

Experimental

The Ni/Al_2O_3 catalysts were prepared by impregnation of γ-alumina (JRC-ALO-3 supplied by Catalysis Society of Japan) with aqueous solution of the nickel salts (nickel acetate, nickel formate, nickel chloride and nickel nitrate) or aqueous ammonia (28%) of a nickel carbonate and the solution was evaporated at 100 °C. The impregnated samples were calcined in air at 450 °C for 2 h and, subsequently, reduced in a stream of hydrogen at 450 °C for 2 h. Typical properties of the support are given in Table 1. Nickel concentration profiles along the diameter of the catalyst cross section were measured by EPMA (JEOL JCXA-733). The catalyst was embedded in a thermoplastic resin. After solidification, raping film sheets were used to grind off the catalyst particles so as to expose the cross section. The sample was coated with a layer of carbon by vacuum deposition. The particle size of nickel was measured by TEM (Hitachi H-9000H). Finely ground catalyst particles were suspended in ethanol and then scooped up with a micromesh. These particles were dried under vacuum and used as a specimen. The reduction behavior of the catalyst was measured by TPR. Typically, 50-mg samples were used. Prior to reduction, each sample was dried for one hour in a stream of helium at 300 °C. On cooling the sample to room temperature, helium was replaced by hydrogen, then, the reactor temperature was raised (1 °C min^{-1}) and the hydrogen consumption was measured. The total nickel content in each catalyst was determined by chelate titration. A sample solution was prepared by dissolving the nickel of the catalyst in hydrochloric acid and filtering.

Table 1. Physical Properties of JRC-ALO-3[7,8]

Composition	γ-alumina
BET surface area/m^2g^{-1}	121
Modal pore diameter /nm	10.0
Specific pore volume/m^3g^{-1}	5.28×10^{-7}
Average diameter/mm	3.0—3.2

Results and Discussion

First, the nickel concentration profile and total nickel contents in the alumina sphere of the prepared Ni/Al_2O_3 using various nickel solution were measured as shown in the Fig. 1. The nickel concentration profile in the support can be classified into two types. In the first type, the nickel atoms were uniformly distributed over the whole of alumina sphere (A and B). In the second type, the nickel atoms were concentrated in the vicinity of the outer surface of alumina sphere (C, D, and E). Further, the band widths of the nickel atom in the second-type concentration profile were changed by the starting source materials. In the case of nickel carbonate, the nickel atoms were sharply distributed on the outer surface of the alumina sphere. The thickness of the nickel band was estimated to be about 100 μm. On the other hand, the position of the nickel band seems to spread toward the center of the alumina sphere when nickel acetate and nickel formate were used. The Ni/Al ratio of impregnant was 50/950 but the total nickel contents of these catalysts were different from those of the starting source materials. The total nickel contents obtained by chelate titration were in good agreement with the analytical data from EPMA response for nickel. The differences of the nickel concentration profile and total nickel contents in the alumina sphere were attributed to the adsorption rate of nickel complex ion into the alumina.[9]

The particle sizes of the nickel metal in the catalysts were observed by TEM as shown in Fig. 2. In the case of the catalysts prepared from nickel nitrate, nickel acetate and nickel chloride, the nickel metal particles were highly dispersed in an even size around 5 nm on the alumina spheres. On the other hand, the nickel metal particles of the catalysts prepared from nickel carbonate and nickel formate were observed in the form of larger crystallites. The nickel concentration profile produced from nickel acetate in alumina sphere was similar to that from nickel formate as shown in Fig. 1, but they differed from one another in the nickel particle size.

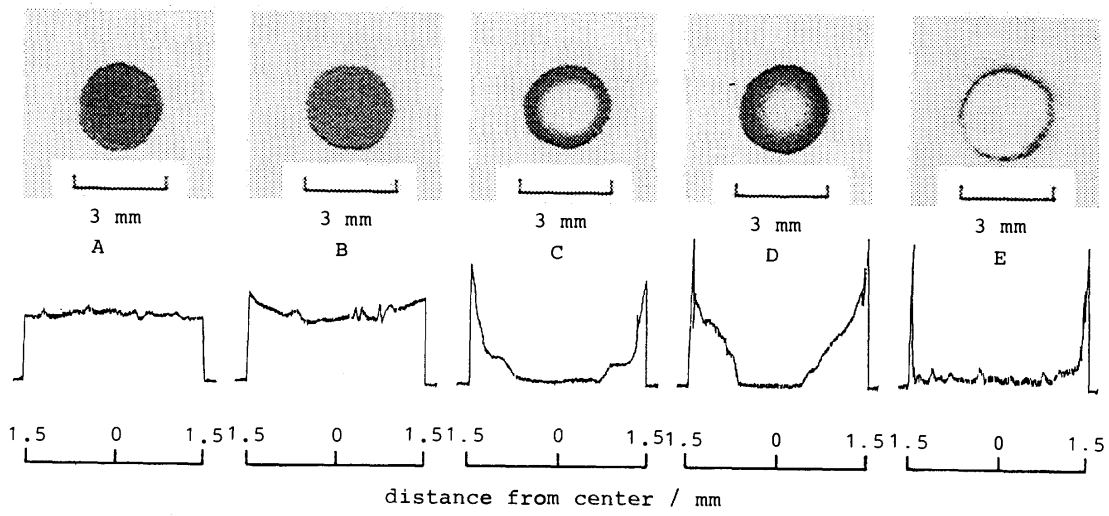

Fig. 1. Distribution of Ni atom in the catalysts measured by EPMA.
A: nickel nitrate (Ni/Al=37/923), B: nickel chloride (Ni/Al=36/924), C: nickel formate (Ni/Al=32/928), D: nickel acetate (Ni/Al=28/972), E: nickel carbonate (Ni/Al=19/981).

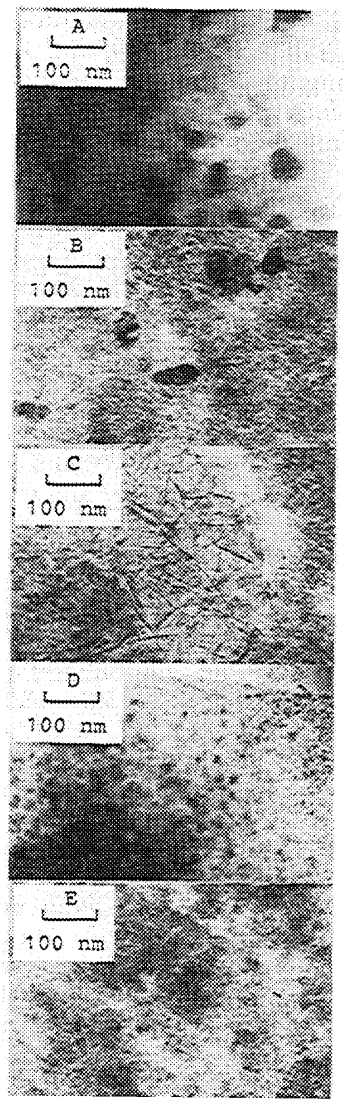

Fig. 2. TEM photograph of Ni in the catalyst reduced at 500 °C for 3 h.
A: nickel formate, B: nickel carbonate, C: nickel chloride, D: nickel acetate, E: nickel nitrate.

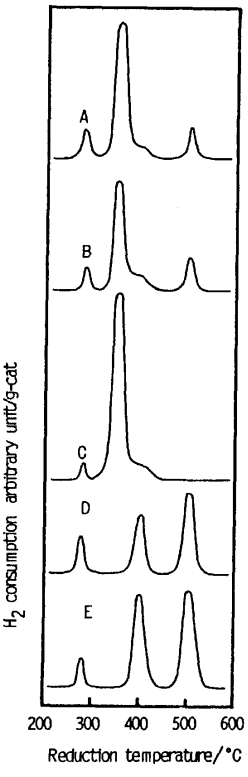

Fig. 3. TPR spectrum of supported nickel catalysts.
A: nickel nitrate, B: nickel acetate, C: nickel chloride, D: nickel formate, E: nickel carbonate.

The chemical interaction between nickel oxide and alumina was measured by TPR. Figure 3 shows the TPR spectrum change in relation to starting nickel source materials. The reduction peak of nickel oxide appeared at 280 °C. The main reduction peaks of the catalysts prepared from nickel nitrate, nickel chloride and nickel acetate were observed at 350 °C and a small peak appeared at 500 °C, while the main reduction peaks of the catalysts prepared from nickel carbonate and nickel formate appeared at 400 and 500 °C. It

was found that the reduction of the catalysts prepared from nickel carbonate and nickel formate became very difficult compared with those prepared from nickel nitrate, nickel chloride and nickel acetate. The results from the morphology investigation on the nickel/γ-alumina catalysts[10] indicated that the difficulty in the reduction of the nickel oxide were responsible for the formation of nickel aluminate precursor and large nickel crystallites were produced by its reduction. According to the experimental results in Figs. 2 and 3, the nickel aluminate precursor was plausibly formed when nickel carbonate and nickel formate were used as starting source materials.

It is concluded that the starting nickel source has the remarkably effects on the nickel concentration profile and nickel particle size in the alumina spheres which are used as a support, when preparing the catalyst by the impregnation method.

References

1) Y. Ogino, *Shokubai [Catalyst]*, **19**, 334 (1977).
2) M. Komiyama, R. P. Merrill, and H. F. Harnsberger, *J. Catal.*, **63**, 35 (1980).
3) E. R. Becker and T. A. Nuttall, "Preparation of Catalysts II," ed by Delmon et al., Elsevir Sci. Pub. Co. (1978), p. 159.
4) Y. Shyr and W. R. Ernst, *J. Catal.*, **63**, 425 (1980).
5) J. K. Gimzewski, B. D. Padalia, and S. Affrossman, *J. Catal.*, **55**, 250 (1978).
6) Y. Uemura, Y. Hatate, and A. Ikari, *J. Chem. Eng. Jpn.*, **20**, 563 (1987).
7) Data-JRC-0001, T. Hattori, *Syokubai [Catalyst]*, **22**, 115 (1980).
8) Data-JRC-0002, K. Mukaida, *Syokubai [Catalyst]*, **22**, 116 (1980).
9) J. C. Summers and S. A. Ausen, *J. Catal.*, **52**, 445 (1978).
10) J. Zielinsky, *J. Catal.*, **76**, 157 (1982).

Hydrogenation of Carbon Dioxide on Unpromoted and Potassium-Promoted Iron Catalysts

Min-Dar LEE,* Jyh-Fu LEE, and Chau-Shang CHANG
Department of Chemical Engineering, National Taiwan University, Taipei, Taiwan 10764, Republic of China
(Received October 7, 1988)

Synopsis. The promotional effect of potassium was studied on catalytic behavior of iron in CO_2 hydrogenation. A higher product selectivity toward light olefins and long-chain hydrocarbons was obtained on promoted catalyst than on unpromoted catalyst. This can be attributed to the enhancement of carburization on iron catalyst by potassium, as evidenced by Mössbauer spectroscopy and temperature-programmed decarburization.

The catalytic hydrogenation of CO has been extensively studied because it is an important step in utilization of coal as a carbon source. However, the hydrogenation of CO_2 has gained considerably less attention.[1-5] Previous studies indicated that the hydrogenation of CO_2 to hydrocarbons (HC) is proceeded via two elementary steps in series.[5-7] CO_2 first reacts with H_2 to form CO and H_2O, so-called reverse water-gas shift (RWGS) reaction, followed by Fischer-Tropsch (F-T) reaction in which CO is further hydrogenated to HC. Since iron-based catalysts are widely used in the industrial shift reaction as well as F-T reaction,[8,9] iron should be a potential catalyst for the hydrogenation of CO_2 to HC. On the other hand, potassium has long been known as an effective promoter of iron-based catalysts for the production of olefins and long-chain hydrocarbons in F-T reaction with enhanced water-gas-shift activity.[10] Accordingly, it is expected that potassium will also exhibit remarkable promotional effect in CO_2 hydrogenation.

In the present work, hydrogenation of CO_2 was carried out on the unpromoted and potassium-promoted iron catalysts. The bulk phase changes of catalysts during reaction were characterized by Mössbauer spectroscopy. Comparison between the relative stabilities of carbon deposits on used catalysts was accomplished by temperature-programmed decarburization. All the experimental evidences are helpful to elucidate the promotional effect of potassium on iron catalyst in CO_2 hydrogenation.

Experimental

Iron oxide was prepared by slowly adding ammonium hydroxide into an aqueous iron(III) nitrate solution until pH of 8.5 was reached. The precipitate was vacuum dried overnight at 393 K and calcined at 773 K for 24 h. To prepare potassium-promoted catalyst (with potassium loading of 3 atom%), calcined iron oxide was impregnated with an aqueous solution of potassium carbonate to incipient wetness followed by further calcination at 773 K for 3 h. Two catalyst samples are designated as Fe and K/Fe, respectively.

Prior to reaction tests, the calcined samples were reduced in situ in flowing hydrogen at 773 K for 15 h. The reactions were carried out in a tubular flow reactor at 593 K under 101 kPa or 1013 kPa, using a H_2/CO_2 (4/1 mole ratio) mixture of 600 cm^3(NTP) $h^{-1}g^{-1}$ (based on unreduced catalysts) as feed gas. Effluent gas from the reactor was analyzed by a gas chromatograph equipped with Porapak Q columns and both thermal conductivity detector (TCD) and flame ionization detector (FID).

In each of the temperature-programmed decarburization (TPDC) runs, the catalyst of 0.1 g was subjected to a H_2/CO_2 feed gas of 10 $cm^3 min^{-1}$ under 101 kPa. After a certain period, the catalyst bed was purged with helium for 2 min followed by quickly cooling down to room temperature. The gas stream was then switched to hydrogen and temperature increased to 773 K at 5 K min^{-1} to evolve carbon deposits on the catalyst. Continuous detection of any H_2-evolved carbon by FID gives a TPDC profile.

All ^{57}Fe-Mössbauer spectra were recorded at room temperature with a ^{57}Co(Rh) source oscillating in constant acceleration mode. The hyperfine spectrum of a natural iron foil was used to calibrate the velocity scale. After computer folding, each spectrum consisted of 512 points and was fitted with Lorentzian lines using a nonlinear regression program.[11]

Results and Discussion

The Mössbauer spectra show a single sextet with a hyperfine field of 330 kOe for both freshly reduced Fe

Table 1. Conversion and Product Selectivity in CO_2 Hydrogenation[a]

Catalyst	Reaction pressure	CO_2 conv.	Yield of CO	Yield of HC	HC distribution/carbon %					Olefin/paraffin ratio in C_2—C_4
	kPa	%	%	%	CH_4	C_2	C_3	C_4	C_{5+}	
Fe	101	21.6	17.1	4.5	66.5	18.3	9.2	3.3	2.7	0.90
Fe	1013	32.0	7.5	24.5	33.1	15.6	15.2	9.9	26.2	0.21
K/Fe	101	19.2	18.7	0.5	59.4	15.8	11.4	5.8	7.6	6.4
K/Fe	1013	34.7	6.3	28.4	19.7	12.6	16.9	14.5	36.3	5.3

a) Reaction conditions: temp=593 K, H_2/CO_2=4/1 (mole ratio), GHSV=600 $cm^3 h^{-1} g^{-1}$. Data were taken after 24 h reaction (101 kPa) and 48 h reaction (1013 kPa).

and K/Fe catalysts, indicating that all iron atoms exist in the form of α-Fe before reaction. The BET surface areas of these two catalysts are nearly the same (14 ± 2 $m^2\ g^{-1}$). However, CO uptake at 195 K by K/Fe catalyst (0.8 $\mu mol\ g^{-1}$) is far less than that by Fe catalyst (4.5 $\mu mol\ g^{-1}$), consistent with the picture in which a large portion of iron surface is covered by potassium.[12]

The conversion and product selectivity of CO_2 hydrogenation on both catalysts are listed in Table 1 for comparison. The promotional effect of potassium was reflected in the higher selectivity toward light olefins and long-chain hydrocarbons on K/Fe catalyst. This catalytic result can be satisfactorily explained from the viewpoint that the carburization (in contrast to hydrogenation) on iron catalyst was enhanced by potassium during CO_2 hydrogenation.

Figure 1 shows the Mössbauer spectra of used catalysts after CO_2/H_2 reactions. During computer fitting, seven sextets attached to four components (α-Fe, Fe_3O_4, θ-Fe_3C, and χ-Fe_5C_2) are taken into consideration. Based on the assumption that the recoil-free fraction of ^{57}Fe nuclei in γ-ray resonance absorption is the same for all components, the percentages of spectral peak areas (see Table 2) represent directly the distribution of iron atoms in individual components.

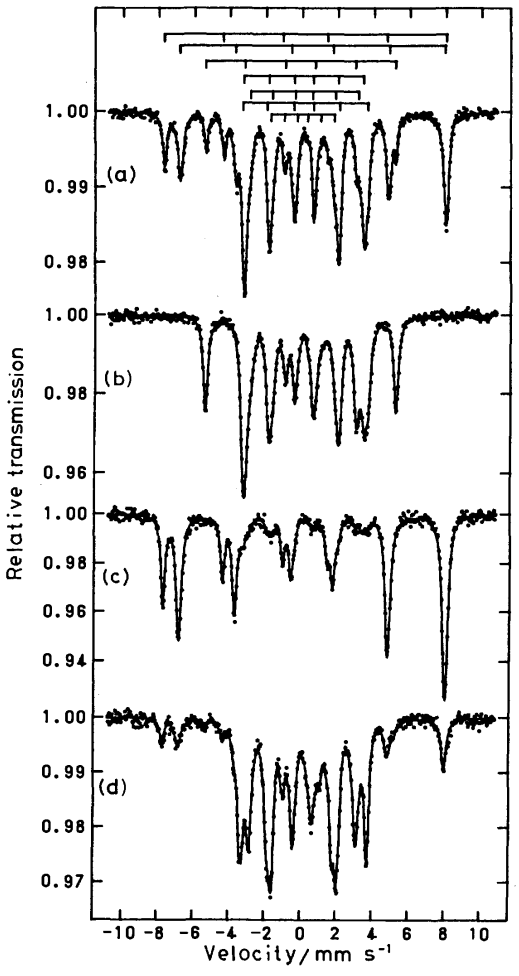

Fig. 1. Mössbauer spectra of (a) Fe and (b) K/Fe catalysts after CO_2/H_2 reaction under 101 kPa for 24 h, and (c) Fe and (d) K/Fe catalysts after CO_2/H_2 reaction under 1013 kPa for 48 h. The seven identifications shown for the (a) spectrum represent, from top down respectively, the tetrahedral and octahedral sites in Fe_3O_4, α-Fe, θ-Fe_3C, and I, II, and III sites in χ-Fe_5C_2.

Metallic iron catalysts will be oxidized (to Fe_3O_4) as well as carburized (to χ-Fe_5C_2 or θ-Fe_3C) during CO_2 hydrogenation. For a given catalyst, high reaction pressure favors the formation of Fe_3O_4. Since H_2O is the common product in both elementary steps (RWGS and F-T reactions) of overall CO_2 hydrogenation, high conversion of CO_2 especially with increased HC yield leads to abundant H_2O production. Therefore, it is believed that the preference for Fe_3O_4 formation under elevated pressure is due to the oxidation of metallic iron by H_2O.

The bulk carburization of iron catalyst is enhanced in the presence of potassium promoter. Not only carbide phases are more preferable on K/Fe catalyst than on Fe catalyst for given reaction conditions, but the relative dominance of carbide phases shifts from θ-Fe_3C to χ-Fe_5C_2. The χ-Fe_5C_2 phase is known to be less stable than θ-Fe_3C phase,[13,14] and its formation requires a lower H_2/CO feed ratio in CO hydrogenation. However, CO is an intermediate product instead of reactant in CO_2 hydrogenation. This in turn leads to a high ratio of H_2/CO on the catalyst surface, which is a favorable condition for θ-Fe_3C formation.

Table 2. Peak Area Percentages of Spectral Contributions Shown in Fig. 1

Spectrum	α-Fe	Fe_3O_4	θ-Fe_3C	χ-Fe_5C_2
(a)	7.4	33.9	33.2	25.5
(b)	28.8	—	25.9	45.3
(c)	—	86.8	6.7	6.5
(d)	2.3	14.1	—	83.6

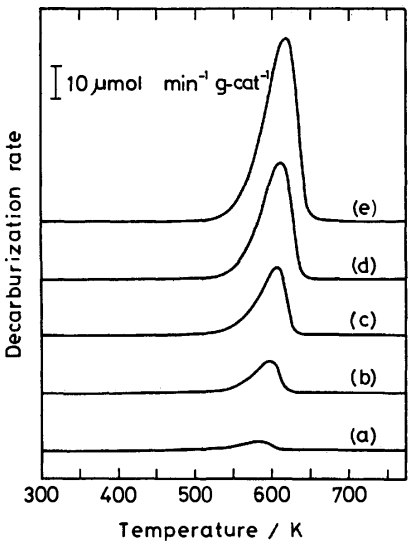

Fig. 2. Temperature-programmed decarburization profiles (with a heating rate of 5 K min^{-1}) of Fe catalyst after CO_2/H_2 reaction for (a) 2, (b) 5, (c) 10, (d) 20, and (e) 40 min.

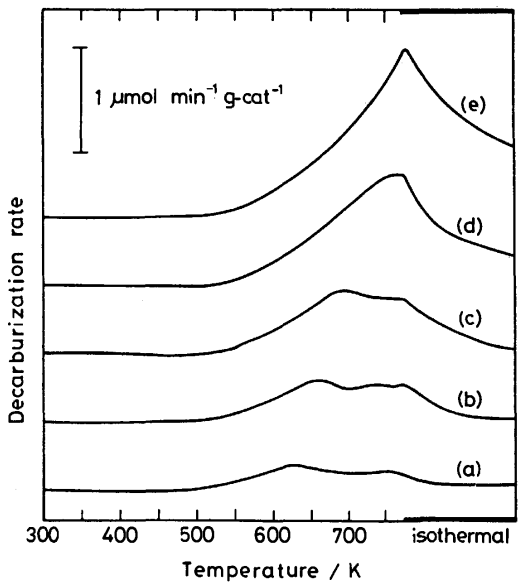

Fig. 3. Temperature-programmed decarburization profiles (with a heating rate of 5 K min^{-1}) of K/Fe catalyst after CO_2/H_2 reaction for (a) 2, (b) 5, (c) 10, (d) 20, and (e) 40 min.

The enhancement of carburization on K/Fe catalyst destroys this condition to some extent, and hence χ-Fe_5C_2 is more likely to form.

The relative stabilities of carbon deposits on used catalysts are also reflected by the peak temperatures of TPDC profiles. The higher peak temperature implies the more stable carbon deposits, and vice versa. Figures 2 and 3 show the TPDC profiles of Fe and K/Fe catalysts, respectively, after subjecting to CO_2/H_2 reaction for various times between 2 and 40 min.

All TPDC profiles for Fe catalyst show a single peak with peak temperature shifting from 587 K to 621 K when reaction time increases from 2 to 40 min. As shown in Fig. 2, most carbon deposits are evolved in the temperature range between 500 K and 650 K. In contrast, multiple peaks can be observed on the TPDC profiles of K/Fe catalyst if reaction time is shorter than 10 min, indicating that more than one forms of carbon deposits exist with different reactivities toward hydrogen. The distribution of carbon deposits with various stabilities makes the TPDC peaks of K/Fe catalyst much broader, regardless of the take-off temperature of TPDC peaks close to that of Fe catalyst. As the reaction time further increases, overlapping between unresolved TPDC peaks tends to combine in a single but even broader peak with peak temperature higher than 770 K. Since the temperature rise was stopped at 773 K in TPDC experiments and then held isothermally at that temperature, the decarburization rate turns to drop due to the decrease of driving force.

In summary, it is no doubt that carbon deposits on K/Fe catalyst are more stable than on Fe catalyst upon comparing the corresponding TPDC peak temperatures. The existence of more stable carbon deposits provides another evidence for the enhancement of carburization on iron catalyst by potassium promoter. This promotional effect of potassium also leads to the preference for bulk phase changes of K/Fe catalyst to carbides rather than oxides, as observed in Mössbauer spectroscopy, and bears the responsibility for the higher product selectivity of light olefins and long-chain hydrocarbons in CO_2 hydrogenation.

The authors wish to thank Dr. Teng-Yuan Dong (Institute of Chemistry, Academia Sinica) for his generosity of providing the Mössbauer spectrometer and assistance in the spectroscopic experiments. Financial support of this work by National Science Council (grant NSC77-0402-E002-05) is gratefully acknowledged.

References

1) G. A. Mills and F. W. Steffgen, *Catal. Rev.*, **8**, 159 (1973).

2) D. J. Dwyer and G. A. Somorjai, *J. Catal.*, **52**, 291 (1978).

3) F. Solymosi and A. Erdohelyi, *J. Mol. Catal.*, **8**, 471. (1980).

4) M. Pijolat, V. Perrichon, M. Primet, and P. Bussiere, *J. Mol. Catal.*, **17**, 367 (1982).

5) G. D. Weatherbee and C. H. Bartholomew, *J. Catal.*, **87**, 352 (1984).

6) J. L. Falconer and A. E. Zagli, *J. Catal.*, **62**, 280 (1980).

7) G. D. Weatherbee and C. H. Bartholomew, *J. Catal.*, **77**, 460 (1982).

8) D. S. Newsome, *Catal. Rev. -Sci. Eng.*, **21**, 275 (1980).

9) M. E. Dry, "Catalysis-Science and Technology," ed by J. R. Anderson and M. Boudart, Springer-Verlag, Berlin (1981), Vol. 1, p.159.

10) J. A. Amelse, L. H. Schwartz, and J. B. Butt, *J. Catal.*, **72**, 95 (1981).

11) J. F. Lee, M. D. Lee, and P. K. Tseng, *Chemistry*, **45**, 50 (1987).

12) D. C. Silverman and M. Boudart, *J. Catal.*, **77**, 208 (1982).

13) J. W. Niemantsverdriet, A. M. van der Kraan, W. L. van Dijk, and H. S. van der Baan, *J. Phys. Chem.*, **84**, 3363 (1980).

14) G. Le Caër, J. M. Dubois, M. Pijolat, V. Perrichon, and P. Bussiere, *J. Phys. Chem.*, **86**, 4799 (1982).

Potentiometric Determination of Some Aliphatic Aldehydes Using the Silver/Sulfide Ion-Selective Electrode

M. Tarek M. ZAKI* and M. H. FAWZY
Department of Chemistry, Faculty of Science, Ain Shams University, Abbassia, Cairo, Egypt
(Received October 14, 1988)

Synopsis. A simple, selective and reproducible method for the potentiometric determination of some aliphatic aldehydes is described. The method is based on oxidation of the aldehydes with silver oxide packed in a column. The formed silver salts of the fatty acids are eluted with water and the silver ion concentration is determined with a silver/sulfide ion-selective electrode using either a calibration graph or a standard addition technique. The effects of experimental variables and the interference of other organic functional groups are investigated. Samples containing up to 5.0 mg aldehyde are analyzed with an average recovery of 98.5% and 98.4% using the proposed techniques, respectively.

Potentiometric methods for aldehyde determination are based on either condensation or oxidation-reduction reactions. In the methods involving condensation reactions, an excess of hydrazine or hydroxyl amine derivatives is added, and the unreacted reagent is back titrated with a suitable titrant. Siggia and Stahl[1] treated aldehydes with excess 1,1-dimethylhydrazine in methanol or ethylene glycol medium. The unused reagent was titrated with hydrochloric acid in methanol. Berka and Zyka[2,3] used 2,4-dinitrophenylhydrazine. The formed hydrazone was separated and the unreacted reagent was titrated with chloramine T in presence of potassium bromide. Moreover, Langmair[4] utilized hydroxylamine hydrochloride as reagent and sodium hydroxide as titrant. However, the former methods lacks selectivity.

On the other hand, Siggia and Segal[5] reported a macro method based on oxidation with Tollens reagent. The residual silver ions were potentiometrically titrated with potassium iodide solution. However, the reagent is unstable and the method is not suitable for adaptation to the micro scale.[6,7]

Application of ion-selective electrodes for end point detection was also reported. Formaldehyde was determined by reaction with iodine-iodide solution in alkaline medium.[8] After acidification, the mixture was titrated with silver nitrate solution using the iodide ion-selective electrode. Moreover, Ma and Hassan[9] reported that the amperometric method of Ikeda[10] for formaldehyde determination with potassium cyanide may be adapted potentiometrically by titrating the unreacted cyanide ions with silver nitrate solution using the cyanide or silver/sulfide ion-selective electrode.

In the present work, the optimum conditions for aliphatic aldehyde determination based on oxidation with silver(I) ions followed by potentiometric measurement using the silver/sulfide ion-selective electrode were investigated. The reagent, silver oxide-butylamine complex, which was recommended by Siggia et al.[11] for the volumetric determination of aldehydes has been tested. However, an invariably low recovery was obtained. To overcome this problem, a potentiometric study based on prior oxidation with silver oxide[12] packed in a column has been carried out. The eluted silver salts of fatty acids were determined with the silver/sulfide ion-selective electrode using either a calibration graph or a known addition technique.

Experimental

Instrumentation and Reagents. An Orion Model EA 920 pH/ISE meter fitted with Orion silver/sulfide ion-selective electrode (Model 94-16) and Orion double-junction reference electrode (Model 90-02) were used for potential measurements.

Silver oxide of 99% purity (Aldrich Chem.) was used to pack two-thirds of a column (1 cm diam. ×15 cm). The filled column was washed several times with twice-distilled water before introducing the samples.

Potassium nitrate solution, 4 M (1 M=1 mol dm^{-3}), was used as ionic strength adjustor (ISA).

Procedure. Introduce 5 ml of the sample solution, containing up to 5.0 mg of the aldehyde in water or 1,4-dioxane, into the column. Elute with water to make a total volume of 40 ml. Collect the eluent in 250-ml beaker. Add 60 ml water and determine the silver ion concentration using the silver/sulfide-double junction reference electrode system by either of the following techniques:

1-Calibration Graph Technique: The electrode calibration graph was established using 100 ml each of the 10^{-1} to 10^{-5} M silver nitrate solution in water or 5% dioxane-water according to the solvent used for the tested sample. To each solution, 2.0 ml of ISA was added before the potential measurement. A linear calibration graph was obtained over the entire range studied.

To the eluted solution, 2.0 ml of ISA was added and the potential was measured. A blank experiment was carried out under identical conditions. The calibration graph was used to determine the silver ion concentration equivalent to the aldehyde sample.

2-Known Addition Technique: Add 2.0 ml of ISA to the eluent, place the electrodes and stir thoroughly. Measure the relative millivolt. Set the reading to zero by turning the calibration control or record the potential reading, if the reading cannot be set to zero. Prepare a standard solution about ten folds as concentrated as the sample concentration under investigation. Add 2.0 ml of ISA to each 100 ml standard. Add 10.0 ml of the standard to the sample and stir thoroughly. Record the potential difference (ΔE). If the meter could not be zeroed in the former step, subtract the second reading from the first to get (ΔE). Calculate the silver ion concentration in the sample which is equivalent to the aldehyde using the equation:

$$C_0=\frac{C_sV_s}{V_0+V_s}\left[10^{-\Delta E/S}-\left(\frac{V_0}{V_0+V_s}\right)\right]^{-1}$$

where C_0 and C_s are the molar concentrations of the sample

Table 1. Potentiometric Determination of Some Aliphatic Aldehydes Using The Silver/Sulfide Ion-Selective Electrode

Sample	Carbonyl group(%)				
	Calcd	Electrode calibration method		Standard addition method	
		Found	Recovery	Found	Recovery
Formaldehyde solution (37 wt.%)	93.33	91.56	98.1	91.44	98.0
		91.58	98.1	91.53	98.1
		91.64	98.2	91.55	98.1
Acetaldehyde	63.64	62.79	98.7	62.69	98.1
		62.85	98.8	62.76	98.6
		62.91	98.9	62.80	98.7
Propion-aldehyde	48.28	47.67	98.7	47.66	98.7
		47.76	98.9	47.72	98.8
		47.81	99.0	47.74	98.9
Butanal	38.89	38.35	98.6	38.29	98.5
		38.36	98.6	38.34	98.6
		38.38	98.7	38.35	98.6
Pentanal	32.56	32.01	98.3	31.98	98.2
		32.05	98.4	31.99	98.2
		32.08	98.5	32.03	98.4
Hexanal	28.00	27.42	97.9	27.37	97.8
		27.48	98.1	27.40	97.9
		27.51	98.3	27.43	98.0

and the standard, V_0 and V_s the corresponding volumes and S is the electrode slope in mV per ten-fold change in concentration. C_0 may also be calculated using the equation:

$$C_0 = QC_s$$

where Q is the value from the known table.[13]

Results and Discussion

The aim of this work was to accomplish the optimum conditions for aliphatic aldehyde determination by oxidation with silver(I) ions. The low recovery obtained using silver oxide-butylamine complex[11] as reagent and silver/sulfide ion-selective electrode for the end point detection, may be attributed to the presence of free amine which affect the sensor membrane. Therefore, an external column packed with silver oxide was utilized as oxidizing agent.

Selection of Conditions. Aliphatic aldehydes are oxidized with silver oxide to the corresponding silver salt of the fatty acids according to the equation:

$$2\ RCHO + 3\ Ag_2O_{(s)} = 2\ RCOOAg + H_2O + 4\ Ag_{(s)}$$

Water, methanol, ethanol, 1-propanol, 2-propanol, and 1,4-dioxane were tested as solvents for aldehyde samples. Water was suitable for aldehydes of low molecular weight. On the other hand, aldehydes of relatively high molecular weight were best dissolved in 1,4-dioxane. Using alcohols as solvents were accompanied by a slight increase in the blank values. This is presumably due to the partial oxidation of this alcohols with silver oxide.

The effect of water volume necessary for eluting the formed fatty acid silver salts was investigated. 20 ml of water was sufficient to elute the formed silver formate or acetate. However, 35 ml of water was required to elute the salts formed by oxidation of higher aldehydes such as pentanal or hexanal. Larger volumes of water than that was accompanied by increasing the blank value due to the solubility of silver oxide. Therefore, 35 ml of water was recommended to elute all samples.

Anal sis of Aldehyde. The results obtained for the analysis of some aldehydes using the calibration graph and the standard addition techniques are summarized in Table 1. Average recoveries of 98.49% and 98.37% with a relative standard deviation of 0.32% and 0.33% were obtained, respectively. On the other hand, the analysis of higher aliphatic aldehydes such as octanal and decanal, in addition to aromatic aldehydes gave low recoveries. This may be due to a nonstoichiometric oxidation with silver oxide or incomplete elution of the formed fatty acid silver salts.

Interferences. The extent of interference from other organic functional groups was investigated. Alcohols (methanol, ethanol, 1-propanol, 2-propanol, and 2-methyl-2-propanol), ketones (acetone, 2-butanone, 3-pentanone, 2-hexanone, and 4-methyl-2-pentanone), amides (formamide, acetamide, and *N,N*-dimethylformamide), imides (succinimide), and hydrogen peroxide did not interfere.

However, acids and esters interfered. Esters undergo partial hydrolysis to form the corresponding fatty acid silver salts. Therefore, a preliminary separation of these compounds was required before aldehyde determination.

References

1) S. Siggia and C. R. Stahl, *Anal. Chem.*, **27**, 1975 (1955).
2) A. Berka and J. Zyka, *Chem. Listy*, **50**, 831 (1956).
3) A. Berka and J. Zyka, *Pharmazie*, **13**, 89 (1958).
4) F. Langmaier, *Kozarstui*, **12**, 140 (1962).

5) S. Siggia and E. Segal, *Anal. Chem.*, **25**, 640 (1962).
6) S. Siggia, "Quantitative Organic Analysis via Functional Groups," 3 rd ed, John Wiley & Sons, New York (1963), pp. 93—97.
7) N. D. Cheronis and T. S. Ma, "Organic Functional Group Analysis by Micro and Semimicro Methods," John Wiley & Sons, New York (1964), p. 154.
8) S. Ikeda, *Anal. Lett.*, **7**, 343 (1974).
9) T. S. Ma and S. S. M. Hassan, "Organic Analysis Using Ion-Selective Electrodes," Academic Press, London (1982), Vol. 2, p. 41.
10) S. Ikeda, *Anal. Chem.*, **46**, 1587(1974).
11) J. A. Mayes, E. J. Kuchar, and A. Siggia, *Anal. Chem.*, **36**, 934(1964).
12) H. C. Bailey and J. H. Knowx, *J. Chem. Soc.*, **1951**, 2741.
13) Model 94-16 Silver/Sulfide Ion-Selective Electrode Instruction Manual, Orion Research.

 © 1989 The Chemical Society of Japan Bull. Chem. Soc. Jpn., 62, 2763—2767 (1989)

1:1:1 Inclusion Compounds of β-Cyclodextrin with Fluorene and Alcohols or Nitriles in Aqueous Solution

Sanyo HAMAI
Department of Physics, Miyazaki Medical College, Kiyotake, Miyazaki 889-16
(Received December 8, 1988)

Fluorene forms a 1:1 inclusion compound (FC) with β-cyclodextrin (CDx) in aqueous solution. From electronic absorption and emission spectra, FC has been found to further associate with alcohol (from ethanol to 1-pentanol) or nitrile (from propionitrile to hexanenitrile) to form a 1:1:1 inclusion compound. An equilibrium constant (K_3) for the formation of the 1:1:1 inclusion compound from FC and alcohol, and that (K_4) from fluorene and a 1:1 inclusion compound of CDx with alcohol have been determined. Upon going from ethanol to 1-pentanol, the value of K_4 increases, reaches a maximum at 1-propanol, and then decreases while K_3 monotonously increases with an increase in the alkyl-chain length of alcohol. For nitriles, K_3 and K_4 have also been evaluated. In this case, the largest K_4 value is seen for propionitrile and butyronitrile, while K_3 increases with increasing the alkyl-chain length of nitrile.

In the β-cyclodextrin (CDx)–alcohol–pyrene and CDx–alcohol–acenaphthene systems, we have found that association occurs between alcohol and a 1:1 inclusion compound of CDx with pyrene or acenaphthene.[1,2] From fluorescence lifetime measurements, Nelson et al. have proposed that 2-methyl-2-propanol is associated with a CDx–pyrene 1:1 inclusion compound.[3] Such behavior of the 1:1 inclusion compound of pyrene or acenaphthene seems to be reasonable since these aromatic guests are too large to bind deeply into the CDx cavity. From comparisons of equilibrium constants for the formation of a ternary 1:1:1 inclusion compound, it was concluded that 1-propanol, among primary alcohols, fits most snugly into the void interior space of the CDx cavity which already accommodates pyrene or acenaphthene.[1,2] These results suggest that the fit of two guest molecules of different kinds into the CDx cavity plays an important role in forming the 1:1:1 inclusion compound.

From a stereochemical point of view, the whole body of a fluorene molecule is anticipated to be deeply incorporated into the cavity, thereby the interior dimension of the cavity being thoroughly occupied by fluorene. Under such circumstances, it seems to be difficult for a 1:1 inclusion compound of CDx with fluorene to associate with an additional alcohol molecule. Thus, in order to further clarify the nature of 1:1:1 inclusion compounds of CDx, we investigated whether or not the CDx–fluorene 1:1 inclusion compound complexes with additional alcohol or nitrile by means of measurements of absorption and fluorescence spectra.

Experimental

Fluorene purchased from Tokyo Kasei was recrystallized twice from ethanol. β-Cyclodextrin (CDx) from Nakarai was recrystallized three times from water. Alcohols (from methanol to hexanol) and nitriles (from acetonitrile to hexanenitrile) were distilled under atmospheric or reduced pressure. Fluorene aqueous solutions were prepared according to the same method as that used for pyrene.[4] The fluorene concentration of sample solutions was (6—7)×10^{-6} mol dm^{-3}. Aerated sample solutions were employed throughout this work. Absorption spectra were run on a Shimadzu UV-260 spectrophotometer. Fluorescence spectra were recorded on a Shimadzu RF-501 spectrofluorometer equipped with a cooled Hamamatsu R-943 photomultiplier, and were corrected for the spectral response of the fluorometer. All measurements were made at 25±0.1 °C, unless otherwise noted.

Results and Discussion

1:1 Inclusion Compound of CDx with Fluorene.

Figure 1 shows the absorption spectra of fluorene aqueous solutions containing various concentrations of CDx. The addition of CDx resulted in red shifts of absorption peaks and the appearance of isosbestic points at 294 and 299 nm. The spectral change is attributed to the formation of a 1:1 inclusion compound (FC) of CDx with fluorene:

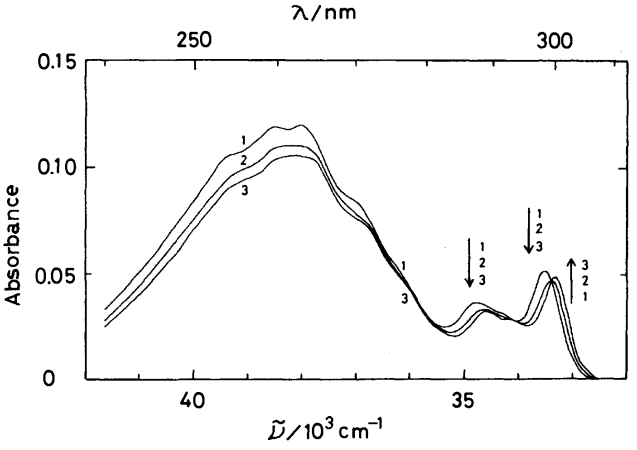

Fig. 1. Absorption spectra of fluorene (ca. 6×10^{-6} mol dm^{-3}) in the presence of CDx. Concentration of CDx: (1) 0 mol dm^{-3}; (2) 8.4×10^{-4} mol dm^{-3}; (3) 4.2×10^{-3} mol dm^{-3}.

$$FL + CDx \underset{}{\overset{K_1}{\rightleftharpoons}} FC, \quad (1)$$

where FL represents fluorene, and K_1 is an equilibrium constant for the formation of FC. From the absorbance change of fluorene,[5] K_1 has been determined to be 1200±100 mol^{-1} dm^3. This value is nearly twice that for naphthalene (685 mol^{-1} dm^3)[5] and one to two orders of magnitude greater than those for pyrene (7.6 mol^{-1} dm^3)[1] and acenaphthene (76±5 mol^{-1} dm^3).[2] Since pyrene and acenaphthene cannot bind deeply into the CDx cavity owing to the steric hindrance, smaller K_1 values are obtained. A naphthalene ring fully enters the cavity,[6] resulting in the relatively large value of K_1. A comparison between these K_1 values suggests that in FC the hydrophobic interaction occurs between CDx and fluorene, i.e., as expected above, the whole body of a nearly prolate fluorene molecule deeply penetrates into the CDx cavity. An examination of a space-filling molecular model supports such a picture of FC. When CDx is added to a fluorene aqueous solution, the intensity ratio of the 304-nm peak to the 312-nm peak in the fluorene fluorescence is enhanced. This change in the fluorescence spectra also shows the complex formation between CDx and fluorene. From the fluorescence intensity change caused by the addition of CDx, a K_1 value (1100±100 mol^{-1} dm^3) similar to that obtained from the absorption method was evaluated.[7]

1:1:1 Inclusion Compounds of CDx with Fluorene and Alcohols. Figure 2 illustrates the absorption spectra of fluorene aqueous solutions containing both CDx (4.2×10^{-3} mol dm^{-3}) and varying amounts of 1-butanol (Bu). Isosbestic points are observed at 256, 261, 286, 290, 298, and 301 nm, and a new shoulder appears at ca. 303 nm, which locates at longer wavelengths than the 0–0 band of fluorene in water or in water containing CDx. Upon cooling to 5 °C, this shoulder becomes a sharp peak at 304 nm. Such spectral changes have never been observed in the absence of CDx. Consequently, the absorption change shown in Fig. 2 can be interpreted in terms of the formation of a ternary inclusion compound composed of CDx, fluorene, and Bu. This conclusion is consistent with Scypinsky and Cline Love's suggestion that CDx, 1,2-dibromoethane, and fluorene forms a ternary complex.[8] Figure 3 exhibits the normalized fluorescence of fluorene in aqueous solutions contain-

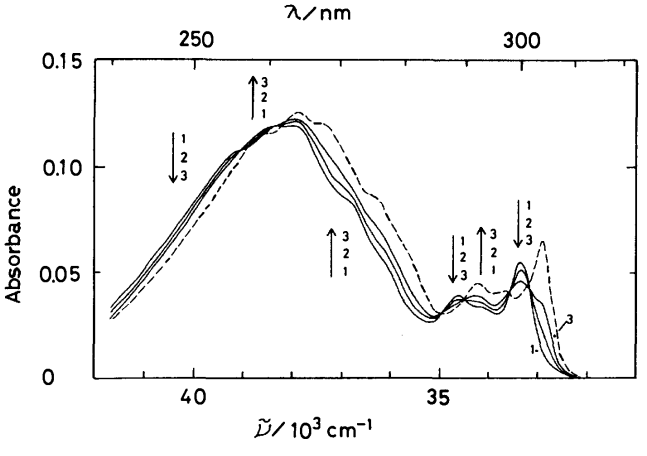

Fig. 2. Absorption spectra of fluorene (ca. 6×10^{-6} mol dm^{-3}) aqueous solutions containing CDx (4.2×10^{-3} mol dm^{-3}) and varying concentrations of Bu at 25 °C and the absorption spectrum (----) of a fluorene solution containing CDx (4.2×10^{-3} mol dm^{-3}) and Bu (1.09×10^{-1} mol dm^{-3}) at 5 °C. Concentration of Bu: (1) 0 mol dm^{-3}; (2) 3.28×10^{-2} mol dm^{-3}; (3) 1.09×10^{-1} mol dm^{-3}.

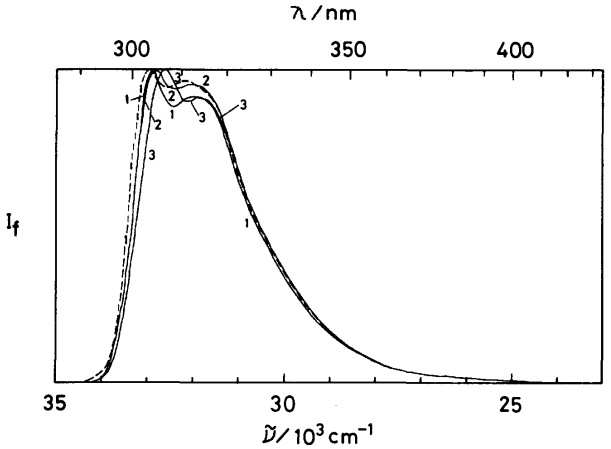

Fig. 3. Normalized fluorescence spectra of fluorene (ca. 6×10^{-6} mol dm^{-3}) aqueous solutions containing CDx (4.2×10^{-3} mol dm^{-3}) and varying concentrations of Bu. For comparison, the normalized fluorescence spectrum (----) of fluorene in aqueous solution is also shown. Concentration of Bu: (1) 0 mol dm^{-3}; (2) 2.19×10^{-2} mol dm^{-3}; (3) 1.09×10^{-1} mol dm^{-3}. λ_{ex}=298 nm.

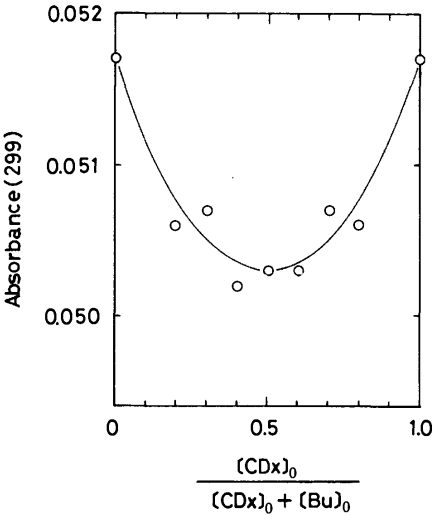

Fig. 4. Continuous variation plot under the condition of $[CDx]_0+[Bu]_0=1\times10^{-2}$ mol dm^{-3}. The observed wavelength is 299 nm. The fluorene concentration is ca. 6.5×10^{-6} mol dm^{-3}.

ing both CDx (4.2×10^{-3} mol dm^{-3}) and varying concentrations of Bu. Upon the addition of Bu, the fluorescence maximum is shifted to longer wavelengths. The red shift in the fluorescence spectrum shown in Fig. 3 corresponds to that in the absorption spectrum in Fig. 2. In order to determine the stoichiometry of the ternary inclusion compound responsible for the red shifts in the absorption and fluorescence spectra, we applied a continuous variation method,[1,4] in which the absorbance at 299 nm was monitored as a function of the molar fraction of CDx under the condition that a sum of the initial concentrations of CDx and Bu was held constant at 1×10^{-2} mol dm^{-3} while the fluorene concentration was fixed. The experimental results are shown in Fig. 4. Although there is some scatter of the data, a minimum at a molar fraction of 0.5 evidently indicates a 1:1 stoichiometry concerning CDx and Bu. When Bu less than 5×10^{-2} mol dm^{-3} is added to a fluorene solution containing CDx (4.2×10^{-3} mol dm^{-3}), the absorbance at 305 nm is proportional to the Bu concentration, indicating that the ternary inclusion compound contains only one Bu molecule. From these results, the ternary inclusion compound can be assigned to a 1:1:1 inclusion compound (FBC) of CDx with fluorene and Bu. Such 1:1:1 inclusion compounds including alcohol have already been reported for the cases of pyrene and acenaphthene.[1,2] The formation of FBC is represented by the following equilibria:

$$\text{Bu} + \text{CDx} \underset{}{\overset{K_2}{\rightleftharpoons}} \text{BC}, \tag{2}$$

$$\text{FC} + \text{Bu} \overset{K_3}{\rightleftharpoons} \text{FBC}, \tag{3}$$

and

$$\text{FL} + \text{BC} \overset{K_4}{\rightleftharpoons} \text{FBC}, \tag{4}$$

where BC is a 1:1 inclusion compound of CDx with Bu, and K_2, K_3, and K_4 are equilibrium constants for the formation of BC, FBC from FC and Bu, and FBC from fluorene and BC, respectively. As in the case of the CDx-alcohol-pyrene system,[1] K_3 can be determined from a comparison of the observed fluorescence intensities, which are a function of the Bu concentration, with curves calculated by assuming three parameters. By using an instrumental constant a, the fluorescence quantum yield ϕ, the molar absorption coefficient ε at the excitation wavelength, and subscripts 1, 2, and 3 which stand for fluorene, FC, and FBC, respectively, one can write the fluorene fluorescence intensity I_f as[1]

$$I_f = A - B/(C + [\text{Bu}]_0), \tag{5}$$

where $A=a\phi_3\varepsilon_3[\text{FL}]_0$, $B=a\{\phi_3\varepsilon_3K_1K_3[\text{CDx}]_0(1+K_1[\text{CDx}]_0)(1+K_2[\text{CDx}]_0)[\text{FL}]_0/K_1K_3[\text{CDx}]_0-(\phi_1\varepsilon_1+\phi_2\varepsilon_2K_1[\text{CDx}]_0)(1+K_2[\text{CDx}]_0)[\text{FL}]_0/K_1K_3[\text{CDx}]_0\}$, and $C=(1+K_1[\text{CDx}]_0)(1+K_2[\text{CDx}]_0)/K_1K_3[\text{CDx}]_0$. Here, subscript 0 refers to the initial concentration. The least-squares fit of a simulation curve was obtained when $A=110$, $B=3.07$ mol dm^{-3}, and $C=0.0573$ mol dm^{-3} (Fig. 5). From this C value, the K_1 value determined in this study, and the K_2 value reported by Matsui and Mochida,[9] K_3 was evaluated to be 22 ± 1 mol^{-1} dm^3. From a relationship $K_1K_3=K_2K_4$, K_4 was estimated to be 1900 ± 200 mol^{-1} dm^3. These K_3 and K_4 values are given in Table 1.

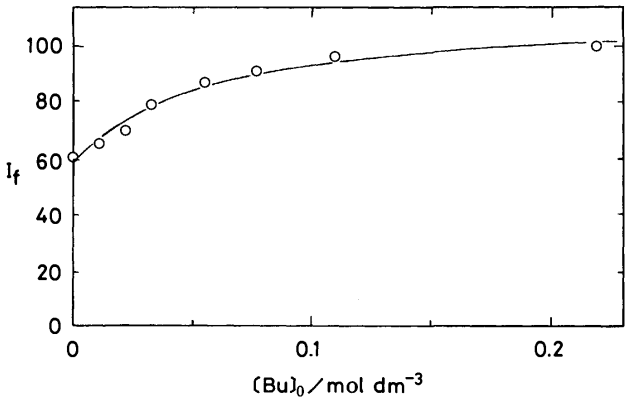

Fig. 5. Comparison between observed fluorescence intensities of fluorene (ca. 6×10^{-6} mol dm^{-3}) and a least-squares fit curve calculated with assumed parameters $A=110$, $B=3.07$ mol dm^{-3}, and $C=0.0573$ mol dm^{-3}. The maximum fluorescence intensity is normalized to 100. $[\text{CDx}]_0=4.2\times10^{-3}$ mol dm^{-3}. $\lambda_{ex}=303$ nm.

The addition of alcohols from ethanol to 1-pentanol to fluorene aqueous solutions with CDx results in an absorption change similar to that shown in Fig. 2, indicating the formation of 1:1:1 inclusion compounds containing alcohol.[10] For alcohols other than Bu, K_3 and K_4 have similarly been evaluated, and are also summarized in Table 1. As the alkyl chain of alcohol is lengthened, K_3 monotonously increases like K_2. On the other hand, the largest K_4 is obtained for 1-propanol, and K_4 is reduced when the alkyl chain of alcohol is shortened or lengthened relative to that of 1-propanol. Such characteristics of K_3 and K_4 are quite similar to those obtained for the CDx-alcohol-pyrene and CDx-alcohol-acenaphthene systems.[1,2] In the 1:1 inclusion compound of pyrene or acenaphthene, the CDx cavity which accommodates pyrene or acenaphthene has a void space, while in the 1:1 inclusion compound of fluorene there is no void dimension inside the cavity since the cavity is fully occupied by fluorene. From the stereochemical standpoint, it is surprising that an additional guest, alcohol, can associate with the CDx-fluorene 1:1 inclusion compound. Therefore, owing to the formation of the 1:1:1 inclusion compound of fluorene, a fluorene molecule within the CDx cavity may protrude from the cavity to some extent to make a void space for an additional alcohol molecule. In the case of fluorene, the K_3 values are two to three orders of magnitude smaller than those for the pyrene or

Table 1. Equilibrium Constants for the Formation of 1:1 and 1:1:1 Inclusion Compounds

	K_2/mol^{-1} dm^3	K_3/mol^{-1} dm^3	K_4/mol^{-1} dm^3
Ethanol	0.93[a]	0.94±0.05	1400±100
1-Propanol	3.72[a]	7.9±0.4	3000±300
1-Butanol	16.6[a]	22±1	1900±200
1-Pentanol	63.1[a]	78±3	1800±200
Propionitrile	3.8±0.3	3.6±0.2	1300±200
Butyronitrile	16±1	15±1	1300±200
Valeronitrile	170±10	86±5	740±130
Hexanenitrile	510±30	120±10	340±60

a) Data of Matsui and Mochida (Ref. 9).

acenaphthene system,[1,2,11] indicating that the complexation reaction between the CDx-fluorene 1:1 inclusion compound and additional alcohol is not so favorable as that between a CDx-pyrene or CDx-acenahthene 1:1 inclusion compound and alcohol. The same is true for K_4.[12]

As mentioned above, at low temperatures the 0-0 absorption band of the 1:1:1 inclusion compound appears at 304 nm. This peak wavelength is rather abnormal because fluorene exhibits the peak of the 0-0 band at 301, 300, 300, 301, 300, 300, 299, and 298 nm in cyclohexane (ε=2.02), 1,4-dioxane (ε=2.21), ethyl acetate (ε=6.02), dichloromethane (ε=9.08), ethanol (ε=24.3), methanol (ε=32.6), acetonitrile (ε=37.5), and water (ε=78.5), respectively. For the S_2 absorption band of pyrene in the CDx-alcohol-pyrene 1:1:1 inclusion compound, the 0-0 band is also located at longer wavelengths than that in any solvent.[1] The abnormally large red shifts of the absorption peaks in the CDx-alcohol-fluorene and -pyrene 1:1:1 inclusion compounds may be interpreted in terms of a kind of microheterogeneous solvent effect. One part of a long fluorene molecule in the 1:1:1 inclusion compound is extruded out of the CDx cavity to the very polar water medium, and the other part of the fluorene molecule resides in the CDx cavity, being in contact with the alkyl chain of an alcohol molecule entering the cavity. Therefore, one end of the fluorene molecule experiences a very polar environment, and the other end of the fluorene molecule is in a relatively nonpolar environment owing to both the hydrophobicity of the inner wall of the CDx cavity and that of the alkyl chain of an alcohol molecule entering the CDx cavity. Under such circumstances, the excited state of fluorene may be lowered in energy relative to that in a uniform environment (neat solvent), since π electrons delocalize more easily in the excited state than in the ground state. As a consequence, the 0-0 band of fluorene in the 1:1:1 inclusion compound is shifted to the red relative to that in any neat solvent.

1:1:1 Inclusion Compounds of CDx with Fluorene and Nitriles. The association of FC with nitriles from propionitrile to hexanenitrile has been confirmed from the observations of absorption and fluorescence spectral changes similar to those for solutions containing alcohol.[13] This finding is consistent with Turro et al.'s suggestion that a ternary complex is formed among CDx, acetonitrile, and 1-halonaphthalene.[14] On the basis of a competition method,[2,9] K_2 values for the nitriles have been evaluated and are listed in Table 1. From comparisons between the observed fluorescence intensities and intensity curves which have been calculated according to Eq. 5, K_3 and K_4 for the nitriles have been determined (Table 1). Both K_2 and K_3 increase as the alkyl chain of nitrile is lengthened. These K_2 and K_3 values are several times greater than those for alcohols possessing the same alkyl group, indicating the stronger hydrophobicity of nitrile than that of alcohol. However, the K_4 values for the nitriles are rather small compared with those for the corresponding alcohols. The largest K_4 is seen both for propionitrile and butyronitrile, and K_4 decreases on going from butyronitrile to hexanenitrile. It should be noted that K_4 for propionitrile with a shorter alkyl chain than 1-propanol, whose K_4 is the largest in the alcohol series, has a maximum value in the nitrile series. These findings may imply that in the 1:1:1 inclusion compound the orientation and/or location of a nitrile molecule within the CDx cavity is slightly different from that of the alcohol molecule.

The author is grateful to Professor Fumio Hirayama for his valuable discussion.

References

1) S. Hamai, *J. Phys. Chem.*, **93**, 2074 (1989).
2) S. Hamai, *J. Am. Chem. Soc.*, **111**, 3954 (1989).
3) G. Nelson, G. patonay, and I. M. Warner, *J. Inclusion Phenom.*, **6**, 277 (1988).
4) S. Hamai, *J. Phys. Chem.*, **92**, 6140 (1988).
5) S. Hamai, *Bull. Chem. Soc. Jpn.*, **55**, 2721 (1982).
6) K. Harata and H. Uedaira, *Bull. Chem. Soc. Jpn.*, **48**, 375 (1975).
7) According to the method of Ref. 1, 302 nm was selected as the excitation wavelength.
8) S. Scypinsky and L. J. Cline Love, *Anal. Chem.*, **56**, 322 (1984).

9) Y. Matsui and K. Mochida, *Bull. Chem. Soc. Jpn.*, **52**, 2808 (1979).

10) No absorption and fluorescence spectral changes are observed when methanol is added to a fluorene solution with CDx.

11) The K_3 values in the CDx-1-propanol-pyrene and CDx-1-propanol-acenaphthene systems are 7600 and 1600 mol^{-1} dm^3, respectively (Refs. 1 and 2).

12) The K_4 values in the CDx-1-propanol-pyrene and CDx-1-propanol-acenaphthene systems are 15000 and 32000 mol^{-1} dm^3, respectively (Refs. 1 and 2).

13) Addition of acetonitrile to a fluorene aqueous solution containing CDx results in no changes in the absorption and fluorescence spectra.

14) N. J. Turro, J. D. Bolt, Y. Kuroda, and I. Tabushi, *Photochem. Photobiol.*, **35**, 69 (1982).

 © 1989 The Chemical Society of Japan Bull. Chem. Soc. Jpn., 62, 2768—2773 (1989) [Vol. 62, No. 9

A Transition Sequence of Complex Oscillations in a Chemical Oscillation Model Showing Chaos

Makoto MORITA, Kazutoshi IWAMOTO, and Manabu SENŌ*
Institute of Industrial Science, University of Tokyo,
7-22-1, Roppongi, Minato-ku, Tokyo 106
(Received January 25, 1989)

A three-variable model system exhibiting complex oscillations was analyzed. Our analysis reveals a bifurcation structure of complex oscillations including chaotic oscillations. The bifurcation structure reproduces well the transition sequences of oscillatory states observed in the experiments of the Belousov–Zhabotinskii reaction and the chlorite oscillators. The transition sequence to chaotic oscillations in our model system shows period-doubling sequences. When the number F is defined as a ratio of the number of large amplitude to the total number of oscillations per period in the complex oscillation, the number constitutes a monotonous, stepwise-increasing function of a control parameter. The sequence of the complex oscillations is described well by the Farey arithmetric. Also, the average flux of reaction was found to change abruptly at the bifurcation points of the complex oscillations.

In recent years much attention has been paid on the complex oscillations and the chaotic oscillations in the oscillating chemical reactions, and numerous experimental and theoretical studies have been made.[1–4] The complex oscillations were first investigated by Belousov and Zhabotinskii,[5] and Hudson et al. reexamined in detail the Belousov–Zhabotinskii (BZ) reaction in a continuous flow reactor and confirmed that the complex oscillations continued steadily.[6,7] Their experiments exhibited various types of complex oscillations and chaotic oscillations depending on the flow rate of the reactant solutions. Similar phenomena have been also observed in various chlorite oscillators.[8,9] Every complex oscillation reported hitherto is composed of a combination of small and large amplitude oscillations per period. Theoretical investigations on the appearance of complex oscillations have been also performed. Especially, studies on the modified Oregonator[10] may be the most representative.[11–14]

In a previous paper we proposed a simple model to explain chemical oscillations.[15] Moreover, with some modification of the original model system, we constituted a new model system showing some complex oscillations consisting of concatenating small and large amplitude oscillations and explained a mechanism for occurrence of such complex oscillations.[16]

Recently, transition sequences of complex oscillations have been observed in careful and detailed experiments.[17–19] To understand these transition sequences of periodic states, theoretical studies have been carried out by means of one-dimensional maps[20–22] and model systems.[23,24] Many experimental and theoretical efforts have been made to establish the theory of bifurcation structures in oscillating chemical reactions, but still now we can say that bifurcation structures including chaotic oscillations have not been adequately understood.

In the present paper we report a bifurcation structure of complex oscillations including chaotic oscillations by analyzing our simple model with three variables. The model exhibits a quite similar transition sequence of the complex oscillations observed in the BZ reaction[6,7,17–19] and the chlorite oscillators.[8,9] All the complex oscillations appear in the region between the singly small amplitude oscillation and the singly large amplitude oscillation. Mode locking is observed in the transition sequence of complex oscillations. And combined complex oscillations and chaotic oscillations were observed between two stable complex oscillations. The transition sequence from a complex to the chaotic oscillation was period doubling. A complex oscillation becomes unstable with an increase in a control parameter value and a 2-cycle period oscillation appears and then, when the parameter increases, 2^2, 2^3,…, 2^k-cycle oscillations appear and finally an aperiodic state (chaotic oscillation) is followed. When the control parameter increases further, the aperiodic state becomes unstable and a 3-cycle oscillations appears. This sequence was predicted by Li and Yorke.[25]

When an oscillatory state is characterized by a number F, the ratio of the number of large amplitude peaks to the total number of peaks per period, F is a monotonous stepwise-increasing function of a control parameter and forms a staircase similar to the so-called "devil's staircase".[26] The transition sequence of complex oscillations is described well by Farey series.[27]

In order to consider meanings of the staircase structure, the average flux of reaction of each oscillatory state was calculated and a distinct relationship between the oscillatory state and the average flux of reaction was found.

The main purpose of this paper is to show the global feature of the bifurcation structure in our model. Details of respective cases will appear somewhere.

The Model

In a previous paper, we proposed a two-variable chemical system exhibiting temporal oscillations.[15] In a succeeding paper of it, a three-variable model system exhibiting complex oscillations was derived by some modification of the original system and its behavior was analyzed.[16] In this paper, the modified system was investigated in order to make clear the bifurcation structure of the complex oscillations including chaotic oscillations. The system is consisting of the following chemical reactions;[16]

$$\mathrm{P} + \mathrm{Z} \xrightarrow{k_1} \mathrm{E} + \mathrm{Z}, \qquad \text{(R1)}$$

$$\mathrm{E} + \mathrm{X} \xrightarrow{k_2} \mathrm{R} + \mathrm{X}, \qquad \text{(R2)}$$

$$\mathrm{A} + 2\mathrm{X} + \mathrm{E} \underset{k_4}{\overset{k_3}{\rightleftharpoons}} 3\mathrm{X} + \mathrm{E}, \qquad \text{(R3)}$$

$$\mathrm{B} + \mathrm{X} \underset{k_6}{\overset{k_5}{\rightleftharpoons}} \mathrm{C}, \qquad \text{(R4)}$$

$$\mathrm{Q} \xrightarrow{k_7} \mathrm{Z}, \qquad \text{(R5)}$$

$$\mathrm{Z} + \mathrm{X} \xrightarrow{k_8} \mathrm{D} + \mathrm{X}, \qquad \text{(R6)}$$

where A, B, P, and Q are reactants, C, D, and R are products and E, X, and Z, are intermediates. In the model the concentrations of all the reactants and the products are assumed to be constant, keeping the system effectively far from equilibrium. For simplicity, the symbols for the chemical species are used also to denote their concentrations. The differential equations describing the dynamic behavior of this model are given by applying the law of mass action to Reactions (R1)—(R6);

$$\frac{dE}{dt} = k_1PZ - k_2EX, \qquad (1)$$

$$\frac{dX}{dt} = k_3AEX^2 - k_4EX^3 - k_5BX + k_6C, \qquad (2)$$

$$\frac{dZ}{dt} = k_7Q - k_8XZ. \qquad (3)$$

k_i's denote forward or backward rate constants for Reactions (R1)—(R6). The numerical values of k_1 through k_8, A, B, C, and Q are given as follows: k_1=1.0, k_2=5.0, k_3=100.0, k_4=50.0, k_5=10.0, k_6=1.0, k_7=0.1, k_8=0.4, A=1.3, B=5.0, C=5.3, and Q=1.0. Equations 1—3 were calculated by the double-precision Runge-Kutta-Gill method with a digital computer. P is set as a control parameter and every calculation was carried out by assigning a proper value of P.

Bifurcation Structures of Complex Oscillations

According to the results of linearized stability analysis, the steady state of the present chemical system is unstable in the region, $1.034<P<14.21$. The differential equations (Eqs. 1—3) were solved numerically to confirm the occurrence of sustained oscillations at these unstable steady states. Complex oscillations formed from combinations of small and large amplitude oscillations appear, as an example is illustrated in Fig. 1. A mechanism for the occurrence of the complex oscillations has been proposed in the preceding paper.[16] Figure 1(a) shows the temporal change of the intermediate X at P=1.13. This complex oscillations is formed by concatenating one large amplitude and four small amplitude oscillations per period. Figure 1(b) shows a three-dimensional view of this complex oscillation. A common feature of the complex oscillations observed in our system is that they consist of periodic repetitions of a basic pattern of a large amplitude oscillation followed by some small amplitude oscillations. Therefore, these typical complex oscillations can be characterized by a number n, the total number of peaks per period. The notation $\pi(n)$ is used hereafter to describe the complex oscillation formed from the combination of one large peak and $(n-1)$ small peaks per period. The oscillation shown in Fig. 1 is $\pi(5)$.

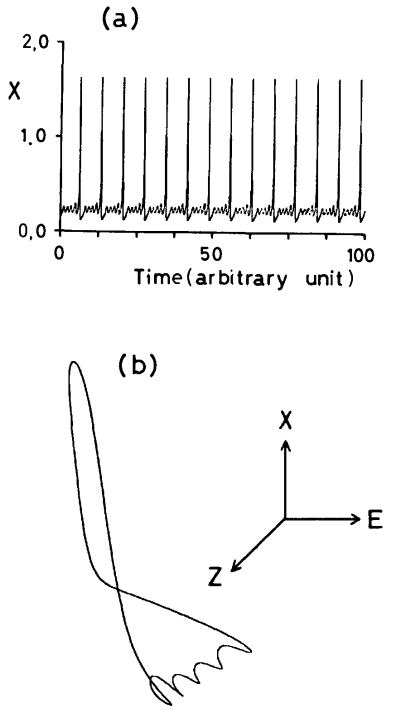

Fig. 1. A behavior of the complex oscillation $\pi(5)$ in our model. (a) Temporal change X vs. time, (b) three dimensional view in the E-X-Z space. P=1.13.

Figure 2 shows the relationship between the number n and the parameter P. With an increase in the value of P, the number of small peaks per period decreases by one. Here, $\pi(1)$ represents a single, large amplitude oscillation. It is noteworthy that the mode locking exerts in these oscillations and the number n is a

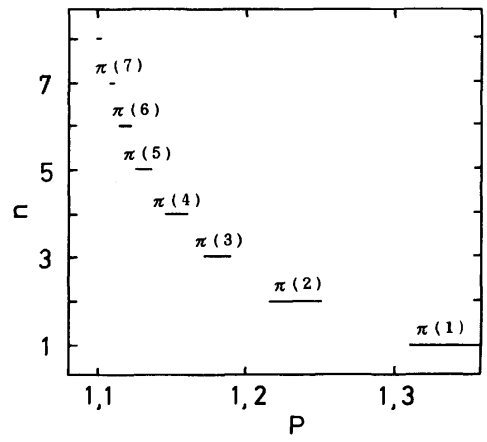

Fig. 2. A mode locking structure of complex oscillations. Relationship between the control parameter P and the number n which characterizes the states of complex oscillations.

staircase-like function of P. The oscillation region of $\pi(n)$ and the transition region between $\pi(n+1)$ and $\pi(n)$ become larger for the smaller number of n.

The property of mode locking has been noticed also in the BZ reaction[17-19] and a one-dimensional map has been utilized to describe the sequence of oscillatory states in the BZ reaction.[20] The mode locking behaviors have been occasionally observed in nonlinear systems having 2-torus attractor,[28-34] even though we do not confirm the existence of two distinct oscillators in these systems.

More complex oscillations appear in the parameter range between $\pi(n)$ and $\pi(n-1)$. They are a periodic oscillation formed from the combination of $\pi(n)$ and $\pi(n-1)$ per period and a chaotic oscillation. Typical examples are shown in Fig. 3. Figure 3(a) shows a periodic oscillation where $\pi(2)$ and $\pi(3)$ appear alternately. Hereafter we call this type oscillation as a combined complex oscillation and designate as $\pi(3)\pi(2)$ for an example. Figure 3(b) shows a more complicated periodic oscillation consisting of a 3-cycle oscillation of $\pi(2)$ and a 1-cycle oscillation of $\pi(3)$ per period. The general notation of these combined complex oscillations is $[\pi(n)]^k[\pi(n-1)]^m$; a periodic oscillation formed from the combination of k-cycle oscillation of $\pi(n)$ and m-cycle oscillation of $\pi(n-1)$. The combined complex oscillation shown in Fig. 3(b) is $[\pi(3)][\pi(2)]^3$. Noteworthily, almost all the combined complex oscillations between the regions of $\pi(n)$ and $\pi(n-1)$ consist of the combination of $\pi(n)$ and $\pi(n-1)$. Moreover, a chaotic oscillation observed in this region consists of aperiodic repetitions of $\pi(n)$ and $\pi(n-1)$, as Fig. 3(c) illustrates. However, there are some exceptional cases where the chaotic oscillations in the region between $\pi(n)$ and $\pi(n-1)$ consist of not only $\pi(n)$ and $\pi(n-1)$ but also $\pi(k)$ with k except for n and $n-1$. An example is shown in Fig. 3(d). On a chaotic oscillation we will explain in detail the bifurcation

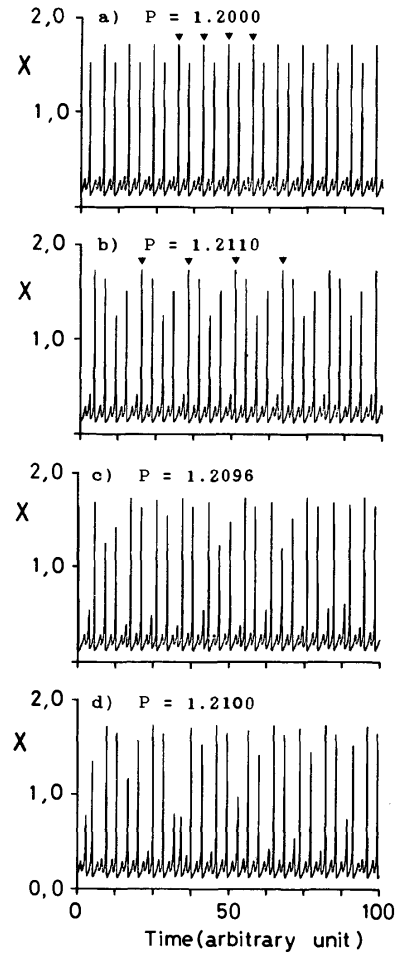

Fig. 3. The combined complex oscillations and the chaotic oscillations. (a) P=1.20: $\pi(3)\pi(2)$, (b) P=1.211: $[\pi(3)][\pi(2)]^3$, (c) P=1.2096 and (d) P=1.21: chaos. Each mark above the oscillations shows the period.

structure in the following papers.

In order to explain the transition sequence including combined complex oscillations and chaotic oscillations, we put a suitable rational between n and $n-1$ to a periodic oscillation of $[\pi(n)]^k[\pi(n-1)]^m$ and plot against P on the n-P two-dimensional phase diagram, as seen in Fig. 4. The mode locking is observed again. The combined complex oscillation of $\pi(n)\pi(n-1)$ occupies a larger region between $\pi(n)$ and $\pi(n-1)$ than other combined complex oscillations of $[\pi(n)]^k[\pi(n-1)]^m$ ($k \neq m$). Every chaotic oscillation takes place in a very limited region. Figure 5 shows an outline of the transition sequence of oscillatory states between $\pi(2)$ and $\pi(1)$. Figure 6 shows the examples of corresponding oscillation states. The oscillation $\pi(2)$ (a) bifurcates successively to $[\pi(2)]^2$ (b), $[\pi(2)]^4$ (c), $[\pi(2)]^8$ (d),$\cdots$, resulting in an aperiodic oscillation (e) formed from $\pi(2)$, as P increases. When P increased beyond over the chaotic region, a 3-cycle oscillation $[\pi(2)]^3$ (f) and a different type chaotic oscillation (g) were found to appear without any period-doubling sequence. The

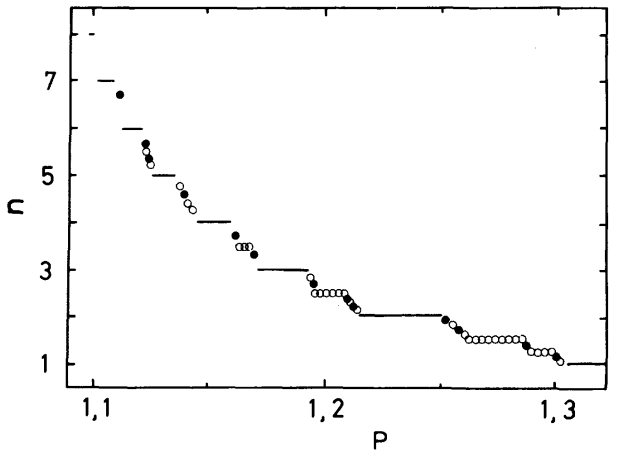

Fig. 4. Relationship between the control parameter P and oscillatory states. Symbols; (—) complex oscillation $\pi(n)$, (○) combined complex oscillation $[\pi(n)]^k[\pi(n-1)]^m$, (●) chaotic oscillation.

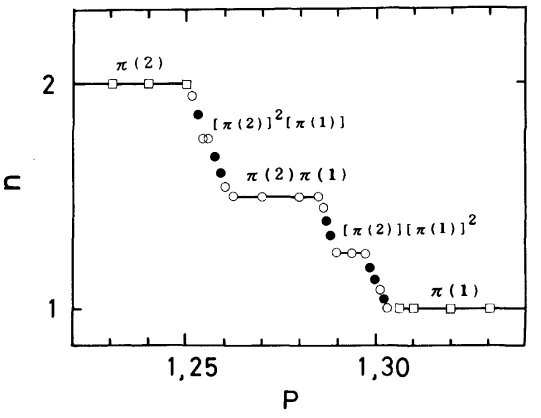

Fig. 5. A sequence of oscillatory states between $\pi(2)$ and $\pi(1)$ by varying the control parameter P. Symbols; (□) complex oscillation $\pi(n)$, (○) combined complex oscillation $[\pi(n)]^k[\pi(n-1)]^m$, (●) chaotic oscillation.

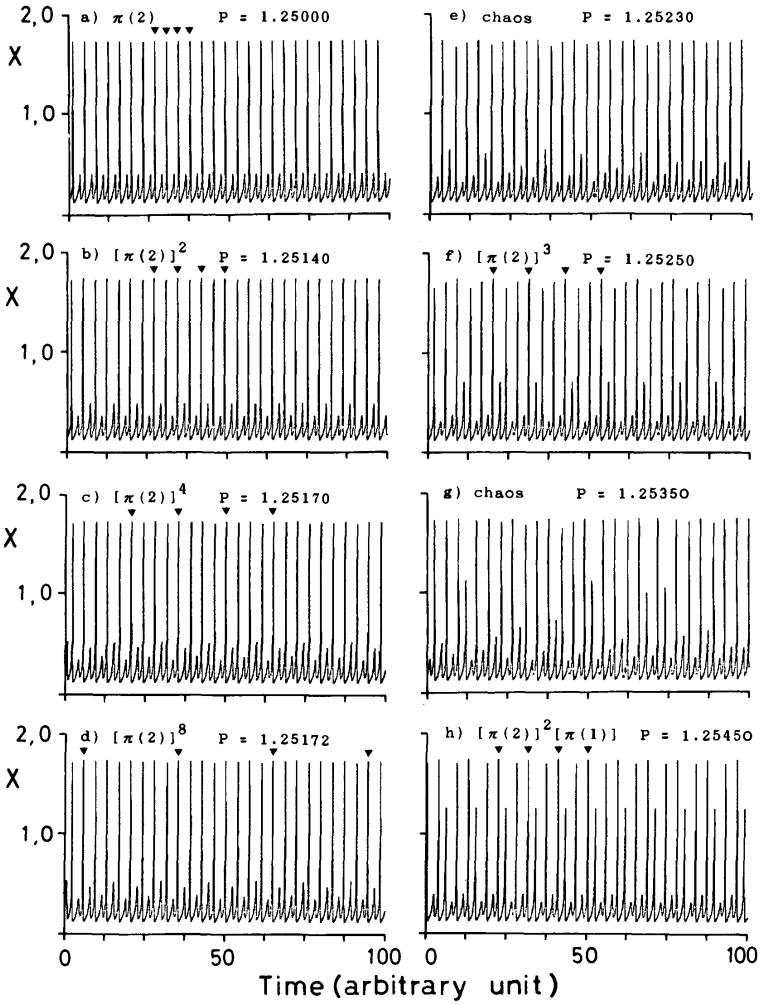

Fig. 6. A transition sequence of oscillations between $\pi(2)$ and $[\pi(2)]^2[\pi(1)]$. Each mark above the oscillations shows the period.

latter chaotic oscillation consists of a combination of $\pi(2)$ and $\pi(1)$. Then, the system leads a combined complex oscillation $[\pi(2)]^2[\pi(1)]$ (h) formed by concatenating $\pi(2)$ and $\pi(1)$, which shows period-doubling as an increase in P till it becomes unstable. After repetitions of these processes, $\pi(2)\pi(1)$ and finally $\pi(1)$ occur.

The transition sequence from $\pi(n)$ to $\pi(n-1)$ with an increasing P can be summarized as follows:

$$\begin{aligned}&\pi(n) \to [\pi(n)]^2 \to [\pi(n)]^4 \to \to \text{chaos} \to [\pi(n)]^3 \\ &\to \text{chaos} \to \to \to [\pi(n)]^k[\pi(n-1)]^m\,(k>m) \to \to \text{chaos} \to \\ &\to \pi(n)\pi(n-1) \to \to \text{chaos} \to \to [\pi(n)]^k[\pi(n-1)]^m\,(k<m) \\ &\to \to \text{chaos} \to [\pi(n-1)]^3 \to \to \text{chaos} \to [\pi(n-1)]^4 \\ &\to [\pi(n-1)]^2 \to \pi(n-1),\end{aligned}$$

where $[\pi(n)]^k$ is a k-cycle oscillation of $\pi(n)$.

According to Maselko and Swinney,[18,19] we define a following number F which characterizes each complex oscillation;

$$F = L/(L + S),$$

where S and L are respectively the numbers of small and large amplitude oscillations per period. For examples, the complex oscillation $\pi(n)$ has the number of $F=1/n$ and the combined complex oscillation $\pi(n)\pi(n-1)$ has $F=2/(2n-1)$. Of course, some of the different oscillations have the same value of F; e.g. both $\pi(2)$ and $[\pi(2)]^2$ have $F=1/2$.

Figure 7 shows the relationship between F and P, where F forms a staircase as a function of P. F equals 1/2 in a discrete wide range of P. The regions having the values of 1/3, 2/3, 1/4, and 3/4 are also clearly distinguishable. $F=1/2$ represents a series of periodic states formed from $\pi(2)^n$, where n=1, 2, 4, 8,·····5, 3 (Sarkovskii sequence).[36] Similarly, 1/3, 2/3, and 1/4, respectively show $\pi(3)^n$, $[\pi(2)\pi(1)]^n$, and $\pi(4)^n$, where n=1, 2, 4, 8,···5, 3. Aperiodic states (chaotic oscillations) are thus included in this figure, but the case shown in Fig. 6(g) is difficult to define its value of F and to show in this figure. This staircase is similar

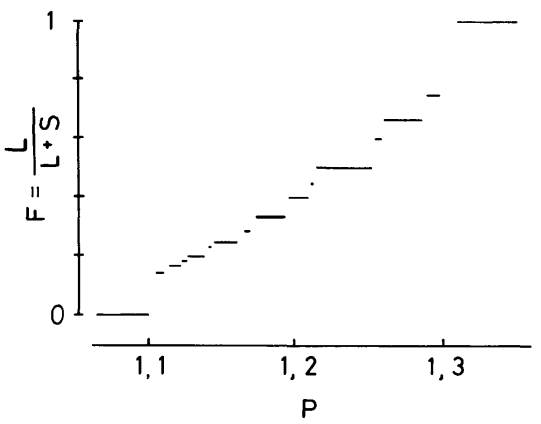

Fig. 7. A staircase behavior of the number F vs. P.

to the "devil's staircase".[26] The devil's staircase has as infinite self-similar staircase structure and is a representative example of fractal, which has been often observed in nonlinear systems. For examples, the one-dimensional Ising model[31] and the sine circle map[32,33] exhibit the devil's staircase.

Recently, Maselko and Swinney have found a similar staircase in the BZ reaction.[18,19] They studied two types of sequences, a complex oscillation composed of two basic patterns and that of three basic patterns. The former sequence is in conformity with the experimental results by Hudson et al. These sequences could be well reproduced in our model.

It has been noticed that the ordering of the number F is related to the Farey series,[18,19,30] when the system has the staircase structure. The Farey series is given by the following procedure; starting with two fractions, 0/1 and 1/1, we get a new fraction according to the following equation.

$$a/b \oplus c/d = (a + c)/(b + d).$$

The first Farey series is 0/1, 1/1, the second is 0/1, 1/2, 1/1, the third is 0/1, 1/3, 1/2, 2/3, 1/1, and so forth. The series of F in Fig. 7 is in a good agreement with the Farey series. It is noteworthy that the complex oscillation having a smaller denominator in the Farey number occupies the wider region. 0/1 and 1/1 represent the single oscillations with a smaller and a larger amplitude, respectively.

Relationship between Oscillatory States and the Average Flux of Reaction

As described above, the transition sequence of complex oscillations in the BZ reaction could be simulated by means of our system. The transition behavior suggests us that there should exist some quantities that change discontinuously at the transition, like entropy or heat capacity in the ordinary phase transition of first or second order. Although it is not yet confirmed that such a quantity exists in the dynamic transition point, we tried to calculate the flux of reaction and examine its relationship to the oscillation states, because the system concerned is a non-equilibrium state far from equilibria and the flux of reaction is one of the essential quantities that characterize the dynamic state of system and determine the entropy production rate. In the case of the one-dimensional Ising model, it has been proved that the staircase structure appears under the conditions that the total energy of the system should be minimized at a given magnetization.[31] Thus, we intend to find a useful quantity like the total energy in the Ising model to explain the staircase structure. Here, we examine the relation between each oscillatory state and its flux of reaction. The average flux of reaction was determined from the integrated flux of the reaction for a

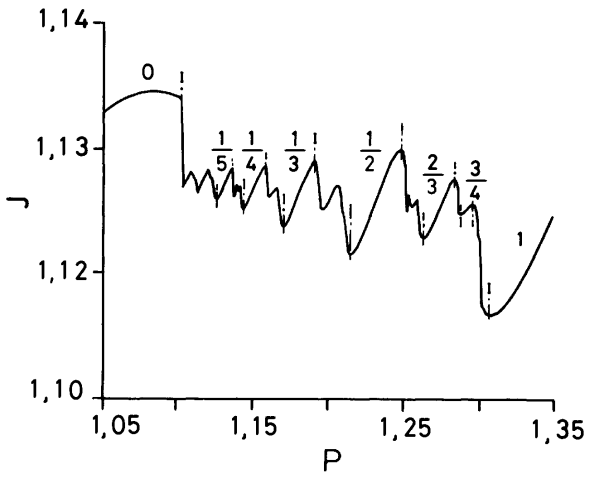

Fig. 8. Relationship between P and average flux of reaction. The values of F for the representative states are given in the figure.

sufficiently long period divided by the integration time.

Figure 8 shows the relationship between P and J, where J is the consuming rate of P ($J=k_1PZ$). Compared with Fig. 7, the average flux J increases monotonously in the region of a (combined) complex oscillation and start to decrease where the period-doubling sequence begins to occur. That is, the inflection point from an increase to a decrease in J coincides perfectly with the starting point of changing from a complex oscillation toward the next one. In some cases where a periodic oscillation changes to a chaotic oscillation without showing any period-doubling sequence, the changes in J are drastic. The value of J would exhibit the same tendency as the value of entropy production rate.[37] Further investigations are needed.

References

1) C. Vidal and A. Pacault, "Nonlinear Phenomena in Chemical Dynamics," Springer, New York (1981).
2) C. Vidal and A. Pacault, "Non-equilibrium Dynamics in Chemical System," Springer, New York (1984).
3) R. J. Field and M. Burger, "Oscillations and Traveling Waves in Chemical System," Wiley, New York (1985).
4) L. Györgyi and R. J. Field, *J. Phys. Chem.*, **92**, 7079 (1988).
5) A. M. Zhabotinskii, *Dokl. Akad. Nauk SSSR*, **157**, 392 (1964).
6) R. A. Schmitz, K. R. Graziani, and J. L. Hudson, *J. Chem. Phys.*, **67**, 3040 (1977).
7) J. L. Hudson, M. Hart, and D. Marinko, *J. Chem. Phys.*, **71**, 160 (1979).
8) M. Orban and I. R. Epstein, *J. Phys. Chem.*, **86**, 3907 (1982).
9) M. Alamgir and I. R. Epstein, *J. Phys. Chem.*, **88**, 2848 (1984).
10) R. J. Field and R. M. Noyes, *J. Chem. Phys.*, **60**, 1877 (1974).
11) K. Showalter, R. M. Noyes, and K. Bar-Eli, *J. Chem. Phys.*, **69**, 2514 (1978).
12) R. D. Janz, D. J. Vanacek, and R. J. Field, *J. Chem. Phys.*, **73**, 3132 (1980).
13) N. Ganapathisubramanian and R. M. Noyes, *J. Chem. Phys.*, **76**, 1770 (1982).
14) J. Rinzel and W. C. Troy, *J. Chem. Phys.*, **76**, 1775 (1982).
15) K. Iwamoto and M. Seno, *J. Chem. Phys.*, **70**, 70, 5851 (1979).
16) K. Iwamoto S. Kawauchi, K. Sawada, and M. Seno, *Bull. Chem. Soc. Jpn.*, **55**, 423 (1982).
17) M. Hourai, Y. Kotake, and K. Kuwata, *J. Phys. Chem.*, **89**, 1760 (1985).
18) J. Maselko and H. L. Swinney, *Phys. Scr.*, **T9**, 35 (1985).
19) J. Maselko and H. L. Swinney, *J. Chem. Phys.*, **85**, 6430 (1986).
20) K. Tomita and I. Tsuda, *Prog. Theor. Phys.*, **64**, 1138 (1980).
21) R. H. Simoyi, A. Wolf, and H. L. Swinney, *Phys. Rev. Lett.*, **49**, 245 (1982).
22) R. J. Baley, G. Mayer-Kress, and J. D. Farmer, *Phys. Lett. A*, **114**, 419 (1986).
23) J. S. Turner, J. C. Roux, W. D. McCormick, and H. L. Swinney, *Phys. Lett. A*, **85**, 9 (1981).
24) J. Rinzel and I. B. Schwartz, *J. Chem. Phys.*, **80**, 5610 (1984).
25) T-Y. Li and J. A. Yorke, *Am. Math. Monthly*, **82**, 985 (1975).
26) B. Mandelbrot, "Fractals: Form, Chance, and Dimension," Freeman, San Fransisco (1977).
27) G. H. Hardy and E. M. Wright, "An Introduction to the Theory of Nmbers," Carendon Press, Oxford (1979).
28) L. D. Harmon, *Kybernetik*, **1**, 89 (1961).
29) J. Nagumo and S. Sato, *Kybernetik*, **10**, 155 (1972).
30) T. Allen, *Physica D*, **6**, 305 (1983).
31) P. Bak and R. Bruinsma, *Phys. Rev. Lett.*, **49**, 249 (1982).
32) M. H. Jensen, P. Bak, and T. Bohr, *Phys. Rev. Lett.*, **50**, 1637 (1983).
33) P. Bak, T. Bohr, and M. H. Jensen, *Phys Scr.*, **T9**, 50 (1985).
34) V. N. Belykh, N. F. Pedersen, and O. H. Soerensen, *Phys. Rev. B*, **16**, 4860 (1978).
35) M. J. Feigenbaum, *J. Stat. Phys.*, **19**, 25 (1978).
36) R. L. Devaney, "An Introduction to Chaotic Dynamical Systems," Benjamin, Cummings (1986).
37) P. Glansdorff and I. Prigogine, "Thermodynamic Theory of Structure, Stability, and Fluctuations," Wiley, New York (1971).

 © 1989 The Chemical Society of Japan Bull. Chem. Soc. Jpn., 62, 2774—2780 (1989)

Transition Sequences of Oscillatory States of a Model Chemical System Showing Chaotic Oscillations

Makoto MORITA, Kazutoshi IWAMOTO, and Manabu SENŌ*
Institute of Industrial Science, University of Tokyo,
7-22-1, Roppongi, Minato-ku, Tokyo 106
(Received March 24, 1989)

The transition sequence from a complex oscillation or a combined complex oscillation to a chaotic oscillation of a three-variable model system of chemical reactions were studied through analyses of the bifurcation diagrams. Period-doubling sequences, discontinuous transitions between two different oscillation states, and intermittency-type pseudo-periodic oscillations were observed. A pseudo-periodic oscillation appears when a combined complex oscillation changes to a new oscillatory state under some transition conditions. By changing the conditions, the discontinuous transition becomes to occur, leading the hysteresis behavior of transition.

Aperiodic behavior (chaotic oscillation) in chemical reactions has been observed in the peroxidase-catalyzed oxidation of NADH,[1] the Belousov-Zhabotinskii (BZ) reaction,[2-11] and the chlorite–thiosulfate reaction.[12,13] Some periodic-chaotic sequences have been carefully examined for the BZ reaction and the chlorite oscillators carried out in a continuous flow stirred tank reactor (CSTR).

A chemical reaction model which exhibits chaotic oscillations was first proposed by Rössler[14] in 1976. The Rössler model is a chemical system with three variables and its chaotic behavior has been fully investigated through numerical calculations. The Oregonator[15] is the most well-known model for the BZ reaction and, however, any attempt to find out chaotic oscillations for the three-variable Oregonator has not yet succeeded. Turner et al. modified the original Oregonator to make up a new model having four variables and showed the appearance of chaotic oscillations.[7] On the other hand, Tomita and Tsuda proved for a three-variable model of the BZ reaction to show chaotic oscillations by introducing flow terms.[17]

Some routes from periodic oscillations to chaotic oscillations have been uncovered; period doubling,[16] intermittency,[18] and quasi-periodicity[19] are typical examples. The intermittency,[8,10] and the quasi-periodicity[20] have been experimentally observed in the BZ reaction. The period-doubling sequence from the oscillating state with a single amplitude to the chaotic state was found experimentally in the BZ reaction by Simoyi et al.[9] and numerically in the modified Oregonator by Ringland and Turner.[21] But the route from a complex oscillation or a combined complex oscillation to a chaotic oscillation is not yet examined.

The BZ reaction is the most well-known experimental system which exhibits chaotic oscillations. Swinney et al. examined in detail the transition sequence using CSTR and found a staircase relationship by plotting the Firing number F against the residence time of the flow reactor as a control parameter. The BZ reaction in CSTR shows complicated oscillations made of L cycles of large amplitude oscillations and S cycles of small amplitude oscillations and the Firing number of the oscillation is defined as $F=L/(L+S)$.

In our preceeding paper,[22] a three-variable model chemical system was studied and its bifurcation structures from a complex oscillation to a chaotic or a combined complex oscillation have been reported. When the transition sequence was displayed by the relationship of the firing number F with a control parameter, according to the way of Swinney et al., the resulting staircase behavior of F is very similar to the staircase diagram observed experimentally in the BZ reaction. This result strongly suggests a similarity of the mathematical structure between the BZ reaction and the present model. Thus, it is expected that the detailed analyses of the present model give us a more detailed prospect of the transition sequence in the BZ reaction.

In this paper, the model chemical system of three variables was studied through numerical calculation and period-doubling sequences from complex or combined complex oscillations to chaotic oscillations was demonstrated. Here, the terms, "complex oscillation" and "combined complex oscillation", are defined as follows.[22] A complex oscillation is an oscillatory state combining of one large amplitude oscillation and $n-1$ small amplitude oscillations. The symbol $\pi(n)$ is used to note this complex oscillation. The term of combined complex oscillation is used for a combination of two or more complex oscillations and the symbol $\pi(m)\pi(n)$ is for a combined complex oscillation consisting of complex oscillations $\pi(m)$ and $\pi(n)$. Now, the detailed structure of transition sequence of the model chemical system will be investigated by using a bifurcation diagram, which is made by plotting the peak height of each pulse in a periodic or an aperiodic state on a two-dimensional phase plane. There appear a period-doubling sequence, a discontinuous transition between a combined complex oscillation and a pseudo-periodic oscillation, and an intermittency-type pseudo-periodic oscillation. The term of "pseudo-periodic oscillation" is hereafter used

when we can not determine whether the oscillation is chaotic or not. A discontinuous change implies usually a hysteresis correlation and coexistence of two different oscillatory states. This phenomenon, which is called birhythmicity, has been found in the experimental[23] and the computational works.[24] However, this is the first paper reporting the birhythmicity between a combined complex oscillation and a pseudo-periodic oscillation.

Chemical Oscillation Model

In the present investigations, the system consisting of the following chemical reactions is considered. This model system has been proposed in a previous paper.[22]

$$\mathrm{P} + \mathrm{Z} \xrightarrow{k_1} \mathrm{E} + \mathrm{Z}, \quad \text{(R1)}$$

$$\mathrm{E} + \mathrm{X} \xrightarrow{k_2} \mathrm{R} + \mathrm{X}, \quad \text{(R2)}$$

$$\mathrm{A} + 2\mathrm{X} + \mathrm{E} \underset{k_4}{\overset{k_3}{\rightleftharpoons}} 3\mathrm{X} + \mathrm{E}, \quad \text{(R3)}$$

$$\mathrm{B} + \mathrm{X} \underset{k_6}{\overset{k_5}{\rightleftharpoons}} \mathrm{C}, \quad \text{(R4)}$$

$$\mathrm{Q} \xrightarrow{k_7} \mathrm{Z}, \quad \text{(R5)}$$

$$\mathrm{Z} + \mathrm{X} \xrightarrow{k_8} \mathrm{D} + \mathrm{X}, \quad \text{(R6)}$$

where A, B, P, and Q are reactants, C, D, and R are products and E, X, and Z are intermediates. Then, three differential equations concerning the concentrations of E, X, and Z will describe the time behavior of the system;

$$\frac{dE}{dt} = k_1PZ - k_2EX, \quad (1)$$

$$\frac{dX}{dt} = k_3AEX^2 - k_4EX^3 - k_5BX + k_6C, \quad (2)$$

$$\frac{dZ}{dt} = k_7Q - k_8XZ. \quad (3)$$

The following values are substituted in respective parameters and the equations are solved numerically by the aid of FACOM M380 (Fujitsu). These values were selected to afford a chaotic behavior of oscillations. The value of P is selected as a variable for the calculation. A=1.3, B=5.0, C=5.3, Q=1.0, k_1=1.0, k_2=5.0, k_3=100.0, k_4=50.0, k_5=10.0, k_6=1.0, k_7=0.1, and k_8=0.4.

Results and Discussion

Period-Doubling Sequence. By solving Eqs. 1—3 numerically, complex oscillations, combined complex oscillations and chaotic oscillations were confirmed to appear in a range $1.08 \leqq P \leqq 1.31$, and the global profile of the transition sequence has been reported in a preceding paper.[22] Some characteristics of transition sequences were studied by the aid of bifurcation diagrams, which are made by plotting the peak value of X of every pulse in an oscillatory state. The bifurcation diagram shown in Fig. 1 is obtained on increasing the value of P stepwise from 1.250 to 1.262. In solving Eqs. 1—3 numerically for each P value, the final values of E, X, and Z in a preceeding step with a given value of P were used for the initial values of the calculation for the next step of P.

Figure 1 shows the transition sequence from the complex oscillation $\pi(2)$ to the combined complex oscillation $\pi(2)\pi(1)$, passing through the combined complex oscillations $[\pi(2)]^2\pi(1)$ and $[\pi(2)]^3\pi(1)$. The notation $[\pi(m)]^i[\pi(n)]^j$ means a combined complex

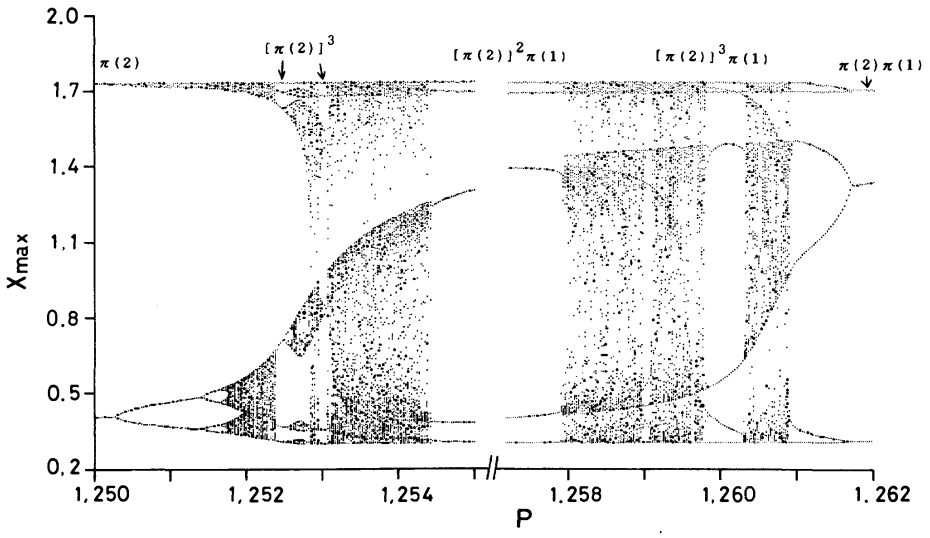

Fig. 1. A bifurcation diagram displaying from $\pi(2)$ to $\pi(2)\pi(1)$. The regimes of respective oscillations are noted.

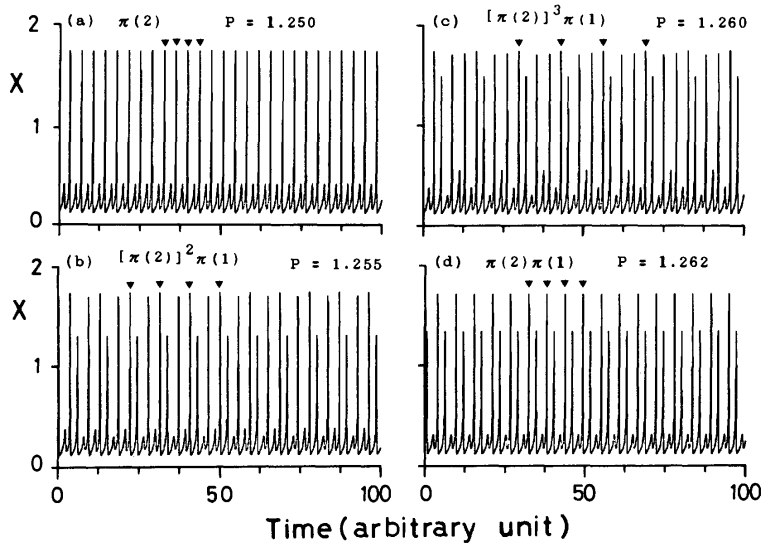

Fig. 2. Representative periodic oscillations designated in Fig. 1. Marks above the oscillations show the period.

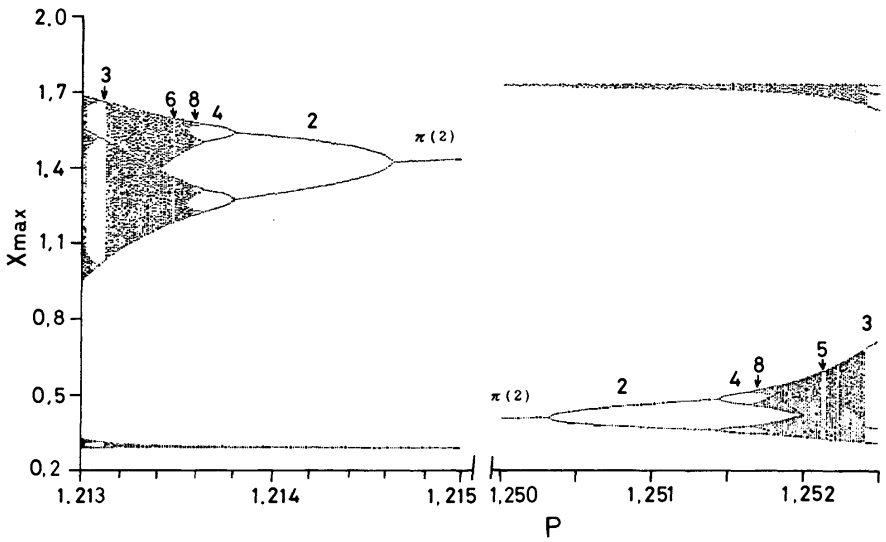

Fig. 3. Period-doubling sequences of the complex oscillation π(2) for increasing and decreasing P. The 2^n-cycle oscillations of π(2) are marked with n. Windows of 6, 5, and 3-cycle oscillations can be seen.

oscillation consisting of i-cycle $\pi(m)$ and j-cycle $\pi(n)$.[22] The oscillation behavior of π(2), $[\pi(2)]^2\pi(1)$, $[\pi(2)]^3\pi(1)$, and $\pi(2)\pi(1)$ are shown in Fig. 2. As shown in the preceding paper,[22] the number F defined as $F=L/(L+S)$ according to Maselko and Swinney,[25] where S and L are respectively the numbers of small and large amplitude oscillations per period, is staircase-like increasing function against P, when only the conspicuous oscillations with large regimes on P are selected. In detail, however, the values of F for the oscillations π(2), $[\pi(2)]^2\pi(1)$, $[\pi(2)]^3\pi(1)$, and $\pi(2)\pi(1)$ with an increase of P are 1/2, 3/5, 4/7, and 2/3, respectively, and this order is not an increasing order. That is, this series of oscillations is out of the rule of staircase-like increasing function of F. Similar trends are occasionally seen in the fine structures of the bifurcation diagram of the present model. Experimentally such a trend has never been observed but probably could be found by a careful experiment.

A period-doubling sequence is clearly seen in Fig. 1. The complex oscillation π(2) appears at $P=1.250$. As P increases, π(2) becomes unstable and diverges to the 2-cycle oscillation of π(2) (i.e. $[\pi(2)]^2$). The right hand figure of Fig. 3 displays an enlarged view of this

region. With a further increase in P, $[\pi(2)]^2$ develops to the 4-cycle oscillation of $\pi(2)$ (i.e. $[\pi(2)]^4$), followed by the higher order 2-cycle oscillations. The range of P of 2^n-cycle oscillation of $\pi(2)$ becomes steeply narrower as n increases, and finally a chaotic oscillation appears. According to Li and Yorke,[26] a chaotic oscillation resulting from the sequence of infinitely high order 2-cycle oscillations is a typical example of the chaotic oscillations. The chaotic oscillations are shown as a diffuse and vertical distribution of dots in the diagram. The bifurcation diagram shown in Fig. 3 is partly broken by "windows" of 6-cycle and 5-cycle oscillations of $\pi(2)$ and is very similar to that of May's system with a typical period-doubling bifurcation.[27]

Feigenbaum[17] showed that an asymptotic limit of the ratio $(P_n-P_{n-1})/(P_{n+1}-P_n)$, where P_n is the parameter value at which the n^{th} doubling bifurcation begins, is a universal number called Feigenbaum's constant, i.e., $\delta=4.6692\cdots$. The values of P_n in the present model are: $P_1=1.250332$, $P_2=1.251452$, $P_3=1.2516700$, $P_4=1.2517154$, and $P_5=1.2517252$. The P_n with $n\geqq 6$ could not be determined. From these values, the ratio $(P_4-P_3)/(P_5-P_4)=4.6\pm0.1$, being fairly in agreement with Feigenbaum's constant.

The bifurcation diagram in the region from $P=1.213$ to 1.215 is shown in the left hand of Fig. 3, where the similar period-doubling bifurcation takes place in a decreasing direction of P. Thus, it was concluded that the complex oscillation $\pi(2)$ changes to a chaotic oscillation through the period-doubling bifurcation with both the increasing and the decreasing directions of P.

For the cases of $\pi(n)$ ($n=1$, 3, 4, 5, and 6), the period-doubling sequences were always observed, so that we can conclude that a complex oscillation diverges to another oscillatory state through a period-doubling sequence. The period-doubling sequence of $\pi(1)$ is clearly seen in Fig. 4.

Intermittency-Type Pseudo-Periodic Oscillation. As the value of P increases up to 1.255, the complex oscillation $\pi(2)$ changes to the combined complex oscillation $[\pi(2)]^2\pi(1)$, where the F value changes from 1/2 to 3/5. That is, the mixing of $\pi(2)$ with $\pi(1)$ should take place after the period-doubling sequence of $\pi(2)$. Similarly, when the combined complex oscillation $[\pi(2)]^2\pi(1)$ changes to the following oscillatory state having a different value of F with an increase in P, the mixing of some oscillatory component into $[\pi(2)]^2\pi(1)$ would take place, resulting in a change in the F value. The bifurcation diagram of Fig. 5 shows a sudden transition at about $P=1.257886$, where $[\pi(2)]^2\pi(1)$ enters into a new oscillatory state. The sudden change in the distribution of dots should be noticed and the period-doubling sequence is not observed in this case. The oscillations before and after the transition are also shown in Fig. 5. After the transition the regular oscillation $[\pi(2)]^2\pi(1)$ is occasionally disturbed by two or three repetitions of irregular oscillation. The irregular oscillation happens to appear intermittently. This type of oscillation is called hereafter as "intermittency-type pseudo-periodic oscillation", because we can not definitely determine whether it is chaotic or not.

Figure 1 shows many transitions which seem to be discontinuous. Some of them were investigated in detail and found to be the transitions with intermittency-type pseudo-periodic oscillations. We can say that this type of transition occurs when a combined complex oscillation changes to a new oscillatory state

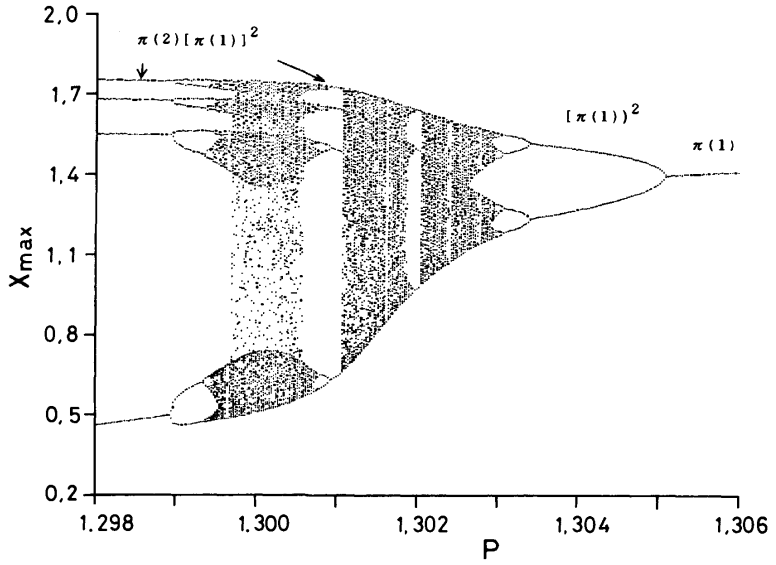

Fig. 4. A bifurcation diagram displaying from $\pi(2)[\pi(1)]^2$ to $\pi(1)$ with the period-doubling sequence of $\pi(1)$.

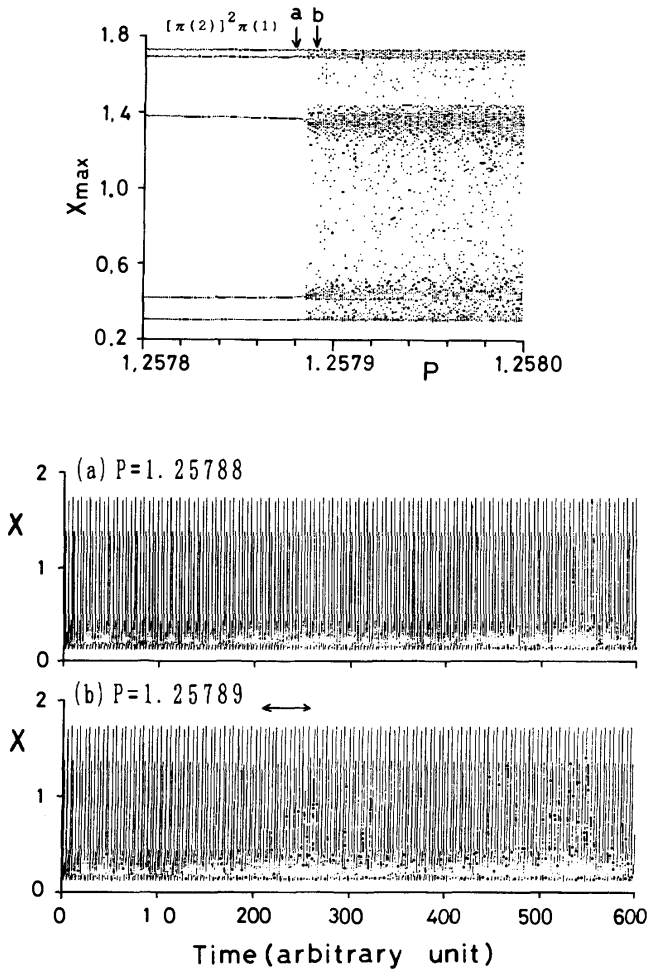

Fig. 5. A bifurcation diagram showing a sudden transition from $[\pi(2)]^2\pi(1)$ to a new oscillatory state and oscillatory behaviors before and after the sudden transition. (a) P=1.25788 and (b) P=1.25789. The bar in (b) indicates the region where $[\pi(2)]^2\pi(1)$ is disturbed.

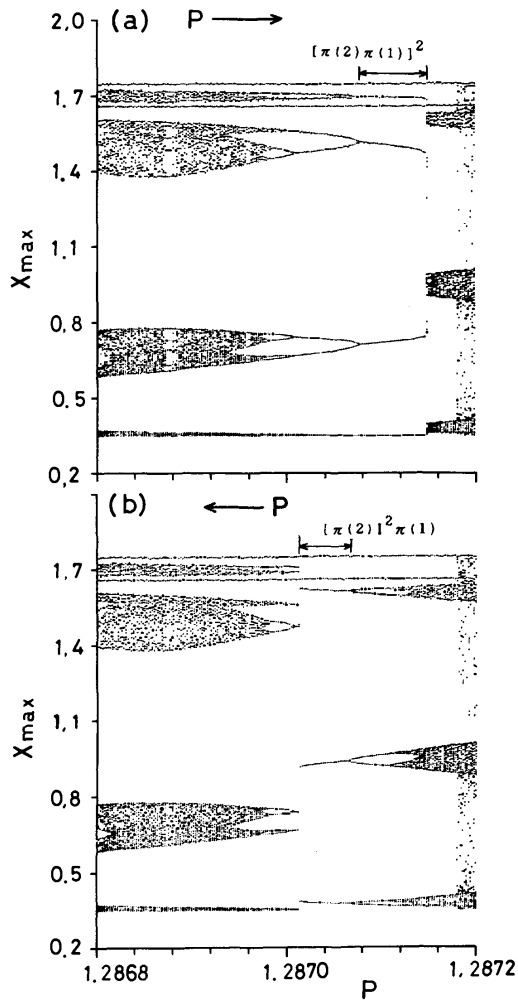

Fig. 6. Dependence of the bifurcation diagram on the direction of change in P. (a) P is increasing, and (b) P is decreasing.

with a different F value. Now we face a question whether the intermittency-type pseudo-periodic oscillation occurs always in a transition state from an oscillatory state to another with a change in F. The answer is that it is not always true. A different type of transition behavior will be shown in the next section.

Birhythmicity. A discontinuous change is observed at about P=1.28714 in a sequence of the combined complex oscillations $\pi(2)\pi(1)$. At this point, the birhythmicity appears and one of two different oscillations is realized depending on the initial conditions of calculation. This result suggests strongly the existence of hysteresis behavior of oscillations as for the changing direction of P. Figure 6 displays the dependence of the bifurcation diagram on the changing direction of P. The transition is discontinuous and hysteresis behavior is clearly shown. Interestingly, the F values of the coexisting oscillations, $[\pi(2)\pi(1)]^2$ and $[\pi(2)]^2\pi(1)$, are different one another and the correlation of F vs. P shows also hysteresis. The transition from $[\pi(2)\pi(1)]^2$ to $[\pi(2)]^2\pi(1)$ occurs at P=1.287148 as P increases, and the reverse transition does at P=1.287012 as P decreases, without showing any intermittency-type pseudo-periodic oscillations.

The hysteresis behavior could be related to a cusp-type catastrophy with a folded phase plane in a three dimensional phase space. Thus, an interpretation of birhythmicity is undertaken with a three-dimensional profile. Figure 7 shows bifurcation diagrams at the discontinuous transition with various values of A. When A=1.286, $[\pi(2)\pi(1)]^2$ changes to $[\pi(2)]^2\pi(1)$, passing through a sudden transition. In this case no hysteresis is observed. When the value of A increases further, the region of pseudo-periodic oscillations becomes narrower and finally disappears, as shown in Fig. 10(b). When the value of A increases further, hysteresis behavior begins to appear.

On the basis of these computations, a schematic profile of the folded phase plane leading these bifurcation diagrams would be drawn as shown in Fig.

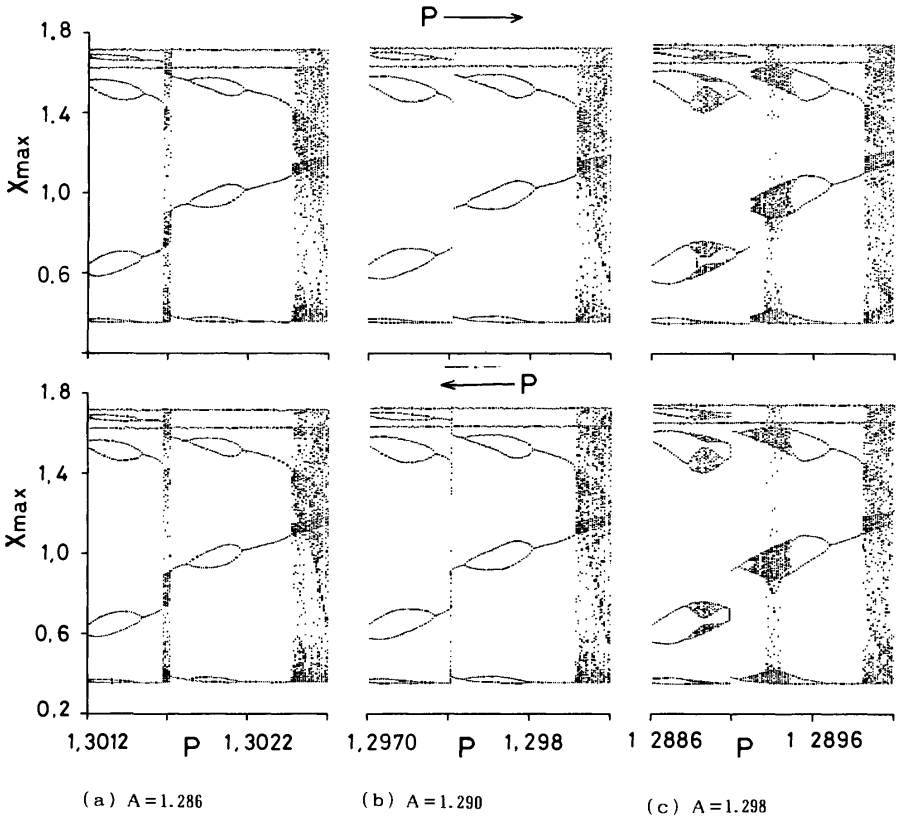

Fig. 7. Bifurcation diagrams with various values of A. In case (a), a sudden transition takes place and no hysteresis is observed. In case (b), the region of intermittecy-type pseudo-periodic oscillation almost disappeared, but no hysteresis is observed. In case (c), a transition accompanied by hysteresis is observed.

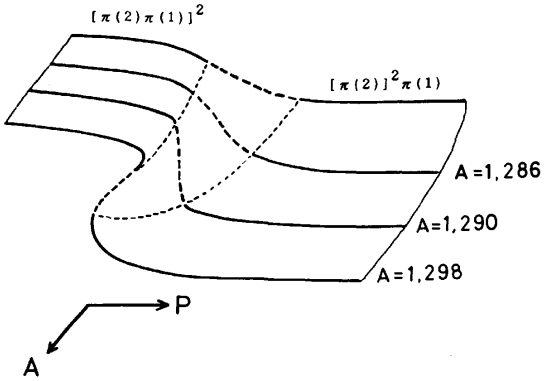

Fig. 8. A phase portrait with a casp catastrophy inferred from the bifurcation diagrams in Fig. 7. The dashed part of each line shows the region of an intermittency-type pseudo-periodic oscillation. The perpendicular coordinate is used to figure the respective states of oscillation.

8. The transition region from $[\pi(2)\pi(1)]^2$ to $[\pi(2)]^2\pi(1)$ is shown by dotted lines. As the value of A increases, the transition region becomes concaved more steeply and finally folded completely between the oscillatory states of $[\pi(2)\pi(1)]^2$ and $[\pi(2)]^2\pi(1)$. Under the latter conditions, the transition between the two combined complex oscillations takes place without showing any pseudo-periodic oscillation, and the birhythmicity is caused by the hysteresis nature of a folded phase plane.

References

1) L. F. Olsen and H. Degn, *Nature (London)*, **267**, 177 (1977).
2) R. A. Schmitz, K. R. Graziani, and L. R. Hudson, *J. Chem. Phys.*, **67**, 3040 (1979).
3) O. E. Rössler and K. Wegman, *Nature (London)*, **271**, 86 (1978).
4) J. L. Hudson, M. Hart, and D. Marinko, *J. Chem. Phys.*, **71**, 1601 (1979); J. L. Hudson and J. C. Markin, *J. Chem. Phys.*, **74**, 6171 (1981).
5) C. Vidal, J. C. Roux, and S. Bachelart, *Ann. N. Y. Acad. Sci.*, **357**, 377 (1980).
6) H. Nagashima, *J. Phys. Soc. Jpn.*, **49**, 2427 (1980).
7) J. S. Turner, J. C. Roux, W. D. McCormick, and H. L. Swinney, *Phys. Lett. A*, **85**, 9 (1981).
8) Y. Pomeau, J. C. Roux, A. Rossi, S. Bachelart, and C. Vidal, *J. Phys. Lett.*, **42**, L271 (1981).
9) R. H. Simoyi, A. Wolf, and H. L. Swinney, *Phys. Rev. Lett.*, **49**, 245 (1982).
10) J. C. Roux, *Physica*, **57D**, 7 (1983).

11) M. Hourai, Y. Kotake, and K. Kuwata, *J. Phys. Chem.*, **89**, 1760 (1985).
12) M. Orban and I. R. Epstein, *J. Phys. Chem.*, **86**, 3907 (1982).
13) J. Maselko and I. R. Epstein, *J. Chem. Phys.*, **80**, 3175 (1984).
14) O. E. Rössler, *Z. Naturforsch.*, **31A**, 259 (1976).
15) R. J. Field and R. M. Noyes, *J. Chem. Phys.*, **60**, 1877 (1974).
16) K. Tomita and I. Tsuda, *Phys. Lett. A*, **79**, 489 (1979).
17) M. J. Feigenbaum, *J. Stat. Phys.*, **19**, 25 (1978); **21**, 669 (1979).
18) Y. Pomeau and P. Monneville, *Commun. Math. Phys.*, **74**, 189 (1980).
19) D. Rand, S. Ostlund, J. Sethna, and E. O. Siggia, *Phys. Rev. Lett.*, **49**, 1982 (1982).
20) F. Argoul, A. Arneodo, P. Richetti, and J. C. Roux, *J. Chem. Phys.*, **86**, 3325 (1987).
21) J. Ringland and J. S. Turner, *Phys. Lett. A*, **105**, 93 (1984).
22) M. Morita, K. Iwamoto, and M. Seno, *Bull. Chem. Soc. Jpn.*, **62**, 2768 (1989).
23) M. Alamgir and I. R. Epstein, *J. Am. Chem. Soc.*, **105**, 2500 (1983).
24) O. Decroly and A. Goldbeter, *Proc. Natl. Acad. Sci. U.S.A.*, **79**, 6917 (1982).
25) J. Maselko and H. L. Swinney, *Phys. Scr.*, **T9**, 35 (1985); *J. Chem. Phys.*, **85**, 6430 (1986).
26) T-Y. Li and J. York, *Am. Math. Monthly*, **82**, 985 (1975).
27) H. A. Lauwerier, in "Chaos", edited by A. V. Holden, Manchester Univ. (1986), p. 39.

 © 1989 The Chemical Society of Japan Bull. Chem. Soc. Jpn., 62, 2781—2788 (1989)

Interactions of Excited Lithium Atom with Molecular Hydrogen. III. Orthogonality Constrained MCSCF+NCI Calculations of Potential Energy Surfaces and Electronic Wave Functions in the Potential Crossing Region

Masayuki TOYAMA,* Takayuki UCHIDE, Toshimasa YASUDA,§
Tokuo KASAI,§§ and Shiro MATSUMOTO
Department of Chemistry, College of Science and Engineering,
Aoyama Gakuin University, Chitosedai, Setagaya-ku, Tokyo 157
(Received January 30, 1989)

A method of calculating the excited state MCSCF electronic wave function by constraining it to be orthogonal to the predetermined ground state wave function was applied to calculate wave functions of the Li-H_2 system near the center of a conical intersection of the lowest two potential energy surfaces. Combined with an additional nonorthogonal configuration interaction process, it has proved to be an efficient method to get systems of wave functions that are continuous throughout whole geometries. Qualitative characters of wave functions near the center of potential crossing previously inferred have been reconfirmed.

Nonadiabatic transition is a key process to all physicochemical phenomena involving electronically excited states. It participates in every process where electronic energy is converted in to other kinds of energy. Its detailed mechanism, particularly how electrons will behave at the moment of transition, is of great theoretical interest.[1-9,18,35,37,38] Quenching of the fluorescence of alkali metal atoms by simple molecules is a prototype of relevant phenomena and suitable for detailed theoretical investigation, and has been the subject of many experimental and theoretical works.[10-43]

Many authors[25-28,41-43] have applied the classical trajectory method to potential energy surfaces calculated by some semiempirical methods. In those studies, discussion was often neglected on the nature of wave functions and detailed shapes of potential surfaces in the nonadiabatic region were often neglected. In ab initio calculation of wave functions[44,47-50,52,53] also, most concern has been given to detailed shapes of potential energy surfaces in their crossing regions and not to the nature of wave functions themselves.

For the Li-H_2 system, ab initio calculations of wave functions using large basis sets have been reported only for limited geometries.[34,36,38] Neither calculation of complete three-dimensional potential hypersurfaces nor analysis of wave functions near the center of their conical intersection[35] has hitherto been carried out by anyone including ourselves, despite their importance for detailed understanding of the nonadiabatic process. This is mainly because, as reported in the preceding paper,[54] direct MCSCF calculations of excited states for such geometries suffer convergence difficulties. Even if fortuitous convergence has been achieved, potential energy surfaces thus obtained often show apparent irregularities near crossing geometry, yielding electron density maps inadequate to excited states. Such cases have usually been treated by the state averaged MCSCF (SA-MCSCF) method.[44-53]† Using the method with weight factor 0.5 for lower accompanying states, we have obtained[54] smooth potential curves for the ground and excited states, but they lie somewhat higher than the corresponding curves obtained by the ordinary MCSCF method. Moreover, we have not been able to obtain SA-MCSCF functions if we use the weight factor 0.0 for lower states. This leaves some ambiguity in wave function obtained. To overcome these difficulties, we have introduced a new alternative method[54] to obtain excited MCSCF wave functions. It amounts to minimizing the energy requiring the function to be orthogonal[55] to a predetermined MCSCF ground state (hereafter, this method will be abbreviated as OC-MCSCF).

OC-MCSCF gives exactly the same function outside the crossing region as the conventional MCSCF method, and gives potential surfaces which seem to stand for smooth interpolations of potential surfaces obtained in the left and right sides of the crossing region, just as the SA-MCSCF method does, but energies are, in general, lower than those obtained by the SA-MCSCF method. The above-mentioned achievement of the present method has been gained by sacrificing, for general C_s geometries,[54] the generalized Brillouin theorem[56] to some extent. (SA-MCSCF functions with nonzero weight factors for lower accompanying states also may not fulfill the theorem.) Moreover, excited MCSCF function(s) in the potential crossing region may, in general, not be properly

§ Present address: Ashigara Research Laboratories, Fuji Photo Film Co., Ltd., Nakanuma, Minamiashigara, Kanagawa 250-01.

§§ Present address: Fujitsu Ltd., 3-21-8, Nishishinbashi, Minato-ku, Tokyo 105.

† Other methods of calculating correlated wave functions, such as Cluster Expansion Methods, CEPA, and MP2, are left aside here, and treatments in the MCSCF domain are discussed.

hamiltonian-orthogonal to the ground MCSCF function independently calculated for the same geometry. Thus, in our scheme,[54] a final nonorthogonal configuration interaction process (NCI) is taken from among all CSF's constituting the pair of ground and excited MCSCF functions. This guarantees the mutual orthogonality and hamiltonian-orthogonality of the final pair of MCSCF functions.

In this paper, we report the whole unified potential surfaces for the Li-H_2 system thus obtained. The nature of wave functions will also be discussed using suitable electron density maps.

Method of Calculation

The geometric parameters are shown in Fig. 1. The basis functions are the same as used in an earlier work.[38] Dill and Pople's 5-21G basis set was used for Li atom, and for H atoms the 4-31G basis set of Ditchfield et al.[58] was augmented by p-polarization functions of exponent 1.0 before use. All calculations were done with C_s symmetry of molecular orbitals. No further symmetry constraint was applied to orbitals even in higher symmetric geometries than C_{2v}. This was necessary to avoid any discontinuities in potential surfaces.[35,38] The selection of CSF was of CAS[59] type. The inactive space consisted of 1a′ orbital, and the active space consisted of (2a′—6a′) and 1a″ orbitals. Orbitals from 7a′ to 15a′ and 2a″, 3a″, and 4a″ were taken to be virtual. The resulting 45 CSF's corresponded to those of the minimal basis full valence calculation.

Ground state MCSCF functions were calculated by the standard one-step Newton-Raphson procedure using an exponetial formalism incorporated with a mode control and a mode damping process.[60] Near the center of the conical intersection of the ground and the excited state potential energy surface, each excited state wave function was calculated with a constraint of being orthogonal to the corresponding ground state wave function, by using a slight modification of the original MCSCF program, as reported in the preceding paper.[54] When the geometry was far from the critical geometry, both the constrained and the unconstrained program gave exactly the same result.

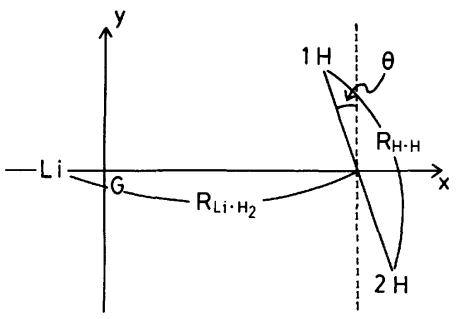

Fig. 1. Geometrical parameters for the Li-H_2 system.

In practice, we adopted the natural orbital expansion for all MCSCF functions to make their expressions unique since CAS wave function forms are invariant to any orbital rotations in the active space.

Then, we adopted the nonorthogonal configuration interaction for all CSF's (45×2=90 in all) constituting the primary pair of ground and excited MCSCF wave functions to get the final expression of states

$$\Psi = \sum_{i=1}^{N} A_i^{(G)} \Phi_i^{(G)} + \sum_{i=1}^{N} A_i^{(E)} \Phi_i^{(E)},$$

where $\Phi_i^{(G)}$'s are the CSF's obtained for the ground MCSCF function, and $\Phi_i^{(E)}$'s are those for the excited MCSCF function. $A_i^{(G)}$'s and $A_i^{(E)}$'s are taken freely to make $<\Psi|H|\Psi>$ stationary under a sole condition of $<\Psi|\Psi>=1$.

Results and Discussion

1 C_{2v} Geometry. (1) Potential Energy Curves in the Immediate Neighborhood of the Center of Intersection: Figure 2 shows the total energies of the system calculated by the method described above along some reaction coordinate defined earlier[38] on the C_{2v} potential energy surface. The solid lines show the results before NCI and the chain lines show those after NCI. The ground state energies (filled circles in Fig. 2) were obtained directly by the usual MCSCF method,

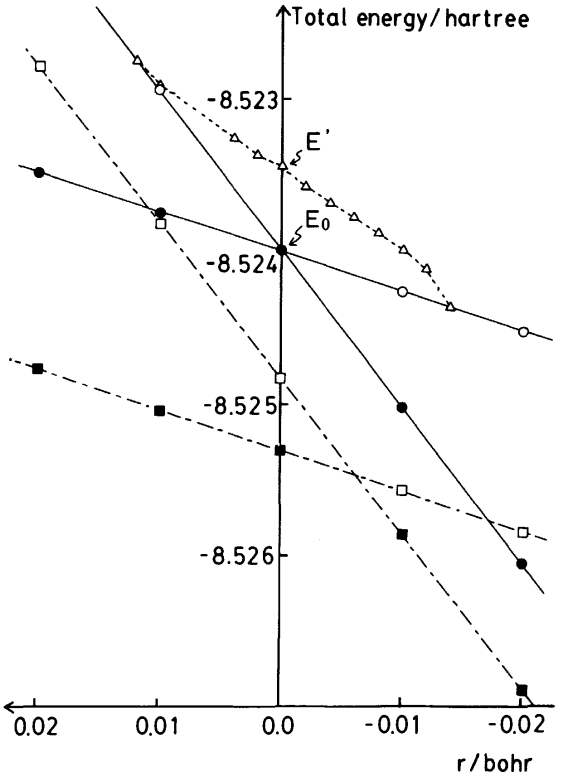

Fig. 2. Comparison of potential energy curves near the point P along the reaction coordinate r calculated by conventional MCSCF: (●, △), OC-MCSCF: (○), OC-MCSCF+NCI: (■, □).

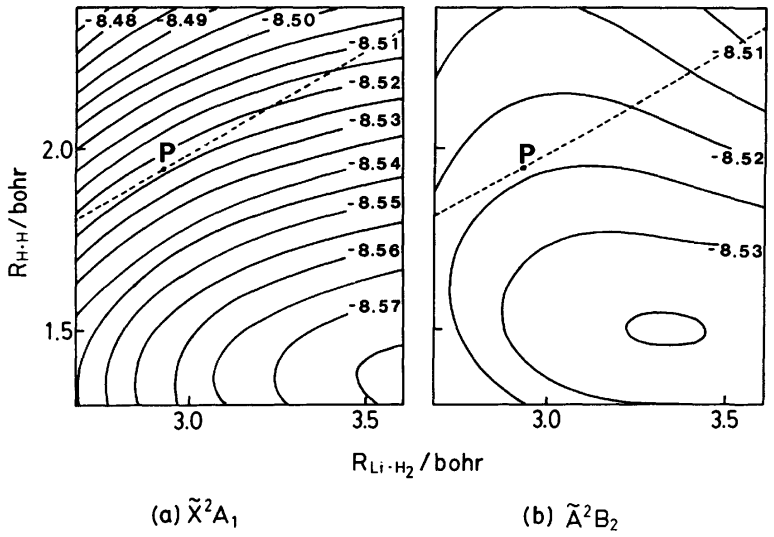

Fig. 3. Contour plots of the two lowest potential energy surfaces near their crossing seam (broken lines). Energies are given in hartrees. *P* is the lowest point on the crossing seam.

while the excited state energies (open circles in Fig. 2) were obtained by OC-MCSCF using the corresponding ground state as reference. As seen in the figure, no irregularities occur in the OC-MCSCF curve as is usually reported in SA-MCSCF calculations.[44,48–50,52,53]†† The open triangles in the figure indicate energies of excited states when the constraint was not applied. When the geometry was relatively far from the *P* point, i.e., $r \gtrsim 0.01$ or $r \lesssim -0.015$ bohr, open triangles fell on the open circles, and the wave functions with and without constraint were identical after the MO's were transformed to natural orbitals. As we see from the 3a′ natural orbital electron density maps in Figs. 5(a) and (b), for example at $r=0$, the symmetry of the wave functions by the method are correctly of C_{2v}, even though no C_{2v} constraint was put on the MO form. The typical energy lowering by the NCI was 7×10^{-4} hartree at the *P* point. For further details see Ref. 54.

(2) C_{2v} Potential Energy Surfaces in the Crossing Region: Figure 3 shows the lowest two potential energy surface contour maps thus obtained for a wider range of geometries around the central point of the crossing region. The broken lines indicate the crossing seam between the surfaces. The location and energy of the *P* point (the lowest point on the seam) are $R_{Li\text{-}H_2}=2.9344$ and $R_{H\text{-}H}=1.9520$ bohr, respectively. It lies 1.1×10^{-3} hartree lower than the energy of $Li(^2P)+H_2(^1\Sigma_g^+)$. The depth of the pond on the excited state potential surface is 1.26×10^{-2} hartree, and its bottom is located at ($R_{Li\text{-}H_2}=3.35$, $R_{H\text{-}H}=1.55$ bohr). These values deviate somewhat from the values of Hobza and Schleyer.[34] The difference may be due mainly to the basis set quality, but may also have resulted from the small NCI size adopted in the work. Even the size of the wave function set used in the present NCI may be sufficient in improving both qualities and some of the energies of MCSCF functions in the vicinity of the potential crossing center, but for other geometries it is rather insufficient. Increasing the size of NCI would have no difficulty and may improve the whole of the unified potential surfaces. The results will be reported in future papers. The main additional task in OC-MCSCF plus NCI procedure over the usual MCSCF procedure is the construction of second order transition density matrix elements between the ground and the excited state. This did not cause any methodological difficulties, but required about 20% extra CPU time over the ordinary procedure in iterations.

It should be noted that we have found a small dip in the C_{2v} ground state potential energy surface. It is located at ($R_{Li\text{-}H_2}=11.8$, $R_{H\text{-}H}=1.4$ bohr) and has a depth of 8.2 μhartree. It probably corresponds to the van der Waals interaction of $Li(^2S)$ and $H_2(^1\Sigma_g^+)$. A minimum also is observed in our $C_{\infty v}$ calculations at ($R_{Li\text{-}H_2}=12.3$, $R_{H\text{-}H}=1.4$ bohr), and its depth is 5.2 μhartree. Hobza and Schleyer[34] also reported a minimum on their potential energy surface for $C_{\infty v}$ symmetry ($R_{Li\text{-}H_2}=11.4$, $R_{H\text{-}H}=1.4$ bohr, 30 μhartree†††).

2 C_s Geometry. The OC-MCSCF method was most effective in computing the excited states in C_s geometries. Figure 4 shows part of the various poten-

†† In this case also, we got smooth SA curves some 5×10^{-3} hartree shifted upwards relative to the OC-MCSCF excited and ground state curves. (cf. Ref. 54)

††† Referring to Table 1 of Ref. 34, we obtain the numerical value for the depth given above, instead of "13 kcal mol^{-1}" given in the text of that paper.

tial curves obtained by three methods, conventional MCSCF, OC-MCSCF, and OC-MCSCF+NCI, when the H_2 molecule was rotated from the C_{2v} geometry of the point P with R_{Li-H_2} and R_{H-H} kept fixed. The actual calculation was started from $\theta=90°$ ($C_{\infty v}$) and proceeded step by step down to $\theta=0°$ by using the converged MC function at a previous geometry as the 0th approximation of iteration. The OC-MCSCF function at $\theta=90°$ was obtained from the function at ($R_{Li-H_2}=3.0$, $R_{H-H}=1.4$ bohr, $\theta=90°$), the latter function being calculated in the opposite direction, i.e., by starting from ($R_{Li-H_2}=3.0$, $R_{H-H}=1.4$ bohr, $\theta=0°$, C_{2v}) and increasing θ up to 90°. At the last geometry, there was no ambiguity in identifying the ground and excited state MCSCF functions since they are sufficiently outside the geometric region where the usual MCSCF procedure shows irregularities.

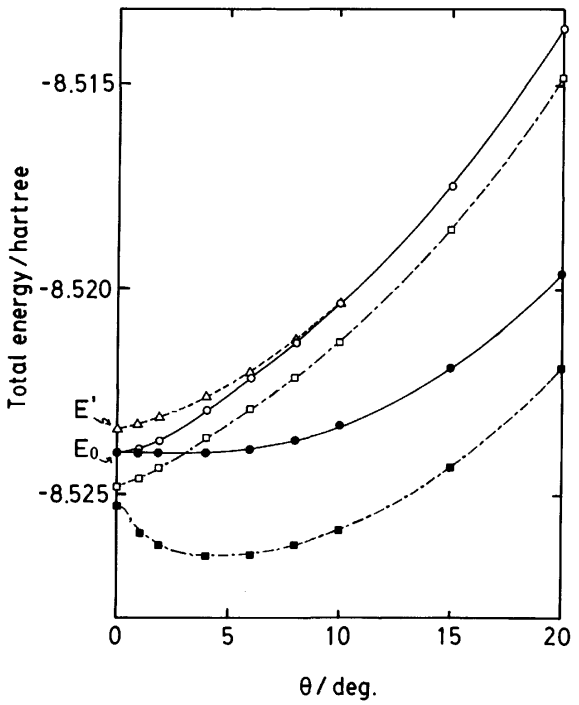

Fig. 4. Potential energy curves of the ground state and the first excited state vs. rotation angle θ from the C_{2v} geometry at point P. R_{Li-H_2} and R_{H-H} are fixed constant. Conventional MCSCF: (●, △), OC-MCSCF: (○), OC-MCSCF+NCI: (■, □).

In Fig. 4, as θ decreases from 20°, the MCSCF excited state curve deviates upward from the OC-MCSCF curve and reaches the energy E', somewhat higher than that of the MCSCF ground state at $\theta=0°$ (E_0). The energy E' is equal to the energy of the excited state obtained by an MCSCF calculation on C_{2v} geometries (E' in Fig. 2). An electron density map analysis also has shown that the MCSCF excited state thus obtained has no correct C_{2v} symmetry. These reveal the inadequateness of the conventional MCSCF method for the central portion of potential crossing geometries. (We have made many other attempts by starting with different 0th approximations or using different algorithms, but none of them has been successful.) On the other hand, the OC-MCSCF curve reaches E_0 just at $\theta=0°$ and there occur no discontinuities between the C_{2v} and C_s potentials. After the MO's were converted to natural orbitals, the OC-MCSCF function at $\theta=0°$ was identical with that obtained in section 1-(1). The 3a'

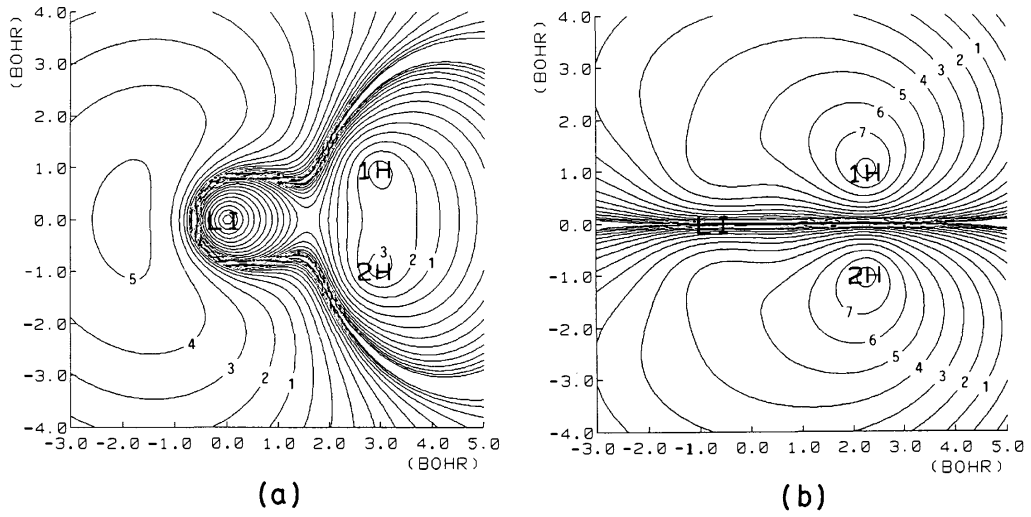

Fig. 5. Contour plots of 3a' natural orbital electron density maps at P (a) the $\tilde{X}^2A_1$ state obtained by conventional MCSCF and (b) $\tilde{A}^2B_2$ state obtained by OC-MCSCF. The numbers 1, 2, ···, and 7 beside the contours indicate electron density of 6.325×10^{-4}, 1.125×10^{-3}, 2.000×10^{-3}, 3.556×10^{-3}, 6.325×10^{-3}, 1.125×10^{-2}, 2.000×10^{-2} electrons bohr^{-3}, respectively.

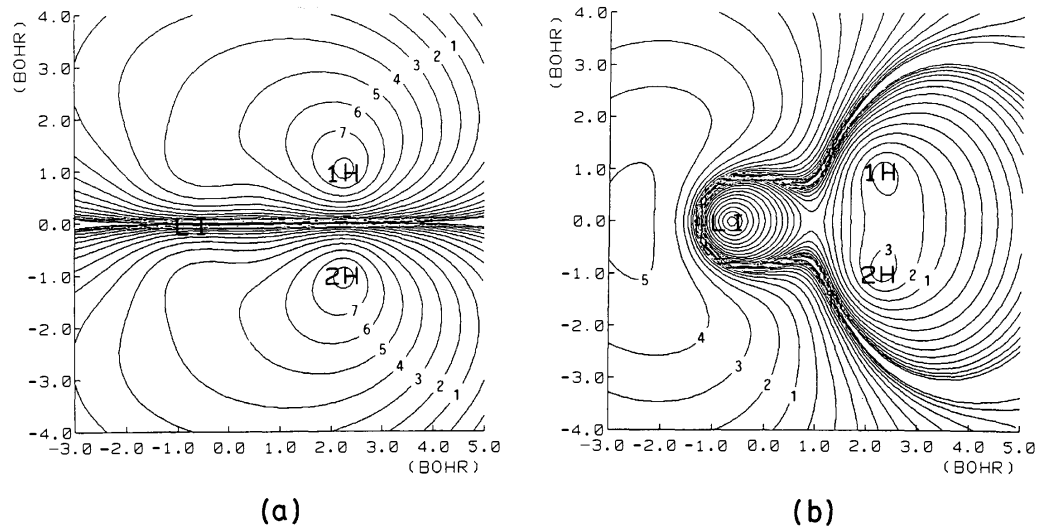

Fig. 6. Similar maps as in Fig. 5, after NCI.

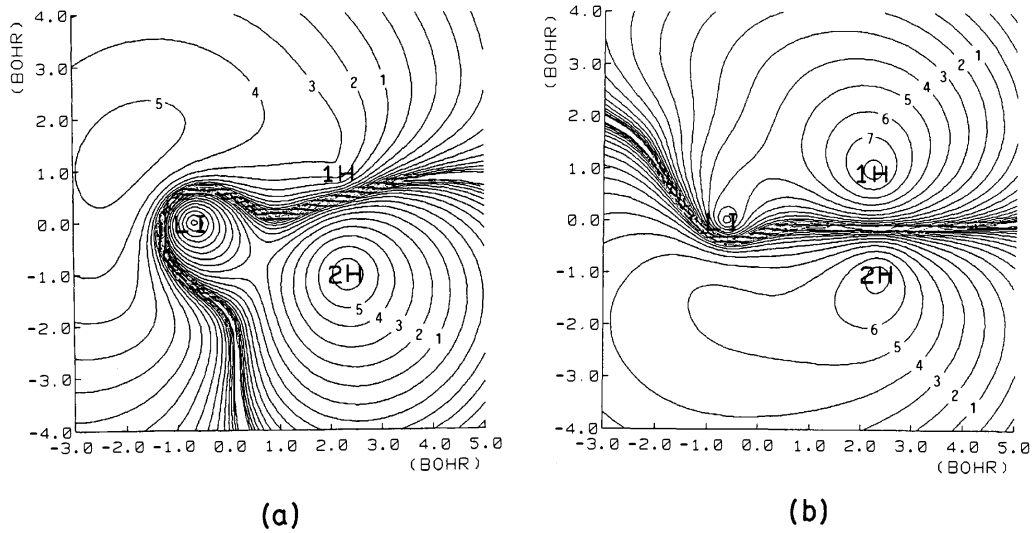

Fig. 7. Contour plots of 3a′ natural orbital electron density maps at a geometry where H_2 is rotated 4.0° from the geometry of P with $R_{Li\text{-}H_2}$ and $R_{H\text{-}H}$. (a) the $1^2A'$ state obtained by conventional MCSCF and (b) $2^2A'$ state obtained by OC-MCSCF. Figures besides contours have the same meaning as in Fig. 6.

natural orbital electron density maps of the ground and excited states are thus identical with Figs. 5(a) and (b), which show the correct symmetry of the functions.

As seen in Fig. 4, the NCI splits the energies of the almost degenerate OC-MCSCF function pair at $\theta=0°$. As a consequence, the intersection of the $^2A_1$ and $^2B_2$ curves in C_{2v} geometry shifts somewhat, as seen in Fig. 2. At the same time, we get small but definite energy improvements (cf. section 1-(1)) at the geometry.

Common to all results reported hitherto,[35,37,38] there is a minimum (at $\theta=5°$ with a depth of 4.4×10^{-3} hartree relative to $\theta=0°$) in the ground state curve, while the excited state curve increases monotonically as θ increases.

Figures 6(a) and (b) are the 3a′ natural orbital electron density maps of the pair states at $\theta=0°$ after NCI. They also show C_{2v} symmetry.†††† Figures 7(a) and (b) show similar density maps taken at $\theta=4.0°$ before NCI. It is seen that both the functions have their own unique natures widely differing from each other. It is a favorable feature for them to be the basis of the succeeding NCI step since as we are inclined to gather a maximum degree of information from the

†††† The interchange between the $^2A_1$ and $^2B_2$ state energies is due to the shift of the P point noted above.

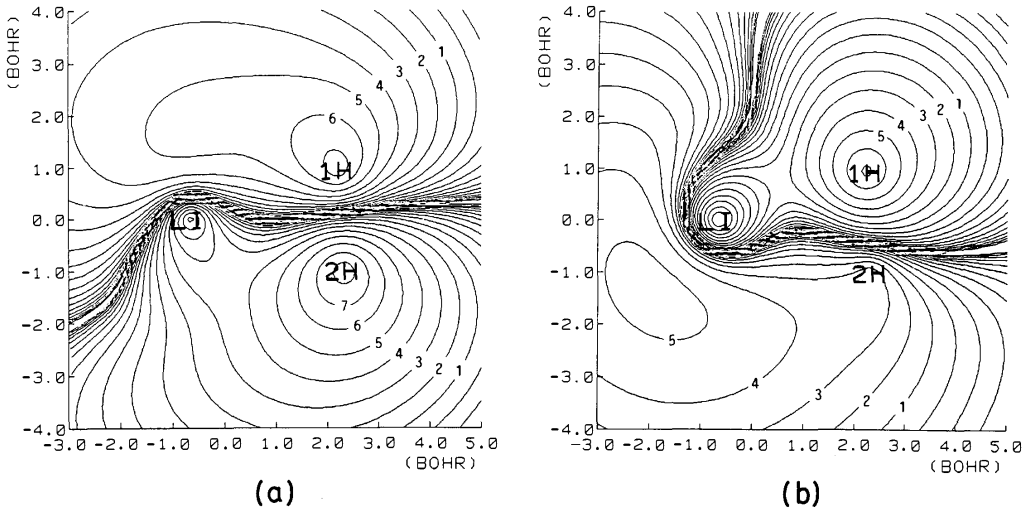

Fig. 8. Similar maps as in Fig. 7, after NCI.

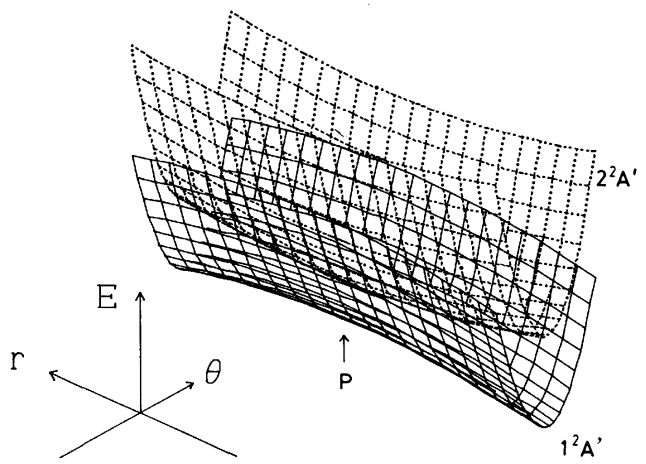

Fig. 9. Computer graphical representation of the $1^2A'$ and $2^2A'$ adiabatic potential energy surfaces in θ and r dimensions near the apex of the conical intersection.

primary MCSCF function of limited size to construct final functions. In this connection, Hosteny and Hagstrom[61] and Petsalakis et al.[62,63] have argued that the effect of NCI may be comparable to that of an ordinary large size CI when the two sets of CSF's differ considerably. Figures 8(a) and (b) are the maps after the NCI. The improvement by NCI of the main features of these maps had turned out not to be very significant,†††† and the features of the final function are in good agreement with those reported earlier for less quantitative calculations (minimal basis valence CAS,[33,35] minimal basis full CI,[37] and SCF+NCI[38] using the same basis set as the present one) with respect to the bonding nature of the shorter Li–H in the ground state and the bonding nature of the longer Li–H in the excited state.

In order to obtain certain cross sections of the three dimensional hypersurfaces, we carried out similar calculations starting with many geometries for the reaction coordinate of section 1-(1). Using some interpolation techniques, these results were combined to give two sheets of potential energy surfaces. Figure 9 is a computer graphical representation of these surfaces. The outlook of these surfaces is very much the same as reported earlier,[35] but it is now more quantitative.

Conclusion

In summary, the OC-MCSCF and the additional NCI procedure described in this and the preceding paper provide an effective means of constructing excited state MCSCF functions and of the corresponding ground state functions in geometries where their potential energy surface fall close to each other or even cross with each other. The potential energy surfaces and the functions themselves connect continuously with the ones calculated by the ordinary MCSCF procedure outside the critical region, and no discontinuities occur between them. The excited state function is strictly orthogonal and hamiltonian orthogonal to its corresponding ground state function. The method is general, and only a little extra work over the ordinary method is required in constructing the second order transition density matrix. Further, by extension of the size of NCI, the method may give us unified MCSCF functions and potential surfaces which are good throughout a wide range of geometries, not restricted to the nonadiabatic region. The geometrical symmetries of the wave functions tested for the present special case seem to be reasonable.

Conclusions reported in earlier papers concerning

†††† The apparent interchange between the characteristics of $1^2A'$ and $2^2A'$ maps is for the same reason as given in the footnote.††††

the behavior of wave functions of the Li-H_2 system in the nonadiabaic region have been reconfirmed in the present more quantitative calculations.

The authors wish to thank Professor Keiji Morokuma of the Institute for Molecular Science and Dr. Shigeki Kato of the University of Tokyo. The calculations were carried out at the Computer Center of the IMS, Okazaki National Research Institutes, at the Computer Center of the University of Tokyo, and at the Information Science Research Center of Aoyama Gakuin University.

References

1) M. Desouter-Lecomte, C. Galloy, J. C. Lorquet, and M. Vaz Pires, *J. Chem. Phys.*, **71**, 3661 (1979), and the preceding papers by the same authors. See also references cited therein.
2) D. Dehareng, X. Chapuisat, J. C. Lorquet, C. Galloy, and G. Rassev, *J. Chem. Phys.*, **78**, 1246 (1983).
3) M. Desouter-Lecomte, D. Dehareng, B. Lehy-Nihant, M. Th. Praet, A. J. Lorquet, and J. C. Lorquet, *J. Phys. Chem.*, **89**, 214 (1985).
4) R. D. Levine, *Bull. Chem. Soc. Jpn.*, **61**, 29 (1988).
5) B. C. Garrett, M. J. Redmon, D. G. Truhlar, and C. F. Melius, *J. Chem. Phys.*, **74**, 412 (1981).
6) B. C. Garrett, D. C. Truhlar, and C. F. Melius, *Phys. Rev. A*, **24**, 2853 (1981).
7) S. Kato, R. L. Jaffe, A. Komornicki, and K. Morokuma, *J. Chem. Phys.*, **78**, 4567 (1983).
8) M. Baer, I. Last, and Y. Shima, *Chem. Phys. Lett.*, **110**, 163 (1984).
9) C. Leforestier, *Chem. Phys. Lett.*, **125**, 373 (1986).
10) J. L. Magee and T. Ri, *J. Chem. Phys.*, **9**, 638 (1941).
11) K. J. Laidler, *J. Chem. Phys.*, **10**, 34 (1942).
12) G. J. Schulz, *Rev. Mod. Phys.*, **45**, 422 (1973).
13) J. R. Barker and R. E. Weston Jr., *J. Chem. Phys.*, **45**, 1427 (1976).
14) I. V. Hertel, H. Hofmann, and K. A. Rost, *Chem. Phys. Lett.*, **47**, 163 (1977).
15) A. Sevin and P. Chaquin, *Chem. Phys.*, **93**, 49 (1985).
16) C. Crepin, J. L. Picque, G. Rahmat, J. Verges, R. Vetter, F. X. Gadea, M. Pelissier, F. Spiegelmann, and J. P. Malrieu, *Chem. Phys. Lett.*, **110**, 395 (1984).
17) P. Herbitz, *Chem. Phys.*, **54**, 131 (1980).
18) P. Botschwina, W. Meyer, I. V. Herterl, and W. Reiland, *J. Chem. Phys.*, **75**, 5438 (1981).
19) D. Papierowska-Kaminski, M. Persico, and V. Bonačić-Koutecký, *Chem. Phys. Lett.*, **113**, 264 (1985).
20) A. Sevin and P. Chaquin, *Chem. Phys.*, **93**, 49 (1985).
21) D. R. Yarkony, *J. Chem. Phys.*, **84**, 3206 (1986).
22) A. Sevin, P. C. Hiberty, and J.-M. Lefour, *J. Chem. Phys.*, **109**, 1845 (1987).
23) D. Poppe, D. Papierowska-Kaminski, and Bonačić-Koutecký, *J. Chem. Phys.*, **86**, 822 (1987).
24) M. M. Gallo and D. R. Yarkony, *J. Chem. Phys.*, **86**, 4990 (1987).
25) D. G. Truhlar, J. W. Duff, N. C. Blais, J. C. Tully, and B. C. Garrett, *J. Chem. Phys.*, **77**, 764 (1982).
26) N. C. Blais and D. G. Truhlar, *J. Chem. Phys.*, **79**, 1334 (1983).
27) N. C. Blais, D. G. Truhlar, and B. C. Garrett, *J. Chem. Phys.*, **78**, 2956 (1983).
28) C. W. Eaker, *J. Chem. Phys.*, **87**, 4532 (1987).
29) D. R. Jenkins, *Proc. R. Soc. London, Ser. A*, **306**, 413 (1968).
30) J. Elward-Berry and J. E. Berry, *J. Chem. Phys.*, **72**, 4510 (1980).
31) C. H. Meller III, K. Schofield, and M. Steinberg, *J. Chem. Phys.*, **72**, 6620 (1980).
32) J. Derouard and N. Sadeghi, *Chem. Phys. Lett.*, **111**, 353 (1984).
33) K. Mizutani, Y. Kuribara, K. Hayashi, and S. Matsumoto, *Bull. Chem. Soc. Jpn.*, **52**, 2184 (1979).
34) P. Hobza and P. R. Schleyer, *Chem. Phys. Lett.*, **105**, 630 (1980).
35) K. Mizutani, T. Yano, A. Sekiguchi, K. Hayashi, and S. Matsumoto, *Bull. Chem. Soc. Jpn.*, **57**, 3368 (1984).
36) J. García-Prieto, W. L. Feng, and O. Novaro, *Chem. Phys. Lett.*, **119**, 128 (1985).
37) K. Mizutani, M. Toyama, K. Taguchi, and S. Matsumoto, *Comput. Chem.*, **9**, 259 (1985).
38) S. Matsumoto, K. Mizutani, A. Sekiguchi, T. Yano, and M. Toyama, *Int. J. Quantum Chem.*, **29**, 689 (1986).
39) P. Saxe and D. R. Yarkony, *J. Chem. Phys.*, **86**, 321 (1987).
40) A. Sevin, P. Chaquin, L. Hamon, and P. C. Hiberty, *J. Phys. Chem.*, **110**, 5681 (1988).
41) J. C. Tully, *J. Chem. Phys.*, **59**, 5122 (1973).
42) C. W. Eaker, *J. Phys. Chem.*, **92**, 3858 (1988).
43) J. C. Tully, "Dynamics of Molecular Collisions," ed by W. H. Miller, Plenum, New York (1976), Part B, pp. 217—267.
44) K. Docken and J. Hinze, *J. Chem. Phys.*, **57**, 4928 (1972).
45) J. Hinze, *J. Chem. Phys.*, **59**, 6424 (1973).
46) C. C. J. Roothaan, J. H. Detrich, and D. G. Hopper, *Int. J. Quantum Chem.*, **S13**, 93 (1979).
47) K. Rudenberg, L. M. Cheung, and S. T. Elbert, *Int. J. Quantum Chem.*, **16**, 1069 (1979).
48) H.-J. Werner and W. Meyer, *J. Chem. Phys.*, **74**, 5794 (1981).
49) R. N. Differnderfer and D. R. Yarkony, *J. Phys. Chem.*, **86**, 5098 (1982).
50) B. Pouilly, B. H. Lengsfield, and D. R. Yarkony, *J. Chem. Phys.*, **80**, 5089 (1984).
51) H.-J. Werner, "Ab Initio Methods in Quantum Chemistry," ed by K. P. Lawley, Wiley, New York (1987), Vol. LXIX, Part II, pp. 1—62.
52) P. Saxe, B. H. Lengsfield III, and D. R. Yarkony, *Chem. Phys. Lett.*, **113**, 159 (1985).
53) M. I. McCarthy, P. Rosmus, H.-J. Werner, P. Botschwina, and V. Vaida, *J. Chem. Phys.*, **86**, 6693 (1987).
54) S. Matsumoto, M. Toyama, T. Yasuda, T. Uchide, and R. Ueno, *Chem. Phys. Lett.*, in Press.
55) H. G. Miller and R. M. Dreizler, *Nucl. Phys. A*, **316**, 32 (1979).
56) A. C. Wahl and G. Das, "Methods of Electronic Structure Theory," ed by H. F. Schaefer III, Plenum, New York (1977), Vol. III, pp. 51—78.
57) J. D. Dill and J. A. Pople, *J. Chem. Phys.*, **62**, 2921 (1975).

58) R. Ditchfield, W. J. Hehre, and J. A. Pople, *J. Chem. Phys.*, **54**, 724 (1971).
59) B. O. Roos, "Methods in Computational Molecular Physics," ed by G. H. F. Diercksen and S. Wilson, D. Reidel Publishing Company, Dordrecht (1983), NATO ASI Series C, Vol. 113, pp. 161—187.
60) J. Olsen, D. L. Yeager, and F. Jørgensen, "Advances in Chemical Physics," ed by I. Prigogine and S. A. Rice, Wiley, New York (1985), Vol. LIV, pp. 1—176.
61) R. P. Hosteny and S. A. Hagstrom, *J. Chem. Phys.*, **58**, 4396 (1973).
62) I. D. Petsalakis, G. Theodorakopoulos, C. A. Nicolaides, R. J. Bunker, and S. D. Peyerinhoff, *J. Chem. Phys.*, **81**, 3161 (1984).
63) I. D. Petsalakis, G. Theodorakopoulos, C. A. Nicolaides, and R. J. Bunker, *J. Chem. Phys.*, **81**, 5952 (1984).

Mechanism of Stabilization of ZnO Photoanodes in High pH Solutions

Eiji KIKUCHI,* Kiminori ITOH,† Tamihiko KATOH,†† and Akira FUJISHIMA
Department of Synthetic Chemistry, Faculty of Engineering, University of Tokyo, Hongo, Bunkyo-ku, Tokyo, 113
†Institute of Environment Science and Technology, Yokohama National University, 156, Tokiwadai, Hodogaya-ku, Yokohama 240
††Department of Applied Chemistry, Nagoya Institute of Technology, Gokiso, Showa-ku, Nagoya 466
(Received February 16, 1989)

Stabilization of ZnO photoanodes was investigated using ZnO thin film electrodes under controlled potential in various pH solutions; the effects of light intensity and agitation were also studied. The photocorrosion of ZnO photoanodes was suppressed at sufficiently cathodic potentials and/or at low light intensity. Agitation of solution also suppressed photocorrosion. On the basis of the experimental results, the mechanism of the stabilization in high pH solutions is discussed and a model is proposed.

Zinc oxide (ZnO) is one of the most popular semiconductor photoelectrodes. Although it shows a large anodic photocurrent, it has been difficult to use ZnO for solar energy conversion[1] or photoelectrochemical synthesis[2-4] because of its photocorrosion.[5-10] We recently showed that ZnO photoanodes could be stabilized in high pH solutions,[11,12] but the mechanism of the stabilization still remains unknown. On the other hand, the photocorrosion of ZnO can be used for other applications such as imaging systems,[13] and micro-processing of ZnO for optoelectric devices.[14,15] In these systems, it is necessary to control film thickness, and therefore speed of the photocorrosion, during the photoetching process. Thus it is still important to understand the details of the mechanism of the photocorrosion of ZnO photoelectrodes. In the present work we studied the effects of pH of the solution, electrode potential, light intensity, and agitation of the solution on the photocorrosion of ZnO photoelectrode. We have developed a new simple technique for monitoring the dissolution of ZnO electrode. ZnO thin films on transparent SnO_2-coated glass were used as photoelectrodes. A change in thickness of the ZnO film was detected by observing a change in interference colors. In addition, the surface morphology could be monitored with a scanning electron microscope. The experimental results are explained in terms of competition between the photocorrosion of ZnO and the oxidation of hydroxide ion in the electrolyte solution.

Experimental

A ZnO thin film was deposited onto a SnO_2-coated glass (Asahi Glass Co., Ltd.) by a spray-pyrolysis technique.[16] Figure 1 shows the structure of the ZnO film electrode. The thickness of the film was estimated to be 200±20 nm. X-Ray diffraction analyses showed that the c-axis was oriented vertically to the surface. The photocorrosion of ZnO was investigated under a controlled bias in a solution of $NaClO_4$ (0.2 mol dm^{-3}) containing an adequate amount of NaOH for pH control. A He-Cd laser (Kinmon Denki Co., Ltd. wavelength 325 nm, output 8 mW) was used as a light source; the diameter of the light beam was controlled with a quartz lens so that the incident photon flux was maintained constant.

The amount of charge passed, C, which resulted in the dissolution of the irradiated spot of the ZnO films, can be calculated as follows:

$$C = \frac{\pi \cdot r^2 \cdot d \cdot D \cdot n \cdot F}{4 \cdot M} \quad (1)$$

Here r is beam diameter, d thickness of the films, D the specific gravity of ZnO, n number of electrons transferred, F the Faraday constant, and M formular weight of ZnO. For $n=2$, $r=1.2\pm0.1$ mm, and $d=200\pm20$ nm, C is 2—4 mC. However, the photocurrent from SnO_2 must be taken into account as a background. Thus, characterization of the electrode surface was carried out after a charge of 5 mC was passed, which took several minutes under the present conditions.

The relation between the interference color and the thickness of the film can be written as follows

$$4 \cdot n \cdot d = (2 \cdot M + 1) \cdot \lambda \quad (2)$$

Here, d is the thickness of the film, n the refractive index of

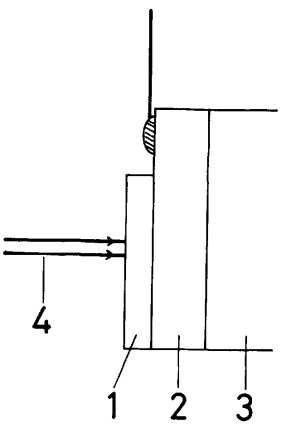

Fig. 1. The structure of the ZnO film electrode. 1: ZnO film, 2: SnO_2 layer, 3: glass substrate, 4: laser beam.

ZnO, λ the wave length of the interference light, and M an integral constant. Since the refractive index of ZnO is about 2.0, $\lambda=8\cdot d$ when $M=0$, and a change in λ of ca. 40—50 nm can be detected by the observation with naked eyes. Thus a thickness change of 5 nm could be easily detected. When the interference color of the irradiated spot was the same as that of the substrate SnO_2 film, it was judged that the ZnO film had completely been removed. When there was no change in the interference color after the irradiation, it was regarded that photocorrosion did not occur. Between these two cases, it was concluded that incomplete photocorrosion had occurred.

Results

Figure 2 shows the typical current-time curves for the following three cases; no ptotocorrosion, incomplete photocorrosion and complete photocorrosion. Since the power of the light beam was 8 mW and the irradiated area was 1.3 ± 10^{-2} cm^2, the light intensity was calculated to be 0.6 W cm^{-2}. The quantum efficiency of the ZnO photoelectrodes used here is 40—70% in ordinary circumstances. However, the total quantum efficiency was decreased to 10—20% under these experimental conditions, because the light intensity was so high that the recombination of the carrier occurred. In addition, I_{ph} was not saturated at the potential regions employed here. Thus, it is reasonable that the I_{ph} values observed here were smaller than that expected from the amount of incident photons. When the photocorrosion did not occur (Fig. 2(a)), I_{ph} was almost constant. Figure 2(b) corresponds to the cases with incomplete photocorrosion. I_{ph} initially showed a large decrease and then became almost constant. These two results imply that reaction other than photocorrosion takes place at the electrode surface. This reaction is the oxidation of OH^- ions to gaseous oxygen. However, we could not visually detect gas evolution because of the small photocurrent. Figure 2(c) shows the case of complete photocorrosion; I_{ph} exhibited a large decrease after an initial small increase. The photocorrosion roughens the electrode surface, and thus increases the surface area. This is the reason why I_{ph} increases at first. The thickness of the ZnO film decreases with the occurrence of photocorrosion, and consequently I_{ph} decreases. A small constant I_{ph} is probably due to I_{ph} from the SnO_2 substrate.

It was found that pH of the solution, electrode

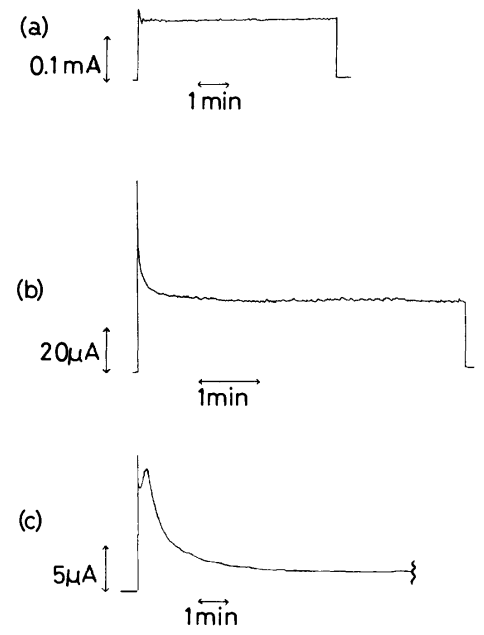

Fig. 2. Typical current-time curves: light intensity 0.6 W cm^{-2}. (a) pH 13, −0.3 V vs. SCE: no photocorrosion. (b) pH 12, −0.1 V vs. SCE: incomplete photocorrosion. (c) pH 11, 0.0 V vs. SCE: complete photocorrosion.

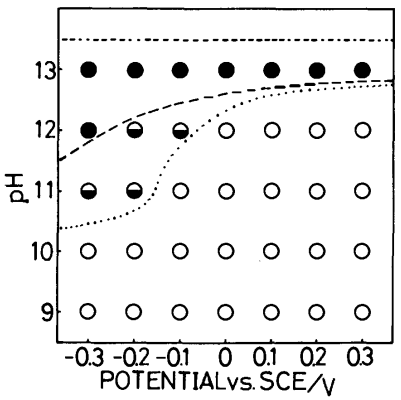

Fig. 3. Summary of the effects of pH and potential. ○: complete photocorrosion. ◒: incomplete photocorrosion. ●: no photocorrosion.

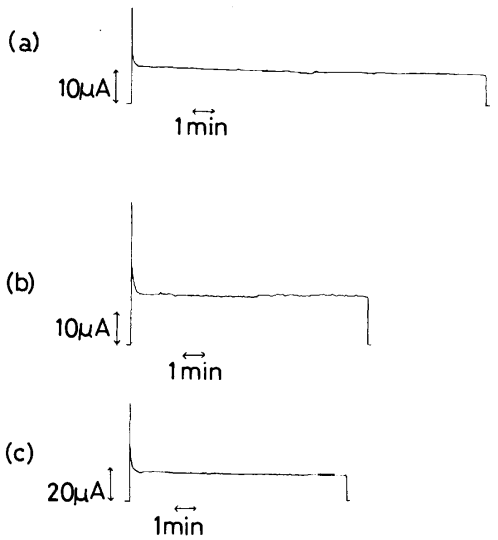

Fig. 4. Photocurrent-time curve in a pH 12 solution, light intensity 0.6 W cm^{-2}. (a) potential −0.3 V vs. SCE. (b) potential −0.2 V vs. SCE. (c) potential −0.1 V vs. SCE.

potential, light intensity and agitation of the solution affected the photocorrosion of ZnO. The effects of the electrode potential and pH of the solution are summarized in Fig. 3 (light intensity 0.6 W cm^{-2}, in stationary solution). The effect of electrode potential was apparent in the region near 0 V vs. SCE. The I_{ph} increases with the electrode potential in this potential region. From pH 7 to 10, the photocorrosion was observed for all the applied potentials. The photocorrosion was incomplete at −0.3 V vs. SCE for pH 11 and at −0.2 to −0.1 V vs. SCE for pH 12. The photocorrosion was not observed at −0.3 V vs. SCE for pH 12 and in the potential region from −0.3 to −0.8 V vs. SCE for pH 13.

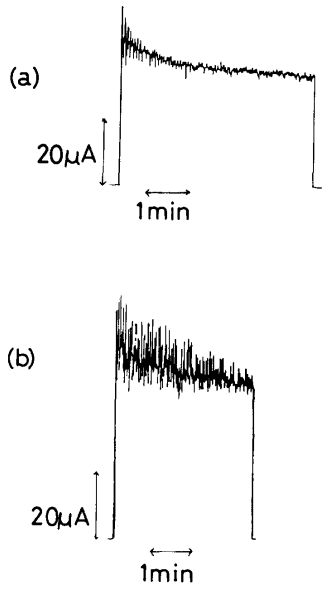

Fig. 5. Photocurrent-time curve in an agitated solution, pH 12, light intensity 0.6 W cm^{-2}. (a) potential −0.1 V vs. SCE. (b) potential 0.0 V vs. SCE.

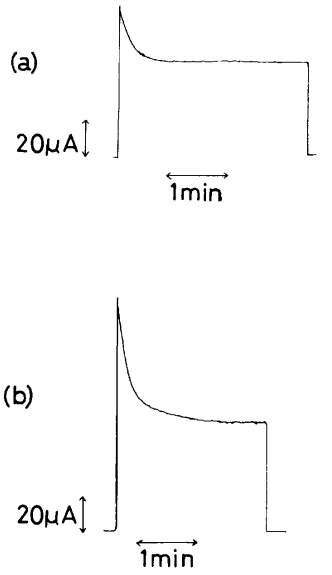

Fig. 6. Photocurrent-time curve in pH 12 solution, light intensity 0.1 W cm^{-2}. (a) Potential −0.1 V vs. SCE. (b) Potential 0.0 V vs. SCE.

The effects of agitation and light intensity are shown in Figs. 4—6. Photocorrosion was observed in a stationary solution of pH 12 when the light intensity was 0.6 W cm^{-2} and the electrode potential was −0.1 V vs. SCE (Fig. 4(c)), but it was not observed when the solution was agitated (Fig. 5(a)) or when the light intensity was 0.1 W cm^{-2} (Fig. 6(a)).

Discussion

Here we consider the competition reaction between the photocorrosion and the oxidation of OH^- ions in order to explain the experimental results observed. The photocorrosion of ZnO and the oxidation of OH^- can be summarized by Eqs. 3—8.

$$ZnO + h\nu \longrightarrow ZnO + p^+ + e^- \tag{3}$$

$$ZnO + 2p^+ \longrightarrow Zn^{2+} + \cdot O \quad \text{(slow)} \tag{4}$$

$$OH^- + p^+ \longrightarrow \cdot OH \quad \text{(slow)} \tag{5}$$

$$Zn^{2+} + nH_2O \longrightarrow Zn^{2+}(H_2O)_n \quad \text{(fast)} \tag{6}$$

$$2\cdot O \longrightarrow O_2 \quad \text{(fast)} \tag{7}$$

$$2\cdot OH \longrightarrow H_2O + 1/2O_2 \quad \text{(fast)} \tag{8}$$

We did not consider the chemical dissolution of ZnO which takes place at extremely high pH and low pH. The rate-determining step of the photocorrosion is given by Eq. 4 and that of the oxidation of OH^- by Eq. 5. Now, we write the rate of the reaction (4) as V_1 and that of the reaction (5) as V_2. According to this model, the current efficiency of the ZnO decomposition, C_d becomes as follows,

$$C_d = \frac{V_1}{V_1 + V_2} \tag{9}$$

The steady state is attained with respect to the surface concentrations of OH^- ion and p^+ when the photocurrent is constant with time. These conditions are satisfied when the thickness of the ZnO films is sufficiently larger than that of the space charge layer, or when the photocorrosion does not occur. The following relations hold under the steady state;

$$I_p = V_1 + V_2 \tag{10}$$

$$f = V_2 \tag{11}$$

Here I_p and f denote the photocurrent density and the current density induced by the flux of OH^- ion, respectively. We obtain the following equation by using Eqs. 9—11.

$$C_d = \frac{I_p - f}{I_p}$$

$$= 1 - \frac{f}{I_p} \quad (12)$$

This analysis shows that C_d is determined by I_p and f. I_p is a function of the electrode potential and the light intensity. The flux f is a function of the thickness of the diffusion layer (d), concentration of OH^- ion in bulk ($[OH^-]_b$) and at surface ($[OH^-]_s$). The conditions where the photocorrosion does not occur, that is, $C_d=0$ can be realized when $I_p=f$. When diffusion along the surface is neglected, f can be approximately expressed as

$$f = \frac{D}{d} \cdot F \cdot ([OH^-]_b - [OH^-]_s) \quad (13)$$

Here D is the diffusion coefficient of OH^- ions, F the Faraday constant. We write the f as f_{max} when $[OH^-]_s$ is zero. Under the conditions where d and $[OH^-]_s$ are constant, f_{max} is constant. When I_p is equal or smaller than f_{max}, $I_p=f$ is approximately realized, and consequently C_d becomes zero. When I_p is larger than f_{max}, $I_p=f$ cannot be realized then $C_d=1-f_{max}/I_p>0$, and photocorrosion occurs.

From the experimental results, we can make a quantitative analysis. The diffusion coefficient of OH^- ion, D, was estimated from the molar conductivity, to be ca. 3×10^{-5} cm^2 s^{-2}. The thickness of diffusion layer, d, can be estimated from the time needed for the photocurrent to become constant. It was ca. 3×10^{-3} cm when the light intensity was 0.6 W cm^{-2} for pH 12 ($[OH^-]_b=1\times10^{-2}$ mol l^{-1}), and photocorrosion was not observed. Under this condition, f_{max} becomes ca. 1×10^{-3} A cm^{-2}. We can compare this estimation with the results of Figs. 4(a) and 4(b). Photocorrosion was not observed for Fig. 4(a) where $I_p=8.8\times10^{-4}$ A cm^{-2}, and photocorrosion was observed for Fig. 4(b) where $I_p=1.2\times10^{-3}$ A cm^{-2}. These results support our competition model.

In an agitated solution of pH 12 (Fig. 5), photocorrosion was not observed even when I_p was 3.0×10^{-3} A cm^{-2} (Fig. 5(a)), but was observed when I_p was 4.2×10^{-3} A cm^{-2} (Fig. 5(b)). This result shows that the f_{max} value was 3—4 times larger than that in a stationary solution. This is because d was decreased by the agitation.

In the case where the light intensity was 0.1 W cm^{-2}, photocorrosion did not occur when I_p was 6.6×10^{-4} A cm^{-2} (Fig. 6(a)), but was observed when I_p was 8.8×10^{-4} A cm^{-2} (Fig. 6(b)). From the time needed for the photocurrent to become constant, d was estimated to be 4×10^{-2} cm, and f_{max} was calculated to be 7×10^{-4} A cm^{-2}. This f_{max} value is smaller than that estimated from Figs. 4(a) and 4(b). In the potential region employed in these experiments, the photocurrent was not saturated, so a large part of the energy of the incident photons was converted into heat. Thus, there was heat convection around the irradiated spot. In a stationary solution, this heat convection reduces the thickness of the diffusion layer. Thus when the light intensity is large, heat convection will be intense and the thickness of the diffusion layer will be small. Hence f_{max} for the light intensity of 0.1 W cm^{-2} became smaller than that for the light intensity of 0.6 W cm^{-2}.

Conclusion

Photocorrosion of ZnO is suppressed when the concentration of OH^- ion at the surface is large or when the concentration of p^+ at the surface is small. These results can be explained in terms of competition reaction between the oxidation of OH^- ion and the photocorrosion of ZnO.

We would like to thank Professor B. H. Loo for his kind advice and appreciate financial support from the Ministry of Education, Science and Culture, Grant-in-Aid.

References

1) A. J. Bard and M. S. Wrighton, *J. Electrochem. Soc.*, **124**, 1706 (1977).
2) J. R. Harbour and M. L. Hair, *J. Phys. Chem.*, **83**, 652 (1979).
3) W. P. Gomes, T. Freund, and S. R. Morrison, *J. Electrochem. Soc.*, **115**, 818 (1968).
4) S. R. Morrison and T. Freund, *J. Chem. Phys.*, **47**, 1543 (1967).
5) H. Gerischer, *J. Electrochem. Soc.*, **113**, 1175 (1966).
6) H. Gerischer, *J. Electroanal. Chem.*, **82**, 133 (1977).
7) T. Kobayashi, H. Yoneyama, and H. Tamura, *Chem. Lett.*, **1979**, 457.
8) S. R. Morrison and T. Freund, *Electrochim. Acta*, **13**, 1343 (1968).
9) J. Domenech and A. Prieto, *J. Phys. Chem.*, **90**, 1123 (1986).
10) K. Micka and H. Gerischer, *J. Electrochem. Soc.*, **38**, 397 (1972).
11) A. Fujishima, T. Katoh, E. Maekawa, and K. Honda, *Bull. Chem. Soc. Jpn.*, **54**, 1671 (1981).
12) J. Lee, T. Katoh, A. Fujishima, and K. Honda, *Bull. Chem. Soc. Jpn.*, **57**, 1179 (1984).
13) M. Okano, K. Itoh, E. Kikuchi, and A. Fujishima, *J. Appl. Phys.*, **62**, 2143 (1987).
14) M. Okano, K. Itoh, A. Fujishima, and K. Honda, *Chem. Lett.*, **1986**, 469.
15) R. Tenne, V. Marcu, and N. Yellin, *Appl. Phys. Lett.*, **45**, 1219 (1984).
16) K. L. Chopra, R. C. Kainthla, D. K. Pandya, and A. P. Thakoor, "Physics of Thin Films," ed by G. Hass, M. H. Francombe, and Y. L. Vossen, Academic Press, New York (1982), Vol. 12, p. 167.
17) D. Bahnememn, A. Henglein, and L. Spanhel, *Faraday Discuss. Chem. Soc.*, **78**, 151 (1984).

The Phase Transition of Quaternary Fluoroalkyl Halide Salts of 1,4-Diazabicyclo[2.2.2]octane

Tohru TERADA, Takashi NOGAMI,* and Yasuhiko SHIROTA
Department of Applied Chemistry, Faculty of Engineering, Osaka University, Yamadaoka, Suita, Osaka 565
(Received April 3, 1989)

The solid-solid phase transition of quaternary halide salts of 1,4-diazabicyclo[2.2.2]octane (DABCO) was investigated by DSC, Raman spectroscopies, and the measurements of the ionic conductivity of the halide anions. The DABCO salts studied are classified into two; one is the salt possessing both fluoroalkyl and alkyl groups, and the other the ones possessing the same fluoroalkyl groups at both ends of the molecule. The former molecule exhibited a gradual increase of the ionic conductivity above the transition temperature. The ionic conductivity of the former molecule was higher than that of the latter molecules and the symmetric quaternary alkyl halide salts of DABCO. These facts were explained by a spacer effect of the fluoroalkyl group. The temperature dependence of the Raman spectra of the former salt established that the fluoroalkyl group was much more rigid than the alkyl group, and that the molecular movement took place mainly at the alkyl group and the DABCO portion in the high temperature phase. One of the latter type of molecules exhibited a conductivity jump around the transition temperature.

The phase transition of a series of quaternary alkyl halide salts of 1,4-diazabicyclo[2.2.2]octane (DABCO) was investigated by DSC, IR and Raman spectroscopies, NMR, and the measurements of the ionic conductivities of halide anions.[1-8] The phase transition of the quaternary DABCO salts containing tetrafluoroborate anion has also been reported recently.[9] These materials exhibit conformational change of the alkyl group in the high temperature phase in the solid. A conductivity jump of the halide anion was observed by up to three orders of magnitude around the transition temperature. These materials also showed the disappearance of optical anisotropy in the high temperature phase, and in some cases they remained in a metastable state after having been heated above the transition temperature and then cooled to room temperature. These switching properties of the ionic conductivities[10] and optical and thermodynamic properties may be applicable to some temperature and memory devices.

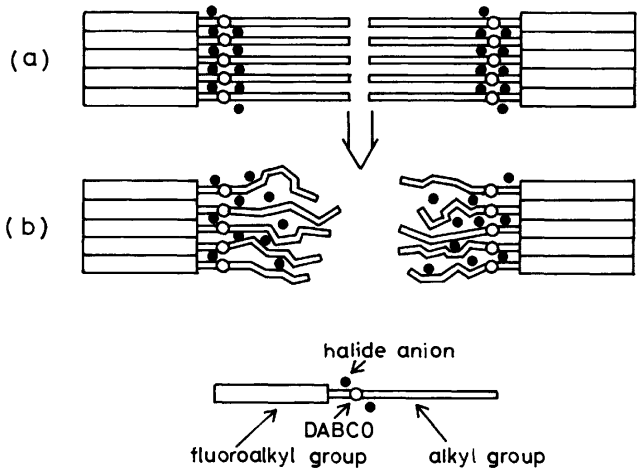

Fig. 1. Schematic drawing of the proposed molecular arrangement, spacer effect, and molecular motion of C_n^F-DABCO-C_n-X_2 in a solid. (a) Low temperature phase, (b) high temperature phase.

A variety of amphipatic materials containing both long alkyl and fluoroalkyl chains as hydrophobic parts were synthesized, and their physicochemical properties investigated.[11] These studies established that the fluoroalkyl and alkyl groups tend to separate from each other in the solid; in other words, the fluoroalkyl chains arrange parallel to one another, and so do the alkyl chains.[12] In general, the fluoroalkyl chain forms a helical structure, and the fluorine atoms surround the C-C backbone.[13] The structural difference of the fluoroalkyl chain from the alkyl chain results in the more rigid structure of the former chain than of the latter. Moreover, the fluoroalkyl group is bulkier than the alkyl group. Thus, the quaternary halide salt of DABCO containing both the fluoroalkyl and the alkyl groups (C_n^F-DABCO-C_n-X_2) may possess the molecular arrangement shown schematically in Fig. 1(a). The bulkier fluoroalkyl groups function as spacers in the solid, so that the less bulky alkyl groups may move relatively freely in the high temperature phase (Fig. 1(b)). On the other hand, the molecular motion of the alkyl group may be retarded in the case

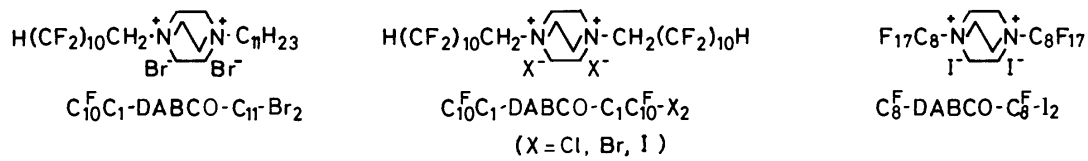

Fig. 2. Quaternary DABCO halide salts.

of the DABCO salts possessing two alkyl groups at both sides of the molecule (C_n-DABCO-C_n-X_2) because of the closed-packed molecular arrangements. Thus, C_n^F-DABCO-C_n-X_2 may show higher halide anion conductivity than C_n-DABCO-C_n-X_2. We are also interested in the difference of the molecular motion between the alkyl and fluoroalkyl groups in the solid. Bearing these assumptions in mind, we have synthesized the two types of quaternary DABCO halide salts shown in Fig. 2; one is a quaternary DABCO bromide salt containing both fluoroalkyl and alkyl groups in the molecule, and the other the symmetric quaternary DABCO halide salts containing two fluoroalkyl groups in the molecule. The names of the molecules in Fig. 2 are abbreviated to $C_{10}^F C_1$-DABCO-C_{11}-Br_2, $C_{10}^F C_1$-DABCO-$C_1 C_{10}^F$-X_2 (X=Cl, Br, I), and C_8^F-DABCO-C_8^F-I_2.

Experimental

$C_{10}^F C_1$-DABCO-C_{11}-Br_2. $H(CF_2)_{10}CH_2OH$ (1.2 g, 2.3 mmol) was dissolved in benzene (50 cm^3) containing several drops of pyridine, and thionyl bromide (0.5 g, 2.4 mmol) wad added dropwise to this solution at 0 °C. The solution was heated gradually to 60 °C, stirred for 8 h at this temperature, and allowed to cool to room temperature. The solvent was distilled out using an evaporator, and the residual white powder was recrystallized from a mixed solvent of benzene and hexane to obtain $H(CF_2)_{10}CH_2Br$ (0.54 g, 40%). Quaternary undecylbromide salt of DABCO (C_{11}-DABCO-Br)[3] (0.7 g) and $H(CF_2)_{10}CH_2Br$ (1.2 g) so obtained were dissolved in benzene (50 cm^3) and the solution was stirred for 24 h at 60 °C, and then cooled by ice. The precipitate was collected, and recrystallized from benzene (22% yield, 0.41 g).

$C_{10}^F C_1$-DABCO-$C_1 C_{10}^F$-Cl_2. $H(CF_2)_{10}CH_2Cl$ was obtained (62% yield) by the same method as the synthesis of $H(CF_2)_{10}CH_2Br$. Thionyl chloride was used instead of thionyl bromide. DABCO (0.06 g, 0.5 mmol) and $H(CF_2)_{10}CH_2Cl$ (0.6 g, 1.1 mmol) were dissolved in benzene (50 cm^3) and the solution was stirred for 12 h at 60 °C. Subsequently the same procedure as that described for the synthesis of $C_{10}^F C_1$-DABCO-C_{11}-Br_2 was adopted (75% yield, 0.49 g).

$C_{10}^F C_1$-DABCO-$C_1 C_{10}^F$-Br_2. This was synthesized by the same method as that described for the corresponding chloride salt (73% yield).

$C_{10}^F C_1$-DABCO-$C_1 C_{10}^F$-I_2. $H(CF_2)_{10}CH_2Cl$ (1.2 g, 2.2 mmol), DABCO (0.12 g, 1.1 mmol), and potassium iodide (2 g, 20 mmol) was dissolved in the mixed solvent of ethanol and water (1:1, 50 cm^3), and the solution was refluxed for 12 h. The precipitate was collected, and recrystallized from benzene (68% yield, 1.0 g).

C_8^F-DABCO-C_8^F-I_2. The ethanol solution (50 cm^3) of $C_8F_{17}I$ (1.2 g, 2.2 mmol) and DABCO (0.12 g, 1.1 mmol) was stirred for 6 h at room temperature.[14] The solution was then cooled by ice to yield a white precipitate. It was collected, and recrystallized from benzene (82% yield, 1.08 g).

Measurements. DSC, and ionic conductivities were measured by the methods described previously.[2] The temperature dependence of the Raman spectra was measured by the method described previously.[7] R-500 Laser Spectrometer (Japan Spectroscopic Co., Ltd.) was used as a monochromator, and a GLS/GLG argon ion laser (514.5 nm) (Nippon Electric Co., Ltd.) as an excitation source. Since all of the materials were unstable above ca. 40 °C in air, all of the measurements were made in a sealed cell under nitrogen atmosphere.

Results and Discussion

DSC Measurements of $C_{10}^F C_1$-DABCO-C_{11}-Br_2. Figure 3 shows the DSC curve of $C_{10}^F C_1$-DABCO-C_{11}-Br_2 measured with a scan rate of 5 °C min^{-1}. It showed an endothermic signal at 38 °C (extrapolated onset temperature) when heated from room temperature. When the sample was cooled after having been heated above 50 °C, a much broader exothermic signal was observed. The succeeding heating/cooling cycles gave signals almost identical with those of Fig. 3. Thus, a phase transition occurred at 38 °C, and the initial low temperature phase recovered gradually when the temperature was lowered from the high temperature phase to room temperature. The transition temperature (T_c), transition enthalpy (ΔH), and transition entropy ($\Delta S=\Delta H/T_c$) are shown in Table 1. This material decomposed at 83 °C in an inert atmosphere. This is a much lower decomposition temperature than that of the corresponding C_{11}-DABCO-C_{11}-Br_2.[2] It may be caused by the weak C-N bond energy between DABCO-nitrogen and the fluoroalkyl carbon due to the inductive effect of the fluoroalkyl group.[14]

Ionic Conductivities of $C_{10}^F C_1$-DABCO-C_{11}-Br_2. The temperature dependence of the ionic conductivities of $C_{10}^F C_1$-DABCO-C_{11}-Br_2 was measured for a compressed pellet sample by an AC impedance method,[2] in order to see the effect of the phase transition on the ionic conductivities. This type of quaternary DABCO-halide salt was found to be a halide anion conductor by the fact that the ionic conductivity did not change at all on applying a DC current if the halide anions were injected from the electrode.[1] Figure 4 shows the plot of the ionic conductivity of $C_{10}^F C_1$-DABCO-C_{11}-Br_2 against the

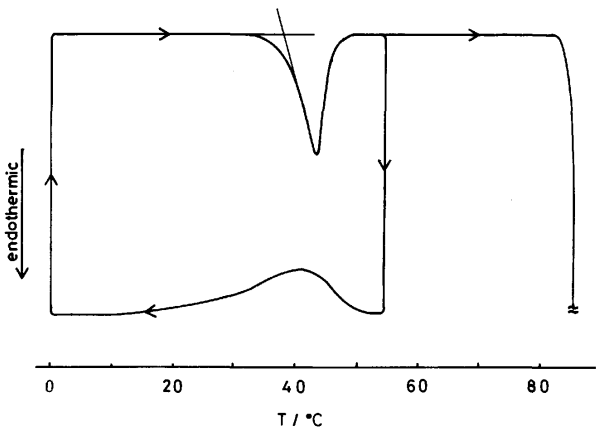

Fig. 3. DSC thermogram of $C_{10}^F C_1$-DABCO-C_{11}-Br_2.

Table 1. Materials, Transition Temperatures (T_c), Transition Enthalpies (ΔH), Transition Entropies (ΔS), and Ratios of Halide Anion Conductivities (σ_h/σ_l) Below and Above Transition Temperatures

Materials	T_c	ΔH	ΔS	σ_h/σ_l
	°C	kJ mol^{-1}	J mol^{-1} K^{-1}	
$C^F_{10}C_1$-DABCO-C_{11}-Br_2	38	38.3	123	a)
$C^F_{10}C_1$-DABCO-$C_1C^F_{10}$-Cl_2	63	109.6	326	120
$C^F_{10}C_1$-DABCO-$C_1C^F_{10}$-Br_2	93	47.5	130	b)
$C^F_{10}C_1$-DABCO-$C_1C^F_{10}$-I_2	96	51.0	138	b)
C^F_8-DABCO-C^F_8-I_2	89	58.3	161	c)

a) Since a gradual increase in the ionic conductivity was observed above the transition temperature, it was difficult to estimate the value of the conductivity jump. b) No conductivity jump was observed. c) Because of the decomposition of the material at a few degrees above the transition temperature, the σ_h/σ_l value could not be estimated.

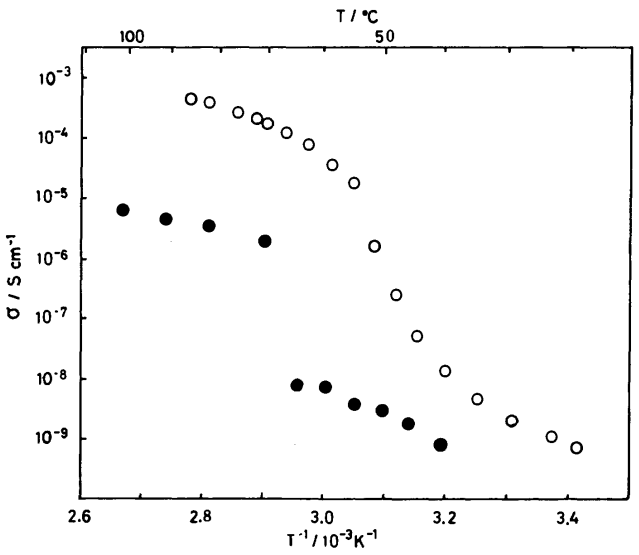

Fig. 4. Temperature dependence of the ionic conductivities of bromide anion. ○ $C^F_{10}C_1$-DABCO-C_{11}-Br_2, ● C_{11}-DABCO-C_{11}-Br_2.

reciprocal temperature. This figure also shows the same plot of C_{11}-DABCO-C_{11}-Br_2 (transition temperature=72 °C[2]) for the sake of comparison. The bromide anion conductivities of $C^F_{10}C_1$-DABCO-C_{11}-Br_2 were always higher than those of C_{11}-DABCO-C_{11}-Br_2, probably due to the spacer effect of the fluoroalkyl group as described in the Introduction (see also Fig. 1). The ionic conductivity of the former material approached to 10^{-3} S cm^{-1} in the high temperature phase, and this value was higher by about two orders of magnitude than those of the symmetric DABCO salts, C_n-DABCO-C_n-Br_2 ($10 \leqq n \leqq 22$).[2] The temperature dependence of the ionic conductivity of $C^F_{10}C_1$-DABCO-C_{11}-Br_2 was different from that of C_{11}-DABCO-C_{11}-Br_2; the latter material showed a conductivity jump by a factor of 630 around the transition temperature.[2] On the other hand, the former material did not show a conductivity jump, but showed a gradual increase of the ionic conductivity in the range of 40—60 °C, which was initiated by the phase transition at 38 °C. These results are explained as follows. In the case of C_{11}-DABCO-C_{11}-Br_2, the alkyl group could not move vigorously due to the closed-packed molecular arrangement in the low temperature phase. When the sample was heated to the transition temperature, the movement of the alkyl chain was released suddenly to give rise to the conductivity jump. On the other hand, the movement of the alkyl chain of $C^F_{10}C_1$-DABCO-C_{11}-Br_2 could be excited more easily due to the spacer effect of the fluoroalkyl group (Fig. 1). Thus, the gradual increase of the ionic conductivity was caused by a facile excitation of the movement of the alkyl group with the elevation of the temperature. This assumption was confirmed by Raman spectroscopy (vide infra).

Raman Spectroscopy of $C^F_{10}C_1$-DABCO-C_{11}-Br_2. Generally, Raman and IR bands broaden as the amount of the thermal motion increases in the solid.[15] In order to clarify the molecular motion in more detail and to relate it to the results of DSC and the measurements of the ionic conductivities, Raman spectra of $C^F_{10}C_1$-DABCO-C_{11}-Br_2 were measured in the low (13 °C) and high (65 °C) temperature phases (Fig. 5). Since the band at 732 cm^{-1} (C-C stretching mode of the fluoroalkyl group)[16] hardly changed at both temperatures, hardly any molecular movement at the fluoroalkyl group accompanied the conformational change. This assumption was confirmed by the almost constant Raman profiles of the CF_2 stretching modes, (1308, 1360, and 1372 cm^{-1}).[16] Slight line broadning was observed at 65 °C for the Raman bands of the CF_2 vibrational modes (306 and 385 cm^{-1}),[16] which indicates that a rotational movement of the fluoroalkyl group was excited to some extent in the high temperature phase.

In contrast to the small change of the Raman bands of the CF_2 vibrational modes, the Raman bands at 1064 and 1132 cm^{-1} (skeltal vibration of the alkyl group[7]) decreased their intensities appreciably in the high temperature phase. This fact suggests that vigorous motions accompany the conformational change occurring at the alkyl group in the high temperature phase.

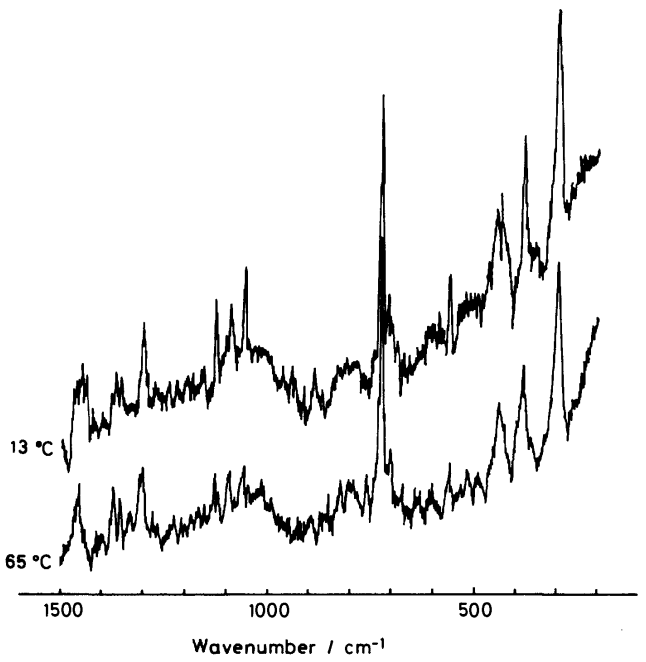

Fig. 5. Raman spectra of $C_{10}^{F}C_1$-DABCO-C_{11}-Br_2 below and above the transition temperature.

As to the Raman bands ascribable to the DABCO portion,[7] the band at 714 cm^{-1} (NC_4 symmetric stretching mode) decreased its intensity at 65 °C, and the band at 890 cm^{-1} (NC_4 degenerate stretching mode) observed in the low temperature phase disappeared almost completely at 65 °C. This suggests that the rotational movement of the DABCO portion was excited in the high temperature phase.

Summarizing the above experimental results, the molecular movement sets in mainly at the alkyl group and DABCO portion at the transition temperature. On the other hand, only a slight rotational movement seems to be excited at the fluoroalkyl group. Thus, the prediction of the molecular motion illustrated in Fig. 1 was confirmed by Raman spectroscopy.

Phase Transition of Symmetric Quaternary Fluoroalkyl Halide Salts of DABCO. The phase transitions of the symmetric quaternary fluoroalkyl halide salts of DABCO, $C_{10}^{F}C_1$-DABCO-$C_1C_{10}^{F}$-X_2 (X=Cl, Br, I), and C_8^F-DABCO-C_8^F-I_2, were also investigated by DSC, Raman spectroscopy, and the measurements of the ionic conductivities of the halide anions in order to compare them with those of $C_{10}^{F}C_1$-DABCO-C_{11}-Br_2 and C_n-DABCO-C_n-X_2. These materials showed reversible DSC signals. Table 1 summarizes the transition temperatures (T_c), transition enthalpies (ΔH), and transition entropies (ΔS) obtained by the DSC measurements in a nitrogen atmosphere. C_8^F-DABCO-C_8^F-I_2 decomposed at 93 °C, just above the transition temperature (89 °C), in an inert atmosphere. The exceptionally instability of C_8^F-DABCO-C_8^F-I_2 may be associated with a weak C-N bond energy caused by an inductive effect of fluorine atoms. Temperature dependences of the halide anion conductivities of $C_{10}^{F}C_1$-DABCO-$C_1C_{10}^{F}$-X_2 (X=Cl, Br, I) were measured, and only the chloride salt showed a conductivity jump (σ_h/σ_l) by a factor of about 120 (Table 1).[17] This value was much smaller than those observed for the corresponding symmetric quaternary alkyl halide salts of DABCO.[2] These facts suggest that the molecular motion of $C_{10}^{F}C_1$-DABCO-$C_1C_{10}^{F}$-X_2 (X=Cl, Br, I) is less vigorous than that of C_{11}-DABCO-C_{11}-X_2 (X=Cl, Br, I) in the high temperature phases. In order to confirm this, the temperature dependence of the Raman spectra of $C_{10}^{F}C_1$-DABCO-$C_1C_{10}^{F}$-Br_2 (not shown here) was measured below and above (16 °C and 103 °C) the transition temperature (93 °C). The Raman band at 732 cm^{-1} (C-C stretching of fluoroalkyl group) hardly changed for the high temperature phase. This suggests that the amount of molecular motion of the fluoroalkyl group is small even for the high temperature phase. Since the Raman intensities ascribable to the $-CH_2$-DABCO-CH_2- portion were weak, no further detailed analysis could be mode. The phase transition may be caused by the molecular motion of $-CH_2$-DABCO-CH_2- portion and/or by the change of the molecular packing in the solid. The small σ_h/σ_l values of $C_{10}^{F}C_1$-DABCO-$C_1C_{10}^{F}$-X_2 (X=Cl, Br, I) could be related to the rigid molecular structure of the fluoroalkyl group.

We are grateful to Professor Shigekazu Kusabayashi and Dr. Shunsuke Takeneka, Faculty of Engineering, Osaka University, for allowing us to use the DSC apparatus. The present work was supported by a Grant-in-Aid for Special Project Research on Chemical Sensors (No. 62217014) from the Ministry of Education, Science and Culture.

References

1) J. Shimizu, T. Nogami, and H. Mikawa, *Solid State Commun.*, **54**, 1009 (1985).

2) J. Shimizu, K. Imamura, T. Nogami, and H. Mikawa, *Bull. Chem. Soc. Jpn.*, **59**, 1443 (1986).

3) K. Imamura, J. Shimizu, and T. Nogami, *Bull. Chem. Soc. Jpn.*, **59**, 2699 (1986).

4) J. Shimizu, K. Imamura, T. Nogami, and H. Mikawa, *Bull. Chem. Soc. Jpn.*, **59**, 3367 (1986).

5) K. Imamura, T. Nogami, and Y. Shirota, *Bull. Chem. Soc. Jpn.*, **60**, 111 (1987).

6) K. Imamura, T. Nogami, and Y. Shirota, *Bull. Chem. Soc. Jpn.*, **60**, 3499 (1987).

7) K. Imamura, T. Nogami, Y. Shirota, T. Ishioka, and M. Kobayashi, *Bull. Chem. Soc. Jpn.*, **60**, 3879 (1987).

8) H. Nakayama, T. Eguchi, N. Nakamura, H. Chihara, T. Nogami, K. Imamura, and Y. Shirota, *Bull. Chem. Soc. Jpn.*, **62**, 399 (1989).

9) T. Terada, T. Nogami, and Y. Shirota, *Bull. Chem. Soc. Jpn.*, **62**, 5 (1989).

10) Optical switching of ionic conductivities has recently

been reported. K. Kimura, T. Suzuki, and M. Yokoyama, *Chem. Lett.*, **1989**, 227.

11) N. Higashi and T. Kunitake, *Maku (Membrane)*, **10**, 138 (1985).

12) T. Kunitake and N. Higashi, *J. Am. Chem. Soc.*, **107**, 692 (1985).

13) C. W. Bunn and E. R. Howell, *Nature (London)*, **174**, 549 (1954).

14) Symmetric quaternary alkyl halide salts of DABCO were usually synthesized by refluxing methanol solution of alkyl halide and DABCO for about 36 h. The much milder condition for the synthesis of C_8^F-DABCO-C_8^F-I_2 exemplifies that a nucleophilic attack of the lone-pair of DABCO nitrogen to the fluoroalkyl carbon takes place more easily than that to the alkyl carbon, due to the inductive effect of fluorine atoms.

15) R. G. Snyder, J. R. Scherer, and B. P. Gaber, *Biochim. Biophys. Acta*, **601**, 47 (1980); Y. Cho, M. Kobayashi, and H. Tadokoro, *J. Chem. Phys.*, **84**, 4643 (1986).

16) C. E. Hathaway and J. R. Nielsen, *J. Chem. Phys.*, **41**, 2203 (1964).

17) This fact corresponds to the largest transition entropy of this material.

 © 1989 The Chemical Society of Japan Bull. Chem. Soc. Jpn., 62, 2798—2801 (1989)

On the Intrinsic Difference between Topological Aromaticity and So-Called Quasi-Aromaticity

Hiroshi ICHIKAWA,* Jun-ichi AIHARA,† and Siegfried DAEHNE††
Hoshi College of Pharmacy, Shinagawa, Tokyo 142
†Department of Chemistry, Faculty of Sciences, Shizuoka University, Shizuoka 422
††Central Institute of Physical Chemistry, Academy of Sciences of the GDR,
1199 Berlin-Adlershof, Rudower Chaussee 5, GDR
(Received April 6, 1989)

In an attempt to understand the intrinsic difference between topological aromaticity and so-called quasi-aromaticity, the authors examined the potential energy and the kinetic energy of electrons in 6-π-acyclic polymethine-like molecules (**5**—**7**), benzene (**8**), and hexatriene (**9**) as a reference structure. Protonation interrupts π conjugation; the energetic difference from the non-protonated structure depends on the conjugative stabilization energy. Such a difference from the reference system corresponds to extra stabilization. Analysis of this difference showed that benzene increases the kinetic energy by interrupting its conjugation more than hexatriene while polymethine-like molecules increase the potential energy by doing so. This indicates that extra stabilizaion in benzene is produced by lowering the kinetic energy of electrons. In marked contrast with this that in polymethine-like molecules is due to lowering the potential energy. Analogous results were obtained in the ten-π-electron systems (**10**—**13**). The authors discussed the inappropriateness of the term "quasi-aromatic" for polymethinic resonance stabilization.

Aromatic compounds have been characterized by the tendency to undergo substitution reactions.[1] Such a characteristic is really applicable to many cyclic conjugated compounds and has been studied topologically[2] as well as by a variety of molecular orbital methods.[3-5] Atoms are arranged in an aromatic compound in such a manner that they induce an appreciable amount of so-called topological resonance energy. This kind of aromaticity will be referred to as topological aromaticity.

It is noteworthy that substitution reactions take place not only in many cyclic but also in some acyclic systems, e.g. some of which not only undergo very easily electrophilic substitution but also nucleophilic substitution followed by a cleavage of the C-C bond.[6] Lloyd and Marshall proposed that molecules should be called quasi-aromatic if they are acyclic conjugated π electron systems with chemical properties typical of aromatic compounds.[7] At the same time Daehne et al. showed that conjugated chain-shaped molecules consisting of n atoms and $n\pm1$ π electrons have unique features which are not comparable to those of aromatic compounds.[8] Therefore, they introduced the term ideal polymethine state to describe the typical properties of resonance stabilized molecular chains. The quantum chemical foundation of this ideal state was given by Fabian and Hartmann.[9] Among such "quasi-aromatics" or "polymethinic" compounds are the 2,3-dihydro-1*H*-1,4-diazepinium salts (**1**),[7,10] α,ω-diazapolymethinium ions (**2**),[8a,11] and transition-metal chelates of diketones (**3**).[12] Noteworthy, however, is that extra stabilization energy scarcely arises from these systems: So-called topological resonance energy is negligible.[13] Recently, Aihara[14] as well as Klein[15] pointed out that quasi-aromatic compounds can be rationalized in terms of Gimarc's topological charge stabilization rule.[16] Our problem is what then is the intrinsic difference between topological aromaticity on the one hand and quasi-aromaticity or polymethinic resonance stabilization or "polymethinicity" on the other hand.

Theory

Molecular energy (E) consists of the electronic energy and the energy of nuclear motion. The kinetic energy of nuclear motion may be treated separately as far as the Born-Oppenheimer approximation operates.[17] Therefore, important energies are the potential energy (V) and the kinetic energy of electrons (T). Those energies can be easily obtained by the ab initio Hartree-Fock theory.

At the optimized structure the system holds the virial relationship, $V=-2T$, as far as all bond lengths, with which the geometry is determined together with bond angles, are optimized with respect to the total energy. As a matter of fact, it is not easy to obtain such a wave function without artificially scaling it. Fortunately, this is not necessary in most case, since we only need the changes of the energy components. For example, the energy difference (by an MO method with any split-valence basis set) between any two sets of geometry-optimized conformations was shown to satisfy the relationship, $\Delta V=-2\Delta T$ (the virial theorem of difference), where ΔT and ΔV are the differences of the kinetic energy and the potential energy.[18c] This shows that the virial errors caused by an inappropriate wave function are cancelled in the differences. The effectiveness of the use of these differences has been discussed in detail[18] and successfully applied in the analyses of π bond formation and conjugations between a π electron system and its substituent.

Now consider a perturbed state such that a proton is loosely put on one of the carbon atoms of the conjugated system. Such a perturbation leads to changes in the total energy and its components, where the simple virial relationship of difference no longer holds, since the system is not in the state of the optimized geometry. Our strategy is to analyze those energy changes by protonation. The basis sets adopted here are 6-31G[19] and 4-31G,[20] which are suitable for the practical analysis of such large molecular systems as those studied here.[18c]

Results and Discussion

Intrinsic Difference of Resonance Stabilizations. We examined the effect of protonation on individual energy terms of π conjugated acyclic compounds (**4**—**7**, **10**, **11**) as well as benzene (**8**) and naphthalene (**12**). Protonation interrupts π conjugation; the difference from the non-protonated structure (ΔE) may depend on the resonance stabilization energy. Analysis of the energy changes in ΔE may reveal the origin of resonance stabilization. In determining the degree of resonance stabilization, e.g. topological aromaticity, of a given compound, one needs the reference structure. The reference structure is considered to have the *standard* conjugation and can be a measure of any type of π conjugation. For cyclic unsaturated hydrocarbons, the linear unsaturated hydrocarbon with the same number of double bonds has once been used as the reference structure.[4] Such a reference structure has later been replaced by a hypothetical structure constructed with bonds of an appropriate infinitely large conjugated system.[2] Although the latter reference structure is desirable, it is not applicable to the present problem. Therefore, we adopted hexatriene (**9**) and decapentaene (**12**) as the reference structures for the six-π-electron and ten-π-electron systems, respectively.

The proton can be placed at any distance from the carbon atom to give a perturbation with shorter distances leading to larger energy changes. Shown in tables are the case where proton was placed 1.2 Å vertically above a carbon atom on the molecular plane (Scheme 2).

Table 1 shows the total energy and its components in the six-π-electron systems. As for the protonated systems only the deviation from the intact systems is recorded. The last column shows the difference in energy from the reference system. In all cases protonation increases the kinetic energy and decreases the potential energy. The latter is larger, resulting in lower total energy by protonation. This is a natural consequence that reflects a localization of π electrons by a broken conjugation.

The energy difference from the reference system is important as is true for determining the degree of aromaticity. Namely, the difference from the reference system corresponds to *extra* stabilization. As shown in

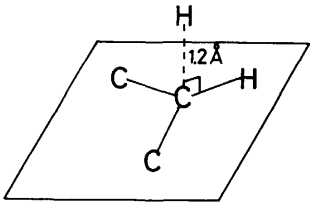

Scheme 2.

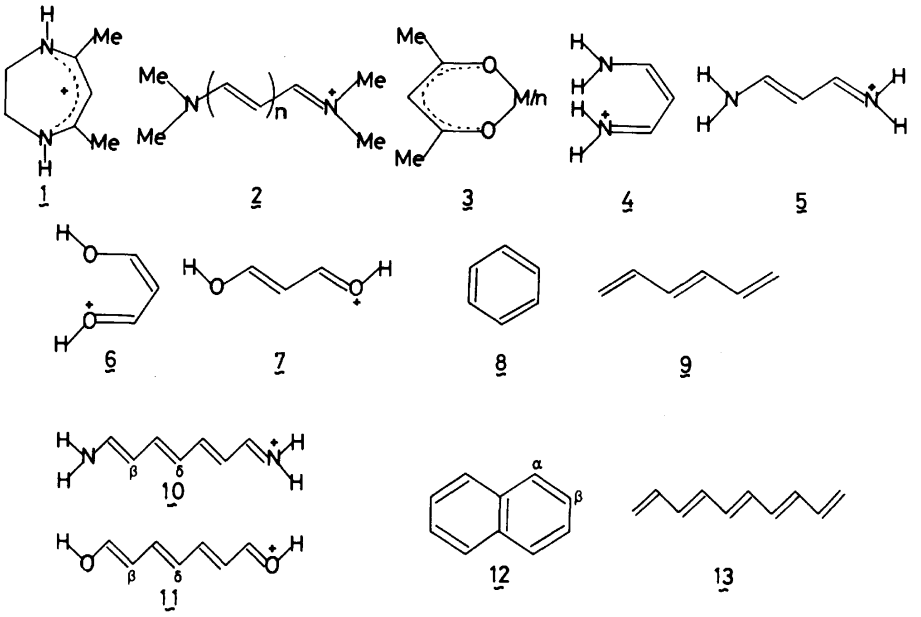

Scheme 1.

the last column of Table 1, benzene increases the kinetic energy by interrupting its conjugation more than hexatriene while acyclic conjugated molecules increase the potential energy by doing so. This indicates that resonance stabilization in benzene is produced by the kinetic energy of electrons. In marked contrast with this, that in polymethine-like molecules is due to the potential energy.

Table 1. Change of Total Energy and Its Components by Protonation in 6π Electron Systems

	Intact[a]	Protonated[b]	Difference[c]
Benzene (**8**)			
E	−230.624489	−0.265263	20
T	230.903329	0.537919	42
V	−461.527818	−0.803182	−22
cis-α,ω-Diaminotrimethinium ion (**4**)			
E	−226.267783	−0.095677	465
T	226.453696	0.399686	−321
V	−452.721480	−0.495463	786
trans-α,ω-Diaminotrimethinium ion (**5**)			
E	−226.285304	−0.100065	454
T	226.479256	0.408643	−297
V	−452.764560	−0.508708	751
cis-α,ω-Dihydroxytrimethinium ion (**6**)			
E	−265.841417	−0.052270	579
T	265.949952	0.352943	−443
V	−531.791369	−0.405213	1022
trans-α,ω-Dihydroxytrimethinium ion (**7**)			
E	−265.843424	−0.046499	594
T	265.969946	0.347787	−457
V	−531.813370	−0.394286	1051
Hexatriene (**9**)[d]			
E	−231.725518	−0.272877	
T	232.011570	0.521786	
V	−463.737088	−0.794663	

a) By 6-31G in terms of au. b) Difference from the intact structure. c) Difference from the hexatriene system (kJ mol^{-1}). d) Proton was put on C_3.

Analogous results for the ten-π-electron systems are presented in Table 2. Possible sites of protonation in **10** and **11** are at β and δ carbons. In harmony with the six-π-electron systems, ten-π-electron polymethines give higher potential energy than the corresponding reference structures by protonation while naphthalene gives higher kinetic energy by protonation.

Concluding Remarks

Ichikawa and Ebisawa reported that thermodynamic stability of a topological aromatic system is given by the lowered kinetic energy of π electrons.[5c] The present results for benzene and naphthalene are in good accord with this interpretation of topological aromaticity. From the present study, we come to the conclusion that the resonance stabilization of acyclic conjugated molecules is intrinsically different from that of topological aromatics. Stabilization of topological aromatics is given by the lowered kinetic energy of π electrons whereas that of acyclic polymethine-like molecules by the potential energy. From the above reason the term "quasi-aromatic" connected with resonance-stabilized chain-shaped molecules seems to us misleading, whereas designation such as ideal polymethine state, polymethinic resonance stabilization, or "polymethinicity" much better describe the situation. We caution, however, against over-emphasizing the charge stabilization rule, because there are

Table 2. Change of Total Energy and Its Components by Protonation in 10π Electron Systems

	Intact[a]	Protonated[b]	Difference[c]	Protonated	Difference
Naphthalene (**12**)		α-Protonation		β-Protonation	
E	−382.810012	−0.286775	−13	−0.280042	5
T	383.334234	0.520290	38	0.518230	33
V	−766.144246	−0.807065	−51	−0.798272	−28
α,ω-Diaminoheptamethinium ion (**10**)		β-Protonation		δ-Protonation	
E	−379.612764	−0.169398	295	−0.176990	275
T	380.035021	0.423839	−215	0.427294	−206
V	−759.647785	−0.593237	510	−0.604284	481
α,ω-Dihydroxyheptamethinium ion (**11**)		β-Protonation		δ-Protonation	
E	−419.155002	−0.127994	404	−0.139094	375
T	419.492695	0.371604	−352	0.387287	−311
V	−838.647697	−0.499597	756	−0.526381	686
Decapentaene (**13**)		C_5-Protonation			
E	−385.036761	−0.282039			
T	385.549432	0.505638			
V	−770.586193	−0.787677			

a) By 4-31G in terms of au. b) Difference from the intact structure. c) Difference from the decapentaene system (kJ mol^{-1}).

two basic phenomenological preconditions of maximum resonance stabilization of chain-shaped molecules,[8,9] i.e., not only certain charge alternation but also maximum bond order equalization.

The authors acknowledge Y. Ebisawa for her technical assistance. The GAUSSIAN 80H program (a HITAC version of GAUSSIAN 80[21]) was used at the Computer Center of the University of Tokyo. The research was financially supported by the Ministry of Education, Science and Culture (Grand-in-Aid for Developmental Scientific Research No. 63540352).

References

1) R. Robinson, *Tetrahedron*, **3**, 323 (1958).
2) J. Aihara, *Bull. Chem. Soc. Jpn.*, **56**, 1935 (1983).
3) By Hückel MO methods: a) R. Breslow and E. Mohasci, *J. Am. Chem. Soc.*, **85**, 431 (1963). b) B. A. Hess, Jr. and L. J. Schaad, *J. Am. Chem. Soc.*, **93**, 302 (1983).
4) By a PPP (Pariser-Parr-Pople) MO method: M. J. S. Dewar and C. de Llano, *J. Am. Chem. Soc.*, **91**, 789 (1969).
5) By ab initio MO methods: a) R. C. Haddon and J. Starnes, *J. Adv. Chem. Ser. A*, **No. 169**, 333 (1978). b) B. A. Hess, Jr. and L. J. Schaad, *J. Am. Chem. Soc.*, **105**, 7500 (1983). c) H. Ichikawa and Y. Ebisawa, *J. Am. Chem. Soc.*, **107**, 1161 (1985).
6) H.-E. Nikolajewski, S. Daehne, B. Hirsch, and E.-A. Jauer, *Angew. Chem., Int. Ed. Engl.*, **5**, 1044 (1966).
7) D. Lloyd and E. R. Marshall, *Chem. Ind. (London)*, **1964**, 1760; *Angew. Chem., Int. Ed. Engl.*, **11**, 404 (1972).
8) a) S. Daehne, *Z. Chem. (Leipzig)*, **5**, 441 (1965). b) S. Daehne and D. Leupold, *Ber. Bunsenges. Phys. Chem.*, **70**, 618 (1966). c) S. Daehne, *Science*, **199**, 1163 (1978).
9) a) J. Fabian and H. Hartmann, *Theoret. Chim. Acta*, **36**, 351 (1975). b) J. Fabian and H. Hartmann, *J. Mol. Struct.*, **27**, 67 (1975).
10) D. Lloyd, H. P. Cleghorn, and D. R. Marshall, *Adv. Heterocycl. Chem.*, **17**, 1 (1974).
11) J. Kucera and Z. Arnold, *Collect. Czech. Chem. Commun.*, **32**, 1704 (1967).
12) J. P. Collman, *Angew. Chem., Int. Ed. Engl.*, **4**, 132 (1965).
13) a) J. Aihara, *J. Am. Chem. Soc.*, **98**, 2750 (1976). b) M. Milun, I. Gutman, and N. Trinajstić, *J. Am. Chem. Soc.*, **99**, 1692 (1977).
14) J. Aihara, *Bull. Chem. Soc. Jpn.*, **60**, 2268 (1987).
15) J. Klein, *Tetrahedron*, **44**, 503 (1988).
16) B. M. Gimarc, *J. Am. Chem. Soc.*, **105**, 1979 (1983).
17) M. Born and J. R. Oppenheimer, *Ann. Phys.*, **84**, 475 (1927).
18) a) H. Ichikawa, Y. Ebisawa, and A. Shigihara, *J. Phys. Chem.*, **92**, 1440 (1988). b) H. Ichikawa, Y. Ebisawa, and K. Sameshima, *Bull. Chem. Soc. Jpn.*, **61**, 659 (1988). c) H. Ichikawa and A. Shigihara, *Bull. Chem. Soc. Jpn.*, **61**, 1837 (1988). See also Ref. 5c.
19) W. J. Hehre, R. Ditchfield, and J. A. Pople, *J. Chem. Phys.*, **56**, 2257 (1972).
20) R. Ditchfield, W. J. Hehre, and J. A. Pople, *J. Chem. Phys.*, **54**, 724 (1971).
21) *QCPE* No. 437 (1982).

 © 1989 The Chemical Society of Japan Bull. Chem. Soc. Jpn., 62, 2802—2806 (1989) [Vol. 62, No. 9

Kinetics and Mechanism of the Substitution of β-Diketonates for Acetylacetonate in Bis(acetylacetonato)(trimethyl phosphate)-dioxouranium(VI)

Yoshiko UDAGAWA, Hiroshi TOMIYASU,* Woo-Sik JUNG,†
Tae Yoon EOM,† and Hiroshi FUKUTOMI††
Research Laboratory for Nuclear Reactors, Tokyo Institute of Technology, O-okayama, Meguro-ku, Tokyo 152
(Received March 1, 1989)

Kinetics of the substitution of β-diketonates for one acetylacetonate in $UO_2(acac)_2tmp$ (acac= acetylacetonate, tmp=trimethyl phosphate) has been studied in tmp by spectrophotometric methods. The reactions proceed through intermediate complexes $UO_2(acac)_2HB$, where HB denotes various β-diketones. The formation of the intermediates are followed by intramolecular proton transfer processes from coordinated HB to one of two acac in $UO_2(acac)_2HB$. The proton-transfer step for various HB can be classified into two groups owing to the difference in the values of rate constants k_2, i.e. the substitutions of Hbza, Hhpd, and Hdbm and those of Hbta, Htta, and Htfa, k_2 of the former group giving the order of $10^{-3}\,s^{-1}$, while that of the latter the order of $10^{-1}\,s^{-1}$, at 25 °C, where Hbza=benzoylacetone, Hhpd=3,5-heptanedione, Hdbm=dibezoylmethane, Hbta=benzoyltrifluoroacetone, Htta=2-thenoyltrifluoroacetone, and Htfa=trifluoroacetylacetone. This can be well explained in view of the acidity of β-diketones. The addition of amphiprotic solvents, such as water and alcohols, accelerates the substitution rates, and the observed first-order rate constant k_{obsd} is expressed by $k_{obsd}=k_2+k_c[solvent]$. In the case of the addition of alcohols, k_c increases in the order: *n*-BuOH<*i*-PrOH<*n*-PrOH<EtOH<MeOH. This is the reverse order of autoprotolysis constants of these alcohols. Kinetic isotope effects k_c^H/k_c^D for the substitution of Hbza in tmp in the presence of H_2O (or D_2O) and CH_3OH (or CH_3OD) were determined to be 2.5 and 1.8, respectively.

In a previous paper,[1] we reported the kinetics of the substitution of dibenzoylmethanate for one acac in $UO_2(acac)_2L$, where L denotes dmso (dimethyl sulfoxide), dmf (*N*,*N*-dimethylformamide) and tmp, and proposed that the reaction started with the formation of an intermediate complex $UO_2(acac)_2Hdbm$, followed by a relatively slow proton-transfer process from coordinated Hdbm to acac. A similar proton-transfer process was also found to control the rates of β-diketonate exchange reactions in U(IV) and Th(IV) complexes.[2-4] However, the rates of these exchange reactions are much faster than those of β-diketonates in dioxouranium(VI) in spite of the similarity of the reaction mechanism.

This paper presents further information on the kinetics of the substitutions of various β-diketonates for acac in $UO_2(acac)_2tmp$. The reaction can be expressed by:

$$UO_2(acac)_2tmp + \beta\text{-diketone} \xrightarrow[\text{in tmp}]{} UO_2(acac)(\beta\text{-diketonato})tmp + Hacac.$$

The effect of water and alcohols on the rates of substitution and the kinetic isotope effects were also investigated. The kinetic results are compared with those of the previous paper.[1]

† Present address: Korea Advanced Energy Research Institute, Chung-Nam, Korea.

†† Present address: Department of Chemistry, Okayama University, Tsushimanaka, Okayama 700.

Experimental

The complex $UO_2(acac)_2tmp$ was synthesized by the same method as described previously.[1] Hacac and tmp were distilled under reduced pressure, and Hbza and Htta were recrystallized from ethanol and methanol, respectively, and dried under vacuum before use. Htfa, Hhpd, and Hbta were used without further purification. Methanol, ethanol, propanol, 2-propanol, and butanol were dried over 3- or 4-A Molecular Sieves. Merck 99.8 atom% deuterium oxide and 98 atom% methanol-d_1 were used. The water content of the solvent was below 5×10^{-3} M (M=mol dm^{-3}) as determined by Karl-Fisher titration after each kinetic run, and this degree of water content has no significant influence on the reaction rates.

The kinetic measurements were carried out on a JASCO UNIDEC-505 spectrophotometer with thermostated cell compartments (±0.2 °C) and 1-cm quartz cells for slow reaction or a Union Giken RA-401 stopped-flow spectrophotometer for fast reactions. The kinetic experiments were done under pseudo-first-order conditions ($[UO_2(acac)_2tmp]\gg[\beta\text{-diketone}]$). The rate of the replacement of one coordinated acac in $UO_2(acac)_2tmp$ was given by $k_{obsd}[\beta\text{-diketone}]_{enol}$, where $[\beta\text{-diketone}]_{enol}$ refers to the concentration of β-diketone in the enol form and k_{obsd} refers to the rate constant for the substitution of each acac. The pseudo-first-order rate constant k_{app} was determined from the slope in plots of $\ln(A_f-A_t)$ versus time t, where A_t and A_f are absorbances at time t and infinity, respectively at the wavelength 440 nm which gives the largest absorption change by the ligand substitution. Since $UO_2(acac)_2tmp$ involves two acac molecules, each suffering the substitution in an equal probability, k_{obsd} is the half of k_{app}. Kinetic runs were performed at least twice.

Results and Discussion

Figure 1 shows that k_{obsd} for the substitution of Hbza for acac in $UO_2(acac)_2tmp$ are independent of the concentrations of complex $[UO_2(acac)_2tmp]$. The values of k_{obsd} at various temperatures are given in Table 1. For the substitution of Htta, k_{obsd} increases linearly with $[UO_2(acac)_2tmp]$ in the low region of $[UO_2(acac)_2tmp]$, but tends to saturate in the high region. However, as seen in Fig. 2, plots of $1/k_{obsd}$ against

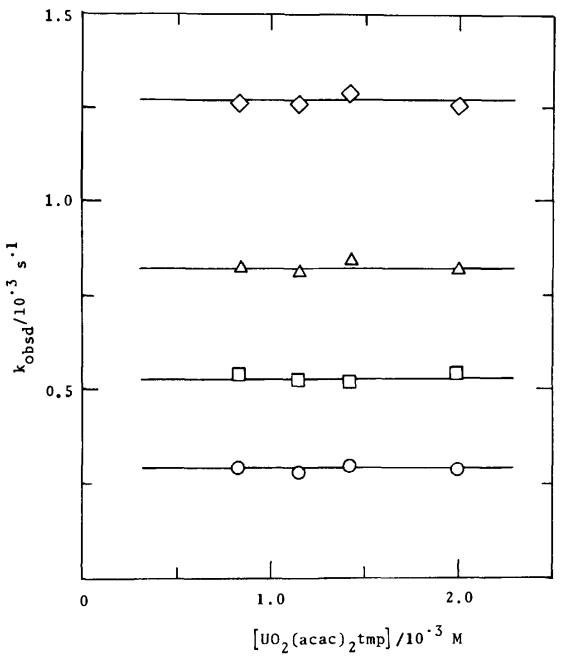

Fig. 1. Plots of k_{obsd} versus $[UO_2(acac)_2tmp]$ for the substitution of Hbza for acac in $UO_2(acac)_2tmp$: (○) 20°C; (□) 24°C; (△) 28°C; (◇) 32°C.

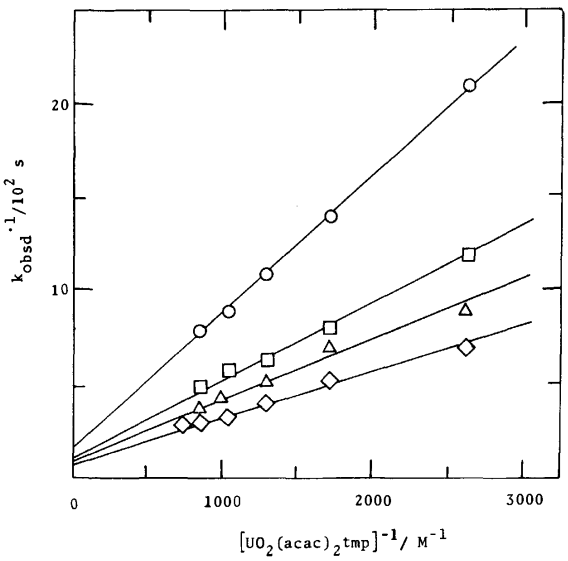

Fig. 2. Plots of $1/k_{obsd}$ versus $1/[UO_2(acac)_2tmp]$ for the substitution of Htta for acac in $UO_2(acac)_2tmp$: (○) 20°C; (□) 24°C; (△) 25°C; (◇) 28°C.

Table 1. Kinetic Data for the Substitution of β-Diketonates for acac in $UO_2(acac)_2tmp$

β-Diketonate	Parameter	Rate or equilibrium constants					ΔH^*	ΔS^*
		20°C	24°C	25°C	28°C	32°C	kJ mol^{-1}	J K^{-1} mol^{-1}
bza	$k_2/10^{-4}$ s^{-1}	2.94±0.21	5.30±0.25		8.20±0.25	12.7±0.3	87.3±4.6	−14.3±15.4
tta	q^{-1} or $k_2/10^{-2}$ s^{-1}	6.65±1.05	7.75±1.95	8.80±2.30	11.7±4.1		48.7±10.0	−102±33
	(q/r) or K_1/M^{-1}	209 ±25	324 ±42	367 ±92	352 ±27			

Table 2. Kinetic Data for the Substitution of β-Diketonates for acac in $UO_2(acac)_2tmp$ at 25 °C

Substitution of tfa		Substitution of hpd		Substitution of bta	
$[UO_2(acac)_2tmp]$	k_{obsd}	$[UO_2(acac)_2tmp]$	k_{obsd}	$[UO_2(acac)_2tmp]$	k_{obsd}
10^{-3} M	10^{-2} s^{-1}	10^{-3} M	10^{-4} s^{-1}	10^{-3} M	10^{-2} s^{-1}
0.384	3.04	1.00	5.70	1.00	5.90
0.574	3.81	2.00	7.95	1.69	6.05
0.768	4.37	2.50	8.50	1.87	6.25
0.958	5.75	4.00	8.65	2.50	7.00
1.00	5.65	5.00	9.15	4.00	7.05
1.69	6.45			5.00	7.20
4.00	8.56	$k_2=(1.11\pm0.06)\times10^{-3}$ s^{-1}		$k_2=(7.55\pm0.04)\times10^{-2}$ s^{-1}	
$k_2=(1.25\pm0.22)\times10^{-1}$ s^{-1}		$K_1=(1.09\pm0.05)\times10^{-3}$ M^{-1}		$K_1=(3.15\pm0.05)\times10^{-3}$ M^{-1}	
$K_1=(7.76\pm0.37)\times10^{-2}$ M^{-1}					

$1/[UO_2(acac)_2tmp]$ give straight lines with intercepts yielding the expression:

$$1/k_{obsd} = q + r/[UO_2(acac)_2tmp] \quad (1)$$

where q and r are constants. The same tendency was observed for the substitutions of Htfa, Hhta, and Hhpd. The data are summarized in Table 2 with the values of q and r.

The results in the present study can be well-explained by a mechanism (Fig. 3) proposed in the previous paper.[1] In this mechanism, the reaction is initiated with the fast equilibrium between UO_2-$(acac)_2tmp$ (**I**) and β-diketone in the enol form HB,[5] followed by the intramolecular proton-transfer process from coordinated HB to one of two chelated acac. According to the neutron diffraction study on UO_2-$(acac)_2Hacac$,[6] Hacac is coordinated to uranium atom via a keto oxygen atom, and the plane of Hacac is located at 32.5 °C to the pentagonal equatorial plane. The structure of intermediate **II** could be similar to that of $UO_2(acac)_2Hacac$. Based on the above mechanism, assuming that the proton-transfer process (k_2 path) is the rate-determining step, k_{obsd} is given by

$$k_{obsd} = k_2K_1[UO_2(acac)_2tmp]/(1 + K_1[UO_2(acac)_2tmp] \quad (2a)$$

or

$$k_{obsd}^{-1} = 1/k_2 + 1/(k_2K_1[UO_2(acac)_2tmp]) \quad (2b)$$

where $K_1=[UO_2(acac)_2HB]/([UO_2(acac)_2tmp][HB])$. In the limiting case $K_1[UO_2(acac)_2tmp]\gg1$, Eq. 2a can be simplified as $k_{obsd}=k_2$, i.e. k_{obsd} is independent of $[UO_2(acac)_2tmp]$. This is the case for the substitution of Hbza. Equation 2b is basically the same as Eq. 1, and parameters k_2 and K_1 are determined by these equations for the substitutions of Htta, Htfa, Hhpd, and Hbta. The results are listed in Tables 1 and 2. In these tables, the substitutions of HB can be classified into two groups owing to the difference of k_2 values: one is the substitutions of Hbza and Hhpd, and the other those of Htta, Htfa, and Htfa, k_2 of these groups being the order of 10^{-3} and 10^{-1} s^{-1}, respectively. The substitution of Hdbm[1] belongs to the former group. Since the k_2 path corresponds to the proton-transfer process from HB to coordinated acac, it is likely that k_2 increases with increasing acidity of HB. The acidity of HB was evaluated from data of pK_a in water-dioxane mixture (75 wt% dioxane) at 30 °C,[7,8] because pK_a of HB was not available in tmp. The values of k_2 at 25 °C and pK_a of HB are summarized in Table 3. In this table the pK_a values are considerably smaller, i.e. HB is more acidic, in the latter group. These facts indicate that the acidity of HB plays an important role for the k_2 process.

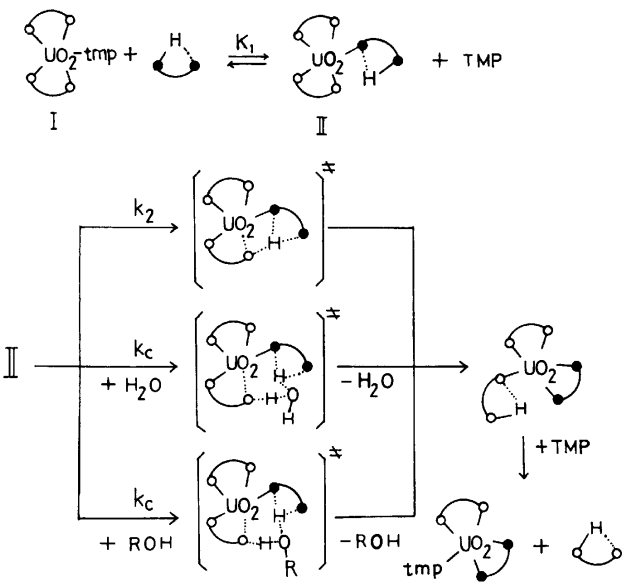

Fig. 3. Possible mechanism of the substitution of β-diketonates for acac in $UO_2(acac)_2tmp$ in tmp. HO⌒O and H●⌒● represent Hacac and β-diketone in the enol form, respectively.

In order to examine the steric hindrance of entering HB for the substitution rate, the substitution of Hbza is compared with that of Hdbm, because Hdbm is

Table 3. Rate Constants k_2 for the Substitution of β-Diketonates for acac in $UO_2(acac)_2tmp$ at 25 °C and pK_a of β-Diketones

β-Diketone	Hbza	Hhpd	Hdbm[a]	Hbta	Htta	Htfa
k_2/s^{-1}	5.66×10^{-4}[b]	1.11×10^{-3}	2.31×10^{-3}	7.55×10^{-2}	8.80×10^{-2}	1.25×10^{-1}
pK_a[c]	12.85	13.7[d]	13.75	9.2	9.1	8.7

a) Ref. 1. b) Calibrated at 25 °C. c) In water-dioxane mixture (75 wt% dioxane) at 30 °C. d) Ref. 7.

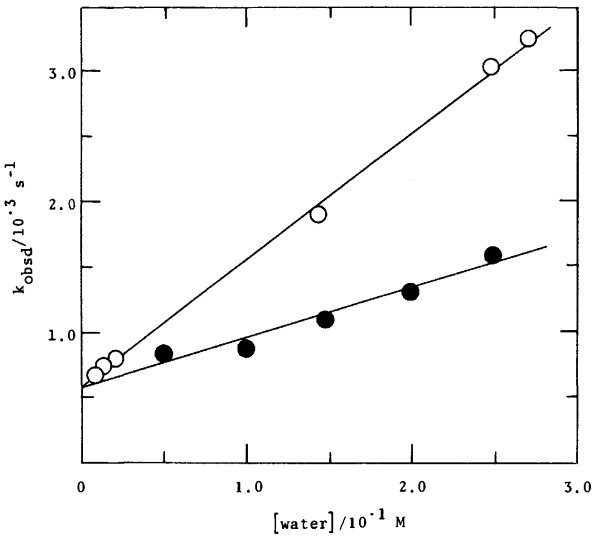

Fig. 4. Plots of k_{obsd} versus [Water] for the substitution of Hbza for acac in $UO_2(acac)_2tmp$ at 25 °C: (○) H_2O; (●) D_2O.

much bulkier in size than Hbza and their pK_a values are similar. In Table 1, k_2 for Hbza is 5.30×10^{-4} s^{-1} at 24 °C, while 2.19×10^{-3} s^{-1} for Hdbm at the same temperature.[1] The results that the rate is even faster for the substitution of the bulkier ligand suggest that the steric hindrance is of no significant effect.

The effect of adding water (<0.3 M) and various alcohols (<0.05 M) on the rates was investigated for the substitution of Hbza. As seen in Fig. 4, k_{obsd} increases linearly with the concentration of H_2O (D_2O). The similar linearlity was also found for all alcohols studied. Therefore, k_{obsd} can be expressed by:

$$k_{obsd} = k_2 + k_c[S] \quad (3)$$

where [S] denotes the concentrations of water and alcohols. The second-order rate constant k_c is listed in Table 4, together with the autoprotolysis constant pK_{auto}. In the case of the addition of alcohols, k_c shows a tendency to decrease with increasing pK_{auto}. This suggests that the k_c process in Fig. 3 is related to the amphiprotic property of alcohols, i.e. the ability of acting as a proton-donor and -acceptor through hydrogen bonding with intermediate **II**. Since K_{auto} is the product of the acidity constant ($ROH=RO^-+H^+$) and the constant for proton accepting equilibrium ($ROH+H^+=ROH_2^{2+}$) expressed by: $K_{auto}=[RO^-][ROH_2^{2+}]$, the role of each individual property of proton-donating or -accepting for the k_c process can not be determined strictly from these data. If the acceptor number[14] is allowed to estimate the acid strength for prototype acids, the acidity of alcohols decreases in the order: MeOH>EtOH>*i*-PrOH, e.g. as a mutter of fact, pK_a of MeOH and EtOH are 16.68 and 18.88, respectively,[9] indicating that the ability of proton donating of alcohols appears to be important. Water seems to behave differently, because the geometric configuration of intermediate II involving water differs from that of the intermediate involving alcohols.

Table 4. Influence of Water and Alcohols on the Rate of the Substitution of bza for acac in $UO_2(acac)_2tmp$ at 25 °C

ROH	k_c / 10^{-2} M^{-1} s^{-1}	pK_{auto}[a] (25 °C)
H_2O	0.99±0.02	14.00
D_2O	0.39±0.06	14.96
MeOH	2.54±0.36	16.7
MeOD	1.42±0.12	
EtOH	2.26±0.10	18.9
n-PrOH	1.08±0.04	19.4
i-PrOH	0.71±0.04	20.8
n-BuOH	0.71±0.03	21.6[b]

a) Ref. 9. b) Ref. 13.

The replacement of adding H_2O and CH_3OH by D_2O and CH_3OD lowers the k_c values (Table 4) and the kinetic isotope effects k_c^H/k_c^D for H_2O/D_2O and CH_3OH/CD_3OD are determined to be 2.5 and 1.8, respectively. These values are substantially small compared with the direct proton transfer in the acac-exchange reaction.[11] Since proton transfers proceed from entering HB to leaving acac through water or alcohols, this indirect proton transfer might reduce the isotope effect in the presence of these amphiprotic solvents, particularly in such cases where proton-donor and -acceptor atoms are unsymmetrically located. This is experimentally evidenced by the fact that the smaller the difference in the acidity between two acids, HX and HY, (i.e. the more symmetrical the transition state) the larger the kinetic isotope effect for the proton-transfer reaction X^- and HY or Y^- and HX.[10]

The activation parameters of the k_2 path for the various β-diketonates are listed in Table 5. Although

Table 5. Activation Parameters for the Proton-Transfer Rate Constant in the Substitution of β-Diketonates for acac in $UO_2(acac)_2L$

	β-Diketonate	L	Solvent	ΔH^* / kJ mol^{-1}	ΔS^* / J K^{-1} mol^{-1}	Ref.
1.	dbm	dmf[a)]	dmf[a)]	31.3	−177	1
2.	dbm	tmp	tmp	50.2	−127	1
3.	dbm	tmp	tmp-nm[b)]	63.4	−77.4	1
4.	bza	tmp	tmp	87.3	−14.3	This work
5.	tta	tmp	tmp	48.7	−102	This work

a) *N*,*N*-Dimethylformamide. b) tmp–nitromethane (1:1, v/v) mixture.

there is no consistency in ΔH^* in a series of the substitutions, the change in k_2 is relatively small. This is attributed to the compensation effect[12] between ΔH^* and ΔS^*, which might be resulted from the polarization of intermediate **II** as acac···$H^{\delta+}$–$B^{\delta-}$, i.e. the larger polarization could reduce the ΔH^* values because of the weakened HB bonds and could make ΔS^* more negative as well owing to an increase of solvation towards the intermediate.

This work is partly supported by a Grant-in-Aid for General Scientific Research No. 62470039 from the Ministry of Education, Science and Culture.

References

1) W.-S. Jung, H. Tomiyasu, and H. Fukutomi, *Inorg. Chem.*, **25**, 2582 (1986).
2) N. Fujiwara, H. Tomiyasu, and H. Fukutomi, *Bull. Chem. Soc. Jpn.*, **57**, 1576 (1984).
3) N. Fujiwara, H. Tomiyasu, and H. Fukutomi, *Bull. Chem. Soc. Jpn.*, **58**, 1386 (1985).
4) H. Fukutomi, H. Ohno, and H. Tomiyasu, *Bull. Chem. Soc. Jpn.*, **59**, 2303 (1986).
5) Y. Ikeda, H. Tomiyasu, and H. Fukutomi, *Bull. Chem. Soc. Jpn.*, **56**, 1060 (1983).
6) M. Lenner, *Acta Crystallogr., Sect. B*, **32**, 2396 (1979).
7) a) L. G. Van Uitert, C. G. Haas, W. C. Fernelius, and B. E. Douglas, *J. Am. Chem. Soc.*, **75**, 455 (1953); b) L. G. Van Uitert, W. C. Fernelius, and F. B. Douglas, *J. Am. Chem. Soc.*, **75**, 457 (1953); c) J. L. Ault, H. J. Harries, and J. Burgess, *J. Chem. Soc., Dalton Trans.*, **1973**, 1095.
8) According to Ref. 7a and 7b, an approximately linear relationship exists between the pK_a value of β-diketone and the mole fraction of dioxane in water–dioxane mixture, i.e. $pK_a=p+qn_2$ (p and q are constants and n_2 is a mole fraction). The pK_a value of Hhpb at $n_2=0.38$ was estimated by using the pK_a value (11.2) at $n_2=0.17$ and assuming that the q value of Hhpd is equal to that of Hacac (11.6) (Ref. 7a).
9) J. F. Coetzee and C. D. Ritchie, "Solute-Solute Interactions," Marcel Dekker, New York (1969).
10) R. P. Bell, "The Proton in Chemistry," Chapman and Hall, London (1973), Chap. 12.
11) Y. Hatakeyama, H. Kido, M. Harada, H. Tomiyasu, and H. Fukutomi, *Inorg. Chem.*, **27**, 992 (1988).
12) K. J. Laidler, "Chemical Kinetics," McGraw-Hill, London (1965).
13) C. Reichardt, "Solvent Effects in Organic Chemistry," Verlag Chemie, Weinheim (1979).
14) V. Gutmann, "The Donor-Acceptor Approach to Molecular Interactions," Plenum Press, New York (1978).

 © 1989 The Chemical Society of Japan Bull. Chem. Soc. Jpn., 62, 2807—2818 (1989)

An X-Ray Diffraction Study on the Stucture of 18-Crown-6 Ether Complexes with Alkali Metal Ions in Aqueous Solution

Kazuhiko OZUTSUMI,§ Masahiko NATSUHARA,† and Hitoshi OHTAKI*
Coordination Chemistry Laboratories, Institute for Molecular Science, Myodaiji, Okazaki 444
†Department of Electronic Chemistry, Tokyo Institute of Technology at Nagatsuta, Nagatsuta-cho 4259, Midori-ku, Yokohama 227
(Received April 14, 1989)

The structure of 1,4,7,10,13,16-hexaoxacyclooctadecane (18-crown-6) and its complexes with alkali metal ions in aqueous solution has been investigated by X-ray diffraction and Raman spectroscopic methods at 25 °C. The X-ray scattering data and Raman spectrum for an aqueous 18-crown-6 solution show that free 18-crown-6 has a conformation of C_i or D_{3d} symmetry. The molecule seems to be flexible and may be present as a mixture of the two conformations in aqueous solution. The structure of the lithium complex was not conclusive because of a weak scattering power of lithium atoms and weak complex formation between lithium ion and 18-crown-6. The sodium 18-crown-6 complex is estimated to have a structure similar to that found in crystal. The 18-crown-6 ring within the complex adopts the C_i conformation, where five oxygen atoms within 18-crown-6 coordinate to sodium ion at the equatorial position and an oxygen atom within 18-crown-6 and a water molecule at the axial one. The structure of the potassium complex is also similar to that in crystal in which the D_{3d} conformation is taken. Potassium ion is located at the center of the mean plane of 18-crown-6 and one or two water molecules solvate potassium ion above and/or below the plane of 18-crown-6. It is suggested that the structure of the caesium complex is with either C_i or D_{3d} symmetry, where caesium ion is apart from the mean plane of 18-crown-6. The rubidium complex was not examined because of a strong fluorescent X-ray emission from rubidium atoms when studied. The 18-crown-6 ring in the sodium and potiassium complexes is rather rigid probably because the cavity of the ring well fits to the metal ions, while the ring coordinating to large caesium ion becomes more flexible than that in the sodium and potassium complexes due to weaker interaction with caesium ion.

Synthetic macrocyclic polyethers (crown ethers) can be good model compounds of ionophores such as nonactin and valinomycin in biological systems because of the similarity in structure and ion selectivity. Metal complexes with polyethers are also useful in organic syntheses since they increase the nucleophilic reactivity of halide ions by solubilizing metal halides in many organic solvents. In these respects, complexation equilibria of metal ions with crown ethers have extensively been investigated in various solvents.[1] Many complexes with crown ethers have also been isolated and their structures in crystal have been determined.[2]

It has been found that the conformational change of valinomycin occurs in the course of complexation with potassium ion in methanol.[3] Crown ethers seem to be similarly flexible in solution and thus the structure determined in crystal may sometimes be different from that in solution. The flexibility of the crown ring may play an important role in the complexation with metal ions. However, thermodynamic quantities of crown ether complexes in solution have been interpreted on the basis of their structures in crystal because of insufficient structural information of the complexes in solution. It has also been shown that the stability constants of crown ether complexes are strongly dependent on properties of solvents.[1] Solvation of the complexes is also an important factor for the stability and reactivity of the complexes as well as the conformation of the ring structure in solution. Thus, we aimed at determining the structure of 1,4,7,10,13,16-hexaoxacyclooctadecane (18-crown-6) complexes with alkali metal ions, as well as the structure of the free ligand, in aqueous solution by employing X-ray diffraction and Raman spectroscopic methods in order to obtain more direct structural information in solution.

The structure of 18-crown-6[4] and its 1:1 complexes with monovalent cations[5-13] has been determined in crystal. Two ring oxygen atoms and two water molecules coordinate to lithium ion in the $LiClO_4 \cdot$(18-crown-6)$\cdot 2H_2O$ crystal.[13] Other cations are all coordinated with six oxygen atoms within 18-crown-6 and the seventh and/or eighth coordination sites of metal ions are occupied by anions in most complexes in crystal. The sites may, however, be occupied by solvent molecules in solution.

The most stable conformation of free 18-crown-6 in an isolated state was evaluated to be the one with C_i symmetry from a molecular mechanical study,[14] and the conformation has also been found in the 18-crown-6 crystal.[4] On the other hand, in aqueous solution the most stable conformation is proposed to be with D_{3d} symmetry by the Monte Carlo simulation.[15] The different structures of the 18-crown-6 ether in solution and in crystal are due to solvation of the compound with water molecules in the former. The C_i conformation was found in the NaSCN–18-crown-6 complex in crystal[7] and the D_{3d} conformation was observed in other 18-crown-6 complexes with monovalent cations including lithium ion.[5,6,8-13] The most

§ Present address: Department of Chemistry, The University of Tsukuba, Tsukuba, Ibaraki 305.

Table 1. Structure of 18-Crown-6 and Its Complexes with Alkali Metal Ions Estimated by Various Methods

Form	Method	Free ligand	Lithium complex	Sodium complex	Potassium complex	Caesium complex
Crystal[a]	X-Ray	C_i	D_{3d}	C_1	D_{3d}	D_{3d}
Methanol[b] solution	Raman	D_{3d}	—	D_{3d}	D_{3d}	D_{3d}
Isolated[c] molecule	Molecular mechanics	C_i	—	C_1	D_{3d}	D_{3d}
Aqueous[d] solution	Monte Carlo simulation	D_{3d}	—	—	—	—

a) Refs. 4, 7, 8, 12, and 13. b) Ref. 18. c) Ref. 14. d) Ref. 15.

Table 2. Composition (mol dm^{-3}), Stoichiometric Volumes V, and Densities ρ of the Sample Solutions

	A	B (M=Li)	C (M=Li)	D (M=Na)	E (M=K)	F (M=Cs)
MCl	—	1.503	1.996	2.023	1.942	1.508
18C6	2.007	1.805	2.105	2.213	1.991	1.832
H_2O	30.76	31.65	27.37	25.28	26.97	29.08
ρ/g cm^{-3}	1.085	1.111	1.134	1.159	1.157	1.262
$V/10^9$ pm^3	0.8272	1.105	0.8320	0.8208	0.8551	1.101
C_{18C6}/C_M	—	1.201	1.055	1.094	1.025	1.215

stable conformation of 18-crown-6 within the sodium and potassium complexes in an isolated state without any hydrated water molecules was found to be C_1 and D_{3d}, respectively, by the molecular mechanical calculations.[14] It is suggested that the D_{3d} conformation is more stable than the C_1 conformation in the potassium complex with two water molecules coordinating to metal ions, while the energy difference between the C_1 and D_{3d} conformations was very small in the sodium complex according to the same method.[14] Thus it is seen that the solvation of 18-crown-6 greatly affects its conformation in solution. The structures of free 18-crown-6 and the complexes in various states reported so far by employing different methods are summarized in Table 1.

Although the conformation of 18-crown-6 in solution has so far been investigated by the dipole moment[16] and Raman spectral measurements,[17,18] no direct structual data of the solvated complexes have been given. An EXAFS measurement for the rubidium complex in solution has been carried out,[19] but the structure analysis is still incomplete. In the present paper we report the structural data of 18-crown-6 complexes with alkali metal ions, except rubidium ion, in aqueous solution studied by the X-ray diffraction method in order to obtain information on both conformation and solvation of the complexes. The structure of the rubidium complex was not determinable by the present method because of a strong fluorescent X-ray radiation. Raman spectroscopic measurements were also carried out to obtain additional information of the structure of the complexes.

Experimental

Preparation of Sample Solutions. NISSO 18-crown-6 (99%) was used without further purification and dried at room temperature under a reduced pressure. Alkali chlorides of reagent grade were recrystallized once from water.

Six sample solutions were prepared for the X-ray diffraction measurements. Solution A was an aqueous 18-crown-6 solution. Solutions B through F were prepared by dissolving alkali chlorides and 18-crown-6 in water. Concentrations of chloride ions in the test solutions were gravimetrically determined as AgCl. Concentrations of alkali metal ions in the solutions were evaluated from the stoichiometry of the salts used. Concentrations of 18-crown-6 were calculated from the weighted amounts of 18-crown-6. Densities of the solutions were measured by using pycnometer. The composition of the solutions is listed in Table 2.

X-Ray Scattering Measurements. X-Ray scattering measurements were performed on a JEOL θ-θ type diffractometer by using Mo $K\alpha$ radiation (λ=71.07 pm). The method of measurements and data treatments were described elsewhere.[20] The accessible range of scattering angle 2θ was from 2° to 140°, which corresponded to the scattering variable s ($=4\pi\lambda^{-1}\sin\theta$) range of 0.3×10^{-2} to 16.6×10^{-2} pm^{-1}. Times required to accumulate 80000 counts were recorded at each angle of 2θ and the measurement was repeated three times over the whole angle range.

The reduced intensities $i(s)$ were obtained by subtracting independent coherent scatterings from the measured intensities $I(s)$ as follows:

$$i(s) = KI(s) - \sum_j n_j[\{f_j(s) + \Delta f_j'\}^2 + (\Delta f_j'')^2], \quad (1)$$

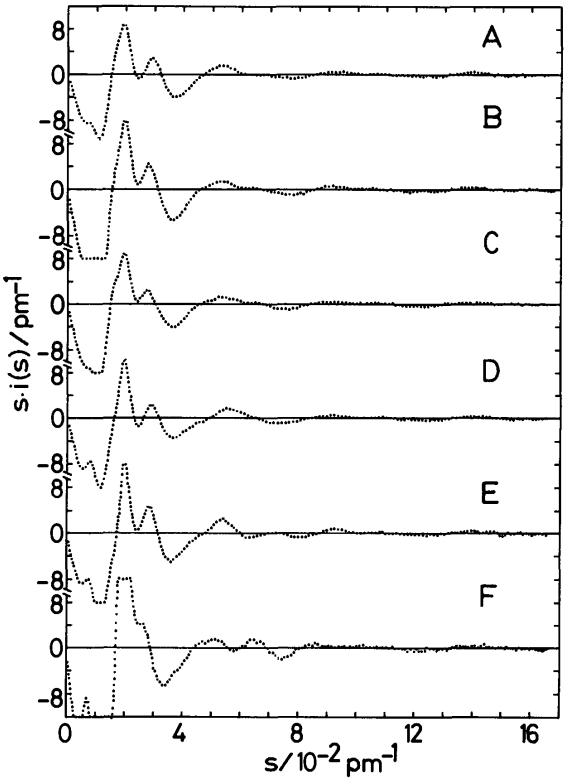

Fig. 1. The reduced intensities multiplied by s for solutions A through F.

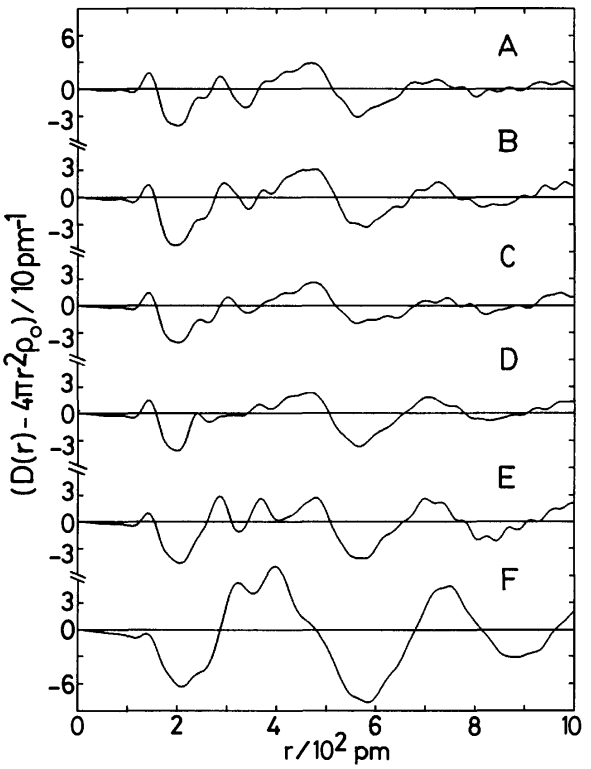

Fig. 2. The differential radial distribution curves, $D(r)-4\pi r^2\rho_0$, for solutions A through F.

where K stands for a normalization factor of the measured intensities to the absolute ones. n_j is the number of atom j in a stoichiometric volume V of the test solutions. $f_j(s)$ represents the atomic scattering factor at s, and $\Delta f_j'$ and $\Delta f_j''$ denote the real and imaginary parts of anomalous dispersion, respectively, of atom j. The reduced intensities multiplied by s for the sample solutions are shown in Fig. 1.

The radial distribution function $D(r)$ was calculated by the Fourier transform of the reduced intensities according to Eq. 2:

$$D(r) = 4\pi r^2 \rho_0 + \frac{2r}{\pi}\int_0^{s_{max}} s\cdot i(s)\cdot M(s)\cdot \sin(rs)\mathrm{d}s, \quad (2)$$

where ρ_0 ($=\{\sum n_j\cdot f_j(0)\}^2/V$) is the average scattering density in a stoichiometric volume of the sample solution and s_{max} represents the maximum s-value attained in the measurement ($s_{max}=16.6\times10^{-2}$ pm^{-1}). The modification function $M(s)$ is given as

$$M(s) = \frac{\sum_j n_j\{(f_j(0)+\Delta f_j')^2+(\Delta f_j'')^2\}}{\sum_j n_j\{(f_j(s)+\Delta f_j')^2+(\Delta f_j'')^2\}}\cdot\exp(-ks^2). \quad (3)$$

The damping factor k was chosen as 100 pm^2 in the present case. The $(D(r)-4\pi r^2\rho_0)$ curves for the test solutions are depicted in Fig. 2.

A least-squares calculation for the refinement of the structure parameters was applied to the reduced intensities so as to minimize the error-square sum U,

$$U = \sum_{s_{min}}^{s_{max}} s^2\{i(s)_{obsd} - i(s)_{calcd}\}^2. \quad (4)$$

The theoretical intensities $i(s)_{calcd}$ arising from the interatomic interactions in the solutions are obtained as follows:

$$i(s)_{calcd} = \sum_{\substack{p\\p\neq q}}\sum_{q} n_{pq}[\{f_p(s)+\Delta f_p'\}\{f_q(s)+\Delta f_q'\}+(\Delta f_p'')(\Delta f_q'')] \times \frac{\sin(r_{pq}s)}{r_{pq}s}\cdot\exp(-b_{pq}s^2), \quad (5)$$

where r_{pq}, b_{pq}, and n_{pq} represent the distance, the temperature factor, and the frequency factor of the atom-pair p-q, respectively.

All calculations were performed by using programs KURVLR[21] and NLPLSQ.[22]

Raman Spectroscopic Measurements. Raman spectra for solutions A through F were measured by JEOL JRS-400T laser Raman spectrophotometer equipped with an Ar^+ ion laser (Spectra-Physics Model 125 laser) using 514.5 nm excited line at the Instrumental Center of the Institute for Molecular Science.

Results and Discussion

Raman Spectra. Figure 3 shows the Raman spectra for solutions A through F. Conformations of C_i, C_1, and D_{3d} symmetry have been known for the 18-crown-6 ring in the crystalline state. The C_i and C_1 conformations have been found in the crystals of pure 18-crown-6 and the NaSCN–18-crown-6 complex, respectively.[4,7] The D_{3d} symmetry is observed in various metal complexes with 18-crown-6 in crys-

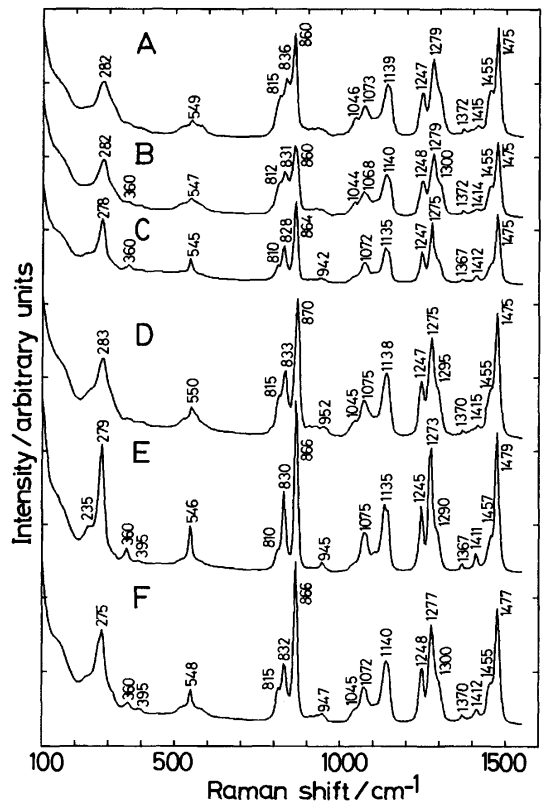

Fig. 3. The Raman spectra for solutions A through F.

tal.[5,6,8-13] The Raman spectrum of pure 18-crown-6 in the solid state which has the conformation of the C_i symmetry has been reported,[17,18] in which strong bands appeared at 271, 320, 415, 580, 824, 868, 892, and 988 cm^{-1}. However, the bands at 320, 415, 580, 824, 892, and 988 cm^{-1} are not observed in the spectrum of the solution sample of free 18-crown-6 (see Fig. 3). On the other hand, the band at 549 cm^{-1} observed for the solution sample is not seen in the spectrum of the crystal having the C_i conformation. No Raman spectroscopic data are available for pure 18-crown-6 with other conformations in the solid state and no direct comparison may be possible between the spectrum of free 18-crown-6 in Fig. 3 and those of metal complexes, because coordination of the ligating atoms of the crown ring to metal ions usually strongly influences vibrational modes of the ligand molecule. It is thus conclusive from the Raman spectra that 18-crown-6 in solution has not the conformation of the C_i symmetry and probably it takes either C_1 or D_{3d} symmetry, or is present as a mixture of the two. This result agrees with the conclusion of the C_i conformation which is the least stable in aqueous solution according to the Monte Carlo simulation for the conformation of 18-crown-6.[15]

The band at 550 cm^{-1} becomes sharper when an alkali metal ion is introduced in the ring (see Fig. 3,B—F).

Table 3. Interatomic Distances (r) below 500 pm and the Frequency Factors (n) of the Relevant Atom-Pairs within 18-Crown-6 of Different Conformations[a]

Interaction	r/pm C_i	C_1	D_{3d}	n
C-H (C_2-H_1)	106	106	106	24
C-O (C_2-O_1)	142	142	142	12
C-C (C_2-C_3)	151	151	151	6
O···H (O_1···H_1)	201	199	199	24
C···H (C_2···H_3)	209	206	205	24
C···O (C_3···O_1)	239	238	237	12
C···C (C_3···C_5)	236	238	235	6
O···H (O_4···H_1)	256	261	253	12
C···H (C_5···H_3)	265	268	258	24
O···O (O_1···O_4)	315	276	281	6
C···C (C_2···C_5)	356	350	366	12
C···O (C_5···O_1)	411	391	412	12
O···O (O_1···O_7)	522	423	485	6
C···C (C_2···C_6)	462	449	473	6
C···O (C_6···O_1)	488	453	499	12

a) The distances are averaged ones.

A composite band around 860 cm^{-1} found in an aqueous 18-crown-6 solution (solution A) consists of two distinct bands at 836 and 860 cm^{-1} and a small peak at 815 cm^{-1}. The highest peak among the three, the band at ca. 860 cm^{-1}, shifts toward the high frequency side when an alkali metal ion is combined with the ligand. The order of the Raman shift is Li<Na>K≈Cs, but it is not very clear when we take into account the uncertaintiy of the measurement (±2 cm^{-1}). However, the shape of the band at 860 cm^{-1} seems to be very closely related to the stabilities of the metal complexes,[23,24] i.e., the sharpness of the peak changes in the order: free <Li<Na<K>Cs. The same trend can also be observed in the band shapes at ca. 280, 550, 1275, and 1475 cm^{-1}.

Radial Distribution Functions. 18-Crown-6 Solution. The radial distribution curve for an aqueous 18-crown-6 solution (solution A) is depicted in Fig. 2,A. Three large peaks appear around 140, 280, and 480 pm in the curve. In order to analyze the radial distribution function of solution A, intramolecular atomic distances for the conformations with C_i, C_1, and D_{3d} symmetry are calculated from the structural data of 18-crown-6,[4] NaSCN-18-crown-6,[7] and KSCN-18-crown-6[8] crystals, respectively. The interatomic distances obtained from the data of RbSCN-18-crown-6[11] and CsSCN-18-crown-6[12] crystals, in both of which the 18-crown-6 molecule adopts the D_{3d} conformation, are almost the same as those estimated from the structure of the KSCN-18-crown-6 crystal. The results are summarized in Table 3. For the sake of convenience in the following discussions, the atoms within an 18-crown-6 molecule are numbered as shown in Fig. 4.

From the table it is seen that the first peak at 140 pm is attributed to the C-H, C-O, and C-C bonds within 18-crown-6 molecules and the O-H bonds within

water molecules. The second peak at 280 pm with a shoulder at 240 pm includes peaks due to nonbonding intramolecular interactions such as $C_2\cdots H_3$, $O_1\cdots H_1$, $C_3\cdots O_1$, $C_3\cdots C_5$, $O_1\cdots O_4$, $O_4\cdots H_1$, and $C_5\cdots H_3$ ones within 18-crown-6 molecules. Conformations of 18-crown-6 are very insensitive to the distances. It should be noted that the C···H and O···H interactions can not be neglected in the course of the analysis in spite of the weak scattering power of hydrogen atom, since the frequency factors for the interactions are very large (Table 3). The large peak around 480 pm is mainly due to various intramolecular interactions of

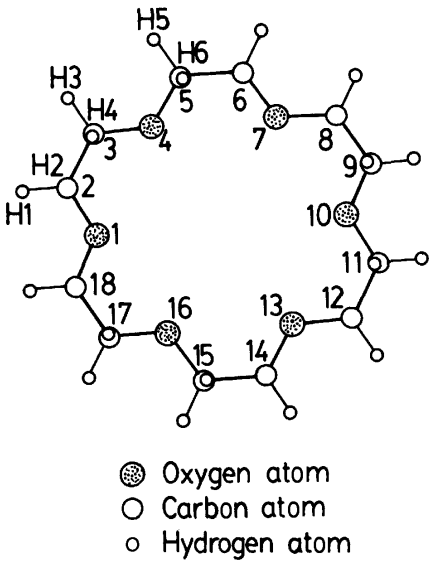

Fig. 4. The numbering of atoms within 18-crown-6.

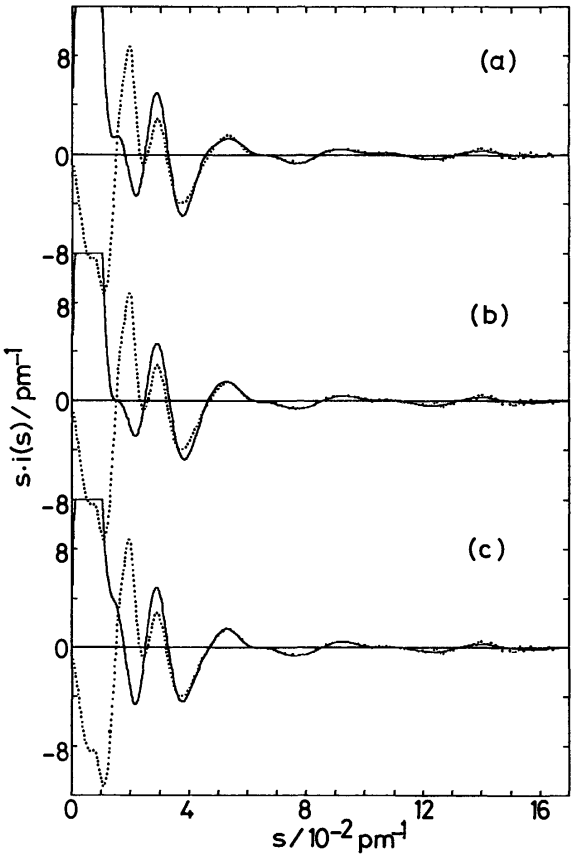

Fig. 5. The $s\cdot i(s)$ curve for solution A. The observed values are shown by the dotted lines and the calculated ones by assuming (a) C_i, (b) C_1, and (c) D_{3d} conformations of 18-crown-6 are drawn by the solid lines.

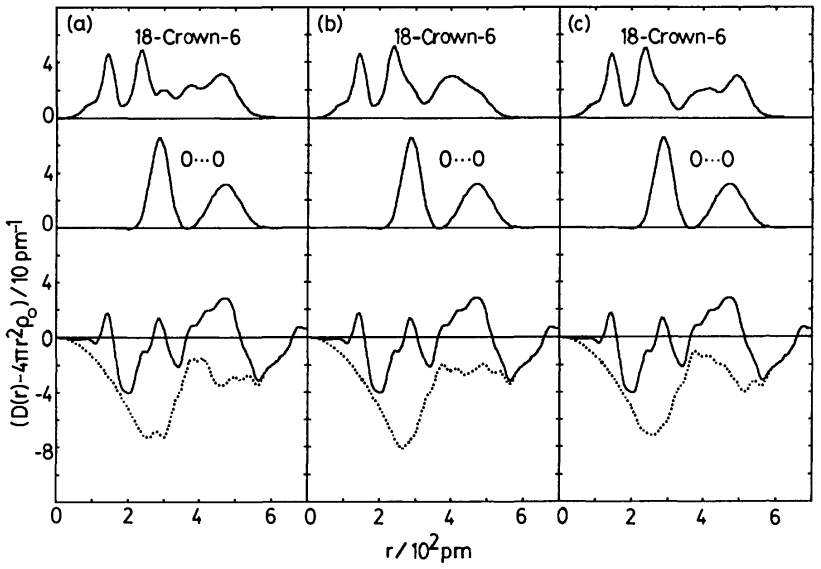

Fig. 6. The $(D(r)-4\pi r^2\rho_0)$ curve for solution A. The peak shapes for intramolecular interactions within 18-crown-6 are calculated on the basis of (a) C_i, (b) C_1, and (c) D_{3d} conformations of 18-crown-6 (upper part). The dotted lines (lower part) represent the residual curves after subtraction of the theoretical peak shapes owing to the intramolecular interactions within 18-crown-6 and the O···O interactions of hydrated 18-crown-6 and of bulk water.

18-crown-6, the distances being varied depending on the conformations of 18-crown-6. The O···O interactions between water molecules in the bulk may appear also around 280 and 460 pm.[25]

In order to draw the theoretical reduced intensities and radial distribution curves by using the parameter values given in Table 3, the root mean square amplitudes Δr_{pq} of the atom-pairs were assumed to be 5% of the corresponding atom-pair distances, which have been evaluated from the results of solution X-ray diffraction measurements so far examined for non-bonding interatomic interactions which have a separation of one to two atoms in between. The temperature factors b_{pq} were thus calculated as $b_{pq}=(\Delta r_{pq})^2/2$. In the course of the calculations, hydration of oxygen atoms in 18-crwon-6 was teken into account on the basis of the hydration model proposed by the Monte Carlo simulation.[15] The O···O contacts of bulk water were also considered.[25] In Figs. 5 and 6 are shown the reduced intensities and radial distribution curves, respectively, thus calculated, all of which reasonably reproduce the experimental ones. Therefore, it is not conclusive which conformation predominantly exists in aqueous solution from the present X-ray scattering data, but the D_{3d} conformation (Fig. 5,C) seems to give the best fit result. According to the Raman spectroscopic measurement described in the preceding section, the C_1 and D_{3d} conformations are possible to be present, and the C_i conformation was not acceptable.

The peaks due to the intramolecular interactions of 18-crown-6 are large and comparable to those for O···O interactions of bulk water, and therefore, we must be careful to analyze peaks due to the intramolecular structure of 18-crown-6 complexes in the following sections with a reasonable evaluation of structure parameters for interactions between water molecules in the bulk, as well as those between atoms in the 18-crown-6 molecule.

LiCl and 18-Crown-6 Solutions. The $s\cdot i(s)$ (Figs. 1,B and C) and $(D(r)-4\pi r^2\rho_0)$ curves (Figs. 2,B and C) of aqueous LiCl solutions with 18-crown-6 (solutions B and C) are analyzed by the similar method to that employed for solution A. The C_i, C_1, and D_{3d} conformations of 18-crown-6 were assumed at each calculation. As pointed out in the preceding section, complexation between lithium ion and 18-crown-6 was weak, and an only part of the whole lithium ions in the solution is trapped into the crown ring. In this calculation hydration of oxygen atoms in 18-crown-6 was not taken into consideration. The octahedral hydration model of chloride ion given in the literature was assumed.[26] The Li–O interactions arising from the hydration of free lithium ion and from the complex between lithium ion and 18-crown-6 were neglected in the course of the calculation because of the weak scattering power of lithium atom and its low concentration in the solution. The results for solution B calculated by using different assumptions of the C_i, C_1, and D_{3d} conformations are shown in Fig. 7 and practically the same results were also obtained for solution C. It may be rather difficult to draw a definite conclusion from the reduced intensities because all cases seem to give similar fits between experimental and calculated results. We may say that the D_{3d} symmetry (Fig. 7,C) gave the best fit result among the three, but this is not conclusive. The Raman spectroscopic data indicated that either the C_1 or D_{3d} conformation or both are possible for the lithium 18-crown-6 complex in solution (see Fig. 3).

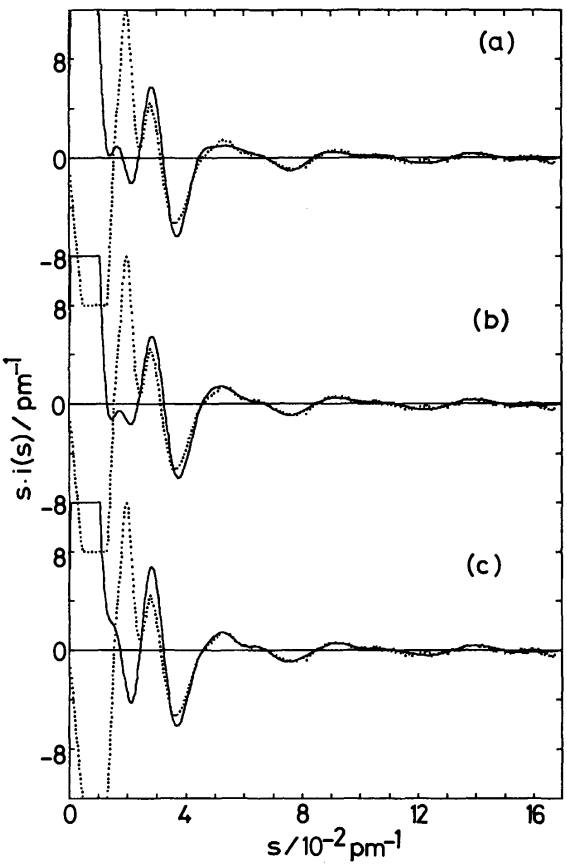

Fig. 7. The $s\cdot i(s)$ curve for solution B. The observed values are shown by the dotted lines and the calculated ones by assuming (a) C_i, (b) C_1, and (c) D_{3d} conformations of 18-crown-6 are drawn by the solid lines.

NaCl and 18-Crown-6 Solution. The $(D(r)-4\pi r^2\rho_0)$ curve for solution D depicted in Fig. 2,D is also analyzed by assuming three structural models (C_i, C_1, and D_{3d}) for the conformation of the 18-crown-6 ring in the sodium complex. In the C_i model sodium ion is located at the center of gravity of the six oxygen atoms in the ring and then is moved along the axis which is perpendicular to the mean plane defined by the six oxygen atoms in 18-crown-6. The position of sodium ion is determined so that the distance between the sodium ion and the nearest oxygen atom is ca. 245 pm,

which is estimated from the peak position in the radial distribution curve (Fig. 2,D). Two hydrated water molecules at the same distance from sodium ion are also taken into consideration in order to explain the peak area at ca. 245 pm. The 18-crown-6 ring in the sodium complex with thiocyanate ion as the counter anion in crystal has the C_i conformation, i.e., sodium ion is surrounded by five oxygen atoms (O_1 to O_{13}) in the equatorial plane and an oxygen atom (O_{16}) and a water molecule coordinate at the axial site.[7] For the D_{3d} conformation two model structures are examined: in one model sodium ion is located at the center of the six oxygen atoms within 18-crown-6 with D_{3d} symmetry, the structure corresponding to that found in KSCN–18-crown-6 crystal[8] and, thus, the Na–O distance is ca. 280 pm. In the other model sodium ion contacts with two oxygen atoms at the distance of 240—250 pm in the mean plane of 18-crown-6. In both cases two hydrated water molecules above and below the plane are taken into consideration.

Among the structure models examined, the theoretical values based on the C_i model gave the best agreement with the experimental ones as shown in Fig. 8. The C_i and D_{3d} models do not fit to the observed curves. From these results we concluded that the structure of the sodium complex in aqueous solution is with the C_i conformation which is similar to that in the solid state with one hydrated water molecule.

The structure parameters of the Na–18-crown-6 complex could not be well refined by a least-squares calculation using reduced intensities because of the low concentration of sodium ion and the relatively weak scattering power of sodium atom, since the contribution of intramolecualr structure of 18-crown-6 to the intensity values is very large.

KCl and 18-Crown-6 Solution. The differential radial distribution curve for solution E (Fig. 2,E) shows two distinct peaks at 280 and 360 pm which are not observable in solutions A through D. The peaks may thus be ascribed to the K–O and K···C interactions within the K–18-crown-6 complex.

The $(D(r)-4\pi r^2\rho_0)$ curve for solution E was

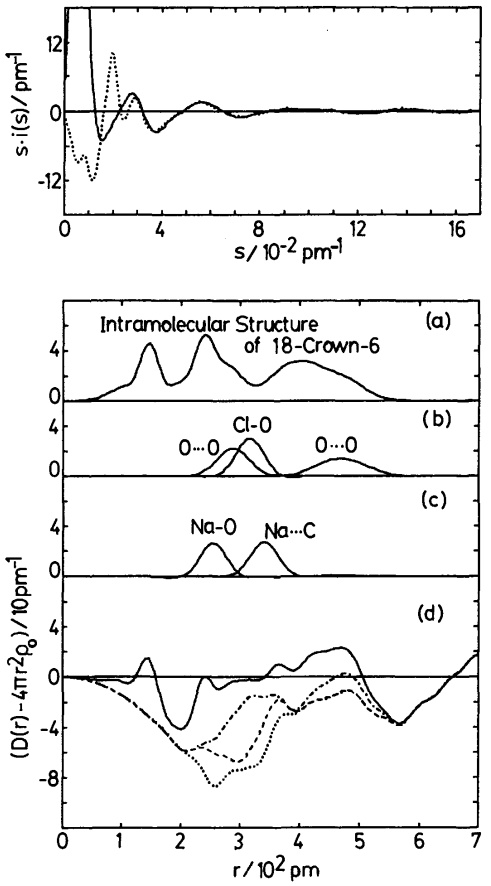

Fig. 8. The $s\cdot i(s)$ and $(D(r)-4\pi r^2\rho_0)$ curves for solution D. The observed $s\cdot i(s)$ values are shown by the dotted line and calculated ones by the solid line (above). The observed radial distribution curve is drawn by the solid line, and chain, dashed, and dotted ones represent the residual curves after subtraction of calculated peak shapes in (a), (b), and (c), respectively (below).

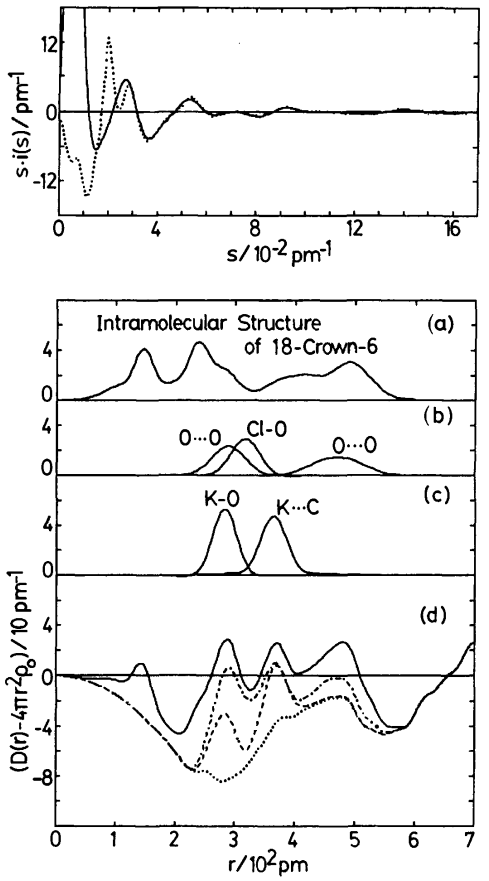

Fig. 9. The $s\cdot i(s)$ and $(D(r)-4\pi r^2\rho_0)$ curves for solution E. The observed $s\cdot i(s)$ values are shown by the dotted line and calculated ones by the solid line (above). The observed radial distribution curve is drawn by the solid line, and chain, dashed, and dotted ones represent the residual curves after subtraction of calculated peak shapes in (a), (b), and (c), respectively (below).

analyzed in a similar manner to that employed in previous sections on the basis of three conformational models of 18-crown-6. For the C_i conformation, the same model as that employed for solution D was used. The distance between potassium ion and the nearest oxygen atom was taken to be ca. 280 pm. In the C_1 model potassium ion was moved along the line which is perpendicular to the mean plane defined by five oxygen atoms within 18-crown-6 through the center of gravity of these atoms, and in the course of this procedure, the K–O distance to the nearest oxygen atom within 18-crown-6 was assumed to be approximately 280 pm which were evaluated from the peak position in the $(D(r)-4\pi r^2 \rho_0)$ curve. The conformation with D_{3d} symmetry was adopted which has been found in the KSCN–18-crown-6 crystal.[8] In all cases two water molecules bound to potassium ion at the distance of ca. 280 pm are taken into account. In these examinations the D_{3d} model gave the best-fit result. In Fig. 9 the reduced intensities and radial distrubution curve drawn on the basis of the D_{3d} model are shown, in which theoretical curves well reproduced the experimental ones. Reduced intensity curves calculated from the C_i and C_1 models gave large discrepancies from the experimental ones. Thus the most plausible structure of the potassium complex was concluded to be the one with D_{3d} symmetry.

Since the contribution of interatomic interactions in 18-crown-6 and in the bulk water to the reduced intensities and radial distribution curve becomes almost comparable to those of K–O and K···C interactions (see Fig. 9), the direct analysis of the curve for the structural parameters of the K–O and K···C interactions may be largely affected by the assumption for the Cl–O distance and the hydration number of chloride ion in aqueous solution, which has been reported to be concentration dependent,[27] as well as for the interatomic interactions in 18-crown-6 and in the bulk water. Therefore, the structure parameters for the potassium 18-crown-6 complex were evaluated by the following procedure: we first subtracted the reduced intensities for solution C containing 2 mol dm^{-3} lithium chloride, in which almost the same concentrations of 18-crown-6, chloride ion, and water molecule as in solution E are contained, from those of solution E. By this procedure the short-range interatomic interactions in 18-crown-6 below 300 pm, hydrated chloride ions and the bulk water, except for those of the metal–oxygen interactions, were eliminated. The contribution of long-range interatomic interactions in 18-crown-6 would entirely be eliminated when the conformation of 18-crown-6 in the potassium complex was the same as that in the lithium complex. Even if their conformations are different, the difference in the long-range interatomic interactions may be small enough to obtain the structure parameters for the potassium complex with a reasonable accuracy, because the contribution of K–O and K···C interactions to the difference reduced intensities $\Delta\{s\cdot i(s)\}$ is much larger. The Li–O and Li···C interactions in case of solution C may be neglected because of the weak scattering power of lithium atom. The difference reduced intensities $\Delta\{s\cdot i(s)\}$ and difference radial distribution curve $\Delta D(r)$ are shown in Fig. 10. The $\Delta D(r)$ curve shows two distinct peaks at 278 and 360 pm which should be due to the K–O and K···C interactions, respectively. The areas under the peaks correspond to ca. seven K–O bonds and ca. twelve K···C interactions.

A least-squares calculation was finally applied to the $\Delta\{s\cdot i(s)\}$ curve in the high-angle region to optimize the structural parameters of the potassium 18-crown-6 complex. The conformation of 18-crown-6 within the potassium complex was assumed to be D_{3d} on the basis of the analysis of the radial distribution curve in the course of the refinements. Two types of the calculations were performed in the refinements: in the type I calculation, the conformation of 18-crown-6 in solution C was assumed to be the same as that in

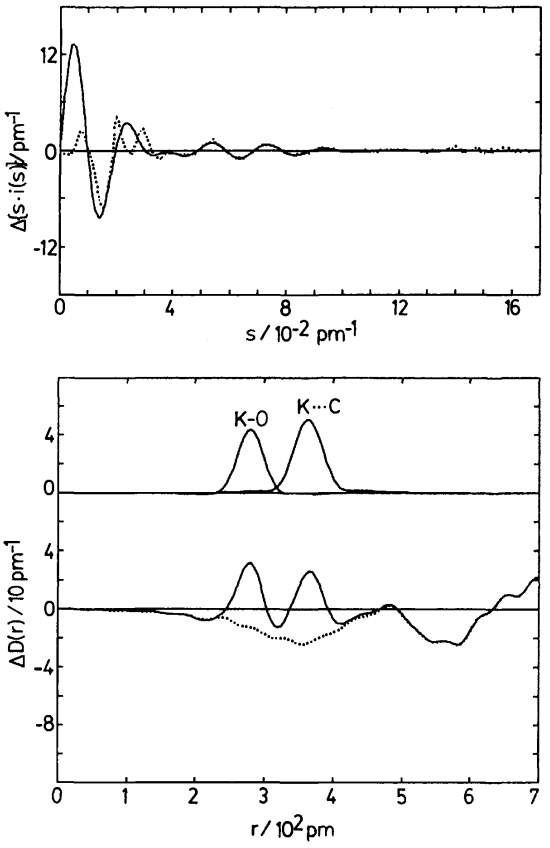

Fig. 10. The difference reduced intensities $\Delta\{s\cdot i(s)\}$ and difference radial distribution curve $\Delta D(r)$ for solution E. The observed $\Delta\{s\cdot i(s)\}$ values are shown by the dotted line and calculated ones by the solid line (above). The observed $\Delta D(r)$ curve is drawn by the solid line and the residual curve after subtraction of calculated peak shapes by the dotted line (below).

Table 4. Least-Squares Refinements for the Structure Parameters of the Potassium 18-Crown-6 Complex in Aqueous Solution with Different Models

Interaction	Parameter	I	II	Proposed length
K-O	r/pm	278(1)	276(1)	277(2)
	$b/10^2$ pm^2	6(1)	12(2)	
	n	5.5(4)	8.2(6)	
K···C	r/pm	363(1)	356(1)	360(4)
	$b/10^2$ pm^2	14(1)	14(1)	
	n	12[a]	12[a]	
	U/pm^{-2}	4.9	5.1	

a) The values were kept constant during the calculation.

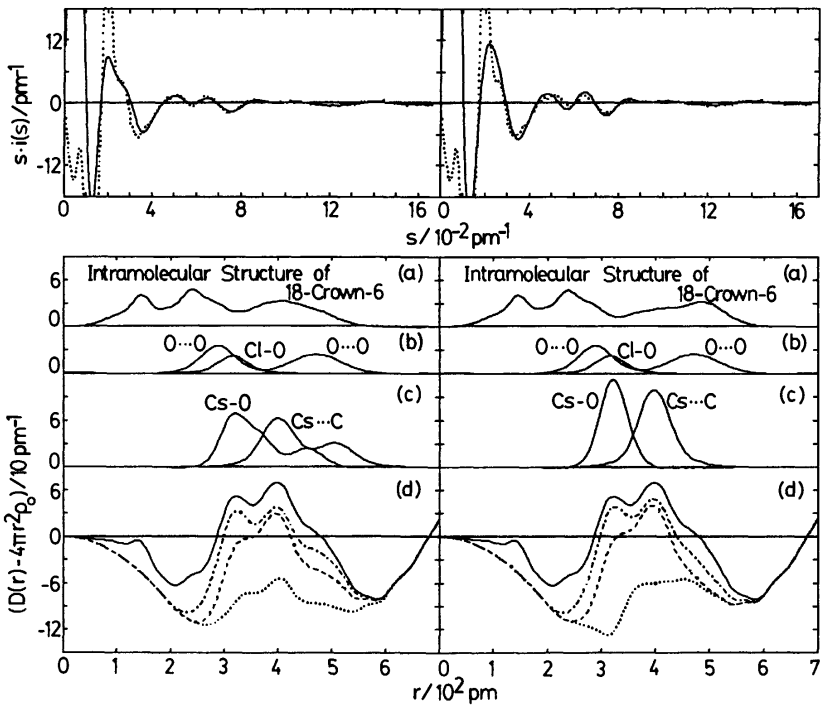

Fig. 11. The $s \cdot i(s)$ and $(D(r)-4\pi r^2\rho_0)$ curves for solution F. The theoretical curves are calculated on the basis of the C_1 (left) and D_{3d} (right) conformations. The observed $s \cdot i(s)$ values are shown by the dotted line and calculated ones by the solid line (above). The observed radial distribution curve is drawn by the solid line, and chain, dashed, and dotted ones represent the residual curves after subtraction of calculated peak shapes in (a), (b), and (c), respectively (below).

solution E (D_{3d} conformation). On the other hand, in the type II treatment, the conformations of 18-crown-6 in solutions C and E were different, the former 18-crown-6 adopting the C_1 conformation, and hence the structural difference between the two complexes must be taken into consideration. The results are summarized in Table 4 and very similar results were obtained by both treatments. The structural difference between lithium and potassium complexes did not thus affect the structure determination of the potassium complex even if their structures were different. The K-O and K···C distances determined are 277(2) and 360(4) pm, respectively, and therefore, potassium ion is located at the center of 18-crown-6. The frequecy factor for the K-O bond is estimated to be 6—8, which suggests that one or two water molecules solvate potassium ion above and/or below the mean plane of 18-crown-6 with D_{3d} symmetry.

CsCl and 18-Crown-6 Solution. The $(D(r)-4\pi r^2\rho_0)$ curve for solution F depicted in Fig. 2,F shows two large peaks around 310 and 390 pm. The peaks are assignable to the Cs-O and Cs···C interactions within the caesium 18-crwon-6 complex.

The radial distribution function for solution F was analyzed by a similar procedure to that employed for solution E. The Cs-O distance to the nearest oxygen atom within 18-crown-6 was set to be 315 pm in the three models examined (C_i, C_1, and D_{3d} models). Two water molecules with the same distance from the caesium ion were also taken into consideration in

order to explain the large area under the peak at 310 pm. Among the structure models examined, both C_1 and D_{3d} models rather reasonably reproduced the experimental values as depicted in Fig. 11. Therefore, it is not conclusive from the result which conformation is taken in the complex. Both can also exist as a mixture of two type conformations in the solution. The latter explanation seems to be likely because Cs–O interactions are rather weak and the Raman bands in the CsCl–18-crown-6 solution are broader than those of KCl–18-crown-6 solution.

The refinement of the structure parameters for the Cs–O and Cs···C interactions within the caesium complex was also performed by the similar method to that applied to the case of the potassium complex. In this case the reduced intensities of solution B were subtracted from those of solution F because the composition of the two solutions is very similar. The difference reduced intensities $\Delta\{s\cdot i(s)\}$ and difference radial distribution curve $\Delta D(r)$ are shown in Fig. 12. In the observed $\Delta D(r)$ curve two large broad peaks are found around 320 and 400 pm owing to the Cs–O and Cs···C interactions, respectively, which are less separated than those for the potassium complex. This suggests that the temperature factors for both Cs–O and Cs···C interactions are larger than those of K–O and K···C interactions. The large temperature factors of the Cs–O and Cs···C pairs certainly arise from their weak interactions, and thus the Cs–O and Cs···C distances may fluctuate to a relatively large extent. In the crystal of CsSCN–18-crown-6 each of the Cs–O and Cs···C distances can be devided into two groups, i.e., three shorter Cs–O distances of 306 pm and three longer ones of 324 pm, and five shorter Cs···C distances of 377 pm and seven longer ones of 398 pm.[12] Therefore, we tried to separate the peaks in the radial distribution curve into four major ones on the basis of the crystallographic data. However, any combination of the interatomic distances and temperature factors was not successful to reproduce the experimental curves by using four kinds of interactions. Three different Cs–O bonds and two different Cs···C interactions, at least, were needed in order to explain the experimental result according to the least-squares calculations for the $\Delta\{s\cdot i(s)\}$ values when we adopted the C_1 conformation of the 18-crown-6 structure. On the other hand, only two interactions, one Cs–O and one Cs···C, were sufficient to interprete the difference reduced intensities of the solution on the basis of the D_{3d} symmetry model (see Table 5).

The structure parameters finally refined by a least-squares calculation using the high-angle region of the $\Delta\{s\cdot i(s)\}$ values are summarized in Table 5. Both models almost equally reproduce the experimental

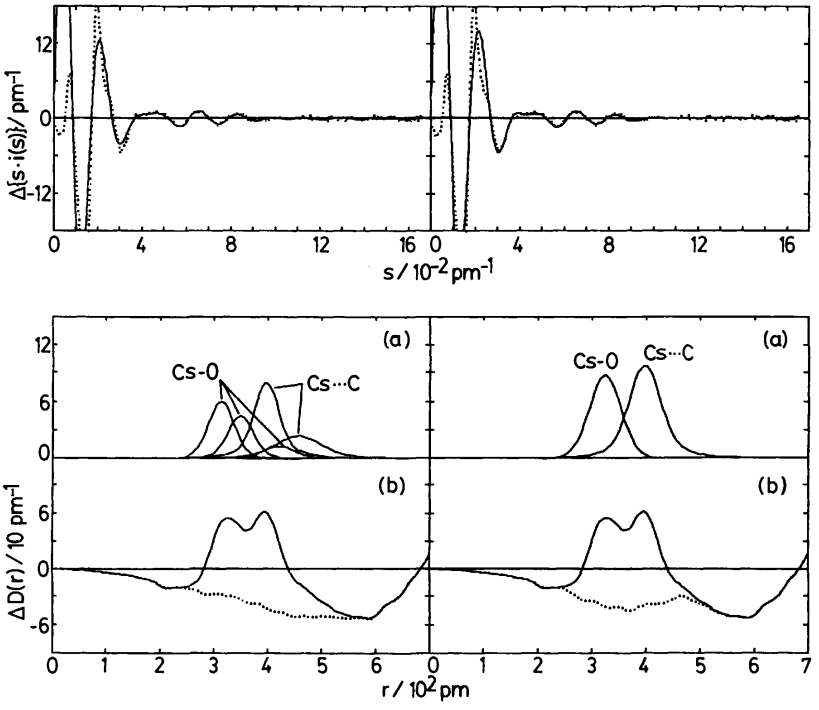

Fig. 12. The difference reduced intensities $\Delta\{s\cdot i(s)\}$ and difference radial distribution curve $\Delta D(r)$ for solution F. The theoretical curves are calculated on the basis of the C_1 (left) and D_{3d} (right) conformations. The observed $\Delta\{s\cdot i(s)\}$ values are shown by the dotted line and calculated ones by the solid line (above). The observed $\Delta D(r)$ curve is drawn by the solid line and the residual curve after subtraction of calculated peak shapes by the dotted line (below).

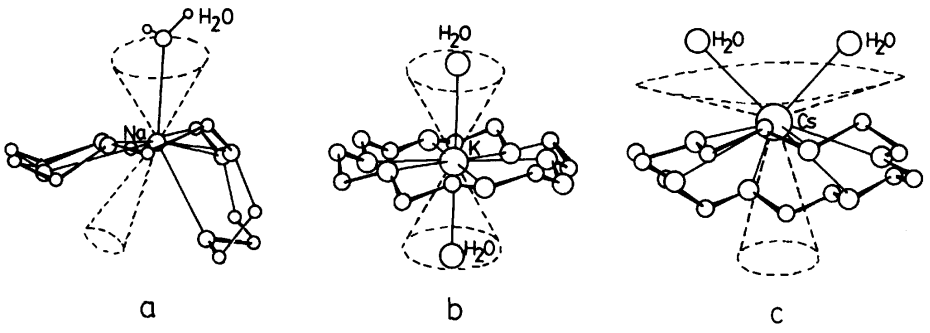

Fig. 13. Proposed structures of hydrated 18-crown-6 alkali metal complexes. Broken lines indicate corn angles above and below the metal ion in the complexes. (a) Sodium complex with C_1 conformation of the 18-crown-6 ring, (b) Potassium complex with D_{3d} conformation, (c) One of the possible structure of the caesium complex which has the D_{3d} conformation.

Table 5. Least-Squares Refinements for the Structure Parameters of the Caesium 18-Crown-6 Complex in Aqueous Solution with Different Models of the Crown-Ring Structure

Interaction	Parameter	C_1	D_{3d}
Cs–O	r/pm	312(2)	321(1)
	$b/10^2$ pm^2	13(2)	27(4)
	n	4[a,b]	7.1(4)
Cs–O	r/pm	348(5)	—
	$b/10^2$ pm^2	13(5)	—
	n	3[a]	—
Cs–O	r/pm	419(43)	—
	$b/10^2$ pm^2	25[a]	—
	n	1[a]	—
Cs···C	r/pm	396(3)	394(1)
	$b/10^2$?pm^2	15(4)	29(2)
	n	8[a]	12[a]
Cs···C	r/pm	453(20)	—
	$b/10^2$ pm^2	71(54)	—
	n	4[a]	—
	$U/10$ pm^{-2}	1.1	1.2

a) The values were kept constant during the calculation. b) The value was varied from 2 to 6 but practically the same Cs–O and Cs···C distances were obtained.

curve. Therefore it is concluded that Cs–18-crown-6 complex with different conformations C_1 and D_{3d} can be present, and the Cs–18-crown-6 complex takes either C_1 or D_{3d} conformation, or has a structure of their mixture in the solution. Since a large caesium ion cannot accommodate in the hole of the 18-crown-6 ring and is located appart from the mean plane of the ring, the ring may be more flexible than that in the sodium and potassium complexes, in which these ions are kept at the center of the ring, and thus, the latter explanation (mixture model) cannot be rejected from the conclusion. Since the frequency factor for the Cs–O bond in the D_{3d} model converged to 7.1(4), the caesium ion may be solvated with one to two water molecules in the solution.

In Fig. 13 plausible structures are depicted for the alkali metal complexes with 18-crown-6 in aqueous solution examined, except fot the lithium complex whose structure was not estimated from the present work. Broken lines in the figure indicate corn angles around the central metal ions which are drawn by taking into account the van der Waals radii of oxygen, carbon, and hydrogen atoms in the 18-crown-6 ring. It is seen from the corn angles, it may be possible that only one water molecule combines with sodium ion in the complex. In the potassium complex, two water molecules can approach the central ion. For the caesium complex, about two water molecules can interact with caesium ion from one side of the crown ring.

The work has been financially supported by the Grant-in-Aid for Scientific Research No. 63612005 (Macromolecular Complexes) from the Ministry of Education, Science and Culture. Computer calculations were carried out at the computer center of the Institute for Molecular Science in Okazaki.

References

1) R. M. Izatt, J. S. Bradshaw, S. A. Iielsen, J. D. Lamb, J. J. Christensen, and D. Sen, *Chem. Rev.*, **85**, 271 (1985).
2) M. R. Truter, *Structure and Bonding*, **16**, 71 (1973).
3) D. J. Patel, *Biochemistry*, **12**, 496 (1973).
4) J. D. Dunitz and P. Seiler, *Acta Crystallogr., Sect. B*, **30**, 2739 (1974); E. Maverrick, P. Seiler, W. B. Schweizer, and J. D. Dunitz, *Acta Crystallogr., Sect. B*, **36**, 615 (1980).
5) J.-P. Behr, P. Dumas, and D. Moras, *J. Am. Chem. Soc.*, **104**, 4540 (1982).
6) O. Nagano, A. Kobayashi, and Y. Sasaki, *Bull. Chem. Soc. Jpn.*, **51**, 790 (1978).
7) M. Dobler, J. D. Dunitz, and P. Seiler, *Acta Crystallogr., Sect. B*, **30**, 2741 (1974).
8) P. Seiler, M. Dobler, and J. D. Dunitz, *Acta Crystallogr., Sect. B*, **30**, 2744 (1974).
9) O. Nagano, *Acta Crystallogr., Sect. B*, **35**, 465 (1979).

10) O. Nagano and Y. Sasaki, *Acta Crystallogr., Sect. B*, **35**, 2387 (1979).
11) M. Dobler and R. P. Phizackerley, *Acta Crystallogr., Sect. B*, **30**, 2746 (1974).
12) M. Dobler and R. P. Phizackerley, *Acta Crystallogr., Sect. B*, **30**, 2748 (1974).
13) P. Groth, *Acta Chem. Scand., Ser. A*, **36**, 109 (1982).
14) G. Wipff, P. Weiner, and P. A. Kollman, *J. Am. Chem. Soc.*, **104**, 3249 (1982); G. Wipff, P. A. Kollman, and J. M. Lehn, *J. Mol. Struct.*, **93**, 153 (1983).
15) G. Ranghino, S. Romano, J. M. Lehn, and G. Wipff, *J. Am. Chem. Soc.*, **107**, 7873 (1985).
16) R. Perrin, C. Decoret, G. Bertholon, and R. Lamartine, *Nouv. J. Chim.*, **7**, 263 (1983).
17) H. Sato and Y. Kusumoto, *Chem. Lett.*, **1978**, 635.
18) H. Takeuchi, T. Arai, and I. Harada, *J. Mol. Struct.*, **146**, 197 (1986).
19) J. Goulon and C. Goulon-Ginet, *Pure Appl. Chem.*, **54**, 2307 (1982).
20) H. Ohtaki, *Rev. Inorg. Chem.*, **4**, 103 (1982).
21) G. Johansson and M. Sandström, *Chem. Scr.*, **4**, 195 (1973).
22) T. Yamaguchi, Doctor Thesis, Tokyo Institute of Technology, March (1978).
23) H. K. Frensdorff, *J. Am. Chem. Soc.*, **93**, 600 (1971).
24) R. M. Izatt, R. E. Terry, B. L. Haymore, L. D. Hansen, N. K. Dalley, A. G. Avondet, and J. J. Christensen, *J. Am. Chem. Soc.*, **98**, 7620 (1976).
25) A. H. Narten, *ORNL-4578* (1970).
26) G. Pálinkás, T. Radnai, and F. Hajdu, *Z. Naturforsch., A*, **35**, 107 (1980).
27) T. Yamaguchi, H. Ohtaki, E. Spohr, G. Pálinkás, K. Heinzinger, and M. M. Probst, *Z. Naturforsch., A*, **41**, 1175 (1986).

 © 1989 The Chemical Society of Japan Bull. Chem. Soc. Jpn., 62, 2819—2823 (1989)

The Thermal Decomposition of Ammonium Strontium *cyclo*-Tri-, *cyclo*-Tetra-, and *cyclo*-Hexaphosphate

Atsushi TAKENAKA,* Itaru MOTOOKA,† and Hiroyuki NARIAI
Department of Industrial Chemistry, Yonago National College of Technology, Otakazuna, Hikona-cho, Yonago, Tottori 683
†Department of Chemistry, Faculty of General Education, Kobe University, Tsurukabuto, Nada-ku, Kobe 657
(Received May 11, 1988)

Ammonium strontium *cyclo*-triphosphate $Sr(NH_4)P_3O_9 \cdot 3H_2O$ [P_{3m}], *cyclo*-tetraphosphate $Sr(NH_4)_2P_4O_{12}$ [P_{4m}], and *cyclo*-hexaphosphate $Sr_2(NH_4)_2P_6O_{18} \cdot 7H_2O$ [P_{6m}] were prepared by a wet method. The thermal decomposition of the *cyclo*-phosphates was investigated by means of TG-DTA, HPLC-FIA, X-ray analysis, and IR spectrometry. Streams of humid air and dry nitrogen gas were used to clarify the effect of humidity on the pyrolysis. The decomposition of the ring structure of P_{3m} and P_{4m} was accompanied by the elimination of ammonia. Although P_{6m} lost some of the waters of crystallization without any change in the structure, the ring was cleaved by the release of the other waters of crystallization. Regardless of the *cyclo*-phosphates, the final crystalline product was β-$Sr(PO_3)_2$, with a long-chain anion. The formation of β-$Sr(PO_3)_2$ was facilitated by water vapor in the cases of P_{3m} and P_{6m}. Unlike the pyrolysis of $(NH_4)_6P_6O_{18} \cdot 1.5H_2O$ and $(NH_4)_4P_4O_{12}$, it was unlikely that P_{3m}, P_{4m}, and P_{6m} were decomposed to produce oligophosphate radicals. They were probably hydrolyzed to oligophosphates; then, polyphosphates were formed by the condensation of the oligophosphates.

In general, the formation and the structure of condensed phosphates depend on the temperature and the time of heating, the cooling rate of the melts, and the pressure of water vapor in the atmosphere.[1-7] Moreover, it is known that the valence and the radius of the constituent metal ion also affect the structures of condensed phosphates.[8]

We reported in a previous paper[9] that ammonium *cyclo*-tetra- and *cyclo*-hexaphosphates decomposed to produce ammonium polyphosphate through some lower-condensed phosphate radicals. If such a mechanism as a radical decomposition-polymerization depends on the radius of the constituent cation, it is of interest to study the thermal decomposition of ammonium metal(II) *cyclo*-phosphate, prepared by replacing the ammonium ion of the ammonium *cyclo*-phosphates with a bivalent metal ion having a radius close to that of the ammonium ion.

Though the strontium ion has a radius somewhat less than that of the ammonium ion,[10] an attempt to produce ammonium strontium *cyclo*-hexaphosphate (P_{6m}) in solution was successful. However, we could not prepare ammonium barium (which has a radius[10] close to that of the ammonium ion) *cyclo*-hexaphosphate by a wet method. Therefore, we chose strontium as the metal ion to substitute for the ammonium ion.

Durif et al. prepared ammonium strontium *cyclo*-tetraphosphate by a solid-state reaction, and then investigated it crystallographically.[11] Ammonium strontium *cyclo*-triphosphate, synthesized through a solid-state reaction, was studied by means of IR spectroscopy by Serazetdinov et al.[12] However, ammonium strontium *cyclo*-hexaphosphate has not yet been reported. The purpose of this work is to study the thermal decomposition of P_{6m}, in connection with the effect of humidity in the atmosphere, as well as the thermal decompositions of ammonium strontium *cyclo*-tri- (P_{3m}) and *cyclo*-tetraphosphate (P_{4m}), both prepared by the wet method.

Experimental

Chemicals. Guaranteed-grade reagents were used unless otherwise stated.

Determination of Strontium, Nitrogen, Phosphorus, and the Water of Crystallization. The strontium was determined by means of a replacement titration technique, in which Mg-EDTA and Eriochrome Black T(EBT) were employed.[13] The nitrogen content was obtained by means of an ammonia-distillation method.[14]

The strontium ions were precipitated as strontium oxalate[15] or removed by the use of a cation-exchange resin, Amberlite IR-120B.[16] Then, phosphates were hydrolyzed with diluted hydrochloric acid.[17] The resultant phosphates were determined colorimetrically.[18]

A sample was mixed with zinc oxide. The mixture was heated to a constant weight at 650 °C.[19] The amount of the water of crystallization could be determined by subtracting the weight loss due to the evolution of ammonia and the water arising from the NH_4^+ ions, calculated from the nitrogen content, from the total weight loss of the mixture.

X-Ray Diffractometry. The X-ray diffraction patterns were recorded on a Rigaku Denki Geigerflex X-ray diffractometer, RAD-IA, using nickel-filtered Cu $K\alpha$ radiation.

Thermal Analysis. About 20 mg of the sample was placed in a platinum pan. The thermal analyses (TG-DTA) were carried out at the heating rate of 2.5 °C min^{-1} on a Rigaku High-temperature-type Thermal Analyser, 8076 D1. The measurements were performed in stationary air or in a stream of dry N_2 gas at 50 cm^3 min^{-1}. The dry N_2 gas was introduced for 30 min before the measurements.

HPLC-Flow Injection Analysis (HPLC-FIA). The ratio of individual phosphates was determined according to the method in the literature.[9]

IR Spectrophotometry. The IR spectra were recorded on a JASCO IR spectrophotometer, IR-700, by the use of a Nujol-mull method.

Thermal Decomposition. The thermal decomposition

Table 1. X-Ray Diffraction Data for Ammonium Strontium *cyclo*-Triphosphate, $Sr(NH_4)P_3O_9 \cdot 3H_2O$

d/Å	Intensity[a]	d/Å	Intensity
7.69	M	2.86	M
7.25	VS	2.83	W
5.90	M	2.81	M
5.68	S	2.79	M
4.77	M	2.76	M
4.46	M	2.74	M
4.39	M	2.66	M
4.35	S	2.62	W
4.09	M	2.58	VW
3.93	M	2.55	VW
3.83	M	2.49	M
3.62	VS	2.47	VW
3.54	S	2.43	VW
3.41	M	2.35	W
3.39	VW	2.34	W
3.14	M	2.32	S
3.05	M	2.28	W
3.00	M	2.24	M

a) VS: Very strong, S: strong, M: medium, W: weak, VW: very weak.

Table 2. X-Ray Diffraction Data for Ammonium Strontium *cyclo*-Hexaphosphate, $Sr_2(NH_4)_2P_6O_{18} \cdot 7H_2O$

d/Å	Intensity[a]	d/Å	Intensity
8.66	S	3.18	W
7.08	W	3.14	VW
6.23	S	3.12	W
6.10	VS	3.01	S
5.79	M	2.94	M
5.53	S	2.89	M
5.43	M	2.84	VW
4.92	W	2.80	VW
4.67	W	2.76	M
4.33	W	2.71	M
4.02	W	2.68	M
3.91	M	2.65	M
3.83	M	2.63	M
3.67	M	2.62	M
3.52	VS	2.56	W
3.40	S	2.51	W
3.34	VW	2.46	S
3.22	S	2.34	M

a) VS: Very strong, S: strong, M: medium, W: weak, VW: very weak.

was carried out in a way similar to that previously reported,[9] although a stream of dry N_2 gas (50 cm^3 min^{-1}) was used instead of that of dry air.

The amount of ammonia evolved by the pyrolysis was determined as follows. The effluent gas (dry nitrogen or humid air) was introduced continuously into 30 cm^3 of a 0.01 mol dm^{-3} sulfuric acid at 50 cm^3 min^{-1}. When the furnace had reached the required temperature, the sample was taken out quickly and the gas (dry nitrogen or humid air) was passed into the acid for a further 10 min to absorb any ammonia remaining in the furnace. The ammonia absorbed in the solution was determined by means of a back-titration technique, using a 0.02 mol dm^{-3} sodium hydroxide solution and Methyl Red as an indicator.

Preparation of Ammonium Strontium *cyclo*-Phosphates. **Ammonium Strontium *cyclo*-Triphosphate Trihydrate $Sr(NH_4)P_3O_9 \cdot 3H_2O$:** Twenty mmol (5.8188 g) of $(NH_4)_3P_3O_9$,[21] prepared by means of the ammoniation of $Na_3P_3O_9 \cdot H_2O$,[22] were dissolved in 80 cm^3 of water. This solution was then mixed with 40 cm^3 (20 mmol) of a 0.5 mol dm^{-3} strontium chloride aqueous solution, and the mixture was stirred for 30 min. The precipitate was filtered off and washed with cold water, 50% (v/v) ethanol–water, and then methanol. The product was air-dried. Found: Sr, 21.88; N, 3.33; P, 23.95; H_2O, 14.28%. Calcd for $Sr(NH_4)P_3O_9 \cdot 3H_2O$: Sr, 22.10; N, 3.53; P, 23.43; H_2O, 13.62%. The X-ray diffraction data are listed in Table 1. Ninety-three per cent of the P atoms were found by HPLC-FIA to be present as *cyclo*-$P_3O_9^{3-}$.

Ammonium Strontium *cyclo*-Tetraphosphate $Sr(NH_4)_2P_4O_{12}$: Fifteen mmol (5.82 g) of anhydrous $(NH_4)_4P_4O_{12}$,[21] obtained from $Na_4P_4O_{12} \cdot 4H_2O$,[23] were dissolved in 60 cm^3 of water. Fifteen-cm^3 (7.5 mmol) of the 0.5 mol dm^{-3} strontium chloride solution was then added, and the mixture was stirred. After 1 h, the precipitate was filtered off, washed, and dried as described above. At least 92% of the P atoms were in the form of *cyclo*-tetraphosphate. The X-ray diffraction pattern was in agreement with that of $Sr(NH_4)_2P_4O_{12}$, reported by Durif et al.[11] The elemental analyses also suggested that the product was anhydrous $Sr(NH_4)_2P_4O_{12}$.

Ammonium Strontium *cyclo*-Hexaphosphate Heptahydrate $Sr_2(NH_4)_2P_6O_{18} \cdot 7H_2O$: Five mmol (3.045 g) of $(NH_4)_6P_6O_{18} \cdot 1.5H_2O$ were dissolved in 30 cm^3 of water.[9] Then the solution was mixed with 20 cm^3 (10 mmol) of the 0.5 mol dm^{-3} strontium chloride solution. The mixture was stirred for 30 min. The precipitate was then filtered off, washed, and dried as above. Found: Sr, 21.87; N, 3.32; P, 23.03; H_2O, 15.57%. Calcd for $Sr_2(NH_4)_2P_6O_{18} \cdot 7H_2O$: Sr, 21.61; N, 3.45; P, 22.91; H_2O, 15.53%. At least 97% of the P atoms were found as *cyclo*-$P_6O_{18}^{6-}$ ions. The X-ray diffraction data are shown in Table 2.

Results and Discussion

Thermal Decomposition of Ammonium Strontium *cyclo*-Triphosphate $Sr(NH_4)P_3O_9 \cdot 3H_2O$. Figure 1 shows the thermal analyses (TG-DTA) in stationary air and in a stream of N_2 gas. Strong endothermic peaks with a weight loss appeared at 130 °C in both atmospheres. In stationary air (humid atmosphere), there was an endothermic peak at about 340 °C and an exothermic peak at about 355 °C. These peaks shifted to 360 and 390 °C respectively in a stream of dry N_2 gas (dry atmosphere).

The amount of the individual phosphate in the products obtained by heating up to the temperature indicated by arrows in Fig. 1, changed as is shown in Fig. 2. The *cyclo*-triphosphate anion of P_{3m} was not decomposed, at least not until 250 °C. Figure 3 represents the amount of ammonia evolved by heating P_{3m}, as a function of the temperature. Since ammonia

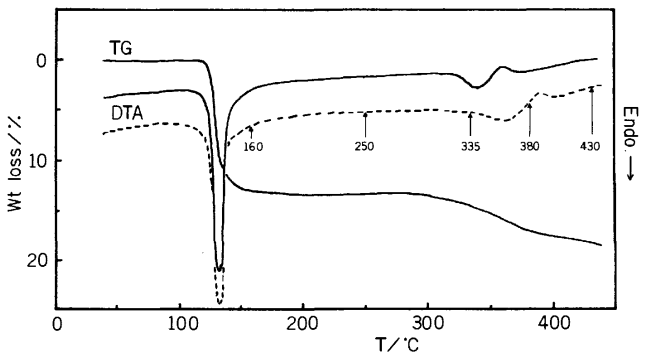

Fig. 1. Thermal analyses of $Sr(NH_4)P_3O_9 \cdot 3H_2O$ in the two different atmospheres. Solid line (—): TG and DTA measured in stationary air, dotted line (---): DTA in a stream of dry N_2 gas.

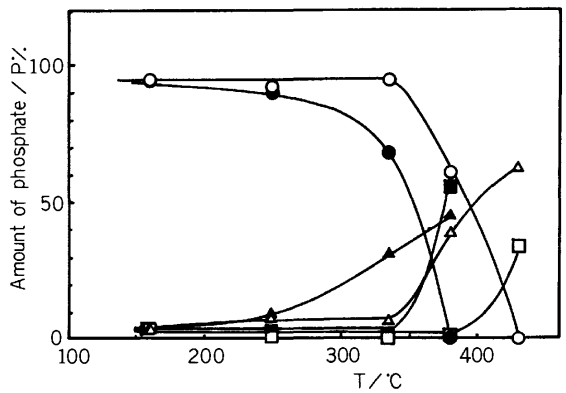

Fig. 2. Amounts of phosphates in the decomposition products of $Sr(NH_4)P_3O_9 \cdot 3H_2O$. ○ and ●: *cyclo*-Triphosphate observed in the dry and the humid atmospheres, respectively; □ and ■: oligophosphates with the chain length less than three, observed in the dry and the humid atmospheres respectively; △ and ▲: polyphosphates with the chain length more than four, in the dry and the humid atmospheres respectively.

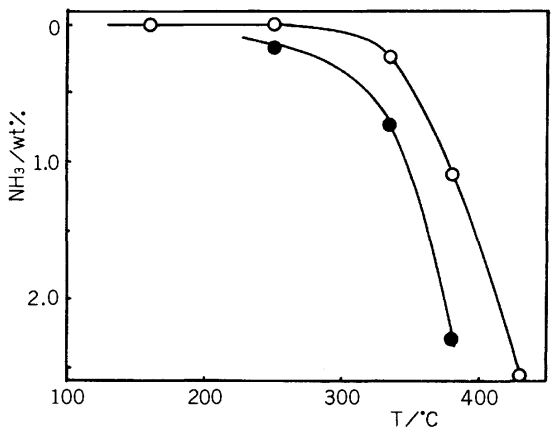

Fig. 3. Amount of ammonia evolved by heating $Sr(NH_4)P_3O_9 \cdot 3H_2O$. ○: Measured in the dry atmosphere, ●: in the humid atmosphere.

was not evolved up to 250 °C in the dry atmosphere, the endothermic peak at 130 °C was attributed to the elimination of the water of crystallization. The corresponding TG-loss (13.1%) was close to the calculated value (13.62%).

Figure 3 shows that the water vapor accelerated the evolution of ammonia. A similar "catalytic effect" of the water vapor was reported in the reaction of calcium oxide with ammonium chloride.[24]

The product obtained by heating up to 380 °C in the dry atmosphere contained many P_{3m} anions, and the evolution of ammonia was clearly observed above 335 °C. It was supposed that not the cleavage of the P_{3m} anions but the evolution of ammonia from P_{3m} caused the endothermic peak at 360 °C.

Since the decomposition of P_{3m} was influenced by the humidity, as is shown in Fig. 2, and since neither an increase in weight nor a corresponding exothermal peak may be seen in Fig. 1, P_{3m} can not be thought to form oligophosphate radicals.[9] Therefore, polyphosphates with a chain length of more than four must be produced through the condensation of oligophosphates.

Considerable ammonia was lost at 380 and 430 °C in the humid and dry atmospheres respectively (Fig. 3). It is expected that the product became acidic and that a vigorous hydrolytic reaction took place at 380 and 430 °C. Obviously, the total quantities of the oligophosphates with a chain length of less than three, which were considered to be the initial hydrolytic products of P_{3m} (or perhaps the oligophosphates are produced from the polyphosphates), were greater at 380 and 430 °C (Fig. 2).

Although the products from 160 to 380 °C under dry conditions did not change X-ray diffractometrically, the sample heated up to 380 °C was somewhat amorphous. The X-ray diffraction pattern of the product obtained by heating up to 430 °C under the dry condition agreed with that of β-$Sr(PO_3)_2$ with a long-chain anion. Consequently, the exothermic peak at 390 °C (or 355 °C for the humid conditions) was attributable to the following reaction (1), although the temperature was lower than 430 °C, as has been observed by Ropp et al.:[20]

$$Sr(PO_3)_2\,[\text{amorphous}] \longrightarrow \beta\text{-}Sr(PO_3)_2\,[\text{crystalline}] \quad (1)$$

The thermal decomposition may be summarized as follows (the water of crystallization was lost at 130 °C):

$$Sr(NH_4)P_3O_9 \cdot 3H_2O \longrightarrow Sr(NH_4)P_3O_9 + 3H_2O \quad (2)$$

Above 335 °C (or 250 °C for the humid conditions), polyphosphates began to form, accompanied by the evolution of ammonia (Figs. 2 and 3). Therefore, the following reaction takes place above that temperature:

$$Sr(NH_4)P_3O_9 \longrightarrow Sr(PO_3)_2\,[\text{amorphous}] + (NH_4)_{1-n}H_n(PO_3)\,[\text{amorphous}] + nNH_3 \quad (3)$$

where $Sr(PO_3)_2$ and $(NH_4)_{1-n}H_n(PO_3)$ are polyphosphates. They are formed through the condensation of oligophosphates. At a higher temperature (430 and 380 °C respectively), because of the loss of ammonia, the hydrolysis becomes vigorous enough to produce an appreciable amount of oligophosphates, as has been mentioned above.

Thermal Decomposition of Ammonium Strontium *cyclo*-Hexaphosphate $Sr_2(NH_4)_2P_6O_{18}\cdot 7H_2O$. Figure 4 shows the results of thermal analyses in the dry and humid atmospheres. The products, heated up to the temperatures indicated by the arrows in Fig. 4, were analyzed. Heating up to 200 °C, irrespective of the conditions, did not cause any ammonia-elimination. Consequently, the two large endothermic peaks below 130 °C and the set of endothermic peaks from 130 to 200 °C were considered to result from the elimination of the water of crystallization. The two large endothermic peaks were shifted to a higher temperature by an enhanced partial pressure of water vapor.

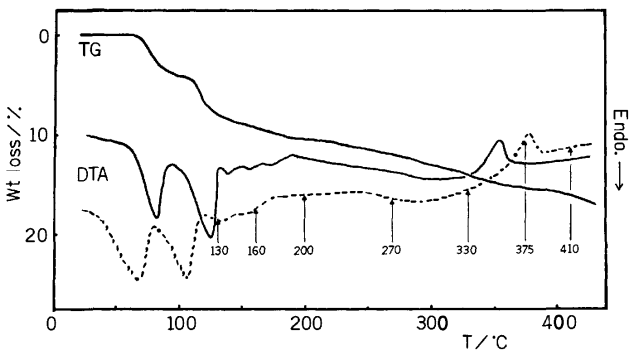

Fig. 4. TG-DTA analyses of $Sr_2(NH_4)_2P_6O_{18}\cdot 7H_2O$ measured in the two different atmospheres. Solid line (—): TG and DTA in stationary air, dotted line (---): DTA in a stream of dry N_2 gas.

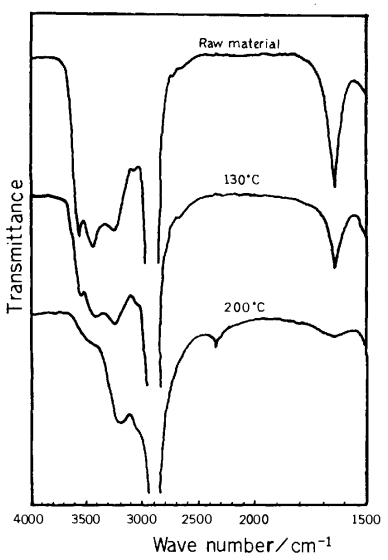

Fig. 5. IR spectra of the products at 130 and 200°C of $Sr_2(NH_4)_2P_6O_{18}\cdot 7H_2O$ in dry atmosphere.

There were absorptions at 3560 cm^{-1} in the IR spectra of P_{6m} and the product heated up to 130 °C (Fig. 5). These absorptions (as high as 3580 cm^{-1}) were attributed to the "interstitial" water molecules, loosely held in the crystal lattice.[25] The sharp and strong band at 1640 cm^{-1} of P_{6m} was also assigned to these water molecules.[25] The "interstitial" water may be identical with the so-called "Zeolitic Water."[26,27] Since the *cyclo*-hexaphosphate anion was not cleaved (Fig. 6), and since the structure of the products did not change X-ray diffractometrically until 130 °C (though the diffraction lines became weak), the endothermic peaks below 130 °C can be regarded as being caused by the elimination of a part of the interstitial water molecules.

The decomposition of P_{6m} was found not to be dependent on the humidity, and neither an increase in weight nor the corresponding exothermic reaction was observed (Figs. 6 and 4). Thus, P_{6m} could not be presumed to produce oligophosphate radicals as in the pyrolysis of $(NH_4)_6P_6O_{18}\cdot 1.5H_2O$.[9] Therefore, it was probably cleaved by hydrolysis. The absorptions at 1640, 3440, and 3560 cm^{-1} almost disappeared in the sample heated to 200 °C (Fig. 5). Consequently, P_{6m} was considered to lose the water of crystallization completely. The appearance of the peak at 2360 cm^{-1}, assigned to P-OH stretching,[25,28] certainly resulted from the hydrolysis.

The exothermic peak at around 375 °C in the dry atmosphere was shifted to a lower temperature (about 350 °C) in the humid atmosphere. The X-ray diffractogram showed that the phase transition from

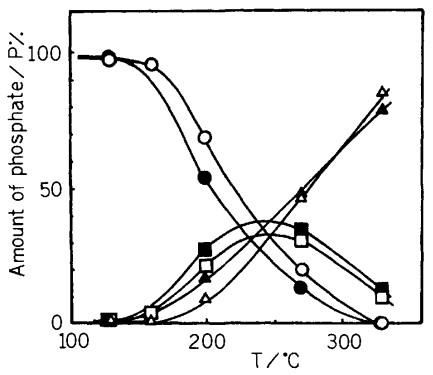

Fig. 6. Amounts of phosphates in the products of $Sr_2(NH_4)_2P_6O_{18}\cdot 7H_2O$. ○ and ●: *cyclo*-Hexaphosphate observed in the dry and the humid atmospheres, respectively; □ and ■: oligophosphates with the chain length less than six, observed in the dry and the humid atmospheres respectively; △ and ▲: polyphosphates with the chain length more than seven, in the dry and the humid atmospheres respectively.

amorphous $Sr(PO_3)_2$ to β-$Sr(PO_3)_2$ was exothermic. McGilvery and Scott reported that water vapor facilitated the crystallization of sodium triphosphate, and that water was considered to promote the diffusion of the sodium ions.[5] In a similar way, the diffusion of the strontium ion in the amorphous phase, which was produced before the exothermic peak, might also be facilitated by water vapor, so that the crystallization of β-$Sr(PO_3)_2$ occurred under the humid conditions at a lower temperature.

Thermal Decomposition of Ammonium Strontium *cyclo*-Tetraphosphate $Sr(NH_4)_2P_4O_{12}$. The thermal analysis shows only the large endothermic peak at about 375 °C; this temperature was not influenced by the humidity. The endothermic peak corresponds to the elimination of ammonia from P_{4m}. The decomposition of P_{4m} was accompanied by the elimination of ammonia—analogously to the cleavage of P_{3m}.

The products above 375 °C always contained β-$Sr(PO_3)_2$. No exothermic peak caused by the transition of amorphous $Sr(PO_3)_2$ to β-$Sr(PO_3)_2$ was recognized; the endothermic peak may be supposed to conceal it.

Compared to the cases of $(NH_4)_6P_6O_{18}\cdot 1.5H_2O$ (215 °C) and $(NH_4)_4P_4O_{12}$ (238 °C),[9] the decomposition temperatures of P_{6m} (330 °C) and P_{4m} (420 °C) were heightened by the replacement of the NH_4^+ ion with the Sr^{2+} ion. The ring anions of all the ammonium strontium *cyclo*-phosphates studied (P_{3m}, P_{4m}, and P_{6m}) decomposed, accompanied by a weight loss. No corresponding exothermic peak attributable to the incorporation of water molecules, suggesting the radical formation,[9] was observed in the respective thermal analysis. The decompositions of $(NH_4)_6P_6O_{18}\cdot 1.5H_2O$ and $(NH_4)_4P_4O_{12}$ to the oligophosphate radicals were not influenced by the humidity,[9] whereas the degradation of P_{3m} and P_{6m} depended on the water vapor (Figs. 2 and 6); thus, P_{3m} and P_{6m} were not supposed to bring about a radical decomposition-polymerization. On the other hand, P_{4m} decomposed irrespective of the humidity. However, its thermal analysis showed no increase in weight and no exothermic peak. Accordingly, P_{4m} also could not be proved to produce oligophosphate radicals thermally. In conclusion, the radical decomposition-polymerization of *cyclo*-phosphates probably has no definite relation to the radius of the constituent cation.

The authors wish to thank Miss Fumine Shitani and Mr. Toshihiro Sumioka, who were students in the present college, for their helpful assistance.

References

1) D. E. C. Corbridge, "Phosphorus: An Outline of Its Chemistry, Biochemistry and Technology," 3rd ed, Elsevier Science, Amsterdam (1985), Chap. 3.
2) S. Ohashi, *Kogyo Kagaku Zasshi*, **66**, 16 (1963).
3) S. Ohashi and T. Nakamura, *Bull. Chem. Soc. Jpn.*, **35**, 498 (1962).
4) E. Thilo and H. Grunze, *Z. Anorg. Allg. Chem.*, **281**, 262 (1955).
5) J. D. McGilvery and A. E. Scott, *Can. J. Chem.*, **32**, 1100 (1954).
6) U. Schülke, R. Kayser, and L. Arndt, *Z. Anorg. Allg. Chem.*, **504**, 77 (1983).
7) H. Nariai, I. Motooka, Y. Kanaji, and M. Tsuhako, *Bull. Chem. Soc. Jpn.*, **60**, 1337 (1987).
8) E. Thilo and I. Grunze, *Z. Anorg. Allg. Chem.*, **290**, 209, 223 (1957).
9) A. Takenaka, I. Motooka, and H. Nariai, *Bull. Chem. Soc. Jpn.*, **60**, 4299 (1987).
10) B. E. Douglas and D. H. McDaniel, "Concepts and Models of Inorganic Chemistry," Blaisdell, Massachusetts (1965), Chaps. 3 and 9.
11) A. Durif, C. Martin, I. Tordjmann, and D. Tranqui, *Bull. Soc. Fr. Mineral. Cristallogr.*, **89**, 439 (1966); *Chem. Abstr.*, **66**, 109201e (1967).
12) D. Z. Serazetdinov, M. Kh. Kim, and A. B. Bekturov, *Vestn. Akad. Nauk Kaz. SSR*, **25**, 56 (1969); *Chem. Abstr.*, **71**, 108537k (1969).
13) W. Biedermann and G. Schwarzenbach, *Chimia*, **2**, 56 (1948); K. Ueno, "Kireto-Tekitei Ho," 11th ed., Nankodo, Tokyo (1965), p. 216.
14) S. Araki, T. Murakami, and S. Suzuki, "Bunseki Kagaku Jikken Shishin," ed by Nippon Bunseki Kagaku Kai, Tokyo Kagaku Dojin, Tokyo (1974), p. 139.
15) Ref. 14, p. 86.
16) "Shin Jikken Kagaku Koza," ed by Nippon Kagaku Kai, Maruzen, Tokyo (1976), Vol. 9(I), p. 183; B. H. Kindt, E. W. Balis, and H. A. Liebhafsky, *Anal. Chem.*, **24**, 1501 (1952).
17) E. J. Griffith, *Anal. Chem.*, **28**, 525 (1956).
18) D. N. Bernhart and A. R. Wreath, *Anal. Chem.*, **27**, 440 (1955).
19) I. Motooka, R. Endo, T. Morikawa, M. Ishizaki, and M. Kobayashi, *Kogyo Kagaku Zasshi*, **70**, 1097 (1967); A. E. Westmann, M. J. Smith, and P. A. Gartaganis, *Can. J. Chem.*, **37**, 1764 (1959).
20) R. C. Ropp, M. A. Aia, C. W. W. Hoffman, T. J. Veleker, and R. W. Mooney, *Anal. Chem.*, **31**, 1163 (1959).
21) R. V. Coates and G. D. Woodard, *J. Chem. Soc.*, **1964**, 1780.
22) H. M. Ondik and J. W. Gryder, *J. Inorg. Nucl. Chem.*, **14**, 240 (1960).
23) R. N. Bell, L. F. Audrieth, and F. Hill, *Ind. Eng. Chem.*, **44**, 568 (1952).
24) R. Remy-Gennete and J. Bourhis, *Bull. Soc. Chim. Fr.*, **1950**, 1162; *Chem. Abstr.*, **45**, 6109i (1951).
25) D. E. C. Corbridge and E. J. Lowe, *J. Chem. Soc.*, **1954**, 493.
26) M. H. Simonot-Grange, *J. Colloid Interface Sci.*, **70**, 231 (1979).
27) A. Thrierr-Sorel, D. Tacquenet, and M. H. Simonot-Grange, *Phosphorus and Sulfur*, **8**, 73 (1980).
28) I. Motooka, G. Hashizume, and M. Kobayashi, *Nippon Kagaku Zasshi*, **87**, 48 (1966).

 © 1989 The Chemical Society of Japan Bull. Chem. Soc. Jpn., 62, 2824—2829 (1989) [Vol. 62, No. 9

Equilibrium and Kinetic Studies of the Iron(III) Complex with *N*-Pyridoxylidene-L-tryptophan: Electronic Absorption and Circular Dichroism Spectral Characteristics, Stability, and Formation and Ligand-Substitution Reaction Mechanisms

Hideyuki KUNO, Ken-ichi OKAMOTO,† Jinsai HIDAKA,† and Hisahiko EINAGA*
Institute of Materials Science, University of Tsukuba, Tsukuba, Ibaraki 305
†Department of Chemistry, University of Tsukuba, Tsukuba, Ibaraki 305
(Received October 24, 1988)

Studies have been made of the electronic absorption and circular dichroism (CD) spectral characteristics, thermodynamic stability, and formation and ligand-substitution reaction kinetics of an iron(III) complex with *N*-pyridoxylidene-L-tryptophan (Hpdx-L-Htrp). The 1:2 (metal:ligand) complex forms in an acidic aqueous solution with the stability constant (β_2) of $\log \beta_2 = 18.38 \pm 0.10$ mol^{-2} dm^6 (0.50 mol dm^{-3} (NaCl), 25 °C). The complex shows a characteristic CD spectrum in the charge-transfer region. The kinetics were studied by a stopped-flow CD method in a 0.50 mol dm^{-3} aqueous NaCl solution at 25 °C. The formation of the complex proceeds through six parallel pathways of Fe^{3+}, $FeOH^{2+}$, and $FeCl^{2+}$ with H_2pdx-L-Htrp$^+$ and H_2pdx-L-trp, with the coordination of the carboxylato group to iron(III) as the rate-determining step. The ligand-substitution reaction of the complex by ethylenediamine-*N*,*N*,*N*′,*N*′-tetraacetic acid depends neither on the entering ligand nor on the hydrogen-ion concentration. The dissociation of a coordinated Hpdx-L-trp$^-$ from [Fe(Hpdx-L-trp)$_2$]$^+$ is concluded to be the rate-determining step. The reaction mechasnisms are discussed in detail.

Metal complexes containing Schiff bases of pyridoxal and optically active amino acids have attracted great attention as reaction intermediates since the pioneering work by Metzler and Snell[1] on the nonenzymatic transamination of the Schiff base of pyridoxal and glutamic acid. This is because these complexes play an important role not only in the transamination, but also in the racemization, decarboxylation, and related reactions, of the amino acids. Many studies have been made since that time of the structures of these Schiff-base complexes of various sorts of metal ions and amino acids; an iron(III) complex with pyridoxal and DL-valine has been isolated in the crystalline state, and its structure has been determined by the X-ray diffraction method.[2] However, little have been known on the reaction kinetics and mechanism as well as on the thermodynamic stability of these complexes.

In the present work, the formation and ligand-substitution reactions of the iron(III) complex with a Schiff base of pyridoxal and L-tryptophan(*N*-pyridoxylidene-L-tryptophan, Hpdx-L-Htrp) were investigated by means of the stopped-flow circular dichroism (CD) method. The iron(III) complex with Hpdx-L-Htrp was chosen here because the Schiff-base ligand forms quantitatively over a wide range of acidities and because the iron(III) complex is stable to coordinated-ligand reactions during a kinetic investigation. The reactions were studied in a 0.50 mol dm^{-3} aqueous sodium chloride solution in order to make it possible to compare the present work's to those in the literature data on *N*-pyridoxylidene-L(and/or D)-amino acids. The reaction mechanisms of the formation and ligand-substitution by ethylenediamine-*N*,*N*,*N*′,*N*′-tetraacetic acid (EDTA, H_4edta) of the iron(III) complex will be discussed in detail.

Experimental

Reagents. The analytical-grade reagents of pyridoxal (as hydrochloride) and L-tryptophan were supplied by the Tokyo Kasei Kogyo Co., Ltd., Tokyo, and the Wako Pure Chemicals Ind., Ltd., Osaka, and by the Kanto Chemical Co., Ltd., respectively. The Hpdx-L-Htrp was prepared by the condensation of pyridoxal and L-tryptophan in an aqueous solution in the usual manner. The ligand was characterized by the elemental analysis. A stock solution of iron(III) was prepared from $(NH_4)Fe(SO_4)_2 \cdot 12H_2O$ and was acidified with the minimum quantity of sulfuric acid necessary to prevent the hydrolysis of iron(III). The absence of traces of iron(II) was checked on the the stock solution by means of a reaction with 2,2′-bipyridine. The other reagents used were of an analytical or equivalent grade.

Measurements. The electronic absorption and CD spectra were recorded on a JASCO spectrophotometer, model UVIDEC-1M, and a JASCO spectropolarimeter, model J-500C. The protonation, stability, and rate constants were determined in a 0.50 mol dm^{-3} aqueous NaCl solution at 25.0±0.1 °C.

The pH of the solution was measured with an Orion Research digital pH meter, model 801A, with glass and saturated calomel electrodes. The hydrogen-ion concentration, $-\log [H^+]$, was calculated from the pH value, pH_{meas}, according to Eq. 1:

$$-\log [H^+] = pH_{meas} + \log f_{H^+} \quad (1)$$

The coefficient, f_{H^+}, was estimated on the basis of the literature procedure[3] by defining a solution containing 0.0100 mol dm^{-3} of HCl and 0.4900 mol dm^{-3} of NaCl at 25 °C as having $-\log [H^+] \equiv 2.00$.

The kinetic runs were carried out on the JASCO spectropolarimeter, to which were attached a stopped-flow apparatus, model SFC-5, a data processor, model DP-500, and a Watanabe Sokki X-Y recorder, model WX-441. The formation reaction was studied at 600 nm by following the

CD-intensity change with the time under the pseudo-first-order kinetic conditions for the metal-ion concentration. The ligand-substitution reaction of the iron(III) complex with Hpdx-L-Htrp by EDTA was studied at the same wavelength under the pseudo-first-order kinetic conditions used for the iron(III) complex concentration. These conditions satisfied the requirement that the CD intensity depends linearly on the concentration of the iron(III) complex with Hpdx-L-Htrp. This complex was stable enough to show no racemization of the coordinated ligand during the kinetic runs.

The observed rate constant, k_{obsd}, was calculated from the slope of the linear relation, $-\ln(\Delta E_t - \Delta E_\infty)$ vs. t, on the basis of Eq. 2:

$$\ln\{(\Delta E_0 - \Delta E_\infty)/(\Delta E_t - \Delta E_\infty)\} = k_{obsd}t \qquad (2)$$

where ΔE_0, ΔE_t, and ΔE_∞ stand for the CD intensities at the initial state, at time t, and at equilibrium, respectively. Good straight lines were obtained for the formation and lignd-substitution reactions for more than three half-life periods.

Results and Discussion

Electronic Absorption and CD Spectra. Figure 1 shows the electronic absorption and the CD spectra of the iron(III) complex, with the corresponding values for Hpdx-L-Htrp and the free ligand shown for the sake of comparison. The iron(III) complex gives new absorption bands as shoulders near 18×10^3 and 23×10^3 cm^{-1} assignable to the $t_{2g}(O_h)\leftarrow\pi$ and $\pi_2^*\leftarrow e_g(O_h)$ charge-transfer transitions, and a shoulder near 28×10^3 cm^{-1} and bands around 35×10^3 cm^{-1} assignable to the $\pi_1^*\leftarrow\pi$ (azomethine chromophore) and $\pi_2^*\leftarrow\pi$ (pyridine and indole ring chromophores) transitions of the coordinated ligand.[4-14] The CD spectrum of the iron(III) complex shows new negative and positive bands at 16.6×10^3 and 19.1×10^3 cm^{-1} in the $t_{2g}(O_h)\leftarrow\pi$ transition region due to a diastereoisomeric pair of the complex, Δ_{LL}-spiral and Λ_{LL}-spiral,[15] with the meridional (mer) coordination[2,16-19] of Hpdx-L-Htrp. The relatively large magnitude of the $\Delta\varepsilon$ on the CD spectrum indicates that one of the diastereoisomers is present in solution in preference to the other and that the CD spectral pattern in the $t_{2g}(O_h)\leftarrow\pi$ transition region reflects the total concentration of the complex.

Hence, the absorption and CD spectral bands in the wavenumber region below 21×10^3 cm^{-1} can be used for the thermodynamic and kinetic studies of the iron(III) complex with Hpdx-L-Htrp.

Stability. The protonation constants of Hpdx-L-Htrp were determined spectrophotometrically for $K_{a(phOH)}$ (=[Hpdx-L-trp$^-$]/[H$^+$][pdx-L-trp^{2-}]) at the absorption maximum of the pdx-L-trp^{2-} species (394 nm) and for $K_{a(pyNH)}$ (=[H$_2$pdx-L-trp]/[H$^+$][Hpdx-L-trp$^-$]) at that of the Hpdx-L-trp$^-$ species (390 nm), exept for $K_{a(COOH)}$ (=[H$_2$pdx-L-Htrp$^+$]/[H$^+$][H$_2$pdx-L-trp]), which was estimated separately (vide infra) because of the very small spectral changes on protonation to the H$_2$pdx-L-trp sepcies. The data are summarized in Table 1.

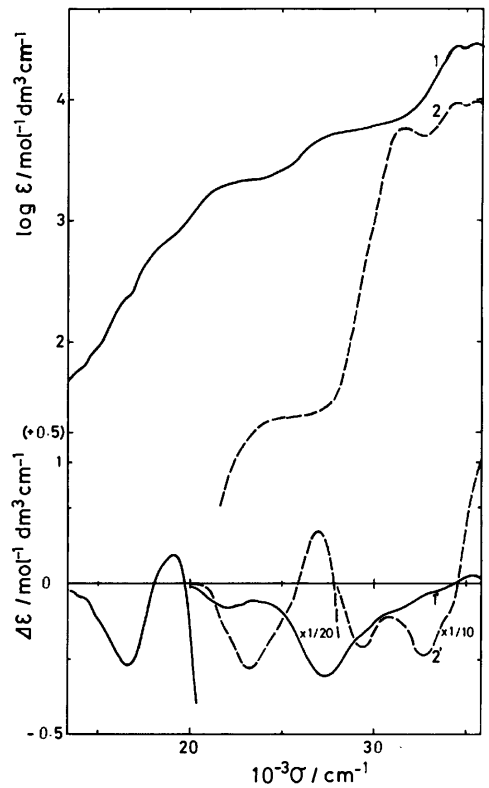

Fig. 1. Electronic absorption and CD spectra of iron(III) complex with Hpdx-L-Htrp in aqueous solution. 1,1': [Fe(Hpdx-L-trp)$_2$]$^+$; and 2,2': H$_2$pdx-L-trp species. The complex was used after isolation as a solid (Anal.($C_{38}H_{38}N_6O_8Cl_2FeCl\cdot H_2O$) C,H,N,Fe).

Table 1. Protonation and Stability Constants

	$\log K_{a(COOH)}$	$\log K_{a(pyNH)}$	$\log K_{a(phOH)}$
	mol^{-1} dm^3	mol^{-1} dm^3	mol^{-1} dm^3
Hpdx-L-Htrp[a]	2.30±0.05	4.10±0.05	8.24±0.05
	$\log\beta_1$	$\log\beta_2$	
	mol^{-1} dm^3	mol^{-2} dm^6	
[Fe(Hpdx-L-trp)$_2$]$^+$	9.65±0.10	18.38±0.10	

0.50 mol dm^{-3} (NaCl), 25 °C. a) The $K_{a(COOH)}$, $K_{a(pyNH)}$, and $K_{a(phOH)}$ of the ligand refer to the protonations at the carboxylate oxygen, pyridyl nitrogen, and phenolate oxygen respectively.

The stability constants of the iton(III) complex with Hpdx-L-Htrp were determined spectrophotometrically at 450 nm under the experimental conditions of $C_L \gg C_M$ (C_L and C_M are the total concentrations of iron(III) and Hpdx-L-Htrp; C_M is of the order of 10^{-4} mol dm^{-3}). By taking into consideration the hydrolysis constant ($\log K^{11}_{OH} = -2.72$ mol dm^{-3} (0.50 mol dm^{-3} ($NaClO_4$), 25 °C; $K^{11}_{OH} = [FeOH^{2+}][H^+]/[Fe^{3+}]$)[20,21] and the chloro complex formation constant ($\log \beta^1_{Cl} = 0.64$ mol^{-1} dm^3 (0.50 mol dm^{-3}(—), 25 °C; $\beta^1_{Cl} = [FeCl^{2+}]/[Fe^{3+}][Cl^-]$)[22] of iron(III), and the protonation constants of Hpdx-L-Htrp, the following relations can be derived[23] for the bis-ligand complex:

$$\log (A_{max} - A)/(A - A_{min}) = 2 \log \{k_{a(phOH)}[H^+] (K_{a(COOH)}[H^+] + 1)\} + \log (1 + K^{11}_{OH}[H^+]^{-1} + \beta^1_{Cl}[Cl^-]) - \log \beta_2 C_L^2 \quad (3)$$

and for the mono-ligand complex:

$$\log (A_{max}' - A)/(A - A_{min}) = \log \{k_{a(phOH)}[H^+] (K_{a(COOH)}[H^+] + 1)\} + \log (1 + K^{11}_{OH}[H^+]^{-1} + \beta^1_{Cl}[Cl^-]) - \log \beta_1 C_L \quad (4)$$

Here, A_{max} stands for the absorbance of a solution in which the bis-ligand complex forms quantitatively: A_{max}', for that of a solution in which the mono-ligand complex forms quantitatively; A_{min}, for that of a solution containing the ligand alone, and A, for that of a solution in which the bis-ligand or the mono-ligand complex and the free ligand coexist.

The experimental data are depicted in Fig. 2. Good linear relations with a slope of unity were obtained above $-\log [H^+]$ of 2.3 (cf. line 1) and below 1.9 (cf. line 2) with a suitable assumption of the value of A_{max}' between the absorbance and the hydrogen-ion-concentration terms of Eqs. 3 and 4, respectively. The stability constants for the bis-ligand complex (β_2) and the mono-ligand complex (β_1) are summarized in Table 1.

The behavior of pyridyl nitrogen during the complex formation should also be discussed. In a weakly acidic aqueous solution, the principal complex formation reaction equilibrium can be expressed as follows ($C_L \gg C_M$):

$$Fe^{3+} + 2\,H_2pdx\text{-}L\text{-}trp \rightleftharpoons [Fe(Hpdx\text{-}L\text{-}trp)_2]^+ + 2H^+ \quad (5)$$

Here, pyridyl nitrogen was assumed still to be protonated in the coordinated ligand, because a reasonable analysis of the experimental data on absorbance vs. the hydrogen-ion concentration based on the formation of $[Fe(pdx\text{-}L\text{-}trp)_2]^-$ and the liberation of four protons per complex instead of Eq. 5 was unsuccessful. This means that the coordination of

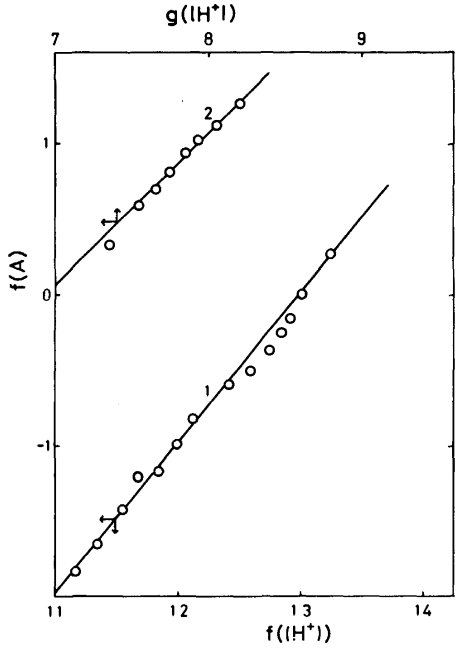

Fig. 2. Dependence of $f(A)$ on $f([H^+])$ and on $g([H^+])$. $f(A) \equiv \log (A_{max} - A)/(A - A_{min})$ or $\log (A_{max}' - A)/(A - A_{min})$, $f([H^+]) \equiv 2 \log \{K_{a(phOH)}[H^+](K_{a(COOH)}[H^+]+1)\} + \log (1 + K^{11}_{OH}[H^+]^{-1} + \beta^1_{Cl}[Cl^-])$, $g([H^+]) \equiv \log \{K_{a(phOH)}[H^+](K_{a(COOH)}[H^+]+1)\} + \log (1 + K^{11}_{OH}[H^+]^{-1} + \beta^1_{Cl}[Cl^-])$, C_L: 2.00×10^{-3} mol dm^{-3}; C_M: 1.25×10^{-4} mol dm^{-3}; 0.50 mol dm^{-3} (NaCl); 25 °C; and λ: 450 nm.

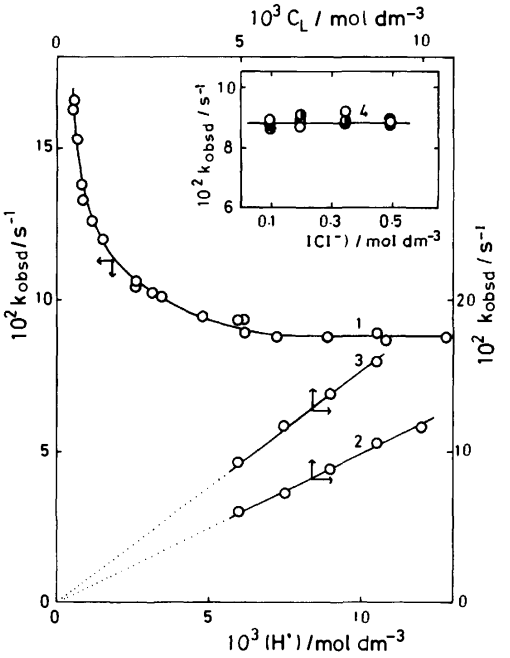

Fig. 3. Dependence of k_{obsd} on $[H^+]$, on C_L, and on $[Cl^-]$. 1: C_L: 7.50×10^{-3} mol dm^{-3}; C_M: 2.50×10^{-4} mol dm^{-3}; 0.50 mol dm^{-3} (NaCl). 2: C_M: 2.50×10^{-4} mol dm^{-3}; $[H^+]$: 1.05×10^{-2} mol dm^{-3}; 0.50 mol dm^{-3} (NaCl). 3: C_M: 2.50×10^{-4} mol dm^{-3}; $[H^+]$: 8.10×10^{-4} mol dm^{-3}; 0.50 mol dm^{-3} (NaCl). 4: C_L: 7.50×10^{-3} mol dm^{-3}; C_M: 2.50×10^{-4} mol dm^{-3}; $[H^+]$: 7.18×10^{-3} (◐), 1.05×10^{-2} (○), and 1.28×10^{-2} mol dm^{-3} (◑); $[NaCl]+[NaClO_4]$: 0.50 mol dm^{-3}. 25 °C; and λ: 600 nm.

Hpdx-L-Htrp to iron(III) has little influence on the basicity of pyridyl nitrogen.

Formation-Reaction Kinetics. Experimental data on the relations between k_{obsd} and $[H^+]$, k_{obsd} and C_L, and k_{obsd} and $[Cl^-]$ under the conditions of $C_L \gg C_M$ are given in Fig. 3. The linear relation between k_{obsd} and C_L at constant $[H^+]$ and $[Cl^-]$ values, which can be extrapolated to the point of origin, indicates that the coordination of the first Hpdx-L-Htrp to iron(III) corresponds to the rate-determining step.

In the formation of the mono-ligand complex as the rate-determining step, six reaction pathways contributing Fe^{3+}, $FeOH^{2+}$, and $FeCl^{2+}$ for the metal ion and H_2pdx-L-Htrp$^+$ and H_2pdx-L-trp for the ligand are possible by taking into consideration the protonation constants of the ligand, the hydrolysis constant of iron(III), and the stability constants of the chloro and the Hpdx-L-Htrp complexes, and the rapid attainment of equilibria for the protolytic processes[3] as compared with the complex formation process. The following rate equation can be derived under the pseudo-first-order kinetic conditions for C_M:

$$d[[Fe(Hpdx\text{-}L\text{-}trp)_2]^+]/dt = k_{obsd}([[Fe(Hpdx\text{-}L\text{-}trp)_2]^+]_\infty - [[Fe(Hpdx\text{-}L\text{-}trp)_2]^+]) \quad (6)$$

$$k_{obsd}(1 + K^{11}_{OH}[H^+]^{-1} + \beta^1_{Cl}[Cl^-])(K_{a(COOH)}[H^+] + 1)\, C_L^{-1} = (k_{31} + k_{21(Cl)}\beta^1_{Cl}[Cl^-])K_{a(COOH)}[H^+] + k_{30} + k_{20(Cl)}\beta^1_{Cl}[Cl^-] + k_{21}K^{11}_{OH}K_{a(COOH)} + k_{20}K^{11}_{OH}[H^+]^{-1} \quad (7)$$

Here, k_{ij} is the rate constant for the reaction pathway of $[Fe(OH)_{3-i}]^{i+}$ (i=2 and 3), and $k_{2i(Cl)}$, that for the pathway of $FeCl^{2+}$ with H_2pdx-L-H$_j$trp^{j+} (j=0 and 1).

The experimental data given in Fig. 3 indicate that k_{obsd} is constant in the case of changes in $[Cl^-]$ within the limits of experimental error and that the k_{obsd} value can be classified by acidity region: that in the higher-acidity region, where the contribution of the pathway of k_{20} can be neglected, and that in the lower-acidity region, where that of the pathways of k_{31} and $k_{21(Cl)}$ can be neglected. Firstly, the data in the higher-acidity region ($-\log [H^+] < 2.4$) were analyzed at a constant $[Cl^-]$ under the assumption of a suitable numerical value of $K_{a(COOH)}$ so that a good linear relation could be obtained between $k_{obsd}(1+K^{11}_{OH}[H^+]^{-1}+\beta^1_{Cl}[Cl^-])(K_{a(COOH)}[H^+]+1)\, C_L^{-1}$ and $[H^+]$. Secondly, by using the $K_{a(COOH)}$ value thus estimated and the intercept, which is equal to the $k_{30}+k_{20(Cl)}\beta^1_{Cl}[Cl^-]+k_{21}K^{11}_{OH}K_{a(COOH)}$ derived from the above relation, the data in the lower-acidity region ($-\log [H^+] > 2.4$) were analyzed for the linear relation between $k_{obsd}(1+K^{11}_{OH}[H^+]^{-1}+\beta^1_{Cl}[Cl^-])(K_{a(COOH)}[H^+]+1)\, C_L^{-1}$ and $[H^+]^{-1}$. Finally, $k_{31}K_{a(COOH)}+k_{21(Cl)}\beta^1_{Cl}K_{a(COOH)}[Cl^-]$ and $k_{30}+k_{21}K^{11}_{OH}K_{a(COOH)}+k_{20(Cl)}\beta^1_{Cl}[Cl^-]$ were plotted against $[Cl^-]$ to obtain the individual rate constant. Those of k_{31}, $k_{31(Cl)}$, k_{20}, $k_{20(Cl)}$, and $k_{30}+k_{21}K^{11}_{OH}K_{a(COOH)}$, the last of which cannot be separated because of the proton ambiguity (vide infra), are summarized in Table 2.

Many kinetic data have been reported[24] for the iron(III) complexes with various sorts of ligands. The rate constant for the pathway of Fe^{3+} with H_2pdx-L-Htrp$^+$, k_{31}, is in close proximity to the constants for the reaction pathways of Fe^{3+} with aliphatic carboxylic acids. This fact indicates that the coordination of Hpdx-L-Htrp to iron(III) proceeds through the donation of the carboxylato group of the amino acid moiety rather than the phenolato group of the pyridoxal moiety, because the analysis of kinetic data by using $K_{a(phOH)}$ instead of $K_{a(COOH)}$ gave an extremely small and unreasonable magnitude of k_{31}. Furthermore, this close proximity in the rate constants substantiates the fact that the rate-determining step of the reaction of iron(III) with Hpdx-L-Htrp lines in the coordination of the first ligand to iron(III), because the rate constants for Fe^{3+} with these carboxylic acid ligands have been determined on the mono(carboxylato)iron(III) complexes.[25-32]

Contrary to k_{31}, k_{20} is considerably smaller than the value of $FeOH^{2+}$ with $ClCH_2COO^-$ (k_{20}: $(4.1\pm0.2)\pm10^4$ mol^{-1} dm^3 s^{-1} (1 mol dm^{-3}($NaClO_4$), 25 °C).[25] The magnitude of k_{20} reflects the fact that the carboxylato group of H_2pdx-L-trp ligand species may not be free, but hydrogen-bonded. There is a possibility of an intramolecular hydrogen bond between the hydroxyl and the carboxylato groups for the enol imine form and also between the imino hydrogen and the carboxylato group for the keto enamine form of Hpdx-L-Htrp. This role of the intramolecular hydrogen bond is substantiated by a comparison of the rate constant for $FeOH^{2+}$ with $ClCH_2COO^-$ (k_{20}: vide supra) with that for $FeOH^{2+}$ with the monoprotonated salicylato ligand (k_{21}: 2.9×10^3 mol^{-1} dm^3 s^{-1} (0.1 mol dm^{-3}

Table 2. Rate Constants for the Iron(III) Complex with Hpdx-L-Htrp

Pathway	k_{ij} / mol^{-1} dm^3 s^{-1}
$Fe^{3+}+H_2$pdx-L-Htrp$^+$ (k_{31})	10.1±0.3
$Fe^{3+}+H_2$pdx-L-trp and $FeOH^{2+}+H_2$pdx-L-Htrp$^+$ ($k_{30}+k_{21}K^{11}_{OH}K_{a(COOH)}$)	21.3±0.6
$FeCl^{2+}+H_2$pdx-L-Htrp$^+$ ($k_{21(Cl)}$)	11.7±0.3
$FeCl^{2+}+H_2$pdx-L-trp ($k_{20(Cl)}$)	11.5±0.3
$FeOH^{2+}+H_2$pdx-L-trp (k_{20})	32.5±0.3
$[Fe(Hpdx\text{-}L\text{-}trp)_2]^+$ ($+H_2O$) ($k_{-3\bar{1}}$)	2.9±0.3[a]

0.50 mol dm^{-3} (NaCl), 25 °C. a) $k_{-3\bar{1}}$/s^{-1}.

($LiClO_4$), 25 °C[31] and (1.4±0.1) $\times 10^4$ mol^{-1} dm^3 s^{-1} (1.0 mol dm^{-3} (KNO_3), 25 °C[32]). The progress of the reaction through the donation of the carboxylato group indicates that there are no fundamental differences in the kinetics of the enol imine and the keto enamine forms of Hpdx-L-Htrp.

The rate constant, $k_{21(Cl)}$, is very close to k_{31}, as can be expected from independence of k_{obsd} on [Cl^-] at constant C_L and [H^+] values. There have been several papers[33-36] concerning with kinetics of Fe^{3+} with Cl^-; the rate-determining step for the formation of $FeCl^{2+}$ from Fe^{3+} and Cl^- has been concluded to be the release of a water molecule from the primary coordination sphere of iron(III).[33,35] The kinetic data (k/mol^{-1} dm^3 s^{-1} ($Fe^{3+}+Cl^-$): 9.4±1.0[33] and 4.8±0.4;[36] and k/s^{-1} ($FeCl^{2+}+H_2O$): 2.3±0.2[33] and 3.2±0.2[36] (1.0 mol dm^{-3},[33] and 1.5 mol dm^{-3} ($NaClO_4$), 25 °C[36]) and the ^{35}Cl and ^{17}O NMR spectral data[34,35] on the exchange of a water molecule and a chloride ion between the primary coordination sphere of the chloro and aqua iron(III) complex species and the bulk solvent establish that the exchange process, together with the protolytic reaction of $Fe^{3+} \rightleftharpoons FeOH^{2+}+H^+$, is rapid enough for us to regard the process as a reversible pre-equilibrium for the kinetic process of Fe^{3+} with Hpdx-L-Htrp. Our experimental data on the close proximity of $k_{21(Cl)}$ to k_{31} support this deduction: The coordinated chloro ligand makes no intrinsic contribution to the coordination reaction kinetics of Hpdx-L-Htrp to iron(III).

The deduction mentioned above indicates that k_{21} can be estimated from the composite rate constants of $k_{30}+k_{21}K_{OH}^{11}K_{a(COOH)}$ given in Table 2, because k_{30} can reasonably be assumed to be equal to $k_{20(Cl)}$. The value of k_{21} thus calculated was 26±6 mol^{-1} dm^3 s^{-1}.

It can be summarized that the formation of the iron(III) complex with Hpdx-L-Htrp proceeds through the parallel pathways of Fe^{3+}, $FeOH^{2+}$, and $FeCl^{2+}$ with H_2pdx-L-Htrp$^+$ and H_2pdx-L-trp via the coordination of the carboxylato group to iron(III) as the mechanistic rate-determining step. This coordination of the carboxylato group follows the rapid coordination of the azomethine nitrogen and the phenolato oxygen to form an intermediate, Fe(Hpdx-L-trp)$^{2+}$, with five- and six-membered fused chelate rings. The coordination of the second Hpdx-L-Htrp to the intermediate proceeds in just the same way as that of the first one, but in a more rapid way as a result of the labilization[3,37] of the remaining coordinated water molecules in Fe(Hpdx-L-trp)$^{2+}$ to complete the thermodynamically more stable [Fe(Hpdx-L-trp)$_2$]$^+$.

Ligand-Substitution Reaction Kinetics. Fe(Hpdx-L-trp)^2]$^+$ gives a ligand-substitution with EDTA to form Fe(edta)$^-$ quantitatively in an acidic aqueous solution under the experimental conditions of $C_{edta} \gg C_M$ and $2C_L > C_M$. The ligand-substitution reaction was of the first order with respect to the starting complex concentration, as has been described in the Experimental section. The relations between k_{obsd} and C_{edta}, between k_{obsd} and [H^+], and between k_{obsd} and C_L are given in Table 3. The k_{obsd} depends neither on C_{edta}, C_L, nor [H^+]; the ligand-substitution reaction proceeds by means of the dissociation of one of the Hpdx-L-trp$^-$ ligands from [Fe(Hpdx-L-trp)$_2$]$^+$ to form Fe(Hpdx-L-trp)$^{2+}$ as an intermediate as the rate-determining step:

Table 3. Kinetic Data of the Ligand-Substitution Reaction

[H^+]	C_{edta}	C_L	k_{obsd}
10^3 mol dm^{-3}	10^2 mol dm^{-3}	10^3 mol dm^{-3}	s^{-1}
0.575	0.500	3.00	2.87
3.24	0.500	3.00	3.20
3.98	0.500	3.00	2.95
5.89	0.500	3.00	3.03
8.71	0.500	3.00	2.96
9.77	0.500	3.00	3.06
4.91	0.250	3.00	2.87
4.91	0.500	3.00	2.91
4.27	1.00	3.00	3.00
5.01	1.00	3.00	2.96
3.98	1.50	3.00	3.23
4.27	1.70	3.00	2.80
4.57	1.75	3.00	2.77
4.57	0.500	2.00	2.94
4.57	0.500	2.50	3.01
4.57	0.500	3.50	3.07
4.57	0.500	4.00	2.86

C_M: 1.00×10^{-4} mol dm^{-3}, 0.50 mol dm^{-3} (NaCl), 25 °C.

$$-d[[Fe(Hpdx\text{-}L\text{-}trp)_2]^+]/dt = k_{obsd}[[Fe(Hpdx\text{-}L\text{-}trp)_2]^+] \quad (8)$$

$$k_{obsd} = k_{-3\bar{1}} \quad (9)$$

The rate constant, $k_{-3\bar{1}}$, as estimated from Table 3, is given in Table 2.

The ligand-substitution reaction of [Fe(Hpdx-L-trp)$_2$]$^+$ with EDTA belongs to a simple aquation, because the reaction is of zeroth order with respect to the entering and leaving ligand concentrations, which fact rules out the liberation of the second ligand from Fe(Hpdx-L-trp)$^{2+}$ or its mixed-ligand complex with EDTA as an intermediate as the rate-determining step. Furthermore, the pathway of [Fe(Hpdx-L-trp)$_2$]$^+$+H^+ and analogous proton-assisted pathways, which are anticipated from the formation reaction kinetics, are impracticable in the present ligand-substitution reaction. Only the pathway of [Fe(Hpdx-L-trp)$_2$]$^+$ (+H_2O) to form Fe(Hpdx-L-trp)$^{2+}$ and Hpdx-L-trp$^-$, the latter of which will rapidly protonate to form H_2pdx-L-trp and H_2pdx-L-Htrp$^+$, is practicable. The mechanistic rate-determining step may be the dissociation from the central metal atom of the carboxylato group of the coordinated ligand in the thermodynamically more stable [Fe(Hpdx-L-trp)$_2$]$^+$ by taking the kinetic characteristics of the formation and the basicity of the ligating groups on Hpdx-L-Htrp into consideration.

In conclusion, *N*-pyridoxylidene-L-tryptophan forms a 1:2 (metal: ligand) complex with iron(III) of a high thermodynamic stability and lability. The coordination of the ligand proceeds through six parallel pathways of Fe^{3+}, $FeOH^{2+}$, and $FeCl^{2+}$ with H_2pdx-L-Htrp$^+$ and H_2pdx-L-trp, with the donation of the carboxylato oxygen to iron(III) as the rate-determining step. This coordinated ligand leaves the central metal atom dissociatively, even in the presence of other multidentate ligands, through the pathway of Fe(Hpdx-L-trp)$^{2+}$ and Hpdx-L-trp$^-$, with cleavage of the carboxylato oxygen-iron(III) bond as the rate-determining step.

References

1) D. E. Metzler and E. E. Snell, *J. Am. Chem. Soc.*, **74**, 979 (1952).
2) H. N. Christensen, *J. Am. Chem. Soc.*, **79**, 4073 (1957).
3) Y. Hara, K. Okamoto, J. Hidaka, and H. Einaga, *Bull. Chem. Soc. Jpn.*, **57**, 1211 (1984).
4) D. Heinert and A. E. Martell, *J. Am. Chem. Soc.*, **85**, 183 (1963).
5) L. Casella and M. Gullotti, *J. Am. Chem. Soc.*, **105**, 803 (1983).
6) J. C. Tomkinson and R. J. P. Williams, *J. Chem. Soc.*, **1958**, 1153.
7) C. K. Jørgensen, *Acta Chem. Scand.*, **16**, 2406 (1962).
8) A. Syamal, *Can. J. Chem.*, **47**, 1693 (1969).
9) H. F. Steger, *J. Inorg. Nucl. Chem.*, **37**, 39 (1975).
10) Y. Matsushima and A. E. Martell, *J. Am. Chem. Soc.*, **89**, 1322 (1967).
11) L. Casella and M. Gullotti, *J. Am. Chem. Soc.*, **10**, 6338 (1981).
12) L. Casella and M. Gullotti, *Inorg. Chem.*, **25**, 1293 (1986).
13) J. S. Griffith, "The Theory of Transition Metal Ions," Cambridge Univ. Press, London (1971), p. 301.
14) A. B. P. Lever, "Inorganic Electronic Spectroscopy," 2nd ed, Elsevier, Amsterdam (1984), pp. 452—453.
15) The *Δ*LL- and *Λ*LL-spiral configurations are defined respectively, on the right-handed and the left-handed spirals of two meridionally chelated Hpdx-L-Htrp ligands around the C_2 axis of the complex.
16) J. F. Cutfield, D. Hall, and T. N. Waters, *J. Chem. Soc., Chem. Commun.*, **1967**, 785.
17) E. H. Abbott and A. E. Martell, *J. Am. Chem. Soc.*, **91**, 6866 (1969); **92**, 5845 (1970).
18) S. Capasso, F. Giordano, C. Mattia, L. Mazzarella, and A. Ripamonti, *J. Chem. Soc., Dalton Trans.*, **1974**, 2228.
19) K. Aoki and H. Yamazaki, *J. Chem. Soc., Chem. Commun.*, **1980**, 363.
20) C. F. Baes, Jr., and R. E. Mesmer, "The Hydrolysis of Cations," Wiley, New York (1976), pp. 229—237.
21) L. G. Sillen and A. E. Martell, "Stability Constants of Metal-Ion Complexes," Chem. Soc., London (1964), Sp. Pub. No. 17, p. 53.
22) R. M. Smith and A. E. Martell, "Critical Stability Constants," Plenum Press, New York (1976), Vol. 4, p. 106.
23) Here, very small molar absorption coefficients of the aqua and hydroxo complex species (cf. Ref. No. 20, p. 232) and of the chloro complex species (cf. Ref. No. 33) of iron(III), compared with those of the iron(III) complex with Hpdx-L-Htrp and the free ligand species at 450 nm, are assumed. For the derivation of Eqs. 3 and 4, consult Ref. No. 3.
24) For example: D. W. Margerum, G. R. Cayley, D. C. Weatherburn, and G. K. Pagenkopf, "Coordination Chemistry," ed by A. E. Martell, Am. Chem. Soc., Washington, D. C. (1978), Vol. 2, pp. 68 and 109—111.
25) B. Perlmutter-Hayman and E. Tapuhi, *J. Coord. Chem.*, **6**, 31 (1976).
26) F. A. Accascina, F. P. Cavasino, and E. D. Dio, *Trans. Faraday Soc.*, **65**, 489 (1969).
27) R. N. Pandey and W. MacF. Smith, *Can. J. Chem.*, **50**, 194 (1972).
28) S. Gouder and J. Stuehr, *Inorg. Chem.*, **13**, 379 (1974).
29) K. Nakamura, T. Tsuchida, A. Yamagishi, and M. Fujimoto, *Bull. Chem. Soc. Jpn.*, **46**, 456 (1973).
30) F. P. Cavasino and E. D. Dio, *J. Chem. Soc. A*, **1970**, 1151.
31) P. G. T. Fogg and R. J. Hall, *J. Chem. Soc. A*, **1971**, 1365.
32) G. Saini and E. Mentasti, *Inorg. Chim. Acta*, **4**, 585 (1970).
33) R. E. Connick and C. P. Coppel, *J. Am. Chem. Soc.*, **81**, 6389 (1959).
34) A. H. Zeltmann and L. O. Morgan, *J. Phys. Chem.*, **70**, 2807 (1966).
35) F. A. Accascina, F. P. Cavascino, and S. D'Alessandro, *J. Phys. Chem.*, **71**, 2474 (1976).
36) B. B. Hasinoff. *Can. J. Chem.*, **54**, 1820 (1976).
37) I. Ohkura, K. Fujiwara, K. Okamoto, J. Hidaka, and H. Einaga, *J. Coord. Chem.*, **13**, 221 (1984).

Redox Behaviors of Glassy Carbon Electrodes Modified with $[Fe_4X_4(YC_6H_4\text{-}p\text{-}t\text{-}C_4H_9)_4]^{2-}$ (X, Y=S and Se) in Water

Koji TANAKA,* Masami NAKAMOTO,† Yoshihisa TARU, and Toshio TANAKA
Department of Applied Chemistry, Faculty of Engineering, Osaka University, Yamada-oka, Suita, Osaka 565
†Osaka Municipal Technical Research Institute, Morinomiya, Joto-ku, Osaka 536
(Received March 24, 1989)

Cyclic voltammograms of glassy carbon electrode modified with iron-sulfur and iron-selenium clusters $(Bu_4N)_2[Fe_4X_4(YC_6H_4\text{-}p\text{-}t\text{-}C_4H_9)_4]$ (X, Y=S, Se) show the stable (2−/3−) redox couple in water, and the peak potentials of those redox waves are shifted by the change of pH due to reversible protonations not only of the oxidized but also of the reduced clusters. The electron transfer between the cluster and the glassy carbon plate is also influenced by the protonation equilibrium. A retardation of the electron transfer caused by the protonation of the cluster may be associated with a reorganization energy required in the redox reaction of the protonated cluster.

Synthetic Fe_4S_4 clusters with arene- and alkanethiolate ligands as models of 4Fe ferredoxins show reversible or pseudo-reversible $[Fe_4S_4]^{2+/+}$ redox couple not only in organic solvents but also in aqueous solutions.[1] On the other hand, some of biological redox reactions mediated by iron sulfur proteins involve a multi-electron transfer process such as NO_3^-[2] and SO_4^{2-}[3]-reductions, CO_2-assimilation,[4] and N_2-fixation.[5] Among those multi-electron reductions, N_2 fixation is especially interested in the viewpoint of the fact that N_2 is reduced with eight electrons to afford NH_3 and H_2, where unstable N_2H_2 is proposed as a reaction intermediate.[6] The construction of a catalytic system which can transport electrons rapidly to the reaction center, therefore, is desired in order to simulate multi-electron reductions involving unstable intermediates, otherwise the reaction intermediate may be decomposed without affording the final reduction product. In accordance with this view, six- and eight-electron reductions of RN_3 (R=CH_2CH_2OH) affording N_2H_4 and NH_3 via N_2H_2 can be achieved by using glassy carbon electrodes modified with $[Fe_6Mo_2S_8(SPh)_9]^{3-}$,[7] $[Fe_3MoS_4(SPh)_3(quinone)]_2^{4-}$,[8] and $[Fe_4S_4(SPh)_4]^{2-}$[8] under the controlled potential electrolysis at −1.25 V vs. SCE in H_2O, whereas the same clusters can catalyze only the two-electron reduction of RN_3 affording RNH_2 and N_2 under the electrolysis at the same potential in a homogeneous MeOH/THF solution. The superiority of the heterogeneous electrolysis to the homogeneous one with respect to a multi-electron reduction of RN_3 may be ascribed to an efficient multi-electron transfer to the cluster directly attached to the electrode in the former. Thus a multi-electron reduction involving unstable reaction intermediates can be achieved by a catalytic system which is provided with the ability of transport multi-electrons rapidly to the reaction center. On the basis of the fact that 4Fe ferredoxins mediate multi-electron transfer processes in biological reductions, synthetic Fe_4S_4 cluster modified electrodes may be applicable as redox catalysts to a wide range of reductions involving a multi-electron process. It seems, therefore, to be very important to elucidate the factor determining the rate of the electron transfer in the cluster-modified electrodes.

Experimental

General Procedure and Materials. All manipulations were carried out under N_2 atmosphere. Iron-sulfur and iron-selenium clusters $(Bu_4N)_2[Fe_4S_4(SC_6H_4\text{-}p\text{-}t\text{-}Bu)_4]$ ($(Bu_4N)_4$-[4FeSS]), $(Bu_4N)_2[Fe_4S_4(SeC_6H_4\text{-}p\text{-}t\text{-}Bu)_4]$ ($(Bu_4N)_2$[4FeSSe]), $(Bu_4N)_2[Fe_4Se_4(SC_6H_4\text{-}p\text{-}t\text{-}Bu)_4]$ ($(Bu_4N)_2$[4FeSeS]), and $(Bu_4N)_2[Fe_4Se_4(SeC_6H_4\text{-}p\text{-}t\text{-}Bu)_4]$ ($(Bu_4N)_2$[4FeSeSe]) were prepared according to a literature.[9] Commercially available guaranteed reagents grades of NaOH and H_3PO_4 were used without further purification. Glassy carbon electrodes modified with a cluster (1×10^{-9}—1×10^{-6}mol cm^{-2}) were prepared by addition of a given amount of a CH_3CN solution of each cluster (1.0 mmol dm^{-3}) on a polished surface of the glassy carbon plates (1.0 cm^2) by syringe techniques and dried for ca. 30 min under dry N_2 stream.[7]

Physical Measurements. Cyclic voltammograms of cluster-modified electrodes were obtained at 298 K in H_2O by using a Hokuto Denko potentialstat HB-401, a Hokuto Denko function generator HB-107, and a Yokogawa Electric X-Y recorder 3077. H_3PO_4–NaOH was used as a supporting electrolyte in aqueous solutions.

Results and Discussion

Cyclic Voltammograms of Glassy Carbon Electrodes Modified with Clusters. It has been reported that Fe_4S_4 clusters attached covalently to a SnO_2 electrode[10] and incorporated in electrode-bound ion-exchange polymer[11] undergo a pseudo-reversible or reversible redox reaction in organic solvents. Compared with those Fe_4S_4 cluster-coated electrodes, the current cluster-modified electrode can be quite easily prepared. The cyclic voltammogram of the glassy carbon electrode modified with $(Bu_4N)_2[Fe_4S_4(SC_6H_4\text{-}p\text{-}t\text{-}Bu)_4]$ ([4FeSS]/GC; 1×10^{-8} mol cm^{-2}) in water (pH 11.9) at 10 mV s^{-1} shows an anodic wave at −0.93 V vs. SCE together with a strong cathodic current at potentials more negative than −1.2 V due to not only the reduction of the cluster modified on the glassy carbon plate but also the evolution of H_2 catalyzed by the

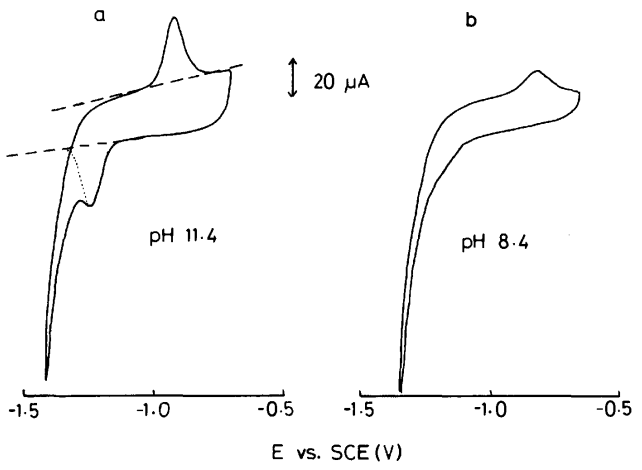

Fig. 1. Cyclic voltammograms of the glassy carbon electrode modified with $(Bu_4N)_2[Fe_4S_4(SC_6H_4\text{-}p\text{-}t\text{-}Bu)_4]$ (1.0×10^{-8} mol dm^{-2}) in H_2O at pH 11.4 (a) and at pH 8.4 (b), dE/dt=10 mV s^{-1}; a dotted line (a) represents the pattern of the anodic wave.

reduced species of the cluster[12] (a solid line in Fig. 1a). The cyclic voltammogram of the [4FeSS/GC] was unchanged essentially even in a multi-scanning for 1 h. Thus, the Fe_4S_4 cluster modified on the GC plates stably undergoes a redox reaction in water. The cathodic wave at −1.24 V is almost superimposable on the anodic one at −0.93 V (a dotted line in Fig. 1a).[13] In addition, the electricity calculated from the area of the anodic wave corresponded to the number of $[4FeSS]^{2-}$ molecules modified on the electrode with the ratio of electron/molecule=1.00±0.02. These results clearly indicate that almost all the clusters undergo the $[4FeSS]^{2-/3-}$ redox reaction (Eq. 1) on the GC plate.

$$[Fe_4S_4(SC_6H_4\text{-}p\text{-}t\text{-}Bu)_4]^{2-} + e^- \rightleftharpoons [Fe_4S_4(SC_6S_4(SC_6H_4\text{-}p\text{-}t\text{-}Bu)_4]^{3-} \quad (1)$$

On the other hand, the change of pH of the aqueous phase from 11.4 to 8.3 causes a shift of the anodic wave from −0.93 to −0.82 V with decreasing the electricity of the wave at the same scanning rate (10 mV s^{-1}). At the same time, the cathodic wave was almost concealed by the anodic shift of the threshold potential of H_2 evolution (Fig. 1b). Such the change of the cyclic voltammogram of [4FeSS]/GC at pH 8.3 results from neither the decomposition nor stripping off the cluster from the GC plate since the cyclic voltammogram of [4FeSS]/GC at pH 11.4 was regenerated when the pH was put back to 11.4. The cyclic voltammograms of glassy carbon electrodes modified with $(Bu_4N)_2[Fe_4S_4(SeC_6H_4\text{-}p\text{-}t\text{-}Bu)_4]$, $(Bu_4N)_2[Fe_4Se_4(SC_6H_4\text{-}p\text{-}t\text{-}Bu)_4]$, and $(Bu_4N)_2[Fe_4Se_4(SeC_6H_4\text{-}p\text{-}t\text{-}Bu)_4]$ ([4FeSSe]/GC, [4FeSeS]/GC, and [4FeSeSe]/GC, respectively) also exhibit the similar pH dependence as that of [4FeSS]/GC in H_2O.

The redox reaction of the Fe_4S_4 cluster-modified electrode is accompanied by the transport of the counter ion of the cluster between the redox center on the GC plate and the contacting aqueous electrolyte solutions. The migration of the counter ion of the cluster for the charge neutrality, therefore, largely influences the stability of the cluster modified electrodes. For example, the cyclic voltammogram of a glassy carbon plate modified with $(Et_4N)_4[Fe_4S_4(SC_6H_5)_4]$ was essentially consistent with that with the [4FeSS]/GC (Fig. 1). The anodic wave of the former, however, was almost disappeared in the multi-scanning cyclic voltammogram for 30 min, while the decrease in the anodic peak current of the glassy carbon electrode modified with $(Bu_4N)_2[Fe_4S_4(SC_6H_5)_4]$ was about 20% in the multi-scanning cyclic voltammogram for 1 h. Thus, a bulky counter ion of the cluster stabilizes the modified electrode. In addition, the Bu_4N^+ salt of the Fe_4S_4 cluster with the terminal ligand $SC_6H_4\text{-}p\text{-}t\text{-}Bu$ in place of SC_6H_5 further improved the stability of the cluster-modified electrode, as described in a previous section. It should be mentioned that the cyclic voltammogram of the Fe_4S_4 cluster-modified electrode did not show any redox couple of the cluster in the case a bulky Bu_4NClO_4 was used as an electrolyte in pure H_2O.[14] This fact clearly indicates that the charge neutrality in the [4FeXY]/GC (X, Y=S, Se) is maintained by the transport of Na^+ from the aqueous NaOH–H_3PO_4 buffer solution rather than that by H^+.[15] If the diffusion coefficient of Na^+ in the [4FeXY]/GC is assumed to be constant in the experimental pH region, the pH dependent cyclic voltammogram of [4FeXY]/GC (see Fig. 1a and 1b) is ascribed to the change of the proton concentrations in the aqueous phase. In accordance with this, not only oxidized but also reduced species of the current clusters undergo reversible protonation reactions in aqueous Triton X-100 micellar and poly[2-(dimethylamino)hexanamide] (PDACA) solutions.[9] The pH dependent redox behavior of the [4FeXY]/GC, therefore, also can be associated with such the reversible protonation of the clusters modified on the GC plate.

Not only the pattern of the cyclic voltammogram but also the peak potentials of the $[4FeXY]^{2-/3-}$ redox couples are altered by the change of proton concentrations in the aqueous phase. The anodic and cathodic peak potentials (E_{pa} and E_{pc}, respectively) of the [4FeXY]/GC at various pH, therefore, are depicted in Fig. 2, where E_{pa} and E_{pc} were determined at the sweep rate 10 mV s^{-1} in order to minimize the effect of the sweep rate on those peak potentials.[16] Although the E_{pc} value in the neutral pH region was not determined accurately due to the cathodic current of the H_2 evolution, the dependence of the E_{pc} values on pH is consistent with that of the E_{pa} on pH; the E_{pa} and E_{pc} values of the [4FeSS]/GC and the [4FeSeS]/GC show a tendency to level off in the pH region lower and higher than around 9.5 and 10.5, respectively and a shift by −60 mV/pH in the intermediate pH region (Fig. 2a).

Such the characteristic curves of Fig. 2a can be explained in terms of the reversible protonation of not only $[4FeXS]^{2-}$ but also $[4FeXS]^{3-}$ (X=S, Se) modified on the GC plate as similar to that of those clusters solubilized in an aqueous PDACA solution.[9] The turning points of Fig. 2a can, therefore, be associated with the pK_a values of the cluster. From the consideration of the basicity of $[4FeXS]^{2-}$ and $[4FeXS]^{3-}$, the protonation of $[4FeXS]^{3-}$ should take place in higher pH region than that of $[4FeXS]^{2-}$. The turning points in the plots of E_{pa} vs. pH (or E_{pc} vs. pH) around pH 10.5 and 9.5 in Fig. 2a, therefore, are assigned to the pK_a^{red} and pK_a^{ox} values of the protonated (3−) and (2−) states of the clusters, respectively. The shift of the E_{pa} and E_{pc} values of the [4FeXS]/GC by −60 mV/pH in the pH region from the pK_a^{red} to pK_a^{ox} values, therefore, is caused by the dissociation of one proton upon the oxidation of the protonated $[4FeXY]^{3-}$ to $[4FeXY]^{2-}$, and the association of one proton to $[4FeXY]^{3-}$ formed by the reduction of $[4FeXY]^{2-}$. On the basis of the preceding discussion, the turning points observed at around 10.5 (Fig. 2b) in the plots of E_{pa} and E_{pc} values of the [4FeXSe]/GC (X=S, Se) against pH can be assigned to their pK_a^{ox} values. The continuous shift by −60 mV/pH of the E_{pa} and E_{pc} values of those clusters above pH 10.5, therefore, is reasonably explained by the pK_a^{red} values of the protonated $[4FeXSe]^{3-}$ (X=S, Se) being larger than 12. It should be noticed that the relation between E_{pa} and E_{pc} of the cluster and pH affords only the information about the difference in the number of protons attached to the (2−) and (3−) states of the cluster. The total number of protons bonded to $[4FeXY]^{2-}$ and $[4FeXY]^{3-}$ is not clear in the present study so that the protonation equilibriums of [4FeXY]/GC are depicted by Scheme 1, where n, E_1, E_2 are the total number of protons bonded to the clusters in a given pH, the redox potential of the $[4FeXY]^{2-/3-}(H^+)_{n-1}$, and that of the $[4FeXY]^{2-/3-}(H^+)_n$.[17]

Table 1 summarizes the pK_a^{red} and pK_a^{ox} of the [4FeXY]/GC obtained from the turning points of the plots of E_{pa}^{ox} vs. pH of Fig. 2 together with those values determined in an aqueous PDACA solution.[9] Although the pK_a^{red} values of the protonated $[4FeXSe]^{3-}$ could not be determined in the present study, the pK_a^{ox} values are divided into two groups; around 9.5 for $[4FeSS]^{2-}$ and $[4FeSeS]^{2-}$, and around 10.5 for $[4FeSSe]^{2-}$

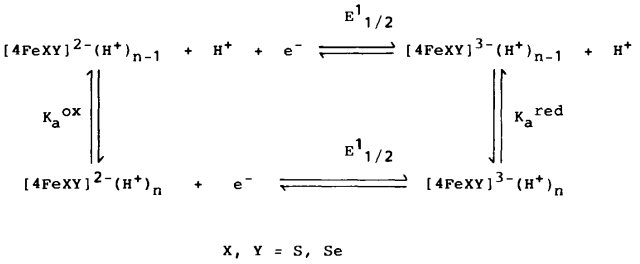

Scheme 1.

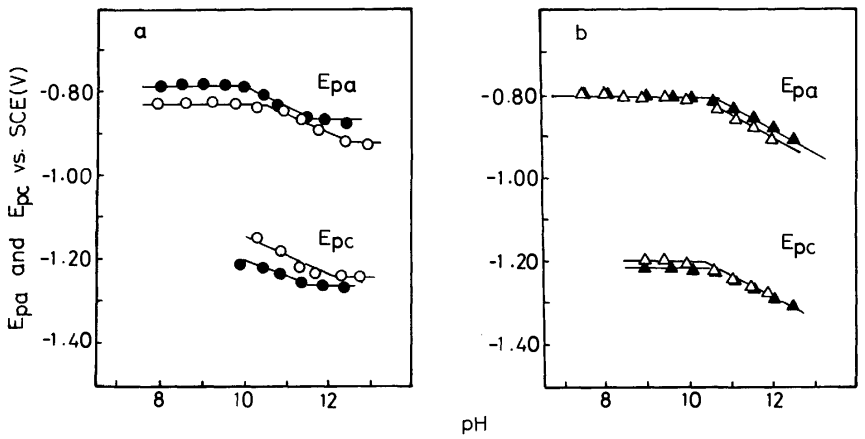

Fig. 2. Plots of peak potentials of the anodic and cathodic waves of the $[4FeXY]^{2-/3-}$ redox couple; X,Y=S,S (○), SeS (●), SSe (△), and SeSe (▲).

Table 1. pK_a Values of the Oxidized and Reduced Cluster Modified on a Glassy Carbon Plate and Solubilized in an Aqueous PDACA Solution

Cluster	pK_a^{ox}	pK_a^{red}
$[Fe_4S_4(SC_6H_4\text{-}p\text{-}t\text{-}Bu)_4]^{2-}$	9.6 (5.9)[a]	11.4 (8.8)
$[Fe_4Se_4(SC_6H_4\text{-}p\text{-}t\text{-}Bu)_4]^{2-}$	9.2 (5.9)	10.5 (7.3)
$[Fe_4S_4(SeC_6H_4\text{-}p\text{-}t\text{-}Bu)_4]^{2-}$	10.4 (6.9)	(8.8)
$[Fe_4Se_4(SeC_6H_4\text{-}p\text{-}t\text{-}Bu)_4]^{2-}$	10.6 (6.7)	(7.3)

a) Values in parentheses are in a PDACA solution.[9]

and [4FeSeSe]$^{2-}$. Such a pK_a^{ox} difference may be explained in terms of the difference of terminal sulfur and selenium rather than that of the Fe_4X_4 core (X=S, Se), suggesting that the protonation of [4FeXY]$^{2-}$ modified on the glassy carbon plate takes place on the terminal sulfur or selenium atom. It is worthy to note that both pK_a^{red} and pK_a^{ox} values of the [4FeXY]/GC are fairly larger than those of the clusters solubilized in aqueous PDACA solution (values in parentheses in Table 1). This result suggests that the hydrophobicity around the cluster modified on the GC plates in H_2O is less than that in an aqueous PDACA solution.

Rate Constants of the Electron Transfer between Clusters and Glassy Carbon Plates. As described in a previous section, the electricity consumed in the anodic and cathodic waves of the [4FeSS]/GC at pH 11.4 is equal to the amount of [4FeSS]$^{2-}$ modified on the GC plates, while the electricity of the anodic wave at pH 8.4 is much smaller than the amount of [4FeSS]$^{2-}$ (Fig. 1). This discrepancy may result from the fact that the reduction of the cluster is followed by H_2 evolution catalyzed by the resultant [4FeXY]$^{3-}$. Even if all the clusters modified on the GC plate participate in the redox reaction, the agreement between the electricity consumed in those redox waves and the amount of [4FeXY]$^{2-}$ modified is realized only when the rate of the electron transfer (k_s) between the cluster and the GC plate is much faster than that of H_2 evolution, otherwise most of electrons transferred to [4FeXY]$^{2-}$ from the GC plates are consumed by H_2 evolution prior to the anodic process of [4FeXY]$^{3-}$ in the GC plate. Accordingly, in a case of k_s being slower than the rate of H_2 evolution, the electricity released in the anodic wave of the [4FeXY]/GC is smaller than the amount of [4FeXY]$^{2-}$ modified on the GC plate. The rate of H_2 evolution apparently increases with decreasing pH. The rate of the electron transfer in the [4FeXY]/GC was evaluated under the assumption that H_2 evolution catalyzed by the reduced cluster does not disturb seriously the rate of the electron transfer.

The values of the peak separation between anodic and cathodic waves (ΔE_p) of an adsorbed species is frequently used as the criterion for kinetics in the electron transfer between the electrode and the redox center. For rapid kinetics in the electron transfer, $\Delta E_p=0$ is expected at any scan rate.[18] The present clusters, however, shows a fairly large ΔE_p values (300—400 mV) even at sweep rate 10 mV s^{-1} (Fig. 1), and both E_{pa} and E_{pc} are dependent on sweep rates. In the present study, both oxidized and reduced clusters are attached to the GC plate. When a redox center in a modified electrode is distributed homogeneously without any special interaction with the neighboring one, the rate constant of electron transfer k_s is expressed by Eq. 2,[19]

$$\log k_s = \alpha \log(1-\alpha) + (1-\alpha)\log \alpha - \log (RT/nFv) - \alpha(1-\alpha)nF\Delta E_p/2.3RT \quad (2)$$

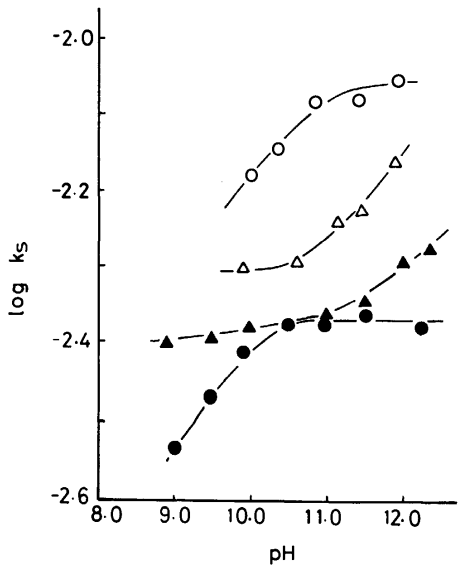

Fig. 3. The rate constant of the electron transfer (k_s) of the [4FeXY]/GC (X,Y=S,Se) at various pH; X,Y=S,S (O), SeS (●), SSe (△), and SeSe (▲).

where α, R, T, n, F, and v are the transfer coefficient, the gas constant, temperature, the Faraday constant, and the sweep rate. The value of α was obtained by the half width of the anodic wave (α=62.5 mV/$\delta_{1/2}$).[20] As mentioned in previous section, the cathodic wave of the (2−/3−) redox couple in the neutral region is almost completely concealed by H_2 evolution catalyzed by the (3−) state of the cluster, the k_s value, therefore, was determined in a limited pH region, where E_{pc} can be determined accurately. The plot of k_s obtained vs. pH is depicted in Fig. 3, which clearly shows the tendency of the decrease of k_s with increasing pH and the presence of the turning points close to the pK_a^{red} and pK_a^{ox} values of each [4FeXY]/GC (compare Fig. 2 with Fig. 3). Taking account the fact that protons in aqueous phase does not function as a counter ion in the redox reaction of the [4FeXY]/GC, the protonation of not only [4FeXY]$^{2-}$ but also [4FeXY]$^{3-}$ may cause a retardation of the rate of the electron transfer. Thus, the decrease of the electricity consumed in the anodic wave with decreasing pH (Fig. 1) may be caused by the retardation of the electron transfer, resulting from the protonation of the [4FeXY]/GC. It has been elucidated that the structure of $[Fe_4S_4(SC_6H_5)_4]^{2-}$ is nearly D_{2d} core symmetry with four short and eight longer Fe-S bonds approximately parallel to and perpendicular to the $\bar{4}$ axis,[21] while that of $[Fe_4S_4(SC_6H_5)_4]^{3-}$ is idealized D_{2d} core symmetry with four long Fe-S bonds approximately parallel to the $\bar{4}$ axis.[22] The similar structural change between [4FeXY]$^{2-}$ and [4FeXY]$^{3-}$ should be caused by the redox reaction of the [4FeXY]/GC. Such a reorganization process involved in the redox reaction of a Fe_4S_4 cluster may hardly influence on the rate of electron transfer in a certain Fe_4S_4 cluster-modified electrode since $[Fe_4S_4(SC_6H_5\text{-}p\text{-}n\text{-}C_8H_{17})_4]^{2-}$ adsorbed

on an Hg electrode undergoes a similar protonation reaction in an aqueous lecithin vesicle solution and exhibits a reversible (2−/3−) redox couple with $\Delta E_p=0$ at any scan rates in neutral and weak acidic conditions.[23] The distinct difference in the rate of the electron transfer in the redox reactions between $[Fe_4S_4(SC_6H_5\text{-}p\text{-}n\text{-}C_8H_{17})_4]^{2-}$ adsorbed on an Hg electrode and $[Fe_4X_4(Y_4C_6H_4\text{-}p\text{-}t\text{-}Bu)_4]^{2-}$ (X, Y=S, Se) modified on a GC plate may be associated with the form of the cluster; the former exists as a monomeric form on the Hg electrode, while the latter exists as the solid form on the GC plate. The rate-determining step of the electron transfer in the present study may, therefore, involve the structural change of the cluster in the solid state. The agreement of the turning points in the plots of k_s vs. pH with the pK_a^{ox} and pK_a^{red} values of those clusters suggests that protonation of the [4FeXY]/GC increases the reoganization energy of the cluster in the solid state.

References

1) B. V. Depamphilis, B. A. Averill, T. Herskovitz, L. Que, Jr., and R. H. Holm, *J. Am. Chem. Soc.*, **96**, 4159 (1974); C. L. Hill, J. Renaud, R. H. Holm, and L. E. Mortenson, *ibid.*, **99**, 2549 (1977).

2) P. Forget, *Eur. J. Biochem.*, **42**, 325 (1974); P. J. Aparicio, D. B. Knaff, and R. malkin, *Archiv. Biochem. Biophys.*, **164**, 102 (1975); R. Cammack, D. B. Hucklesby, and E. J. Hewitt, *Biochem. J.*, **171**, 519 (1978); J. A. Christner, E. Munck, P. A. Janick, and L. M. Siegel, *J. Biol. Chem.*, **254**, 2098 (1981); P. Greenbaum, K. N. Prodouz, and R. H. Garrett, *Biochim. Biophys. Acta*, **526**, 52 (1978).

3) J. P. Lee and H. Peck, *Biochem. Biophys. Res. Commun.*, **45**, 583 (1971); L. M. Siegel, "Mechanism of Oxidizing Enzymes," ed by T. P. Singer and R. N. Ondarza Elsevier, Amsterdam, pp. 201—214 (1978); L. M. Siegel, D. S. Davis, and H. Kamin, *J. Biol. Chem.*, **249**, 1572 (1974).

4) R. S. Wolfe and I. J. Higgins, *Int. Rev. Biochem.*, **21**, 267 (1979); P. A. Scherer and R. K. Thauer, *Eur. J. Biochem.*, **85**, 125 (1978).

5) R. H. Burris, "Nitrogen Fixation," ed by W. E. Newton and W. H. Orme-Johnson, (1980), Vol. 1; W. G. Zumft, L. E. Mortenson, and G. Palmer, *Eur. J. Biochem.*, **46**, 525 (1974); R. R. Eady and J. R. Postgate, *Nature (London)*, **249**, 805 (1974).

6) R. N. F. Thorneley, R. R. Eady, and D. J. Lowe, *Nature (London)*, **272**, 557 (1978).

7) S. Kuwabata, K. Tanaka, and T. Tanaka, *Inorg. Chem.*, **25**, 1691 (1986).

8) K. Tanaka, S. Uezumi, and T. Tanaka, *J. Chem. Soc., Dalton Trans.*, in press.

9) M. Nakamoto, K. Tanaka, and T. Tanaka, *Bull. Chem. Soc. Jpn.*, **61**, 4099 (1988).

10) R. J. Burt, G. J. Leight, and C. J. Pickett, *J. Chem. Soc., Chem. Commun.*, **1976**, 940.

11) J-C. Moutet and C. J. Pickett, *J. Chem. Soc., Chem. Commun.*, **1989**, 188.

12) G. Christou, R. V. Hageman, and R. H. Holm, *J. Am. Chem. Soc.*, **102**, 7600 (1980); T. Yamamura, G. Christou, and R. H. Holm, *Inorg. Chem.*, **22**, 187 (1984).

13) In the case the amount of the cluster on the GC plate is more than 10^{-6} mol cm^{-2}, the electricity in the anodic wave of the [4FeSS]/GC is fairly smaller than the expected value even at pH 11.4 due to a poor conductivity of the cluster.

14) $(Bu_4N)_2$[4FeSS] is irreversibly oxidized around 0 V vs. SCE in DMF. However, the [4FeSS]/GC showed no anodic wave at potentials more positive than 0 V vs. SCE in H_2O, since Bu_4N^+ may be completely fixed on the GC plate.

15) The reduction of $(Bu_4N)_2$[4FeSS] on the GC plate results in the formation of $(Bu_4N)_2Na$[4FeSS].

16) Both E_{pa} and E_{pc} values depend on the sweep rate, but the turning points of Fig. 2 is essentially independent on the sweep rates in the range of 10 to 100 mV s^{-1}.

17) The half wave potential for the overall electrode reaction can be written as follows;[9]

$$E_{1/2} = E^1_{1/2} + (RT/F)\ln[K_{ox}(K_{red} + [H]^+)/(K_{red}(K_{ox} + [H]^+))]$$

or

$$E_{1/2} = E^2_{1/2} + (RT/F)\ln[(K_{red} + [H]^+)/(K_{ox} + [H]^+)]$$

18) R. F. Lane and A. T. Hubbard, *J. Phys. Chem.*, **77**, 1401 (1973); E. Laviron, *J. Electroanal. Chem.*, **100**, 263 (1979); H. Angerstein-Kozlowska, J. Klinger, and B. E. Conway, *ibid.*, **75**, 45 (1977).

19) E. Laviron, *J. Electroanal. Chem.*, **101**, 19 (1979).

20) E. Laviron, *J. Electroanal. Chem.*, **51**, 355 (1974); the value α was in the range 0.39 to 0.46 for the [4FeSS]/GC, 0.38 to 0.42 for the [4FeSSe]/GC, 0.42 to 0.50 for the [4FeSeS]/GC, and 0.38 to 0.43 for the [4FeSeSe]/GC. No clear relation between these values and pH was observed.

21) L. Que, Jr., M. A. Bobrik, J. A. Ibers, and R. H. Holm, *J. Am. Chem. Soc.*, **96**, 4160 (1974).

22) E. Laskowski, R. B. Frankel, W. O. Gillum, G. C. Papaefthymiou, J. Renaud, J. A. Ibers, and R. H. Holm, *J. Am. Chem. Soc.*, **100**, 5322 (1978).

23) K. Tanaka, M. Masanaga, and T. Tanaka, *J. Am. Chem. Soc.*, **108**, 5448 (1986).

 © 1989 The Chemical Society of Japan Bull. Chem. Soc. Jpn., 62, 2835—2843 (1989)

Synthesis and Chromogenic Properties of Disulfonated (1-Naphthyl)(2-quinolyl)-methanone 5-Nitro-2-pyridylhydrazone and Its Application to the Spectrophotometric and Analogue-Derivative Spectrophotometric Determination of Trace Amounts of Zinc†

Hajime ISHII,* Katsunori KOHATA, Tsugikatsu ODASHIMA, and Yoshiaki KAWAMONZEN
Chemical Research Institute of Non-Aqueous Solutions, Tohoku University, Katahira, Sendai, Miyagi 980
(Received March 25, 1989)

A water-soluble hydrazone, disulfonated (1-naphthyl)(2-quinolyl)methanone 5-nitro-2-pyridylhydrazone (NQNPH), in which one nitro group and two sulfo groups are introduced for the purpose of increasing sensitivity and solubility in water, has been synthesized and its chromogenic property and reactivity with metal ions investigated. NQNPH reacts with various metal ions including zinc(II) to form 1:2 (metal:ligand) colored stable complexes with high molar absorptivities. On this basis, sensitive and practical spectrophotometric and analogue-derivative spectrophotometric methods for the determination of trace amounts of zinc with NQNPH have been proposed. The zinc(II)–NQNPH complex is formed quantitatively in the pH range 6.9—9.6 and its absorption spectrum shows an absorption maximum at 516 nm. Beer's law is obeyed over the range 0.07—1.5 ppm of zinc and the apparent molar absorptivity of the complex is 4.33×10^4 dm^3 mol^{-1} cm^{-1} at 516 nm. The proposed method was applied to the determination of zinc in Kuroko and water samples, with satisfactory results. In addition, the acid dissociation constants of NQNPH and the overall formation constant of its zinc complex were also determined spectrophotometrically.

In the course of a series of studies on the synthesis of hydrazone compounds as highly sensitive and selective reagents and their analytical application, recently we synthesized five kinds of water-soluble hydrazones derived from 2-(3-sulfobenzoyl)pyridine[1,2] and reported that one of them, (2-pyridyl)(3-sulfophenyl)-methanone 2-pyrimidylhydrazone, is a very useful reagent for the determination of iron at sub-ppm levels by spectrophotometry[1] and flow injection analysis.[3] Furthermore, we also synthesized a series of water-soluble hydrazones, in which various substituents were introduced to the 5-position of the pyridine ring in the hydrazine moiety of (2-pyridyl)(3-sulfophenyl)-methanone 2-pyridylhydrazone synthesized by Going et al.,[4] and found that, of those hydrazones, (2-pyridyl)(3-sulfophenyl)methanone 5-nitro-2-pyridyl-hydrazone having an electron-withdrawing nitro group is a very favorable spectrophotometric reagent in both sensitivity and selectivity for the determination of metals, especially for that of cobalt.[5]

In the work presented here disulfonated (1-naphthyl)-(2-quinolyl)methanone 5-nitro-2-pyridylhydrazone (NQNPH) which has one nitro group and two sulfo groups in its molecule was synthesized from a viewpoint of the development of the hydrazone reagent which is more soluble in water as well as sensitive to metal ions and properties of the hydrazone and its metal complexes were investigated in detail. On the basis of the results, a spectrophotometric method for the determination of trace amounts of zinc has been developed and applied successfully to the determination of zinc in Kuroko, a kind of mineral containing copper, lead and zinc as major constituents, and water samples, as examples. Further, the proposed method could be made more sensitive by the introduction of an analogue-derivative spectrophotometric technique.

† Presented in part at the 48th Symposium on Analytical Chemistry, Toba, June, 1987.

Experimental

Synthesis of NQNPH. NQNPH was synthesized according to Scheme 1 as follows.

Synthesis of 2-(1-Naphthoyl)quinoline (3): Manganese dioxide (activated under vacuum at 110 °C for 2 days, 67.6 g, 0.773 mol) was added to the chloroform solution (300 cm^3) of (1-naphthyl)(2-quinolyl)methanol (9.6 g, 0.034 mol) which was obtained by the Grignard method[6] using 1-bromonaphthalene (**2**) (16.6 g, 0.773 mol), magnesium turnings (3.86 g, 0.159 mol) and 2-quinolinecarbaldehyde (**1**) (10.5 g, 0.067 mol).[7] The reaction mixture was refluxed for 5 h. After cooling the mixture was filtered through a Celite pad and concentrated to yield a yellow solid, which was

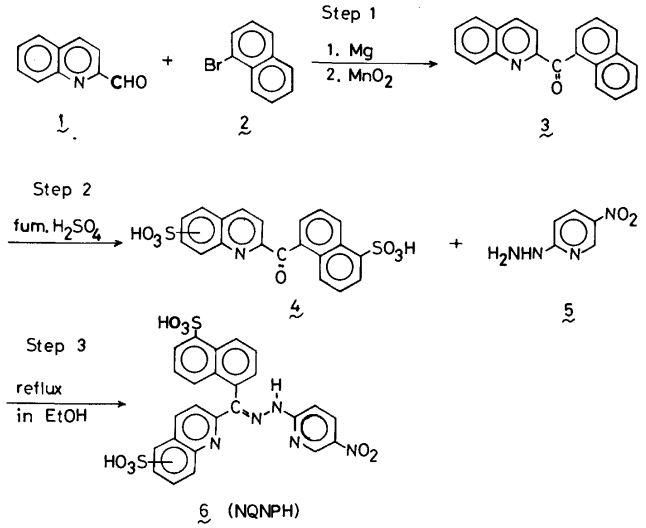

6 (NQNPH)

Scheme 1.

recrystallized from benzene to give a pure pale yellow 2-(1-naphthoyl)quinoline (**3**) [9.21 g (92.8%)]. Mp: 139 °C. Found: C, 84.76; H, 4.81; N, 5.39%. Calcd. for $C_{20}H_{13}ON$: C, 84.78; H, 4.63; N, 5.65%. IR (KBr): $\nu_{C=O}$ 1650 cm^{-1}.

Synthesis of Disulfonated 2-(1-Naphthoyl)quinoline (4): 2-(1-Naphthoyl)quinoline (**3**) (6 g, 0.021 mol) and fuming sulfuric acid (25% SO_3, 30 cm^3) were placed in a round bottom flask with a tight stopper and the mixture was stirred at 90 °C for 138 h. Fuming sulfuric acid (20 cm^3) was added, the temperature was raised to 110 °C and the stirring was continued for additional 72 h. Furthermore fuming sulfuric acid (10 cm^3) was added. After the stirring was continued for additional 27 h, the reaction mixture was cooled and cautiously poured into ethanol (120 cm^3) under cooling. Addition of ethyl acetate (6 dm^3) with sufficient stirring caused the precipitate as a dark brown solid. The mixture was filtered, washed with acetone and dried overnight at 60 °C under reduced pressure to yield a dark brown solid (**4**) (13 g), which still contained water and sulfuric acid. This material was used in the next step without purification. IR (KBr): $\nu_{C=O}$ 1670 cm^{-1}, ν_{SO_2} 1240—1140, 1040—1020 cm^{-1}.

Synthesis of Disulfonated (1-Naphthyl)(2-quinolyl)-methanone 5-Nitro-2-pyridylhydrazone (NQNPH) (6): 5-Nitro-2-pyridylhydrazine (**5**) (2.09 g, 0.014 mol) in hot ehtanol (450 cm^3) was added to a hot ethanol solution (100 cm^3) of disulfonated 2-(1-naphthoyl)quinoline (**4**) (7 g) and the mixture was refluxed for 5 h. After cooling a dark brown solid was obtained by concentration of the mixture. This solid was purified in a column of silica gel by elution with 2-propanol–ethyl acetate–water (2+3+1, v/v). Appropriate fractions [R_f=0.42 in 2-propanol–ethyl acetate–water (2+3+2, v/v)] were collected and concentrated to afford an orange yellow solid. This purification was repeated for several times to give 3.5 g in total. Mp>350 °C, IR (KBr): $\nu_{C=O}$ 1670 cm^{-1} (disappeared), ν_{NO_2} 1540, 1340 cm^{-1}, ν_{SO_2} 1240—1180, 1040 cm^{-1}.

Reagents. All reagents used were of analytical-reagent grade unless stated otherwise. All solutions were prepared with distilled, deionized water.

NQNPH solution. A 1.25×10^{-3} M (1 M=1 mol dm^{-3}) aqueous solution was prepared using synthesized NQNPH. This solution was standardized by photometric titration with a standard copper(II) solution at pH 5.5 and at 530 nm.

Standard zinc(II) solution. A 1×10^{-2} M stock solution was prepared by dissolving metallic zinc (99.999% pure) in a sufficient volume of hydrochloric acid (1+1) to give an acidity of about 0.1 M in the final solution. Working solutions were prepared by dilution of this solution with water.

Buffer solutions. 1 M Chloroacetic acid–1 M sodium chloroacetate, 1 M acetic acid–1 M sodium acetate, 0.5 M tris(hydroxymethyl)aminomethane–0.5 M hydrochloric acid, 1 M aqueous ammonia–1 M ammonium chloride or 0.5 M boric acid–0.5 M sodium carbonate system was used according to the pH value required.

Apparatus. For measurements of the absorbance, the absorption spectrum and the derivative absorption spectrum, the same instruments as those stated in an earlier paper[5] were used. Infrared spectra were obtained on a JASCO A-3 IR spectrometer. Thin-layer chromatography (TLC) was carried out on 0.2-mm E. Merck 60F-254 precoated silica-gel plates. For column chromatography, E. Merck silica gel 60 (70—230 mesh) was used.

Procedures. Determination of Zinc by Ordinary Spectrophotometry: Place a sample or standard solution containing up to 30 μg of zinc(II) in a 25-cm^3 calibrated flask. Add 5 cm^3 of 0.5 M tris(hydroxymethyl)aminomethane–0.5 M hydrochloric acid buffer solution (pH 7.2), suitable masking agents if necessary and 2 cm^3 of 1.25×10^{-3} M NQNPH solution, and dilute to the mark with water. After allowing to stand for about 10 min, measure the absorbance of the resultant solution at 516 nm against a reagent blank prepared under the same conditions using 1-cm cells.

Determination of Zinc by Second-Derivative Spectrophotometry: When the zinc content of the solution prepared by the procedure described under ordinary spectrophotometry is too low to give a measureable absorbance, record the second-derivative spectrum from 600 to 400 nm against a reagent blank by using a combination of both first- and second-order differentiation circuits (No. 6 of Refs. 8 and 9) and a scan speed of 300 nm min^{-1} and measure the second-derivative absorbance (the vertical distance from a peak to a trough or that from the base line to a trough of the peak).

Dissolution and Pretreatment of Kuroko Samples: Decompose sample and prepare the sample solution according to JIS method:[10] To 10—40 mg of sample add 15 cm^3 each of concentrated nitric and hydrochloric acids and heat to decompose the sample. Add 2 cm^3 of sulfuric acid (1+1) and evaporate to dryness. After cooling to room temperature, dissolve the residue in about 50 cm^3 of hydrochloric acid (1+50), heat for a few minutes to dissolve the soluble salts, filter into a 200-cm^3 calibrated flask, wash with hot water, and dilute to the mark with water after cooling to room temperature. Use an appropriate aliquot of the resultant solution to the determination.

Results and Discussion

Identification of the Hydrazone. Identification of the product was carried out at two stages in the course of synthesis.

Disulfonated 2-(1-Naphthoyl)quinoline (4): A TLC test on the product obtained at step 2 revealed that the product consists of two position isomers of the sulfo group on quinoline ring [R_f=0.26 and 0.18 respectively in 2-propanol–ethyl acetate–water (2+3+2, v/v)]. The faster-migrating product was obtained mainly on a reaction mixture sulfonated for 23 h and decreased gradually with the addition of fuming sulfuric acid and the passage of time. On the other hand, the slower-migrating one increased gradually and became main finally. The faster- and slower-migrating products presumed to be 2-(5-sulfo-1-naphthoyl)-5-quinolinesulfonic acid and 2-(5-sulfo-1-naphthoyl)-8-quinolinesulfonic acid, respectively, because 5-sulfoquinoline migrated faster (R_f=0.45) than 8-sulfoquinoline (R_f=0.39) in 2-propanol–ethyl acetate–water (2+3+2, v/v). However, the position of sulfo group on quinoline ring could not be decided.

NQNPH (6): Neither of the elemental analysis, the determination of water content by Karl Fischer's

method, the mass spectrum (FAB) and the NMR spectrum of the final product gave reliable results in spite of trials because the product is hygroscopic and has large molecular weight and two sulfo groups. However, the hydrolysis of this product with concentrated nitric acid at room temperature for two days gave the starting ketone, disulfonated 2-(1-naphthoyl)-quinoline (**4**). On the basis of the result, this product is presumed to be a target hydrazone.

The number of sulfo groups of NQNPH (**6**) was determined by the ion-pair extraction method with zephiramine as an ion-pair-forming reagent, that is, solutions of pH 7.8 containing a fixed amount of NQNPH and various amounts of zephiramine were shaken for 24 h with an equal volume of benzene to the aqueous phase and then the absorbances of the organic and aqueous phases were measured, in which the absorbance of the latter was measured after the addition of sufficient amounts of zinc(II) as a color-forming reagent. The results are shown in Fig. 1, from

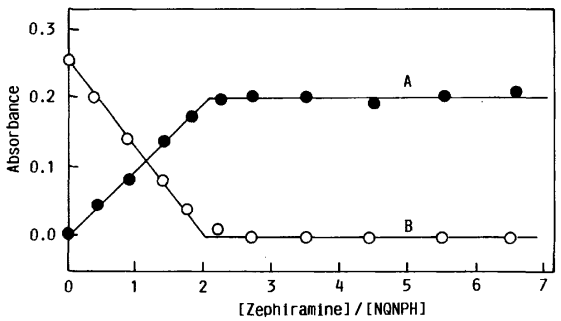

Fig. 1. Determination of the number of sulfo groups of NQNPH by the ion-pair extraction method. NQNPH, 7.2×10^{-5} M; pH 7.8; shaking time, 24 h. A, Benzene phase measured at 430 nm against benzene; B, water phase measured at 516 nm against water.

which the composition of the ion pair of NQNPH and zephiramine is found to be 1:2. This indicates that the number of sulfo groups of NQNPH is two.

Properties and Characteristics of the Hydrazone. NQNPH is hygroscopic, but remains unchanged for more than one year when stored in a desiccator. It is very soluble in water as expected beforehand and also soluble in polar solvents such as ethanol, *N*,*N*-dimethylformamide, and dimethyl sulfoxide, but insoluble in less or nonpolar solvents. Its aqueous solution is very stable.

As is apparent from the structure, NQNPH is a tribasic acid as well as a triacidic base, having six dissociable hydrogens in acidic solutions above 1 M. However, in less acidic solutions, the de-protonations from the C=N nitrogen and the sulfo groups are complete. Hence NQNPH exists in solution in any of the following forms, depending on pH:

$$H_3L \overset{K_{a4}}{\rightleftharpoons} H_2L^- \overset{K_{a5}}{\rightleftharpoons} HL^{2-} \overset{K_{a6}}{\rightleftharpoons} L^{3-} \quad (1)$$

where L denotes the undissociable part of the hydrazone and K_{a4}, K_{a5}, and K_{a6} are the acid dissociation constants.

The acid dissociation constants were determined spectrophotometrically at ionic strengths of 0.2 for K_{a5} and K_{a6} and 3.0 for K_{a4}, and at 25±0.1 °C. The values obtained for K_{a4}, K_{a5}, and K_{a6} were $10^{-0.80}$, $10^{-4.80}$, and $10^{-10.93}$, respectively. The K_{a4} and K_{a5} may be assigned to the de-protonation of the protonated pyridine-nitrogen and quinoline-nitrogen, respectively, whereas the K_{a6} corresponds to that of the secondary amino group. The contribution of the electron-withdrawing nitro group on the pyridine ring to the value of K_{a4} is found to be remarkable. A species distribution diagram of NQNPH prepared on the basis of these acid dissociation constants is shown in Fig. 2.

Table 1. Reactivity of NQNPH with Metal Ions

Metal ion	pH 4		pH 7		pH 10	
	λ_{max}/nm	ε/M^{-1} cm^{-1}	λ_{max}/nm	ε/M^{-1} cm^{-1}	λ_{max}/nm	ε/M^{-1} cm^{-1}
Ag(I)	—	—	—	—	515	32800
Cd(II)	—	—	519	18700	519	47100
Co(II)	521	1000	521	37400	521	20300
Cr(III)	—	—	—	—	515	2700
Cr(VI)	—	—	—	—	525	5700
Cu(II)	530	33900	530	33900	530	28400
Fe(II)	—	—	513	41100	498	14200
Fe(III)	—	—	500	3100	—	—
Hg(II)	494	7800	485	8600	445	17700
Mn(II)	—	—	519	2600	519	44900
Ni(II)	524	2900	524	47100	524	42000
Pb(II)	—	—	525	15600	—	—
Pd(II)	592	22000	592	22000	592	21100
Ti(IV)	—	—	—	—	—	—
V(IV)	—	—	—	—	510	4000
V(V)	—	—	—	—	490	1500
Zn(II)	—	—	516	43300	516	41400

Standing time: 30 min.

Reactivity of the Hydrazone. The reactivity of NQNPH with various metal ions at pH 4, 7, and 10 were investigated, the results being summarized in Table 1. NQNPH is found to react with cadmium(II), cobalt(II), copper(II), iron(II), nickel(II), palladium(II), zinc(II), etc. to form colored stable complexes with high molar absorptivities. So the complexation reaction of NQNPH with these metal ions was investigated somewhat in detail. Absorption spectra of the complexes are shown in Fig. 3. Experimental results concerning the effect of pH on the complexations are indicated in Fig. 4. Absorption maxima of the complexes and optimum pH ranges for the complexations obtained from these results are summarized in Table 2 along with apparent molar absorptivities and compositions of the complexes determined by both the continuous variation and the molar ratio methods. These results suggest that NQNPH may be useful for the sensitive determination of these metals. Hence conditions for the complexation with zinc(II) and spectrophotometric determination of zinc at sub-ppm levels utilizing this complexation were investigated in detail at the outset in the subsequent work.

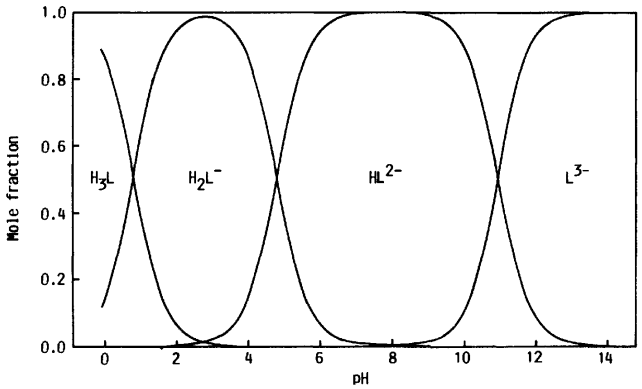

Fig. 2. Species distribution diagram of NQNPH.

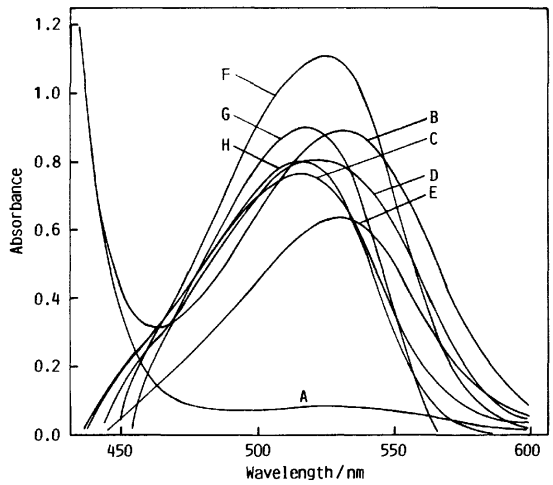

Fig. 3. Absorption spectra of (A, B) NQNPH and (C–H) its metal complexes. NQNPH, 2.50×10^{-4} M; metal ions, 1.87×10^{-5} M; pH, 7.5 (except for 9.0 for B and G); standing time, 30 min (except for 12 h for F); reference—A and B, water; C—H, reagent blank. A and B, NQNPH (reagent blank) at pH 7.5 and 9.0, respectively; C, iron(II); D, cobalt(II); E, copper(II); F, nickel(II); G, cadmium(II); H, zinc(II) complex.

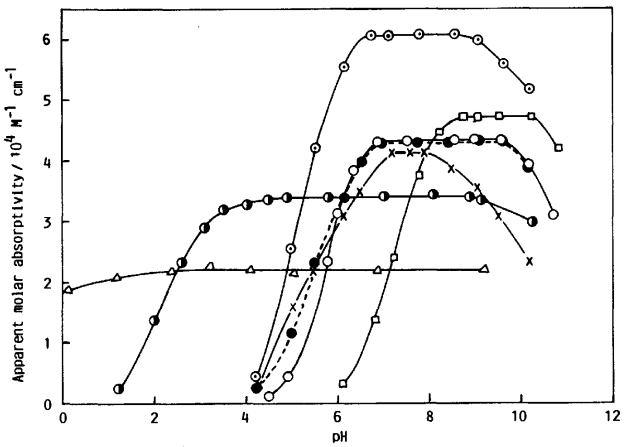

Fig. 4. Effect of pH on the complexation. Reference, reagent blank.

	Complex	Standing time	Wavelength	[NQNPH]/[Metal]
—□—	Cd(II) complex	30 min	519 nm	17.3
—●—	Co(II) complex	1 h	521 nm	17.9
—◑—	Cu(II) complex	30 min	530 nm	19.8
—×—	Fe(II) complex	30 min	513 nm	17.0
—⊙—	Ni(II) complex	12 h	524 nm	18.1
—△—	Pd(II) complex	30 min	592 nm	4.7
—○—	Zn(II) complex	30 min	516 nm	9.5

Table 2. Properties of Metal-NQNPH Complexes and Optimum pH Ranges for the Complexations

Complex	Absorption maximum/nm	Apparent molar absorptivity/M^{-1} cm^{-1}	Composition (metal: ligand)	Optimum pH range
Cd(II)-NQNPH	519	47100	1:2	8.7—10.2
Co(II)-NQNPH	521	43000	1:2	7.0— 9.6
Cu(II)-NQNPH	530	33900	1:2	4.9— 8.9
Fe(II)-NQNPH	513	41100	1:2	7.2— 7.9
Ni(II)-NQNPH	524	60600	1:2	6.7— 8.6
Pd(II)-NQNPH	592	22000	1:2	2.8— 9.2
Zn(II)-NQNPH	516	43300	1:2	6.9— 9.6

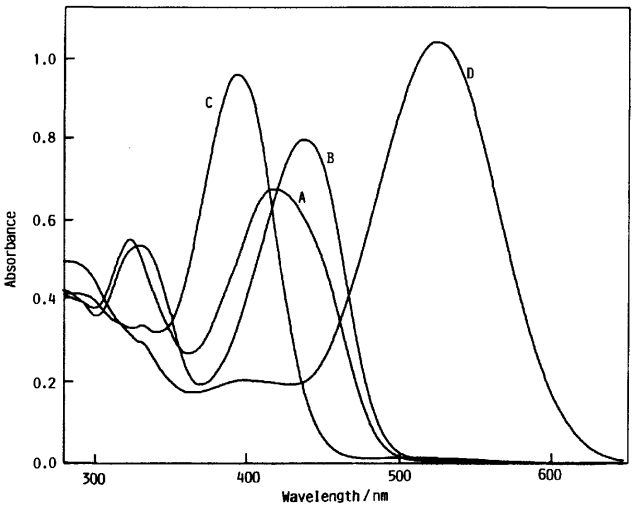

Fig. 5. Absorption spectra of NQNPH at pH (A), 0; (B), 3; (C), 8; and (D), 13.7. NQNPH, 4.1×10^{-5} M; reference, water.

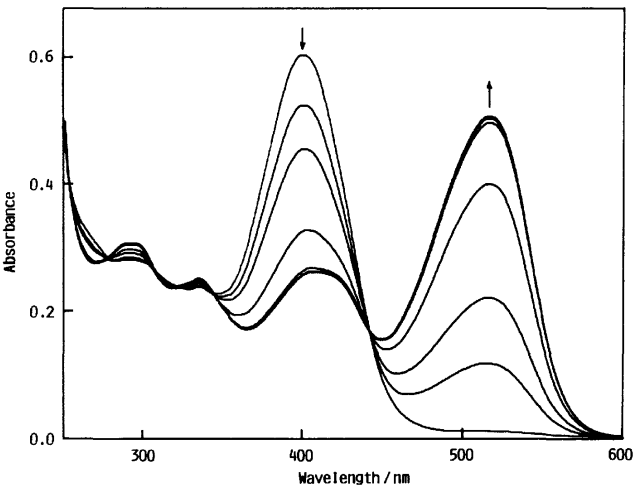

Fig. 6. Absorption spectra of the zinc(II)-NQNPH system. NQNPH, 2.3×10^{-5} M; pH, 7.0; reference, water. Arrows indicate spectral trends observed when changing the NQNPH to zinc(II) ratio from 1:0 to 1:3.2.

Studies of the Zinc(II)-NQNPH System. Absorption Spectra: Figure 5 shows absorption spectra of NQNPH at pH 0, 3, 8, and 13.7, in which spectra A, B, C, and D correspond to H_3L, H_2L^-, HL^{2-}, and L^{3-},

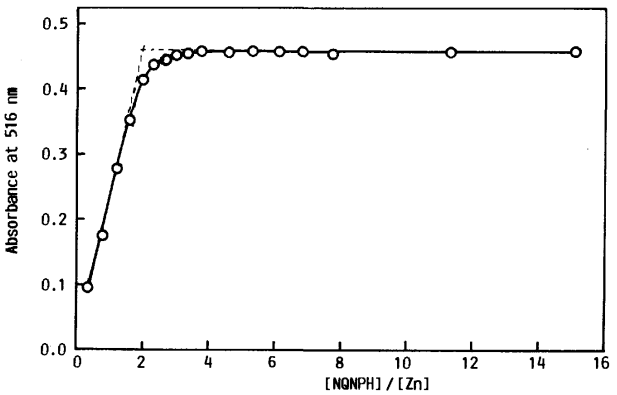

Fig. 7. Effect of NQNPH concentration. Zn(II), 693 ppb (1.1×10^{-5} M); pH, 7.2; reference, reagent blank.

respectively, taking Fig. 2 into consideration. Figure 6 exhibits the spectral change in the complexation between zinc(II) and NQNPH at pH 7.0, from which it is found that the absorption maximum shifts from 400 to 516 nm on complexation. In addition, the absorption due to NQNPH itself is very small at the latter wavelength, which is favorable for the zinc determination.

Effect of pH: As shown in Fig. 4 and Table 2, a constant and maximum absorbance is obtained over the pH range 6.9—9.6. The use of tris(hydroxymethyl)-aminomethane-hydrochloric acid buffer (pH 7.2) is recommended because the phosphate buffer interferes with the zinc determination.

Effect of NQNPH Concentration: The effect of the NQNPH concentration on the complexation was investigated. The results was shown in Fig. 7, from which it is found that a 4-fold molar excess of NQNPH is necessary for the complete complexation and an excess of NQNPH does not interfere. In addition, this result suggests the formation of a 1:2 (metal: ligand) complex.

Stability of the Complex: Under the recommended conditions, zinc(II) reacts almost instantaneously with NQNPH to form a complex at room temperature. The complex formed is very stable, the absorbance remaining constant even after 20 h.

Calibration Graph, Sensitivity and Precision: A linear calibration graph passing through the origin

Table 3. Tolerance Limits for Other Metal Ions in the Determination of 15.9 μg of Zinc

Tolerance limit		No masking agent added	Masking agent added
Above	1000 μg	Mg(II), Cr(VI)	Ag(I),[a] Hg(II)[a]
	500 μg	Ca(II), V(V)	
	200 μg	Al(III)	Fe(III),[b] Cu(II)[c]
	100 μg	Cr(III)	
	50 μg	Ti(IV)	V(IV),[d] Mn(II),[b] Pd(II),[c] Pd(II)[a]
	20 μg		Co(II),[e] Ni(II),[f] Cd(II)[a]
	10 μg	Mn(II), Ag(I), Hg(II)	V(IV),[b] Co(II)[f]
	5 μg	V(IV)	
	2 μg	Pd(II), Pb(II)	
	1 μg	Fe(III), Cd(II)	
Below	1 μg	Fe(II), Co(II), Ni(II), Cu(II)	
Above	100 mg	Br^-, Cl^-, I^-, ClO_4^-, NO_3^-, SCN^-, SO_4^{2-}, Acetate	
	50 mg	F^-, $S_2O_3^{2-}$	
	20 mg	Tartrate	
	10 mg	PO_4^{3-}	
	1 mg	Oxalate	
Below	1 mg	Citrate, EDTA	

a) 3 ml of 50% potassium iodide solution was added. b) 4 ml of 4% sodium fluoride solution was added. c) 5 ml of 10% thiourea solution was added. d) 1 ml of 2.5% sodium tartrate solution was added. e) 1 ml of 10% sodium perborate solution and 1.5 ml of sodium acetate solution were added. f) 0.7 ml of 5×10^{-3} M *N*-(dithiocarboxy)sarcosine solution was added.

was obtained by the recommended procedure. The equation for the line obtained by a least-squares treatment was

$$\text{Zn(ppm)} = 1.51A \quad (2)$$

where A is the absorbance. The optimum range for the zinc determination is 0.1—1.5 ppm in the solution measured. The apparent molar absorptivity calculated from Eq. 2 is 4.33×10^4 M^{-1} cm^{-1}.

Ten standard solutions containing 638 ppb of zinc(II) were analyzed by the recommended procedure. The results gave a relative standard deviation of 0.29%.

Effect of Diverse Ions: The effect of diverse ions on the determination of zinc were studied by adding a known amount of the ion in question to a solution containing 15.9 μg of zinc(II) and following the recommended procedure. An error of ±3% in the absorbance reading was considered tolerable. The results are summarized in Table 3. Many ions including cadmium(II), cobalt(II), copper(II), iron(II and III), lead(II), manganese(II), mercury(II), nickel(II), palladium(II), silver(I), vanadium(IV), oxalate, citrate, and EDTA interfered with the determination when no masking agent is added, but the other ions scarcely or did not interfere. Of these interfering ions, iron(III), manganese(II) and a small amount of vanadium(IV) can be masked with sodium fluoride, cadmium(II), lead(II), mercury(II), and silver(I) with thiourea, nickel(II) and a small amount of cobalt(II) with *N*-(dithiocarboxy)sarcosine, vanadium(IV) with sodium tartrate, and cobalt(II) with sodium perborate and ammonium acetate.

In addition, the removal of interferences caused by several ions which coexist at the same time was also examined. For example, a calibration graph prepared in the presence of each 30 μg of copper(II), iron(III), and lead(II) and by using thiourea, sodium fluoride, and potassium iodide as masking agents for these ions was in good agreement with that prepared in the absence of these interferents within an error of 3%. This suggests that the selectivity in the proposed method can be improved enough to apply it to the analysis of practical samples.

Use of Analogue-Derivative Spectrophotometry to Improve Sensitivity. Derivative spectrophotometry using the analogue differentiation circuit enhances the sensitivity of ordinary spectrophotometry,[8,9] so second-derivative spectrophotometry was applied here to the determination of zinc.

Selection of Conditions for Measurements: In second-derivative spectrophotometry both the time constant of the analogue differentiation circuit and the scan speed of the spectrophotometer considerably affect the sensitivity and selectivity, so both need to be optimized to give a well resolved large peak. Figure 8 shows the second-derivative spectra of the zinc(II)–NQNPH complex measured with various scan speeds and circuit numbers. A combination of circuit No. 6 (which has the largest time constant, 2.0 s, the time constant increasing with circuit number in our apparatus) and a scan speed of 300 nm min^{-1} was found to give the best sensitivity and resolution (i.e., selectivity) for the zinc determination.

Calibration Graph: The calibration graph prepared under the recommended conditions by plotting the second-derivative absorbance versus the zinc concentration is linear and passes through the origin

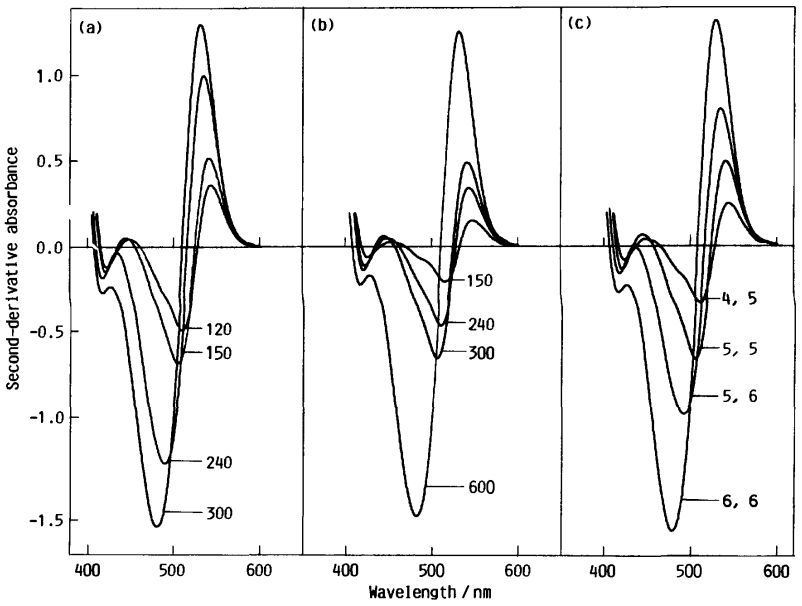

Fig. 8. Influence of (a), (b) scan speed [with circuits all No. 6 in (a) and all No. 5 in (b)] and (c) circuit number (with scan speed 300 nm min^{-1}) on second-derivative spectra of zinc(II)-NQNPH complex solution. Zn(II), 319 ppb (4.9×10^{-6} M); NQNPH, 1.0×10^{-4} M; pH, 7.2; reference, reagent blank. Numerical values indicate scan speeds in (a) and (b) and first- and second-differentiation circuits in (c).

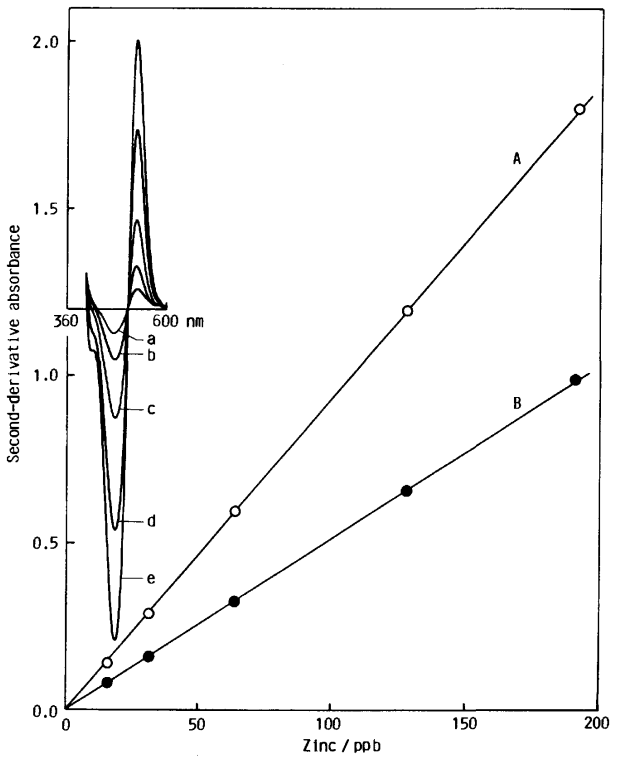

Fig. 9. Calibration graph for zinc in second-derivative spectrophotometry. A, Peak-to-trough values plotted; B, base line-to-trough values plotted. Circuits, all No. 6; scan speed, 300 nm min^{-1}; slit width, 1 nm; recorder sensitivity, ×1; reference, reagent blank; NQNPH, 1.0×10^{-4} M. Zn(II)—a, 15.9; b, 31.9; c, 63.8; d, 128; and e, 191 ppb.

when either the peak to trough values or the base line to trough values are plotted, as shown in Fig. 9. The equation for the lines were

$$\text{Zn(ppb)} = 107D \quad (3)$$

$$\text{Zn(ppb)} = 194D \quad (4)$$

where D is the second-derivative absorbance converted into absorbance. It will be seen that zinc at levels as low as 16 ppb can easily be determined in this way.

Practical Applications. To confirm the usefulness of the proposed method, zinc in Kuroko and water samples was determined. The results are summarized in Table 4 together with those by atomic absorption spectrometry carried out for comparison. Both sets of results are in good agreement.

Composition of the Complex. The molar composition of the zinc(II)-NQNPH complex formed under the conditions for the determination of zinc was examined by both the molar ratio and the continuous variation methods. Both method indicated the formation of a 1 : 2 (metal : ligand) complex. As an example, the result by the continuous variation method is shown in Fig. 10.

Formation Constant of the Complex. The formation constant of the zinc(II)-NQNPH complex formed under the recommended conditions was determined spectrophotometrically by the equilibrium shift method.[11]

Table 4. Determination of Zinc in Kuroko and Water Samples

Sample	Zinc content		
	Proposed method		Atomic absorption method[a]
	Individual values	Average	
Kuroko A	19.4% 18.8%	19.1%	19.0%
Kuroko B	9.19% 8.90%	9.05%	9.07%
Tap water	34 ppb 34 ppb 33 ppb	34 ppb	35 ppb[b]
Hirose river water	18 ppb 19 ppb 19 ppb	19 ppb	20 ppb[b]

a) By JIS K-0102 (1981) p. 155. b) Before the determination samples were concentrated by evaporation to 1/20 of the initial volume.

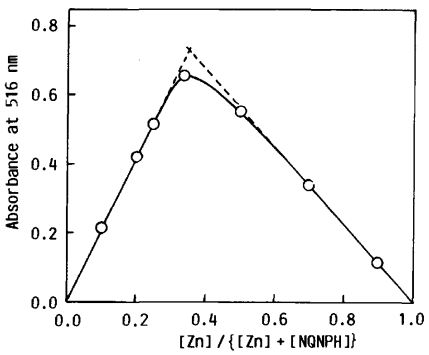

Fig. 10. Continuous variation graph for the zinc(II)–NQNPH system. [Zn]+[NQNPH]=4.88×10⁻⁵ M; pH, 7.2; reference, reagent blank.

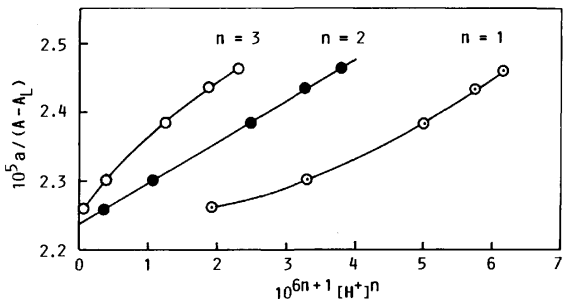

Fig. 11. Plots of $a/(A-A_L)$ versus $[H^+]^n$. Zn(II) (=a), 9.75×10⁻⁶ M; NQNPH (=b), 3.39×10⁻⁴ M; wavelength, 516 nm; ionic strength, 0.2 ($NaClO_4$); temperature, 25±0.1 °C.

The complexation equilibrium between zinc(II) and NQNPH may be expressed as

$$Zn^{2+} + nHL^{2-} \rightleftharpoons ZnL_n^{(3n-2)-} + nH^+ \quad (5)$$

$$K_{eq} = [ZnL_n^{(3n-2)-}][H^+]^n/[Zn^{2+}][HL^{2-}]^n \quad (6)$$

where K_{eq} denotes the equilibrium constant of the complexation reaction. If the initial concentration of the ligand, b, is much higher than that of the metal ion, a, Eq. 6 can be approximated as

$$K_{eq} = x[H^+]^n/(a-x)b^n \quad (7)$$

where x is the equilibrium concentration of the complex formed. As described above, the system obeys Beer's law additively over the wavelength range of interest, it can be deduced that

$$A = \varepsilon_L(b-nx) + \varepsilon_C x \quad (8)$$

where ε_L and ε_C are molar absorptivities of the ligand and the complex at a specified wavelength, respectively, and A is the total absorbance of the solution. From Eqs. 7 and 8, Eq. 9 can finally be obtained:

$$a/(A-A_L) = [H^+]^n/(\varepsilon_C - n\varepsilon_L)K_{eq}b^n + 1/(\varepsilon_C - n\varepsilon_L) \quad (9)$$

where A_L is the absorbance of the solution of the ligand alone. Equation 9 implies that at constant values of a and b there should be a linear relationship between the terms $a/(A-A_L)$ and $[H^+]^n$, from which the value of n can be estimated. Such a relation was experimentally obtained when assuming n is equal to 2, as shown in Fig. 11. This reveals the formation of a 1:2 (metal:ligand) complex, which is in accordance with the result by the continuous variation method indicated above. Thus the complexation reaction of zinc(II) with NQNPH may reasonably be expressed as

$$Zn^{2+} + 2HL^{2-} \rightleftharpoons ZnL_2^{4-} + 2H^+ \quad (5')$$

$$K_{eq} = [ZnL_2^{4-}][H^+]^2/[Zn^{2+}][HL^{2-}]^2 \quad (6')$$

The value of K_{eq} obtained from Eq. 9 and the

experimental data when assuming $n=2$ in Fig. 11 was $10^{-4.49}$.

The overall formation constant, β_2, of the complex defined by

$$Zn^{2+} + 2L^{3-} \rightleftharpoons ZnL_2^{4-} \quad (10)$$

$$\beta_2 = [ZnL_2^{4-}]/[Zn^{2+}][L^{3-}]^2 \quad (11)$$

can be calculated from the values of K_{eq} and the acid dissociation constant of the ligand, K_{a6}, as follows:

$$\beta_2 = K_{eq}/K_{a6}^2 = 10^{-4.49}/(10^{-10.93})^2 = 10^{17.37}$$

Conclusion

A water-soluble hydrazone, NQNPH, was synthesized and its chromogenic properties and reactivity with metal ions were investigated. This hydrazone, the synthesis of which was somewhat complicated, was very soluble in water as expected beforehand and reacted with transition metal ions to give complexes with high molar absorptivities as well as water-soluble hydrazones reported earlier by us.[1,2,5] On the basis of results of fundamental experiments, spectrophotometric and analogue-derivative spectrophotometric methods for the determination of trace amounts of zinc have been proposed and applied successfully to the analysis of mineral and water samples. The proposed methods offer the advantages of simplicity, rapidity, reasonable selectivity and high sensitivity. Very high sensitivity was attained on employing second-derivative spectrophotometry. In addition, the acid dissociation constants of NQNPH and the formation constant of the zinc(II)–NQNPH complex were determined spectrophotometrically.

References

1) T. Aita, T. Odashima, and H. Ishii, *Analyst*, **109**, 1139 (1984).
2) H. Ishii, T. Odashima, and T. Aita, *Nippon Kagaku Kaishi*, **1985**, 1770.
3) H. Ishii, M. Aoki, T. Aita, and T. Odashima, *Anal. Sci.*, **2**, 125 (1986).
4) J. E. Going and C. Sykora, *Anal. Chim. Acta*, **70**, 127 (1974).
5) T. Odashima, T. Kikuchi, W. Ohtani, and H. Ishii, *Analyst*, **111**, 1383 (1986).
6) H. Gilman and F. Schul, *Org. Synth.*, Coll. Vol. 2, 425 (1943).
7) H. Kaplan, *J. Am. Chem. Soc.*, **63**, 2654 (1941).
8) H. Ishii and H. Koh, *Nippon Kagaku Kaishi*, **1980**, 203.
9) H. Ishii and K. Satoh, *Fresenius Z. Anal. Chem.*, **312**, 114 (1982).
10) JIS, M-8124 (1965).
11) Y. Oka, "Jikken Kagaku Koza," Continued Vol. 7, ed. by Nippon Kagakukai, Maruzen (1966), p. 210.

A Highly Sensitive Fiber-Optic Immunosensor Using a Metal-Complex Compound as a Chemiluminescent Catalyst

Tadashi HARA,* Kazuhiko TSUKAGOSHI, Akihiro ARAI, and Yuji IMASHIRO
Department of Chemical Engineering, Faculty of Engineering, Doshisha University, Karasuma Imadegawa, Kamigyo-ku, Kyoto 602
(Received March 28, 1989)

A highly sensitive fiber-optic immunosensor using an antibody-immobilized optical fiber was developed and introduced into a chemiluminescence complex catalyst immunoassay (CLCCIA) which had been reported by the authors in a previous paper. After optimization of the experimental conditions, human serum albumin as model protein was determined by both competitive immunoassay and sandwich immunoassay, using the fiber-optic immunosensor. Human serum albumin could be determined in the concentration range 1×10^{-4}—1×10^{-1} g dm^{-3} with a lower limit of 400 pg by competitive immunoassay while in the concentration range 1×10^{-5}—1×10^{-1} g dm^{-3} with a lower limit of 40 pg by sandwich immunoassay. The new fiber-optic immunosensor developed by the authors can be characterized as follows: 1) Highly sensitive for the determination of a small amount of protein, 2) applicable to a wide concentration range of protein sample, 3) feasible with a microvolume of sample, 4) suitable for automated operation, and 5) excellent regarding safety, cost, and treatment.

A new immunoassay, chemiluminescence complex catalyst immunoassay (CLCCIA), in which iron(III) 2,9,16,23-tetrakis(chlorocarbonyl)phtalocyanine (TCCP-Fe(III)) was used as a labeling agent, was previously developed by the authors[1-3] using the fact that TCCP-Fe(III) markedly accelerates the chemiluminescene (CL) reaction between 5-amino-2,3-dihydro-1,4-phthalazinedione (luminol) and hydrogen peroxide (H_2O_2). Their immunoassays were carried out by a batchwise method, a flow-through method, and a chromatographic method using antibody-immobilized glass beads. The CLCCIA was highly sensitive and superior regarding safety, cost, and easy treatment to radioimmunoassay and enzyme immunoassay.

An optical fiber has recently been applied to a chemical sensor and a biosensor since the optical fiber makes in situ and in vivo measurements possible and allows very weak light to transfer without any accompanying light loss. However, a few reports have been published with regard to a fiber-optic immunosensor in which an antibody is directly immobilized on the plain end of an optical fiber,[4,5] or a CL reaction is used for the determination of an antigen.[6-8]

In the present study, an attempt was made to develop a new fiber-optic immunosensor using an antibody-immobilized optical fiber and to introdue it into CLCCIA. The fiber-optic immunosensor gave satisfactory results regarding sensitivity for detection, concentration range for determination, amount of sample, and cost.

Experimental

Reagents. All reagents were of commercially available special grade. Ion-exchanged water was distilled before use.

A 1.0×10^{-3} mol dm^{-3} luminol solution contained 1.8×10^{-1} mol dm^{-3} sodium carbonate, 2.0×10^{-1} mol dm^{-3} sodium hydrogencarbonate, and 1.0×10^{-3} mol dm^{-3} ethylenediaminetetraacetic acid (EDTA). A 7.5×10^{-3} mol dm^{-3} H_2O_2 solution was prepared by diluting 30 wt% H_2O_2 with water.

Since the purpose of the present study was to describe the establishment of a new immunoassay methodology, all experiments were carried out using easily available and inexpensive human serum albumin (HSA) as model protein. Rabbit anti-HSA (DAKO) was used without further purification. HSA (MilesLabolatories, Inc.), bovine serum albumin (BSA)(Sigma Chemical Co.), human serum γ-globulin-(HγG)(Sigma Chemical Co.), bovine serum γ-globulin (BγG) (Sigma Chemical Co.), bovine serum α-globulin (BαG) (INC Pharmaceuticals, Inc.), and ovalbumin (Ova)(Sigma Chemical Co.) were dissolved and diluted with a phoshate buffer solution consisting of 2.78×10^{-3} mol dm^{-3} potassium dihydrogenphosphate, 5.56×10^{-3} mol dm^{-3} disodiumhydrogenphosphate, and 0.05 wt% sodium azide (pH 7.3) (Buff-A) or a Buff-A containing 1 wt% BSA (Buff-B).

Iron(III) 2,9,16,23-tetracarboxyphtalocyanine (TCP-Fe(III)) and TCCP-Fe(III) were synthesized as described in the previous paper.[1,9] TCCP-Fe(III) was used as a labeling reagent. TCP-Fe(III) was used to optimize the conditions for the measurement of the CL intensity because TCCP-Fe(III) was hydrolyzed in water and changed to TCP-Fe(III).

Preparation of labeled HSA and labeled anti-HSA were carried out as described in previous papers.[1,3] The concentrations of these albumins were determined on the basis of the calibration curves of their absorbance.

Preparation of the Optical Fiber Immobilized with Anti-HSA. The plain end of an optical fiber (GC. 800/1000L, Fujikura Co.; 1 mm i.d.×5 cm) was polished with a sand paper (1200 CC-CW, SANKYO RIKAGAKU Co.) and was followed by the immobilization of anti-HSA, as described in the literature.[4,10] After the end part of an optical fiber was activated by strong mineral acid, the surface was treated by 3-(2,3-epoxypropoxy)propyltrimethoxysilane, and anti-HSA was immobilized by a periodic acid method on the surface, followed by the reduction of the imine-type bond to the amine-type bond by sodium borohydride. The antibody-immobilized optical fiber, thus obtained, was washed by Buff-A and stored at 4 °C in Buff-B. According to the present procedure, 160 pieces of antibody-immobilized optical fibers were obtained using 10 mg of antibody.

Apparatus and Procedure. Both the competitive immunoassay and sandwich immunoassay are schematically shown in Fig. 1.

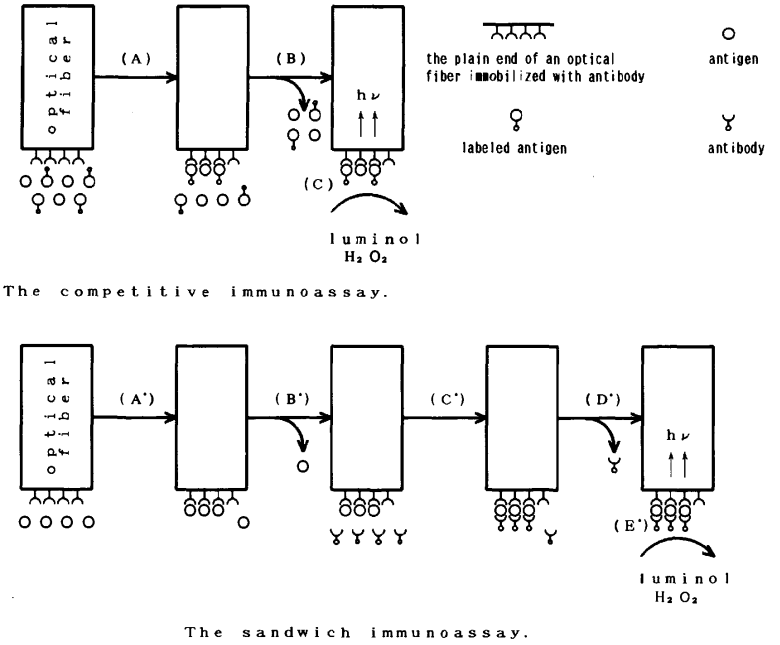

Fig. 1. Schematic diagram of the immunoassay. (A),(A'),(C'): Antigen-antibody reaction, (B),(B'),-(D'): separation of bound and free fractions, and (C),(E'): measurement of CL intensity.

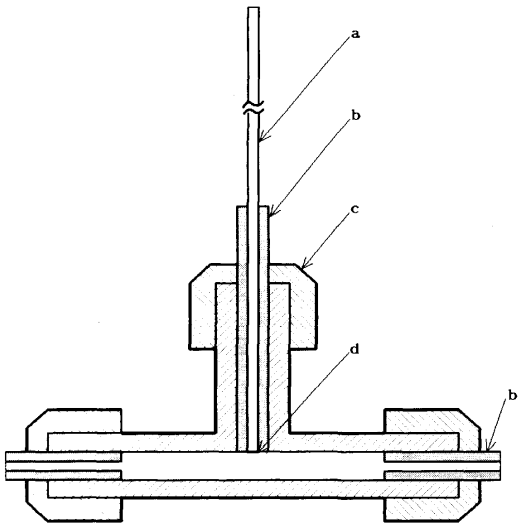

Fig. 2. The cell set with an optical fiber. a: optical fiber, b: silicone tube (3 mm o.d.×1 mm i.d.), c: Teflon-made three-way joint (3 mm i.d.), and d: immobilized antibody.

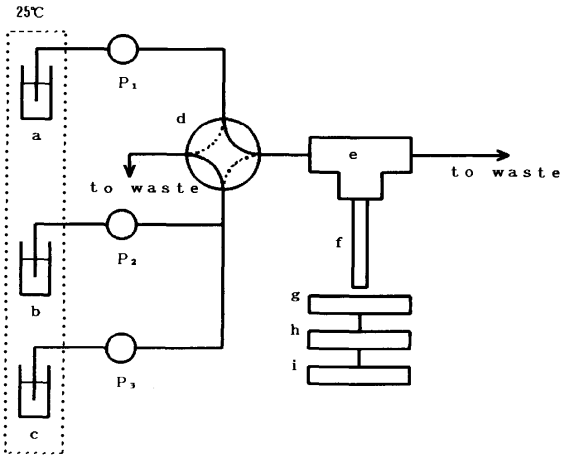

Fig. 3. Schematic flow diagram of a fiber-optic immunosensor. a: Buffer solution, b: H_2O_2 solution, c: luminol solution, d: four-way cock, e: cell, f: optical fiber, g: photomultiplier, h: photoncounter, i: integrator, and P_1, P_2, P_3: pump.

Competitive immunoassay was carried out as follows: The end part of an antibody-immobilized optical fiber was immersed in a mixed solution containing 2.4 ng of labeled HSA in 4 mm^3 of Buff-B and a definite amount of HSA in 4 mm^3 of Buff-B, and was made to react with antigen (HSA) in the mixed solution at 4 °C for 2 hours (A). The optical fiber was twice washed with 50 mm^3 of Buff-C (2.78×10^{-3} mol dm^{-3} potassium dihydrogenphosphate, 5.56×10^{-3} mol dm^{-3} disodium hydrogenphosphate) (B) and positioned in the cell as shown in Fig. 2. Sandwich immunoassay was carried out as follows: The end part of an antibody-immobilized optical fiber was immersed in a solution containing a definite amount of HSA in 4 mm^3 Buff-B, and was made to react with antigen (HSA) in the solution at 25 °C for 2 hours (A'). The optical fiber was twice washed with 50 mm^3 of Buff-B (B') and was made to react with 12 ng of labeled HSA in 4 mm^3 of Buff-A at 4 °C for 4 hours (C'). The optical fiber was positioned in the cell as shown in Fig. 2 after washing twice with 50 mm^2 Buff-C (D').

The CL emitted from the surface of the optical fiber set to the cell was measured ((C) and (E')) in accordance with the following procedure: The measurement of the CL intensity was made using the immunosensor system shown in Fig. 3 in which all the tubes and connectors were made of Teflon. Each solution of Buff-C (a), H_2O_2 (b), and luminol (c) was fed at a flow rate of 1.5, 0.25, and 0.25 cm^3 min^{-1} by means of pumps (P_1), (P_2), and (P_3) (Atto, SJ1211). The optical fiber set to the cell was washed with Buff-C for 1 min and fed with a mixed solution of H_2O_2 and luminol by operating a four-way cock (d). The CL emitted from the surface of the optical fiber was immediately detected with the photon-counter (h) and was integrated for 1 min with the integrator (i) to give the CL intensity as a peak area (V s).

Results and Disccusion

Determination of Analysis Conditions. An adequate investigation was not made in previous studies,[1-3,9] regarding the type and pH of the buffer solution used for a luminol solution in the lunimol-H_2O_2-TCP-Fe(III) system. To improve the sensitivity of immunoassay, a CL system by which TCP-Fe(III) could be determined more sensitively was necessary. Then, the type and pH used for a luminol solution were optimized. The apparatus used for this experiment is shown schematically in Fig. 4. Each solution of luminol, H_2O_2 and carrier(Buff-C) was fed at a flow rate of 2.0, 2.0, and 0.5 $cm^{-3}min^{-1}$. A 50 mm^3 portion of a 1.0×10^{-8} mol dm^3 TCP-Fe(III) catalyst solution was injected into the line of carrier solution through the sampling loop and six-way cock. The CL intensity of the solution passing through the flow-cell (0.8 mm i.d.×45 cm; poly (vinyl chloride) tube) was detected with a photoncounter and recorded on a recoder. The peak area obtained by injecting the catalyst sample solution was integrated with the integrator to give the CL intensity as a peak area (V s). As can be seen from the experimental results (Fig. 5) obtained using the above-mentioned apparatus, the CL intensity showed a maximum value when a 0.2 mol dm^{-3} carbonate buffer solution (pH 10.8) was used. Since the value of the base line which corresponded to the CL intensity due to both a luminol solution and a H_2O_2 solution in the absence of a catalyst solution was large, a 1.0×10^{-2}—1.0×10^{-4} mol dm^{-3} EDTA solution was added to a luminol solution so as to minimize the value of the base line. The relationship between the EDTA concentration and the value of the base line or the CL intensity of a TCP-Fe(III) catalyst solution was obtained. The addition of the EDTA solution lowered the value of the base line by one-hundred times, but had almost no affect on the catalytic activity of the

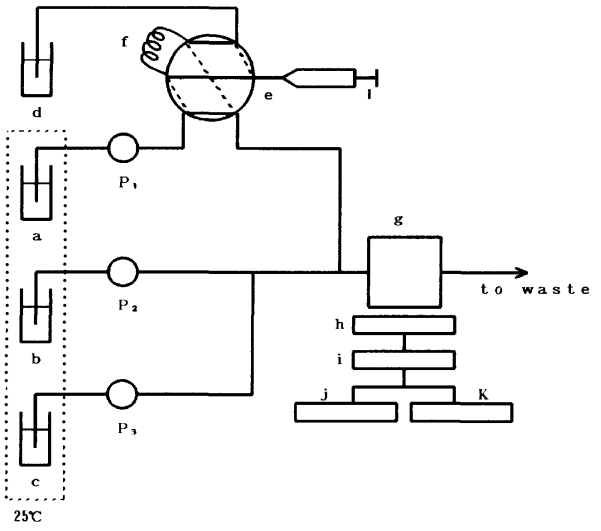

Fig. 4. Flow-injection system.
a: Buffer solution, b: H_2O_2 solution, c: luminol solution, d: sample solution, e: six-way cock, f: sampling loop, g: flow-cell, h: photomultiplier, i: photon-counter, j: recorder, k: integrator, l: syringe, and P1, P2, P3: pump.

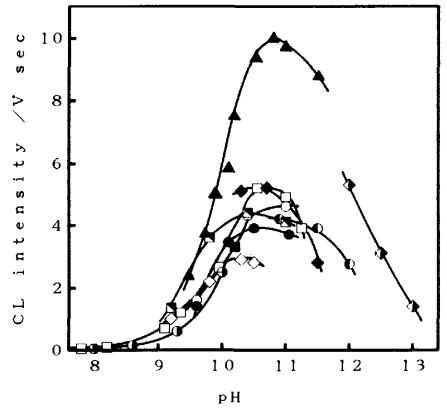

Fig. 5. Effect of various buffer solutions on the CL intensity of the luminol-H_2O_2 system.
■: H_3BO_3-KOH buffer, ◪: $Na_2B_4O_7$-Na_2CO_3 buffer, □: H_3BO_3-KCl-Na_2CO_3 buffer, ◇: $Na_2B_4O_7$-NaOH buffer, ◆: NaOH-KCl buffer, ◆: HCl-Na_2CO_3 buffer, O: $NaHCO_3$-NaOH buffer, ◐: Na_2HPO_4-NaOH buffer, ◑: H_3BO_3-KCl-NaOH buffer, ▲: 0.2 mol dm^{-3} (Na_2CO_3-$NaHCO_3$) buffer, and ●: 0.02 mol dm^{-3} (Na_2CO_3-$NaHCO_3$) buffer.

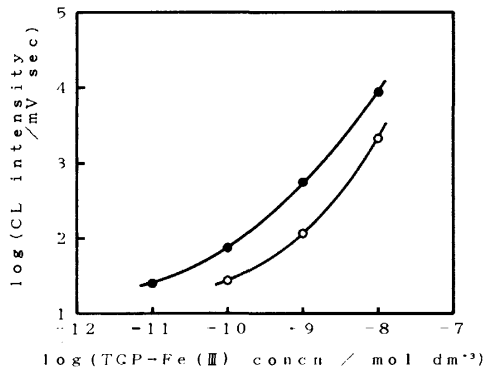

Fig. 6. The relationship between concentration of TCP-Fe(III) and CL intensity.
●: The present luminol solution and O: the conventional luminol solution.

TCP-Fe(III) solution. Therefore, the detection limit of TCP-Fe(III) using the present luminol solution consisting of 1.0×10^{-3} mol dm^{-3} EDTA in a 0.2 mol dm^{-3} carbonate buffer solution (pH 10.8), was about one-tenth that of TCP-Fe(III) using the luminol solution mentioned in a previous paper.[3] Two calibration curves for TCP-Fe(III) using the present luminol solution and same luminol solution as in the previous paper[3] were shown in Fig. 6.

The relationship between the CL intensity and the flow rate of a 1:1 mixed solution of a luminol solution and a H_2O_2 solution was examined by the measuring system shown in Fig. 3. In this experiment the CL emitted from an antibody-immobilized optical fiber, which had been made to react with 4 mm^3 of 1.0×10^{-2} g dm^{-3} labeled HSA at 4 °C for 20 min, was measured for 1 min at various flow rates of the 1:1 mixed solution of a luminol solution and a H_2O_2 solution. The maxium CL intensity was observed when the flow rate of the 1:1 mixed solution was 0.5 cm^3 min^{-1}; the change of the CL intensity in the flow rate range of 0.1—2.0 cm^3 min^{-1} was within 10%. A flow rate of 0.5 cm^3 min^{-1} was used for the experiment.

The relationship between the repetitive use and the activity change of an antibody-immobilized optical fiber was examined as follows: The antibody-immobilized optical fiber was made to react with 4 mm^3 of 1.0×10^{-2} g dm^{-3} labeled HSA at 4 °C for 20 min and the CL emitted from the optical fiber was measured for 1 min. Then, the labeled HSA was eluted with a 8.0×10^{-3} mol dm^{-3} hydrochloric acid —3.0×10^{-2} mol dm^{-3} potassium chloride buffer solution (pH 2.3), and the antibody-immobilized optical fiber was subjected to the next immune reaction, followed by measuring (using a similar method as before) the CL. This operation was repeated severall times. According to the obtained results, about a 20% reduction of the CL intensity was observed for one-time use. A newly prepared antibody-immobilized optical fiber was used for every measurement in the present study.

The conditions necessary for the immune reaction (A) in competitive and the immune reaction (C′) in sandwich immunoassay were chosen by taking the reaction time and nonspecific adsorption into consideration,[11,12] as follows: Immune reaction (A) 3.0×10^{-3} g dm^{-3} labeled HSA, 4 °C, and 2 hours; immune reaction (C′) 3.0×10^{-2} g dm^{-3} labeled anti-HSA, 4 °C, and 4 hours.

The relationship between the reaction time and the CL intensity was examined for the immune reaction (A′) in sandwich immunoassay. The immune reaction (A′) was found to almost attain equilibrium in 2 hours. Therefore, the immnue reaction (A′) in the subsequent experiment was carried out for 2 hours. The relationship between the sample amount used for sandwich immunoassay and the CL intensity was examined. The CL intensity was nearly definite for a sample solution of more than 4 mm^3. Therefore, a 4 mm^3 sample solution was used in the subsequent experiment.

Calibration Curve of HSA. The calibration curve for HSA was obtained by competitive immunoassay under the optimized conditions mentioned above (Fig. 7). HSA could be determined in the concentration range 1×10^{-4}—1×10^{-1} g dm^{-3}, with a lower limit of 400 pg. The coefficient of variation for five analyses of a 1.0×10^{-3} g dm^{-3} HSA solution was 6.5%.

The calibration curve for HSA was also obtained by sandwich immunoassay under the optimized conditions mentioned above (Fig. 8). HSA could be determined in the concentration range 1×10^{-5}—1×10^{-1} g dm^{-3}, with the lower limit of 40 pg. The

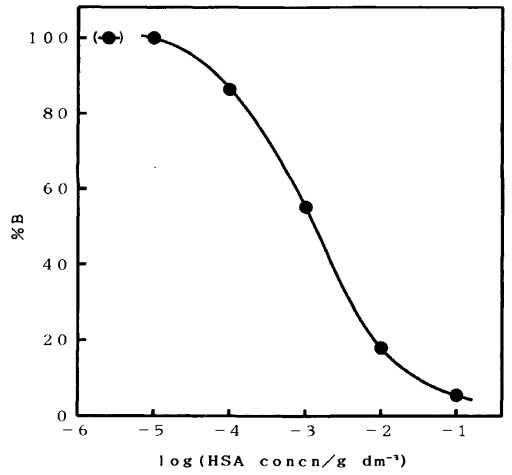

Fig. 7. Calibration curve for HSA obtained by the competitive immunoassay.
$\%B=\{(I_s-I_{ba})/(I_{b1}-I_{ba})\}\times100$. I_s, I_{b1}: CL intensity of the sample in the presence or absence of HSA, I_{ba}: CL intensity of background, and (-●-): Blank value.

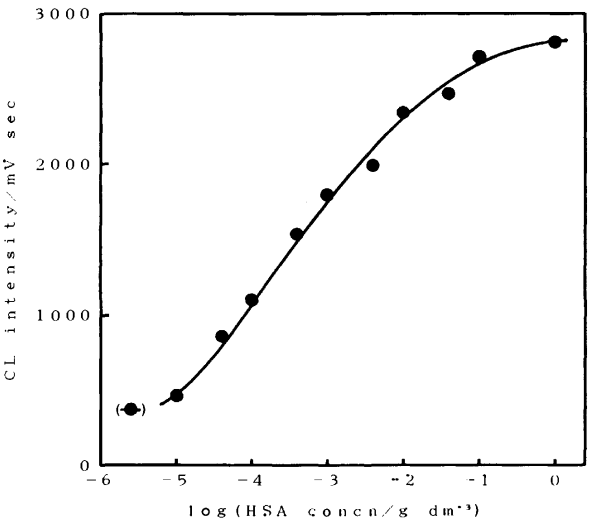

Fig. 8. Calibration curve for HSA obtained by the sandwich immunoassay. (-●-): Blank value.

Table 1. Selectivity of a Fiber-Optic Immunosensor

Protein	Relative CL intensity
HSA	1.00
HγG	0.14
BγG	0.07
BγG	0.00
Ova	0.00

Protein concn=1.0×10^{-2} g dm^{-3}.

coefficient of variation for five analyses of a 1.0×10^{-3} g dm^{-3} HSA solution was 5.0%. Though sandwich immunoassay was a tedious method, it was about 10 times more sensitive than competitive immunoasay.

Selectivity. The selectivity of the fiber-optic immunosensor in sandwich immunoassay was examined by measuring the adsorption amount of various proteins onto an anti-HSA immobilized optical fiber (Table 1). Each 1.0×10^{-2} g dm^{-3} of protein was used throughout this experiment and the relative CL intensity was shown based on the CL intensity of HSA (=1.00). As can be seen from Table 1, BαG and Ova showed no nonspecific adsorption, whereas HγG and BγG showed somewhat nonspecific adsorption with values of 0.14 and 0.07. Such nonspecific adsorption would be decreased by the ues of a monoclonal antibody, since a polyclonal antibody was used in the present experiment.

Comparison with Other Methods. The method for the determination of protein, which is based on the combination of CLCCIA and an immune column, has already been reported by the authors.[3] The concentration range for the determination of protein, the detection limit, and the sample amount necessary for the determination mentioned in the paper[3] were 2.5×10^{-5}—5×10^{-3} g dm^{-3}, 5 ng, and 200 mm^3, while those in the sandwich immunoassay in the present study were 1×10^{-5}—1×10^{-1} g dm^{-3}, 40 pg, and 4 mm^3.

Sepaniak et al. reported the determination of IgG in the concentration range 3.7×10^{-4}—1.8×10^{-1} g dm^{-3} by use of a fiber-optic immunosensor (D-I)[4] with fluorescence detection in which an antibody was directly immobilized on the plain end of an optical fiber. Aizawa et al. also reported the determination of protein in the concentration range 6.9×10^{-2}—2.1 g dm^{-3} HSA using a fiber-optic immunosensor (D-II)[6,7] with electro-chemical luminescence detection and in the concentration range 1×10^{-6}—1×10^{-2} g dm^{-3} IgG they used a fiber-optic immunosensor (D-III)[8] with chemiluminescence detection, in which an aromatic hydrocarbon or enzyme was used as a labeling agent, though the antibody was not directly immobilized on an optical fiber. In the present study, a highly sensitive immunosensor using an optical fiber immobilized with antibody directly on its plain end was newly developed; it was introduced into CLCCIA using a synthetic metal-complex catalyst for CL reaction as a labeling agent. The sensitivity of the present method was inferior to that of D-III but superior to those of D-I and D-II by more than 10 times.

The new fiber-optic immunosensor was characterized by the followings: 1) Highly sensitive for the determination of a small amount of protein, 2) applicable to a wide concentration range of protein sample, 3) feasible with a microvolume of sample, 4) suitable for the automation of operation, and 5) excellent regarding safety, cost, and treatment.

The authors wish to thank Mr. Masakatsu Imaki (Horiba, Ltd.) for providing the apparatus necessary for the present study.

The present study was supported by a Grant-in-Aid for General Scientific Research No. 63550567 from the Ministry of Education, Science and Culture.

References

1) T. Hara, M. Toriyama, and K. Tsukagoshi, *Bull. Chem. Soc. Jpn.*, **56**, 2965 (1983).

2) T. Hara, M. Toriyama, and K. Tsukagoshi, *Bull. Chem. Soc. Jpn.*, **57**, 587 (1984).

3) T. Hara, M. Toriyama, and M. Imaki, *Bull. Chem. Soc. Jpn.*, **58**, 1299 (1985).

4) B. J. Tromberg, M. J. Sepaniak, T. Vo-Dinh, and G. D. Griggin, *Anal. Chem.*, **59**, 1226 (1987).

5) R. D. Petrea, M. J. Sepaniak, and T. Vo-Dinh, *Talanta*, **35**, 139 (1988).

6) Y. Ikariyama, H. Kunoh, and M. Aizawa, *Biochem. Biophys. Res. Commun.*, **128** (1985).

7) M. Aizawa, Y. Ikariyama, M. Tanaka, and H. Shinohara, *Pro-Electrochem. Soc.*, **1987**, 362.

8) M. Aizawa, *Protein, Nucleic Acid and Enzyme, Bessatsu*, No. 31, 272 (1987).

9) T. Hara, M. Toriyama, and K. Tsukagoshi, *Bull. Chem. Soc. Jpn.*, **56**, 2267 (1983).

10) J. R. Sportsman and G. S. Wilson, *Anal. Chem.*, **52**, 2013 (1980).

11) N. Hibi and H. Hirai (1978) in Enzyme immunoassay (E. Ishikawa, T. Kawai, and K. Miyai) pp. 136—146, Igaku-shoin, Tokyo.

12) E. Ishikawa, "Koso-meneki-sokutei-ho no saishin-gijutsu to monokuronaru-kotai heno oyo no jissai", Kogaku-joho-senta.

 © 1989 The Chemical Society of Japan Bull. Chem. Soc. Jpn., 62, 2849—2853 (1989)

Temperature Dependence and Decay Kinetics of the High-Energy Band in DPH Fluorescence

Shoji YAMASHITA,* Aurthur G. SZABO,† and P. CAVATORTA†
Institute of Biophysics, Faculty of Agriculture, Kyushu University, Higashiku, Hakozaki, Fukuoka 812
†Division of Biological Sciences, National Research Council Canada, Ottawa, Canada K1A0R6
(Received February 18, 1989)

The temperature dependence and associated decay kinetics of the high energy band centered at 380 nm in the fluorescence spectrum of 1,6-diphenyl-1,3,5-hexatriene in a nonpolar solvent were investigated. Below 150 K the emission intensity at 380 nm relative to that of a sharp band near 400 nm was very small. Above this temperature the intensity at 380 nm increased with increasing temperature. The fluorescence decay analysis of this band showed two components with decay times of 62 ps and 13.4 ns. The 62 ps component was assigned to the prompt fluorescence of the S2 (1Bu*) state and 13.4 ns component to a delayed type fluorescence from the same state after establishment of a thermal equilibrium with lower S1 (1Ag*) state.

When a molecule is used as a fluorescence probe in biological systems it is essential that its photophysical properties are clearly understood so that the information provided by the probe is correct and most useful. 1,6-Diphenyl-1,3,5-hexatriene (DPH) has been employed as a fluorescence probe for the elucidation of the order and dynamics of membrane systems.[1-3] It is representative of the diphenyl derivatives of linear polyenes and considerable data about their photophysical properties have been reported.[4,5] It has been adequately shown that DPH has anomalous fluorescence properties.[6] The fluorescence properties of DPH has a large Stokes shift and its radiative lifetime when estimated from Strickler-Berg relationships[7] is far smaller than that obtained experimentally.[8] A large number of investigations of DPH photophysics have been directed at understanding origin of these anomalies. It has been shown that the 1Ag* state is the emitting state.[9] Birks and co-workers[10] suggested that the fluorescence occured from the symmetrically forbidden 1Ag*-1Ag transition, which borrowed intensity from the dipole allowed 1Bu*-1Ag transition. They proposed that the energy difference between the 1Bu* and 1Ag* state and conformational changes in the excited state were controlling factors for the photophysical processes of diphenylpolyenes such as diphenylbutadiene (DPB) and diphenyloctatetraene (DPO). While this rationalization appears to be reasonable, Alford, Palmer,[11,12] Itoh and Kohler[13] in their investigations of the fluorescence spectra of DPH and its derivatives assigned a band near 380 nm to the 1Bu*-1Ag transition. Furthermore, recent picosecond transient absorption studies on DPH suggested a thermal equilibrium exists between the S2 and S1 states.[14] In this report we present a detailed study of the temperature dependence and fluorescence decay kinetics of the high enegry band.

Materials and Methods

all-trans-1,6-Diphenyl-1,3,5-hexatriene (Sigma Chemical Co. St. Louis Mo.) was purified by vacuum sublimation. Its purity and photochemical decomposition was checked by measuring its absorption spectrum before and after any fluorescence measurements. Methylcyclohexane (MCH) (Distilled in glass quality, Caledon Lab, Georgetown, Ont) was used without further purification and shown to be free of any fluorescence impurities.

Fluorescence decay measurements were performed with a frequency doubled Spectra-Physics synchronously pumped and cavity dumped laser system (E_x=295 nm or 310 nm) and methods of time correlated single photon counting techniques. The instrumentation and the methods of data analysis used have been described in detail.[15] The emission bandpass was 4 nm. A Perkin-Elmer MPF-44A spectrofluorometer equipped with a DCSU-2 microprocessor correction unit was used for measurement of the fluorescence spectra. The fluorometer was connected through an analog to digital converter to a Commodore PET minicomputer for the storage and manipulation of the fluorescence spectra. The fluorometer was equipped with a thermostable cell holder. Low temperature (<0 °C) spectra were recorded using a NRCC built quartz Dewar assembly the temperature of which was controlled by blowing cold nitrogen gas into the Dewar. The samples in this latter case were in a suprasil quartz tube. The excitation and emission bandpasses were 2 nm and 2 nm respectively. All samples were deoxygenated by flushing with oxygen free nitrogen. Absorption spectra were measured on Cary 118 spectrophotometer.

Results

The fluorescence spectrum of DPH in a MCH glass at 77 K has three sharp bands at 397, 425, and 445 nm and a shoulder at 480 nm (Fig. 1). Above 147 K the MCH solution is liquid. The spectrum at 150 K again has three sharp transitions at 401, 426, and 450 nm which are red shifted relative to the bands in the 77 K spectrum. At 150 K and 77 K the emission intensity between 360 nm and 390 nm was negligible when

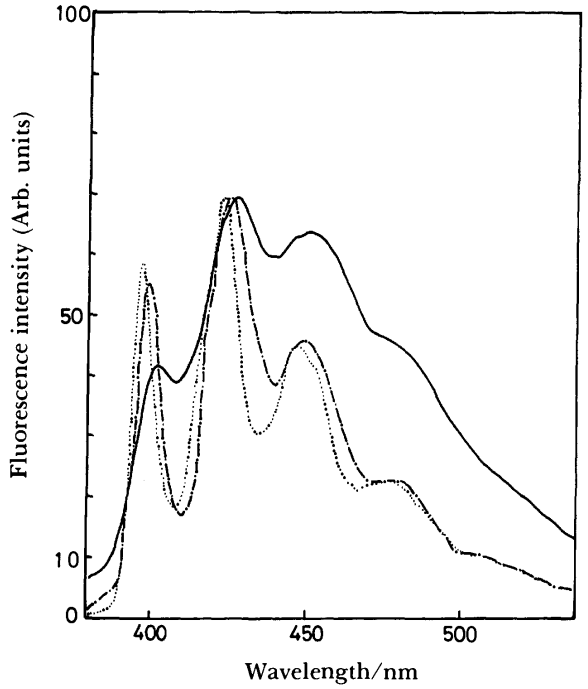

Fig. 1. Fluorescence spectra of DPH in MCH. -----; 77 K, ----; 150 K, —; 293 K.

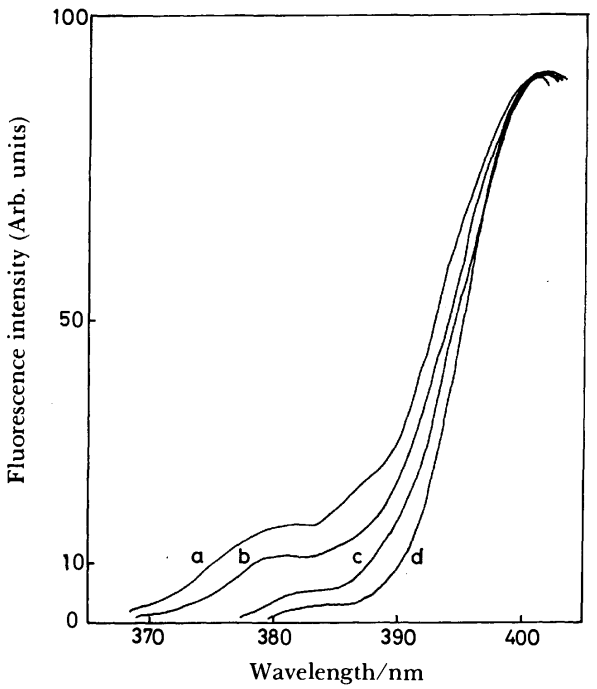

Fig. 2. Temperature dependence of high energy band of DPH fluorescence spectrum in MCH, a; 313 K, b; 279 K, c; 233 K, d; 183 K.

compared to the intensity of the band above 390 nm. As the temperature increased the position of the bands remained constant, however the band widths broadened and the intensities of the long wavelength bands (426, 450, and 482 nm) increased. At the same time, a shoulder became evident at a wavelength below the

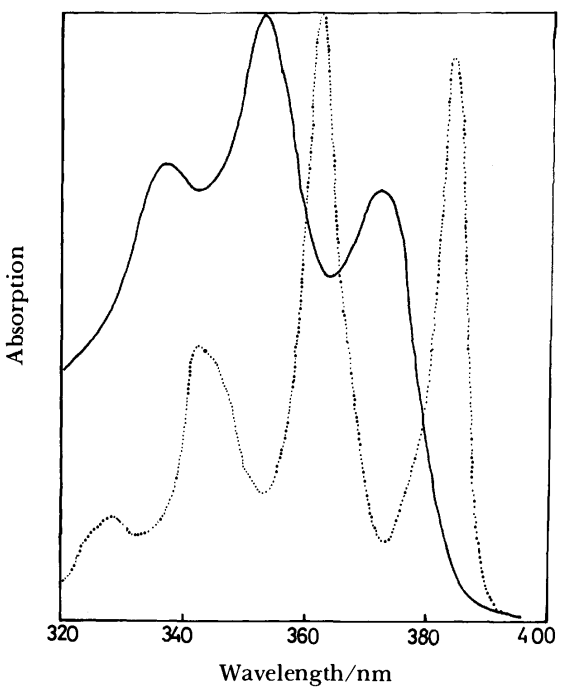

Fig. 3. Absorption spectra of DPH in MCH at 77 K (-----) and 293 K (—). See text.

400 nm band. Figure 2 shows the high energy edge of the DPH fluorescence spectrum in MCH solution at 183, 233, 279, and 313 K. The emission intensity in this region increased as the temperature increased. The peak position and the band width of the high energy emission band, measured at 279 K was estimated to be 380 nm and 970 cm^{-1} respectively by curve fitting assuming Gaussian band shapes. Because of the broadening of the 400 nm band, it is difficult to determine the precise peak position of the high energy band at high temperature. But this band apparently undergoes a shift to the lower energy side with decreasing temperature. This contrasts with the behavior of the main fluorescence bands above 400 nm.

The absorption spectrum of DPH in MCH at 77 K has sharp bands at 327, 342, 362, and 384 nm and no absorption was detected around 400 nm (Fig. 3). Usually the excitation spectrum is used for the investigation of absorbance at 77 K. But that is correct only when the sample concentration is extremely low. The spectrum shown in Fig. 3 was obtained from the intersection of the straight line log $(I(\lambda)/I(\lambda_0))$-[DPH] plot of the following equation

$$\log\{I(\lambda)/I(\lambda_0)\} = \log\{\varepsilon(\lambda)/\varepsilon(\lambda_0)\} - \{\varepsilon(\lambda) - \varepsilon(\lambda_0)\}cd$$

where $I(\lambda)$ and $I(\lambda_0)$ are fluorescence intensities excited by λ and λ_0 and ε, c and d are absorption coefficient, DPH concentration and optical path length, respectively.[16] The absorption spectrum of DPH at temperature above 293 K has peaks at 337 nm, at 353 nm and 372 nm which are blue shifted relative to the 77 K

Table 1. Fluorescence Decay Parameters for DPH in MCH at 293 K, A_1 and A_2; Normalized Preexponential Factors, F_1 and F_2; Fractional Contributions

F_m/nm	T_1/ns	T_2/ps	A_1	A_2	F_1	F_2
373	13.38	62	0.167	0.833	0.978	0.022
377	13.38	62	0.268	0.732	0.988	0.012
380	13.38	62	0.357	0.643	0.992	0.008
383	13.38	62	0.375	0.625	0.992	0.008
387	13.38	62	0.449	0.551	0.994	0.006
390	13.38	62	0.557	0.443	0.996	0.004
393	13.38	62	0.817	0.188	0.999	0.001
397	13.40					
400	13.40					
400<	13.40					

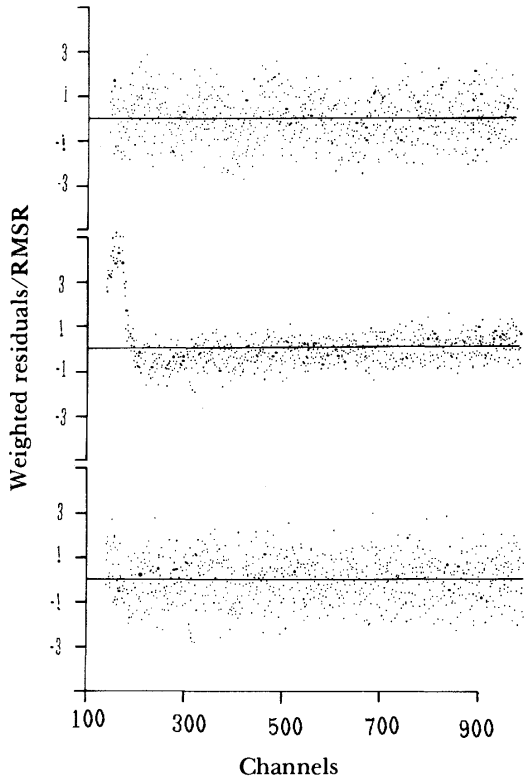

Fig. 4. Plots of weighted residuals/RMSR after iterative convolution of the DPH fluorescence in MCH at 293 K for the best fits (upper) single exponential function at 430 nm, (middle) single exponential function at 380 nm, (lower) double exponential at 380 nm. 10 ps/channel.

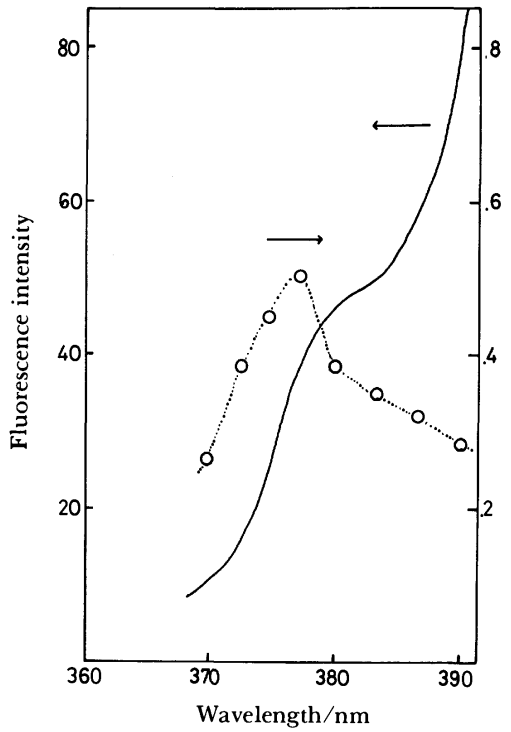

Fig. 5. Fluorescence spectrum of 62 ps component of DPH in MCH at 293 K, solid curve; high energy band of the DPH fluorescence. Broken curve; calculated fluorescence intensities of 62 ps component.

spectrum. As reported earlier[8] these bands undergo small shifts to higher energy with increasing temperature. The emission band at the high energy edge (380 nm) overlaps the lowest energy band of the absorption spectra.

The fluorescence decay of DPH in MCH was measured over the full spectral region. Between 400 nm and 550 nm the fluorescence decayed with single exponential decay kinetics (Fig. 4 upper). Below 400 nm, in the high energy fluorescence spectral region, DPH showed the double exponential decay kinetics (Fig. 4 middle and lower) with lifetimes of 13.38 ns (T_1) and 62 ps (T_2). The fluorescence decay parameters of DPH are summarized in Table 1. Because T_2 is short and its fractional fluorescence is small, close attention was paid to eliminate the possibility that this component was due to light scattering or emission from quartz cuvette or solvent impurities. From the relation between the steady state fluorescence intensity, $F_{ss}(\lambda)$ and the fluorescence decay kinetics, the fast decay component $F_s(\lambda)$ is extracted as follows,

$$F_s(\lambda) = F_{ss}(\lambda)R(\lambda)\ T_2/(R(\lambda)\ T_2 + T_1)$$

where $R(\lambda)$ is the ratio of the normalized preexponential factor. The time resolved spectrum of DPH fluorescence in the high energy spectral region gives a

clear peak at 377 nm (Fig. 5). This peak position is coincident with the high energy peak of the steady state DPH fluorescence spectra estimated by a curve fitting procedure. In experiments using the third harmonics (353 nm) from the neodymium laser it was observed that the fluorescence of DPH had a decay component which decayed to 70 percent of the maximum fluorescence within 30 ps after excitation.[17] This component corresponds to the 62 ps component which we observed. The time evolution of the transient absorption spectra of DPH shown by Rullière and Declémy supports the assignment of the fast decay component of DPH fluorescence to the S_2-S_0 transition.[14]

Discussion

Because the 1Ag*-1Ag transition is symmetrically forbidden, it is presumed that the absorption spectrum of DPH is due to the 1Bu*-1Ag transition. Therefore the spectral overlap at temperature 150 K in the 380 nm region would support the assignment of this latter emission band originating from the 0-0 level of the same transition. Further since the 1Ag* state is lower in energy than the 1Bu* state in DPH in nonpolar solvents the 401 nm band in the 150 K fluorescence spectrum can be assigned to the 0-0 band of the 1Ag*-1Ag transition.

We agree that the increase in the 380 nm fluorescence intensity with temperature is indicative, as Alford and Palmer suggested, requires that a thermal equilibrium be established between the S_2 (1Bu*) and S_1 (1Ag*) states. Using the data obtained at several different temperatures it is possible to estimate the energy difference between these states from the relationship proposed by Parker[18]:

$$I(380)/I(401) = A\exp(-E_0/kT)$$

where $I(380)$ and $I(401)$ represent the fluorescence intensities at 380 nm and 401 nm respectively, A is a temperature independent constant which include a frequency factor and a radiative lifetime, and the other terms, k, and T have their usual definitions. A plot of the natural logarithm of the intensity ratio against $1/T$ is shown in Fig. 6; an excellent straight line was obtained with a slope having a value for E_0=630 cm^{-1} (0.078 eV). This value is coresponds to the energy difference E(1Bu*)−E(1Ag*) of DPH in hexane at zero temperature reported by Itoh and Kohler.[13] The energy difference between the 1Bu* and 1Ag* state can also be estimated from the 0-0 bands of the fluorescence spectra. This gives a value of 840 cm^{-1} which is in close agreement with the value obtained above. It is noteworthy that Cehelnik et al. in a study of the temperature quenching of the fluorescence of DPH in MCH (E_m=400 nm) found a value of 7.1 kJ mol^{-1} (596 cm^{-1}) which is close to the value which we report

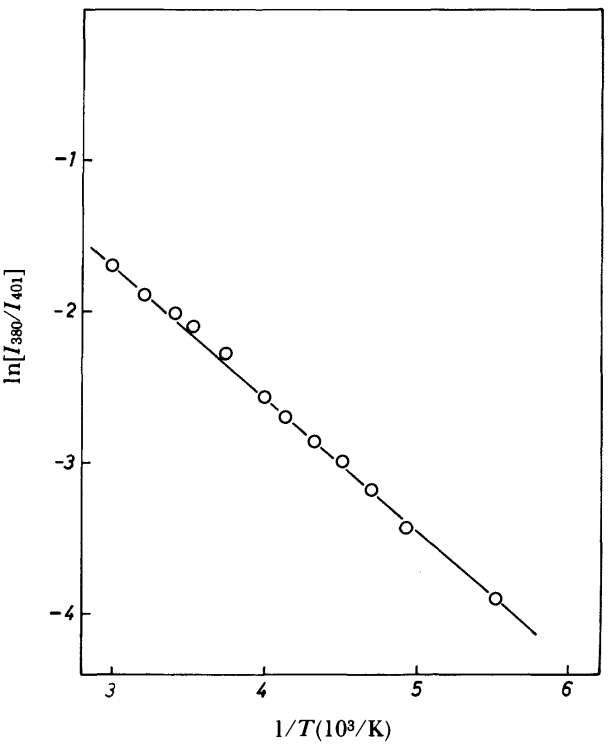

Fig. 6. Plot of ln (I_{380}/I_{401}) against $1/T$, I_{380} and I_{401} are fluorescence intensities at 380 and 401 nm, respectively.

herein. This is strong evidence that the main nonradiative deactivation pathway of the 1Ag* state is a thermally activated process occuring through the 1Bu* state.

We propose that the fluorescence decay results may be rationalized according to the following scheme. We attribute the 62 ps component, which is only observed at wavelengths below 400 nm, to prompt emission from the initially excited 1Bu* state. We have not been able to detect any evidence of a short component at longer wavelengths. This may be due either to the lack of such a contribution at lower energies or to a very small contribution (<0.2% of a 13.40 ns component) which cannot be detected. The signal 13.4 ns component which is observed above 400 nm is assigned to the emission from the 1Ag* state. The 13.4 ns component, which is observed below 400 nm, is attributed to a delayed type emission from the 1Bu* state after thermal repopulation from the 1Ag* state. At present we cannot rule out the possibility that the fluorescence above 400 nm includes 1Bu* emission. If it did however we might expect to detect a 62 ps component due to the prompt fluorescence from this state. As stated above this might make a negligible contribution to the fluorescence in this region.

The value of the radiative lifetime, τ_r, of DPH from the 1Bu*-1Ag transition, estimated by the Strickler-Berg method was 1.6 ns. The short lifetime, 62 ps, in these experiment is much less than the theoretical

value. However, it is reasonable to attribute the shorter value to internal conversion processes between the 1Bu* and 1Ag* states.

In summary we have resolved the temporal behavior of the 380 nm transition and have confirmed the assignment of this band as the 1Bu*–1Ag transition. The model of a thermal equilibrium between the S_2 (1Bu*) and S_1 (1Ag*) excited state is consistent with all the data. We consider that their relationship and the role they play in the photophysical processes in DPH are clarified so that a better understanding of these processes in lipid system where DPH is used as a probe of order and dynamics is possible.

References

1) M. Shinitzky and Y. Barenholtz, *Biochim. Biophys. Acta*, **515**, 367 (1978).
2) C. Zannoni, A. Arcioni, and P. Cavatorta, *Chem. Phys. Lipid*, **32**, 179 (1983).
3) R. E. Dale, "Time resolved fluorescence spectroscopy in biochemistry and biology," R. B. Cundallg and R. E. Dale, Plenum Press (1983), p. 555.
4) B. Hudson and B. Kohler, *Ann. Rev. Phys. Chem.*, **25**, 437 (1974).
5) B. Hudson, B. Kohler, and K. Schilten, *Excited State*, **6**, 1 (1982).
6) J. B. Birks and D. J. S. Birch, *Chem. Phys. Lett.*, **31**, 608 (1975).
7) S. J. Strickler and R. A. Berg, *J. Chem. Phys.*, **37**, 814 (1962).
8) E. D. Cehelnik, R. B. Cundall, J. R. Lockwood, and T. F. Palmer, *J. Phys. Chem.*, **79**, 1369 (1975).
9) J. B. Birks, G. N. R. Triphati, and M. D. Rumb, *Chem. Phys. Lett.*, **33**, 185 (1978).
10) J. B. Birks, *Chem. Phys. Lett.*, **54**, 430 (1978).
11) P. C. Alford and T. F. Palmer, *Chem. Phys. Lett.*, **86**, 248 (1982).
12) P. C. Alford and T. F. Palmer, *J. Chem. Soc., Faraday Trans. 2*, **79**, 433 (1983).
13) T. Itoh and B. E. Kohler, *J. Phys. Chem.*, **91**, 1760 (1987).
14) C. Rulliere and A. Declemy, *Chem. Phys. Lett.*, **135**, 213 (1987).
15) M. Zuker, A. G. Szabo, L. Bramall, D. T. Krajcarski, and B. Sellinger, *Rev. Sci. Instrum.*, **56**, 14 (1985).
16) T. Ikeyama and T. Azumi, *J. Chem. Phys.*, **76**, 5672 (1982).
17) T. C. Felder, K. Choi, and M. R. Topp, *Chem. Phys.*, **64**, 175 (1982).
18) C. A. Parker, "The Triplet State," ed by A. B. Zahlan, Cambridge University Press (1967), p. 353.

The Addition of the Cyanide Ion to the *N*-Methyl-3-carbamoylpyridinium Ion in Reversed Micelles

Ayako GOTO* and Hiroshi KISHIMOTO†
Department of Chemistry, University of Shizuoka, 395 Yada, Shizuoka 422
†Faculty of Pharmaceutical Sciences, Nagoya City University, Tanabe-dori, Mizuho-ku, Nagoya 467
(Received February 22, 1989)

The addition reaction of the cyanide ion to the *N*-methyl-3-carbamoylpyridinium ion was carried out in reversed micelle systems, and the functions of the electric charge of surfactants and of the entrapped water in the micelle were studied by measuring the rate and equilibrium constants. Reversed micelles formed by hexadecyltrimethylammonium bromide (HTAB), a cationic surfactant, not only enhanced the reaction, but also stabilized the product, 4-cyano-1,4-dihydro-*N*-methylnicotinamide (P), which is thermodynamically unstable in aqueous media. This was in contrast to sodium 1,2-bis(2-ethylhexyloxycarbonyl)ethanesulfonate (AOT), an anionic surfactant, reversed micelles. In both reversed micelle systems the reaction could be controlled by varying the water content, although neither is favorable for the reaction at a higher water content. From the distribution measurements and spectroscopic studies, it can be suggested that the reaction occurred preferably in the micellar phase, especially in the water pool. Three kinds of effects were proposed for interpreting the enhancement as compared to the reaction in aqueous systems. The first was the local concentration of reaction species in the water pools, and the second was the lower micropolarity of water pools. The third concerned the electric nature of the surfactant and reactant ions.

The active site of enzyme provides a specific microenvironment, one in which the nature of the medium, such as the pH, the polarity and the viscosity, is quite different from that of bulk water, resulting in the enhancement of the reactivity of the substrates. Thus, the reaction pathway, the rate, and the equilibrium of an enzyme-substrate complex reaction can be controlled by adjusting the physicochemical conditions of the microenvironment.[1] From the physicochemical point of view, the issue of the microenvironment is very interesting to study.

Some reversed micelles[2-5] afford to substrates a microenvironment similar to that afforded by enzymes, because the water in the interior cores of reversed micelles is considered to be less polar and more viscous than in the bulk phase, so that the water pools in the reversed micelles might subrogate the active sites of enzymes for substrates. It has also been proposed, for the reversed micelles formed out of some kinds of functionalyzed surfactants, that the interfaces between the water pools and the hydrophilic groups of the surfactants inside of the micelles are activated and that the inner surfaces of the micelles can mimic the active sites of enzymes.[6] It must be noted here that, contrary to the cases of aqueous micelle systems, in reversed micelle systems the reactivity of substrates can easily be controlled by changing the content of water in the systems and by adjusting the physicochemical properties of the water in the pools.

Baumrucker et al.[7] and Bunton et al.[8] found that the rate and equilibrium constants for the addition of cyanide ion to a series of *N*-alkyl-3-carbamoylpyridinium ions remarkably increased in aqueous micelle systems with normal alkyltrimethylammonium salts and 3-(dodecyldimethylammonio)-1-propanesulfonate as surfactants.

In this work, we wish to report on an addition reaction similar to the one mentioned above, but carried out in some reversed micelle systems. As a reacting cation, the water-soluble *N*-methyl-3-carbamoylpyridinium (S^+) ion was used. The stoichiometric relation is shown by Eq. 1. We examined the functions of the electric charge of the surfactants and the entrapped water in the micelles by measuring the rate and equilibrium constants of the reactions as well as the stability of the product, the i.e., 4-cyano-1,4-dihydro-*N*-methylnicotinamide or simply, the 4-cyano adduct (P).

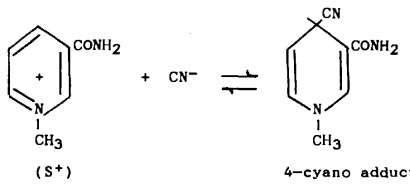

(1)

Experimental

Materials. The *N*-methyl-3-carbamoylpyridinium chloride (S) was obtained from Wako Chemicals and was twice recrystallized from methanol (MeOH). The water used was distilled by the use of an all-glass distillation apparatus. The sodium cyanide was of reagent grade. The chloroform and 2,2,4-trimethylpentane (isooctane) were dried and stored over a type 4A Molecular Sieve which had been activated by heating at 200 °C under reduced pressure for several hours and, then cooled in vacuo over silica gel; they were used as soon as possible.

The hexadecyltrimethylammonium bromide (HTAB), the cationic surfactant, was commercially obtained and was twice recrystallized from acetone–MeOH. The sodium 1,2-bis(2-ethylhexylcarbonyl)ethane sulfonate (AOT), the anionic surfactant, was obtained from Nikko Chemicals; its purity was more than 99.9%. Both the surfactants were dried at 60 °C in vacuo over P_2O_5 and used immediately.

Preparation of Solutions I and II. Each reversed micelle

system was formed by adding a ternary mixture of an organic solvent, a surfactant, and S (Solution I) to a quaternary mixture of an organic solvent, water, a surfactant, and NaCN (Solution II). The HTAB was dissolved in chloroform/isooctane mixture (3:2 volume ratio). The AOT was dissolved in isooctane. Each solution will hereafter be denoted as a mother solution.

Then, to prepare Solution I, a relatively small amount of the S/MeOH solution was dissolved in the mother solution. The concentration of HTAB or AOT in the mother solution before dissolving the S/MeOH solution was always kept at 0.2 M (1 M=1 mol dm^{-3}). The concentration of S in Solution I was in the range from 2 to 4×10^{-4} M, corresponding to the amount and concentration of the MeOH solution of S. The content of MeOH was within a 0.5% volume ratio. Special care was taken to exclude moisture during the above procedures. To prepare Solution II, various amounts of NaCN aqueous solutions were added, solubilized in the mother solution, and kept at 1×10^{-2} M. However, the molar ratio of water to HTAB or AOT in this solution was variable.

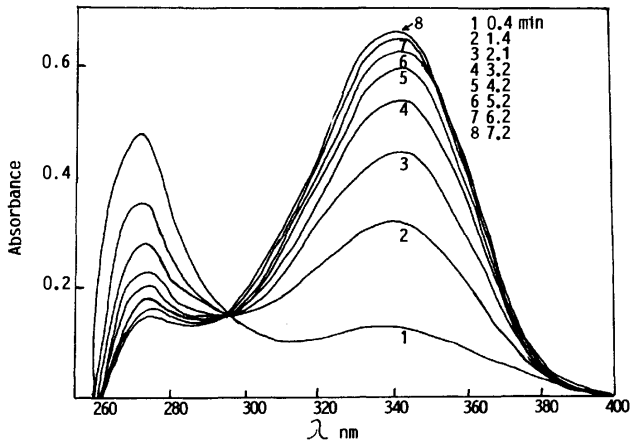

Fig. 1. Ultraviolet spectra of HTAB reversed micelle solution containing *N*-methyl-3-carbamoylpyridinium chloride and sodium cyanide at various reaction time. [HTAB]=0.2 M, R=2.7, $[NaCN]_{aq}$= 0.06 M.

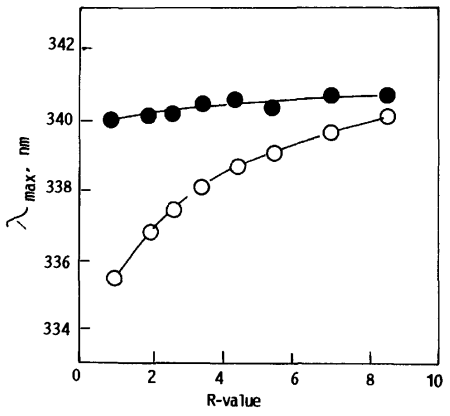

Fig. 2. The wavelength of maximum absorption, λ_{max}, of 4-cyano-1,4-dihydro-*N*-methylnicotinamide, P, in reversed micelles. ●, 0.2 M HTAB; ○, 0.2 M AOT.

By mixing equal amounts of Solutions I and II, we prepared the system for Reaction 1. In Solution II and the resultant reaction system, water was estimated to induce the formation and/or the growth of reversed micelles, which might not have appeared or developed yet, in the mother solution and also in Solution I. Solutions I and II as well as their mixed systems were found to be transparent and colorless.

Kinetics. Kinetic measurements were carried out spectrophotometrically with the aid of a Shimazu UV-265 spectrophotometer thermoregulated at 25±0.1 °C. The addition reaction (Reaction 1) was followed by measuring the OD (optical density) at 340 nm, where the absorption maximum of the reaction product, P, was found nearby, as is shown in Fig. 1. Although the wavelength of maximum absorption, λ_{max}, of P depended upon the composition of the reaction system, its variation was rather slight (Fig. 2) and, was considered to be tolerable in fixing the measured wave length of absorption at 340 nm for the kinetic study.

The reaction was initiated by the addition of 1.5 ml of a substrate solution (Solution I) to 1.5 ml of a cyanide solution (Solution II) in a moisture-proof cell in the spectrophotometer.

Distribution Measurement. The distribution of S between chloroform and aqueous phase was examined as follows, although the organic phase was different from that in the reversed micelle systems. Aqueous solutions of S with concentrations of 3×10^{-4}, 3×10^{-3}, and 3×10^{-2} M were prepared. Equal volumes of one of the aqueous solutions and chloroform were mixed in a vial, which was then sealed with a screw cap and vigorously shaken for about 12 hours at 25 °C. After the vial has been allowed to stand until the two liquid phases had completely separated, the solute concentration in the aqueous phase was determined spectrophotometrically.

Results and Discussion

Rate and Equilibrium Constants of the Addition Reaction in Reversed Micelles. In the reaction mixture, the initial concentrations S^+ and cyanide ions, $[S^+]^i$ and $[CN^-]^i$, were $1—2\times10^{-4}$ M and 5×10^{-3} M respectively. Within 30 min, all the reactions were regarded as having reached their final states, as may be seen in Figs. 1 and 3a. In aqueous systems, a remarkable spectral shift from 340 nm to 320 nm, which suggested the formation of the 2- or 6-cyano adduct, were observed.[9] However, in reversed micelle systems, no spectral change was observed, even after 2 hours, suggesting that less rearrangement of the 4-cyano adduct to the 6- or 2-cyano adduct occurs. Since $[CN^-]^i$ was sufficiently higher than $[S^+]^i$, Reaction 1 was expected to proceed with a pseudo first order in the earlier stage of the reaction. To examine this expectation, we traced the reaction in the plot of log ($OD^f_{340}-OD_{340}$) vs. time, where OD_{340} is the measured optical density at 340 nm and where OD^f_{340} denotes the value of OD_{340}, when the reaction was estimated to be at its final state. As may be seen in Fig. 3b, all the plots were linear with a correlation

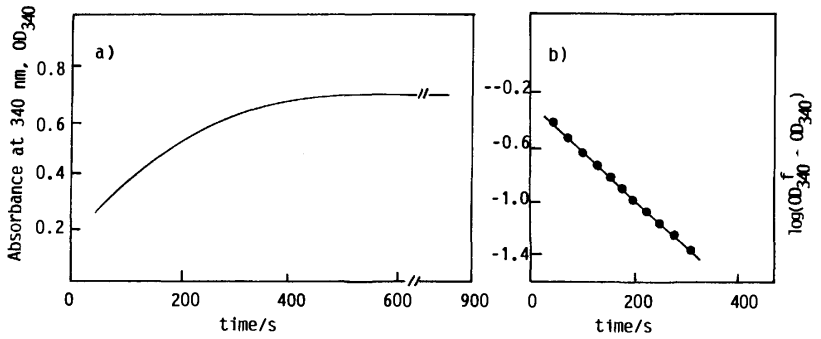

Fig. 3. Determination of first-order rate constants for the addition reaction. a) Absorption change at 340 nm at time; b) Plots of log (OD^{f}_{340}—OD_{340}) against time.

coefficient of 0.998 or over. Therefore, Reaction 1 in this work might be analyzed, at least mathematically, according to a pseudo first order rate equation with respect to the S^+ ion. The rate constant, k_{ob}, can be given as the negative slope of the above-mentioned plot.

The reversibility of Reaction 1 was examined as follows. When the reaction was considered to be practically completed after 30 min, we added a small amount of 1 M acetic acid and found that the absorbance at 265 nm increased according to the decrease in $[CN^-]$. Also, we found that the absorbance at 340 nm increased when we added NaCN. From the above results, we could conclude that the reaction is reversible. Therefore, the effect of the backward reaction on k_{ob} was considered. According to Lindquist and Cordes,[9] who worked on the reversible addition reaction of the CN^- ion to the 4-position of the *N*-methyl-3-carbamoylpyridinium ion in the aqueous micelle systems, we have:

$$k_2 = k_{ob}/([CN^-] + K^{-1}), \quad (2)$$

where K is the equilibrium constant of Reaction 1 and can be given by Eq. 3 in terms of the equilibrium concentrations of the P, CN^-, and S^+ ions, which are written as $[P]^{eq}$, $[CN^-]^{eq}$, and $[S^+]^{eq}$ respectively.

$$K = [P]^{eq}/([CN^-]^{eq}\cdot[S^+]^{eq}) \quad (3)$$

Here, the quantities, k_2, k_{ob}, and K must be the apparent ones, because these values were determined on the basis of the concentrations of the reacting species, which were evaluated over the total volume of the system, while the systems in this work are heterogeneous from the microscopical point of view and so the chemical species would be unevenly distributed or localized.

When $[CN^-]^i$ is sufficiently higher than $[S^+]^i$, the value of $[CN^-]^{eq}$ in Eq. 3 can be approximately substituted by a constant, $[CN^-]^i$. The ratio of $[P]^{eq}$ to $[S^-]^{eq}$ is approximately equal to the ratio, $OD^{f}_{340}/(\varepsilon_{340}\cdot[S^+]^i - OD^{f}_{340})$, at the reaction equlibrium. The symbol ε_{340} represents the molar extinction coefficient of P at 340 nm. For the value of OD_{340} at the reaction equilibrium, we adopted the value of OD^{f}_{340}. The value of ε_{340}, which is considered to be constant through each measurement, was determined following the usual procedure from the relationship between the absorbance of P at 340 nm and that of the S^+ ion at 265 nm in the course of the reaction, where the isosbestic point was always observed. This also indicates that Reaction 1 proceeds stoichiometrically in reversed micelles, while the succeeding reaction scarcely proceeds at all, reflecting the formation of the 2- or 6-cyano adduct.

Equation 3 reduced to Eq. 4 for the experimental determination of K:

$$K = OD^{f}_{340}/(\varepsilon_{340}\cdot[S^+]^i - OD^{f}_{340})[CN^-]^i \quad (4)$$

Then, we estimated the value of k_2 for each course of reaction, according to Eq. 2. As k_{ob} and $[CN^-]$, we adopted, respectively, the value of k_{ob} in the earlier stage of reaction and the value of $[CN^-]^i$.

We estimated the values of k_2 and K in the reversed micelle systems under the initial conditions that the concentrations of the surfactant and the CN^- ion were 0.2 M and 5×10^{-3} M respectively. The ratio of the water to the surfactant, R, was varied from less than unity to nearly ten. We show the plots of k_2 and K vs. R in Figs. 4 and 5. It was found that the formation of P is greatly favored in the reversed micelles, especially with smaller R values, compared with the reaction in pure water, where k_2 and K are estimated to be 0.016 $M^{-1}s^{-1}$ and 0.238 M^{-1} respectively.[9] In the reversed micelle systems with HTAB or AOT as the surfactant, the value of k_2 reached a thousand times or a hundred times, respectively, as much as the value in pure water, while a several or ten thousand-fold increase in K was estimated at the maximum. However, the values of k_2 and K both decreased with

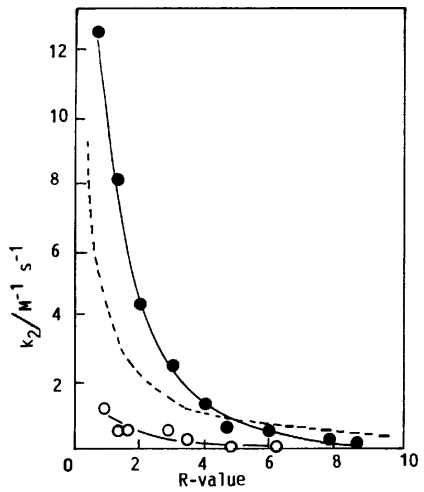

Fig. 4. Second-order rate constants, k_2, for the addition reaction in reversed micelles as a function of R-value at 25 °C. ●, 0.2 M HTAB; ○, 0.2 M AOT; broken line, a theoretical plot which took account of the localization effect of reactants.

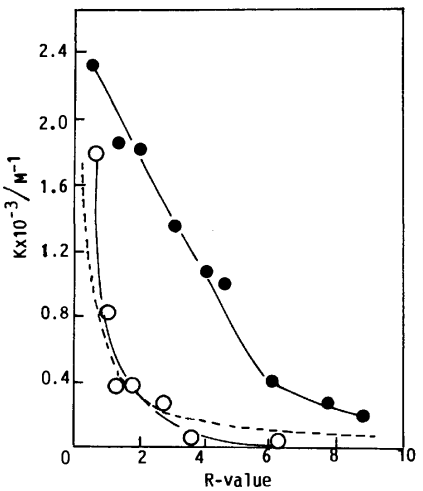

Fig. 5. Equilibrium constants, K, for the addition reaction in reversed micelles as a function of R-value at 25 °C. ●, 0.2 M HTAB; ○, 0.2 M AOT; broken line, a theoretical plot which took account of the localization effect of reactants.

the increase in R, as is seen in Figs. 4 and 5. The inconstancy of k_2 and K may be interpreted as reflecting the heterogeneity of the reversed micelle systems and the nature of the microenvironment surrounding each chemical species concerned.

Location of the Addition Reaction in the Reversed Micelle Systems. From the thermodynamic or macroscopic point of view, the presence of micelle yields no new phase. However, in order to elucidate the nature of any reaction concerned with the micelle, we should discuss the reaction from the microscopic point of view, which divides the reaction system into a number of subphases. For Reaction 1, therefore, we divided each reversed micelle system into two subphases, i.e.,

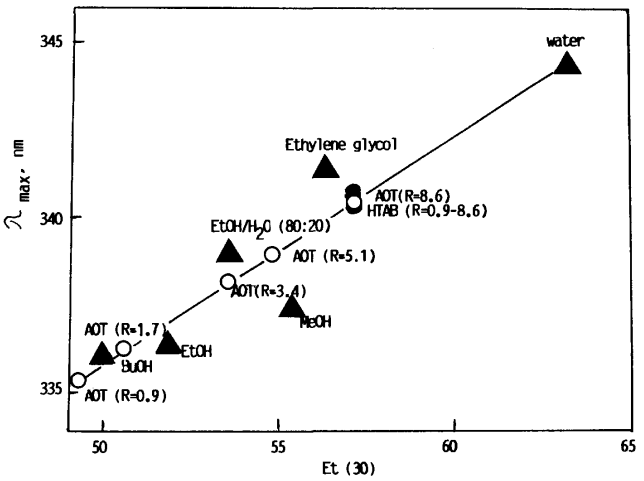

Fig. 6. Absorption maxima of 4-cyano-1,4-dihydro-*N*-methylnicotinamide, P, in several solvents as a function of the Dimroth's solvent-polarity parameter, Et(30). ▲, various solvents; ●, 0.2 M HTAB; ○, 0.2 M AOT.

the bulk phase and a pseudophase in colloidal dispersion. The former phase consists of an organic medium and various solutes, while the latter one, hereafter called the "micellar phase", consists mainly of a surfactant, water, and solutes. A small amount of a surfactant is dissolved in the bulk phase, with its concentration at cmc. The micellar phase will be subdivided into the outer shell, which mainly consists of the surfactant, and the water pool. In the detailed discussion, the water will be distinguished between that bound to the ionic heads of the surfactants at the inner surface of the micelle and the other water which constitutes the water pool.[10] Here, we will call the former the "interface zone", and the latter, the "center zone".

In the distribution measurements of S, the concentration ratio of the S^+ ion in chloroform to water was found to be less than 0.05. The ratio for the CN^- ion may be expected to be much less than that for the S^+ ion, in view of the more polar structure of the CN^- ion than the S^+ ion. Therefore, the greater parts of the reactants, the S^+ and CN^- ions, were estimated to be present preferably in the micellar phase, especially in the water pool.

To estimate the location of P in reversed micelle systems, we applied to these systems the relation between the value of λ_{max} and the polarity of the surrounding medium adjacent to P. First, Reaction 1 was carried out in various solvents, and the value of the λ_{max} of P was measured. The value in each solvent was then plotted against the Dimroth's solvent polarity parameter, Et(30), as is shown by the solid triangles in Fig. 6.[11] From the values of the λ_{max} of P in various HTAB or AOT reversed micelle systems, as may be seen in Fig. 2, we could read the corresponding values of Et(30) of the reversed micelle systems on the

calibration line in Fig. 6.

Since the reversed micelle system is microscopically heterogeneous, the Et(30) value of a reversed micelle system is considered to be the average of the Et(30) values for the microenvironments. Therefore, the estimated value of Et(30) from the measurement of λ_{max} would approximately disclose the average location of P.

In the HTAB reversed micelle systems with various R values, it was found that the λ_{max} of P or Et(30) remains nearly constant halfway between water and MeOH (Figs. 2 and 6). In other words, the environment around P is like the MeOH–water mixture in terms of the polarity. Concerning the polarity of the MeOH–water mixture, we show the plots of the λ_{max} of P in the mixture against its composition in Fig. 7. According to Sunamoto et al.,[5b] the micropolarity of the water pool in HTAB reversed micelles with smaller values of R can be estimated to be near to that of MeOH from the fluorescence maximum of *O*-methylpyranine. Therefore, it seems that it can be roughly concluded that the P in the HTAB reversed micelle systems is in the water pool. The question is where P exists inside the water pool with respect to its microscopic location. If P is dissolved homogeneously throughout in the water pool, the value of the λ_{max} of P in the HTAB reversed micelle systems would vary between those in MeOH and water with the variation in R, since the nature of the water pool must approach that of the bulk water with the increase in R, while approaching that of MeOH with the decrease in R. The results shown in Figs. 2 and 6 deviate the homogeneous distribution of P in the water pool. Also, it can be deduced, from an argument similar to that above, that P is not concentrated in the center zone of the water pool. The true situation is possibly some kind of localized concentration of P near the interface zone of the water pool, and the interface zone is not much affected by the variation in R. The penetration of P into the palisade layer of the surfactant might be a result of the electrically neutral and hydrophobic nature of P. The nearly constant value of λ_{max} has previously been explained. The fact that the value of λ_{max} of P in the HTAB reversed micelles is not the same as that in MeOH, but lies halfway between those in MeOH and water, suggests that the value of λ_{max} depends not only on the polarity of the medium, but also on the specific interaction between solute and medium. Thus, the result on *O*-methylpyranine seems to differ somewhat from the result on P in this work.

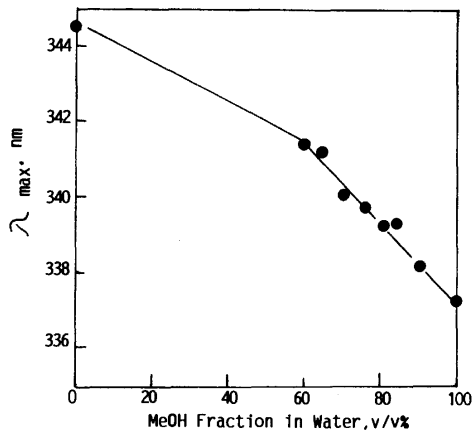

Fig. 7. The wavelength of maximum absorption, λ_{max}, of 4-cyano-1,4-dihydro-*N*-methylnicotinamide, P, in mixed solvents of MeOH–H_2O.

In the AOT reversed micelle systems, the dependency of λ_{max} or Et(30) on R was remarkable in comparison with the HTAB reversed micelle systems. Also, it was found that the λ_{max} in the AOT systems is always shorter than in the HTAB systems and that the microenvironment of P in the AOT systems is lower in polarity than that in the HTAB systems. Sunamoto et al.[5b] estimated that the polarity of water pools in the AOT reversed micelles is intermediate between those of MeOH and water, while that in the HTAB reversed systems is nearly that of MeOH, as has already been mentioned. In other words, the polarity of the water pools themselves in the AOT reversed micelles is higher than that in the HTAB reversed micelles; this is contrary to the case of the microenvironment of P. From the above facts, it can be deduced that the greater of the P in the AOT reversed systems is much more concentrated in the interface zone of the water pool, and is surrounded by a more nonpolar or hydrophobic environment, than in the HTAB reversed systems. That is, the P in an AOT micelle might exist mainly in or near the palisade layer of the surfactant, with its polar head turned toward the center of the water pool. The remarkable variation in the λ_{max} of P with the variation of R suggests a gradual change in the surfactant shell of the AOT micelle, which forms entirely, or at least in large part, of the microenvironment of P. It seems most likely that an increase or decrease in R is accompanied by an increase or decrease of the micellar size, which causes the molecular packing of the surfactant shell to tighten or loosen. In the micelle of a smaller size, which is supposed to have a more loosely packed shell, P must penetrate more deeply inside the surfactant shell or the palisade layer of the micelle.

From the location of the reaction species, the main fields of the forward and backward processes in Reaction 1 were identified approximately as follows. The forward reaction, in which S^+ and CN^- ions are the principal species, proceeds in the interior of the water pool, while the backward one, with the P proceeds in the outer sphere of the water pool. The discrepancy in site between the two opposing reactions might require some modification of Eqs. 2 and 3, which need the same sites for both reactions. Therefore, the following discussion of the values of k_2 and K,

which are based on Eqs. 2 and 3, might be regarded as rather qualitative and might have to be modified by taking into account, e.g., the transport or the diffusion process of the reaction species between the different sites.

Factors Responsible for the Enhancement of the Addition Reaction in Reversed Micelle Systems. Three kinds of effects may be proposed for interpreting the enhancement of the addition reaction in the reversed micelle systems as compared to that in the aqueous systems. The first is the local concentration of reaction species in the water pool rather than in the whole volume of each system. When the reaction is a bimolecular process, as it was in this work, the localization of the reaction species results in the enhancement of the reaction rate and equilibrium (k_2 and K) by the factor of the effective concentration to nominal, e.g., by a multiplication factor of about 300 and 40 times for R at 1 and 10 respectively.

The actual enhancement deviated more or less from the expectation; we took account of the concentration effect and adopted the values obtained by Lindquist and Cordes[9] for the reaction in pure water as the basis of comparison. The expected values are shown in Figs. 4 and 5. The deviation differed in degree between the results in the HTAB and AOT systems. Since S^+ and CN^- are presumed to be dissolved in the water pool, the difference in the reaction constants between the HTAB and AOT systems can be partly attributed to the difference in nature between the water pools of the two systems. As has already been established,[5b] the micropolarity of the water pools at a small water content is near to that of MeOH for the HTAB reversed micelles and intermediate between those of MeOH and water for the AOT reversed micelles. The lower micropolarity of the water pools seems to contribute to the enhancement of the reaction in the HTAB systems. Although Lamborg et al.[16] have reported that the addition of a 1-methylpyridinium compound with the cyanide ion was strongly dependent upon the dielectric constant of the solvent, it has not yet been studied quantitatively. Therefore, in order to examine the relation between the polarity of a medium and the reactivity, we measured the values of k_2 and K of the addition reaction in the mixed solvents of MeOH and water, as is shown in Figs. 8 and 9. As the fraction of MeOH in the solvent, i.e., the polarity of the medium, approaches that of pure MeOH, the values of k_2 and K were found to increase with the acceleration. Thus, the significantly high values of k_2 and K in the HTAB systems at lower R were elucidated, at least quantitatively. For the AOT systems, the effect of the micropolarity of the water pools on the addition reaction seems to be negligible, judging from the results in Figs. 8 and 9, which shar the polarity halfway between MeOH and water.

The third effect is connected with the electric nature

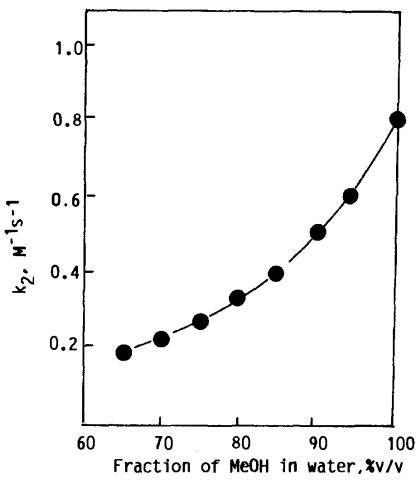

Fig. 8. Second-order rate constants, k_2, for the addition reaction in MeOH–H_2O mixed solvents at 25 °C.

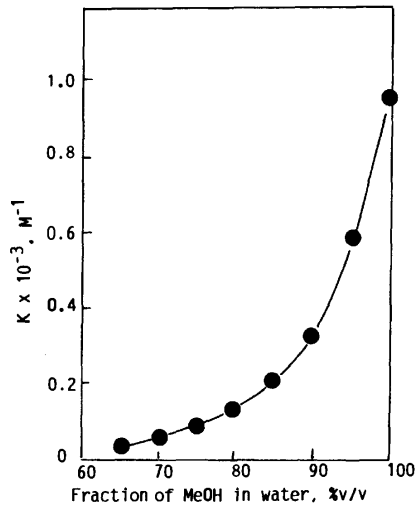

Fig. 9. Equilibrium constants, K, for the addition reaction in MeOH–H_2O mixed solvents at 25 °C.

of the surfactant and the reactant ions. No doubt, the electrostatic attraction and/or repulsion between various ions plays a principal role in determining the spatial distribution of the reactant ions in the water pools and will affect the addition reaction. It can be supposed in each HTAB reversed micelle that the S^+ and CN^- ions are concentrated in the center zone and near the interface zone of the water pool due to the electrostatic repulsion and to the attraction with the cationic head of the surfactant respectively. The above situation might serve to attenuate the first and second kinds of effects, i.e., localized concentration of the reactants and the lowering of the polarity of microenvironment, on the reaction in the reversed micelle systems with relatively large R values. However, with a decrease in R, the concentration of CN^- ions will soon become saturated in the interface zone and increase throughout the region of the water pool, since [CN^-] in this work

is set relatively high (5×10^{-3} M). Then, the above-mentioned attenuating effect will disappear. With a very small R, the repulsion between the S^+ ion and the cationic head might promote the forward reaction, that is, a charge neutralization, and result in a significant increase in k_2 and K.

Similarly to the case of the HTAB systems, but with the inverse type of ionic distribution, it can be supposed in each AOT micelle that the CN^- and S^+ ions have a tendency to concentrate in the center zone and near the interface zone of the water pool respectively. At higher R values, the divided concentrations of both reactant ions would contribute to the values of k_2 and K in the AOT reversed micelle systems, much like those in the HTAB systems. At very small R values, the situation must be the same as between both kinds of reversed micelle systems; i.e., there is a significant increase in k_2 and K. However, in the intermediate region of R, there are some differences between the two reversed micelle systems in the distribution patterns of the ions in the water pools. In other words, the saturation of CN^- ions in the center zone of the water pool in the AOT systems may be expected to occur somewhat later than the saturation in the interface zones of the HTAB systems. The difference in porofile between the plots for the HTAB and AOT systems, as is seen in Figs. 4 and 5, is considered to be due to the differences in R for the saturation of CN^- ions between the respectively preferred zones.

The Stability of the 4-Cyano Adduct in Reversed Micelles. Lindquist and Cordes[9] reported that the peak near 345 nm slowly decreased in magnitude, while, at the same time, a new absorption peak appeared near 305 nm together with increased absorption near 265 nm, they suggested that the spectral shift might be a rearrangement of P to the 6- and 2-cyano adduct, as has already been described. Therefore, it was supposed that P is not stable thermodynamically in an aqueous medium.[9] It can be considered that the stability of P in MeOH is higher than in an aqueous medium, but such a spectral shift was observed in concentrated MeOH (95%) after 48 hours (Fig. 10). As the water fraction in the mixed solvents of MeOH–H_2O increased, a remarkable shift from 340 to 310 nm was observed. The 4-cyano adduct, P, formed in AOT reversed micelles was relatively stable, thus making it possible to estimate the equilibrium constant approximately, but a distinct spectral shift was observed after 2 hours (Fig. 10). It was supposed that AOT itself acts against the P as a base, resulting in the formation of nitrile.[14]

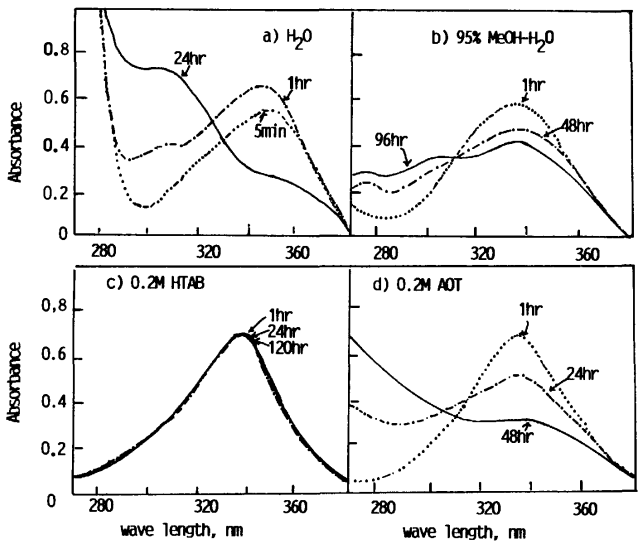

Fig. 10. Ultraviolet spectra for solutions containing initially *N*-methyl-3-carbamoylpyridinium chloride and sodium cyanide. a) H_2O; [S]=6.3×10^{-4} M, [NaCN]=5.0×10^{-1} M, b) 95%MeOH–H_2O, c) 0.2 M HTAB (R=1.0) and d) 0.2MAOT (R=1.0); [S]= 1.5×10^{-4} M, [NaCN]=5.0×10^{-3} M.

On the other hand, such a spectral shift was not observed in HTAB reversed micelles even after they had stood 5 days. It can thus be concluded that the P in HTAB reversed micelles is especially stable. This shows that the microenvironment surrounding the P in HTAB reversed micelles contributes to the stability of the P, most likely because of the specific nature of the water pool.

In conclusion, it became evident that the reaction field provided by HTAB reversed micelles not only enhanced the addition reaction, but also stabilized the P, which is thermodynamically unstable in an aqueous medium. This is in contrast to the AOT reversed micelle system. These results might be related to the postulate that a cationic charge, such as the lysine residue of alcohol dehydrogenase located very close to the bound NADH may protect the NADH from hydration decay.[15] Therefore, it is not too much to say that the HTAB reversed micelle systems provide a field advantageous for synthesizing the dihydro compounds, for the dihydro-compounds produced by the addition of the cyanide ion to pyridinium salt or isoquinolinium salt are usually less stable and can not easily be isolated.[12,17]

Also, it should be noted that reversed micelle systems can control the addition reaction by varying the water content, although they may be unfavorable for reactions at higher water contents.

References

1) M. I. Page, "The Chemistry of Enzyme Action," Elsevier (1984).

2) J. H. Fendler, E. J. Fendler, P. T. Medary, and V. A. Woods, *J. Am. Chem. Soc.*, **94**, 7288 (1972).

3) J. H. Fendler and E. J. Fendler, "Catalysis in Micellar and Macromolecular Systems," Academic Press (1975).

4) J. H. Fendler, "Membrane Mimetic Chemistry," A Wiley-Interscience (1982), p. 48.

5) a) J. Sunamoto, K. Iwamoto, M. Akutagawa, M.

Nagase, and H. Kondo, *J. Am. Chem. Soc.*, **104**, 4904 (1982). b) J. Sunamoto, K. Iwamoto, S. Nagamatsu, and H. Kondo, *Bull. Chem. Soc. Jpn.*, **56**, 2469 (1983). c) J. Sunamoto, H. Kondo, and K. Akimaru, *Chem. Lett.*, **1978**, 821. d) J. Sunamoto, H. Kondo, J. Kikuchi, H. Yoshinaga, and S. Takei, *J. Org. Chem.*, **48**, 2423 (1983). e) J. Sunamoto and D. Horiguchi, *Nippon Kagaku Kaishi*, **1980**, 475.

6) a)L. J. Magid, "Reversed Micelles," ed by P. L. Luisi and B. E. Straub, Plenum Press (1984), p. 95. b)K. Konno, M. Tosaka, and A. Kitahara, *J. Colloid Interface Sci.*, **86**, 288 (1982).

7) a) J. Baumrucker, M. Calzadilla, M. Centeno, G. Lehrmann, M. Urdaneta, P. Lindquist, D. Dunham, P. Price, B. Sears, and E. H. Cordes, *J. Phys. Chem.*, **74**, 1152 (1970). b) J. Baumrucker, M. Calzadilla, M. Centeno, G. Lehrmann, M. Urdaneta, P. Lindquist, D. Dunham, M. Price, B. Sears, and E. H. Cordes, *J. Am. Chem. Soc.*, **94**, 8164 (1972).

8) C. A. Bunton, L. S. Romsted, and C. Thamarit, *J. Am. Chem. Soc.*, **102**, 3900 (1980).

9) R. N. Lindquist and E. H. Cordes, *J. Am. Chem. Soc.*, **90**, 1269 (1968).

10) H. Kondo, I. Miwa, and J. Sunamoto, *J. Phys. Chem.*, **86**, 4826 (1982).

11) D. R. C. Reichardt, *Angew. Chem., Int. Ed. Engl.*, **4**, 29 (1965).

12) R. E. Lyle and G. J. Ganthier, *Tetrahedron Lett.*, **1965**, 4165.

13) M. Zulauf and H. F. Eicke, *J. Phys. Chem.*, **83**, 480 (1979).

14) W. E. Feely and E. M. Beavers, *J. Am. Chem. Soc.*, **81**, 4004 (1958).

15) S. Shinkai, R. Ando, and T. Kunitake, *Bull. Chem. Soc. Jpn.*, **49**, 3652 (1976).

16) M. R. Lamborg, R. M. Burton, and N. O. Kaplan, *J. Am. Chem. Soc.*, **79**, 6173 (1957).

17) A. S. Pietro, *J. Biol. Chem.*, **217**, 579 (1955).

Limitation of Absorbance Measurement by Using Photoacoustic Method

Masahide TERAZIMA* and Tohru AZUMI
Department of Chemistry, Faculty of Science, Tohoku University, Sendai 980
(Received March 3, 1989)

The solute dependence of the photoacoustic (PA) signal intensity has been examined. The results show that the PA signal intensity depends not only on the released energy, but also on the nature of the solute. This means that the absorbance of an unknown sample cannot be precisely measured by comparing the PA signal intensity with that of a standard solution containing a different solute.

Photothermal techniques, such as thermal lens (TL)[2,3] and photoacoustic (PA),[4-6] have been utilized for the sensitive detection of weak absorptions. In order to obtain absorptivity in a quantitative manner, the light energy absorbed by a solution should be obtained from the signal intensity. However, since the TL and PA signal intensities depend on the various physical properties of the solution (vide infra) and experimental conditions, it is extremely difficult, if not impossible, to determine the absorbed energy from the signal intensity. In view of this difficulty, one usually tries to estimate the absorbed energy by comparing the signal intensity with that of a standard sample of known absorbance.[4-15] This comparison method is based on the theoretical expectation[4-8] that, provided that the proper correction for the energy loss due to radiative emission and photochemical reaction is made, the signal intensity should be proportional only to the absorbed energy in the series of experimental data obtained with the same experimental setup. In particular, since the signal intensity of the sample is compared with that of the standard solution, which usually contains a different solute, the signal intensity should not depend on the nature of the solute if the released energy is identical.

Even though this comparison method is frequently used in both the PA and TL methods,[4-15] we found in a previous study that the absorbance of a sample cannot be precisely measured, at least by the TL method.[1] This result was based on the fact that the TL signal intensity depends not only on the releasing energy but also on the nature of the solute. Namely, the assumption which is essential for the capability of the quantitative measurement has been revealed to be invalid. We have suggested that the solute dependence of the TL signal comes from the vibrational mode dependence of the vibration to the translation energy transfer rate.[1]

As an extension of this TL experiment, we attempted in the present work to study the PA signal and its correlation with the TL signal by using a simultaneous PA and TL measuring system. As described in detail below, we found that the PA signal intensity also depends on the solute. This means that the PA signal intensity of a solution cannot be calibrated by using a standard sample solution containing a different solute.

Experimental

The apparatus of the TL experiment described previously[1] was modified so as to perform simultaneous measurements of both the TL and PA signals (Fig. 1). For the PA detector, a piezoelectric transducer (PZT) of a lead zirconate-lead titanate cylinder (Tohoku Kinzoku Co. N-6) poled axially was used. It was mounted inside a metal case, essentially the same as designed by Patel and Tam.[17] The transducer was directly attached to the wall of the square cell from the outside with a thin vacuum grease layer to facilitate acoustic coupling. The signal from the transducer was amplified by a wide-band preamplifier (PAR, Model 115) with a voltage gain of 10. The signal from the amplifier was fed into a transient digitizer (Iwatsu Co., DM901) and averaged by a microcomputer (NEC, PC-9801). For the excitation light source, a nitrogen laser (Molectron UV-24) was used. The laser power was 3 μJ/pulse. In the case of 400-nm excitation, a dye laser (Molectron, DLII-14P) pumped by the nitrogen laser was used for the light source. The laser beam, focused using a 20-cm focal-length lens, passed through the sample cell at the distance 5 mm from the PA detector. Since the PA signal intensity slightly depended on the volume of the sample in the cell, we use a fixed volume (3.5 cm^3) of the sample for the measurement.

Chemicals and purification procedures were the same as previously reported.[1] The concentrations of the sample solutions were adjusted so that the absorbance at 337.1 nm

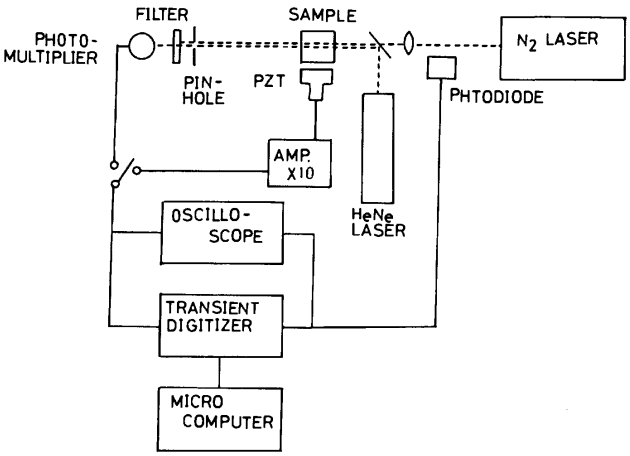

Fig. 1. Block diagram of the experimental setup for thermal lens and photoacoustic measurement in simultaneously.

was 0.1±0.01. Therefore, the concentration of each solution varied, depending on the molar extinction coefficient at 337.1 nm.

Method

If the assumptions described below are satisfied, the electronic signal from a PZT is given by[8,9]

$$I_{PA} = K\frac{v^2\beta}{C_P}(1 - 10^{-A})H, \quad (1)$$

where K is a constant that depends on the geometrical parameters as well as on the response properties of the PZT, but not on the nature of the solute. Further, C_p, β, A, and v denote the molar heat capacity at constant pressure, the thermal expansion coefficient, the absorbance of the sample, and acoustic velocity, respectively. The factor $(1-10^{-A})H$ represents the releasing energy from the sample as the radiationless transition. H is expressed by[1]

$$H = H_0\left(1 - \frac{E_s}{E_{ex}}\phi_f - \frac{\Delta H}{E_{ex}}\phi_{reac}\right), \quad (2)$$

where E_{ex}, E_s, and H_0 are the photon energy of the pulsed laser, the photon energy of the fluorescence, and the laser power which is used to excite the solute, respectively. Further, ϕ_f is the quantum yield of the fluorescence and ϕ_{reac} is a quantum yield of the photochemical reaction. The quantity ΔH is the enthalpy difference between the reactant and the product. For air-saturated samples, any radiative decay due to phosphorescence can be neglected.

The assumptions which were used to derive Eq. 1 are as follows:[8,9]

(a) A thin cylindrical excitation (week absorption of the sample),

(b) $w^2/D \gg t_a$, (3)

(c) $t_a \gg t_p$, (4)

and

(d) $t_a \gg t_{nr}$. (5)

Here t_p, t_{nr}, and t_a are the pulse length of the excitation laser, the relaxation time from the excited state, and an acoustic transit time to travel across the laser illuminated region in the sample, respectively. Further, D and w are the thermal diffusion coefficient and the laser spot size, respectively.

The PA signal intensity should be solute independent as long as Eq. 1 is valid, since Eq. 1 was derived from thermodynamic equations, in which there are no solute dependent factors. Previously, investigators have taken it for granted that Eq. 1 is valid for many molecules under real experimental conditions. Our goal in this study was to check whether or not Eq. 1 is valid under our experimental condition. We define the corrected signal intensity as

$$S_{PA} = I_{PA}/(1 - 10^{-A})H = K\frac{v^2\beta}{C_p}. \quad (6)$$

If the thermal properties (β, C_v, v) of a solution are essentially identical to those of the solvent, S_{PA} should not depend on the solutes as long as Eq. 1 is valid. We measured S_{PA} for many organic solutes in the same solvent (benzene).

The TL signal intensity (I_{TL}) and the corrected intensity (S_{TL}), defined previously,[1] are given here again for convenience:

$$I_{TL} = \frac{I(t=0) - I(t=\infty)}{I(t=0)} \quad (7)$$

and

$$S_{TL} = I_{TL}/(1 - 10^{-A})H, \quad (8)$$

where $I(t=0)$ and $I(t=\infty)$ are the intensity of the cw monitoring laser just after the solute is excited by the pulsed laser and that after the sufficiently long time compared with the heat diffusion time in the solution, respectively.

Results

A typical PA siganl is shown in Fig. 2. There is no detectable signal from the pure solvent; we therefore conclude that there is no signal from the wall of the cell or due to scattered light. The peak height of the first minimum in the PA signal is an arbitrary measure of the amplitude of the signal (I_{PA})(Fig. 2), because the first maximum peak is easily disturbed by the electric noise coming from the excitation laser. The relative I_{PA}

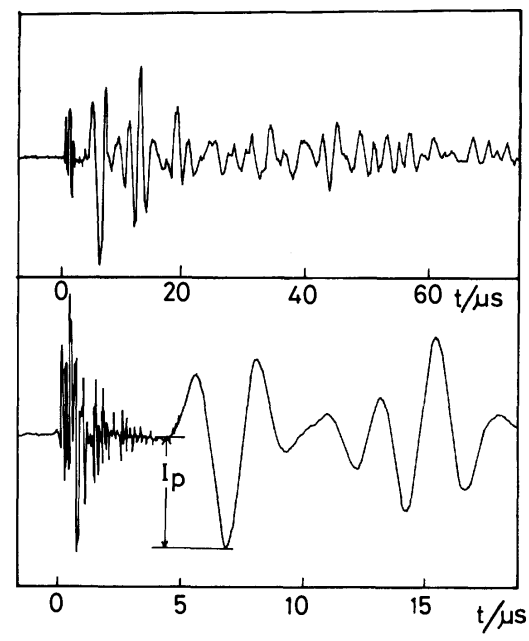

Fig. 2. Single pulse trace of the PA signal. The signal intensity (I_{PA}) which we measured is also represented.

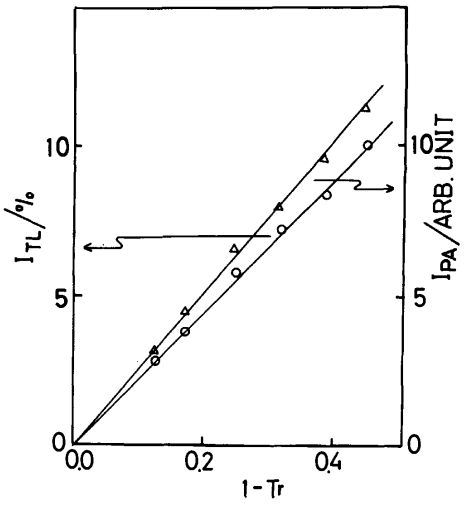

Fig. 3. Plot of the thermal lens and photoacoustic signal intensity vs. $(1-T_r)$, where T_r is the transmittance of the benzophenone in benzene at 337.1 nm.

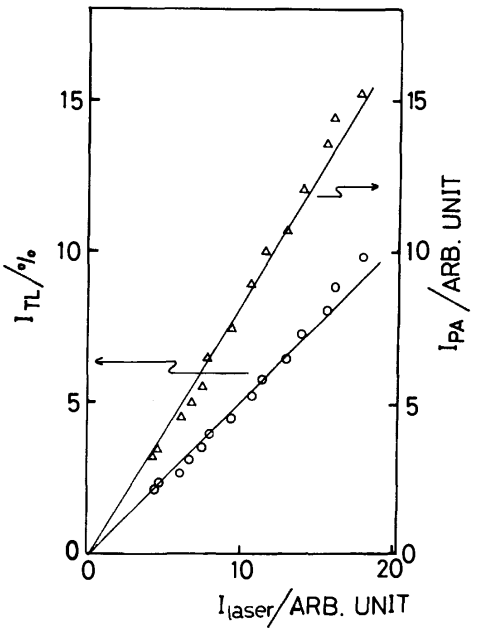

Fig. 4. Plot of the thermal lens and photoacoustic signal intensity vs. the excitation laser power for benzophenone in benzene.

values were reproducible within 5%.

First, we checked the linerity of our system for the PA and TL measurements. Figure 3 shows the signal intensity of PA and TL against $(1-10^{-A})$. The linear dependence of the PA and TL signal intensities on the laser power is shown in Fig. 4. Within the range of concentrations and laser powers which we used there was no saturation effect. These results rationalize the validity of Eq. 6.

Table 1 summarizes the relative PA (S^r_{PA}) and TL(S^r_{TL}) signal intensities observed for various solutes in benzene. The signal intensity of benzophenone is set to be 1.00; that is,

$$S^r_{PA} = S_{PA}(\text{sample})/S_{PA}(\text{benzophenone})$$

and

$$S^r_{TL} = S_{TL}(\text{sample})/S_{TL}(\text{benzophenone}).$$

The correction parameters for fluorescence and photochemical reactions are the same as those listed previously.[1)]

Table 1. The Corrected TL (S_{TL}) and PA (S_{PA}) Signal Intensity for Various Solutes in Benzene
S_{PA} and S_{TL} of benzophenone is set to be 1.00.

Solute	S_{PA}	S_{TL}
Benzophenone	1.00	1.00
Anthracene	0.98	1.10
Phenanthrene	1.00	1.03
Stilbene	0.92	0.65
9,10-Dibromoanthracene	0.83	0.92
9,10-Anthraquinone	0.83	0.73
Fluorenone	0.79	0.90
Biacetyl	0.83	0.99
Tetrachloro-*p*-benzoquinone	0.62	0.83
1,2-Naphthoquinone	0.81	0.83
1,4-Naphthoquinone	0.97	0.83
Benzil	0.85	0.83
1-Amino-9,10-anthraquinone	0.76	0.75
9,10-Phenanthraquinone	0.70	0.83
Quinoxaline	0.68	0.82
Phthalazine	0.88	0.76
Quinoline	0.81	0.81
Isoquinoline	1.00	0.89
Phenazine	0.81	0.91
9,10-Diazaphenanthrene	0.96	0.89
Azobenzene	0.85	0.60
3,3′-Dimethylazobenzene	0.81	0.59
p-Nitrophenol	1.00	0.84
p-Nitroaniline	0.96	0.69
o-Nitroaniline	0.86	0.61
Nitrodiphenylamine	0.97	0.70

Discussion

The Validity of Eq. 1. According to Eq. 1, the PA signal intensity should be proportional to the releasing energy. Further, if the releasing energy, experimental configuration and thermal properties (β, v, C_p) are identical, the PA signal intensity should be identical. The results listed in Table 1 are, however, inconsistent with this prediction.

Before we doubt the validity of Eq. 1, we should check the solute dependence of the factors which affect the signal intensity. We will first check the thermal properties of the solutions. In dilute solutions, as in this case, the thermal properties of the solution are considered to be almost identical to those of the pure solvent. Actually, we have already confirmed that the thermal properties which affect the TL signal intensity (thermal diffusivity, thermal conductivity and dn/dT; where n and T denote the refractive index and temperature, respectively) are almost identical to those

Table 2. The PA Signal Intensity (I_{PA}) of Mixed Solutions to Examine the Solute Effect on the Thermal Properties of the Solvent
The excitation wavelength is 400.0 nm. I_{PA} of 9,10-dibromoanthracene (DBA) is set to be 1.00 as reference.

	I_{PA}
9,10-Dibromoanthracene (DBA)	1.00
DBA+anthracene	0.95
DBA+benzophenone	0.99
DBA+quinoxaline	0.95
DBA+stilbene	0.98

of the pure solvent.[1] Here, we examine whether the thermal properites which affect the PA signal (β, v, C_p) are similarly identical to those of a pure solvent.

The principle is as follows: If the thermal properties of a solution are different from those of a pure solvent upon adding a solute (solute A), the PA signal intensity which comes from another solute (solute B) with solute A should be different from that of solute B without solute A. We used 9,10-dibromoanthracene (DBA) as solute B. We choose benzophenone, stilbene, quinoxaline, and anthracence for solute A. A dye laser at 400 nm was used to excite only solute B, not solute A. Note that only DBA possesses an absorption band at 400 nm. We prepared two kinds of solutions. One solution contained only solute B, whose absorbance at 400 nm was adjusted to 0.1. The other solution contained solute B of the same concentration as solute A, whose absorbance at 337.1 nm was adjusted to 0.1, identical to the previous experiment (Table 1). If the PA signal intensity of the solution contained both A and B is different from that of the solution contained only solute B, it means that solute A changes the thermal properties of the solution from those of a pure solvent. The observed S_{PA}, summarized in Table 2, does not depend on whether or not solute A is contained within the experimental error. This result shows that the thermal properties which affect the PA signal intensity are almost identical to those of a pure solvent. Therefore, the solute dependence (Table 1) cannot be explained by the solute effect on the thermal properties of the solvent.

Other trivial factors, such as multiphoton and/or transient absorption and scattering processes, can be neglected under our conditions, as confirmed previously.[1]

The S_{TL} values listed in Table 1 are almost identical to the values reported in Ref. 1. In that paper, we conclude that the dissipation of thermal energy as pressure waves does not play an important role in the solute dependence of the TL signal intensity. If the thermal energy dissipation as pressure waves is the origin of the solute dependence of the TL signal, a solute which gives a small S_{TL} should give a large S_{PA}. However, such a negative correlation was not found, as shown in Fig. 5. This result supports the previous

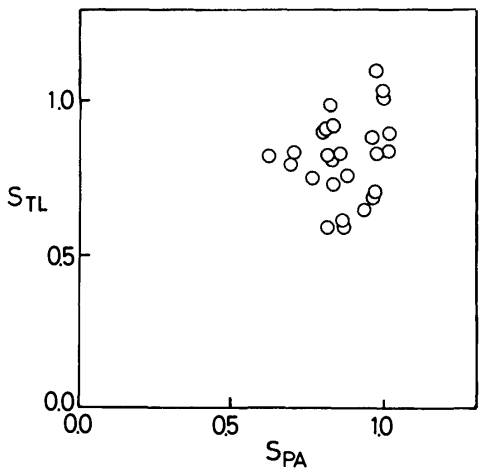

Fig. 5. Plot of the corrected TL (S_{TL}) vs. PA (S_{PA}) signal intensity for various solutions listed in Table 1.

conclusion.[1]

The Origin of the Solute Dependence. According to the above discussion, the solute dependence of S_{PA} means that Eq. 1 does not hold under our experimental conditions. In this section, we discuss the origin of the solute dependence by checking the assumptions on which Eq. 1 is based.

Under our experimental conditions, the first (a thin cylindrical excitation), the second (Eq. 3) and the third (Eq. 4) assumptions were considered to be adequate on the basis of parameters $w \approx 1$ mm, $D \approx 10^{-3}$ cm^2 s^{-1}, $t_a \approx 4 \times 10^{-7}$ s, and $t_p \approx 1 \times 10^{-8}$ s. Furthermore, these conditions should not depend on the nature of the solute, as considered in the previous section (Table 2). Therefore, the solute dependence is not due to a violation of these conditions. The factor t_{nr} of Eq. 5 represents the relaxation time of the energy transfer from the electronic energy of the solute to the translational energy of the solvent. If t_{nr} is longer than 500 ns, this quantity can be measured from the rise time of the TL signal and the adequacy of the fourth condition checked. Unfortunately, we found that the rise times of the TL signal of these solutions which we investigated are determined by the time constant of the TL signal (500 ns) in our experimental apparatus. We can therefore only say that t_{nr} is shorter than 500 ns. Although we cannot conclude the invalidity of the fourth condition exclusively, we may suggest that the remaining condition, i.e. the fourth condition (Eq. 5), could be the reason for the solute dependence; namely, the fourth condition does not hold for some solutes. The experimental support for this assumption is now in progress.

The observed solute dependence of the PA signal intensity means that the quantitative measurement by the PA method using a reference solute is not precious. In order to measure the absorbance precisely, the solute of the reference sample should be the same

solute as the sample, or the solute-dependent factor should be corrected before the PA signal intensity is compared. For practical purposes, we suggest that the signal intensity of the PA signal should be expressed empirically be

$$I_{PA} = K' \frac{v^2 \beta}{C_p} (1 - 10^{-A})H, \quad (9)$$

where K' depends on the nature of the solute.

Conclusion

Our experimental results show that not only the TL signal but also the PA signal intensity depends on the solute, even if the releasing energy and the experimental configuration are identical. This fact means that absorbance measurements by the TL and PA method are not precious unless the signal intensity is calibrated using the same solute.

The authors are grateful to Mr. Makoto Kobayashi and Miss. Michiko Horiguchi for technical assistance.

References

1) M. Terazima, M. Horiguchi, and T. Azumi, *Anal. Chem.*, in press.

2) H. L. Fang and R. L. Swofford, "Ultrasensitive Laser Spectroscopy," ed by D. S. Klinger, Academic Press, New York (1983).

3) M. E. Long, R. L. Swofford, and A. C. Albrecht, *Science*, **191**, 183 (1976).

4) P. A. Tam, "Ultrasensitive Laser Spectroscopy," ed by D. S. Kliger, Academic Press, New York (1983).

5) V. P. Zharov and V. S. Letokhov, "Laser Optoacoustic Spectroscopy," Springer-Verlag, (1985).

6) C. K. N. Patel and A. C. Tam, *Appl. Phys. Lett.*, **34**, 467 (1979).

7) Y. Kohanzadeh, J. R. Whinnery, and M. M. Carroll, *J. Acoust. Soc. Am.*, **57**, 67 (1976).

8) C. K. N. Patel and A. C. Tam, *Rev. Mod. Phys.*, **53**, 517 (1981).

9) E. T. Nelson and C. K. N. Patel, *Opt. Lett.*, **6**, 354 (1981).

10) A. C. Tam, C. K. N. Patel, and R. J. Kerl, *Opt. Lett.*, **4**, 81 (1979).

11) C. K. N. Patel and A. C. Tam, *Chem. Phys. Lett.*, **62**, 511 (1979).

12) S. J. Komorowski, Z. R. Grabowski, and W. Zielenkiewicz, *J. Photochem.*, **30**, 141 (1985).

13) G. F. Kirikbright, *Adv. Lumines. Spectrosc.*, **1985**, 55.

14) H. L. Fang, T. L. Gustafson, and R. L. Swofford, *J. Chem. Phys.*, **78**, 1663 (1983).

15) J. H. Brannon and D. J. Magde, *Chem. Phys.*, **82**, 706 (1978).

16) J. K. Rice and R. W. Anderson, *J. Chem. Phys.*, **90**, 6793 (1986).

17) A. C. Tam and C. K. N. Pate, *Opt. Lett.*, **5**, 27 (1980). *Appl. Opt.*, **18**, 3348 (1979).

 © 1989 The Chemical Society of Japan Bull. Chem. Soc. Jpn., 62, 2867—2874 (1989)

Studies of Collectors. XI.[1] The Preparation of Cyclic Polyamine-Type Surfactants and Application to Ion-Flotation Collectors

Kimiho YAMADA, Yoshifumi KOIDE,* Hiroshi YAMANOKUCHI, Masaki OHMURA, and Hideto SHOSENJI

Department of Applied Chemistry, Faculty of Engineering, Kumamoto University, Kurokami, Kumamoto 860

(Received April 3, 1989)

Inclusion-type surfactants bearing cyclic dioxopolyamine ($R_n$doN$_4$, $R_n$doN$_5$) or cyclic polyamine ($R_{12}N_4$, 2.4R-N$_6$, Ls6.8N$_6$) were prepared and then investigated as ion-flotation collectors. The surface tensions of the surfactant solutions were 30—40 dyn cm^{-1}. The molecular areas of the surfactants in the aqueous solutions, as calculated from the Gibbs adsorption isotherm, were discussed in connection with the structures of the $R_n$doN$_4$ and its Cu^{2+} complex. Heavy metal ions were floated with $R_n$doN$_4$ or $R_n$doN$_5$. The highest floatabilities of Cu^{2+} and Ni^{2+} were in the pH range of 10—12, while that of Fe^{3+} was in the pH range of 6—10. Furthermore, similar characteristics of the metal floatabilities were obtained by using $R_{12}N_4$ and alkylated linear polyamine. The flotation using $R_n$doN$_4$ or $R_n$doN$_5$ was done by the complex formation, but that using $R_{12}N_4$ or 2.4R-N$_6$ was done by the neutralization of the complex with OH^-. The selectivities in pH 4—8 were $Cu^{2+}>Ni^{2+}>Fe^{3+}>Zn^{2+}$ when $R_n$doN$_4$ was used and $Fe^{3+}>Cu^{2+}>Ni^{2+}>Zn^{2+}$ when $R_n$doN$_5$ was used.

Inclusion compounds, such as cyclodextrin[2] and crown ether, have recently been reported as new functional materials.[3] These compounds form stable complexes, and the complex formations are highly selective. Some amphiphilic crown ethers have been prepared, and their alkali metal complexes have been examined as phase-transfer catalysts.[4]

Moreover, specific chelating surfactants have been applied to ion-flotation collectors.[5] High selectivity is usually a matter of great importance in ion-flotation. Therefore, the inclusion compounds capable of capturing such heavy metal ions as cyclic polyamine, particularly the dianion-type ligand of cyclic dioxopolyamine, which forms an uncharged complex with Cu^{2+} and Ni^{2+},[6] are very attractive. The capturing ability becomes more effective upon the introduction of a long alkyl group, because the ligand is densely adsorbed at the gas-liquid interface of the bubble; thus, the heavy metal ions must be highly concentrated on the ligand-condensed foams. In this study, the long-alkyl-substituted cyclic dioxopolyamines and cyclic polyamines are prepared, and their surface activities and their characteristics as ion-flotation collectors are investigated.

N-Alkylethylenediamine and *N*-dodecyldiethylenetriamine have previously been used as ion-flotation collectors.[7] However, ion-flotation collectors of cyclic polyamine-type surfactants have not yet been investigated, except for 1,4,8,11-tetraazacyclotetradecane, used as a carrier in the transportation.[6,8]

Experimental

Materials. Long-alkyl-substituted cyclic dioxopolyamines were prepared by reference to the method described in the literature.[9] The condensation of dimethyl alkylmalonate[10] with 3,7-diazanonane-1,9-diamine[11] gave the cyclic dioxohexamine derivatives (R_{12}doN$_4$, R_{18}doN$_4$), while the condensation with 3,6,10-triazaundecane-1,11-diamine gave the cyclic dioxopentamine derivatives (R_{12}doN$_5$, R_{18}doN$_5$). The preparation of the cyclic dioxohexamine bearing a dodecyl group, R_{12}doN$_4$, was done as follows: 0.1 mol of 3,7-diazanonane-1,9-diamine and 0.1 mol of dimethyl dodecylmalonate were dissolved in 100 cm^3 of methanol, after which the mixture was refluxed for 5 d. The resulting white precipitates, R_{12}doN$_4$, was purified by recrystallization from acetone. Yield, 30%. R_{18}doN$_4$ and $R_n$doN$_5$ were prepared by a similar procedure; the R_{12}doN$_5$ and R_{18}doN$_5$ were deposited out by adding hydrochloric acid, and then the precipitate was recrystallized from 50% methanol. Yields: R_{18}doN$_4$, 28%; R_{12}doN$_5$, 25%; R_{18}doN$_5$, 35%. Their structures were confirmed by the IR spectra (Shimadzu IR-408), the ^{1}H NMR spectra (JEOL JMN-MH-100), and elementary analyses (Yanako CHN Corder MT-3). Mp: R_{12}doN$_4$ 85—88 °C, R_{18}doN$_4$ 99—102 °C, R_{12}doN$_5$·3HCl 184—188 °C, R_{18}doN$_5$·3HCl 235—240 °C. IR (KBr): ν_{NH} 3300, ν_{CH} 2900, ν_{CO} 1650, δ_{NH} 1540, δ_{CH} 1460 cm^{-1}. ^{1}H NMR: $R_n$doN$_4$ in $CDCl_3$ δ=0.9 (3H, t, CH_3-CC-), 1.3 (methylene in alkane), 1.8 (4H, -CCH$_2$C-, -CCH$_2$C<), 2.7 (8H, -CCH$_2$NCH$_2$C-), 3.2—3.4 {5H, -COCH(C-)CO-, -CONCH$_2$C-}; $R_n$doN$_5$·3HCl in D_2O δ=0.8 (3H, t, CH_3CC-), 1.3 (methylene in alkane), 1.8 (2H, -CCH$_2$C<), 3.0 {H, -COCH(C-)CO-}, 3.4 (4H, -CONCH$_2$C-), 3.5—3.6 (12H, -CCH$_2$N$^+$CH$_2$C-). R_{12}doN$_4$ Found: C, 63.89; H, 10.70; N, 13.15%; Calcd for $C_{22}H_{44}O_2N_4\cdot 0.9H_2O$: C, 63.89; H, 11.18; N, 13.54%. R_{18}doN$_4$ Found: C, 65.85; H, 11.32; N, 11.08%; Calcd for $C_{28}H_{56}N_4O_2\cdot 1.7H_2O$: C, 65.74; H, 11.71; N, 10.96%. R_{12}doN$_5$·3HCl Found: C, 50.82; H, 9.35; N, 12.28%; Calcd for $C_{23}H_{47}O_2N_5\cdot 3HCl\cdot 0.5H_2O$: C, 50.82; H, 9.45; N, 12.88%. R_{18}doN$_5$·3HCl Found: C, 56.13; H, 9.84; N, 11.04%; Calcd for $C_{29}H_{53}N_5O_2\cdot 3HCl$: C, 56.79; H, 9.22; N, 11.42%.

Cyclic tetramine bearing a dodecyl group, $R_{12}N_4$, was prepared from the R_{12}doN$_4$. The R_{12}doN$_4$ was reduced with a large excess of a reductant, B_2H_6, in refluxing tetrahydrofuran for 24 h. After the treatment with hydrochloric acid, the salts ($R_{12}N_4\cdot 4HCl$) were recrystallized from 80% methanol. Yield, 25%. $R_{12}N_4\cdot 4HCl$ Mp: 218—221 °C. IR (KBr): ν_{NH} 3300, ν_{CH} 2900, δ_{NH} 1610, δ_{CH} 1450, ν_{CN} 1050—1030 cm^{-1}. ^{1}H NMR (CF_3COOH): δ=0.9 (3H, t, CH_3CC-), 1.3—1.9 (methylene and methylidyne in alkane), 3.6—3.9 (16H,

$-CCH_2N^+CH_2C-$). $R_{12}N_4$ Found: C, 51.54; H, 9.86; N, 10.11%; Calcd for $C_{22}H_{48}N_4 \cdot 4HCl$: C, 51.32; H, 10.20; N, 10.89%.

Cyclic hexamine, [18]aneN$_6$, was prepared according to the procedure described in the literature.[12,13] [18]aneN$_6$ Found: C, 28.55; H, 7.61; N, 16.44%; Calcd for $C_{12}H_{30}N_6 \cdot 6HCl \cdot 1.5H_2O$: C, 28.55; H, 7.80; N, 16.64%. The [18]aneN$_6$ bearing 2.4 mol of the dodecanoyl groups, 2.4R-N$_6$, was obtained by the treatment of [18]aneN$_6$ with a 2.8-fold mol portion of dodecanoyl chloride. The number of the side chain was determined by the ratios based on the ^{1}H NMR spectra and the elementary analyses. ^{1}H NMR ($CDCl_3$): δ=0.9 (3H, t, CH_3CC-), 1.2 (methylene in alkane), 2.7—3.4 (24H, $-NCH_2CH_2N-$). 2.4R-N$_6$ Found: C, 67.57; H, 11.31; N, 11.44%; Calcd for $C_{40.8}H_{82.8}N_6O_{2.47} \cdot 0.8HCl$: C, 67.58; H, 11.62; N, 11.59%.

A telomer bearing 6.8 mol of [18]aneN$_6$, Ls6.8N$_6$, was derived from an acrylic acid-type telomer (LsnAc). The LsnAc was prepared by the radical telomerization of acrylic acid by a procedure similar to that described previously;[14] it was refined by reprecipitations with hexane after having been dissolved in ether, after which the insoluble telomer in the ether was filtered off. The conditions of telomerization are shown in Table 1. The molar ratios of 1-dodecanethiol to acrylic acid (β) are correlated to the polymerization degrees (Pn), because the chain transfer of the growing radical to 1-dodecanethiol is affected by the β. The Pn of the telomers were: $Pn^{-1}=0.71\times\beta-0.018$ (insoluble in ether); $Pn^{-1}=0.71\times\beta+0.090$ (soluble in ether). The structures of the telomers were determined by IR, ^{1}H NMR, and elementary analyses. An example (Ls8.5Ac) is as follows; IR (KBr): ν_{CH} 2900, ν_{CO} 1700 cm^{-1}; ^{1}H NMR{DCON(CD_3)$_2$}: δ=0.9 (3H, t, CH_3CC-), 1.3 (methylene in alkane), 10 (8.5H, -COOH); Ls8.5Ac Found: C, 54.9; H, 7.58%; Calcd for $C_{12}H_{25}S(CH_2CHCOOH)_{8.5}H$: C, 55.26; H, 7.43%. Then, the carboxyl groups of Ls8.5Ac were converted into chloroformyl groups by treatment with an excess of thionyl chloride.[15] The conversion was confirmed by IR (KBr) and ^{1}H NMR spectroscopy. The ν_{CO} frequencies, based on the carboxyl group (1700 cm^{-1}), were shifted to high ν_{CO} frequencies based on the chloroformyl group (1750—1800 cm^{-1}), and the proton signal of the carboxyl group (δ=10) disappeared. The telomer bearing 8.5 mol of chloroformyl groups was treated with an amount of [18]aneN$_6$ equimolar to the unit chloroformyl group in a refluxing toluene solution. After the toluene has been evaporated, the residue was washed with cold water and then acetone. The structure of the telomer bearing 6.8 mol of [18]aneN$_6$, Ls6.8N$_6$1.7Ac, was confirmed by IR, ^{1}H NMR, and elementary analyses. IR (KBr): ν_{CO} 1630 cm^{-1}; ^{1}H NMR(D_2O): δ=0.9 (3H, t, CH_3CC-), 1.2 (methylene in alkane), 3.8 (methylene in [18]aneN$_6$), the ratio of [18]aneN$_6$ to the dodecyl group, as determined by the peak areas, was 6.8; Ls6.8N$_6$1.7Ac Found N/C ratio(%/%)=0.42: Calcd for $C_{12}H_{25}S(CH_2CHCOC_{12}H_{29}N_6)_{6.8}(CH_2CHCOOH)_{1.7}H \cdot 5HCl$ N/C(%/%)=0.40.

The abbreviations of these cyclic polyamine-type surfactants are shown in Fig. 1.

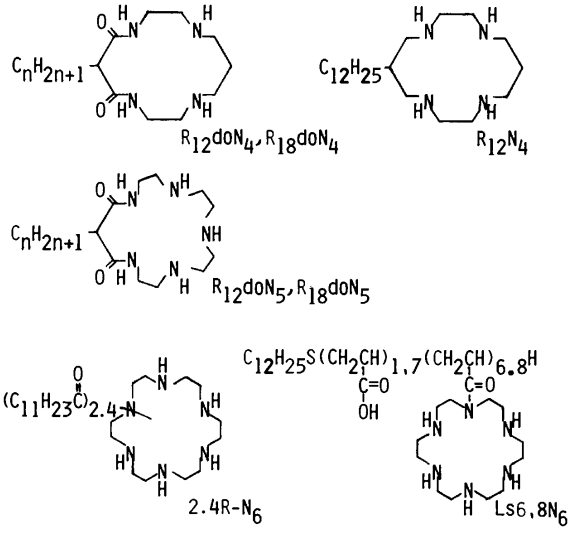

Fig. 1. The structures and the abbreviations.

Table 1. Preparation of the Telomer, LsnAc

	Conditions of reaction[a]		Products[b]		
	LSH	β	Abbreviation	Yield	Pn
	mol	mol mol^{-1}		wt%	
1	0.02	0.05	Insol Ls23.6Ac	65.2	23.6
			Sol Ls8.5Ac	13.9	8.5
2	0.04	0.10	Insol Ls16.3Ac	46.2	16.3
			Sol Ls5.5Ac	7.0	5.5
3	0.06	0.15	Insol Ls13.9Ac	19.0	13.9
			Sol Ls5.9Ac	10.0	5.9
4	0.08	0.20	Insol Ls14.3Ac	29.5	14.3
			Sol Ls3.8Ac	11.8	3.8
5	0.12	0.30	Sol Ls3.2Ac	16.7	3.2

a) Acrylic acid, 0.4 mol; LSH: 1-Dodecanethiol, β=LSH/(acrylic acid); 2,2′-azobisisobutyronitrile, 0.289 g; ethanol, 300 cm^3. Temp: 78 °C, time: 3 h. b) Sol: Telomer soluble in ether, Insol: telomer insoluble in ether. Pn: Polymerization degree.

Apparatus and Procedures. The flotation apparatus was the same as that previously reported.[5] The cyclic polyamine-type surfactant was added to 500 cm^3 of a metal solution (Cu^{2+}, Ni^{2+}, Fe^{3+}, Zn^{2+}, Hg^{2+}) in a flotation vessel, and then air was introduced into the solution through a sintered-glass disk (No. 4) at the bottom of the vessel at the rate of 30—40 cm^3 min^{-1} for 20 min. The floatabilities of the metal ions were calculated using the following formula:

$$F(\%) = \frac{a_0 - a_1}{a_0} \times 100$$

where a_0 and a_1 denote the initial and final metal concentrations respectively.

Results and Discussion

Surface Activities of R_ndoN_4. The synthesized compounds bear a hydrophobic long alkyl group and a hydrophilic polyamine residue, so the surface activities were investigated. The surface tension of the $R_{12}doN_4$ solution, as measured by a Wilhelmy (Shimadzu ST-1) surface tension balance, is shown in Fig. 2 (1 dyn=1×10^{-5} N). The lowering of the surface tension was more at pH 10 or in the presence of Cu^{2+}, as compared with that at pH 4. The lowering ceased in about 10 h, and the value become nearly constant. Therefore, the following measurements were carried out until the surface tension became constant (longer than 10 h).

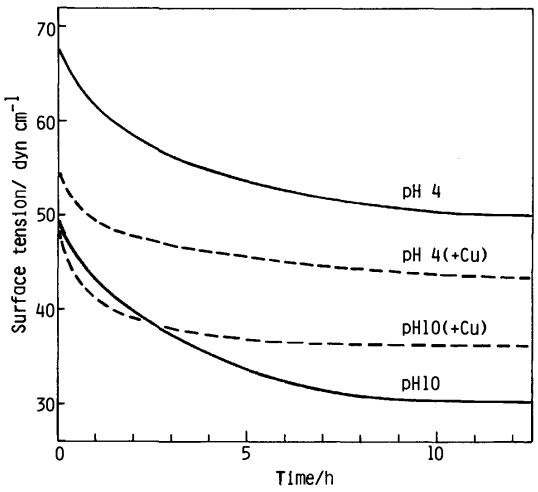

Fig. 2. Surface tension curves of $R_{12}doN_4$ at 20°C.
Concn at pH 4: [$R_{12}doN_4$]=4.8×10^{-5} mol dm^{-3}, [$R_{12}doN_4$]+[Cu^{2+}]=(4.7+4.7)×10^{-5} mol dm^{-3}.
Concn at pH 10: [$R_{12}doN_4$]=6.3×10^{-5} mol dm^{-3}, [$R_{12}doN_4$]+[Cu^{2+}]=(4.8+4.8)×10^{-5} mol dm^{-3}.

The relations between the surface tension and the concentration of R_ndoN_4 are shown in Fig. 3. $R_{12}doN_4$ at pH 10 had an excellent ability to lower the surface tension. The critical micellar concentration (cmc) was 1×10^{-4} M (1 M=1 mol dm^{-3}); this was confirmed also by the conductometric titration. However, the cmc at pH 4 was not observed in concentrations below 3.8×10^{-4} M. The $R_{12}doN_4$ in the presence of Cu^{2+} had an excellent lowering ability, and the surface tensions at pH 4 and 10 were nearly the same in value. $R_{18}doN_4$ was soluble in a solution acidic enough for its surface tension to be measured, but not at pH 10. The addition of Cu^{2+} to the $R_{18}doN_4$ solution made the surface tension lower, even at pH 10, and the two surface-tension curves at pH 4 and 10 became nearly the same.

The $R_{12}doN_4$-Ni^{2+} complex had as much lowering ability as the Cu^{2+} complex. However, the Fe^{3+} complex at pH 10 was deposited, and the surface tension was not lowered so much {[$R_{12}doN_4$]+[Fe^{3+}]=(4.7+4.7)×10^{-5} M: 42 dyn cm^{-1}, which is not shown in the figure}. The formation of the Cu^{2+} and Ni^{2+} complexes was confirmed over the pH range of 4.5—10,[16] but that of the Fe^{3+} complex has not yet been confirmed. The Fe^{3+} complex would be less stable and

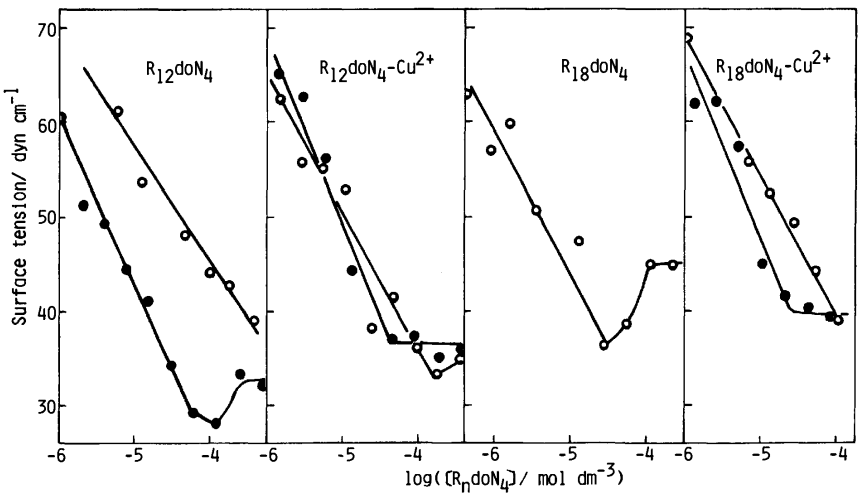

Fig. 3. Relations between surface tension and concn of R_ndoN_4. [R_ndoN_4]=[Cu^{2+}], temp: 20°C. ○: pH 4, ●: pH 10.

Table 2. Surface Activities of R_ndoN_4 and R_ndoN_4-Cu^{2+} Complexes[a)]

	pH 4			pH 10		
	γ_{cmc}	cmc	S	γ_{cmc}	cmc	S
	dyn cm^{-1}	$\times10^{-4}$ M	$Å^2$ mol^{-1}	dyn cm^{-1}	$\times10^{-4}$ M	$Å^2$ mol^{-1}
$R_{12}doN_4$	<39	3.8<	82	32	1	57
$R_{12}doN_4$+Cu^{2+}	35	2	66	36	0.5	46
$R_{18}doN_4$	45	0.3	77		Insoluble	
$R_{18}doN_4$+Cu^{2+}	<39	1.3<	67	40	0.3	48

a) Wilhelmy surface-tension balance; temp: 20°C.

so would be hydrolyzed easily, or the $R_{12}doN_4$ might bind to the Fe^{3+} hydroxide.

The surface-tension curves of hydrophilic R_ndoN_5 were located in higher concentrations than the curves of R_ndoN_4. The relations of the surface tension between the $R_{12}doN_5$, the $R_{18}doN_5$, and their Cu^{2+} complexes were similar to those between the corresponding $R_{12}doN_4$, $R_{18}doN_4$, and their Cu^{2+} complexes.

Molecular Area. The surfactants (R_ndoN_4 and its Cu^{2+} complex) are oriented on the surface layer of the solutions. Therefore, the mole numbers of the vertical surfactants(Γ) per unit area (cm^2) were calculated from the Gibbs adsorption isotherm on the basis of the lowering of the surface tension(γ):[17]

$$\Gamma = \frac{1}{RT} \times \frac{d\gamma}{d \ln C}$$

Then, the areas of the cross-section of a surfactant molecule were calculated from the mole number. The areas (S) are shown in Table 2, together with their surface activities. The S values when soluble in water lead to a small error. However, it is reasonable to estimate the relative areas in connection with the structures of the R_ndoN_4 and its Cu^{2+} complex.

The areas of $R_{12}doN_4$ were 82 $Å^2$ mol^{-1} at pH 4 and 57 $Å^2$ mol^{-1} at pH 10; that of $R_{18}doN_4$ was 77 $Å^2$ mol^{-1} at pH 4, but has unmeasured at pH 10. The $R_{12}doN_4$ and $R_{18}doN_4$ in the acidic solution of pH 4 are cationic. Therefore, the area of $R_{12}doN_4$ at pH 4 would be widened because of the solvation and the electrostatic repulsion, while the area of $R_{18}doN_4$ at pH 4 would become narrower than that of $R_{12}doN_4$ at pH 4 because of the additional aggregation based on the van der Waals force of a longer alkyl chain.

The area of R_ndoN_4 in the presence of Cu^{2+} became smaller than that in the absence of Cu^{2+}. The $R_{12}doN_4$-Cu^{2+} and $R_{18}doN_4$-Cu^{2+} complexes had nearly the same S values, and the two areas at pH 10 (46—48 $Å^2$ mol^{-1}) were smaller than those at pH 4 (66—67 $Å^2$ mol^{-1}). Dioxo[14]aneN_4 is known to form the uncharged Cu^{2+} complex above pH 4.5.[16] Therefore, the R_ndoN_4 at pH 10 would form the uncharged Cu^{2+} complex with a tighter aggregation.

Thus, it was proved that the long-alkyl-substituted cyclic dioxopolyamine and its metal complexes have the ability to lower the surface tension.

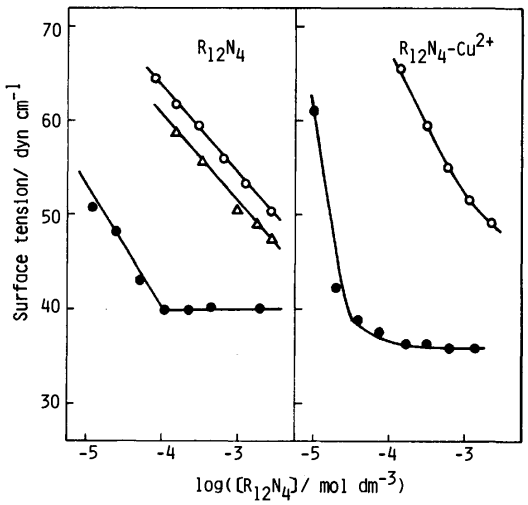

Fig. 4. Surface tension of $R_{12}N_4$. $[R_{12}N_4]$=$[Cu^{2+}]$, temp: 20°C. ○: pH 4, △: pH 7, ●: pH 10.

Surface Activities of $R_{12}N_4$. The reduction product of $R_{12}doN_4$, $R_{12}N_4$, also made the surface tension lower. The surface tension, as measured by Du Noüy surface-tension balance, is shown in Fig. 4. At pH 4 and 7, the surface tension lowered with the increase in the concentration, and the cmc was not observed over the concentration range below 3×10^{-3} M. The surface tension at pH 10 fell to 40 dyn cm^{-1}, and the cmc was nearly 10^{-4} M. The addition of Cu^{2+} lowered the surface tension a little, and the cmc at pH 10 shifted to a lower concentration. The calculated S values of $R_{12}N_4$ were 95 $Å^2$ mol^{-1} at pH 4 and 66 $Å^2$ mol^{-1} at pH 10, while those of the Cu^{2+} complex were 48—53 $Å^2$ mol^{-1} at pH 4 and 39 $Å^2$ mol^{-1} at pH 10. The 2.4R-N_6 and Ls6.8N_6 showed a lowering of the surface tension (2.4R-N_6 34—37 dyn cm^{-1}, Ls6.8N_6 42 dyn cm^{-1}); their Cu^{2+} complexes had a similar surface tension. The S values at pH 7 were 72 $Å^2$ mol^{-1} for 2.4R-N_6 and 42 $Å^2$ mol^{-1} for the Cu^{2+} complex. The differences in the areas are probably caused by the tightness of the aggregation based on the complex formation. However, the S values of Ls6.8N_6 and its Cu^{2+} complex were both 92 $Å^2$ mol^{-1} at pH 7. The same wide areas are probably caused by the weak

aggregation based on the similar great repulsion of the 1.7 mol of carboxylate ion in Ls6.8N_6 and its Cu^{2+} complex.

Ion-Flotation. The four metal ions (Cu^{2+}, Ni^{2+}, Fe^{3+}, Zn^{2+}) in water were separated by the method of ion-flotation using these surfactants. $R_{12}doN_4$ and $R_{18}doN_4$ showed almost the same floatabilities of the metal ions, as is shown in Fig. 5. The dioxo[14]aneN_4-metal complexes when the equimolar dioxo[14]aneN_4 was added to the 10^{-4} M of the metal ion were calculated from the data of the stability constants.[18] The 1:1 species were in the pH range above 4.6 for Cu^{2+} and above 7 for Ni^{2+}. Therefore, the alkylated R_ndoN_4 would complex and float with Cu^{2+} or Ni^{2+} in that pH region. R_ndoN_5 exhibited slightly different floatabilities from those obtained by using R_ndoN_4, e.g., Fe^{3+} in pH 5—6 (Fig. 6). R_ndoN_5 is more hydrophilic than R_ndoN_4, so that the differences in the floatabilities are caused by their HLB.

The collector characteristics of the alkylated reduction product ($R_{12}N_4$) and the polyalkylated 2.4R-N_6 ([18]aneN_6 bearing 2.4 mol of dodecyl groups) are shown in Fig. 7. The stability constants (log K) of the cyclic polyamine-Cu^{2+} complexes are known to be far greater than those of the cyclic dioxopolyamine-Cu^{2+} complexes.[18,19] The pk_a and log K(Cu^{2+} complex) have been reported as follows: dioxo[14]aneN_4 pk_{a1} 5.97, pk_{a2} 9.57, log K 1.0; dioxo[16]aneN_5 $pk_{a1}<2$, pk_{a2} 8.69, pk_{a3} 9.01;[18] [14]aneN_4 pk_{a1} 0.9, pk_{a2} 1.61, pk_{a3} 10.62, pk_{a4} 11.59, log K 27.2; [18]aneN_6 pk_{a1} ca. 1, pk_{a2} ca. 2, pk_{a3} 4.30, pk_{a4} 9.01, pk_{a5} 9.51, pk_{a6} 10.46, log K 21.6.[19]

Then, the stabilities of the $R_{12}doN_4$-Cu^{2+} and $R_{12}N_4$-Cu^{2+} complexes were confirmed by pH titration with a NaOH solution. The titration curves of the $R_{12}doN_4$ and $R_{12}N_4$ showed the end points based on the acid dissociation (pk_a) at two and four equimolar quantities of NaOH respectively. From the two pH-titration curves in the presence of Cu^{2+}, it was concluded that the Cu^{2+} complex of $R_{12}N_4$ is far more stable than the complex of $R_{12}doN_4$, while the $R_{12}doN_4$ forms uncharged complexes with divalent Cu^{2+}.

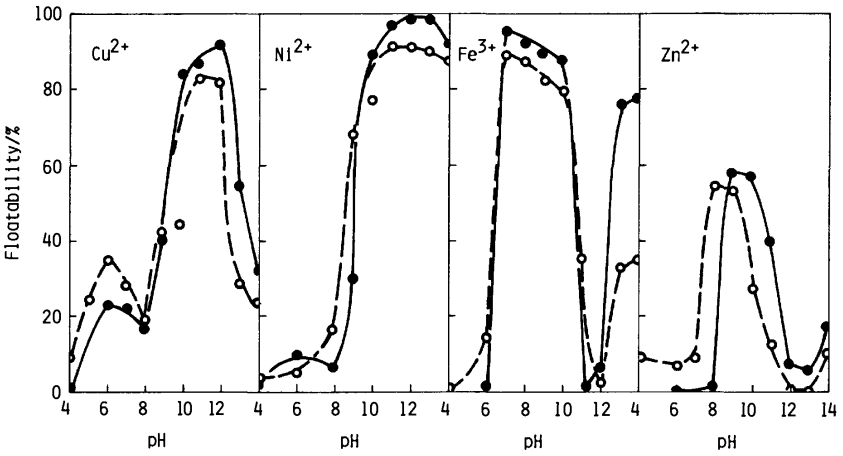

Fig. 5. Flotation by using R_ndoN_4. [Metal ion], [R_ndoN_4]=10^{-4} mol dm^{-3}. O: $R_{12}doN_4$, ●: $R_{18}doN_4$.

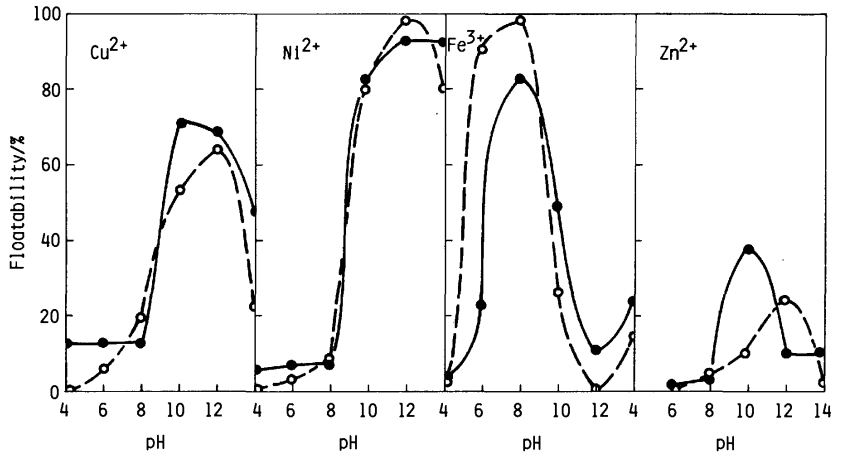

Fig. 6. Flotation by using R_ndoN_5. [Metal ion], [R_ndoN_5]=10^{-4} mol dm^{-3}. O: $R_{12}doN_5$, ●: $R_{18}doN_5$.

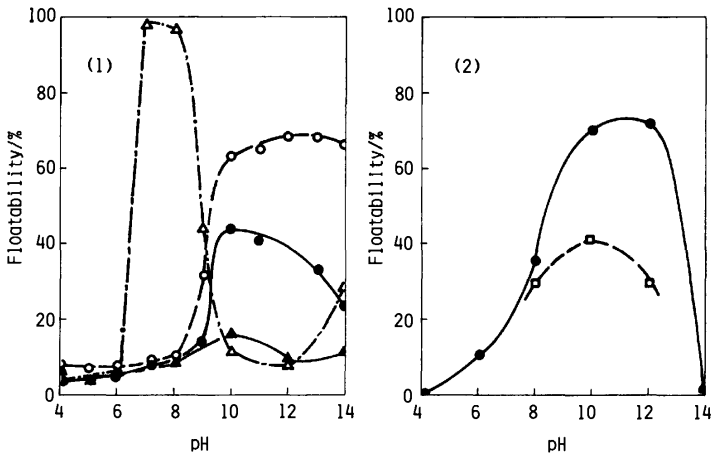

Fig. 7. Flotation by using $R_{12}N_4$ and 2.4R-N_6. (1): [Metal ion], $[R_{12}N_4]=10^{-4}$ mol dm^{-3}. (2): [Metal ion], [2.4R-N_6]$=3\times10^{-5}$ mol dm^{-3}. ●: Cu^{2+}, O: Ni^{2+}, △: Fe^{3+}, ▲: Zn^{2+}, □: Hg^{2+}.

Therefore, the pk_a values of $R_n$doN$_4$, $R_n$doN$_5$, $R_{12}N_4$, and 2.4R-N_6, and the log$K$ values of their metal complexes, are comparable to those of the corresponding cyclic dioxopolyamine, cyclic polyamine, and the metal complexes.

However, neither Cu^{2+} nor the other metal ions was floated so highly by using $R_{12}N_4$, and the floatability of Cu^{2+} by using 2.4R-N_6 in the alkaline region was similar to that when $R_n$doN$_4$ or $R_n$doN$_5$ was used. The floatable $R_{12}N_4$-metal and 2.4R-N_6-metal complexes in that alkaline region are the neutralized species with OH^-. The telomer bearing 6.8 mol of [18]aneN$_6$, Ls6.8N$_6$, formed soluble metal complexes and did not make the metal ions float.

Thus, the variation in the complex forms, that is, the variation in their HLB values, fairly affected the floatabilities. The floated complexes were surface-active. The HLB values were calculated according to the Oda equation[20] on the basis of the postulated structures. The HLB values were R_{12}doN$_4$-Cu 9, R_{12}doN$_5$-Cu 10, and $(R_{12}N_4\text{-Cu})^{2+}\cdot2(OH)^-$ 14. The values of the complexes proved to be in the HLB range of 4—14 suitable for ion flotation, as has been reported previously.[21] Therefore, they must be floated.

Flotation Using Polyamine. *N*-Alkylethylenediamine and *N*-dodecyldiethylenetriamine have been placed in an ion-flotation collector.[7] The complexation of the cyclic polyamine differs much from that of the linear polyamine. Therefore, the collector characteristics of the alkylated cyclic polyamines were compared with those of the linear polyamine-type surfactants. The flotation of Cu^{2+} is shown in Fig. 8.[7,22] All the floatabilities were roughly similar, in spite of the great differences in the stability constants. The Cu^{2+} complexes of linear polyamines should be neutralized with OH^- in the alkaline region, and then the complexes come to be in the HLB range of 4—14.

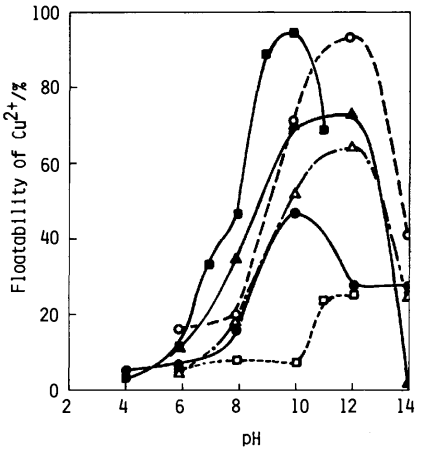

Fig. 8. Flotation of Cu^{2+} by using polyamine-type surfactants. O: R_{12}doN$_4$, △: R_{12}doN$_5$, ●: $R_{12}N_4$, ▲: 2.4R-N_6, □: *N*-dodecylethylenediamine, ■: *N*-dodecyldiethylenetriamine.

Therefore, the complexes should be floated in the alkaline region, and all the collector characteristics will resemble each other.

Selectivity. The selectivity of metal ions is a matter of great practical importance in separation. Therefore, the selective flotation from a metal-ion mixture (Fe^{3+}, Cu^{2+}, Ni^{2+}, Zn^{2+}) was examined. The flotations by using R_{18}doN$_4$ and R_{18}doN$_5$ in pH 4—8 are shown in Fig. 9. The selectivities by using R_{18}doN$_4$ or R_{12}doN$_4$ were $Cu^{2+}>Ni^{2+}>Fe^{3+}>Zn^{2+}$; this order differed from that by using R_{18}doN$_5$ or R_{12}doN$_5$ ($Fe^{3+}>Cu^{2+}>Ni^{2+}>Zn^{2+}$). The coordination numbers of Cu^{2+} and Fe^{3+} are usually 4 and 6 respectively. Therefore, it was considered that the $R_n$doN$_4$-Cu^{2+} complex was saturated, while the $R_n$doN$_5$-Cu^{2+}, R_{18}doN$_4$-Fe^{3+}, and R_{18}doN$_5$-Fe^{3+} complexes (or compounds) were not. The unsaturated R_{18}doN$_5$-Cu^{2+}

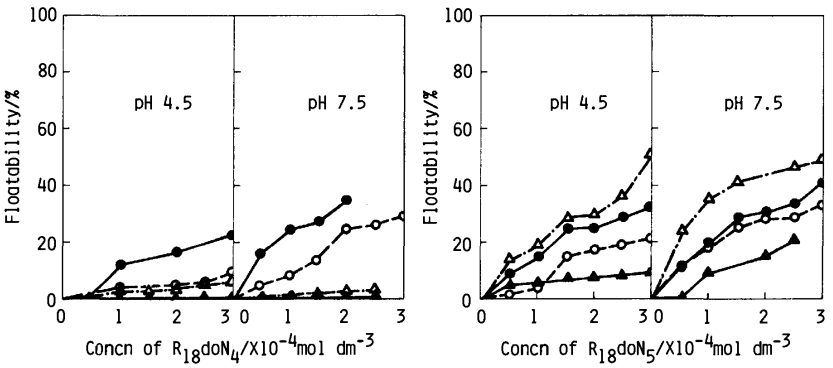

Fig. 9. Selectivities using $R_{18}doN_x$ at pH 4.5 and 7.5. Metal ions mixture: Cu^{2+}, Ni^{2+}, Fe^{3+}, Zn^{2+} (each 10^{-4} mol dm^{-3}). ●: Cu^{2+}, ○: Ni^{2+}, △: Fe^{3+}, ▲: Zn^{2+}.

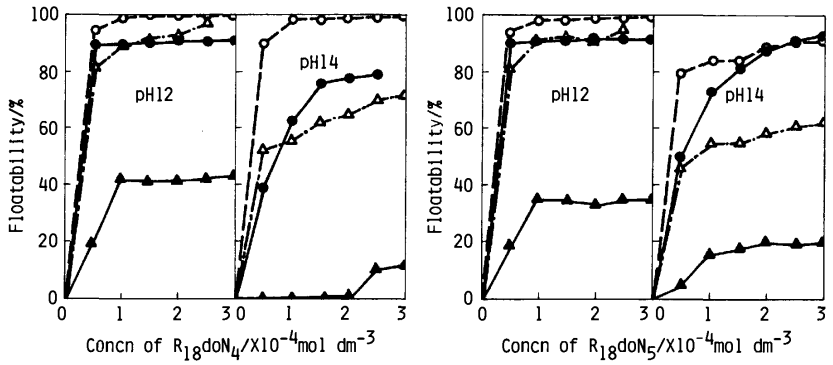

Fig. 10. Selectivities using $R_{18}doN_x$ in alkaline. Metal ions mixture: Cu^{2+}, Ni^{2+}, Fe^{3+}, Zn^{2+} (each 10^{-4} mol dm^{-3}). ●: Cu^{2+}, ○: Ni^{2+}, △: Fe^{3+}, ▲: Zn^{2+}.

complex is more hydrophilic than the saturated $R_{18}doN_4$-Cu^{2+} complex, because of its one more amine. Moreover, the unsaturated Fe^{3+} complexes are cationic and are hydrolyzed easily above pH 3—4. The cationic $R_{18}doN_4$ and $R_{18}doN_5$ might bind to the colloidal Fe^{3+} hydroxide. Therefore, the $R_{18}doN_4$-Cu^{2+} complex would be more hydrophobic than the $R_{18}doN_4$-Fe^{3+} compound. This tendency agreed with the hydrophobic properties in the surface tension; that is, the lowering of the surface tension of the hydrophobic $R_{12}doN_4$-Cu^{2+} complex at pH 4 (Fig. 3) began at a lower concentration of $R_{12}doN_4$ than did that of the $R_{12}doN_4$-Fe^{3+} compound at pH 4 (the surface-tension curve, which is not shown, was nearly the same as the curve of the $R_{12}doN_4$ in the absence of Fe^{3+}). On the other hand, the $R_{18}doN_5$-Fe^{3+} complex, the cyclic dioxopentamine compound, should be less hydrophilic than the Cu^{2+} complex. Therefore, the hydrophobic Cu^{2+} and Fe^{3+} complexes would be selectively floated by using R_ndoN_4 and R_ndoN_5 respectively. However, the same selectivities were observed in the pH range of 12—14, even though the floatabilities (Ni^{2+}>Cu^{2+}>Fe^{3+}>Zn^{2+}) were high, as is shown in Fig. 10. Metal ions form polyhydroxo complexes in a strongly alkaline solution. The log K values of the metal-hydroxo complexes are Ni^{2+} 3.08, Cu^{2+} 6.66, Fe^{3+} 11.17, and Zn^{2+} 5.04;[23] the Ni^{2+} hydroxide is the least stable among these metal ions. Therefore, the conditional stability constants of the $R_{18}doN_4$-Ni^{2+} and the $R_{18}doN_5$-Ni^{2+} complexes in the pH range of 12—14 would become the largest, and then Ni^{2+} would be floated most. Figures 5 and 6 also illustrate that the hydrophobic properties (HLB) of the Cu^{2+} and Fe^{3+} complexes developed in the floatabilities at pH 5—6, while the stabilities of the Ni^{2+} complex developed in the floatabilities above pH 12. On the other hand, the Cu^{2+} was extracted and transported selectively by using $R_{16}doN_4$ from a mixture of Cu^{2+}, Fe^{3+}, Ni^{2+}, and Zn^{2+} because of the formation of the most stable complex.[6] Therefore, the selectivities in the ion-flotaion markedly differed from those in the extraction and transportation.

Thus, it is concluded that the cyclic polyamine-type surfactants have excellent surface-activities and that the flotation using the cyclic dioxopolyamine-type surfactant was done by means of the complex formation, while that using the cyclic polyamine or linear polyamine was done by means of the neutralization of

the complex with OH^-. Furthermore, the selective flotation has been proved to be attributable to the hydrophobic properties (smaller HLB) of the metal complexes in the HLB range of 4—14 rather than to the stability.

The authors are grateful to Assistant Professor Akinori Jyo for his useful suggestions and to Mr. Shunji Hayashi and Mr. Norihito Maehara for their help in the experiments.

References

1) Part X: Y. Koide, M. Uchino, H. Shosenji, and K. Yamada, *Bull. Chem. Soc. Jpn.*, submitted for publication.
2) W. Takagi, *Yukagaku*, **37**, 394 (1988).
3) E. Kimura, *Yuki Gosei Kagaku Kyokai Shi*, **44**, 871 (1986).
4) S. Inokuma, D. Ito, W. Kobori, and T. Kuwamura, *Yukagaku*, **37**, 668 (1988).
5) Y. Koide, M. Uchino, and K. Yamada, *Bull. Chem. Soc. Jpn.*, **60**, 3477 (1987).
6) E. Kimura, C. A. Dalimunte, A. Yamashita, and R. Machida, *J. Chem. Soc., Chem. Commun.*, **1985**, 1041.
7) K. Yamada, Y. Koide, F. Koga, K. Izumi, and A. Hongo, *Nippon Kagaku Kaishi*, **1977**, 575.
8) E. Kimura, Y. Lin, R. Machida, and H. Zenda, *J. Chem. Soc., Chem. Commun.*, **1986**, 1020.
9) I. Tabushi, Y. Taniguchi, and H. Kato, *Tetrahedron Lett.*, **1977**, 1049.
10) R. Adams and R. M. Kamm, *Org. Synth.*, **I**, 250 (1941).
11) J. V. Alphen, *Recl. Trav. Chim. Pays-Bas*, **55**, 835 (1936).
12) M. Micheloni, P. Paoletti, and A. Poggi, *J. Chem. Soc., Dalton Trans.*, **1982**, 61.
13) W. L. Smith, J. D. Ekstrand, and K. N. Raymound, *J. Am. Chem. Soc.*, **100**, 3539 (1978).
14) K. Yamada and Y. Koide, *Yukagaku*, **30**, 2 (1981).
15) B. Helfevich and W. Schaefev, *Org. Synth.*, **I**, 147 (1941).
16) L. Fabbrizzi, F. Forlini, A. Perotti, and B. Seghi, *Inorg. Chem.*, **23**, 807 (1984).
17) T. Kondo, "Kaimenkagaku," Sankyo Shuppan, Tokyo (1968), p. 18.
18) E. Kimura, R. Machida, and M. Kodama, *J. Am. Chem. Soc.*, **106**, 5497 (1984).
19) M. Kodama, E. Kimura, and S. Yamaguchi, *J. Chem. Soc., Dalton Trans.*, **1980**, 2536.
20) R. Oda and K. Teramura, "Kaimen-kasseizai No Gosei To Sonooyo," Makishoten, Tokyo (1962), p. 501.
21) Y. Koide, K. Izumi, K. Okuzono, and K. Yamada, *Nippon Kagaku Kaishi*, **1980**, 742.
22) G. Izumi, M. Sato, S. Shoji, and K. Oikawa, *Bull. Chem. Soc. Jpn.*, **49**, 1727 (1976).
23) R. M. Smith and A. E. Martell, "Critical Stability Constants," Vol. 4, Plenum Press (1976).

 © 1989 The Chemical Society of Japan Bull. Chem. Soc. Jpn., 62, 2875—2879 (1989)

Effects of Polysubstitution on Mesomorphic Properties: Chloro and Methyl Derivatives of *N*-[4-(4-Substituted benzoyloxy)benzylidene]anilines

Hiroyuki HASEGAWA, Tatsuya MASUDA, Yoshio MATSUNAGA,*
Sachiko SEO, and Kazuaki YASUHARA
Department of Chemistry, Faculty of Science, Hokkaido University, Sapporo 060
(Received April 12, 1989)

The effects of mono-, di-, and trichloro substitution of the aniline moiety on the nematic-isotropic transition temperature of *N*-[4-(4-X-substituted benzoyloxy)benzylidene]anilines, where X=CH_3O, CH_3, or Cl, have been studied, while paying particular attention to the vicinal chlorines. While the substituent on the 2 or 3 position of the aniline moiety lowers the transition temperature of the parent compound and the 4-chloro derivative, the 2,3-dichloro derivative shows a temperature higher than that of either the 2- or 3-chloro derivative. Moreover, the transition temperature of the 2,3,4-trichloro derivative exceeds that of the 3,4-dichloro derivative and is a little below that of the 2,4-dichloro isomer. In contrast, the introduction of 4-substituent increases the temperature, regardless of the position(s) of the other substituent(s). Methyl substitution exerts effects closely similar to those described above.

The effects of polysubstitution on mesomorphic thermal stabilities have been the subjects of many studies.[1] These studies have demonstrated that lateral substitution of a mesomorphic compound causes a pronounced lowering of the mesomorphic transition temperature. Therefore, the increased intermolecular separation seems to decrease the intermolecular cohesion to an extent outweighing any enhancement in these cohesive forces arising from increased polarity and polarizability. It has been concluded that the effects of two substituents are approximately additive.[2] However, Young et al. have noted that the transition temperature drops more slowly with each additional substituent when the molecule contains three or four substituents.[3] A survey of the literatures revealed that the substituents in almost all cases are located on different aromatic rings or are not bonded to the neighboring carbon atoms if they are located on the same ring. The work by Panse et al. on 4-(4-alkoxybenzoyloxy)-4′-alkylazobenzenes includes some exceptional cases.[4] For instance, the nematic–isotropic (N-I) transition temperature of the 2,3-dimethyl derivative was recorded to be 215 °C when the terminal substituents were butoxyl and butyl groups, respectively. This value is appreciably higher than that of the corresponding 3-methyl derivative, 183 °C. Moreover, the effects of two lateral cyano groups introduced into the neighboring positions on the mesomorphic behavior of four esters were described by Osman.[5] He concluded that the second substituent has little effect on the clearing point since it fills the space produced by the introduction of the first one and does not increase the intermolecular separation.

We have undertaken systematic examinations of the effects of substituents attached to the neighboring carbon atoms in the same benzene ring on the thermal stability of mesophases. As the decreases in thermal stability of the mesophase by the introduction of lateral substituent(s) are often large, the thermal stabilities of mesophases and the temperature ranges over which the mesophases exist must be considerable, if one is to study the effects of di- and polysubstitution upon the mesomorphic transition temperatures. For this purpose, we have chosen *N*-[4-(4-substituted benzoyloxy)benzylidene]anilines (**1**) as the parent compounds and methyl and/or chloro substituent(s) to be introduced to the aniline moieties. The van der Waals radii of these two substituents are about 0.23 and 0.18 nm respectively; however, the difference in the radius is almost cancelled by the difference in the ring-X bond length; these two are expected to affect the thermal stability of mesophase nearly to the same extent when they are employed as lateral substituents.[1] The stable or metastable nematic phase may hopefully be detected with the selected compounds, since *N*-[4-(4-methoxybenzoyloxy)benzylidene]-4-methylaniline has been reported to exhibit a nematic phase over the temperature range from 129 to 274.5 °C and the 4-chloro analog from 165 to 274 °C.[6,7]

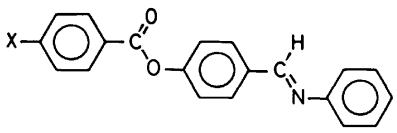

1

Experimental

Materials. 4-(4-X-substituted benzoyloxy)benzaldehydes were prepared by reacting 4-X-substituted benzoyl chlorides and 4-hydroxybenzaldehyde in the presence of pyridine. The Schiff's bases were synthesized by condensing the above-mentioned benzaldehydes with appropriate anilines in ethanol. The products were recrystallized from ethanol, benzene, or the mixtures until constant transition temperatures were obtained.

Measurements. Transition temperatures were determined by calorimetric curves recorded with a Rigaku Thermoflex differential scanning calorimeter at a heating or cooling rate of 5 °C min^{-1}. Enthalpy changes were estimated by comparing the peak areas with that due to the melting of indium, 3.26 kJ mol^{-1}. When no mesophase was detectable,

the virtual transition temperature was estimated by the extrapolation of the clearing point curve in the binary system with 4,4′-azoxydianisole.

Results and Discussion

The transition temperatures and the associated enthalpy changes of the monofluoro, monochloro, monobromo, monoiodo, and monomethyl derivatives of *N*-[4-(4-methoxybenzoyloxy)benzylidene]aniline (X=CH_3O) are summarized in Table 1. Here, crystalline, nematic, and isotropic phases are denoted by K, N, and I respectively. Gray and Worrall have shown that the clearing point (N-I transition temperature) of 3′-substituted 4′-octyloxybiphenyl-4-carboxylic acids decreases smoothly with increasing the molecular breadth.[8] Gray and his coworkers have also studied the mesomorphic properties of 2′- and 3′-X-substituted 4-[(4-alkoxybenzylidene)amino]biphenyls.[9] The 2′-isomers give much larger depressions of the clearing point because of a twisting effect superimposed on a broadening effect. In our case, a twisting effect is essentially absent and the substituent on the 2 position of the aniline moiety may be less exposed than that on the 3 position, because the lines defining the molecular breadth have their positions determined by the stereochemistry of the -COO- and -CH=N- units. The substituent on the 3 position is so effective in reducing the temperature that the mesophase is eliminated when chlorine, bromine, and iodine atoms are employed. In these cases, the virtual transition temperature estimated by the extrapolation of the clearing point curve in the binary system with 4,4′-azoxydianisole is listed in Table 1. As a result, the depression of the clearing point by the 2-chloro substituent was found to be 59 °C and that by the 3-substitution 82 °C. The methyl substitution results in similar differences.

Table 2 presents the transition temperatures and the associated enthalpy changes of the dichloro and trichloro derivatives of *N*-[4-(4-methoxybenzoyloxy)-benzylidene]aniline. The change in the clearing point by the chloro substituents is well demonstrated by the diagram shown in Fig. 1a. The 4-substitution promotes the thermal stability of the mesophase in the 2-chloro, 3-chloro, and 2,3-dichloro derivatives. The extents are not much different from that found with the parent compound. Furthermore, the depression of the transition temperature of the 4-chloro derivative by the 2- or 3-substitution appears to be similar to those arising from the substitution on the parent compound. Thus, the effects are approximately additive in these cases. Serious deviations from the additivity rule are clearly seen when the thermal stability of mesophase is compared between the 2,3-dichloro derivative and the 2- or 3-chloro derivative, and also between the 2,3,4-trichloro derivative and the 2,4- or 3,4-dichloro derivative. Namely, the 2,3-dichloro derivative exhibits a temperature higher than either the 2-chloro or the 3-chloro derivative. Stabilization by the second substituent is about twice as large when the first one is located on the 3 position. A similar, but less pronounced, tendency is found among the trichloro and dichloro derivatives mentioned above.

While the clearing point of the monomethyl derivative is close to that of the corresponding monochloro derivative, the difference is somewhat larger among the disubstituted compounds (see Table 2). The changes in the transition temperature by methyl substitution are summarized in Fig. 1b. It may be noted that all of the compounds employed in this

Table 1. Transition Temperatures (°C) and Enthalpy Changes (kJ mol^{-1}) of 2-, 3-, and 4-Substituted *N*-[4-(4-Methoxybenzoyloxy)benzylidene]anilines[a]

Substituent	K	N	I
None	129 (31)	177 (0.4)	
2-F	135 (39)	145 (0.3)	
2-CH_3	150 (41)	[121 (0.2)]	
2-Cl[b]	129 (34)	[118 (0.3)]	
2-Br	140 (34)	[105 (0.2)]	
2-I	133 (36)	[81 (0.2)]	
3-F	135 (39)	150 (0.4)	
3-CH_3	111 (34)	[88 (0.1)]	
3-Cl	160 (47)	[95[c]]	
3-Br	159 (36)	[60[c]]	
3-I	132 (33)	[57[c]]	
4-F	131 (32)	255 (0.8)	
4-CH_3[d]	129 (28)	278 (1.1)	
4-Cl[e]	172 (27)	285 (1.6)	
4-Br	187 (38)	280 (0.9)	
4-I	202 (21)	274 (0.4)	

a) The latter quantities are in parentheses. b) 133 and 120 °C by Vora and Patel (Ref. 7). c) The virtual transition temperature estimated by the extrapolation of the clearing point curve in the binary system with 4,4′-azoxydianisole. d) 129 and 274.5 °C by Dave and Kurian (Ref. 6). e) 165 and 274 °C by Vora and Patel (Ref. 7).

Table 2. Transition Temperatures (°C) and Enthalpy Changes (kJ mol^{-1}) of Di- and Trisubstituted *N*-[4-(4-Methoxybenzoyloxy)benzylidene]anilines[a]

Substituents	K	N	I
2,3-Cl_2	147 (29)	[139 (0.3)]	
2,4-Cl_2	143 (43)	231 (2.1)	
3,4-Cl_2	201 (22)	[192 (0.5)]	
2,3,4-Cl_3	183 (42)	222 (0.4)	
2,3-$(CH_3)_2$	126 (31)	158 (0.4)	
2,4-$(CH_3)_2$	142 (36)	222 (0.8)	
3,4-$(CH_3)_2$	118 (26)	182 (0.5)	
2-CH_3-3-Cl	139 (31)	149 (0.4)	
3-Cl-4-CH_3	159 (44)	191 (0.4)	

a) The latter quantities are in parentheses.

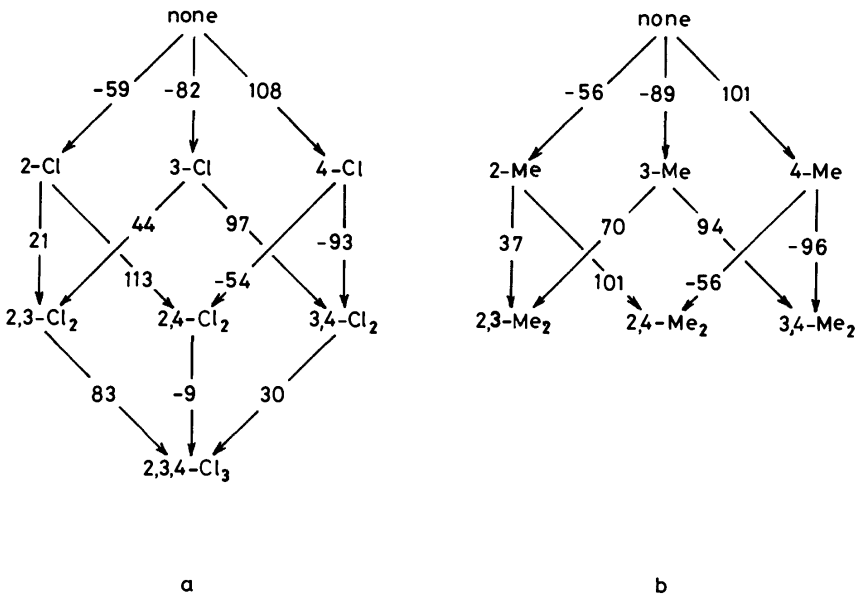

Fig. 1. The change in the clearing point (°C) of *N*-[4-(4-methoxybenzoyloxy)benzylidene]aniline by (a) chloro and (b) methyl substitution.

figure exhibit a stable or metastable mesophase; in other words, all of the transition temperatures are measurable. The mesophase is promoted by 4-methyl substitution as much as by the 4-chloro substitution presented in Fig. 1a. Moreover, the phase of the 4-methyl derivative is destabilized by 2- or 3-methyl substitution to an extent which is well compared with that given by the corresponding chloro derivative. Since the 2,3-dimethyl derivative exhibits an N-I transition temperature higher by 19 °C than the 2,3-dichloro derivative, the deviation from the additivity rule observed in Fig. 1b is more striking than that given in Fig. 1a.

The resemblance in the mesomorphic behavior between the chloro and methyl derivatives indicates that dispersive forces play a major role compared with dipole attractive forces, as pointed out by Osman.[5] This conclusion is supported by our additional data on the 2-methyl-3-chloro and 3-chloro-4-methyl derivatives. Their clearing points are in the order; 2,3-dichloro<2-methyl-3-chloro<2,3-dimethyl and 3,4-dimethyl<3-chloro-4-methyl<3,4-dichloro, respectively.

The thermodynamic data for compounds with X=CH_3 are presented in Table 3 and the changes in the clearing point are given in Fig. 2a. As the 2-chloro, 3-chloro, and 2,3-dichloro derivatives are not mesogenic, the changes involving these derivatives may not be very accurate. Nevertheless, the general feature in Fig. 2a is in good agreement with those found in Figs. 1a and b. The enhancement in the thermal stability of mesophase by the 4-chloro substituent seems to be more pronounced than that in the previously-described series. As demonstrated by the clearing points of the 4-chloro, 2,4-dichloro, and 3,4-dichloro derivatives, the 3-chloro substituent is more efficient to reduce the clearing point than the 2-chloro substituent. The difference in the clearing point between the 2,3,4-trichloro derivative and the 2,4-dichloro or 3,4-dichloro derivative contrasts markedly with the above-mentioned and definitely indicates that the anomaly is caused by the substituents located at the 2 and 3 positions. It must be added that the 2-methyl-3-chloro derivative is not mesogenic in conformity with the behavior of the 2,3-dichloro derivative. The clearing

Table 3. Transition Temperatures (°C) and Enthalpy Changes (kJ mol^{-1}) of Mono-, Di-, and Trisubstituted *N*-[4-(4-Methylbenzoyloxy)benzylidene]anilines[a]

Substituent(s)	K		N		I
None	.	142 (35)	[.	124 (0.3)]	.
2-Cl	.	165 (37)	[.	76[b]]	.
3-Cl	.	138 (38)	[.	63[b]]	.
4-Cl	.	169 (29)	.	257 (0.6)	.
2,3-Cl_2	.	152 (37)	[.	85[b]]	.
2,4-Cl_2	.	166 (37)	.	197 (0.6)	.
3,4-Cl_2	.	152 (41)	.	155 (0.3)	.
2,3,4-Cl_3	.	176 (33)	.	190 (0.5)	.
2-CH_3-3-Cl	.	153 (44)	[.	102[b]]	.
3-Cl-4-CH_3	.	133 (28)	.	149 (0.3)	.

a) The latter quantities are in parentheses. b) The virtual transition temperature estimated by the extrapolation of the clearing point curve in the binary system with 4,4′-azoxyldianisole.

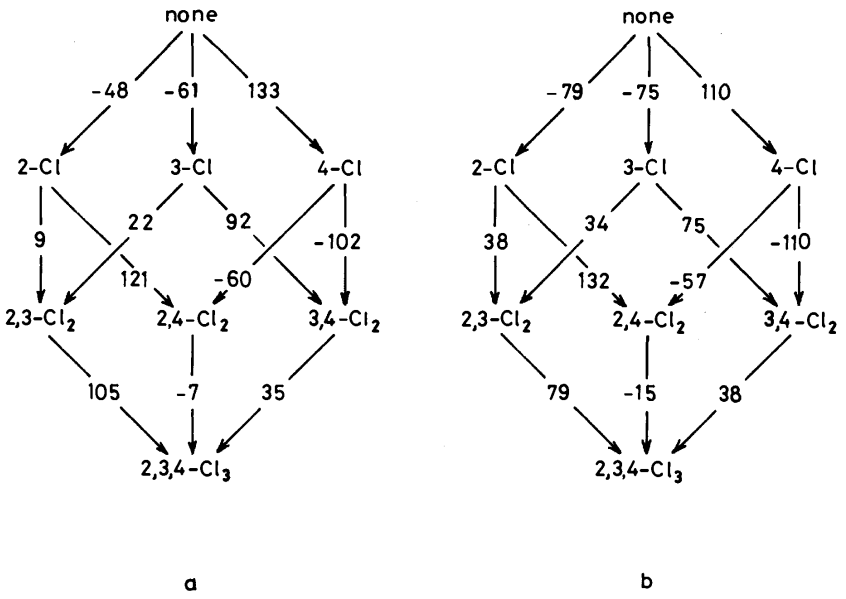

Fig. 2. The change in the clearing point (°C) by chloro substitution of *N*-[4-(4-X-substituted benzoyloxy)benzylidene]aniline; (a) X=CH_3 and (b) X=Cl.

Table 4. Transition Temperatures (°C) and Enthalpy Changes (kJ mol^{-1}) of Mono-, Di-, and Trisubstituted *N*-[4-(4-Chlorobenzoyloxy)benzylidene]anilines[a]

Substituent(s)	K		N		I
None	.	158 (39)	[.	146 (0.4)]	.
2-Cl	.	137 (35)	[.	67[b]]	.
3-Cl	.	146 (28)	[.	71[b]]	.
4-Cl	.	146 (28)	.	256 (1.0)	.
2,3-Cl_2	.	170 (43)	[.	105[b]]	.
2,4-Cl_2	.	147 (33)	.	199 (0.6)	.
3,4-Cl_2	.	135 (36)	.	146 (0.3)	.
2,3,4-Cl_3	.	155 (34)	.	184 (0.5)	.
2-CH_3-3-Cl	.	155 (37)	[.	86 (0.4)]	.
3-Cl-4-CH_3	.	145 (38)	.	161 (0.3)	.

a) The latter quantities are in parentheses. b) The virtual transition temperature estimated by the extrapolation of the clearing point curve in the binary system with 4,4'-azoxyldianisole.

point given by the 3-chloro-4-methyl derivative is lower than that of the 3,4-dichloro derivative.

Table 4 summarizes the effect of chloro substitution on the mesomorphic behavior of compounds with X=Cl. These compounds are unique in the sense that all the substituents are chlorine atoms. This situation is reflected by some irregularities in the thermal behavior. Compared with the compound listed in Table 3, the clearing point of the parent compound is higher by 22 °C. In contrast, the mesophase of the 3,4-dichloro derivative in the present series is transformed into an isotropic liquid at a temperature lower by 9 °C and that of the 2,3,4-trichloro derivative by 6 °C. The clearing point exhibited by the remaining two, the 4-chloro and 2,4-dichloro derivatives, is almost the same as that of the corresponding methyl compound. Thus, the compounds carrying only chloro substituents do not seem follow the well-known order of nematic group efficiency for terminal substituents.

The thermal stability of mesophase varies by the substitution as shown in Fig. 2b. In this series too, no mesophase is detectable for the 2-chloro, 3-chloro, and 2,3-dichloro derivatives. It seems to be reasonable to see that the clearing point of the 2,4-dichloro derivative is much higher than that of the 3,4-dichloro derivative. Therefore, the observation that the 2-chloro and 3-chloro substituents contribute nearly equally in reducing the clearing point of the parent compound looks very strange and might be ascribed to the uncertainties in the virtual clearing points of these chloro derivatives. Even so, the anomalously high thermal stabilities in the 2,3-dichloro and 2,3,4-trichloro derivatives are firmly demonstrated by this diagram.

The following general comments may be made about the results presented in this work. The terminal substituent (the substituent on the 4 position) promotes the thermal stability of mesophase irrespective of the presence of a lateral substituent, even when the latter is bonded to the neighboring carbon atom. In these cases, the effects of the terminal and lateral

substituents are roughly additive. When two lateral substituents are bonded to the neighboring carbon atoms (the 2 and 3 positions), the effects deviate greatly from the additivity rule. The second substituent is accommodated, more or less, in the space produced by the introduction of the first one; therefore, it may be possible that the enhancement of the intermolecular cohesion arising from the increased polarizability outweighs the decrease in the cohesion due to the increased intermolecular separation. If the nature of substituents is markedly different from that in the compounds studied here, the outcome may become less significant, as reported by Osman.[5]

The presence of a short-range order of the molecular positions in the nematic phase, such as the smectic C-type and one-dimensional correlation along the nematic director, has been pointed out in addition to the long-range orientational order along the director.[10,11] Furthermore, a molecule with a polar terminal substituent is known to exhibit a strong tendency to molecular association.[12] The terminal substituents employed in the present work are so different in polarity from each other that the favorable relative arrangement of the molecules in the nematic phase may not be identical. Consequently, it seems reasonable that compounds carrying X=Cl exhibit a thermal behavior somewhat anomalous compared with those carrying the other substituents.

This work was supported by a Grant-in-Aid for Scientific Research No. 60470001 from the Ministry of Education, Science and Culture.

References

1) G. W. Gray, "Liquid Crystals and Plastic Crystals," ed by G. W. Gray and P. A. Winsor, Ellis Horwood, Chichester (1974), pp. 125—136.

2) J. Byron, G. W. Gray, and B. M. Worrall, *J. Chem. Soc.*, **1965**, 3706.

3) W. R. Young, I. Haller, and D. C. Green, *J. Org. Chem.*, **23**, 3707 (1972).

4) D. G. Panse, B. V. Bapat, and B. B. Ghatge, *Indian J. Chem., Sect. B*, **21**, 66 (1982).

5) M. A. Osman, *Mol. Cryst. Liq. Cryst.*, **128**, 45 (1985).

6) J. S. Dave and G. Kurian, *Mol. Cryst. Liq. Cryst.*, **42**, 175 (1977).

7) R. A. Vora and D. N. Patel, *Mol. Cryst. Liq. Cryst.*, **103**, 127 (1983).

8) G. W. Gray and B. M. Worrall, *J. Chem. Soc.*, **1959**, 1545.

9) D. J. Byron, G. W. Gray, A. Ibbotson, and B. M. Worrall, *J. Chem. Soc.*, **1963**, 2246.

10) A. de Vries, *Mol. Cryst. Liq. Cryst.*, **10**, 219 (1970).

11) A. S. Paranjpe, K. Usha Deniz, P. S. Parvathanathan, V. Amirthalingam, and K. V. Muralidharan, *Mol. Cryst. Liq. Cryst.*, **149**, 79 (1987).

12) A. J. Leadbetter, R. M. Richardson, and C. N. Colling, *J. Phys. (Paris)*, **36**, Cl-37 (1975).

Determination of Individual Partial Molar Volumes of Ions in Water from Measurements of Ultrasonic Vibration Potentials

Nobuo TAKENAKA and Kiyoshi ARAKAWA*
Research Institute of Applied Electricity, Hokkaido University, Sapporo 060
(Received April 27, 1989)

A new apparatus for measurements of ionic vibration potentials generated by the propagation of ultrasonic waves through electrolyte solutions was constructed, and used for the determination of partial molar volumes of ions in aqueous solutions of uni-univalent electrolytes. The apparatus, based on the method of ultrasonic vibration potentials (Zana and Yeager), was improved in two points through the introduction of the Doppler effect: a small measuring cell (about 50 cm^3) and very low noises (50 nV). Then, measurements of temperature variation of ultrasonic vibration potentials have become possible. Partial molar volumes of hydrogen, alkali metal, and halide ions in water were determined in the range of temperature, 15—45 °C.

The ionic partial molar volume has turned out to be a very useful tool in elucidating the nature of ion-solvent interactions in electrolyte solutions.[1,2] For the direct experimental determination of partial molar volumes of individual ions, the method of ultrasonic vibration potentials (UVP) has been found to be the still unique experimental means available to obtain those data. The theoretical basis of the method of UVP was given by Debye,[3] and others,[4,5] formerly, and Zana and Yeager[6] constructed the experimental apparatus for the measurements of UVP in 1967.

In the apparatus used by Zana et al.[6,7] the measuring unit was, however, too large in its size and therefore measurements have been confined near room temperature only. Then, we have undertaken to improve the experimental method of UVP given first by Zana and others, especially aiming at obtaining the data at various temperatures.

Theory and Experimental Procedures

Theory. In a sound field the difference in the dynamical responses between cations and anions within an electrolyte solution produces an alternating potential (ionic vibration potential/ultrasonic vibration potential).

The forces acting on an ion (the jth type) within the solution are expressed as follows,[3,6]

$$e_jE - \mu_j(u_j - u_0) + d_0v_j\frac{\partial u_0}{\partial t} = m_j\frac{\partial u_j}{\partial t}. \quad (1)$$

m_j, e_j, v_j, and u_j, is the mass, the charge, the volume, and the velocity of the ion, respectively. μ_j is the frictional coefficient acting on the ion, d_0 and u_0 the density and the velocity of the solvent molecule, E the strength of the field, and t time.

The Poisson equation is

$$\varepsilon\frac{\partial E}{\partial x} = \Sigma n_je_j, \quad (2)$$

where ε is the permittivity of the medium, n_j the number density of the jth ions, and x the coordinate (the propagation distance of the sound wave), and the equation of continuity becomes

$$\frac{\partial n_j}{\partial t} + \frac{\partial(n_ju_j)}{\partial x} = 0. \quad (3)$$

The velocity of the ion and solvent in the sound field is expressed as

$$u_j = a_je^{i(\omega t - kx)}, \quad (4a)$$

$$u_0 = a_0e^{i(\omega t - kx)}, \quad (4b)$$

where ω and k is the angular frequency and the propagation constant of the sound wave, and $k=\omega/c$ (c; sound velocity). Here, we define α_j as

$$\alpha_j = \frac{a_jm_j - a_0d_0v_j}{m_j - d_0v_j} = \frac{a_jm_j - a_0d_0v_j}{w_j}, \quad (5)$$

and the UVP becomes

$$\Phi = -\int E\mathrm{d}x = \Phi_0e^{i(\omega t - kx)}. \quad (6)$$

In the following we treat the case of solutions of uni-univalent electrolyte, where suffixes 1 and 2 denote cations and anions, respectively. Then we can derive the equation of UVP from Eqs. 1—6[6]

$$\Phi_0F = c(\alpha_1W_1t_1 - \alpha_2W_2t_2)f(\omega), \quad (7)$$

and

$$f(\omega) = (\sigma/\varepsilon\omega)/[1 + (\sigma/\varepsilon\omega)^2]^{1/2},$$

where F is the Faraday constant, σ the electrolytic conductivity, and t_i (i=1,2) the transport number at the concentration. When the concentration is not so extremly dilute and the sound frequency is not so high, $f(\omega)$ is safely regarded as $f(\omega)=1$[3] and the factor in Eq. 7 can be eliminated. In Eq. 7 W_i (i=1,2) originally defined in Eq. 5 is expressed as molar quantities.

Here, according to Zana et al.,[6] we use following notations with respect to the molar mass of solvated ions,

$$M_i = M_{i0} + M_{iw}, \quad i = 1, 2, \quad (8)$$

where M_{i0} is the molar mass of bare ions and M_{iw} that of solvents solvated to ions. Then, apparent molar volumes of ions φ_i are

$$\varphi_i = V_i - M_{iw}/d_0, \quad i = 1, 2, \tag{9}$$

and the apparent molar volume of the salts φ is

$$\varphi = \varphi_1 + \varphi_2.$$

From Eqs. 7, 8, and 9,

$$\varphi_1 = \frac{1}{d_0(\alpha_1 t_1 + \alpha_2 t_2)} \times [\alpha_1 t_1 M_{10} - \alpha_2 t_2 M_{20} + d_0 \alpha_2 t_2 \varphi - \frac{\Phi_0 F}{c}], \tag{10a}$$

$$\varphi_2 = \frac{1}{d_0(\alpha_1 t_1 + \alpha_2 t_2)} \times [\alpha_2 t_2 M_{20} - \alpha_1 t_1 M_{10} + d_0 \alpha_1 t_1 \varphi + \frac{\Phi_0 F}{c}]. \tag{10b}$$

At this step, if we take for

$$\alpha_1 = \alpha_2 = a_0 \quad (\text{this means } a_1 = a_2 = a_0), \tag{11}$$

Eqs. 10 become

$$\varphi_1 = \frac{1}{d_0}(t_1 M_{10} - t_2 M_{20}) + t_2 \varphi - \frac{\Phi_0 F}{a_0 d_0 c}, \tag{12a}$$

$$\varphi_2 = \frac{1}{d_0}(t_2 M_{20} - t_1 M_{10}) + t_1 \varphi + \frac{\Phi_0 F}{a_0 d_0 c}. \tag{12b}$$

Eqs. 12a and 12b are quite identical with those given and used by Zana et al.[6,7] The introduction of the assumption, Eq. 11, means an approximation that, in the derivation of Eqs. 12, the factor $\partial u_j/\partial t$ in the right hand side of Eq. 1 is replaced by $\partial u_0/\partial t$ at this step. Then we adopt here another approximation instead of Eq. 11 as follows,

$$\alpha_1 = \alpha_2 = \alpha \quad (\neq a_0). \tag{13}$$

Using Eq. 13, Eqs. 10a and 10b become respectively

$$\varphi_1 = \frac{1}{d_0}(t_1 M_{10} - t_2 M_{20}) + t_2 \varphi - \frac{\Phi_0 F}{\alpha d_0 c}, \tag{14a}$$

$$\varphi_2 = \frac{1}{d_0}(t_2 M_{20} - t_1 M_{10}) + t_1 \varphi + \frac{\Phi_0 F}{\alpha d_0 c}. \tag{14b}$$

We use Eqs. 14a and 14b here instead of Eqs. 12a and 12b. That is, we measure Φ_0 for two electrolyte solutions containing common ions, for example, NaCl and LiCl, at the same concentration and from the two values of Φ_0, using Eqs. 14a and 14b, we can determine the magnitudes of φ_{Na^+}, φ_{Li^+}, φ_{Cl^-}, and α.

Apparatus and Experimental Procedures. The block diagram of the apparatus constructed is shown in Fig. 1. A 1 MHz ultrasonic wave is propagated in the cell through a transducer by excitation from the 1 MHz oscillator, and the UVP is produced within the sample solution. The detector consists of two iridium needles (0.127 mm ϕ) held parallel. In order to detect the UVP, it is rotated in the sample and fixed at an angle where the distance between two needles along the sound wave becomes $\lambda/2$ (λ: the wavelength of the sound wave), and then, as the result of the Doppler effect of the ultrasonic wave by moving the cell back and forth with a constant velocity of $10^{-6}c$, the UVP of $2\Phi_0$ (frequency 1 M±1 Hz) is produced in the sample and detected between two needles.

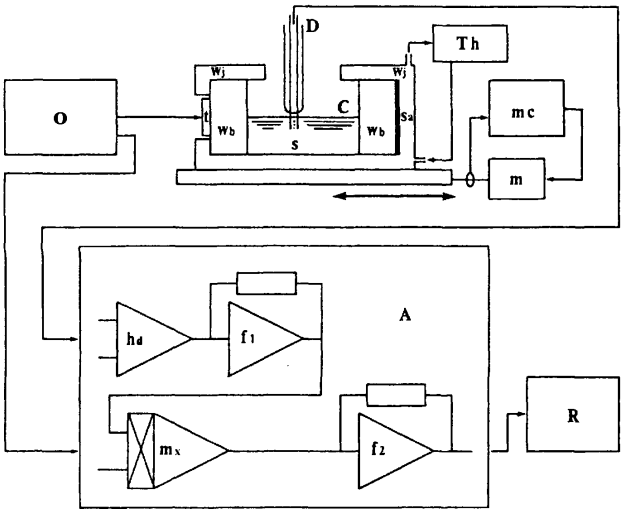

Fig. 1. Block diagram of the apparatus. O: oscillator, C: cell; t transducer (20 mmϕ, ceramics), s sample, w_b buffer (water), s_a sound absorber (butyl rubber), w_j water jacket, m motor, mc motor controller, D: detector, A: amplifier; h_d high input impedance differential amplifier, m_x mixer, f_1 bandpass filter (1 MHz), f_2 bandpass filter (1 Hz), R: recorder, T_h: thermostat.

In the detecting device circuit, the UVP, via a high input impedance amplifier, is mixed with a direct output from the oscillator, and then, is converted to a 1 Hz wave and 2 M±1 Hz wave, where the leakage from power sources is converted to a non-alternating current drift and 2 MHz wave. These all waves are lead to a bandpass filter with a central frequency of 1 Hz, and we can easily take out the 1 Hz component only from the UVP. This 1 Hz component is recorded by a recorder of ordinary type, where the total gain of 5000 is required in the amplification device on the whole.

In the device described above, a part of the differential amplifier with high input impedance is shown in Fig. 2.

A typical pattern of UVP recorded for a solution of NaI is shown in Fig. 3. The wave shows the UVP after frequency conversion to 1 Hz. The straight broken line in the figure shows the position of the cell in its movement: the point (a) denotes the starting point and the point (b) the end point. If the cell comes to the end of the path, the cell is stopped and the UVP vanishes. The UVP pattern at the right half in Fig. 3, shows that

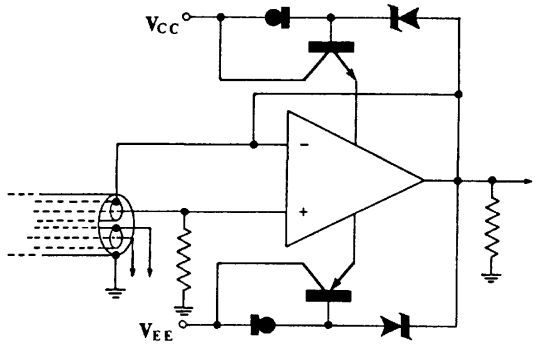

Fig. 2. A part of high input impedance differential amplifier. The amplifier made by a combination of bootstrap and driven shield circuit.

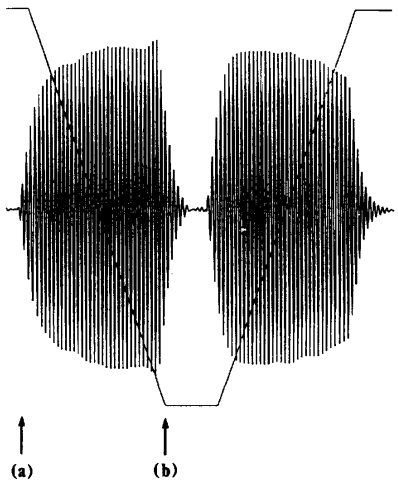

Fig. 3. Typical pattern of UVP recorded (NaI, 0.01 mol dm^{-3}).

on the backward shift of the cell.

The noise level in our device is below 50 nV. This noise level is of the order of 1/100, or so, of that observed in the apparatus used by Zana and Yeager.[6,7]

Results and Discussion

We have chosen a pair of salts, LiCl and NaCl, as a standard pair of samples to be measured in the present experiment according to the theoretical procedure using Eqs. 14a and 14b. In applying the procedure, the effectiveness of the approximation, Eq. 13, must be taken into consideration. Too large values of Φ_0 are supposed to violate the approximation. Then, the magnitude of Φ_0 should be not too large. The pair of LiCl and NaCl fits the condition in addition to the merit that the Φ_0 for the pair is determined with high accuracy.

We measured the magnitudes of UVP, Φ_0, for the NaCl solution as well as for the LiCl solution at the same concentrations, and determined the values of φ_{Na^+}, φ_{Li^+}, φ_{Cl^-}, and Φ_0/α. The observed values of Φ_0 at 15—45 °C are given in Table 1. The accuracy of those at $C>0.1$ mol dm^{-3}, is found to be smaller than ±5%. The magnitudes of Φ_0 and Φ_0/α at 25 °C are shown in Fig. 4. The increasing trend of UVP with decrease of concentration at low concentrations, $C\leqq 0.1$ mol dm^{-3}, is clearly seen in the figure, which was pointed out by Hunter et al.[8,9] previously. Then for the analysis below, we used the data at $C>0.1$ mol dm^{-3}, where, with respect to the transport number of ions and the apparent molar volume of salts, literature values were used.[10–15] The literature values of transport numbers and apparent molar volumes are shown in Table 2.

The values of φ_{Li^+}, φ_{Na^+}, φ_{Cl^-}, and α obtained at 25 °C are given in Table 3. The magnitudes of φ_{Na^+}, at

Table 1. Observed UVP

Solute	θ/°C	$\lvert 2\Phi_0\rvert$/μV								
		C/mol dm^{-3}								
		0.01	0.05	0.10	0.125	0.15	0.175	0.20	0.225	0.25
LiCl	15	4.1$_8$	3.1$_0$	2.5$_0$	2.4$_5$	2.4$_5$	2.4$_8$	2.5$_0$	2.5$_3$	2.5$_5$
	25	4.3$_9$	4.3$_2$	2.6$_6$	2.6$_6$	2.6$_7$	2.6$_9$	2.6$_9$	2.7$_1$	2.7$_4$
	35	4.9$_0$	3.6$_7$	2.9$_5$	2.7$_4$	2.7$_6$	2.8$_2$	2.8$_5$	2.8$_7$	2.9$_3$
	45	4.8$_2$	3.6$_7$	3.0$_2$	3.0$_5$	3.1$_0$	3.1$_5$	3.1$_7$	3.2$_0$	3.2$_5$
NaCl	15	2.5$_9$	1.9$_4$	1.8$_0$	1.8$_0$	1.7$_8$	1.7$_7$	1.7$_6$	1.7$_5$	1.7$_4$
	25	2.6$_6$	2.2$_3$	2.0$_3$	2.0$_2$	1.9$_8$	1.9$_6$	1.9$_4$	1.9$_3$	1.9$_2$
	35	2.6$_6$	2.3$_0$	2.0$_9$	2.0$_8$	2.0$_8$	2.0$_7$	2.0$_6$	2.0$_5$	2.0$_6$
	45	3.1$_0$	2.5$_2$	2.3$_4$	2.3$_4$	2.3$_3$	2.3$_2$	2.3$_2$	2.3$_0$	2.3$_1$

Table 2. Values of Transport Numbers and Apparent Molar Volumes at 25 °C

	C/mol dm^{-3}	0.125	0.15	0.175	0.20	0.225	0.25	Ref.
LiCl	t^+	0.305	0.302	0.300	0.298	0.296	0.294	10, 15
NaCl	t^+	0.379	0.377	0.376	0.374	0.373	0.372	10
LiCl	φ_{LiCl}/cm^3 mol^{-1}	17.53	17.58	17.63	17.67	17.72	17.76	13
NaCl	φ_{NaCl}/cm^3 mol^{-1}	17.29	17.36	17.42	17.47	17.52	17.57	13, 14

Table 3. Apparent Molar Volumes of Ions at 25°C

C/mol dm^{-3}	0	0.125	0.15	0.175	0.20	0.225	0.25
φ_{Cl^-}/cm^3 mol^{-1}	22.9±0.3	23.4±0.2	23.4±0.2	23.5±0.2	23.5±0.2	23.6±0.2	23.6±0.2
φ_{Li^+}/cm^3 mol^{-1}	−6.0±0.3	−5.8±0.2	−5.8±0.2	−5.8±0.2	−5.8±0.2	−5.8±0.2	−5.8±0.2
φ_{Na^+}/cm^3 mol^{-1}	−6.3±0.3	−6.1±0.2	−6.1±0.2	−6.0±0.2	−6.0±0.2	−6.0±0.2	−6.0±0.2
α/cm s^{-1}		1.88	1.87	1.87	1.87	1.88	1.89

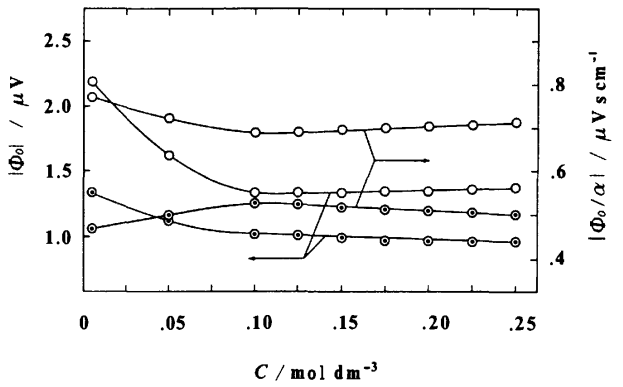

Fig. 4. Concentration dependence of $|\Phi_0|$ and $|\Phi_0/\alpha|$ at 25°C. ⊙: NaCl, O: LiCl.

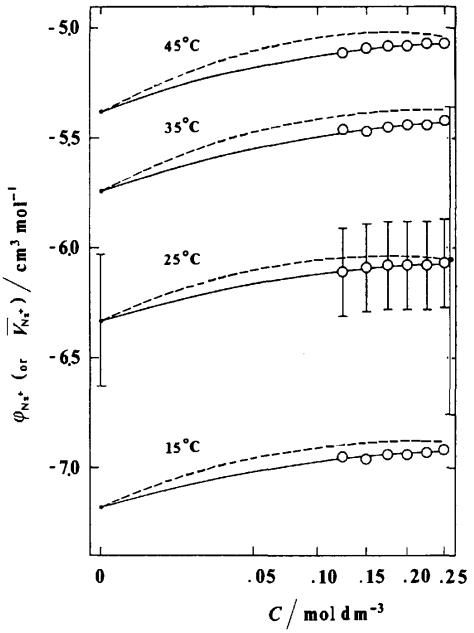

Fig. 5. Concentration dependence of φ_{Na^+} at various temperatures. O: observed, —: best fitted by the formula (15), ------: $\overline{V}_{Na^+}$ calculated by the formula in Ref. 2; $\overline{V}_{Na^+}=\varphi^0_{Na^+}+(3/2)A\sqrt{C}+BC$.

various temperatures are given as circles in Fig. 5, where the thin solid lines and dashed lines represent the values determined according to the best-fit procedure with the following formula[2] and those of the partial molar volumes obtained.

$$\varphi_{Na^+} = \varphi^0_{Na^+} + \frac{A}{2}\sqrt{C} + BC, \qquad (15a)$$

Table 4. Comparison of Values for Partial Molar Volumes at Infinite Dilution at 25°C

Ions	$\overline{V}^0_{ion}$/cm^3 mol^{-1}		
	This work	Zana-Yeager	Hirakawa
H^+	−5.0±0.3	−5.4±0.2	(−6.26—−0.32)
Li^+	−6.0±0.3	−11.2±1.2	(−13.02—−1.29)
Na^+	−6.3±0.3	−7.4±1.9	(−9.46—−1.45)
K^+	3.9±0.3	3.4±0.6	(3.56— 9.23)
Rb^+	9.0±0.3	9.0±0.7	(7.50— 17.0)
Cs^+	16.2±0.3	15.5±0.3	(10.25— 24.90)
F^-	3.9±0.3	3.3±1.0	(−4.47— 4.05)
Cl^-	22.9±0.3	23.7±1.2	(14.0 — 23.21)
Br^-	29.8±0.3	30.2±0.2	(17.68— 30.13)
I^-	41.1±0.5	41.4±0.9	(33.47— 40.95)

$$A = F^2 e \frac{10^2}{2\pi}\left(\frac{1}{20\varepsilon RT}\right)^{1/2}\left(\frac{\partial \ln\varepsilon}{\partial p} - \frac{\beta}{3}\right), \qquad (15b)$$

where A is the Debye-Hückel constant, B the material constant, β the isothermal compressibility.

The accuracy of each quantity is ±0.2, ±0.3, ±0.7** cm^3 mol^{-1} for φ_{ion}, φ^0_{ion} ($\equiv\overline{V}^0_{ion}$), and $\overline{V}_{ion}$ respectively.

The magnitudes of $\overline{V}^0_{Li^+}$, $\overline{V}^0_{Na^+}$, and $\overline{V}^0_{Cl^-}$ thus determined as well as those for other ions obtained from the values and $\overline{V}^0$ (partial molar volume of salts at infinite dilution) are given in Table 4, together with those of Zana-Yeager and Hirakawa[16] for comparison. Hirakawa constructed an apparatus for the measurement of the sedimentation potential in ionic solutions and obtained individual ionic partial molar volumes. The method of the sedimentation potential is essentially identical with the method of ultrasonic vibration potentials in principle, though vibration frequency is 100 Hz.[16]

As seen in Table 4, the values of the present work are found to be coincided with those of Zana and Yeager within the deviation of 1 cm^3 mol^{-1}, except for the case of Li^+. In the case of $\overline{V}^0_{Li^+}$, the absolute magnitudes of the values are found to deviate each other. Zana-Yeager's value of $|\overline{V}^0_{Li^+}|$ is clearly too large, being taken into consideration of the fact that in the case of the values of $\overline{V}^0_{Cl^-}$ as a counter ion, those of ours and Zana-Yeager's coincide within experimental errors. In Table 5, the present data are compared with the values calculated by the empirical formula of Mukerjee[17] and

** The accuracy of $\overline{V}_{ion}$ depends on the concentration. This value is that at C=0.25 mol dm^{-3}.

Table 5. Comparison of Values for Partial Molar Volumes with those from Empirical Formula

Ions	$\bar{V}^0_{ion}$/cm^3 mol^{-1}		
	This work	Mukerjee	Conway et al.
H^+	−5.0	−4.5	−6.0
Li^+	−6.0	−5.2	−6.9
Na^+	−6.3	−5.7	−7.3
K^+	3.9	4.5	2.9
Rb^+	9.0	9.5	8.1
Cs^+	16.2	16.9	15.2
F^-	3.9	2.1	4.8
Cl^-	22.9	22.3	23.9
Br^-	29.8	29.2	30.9
I^-	41.1	40.8	42.2

Table 6. Partial Molar Volumes of Ions at Infinite Dilution at Various Temperature

Ions	$\bar{V}^0_{ion}$/cm^3 mol^{-1}			
	15°C	25°C	35°C	45°C
H^+	−5.3	−5.0	−4.7	−4.6
Li^+	−6.1	−6.0	−6.1	−6.1
Na^+	−7.2	−6.3	−5.7	−5.4
K^+	3.2	3.9	4.3	4.5
Rb^+	8.2	9.0	9.4	9.8
Cs^+	15.2	16.2	16.8	17.3
Cl^-	22.8	22.9	23.0	23.0
Br^-	29.7	29.8	30.3	30.4
I^-	40.7	41.1	42.0	42.4

that of Conway et al.[18] The coincidence is fairly good on the whole.

Concerning the temperature dependence of partial molar volumes of ions at infinite dilution, the values for univalent ions at various temperatures are given in Table 6, where the accuracy of those is ±0.3 cm^3 mol^{-1} throughout all the temperature range observed. As seen in the table, the values for alkali metal ions except for Li^+ are clearly observed to increase with increasing temperature as well as those for H^+, while those for Li^+ and Cl^- are held to be nearly constant in this temperature range. For other halide ions, Br^- and I^-, the values increase very slowly with increase of temperature.

References

1) H. L. Friedman and C. V. Krishnan, "Water," ed by F. Franks, Plenum Press, New York (1973), Vol. 3, Chap. 1.
2) F. J. Millero, "Water and Aqueous Solutions," ed by R. A. Horne, Wiley-Interscience, New York (1972), Chap. 13.
3) P. Debye, *J. Chem. Phys.*, **1**, 13 (1933).
4) J. J. Hermans, *Philos. Mag.*, [7] **25**, 426; [7] **26**, 674 (1938).
5) J. Bugosh, E. Yeager, and F. Hovorka, *J. Chem. Phys.*, **15**, 592 (1947).
6) R. Zana and E. Yeager, *J. Phys. Chem.*, **71**, 521 (1967).
7) R. Zana, G. A. Lage, and C. M. Criss, *J. Soln. Chem.*, **9**, 667 (1980).
8) A. N. Hunter, *Proc. Phys. Soc., (London)*, **71**, 847 (1958).
9) A. N. Hunter and T. B. Jones, *Proc. Phys. Soc., (London)*, **80**, 795 (1962).
10) H. S. Harned and B. B. Owen, "The Physical Chemistry of Electrolytic Solutions," Reinhold Book Corp. New York (1958), Chap. 6.
11) F. J. Millero, "Water and Aqueous Solutions," ed by R. A. Horne, Wiley-Interscience, New York (1972), Addendum to Chap. 13.
12) L. A. Dunn, *Trans. Faraday Soc.*, **64**, 1898; 2951 (1968).
13) J. E. Desnoyers, M. Arel, G. Perron, and C. Jolicoeur, *J. Phys. Chem.*, **73**, 3346 (1969).
14) F. J. Millero, *J. Phys. Chem.*, **74**, 356 (1970).
15) T. Isono, *Rikagaku Kenkyusho Hokoku*, **56**, 103 (1980).
16) H. Hirakawa, *J. Phys. Chem.*, **91**, 3452 (1987).
17) P. Mukerjee, *J. Phys. Chem.*, **65**, 740; 744 (1961).
18) B. E. Conway, R. E. Verrall, and J. E. Desnoyers, *Trans. Faraday Soc.*, **62**, 2738 (1966).

 © 1989 The Chemical Society of Japan Bull. Chem. Soc. Jpn., 62, 2885—2889 (1989)

Solvent Extraction of Uni- and Bivalent Metal Picrates with 16-Crown-5 into Benzene

Yasuyuki TAKEDA,* Tokutaro KIMURA, Yoshihiro KUDO, Hiroaki MATSUDA, Yoshihisa INOUE,† and Tadao HAKUSHI††

Department of Chemistry, Faculty of Science, Chiba University, Yayoi-cho, Chiba 260
†Basic Research Laboratory, Himeji Institute of Technology, 2167 Shosha, Himeji, Hyogo 671-22
††Department of Applied Chemistry, Himeji Institute of Technology, 2167 Shosha, Himeji, Hyogo 671-22

(Received April 22, 1989)

Distribution constant ($K_{D,L}$) of 16-crown-5 (16C5) and overall extraction equilibrium constants (K_{ex}) of uni- and bivalent metal picrates with 16C5 were determined between benzene and water at 25 °C. The K_{ex} values were analyzed by four fundamental equilibria, extraction constant of picric acid, $K_{D,L}$, formation constant in water and ion-pair extraction constant ($K_{ex,ip}$) with a picrate ion of the 16C5-metal ion complex. The K_{ex} value of 16C5 for the uni- and bivalent metal ions decreases in the order $Ag^+ > Na^+ > Tl^+ > K^+ > Rb^+ > Cs^+ > Li^+$ and $Pb^{2+} > Ba^{2+} \geq Sr^{2+} > Ca^{2+}$, respectively. Size-fit relationship holds for extraction-selectivity of 16C5 toward alkali metal ions, but it does not hold for that toward alkaline earth metal ions. Factors influencing extractability and extraction-selectivity of 16C5 for metal ions were discussed from the viewpoint of molecular grounds. $K_{ex,ip}$ value of 16C5 varies with a cation of the same charge held in the cavity. $K_{ex,ip}$ values of 16C5-metal picrate complexes were compared with those of 15-crown-5-metal picrate complexes. Various effects on ion-pair extractability of a 16C5-metal ion complex with a picrate anion were explained.

16-Crown-5 (16C5) and 15-crown-5 (15C5) have the same number of donor oxygen atoms. However, 15C5 has a symmetrical structure, whereas 16C5 has a less symmetrical structure, which is caused by an introduction of an extra methylene group into the 15C5 ring. It has been reported that 16C5 shows much higher selectivity for Na^+ among alkali metal ions than 15C5 in both homogeneous[1] and liquid-liquid extraction systems.[2] The higher selectivity of 16C5 for Na^+ was explained in terms of cavity size and orientation of the donor oxygen atoms through examination of CPK molecular models; namely, Na^+ is better accommodated in the cavity of 16C5 than in the cavity of 15C5, and the donor oxygen atoms of 16C5 arrange more nicely around Na^+ compared with 15C5.

In this study, in order to clarify the role of 16C5 in the metal ion-extraction process, overall extraction equilibrium constants of uni- and bivalent metal picrates with 16C5 were determined between benzene and water at 25 °C and analyzed by four constituent equilibria. The data on 16C5 were compared in detail with those of 15C5.

Experimental

Materials. The preparation of 16C5 was just the same as that described in the previous paper.[2a] Benzene, picric acid, $LiOH \cdot H_2O$, NaOH, KOH, $AgNO_3$, $TlNO_3$, $Mg(NO_3)_2 \cdot 6H_2O$, $Ca(NO_3)_2 \cdot 4H_2O$, $Sr(OH)_2 \cdot 8H_2O$, $Ba(OH)_2 \cdot 8H_2O$, and $Pb(NO_3)_2$ were analytical-grade reagents. Rubidium and caesium hydroxides were reagent-grade. Benzene was washed three times with distilled water. The purities of $AgNO_3$ and the other nitrates were determined by KCl and EDTA titrations, respectively. The concentrations of solutions of the hydroxides and picric acid were determined by neutralization titration.

The experimental procedures were almost the same as those described in previous papers.[3,4] Extractions were conducted at 25±0.2 °C. Concentrations of 16C5, metal salts, and picric acid were 2.8×10^{-5}—7.9×10^{-2} M (1 M= 1 mol dm^{-3}), 4.1×10^{-3}—1.8×10^{-1} M, and 3.3×10^{-3}—1.1×10^{-2} M, respectively. For nitrate and Cs systems, the extractions were carried out at pH 2.2—2.9. For all the other systems, the extractions were performed at pH 6.8—12.1.§ Concentrations of extracted Li, Na, K, Sr, and Ba were determined by a UV-spectrophotometer; those of extracted Rb, Cs, Ag, Tl, Ca, and Pb were determined by an atomic absorption spectrophotometer. It was impossible to extract any Mg into the benzene phase.

The Distribution Coefficient of 16C5. A 13 ml benzene solution of 16C5 (2.6×10^{-5}—1.5×10^{-3} M) and an equal volume of distilled water in a stoppered glass tube (volume 30 ml) were shaken in a thermostated water bath at 25± 0.2 °C for 2 h and centrifuged. A portion 12 ml of the benzene phase and an equal volume of an aqueous solution (pH 10.7—11.3) containing NaOH (1.1×10^{-1} M) and picric acid (1.0×10^{-1} M) were placed in a stoppered glass tube (No. 1), agitated, and centrifuged. A portion ($12-2n$) ml of the aqueous phase in the stoppered glass tube (No. n) and an equal volume of benzene were placed in a stoppered glass tube (No. $(n+1)$), shaken, and centrifuged. This procedure was repeated until $n=4$. The picrate in the benzene phase in the stoppered glass tube (No. n) was back-extracted into ($12-2n$) ml of 0.01 M NaOH aqueous solution (volume ratio 1:1), and the picrate concentration was determined spectrophotometrically ($\lambda_{max}=356$ nm, $\varepsilon=1.45\times10^4$ cm^{-1} M^{-1}). This procedure was repeated until $n=5$. The total concentration of the extracted 16C5-sodium picrate complex in a series of these extractions was calculated. The total concentration of the extracted 16C5 complex was assumed to be equal to the concentration of 16C5 which distributed itself into the 13 ml benzene phase. The distribution coefficient value of 16C5 is 0.397±0.004, which is the average of 22 measurements.

Results

In an equilibrium between a benzene solution of a

§ These experiments were designed to study extraction of a 1:1 16C5:metal ion complex with a picrate ion.

crown ether (L) and an aqueous solution of a metal ion (M^{m+}) and a picrate ion (A^-), the equilibrium constants are defined as

$$K_{ex} = [MLA_m]_o[H^+]^m/[M^{m+}][L]_o[HA]_o^m, \quad (1)$$

$$K_{D,L} = [L]_o/[L], \quad (2)$$

$$K_{ex}(HA) = [HA]_o/[H^+][A^-], \quad (3)$$

$$K_{ML} = [ML^{m+}]/[M^{m+}][L], \quad (4)$$

$$K_{ex,ip} = [MLA_m]_o/[ML^{m+}][A^-]^m, \quad (5)$$

where the subscript "o" and the lack of subscript denote the organic and the aqueous phase, respectively. The overall extraction equilibrium constant (K_{ex}) can be written as

$$K_{ex} = K_{ML}K_{ex,ip}K_{D,L}^{-1}K_{ex}(HA)^{-m}. \quad (6)$$

The distribution ratio of the metal is represented by

$$D = [MLA_m]_o/([M^{m+}] + [ML^{m+}]). \quad (7)$$

In the case of $[M^{m+}] \gg [ML^{m+}]$, Eq. 7 is transformed into

$$D = K_{ex}K_{ex}(HA)^m[L]_o[A^-]^m. \quad (8)$$

For the univalent metal ion system, $\log(D/[A^-])$ vs. $\log[L]_o$ plot in Fig. 1 shows a straight line with a slope of 1 in every case. This indicates that 16C5 forms a 1:1 complex with the univalent metal ion. For the bivalent metal ion system, $\log(D/[A^-]^2)$ vs. $\log[L]_o$ plot in Fig. 2 always shows a line with a slope of 1. This indicates that 16C5 forms a 1:1 complex with the bivalent metal ion.

From the mass balances, $[L]_o$, $[M^{m+}]$, and $[HA]_o$ are given by

$$[L]_o = ([L]_t - [MLA_m]_o)/(\alpha + \beta[M^{m+}]), \quad (9)$$

$$[M^{m+}] = ([M]_t - [MLA_m]_o)/(1 + \beta[L]_o), \quad (10)$$

$$[HA]_o = ([HA]_t - m[MLA_m]_o)/\{1 + ([H^+]^{-1} + K_{HA})K_{ex}(HA)^{-1}\}, \quad (11)$$

where the subscript "t" denotes the total concentration, $\alpha = 1 + K_{D,L}^{-1}$, and $\beta = K_{ML}K_{D,L}^{-1}$. For all the systems except for the cases of Li^+, Rb^+, Cs^+, and Ca^{2+}, K_{ex} values were determined by using $[L]_o$ values of Eq. 9, $[M^{m+}]$ values of Eq. 10, and $[HA]_o$ values of Eq. 11; for the Li^+, Rb^+, Cs^+, and Ca^{2+} systems, K_{ex} values were determined, neglecting the terms, $\beta[M^{m+}]$ of Eq. 9 and $\beta[L]_o$ of Eq. 10. Values of $K_{ex}(HA)$ and K_{HA} at 25 °C are 247[3] and 1.9$_5$,[5] respectively, where K_{HA} is an association constant of picric acid in water and $K_{HA} = [HA]/[H^+][A^-]$. Equilibrium constants are summarized in Table 1.

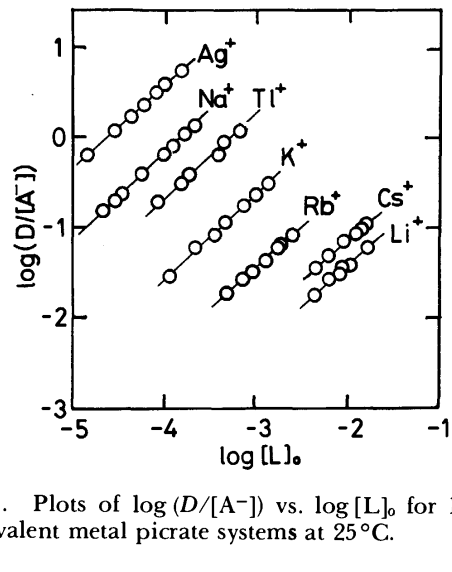

Fig. 1. Plots of $\log(D/[A^-])$ vs. $\log[L]_o$ for 16C5–univalent metal picrate systems at 25 °C.

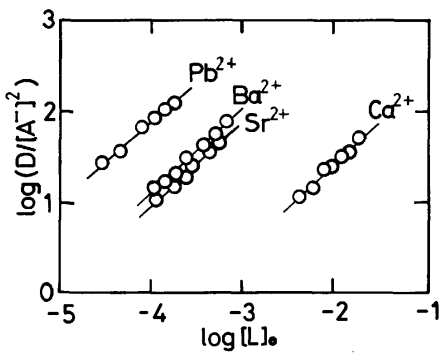

Fig. 2. Plots of $\log(D/[A^-]^2)$ vs. $\log[L]_o$ for 16C5–bivalent metal picrate systems at 25 °C.

Discussion

$\log K_{D,L}$ values at 25 °C of 12-crown-4 (12C4), 15C5, and 18-crown-6 (18C6) between benzene and water are −0.82,[8] -0.80_6,[3,4] and -1.19_8,[3,4] respectively. From $\log K_{D,L}$ values of 12C4, 15C5, 18C6, and 16C5, the contribution of an ether oxygen atom to $\log K_{D,L}$ (Π_o) at 25 °C between benzene and water can be evaluated by using the Π_{CH_2} value (0.48_5[9]), where Π_{CH_2} is the contribution of a methylene group to extraction constants of ion pairs of tetraalkylammonium ions with picrate anions at 25 °C between benzene and water; namely, $\Pi_o = (\log K_{D,L} - \Pi_{CH_2} \times a)/b$, a and b denoting the number of methylene groups and ether oxygen atoms, respectively. Π_o values are −1.17, -1.13_1, -1.16_9, and −1.147 for 12C4, 15C5, 18C6, and 16C5, respectively. They are nearly equal. The Π_o value is −1.15 on the average. From these empirical parameters, the $\log K_{D,L}$ value of 16C5 at 25 °C between benzene and water can be estimated to be -0.41_5. This is in accord with the experimental $\log K_{D,L}$ value of 16C5 (-0.401 ± 0.004).

The difference in $\log K_{D,L}$ values between 16C5 and

Table 1. Summary of Equilibrium Constants at 25 °C

Crown ether	$\log K_{D,L}$	Cation	Ionic radius (Å)[a]	$\log K_{ex}$	$\log K_{ML}$	$\log K_{ex,ip}$
16C5	−0.401±0.004	Li^+	0.74	−1.74±0.02	—	—
		Na^+	1.02	1.474±0.005	0.78[6]	2.68
		K^+	1.38	0.041±0.009	0.4[6]	1.63
		Rb^+	1.49	−0.84±0.01	—	—
		Cs^+	1.70	−1.49±0.03	—	—
		Ag^+	1.15	2.235±0.009	1.10[6]	3.13
		Tl^+	1.50	0.96±0.02	0.73[6]	2.22
		Ca^{2+}	1.00	−1.26±0.06	—	—
		Sr^{2+}	1.13	0.00±0.03	2.08[6]	2.61
		Ba^{2+}	1.36	0.07±0.02	1.84[6]	2.92
		Pb^{2+}	1.19	1.16±0.03	0.74[6]	4.81
15C5	−0.80[3,4]	Li^+		−1.10[4]	—	—
		Na^+		1.51[4]	0.70[7]	2.40[4]
		K^+		0.19[4]	0.74[7]	1.04[4]
		Rb^+		−0.25[4]	0.62[7]	0.72[4]
		Cs^+		−0.49[4]	0.8[7]	0.30[4]
		Ag^+		2.06[4]	0.94[7]	2.71[4]
		Tl^+		1.41[4]	1.23[7]	1.77[4]
		Ca^{2+}		−1.07[3]	—	—
		Sr^{2+}		0.91[3]	1.95[7]	2.94[3]
		Ba^{2+}		0.41[3]	1.71[7]	2.68[3]
		Pb^{2+}		1.67[3]	1.85[7]	3.80[3]

a) R. D. Shannon and C. T. Prewitt, *Acta Crystallogr., Sect. B*, **25**, 925 (1969).

15C5 corresponds to Π_{CH_2}. It is interesting that the difference (0.40[5]) between the two neutral crown ethers is consistent with the Π_{CH_2} value (0.48[5]) determined by ion-pair extraction constants of tetraalkylammonium picrates.

Table 1 shows that $\log K_{ex}$ value of 16C5 for the univalent metal ions decreases in the order $Ag^+>Na^+>Tl^+>K^+>Rb^+>Cs^+>Li^+$. This indicates that, for the alkali metal ions, the more closely the metal ion fits into the 16C5 cavity (cavity radius 0.9 Å[1]), the more extractable the 16C5-metal ion complex is (size-fit concept); Ag^+, which has a more favorable size for the 16C5 cavity than Tl^+, is more extractable with 16C5 than Tl^+. The $\log K_{ex}$-value sequence of 16C5 for the univalent metal ions is identical with that of 15C5. However, 16C5 shows higher extraction selectivity for Ag^+ and Na^+ than for the other univalent metal ions, compared with 15C5; furthermore, extraction selectivity of 16C5 is higher for Ag^+ than for Na^+, compared with 15C5. For univalent metals M_1 and M_2, and crown ethers L_1 and L_2, $\Delta(\Delta\log K_{ex}(M_1-M_2))(L_1-L_2)$, $\Delta(\Delta\log K_{ML}(M_1-M_2))(L_1-L_2)$, and $\Delta(\Delta\log K_{ex,ip}(M_1-M_2))(L_1-L_2)$ are defined as follows; $\Delta(\Delta\log K_{ex}(M_1-M_2))(L_1-L_2)=(\Delta\log K_{ex}(M_1-M_2))_{L_1}-(\Delta\log K_{ex}(M_1-M_2))_{L_2}$, where $(\Delta\log K_{ex}(M_1-M_2))_L=(\log K_{ex}(M_1))_L-(\log K_{ex}(M_2))_L=(\Delta\log K_{ML}(M_1-M_2))_L+(\Delta\log K_{ex,ip}(M_1-M_2))_L$, where $(\Delta\log K_{ML}(M_1-M_2))_L=\log K_{M_1L}-\log K_{M_2L}$ and $(\Delta\log K_{ex,ip}(M_1-M_2))_L=(\log K_{ex,ip}(M_1))_L-(\log K_{ex,ip}(M_2))_L$, where $(\log K_{ex}(M))_L$ and $(\log K_{ex,ip}(M))_L$ are $\log K_{ex}$ and $\log K_{ex,ip}$ of a L-MA complex, respectively. $\Delta(\Delta\log K_{ML}(M_1-M_2))(L_1-L_2)=(\Delta\log K_{ML}(M_1-M_2))_{L_1}-(\Delta\log K_{ML}(M_1-M_2))_{L_2}$. $\Delta(\Delta\log K_{ex,ip}(M_1-M_2))(L_1-L_2)=(\Delta\log K_{ex,ip}(M_1-M_2))_{L_1}-(\Delta\log K_{ex,ip}(M_1-M_2))_{L_2}$. Thus, $\Delta(\Delta\log K_{ex}(M_1-M_2))(L_1-L_2)=\Delta(\Delta\log K_{ML}(M_1-M_2))(L_1-L_2)+\Delta(\Delta\log K_{ex,ip}(M_1-M_2))(L_1-L_2)$. Both positive $\Delta(\Delta\log K_{ML}(Ag-Na))(16C5-15C5)$ and $\Delta(\Delta\log K_{ex,ip}(Ag-Na))(16C5-15C5)$ values are responsible for higher extraction selectivity of 16C5 for Ag^+ than for Na^+, compared with 15C5.§§ 16-Crown-5 shows higher extraction selectivity for Ag^+ or Na^+ than for Tl^+ and K^+ in comparison with 15C5. This is attributed to the fact that, although $\Delta(\Delta\log K_{ex,ip}(M_1-M_2))(L_1-L_2)$ value is negative, $\Delta(\Delta\log K_{ML}(M_1-M_2))(L_1-L_2)$ value is positive and $\Delta(\Delta\log K_{ML}(M_1-M_2))(L_1-L_2)$ is larger than $|\Delta(\Delta\log K_{ex,ip}(M_1-M_2))(L_1-L_2)|$ (M_1=Ag or Na; M_2=Tl or K; L_1=16C5 and L_2=15C5). From the above discussion, it can be concluded that higher extraction selectivity of 16C5 for Ag^+ than for Na^+, Tl^+, and K^+ and that for Na^+ than for Tl^+ and K^+ in comparison with 15C5 are dependent on higher selectivity in water of 16C5 for Ag^+ than for Na^+, Tl^+, and K^+ and that for Na^+ than for Tl^+ and K^+, compared with 15C5, respectively.

$\log K_{ex}$-, $\log K_{ML}$-, and $\log K_{ex,ip}$-value sequences of 16C5 for Na^+, K^+, Ag^+, and Tl^+ are identical ($Ag^+>Na^+>Tl^+>K^+$), whereas it does not hold for

§§ Detailed explanations are as follows. The difference in $\log K_{ML}$ values of 16C5 between Ag^+ and Na^+ (0.32) is larger than the corresponding difference of 15C5 (0.24). The difference in $\log K_{ex,ip}$ values of 16C5 between Ag^+ and Na^+ (0.45) is larger than the corresponding difference of 15C5 (0.31). These two positive contributions are responsible for the fact that the difference in $\log K_{ex}$ values of 16C5 between Ag^+ and Na^+ (0.761) is larger than the corresponding difference of 15C5 (0.55).

15C5.

For a given metal ion, the following relationship can be derived from Eq. 6;

$$\log\{K_{ex}(L_1)/K_{ex}(L_2)\} = \log(K_{ML_1}/K_{ML_2}) + \log\{K_{ex,ip}(L_1)/K_{ex,ip}(L_2)\} - \log(K_{D,L_1}/K_{D,L_2}). \quad (12)$$

16-Crown-5 shows lower extractability for the univalent metal ion except for Ag^+ than does 15C5 (Table 1). For Na^+, K^+, and Tl^+, this is ascribed to the fact log $(K_{D,L_1}/K_{D,L_2})$>log (K_{ML_1}/K_{ML_2})+log $\{K_{ex,ip}(L_1)/K_{ex,ip}(L_2)\}$; greater extractability of 16C5 for Ag^+ than that of 15C5 is attributable to the fact that log $\{K_{ex,ip}(L_1)/K_{ex,ip}(L_2)\}$>log $(K_{D,L_1}/K_{D,L_2})$ and the log (K_{ML_1}/K_{ML_2}) value is positive, where L_1=16C5 and L_2=15C5.

log K_{ex}-value sequences of 16C5 for the bivalent metal ions are $Pb^{2+}>Ba^{2+}\geq Sr^{2+}>Ca^{2+}$ (Table 1). The size-fit concept does not hold for the extractability of 16C5 for the alkaline earth metal ions. Although stability of the 16C5–Pb^{2+} complex in water is much lower than that of 16C5–Sr^{2+} and Ba^{2+} complexes, the 16C5–Pb^{2+} complex is the most extractable among all the 16C5–bivalent metal ion complexes. This is entirely due to much the largest log $K_{ex,ip}$ value of the 16C5–Pb^{2+} complex. log K_{ex}-value sequence of 16C5 for the bivalent metal ions except for Ba^{2+} is identical with that of 15C5. The value of $(\Delta\log K_{ML}(Sr-Ba))_L+(\Delta\log K_{ex,ip}(Sr-Ba))_L$ is negative when L=16C5 and positive when L=15C5, which are responsible for the slightly larger log K_{ex} value of Ba^{2+} of 16C5 than that of Sr^{2+} and the smaller log K_{ex} value of Ba^{2+} of 15C5 than that of Sr^{2+}, respectively.

Extractability of 16C5 for the bivalent metal ion is lower than that of 15C5. It can be seen from Table 1 and Eq. 12 that, for Sr^{2+}, Ba^{2+}, and Pb^{2+}, the term log $(K_{D,L_1}/K_{D,L_2})$ plays a very important role in the lower extractability of 16C5 compared with 15C5, where L_1=16C5 and L_2=15C5; namely, the smaller log K_{ex} value of 16C5 than that of 15C5 is largely or completely due to the higher lipophilicity of 16C5 compared with 15C5.

log $K_{ex,ip}$ value of 16C5 varies with a cation of the same charge (Table 1). The same trend is found for 15C5.

From Gibbs free energies of hydration ($\Delta G_h°$/kJ mol^{-1}) of Na^+ (−411.3) and K^+ (−338),[10] the interaction of Na^+ with water is much stronger than that of K^+. The interaction with water of Na^+ trapped in the 16C5 cavity is expected to be stronger than that of K^+. Association constant of Na^+ with a picrate ion in water is smaller than that of K^+.[11] Association constant with a picrate ion of Na^+ trapped in the 16C5 cavity is expected to be smaller than that of K^+. Hence, $K_{ex,ip}$ value of the Na^+–16C5 complex is anticipated to be smaller than that of the K^+ complex. However, $K_{ex,ip}$ value of 16C5 is larger for Na^+ than for K^+ (Table 1). From the structure of the 16C5 complex with the univalent metal ion trapped in the cavity, anion- and solvent-contact are possible in respective directions perpendicular to the plane of the 16C5 ring. Consequently, it is concluded from the above discussion that the larger $K_{ex,ip}$ value of the Na^+–16C5 complex than that of the K^+ complex is ascribed to negligible effect of water on association of the Na^+–16C5 complex with a picrate ion and/or weak interaction with water of the Na^+ complex. The same discussion holds for the cases of 15C5–Na^+ and –K^+ complexes. A Na^+ ion has a more suitable size for the 16C5 cavity than does a Ag^+ ion; $-\Delta G_h°$ of Ag^+ (479.1 kJ mol^{-1})[10] is larger than that of Na^+; but, $K_{ex,ip}$ value of 16C5 is greater for Ag^+ than for Na^+. The larger $K_{ex,ip}$ value of the Ag^+–16C5 complex may be attributed to the specific interaction with benzene of the Ag^+ ion[12] in the 16C5 complex and stronger association with a picrate ion and/or weaker interaction with water of the Ag^+ complex compared with the case of the Na^+ complex. The same discussion holds for the cases of 15C5–Na^+ and –Ag^+ complexes.

For a crown ether–bivalent metal ion complex, two picrate anion-contacts with the cation are possible in respective directions perpendicular to the plane of the ring. Sr^{2+} and Pb^{2+} are nearly equal in size and larger than the 16C5- and 15C5-cavity. Therefore, it can be considered that the size of the MLA_2 complex of Pb^{2+} is nearly equal to that of the corresponding MLA_2 complex of Sr^{2+}. $-\Delta G_h°$ values of Sr^{2+} (1447 kJ mol^{-1})[10] and Pb^{2+} (1497 kJ mol^{-1})[10] are almost the same. However, in each case of 16C5 and 15C5, $K_{ex,ip}$ is greater for Pb^{2+} than for Sr^{2+}. This is probably attributable to stronger interaction with the two picrate anions of the Pb^{2+} complex compared with the corresponding Sr^{2+} complex.

From Table 1, $K_{ex,ip}$ value of a univalent metal ion increases with an increase in the size of crown ether (15C5<16C5); but, it is not always true for the cases of the bivalent metal ions. The difference in log $K_{ex,ip}$ values of a univalent metal ion between 16C5 and 15C5 is 0.28—0.59, which is roughly constant. This indicates that an increment of log $K_{ex,ip}$ value per a methylene group is about 0.44 (on the average), which is nearly equal to the Π_{CH_2} value (0.48_5). $K_{ex,ip}$ consists of two fundamental equilibria, namely, $K_{ex,ip}=K_{MLA}K_{D,MLA}$ ($K_{MLA}=[MLA]/[ML^+][A^-]$, $K_{D,MLA}=[MLA]_o/[MLA]$). Since $K_{D,MLA}$ is a partition constant of a neutral complex MLA between benzene and water, an increment of log $K_{D,MLA}$ per a methylene group is evaluated to be about 0.49 on the basis of Π_{CH_2} value (0.48_5). It thus appears from the above discussion that log K_{MLA} values of 16C5 and 15C5 complexes with the same univalent metal ion are roughly equal.

Since MLA_2 is a neutral complex, the K_{D,MLA_2} value probably increases with an increase in the size of the crown ether (15C5<16C5), where $K_{D,MLA_2}=[MLA_2]_o/[MLA_2]$. The differences in log $K_{ex,ip}$ values between

16C5 and 15C5 for Pb^{2+} and Ba^{2+} are larger than and are comparable to the Π_{CH_2} value, respectively. This indicates that K_{MLA_2} values of 16C5 for Pb^{2+} and Ba^{2+} are greater than and roughly equal to those of 15C5, respectively, where $K_{MLA_2}=[MLA_2]/[ML^{2+}][A^-]^2$. Whereas, the log $K_{ex,ip}$ value of the 16C5–Sr^{2+} complex is smaller than that of the 15C5–Sr^{2+} complex. This indicates that the K_{MLA_2} value of the 16C5 complex is much smaller than that of the 15C5 complex.

For 15C5, log $K_{ex,ip}$ value of Sr^{2+} is larger than that of Ba^{2+}; but, the reverse is found for 16C5. It seems that, in each case of 16C5 and 15C5, the MLA_2 complexes of Sr^{2+} and Ba^{2+} are almost the same in size. Therefore, K_{D,MLA_2} values of Sr^{2+} and Ba^{2+} of the same crown ether can be expected to be nearly equal. It thus appears that the K_{MLA_2} value of Sr^{2+} for 15C5 is greater than that of Ba^{2+}, whereas the reverse is true for 16C5, which is caused by an extra methylene group in the 16C5 ring.

We thank Mr. Masanao Nagamori of this laboratory for his experimental assistance.

References

1) Y. Takeda, K. Katsuta, Y. Inoue, and T. Hakushi, *Bull. Chem. Soc. Jpn.*, **61**, 627 (1988).

2) a) M. Ouchi, Y. Inoue, H. Sakamoto, A. Yamahira, M. Yoshinaga, and T. Hakushi, *J. Org. Chem.*, **48**, 3168 (1983); b) M. Ouchi, Y. Inoue, T. Kanzaki, and T. Hakushi, *ibid.*, **49**, 1408 (1984).

3) Y. Takeda and H. Kato, *Bull. Chem. Soc. Jpn.*, **52**, 1027 (1979).

4) Y. Takeda and H. Goto, *Bull. Chem. Soc. Jpn.*, **52**, 1920 (1979).

5) "Dissociation Constants of Organic Acids in Aqueous Solution," ed by G. Kortün, W. Vogel, and K. Andrussov, Butterworths, London (1961).

6) Y. Takeda et al., unpublished data.

7) R. M. Izatt, R. E. Terry, B. L. Haymore, L. D. Hansen, N. K. Dalley, A. G. Avondet, and J. J. Christensen, *J. Am. Chem. Soc.*, **98**, 7620 (1976).

8) Y. Takeda, *Bull. Chem. Soc. Jpn.*, **53**, 2393 (1980).

9) Y. Takeda and Y. Matsumoto, *Bull. Chem. Soc. Jpn.*, **60**, 2313 (1987).

10) H. L. Friedman and C. V. Krishnan, "Water," ed by F. Franks, Plenum, New York (1973), Vol. 3, p. 55.

11) M. Yamane, T. Iwachido, and K. Tōei, *Bull. Chem. Soc. Jpn.*, **44**, 745 (1971).

12) Y. Takeda, M. Nemoto, and S. Fugiwara, *Bull. Chem. Soc. Jpn.*, **55**, 3438 (1982).

A Simple and Rugged Home-Built Scanning Tunneling Microscope for Operation in Both Air and Liquid

Kenji SAKAMAKI,* Kiminori ITOH, Akira FUJISHIMA,*
Yohichi GOHSHI,† and Hidemoto NAKAGAWA††
Department of Synthetic Chemistry, Faculty of Engineering, The University of Tokyo, 7-3-1, Hongo, Bunkyo-ku, Tokyo 113
†Department of Industrial Chemistry, Faculty of Engineering, The University of Tokyo, 7-3-1, Hongo, Bunkyo-ku, Tokyo 113
††Nakagawa Applied Research, 6-10-7, Megurohoncho, Meguro-ku, Tokyo 152
(Received April 27, 1989)

A simple, rugged home-built scanning tunneling microscope for operation in both air and liquid that uses a Z-stage micrometer to provide coarse mechanical positioning is described. The construction of this STM was accomplished at low cost without precision machining. The tunneling current is typically acquired within 10—15 minutes. The atomic resolving power of our STM has been demonstrated by a cleaved HOPG at a 15-Hz scanning rate in air. There was no use of plate-stack-type isolators, due to the high rigidness of the tunneling unit. The STM image of a HOPG in ultrapure water was also observed with a glass-coated tip. Images of a pc-Ag electrode in 0.1 mol dm^{-3} KCl demonstrate stable operation in a liquid solution. The lateral drift was shown to be less than 0.13 nm min^{-1} for operation in liquid, estimated by subsequent imaging of the same area. This STM is easy to handle and has a suitable design for in situ electrode surface characterization.

Scanning tunneling microscope (STM) and associated techniques are beginning to be incorporated into the field of electrochemistry. To date, surface chemistry is poorly understood on account of the limited measuring conditions and resolving power of available tools. The currently developing scanning tunneling microscope is a suitable instrument for investigating the surfaces of conducting materials at the nanometer scale under various environments.[1] A number of designs for scanning tunneling microscopes (STMs) have been published since the pioneering work of Binnig and Rohrer.[2] Among them, Sonnenfeld and Hansma[3] have demonstrated that STM could be used to study surfaces immersed in liquid solutions. The investigations of Hansma's group have opened up the field for in situ observations of surface structures at the solid/liquid interface.[4] Bard et al.,[5] Arvia et al.,[6] and Itaya et al.[7] were the first groups to apply the STM in the field of electrochemistry. Considerable attention has recently been focused on in situ observations.[8] To apply STM to the particular interests of electrochemistry, suitable STM needs to be constructed. Much effort has been expended on ingenious designs of STM. However, the construction of our STM was accomplished at low cost without precision machining. Here, we present the design of a simple, rugged home-built STM for operation in both air and liquid. It has a suitable design for studying electrochemical processes in situ. The emphasis of this paper is on the STM itself.

Experimental

Tunnel Unit Design. The basic principle for construction of a tunneling unit is simplicity and rigidness. Figure 1 shows a schematic illustration of our tunneling unit. The unit comprises essentially two main parts. The lower part is a high-precision, vertical-translation Z-stage (Σ-303-(2), Sigmakohki Co., Ltd., Japan) and a four-legged piezoactuator (Fuji Ceramics, Co., Ltd., Japan) which is attached to a motionless part of the Z-stage. The upper part is a tripod scanner fixed inside a stainless-steel enclosure which is rigidly screwed to the stage. At the top of the unit, a current-sensitive preamplifier is installed so as to decrease electronic noise. Our unit has several advantages: (1) no precision machining is required, (2) unit fabrication can be accomplished at low cost, (3) exchanging both the tip and the sample is facile, (4) different areas can be observed by sliding the enclosure across the stage, and (5) for operation in liquid, the tip approaches the vertical direction from above the sample.

Tunneling Tip and Sample Setting. Commercially available Pt-Ir tips with a diameter 250 μm (Longreach Scientific Resources Co., Ltd., USA) were used. This type tip was slightly bent and mounted within a steatite tip holder by inserting it into a steel tube made from a hypodermic needle. A sample is attached with silver paint to

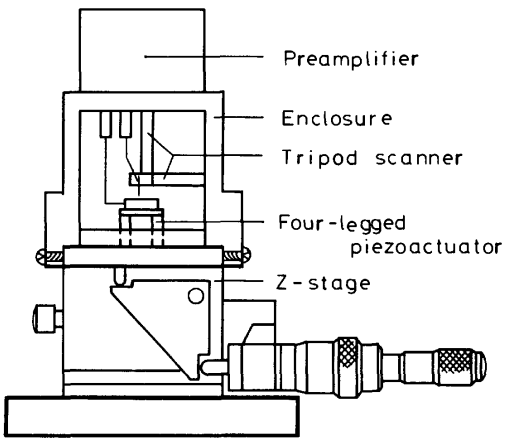

Fig. 1. A schematic cross-sectional view of the tunnel unit.

quartz glass which is glued with epoxy to the top of a four-legged piezoactuator.

Coarse and Fine Adjustment. The Z-stage micrometer with a 0.5 μm resolution provides a simple coarse adjustment mechanism that brings the tip into the operating range of the four-legged piezoactuator, while being observed by an optical microscope of 100 magnification. After coarse positioning the tip mechanically with the Z-stage micrometer from the sample, the Z-stage is clamped by a screw so as to prevent any backlash. The tunneling current is automatically detected by raising the sample under the control of the four-legged piezoactuator in connection with a personal computer (PC98VX4, NEC, Japan) while operating a feedback control of the Z-piezoactuator. The four-legged piezoactuator provides displacements from −2.0 μm to +2.0 μm by a stable dc voltage source (M107, Systron Donner, USA) with an accuracy of 0.002%. The feedback voltage applied to the Z-piezoactuator is in the range between +250 V to −250 V, determined by the feedback gain. The full voltage range of the feedback response of the Z-piezoactuator corresponds to a tip motion of 1.0 μm. The tunneling current is typically acquired within 10—15 minutes without crashing the tip into the sample; no additional precision mechanisms are employed.

3-Dimension Scanning. Prototype tripod piezoelectric actuators (three orthogonal piezoelectric rods) are being used for a 3-dimensional scanner. *X*, *Y*, and *Z* PZT-piezoelectric arms ((C-8), Fuji ceramics Co., Ltd., Japan) have the same characteristics with a resonance frequency of 140 kHz, an electrostatic capacity of 180 pF, and a curie temperature of 210 °C. The three (*X*, *Y*, *Z*) piezoelectric arms are attached to a steatite ($MgO \cdot SiO_2$) tip holder with epoxy. Calibration of the piezoelectric sensitivity is performed by the STM image of a highly oriented pyrolytic graphite (HOPG), as described later. Its sensitivity is 2.0 nm V^{-1}.

Vibration Isolation. Vibration isolation is provided by an air-suspension table with a resonance frequency of 1.8 and 2 Hz in the vertical and horizontal directions, respectively. The suitability of vibration isolation for our STM operation was checked with the cooperation of Meiritsuseiki Co., Ltd., Japan using an FFT analyser. A 15-kg circular weight is located on the air-suspension table; the tunneling unit sits on top of it. Neither a plate-stack type isolator nor a coil-spring type isolator was necessary, due to the high rigidness of the tunneling unit. The unit was installed in a shield box in order to avoid any acoustic or electronic noise.

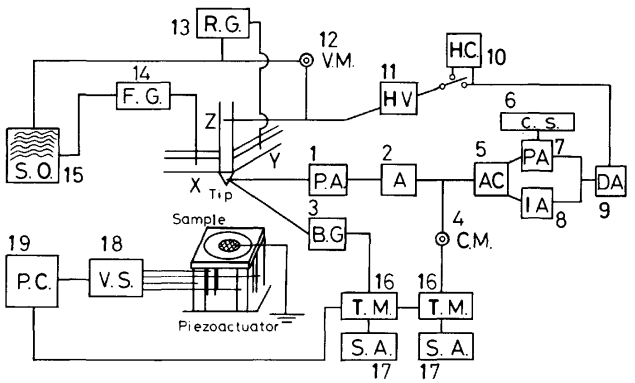

Fig. 2. A block diagram of the electronic setup of STM. 1: preamplifier, 2: amplifier, 3: tunnel bias generator, 4: tunneling current monitor, 5: absolute value circuit, 6: tunnel current setting, 7: proportional amplifier, 8: integrated amplifier, 9: differential amplifier, 10: feedback hold circuit, 11: high voltage source, 12: feedback voltage monitor, 13: ramp generator, 14: function generator, 15: storage oscilloscope, 16: transient memory, 17: signal averager, 18: stable DC voltage source, 19: personal computer.

Electronics. Figure 2 shows a block diagram of the electronic setup of STM and tunneling spectroscopy. Our electronic setup differs from the commonly used types mainly regarding three aspects: (1) the sample is a ground for all the electronics, (2) the tunneling bias is applied to the tip, and (3) the tunneling current is detected from the tip. The scanning rate in the X-direction can be changed from 0.1 Hz to 100 Hz by a function generator (FG-143, NF Electronic Instruments INC., Japan). A ramp generator was used for Y-scanning. Our STM is operated in an analog mode and images are monitored on a storage oscilloscope. It also has a computerized arrangement for tunneling spectroscopy, using a feedback hold mode at a point (Fig. 2). The tunneling current and bias are monitored by two transient memories (S210, Autonics, Japan); each is averaged by an averager (F601, Autonics, Japan). The digital data is transferred to a personal computer and can be calculated numerically. The surface density of states of a TiO_2(110) single crystal obtained by tunneling spectroscopy using our STM setup is discussed elsewhere.[9]

Sample. As a standard sample for STM study,[10] a cleaved HOPG single crystal (Nippon Carbon, Co., Ltd., Japan) was used to examine the resolving power of our STM.

Results and Discussion

STM Images in Air. In Figs. 3(a) and (c) we display images of a HOPG in air at a frequency of 5 and 15 Hz in the *X*-direction, respectively. These images were taken with a constant current mode over an area of 1.4×1.4 nm^2. The tunneling bias and current were set at +10 mV (tip positive) and 1 nA, respectively. The STM image (Fig. 3(a)) shows the atomic structure of graphite. It coincides with the surface crystallographic structure[11] in the same area depicted in Fig. 3(b). The geometrical configuration of the carbon atoms of graphite have three sites (Fig. 3(b)). At site A (●) the atoms in the two uppermost layers are atop. At site B (●) there is only an atom in the upper layer; at site C (○) the atom is only in the underneath layer.[10,11] The STM images in Figs. 3(a) and (c) show the atomic configuration of B site of graphite.[12] Therefore, our STM has a resolving power better than 0.25 nm in the lateral direction and 0.10 nm in the vertical direction, respectively. The STM has an atomic resolving power at a high X scanning rate (15 Hz) due to the rigidness of the tunneling unit (Fig. 3(c)). The time required for imaging was only 5 seconds. To observe the atomic corrugation, the rigid setting of the tunneling tip was a dominant factor. It is noteworthy that any dust attached to the tip of the needle or a sample can be stripped by flowing N_2 before imaging. We also in-

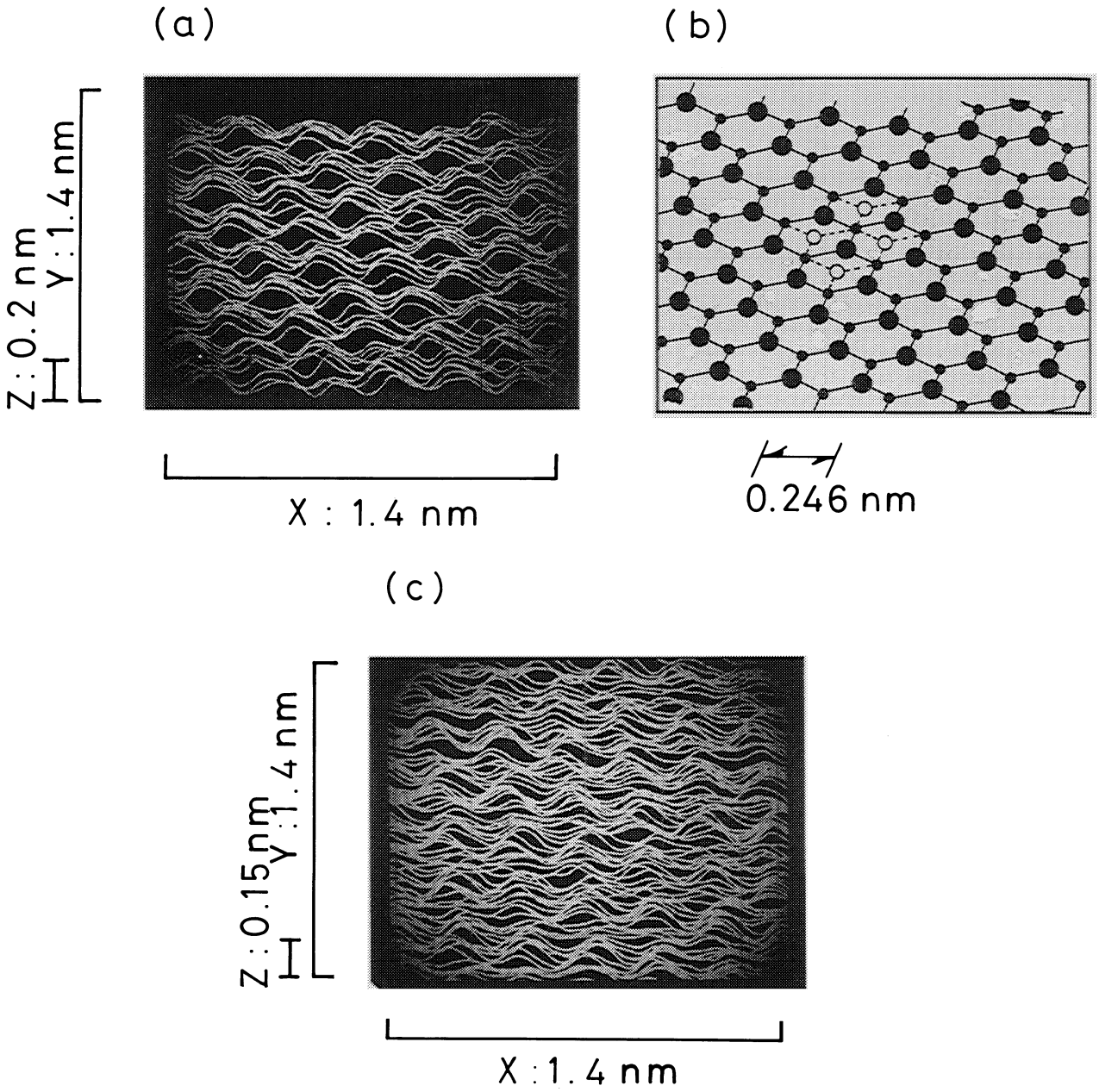

Fig. 3. Constant current images of a HOPG in air observed at a frequency of 5 Hz (a) and 15 Hz (c), respectively. Measuring conditions (1 nA, +10 mV (tip positive)). (b) is the surface crystallographic structure of graphite. A, B and C site are denoted •, ●, and ○, respectively.

vestigated the surface morphology of a polycrysalline (pc-) Ag (99.88%, The Japan Lamp Industies Co., Ltd.) in air. It is difficult to mechanically polish a soft metal like Ag with a SiO_2 powder because the SiO_2 abrasive sticks to the surface. In this work mechanical polishing was accomplished with wet lapping films containing alumina powder (9, 3, 1, 0.3 μm grain size) using Newdaiyalap (ML-451) with the cooperation of Maruto Co., Ltd., Japan. Figures 4(a) and (b) are STM images of pc-Ag in air at ambient pressure. Figure 4(b) was obtained by sliding the enclosure across the Z-stage after the observation of Fig. 4(a). A shallow surface was captured in the STM image (Fig. 4(a)); the surface was nearly flat over an area of $25 \times 20\ nm^2$. At different regions of the same sample (Fig. 4(b)), a 2-nm step as well as a tableland structure can be seen. Under air and ambient pressure, our STM draws the same profile of the surface during about 20 minutes.

STM Images in Liquids. To test the operation

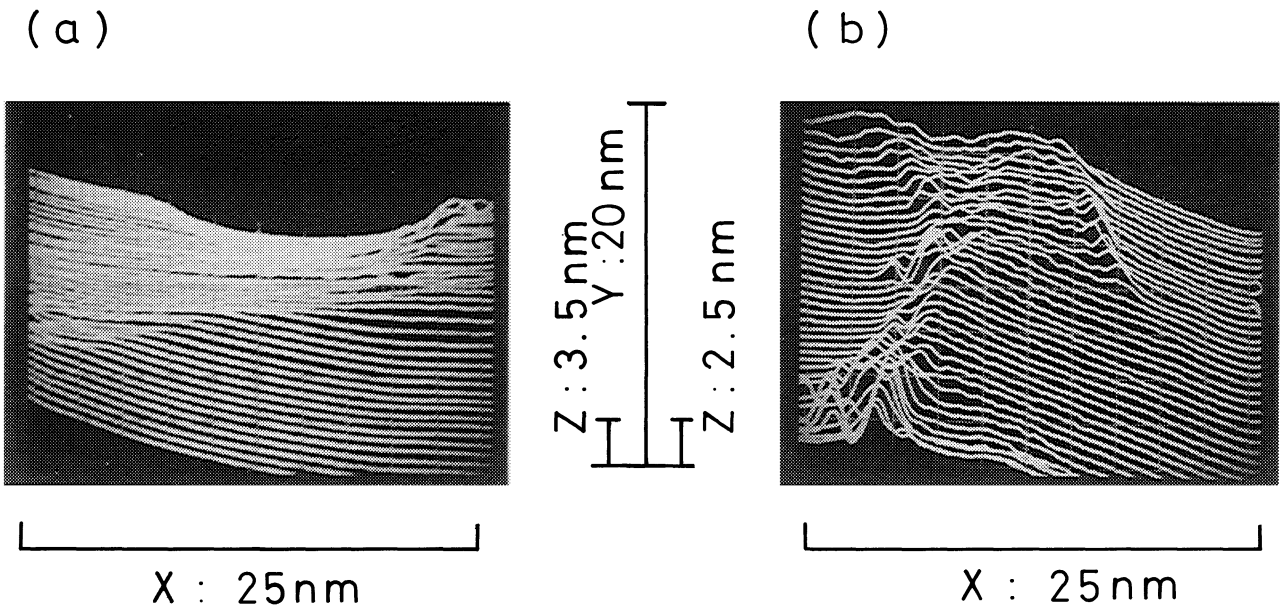

Fig. 4. STM images of a mechanically polished pc-Ag electrode in air. Measuring conditions 1 nA, +200 mV (tip positive), scan rate: 2 Hz). (a) and (b) were observed at different area.

in liquid we examined the HOPG sample in ultrapure water (UHQ, ELGA). Glass-coated Pt–Ir tips (Longreach Scientific Resources, USA) were used for measurements in liquid solutions. The exposed tip areas were determined by an electrochemical method[13] with an oxidation-limiting current of 1 m mol dm^{-3} of ferrocene in acetonitrile containing 0.2 m mol dm^{-3} TBAP. The exposed areas ranged typically between about 80 and 2 μm^2.[14] The glass-coated tip was rinsed in concd H_2SO_4 for 1 hour and ultra-pure water before use. The cleaved HOPG plate (5 mm×5 mm×1 mm thick) was attached to a Cu plate with silver paint. The exposed area of the Cu plate was covered with epoxy. A Teflon sheet (10 mm×10 mm×4 mm thick) with a hole of 8 mm diameter was attached above sample with epoxy. After the cell was carefully rinsed in 0.1 mol dm^{-3} H_2SO_4 and ultra-pure water, it was set on the four-logged piezoactuator with silver paint. Figure 5 shows the STM image (constant current mode) of the HOPG in the area of 1.3×1.7 nm^2 in ultrapure water. The tunneling current and bias were set at 8 nA and +10 mV (tip positive), respectively. The *X* scan rate (0.35 Hz) was reduced compared to the measuring condition under air in order to avoid any sway of water during tip scanning. The atomic corrugation of the HOPG was slightly distorted. The main reason of this distortion is the surface tension of water. The grass-coated tip was pulled by this force in the direction to the sample surface. A firm setting of the glass-coated tip is necessary in order to gain a good STM image under liquid with respect to the measurements under air. Following the above experiment, we examined a

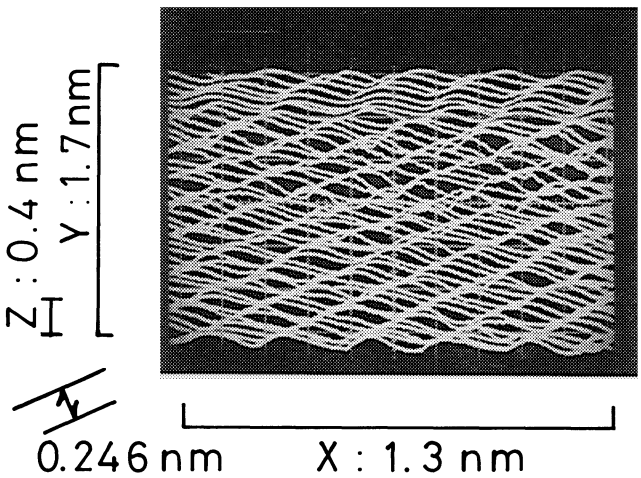

Fig. 5. STM image of a HOPG in ultra water. Measuring conditions (8 nA, +10 mV (tip positive), scan rate: 0.35 Hz).

pc-Ag surface in 0.1 mol dm^{-3} KCl. An Ag electrode cell was made with Teflon sheet. The cell was carefully rinsed in acetone and distilled water. Any electrochemical current was less than 100 pA in 0.1 mol dm^{-3} KCl and was suppressed by a factor of 50 under the tunneling current (5 nA) and the tunnel bias (+200 mV: tip positive). Figures 6(a) and (b) are STM images of a pc-Ag in 0.1 mol dm^{-3} KCl. Figure 6(b) was observed 10 minutes after the observation of Fig. 6(a). About a 2.5 nm "mountain range" structure in the top left-side and a small "hill" in the bottom right-side were found in both STM images. The long-term

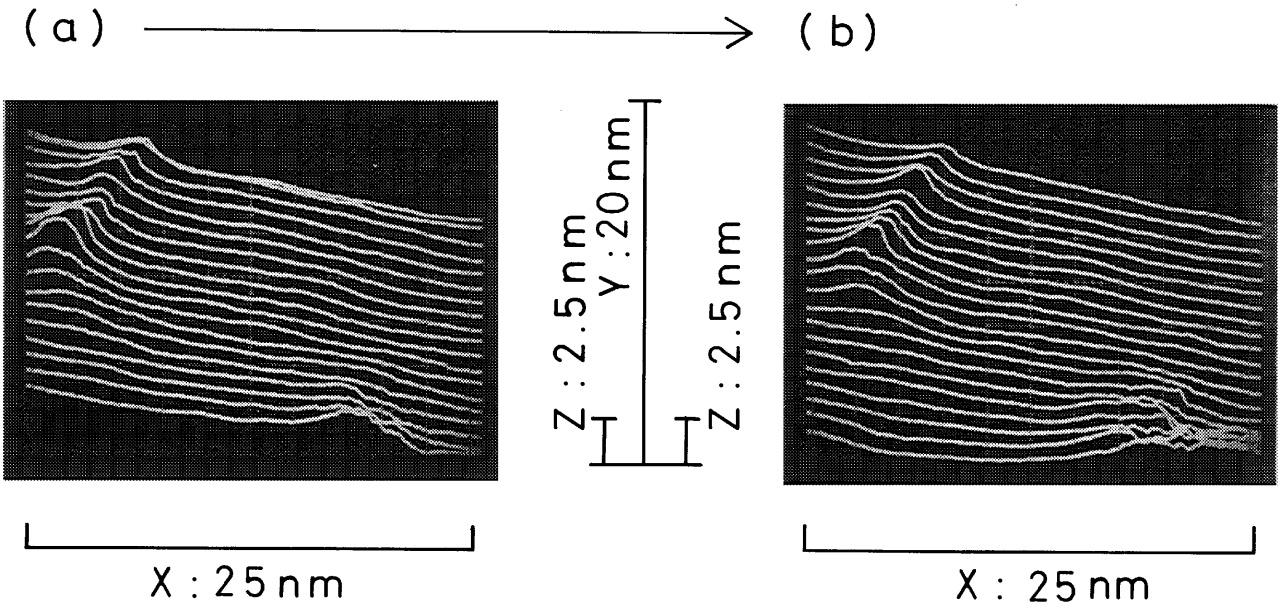

Fig. 6. STM images of a mechanically polished pc-Ag electrode in 0.1 mol dm^{-3} KCl. (b) was observed 10 minutes after the observation of (a). Measuring conditions (5 nA, +200 mV (tip positive), scan rate: 1 Hz).

stability of our STM in liquid is demonstrated as shown in Fig. 6. A lateral drift of less than ca. 0.13 nm min^{-1} in a salt water solution was estimated by subsequent imaging of the same area. For operation in liquid, it is necessary to rinse both the sample and the glass-coated tip carefully. In order to compare STM images observed in air and liquid, the following experiment was carried out. First, the surface of a pc-Ag electrode was imaged in air (Fig. 7(a)). After imaging in air, the tip was raised above the sample. A solution of 0.1 mol dm^{-3} KCl was carefully poured into the cell with Microsyringe (HAMILTON). The surface in the same area was then imaged in 0.1 mol dm^{-3} KCl (Fig. 7(b)). The X scan frequency of Figs. 7(a) and (b) were 2 and 1 Hz, respectively. The other measuring conditions were the same. A "mountain range" structure can be seen in both images (Figs. 7(a) and (b)). Both images draw the same surface profile, except for the offset. The appearance of a "hillock" in the top left-side in Fig. 7(b) was caused by drift when the liquid was poured into the cell. However, the "mountain range" in 0.1 mol dm^{-3} KCl (Fig. 7(b)) was higher than that in air (Fig. 7(a)) due to a current without a tunneling current. It seems that the more the exposed tip area is decreased, the greater does the resolving power of STM in the liquid solution increase. In addition, the large-area STM images of a pc-Ag have "island-like" structures.[15,16] The characterization of an electrochemically modified (ORC treatment) pc-Ag electrode with or without pyridine molecules in connection with surface-enhanced Raman scattering (SERS) has been discussed elsewhere.[15,16]

In conclusion, the rigid construction of an STM unit has demonstrated the atomic resolving power in both air and liquid solutions without additional precision mechanisms and careful vibration isolation. The STM is easy to handle and has a suitable design for in situ electrode surface characterization.

One part of this work was presented at the STM(II) meeting under Thin Film and Surface Physics of the Japan Society of Applied Physics, Dec., 12—14, 1988 at Atagawa, Japan.

One of the authors (K. S.) greatly acknowledges instructive discussions with Prof. Kingo Itaya (Tohoku Univ.) and Prof. Toshio Sakurai (Tokyo Univ.), and Prof. Osamu Nishikawa (Tokyo Institute of Technology) when he visited their laboratories. In addition, K. S. is grateful to Dr. Ichiro Otsuka (Tohoku Dental. Univ.) for useful discussions.

References

1) G. Binnig and H. Rohrer, *Rev. Mod. Phys.*, **59**, 615 (1987).

2) G. Binnig and H. Rohrer, *Helv. Phys. Acta*, **55**, 726 (1982).

3) R. Sonnenfeld and P. K. Hansma, *Science*, **232**, 211 (1986).

4) R. Sonnenfeld and B. C. Schardt, *Appl. Phys. Lett.*, **49**, 1172 (1986); R. Sonnenfeld, J. Schneir, B. Drake, P. K. Hansma, and D. E. Aspnes, *Appl. Phys. Lett.*, **50**, 1742 (1987); P. K. Hansma, V. B. Elings, O. Marti, and C. E. Bracker, *Science*, **242**, 209 (1988) and reference therein.

5) H-Y Liu, F-R F. Fan, C. W. Lin, and A. J. Bard, *J. Am.*

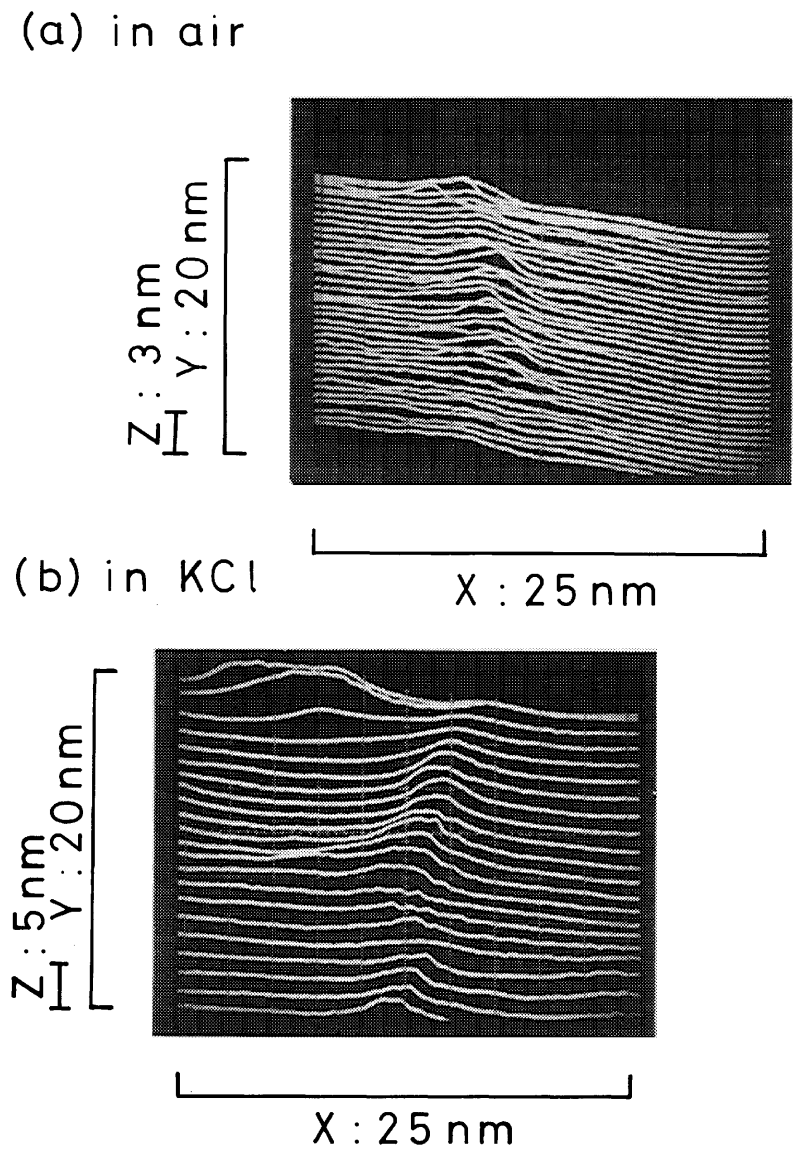

Fig. 7. STM images of a pc-Ag in air (a) and in 0.1 mol dm^{-3} KCl (b) in the same area. Measuring conditions (5 nA, +200 mV (tip positive), scan rate: 2 Hz (a), 1 Hz (b)).

Chem. Soc., **108**, 3839 (1986); O. E. Husser, D. H. Craston, and A. J. Bard, *J. Vac. Sci. Technol.*, **B6**, 1873 (1988); A. J. Bard, F-R F. Fan, J. Kwak, and O. Lev, *Anal. Chem.*, **61**, 132 (1989), and reference therein.

6) J. Gómez, L. Vázquez, A. M. Baró, N. García, C. L. Perdriel, W. E. Triaca, and A. J. Arvia, *Nature (London)*, **323**, 612 (1986); L. Vázquez, J. Gómez, A. M. Baró, N. García, M. L. Marcos, J. G. Velasco, J. M. Vara, A. J. Arvia, J. Presa, A. García, and M. Aguilar, *J. Am. Chem. Soc.*, **109**, 1730 (1987).

7) K. Itaya, S. Sugawara, and K. Higaki, *J. Phys. Chem.*, **92**, 6714 (1988); K. Itaya and E. Tomita, *Surf. Sci.*, **201**, L507 (1988) and reference therein.

8) S. Morita, I. Otsuka, T. Okada, H. Yokoyama, T. Iwasaki, and N. Mikoshiba, *Jpn. J. Appl. Phys.*, **26**, L1853 (1987); J. Wiechers, T. Twomey, D. M. Kolb, and R. J. Behm, *J. Electroanal. Chem.*, **248**, 451 (1988); P. Lustenberger, H. Rohrer, R. Christoph, and H. Siegenthaler, *J. Electroanal. Chem.*, **243**, 225 (1988); M. M. Dovek, M. J. Heben, C. A. Lang, N. S. Lewis, and C. F. Quate, *Rev. Sci. Instrum.*, **59**, 2333 (1988); M. H. J. Hottenhuis, M. A. H. Mickers, J. W. Gerriten, and J. P. Van Der Eerden, *Surf. Sci.*, **206**, 259 (1988); K. Uosaki and H. Kita, *J. Electroanal. Chem.*, **259**, 301 (1989).

9) K. Sakamaki, K. Itoh, A. Fujishima, and Y. Gohshi, *The Review of Polarography*, **33**, 53 (1987). *Surf. Sci.*, in press., *J. Vac. Sci. Technol.*, **A**, in press.

10) Sang-Il Park and C. F. Quate, *Appl. Phys. Lett.*, **48**, 112 (1986); H. Bando, N. Morita, H. Tokumoto, W. Mizutani, K. Watanabe, A. Honma, S. Wakiyama, M. Shigeno, K. Endo, and K. Kajimura, *J. Vac. Sci. Technol.*, **A6**, 344 (1988).

11) A. Selloni, P. Carnevali, E. Tosatti, and C. D. Chen, "Proceedings of the 17th International Conference on the Physics of Semiconductors," edited by J. D. Chadi and W. A. Harrison, Springer, New York (1985), p. 11.

12) I. P. Batra and S. Ciraci, *J. Vac. Sci. Technol.*, **A6**, 313

(1988).

13) R. M. Wightman, *Science*, **240**, 415 (1988); K. R. Wehmeyer and R. M. Wightman, *Anal. Chem.*, **57**, 1989 (1985); S. Pons and M. Fleischmann, *Anal. Chem.*, **59**, 1391A (1987); T. Kuwana, D. E. Bublitz, and G. Hoh, *J. Am. Chem. Soc.*, **82**, 5811 (1960).

14) The exposed areas of the glass-coated tips were determined as a hemispherical microvoltammetric electrode with the Eq. $i_d=2\pi nFDCr$ where i_d is the limiting steady-state current and r is the radius of the electrode and the other terms have their usual meaning (Ref. 13).

15) S. Matsunaga, B. H. Loo, K. Sakamaki, A. Fujishima, and Y. Gohshi, Abstract of the 58th spring meeting of Chemical Society of Japan, Kyoto, 1989, p. 758.

16) K. Sakamaki, B. H. Loo, and A. Fujishima, The 4th International Conference on STM/TS, Oarai, Ibaraki, Japan, 1989. pp. 3—47., K. Sakamaki, K. Itoh, A. Fujishima, and Y. Gohshi, *J. Vac. Sci. Technol.*, **A**, in press.

 © 1989 The Chemical Society of Japan Bull. Chem. Soc. Jpn., 62, 2897—2901 (1989)

Racemization of Phenylalanine Coordinated to Bis(2,2′-bipyridine)-ruthenium(II) Complexes in Basic Aqueous Solutions

Takashi NAGAI
Laboratory of Chemistry, Nippon Medical School, Kosugi-chou, Nakahara-ku, Kawasaki 211
(Received January 31, 1989)

Racemization of the phenylalaninato ligand in Λ- and Δ-$[Ru(phe)(bpy)_2]^+$ (phe; phenylalaninate anion, bpy; 2,2′-bipyridine) complexes was found in basic aqueous solutions. It was proceeding without conformational change around the ruthenium ion in the dark. The equilibrium and rate constants of the racemization were determined in basic solutions at 100 °C. The reaction was base-catalyzed and not affected by photoexcitation of the complex ions.

The photochemical inversion of diastereoisomers of $[Ru(S\text{-am})(bpy)_2](ClO_4)_n$ (am; amino acidate anion) has been studied by Vagg et al.[1-5] They have reported that in aqueous solutions these complexes are photolabile and the inversion reaction around the metal ion occurs on irradiation of light. By contrast, these complexes are markedly stable in darkness: No inversion occurs even on boiling the complexes in aqueous solutions for a few hours. However, we found that the coordinated phenylalanine in $[Ru(phe)(bpy)_2]^+$ ion was gradually racemized in basic solutions in the dark. The rate and equilibrium constants of the racemization at 100 °C were determined by the use of the chromatographic method. Moreover, effects of photoexcitation of the complexes on the racemization were examined by light irradiation during the reaction.

Experimental

All materials used were of reagent grade, and used without further purification. The UV-visible spectra were obtained with a HITACHI 340 spectrophotometer. Circular dichroism (CD) spectra were obtained using a JASCO J-500 spectrophotometer.

Λ- and Δ-[Ru(*S*-phe)(bpy)$_2$]ClO$_4$ Hydrates. The mixture of Λ- and Δ-isomers was prepared and partially resolved by Vagg et al.[1,4] However, we prepared it by a different way and resolved it completely to obtain perchlorates of the Λ- and Δ-forms.

cis-$[Ru(CO_3)(bpy)_2]\cdot 3H_2O$[6] (1 g) was dissolved in 200 cm^3 of hot water, and (*S*)-phenylalanine (0.4 g) was added. The solution was stirred at 50 °C for 25 min in the dark. The deep-red solution was cooled, and then added on a short column (12.5 cm height×2.5 cm diameter) of SE-Toyopearl.[7] The adsorbed complexes were eluted with 0.2 mol dm^{-3} Na_2SO_4 to remove minor impurities. The main adsorption band was eluted, and the complexes in the eluate were precipitated by adding an excess of $NaClO_4$. The dark-red precipitate was filtered, washed with a small amount of water, and air-dried (yield 1.2 g).

The precipitate (0.7 g) was dissolved in 400 cm^3 of water, and placed on a column (56 cm height×2.6 cm diameter) of SE-Toyopearl. The adsorbed complex cations were washed with water and then eluted with 0.05 mol dm^{-3} sodium (*R*,*R*)-tartrate to develop two adsorption bands by the recycle chromatographic technique. The two bands were eluted separately, and each eluate was evaporated to about one-tenth of the initial volume by a rotary evaporator at about 40 °C, and then methanol was added to remove sodium (*R*,*R*)-tartrate. The filtrates were evaporated to take off the methanol, and dark-red crystals were precipitated by adding $NaClO_4$. The products were filtered off, washed with a small amount of water and dried under vacuum. All the above procedures were performed in the dark. The assignment of the absolute configuration of the complexes was determined by the sign of the peaks at about 290 nm of the CD spectrum in accordance with Vagg's report.[1] The products from the first and second adsorption bands were assigned to Δ- and Λ-isomers, respectively, and were used as the standard samples for measuring absorption and CD spectra in kinetic experiments.

Δ-Isomer. Found: Ru, 15.10; C, 49.04; H, 3.76; N, 9.86%. Calcd for Δ-$[Ru(S\text{-phe})(bpy)_2]ClO_4\cdot H_2O$: Ru, 14.54; C, 50.11; H, 4.06; N, 10.08%. ABS (H_2O) 492 nm (ε 9250); CD (H_2O) 350 nm (Δε −13.7). Λ-Isomer. Found: Ru, 13.60; C, 46.81; H, 3.57; N, 9.50%. Calcd for Λ-$[Ru(S\text{-phe})(bpy)_2]ClO_4\cdot 3H_2O$: Ru, 13.82; C, 47.64; H, 4.41; N, 9.58%. ABS (H_2O) 492 nm (ε 9250); CD (H_2O) 350 nm (Δε 16.1).

Starting Materials of Kinetic Experiments. A solution containing *cis*-$[Ru(CO_3)(bpy)_2]$ and (*S*)-phenylalanine was refluxed for 20 min at 100 °C. After cooling, a dark-red product was precipitated by adding $NaClO_4$. The product was identified as $[Ru(phe)(bpy)_2]ClO_4\cdot 2H_2O$ by the spectrophotometric methods, and it was found by the chromatographic separation that the product comprised four isomers which consisted of two predominant ones, Λ- and Δ-[Ru(*S*-phe)$(bpy)_2$]$ClO_4\cdot 2H_2O$, and two minor ones, Λ- and Δ-[Ru(*R*-phe)$(bpy)_2$]$ClO_4\cdot 2H_2O$, because of partial racemization of the coordinated phenylalanine.[8] This product was used as starting materials in the following experiments.

Rate Determination Procedures. The starting materials, $[Ru(phe)(bpy)_2]ClO_4\cdot 2H_2O$, of 0.2—0.25 mmol were dissolved in 100 cm^3 of a refluxing Sørensen buffer solution (0.05 mol dm^{-3} borax–0.1 mol dm^{-3} NaOH) at (100±2) °C in an atmosphere of nitrogen in darkness. In the case of a typical experiment, a 10 cm^3 aliquot of the reaction solution was taken out after 1 and 2 hours later and cooled in ice. The solution was added on a column (27 cm height×2 cm diameter) of SE-Toyopearl. The adsorbed complex cations were eluted with 0.1 mol dm^{-3} sodium (*R*,*R*)-tartrate, and completely resolved into two isomeric groups. One group contained Δ-$[Ru(S\text{-phe})(bpy)_2]^+$ (Δ-*S*) and Λ-$[Ru(R\text{-phe})(bpy)_2]^+$ (Λ-*R*) ions which were first eluted, and another contained Λ-$[Ru(S\text{-phe})(bpy)_2]^+$ (Λ-*S*) and Δ-[Ru(*R*-phe)-

$(bpy)_2]^+$ (Δ-R) ions which were secondly eluted. Decomposition products were negligible. An absorbance at 492 nm (ε=9250 for all of four isomers) gave the total concentration of the complexes, and a circular dichroism at 350 nm ($\Delta\varepsilon$=−13.7 for Δ-S, 16.1 for Λ-S, 13.7 for Λ-R, and −16.1 for Δ-R) reflected a ratio of the concentrations between two enantiomers in each eluate. The fractions of each isomer to the total complex ions were calculated from these spectrophotometric data and volumetric ratio of the two eluates as shown in Table 1. The data at t=0 were obtained from the chromatographic separation of the starting complex solution which was not refluxed. The data at equilibria were obtained from the refluxing solutions at pH 9.03 and 8.64 for 10 and 45 h, respectively. These reaction periods were more than ten times of half-lives estimated with effective rate constants (vide infra).

As regards racemization of the coordinated phenylalanine, the pseudo first-order rate constants, k_{AD}, k_{BD}, k_{AL}, and k_{BL}, were defined as follows:

$$\Delta\text{-}S \underset{k_{BD}}{\overset{k_{AD}}{\rightleftharpoons}} \Delta\text{-}R, \tag{1}$$

$$\Lambda\text{-}R \underset{k_{BL}}{\overset{k_{AL}}{\rightleftharpoons}} \Lambda\text{-}S. \tag{2}$$

In the present experiments, the fractions of the four isomers were obtained for each reaction time, and hence two integrated rate equations were yielded independently from both rates of disappearance of the reactant and appearance of the product with regard to one of the reversible reactions. The two expressions for the effective rate constant, k_{eff}, defined as sum of the rate constants for the forward and reverse directions of reaction (1), are

$$k_{eff} = \frac{1}{t}\cdot\ln\left(\frac{P[\Delta\text{-}S]_0 - P[\Delta\text{-}S]_e}{P[\Delta\text{-}S]_t - P[\Delta\text{-}S]_e}\right) \tag{3}$$

and

$$k_{eff} = \frac{1}{t}\cdot\ln\left(\frac{P[\Delta\text{-}R]_0 - P[\Delta\text{-}R]_e}{P[\Delta\text{-}R]_t - P[\Delta\text{-}R]_e}\right), \tag{4}$$

where P[A] is the fraction of A, and subscripts 0 and e refer to zero time and equilibrium conditions, respectively. The values evaluated by the two equations almost agreed with each other, and thereupon the mean value was adopted as k_{eff}. The rate constants, k_{AD} and k_{BD}, were calculated by

$$k_{eff} = k_{AD} + k_{BD} = k_{BD}\cdot(1 + K), \tag{5}$$

where K is the equilibrium constant defined as

$$K = P[\Delta\text{-}R]_e/P[\Delta\text{-}S]_e = P[\Delta\text{-}S]_e/P[\Delta\text{-}R]_e. \tag{6}$$

The each value of the fractions at equilibria ($P[\Delta\text{-}S]_e$, $P[\Delta\text{-}R]_e$, $P[\Lambda\text{-}S]_e$, and $P[\Lambda\text{-}R]_e$) was assumed to be the same for all runs at various pHs. The mean values of the corresponding fractions at pH 8.64 and 9.03 were adopted as the values at equilibria, and used to calculate the rate and equilibrium constants. The other rate constants, k_{AL} and k_{BL}, were similarly derived by using the fractions of the isomers in reaction (2). The values of each rate constant were calculated corresponding to two reaction times other than at equilibrium, and they were the same at respective pH values. The mean observed values of k_{AD}, k_{BD}, k_{AL}, and k_{BL} are summarized in Table 2.

The pH values at the reaction temperature, (100±2) °C, were estimated by extrapolation of the pH values measured at room temperature to those at 100 °C by reference to the temperature dependence data of pH of Sørensen buffer solution.

Experiments on effects of photoexcitation were carried out at pH 9.03. Light from 300 W short-arc type Xe lamp was focused on an area of about 4 cm diameter, and irradiated to the refluxing solution through a Pyrex glass vessel.

Results and Discussion

Table 1 shows that the (S)-phenylalaninato complexes, Δ-S and Λ-S, were predominant components of the starting materials. As the racemization of the coordinated phenylalanine proceeded, the fractions of the (R)-phenylalaninato complexes, $P[\Delta\text{-}R]$ and $P[\Lambda\text{-}R]$, increased. From Table 1, it is also seen that the fraction of Δ-isomers, $P[\Delta]$, or that of Λ-ones, $P[\Lambda]$, was always constant for all the dark reactions. Preliminary experiments revealed that no inversion around the metal ion was detected even though an isomer was refluxed in a neutral aqueous solution for four hours in the dark, and the results were the same with those by Vagg et al.[5] From such observations, we assumed the dark reaction paths as illustrated in Scheme 1.

Scheme 1 expresses that racemization occurs only on the amino carboxylato ligand (paths I and II), while the paths of the inversion reaction (paths III and IV) are intercepted by some energy barriers. Absence of the reactions through the paths III and IV was supported by the fact that both fractions of Δ- and Λ-isomers, $P[\Delta]$ and $P[\Lambda]$, were maintained constant in addition to the total concentration of the complexes. The enantiomers, Δ-S and Λ-R or Δ-R and Λ-S, are energetically equivalent. At equilibria the ratios of the fractions of the enantiomers, ($P[\Delta\text{-}S]_e/P[\Lambda\text{-}R]_e$) and ($P[\Delta\text{-}R]_e/P[\Lambda\text{-}S]_e$), were not unity but equal to ($P[\Delta]/P[\Lambda]$), which was always constant at 0.92±0.01 for the dark reactions. This is also explainable as a result of absence of the paths III and IV.

For each pH, the values of k_{AD} and k_{BD} agree with k_{AL} and k_{BL}, respectively, within experimental errors as shown in Table 2. Hence it is confirmed that the paths I and II are statically and dynamically identical reactions. Then the pseudo first-order rate constants k_A will be used for k_{AD} and k_{AL}, and k_B for k_{BD} and k_{BL} in the following. Since the stability of the two isomers in path I or II differed from each other, the magnitude of k_A did not coincide with that of k_B in each pH. It is suggested that Λ-S (or Δ-R) is more stable than Δ-S (or Λ-R), because k_A is greater than k_B. This is consistent with Vagg's report.[4,5] He has described that the main

Table 1. Fractions of the Isomers during the Racemization at 100 °C

pH[a]	t/min	$P[\Delta\text{-}S]$[b]	$P[\Delta\text{-}R]$	$P[\Lambda\text{-}S]$	$P[\Lambda\text{-}R]$	$P[\Delta]$[c]	$P[\Lambda]$
—	0	0.440	0.043	0.490	0.027	0.483	0.517
—	0	0.445	0.041	0.492	0.023	0.486	0.515
8.25	122	0.407	0.072	0.470	0.051	0.479	0.521
	241	0.382	0.097	0.462	0.060	0.479	0.522
8.64	60	0.403	0.078	0.468	0.051	0.481	0.519
	120	0.366	0.113	0.451	0.070	0.479	0.521
	2700(∞)	0.169	0.312	0.340	0.180	0.481	0.520
9.03	60	0.288	0.188	0.410	0.114	0.476	0.524
	120	0.220	0.257	0.371	0.152	0.477	0.523
	600(∞)	0.166	0.315	0.339	0.180	0.481	0.519
9.24	60	0.241	0.240	0.376	0.143	0.481	0.519
	120	0.189	0.287	0.349	0.175	0.476	0.524
9.69	30	0.219	0.257	0.361	0.163	0.476	0.524
	60	0.179	0.298	0.346	0.177	0.477	0.523
9.03[d]	60	0.258	0.177	0.457	0.108	0.435	0.565
	120	0.223	0.246	0.381	0.150	0.469	0.531

a) Extrapolated values at 100 °C. b) Fraction of $[\Delta\text{-}S]$ to the total concentration of the complex ions. c) Fraction of $([\Delta\text{-}S]+[\Delta\text{-}R])$ to the total concentration of the complex ions. The mean value of $P[\Delta]$ is 0.479±0.003, and that of $P[\Lambda]$ 0.521±0.003 for the dark reactions. d) Under irradiation of Xe light.

Table 2. Racemization Rate Constants/10^{-5} s^{-1} at 100 °C

pH	k_{AD}	k_{AL}	k_{BD}	k_{BL}
8.25	1.1±0.1	1.3±0.3	0.59±0.05	0.68±0.02
8.64	2.8±0.2	3.0±0.2	1.5 ±0.1	1.6 ±0.1
9.03	15 ±1	15 ±1	7.7 ±0.3	7.9 ±0.5
9.24	23 ±1	27 ±3	12 ±1	14 ±1
9.69	57 ±4	70 ±10	30 ±2	37 ±5

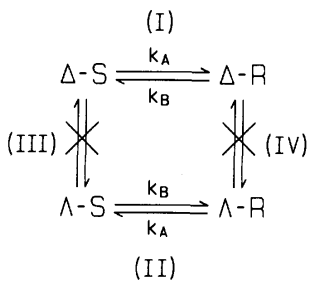

Scheme 1. Reaction paths for the dark system.

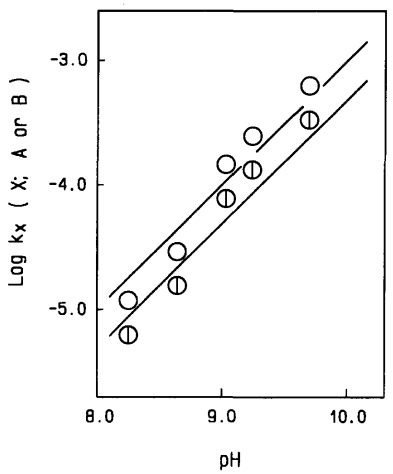

Fig. 1. Logarithms of the racemization rate constants k_A (○) and k_B (◑) vs. pH. Lines are drawn with slope of 1.0.

factor to determining the stability of these complex species is the steric interaction between one of the bipyridine protons and amino acid side chain.

In Table 2, the rate constants at pH 9.03 are greater than the corresponding ones at pH 8.64 by a factor about 5. On the other hand, in Table 1, the equilibrium constants evaluated by Eq. 6 for these pH values are the same (K=1.9) and independent of pH. These results indicate that this is base-catalyzed reaction. Logarithms of k_A and k_B are plotted against pH in Fig. 1. The plots are linear and both slopes can be regarded as unity, and it is indicated that the racemization rates are the first-order with respect to OH^- concentration. Hence, the expressions for the rate law are

Table 3. Reactions at Room Temperature (23—24°C)

	P[Δ-S]	P[Δ-R]	P[Λ-S]	P[Λ-R]	P[S]	P[R]
Irradiated	0.383	0.061	0.510	0.045	0.894	0.106
Nonirradiated	0.420	0.062	0.475	0.043	0.895	0.105

pH of the solution: 10.70; The reaction time: 2.3 h for both the irradiated and the nonirradiated reactions.

$$R_A = k_A'[OH^-][\Delta\text{-}S] = k_A'[OH^-][\Lambda\text{-}R] \quad (7)$$

and

$$R_B = k_B'[OH^-][\Lambda\text{-}S] = k_B'[OH^-][\Delta\text{-}R], \quad (8)$$

where R_A and R_B represent the rates for the faster and slower reactions, respectively, and k_A' and k_B' are the corresponding second-order rate constants. The values of k_A' and k_B' are derived from k_A and k_B,[9] as follows:

$$k_A' = (0.19 \pm 0.07)\ \text{mol}^{-1}\cdot\text{dm}^3\cdot\text{s}^{-1},$$

$$k_B' = (0.10 \pm 0.04)\ \text{mol}^{-1}\cdot\text{dm}^3\cdot\text{s}^{-1} \quad (\text{at } 100\,^\circ\text{C}).$$

Bada[11] has determined the racemization rate of free phenylalanine at pH 7.6:

$$\log k(\text{year}^{-1}) = 17.05 - 6208/T.$$

When T is 373 K, k is evaluated to $8.1\times10^{-8}\ \text{s}^{-1}$. On the other hand, extrapolation of the present data to pH 7.6 gives $k_A \simeq 4.4\times10^{-6}\ \text{s}^{-1}$ and $k_B \simeq 2.3\times10^{-6}\ \text{s}^{-1}$. These values of k_A and k_B are ca. 50 and ca. 30 times greater than the rate constant of free phenylalanine, respectively.

Widely, the rate of racemization of amino acids chelated to a metal ion or in proteins and peptides are of the first-order with respect to hydroxide ion concentration, while the free amino acids racemize with a small pH dependence in basic solutions.[10-12] Accordingly, the present results suggest that the coordinated phenylalanine racemizes without breaking bonds to the ruthenium ion. As for reaction mechanism, it would be the same as generally recognized base-catalyzed one: α-proton is abstracted by hydroxide ion to form a planar carbanion intermediate.[10-15]

When light was irradiated on the reaction system, the rapid reaction paths III and IV in Sheme 1 were induced. On the assumption that the equilibria for paths III and IV are established rapidly enough as compared to paths I and II, the system is apparently written by

$$S_{\text{total}} \underset{k_{ap}}{\overset{k_{ap}}{\rightleftarrows}} R_{\text{total}}, \quad (9)$$

where S_{total} refers (Δ-S+Λ-S) and R_{total} does (Δ-R+Λ-R), and k_{ap} is the apparent first-order rate constant. If the light has no effect on the paths I and II, k_{ap} can be yielded by using k_A and k_B for the dark reaction system. The relationship is expressed by

$$k_{ap} = (k_A + k_B\cdot K_{inv})/(K_{inv} + 1), \quad (10)$$

where K_{inv} is equilibrium constant for the inversion reaction paths III and IV and defined as

$$K_{inv} = P[\Lambda\text{-}S]_e/P[\Delta\text{-}S]_e = P[\Delta\text{-}R]_e/P[\Lambda\text{-}R]_e. \quad (11)$$

Considering energetic relationship of the isomers, K_{inv} is essentially the same with K for the racemization of the coordinated amino acid. The values of the rate constants of the dark reaction under pH 9.03, $k_A = 1.5\times10^{-4}\ \text{s}^{-1}$ and $k_B = 7.8\times10^{-5}\ \text{s}^{-1}$, and equilibrium constant, $K_{inv} = K = 1.9$, are substituted in Eq. 10 to yield $1.0\times10^{-4}\ \text{s}^{-1}$ for k_{ap}. On the other hand, k_{ap} was determined to be $9.9\times10^{-5}\ \text{s}^{-1}$ by using data under irradiation of light in Table 1. The two values agree very well with each other.

Effects of the irradiation on the racemization were also examined with solutions at pH 10.70 at room temperature where no racemization was expected to take place in the dark. Results in Table 3 show that the racemization is not caused even by the irradiation, although the inversion around the metal ion occured.

It is concluded that the racemization of the coordinated amino acid proceeds independently of the photoexcitation of the complex ions. Commonly, the racemization rate of an amino acid increases with increasing stability of the carbanion intermediate. The extent of the stability is influenced greatly by the electron-withdrawing power of the metal ion in complexes, when amino acid is chelated as a bidentate.[10,15] Photoexcited states of complexes such as ones studied have been considered to be ^{3}(MLCT) and (dd) excited states[16] which bring some electron deficient state on the central metal ion and some distortion on metal-ligand bonds, respectively. The excited states cause secondary reactions such as the photosensitized one and ligand substitutions. However, the present studies indicate that effects of the photoexcited states of the complexes are limited in the bis(2,2′-bipyridine)ruthenium moiety and do not extend to the α-carbon of the amino carboxylato ligand or events concerning the excited states are much faster than the racemization.

References

1) R. S. Vagg and P. A. Williams, *Inorg. Chim. Acta*, **51**, 61 (1981).

2) R. S. Vagg and P. A. Williams, *Inorg. Chem.*, **22**, 355 (1983).

3) F. S. Stephens, R. S. Vagg, and P. A. Williams, *Inorg. Chim. Acta*, **72**, 253 (1983).

4) T. J. Goodwin, P. A. Williams, and R. S. Vagg, *Inorg. Chim. Acta*, **83**, 1 (1984).

5) R. S. Vagg, *J. Proc. Roy. Soc. N. S. Wales*, **117**, 99 (1984).

6) E. C. Johnson, B. P. Sullivan, D. J. Salmon, S. A. Adeyemi, and T. J. Meyer, *Inorg. Chem.*, **17**, 2211 (1978); M. Tanaka, T. Nagai, E. Miki, K. Mizumachi, and T. Ishimori, *Nippon Kagaku Kaishi*, **1979**, 1112.

7) M. Fujita, Y. Yoshikawa, and H. Yamatera, *Chem. Lett.*, **1982**, 437.

8) When a mixed solution of *cis*-$[Ru(CO_3)(bpy)_2]$ and (*S*)-phenylalanine was refluxed for 20 h, it was found that phenylalaninato ligands in $[Ru(phe)(bpy)_2]ClO_4 \cdot 2H_2O$ isolated had been racemized completely.

9) The k_x' (x; A or B) is determined by

$$k_x' = k_x \cdot [H^+]/K_w$$

The value 5.8×10^{-13} mol^2 dm^{-6} was adopted for ion product of water, K_w, at 100 °C from L. G. Sillén and A. E. Martell, "Stability Constant of Metal-Ion Complexes," Spec. Publ. No. 17, The Chemical Society, London (1964), p. 39.

10) J. L. Bada and R. A. Schroeder, *Naturwissenschaften*, **62**, 71 (1975).

11) J. L. Bada, *Adv. Chem. Ser.*, **106**, 309 (1971).

12) G. G. Smith and R. C. Evans, "Biogeochemistry of Amino Acids," ed by P. E. Hare, T. C. Hoering, and K. King, Wiley Interscience, New York (1980), pp. 257—282.

13) D. A. Buckingham, L. G. Marzilli, and A. M. Sargeson, *J. Am. Chem. Soc.*, **89**, 5133 (1967).

14) A. Pasini and L. Casella, *J. Inorg. Nucl. Chem.*, **36**, 2133 (1974).

15) G. G. Smith, A. Khatib, and G. S. Reddy, *J. Am. Chem. Soc.*, **105**, 293 (1983).

16) T. J. Meyer, *Pure Appl. Chem.*, **58**, 1193 (1986).

A Structural Study of a Series of Bis(2,3-alkanedione dioximato)-nickel(II) Complexes in the Crystal and the Liquid States by X-Ray Absorption Spectroscopy

Seiichi YAMASHITA, Yoshio YANASE, Toshio YAMAGUCHI, and Hisanobu WAKITA*
Department of Chemistry, Faculty of Science, Fukuoka University, Nanakuma, Jonan-ku, Fukuoka 814-01
(Received March 1, 1989)

The structures of a series of bis(2,3-alkanedione dioximato)nickel(II) complexes, [Ni(R,R′-dioxH)$_2$], with dioxH=C(=NOH)-C(=NO), R and R′=H(**A**), R=CH_3 and R′=H(**B**), CH_3(**C**), C_2H_5(**D**), n-C_3H_7(**E**), n-C_4H_9(**F**), n-C_5H_{11}(**G**), n-C_6H_{13}(**H**), or n-$C_{10}H_{21}$(**I**), were investigated in crystals, pyridine solution, and melt (160 °C) by means of extended X-ray absorption fine structure (EXAFS) and X-ray absorption near edge structure (XANES), magnetic susceptibility, and UV/visible spectra. The magnetic susceptibility of complexes **C**, **F**, and **H** in crystals revealed a diamagnetic character. The electronic spectra of crystalline samples **E**, **F**, and **H** changed with the alkyl substituents of the glyoximato ligands, while the corresponding spectra in a pyridine solution were very similar to each other, independent of the glyoximato ligands. The EXAFS data showed that the average Ni-N distance within nickel(II) glyoximato complexes is 1.85—1.88 Å, practically independent of the alkyl substituents of the glyoximato ligands. The XANES spectra were found to correlate with the molecular packing structures of nickel(II) glyoximato complexes in crystals, pyridine solutions, and melt.

A series of 2,3-alkanedione dioximes are known as a good precipitant for Ni(II) and Pd(II) ions. The crystal structures of bis(2,3-alkanedione dioximato) nickel(II) complexes (Fig. 1) were reported for bis(dioximato)nickel(II), [Ni(gH)$_2$],[1] bis(2,3-butanedione dioximato)nickel(II), [Ni(dmgH)$_2$],[2] and bis(2,3-pentanedione dioximato)nickel(II), [Ni(emgH)$_2$].[3] In the crystal structure of [Ni(dmgH)$_2$], planar Ni(II) complexes are stacked face to face along the c-axis to form Ni···Ni linear chains;[4] hereafter, this molecular packing structure is referred to as the cross-type[5] ((b) and (d) in Fig. 2). On the other hand, for the crystal structures of [Ni(gH)$_2$] and [Ni(emgH)$_2$], planar Ni(II) complexes are arrayed like the slats of a venetian blind; this molecular packing structure is referred to as the blind-type[5] ((a) and (c) in Fig. 2). The molecular packing structure of the blind-type for [Ni(emgH)$_2$] complex is transformed into the cross-type by heating.[5] On the other hand, bis(2,3-alkanedione dioximato)-nickel(II) complexes in pyridine, acetone, and alcohols solutions show the same red-orange color as that in the crystalline state,[6] suggesting that no solvent molecule coordinates to a central nickel(II) ion. Moreover, [Ni(R,R′-dioxH)$_2$] complexes with long alkyl chains R′ (**E**—**I**) can be melted and sublimed by heating.

In spite of the above interesting phenomena, there are no comprehensive structural analyses of a series of bis(2,3-alkanedione dioximato)nickel(II) complexes in crystals, solution, and melt. In the present paper, the structures of the [Ni(R,R′-dioxH)$_2$] complexes given in Table 1 have been investigated in solid, pyridine solution, and melt by EXAFS[7] and XANES[8] spectra, magnetic susceptibility,[9] and UV/visible spectral measurements, in particular, to examine the effect of the length of the alkyl chains in glyoximato ligands on the molecular structure of the Ni(II) complexes and to reveal structural differences between the Ni(II) complexes in the three states.

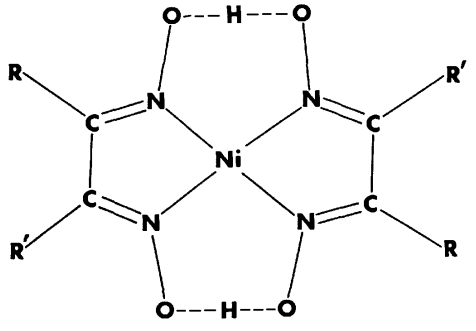

Fig. 1. Molecular structure of [Ni(R,R′-dioxH)$_2$].

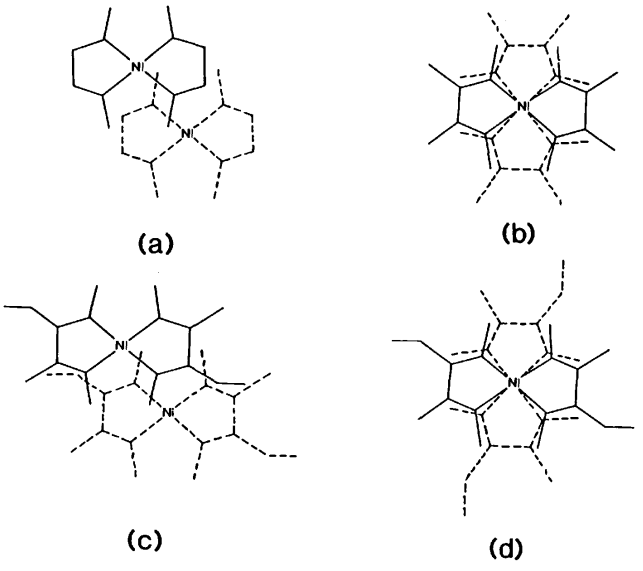

Fig. 2. Molecular packing structures for crystals of [Ni(R,R′-dioxH)$_2$]. (a) The blind-type for [Ni(gH)$_2$],[1] (b) the cross-type for [Ni(dmgH)$_2$],[2] (c) the blind-type for [Ni(emgH)$_2$],[3] and (d) the cross-type for thermally transformed [Ni(emgH)$_2$].[3]

Experimental

Sample Preparation. A series of 2,3-alkanedione dioximes were prepared as reported in the literature[5] and recrystallized from a mixture of methanol and chloroform.

Bis(2,3-alkanedione dioximato)nickel(II) complexes (Table 1) were prepared in the following manner. An aqueous solution, saturated with $[Ni(CH_3COO)_2]4H_2O$, was added to a hot concentrated methanol solution of a dioxime ligand. The complex formed was recrystallized more than five times from a mixture of methanol and chloroform, and then dried in a vacuum desiccator. They were identified by ^{13}C NMR spectrometry, X-ray powder diffractometry and thermal analysis.

Magnetic Susceptibility Measurements. For crystalline powder of complexes **C**, **F**, and **H**, and a pyridine solution and melt of complex **F**, the magnetic susceptibility was measured by a hand-made thermomagnetic analysis (TMA) system equipped with a temperature control unit,[9] The voltage, the electric current, and the intensity of the magnetic field used in the measurements were 50 V, 7A, and 1.6 T, respectively. A reference compound used for calibration of TMA was powdery $[Ni(en)_3]S_2O_3$, which had been purified by recrystallization from water twice.

UV/Visible Spectral Measurements. UV/visible spectra were measured over the wavelength from 400 to 600 nm with a Hitachi spectrophotometer U-3200. The opal method was used for crystalline samples, while the liquid film method was employed for pyridine solutions.

X-Ray Absorption Measurements. X-Ray absorption measurements were performed at the BL-10B station of the Synchrotron Radiation Research Facility (the Photon Factory) in the National Laboratory for High Energy Physics (KEK). X-Ray absorption data were collected in the range from ca. 400 eV on the lower energy side of the nickel *K*-edge (8331.7 eV) to ca. 1800 eV on the higher energy side.

Table 1. Composition of $[Ni(R,R'\text{-dioxH})_2]$

	Complex	R	R′
A	$[Ni(gH)_2]$	H	H
B	$[Ni(mgH)_2]$	CH_3	H
C	$[Ni(dmgH)_2]$	CH_3	CH_3
D	$[Ni(emgH)_2]$	CH_3	C_2H_5
E	$[Ni(mprgH)_2]$	CH_3	n-C_3H_7
F	$[Ni(bmgH)_2]$	CH_3	n-C_4H_9
G	$[Ni(mpegH)_2]$	CH_3	n-C_5H_{11}
H	$[Ni(hxmgH)_2]$	CH_3	n-C_6H_{13}
I	$[Ni(decmgH)_2]$	CH_3	n-$C_{10}H_{21}$

The time to collect X-ray photons was 2 seconds at each measuring point. Crystalline samples were measured in a pellet form after powdering crystals with an agate mortar. Pyridine solution samples, prepared by dissolving crystalline Ni(II) complexes in distilled pyridine, were measured with a polyethylene pouch sandwiched by polyacrylate holders. Melting samples were measured at 160 °C by use of a metallic cell on a hot-plate.

EXAFS spectra were analysed as previously reported.[7] The structural parameters (the interatomic distance, the mean-square displacement, and the coordination number) were determined by a curve fitting method applied to Fourier filtered EXAFS spectra. The basic formula are described below.

The observed EXAFS spectrum, $\chi_{obsd}(k)$, is Fourier transformed to a function, $F(r)$, by the following equation.

$$F(r) = \int_{k_{min}}^{k_{max}} k^3 \cdot \chi_{obsd}(k) \cdot \exp(2ikr)\mathrm{d}k \quad (1)$$

$$= F_{re}(r) + iF_{im}(r), \quad (2)$$

where k is the photoelectron wavenumber, $F_{re}(r)$ and $F_{im}(r)$ are the real and imaginary parts of the $F(r)$ function, respectively. k_{max} and k_{min} are the upper and lower k-values used in the transform. The radial function, $|F(r)|$, is given as

$$|F(r)| = [F_{re}(r)^2 + F_{im}(r)^2]^{1/2}. \quad (3)$$

The calculated EXAFS spectrum, $\chi_{calcd}(k)$, is given as

$$\chi_{calcd}(k) = \sum_j [N_j/(k \cdot r_j^2)] \cdot |f_j(\pi, k)| \cdot \sin(2kr_j + \phi_j(k)) \cdot \exp(-2r_j/\lambda_j) \cdot \exp(-2\sigma_j^2 k^2), \quad (4)$$

where r_j is the distance from an absorbing to backscattering atoms in the j-th coordination shell, N_j the number of the backscattering atoms at r_j, σ_j^2 the mean square displacement, and λ_j the mean free path. $|f_j(\pi,k)|$ and $\phi_j(k)$ are, respectively, the backscattering amplitude and the phase shift of the atoms in the j-th shell. A curve fitting is performed to minimize an error-square sum, U, as

$$U = \sum[k^3 \cdot \chi_{filt}(k) - k^3 \cdot \chi_{calcd}(k)]^2, \quad (5)$$

where $\chi_{filt}(k)$ is the Fourier backfiltered EXAFS spectrum.

Results

Magnetic Susceptibilities. The measured magnetic susceptibility of complexes **C**, **F**, and **H** is listed in Table 2. In the case of crystalline samples **C**, **F**, and **H**,

Table 2. Magnetic Susceptibility Measured for Complexes **C**, **F**, and **H**. χ_{Ni}, μ_B, and T Are the Magnetic Susceptibility Per Mole of Ni Atom, Bohr Magneton, and Temperature Measured, Respectively

	Sample		$\chi_{Ni}/10^{-6}$ cm^3 mol^{-1}	μ_B/BM	T/°C
C	$[Ni(dmgH)_2]$	Crystal	−34.0		20
F	$[Ni(bmgH)_2]$	Crystal	−27.0		20
		Melt	4.45	0.12	160
		Solution[a]	125	0.54	20
H	$[Ni(hxmgH)_2]$	Crystal	−22.6		20

a) Pyridine solution.

the magnetic susceptibility per mole of Ni, χ_{Ni}, measured at 20 °C was all negative. On the other hand, the χ_{Ni} values of a melt of sample **F** at 160 °C and of a pyridine solution of sample **F** at 20 °C became both slightly positive.

UV/Visible Spectra. Figure 3 shows the electronic spectra for complexes **E**, **F**, and **H** in crystals and pyridine solutions. The spectra of the crystalline samples (solid lines in the figure) show different d–d transition bands in the wavelength range from 430 to 550 nm, depending on the complexes. For the corresponding pyridine solutions, however, all spectra (dashed lines) resemble each other with a shoulder at about 480 nm.

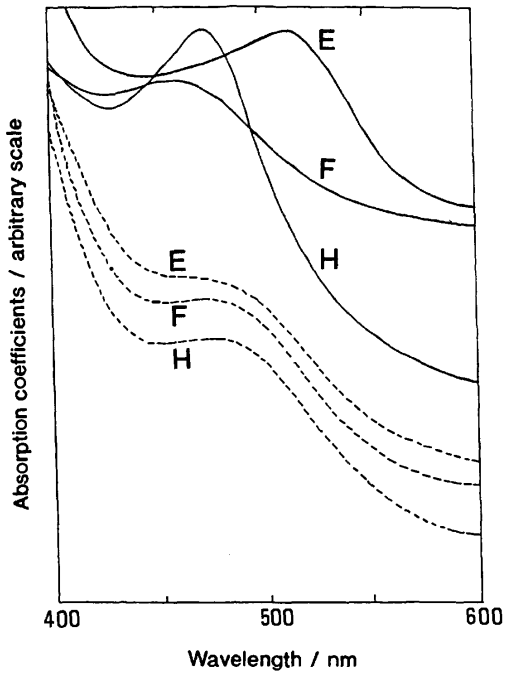

Fig. 3. UV/visible spectra of complexes **E**, **F**, and **H**. Solid lines; crystal, dashed lines; pyridine solution.

EXAFS Analysis. Figures 4 and 5 show the experimentally obtained $k^3\chi(k)$ curves of the crystalline powder of complexes **A**—**I**, and of pyridine solutions and melts of complexes **E**, **F**, and **H** respectively. The corresponding radial function curves (uncorrected for the phase shift) are shown in Figs. 6 and 7; the k range used in the Fourier transform was from 4.5 to 14.0 Å^{-1} for all the spectra. The prominent first peak at about 1.5 Å in each radial function is ascribable to Ni–N interactions within [Ni(R,R′-dioxH)$_2$] complexes. The second and third peaks observed at 2.5—4.0 Å should be ascribed to nonbonded Ni···C and Ni···O interactions within the complexes. The peaks appearing beside the sharp Ni–N peak are the side lobe.

In order to obtain the structural parameters of the Ni–N interactions, Fourier filtered EXAFS spectra were extracted for the first peak from 1.1 to 1.9 Å in the radial functions. Subsequently, the theoretical function of Eq. 4 was fitted to the filtered spectra from 5.5 to 13.0 Å^{-1} in the k space. The backscattering amplitude and phase shift for the Ni–N interaction were determined by a least-squares method for reference compound of known structure **A**. In the fits

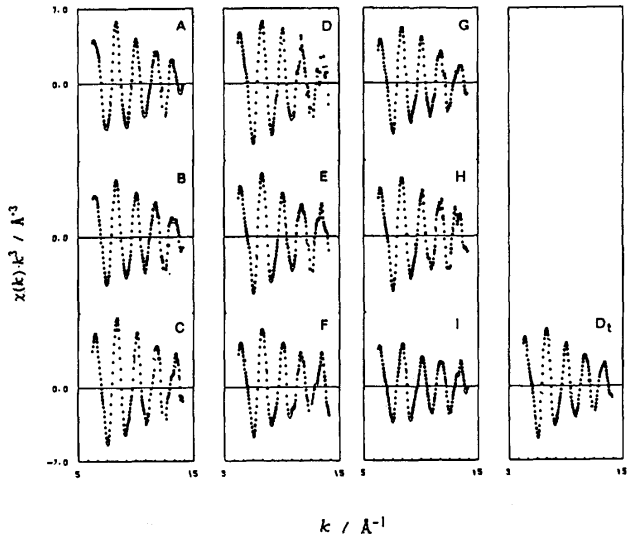

Fig. 4. Observed EXAFS, $k^3\chi(k)$, spectra for crystalline samples **A**—**I** and $\mathbf{D}_t$. $\mathbf{D}_t$ is thermally transformed crystal **D**.

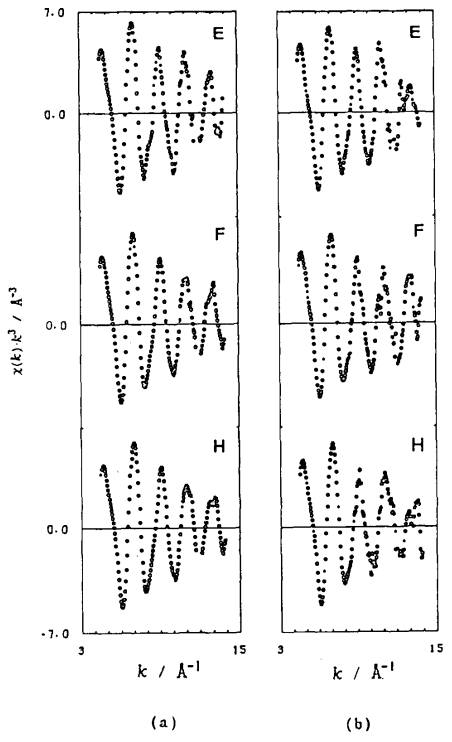

Fig. 5. Observed EXAFS, $k^3\chi(k)$, spectra for solutions and melts of complexes **E**, **F**, and **H**. (a) Pyridine solutions (b) melts (160 °C).

Table 3. Ni–N Interatomic Distances in Crystal, Pyridine Solution, and Melt Obtained from the EXAFS Analysis on the Basis of the One-Shell Model for the Ni–N Interactions. The Values in Parentheses Are X-Ray Diffraction Data

	Complex	r/Å		
		Crystal	Solution[a]	Melt[b]
A	$[Ni(gH)_2]$[c]	1.88 (1.87,[d] 1.88[d])		
B	$[Ni(mgH)_2]$	1.88		
C	$[Ni(dmgH)_2]$	1.87 (1.87,[e] 1.90[e])		
D	$[Ni(emgH)_2]$	1.85 (1.83,[f] 1.88[f])		
$\mathbf{D_t}$	$[Ni(emgH)_2]$[g]	1.88		
E	$[Ni(mprgH)_2]$	1.88	1.88	1.88
F	$[Ni(bmgH)_2]$	1.88	1.87	1.88
G	$[Ni(mpegH)_2]$	1.88		
H	$[Ni(hxmgH)_2]$	1.88	1.86	1.88
I	$[Ni(decmgH)_2]$	1.86		

a) Pyridine solution. b) Measured at 160°C. c) Structure standard. d) Ref. 1. e) Ref. 2 (poor R-value=0.16). f) Ref. 3. g) Thermally transformed crystal **D**.

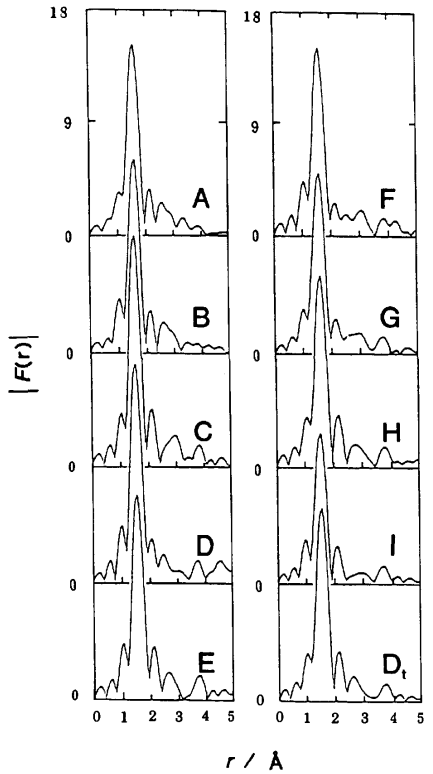

Fig. 6. The radial functions, $|F(r)|$, for crystalline samples **A**—**I** and $\mathbf{D_t}$. $\mathbf{D_t}$ is thermally transformed crystal **D**.

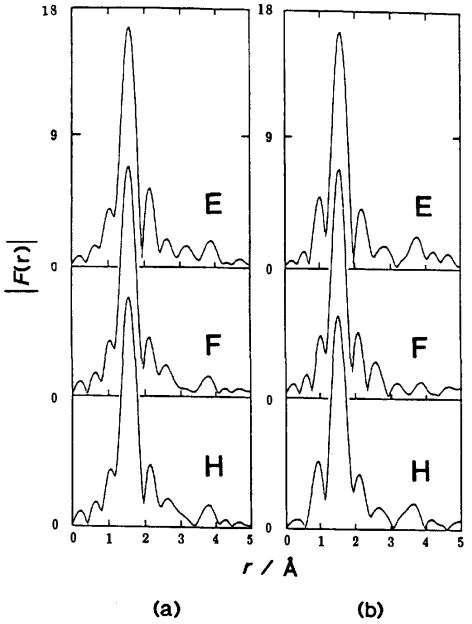

Fig. 7. The radial functions, $|F(r)|$, for solutions and melts of complexes **E**, **F**, and **H**. (a) Pyridine solutions (b) melts (160°C).

different Ni–N interactions in the crystal (1.87 and 1.88 Å) were treated as one-shell since the difference in the Ni–N distances was within the uncertainties in the EXAFS analysis; the average bond distance and the coordination number were fixed at 1.88 Å and 4,[1] respectively.

Table 3 summarizes the Ni–N interatomic distance within the complexes in crystals, pyridine solutions, and melts obtained from the curve-fittings. The Ni–N bond lengths fall within 1.85 — 1.88 Å independent of the alkyl substituents and the sample states.

In the curve fits of the Ni–N interactions for complexes **E**, **F**, and **H** in pyridine solutions the coordination numbers of four and six were tested for Ni(II)-coordination; the best fit was obtained only when the coordination number was four. This result shows that no pyridine molecules coordinate to a central nickel(II) ion. Therefore, in subsequent curve fits of pyridine solutions of complexes **E**, **F**, and **H** the coordination number was kept constant at four.

XANES Patterns. Figures 8 and 9 show, respectively, the XANES curves for crystals of complexes **A**—**I** and for pyridine solutions and melts of complexes **E**, **F**, and **H**. The XANES curves in the X-ray energy range from 8310 to 8380 eV can be classified into three kinds of patterns, which are referred subsequently to as α-, β-, and γ-patterns. In the three kinds of XANES

patterns were observed a pre-edge peak at 8330 eV and two peaks at 8348—8362 eV. The α-, β-, and γ-patterns correspond, respectively, to that of crystalline samples **A**, **B**, and **D**, that of crystalline samples **C**, **E**—**I**, and $\mathbf{D}_t$, and that of solution samples **E**, **F**, and **H**.

The α-pattern was characteristic of a shoulder at 8336 eV, while the β-pattern had a sharp peak at 8335 eV and a shoulder at 8342 eV. On the other hand, the γ-pattern observed for the pyridine solutions showed no distinct peak at 8335—8345 eV, but appreciable shoulders at 8337 and 8342 eV. The XANES curves of the melts of complexes **E**, **F**, and **H** showed the β-pattern.

Discussion

Crystalline State. As seen in Table 3, the Ni–N interatomic distances for crystalline samples **B**—**I** do not change significantly with the length of the alkyl substituents in the glyoximato ligands. In addition, the magnetic susceptibility (Table 2) of crystalline samples **C**, **F**, and **H** is all negative; thus, these [Ni(R,R′-dioxH)$_2$] complexes are diamagnetic in crystals. These experimental results indicate that the square planar NiN_4 skeleton within a series of the [Ni(R,R′-dioxH)$_2$] complexes is not significantly distorted in the solid state.

However, the XANES patterns (Fig. 8) of the crystalline [Ni(R,R′-dioxH)$_2$] complexes have shown different features (the α- and β-types) as mentioned in the previous section. The pre-edge peak due to the 1s→3d electron transition of nickel(II) ion observed at 8330 eV in all spectra does not show any remarkable change with respect to the shape and peak position. This fact indicates that the oxidation state of nickel atom in crystalline samples **B**—**I** is very similar to

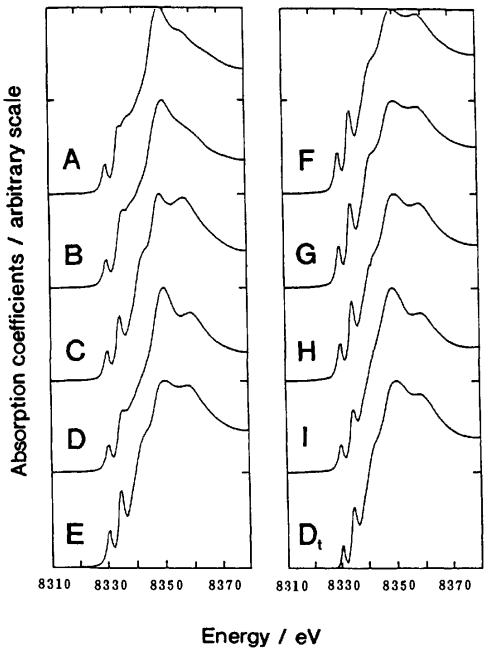

Fig. 8. The XANES spectra of crystalline samples **A**—**I** and $\mathbf{D}_t$. $\mathbf{D}_t$ is thermally transformed crystal **D**.

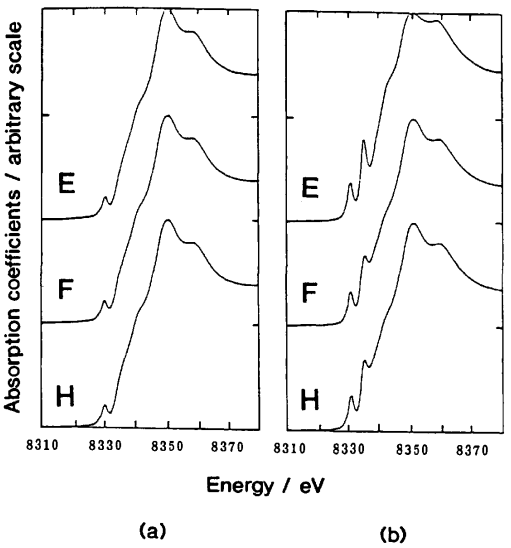

Fig. 9. The XANES spectra of solutions and melts of complexes **E**, **F**, and **H**. (a) Pyridine solutions, (b) melts (160°C).

Table 4. Packing Structures and XANES Patterns (Figs. 8 and 9) Found for [Ni(R,R′-dioxH)$_2$] Complexes in Crystals, Melts, and Pyridine Solutions. The α, β, and γ Refer to the Packing Types Described in the Text

	Complex	Crystal		Solution[a]	Melt[b]
		Packing	XANES	XANES	XANES
A	[Ni(gH)$_2$]	Blind	α		
B	[Ni(mgH)$_2$]		α		
C	[Ni(dmgH)$_2$]	Cross	β		
D	[Ni(emgH)$_2$]	Blind	α		
$\mathbf{D}_t$	[Ni(emgH)$_2$][c]	Cross	β		
E	[Ni(mprgH)$_2$]		β	γ	β
F	[Ni(bmgH)$_2$]		β	γ	β
G	[Ni(mpegH)$_2$]		β		
H	[Ni(hxmgH)$_2$]		β	γ	β
I	[Ni(decmgH)$_2$]		β		

a) Pyridine solution. b) Measured at 160°C. c) Thermally transformed crystal **D**.

each other, independent of the length of the alkyl chains in glyoximato ligands. Therefore, the variation of the XANES curves may be due to the change in the electronic state of nickel(II) ion influenced by neighboring atoms: the change in the symmetry around Ni(II) ion and/or different multiple scattering processes arising from different surroundings of Ni(II) ion in the complexes, i.e. different crystal packings.

Table 4 compares the crystal packing structures of Ni(II) glyoximato complexes with their XANES patterns. According to the crystal structures reported,[1-3] the packing form of complexes **A** and **D** is of the blind-type ((a) and (c) in Fig. 2); the corresponding XANES curves show the α-pattern. On the other hand, complexes **C** and $\mathbf{D}_t$ have the cross-type packing structure ((b) and (d) in Fig. 2); their XANES curves belong to the β-pattern. The crystal structures of complexes **B** and **E**—**I** are not available in the literature. X-Ray diffraction patterns were measured for all the powdered samples **A**—**I**, but none of these was found to be isomorphic; thus the packing structures of complexes **B** and **E**—**I** could not be estimated from the X-ray powder patterns. It is suggested, however, from UV/visible spectral measurements[5] that the crystal packing of complex **E** is similar to that of complex **C** with the cross-type packing structure.

In spite of the above limited number of the crystal structures reported for [Ni(R,R′-dioxH)$_2$] complexes, we may discuss the correlation between the XANES patterns and the packing types in the crystal structure. As seen in Fig. 2, in the case of the packing structure of the blind-type, the axial sites above and below a central Ni atom are occupied by light (oxygen, nitrogen, and carbon) atoms, while for the packing structure of the cross-type nickel atoms in other layers are above and below a central Ni(II) ion. Thus, the different feature in the XANES spectra shown in Figs. 8 and 9 is probably ascribed to the different types of the interactions between an Ni(II) ion and the atoms present above and below the Ni(II) ion since the electronic state of Ni(II) glyoximato complexes or the multiple scattering process through different backscattering atoms will change. This conclusion is also supported from the experimental finding that the γ-pattern is observed for all pyridine solutions (Fig. 9), in which no pyridine molecule directly coordinates to a central nickel(II) ion.

On the basis of the above relation between the XANES patterns and the packing types we may presume a packing structure of the other complexes whose crystal structures are not known. Since the XANES curve of complex **B** shows the α-pattern, the complex probably has the blind-type packing structure. Similarly, from the XANES curves of complexes **E**—**I** showing the β-pattern, the packing structure of the complexes may be of the cross-type.

Solutions and Melts. Unlike the crystalline compounds, the solution and melt of sample **F** showed a slightly positive value (0.54 and 0.12 BM) of their magnetic susceptibility (Table 2). The positive magnetic susceptibility of bis(2-propanedione dioximato)nickel(II) in pyridine solution was reported to be 1.5 BM.[10]

In pyridine solutions the electronic spectra of the three complexes (**E**, **F**, and **H**) resemble each other (Fig. 3), independent of the length of the alkyl substituents, so do the XANES spectra (Fig. 9). From these experimental findings the complexes **E**, **F**, and **H** may have a similar NiN_4 moiety in pyridine solutions.

For melts of complexes **E**, **F**, and **H**, the Ni–N interatomic distances and the XANES patterns are similar to those in crystals (Table 3). The XANES spectra of the melts show the β-pattern, suggesting that the complex molecules in the melts still retain cross-type packing structure, similar to that found in the corresponding crystals.

The authors wish to thank Dr. Masaharu Nomura for his advice in the X-ray absorption spectral measurements and Dr. Mikiya I for his help in preparation of the compounds. This work has been performed under the approval of the Photon Factory Program Advisory Committee (Proposal No. 86-008). All the calculations were performed with an FACOM M-380 R computer at the Computer Center of Fukuoka University.

References

1) M. Calleri and G. Ferraris, *Acta Crystallogr.*, **22**, 468 (1967).

2) L. E. Godycki and R. E. Rundle, *Acta Crystallogr.*, **6**, 487 (1953).

3) R. H. Bowers, C. V. Banks, and R. A. Jacobson, *Acta Crystallogr., Sect. B*, **28**, 2318 (1972); A. G. Sharpe and D. B. Wakefield, *J. Chem. Soc.*, **1957**, 281; B. Egneus, *Anal. Chim. Acta*, **48**, 291 (1969).

4) S. Yamada and R. Tsuchida, *Bull. Chem. Soc. Jpn.*, **27**, 156 (1954); C. V. Banks and D. W. Barnum, *J. Am. Chem. Soc.*, **80**, 3579 (1958); J. C. Zahner and H. G. Drickamer, *J. Chem. Phys.*, **33**, 1625 (1960); C. V. Banks and S. Anderson, *Inorg. Chem.*, **2**, 112 (1963).

5) M. I, H. Wakita, and I. Masuda, *Bull. Chem. Soc. Jpn.*, **56**, 1627 (1983).

6) S. Shinra, *Kagaku*, **19**, 939 (1963).

7) Y. Tajiri and H. Wakita, *Bull. Chem. Soc. Jpn.*, **59**, 2285 (1986); Y. Tajiri and H. Wakita, *Nippon Kagaku Kaishi*, **11**, 1531 (1986); "EXAFS Spectroscopy," ed by B. K. Teo and D. C. Joy, Plenum Press, New York (1981).

8) "EXAFS and Near Edge Structure," ed by A. Bianconi, L. Incoccia, and S. Stipcich, Springer Series in Chemical Physics 27 of International Conference, Tokyo (1982).

9) K. Miyokawa and I. Masuda, *Fukuoka Univ. Sci. Rep.*, **10**, 85 (1980).

10) J. B. Willis and D. P. Mellor, *J. Am. Chem. Soc.*, **69**, 1237 (1947).

A Modified Vapor Saturation Method for Preparing Aqueous Solutions of Solid Aromatic Hydrocarbons

Isao SANEMASA,* Kazunari ISHIBASHI, Masaya KUMAMARU, and Toshio DEGUCHI
Department of Chemistry, Faculty of Science, Kumamoto University, Kurokami 2-39-1, Kumamoto 860
(Received April 3, 1989)

An excess quantity of a solid hydrocarbon is dispersed in water, and then air is bubbled through the aqueous phase to produce the solute vapor. The vapor is introduced into a separate water phase and circulated in a closed system. Aqueous solutions saturated with some solid aromatic hydrocarbons can be prepared in a relatively short time without any need to remove solute microcrystals. It can be confirmed whether the solubility obeys Henry's law. The present method provides us with rough enthalpy of sublimation of a solute if its solubility follows Henry's law. Biphenyl, naphthalene, phenanthrene, and anthracene were examined as solutes.

We recently proposed a method to prepare aqueous solutions saturated with solid aromatic hydrocarbons.[1] The principle is as follows: a solid solute is added in excess to a suitable organic solvent so that a part of the solute is always present in solid state in the solvent, then, air is bubbled through the solvent, and the resulting vapor is introduced into water to circulate in a closed system. It was found that 1-octanol was the most suitable solvent for preparing aqueous solutions saturated with solid aromatic hydrocarbons.

The present work concerns a modification of the previous method. The organic solvent was not used here, but water was used to disperse solid solutes. This work aims to see whether or not the modification is successful and, if successful, to confirm whether Henry's law holds for some solid aromatic hydrocarbons.

Experimental

Materials. The solid aromatic hydrocarbons used as solutes are the same as those examined in the previous paper.[1] Distilled deionized water was used throughout this work.

Apparatus and Procedures. The apparatus used for preparing aqueous solutions saturated with solute vapor is essentially the same as that previously used,[2] except for some minor modification. The apparatus was composed of two main glass parts: a pear-shaped long-necked vessel of 50 cm^3 capacity in which ca. 0.5 g of solid hydrocarbon roughly powdered by agate mortar was placed together with ca. 20 cm^3 water (we call this vessel the "solute reservoir") and a separatory funnel of 200 cm^3 capacity in which 150 cm^3 water was placed (we call this funnel the "solubility flask"). These two vessels were connected with glass and Teflon tubes incorporated with a Viton diaphragm airpump (Iwaki Type AP-32 Z) and a round-bottom flask of 200 cm^3 capacity to trap fine solute powders.

The temperature of the solubility flask was held at 25±0.1 °C by circulating water from a thermostated water bath through a jacket surrounding the funnel. The solute reservoir and the trap-flask were immersed in a separate water bath kept constant at any desired temperature below 25 °C. The temperature of a chamber containing the assembled apparatus was always kept higher than that of the solute reservoir.

By means of the pump, air was bubbled at a flow rate of ca. 0.5 $dm^3\ min^{-1}$ through the solute reservoir via a glass capillary, and the resulting solute (and water) vapor was introduced through the trap-flask into water in the solubility flask to disperse via a glass capillary, and circulated in the closed system. After solubility equilibrium was attained, a suitable portion of the aqueous solution was transferred from the separatory funnel into a glass test tube, in which a 5 cm^3 portion of cyclohexane had previously been placed, and weighed; prior to the operation of stopcock attached to the funnel bottom, the funnel position was slightly lowered so as to allow air to enter the funnel through its top opening. Extractions were made after diluting the aqueous phase to 20 cm^3 with water.

The cyclohexane extract, after dehydrated with anhydrous sodium sulfate, was analyzed by UV absorption (biphenyl: 247.5, naphthalene: 285, phenanthrene: 250, anthracene: 251.5 nm) with a Hitachi 100-50 spectrophotometer and by fluorescence for anthracene (excitation 253.6, emission 378 nm) with a JASCO FP-770 spectrofluorometer.

For each solute, a calibration curve was prepared by extracting a 5 cm^3 portion of the standard cyclohexane solution containing a known amount of the solute with 20 cm^3 water.

Results and Discussion

The Time Required for Saturating Water with Solute Vapor. The circulation rate of solute vapor may affect the time for attaining the equilibrium solubility, and high circulation rates are desirable to reduce the time required. In the present work, however, the circulation rate was suppressed to be moderate, because at higher circulation rates extraordinarily high "solubility" values were sometimes observed probably due to accidental contamination with solute fine powders. The time necessary to saturate is as follows: 1 h for biphenyl and naphthalene, 6 h for phenanthrene, and 20 h for anthracene.

The term "equilibrium solubility" is used in this paper to describe the solubility obtained under the condition that the temperature of the solute reservoir differs from that of the solubility flask.

The equilibrium solubility can be attained from both directions: approaches from either lower or

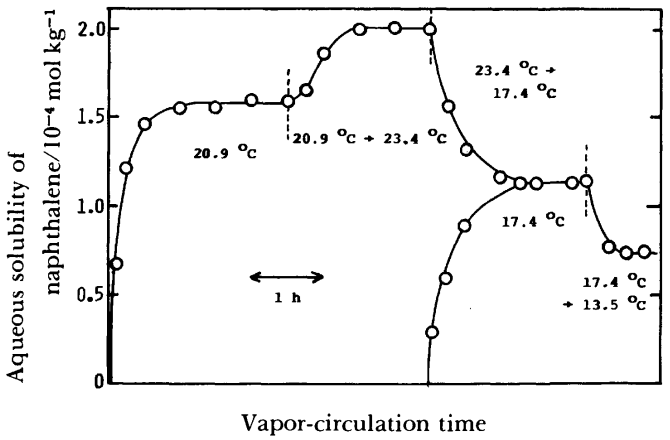

Fig. 1. Equilibrium solubility vs. vapor-circulation time. The temperature of solute reservoir in which solid naphthalene had been placed together with water was set as specified in Figure, while that of solubility flask was held constant at 25 °C.

Table 1. Equilibrium Solubility of Solid Aromatic Hydrocarbons in Water at 25 °C

Temperature of solute	Solute vapor pressure[a]	Equilibrium solubility[b]
°C	Pa	mol kg^{-1}
Biphenyl		
13.7	0.311	1.35×10^{-5}
20.1	0.621	2.60
23.1	0.852	3.48
24.9	1.03	4.25
Naphthalene		
16.6	4.60	1.05×10^{-4}
20.5	6.95	1.54
23.1	9.07	1.99
24.9	10.88	2.38
Anthracene		
10.9	1.08×10^{-4}	$0.329(0.389)\times10^{-7}$
15.2	2.06	0.646(2.22)
19.1	3.62	1.09(3.03)
20.7	4.55	1.21(3.30)
22.1	5.55	1.49(3.69)
23.1	6.38	1.64(3.80)
24.1	7.34	1.83(4.11)
24.8	8.08	2.08(4.10)
24.9	8.19	2.20(4.33)
Phenanthrene		
15.4	0.711×10^{-2}	2.34×10^{-6}
20.7	1.36	4.09
21.9	1.57	4.33
23.0	1.79	5.18
24.2	2.07	5.91
25.0	2.27	6.22

a) The vapor pressure data of biphenyl,[3] naphthalene,[4] anthracene,[5] and phenanthrene,[5] are taken from the literature. b) Values of anthracene in the parentheses were obtained by UV absorption measurements, and these values are unreliable for the solubility data owing to some unknown impurities present in this hydrocarbon (see Text).

higher vapor pressure. This is illustrated in Fig. 1, which shows how naphthalene concentration in water at 25 °C varies with the circulation time after the temperature of the solute reservoir was changed.

Equilibrium Solubility and Solute Vapor Pressure. In Table 1 are given the equilibrium solubility values obtained under the experimental condition that the temperature of the solute reservoir was varied while that of the solubility flask was held constant at 25 °C. The equilibrium solubility of each solute is found to be proportional to the solute vapor pressure (Fig. 2). That is, solubility obeys Henry's law

$$P = K_H X_2, \quad (1)$$

where P is the partial pressure of the solute, X_2 is the mole fraction of the dissolved solute, and K_H is the Henry's law constant. Here, the solute in water being in equilibrium with the solid solute in the solute reservoir, we have taken the partial pressure of the solute to be equal to the vapor pressure of pure solid at the temperature of the solute reservoir. The vapor pressure at any desired temperature of each solid hydrocarbon, biphenyl,[3] naphthalene,[4] anthracene,[5] and phenanthrene,[5] has been estimated from the literature. The Henry's law constant at 25 °C and the aqueous solubility in mol kg^{-1} determined from K_H are summarized in Table 2. The solubility thus determined for the solute studied in this work is in reasonable agreement with that reported in our previous work and that cited therein.[1]

The Aqueous Solubility of Anthracene. In the beginning of this work, the anthracene solubility has been measured by the UV absorption method. Then, it appeared, as can be seen from Table 1, that the equilibrium solubility plotted against the anthracene vapor pressure, does not follow Henry's law, and that the solubility at 25 °C, 4.33×10^{-7} mol kg^{-1}, is two times larger than our previous value. We, then, adopted the fluorescence method to determine the concentration of anthracene, and found that Henry's law holds for this solute and that the solubility is in a reasonable agreement with our previous value.[1] We speculate that this is caused by some impurities present in anthracene and that the impurity is volatile and responds to UV absorption, but not to fluorescence measurements. The present method uses water as the disperse medium, and hence, some impurities are readily volatilized and dissolved into the separate water phase.

As was noted in the previous paper,[1] the literature data of anthracene solubility can be grouped into two well-defined values: 2.5 and 4.2×10^{-7} mol dm^{-3}. The lower value has been reported by researchers who adopted either the fluorescence technique[6] or the combination of HPLC-separation and absorption measurement.[7] This clearly indicates that some impurities are responsible for the higher solubility

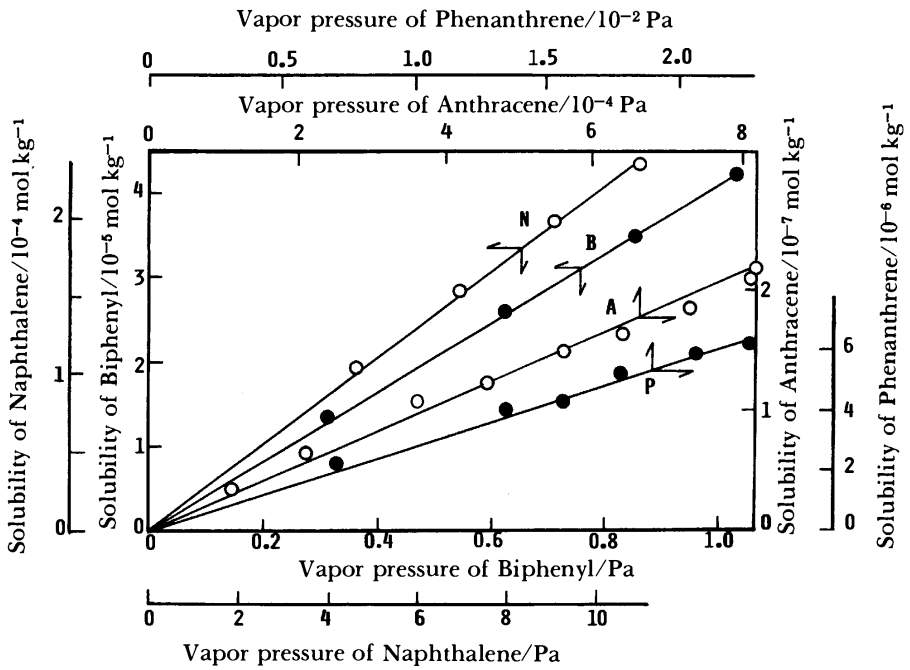

Fig. 2. Equilibrium solubility vs. solute vapor pressure. Biphenyl (B), naphthalene (N), anthracene (A), and phenanthrene (P).

Table 2. Henry's Law Constant and Aqueous Solubility at 25 °C

Solute	$P^{a)}$	$K_H{}^{b)}$	$S^{c)}$
	Pa	Pa	mol kg^{-1}
Biphenyl	1.04	1.34×10^{6}	4.30×10^{-5}
Naphthalene	10.98	2.52×10^{6}	2.42×10^{-4}
Anthracene	8.31×10^{-4}	2.11×10^{5}	2.18×10^{-7}
Phenanthrene	2.27×10^{-2}	1.96×10^{5}	6.45×10^{-6}

a) The vapor pressure of solid hydrocarbon at 25 °C taken from the literature. b) Henry's law constant determined in this work. c) The solubility of hydrocarbon in water estimated from K_H.

value of anthracene. May et al., who used the latter technique, assumed the impurity to be phenanthrene. If it is true, so long as the fluorescence technique is used, the presence of phenanthrene would increase considerably the apparent solubility of anthracene owing to the relatively high solubility of phenanthrene which also has fluorescence. We have analyzed both the cyclohexane extract of aqueous solution saturated with the vapor of anthracene and the cyclohexane solution of this solid hydrocarbon by gas chromatography (Shimadzu GC-14A, detector: FID, column packing: BBBT, temperature: 195 °C). As the result, phenanthrene was detected in neither of the cases.

In our previous study, where the UV absorption technique was employed, the value close to the present fluorescence result was obtained. This is probably due to that the impurities in the solid anthracene are soluble in such an organic solvent as 1-octanol. That is, they remain soluble in 1-octanol, while volatile in water.

The Utility of the Vapor Saturation Method. The use of a disperse medium is favorable for generating the vapor of the solute which exists as solid at ordinary temperatures. For this purpose, benzene and cyclohexane cannot be used,[1] but either 1-octanol or water is suitable. When water is used as the disperser, care should be taken, as was just mentioned above, of volatile impurities which might be present in the solid solute. The use of water as the disperser, however, makes the solubility system much simple, because the influence of 1-octanol, which is also dissolved in water, need not be considered.

We have studied aqueous solubility of volatile nonelectrolytes such as metallic mercury,[8] benzene and alkylbenzenes,[2] and iodine,[9] and demonstrated that the solute vapor circulation method is useful to determine experimentally whether the solute follows Henry's law. This is also the case for the solid aromatic hydrocarbons studied here. The present method has a potential application to such studies that

association of some hydrophobic solutes with aromatic hydrocarbons is to be determined in water by measuring the change of the solubility of aromatics.

The influence of temperature on the vapor pressure of a solid is given by the well-known equation

$$\mathrm{d} \ln P/\mathrm{d}T = \Delta H_{sub}/(RT^2), \quad (2)$$

where P is the sublimation vapor pressure, ΔH_{sub} is the enthalpy of sublimation, and T and R have usual meaning. As the concentration of a solid solute in the aqueous phase increases, the solute crystallizes out when the partial pressure of the solid solute equals its sublimation vapor pressure. This is the case for what happens in the solute reservoir in our present approach. We, therefore, take the vapor pressure, P, which appears in Eqs. 1 and 2, equal to each other in its physical quantity. Then, by combining Eqs. 1 and 2, ΔH_{sub} can be estimated for a solid hydrocarbon. Here, it is assumed that ΔH_{sub} is independent of temperature over the range studied. For each solute studied in this work, $\log X$ was plotted against T^{-1} (Fig. 3), and we get a straight line with a slope which corresponds to $-\Delta H_{sub}/(2.303\times8.314)$. The ΔH_{sub} value thus estimated over the temperature range of 15 to 25 °C is given in Table 3 together with some literature data. Reasonable agreements are found between data of this and the preceding works except for phenanthrene.

Two techniques have been used to prepare aqueous

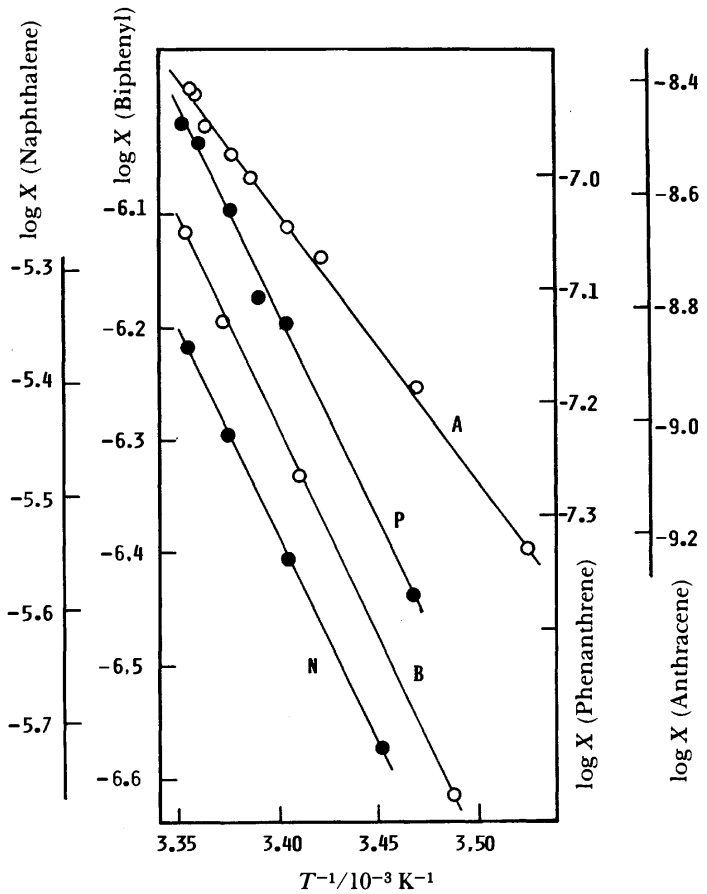

Fig. 3. $\log X$ vs. T^{-1}. X: equilibrium solubility at 25°C in mole fraction; T: absolute temperature of solute; biphenyl (B), naphthalene (N), anthracene (A), and phenanthrene (P).

Table 3. The Enthalpy of Sublimation Estimated from Equilibrium Solubility Over 15—25 °C

Solute	ΔH_{sub}/kJ mol^{-1}			
	This work	Literature data		
Biphenyl	72.4	72.8,[11]	75.8[3]	
Naphthalene	71.0	72.4,[5]	72.6,[12]	75.8[13]
Anthracene	90.9	91.8,[13]	103.8,[3]	104.5[12]
Phenanthrene	73.3	86.6,[3]	92.5,[12]	95.0[13]

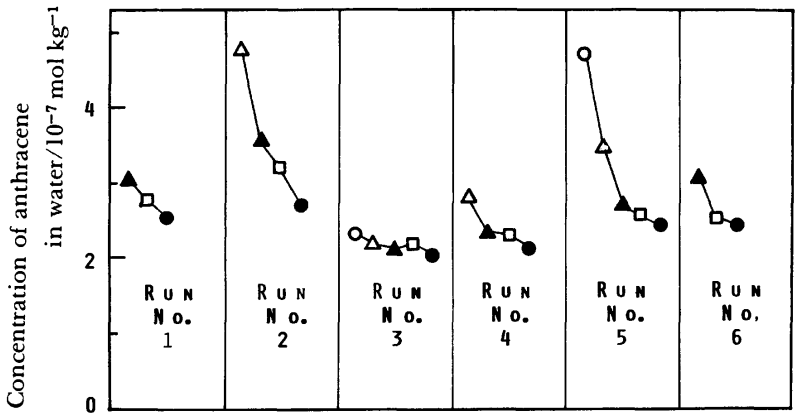

Fig. 4. Concentration of anthracene in water prepared by "shake-flask" technique, six replicated runs. The solid anthracene was stirred in water, and then, allowed to stand for 5(○), 7(△), 9(▲), 11(□), and 14 days(●).

solutions saturated with liquid or solid solutes: one is called "generator column,"[7] and the other "shake-flask." These techniques make the solute phase directly contact with water. The latter technique, most widely used for solubility studies, requires a long time to attain the solubility equilibrium and, subsequently, to settle the excess solute phase. In this work, we have also prepared aqueous solutions of anthracene by the conventional shake-flask method using the device described elsewhere,[10] to check the value obtained by the present solute vapor circulation method. The results of fluorescence measurements in six replicated runs are shown in Fig. 4. After an excess quantity of the solid hydrocarbon had been stirred in water for 24 h at 25 °C, the mixture was allowed to stand in the thermostated bath for two weeks, during which a portion of the aqueous phase was withdrawn periodically via a side-arm attached to the device. It was found that the solubility value approaches on standing for quite a long time the value obtained by the vapor circulation method. A "clear" aqueous phase appeared after the mixture was allowed to stand overnight. Nevertheless, considerably high "solubility" was observed. This is probably due to dispersion rather than true dissolution.

Advantages of the present method are (1) saturated solutions can be prepared in a relatively short time and (2) the removal of the excess solute phase is not required.

References

1) M. Akiyoshi, T. Deguchi, and I. Sanemasa, *Bull. Chem. Soc. Jpn.*, **60**, 3935 (1987).
2) I. Sanemasa, M. Araki, T. Deguchi, and H. Nagai, *Bull. Chem. Soc. Jpn.*, **55**, 1054 (1982).
3) A. Aihara, *Nippon Kagaku Zasshi*, **76**, 492 (1955).
4) L. Fowler, W. N. Trump, and C. E. Vogler, *J. Chem. Eng. Data*, **13**, 209 (1968).
5) R. S. Bradley and T. G. Cleasby, *J. Chem. Soc.*, **1953**, 1690.
6) F. P. Schwarz, *J. Chem. Eng. Data*, **22**, 273 (1977).
7) W. E. May, S. P. Wasik, and D. H. Freeman, *Anal. Chem.*, **50**, 175 (1978).
8) I. Sanemasa, *Bull. Chem. Soc. Jpn.*, **48**, 1795 (1975).
9) I. Sanemasa, T. Kobayashi, C. Y. Piao, and T. Deguchi, *Bull. Chem. Soc. Jpn.*, **57**, 1352 (1984).
10) I. Sanemasa, M. Kumamaru, K. Ishibashi, and T. Deguchi, *Bull. Chem. Soc. Jpn.*, **62**, 1061 (1989).
11) N. F. H. Bright, *J. Chem. Soc.*, **1951**, 624.
12) C. G. de Kruif, *J. Chem. Thermodyn.*, **12**, 243 (1980).
13) W. J. Sonnefeld, W. H. Zoller, and W. E. May, *Anal. Chem.*, **55**, 275 (1983).

 © 1989 The Chemical Society of Japan Bull. Chem. Soc. Jpn., 62, 2913—2918 (1989)

Hexacarbonylmolybdenum(0)-Induced Dechalcogenization of Allylic Sulfides, Sulfones, and Selenides: Nucleophilic Substitution and Reductive Dechalcogenization

Yoshiro MASUYAMA,* Kohji YAMADA, Soh-hei SHIMIZU, and Yasuhiko KURUSU
Department of Chemistry, Faculty of Science and Technology, Sophia University, Kioicho, Chiyoda-ku, Tokyo 102
(Received February 13, 1989)

Hexacarbonylmolybdenum(0)-induced dechalcogenization of allylic sulfides **I**, sulfones **II**, and selenides **III** in refluxing dioxane, which led to nucleophilic substitutions with carbon nucleophiles. Attack of the relatively bulky nucleophile, 2-ethoxycarbonyl-2-sodiocyclopentanone occurred regioselectively at the less substituted end of the allyl unit after the dechalcogenization to give only one isomer. Attack of diethyl sodiomalonate to **I** and **III** occurred preferentially at γ-position, and that to **II** occurred preferentially at the more substituted end of the allyl unit after the desulfonylation. In the absence of the carbon nucleophiles, treatment of **I**, **II**, and **III** with $Mo(CO)_6$ in refluxing dioxane caused reductive dechalcogenization. Addition of H_2O accelerated the reductive dechalcogenization.

Organochalcogenides have made a great contribution to organic synthesis, due to the ability of the chalcogenide group to stabilize the adjacent carbanion.[1,2] In particular, allylic chalcogenides have been widely applied to the reactions with various electrophiles as reagents for three carbon homologation.[3] Since the chalcogenide-functional groups are rarely present in the final synthetic target, removal of the functional groups becomes an important subject. The representative removal methods are (1) β-elimination of the sulfide and selenide via oxidation[1,2] and of the sulfone under basic conditions[1,4] and (2) reductive defunctionalization of all groups with metal reagents.[1,5] The organochalcogen groups have not been generally utilized as the leaving groups in the nucleophilic substitutions with carbon nucleophiles. Use of a metal reagent, which has oxidizing-ability, may permit the nucleophilic substitution.[6] Hexacarbonylmolybdenum [$Mo(CO)_6$] seems to have both oxidizing and reducing abilities, since molybdenum has a variety of oxidation states between −2 and +6. In addition, molybdenum has thiophilicity. Thus, $Mo(CO)_6$ becomes an effective reagent for both the rare nucleophilic substitution (oxidation) and the reductive defunctionalization (reduction) of organosulfur compounds. The objective of our study is the development of an approach to this subject which has been achieved in allylic systems such as allylic sulfides and sulfones (Eq. 1).[7]

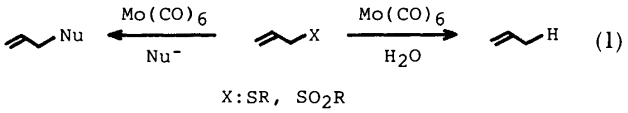

(1)

The early applications of the transition metal-promoted substitutions are represented by the nickel-catalyzed reaction of the allylic sulfides with Grignard reagents[8] and the palladium- or molybdenum-catalyzed reaction of the allylic sulfones with active methylene compounds.[9] These metal-promoted substitutions probably proceed via π-allylmetal complexes (Eq. 2).

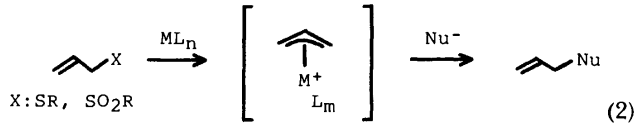

(2)

In both the nucleophilic substitutions and the reductive defunctionalizations of allylic sulfides, sulfones, and selenides with $Mo(CO)_6$, the properties of these organochalcogen groups should affect the coordination of olefins to molybdenum, namely the formation of π-allylmolybdenum complexes, to exhibit unique regiochemistry in the reaction of the allylic moieties.

Results and Discussion

Nucleophilic Substitution. The $Mo(CO)_6$-induced nucleophilic substitution of allylic sulfides **I**, sulfones **II**, or selenides **III** with carbon nucleophiles, diethyl sodiomalonate (**1**) or 2-ethoxycarbonyl-2-sodiocyclopentanone (**2**) proceeded in refluxing dioxane under a nitrogen atmosphere to afford allylic alkylation products. The results are summarized in Table 1. In the reactions of **I** at 110 °C, use of dioxane as a solvent exhibited higher yield than that in solvents such as DMF and toluene, while the reaction did not occur in refluxing THF or benzene. Reactivity of **II** and **III** seems to be slightly higher than that of **I** in the nucleophilic substitution. Using any allylic compound mentioned above, the relatively bulky nucleophile **2** attacked regioselectively at the less substituted end of the allyl unit after the defunctionalization to produce only one isomer **IV** (Entries 4—7, 22—25, 35—38), as

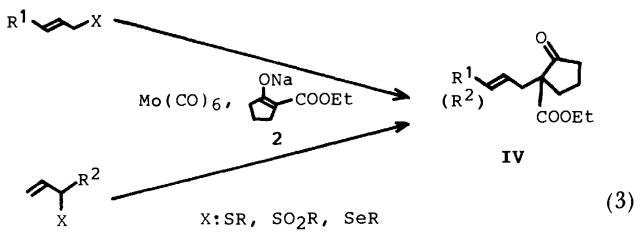

(3)

shown in Eq. 3. The attack of nucleophile **1** to **I** occurred at γ-position (product **VI**) in preference to

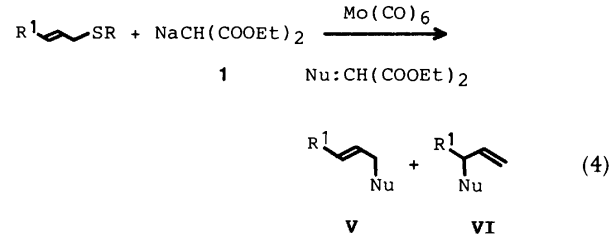

(4)

α-position (product **V**) even in γ-substituted allyl sulfides (Entries 9, 10, 12, 13, Eq. 4). However, any steric hindrance of bulky substituent on γ-carbon should reduce the regioselectivity. The low reactivity of α-substituted allyl sulfides toward **1** is presumably attributable to preferential complexation of **1** and $Mo(CO)_6$,[10] since the bulky α-substituent disturbs that of the allyl sulfides and $Mo(CO)_6$. Thus, the results demonstrate that the reaction proceeds not via π-allylmolybdenum intermediate but via coordination of

Table 1. Nucleophilic Substitutions

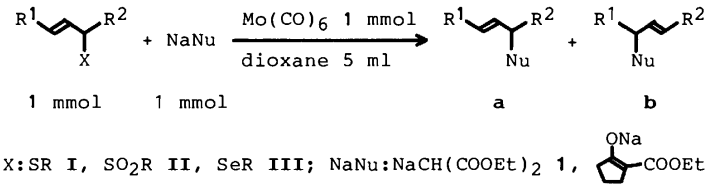

Entry	Allylic compound R¹	R²	X	NaNu	Time / h	Product	Yield[a] / %	Ratio[b] a : b
1	H	H	SPh	**2**	16	**3**	67	—
2	H	H	SPh	**2**	24	**3**	40[c]	—
3	H	H	SPh	**2**	67	**3**	23[d]	—
4	CH_3	H	SPh	**2**	40	**4**	75	100 0
5	Ph	H	SPh	**2**	47	**5**	52	100 0
6	H	$PhCH{=}CHCH_2$	SPh	**2**	41	**6**	48	0 100
7	H	$CH_3(CH_2)_3$	S-2-Py	**2**	63	**7**	47	0 100
8	$-(CH_2)_3-$		S-2-Py	**2**	34	**8**	22	—
9	CH_3	H	SPh	**1**	48	**9**	48	27 73
10	Ph	H	SPh	**1**	72	**10**	32	50 50
11	CH_3	CH_3	SPh	**1**	65	**11**	35	—
12	CH_3	$CH_3(CH_2)_3$	SPh	**1**	65	**12**	11	30 70
13	H	$CH_3(CH_2)_3$	SPh	**1**	72	**13**	6	0 100
14	H	H	SO_2Tol	**1**	20	**14**	29(14)[e]	—
15	H	H	SO_2Tol	**1**	24	**14**	12(30)[d,e]	—
16	H	H	SO_2Tol	**1**	68	**14**	36(35)[e,f]	—
17	CH_3	H	SO_2Tol	**1**	59	**9**	54	30 70
18	Ph	H	SO_2Tol	**1**	63	**10**	50	35 65
19	H	$CH_3(CH_2)_3$	SO_2Ph	**1**	66	**13**	32	100 0
20	H	$PhCH_2$	SO_2Ph	**1**	41	**15**	37	100 0
21	H	H	SO_2Tol	**2**	60	**3**	44	—
22	CH_3	H	SO_2Tol	**2**	60	**4**	48	100 0
23	Ph	H	SO_2Tol	**2**	45	**5**	24	100 0
24	H	$CH_3(CH_2)_3$	SO_2Ph	**2**	42	**7**	46	0 100
25	H	$PhCH_2$	SO_2Ph	**2**	45	**16**	41	0 100
26	H	H	SePh	**1**	41	**14**	53	—
27	H	H	SePh	**1**	96	**14**	19[g]	—
28	H	H	SePh	**1**	32	**14**	47[d]	—
29	CH_3	H	SePh	**1**	48	**9**	75	27 73
30	Ph	H	SePh	**1**	87	**10**	49	37 63
31	H	CH_3	SePh	**1**	62	**9**	36	58 42
32	H	$CH_3(CH_2)_3$	SePh	**1**	52	**13**	35	50 50
33	H	H	SePh	**2**	15	**3**	57	—
34	H	H	SePh	**2**	96	**3**	10[g]	—
35	CH_3	H	SePh	**2**	32	**4**	67	100 0
36	Ph	H	SePh	**2**	50	**5**	22	100 0
37	H	CH_3	SePh	**2**	62	**4**	60	0 100
38	H	$CH_3(CH_2)_3$	SePh	**2**	16	**7**	46	0 100

a) Isolated yields of mixtures of **a** and **b**. b) Ratio of isomers was determined by ^1H NMR (FX-200 and GX-270). c) DMF was used as a solvent. d) Toluene was used as a solvent. e) Figures in parentheses are yields of diallylated product. f) Two equivalents of **II** were used. g) THF was used as a solvent.

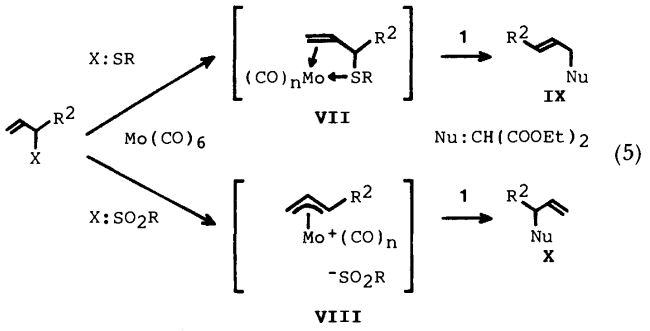

(5)

a sulfenyl group to molybdenum (chelate intermediate **VII**) (Eq. 5). Attack of **1** to α-substituted allyl sulfones occurred regioselectively at α-position, which is the more substituted end of the allyl unit, after the desulfonylation, contrary to the case of α-substituted allyl sulfides (Entries 19, 20, Eq. 5). Therefore, the intermediate derived from **II** and $Mo(CO)_6$ should be different from that derived from **I** and $Mo(CO)_6$. Since the nucleophilic substitution of π-allylmolybdenum complex, derived from allylic acetate and $Mo(CO)_6$, with dimethyl sodiomalonate has preferentially occurred at the more substituted end of the allyl unit,[10–12] π-allylmolybdenum intermediate **VIII** may be produced by the reaction of **II** with $Mo(CO)_6$, similarly to the case of π-allylpalladium complex prepared by that of **II** with $Pd(PPh_3)_4$ (Eq. 5).[9,13] In the case of γ-substituted allyl sulfones, the preparation of **VIII** may compete with that of the sulfide-like intermediate to afford the mixture of **a** and **b**, because bulky substituents on an olefin hindered π-coordination of the olefin (Entries 17, 18). γ-Substituted allyl selenides preferentially reacted with **1** at γ-position (Entries 29, 30). In contrast with α-substituted allyl sulfides, the γ-regioselective attack of **1** to α-substituted allyl selenides was not detected (Entries 31, 32). α-Substituted allyl selenides **XI** in refluxing dioxane easily caused [1,3] allylic shift of benzeneselenenyl group to produce γ-substituted allyl selenides **XII**.[14] In the reaction of **XI** with **1** in the presence of $Mo(CO)_6$, the [1,3] allylic shift should occur in preference to the nucleophilic substitution. Thus, the apparent attack of **1** at α-position of **XI** probably increased (Entries 31, 32, Eq. 6).

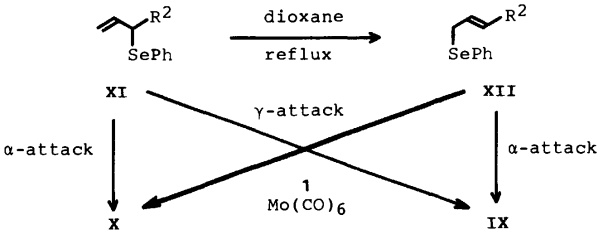

(6)

Reductive Dechalcogenization. The results of reductive dechalcogenization of 1-(3,4-methylenedioxybenzyl)allyl derivatives **17**, **18**, and **19** with $Mo(CO)_6$ are summarized in Table 2. These results demonstrated that reductive deselenenylation of allylic selenides with $Mo(CO)_6$ was easier than the corresponding reductive desulfenylation or desulfonylation. The addition of H_2O (or D_2O) accelerated the reductive dechalcogenization. Product **20c** was probably produced by the isomerization of **20b** with $Mo(CO)_6$, because elongation of the reaction time led to the increase of **20c**. Both the results of regioselectivity in deuteration with D_2O and the ratios of deuteration to protonation suggested that reaction mechanism of the reductive desulfonylation was different from that of

Table 2. Reductive Dechalcogenization of **17**, **18**, and **19**

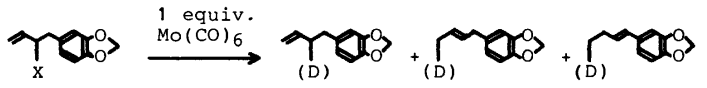

X:SPh **17**
SO_2Tol **18**
SePh **19**

20a **20b** **20c**

Entry	Substrate	Additive	Equiv.	Time h	Yield[a] %	Ratio[b] a : b[c] : c
1	**17**	—		40	34	10 : 90
2	**17**	D_2O	5	20	56[d]	50 : 50
3	**17**		5	35	48	11 : 89
4	**18**	—		40	38	27 : 43 : 30
5	**18**	D_2O	5	19	65[e]	22 : 43 : 35
6	**19**	—		21	81	6 : 32 : 62
7	**19**	D_2O	5	19	80[f]	4 : 61 : 35

a) Isolated yields of a mixture of **20a**, **20b**, and **20c**. b) Ratio of isomers was determined by ^1H NMR (FX-200 or GX-270). c) The *E*/*Z* ratio of **20b** was ca 3/1 in every case. d) Complete deuteration occurred. e) The ratios of deuteration to protonation in every isomer were 13—15%. f) The ratios of deuteration to protonation in every isomer were 35—40%.

the reductive desulfenylation. The intermediates in the reductive dechalcogenizations seem to be the same as those in the corresponding nucleophilic substitutions. Deuteration scarcely occurred in the desulfenylation of **17** without H_2O in refluxing dioxane-d_8.[15]

The reductive desulfenylation of substrate **21**[16] proceeded more rapidly to give only one regioisomer **22** (Eq. 7). Even in the presence of nucleophile **1**, **21**

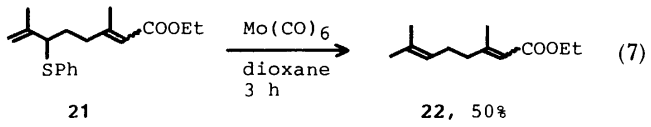

21 22, 50% (7)

did not cause nucleophilic substitution but did cause reductive desulfenylation. 1-Benzyl-3-phenylallyl sulfide **23** did not react with $Mo(CO)_6$, but the corresponding sulfone **24** caused reductive desulfonylation in the presence of H_2O to give **25a** and **25b** (Eq. 8). In

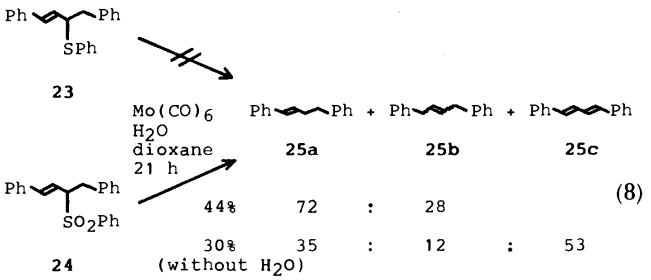

(8)

absence of H_2O, main product of the reaction was diene **25c**. Considering the ease of alkylation of allylic sulfones, the reductive desulfonylation could be applied to organic synthesis of alkene derivatives. This desulfonylation was applied to the synthesis of squalene (**27**) from allylic sulfone **26**[17] (Eq. 9).[18]

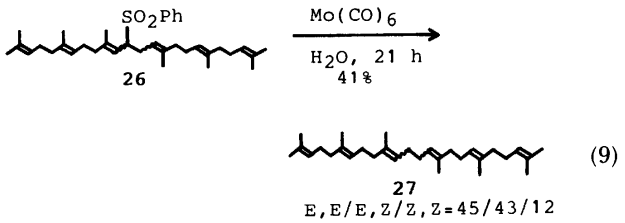

(9)

Cinnamyl phenyl selenide (**28**) did not cause the reductive deselenenylation in refluxing dioxane, but caused reductive allylic homocoupling at 100 °C in HMPA (Eq. 10). The reductive deselenenylation of

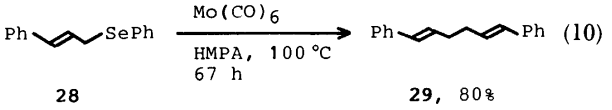

(10)

allylic selenide having trisubstituted olefin, farnesyl phenyl selenide (**30**), easily occurred in refluxing dioxane to give triene isomers **31a** and **31b** (Eq. 11).

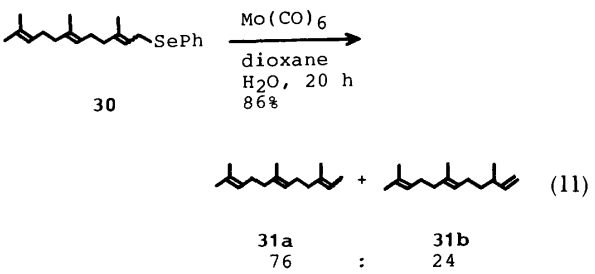

(11)

Conclusion

Hexacarbonylmolybdenum-induced dechalcogenization of allylic sulfides, sulfones, and selenides, which led to nucleophilic substitution with carbon nucleophiles and reduction without the carbon nucleophiles. Yields in the nucleophilic substitution were not so high, since reductive dechalcogenization presumably occurred even in the presence of the carbon nucleophiles. $Mo(CO)_6$ could thus be used as both an oxidizing agent and a reducing agent in the dechalcogenization. The reactivity of sulfonyl and selenenyl groups with $Mo(CO)_6$ seems to be higher than that of sulfenyl groups with $Mo(CO)_6$. The regiochemistry in both the nucleophilic substitution and the reduction of allylic sulfones was different from that in reactions of both allylic sulfides and selenides. The intermediate should hence be different for allylic sulfones and for allylic sulfides and selenides. Both reactions of allylic sulfones probably proceeded via π-allylmolybdenum intermediates. In contrast with allylic sulfones, allylic sulfides and selenides should not form the corresponding π-allylmolybdenum intermediates, since the coordination of sulfenyl and selenenyl groups to molybdenum center was stronger than that of olefinic moiety.

Experimental

General. $Mo(CO)_6$ was purchased from Strem Chemicals, Inc. Benzenethiol, 2-pyridinethiol, sodium benzenesulfinate, sodium *p*-toluenesulfinate, 3-bromo-1-propene, 3-chloro-1-phenyl-1-propene, 1-chloro-2-butene, 3-chloro-2-methyl-1-propene, 1-iodobutane, iodomethane, benzyl bromide, diethyl malonate, methyl vinyl ketone, and ethyl diethoxyphosphinylacetate were purchased from Tokyo Chemical Industry Co., Ltd. Diphenyl diselenide was prepared by the reaction of phenylmagnesium bromide with selenium, followed by oxidation. 2-(Ethoxycarbonyl)-cyclopentanone was prepared by the Dieckmann condensation. Allyl and γ-substituted allyl sulfides, sulfones, and selenides were prepared by reactions of allylic halides with sodium thiolates, sulfinates, and selenolates, respectively. α-Substituted allyl sulfides and selenides were prepared by alkylation of the anion of the corresponding allylic compounds with alkyl halides.[3] α-Substituted allyl sulfones were prepared by molybdenum-catalyzed oxidation of the corresponding allylic sulfides with H_2O_2. Sodium hydride and potassium hydride were employed after removal of mineral oil from 60 wt.% dispersion NaH and 35 wt.% dispersion KH, respectively (Wako Pure Chemical Industries,

Ltd.). Sodium borohydride was purchased from Wako Pure Chemical Industries, Ltd. Dioxane, tetrahydrofuran, and toluene were distilled from sodium benzophenone ketyl. Purification of products was carried out by means of column chromatography (E. Merck, Silica gel 60). IR spectra were recorded on a Hitachi 260-50 spectrophotometer, ^{1}H NMR spectra on Hitachi R-22 and Jeolco FX-200 and GX-270 spectrometers, and mass spectra on a Jeolco JMS-D300 spectrometer.

General Procedure of Nucleophilic Substitution. To a solution of carbanion derived from diethyl malonate (0.16 g, 1.0 mmol) or 2-(ethoxycarbonyl)cyclopentanone (0.16 g, 1.0 mmol) with sodium hydride (29 mg, 1.2 mmol) in dry dioxane (5 ml) were added allylic compounds **I**, **II**, or **III** (1 mmol) and Mo(CO)$_6$ (1.1 mmol). This mixture was refluxed for 16—87 h under nitrogen atmosphere. The reaction mixture was diluted with chloroform (30 ml) and a precipitate was removed from the mixture by filtration. Evaporation of solvents and purification by column chromatography on silica gel using hexane/ethyl acetate (7/1) as eluent gave the product.

2-Ethoxycarbonyl-2-(2-propenyl)cyclopentanone (**3**): IR and ^{1}H NMR spectra corresponded with those of the authentic sample.[19]

2-[(*E*)-2-Butenyl]-2-(ethoxycarbonyl)cyclopentanone (**4**): IR and ^{1}H NMR spectra corresponded with those of the authentic sample.[19]

2-Ethoxycarbonyl-2-[(*E*)-3-phenyl-2-propenyl]cyclopentanone (**5**): IR (neat) 1750, 1715, 1220, 1150, 1020, 740, 690 cm^{-1}. ^{1}H NMR ($CDCl_3$) δ=1.25 (t, J=7.18 Hz, 3H), 1.85—2.87 (m, 8H), 4.16 (q, J=7.18 Hz, 2H), 6.09 (dt, J=15.7, 7.53 Hz, 1H), 6.45 (d, J=15.7 Hz, 1H), 7.15—7.36 (m, 5H). The IR and ^{1}H NMR spectra corresponded with those of one regioisomer of the authentic sample.[19]

2-Ethoxycarbonyl-2-(6-phenyl-2,5-hexadienyl)cyclopentanone (**6**): IR (neat) 1750, 1720, 1220, 1150, 1020, 740, 690 cm^{-1}. ^{1}H NMR (CCl_4) δ=1.21 (t, J=7.0 Hz, 3H), 1.74—2.70 (m, 8H), 2.84 (br. t, J=5.4 Hz, 2H), 4.06 (q, J=7.0 Hz, 2H), 5.16—5.68 (m, 2H), 6.01 (dt, J=15.4, 5.4 Hz, 1H), 6.28 (d, J=15.4 Hz, 1H), 7.02—7.32 (m, 5H). MS (70 eV) m/z (rel intensity) 312 (M^+; 0.4), 199 (39), 198 (48), 156 (100), 141 (32), 117 (79), 115 (41), 104 (54), 91 (76). Calcd for $C_{20}H_{24}O_3$: M, 312.1724. Found: m/z 312.1717.

2-Ethoxycarbonyl-2-(2-heptenyl)cyclopentanone (**7**): IR (neat) 1750, 1720, 1220, 1155 cm^{-1}. ^{1}H NMR (CCl_4) δ=0.89 (br. t, J=6.5 Hz, 3H), 1.24 (t, J=7.0 Hz, 3H), 1.22—1.42 (m, 4H), 1.75—2.70 (m, 10H), 4.15 (q, J=7.0 Hz, 2H), 5.06—5.70 (m, 2H). MS (70 eV) m/z (rel intensity) 252 (M^+; 6.8), 179 (41), 156 (91), 121 (100), 110 (44), 55 (43). Calcd for $C_{15}H_{24}O_3$: M, 252.1724. Found: m/z 252.1727.

2-(2-Cyclohexenyl)-2-(ethoxycarbonyl)cyclopentanone (**8**): IR (neat) 1750, 1720, 1220, 1155 cm^{-1}. ^{1}H NMR (CCl_4) δ=1.21 (t, J=7.0 Hz, 3H), 1.42—2.54 (m, 12H), 2.84—3.22 (br, 1H), 4.08 (q, J=7.0 Hz, 2H), 4.97—5.41 (m, 1H), 5.52—5.78 (m, 1H).

A mixture of diethyl 2-butenylmalonate and diethyl 1-methyl-2-propenylmalonate (**9**) (Entry 9 in Table 1): IR (neat) 1740, 1635, 1260, 1220, 1175, 1145, 1030 cm^{-1}. ^{1}H NMR ($CDCl_3$) δ=1.11 (d, J=6.84 Hz, 2.19H), 1.25, 1.27 (2t, J=7.18 Hz, 6H), 1.64 (d, J=6.22 Hz, 0.81H), 2.54—2.69 (m, 0.54H), 2.88—3.00 (m, 0.73H), 3.27 (d, J=8.89 Hz, 0.73H), 3.36 (t, J=7.70 Hz, 0.27H), 4.17, 4.22 (2q, J=7.18 Hz, 4H), 5.01 (dd, J=10.2, 2.60 Hz, 0.73H), 5.09 (dd, J=17.5, 2.60 Hz, 0.73H), 5.20—5.62 (m, 0.54H), 5.79 (ddd, J=17.5, 10.2, 7.86 Hz, 0.73H). MS (70 eV) m/z (rel intensity) 214 (M^+; 5.6), 141 (100), 140 (35), 123 (44), 113 (32), 112 (53), 95 (30), 55 (47). Calcd for $C_{11}H_{18}O_3$: M, 214.1204. Found: m/z 214.1198.

A mixture of diethyl 3-phenyl-2-propenylmalonate and diethyl 1-phenyl-2-propenylmalonate (**10**) (Entry 10 in Table 1): IR (neat) 1745, 1730, 1255, 1225, 1170, 1150 cm^{-1}. ^{1}H NMR ($CDCl_3$) δ=1.25 (t, J=7.18 Hz, 6H), 2.80 (dd, J=7.52, 7.18 Hz, 1H), 3.49 (t, J=7.52 Hz, 0.5H), 3.83 (d, J=10.9 Hz, 0.5H), 4.06—4.15 (m, 0.5H), 4.20 (q, J=7.18 Hz, 4H), 5.07 (d, J=10.2 Hz, 0.5H), 5.12 (d, J=17.0 Hz, 0.5H), 6.00 (ddd, J=17.0, 10.2, 8.12 Hz, 0.5H), 6.15 (dt, J=15.7, 7.18 Hz, 0.5H), 6.47 (d, J=15.7 Hz, 0.5H), 7.15—7.35 (m, 5H). MS (70 eV) m/z (rel intensity) 276 (M^+; 5.9), 203 (100), 175 (21), 129 (48), 117 (92), 115 (29). Calcd for $C_{16}H_{20}O_4$: M, 276.1360. Found: m/z 276.1358.

Diethyl 1-methyl-2-butenylmalonate (**11**): IR (neat) 1730, 1240, 1150 cm^{-1}. ^{1}H NMR (CCl_4) δ=1.00 (d, J=7.0 Hz, 3H), 1.21 (br. t, J=7.0 Hz, 6H), 1.58 (d, J=4.5 Hz, 3H), 2.64—2.86 (m, 1H), 3.02 (d, J=7.5 Hz, 1H), 4.05, 4.08 (2d, J=7.0 Hz, 4H), 5.00—5.67 (m, 2H).

A mixture of diethyl 1-butyl-2-butenylmalonate (**12**): IR (neat) 1730, 1240, 1150 cm^{-1}. ^{1}H NMR (CCl_4) δ=0.70—1.08 (br, 3H) 1.03 (d, J=6.0 Hz, 2.1H), 1.15—1.74 (m, 10.6H), 1.61 (d, J=5.6 Hz, 0.9H), 1.74—2.14 (m, 1.4H), 2.44—3.02 (m, 1H), 3.02—3.21 (m, 1H), 3.92—4.26 (m, 4H), 5.00—5.56 (m, 2H).

A mixture of diethyl 1-butyl-2-propenylmalonate and diethyl 2-heptenylmalonate (**13**) (Entry 32 in Table 1): IR (neat) 1750, 1725, 1240, 1150 cm^{-1}. ^{1}H NMR ($CDCl_3$) δ=0.80—0.95 (br, 3H), 1.15—1.45 (m, 11H), 1.95—2.03 (m, 1H), 2.57 (dd, J=6.60, 6.30 Hz, 1H), 2.83—2.90 (m, 0.5H), 3.30—3.42 (m, 1H), 4.18 (q, J=7.18 Hz, 4H), 5.03—5.14 (m, 1H), 5.25—5.74 (m, 1.5H). MS (70 eV) m/z (rel intensity) 256 (M^+; 6.5), 199 (81), 183 (83), 165 (42), 161 (30), 160 (100), 155 (30), 153 (38), 140 (34), 133 (36), 127 (39), 125 (43), 115 (31), 81 (37), 67 (34), 55 (87). Calcd for $C_{14}H_{24}O_4$: M, 256.1673. Found: m/z 256.1677.

Diethyl 2-propenylmalonate (**14**): IR (neat) 1725, 1270, 1115 cm^{-1}. ^{1}H NMR ($CDCl_3$) δ=1.27 (t, J=7.18 Hz, 6H), 2.61—2.67 (m, 2H), 3.42 (t, J=7.52 Hz, 1H), 4.20 (q, J=7.18 Hz, 4H), 5.06 (dd, J=10.3, 2.60 Hz, 1H), 5.12 (dd, J=17.1, 2.60 Hz, 1H), 5.78 (ddt, J=17.1, 10.3, 6.83 Hz, 1H). MS (70 eV) m/z (rel intensity) 200 (M^+; 3.0), 182 (30), 153 (39), 127 (40), 109 (36), 105 (100), 98 (32), 93 (29), 81 (27), 77 (53). Calcd for $C_{10}H_{16}O_4$: M, 200.1048. Found: m/z 200.1045.

Diethyl 1-benzyl-2-propenylmalonate (**15**): IR (neat) 1730, 1230, 1150 cm^{-1}. ^{1}H NMR (CCl_4) δ=1.21 (t, J=6.8 Hz, 6H), 2.43—2.92 (m, 3H), 3.25 (d, J=6.0 Hz, 1H), 4.09 (2q, J=6.8 Hz, 4H), 4.72—4.95 (m, 2H), 5.46—5.90 (m, 1H), 6.93—7.24 (m, 5H).

2-Ethoxycarbonyl-2-(4-phenyl-2-butenyl)cyclopentanone (**16**): IR (neat) 1745, 1720, 1220, 1150, 750, 700 cm^{-1}. ^{1}H NMR (CCl_4) δ=1.17 (t, J=7.2 Hz, 3H), 1.63—2.70 (m, 8H), 3.24 (d, J=6.4 Hz, 2H), 4.03 (q, J=7.2 Hz, 2H), 5.10—5.75 (m, 2H), 6.90—7.25 (m, 5H). MS (70 eV) m/z (rel intensity) 286 (M^+; 0.1), 131 (16), 130 (100), 129 (13), 121 (11), 91 (20). Calcd for $C_{18}H_{22}O_3$: M, 286.1568. Found: m/z 286.1565.

General Procedure of Reductive Dechalcogenization. A solution of allylic compound **I**, **II**, or **III** (1 mmol), Mo(CO)$_6$ (1.1 mmol), and H_2O (5 mmol) in dioxane (7 ml) was refluxed for 3—40 h under nitrogen atmosphere. The reaction mixture was diluted with chloroform (40 ml) and

precipitate material was removed from the mixture by filtration. Evaporation of solvents and purification by column chromatography on silica gel using hexane or hexane/ethyl acetate as eluent gave the product.

A mixture of 4-(3,4-methylenedioxyphenyl)-1-butene (**20a**), 1-(3,4-methylenedioxyphenyl)-2-butene (**20b**), and 1-(3,4-methylenedioxyphenyl)-1-butene (**20c**): ^{1}H NMR ($CDCl_3$) **20a**: δ=2.33 (m, 2H), 2.62 (t, J=7.42 Hz, 2H), 4.97 (br. d, J=10.9 Hz, 1H), 5.02 (br. d, J=18.0 Hz, 1H), 5.76—5.88 (m, 1H), 5.91 (s, 2H), 6.60 (br, 1H), 6.63 (br, 2H), **20b**: δ=1.67 (br. d, J=5.10 Hz, 3H), 3.22, 3.31 (E/Z=81/19, 2d, J=5.10, 5.79 Hz, 2H), 5.49—5.56 (m, 2H), 5.92 (s, 2H), 6.67 (br, 2H), 6.71 (s, 1H), **20c**: δ=1.07 (t, J=7.52 Hz, 3H), 2.19 (m, 2H), 5.90 (s, 2H), 6.08 (dt, J=15.6, 6.33 Hz, 1H), 6.28 (d, J=15.6 Hz, 1H), 6.73 (br, 2H), 6.89 (br, 1H). MS (70 eV) m/z (rel intensity) 176 (M^+, 93), 161 (29), 131 (100), 103 (46), 77 (22). Calcd for $C_{11}H_{12}O_2$: M, 176.0836. Found: m/z 176.0836.

Ethyl 3,7-dimethyl-2,6-octadienoate (**22**): ^{1}H NMR (CCl_4) δ=1.21 (t, J=7.2 Hz, 3H), 1.56 (s, 3H), 1.64 (s, 3H), 1.90—2.30 (m, 4H), 2.09 (s, 3H), 4.02 (q, J=7.2 Hz, 2H), 5.00 (m, 1H), 5.51 (br, 1H). The NMR spectrum corresponded with that of the authentic sample derived from 6-methyl-5-hepten-2-one and ethyl diethoxyphosphinylacetate with t-BuOK.

A mixture of stereoisomers of squalene (**27**): ^{1}H NMR ($CDCl_3$) δ=1.60, 1.68 (2s, 24H), 1.90—2.15 (m, 20H), 5.03—5.19 (m, 6H). The NMR spectrum corresponded with that of an authentic sample.[20] The isomer ratio was determined by GLPC [5% OV-17/Chromosorb W (AW-DMCS), 60—80 mesh, 2 m, He, 200 °C].[20]

1,6-Diphenyl-1,5-hexadiene (**29**): IR (KBr) 1590, 1480, 1180, 1065, 1015, 735 cm^{-1}. ^{1}H NMR (CCl_4) δ=2.23—2.38 (br, 4H), 6.07 (dt, J=16.0, 5.8 Hz, 2H), 6.35 (t, J=16.0 Hz, 2H), 6.90—7.25 (m, 10H). The IR and NMR spectra and retention time of GLPC [5% OV-17/Chromosorb W (AW-DMCS), 60—80 mesh, 2 m, He, 230 °C] corresponded with those of an authentic sample.[20]

A mixture of 2,6,10-trimethyl-2,6,10-dodecatriene (**31a**) and 3,7,11-trimethyl-1,6,10-dodecatriene (**31b**): IR (neat) 2960, 2920, 970 cm^{-1}. ^{1}H NMR ($CDCl_3$) δ=0.95 (d, J=6.96 Hz, 0.72H), 1.53—1.75 (m, 14.0H), 1.90—2.20 (br, 7.8H), 4.90 (dd, J=9.60, 2.20 Hz, 0.24H), 4.95 (d, J=16.0 Hz, 0.24H), 5.11 (t, J=5.38 Hz, 2H), 5.20 (q, J=6.70 Hz, 0.76H), 5.68 (ddd, J=16.0, 9.60, 7.80 Hz, 0.24H). MS (70 eV) m/z (rel intensity) 206 (M^+, 6), 137 (14), 123 (14), 81 (62), 69 (100), 55 (18). Calcd for $C_{15}H_{26}$: M, 206.2033. Found: m/z 206.2033.

References

1) "Comprehensive Organic Chemistry," ed by D. N. Jones, Pergamon, Oxford (1979), Vol. 3, Chaps. 11 and 12.

2) C. Paulmier, "Selenium Reagents and Intermediates in Organic Synthesis," Pergamon, Oxford (1986).

3) J. F. Biellmann and J. B. Ducep, *Org. React.*, **27**, 1 (1982).

4) P. D. Magnus, *Tetrahedron*, **33**, 2019 (1977).

5) M. Hudlicky, "Reductions in Organic Chemistry," Ellis Horwood, Chichester (1984), p. 86.

6) B. M. Trost and M. R. Ghadiri, *J. Am. Chem. Soc.*, **106**, 7260 (1984); **108**, 1098 (1986).

7) Preliminary reports: a) Y. Masuyama, K. Yamada, and Y. Kurusu, *Tetrahedron Lett.*, **28**, 443 (1987); b) Y. Masuyama, K. Yamada, and Y. Kurusu, *Chem. Express*, **2**, 687 (1987).

8) H. Okamura and H. Takei, *Tetrahedron Lett.*, **1979**, 3425.

9) B. M. Trost, *Bull. Chem. Soc. Jpn.*, **61**, 107 (1988).

10) B. M. Trost and M. Lautens, *J. Am. Chem. Soc.*, **105**, 3343 (1983).

11) B. M. Trost and M. Lautens, *J. Am. Chem. Soc.*, **104**, 5543 (1982).

12) I. Minami, I. Shimizu, and J. Tsuji, *J. Organomet. Chem.*, **296**, 269 (1985).

13) In order to detect π-allylmolybdenum intermediate **VIII**, ^{1}H NMR spectroscopic investigation was carried out in the reaction of allyl tolyl sulfone with $Mo(CO)_6$ in dioxane at 100 °C. The formation of **VIII** was not confirmed, since the reductive desulfonylation probably occurred rapidly. In a case of allyl phenyl sulfide, neither chelate intermediate **VII** nor π-allyl intermediate was detected.

14) a) K. B. Sharpless and R. F. Lauer, *J. Am. Chem. Soc.*, **94**, 715 (1972); b) K. B. Sharpless and R. F. Lauer, *J. Org. Chem.*, **37**, 3973 (1972). A typical procedure of the [1,3] allylic shift of benzeneselenenyl group is as follows: 4-(3,4-methylenedioxyphenyl)-3-phenylseleno-1-butene (3.3 g, 10 mmol) was stirred for 23 h in refluxing dioxane. Evaporation of dioxane and purification by column chromatography (Wakogel C-200, hexane/AcOEt=20/1) gave 1-(3,4-methylenedioxyphenyl)-4-phenylseleno-2-butene (2.8 g, 85%). The [1,3] allylic shift of benzenesulfenyl group in α-substituted allyl sulfides did not occur under the same conditions; see: P. Brownbridge and S. Warren, *J. Chem. Soc., Chem. Commun.*, **1975**, 820.

15) In the reductive desulfenylation without adding H_2O, proton source was not detected.

16) Preparation of **21** was carried out in the following manner:

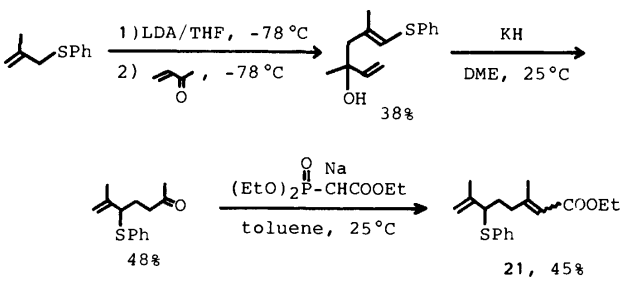

17) The isomer ratio (*E,E/E,Z/Z,E/Z,Z*) of allylic sulfone **26** was not determined by ^{1}H NMR.

18) P. A. Grieco and Y. Masaki, *J. Org. Chem.*, **39**, 2135 (1974).

19) Y. Masuyama, Y. Kurusu, and K. Segawa, *J. Mol. Catal.*, **40**, 183 (1987).

20) Y. Masuyama, K. Otake, and Y. Kurusu, *Bull. Chem. Soc. Jpn.*, **60**, 1527 (1987).

 © 1989 The Chemical Society of Japan Bull. Chem. Soc. Jpn., 62, 2919—2922 (1989)

A New Synthesis of 3-Hydroxy-2,5-dialkyl-1,4-benzoquinone from 3-Halo-3,6-dialkyl-1,2-cyclohexanedione Using Iodine-Copper(II) Acetate

C. Akira HORIUCHI* and Yasuto SUZUKI
Department of Chemistry, Rikkyo (St. Paul's) University, Nishi-Ikebukuro, Toshima-ku, Tokyo 171
(Received February 25, 1989)

The reaction of 3-iodo-3,6-dialkyl-1,2-cyclohexanedione (**2**) with iodine-copper(II) acetate in acetic acid-water (5:1) at 80 °C gave the respective 3-hydroxy-2,5-dialkyl-1,4-benzoquinone in 38—80% yields. On the other hand, the reaction of **2** with copper(II) acetate in acetic acid-water (10:1) under refluxing afforded the respective 3,3′-dihydroxy-2,2′,5,5′-tetraalkyl-4,4′-diphenoquinone (**5**) in 41—85% yields. In the case of 3-bromo-3,6-dialkyl derivative (**3**) with copper(II) acetate, the diphenoquinone derivatives and 3-hydroxy-2,5-dialkyl-1,4-benzoquinone were obtained.

3-Hydroxy-2,5-dialkyl-1,4-benzoquinones are important as intermediates,[1-4] and hydroxy-1,4-benzoquinone derivatives are known as natural products.[5-9] Much work has been reported on the syntheses of 3-hydroxy-2,5-dialkyl-1,4-benzoquinone.[1,2,10,11] However, all of these methods give only a low yield and involve several steps in preparing the starting materials. Diphenoquinone derivatives and 3,3′-dihydroxy-4,4′-diphenoquinones, both those having and not having alkyl groups, are often used as dyes, possessors of biological activity, electron acceptors, and synthetic intermediates.[12] 3,3′-Dihydroxy derivatives are prepared by one of the following methods: the reaction of 2-hydroxy-5-methoxybenzaldehyde with hydrogen peroxide-sodium hydroxide;[13] the reaction of 3-hydroxy-2,5-dimethyl-1,4-benzoquinone with boron trifluoride etherate;[3] or the Ullmann Reaction of 4-iodoveratrole.[14] Though these methods involve several steps to prepare the starting materials, they have been little afforded 3,3′-dihydroxy-2,2′,5,5′-tetraalkyl-4,4′-diphenoquinone. There has been no information concerning a direct synthesis from the cyclic 1,2-diketone derivative. In connection with our studies, we have found that iodine-copper(II) acetate in acetic acid is a useful reagent for the syntheses of some iodo compounds.[16] In a previous paper[17] we reported on a new synthesis of 3-hydroxy-2,5-dialkyl-1,4-benzoquinones using iodine-copper(II) acetate.

In the present paper we would like to report that the reaction of 3-bromo- and 3-iodo-3,6-dialkyl-1,2-cyclohexanedione with iodine-copper(II) acetate or copper(II) acetate in acetic acid-water gave the corresponding 3-hydroxy-2,5-dialkyl-1,4-benzoquinone or 3,3′-dihydroxy-2,2′,5,5′-tetraalkyldiphenoquinone, respectively.

The reaction of **2c—2e** with iodine (0.5 mol equiv)-copper(II) acetate (1.0 mol equiv) in acetic acid-water (5:1) at 80 °C for 5 h gave the 3-hydroxy-2,5-dialkyl-1,4-benzoquinone (47% for **4c**; 67% for **4d** and **4′d**; and 38% for **4e**). These 1,4-benzoquinones showed IR absorption at 3288—3296 (OH), 1656—1668 (C=O), 1634—1640 (C=O), and 1614—1616 cm^{-1} (C=C) in their IR spectra. The IR and UV spectra indicated that they had *p*-quinonoid structures with a hydroxyl group in the molecule. The ^1H NMR spectra of these hydroxy-1,4-benzoquinones (**4c—4e**) showed a doublet at δ 6.42 (J=0.70 Hz) for **4c**, a triplet at δ 6.49 (J=1.71 Hz) for **4d**, and a triplet at δ 6.46 (J=1.0 Hz) for **4e** assignable to the C_6-H. Compound **4′d** showed a doublet at δ 2.07 (J=1.71 Hz) and a triplet at δ 6.49 (J=1.71 Hz) in the ^1H NMR spectrum. Therefore, **4c**, **4d**, and **4e** were presumed to be 3-hydroxy-2,5-dialkyl-1,4-benzoquinone and **4′d** was presumed to be 5-hydroxy derivative. These were also supported by the ^{13}C NMR spectral data.

The reaction of 3-iodo-1,2-diketone (**2a**, **2b**, **2c**, **2d**, and **2e**) with copper(II) acetate (1.5 mol equiv.) in acetic acid-water (10:1) under refluxing for 4 h yielded reddish crystals (**5a**, **5b**, **5c**, **5d**, and **5e**) in a 41—82% yield, and 3-hydroxy-1,4-benzoquinones (**4a**, **4b**, **4c**, and **4e**) in a 3—14% yield. These compounds showed absorption at 3440—3480 (OH), 1650—1654 (C=O), 1636—1642 (C=O), and 1594—1600 cm^{-1} (C=C) in their IR spectra. The ^1H NMR spectra of these compounds showed a singlet at δ 6.89—7.00 due to the CH of the *p*-quinonoid structure. The UV spectra showed absorption at 406 nm due to diphenoquinone.

On the basis of the IR, ^1H NMR, UV, and HRMS spectral data for **5a**, **5b**, **5c**, **5d**, and **5e**, the structures of these diphenoquinones were determined to be 3,3′-dihydroxy-2,2′,5,5′-tetraalkyl-4,4′-diphenoquinone.

Table 1. Products and Isolated Yields (%) in the Reaction of 3-Iodo-1,2-cyclohexanedione (**2a—2e**) with Iodine-Copper(II) Acetate

$$2 \xrightarrow[\text{AcOH-H}_2\text{O}]{\text{I}_2\text{-Cu(OAc)}_2} 4$$

Substrate	Products (%)
2a	**4a** (80)
2b	**4b** (50) **7b** (34)
2c	**4c** (47)
2d	**4d**,**4′d** (67)[a]
2e	**4e** (38)

a) **4d**:**4′d**=60:40.

Table 2. Products and Isolated Yields (%) in the Reaction of 3-Iodo- (**2a**—**2e**) and 3-Bromo-1,2-cyclohexanedione (**3a**—**3e**) with Copper(II) Acetate

$$\textbf{2 or 3} \xrightarrow[\text{AcOH-H}_2\text{O}]{\text{Cu(OAc)}_2} \textbf{4 + 5}$$

Substrate	Products (%)	
2a	**4a** (3)	**5a** (43)
2b	**4b** (5)	**5b** (41)
2c	**4c** (12)	**5c** (82)
2d	**4d** (1)	**5d** (72)
2e	**4e** (14)	**5e** (44)
3a,3'a	**4a** (19)	**5a** (25)
3b	**4b** (22)	**5b** (21)
3c	**4c** (16)	**5c** (16)
3d,3'd	**4d,4'd** (8)[a]	**5d** (60)
3e	**4e** (15)	**5e** (41)

a) **4d**:**4'd**=59:41.

These were also supported by the ^{13}C NMR spectral data. The oxidation of 3,3',4,4'-tetrahydroxy-2,2',5,5'-tetraalkylbiphenyl (**8a** and **8b**) produced as an intermediate with copper(II) acetate yielded the diphenoquinone derivative (**5a** and **5b**).

On the other hand, to investigate the properties of other halogen, the reaction of 3-bromo-1,2-diketone (**3a**, **3b**, **3c**, **3d**, and **3e**) with copper(II) acetate was carried out. These reactions gave the hydroxyquinone (8—22%) and diphenoquinone (16—60%). In the case of diosphenol (**1a**) with bromine-copper(II) acetate, the hydroxyquinone (**4a**) (21%) was obtained. It seemed that these results indicated our previously proposed reaction pathway: 3-iodo-3,6-dialkyl-1,2-diketone⟶3,6-dialkyl-1,2-benzenediol⟶4-iodo derivative⟶4-hydroxy-1,2-diketone⟶3-hydroxy-1,4-benzoquinone. It is assumed that copper(I) iodide can not recycle, but copper(II) bromide is given by the reaction of copper(I) bromide and hydrogen bromide produced with oxygen in the air. Therefore, in the case of 3-bromo-1,2-diketone, it seemed that a considerable sum of hydroxy-1,4-benzoquinone was yielded by the reaction pathway mentioned above. In the absence of halogen, the coupling reaction occurs preferentially, rather than the following pathway: halogenation⟶hydrolysis⟶oxidation.

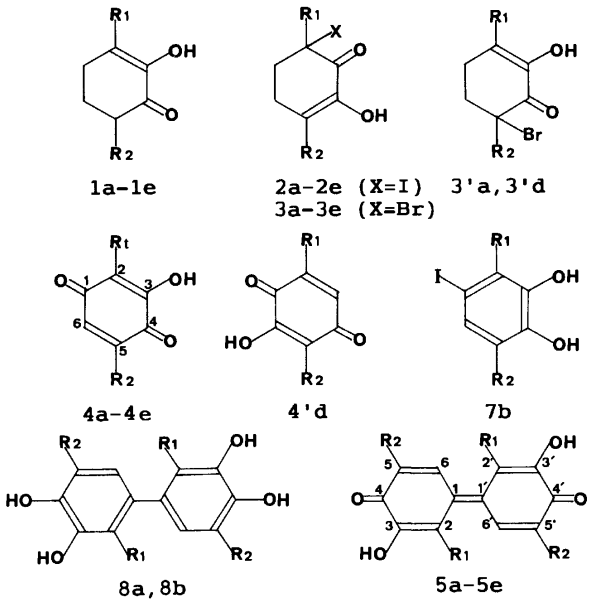

a:R_1=Me, R_2=i-Pr
b:R_1=R_2=Me
c:R_1=Me, R_2=Cyclohexyl
d:R_1=Me, R_2=Et
e:R_1=R_2=Et

Experimental

All the melting points are uncorrected. The IR apectra were measured using a Hitachi Model 270-30 grating infrared spectrometer. The NMR spectra were measured using JEOL FX 200 Model Spectrometer in deuteriochloroform with TMS as an internal standard. The high-resolution mass spectra were recorded at 75 eV on a JEOL JMS-O1SG-2 instrument with a direct inlet.

3,6-Dialkyl-1,2-cyclohexanedione (1a—1e). These compounds (**1a**—**1e**) were synthesized by the methods described in the literature.[18]

3-Iodo-3,6-dialkyl-1,2-cyclohexanedione (2a—2e). Diosphenol (**1a**) (0.50 g) in acetic acid-water (5:1) (48 ml) was treated with iodine (0.80 g) and copper(II) acetate (0.65 g) at room temperature for 8 h. The precipitated copper(I) iodide was removed by filtration, and the solvent was then removed under reduced pressure. The residue was poured into water and extracted with ether. The ethereal solution was washed successively with aqueous sodium hydrogencarbonate and with water, dried, and concentrated. Crystallization of the residue from ethanol gave needles of **2a** (0.80 g) (83%), mp 85—87 °C.[17]

2b: Yield 80%, mp 109—110 °C.[17]

2c: Yield 76%, mp 97—98 °C; IR (KBr): 3440, 1658, and 1624 cm^{-1}; ^{1}H NMR ($CDCl_3$): δ=2.11 (s, 3H), 2.75 (m, 1H), and 6.10 (s, 1H); ^{13}C NMR ($CDCl_3$): δ=190.6, 138.8, 138.2, 46.0, 41.6, 38.8, 30.9, 30.0, 29.4, 26.2, 26.1, 26.0, and 25.4. Found: *m/z* 334.042. Calcd for $C_{13}H_{19}O_2I$: M, 334.043.

2d: Yield 67%; mp 81—83 °C; IR (KBr): 3440, 1670, and 1626 cm^{-1}; ^{1}H NMR ($CDCl_3$): δ=0.96 (t, 3H), 1.94 (s, 3H), 2.04 (m, 2H), and 6.10 (s, 1H); ^{13}C NMR ($CDCl_3$): δ=189.4, 140.7, 130.0, 54.8, 37.1, 34.8, 30.8, 17.0, and 11.4. Found: *m/z* 279.995. Calcd for $C_9H_{13}O_2I$: M, 279.996.

2e: Yield 67%, mp 81—83 °C; IR (KBr): 3428, 1662, and 1630 cm^{-1}; ^{1}H NMR ($CDCl_3$): δ=1.00 (t, 3H), 1.10 (t, 3H), 1.93 (m, 2H), 2.40—2.55 (m, 2H), and 6.12 (s, 1H); ^{13}C NMR ($CDCl_3$): δ=189.8, 140.1, 135.0, 55.0, 37.2, 34.8, 28.4, 24.0, 11.5, and 11.3. Found: *m/z* 294.012. Calcd for $C_{10}H_{15}O_2I$: M, 294.012.

3-Bromo-3,6-dialkyl-1,2-cyclohexanedione (3a—3e). Diosphenol (**1a**) (1.00 g) in acetic acid (50 ml) was treated with bromine (0.997 g) at room temperature for 5 min. After the usual work-up, the resulting oil, upon crystallization from ethanol, gave mixtures (60:40) of 3-bromo- (**3a**) and 6-bromo-3-methyl-6-isopropyl-1,2-cyclohexanedione (**3'a**) (1.440 g) (98%), mp 51—53 °C; IR (KBr): 3440, 1660, and 1634 cm^{-1}; ^{1}H NMR ($CDCl_3$): δ=0.93 (d, 3H), 1.06 (d, 3H), 1.10 (d, 3H), 1.17 (d, 3H), 1.92 (s, 3H), 1.94 (d, 3H), 2.81 (m, 1H), 3.17 (m,

1H), 6.08 (s, 1H), and 6.14 (s, 1H); ^{13}C NMR ($CDCl_3$): δ=188.9, 187.9, 141.7, 139.7, 139.4, 130.5, 39.4, 34.7, 29.9, 28.1, 28.0, 27.9, 21.8, 19.9, 19.4, 18.3, 18.1, and 17.1. Found: *m/z* 246.027. Calcd for $C_{11}H_{15}O_2Br$: M, 246.026.

3b: Yield 95%; mp 99—101 °C; IR (KBr): 3436, 1668, and 1632 cm^{-1}; ^{1}H NMR ($CDCl_3$): δ=1.940 (s, 3H), 1.942 (s, 3H), and 6.05 (br s, 1H); ^{13}C NMR ($CDCl_3$): δ=188.2, 140.8, 131.0, 61.1, 39.2, 28.6, 27.9, and 17.1; MS *m/z* 218 (M^+) and 220 (M+2).

3c: Yield 79%; mp 107—108 °C; IR (KBr): 3440, 1668, and 1630 cm^{-1}; ^{1}H NMR ($CDCl_3$): δ=1.92 (s, 3H), 2.80 (m, 1H), and 6.04 (s, 1H); ^{13}C NMR ($CDCl_3$): δ=188.9, 139.5, 134.8, 61.1, 39.4, 38.8, 29.9, 29.5, 27.9, 26.18, 26.12, 26.06, and 22.8. Found: *m/z* 286.051. Calcd for $C_{13}H_{19}O_2Br$: M, 286.057.

3d, 3′d: Yield 89% (**3d**:**3′d**=60:40); mp 67—70 °C, 75—77 °C; IR (KBr): 3444, 1668, 1641, and 1630 cm^{-1}; ^{1}H NMR ($CDCl_3$): δ=1.02 (t, 3H), 1.10 (t, 3H), 1.94 (s, 3H), 1.95 (s, 3H), 6.04 (s, 1H), and 6.08 (s, 1H); ^{13}C NMR ($CDCl_3$): δ=188.6, 188.0, 141.3, 140.1, 136.2, 130.8, 67.0, 61.2, 39.4, 35.1, 32.4, 28.3, 27.9, 26.1, 24.1, 17.1, 11.3, and 9.6. Found: *m/z* 232.006. Calcd for $C_9H_{13}O_2Br$: M, 232.010.

3e: Yield 99%; 86—89 °C; IR (KBr): 3436, 1668, and 1632 cm^{-1}; ^{1}H NMR ($CDCl_3$): δ=1.02 (t, 3H), 1.10 (t, 3H), 1.98 (m, 2H), 2.45—2.57 (m, 2H), and 6.02 (s, 1H); ^{13}C NMR ($CDCl_3$): δ=188.4, 140.7, 136.0, 67.1, 35.2, 32.4, 25.8, 24.1, 11.3, and 9.6. Found: *m/z* 246.024. Calcd for $C_{10}H_{13}O_2Br$: M, 246.026.

Reaction of 3-Iodo-3-methyl-6-isopropyl-1,2-cyclohexanedione (2a) with Iodine-Copper(II) Acetate in Acetic Acid-Water. A mixture of **2a** (200 mg), iodine (160 mg), and copper(II) acetate monohydrate (140 mg) in acetic acid-water (5:1) (12 ml) was stirred at 80 °C for 5 h. The precipitated copper(I) iodide was removed by filtration, and the solvent was then removed under reduced pressure. The residue was poured into water and extracted with ether. The ethereal solution was washed successively with aqueous sodium hydrogencarbonate and with water, dried, and concentrated. Crystallization of the residue from ethanol gave needles of **4a** (150 mg) (80%), mp 167—168 °C (lit,[17] 167—168 °C). The IR and ^{1}H and ^{13}C NMR spectra[15] were identical with those of an authentic sample.

4b: Yield 50%; mp 138—140 °C (lit,[10] 141—142 °C). The IR and ^{1}H NMR spectra were identical with those of an authentic sample.

4c: Yield 47%; mp 130—132 °C; IR (KBr): 3296, 1668, 1640, and 1614 cm^{-1}; UV (EtOH): 270 (ε 1.08×10^4) and 425 nm (ε 0.97×10^3); ^{1}H NMR ($CDCl_3$): δ=1.92 (s, 3H), 2.65 (m, 1H), 6.16 (s, 1H), and 6.42 (d, *J*=0.70 Hz, 1H); ^{13}C NMR ($CDCl_3$): δ=194.0, 178.7, 151.7, 141.8, 132.3, 117.1, and 7.8. Found: *m/z* 220.112. Calcd for $C_{13}H_{16}O_3$: M, 220.110.

4d, 4′d: Yield 67% (**4d**:**4′d**=60:40); mp 124—126 °C; IR (KBr): 3288, 1658, 1634, and 1616 cm^{-1}; UV (EtOH): 266 (ε 1.31×10^4) and 405 nm (ε 1.39×10^3); ^{1}H NMR ($CDCl_3$): δ=1.07 (t, 3H), 1.15 (t, 3H), 1.94 (s, 3H), 2.07 (d, *J*=1.71 Hz, 3H), 2.40—2.54 (m, 4H), 6.49 (t, *J*=1.71 Hz, 1H), and 7.02 (br s, 2H); ^{13}C NMR ($CDCl_3$): δ=184.4, 183.7, 151.4, 146.3, 133.6, 117.1, 21.4, 12.6, and 7.9 (for **4d**); δ=184.4, 183.7, 150.9, 141.0, 135.4, 122.6, 16.1, 14.8, and 11.6 (for **4′d**). Found: *m/z* 166.065. Calcd for $C_9H_{10}O_3$: M, 166.063.

4e: Yield 38%; mp 115—116 °C; IR (KBr): 3288, 1656, 1634, and 1614 cm^{-1}; UV (EtOH): 266 (ε 1.31×10^4) and 405 nm (ε 1.39×10^3); ^{1}H NMR ($CDCl_3$): δ=1.00 (m, 6H), 2.48 (m, 4H), 6.46 (t, *J*=1.0 Hz, 1H), and 6.98 (s, 1H); ^{13}C NMR ($CDCl_3$): δ=187.6, 183.9, 150.8, 146.1, 133.8, 122.5, 21.4, 16.1, 12.6, and 11.6. Found: *m/z* 180.080. Calcd for $C_{10}H_{12}O_3$: M, 180.079.

Reaction of 3-Isopropyl-6-methyl-1,2-benzenediol (6) with Iodine-Copper(II) Acetate in Acetic Acid-Water (5:1). A mixture of **6** (109 mg), iodine (173 mg), and copper(II) acetate monohydrate (130 mg) in acetic acid-water (5:1) (12 ml) was stirred at 80 °C for 1 h. After the usual work-up, the resulting oil, upon crystallization from ethanol, gave **4a** as needles (101 mg), mp 167—168 °C.

Reaction of 4-Iodo-3,6-dimethyl-1,2-benzenediol (7d) with Iodine-Copper(II) Acetate in Acetic Acid-Water. A mixture of **7** (3.0 mg), iodine (1.5 mg), and copper(II) acetate (2.2 mg) in acetic acid-water (5:1) (0.3 ml) was stirred at 80 °C for 4 h. After the usual work-up, the resulting oil, upon crystallization from ethanol, gave **4b** as needles (0.9 mg), mp 138—140 °C.

Reaction of 3-Iodo-3-methyl-6-isopropyl-1,2-cyclohexanedione (2a) with Copper(II) Acetate in Acetic Acid-Water. 3-Iodo-1,2-diketone (**2a**) (300 mg) in acetic acid-water (10:1) (25 ml) was treated with copper(II) acetate (305 mg) under refluxing for 4 h. The precipitated copper(I) iodide was removed by filtration, and the solvent was then removed under reduced pressure. The residue was poured into water and extracted with chloroform. After a similar work-up, the resulting oil (217 mg) was chromatographed on silica gel (25 g). Elution with benzene-chloroform (5:1) (120 ml) gave 3-hydroxythymo-1,4-quinone (**4a**) as needles (6 mg) from ethanol, mp 167—168 °C. The second fraction, eluted by the same solvent (320 ml) gave 3,3′-dihydroxy-2,2′-dimethyl-5,5′-diisopropyl-4,4′-diphenoquinone (**5a**) as needles (72 mg) from ethanol, mp 238—240 °C; IR (KBr): 3470, 1650, 1640, 1594, and 840 cm^{-1}; UV ($CHCl_3$): 245 (ε 1.09×10^4) and 406 nm (ε 4.57×10^3); ^{1}H NMR ($CDCl_3$): δ=1.32 (t, 12H), 1.60 (br s, 2H), 2.08 (s, 3H), 2.36 (s, 3H), 3.46 (m, 2H), and 7.00 (s, 2H); ^{13}C NMR ($CDCl_3$): δ=179.5, 149.4, 135.0, 126.0, 124.4, 121.2, 26.7 (24.6), 22.7 (20.2), and 14.7. Found: *m/z* 328.168. Calcd for $C_{20}H_{24}O_4$: M, 328.168.

Reaction of 3-Iodo-3,6-dimethyl-1,2-cyclohexanedione (2b) with Copper(II) Acetate in Acetic Acid-Water. By practically the same method as that in the case of **2a** above, **2b** (300 mg) was treated with copper(II) acetate. After the usual work-up, the resulting oil (185 mg) was chromatographed on silica gel (25 g). Elution with benzene-chloroform (5:1) (250 ml) gave 3-hydroxy-2,5-dimethyl-1,4-benzoquinone (**4b**),as needles (9 mg) from ethanol, mp 138—140 °C. The second fraction, eluted by the same solvent (160 ml) gave 4-iodo-3,6-dimethyl-1,2-benzenediol (**7**) as needles (14 mg) from ethanol, mp 88—90 °C.[17] The third fraction, eluted by the same solvent (200 ml), on crystallization from ethanol gave 3,3′-dihydroxy-2,2′,5,5′-tetramethyl-4,4′-diphenoquinone (**5b**) as reddish needles (64 mg), mp 238—239 °C; IR (KBr): 3450, 1654, 1642, 1606, and 836 cm^{-1}; UV ($CHCl_3$): 246 (ε 1.96×10^4) and 406 nm (ε 8.87×10^3); ^{1}H NMR ($CDCl_3$): δ=1.59 (br s, 6H), 2.12 (s, 6H), 2.40 (s, 6H), and 6.96 (s, 2H); ^{13}C NMR ($CDCl_3$): δ=181.8, 150.0, 139.5, 131.1, 126.4, 124.6, 14.7, and 7.7. Found: *m/z* 272.104. Calcd for $C_{16}H_{16}O_4$: M, 272.105.

Reaction of 3-Iodo-6-cyclohexyl-3-methyl-1,2-cyclohexanedione (2c): The 3-iodo-1,2-dione (**2c**) (275 mg) in acetic acid-water was treated with copper(II) acetate to give 23 mg

of **4c** and 147 mg of **5c**.

5c: Reddish needles; mp 237—240 °C; IR (KBr): 3480, 1654, 1642, 1594, and 840 cm^{-1}; UV ($CHCl_3$): 244 (ε 1.92×10^4) and 406 nm (ε 8.16×10^3); ^1H NMR ($CDCl_3$): δ=1.61 (br s, 2H), 2.07 (s, 3H), 2.35 (s, 3H), 3.11 (m, 2H), and 6.98 (s, 2H); ^{13}C NMR ($CDCl_3$): δ=177.3, 148.0, 132.2, 124.5, 123.1, 120.5, and 7.8. Found: *m/z* 408.230. Calcd for $C_{26}H_{32}O_4$: M, 408.230.

Reaction of 3-Iodo-6-ethyl-3-methyl-1,2-cyclohexanedione (2d): The 3-iodo-1,2-dione (**2d**) (85 mg) in acetic acid–water was treated with copper(II) acetate. After a similar work-up, the resultant oil was chromatographed on silica gel (25 g). Elution with benzene–chloroform (10:1) (150 ml) gave 3,3′-dihydroxy-5,5′-diethyl-2,2′-dimethyl-4,4′-diphenoquinone (**5d**) as reddish needles (33 mg), mp 184—187 °C; IR (KBr): 3440, 1652, 1625, 1600, and 840 cm^{-1}; UV ($CHCl_3$): 245 (ε 2.18×10^4) and 406 nm (ε 9.57×10^3); ^1H NMR ($CDCl_3$): δ=1.15 (t, 3H), 1.28 (t, 3H), 1.54 (s, 2H), 2.11 (s, 3H), 2.38 (s, 3H), 2.64 (q, 2H), 2.77 (q, 2H), and 6.95 (s, 2H); ^{13}C NMR ($CDCl_3$): δ=179.2, 149.1, 135.8, 130.2, 124.1, 121.1, 22.4, 14.7, and 7.8. Found: *m/z* 300.135. Calcd for $C_{18}H_{20}O_4$: M, 300.136.

Reaction of 3-Iodo-3,6-diethyl-1,2-cyclohexanedione (2e): The 3-iodo-1,2-dione (**2e**) (483 mg) in acetic acid–water was treated with copper(II) acetate to give 44 mg of **4e** and 115 mg of **5e**.

5e: Reddish needles; mp 185—188 °C; IR (KBr): 3454, 1654, 1636, 1598, and 848 cm^{-1}; UV ($CHCl_3$): 245 (ε 2.18×10^4) and 406 nm (ε 9.46×10^3); ^1H NMR ($CDCl_3$): δ=1.15 (t, 6H), 1.31 (t, 6H), 1.71 (br s, 2H), 2.65 (q, 4H), 2.79 (q, 4H), and 6.89 (s, 2H); ^{13}C NMR ($CDCl_3$): δ=178.5, 148.6, 135.4, 129.9, 124.0, 120.6, 22.2, 15.9, 14.0, and 12.6. Found: *m/z* 328.168. Calcd for $C_{20}H_{24}O_4$: M, 328.168.

Reaction of 3,3′,4,4′-Tetrahydroxy-2,2′,5,5′-tetraalkylbiphenyl (8a,8b) with Copper(II) Acetate. The tetrahydroxybiphenyl (**8a** and **8b**) (50 mg) in acetic acid–water was treated with copper(II) acetate. After the usual work-up, crystallization from ethanol afforded needles of **5a** (46 mg), mp 238—240 °C and **5b** (44 mg), mp 238—239 °C.

Reaction of Diosphenol (1a) with Bromine and Copper(II) Acetate in Acetic Acid–Water. The diosphenol (**1a**) (600 mg) in acetic acid–water (5:1) (60 ml) was treated with bromine (570 mg) and copper(II) acetate (712 mg) under refluxing for 5 h. After the usual work-up, the resulting oil (552 mg) was chromatographed on silica gel (25 g). Elution with benzene–ether (10:1) (220 ml) gave **4a** as needles (134 mg), mp 167—168 °C.

Reaction of 3-Bromo-3,6-dialkyl-1,2-cyclohexanedione (3a—3e) with Copper(II) Acetate in Acetic Acid–Water. General Procedure. A mixture of 3-bromo-1,2-diketone (**3a—3e**) (1.00×10^{-3} mol), copper(II) acetate monohydrate (1.50×10^{-3}mol), and acetic acid–water (10:1) (16.5 ml) was stirred under refluxing for 4 h. After the usual work-up, the resulting oil was chromatographed on silica gel. Elution with benzene–chloroform (4:1) gave orange and reddish crystals from ethanol. These results are summarized in Table 2.

We are indebted to Research Laboratories of Toyo Jozo Co., Ltd. and Associate Professor Sukekatsu Nozaki, Josai University, for their measurements of the high resolution mass spectra. Thanks are also due to Associate Professor Yoshio Koike and Mr. Toshio Takayama, Kanagawa University, for the measurement of FT-NMR spectra.

References

1) F. M. Dean, P. G. Jones, and P. Sidisunthorn, *J. Chem. Soc.*, **1962**, 5186.
2) J. F. Corbett, *J. Chem. Soc. C*, **1970**, 1912.
3) H. Musso, U. V. Gizycki, U. Zahorszky, and D. Bormann, *Justus Liebigs Ann. Chem.*, **676**, 10 (1964).
4) H. W. Moore and R. J. Wikholm, *J. Chem. Soc., Chem. Commun.*, **1971**, 1073.
5) E. M. Chamberlain and S. Dagley, *Biochem. J.*, **110**, 755 (1968).
6) J. A. Croft, E. Ritchie, and W. C. Taylar, *Aust. J. Chem.*, **29**, 1979 (1976).
7) F. Kogl and A. G. Boer, *Recl. Trav. Chim. Pays-Bas*, **54**, 779 (1935).
8) K. L. Colson, L. M. Jackman, T. Jain, G. Simolike, and J. Keeler, *Tetrahedron Lett.*, **26**, 4579 (1985).
9) K. Nakanishi, T. Goto, S. Ito, S. Natori, and S. Nozoe, "Natural Products Chemistry," Academic Press Inc., New York and London (1975), Vol. 2, pp. 226—227; T. K. Devon and A. I. Scott, "Handbook of Naturally Occurring Compound," Academic Press Inc., New York, San Francisco and London (1975), Vol. I, pp. 229—236.
10) C. Estable, M. I. Ardao, N. P. Brasil, and L. F. Fieser, *J. Am. Chem. Soc.*, **77**, 4942 (1955); L. F. Fieser and M. I. Ardao, *ibid.*, **78**, 774 (1956).
11) R. H. Eastman and J. C. Selover, *J. Am. Chem. Soc.*, **76**, 4118 (1954).
12) H-D. Becker, "The Chemistry of the Quinoid Compounds," ed by S. Patai, John Wiley & Sons, New York (1974), Chap. 7; D. H. R. Barton and W. D. Ollis, "Comprehensive Organic Chemistry," ed by J. F. Stoddart, Pergamon Press, Oxford (1979), Vol. 1, pp. 1213—1227.
13) L. Horner and K-H. Weber, *Chem. Ber.*, **96**, 1568 (1963).
14) H. Musso and H. Pietsch, *Chem. Ber.*, **100**, 2854 (1967).
15) P. Joseph-Nathan, D. Abramo-Bruno, and D. A. Ortega, *Org. Magn. Reson.*, **15**, 311 (1981).
16) C. A. Horiuchi and J. Y. Satoh, *Synthesis*, **1981**, 312; C. A. Horiuchi and J. Y. Satoh, *J. Chem. Soc., Chem. Commun.*, **1982**, 671; C. A. Horiuchi and J. Y. Satoh, *Bull. Chem. Soc. Jpn.*, **57**, 2691 (1984); C. A. Horiuchi and J. Y. Satoh, *Chem. Lett.*, **1984**, 1509; C. A. Horiuchi, A. Haga, and J. Y. Satoh, *Bull. Chem. Soc. Jpn.*, **59**, 2459 (1986); C. A. Horiuchi and J. Y. Satoh, *ibid.*, **60**, 426 (1987); C. A. Horiuchi and J. Y. Satoh, *Chem. Lett.*, **1988**, 1219.
17) C. A. Horiuchi, Y. Suzuki, M. Takahashi, and J. Y. Satoh, *Chem. Lett.*, **1987**, 393.
18) M. Utaka, S. Matsushita, and A. Takeda, *Chem. Lett.*, **1980**, 779.

 © 1989 The Chemical Society of Japan Bull. Chem. Soc. Jpn., 62, 2923—2931 (1989)

Implications of Unusual Population Ratios in Rotational Isomers of 9-(4-Substituted Benzyl)-8,13-dichloro-1,4-dimethyltriptycenes and 4-Substituted 9-Benzyl-8,13-dichloro-1-methyltriptycenes: $CH_3\cdots\pi$ Hydrogen Bond[1)]

Yasufumi NAKAI, Katsuya INOUE, Gaku YAMAMOTO, and Michinori ŌKI*,#
Department of Chemistry, Faculty of Science, The University of Tokyo, Bunkyo-ku, Tokyo 113
(Received February 28, 1989)

Population ratios of rotational isomers in substituted 9-benzyl-8,13-dichloro-1-methyltriptycenes were examined by equilibration in solution. The *sc* isomers increase in their populations as the electron density on the 9-benzyl group increases and the acidity of the 1-methyl group increases. The *sc/ap* ratios were larger than 2, the statistical value, in all the compounds examined, except the 4-nitrobenzyl compound. By contrast, MM2 calculations show that the *sc* isomers are less stable than the *ap* by ca. 1 kcal mol^{-1}. This discrepancy together with the substitutent effects on populations of the rotamers are attributed to the presence of $CH_3\cdots\pi$ interactions in the *sc* forms that stabilize the system mainly by charge-transfer interactions but are not included in the MM2 calculations.

Since the π-systems act as base, though weak,[2)] it is possible to observe the presence of OH–π hydrogen bond[3)] and NH–π hydrogen bond.[4)] Because of the weakness of the basicity of the π-system, the proton donor must be rather strong to manifest the XH–π hydrogen bond. Since the CH group is a weak electron-acceptor, the CH–π interactions are seldom observed unless the C–H group is a strong acid: the presence of the interactions between the acetylenic CH group and π-systems has been reported.[5)]

Although the presence of hydrogen bond involving the CH group as an electron acceptor has been reported in various cases,[6)] evidence for the presence is often not decisive: in many cases, if a C–H group and an electron donor are placed within the sum of their van der Waals radii in crystals, the result is taken to imply the presence of the hydrogen bond.[7)] In solution, the situation is more complicated than in the solid, because there is no means to determine the distance between the two groups concerned.

Hirota and Nishio have worked for a long time in this area. Once they believed that the unusual population ratios of rotamers in 1-alkyl-2-arylethane derivatives were the indication of the presence of the CH–π interactions but later they interpreted the results by dispersion forces because MM2 calculations could reproduce the population ratios of those compounds.[8)] Although they recently reported that they observed the CD–π hydrogen bond in 2-methyl-4-phenyl-3-pentanone-2*d* by infrared spectroscopy, their experimental results are so unusual from the normal sense of hydrogen bond that it is not possible to take the results as firm evidence for the presence of the CH–π hydrogen bond: the C–D stretching absorption due to the hydrogen-bonded form appears at a higher frequency than the non-hydrogen-bonded C–D stretching and the hydrogen-bonded form is less stable than the non-hydrogen-bonded form.[9)] However, the CH–π hydrogen bond is theoretically possible, though weak.[10,11)]

It is understood that, because of the very weak nature of the CH–π hydrogen bond, if after all present, strong evidence for the presence of the CH–π hydrogen bond is difficult to obtain. The N–H stretching absorption is known not to be affected by the NH–π hydrogen bond.[12)] The CH–π hydrogen bond, being still weaker than the NH–π, is expected to not affect the C–H stretching absorption, though it is possible that the C–H stretching appears at a higher frequency than the normal C–H stretching because of the congestion.[13)] Although appearance of abnormal population ratios of rotational isomers can be taken as evidence for the presence of attractive interactions, like the *sc* isomers of 1,2-ethanedithiol,[14)] this kind of effect is manifested only when the attractive interaction is stronger than repulsive interactions in the very conformation. Because of the weak nature of the CH–π interaction, the interaction may not overcome the repulsive van der Waals interactions in a given conformer in which the CH–π interaction is possible. To observe enhanced populations due to weak CH–π interactions, we must design a system in which the van der Waals repulsion can be eliminated or balanced in various conformations.

It is not possible, of course, to construct such a system, but it is possible to construct a system that nearly conforms to the conditions mentioned above. That is the 1,9-disubstituted triptycenes (**1**). In this

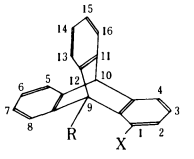

1

system, the atoms beta to the C_9 in the 9-substituent is placed unusually closely to the 1-substituent. X-Ray

Present address: Department of Chemistry, Faculty of Science, Okayama University of Science, Ridaicho, Okayama 700.

crystallographic data reveal that the distance is ca. 3.0 Å,[15] which is well within the sum of the van der Waals radii of the two groups concerned. If the 9-substituent is a primary alkyl group, it can rotate to assume another conformation, in which the atom beta to the 9-position is *ap* to the 1-substituent, when the distance between the substituent and the peri-carbon (8 or 13) is ca. 3.2 Å,[16] which is again within the sum of the van der Waals radii of the groups concerned. Although it is true that the distance between the two groups in the *ap* position is indeed a little longer than that in the *sc*[17] and the van der Waals replusion is more severe in the *sc* conformation than in the *ap*, yet it is also true that even in the *ap* conformation the van der Waals repulsion is severe, even though we neglect the presence of a hydrogen atom attached to the peri-carbon. Thus in this system, it can be expected that the severe van der Waals repulsion in the *sc* form is nearly equalled by that in the *ap*. Thus a weak interaction may be observed in this system as the unusual population ratios: that is, the *sc* form may be favored irrespective of the fact that sterically it is less favored.

The reason why we could report the presence of weak molecular interactions by taking advantage of this system is indeed the feature of the structures mentioned above. It was possible to detect charge-transfer interactions between a methoxy-oxygen and benzene rings that do not carry electronegative groups,[18] those between a chloro or a methoxy-oxygen and a carbonyl group,[19] those between a methoxy-oxygen and a CH_2X group where the X is an electronegative group,[20] and $CH_3\cdots O$ hydrogen bond.[21] It is quite natural to expect that the system could be useful in manifesting the CH-π interactions.

We have had several experiences that might be explained by the presence of the $CH_3\cdots\pi$ interactions in the 1,9-disubstituted triptycenes. In 1,4-dimethyl-9-(1-methyl-2-propenyl)triptycene (**2**), the population ratio, *sc*/*ap*, of the rotamers is 1.52, whereas the ratio is ca. 0.8 when the 1-substituent of comound **2** is switched to a chloro, a bromo, or a methoxyl.[22] We have pointed out a possibility that the results might imply the presence of the CH-π hydrogen bond, although it is possible to argue that the unusual population could be caused by the bulkiness of the methyl group in the 9-substituent.

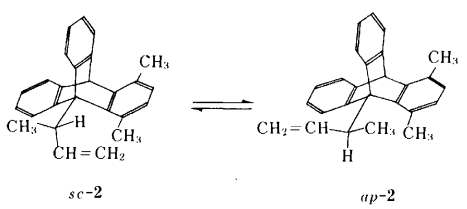

sc-2 *ap*-2

In 9-substituted 8,13-dichloro-1,4-dimethyltriptycenes (**3**), the *sc*/*ap* value is 2.0 or more if the 9-substituent carries a π-system beta to the 9-position, but it becomes 0.75 when the beta-substituent is a methyl.[23] Although it is possible again to argue that the results can be attributed to the steric repulsion due to the fact that a methyl is larger than a chloro and than a π-system, it is possible also to assume that the results are the indication that the *sc* conformation is stabilized by the presence of the CH-π interactions. Although the charge-transfer interaction between the chloro group and the π^*-system of the substituent may be claimed to be the cause, this interaction should favor the *ap* conformation rather than the *sc*.

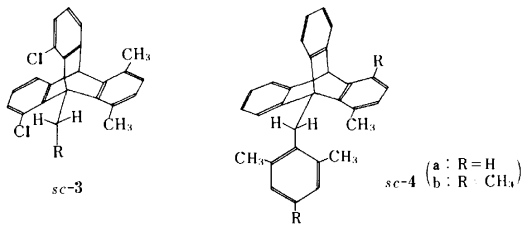

sc-3 *sc*-4 (a : R=H, b : R=CH3)

Another encouraging factor for the assumption of the presence of the CH-π interactions in this system is the failure of an empirical force field calculation in predicting the correct relative stability of the *sc* and the *ap* rotamers of 9-benzyl-1-methyltriptycene derivatives (**4**). Mislow and his co-workers calculated the stability by the empirical method to find that the *ap* conformer of 1-methyl-9-(2,6-dimethylbenzyl)triptycene (**4a**) is more stable than the *sc* form by 0.6 kcal mol^{-1} (1 cal=4.184 J). The experiment on the conformers of 1,4-dimethyl-9-(2,4,6-trimethylbenzyl)triptycene (**4b**) shows, in contrast, that the *sc* isomer is more stable than the *ap* by 0.8 kcal mol^{-1} or more.[24] The discrepancy may be taken as that the calculation is not reliable in this kind of congested molecules, but our experiences show that the calculations give correct tendency, though the value itself may not be correct.[25] It may indicate the presence of the CH-π interactions, because this type of charge-transfer interactions are not taken care of by the empirical calculations. We have thus felt that the assumption that the CH-π interactions are observed in this system is worthwhile to examine. This paper reports the results of such an examination.

We have selected the system of 9-benzyl-8,13-dichloro-1-methyltriptycenes for two reasons. One is that the system gives stable rotational isomers that can be separated at room temperature.[23] The advantage of this system is that we can equilibrate the rotational isomers by the classical method which is believed to afford reliable data. The other is that the chloro and the methyl groups are similar in size. This should give similar steric circumstances for both the *sc* and *ap* rotamers and the cancellation of the van der Waals repulsion in both rotamers is better than the case where there are no substituents in the 8,13-positions. The system involves two series of compounds: one is 9-(4-substituted benzyl)-1,4-dimethyltriptycenes which

provide a variety of electron densities in the benzyl group and the other is 4-substituted 9-benzyl-1-methyltriptycenes which provide a variety of acidities of the 1-methyl group.

Syntheses

The method of synthesis of 1,4-dimethyl-9-(4-nitrobenzyl)triptycene (**7**) is essentially the same with that of the unsubstituted compound that has been published.[23] 4,5-Dichloro-9-anthrone (**5**) was treated with *p*-nitrobenzyl chloride and aqueous potassium hydroxide and the product was reduced with sodium tetrahydroborate and then dehydrated in the presence of phosphorus pentaoxide to afford 1,8-dichloro-9-(4-nitrobenzyl)anthracene (**6**). Treatment of the anthracene (**6**) with 3,6-dimethylbenzyne which was produced in situ from 3,6-dimethylanthranilic acid gave 8,13-dichloro-1,4-dimethyl-9-(4-nitrobenzyl)triptycene (**7**). Hydrogenation of the triptycene (**7**) in the presence of platinum oxide followed by methylation afforded 8,13-dichloro-9-[4-(dimethylamino)benzyl]-1,4-dimethyltriptycene (**8**).

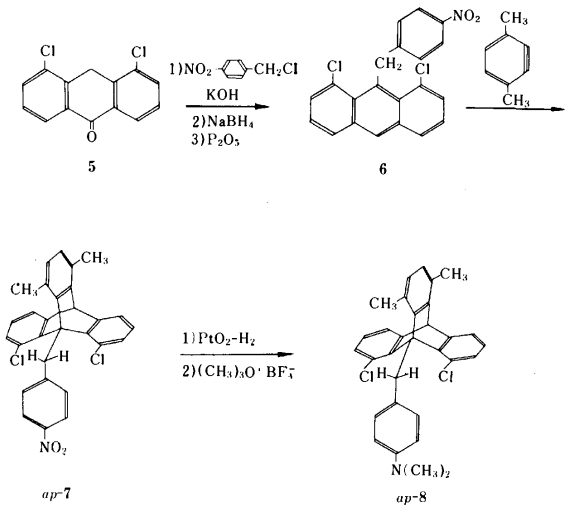

Similarly 9-benzyl-1,8-dichloroanthracene (**9**) was treated with 3-methylbenzyne which was generated from 3-methylanthranilic acid to afford a mixture of 9-benzyl-8,13-dichloro-1-methyltriptycene (**10**) and its 4-methyl isomer (**11**). The assignment of the structures of **10** and **11** bases on the ^{1}H NMR data: the chemical shift of the methyl protons in the *sc* form of **10** is higher than that of **11** due to the ring current effect of the benzyl-benzene ring.

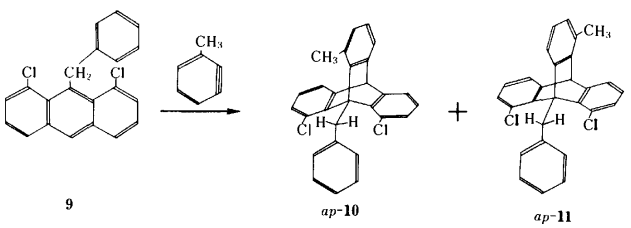

Treatment of 9-benzyl-8,13-dichloro-1,4-dimethyltriptycene (**12**) with *N*-bromosuccinimide afforded 9-benzyl-4-bromomethyl-8,13-dichloro-1-methyltriptycene (**13**) and 9-benzyl-1-bromomethyl-8,13-dichloro-1-methyltriptycene (**14**) together with other products. The identification of **13** and **14** was carried out again with the use of the chemical shift data of the methyl and the bromomethyl protons in ^{1}H NMR spectra that reflected the anisotropy effect of the benzyl-benzene ring. The 4-bromomethyl compound (**13**) was hydrolyzed and then oxidized with the Jones reagent to afford 9-benzyl-8,13-dichloro-4-carboxy-1-methyltriptycene (**15**). Compound **15** was methylated to give the methyl ester (**16**). Treatment of compound **15** with thionyl chloride followed by that with ammonia and then phosphorus pentaoxide afforded the corresponding nitrile (**17**).

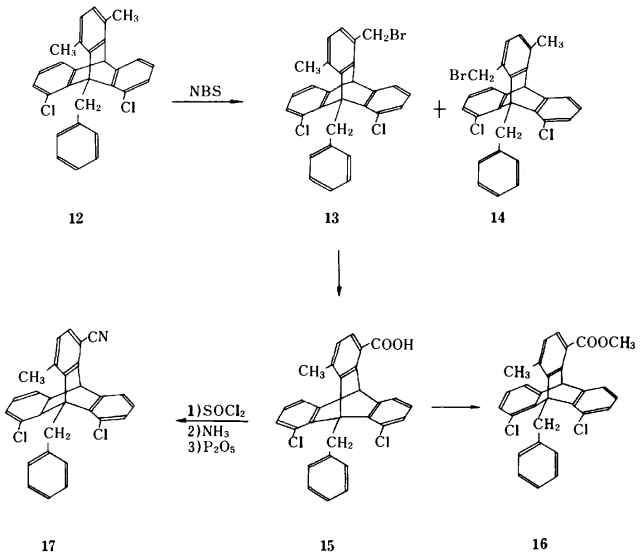

Results and Discussion

The isomerization was carried out by heating solutions of the compounds in chloroform-*d* unless otherwise mentioned. The assignment of the conformations was performed by observing the singlet signal for the *ap* form and the AB quartet for the *sc* form in

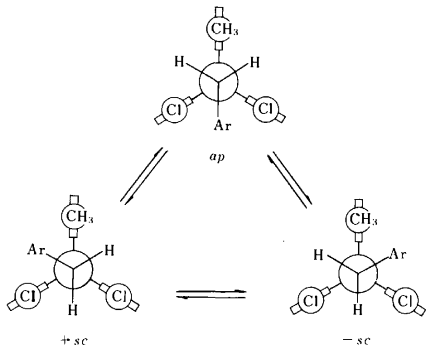

Scheme 1. Rotational circuit.

the ^{1}H NMR spectra of the benzylic methylene protons as is clearly understood from the Newman-type projection in Scheme 1.

Although only one isomer was isolated by chromatography, the identity of the other isomer was confirmed by equilibration as well as their ^{1}H NMR spectra. The populations of isomers were estimated by the ^{1}H NMR spectra at 270 MHz. The equilibration data at 54 °C for the rotamers of the compounds in question are compiled in Tables 1 and 2 together with some relevant data.

In principle, the populations of one isomer can increase, if the rotamer is stabilized by an attractive interaction, or if other isomers are destabilized by a repulsive interaction or by structural deformation of the molecule. Although it is difficult to diagnose which is the case in general, the rotational barrier will give a clue for the diagnosis in this case because the transition state energy for rotation in the series of compounds can be assumed little different, if we take molecular interactions in the transition state only. Thus we decided to compare the barrier to rotation in the nitro compound (**7**) with that in the unsubstituted (**12**).[23] The kinetic data for the isomerization of the nitro compound (**7**) are compiled in Table 3.

The rate constants for isomerization, *sc*→*ap*, are ca. 1.7 times larger for the unsubstituted compound (**12**) than the nitro (**7**), whereas those for the *ap*→*sc* process are ca. 2.5 times faster for the former than the latter. Although *ap*-**7** isomerizes more sluggishly than *ap*-**12**, the tendency is also true for the *sc* conformer. The results may be interpreted to mean that the *sc* form of the nitro compound (**7**) is not specially destabilized, though its population decreases relatively from the unsusbstituted compound (**12**). We assume, therefore, that the population change in the series of compounds is mainly caused by repulsive and attractive interactions within the molecules without significant structural changes.

The main attractive forces and repulsive forces that may affect the populations of rotamers are van der Waals attractive force (dispersion force), charge-transfer interactions, van der Waals repulsions, and Coulombic interactions, both attractive and repulsive.

The data in Table 1 clearly indicate that, as the electron density on the benzyl-benzene ring increases, the *sc* form becomes favored. The results cannot be explained by the van der Waals repulsion because the high electron density on the benzyl-benzene means the bulkier π-system than the low electron-density one and

Table 1. Equilibrium Constants of the Rotational Isomers in 9-(4-Substituted benzyl)-8,13-dichloro-1,4-dimethyltriptycenes at 54.0 °C in $CDCl_3$ and Electron Densities on the Benzyl-Benzene Ring

Compd	Subst	K ($\pm sc/ap$)	Electron density[a]
8	$N(CH_3)_2$	2.87±0.10	−0.0370
12	H	2.30±0.04	0.0
7	NO_2	1.52±0.04	0.0714

a) π-Electron density at the 4-position as calculated by the CNDO method for monosubstituted benzenes.[26]

Table 2. Equilibrium Constants of the Rotational Isomers in 4-Substituted 9-Benzyl-8,13-dichloro-1-methyltriptycenes in $CDCl_3$ at 54.0 °C and Substituent Constants

Compd	Subst	K ($\pm sc/ap$)	Substituent constant (para)[27]
12	CH_3	2.30±0.04	−0.129
10	H	2.22±0.06	0.00
16	$COOCH_3$	4.09±0.16	0.385
17	CN	3.42±0.14	0.674

Table 3. Kinetic Data for the Isomerization of Rotamers in 8,13-Dichloro-1,4-dimethyl-9-(4-nitrobenzyl)triptycene in $CDCl_3$[a]

Temperature/°C	$k_{-1}/10^{-5}$ s^{-1}	$\Delta G^{\ddagger}$/kcal mol^{-1}	K ($\pm sc/ap$)
69.0	22.9	25.8	1.66
62.0	10.8	25.8	1.63
54.0	4.38	25.7	1.53
49.0	2.44	25.7	1.43

a) $ap \underset{k_{-1}}{\overset{2k_1}{\rightleftharpoons}} sc$ $\quad K=2k_1/k_{-1}$

$\Delta H^{\ddagger} = 23.8 \pm 1.2$ kcal mol^{-1}

$\Delta S^{\ddagger} = -5.8 \pm 3.7$ cal mol^{-1} K^{-1}

the methyl group is larger than the chloro group. In consideration of the Coulombic interactions, we may consider the bond dipoles of the C–Cl and the substituted benzene rings, because other parts of the molecule are hydrocarbons. Since the distance between the C–Cl bonds and the substituted benzyl-benzene rings are different in the *sc* form from those in the *ap*, the Coulombic interactions may change in one isomer from the other. However, to the first approximation, we neglect the difference, because the directions of the dipole of the substituted benzenes, 60° or 120°, relative to the C–Cl bonds do not change irrespective of the kind of rotamers. The dispersion force may be neglected to the first approximation from being the main factor that manifests the observed rotamer ratios, because the dispersion force is dependent on the polarizability and the ionization potential:[28] the high electron density means the high polarizability as well as the low ionization potential. In addition, we are comparing the rotamer distributions in a series of compounds: the comparison may cancel the change in the dispersion force. Thus the charge-transfer interactions between the CH_3 group and the π-system remain as a strong candidate that favors the *sc* conformation over the *ap*. However, it is possible to argue that, since the charge-transfer interaction[18] between the chloro group and the π^*-system of the benzyl group is expected to be stronger in the *ap* conformation than in the *sc*, especially in the case with electronegative substituents, the results are attributed to this type of charge-transfer. The argument cannot be ruled out by the data in Table 1.

The data in Table 2 suggest that, by and large, the *sc/ap* value increases as the 4-substituent becomes electronegative. Since the bulkiness of the 1-methyl group will not substantially change irrespective to the change in the electron density at the 1-position, the results cannot be explained by the van der Waals repulsions. Van der Waals attraction may also be neglected as a main factor that favors the *sc* form because the change in the force may again be small. The Coulombic interactions cannot be the factor that mainly controls the rotamer populations in this case because the dipole introduced by the 4-substituent must contribute equally to both the *sc* and *ap* rotamers. The results as well exclude the possibility that the charge-transfer interaction between the chloro substituent and the π^*-system is the main cause for the observed population ratios: if it were the case, the 4-substituent should affect the population ratios little. Thus the results strongly support the claim that we have observed the presence of the $CH_3\cdots\pi$ interactions.

Although the general trend that, as the acidity of the 1-methyl group becomes high, the *sc* form becomes favored relative to the *ap* form is apparent, close examination reveals some irregularities: the *K* value for the 4-methyl compound (**12**) is larger than that for the unsubstituted compound (**10**) and the *K* value for the 4-cyano compound (**17**) is smaller than that for the 4-methoxycarbonyl compound (**16**), even though the 4-methyl group increases the electron density on the 1-methyl group more than the 4-hydrogen and a cyano group is more electron-attracting than a methoxycarbonyl. We suspected that a small difference in dipole moments of the rotamers involved might be responsible to the irregular trend in the population ratios.

MM2 calculations show that the dipole moments of the rotamers of 9-benzyl-8,13-dichloro-1,4-dimethyltriptycene are indeed different, though the difference is small: *sc* 3.231 D and *ap* 3.157 D (1 D=3.3356×10^{-30} C m). Introduction of a substituent instead of the methyl at the 4-position will change the difference in the dipole moments of the rotamers. Thus we examined the solvent effect on the rotamer populations. The *sc/ap* values in dimethyl-d_6 sulfoxide were obtained as follows at 54.0 °C: 4-CH_3 2.0, 4-H 1.8, 4-CH_3OCO 3.0, 4-CN 2.4. Thus the *K* values all decrease in dimethyl sulfoxide relative to the value in chloroform and the irregular tendency is repeated. Thus at least dipole moments of the molecules are not the factors that cause the irregularities. Although further study is needed to clarify the point, the irregularities must be caused by the factors we have neglected in the discussion.

The total steric energies of the 4-substituted 9-benzyl-8,13-dichloro-1-methyltriptycenes as calculated by the MM2 method are shown in Table 4. The interesting point here is the fact that the *ap* forms of the series of comounds are ca. 1.0 kcal mol^{-1} more stable than the corresponding *sc* forms by calculations, irrespective of the kind of substituents, in sharp contrast to the experimental observation that the *sc* forms are more favored than the statistical value. From our experience in MM2 calculations, we under-

Table 4. Total Steric Energies of 4-Substituted 9-Benzyl-8,13-dichloro-1-methyltriptycene Rotamers as Calculated by MM2 Method

Compd	Subst	*ap*/kcal mol^{-1}	*sc*/kcal mol^{-1}	ΔE/kcal mol^{-1}
12	CH_3	28.462	29.539	1.077
10	H	28.208	29.216	1.008
16	$COCH_3$[a]	37.275	38.259	0.984
17	CN	27.397	28.445	1.052

a) This substituent was used instead of the methoxycarbonyl group, because the parameters for the latter were not available.

stand that the absolute values obtained by the method may not be reliable in the series of congested triptycenes, even for the ground states. However, it is also true that the relative values and the tendency of the stability of the ground state molecules are reproducible by the MM2 calculations.[25] Therefore, we believe the discrepancy between the MM2 calculations and the experimental results is significant. Since MM2 calculations take care of dispersion forces and the dipole interactions, the discrepancy must be attributed to the forces other than those mentioned. Thus the charge-transfer interactions are the most likely factor that stabilizes the *sc* form.

We conclude that the *sc* form of the triptycenes described in this paper is stabilized by the $CH_3\cdots\pi$ interactions. Although the $CH\cdots\pi$ interactions are known to be very weak by theoretical studies,[10,11] there are two points that render the observation of the presence of the $CH_3\cdots\pi$ interactions possible. They are the proximity of the two groups concerned that makes overlap of the orbitals concerned more effective than the normal cases and the near-cancellation of the repulsive forces in the triptycene rotamers due to the highly congested state in both rotamers. The unusual population ratios described in the introduction of this paper is now believed to include the contribution of this type of interactions at least to some extent. Although observation of normal hydrogen bonding is resulted by various factors including dipole interactions, charge transfer, and repulsive interactions, the contribution of dipole moment is rather small in the case of C–H bonds.[11] Thus the results presented in this paper can be the basis that there is the $CH_3\cdots\pi$ hydrogen bond in which charge transfer is the main stabilizing factor.

Experimental

Kinetics of Isomerization. The 4-nitrobenzyl compound (**7**) (*sc* or nearly pure *ap*) was dissolved in chloroform-*d* to make up ca. 1% (w/v) solutions. The kinetic data were obtained as described previously.[29] The analyses of the starting material and the product were performed by using a Waters HPLC apparatus (microporasil and hexane) equipped with a UV detector, *p*-nitrotoluene being used as an internal standard. The data were processed by assuming a reversible first order reaction.

Equilibration of Rotamers. The triptycenes were dissolved in either chloroform-*d* or dimethyl-d_6 sulfoxide to make up ca. 1% (w/v) solutions. The solution was sealed in an NMR sample tube and was heated by immersing into a boiling acetone bath. The populations of the rotamers were determined by integration of the methyl signals, of which assignment was confirmed by consulting the intensities of the signals due to benzylic methylene protons, in ^{1}H NMR spectra recorded on a JEOL GX270 spectrometer which operated at 270 MHz. The integration was carried out for several times and the data were treated statistically.

MM2 Calculations. The calculations were carried out with the use of an available program[30] by a HITAC M-280H computer at the Computer Center of the University of Tokyo. The parameters used for the chloro substituents were those reported from this laboratory some time ago.[31] Structural features of 1,9-disubstituted triptycenes, such as sharpening of the pyramid of which apex is C_9 with a base made up by C_{9a}–C_{8a}–C_{12} and widening of the dihedral angle that is made by two benzeno bridges flanking the beta atom of the 9-substituent (a phenyl in the cases described here), were reproducible.

4,5-Dichloro-10-(4-nitrobenzyl)anthrone. To a boiling solution of 3.29 g (12.5 mol) of 4,5-dichloroanthrone (**5**)[32] and 2.14 g (12.5 mmol) of *p*-nitrobenzyl chloride in 100 mL of methanol, was added 1.0 g (ca. 15 mmol) of potassium hydroxide (ca. 85% pure) in 40 mL of methanol in 2 h under a nitrogen atmosphere. The reaction mixture was allowed to cool with stirring and the precipitate was removed by filtration. The solvent was evaporated from the filtrate and the residue was recrystallized from tetrahydrofuran–methanol to afford pale yellow crystals, mp 200—201 °C, in 4.05 g (81%) yield. Found: C, 63.25; H, 3.30; N, 3.60; Cl, 17.33%. Calcd for $C_{21}H_{13}Cl_2NO_3$: C, 63.34; H, 3.29; N, 3.52; Cl, 17.80%. ^{1}H NMR ($CDCl_3$) δ=3.49 (2H, d, J=4.5 Hz), 5.41 (1H, t, J=4.5 Hz), 6.18 (2H, d, J=8.6 Hz), 7.2—8.0 (8H, m).

1,8-Dichloro-9-(4-nitrobenzyl)anthracene (6). To a solution of 5.58 g (14.0 mmol) of the foregoing anthrone in 200 mL of methanol, was added 3.0 g (79 mmol) of sodium tetrahydroborate in 3 portions with 10 min intervals. The mixture was stirred for further 10 min and the solvent was evaporated. The residue was treated with water and extracted with chloroform. The extract was dried over magnesium sulfate and the solvent was evaporated to give oily 4,5-dichloro-10-(4-nitrobenzyl)-9-anthranol which was apparently one isomer of the possible two according to the ^{1}H NMR spectrum ($CDCl_3$): δ=2.49 (1H, d, J=10.2 Hz), 3.21 (2H, d, J=5.6 Hz), 4.43 (1H, d, J=10.2 Hz), 5.18 (1H, t, J=5.6 Hz), 6.59 (2H, d, J=8.9 Hz), 7.1—7.6 (6H, m), 7.81 (2H, d, J=8.9 Hz).

The anthranol in 100 mL of carbon tetrachloride was heated with 15 g of phosphorus pentaoxide for 15 min. The solid was removed by filtration and was washed with hot carbon tetrachloride. The combined carbon tetrachloride solution was evaporated and the residue was submitted to silica-gel chromatography (hexane–dichloromethane eluent) to yield 1.23 g (23%) of the desired product which was purified by recrysallization from dichloromethane–hexane. Bright yellow crystals, mp 184—185 °C. Found: C, 66.14; H, 3.66; N, 3.73; Cl, 18.50%. Calcd for $C_{21}H_{13}Cl_2NO_2$: C, 65.59; H, 3.43; N, 3.66; Cl, 18.55%. ^{1}H NMR ($CDCl_3$) δ=5.71 (2H, s), 6.8—8.0 (10H, m), 8.45 (1H, s).

8,13-Dichloro-1,4-dimethyl-9-(4-nitrobenzyl)triptycene (7). To a boiling solution of 2.38 g (6.23 mmol) of the anthracene (**6**) and 6.0 mL (45 mmol) of isopentyl nitrite in 150 mL of dichloromethane were simultaneously added a solution of 3.00 g (18.2 mmol) of 3,6-dimethylanthranilic acid[33] in 80 mL of dichloromethane and that of 3.0 mL (22 mmol) of isopentyl nitrite in 20 mL of dichloromethane from two separatory funnels under a nitrogen atmosphere in 40 min and the whole was refluxed for 20 min. The solvent was evaporated and the residue was submitted to chromatography on silica gel (hexane–dichloromethane eluent). The

product was recrystallized from dichloromethane–hexane and was found to be a mixture of ca. 1:6 *sc* and *ap* isomers. Yield was 2.40 g (79%). Attempted purification of the *ap* isomer by recrystallization resulted in failure because the operation enriched the *sc* isomer. The *sc* isomer was obtained by chromatography (hexane–dichloromethane eluent) of the thermally equilibrated mixture of *sc* and *ap* forms on alumina, the mixture being obtained by heating a tetrahydrofuran solution under reflux for 6 h. The melting point was >300 °C. Found: C, 71.39; H, 4.55; N, 3.13; Cl, 14.34%. Calcd for $C_{29}H_{21}Cl_2NO_2$: C, 71.61; H, 4.35; N, 3.13; Cl, 14.58%. ^{1}H NMR ($CDCl_3$) δ=2.09 (3H, s), 2.58 (3H, s), 5.40 and 5.85 (2H, ABq, J=19.3 Hz), 5.60 (1H, s), 6.55—7.40 (9H, m), 7.65—7.8 (2H, m), 8.2—8.3 (1H, m).

The following ^{1}H NMR data ($CDCl_3$, δ) of the *ap* form were collected: 2.43 (3H, s), 2.84 (3H, s), 5.60 (2H, s), 5.64 (1H, s), 6.7—7.4 (9H, m), 7.65—7.8 (2H, m), 8.2—8.3 (1H, m).

8,13-Dichloro-9-[4-(dimethylamino)benzyl]-1,4-dimethyltriptycene (8). A suspension of 667 mg (1.37 mmol) of the nitrobenzyltriptycene (**7**, *sc*/*ap*=1.0) in 1:1 (v/v) dioxane–acetic acid was shaken under a hydrogen atmosphere in the presence of ca. 60 mg of platinum(IV) oxide for 12 h. For completion of the hydrogenation, it was necessary to add another portion of platinum oxide (60 mg) and to shake under hydrogen for 24 h. After removal of the catalyst by filtration, the solvents were evaporated and the residue was treated with aqueous sodium hydrogencarbonate. The mixture was extracted with dichloromethane and the solution was dried over magnesium sulfate. The product, after evaporation of the solvent, was used directly for the next reaction. The following ^{1}H NMR data were collected ($CDCl_3$, δ): *sc* form 2.19 (3H, s), 2.53 (3H, s), 3.38 (2H, br s), 5.13 and 5.57 (2H, ABq, J=18.9 Hz), 5.55 (1H, s), 6.1—7.4 (12H, m); *ap* form 2.37 (3H, s), 2.81 (3H, s), 3.38 (2H, br s), 5.37 (2H, s), 5.57 (1H, s), 6.1—7.4 (12H, m).

Trimethyloxonium tetrafluoroborate[34] (ca. 300 mg or ca. 2 mmol) was added to a solution of 625 mg (1.37 mmol) of the amine in 15 mL of dichloromethane and the mixture was stirred for 2 h at room temperature. The mixture was poured into a saturated solution of sodium hydrogencarbonate in water and then the aqueous layer was extracted with dichloromethane. After drying over magnesium sulfate, the solvent was evaporated and the residue was treated again with the Meerwein reagent as above. The product was chromatographed on alumina (hexane–dichloromethane eluent) to give 422 mg (64%) of the desired product, which was a mixture (*sc*/*ap*=2.0) of the rotamers.

The *sc* isomer was obtained in a pure form by semi-preparative HPLC (microporasil, 20:1 hexane-chloroform eluent), mp 280 °C (decomp). Found: C, 76.74; H, 5.32; N, 2.86; Cl, 14.43%. Calcd for $C_{31}H_{27}Cl_2N$: C, 76.86; H, 5.62; N, 2.89; Cl, 14.64%. ^{1}H NMR ($CDCl_3$) δ=2.19 (3H, s), 2.56 (3H, s), 2.87 (6H, s), 5.15 and 5.60 (2H, ABq, J=18.2 Hz), 5.56 (1H, s), 6.15—6.25 (2H, m), 6.5—7.4 (10H, m).

The following ^{1}H NMR data ($CDCl_3$, δ) of the *ap* form were collected: 2.41 (3H, s), 2.85 (3H, s), 2.88 (6H, s), 5.38 (2H, s), 5.58 (1H, s), 6.15—6.25 (2H, m), 6.5—7.4 (10H, m).

9-Benzyl-8,13-dichloro-1-methyltriptycene (10). 9-Benzyl-1,8-dichloroanthracene[23] (4 mmol) was similarly treated with 3-methylanthranilic acid[35] (9 mmol) and isopentyl nitrite in dichloromethane as described for the preparation of the nitro compound (**7**). The reaction afforded, after chromatography on silica gel (hexane–dichloromethane eluent), a 3:2:8 mixture of *sc*-**10**, *ap*-**10**, and 9-benzyl-8,13-dichloro-4-methyltriptycene (**11**). Most of the 4-methyl isomer (**11**) was removed by filtration after letting a solution of the mixture in dichloromethane to stand to evaporate the solvent. The filtrate was submitted to gel permeation chromatography (chloroform solvent) to separate **10** from **11**. The mixture of rotamers of **10** was resubmitted to GPC. Recycling 40 times did not give any of the pure rotamers. Recrystallization of the *sc*-enriched portion from 1:1 dichloromethane–hexane afforded crystals which consisted of 8:3 *sc* and *ap* rotamers and melted at 249.5—251.0 °C. Found: C, 78.36; H, 4.68; Cl, 16.88%. Calcd for $C_{28}H_{20}Cl_2$: C, 78.69; H, 4.72; Cl 16.59%. The following ^{1}H NMR data ($CDCl_3$, δ) were collected. *sc*: 2.17 (3H, s), 5.27 and 5.76 (2H, ABq, J=19.1 Hz), 6.4—7.7 (14H, m). *ap*: 2.89 (3H, s), 5.26 (1H, s), 5.51 (2H, s), 6.4—7.7 (14H, m).

The 4-methyl isomer (**11**) was submitted to recrystallization from 1:1 dichloromethane–hexane to give analytical sample, mp 227.0—228.0 °C. Found: C, 78.62; H, 4.89; Cl 16.82%. Calcd for $C_{28}H_{20}Cl_2$: C, 78.69; H, 4.72; Cl, 16.59%. This compound apparaently crystallized as *sc* forms. ^{1}H NMR ($CDCl_3$, 25 °C) δ=2.58 (3H, s), 5.60 (1H, s), 4.88 and 5.95 (2H, ABq, J=18.2 Hz), 6.50 (1H, br s), 6.7—7.5 (12 H, m), 7.58 (1H, br s). ^{1}H NMR spectra at other temperatures suggest that the isolated rotation of the benzylic phenyl group at −40 °C is slow but is taking place slowly at room temperature, whereas rotation about the C_9-to-substituent bond begins to take palce at 55 °C in chloroform-*d*: at −40 °C, δ=2.58 (3H, s), 5.60 (1H, s), 4.88 and 5.95 (2H, ABq, J=18.1 Hz), 6.49 (1H, d, J=8.5 Hz), 6.7—7.5 (12H, m), 7.68 (1H, d, J=8.5 Hz); at 55 °C, δ=2.57 (3H, s), 4.80 (1H, br d), 5.58 (1H, s), 5.94 (1H, br d), 6.6—7.4 (14H, m).

9-Benzyl-4-bromomethyl-8,13-dichloro-1-methyltriptycene (13). A mixture of 1.01 g (2.29 mmol) of 9-benzyl-8,13-dichloro-1,4-dimethyltriptycene (**12**)[23] (*sc*/*ap*=1.0), 0.45 g (2.5 mmol) of *N*-bromosuccinimide and a small amount of dibenzoyl peroxide in 60 mL of carbon tetrachloride was heated under reflux for 4 h. The mixture was cooled and the insoluble materials were removed by filtration. The solvent was evaporated in vacuo from the filtrate and the residue was submitted to chromatography on silica gel with the use of a medium-pressure liquid chromatograph (hexane–dichloromethane eluent). The order of elution was the unreacted material, *sc*-**13**, *ap*-**13**, *sc*-**14**, and *ap*-**14**. The total yield of *sc*-**13** and *ap*-**13** was 0.39 g (33%). The mixture of *sc*- and *ap*-**13** (*sc*/*ap*=2.0) was resubmitted to the medium-pressure chromatography to afford pure *sc*-**13**, mp 247.5—248.5 °C. Found: C, 66.89; H, 4.37; Cl, 13.58; Br, 15.30%. Calcd for $C_{29}H_{21}BrCl_2$: C, 66.95; H, 4.07; Cl, 13.63; Br, 15.36%. ^{1}H NMR ($CDCl_3$) δ=2.18 (3H, s), 4.73 and 4.85 (2H, ABq, J=10.3 Hz), 5.28 and 5.76 (2H, ABq, J=18.7 Hz), 5.77 (1H, s), 6.42 (1H, br d, J=8.1 Hz), 6.62 (1H, d, J=8.1 Hz), 6.8—7.6 (11H, m). The *ap*-**13** afforded the following ^{1}H NMR data ($CDCl_3$, δ): 2.89 (3H, s), 4.62 (2H, s), 5.51 (2H, s), 5.79 (1H, s), 6.42 (1H, br d, J=8.1 Hz), 6.62 (1H, d, J=8.1 Hz), 6.8—7.6 (11H, m).

9-Benzyl-4-carboxy-8,13-dichloro-1-methyltriptycene (15). To a solution of compound **13** (*sc*/*ap*=2.0, 268 mg or 0.514 mmol) in 10 mL of dimethyl sulfoxide, was added

2 mL of water and the whole was heated at 90—100 °C for 4 h. The mixture was poured into water and extracted with dichloromethane. The extract was dried over magnesium sulfate and the solvent was evaporated. The residue was taken up in 6 mL of acetone and, to this solution, the Jones reagent[36] was added at room temperature until the yellow color of Cr(VI) became persistent. The mixture was stirred for further 30 min at room temperature and the excess of the Cr(VI) was reduced with ethanol. The solid was removed by filtration and the filtrate was poured into water. The mixture was extracted with dichloromethane and the extract was dried over magnesium sulfate. Evaporation of the solvent afforded practically pure **15**, which was directly used for the next reaction, in 229 mg (95%) yield. The *sc*/*ap* value was 4.0. The following ^{1}H NMR data were collected ($CDCl_3$, δ): *sc* 2.28 (3H, s), 5.34 and 5.81 (2H, ABq, J=19.4 Hz), 6.35—6.4 (1H, m), 6.7—7.75 (14H, m); *ap* 2.98 (3H, s), 5.55 (2H, s), 6.35—6.4 (1H, m), 6.7—7.75 (14H, m).

9-Benzyl-8,13-dichloro-4-methoxycarbonyl-1-methyltriptycene (16). To a solution of 244 mg (0.517 mmol) of the carboxylic acid (**15**, *sc*/*ap*=4.0) in 15 mL of dichloromethane, was added diazomethane in ether,[37] prepared from *N*-methyl-*N*-nitroso-*p*-toluenesulfonamide, until the solution bore yellow tinge and then the mixture was stirred for 10 min at room temperature. The excess of diazomethane was destroyed with acetic acid and the mixture was poured into aqueous sodium hydrogencarbonate. The mixture was extracted with dichloromethane and the extract was dried over magnesium sulfate. The solvent was evaporated and the residue was submitted to preparative TLC (silica gel, hexane–dichloromethane eluent) to afford 211 mg (84%) of the desired product. The *sc* isomer was isolated by medium-pressure chromatography (silica gel, hexane-dichloromethane eluent). Mp 218.5—224.5 °C. Found: C, 74.42; H, 4.82; Cl, 14.40%. Calcd for $C_{30}H_{22}Cl_2O_2$: C, 74.23; H, 4.52; Cl, 14.61%. ^{1}H NMR ($CDCl_3$) δ=2.24 (3H, s), 4.00 (3H, s), 5.32 and 5.79 (2H, ABq, J=19.1 Hz), 6.3—6.4 (1H, m), 6.65—7.6 (13H, m).

ap-**16** exhibited the following ^{1}H NMR data ($CDCl_3$, δ): 2.94 (3H, s), 3.94 (3H, s), 5.52 (2H, s), 6.3—6.4 (1H, m), 6.65—7.6 (13H, m).

9-Benzyl-8,13-dichloro-4-cyano-1-methyltriptycene (17). To a suspension of 229 mg (0.486 mmol) of the acid (**15**) (*sc*/*ap*=4.0) in 10 mL of benzene was added 0.20 mL (2.7 mmol) of thionyl chloride. The mixture was stirred at room temperature for 1 h and then heated under reflux for 4 h. The benzene and the excess of the thionyl chloride were removed in vacuo and the residue was taken up in 2.5 mL of tetrahydrofuran. The solution was treated with 2 mL of concentrated aqueous ammonia for 2 h with ice-cooling. The whole was poured into water and extracted with dichloromethane. The extract was dried over magnesium sulfate and the solvent was evaporated. The residue, taken up in 10 mL of toluene, was heated with 2 g of phosphorus pentaoxide for 2 h under reflux. The solid was removed by filtration from the cooled mixture and the solvent was evaporated from the filtrate. The residue was submitted to preparative TLC (silica gel, hexane–dichloromethane eluent) to give 95 mg (43%) of the desired product (*sc*/*ap*=3.0). The *sc* form was separated by medium-pressure chromatography (silica gel, hexane–dichloromethane), mp 300.5—301.0 °C. Found: C, 76.82; H, 4.02; N, 2.93; Cl, 15.49%. Calcd for $C_{29}H_{19}Cl_2N$: C, 77.00; H, 4.23; N, 3.10; Cl, 15.67%. ^{1}H NMR ($CDCl_3$) δ=2.22 (3H, s), 5.25 and 5.79 (2H, ABq, J=19.4 Hz), 5.83 (1H, s), 6.3—6.4 (1H, m), 6.75—7.6 (12H, m). IR (KBr disc): 2225 cm^{-1}.

The following ^{1}H NMR data for *ap*-**17** were recorded ($CDCl_3$, δ): 2.94 (3H, s), 5.50 (2H, s), 5.80 (1H, s), 6.3—6.4 (1H, m), 6.75—7.6 (12H, m).

This work was partially supported by a Grant-in-Aid (No. 62303004) for Fundamental Scientific Research of the Ministry of Education, Culture and Science.

References

1) A preliminary note has been published: Y. Nakai, G. Yamamoto, and M. Ōki, *Chem. Lett.*, **1987**, 89.

2) H.-H. Perkampus, *Adv. Phys. Org. Chem.*, **4**, 195 (1966).

3) M. Ōki and T. Yoshida, *Bull. Chem. Soc. Jpn.*, **44**, 1136 (1971) and earlier papers.

4) M. Ōki and K. Mutai, *Bull. Chem. Soc. Jpn.*, **39**, 809 (1966) and earlier papers: I. Suzuki, M. Tsuboi, and T. Shimanouchi, *Spectrochim. Acta*, **16**, 467 (1960).

5) C. D. Brand, G. Eglinton, and J. Tyrrell, *J. Chem. Soc.*, **1965**, 5914.

6) R. D. Green, "Hydrogen Bonding by C-H Groups," John-Wiley, New York (1974).

7) R. Taylor and O. Kennard, *J. Am. Chem. Soc.*, **104**, 5063 (1982).

8) M. Hirota, K. Abe, H. Suezawa, and M. Nishio, *J. Mol. Struct.*, **126**, 455 (1985).

9) M. Karatsu, H. Suezawa, K. Abe, M. Hirota, and M. Nishio, *Bull. Chem. Soc. Jpn.*, **59**, 3529 (1986).

10) K. Abe, M. Hirota, and K. Morokuma, *Bull. Chem. Soc. Jpn.*, **58**, 2713 (1985).

11) T. Takagi, A. Tanaka, S. Matsuo, H. Maezaki, M. Tani, H. Fujiwara, and Y. Sasaki, *J. Chem. Soc. Perkin Trans. 2*, **1987**, 1015.

12) K. Moriyama, N. Nakamura, M. Nakamura, and M. Ōki, *Gazz. Chim. Ital.*, **117**, 655 (1987).

13) L. de Vries and P. R. Ryason, *J. Org. Chem.*, **26**, 621 (1961).

14) S. L. Barkowski, L. Hedberg, and K. Hedberg, *J. Am. Chem. Soc.*, **108**, 6898 (1986).

15) M. Mikami, T. Toriumi, K. Konno, and Y. Saito, *Acta Crystallogr., Sect. B*, **31**, 2474 (1975).

16) N. Nogami, M. Ōki, S. Sato and Y. Saito, *Bull. Chem. Soc. Jpn.*, **55**, 3580 (1982).

17) Since we neglect the presence of the peri-hydrogen in discussing the distance because of the uncertainty of the positions of the hydrogen atoms obtained by X-ray analysis, the distance between the beta atom of the 9-substituent and the peri-positions in the *ap* form may be even closer than the value mentioned above. However, it is also true that a bulky substituent prefers the *ap* position in the rotational isomers of the triptycene series. See the following paper for the references: M. Ōki, N. Takiguchi, S. Toyota, G. Yamamoto, and S. Murata, *Bull. Chem. Soc. Jpn.*, **61**, 4295 (1988).

18) F. Suzuki and M. Ōki, *Bull. Chem. Soc. Jpn.*, **48**, 596 (1975).

19) M. Ōki, G. Izumi, G. Yamamoto, and N. Nakamura, *Bull. Chem. Soc. Jpn.*, **55**, 159 (1982).

20) G. Izumi, G. Yamamoto, and M. Ōki, *Bull. Chem. Soc. Jpn.*, **54**, 3064 (1981).
21) Y. Tamura, G. Yamamoto, and M. Ōki, *Bull. Chem. Soc. Jpn.*, **60**, 1781, 3789 (1987).
22) H. Kikuchi, S. Hatakeyama, G. Yamamoto, and M. Ōki, *Bull. Chem. Soc. Jpn.*, **54**, 3832 (1981).
23) G. Yamamoto and M. Ōki, *Bull. Chem. Soc. Jpn.*, **57**, 2219 (1984).
24) R. S. Nachbar, Jr., W. D. Hounshell, V. A. Naman, O. Wennerström, A. Guenzi, and K. Mislow, *J. Org. Chem.*, **48**, 1227 (1983).
25) T. Tanaka, K. Yonemoto, Y. Nakai, G. Yamamoto, and M. Ōki, *Bull. Chem. Soc. Jpn.*, **61**, 3239 (1988); T. Tanaka, Y. Tanaka, T. Tanuma, G. Yamamoto, and M. Ōki, *ibid.*, 4305.
26) P. Lazzaretti and F. Taddei, *Org. Magn. Reson.*, **3**, 283 (1971).
27) H. van Bekkum, P. E. Verkade, and B. M. Wepster, *Recl. Trav. Chim. Pays-Bas*, **78**, 815 (1959).
28) T. Kihara, "Bunshikanryoku (Intermolecular Forces)," Iwanami, Tokyo (1976); M. Rigby, E. B. Smith, W. A. Wakeham, and G. C. Maitland, "The Forces between Molecules," Oxford Claredon Press, Oxford (1986), pp. 10, 11.
29) G. Yamamoto and M. Ōki, *Bull. Chem. Soc. Jpn.*, **54**, 473 (1981).
30) N. L. Allinger, *J. Am. Chem. Soc.*, **99**, 8127 (1977); N. L. Allinger and Y. H. Yuh, QCPE, No. 395; Modification by E. Osawa which is stored at Computer Center of the University of Tokyo Program Library.
31) G. Yamamoto and M. Ōki, *Bull. Chem. Soc. Jpn.*, **58**, 1690 (1985).
32) E. de B. Barnett, J. W Cook, and M. A. Mathews, *Recl. Trav. Chim. Pays-Bas*, **45**, 68 (1926).
33) G. Gronowitz and G. Hansen, *Arkiv Kemi*, **27**, 145 (1967).
34) T. J. Curphey, *Org. Synth.*, **51**, 142 (1971).
35) F. Mayer, W. Schäfer, and J. Rosenbach, *Arch. Pharm.*, **267**, 571 (1929).
36) L. F. Fieser and M. Fieser, "Reagents for Organic Synthesis," Vol. I, John-Wiley, New York (1967), p. 142.
37) Th. J. de Boer and H. J. Backer, *Org. Synth.*, Coll. Vol. IV, 250 (1963).

Synthetic Photochemistry. LI.[1] Structure Elucidation of the Pyrolysates Formed by "Retro-Benzilic Acid Rearrangement" of the Proto-Photocycloadducts of Methyl 2,4-Dioxopentanoate-Olefins

Toshihide HATSUI, Chitoshi NOJIMA,† and Hitoshi TAKESHITA*
Institute of Advanced Material Study, 86, Kyushu University, Kasuga-koen, Kasuga, Fukuoka 816
†Graduate School of Engineering Sciences, 39, Kyushu University, Kasuga-koen, Kasuga, Fukuoka 816
(Received March 1, 1989)

Pyrolysates obtained from the proto-photoadducts of methyl 2,4-dioxopentanoate with olefins were shown to be 3-acetyl-1,2-cyclopentanedione derivatives. One-pot formation of polyfunctionalized cyclopentane derivatives via a photocycloaddition has no precedence. Intentional preparation of the ring system was also achieved by a diethyl azodicarboxylate–triphenylphosphine treatment of the proto-adducts.

During our studies of the photochemical cycloadditions of methyl 2,4-dioxopentanoate with various olefins, we noticed the formation of by-products in variable yields. This paper deals with their structure elucidation.

As previously reported,[2] irradiation of methyl 2,4-dioxopentanoate (**1**) with isoprene (**2**) in ethyl acetate by means of a 400-W high-pressure mercury lamp through a Pyrex glass filter at 0 to 5 °C caused a smooth photocycloaddition to give photoadducts. When the whole mixture was thermolyzed at 180 °C, a new polar by-product (**3**) was isolated in 7% yields together with the expected 1,5-diketones (**4** and **5**) and a decarbonylated ene-reaction product (**6**),[3] 35, 15, and 14% yields, respectively. Upon treatment with ethereal diazomethane, **3** gave a methyl derivative (**7**) in good yield. On the basis of the molecular compositions, **3** and **7** were shown to be derived from 1 : 1-adducts of **1** to **2**. The IR spectrum of **7** revealed two carbonyl stretching bands at 1710 and 1660 cm^{-1}, while the ^1H NMR of **3** disclosed the presence of chelated β-hydroxy α,β-unsaturated ketone functions, δ=13.55. Both **3** and **7** revealed low-field shifted acetyl methyl signals at 2.39 and 2.51 in the ^1H NMR spectra. Other than these, there are signals ascribable to a singlet methyl on the sp^3-carbon and three olefinic protons. Therefore, **3** and **7** were deduced to be five-membered carbocyclic derivatives.

In order to detect corresponding thermolysate from isomeric proto-cycloadduct (**A'**), the entire reaction mixture was at first briefly treated with aqueous sodium hydrogen carbonate, methylated with diazomethane, and chromatographed on a silica-gel column.

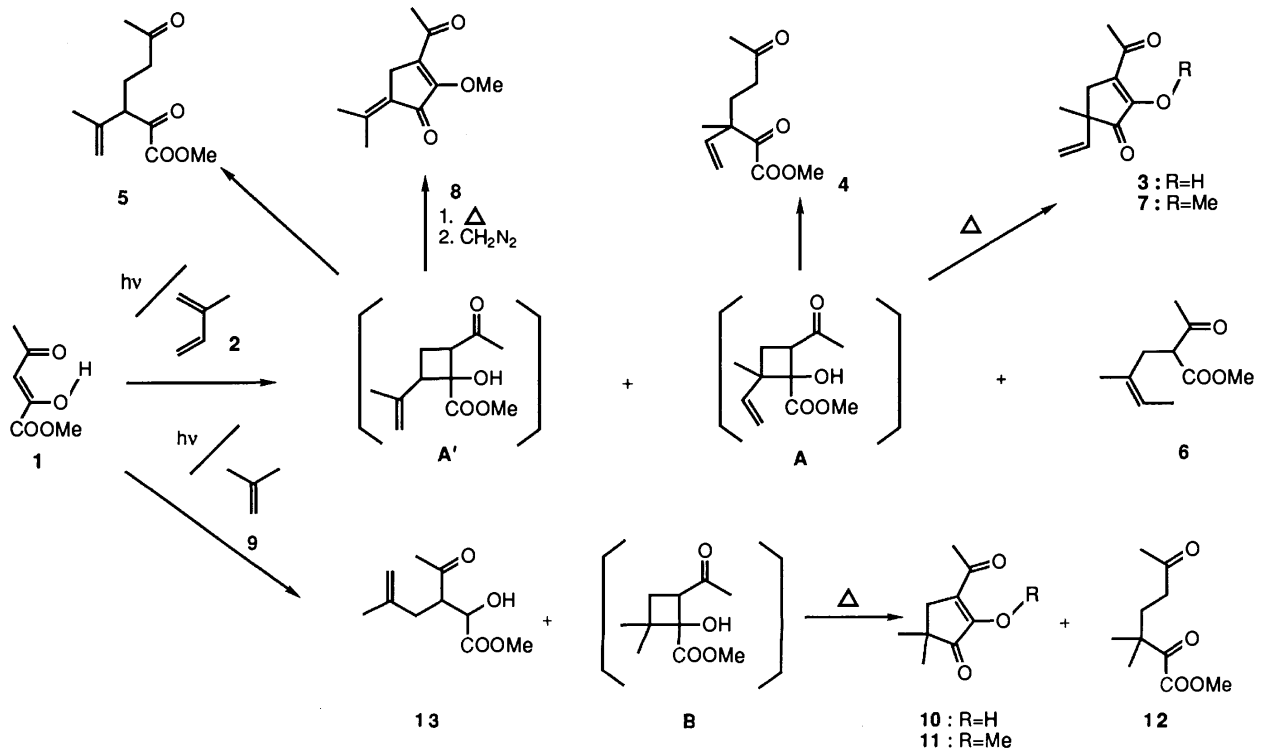

Scheme 1.

Indeed, together with **7** and **6**, a cyclopentenone derivative (**8**), in 0.8% yield, was isolated. The ^{1}H NMR spectrum of **8** revealed signals at 1.94 and 2.32 (each 3H, s), the latter of which suffered strong anisotropic and electric-field effects from the neighboring cisoid carbonyl group, indicating the presence of an isopropylidene group. The yield of **8** was much smaller than expected from the ratio of **4**:**5** (**7**:**8**=9:1; **4**:**5**=23:13). Therefore, the formation of this type of by-products is favorable for the photoadducts of 1,1-disubstituted ethenes.

Indeed, the photocycloaddition of **1** with 2-methylpropene (**9**)[4] gave a similar pyrolytic product (**10**) in 6% yield, which was characterized as a methyl derivative (**11**). The normal photoproduct (**12**) was isolated in 16% yield together with an ene-reaction product (**13**), whose structure was elucidated from the NMR evidence.

When **10** was treated with alkaline hydrogen peroxide[5] at room temperature, two acidic compounds were formed and their methyl esters were identified as dimethyl 4-acetyl-2,2-dimethylglutarate (**14**) and its decarboxylated methyl 2,2-dimethyl-5-oxohexanoate (**15**) by the NMR spectral analysis. The latter, **15**, was also formed by similar oxidation of **4**. Thus, the structure **11** must be 3-acetyl-2-methoxy-5,5-dimethyl-2-cyclopenten-1-one. Consequently, **3** and **10** should be derived from the proto-photoadducts (**A** and **B**) by a "retro-benzilic acid rearrangement"-type ring enlargement.

After deduction of the structures, our attention turned to a method for improving their formation. When the reaction mixture from **1** and **2** was treated with diethyl azodicarboxylate and triphenylphosphine[6] in ether at room temperature, the yields of **7** improved to 18% yield together with the expected **4** and **5**, in 28 and 13% yields, respectively. However, this alternative method was not always preferable; sometimes, the yields of cyclopentenones were lower than those of the pyrolytic workup. Nevertheless, by this alternative method, methyl ethers can be obtained directly by dehydration.

In addition, **1** and indene (**16**) gave, after similar irradiation and thermal treatment, the same type of methyl ethers (**17** and **18**) in 18 and 3% yields, respectively, along with the expected 2,6-dioxo ester (**19**) and previously undetected isomeric 2,6-dioxo ester (**20**).[7] The ^{1}H NMR spectrum of **17** revealed signals due to a methylene group and two methine protons, and the ^{13}C NMR showed two carbonyl carbon signals, suggesting the same carbon skeleton with **7**. The structure of **20** was deduced from an unequivocal

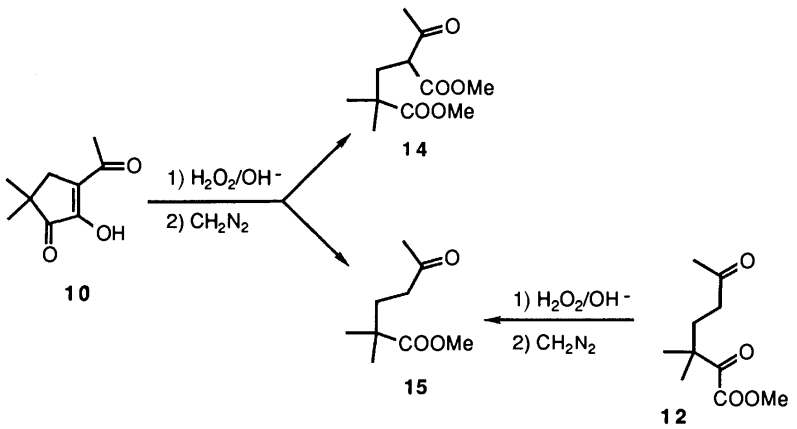

Scheme 2.

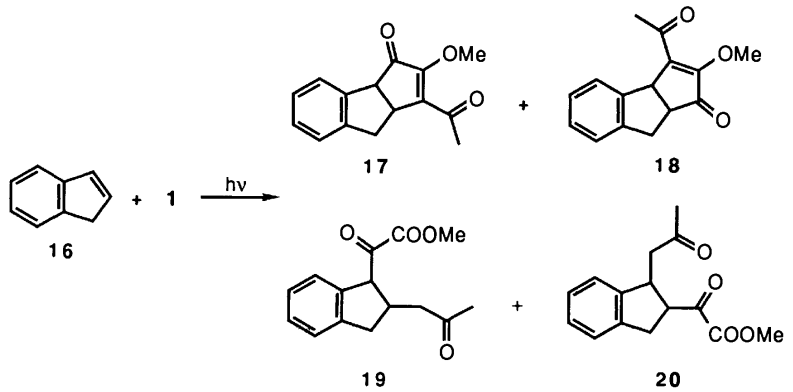

Scheme 3.

analysis of its ^{1}H NMR spectrum; i.e., the methylene protons adjacent to the acetyl group appear at 2.59 and 2.80 with mutual spin coupling of 18.7 Hz and additional coupling with a methine proton at 4.03. The coupling pattern of the methine proton, ddd (J=7.9, 7.8, 5.2 Hz), confirmed it to be benzylic.

Similar types of secondary products were obtained from various proto-photocycloadducts of **1** with olefins (Scheme 4). Namely, both conjugated olefins, cyclopentadiene (**21**),[8] and 2,3-dimethylbutadiene(**22**), and the isolated olefins, cyclopentene (**23**),[8] 2-methyl-2-butene (**24**), 2,3-dimethyl-2-butene (**25**), and 1-methylcyclohexene (**26**), respectively afforded the products in low, but reproducible, yields. They were characterized as methyl ethers after treatment with diazomethane. The physical properties of these products (**27** to **42**) are summarized in the experimental section. The yields of the rearranged compounds were relatively high, especially those from 1,1-disubstituted ethenes, which make the α-carbons to the α-hydroxy ester function quaternary in the proto-photoadducts. Occasionally, we have characterized other secondary products derived from the proto-adducts; one notable feature is methyl 2-(2-alkenyl)-3-oxobutyrates (**6** and **31**), from **2** and **22**, via photochemical retro-Prins cleavage,[3] and pyrolytic decarbonylation. These facts further showed the stability of these β-acetylcyclobutanol derivatives under the conditions mentioned above. An extreme case was a reaction with **25**; the proto-product, **38**, was detected in the photoproduct mixture, where expected diketone, **37**, was formed only after the thermolysis. The photoproducts from these olefins are listed in Scheme 4.

For a further confirmation of the rearranged structures, we carried out a two-dimensional C–H correlation NMR spectrum (C–H COSY) and long-

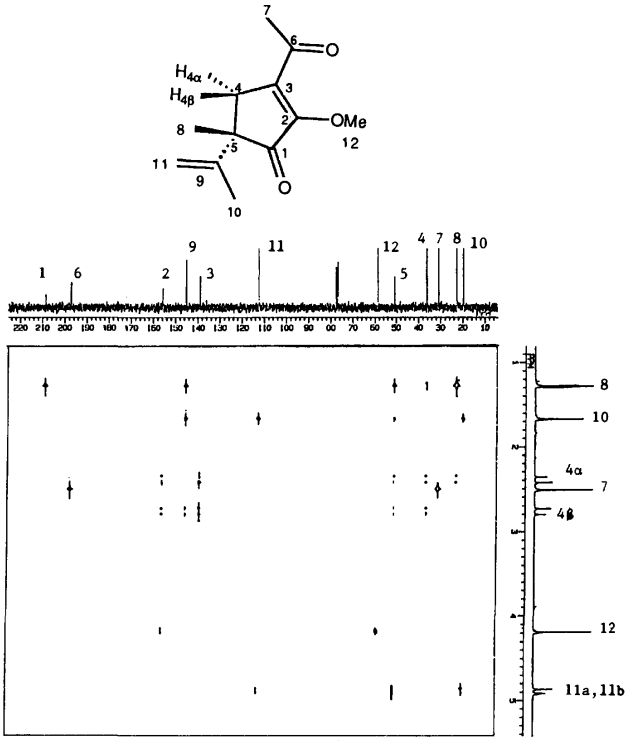

Fig. 1. Long-range C–H COSY spectrum of **29**. (Experimental conditions: observed frequency, 67.8 MHz; data points, 4 KX256; repetition, 80 scans; polarization transfer delay (τ_1), 50 ms (corresponding to J_{CH}=10 Hz) with second delay for proton decoupling (τ_2), 25 ms).

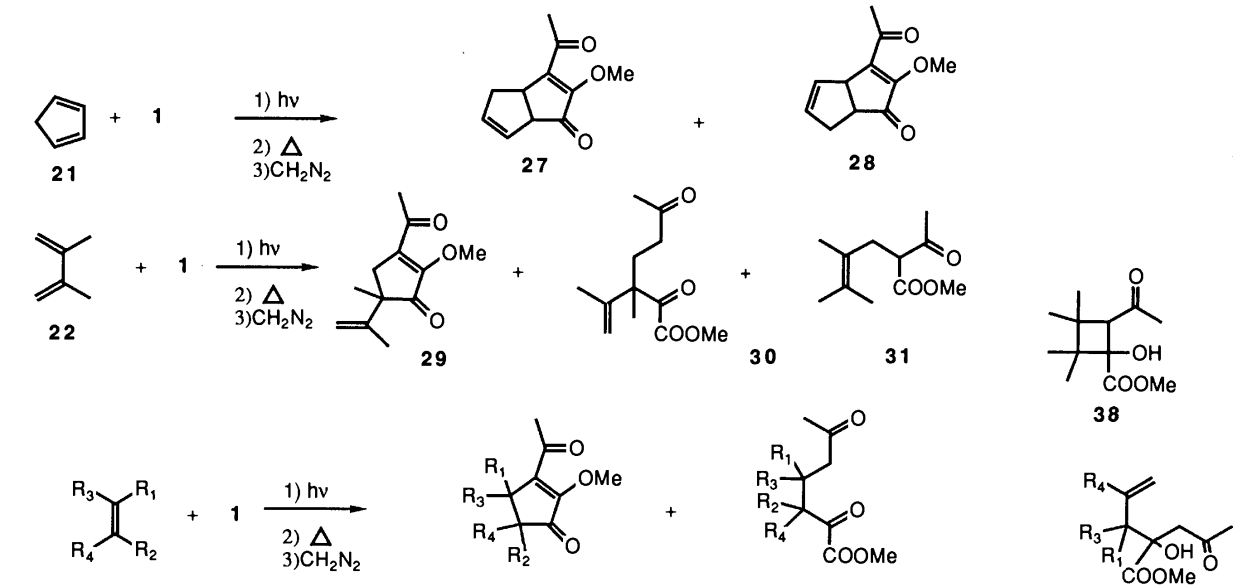

23 : R_1=R_2=H, R_3+R_4=$(CH_2)_3$
24 : R_1=H, R_2=R_3=R_4=Me
25 : R_1=R_2=R_3=R_4=Me
26 : R_1=H, R_2=Me, R_3+R_4=$(CH_2)_4$

32 : R_1=R_2=H, R_3+R_4=$(CH_2)_3$
34 : R_1=H, R_2=R_3=R_4=Me
36 : R_1=R_2=R_3=R_4=Me
40 : R_1=H, R_2=Me, R_3+R_4=$(CH_2)_4$

33 : R_1=R_2=H, R_3+R_4=$(CH_2)_3$
35 : R_1=H, R_2=R_3=R_4=Me
37 : R_1=R_2=R_3=Me
41 : R_1=H, R_2=Me, R_3+R_4=$(CH_2)_4$

39 : R_1=R_3=R_4=Me
42 : R_1=H, R_3+R_4=$(CH_2)_4$

Scheme 4.

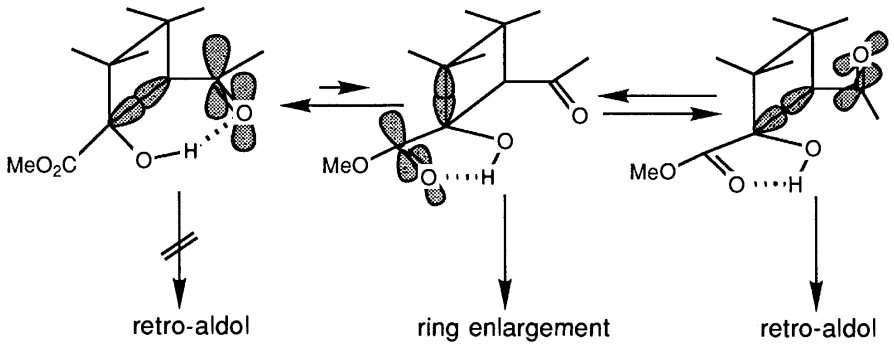

Scheme 5.

range C–H COSY analyses with **29** from the photo-adduct of **1** with **22**. The methoxyl proton signal revealed a correlation with an sp^2-carbon at δ=155.6 and the singlet methyl signal at 1.28 revealed a correlation with the carbonyl carbon signal at 208.4. Clearly, this carbonyl group exists at the α-position of the quaternary carbon bearing the methyl group; the methoxyl group is on the enol system (Fig. 1).

It is interesting that the formation of the by-products described in this paper constitutes a one-pot formation of the cyclopentane derivatives which carry several functional groups. Although a practical synthetic method of functional cyclopentane derivatives from various photocycloadducts of **1** has been developed by titanium(II) chloride condensation,[9] the derivatives described in this paper possess a different substitution pattern.[10] An improvement in the yields will be our next aim, for which the use of high-concentration conditions with olefins is favorable, as shown in the large-scale preparation of **3** (see Experimental); at present, about 50% of the proto-cycloadducts could be converted to the acetylcyclopentenone derivatives, according to a comparison of the product distributions.

Finally, it is also noteworthy that those sufficiently inert proto-cycloadducts of **1** towards retro-aldolization carry heavy substituents. The stable conformation of the proto-adduct is one having hydrogen bonding between the hydroxyl proton and carbonyl oxygen of the acetyl group, which is supported by a chemical shift of the hydroxy proton of **38** to at as low as δ=5.12. In this conformation, however, a retro-aldol reaction is stereoelectronically unfavored due to the perpendicular geometry of the C=O π-orbital and the breaking C–C bond. A steric repulsion from the adjacent substituents makes the orientation of methoxycarbonyl group favorable for ring enlargement, and the acetyl group was inhibited to change the conformation to one having the C=O π-orbital parallel to the breaking C–C bond in the retro-aldol process. This is one reason why the heavily substituted olefins give proto-photoadducts[11] and their transformation products.

Experimental

Elemental analyses were performed by Miss S. Hirashima, of Institute of Advanced Material Study, Kyushu University. The NMR spectra were measured in $CDCl_3$ with an FX 100 Model and a GSX 270H Model spectrometers, JEOL, and the chemical shift were expressed in δ values. The mass spectra were measured with a OISG-2 spectrometer, JEOL. IR spectra were measured with a Jasco IR-A 102 Model spectrometer as KBr disks, inserted liquid films, or in $CHCl_3$ solutions. The oxygen-free solvents for irradiations were obtained by careful distillation under an N_2 atmosphere.

Photoproducts of Low-Temperature Irradiation of 1 and 2. Isolation of 7 and 8. An EtOAc solution (30 cm^3) of **1** (480 mg) and **2** (11 cm^3) was irradiated by means of a 400-W high-pressure mercury lamp at −60 °C for 6 h. Then, the irradiation was stopped at the 74%-consumption of **1** (UV spectrometry) and the mixture was heated at 180 °C for 1 h, and the mixture was, after methylation with CH_2N_2, chromatographed on a silica-gel column to give **7** [a pale yellow oil, 34 mg; 7%. Found: *m/z*, 194.0941 (M^+). Calcd for $C_{11}H_{14}O_3$: 194.0942. ^{1}H NMR δ=1.26 (3H, s), 2.46 (1H, d, J=17.8 Hz), 2.51 (3H, s), 2.77 (1H, d, J=17.8 Hz), 4.17 (3H, s), 5.13 (1H, d, J=10.7 Hz), 5.14 (1H, d, J=17.3 Hz), and 5.78 (1H, dd, J=17.3, 10.7 Hz). ^{13}C NMR δ=22.4, 30.9, 35.9, 48.5, 58.6, 114.6, 138.1, 139.8, 155.1, 197.0, and 207.3. IR ν: 2950, 1710, 1660, 1610, 1380, 1220, 1180, 1040, 1020, and 920 cm^{-1}], **8** [yellow crystals, mp 110—111 °C, 4 mg; 0.8%. Found: *m/z*, 194.0982 (M^+). Calcd for $C_{11}H_{14}O_3$: 194.0942. ^{1}H NMR δ=1.94 (3H, s), 2.32 (3H, s), 2.50 (3H, s), 3.09 (2H, s), and 4.26 (3H, s). ^{13}C NMR δ=20.7, 22.9, 27.5, 30.9, 58.7, 127.5, 132.3, 152.2, 159.4, 192.3, and 197.4. IR ν: 2900, 1685, 1655, 1635, 1600, 1440, 1390, 1280, 1230, 1180, 1150, 1020, 950, 900, and 810 cm^{-1}], **4** (181 mg; 35%), **5** (79 mg; 15%), and decarbonylated **6** [a colorless oil, 63 mg; 14%. Found: *m/z*, 184.1101(M^+). Calcd for $C_{10}H_{16}O_3$: 184.1167. ^{1}H NMR δ=1.58 (3H, dq, J=7.0, 1.5 Hz), 1.67 (3H, q, J=1.5 Hz), 2.23 (3H, s), 2.56 (1H, dd, J=13.9, 7.3 Hz), 2.66 (1H, dd, J=13.9, 8.1 Hz), 3.64 (1H, dd, J=8.1, 7.3 Hz), 3.72 (3H, s), and 5.32 (1H, qm, J=7.0 Hz). ^{13}C NMR δ=13.4, 22.9, 29.1, 30.1, 52.4, 57.6, 122.7, 131.4, 170.2, and 202.8. IR ν: 2970, 2930, 1750, 1720, 1440, 1360, 1270, 1240, 1210, and 1150 cm^{-1}].

Large-Scale Irradiation of 1 with 2. A mixture of **1** (11.4 g) and **2** (150 cm^3) was irradiated by means of a 400-W high-pressure mercury lamp through a Pyrex-glass filter at 0 °C under an N_2 atmosphere. After 13 h, the mixture was

distilled in vacuo; the distillate solidified spontaneously was recrystallized from MeOH to give **3** [colorless crystals, mp 63—64 °C, 3.22 g; 22.7%. Found: C, 66.49; H, 6.75%. Calcd for $C_{10}H_{12}O_3$: C, 66.65; H, 6.71%. ^{1}H NMR δ=1.31 (3H, s), 2.39 (3H, s), 2.56 (1H, d, J=15.5 Hz), 2.86 (1H, d, 15.5 Hz), 5.12 (1H, dd, J=10, 0.5 Hz), 5.13 (1H, dd, J=17.5, 0.5 Hz), 5.80 (1H, dd, J=17.5, 10 Hz), and 13.55 (1H, br). ^{13}C NMR δ=23.5, 28.4, 36.5, 48.4, 114.8, 128.6, 139.2, 157.3, 201.3, and 205.3. IR ν: 3300, 1730, 1230, 930 cm^{-1}]. Silica-gel column chromatography of the residual mass in the bottom gave **4** (3.33 g; 20%),[2] and **5** (1.74 g; 10.4%).[2]

The CH_2N_2-Treatment of 3. Formation of 7. An ethereal solution (10 cm^3) of **3** (69 mg) was treated with an ethereal solution (10 cm^3) of CH_2N_2 to give **7** (70 mg; 94%).

Isolation of the Photoadducts from 1 and 2-Methylpropene (9).[5] Similarly, an EtOAc solution (50 cm^3) of **1** (960 mg) and **9** (1.2 g) was irradiated at −60 °C for 6 h to show 85%-consumption of **1**. One half of the mixture was diluted with *p*-cymene and refluxed for 1 h. After methylation with CH_2N_2, silica-gel column chromatography of the mixture gave **11** [a colorless oil, 39 mg; 8%. Found: m/z 182.0932 (M^+). Calcd for $C_9H_{12}O_3$: 182.0942. ^{1}H NMR δ=1.13 (6H, s), 2.45 (2H, s), 2.50 (3H, s), and 4.18 (3H, s). ^{13}C NMR δ=25.2 (2C), 30.8, 37.8, 41.8, 58.4, 138.3, 155.0, 197.2, and 210.8. IR ν: 2970, 2940, 2880, 1710, 1660, 1610, 1460, 1420, 1385, 1240, 1205, 1165, 1130, 1040, 960, 920, and 820 cm^{-1}], together with the ordinary product, **12** [a colorless oil, 144 mg; 25%. Found: m/z, 201.1125 (M^++1). Calcd for $C_{10}H_{17}O_4$: 201.1126. ^{1}H NMR δ=1.23 (6H, s), 1.94 (2H, dt, J=7.9, 1.5 Hz), 2.15 (3H, s), 2.40 (2H, tm, J=7.9 Hz), and 3.86 (3H, s). ^{13}C NMR δ=23.6 (2C), 29.9, 32.4, 38.8, 45.5, 52.4, 164.0, 201.1, and 207.7. IR ν: 2960, 1740, 1710, 1440, 1280, 1240, 1160, 1050, and 1030 cm^{-1}].

The rest of the mixture was directly chromatographed on a silica-gel column to give **13** [a colorless oil, 24 mg; 4%. Found: m/z 200.1045 (M^+). Calcd for $C_{10}H_{16}O_4$: 201.1048. ^{1}H NMR δ=1.82 (3H, br s), 2.21 (3H, s), 2.48 (2H, dm, J=7.7 Hz), 3.21 (1H, dt, J=7.7, 3.3 Hz), 3.35 (1H, dm, J=8.1 Hz), 3.85 (3H, s), 4,25 (1H, dd, J=8.1, 3.3 Hz), 4.87 (1H, br s), and 4.93 (1H, br s). ^{13}C NMR δ=22.2, 29.2, 36.0, 52.6, 52.7, 70.8, 113.8, 141.5, 174.2, and 211.0. IR ν: 3500, 2950, 1740, 1720, 1440, 1360, 1270, 1210, 1110, and 890 cm^{-1}], together with **12** (215 mg; 38%).

Hydrolysis of 11 to 10. An EtOH solution of **11** (48 mg) containing 2 M HCl (2 cm^3; 1 M=1 mol dm^{-3}) was refluxed for 1 h to give **10** [colorless needles, mp 98—100 °C, 43 mg; 96%. Found: C, 64.44; H, 7.13%. Calcd for $C_9H_{12}O_3$: C, 64.27; H, 7.19%. ^{1}H NMR δ=1.20 (6H, s), 2.40 (3H, s), 2.58 (2H, s), and 10.00 (1H, br s). ^{13}C NMR δ=25.2 (2C), 28.2, 38.4, 41.9, 128.4, 157.7, 201.8, and 208.4. IR ν: 3320, 2970, 1715, 1640, 1430, 1360, 1265, 1230, 1110, and 690 cm^{-1}].

Alkaline H_2O_2-Oxidation of 10 and Subsequent Methylation. Characterization of Dimethyl 4-Acetyl-2,2-dimethylglutarate (14) and Methyl 2,2-Dimethyl-5-oxohexanoate (15). An MeOH solution (3 cm^3) of **10** (8.4 mg) containing NaOH (13 mg) was treated with 35%-H_2O_2 (25 mg) at room temperature for 1 h. The mixture was then diluted with aq Na_2CO_3 and extracted with ether. The aqueous layer was acidified with dil HCl, and extracted with EtOAc, and methylated with ethereal CH_2N_2. Silica-gel column chromatography of the mixture afforded **15** [a colorless oil, 1.2 mg; 14%. Found: m/z, 172.1091 (M^+). Calcd for $C_9H_{16}O_3$: 172.1099. ^{1}H NMR δ=1.17 (6H, s), 1.81 (2H, m), 2.15 (3H, s), 2.40 (2H, m), and 3.67 (3H, s). ^{13}C NMR 25.1 (2C), 30.0, 33.9, 39.5, 41.6, 51.8, 177.9, and 208.3] and **14** [a colorless oil, 5.8 mg; 50%. Found: m/z, 231.1215 (M^++1). Calcd for $C_{11}H_{19}O_5$: 231.1231. ^{1}H NMR δ=1.18 (6H, s), 2.12 (1H, dd, J=14.7, 6.6 Hz), 2.22 (1H, dd, J=14.7, 5.1 Hz), 2.26 (3H, s), 3.55 (1H, dd, J=6.6, 5.1 Hz), 3.65 (3H, s), and 3.73 (3H, s). ^{13}C NMR δ=24.8, 25.7, 29.0, 37.5, 41.7, 51.9, 52.6, 56.4, 170.4, 177.4, and 202.4. IR ν: 2960, 1720, 1440, 1360, 1290, 1250, 1200, 1160, and 980 cm^{-1}].

H_2O_2-Oxidation of 12. An MeOH solution of **12** (20 mg) was briefly treated with 35%-H_2O_2 at room temperature for 10 min. The mixture was diluted with aq Na_2CO_3, from which neutral compound was removed by extraction with ether. After acidifying the aqueous solution with dil HCl, the acidic compounds were methylated with CH_2N_2, and collected via a silica-gel column chromatography to give **15**, which was identical with the sample obtained from **10** in every respect.

Isolation of 6 from the Photoproduct Mixture of 1 and 2 by Means of PPh_3-Diethyl Azodicarboxylate. The photoproduct mixture, immediately after the irradiation was treated with $(NCOOEt)_2$ and PPh_3 in ether (10 cm^3) at room temperature. The mixture was then diluted with ether and water, and extracted with ether. Silica-gel column chromatography of the organic extract afforded **6** (119 mg; 18%), which was identical with the authentic sample, together with **4** (189 mg; 27%) and **5** (95 mg; 13%).

Isolation of the Photoproducts of 1 and Indene (16).[6] Smilarly, an EtOAc solution (50 cm^3) of **1** (960 mg) and **16** (2.32 g) was irradiated at −60 °C for 6 h. The mixture was then divided into two parts. One of them was diluted with *p*-cymene (6 cm^3), and refluxed for 1 h. After methylation with CH_2N_2 silica-gel column chromatography of this mixture gave **17** [yellow crystals, mp 81—82 °C, 43 mg; 8%. Found: C, 74.44; H, 5.83%. Calcd for $C_{15}H_{14}O_3$: C, 74.36; H, 5.82%. ^{1}H NMR δ=2.47 (3H, s), 2.85 (1H, ddd, J=17.9, 3.3, 1.4 Hz), 3.45 (1H, dd, J=17.9, 10.0 Hz), 3.83 (1H, ddd, 10.0, 6.5, 3.3 Hz), 3.94 (1H, dd, J=6.5, 1.1 Hz), 4.15 (3H, s), and 7.14—7.50 (4H, m). ^{13}C NMR δ=31.3, 36.9, 55.1, 58.6, 124.9, 125.4, 127.0, 128.3, 137.5, 142.9, 143.1, 156.1, 197.2, and 204.1. IR ν: 3000, 2940, 2850, 1710, 1660, 1610, 1600, 1450, 1380, 1270, 1160, 1130, 1070, and 740 cm^{-1}] and **18** [a yellow oil, 16 mg; 3%. Found: m/z, 242.0948 (M^+). Calcd for $C_{15}H_{14}O_3$: 242.0942. ^{1}H NMR δ=2.51 (3H, s), 3.22—3.76 (3H, m), 4.16 (3H, s), 4.75 (1H, d, J=5.9 Hz), and 7.17—7.43 (4H, m). ^{13}C NMR δ=31.4, 33.3, 45.5, 48.0, 58.6, 125.1, 126.2, 127.0, 127.8, 141.5, 142.8, 143.6, 156.6, 197.4, and 208.1].

The rest of the photoproduct mixture was immediately passed through a silica-gel column to give the ordinary type products, **19**[6] and newly characterized **20** [a colorless oil, 17 mg; 3%. Found: m/z, 260.1041 (M^+). Calcd for $C_{15}H_{16}O_4$: 260.1048. ^{1}H NMR δ=2.06 (3H, s), 2.59 (1H, dd, J=18.7, 5.2 Hz), 2.80 (1H, dd, J=18.7, 7.8 Hz), 2.97 (1H, dd, J=16.1, 7.8 Hz), 3.34 (1H, dd, J=16.1, 10.0 Hz), 3.93 (3H, s), 4.03 (1H, ddd, J=7.9, 7.8, 5.2 Hz), 4.48 (1H, ddd, J=10.0, 7.9, 7.8 Hz), and 7.1—7.2 (4H, m). ^{13}C NMR δ=30.2, 33.4, 42.8, 45.2, 49.3, 53.2, 123.8, 124.7, 127.2, 127.4, 140.6, 144.4, 161.2, 194.7, and 207.8. IR ν: 2940, 1715, 1430, 1360, 1260, 1160, 1080, 750 cm^{-1}].

Isolation of Photoproducts from 1 and Cyclopentadiene (21).[7] Similarly, an EtOAc solution (30 cm^3) of **1** (480 mg) and **21** (660 mg) was irradiated at −60 °C for 6 h. The mixture was then diluted with *p*-cymene (6 cm^3) and

refluxed for 1 h. The mixture, after treatment with CH_2N_2, was chromatographed on a silica-gel column to give **27** [yellow crystals, mp 71—72 °C, 48 mg; 13%. Found: C, 69.00; H, 6.39%. Calcd for $C_{11}H_{12}O_3$: C, 68.74; H, 6.29%. ^{1}H NMR δ=2.15 (1H, br), 2.48 (3H, s), 2.85 (1H, br), 3.47 (1H, br), 3.57 (1H, m), 4.17 (3H, s), 5.63 (1H, m), and 5.74 (1H, m). ^{13}C NMR δ=31.3, 36.0, 37.3, 56.6, 58.6, 126.4, 133.8, 143.1, 155.8, 197.2, and 205.1] and **28** [as a mixture with **27**. 16 mg; ca. 4%. ^{1}H NMR δ=2.48 (3H, s), 2.54 (1H, br m), 2.63 (1H, br m), 3.03 (1H, m), 4.01 (1H, m), 4.17 (3H, s), 5.58 (1H, m), and 5.86 (1H, m)]. No other photoproduct was isolated by this work up.

Isolation of the Photoproducts from 1 and 2,3-Dimethylbutadiene (22). Similarly, an EtOAc solution (30 cm^3) of **1** (480 mg) and **22** (820 mg) was irradiated at −60 °C for 6 h to show 65%-consumption of **1**. The mixture was then diluted with *p*-cymene, and refluxed for 1 h. Silica-gel column chromatography of the methylated mixture afforded **29** [a pale-yellow oil, 27 mg; 6%. Found: *m/z*, 208.1102 (M^+). Calcd for $C_{12}H_{16}O_3$: 208.1099. ^{1}H NMR δ=1.28 (3H, s), 1.67 (3H, dd, *J*=1.5, 0.7 Hz), 2.39 (1H, d, *J*=18 Hz), 2.51 (3H, s), 2.76 (1H, d, *J*=18 Hz), 4.18 (3H, s), 4.87 (1H, q, *J*=0.7 Hz), 4.91 (1H, q, *J*=1.5 Hz). ^{13}C NMR δ=19.6, 22.6, 30.8, 36.1, 50.7, 58.5, 112.3, 138.8, 145.0, 155.6, 197.0, and 208.4. IR ν: 2950, 1700, 1660, 1610, 1380, 1220, 1180, 1160, 1140, 1020, 930, and 890 cm^{-1}] together with the ordinary product **30** [a colorless oil, 162 mg; 33%. Found: *m/z*, 226.1205 (M^+). Calcd for $C_{12}H_{18}O_4$: 226.1204. ^{1}H NMR δ=1.33 (3H, s), 1.73 (3H, s), 2.01—2.12 (2H, m), 2.13 (3H, s), 2.31—2.37 (2H, m), 3.79 (3H, s), 4.85 (1H, br m), and 5.08 (1H, br s). ^{13}C NMR δ=19.8, 20.0, 28.6, 30.0, 38.4, 52.3, 54.5, 114.8, 144.1, 163.2, 198.2, and 207.8. IR ν: 2950, 1740, 1720, 1640, 1440, 1360, 1280, 1160, 1020, and 900 cm^{-1}] and decarbonylated **31** [a colorless oil, 116 mg; 29%. Found: *m/z*, 198.1248 (M^+). Calcd for $C_{11}H_{18}O_3$: 198.1256. ^{1}H NMR δ=1.63 (6H, s), 1.66 (3H, s), 2.21 (3H, s), 2.58 (1H, dd, *J*=14.3, 8.7 Hz), 2.67 (1H, dd, *J*=14.3, 6.7 Hz), 3.61 (1H, dd, *J*=8.7, 6.7 Hz), and 3.71 (3H, s). ^{13}C NMR δ=18.0, 20.4, 20.8, 29.2, 33.1, 52.3, 58.1, 123.2, 127.9, 170.4, and 203.2. IR ν: 2950, 2920, 1740, 1720, 1430, 1355, 1265, 1220, 1190, and 1150 cm^{-1}].

Isolation of Photoproducts from 1 and Cyclopentene (23).[7] Similarly, an EtOAc solution (30 cm^3) of **1** (480 mg) and **23** (680 mg) was irradiated at −60 °C for 6 h; during that period 23% of **1** was consumed. The mixture was then diluted with *p*-cymene and refluxed for 1 h. Silica-gel column chromatography of the methylated mixture afforded **32** [yellow oil, 8 mg; 5%. Found: *m/z*, 194.0944 (M^+). Calcd for $C_{11}H_{14}O_3$: 194.0942. ^{1}H NMR δ=1.3 (1H, br), 1.5—1.9 (5H, m), 2.47 (3H, s), 2.71 (1H, ddd, *J*=9, 6, 2 Hz), 3.38 (1H, *J*=9, 6, 2 Hz), and 4.16 (3H, s). ^{13}C NMR δ=24.4, 29.6, 30.4, 31.3, 38.8, 49.1, 58.5, 143.7, 157.1, 197.3, and 209.2. IR ν: 2950, 2870, 1710, 1660, 1600, 1410, 1380, 1320, 1220, 1180, 1135, 1105, 1080, 1060, 1010, 960, 930, and 910 cm^{-1}] and the ordinary product **33**[7] [a colorless oil, a trace amount. ^{13}C NMR δ=23.5, 28.0, 30.2, 32.6, 38.2, 44.6, 48.8, 53.0, 161.9, 196.6, and 208.3].

Isolation of the Photoproducts from 1 and 2-Methyl-2-butene (24). Similarly, **1** (480 mg) and **24** (700 mg) were irradiated at −60 °C for 6 h to consume 28% of **1**. The mixture was then refluxed in a *p*-cymene solution, and then chromatographed on a silica-gel column to give **34** [a pale-yellow oil, 30 mg; 16%. Found: *m/z*, 196.1089 (M^+). Calcd for $C_{11}H_{16}O_3$: 196.1099. ^{1}H NMR δ=1.04 (3H, d, *J*=7.0 Hz), 1.05 (3H, s), 1.12 (3H, s), 2.48 (3H, s), 2.79 (1H, q, *J*=7.0 Hz), and 4.14 (3H, s). ^{13}C NMR δ=16.5, 19.3, 27.6, 31.6, 41.0, 46.4, 58.5, 143.6, 154.9, 197.6, and 210.7. IR ν: 2975, 1710, 1660, 1610, 1450, 1380, 1235, 1160, 1130, 1030, and 940 cm^{-1}] and expected **35** [a colorless oil, 44 mg; 22%. Found: *m/z*, 214.1213 (M^+). Calcd for $C_{11}H_{18}O_4$: 214.1205. ^{1}H NMR δ=0.89 (3H, d, *J*=6.6 Hz), 1.12 (3H, s), 1.19 (3H, s), 2.14 (3H, s), 2.21 (1H, dd, *J*=16.9, 10.3 Hz), 2.41 (1H, dd, *J*=16.9, 2.8 Hz), 2.62 (1H, br m), and 3.85 (3H, s). IR ν: 2980, 1740, 1720, 1710, 1365, 1280, 1220, 1050, 1030, and 750 cm^{-1}].

Fractionation of the Photoproducts from 1 and 2,3-Dimethyl-2-butene (25). Similarly, an EtOAc solution (30 cm^3) of **1** (480 mg) and **25** (840 mg) was irradiated at −60 °C for 6 h to consume 33% of **1**. The mixture was then diluted with *p*-cymene and refluxed for 1 h. Silica-gel column chromatography of the methylated mixture afforded **36** [a pale-yellow oil, 35 mg; 15%. Found: *m/z* 210.1246 (M^+). Calcd for $C_{12}H_{18}O_3$: 210.1255. ^{1}H NMR δ=1.05 (6H, s), 1.17 (6H, s), 2.45 (3H, s), and 4.08 (3H, s). ^{13}C NMR δ=21.4 (2C), 24.2 (2C), 32.5, 43.1, 51.5, 58.5, 145.7, 155.2, 198.6, and 210.2. IR ν: 2975, 1710, 1670, 1600, 1450, 1370, 1280, 1210, 1160, and 1090 cm^{-1}], and a mixture (55 mg) of **37** [ca. 7%. ^{1}H NMR δ=1.13 (6H, s), 1.22 (6H, s), 2.15 (3H, s), and 2.56 (2H, s), and 3.84 (3H, s)], and **39** [17%. ^{1}H NMR δ=1.15 (3H, s), 1.18 (3H, s), 1.84 (3H, dd, *J*=1.3, 0.8 Hz), 2.15 (3H, s), 2.85 (1H, d, *J*=17.4 Hz), 3.15 (1H, d, *J*=17.4 Hz), 3.73 (3H, s), 3.81 (1H, s), 4.82 (1H, quint, *J*=0.8 Hz), and 4.96 (1H, qq, *J*=1.3, 0.8 Hz). ^{13}C NMR δ=22.5, 23.3, 23.6, 30.9, 44.8, 47.5, 52.3, 113.6, 149.9, 175.1, and 208.4].

Without a thermal treatment of the mixture, silica-gel column chromatography gave none of the expected **37**, but proto-product **38** [ca. 25%. ^{1}H NMR δ=0.97 (3H, s), 1.03 (3H, s), 1.19 (3H, s), 1.23 (3H, s), 2.13 (3H, s), 3.56 (1H, s), and 5.12 (1H, s). ^{13}C NMR δ=16.0, 21.5, 21.6, 24.8, 31.0, 42.0, 44.4, 52.0, 54.1, 80.2, 172.4, and 212.0] and ene-product **39** (12%). However, the isolation of these compounds was unsuccessful.

Isolation of the Photoproducts from 1 and 1-Methylcyclohexene (26). Similarly, an EtOAc solution (30 cm^3) of **1** (960 mg) and **26** (1.9 g) was irradiated at −60 °C for 6 h to consume 28% of **1**. One half of the mixture was then diluted with *p*-cymene, and refluxed for 1 h. Silica-gel column chromatography of the methylated mixture gave **40** [pale-yellow oil, 5 mg; 2%. Found: *m/z*, 222.1279 (M^+). Calcd for $C_{13}H_{18}O_3$: 222.1255. ^{1}H NMR δ=1.05 (3H, s), 1.1—1.3 (3H, m), 1.3—1.45 (2H, m), 1.5 (1H, br), 1.9 (1H, br), 2.48 (3H, s), 2.73 (1H, dd, *J*=7.5, 5.6 Hz), and 4.15 (3H, s). ^{13}C NMR δ=20.2, 20.3, 26.3, 27.9, 30.3, 31.3, 42.6, 46.9, 58.5, 143.0, 155.7, 197.4, and 210.5. IR ν: 2950, 2880, 1710, 1660, 1605, 1450, 1420, 1380, 1220, 1170, 1140, 1080, 1020, 960, 910, and 800 cm^{-1}] and the ordinary product, **41** [a colorless oil, a trace amount. Found: *m/z*, 241.1475 (M^++1). Calcd for $C_{13}H_{21}O_4$: 241.1439. ^{1}H NMR δ=1.29 (3H, s), 1.3—1.7 (7H, m), 2.04—2.16 (2H, m), 2.14 (3H, s), 2.52 (1H, dd, *J*=17.8, 9.5 Hz), 2.73 (1H, dd, *J*=17.8, 2.6 Hz), and 3.83 (3H, s). ^{13}C NMR δ=22.7, 23.5, 24.6, 27.8, 30.7, 35.1, 39.8, 44.9, 49.3, 52.3, 164.2, 201.8, and 208.1. IR ν: 2940, 2860, 1740, 1450, 1360, 1280, 1260, 1160, 1040, and 1010 cm^{-1}].

The rest of the photoreaction mixture was treated without thermolysis and chromatographed on a silica-gel column to give **41** (15 mg; 6%) and an ene-product, **42** [a colorless oil, 12 mg; 5%. Found: *m/z*, 240.1363 (M^+). Calcd for $C_{13}H_{20}O_4$: 240.1360. ^{1}H NMR δ=1.25—1.85 (6H, m), 2.11—2.22 (2H, m), 2.23 (3H, s), 2.94 (1H, dm, *J*=11.7 Hz), 3.36 (1H, dd,

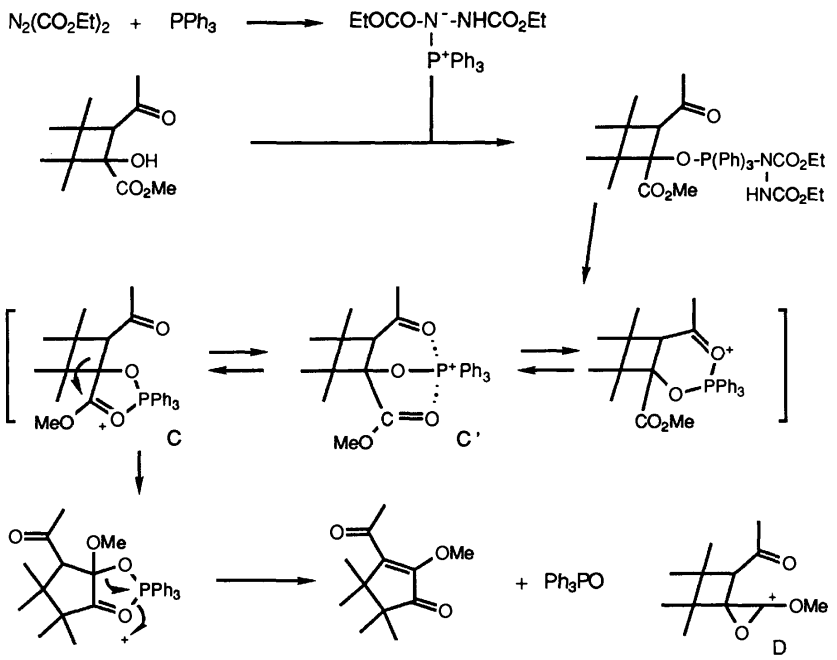

Scheme 6.

J=11.7, 2.6 Hz), 3.47 (1H, d, J=8.8 Hz), 3.77 (3H, s), 4.28 (1H, dd, J=8.8, 2.6 Hz), 4.87 (2H, br s). ^{13}C NMR δ=21.9, 28.3, 30.5, 32.3, 32.9, 41.9, 52.6, 53.0, 70.8, 111.0, 147.7, 194.4, and 213.2. IR ν: 3500, 2930, 2860, 1740, 1720, 1440, 1360, 1250, 1220, 1160, and 1100 cm^{-1}].

References

1) Part L: A. Mori, N. Nishiyama, Y. Kohguchi, H. Shinka, and H. Takeshita, *Bull. Chem. Soc. Jpn.*, **62**, 1666 (1989).

2) H. Takeshita, T. Hatsui, and T. Masuda, *Kyushu Daigaku Sogo Rikogaku Kenkyuka Hokoku*, **1**, 35 (1979); H. Takeshita, T. Hatsui, N. Kato, T. Masuda, and H. Tagoshi, *Chem. Lett.*, **1982**, 1153.

3) Formation of **6** and **31** can be explained as the result of photochemical retro-Prins cleavage of their proto-cycloadducts as already described in our previous paper (H. Takeshita, K. Komiyama, and K. Okaishi, *Bull. Chem. Soc. Jpn.*, **58**, 2725 (1985)). However, for the present case, subsequent refluxing in *p*-cymene for 1 h caused spontaneous decarbonylation of the α-keto ester moiety to result in these products. Furthermore, it is interesting that 3-substituted 2,6-dioxoheptanoates were stable toward thermal decarbonylation under those conditions.

4) This olefin was employed for the synthesis of deoxytrisporone via the cycloaddition with methyl 2,4-dioxohexanoate. See H. Takeshita, S. Hatta, and T. Hatsui, *Bull. Chem. Soc. Jpn.*, **57**, 619 (1984).

5) E. Kyburz, B. Riniker, H. R. Schenk, H. Heusser, and O. Jeger, *Helv. Chim. Acta*, **36**, 1891 (1953); W. Baker, H. F. Bondy, J. Gumb, and D. Miles, *J. Chem. Soc.*, **1953**, 1615.

6) Triphenylphosphine-dimethylazodicarboxylate is a mild and neutral dehydrating agent leading to esters, lactones, cyclic esters and amines by activating the hydroxyl group (O. Mitsunobu, *Synthesis*, **1986**, 1). We are grateful to a referee who called our attention to a novelty of present application in respect of carbonyl group activation for dehydration. The reaction is likely to proceed via penta- or hexa-coordinated phosphorane intermediate (**C** or **C'**) rather than via oxiranyl cation (**D**) by participation of neighboring carbonyl group. Stereochemical feature is similar to that in pyrolytic dehydration (Scheme 6).

7) H. Takeshita, A. Mori, and T. Toyonaga, *Kyushu Daigaku Seisan Kagaku Kenkyusho Hokoku*, **64**, 25 (1976).

8) H. Takeshita, A. Mori, and Y. Toyonaga, *Bull. Chem. Soc. Jpn.*, **48**, 307 (1975).

9) N. Kato, K. Nakanishi, and H. Takeshita, *Bull. Chem. Soc. Jpn.*, **59**, 1125 (1986); H. Takeshita and N. Kato, *Yuki Gosei Kagaku Kyokai Shi*, **44**, 1081 (1986).

10) We should point out that, indeed, the metacycloaddition of benzene derivatives (P. A. Wender and G. B. Dreyer, *J. Am. Chem. Soc.*, **104**, 5805 (1982)) should belong to this category. Or, even photodimerization of phenylethyne to 1-phenylazulene (D. Bryce-Smith and J. E. Lodge, *J. Chem. Soc.*, **1963**, 15) and photoisomerization of barrelene to semibullvalene (H. E. Zimmermann, and G. L. Grunewald, *J. Am. Chem. Soc.*, **88**, 183 (1966)) are the cases. More versatile example was the intramolecular hydrogen abstraction and cyclization of α-diketones to acyloin derivatives (R. Bishop and N. K. Hamer, *J. Chem. Soc. C*, **1970**, 1193), though it is not the cycloaddition.

11) During our total synthesis of cuparene, such proto-product (**i**) from **1** and *p*-isopropenyltoluene was indeed isolated. See H. Takeshita, A. Mori, and S. Nakamura, *Bull. Chem. Soc. Jpn.*, **57**, 3152 (1984).

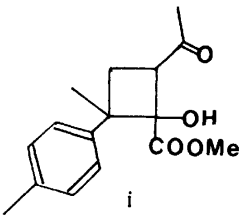

 © 1989 The Chemical Society of Japan Bull. Chem. Soc. Jpn., 62, 2939—2941 (1989)

Ozonization of Thio- and Azauracils

Masaki MATSUI,* Kazusaki KAMIYA, Shigeo KAWAMURA,
Katsuyoshi SHIBATA, and Hiroshige MURAMATSU
Department of Chemistry, Faculty of Engineering, Gifu University, 1-1 Yanagido, Gifu 501-11
(Received March 3, 1989)

The reactions of 2-thiouracils and azauracils with ozone have been examined. 2-Thiouracils were ozonized to give the corresponding 4(3*H*)-pyrimidinones and uracils. Ozone attacks the thiocarbonyl moiety and the desulfurization process to give 4(3*H*)-pyrimidinones competes with the oxidation process to give uracils. 5-Azauracil was stable for ozone, while 6-azauracil readily reacted with ozone to give parabanic acid.

The ozonization of the C=S moiety has been reported to give the corresponding C=O and/or C=S=O moieties.[1] Interestingly, in our study on the ozonization of pyrimidine bases, 2-thiouracils were found to give 4(3*H*)-pyrimidinones as the main products. This is the first report on the transformation of C=S into the C–H moiety by ozone. The reaction of azauracils with ozone was also investigated.

Experimental

Instruments. Ozone was generated with a Nihon Ozon 0-1-2 ozonizer. Melting points were measured by a Yanagimoto micro melting point apparatus and uncorrected. NMR and mass spectra were recorded on JEOL JNM-GX 270 FT NMR and Shimadzu QP-1000 mass spectrometers, respectively. High-performance liquid chromatography was performed on a Jasco Familic 100N liquid chromatograph.

Materials. Uracil (**1a**) and azauracils (**11** and **12**) were purchased from Tokyo Kasei Kogyo Co., Ltd. and used without further purification. Thiouracils (**3a—g** and **5**), dithiouracil (**6**) and 2-methylthio-4(3*H*)-pyrimidinone (**7**) were synthesized as described in the literature. Their melting points and spectral data are as follows:

2-Thiouracil (**3a**): mp >300 °C (lit,[2] 340 °C); ^{1}H NMR (DMSO-d_6) δ=5.81 (d, J=7 Hz, 1H), 7.40 (d, J=7 Hz, 1H), 12.37 (br. s, 2H); MS (70 eV) m/z (rel intensity) 128 (M^+, 100).

5-Methyl-2-thiouracil (**3b**): mp 265—267 °C (lit,[3] 265—267 °C); ^{1}H NMR (DMSO-d_6) δ=1.77 (s, 3H), 7.31 (s, 1H), and 12.29 (br. s, 2H); MS(70 eV) m/z (rel intensity) 142 (M^+, 80) and 55 (100).

5-Ethyl-2-thiouracil (**3c**): mp 191—192 °C (lit,[4] 190—192 °C); ^{1}H NMR (DMSO-d_6) δ=1.01 (t, J=7 Hz, 3H), 2.21 (q, J=7 Hz, 2H), 7.21 (s, 1H), and 12.35 (br. s, 1H); MS (70 eV) m/z (rel intensity) 156 (M^+, 100).

6-Methyl-2-thiouracil (**3d**): mp >300 °C (lit,[4] >300 °C); ^{1}H NMR (DMSO-d_6) δ=2.06 (s, 3H), 5.68 (s, 1H), and 12.27 (br. s, 2H); MS (70 eV) m/z (rel intensity) 142 (96) and 44 (100).

3-Methyl-2-thiouracil (**3e**): mp 272—273 °C; ^{1}H NMR (DMSO-d_6) δ=3.52 (s, 3H), 5.94 (d, J=8 Hz, 1H), 7.44 (d, J=8 Hz, 1H), and 12.60 (br. s, 1H); MS (70 eV) m/z (rel intensity) 142 (M^+, 100).

1-Methyl-2-thiouracil (**3f**): mp 229 °C (lit,[5] 228 °C); ^{1}H NMR (DMSO-d_6) δ=3.56 (s, 3H), 5.91 (d, J=8 Hz, 1H), 7.83 (d, J=8 Hz, 1H), and 12.58 (br. s, 1H); MS (70 eV) m/z (rel intensity) 142 (M^+, 72) and 42 (100).

1,3-Dimethyl-2-thiouracil (**3g**): mp 104 °C (lit,[6] 103 °C); ^{1}H NMR (DMSO-d_6) δ=3.56 (s, 3H), 3.65 (s, 3H), 6.05 (d, J=8 Hz, 1H), and 7.97 (d, J=8 Hz, 1H); MS (70 eV) m/z (rel intensity) 156 (M^+, 72) and 42 (100).

4-Thiouracil (**5**): mp >300 °C (lit,[7] 317—321 °C); ^{1}H NMR (DMSO-d_6) δ=5.74 (d, J=8 Hz, 1H), 7.38 (d, J=8 Hz, 1H), and 12.20 (br. s, 2H); MS (70 eV) m/z (rel intensity) 128 (M^+, 100).

2,4-Dithiouracil (**6**): mp 267—273 °C (lit,[8] 265—275 °C); ^{1}H NMR (DMSO-d_6) δ=6.50 (d, J=7 Hz, 1H), 7.26 (d, J=7 Hz, 1H), 12.87 (br. s, 1H), and 13.62 (br. s, 1H); MS (70 eV) m/z (rel intensity) 144 (M^+, 100).

2-Methylthio-4(3*H*)-pyrimidinone (**7**): mp 190—192 °C (lit,[9] 198—199 °C); ^{1}H NMR (DMSO-d_6) δ=2.54 (s, 3H), 6.12 (d, J=7 Hz, 1H), and 7.89 (d, J=7 Hz, 1H); MS (70 eV) m/z (rel intensity) 142 (M^+, 100).

The purity of used materials was checked by TLC (SiO_2, AcOEt:Me_2CHOH:H_2O=75:16:9).

Ozonization Reaction. Ozonization was carried out with an ozone-oxygen mixture (O_3: 0.22 mmol min^{-1}, O_2: 200 ml min^{-1}) on 2 mmol of substrate in 100 ml of acetic acid at room temperature. The end point of the reaction was monitored by TLC (SiO_2, AcOEt:Me_2CHOH:H_2O=75:16:9). In order to remove the dissolved ozone, nitrogen gas (100 ml min^{-1}, 10 min) was bubbled into the solution, which was allowed to stand overnight. The disappearance of peroxide activity was checked by a KI test. The solution was concentrated on a rotary evaporator and chromatographed on preparative TLC (SiO_2, AcOEt:Me_2CHOH:H_2O=75:16:9). The isolated products were identified on the basis of their spectral data shown below: 5-Methyluracil (**1b**): mp >300 °C (lit,[10] 313—314 °C); ^{1}H NMR (DMSO-d_6) δ=1.71 (s, 3H), 7.24 (s, 1H), 10.57 (br. s, 1H), and 10.99 (br. s, 1H); MS (70 eV) m/z (rel intensity) 126 (M^+, 39) and 55 (100).

5-Ethyluracil (**1c**): mp 290 °C (lit,[11] 300—303 °C); ^{1}H NMR (DMSO-d_6) δ=0.99 (t, J=7 Hz, 3H), 2.16 (q, J=7 Hz, 2H), 7.16 (d, J=7 Hz, 1H), 10.61 (br. s, 1H), and 10.97 (br. s, 1H); MS (70 eV) m/z (rel intensity) 140 (M^+, 100).

6-Methyluracil (**1d**): mp >300 °C (lit,[12] 340 °C); ^{1}H NMR (DMSO-d_6) δ=2.00 (s, 3H), 5.31 (s, 1H), and 10.82 (br. s, 2H); MS (70 eV) m/z (rel intensity) 126 (M^+, 29) and 42 (100).

3-Methyluracil (**1e**): mp 169 °C (lit,[13] 174—175 °C); ^{1}H NMR (DMSO-d_6) δ=3.12 (s, 3H), 5.57 (d, J=7 Hz, 1H), 7.39 (dd, J=7 and 6 Hz, 1H), and 10.97 (br. s, 1H); MS (70 eV) m/z (rel intensity) 126 (M^+, 90) and 69 (100).

1-Methyluracil (**1f**): mp 178—182 °C (lit,[14] 232 °C); ^{1}H NMR (DMSO-d_6) δ=3.23 (s, 3H), 5.50 (dd, J=8 and 2 Hz, 1H), 7.58 (d, J=8 Hz, 1H), and 11.07 (br. s, 1H); MS (70 eV) m/z (rel intensity) 126 (M^+, 52) and 42 (100).

1,3-Dimethyluracil (**1g**): mp 122—123 °C (lit,[15] 122—124 °C); ^{1}H NMR (DMSO-d_6) δ=3.14 (s, 3H), 3.29 (s, 3H),

5.65 (d, J=8 Hz, 1H), and 7.65 (d, J=8 Hz, 1H); MS (70 eV) m/z (rel intensity) 140 (M^+, 91) and 42 (100).

1-Formyl-5-hydroxyhydantoin (**2**): mp 153—155 °C; ^{1}H NMR (DMSO-d_6) δ=5.47 (d, J=8 Hz, 1H), 7.56 (d, J=8 Hz, 1H, exchanges with D_2O), 8.95 (s, 1H), and 11.70 (br. s, 1H, exchanges with D_2O); ^{13}C NMR (DMSO-d_6) δ=75.8 (d), 154.2 (s), 158.9 (d), and 171.1 (s); MS (70 eV) m/z (rel intensity) 144 (M^+, 5), 116 (54), and 88 (100); MS (CI, 200 eV, isobutane) m/z 145 (MH^+, 100%); Found: m/z 144.0175. Calcd for $C_4H_4N_2O_4$: M^+, 144.0171.

4(3*H*)-Pyrimidinone (**4a**): mp 160—163 °C (lit,[16] 163—164 °C); ^{1}H NMR (DMSO-d_6) δ=6.31 (d, J=7 Hz, 1H), 7.89 (d, J=7 Hz, 1H), 8.16 (s, 1H), and 12.54 (br. s, 1H); ^{13}C NMR (DMSO-d_6) δ=115.9 (d), 150.5 (d), and 161.3 (s); MS (70 eV) m/z (rel intensity) 96 (M^+, 100).

5-Methyl-4(3*H*)-pyrimidinone (**4b**): mp 145—147 °C (lit,[17] 153—154 °C); ^{1}H NMR (DMSO-d_6) δ=2.13 (s, 3H), 7.89 (s, 1H), and 8.18 (s, 1H); ^{13}C NMR (DMSO-d_6) δ=13.7 (q), 126.7 (s), 148.8 (d), 152.1 (d), and 163.3 (s); MS (70 eV) m/z (rel intensity) 110 (M^+, 100).

5-Ethyl-4(3*H*)-pyrimidinone (**4c**): mp 88—90 °C; ^{1}H NMR (DMSO-d_6) δ=1.22 (t, J=7 Hz, 3H), 2.53 (q, J=7 Hz, 2H), 7.90 (s, 1H), 8.27 (s, 1H), and 9.39 (s, 1H); ^{13}C NMR (DMSO-d_6) δ=12.4 (q), 20.8 (t), 131.1 (s), 147.0 (d), 150.0 (d), and 164.0 (s); MS (70 eV) m/z (rel intensity) 124 (M^+, 100).

6-Methyl-4(3*H*)-pyrimidinone (**4d**): mp 145—147 °C (lit,[18] 149—150 °C); ^{1}H NMR (DMSO-d_6) δ=2.17 (s, 3H), 6.16 (s, 1H), and 8.08 (s, 1H); ^{13}C NMR (DMSO-d_6) δ=23.0 (q), 112.6 (d), 149.2 (d), 160.8 (d), and 164.3 (s); MS (70 eV) m/z (rel intensity) 110 (M^+, 100).

3-Methyl-4(3*H*)-pyrimidinone (**4e**): mp 118—120 °C (lit,[19] 121—122 °C); ^{1}H NMR (DMSO-d_6) δ=3.32 (s, 3H), 6.49 (d, J=7 Hz, 1H), 7.90 (d, J=7 Hz, 1H), and 8.21 (s, 1H); MS (70 eV) m/z (rel intensity) 110 (M^+, 42) and 42 (100).

Parabanic acid (**13**): mp 236—240 °C (lit,[20] 238—244 °C); ^{1}H NMR (DMSO-d_6) δ=11.75 (br. s, 2H); MS (70 eV) m/z (rel intensity) 114 (M^+, 72), 86 (64), and 43 (100). The purity of all products was checked by TLC (SiO_2, AcOEt:Me_2CHOH:H_2O=75:16:9). Analysis of products was carried out by HPLC (SS-10, AcOEt:Me_2CHOH:H_2O=75:16:9, 254 nm).

Results and Discussion

The ozonization reactions of uracil (**1a**), 2-thiouracils (**3a—d**), 4-thiouracil (**5**), and 2,4-dithiouracil (**6**) are summarized in Table 1. The reaction of uracil (**1a**) gave 1-formyl-5-hydroxyhydantoin (**2**) in a 29% yield (Run 1). Interestingly, the reaction of 1-unsubstituted 2-thiouracils **3a—e** under the same conditions gave the corresponding uracils **1a—e** and 4(3*H*)-pyrimidinones **4a—e** in 7—37 and 48—72% yields, respectively (Runs 2—6). The reaction of 1-methyl-2-thiouracils **3f,g** preferentially gave 1-methyluracils **1** in 19 and 47% yields, respectively (Runs 7 and 8). The ozonization of 4-thiouracil (**5**) gave only uracil (**1a**) in a 41% yield (Run 9). In the case of insoluble

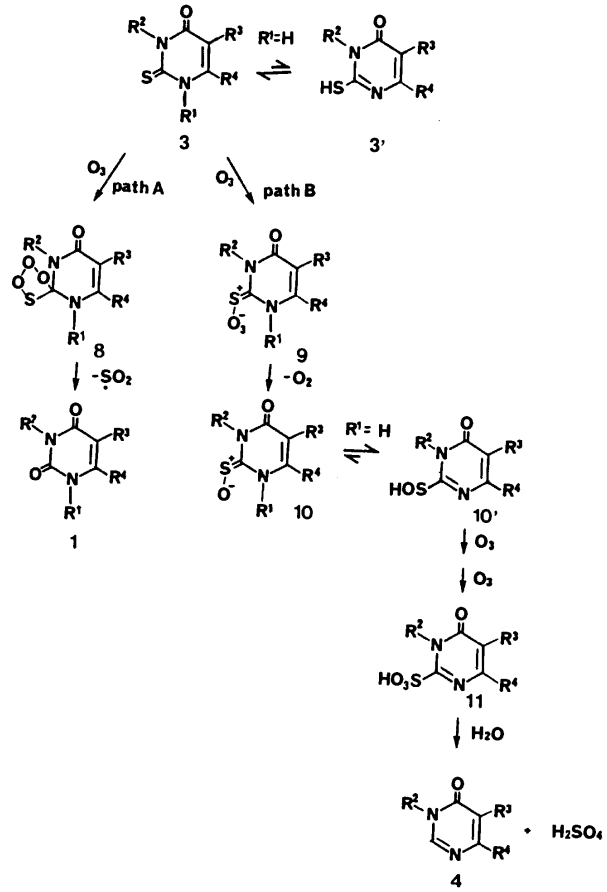

Scheme 1.

Table 1. Ozonization of Thiouracils[a]

Run	Substrate	Substituent				Time	Conv.	Yield/%		
		R^1	R^2	R^3	R^4	min	%	**1**	**2**	**4**
1	**1**					20	99	—	29	—
2	**3a**	H	H	H	H	15	97	18	0	68
3	**3b**	H	H	Me	H	10	98	7	0	58
4	**3c**	H	H	Et	H	12	92	7	0	48
5	**3d**	H	H	H	Me	9	97	37	0	56
6	**3e**	H	Me	H	H	6	97	25	0	72
7	**3f**	Me	H	H	H	6	92	19	0	0
8	**3g**	Me	Me	H	H	5	93	47	0	0
9	**5**					8	87	41	Trace	0
10	**6**					50[b]	98	4	0	4

a) Ozonization was carried out with an ozone-oxygen mixture (O_3: 0.22 mmol min^{-1}, O_2: 200 ml min^{-1}) on 2 mmol of substrate in 100 ml of acetic acid at room temperature. b) 2,4-Dithiouracil (**6**) is insoluble in acetic acid under the conditions.

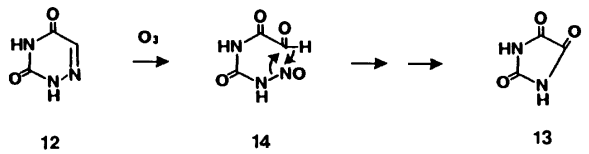

12 14 13

Scheme 2.

2,4-dithiouracil (**6**) in acetic acid, the reaction gave small amounts of uracil (**1a**) and 4(3*H*)-pyrimidinone (**4a**) (Run 10).

A proposed path for the formation of uracils **1** and 4(3*H*)-pyrimidinones **4** is shown in Scheme 1. It is clear that ozone preferentially attacks the thiocarbonyl moiety of 2-thiouracils **3** rather than the olefinic 5-6 bond. 2-Thiouracils **3** can be in equilibrium with the thiol form **3'** in solution. It has been reported that the thione form **3** is predominant under acidic conditions.[21] Besides the ozonization of 2-methylthio-4(3*H*)-pyrimidinone (**7**), which exists in thiol form, was complicated and gave neither uracil nor 4(3*H*)-pyrimidinone. Therefore, it is concluded that ozone reacts with the thione form **3**. In the ozonization of thiocarbonyl moiety, both 1,3-dipolar cycloaddition and electrophilic attack of ozone have been proposed.[1] In the cases of 1-unsubstituted 2-thiouracils **3a—e**, the former to give uracils **1a—e** competes with the latter to afford 4(3*H*)-pyrimidinones **4a—e**. 1,3-Dipolar cycloaddition of ozone to the C=S moiety gives the ozone-adduct **8** followed by the elimination of sulfur dioxide to give uracils **1** (path A). Electrophilic ozone attack on the S-atom gives the ozone-adduct **9** followed by deoxygenation to give sulfine **10**, which is in equilibrium with sulfenic acid **10'** (path B). This intermediate **10'** is further oxidized to give sulfonic acid **11**. Since a small amount of water is contained in the solvent, the sulfonic acid **11** is desulfurized to give 4(3*H*)-pyrimidinones **4a—e**. After the ozonization of 2-thiouracil (**3a**), the pH value of the solution was 1.5 and a sulfate ion was detected by the barium chromate-diphenylcarbonohydrazide method.[22] In the cases of 1-substituted 2-thiouracils **3f,g**, uracils **1f,g** are preferentially obtained via path A, because no equilibrium between sulfine **10** and sulfenic acid **10'** exists and the sulfines **10f,g** are further ozonized to give unidentified products. In the case of **3f**, 1-methyl-4(1*H*)-pyrimidinone was not detected.

5-Azauracil (**11**) was very stable for ozone under the same conditions, while 6-azauracil (**12**) readily reacted with ozone to give parabanic acid (**13**) in a 34% yield. Similarly, 5-azacytosine was stable for ozone, while 6-azacytosine readily reacted with ozone to give unidentified several compounds in low yields. A mechanism for the ozonization of 6-azauracil (**12**) is proposed in Scheme 2. The reaction of C=N bond with ozone gives the corresponding carbonyl and nitroso compounds.[23] The ozonization of 5-6 bond of 6-azauracil (**12**) may give the intermediate **14**, followed by the elimination of HNO (or HNO_2) to give parabanic acid (**13**). Nitrite and/or nitrate ions were detected by a sulfuric acid–iron(II) sulfate method.[24]

References

1) B. Zwanenburg and W. A. Janssen, *Synthesis*, **1973**, 617; N. H. Nilsson and A. Senning, *Angew. Chem., Int. Ed. Engl.*, **11**, 295 (1972).

2) H. L. Wheeler and L. M. Liddle, *Am. Chem. J.*, **40**, 547 (1908).

3) H. Vorbruggen and P. Strehlke, *Chem. Ber.*, **106**, 3039 (1973).

4) G. W. Anderson, I. F. Halverstadt, W. H. Miller, and R. O. Roblin, *J. Am. Chem. Soc.*, **67**, 2197 (1945).

5) G. Shaw and R. N. Warrener, *J. Chem. Soc.*, **1958**, 153.

6) K. Hirota, K. A. Watanabe, and J. J. Fox, *J. Org. Chem.*, **43**, 1193 (1978).

7) D. J. Brown and K. Shinozuka, *Aust. J. Chem.*, **33**, 1147 (1980).

8) D. J. Brown, *J. Soc. Chem. Ind.*, **69**, 353 (1950).

9) H. L. Wheeler and H. F. Merriam, *Am. Chem. J.*, **29**, 478 (1903).

10) H. W. Scherp, *J. Am. Chem. Soc.*, **68**, 912 (1946).

11) J. H. Burckhalter and H. C. Scarborugh, *J. Am. Pharm. Assoc.*, **44**, 545 (1955).

12) M. M. Endicott and T. B. Johnson, *J. Am. Chem. Soc.*, **63**, 1286 (1941).

13) T. B. Johnson and F. W. Heyl, *Am. Chem. J.*, **37**, 628 (1907).

14) H. L. Wheeler and T. B. Johnson, *Am. Chem. J.*, **37**, 30 (1907).

15) K. J. Kolonko, R. H. Shapiro, R. M. Barkley, and R. E. Sievers, *J. Org. Chem.*, **44**, 3769 (1979).

16) L. Bauer, G. E. Wright, B. A. Mikrut, and C. L. Bell, *J. Heterocycl. Chem.*, **2**, 447 (1965).

17) D. J. Brown, *Aust. J. Chem.*, **21**, 243 (1968).

18) H. M. Foster and H. R. Sbyder, *Org. Synth.*, **35**, 80 (1955).

19) J. P. Jonak, G. C. Hopkins, H. J. Minnemeyer, and H. Tieckelmann, *J. Org. Chem.*, **35**, 2512 (1970).

20) T. B. Johnson and R. B. Flint, *J. Am. Chem. Soc.*, **53**, 1082 (1931).

21) G. B. Elion, W. S. Ide, and G. H. Hitchings, *J. Am. Chem. Soc.*, **68**, 2137 (1946); D. Shugar and J. J. Fox, *Bull. Soc. Chim. Belg.*, **61**, 293 (1952).

22) I. Ishizaki, S. Utsumi, K. Hagino, T. Tarutani, and T. Ozawa, *Bull. Chem. Soc. Jpn.*, **30**, 847 (1957).

23) A. H. Liebel, R. E. Erickson, C. J. Abshire, and P. S. Bailey, *J. Am. Chem. Soc.*, **82**, 1801 (1960).

24) "Bunsekikagakubinran," Maruzen, Tokyo (1961), p. 223.

Generation of Enolates from α,β-Epoxy Sulfoxides with Lithium Dimethylcuprate: A Novel Synthesis of Aldols and Some Trial to Trap the Enolates[1)]

Tsuyoshi SATOH, Atsushi SUGIMOTO, Masayuki ITOH, and Koji YAMAKAWA*
Faculty of Pharmaceutical Sciences, Science University of Tokyo,
Ichigaya-funagawara-machi, Shinjuku-ku, Tokyo 162
(Received March 17, 1989)

Enolates were generated from α,β-epoxy sulfoxides using lithium dimethylcuprate as an electron-transfer reagent. The enolates were trapped with several electrophiles, in which aldehydes reacted with the generated enolates giving aldols in good yields with high regioselectivity.

Enolates are the most fundamental intermediates in the chemistry of carbon–carbon bond formation. Such famous reactions as acetoacetic ester synthesis, aldol condensation, Claisen reaction, Dieckman condensation, Perkin reaction, and Robinson annulation are known to take place through enolates.[2)] Usually, enolates are generated from carbonyl compounds with strong bases, such as sodium hydride, metal alkoxides, or lithium diisopropylamide (LDA). In modern organic syntheses some other methods for the generation of metal enolates have been reported.[3)]

We recently reported novel synthetic methods from 1-chloroalkyl aryl sulfoxides and carbonyl compounds through α,β-epoxy sulfoxides **1**.[4)] In a study it was found that the β-position of **1** shows quite a high reactivity to various kinds of nucleophiles. In a search for another nucleophiles we found that lithium dialkylcuprates reacts with α,β-epoxy sulfoxides **1** to give enolates **2** (Scheme 1).

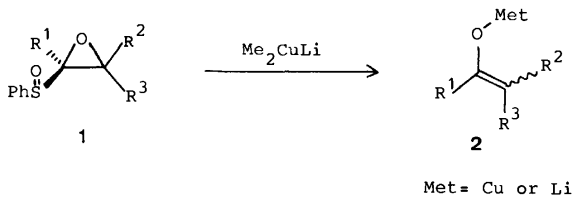

Scheme 1.

In this paper we report on details concerning a novel method for the generation of enolates **2** from **1** with lithium dimethylcuprate (Me_2CuLi) and the synthesis of aldols from **1**.[5)] We also refer to some trials to trap the generated enolates with *t*-butyldimethylsilyl chloride, acetyl chloride, and ethyl chloroformate.

Results and Discussion

The nucleophilic ring-opening of oxiranes by organocopper reagents is a very useful method for carbon–carbon bond formation.[6)] In some cases, however, the reaction of oxiranes with organocopper reagents shows a somewhat different aspect due to the electron-transferable nature of the reagents.[7)] For instance, Tamao et al. recently reported the deoxygenation of α,β-epoxy silanes with Grignard reagents catalyzed by copper giving vinylsilanes.[8)] This reaction was thought to proceed through a one-electron transfer from an organocopper reagent.

The treatment of α,β-epoxy sulfoxide **3**,[9)] which was synthesized from 1-chlorobutyl phenyl sulfoxide and benzaldehyde, was carried out with two equivalents of Me_2CuLi in ether at 0 °C for 3 h. The reaction was quenched with aqueous NH_4Cl to give 1-phenyl-2-pentanone **4** in 77% yield as the sole product. Interestingly, no methylated product was obtained. Among the alkylcopper reagents studied (Me_2CuLi, Bu_2CuLi, $Bu_2CuCNLi$, $Et_2CuMgBr$) Me_2CuLi was found to be the most useful. As a copper source,

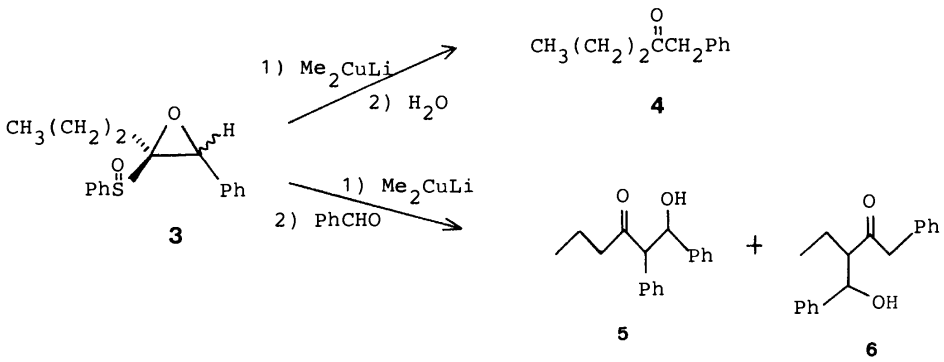

Scheme 2.

Table 1. Trapping the Generated Enolates from α,β-Epoxy Sulfoxides (**7** and **8**) with Electrophiles

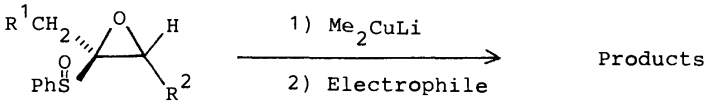

7 $R^1=(CH_2)_5CH_3$; $R^2=Rh$
8 $R^1=Ph$; $R^2=(CH_2)_5CH_3$

Entry	α,β-Epoxy sulfoxide	Electrophile (equiv.)	Conditions[a]	Product	Yield[b] %
1	**7**	TBDMS-Cl (5)	Et_3N, HMPA 0°C—r.t. 9 h	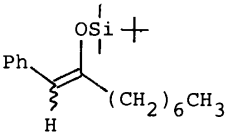 **9**	90
2	**8**	TBDMS-Cl (5)	Et_3N, HMPA 0°C—r.t. 17 h	**9**	85
3	**7**	CH_3COCl (10)	0°C (1.5 h) then r.t. 1 h	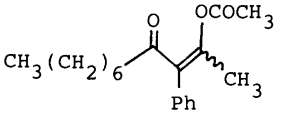 **10**	53
4	**8**	CH_3COCl (10)	0°C, 1.5 h	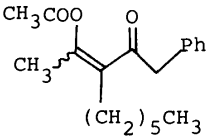 **11**	30
5	**7**	ClCOOEt (5)	0°C, 1.5 h	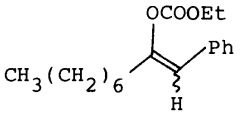 **12**	50
6	**8**	ClCOOEt (5)	0°C, 1 h	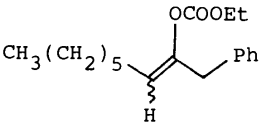 **13**	81

a) All reactions were carried out with three equivalents of Me_2CuLi in dry ether at 0°C then quenched with electrophile. b) Isolated yield after silica-gel column chromatography.

copper(I) bromide–dimethyl sulfide complex (CuBr·SMe_2)[10] was found to be the most effective. We thought that this reaction took place through an enolate. Indeed, by quenching the reaction with benzaldehyde instead of water, a mixture of aldols (**5** and **6**; **5**:**6**=1:4) was obtained in 41% yield (Scheme 2).[11]

In order to obtain further proof of the enolates, the reaction was carried out with other electrophiles using **7** and **8** as the α,β-epoxy sulfoxides. The reason for using **7** and **8** was to clarify the reactivity and regioselectivity of the generated enolates (Table 1).

Quenchig the enolates generated from **7** and **8** with chlorotrimethylsilane gave a mixture of silyl enol ethers; however their isolation was found to be difficult. With *t*-butyldimethylsilyl chloride, both enolates derived from **7** and **8** selectively gave a stereoisomeric mixture of silyl enol ether **9** in good yield, though the reaction was found to have no regiospecificity (Entries 1 and 2). The reaction of the enolates with acetyl chloride was somewhat interesting: it gave diacylated products (**10** and **11**) with high regioselectivity, though yields were not satisfactory (Entries 3 and 4). The reaction of the enolates with ethyl chloroformate regioselectively gave the enol carbonates (**12** and **13**) in moderate to good yields (Entries 5 and 6).

With some results of trapping the enolates with electrophiles in hand, our attention was again focused

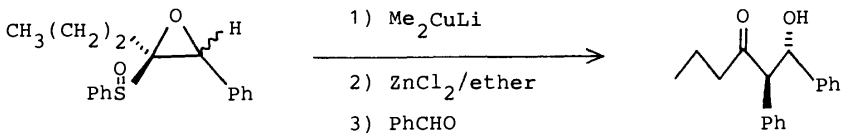

3 Scheme 3. 5

Table 2. Synthesis of Aldols from α,β-Epoxy Sulfoxides with Me_2CuLi and Carbonyl Compounds in the Presence of $ZnCl_2$

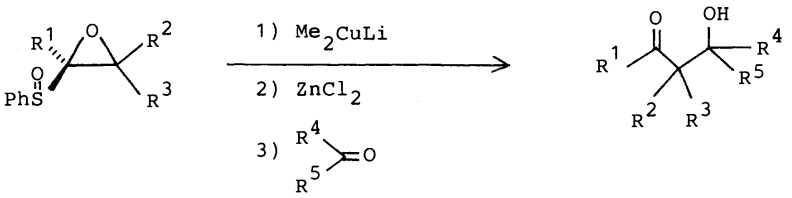

Entry	α,β-Epoxy sulfoxide R¹	R²	R³	Carbonyl compound R⁴	R⁵	Time[a]	Aldol		Yield[b] %
1	$PhCH_2$	CH_3	H	Ph	H	1.5 h[c]	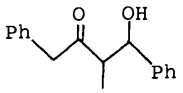	**14**[e]	80
2	$PhCH_2$	CH_3	H	CH_3CH_2	H	1.5 h[c]	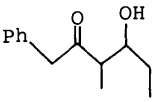	**15**[e]	79
3	$PhCH_2$	CH_3CH_2	H	Ph	H	2 h	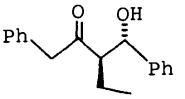	**16**	53
4	$PhCH_2$	$CH_3(CH_2)_5$	H	Ph	H	7 h	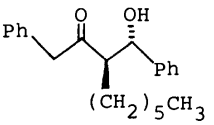	**17**	60
5	$PhCH_2$	$CH_3(CH_2)_4$	H	Ph	H	4 h	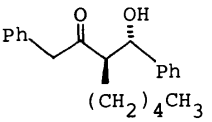	**18**	74
6	$CH_3(CH_2)_6$	Ph	H	Ph	H	30 min	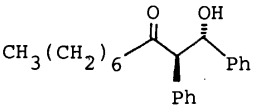	**19**	70
7	$CH_3(CH_2)_6$	Ph	H	CH_3	CH_3	30 min	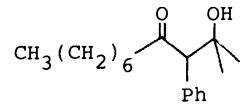	**20**	52[f]
8	$CH_3(CH_2)_2$	Ph	H	Ph	H	40 min	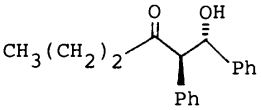	**5**	74
9	$PhCH_2$	CH_3	CH_3	Ph	H	2 d[d]	—[g]		—
10			H	—	—	2 h[c]	—[h]		—

a) All reactions were carried out in ether at 0°C. Unless otherwise noted, 3 equivalents of Me_2CuLi were used. b) Isolated yield. c) 4 equivalents of Me_2CuLi were used. d) 5 equivalents of Me_2CuLi were used. e) Threo/erythro=2/1. f) This reaction gave **20** with 1-phenyl-2-nonanone (39%). g) This reaction did not give aldol but 3-methyl-1-phenyl-2-butanone[4a] in 68% yield. h) The α,β-epoxy sulfoxide did not react with Me_2CuLi.

on the result with the carbonyl compound described above. As shown in Scheme 2, quenching the enolate obtained from **3** with benzaldehyde gave aldols **5** and **6** without regioselectivity. We thought that it is possible to obtain aldols with high regioselectivity if the reaction is carried out with some additives. House demonstrated that zinc chloride is quite useful as an additive for controling the aldol condensation.[12]

α,β-Epoxy sulfoxide **3** was treated with three equivalents of Me_2CuLi in ether at 0 °C for 40 min. After all of the starting materials disappeared, two equivalents of $ZnCl_2$ in ether[12a] followed by benzaldehyde were added to the reaction mixture. The desired aldol reaction took place quite smoothly to give **5** in 74% yield (Scheme 3). The stereochemical assignment of **5** was made by an examination of the vicinal coupling constant in the ^1H NMR. The coupling constant (J=9 Hz) of the proton at the carbon bearing a hydroxyl group clearly indicated that **5** was threo diastereomer.[12b,13] Though a trace amount of the erythro isomer was observed on ^1H NMR, this reaction was found to take place with complete regioselectivity. The representative examples of the synthesis of aldols from α,β-epoxy sulfoxides with Me_2CuLi and carbonyl compounds are listed in Table 2.

The important characteristics of the results shown in Table 2 are as follows: 1) The α,β-epoxy sulfoxides having a hydrogen at the β-carbon (R^3=H; they were synthesized from aldehydes) reacted smoothly with Me_2CuLi to give enolates in high yields, except Entry 10. 2) The α,β-epoxy sulfoxides having a branch at C-1 of R^1 showed quite a low reactivity with Me_2CuLi (Entry 10). 3) The α,β-epoxy sulfoxides having a phenyl group at the β-carbon showed a much higher reactivity with Me_2CuLi than other α,β-epoxy sulfoxides (Entries 6—8). 4) β-Disubstituted α,β-epoxy sulfoxide reacted very sluggishly with Me_2CuLi, giving enolate; however, the reaction of this enolate with benzaldehyde gave a complex mixture (Entry 9). 5) *threo*-Aldols were obtained exclusively or predominantly. 6) Acetone gave aldol in low yield (Entry 7). 7) In Entries 3, 8 and 4, 6, regioisomers of aldols (**16**, **5** and **17**, **19**, respectively) were synthesized in pure form; these results mean that these reactions are a kind of the directed aldol reaction.[3]

The possible mechanism of these reactions can be proposed as follows (Scheme 4). One electron transfer from Me_2CuLi to the α,β-epoxy sulfoxide **1** gives an anion radical intermediate **A**, which receives a second electron from Me_2CuLi to give a dianion intermediate **B**. Then elimination of the phenylsulfinyl group takes place to afford an enolate **C**. The enolate is trapped with electrophiles to give the product described in this paper. The stereochemistry of **C** in the aldol reaction is worth noting. Both isomers of the α,β-epoxy sulfoxides equally react with Me_2CuLi followed by aldehydes to afford *threo*-aldols. From these selectivities of the reaction, it can be presumed that the stereochemistry of the enolates is *E*, as shown in Scheme 4.[14]

Even though the reaction gave aldols with some limitation, we believe that the present method will prove to be valuable in the synthesis of aliphatic aldols with high regioselectivity.

Experimental

All melting points are uncorrected. The IR spectra were measured directly on a NaCl plate or KBr disks with a Hitachi 215 spectrometer. ^1H NMR spectra were measured in a $CDCl_3$ solution with a JEOL FX-100 spectrometer or Hitachi R-24B spectrometer using Me_4Si as an internal standard. Electron-impact mass spectra (MS) were obtained on a Hitachi M-80 double-focusing spectrometer at 70 eV by direct insertion. Silica gel BW-127 ZH (Fuji-Devison) containing a 2% fluoresence reagent (254) and a quartz column were used for column chromatography; products showing ultraviolet (UV) absorption were detected by UV

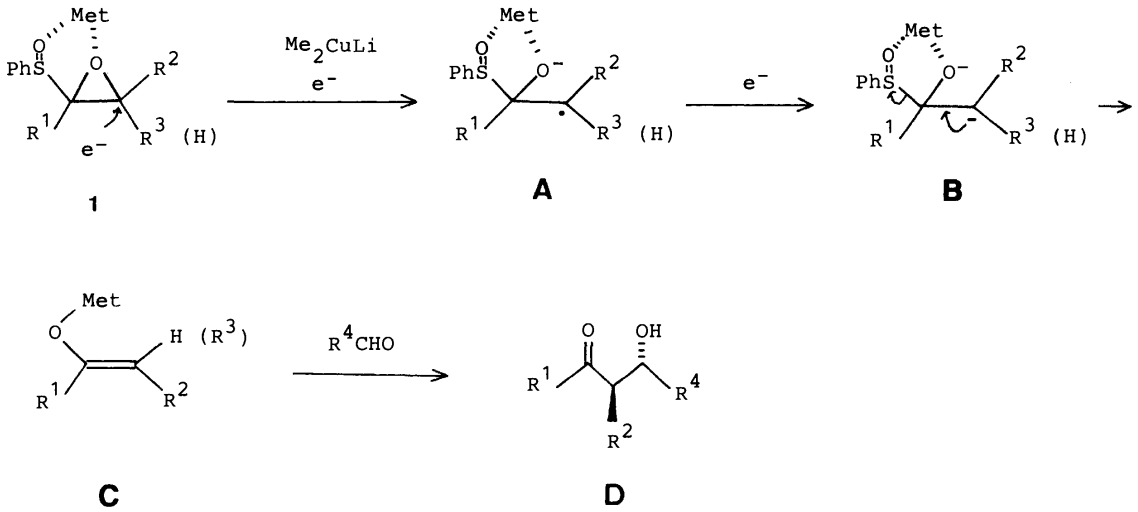

Scheme 4.

irradiation. Ether and THF were dried with benzophenone ketyl and distilled.

α,β-Epoxy Sulfoxides. All α,β-epoxy sulfoxides, except for **8** and the α,β-epoxy sulfoxide in Table 2 (Entry 3), were reported previously.[4,9] Two new α,β-epoxy sulfoxides were prepared from the aldehydes and 1-chloro-2-phenylethyl phenyl sulfoxide through chlorohydrins in the usual way.[4]

2,3-Epoxy-1-phenyl-2-phenylsulfinylpentane (Entry 3 in Table 2). *Z*-Isomer: Colorless semisolid, 44% overall yield. IR (neat): 1080 and 1050 (SO) cm^{-1}; ^1H NMR δ=1.10 (3H, t, *J*=6 Hz), 1.99 (2H, m), 2.52 (1H, d, *J*=15 Hz), 2.62 (1H, t, *J*=6 Hz), 3.55 (1H, d, *J*=15 Hz), and 6.8—7.9 (10H, m); MS *m/z* (%) 286 (M^+, 0.5), 161 (9), 126 (13), and 91 (100); Found: *m/z* 286.1023. Calcd for $C_{17}H_{18}O_2S$: M, 286.1026. *E*-Isomer: Colorless oil, 40% overall yield. IR (neat): 1080 and 1050 (SO) cm^{-1}; ^1H NMR δ=1.00 (3H, t, *J*=6 Hz), 1.58 (2H, m), 3.02 (2H, s), 3.68 (1H, t, *J*=6 Hz), and 6.8—7.9 (10H, m); MS *m/z* (%) 286 (M^+, 0.3), 161 (10), 126 (14), and 91 (100); Found: *m/z* 286.1017. Calcd for $C_{17}H_{18}O_2S$: M, 286.1025.

2,3-Epoxy-1-phenyl-2-phenylsulfinylnonane (8). *Z*-Isomer: Colorless oil, 43% overall yield. IR (neat): 1080 and 1050 (SO) cm^{-1}; ^1H NMR δ=0.90 (3H, t, *J*=6 Hz), 1.0—2.2 (10H, m), 2.53 (1H, d, *J*=15 Hz), 2.65 (1H, t, *J*=6 Hz), 3.58 (1H, d, *J*=15 Hz), and 6.7—7.9 (10H, m); MS *m/z* (%) 342 (M^+, trace), 217 (9), 126 (12), and 91 (100); Found: *m/z* 342.1655. Calcd for $C_{21}H_{26}O_2S$: M, 342.1653. *E*-Isomer: Colorless oil, 41% overall yield. IR (neat): 1080 and 1050 (SO) cm^{-1}; ^1H NMR δ=0.88 (3H, t, *J*=6 Hz), 1.0—1.7(10H, m), 3.04 (2H, s), 3.70 (1H, t, *J*=6 Hz), and 7.0—7.8 (10H, m); MS *m/z* (%) 342 (M^+, trace), 217 (9), 126 (11), and 91 (100); Found: *m/z* 342.1662. Calcd for $C_{21}H_{26}O_2S$: 342.1652.

1-Phenyl-2-pentanone (4). A solution of **3** (90 mg; 0.28 mmol) in 1 ml of dry ether was added to a solution of Me_2CuLi (0.56 mmol; prepared from MeLi and $CuBr \cdot SMe_2$ in ether at 0 °C) in ether (3 ml) at 0 °C under N_2. The reaction mixture was stirred at 0 °C for 3 h; the reaction was then quenched with sat. aq. NH_4Cl. The solution was extracted with ether and the organic layer was washed with sat. aq. NH_4Cl. The usual work-up followed by silica-gel column chromatography afforded 35 mg (77%) of **4** as a colorless oil. IR (neat): 1710 (CO) cm^{-1}; ^1H NMR δ=0.96 (3H, t, *J*=7 Hz), 1.58 (2H, m), 2.41 (2H, t, *J*=7 Hz), 3.66 (2H, s), and 7.0—7.4 (5H, m); MS *m/z* (%) 162 (M^+, 18), 91 (48), and 71 (100); Found: *m/z* 163.1062. Calcd for $C_{11}H_{14}O$: M, 163.1076.

2-(*t*-Butyldimethylsiloxy)-1-phenyl-1-nonene (9). A solution of **7** (69 mg; 0.2mmol) in 1 ml of dry ether was added to a solution of Me_2CuLi (0.6 mmol) in 1.5 ml of ether at 0 °C under N_2. The reaction mixture was stirred at 0 °C for 40 min. To the reaction mixture was added a solution of Et_3N (1 mmol) in 4 ml of dry THF followed by a solution of *t*-butyldimethylsilyl chloride (1 mmol) and HMPA (1 mmol) in 2 ml of THF. The solution was stirred at room temperature for 9 h. The reaction was quenched with H_2O and the whole was extracted with ether. The usual work-up followed by silica-gel column chromatography gave 60 mg (90%) of **9** (a mixture of *E/Z*=1/2) as a colorless oil. IR (neat): 1650 and 1255 cm^{-1}; ^1H NMR δ=−0.04, 0.00 (each 3H, s), 0.81 (9H, s), 0.7—1.0 (3H, m), 1.0—1.6 (12H, m), 2.08 (t, *J*=7 Hz, *E*-isomer), 2.32 (t, *J*=7 Hz, *Z*-isomer), 5.31 (s, vinyl-H, *Z*-isomer), 5.64 (s, vinyl-H, *E*-isomer), and 7.0—7.5 (5H, m); MS *m/z* (%) 332 (M^+, 25), 275 ($[M-C_4H_9]^+$, 100), and 191 (18); Found: *m/z* 332.2530. Calcd for $C_{21}H_{36}OSi$: M, 332.2527.

α,β-Epoxy sulfoxide **8** gave the same product on treatment with Me_2CuLi followed by *t*-butyldimethylsilyl chloride.

2-Acetoxy-3-phenyl-2-undecen-4-one (10). A solution of **7** (103 mg; 0.3 mmol) in 1 ml of ether was added to a solution of Me_2CuLi (0.9 mmol) in 2 ml of ether at 0 °C under N_2. The reaction mixture was stirred at 0 °C for 30 min. To this reaction mixture was added acetyl chloride (3 mmol); the mixture was first stirred at 0 °C for 1.5 h and then at room temperature for 1 h. The reaction was quenched with 1% aq. ammonia and the whole was extracted with ether. The usual work-up followed by silica-gel column chromatography afforded 48 mg (53%) of **10** as a colorless oil. Single isomer; *E/Z* not determined. IR (neat): 1770 and 1700 (CO) cm^{-1}; ^1H NMR δ=0.85 (3H, t, *J*=6 Hz), 1.0—1.6 (10H, m), 1.92 (3H, s), 2.19 (2H, m), 2.21 (3H, s), and 7.1—7.5 (5H, m); MS *m/z* (%): 302 (M^+, 6), 260 ($[M-C_2H_2O]^+$, 19), 242 (20), 176 (71), 161 (92), and 43 (100); Found: *m/z* 302.1880. Calcd for $C_{19}H_{26}O_3$: M, 302.1880.

2-Acetoxy-3-hexyl-5-phenyl-2-penten-4-one (11). A similar treatment of **8** with Me_2CuLi followed by acetyl chloride gave **11** as a *E/Z*-mixture (1:1) in 30% yield. Colorless oil; IR (neat): 1760 and 1690 (CO) cm^{-1}; ^1H NMR δ=0.86 (3H, t, *J*=6 Hz), 1.0—1.6 (8H, m), 1.8—2.5 (8H, m), 3.76, 3.83 (each bs, 2H, $PhC\underline{H_2}CO$-), and 7.0—7.4 (5H, m); MS *m/z* (%) 302 (M^+, 1), 260 ($[M-C_2H_2O]^+$, 2), 211 ($[M-PhCH_2]^+$, 16), and 169 (100); Found: *m/z* 302.1904. Calcd for $C_{19}H_{26}O_3$: M, 302.1881.

2-Ethoxycarbonyloxy-1-phenylnonene (12). A solution of **7** (69 mg; 0.2 mmol) in 1 ml of ether was added to a solution of Me_2CuLi (0.6 mmol) in 1.5 ml of ether at 0 °C under N_2. The reaction mixture was stirred at 0 °C for 30 min; then ethyl chloroformate (1 mmol) was added. The reaction mixture was stirred at 0 °C for 1.5 h; then the reaction was quenched with 1% aq. ammonia. The usual work-up followed by silica-gel column chromatography gave 30 mg (50%) of **12** (a mixture of *E/Z*; *E/Z*=2/1) as a colorles oil. IR (neat): 1765 (CO) and 1240 (COC) cm^{-1}; ^1H NMR δ=0.85 (3H, m, CH_3), 1.0—1.7 (13H, m), 2.28—2.60 (2H, m, $C=CC\underline{H_2}$), 4.0—4.2 (2H, m, $OC\underline{H_2}CH_3$), 5.90 (s, vinyl-H; Z), 6.33 (s, vinyl-H, E), and 7.0—7.5 (5H, m); MS *m/z* (%) 290 (M^+, 11), 218 ($[M-C_3H_4O_2]^+$, 21), 199 (15), 134 (43), and 91 (100); Found: *m/z* 290.1895. Calcd for $C_{18}H_{26}O_3$: M, 290.1881.

2-Ethoxycarbonyloxy-1-phenyl-2-nonene (13). A similar treatment of **8** with Me_2CuLi followed by ethyl chloroformate gave **13** as a *E/Z*-mixture (*E/Z*=3/2) in 81% yield. Colorless oil; IR (neat): 1760 (CO) and 1250 (COC) cm^{-1}; ^1H NMR δ=0.86 (3H, m, CH_3), 1.0—1.6 (11H, m), 1.6—2.1 (2H, m), 3.52 (3/5H, s, $PhC\underline{H_2}$), 3.85 (2/5H, s, $PhC\underline{H_2}$), 4.0—4.4 ($OC\underline{H_2}$–, and vinyl-H (*Z*), m), 4.95 (3/5H, t, *J*=7 Hz, vinyl-H (*E*)), and 7.0—7.6 (5H, m); MS *m/z* (%) 290 (M^+, 2), 207 (34), and 91 (100); Found: *m/z* 290.1893. Calcd for $C_{18}H_{26}O_3$: M, 290.1881.

General Procedure for the Preparation of Aldols from α,β-Epoxy Sulfoxides with Me_2CuLi Followed by Carbonyl Compounds: The synthesis of (1*R**,2*S**)-1-hydroxy-1,2-diphenyl-3-hexanone **5** from **3** is described. A solution of **3** (97 mg; 0.3 mmol) in 1 ml of ether was added to a solution of Me_2CuLi (0.9 mmol) in 2 ml of ether at 0 °C under N_2. The solution was stirred at 0 °C for 40 min. To this reaction

mixture was added a solution of $ZnCl_2$ in ether (0.6 mmol) followed by benzaldehyde (0.33 mmol). The reaction mixture was stirred for 10 min; then the reaction was quenched with sat. aq. NH_4Cl. The solution was extracted with ether-benzene. The usual work-up followd by column chromatography gave 67 mg (74%) of **5** as colorless needles. Mp 48.5—50.5 °C (AcOEt-hexane); IR (KBr): 3400 (OH) and 1705 (CO) cm^{-1}; ^1H NMR δ=0.81 (3H, t, J=7 Hz), 1.56 (2H, sextet, J=7 Hz), 2.37 (2H, t, J=7 Hz), 3.93 (1H, d, J=9 Hz), 5.18 (1H, d, J=9 Hz), and 6.7—7.3 (10H, m); MS m/z (%) 250 ($[M-H_2O]^+$, 0.8), 207 (0.5), 162 (28), and 70 (100); Found: C, 80.62; H, 7.51%. Calcd for $C_{18}H_{20}O_2$: C, 80.56; H, 7.51%.

4-Hydroxy-3-methyl-1,4-diphenyl-2-butanone (14). A threo/erythro (2/1) mixture; colorless oil; 80% yield. IR (neat): 3450 (OH) and 1720 (CO) cm^{-1}; ^1H NMR δ=0.88 (d, J=7 Hz threo), 1.07 (d, J=7 Hz, erythro), 2.8—3.2 (1H, m), 3.58 (s, PhC$\underline{H}_2$, erythro), 3.74 (s, PhC$\underline{H}_2$, threo), 4.69 (bd, J=9 Hz, threo), 4.90 (d, J=5 Hz, erythro), and 6.9—7.4 (10H, m); MS m/z (%): 254 (M^+, 4), 180 (6), 163 ($[M-PhCH_2]^+$, 17), 148 (44), and 107 (100); Found: m/z 254.1302. Calcd for $C_{17}H_{18}O_2$: M, 254.1305.

4-Hydroxy-3-methyl-1-phenyl-2-hexanone (15). A threo/erythro (2/1) mixture; colorless oil; 79% yield. IR (neat): 3475 (OH) and 1715 (CO) cm^{-1}; ^1H NMR δ=0.90 (3H, t, J=7 Hz), 1.12 (d, J=7 Hz, erythro), 1.13 (d, J=7 Hz, threo), 1.2—1.7 (2H, m), 2.5—2.9 (1H, m), 3.4—3.8 (1H, m), 3.77 (2H, s), and 7.0—7.4 (5H, m); MS m/z (%) 206 (M^+, 10), 148 ($[M-C_3H_6O]^+$, 13), 115 (72), and 91 (100); Found: m/z 206.1311. Calcd for $C_{13}H_{18}O_2$: M, 206.1305.

(3*R,4*S**)-3-Ethyl-4-hydroxy-1,4-diphenyl-2-butanone (16).** Colorless crystals; 53% yield; mp 59—60.5 °C (AcOEt-hexane). IR (KBr): 3405 (OH) and 1720 (CO) cm^{-1}; ^1H NMR δ=0.73 (3H, t, J=7 Hz), 1.1—1.8 (2H, m), 2.8—3.1 (1H, m), 3.63 (2H, s), 4.77 (1H, d, J=7 Hz), and 6.9—7.4 (10H, m); MS m/z (%) 268 (M^+, 2), 239 ($[M-C_2H_5]^+$, 1), 177 (22), 162 (25), and 91 (100); Found: C, 80.38; H, 7.51%. Calcd for $C_{18}H_{20}O_2$: C, 80.56; H, 7.51%.

(3*R,4*S**)-3-Hexyl-4-hydroxy-1,4-diphenyl-2-butanone (17).** Colorless crystals; 60% yield; mp 62—63 °C (AcOEt-hexane). IR (KBr): 3400 (OH) and 1715 (CO) cm^{-1}; ^1H NMR δ=0.83 (3H, t, J=6 Hz), 0.9—1.8 (10H, m), 2.84—3.16 (1H, m), 3.61 (2H, s), 4.76 (1H, d, J=8 Hz), and 6.9—7.4 (10H, m); MS m/z (%) 324 (M^+, 0.6), 233 ($[M-PhCH_2]^+$, 6), 215 (4), 187 (8), and 127 (100); Found: C, 81.36; H, 8.77%. Calcd for $C_{22}H_{28}O_2$: C, 81.44; H, 8.71%.

(3*R,4*S**)-4-Hydroxy-3-pentyl-1,4-diphenyl-2-butanone (18).** Colorless crystals; 74% yield; mp 70—71.5 °C (AcOEt-hexane). IR (KBr): 3400 (OH) and 1720 (CO) cm^{-1}; ^1H NMR δ=0.79 (3H, t, J=6 Hz), 0.9—1.8 (8H, m), 2.84—3.16 (1H, m), 3.61 (2H, s), 4.75 (1H, d, J=8 Hz), and 6.9—7.4 (10H, m); Ms m/z (%) 310 (M^+, 1), 219 ($[M-PhCH_2]^+$, 12), 173 (15), and 113 (100); Found: C, 81.17; H, 8.45%. Calcd for $C_{21}H_{26}O_2$: C, 81.25; H, 8.44%.

(1*R,2*S**)-1-Hydroxy-1,2-diphenyl-3-decanone (19).** Colorless crystals; 70% yield; mp 55.5—57 °C (AcOEt-hexane). IR (KBr): 3400 (OH) and 1705 (CO) cm^{-1}; ^1H NMR δ=0.84 (3H, t, J=6 Hz), 0.9—1.7 (10H, m), 2.38 (2H, t, J=7 Hz), 3.93 (1H, d, J=9 Hz), 5.18 (1H, J=9 Hz), and 6.8—7.4 (10H, m); MS m/z (%) 306 ($[M-H_2O]^+$, 1), 218 ($[M-C_7H_6O]^+$, 23), 180 (13), 127 (80), and 57 (100); Found: C, 81.62; H, 8.81%. Calcd for $C_{22}H_{28}O_2$: C, 81.44; H, 8.71%.

2-Hydroxy-2-methyl-3-phenyl-4-undecanone (20). Colorless oil; 52% yield. IR (neat): 3520 (OH) and 1700 (CO) cm^{-1}; ^1H NMR δ=0.84 (3H, t, J=6 Hz), 0.99 (3H, s), 1.0—1.8 (10H, m), 1.33 (3H, s), 2.36 (2H, t, J=7 Hz), 3.69 (1H, s), and 7.27 (5H, s); MS m/z (%) 216 ($[M-H_2O]^+$, 2), 218 ($[M-C_3H_6O]^+$, 98), and 127 ($[M-C_{10}H_{13}O]^+$, 100).

The authors are grateful to Dr. Mikio Takeda, Tanabe Seiyaku Co., Ltd. for elemental analyses and Miss Noriko Sawabe and Mrs. Tomoko Akiyama of this laboratory for NMR and MS measurements. This work was supported in part by the Grant-in-Aid for Scientific Research from the Ministry of Education, which is gratefully acknowledged.

References

1) α,β-Epoxy sulfoxides as useful itermediates in organic synthesis. 23. Part 22: T. Satoh, T. Sato, T. Oohara, and K. Yamakawa, *J. Org. Chem.*, in press.

2) J. March, "Advanced Organic Chemistry," 2 nd ed. McGraw-Hill Book Company, New York (1977); B. P. Mundy and M. G. Ellerd, "Name Reactions and Reagents in Organic Synthesis," John Wiley and Sons, New York (1988).

3) T. Mukaiyama, *Org. React.*, **28**, 228 (1982).

4) a) T. Satoh, Y. Kaneko, T. Izawa, K. Sakata, and K. Yamakawa, *Bull. Chem. Soc. Jpn.*, **58**, 1983 (1985); b) T. Satoh, T. Kumagawa, and K. Yamakawa, *ibid.*, **58**, 2849 (1985); c) T. Satoh, Y. Kaneko, K. Sakata, and K. Yamakawa, *ibid.*, **59**, 457 (1986); d) T. Satoh, A. Sugimoto, K. Yamakawa, *Chem. Pharm. Bull.*, **35**, 4632 (1987); e) T. Satoh, K. Iwamoto, A. Sugimoto, and K. Yamakawa, *Bull. Chem. Soc. Jpn.*, **61**, 2109 (1988) and references cited therein.

5) The preliminary communication of this study: T. Satoh, A. Sugimoto, M. Itoh, and K. Yamakawa, *Tetrahedron Lett.*, **30**, 1083 (1989).

6) R. W. Herr, D. M. Wieland, and C. R. Johnson, *J. Am. Chem. Soc.*, **92**, 3813 (1970); G. H. Posner, *Org. React.*, **22**, 253 (1975); J. P. Marino and D. M. Floyd, *Tetrahedron Lett.*, **1979**, 675; A. Alexakis, G. Cahiez, and J. F. Normant, *Tetrahedron*, **36**, 1961 (1980); A. Ghribi, A. Alexakis, and J. F. Normant, *Tetrahedron Lett.*, **25**, 3075 (1984); B. H. Lipshutz, R. S. Wilhelm, J. A. Kozlowski, and D. Parker, *J. Org. Chem.*, **49**, 3928 (1984); J. M. Chong and K. B. Sharpless, *Tetrahedron Lett.*, **26**, 4683 (1985).

7) H. O. House, *Acc. Chem. Res.*, **9**, 59 (1976); E. C. Ashby and D. Coleman, *J. Org. Chem.*, **52**, 4554 (1987).

8) K. Tamao, E. Nakajo, and Y. Ito, *J. Org. Chem.*, **53**, 414 (1988).

9) T. Satoh, A. Sugimoto, and K. Yamakawa, *Chem. Pharm. Bull.*, **37**, 184 (1989).

10) H. O. House, C-Y. Chu, J. M. Wilkins, and M. J. Umen, *J. Org. Chem.*, **40**, 1460 (1975).

11) Both *E*- and *Z*-isomer of the α,β-epoxy sulfoxides **3** showed the same reactivity with Me_2CuLi.

12) a) H. O. House, D. S. Crumrine, A. Y. Teranishi, and H. D. Olmstead, *J. Am. Chem. Soc.*, **95**, 3310 (1973); b) K. K. Heng and R. A. J. Smith, *Tetrahedron*, **35**, 425 (1979).

13) R. Baker, J. L. Castro, and C. J. Swain, *Tetrahedron Lett.*, **29**, 2247 (1988).

14) W. Carruthers, "Some Modern Methods of Organic Synthesis," 3rd ed., pp. 48—63, Cambridge University Press, Cambridge (1986).

A High Cis-Stereoselectivity in the Hydrogenation of 6-*t*-Butyltetrahydropyran-3-one and 2-*t*-Butyl-1,3-dioxan-5-one

Yasuhisa SENDA,*,† Toshiyuki TERASAWA, Jun-ichi ISHIYAMA, Shin-ichi KAMIYAMA, and Shin IMAIZUMI
Department of Engineering Science, Faculty of Engineering, Tohoku University, Aoba, Sendai 980
(Received April 20, 1989)

Stereochemistry in the hydrogenation of 4-*t*-butylcyclohexanone and the corresponding oxa- and dioxacyclohexanone was examined. A high cis selectivity was observed in the latter two compounds regardless of the catalyst metals used here. These results were explained in terms of intramolecular n_O–π_{CO} interaction, which was supported by ^{13}C NMR chemical shifts of the carbonyl carbons and CNDO/2 calculation.

The stereochemistry of hydrogenation of an unsaturated bond is frequently controlled by a heteroatom in a molecule. For instance, in allylic alcohols and ethers, hydrogens come into the unsaturated bond from the same side as the oxygen atom of the hydroxyl or the alkoxyl group. This is attributed to an interaction of the oxygen atom through the lone pair with the catalyst surface. This is called as the "directing effect" or "anchor effect".[1] However, in some cases, this effect does not necessarily appear. For methylene-1,3-dioxanes in which oxygen atoms and the double bond are placed at an appropriate position, the stereochemistry of the hydrogenation is such that the hydrogens add from the side opposite to the oxygen lone pair. This is interpreted in terms of intramolecular interaction between the nonbonding orbital of the oxygen and the olefinic π-orbital.[2]

In this paper, in order to investigate how the effect of an oxygen atom appears in the hydrogenation of cyclic ketones, 6-*t*-butyltetrahydropyran-3-one (**1**) and 2-*t*-butyl-1,3-dioxan-5-one (**2**) were hydrogenated in ethanol over several Group VIII transition metal catalysts and the stereochemistry was compared with that of 4-*t*-butylcyclohexanone (**3**). The results of the hydrogenation are tabulated in Table 1.

In the hydrogenation of **1** and **3**, Pd and Rh black catalysts behaved somewhat differently from other metal catalysts used in the present study. The main products of hydrogenation from **3** were saturated alcohol on Rh catalyst (Fig. 2) and saturated ether on Pd catalyst (Fig. 3) similar as the results obtained by Nishimura et al.[3] On the contrary, the saturated alcohol was the main products of hydrogenation from **1** on Pd catalyst under the same reaction conditions (Fig. 1).

Table 1. Hydrogenation[a] and Complex Metal Hydride Reduction[b] of 6-*t*-Butyltetrahydropyran-3-one (**1**), 2-*t*-Butyl-1,3-dioxan-5-one (**2**) and 4-*t*-Butylcyclohexanone (**3**)

		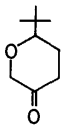 (**1**)	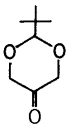 (**2**)	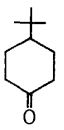 (**3**)
Catalyst	Weight/mg			
Raney Co	1000	80	91	56
Raney Ni	1000	89	97	71
Ru-black	20	90	91	77
Rh-black	20	94	100	—[c]
Pd-black	20	96[d]	100	—[e]
Os-black	20	66	67	55
Ir-black	20	70	88	58
Pt-black	20	81	90	32
$LiAlH_4$		8	7	7
$NaBH_4$		9	6	15

a) Values are cis% of alcohols produced when 50% of substrates were consumed. Substrate; 0.5 mmol, solvent (ethanol); 3 ml, ambient temperature under atmospheric pressure of hydrogen. b) Values are cis% of alcohols. Substrate 1 mmol, complex metal hydride; 0.25 mmol, solvent (ether with $LiAlH_4$ and 2-propanol with $NaBH_4$); 10 ml at 0 °C. c) Acetal, 98%. d) Acetal, 85%. e) Acetal and ethers, 100%.

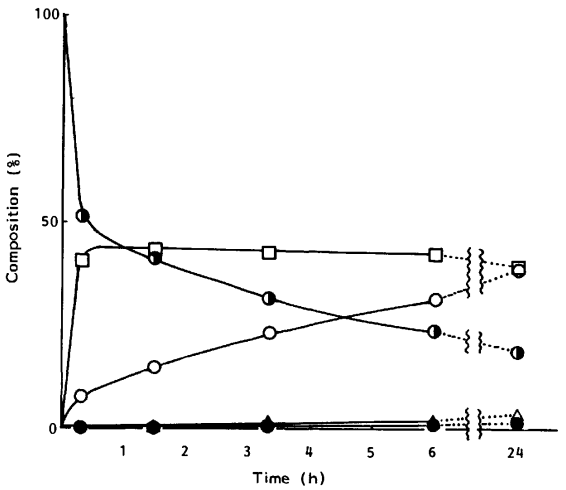

Fig. 1. Hydrogenation of 6-*t*-butyltetrahydropyran-3-one (**1**) over Pd-black catalyst: ◑; **2**, □; 6-*t*-butyltetrahydropyran-3-one diethyl acetal, △; *cis*-6-*t*-butyl-1-ethoxytetrahydropyran, ○; *cis*-6-*t*-butyltetrahydropyran-3-ol, ●; *trans*-6-*t*-butyltetrahydropyran-3-ol.

† Present address: Department of Chemistry, Faculty of Science, Yamagata University, Koshirakawa, Yamagata 990.

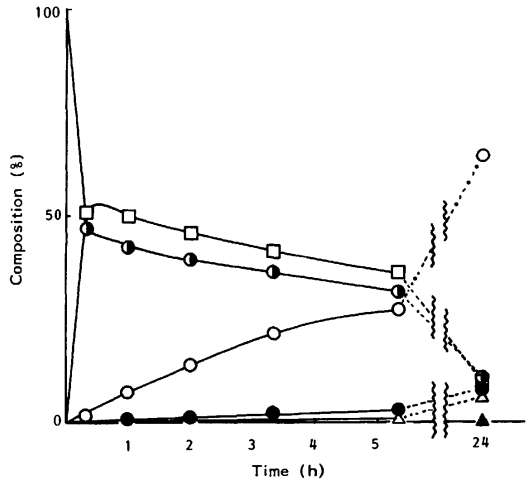

Fig. 2. Hydrogenation of 4-*t*-butylcyclohexanone (**3**) over Rh-black catalyst: ◑; **3**, □; 4-*t*-butylcyclohexanone diethyl acetal, △; *cis*-1-*t*-butyl-4-ethoxycyclohexane, ▲; *trans*-1-*t*-butyl-4-ethoxycyclohexane, ○; *cis*-4-*t*-butylcyclohexanol, ●; *trans*-4-*t*-butylcyclohexanol.

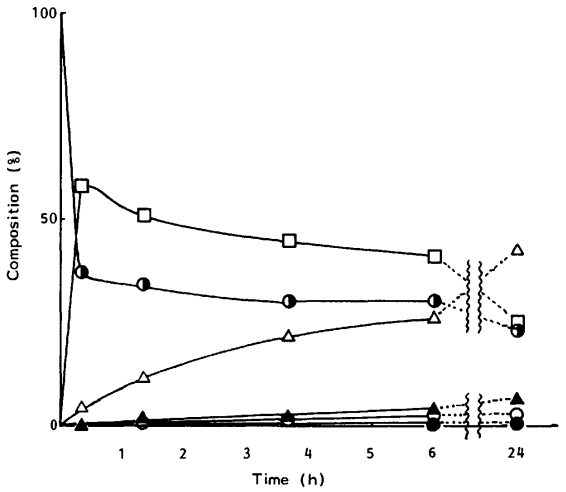

Fig. 3. Hydrogenation of 4-*t*-butylcyclohexanone (**3**) over Pd-black catalyst: ◑; **3**, □; 4-*t*-butylcyclohexanone diethyl acetal, △; *cis*-1-*t*-butyl-4-ethoxycyclohexane, ▲; *trans*-1-*t*-butyl-4-ethoxycyclohexane, ○; *cis*-4-*t*-butylcyclohexanol, ●; *trans*-4-*t*-butylcyclohexanol.

The stereochemistry of the hydrogenation of **3** over Group VIII transition metal black catalysts has been investigated in detail and was interpreted in terms of the Horiuti-Polanyi mechanism which is one of the most satisfactory theories.[4] The change in the product-controlling step depending on the catalysts coincides with a change in the ratio of the product. The Horiuti-Polanyi formulation of the mechanism of hydrogenation of unsaturated bonds may be represented by four elementary reactions, dissociation of hydrogen, adsorption of the substrate on the catalyst, first hydrogen transfer to the adsorbed species,

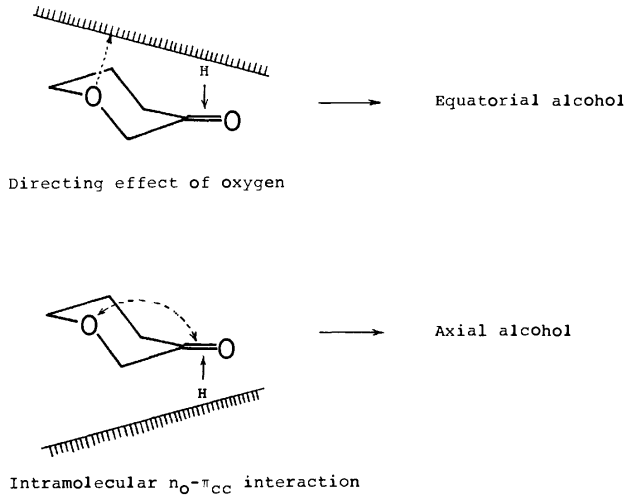

Scheme 1.

and second hydrogen transfer to the half-hydrogenated intermediate. The proportion of the stereoisomeric products will depend upon which of the elementary reactions is a product controlling step, because the geometry and/or composition of the several possible transition states differ from one another. When the product controlling step is the adsorption of the substrate on the catalyst or the first hydrogen transfer from the catalyst to the adsorbed species, the stereochemistry of the reaction is controlled by the interaction between the substrate and the catalyst. On the other hand, when the product controlling step is the second hydrogen transfer from the catalyst to the half-hydrogenated species, the stereochemistry is controlled by the relative stabilities of the two epimeric half-hydrogenated species.

The hydrogenation of **3** gave an excess cis product (55—77%) except in the case of Pt black on which the more stable one of the two possible products was predominant. This indicates that the stereochemistry is controlled by the steric interaction between the substrate and the catalysts other than Pt black catalysts.[5] Significantly high cis stereoselectivity was observed in the hydrogenation of **1** and **2** which contain the oxygen atom/atoms in the β-position with respect to the carbonyl carbon. Since geometries of the 1,3-dioxane and the tetrahydropyran skeleton are similar to the cyclohexane ring, formation of the trans products (equatorial alcohol) is expected by the introduction of the oxygen atom/atoms (Scheme 1).[1] The reaction, however, proceeded selectively to give cis saturated products. Such a high cis selectivity in the oxygen-containing substrates has been found in the hydrogenation of 2-*t*-butyl-5-methylene-1,3-dioxane and 2-*t*-butyl-5-methylenetetrahydropyran.[2]

In order to obtain information on the structure of these molecules, the substrates were subjected to ^{13}C NMR spectroscopy. The chemical shifts were tabulated in Table 2. The chemical shifts of the

Table 2. Carbon-13 Chemical Shifts of 6-*t*-Butyltetrahydropyran-3-one (**1**), 2-*t*-Butyl-1,3-dioxan-5-one (**2**), 4-*t*-Butylcyclohexanone (**3**) and the Hydrogenation Products of **1** and **2** in $CDCl_3$ (δ)

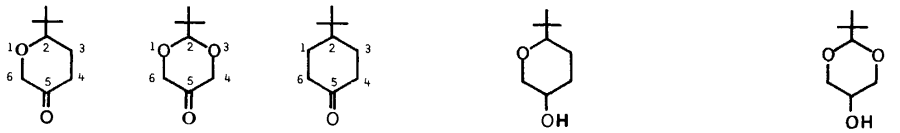

Cis	(**1**)	(**2**)	(**3**)	Cis	Trans	Cis	Trans
C-1	—	—	27.6	—	—	—	—
C-2	83.6	105.8	46.8	86.1	85.4	108.0	107.4
C-3	24.3	—	27.6	20.0	24.6	—	—
C-4	74.8	73.3	41.3	73.2	73.2	71.9	71.7
C-5	208.8	204.9	212.2	64.8	66.3	64.1	61.5
C-6	37.1	73.3	41.3	30.3	33.0	71.9	71.7
$(CH_3)_3\underline{C}$	34.3	35.3	32.5	34.3	33.8	35.0	29.6
$(\underline{C}H_3)_3C$	25.9	26.9	27.6	25.9	26.2	24.5	24.8

Table 3. Differences in β-Carbon Resonances between Oxygen Containing Heterocycles and the Corresponding Carbocyclic Compounds (ppm)

	β
	−1.1
	−1.0
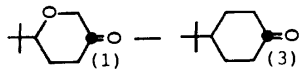	−3.4
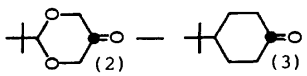	−7.3
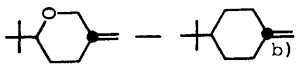	−5.2
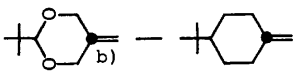	−10.0

The chemical shifts were taken from a) J. B. Stothers, "Carbon-13 NMR Spectroscopy," Academic Press Inc., New York (1972). b) Ref. 2.

carbonyl carbons were compared with those of the carbo-cyclic carbonyl compounds. When the oxygen atom/atoms were introduced in the cyclohexane ring, the shift effect of the oxygen on the β carbon was found to be −1.1 ppm for tetrahydropyran and −1.0 for 1,3-dioxane. Much larger high field shifts of carbonyl carbons which are β to the oxygen atom were practically observed in **1** and **2** (−3.4 ppm for **1** and −7.3 ppm for **2**, respectively) as shown in Table 3. Experimentally it has been found that the effects of substituents on ^{13}C chemical shifts are largely additive. Such high field shifts of the carbonyl carbons in an unsaturated system compared to a saturated one by the introduction of an oxygen atom/atoms indicate electron delocalization of π-electrons similar to those with 2-*t*-butyl-5-methylene-1,3-dioxane[2] and 2-*t*-butyl-5-methylenetetrahydropyran (Table 3). This implies an interaction between the oxygen lone pair and the carbon–oxygen double bond.

The semi-empirical calculations of **1**, **2**, and **3** were performed to compare the electron density of the carbonyl group by the CNDO/2 method which was successful in predicting the electron density of the double bond. Total and π-electron densities of the carbonyl group in each of the most stable chair conformations were obtained and the difference in electron densities can be calculated between compounds containing oxygen and the corresponding cyclohexanone. The δD_T (difference in the total electron density) values for carbonyl carbon are +0.0211 for **1** and +0.0425 for **2**, and for carbonyl oxygen are −0.0157 for **1** and −0.0301 for **2** compared to **3**. The δD_π (difference in the π-electron density) values for carbonyl carbon are +0.0103 for **1** and +0.0193 for **2**, and for carbonyl oxygen are −0.0203 for **1** and −0.0375 for **2** compared to **3** (Table 4). A good correlation was found between the δD values of the electron density and the $\Delta\delta$ values of the ^{13}C NMR chemical shifts. The carbonyl carbon resonances moved to a higher field with an increase in the electron density. Such calculations also support the presence of intramolecular orbital interaction between the oxygen atom and the unsaturated bond.

A high cis (axial alcohol) selectivity observed in the hydrogenation of **1** and **2** implies significant control exerted by the oxygen participation on the transition state of the adsorption of the substrate. The non-bonded electrons of the oxygen can stabilize any incipient charge which might result from a π-donation of an unsaturated carbon–oxygen bond on the metal surface. The enhanced effective electronegativity of the oxygen, therefore, induces the back-donation from the metal surface to the π^*-orbital of the carbonyl.

Table 4. Total and π-Electron Densities (D_T, D_π) of Carbonyl Group in 6-*t*-Butyltetrahydropyran-3-one (**1**), 2-*t*-Butyl-1,3-dioxan-5-one, and 4-*t*-Butylcyclohexanone (**3**) by CNDO/2 Calculation

		C=O				C=*O*		
(1)	D_T	3.7673	δD_T	0.0211	D_T	6.2529	δD_T	−0.0157
	D_π	0.8288	δD_π	0.0103	D_π	1.2335	δD_π	−0.0203
(2)	D_T	3.7887	δD_T	0.0425	D_T	6.2385	δ_T	−0.0301
	D_π	0.8378	δD_π	0.0193	D_π	1.2163	δD_π	−0.0375
(3)	D_T	3.7462			D_T	6.2686		
	D_π	0.8185			D_π	1.2538		

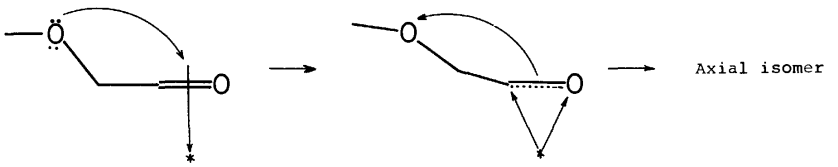

Scheme 2.

This results in a predominant adsorption from the equatorial side of the molecule (Schemes 1 and 2). Similarly, anchimeric assistance by long-range oxygen participation has also been found in the solvolytic reaction of 9-oxabicyclo[4.2.1]nonan-2-yl brosylates[6] and in some electrophilic reactions of 8-oxabicyclo-[4.3.0]non-3-enes.[7]

Chemical reduction with $LiAlH_4$ and $NaBH_4$ was also examined, and its stereochemistry made a sharp contrast with that of the hydrogenation (Table 1). Stereoselective formation of equatorial alcohols from **1** and **2** was consistent with the reduction of 2-phenyl-1,3-dioxan-5-one which was reported by Jochims et al.[8]

Experimental

6-*t*-Butyltetrahydropyran-3-one (1). The compound, **1** was prepared following two methods. (I) According to the method of Ancelmi et al.[9] by using trimethylacetaldehyde and 3-buten-1-ol as starting materials. (II) The hydroboration of 2-*t*-butyl-5,6-dihydro-4*H*-pyran which was prepared by the method of Anderson and Sepp[10] followed by the oxidation with pyridinium chlorochromate; bp 92—94 °C (12 mmHg; 1 mmHg≈133.322 Pa); ^{1}H NMR ($CDCl_3$) δ=0.95 (9H, s), 1.6—3.4 (5H, m), 3.95 (1H, bs), 4.05 (1H, bs). Found: C, 68.92; H, 10.37%. Calcd for $C_9H_{16}O_2$: C, 69.19; H, 10.32%.

2-*t*-Butyl-1,3-dioxan-5-one (2).[11] 2-*t*-Butyl-5-hydroxymethyl-5-nitro-1,3-dioxane[12] was converted to **2** by the hydrogenation of nitro group followed by sodium periodate oxidation.

Metal Black Catalyst. The metal black catalysts were prepared from the corresponding metal chloride or metal oxides by the methods reported in the literature.[13,14]

Catalytic Hydrogenation. The substrate (0.5 mmol) was stirred under hydrogen atmosphere in 3 ml ethanol at room temperature over a weighed catalyst. The reaction was followed gas chromatographically by analyzing aliquots of the reaction mixture at appropriate time intervals. The cis products from **1** and **2** over Rh catalyst were subjected to ^{13}C NMR analysis (the epimeric purity was 94 and 100%, respectively).

Metal Hydride Reduction. To a solution of 0.25 mmol of complex metal hydride in ether ($LiAlH_4$) or in 2-propanol ($NaBH_4$), ketone (1 mmol) was added at 0 °C. After the reaction mixture had been stirred for 30 min, water was added and the solution was subjected to gas chromatography. The trans products from **1** and **2** on $LiAlH_4$ reduction were subjected to ^{13}C NMR analysis (the epimeric purity was 92 and 93%, respectively).

NMR and Gas Chromatographic Analyses. ^{1}H NMR spectra were obtained with a JEOL JNM-MH-100 spectrometer and ^{13}C NMR spectra were obtained with a JEOL JNM-FX-60-Q spectrometer. Gas chromatographic analyses were performed with Hitachi 164 with a Goley column of PEG 4000 (45 m×0.25 mm for the products from **1** and **3**, and 30 m×0.25 mm for the products from **2**) at 130 °C.

References

1) M. C. Dart and H. B. Henbest, *J. Chem. Soc.*, **1960**, 3563; C. P. Rader, G. E. Wicks, Jr., R. L. Young, Jr., and H. S. Aaron, *J. Org. Chem.*, **29**, 2252 (1964); T. J. Howard, *Chem. Ind. (London)*, **1963**, 1899; T. J. Howard and B. Morley, *Chem. Ind. (London)*, **1967**, 73; S. Mitsui, Y. Senda, and H. Saito, *Bull. Chem. Soc. Jpn.*, **39**, 694 (1966); S. Mitsui, M. Ito, A. Nanbu, and Y. Senda, *J. Catal.*, **36**, 119 (1975).

2) J-I. Ishiyama, Y. Senda, and S. Imaizumi, *J. Chem. Soc., Perkin Trans. 2*, **1982**, 71; J-I. Ishiyama, S. Kamiyama, Y. Senda, and S. Imaizumi, *Chem. Ind. (London)*, **1988**, 466.

3) S. Nishimura and T. Itaya, *J. Chem. Soc., Chem. Commun.*, **1967**, 422; S. Nishimura, S. Iwafune, T. Nagura,

Y. Akimoto, and M. Uda, *Chem. Lett.*, **1985**, 1275.

4) S. Siegel and B. Dmukovsky, *J. Am. Chem. Soc.*, **84**, 3132 (1962); and the references cited therein.

5) S. Mitsui, H. Saito, Y. Yamashita, M. Kaminaga, and Y. Senda, *Tetrahedron*, **29**, 1531 (1973): S. Nishimura, M. Ishige, and M. Shiota, *Chem. Lett.*, **1977**, 535.

6) L. A. Paquett and P. C. Storm, *J. Am. Chem. Soc.*, **94**, 4295 (1970).

7) B. P. Mundy and R. D. Otzenberger, *J. Org. Chem.*, **37**, 677 (1972).

8) Y. M. Kobayashi, J. Lambrecht, J. C. Jochims, and U. Burkert, *Chem. Ber.*, **111**, 3442 (1978).

9) C. Ancelmi, G. Berti, G. Catelani, L. Lecce, and L. Monti, *Tetrahedron*, **33**, 2271 (1977).

10) C. B. Anderson and D. T. Sepp, *J. Org. Chem.*, **33**, 3272 (1968).

11) A. A. Marei and R. A. Raphael, *J. Chem. Soc.*, **1960**, 886.

12) A. Scattergood and A. L. MacLean, *J. Am. Chem. Soc.*, **71**, 4153 (1949).

13) S. Nishimura, M. Katagiri, T. Watanabe, and M. Uramoto, *Bull. Chem. Soc. Jpn.*, **44**, 166 (1971).

14) K. Tanaka, Y. Takagi, O. Nomura, and I. Kobayashi, *J. Catal.*, **35**, 23 (1974).

 © 1989 The Chemical Society of Japan Bull. Chem. Soc. Jpn., 62, 2953—2959 (1989)

Syntheses and Some Reactions of Trimethylsilylated Dinitrogen Complexes of Tungsten and Molybdenum[1)]

Keiko KOMORI, Seiya SUGIURA, Yasushi MIZOBE,
Masaki YAMADA, and Masanobu HIDAI*
Department of Synthetic Chemistry, Faculty of Engineering, The University of Tokyo,
Hongo, Bunkyo-ku, Tokyo 113
(Received May 9, 1989)

A series of new trimethylsilyldiazenido complexes [MX(NNSiMe$_3$)(L)$_4$] (M=Mo: X=I; M=W: X=CF_3SO_3; L=PMe_2Ph or 1/2 dpe; dpe=$Ph_2PCH_2CH_2PPh_2$) and trimethylsilylhydrazido(2−) complexes [MX$_2$(NNHSiMe$_3$)-(PMe_2Ph)$_3$] (M=Mo: X=I or Br; M=W: X=CF_3SO_3) and [MX(NNHSiMe$_3$)(dpe)$_2$]X (M=Mo: X=I; M=W: X=CF_3SO_3) were prepared by treatment of dinitrogen complexes *cis*-[M(N$_2$)$_2$(PMe_2Ph)$_4$] or *trans*-[M(N$_2$)$_2$(dpe)$_2$] with Me$_3$SiX in benzene. The trimethylsilyl groups on the terminal nitrogen atoms were easily replaced by hydrogen by the reaction with MeOH or H_2O, affording, for example, diazenido and hydrazido(2−) complexes such as [WI(NNH)(dpe)$_2$] and [WI$_2$(NNH$_2$)(PMe_2Ph)$_3$] from [WI(NNSiMe$_3$)(dpe)$_2$] and *mer*-[WI$_2$(NNHSiMe$_3$)-(PMe_2Ph)$_3$], respectively. When reduced with excess Na in THF under N_2, complexes *trans*-[MI(NNSiMe$_3$)-(PMe_2Ph)$_4$] (M=Mo or W) and *mer*-[WI$_2$(NNHSiMe$_3$)(PMe_2Ph)$_3$] gave (Me$_3$Si)$_2$NH and NH_3 in substantial yields, accompanied by the regeneration of the parent dinitrogen complexes. Additional amount of NH_3 was obtained by the hydrolysis of the evaporated reaction mixture residue.

As the first demonstrated example of the Si–N bond formation from coordinated dinitrogen, we have recently reported the reaction of a series of tungsten dinitrogen complexes of the type [W(N$_2$)$_2$(L)$_4$] (L=tertiary phosphines) with Me$_3$SiI to give trimethylsilyldiazenido (NNSiMe$_3$) and trimethylsilylhydrazido(2−) (NNHSiMe$_3$) complexes, together with the X-ray structures of *trans*-[WI(NNSiMe$_3$)(PMe_2Ph)$_4$] (**1**) and *mer*-[WI$_2$(NNHSiMe$_3$)(PMe_2Ph)$_3$] (**2**).[2)] Here we wish

cis-[W(N$_2$)$_2$(PMe_2Ph)$_4$] (**5**) $\xrightarrow{Me_3SiI}$ *trans*-[WI(NNSiMe$_3$)(PMe_2Ph)$_4$] (**1**)

$\xrightarrow{Me_3SiI/HI}$ *mer*-[WI$_2$(NNHSiMe$_3$)(PMe_2Ph)$_3$] (**2**)

to report the results of the reaction of molybdenum dinitrogen complexes *cis*-[Mo(N$_2$)$_2$(PMe_2Ph)$_4$] (**3**) and *trans*-[Mo(N$_2$)$_2$(dpe)$_2$] (**4**, dpe=$Ph_2PCH_2CH_2PPh_2$) with Me$_3$SiI as well as the trimethylsilylation of tungsten dinitrogen complexes *cis*-[W(N$_2$)$_2$(PMe_2Ph)$_4$] (**5**) and *trans*-[W(N$_2$)$_2$(dpe)$_2$] (**6**) by using $CF_3SO_3SiMe_3$. Some properties and reactivities of trimethylsilylated dinitrogen complexes are also described.

Results and Discussion

Preparation of New Trimethylsilylated Dinitrogen Complexes. When treated with 1 equiv of Me$_3$SiI in benzene under rigorously dry conditions, complex **3** gave the trimethylsilyldiazenido complex *trans*-[MoI-(NNSiMe$_3$)(PMe_2Ph)$_4$](**7**) in moderate yield. Complex **3** is more reactive than its tungsten analogue **5**. Thus, the reaction proceeds smoothly even at room temperature, whereas complex **5** does react with Me$_3$SiI around 50 °C. In the case of complex **4**, the reaction is much slower than that of complex **3** under the same conditions and the reaction must be carried out at 50 °C by using 2 equiv of Me$_3$SiI to obtain [MoI-(NNSiMe$_3$)(dpe)$_2$]. As described in the preceding paper,[2)] removal of HI generated in situ by the reaction of Me$_3$SiI and adventitious moisture is necessary to isolate these trimethylsilyldiazenido complexes. On the other hand, if the freeze-pump-thaw cycles to remove HI are omitted, complexes **3** and **4** reacted with Me$_3$SiI (ca. 1.5 equiv for complex **3** and ca. 2 equiv for complex **4**) to give trimethylsilylhydrazido(2−) complexes *mer*-[MoI$_2$(NNHSiMe$_3$)(PMe_2Ph)$_3$](**8**) and [MoI-(NNHSiMe$_3$)(dpe)$_2$]I, respectively, although the isolated yields of these complexes were low. These

[Mo(N$_2$)$_2$(L)$_4$] (**3**: L = PMe_2Ph; **4**: L = 1/2dpe)
$\xrightarrow{Me_3SiI}$ [MoI(NNSiMe$_3$)(L)$_4$]
$\xrightarrow{Me_3SiI/HI}$ [MoI$_2$(NNHSiMe$_3$)(L)$_3$] (L = PMe_2Ph) or [MoI(NNHSiMe$_3$)(L)$_4$]I (L = 1/2dpe)

trimethylsilylated dinitrogen complexes of molybdenum are less stable than the corresponding tungsten complexes and decompose slowly at room temperature even when stored under an inert atmosphere in a solid state. The lower isolated yields of the molybdenum complexes than those of the tungsten analogues presumably result from the lower stability observed for the molybdenum complexes.

Spectroscopic data of the trimethylsilyldiazenido and trimethylsilylhydrazido(2−) complexes are shown in Table 1, which correspond well to those of tungsten complexes reported previously (Table 2). It is interesting to note that the trimethylsilyldiazenido complexes of molybdenum show ν(NN) bands at higher frequencies and ν(SiN) bands at lower frequencies than the corresponding tungsten analogues. According to the results of the X-ray analyses of complex **1** which demonstrate the linear W–N–N linkage and the unusually short Si–N bond length in the tri-

Table 1. IR and ^{1}H NMR Data of Trimethylsilylated Dinitrogen Complexes of Molybdenum

Complex	IR[a]				^{1}H NMR[b]
	ν(NN)	δ(CH_3Si)	ν(SiN)	ν(NH)	
trans-[MoI($NNSiMe_3$)(PMe_2Ph)$_4$] (**7**)	1610	1245	855	—	0.46 (s, 9H, $SiCH_3$) 1.65 (s, 24H, PCH_3)
[MoI($NNSiMe_3$)(dpe)$_2$]	1660	1230	850	—	c)
mer-[MoI_2($NNHSiMe_3$)(PMe_2Ph)$_3$] (**8**)	1345	1255	844	3240	0.04 (s, 9H, $SiCH_3$) 1.39 (d, 6H, PCH_3) 2.25 (t, 6H, PCH_3) 2.29 (t, 6H, PCH_3) 3.60 (s, 1H, NH)
mer-[MoI_2($^{15}N^{15}NHSiMe_3$)(PMe_2Ph)$_3$]	1308	1255	844	3240	d)
[MoI($NNHSiMe_3$)(dpe)$_2$]I·C_6H_6	1340[f]	1246	843	e)	0.34 (s, $SiCH_3$) 2.64 (broad s, PCH_2) 2.76 (broad s, PCH_2)
mer-[$MoBr_2$($NNHSiMe_3$)(PMe_2Ph)$_3$]	1341	1251	842	3180	d)

a) cm^{-1}; KBr disks. b) δ; C_6D_6 solution; referred to a trace of C_6H_6 in C_6D_6 at δ 7.25; phenyl protons are omitted. c) Practically insoluble in benzene. d) Not measured. e) Not assignable. f) Very weak.

Table 2. IR and ^{1}H NMR Data of Trimethylsilylated Dinitrogen Complexes of Tungsten

Complex	IR[a]				^{1}H NMR[b]
	ν(NN)	δ(CH_3Si)	ν(SiN)	ν(NH)	
trans-[W(CF_3SO_3)($NNSiMe_3$)(PMe_2Ph)$_4$][c]	1565	d)	880	—	0.40 (s, 9H, $SiCH_3$) 1.60 (s, 24H, PCH_3)
[W(CF_3SO_3)($NNSiMe_3$)(dpe)$_2$]	1638 1665	d)	855	—	e)
mer-[W(CF_3SO_3)$_2$($NNHSiMe_3$)(PMe_2Ph)$_3$]	1375	d)	845	3255	0.13 (s, 9H, $SiCH_3$) 1.19 (d, 6H, PCH_3) 1.70 (t, 6H, PCH_3) 1.91 (t, 6H, PCH_3) 4.47 (s, 1H, NH)
[W(CF_3SO_3)($NNHSiMe_3$)(dpe)$_2$][CF_3SO_3]	d)	d)	850	3230	0.21 (s, 9H, $SiCH_3$) 2.59 (broad s, PCH_2) 2.72 (broad s, PCH_2) 5.31 (s, NH)
trans-[WI($NNSiMe_3$)(PMe_2Ph)$_4$] (**1**)[f]	1580	1246	873	—	0.47 (s, 9H, $SiCH_3$) 1.73 (s, 24H, PCH_3)
[WI($NNSiMe_3$)(dpe)$_2$][f]	1621	1246	868	—	c)
mer-[WI_2($NNHSiMe_3$)(PMe_2Ph)$_3$] (**2**)[f]	1360	1254	842	3250	−0.02 (s, 9H, $SiCH_3$) 1.46 (d, 6H, PCH_3) 2.13 (s, 1H, NH) 2.29 (2t, 12H, PCH_3)
[WI($NNHSiMe_3$)(dpe)$_2$]I[f]	1355	1248	842	3195	c)

a) cm^{-1}; KBr disks. b) δ; C_6D_6 solution; referred to a trace of C_6H_6 in C_6D_6 at δ 7.25; phenyl protons are omitted. c) ^{31}P NMR: singlet at −16 ppm from H_3PO_4. d) Obscured by the strong absorbances of CF_3SO_3 ligands. e) Practically insoluble in benzene. f) Ref. 2.

methylsilyldiazenido moiety, we previously proposed the presence of the contribution of structure **II** toward structure **I** considering the back donation from the metal.[2] The IR data described above indicate that the structure **II** contributes to a greater extent in the tungsten complexes than in the molybdenum analogues. This trend can be well explained by the stronger electron-donating ability of tungsten compared with molybdenum, which is commonly observed.

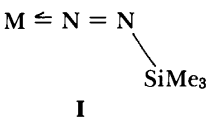

I

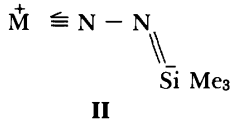

II

In contrast, trimethylsilylhydrazido(2−) complexes of molybdenum show ν(NN)[3] at lower frequencies in the IR spectra than those of the tungsten analogues. In this case also, the greater electron density is presumably donated into the π orbital(s) that spread(s) from the metal to the Si atom via the two nitrogen atoms for the tungsten complexes than the molybdenum analogues. However, this results in an increase of the N–N bond order in contrast to the above trimethylsilyldiazenido complexes. Thus, the structure of the trimethylsilylhydrazido(2−) ligand may best be described as **III**.

When treated with Me_3SiBr in place of Me_3SiI, complex **3** gave the corresponding trimethylsilylhydrazido-

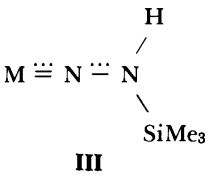

III

(2−) complex *mer*-[$MoBr_2(NNHSiMe_3)(PMe_2Ph)_3$] in low yield. However, no silylated complexes were obtained in the case of complex **5** under the same conditions. On the other hand, complex **5** can be readily converted into trimethylsilylhydrazido(2−) complex *mer*-[$W(CF_3SO_3)_2(NNHSiMe_3)(PMe_2Ph)_3$] by treatment with 3 equiv of $CF_3SO_3SiMe_3$. The reaction proceeded smoothly in benzene at room temperature. However, the trials to isolate the trimethylsilyldiazenido complex *trans*-[$W(CF_3SO_3)(NNSiMe_3)(PMe_2Ph)_4$] by using 1.5 equiv of $CF_3SO_3SiMe_3$ were not successful except for only one run. This is probably because the removal of CF_3SO_3H from $CF_3SO_3SiMe_3$ is very difficult compared to HI. As shown in Table 2, the IR and NMR data are consistent with the above structures. Treatment of complex **6** with 6 equiv of $CF_3SO_3SiMe_3$ at room temperature afforded a mixture of the trimethylsilyldiazenido complex [$W(CF_3SO_3)(NNSiMe_3)(dpe)_2$] and the trimethylsilylhydrazido(2−) complex [$W(CF_3SO_3)(NNHSiMe_3)(dpe)_2$][$CF_3SO_3$]. Appearance of two ν(NN) bands in the IR spectrum of the former complex probably results from the existence of two isomeric forms, for example cis and trans, in this complex. However, this compound is practically insoluble in common NMR solvents and further characterization of this complex was abandoned.

As described above, trimethylsilylhydrazido(2−) complexes can be isolated as the major products in the presence of HX (X=Br, I, CF_3SO_3) that is formed by the reaction of Me_3SiI or $CF_3SO_3SiMe_3$ with adventitious water. This is supported by the fact that when Me_3SiI (3 mol/W atom) in benzene was treated with MeOH (0.8 mol/W atom) first to generate HI in situ and then complex **5** was added to this mixture, the yield of complex **2** increased to 70%. Although this shows that the presence of HX is essential to form trimethylsilylhydrazido(2−) complexes, two reaction pathways are possible as shown below. The pathway which proceeds via [$MX(NNSiMe_3)(L)_4$] is supported by the fact that treatment of complex **1** with 1 equiv of HCl gas gave the trimethylsilylhydrazido(2−) complex [$WClI(NNHSiMe_3)(PMe_2Ph)_3$] which showed ν(NN) and ν(SiN) bands at 1334 and 845 cm^{-1} in its IR spectrum, respectively. On the other hand, the fact that an isolated diazenido complex [$WI(NNH)(dpe)_2$] reacted with Me_3SiI to give [$WI(NNHSiMe_3)(dpe)_2$]I in about 70% yield is indicative of the presence of the other pathway that includes the formation of diazenido complexes (MNNH) and the successive reaction with Me_3SiX. Thus both pathways are possible at present and the reaction course may depend upon the nature of the metals, the phosphines and the trimethylsilylating reagents. At least for the formation of complex **8**, the upper reaction pathway seems more plausible, since complex **7** was isolated as the major product from the reaction of complex **3** with Me_3SiI (2 mol/Mo atom) in the presence of 0.8 equiv of MeOH, whereas the formation of complex **8** was enhanced by the addition of 1.7 equiv of MeOH.

Reaction of Trimethylsilylated Dinitrogen Complexes with Water and Alcohols. As is well-known, trimethylsilyl group has a strong affinity with a fluoride anion and an oxygen atom. Thus, the reaction of complexes **1** and **2** with [n-Bu_4N]F were tried, but the purification of the products for full characterization was not successful. In contrast, treatment of complex **2** with about 4 equiv of water in benzene afforded the hydrazido(2−) complex *mer*-[$WI_2(NNH_2)(PMe_2Ph)_3$] (**9**) in 89% yield, as was expected. The similar reaction with a slightly excess of MeOH also resulted in the formation of complex **9** in 66% yield. Furthermore, the trimethylsilyldiazenido complex [$WI(NNSiMe_3)(dpe)_2$] reacted similarly with an almost stoichiometric amount of MeOH to give the diazenido complex [$WI(NNH)(dpe)_2$]. This is the only demonstrated method to derive diazenido complexes from dinitrogen complexes except for the reaction of hydrazido(2−) complexes with weak bases.[4] Diazenido complexes are regarded as an initial intermediate stage to reach ammonia and hydrazine from dinitrogen complexes. Although a series of diazenido complexes of type [$MX(NNH)(dpe)_2$] (M=W: X=F, Cl, Br; M=Mo: X=F, Br) are prepared by the reaction of the corresponding hydrazido(2−) complexes with weak bases, diazenido complexes with PMe_2Ph ligands

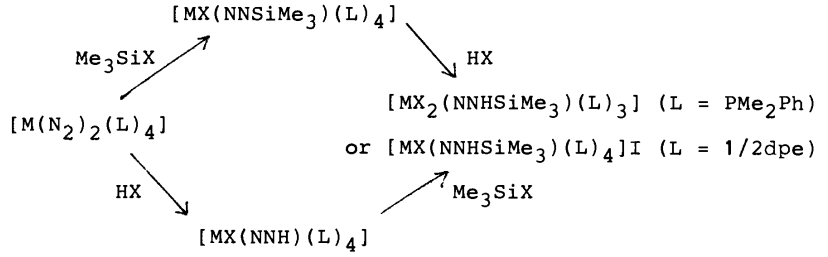

are not yet known. Therefore the reaction of complex **1** with water or MeOH was performed. However, the isolated product was only complex **9** (35% yield) for the former and *trans*-[WI(NNH_2)(PMe_2Ph)$_4$]I (15% yield) for the latter, respectively, and the formation of the diazenido complex [WI(NNH)(PMe_2Ph)$_4$] was not observed. It may be presumed that the diazenido complex initially formed was so unstable that it was converted into the hydrazido(2−) complex(es) by the disproportionation reaction. Formation of the dinitrogen complex **5** from the reaction of complex **1** with MeOH may support this reaction pathway, although the yield of complex **5** was quite low.

Redox Properties of Trimethylsilyldiazenido and Trimethylsilylhydrazido(2−) Complexes. Cyclic voltammograms of complexes **1** and **2** were recorded in THF-0.1 M [*n*-Bu_4N][BF_4] under Ar by using glassy carbon, Pt wire and Ag wire immersed in the electrolyte as the working, counter, and reference electrodes, respectively. Under the present conditions, one-electron transfer between (η^5-C_5H_5)$_2$Fe and (η^5-C_5H_5)$_2$Fe$^+$ occurs at the potential of +0.56 V. The solution of the trimethylsilyldiazenido complex **1** shows the irreversible oxidation wave at +1.16 V, which gradually weakened and shifted to the negative direction by the repetitive scans. During these scans appeared the new anodic and cathodic waves at +0.53 and +0.16 V, which may correspond to the redox processes assignable to the species generated by the irreversible oxidation of complex **1**. By the scan to the negative direction from 0 V, no distinctive reduction peaks were observed, although the reduction current itself increased significantly at the potentials below −1.8 V. On the other hand, the trimethylsilylhydrazido(2−) complex **2** shows the irreversible reduction and oxidation waves at −2.1 and +0.82 V, respectively.

Reduction of Trimethylsilylated Dinitrogen Complexes with Sodium Metal and Sodium Hydride. Several attempts have been made to reduce hydrazido(2−) and dialkylhydrazido(2−) complexes to obtain nitrogenous compounds, regenerating the parent dinitrogen complexes at the same time.[5,6] Now we have found that treatment of complex **1** with excess Na sand (0.5—1 mm diameter) in THF at 30 °C under Ar gave $(Me_3Si)_2NH$ and NH_3 in substantial yields, accompanied by the formation of free and coordinated dinitrogen. After hydrolysis of the evaporated reaction mixture residue, additional amount of NH_3 was detected in moderate yield. The total nitrogen balance of the products based on complex **1** as a unit of dinitrogen was 0.95. When this reaction was carried out under N_2, the parent dinitrogen complex **5** was regenerated in 55% yield. The reactions with Na metal proceeded analogously for the molybdenum trimethylsilyldiazenido complex (**7**), the results of which are summarized in Table 3.

$$\textit{trans}\text{-[MI(NNSiMe}_3\text{)(P)}_4\text{]} \xrightarrow[\text{THF}]{\text{Na}} N_2 + [M(N_2)_2(P)_4] + (Me_3Si)_2NH + NH_3 + NaNH_2 + (Me_3Si)NHNa + (Me_3Si)_2NNa + \cdots\cdots \quad (M = Mo, W;\ P = PMe_2Ph) \qquad (1)$$

About a half of the nitrogen atoms in the trimethylsilyldiazenido complexes are converted into the N_1 products in this reaction system, with the remainder forming N_2 gas (Eq. 1). Among these products, $(Me_3Si)_2NH$ might be formed by the disproportionation reaction between two unstable Me_3SiNH_2 molecules, the protons of which may be derived from THF and/or a trace amount of H_2O still remaining despite the employment of rigorously dry conditions. Major N_1 products which were detected as NH_3 after hydrolysis are presumably present as the sodium salts such as $NaNH_2$, $Me_3SiNHNa$, or $(Me_3Si)_2NNa$, since the addition of Et_3SiCl to the reaction mixture of complex **1** with Na for 22 h resulted in the formation of Et_3SiNH_2, $(Me_3Si)NH(SiEt_3)$, $(Et_3Si)_2NH$, and $(Me_3$-

Table 3. Reduction of Trimethylsilylated Dinitrogen Complexes[a]

Complex	Atm.	Yield (per metal atom)				
		$(Me_3Si)_2NH$[b]	NH_3		N_2	
			Free	After hydrol.[c]	Free	Coordinated[d]
trans-[WI($NNSiMe_3$)(PMe_2Ph)$_4$] (**1**)	Ar	0.07	0.18	0.67	0.23	0.24
trans-[WI($NNSiMe_3$)(PMe_2Ph)$_4$] (**1**)	N_2	0.03	Trace	0.55	—	e)
trans-[MoI($NNSiMe_3$)(PMe_2Ph)$_4$] (**7**)	Ar	0.09	0.16	0.64	0.50	Trace
trans-[MoI($NNSiMe_3$)(PMe_2Ph)$_4$] (**7**)	N_2	0.11	0.11	0.88	—	e)
trans-[WI($NNSiMe_3$)(PMe_2Ph)$_4$] (**1**)[f]	Ar	0.06	0.65	0.01	0.52	0
trans-[MoI($NNSiMe_3$)(PMe_2Ph)$_4$] (**7**)[f]	Ar	0.05	0.13	0.11	0.50	0.05
mer-[WI_2($NNHSiMe_3$)(PMe_2Ph)$_3$] (**2**)	Ar	0.06	0.02	0.83	0.11	0.14
mer-[WI_2($NNHSiMe_3$)(PMe_2Ph)$_3$] (**2**)	N_2	Trace	0.04	1.00	—	g)

a) Reaction conditions: complex, 0.14—0.17 mmol; THF, 5 ml; Na sand (0.5—1 mm diameter), 20 equiv of M atom; 30 °C, 22 h, in the dark. b) Determined by GLC. c) Not including free NH_3. In each run N_2H_4 was detected in low yields after distillation (ca. 0.06 mol per metal atom). d) Determined by GLC after thermal decomposition and/or by the IR spectrum of the evaporated residue. e) The parent dinitrogen complexes *cis*-[W(N_2)$_2$(PMe_2Ph)$_4$] (**5**) and *cis*-[Mo(N_2)$_2$(PMe_2Ph)$_4$] (**3**) were recovered in 55 and 45% yields, respectively, determined by the IR method. f) NaH was used in place of Na sand. g) *cis*-[W(N_2)$_2$(PMe_2Ph)$_4$] (**5**) were recovered in 36% yield.

$Si)_2N(SiEt_3)$ in the yields of 9%, 21%, 19%, and 6% per W atom, respectively. On the other hand, when complexes **1** and **7** were reduced with Na under Ar in the presence of excess Me_3SiCl, $(Me_3Si)_3N$ was formed as the principal product in the yields of 0.42 mol and 0.75 mol per metal atom, respectively. Based on these observations the catalytic conversion of molecular nitrogen into silylamines has been achieved very recently and details of this work have been reported separately.[7]

Reduction of the trimethylsilylhydrazido(2−) complex **2** with Na metal under the similar reaction conditions also produced $(Me_3Si)_2NH$ and NH_3 in substantial yields together with free N_2 and the parent dinitrogen complex **5** as shown in Table 3. Further NH_3 was detected in moderate yield after following hydrolysis. By the similar treatment under a nitrogen atmosphere, the recovery of the dinitrogen complex **5** increased to 36% per W atom.

When NaH was used as a reducing agent under Ar, about a half of the nitrogen atoms in complexes **1** and **7** were converted into gaseous N_2 and total yields of NH_3 resulting from the remaining nitrogen atoms did not exceed those obtained by the reactions using Na metal.

Experimental

Ganeral. All experiments were carried out under dry nitrogen atmosphere. All solvents were rigorously dried by Na wire or Na–benzophenone ketyl and distilled just before use. Complexes **1**,[2] **2**,[2] **4**,[8] **5**,[8,9] **6**,[8,10] and Me_3SiI[11] were prepared according to the literature methods. Trimethylsilyl triflate commercially obtained was used after being degassed. The IR spectra were recorded on a Hitachi 215 or a Shimadzu IR-400 spectrometer and ^1H and ^{31}P NMR spectra were on a JEOL JMN-GX-400 spectrometer. Quantitative analyses using GLC were carried out on a Hitachi K23, a Shimadzu GC-8A or a GC-14A Gas Chromatograph. GC-MS analyses were performed on a Shimadzu GC-MS QP-1000 spectrometer. Electrochemical measurements were carried out at ambient temperature under Ar by using Hokuto Denko instrumentation (HA-501 Potentiostat, and HB-105 Function Generator), a glassy-carbon working electrode, and a platinum wire counter electrode. Potentials were measured vs. a pseudo-reference electrode of a silver wire immersed in the electrolyte (0.1 M $[n\text{-}Bu_4N][BF_4]$–THF). The cyclic voltammogram recorded under these conditions with the scan rate of $0.2\ V\ s^{-1}$ showed the oxidation potential of ferrocene at $E_{1/2}$=+0.52 V.

Preparation of *cis*-$[Mo(N_2)_2(PMe_2Ph)_4]$(3). The reported method[8] was modified as follows. The mixture of Mg turnings (6 g) and a piece of I_2 was heated at 150 °C with stirring under reduced pressure for 2 h. After cooling to room temperature, THF (100 ml) and PMe_2Ph (2.85 ml, 20.0 mmol) were added. Then $MoCl_5$ (1.36 g, 5.00 mmol) was added slowly with stirring. The color of the reaction solution changed from pale brown to dark brown. After stirring overnight under N_2 (1 atm) the resultant mixture was filtered and the filtrate was dried up. The dark sticky residue was washed with MeOH, extracted with ether (200 ml) and the extract was cooled down to −20 °C. The yellow crystals deposited were filtered off, washed successively with hexane, MeOH, and ether, and then dried in vacuo (1.2 g, 32%).

The ^{15}N complex *cis*-$[Mo(^{15}N_2)_2(PMe_2Ph)_4]$ was prepared from complex **3** according to the published method.[12]

Preparation of *trans*-$[MoI(NNSiMe_3)(PMe_2Ph)_4]$ (7). Into a solution of Me_3SiI (32 μl, 0.225 mmol) in benzene (5 ml) carefully degassed by freeze (at −50 °C)-pump-thaw cycles was added complex **3** (165 mg, 0.234 mmol) and the resultant yellow solution was stirred for 8 h at room temperature in the dark. Trap to trap condensation of hexane (6 ml) on the red product solution gave red crystals, which were filtered off, washed with hexane and then dried in vacuo (57 mg, 28%). Found: C, 47.25; H, 6.51; N, 2.94; I, 13.98%. Calcd for $C_{35}H_{53}N_2IP_4SiMo$: C, 47.95; H, 6.11; N, 3.19; I, 14.41%.

Preparation of $[MoI(NNSiMe_3)(dpe)_2]$. Into a solution of Me_3SiI (80 μl, 0.56 mmol) in benzene (8 ml) carefully prepared as above was added complex **4** (270 mg, 0.284 mmol). After stirring overnight at 50 °C in the dark, the yellow orange suspension was reduced in volume to a half in vacuo. After trap to trap condensation of hexane (6 ml) on it, the yellow solid deposited was filtered off and dried in vacuo (42 mg, 13%). Found: C, 57.87; H, 4.94; N, 1.49%. Calcd for $C_{55}H_{57}N_2IP_4SiMo$: C, 58.94; H, 5.13; N, 1.49%.

Preparation of *mer*-$[MoI_2(NNHSiMe_3)(PMe_2Ph)_3]$ (8). Into a solution of complex **3** (154 mg, 0.219 mmol) in benzene (5 ml) was added Me_3SiI (49 μl, 0.344 mmol) and the mixture was stirred for 12 h at room temperature in the dark. The deep red solution obtained was filtered and hexane (10 ml) was added to the filtrate by trap to trap condensation. The black crystals precipitated were filtered off, washed with hexane and dried in vacuo (8 mg, 4%). Found: C, 37.10; H, 4.86; N, 2.77; I, 28.72%. Calcd for $C_{27}H_{43}N_2I_2P_3SiMo$: C, 37.43; H, 5.01; N, 3.23; I, 29.29%.

Addition of MeOH (20 μl, 0.493 mmol) into a mixture of Me_3SiI (80 μl, 0.562 mmol) and benzene before reaction with complex **3** (200 mg, 0.284 mmol) increased the yield of complex **8** to 15%.

Preparation of $[MoI(NNHSiMe_3)(dpe)_2]I\cdot C_6H_6$. Into a suspension of complex **4** (502 mg, 0.529 mmol) in benzene (10 ml) was added Me_3SiI (150 μl, 1.05 mmol) and the mixture was stirred for 20 h at 40 °C in the dark. The red product solution was separated from unreacted complex **4** by filtration and hexane (15 ml) was added to the filtrate. Dark yellow crystals deposited were filtered off, washed with hexane, and then dried in vacuo (93 mg, 13%). Found: C, 55.41; H, 5.22; N, 2.10; I, 18.18%. Calcd for $C_{61}H_{64}N_2I_2P_4SiMo$: C, 55.21; H, 4.87; N, 2.11; I, 19.12%.

Preparation of *mer*-$[MoBr_2(NNHSiMe_3)(PMe_2Ph)_3]$. Into a mixture of Me_3SiBr (38 μl, 0.29 mmol) and benzene (7 ml), complex **3** (122 mg, 0.173 mmol) was added to give a yellow solution. After 4 h, the red solution obtained was concentrated and hexane (5 ml) was condensed on it by trap to trap method. On cooling at −18 °C, red crystals precipitated together with crystals of the parent complex **3**. Only the red crystals were collected, washed with hexane and dried in vacuo (5 mg, 4%). Found: C, 42.01; H, 5.55; N, 3.54; Br, 20.73%. Calcd for $C_{27}H_{43}N_2Br_2P_3SiMo$: C, 41.98; H, 5.62; N, 3.62; Br, 20.69%.

Treatment of *cis*-$[W(N_2)_2(PMe_2Ph)_4]$(5) with $CF_3SO_3SiMe_3$.

Into a solution of complex **5** (283 mg, 0.358 mmol) in benzene (5 ml) was added $CF_3SO_3SiMe_3$ (0.195 ml, 1.01 mmol). After stirring for 10 h at room temperature, the resultant red solution was reduced in volume to about a quarter. Trap to trap condensation of hexane (7.5 ml) on it gave red needles of the trimethylsilylhydrazido(2−) complex *mer*-[$W(CF_3SO_3)_2(NNHSiMe_3)(PMe_2Ph)_3$], which were filtered off, washed with hexane and dried in vacuo. (196 mg, 37%). Found: C, 34.42; H, 4.53; N, 2.81%. Calcd for $C_{29}H_{43}O_6N_2F_6S_2P_3SiW$: C, 34.87; H, 4.35; N, 2.81%.

Analogous treatment of complex **5** with 1.5 equiv of $CF_3SO_3SiMe_3$ in benzene gave the trimethylsilyldiazenido complex *trans*-[$W(CF_3SO_3)(NNSiMe_3)(PMe_2Ph)_4$] only once in low yield but all other trials to reproduce this run were unsuccessful probably due to the impurity such as CF_3SO_3H present in the commercially obtained $CF_3SO_3SiMe_3$. Found: C, 44.18; H, 5.44; N, 2.25%. Calcd for $C_{36}H_{53}O_3N_2F_3P_4SSiW$: C, 43.82; H, 5.41; N, 2.84%.

Preparation of [$W(CF_3SO_3)(NNSiMe_3)(dpe)_2$] and [$W(CF_3SO_3)(NNHSiMe_3)(dpe)_2$][$CF_3SO_3$]. Into a suspension of complex **6** (246 mg, 0.237 mmol) in benzene (10 ml) was added $CF_3SO_3SiMe_3$ (0.27 ml, 1.5 mmol) and the mixture was stirred overnight. The resultant orange solution was concentrated to about a half volume and trap to trap condensation of hexane to it gave a mixture of a yellow solid and orange crystals. Removal of the slurry containing the yellow solid remained the orange crystals of the trimethylsilyldiazenido complex, which was washed with hexane and dried (231 mg, 79%). Found: C, 54.88; H, 4.68; N, 2.00%. Calcd for $C_{56}H_{57}O_3N_2F_3SP_4SiW$: C, 54.63; H, 4.68; N, 2.27%. The trimethylsilylhydrazido(2−) complex was isolated by filtration of the separated yellow slurry (42 mg, 13%). Found: C, 48.34; H, 3.90; N, 1.17%. Calcd for $C_{57}H_{58}O_6N_2F_6S_2P_4SiW$: C, 49.57; H, 4.24; N, 2.03%.

Reaction of *trans*-[$WI(NNSiMe_3)(PMe_2Ph)_4$] (1) with HCl Gas. Onto a frozen solution of complex **1** (158 mg, 0.164 mmol) in benzene (10 ml) was condensed HCl gas (107 ml/28 mmHg/22.5 °C, 0.163 mmol; 1 mmHg≈133.322 Pa) at −196 °C. The mixture was slowly warmed to room temperature and stirred for 24 h. The red product solution was concentrated to about 2 ml in vacuo and hexane (6 ml) was added to it by trap to trap condensation. The yellow solid of *mer*-[$WClI(NNHSiMe_3)(PMe_2Ph)_3$] was filtered off, washed with hexane and dried in vacuo (92 mg, 64%). IR (KBr disk): ν(NN), 1334; $\delta(Me_3Si)$, 1245; ν(SiN), 845 cm^{-1}.

Reaction of [$WI(NNH)(dpe)_2$] with Me_3SiI. Into a suspension of [$WI(NNH)(dpe)_2$] (207 mg, 0.182 mmol) in benzene (10 ml) was added Me_3SiI (54 μl, 0.379 mmol). The color of the mixture gradually changed from yellow to orange. After stirring for 6 h, the orange solid was filtered off, washed with hexane and dried in vacuo (199 mg). Major component of this solid was [$WI(NNHSiMe_3)(dpe)_2$]I, the yield of which was estimated to be about 70% by the IR spectrum. Further purification of the product was not successful because of its low solubility.

Reaction of *trans*-[$WI(NNSiMe_3)(PMe_2Ph)_4$] (1) with Water. Into a solution of complex **1** (119 mg, 0.123 mmol) in benzene was added H_2O (2.2 μl, 0.122 mmol) and the mixture was stirred for 17 h in the dark at room temperature. The red solution obtained was concentrated to about 1 ml and hexane (6 ml) was added to it. The brown solid deposited was filtered off and precipitated again from benzene/hexane. The yellow solid isolated was characterized as complex **9** by the IR spectrum and the analytical data (38 mg, 35%). Found: C, 33.01; H, 4.01; N, 3.07%. Calcd for $C_{24}H_{35}N_2I_2P_3W$: C, 32.67; H, 4.01; N, 3.18%.

Reaction of *mer*-[$WI_2(NNHSiMe_3)(PMe_2Ph)_3$] (2) with Water. Analogous treatment of complex **2** (112 mg, 0.116 mmol) in benzene (10 ml) with H_2O (7.5 μl, 0.414 mmol) gave the product suspension. The yellow solid separated by filtration was characterized as complex **9** by the IR spectrum (91 mg, 89%).

Reaction of *mer*-[$WI_2(NNHSiMe_3)(PMe_2Ph)_3$] (2) with MeOH. Into a solution of complex **2** (254 mg, 0.266 mmol) in benzene (5 ml) was added MeOH (13 μl, 0.322 mmol). The red solution changed rapidly to the brown suspension. After stirring for 20 h in the dark, complex **9** produced was filtered off, washed with benzene and dried in vacuo (145 mg, 66%).

Reaction of [$WI(NNSiMe_3)(dpe)_2$] with MeOH. Into a suspension of [$WI(NNSiMe_3)(dpe)_2$] (220 mg, 0.182 mmol) in benzene (15 ml) was added MeOH (7.8 μl, 0.193 mmol). After stirring for 35 h, the resultant suspension was filtered and the deep yellow solution obtained was concentrated to about 3 ml. Addition of hexane (7 ml) gave dark red crystals of [$WI(NNH)(dpe)_2$], which were filtered off, washed with hexane and dried in vacuo (42 mg, 20%). Found: C, 55.01; H, 4.30; N, 2.09; I, 11.54%. Calcd for $C_{52}H_{49}N_2IP_4W$: C, 54.94 H, 4.35; N, 2.46; I, 11.16%. IR (KBr disk): ν(NN), 1900 cm^{-1}.

Reaction of *trans*-[$WI(NNSiMe_3)(PMe_2Ph)_4$] (1) with MeOH. Analogous treatment of complex 1 (212 mg, 0.220 mmol) with MeOH (13 μl, 0.322 mmol) gave the brown solid of *trans*-[$WI(NNH_2)(PMe_2Ph)_4$]I (34 mg, 15%). From the filtrate were obtained small amounts of complexes **5** and **9**. However, isolation and characterization of the major product from this reaction mixture were not successful.

Reduction of Trimethylsilylated Dinitrogen Complexes. under Ar with Na: Onto a frozen mixture of THF (5—6 ml) and Na sand (0.5—1 mm diameter, ca. 20 mol excess) in a rigorously dried Schlenk tube with a volume of 35—40 ml, complex **1**, **2**, or **7** (0.12—0.17 mmol) and nonane as an internal standard were added under Ar. The mixture was warmed slowly and then stirred for 22 h in the dark at 30 °C. After determining the amounts of the evolved N_2 in the gaseous phase (Molecular Sieve 13X, 80—100 mesh, 3 mm ϕ×2.0 m stainless column) and $(Me_3Si)_2NH$ in the liquid phase (Silicone KF-96, 5% on Chromosorb W(AW-DMCS), 60—80 mesh, 2.6 mm ϕ×2.0 m glass column) by GLC, volatile materials were condensed into another Schlenk tube immersed in liquid nitrogen from the reaction mixture which was cooled down to −30—−40 °C to avoid the evaporation of $(Me_3Si)_2NH$. The trapped materials including free ammonia were treated with aqueous H_2SO_4 solution (0.5 mol dm^{-3}, 10 ml) and NH_3 was analyzed quantitatively by the indophenol method. As for the evaporated residue, the amount of the coordinated dinitrogen was determined by comparing the intensities of the ν(NN) band at 1910 cm^{-1} and the band at 1430 cm^{-1} assigned to the phenyl group in PMe_2Ph ligand and/or by the GLC analysis of the evolved N_2 gas after thermal decomposition of the residue at 160—170 °C for 1 h. After these procedure, the residue was treated with an aqueous KOH solution (40%, 10 ml) and NH_3 and N_2H_4 distilled into an aqueous H_2SO_4 solution were analyzed by indophenol and *p*-dimethylaminobenzaldehyde reagents, respectively.

Under N_2 with Na: The similar procedure to the reduction under Ar was carried out except for the determination of evolved N_2 gas by GLC.

Under Ar with NaH: The similar procedure was undertaken except that NaH (ca. 20 mol excess) was used in place of Na sand.

Reaction with Et_3SiCl after Reduction. After the similar treatment of complex **1** (141 mg, 0.146 mmol) with Na microdispersion (62 mg, 2.71 mmol) adding decane as an internal standard, the amount of $(Me_3Si)_2NH$ determined by GLC was 0.11 mol per W atom (Silicone OV-17, 5% on Chromosorb W(AW-DMCS), 60—80 mesh, 2.6 mmϕ×2.0 m glass column). Then Et_3SiCl (356 mg, 2.43 mmol) was added to the solution. After stirring for 2 days at room temperature, the amounts of Et_3SiNH_2, $(Me_3Si)NH(SiEt_3)$ (Silicone OV-17, 5% on Chromosorb W(AW-DMCS), 60—80 mesh, 2.6 mmϕ×2.0 m glass column), $(Et_3Si)_2NH$ and $(Me_3Si)_2N(SiEt_3)$ (Shimadzu HiCap-CBP10-M25-025, capillary column) in the solution were determined by GLC.

Reduction of *trans*-[MoI(NNSiMe$_3$)(PMe$_2$Ph)$_4$] (7) and *trans*-[WI(NNSiMe$_3$)(PMe$_2$Ph)$_4$] (1) with Na in the Presence of Excess Me_3SiCl. Into a degassed mixture of Na microdispersion (8—10 μm diameter, ca. 20 mol excess) and Me_3SiCl (ca. 20 mol excess) in THF (5 ml) at −78 °C, *mer*-[MoI(NNSiMe$_3$)(PMe$_2$Ph)$_4$] (**7**) (123 mg, 0.128 mmol) was added under Ar. After stirring for 22 h at room temperature in the dark, the unreacted Me_3SiCl and about a half of THF were removed by trap-to-trap method. Then the yield of $(Me_3Si)_3N$ in the residue was determined by GLC (Silicone OV-225, 2% on Chromosorb W(AW-DMCS), 80—100 mesh, 2.6 mmϕ×2.0 m glass column) using nonane as an internal standard (0.75 mol per Mo atom). In the presence of excess Me_3SiCl, the quantitative GLC analysis of $(Me_3Si)_3N$ was not successful under the conditions we examined.

By the similar treatment of complex **1**, $(Me_3Si)_3N$ was produced in the yield of 0.42 mol per W atom.

The financial support by the Ministry of Education of Japan and the Asahi Glass Foundation of Engineering Technology is greatly appreciated.

References

1) Preparation and Properties of Molybdenum and Tungsten Dinitrogen Complexes. 26. Part 25: see Ref. 7.

2) M. Hidai, K. Komori, T Kodama, D.-M. Jin, T. Takahashi, S. Sugiura, Y. Uchida, and Y. Mizobe, *J. Organomet. Chem.*, **272**, 155 (1984).

3) Although no IR bands assignable to ν(NN) were reported for the hydrazido(2−) and organohydrazido(2−) complexes of molybdenum and tungsten containing (NNRR′) ligands (R, R′=H,[9] alkyl,[13,14] aroyl[14]) except for the case of R=acetyl and R′=H (M=W: 1368 cm^{-1}),[14] trimethylsilylhydrazido(2−) complexes reported here show ν(NN) bands at around 1350 cm^{-1}, assignment of which was demonstrated by the fact that the band at 1345 cm^{-1} for complex **8** shifted to 1308 cm^{-1} on ^{15}N substitution.

4) J. Chatt, A. J. Pearman, and R. L. Richards, *J. Chem. Soc., Dalton Trans.*, **1976**, 1520.

5) C. J. Pickett, K. S. Ryder, and J. Talarmin, *J. Chem. Soc., Dalton Trans.*, **1986**, 1453.

6) W. Hussain, G. J. Leigh, and C. J. Pickett, *J. Chem. Soc., Chem. Commun.*, **1982**, 747.

7) K. Komori, H. Oshita, Y. Mizobe, and M. Hidai, *J. Am. Chem. Soc.*, **111**, 1939 (1989).

8) W. Hussain, G. J. Leigh, H. M.-Ali, C. J. Pickett, and D. A. Rankin, *J. Chem. Soc., Dalton Trans.*, **1984**, 1703.

9) J. Chatt, A. J. Pearman, and R. L. Richards, *J. Chem. Soc., Dalton Trans.*, **1974**, 2074.

10) J. R. Dilworth and R. L. Richards, *Inorg. Synth.*, **20**, 119 (1980).

11) M. E. Jang and M. A. Lyster, *Org. Synth.*, **59**, 35, (1979).

12) J. Chatt, A. J. Pearman, and R. L. Richards, *J. Chem. Soc., Dalton Trans.*, **1977**, 1852.

13) D. C. Busby, T. A. George, S. D. Allen Iske, Jr., and S. D. Wagner, *Inorg. Chem.*, **20**, 22 (1981).

14) J. Chatt, A. A. Diamantis, G. A. Heath, N. E. Hooper, and G. J. Leigh, *J. Chem. Soc., Dalton Trans.*, **1977**, 688.

$2^A,2^B$-, $2^A,2^C$-, and $2^A,2^D$-Bis-*O*-(*p*-tolylsulfonyl)-β-cyclodextrins

Kahee FUJITA,* Takashi ISHIZU, Kyoko OSHIRO, and Ken-ichi OBE
Faculty of Pharmaceutical Sciences, Fukuyama University, Sanzo, Higashimura-cho, Fukuyama 729-02
(Received May 11, 1989)

A mixture of the title ditosylates was prepared by the reaction of β-cyclodextrin with dibutyltin oxide and tosyl chloride. Each ditosylate was isolated by reversed-phase column chromatography and the structure was assigned on the basis of conversion into a known compound or hydrolysis with Taka amylase A.

The introduction of two functional groups at the desired positions of cyclodextrins is an approach to the construction of enzyme (or receptor) mimics.[1-5] In this context the study of specific disulfonylation is important.

Tabushi et al.[6-9] reported the specific 6,6-di-*O*-sulfonylation of β-cyclodextrin (β-CD) and Boger and Knowles[10] demonstrated nonspecific 6,6,6-tri-*O*-sulfonylation of α-cyclodextrin (α-CD) but only the $6^A,6^C,6^E$ isomer was identified. Fujita et al.[11-14] prepared poly-6-*O*-sulfonylated α(or β or γ)-cyclodextrins by nonspecific sulfonylation.

Since Breslow et al.[15] demonstrated that β-CD modified with a pyridoxamine moiety on its secondary hydroxyl side[15] produced amino acids with opposite chirality to that produced from the corresponding 6-*O*-modified β-CD[16] in transamination reactions, disulfonylation of the secondary hydroxyl groups has been a challenging problem. However, there are few reliable methods for the specific sulfonylation of 3-OH or 2-OH.

Fujita et al.[17] reported the preparation of 3-*O*-sulfonylated α- or β-CD by reaction with 2-naphthalenesulfonyl chloride in alkaline aqueous acetonitrile and its application for the preparation of $3^A,3^C$- and $3^A,3^D$-di-*O*-sulfonylated β-CDs.

Three methods have been reported for the 2-*O*-sulfonylation of β-CD. (a) Ueno and Breslow[18] prepared 2-*O*-(*p*-tosyl)-β-CD by the reaction of β-CD with *m*-nitrophenyl *p*-tosylate in alkaline aqueous *N,N*-dimethylformamide. (b) Fujita et al. reported that the reaction of α- or β-CD with *m*-nitrobenzenesulfonyl chloride[19] or 1-naphthalenesulfonyl chloride[20] in alkaline aqueous solution gave the corresponding 2-*O*-sulfonates. The reaction with *m*-nitrobenzenesulfonyl chloride was used to synthesize $2^A,2^X$-di-*O*-sulfonyl-α-CDs (X=B, C, and D). However, the reaction with 1-naphthalenesulfonyl chloride gave a low yield of 2-*O*-sulfonyl β-CD and the rate of reaction was too slow to allow further sulfonylation because of the competitive epoxidation of the monosulfonate. (c) Murakami et al.[21] reported the preparation of a 2-*O*-sulfonate by the use of dibutyltin oxide and the corresponding sulfonyl chloride in *N,N*-dimethylformamide.[22] Methods (a) and (b) did not allow accumulation of the disulfonates since the 2-*O*-sulfonylated β-CDs were converted into the epoxide, $(2^AS,3^AS)$-$2^A,3^A$-anhydro-β-CD.

Method (c), on the other hand, is carried out in dry *N,N*-dimethylformamide and offers a promise for the preparation of 2,2-di-*O*-sulfonylated β-CDs. We now describe its use for the preparation of $2^A,2^B$-, $2^A,2^C$-, and $2^A,2^D$-bis-*O*-(*p*-tosyl)-β-CDs by the reaction of β-CD.

Results and Discussion

Following the reaction of β-CD with dibutyltin oxide and *p*-toluenesulfonyl chloride in *N,N*-dimethylformamide, reversed-phase column chromatography of the products gave, in order of elution in reversed-phase HPLC, 2-*O*-*p*-tosyl (9.4%), $2^A,2^D$- (**1**, 3.6%), $2^A,2^C$- (**2**, 2.6%), and $2^A,2^B$-bis-*O*-(*p*-tosyl) (**3**, 1.8%) derivatives (Scheme 1). That **1**—**3** were ditosylates was confirmed by their fast-atom bombardment (hereafter abbreviated to FAB) mass spectra and by their

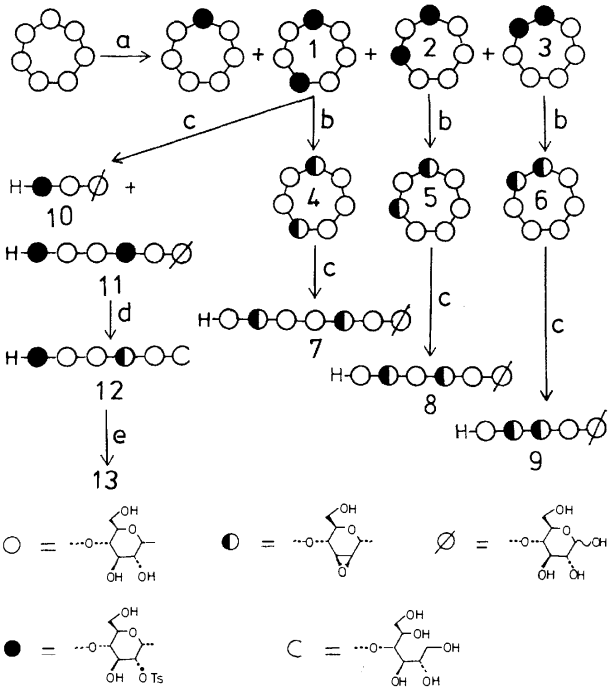

Scheme 1. Preparation and determination of the structure of $2^A,2^X$-bis-*O*-(*p*-tosyl)-β-cyclodextrins (**1**—**3**): (a) *p*-toluenesulfonyl chloride–Bu_2SnO–*N,N*-dimethylformamide, (b) $Ba(OH)_2$, (c) Taka amylase A, (d) $NaBH_4$, (e) Ac_2O–pyridine.

^{13}C NMR spectra which showed that two of the ^{13}C resonances were shifted up-field (see Experimental). However, the ^{13}C NMR spectra were not helpful in determining the regiochemistry of the sulfonylations.

Fujita et al.[19] reported that $2^A,2^X$-di-*O*-sulfonyl-α-CDs (X=B, C, and D) were converted easily into the corresponding ($2^AS,3^AS:2^XS,3^XS$)-$2^A,3^A:2^X,3^X$-dianhydro-α-CDs by treatment with aqueous alkali and that ($2^AS,3^AS:2^CS,3^CS$)-$2^A,3^A:2^C,3^C$-dianhydro-α-CD and ($2^AS,3^AS:2^BS,3^BS$)-$2^A,3^A:2^B,3^B$-dianhydro-α-CD were hydrolyzed by Taka amylase A to give ($2''S,3''S:2''''S,3''''S$)-$2'',3'':2'''',3''''$-dianhydromaltohexaose and ($2''S,3''S:2'''S,3'''S$)-$2'',3'':2''',3'''$-dianhydromaltopentaose, respectively, whereas ($2^AS,3^AS:2^DS,3^DS$)-$2^A,3^A:2^D,3^D$-dianhydro-α-CD was unaffected.

Following these procedures, **1**—**3** were treated with aqueous $Ba(OH)_2$ to give the corresponding diepoxides **4**—**6**. Although the ^{13}C NMR spectra of **4**—**6** were different from each other, they did not allow the structures to be assigned. The diepoxides **4**—**6** were hydrolyzed by Taka amylase A to give diepoxides (**7**—**9**) of maltoheptaose, maltohexaose, and maltopentaose, respectively, together with glucose (Scheme 1). The FAB mass spectra of **7**—**9** contained the corresponding molecular ions (see Experimental). The structures ($2''S,3''S:2''''S,3''''S$)-$2'',3'':2'''',3''''$-dianhydromaltohexaose and ($2''S,3''S:2'''S,3'''S$)-$2'',3'':2''',3'''$-dianhydromaltopentaose were assigned to **8** and **9**, respectively, by comparing the FAB mass spectra and retention times in reversed-phase HPLC with those of the authentic compounds which were prepared from ($2^AS,3^AS:2^XS,3^XS$)-$2^A,3^A:2^X,3^X$-dianhydro-α-CDs (X=B and C) as described above.[19] Therefore, **2** and **3** are the $2^A,2^C$- and $2^A,2^B$-ditosylate, respectively. Since there are only three 2,2-disulfonates, **1** must be the $2^A,2^D$ isomer and this was confirmed as follows.

Hydrolysis of 2-*O*-arylsulfonyl-β-CDs by Taka amylase A gives[20] $2''$-*O*-(arylsulfonyl)maltotrioses (**10**). However, enzymic hydrolysis of **1** gave the expected known compound **10**[20] only as a minor product. The major product was **11**. Reduction of **11** with aqueous $NaBH_4$ gave **12**, the FAB mass spectrum of which contained ($M+H^+$) ion at *m/z* 1129 demonstrating that one of the two tosylated sugar units had been converted into an epoxide and that the end group was a hexitol moiety. Treatment of **12** with acetic anhydride in pyridine gave the octadecaacetate **13**, the FAB mass spectral fragmentation of which (Scheme 2) demonstrated the tosyl and the epoxy groups were located at the first and fourth glucose units, respectively. Therefore, the identity of **1** is confirmed as $2^A,2^D$-bis-*O*-(*p*-tosyl)-β-CD.

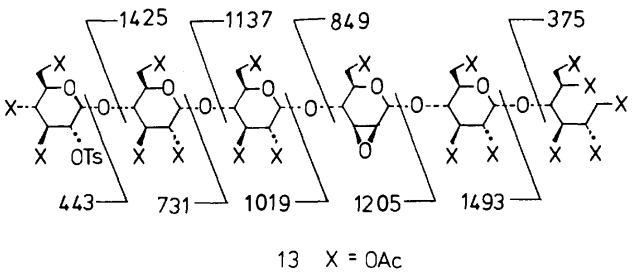

13 X = OAc

Scheme. 2. FAB mass spectral fragmentation pattern of **13**.

The ditosylates **1**—**3** may serve as starting materials for the synthesis of specifically bifunctionalized β-CDs.

Experimental

General. ^{13}C NMR spectra were determined with a JEOL FX 100 (25 MHz) spectrometer. FAB mass spectra were recorded with a JEOL DX-300 data system. Merck Lobar prepacked columns of LiChroprep Rp18 (A 10 mm×240 mm and B 25 mm×310 mm) and Rp8 (C 37 mm×440 mm) were used for reversed-phase column chromatography. HPLC was performed on a HITACHI L-3000 instrument with a column (4.6 mm×250 mm) of TSKgel ODS-80TM (5 μm, TOSOH).

Preparation and Isolation of $2^A,2^X$-Bis-*O*-(*p*-tosyl)-β-CDs (1—3, X=B—D). A mixture of β-cyclodextrin (5.25 g, 4.63 mmol) and dibutyltin oxide (11.52 g, 46.3 mmol) in anhydrous *N,N*-dimethylformamide (35 mL) was stirred at 95—100 °C for 2 h under nitrogen. The mixture was cooled to 0 °C, triethylamine (5.61 g, 55.5 mmol) was added, followed dropwise by a solution of *p*-toluenesulfonyl chloride (8.84 g, 46.3 mmol) in anhydrous *N,N*-dimethylformamide (10 mL). The mixture was stirred for 10 h at room temp and then concentrated in vacuo to 20 mL. The residual yellow syrup was stirred vigorously with acetone (500 mL) for 20 min, the solid was collected, washed with acetone, and dried in vacuo. A solution in water (250 mL) was filtered and chromatographed on column C. After elution with aqueous 20% methanol (1 L), gradient elution from aqueous 30% methanol (1 L) to aqueous 60% methanol (1 L) was applied to give 2-*O*-(*p*-tosyl)-β-CD (561 mg, 9.4%) and a mixture of $2^A,2^X$-bis-*O*-(*p*-tosyl)-β-CDs (X=B—D). The mixture was concentrated in vacuo and chromatographed on column B with gradient elution from aqueous 40% methanol (1 L) to aqueous 60% methanol (1 L) to give $2^A,2^D$-(**1**, 240 mg, 3.6%), $2^A,2^C$-(**2**, 174 mg, 2.6%), and $2^A,2^B$-bis-*O*-(*p*-tosyl)-β-CD (**3**, 122 mg, 1.8%). ^{13}C NMR (Me_2SO-d_6, internal Me_4Si, characteristic nonaromatic carbons), **1** δ=59.8, 69.1, 71.9, 72.2, 72.9, 79.5, 81.4, 98.1 (two shifted C-1 resonances), 101.8, **2** δ=59.7, 69.2, 70.2, 72.0, 72.8, 79.6, 80.9, 81.4, 98.1 (two shifted C-1 resonances), 101.8, **3** δ=59.8, 68.8, 69.1, 71.9, 72.9, 79.2, 80.2, 81.1, 81.5, 97.1 (a shifted C-1 resonance), 97.7 (a shifted C-1 resonance), 101.8; FABMS *m/z* **1** 1443 ($M+H^+$), **2** 1443 ($M+H^+$), **3** 1443 ($M+H^+$).

Epoxidation of $2^A,2^X$-Bis-*O*-(*p*-tosyl)-β-CDs (1—3, X=B—D). A solution of **1** (30.8 mg) in 0.05 M $Ba(OH)_2$ (3 mL; 1 M=1 mol dm^{-3}) was stirred at room temperature for 1.5 h, then neutralized with 0.5 M H_2SO_4, filtered, applied to a column (2.6 cm×90 cm) of Bio-Gel P-2 (200—400 mesh, Bio-Rad Laboratories), and eluted with water to give ($2^AS,3^AS:2^DS,3^DS$)-$2^A,3^A:2^D,3^D$-dianhydro-β-CD **4** (23.1 mg, 74%).

Similarly, **2** (15.0 mg) and **3** (25.2 mg) gave ($2^AS,3^AS:2^CS,3^CS$)-$2^A,3^A:2^C,3^C$-dianhydro-β-CD (**5**, 11.3 mg, 84.8%) and ($2^AS,3^AS:2^BS,3^BS$)-$2^A,3^A:2^B,3^B$-dianhydro-β-CD (**6**, 17.8 mg, 97.8%),

respectively. ^{13}C NMR [D_2O, internal $Me_3Si(CH_2)_3SO_3Na$, characteristic absorptions] **4** δ=51.7, 56.5, 62.7, 63.5, 74.3, 75.0, 82.2, 82.6, 83.1, 100.0, 100.2, 103.9, **5** δ=51.9, 56.6, 62.7, 63.4, 74.3, 74.6, 82.3, 82.7, 83.2, 100.1, 103.6, 104.1, **6** δ=51.7, 52.2, 56.7, 62.8, 63.4, 74.4, 75.6, 82.8, 83.3, 99.0, 100.2, 103.0, 104.1; FABMS *m/z* **4** 1121 ($M+Na^+$), 1137 ($M+K^+$), **5** 1121 ($M+Na^+$), **6** 1099 ($M+H^+$), 1137 ($M+K^+$).

Hydrolysis of (2^A*S*,3^A*S*:2^X*S*,3^X*S*)-2^A,3^A:2^X,3^X-dianhydro-β-CD (4—6, X=B—D) with Taka Amylase A. A solution of (36 mg) and Taka amylase A [α-amylase Type X-A (Sigma), 36 mg] in 0.2 M acetate buffer (3 mL, pH 5.5) containing 0.01 M $CaCl_2$ was kept at 40 °C for 2 days, then heated at 100 °C for 10 min, filtered, applied to a column (2.6 cm×90 cm) of Bio-Gel P-2 and eluted with water to give (2″*S*,3″*S*:2⁗*S*,3⁗*S*)-2″,3″:2⁗,3⁗-dianhydromaltoheptaose (**7**, 17.6 mg, 48.2%).

Similarly, **5** (26 mg) and **6** (59 mg) gave (2″*S*,3″*S*:2⁗*S*,3⁗*S*)-2″,3″:2⁗,3⁗-dianhydromaltohexaose (**8**, 6.0 mg, 26.5%) and (2″*S*,3″*S*:2‴*S*,3‴*S*)-2″,3″:2‴,3‴-dianhydromaltopentaose (**9**, 32.0 mg, 88.8%), respectively. FABMS *m/z* **7** 1117 ($M+H^+$), 1139 ($M+Na^+$), **8** 955 ($M+H^+$), 977 ($M+Na^+$), 993 ($M+K^+$), **9** 793 ($M+H^+$), 815 ($M+Na^+$).

Hydrolysis of 2^A,2^D-Bis-*O*-(*p*-tosyl)-β-CD 1 with Taka Amylase A. A solution of **1** (60 mg) and Taka amylase A (180 mg) in 0.2 M acetate buffer (8 mL, pH 5.5) containing 0.01 M $CaCl_2$ was kept at 40 °C for 2 days, then worked-up as described above. The filtrate was chromatographed on column A. After elution of aqueous 5% methanol (50 mL), gradient elution from aqueous 10% methanol (500 mL) to aqueous 50% methanol (500 mL) was applied to give 2″-*O*-(*p*-tosyl)maltotriose (**10**, 9 mg, 32.9%) and 2″,2⁗″-bis-*O*-(*p*-tosyl)maltohexaose (**11**, 36.0 mg, 66.7%). FABMS *m/z* **10** 659 ($M+H^+$), 681 ($M+Na^+$), **11** 1299 ($M+H^+$), 1321 ($M+Na^+$).

Reduction of 2″,2⁗″-Bis-*O*-(*p*-tosyl)maltohexaose 11 with $NaBH_4$. A solution of **11** (15.5 mg) in aqueous 1% $NaBH_4$ (5 mL) was kept at room temp for 16 h, then neutralized with aqueous 5% HCl, filtered, and chromatographed on column A with gradient elution from aqueous 20% methanol (500 mL) to aqueous 50% methanol (500 mL) to give *O*-2-*O*-(*p*-tosyl)-α-D-glucopyranosyl-(1→4)-*O*-α-D-glucopyranosyl-(1→4)-*O*-α-D-glucopyranosyl-(1→4)-*O*-[(2*S*,3*S*)-2,3-anhydro-α-D-glucopyranosyl]-(1→4)-*O*-α-D-glucopyranosyl-(1→4)-D-glucitol (**12**, 7.5 mg, 55.9%). FABMS *m/z* 1129 ($M+H^+$).

A solution of **12** (3 mg) was treated conventionally with acetic anhydride (1.5 mL) in pyridine (1.5 mL) at room temp for 2 days. The crude product was purified by reversed-phase HPLC with gradient elution from aqueous 50% CH_3CN to aqueous 80% CH_3CN to give *O*-2-*O*-(*p*-tosyl)-α-D-glucopyranosyl-(1→4)-*O*-α-D-glucopyranosyl-(1→4)-*O*-α-D-glucopyranosyl-(1→4)-*O*-[(2*S*,3*S*)-2,3-anhydro-α-D-glucopyranosyl]-(1→4)-*O*-α-D-glucopyranosyl-(1→4)-D-glucitol octadecaacetate (**13**). FABMS *m/z* 1885 ($M+H^+$) (see Scheme 2).

We thank Japan Maize Products Co., Ltd. for a generous gift of β-cyclodextrin.

References

1) R. Breslow, J. B. Doherty, G. Guillot, and C. Lipsey, *J. Am. Chem. Soc.*, **100**, 3227 (1978).
2) R. Breslow, P. Bovy, and C. L. Hersh, *J. Am. Chem. Soc.*, **102**, 2115 (1980).
3) I. Tabushi and Y. Kuroda, *J. Am. Chem. Soc.*, **106**, 4580 (1984).
4) I. Tabushi, Y. Kuroda, M. Yamada, H. Higashimura, and R. Breslow, *J. Am. Chem. Soc.*, **107**, 5545 (1985).
5) I. Tabushi, Y. Kuroda, and T. Mizutani, *J. Am. Chem. Soc.*, **108**, 4514 (1986).
6) I. Tabushi, K. Shimokawa, N. Shimizu, H. Shirakata, and K. Fujita, *J. Am. Chem. Soc.*, **98**, 7855 (1976).
7) I. Tabushi, Y. Kuroda, K. Yokota, and L. C. Yuan, *J. Am. Chem. Soc.*, **103**, 711 (1981).
8) I. Tabushi and L. C. Yuan, *J. Am. Chem. Soc.*, **103**, 3574 (1981).
9) I. Tabushi, T. Nabeshima, K. Fujita, A. Matsunaga, and T. Imoto, *J. Org. Chem.*, **50**, 2638 (1985).
10) J. Boger, D. G. Brenner, and J. R. Knowles, *J. Am. Chem. Soc.*, **101**, 7630 (1979).
11) K. Fujita, A. Matsunaga, and T. Imoto, *J. Am. Chem. Soc.*, **106**, 5740 (1984).
12) K. Fujita, H. Yamamura, A. Matsunaga, T. Imoto, T. Fujioka, and K. Mihashi, *J. Am. Chem. Soc.*, **108**, 4509 (1986).
13) K. Fujita, A. Matsunaga, and T. Imoto, *Tetrahedron Lett.*, **25**, 5533 (1984).
14) K. Fujita, H. Yamamura, T. Imoto, T. Fujioka, and K. Mihashi, *J. Org. Chem.*, **53**, 1943 (1988).
15) R. Breslow and A. W. Czarnik, *J. Am. Chem. Soc.*, **105**, 1390 (1983).
16) R. Breslow, M. Hammond, and M. Lauer, *J. Am. Chem. Soc.*, **102**, 421 (1980).
17) K. Fujita, T. Tahara, T. Imoto, and T. Koga, *J. Am. Chem. Soc.*, **108**, 2030 (1986).
18) A. Ueno and R. Breslow, *Tetrahedron Lett.*, **23**, 3451 (1982).
19) K. Fujita, S. Nagamura, T. Imoto, T. Tahara, and T. Koga, *J. Am. Chem. Soc.*, **107**, 3233 (1985).
20) K. Fujita, T. Tahara, S. Nagamura, I. Imoto, and T. Koga, *J. Org. Chem.*, **52**, 636 (1987).
21) T. Murakami, K. Harata, and S. Morimoto, *Tetrahedron Lett.*, **28**, 321 (1987).
22) Hexakis(2,6-di-*O*-benzoyl)-α-cyclodextrin was regioselectively prepared by the reaction of α-cyclodextrin with bis(tributylstannyl) oxide followed by the reaction with benzoyl chloride. Substitution of benzoyl chloride with tosyl chloride in this reaction must give hexakis(2,6-di-*O*-tosyl)-α-cyclodextrin regioselectively as suggested by the authors: T. Ogawa and M. Matsui, *Carbohydr. Res.*, **56**, C1 (1977).

 © 1989 The Chemical Society of Japan Bull. Chem. Soc. Jpn., 62, 2963—2967 (1989)

Catalytic Intermolecular Hydrogen Transfer with Photogenerated Hydride Transient $CoH[PPh(OEt)_2]_3$

Masayoshi ONISHI,* Masahiko MATSUDA, Isato TAKAKI,
Katsuma HIRAKI, and Shigero OISHI*,†
Department of Industrial Chemistry, Faculty of Engineering, Nagasaki University,
Bunkyo-machi, Nagasaki 852
†Department of Chemistry, School of Hygienic Sciences, Kitasato University,
Kitasato, Sagamihara, Kanagawa 228
(Received May 11, 1989)

Pyrex-filtered photoirradiation of a thermally inert complex $CoH[PPh(OEt)_2]_4$ generated a coordinatively unsaturated active hydride species "$CoH[PPh(OEt)_2]_3$" ($CoHP_3$), which catalyzed hydrogen transfer from secondary alcohols to carbonyl compounds, such as ketones. Study of initial reaction-rate dependence of the hydrogen transfer on complex and substrate concentrations indicated that the reaction was initiated by coordination of the carbonyl compounds to the photogenerated $CoHP_3$ species, and these coordination was confirmed by the decay analysis of the transient $CoHP_3$ absorbance observed after laser flash photolysis. In addition, the rate-determining step of the hydrogen-transfer reaction was associated with the hydride transfer to the carbonyl carbon, at the stage of the transformation of hydrido (ketone or aldehyde) cobalt into alkoxo intermediate. Second-order coordination-rate constants k' of aldehydes and ketones to $CoHP_3$ ranged from 10^5 to 10^3 M^{-1} s^{-1}. The constants k' of aldehydes were considerably larger than those of ketones, where substantial steric repulsion by the bulky substituents introduced in place of the aldehyde hydrogen, was presumed to hinder the $CoHP_3$ approach to the carbonyl group.

Transition-metal hydride complexes have become an important class of compounds in organometallic chemistry, which play a key role in many homogeneous catalytic reactions[1] and have promise also in hydrogen and energy storage systems.[2] Moreover, their photochemical properties[3] have recently received much attention in view of photochemical hydrogen production from water[2a,b] and of photogeneration of highly reactive organometallic fragments.[4]

The hydridophosphonitecobalt(I) complex $CoH[PPh(OEt)_2]_4$ ($CoHP_4$) with an 18-electron configuration is thermally inert. However, Pyrex-filtered photoirradiation of the complex dissociates a phosphonite ligand $PPh(OEt)_2$ (P) from cobalt efficiently without cleavage of the hydrido–cobalt bond, and produces a coordinatively unsaturated transient of the hydride species "$CoH[PPh(OEt)_2]_3$" ($CoHP_3$).[5] The quantum yield for the $CoHP_3$ photogeneration is almost 1.0 at 337 nm.[5b] Furthermore, the species has shown high catalytic activities in double-bond migration of some allylic compounds such as *N,N*-diethylallylamine, and laser flash photolysis displayed the substrate coordination through C=C double bond to the species.[5c]

We now report the photoassisted intermolecular hydrogen transfer from secondary alcohols to carbonyl compounds such as ketones, as an another example of the catalytic reactions by the photogenerated $CoHP_3$ species. Some aspects of this work have appeared in a preliminary communication.[6]

Catalytic transfer hydrogenation using organic compounds as hydrogen sources seems to remain of current interest and secondary alcohols have most often been employed as the sources.[1b,7] In these reactions, homogeneous catalyst have been widely used, such as $RhCl(PPh_3)_3$, $RhH(PPh_3)_4$, $RuCl_2(PPh_3)_3$, and $RuH_2(PPh_3)_4$.[7] However, there were only a few descriptions on the hydrogen transfer catalyzed by photogenerated reactive organometallic species.[8]

Experimental

Materials and General Procedures. The complex $CoH[PPh(OEt)_2]_4$, $CoHP_4$ was prepared by the literature methods.[9] Benzene was treated with concentrated sulfuric acid until thiophene-free. After water washing, it was dried over anhydrous magnesium sulfate, and distilled from sodium under nitrogen. Toluene was purified similarly. For continuous irradiation, a high-pressure mercury lamp (400 W) was used with a Pyrex filter, and reactant solutions were placed at about 45 mm from the lamp.

Catalytic Hydrogen Transfer and Product Analyses. Benzene solutions (5 cm^3) of $CoHP_4$ and substrates were degassed by freeze-pump-thaw cycles in a Pyrex Schlenk tube (18 mm^{ϕ}). After standing the solutions at 30 °C in the dark or under irradiation to proceed catalytic hydrogen transfer, the reaction mixture was analyzed by Shimadzu GC-8AIT(TCD) and GC-8APF(FID) gas chromatographs with Molecular Sieve 5A, polyethylene glycol 20M, Silicone SE-30, tetrakis-*O*-(2-cyanoethyl)pentaerythritol, and Thermon 3000 columns, together with JEOL model JMS-DX303 GC-mass and JNM-GX-400 NMR spectrometers. Other catalytic reactions described in this paper were conducted similarly.

Laser Flash Photolysis. A Molectron UV-400 nitrogen laser was used for excitation. A right-angle optical system using a 1×1 cm Pyrex cell was employed for the excitation-analysis set-up. The kinetic spectrophotometer and data collection system are described elsewhere.[10] Samples were deaerated by bubbling with argon for 20 min or by several freeze-pump-thaw cycles after transfer of solvent from a reservoir, containing

$LiAlH_4$, using a vacuum line. Second-order rate constants were obtained from the plots of pseudo-first-order rate constants vs. the substrate concentrations, and regarded as accurate to within ca. 10%.

Results and Discussion

Intermolecular Hydrogen Transfer from Secondary Alcohols to Ketones. The $CoHP_4$ complex was mixed with 50-fold moles of cyclohexanone and 1-phenylethanol in benzene, and the solution was irradiated at 30 °C for 8 h by use of a high-pressure Hg lamp with a Pyrex filter. Hydrogen transfer occurred from 1-phenylethanol to cyclohexanone affording acetophenone and cyclohexanol, and virtual stoichiometric relationship was found to hold among these four organic compounds.[6] The reaction mixture gave

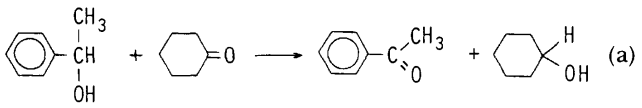

(a)

a value of 0.77 for the molar ratio of cyclohexanol formed to that of cyclohexanone charged. Similar photocatalytic hydrogen transfer was performed also from cyclohexanol to acetophenone (i.e., backward hydrogen-transfer reaction of (a)), and afforded the reaction mixture of comparable composition to that of the forward hydrogen-transfer reaction, indicating equilibration among these alcohols and ketones.[6] Formation of pinacols and their derivatives was not observed under the present reaction conditions. No other products were detected on the basis of gas chromatography except a small amount of dissociated phosphonite and only trace of molecular hydrogen (less than 2% yield relative to $CoHP_4$).

In the absence of $CoHP_4$, the hydrogen transfer did not proceed even under irradiation, and addition of free phosphonite did not change the situation either. In the dark, the cobalt complex did not cause the hydrogen transfer at 30 °C in benzene at all. Accordingly, the hydrogen transfer of the present system was determined to be photoassisted. In consideration of the fact that the present hydrogen transfer proceeded only under photoirradiation of $CoHP_4$ and ceased immediately upon interruption of irradiation, it was evident that the photogenerated hydride species $CoHP_3$ played an important role in the catalytic cycle of the present hydrogen transfer, similarly to the photoassisted reactions of the olefin double-bond migration reported previously.[5a,c]

Dependence of the Hydrogen-Transfer Reaction-Rates on Concentrations of the Cobalt Complex and Substrates. For benzene solutions of 0.82 M†† 1-phenylethanol and cyclohexanone, the initial reaction rate of the hydrogen transfer became larger as the concentration of $CoHP_4$ increased from 0.16× to 0.82×10^{-2} M (Fig. 1). However, in the range above 0.82×10^{-2} M, the initial reaction rate did not change so much upon the further increase in the $CoHP_4$ concentration, and the rate seemed to approach one asymptotic value. This finding was attributed to the saturated photogeneration of the hydride $CoHP_3$ species due to total absorption of the incident light. Similar phenomenon was noticed also in the conversion of cyclohexanone to cyclohexanol after 4 h.

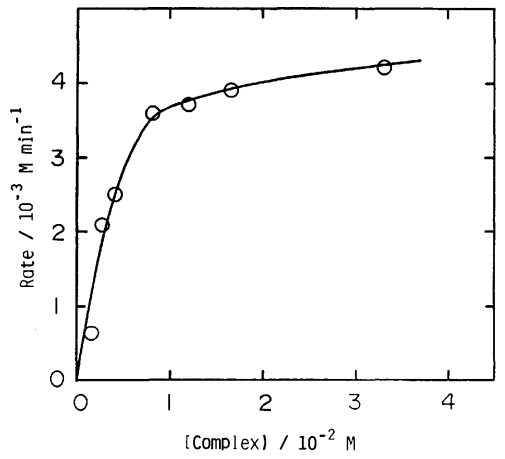

Fig. 1. Dependence of the initial rate of hydrogen transfer on the $CoH[PPh(OEt)_2]_4$ concentration. 1-Phenylethanol, 0.82 M; cyclohexanone, 0.82 M.

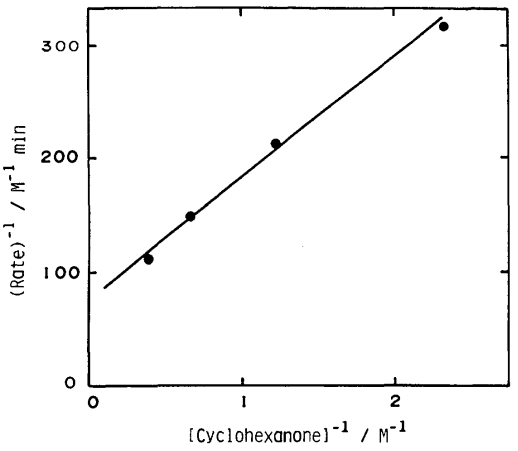

Fig. 2. Double reciprocal plots of the initial reaction rate against the cyclohexanone concentration. $CoH[PPh(OEt)_2]_4$, 0.0165 M; 1-phenylethanol, 0.82 M.

At the fixed concentrations of $CoHP_4$ (1.65×10^{-2} M) and 1-phenylethanol (0.82 M), we studied concentration effects of the cyclohexanone charged, and found that the reciprocal initial reaction rate bore a linear relationship with the reciprocal

$$\left[\frac{d[Y]}{dt}\right]_{t=0}^{-1} = \frac{1}{V} + \frac{K_m}{V} \times [S]_{t=0}^{-1},$$

S=cyclohexanone, t=time, Y=cyclohexanol,

$V=1.28\times10^{-2}$ M min^{-1}, $K_m=1.32$ M, Correlation coefficient=0.997

†† 1 M=1 mol dm^{-3}.

concentration of the cyclohexanone charged (Fig. 2). On the contrary, the initial reaction rate was practically independent of the concentration of 1-phenylethanol charged, as shown in Fig. 3, where the concentration ranged from 0.4 to 2.5 M.

As for the mechanism of the present hydrogen transfer, we propose the reaction pathway, which involves initial coordination of ketone to the $CoHP_3$ species photogenerated and the hydride transfer to the carbonyl carbon in ketone, forming an alkoxo intermediate. Subsequent reaction of the intermediate takes place with reactant alcohol to release product alcohol converted from the charged ketone, accompanied by transformation into another intermediate with the alkoxo group of the reactant alcohol. The latter intermediate is expected to afford product ketone and to regenerate the catalytic hydride $CoHP_3$ species through β-hydrogen elimination. As mentioned above (Fig. 2), the linear relationship was observed on the double reciprocal plots of the initial reaction rates and the concentrations of the ketones charged, in sharp contrast to the case of the alcohols where their concentrations did not affect significantly the initial reaction rates in the concentration range under discussion. By analogy with the Michaelis-Menten model,[11] this result supported coordination equilibrium of ketones to $CoHP_3$ in our proposed reaction pathway. Moreover, pulsed laser photolysis of $CoHP_4$ was performed in the presence of some substrates used in this study, and confirmed ketone coordination to the photogenerated $CoHP_3$ species (vide infra).

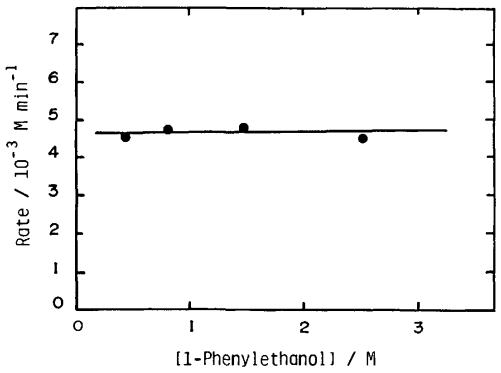

Fig. 3. Dependence of the initial reaction rate on the 1-phenylethanol concentration. CoH[PPh(OEt)2]4, 0.0165 M; cyclohexanone, 0.82 M.

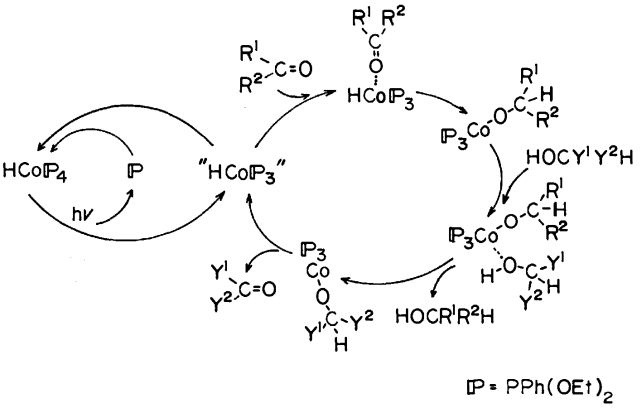

Hydrogen Transfer to 4-Alkyl-Substituted Cyclohexanones. 4-Alkyl-substituted cyclohexanones were employed as hydrogen acceptors in the photoassisted hydrogen-transfer reaction with the cobalt complex, to study stereoselectivity in reduction of the carbonyl groups. The hydrogen-transfer reaction of 1-phenylethanol with 4-methylcyclohexanone in benzene for 4 h gave 4-methylcyclohexanols with the cis/trans isomer ratio of about 2.1 in a 65% conversion, whereas similar reaction of neat 2-propanol showed the cis/trans ratio of 2.4 with the 87% conversion. For 4-*t*-butylcyclohexanone, the hydrogen-transfer reaction of 1-phenylethanol in benzene proceeded slowly to give 2.2 and 19% for the cis/trans value and the conversion, respectively. Free-energy difference between cis and trans 4-*t*-butylcyclohexanols has been described to be about 0.5 kcal mol^{-1},[12] which led to a value of 0.43 for the cis/trans ratio in the thermodynamically equilibrated state at 30 °C. It was determined that the present photoassisted hydrogen transfer with $CoHP_4$ afforded kinetically controlled product composition rather than thermodynamically controlled one, and preferred formation of thermodynamically less stable cis isomers. During the course of the probable transformation of hydrido(4-alkylcyclohexanone)cobalt species to cis and trans (4-alkylcyclohexyloxy)cobalt through hydride transfer to the carbonyl carbon, steric

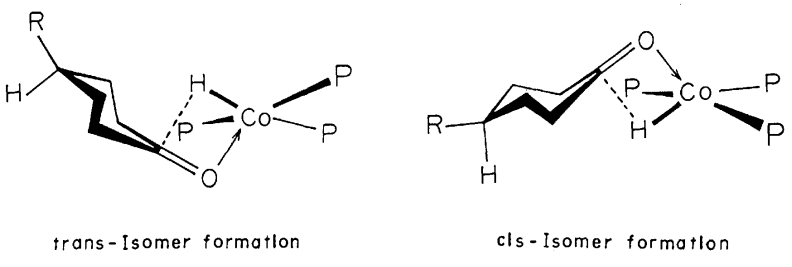

Fig. 4. Formation of trans and cis 4-substituted cyclohexanols.

approach control was presumed to prefer less sterically hindered pathway effectively, which afforded axial i.e. cis cyclohexanols.

Hydrogen Transfer to *p*-Substituted Benzaldehydes. In the hope to obtain some further clues to the present reaction mechanism, we performed the hydrogen transfer from neat 2-propanol to some *p*-substituted benzaldehydes, and studied substituent effect on the initial formation rates of the corresponding benzyl alcohols. Figure 5 shows good linear relationship of the logarithmic formation rates with the respective Hammett substituent constants σ_p^+. The reaction constant (the gradient of the linear relationship) ρ and the correlation coefficient were 1.348 and 0.997, respectively. Positive reaction constant ρ implys that the rate was enhanced by withdrawal of electron density from the reaction site. In connection with the above-described observation of the kinetically controlled hydrogen transfer to 4-alkyl-substituted cyclohexanones, this fact led us to conclude that the important rate-determining step was the hydride transfer to the carbonyl carbon with partial positive charge, at the stage of the transformation of hydrido-(aldehyde or ketone)cobalt into alkoxocobalt intermediate.[13] Subsequent reaction of the alkoxo intermediate with secondary reactant alcohols was assumed to be fast, in conformity with the finding that the initial hydrogen-transfer rate was not dependent apparently on the concentration of secondary alcohols charged (Fig. 3).

Laser Flash Photolysis and Substrate Coordination to $CoHP_3$. Laser flash photolysis of $CoHP_4$ was performed at 337 nm using a nitrogen laser in the presence of some substrates, such as cyclohexanone and 1-phenylethanol in benzene at room temperature. In the time-resolved absorption spectra, we monitored the decay of the transient bands of photogenerated $CoHP_3$ at 580 and 760 nm, due to recombination with free phosphonite and to substrate coordination. Table 1 summarizes the second-order coordination-rate constants k' of these and some related substrates.[5c,14]

$$-\frac{d[CoHP_3]}{dt} = k[CoHP_3][P] + k'[CoHP_3][\text{Substrate}]$$

P=$PPh(OEt)_2$, $k=1.4\times10^8\,M^{-1}s^{-1}$

The constants k' of ketones and aldehydes ranged from 10^5 to $10^8\ M^{-1}\ s^{-1}$, whereas those of the secondary alcohols were very small and undetermined explicitly. Therefore, this result confirmed the ketone coordination to the photogenerated $CoHP_3$ species, in the above-described reaction pathway concerning the photoassisted hydrogen transfer with $CoHP_4$. Moreover, Table 1 shows the constants k' of aldehydes were considerably larger than those of ketones. When the photogenerated $CoHP_3$ species approach the carbonyl groups in these compounds, interaction of the species was initiated with the HOMO of the groups, which expand mainly over the sp^2-hybrid plane,[15] as illustrated in Fig. 6. In the case of aldehydes, the $CoHP_3$ species can approach the carbonyl group easily through the less hindered side including the aldehyde hydrogen on the hybrid plane. However, in the case of ketones, substantial steric repulsion by the bulky

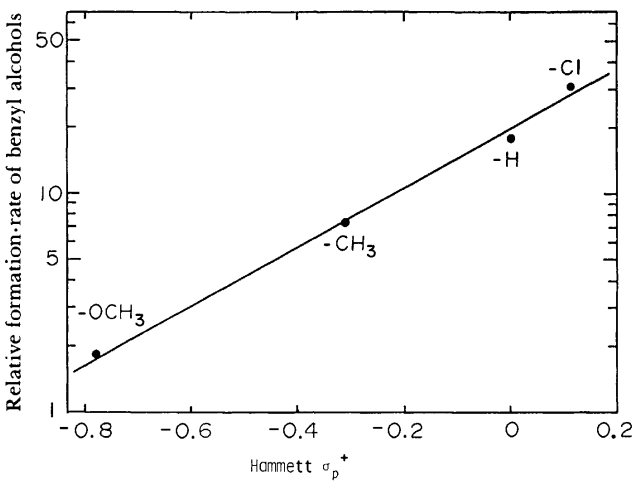

Fig. 5. Plots of the logarithmic formation rate of *p*-substituted benzyl alcohols against Hammett σ_p^+. $CoH[PPh(OEt)_2]_4$, 5×10^{-3} M; *p*-substituted benzaldehyde, 0.2 M; solvent, 2-propanol; temperature, 30°C.

Table 1. Second-Order Rate Constants k' ($M^{-1}\ s^{-1}$) for Coordination

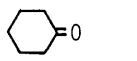	8.6×10^5	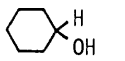	Negligible
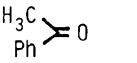	3.2×10^5	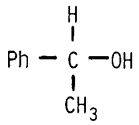	Negligible
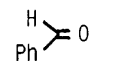	1.6×10^8	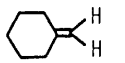	9.4×10^6
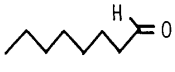	1.1×10^8	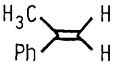	9.1×10^6

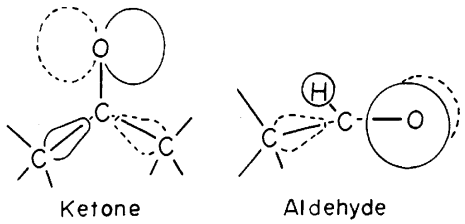

Fig. 6. Pictorial representation of the HOMO (n) orbitals of the carbonyl groups.

substituents introduced in place of the aldehyde hydrogen, was presumed to hinder the $CoHP_3$ approach to the carbonyl group. Steric factor was described previously to be dominant in the magnitude of the constants k' for aliphatic amines.[14]

It is noteworthy also that methylenecyclohexane showed a comparable value of the rate constant to that of 2-phenylpropene, whereas the constant of cyclohexanone was larger than that of acetophenone by a factor of ca. 2.7. In the cases of the former two substrates of olefins, the $CoHP_3$ species was attracted by the olefinic π-bond electrons and approached the axial site over the sp^2-hybrid plane of the two double-bonded carbons. On the other hand for the ketones, the species approached the HOMO expanded mainly over the sp^2-hybrid plane of the carbonyl groups, and steric factor was assumed to work in this planar approach process.

Concluding Remarks

Photogenerated hydride transient $CoHP_3$ catalyzed intermolecular hydrogen transfer from secondary alcohols to carbonyl compounds such as ketones. The catalytic reaction was initiated by coordination of the carbonyl compounds to $CoHP_3$. The rate-determining step was associated with the hydride transfer to the carbonyl carbon, at the stage of the transformation of hydrido(ketone or aldehyde)cobalt into alkoxo intermediate.

These studies were partially supported by the Iwatani Naoji Foundation's Research Grant. LFP was done at Radiation Laboratory, University of Notre Dame. S. O. thanks the Office of Basic Energy Sciences of the Department of Energy, U.S.A. The authors are grateful to Mr. Shoji Takahira for his technical assistance.

References

1) a) R. H. Crabtree, "The Organometallic Chemistry of the Transition Metals," John Wiley & Sons, New York (1988); b) J. P. Collman and L. S. Hegedus, "Principles and Applications of Organotransition Metal Chemistry," University Science Books, Mill Valey, California (1980).

2) a) P. K. Eidem, A. W. Maverick, and H. B. Gray, *Inorg. Chim. Acta*, **50**, 59 (1981); b) V. Balzani, L. Moggi, M. F. Manfrin, F. Bolletta, and M. Gleria, *Science*, **189**, 852 (1975); c) K. J. Brewer, W. R. Murphy, Jr., K. J. Moore, E. C. Eberle, and J. D. Petersen, *Inorg. Chem.*, **25**, 2470 (1986); d) T. Yoshida and S. Otsuka, *Adv. Chem. Ser.*, **196**, 135 (1982).

3) G. L. Geoffroy and M. S. Wrighton, "Organometallic Photochemistry," Academic Press, New York (1979).

4) a) M. S. Wrighton, J. L. Graff, R. J. Kazlauskas, J. C. Mitchener, and C. L. Reichel, *Pure Appl. Chem.*, **54**, 161 (1982); b) W. Strohmeier and G. Csontos, *J. Organomet. Chem.*, **67**, C27 (1974); c) J. L. Graff, T. J. Sobieralski, M. S. Wrighton, and G. L. Geoffroy, *J. Am. Chem. Soc.*, **104**, 7526 (1982); d) A. H. Janowicz and R. G. Bergman, *ibid.*, **105**, 3929 (1983); e) P. Bergamini, S. Sostero, and O. Traverso, *J. Organomet. Chem.*, **299**, C11 (1986); f) H. L. Conder, A. R. Courtney, and D. DeMarco, *J. Am. Chem. Soc.*, **101**, 1606 (1979); g) F. D. Miller and R. D. Sanner, *Organometallics*, **7**, 818 (1988); h) W. D. Jones and F. J. Feher, *J. Am. Chem. Soc.*, **106**, 1650 (1984); i) A. J. Kunin and R. Eisenberg, *ibid.*, **108**, 535 (1986); j) H. Kletzin and H. Werner, *Angew. Chem., Int. Ed. Engl.*, **22**, 873 (1983).

5) a) M. Onishi, K. Hiraki, M. Matsuda, and T. Fukunaga, *Chem. Lett.*, **1983**, 261; b) S. Oishi, K. Tajime, A. Hosaka, and I. Shiojima, *J. Chem. Soc., Chem. Commun.*, **1984**, 607; c) M. Onishi, S. Oishi, M. Sakaguchi, I. Takaki, and K. Hiraki, *Bull. Chem. Soc. Jpn.*, **59**, 3925 (1986).

6) M. Onishi, M. Matsuda, and K. Hiraki, *Chem. Lett.*, **1984**, 1157.

7) a) B. R. James, *Adv. Organomet. Chem.*, **17**, 319 (1979), and references cited therein; b) P. A. Chaloner, "Handbook of Coordination Catalysis in Organic Chemistry," Butterworths, London (1986).

8) a) R. G. Salomon and N. E. Sanadi, *J. Am. Chem. Soc.*, **97**, 6214 (1975); b) R. Damico and T. J. Logan, *J. Org. Chem.*, **32**, 2356 (1967).

9) D. Titus, A. A. Orio, and H. B. Gray, *Inorg. Synth.*, **13**, 117 (1979).

10) a) P. K. Das, M. V. Encinas, R. D. Small, Jr., and J. C. Scaiano, *J. Am. Chem. Soc.*, **101**, 6965 (1979); b) V. Nagarajan and R. W. Fessenden, *J. Phys. Chem.*, **89**, 2330 (1985).

11) A. Nakamura and M. Tsutsui, "Principles and Applications of Homogenous Catalysis," John Wiley & Sons, New York (1980).

12) E. L. Eliel, N. L. Allinger, S. J. Angyal, and G. A. Morrison, "Conformational Analysis," John Wiley & Sons, New York (1965).

13) The present authors did not agree with one-step addition model of the hydrido-cobalt bond to the carbonyl group through possible four-centered transition state, but supported stepwise addition model, i.e. coordination of the group to cobalt via oxygen atom and subsequent hydride transfer to the carbonyl carbon, in view of the following matters; (1) Observed double-reciprocal linear relationship between the initial hydrogen-transfer rates and ketone concentrations charged (Fig. 2), indicating coordination equilibrium of ketones to $CoHP_3$. (2) Spatial distribution of HOMO in the carbonyl groups (Fig. 6).

14) M. Onishi, I. Takaki, K. Hiraki, and S. Oishi, *J. Chem. Soc., Dalton Trans.*, **1988**, 2675.

15) W. L. Jorgensen and L. Salem, "The Organic Chemist's Book of Orbitals," Academic Press, New York (1973).

Rhodium Catalyzed Hydrogenation of Quinolines and Isoquinolines under Water-Gas Shift Conditions

Shun-Ichi MURAHASHI,* Yasushi IMADA, and Yoshiaki HIRAI
Department of Chemistry, Faculty of Engineering Science, Osaka University, Machikaneyama, Toyonaka, Osaka 560
(Received May 12, 1989)

Wide variety of quinolines and isoquinolines can be hydrogenated selectively in the nitrogen-containing ring by means of carbon monoxide and water in the presence of catalytic amount of rhodium carbonyl cluster. These reactions provide a useful method for the preparation of 1,2,3,4-tetrahydroquinolines and 1,2,3,4-tetrahydroisoquinolines which are key intermediates for the synthesis of isoquinoline alkaloids and other biologically active nitrogen compounds.

Polynuclear nitrogen heteroaromatic compounds, such as quinolines and isoquinolines are much contained in coal, oil shale, and tar sands.[1] Selective hydrogenation of these nitrogen heteroaromatics provides potential means for utilization of these natural resources, and various synthetic key intermediates can be obtained. 1,2,3,4-Tetrahydroquinoline derivatives are synthetic intermediates for drugs,[2] agrochemicals,[3] and dyes,[4] while 1,2,3,4-tetrahydroisoquinoline derivatives are useful precursors of isoquinoline alkaloids.[5] Water-gas shift reactions are of importance in view of energy problem because hydrogen can be generated from water and carbon monoxide, which is readily available from low-grade carbonaceous materials such as coal, oil shale, tar sands, and lignite.[6] The metal hydride species which are formed as intermediates of water-gas shift reactions, can be used directly as reducing agents. Therefore, the reduction of various substrates such as nitroarenes, carbonyl compounds, and α,β-unsaturated ketones and nitriles have been studied under water-gas shift conditions.[7]

We have found that hydrogenation of wide variety of quinolines and isoquinolines can be performed selectively under water-gas shift conditions as depicted by Eqs. 1 and 2.[8] The results are different from those obtained from the catalytic hydrogenations of nitrogen aromatics under molecular hydrogen.[9,10] Reduction of nitrogen heteroaromatics using carbon monoxide and water has been studied. Laine[11] reported that the reduction of pyridine to piperidine was catalyzed by rhodium complex. Fish and Kaezs reported that $Fe(CO)_5$[12,13] and $Mn_2(CO)_8(PBu_3)_2$[12] catalyzed the hydrogenation reaction in the presence of base such as KOH. As compared with these reports, we describe the full details of our reactions, which can be utilized for the selective hydrogenation of various types of substituted quinolines and isoquinolines.

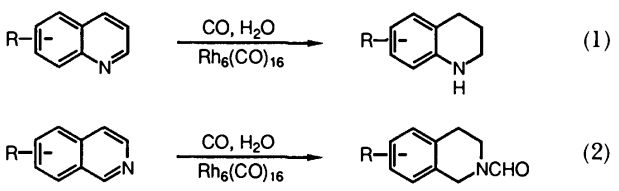

Results and Discussion

Hydrogenation of Quinolines. Quinolines are hydrogenated selectively in the nitrogen containing ring to give 1,2,3,4-tetrahydroquinolines under water-gas shift conditions. The catalytic activity of various metal carbonyls was examined with respect to the reaction of quinoline (**1**). The representative results are shown in Table 1. Rhodium carbonyl cluster $Rh_6(CO)_{16}$ gave the best results. The exclusive product detected during the reaction was 1,2,3,4-tetrahydroquinoline (**2**), and neither 5,6,7,8-tetrahydroquinoline nor decahydroquinoline were obtained. Rhodium clusters such as $Rh_4(CO)_{12}$ and $[Rh(COD)Cl]_2$ and ruthenium clusters such as $Ru_3(CO)_{12}$ gave good results. Other metal carbonyls such as $W(CO)_6$ and $Fe(CO)_5$ did not produce the hydrogenated product under the present conditions. Although $Fe(CO)_5$ has been reported to be an active catalyst for the hydrogenation of quinoline in the presence of KOH,[13] the catalytic activity was not

Table 1. Catalytic Activity of Various Metal Complexes for the Hydrogenation of **1**[a]

Entry	Catalyst	Amount/mol%	Convn.[b]/%	Yield[b]/%
1	$Rh_6(CO)_{16}$	0.81	100	97
2	$Rh_4(CO)_{12}$	1.2	80	75
3	$[Rh(COD)Cl]_2$	2.4	65	62
4	$Ru_3(CO)_{12}$	1.6	70	65
5	$W(CO)_6$	3.3	0	0
6	$Fe(CO)_5$	3.3	0	0

a) A mixture of quinoline (2.31 mmol), water (0.5 ml), and catalyst in 2-methoxyethanol (2 ml) was heated at 150 °C for 12 h under the pressure of CO (56 kg cm^{-2}). b) Determined by GLC analysis.

observed under the present conditions. The addition of bases enhances the catalytic activity of transition metal carbonyls under water-gas shift conditions.[14] The key point of the present reaction is that quinolines behave as bases to enhance the hydrogenation and are also reduced regioselectively in the nitrogen-containing ring. Most of the solvents examined such as, 2-methoxyethanol, toluene, dioxane, and dimethylformamide gave good results; however, chloroform retarded the reaction. Without a solvent **2** was obtained in low yields.

The representative results of the hydrogenation of quinolines under water-gas shift conditions are summarized in Table 2. In general, 1,2,3,4-tetrahydroquinolines are obtained selectively under the present reaction conditions. Substituted quinolines have been recovered under the conditions using $Fe(CO)_5$ catalyst.[13] It is noteworthy that 4-methylquinoline (**4**) can be converted into 4-methyl-1,2,3,4-tetrahydroquinoline (**5**) selectively (Entry 3) under the present water-gas shift conditions. In the nickel catalyzed hydrogenation of methyl substituted quinolines with molecular hydrogen, substituent on the benzene ring leads to exclusive formation of 1,2,3,4-tetrahydroquinolines, while substituent loading of the pyridine ring favors the formation of 5,6,7,8-tetrahydro compounds.[15] Typically, tetrahydroquinoline **5** was obtained selectively in 91% yield under the present reaction conditions. However, catalytic hydrogenation of **4** afforded a mixture of **5** and 4-methyl-5,6,7,8-tetrahydroquinoline (**6**) in 33% and 66% yields, respectively. The $Rh_6(CO)_{16}$ catalyzed hydrogenation of **4** under hydrogen (10 kg cm^{-2}) also gave **6** exclusively

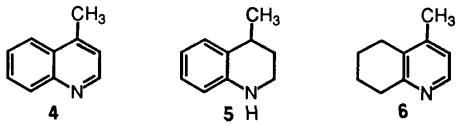

(50% conversion). Moreover, the hydrogenation of 2,4-dimethylquinoline (**10**) under the present conditions gave 2,4-dimethyl-1,2,3,4-tetrahydroquinoline (**11**) exclusively in 89% yield (Entry 6), while the hydrogenation of **10** with nickel catalyst under molecular hydrogen gave **11** only in 20% yield along with 80% of 5,6,7,8-tetrahydroquinoline.[15] The cis/trans ratio of

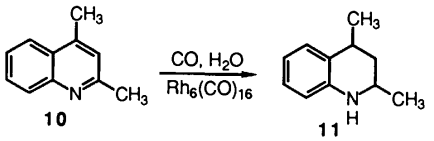

Table 2. Hydrogenation of Methyl Substituted Quinolines under Water-Gas Shift Conditions[a]

Entry	Quinoline	Tetrahydroquinoline	Yield[b]/%
1	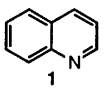	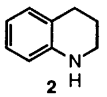	97
2	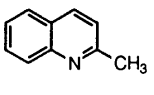	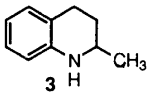	95
3	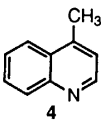	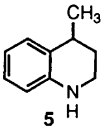	91
4	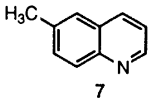	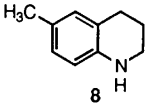	96
5	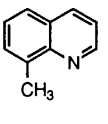	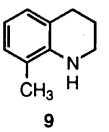	90
6	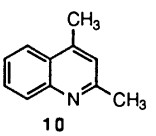	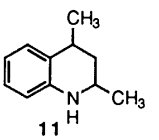	89[c]

a) A mixture of quinoline (2.31 mmol), $Rh_6(CO)_{16}$ (0.0188 mmol), and water (0.5 ml) in 2-methoxyethanol (2 ml) was heated at 150 °C for 24 h under the pressure of CO (56 kg cm^{-2}). b) Isolated yield. c) *cis*-**11**/*trans*-**11**=7/3.

Table 3. Hydrogenation of Substituted Quinolines under Water-Gas Shift Conditions[a]

Entry	Quinoline	Tetrahydroquinoline	Yield[b]/%
1	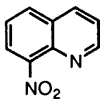 **12**	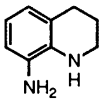 **13**	81[c]
2	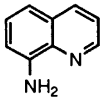 **14**	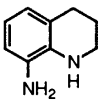 **13**	84
3	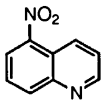	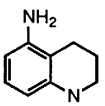 **15**	85
4	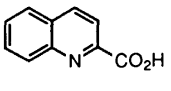	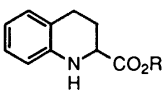 **16** R = $CH_2CH_2OCH_3$	61
5	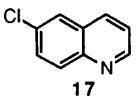 **17**	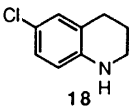 **18**	91[d]
6	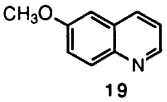 **19**	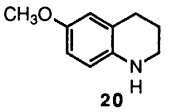 **20**	94

a) A mixture of quinoline (2.31 mmol), $Rh_6(CO)_{16}$ (0.0188 mmol), and water (0.5 ml) in 2-methoxyethanol (2 ml) was heated at 150 °C for 24 h under the pressure of CO (56 kg cm^{-2}). b) Isolated yield. c) Reaction time was 48 h. d) Reaction time was 12 h.

11 was determined to be 7/3 on the basis of ^1H and ^{13}C NMR analyses.

Quinolines bearing other functional groups also undergo the hydrogenation on the pyridine ring to give the corresponding 1,2,3,4-tetrahydroquinolines. These results are summarized in Table 3. 8-Nitroquinoline (**12**) was reduced under the rhodium catalyzed water-gas shift conditions (48 h) to give 8-amino-1,2,3,4-tetrahydroquinoline (**13**) exclusively (Entry 1), while the same reaction of **12** for shorter time (24 h) gave **13** and 8-aminoquinoline (**14**) in 61% and 16% yields, respectively. 8-Aminoquinoline **14** was also converted into **13** highly efficiently (Entry 2). Therefore, the reduction of the nitro group of **12** proceeds faster than that of the pyridine ring. 5-Aminoquinoline was also converted into 5-amino-1,2,3,4-tetrahydroquinoline (**15**) (Entry 3). The reaction of 2-quinolinecarboxylic acid afforded 2-methoxyethyl 1,2,3,4-tetrahydroquinoline-2-carboxylate (**16**) (Entry 4), which was formed by hydrogenation followed by esterification with 2-methoxyethanol. 6-Chloroquinoline (**17**) was converted into 6-chloro-1,2,3,4-tetrahydroquinoline (**18**) selectively without cleavage of carbon–halogen bond (Entry 5). By using this product, various functional groups can be introduced at 6-position of tetrahydroquinolines.

The tetrahydroquinolines thus obtained are valuable synthetic intermediates. Tungstate catalyzed oxidation of tetrahydroquinolines with hydrogen peroxide gives the corresponding hydroxamic acids,[16] which show antibacterial activity[17] and also are precursors of biologically active compounds, such as 3,4-dihydrocarbostyril compounds. Typically, the treatment of tetrahydroquinoline **8**, which was obtained from **7** in 96% yield, with aqueous 30% hydrogen peroxide in the presence of catalytic amount of Na_2WO_4 gave 1-hydroxy-6-methyl-1,2,3,4-tetrahydroquinolin-2-one (**21**)

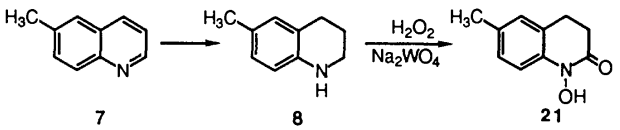

7 8 **21**

in 82% yield. Amino-1,2,3,4-tetrahydroquinolines are useful precursors of hair coloring compositions[4] and fungicides.[18] Treatment of **13** with diethyl carbonate in acetic acid gave 1,2,5,6-tetrahydroimidazoquinolin-2-one **22**.[18] Furthermore, the reaction of **5** with

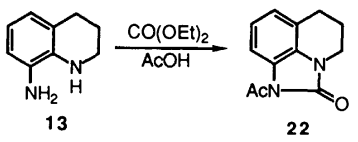

13 22

bromoacetyl bromide followed by intramolecular alkylation gives 1,2,5,6-tetrahydropyrroloquinolin-2-one **24**, which has pharmacological activity and has been used as CNS depressant agents.[19]

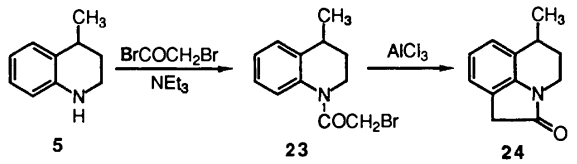

5 23 24

Next, the reactivity of four 6-substituted quinolines, that is, quinoline (**1**), 6-methylquinoline (**7**), 6-chloroquinoline (**17**), and 6-methoxyquinoline (**19**) was compared. The results are listed in Table 4. Quinolines **1** and **17** were reduced completely within 5 h; however, the conversion of quinolines **7** and **19** were only 30% and 35% after 5 h and 70% and 80% after 10 h, respectively. The rate difference seems to reflect electronic requirement of substituents at the 6-position. Thus, electron withdrawing substituents such as chloro group accelerate the reaction, while electron donating substituents retard the reactivity.

Table 4. Reactivity of Quinolines **1**, **7**, **17**, and **19** for the Hydrogenation[a]

Run time	Convn. of quinolines[b]/%			
	1	**17**	**7**	**19**
5 h	>98	>98	30	35
12 h			70	80
24 h			>98	>98

a) A mixture of quinoline (2.31 mmol), $Rh_6(CO)_{16}$ (0.0188 mmol), and water (0.5 ml) in 2-methoxyethanol (2 ml) was heated at 150 °C under the pressure of CO (56 kg cm^{-2}). b) Determined by 270 MHz ^{1}H NMR analysis.

Hydrogenation of Isoquinolines. Isoquinolines were converted into *N*-formyl-1,2,3,4-tetrahydroisoquinolines under the same conditions. Typically, the reaction of isoquinoline gave *N*-formyl-1,2,3,4-tetrahydroisoquinoline (**25**) in 69% isolated yield. When the same reaction was carried out for shorter reaction time, a mixture of **25** and 1,2,3,4-tetrahydroisoquinoline (**26**) was obtained, indicating that initial formation of **26** and subsequent *N*-formylation. The *N*-formylation of tetrahydroisoquinoline **26** may be due to higher basicity of nitrogen of **26** in comparison with **2**. Indeed, **25** was obtained from **26** in 76% yield under the same conditions. The representative results of the hydrogenation of isoquinolines are summarized in Table 5. It is noteworthy that benzyloxy group torelates the reaction, although benzyloxy group is readily removed by reductive cleavage under usual hydrogenation conditions. Thus, 6-benzyloxy-7-methoxyisoquinoline was converted into the corresponding *N*-formyl-6-benzyloxy-7-methoxy-1,2,3,4-tetrahydroisoquinoline (**27**) (Entry 2).

N-Formyltetrahydroisoquinolines thus obtained can be readily converted into *N*-methyltetrahydroisoquinolines upon treating with $LiAlH_4$. Thus, the reduction of **27** with $LiAlH_4$ gave 6-benzyloxy-7-methoxy-*N*-methyl-1,2,3,4-tetrahydroisoquinoline (**29**) selectively in 83% yield. *N*-Formyl group on 1,2,3,4-tetrahydroisoquinolines can be removed readily by acid catalyzed hydrolysis. Thus, when *N*-formyl compound **27** was allowed to react with sulfuric acid in methanol (1/9) at

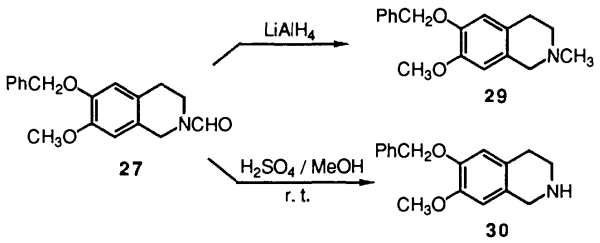

27 29 30

Table 5. Hydrogenation of Isoquinolines under Water-Gas Shift Conditions[a]

Entry	Isoquinoline	Tetrahydroisoquinoline	Yield[b]/%
1	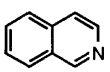	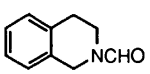 **25**	69
2	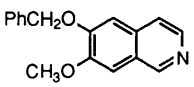	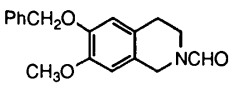 **27**	65
3	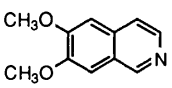	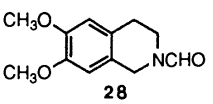 **28**	66

a) A mixture of isoquinoline (2.31 mmol), $Rh_6(CO)_{16}$ (0.0188 mmol), and water (0.5 ml) in 2-methoxyethanol (2 ml) was heated at 150 °C for 24 h under the pressure of CO (56 kg cm^{-2}). b) Isolated yield.

room temperature, 6-benzyloxy-7-methoxy-1,2,3,4-tetrahydroisoquinoline (**30**) was obtained in 95% yield. 6,7-Dimethoxy-1,2,3,4-tetrahydroisoquinoline (**31**) was also obtained upon hydrolysis of *N*-formyl-6,7-dimethoxy-1,2,3,4-tetrahydroisoquinoline (**28**) in 96% yield.

The tetrahydroisoquinolines thus obtained are quite useful synthetic intermediates. Introduction of substituents at position 1 of tetrahydroisoquinolines can be performed readily by using our recently developed methods, that is, oxidation of secondary amines to give either imines[20] or nitrones[21] and subsequent treatment of these intermediates with nucleophiles as shown in Scheme 1.

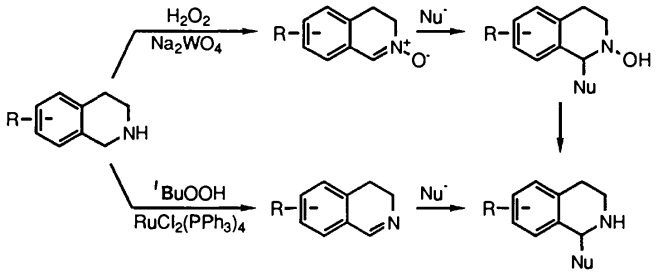

Scheme 1.

Mechanisms. The hydrogenation of quinoline **1** using deuterium oxide in place of water in toluene was examined. The product of deuterated 1,2,3,4-tetrahydroquinoline was analyzed by 270 MHz ^{1}H NMR spectroscopy, and the results were shown in Scheme 2. The product obtained after 5 h had 1.2 deuteriums at position 2, 1.0 deuterium at position 3, 1.2 deuteriums at position 4, and 0.2 deuterium at each positions 5 and 8. The product obtained after 24 h had 1.7 deuteriums at position 2, 1.0 deuterium at position 3, 1.2 deuteriums at position 4, and 0.9 deuterium at each positions 5 and 8. When 1,2,3,4-tetrahydroquinoline (**2**) was subjected to the same conditions for 5 h, the product had 0.1 deuterium at position 2 and 0.8 deuterium each at positions 5 and 8, and no deuterium incorporation was observed at positions 3 and 4 as shown in Scheme 3. Thus, water must be the hydrogen source in the present hydrogenation reaction, and each 1.0 deuterium was introduced at the positions of 2, 3, and 4. The deuterium incorporation at positions 5 and 8 may be due to the exchange of the aromatic hydrogen of **2** rather than **1**. The deuterium incorporation at positions 5 and 8 in **2** is noteworthy, although specific reason has not been clarified yet. The deuterium incorporation at position 2 in **2** is derived from dehydrogenation–hydrogenation process of **2** via intermediacy imine metal complex.[22,23]

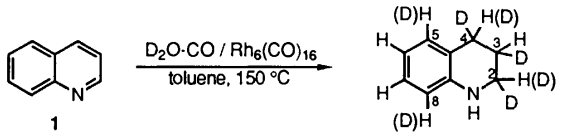

position	2	3	4	5	8
5 h	1.2	1.0	1.2	0.2	0.2
24 h	1.7	1.0	1.2	0.9	0.9

Scheme 2.

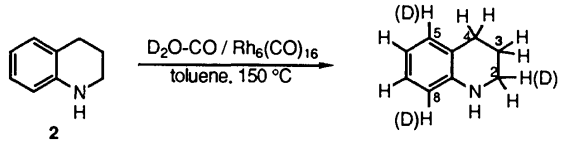

position	2	3	4	5	8
5 h	0.1	0	0	0.8	0.8

Scheme 3.

Although the exact nature of the active species still remains unspecified, a hydrido rhodium carbonyl species[24] seems to be the active catalyst. Recently Fish[25] reported that **1** reacts with mononuclear rhodium dication complex to form N-bounded rhodium–quinoline complex, while **2** complexes with π-bonding rather than N-bonding. Laine[26] and Fish[27] isolated ruthenium–quinoline complexes by the reaction of **1** with $Ru_3(CO)_{12}$, and the structure of the complexes has been characterized as triangle of ruthenium atoms with **1** bound to the cluster to the nitrogen and the 2-carbon atoms. The catalytic cycle is rationalized by assuming Scheme 4. The first step is the coordination of quinoline to the rhodium catalyst to give the N-bounded rhodium–quinoline complex **32**. Water-gas shift reactions induced by rhodium and ruthenium catalysts are promoted by amines, and hence amine-coordinated complexes have been considered to be active species.[14a,c] The water-gas shift reaction gives quinoline-coordinated rhodium hydride species **34**. Subsequent intramolecular addition of nitrogen-bounded rhodium hydride to the pyridine ring of

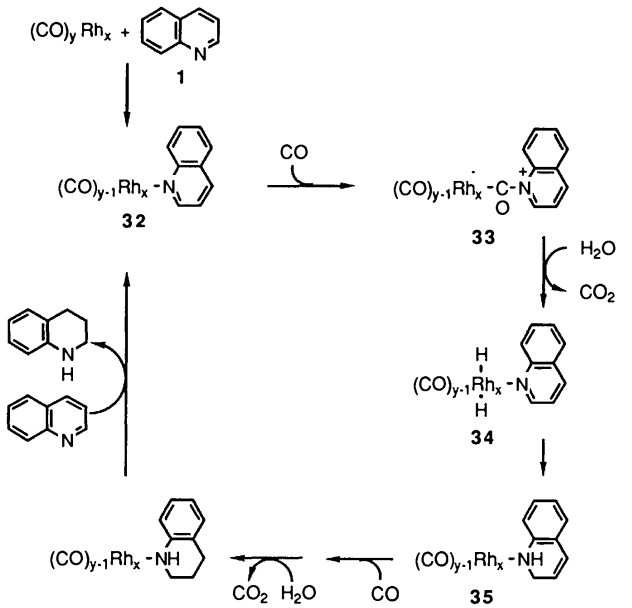

Scheme 4.

quinoline results in regioselective reduction to give **35**, Similar reaction of **35** with carbon monoxide and water gives 1,2,3,4-tetrahydroquinoline along with **32**.

In summary, the rhodium carbonyl cluster catalyzes the hydrogenation of a wide variety of quinolines by means of water and carbon monoxide. The hydrogenation proceeds regioselectively to give 1,2,3,4-tetrahydroquinolines efficiently. Similar treatment of isoquinolines affords the corresponding *N*-formyl-1,2,3,4-tetrahydroisoquinolines.

Experimental

General. All melting points were determined in capillary tubes and are uncorrected. IR spectra were recorded on a Hitachi 215 spectrometer. NMR spectra were obtained on JEOL JNM PMX-60SI (60 MHz for ^1H) and JEOL JNM GSX-270 (270 MHz for ^1H and 67.9 MHz for ^{13}C) spectrometers; chemical shifts (δ) were expressed in parts per million down field from tetramethylsilane. Analytical GLC evaluations of products mixtures were carried out on Shimadzu GC-9A flame ionization gas chromatograph by using a 1 m×4 mm analytical column (10% SE-30 on 60—80 mesh Uniport HP). Preparative TLC was performed on glass plates coated with Merck silica gel 60 PF_{254} (art. 7747). Mass spectra were obtained on a Hitachi RMS-4 or Shimadzu GCMS-QP1000 mass spectrometers. Elemental analyses were performed on a Yanagimoto MT-3 CHN corder.

Materials. $Rh_6(CO)_{16}$ (Nippon Engelhald Co., Ltd.) and other metal catalysts were commercially available and used as received, except $Fe(CO)_5$ which was distilled prior to use and $Mo(CO)_6$ which was sublimed prior to use. 2-Methoxyethanol was commercially available and used as received. Quinolines and isoquinolines were commercially available and used as received except 8-aminoquinoline, 5- and 8-nitroquinoline,[28] 6-benzyloxy-7-methoxyisoquinoline, and 6,7-dimethoxyisoquinoline[29] which were prepared according to the reported procedure.

Catalytic Activity of Various Metal Complexes. A mixture of quinoline (**1**), metal complex, H_2O (0.5 mL), and 2-methoxyethanol (2 mL) was heated at 150 °C for 12 h in a 10-mL stainless-steel autoclave under the pressure of CO (56 kg cm^{-2}). The conversion of **1** and the yield of 1,2,3,4-tetrahydroquinoline (**2**) were determined by the GLC analysis of the reaction mixture using an internal standard (dodecane). The results with various catalysts are shown in Table 1.

General Procedure for Hydrogenation of Quinolines and Isoquinoline under Water-Gas Shift Conditions. In a 10-mL stainless-steel autoclave equipped with a magnetic stirring bar were placed quinoline (2.31 mmol), $Rh_6(CO)_{16}$ (0.020 g, 0.0188 mmol), H_2O (0.5 mL, 27.8 mmol), and 2-methoxyethanol (2.0 mL). The autoclave was sealed and degassed by three 5 kg cm^{-2} pressurization/depressurization cycles with CO. The autoclave was then charged to 56 kg cm^{-2} of CO and heated with stirring a 150 °C for 24 h. After the autoclave was cooled to room temperature, the pressure was released. The reaction mixture was taken up with chloroform and filtered through a pad of Florisil (3 g, 14×55 mm). After removal of the solvent under reduced pressure, the product was purified by means of silica-gel column chromatography (ca. 5 g, eluents are described below) or Kugelrohr distillation. These results are summarized in Tables 2, 3, and 5.

1,2,3,4-Tetrahydroquinoline (2): Bp 126—127 °C/3 mmHg (1 mmHg≈133.3 Pa) (Kugelrohr); R_f 0.83 (SiO_2, ethyl acetate); ^1H NMR ($CDCl_3$, 270 MHz) δ=1.91 (2H, tt, J=6.3 and 5.8 Hz, H^3), 2.74 (2H, t, J=6.3 Hz, H^4), 3.26 (2H, t, J=5.8 Hz, H^2), 3.76 (1H, br-s, NH), 6.43 (1H, d, J=7.4 Hz, H^8), 6.58 (1H, t, J=7.2 Hz, H^6), and 6.90—6.98 (2H, m, H^5 and H^7).

Found: C, 81.26; H, 8.34; N, 10.41%. Calcd for $C_9H_{11}N$: C, 81.16; H, 8.33; N, 10.52%.

2-Methyl-1,2,3,4-tetrahydroquinoline (3): Bp 126 °C/5 mmHg (Kugelrohr); R_f 0.69 (SiO_2, ethyl acetate-hexane=1:4); IR (neat) 3400 (NH), 2940, 2860, 1615, 1500, 1320, and 775 cm^{-1}; ^1H NMR ($CDCl_3$, 270 MHz) δ=1.19 (3H, d, J=6.3 Hz, CH_3), 1.57 (1H, dddd, J=12.8, 11.4, 9.9, and 5.5 Hz, H^{3a}), 1.91 (1H, dddd, J=12.8, 5.6, 3.5, and 2.9 Hz, H^{3e}), 2.71 (1H, ddd, J=16.4, 5.5, and 3.5 Hz, H^{4e}), 2.83 (1H, J=16.4, 11.4, and 5.6 Hz, H^{4a}), 3.38 (1H, ddq, J=9.9, 6.3, and 2.9 Hz, H^2), 3.60 (1H, br-s, NH), 6.45 (1H, dd, J=8.1 and 1.2 Hz, H^8), 6.59 (1H, ddd, J=7.3, 7.3, and 1.2 Hz, H^6), and 6.90—6.99 (2H, m, H^5 and H^7); ^{13}C NMR ($CDCl_3$, 67.9 MHz) δ=22.6, 26.6, 30.2, 47.2, 114.0, 117.0, 121.1, 126.7, 129.3, and 144.8.

Found: C, 81.36; H, 8.80; N, 9.43%. Calcd for $C_{10}H_{13}N$: C, 81.58; H, 8.90; N, 9.52%.

4-Methyl-1,2,3,4-tetrahydroquinoline (5): Bp 150 °C/5 mmHg (Kugelrohr); IR (neat) 3400 (NH), 2960, 2860, 1610, 1585, 1500, 1360, 1315, 1070, and 740 cm^{-1}; ^1H NMR ($CDCl_3$, 270 MHz) δ=1.25 (3H, d, J=7.1 Hz, CH_3), 1.62 (1H, dddd, J=12.8, 6.4, 6.4, and 3.8 Hz, H^{3e}), 1.92 (1H, J=12.8, 8.2, 5.3, and 4.2 Hz, H^{3a}), 2.80—2.92 (1H, m, H^4), 3.17 (1H, ddd, J=11.2, 6.4, and 4.2 Hz, H^{2e}), 3.25 (1H, ddd, J=11.2, 8.2, and 3.8 Hz, H^{2a}), 3.75 (1H, br-s, NH), 6.39 (1H, dd, J=7.9 and 1.2 Hz, H^8), 6.59 (1H, ddd, J=7.5, 7.5, and 1.2 Hz, H^6), 6.92 (1H, ddd, J=7.9, 7.5, and 1.2 Hz, H^7), and 7.01 (1H, d, J=7.5 Hz, H^5); ^{13}C NMR ($CDCl_3$, 67.9 MHz) δ=22.6, 29.9, 30.2, 39.0, 114.1, 116.8, 126.5, 126.7, 128.3, and 144.3; mass spectrum (80 eV), m/z (relative intensity) 147 (M^+, 44), 146 (M^+-1, 10), 133 (100), and 118 (26).

Found: C, 81.46; H, 8.95; N, 9.46%. Calcd for $C_{10}H_{13}N$: C, 81.58; H, 8.90; N, 9.52%.

6-Methyl-1,2,3,4-tetrahydroquinoline (8): Bp 144—145 °C/5 mmHg (Kugelrohr); IR (neat) 3350 (NH), 3000, 2900, 2830, 1610, 1510, 1260, and 800 cm^{-1}; ^1H NMR ($CDCl_3$, 270 MHz) δ=1.87—1.96 (2H, m, H^3), 2.19 (3H, s, CH_3), 2.72 (2 H, t, J=6.5 Hz, H^4), 3.25 (2H, t, J=5.5 Hz, H^2), 3.51 (1H, br-s, NH), 6.38 (1H, d, J=8.5 Hz, H^8), and 6.75—6.78 (2H, m, H^5 and H^7); ^{13}C NMR ($CDCl_3$, 67.9 MHz) δ=20.4, 22.5, 26.9, 42.2, 114.5, 121.6, 126.2, 127.3, 130.1, and 142.4.

Found: C, 81.64; H, 8.80; N 9.44%. Calcd for $C_{10}H_{13}N$: C, 81.58; H, 8.90; N, 9.52%.

8-Methyl-1,2,3,4-tetrahydroquinoline (9): Bp 148—150 °C/5 mmHg (Kugelrohr); R_f 0.79 (SiO_2, ethyl acetate); IR (neat) 3400 (NH), 2930, 2840, 1600, 1490, 1360, 1310, 1270, 1190, 1110, 750, and 730 cm^{-1}; ^1H NMR ($CDCl_3$, 270 MHz) δ=1.92 (2H, tt, J=6.4 and 5.5 Hz, H^3), 2.05 (3H, s, CH_3), 2.77 (2H, t, J=6.4 Hz, H^4), 3.34 (2H, t, J=5.5 Hz, H^2), 3.60 (1H, br-s, NH), 6.54 (1H, dd, J=7.4 and 7.4 Hz, H^6), and 6.80—6.88 (2H, m, H^5 and H^7); ^{13}C NMR ($CDCl_3$, 67.9 MHz) δ=17.1, 22.1, 27.3, 42.3, 116.4, 120.8, 121.1, 127.3, 127.8, and 142.7.

Found: C, 81.60; H, 8.87; N, 9.41%. Calcd for $C_{10}H_{13}N$: C, 81.58; H, 8.90; N, 9.52%.

2,4-Dimethyl-1,2,3,4-tetrahydroquinoline (11): Bp 143—144 °C/4 mmHg (Kugelrohr); R_f 0.70 (SiO_2, ethyl acetate);

IR (neat) 3370 (NH), 3040, 2960, 2850, 1610, 1580, 1480, 1300, 1260, 1170, 1160, 1130, 1040, and 840 cm^{-1}; ^1H NMR ($CDCl_3$, 270 MHz) δ=1.17 (3H×0.7, d, J=6.2 Hz, cis-2-CH_3), 1.19 (3H×0.3, d, J=6.2 Hz, trans-2-CH_3), 1.26 (3H×0.3, d, J=7.2 Hz, trans-4-CH_3), 1.31 (3H×0.7, d, J=6.7 Hz, cis-4-CH_3), 1.34 (1H×0.7, ddd, J=12.8, 11.2, and 11.1 Hz, cis-H^{3a}), 1.636 (1H×0.3, dd, J=6.5 and 4.0 Hz, trans-H^{3a}), 1.638 (1H×0.3, dd, J=7.5 and 5.0 Hz, trans-H^{3e}), 1.91 (1H×0.7, ddd, J=12.8, 5.3, and 2.6 Hz, cis-H^{3e}), 2.80—3.00 (1H, m, H^4), 3.30—3.55 (1H, m, H^2), 3.47 (1H, br-s, NH), 6.44 (1H×0.7, dd, J=7.9 and 1.2 Hz, cis-H^8), 6.47 (1H×0.3, dd, J=7.9 and 1.2 Hz, trans-H^8), 6.58—6.66 (1H×0.3, m, trans-H^6), 6.64 (1H×0.7, ddd, J=7.6, 7.5, and 1.2 Hz, cis-H^6), 6.91—6.99 (1H×0.3, m, trans-H^7), 6.96 (1H×0.7, ddd, J=7.9, 7.5, and 1.2 Hz, cis-H^7), 6.99—7.04 (1H×0.3, m, trans-H^5), and 7.12 (1H×0.7, ddd, J=7.6, 1.2, and 1.2 Hz cis-H^5); ^{13}C NMR ($CDCl_3$, 67.9 MHz) δ=20.3 (cis-4-CH_3), 22.7 (2-CH_3), 24.8 (trans-4-CH_3), 30.1 (trans-C^4), 30.8 (cis-C^4), 37.1 (trans-C^3), 40.6 (cis-C^3), 42.3 (trans-C^2), 47.3 (cis-C^2), 113.9 (cis-C^8), 114.0 (trans-C^8), 116.9 (trans-C^6), 117.2 (cis-C^{6a}), 126.2 (C^{4a}), 126.6 (trans-C^7), 126.7 (cis-C^7), 126.8 (cis-C^5), 129.1 (trans-C^5), 144.1 (trans-C^{8a}), and 144.7 (cis-C^{8a}).

Found: C, 82.05; H, 9.39; N, 8.57%. Calcd for $C_{11}H_{15}N$: C, 81.93; H, 9.38; N, 8.69%.

8-Amino-1,2,3,4-tetrahydroquinoline (13): Bp 172 °C/5 mmHg (Kugelrohr); R_f 0.62 (SiO_2, ethyl acetate); IR (neat) 3330 (NH), 3050, 2930, 2850, 1600, 1500, 1330, 1290, 1250, 1180, 1100, 990, 760, and 730 cm^{-1}; ^1H NMR ($CDCl_3$, 60 MHz) δ=1.65—2.15 (2H, m, H^3), 2.73 (2H, t, J=6.0 Hz, H^4), 3.13 (3H, br-s, NH and NH_2), 3.10—3.43 (2H, m, H^2), and 6.50 (3H, s, ArH).

Found: C, 72.85; H, 8.20; N, 18.73%. Calcd for $C_9H_{12}N_2$: C, 72.94; H, 8.16; N, 18.90%.

5-Amino-1,2,3,4-tetrahydroquinoline (15): Mp 102 °C; R_f 0.76 (SiO_2, ethyl acetate); IR (Nujol) 2870, 1580, 1340, 1250, 1170, 1130, and 760 cm^{-1}; ^1H NMR ($CDCl_3$, 270 MHz) δ=2.00 (2H, tt, J=6.6 and 5.4 Hz, H^3), 2.47 (2H, t, J=6.6 Hz, H^4), 3.23 (2H, t, J=5.4 Hz, H^2), 3.52 (3H, br-s, NH and NH_2), 5.99 (1H, d, J=7.9 Hz), 6.07 (1H, d, J=7.9 Hz), and 6.79 (1H, dd, J=7.9 and 7.9 Hz, H^7); ^{13}C NMR ($CDCl_3$, 67.9 MHz) δ=21.5, 22.4, 41.4, 104.7, 105.6, 106.8, 127.0, 144.9, and 145.8.

Found: C, 72.77; H, 8.13; N, 18.82%. Calcd for $C_9H_{12}N_2$: C, 72.94; H, 8.16; N, 18.90%.

2-Methoxyethyl 1,2,3,4-Tetrahydroquinoline-2-carboxylate (16): Bp 230—232 °C/7 mmHg (Kugelrohr); R_f 0.81 (SiO_2, ethyl acetate); IR (neat) 3400 (NH), 2930, 1740 (C=O), 1610, 1590, 1500, 1200, 1120, 1040, and 740 cm^{-1}; ^1H NMR ($CDCl_3$, 270 MHz) δ=2.01 (1H, dddd, J=12.9, 8.9, 8.9, and 5.5 Hz, H^{3a}), 2.31 (1H, dddd, J=12.9, 5.6, 5.6, and 3.8 Hz, H^{3e}), 2.74 (1H, ddd, J=16.5, 5.6, and 5.5 Hz, H^{4e}), 2.83 (1H, J=16.5, 8.9, and 5.6 Hz, H^{4a}), 3.38 (3H, s, OCH_3), 3.61 (2H, t, J=4.7 Hz), 4.0 (1H, br, NH), 4.08 (1H, dd, J=8.9 and 3.8 Hz, H^2), 4.33 (2H, t, J=4.7 Hz), 6.58 (1H, dd, J=7.9 and 0.9 Hz, H^8), 6.64 (1H, ddd, J=7.4, 7.3, and 1.2 Hz, H^6), and 6.92—7.03 (2H, m, H^5 and H^7); ^{13}C NMR ($CDCl_3$, 67.9 MHz) δ=24.7, 25.8, 53.9, 59.0, 64.2, 70.3, 114.6, 117.6, 120.5, 127.0, 129.1, 143.0, and 173.3.

Found: C, 66.31; H, 7.27; N, 5.85%. Calcd for $C_{13}H_{17}NO_3$: C, 66.35; H, 7.30; N, 5.95%.

6-Chloro-1,2,3,4-tetrahydroquinoline (17): Reaction time was 12 h: IR (neat) 3400 (NH), 2930, 2840, 1600, 1580, 1495, 1470, 1350, 1300, 1270, 1180, 1080, 950, 890, and 800 cm^{-1}; ^1H NMR ($CDCl_3$, 270 MHz) δ=1.89 (2H, tt, J=6.4 and 5.5 Hz, H^3), 2.71 (2H, t, J=6.4 Hz, H^4), 3.26 (2H, t, J=5.5 Hz, H^2), 3.75 (1H, br-s, NH), 6.36 (1H, dd, J=7.2 and 1.7 Hz, H^8), and 6.86—6.91 (2H, m, H^5 and H^7); ^{13}C NMR ($CDCl_3$, 67.9 MHz) δ=21.6, 26.8, 41.7, 115.0, 120.8, 122.7, 126.3, 128.9, and 143.3.

17·HCl: Found: C, 52.89; H, 5.39; N, 6.82; Cl, 34.35%. Calcd for $C_9H_{11}NCl_2$: C, 52.97; H, 5.43; N, 6.86; Cl, 34.74%.

6-Methoxy-1,2,3,4-tetrahydroquinoline (20): Bp 162—168 °C/6 mmHg (Kugelrohr); IR (neat) 3380 (NH), 2940, 2840, 1520, 1470, 1300, 1260, 1240, 1200, 1160, 1040, and 810 cm^{-1}; ^1H NMR ($CDCl_3$, 270 MHz) δ=1.86—1.95 (2H, m, H^3), 2.73 (2H, t, J=6.5 Hz, H^4), 3.20—3.25 (2H, m, H^2), 3.43 (1H, br-s, NH), 3.71 (3H, s, OCH_3), 6.42 (1H, d, J=8.4 Hz, H^8), and 6.53—6.60 (2H, m, H^5 and H^7); ^{13}C NMR ($CDCl_3$, 67.9 MHz) δ=22.5, 27.2, 42.4, 55.8, 113.0, 115.0, 115.6, 122.9, 138.9, and 151.9.

Found: C, 73.68; H, 8.08; N , 8.46%. Calcd for $C_{10}H_{13}NO$: C, 73.59; H, 8.03; N, 8.58%.

2-Formyl-1,2,3,4-tetrahydroquinoline (25): R_f 0.44 (SiO_2 ethyl acetate); IR (neat) 2850, 1660 (C=O), 1440, 1400, 1190, 930, and 750 cm^{-1}; ^1H NMR ($CDCl_3$, 60 MHz) δ=2.90 (2H, t, J=6.0 Hz, H^4), 3.58 (2H×0.6, t, J=6.0 Hz, H^3), 3.73 (2H×0.4, t, J=6.0 Hz, H^3), 4.47 (2H×0.4, s, H^1), 4.62 (2H×0.6, s, H^1), 7.00 (4H, s, ArH), 8.10 (1H×0.6, s, NCHO), and 8.15 (1H×0.4, s, NCHO).

Found: C, 74.41; H, 6.80; N, 8.55%. Calcd for $C_{10}H_{11}NO$: C, 74.51; H, 6.88; N, 8.69%.

2-Formyl-6-benzyloxy-7-methoxy-1,2,3,4-tetrahydroisoquinoline (27): IR (neat) 2940, 1665 (C=O), 1620, 1520, 1450, 1260, 1225, 1115, 1020, 860, 750, and 700 cm^{-1}; ^1H NMR ($CDCl_3$, 270 MHz) δ=2.72 (2H×0.4, t, J=6.1 Hz, H^4), 2.75 (2H×0.6, t, J=5.9 Hz, H^4), 3.57 (2H×0.6, t, J=5.9 Hz, H^3), 3.74 (2H×0.4, t, J=6.1 Hz, H^3), 3.84 (3H×0.6, s, OCH_3), 3.85 (3H×0.4, s, OCH_3), 4.44 (2H×0.4, s, H^1), 4.59 (2H×0.6, s, H^1), 5.10 (2H, s), 6.59 (1H×0.4, s), 6.62 (2H×0.6, s), 6.65 (1H×0.4, s), 7.26—7.45 (5H, m, Ph), 8.16 (1H×0.6, s, NCHO), and 8.22 (1H×0.4, s, NCHO); ^{13}C NMR ($CDCl_3$, 67.9 MHz) δ=27.5, 29.2, 38.0, 42.0, 43.3, 47.1, 56.18, 56.24, 71.25, 71.32, 109.5, 110.0, 114.7, 114.8, 124.5, 124.7, 125.5, 126.4, 127.3, 127.86, 127.90, 128.5, 137.0, 137.1, 147.1, 148.9, 161.1, and 161.5; mass spectrum (80 eV), m/z (relative intensity) 297 (M^+, 4), 265 (3), 206 (M^+-CH_2Ph, 5), 178 (5), and 91 (100).

Found: C, 72.97; H, 6.68; N, 4.63%. Calcd for $C_{18}H_{19}NO_3$: C, 72.71; H, 6.44; N, 4.71%.

2-Formyl-6,7-dimethoxy-1,2,3,4-tetrahydroisoquinoline (28) Mp 127—128 °C; R_f 0.26 (SiO_2, ethyl acetate); ^1H NMR ($CDCl_3$, 270 MHz) δ=2.79 (2H×0.4, t, J=6.1 Hz, H^4), 2.83 (2H×0.6, t, J=5.8 Hz, H^4), 3.63 (2H×0.6, t, J=5.8 Hz, H^3), 3.78 (2H×0.4, t, J=6.1Hz, H^3), 3.85 (6H×0.6, s, OCH_3), 3.86 (6H×0.4, s, OCH_3), 4.47 (2H×0.4, s, H^1), 4.61 (2H×0.6, s, H^1), 6.58 (1H×0.4, s), 6.60 (2H×0.6, s), 6.62 (1H×0.4, s), 8.19 (1H×0.6, s, NCHO), and 8.25 (1H×0.4, s, NCHO); ^{13}C NMR ($CDCl_3$, 67.9 MHz) δ=27.6, 29.3, 38.1, 42.0, 43.4, 47.1, 56.0, 56.05, 56.10, 108.9, 109.4, 111.7, 112.0, 123.8, 124.0, 125.4, 126.4, 148.0, 148.2, 148.3, 161.1, and 161.6.

Found: C, 65.02; H, 6.76; N, 6.07%. Calcd for $C_{12}H_{15}NO_3$: C, 65.13; H, 6.85; N, 6.33%.

Hydrogenation of 4 Using Molecular Hydrogen. A mixture of **4** (1.57 g, 11.0 mmol) and $Rh_6(CO)_{16}$ (0.024 g, 0.023 mmol) was heated at 200 °C for 20 h under the pressure of H_2 (10 kg cm^{-2}). After cooling to room temperature, the reaction mixture was taken up with ether and filtered. After removal of the solvent under reduced pressure, silica-gel column chromatography (ethyl acetate–hexane=3:7) afforded

4-methyl-5,6,7,8-tetrahydroquinoline (**6**) (0.680 g, 47%): R_f 0.50, (SiO_2, ethyl acetate); ^1H NMR ($CDCl_3$, 270 MHz) δ=1.82—1.88 (4H, m, H^6 and H^7), 2.20 (3H, s, CH_3), 2.64 (2H, t, J=6.1 Hz), 2.91 (2H, t, J=6.1 Hz), 6.89 (1H, d, J=4.8 Hz, H^3), and 8.22 (1H, d, J=4.8 Hz, H^2); ^{13}C NMR ($CDCl_3$, 67.9 MHz) δ=18.8, 22.86, 22.91, 25.8, 33.0, 122.6, 131.1, 145.8, 146.1, and 156.7.

Oxidation of 8 to 1-Hydroxy-6-methyl-1,2,3,4-tetrahydroquinolin-2-one (21): To a mixture of **8** (0.270 g, 1.83 mmol) and sodium tungstate monohydrate (0.012 g, 0.04 mmol) in methanol (25 mL) was added dropwise 30% aqueous hydrogen peroxide (0.62 mL, 6.0 mmol) at 0 °C under nitrogen. The reaction mixture was stirred at room temperature for 24 h. After removal of methanol under reduced pressure, the solidified dark brown residue was extracted with dichloromethane (10 mL×4). The combined extracts were dried over sodium sulfate and evaporated. Silica-gel column chromatography (20×80 mm, dichloromethane–ether=9:1) gave **21** (0.267 g, 82%): mp 137.8—138.5 °C; R_f 0.35 (SiO_2, ether); IR (Nujol) 2900 (O-H), 1645 (C=O), 1285, 1245, 1215, 1080, 1025, 975, 890, 850, 820, and 740 cm^{-1}; ^1H NMR ($CDCl_3$, 270 MHz) δ=2.30 (3H, s, CH_3), 2.72 (2H, dd, J=7.7 and 7.0 Hz, H^3), 2.90 (2H, dd, J=7.7 and 7.0 Hz, H^4), 6.95 (1H, s, H^5), 7.08 (1H, d, J=8.1 Hz), 7.25 (1H, d, J=8.1 Hz), and 8.0—10.0 (1H, br, OH); ^{13}C NMR ($CDCl_3$, 67.9 MHz) δ=20.7, 24.6, 30.0, 113.0, 123.4, 128.08, 128.11, 133.4, 134.8, and 164.7.

Found: C, 67.88; H, 6.22; N, 7.83%. Calcd for $C_{10}H_{11}NO_2$: C, 67.78; H, 6.26; N, 7.91%.

Synthesis of 1-Acetyl-1,2,5,6-tetrahydro-4*H*-imidazo[4,5,1-*ij*]quinolin-2-one (22). In a 25-mL round-bottomed flask equipped with a reflux condenser were placed **13** (0.148 g, 1.00 mmol), diethyl carbonate (0.13 mL, 1.07 mmol), and acetic acid (5 mL). The mixture was stirred at 100 °C for 3 h. The reaction mixture was cooled to room temperature, basified with dilute aqueous ammonia, and extracted with chloroform (10 mL×3). The combined extracts were dried over sodium sulfate and evaporated. The residue was chromatographed on silica gel (20×80 mm, ethyl acetate–hexane=1:1 and methanol) to afford **22** (0.102 g, 49%) along with unreacted **13** (0.031 g, 21%). Thus, the yield based on consumed **13** is 62%: R_f 0.69 (SiO_2, methanol); ^1H NMR ($CDCl_3$, 60 MHz) δ=2.10 (2H, tt, J=5.5 and 6.0 Hz, H^5), 2.43 (3H, s, $NCOCH_3$), 2.85 (2H, t, J=5.5 Hz, H^6), 3.90 (2H, t, J=6.0 Hz, H^4), and 6.97—7.47 (3H, m, ArH); mass spectrum (70 eV), m/z (relative intensity) 172 (M^+-COCH_3, 100), 171 (90), 144 (14), and 130 (30).

Synthesis of 6-Methyl-1,2,5,6-tetrahydro-4*H*-pyrrolo[3,2,1-*ij*]quinolin-2-one (24). In a 50-mL round-bottomed flask were placed tetrahydroquinoline **5** (0.294 g, 2.00 mmol), bromoacetyl bromide (0.20 mL, 2.30 mmol), triethylamine (0.3 mL, 2.15 mmol), and benzene (10 mL). The reaction mixture was stirred at room temperature under argon atmosphere for 3 h. The resulting mixture was washed with water (10 mL×3) and dried over magnesium sulfate. After removal of the solvent under reduced pressure, column chromatography on silica gel (18×60 mm, ethyl acetate–hexane=1:1) gave 1-bromoacetyl-4-methyl-1,2,3,4-tetrahydroquinoline (**23**) (0.512 g, 96%).

In a 50-mL round-bottomed flask were placed **23** (0.128 g, 0.478 mmol) and aluminum chloride (0.190 g, 1.43 mmol). After the mixture was heated at 150 °C for 30 min, crushed ice was added to the reaction mixture. The resulting mixture was made alkaline with dilute aqueous ammonia and extracted with chloroform (10 mL×3). Combined organic layers were dried over magnesium sulfate. After removal of the solvent under reduced pressure, the residue was sublimed (110 °C, 5 mmHg, 10 h) to give **24** (0.058 g, 65%). **23**: R_f 0.91 (SiO_2, ethyl acetate); IR (neat) 2950, 2870, 1730, 1650, 1580, 1490, 1380, 1200, 1120, and 750 cm^{-1}; ^1H NMR ($CDCl_3$, 60 MHz) δ=1.26 (3H, d, J=6.0 Hz, CH_3), 1.90—2.30 (2H, m, H^3), 2.47—3.03 (1H, m, H^4), 3.70 (2H, t, J=5.0 Hz, H^2), 4.00 (2H, s, $COCH_2$), and 7.00—7.50 (4H, m, ArH). **24:** R_f 0.61 (SiO_2, ethyl acetate); ^1H NMR ($CDCl_3$, 270 MHz) δ=1.34 (3H, d, J=7.1 Hz, CH_3), 1.72 (1H, dddd, J=13.7, 8.7, 8.6, and 4.4 Hz, H^{5a}), 2.06 (1H, J=13.7, 6.7, 4.4, and 4.2 Hz, H^{5e}), 2.90—3.03 (1H, m, H^6), 3.50 (2H, s, H^1), 3.63 (1H, ddd, J=13.2, 8.6, and 4.2 Hz, H^{4a}), 3.85 (1H, ddd, J=13.2, 6.7, and 4.4 Hz, H^{4e}), 6.95 (1H, dd, J=7.6 and 7.6 Hz, H^8), and 7.05—7.12 (2H, m, H^7 and H^9); ^{13}C NMR ($CDCl_3$, 67.9 MHz) δ=19.9, 29.3, 29.4, 36.7, 37.1, 122.0, 122.2, 123.3, 125.1, 125.2, 141.7, and 174.1.

Found: C, 76.62; H, 6.98; N, 7.50%. Calcd for $C_{12}H_{13}NO$: C, 76.96; H, 7.01; N, 7.48%.

Hydrogenation of 1 by Using Deuterium Oxide. The reaction of **1** with D_2O was carried out according to the general procedure by using toluene in place of 2-methoxyethanol. The product was analyzed by 270 MHz ^1H NMR and the results were shown in Scheme 2.

Preparation of 6-Benzyloxy-7-methoxy-2-methyl-1,2,3,4-tetrahydroisoquinoline (29). In a 200-mL three-necked flask equipped with a reflux condenser and a dropping funnel were placed lithium aluminum hydride (0.339 g, 0.892 mmol) and anhydrous tetrahydrofuran (15 mL). To the suspension was added cautiously a solution of **27** (1.34 g, 4.51 mmol) in anhydrous tetrahydrofuran (26 mL). After addition was complete, the reaction mixture was refluxed for 15 h. Stirring was continued while the mixture was cooled in an ice bath and a saturated aqueous solution of sodium sulfate was added cautiously until the hydrogen evolution ceased. The mixture was then filtered and evaporated to afford **29** (1.06 g, 83%). An analytical sample after recrystallization from hexane showed following properties: mp 93—94 °C; IR (Nujol) 3300 (N-H), 1610, 1520, 1225, 1130, 1010, 750, and 700 cm^{-1}; ^1H NMR ($CDCl_3$, 270 MHz) δ=2.44 (3H, s, CH_3), 2.64 (2H, t, J=5.9 Hz), 2.78 (2H, t, J=5.9 Hz), 3.50 (2H, s, H^1), 3.83 (s, 3H, OCH_3), 5.09 (2H, s, OCH_2Ph), 6.53 (1H, s), 6.63 (1H, s), and 7.25—7.50 (5H, m, Ph); ^{13}C NMR ($CDCl_3$, 67.9 MHz) δ=28.7, 46.0, 52.9, 56.2, 57.6, 71.3, 110.2, 114.7, 125.9, 127.37, 127.41, 127.7, 128.5, 137.4, 146.9, and 148.1.

Preparation of 6-Benzyloxy-7-methoxy-1,2,3,4-tetrahydroisoquinoline (30). In a 50-mL round-bottomed flask were placed **28** (0.947 g, 3.18 mmol) and a mixture of sulfuric acid and methanol (1/9) (20 mL). After the mixture was stirred at room temperature for 48 h, the solution was basified with diluted aqueous ammonia. After methanol was removed under reduced pressure, the resulting aqueous solution was extracted with chloroform (10 mL×3). The combined organic layers were dried over sodium sulfate and evaporated to give **30**: mp 78 °C; ^1H NMR ($CDCl_3$, 270 MHz) δ=1.81 (1H, br-s, NH), 2.64 (2H, t, J=5.8 Hz), 3.08 (2H, t, J=5.8 Hz), 3.83 (3H, s, OCH_3), 3.93 (2H, s, H^1), 5.10 (2H, s, OCH_2Ph), 6.53 (1H, s), 6.61 (1H, s), and 7.25—7.46 (5H, m, Ph); ^{13}C NMR ($CDCl_3$, 67.9 MHz) δ=28.6, 44.0, 48.0, 56.2, 71.4, 110.0, 115.3, 126.7, 127.3, 127.8, 128.5, 128.6, 137.4, 146.8, and 148.2; mass spectrum (80 eV), m/z (relative intensity) 269

(M^+, 9), 178 (M^+-CH_2Ph), 150 (27), and 91 (100).

Found: C, 75.49; H, 7.12; N, 5.04%. Calcd for $C_{17}H_{19}NO_2$: C, 75.81; H, 7.11; N, 5.20%.

6,7-Dimethoxy-1,2,3,4-tetrahydroisoquinoline (31). ^1H NMR ($CDCl_3$, 270 MHz) δ=2.02 (1H, br-s, NH), 2.71 (2H, t, J=5.9 Hz, H^4), 3.12 (2H, t, J=5.9 Hz, H^3), 3.83 (3H, s, OCH_3), 3.84 (3H, s, OCH_3), 3.94 (2H, s, H^1), 6.51 (1H, s), and 6.58 (1H, s); ^{13}C NMR ($CDCl_3$, 67.9 MHz) δ=28.7, 44.0, 48.0, 56.0, 109.3, 112.2, 126.6, 127.8, 147.4, and 147.6.

References

1) D. McNeil, "Chemistry of Coal Utilization, Second Suppl. Vol.," ed by M. A. Elliott, Wiely, New York (1981), p. 1003.

2) A. Ferranti, L. Garuti, G. Giovanninetti, R. Gaggi, P. Roncada, and P. Nardi, *Farmaco, Ed. Sci.*, **42**, 237 (1987); G. C. Wright and D. E. Portlock, Ger. Offen. 3004370 (1980); *Chem. Abstr.*, **93**, 239262u (1980).

3) Y. Kurahashi, K. Shiokawa, T. Goto, S. Kagabu, A. Kamochi, K. Moriya, and H. Hayakawa, Eur. Patent 173208 (1986); *Chem. Abstr.*, **105**, 78937s (1986).

4) D. Rose, P. Busch, and E. Lieske, Ger. Offen. 2714955 (1978); *Chem. Abstr.*, **90**, 43672w (1979).

5) For review: M. Shamma and J. L. Moniot, "Isoquinoline Alkaloids Research," Plenum, New York (1978).

6) R. M. Laine and R. B. Wilson, Jr., "Aspects of Homogeneous Catalysis Vol 5," ed by R. Ugo, Reidel, Dordrecht, Holland (1984), p. 217.

7) a) R. Pettit, K. Cann, T. Cole, C. H. Mauldin, and W. Slegeir, *Adv. Chem. Ser.*, **173**, 121 (1979); b) P. Escaffre, A. Thorez, and P. Kalck, *J. Mol. Catal.*, **33**, 87 (1985).

8) S.-I. Murahashi, Y. Imada, and Y. Hirai, *Tetrahedron Lett.*, **28**, 77 (1987).

9) For review: M. Freifelder, *Adv. Catal.*, **14**, 203 (1963); P. Rylander, "Catalytic Hydrogenation in Organic Syntheses," Academic Press, New York (1979), p. 213.

10) a) R. H. Fish, J. L. Tan, and A. D. Thormodsen, *J. Org. Chem.*, **49**, 4500 (1984); b) R. H. Fish, J. L. Tan, and A. D. Thormodsen, *Organometallics*, **4**, 1743 (1985).

11) a) R. M. Laine, D. W. Thomas, and L. W. Cary, *J. Org. Chem.*, **44**, 4964 (1979); b) R. M. Laine, D. W. Thomas, and L. W. Cary, *J. Am. Chem. Soc.*, **104**, 1763 (1982).

12) R. H. Fish, A. D. Thormodsen, and G. A. Cremer, *J. Am. Chem. Soc.*, **104**, 5234 (1982).

13) a) T. J. Lynch, M. Banah, M. McDougall, and H. D. Kaesz, *J. Mol. Catal.*, **17**, 109 (1982); b) T. J. Lynch, M. Banah, H. D. Kaesz, and C. R. Porter, *J. Org. Chem.*, **49**, 1266 (1984).

14) a) R. C. Ryan, G. M. Wilemon, M. P. Dalsanto, and C. U. Pittman, Jr., *J. Mol. Catal.*, **5**, 319 (1979); b) K. Kaneda, M. Hiraki, K. Sano, T. Imanaka, and S. Teranishi, *ibid.*, **9**, 227 (1980); c) W. A. R. Slegeir, R. S. Sapienza, and B. Easterling, *ACS Symp. Ser.*, **152**, 325 (1981).

15) J. von Braun, W. Gmelin, and A. Schultheiss, *Chem. Ber.*, **56**, 1338 (1923).

16) S.-I. Murahashi, T. Oda, T. Sugahara, and Y. Masui, *J. Chem. Soc., Chem. Commun.*, **1987**, 1471.

17) R. T. Coutts, D. Noble, and D. G. Wibberley, *J. Pharm. Pharmacol.*, **16**, 773 (1964).

18) S. Inoue, N. Yamashita, and T. Uematsu, Jpn. Kokai Tokkyo Koho 79-132232 (1979); *Chem. Abstr.*, **92**, 105843e (1980).

19) G. E. Hardtmann, U.S. Patent 4015005 (1977); *Chem. Abstr.*, **87**, 39306a (1977).

20) a) H. Mitsui, S. Zenki, T. Shiota, and S.-I. Murahashi, *J. Chem. Soc., Chem. Commun.*, **1984**, 874; b) S.-I. Murahashi and T. Shiota, *Tetrahedron Lett.*, **28**, 2383 (1987); c) S.-I. Murahashi and T. Shiota, *ibid.*, **28**, 6469 (1987).

21) S.-I. Murahashi, T. Naota, and H. Taki, *J. Chem. Soc., Chem. Commun.*, **1985**, 613.

22) S.-I. Murahashi, N. Yoshimura, T. Tsumiyama, and T. Kojima, *J. Am. Chem. Soc.*, **105**, 5002 (1983).

23) C. W. Jung, J. D. Fellmann, and P. E. Garrou, *Organometallics*, **2**, 1042 (1983).

24) R. M. Laine, *J. Am. Chem. Soc.*, **100**, 6451 (1978).

25) R. H. Fish, H.-S. Kim. J. E. Babin, and R. D. Adams, *Organometallics*, **7**, 2250 (1988).

26) A. Eisenstadt, C. M. Giandomenico, M. F. Frederick, and R. M. Laine, *Organometallics*, **4**, 2033 (1985).

27) R. H. Fish, T.-J. Kim, J. L. Stewart, J. H. Bushweller, R. K. Rosen, and J. W. Dupon, *Organometallics*, **5**, 2193 (1986).

28) V. M. Dziomko and I. A. Krasavin, *Khim. Geteroskil.*, **1967**, 281.

29) A. J. Birch, A. H. Jackson, and V. R. Shanon, *J. Chem. Soc., Perkin Trans. 1*, **1974**, 2185.

 © 1989 The Chemical Society of Japan Bull. Chem. Soc. Jpn., 62, 2977—2980 (1989)

(−)-(9Z)-1,9-Heptadecadiene-4,6-diyn-3-ol as a Principal Component of the Resinous Sap of Evodiopanax innovans Nakai, Japanese Name, Takanotsume, and Its Role in an Ancient Golden Varnish of Japan[1)]

Akira TERADA,* Yasuhiro TANOUE, and Daishiro KISHIMOTO
Department of Chemistry, Faculty of Engineering, Kyushu Institute of Technology, Tobata, Kitakyushu 804
(Received November 30, 1988)

(−)-(9Z)-1,9-Heptadecadiene-4,6-diyn-3-ol was for the first time isolated in high yield (29%) from the resinous sap of Evodiopanax innovans Nakai, Araliaceae. This compound has been associated with the main polymerizable component of an ancient golden varnish. It has also been associated with a phytoalexin and a defense material which produces a water-insoluble coating film by photopolymerization under sunlight for a Takanotsume tree upon being wounded.

(−)-(9Z)-1,9-Heptadecadiene-4,6-diyn-3-ol, also called panaxynol,[2)] falcarinol,[3)] and carrotatoxin,[4)] was first isolated in high yield as the main component of the resinous sap of the Takanotsume tree; it was previously used as one of the GONZETSU paints in Japan. GONZETSU was a golden-colored, anticorrosive paint varnish (photopolymerizable by sunlight) used for armor suits and helmets in ancient Japan, Korea, and China.[5)] GONZETSU paint used in ancient Japan had been named as KOSHIABURA and was thought to be the resinous sap of the Koshiabura tree (Acanthopanax sciadophylloides French et. Sav., Araliaceae),[6)] though its correct origin remained unproven until recently.[7)]

Terada[8)] studied the historical documents concerning GONZETSU, as well as the floras of the Koshiabura tree and similar trees such as Kakuremino and Takanotsume trees, Araliaceae in Japan. He also investigated the chemical constituents of their resinous saps, arriving at the conclusion that in Korea and China during the T′ang dynasty the GONZETSU was called ŌSHITSU (yellow varnish), the resinous saps of trees of the Dendropanax genus (Araliaceae family; these plants belong to one and the same genus of Japanese Kakuremino tree, namely, Dendropanax morbifera Leb., in Korea, and Dendropanax chevalieri (Viquier) Merr., in Chechiang-Sheny of China). He also concluded that in Japan the resinous saps of trees of Koshiabura, Takanotsume, and Kakuremino (Dendropanax trifidus Makino) were used for the same purpose.[9)] The saps of the former two were the indigenous Japanese golden varnish GONZETSU; their fast-drying abilities were so valuable that they were exported to T′ang and Po-hai in ancient times.[9)] All of them were called either GONZETSU or KOSHIABURA in Japan, and were photosensitive paints which could harden under sunlight irradiation.[9)]

We have already reported on the chemical constituents of the resinous saps of Koshiabura and Japanese Kakuremino,[10,11)] and recently found that they contained polyacetylenic compounds.[12)] The present report deals with the detection of a polyacetylenic compound((−)-(9Z)-1,9-heptadecadiene-4,6-diyn-3-ol) as the main component of Takanotsume resinous sap as well as its sunlight polymerization and biological roles.

Results and Discussion

The ethanolic extract of Takanotsume sap (**1**) was a red brown oil, and showed conjugated polyacetylenic absorption bands in IR and UV which implied an ene-diyne conjugated system.[13)] Since this sample accompanied many mono- and sesquiterpenes and polymers and was very labile, catalytic hydrogenation at ordinary temperature and pressure was carried out and gave white crystals: $C_{17}H_{36}O$, mp 51.5—52 °C in 27% yield. ^{13}C NMR and other analytical evidence showed that this was 3-heptadecanol (**2**).

Repeated TLC separations of the crude sample (**1**) of polyacetylenes afforded an analytical sample, $C_{17}H_{24}O$ (**3**) in 29% yield, which showed $[\alpha]_D^{18}$ −36.93°; the IR spectrum was identical with that of (−)-(9Z)-1,9-heptadecadiene-4,6-diyn-3-ol, panaxynol, isolated and identified already by Takahashi et al.[2a)] from the Ginseng root (Panax ginseng C. A. Meyer) in 0.1% yield. This was also identical with the carrotatoxin isolated in a trace amount (between 10 and 20 ppm) as a natural toxicant from vegetable carrot (Daucus carota L.) by Crosby and Aharonson,[4)] and with falcarinol from Falcaria vulgaris Bernh and from many other Umbelliferae by Bohlmann et al.[3)] All of them were shown to be the same compound by Bently et al.[14)]

The MnO_2 oxidation of **3** resulted in the formation of (9Z)-1,9-heptadecadiene-4,6-diyn-3-one (**4**), also proving the existence of **3** in Takanotsume sap.

Compound **3** polymerizes in sunlight to produce a golden, transparent, hard film that is insoluble in solvents. In general, a conjugated polyacetylenic compound quickly polymerizes under daylight[15)] or UV-light irradiation,[16)] and the following polymer structure, like **5** in Fig. 1 for example, may be typical in the case of the conjugated diacetylene (**3**).[16)] Upon polymerization, the carbon-carbon double bonds in the R and R′ groups (Fig. 1) may be co-operative dur-

ing polymerization. The IR- and UV-absorption spectra of the dried film **5** are shown in Figs. 2 and 3, respectively, along with those of **3**.

The IR-absorption bands of the monomer **3** at 2255 (C≡C–C≡C, strong), 983 and 929 (vinyl), and 692 cm^{-1} (C=C, cis) were absent in the polymer film (**5**). Moreover, new characteristic bands of the polymer (**5**) appeared at 2195, 2155, and 2120 (C≡C–C=C, conjugated, all weak), and at 979 and 955 cm^{-1} (C=C, conjugated). Tieke et al. ascribed these phenomena to the C≡C-streching modes of the polymer backbone with various C–C-skeleton motions, judged from a large number of small peaks around them.[18] In addition, the structure of the polymer was supported by the finding of Baughman et al. that the polymer backbone was best represented by $(=C-C\equiv C-C=)_n$ from its Raman spectra.[19] These facts show that the polymer backbone is built up by a structure like **5** in Fig. 1.

The UV of polymer **5** in Fig. 3 shows a bathochromic shift and the polymer color is, therefore, a golden-yellow. Usually, to make Langmuir–Blodgett multilayers a number of conjugated diacetylenes are employed in solid state polymerization by irradiation of the UV light from a high-pressure mercury lamp; the

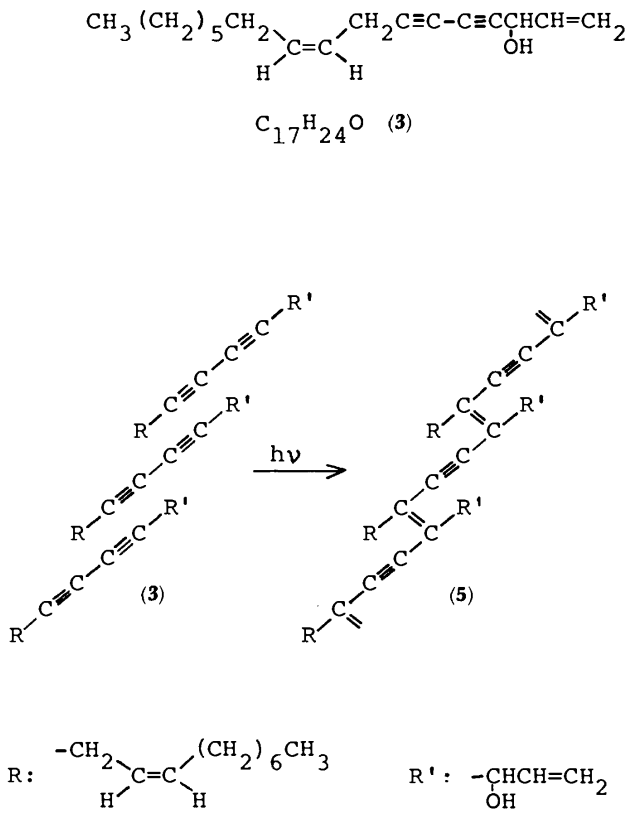

Fig. 1. Photopolymerization of **3**.

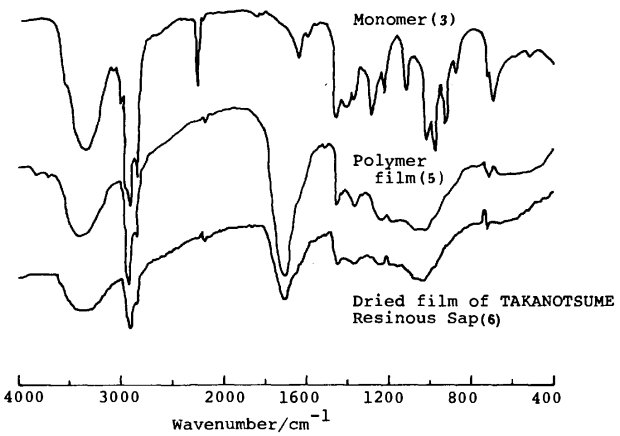

Fig. 2. IR of monomer **3**, polymer **5**, and dried film of TAKANOTSUME resinous sap.

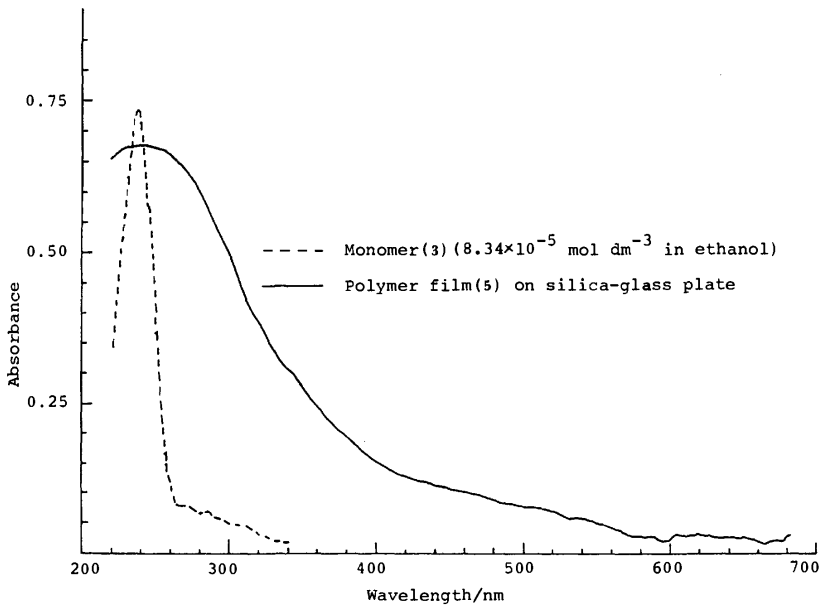

Fig. 3. UV of monomer **3** and polymer **5**.

reactions come to completion within a few minutes. These polymerizations proceed topochemically without any destruction of the layer structures, and appear as deep purple; this color changes irreversibly to red upon treatment with ethanol or chloroform.[16] Because the net-worked insoluble polymer **5**, which we obtained in this study, is not such a high-molecular-weight one and does not have such a stereoregularity, it therefore shows a golden-yellow color owing to the short-distance conjugation of carbon–carbon double and triple bonds in the polymer backbone. Krieger said that a polymer having a highly planar backbone is blue, that a slightly planar one is red, and that a highly nonplanar one is yellow.[20]

We also show the IR of a dried fim of Takanotsume sap in Fig. 2-**6**. This is almost the same with that of the polymer **5**.

The above-mentioned facts prove that this sap would be one of the old GONZETSU paint-compounds which made the old armors and helmets golden-colored, waterproof and anticorrosive.

Yoshioka et al.[21] have reported that the hexane extract of Takanotsume stems showed no conjugated polyacetylenic compound on its UV-spectral detection. Thus, our finding that compound **3** occurs only upon cutting the bark to obtain sap would suggest that this is a phytoalexin which can be used as an antiseptic. Dewit and Kodde have reported this compound **3**, falcarinol, as a phytoalexin, which was found in tomato (Lycopersicon esculentum) after incubation with Cladosporium fulvum.[22] Harding and Heale have found falcarinol to be one of the inhibitory compounds in the induced resistance response of carrot root slices; the compound was active against Botrysis cinerea.[23] We also suppose that the compound **3** that we obtained here acts effectively as defensive-type substance through a phytoalexin and also by forming a coating film over a raw wound. These phenomena suggest that compound **3** would play a similar role to Japanese lacquer urushiol found in the sap of Rhus verniciflua Stokes.

Otsuka et al. have found a strong inhibitory activity of the chloroform extract of roots of Panax ginseng C. A. Meyer against the formation of granulation tissue and proved that compound **3** and linoleic acid were the major active components.[24]

In Japan, especially in Northeast districts (Tohoku), some people have a well-established custom of eating the young leaves of Takanotsume. They also feed domestic animals the leaves since the tree is of little importance these days. Yasue et al.[25] have reported an accident in which some goats were poisened after eating this food. We suppose that since many polyacetylenic compounds are well known to be poisonous to fish,[26] and that compound **3** has been found as a natural toxicant by Crosby and Aharonson,[4] such a poisoning might suggest an accumulation of compound **3** as well as closely related polyacetylenic compounds in their food leaves.

We also conclude again that the occurrence of a great quantity of compound **3** in a wounded Takanotsume tree is for phytoalexin and serves as a barrier against the raw wound through polymerization; it then makes its own cure.

Experimental

Infrared and ultraviolet absorption spectra were recorded on Hitachi 260-30 infrared and Hitachi 139 UV spectrophotometers, respectively. ^1H and ^{13}C NMR spectra were obtained on a JEOL JNM-FX 60 spectrometer operated at 60 and 15.04 MHz, respectively. Mass spectra were determined on a JEOL DX-300 spectrometer. Mp's(corrected) were determined on a Yanagimoto micromelting point apparatus. TLC separations were performed by silica gel(Merck, 60 PF).

Ethanolic Extract of Takanotsume sap. Takanotsume sap was dissolved in ethanol, filtered and concentrated under diminished pressure to give an orange-yellow oil (**1**). IR (neat) 3380 (broad, OH), 2250 (sharp, -C≡C-), 2230 (weak, -C≡C-), 1640 (-C=C-), and 698 cm^{-1} (cis -CH=CH-). The benzene extract of **1** showed the UV_{max} (methanol) at 228, 237, 254, 269, and 285 nm. This orange-yellow oil (**1**) spread on a glass plate was dried under sunlight irradiation for half an hour,[1] resulting in the formation of a golden-colored, transparent, hard film.

Catalytic Hydrogenation of Ethanolic Extract of Takanotsume sap. Upon hydrogenation using a platinum black catalyst in ethanol under ambient temperature and atmospheric pressure, 1.740 g of the ethanolic extract (**1**) absorbed 551.6 ml of hydrogen and yielded 27% of white crystals, mp 51.5—52 °C, after purifications by silica-gel column chromatography and recrystallization from ethanol. The ^{13}C NMR data showed that this compound was an open chain alcohol, 3-heptadecanol (lit, mp 54—54.5 °C,[2a] 44—46 °C,[4]) and the IR spectral data well agreed with those reported.[4] IR (KBr) 3320, 3220 (each OH), 1473 (CH_2), 1380, 1348 (each CH_3), 1139 (OH), 948, and 723 cm^{-1}; MS *m/z* 256 (M^+), 238 ($M^+ - H_2O$), 227 ($M^+ - CH_3CH_2$), 197 ($C_{14}H_{29}$), 59 ($C_2H_5CH(OH)$); ^{13}C NMR ($CDCl_3$) δ=9.9 (q, C-1), 14.2 (q, C-17), 22.7 (t, C-16), 25.8 (t, C-5), 29.4 (t, C-6, C-14), 29.7 (t, C-7—C-13), 30.2 (t, C-2), 32.0 (t, C-15), 37.0 (t, C-4), and 73.4 (d, C-3). Found: C, 79.57; H, 14.34%. Calcd for $C_{17}H_{36}O$: C, 79.61; H, 14.15%.

Isolation of 3. An ethanolic extract of a fresh Takanotsume sap was repeatedly chromatographed by TLC and gave 29% of a light-yellow oil (**3**) (R_f=0.33, $CHCl_3$), $[\alpha]_D^{18}$ −36.93° (*c* 0.77, $CHCl_3$) (lit, −25.2°).[2a] UV(95%C_2H_5OH) λ_{max} 238 (ε=8700); IR (neat) 3330 (OH), 3090, 3020 (C=C-H), 2255 (C≡C), 1638 (C=C), 1118 (OH), 1015, 983, 930 (vinyl), and 698 cm^{-1} (cis -CH=CH-);[2d] MS *m/z* 244 (M^+, 6%) and 159 ($M^+ - [-(CH_2)_5CH_3]$); ^1H NMR ($CDCl_3$) δ=0.81 (3H, m, CH_3), 1.28 (10H, m, CH_2×5), 2.0 (2H, m, =CH-C<u>H</u>$_2$-), 3.12 (2H, d, *J*=6 Hz, ≡CC<u>H</u>$_2$-CH=), 4.88 (1H, d, *J*=4.8 Hz, C<u>H</u>OH), 5.4 (2H, m, vinyl CH_2=), 5.85 (1H, ddd, *J*=4.8, 9.4, 17 Hz, vinyl), and 5.45 (2H, m, -CH=CH-). Found: C, 83.08; H, 9.62%. Calcd for $C_{17}H_{24}O$: C, 83.55; H, 9.80%.

(9Z)-1,9-Heptadecadiene-4,6-diyn-3-one (4). By the procedure of Takahashi and Yoshikura,[2b] MnO_2 oxidation of 80 mg of **3** in hexane afforded 41 mg of a pure sample of **4**

after the usual work-up, a yellow oil. The IR was identical with those of Takahashi and Yoshikura[2b] and Bohlmann et al.[27] IR (neat) 3010 (C=CH), 2240 (C≡C), 1642 (C=O), 1614(C=C), 1462, 1402, 1311, 1272, 1163, 1078, 982, and 967 (vinyl), 905, 795, 703, and 686 cm^{-1} (cis C=C). There was no appearance of an OH band in the 3500—3300 cm^{-1} region.

Photopolymerization of 3. A sample of **3** was spread to a thickness of 20 μm on a glass plate using an applicator, and exposed directly to the sun for 1 h. Polymerization was almost completed within this time and the color changed to golden yellow (Fig. 1). The dried film showed 33 in hardness according to a Swoad-Rocker Hardness test (the hardness of the standard glass plate is provided as 100).[17] The IR and UV spectra are shown in Figs. 2 and 3, respectively.

References

1) Presented partially at the 55th Annual Meeting of the Chemical Society of Japan (Fukuoka, Oct. 16, 1987) by A. Terada, Y. Tanoue, and D. Kishimoto; and at the 10th Annual Meeting of the Association of Scientific Research on Historic and Artistic Works of Japan (Tokyo, May 21, 1988) by A. Terada. Paper XII on Synthesis of Urushi-Analogous Compounds, for previous papers, see Ref. 9.

2) a) M. Takahashi, K. Isoi, Y. Kimura, and M. Yoshikura, *J. Pharm. Soc. Jpn.*, **84**, 752 (1964). b) M. Takahashi and M. Yoshikura, *ibid.*, **84**, 757 (1964). c) **86**, 1051 (1966). d) **86**, 1053 (1966).

3) F. Bohlmann, U. Niedballa, and K. Rode, *Chem. Ber.*, **99**, 3552 (1966).

4) D. G. Crosby and N. Aharonson, *Tetrahedron*, **23**, 465 (1967).

5) A. Terada, *Sci. Antiq.*, **26**, 1 (1981).

6) S. Minamoto, "Wamyo-ruiju-sho," **15** (931—938), ed by A. Masamune, Kazama Publ. Co., Tokyo (1954), p. 14.

7) E. Matsui, *Sci. Antiq.*, **22**, 48 (1978).

8) A. Terada, *Kagakushi Kenkyu*, Series II, **21**, 65 (1982).

9) A. Terada, *Kagakushi Kenkyu*, Series II, **25**, 129 (1986).

10) A. Terada and A. Higashi, *Sci. Antiq.*, **25**, 25 (1980).

11) A. Terada, Y. Tanoue, S. Inadomi, and A. Higashi, Abstracts of the Ube Meeting of the Chemical Society of Japan, October 1979, p. 112.

12) A. Terada, Y. Tanoue, and S. Shimamoto, unpublished work.

13) F. Bohlmann, T. Burkhardt, and C. Zdero, "Naturally Occurring Acetylenes," Academic press, London (1973), p. 4.

14) R. K. Bently, D. Bhattachavjee, E. R. H. Jones, and V. Thaller, *J. Chem. Soc. (C)*, **1969**, 685.

15) F. Bohlmann, *Chem. Ber.*, **86**, 657 (1953).

16) B. Tieke, G. Lieser, and G. Wegner, *J. Polym. Sci., Polym. Chem. Ed.*, **17**, 1631 (1979).

17) "Toryo Handbukku (Hand Book of Paints)," 2nd ed., ed by S. Iwai, Sangyo Tosho publ. Co., Tokyo (1960), p. 623.

18) B. Tieke, H.-J. Graf, G. Wegner, B. Naegele, H. Ringsdolf, A. Banerjie, D. Day, and J. B. Lando, *Colloid Polym. Sci.*, **255**, 521 (1977).

19) R. H. Baughman, J. D. Witt, and K. C. Yee, *J. Chem. Phys.*, **60**, 4755 (1974).

20) J. H. Krieger, *Chem. Eng. News*, **1980**, Aug. 4, 24.

21) I. Yoshioka, T. Kimura, H. Imagawa, and K. Takura, *J. Pharm. Soc. Jpn.*, **86**, 1216 (1966).

22) P. J. G. M. Dewit and E. Kodde, *Physiological Plant Pathology*, **18**, 143 (1981).

23) V. K. Harding and J. B. Heale, *Physiological Plant Pathology*, **18**, 7 (1981).

24) H. Otsuka, T. Komiya, S. Fujioka, M. Goto, Y. Hiramatsu and H. Fujimura, *J. Pharm. Soc. Jpn.*, **101**, 1113 (1981).

25) M. Yasue, M. Itaya, M. Inagaki, H. Katayama, and N. Kawamura, *J. Pharm. Soc. Jpn.*, **87**, 247 (1967).

26) "Seibutsu Kassei Tennen Busshitsu," (Natural Products having Bioactivities), ed by S. Shibata, Ishiyaku publ. Co., Tokyo (1979), p. 283.

27) F. Bohlmann, C. Arndt, H. Bornowski, and K. Kleine, *Chem. Ber.*, **94**, 958 (1961).

 © 1989 The Chemical Society of Japan Bull. Chem. Soc. Jpn., 62, 2981—2988 (1989)

The Catalytic Degradation Reaction of Polypropylene with Silica-Alumina

Yumiko ISHIHARA,* Hidesaburo NANBU, Chiemi IWATA,
Tadashi IKEMURA, and Tomoyuki TAKESUE
Department of Industrial Chemistry, College of Science and Technology, Nihon University,
1-8, Kanda-Surugadai, Chiyoda-ku, Tokyo 101
(Received March 2, 1989)

A detailed analysis was carried out on the catalytic degradation of polypropylene with silica-alumina, using a glass tube reactor (25ϕ×150 mm) at 180 to 300 °C and a N_2 flow rate of 120 ml min^{-1} over a period of 5 to 120 minutes. The ratio of C/S was from 0.1 to 6.0. The molecular weight of PP decreased slightly at about 160 °C by cationic degradation, but the decrease started at about 200 °C by radical degradation (without catalyst). The main chain of PP was remarkable weakened by the catalytic degradation with silica-alumina. Analysis of degradation products by ^{13}C NMR, FD-MS and variation in chain scission number clearly indicated the catalytic degradation of PP to occur in two stages. The first stage at low temperature is initiated by the addition of a proton released from the catalyst to weak links in the main chain. The second stage at high temperature occurs by attack a low-molecular-weight carbonium ion of the saturated degraded oligomer. These ions are closely involved in the production of irregular structural oligomers and their redegradation.

The degradation reaction of polymer is important for the synthesis of materials by polymeric reactions starting from a high polymer and studying the molecular design of functional, heat-resistant polymers and the stabilization of a general-purpose polymers.

Many studies in this area, especially on pyrolytic radical reactions, have been reported. However, only a few studies have been carried out cationic and anionic degradation reactions of polymers in the presence of a catalyst. A study using an oligomer fraction produced by degradation of polypropylene (briefly "PP") as a lubricating oil has been conducted.[1] The catalytic degradation of PP,[2,3] and reactions of nylon, polyisobutylene (briefly "PIB"), and polystyrene (briefly "PS")[4-6] have been recently studied. Gasification reactions are studied to determine the yields and composition of volatile matter while PP, PIB, nylon, and PS reactions are investigated to clarify main chain skeleton reactions as polymeric reactions.

The authors found unusual polymeric reactions of the latter type to take place. For instance, a unique polyindan[6] can be produced at high yield in the catalytic reaction of PS with aluminum chloride and the multibranched ethylene oligomer is produced in the catalytic reaction of polyethylene (briefly "PE") with silica-alumina.[7]

The above cationic degradations are remarkably different from conventional pyrolytic radical reactions. It is not possible to synthesis the polyindan and the multibranched oligomer mentioned above either by a radical reaction nor by ordinary monomer polymerization. The cationic and anionic degradation reactions of polymers may thus possibly hold promise for the synthesis of new materials. And considerable research should be directed to the basic cationic and anionic degradation reactions of polymers as pyrolytic radical reaction. The authors consequently conducted fundamental research on the cationic degradation reactions of polymers and the catalytic degradation of general-purpose polymers.

Experimental

The sample used for this study was prepared by pulverizing a commercially available isotactic PP (Biscol 330P manufactured by Sanyo Kasei; isotacticity; 90%; and $\bar{M}_n$ (by viscosity method)=16000), to 60 mesh or under, extracting in with heptane in a Soxlet extractor, for 6 hours and drying at 40 °C for 72 hours under vacuum.

The catalyst was prepared by pulverizing a commercially available silica-alumina catalyst (N-631L manufactured by Nikki Chemical; alumina content: 13 wt%) to a 100 mesh or less sintering it at 540 °C for 3 hours and then drying it in a flow of dried air. The activity of the catalyst was measured by butylamine titration.[8,9]

Experimental Operation and Procedure. A Pyrex glass tube reactor (outer diameter: 25 mm and length: 150 mm) connected to traps for recovering gaseous and liquid products as shown in Fig. 1 was used.

The experimental procedure was as follows: 2 g each of the sample and the catalyst were mixed by stirring at different temperatures and timings and 0.6 to 2 g of the sample and 0.2 to 4 g of the catalyst were mixed by stirring with different concentrations of the catalyst. The mixture was put in a

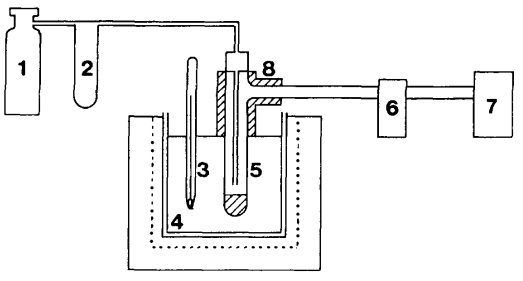

Fig. 1. Apparatus for the catalytic degradation: (1) N_2 cylinder, (2) manometer, (3) thermometer, (4) metal bath, (5) reactor, (6) trap for liquid fraction, (7) trap for gaseous product, (8) asbestos.

reactor; the reaction a value was maintained from 180 to 300 °C in an oil or metal bath; nitrogen was passed through the reactor at a flow rate of 120 ml min^{-1} for 5 to 120 minutes and the ratio of catalyst to sample (C/S) was varied from 0.1 to 6.

Analytical Method. A gas-liquid chromatograph (GC-8A of Shimadzu) was used.

The gaseous product was qualitatively analyzed by a comparison with the retention time of the standard gas and quantitatively analyzed by the absolute calibration curve method.[10]

A FT-IR spectrometer (Fourier transform infrared spectrophotometer of Nihon Denshi) was used. The range of wavelength for measurement was from 4000 to 400 cm^{-1}.

Parameter of the starting PP sample were determined by the Fourier transform infrared spectroscopic method.

Field desorption- (FD-) and field ionization-mass spectrometers (FI-MS) (RMU-7M of Hitachi) were used. The molecular weight distribution of the oligomer was determined by FD-MS. The molecular weight of low- and high-boiling fractions in the liquid product were determined by FI- and FD-MS, respectively.

The measuring conditions are shown in Table 1.

^1H and ^{13}C NMR (JUM FX-100 of Nihon Denshi) were used. The resonance frequencies of ^1H and ^{13}C NMR were 99.6 and 25.05 MHz, respectively.

The PP sample dissolved in 1,2,4-trichlorobenzene, benzene-*d* as the internally locking agent of the magnetic field and a small amount of hexamethyldisiloxane (HMDS) as the internal standard material were introduced into a 5 mm-NMR tube which was then deaereated by freezing, followed by a complete substitution with nitrogen and sealing. The oligomer dissolved in chloroform-*d* and a small amount of tetramethylsilane (TMS) as the internal standard material were put in a 5 mm-NMR tube.

The measuring conditions of ^1H and ^{13}C NMR are the same as in the previous paper.[10]

Table 1. Operational Conditions for FD- and FI-MS

	FD-MS	FI-MS
Sample	Oligomer, Liquid	Liquid
Total scan No.	79	64
Data format	3	3
Sampling period	25 μs	25 μs
Rescan duration	1.2 s	1.2 s
Threshold	100	100
Acquiring range	0—10000 min	0—10000 min
Cathode voltage	−3 kV	−3 kV
Emitter current	0—30 mA (3 mA min^{-1})	0 mA
Disk	87%	86%

Table 2. Chemical Shift Parameters of Lindeman-Adams

S	*Bs*	*M*	*Asm*	γs	Δs
1	6.80	2	9.56	−2.99	0.49
		3	17.83		
		4	25.48		
2	15.34	2	9.75	−2.69	0.25
		3	16.70		
		4	21.43		
3	23.46	2	6.60	−2.07	0
		3	11.14		
		4	14.70		
4	27.77	2	2.26	+0.68	0
		3	3.96		
		4	7.35		

Method for the Assignment of ^{13}C NMR Signal. The addition rules of Grant-Paul,[11] Randall,[12] and Lindeman-Adams[13] are generally used for assigning ^{13}C NMR signals. In particular, the addition rule Grant-Paul is used for the ^{13}C NMR signal of PP. Nishioka et al.[14] calculated the average values of standard deviations in the structures with ethyl to hexyl or higher side chains.

In contrast, the addition rule of Lindeman-Adams has the following advantages: the standard deviation from the Lindeman-Adams method is intermediate between the values obtained from these three methods and the calculated value of a quaternary carbon atom can be obtained. Accordingly, in the present study, the addition rule of Lindeman-Adams was used mainly. For comparison, both these addition rules were used.

The addition rule is expressed as follows:

$$\delta c(K) = Bs + \sum^{4} D_M A_{SM} + \gamma_S N_3 + \Delta S N_4$$

where *B*, *A*, γ, and Δ=the respective additive parameters for the α-, β-, γ-, and δ-positions of C-k, *s*=number of carbon atoms directly bonding to C-k, D_M=total M carbon atoms bonding to C-k, and Nk3 (Nk4)=number of carbon atoms three (four) bonds away from C-k, that is, the γ-carbon atom (δ-carbon atom).

The parameters used in the addition rules are shown in Table 2.

Results and Discussion

Variation in the Number of Chain Scission of Polypropylene. Variation in the molecular weight of the main of PP was measured to examine its catalytic degradation reaction when using a silica-alumina catalyst.

The results are shown in Fig. 2. Decreasing molecular weight in the thermal degradation with non catalyst was observed at 200 °C. But, in the degradation of PP with the catalyst, the molecular weight sharply decreased from 16000 to 10000 at lower temperature in the experiment on variation in reaction temperature (open symbol). It slowly decreased from 10000 to 7500 at higher temperature. These trends are more pronounced for variation in time (closed symbol). The decrease in molecular weight at the early stage (lower temperature) of the catalytic degradation reaction thus appears to differ from that at the late stage (higher temperature).

The results are expressed as change in the number of main-chain scissions by rearranging the above results is shown in Table 3. The number of chain scissions was 0.45 from 180 to 220 °C, and 0.3 to 0.38 from 220 to 280 °C. Thus, the molecular weight decreased more sharply at the early stage. The number of chain scissions was 0.44 in the period from zero to 40

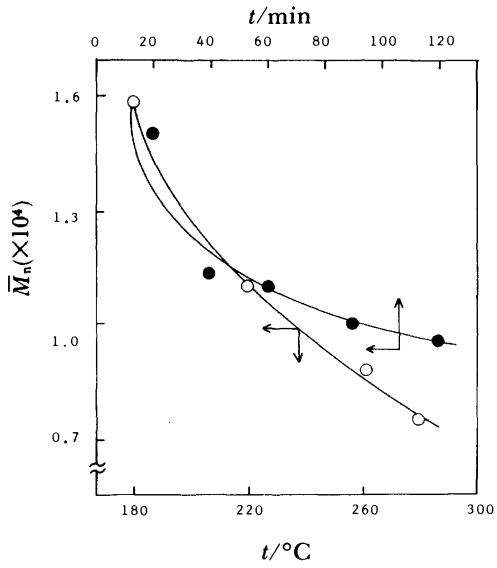

Fig. 2. Changes in the molecular weight ($\bar{M}_n$) of the degraded polymer. O: temp., ●: time.

Table 3. The Number of Main-Chain Scission of Catalytic Degraded Polymer

t/°C	180	220	260	280
Number of main-chain-scission	0	0.45	0.75	1.13

t/min	20	40	60	90	120
Number of main-chain-scission	0.06	0.44	0.48	0.56	0.60

Reaction conditions; time=60 min, C/S=1
Reaction conditions; temp=220°C, C/S=1.

minutes, and 0.14, only a third of the former in the period from 40 to 120 minutes. Chain scission thus takes place, more rapidly at the early stage than late stage. The molecular weight decreasing reaction at the early stage differed from that at the late stage.

The molecular weight decreasing reaction of PS was similar to the above reaction.

The molecular weight of PS decreased rapidly at the early stage and slowly at the late stage.[15] This rapid decrease is attributed to a low activation energy reaction caused by weak links in the main chain.[16] Since these weak links are more distinct in the main chain of PP than in that of PS, the initial reaction is possibly initiated by low activation energy in the same manner as in PS. It is thus likely, that the rapid decrease in molecular weight is caused by weak links in the same way as in PS. The weak links in the sample of this study are illustrated in Fig. 9.

These two molecular weight decreasing reactions were analyzed in terms of change in degraded product composition.

Yields of Degradation Products vs. Reaction Conditions. Figure 3 shows variation in the yields of the four main fractions, gas, liquid, grease (oligomer), and wax (low polymer). Another important product was carbon deposited on the catalyst.

The yield of wax (low polymer) linearly decreased with increase in reaction temperature, while that of the liquid sharply increases.

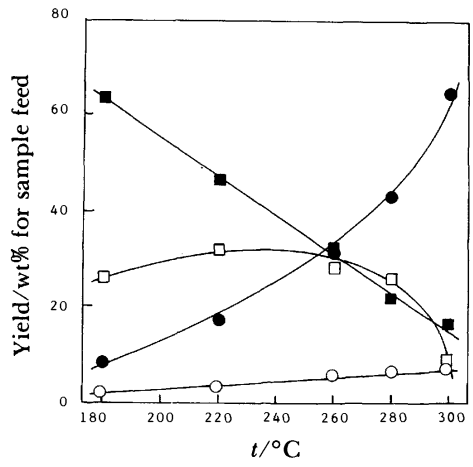

Fig. 3. Catalytic degradation product yield from PP. O: gas, ●: liquid, □: oligomer, ■: polymer. Reaction conditions: 60 min, C/S=1.

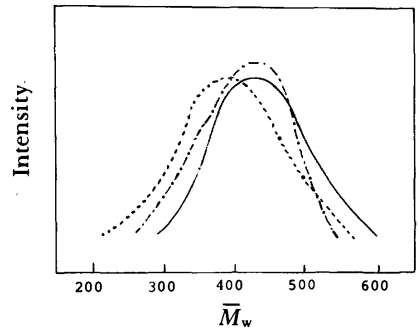

Fig. 4. $\bar{M}_w$ distribution of the propylene oligomer (liquid fraction) formed by catalytic degradation of PP. —: 220°C, ------: 260°C, ------: 280°C. Reaction conditions: 60 min, C/S=1.

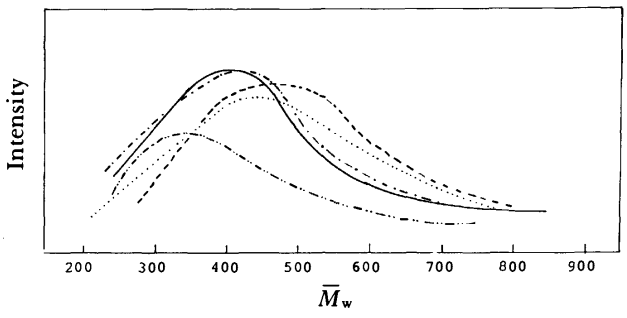

Fig. 5. $\bar{M}_w$ distribution of the propylene oligomer (grease fraction) formed by catalytic degradation of PP. ------: 180°C, —: 220°C, ------: 260°C, ·····: 280°C, ------: 300°C. Reaction conditions: 60 min, C/S=1.

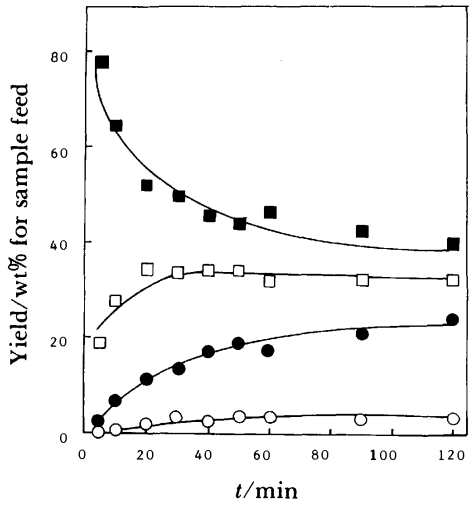

Fig. 6. Catalytic degradation product yield from PP. O: gas, ●: liquid, □: oligomer, ■: polymer. Reaction conditions: 220 °C, C/S=1.

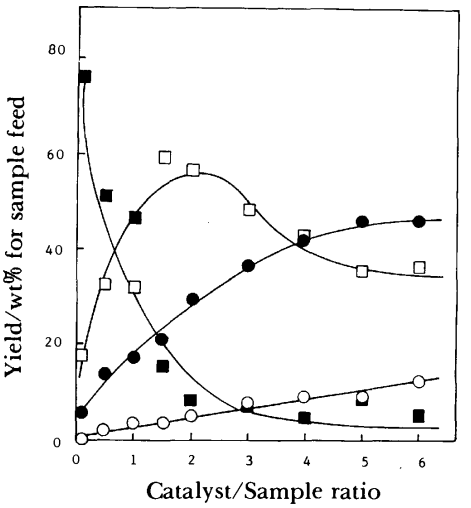

Fig. 7. Catalytic degradation product yield from PP. O: gas, ●: liquid, □: oligomer, ■: polymer. Reaction conditions: 220 °C, 60 min.

The results of FD-MS in Figs. 4 and 5 indicate the molecular weight distributions of the liquid and oligomer (mixture of grease and wax) fractions produced at 280 °C from 200 to 600, mainly at 360 and from 200 to 900, mainly at 450. Figure 4 shows the fraction (shown as····) produced at higher temperature to have a lower molecular weight, while that (shown as——) produced at lower temperatures, a higher molecular weight. Since the exhaust fume temperature in the higher temperature reaction system was high, the high boiling heavier fraction (oligomer) formed could flow out of the system. Phenomena such as reflux and redegradation way occur in the lower temperature reaction system, since the heavier fraction can hardly flow out. The molecular weight of the higher temperature reaction product should thus be higher than that of the lower temperature reaction product. This however, is the reverse of the above theory and at variance with the concept based on the boiling point of the reaction product in the reaction system.

This variance, however, may be resolved by considering that the oligomer redegradation to proceed at high temperature and the recombination-addition reactions of low-boiling products formed to occur during reflux in the long residence time at low temperature. Consequently, the molecular weights of the products become higher than those of products formed at high temperature. The molecules of a degradation product from an oligomer are smaller than those of the oligomer itself, and thus they move more easily toward the catalyst, should be more readily degraded and recombined. Evidence for this view is shown in Figs. 7 and 8.

The above results show PP to hardly be depolymerized in the catalytic degradation reaction, but to be

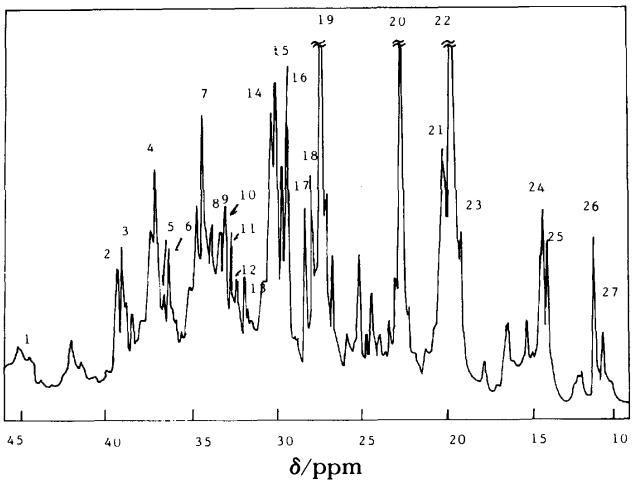

Fig. 8. ^{13}C NMR spectrum of the propylene oligomer (grease fraction). Reaction conditions: 220 °C, 60 min, C/S=1.

degraded through random scission. The yield of the component (propylene) produced by the depolymerization of PP was only 0.35 wt% the total yield.

The decrease in molecular weight of the main chain dominates at the early stage of the reaction mentioned above, while volatile matter is vigorously produced at the late stage. The catalytic degradation of PP was confirmed to occur in two stages remarkably different from each other. This reaction is similar to that of PS degradation. However, most of the reaction products in the latter half of the reaction of PS are olefinic monomers derived from depolymerization, while those of PP comprise a low-boiling liquid mixture of saturated hydrocarbons containing recombination and addition products as was shown by NMR analysis (in the later section).

The relationships among the four main fractions

and reaction time are shown in Fig. 6. They were all essentially the same the composition of each reaction product attained equilibrium during the catalytic degradation reaction. Each product thus appears to be formed in a simple reaction process. This, however, should be considered in relation to the catalyst concentration.

Variation in Degradation Products with Catalyst Concentration. The effect of the concentration of the catalyst was examined to elucidate the relationship between its activity and degradation. The results are shown in Fig. 7. The oligomer was degraded more than the liquid at a high concentration of catalyst (C/S=3) and the yield of polymer remarkably decreased as C/S exceeded 2 and the decrease was approximately 5.1 wt% at C/S of 4. The degradation reaction thus depends mainly the reaction temperature and catalytic concentration.

Since the oligomer with high-molecular mobility comes into contact more easily with the catalyst than the polymer with low molecular mobility and the oligomer is more rapidly degraded than the polymer an at extremely high concentration of catalyst, the yield of the oligomer is likely to drop. The yield of the oligomer, however, was not so much reduced as that of the polymer. The yield of gas and liquid should increase since the degradation reaction is accelerated more with increase in the concentration of catalyst. The yield of the oligomer did not decrease as shown in Fig. 7. This is probably because the oligomer was produced not only by degradation of the polymer but also by recombination or addition reaction of low-molecular components such as gaseous and liquid fractions. These results are essentially the same as those shown in Fig. 4.

These recombination reactions were confirmed by the chemical structures of the degraded products and the reaction of a model compound, 1-pentadecene. Thus, most of the olefin groups of the model compound are recombined, leading to increased molecular weight.[17] The reaction was quite different from the radical degradation reaction and characterized the cationic polymer degradation with the silica-alumina catalyst.

Table 4. Chemical Shift (ppm) Observed from ^{13}C NMR Spectrum of the Propylene Oligomer

Peak No.	δ	Peak No.	δ
1	44.56	15	29.77
2	39.39	16	29.41
3	39.10	17	28.36
4	37.16	18	28.00
5	36.69	19	27.42
6	36.40	20	22.66
7	34.40	21	20.31
8	33.93	22	19.73
9	33.41	23	19.26
10	33.11	24	14.44
11	32.76	25	14.15
12	32.53	26	11.39
13	32.00	27	10.92
14	30.41		

Reaction conditions; 220°C, 60 min, C/S=1.

NMR Analysis of Degradation Products. Figure 8 illustrates the ^{13}C NMR spectrum of the oligomer

Table 5. Chemical Shifts Observed by ^{13}C NMR and Calculated

Branched species	Carbon No.	Calcd[a] (ppm)	Peak No.[b]
(a)			
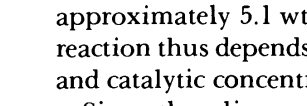	1	22.62	6
	2	25.92	7
	3	46.55	1
	4	28.38	5
	5	20.63	8
(b)			
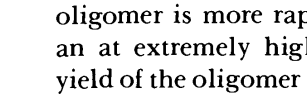	1	14.35	10
	2	19.96	9
	3	39.60	2
	4	30.45	3
	5	20.12	8
(c)			
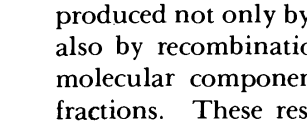	1	7.88	27
	2	31.64	13
	3	33.65	9
	4	27.28	19
(d)			
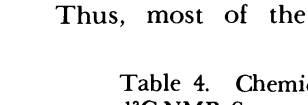	1	14.84	24
	2	17.27	23
	3	44.33	1
	4	34.44	7
	5	27.77	19
(e)			
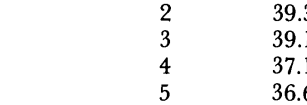	1	19.14	23
	2	32.53	12
	3	37.06	4
	4	16.64	24
(f)			
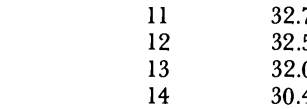	1	10.87	27
	2	29.85	15
	3	32.52	11
	4	19.63	22

a) Chemical shifts calculated by Lindeman-Adams method. b) Peak No. in ^{13}C NMR spectrum of Fig. 8.

fraction produced at the late stage. The spectrum of the liquid fraction was nearly equal to that of the oligomer. The chemical structures of the products were assigned by calculation of the formulas.[11-13] The signals of the chain ends and chain skeletons of the main components are shown in Table 4. The relationship between the detailed structures and their signals are shown in Table 5.

The chemial structures of the chain ends of the oligomer and liquid include the following six types:

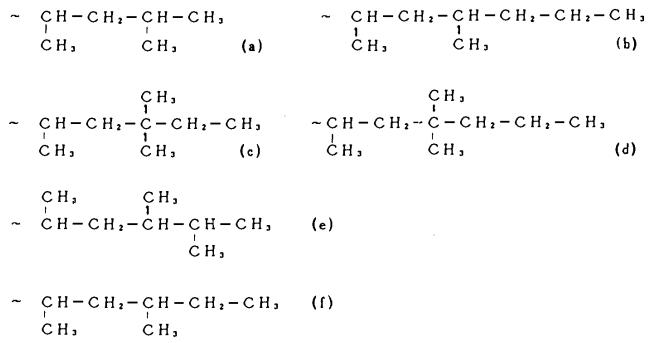

Thus, the formation of these chain ends can be resonably explained on the basis of the following reaction schemes:

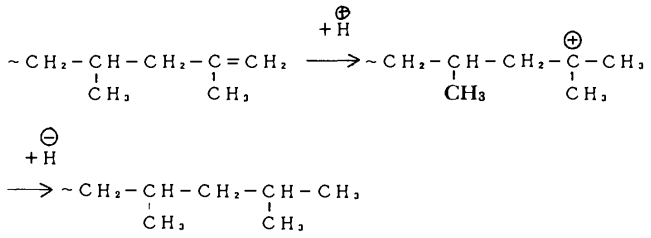

Scheme 1.

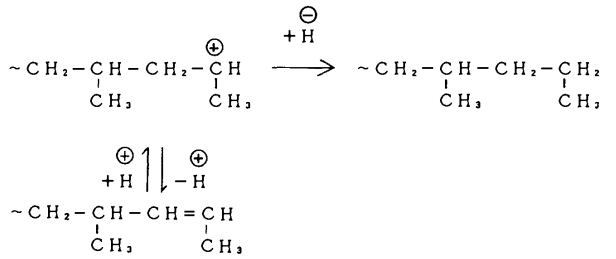

Scheme 2.

These chain end olefins with high affinity for protons are hydrogenated or saturated by the addition of a low-molecular-weight carbonium ion intermediate and the hydride ion ($\overset{\ominus}{H}$). The results of qualitative analysis indicated the chain ends of degradation products to be approximately hydrogenated. Moreover, the chain end of the degraded polymer includes only two types, (a) and (b), which are extremely simple compared to those of the oligomer and liquid. These two types of ends are also the main chain end structures of the oligomer fractions.

It is clear from the end structure of the main chain that main chain scission of the polymer is caused mainly by β-scission of the tertiary carbonium ion produced on the main chain according to the following scheme:

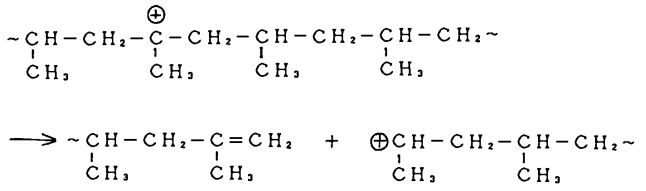

Scheme 3.

It was confirmed that the quaternary carbon atoms in (c) and (d) structures are produced in the oligomer and liquid fractions unlike those in the normal end structure. All these quaternary carbon atoms are found only in components produced in a high-temperature reaction. This proves that the oligomer and liquid fractions are produced by recombination of the low-molecular gaseous and liquid fractions. But they are not formed as internal carbon atoms in backbone chains and are located in the vicinity of the chain ends.

The concentration of quaternary carbon atoms seem high, considering the ratio of intensities of spectra. The chain end olefin (>C=CH$_2$ Scheme 1) is immediately attacked by a proton released from the catalyst or by a reaction intermediate possessing a tertiary carbonium ion formed from olefinic products consisting of the gaseous and liquid fractions.

The analytical results of the chemical structure of a catalytically degraded product of PP indicated the carbonium ion produced on the main chain to cause β-scission, and both the chain end olefin and the chain end high-molecular-weight carbonium ion to be saturated by hydrogenation or addition of activated low-molecular component.

The catalytic degradation reaction of PP occurs in two stages. The first stage is a low-temperature reaction initiated by the addition of a proton released from the catalyst to weak links in the main chain. The reaction should proceed using low activation energy. The formation of the carbonium ion on the main chain takes place at weak links in PP, which are the following functional groups included in the main chain.[18,19] These weak links in the starting sample in this study are shown by the FT-IR spectrum in Fig. 9. The functional groups confirmed in the sample are shown in the 1, 2, and 3 in figure. [1,2: >C=O, (1758, 1689 cm^{-1}), 3: olefin group, (1646 cm^{-1})]

These groups are easily attacked by protons, producing an on-chain a molecular weight decrease.

The second stage should be initiated by a higher activation energy than in the first stage reaction at high temperature. The chain ends of the oligomer

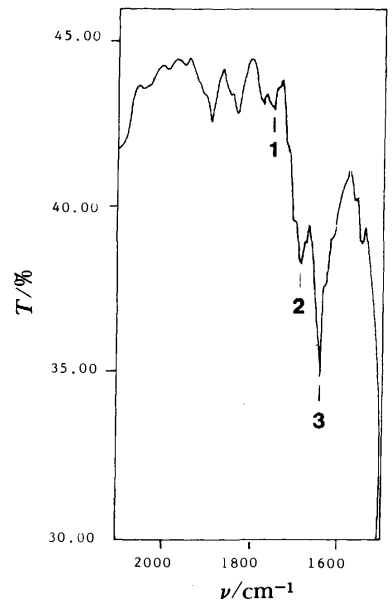

Fig. 9. FT-IR spectrum of the starting polypropylene

produced by the catalytic degradation reaction are saturated because the weak links (functional groups) were eliminated at the first stage of reaction. The oligomer is thus, chemically stable and contains no functional groups with affinity for a proton. The reaction which produces the on-chain carbonium ion causing the decrease in molecular weight of the saturated oligomer should require an extremely high activation energy. There is a wide difference in the activation energies required for producing the on-chain carbonium ion between the first and second stages of the reaction. Accordingly, the decreasing rate of molecular weight was determind in the two stages.

The results from variation in yields of the four fraction produced, FD-MS of liquid fraction and the determination of quaternary carbon atom by NMR indicate the lower molecular components including the liquid fraction to participate in the recombination reaction at low temperature but not the higher molecular weight components including the oligomer and polymer. The redegradation reaction of the chemically stable paraffinic oligomer is initiated by the intermolecular reaction with the intermediates of low-molecular-weight carbonium ion.

That is, in the reaction at high temperature, these ionic intermediates are formed by proton addition with olefinic gaseous and liquid products and also attack the on-chain tertiary carbon atoms of a saturated oligomer and degraded polymers. The activation energy of the reaction should be higher than that of the weak links.

These ionic intermediates are saturated by hydride ions extracted from the oligomer and polymer chains. Consequently, chain tertiary carbonium ions are again produced on the paraffinic oligomer and degraded polymers chains.

The intermolecular rearrangement of carbonium ions takes place on the surface of the catalyst. These reactions certainly require much higher activation energies than the addition reaction of protons to the weak links. The reaction of the intermolecular rearrangement of carbonium ion in the latter takes place as follows:

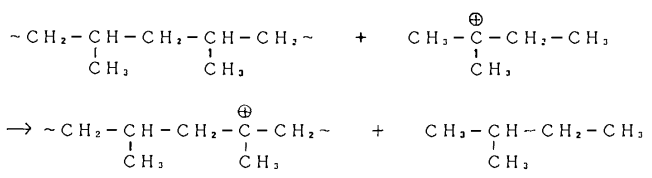

Scheme 4.

The schematic process of the catalytic degradation of PP using a silica-alumina catalyst involves the production of the on-chain carbonium ion initiated by the addition of protons to the weak links at the early stage and production of on-chain carbonium ion by the intermolecular rearrangement reaction of the low-molecular-weight carbonium ionic intermediates with tertiary carbon atoms in paraffinic oligomers at the late stage. The carbonium ionic intermediates of the low-molecular-weight fractions produced recombine with the low-molecular-weight olefinic fractions to increase the concentration of the oligomer fraction. In particular, it is clear that the intermediate of the low-molecular-weight tertiary carbonium ion is equally involved in the production of oligomer fraction with irregular structures. These reactions are quite different from the pyrolytic radical reaction of PP in which recombination of volatile matter is not important.[20]

References

1) N. M. Seidov, *Azerb. Neft. Khoz.*, **1987**, 47.
2) Y. Uemichi, A. Ayame, T. Yoshida, and H. Kanoh, *J. Jpn. Petrol. Inst.*, **23**, 35 (1980).
3) G. Audisio, *J. Anal. Appl. Pyrolysis*, **8**, 87 (1985).
4) M. Langhamer and I. Luederwald, *Makromol. Chem.*, **187**, 829 (1986).
5) S. R. Ivanova, I. Yu. Ponedel'kina, and T. V. Romanko, *Vysokomol. Soedin., Ser. A*, **28**, 1217 (1986).
6) H. Nanbu, Y. Sakuma, Y. Ishihara, T. Takesue, and T. Ikemura, *Polym. Degrad. Stab.*, **19**, 61 (1987).
7) H. Nanbu, Y. Ishihara, H. Honma, T. Takesue, and T. Ikemura, *Nippon Kagaku Kaishi*, **1987**, 765.
8) M. W. Tamele, *Disc. Faraday Soc.*, **8**, 270 (1960).
9) K. Tanabe and T. Takeshita, "San-Enki-Shokubai," Sangyo Tosho, (1967), p. 165.
10) Y. Ishihara, H. Nanbu, T. Ikemura, and T. Takesue, *J. Appl. Polym. Sci.*, in press.
11) D. M. Grant and E. G. Paul, *J. Am. Chem. Soc.*, **86**, 2984 (1964).
12) J. C. Randall, *J. Polym. Sci., Polym. Chem. Ed.*, **13**, 901

(1975).
13) L. P. Lindeman and J. Q. Adams, *Anal. Chem.*, **43**, 1245 (1971).
14) A. Nishioka, Y. Mukai, M. Ouchi, and T. Imanari, *Bunseki Kagaku*, **29**, 774 (1980).
15) G. G. Cameron and N. Grassie, *Polymer*, **2**, 367 (1961).
16) H. H. G. Jellink, *J. Polym. Sci.*, **4**, 13 (1949).
17) Y. Ishihara, T. Narizuka, and T. Takesue, *Polym. Prepr. Jpn.*, **36**, 1589 (1987).
18) Y. Kato, D. J. Carlsson, and D. M. Wiles, *J. Appl. Polym. Sci.*, **13**, 1447 (1969).
19) W. S. Subowo, *J. Polym. Sci., Polym. Chem. Ed., Part A*, **24**, 1351 (1986).
20) Y. Tsuchiya and K. Sumi, *J. Polym. Sci., Part A*, **7**, 1599 (1969).

Reinvestigation of the Nontotally Symmetric g-Type Normal Vibrations of [$^1H_4$]- and [$^2H_4$]Pyrazines

Toshikazu HIEIDA, Masayoshi MAEHARA, Yoshinori NIBU,
Hiroko SHIMADA,* and Ryoichi SHIMADA†
Department of Chemistry, Faculty of Science, Fukuoka University, Nanakuma, Jonan-ku, Fukuoka 814-01
†Department of Chemistry, Faculty of Science, Kyushu University 33, Hakozaki, Higashi-ku, Fukuoka 812
(Received January 28, 1989)

Synopsis. The assignment of the nontotally symmetric g-type normal vibrations of [$^1H_4$]- and [$^2H_4$]pyrazines was reinvestigated through the analyses of the single vibronic level fluorescence spectrum. The assignment given in this work was consistent with the assignment made based on the polarization behavior of the phosphorescence spectrum.

In spite of a large number of works made on the assignment of the normal vibrations of pyrazine the assignment given for some of the nontotally symmetric vibrations has not been established yet.[1-7] Many workers made the assignment through the analyses of the Raman and infrared spectra.[1-4] Udagawa et al.[5] and McDonald and Rice[6] studied the assignment based on the analyses of the single vibronic level (SVL) fluorescence spectra and Azumi et al.[7,8] studied the assignment based on the polarization behavior of the phosphorescence spectrum. Their results are summarized in Table 1. The assignment given for the totally symmetric and ν_{10a} vibrations is established based on the various experimental results, while the assignment given for the ν_4, ν_5, and ν_{6b} is not consistent with each other.

Since the reasonable and definite assignment of the normal vibrations is very important for the study of the nature of the electronic excited states, the assignment of the ν_4, ν_5, and ν_{6b} vibrations is reinvestigated through the analyses of the SVL fluorescence and polarized Raman spectra of [$^1H_4$]- and [$^2H_4$]pyrazines in this work.

Experimental

Material. [$^2H_4$]Pyrazine was synthesized by exchange reaction of [$^1H_4$]pyrazine with D_2O using palladium asbestos as a catalyst. The sample was purified by repeated vacuum distillation.

Optical Measurements. The SVL fluorescence spectra were observed in vapor and in supersonic free jets. The excitation light source was a frequency doubled dye laser pumped by the second harmonic of a YAG laser (Qunta-Ray PDL-II DCR-11). The fluorescence spectrum dispersed by a 1.26 m monochromator (Spex. 1269) was detected by a photomultiplier tube (EMI 9789QB) and the signal was processed by a gated integrator (Stanford Research Systems SR 250).

The polarized Raman spectrum was observed with a laser Raman spectrophotometer (Jeol 400T) and the 514.5 nm beam from an Ar^+ ion laser, whose power was adjusted low enough because of high sublimation property of the pyrazine crystal. A single crystal grown by the Bridgman method was cut along the cleavage (101) plane, which will be referred to as the bc′ plane, where the c′ axis is taken to be inclined counterclockwise by 57.6° from the c axis in the ac plane.[9] The bb, c′c′, and bc′ polarized Raman spectra were observed by the back scattering method in the same way as described previously,[10] where the first and second letters refer to the polarization directions of the excitation and scattering lights, respectively.

Results and Discussion

Fluorescence Spectrum. The fluorescence excitation spectra of [$^1H_4$]- and [$^2H_4$]pyrazines observed in supersonic free jets are given in Fig. 1. The

Table 1. Nontotally Symmetric g-Type Normal Vibrations of [$^1H_4$]- and [$^2H_4$]Pyrazines in the Ground State

	[$^1H_4$]Pyrazine						[$^2H_4$]Pyrazine					
	b_{1g}	b_{2g}		b_{3g}			b_{1g}	b_{2g}		b_{3g}		
	ν_{10a}	ν_4	ν_5	ν_{8b}	ν_3	ν_{6b}	ν_{10a}	ν_4	ν_5	ν_{8b}	ν_3	ν_{6b}
Simmons[a]	757	703	918.6	1524	1118	516	580	678	721.1	1505		
Califano[b]	925	703	753	1523	1350	641	724					
Sbrana[c]	952	754	983	1520	1361	697	740	649	842	1501	1038	672
Zarembowitch[d]	927	756	983	1525	1346	704						
Udagawa[e]	919	660	756				721	590	651			
McDonald[f]	918	705	757			662						
Azumi[g,h]	929	756	971			692	726	645	844			679
This work												
Fluorescence	921	755	965			704	725	648	841			687
Raman	943	756	978	1523	1360	700	735	648	840	1503	1037	674
						697						671

(in cm^{-1} units)

a, b, c, d, e, f, g, and h are taken from Refs. 1, 2, 3, 4, 5, 6, 7, and 8, respectively (see the text).

assignment made on the vibronic bands is the same as that given by Udagawa et al.[5] except for the band at $0^0+509\,cm^{-1}$ in the [$^1H_4$]pyrazine spectrum and the weak band at $0^0+473\,cm^{-1}$ in [$^2H_4$]pyrazine, which was newly detected in this work. The SVL fluorescence spectra generated by pumping to the 0^0 level at 30875 (31032) cm^{-1}, to the $10a^1$ level at $0^0+383\,cm^{-1}$ ($0^0+293\,cm^{-1}$), and to the level at $0^0+509\,cm^{-1}$ ($0^0+473\,cm^{-1}$) are given in Fig. 2, where the first number refers to the frequency for [$^1H_4$]pyrazine and the number in parentheses to that for [$^2H_4$]pyrazine. The assignment given for the vibronic bands in the 0^0 and $10a^1$ SVL fluorescence spectra is exactly the same as that given by Udagawa et al. and McDonald and Rice, except for the bands at $0^0-755\,cm^{-1}$ and $10a^1-704\,cm^{-1}$ ($0^0-648\,cm^{-1}$, $0^0-886\,cm^{-1}$, $0^0-1008\,cm^{-1}$, and $10a^1-687\,cm^{-1}$). In the 0^0 SVL spectrum of pyrazine the 0_0^0 and totally symmetric vibronic bands showed parallel band envelope in correspondence with the out-of-plane transition moments, while the vibronic bands at $0^0-755\,cm^{-1}$ and $0^0-921\,cm^{-1}$ ($0^0-648\,cm^{-1}$ and $0^0-725\,cm^{-1}$) showed perpendicular band envelope as observed by Udagawa et al. This indicates that these vibronic bands are induced by the vibronic coupling through certain out-of-plane vibrations. Since the frequencies of 921 (725) cm^{-1} was already assigned to the ν_{10a} vibration of b_{1g} species,[5,6] the frequency of 755 (648) cm^{-1} should be assigned to one of the normal vibrations of b_{2g} species in the ground state.

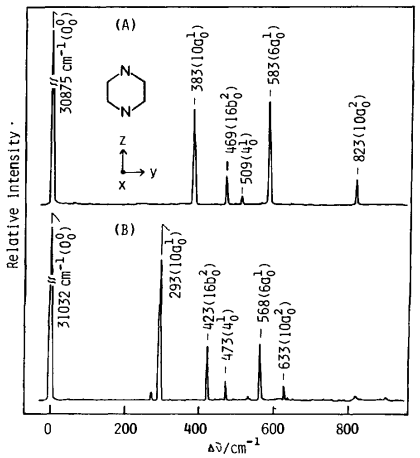

Fig. 1. Fluorescence excitation spectra of [$^1H_4$]- (A) and [$^2H_4$]- (B) pyrazines. The difference in wavenumber from the 0-0 band is expressed by $\Delta\tilde{\nu}$.

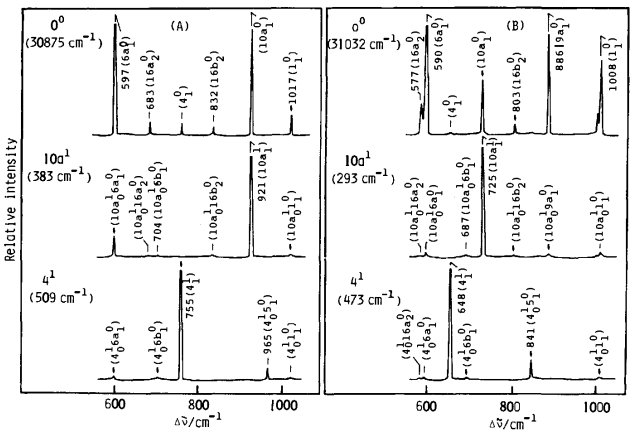

Fig. 2. SVL fluorescence spectra of [$^1H_4$]- (A) and [$^2H_4$]- (B) pyrazines. Excited level is indicated in the left hand side of the each spectrum. The difference in wavenumber from the exciting light is expressed by $\Delta\tilde{\nu}$.

In the $0^0+509\,cm^{-1}$, which will be written as ν_{509}, SVL spectrum of [$^1H_4$]pyrazine several bands were newly detected at $\nu_{509}-597\,cm^{-1}$, $\nu_{509}-704\,cm^{-1}$, and $\nu_{509}-965\,cm^{-1}$ in the fundamental vibrational region in addition to the band at $\nu_{509}-755\,cm^{-1}$ which was assigned to the 5_1^1 band by Udagawa and McDonald. In the $0^0+473\,cm^{-1}$ (ν_{473}) SVL spectrum of [$^2H_4$]pyrazine several bands were clearly observed at $\nu_{473}-577\,cm^{-1}$, $\nu_{473}-590\,cm^{-1}$, $\nu_{473}-648\,cm^{-1}$, $\nu_{473}-687\,cm^{-1}$, and $\nu_{473}-841\,cm^{-1}$. The assignment for the vibronic bands involving a_g vibrations was made straightforwardly by comparing the bands with the 0^0 SVL spectra and is given in Fig. 2.

For the nontotally symmetric vibrations the potential minimum would not change upon excitation and therefore the overlap integral of the vibrational wave functions of the ground and excited states $\langle X_i|X_j'\rangle$, which governs the transition probability, is close to δ_{ij}. Thus, the fact that the intensity of the band at $\nu_{509}-755\,cm^{-1}$ became strongest in the [$^1H_4$]pyrazine spectrum when the $0^0+509\,cm^{-1}$ level was excited indicates that the $509\,cm^{-1}$ band should be ascribed to the b_{2g} vibration in the $^3B_{3u}$ (n, π^*) state as indicated by Udagawa and McDonald. Similarly the fact that the intensity of the $\nu_{473}-648\,cm^{-1}$ band became strongest in the [$^2H_4$]pyrazine spectrum when the $0^0+473\,cm^{-1}$ level was excited indicates that the frequency of $473\,cm^{-1}$ should be assigned to the upper state b_{2g} vibration.

It was shown that two normal modes that belong to the same symmetry species and are effective to the vibronic coupling concerning to a certain electronic transition can exhibit Duschinski effect. In pyrazine the vibronic coupling between the $^1B_{3u}$ (n, π^*) and $^1B_{1u}$ (π, π^*) states can be induced through the ν_4 and ν_5 vibrations of b_{2g} species. The observations that the $\nu_{509}-965\,cm^{-1}$ ($\nu_{473}-841\,cm^{-1}$) band is the second strongest band in the fundamental vibrational region of the $0^0+509\,cm^{-1}$ ($0^0+473\,cm^{-1}$) SVL spectrum while the vibronic band involving the frequency of 965 (841) cm^{-1} was hardly detected in the 0^0 SVL spectrum and could not be detected in the $10a^1$ SVL spectrum as shown in Fig. 2 suggest that (1) the 965 (841) cm^{-1} band can be classified into the same symmetry species as that of the 755 (648) cm^{-1} band, (2) the 755 and 965 (648 and 841) cm^{-1} bands can be assigned to the ν_4 and ν_5 vibrations in the ground state, respectively, and (3) the 509 (473) cm^{-1} band can be assigned to the ν_4 vibration in the $^1B_{3u}$ (n, π^*) state.

The vibronic band involving the frequency of 704 (687) cm^{-1} was not observed in the 0^0 SVL spectrum but observed clearly in the $10a^1$ and 4^1 SVL spectra. Symmetry consideration suggests that this frequency

Table 2. Squares of Relative Values of Elements of the Raman Tensor for Pyrazine Crystal

	b_{1g}	b_{2g}	b_{3g}
$(A_{b\,b})^2$	0.50	0.00	0.00
$(A_{c'\,c'})^2$	0.04	0.12	0.70
$(A_{b\,c'})^2$	0.14	0.61	0.10

can be ascribed to one of the b_{3g} vibrations. The study of the normal vibrations of pyridine[11] and pyrimidine[12] suggests that the frequencies of 886 and 1008 cm^{-1} observed in the fluorescence spectrum of [$^2H_4$]pyrazine should be assigned to the ν_{9a} and ν_1 vibrations, respectively, although Udagawa et al. assigned these to the ν_1 and ν_{9a} vibrations, respectively.

The assignment given in this work for the vibronic bands observed in the fluorescence excitation and SVL fluorescence spectra is given in Figs. 1 and 2 and Table 1.

Polarized Raman Spectrum. Pyrazine crystallizes in the orthorhombic space group P_{mnn} with two molecules in the unit cell.[9] The matrix elements of the Raman tensor of the pyrazine crystal was calculated based on the simple oriented gas model approximation. The squares of relative values of the elements of the Raman tensor are given in Table 2. The bb, bc', and c'c' polarized Raman spectra of the [$^1H_4$]- and [$^2H_4$]pyrazine crystals are shown in Fig. 3. In the bb spectrum the Raman bands were observed at 1582 (1540), 1250 (899), 1017 (1003), 598 (591), and 943 (735) cm^{-1}. The first four bands can be assigned to the totally symmetric vibrations as already established by various workers. The band at 943 (735) cm^{-1} can be assigned to the ν_{10a} vibration based on the SVL fluorescence spectrum but the observed polarization behavior of this Raman band was not consistent with the expected behavior given in Table 2.

The Raman bands at 978 (840) and 756 (648) cm^{-1} observed in the c'c' and bc' spectra can be assigned to the ν_5 and ν_4 vibrations based on the SVL fluorescence spectrum, respectively, but the polarization behavior of these Raman bands did not entirely coincide with the expected behavior. The Raman bands at 1523 (1503), 1360 (1037), and 700 (674) cm^{-1} were observed in the c'c' and bc' spectra. The last band splits into doublets at 700 and 697 (674 and 671) cm^{-1} in the crystal, which may be caused by the factor group splitting. The first two Raman bands can be assigned to the ν_{8b} and ν_3 vibrations of the in-plane vibration of b_{3g} species, respectively, because of their higher frequencies than 1000 cm^{-1}. The last Raman band can be assigned to the ν_{6b} vibration of b_{3g} species because the corresponding frequency was not observed in the 0^0 SVL fluorescence spectrum but observed in the $10a^1$ and 4^1 SVL spectra. The observed polarization behavior of these b_{3g} vibrations did not entirely coincide with the expected one. The inconsistency of the observed and expected polarization behavior of the Raman bands may be ascribed to the characteristics in the pyrazine crystal which is invariably twinned on the (101) plane as indicated by Wheatley,[9] and therefore this suggests that the simple oriented gas model approximation cannot be applied to the analysis of the polarized Raman spectrum of the pyrazine crystal. Polarization behavior of the Raman bands can only give a reasonable evidence for the Raman bands observed in the bb spectrum being assigned to the a_g or b_{1g} vibration but not to the b_{2g} and b_{3g} vibrations since the vanishing values of the matrix elements for the b_{2g} and b_{3g} vibrations in the bb spectrum given in Table 2 result from the fact that the molecular z axis is parallel to the crystal a axis. The assignment made in this work, which is given in Figs. 2 and 3 and Table 1, is completely coincided with that made by Azumi et al. based on the polarized phosphorescence spectra of [$^1H_4$]- and [$^2H_4$]pyrazines.[7,8]

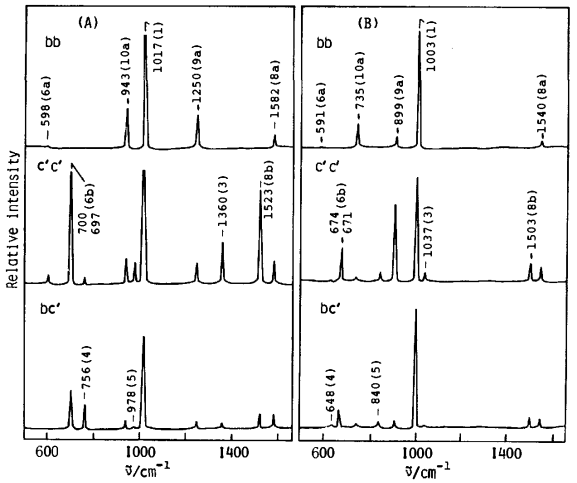

Fig. 3. Polarized Raman spectra of [$^1H_4$]- (A) and [$^2H_4$]- (B) pyrazine single crystals.

References

1) J. D. Simmons, K. K. Innes, and G. M. Begun, *J. Mol. Spectrosc.*, **14**, 190 (1964).
2) S. Califano, G. Adembri, and G. Sbrana, *Spectrochim. Acta*, **20**, 385 (1964).
3) G. Sbrana, V. Schettino, and R. Righini, *J. Chem. Phys.*, **59**, 2441 (1973).
4) J. Zarembowitch and L. Bokobza-Sebagh, *Spectrochim. Acta, Part A*, **32**, 605 (1976).
5) Y. Udagawa, M. Ito, and I. Suzuka, *Chem. Phys.*, **46**, 237 (1980).
6) D. McDonald and S. A. Rice, *J. Chem. Phys.*, **74**, 4893 (1981).
7) K. Matsuzaki, M. Sasaki, and T. Azumi, *J. Chem. Phys.*, **65**, 3326 (1976).
8) F. Kotani and T. Azumi, *J. Chem. Phys.*, **77**, 2757 (1982).
9) P. J. Wheatley, *Acta Crystallogr.*, **10**, 182 (1957).
10) T. Hieida, M. Masayoshi, Y. Nibu, H. Shimada, and R. Shimada, *Bull. Chem. Soc. Jpn.*, **62**, 925 (1989).
11) K. N. Wong and S. D. Colson, *J. Mol. Spectrosc.*, **104**, 129 (1984).
12) M. Umemoto, T. Ogata, H. Shimada, and R. Shimada, *Bull. Chem. Soc. Jpn.*, **57**, 3300 (1984).

Formation of Magnesium and Chloroaluminium Phthalocyanine Thin Films Exhibiting an Intense Near-Infrared Absorption by Electrolysis of Surfactants with Ferrocenyl Moiety

Tetsuo SAJI
Department of Chemical Engineering, Tokyo Institute of Technology, Ohokayama, Meguro-ku, Tokyo 152
(Received February 6, 1989)

Synopsis. Magnesium or chloroaluminium phthalocyanine (**1** and **2**) was dispersed to the micellar solution formed by a non-ionic surfactant with ferrocenyl moiety (**3**). The thin films prepared by the controlled-potential electrolysis of the micellar solution exhibited an intense near-infrared absorption.

In recent years extensive researches have been carried out on organic compounds for laser recording materials.[1] The sublimed films of phthalocyanine compounds usually exhibit no strong absorption in the wavelength region over 800 nm of use for a laser diode light source.[2] After acid, organic solvent, or thermal treatments, the sublimed films of magnesium, aluminium, and vanadyl phthalocyanines show strong absorption in the near-infrared region.[3-6]

Recently, we have presented a novel technique for electrochemical formation of an organic thin film by electrolysis of cationic surfactants with ferrocenyl moiety (micelle disruption method).[7] We further reported thin films of phthalocyanine compounds MPc (M=H_2, Cu) by electrolysis of non-ionic surfactants with a ferrocenyl moiety (**3**), and showed that crystalline forms of CuPc thin films prepared by this technique are identical with those of CuPc powders dispersed in an aqueous solution of the surfactant.[8,9] The author will report the preparation of thin films of magnesium and chloroaluminium phthalocyanines (**1** and **2**) using this technique, which have an intense absorption peak in the near-infrared region and have been proposed as candidates for laser recording materials.[1]

Experimental

1 was obtained from Tokyo Kasei Co. **2** was given by Nippon Shokubai Kagaku Kogyo Co. The surfactant used was poly(oxyethylene) (**13**) 11-ferrocenylundecyl ether (average molecular weight≒900) (**3**).[10] The micellar solution of **1** was prepared in the following manner: An aqueous solution containing 1 mM **3**, 0.1 M LiBr, and 5 mM **1** was sonicated for 10 min and stirred for three days. This solution was allowed to stand for overnight. The supernatant of this

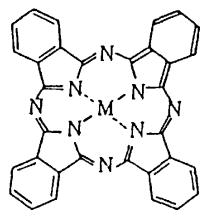

1, M=Mg
2, M=AlCl

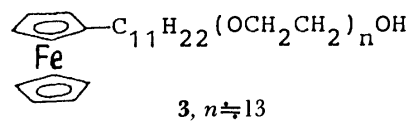

3, n≒13

solution was used for preparing the films. The test solution for electronic absorption measurements was prepared by diluting this solution. The micellar solution of **2** was prepared in the same manner as that of **1**.

Controlled-potential electrolysis was done for of an aqueous solution containing 3.2 mM **1**, 1.0 mM **3**, and 0.1 M LiBr by indium tin oxide (ITO) electrode maintained at +0.50 V vs. SCE with slow stirring. When 2.0 mM **3** solution was used, **1** film did not grow up. If **3** is present in the solution which is unadsorbed on the surfaces of **1** particles, the film formation seems to be disturbed. After a definite amount of current passed through ITO electrode, the electrode was air-dried at room temperature overnight, then rinsed with distilled water. Electrochemical measurements were carried out at 25 °C under a nitrogen atmosphere.

Results and Discussion

Figure 1 shows the electronic absorption spectrum of 1.0 mM (1 M=1 mol dm^{-3}) aqueous solution of **1** (a), and that of **1** in ethanol solution (b). The absorption peaks in spectrum (b) are the same as those previously reported[11] and are attributable to the

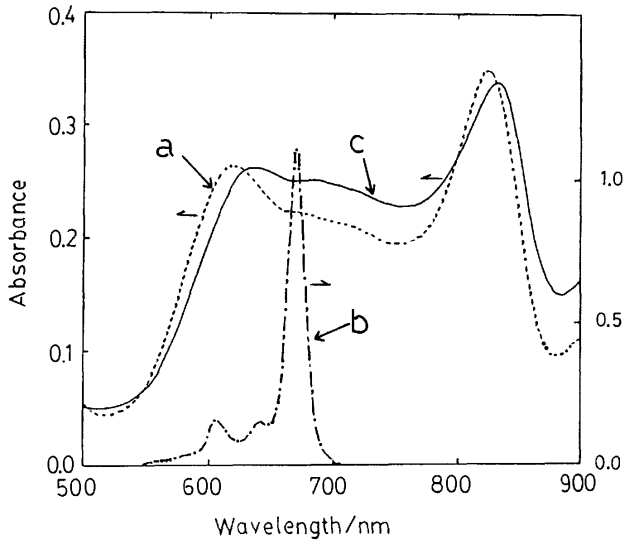

Fig. 1. Electronic absorption spectra of **1** in 1 mM **3**, and 0.1 M LiBr aqueous solution (a), in ethanol solution (b), and **1** film prepared by electrolysis of an aqueous solution containing 1 mM **3**, 3.2 mM **1**, and 0.1 M LiBr at ITO electrode maintained at +0.5 V vs. SCE for 1 h (c).

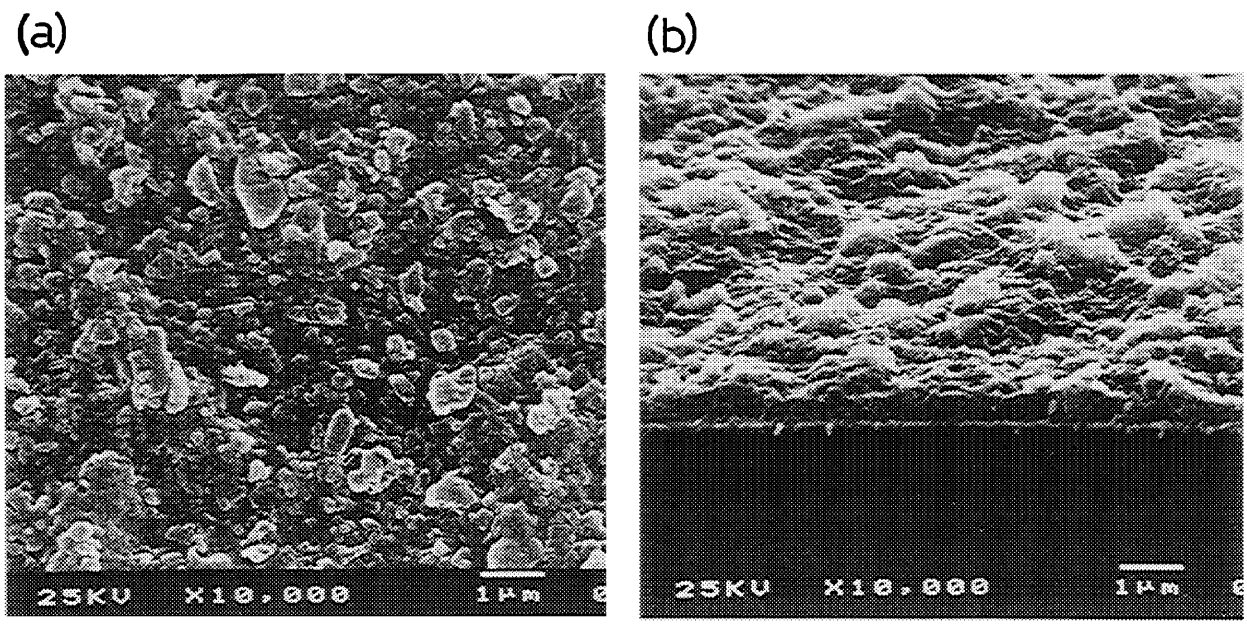

Fig. 2. SEM top (a) and cross sectional (b) views of **1** film prepared by the electrolysis of an aqueous solution containing 3.2 mM **1**, 1.0 mM **3**, and 0.1 M LiBr at ITO electrode maintained at +0.5 V vs. SCE for 14 h.

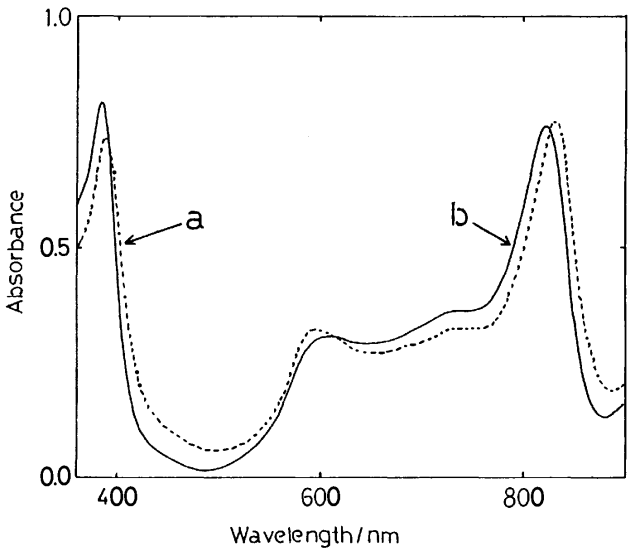

Fig. 3. Electronic absorption spectra of **2** in aqueous solution containing 2.0 mM **3** and 0.1 M LiBr (a), and **2** film prepared by the electrolysis of the same solution at ITO electrode maintained at +0.5 V vs. SCE for 3 h (b).

monomer.[12] The spectrum (a) consisting of a broad intense near-infrared peak at 827 nm suggests that the molecules of **1** in micellar solution exist in aggregates (particles).

The absorption spectrum of **1** film on the ITO electrode prepared by the electrolysis for 1 h consists of a broad intense near-infrared peak at 830 nm (Fig. 1-c).

Figure 2 shows the scanning electron micrographs (SEM) of the film on ITO. The crystals less than 1 μm in length were formed as shown in this figure. The SEM of the cross section of the film shows that the film thickness is approximately 0.5 μm (Fig. 2). This film thickness was easily controlled by changing the electrolysis time.

Figure 3-a shows the electronic absorption spectrum of **2** in 2.0 mM **3** (Fig. 3-b). The spectrum consists of an intense near-infrared peak at 828 nm. The thin film of **2** was prepared by the same method as that of **1**. The electronic absorption spectrum of **2** film (Fig. 3-b) consisted of an intense near-infrared peak at 822 nm.

Such near-infrared peaks of **1** and aluminium-phthalocyanine derivatives have been reported in the cases of treating these sublimed films with organic solvents.[3,4] These phenomena have been ascribed to a crystal form change, followed by dissolving of these compounds in the organic solvent. The formation of the films in our studies which show near-infrared peaks is relevant to the process of preparing these films: The cyrstal form of the particles dispersed in the surfactant solution is maintained in that of the film deposited on ITO electrode, because the electronic absorption spectrum of the film is similar to that of the micellar solution (Figs. 1 and 3).

The experimental results indicate that such an electrochemical method will give a technique for preparing **1** and **2** films which show near-infrared peaks without any further treatment.

We would like to thank Rokuro Ohki for the electron micrographs.

References

1) N. C. Khe and M. Aizawa, *Nippon Kagaku Kaishi,*

1986, 393; references therein.
2) E. A. Lucia and F. D. Verderance, *J. Chem. Phys.*, **48**, 2674 (1968).
3) A. M. Hor and R. O. Loutfy, *Thin Solid Films*, **106**, 291 (1983).
4) K. Arishima, H. Hiratsuka, A. Tate, and T. Okada, *Appl. Phys. Lett.*, **40**, 279 (1982).
5) L. H. Dao and G. Perrier, *Chem. Lett.*, **1986**, 1259; G. Perrier and L. H. Dao, *J. Electrochem. Soc.*, **134**, 1148 (1987).
6) C. H. Griffith, M. S. Walker, and Goldstein, *Mol. Cryst. Liq. Cryst.*, **33**, 149 (1976).
7) K. Hoshino and T. Saji, *J. Am. Chem. Soc.*, **109**, 5881 (1987); *Chem. Lett.*, **1987**, 1439; **1988**, 547.
8) T. Saji, *Chem. Lett.*, **1988**, 693.
9) T. Saji and Y. Ishii, *J. Electrochem. Soc.*, in press.
10) Poly(oxyethylene) (**13**) 11-ferrocenylundecyl ether is now available from Dojindo Laboratories. The results obtained by using this surfactant were almost the same as those using **3**.
11) B. D. Beerzir, *Russ. J. Phys. Chem.*, **36**, 258 (1962).
12) K. Bernauer and S. Fallab, *Helv. Chim. Acta*, **44**, 1287 (1961).

Effect of α-Cyclodextrin on the Electrochemistry of (Ferrocenylmethyl)-dodecyldimethylammonium Bromide at a Glassy Carbon Electrode

Marcin OPALLO,† Nagao KOBAYASHI,* Tetsuo OSA,*
Hiroshi YAMADA,†† and Shinji ONODERA††
Pharmaceutical Institute, Tohoku University, Aobayama, Sendai 980
††Chemical Research Institute of Non-Aqueous Solutions, Tohoku University, Katahira, Sendai 980
(Received February 18, 1989)

Synopsis. The influence of α-cyclodextrin (α-CD) on the electrochemistry of (ferrocenylmethyl)dodecyldimethylammonium bromide (**I**) was studied with a glassy carbon (GC) electrode. α-CD increases the apparent diffusion coefficient of **I**. This unusual effect is explained in terms of disruptive effect of α-CD on **I**'s aggregates. α-CD also influences, to some extent, **I**'s adsorption onto GC electrode when adsorbed from its micromolar aqueous solution.

The electrochemistry of redox active surfactants in aqueous solution has received some attention in the last few years.[1-5] Furthermore, their spontaneous aggregation on the surface of solid electrodes has recently been reported.[6-8]

Cyclodextrins (CDs) are torus shaped cyclic oligosaccharides having a hydrophobic cavity and a hydrophilic exterior. They can function as hosts for hydrophobic moieties of molecules dissolved in aqueous medium.[9] When CDs are added to a surfactant solution, they cause a decrease in the hydrophobicity of the solution. This is due to the inclusion of the hydrophobic alkyl chain of surfactant into the hydrophobic CD cavity.[10,11] Also, the solubility of a few electroreduced surfactants is known to increase by the presence of CD.[12,13]

In this report we show how α-CD influences the electrochemistry of redox active surfactants in aqueous solution. Although the effect of CDs on the behavior of redox inactive chromophore molecules in solution can be evaluated by, for example, UV-visible absorption and induced circular dichroism spectroscopies, that of redox active species can be examined by electrochemical methods, too. It appears not insignificant to show such an example. We chose here a functional surfactant with ferrocene (Fc) moiety, i.e. $FcCH_2N^+(CH_3)_2C_{12}H_{25}Br^-$ (**I**) and studied its properties and behavior in terms of electrochemistry. This molecule aggregates because it contains a long alkyl chain,[6] but is different from often studied viologen surfactants,[7,8] with which attractive interactions between viologen moieties may also cause aggregation.[14] The choice of α-CD, which is composed of six glucose units and has among CDs the smallest hydrophobic cavity with diameters of 0.47—0.52 nm,[9] is to lessen the probability of inclusion of the ferrocene moiety into the cyclodextrin cavity.

Experimental

Materials. **I** was synthesized by the reaction of [(dimethylamino)methyl]ferrocene (Aldrich) with dodecyl bromide (Tokyo Kasei) according to the literature.[1] The product was identified by elementary analysis. Found: C, 60.22; H, 8.70; N, 2.77%. Calcd for $C_{25}H_{42}NFeBr$: C, 60.08; H, 8.62; N, 2.85%. Li_2SO_4 was an extra pure reagent and was used as received. The water used for preparation of electrolyte solutions and sonication of electrodes was purified by a water purifier RO-10C (Tokyo Rikakikai Co., Ltd.).

Equipment and Procedures. Cyclic voltammetry and potential step chronoamperometry were performed using a potentiostat/galvanostat HA-501, an arbitrary function generator HB-105 (both Hokuto Denko), and a 3036 XY recorder (Yokogawa) connected with a water-jacketed three-compartment electrochemical cell at 25 °C. A spiral made of platinum wire served as the counter electrode and a saturated calomel electrode (SCE) as a reference one. As a working electrode a GC (Tokai Carbon GC-20) disc (0.071 cm^2 area) mounted in Teflon was used. It was polished using 0.3 and 0.05 μm β-alumina (Buehler). Each polishing step was followed by rinsing and sonication with water for more than 10 min. Then the electrode was immersed into a nitrogen-saturated solution and electrochemical measurements were performed. Apparent redox potentials (E°_{app}) were determined from cyclic voltammograms as midpotentials of cathodic and anodic peak potentials. Apparent diffusion coefficients (D_{app}) were determined by potential step chronoamperometry[15] by assuming one-electron process. The error of the above parameters was estimated to be 10 mV for E°_{app} and less than 20% for D_{app}.

Circular dichroism spectra were recorded on a JASCO-400X spectropolarimeter connected with a cell having an optical path of 10 mm.

Results and Discussion

The cyclic voltammograms recorded for the 2 mM (1 M=1 mol dm^{-3}) **I** and 0.2 M Li_2SO_4 aqueous solution in the absence and presence of 10 mM α-CD are presented in Fig. 1. It is obvious that **I** adsorbs weakly onto GC as onto Pt electrode.[1] The value of E°_{app} (0.427 V) determined in this particular case as being 0.029 V more positive than the cathodic peak potential, is within the error of experiment, being the same as in the case of Pt electrode.[1]

When the above experiment was performed in the 10 mM α-CD solution, the shape of the anodic peak changed. The 60 mV difference between cathodic and anodic peak potentials and the linear dependence of peak currents on the square root of scan rates in the scan rate range 0.01—0.2 V s^{-1} indicate that this couple is associated with a one-electron process, controlled by mass transport to the electrode.[15] The decrease in the anodic peak current, the shift of E°_{app} by 0.020 V in the anodic direction, and the slight increase in cathodic current in comparison to those determined in the absence of α-CD may be caused by a complexation

† On leave from the Institute of Physical Chemistry of Polish Academy of Sciences, Warszawa, Poland.

with α-CD and its influence on I's aggregation (see below).

The concentration dependences ($0.2 \leqq [\mathbf{I}] \leqq 4$ mM) of D_{app} and E°_{app} of **I** in the 10 mM α-CD and 0.2 M Li_2SO_4 aqueous solution are shown in Fig. 2. The D_{app} decreases slightly with the increase in [**I**] but it is larger than that in the absence of α-CD, except in the 0.2 mM **I** solution (compare also with Fig. 2 in Ref. 1). This behavior is opposite to that generally observed.[16] It has been shown that D_{app} is lower when molecules of redox probe aggregate than when aggregation does not occur.[1] Therefore, the effect of α-CD on the D_{app} of **I** may be caused by its disruptive effect on I's micelles (the twofold increase in critical micelle concentration (cmc) of tetraalkylammonium surfactants in the presence of CD has been explained similarly[10,11]).

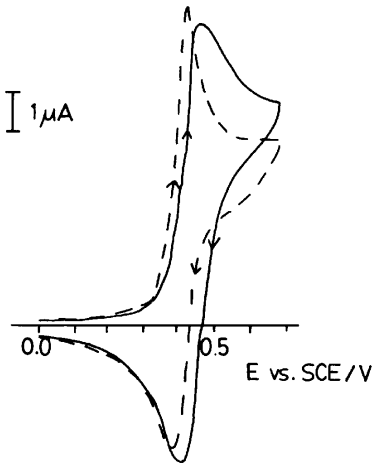

Fig. 1. The cyclic voltammograms recorded in 2 mM solution of **I** in 0.2 M Li_2SO_4 aqueous solution at GC electrode with scan rate 0.1 V s^{-1} (broken line). The same with 10 mM α-CD (solid line).

The D_{app} value estimated at the maximum concentration of **I** in the presence of α-CD is about 20% higher than that estimated in the absence of α-CD.[1] This may be due to the higher value of cmc as well as the smaller molecular weight of micelles in the presence of α-CD (the cmc values of **I** in the 0.2 M Li_2SO_4 in the absence and presence of α-CD are estimated to be, at 25 °C, ca. 0.5 mM[1] and ca. 2 mM (from Fig. 2), respectively). The D_{app} value estimated for the 0.2 mM solution of **I** is smaller than that estimated in the absence of α-CD. At this concentration **I** does not form aggregates[1] and this decrement in D_{app} may be ascribed only to CD complex formation.[16] The dependence of E°_{app} on [**I**] is similar to that evaluated in the absence of α-CD,[1] but E°_{app} is slightly shifted in the anodic direction. The anodic shift of E°_{app} in the 0.2 mM solution of **I** may indicate a stronger complexation of the reduced form of **I** by α-CD. At higher concentrations of **I**, the concentration dependence of E°_{app} may be caused by both aggregation and complexation.

Circular dichroism is induced when a chromophore is trapped in the cavity of CDs.[17] Accordingly, the lack of circular dichroism signals in the range of 200—500 nm in the 0.5 mM **I** and 10 mM α-CD solution indicates that the ferrocene chromophore is not included into the α-CD cavity.

The influence of CD on the surface aggregation of redox surfactants in solution has recently been mentioned.[8] Therefore, we performed a similar experiment with **I**. The cyclic voltammograms recorded at $[\mathbf{I}]/\mu M = 30$ in the 0.2 M Li_2SO_4 solution are presented in Fig. 3A. The linear dependence of anodic and cathodic peak currents (after subtraction of the current recorded in the electrolyte solution) on scan rate in the range 0.01—0.2 V s^{-1} indicates that **I** adsorbs onto the GC electrode from this solution. The E°_{app} value (+0.49 V) of the $\mathbf{I}^{0/+1}$ couple is shifted in the anodic direction by 0.13 V relative to that determined

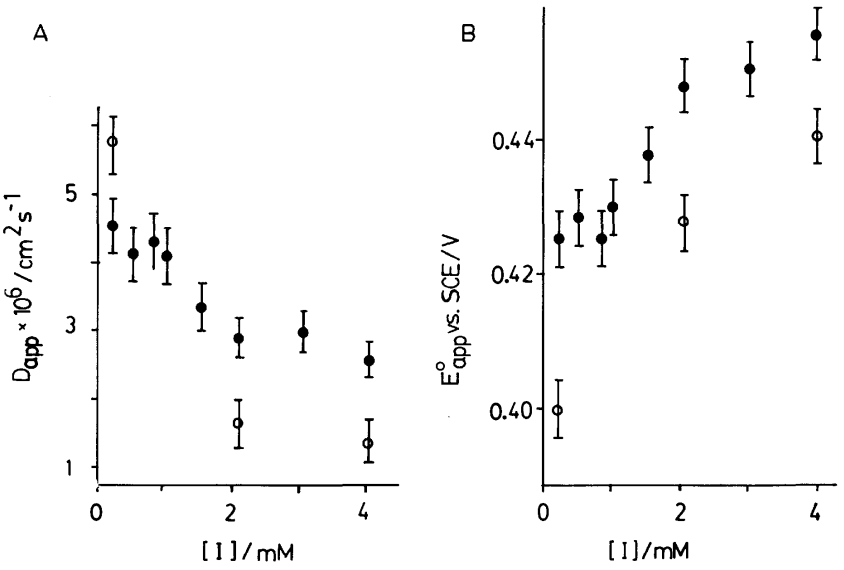

Fig. 2. The dependence of (A) D_{app} of **I** and (B) E°_{app} of $\mathbf{I}^{0/+1}$ couple on [**I**] in aqueous 0.2 M Li_2SO_4 (○). The same with 10 mM α-CD (●).

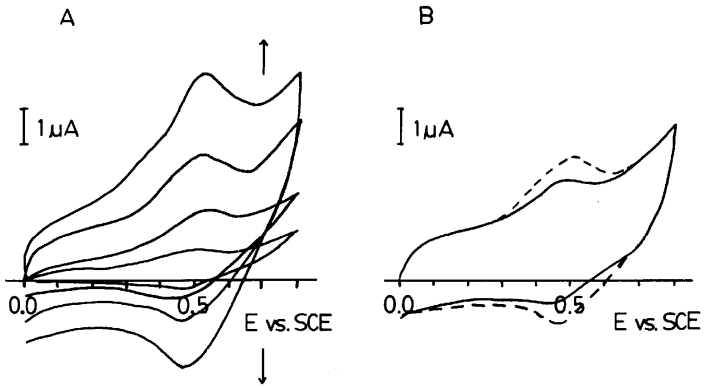

Fig. 3. The cyclic voltammograms recorded at GC electrode in 0.2 M Li_2SO_4 solution containing 30 μM of **I** (A) with scan rates 0.025, 0.05, 0.1, and 0.2 V s^{-1}, and (B) with the scan rate 0.1 V s^{-1} in the absence (broken line) and presence (solid line) of 0.5 mM α-CD.

for ferrocenyltrimethylammonium cation (0.36 V vs. SCE[18]). This indicates that, of the two redox forms, the oxidized one is more weakly bonded to the electrode. This may be caused by stronger repulsive interactions among head groups in the oxidized species of **I**. The differences between the anodic and cathodic peak potentials are equal to 0.04—0.06 V and their half widths (though difficult to estimate) are larger by more than 0.07 V than the theoretical value (0.091 V[19]). This indicates that the layer cannot be regarded as tightly packed, although the area per molecule (about 50 nm^2) is similar to that reported for the monolayer of (ferrocenylmethyl)octadecyldimethylammonium cations deposited on Au electrode by the Langmuir-Blodgett technique.[20]

When the experiments described above were performed in the 0.5 mM α-CD solution, i.e. at [α-CD]/[**I**]=17 (Fig. 3B), both the anodic and cathodic peak currents decreased by ca. 50%, and when [α-CD] was increased to ca. 10 mM ([α-CD]/[**I**]=ca. 3333), the two peaks disappeared. This behavior is different from that of viologen surfactant where 10-fold excess of α-CD was enough to prevent the surface aggregation onto Au electrode.[8] The formation constant of alkyl chain surfactant-α-CD complexes are about 10^3 dm^3 mol^{-1},[10,11] and it does not depend on the length of alkyl chain of surfactants when the chain contains more than 10 carbon atoms.[11] Therefore, it seems reasonable to assume a similar formation constant for **I**-α-CD complexes. If so, in the above experiments more than 90% of **I**'s molecules are considered to be complexed with α-CD. In spite of such a high degree of complexation, the decrease of adsorption is slight compared with other systems.[8] This may indicate the presence of some attractive interactions between **I** and hydrophilic GC surface. The lock of circular dichroism signals suggests no inclusion of ferrocenyl moiety. Accordingly, if some interaction exists between the electrode surface and **I**, **I**'s ferrocenyl group would be participating in the interaction.

M. Opallo acknowledges the financial support from the Ministry of Education, Science and Culture.

References

1) T. Saji, K. Hoshino, and S. J. Aoyagui, *J. Am. Chem. Soc.*, **107**, 6865 (1985).
2) K. Hoshino and T. Saji, *Chem. Lett.*, **1987**, 1439.
3) K. Hoshino and T. Saji, *J. Am. Chem. Soc.*, **109**, 5889 (1987).
4) T. Saji, *Chem. Lett.*, **1988**, 693.
5) K. Hoshino, M. Goto, and T. Saji, *Chem. Lett.*, **1988**, 548.
6) J. Facci, *Langmuir*, **3**, 525 (1987).
7) C-W. Lee and A. J. Bard, *J. Electroanal. Chem. Interfacial Electrochem.*, **239**, 441 (1988).
8) A. Diaz and A. E. Kaifer, *J. Electroanal. Chem. Interfacial Electrochem.*, **249**, 333 (1988).
9) W. Saenger, *Angew. Chem., Int. Ed. Engl.*, **19**, 344 (1980).
10) T. Okubo, H. Kitano, and N. Ise, *J. Phys. Chem.*, **80**, 2661 (1976).
11) I. Satake, T. Ikenoue, T. Takeshita, K. Hayakawa, and T. Maeda, *Bull. Chem. Soc. Jpn.*, **58**, 2746 (1985).
12) A. Yasuda, H. Kondo, H. Itabashi, and J. Seto, *J. Electroanal. Chem. Interfacial Electrochem.*, **210**, 265 (1987).
13) A. Diaz, P. A. Quintela, J. M. Schuette, and A. E. Kaifer, *J. Phys. Chem.*, **92**, 3537 (1988).
14) C. L. Bird and A. T. Kuhn, *Chem. Soc. Rev.*, **10**, 49 (1980).
15) A. J. Bard and L. R. Faulkner, "Electrochemical Methods," John Wiley & Sons, Inc., New York (1980).
16) T. Matsue, T. Osa, and D. H. Evans, *J. Inclusion Phenom.*, **2**, 547 (1984).
17) N. Kobayashi, S. Minato, and T. Osa, *Makromol. Chem.*, **184**, 2123 (1984) and Refs. 12—17 therein.
18) R. Szentirmay, P. Yeh, and T. Kuwana, "Electrochemical Studies of Biological Systems," ed by D. T. Sawyer, *ACS Symp. Ser.*, **38**, Washington DC, 152 (1977).
19) A. P. Brown and F. C. Anson, *Anal. Chem.*, **49**, 1589 (1977).
20) J. S. Facci, F. A. Fatcigno, and J. M. Gold, *Langmuir*, **2**, 736 (1986).

Dielectric Properties of Dehydrated Ca_1Na_{10}-A and Na_{12}-A Zeolites

Tatsuo OHGUSHI,* Kenji NONAKA, Hiroyuki YOSHIDA, and Tetsuo TAKAISHI
Department of Materials Science, Toyohashi University of Technology, Toyohashi 440
(Received February 14, 1989)

Synopsis. Dielectric properties of completely dehydrated Ca_1Na_{10}-A and Na_{12}-A zeolites were studied. The properties of Ca_1Na_{10}-A bore close parallels to those of Na_{11}-ZK4 having almost the same cation distribution as Ca_1Na_{10}-A. The properties of Na_{12}-A were markedly different from those of Ca_1Na_{10}-A and the unusual behavior of the zeolite were attributed to a larger mobility of Na^+ ion on the 4-ring site.

Properties of Ca_xNa_{12-2x}-A zeolites ($0 \leq x \leq 6$) have been widely investigated, e.g., heats of gas-adsorption,[1] reactivities of oxygen in zeolite framework,[2] and heat-resistivities.[3] These properties of the zeolite at composition of $x=0$ were markedly different from those at $x \geq 1$ and the differences were correlated to the Na^+ ion near a 4-membered oxygen ring (abbreviated as 4-ring Na^+ ion), since the zeolite contains the 4-ring Na^+ ion at $x=0$ but not at $x \geq 1$ (Table 1). The unusual behavior of the 4-ring Na^+ ion may be directly studied by dielectric measurements, and thus the dielectric properties of Na_{12}-A and Ca_1Na_{10}-A were measured and compared with each other. It is one objective of the present work to study the unusual properties of Na_{12}-A.

Another subject is to investigate the similarities of the dielectric properties of the Ca_1Na_{10}-A and Na_{11}-ZK4 zeolites. Zeolite A is isostructural with zeolite ZK4, and Ca_1Na_{10}-A has the same cation distribution as Na_{11}-ZK4, except for a Ca^{2+} ion being used in the place of a Na^+ ion near a 6-ring (Table 1). Thus, the dielectric properties of Ca_1Na_{10}-A are expected to be similar to those observed in Na_{11}-ZK4.[7]

Experimental

The apparatus and the procedures used in the dielectric measurements were the same as in a previous paper.[8] A commercial 4A zeolite, $Na_{11.8}(AlO_2)_{11.8}(SiO_2)_{12.2} \cdot nH_2O$ (abbreviated as Na_{12}-A), was ion-exchanged with 0.1 mol dm^{-3} solution of $(CH_3COO)_2Ca$ at 353±0.5 K for 3 d, and the cation composition of zeolite after ion-exchange was determined to be $Ca_{1.05}Na_{9.7}(AlO_2)_{11.8}(SiO_2)_{12.2}$ (Ca_1Na_{10}-A), by EDTA titration of the ion exchange solution and from the material balance.

Complex dielectric constants ($\varepsilon^* = \varepsilon' - i\varepsilon''$) were measured as functions of frequency f and temperature T, in the ranges of 20—2×10^6 Hz and 273—653 K for Ca_1Na_{10}-A, and 50—2×10^6 Hz and 163—363 K for Na_{12}-A. In the present work, we did not require the absolute value of the dielectric constant and did not make the correction for the packing density of the sample disk, because we were concerned only with its dependence on the frequency and temperature.

Table 1. Cation Distribution[4-6]

Composition	8-Ring 3[a]	6-Ring 8[a]	4-Ring 12[a]
Na_{12}-A	3 Na^+	8 Na^+	1 Na^+
Ca_1Na_{10}-A	3 Na^+	1 Ca^{2+}+7 Na^+	0
Na_{11}-ZK4	3 Na^+	8 Na^+	0

a) Number of ring per pseudo unit cell. Each ring can accommodate only one cation.

Results

Spectra of the loss tangent for Ca_1Na_{10}-A are shown in Fig. 1, which contain two main losses, a loss peak in a higher frequency region and a peak-less loss in a lower region. A frequency, f_{tan}, at the peak of the loss tangent was determined and the activation energy, E_{tan}, of cation jump was found to be 87±2 kJ mol^{-1} from the slope of the plots of $\ln f_{tan}$ vs. $1/T$.

Cole-Cole plots (Fig. 2) showed, in a larger ε' region, a steep rise of ε''_{obs} which is usually attributed to a conductivity loss[9-11] (subscript obs denotes observed

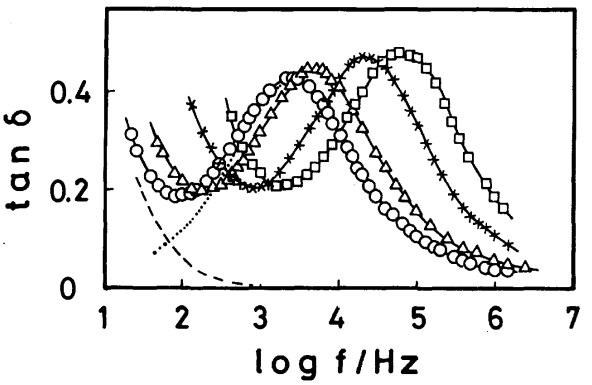

Fig. 1. Spectra of dielectric loss tangent for Ca_1Na_{10}-A zeolite. □: 657.7 K, ✳: 614.4 K, △: 566.8 K, ○: 543.8 K. Broken line for loss tangent of conduction, $\tan\delta_c = \varepsilon''_c/\varepsilon'_{obs}$, at 543.8 K ($\varepsilon''_c = \sigma/2\pi f\varepsilon_0$ with $\sigma = 2.1\times10^{-8}$ S m^{-1}). Dotted line for loss tangent of relaxation, $\tan\delta_r = \tan\delta_{obs} - \tan\delta_c$, at 543.8 K. Subscript obs denotes observed values.

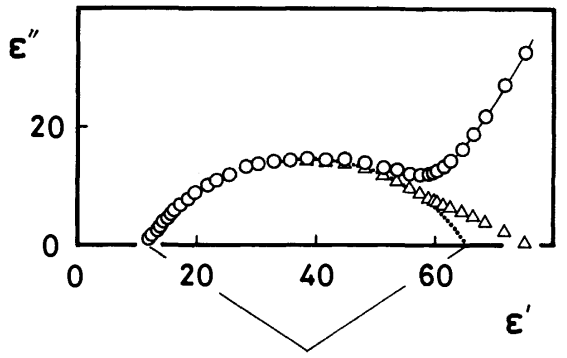

Fig. 2. Cole-Cole plots for Ca_1Na_{10}-A zeolite at 614.4 K. ○: ε''_{obs} vs. ε'_{obs}, △: ε''_r vs. ε'_{obs} ($\varepsilon''_r = \varepsilon''_{obs} - \varepsilon''_c$, $\varepsilon''_c = \sigma/2\pi f\varepsilon_0$ with $\sigma = 1.8\times10^{-7}$ S m^{-1}). Dotted line for Cole-Cole circular arc best fitted to ε''. Subscript obs denotes observed values.

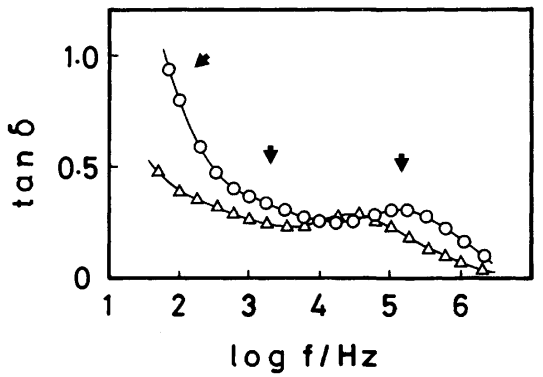

Fig. 3. Spectra of dielectric loss tangent for Na_{12}-A zeolite. O: 363.2 K, Δ: 331.0 K. Arrows denote losses in each frequency region of spectrum at 363.2 K, losses in the lower, middle and higher frequency regions.

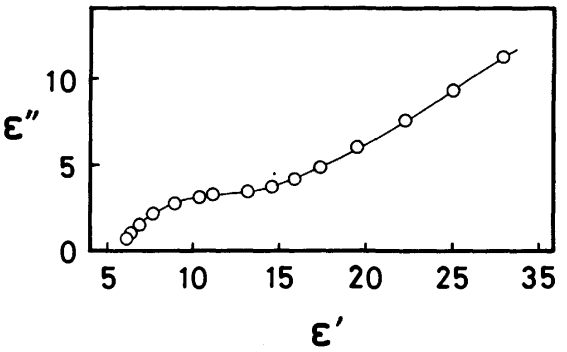

Fig. 4. Cole-Cole plots for Na_{12}-A zeolite at 363.2 K.

values). The loss part in the larger ε' region was described with the equation of the conductivity loss, $\varepsilon_c''=\sigma/2\pi f\varepsilon_0$, and was thereby assigned to the conductivity loss, where ε_c'' and ε_0 are the conductivity loss and the permittivity of vacuum, respectively, and σ an apparent dc conductivity. A plot of $\ln\sigma$ vs. $1/T$ gave $E_c=83\pm4$ kJ mol^{-1} for the conduction process. The observed loss was corrected for by subtracting the conductivity loss. The plots of ε_r'' $(=\varepsilon_{obs}''-\varepsilon_c'')$ vs. ε_{obs}' were well described with a single circular arc, except for the larger ε' region, as shown in Fig. 2. Hence, we concluded that the main part of ε_r'' contains only one relaxation loss. For the relaxation process, the activation energy, E_r, and the frequency factor, ω_0, were determined from plots of $\ln f_r$ vs. $1/T$, where f_r is the frequency at the maximum value of ε_r'' and ω_0 is defined as $\ln f_r=\ln\omega_0/2\pi-E_r/RT$. Their values were $E_r=87\pm3$ kJ mol^{-1} and $\log\omega_0=12.0\pm0.4$. If a relaxation process and a conduction process contain the same cation-jump, the equation of $E_r-E_c=RT$ holds true.[8] The present values of E_r and E_c satisfy this relationship, and thus it was concluded that both processes involve the same cation jump.

For Na_{12}-A zeolite, both ε_{obs}' and ε_{obs}'', at $T>400$ K, were too large to give useful data for analysis. The measurements were thereby limited to temperatures lower than 363 K. Representative spectra of the loss tangent and Cole-Cole plots are given in Figs. 3 and 4, respectively. The spectra of the loss tangent show that there are three kinds of losses, a loss peak in the higher frequency region, a large peak-less loss in the lower region, and a small loss in the middle region, though the last is less clear. The large loss in the larger ε' region, in Fig. 4, may be due to conduction. However, the loss part was not evaluated with the equation of conductivity loss owing to the loss in the middle region. Thus the Cole-Cole curve could not be separated into separate components. The activation energy of cation jump was thereby determined only from the spectra of loss tangent, and was $E_{tan}=48\pm4$ kJ mol^{-1}.

Discussion

Let us consider cation-jumps causing the losses observed in Ca_1Na_{10}-A. Allowed cation-jumps in Ca_1Na_{10}-A can be deduced from the cation distribution in the zeolite, since only jumps to sites unoccupied by cations are allowed. The cation distribution is essentially the same as in Na_{11}-ZK4 and thus the same type of cation-jumps as in Na_{11}-ZK4 are allowed, namely a jump from the 8- or 6-ring site to the 4-ring site, a jump from the 8-ring site to the neighboring sites in the same ring, and a jump between the 6-ring sites in the large cage side and in the soadalite cage side.[7] In the allowed jumps, the jump which can cause both relaxation and conductivity losses is only the jump of Na^+ ion between the 8- and 4-ring sites, since the cation can escape from the unit cell dimension only by repeating the jump of the 8-ring site → 4-ring site → another 8-ring site. Thus both relaxation and conductivity losses observed in Ca_1Na_{10}-A are assigned to the jump of Na^+ ion between the 8-ring and 4-ring sites.

The relaxation loss is characterized by $E_{tan}=87\pm2$ kJ mol^{-1}, $E_r=87\pm3$ kJ mol^{-1}, and $\log\omega_0=12.0\pm0.4$, and the conductivity loss by $E_c=83\pm4$ kJ mol^{-1}. These characteristics are respectively close to those for Na_{11}-ZK4 ($E_{tan}=89\pm2$ kJ mol^{-1}, $E_r=91\pm3$ kJ mol^{-1}, $\log\omega_0=12.1\pm0.4$ for the relaxation loss assigned to the jump between the 8- and 4-ring sites, and $E_c=86\pm4$ kJ mol^{-1} for the conductivity loss attributed to the jump of 8-ring → 4-ring → another 8-ring).[7] Hence, we can conclude that the dielectric properties of Ca_1Na_{10}-A bear close parallels to those of Na_{11}-ZK4.

In Na_{12}-A, the loss peak was observed at a lower temperature range of 273—363 K. Such a loss was not observed in Ca_1Na_{10}-A and Na_{11}-ZK4 zeolites lacking the 4-ring Na^+ ion. The loss is thereby peculiar to Na_{12}-A and is correlated to jumps of the 4-ring Na^+ ion. There are two kinds of jumps related to the 4-ring Na^+ ion, that is, one is the jump from the 4-ring site to the neighboring 4-ring site and another is the modification of the jump, from the 8- or 6-ring site to the 4-ring site, by the 4-ring Na^+ ion. If the Na^+ ion on the 4-ring site jumps to the nearest 4-ring site, the activation energy of the jump may be as small as $E_{tan}=48$ kJ mol^{-1}, since the cation has a weak affinity to the 4-ring site.[4,12] Thus the loss peak is most probably assigned to the jump of Na^+ ion between the 4-ring sites.

Conclusion

It was confirmed that the dielectric properties of Ca_1Na_{10}-A and Na_{11}-ZK4 zeolites are, in both the characteristic values and the jump mechanism, close to each other. The zeolite Na_{12}-A showed "unusual" behaviors also in dielectric properties. As can be seen from the small activation energy of jump of the 4-ring Na^+ ion, the unusual behavior has its origin in a larger mobility of the Na^+ ion on the 4-ring site.

References

1) T. Masuda, K. Tsutsumi, and H. Takahashi, *J. Colloid Interface Sci.*, **77**, 232 (1980).
2) T. Takaishi and A. Endoh, *J. Chem. Soc., Faraday Trans. 1*, **83**, 411 (1987).
3) T. Ohgushi and M. Miyoshi, *Chem. Lett.*, **1989**, 693.
4) T. Takaishi, Y. Yatsurugi, A. Yusa, and T. Kuratomi, *J. Chem. Soc., Faraday Trans. 1*, **71**, 97 (1975).
5) A. Yusa, T. Ohgushi, and T. Takaishi, *J. Phys. Chem. Solids*, **38**, 1233 (1977).
6) D. W. Breck, "Zeolite Molecular Sieves," John Wiley & Sons, New York (1974), p. 179.
7) T. Ohgushi, K. Nonaka, and T. Watanabe, *Bull. Chem. Soc. Jpn.*, **61**, 1797 (1988).
8) T. Ohgushi, *Bull. Chem. Soc. Jpn.*, **61**, 1109 (1988).
9) R. M. Barrer and E. A. Saxon-Napier, *Trans. Faraday Soc.*, **58**, 145, 156 (1962).
10) B. Morris, *J. Phys. Chem. Solids*, **30**, 73 (1969).
11) R. A. Schoonheyt and W. Wild, *J. Chem. Soc., Faraday Trans. 1*, **70**, 2132 (1974).
12) K. O. Koh and M. S. Jhon, *Zeolites*, **5**, 313 (1985).

Absence of the Enhanced Methanation Activity of Ni/TiO_2 in the SMSI State as Examined with Pulse Surface Reaction Rate Analysis

Toshiaki MORI,* Kenzi SUZUKI, Masahiro SAITO,†
Tadashi HATTORI,†† and Yuichi MURAKAMI††
Government Industrial Research Institute, Nagoya, Hirate-cho, Kita-ku, Nagoya 462
†National Research Institute for Pollution and Resources, Yatabe-cho, Tsukuba 305
††Department of Synthetic Chemistry, Faculty of Engineering, Nagoya University, Chikusa-ku, Nagoya 464
(Received April 18, 1989)

Synopsis. From rate measurements with pulse surface reaction rate analysis, it was found that the methanation activity of Ni/TiO_2 was the same both in the SMSI and in the normal states.

On high-temperature reduction (namely at 773 K), titania-supported metals exhibit an interesting phenomenon which is known as a strong metal-support interaction (SMSI).[1] As a result of SMSI, a large part of the chemisorption ability for H_2 or CO is lost without any agglomeration of a supported metal.[2] While most reactions in which hydrogen is involved are suppressed on the catalyst in the SMSI state, it has been found that the hydrogenation of CO or methanation is enhanced by SMSI.[3] This enhanced activity was measured on the basis of the turnover frequency (TOF), which is determined by dividing the rate by the number of adsorption sites. The suppression of chemisorption, however, makes it difficult to count precisely the number of adsorption sites. Indeed, there seems to be controversy over the enhanced activity of the SMSI catalyst for CO hydrogenation.[4]

Different from the conventional TOF, we have found that pulse surface reaction rate analysis (PSRA) is relevant in examining the activity enhancement of the SMSI catalyst for CO hydrogenation.[5] Since adsorbed CO is an initial reacting species under conditions of PSRA, the CO adsorption step is not involved in this rate analysis. Therefore, if the number of adsorbed CO molecules is decreased only by methanation, but not by desorption, we can determine directly the rate constant per active site without any information about the number of active sites from the analysis of the dynamic behavior of the adsorbed CO or the CH_4 produced.[6] PSRA has a further advantage: the rate for the initial state of a catalyst can be measured with minimal influence of the H_2O produced, which can destroy the SMSI state.[7] In the previous study, by using PSRA, we revealed that SMSI increased the activity for the hydrogenation of adsorbed CO on titania-supported Pt and Pd, but not on titania-supported Rh, Ru, and Ir.[5] Compared to noble metals, studies about the effect of SMSI on CO hydrogenation over titania-supported base metals are limited.[3,4] In the present study, selecting Ni as the base metal, we examined the effect of SMSI on the hydrogenation of adsorbed CO on the basis of the rate constant per active site determined by PSRA.

Experimental

Catalyst. Ni/TiO_2 catalyst (metal loading, 20 wt%) was prepared by impregnating TiO_2 (Nippon Aerosil, P-25) with an aqueous solution of $Ni(NO_3)_2$ followed by drying and subsequent calcination. Before making rate and chemisorption measurements, the catalyst was reduced at different temperatures for 4 h. In order to obtain information about the extents both of reduction and of sintering, X-ray powder diffraction measurements were made using a Shimadzu Cu $K\alpha$ diffractometer (Shimadzu XD-3A).

Rate and Chemisorption Measurements. For the hydrogenation of adsorbed CO, the rate constant per active site was determined by PSRA in the manner described elsewhere.[5,6] The amount of CO chemisorbed on the catalyst was determined at 300 K using a conventional pulse adsorption apparatus.

Results and Discussion

Figure 1 shows the X-ray diffraction patterns for

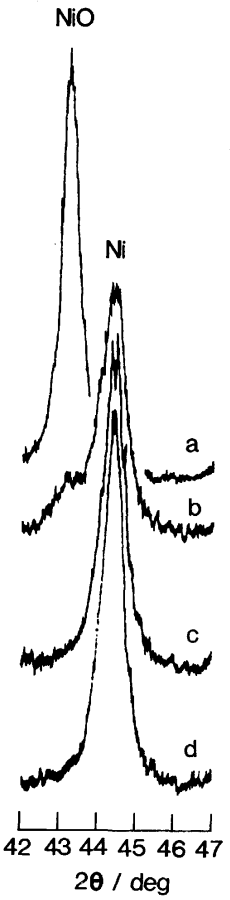

Fig. 1. X-Ray powder diffraction patterns for unreduced (a) and reduced Ni/TiO_2 catalysts. Reduction temperature: 573 K (b), 673 K (c), and 773 K (d).

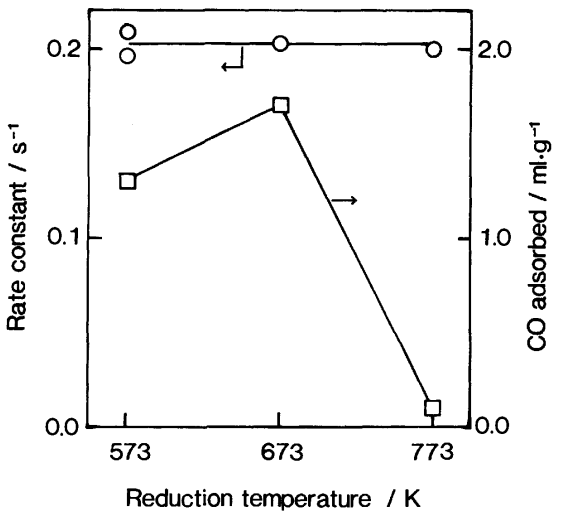

Fig. 2. Amount of CO adsorbed (□) and the rate constant per active site (○) on Ni/TiO_2 against the reduction temperature. Catalyst weight; 100 mg, reaction temperature; 453 K, flow rate of carrier gas; 40 cm^3 min^{-1}, amount of CO pulsed; 10 mm^3.

unreduced and reduced catalysts. Although most NiO is changed into Ni metal after reduction at 573 K, some of the NiO still remains unreduced. After reduction both at 673 and at 773 K, on the other hand, the NiO diffraction peak disappears, implying that complete reduction occurs. It is furthermore observable from X-ray diffraction patterns that the peak width at half height is almost the same at all reduction temperatures examined. This suggests that the particle size is hardly altered after reduction below 773 K.

The amount of CO adsorbed is shown in Fig. 2 as a function of the reduction temperature. A considerable amount of CO is adsorbed on the catalyst after reduction at 573 and 673 K, although the amount is smaller on reduction at 573 K than at 673 K. The lower amount of CO chemisorption on reduction at 573 K is ascribable to the incomplete reduction, as the X-ray diffraction shows (see Fig. 1). Contrary to this, CO chemisorption is suppressed almost completely after reduction at 773 K. Since reduction at 773 K did not cause the agglomeration of supported Ni metal particles, as described above, the drastic suppression of CO chemisorption should be attributed to SMSI.

Under experimental conditions of PSRA, a small amount of CO (usually 10 mm^3) pulsed via the H_2 carrier gas was immediately adsorbed on the catalyst and then hydrogenated selectively to CH_4. Analysis of the dynamics of the CH_4 produced permits us to determine the rate constant per active site.[5,6] The rate constant determined is also shown in Fig. 2 as a function of the reduction temperature. The rate constant is almost constant irrespective of the reduction temperature. Taking into account the fact that reduction at 773 K induces the SMSI state in the Ni/TiO_2, the results in Fig. 2 clearly indicates that the SMSI of this catalyst does not increase the rate constant per active site for the hydrogenation of adsorbed CO. It is interesting to compare the present results with the one previously obtained on noble metals.[5] Titania-supported Ni is very similar to titania-supported Rh, Ru, and Ir in a sense that their SMSI does not increase the activity for the hydrogenation of adsorbed CO.

It is now accepted that SMSI results from migration of TiO_x-suboxide species, formed by high-temperature reduction, onto the metal particles.[8] The suppression of CO chemisorption results from site blocking by the migrated TiO_x-suboxide, by which the number of adsorption sites is decreased. The influence of SMSI on CO hydrogenation has been attributed to this TiO_x-suboxide.[9] The suboxide takes part in C–O bond dissociation by bond formation between a titanium ion in a partially reduced state and an oxygen end of an adsorbed CO species. Due to the high affinity of the titanium ion in the reduced state for an oxygen atom, a C–O bond is readily dissociated, leading to an increase in the activity for CO hydrogenation. Since our Ni/TiO_2 is in the SMSI state after reduction at 773 K, the TiO_x-suboxide should be present on Ni metal particles. Nevertheless, this suboxide did not increase the activity for the hydrogenation of adsorbed CO. We have previously presented a possible explanation for the effect of the TiO_x-suboxide: the suboxide effectively takes part in the C–O bond dissociation on such a metal as Pt or Pd exhibiting a relatively low activity for CO hydrogenation. However, it does not work on a metal with high activity like Rh or Ru.[5] This may also explain the absence of the enhanced activity of Ni/TiO_2 in the SMSI state, because Ni is known to be one of the most active metals for CO hydrogenation.[10] This may again support our previous explanation.

References

1) S. J. Tauster, S. C. Fung, R. T. K. Baker, and J. A. Horsley, *Science*, **211**, 4487 (1981); "Studies in Surface Science and Catalysis," ed by B. Imelik et al., Elsevier, Amsterdam (1982), Vol. 11; G. C. Bond and R. Burch, "Catalysis (Specialist Periodical Reports)," The Chemical Society, London (1983), Vol. 6, pp. 27—60.

2) S. J. Tauster, S. C. Fung, and R. L. Garten, *J. Am. Chem. Soc.*, **100**, 170 (1978).

3) M. A. Vannice and R. L. Garten, *J. Catal.*, **56**, 236 (1978); S.-Y. Wang, S. H. Moon, and M. A. Vannice, *ibid.*, **71**, 167 (1981); M. A. Vannice and C. C. Twu, *ibid.*, **82**, 213 (1983); J. S. Rieck and A. T. Bell, *ibid.*, **99**, 262 (1986).

4) R. Burch and A. R. Flambard, *J. Catal.*, **78**, 389 (1982); J. D. Bracey and R. Burch, *ibid.*, **86**, 384 (1984).

5) S. Taniguchi, T. Mori, Y. Mori, T. Hattori, and Y. Murakami, *J. Catal.*, **116**, 108 (1989).

6) T. Mori, H. Masuda, H. Imai, A. Miyamoto, S. Baba, and Y. Murakami, *J. Phys. Chem.*, **86**, 2753 (1982); T. Mori, H. Masuda, H. Imai, A. Miyamoto, R. Hasebe, and Y. Murakami, *ibid.*, **87**, 3648 (1983); T. Mori, A. Miyamoto, H. Niizuma, N. Takahashi, T. Hattori, and Y. Murakami, *ibid.*, **90**, 109 (1986).

7) K. Kunimori, S. Matsui, and T. Uchijima, *Chem. Lett.*, **1985**, 359; J. B. F. Anderson and R. Burch, *Appl. Catal.*, **21**, 179 (1986).

8) P. Meriaudeau, J. F. Dutel, M. Defaux, and C. Naccache, "Studies on Surface Science and Catalysis," ed by B. Imelik et al., Elsevier, Amsterdam (1982), Vol. 11, pp. 95—104; J. Santos, J. Phillips, and J. A. Dumesic, *J. Catal.*, **81**, 147 (1983); D. E. Resasco and G. L. Haller, *ibid.*, **82**, 279 (1983); H. R. Sadeghi and V. E. Henrich, *ibid.*, **87**, 279 (1984).

9) M. A. Vannice and C. Sudhakar, *J. Phys. Chem.*, **88**, 2429 (1984); W. M. H. Sachtler, in "Proc. 8th Internat. Congr. Catal., Berlin, 1984," Verlag Chemie, Weinheim (1984), Vol. V, pp. 151—173.; M. E. Levin, M. Salmeron, A. T. Bell, and G. A. Somorjai, *J. Catal.*, **106**, 401 (1987).
10) M. A. Vannice, *Catal. Rev.-Sci. Eng.*, **14**, 153 (1976).

Molecular Aggregation Structure of Barium Stearate Monolayer Based on Electron Microscopy

Tisato KAJIYAMA,* Kazuo UMEMURA, Motoko UCHIDA, Yushi OISHI, and Ryutaro TAKEI†
Department of Applied Chemistry, Faculty of Engineering, Kyushu University,
6-10-1 Hakozaki, Higashi-ku, Fukuoka 812
(Received May 18, 1989)

Synopsis. Aggregation structure of barium stearate monolayers prepared from a benzene solution at various surface pressures was investigated by using a transmission electron microscope. Two-dimensional crystallites of the monolayer were formed even at the surface pressure of 0 $mN \cdot m^{-1}$. The monolayer crystallites on the water surface became a continuous phase at 25 $mN \cdot m^{-1}$ and collapsed at 40 $mN \cdot m^{-1}$. The surface pressure-area isotherm represents an aggregating process of the small two-dimensional crystallites on the water surface, instead of a generally accepted concept on phase transitions among gas, liquid, and solid phases.

It has been generally accepted on the basis of π-A isotherm behavior that monolayer on the water surface is homogeneous at every surface pressure and also that the gaseous monolayer state at very low surface pressure converts into the liquid expanded one, liquid condensed one and finally the solid monolayer state with increasing surface pressure on the water surface. To ascertain this concept, morphology for monolayers prepared from various amphiphiles has been studied.[1-6] However, there has been no morphological observation with diffraction experiment for phase assignment of monolayers at various surface pressures.

In this study, the aggregation structure of barium stearate monolayer transferred onto a substrate at various surface pressures was investigated on the basis of electron microscopic observations, a bright field electron micrograph and an electron diffraction, ED pattern.

Experimental

Benzene solution of stearic acid was prepared at the concentration of 3.5×10^{-3} $mol \cdot l^{-1}$. The monolayer was spread on the water subphase containing 3×10^{-5} $mol \cdot l^{-1}$ of $BaCl_2$ and 4×10^{-4} $mol \cdot l^{-1}$ of $KHCO_3$ and then, compressed to a given surface pressure at the barrier speed of 48 $mm \cdot min^{-1}$. The subphase temperature, T_{sp} was maintained at 290±0.5 K. The monolayer was transferred onto a substrate by a horizontal lifting method at the surface pressure of 0 $mN \cdot m^{-1}$ or by a vertical lifting method at 10, 25 and 40 $mN \cdot m^{-1}$. The transfer rate was 10 $mm \cdot min^{-1}$. The prepared substrate was Formvar-covered electron microscope grids (200-mesh).[2] It was confirmed by an electron micrograph and an ED pattern that the substrate surface was smooth and the substrate itself was in an amorphous state. Therefore, this substrate was suitable for observation of the monolayer structure by using an electron microscope. Transmission electron micrographs were taken with a Hitachi H-500 electron microscope, operated at 75 kV and a beam current of 2.5 μA. Pt-carbon was vapor-deposited onto the monolayer samples with shadowing angle of 23°.

† On leave from Asahi Glass Electronic Products R&D Center Co., Ltd., Yokohama 221.

Results and Discussion

Figure 1 shows the surface pressure-area (π-A) isotherm for barium stearate monolayers spread on the buffered water at T_{sp} of 290 K. This temperature was much lower than the melting temperature, T_m of the monolayer which was estimated from the T_{sp} dependence of the maximum area modulus of the monolayer.[7] This isotherm showed a rapid rise of surface pressure with decreasing surface area. On the basis of a generally accepted concept, this π-A behavior is interpreted as that a gas state monolayer at very low surface pressure converts into a solid state monolayer at higher surface pressure without appearance of a liquid expanded state monolayer. The limiting area for the monolayer was 0.21 $nm^2 \cdot molecule^{-1}$. The value was close to the area of 0.20 $nm^2 \cdot molecule^{-1}$ which corresponded to the occupied cross-sectional area of closely packed hydrocarbon chains.

Figure 2 shows the bright field electron micrographs and the ED patterns of barium stearate monolayers which were spread from a benzene solution on the water surface and also, were transferred at the surface pressures of (a) 0, (b) 10, (c) 25, and (d) 40 $mN \cdot m^{-1}$. The transfer ratios at 10, 25, and 40 $mN \cdot m^{-1}$ were 0.9, 1.0, and 1.7, respectively. The direction of Pt-C shadowing is shown by an arrow. At 0 $mN \cdot m^{-1}$ (a), many isolated domains were observed in the bright field image. At 10 $mN \cdot m^{-1}$ (b), these domains covered almost all region of the water surface. The bright field image of the monolayer at 25 $mN \cdot m^{-1}$ (c) exhibited the fairly uniform, smooth, and continuous monolayer. The bright field image at 40 $mN \cdot m^{-1}$ (d) showed heterogeneous aggregation which was composed of

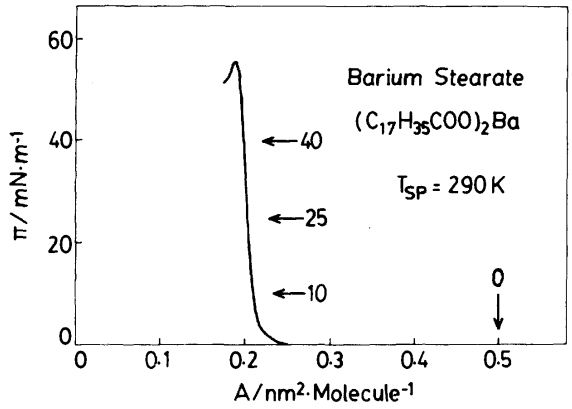

Fig. 1. π-A isotherm of barium stearate monolayer.

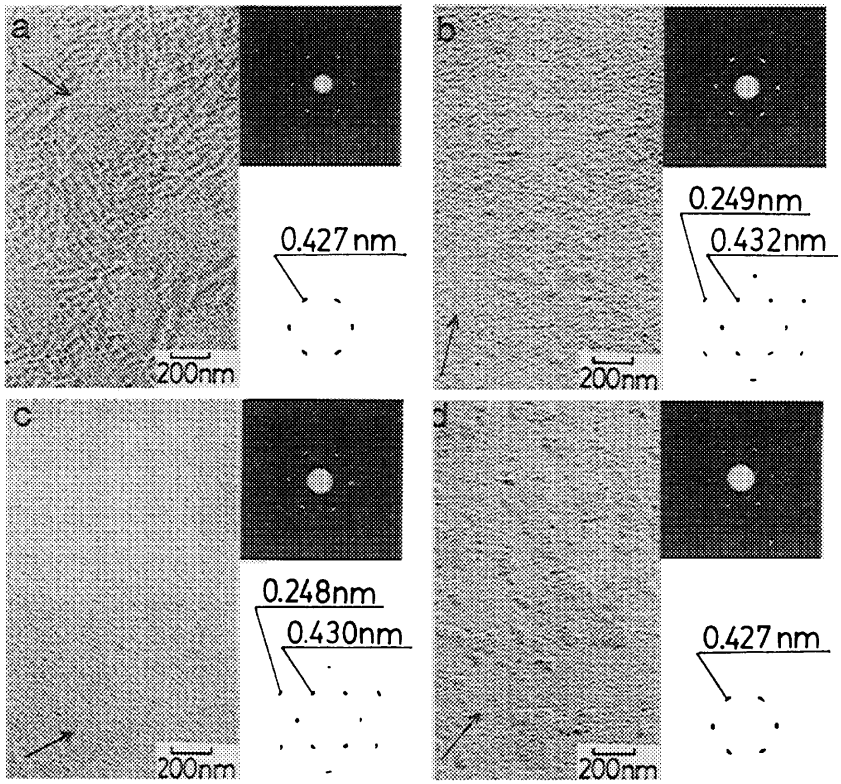

Fig. 2. Electron micrographs and electron diffraction patterns of barium stearate monolayers transferred at (a) 0 $mN \cdot m^{-1}$, (b) 10 $mN \cdot m^{-1}$, (c) 25 $mN \cdot m^{-1}$, and (d) 40 $mN \cdot m^{-1}$.

partially overlapped domains due to collapse of the monolayer. Figure 2(d) indicates that the monolayer starts to collapse at a lower surface pressure than the generally defined collapse pressure as the peak of the π-A isotherm. This partial collapse of monolayer cause the excess transfer of monolayer with the transfer ratio of 1.7 more than 1. The height of these overlapped domains was evaluated to be 5 nm from the shadowed length of Pt-C. Since the value of 5 nm corresponds to the thickness of a double layer of barium stearate, the monolayer collapses in a similar mechanism proposed by Ries.[8]

Every ED pattern of the monolayers transferred at the surface pressures of 0, 10, 25, and 40 $mN \cdot m^{-1}$ exhibited sharp crystalline spots with the spacing of 0.43 nm as shown in Fig. 2. At 10 and 25 $mN \cdot m^{-1}$, the crystalline spots with the spacing of 0.25 nm which is $1/\sqrt{3}$ of the spacing of 0.43 nm, were also observed in the ED patterns. These results indicate that the ED patterns are analyzed as a hexagonal structure and that the spacings of 0.43 and 0.25 nm are assigned to $(10\bar{1}0)$ and $(11\bar{2}0)$ reflections, respectively. When one molecule is assigned to the unit cell, the surface area occupied is estimated to be 0.21 $nm^2 \cdot molecule^{-1}$ which agrees with that found from the extrapolation of the π-A isotherm. It should be noted that the domains observed in the bright field image are in a crystalline state even at 0 $mN \cdot m^{-1}$ and also, that monolayer crystallites in a fairly wide area (corresponding to an electron beam diameter of several μm) aggregate with the crystallographically same orientation. Therefore, it is reasonable to consider that small two-dimensional crystallites grow right after spreading a solution on the water surface. The reason why crystallites arrange along their crystallographic direction on the water surface, is unknown at present. However, it is expected that crystallographic sintering at the boundary surfaces was caused from fusion or recrystallization at a higher surface pressure of 25 or 40 $mN \cdot m^{-1}$, resulting in formation of a large homogeneous two-dimensional single crystal (monolayer). For obtaining a larger single crystalline monolayer, it is necessary to anneal the monolayer on the water surface after compressing it to the surface pressure where the monolayer is morphological homogeneous.

The aggregation state of monolayer domains during compression is schematically shown in Fig. 3 in the case of T_{sp} lower than T_m. Barium stearate molecules form two-dimensional crystallites right after spreading a solution (at π_0) as mentioned above. The schematic crystallites are represented by the hatched domains in Fig. 3. The free area (white space) presented among crystallites is reduced with decreasing the surface area from A_0 to A_1. Contact between crystallites gives rise to an increase in surface pressure (at π_1). Monolayer crystallites in surface pressure range between π_1 and π_2 gather closer, resulting in the formation of a large-area monolayer at π_2. At a higher surface pressure than π_2,

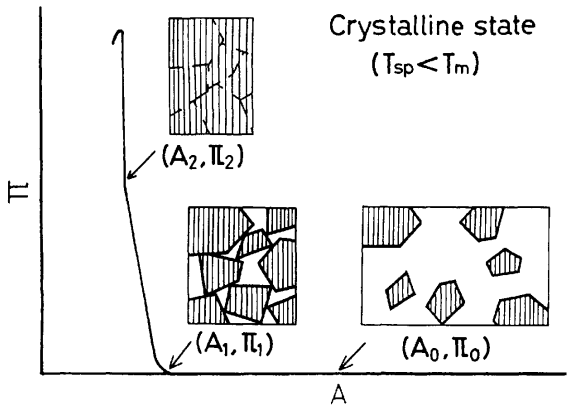

Fig. 3. Schematic representation of aggregation structure of monolayer during compression.

the monolayer starts to collapse locally, even though the surface pressure is lower than the generally defined collapse pressure as the peak of the π-A isotherm. Thus, in the case of barium stearate, a compression process on the water surface corresponds to an aggregation one of monolayer crystallites formed right after spreading a solution. The similar concept was also proposed by other researchers, on the basis of microscopic observations for a polydiacetylene monolayer,[9] dialkylammonium monolayer[10] and fatty acids or these salts.[11]

Conclusion

It became apparent that a molecular aggregation state in the barium stearate monolayer is quite different from the generally accepted concept based on the π-A isotherm. Barium stearate molecules aggregate in a crystalline state even at zero surface pressure when the subphase temperature is lower than the melting temperature of the monolayer. Therefore, the π-A isotherm represents an aggregating process of small two-dimensional crystallites on the water surface.

References

1) H. E. Ries, Jr., and W. A. Kimball, *Nature (London)*, **181**, 901 (1958); *idem*, *J. Phys. Chem.*, **59**, 94 (1955).
2) S. Fereshtehkhou, R. D. Neuman, and R. Ovalle, *J. Colloid Interface Sci.*, **109**, 385 (1986).
3) E. Sheppard, R. P. Bronson, and N. Tcheurekdjian, *J. Colloid Sci.*, **19**, 833 (1964); E. Sheppard, R. P. Bronson, and N. Tcheurekdjian, *J. Colloid Sci.*, **20**, 755 (1965).
4) R. D. Neuman, *J. Colloid Interface Sci.*, **56**, 505 (1976).
5) J. A. Spink, *J. Colloid Interface Sci.*, **23**, 9 (1967).
6) M. Losche, J. Rale, A. Fisher, B. U. Rucha, W. Knell, and H. Möhwald, *Thin Solid Films*, **117**, 269 (1980).
7) T. Kajiyama, N. Morotomi, M. Uchida, and Y. Oishi, *Chem. Lett.*, **1989**, 1047.
8) H. E. Ries, Jr., *J. Colloid Interface Sci.*, **16**, 361 (1961).
9) K. Miyano and A. Mori, *Polym. Prepr. Jpn.*, **36**, E29 (1987).
10) M. Shimomura, K. Fujii, P. Karg, W. Frey, E. Sackmann, P. Meller, and H. Ringsdorf, *Jpn. J. Appl. Phys.*, **27**, L1761 (1988).
11) N. Uyeda, M. Matsumoto, Y. Fujiyoshi, K. Aoyama, and T. Takenaka, *Polym. Prepr. Jpn.*, **36**, E30 (1987).

Evaluation of Oxidation of Vegetable Oils by Pyrolytic Sulfurization Gas Chromatography

Itsuro KAWAI* and Tadashi HARA†
Department of Applied Physics and Chemistry, Fukui Institute of Technology, Gakuen-3chome, Fukui 910
†Department of Chemical Engineering, Faculty of Engineering, Doshisha University, Karasuma Imadegawa, Kamigyo-ku, Kyoto 602
(Received November 29, 1988)

Synopsis. Oxygen determination by pyrolytic sulfurization gas chromatography[1-5] was applied to observe the degree of oxidation of vegetable oils. Oxidation deterioration of vegetable oil and the effect of antioxidants were evaluated.

Elemental analysis by use of pyrolytic sulfurization gas chromatography (PSGC), adopting the sulfur combustion method instead of the conventional oxygen combustion, has its prime feature in its ability to determine the oxygen content of a sample together with the contents of other constituent elements. This report deals with a study on the oxidation of vegetable oils performed as an application of this advantageous oxygen determination by PSGC. Both the oxidation deterioration of vegetable oils and the effect of antioxidants on it were investigated.

Experimental

Reagents. The sulfur used as a reaction agent together with a sample was obtained by purifying[6] commercially available sulfur (chemically pure) by the Bacon-Fanelli method. Drying oils (linseed, and soybean oils), a semidrying oil (sesame oil) and nondrying oils (olive, and castor oils) as the sample oils were obtained commercially. The aromatic antioxidants (*t*-butylhydroquinone, propyl gallate, and hydroquinone) were of JIS special grade quality.

Apparatus. A sampler, a displacement apparatus and an electric furnace were used. Gas chromatograms were taken on a Shimadzu GC-4B gas chromatograph.

Procedure. The oxidation test of the vegetable oils was made as follows: A sample oil (25 ml) was introduced into a 50 ml round-bottom flask, and oxidized by bubbling oxygen gas into it at a flow rate of 180 ml min^{-1} under agitation at 1400 rpm. At fixed time intervals after the start of the reaction, specimens (about 0.5 mg) were taken out and subjected to elemental analysis by PSGC. The measurements were made at different temperatures between 50 and 150 °C. Each type of drying, semidrying, and nondrying oils was used as the sample vegetable oil.

For the examination of the effect of antioxidants, sample oils containing 8.2×10^{-4} mol l^{-1} of antioxidants were used, and analysis by PSGC was made in the same way as for the oxidation test described above. The antioxidants used were aromatics.

The analytical conditions of PSGC were as follows: About 0.5 mg of a vegetable oil and 5 mg of sulfur were sampled into an ampoule, and allowed to react at a high temperature under a pressurized helium atmosphere. The reaction products were subjected to gas chromatography under the following conditions: Porapak QS 150 cm×4ϕ Teflon, Chromosorb 104 50 cm×4ϕ Teflon; column temperature 85 °C; carrier gas He 50 ml min^{-1}; and detector TCD.

Results and Discussion

Fats and oils generally consist of glycerides, which are susceptible to oxidation when they are of unsaturated types. Most of vegetable oils, in particular, strongly tend to be oxidized because of their being unsaturated glycerides.

Under the conditions adopted, the pyrolytic sulfurization products from vegetable oils were limited to three species (H_2S, COS, CS_2) regardless of the kinds of vegetable oil:

$$\text{Vegetable oil (C, H, O)} \xrightarrow[\text{Sulfur}]{950\,^\circ\text{C}} [H_2S, COS, CS_2]$$

where carbon contained in the sample was converted to carbonyl sulfide (COS) and carbon disulfide (CS_2); hydrogen to hydrogen sulfide (H_2S); and oxygen wholly to carbonyl sulfide (COS). Figure 1 shows the oxidation curves derived from the pyrograms, at an oxidation temperature of 100 °C, of typical vegetable oils. According to this figure, castor oil and sesame oil underwent no change under the conditions adopted for oxidation, conceivably because castor oil consists primarily of the triglyceride of hard-to-oxidize ricinoleic acid and sesame oil is accompanied by natural antioxidants. Elemental analysis data by PSGC of vegetable oils are shown in Table 1.

Figure 2 shows the oxidation curves for soybean oil

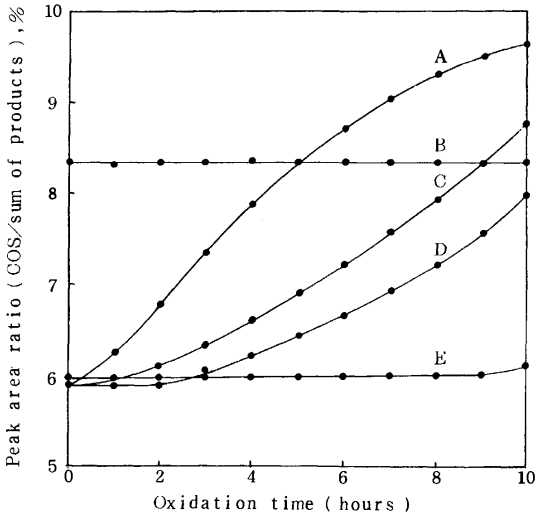

Fig. 1. Oxidation curves of vegetable oils.
Reaction temperature: 100 °C. A: linseed oil, B: castor oil, C: soybean oil, D: olive oil, and E: sesame oil.

Table 1. Analytical Results of Vegetable Oils

Sample	Oxidation time /h	Found (%)		
		C	H	O
Linseed oil	0	78.73	10.96	10.31
	10	73.81	10.17	16.02
Soybean oil	0	78.20	11.19	10.61
	10	74.15	10.90	14.95
Sesame oil	0	77.97	11.37	10.66
	10	77.78	11.43	10.79
Olive oil	0	78.07	11.43	10.50
	10	74.97	11.29	13.77
Castor oil	0	74.09	11.50	14.41
	10	74.60	11.08	14.32

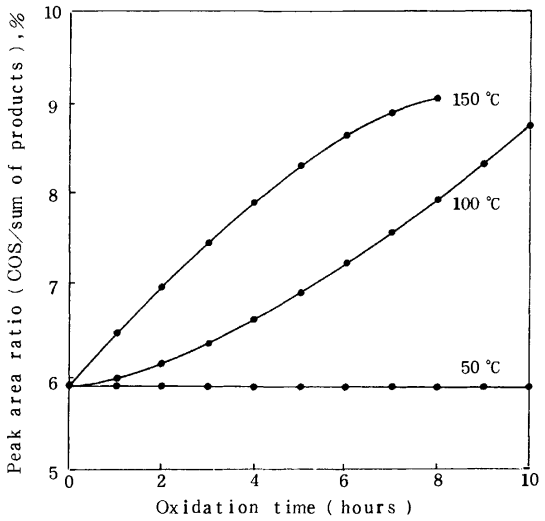

Fig. 2. Oxidation curves of soybean oil.

at varied oxidation temperatures of 50 °C, 100 °C, and 150 °C. As can be seen from this figure, oxidation of vegetable oils is markedly accelerated by the rise of temperature as with general chemical reactions.

The effect of antioxidants on the oxidation of vegetable oils was also investigated. Figure 3 shows the effects of antioxidants on the oxidation rate of soybean oil. The oxidation temperature was 100 °C and the concentration of each antioxidant was 8.24×10^{-4} mol l^{-1}. The same procedure may be applied to other vegetable oils. Figure 4 shows the effect of the concentration of the antioxidant (*t*-butylhydroquinone) on the induction period for soybean oil. The oxidation temperature was 100 °C. Figure 4 indicates that the induction period reaches a maximum when the concentration of *t*-butylhydroquinone is approximately 150 ppm. This procedure may be applied to other antioxidants.

One of the known methods for examining the degree of oxidation of a fat or an oil comprises measuring the weight gain caused by a reaction between the sample fat or oil and oxygen. The data obtained by this method agree well with the analytical data determined by PSGC.

The coefficient of variation in the peak area ratio of each sample vegetable oil calculated by effecting the

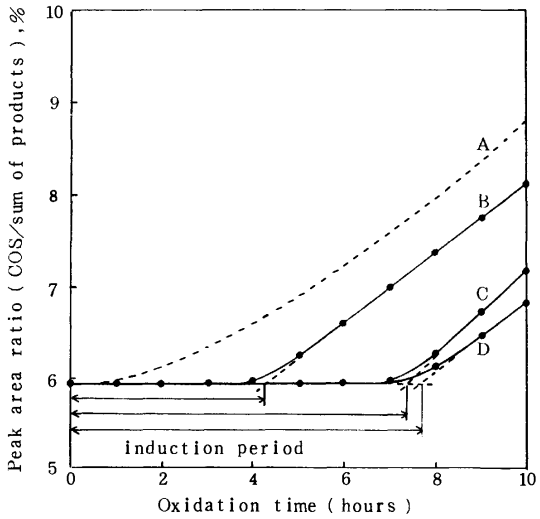

Fig. 3. Effect of antioxidants on the rate of oxidation of soybean oil.
Reaction temperature: 100 °C, and antioxidant concentration: 8.24×10^{-4} mol l^{-1}. A: oil alone, B: oil plus *t*-butylhydroquinone, C: oil plus propyl gallate, and D: oil plus hydroquinone.

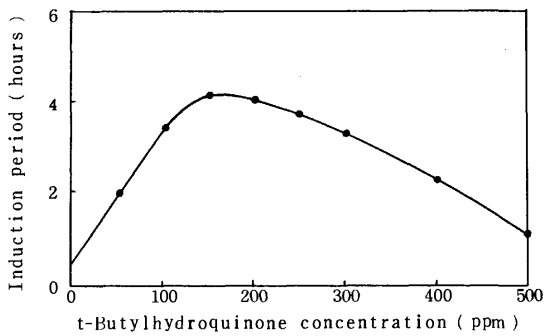

Fig. 4. Relationship between induction period and *t*-butylhydroquinone concentration for soybean oil.
Reaction temperature: 100 °C.

determination by PSGC six times did not exceed 0.5%. In view of this coefficient value, the method of this study can be considered fully suitable for oxidation tests on vegetable oils.

From the findings described above, this method can be considered useful in estimating the oxidation deterioration of vegetable oils and the effect of antioxidants on it. It can also be useful for food analyses and food control of fats and oils, because most of the vegetable oils for home use consist primarily of unsaturated glycerides susceptible to oxidation.

References

1) T. Hara and S. Ito, *Bull. Chem. Soc. Jpn.*, **44**, 2427 (1971).

2) K. Tsuji, K. Fujinaga, and T. Hara, *Bull. Chem. Soc. Jpn.*, **50**, 2292 (1977).

3) T. Hara, K. Fujinaga, and K. Tsuji, *Bull. Chem. Soc. Jpn.*, **51**, 1110 (1978).
4) T. Hara, K. Fujinaga, and F. Okui, *Bull. Chem. Soc. Jpn.*, **53**, 951 (1980).
5) I. Kawai and T. Hara, *Bull. Chem. Soc. Jpn.*, **58**, 3625 (1985).
6) T. Hara, K. Fujinaga, K. Tsuji, and F. Okui, *Bull. Chem. Soc. Jpn.*, **51**, 3079 (1978).

Sulfur Pressure Control in an H_2-Sulfur Vapor System

Hiroaki WADA
National Institute for Research in Inorganic Materials, Namiki 1-1, Tsukuba, Ibaraki 305
(Received December 17, 1988)

Synopsis. A direct sulfur pressure control method by a N_2-sulfur vapor system was modified by using an H_2-sulfur vapor system. A ratio of H_2S/H_2 in the atmosphere was found to be controlled very well in the range from 10^{-2} to 10^{-4} only by the temperature regulation.

A direct sulfur pressure control method by using a N_2-sulfur vapor system has been recently devised and applied to the equilibrium studies of several transition metal sulfides.[1-5] However, this has disadvantage that the lower limit of partial pressure of sulfur available is restricted to 10^{-4} atm because of shortage of accuracy in determination of sulfur content. An attempt has been made to control the partial pressure of sulfur more precisely by using an H_2-sulfur vapor system under the same conditions. This note is concerned with the experimental results obtained in the H_2-sulfur vapor system.

Experimental

Sulfur Pressure Control. The apparatus used for the equilibrium study is shown schematically in Fig. 1. All this apparatus is constructed of quartz glass. The heating systems are the same ones as those described in the previous paper.[2] Several hundred grams of sulfur (purity: 99.9999%) was kept in the round-bottom reservoir. After passing hydrogen gas through the apparatus for 12 h, sulfur was heated and changed to the molten state. Prior to use, the hydrogen gas was purified using DEOXO purifier (Engelhard Co.) in order to remove oxygen and water impurities. The saturated sulfur vapor over molten sulfur was transported to the upper part of the apparatus by hydrogen gas at a constant rate (3 cm^3 of H_2/s). The central zone of part B was held at the minimum temperature in all this apparatus so that the transported sulfur vapor from the reservoir became supersaturated and excess sulfur was condensed on the wall. Only sulfur vapor equilibrated at the minimum temperature zone (width: 10 cm) was carried to the upper part of apparatus. Then the sulfur was changed to hydrogen sulfide at temperatures higher than 773 K according to the reaction of $2H_2+S_2=2H_2S$. A desired partial pressure of hydrogen sulfide was easily obtained by controlling the temperature within ±0.5 K at the minimum temperature zone. At the outlet, L, hydrogen sulfide was absorbed in 0.8 M NaOH solution (1 M=1 mol dm^{-3}) and oxidized by H_2O_2 to SO_4^{2-} ion. Finally, the sulfur content was determined gravimetrically as $BaSO_4$.

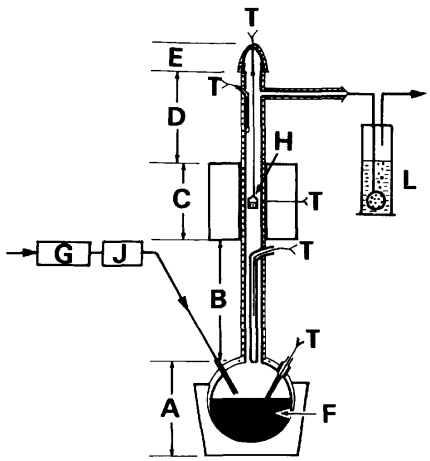

Fig. 1. Schematic diagram of apparatus. The heating systems are divided into five parts from A to E. A: Heating mantle. B: Nichrome wire (0.8 mm) is used for a winding to maintain the minimum temperature zone over the central portion of B. C: Reaction furnace. Pt-40% Rh wire (0.8 mm) is used. D: Nichrome wire (0.45 mm) is used. E: The cap is wound with Nichrome wire (0.8 mm). F: Sulfur. G: DEOXO purifier. H: Sulfide sample is suspended from the cap by strands of thin platinum wire (0.2 mm). J: Mass flow controller (SEC 310). L: NaOH solution. T: Chromel-alumel thermocouples.

Results and Discussion

The experimental results of the sulfur pressure measurements, in terms of the amount of collected sulfur at L, are presented in Table 1 and Fig. 2. The relationship between the total amount of sulfur brought by unit volume of hydrogen and the temperature of the minimum temperature zone is given very well by the following formula (least squares treatment): $\log(W/\mathrm{g\,dm^{-3}})=-4294/(T/\mathrm{K})+7.1852$, where the amount of collected sulfur is represented as W in g. The previous experimental data obtained in the N_2-sulfur vapor system[2] are also shown in Fig. 2 for comparison. Both data exhibit very similar linear relationships except for small difference in the absolute values. This fact indicates clearly that the sulfur pressure was controlled precisely by the temperature regulation at the minimum temperature

Table 1. Relationships between the Temperature of Minimum Temperature Zone, Weight of $BaSO_4$ and the Mass Flow Rate of Sulfur

Temperature / K	Weight of $BaSO_4$ / mg h^{-1}	Mass flow rate of sulfur (g dm^{-3} of H_2)
370	2.72	3.48×10^{-5}
385	9.30	1.19×10^{-4}
386	9.88	1.26×10^{-4}
394	16.50	2.08×10^{-4}
402	23.95	3.06×10^{-4}
403	26.60	3.40×10^{-4}
413	53.68	6.78×10^{-4}
422	74.55	9.54×10^{-4}
423	88.20	1.13×10^{-3}
472	887.79	1.19×10^{-2}

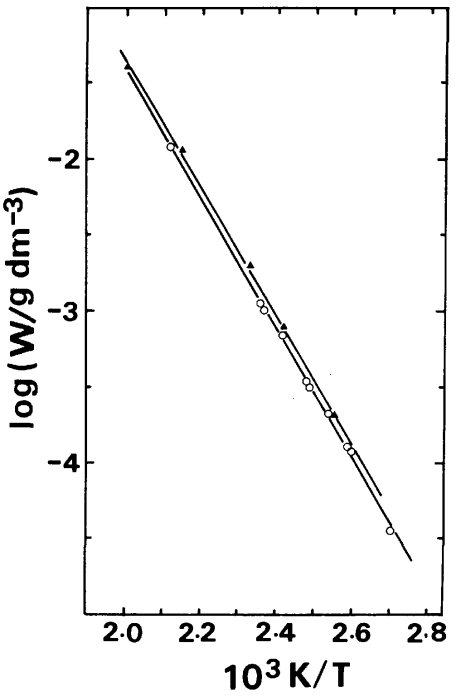

Fig. 2. Plot of log (W/g dm^{-3}) versus $1/T$. ○: H_2–sulfur vapor system, ▲: N_2–sulfur vapor system.

zone in the selected experimental system. The slightly lower values for the data points in the H_2–sulfur vapor system may be due to incomplete transportation of sulfur. One of the possible explanations for this phenomenon may be related to the fact that the viscosity of H_2 gas is much lower than that of N_2 gas.

According to Richardson and Jeffes,[6] the free energy for the reaction

$$H_2(g) + \frac{1}{2}S_2(g) = H_2S(g) \qquad (1)$$

is given by the following equation

$$\Delta G^\circ = -21570 + 11.79T. \qquad (2)$$

The equilibrium of Eq. 1 is represented as follows by using the equilibrium constant K

$$\log K = -\frac{\Delta G^\circ}{RT} = \log \frac{P_{H_2S}}{P_{S_2}^{1/2} P_{H_2}} . \qquad (3)$$

Rearranging Eq. 3, we obtain the following equation

$$\log P_{S_2} = 2\log \frac{P_{H_2S}}{P_{H_2}} + \frac{2\Delta G^\circ}{RT} . \qquad (4)$$

By varying the temperature of the minimum temperature zone H_2S/H_2 ratio could be varied between 10^{-2} and 10^{-4}. The assumptions were made to calculate the sulfur pressure that the sulfur species present in the gas phase is only the diatomic molecule S_2 and that the equilibrium has been established on the reaction Eq. 1 at the high temperatures. Corresponding to the variation of H_2S/H_2, $\log P_{S_2}$ was estimated to range from −8.54 to −12.54 at 973 K.

In an application of this method iron Chevrel phase compound $Fe_{1.25}Mo_6S_{7.75}$ has been subjected to an equilibrium study at 1273 K. The rhombohedral phase of $Fe_{1.25}Mo_6S_{7.75}$ was found to be stable in the range $-7.44 < \log P_{S_2} < -5.35$.

References

1) M. Wakihara, T. Uchida, and M. Taniguchi, *Mater. Res. Bull.*, **11**, 973 (1976).
2) H. Wada, *Bull. Chem. Soc. Jpn.*, **51**, 1368 (1978).
3) H. Wada, *Bull. Chem. Soc. Jpn.*, **52**, 2130 (1979).
4) H. Wada, *Bull. Chem. Soc. Jpn.*, **53**, 668 (1980).
5) H. Wada, *Bull. Chem. Soc. Jpn.*, **53**, 1173 (1980).
6) F. D. Richardson and J. H. E. Jeffes, *J. Iron Steel Inst.*, **171**, 165 (1952).

Mixed-Valence States in TCNQ Salts of 1′,1‴-Dibutyl-, 1′,1‴-Dipentylbiferrocene and Their Mixed Crystals

Satoru NAKASHIMA and Hirotoshi SANO*
Department of Chemistry, Faculty of Science, Tokyo Metropolitan University, Fukasawa, Setagaya-ku, Tokyo 158
(Received January 20, 1989)

Synopsis. Mixed-valence states in TCNQ salts of 1′,1‴-dibutyl-, 1′,1‴-dipentylbiferrocene and their mixed crystals were investigated by Mössbauer spectroscopy. It was found that a valence delocalization of the mixed crystals was affected by the host lattice.

It is known that mixed-valence states of biferrocene derivatives are affected by counter anions,[1,2] and that intermolecular interactions play an important role in the mixed-valence states. It is also known that introduction of aromatic planar molecules as counter anions provides an interesting series of mixed-valence biferrocene derivatives.[3,4] In the present study, mixed-valence states in 7,7,8,8-tetracyanoquinodimethane (TCNQ) salts of 1′,1‴-dibutyl-, 1′,1‴-dipentylbiferrocene and their mixed crystals were inverstigated by means of Mössbauer spectroscopy.

Experimental

Materials. 1′,1‴-Dibutyl-,[5] 1′,1‴-dipentylbiferrocene,[6] and their TCNQ salts[3] were prepared according to the method previously reported. It was found from elemental analysis that the TCNQ salts consist of binuclear ferrocene and TCNQ in a molar ratio of 1:3. Found: C, 70.13; H, 4.25; N, 14.92%. Calcd for 1′,1‴-dibutylbiferrocenium$^+$(TCNQ)$_3^-$, $Fe_2C_{64}H_{46}N_{12}$: C, 70.21; H, 4.24; N, 15.35%. Found: C, 70.71; H, 4.69; N, 14.95%. Calcd for 1′,1‴-dipentylbiferrocenium$^+$(TCNQ)$_3^-$, $Fe_2C_{66}H_{50}N_{12}$: C, 70.60; H, 4.49; N, 14.97%. Mixed crystals were obtained by the following method. A mixture of 1′,1‴-dipentylbiferrocene (40.1 mg, 7.86×10^{-5} mol), and TCNQ (98.6 mg. 4.83×10^{-4} mol) was refluxed for 5 hours in 50 ml of acetonitrile under nitrogen and kept in a freezer for one night. Precipitates were filtered and collected as mixed crystals **1**. The filtrate was kept in the freezer for one night. Precipitates were filtered and collected as mixed crystals **2**. Found for mixed crystals **1**: C, 69.99; H, 4.34; N. 15.44%. Found for mixed crystals **2**: C, 70.12; H, 4.46; N, 15.24%. Calcd for 1:1 mixed crystals, $(Fe_2C_{28}H_{34})_{0.5}$-$(Fe_2C_{30}H_{38})_{0.5}(C_{12}H_4H_4)_3$=$Fe_2C_{65}H_{48}N_{12}$: C, 70.41; H, 4.36; N, 15.16%. It is found that the products consist of the sum of two kinds of binuclear ferrocenes (1′,1‴-dibutylbiferrocene+1′,1‴-dipentylbiferrocene) and TCNQ in the molar ratio of (ca. 0.5+ ca. 0.5): 3. It is difficult to determine definitely the ratio of 1′,1‴-dibutylbiferrocene to 1′,1‴-dipentylbiferrocene in the mixed crystals **1** and **2** from the elemental analysis data, because the difference between the butyl substituent and the pentyl substituent is small in the salts which have large molecular weight. X-Ray diffraction patterns of 1′,1‴-dipentylbiferrocenium$^+$(TCNQ)$_3^-$ shown in Fig. 1 are similar as a whole, suggesting that the salts are isomorphous and make a mixed crystal. The slight difference observed between them can be attributed to the difference of the alkyl group in their cations. The patterns of the mixed crystals **1** are more similar to 1′,1‴-dibutylbiferrocenium$^+$(TCNQ)$_3^-$, while those of mixed crystals **2** to 1′,1‴-dipentylbiferrocenium$^+$(TCNQ)$_3^-$, showing that mixed crystals **1** contain more 1′,1‴-dibutylbiferrocenium than dipentylbiferrocenium and mixed crystals **2** more 1′,1‴-dipentylbiferrocenium than dibutylbiferrocenium than dibutylbiferrocenium. The possibility to be a mixture but not to be mixed crystals is also rejected, based on the results on the Mössbauer spectra measurements (see Results and Discussion).

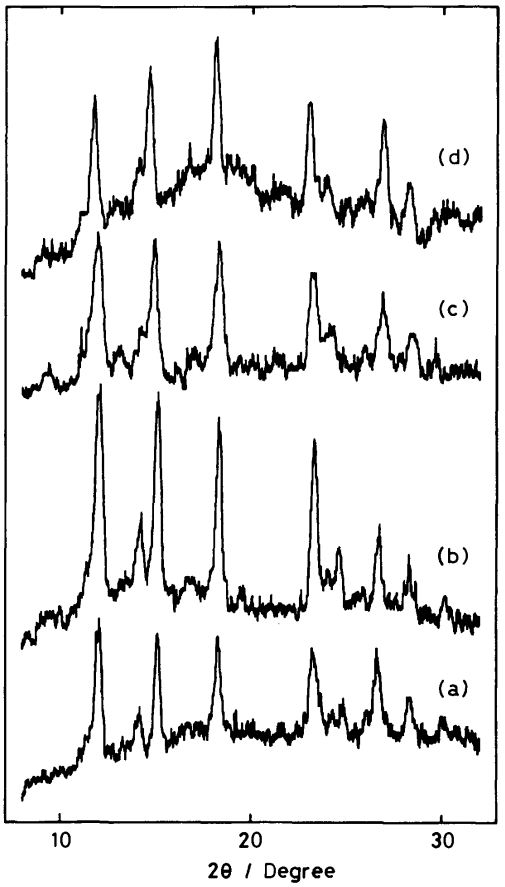

Fig. 1. X-Ray powder patterns (Cu K_α) for (a) 1′,1‴-dibutylbiferrocenium$^+$ (TCNQ)$_3^-$, (b) mixed crystals **1**, (c) mixed crystals **2**, and (d) 1′1‴-dipentylbiferrocenium$^+$ (TCNQ)$_3^-$.

Mössbauer Spectroscopic Measurements. A ^{57}Co(Rh) source moving in a constant-acceleration mode was used for Mössbauer spectroscopic measurements. Mössbauer spectra were obtained by using an Austin Science Associates Mössbauer spectrometer and a proportional counter. Isomer shift values were referred to metallic iron foil. Mössbauer parameters were obtained by least-squares fitting to Lorentian peaks.

Results and Discussion

Mössbauer spectra of 1′,1‴-dibutyl- and 1′,1‴-dipentylbiferrocenium$^+$(TCNQ)$_3^-$ are shown in Figs. 2 and 3, respectively. The Mössbauer spectrum of 1′,1‴-dibutylbiferrocenium$^+$(TCNQ)$_3^-$ at 5 K shows a

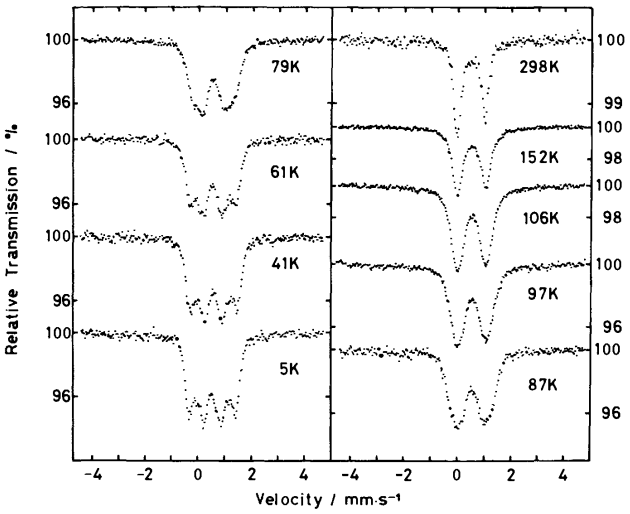

Fig. 2. Mössbauer spectra of 1′,1‴-dibutylbiferrocenium$^+$ $(TCNQ)_3^-$.

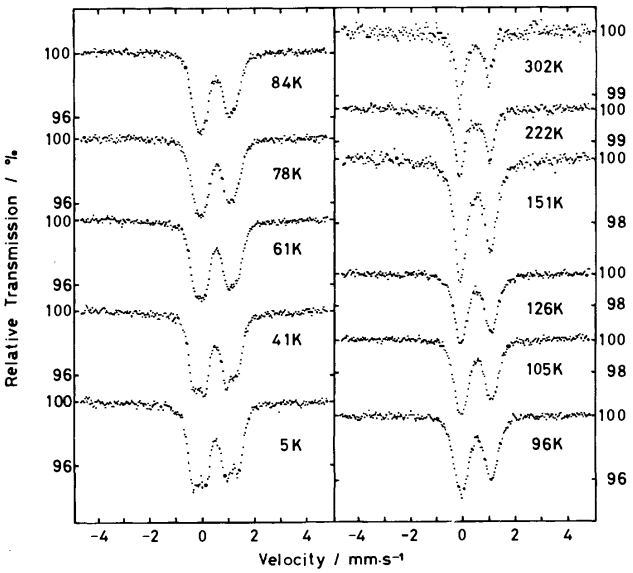

Fig. 4. Mössbauer spectra of mixed crystals **1**.

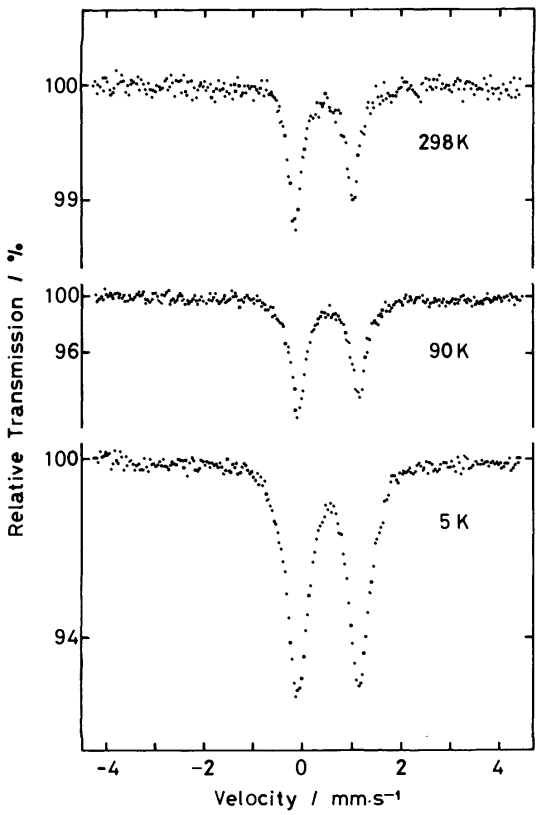

Fig. 3. Mössbauer spectra of 1′,1‴-dipentylbiferrocenium$^+$ $(TCNQ)_3^-$.

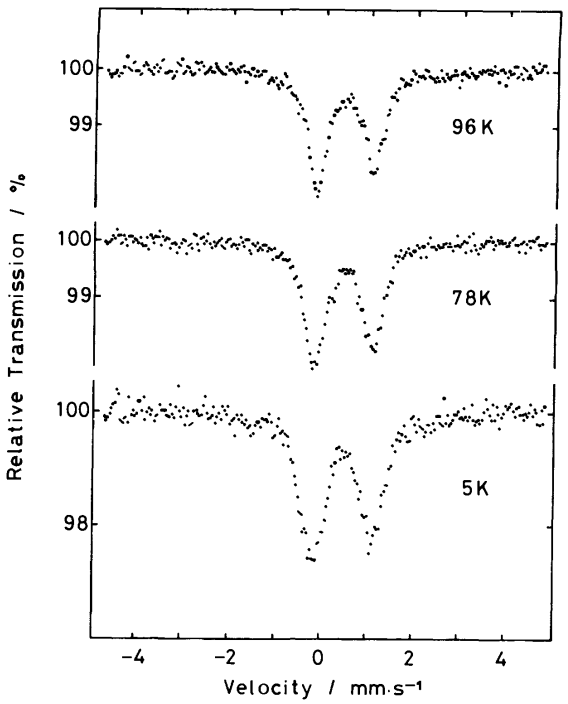

Fig. 5. Mössbauer spectra of mixed crystals **2**.

main component ascribed to a trapped-valence state together with a small component of averaged-valence state. The relative intensity of the doublet for the averaged-valence state increases with increasing temperature, as observed in 1′,1‴-bis(*o*-methylbenzyl)biferrocenium$^+$ $TCNE^-$ (TCNE=tetracyanoethylene).[4] 1′,1‴-Dipentylbiferrocenium$^+$ $(TCNQ)_3^-$ shows only the component of averaged-valence state in the whole temperature range from 5 to 298 K.

Mössbauer spectra of mixed crystals **1** and **2** are shown in Figs. 4 and 5, respectively, and the quadrupole splitting (Q. S.) values of all the salts studied in the present study are summarized in Fig. 6. Although the temperature dependence of the mixed-valence states in mixed crystals **1** is classified into a so-called coexisting type, as in the case of 1′,1‴-dibutylbiferrocenium$^+$$(TCNQ)_3^-$. The Q. S. value at 5 K (0.74 mm s^{-1}) of mixed crystals **1** is different from the value (0.55 mm s^{-1}) of 1′,1‴-dibutylbiferrocenium$^+$ $(TCNQ)_3^-$ at 5 K. In the coexisting region of the trapped- and averaged-valence state (at 5—126 K) in 1′,1‴-dibutylbiferrocenium$^+$$(TCNQ)_3^-$, the Q. S. val-

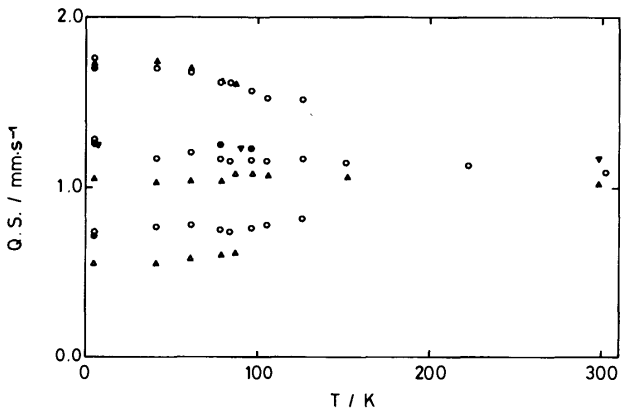

Fig. 6. Temperature dependences in the Q. S. values of 1′,1‴-dibutylbiferrocenium$^+$ $(TCNQ)_3^-$ (△), 1′,1‴-dipentylbiferrocenium$^+$ $(TCNQ)_3^-$ (▽), mixed crystals **1** (○), and mixed crystals **2** (●).

ues of the iron atoms in the averaged-valence state are close to an averaged value of the Q. S. values for the ferrocene-like doublet and ferrocenium-like doublet of their trapped-valence state and almost equal to the value at 302 K. The Q. S. values of the iron atoms in the averaged-valence state for mixed crystals **1** (e.g., 1.09 mm s^{-1} at 302 K) show averaged values of the values of 1′,1‴-dibutylbiferrocenium$^+$ $(TCNQ)_4^-$ (e.g., 1.02 mm s^{-1} at 298 K) and 1′,1‴-dipentylbiferrocenium$^+$ $(TCNQ)_3^-$ (e.g., 1.17 mm s^{-1} at 298 K) as expected for mixed crystals. The results reject the possibility of a mixture of the two salts obtained for the mixed crystals **1** because no line-broadening is found at higher temperatures. Mixed-valence states in mixed crystals **2** are similar to those in 1′,1‴-dipentylbiferrocenium$^+(TCNQ)_3^-$, although a small component assigned to the trapped-valence state coexists at 5 K. The Q. S. values of the trappped-valence state (1.79 mm s^{-1} and 0.72 mm s^{-1} at 5 K) are similar to those of mixed crystals **1** and are different from those of 1′,1‴-dibutylbiferrocenium$^+(TCNQ)_3^-$. The results found in the mixed crystals **2** also reject the possibility of a mixture of the component salts.

The results obtained in the present study indicate that the valence delocalization is affected by the crystal lattice, which is predominantly under the control of the host component, 1′,1‴-dibutylbiferrocenium$^+$ $(TCNQ)_3^-$ in mixed crystals **1** and of 1′,1‴-dipentylbiferrocenium$^+(TCNQ)_3^-$ in mixed crystals **2**.

We thank the Ministry of Education, Science and Culture of Japan for supporting a part of this work under a Grant-in-Aid for Scientific Research (No. 62790155).

References

1) T.-Y. Dong, T. Kambara, and D. N. Hendrickson, *J. Am. Chem. Soc.*, **108**, 4423, 5857 (1986).
2) M. Kai, M. Katada, and H. Sano, *Chem. Lett.*, **1988**, 1523.
3) S. Nakashima, S. Iijima, I. Motoyama, M. Katada, and H. Sano, *Hyperfine Interations*, **40**, 315 (1988).
4) S. Nakashima, Y. Masuda, and H. Sano, *Chem. Lett.*, **1988**, 1851.
5) S. Nakashima, Y. Masuda, I. Motoyama, and H. Sano, *Bull. Chem. Soc. Jpn.*, **60** 1673 (1987).
6) S. Nakashima, M. Katada, I. Motoyama, and H. Sano, *Bull, Chem. Soc. Jpn.*, **60**, 2253 (1987).

Preparation and Characterization of Triethylenetetramine Cobalt(III) Complexes with 1,2-Ethanedithiolate or 1,2-Ethanedisulfinate

Takumi KONNO,* Hideki UMEHARA, Ken-ichi OKAMOTO, and Jinsai HIDAKA
Department of Chemistry, University of Tsukuba, Tsukuba, Ibaraki 305
(Received April 14, 1989)

Synopsis. Triethylenetetramine (trien) cobalt(III) complexes with 1,2-ethanedithiolate (edt) or 1,2-ethanedisulfinate (edsi) were prepared and characterized by absorption, CD, and ^{13}C NMR spectra. Each of the two complexes gave three possible geometrical isomers (cis-α, cis-β-*RR,SS*, and cis-β-*RS,SR*) which were separated and optically resolved by fractional crystallization and/or column chromatography.

In a previous paper[1] we reported the stereochemistry of triethylenetetramine (trien) cobalt(III) complexes with 1,3-propanedithiolate (pdt; $^{-}S(CH_2)_3S^{-}$) or 1,3-propanedisulfinate (pdsi; $^{-}O_2S(CH_2)_3SO_2^{-}$). Both complexes produced only the cis-α isomer, although three geometrical isomers (cis-α, cis-β-*RR,SS*, and cis-β-*RS,SR*)[2] are possible for the [Co(bidentate-*S,S*)(trien)]$^{+}$-type complexes. This note discusses the preparation and resolution of the trien cobalt(III) complexes with 1,2-ethanedithiolate (edt; $^{-}S(CH_2)_2S^{-}$) or 1,2-ethanedisulfinate (edsi; $^{-}O_2S(CH_2)_2SO_2^{-}$); three possible geometrical isomers were formed for each of the two complexes. These isomers were characterized on the basis of absorption, CD, and ^{13}C NMR spectra compared with those of the corresponding pdt and pdsi isomers.

Experimental

(1) Preparation and Resolution of Complexes. a) [Co(edt)(trien)]X (X=ClO_4 and I). To an ice-cold solution containing 3.1 g (0.01 mol) of *cis*-α- or *cis*-β-[$CoCl_2$(trien)]Cl[3] in 60 cm^3 of water was added an ice-cold solution containing 0.95 g (0.01 mol) of 1,3-propanedithiol in a mixture of a 1 mol dm^{-3} NaOH aqueous solution (20 cm^3) and methanol (20 cm^3). The mixture was stirred for 1 h in an ice bath. After removing the precipitate by filtration, to the filtrate was added 20 cm^3 of a saturated $NaClO_4$ solution; this mixture was kept in a refrigerator for 5 h. The precipitate which appeared was filtered off again. The filtrate was concentrated to one half its volume with a rotary evaporator below 25 °C and kept in a refrigerator overnight. The resulting black complex was collected by filtration and recrystallized from a small amount of water. It was found from absorption and ^{13}C NMR spectral measurements that this complex contained a mixture of *cis*-α-, *cis*-β-*RR,SS*-, and *cis*-β-*RS,SR*-[Co(edt)(trien)]$^{+}$. Attempts to separate the isomers using column chromatography were unsuccessful because of decomposition in the column. Yield: 64%. Found: C, 23.96; H, 5.63; N, 14.07%. Calcd for [Co(edt)(trien)]ClO_4=$C_8H_{22}N_4O_4S_2ClCo$: C, 24.22; H, 5.59; N, 14.12%.

The iodide salt was precipitated using 20 cm^3 of a saturated NaI solution instead of a saturated $NaClO_4$ solution. Black tetragonal crystals were obtained by recrystallization from a small amount of water. It was found from absorption and ^{13}C NMR spectral measurements that these crystals contained only the cis-α isomer. Yield: 20%. Found: C, 22.61; H, 5.27; N, 13.22%. Calcd for [Co(edt)(trien)] I=$C_8H_{22}N_4S_2CoI$: C, 22.64; H, 5.22; N, 13.20%

An excess amount (0.5 g) of $Na_2[Sb_2(d\text{-tart})_2]\cdot 5H_2O$ (*d*-tart=*d*-tartrate) was added with stirring to a solution containing 0.1 g of *cis*-α-[Co(edt)(trien)]I in 10 cm^3 of water. After the solution was stirred for 3 min at room temperature, 3 cm^3 of ethanol was added in an ice bath; the resulting black-brown precipitate of the $(-)_{580}^{CD}$-cis-α isomer was collected by filtration. The H_2O_2 oxidation product of the $(-)_{580}^{CD}$-cis-α showed identical absorption spectrum and CD patterns with $(-)_{460}^{CD}$-*cis*-α-[Co(edsi)(trien)]$^{+}$ (A-2 isomer) described in b), though the CD intensity of the former complex was smaller than that of the latter. This indicates that *cis*-α-[Co(edt)(trien)]$^{+}$ was partially resolved; the CD intensity of the $(-)_{580}^{CD}$-cis-α isomer is shown by an arbitrary scale in Fig. 1.

b) [Co(edsi)(trien)]ClO_4. An excess amount (8 cm^3) of a 5% H_2O_2 solution was added to a solution containing 0.5 g of [Co(edt)(trien)]ClO_4 in 20 cm^3 of water, followed by 1 cm^3 of a 30% $HClO_4$ solution. The mixture was stirred for 1 h in an ice bath and then kept in a refrigerator overnight. The resulting yellow powder (A-1) was collected by filtration. The filtrate was concentrated to one half its volume with a rotary evaporator below 24 °C and kept in a refrigerator overnight. After the yellow powder (A-1) was again removed by filtration, the filtrate was concentrated to one half its volume and kept in a refrigerator overnight. The deep-yellow needle crystals (A-2) which appeared were collected by filtration. Each of the A-1 and A-2 complexes was recrystallized from a small amount of water. It was found from the absorption and ^{13}C NMR spectral measurements that the A-1 complex contained a mixture of *cis*-β-*RR,SS*- and *cis*-β-*RS,SR*-[Co(edsi)(trien)]$^{+}$ and the A-2 one contained the cis-α isomer. A-1 complex: Yield: 28%. A-2 complex: Yield: 13%. Found for A-2: C, 20.15; H, 5.03; N, 11.65%. Calcd for [Co(edsi)(trien)]$ClO_4\cdot H_2O$=$C_8H_{22}N_4O_8S_2ClCo\cdot H_2O$: C, 20.07; H, 5.05; N, 11.70%.

An aqueous solution of the A-1 complex (cis-β-*RR,SS* and cis-β-*RS,SR*) was poured onto a Dowex 50W-X8 column (Na^{+} form, 200—400 mesh, 3 cm×20 cm). After sweeping the column with water, the adsorbed band was eluted with a 0.075 mol dm^{-3} $K_2[Sb_2(d\text{-tart})_2]$ solution. Two pairs of yellow bands, B-1 and B-2, were eluted in this order. It was found from the ^{13}C NMR spectral measurements that the earlier moving pair (B-1) contained *cis*-β-*RR,SS*-[Co(edsi)(trien)]$^{+}$ and the later moving one (B-2) contained the cis-β-*RS,SR* isomer. The formation ratio of the two isomers, B-1 (cis-β-*RR,SS*): B-2 (cis-β-*RS,SR*), was about 4:1. For each of the two pairs, the earlier moving and the later moving bands contained the $(-)_{470}^{CD}$ and $(+)_{470}^{CD}$ isomers respectively. The $(-)_{470}^{CD}$ isomer of B-1 (cis-β-*RR,SS*) was isolated as the perchlorate salt. The B-2 (cis-β-*RS,SR*) isomer was not isolated because of its poor yield, and the concentration of this isomer was evaluated by the method of plasma emission spectral analysis. Found for $(-)_{470}^{CD}$ B-1 isomer: C, 20.12; H, 5.06; N, 11.68%. Calcd for [Co(edsi)(trien)]$ClO_4\cdot H_2O$: C, 20.07; H, 5.07; N, 11.70%.

When the A-2 (cis-α) complex was chromatographed on a Dowex 50W-X8 column (Na^{+} form, 200—400 mesh, 3.0 cm× 20 cm) eluting with a 0.075 mol dm^{-3} $K_2[Sb_2(d\text{-tart})_2]$ solution, two deep yellow bands of the $(-)_{460}^{CD}$ and $(+)_{460}^{CD}$ isomers were eluted in this order. Each eluate was converted into the perchlorate salt using a QAE-Sephadex A-25 column (ClO_4^{-}

form, 2.5 cm×20 cm). The concentration of each isomer was evaluated on the basis of the absorption spectral datum of the racemic perchlorate salt.

(2) Measurements. The electronic absorption spectra were recorded on a JASCO UVIDEC-1 or UVIDEC-610 spectrophotometer and the CD spectra on a JASCO J-20 spectropolarimeter. All measurements were carried out in aqueous solution at room temperature. The concentration of *cis*-β-*RS,SR*-[Co(edsi)(trien)]$^+$ (B-2 isomer) was determined with a Jarrel-Ash Model-975 Plasma Atom Comp ICP spectrometer. The ^{13}C NMR spectra were recorded in deuterium oxide on a JEOL JNM-FX-100 NMR spectrometer at the probe temperature. Sodium 4,4-dimethyl-4-silapentane-1-sulfonate was used as an internal reference.

Results and Discussion

Three geometrical isomers (cis-α, cis-β-*RR,SS*, and cis-β-*RS,SR*)[2] are possible for each of [Co(edt)(trien)]$^+$ and [Co(edsi)(trien)]$^+$. The absorption spectrum of [Co(edt)(trien)]$^+$ isolated as the perchlorate or iodide salt is similar to that of *cis*-α-[Co(pdt)(trien)]$^+$ [1] in the whole region (Fig. 1). The edt complex exhibits the sulfur-to-metal charge transfer (SMCT) band at ca. 35×10^3 cm^{-1}, which is composed of two components. This absorption spectral behavior is characteristic for the cis(*S*)-type cobalt(III) complexes with two thiolato donor atoms.[4-7] For the three isomers of [Co(edsi)-(trien)]$^+$, which were derived from the perchlorate salt of [Co(edt)(trien)]$^+$ by the H_2O_2 oxidation reaction, the absorption spectral behavior agrees well with that of *cis*-α-[Co(pdsi)(trien)]$^+$ [1] in the whole region (Fig. 2). It has been established by X-ray structural analysis that the pdsi in *cis*-α-[Co(pdsi)(trien)]$^+$ coordinates through two sulfur atoms.[1] Accordingly, the present edsi complex can be assigned to the *S,S*-bonded isomer having the cis(*S*) geometry. The absorption spectrum of the edsi complex also shows an intense SMCT band consisting of two components at ca. 34×10^3 cm^{-1}.

The iodide salt of [Co(edt)(trien)]$^+$ exhibits four ^{13}C NMR signals at δ 36.84, 46.54, 57.86, and 58.83 due to the eight methylene carbon atoms in the complex, indicating the C_2 symmetry. Further, the H_2O_2 oxidation of the iodide salt gave *cis*-α-[Co(edsi)(trien)]$^+$ (A-2 complex, vide infra). A similar oxidation reaction of the thiolato cobalt(III) complexes has proceeded with retention of the geometrical configuration to form the sulfinato complexes.[1,8] These facts suggest that the iodide salt of [Co(edt) trien)]$^+$ is the cis-α isomer. The perchlorate salt of [Co(edt)(trien)]$^+$ shows twenty ^{13}C NMR signals in the region of δ 35—60, of which four signals are the same as those of the iodide salt. The H_2O_2 oxidation of the perchlorate salt produced *cis*-α-, *cis*-β-*RR,SS*-, and *cis*-β-*RS,SR*-[Co(edsi)(trien)]$^+$ (vide infra). Therefore, it is probable that the perchlorate salt of [Co(edt)(trien)]$^+$ is a mixture of the cis-α, cis-β-*RR,SS*, and cis-β-*RS,SR* isomers. In the ^{13}C NMR spectra of [Co(edsi)(trien)]$^+$ containing eight methylene carbon atoms, the A-1 and A-2 complexes exhibit fifteen and four (δ 45.61, 45.72, 58.78, and 59.65) signals respectively. The A-1 complex was separated into two isomers, B-1 and B-2, which show eight ^{13}C NMR signals (δ 43.83, 50.44, 51.68, 52.33, 56.12, 57.53, 58.40, and 60.68 for B-1, and δ 45.13, 47.84, 53.09, 53.20, 57.26, 59.43, 59.70, and 60.68 for B-2). These results indicate that the A-1 complex is a mixture of the cis-β-*RR,SS* and cis-β-*RS,SR* isomers (C_1 symmetry), while the A-2 complex is the cis-α isomer (C_2 symmetry). The ^{13}C NMR signals of the B-1 isomer appear at higher magnetic fields than those of the B-2 isomer. For [Co(NH$_3$)$_2$(trien)]$^{3+}$ [9] and [Co(CN)$_2$(trien)]$^+$,[10] the cis-β-*RR,SS* isomer commonly shows ^{13}C NMR signals at higher magnetic fields than those of the cis-β-*RS,SR* isomer. Therefore, it is tentatively assigned that the B-1 and B-2 isomers take

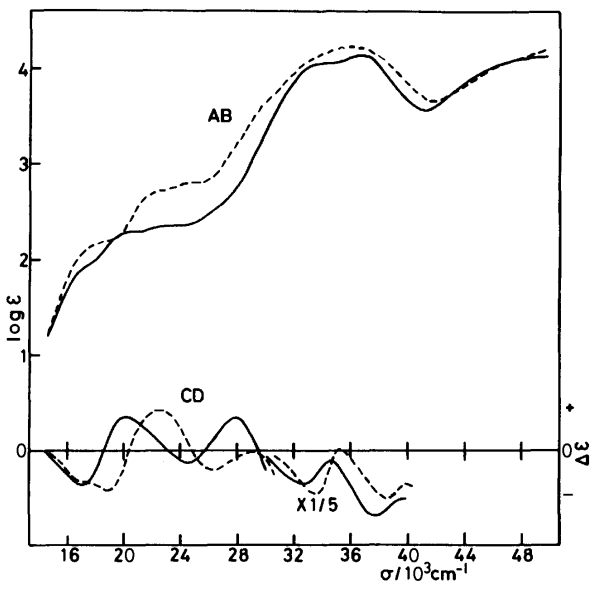

Fig. 1. Absorption and CD spectra of Δ-(−)$^{CD}_{580}$-*cis*-α-[Co(edt)(trien)]$^+$ (——) and Δ-*cis*-α-[Co(pdt)(trien)]$^+$ (-----). CD scale is arbitrary.

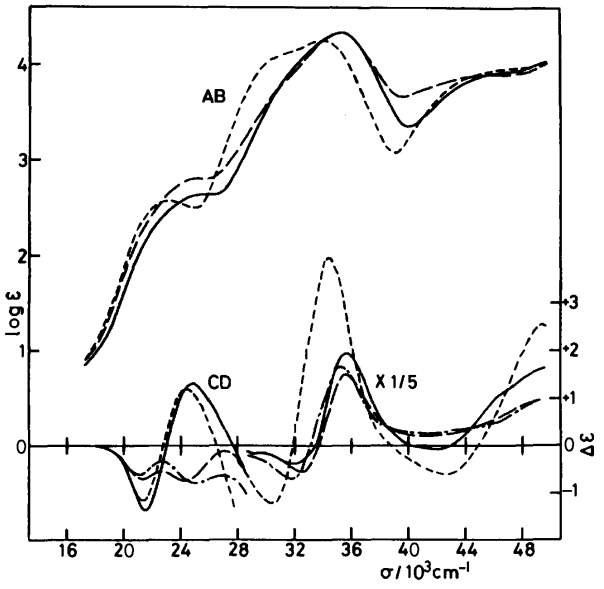

Fig. 2. Absorption and CD spectra of Δ-(−)$^{CD}_{460}$-*cis*-α-(——), Δ-(−)$^{CD}_{470}$-*cis*-β-*RR*- (———), Δ-(−)$^{CD}_{470}$-*cis*-β-*RS*-[Co(edsi)(trien)]$^+$ (—·—·—), and Δ-*cis*-α-[Co(pdsi)-(trien)]$^+$ (-----).

the cis-β-*RR,SS* and cis-β-*RS,SR* configurations respectively. The assignment for the two cis-β isomers is supported from a 4:1 formation ratio of the *RR,SS* (B-1) isomer to the *RS,SR* (B-2) isomer, which is an usual trend observed for $[CoX_2(trien)]^{n+}$ (X_2=$NH_2CH_2CO_2^-$,[11] $2NH_3$,[9] $2CN^-$,[10] and $2NCS^-$ [12]).

As shown in Fig. 2, the CD spectrum of $(-)_{460}^{CD}$-*cis*-α-[Co(edsi)(trien)]$^+$ is similar to that of Δ-*cis*-α-[Co(pdsi)(trien)]$^+$ over the whole region, whose absolute configuration has been determined by X-ray structural analysis.[1] Therefore, the $(-)_{460}^{CD}$-cis-α edsi isomer is assignable to the Δ configuration. The CD spectra of $(-)_{470}^{CD}$-*cis*-β-*RR,SS*- and $(-)_{470}^{CD}$-*cis*-β-*RS,SR*-[Co(edsi)(trien)]$^+$ quite resemble each other, showing the two negative CD bands in the first absorption band region (18—28$\times10^3$ cm^{-1}) and a negative and a positive band from lower energy in the SMCT band region (28—38$\times10^3$ cm^{-1}) (Fig. 2). This CD spectral pattern is the same as that of Δ-$(-)_{460}^{CD}$-*cis*-α-[Co(edsi)(trien)]$^+$, except for some deviation at the higher-energy side in the first absorption band region, suggesting that the two $(-)_{470}^{CD}$-cis-β edsi isomers also take the Δ configuration (Δ-cis-β-*RR* and Δ-cis-β-*RS*). The CD spectrum of $(-)_{580}^{CD}$-*cis*-α-[Co(edt)(trien)]$^+$ is similar to that of Δ-*cis*-α-[Co(pdt)(trien)]$^+$ [1] in the SMCT band regions (30—40$\times10^3$ cm^{-1}), although the intensities are shown by an arbitrary scale (Fig. 1). Furthermore, the oxidation product of $(-)_{580}^{CD}$-*cis*-α-[Co(edt)(trien)]$^+$ showed an identical CD pattern with that of Δ-*cis*-α-[Co(edsi)(trien)]$^+$. Accordingly, it is reasonable to assign that the $(-)_{580}^{CD}$-cis-α edt isomer takes the Δ configuration.

References

1) K. Okamoto, H. Umehara, and J. Hidaka, *Bull. Chem. Soc. Jpn.*, **60**, 2875 (1987).

2) D. P. Schaefer and G. R. Brubaker, *Inorg. Chem.*, **8**, 1794 (1969).

3) A. M. Sargeson and G. H. Seale, *Inorg. Chem.*, **6**, 787 (1967).

4) K. Wakayama, K. Okamoto, H. Einaga, and J. Hidaka, *Bull. Chem. Soc. Jpn.*, **56**, 1995 (1983).

5) K. Okamoto, K. Wakayama, H. Einaga, S. Yamada, and J. Hidaka, *Bull. Chem. Soc. Jpn.*, **56**, 165 (1983).

6) K. Yamanari, N. Takeshita, and Y. Shimura, *Bull. Chem. Soc. Jpn.*, **57**, 1227 (1984).

7) K. Yamanari, N. Takeshita, and Y. Shimura, *Bull. Chem. Soc. Jpn.*, **57**, 2852 (1984).

8) T. Konno, K. Okamoto, H. Einaga, and J. Hidaka, *Bull. Chem. Soc. Jpn.*, **58**, 1119 (1985), and references sited therein.

9) S. Utsuno, Y. Yoshikawa, and Y. Tahata, *Inorg. Chem.*, **24**, 2724 (1985).

10) Y. Nokami, M. Irimichi, Y. Tahata, and S. Utsuno, presented at the 31st symposium on the Coordination Chemistry of Japan, Sendai, 1981, Abstract No. 3B14.

11) D. A. Buckingham, M. Dwyer, G. J. Gainford, V. J. Ho, L. G. Marjilli, W. T. Robinson, A. W. Sargeson, and K. R. Turnbull, *Inorg. Chem.*, **14**, 1739 (1975).

12) Y. Sakai, Y. Nokami, H. Kanno, and S. Utsuno, *Chem. Lett.*, **1981**, 371.

Reactive Langmuir-Blodgett Membrane for Biosensor Applications. Use of Succinimidyl Behenoate-Based Membranes as Support for Covalently Immobilizing α-Chymotrypsin

Jun-ichi ANZAI, Shouryu LEE, and Tetsuo OSA*
Pharmaceutical Institute, Tohoku University, Aobayama, Sendai 980
(Received May 1, 1989)

Synopsis. Succinimidyl behenoate was synthesized to prepare Langmuir-Blodgett (LB) membranes which possess reactive groups on the surface. The surface of the succinimidyl behenoate-based LB membrane could be covalently modified with α-chymotrypsin, for the purpose of biosensor applications.

Several groups have reported the use of Langmuir-Blodgett (LB) membranes for preparing enzyme sensors.[1-5] A prerequisite to construction of LB membrane-based enzyme sensors is to immobilize enzymes on or in the LB membrane deposited previously, or to deposit enzyme-containing monolayer using, for example, Fromherz-type trough. We have prepared an enzyme sensor by immobilizing penicillinase through adsorption on the surface of LB membrane deposited on a pH-sensitive field effect transistor (pH-ISFET). Penicillinase, fortunately, could be tightly adsorbed, through electrostatic or hydrophobic force of attraction, to the surface of the LB membrane. However, it is not always possible for enzymes to be adsorbed to the LB membrane surface without deactivation. In fact, we have observed poor reproducibility in potentiometric response for the pH-ISFETs covered with LB membranes adsorbing urease, trypsin, and α-chymotrypsin, presumably due to desorption or deactivation of enzymes. For these reasons, we have developed a reactive LB membrane which can covalently bind enzymes on the surface, using a fatty acid active ester, succinimidyl behenoate (**1**), as a membrane-forming amphiphile.

This paper reports the immobilization of α-chymotrypsin on the surface of LB membrane containing **1** which is deposited on the pH-ISFET and its use as an enzyme sensor.

Experimental

Materials. Succinimidyl behenoate (**1**) was prepared from *N*-hydroxysuccinimide (1.2 g) and behenic acid (3.4 g) in 50 ml chloroform using dicyclohexylcarbodiimide (2.1 g) as coupling reagent. The crude product was purified by repeated recrystallization from ethanol. 3.2 g (73%). Mp 98—99 °C. Found; C, 71.46; H, 10.59; N, 3.36%. Calcd for $C_{26}H_{47}NO_4$; C, 71.35; H, 10.82; N, 3.20%.

α-Chymotrypsin (EC 3.4.21.1) was obtained from Sigma Co. *N*-Acetyltyrosine ethyl ester (ATEE) was purchased from Research Organics Inc.

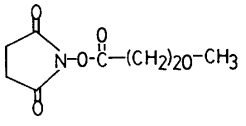

Chart 1. Succinimidyl behenoate **1**.

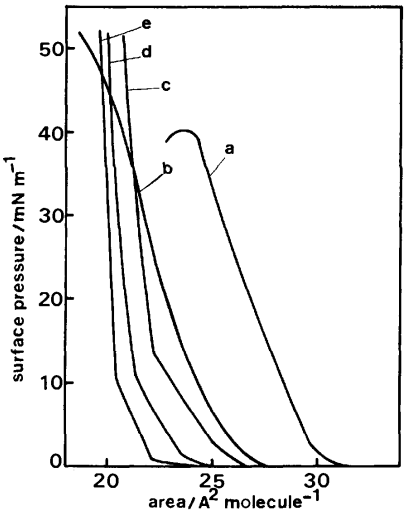

Fig. 1. π-*A* isotherms of **1** and **1**/1-octadecanol mixed monolayers on water at 17 °C. The contents of **1** in the monolayers were 100(a), 90(b), 40(c), 10(d), and 0 w/w%(e).

The procedure for the fabrication and the pH response of the pH-ISFET used are described elsewhere.[6,7]

Sensor Fabrication. The **1** or **1**/1-octadecanol mixed monolayer was spread with benzene on an aqueous subphase in a Langmuir trough (Kyowa Kaimenkagaku Co.). The water subphase was adjusted at ca. pH 7 with $BaCl_2$ and $KHCO_3$. The monolayer was deposited on the pH-ISFET precoated with 11-layer octadecanoic acid LB membrane, by dipping the probe vertically through the monolayer at 25 mN m^{-1}. After the monolayer had been removed from water surface, the probe was pulled up. By this treatment, the active ester groups should be located at the uppermost surface of the deposited LB layer, and, therefore, the surface is reactive to nucleophilic group such as amine. The deposition behavior of **1** and **1**/1-octadecanol membranes was elucidated by the deposition on the glass plate precoated with octadecanoic acid LB layer (1 cm×3 cm), since the small area of the pH-ISFET (ca. 1 mm×3 mm) inhibited precise measurement of deposition ratio.

The LB membrane-coated pH-ISFET, thus prepared, was immersed in a 0.5% α-chymotrypsin solution (1 mM phosphate buffer, pH 7.5, 1 M=1 mol dm^{-3}) for 4 h, in order to bind the enzyme onto the surface of LB membrane. The enzyme sensors prepared were rinsed thoroughly with the working buffer before use.

Results and Discussion

In Fig. 1, we display π-*A* diagrams of **1** monolayer together with the mixed monolayers of **1** and 1-octadecanol spread on water surface at 17 °C. Al-

though the **1** monolayer can be compressed up to about 40 mN m^{-1}, the π-A diagram does not afford clear indication of the formation of condensed monolayer of **1**. Basically the same π-A diagram as **1** was observed for the mixed monolayer with 90 w/w% **1**. These monolayers may assume expanded phase, not condensed one. On the other hand, the mixed monolayers with lower **1** content (10 and 40%) exhibited π-A diagrams with transition pressures at 11 — 14 mN m^{-1}, which are similar to that of 1-octadecanol monolayer, indicative of the formation of stable condensed phase.

We examined the deposition property of the monolayer on the glass plate precoated with octadecanoic acid LB layers. The deposition ratios of the **1** and mixed monolayers were measured by dipping the glass plate into the water subphase through the monolayer at 25 mN m^{-1}. The deposition ratios thus measured were 1.9 for **1** monolayer and 1.3, 1.0, and 1.1 for the mixed monolayers with **1** content of 90, 40, and 10%, respectively. Unexpectedly high values of deposition ratios for the monolayers of higher **1** content might come from the expanded nature of the **1** and 90% **1** monolayers on the water surface at 25 mN m^{-1}.

Figure 2 shows a typical response of the α-chymotrypsin-immobilized pH-ISFET which was prepared by the use of the probe covered with the mixed LB layer (**1** content; 90 w/w%) as well as a pH response of bared pH-ISFET. The potentiometric response of immobilized pH-ISFET became slow to compare with that of bared pH-ISFET. However, the probe exhibited a potentiometric response to *N*-acetyltyrosine ethyl ester (ATEE) (a model substrate of α-chymotrypsin), showing that the enzyme was immobilized without deactivation and catalyzed hydrolysis reaction of ATEE to change pH value at the surface of the pH-ISFET gate as follows:

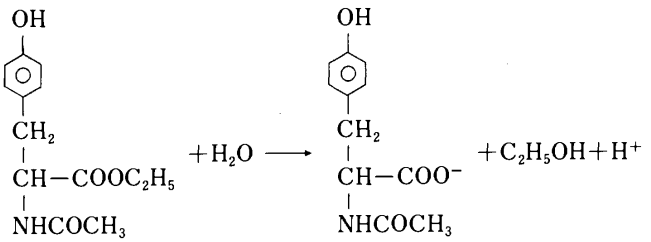

ATEE

It is thought that amino residues in the enzyme attacked the active ester of LB layer to form amide linkage between them, in view of the fact that succinimidyl esters are widely used for modifying proteins[8] and covalently binding proteins on the solid support.[9] The potentiometric response of the sensor was fairly reproducible.

We also tried to immobilize α-chymotrypsin on the surface of 1-octadecanol LB layer deposited on the pH-ISFET, by immersing the probe in the enzyme solution (0.5%) in a similar manner. After rinsing the probe with the working buffer for ca. 1 h, we measured the potentiometric response of the sensor to 2 mM ATEE repeatedly and found that the ΔE_{gs} value

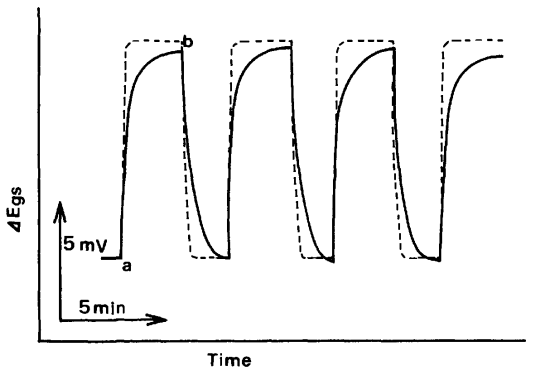

Fig. 2. A typical response of the α-chymotrypsin-immobilized ISFET for *N*-acetyltyrosine ethyl ester. The probe was immersed in the ATEE solution (2 mM) (a) and buffer solution (b). 2 mM buffer (pH 8.0) was used. High concentration samples (above 2 mM) of ATEE could not be prepared due to the low solubility. A response of bared pH-ISFET from pH 8.0 buffer to pH 7.8 buffer is shown in dashed line (---).

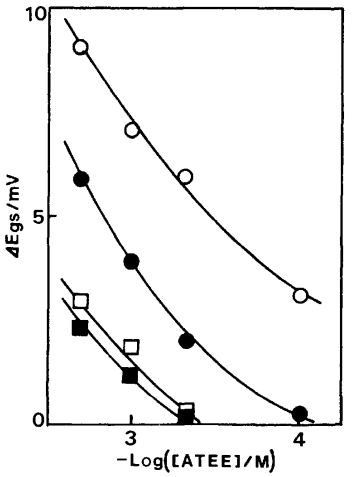

Fig. 3. Effects of **1** content in the LB membrane on the response of the sensor. The contents of **1** were 90(—○—), 40(—●—), 10(—□—), and 0 w/w%(—■—). 2 mM buffer (pH 8.0) was used. High concentration samples (above 2 mM) of ATEE could not be prepared due to the low solubility.

reduced gradually during the repeated use; ΔE_{gs}= ca. 2 mV after 4 measurements (data not shown). This clearly shows the essential role of the active ester to bind enzyme effectively.

The effects of **1** content in the mixed LB membrane on the response of the α-chymotrypsin-immobilized pH-ISFET were examined (Fig. 3). The potentiometric response was enhanced with increasing the **1** content in the LB membrane. This may be due to enchanced enzyme loading on the surface of higher **1** content. A small portion of enzyme seems to be adsorbed to the surface without formation of amide linkage, judging from the fact that the sensor prepared by the use of 1-octadecanol LB membrane showed a little response. The pure **1** LB layer was omitted from

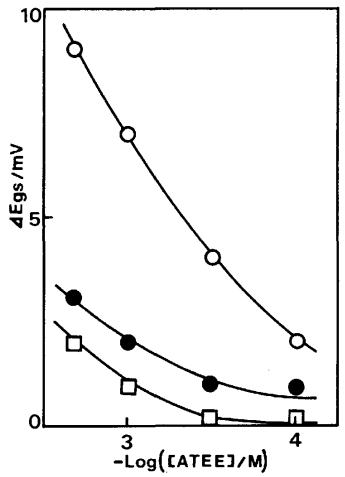

Fig. 4. Effects of pH of the sample solution on the response of the sensor. The pH values of the solutions were 8.0(—○—), 7.0(—●—), and 6.0(—□—).

the consideration, because the nonordered surface structure in deposited **1** layer was suggested by the anomalously high value of deposition ratio.

Figure 4 shows the response of the sensor prepared by the use of 90% **1** mixed LB membrane in pH 6, 7, and 8. The potentiometric response was higher in pH 8 medium, but, in pH 6 and 7 media, the response was lower. This may be due to the fact that the optimum pH of α-chymotrypsin is pH 8.0.[10]

It is a problem in the present method that the long-term stability of α-chymotrypsin immobilized is not satisfactory, which seems to depend on the conditions of measurement and storage. For instance, the catalytic activity of the sensor disappeared in a few days even if the sensor was stored in a 2 mM phosphate buffer (pH 8.0) at 4 °C. However, the long-term stability may be enhanced by the more suitable design of the LB membrane surface and the improvement of the storage conditions.

Thus, we have shown that succinimidyl behenoate is a useful material for the preparation of reactive LB membrane which can bind enzyme covalently on the surface, for the biosensor applications.

This work was supported in part by Grant-in-Aid for Special Project Research (No. 63108002) from the Ministry of Education, Science and Culture.

References

1) J. Anzai, K. Furuya, C-W. Chen, T. Osa, and T. Matsuo, *Anal. Sci.*, **3**, 271 (1987).
2) J. Anzai, J. Hashimoto, T. Osa, and T. Matsuo, *Anal. Sci.*, **4**, 247 (1988).
3) M. Sriyudthsak, H. Yamagishi, and T. Moriizumi, *Thin Solid Films*, **160**, 463 (1988).
4) H. Tsuzuki, T. Watanabe, Y. Okawa, S. Yoshida, S. Yano, K. Koumoto, M. Komiyama, and Y. Nihei, *Chem. Lett.*, **1988**, 1265.
5) J. Anzai, S. Lee, and T. Osa, *Makromol. Chem., Rapid Commun.*, **10**, 167 (1989).
6) T. Matsuo and M. Esashi, *Sensors Actuators*, **1**, 77 (1981).
7) J. Anzai, T. Kusano, T. Osa, H. Nakajima, and T. Matsuo, *Bunseki Kagaku*, **33**, E131 (1984).
8) M. Leonard and E. Dellacherie, *Biochim. Biophys. Acta*, **791**, 219 (1984).
9) S. D. Caras, D. Petelenz, and J. Janata, *Anal. Chem.*, **57**, 1920 (1985).
10) "Koso Handbook," ed by S. Akabori, Asakurashoten, Tokyo (1973), p. 544.

Preparation of Bicyclic Crown Ethers Containing Amide Groups: Coordination of the Oxygen Atoms of the Amide Groups

Takeshi KUMAGAI and Sadatoshi AKABORI*
Department of Chemistry, Faculty of Science, Toho University, Funabashi, Chiba 274
(Received October 29, 1988)

Synopsis. 9,12,23,26,31,36-Hexaoxa-1,6,15,20-tetraaza-3,4:17,18-dibenzotricyclo[18.8.5.5^{6,15}]octatriaconta-3,17-diene-2,5,16,19-tetraone (**7a**) was obtained by the reaction of phthaloyl dichloride with 1,4,10-trioxa-7,13-diazacyclopentadecane in 38% yield, and related compounds were prepared by a similar method. Compound **7a** showed high extraction abilities toward alkali, alkaline earth, and other metal cations (Ag^+, Tl^+, and Pb^{2+}), especially lithium and sodium cations.

Diazacrown ethers are well-known as complexing agents toward alkali and alkaline earth metal cations.[1] Especially, the complexing abilities of cryptand-type bicyclic crown ethers toward alkaline earth metal cations are considerably high.[2] We previously reported that cyclobutane-incorporated diazacrown ether **1**[3,4] had high complexing abilities toward alkali, alkaline earth, and other metal cations (Ag^+, Co^{2+}, Ni^{2+}, and Cu^{2+}) without remarkable selectivities. The structures of the complexes of cyclobutane-incorporated diazacrown ether **1** with lithium and/or mercury(II) were revealed by X-ray analyses.[3,4] The results suggested that the metal cation was not incorporated into the cavity of the crown ether moiety, but was coordinated by the oxygen atoms of the two amide groups. On the other hand, Vögtle et al.[5] isolated the 1:1 complexes of diazacrown ethers **2c**, **2d**, **3c**, and **3d** with Na^+ or K^+, and suggested that the metal cation was incorporated into the cavity of the crown ether moiety. However, they did not discuss the complexing ability of diamide **2a**, **2b**, **3a**, and **3b**. Noting these results, we were interested in the complexing abilities of the crown ethers containing amide groups. We therefore prepared the novel azacrown ethers **6b**, **6d**, **7a**, and **7c** in order to discuss their complexing abilities and the structures of their metal complexes.

Results and Discussion

Compound **7a** was prepared by the reaction of 1,4,10-trioxa-7,13-diazacyclopentadecane (**4a**) with phthaloyl dichloride (**5**) in the presence of triethylamine in 38% yield. Also, the compounds **6b**, **6d**, and **7c** were prepared by the similar methods, as described above. However, in these reactions compounds **6a**, **6c**, **7b**, and **7d** were not obtained. The ^1H NMR spectrum of **6b** showed the signals of methylene protons in the δ=4.38 to 2.88 region as a considerably complicated splitting pattern. The 2D COSY ^1H NMR spectrum of **6d** showed an interesting spectral pattern. As shown in Fig. 1, four protons (Ha and Hb), which were expected to be equivalent, appeared as four independent peaks. The signals of two protons (Ha), which are methylene protons adjacent to the nitrogen atoms and also close to the oxygen atoms of the carbonyl group, appeared at δ=4.36 (t, J=4.3 Hz, 1H) and 4.32 (t, J=4.3 Hz, 1H), whereas the other protons (Hb), which are attached to the same carbon atoms, are shifted upfield to δ=2.95 (q, J=3.8 Hz, 1H) and 2.91 (q, J=3.8 Hz, 1H). From the Corey-Pauling-Koltom

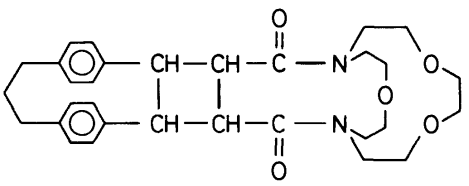

1

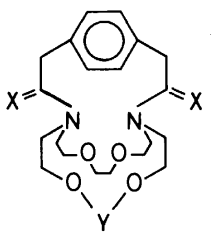

2

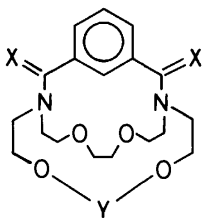

3

a : X = O , Y = $-CH_2CH_2-$
b : X = O , Y = o-phenylene
c : X = H_2 , Y = $-CH_2CH_2-$
d : X = H_2 , Y = o-phenylene

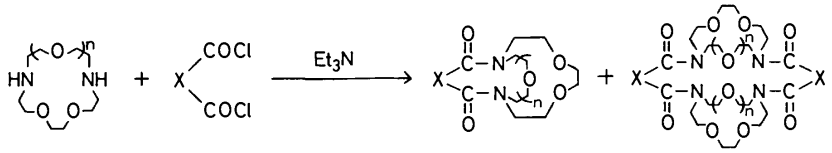

4 5 6 7

a : n = 1 a : X = o-phenylene
b : n = 2 b : X = $-CH_2CH_2-$

a : X = o-phenylene , n=1
b : X = o-phenylene , n=2
c : X = $-CH_2CH_2-$, n=1
d : X = $-CH_2CH_2-$, n=2

(CPK) molecular model, these unusual shifts of the methylene protons were attributed to a steric compression between the carbonyl group and the methylene protons adjacent to nitrogen atoms.[3] However, in the ^{1}H NMR spectra of **7a** and **7c**, the signals of the methylene protons did not give a well-separated pattern; therefore, those signals could not be assigned. The CPK molecular models suggest that the structures of **7a** and **7c** were sterically very crowded and that the mobility of the molecule was obstructed at ambient temperature.

The reaction of **6b** with mercury(II) thiocyanate gave 1:2 complex **8** in 22% yield, and its composition was defined by elemental analysis. In the ^{1}H and ^{13}C NMR spectra, however, only slight differences in the chemical shifts between **6b** and **8** were observed. In the ^{13}C NMR spectra, the chemical shift differences of all carbon atoms between compound **6b** and complex **8** were less than 1.0 ppm. The signals showed that the greatest chemical shift difference was due to the carbonyl carbon atoms, though only 0.98 ppm. These results suggested that if the crown ether moiety and the oxygen atoms of the amide groups are concerned with complexation, coordination becomes presumably very weak.

In the IR spectra, $\nu_{C=O}$ (1616 cm^{-1}) of **8** was shifted to a low wavenumber compared with that (1624 cm^{-1}) of **6b**, and $\nu_{C\equiv N}$ of **8** appeared at 2100 and 2075 cm^{-1}, whereas that of $Hg(SCN)_2$ showed only one absorption band at 2120 cm^{-1}. These results suggested a coordination of the oxygen atoms of the amide groups and the presence of the two kinds of thiocyanate anions. As shown in Fig. 2, the structure of complex **8** was thought to be such that the first of the two mercury atoms is coordinated by the two oxygen atoms of the amide groups, while the second is coordinated by the two nitrogen atoms of the thiocyanate anions of the first one, besides each of the counter anions.

The extraction abilities of the compounds **6b**, **6d**, **7a**, and **7c** toward alkali, alkaline earth, and other metal cations were determined by a method described by Pedersen.[6] However, this determination was carried out using a concentration of azacrown ethers of 7.0×10^{-3} mol dm^{-3}, instead of 7.0×10^{-4} mol dm^{-3}, in order to define the ion selectivities of these azacrown ethers. The results are summarized in Table 1. Compounds **6b** and **7a** showed significant extraction abilities toward alkali and alkaline earth metal cations. Especially, **7a** showed high selectivities toward Li^+(39%) and Na^+(65%). Also **7a** showed high extraction abilities toward Ag^+(49%), Tl^+(42%), and Pb^{2+}(24%). However, **6d** and **7c** showed low extraction

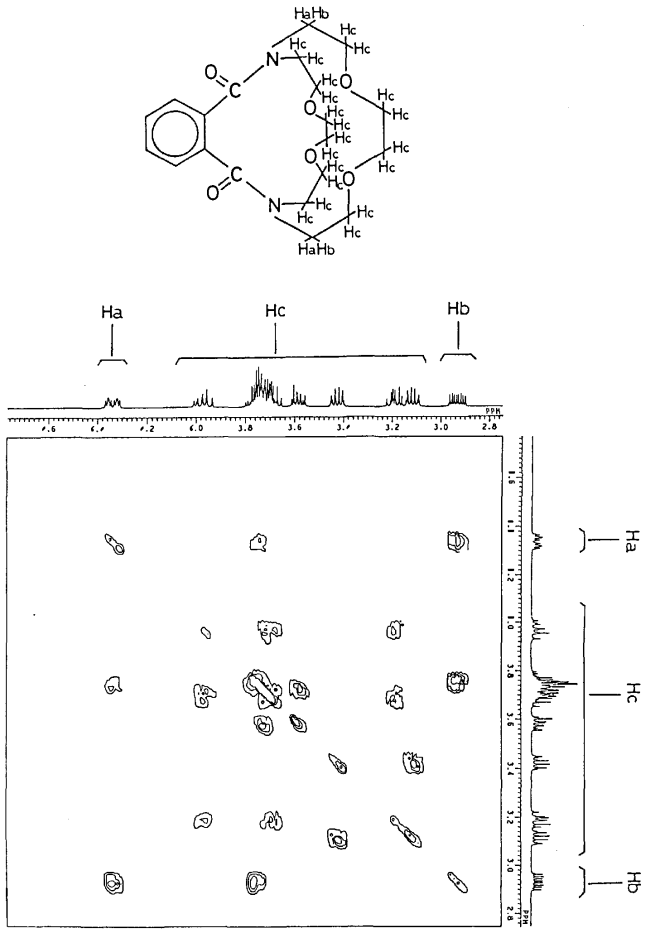

Fig. 1. 400 MHz 2D COSY ^{1}H NMR Spectrum of **6b**.

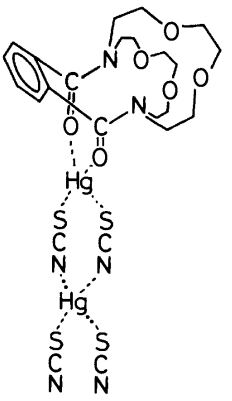

Fig. 2.

Table 1. Extraction of Metal Picrates from the Aqueous to the Organic Phase (%)[a]

Compd	Li^+	Na^+	K^+	Rb^+	Cs^+	Mg^{2+}	Ca^{2+}	Sr^{2+}	Ba^{2+}	Ag^+	Tl^+	Pb^{2+}
6b	13	13	13	12	12	9	11	11	11	30	43	18
6d	4	5	5	4	3	1	5	7	21	19	61	35
7a	39	65	22	22	23	21	22	21	21	49	42	24
7c	3	2	1	2	3	1	2	2	2	28	19	4

a) Solvent: Water and dichloromethane (equal volumes). Azacrown ether=7.0×10^{-3} mol dm^{-3}. Picric acid=7.0×10^{-5} mol dm^{-3}. Metal nitrate=0.1 mol dm^{-3}.

abilities and selectivities toward alkali and alkaline earth metal cations, although they showed high extraction abilities toward Ag^+, Tl^+, and Pb^{2+} cations. Restricted to alkali and alkaline earth metal cations, the significant extraction abilities of **6b** and **7a** may be attributed to an increased basicity of the carbonyl oxygen atoms due to the presence of the *o*-phenylene group. Furthermore, the lower complexing abilities of **6b** toward alkali and alkaline earth metal cations compared with those found in **7a** were presumably caused by difference in the number of carbonyl oxygen atoms. Therefore, compound **7b**, which contains four carbonyl groups as the binding site, showed a stronger affinity toward alkali and alkaline earth metal cations than those of compound **6b**, which contains two carbonyl groups.

Experimental

The melting points were uncorrected. The IR spectra were measured on a JASCO IRA-2 Diffraction Grating Infrared Spectrometer. The ^1H and ^{13}C NMR spectra were obtained on a JEOL GX400 Spectrometer, with TMS as an internal standard. Solvent extraction was carried out according to the method reported previously.[7]

Materials. All reagents and solvents were either commercial or prepared by the usual methods.

The Reaction of 4 with 5. To a solution of triethylamine (1.50 g, 15 mmol) in benzene (400 cm^3), the solution of phthaloyl dichloride (**5a**) (1.02 g, 5.0 mmol) in benzene (100 cm^3) and 1,4,10,13-tetraoxa-7,16-diazacyclooctadecane (**4b**) (1.00 g, 4.6 mmol) in benzene (100 cm^3) were added dropwise at the same rate over a period of 6 h and then stirred for 19 h at room temperature. The precipitated triethylamine hydrochloride was filtered off, and the filtrate was washed with aqueous 10% hydrochloric acid and then water. The mixture was dried by anhydrous magnesium sulfate and concentrated in vacuo. The residue was chromatographed on activated alumina using ethyl alcohol as an eluant. The first fraction was collected and the solvent was removed in vacuo. The residue was recrystallized from benzene to give **6b** as a colorless powder in 13% yield. Mp 216.0—217.0 °C. Found: C, 61.21; H, 7.27; N, 7.12%. Calcd for $C_{20}H_{28}N_2O_6$: C, 61.21; H, 7.19; N, 7.14%. MS (70 eV) *m/z* 392 (M^+). ^1H NMR (CD_3CN) δ=7.45—7.37 (m, 4H), 4.36 (t, *J*=4.3 Hz, 1H), 4.32 (t, *J*=4.3 Hz, 1H), 4.01—3.93 (m, 2H), 3.80—3.65 (m, 10H), 3.61—3.56 (m, 2H), 3.45—3.40 (m, 2H), 3.22—3.16 (m, 2H), 3.14—3.09 (m, 2H), 2.95 (q, *J*=3.8 Hz, 1H), 2.91 (q, *J*=3.8 Hz, 1H). ^{13}C NMR (CD_3CN) δ=169.76 (C=O), 136.47 (bridgehead-C), 129.35 (aromatic-Cβ), 128.98 (aromatic-Cα), 72.71, 70.74, 70.43, 70.16 (-CH_2O-), 51.66, 47.28 (-CH_2N-). IR (KBr disk) 1627, 1163, 1138, 1125, and 1115 cm^{-1}.

6d, Yield 12%. Mp 163.0—165.0 °C. Found: C, 55.89; H, 8.24; N, 8.12%. Calcd for $C_{16}H_{28}N_2O_6$: C, 55.80; H, 8.19; N, 8.13%. MS (70 eV) *m/z* 344 (M^+). ^1H NMR($CDCl_3$) δ=4.50 (t, *J*=5.2 Hz, 1H), 4.47 (t, *J*=5.2 Hz, 1H), 3.98 (t, *J*=6.0 Hz, 1H), 3.94 (t, *J*=6.0 Hz, 1H), 3.82—3.56 (m, 12H), 3.35—3.28 (m, 2H), 3.04 (t, *J*=5.8 Hz, 1H), 3.00 (t, *J*=5.2 Hz, 1H), 2.67 (t, *J*=4.9 Hz, 1H), 2.63 (t, *J*=4.9 Hz, 1H), 2.50—2.43 (m, 2H), 2.17 (s, 4H). IR (KBr disk) 1632, 1133, and 1118 cm^{-1}.

7a, Yield 38%. Mp 281.0—283.0 °C. Found: C, 60.76; H, 6.81; N, 7.63%. Calcd for $C_{36}H_{48}N_4O_{10}\cdot H_2O$: C, 60.49, H, 7.05; N, 7.84%. MS (70 eV) *m/z* 696 (M^+). ^1H NMR ($CDCl_3$) δ=7.52—7.31 (m, 8H), 4.75—2.58 (m, 38H), 1.68 (br, 2H). IR (KBr disk) 1618, 1191, and 1100 cm^{-1}.

7c, Yield 28%. Mp 239.0—240.0 °C. Found: C, 54.70; H, 8.35; N, 9.16%. Calcd for $C_{28}H_{48}N_4O_{10}\cdot 1/6C_6H_6$: C, 54.79; H, 8.05; N, 9.13%. MS (70 eV) *m/z* 600 (M^+). ^1H NMR ($CDCl_3$) δ=4.60—3.23 (m, 40H), 2.71 (br, 16H). IR (KBr disk) 1619, 1188, 1142, and 1122 cm^{-1}.

Isolation of Complex 8. Compound **6b** (20 mg, 5.1×10^{-5} mol) in acetonitrile (3 cm^3) was added to the solution of $Hg(SCN)_2$ (32 mg, 10.2×10^{-5} mol) in acetonitrile (3 cm^3) and the mixture was concentrated to 3 cm^3. The mixture was cooled in a refrigerator and precipitated colorless crystals were obtained in 22% yield. Mp 169.0—170.0 °C. Found: C, 28.09; H, 2.75; N, 8.19%. Calcd for $C_{24}H_{28}Hg_2N_6O_6S_4$: C, 28.09; H, 2.78; N, 8.23%. ^1H NMR (CD_3CN) δ=7.39—7.47 (m, 4H), 4.37 (q, *J*=2.9 Hz, 1H), 4.33 (q, *J*=2.9 Hz, 1H), 4.02—3.93 (m, 2H), 3.81—3.66 (m, 2H), 3.61—3.56 (m, 10H), 3.45—3.40 (m, 2H), 3.23—3.18 (m, 2H), 3.15—3.10 (m, 2H), 2.96 (q, *J*=3.7 Hz, 1H), 2.93 (q, *J*=3.7 Hz, 1H). ^{13}C NMR (CD_3CN) δ=170.74 (C=O), 135.87 (bridgehead-C), 129.77 (aromatic-Cβ), 129.07 (aromatic-Cα), 114.75 (SCN), 72.67, 70.54, 70.10, 69.96 (-CH_2O-), 51.83, 47.71 (-CH_2N-). IR (KBr disk) 2100, 2075, 1616, 1124, and 1104 cm^{-1}.

The present work was partially supported by a Grant-in-Aid for Scientific Research No. 63540414 from the Ministry of Education, Science and Culture.

References

1) M. R. Truter and C. J. Pedersen, *Endeavour*, **30**, 142 (1971). B. Dietrich, J. M. Lehn, and J. P. Sauvage, *Tetrahedron Lett.*, **1969**, 2885, 2888.

2) F. De Jong and D. N. Reinhoudt, "Stability and Reactivity of Crown-ether Complexes," Academic Press, New York (1981).

3) S. Akabori, T. Kumagai, Y. Habata, and S. Sato, *J. Chem. Soc., Chem. Commun.*, **1988**, 661.

4) S. Akabori, T. Kumagai, Y. Habata, and S. Sato, *J. Chem. Soc., Perkin Trans. 1*, in press.

5) E. Buhleier, W. Wehner, and F. Vögtle, *Chem. Ber.*, **112**, 546 (1979). W. Wehner and F. Vögtle, *Tetrahedron Lett.*, **1976**, 2603.

6) C. J. Pedersen, *Federation Proceedings*, **27**, 1305 (1968).

7) S. Akabori, T. Kumagai, Y. Habata, and S. Sato, *Bull. Chem. Soc. Jpn.*, **61**, 2459 (1988).

Synthesis of the 1*H*,5*H*-Naphtho[1,8-*ef*][1,3]dithiocin System

Toshihiro KAMADA,* Yasuo GAMA, and Nobuhide WASADA
National Chemical Laboratory for Industry, Higashi-1, Tsukuba, Ibaraki 305
(Received February 28, 1989)

Synopsis. The titled new pericyclized naphthalene system has been prepared in four steps from 1,8-naphthalenedicarboxylic anhydride in an overall yield of 35—78%. The key step in the synthesis employed a dithioacetal-cyclization reaction of 1,8-bis(mercaptomethyl)naphthalene with carbonyl compounds using boron trifluoride etherate as a catalyst.

Previously, we reported the synthesis of the 8,9,10,11-tetrahydro-7*H*-cycloocta[*de*]naphthalene system (**1**).[1,2] The successful synthesis of the carbocyclic ring of the eight-membered pericyclized naphthalene system has led us to investigate further the synthesis of heterocyclic analogs of this family of molecules. In this paper, a synthesis of new peri ring system, 1*H*,5*H*-naphtho[1,8-*ef*][1,3]dithiocin (**2**) is reported.

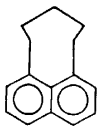

1

Lithium aluminum hydride reduction of the commercially available 1,8-naphthalenedicarboxylic anhydride readily gave 1,8-bis(hydroxymethyl)naphthalene (**3**) (85% yield).[2] Bromination of **3** with phosphorus tribromide in dioxane produced the dibromide **4** (94% yield), which, on treatment with thiourea, was converted to the dithiol **5** (99% yield).[3] Our approach to synthesis of the 1*H*,5*H*-naphtho[1,8-*ef*][1,3]dithiocin system then utilized a dithioacetal-cyclization reaction between **5** and carbonyl compounds. The reactions were carried out with a variety of aldehydes and ketones in chloroform using boron trifluoride etherate as a catalyst. Thus, treatment of **5** with paraformaldehyde (**6a**) yielded 1*H*,5*H*-naphtho[1,8-*ef*][1,3]dithiocin (**2a**) (44% yield) with the desired 1,3-dithiocin peri ring. Similarly, from paraldehyde (**6b**) and benzaldehyde (**6c**) were obtained 3-monosubstituted derivatives of **2a**—i.e., 3-methyl- (**2b**) (69% yield) and 3-phenyl- (**2c**) (97% yield) 1*H*,5*H*-naphtho[1,8-*ef*]dithiocins, respectively. Furthermore, ketones also underwent a ready dithioacetalization reaction on treatment with **5** to give rise to 3,3-disubtituted derivatives of **2a**—i.e., from acetone (**6d**), 2-butanone (**6e**), and acetophenone (**6f**) were obtained 3,3-dimethyl- (**2d**) (70% yield), 3-ethyl-3-methyl- (**2e**) (81% yield), and 3-methyl-3-phenyl- (**2f**) (60% yield) 1*H*,5*H*-naphtho[1,8-*ef*][1,3]dithiocins, respectively.

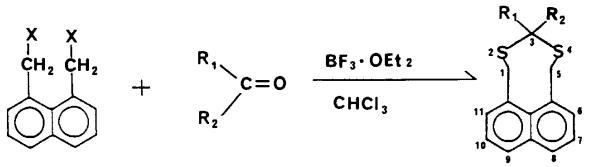

3; X = OH
4; X = Br
5; X = SH

6a—f

2a—f

a; $R_1 = R_2 = H$
b; $R_1 = CH_3$, $R_2 = H$
c; $R_1 = C_6H_5$, $R_2 = H$
d; $R_1 = R_2 = CH_3$
e; $R_1 = C_2H_5$, $R_2 = CH_3$
f; $R_1 = CH_3$, $R_2 = C_6H_5$

All the products obtained (**2a—f**) are listed in Table 1. Each of these new compounds gave elemental analysis and spectra (IR, NMR, MS) identical with its structure. (See Experimental).

Experimental

General. Melting points were taken on a microscopic hot-stage melting-point apparatus and are uncorrected. The R_f values were obtained on Merck Silica gel $60F_{254}$ (0.2 mm) with benzene as a solvent. The IR spectra were measured with a JASCO IR-G spectrometer using Nujol mulls calibrated with polystyrene. The ^1H NMR spectra were determined on a JEOL C-60 spectrometer (at 60 MHz) using chloroform-*d* as a solvent (ca. 10% solution) and tetramethylsilane as an internal standard. Mass spectra were obtained with a JEOL-01SG-2 instrument with a direct-inlet system operating at 75 eV.

1,8-Bis(hydroxymethyl)naphthalene (3). This was prepared from 1,8-naphthalenedicarboxylic anhydride in 85% yield as described previously.[2]

1,8-Bis(bromomethyl)naphthalene (4). This was ob-

Table 1. Synthesis of 1*H*,5*H*-Naphtho[1,8-*ef*][1,3]dithiocins (**2a**—f) from 1,8-Bis(mercaptomethyl)naphthalene (**5**) and Carbonyl Compounds (**6**)

Carbonyl compound (**6**)	R_1	R_2	Product (**2**)	Yield/%
Paraformaldehyde (**6a**)	H	H	**2a**	44
Paraldehyde (**6b**)	CH_3	H	**2b**	69
Benzaldehyde (**6c**)	C_6H_5	H	**2c**	97
Acetone (**6d**)	CH_3	CH_3	**2d**	70
2-Butanone (**6e**)	C_2H_5	CH_3	**2e**	81
Acetophenone (**6f**)	CH_3	C_6H_5	**2f**	60

tained in a more excellent yield than that reported[4] by using the procedure described below.

To a stirred suspension of the diol **3** (20.435 g) in dioxane (100 ml) was slowly added phosphorus tribromide (30 ml) at room temperature. After 25 h, water (300 ml) was added under cooling to decompose the excess reagent, and the resulting mixture, after further addition of water (1200 ml), was stirred at room temperature for an additional 1 h. The solid precipitated was then collected by filtration and crystallized from benzene to give the dibromide **4** (35 g, 94%) as colorless crystals; mp 131.5—132 °C (lit,[4] mp 130—131.5 °C); MS, *m/z* 314 (M^+=$C_{12}H_{10}Br^{79}Br^{81}$).

1,8-Bis(mercaptomethyl)naphthalene (5). This was prepared by a modification of the procedure previously reported.[3]

A mixture of the dibromide **4** (34.54 g) and thiourea (17.6 g) in 95% ethanol (580 ml) was boiled under reflux over a period of 4 h. After cooling the white precipitate of bis(isothiouronium) salt was collected. The salt was then added to a nitrogen-degassed solution of potassium hydroxide (180 g) in water (350 ml) and refluxed under nitrogen atmosphere for 1 h. After cooling and washing with benzene, the aqueous alkaline solution was slowly added with ice-cooling to a nitrogen-degassed 6 M-aqueous hydrochloric acid (1 M=1 mol dm^{-3}). The resulting cloudy solution was stirred for 30 min at room temperature. The white solid precipitated was collected by filtration to provide the dithiol **5** (23.8 g, 99%); mp 79—81 °C (lit,[3] mp 80—80.5 °C); IR (Nujol) 2557 cm^{-1} (S-H); ^1H NMR ($CDCl_3$) δ=1.84 (2H, t, J=6.1 Hz, SH), 4.42 (4H, d, J=6.1 Hz, $ArCH_2SH$), 7.36—7.91 (6H, m, ArH); MS, *m/z* 220 (M^+). This was shown (by IR, ^1H NMR, TLC) to be pure enough and employed without further purification for the following reactions.

Preparation of 1*H*,5*H*-Naphtho[1,8-*ef*][1,3]dithiocins (2a—f) by Reaction of the Dithiol 5 with Paraformaldehyde (6a), Paraldehyde (6b), Benzaldehyde (6c), Acetone (6d), 2-Butanone (6e), and Acetophenone (6f). General Procedure. To a stirred and cooled (0 °C) solution of the dithiol **5** (0.5 mmol) and aldehyde or ketone **6** (0.5 mmol) in chloroform (10 ml) there was added boron trifluoride etherate (2 mmol) under nitrogen atmosphere. After the mixture had been stirred at 0 °C for 2 h, it was allowed to warm to room temperature and was stirred for an additional 18 h. Water was then added and the mixture was extracted with ether. The ether layer was washed successively with 10% aqueous sodium hydroxide solution and water, and was evaporated after drying over magnesium sulfate. The resulting solid was purified by recrystallization from ethanol to afford the pure dithioacetal **2**.

1*H*,5*H*-Naphtho[1,8-*ef*][1,3]dithiocin (2a); colorless needles; mp 180.5—181 °C; R_f 0.51 (SiO_2/benzene); IR (Nujol) 3025, 1600, 1510, 835, 780, 770 cm^{-1}; ^1H NMR ($CDCl_3$) δ=3.55 (2H, s, C_9-CH_2), 4.69 (4H, broad signal, $ArCH_2$), 7.41—7.94 (6H, m, ArH); MS, *m/z* (relative intensity), 232 (M^+, 69), 186 (36), 185 (M^+—CH_3S, 100), 172 (96), 171 (61), 153 (70), 152 (51); Found: C, 67.29; H, 5.02%. Calcd for $C_{13}H_{12}S_2$: C, 67.19; H, 5.21%.

3-Methyl-1*H*,5*H*-naphtho[1,8-*ef*][1,3]dithiocin (2b); colorless microcrystals; mp 133.5—137 °C; R_f 0.52 (SiO_2/benzene); IR (Nujol) 3040, 1600, 1510, 830, 770 cm^{-1}; ^1H NMR ($CDCl_3$) δ=1.36 (3H, d, J=7.1 Hz, CH_3), 3.92 (2H, ABd, J=14.3 Hz, $ArCH_2$), 4.10 (1H, q, J=7.1 Hz, C_9-H), 5.53 (2H, ABd, J=14.3 Hz, $ArCH_2$), 7.40—7.93 (6H, m, ArH); MS, *m/z* (relative intensity), 246 (M^+, 65), 186 (49), 185 (M^+—C_2H_5S, 100), 172 (61), 171 (53), 153 (67), 152 (43), 74 (22). Found: C, 68.30; H, 5.91%. Calcd for $C_{14}H_{14}S_2$: C, 68.24; H, 5.73%.

3-Phenyl-1*H*,5*H*-naphtho[1,8-*ef*][1,3]dithiocin (2c); colorless microcrystals; mp 192.5—193.5 °C; R_f 0.53 (SiO_2/benzene); IR (Nujol) 3050, 1600, 1495, 835, 770, 725, 695 cm^{-1}; ^1H NMR ($CDCl_3$) δ=4.03 (2H, ABd, J=14.6 Hz, $ArCH_2$), 5.17 (1H, s, C_9-H), 5.68 (2H, ABd, J=14.6 Hz, $ArCH_2$), 7.26 (5H, s, Phenyl H), 7.45—7.98 (6H, m, Naphthalene H); MS, *m/z* (relative intensity), 308 (M^+, 40), 186 (M^+—C_7H_6S, 100), 185 (94), 171 (37), 153 (65), 136 (36), 135 (35). Found: C, 73.75; H, 5.40%. Calcd for $C_{19}H_{16}S_2$: C, 73.98; H, 5.23%.

3,3-Dimethyl-1*H*,5*H*-naphtho[1,8-*ef*][1,3]dithiocin (2d); colorless microcrystals; mp 152—152.5 °C; R_f 0.42 (SiO_2/benzene); IR (Nujol) 3030, 1600, 1505, 825, 770, 765 cm^{-1}; ^1H NMR ($CDCl_3$) δ=1.80 (6H, s, CH_3), 4.43 (4H, s, $ArCH_2$), 7.25—7.87 (6H, m, ArH); MS, *m/z* (relative intensity), 260 (M^+, 48), 186 (73), 185 (M^+—C_3H_6S, 100), 171 (47), 153 (82), 152 (55), 88 (81). Found: C, 69.31; H, 6.00%. Calcd for $C_{15}H_{16}S_2$: C, 69.18; H, 6.19%.

3-Ethyl-3-methyl-1*H*,5*H*-naphtho[1,8-*ef*][1,3]dithiocin (2e); colorless crystals; mp 154—155 °C; R_f 0.49 (SiO_2/benzene); IR (Nujol) 3020, 1605, 1510, 825, 775, 765 cm^{-1}; ^1H NMR ($CDCl_3$) δ=1.10 (3H, t, J=7.0 Hz, ethyl-CH_3), 1.65 (3H, s, CH_3), 2.10 (2H, q, ethyl-CH_2), 4.43 (4H, s, $ArCH_2$), 7.29—7.95 (6H, m, ArH); MS, *m/z* (relative intensity), 274 (M^+, 27), 186 (M^+—C_4H_8S, 100), 185 (92), 171 (51), 153 (88), 152 (61), 102 (51). Found: C, 69.85; H, 6.85%. Calcd for $C_{16}H_{18}S_2$: C, 70.02; H, 6.61%.

3-Methyl-3-phenyl-1*H*,5*H*-naphtho[1,8-*ef*][1,3]dithiocin (2f); colorless microcrystals; mp 182.5—184.5 °C; R_f 0.54 (SiO_2/benzene); IR (Nujol) 3050, 1600, 1510, 825, 770, 760, 695 cm^{-1}; ^1H NMR ($CDCl_3$) δ=1.81 (3H, s, CH_3), 4.23 (4H, s, $ArCH_2$), 7.28—8.22 (11H, m, ArH); MS, *m/z* (relative intensity), 322 (M^+, 46), 186 (98), 185 (M^+—C_8H_9S, 100), 171 (45), 153 (84), 152 (55), 150 (73), 149 (60). Found: C, 74.59; H, 5.40%. Calcd for $C_{20}H_{18}S_2$: C, 74.49; H, 5.63%.

References

1) T. Kamada, *Bull. Chem. Soc. Jpn.*, **52**, 170 (1979).
2) T. Kamada, N. Wasada, and O. Yamamoto, *Bull. Chem. Soc. Jpn.*, **49**, 275 (1976).
3) T. Kamada, Jpn. Kōkai Tokkyo Koho, JP76 86453; *Chem. Abstr.*, **86**, 43448v (1977).
4) E. D. Bergmann and J. Szmuszkovic, *J. Am. Chem. Soc.*, **75**, 2760 (1953).

Asymmetric Alkylation of β-Keto Esters with Alkylsulfonium Salts Containing a Sugar Group

Kazuyuki UMEMURA, Haruo MATSUYAMA,* Michio KOBAYASHI, and Nobumasa KAMIGATA
Department of Chemistry, Faculty of Science, Tokyo Metropolitan University, Fukazawa, Setagaya-ku, Tokyo 158
(Received March 4, 1989)

Synopsis. The asymmetric alkylation of 2-methoxycarbonyl-1-indanone (**2**) and ethyl 2-methylacetoacetate (**5**) with an alkylsulfonium salt containing a sugar group were investigated. (*S*)-Ethyl 2-allyl-2-methylacetoacetate (**6b**) was obtained with up to 25% optical purity on alkylation of the enolate ion of **5** using the allyl(*p*-tolyl)sulfonio D-glucoside derivative (**1h**).

S-Adenosylmethionine (AdoMet) is an important biological methylating agent, which is the source of the methyl groups of such compounds as DNA, RNA, proteins, and biogenic amines.[1] A few stereochemical studies have been reported on the methylation reaction of phenolic oxygens with *S*-adenosylmethionine via S_N2-type process in enzymic systems.[2] In recent years, a few studies have been published on the alkylation reaction of oxygen nucleophiles such as carboxylate, nitrogen nucleophiles such as amines, and carbon nucleophiles (e.g. enolate ions of β-keto esters) with racemic alkylsulfonium salts.[3] More recently, we have reported the first examples of asymmetric alkylation of β-keto esters with optically active alkylsulfonium salts.[4] We now describe herein the synthesis of alkylsulfonium salts containing sugar groups, since *S*-adenosylmethionine has a sugar group at the α-position of the sulfur atom. The asymmetric alkylation of cyclic and acyclic β-keto esters using the sulfonium salts is also described.[5]

Alkylsulfonium salts containing sugar groups (**1a**—**k**) were prepared from D-glucose. The sulfonium salts (**1e** and **1i**) were shown to be diastereomeric mixtures on the sulfur atom by ^1H NMR analysis (see Experimental section). They could not be separated by recrystallization.

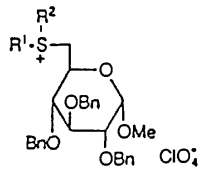

	R^1	R^2		R^1	R^2
1a:	CH_3	CH_3	**1g**:	NO_2–C_6H_4	C_2H_5
1b:	C_2H_5	C_2H_5	**1h**:	CH_3–C_6H_4	$CH_2CH{=}CH_2$
1c:	C_2H_5	CH_3	**1i**:	Cl–C_6H_4	CH_2–C_6H_5
1d:	CH_3–C_6H_4	CH_3	**1j**:	CH_3–C_6H_4	CH_2–C_6H_5
1e:	NO_2–C_6H_4	CH_3	**1k**:	Cl–C_6H_4	$CH_2CH{=}CH_2$
1f:	CH_3–C_6H_4	C_2H_5			

2-Methoxycarbonyl-1-indanone (**2**) was alkylated with a dimethylsulfonio D-glucoside derivative (**1a**) in the presence of anhydrous potassium carbonate in dichloromethane at room temperature for 3 days (Eq. 1). Purification of the reaction mixture by silica-gel chromatography gave *C*-methylated product, (*R*)-(+)-2-methyl-2-methoxycarbonyl-1-indanone (**3a**) (71% yield; o.p. 4.1%),[4] and the *O*-methylated product, **4a** (9% yield). In a similar manner, alkylation of **2** with diethylsulfonio D-glucoside derivative (**1b**) gave the *C*-ethylated product (*R*)-(+)-**3b** (77% yield; o.p. 4.7%),[4] and the *O*-ethylated product **4b** (12% yield).

When the methyl(*p*-tolyl)sulfonio D-glucoside derivative (**1d**) was employed for the reaction with **2**, only the methyl group was introduced to the α-carbon and oxygen atom of **2** to give **3a** and **4a**, respectively. The major product **3a** was also optically active with *R*-configuration.

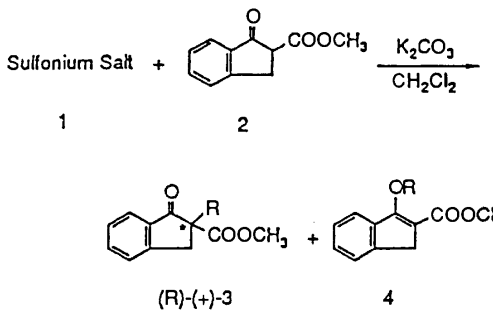

(1)

Similarly, the alkylation of **2** with the methyl(*p*-nitrophenyl)sulfonio D-glucoside derivative (**1e**) gave (*R*)-(+)-**3a** (78% yield; o.p. 6.6%) and product **4a** in 10% yield (Entry 4). Alkylation with arylethylsulfonium salts (**1f** and **1g**) gave (*R*)-(+)-**3b** in 71% yield (o.p. 5.3%) and (*R*)-(+)-**3b** in 74% yield (o.p. 11.9%), respectively (Entries 5 and 6). As shown in Entry 7, the exclusive *C*-allylation of **2** occurred without being accompanied by *O*-allylation. No significant effects on the optical yields were observed when the para-substituent on the aromatic ring was changed from a methyl group (**1d** and **1f**) to a nitro group (**1e** and **1g**).

The alkylation of ethyl 2-methylacetoacetate (**5**)

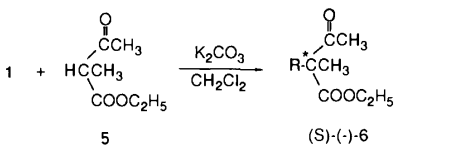

(2)

with alkylsulfonium salts containing sugar group **1** was also investigated (Eq. 2).

When ester **5** was alkylated with sulfonium salt (**1i**), it afforded the *C*-benzylated product (*S*)-(−)-**6a** in 49% yield (o.p. 4.7%).[6] Similarly, allylation of **5** with sulfonium salt (**1h**) gave *C*-allylated products (*S*)-(−)-**6b** in 18% yield (o.p. 25.0%). The results are sum-

Table 1. Alkylation of **2** with Alkylsulfonium Salts **1**

Entry	Sulfonium salt	Product **3** Yield[a]/%	$[\alpha]_D$/deg. ($CHCl_3$)	o.p./% (confn)	Yield[a] of **4** %
1	**1a**	**3a** 71	+0.87	4.1 (*R*)	**4a** 9
2	**1b**	**3b** 77	+3.5	4.7 (*R*)	**4b** 12
3	**1d**	**3a** 78	+2.2	10.4 (*R*)	**4a** 12
4	**1e**	**3a** 78	+1.4	6.6 (*R*)	**4a** 10
5	**1f**	**3b** 71	+3.9	5.3 (*R*)	**4b** 15
6	**1g**	**3b** 74	+8.8	11.9 (*R*)	**4b** 14
7	**1h**	**3c** 89	+8.1		— —

a) Isolated yield.

Table 2. Alkylation of **5** with Alkylsulfonium Salts **1**

Entry	Sulfonium salt	Product **6** Yield[a]/%	$[\alpha]_D$/deg. ($CHCl_3$)	o.p./% (confn)
8	**1i**	**6a** 49	−3.0	4.7 (*S*)
9	**1j**	**6a** 54	−1.8	2.8 (*S*)
10	**1k**	**6b** 65	−2.2	7.4 (*S*)
11	**1h**	**6b** 18	−7.4	25.0 (*S*)

a) Isolated yield.

marized in Table 2.

As shown in Tables 1 and 2, we have achieved asymmetric alkylation using alkylsulfonium salts containing sugar groups, although this method has shown only a small enrichment of one enantiomer by an asymmetric induction effect. Two factors may be considered to explain this asymmetric induction: that is, the chiral transfer from the chiral sulfur atom of the sulfonium salt and the steric control by the sugar moiety. The former factor is not clear, since small asymmetric inductions were observed for the alkylation of **2** with dimethyl- and diethylsulfonium salts (**1a** and **1b**) and alkylarylsulfonium salts (**1e** and **1i**), although **1e** and **1i** were 1:1 diastereomeric mixtures. Accordingly, this asymmetric alkylation is mainly attributable to the steric control by the sugar portion when the enolate ion of **2** attacks at the alkyl carbon atom of the sulfonium salt via an S_N2 process. The S_N2 mechanism is supported by the fact that the ratio of *C*-methylated and *C*-ethylated product of **2** with ethylmethylsulfonium salt (**1c**) was 2.8:1.[7,8]

Experimental

The procedure for the preparation of sulfonium salts **1** is outlined in Scheme 1.

Preparation of Methyl 6-*O*-Tosyl-2,3,4-tri-*O*-benzyl-α-D-glucopyranoside (9). A mixture of methyl 4,6-*O*-benzylidene-2,3-di-*O*-benzyl-α-D-glucopyranoside (**7**) (4.78 g), was prepared from D-glucose by the ordinary procedures, and lithium aluminum hydride (764 mg) in 55 cm^3 of dry CH_2Cl_2–Et_2O (7:4) was stirred and heated to reflux. After the addition of aluminum chloride (2.68 g) in 15 cm^3 of dry ether, the solution was refluxed again for 3 h to give methyl 2,3,4-tri-*O*-benzyl-α-D-glucopyranoside (**8**) (4.67 g, 99% yield). To a pyridine solution (10 cm^3) of **8** (2.03 g) was added *p*-toluenesulfonyl chloride (1.27 g) at 0 °C, and the mixture

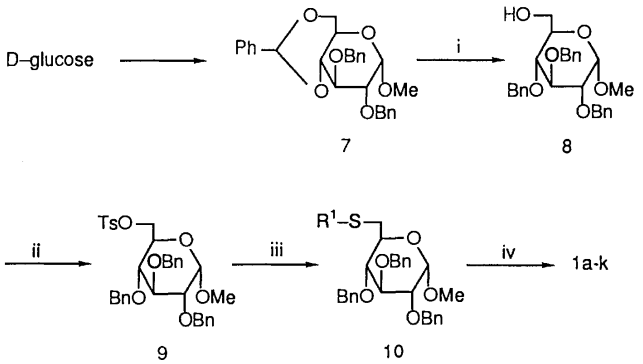

Scheme 1. Reagents: i, $LiAlH_4$–$AlCl_3$, CH_2Cl_2–Et_2O; ii, TsCl, pyridine; iii, R^1SH, EtOH–NaOEt; iv, R^2X–$AgClO_4$, CH_3CN.

was stirred for 1 day at room temperature to give methyl 6-*O*-tosyl-2,3,4-tri-*O*-benzyl-α-D-glucopyranoside (**9**) (2.59 g, 96% yield); $[\alpha]_D$+24.8° (*c* 2.26, $CHCl_3$); ^1H NMR ($CDCl_3$) δ=2.24 (3H, s), 3.17 (3H, s), 3.23—4.93 (13H, m), 6.92—7.83 (19H, m); MS, *m/z* 618 (M^+); HRMS, Calcd for $C_{35}H_{38}O_8S$: M, 618.2286. Found: *m/z* 618.2260.

General Procedure for the Synthesis of 6-Deoxy-6-[alkylthio (or arylthio)]-α-D-glucopyranoside (10). The thiol (5 mmol) was added to an ethanol solution of sodium ethoxide with stirring. The mixture was cooled to 0 °C and **9** (4 mmol) was added to it. The reaction mixture was stirred for 1 h at 0 °C and for 24 h at room temperature to give 6-deoxy-6-[alkylthio (or arylthio)]-α-D-glucopyranoside (**10a—d**).

Methyl 6-Deoxy-6-(*p*-tolylthio)-2,3,4-tri-*O*-benzyl-α-D-glucopyranoside (10a): 69% yield; colorless syrup; ^1H NMR ($CDCl_3$) δ=2.24 (3H, s), 3.32 (3H, s), 2.67—5.04 (7H, m), 4.38—5.04 (6H, m), 6.92 and 7.14 (4H, A_2B_2, *J*=8.4 Hz), 7.20 (15H, br-s); $[\alpha]_D$+22.3° (*c* 1.73, $CHCl_3$); MS, *m/z* 570 (M^+); Calcd for $C_{35}H_{38}O_5S$: C, 73.68, H, 6.72%. Found: C, 73.53, H, 6.79%.

Methyl 6-Deoxy-6-(*p*-nitrophenylthio)-2,3,4-tri-*O*-benzyl-α-D-glucopyranoside (10b): 86% yield; colorless syrup; ^1H NMR ($CDCl_3$) δ=3.13—3.93 (6H, m), 3.28 (3H, s), 4.41—4.90 (6H, m), 5.06 (1H, d, *J*=3.6 Hz), 6.98 and 7.90 (4H, A_2B_2, *J*=8.4 Hz), 7.20 (15H, br-s); $[\alpha]_D$+24.1° (*c* 3.52, $CHCl_3$); MS, *m/z* 601 (M^+); HRMS, Calcd for $C_{34}H_{35}O_7NS$: M, 601.2132. Found: *m/z* 601.2238.

Methyl 6-Deoxy-6-(*p*-chlorophenylthio)-2,3,4-tri-*O*-benzyl-α-D-glucopyranoside (10c): 96% yield; colorless syrup; ^1H NMR ($CDCl_3$) δ=2.60—3.96 (6H, m), 3.23 (3H, s), 3.32—4.73 (6H, m), 4.93 (1H, d, *J*=3.8 Hz), 7.00—7.10 (19H, m); $[\alpha]_D$+29.6° (*c* 1.95, $CHCl_3$); MS, *m/z* 590 (M^+); HRMS,

Calcd for $C_{34}H_{35}O_5SCl$: M, 590.1892. Found: *m/z* 590.1938.

Methyl 6-Deoxy-6-(methylthio)-2,3,4-tri-*O*-benzyl-α-D-glucopyranoside (10d): 89% yield; colorless syrup; ^1H NMR ($CDCl_3$) δ=2.02 (3H, s), 2.32—2.83 (2H, m), 3.05—3.97 (3H, m), 3.29 (3H, s), 4.37—4.75 (7H, m), 4.92 (1H, d, *J*=4.0 Hz), 7.07 (10H, br-s), 7.12 (5H, br-s); $[\alpha]_D$+36.4° (*c* 5.77, $CHCl_3$); MS, *m/z* 494 (M^+); HRMS, Calcd for $C_{29}H_{34}O_5S$: M, 494.2126. Found: *m/z* 494.2153.

Methyl 6-Deoxy-6-(ethylthio)-2,3,4-tri-*O*-benzyl-α-D-glucopyranoside (10e): 92% yield; colorless syrup; ^1H NMR ($CDCl_3$) δ=1.33 (3H, t, *J*=6.4 Hz), 2.37—2.87 (2H, m), 2.56 (2H, q, *J*=6.4 Hz), 3.68 (3H, s), 3.20—4.12 (3H, m), 4.83—4.47 (7H, m), 5.05 (1H, d, *J*=4.2 Hz), 7.23 (5H, s), 7.27 (10H, s); $[\alpha]_D$+40.0° (*c* 1.63, $CHCl_3$); MS, *m/z* 507 (M^+-1); HRMS, Calcd for $C_{30}H_{35}O_5S$ (M^+-1): 507.2204. Found: *m/z* 507.2208.

General Synthetic Procedure for Alkylaryl- and Dialkylsulfonium Salts Containing a Sugar Group (1a—k). To a mixture of silver perchlorate (2.5 g, 12 mmol) and sulfide **10** (12 mmol) in acetonitrile (15 cm^3) was added slowly an acetonitrile solution (5 cm^3) of alkyl iodide (60 mmol) at 0 °C. The mixture was stirred for 2 days at room temperature to give perchlorate salts of alkylaryl- and dialkylsulfonium containing sugar group (**1a—k**).

Perchlorate Salt of Methyl 6-Deoxy-6-(dimethylsulfonio)-2,3,4-tri-*O*-benzyl-α-D-glucopyranoside (1a): 90% yield; colorless syrup; ^1H NMR ($CDCl_3$) δ=2.72 (3H, s), 2.81 (3H, s), 3.33 (3H, s), 3.17—4.07 (6H, m), 4.40—5.03 (7H, m), 7.23 (15H, br-s); $[\alpha]_D$+59.5° (*c* 2.55, $CHCl_3$). **1b**: 73% yield; colorless syrup; ^1H NMR ($CDCl_3$) δ=1.32 (3H, t, *J*=7.2 Hz), 1.36 (3H, t, *J*=7.2 Hz), 3.11—4.09 (10H, m), 3.33 (3H, m), 4.23—5.10 (7H, m), 7.23 (15H, br-s); $[\alpha]_D$+31.9° (*c* 8.63, $CHCl_3$). **1c**: 99% yield; Mp 131—132 °C; ^1H NMR ($CDCl_3$) δ=1.30 (3H, t, *J*=7.0 Hz), 2.73 (3H, s), 3.10—4.07 (8H, m), 3.30 (3H, s), 4.37—4.87 (6H, m), 4.93 (1H, d, *J*=6.6 Hz), 7.22 (15H, br-s); $[\alpha]_D$+58.9° (*c* 1.0, $CHCl_3$); Calcd for $C_{31}H_{39}O_9SCl$: C, 59.74, H, 6.32%. Found: C, 59.97, H, 6.71%. **1d**: 86% yield; colorless syrup; ^1H NMR (acetone-d_6) δ=2.40 (3H, s), 3.28 (3H, s), 3.37 (3H, s), 3.50—4.98 (13H, m), 7.20 (15H, br-s), 7.46 and 7.90 (4H, A_2B_2, *J*=8.4 Hz); $[\alpha]_D$+55.6° (*c* 1.18, acetone). **1e**: 82% yield; colorless syrup; ^1H NMR (acetone-d_6) δ=3.23 (1.5H, s), 3.29 (1.5H, s), 3.33 (3H, s), 3.15—4.20 (6H, m), 4.35—5.12 (7H, m), 7.15 (15H, br-s), 7.92 and 8.26 (4H, A_2B_2, *J*=8.0 Hz); $[\alpha]_D$+39.1° (*c* 1.08, acetone). **1f**: 91% yield; colorless syrup; ^1H NMR ($CDCl_3$) δ=1.20 (3H, t, *J*=7.2 Hz), 2.42 (3H, s), 3.23 (3H, s), 3.30—5.00 (15H, m), 7.22 (15H, br-s), 7.30 and 7.60 (4H, A_2B_2, *J*=8.2 Hz); $[\alpha]_D$+43.4° (*c* 2.17, acetone). **1g**: 68% yield; colorless syrup; ^1H NMR ($CDCl_3$) δ=1.52 (3H, t, *J*=8.0 Hz), 3.28 (3H, s), 3.13—4.16 (8H, m), 4.33—5.10 (7H, m), 7.13 (15H, br-s), 7.90 and 8.23 (4H, A_2B_2, *J*=8.0 Hz); $[\alpha]_D$+54.0° (*c* 1.04, acetone). **1h**: 99% yield; colorless syrup; ^1H NMR ($CDCl_3$) δ=2.38 (3H, s), 3.17 (3H, s), 3.13—4.00 (6H, m), 4.16—4.87 (9H, m), 5.33—5.60 (3H, m), 6.93 and 7.61 (4H, A_2B_2, *J*=8.0 Hz), 7.20 (15H, br-s); $[\alpha]_D$+38.3° (*c* 3.39, acetone). **1i**: 75% yield; colorless syrup; ^1H NMR ($CDCl_3$) δ=3.13 (1.5H, s), 3.21 (1.5H, s), 3.31—4.17 (6H, m), 4.27—5.03 (9H, m), 7.07—7.67 (24H, m); $[\alpha]_D$+17.3° (*c* 8.5, $CHCl_3$). **1j**: 85% yield; colorless syrup; ^1H NMR ($CDCl_3$) δ=2.38 (3H, s), 3.25 (3H, s), 3.47—4.97 (15H, m), 7.10—7.33 (20H, m), 7.45 and 7.88 (4H, A_2B_2, *J*=8.4 Hz); $[\alpha]_D$+38.2° (*c* 2.31, $CHCl_3$). **1k**: 92% yield; colorless syrup; ^1H NMR ($CDCl_3$) δ=3.19 (3H, s), 3.16—4.03 (7H, m), 4.17—5.10 (8H, m), 5.31—5.61 (3H, m), 6.95—7.80 (19H, m); $[\alpha]_D$+42.3° (*c* 1.53, $CHCl_3$).

General Procedure for Asymmetric Alkylation of β-Keto Ester 2 (or 5) with 1. A mixture of alkylsulfonium salts **1** (1 mmol), β-keto ester **6** (or **8**) (1 mmol) and anhydrous potassium carbonate (1.3 mmol) was stirred in dry dichloromethane (10 cm^3) at room temperature for 3 days. After filtration of insoluble materials, the alkylated products of the β-keto ester were purified by column chromatography (silica gel) and GPC. The optical purity and the absolute configuration were determined by ^1H NMR analysis for compound **3b** in the presence of chiral shift reagent ($Eu(hfc)_3$) and by HPLC analysis for compound **3a**, using an optically active column (DAICEL CHEMICAL CHIRALCEL CA-1; methanol as eluent): the results are listed in Table 1. The structures of **6a** and **6b** were determined on the basis of the following spectroscopic data and their optical purity and absolute configuration were determined in comparison with authentic samples.[6]

Ethyl 2-Benzyl-2-methylacetoacetate (6a); ^1H NMR ($CDCl_3$) δ=1.18 (3H, s), 1.18 (3H, t, *J*=7.0 Hz), 2.03 (3H, s), 3.03 (2H, d, *J*=5.0 Hz), 4.06 (2H, q, *J*=7.0 Hz), 6.90—7.23 (5H, m); MS, *m/z* 234 (M^+); HRMS, Calcd for $C_{14}H_{18}O_3$: M, 234.1255. Found: *m/z* 234.1248.

Ethyl 2-Allyl-2-methylacetoacetate (6b); ^1H NMR ($CDCl_3$) δ=1.23 (3H, s), 1.25 (3H, t, *J*=7.0 Hz), 2.03 (3H, s), 2.45 (2H, d, *J*=6.4 Hz), 4.03 (2H, q, *J*=7.0 Hz), 4.77—5.90 (3H, m); MS, *m/z* 184 (M^+); HRMS, Calcd for $C_{10}H_{16}O_3$: M, 184.1099. Found: *m/z* 184.1069.

References

1) G. A. Maw, "The Chemistry of the Sulfonium Group," ed by C. J. M. Stiring and S. Patai, John Wiley & Sons, New York (1981), pp. 703—770.

2) L. D. Zydowsky, T. M. Zydowsky, E. S. Hass, J. W. Brown, J. N. Reeve, and H. G. Floss, *J. Am. Chem. Soc.*, **109**, 7922 (1987).

3) B. J. McBride, M. E. Garst, and M. Hopkins, *J. Org. Chem.*, **49**, 1824 (1984); B. Badet, M. Julia, and M. Ramirez-Munz, *Synthesis*, **1980**, 926.

4) M. Kobayashi, K. Umemura, N. Watanabe, and H. Matsuyama, *Chem. Lett.*, **1985**, 1067; M. Kobayashi, K. Umemura, and H. Matsuyama, *ibid.*, **1987**, 327; K. Umemura, H. Matsuyama, N. Watanabe, M. Kobayashi, and N. Kamigata, *J. Org. Chem.*, **54**, 2374 (1989).

5) The direct alkylation of **2** using the AdoMet (*S*-adenosyl-5′-L-methionine sulfate, *p*-toluenesulfonate (from Yeast), purchased from Tokyo Kasei Kogyo Co., Ltd.) was examined under similar conditions (K_2CO_3, dimethyl sulfoxide). However, no alkylation product corresponding to **3** was obtained.

6) H. Hermann and H. Wynberg, *J. Org. Chem.*, **44**, 2238 (1979); K. Tomioka, K. Ando, Y. Takamasa, and K. Koga, *J. Am. Chem. Soc.*, **106**, 2718 (1984).

7) Ethylmethylsugarsulfonium salt (**1c**) ($[\alpha]_D$+42.4° (*c* 2.8, $CHCl_3$)) was obtained as crystals and the salt was recrystallized from acetonitrile–ether several times to give the optically active sulfonium salt on the sulfonium sulfur atom ($[\alpha]_D$+58.9° (*c* 1.0, $CHCl_3$)); d.e. 86% determined by ^1H NMR (300 MHz, $CDCl_3$) analysis of sulfonium salt **5c**: the diastereomeric methyl groups on the sulfonium sulfur atom were observed at δ 2.78 and 2.86 and the ratio of diastereomeric methyl groups is 7:93. However, the absolute configuration was not yet determined. The alkylation of **2** with optically active sulfonium salt **5c** (d.e. 86%) under the similar conditions (K_2CO_3, CH_2Cl_2) gave the *C*-methylated product (*R*)-(+)-**3a** (56% yield; o.p. 19.8%) and the *C*-ethylated product (*R*)-(+)-**3b** (21% yield; o.p. 12.6%).

8) H. Matsuyama, H. Minato, and M. Kobayashi, *Bull. Chem. Soc. Jpn.*, **48**, 3287 (1975).

An Exceptionally-Large Negative Halochromism in 2-(4-Ethoxycarbonylphenyl)-2,3-dihydro-3,3-dimethyl-5,6-cycloheptapyrazoledione, a Hinopurpurin Derivative

Akira MORI,* Zhi-Hong LI,† and Hitoshi TAKESHITA*
Institute of Advanced Material Study, 86, Kyushu University, Kasuga-koen, Kasuga, Fukuoka 816
†Graduate School of Engineering Sciences, 39, Kyushu University, Kasuga-koen, Kasuga, Fukuoka 816
(Received March 17, 1989)

Synopsis. 2-Aryl-2,3-dihydro-3,3-dimethyl-5,6-cycloheptapyrazolediones with an electron-releasing group at C-4 on the benzene ring showed a bathochromic shift in acid solution, whereas the 4-ethoxycarbonylphenyl derivative showed a negative halochromism; 484 nm in ethyl acetate, 517, 566, and 600(sh) nm in trifluoroacetic acid, and 455 nm in concd sulfuric acid.

It is well-known that azo compounds in acidic solution show absorption maxima normally at longer wavelengths than those in neutral solution.[1] However, 4′-diazonio-4-(dimethylamino)azobenzene[2] and 4-(diethylamino)-4′-(tricyanovinyl)azobenzene[3] are outstanding in view of their negative halochromism, i.e., the absorption in acidic solution is at shorter wavelengths than that in neutral solution. We will describe here a new example showing a remarkably large negative halochromism.

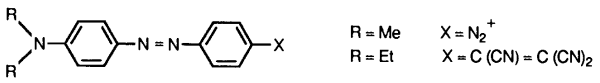

Scheme 1.

2-Aryl-2,3-dihydro-3,3-dimethyl-5,6-cycloheptapyrazolediones, hinopurpurins (**1**), prepared from 4-isopropyltropolone and benzene diazonium salts,[4] are known to be stable dyes. Table 1 summarizes the oxidation-reduction potentials ($E^1_{1/2}$ and $E^2_{1/2}$), determined by cyclic voltammetry (CV), and the maxima of the visible absorption spectra. The remote substituents on the benzene ring influence both the potentials and the maxima. Since **1** can be regarded as a masked *p*-tropoquinone, the shapes of the voltammograms, as shown in Fig. 1, might be similar to those of *p*-tropoquinone derivatives.[5,6] This was indeed observed and the more electron-attractive the substituent, the higher were the potentials $E^1_{1/2}$ and $E^2_{1/2}$.

The absorption of **1a** did not change much on changing the solvent. However, the positions of the absorption of **1c** and **1d** were largely dependent on the solvent. Compounds **1b** and **1c** showed positive halochromism; i.e., 13 nm for **1b** and ca. 70 nm for **1c** between chloroform and concd sulfuric acid.

On the other hand, the absorption of **1d** showed a bathochromic shift (ca. 60 nm) in trifluoroacetic acid, whereas in concd sulfuric acid an unusually large negative shift was observed (111 nm between trifluoroacetic acid and concd sulfuric acid and 29 nm between ethyl acetate and concd sulfuric acid) with a decrease of the peak intensity. The wavelength of the absorption peak was ca. 30 nm shorter than that of **1a** in concd sulfuric acid and that of **1d** in ethyl acetate. This negative halochromism of **1d** was also observed in acidic methanol solutions. The reversibility of this color change was confirmed by changes of the acidity of methanol solutions.

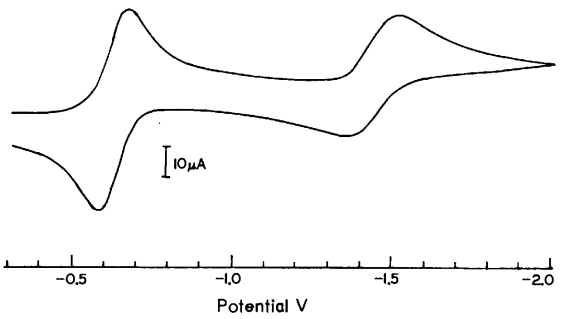

Fig. 1. CV curve of **1d**.

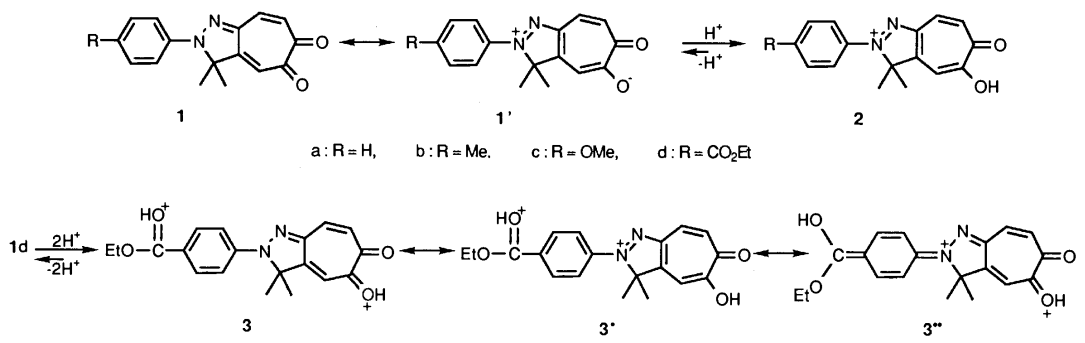

Scheme 2.

Table 1. Oxidation-Reduction Potentials[a] and Maxima of Visible Absorption Bands

	1a	1b	1c	1d
$E^1_{1/2}$	−0.73	−0.75	−0.81	−0.62
$E^2_{1/2}$	−1.45	−1.59	−1.69	−1.43
H_2SO_4	488(25000)	523(35100)	588(46700)	455(27200)
	468(28100)	511(33900)	577(40600)	
CF_3COOH	585(9900, sh)	604(11700, sh)	634(13000, sh)	600(20300, sh)
	500(28200)	516(33400)	562(31400)	566(26600)
				517(31600)
$CHCl_3$	502(34900)	510(34300)	517(24100)	507(42400)
CH_3OH	503(37100)	510(35800)	520(11100)	505(41400)
AcOEt	483(32400)	490(28200)	495(16800)	484(40900)

a) The CV were measured in anhydrous DMF with 0.1 M $(n\text{-Bu})_4NBF_4$ using Pyrex-glass sealed Pt wire as working and counter electrodes and standard Ag/AgCl as a reference electrode at 22—23 °C under N_2 atmosphere with a scan rate of 100 mV s^{-1}.

These phenomena could be explained as follows: There exist the following mesomeric forms (**1** and **1′**). In the ground state, the neutral form is predominant, whereas the ionic form is favored in the excited state. Since a large increase in the dipole moment of the molecule can be expected during the excitation, the energy level of the excited state will be markedly lowered, causing a bathochromic shift.[7] Furthermore, the protonated form (**2**) of **1** seems to be more stable than the neutral one due to the disappearance of the dipole repulsion on the α-diketone part and the formation of a tropolone structure. The electron-releasing substituents on the benzene ring assist this protonation to cause a bathochromic shift as observed in **1b** and **1c**. In the case of **1d**, the ethoxycarbonyl part might be also protonated in concd sulfuric acid. The doubly protonated species **3**, where charges are located at two terminal oxygens, has mesomeric forms such as **3′** and **3″**, the latter of which is a polar and less stable *p*-benzoquinone methide derivative. Accordingly, the excited state is more strongly destabilized than the ground state and the maxima of the absorption would become shorter than those of the neutral form.[7]

In view of recent interest in organic dyes for functional compounds, a rare negative halochromism with exceptionally large differences observed in easily available nonbenzenoid dyes is particularly noteworthy. Furthermore, azo compounds as functional dyes, recently became less attractive in view of their chemical instability; however, the present dyes, hinopurpurins, are stable towards air, light, and acid and base under ordinary conditions, having ring-closed to 5*H*-pyrazole system, and are promising materials.

Experimental

Preparation of Hinopurpurins. To a pyridine solution (5 cm^3) of 4-isopropyltropolone (400 mg, 2.44 mmol) was added drop by drop an aqueous solution of a diazotized amine (3 mmol) at 0 °C to 5 °C with stirring for 2 h. After the solution was diluted with water (40 cm^3), the precipitate was filtered and dried. An EtOH solution of 5-diazonio-4-isopropyltropolone was refluxed for 4 h and cooled to yield crystals by filtration.

1a: Reddish needles, 42%, mp 154—155 °C (from acetone-hexane; lit,[4] mp 148 °C); ^1H NMR ($CDCl_3$)[8] δ=1.75 (6H, s), 6.42 (1H, s), 6.75 (1H, d, *J*=12.1 Hz), 7.32 (1H, t, *J*=7.3 Hz), 7.46 (2H, dd, *J*=9.2, 7.3 Hz), 7.56 (2H, d, *J*=9.2 Hz), and 7.57 (1H, d, *J*=12.1 Hz); ^{13}C NMR ($CDCl_3$) δ=27.8 (2C), 75.7, 116.3, 119.4 (2C), 126.8, 127.4, 129.8 (2C), 132.7, 139.5, 142.9, 157.4, 182.7, and 184.3.

1b: Greenish needles, 52%, mp 256—267 °C (decomp) (from EtOH; lit,[4] mp 244 °C); ^1H NMR (pyridine-d_5) δ=1.60 (6H, s), 2.28 (3H, s), 6.70 (1H, s), 6.83 (1H, d, *J*=12.1 Hz), 7.27 (2H, d, *J*=8.4 Hz), 7.57 (2H, d, *J*=8.4 Hz), and 7.62 (1H, d, *J*=12.1 Hz); ^{13}C NMR (pyridine-d_5) δ=20.7, 27.2 (2C), 76.0, 116.7, 119.9 (2C), 127.3, 130.5 (2C), 132.6, 136.7, 137.7, 142.8, 157.4, 183.3, and 185.1.

1c: Greenish needles, 47%, mp 228—229 °C (from EtOH; lit,[4] 228—229 °C); ^1H NMR ($CDCl_3$) δ=1.69 (6H, s), 3.86 (3H, s), 6.40 (1H, s), 6.72 (1H, d, *J*=12.5 Hz), 6.99 (2H, d, *J*=9.2 Hz), 7.45 (2H, d, *J*=9.2 Hz), and 7.55 (1H, d, *J*=12.5 Hz); ^{13}C NMR ($CDCl_3$) δ=27.7 (2C), 55.7, 76.3, 114.9 (2C), 116.0, 122.2 (2C), 126.8, 132.6, 132.8, 142.5, 156.9, 159.0, 182.7, and 184.3.

1d: Greenish needles, 56%, mp 200—201 °C (from AcOEt-hexane); ^1H NMR ($CDCl_3$) δ=1.41 (3H, t, *J*=7.3 Hz), 1.81 (6H, s), 4.40 (2H, q, *J*=7.3 Hz), 6.43 (1H, s), 6.73 (1H, d, *J*=12.1 Hz), 7.57 (1H, d, *J*=12.1 Hz), 7.62 (2H, d, *J*=9.2 Hz), and 8.11 (2H, d, *J*=9.2 Hz); ^{13}C NMR ($CDCl_3$) δ=14.4, 27.7 (2C), 61.2, 74.9, 117.0, 117.3 (2C), 127.4, 128.4, 131.3 (2C), 132.5, 142.7, 143,7, 157.4, 165.7, 182.7, and 184.2; IR (KBr) 3000—2850, 1700, 1600, 1375, 1275, and 910 cm^{-1}; UV (MeOH) 283 (ε 9600), 302 (5900), 326 (7000), 384 (1400), and 505 nm (41400).

Found: C, 67.61; H, 5.27; N, 8.28%. Calcd for $C_{19}H_{18}N_2O_4$: C, 67.44; H, 5.36; N, 8.28%.

References

1) G. E. Lewis, *Tetrahedron*, **10**, 129 (1960).
2) L. M. Yagupol'skii and L. Z. Gandel'sman, *Zh. Obshch. Khim.*, **37**, 2101 (1967); *Chem. Abstr.*, **68**, 31029z.
3) K. Y. Chu and J. Griffiths, *Tetrahedron Lett.*, **1976**, 405.
4) T. Nozoe, T. Ikemi, and T. Ozeki, *Proc. Jpn. Acad.*, **31**, 455 (1955); T. Nozoe, E. Sebe, and S. Ebine, *ibid.*, **26**, 24 (1950).
5) A. Mori, T. Kusaba, Y. Isayama, and H. Takeshita, *Chem. Lett.*, **1986**, 155.
6) A. Mori, S. Hirayama, Y. Goto, and H. Takeshita, *Bull. Chem. Soc. Jpn.*, **61**, 1029 (1988).
7) W. Liptay, *Angew. Chem., Int. Ed. Engl.*, **8**, 177 (1969).
8) NMR spectra were measured with JEOL FX 100 Model and GSX 270 H Model spectrometers.

Reaction of Methyl 2,3,5,6,11,11b-Hexahydro-3-oxo-1*H*-indolizino[8,7-*b*]indole-5-carboxylate and Its Derivatives with *N*-Bromosuccinimide

Hajime IRIKAWA,* Susumu MUTOH, Masahiro UEHARA, and Yasuaki OKUMURA
Department of Chemistry, Faculty of Science, Shizuoka University, Ohya, Shizuoka 422
(Received April 13, 1989)

Synopsis. Methyl 2,3,5,6,11,11b-Hexahydro-3-oxo-1*H*-indolizino[8,7-*b*]indole-5-carboxylate was converted into the tetrahydro, dihydro, and dehydro esters using *N*-bromosuccinimide. On treatment with acetic acid, the 6a-bromo indolenine derivative bearing a substituent on C-11b gave a mixture of 8- and 9-bromo compounds by migration of the bromine to the benzene ring, while the corresponding 6a-chloro derivative afforded the oxindole.

In the preceding paper, we reported the isolation of 2,3,5,6,11,11b-hexahydro-3-oxo-1*H*-indolizino[8,7-*b*]-indole-5-carboxylic acid and the 5,11b-dicarboxylic acid as the methyl esters **1** and **2** from *Clerodendron trichotomum* Thunb. The conversion of **1** into a blue pigment, trichotomine dimethyl ester (**3**), was achieved using *N*-bromosuccinimide (NBS) in *t*-BuOH, and the formation of **3** was suggested to proceed via the $\Delta^{1,11b}$-tetrahydro ester **4** derived from **5**.[1] The versatility of 3-halo-3*H*-indoles as intermediates in indole alkaloid synthesis is well documented in the literature.[2] This paper deals with the dehydrogenation of **1** by treatment with NBS and the reaction of 6a-halo derivatives **6a**, **b**, obtained from **2**, with acetic acid.

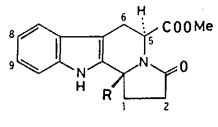

1 R=H
2 R=COOMe

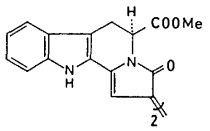

3

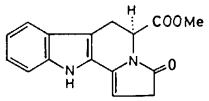

4

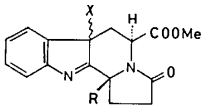

5 X=Br R=H
6a X=Br R=COOMe
6b X=Cl R=COOMe

Bromination of **1** with NBS in CH_2Cl_2 in the presence of K_2CO_3 followed by treatment with triethylamine (Et_3N) gave the $\Delta^{5,6}$-tetrahydro ester **7**. On the other hand, treatment of **1** with NBS in CH_2Cl_2 afforded **4**, from which Iwadare et al. synthesized **3** by autoxidation.[3] The formation of **4** from the initially formed **5** must be catalyzed by hydrogen bromide evolved and supports the intermediacy of **4** in the conversion of **1** into **3** with NBS in *t*-BuOH.

On heating with 5% palladium charcoal in toluene, **7** underwent dehydrogenation to the dihydro ester **8** (UV 329 nm, ε 10500), while on treatment with excess NBS in Et_3N–CH_2Cl_2 at 0 °C for 15 min, **7** was dehydrogenated to **8** and the dehydro ester **9** (UV 376 nm, ε 12800). In the latter reaction, a 6a-bromo derivative formed from **7** seems to undergo dehydrobromination to **8**, which might afford **9** by allylic bromination at C-1 followed by dehydrobromination. In the presence of MeOH, treatment of **7** with NBS in THF afforded the β-carboline **10** (UV 343 nm, ε 4000) presumably by methanolysis of the intermediate **8**. Compounds **8** and **9** were identical with those prepared in the following way. On heating with 2,3-dichloro-5,6-dicyano-*p*-benzoquinone in benzene, **1** underwent dehydrogenation to **9**, which gave **8** by catalytic reduction.

The properties of 6a-halo derivatives **6a**, **b** obtained from **2** were examined, since **6a**, **b** had a methoxycarbonyl group on C-11b and could not undergo such dehydrogenation reactions mentioned above.

Bromination of **2** with NBS gave **6a** as crystals (^{13}C NMR δ=56.5, C-6a). On treatment with Et_3N, **6a** gave the $\Delta^{5,6}$ diester **11**. On the other hand, treatment of **6a** with acetic acid afforded a separable mixture of bromo diesters **12** and **13** in a ratio of 2:5. The presence of bromine on C-8 of **12** and on C-9 of **13** was suggested from the ^1H NMR spectrum of **12** and **13**. The structure **13** was assigned to the major product, since the carbamate **14** formed from **13** with methyl chloroformate showed a singlet of C_{10}-proton at low field (δ=8.20) in the ^1H NMR spectrum. In 3-bromo-3*H*-indoles, migration of the bromine to the benzene ring was reported in the literature.[4] On further

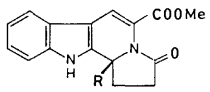

7 R=H
11 R=COOMe

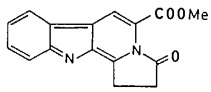

8

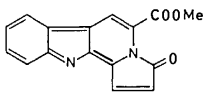

9

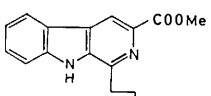

10

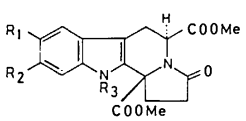

12 R_1=Br R_2=R_3=H
13 R_1=R_3=H R_2=Br
14 R_1=H R_2=Br R_3=COOMe
15 R_1=R_2=Br R_3=H

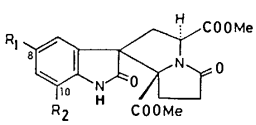

16 R_1=R_2=H
17 R_1=R_2=Cl
18 R_1=Cl R_2=H

treatment with NBS and then with acetic acid, the mixture of **12** and **13** yielded the 8,9-dibromo diester **15**.

After chlorination of **2** with *t*-butyl hypochlorite (*t*-BuOCl), the resulting **6b** was treated with acetic acid to afford the oxindole **16** (^{13}C NMR δ=58.9, C-6a). On treatment with *t*-BuOCl in EtOH-CH_2Cl_2, **2** gave the dichloroxindole **17**. The formation of **17** was rationalized by indole-oxindole rearrangement to **16** followed by chlorination of the benzene ring,[5] since **16** gave the chloroxindole **18** on treatment with *t*-BuOCl and then with EtOH, and **18** yielded **17** with *t*-BuOCl in EtOH-CH_2Cl_2.

Experimental[6]

Preparation of 7. To a stirred mixture of **1** (284 mg, 1.0 mmol), K_2CO_3 (0.50 g) and CH_2Cl_2 (30 ml) cooled to 0 °C was added dropwise a solution of NBS (214 mg, 1.2 mmol) in CH_2Cl_2 (10 ml). After stirring at 0 °C for 10 min, Et_3N (5 ml) was added. The mixture was stirred at room temperature for 7 h, and then filtered. The filtrate was concentrated under reduced pressure to leave a residue, which was dissolved in $CHCl_3$. The solution was washed with water, dried over Na_2SO_4, and concentrated under reduced pressure. Separation of the residue by column chromatography (SiO_2-$CHCl_3$) gave **7** (163 mg, 68% based on reacted **1**) and **1** (42 mg). **7**: mp 253—256 °C (MeOH); ^{1}H NMR (CD_3COCD_3) δ=2.28—3.00 (4H, m), 3.76 (3H, s), 5.30 (1H, m), 7.13—7.77 (4H, m), 7.47 (1H, s), and 10.95 (1H, br s). Found: *m/z* 282.1027. Calcd for $C_{16}H_{14}N_2O_3$: M, 282.1004.

Preparation of 4. To a stirred solution of **1** (142 mg, 0.50 mmol) in CH_2Cl_2 (30 ml) cooled to 0 °C was added dropwise a solution of NBS (134 mg, 0.75 mmol) in CH_2Cl_2 (10 ml). After stirring at 22 °C for 1 h, the solution was washed successively with water, aqueous $NaHCO_3$, and brine, and then dried over Na_2SO_4. Evaporation of the solvent and separation of the products by column chromatography (SiO_2-$CHCl_3$) gave **4**[3] (62 mg, 44%).

Dehydrogenation of 7. A mixture of **7** (50 mg), 5% Pd-C (20 mg) and toluene (70 ml) was refluxed with stirring for 10 h, and then filtered. Evaporation of the solvent and separation of the products by column chromatography (SiO_2, 1 vol% MeOH-$CHCl_3$) gave **8** (27 mg, 54%): mp 257—259 °C ($CHCl_3$-hexane); UV 240 (ε 49200), 264 (21700), 283 (sh, 14600), 317 (8880), and 329 nm (10500); ^{1}H NMR δ=3.26 (2H, t, *J*=7.6 Hz), 3.60 (2H, t, *J*=7.6 Hz), 4.08 (3H, s), 7.51—8.57 (4H, m), and 8.67 (1H, s). Found: *m/z* 280.0864. Calcd for $C_{16}H_{12}N_2O_3$: M, 280.0847.

Reaction of 7 with NBS. To a stirred solution of **7** (28 mg, 0.10 mmol) in Et_3N-CH_2Cl_2 (0.2—20 ml) cooled to 0 °C was added NBS (71 mg, 0.40 mmol). The solution was stirred at 0 °C for 15 min, and worked up in the usual way. Separation of the products by PTLC (SiO_2, 3 vol% MeOH-$CHCl_3$) afforded **8** (1 mg, 4%) and **9** (8 mg, 30%). **8** was identical with that obtained above by ^{1}H NMR and TLC comparisons. **9**: mp 272—273 °C ($CHCl_3$-hexane); UV 214 (ε 28800), 246 (32000), 268 (20100), 305 (sh, 7020), 345 (sh, 8820), 359 (14000), and 376 nm (12800); ^{1}H NMR δ=4.13 (3H, s), 7.05 (1H, d, *J*=9.9 Hz), 7.57—8.70 (4H, m), 8.17 (1H, d, *J*=9.9 Hz), and 8.88 (1H, s); MS *m/z* 278 (M^+). Anal. ($C_{16}H_{10}N_2O_3$) C, H, N.

Preparation of 10. To a stirred solution of **7** (20 mg, 0.07 mmol) in MeOH-THF (2—10 ml) cooled to 0 °C was added NBS (15 mg, 0.08 mmol). The solution was stirred at 0 °C for 30 min, and diluted with AcOEt (100 ml). The solution was worked up in the usual way to give **10** (15 mg, 68%): mp 179—181 °C ($CHCl_3$-hexane); UV 219 (ε 17000), 237 (24100), 270 (35900), 303 (7360), 330 (4430), and 343 nm (4000); ^{1}H NMR δ=2.99 (2H, t, *J*=6.4 Hz), 3.53 (2H, t, *J*=6.4 Hz), 3.67 (3H, s), 4.05 (3H, s), 7.32—8.18 (4H, m), 8.78 (1H, s), and 9.61 (1H, br s). Found: *m/z* 312.1116. Calcd for $C_{17}H_{16}N_2O_4$: M, 312.1109.

Dehydrogenation of 1. A mixture of **1** (284 mg, 1 mmol), DDQ (0.91 g, 4.0 mmol) and benzene (300 ml) was refluxed with stirring for 5 h, and filtered. The filtrate was worked up in the usual way. Separation of the products by column chromatography (SiO_2, 1 vol% MeOH-$CHCl_3$) gave **9** (79 mg, 28%), which was found to be identical with that obtained above by IR and ^{1}H NMR comparisons.

Catalytic Reduction of 9. A mixture of **9** (150 mg, 0.54 mmol), PtO_2 (30 mg), and dioxane (220 ml) was stirred under hydrogen atmosphere at room temperature overnight, and filtered. Evaporation of the solvent and separation of the residue by column chromatography (SiO_2-$CHCl_3$) gave **8** (125 mg, 83%), which was identical with that obtained above by IR and ^{1}H NMR comparisons.

Preparation of 6a. To a solution of **2** (342 mg, 1.0 mmol) in $CHCl_3$ (30 ml) was added a solution of NBS (196 mg, 1.1 mmol) in $CHCl_3$ (30 ml). The solution was kept at room temperature for 15 min and worked up in the usual way. Crystallization from $CHCl_3$-hexane gave **6a** (395 mg, 94%): mp 130—132 °C (decomp); ^{13}C NMR δ=29.5 (t), 29.8 (t), 33.1 (t), 49.4 (d), 52.6 (q), 53.1 (q), 56.5 (s), 67.4 (s), 122.1 (d), 123.3 (d), 127.6 (d), 130.5 (d), 138.5 (s), 152.1 (s), 168.3 (s), 169.7 (s), 175.2 (s), and 178.4 (s). Without further purification, **6a** was subjected to the next experiment.

Preparation of 11. A solution of **6a** (43 mg) in Et_3N-CH_2Cl_2 (0.5—1 ml) was allowed to stand at room temperature for 2 d, and concentrated under reduced pressure. Separation of the residue by PTLC (SiO_2-AcOEt) gave **11** (10 mg, 29%) and **2** (20 mg, 57%). **11**: mp 231—233 °C ($CHCl_3$-hexane); ^{1}H NMR δ=2.39—3.03 (4H, m), 3.70 (3H, s), 3.89 (3H, s), 7.20—7.67 (4H, m), 7.50 (1H, s), and 8.97 (1H, br s). Found: *m/z* 340.1061. Calcd for $C_{18}H_{16}N_2O_5$: M, 340.1058.

Preparation of 12 and 13. A solution of **6a** (210 mg) in AcOH (10 ml) was kept at 20 °C for 22 h, and concentrated under reduced pressure to leave an oil, which was dissolved in $CHCl_3$. The solution was washed with aqueous $NaHCO_3$ and dried over Na_2SO_4. Evaporation of the solvent gave an oil, which contained **12** and **13** in a ratio of 2:5 (determined by ^{1}H NMR). Separation of the products by column chromatography (SiO_2-$CHCl_3$) and PTLC (SiO_2, AcOEt-hexane, 2:1) gave **12** (26 mg, 12%) and **13** (89 mg, 42%). **12**: mp 186—188 °C ($CHCl_3$-hexane); ^{1}H NMR δ=2.17—2.98 (4H, m), 3.05 (1H, dd, *J*=16.0 and 7.0 Hz), 3.23 (1H, dd, *J*=16.0 and 1.8 Hz), 3.61 (3H, s), 3.85 (3H, s), 5.48 (1H, dd, *J*=7.0 and 1.8 Hz), 7.23 (C_{10}-H, d, *J*=8.6 Hz), 7.29 (C_9-H, dd, *J*=8.6 and 1.8 Hz), 7.62 (C_7-H, d, *J*=1.8 Hz), and 8.55 (1H, br s). Found: *m/z* 420.0320. Calcd for $C_{18}H_{17}N_2O_5Br$: M, 420.0320.

13: mp 176—178 °C (MeOH); ^{1}H NMR δ=2.17—2.98 (4H, m), 3.08 (1H, dd, *J*=16.1 and 7.3 Hz), 3.27 (1H, dd, *J*=16.1 and 1.2 Hz), 3.63 (3H, s), 3.86 (3H, s), 5.49 (1H, dd, *J*=7.3 and 1.2 Hz), 7.16 (C_8-H, dd, *J*=8.4 and 1.8 Hz), 7.32 (C_7-H, d, *J*=8.4 Hz), 7.37 (C_{10}-H, d, *J*=1.8 Hz), and 8.65 (1H, br s). Found: *m/z* 420.0300. Calcd for $C_{18}H_{17}N_2O_5Br$: M, 420.0320.

Conversion of 13 into 14. To a stirred solution of **13** (68 mg, 0.16 mmol) in DMF (3 ml) was added NaH (20 mg, 0.9 mmol). After stirring at room temperature for 20 min, methyl chloroformate (0.1 ml) was added. The mixture was stirred at room temperature for 2 h, and then poured into

aqueous NH_4Cl. The solution was worked up in the usual way to give **14** (50 mg, 65%): mp 112—114 °C (MeOH); ^1H NMR δ=2.03—3.33 (4H, m), 2.95 (1H, dd, J=16.5 and 8.1 Hz), 3.59 (1H, d, J=16.5 Hz), 3.64 (3H, s), 3.68 (3H, s), 4.03 (3H, s), 5.47 (1H, d, J=8.1 Hz), 7.38 (C_7-H, d, J=8.1 Hz), 7.44 (C_8-H, dd, J=8.1 and 1.6 Hz), and 8.20 (C_{10}-H, s). Found: m/z 478.0361. Calcd for $C_{20}H_{19}N_2O_7Br$: M, 478.0374.

Preparation of 15. As described above, a solution of **2** (103 mg, 0.30 mmol) in $CHCl_3$ (20 ml) was treated with a solution of NBS (59 mg, 0.33 mmol) in $CHCl_3$ (20 ml) to give **6a** quantitatively. Without crystallization, **6a** was dissolved in AcOH (10 ml) to yield a mixture of **12** and **13**. In the same way as mentioned above, the mixture of **12** and **13** was again treated with NBS (59 mg) and then AcOH (10 ml) to give **15** (95 mg, 63%): mp 232—233 °C (MeOH); ^1H NMR δ=2.18—2.99 (4H, m), 3.05 (1H, dd, J=16.1 and 7.3 Hz), 3.23 (1H, dd, J=16.1 and 0.7 Hz), 3.66 (3H, s), 3.88 (3H, s), 5.49 (1H, dd, J=7.3 and 0.7 Hz), 7.29 (C_{10}-H, s), 7.69 (C_7-H, s), and 8.90 (1H, br s). Found: m/z 497.9439. Calcd for $C_{18}H_{16}N_2O_5Br_2$: M, 497.9426.

Preparation of 16. To a solution of **2** (20 mg) in CH_2Cl_2 (2 ml) was added t-BuOCl (3 drops). The solution was kept at room temperature for 10 min and concentrated under reduced pressure to give **6b** quantitatively: ^{13}C NMR δ=29.5 (t), 33.3 (t), 48.6 (d), 52.6 (q), 53.0 (q), 67.1 (s), 67.5 (s), 122.0 (d), 123.1 (d), 127.7 (d), 130.7 (d), 137.9 (s), 152.8 (s), 168.5 (s), 170.0 (s), 175.2 (s), and 177.8 (s). Without further purification, **6b** was dissolved in AcOH (0.5 ml). The solution was allowed to stand at room temperature for 3 h and concentrated under reduced pressure. The residue was worked up in the usual way to give **16** (20 mg, 95%): mp 267—268 °C (MeOH); ^{13}C NMR δ=23.7 (t), 32.4 (t), 38.7 (t), 52.6 (q), 56.8 (d), 58.9 (s), 78.1 (s), 110.7 (d), 122.7 (d), 123.9 (d), 124.7 (s), 129.7 (d), 141.5 (s), 170.8 (s), 171.5 (s), 177.3 (s), and 179.1 (s). Found: m/z 358.1147. Calcd for $C_{18}H_{18}N_2O_6$: M, 358.1163.

Preparation of 17. To a solution of **2** (162 mg) in EtOH-CH_2Cl_2 (0.5—30 ml) was added t-BuOCl (1 ml). The solution was allowed to stand at room temperature for 2 d and concentrated under reduced pressure to give **17** (142 mg, 70%): mp 266—267 °C (EtOH); ^1H NMR (DMSO-d_6) δ= 1.70—2.95 (6H, m), 3.72 (6H, s), 4.78 (1H, t, J=8.4 Hz), 6.84 (C_7-H, d, J=1.8 Hz), 7.53 (C_9-H, d, J=1.8 Hz), and 11.38 (1H, br s). Found: m/z 426.0381. Calcd for $C_{18}H_{16}N_2O_6Cl_2$: M, 426.0383.

Preparation of 18. To a solution of **16** (14 mg) in CH_2Cl_2 (5 ml) was added t-BuOCl (2 drops). The solution was allowed to stand at room temperature for 18 h and concentrated under reduced pressure. Crystallization of the residue from EtOH gave **18**, mp >300 °C, (13 mg, 87%): ^1H NMR (DMSO-d_6) δ=1.70—2.90 (6H, m), 3.70 (6H, s), 4.77 (1H, t, J=8.4 Hz), 6.82 (C_7-H, d, J=2.1 Hz), 6.88 (C_{10}-H, d, J=8.4 Hz), 7.32 (C_9-H, dd, J=8.4 and 2.1 Hz), and 10.87 (1H, br s). Anal. ($C_{18}H_{17}N_2O_6Cl$) C, H, N.

Preparation of 17 from 18. To a mixture of **18** (24 mg) and EtOH-CH_2Cl_2 (0.1—10 ml) was added t-BuOCl (0.2 ml). The mixture was stirred at room temperature for 2 d and worked up as described above to give **17** (20 mg, 77%), which was found to be identical with that obtained as above.

References

1) H. Irikawa, Y. Toyoda, H. Kumagai, and Y. Okumura, *Bull. Chem. Soc. Jpn.*, **62**, 880 (1989).
2) M. Ikeda and Y. Tamura, *Heterocycles*, **14**, 867 (1980).
3) S. Iwadare, Y. Shizuri, K. Yamada, and Y. Hirata, *Tetrahedron*, **34**, 1457 (1978).
4) T. Hino, M. Endo, M. Tonozuka, Y. Hashimoto, and M. Nakagawa, *Chem. Pharm. Bull.*, **25**, 2350 (1977).
5) T. A. Foglia and D. Swern, *J. Org. Chem.*, **33**, 4440 (1968).
6) For the instruments used see Ref. 1.

A Synthetic Route to (±)-Humulone

Heitaro OBARA,* Jun-ichi ONODERA, Yoshihisa MACHIDA, and Shuji YADA
Department of Applied Chemistry, Faculty of Engineering, Yamagata University, Yonezawa 992
(Received April 14, 1989)

Synopsis. The synthesis of (±)-humulone was achieved by the prenylation of 2,3,4,6-tetrahydroxyisovalerophenone with 1-bromo-3-methyl-2-butene.

Humulone, an antibiotic and bitter costituent of hop (*Humulus lupulus* L.), was first isolated by Lintner and Schnell[1] in 1904; the structure was determined to be 3,5,6-trihydroxy-4,6-bis(3-methyl-2-butenyl)-2-(3-methyl-1-oxobutyl)-2,4-cyclohexadien-1-one (**6**) by the synthesis of its racemate[2] and on the basis of its spectral data.[3]

However, the method for synthesizing (±)-humulone is not applicable to the preparative purpose because of the tedious procedure and poor yield.[2] In this paper we wish to report a new synthetic route to (±)-humulone.

We first succeeded in the synthesis of model compounds of **6**, 3,5,6-trihydroxy-2-acetyl-4,6-dimethyl- and 3,5,6-trihydroxy-2-acetyl-4,6-diethyl-2,4-cyclohexadien-1-one (**3** and **4**), by the di-*C*-alkylation of 2,3,4,6-tetrahydroxyacetophenone (**2**)[4] with methyl or ethyl iodide in the presence of sodium hydride in dimethyl sulfoxide. This method was applied to the convenient synthesis of (±)-**6**.

(±)-Humulone was synthesized by the prenylation of 2,3,4,6-tetrahydroxyisovalerophenone (**5**) obtained by the acylation of 1,2,3,5-benzenetetrol (**1**)[5] with isovaleryl chloride by Friedel-Crafts reaction. The acylation of **1** with isovaleronitrile by the Hoesch reaction did not succeed. The IR and ^{1}H NMR spectra of this synthetic humulone and its *o*-phenylenediamine complex were identical with those of natural specimens.

It is assumed that this synthetic method is applicable to the preparation of such other hop constituents as cohumulone[6] or adhumulone.[7]

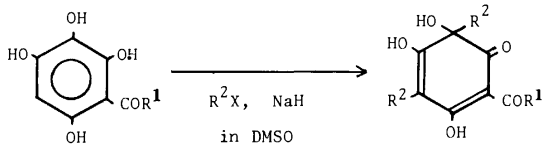

2 R^1 = Me
5 R^1 = $-CH_2CH<^{Me}_{Me}$

3 R^1 = R^2 = Me
4 R^1 = Me, R^2 = Et
6 R^1 = $-CH_2CH<^{Me}_{Me}$,
R^2 = $-CH_2CH=C<^{Me}_{Me}$

Experimental

The UV and IR spectra were recorded with Hitachi 100-50 spectrophotometer and Hitachi 215 spectrophotometers, respectively. The mass spectra were recorded with a Hitachi RMU-6M mass spectrometer. ^{1}H and ^{13}C NMR spectra were recorded with Hitachi R-600 spectrometer and Hitachi R-90H spectrometers using tetramethylsilane as an internal standard, respectively.

3,5,6-Trihydroxy-2-acetyl-4,6-dimethyl-2,4-cyclohexadien-1-one (3). To a mixture of **2** (3.68 g) and sodium hydride (1.6 g) in dry dimethyl sulfoxide (150 ml) was added methyl iodide (9.0 g) under cooling with cold water; the mixture was then stirred for 3 h at room temperature. The reaction mixture was poured into cold dilute hydrochloric acid and extracted with ethyl acetate. The extract was chromatographed on a column of silica gel with carbon tetrachloride–ethyl acetate–acetic acid (60:30:1) to afford **3** (2.36 g, 57%). Mp 153—154 °C (lit,[8] 150.5—151.5 °C). MS *m/z* 212 (M^+). ES λ_{max} (EtOH) 229, 321, and 358 nm (log ε=4.18, 4.09, and 4.01). IR (KBr) ν 3400, 3250, and 1660 cm^{-1}. ^{1}H NMR ($CDCl_3$) δ=1.58 and 1.84 (each 3H, s), 2.57 (3H, s), and 18.42 (1H, s). Found: C, 56.56, H, 5.74%, Calcd for $C_{10}H_{12}O_5$: C, 56.60, H, 5.70%.

3,5,6-Trihydroxy-2-acetyl-4,6-diethyl-2,4-cyclohexadien-1-one (4). Compound **4** (0.2 g, 17%) was obtained from **2** (0.92 g), sodium hydride (0.4 g), and ethyl iodide (2.34 g) by way of **3** as described above. Mp 106—107 °C. MS *m/z* 240 (M^+). ES λ_{max} (EtOH) 229, 322, and 358 nm (log ε=4.19, 4.08, and 3.97). IR (KBr) ν 3350, 3250, and 1660 cm^{-1}. ^{1}H NMR ($CDCl_3$) δ=0.97 (6H, m), 1.86 and 2.35 (each 2H, m), 2.52 (3H, s), 18.59 (1H, s). Found: C, 59.93, H, 6.89%, Calcd for $C_{12}H_{16}O_5$: C, 59.97, H, 6.71%.

2,3,4,6-Tetrahydroxyisovalerophenone (5). To a mixture of **1**[5] (9.0 g) and anhydrous aluminium chloride (10.0 g) in nitrobenzene (100 ml) was added isovaleryl chloride (6.6 g) at 0 °C; the mixture was then stirred for 3 days at room temperature. The reaction mixture was poured into cold 10% hydrochloric acid and extracted with ether. The ether was distilled away and the remaining nitrobenzene was taken off by steam distillation. The residue was chromatographed on a column of silica gel with benzene–ethyl acetate (3:1) to give **5** (4.44 g, 38%). Mp 167—168 °C. MS *m/z* 226 (M^+). ES λ_{max} (EtOH) 237 and 298 nm (log ε=3.94 and 4.28). ^{1}H NMR (DMSO-d_6) δ=0.92 (6H, d, J=7.0 Hz), 2.18 (1H, m), 2.90 (2H, d, J=7.0 Hz), 5.89 (1H, s), 11.12 and 12.19 (each 1H, s). Found: C, 58.55, H, 6.40%, Calcd for $C_{11}H_{14}O_5$: C, 58.40, H, 6.24%.

(±)-Humulone. To a mixture of **5** (2.0 g) and sodium hydride (0.64 g) in dry dimethyl sulfoxide (60 ml) was added 1-bromo-3-methyl-2-butene (2.8 g) under cooling with cold water; the mixture was then stirred for 2 h at room temperature. The reaction mixture was poured into cold dilute hydrochloric acid and extracted with ethyl acetate. The extract was chromatographed on silica gel with benzene–methyl acetate–acetic acid (300:20:1) to give (±)-**6** (1.06 g, 33%) as viscous pale brown oil. MS *m/z* 362 (M^+). ES λ_{max} (EtOH) 228, 327, and 356 nm (log ε=4.15, 4.03, and 3.95). IR (CCl_4) ν 3370, 2970, 2870, 1660, 1530, 1460, 1355, 1340, 1290, 1240, 1215, 1170, and 1100 cm^{-1}. ^{1}H NMR ($CDCl_3$) δ=0.98 and 1.02 (each 3H, d, J=7.0 Hz), 1.54 and 1.69 (12H, s), 2.17 (1H, m), 2.50, 2.70, and 3.09 (each 2H, d, J=7.0 Hz), 5.08 (2H, m), 18.89 (1H, s). ^{13}C NMR ($CDCl_3$) δ=17.7 and 17.8 (each q), 21.1 (d), 22.5, 22.8, 25.7, and 25.9 (each q), 26.4, 42.6, and 46.3 (each t), 78.8, 105.9, and 109.3 (each s), 115.7 and 121.0 (each d), 132.0, 137.9, 167.6, 190.6,

195.0, and 200.0 (each s). The IR and ^{1}H NMR spectra of this compound were completely identical with those of natural (−)-humulone.

(−)-Humulone. Natural humulone-*o*-phenylenediamine complex (0.5 g, mp 103 — 104 °C) was chromatographed on a column of silica gel with benzene–methyl acetate–acetic acid (300:20:1) as an eluent to give **(−)-humulone** (0.2 g), $[\alpha]_D$=−136.0° (*c* 1.39, chloroform), as a pale brown viscous solid.

***o*-Phenylenediamine Complex of (±)-6.** A mixed solution of **(±)-6** (167 mg) and *o*-phenylenediamine (50 mg) in benzene (7 ml) was allowed to stand overnight in a refrigerator. The resulting precipitate was recrystallized from benzene to afford the complex (42 mg, 20%) as light-yellow needles. Mp 104 — 105 °C (lit,[2] mp 105 — 106 °C). The IR and ^{1}H NMR spectra of this complex were completely identical with those of the natural specimen.

The authors express to their thanks to Mr. Masahiro Kowaka of KIRIN Brewery Co., Ltd., for his kind gift of natural sample. We are also grateful to Miss Mamiko Masuzawa and Mr. Kazuhiro Nagahara for their technical assistance.

References

1) C. J. Lintner and J. Schnell, *Z. Ges. Brauw.*, **1904**, 668.
2) W. Riedle, *Chem. Ber.*, **85**, 692 (1952).
3) D. De Keukeleile and M. Verzele, *Tetrahedron*, **26**, 385 (1970).
4) H. Obara, J. Onodera, Y. Kurihara, and F. Yamamoto, *Bull. Chem. Soc. Jpn.*, **51**, 3627 (1978).
5) J. Onodera and H. Obara, *Nippon Kagaku Kaishi*, **1973**, 1808.
6) F. L. Rigby and J. L. Bethune, *J. Chem. Soc.*, **1954**, 3400; M. Verzele, *Bull. Soc. Chim. Belg.*, **64**, 70 (1955).
7) F. L. Rigby and J. L. Bethune, *J. Am. Chem. Soc.*, **77**, 2828 (1955).
8) T. W. Campbell and G. M. Coppinger, *J. Am. Chem. Soc.*, **73**, 1849 (1951).

New Approaches to Tetracyanoquinodimethane

Shunro YAMAGUCHI,* Kazuyuki MIYAMOTO, and Terukiyo HANAFUSA
The Institute of Scientific and Industrial Research, Osaka University, Ibaraki, Osaka 567
(Received April 25, 1989)

Synopsis. New synthetic methods of tetracyanoquinodimethane from terephthaloyl dichloride were presented. Conversion of terephthaloyl dichloride to 1,4-bis(dicyanobenzoyloxymethyl)benzene, followed by debenzoyloxylation and succeessive oxidation afforded TCNQ.

Tetracyanoquinodimethane (TCNQ) is an excellent electron acceptor and readily forms conducting charge-transfer complexes with various donors. Owing to the electrical properties of TCNQ charge-transfer complexes, several approaches to TCNQ have been developed[1] We wish to report the synthetic method of TCNQ from terephthaloyl dichloride in a few steps. Terephthaloyl dichloride was converted to terephthaloyl dicyanide (**3**) with copper(I) cyanide. The reaction of terephthaloyl dicyanide with potassium cyanide and benzoyl chloride under ultrasonic irradiation[2] yielded 1,4-bis(dicyanobenzoyloxymethyl)benzene (**4**). Compound **4** was also prepared by the treatment of terephthaloyl dichloride with potassium cyanide, benzoyl chloride, and 18-crown-6[3] in dichloromethane and water. These reactions were carried out under heterogeneous conditions. Conversion of compound **4** to TCNQ was achieved by four methods. i) Benzoyloxy group of compound **4** was removed electrochemically[4] to give 1,4-bis(dicyanomethyl)-benzene ($TCNQH_2$), and $TCNQH_2$ was oxidized with *N*-iodosuccinimide (NIS) to afford TCNQ. ii) Reduction of compound **4** with zinc dust in acetic acid, followed by the oxidation with *N*-iodosuccinimide gave TCNQ. iii) Conversion of compound **4** to TCNQ was effected with triphenylphosphine-bromine complex in chlorobenzene. iv) Flash pyrrolysis of compound **4** under reduced pressure also afforded TCNQ.

In these approaches, it may be noted that the starting material is terephthaloyl dichloride, all reagents are inexpensive, and the cyanation reagents are easy to handle.

Experimental

Melting points were uncorrected. IR spectra were obtained on Hitachi 260—10 spectrophotometer. ^1H NMR spectra were measured on a Bruker AM360 instrument and the chemical shifts are given in δ-values with respect to TMS used as internal standard. Mass spectra were taken on a JMS-DX300 mass spectrometer.

Terephthaloyl Dicyanide (3). The mixture of terephthaloyl dichloride (50.0 g, 0.25 mol) and CuCN (46.3 g, 0.52 mol) in dry acetonitrile (500 ml) was refluxed overnight. After removal of volatiles, the resulting residue was extracted with hot benzene (100 ml×3). The combined organic layer was evaporated and the resulting residue was sublimed under reduced pressure (1 Torr; 1 Torr=133.322 Pa, 100 °C) to give 42.1 g of a colorless powder. Yield 87%. Mp 142—145 °C (lit,[5] 140—142 °C).

1,4-Bis(dicyanobenzoyloxymethyl)benzene (4). The mixture of terephthaloyl dicyanide (1.0 g, 5.6 mmol), KCN (1.8 g, 27.6 mmol), and benzolyl chloride (4.0 g, 28.5 mmol) in dry acetonitrile (6.5 ml) was placed in a test tube fitted with a screw cap. Ultrasound irradiation of the mixture was performed at 50 °C for 3.5 h, immersed in an ultrasonic cleaner. The insoluble materials were filtered off and the filtrate was condensed under reduced pressure. The resulting residue was purified by silica-gel chromatography and recrystallized from acetonitrile to give 1.5 g, of colorless prisms. Yield 60%. Mp 232—235 °C, IR (KBr disk) 2245, 1740 cm^{-1}, ^1H NMR ($CDCl_3$) δ=8.13 (3 4H), 8.08—7.55 (m 10H). MS (*m/z*) M^+ 446. Calcd for $C_{26}H_{14}O_4N_4$: C, 69.95; H, 3.16; N, 12.55%. Found: C, 69.81; H, 3.23; N, 12.65%.

A mixture of terephthaloyl dicyanide (5.0 g, 27.8 mmol), KCN (9.0 g, 0.14 mmol), benzolyl chloride (20 g, 0.14 mmol), and 18-crown-6 (360 mg, 1.38 mmol) in dry acetonitrile (50 ml) and water (0.08 ml) was stirred for 5 h at room temperature. The insoluble materials were filtered off. After the same procedure mentioned above, 5.6 g of colorless prisms were obtained. Yield 45%. Mp 232—235 °C.

Tetracyanoquinodimethane (1). i) A 100 ml H-type divided electrolysis cell was fitted with a Pb anode and a carbon cathode. A solution of compound **4** (89 mg, 0.2 mmol) and tetraethylammonium tosylate (3.01 g, 10.6 mmol) in concd H_2SO_4 (0.2 ml) and CH_2Cl_2 (20 ml) was placed in the cathodic compartment and in the anodic compartment was placed the solution of tetraethylammonium tosylate (3.01 g, 10.6 mmol) in CH_2Cl_2 (20 ml). The stirred catholyte was electrochemically reduced at 20 mA (current density 6.7 mA cm^{-2}) with N_2 bubbling. After 4.2 mol^{-1} of electricity was passed through the reaction system, the catholyte was taken into a 50 ml round-bottomed flask, to which was added *N*-iodosuccinimide (90 mg, 4.0 mmol). The reaction mixture was stirred for 30 min, washed with H_2O (10 ml×2), dried over anhydrous Na_2SO_4, and the solvent was evaporated. The residue was purified by silica-gel chromatography to give 29 mg of orange microcrystals. Yield 71%. Mp 293—294 °C (lit;[1] 291—293 °C). ^1H NMR ($CDCl_3$) δ=7.38 (s, 4H). IR (Nujol) 2230 cm^{-1}.

ii) To a solution of compound **3** (100 mg, 0.22 mmol) in acetic acid (10 ml) and THF (10 ml) was added Zn dust (2.0 g). After stirring for 10 min at room temperature, the insoluble materials were filtered off and the filtrate was concentrated. The resulting residue was dissolved in acetonitrile

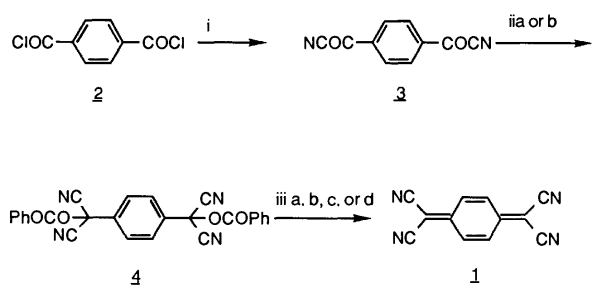

i) CuCN. ii a) KCN, PhCOCl, Ultra sound, ii b) KCN, PhCOCl, PTC
iii a) Electrolysis, NIS. iii b) Zn-AcOH, NIS, iii c) Ph_3PBr_2, iii d) pyrrolysis

Scheme 1. Approaches to TCNQ from terephthaloyl dichlonide.

(10 ml). To the solution was added NIS (120 mg, 0.53 mmol). The reaction mixture was stirred for 30 min at room temperature and then the solvent was evaporated. The residue was purified by silica-gel chromatography to afford 21 mg of orange microcrystals. Yield 46%. Mp 293—294 °C.

iii) To a solution of Ph_3P (131 mg, 0.50 mmol) in chlorobenzene (10 ml) was added bromine (88 mg, 0.55 mmol) and pale yellow crystals were formed. After the addition of compound **3** (100 mg, 0.55 mmol), the mixture was heated for 5 h. Removal of volatiles and purification of the residue by silica-gel chromatography gave 22 mg of orange microcrystals. Yiled 49%. Mp 293—294 °C.

iv) Compound **3** (100 mg, 0.22 mmol) was placed in a Pyrex tube of 0.8 mm diameter. The tube was heated at 750 °C under reduced pressure (0.3 Torr). The sublimated products were dissolved in dichloromethane and purified by chromatography to yield 9 mg of orange microcrystals. Yiled 19%. Mp 293—294 °C.

We wish to thank Dr. Ikuzo Nishiguchi, Osaka Municipal Technical Research Institute for providing tetraethylammonium tosylate.

References

1) D. S. Acker, R. J. Harder, W. R. Hertler, W. Mahler, L. B. Merby, R. E. Benson, and W. E. Mochel, *J. Am. Chem. Soc.*, **82**, 6408 (1960); R. C. Wheland and E. L. Martin, *J. Org. Chem.*, **21**, 3101 (1975); H. Suzuki, T. Kobayashi, and A. Osuka, *Chem. Lett.*, **1983**, 589; M. Uno, K. Seto, M. Masuda, and S. Takahashi, *Tetrahedron Lett.*, **26**, 1533 (1985); S. Yamaguchi and T. Hanafusa, *Chem. Lett.*, **1985**, 685.

2) T. Ando, T. Kawata, J. Yamawaki, and T. Hanafusa, *Synthesis*, **1983**, 637.

3) K. E. Koenig and W. P. Weber, *Tetrahedron Lett.*, **1974**, 2275.

4) I. Nishiguchi, *Yuki Gosei Kagaku Kyokai Shi*, **43**, 617 (1985).

5) G. Blackstock, *J. Am. Chem. Soc.*, **34**, 1082 (1912).

An Improved Synthetic Method of (*S*)-2-Alkoxypropanals from Ethyl (*S*)-Lactate

Yuko KOBAYASHI, Mitsuru TAKASE,† Yoshio ITO, and Shiro TERASHIMA*
Sagami Chemical Research Center, Nishi-Ohnuma, Sagamihara, Kanagawa 229
†Technical Research Laboratory, Nihongi Plant, Nippon Soda Co., Ltd.,
Fujisawa, Nakago-Mura, Nakakubiki-gun, Niigata 949-23
(Received May 11, 1989)

Synopsis. The title synthetic method which undergoes without racemization, was explored employing sequential amidolysis with a secondary amine, alkylation with an alkyl halide under basic conditions, and reduction with sodium bis(methoxyethoxy)aluminium hydride.

In connection with our ongoing project on the synthesis of the carbapenem key intermediate (**1**),[1] a large quantity of optically pure (*S*)-2-benzyloxypropanal (**2a**)[2] was required as a synthetic intermediate. Initially, the requisite aldehyde (**2a**) could be prepared without racemization by benzylation of commercially available inexpensive ethyl (*S*)-lactate (**3**) with benzyl trichloroacetimidate followed by reduction of formed ethyl (*S*)-2-benzyloxypropionate (**4**) with diisobutylalminium hydride.[1] However, this synthetic scheme turned out to be unrewarding for a large scale preparation of **2a** since the reagent for benzylation is highly expensive. Accordingly, an alternative efficient method was sought which can readily produce **2a** by using inexpensive reagents.

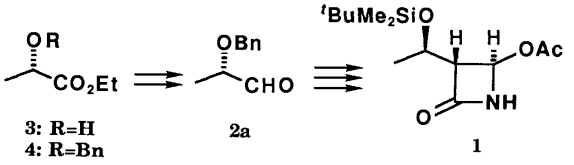

3: R=H
4: R=Bn
2a
1

While it has been uncovered that direct benzylation of **3** under basic conditions such as those employing benzyl bromide and sodium hydride in *N*,*N*-dimethylformamide, gives a low yield[3] of **4** and accompanies considerable racemization,[2c] we have now found that **2a** can be readily prepared without racemization by sequential amidolysis of **3** with a secondary amine, benzylation of the formed (*S*)-*N*,*N*-dialkyllactamide under basic conditions, and reduction of the amide group into an aldehyde moiety.

According to the reported method[4] with some modifications, preparation of (*S*)-*N*,*N*-dimethyllactamide (**5**) could be readily achieved in 93% yield by heating a mixture of **3** and liquid dimethylamine in a sealed tube at 70 °C. Benzylation of **5** was effected smoothly by treating with benzyl chloride and sodium hydride[5] or with benzyl chloride and sodium hydroxide[6] under usual phase-transfer conditions, giving rise to the *O*-benzyl derivative (**7a**) in 88 or 86% yield, respectively. Reduction of **7a** with sodium bis(2-methoxyethoxy)aluminium hydride (Vitride®),[7] furnished **2a** in 90% yield.

Since it had been reported that **2a** shows no constant value on measurement of the optical rotation due to its rapid hydration by moisture present in a solvent or air,[2a] determination of the optical purity of **2a** thus

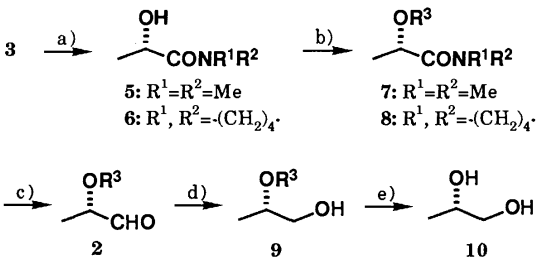

a: R^3=Bn, **b**: R^3=*p*-$ClC_6H_4CH_2$,
c: R^3=*p*-$MeOC_6H_4CH_2$, **d**: R^3=$BnOCH_2$

a) For **5**, Me_2NH, 70°C, 93%. For **6**, see text. b) For **7**, RCl-NaH in DMF-THF, 0°C, 88% (for **7a**), 76% (for **7b**), 75% (for **7c**), 62% (for **7d**), or BnCl-aqNaOH, $BnBu_3NCl$ (cat.), 86% (for **7a**). For **8a**, see text. c) Vitride in THF-toluene, 0°C, 90% (for **2a**), 89% (for **2b**), 80% (for **2c**), 84% (for **2d**). d) $NaBH_4$, in EtOH, 0°C, 89% (for **9a**), 95% (for **9b**), 99% (for **9c**), 85% (for **9d**). e) H_2-Pd/C, HCl (cat.), 70% (from **9a**), 56% (from **9b**), 60% (from **9c**).

obtained was attempted at the stage of (*S*)-2-benzyloxy-1-propanol (**9a**). Thus, treatment of **2a** with sodium borohydride followed by acylation of **9a** with (*R*)- and (*S*)-2-methoxy-3,3,3-trifluoro-2-phenylpropionyl chloride (MTPACl),[8] yielded the (*R*)- and (*S*)-MTPA esters of **9a**, respectively. As the ^1H NMR spectrum of the (*R*)-MTPA ester showed no signals corresponding to those of the (*S*)-MTPA ester, it appeared obvious that **2a** could be produced without racemization.

Taking into account the reagents required for converting **3** into **2a**, the explored synthetic route is undoubtedly more economical than the previous method and can be readily applied to a large scale preparation of **2a**.

In order to extend the developed synthetic scheme to general preparation method of various types of (*S*)-2-alkoxypropanals (**2**) whose protective groups could be introduced under basic conditions, syntheses of **2b—d** were next examined. Thus, alkylation of **5** with *p*-methoxybenzyl chloride, *p*-chlorobenzyl chloride, or benzyloxymethyl chloride,[9] followed by reduction of the *O*-alkyl derivatives (**7b—d**) with Vitride®, smoothly produced **2b—d** in a similar manner to that described for the preparation of **2a**. Since (*S*)-1,2-propanediol (**10**) obtained from **2b**,c by sequential reduction with sodium borohydride and hydrogenolysis exhibited the same optical rotation values as that of **10** independently synthesized from **9a**, it appeared obvious that **2b**,c could be prepared without racemization similarly to **2a**.[10]

As mentioned above, we have succeeded in developing an efficient synthetic method of **2a** required for the synthesis of the carbapenem key intermediate and in extending the explored synthetic scheme to general preparation method of (*S*)-2-alkoxypropanals such as

2b—d.[11] Throughout these studies, **5** was solely used as the substrate for protection of the alcoholic functionality. However, it can be readily realized that (*S*)-*N*,*N*-tetramethylenelactamide (**6**) accessible from **3** and pyrrolidine can be utilized similarly to **5**. The successful preparation of **2a** from **6** by way of the *O*-benzyl derivative (**8a**) has already been briefly mentioned in the separate paper reporting an efficient synthesis of the carbapenem key intermediates.[1b]

Experimental

(*S*)-*N*,*N*-Dimethyllactamide (5). Anhyd dimethylamine (18.0 g, 0.400 mol) was added to **3** (39.6 g, 0.335 mol) in a sealed tube at 0 °C. The mixture was stirred in a sealed tube at 70 °C for 1 d and excess dimethylamine and resulting ethanol were removed in vacuo to afford an oily residue. Additional amount of anhyd dimethylamine (10.0 g, 0.222 mol) was added to the residue and the mixture was further stirred in a sealed tube at 70 °C for 1 d to complete the amidolysis. After complete removal of excess dimethylamine and resulting ethanol in vacuo, the oily residue was purified with distillation (77 °C, 1 mmHg, 1 mmHg=133.322 Pa) to afford **5** as a colorless oil (36.4 g, 93%), $[\alpha]_D^{20}$ +0.98° (*c* 2.03, $CHCl_3$). IR (neat): 3450, 3000, 2950, 1640, 1510, 1450, 1380, 1260, 1120, 1030 cm^{-1}. ^1H NMR ($CDCl_3$): δ=1.33 (3H, d *J*=6.6 Hz, Me), 2.99 (6H, s, NMe_2), 3.66 (1H, bs OH), 4.46 (1H, dq, *J*=6.6 Hz, CH). MS *m/z*: 117 $(M)^+$, 73 $(M-NMe_2)^+$.

(*S*)-*N*,*N*-Dimethyl-2-benzyloxypropionamide (7a). a) Preparation with Sodium Hydride and Benzyl Chloride. A solution of **5** (8.12 g, 69.3 mmol) in THF (10 ml) was added slowly to a suspension of sodium hydride (2.00 g, 83.3 mmol) in THF (50 ml) and DMF (36 ml) at 0 °C with vigorous stirring. After stirring for 2 h, the mixture was diluted with THF (15 ml) and DMF (8 ml) and stirred vigorously for additional 6.5 h. Benzyl chloride (8.80 ml, 76.5 mmol) was added to the mixture at 0 °C, and stirring was continued at the same temperature overnight. The resulting mixture was diluted with H_2O (50 ml) and extracted with AcOEt. The combined extracts were washed with satd aq NaCl and dried over anhyd $MgSO_4$. After filtration and concentration in vacuo, the residue was purified with distillation (140 °C, 1 mmHg) to give **7a** as a colorless oil (11.3 g, 88%), $[\alpha]_D^{20}$ −51.5° (*c* 2.90, $CHCl_3$). IR (neat): 3500, 3000, 2950, 1660, 1500, 1458, 1402, 1260, 1118, 700 cm^{-1}. ^1H NMR ($CDCl_3$): δ=1.42 (3H, d, *J*=6.6 Hz Me), 2.95, 3.03 (6H, two s, NMe_2), 4.34 (1H, q, *J*=6.7 Hz. CH), 4.40, 4.60 (2H, two d, *J*=each 11.7 Hz, $\underline{CH_2}Ph$), 7.32 (5H, s, Ph), MS *m/z*: 208 $(M+1)^+$, 135 $(M-\overline{CO}NMe_2)^+$.

b) Preparation with Sodium Hydroxide and Benzyl Chloride in the Presence of a Phase-Transfer Catalyst. Benzyltributylammonium chloride (0.156 g, 0.500 mmol), benzyl chloride (1.52 g, 12.0 mmol), and aq NaOH (50%, 2.80 g, 35.0 mmol) were successively added to a solution of **5** (1.17 g, 10.0 mmol) in CH_2Cl_2 (5.0 ml) at rt. After being vigorously stirred for 12 h, the mixture was diluted with CH_2Cl_2 (10 ml) and H_2O (5 ml). The aqueous layer was separated and the organic layer was washed successively with 1 mol dm^{-3} HCl, and satd aq NaCl, then dried over anhyd $MgSO_4$. After filtration and concentration in vacuo, the residue was purified with column chromatography (SiO_2, hexane–AcOEt 2:3) to give **7a** as a colorless oil (1.78 g, 86%). The ^1H NMR spectrum of this sample were identical with those of **7a** obtained in a).

(*S*)-*N*,*N*-Dimethyl-2-(*p*-chlorobenzyloxy)propionamide (7b). Treatments of **5** (0.828 g, 7.06 mmol) with *p*-chlorobenzyl chloride (1.37 g, 8.51 mmol) under the same conditions as described for the procedure a) of the preparation of **7a** from **5**, gave **7b** as a colorless oil (1.30 g, 76%) after purification with column chromatography (SiO_2, hexane–AcOEt 3:7). $[\alpha]_D^{20}$ −47.2° (*c* 2.05, $CHCl_3$). IR (neat): 3500, 3000, 2950, 1655, 1498, 1400, 1105, 1018, 810 cm^{-1}. ^1H NMR ($CDCl_3$): δ=1.43 (3H, d, *J*=6.8 Hz, Me), 2.96, 3.01 (6H, two s, NMe_2), 4.34 (1H, q, *J*=6.9 Hz, CH), 4.35, 4.56 (2H, two d, *J*=each 11.7 Hz, $\underline{CH_2}Ar$), 7.29 (4H, s, C_6H_4). MS *m/z*: 242 $(M+1)^+$, 125 $(CH_2C_6H_4Cl)^+$.

(*S*)-*N*,*N*-Dimethyl-2-(*p*-methoxybenzyloxy)propionamide (7c). (*S*)-*N*,*N*-Dimethyllactamide (**5**) (0.828 g, 7.06 mmol) was treated with *p*-methoxybenzyl chloride (1.37 g, 8.51 mmol) under the same conditions as described for the procedure a) of the preparation of **7a** from **5**, afforded **7c** as a colorless oil (1.17 g, 75%) after purification with column chromatography (SiO_2, hexane–AcOEt 1:1). $[\alpha]_D^{20}$ −55.6° (*c* 2.03, $CHCl_3$). IR (neat): 3550, 2950, 1650, 1242, 1100, 1030, 820 cm^{-1}. ^1H NMR ($CDCl_3$): δ=1.41 (3H, d, *J*=6.8 Hz, Me), 2.95, 3.05 (6H, two s, NMe_2), 3.80 (3H, s, OMe), 4.32 (1H, q, *J*=6.8 Hz, CH), 4.34, 4.53 (2H, two d, *J*=each 10.6 Hz, $\underline{CH_2}Ar$), 6.85, 7.26 (4H, two d, *J*=8.8 Hz, C_6H_4). MS *m/z*: 238 $(M+1)^+$, 198 $(M-NMe_2)^+$, 121.

(*S*)-*N*,*N*-Dimethyl-2-(benzyloxymethoxy)propionamide (7d). Treatments of **5** (0.847 g, 7.23 mmol) with benzyloxymethyl chloride (1.21 ml, 8.70 mmol) under the same conditions as described for the procedure a) of the preparation of **7a** from **5**, gave **7d** as a colorless oil (1.07 g, 62%) after purification with column chromatography (SiO_2, hexane–AcOEt 3:2). $[\alpha]_D^{20}$ −64.4° (*c* 2.62, $CHCl_3$). IR (neat): 3550, 3120, 3000, 1665, 1518, 1462, 1418, 1120, 1050, 760, 718 cm^{-1}. ^1H NMR ($CDCl_3$): 1.40 (3H, d, *J*=6.8 Hz, Me), 2.94, 3.04 (6H, two s, NMe_2), 4.61 (1H, q, *J*=6.8 Hz, CH), 4.63 (2H, s, OCH_2O), 4.74, 4.84 (2H, two d, *J*=each 7.8 Hz, $\underline{CH_2}Ph$), 6.85, 7.26 (4H, two d, *J*=8.8 Hz, C_6H_4). MS *m/z*: 238 $(M+1)^+$, 198 $(M-NMe_2)^+$, 121.

(*S*)-2-Benzyloxypropanal (2a). General procedure for the reduction with Vitride®. A 1.07 mol dm^{-3} solution of Vitride® in a mixture of toluene and THF (1.60 ml, 3.20 mmol) was added slowly to a solution of **7a** (1.12 g, 5.39 mmol) in THF (15 ml) at 0 °C. After stirring at the same temperature for 2.5 h, the reaction mixture was poured into 1 mol dm^{-3} HCl (15 ml) cooled in an ice bath and extracted with CH_2Cl_2. The combined extracts were washed successively with 0.3 mol dm^{-3} HCl, satd aq NaCl, satd aq $NaHCO_3$, and satd aq NaCl, then dried over anhyd $MgSO_4$. Filtration and concentration in vacuo gave a residue which was purified with bulb-to-bulb distillation (100 °C, 1 mmHg) to give **2a** as a colorless oil (0.800 g, 90%). IR (neat): 3470, 3058, 3000, 2950, 1740, 1500, 1456, 1380, 1210, 1100, 741, 702 cm^{-1}. ^1H NMR ($CDCl_3$): 1.32 (3H, d, *J*=6.8 Hz,Me), 3.88 (1H, dq, *J*=1.8, 6.8 Hz, Me$\underline{CH}$), 4.62 (2H, s, $\underline{CH_2}Ph$), 7.35 (5H, s, Ph), 9.66 (1H, d *J*=1.8 Hz,CHO). MS *m/z*: 181 $(M+OH)^+$, 135 $(M-CHO)^+$.

(*S*)-(*p*-Chlorobenzyloxy)propanal (2b). Reduction of **7b** (0.800 g, 3.31 mmol) performed in a similar manner to that described for the preparation of **2a**, gave **2b** as a colorless oil (0.586 g, 89%) after purification with column chromatography (SiO_2, hexane–AcOEt 97:3). IR (neat): 2990, 2860, 1738, 1490, 1082, 1010, 802 cm^{-1}. ^1H NMR ($CDCl_3$): δ=1.34 (3H, d, *J*=7.0 Hz, Me), 3.88 (1H, dq, *J*=1.7, 7.0 Hz, CH), 4.51, 4.65 (2H, two d, *J*=each 11.9 Hz, $\underline{CH_2}Ar$), 7.31 (4H, s, C_6H_4), 9.66 (1H, d, *J*=1.5 Hz, CHO). MS *m/z*: 169 $(M-CHO)^+$, 125 $(CH_2C_6H_4Cl)^+$.

(*S*)-(*p*-Methoxybenzyloxy)propanal (2c). Treatment of **7c** (0.427 g, 1.80 mmol) under the conditions similar to those described for the reduction of **7a** afforded **2c** as a colorless oil (0.278 g, 80%) after purification with column chromatography (SiO_2, hexane–AcOEt 24:1). IR (neat): 2950, 2850, 1728, 1610, 1518, 1250, 1030, 820 cm^{-1}. ^1H NMR ($CDCl_3$): δ= 1.30 (3H, d, *J*=7.0 Hz,Me), 3.80 (3H, s, MeO), 3.90 (1H, dq, *J*=1.8, 7.0 Hz, CH), 4.55 (2H, s, $\underline{CH_2}Ar$), 6.88, 7.29 (4H, two

d, J=8.8 Hz, C_6H_4), 9.62 (1H, d, J=1.8 Hz, CHO). MS m/z: 194 $(M)^+$, 121 $(M-CH_2C_6H_4OMe)^+$.

(*S*)-(Benzyloxymethoxy)propanal (2d). Reduction of **7d** (0.724 g, 3.05 mmol) carried out in a similar manner to that described for the preparation of **2a**, gave **2d** as a colorless oil (0.500 g, 84%) after purification with column chromatography (SiO_2, hexane–AcOEt 24:1—4:1). IR (neat): 3050, 2900, 1738, 1450, 1380, 1040, 740, 700 cm^{-1}. ^1H NMR ($CDCl_3$): δ=1.32 (3H, d, J=6.8 Hz, Me), 4.10 (1H, dq, J=1.5, 6.8 Hz, CH), 4.67 (2H, s, OCH_2O), 4.86 (2H, s, $\underline{CH_2}Ph$), 7.33 (5H, s, Ph), 9.64 (1H, d, J=1.5 Hz, CHO). MS m/z: 165 $(M-CHO)^+$.

(*S*)-2-Benzyloxy-2-propanol (9a). General procedure for the reduction with sodium borohydride. Sodium borohydride (0.166 g, 4.39 mmol) was added to a solution of **2a** (0.282 g, 1.72 mmol) in EtOH (2 ml) at 0 °C. After stirring for 2 h at the same temperature, the mixture was diluted with 1 mol dm^{-3} HCl to decompose the excess reducing agent and extracted with AcOEt. The combined extracts were washed successively with satd aq NaCl, satd aq $NaHCO_3$ and satd aq NaCl, then dried over anhyd $MgSO_4$. Filtration and concentration in vacuo gave an oily residue which was purified with column chromatography (SiO_2, hexane–AcOEt 4:1) to give **9a** as a colorless oil (0.272 g, 95%), $[\alpha]_D^{20}$ +44.7° (c 3.47, $CHCl_3$) [lit,[2b] $[\alpha]_D^{25}$ +43.1° (c 3, $CHCl_3$) lit,[2c] $[\alpha]_D$ +45.86° (c 6.4, $CHCl_3$)]. IR (neat): 3450, 3050, 2970, 2940, 2870, 1950, 1880, 1818, 1500, 1450, 1050, 700 cm^{-1}. ^1H NMR ($CDCl_3$): δ=1.15 (3H, d, J=6.0 Hz, Me), 2.41 (1H, bs, OH), 3.51—3.65 (3H, m, $CHCH_2O$), 4.44, 4.63 (2H, two d, J=each 11.7 Hz, $\underline{CH_2}Ph$), 7.31 (5H, bs, Ph). MS m/z: 166 $(M)^+$, 91, 65. The optical purity of this sample was determined by comparing the ^1H NMR spectra of its (*R*)- and (*S*)-MTPA esters prepared according to the method reported by Mosher et al.[8] The (*R*)- and (*S*)-MTPA esters of **9a** were obtained in 72% and 66% yields, respectively. The (*R*)-MTPA ester of **9a**: $[\alpha]_D^{20}$ +45.7° (c 1.35, $CHCl_3$). IR (neat): 3000, 2950, 1745, 1445, 1270, 1240, 1162, 1020, 700 cm^{-1}. ^1H NMR ($CDCl_3$): δ=1.21 (3H, d, J=6.4 Hz, Me), 3.54 (3H, dd, J=1.3, 2.4 Hz, MeO), 3.78—3.90 (1H, m, CH), 4.29—4.39 (2H, m, $CH\underline{CH_2}O$), 4.52 (2H, s, $\underline{CH_2}Ph$), 7.23—7.62 (10H, m, Ph×2). MS m/z: 382 $(M)^+$, 244. The (*S*)-MTPA esters of **9a**: $[\alpha]_D^{20}$ −32.7° (c 2.24, $CHCl_3$). IR (neat): 3000, 2950, 1742, 1442, 1270, 1240, 1160, 1020, 695 cm^{-1}. ^1H NMR ($CDCl_3$): δ=1.20 (3H, d, J=6.4 Hz, Me), 3.53 (3H, dd, J=1.2, 2.3 Hz, MeO), 3.77—3.90 (1H, m, CH), 4.33 (2H, d, J=5.7 Hz, $CH\underline{CH_2}O$), 4.51 (2H, s, $\underline{CH_2}Ph$), 7.22—7.61 (10H, m, Ph×2). MS m/z: 382 $(M)^+$, 244. The ^1H NMR spectrum of the (*R*)-MTPA ester showed no signals corresponding to the (*S*)-MTPA ester. Accordingly, it appeared obvious that **2a** could be prepared from **3** without racemization.

(*S*)-2-(*p*-Chlorobenzyloxy)-1-propanol (9b). Reduction of **2b** (0.408 g, 2.05 mmol) performed as described for the preparation of **9a** from **2a**, gave **9b** as a colorless oil (0.390 g, 95%) after purification with column chromatography. $[\alpha]_D^{20}$ +36.8° (c 1.72, $CHCl_3$). IR (neat): 3450, 2950, 1918, 1610, 1500, 1100, 890 cm^{-1}. ^1H NMR ($CDCl_3$): δ=1.17 (3H, d, J=6.2 Hz, Me), 2.00 (1H, bs, OH), 3.48—3.73 (3H, m, $CHCH_2O$), 4.44, 4.63 (2H, two d, J=each 11.8 Hz, $\underline{CH_2}Ar$), 7.31 (4H, bs, C_6H_4). MS m/z: 200 $(M)^+$, 125 $(CH_2C_6H_4Cl)^+$.

(*S*)-2-(*p*-Methoxybenzyloxy)-1-propanol (9c). Treatments of **2c** (0.216 g, 1.11 mmol) under the same conditions as described for the preparation of **9a** from **2a**, gave **9c** as a colorless oil (0.217 g, 99%) after purification with column chromatography. $[\alpha]_D^{20}$ +41.2° (c 4.10, $CHCl_3$). IR (neat): 3450, 2950, 1610, 1510, 1242, 1030, 820 cm^{-1}. ^1H NMR ($CDCl_3$): δ=1.15 (3H, d, J=5.2 Hz, Me), 2.20 (1H, br, OH), 3.44—3.74 (3H, m, $CHCH_2O$), 3.79 (3H, s, OMe), 4.38, 4.52 (2H, two d, J=each 11.2 Hz $\underline{CH_2}Ar$), 6.87, 7.26 (4H, two d, J=8.6 Hz, C_6H_4). MS m/z: 196 $(M)^+$, 152, 137.

(*S*)-2-(*p*-Benzyloxymethoxy)-1-propanol (9d). Reduction of **2d** (0.431 g, 2.17 mmol) under the same conditions described for the preparation of **9a** from **2a**, afforded **9d** as a colorless oil (0.361 g, 85%) after purification with column chromatography. $[\alpha]_D^{20}$ +51.8° (c 1.51, $CHCl_3$). IR (neat): 3460, 2950, 2900, 1458, 1380, 1040, 700 cm^{-1}. ^1H NMR ($CDCl_3$): δ=1.18 (3H, d, J=6.4 Hz, Me), 2.61 (1H, bs, OH), 3.53 (2H, m, $\underline{CH_2}OH$), 3.86 (1H, m, CH), 4.65 (2H, s, OCH_2O), 4.85 (2H, s, $\underline{CH_2}Ph$), 7.34 (5H, s, Ph). MS m/z: 181 $(M-Me)^+$, 165 $(M-CH_2OH)^+$.

(*S*)-1,2-Propanediol (10). Palladium on carbon (10%, 25.8 mg) and one drop of 5 mol dm^{-3} solution of HCl in EtOH were added to a solution of **9a** (0.204 g, 1.23 mmol) in EtOH (3 ml) and the mixture was stirred under a hydrogen atmosphere for 1 h. The catalyst was filtered off and the filtrate was concentrated in vacuo. The concentration residue was purified with bulb-to-bulb distillation (110 °C, 18 mmHg) to give **10** as a colorless oil (65.0 mg, 70%). By the same procedure as described above, **9b, c** could be derived to **10** (56% from **9b** and 60% from **9c**). $[\alpha]_D^{20}$ +27.4° (c 3.00, $CHCl_3$) (from **9a**), $[\alpha]_D^{20}$ +27.5° (c 2.38, $CHCl_3$) (from **9b**), $[\alpha]_D^{20}$ +28.0° (c 2.31, $CHCl_3$) (from **9c**), [lit,[12] $[\alpha]_D^{24.2}$ +30.0° (c 3.00, $CHCl_3$)]. These specific rotation values clearly confirmed that no racemization had taken place during the preparation of **2b,c** from **3**. IR (neat): 3400, 3000, 2950, 1650, 1140, 1040, 840 cm^{-1}. ^1H NMR ($CDCl_3$): δ=1.15 (3H, d, J=6.4 Hz, Me), 3.10 (2H, bs, OH×2), 3.38—3.99 (3H, m, $\underline{CHCH_2}O$). MS m/z: 61 $(M-Me)^+$, 59 $(M-OH)^+$.

References

1) a) Y. Ito, T. Kawabata, and S. Terashima, *Tetrahedron Lett.*, **27**, 5751 (1986); b) Y. Ito, Y. Kobayashi, T. Kawabata, M. Takase, and S. Terashima, *Tetrahedron*, in press.

2) a) D. C. Baker and L. D. Hawkins, *J. Org. Chem.*, **47**, 2179 (1982); b) J. Mulzer and A. Angermann, *Tetrahedron Lett.*, **24**, 2843 (1983); c) K. Takai and C. H. Heathcock, *J. Org. Chem.*, **50**, 3247 (1985).

3) S. K. Massad, L. D. Hawkins, and D. C. Baker, *J. Org. Chem.*, **48**, 5180 (1983).

4) K. Freudenberg, W. Kuhn, and I. Bumann, *Ber.*, **63**, 2380 (1930).

5) Since the sodium alkoxide prepared from **5** and sodium hydride was found to be fairly unstable at rt, it should be treated blow 0 °C.

6) Sodium hydroxide was used as an aqueous solution or as a powder.

7) V. Bazant, M. Capka, M. Cerny, V. Chvalovsky, K. Kochloefl, M. Kraus, and J. Málek, *Tetrahedron Lett.*, **1968**, 3303.

8) J. A. Dale, D. L. Dull, and H. S. Mosher, *J. Org. Chem.*, **34**, 2543 (1969).

9) The *O*-allyl derivative (**7**: R^3=allyl) was similarly prepared in 71% yield by treating **5** with sodium hydride and allyl chloride though the corresponding propanal derivative (**2**: R^3=allyl) could not be obtained by the subsequent reduction.

10) Since hydrogenolysis of **9d** produced by the reduction of **2d** with sodium borohydride turned out to be unsuccessful, the optical purity of **2d** could not be rigorously ascertained. However, based on the results obtained for **2a—c**, **2d** prepared from **5** by way of **7d** was expected to be optically pure.

11) Application of this methodology to the synthesis of (*R*)- or (*S*)-3-benzyloxybutanal, one of the useful chiral building blocks, from commercially available methyl (*R*)- or (*S*)-3-hydroxybutyrate, resulted in exclusive formation of the elimination product (the crotonamide derivative) in the step of benzylation.

12) N. Shieh and C. C. Price, *J. Org. Chem.*, **24**, 1169 (1959).

A Novel Use of the Ionic Hydrosilation in the Synthesis of Carbapenem Key Intermediate

Yuko KOBAYASHI, Yoshio ITO, and Shiro TERASHIMA*
Sagami Chemical Research Center, Nishi-Ohnuma, Sagamihara, Kanagawa 229
(Received May 18, 1989)

Synopsis. The ionic hydrosilation of the 3-acetyl-2-azetidinone derivative in the presence of boron trifluoride etherate was found to effect highly stereoselective reduction of the acetyl group (at most, 17:1), giving rise to the desired 3-[(*R*)-1-hydroxyethyl]-2-azetidinone derivative as a major product. Simultaneous reductive removal of the bis(*p*-methoxyphenyl)methyl group was also observed depending upon the reaction conditions.

We have recently succeeded in exploring an efficient synthetic route to the important carbapenem key intermediate (**1**) starting from commercially available and inexpensive ethyl (*S*)-lactate (**2**).[1] Thus, the 3-acetyl-2-azetidinone derivative (**4**) bearing the desired absolute stereochemistry could be produced stereoselectively by the [2+2]-cycloaddition of the chiral imine (**3**) derived from **2** with diketene. Subsequent reduction of **4** with K-selectride® or potassium triethylhydroborate according to the reported procedures,[2] afforded the 3-[(*R*)-1-hydroxyethyl]-2-azetidinone (**5a**) in a highly stereoselective manner, from which **1** could be readily elaborated by way of the *N*-unprotected 2-azetidinone and the 3-[(*R*)-1-(*t*-butyldimethylsilyloxy)ethyl]-2-azetidinone derivatives (**5b** and **5c**).

Since a number of the methods which may effect stereoselective reduction of **4** to **5a** are limited[3,4] and the reducing agents so far examined by us seem to be fairly expensive, another efficient reduction method was sought which can produce **5a** from **4** highly stereoselectively. After numerous experimentations surveying various reducing agents, we found that the ionic hydrosilation[5] of **4** underwent in a highly stereoselective manner, affording a good yield of **5a** or **5b** depending upon the reaction conditions.

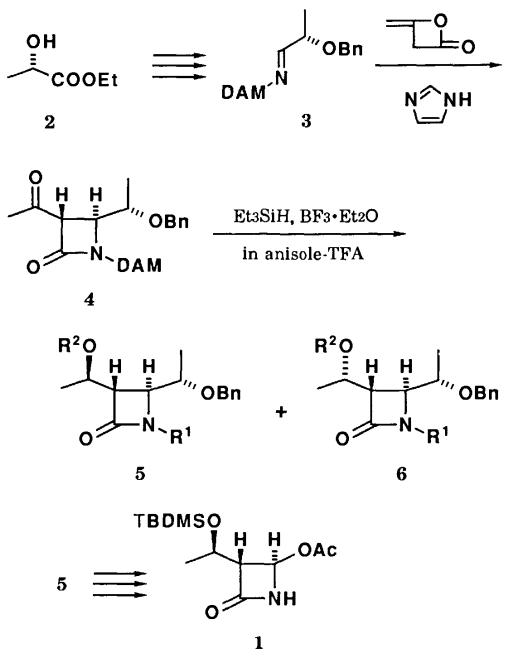

DAM=(*p*-MeOC$_6$H$_4$)$_2$CH

a: R^1=DAM, R^2=H, b: R^1=R^2=H, c: R^1=H, R^2=TBDMS

Thus, when **4** was treated with triethylsilane in a mixture of trifluoroacetic acid (TFA) and anisole in the presence of a catalytic amount of boron trifluoride etherate ($BF_3 \cdot Et_2O$) (0.08 equivalent to the amount of triethylsilane used) at −10 °C, a mixture of **5a** and the 3-[(*S*)-1-hydroxyethyl]-2-azetidinone (**6a**) could be obtained in 71% combined yield along with a small amount of the mixture of **5b** and **6b** (10% combined yield). The formation ratio of **5a** to **6a** was determined as 8:1 by comparing the ^{1}H NMR spectrum of the mixture with those of authentic samples of **5a** and **6a**.[1] On the other hand, treatment of **4** with a mixture of TFA and anisole in the presence of $BF_3 \cdot Et_2O$ (0.35 equivalent to the amount of triethylsilane used) at 0 °C was found to effect simultaneous stereoselective reduction of the acetyl group and reductive removal of the bis(*p*-methoxyphenyl)methyl (DAM) group, giving rise to a mixture of **5b** and **6b** in 64% combined yield. The latter hydrosilation conditions is anticipated to be more severe than the former. The ratio of **5b** and **6b** could be determined as 17:1 by the ^{1}H NMR spectrum after conversion to a mixture of the *t*-butyldimethylsilyl (TBDMS) ethers (**5c** and **6c**). Independent syntheses of **6b**,**c** from **6a** which had already been converted to **5a** by the Mitsunobu reaction,[1] could rigorously establish the stereochemistries of **6b**,**c**.

In these ionic hydrosilation reactions, TFA and $BF_3 \cdot Et_2O$ were found to be essential. Thus, complex mixtures of the decomposition products were always produced in the absence of $BF_3 \cdot Et_2O$ probably due to slowdown of the reaction rate. Uses of other Lewis acids such as boron tribromide or titanium tetrachloride in place of $BF_3 \cdot Et_2O$ were shown to be unrewarding, giving rise to complex decomposition products. Additionally, the ionic hydrosilation reactions attempted using trichloroacetic acid or acetic acid as a protic acid in place of TFA resulted in simple recovery of **4**.

Thus, it appeared that the ionic hydrosilation holds promise as an effective method for reducing the acetyl group of **4** to the (*R*)-1-hydroxyethyl group in a highly stereoselective manner and affords a good yield of **5a** or **5b** depending upon the reaction conditions.[6] Furthermore, direct synthesis of **5b** from **4** may have high practical value since the DAM group of **5a** is removable only by oxidation with fairly expensive

cerium(IV) ammonium nitrate (CAN).

Experimental

General. All melting points were determined with a Yamato MP-21 melting point apparatus and were uncorrected. Measurements of optical rotaions were performed with a Horiba SEPA-200 automatic digital polarimeter. IR spectral measurements were carried out with a JASCO A-202 diffraction grating infrared spectrometer. ^{1}H NMR spectra were recorded with a Hitachi R-90H (90 MHz) and a Bruker AM spectrometer (400 MHz). All signals were expressed as ppm downfield from tetramethylsilane used as an internal standard (δ-value). Wakogel C-200 and C-300 kieselgel 60 were used as an adsorbent for column chromatography.

(3*S*,4*S*)-4-[(*S*)-1-Benzyloxyethyl]-1-[bis(*p*-methoxyphenyl)-methyl]-3-[(*R*)-1-hydroxyethyl]-2-azetidinone and Its 3-[(*S*)-1-Hydroxyethyl] Isomer (5a and 6a). Trifluoroacetic acid (0.640 ml, 8.31 mmol) and $BF_3 \cdot Et_2O$ (6.0 µl, 0.049 mmol) were added to a mixture of **4** (98.1 mg, 0.207 mmol), anisole (68.0 µl, 0.626 mmol), and triethylsilane (0.100 ml, 0.626 mmol) at −10 °C. After stirring at −25 °C for 1.5 h, the mixture was concentrated in vacuo and the concentration residue was diluted with aqueous NaOH and ether. The organic layer was separated and washed successively with 1 mol dm^{-3} HCl and saturated aqueous NaCl, then dried over anhydrous $MgSO_4$. Filtration and concentration in vacuo gave an oily residue, which was purified with column chromatography (SiO_2, CH_2Cl_2–AcOEt 1:0—2:1) to give a mixture of **5a** and **6a** (69.6 mg, 71%) from the less polar fraction. The ratio of **5a** to **6a** could be calculated as 8:1 by comparing the ^{1}H NMR spectrum of the mixture with those of authentic samples of **5a** and **6a**.[1)] A mixture of **5b** and **6b** (4.9 mg, 10%) was also isolated as the minor products from the more polar fraction. Comparison of the ^{1}H NMR spectrum of the mixture with those of pure samples of **5b** and **6b** (vide infra) obviously established the structures of the products (**5b** and **6b**).

(3*S*,4*S*)-4-[(*S*)-1-Benzyloxyethyl]-3-[(*R*)-1-hydroxyethyl]-2-azetidinone and Its 3-[(*S*)-1-Hydroxyethyl] Isomer (5b and 6b). Trifluoroacetic acid (0.690 ml) and $BF_3 \cdot Et_2O$ (25.0 µl, 0.203 mmol) were added to a mixture of **4** (0.106 g, 0.223 mmol), anisole (73.0 µl, 0.672 mmol), and triethylsilane (0.107 ml, 0.670 mmol) at 0 °C. After stirring at the same temperature overnight, the mixture was concentrated in vacuo and the residue was diluted with saturated aqueous $NaHCO_3$ and AcOEt. The organic layer was separated, washed successively with 1 mol dm^{-3} HCl and saturated aqueous NaCl, then dried over anhydrous $MgSO_4$. Filtration and concentration in vacuo gave an oily residue, which was purified with column chromatography (SiO_2, CH_2Cl_2–AcOEt 2:1) to give a mixture of **5b** and **6b** (35.5 mg, 64%). The stereochemistries of the reduction products were determined by converting the mixture of **5b** and **6b** to that of **5c** and **6c** in 84% yield under the same conditions as described for silylation of a pure sample of **6b** with *t*-butylchlorodimethylsilane. As **5c** had been obtained from **5a** by way of **5b**,[1)] an authentic sample of **6c** was prepared by silylation of a pure sample of **6b** (vide infra). The ratio of **5b** to **6b** could be calculated as 17:1 by the integration ratio of C_3-H in the ^{1}H NMR spectrum of the mixture (vide infra). A single recrystallization of the mixture of **5b** and **6b** from hexane–AcOEt readily afforded a pure sample of **5b**, mp 130.5 °C and $[\alpha]_D^{25}$+66.2° (*c* 1.24, $CHCl_3$) [lit,[1b)] mp 129—130 °C and $[\alpha]_D^{25}$+61.5° (*c* 1.45, $CHCl_3$)]. IR and ^{1}H NMR spectrum of this sample were also identical with those reported.[1b)] An authentic sample of **6b** was prepared by oxidation of **6a** with cerium(IV) ammonium nitrate (vide infra).

(3*S*,4*S*)-4-[(*S*)-1-Benzyloxyethyl]-3-[(*S*)-1-hydroxyethyl]-2-azetidinone (6b). Cerium(IV) ammonium nitrate (0.122 g, 0.222 mmol) was added to a solution of an authentic sample of **6a**[1)] (32.1 mg, 0.0675 mmol) in H_2O–MeCN (1:9) (0.2 ml) at −10 °C. The mixture was stirred vigorously at the same temperature for 2 h, then diluted with 1 mol dm^{-3} NaOH (0.45 ml). After stirring at rt for 1 h, the mixture was extracted with AcOEt. The combined organic extracts were washed with saturated aqueous NaCl, dried over anhydrous $MgSO_4$, filtered, and concentrated in vacuo. The concentration residue was purified with column chromatography (SiO_2, hexane–AcOEt 2:3) to give **6b** (9.9 mg, 60%). ^{1}H NMR ($CDCl_3$): 1.22 (3H, d, *J*=5.7 Hz, MeCHOBn), 1.31 (3H, d, *J*=6.4 Hz, MeCHOH), 2.2—2.4 (1H, br, OH), 2.84 (1H, m, C_3-H), 3.4—3.5 (2H, m, CHOBn and C_4-H), 4.07 (1H, m, CHOH), 4.41, 4.68 (2H, two d, *J*=11.9 Hz, PhCH$_2$), 6.20 (1H, bs, NH), 7.32 (5H, s, C_6H_5). This sample was used as an authentic sample of **6b** (vide supra).

(3*S*,4*S*)-4-[(*S*)-1-Benzyloxyethyl]-3-[(*S*)-1-(*t*-butyldimethylsilyloxy)ethyl]-2-azetidinone (6c). Imidazole (10.0 mg, 0.147 mmol) and *t*-butylchlorodimethylsilane (15.0 mg, 0.0995 mmol) were added to a solution of an authentic sample of **6b** (5.5 mg, 0.022 mmol) in DMF (0.1 ml). After stirring for 1 h, the mixture was diluted with H_2O and extracted with ether. The combined extracts were washed with saturated aqueous NaCl and dried over anhydrous $MgSO_4$. Filtration and concentration in vacuo gave a residue, which was purified with column chromatography (SiO_2, CH_2Cl_2) to give **6c** (7.8 mg, 98%). ^{1}H NMR ($CDCl_3$): 0.07 (6H, s, Me_2Si), 0.88 (9H, s, Me_3CSi), 1.22 (3H, d, *J*=6.2 Hz, MeCHOBn), 1.29 (3H, d, *J*=6.4 Hz, MeCHOSi), 2.88 (1H, m, C_3-H), 3.50 (2H, m, CHOBn and C_4-H), 4.17 (1H, m, CHOSi), 4.40, 4.67 (2H, two d, *J*=11.7 Hz, PhCH$_2$), 6.00 (1H, bs, NH), 7.32 (5H, s, C_6H_5). This was used as an authentic sample of **6c** (vide supra).

References

1) a) Y. Ito, T. Kawabata, and S. Terashima, *Tetrahedron Lett.*, **27**, 5751 (1986); b) Y. Ito, Y. Kobayashi, T. Kawabata, M. Takase, and S. Terashima, *Tetrahedron*, in press.

2) a) F. A. Bouffard and B. G. Christensen, *J. Org. Chem.*, **46**, 2208 (1981); b) Y. Ito, T. Katsuki, and M. Yamaguchi, *Tetrahedron Lett.*, **26**, 4643 (1985).

3) a) W. Durckheimer, J. Blumback, R. Lattrell, and K. H. Scheunemann, *Angew. Chem., Int. Ed. Engl.*, **24**, 180 (1985); T. Kametani, K. Fukumoto, and M. Ihara, *Heterocycles*, **17**, 463 (1982).

4) It has been reported that reduction of a 3-acetyl-2-azetidinone derivative with a combination of diisopropylamine-borane complex and magnesium trifluoroacetate can proceed highly stereoselectively. S. Karady, J. S. Amato, R. A. Reamer, and L. M. Weinstock, *J. Am. Chem. Soc.*, **103**, 6765 (1981).

5) D. N. Kursanov, Z. N. Parnes, and N. M. Loim, *Synthesis*, **1974**, 633.

6) To our knowledge, this reaction represents the first example where the ionic hydrosilation reaction has effected reductive removal of the protecting group present at the nitrogen atom of 2-azetidinone.

A Facile Preparation of 7-(Substituted amino)-6*H*-pyrrolo[3,4-*d*]-pyrimidine Derivatives[1)]

Michihiko NOGUCHI,* Yasutoshi KIRIKI, and Shoji KAJIGAESHI
Department of Industrial Chemistry, Faculty of Engineering, Yamaguchi University, Tokiwadai, Ube 755
(Received May 15, 1989)

Synopsis. 6-Phenyl-7-(substituted amino)-6*H*-pyrrolo[3,4-*d*]pyrimidine-2,4(1*H*,3*H*)-diones **3** were obtained by the reaction of 5-formyl-1,3-dimethyl-6-[(substituted amino)-methyl]-2,4(1*H*,3*H*)-pyrimidinediones (**1**) with aniline (**2a**).

Recently, we reported a one-pot preparation of 6,7-dihydropyrido[3,4-*d*]pyrimidine-2,4(1*H*,3*H*)-dione derivatives (**D**) from the reaction of 5-formyl-1,3,6-trimethyl-2,4(1*H*,3*H*)-pyrimidinedione (**A**) with primary amines.[2)] The cycloaddition reaction of 5,6-dihydro-5,6-bis(methylene)-2,4(1*H*,3*H*)-pyrimidinedione **B**, generated via 1,5-hydrogen shift of **A**, and aldimines from **A** and amines yielding 5,6,7,8-tetrahydropyrido[3,4-*d*]pyrimidine-2,4(1*H*,3*H*)-dione **C** was the key step in this pyridopyrimidine synthesis.

In the continuation of the investigations on the preparation of fused pyrimidines, we wish to describe here a facile preparation of 7-(substituted amino)-6*H*-pyrrolo[3,4-*d*]pyrimidine-2,4(1*H*,3*H*)-dione derivatives from the reaction of 5-formyl-1,3-dimethyl-6-[(substituted amino)methyl]-2,4(1*H*,3*H*)-pyrimidinedione with primary amines.

Results and Discussion

The reaction of 5-formyl-1,3-dimethyl-6-(morpholinomethyl)-2,4(1*H*,3*H*)-pyrimidinedione (**1a**) with aniline (**2a**) in benzene under reflux afforded 1,3-dimethyl-7-morpholino-6-phenyl-6*H*-pyrrolo[3,4-*d*]pyrimidine-2,4(1*H*,3*H*)-dione (**3a**) in 59% yield. The reaction of other 5-formyl-6-[(substituted amino)methyl]-2,4(1*H*,3*H*)-pyrimidinediones (**1**) with aniline (**2a**) was also examined. The reaction patterns depended on the kind of the substituted amino groups; the reaction of 6-[(1-pyrrolidinyl)methyl]- (**1b**) afforded only **3b**, the same type product as **3a**, while the reaction of 6-[(diethylamino)methyl]- (**1c**) and 6-[(*N*-methylanilino)methyl]- (**1d**) afforded 1,3-dimethyl-6-phenyl-6*H*-pyrrolo[3,4-*d*]pyrimidine-2,4(1*H*,3*H*)-dione (**4**)[3)] as a major product together with the corresponding 7-(substituted amino) derivatives **3c** and **3d**, respectively.

The structural elucidation of pyrrolopyrimidines **3** was accomplished on the basis of their spectral data comparing with those of **4**.

A pathway for these pyrrolopyrimidines **3** and **4** can be explained by the analogy to that for pyrido[3,4-*d*]pyrimidines **C** from **A** and primary amines. The 1,5-hydrogen shift of the aldimine **E** from **1** and aniline (**2a**) affords a 5-anilinomethylene-5,6-dihydro-6-[(substituted amino)methylene]-2,4(1*H*,3*H*)-pyrimidinedione intermediate (**F**). The 1,5-cyclization of **F** leads to a 6,7-dihydro-5*H*-pyrrolo[3,4-*d*]pyrimidine-2,4(1*H*,3*H*)-dione (**G**). The dehydrogenation of **G** gives the 7-(substituted amino) derivatives **3**, while the deamination of **G** gives pyrrolopyrimidine **4**.

The above pathway for the formation of **G** is related to that for 6-tosylamino-6*H*-pyrrolo[3,4-*d*]pyrimidine synthesis by the reaction of 1,2,3,4-tetrahydro-6-bromomethyl-1,3-dimethyl-2,4-dioxo-5-pyrimidinecarbaldehyde tosylhydrazone with triethylamine, in which the 1,5-cyclization of 1-azapentadienyl anion was proposed.[3)] The dehydrogenation of **G** leading to **3** is much of interest, because another process, the deamination leading to **4**, seems to be a favorable one. Although a plausible explanation for the results is not found yet, we suggest that the substituted amino group at the 7-position might stabilize the 6*H*-pyrrolo[3,4-*d*]pyrimidine system.

In order to survey the usefulness of this method, the

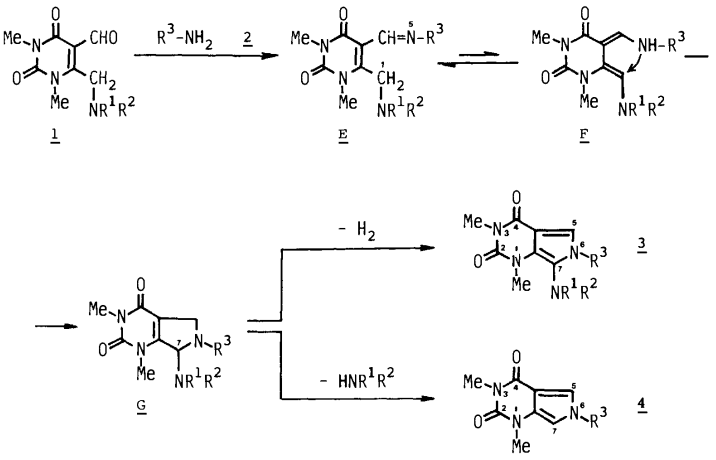

Scheme 1.

Table 1. Reaction of 5-Formyl-6-(substituted amino)methyl-2,4(1*H*,3*H*)-pyrimidinediones **1** with Primary Amines **2**[a]

3	R^1	R^2	R^3	Yield/%[b]	4 Yield/%[b]
3a	$-(CH_2)_2-O-(CH_2)_2-$		Ph	69	—
3b	$-(CH_2)_4-$		Ph	59	—
3c	Et	Et	Ph	33	53
3d	Me	Ph	Ph	23	59
3e	$-(CH_2)_2-O-(CH_2)_2-$		C_6H_4-OMe(*p*)	65	—
3f	$-(CH_2)_2-O-(CH_2)_2-$		C_6H_4-Me(*p*)	66	—
3g	$-(CH_2)_2-O-(CH_2)_2-$		C_6H_4-Br(*p*)	64	—
3h	$-(CH_2)_2-O-(CH_2)_2-$		C_6H_4-Cl(*p*)	65	—
3i	$-(CH_2)_2-O-(CH_2)_2-$		1-Naphthyl	50	—
3j	$-(CH_2)_2-O-(CH_2)_2-$		Benzyl	32	—

a) In dry benzene under reflux for 2 d. b) Based on isolated products.

reaction of **1a** with arylamines and benzylamine were examined. In these reaction the 7-(substituted amino)-6*H*-pyrrolo[3,4-*d*]pyrimidine-2,4(1*H*,3*H*)-diones **3e—j** were obtained in good to fair yields. These results are summarized in Table 1.

Although much attention has been focused on the pharmacological potentialities of pyrrolo[3,4-*d*]pyrimidine derivatives, few reports on their preparation were found.[3-5] We believe that our method based on the 1,5-cyclization of 5-anilinomethylene-5,6-dihydro-6-[(substituted amino)methylene]-2,4(1*H*,3*H*)-pyrimidinediones serves as a new entry into 7-(substituted amino)-6*H*-pyrrolo[3,4-*d*]pyrimidines.

Experimental[6]

The new starting materials **1b** and **1c** were prepared from the reaction of 5-formyl-1,3-dimethyl-6-bromomethyl-2,4-(1*H*,3*H*)-pyrimidinedione and corresponding amines similarly to the reported method.[3]

5-Formyl-1,3-dimethyl-6-[(1-pyrrolidinyl)methyl]-2,4(1*H*,3*H*)-pyrimidinedione (1b): Mp 123—125 °C. Found: C, 57.42; H, 7.00; N, 16.43%. Calcd for $C_{12}H_{17}N_3O_3$: C, 57.35; H, 6.82; N, 16.72%.

6-[(Diethylamino)methyl]-5-formyl-1,3-dimethyl-2,4(1*H*,3*H*)-pyrimidinedione (1c): 73—74 °C. Found: C, 57.14; H, 7.83; N, 16.64%. Calcd for $C_{12}H_{19}N_3O_3$: C, 56.90; H, 7.56; N, 16.59%.

The Reaction of 1 with Aniline (2a). General Procedure: The solution of **1c** (1 mmol) and aniline (**2a**)(1 mmol) in dry benzene (5 mL) was heated under reflux for 2 d, and the solvent was evaporated to dryness. The residue was subjected to column chromatography on silica gel to afford 109 mg (33%) of **3c** as elution of benzene/chloroform (1/1) to chloroform and 154 mg (53%) of **4** as elution of chloroform/ethyl acetate (4/1), respectively.

1,3-Dimethyl-7-morpholino-6-phenyl-6*H*-pyrrolo[3,4-*d*]pyrimidine-2,4(1*H*,3*H*)-dione (3a): Colorless prisms (benzene-ethanol); mp 218—219 °C; IR (KBr) cm^{-1}: 1690, 1640(CO); ^1H NMR ($CDCl_3$) δ=2.8—3.0, 3.4—3.7 (4H, each, 2m, $-CH_2-$), 3.40, 3.67 (3H, each, 2s, $-CH_3$), 7.19 (3H, s, 5-H), 7.3—7.6 (8H, total, m and s, phenyl and benzene); ^{13}C NMR ($CDCl_3$) δ=27.8, 31.5, 52.8, 67.0, 104.9 (4a-C), 118.2 (5-C), 120.8 (7a-C), 123.8 (7-C), 127.7, 128.3, 129.2 (benzene), 129.4, 139.3, 152.5 (2-C), 160.0 (4-C); MS *m/z*: 340 (M^+). Found: C, 66.79; H, 6.07; N, 14.81%. Calcd for $C_{18}H_{20}N_4O_3 \cdot 1/2C_6H_6$: C, 66.47; H, 6.12; N, 14.76%.

1,3-Dimethyl-6-phenyl-7-(1-pyrrolidinyl)-6*H*-pyrrolo[3,4-*d*]pyrimidine-2,4(1*H*,3*H*)-dione (3b): Colorless plates (hexane-ethanol); mp 226—227 °C; IR (KBr) cm^{-1}: 1680, 1640 (CO); ^1H NMR ($CDCl_3$) δ=1.6—1.8, 2.9—3.1 (4H, each, 2 m, $-CH_2-$), 3.41, 3.56 (3H, each, 2s, $-CH_3$), 7.28 (1H, s, 5-H), 7.3—7.6 (5H, m, phenyl); ^{13}C NMR ($CDCl_3$) δ=26.1, 27.8, 30.3, 53.4, 104.9, (4a-C), 117.2 (5-C), 120.2 (7a-C), 121.9 (7-C), 126.3, 128.5, 129.2, 139.0, 152.6 (2-C), 160.2 (4-C); MS *m/z*: 324 (M^+). Found: C, 66.77; H, 6.20; N, 17.26%. Calcd for $C_{18}H_{20}N_4O_2$: C, 66.65; H, 6.22; N, 17.27%.

7-(Diethylamino)-1,3-dimethyl-6-phenyl-6*H*-pyrrolo[3,4-*d*]pyrimidine-2,4(1*H*,3*H*)-dione (3c): Pale yellow prisms (hexane-ethanol); mp 164—166 °C; IR (KBr) cm^{-1}: 1690, 1650(CO); ^1H MNR ($CDCl_3$) δ=0.96 (6H, t, $-CH_3$, J=7 Hz), 2.88 (4H, q, $-CH_2-$, J=7 Hz), 3.45, 3.68 (3H, each, 2s, $-CH_3$), 7.29 (1H, s, 5-H), 7.3—7.6 (5H, m, phenyl); ^{13}C NMR ($CDCl_3$) δ=13.5, 27.8, 31.1, 48.8, 104.8 (4a-C), 118.0 (5-C), 121.2 (7a-C), 122.5 (7-C), 127.0, 128.9, 129.1, 139.8, 152.7 (2-C), 160.3 (4-C); MS *m/z*: 326 (M^+). Found: C, 66.40; H, 6.91; N, 17.34%. Calcd for $C_{18}H_{22}N_4O_2$: C, 66.24; H, 6.79; N, 17.16%.

1,3-Dimethyl-7-(*N*-methylanilino)-6-phenyl-6*H*-pyrrolo[3,4-*d*]pyrimidine-2,4(1*H*,3*H*)-dione (3d): Colorless prisms (hexane-ethanol); mp 168—170 °C; IR (KBr) cm^{-1}: 1690, 1640 (CO); ^1H MNR ($CDCl_3$) δ=3.00, 3.28, 3.47 (3H, each, 3s, $-CH_3$), 6.6—7.5 (10H, m, phenyl), 7.54 (1H, s, 5-H); ^{13}C NMR ($CDCl_3$) δ=27.9, 30.2, 40.0, 105.5 (4a-C), 112.5 (5-C), 117.5 (7a-C), 122.2 (7-C), 118.0, 118.8, 125.2, 128.5, 129.4, 129.5, 137.8, 149.1, 152.3 (2-C), 159.9 (4-C); MS *m/z*: 360 (M^+). Found: C, 70.31; H, 5.61; N, 15.62%. Calcd for $C_{21}H_{20}N_4O_2$: C, 69.98; H, 5.59; N, 15.55%.

6-(*p*-Methoxyphenyl)-1,3-dimethyl-7-morpholino-6*H*-pyrrolo[3,4-*d*]pyrimidine-2,4(1*H*,3*H*)-dione (3e): Pale yellow prisms (hexane-ethanol); mp 192—194 °C; IR (KBr) cm^{-1}: 1690, 1650(CO); ^1H MNR ($CDCl_3$) δ=2.9—3.2, 3.5—3.8 (4H, each, 2m, $-CH_2-$), 3.50, 3.78, 3.99 (3H, each, 3s, $-CH_3$), 7.13 (1H, s, 5-H), 7.2—7.5 (4H, m, phenyl); ^{13}C NMR ($CDCl_3$) δ=27.8, 31.4, 52.8, 55.6, 67.0, 104.6 (4a-C), 114.3, 118.5 (5-C), 120.4 (7a-C), 124.0 (7-C), 128.8, 131.9, 152.5 (4-C), 160.0 (2-C), 160.2; MS *m/z*: 370 (M^+). Found: C, 61.62; H, 5.81; N, 15.00%. Calcd for $C_{19}H_{22}N_4O_4$: C, 61.61; H, 5.99; N, 15.13%.

1,3-Dimethyl-7-morpholino-6-(*p*-tolyl)-6*H*-pyrrolo[3,4-*d*]pyrimidine-2,4(1*H*,3*H*)-dione (3f): Colorless plates (hexane-ethanol); mp 218—219 °C; IR (KBr) cm^{-1}: 1690, 1650 (CO); ^1H NMR ($CDCl_3$) δ=2.48 (3H, s, $-CH_3$), 2.8—3.2, 3.4—3.7 (4H, each, 2m, $-CH_2-$), 3.44, 3.72 (3H, each, 2s, $-CH_3$), 7.20 (1H, s, 5-H), 7.2—7.4 (4H, m, phenyl); ^{13}C NMR ($CDCl_3$) δ=21.2, 27.8, 31.4, 52.8, 67.0, 104.7 (4a-C), 118.3 (5-C), 120.6 (7a-C), 123.8 (7-C), 127.4, 129.8, 136.8, 139.6, 152.5 (4-C), 160.0 (2-C); MS *m/z*: 354 (M^+). Found: C, 64.26; H, 6.30; N, 15.69%. Calcd for $C_{19}H_{22}N_4O_3$: C, 64.39; H, 6.26; N, 15.81%.

6-(*p*-Bromophenyl)-1,3-dimethyl-7-morpholino-6*H*-pyrrolo[3,4-*d*]pyrimidine-2,4(1*H*,3*H*)-dione (3g): Pale yellow

prisms (hexane-ethanol); mp 207—209 °C; IR (KBr) cm^{-1}: 1700, 1650 (CO); ^1H NMR ($CDCl_3$) δ=2.8—3.1, 3.4—3.7 (4H, each, 2m, $-CH_2-$), 3.39, 3.66 (3H, each, 2s, $-CH_2-$), 7.16 (1H, s, 5-H), 7.2—7.3, 7.6—7.7 (2H each, 2m, phenyl); ^{13}C NMR ($CDCl_3$) δ=27.9, 31.7, 52.9, 67.0, 105.3 (4a-C), 118.0 (5-C), 121.0 (7a-C), 123.4, 123.6 (7-C), 129.2, 132.5, 138.3, 152.4 (4-C), 159.8 (2-C); MS *m/z*: 420, 418 (M^+). Found: C, 51.64; H, 4.58; N, 13.16%. Calcd for $C_{18}H_{19}N_4O_3Br$: C, 51.56; H, 4.57; N, 13.36%.

6-(*p*-Chlorophenyl)-1,3-dimethyl-7-morpholino-6*H*-pyrrolo-[3,4-*d*]pyrimidine-2,4(1*H*,3*H*)-dione (3h): Pale yellow prisms (hexane-ethanol); mp 206—208 °C; IR (KBr) cm^{-1}: 1700, 1650 (CO); ^1H NMR ($CDCl_3$) δ=2.8—3.2, 3.3—3.8 (4H, each, 2m, $-CH_2-$), 3.48, 3.75 (3H, each, 2s, $-CH_3$), 7.30 (1H, s, 5-H), 7.4—7.7, 7.4—7.7 (4H, m, phenyl); ^{13}C NMR ($CDCl_3$) δ=27.9, 31.7, 52.8, 67.0, 105.3 (4a-C), 118.1 (5-C), 121.0 (7a-C), 123.7 (7-C), 128.9, 129.5, 135.5, 137.8, 152.4 (2-C), 159.9 (4-C); MS *m/z*: 376, 374 (M^+). Found: C, 57.86; H, 5.13; N, 14.95%. Calcd for $C_{18}H_{19}N_4O_3Cl$: C, 57.68; H, 5.11; N, 14.95%.

1,3-Dimethyl-7-morpholino-6-(1-naphthyl)-6*H*-pyrrolo[3,4-*d*]pyrimidine-2,4(1*H*,3*H*)-dione (3i): Pale yellow plates (ethanol); mp 231—232 °C; IR (KBr) cm^{-1}: 1690, 1660 (CO); ^1H NMR ($CDCl_3$) δ=2.9—3.1, 3.2—3.5 (4H, each, 2m, $-CH_2-$), 3.48, 3.74 (3H, each, 2s, $-CH_3$), 7.30 (1H, s, 5-H), 7.4—8.2 (7H, m, aromatic); ^{13}C NMR ($CDCl_3$) δ=27.9, 31.5, 52.1, 53.0, 66.9, 67.0, 105.0 (4a-C), 119.3 (5-C), 120.4 (7a-C), 122.4, 124.9, 125.0 (7-C), 126.2, 127.1, 127.8, 128.3, 130.2, 131.5, 133.9, 135.8, 152.5 (2-C), 160.1 (4-C); MS *m/z*: 390 (M^+). Found: C, 67.63; H, 5.68; N, 14.34%. Calcd for $C_{22}H_{22}N_4O_3$: C, 67.67; H, 5.68; N, 14.35%.

6-Benzyl-1,3-dimethyl-7-morpholino-6*H*-pyrrolo[3,4-*d*]pyrimidine-2,4(1*H*,3*H*)-dione (3j): Colorless plates (benzene-ethanol); mp 192—193 °C; IR (KBr) cm^{-1}: 1700, 1650 (CO); ^1H NMR ($CDCl_3$) δ=2.8—3.1, 3.5—3.8 (4H, each, 2m, $-CH_2-$), 3.37, 3.60 (3H, each, 2s, $-CH_3$), 5.17 (2H, s, $-CH_2-$), 7.18 (1H, s, 5-H), 7.2—7.5 (5H, m, phenyl); ^{13}C NMR ($CDCl_3$) δ=27.8, 32.3, 51.2, 52.5, 67.3, 104.2 (4a-C), 117.3 (5-C), 121.5 (7a-C), 121.9 (7-C), 126.3, 128.1, 129.0, 136.8, 152.4 (2-C), 160.0 (4-C); MS *m/z*: 354 (M^+). Found: C, 64.34; H, 6.30; N, 15.76%. Calcd for $C_{19}H_{22}N_4O_3$: C, 64.39; H, 6.26; N, 15.81%.

1,3-Dimethyl-6-phenyl-6*H*-pyrrolo[3,4-*d*]pyrimidine-2,4-(1*H*,3*H*)-dione (4): Colorless prisms (ethanol); mp 194—196 °C (lit,[3] 194—196 °C).

References

1) Studies on Fused Pyrimidine Derivatives. Prat V. Part IV of this series: M. Noguchi, K. Sakamoto, S. Nagata, and S. Kajigaeshi, *Chem. Express*, to be submitted.

2) M. Noguchi, K. Sakamoto, S. Nagata, and S. Kajigaeshi, *J. Heterocycl. Chem.*, **25**, 205 (1988).

3) K. Hirota, Y. Yamada, T. Aso, and S. Senda, *Chem. Pharm. Bull.*, **29**, 1525 (1981).

4) For a review: V. Amarnath and R. Madhav, *Synthesis*, **1974**, 837.

5) T. Murata and K. Ukawa, *Chem. Pharm. Bull.*, **22**, 1212 (1974); G. Tarzia, G. Panzone, P. Carminati, P. Schiatti, and D. Selva, *Farmaco, Ed. Sci.*, **31**, 81 (1976); G. Tarzia, G. Panzone, *Gazz. Chim. Ital.*, **108**, 591 (1978); P. L. Southwick, R. Madhav, V. Amarnath, and T. Scheradsky, *Nucl. Acid Chem.*, **1**, 141 (1978); G. Tarzia, G. Panzone, P. Schiatti, and D. Selva, *Farmaco, Ed. Sci.*, **34**, 316 (1979); R. Madhav. C. A. Snyder, and P. L. Southwick, *J. Heterocycl. Chem.*, **17**, 1231 (1980).

6) The general experimental procedures were the same as in Part III.[2]

A Facile Halogenative Cyclization of 4-(2-Benzothiazolyldithio)azetidinones (Kamiya's Disulfide) into 2β-(Halomethyl)penams in a Two Layer System

Hideo TANAKA, Motoaki TANAKA, Sho-zo YAMADA,† Akira NAKAI, Hisashi OHBAYASHI,† Tadafumi TERADA,† and Sigeru TORII*

Department of Applied Chemistry, Faculty of Engineering, Okayama University, Tsushima-naka, Okayama 700
†Chemical Synthesis Research Laboratory, Taiho Pharmaceutical Co., Ltd., Kodama, Saitama 367-02

(Received May 24, 1989)

Synopsis. Chlorinative cyclization of 4-(2-benzothiazolyldithio)azetidinones into 2β-(chloromethyl)penams has been successfully performed by treatment with aqueous sodium nitrite in a two-layer solution comprising aqueous hydrochloric acid and dichloromethane layers. Similarly, the corresponding 2β-(bromomethyl)penams can be obtained by use of aqueous hydrobromic acid in place of aqueous hydrochloric acid.

The nucleophilic substitution of the chlorine atom of 2β-(chloromethyl)penams **3** (X=Cl)[1] is a promising procedure for the synthesis of various 2β-(substituted methyl)penams and 3β-substituted cephams.[1c,2] The 2β-(chloromethyl)penams **3** (X=Cl) has been prepared by a two-step operation involving thermolysis of penicillanate 1-oxides **1** with 2-mercaptobenzothiazole leading to Kamiya's disulfide **2**[1a] and subsequent chlorinative cyclization with chlorine and copper(II) chloride (Scheme 1).[1a-c] In a practical sense, however, the hitherto known methods for the latter step (**2**—**3**) suffer from inevitable disadvantages due to the contamination of overchlorination products and/or difficulties in removing copper complexes generated in the reaction. Therefore, we needed a new device for the chlorinative cyclization of 4-(2-benzothiazolyldithio)-azetidinones **2** in high product selectivities without the tedious workup process. For this purpose, we have elaborated a unique two-layer system, comprising aqueous sodium nitrite-hydrochloric acid and dichloromethane as illustrated in Scheme 2 in which the chlorinative cyclization of **2** can be performed smoothly to afford **3** (X=Cl) in satisfactory yields.

The present method is characterized by the simple operation and the high yield of the product **3** (X=Cl). Into the two-layer solution comprising a dichloromethane solution of 4-dithioazetidinones **2** (R^1=R^2=H) and aqueous 22% hydrochloric acid was added portionwise aqueous 8% sodium nitrite. After being stirred for a few hours, the organic layer was separated and worked up in a conventional manner to afford 2β-(chloromethyl)-penams **3a**—**c** (R^1=R^2=H, X=Cl) together with bis(2-benzothiazoyl) disulfide **4** in good yields, (Table 1, Entries 1—3). Undesired side products, e.g. overchlorina-

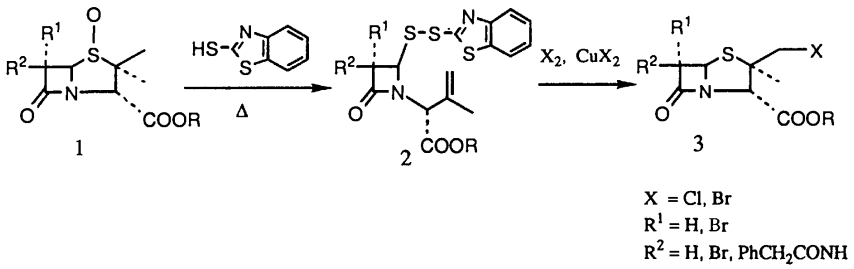

Scheme 1.

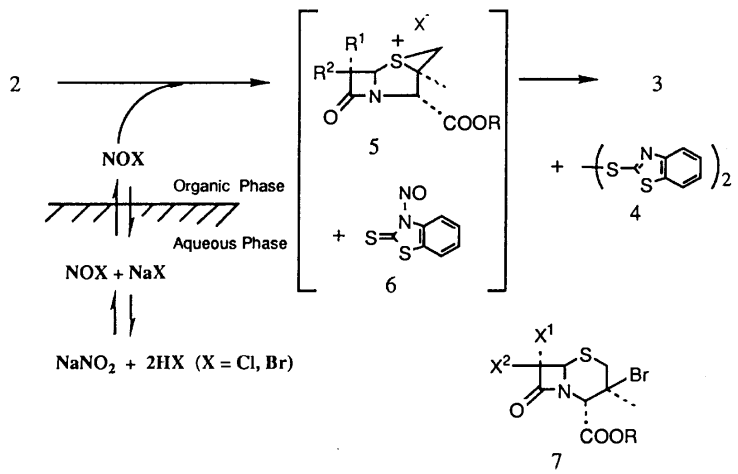

Scheme 2.

Table 1. A Facile Synthesis of 2β-(Halomethyl)penams **3**[a]

Entry	4-Dithioazetidinone				Time	Product		Yield[c]
	2	R^1	R^2	R[b]	h	**3**	X	%
1	**2a**	H	H	PNB	2	**3a**	Cl	91
2	**2b**	H	H	PMB	2	**3b**	Cl	92
3	**2c**	H	H	$CHPh_2$	2	**3c**	Cl	92
4	**2d**	Br	H	PNB	3	**3d**	Cl	91
5	**2e**	Br	Br	PMB	5	**3e**	Cl	93
6	**2f**	Br	Br	$CHPh_2$	5	**3f**	Cl	95
7	**2g**	H	$PhCH_2CONH$	CH_2Ph	2	**3g**	Cl	91
8	**2a**	H	H	PNB	1	**3h**	Br	77(99)[d]
9	**2e**	Br	Br	PMB	5	**3i**	Br	95

a) Carried out with 8% aqueous sodium nitrite (1.1—2 equiv) in 22% hydrochloric acid (or 10% hydrobromic acid) and dichloromethane. b) PNB: *p*-nitrobenzyl; PMB: *p*-methoxybenzyl. c) Isolated yields. d) A mixture of **3h** and **7h** (56/44) was obtained after column chromatography.

tion products or β-lactam ring-opened products were not detected in the crude products. The isolation of the product **3** from the disulfide **4** can be easily performed by a fractional recrystallization from acetone and/or methanol.

The chlorinative cyclization of various 4-dithioazetidinones derivatives **2** was similarly performed in the two layer system (Entries 4—9). 3-Bromo-, 3,3-dibromo-, and 3-(phenylacetamido)azetidinones **2d—g** were transformed to the corresponding penicillanates **3d—g** in good yields.

In addition, the two-layer system can be applied successfully to the preparation of the corresponding 2β-(bromomethyl)penams **3** (X=Br) by use of hydrobromic acid in place of hydrochloric acid. The 2β-(bromomethyl)penams **3** are very susceptible to isomerization to 3β-bromocepham **7**; indeed, upon the chromatography on a silica gel, **3h** (R^1=R^2=H, X=Br) was partly isomerized to a mixture of **3h** and **7h** (55/44). Fortunately, pure 2β-(bromomethyl)penams **3** were obtained by fractional recrystallization from acetone and/or ether immediately after the reaction.

Although the reaction mechanism has not yet been clarified, nitrosyl halide (NOX) generated in the aqueous phase seems to play a significant role; thus, in an aqueous phase, sodium nitrite would react with hydrogen halide to generate nitrosyl halide, which moves to the organic phase and reacts with 4-dithioazetidinones **2**, generating tricyclo sulfonium ion **5** and nitroso intermediate **6**. In turn, the former would produce 2β-(halomethyl)penam **3** by the attack of halide ion on the 2β-methylene carbon of **5**, while the latter would undergo disproportionation and/or further reaction with 4-dithioazetidinones **2** to give dimer **4**.

Experimental

Melting points were determined with a Thomas-Hoover capillary apparatus and are uncorrected. IR spectra were recorded on a JASCO IRA-1 grating spectrophotometer. ^{1}H NMR spectra were taken on a Hitachi R-24 (60 MHz) and a JEOL MX-100 spectrometers (100 MHz) using tetramethylsilane as an internal standard. Mass spectra were obtained on a JEOL JMS-DX303 spectrometer. Microanalyses were performed in our laboratory.

General Procedure for Synthesis of 2β-(Chloromethyl)penams (Table 1, Entries 1—7). ***p*-Nitrobenzyl 2β-(Chloromethyl)-2α-methylpenam-3α-carboxylate (3a):** To a solution of *p*-nitrobenzyl [(*R*)-4-(2-benzothiazol-2-yldithio)-2-oxo-1-azetidinyl]isopropenylacetate (**2a**) (501 mg, 1 mmol) in dichloromethane (4 ml) and 22% hydrochloric acid (4 ml) was added sodium nitrite (76 mg, 1.1 mmol) in water (1 ml) portionwise at 0 °C. The stirring was continued for 2 h at 0 °C. The precipitates bis(2-benzothiazolyl) disulfide (**4**) were filtered and washed with a small amount of dichloromethane. The filtrates and washing were combined, washed with water, aqueous sodium hydrogencarbonate, and brine, and dried (Na_2SO_4). After concentration in vacuo, the residue was taken up with a small amount of acetone and insoluble materials were filtered off. The filtrate was again concentrated in vacuo and the residue was crystallized from ether to afford **3a**[1c] (337 mg, 91%); mp 104—105 °C; IR (KBr) 1780, 1775 cm^{-1}; ^{1}H NMR ($CDCl_3$) δ=1.49 (s, 3H, CH_3), 3.15 (dd, *J*=2 and 16 Hz, 1H, 6-H), 3.63 (dd, *J*=4 and 16 Hz, 1H, 6-H), 3.60 (s, 2H, CH_2Cl), 5.12 (s, 1H, 3-H), 5.30 (s, 2H, OCH_2), 5.40 (dd, *J*=2 and 4 Hz, 5-H), 7.57 (d, *J*=8 Hz, 2H, aromatic H), 8.26 (d, *J*=8 Hz, 2H, aromatic H).

***p*-Methoxybenzyl 2β-Chloromethyl-2α-methylpenam-3α-carboxylate (3b):** IR (Neat) 1790, 1750 cm^{-1}; ^{1}H NMR ($CDCl_3$) δ=1.43 (s, 3H, CH_3), 3.09 (dd, *J*=2 and 16 Hz, 1H, 6-H), 3.60 (dd *J*=4 and 16 Hz, 1H, 6-H), 3.59 (s, 2H, CH_2Cl), 3.81 (s, 3H, OCH_3), 5.01 (s, 1H, 3-H), 5.14 (s, 2H, OCH_2), 5.37 (dd, *J*=2 and 4 Hz, 1H, 5-H), 6.89 (d, *J*=9 Hz, 2H, aromatic H), 7.32 (d, *J*=9 Hz, 2H, aromatic H); FAB-MS *m/z* 378 $(M-Na)^+$.

Benzhydryl 2β-Chloromethyl-2α-methylpenam-3α-carboxylate (3c):[1c] IR (Neat) 1780, 1745 cm^{-1}; ^{1}H NMR ($CDCl_3$) δ=1.33 (s, 3H, CH_3), 3.60 (s, 2H, CH_2Cl), 3.11 (dd, *J*=2 and 16 Hz, 1H, 6-H), 3.76 (dd, *J*=4 and 16 Hz, 1H, 6-H), 5.13 (s, 1H, 3-H), 5.40 (dd, *J*=2 and 4 Hz, 5-H), 6.94 (s, 1H, $CHPh_2$), 7.35 (s, 10H, aromatic H).

***p*-Nitrobenzyl 6β-Bromo-2β-chloromethyl-2α-methylpenam-3α-carboxylate (3d):**[1c] Mp 111—113 °C; IR (KBr) 1800, 1750 cm^{-1}; ^{1}H NMR ($CDCl_3$) δ=1.49 (s, 3H, CH_3), 3.48, 3.66 (ABq, *J*=12 Hz, 2H, CH_2Cl), 4.83 (d, *J*=1.3 Hz, 1H, 6-H), 5.15 (s, 1H, 3-H), 5.27, 5.38 (ABq, *J*=9 Hz, 2H, OCH_2) 5.47 (d, *J*=1.3 Hz, 1H, 5-H), 7.57 (d, *J*=9 Hz, 2H, aromatic H), 8.27 (d, *J*=9 Hz, 2H, aromatic H).

***p*-Methoxybenzyl 6,6-Dibromo-2β-chloromethyl-2α-methylpenam-3α-carboxylate (3e):** IR (Neat) 1795, 1735 cm^{-1}; ^{1}H NMR ($CDCl_3$) δ=1.40 (s, 3H, CH_3), 3.55 (s, 2H, CH_2Cl), 3.77 (s, 3H, OCH_3), 5.01 (s, 1H, 3-H), 5.12 (s, 2H, OCH_2), 5.75 (s, 1H, 5-H), 6.82 (d, *J*=9 Hz, 2H, aromatic H), 7.24 (d, *J*=9 Hz, 2H, aromatic H); FAB-MS *m/z* 536 $(M+Na)^+$.

Benzhydryl 6,6-Dibromo-2β-chloromethyl-2α-methylpenam-

3α-carboxylate (3f): IR (Neat) 1810, 1760 cm^{-1}; ^1H NMR ($CDCl_3$) δ=1.31 (s, 3H, CH_3), 3.52, 3.68 (ABq, J=12 Hz, 2H, CH_2Cl), 5.16 (s, 3H, 3-H), 5.85 (s, 1H, 5-H), 6.94 (s, 1H, $CHPh_2$), 7.35 (s, 10H, aromatic H); FAB-MS m/z 582 $(M+Na)^+$.

Benzyl 2β-Chloromethyl-2α-methyl-6β-(phenylacetamido-penam-3α-carboxylate (3g):[3] IR ($CHCl_3$) 3410, 1780, 1775, 1680 cm^{-1}; ^1H NMR ($CDCl_3$) δ=1.62 (s, 3H, CH_3), 3.37, (s, 2H, $PhCH_2CO$), 3.59 (s, 2H, CH_2Cl), 5.02 (s, 1H, 3-H), 5.14 (s, 2H, OCH_2), 5.45—5.70 (m, 2H, 5-H and 6-H), 6.38 (d, J=8 Hz, 1H, NH), 7.27 (s, 5H, aromatic H), 7.32 (s, 5H, aromatic H).

***p*-Nitrobenzyl 2β-Bromomethyl-2α-methylpenam-3α-carboxylate (3h):** To a solution of **2a** (501 mg, 1 mmol) in dichloromethane (10 ml) and 10% hydrobromic acid (4 ml) was added sodium nitrite (76 mg, 1.1 mmol) in water (1 ml) portionwise at 0 °C. The stirring was continued for 1 h at 0 °C. The precipitates bis(2-benzothiazolyl) disulfide (**4**) were filtered and washed with a small amount of dichloromethane. The filtrate and washings were combined, washed with water, aqueous sodium hydrogencarbonate, and brine, and dried (Na_2SO_4). After concentration in vacuo, the residue was taken up with a small amount of acetone, and insoluble materials were filtered off. The filtrate was concentrated and crystallized from ether to afford **3f**[1c] (320 mg, 77%); mp 80—82 °C; IR (KBr) 1790, 1760 cm^{-1}; ^1H NMR ($CDCl_3$) δ=1.53 (s, 3H, CH_3), 3.15 (dd, J=2 and 16 Hz, 1H, 6-H), 3.57 (s, 2H, CH_2Br), 3.65 (dd, J=4 and 16 Hz, 1H, 6-H), 5.18 (s, 1H, 3-H), 5.31 (s, 2H, OCH_2), 5.43 (dd, J=2 and 4 Hz, 1H, 5-H), 7.57 (d, J=9 Hz, 2H, aromatic H), 8.26 (d, J=9 Hz, 2H, aromatic H).

In a similar manner, **3i** was obtained.

***p*-Methoxybenzyl 6,6-Dibromo-2β-bromomethyl-2α-methyl-penam-3α-carboxylate (3i):** Mp 111—113 °C; IR (KBr) 1800, 1750 cm^{-1}; ^1H NMR ($CDCl_3$), δ=1.44 (s, 3H, CH_3), 3.54 (s, 2H, CH_2Br), 3.80 (s, 3H, OCH_3), 5.11 (s, 1H, 3-H), 5.16 (s, 2H, OCH_2), 5.85 (s, 1H, 5-H), 6.69 (d, J=9 Hz, 2H, aromatic H), 7.32 (d, J=9 Hz, 2H, aromatic H). Found: C, 34.42; H, 2.83; N, 2.53%. Calcd for $C_{16}H_{16}Br_3NO_4S$: C, 34.56; H, 2.90; N, 2.52%.

References

1) a) T. Kamiya, T. Teraji, Y. Saito, M. Hashimoto, O. Nakaguchi, and T. Oku, *Tetrahedron Lett.*, **1973**, 3001; b) H. Tanida, T. Tsuji, T. Tsushima, H. Ishitobi, T. Irie, T. Yano, H. Matsumura, and K. Tori, *ibid.*, **1975**, 3303; C) R. G. Micetich, S. N. Maiti, P. Spevak, M. Tanaka, T. Yamazaki, and K. Ogawa, *Synthesis*, **1986**, 292; d) Y. Hamashima, S. Yamamoto, S. Uyeo, M. Yoshioka, M. Murakami, H. Ona, Y. Nishitani, and W. Nagata, *Tetrahedron Lett.*, **1979**, 2595; e) W. J. Gottstein, L. B. Crast, Jr., R. G. Graham, U. J. Hayner, and D. N. McGregor, *J. Med. Chem.*, **24**, 1531 (1981).

2) a) T. Kamiya, T. Teraji, M. Hashimoto, O. Nakaguchi, and T. Oku, Ger, Offen. 2352199 (1974); *Chem. Abstr.*, **81**, 25687q (1974); b) H. Tanaka, M. Tanaka, A. Nakai, S. Yamada, N. Ishida, T. Ohtani, and S. Torii, *J. Antibiotic.*, **41**, 579 (1988); c) H. Tanaka, M. Tanaka, A. Nakai, S. Yamada, H. Ohbayashi, T. Ohno, and S. Torii, *Chem. Express*, **3**, 618 (1988).

3) H. Tanida and T. Tsuji, Ger. Offen. 2333256 (1974); *Chem. Abstr.*, **80**, 95976m (1974).

Efficient Reduction of 2-Haloacetophenone Derivatives to the Corresponding Halohydrins by 9,10-Dihydro-10-methylacridine in the Presence of Titanium Tetrachloride. Comparison with the Reduction in the Presence of Perchloric Acid

Seiji MOCHIZUKI, Shunichi FUKUZUMI,* and Toshio TANAKA
Department of Applied Chemistry, Faculty of Engineering, Osaka University, Suita, Osaka 565
(Received May 31, 1989)

Synopsis. 2-Haloacetophenone derivatives are reduced by an acid-stable NADH model compound, 9,10-dihydro-10-methylacridine, in the presence of $HClO_4$ in acetonitrile at 335 K to yield 10-methylacridinium ion and the parent acetophenone derivatives as well as halohydrins, while the reduction of 2-haloacetophenone derivatives in the presence of $TiCl_4$ in dichloromethane undergoes much more readily even at 298 K to yield the corresponding halohydrins selectively.

Acid catalysis is known to play an essential role in the efficient enzymatic reduction of carbonyl compounds by dihydronicotinamide adenine dinucleotide (NADH).[1] The catalytic center of the enzyme, zinc ion, is believed to act as a Lewis acid rather than a Brönsted acid.[1] Ohno et al.[2] reported that benzaldehyde is reduced to benzyl alcohol by an acid-stable NADH model compound, 1,2,4-trimethyl-3-(α-methylbenzylcarbamoyl)-1,4-dihydroquinoline, in the presence of a Lewis acid ($TiCl_4$ or $AlCl_3$) in tetrahydrofuran at room temperature in 12 h. The reduction of benzaldehyde derivative by acid-stable NADH model compounds is known to be catalyzed also by a Brönsted acid.[3,4]

We have recently reported that various nonactivated ketones[5] and α-halo ketones[6] can be reduced by an acid-stable NADH model compound, 9,10-dihydro-10-methylacridine ($AcrH_2$), in the presence of a Brönsted acid ($HClO_4$) in acetonitrile at 335 K to yield the corresponding halo alcohols and the parent ketones, respectively. The present work reports the comparison of the reactivities as well as the products in the reduction of 2-haloacetophenone derivatives by $AcrH_2$ in the presence of a Lewis acid ($TiCl_4$) with those in the presence of a Brönsted acid ($HClO_4$).

Experimental

Materials. 9,10-Dihydro-10-methylacridine ($AcrH_2$) was prepared from 10-methylacridinium iodide ($AcrH^+I^-$) by the reduction with $NaBH_4$ in methanol, and purified by recrystallization from methanol.[7] The dideuterated compound, [9,9-$^2H_2$]-9,10-dihydro-10-methylacridine ($AcrD_2$), was prepared from 10-methyl-9-acridone by the reduction with $LiAlD_4$.[8] 2-Bromoacetophenone and 2-chloroacetophenone were obtained commercially and purified by the standard methods.[9] 2-Bromo-4′-methoxyacetophenone and 2-bromo-4′-cyanoacetophenone were prepared from bromination of the corresponding acetophenone derivatives in methanol.[10] Styrene bromohydrins was prepared by the reaction of styrene with *N*-bromosuccinimide in water according to the literature.[11] Titanium tetrachloride, dichloromethane, and acetonitrile-d_3 were obtained commercially and used without further purification. Perchloric acid (70%) was obtained from Wako Pure Chemicals.

Reaction Procedure. Typically, $AcrH_2$ (6.0×10^{-5} mol) was added to an NMR tube that contained a deaerated acetonitrile-d_3 (CD_3CN) solution (0.60 cm^3) of 2-haloacetophenone (1.8×10^{-4} mol) and $HClO_4$ (1.8×10^{-4} mol). After the reactant solution was deaerated again by a stream of argon and sealed, the NMR tube was immersed in a water bath which was thermostatted at 335 K. In the case of the reduction of 2-haloacetophenone by $AcrH_2$ in the presence of $TiCl_4$, 2-haloacetophenone (2.0×10^{-3} mol) was firstly added to a deaerated solution of CD_2Cl_2 (0.05 cm^3) containing $AcrH_2$ (5.0×10^{-4} mol), and then $TiCl_4$ (1.3×10^{-3} mol) was added to the 2-haloacetophenone–$AcrH_2$ system under a stream of argon. The reaction was carried out also by changing the order of addition; $TiCl_4$ was firstly added to a CD_2Cl_2 solution of $AcrH_2$, and then 2-haloacetophenone was added to the $AcrH_2$–$TiCl_4$ system. The reaction was quenched by the addition of water (2.0×10^{-3} mol) after 2 min. The product yields were determined from the ^1H NMR spectra in CD_3CN (0.50 cm^3) by comparing with those of the authentic samples.[6] The NMR spectra were recorded using a Japan Electron Optics JNM-PS-100 NMR spectrometer (100 MHz).

Results and Discussion

An NADH model compound ($AcrH_2$) shows no reactivity towards 2-haloacetophenone ($PhCOCH_2X$; X=Br, Cl) in the dark at 335 K. When $HClO_4$ is added to the $AcrH_2$–$PhCOCH_2X$ system, $PhCOCH_2X$ is reduced by $AcrH_2$ at 335 K to yield 10-methylacridinium ion ($AcrH^+$) and acetophenone (Eq. 1) as well as

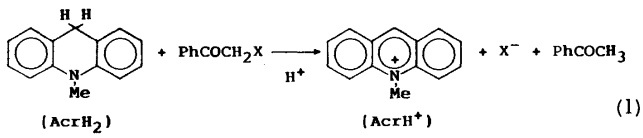

(1)

α-(halomethyl)benzenemethanol (Eq. 2). 2-Haloacetophenone is reduced by $AcrH_2$ much more readily even

$$ArcH_2 + PhCOCH_2X + H^+ \longrightarrow AcrH^+ + PhCH(OH)CH_2X \quad (2)$$

at 298 K in the presence of $TiCl_4$ in dichloromethane, and the corresponding halohydrin, α-(halomethyl)-benzenemethanol is obtained selectively in 70—80% yield with no dehalogenated compound in 2 min, when the reaction is quenched by water. Such selective formation of halohydrin seems interesting since the model systems that have so far been reported for the reduction of α-halo ketones undergo the reductive dehalogenation to yield parent ketones,[12] although the enzyme-mediated reduction of 2-haloacetophenone is known to yield the corresponding halo-

Table 1. Reduction of 2-Haloacetophenone Derivatives (2.0×10^{-3} mol) by $AcrH_2$ and $AcrD_2$ (5.0×10^{-4} mol) in the Presence of $TiCl_4$ (1.3×10^{-3} mol) in Dichloromethane (0.05 cm^3) at 298 K, Compared with the Reduction of the Same Substrates (1.8×10^{-4} mol) by $AcrH_2$ and $AcrD_2$ (6.0×10^{-5} mol) in the Presence of $HClO_4$ (1.8×10^{-4} mol) in Acetonitrile (0.6 cm^3) at 335 K

Substrate	Reductant	Acid	Time	Product yield/%
$PhCOCH_2Br$	$AcrH_2$	$TiCl_4$	2 min	$PhCH(OH)CH_2Br$(80) $AcrH^+$(80)
$PhCOCH_2Br$	$AcrH_2$	$HClO_4$	11 h	$PhCOCH_3$(82) $PhCH(OH)CH_2Br$(14) $PhCH(OH)CH_3$(4) $AcrH^+$(100)
$PhCOCH_2Cl$	$AcrH_2$	$TiCl_4$	2 min	$PhCH(OH)CH_2Cl$(70) $AcrH^+$(77)
$PhCOCH_2Cl$	$AcrH_2$	$HClO_4$	110 h	$PhCOCH_3$(36) $PhCH(OH)CH_2Cl$(49) $PhCH(OH)CH_3$(14) $AcrH^+$(100)
$PhCOCH_2Br$	$AcrD_2$	$TiCl_4$	2 min	$PhCD(OH)CH_2Br$(75) $AcrD^+$(80)
$PhCOCH_2Br$	$AcrD_2$	$HClO_4$	43 h	$PhCOCH_3$(90) $PhCD(OH)CH_2Br$(7) $PhCD(OH)CH_3$(trace) $AcrD^+$(100)
$PhCOCH_2Cl$	$AcrD_2$	$TiCl_4$	2 min	$PhCD(OH)CH_2Cl$(44) $AcrD^+$(70)
	$AcrD_2$	$HClO_4$	200 h	$PhCOCH_3$(57) $PhCD(OH)CH_3$(27) $PhCD(OH)CH_3$(9) $AcrD^+$(100)
4′-$MeOC_6H_4COCH_2Br$	$AcrH_2$	$TiCl_4$	2 min	4′-$MeOC_6H_4CH(OH)CH_2Br$(52) $AcrH^+$(60)
4′-$MeOC_6H_4COCH_2Br$	$AcrH_2$	$HClO_4$	4 h	4′-$MeOC_6H_4COCH_3$(48) 4′-$MeOC_6H_4CH(OH)CH_3$(46) 4′-$MeOC_6H_4CH(OH)CH_3$(6) $AcrH^+$(100)
4′-$CNC_6H_4COCH_2Br$	$AcrH_2$	$TiCl_4$	2 min	4′-$CNC_6H_4CH(OH)CH_2Br$(50) $AcrH^+$(68)
4′-$CNC_6H_4COCH_2Br$	$AcrH_2$	$HClO_4$	7 h	4′-$CNC_6H_4COCH_3$(95) 4′-$CNC_6H_4CH(OH)CH_3$(5) $AcrH^+$(100)
$PhCOCH(C_2H_5)Br$	$AcrH_2$	$TiCl_4$	2 min	$PhCH(OH)CH(C_2H_5)Br$(6) $AcrH^+$(80)
$PhCOCH(C_2H_5)Br$	$AcrH_2$	$HClO_4$	100 h	$PhCOC_3H_7$(92) $PhCH(OH)CH(C_2H_5)Br$(6) $AcrH^+$(100)
$PhCOCH(C_8H_{17})Br$	$AcrH_2$	$TiCl_4$	2 min	$PhCH(OH)CH(C_8H_{17})Br$(10) $AcrH^+$(73)
$PhCOCH(C_8H_{17})Br$	$AcrH_2$	$HClO_4$	200 h	$PhCOC_9H_{19}$(55) $AcrH^+$(100) $PhCH(OH)CH(C_8H_{17})Br$(45)
None	$AcrH_2$	$TiCl_4$	2 min	$AcrH^+$(50)

hydrin selectively.[13]

The reaction conditions and the yields of products are compared for the reduction of various 2-haloacetophenone derivatives by $AcrH_2$ in the presence of $HClO_4$ with those in the presence of $TiCl_4$ as shown in Table 1. The much higher reaction temperature and more prolonged reaction time are required for the reactions in the presence of $HClO_4$ brought to completion than those in the presence of $TiCl_4$. In the reduction of $PhCOCH_2X$ (X=Br, Cl) by $AcrH_2$ in the presence of $TiCl_4$, the yield of the oxidized product $AcrH^+$ is about the same as that of the reduced product, $PhCH(OH)CH_2X$ (Table 1). The prolonged reaction time (e.g., 10 min) did not improve the product yields.

When $AcrH_2$ is replaced by the 9,9-dideuterated analogue ($AcrD_2$) in the reduction of 2-haloacetophenone in the presence of $HClO_4$ and also in the reduction in the presence of $TiCl_4$, the deuterium is incorporated into α-(halomethyl)benzenemethanol in both cases (Table 1). In the case of the reduction in the presence of $HClO_4$, however, no deuterium is incorporated into the dehalogenated product, acetophenone. The acetophenone is further reduced by $AcrH_2$ to yield small amount of the corresponding alcohol in which the deuterium is incorporated (Table 1). The substitution of the α-carbon of $PhCOCH_2Br$ with an alkyl group for the reduction in the presence of $TiCl_4$ results in significant decrease in the yield of halohydrin, accompanied by the recovery of the reactant, although the yield of $AcrH^+$ is rather constant (Table 1).

In the absence of 2-haloacetophenone as well, $AcrH_2$ is readily oxidized by $TiCl_4$ to yield $AcrH^+$ (Table 1). In addition, no appreciable reduction of 2-haloacetophenone occurs upon the reversed addition; $AcrH_2$ is added to a dichloromethane solution of $TiCl_4$ firstly and then 2-haloacetophenone is added to the $AcrH_2$–$TiCl_4$ system. Thus, the reduction of $TiCl_4$ by $AcrH_2$ may take place firstly, and then a reduced titanium species, which would decompose in the absence of active substrates, may reduce 2-haloacetophenone derivatives to the corresponding halohydrins. The reduced titanium species may not be $TiCl_3$, since $TiCl_3$ is known to bring about reductive dehalogenation of 2-haloacetophenone to yield acetophenone exclusively.[14] In general, a Lewis acid such as $TiCl_4$ is known to activate carbonyl compounds in the reductions by various reductants.[15] Thus, a hydride transfer from $AcrH_2$ to 2-haloacetophenone may be mediated by $TiCl_4$ and facilitated by the interaction of α-halo ketones with $TiCl_4$. At present, however, the detection of a possible mediator such as a titanium hydride species by a low-temperature ^1H NMR measurement was unsuccessful. Other Lewis acids such as $SnCl_4$, $BF_3\cdot OEt_2$, and $AlCl_3$ were not effective for the reduction of α-halo ketones to halohydrins by $AcrH_2$.

References

1) H. Eklund and C.-I. Bränden, "Zinc Enzymes," ed by T. G. Spiro, Wiley-Interscience, New York (1983), Chap. 4.

2) A. Ohno, Y. Ishikawa, S. Ushida, and S. Oka, *Tetrahedron Lett.*, **23**, 3185 (1982).
3) S. Shinkai, H. Hamada, and O. Manabe, *Tetrahedron Lett.*, **1979**, 1397.
4) S. Fukuzumi, M. Ishikawa, and T. Tanaka, *J. Chem. Soc., Chem. Commun.*, **1985**, 1069; *Tetrahedron*, **42**, 1021 (1986).
5) S. Fukuzumi, M. Chiba, and T. Tanaka, *Chem. Lett.*, **1989**, 31.
6) S. Fukuzumi, S. Mochizuki, and T. Tanaka, *J. Am. Chem. Soc.*, **111**, 1497 (1989).
7) R. M. G. Roberts, D. Ostović, and M. M. Kreevoy, *Faraday Discuss. Chem. Soc.*, **74**, 257 (1982); S. Fukuzumi, S. Koumitsu, K. Hironaka, and T. Tanaka, *J. Am. Chem. Soc.*, **109**, 305 (1987).
8) P. Karrer, L. Szabo, H. J. V. Krishna, and R. Schwyzer, *Helv. Chim. Acta*, **33**, 294 (1950); D. Ostović, R. M. G. Roberts, and M. M. Kreevoy, *J. Am. Chem. Soc.*, **105**, 7629 (1983).
9) D. D. Perrin, W. L. F. Armarego, and D. R. Perrin, "Purification of Laboratory Chemicals," Pargamon Press, New York (1968).
10) R. E. Lutz, R. K. Allison, G. Ashburn, P. S. Bailey, M. T. Clark, J. F. Codington, A. J. Deinet, J. A. Freek, R. H. Jordan, N. H. Leake, T. A. Martin, K. C. Nicodemus, R. J. Rowlett, Jr., N. H. Shearer, Jr., J. D. Smith, and J. W. Wilson, III, *J. Org. Chem.*, **12**, 617 (1947).
11) C. O. Guss and R. Rosenthal, *J. Am. Chem. Soc.*, **77**, 2549 (1955).
12) H. Inoue, R. Aoki, and E. Imoto, *Chem. Lett.*, **1974**, 1157.
13) D. D. Tanner and A. R. Stein, *J. Org. Chem.*, **53**, 1642 (1988).
14) A. Clerici and O. Porta, *Tetrahedron Lett.*, **28**, 1541 (1987).
15) T. Mukaiyama, K. Banno, and K. Narasaka, *J. Am. Chem. Soc.*, **96**, 7503 (1974); A. Hosomi and H. Sakurai, *Tetrahedron Lett.*, **1976**, 1295; Y. Yamamoto and J. Yamada, *J. Am. Chem. Soc.*, **109**, 4395 (1987).

The Selectivity of Sulfided NiW/Al_2O_3 Catalyst in the Hydrodesulfurization of Dibenzothiophene

Masatoshi NAGAI
Department of Chemical Engineering, Faculty of Technology, Tokyo University of Agriculture and Technology, Koganei, Tokyo 184
(Received March 17, 1989)

Synopsis. The selectivity of a sulfided NiW/Al_2O_3 catalyst for hydrodesulfurization has been studied at 300°C and 10.1 MPa total pressure. The presence of oxygen and sulfur compounds depressed the desulfurization of dibenzothiophene, but not the hydrogenation. The addition of large amounts of acridine improved the catalytic activity significantly for the desulfurization of dibenzothiophene to biphenyl while preventing hydrogenation.

The hydrodesulfurization of petroleum residue is widely practiced and the need for a similar technology for coal-derived liquids is well recognized. Heavy feedstocks contain small amounts of nitrogen compounds and sulfur compounds as impurities. Catalyst poisoning by nitrogen compounds is a serious problem during hydroprocessing treatment.

Several researchers have studied the effect of nitrogen compounds on the hydrodesulfurization reactions in order to obtain more detailed information about the poisoning mechanism. A previous study[1] revealed that the presence of nitrogen compounds depressed the hydrogenation of dibenzothiophene on a sulfided Mo/Al_2O_3 catalyst. Neither an increase in the conversion, nor an improvement in the catalytic activity for the desulfurization, was observed during the reaction. Cowley and Massoth[2] also found that the addition of pyridine greatly decreased the conversion of thiophene on a sulfided Mo/Al_2O_3 catalyst. Moreover, Urimoto and Sakikawa[3] reported that the presence of pyridine inhibited the hydrodesulfurization activity of MoS_2, WS_2, CoS, and NiS catalysts. Thus, the presence of nitrogen compounds greatly decreased the conversion, and diminished the catalytic activity of the molybdenum (or nickel or tungsten) sulfided catalyst which did not contain any promoting metals.

However, we have studied the poisoning effect of nitrogen compounds on the hydrodesulfurization of dibenzothiophene on a sulfided $NiMo/Al_2O_3$[4] and NiW/Al_2O_3[5] catalyst and found that the presence of large amounts of acridine markedly enhanced the desulfurization activity of the catalysts, together with a decrease in the hydrogenation activity. The behavior of these catalysts appeared to be different from the sulfided Mo/Al_2O_3 catalysts or metal sulfide catalysts without a promoter in the presence of nitrogen compounds.

In the present work, the hydrodesulfurization of dibenzothiophene on the sulfided NiW/Al_2O_3 catalyst at 300°C and 10.1 MPa total pressure was investigated in the presence of CS_2 and xanthene as well as acridine. The selectivity of the sulfided NiW/Al_2O_3 catalyst for hydrogenation and desulfurization is discussed.

Experimental

Acridine (Ultra pure grade, Tokyo Kasei Chemical), dibenzothiophene, xanthene and carbon disulfide (Extra pure grade), and xylene (Chemically pure grade) were used without purification. Hydrogen (99.9%, To-Ei Chemical) was passed through 13X Molecular Sieves before use. Hydrogen sulfide (99.5%) was used without purification.

Two grams of a NiW/Al_2O_3 (6.5%, NiO and 21% WO_3, Ketjenfine; 14—20 mesh) were packed into the central portion (length 3.6 cm) of the reactor and were oxidized in air at 450°C for more than 24 h. The catalyst was reduced in situ at 400°C for 4 h at a pressure of 10.1 MPa of hydrogen, then at 30 L h^{-1}. After presulfidation, the catalyst was sulfided at a 10% H_2S/H_2 atmosphere, then at 30 L h^{-1} and 400°C for 3 h. The experiment was carried out in a continuous-flow microreactor at 300°C and 10.1 MPa total pressure. The hydrogen (gas ntp)/dibenzothiophene ratio was 320. The weight hourly space velocity (WHSV) was 7.5. After a solution containing 5 wt% dibenzothiophene in xylene was introduced into the reactor, a steady state was achieved within about 3 h. This standard condition was run before the start of each set of experiments with a particular additive.

When measuring the selective effect on the hydrodesulfurization by an additive, a series of feeds containing increasing concentrations of additive was used. The catalyst attained steady activity within about 1 h when additive concentrations were increased. The liquid products were separated by a high-pressure separator into gaseous products. The liquid products, which had higher boiling points than xylene, were analyzed by FID gas chromatography. Biphenyl, cyclohexylbenzene, and 2-ethylbicyclo[4.4.0]decane were identified by comparisons with data from authentic samples by GC and high-resolution mass spectrometry. The hydrogenated dibenzothiophene compounds, cyclohexylbenzene and methyl- and dimethyl dibenzothiophene, were analyzed by GC-MS.

Results and Discussion

Promoting Effect of Acridine. The change in the product distribution in dibenzothiophene hydrodesulfurization in the presence of acridine at 300°C and 10.1 MPa total pressure is shown in Fig. 1. The concentrations of the unreacted dibenzothiophene and cyclohexylbenzene remained constant at 0.1 wt% of acridine, though but further additions led to a great increase in the conversion of dibenzothiophene. This observation indicates that a large amount of acridine enhances the selective desulfurization of dibenzothiophene to biphenyl and depresses hydrogenation. Above 320°C, conversion is not influenced by acridine. This appears to be caused either by diffusional limitations or by a competitive C–N hydrogenolysis of perhydroacridine, which is formed from acridine hydrogenation.

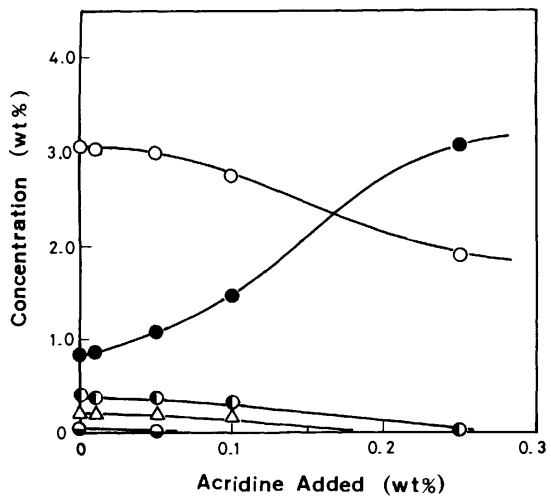

Fig. 1. Change in the product distribution of dibenzothiophene hydrodesulfurization on the addition of acridine at 300 °C. ◒, Methyl- and dimethyldibenzothiophene; ○, Dibenzothiopohene; ●, biphenyl; △, cyclohexylbenzene; ◐, 1,1′-bicyclohexyl, hydrogenated dibenzothiophenes, and other hydrocarbons which have higher boiling point than 1,1′-bicyclohexyl.

The addition of acridine greatly improved the carbon material balance on dibenzothiophene, even at higher temperatures, since the formation of the many small amounts of by-products decreased. The material balance was initially 29 and 57% at 320 and 360 °C, respectively, but rose to 80% after the addition of acridine.

Several authors have proposed shcemes for the electron-transfer reactions between nickel and tungsten ions responsible for generating the desulfurization sites.[1-8] Ni(II) ions should be more easily reduced than WS_2 by hydrogen:

$$\mathrm{Ni(II)} + \mathrm{e} = \mathrm{Ni(I)} \quad (1)$$

and

$$\mathrm{Ni(I)} + \mathrm{W(IV)} = \mathrm{Ni(II)} + \mathrm{W(III)}. \quad (2)$$

The removal of sulfur from dibenzothiophene by W(III) could be followed by reduction with hydrogen to complete the catalytic cycle

$$2\mathrm{W(III)} + \mathrm{RS} + (\mathrm{H_2}) = 2\mathrm{W(IV)} + \mathrm{RH_2} + \mathrm{S^{2-}}, \quad (3)$$

$$\mathrm{S^{2-}} + 4\mathrm{W(IV)} = 1/8\mathrm{S_8} + 4\mathrm{W(III)}, \quad (4)$$

or

$$2\mathrm{S^{2-}} + 2\mathrm{H_2} + 4\mathrm{W(IV)} = 2\mathrm{H_2S} + 4\mathrm{W(III)}. \quad (5)$$

The addition of acridine yielded sulfur in solution as well as a high desulfurization activity to the catalyst. When the reaction solution in the presence of 0.25 wt% acridine was cooled to 0 °C, the solution changed from colorless to orange. Sulfur precipitated from the solution within a couple of days. The orange color was caused by amine complexes,[9] such as hydrogenated acridine compounds with sulfur. The amines, to which acridine was easily hydrogenated, appears to help with the formation of sulfur from a sulfide anion to form an active site W(III) and/or with the desorption of hydrogen sulfide.

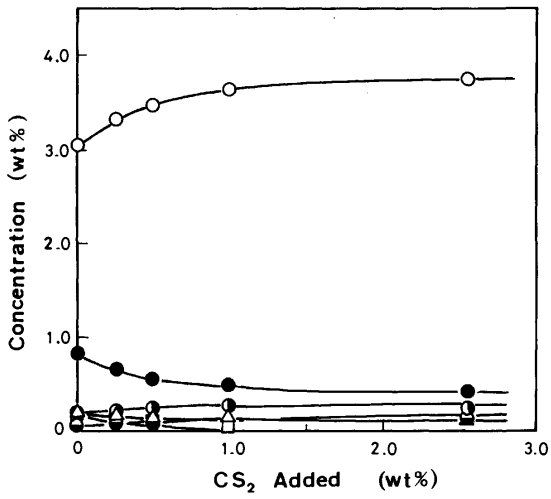

Fig. 2. Effect of CS_2 on product distribution of dibenzothiophene hydrodesulfurization at 300 °C. ◑, Hydrogenated dibenzothiophene compounds; □, 1,1′-bicyclohexyl and other hydrocarbons which have higher boiling point than 1,1′-bicyclohexyl. See Fig. 1 for the other symbols.

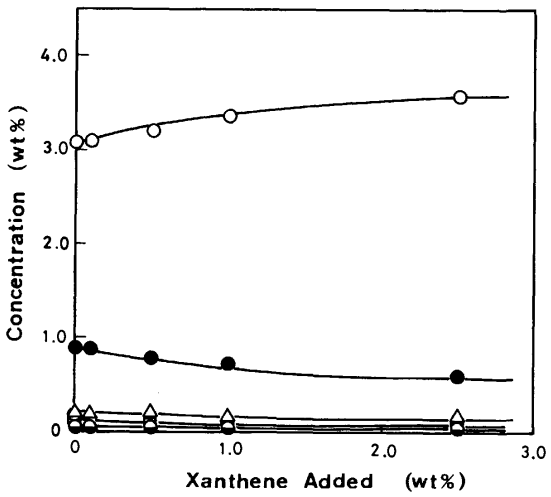

Fig. 3. Effect of xanthene on product distribution of dibenzothiophene hydrodesulfurization at 300 °C. See Fig. 1 for the symbols.

Depressing Effect of Carbon Disulfide and Xanthene. Figure 2 shows the effect of CS_2 on dibenzothiophene hydrodesulfurization at 10.1 MPa and 300 °C. The presence of CS_2 apparently depressed the desulfurization of dibenzothiophene to biphenyl and of hexahydrodibenzothiophene to cyclohexylbenzene. This result gives rise to an increase in concentration of tetrahydro- and hexahydrodibenzothiophene before desulfurization. The presence of an added sulfur compound depresses the desulfurization reaction along with a competitive adsorption of both dibenzothiophene and the hydrogenated compounds, but does not depress the hydro-

genation. Singhal et al.[10] and Broderick et al.[11] also found that H_2S (generated from CS_2) did not inhibit dibenzothiophene hydrogenation on the sulfided $CoMo/Al_2O_3$ catalysts.

The concentrations of methyl- and dimethyl dibenzothiophene was increased by the addition of CS_2. This result indicates that the presence of CS_2 enhanced the alkylation of dibenzothiophene and hampered the desulfurization. These compounds were produced in the reaction with the Co/HY zeolite catalyst,[12] which had stronger acid sites. Therefore, the sulfided NiW/Al_2O_3 catalyst appears to have stronger acid sites than the sulfided $NiMo/Al_2O_3$, $CoMo/Al_2O_3$, and Mo/Al_2O_3 catalysts.

The change in the products of dibenzothiophene hydrodesulfurization in the presence of xanthene at 300°C is shown in Fig. 3. The presence of xanthene depressed the formation of both biphenyl and cyclohexylbenzene with decreasing the conversion of dibenzothiophene, while methyldibenzothiophenes remained unchanged. Thus, the inhibitory effect of an oxygen compound on the sulfided NiW/Al_2O_3 catalyst closely parallels that of CS_2, except for an enhancement of the alkylation of dibenzothiophene.

These results indicated that there are two different sites on the sulfided NiW/Al_2O_3 catalyst; hydrogenation and desulfurization sites. Hydrogenation sites were inhibited by acridine but neither by CS_2 nor by xanthene, whereas desulfurization sites were promoted by acridine. The presence of a nitrogen compound promotes the catalytic activity of the sulfided NiW/Al_2O_3 catalyst for the desulfurization.

References

1) M. Nagai and T. Kabe, *J. Catal.*, **81**, 440 (1983).
2) S. W. Cowley and F. E. Massoth, *J. Catal.*, **51**, 291 (1978).
3) H. Urimoto and N. Sakikawa, *J. Jpn. Pet. Inst.*, **15**, 926 (1972).
4) M. Nagai, *Ind. Eng. Chem. Prod. Res. Dev.*, **24**, 91 (1985).
5) M. Nagai, *Chem. Lett.*, **1989**, 1023.
6) D. S. Thakur and B. Delmon, *J. Catal.*, **91**, 308 (1985).
7) D. S. Thakur, P. Grange, and B. Delmon, *J. Catal.*, **91**, 318 (1985).
8) R. J. H. Voorhoeve and J. C. M. Stuiver, *J. Catal.*, **23**, 228, 243 (1971).
9) S. Oae, "Yuki Iou Kagoubutsu No Kagaku," Kagakudojin, Kyoto (1968), Chap. 2; W. S. Pryor, "Mechanism of Sulfur Reactions," McGraw-Hill, New York (1962), p. 11.
10) G. H. Singhal, R. L. Espino, J. E. Sobel, and G. A. Huff, Jr., *J. Catal.*, **67**, 457 (1981).
11) D. H. Broderick, A. V. Sapre, B. C. Gates, H. Kwart, and G. C. A. Schuit, *J. Catal.*, **91**, 308 (1985).
12) M. Nagai, S. Obata, M. Yamada, and N. Sakikawa, *Nippon Kagaku Kaishi*, **1976**, 956.

Isomerization of 1-Butene on High-Temperature-Chlorinated Alumina

Akimi AYAME* and Goro SAWADA†
Department of Industrial Chemistry, Muroran Institute of Technology,
27-1 Mizumoto, Muroran, Hokkaido 050
(Received February 25, 1989)

Regarding aluminas chlorinated at 973—1223 K, which have only a Lewis acidic character without hydroxyl groups and basic sites, the IR spectra of the adsorbed 1-butene were measured and the isomerization of 1-butene and *cis*-2-butene was performed at 273—323 K. The obtained results were compared with those for aluminas dehydrated at the same temperatures. The IR spectra of the adsorbed 1-butene well resembled that of *cis*-2-butene, including the absence of peaks due to double-bond and π-allyl carbanion species, observed even after outgassing at 473 K. During isomerization at 273 K, the initial isomerization reaction rates and cis/trans ratios were greater than those for dehydrated alumina. The ratio decreased rapidly with increasing reaction temperature. The specific reaction rates and the ratio were independent of the chlorination temperature. In the isomerization of *cis*-2-butene the most thermodynamically unstable molecule, 1-butene, was formed preferentially. The obtained results could be interpreted by an isomerization mechanism through a doubly bonded intermediate, i.e., the allylic butenyl cation.

A high-temperature treatment of aluminas in air and/or in vacuo removes water molecules from the surfaces, resulting in aluminium cations with unsaturated coordination, isolated hydroxyl groups and oxygen anions on the surfaces. Consequently, Lewis acid, Brønsted acid and basic sites are formed.[1-5] On the other hand, it is known that by chlorination with hydrogen chloride, carbon tetrachloride, aluminium trichloride, and gaseous chlorine below 823 K the Lewis and Brønsted acid sites on γ and η-aluminas can be enhanced.[6-11] The effects are interpreted in terms of a decrease in the electron density of aluminium atoms which are directly linked to chlorine **I** or in the nearest position to the aluminium atom linked to chlorine **II**.

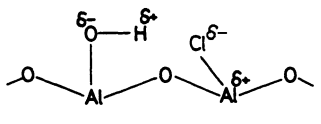

[I]

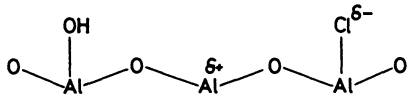

[II]

The authors studied the chlorination of γ-aluminas with dry chlorine at 773—1273 K as well as the surface characteristics of treated aluminas.[12] Chlorination effectively removed surface hydroxyl groups and sulfate ions. The obtained alumina surface had chlorine atoms (2—3 nm^{-2}) bonded with the tetrahedral aluminium cation, leading to the formation of strong Lewis acid sites with $H_0 \leqq -14.52$ and yielding intense IR peaks at 1628 and 1453 cm^{-1} in pyridine adsorption. The surface was, however, unable to form carbonate and bicarbonate ions in carbon dioxide adsorption. In the 1,2-epoxypropane isomerization, allyl alcohol promoted by an acid-base bifunctional catalysis was not produced, whereas the abstraction of an oxygen atom from the epoxide molecule by strong Lewis acid site took place in addition to the formation of propionaldehyde and acetone. Even in hydrogen chloride adsorption, there was no evidence for the formation of hydroxyl groups and water molecules.[13] These experimental results undoubtedly indicated that on high-temperature-chlorinated aluminas Brønsted acid and strong basic sites were absent; only

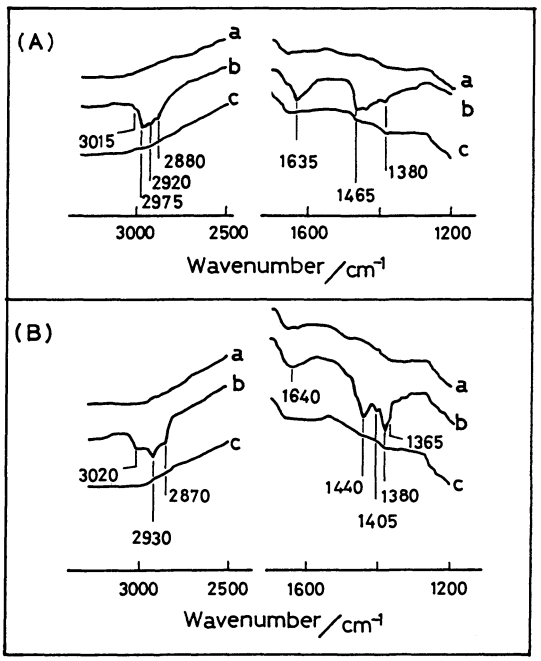

Fig. 1. IR spectra of (A) 1-butene and (B) *cis*-2-butene on alumina (ALO-4) dehydrated at 1073 K. (a) Background; (b) after exposed to 1-butene under 40 Torr for 15 min at room temperature; (c) after outgassing at room temperature for 30 min.

† Present address: Maruzen Petrochemical Co., Ltd., 3 Goi-Minami-Kaigan, Ichihara, Chiba 290.

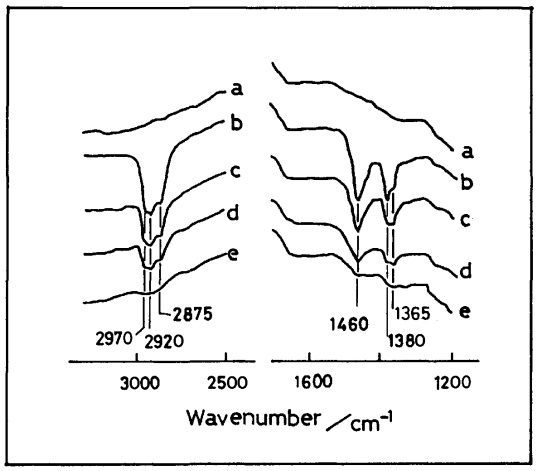

Fig. 2. IR spectra of 1-butene on alumina (ALO-4) chlorinated at 1073 K. (a) Background; (b) after exposed to 1-butene under 40 Torr for 15 min at room temperature; after outgassing for 30 min at (c) room temperature, (d) 373 K, and (e) 473 K.

Lewis acid sites were present. In addition, the strong Lewis acid sites tightly adsorbed benzene to form a π-complex with λ_{max}=294 nm and chloropropanes to the π-allyl cation, respectively, and promoted the isomerization of butane and cyclohexane to 2-methylpropane and methylcyclopentane with 100% selectivity, respectively, at 303 K.[13,14] Consequently, the chlorinated alumina is expected to be a solid Lewis superacid and to be used instead of homogeneous Lewis acids.

In the present work, in order to reveal the catalytic properties of chlorinated alumina, the infrared spectra of adsorbed 1-butene were measured and compared with those for the dehydrated aluminas; also, the isomerization of 1-butene and *cis*-2-butene was carried out. In this paper the 1-butene isomerization mechanism on a pure Lewis acidic surface is also discussed.

Experimental

Cylindrical γ-alumina JRC-ALO-4 (JRC represents the Japan Reference Catalyst[15]) was first crushed and sieved to obtain 16—32 and 100—150 mesh fractions; these were then washed with pure water and dried. Self-supported disks (13 mmϕ) prepared with the 100—150 mesh fraction were used in IR measurements and the 16—32 fraction in catalytic reactions. Commercial chlorine (Nissan Shoji Co., 99.4%) was purified by vacuum distillation, and 1-butene and *cis*-2-butene (Takachiho Chemicals, 99.0%) were used without special purification.

Chlorination of the samples was carried out with 100 Torr (1 Torr≈133.322 Pa) chlorine gas at temperatures between 973 and 1223 K for 1 h and then outgassed. Prior to chlorination, the samples were dehydrated at 773 K for 1 h in vacuo. During chlorination, an IR in situ cell made of a quartz glass tube and a highly pure alumina ceramics tube of 8 mmϕ i.d. (SSA-S, Nippon Ceramics Co.) were used. IR spectra were measured at room temperature using a Hitachi 215 transmission spectrometer. Isomerization reactions of 1-butene and *cis*-2-butene were performed using a fixed bed-closed circular reactor with a volume of about 550 ml. The reactant mixture comprised 1-butene (10 vol%) and helium (99.99% in purity; 90 vol%). The total pressure of the mixture was 300 Torr. The reactor comprised a U-type Pyrex glass tube (4 mmϕ i.d.) and the catalyst (0.1 g) supported by glass wool. The reaction temperature was between 273 and 323 K, and the reactant and product gases were analyzed by a gas chromatograph equipped with a column packed with propylene carbonate (15 wt%/Chromosorb G).

Results and Discussion

IR Spectra. The IR spectra of 1-butene and *cis*-2-butene adsorbed on the alumina dehydrated at 1073 K (Fig. 1). Spectrum b agreed with that on magnesium oxide pretreated at 773 K (reported by Baird and Lunsford[16]). In the spectra of 1-butene, the two peaks at 3015 and 1635 cm^{-1} were assigned to the terminal =C-H and the double-bond stretching vibrations, respectively. For *cis*-2-butene, these peaks appeared at 3020 and 1640 cm^{-1}. The 1405 cm^{-1} peak was due to the C-H deformation vibration of -CH=CH- in the cis configuration. A doublet band consisting of 1380 and 1365 cm^{-1} peaks was assigned to the resonating symmetrical deformation vibration of the C-H bond of two methyl groups in such hydrocarbon molecules as a molecule-like isopropyl group. All of the peaks described above were almost eliminated by outgassing at room temperature for 30 min. Figure 2 shows the IR spectra of the 1-butene adsorbed on alumina chlorinated at 1073 K. The spectra are very similar to that for *cis*-2-butene physically adsorbed on dehydrated alumina, also observed after outgassing at 473 K for 30 min. However, the peaks assigned to the double bond completely disappeared, the 1440 cm^{-1} peak due to the C-H deformation vibration was shifted to 1460 cm^{-1}, and a new 2970 cm^{-1} peak due to the C-H stretching vibration of the methyl group appeared. Further, the intensity ratio of the 1380 to 1460 cm^{-1} peak was 0.6—0.7, which was in accord with that for *cis*-2-butene (Fig. 1). These results indicate that 1-butene was strongly adsorbed on the strong Lewis acid sites to form such adsorbed species as **III** or **IV** via an intermolecular hydrogen-transfer reaction.

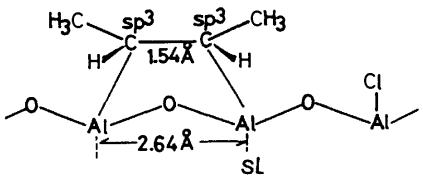

[III]

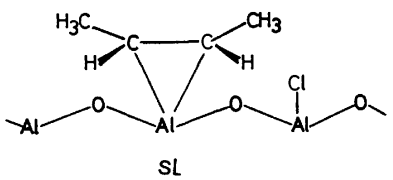

[IV]

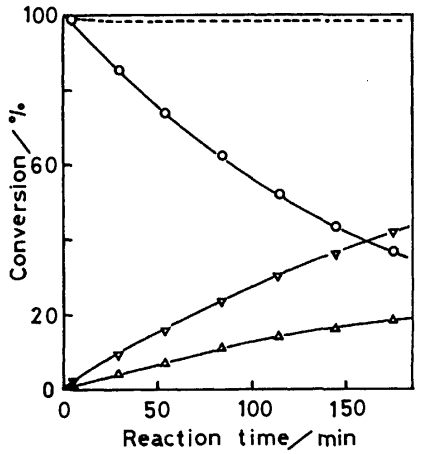

Fig. 3. Isomerization of 1-butene at 323 K on ALO-4 dehydrated at 1073 K. (○) 1-butene; (△) *cis*-2-butene; (▽) *trans*-2-butene; (----) total butenes.

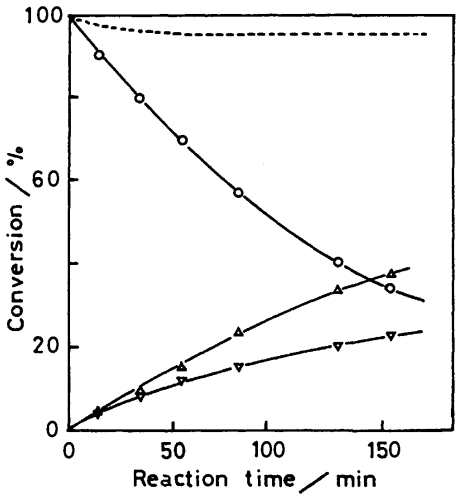

Fig. 4. Isomerization of 1-butene at 323 K on ALO-4 chlorinated at 1073 K. (○) 1-butene; (△) *cis*-2-butene; (▽) *trans*-2-butene; (----) total butene.

Geometrically, form **III** would be favorable, where *sL* indicates a possible strong Lewis acid site enhanced by chlorine bonding to the tetrahedral aluminium cation. In addition, the adsorbed species was likely to be desorbed at a higher reaction temperature, since the clear peaks assigned to oligomers or polymers were not observed. Along with the 1-butene adsorption, a new appearance of OH bands and peaks due to allylic species, which might arise from dissociation of the butene molecule, were undetected. However, on the dehydrated sample a small shift in the OH band to the low-frequency side was observed.

Isomerization of 1-Butene. Table 1 summarizes the initial isomerization reaction rates and obtained cis/trans ratios. The time courses of gas composition when a large conversion of 1-butene was obtained are shown in Figs. 3 and 4. The compositions were far apart from the thermodynamical equilibrium values of butenes: 4.1/70.7/25.2 for 1-butene/*trans*-2-butene/*cis*-2-butene. In every run, a loss in carbon balance was observed. An irreversibly adsorbed amount for 120 min decreased with an increasing reaction time and treatment temperature, being 1—7 and 3—15 mol% of 1-butene for the dehydrated and chlorinated aluminas, respectively. At every reaction temperature, the isomerization rates and cis/trans ratios for the chlorinated aluminas were greater than those for the dehydrated aluminas. Each reaction rate indicated a maximum at a chlorination temperature between 973 and 1073 K. The chlorination temperature dependence was very similar to that of the chlorine content for chlorinated alumina JRC-ALO-2.[12] The surface area decreased as a result of chlorination, as well as with an increase in the chlorination temperature. Consequently, the differences in the reaction rates between the two kinds of treated aluminas became increasingly large with increasing temperature. However, the specific isomerization rates and the cis/trans ratios were almost independent of the chlorination temperature (Fig. 5). Only the specific

Table 1. Initial Reaction Rates and Cis/Trans Ratios in 1-Butene Isomerization on Aluminas (ALO-4) Dehydrated and Chlorinated at High Temperatures above 973 K

Catalyst (0.1 g)	Treatment temperature/K	Initial isomerization rates/mol (g·s)$^{-1}$10^{7}											
		973			1073			1173			1223		
	Reaction temperature/K	273	296	323	273	296	323	273	296	323	273	296	323
Chlorinated ALO-4	*cis*-2-Butene	2.03	4.39	3.89	2.34	4.17	4.28	1.66	3.30	3.56	0.95	2.79	2.80
	trans-2-Butene	0.34	1.19	2.91	0.38	1.09	2.79	0.26	0.95	2.32	0.15	0.76	1.62
	cis/trans ratio	5.97	3.69	1.33	6.16	3.84	1.53	6.31	3.47	1.53	6.33	3.67	1.73
	Surface area/m^{2}g^{-1}		139			139			115			88	
Dehydrated ALO-4	*cis*-2-Butene	0.22	0.92	1.31	0.44	1.34	2.15	0.43	0.93	1.64	0.26	1.01	1.33
	trans-2-Butene	0.06	0.51	2.59	0.13	0.62	4.55	0.12	0.35	2.27	0.08	0.38	0.82
	cis/trans ratio	3.57	1.80	0.51	3.47	2.14	0.47	3.50	2.67	0.72	3.37	2.60	1.62
	Surface area/m^{2}g^{-1}		157			160			152			145	

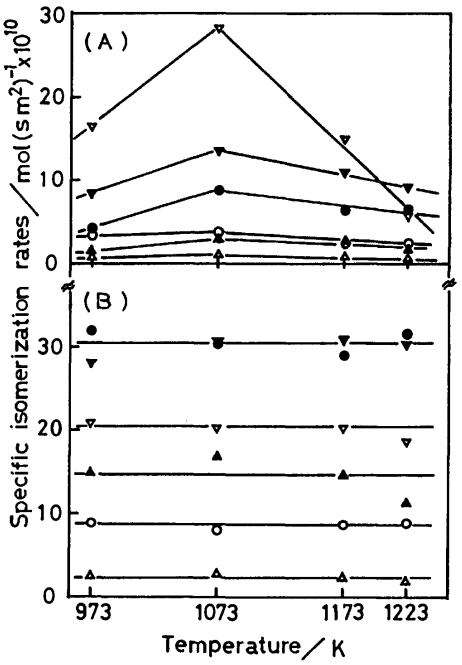

Fig. 5. Treatment temperature dependences of the isomerization reaction rates of 1-butene for (A) dehydrated and (B) chlorinated alumina (ALO-4). Reaction temperatures—273 K (▲ cis, △ trans); 296 K (● cis, ○ trans); 323 K (▼ cis, ▽ trans).

rate to *cis*-2-butene at 273 K varied with the chlorination temperature. This variation seems to reflect an unstable surface state caused by the accumulation of *cis*-2-butene tightly adsorbed in form **III** or **IV**. The number of chlorine atoms per unit surface area was almost constant (2.5 nm^{-2}) and did not depend on the chlorination temperature.[13] This result suggests that 1-butene isomerization is mainly catalyzed by the strong Lewis acid site, "*sL*".

Isomerization of *cis*-2-Butene. The isomerization of *cis*-2-butene was carried out at 273 K under the same reaction conditions as 1-butene (Table 2). The most unstable molecule, 1-butene, among the butenes was formed at 3.2—4.4 times the reaction rates for the dehydrated aluminas. However, the *trans*-2-butene formation rates for the two kinds of catalysts were of the same order. The trans/1 ratios (0.7—1.4) were abnormally small, being smaller than those for the dehydrated aluminas. Such low trans/1 ratios indicate that the rotation of the ^{2}C-^{3}C axis of adsorbed *cis*-2-butene is remarkedly depressed on chlorinated aluminas.

Mechanism. The cis/trans ratio and the trans/1 ratio obtained for dehydrated aluminas were almost in accord with the results reported by Gerberich and Hall and explained by the acid-base bifunctional and geometric isomerization mechanism via allylic butenyl ion intermediate.[17] Basset et al. reported that the π electrons of the double bond were delocalized to yield a dipole intermediate with partially negative and positive charges on ^{1}C and ^{4}C, respectively; they concluded that the repulsion between the positive methyl group and aluminium cation took place to give the high trans/1 ratio in *cis*-2-butene isomerization.[18] In addition, they explained the low trans/1 ratio for carbon tetrachloride-treated alumina by the classical carbonium ion mechanism. However, the cis/trans ratio in the 1-butene isomerization with the carbonium ion mechanism should be close to unity.[17,19] Regarding the chlorinated alumina which Basset et al. employed, oxygen ions with an electron-donor property, weak basic sites and strong Lewis acid sites were present because of adoption of a low chlorination temperature, 473 K.[18] In order to effectively eliminate hydroxyl groups and strong basic sites from the surfaces, a chlorination temperature of at least above 973 K was required.[12] On alumina chlorinated at such temperatures, the strong Lewis acid sites, "*sL*", were enhanced by chlorine bonding to aluminium cations; other weak sites were present. The presence of weak basic sites which would compensate the acidity is not necessarily denied. However, the surface had no ability to adsorb carbon dioxide to form carbonate and bicarbonate ions. In the adsorption of hydrogen chloride, a new OH stretching band at 3700 cm^{-1} and a deformation band of the O-H bond of H_2O at 1600 cm^{-1} clearly appeared on the dehydrated sample,

Table 2. Initial Reaction Rates and Trans/1 Ratio in *cis*-2-Butene Isomerization

Catalyst (0.1 g)	Treatment tempertature /K	Reaction temperature /K	Initial rates/mol $(g \cdot m^2)^{-1} \times 10^{10}$		Trans
			trans-2-Butene	1-Butene	1
Chlorinated	1073	273	2.45	1.80	1.38
	1173	273	1.91	2.61	0.73
ALO-4		296	6.52	3.84	1.71
		323	19.5	5.30	5.52
	1223	273	2.04	2.84	0.74
Dehydrated	1073	273	2.81	0.56	5.02
	1173	273	1.97	0.59	3.33
ALO-4		296	11.7	1.97	6.00
		323	15.5	2.11	7.49
	1223	273	2.07	0.76	2.74

whereas on the chlorinated sample both bands were entirely undetected.[13] These results indicate the complete absence of oxygen ions and hydroxyl groups having an electron-donor character.

The cis/trans ratios obtained on the Lewis acidic surfaces (Table 1) were very great, being rather similar to those for basic metal oxides.[16,20] Dent and Kokes[21] and Chang et al.[22] studied the isomerization and adsorption of 1-butene on a partially dehydrated zinc oxide and concluded that the cis/trans ratio was 10.5 and the adsorbed butene formed a π-allyl carbanion species, which showed absorption peaks at 1550—1572 cm^{-1}. In addition, they confirmed, along with the π-allyl bands, the appearance of a new OH band at 3587 cm^{-1} arising from the dissociation of adsorbed butene, which was caused by strong basic sites. In the present study, there was no evidence for the formation of the π-allyl species or new OH groups. Thus, a mechanism involving a π-allyl carbanion intermediate is very difficult to justify for isomerization on chlorinated aluminas. Further, although the IR peaks assigned to the π-allyl cation can not be observed in Fig. 2, as well as in the case of more longer-time adsorption, it was ascertained that the adsorption of chloropropanes yielded an intense peak at 1533—1535 cm^{-1} due to the cation.[12] This indicates that the strong Lewis acid site abstracts, as a hydride ion, an allylic hydrogen of propene formed from chloropropanes by dehydrochlorination. Consequently, the high selectivity of 1-butene to *cis*-2-butene, as shown in Table 1, is considered to be illustrated by a mechanism via a doubly bonded intermediate, butenyl cation, similar to that presented by Tanaka and Ogasawara[8] (Fig. 6). The 1-butene molecule can approach very closely to the "*sL*" site because of the absence of hydroxyl groups and basic oxygen ions with a large electron cloud. The "*sL*" site abstracts the hydrogen atom on allylic carbon and the adjacent Lewis acid site attracts the terminal methylene carbon. When the intermediate **V** shifts to **VI**, the hybrid orbital of ^3C changes from sp^3 to sp^2. At the same time, the methyl group goes away from the surface due to its large electron cloud and the ^2C moves upward. Subsequently, during the shifting of π-electrons, the cis configuration would be completed. The IR spectra of 1-butene adsorbed on the "*sL*" site, coinciding with that of *cis*-2-butene, completely lost its double-bond character. This shows that a hydride shift and a ^2C-^3C axis rotation take place very fast. Intermediate **III**, corresponding to the spectra in Fig. 2, seems to be the most stable configuration of 1-butene and *cis*-2-butene molecules which approach very close to the surface, since two methyl groups on the same side are permitted to move somewhat away from the surface. The butenyl cation mechanism would lead to the high cis/trans ratio. The experimental value was about 6. Similar results were reported by Gerberich and Hall (about 5) regarding fluoridized alumina[17] and Tanaka and Ogasawara (about 6) regarding hydrogen chloride-treated alumina.[8] For *cis*-2-butene isomerization, intermediate **III** is first formed; however, the formation of a ^2C-^3C axis at rotation to give *trans*-2-butene is more difficult than a hydride shift from ^1C to ^3C, since the interaction between the "*sL*" site and the *cis*-2-butene molecule is very strong. The lower trans/1 ratios therefore seem to have been obtained. At high reaction temperatures, doubly bonded intermediate **III** would become easy to shift to a singly bonded *s*-butyl cation, i.e., trans configuration. Consequently, with increasing reaction temperature, the cis/trans ratio and the trans/1 ratio seem to decrease and increase, respectively.

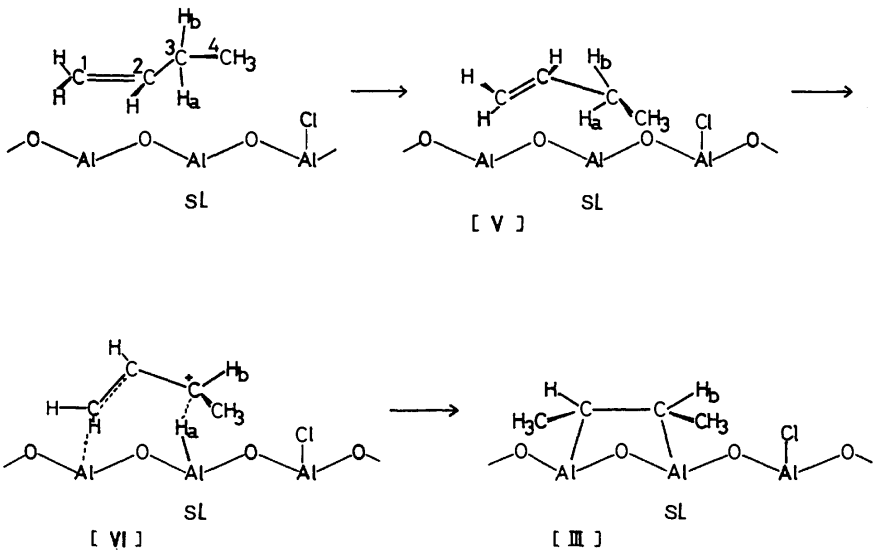

Fig. 6. Possible isomerization mechanism on the chlorinated aluminas.
The *sL* represents a possible strong Lewis acid site.

References

1) E. Parry, *J. Catal.*, **2**, 371 (1963).
2) J. B. Peri, *J. Phys. Chem.*, **69**, 220 (1965).
3) J. B. Peri, *J. Phys. Chem.*, **69**, 231 (1965).
4) C. Morterra, S. Coluccia, A. Chiorino, and F. Boccuzzi, *J. Catal.*, **54**, 348 (1978).
5) "Kinzoku Sanka-butsu to Sono Shokubai Sayo," ed. by T. Seiyama, Kodan-sha-VHC, Tokyo (1979), p. 106.
6) J. B. Peri, *J. Phys. Chem.*, **70**, 1482 (1965).
7) M. Tanaka and S. Ogasawara, *J. Catal.*, **16**, 157 (1970).
8) M. Tanaka and S. Ogasawara, *J. Catal.*, **16**, 164 (1970).
9) A. Melchor, E. Garbowski, M. V. Mathieu, and M. Primet, *J. Chem. Soc., Faraday Trans. 1*, **82**, 1893 (1986).
10) E. Garbowski and M. Primet, *J. Chem. Soc., Faraday Trans. 1*, **83**, 1469 (1987).
11) M. Marczewski, M. Derewinski, and S. Malinowski, *Can. J. Chem. Eng.*, **61**, 93 (1983).
12) A. Ayame, G. Sawada, H. Sato, G. Zhang, T. Ohta, and T. Izumizawa, *Appl. Catal.*, **48**, 25 (1989).
13) A. Ayame, T. Izumizawa, and H. Kakizaki, Proceedings of Acid-Base Catalysis Intern. Symp., ed. by K. Tanabe, Kodan-sha-VHC, Tokyo (1989), p. 371.
14) A. Ayame and T. Izumizawa, *J. Chem. Soc., Chem. Commun.*, **1989**, 645.
15) The Committee on Reference Catalysts (Catal. Soc. Jpn.), *Shokubai*, **22**, 410 (1980).
16) M. J. Baird and J. H. Lunsford, *J. Catal.*, **26**, 440 (1972).
17) H. R. Gerberich and W. K. Hall, *J. Catal.*, **5**, 99 (1966).
18) J. Basset, F. Figueras, M. V. Mathieu, and M. Prettre, *J. Catal.*, **16**, 53 (1970).
19) K. Tanabe, "Shokubai no Hataraki," Kagaku-dojin, (1979).
20) T. Okuhara and M. Misono, *Shokubai*, **25**, 279 (1983).
21) A. L. Dent and R. J. Kokes, *J. Phys. Chem.*, **75**, 487 (1971).
22) C. C. Chang, W. C. Conner, and R. J. Kokes, *J. Phys. Chem.*, **77**, 1957 (1973).

 © 1989 The Chemical Society of Japan Bull. Chem. Soc. Jpn., 62, 3061—3068 (1989)

High-Resolution Solid-State ^{31}P NMR of Alkali Phosphates

Shigenobu HAYASHI* and Kikuko HAYAMIZU
National Chemical Laboratory for Industry, Tsukuba, Ibaraki 305
(Received March 27, 1989)

High-resolution solid-state ^{31}P NMR spectra have been measured for inorganic alkali phosphates with different condensations in the PO_4 units, and the isotropic chemical shift and anisotropy have been determined. The isotropic chemical shifts in alkali orthophosphates do not correlate directly with the cation size. The hydration effects have been carefully examined by means of a ^1H decoupling experiment and by the heat treatment of the materials, accompanied by thermogravimetric analysis. Hydration causes an upfield shift in Na_3PO_4, K_3PO_4, and $Na_4P_2O_7$, while it causes a downfield shift in Rb_3PO_4 and Cs_3PO_4. All the five peaks observed in the $K_4P_2O_7$ sample can be ascribed to anhydrous species; this is in contrast to the findings of previous works. The field-dependence experiments definitely demonstrate that the splittings in $K_4P_2O_7$ and $(KPO_3)_n$ are caused by inequivalent sites.

High-resolution solid-state NMR using magic-angle sample spinning (MAS)[1,2] has been used in a variety of fields recently.[3] Inorganic phosphates are constructed of PO_4 units, which are connected with each other by the sharing of their oxygen atoms. The PO_4 condensation can be expected to be identified by using ^{31}P MAS NMR, much as the SiO_4 condensation is identified by means of ^{29}Si MAS NMR.[4]

Several groups have studied ^{31}P MAS NMR in inorganic phosphates. Rothwell et al.[5] have studied some solid calcium phosphates as examples of mineralized tissues. Andrew et al.[6] and later Haubenreisser et al.[7] and Burlinson et al.[8] have studied sodium triphosphate. Grimmer and Haubenreisser[9] have reported the chemical shifts of PO_4 groups in potassium phosphates with different condensations. Duncan and Douglass[10] have studied several condensed phosphates. Mudrakovskii et al.[11] have measured the spectra of various I—IV-group orthophosphates and pyrophosphates. Turner et al.[12] have studied various orthophosphates and have tried to relate the chemical-shift values with some structural parameters. Prabhakar et al.[13] have measured the spectra of some sodium and potassium phosphates. As reviewed above, data on the ^{31}P MAS NMR spectra of alkali phosphates have been accumulated to some extent. However, the observed lines have not been assigned completely, and there remain some controversies in the assignments.

In the present work, we have measured the ^{31}P MAS NMR spectra of inorganic alkali phosphates and have determined the isotropic chemical shift and its anisotropy, being careful to take account of the effect of the hydration on the chemical-shift parameters. Since the aim of this paper is to present reliable data, we have attempted various measurements, such as ^1H dipolar decoupling and magnetic-field dependence, as well as the heat treatment of the materials.

Experimental

Materials. The materials were purchased from Nacalai Tesque, Inc. (Kyoto, Japan), unless otherwise noted. The $K_4P_2O_7$ was also obtained from the Aldrich Chemical Co. (Milwaukee, U. S. A.); the $Na_5P_3O_{10}$, from Wako Pure Chemical Industries, Ltd. (Osaka, Japan), and the $Rb_3PO_4 \cdot 4H_2O$ and $Cs_3PO_4 \cdot 2.4H_2O$, from the Soekawa Chemicals Co., Ltd. (Tokyo, Japan). The $Na_5P_3O_{10}$ and $K_5P_3O_{10}$ were also synthesized by heating mixtures of M_2HPO_4 and MH_2PO_4 (M=Na, K) at 550 °C.[14] The contents of water in the hydrated materials were checked by means of thermogravimetric analysis (TG). Their anhydrous samples were prepared by heating the hydrated phosphates at the evolution temperatures determined by TG. Three samples, $Na_6P_4O_{13}$, $(NaPO_3)_6$, and $(NaPO_3)_n$, are amorphous, as checked by powder X-ray diffraction.

NMR Measurements. The NMR spectra were measured mostly by the use of a Bruker MSL400 pulsed spectrometer, whose ^{31}P resonance frequency (ν_0) was 161.98 MHz. A JEOL FX200 pulsed spectrometer (ν_0=80.76 MHz) was also used to check the field dependence of the spectra. The probes were doubly tuned to ^{31}P and ^1H resonances, being capable of MAS (magic-angle sample spinning). The chemical shifts are given with respect to 85% H_3PO_4, with the higher-frequency side (i.e., the downfield side) being expressed as positive.

The ordinary single-pulse sequence was used. Typical measuring conditions were $\pi/4$ for the flip angle of the pulse and 10—20 s for the repetition time. A ^1H dipolar decoupling experiment was always performed to check the effect of the ^1H spins.

Since the ^{31}P nucleus has a large chemical-shift anisotropy in many cases, the isotropic peaks are accompanied by many spinning sidebands, especially in high magnetic fields such as used in this work. The isotropic peaks were identified by changing the spinning rate of the sample. The principal values of the chemical-shift tensor were evaluated from the intensities of the spinning sidebands by using the graphical method proposed by Herzfeld and Berger.[15] Q_n in the text denotes that the PO_4 unit shares n oxygen atoms with other PO_4 units. The accuracy of the isotropic chemical shift is about ±0.2 ppm, while that of the principal values of the shift tensor is about ±5 ppm.

Results and Discussion

Orthophosphates (Q_0). In orthophosphates, the PO_4 units are isolated from each other; they are denoted as Q_0. Some typical ^{31}P MAS NMR spectra

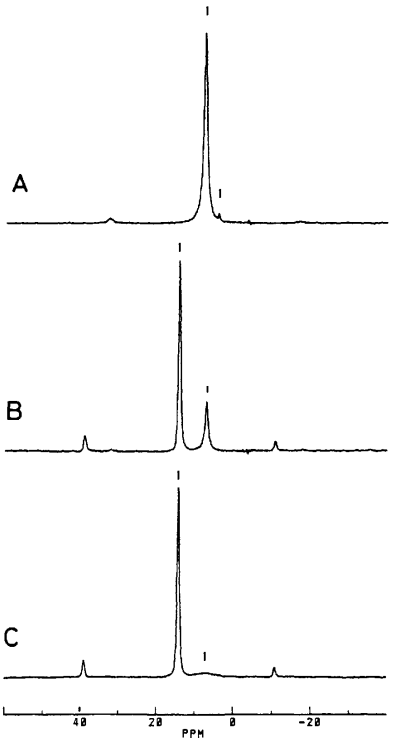

Fig. 1. ^{31}P MAS NMR spectra at ν_0=161.98 MHz of $Na_3PO_4 \cdot 10H_2O$ with ^1H dipolar decoupling (A) and its dehydrated sample with (B) and without (C) decoupling. Bars on top of the peak indicate the isotropic peaks.

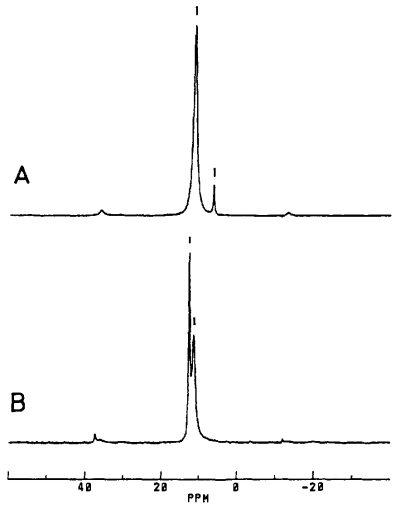

Fig. 2. ^{31}P MAS NMR spectra with ^1H dipolar decoupling of (A) $K_3PO_4 \cdot 3H_2O$ and (B) its dehydrated sample measured at ν_0=161.98 MHz. Bars on top of the peak indicate the isotropic peaks.

of alkali orthophosphates are shown in Figs. 1—3, while the parameters obtained are summarized in Table 1. Impurity peaks are usually omitted from the table if they can be identified. The procedures of the peak assignments will be described below, starting from the lightest cation.

Anhydrous Li_3PO_4 has an isotropic chemical shift

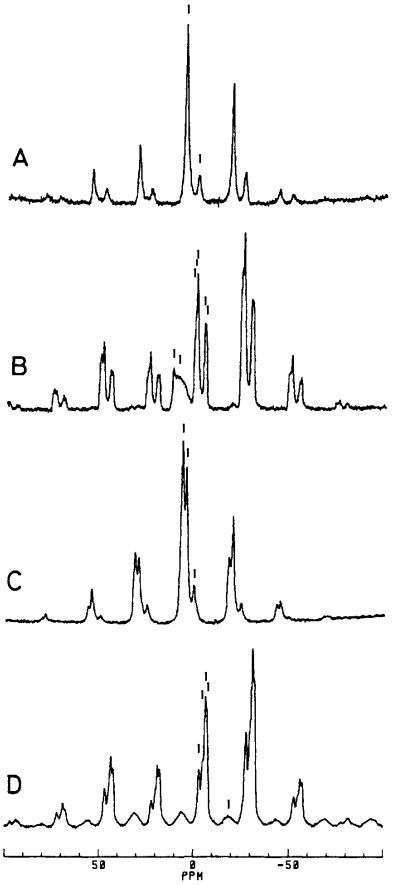

Fig. 3. ^{31}P MAS NMR spectra at ν_0=161.98 MHz of (A) $Rb_3PO_4 \cdot 4H_2O$ with decoupling, (B) its dehydrated sample without decoupling, (C) $Cs_3PO_4 \cdot 2.4H_2O$ with decoupling and (D) its dehydrated sample without decoupling. Bars on top of the peak indicate the isotropic peaks.

of 10.8 ppm, and its tensor is almost isotropic (spectra are not shown).

$Na_3PO_4 \cdot 10H_2O$ has an isotropic chemical shift of 7.7 ppm (Fig. 1A). The thermogravimetric analysis indicates that this sample has the above composition rather than that of $Na_3PO_4 \cdot 12H_2O$ nominated by the supplier. This peak interacts with the ^1H spins in the hydrated water through the dipole-dipole interaction. Another, very small peak is observed at 4.0 ppm; it does not interact with the ^1H spins. This peak disappears after the heat treatment at 210 °C and might be ascribed to much-hydrated species. Heavy hydration is considered to enhance the motion of the PO_4 unit, which can make the time average of the dipole-dipole interaction zero. The sample dehydrated at 210 °C for 0.5 h has isotropic peaks at 14.0 and 6.7 ppm (Fig. 1B). The 14.0 ppm peak is free from the dipolar interaction with the ^1H spins, while the 6.7 ppm peak interacts with the ^1H spins, as is demonstrated in Fig. 1C. The 14.0 ppm peak can be ascribed to anhydrous Na_3PO_4, and the 6.7 ppm peak, to the rehydrated material, $Na_3PO_4 \cdot 10H_2O$.

$K_3PO_4 \cdot 3H_2O$ has an isotropic chemical shift of 11.3

Table 1. Orthophosphates (Q_0)[a]

Compound	δ_i	δ_1	δ_2	δ_3	$\Delta\delta$	η	Ref.
	ppm	ppm	ppm	ppm	ppm		
Li_3PO_4	10.8	—	—	—	N[b]	NM[c]	This work
	10.8	—	—	—	NM	NM	12
	10.0	—	—	—	0	0	11
$Na_3PO_4 \cdot 10H_2O$	7.7	—	—	—	N	NM	This work
$Na_3PO_4 \cdot 12H_2O$	7.8	—	—	—	NM	NM	12
Na_3PO_4	14.0	—	—	—	N	NM	This work
	13.0	—	—	—	0	0	11
	13.7	—	—	—	NM	NM	13
$K_3PO_4 \cdot 3H_2O$	11.3	—	—	—	N	NM	This work
K_3PO_4	12.5	—	—	—	N	NM	This work
	11.7	—	—	—	0	0	9
$Rb_3PO_4 \cdot 4H_2O$	5.6	−25	−25	66	91	0	This work
	−1.2[d]	−49	−27	72	110	0.30	
Rb_3PO_4[e]	0.5						This work
	−0.2	−41	−41	78	119	0	
	−0.9						
	−5.2	−45	−45	74	119	0	
	−5.6						
$Cs_3PO_4 \cdot 2.4H_2O$	6.3	—	—	—	NM[f]	NM	This work
	4.2	—	—	—	NM[f]	NM	
	−0.1[d]	−49	−5	54	81	0.81	
Cs_3PO_4[e]	−3.1						
	−5.1	−45	−45	71	116	0	This work
	−6.4						
	−7.1						

a) The following definitions are used; δ_i: isotropic shift, δ_1, δ_2, and δ_3: principal values of the shift tensor, $\Delta\delta$: shift anisotropy, and η: asymmetry factor in the shift tensor.

$$|\delta_3-\delta_i| \geqq |\delta_1-\delta_i| \geqq |\delta_2-\delta_i| \qquad \delta_i=(\delta_1+\delta_2+\delta_3)/3$$
$$\Delta\delta=\delta_3-(\delta_1+\delta_2)/2 \qquad \eta=(\delta_2-\delta_1)/(\delta_3-\delta_i)$$

b) Negative; its absolute value is less than 30 ppm. c) Not measured. d) Anhydrous species. e) Condensed phosphates might be present. f) Overlapping of the signals prevents accurate estimation.

ppm (Fig. 2A) which interacts with the ^{1}H spins. Another, small peak observed at 6.2 ppm might be ascribed to much-hydrated species, since it does not interact with ^{1}H and disappears after heat treatment at 300 °C. The sample dehydrated at 300 °C for 4.5 h has shifts of 12.5 and 11.3 ppm (Fig. 2B). The interaction with the ^{1}H spins is not found in the former peak, which can be ascribed to anhydrous K_3PO_4. On the other hand, the 11.3 ppm peak does interact with the ^{1}H spins and so can be ascribed to $K_3PO_4 \cdot 3H_2O$.

The above orthophosphates and their hydrates have little anisotropy (less than 30 ppm). The obtained shift parameters agree very well with some of the literature data, as is shown in Table 1. The presence of the rehydrated species in the dehydrated samples suggests that the anhydrous compounds are easily hydrated to form $Na_3PO_4 \cdot 10H_2O$ and $K_3PO_4 \cdot 3H_2O$, while such partially hydrated species as $Na_3PO_4 \cdot nH_2O$ (n=1—9) and $K_3PO_4 \cdot mH_2O$ (m=1,2) are not stable.

The $Rb_3PO_4 \cdot 4H_2O$ sample has two isotropic peaks, at 5.6 and −1.2 ppm (Fig. 3A). The former interacts with the ^{1}H spins, whereas the latter does not. This indicates that the 5.6 ppm peak can be ascribed to a hydrated species like $Rb_3PO_4 \cdot 4H_2O$ and the −1.2 ppm peak, to anhydrous Rb_3PO_4. The sample dehydrated at 400 °C for 2 h has seven isotropic peaks (Fig. 3B), none of which interact with the ^{1}H spins. The peaks at 0.5, −0.2, −0.9, −5.2, and −5.6 ppm can be ascribed to Rb_3PO_4, and the other small peaks at 11.3 and ca.7 ppm, to impurities. The broad linewidth of the 7 ppm peak suggests that a small amount of the amorphous phase was created by the heat treatment.

The $Cs_3PO_4 \cdot 2.4H_2O$ sample has three isotropic peaks (Fig. 3C). The 6.3 and 4.2 ppm peaks interact with the ^{1}H spins and can be ascribed to hydrated species. On the other hand, the −0.1 ppm peak does not interact with the ^{1}H spins and can be ascribed to anhydrous species. The sample dehydrated at 400 °C for 1.3 h has peaks at −3.1, −5.1, −6.4, −7.1, and −19 ppm (Fig. 3D). The peaks other than −19 ppm might be ascribed to Q_0, but the presence of the −19 ppm peak (Q_2) suggests that condensation was encouraged by the heat treatment. The broad linewidth of this peak suggests that an amorphous phase is formed.

In summary, the isotropic chemical shift does not

correlate with the cation radius directly in alkali orthophosphates. Hydration causes upfield shifts in Na_3PO_4 and K_3PO_4, while it leads to downfield shifts in Rb_3PO_4 and Cs_3PO_4. The shift tensors are not isotropic in the orthophosphates with larger cation sizes.

The crystal structure of the hydrated compounds has been studied for $Na_3PO_4 \cdot 12H_2O$.[16] Water molecules coordinate to the Na^+ ion, forming octahedra centered on the Na^+ ion. The PO_4^{3-} ion interacts with the Na^+ ion indirectly through the hydrated water. Thus, the chemical shift of the hydrated compound approaches the value of a Na_3PO_4 aqueous solution ranging from 5.4 to 6.0 ppm.[17] Also, in the other hydrated orthophosphates, water molecules are considered to coordinate to the cations, approaching the shift values near to that of an aqueous solution.

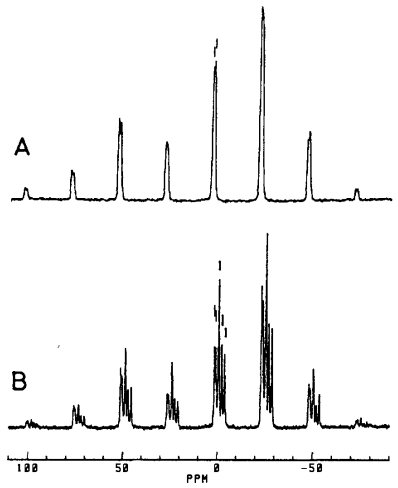

Fig. 4. ^{31}P MAS NMR spectra without ^1H dipolar decoupling of (A) $Na_4P_2O_7$, and (B) $K_4P_2O_7$, measured at ν_0=161.98 MHz. Bars on top of the peak indicate the isotropic peaks.

Pyrophosphates (Q_1-Q_1). Two PO_4 units are connected by sharing one oxygen atom in pyrophosphates. Figure 4 shows the spectra of pyrophosphates; the results are summarized in Table 2.

$Na_4P_2O_7$ has doublet peaks, whose isotropic chemical shifts were 3.0 and 2.2 ppm (Fig. 4A). No splitting was observed at the lower frequency of 80.76 MHz. Thus, the field-dependence measurement failed to elucidate the origin of the splitting. Duncan and Douglass[10] and Prabhakar et al.[13] have reported similar doublets. Duncan and Douglass[10] have interpreted, based on the X-ray diffraction study,[18] that this splitting is caused by inequivalent sites. The magnitudes of the splitting were found to be 1.2 ppm (100 Hz) at 81.015 MHz by Duncan and Douglass,[10] 1.1 ppm (130 Hz) at 121.495 MHz by Prabhakar et al.,[13] and 0.73 ppm (120 Hz) at 161.98 MHz by authors. The ^{31}P-^{31}P scalar coupling in solution is about 20 Hz,[17] much smaller than the observed splitting. Thus, we consider that the interpretation proposed by Duncan and Douglass is most reasonable. In other words, the two Q_1 units in the same Q_1-Q_1 group have different chemical shifts.

$Na_4P_2O_7 \cdot 10H_2O$ shows a similar splitting. The isotropic peaks are observed at −1.4 and −2.3 ppm. The two peaks show interaction with the ^1H spins, and the hydration causes an upfield shift in this compound. Water molecules take part in the sodium coordination, forming octahedra centered on the sodium cation.[19,20] The $P_2O_7^{4-}$ anion interacts with the octahedra through hydrogen bonds. Thus, the chemical shift of the hydrated compound approaches the value of the $Na_4P_2O_7$ aqueous solution (−5.5 to −7 ppm).[17]

On the other hand, five isotropic peaks are observed in $K_4P_2O_7$ (Fig. 4B). Their chemical shifts are 1.4, 0.7, −0.9, −2.5, and −4.0 ppm, and their intensity ratios are approximately 1 : 1 : 2 : 1 : 1. The field-

Table 2. Pyrophosphates (Q_1-Q_1)[a]

Compound	δ_i	δ_1	δ_2	δ_3	$\Delta\delta$	η	Ref.
	ppm	ppm	ppm	ppm	ppm		
$Na_4P_2O_7$	3.0, 2.2	−40	−40	89	129	0	This work
	2.4, 1.2	−37	−37	80	117	0	10
	2.1, 3.2	—	—	—	NM	NM	13
$Na_4P_2O_7 \cdot 10H_2O$	−1.4, −2.3	−38	−38	70	108	0	This work
$K_4P_2O_7$-I	1.4	−43	−43	89	132	0	This work
	−4.0	−44	−44	77	121	0	
-II	0.7	−43	−43	87	130	0	
	−2.5	−40	−40	73	113	0	
-III	−0.9	−40	−40	78	118	0	
$K_4P_2O_7$	−0.3, −2.2[b]	—	—	—	126	0	9
	−2.4, −4.9[c]						
$K_4P_2O_7$	0.9, 0.0[b]	−43	−43	82	125	0	10
	−1.8						
	−3.3, −4.8[c]						

a) Symbols have the same meanings as in Table 1. b) Ascribed to $K_4P_2O_7$ according to the reference. c) Ascribed to $K_4P_2O_7 \cdot 3H_2O$ according to the reference.

dependence measurements definitely demonstrate that the five lines can be ascribed to inequivalent sites. The ^{1}H dipolar decoupling has no effect on the spectra, which indicates that no effective hydration takes place. None of the five lines change a position or intensity after heat treatment at 150 °C for 1 h. Therefore, all five lines can be ascribed to inequivalent sites in anhydrous $K_4P_2O_7$.

The sample obtained from Aldrich gives the same results as to the position, but the relative intensities of peaks differ from those in Nacalai's sample. Based on the principle that the intensity ratio of the peaks belonging to the same phase is constant, a detailed examination of the intensities suggests that three phases are mixed in these samples. The first phase has peaks at 1.4 and −4.0 ppm; the second, at 0.7 and −2.5 ppm, and the third, at −0.9 ppm. The Q_1 units in the same Q_1-Q_1 group have different chemical shifts in the first two phases, while they have the same chemical shift in the third phase.

On the other hand, Grimmer and Haubenreisser[9] have observed four lines— at −0.3, −2.2, −2.4, and −4.9 ppm. They tentatively ascribed the former two lines to anhydrous $K_4P_2O_7$, and the latter two, to $K_4P_2O_7 \cdot 3H_2O$. Duncan et al.[10] reported results similar to ours, but they ascribed their lines according to Grimmer and Haubenreisser,[9] except for the −1.8 ppm line. The above two groups gave the average parameters of anisotropy, probably because the lines were not well resolved. On the other hand, we can determine the anisotropy parameters of each line, since the lines are well separated.

Triphosphates (Q_1-Q_2-Q_1). Three PO_4 units are connected linearly in triphosphates. Figure 5 shows the spectra of triphosphates, and Table 3 summarizes the results.

Both the commercial and synthesized $Na_5P_3O_{10}$ samples have two isotropic peaks at 5.1 and −5.6 ppm; their intensities are 2.2 : 1 (Fig. 5A). The 5.1 ppm and the −5.6 ppm peaks can be ascribed to the end-chain (Q_1) and middle-chain (Q_2) PO_4 groups respectively.[6-8] The third sets of peaks, observed at 3.0 and 2.2 ppm, can be ascribed to the $Na_4P_2O_7$ contained as an impurity.

The synthesized $K_5P_3O_{10}$ sample has at least eight isotropic peaks— at 1.4, 0.3, −0.7, −2.7, −3.7, −16.3, −18.7, and −19.8 ppm (Figs. 5B and 5D). The three strong peaks can be ascribed to Q_1 (−0.7 and −3.7 ppm) and Q_2 (−18.7 ppm) in the Q_1-Q_2-Q_1 unit. The remaining, small peaks can be ascribed to other phases.

On the other hand, the commercial sample has at least six isotropic peaks— at 7.6, 6.8, −0.7, −3.5, −5.3, and −18.6 ppm (Figs. 5C and 5E). Upon the use of

Table 3. Triphosphates (Q_1-Q_2-Q_1)[a]

Compound	δ_i	δ_1	δ_2	δ_3	$\Delta\delta$	η	Q_n	Ref.
	ppm	ppm	ppm	ppm	ppm			
$Na_5P_3O_{10}$	5.1	−62	−32	109	156	0.29	Q_1	This work
	−5.6	79	24	−120	−172	0.48	Q_2	
$Na_5P_3O_{10}$	5.6	—	—	—	NM	NM	Q_1	6
	−6.2	—	—	—	NM	NM	Q_2	
$Na_5P_3O_{10}$-I	1.2	—	—	—	140	0.38	Q_1	7
	−8.0	—	—	—	−185	0.36	Q_2	
-II	4.6	—	—	—	159	0.29	Q_1	
	−6.6	—	—	—	−169	0.40	Q_2	
$Na_5P_3O_{10}$-II	4.0	−62	−37	113	163	0.23	Q_1	8
	−5.7	79	22	−118	−169	0.51	Q_2	
$K_5P_3O_{10}$ -I	−0.7	−64	−34	96	145	0.31	Q_1	This work
(Synth.)	−3.7	−70	−38	97	151	0.32	Q_1	
	−18.7	77	14	−147	−193	0.49	Q_2	
-II	1.4	—	—	—	NM	NM	Q_1	
	0.3	—	—	—	NM	NM	Q_1	
	−2.7	—	—	—	NM	NM	Q_1	
	−16.3	—	—	—	NM	NM	Q_2	
	−19.8	—	—	—	NM	NM	Q_2	
$K_5P_3O_{10}$	7.4[b]	−35	−21	77	105	0.20	Q_1	This work
(Commercial)	−0.7	−62	−38	98	148	0.24	Q_1	
	−3.5[c]	−67	−33	90	140	0.36	Q_1	
	−5.3[b]	−71	−17	72	116	0.70	Q_1	
	−18.6	79	13	−147	−193	0.51	Q_2	
$K_5P_3O_{10}$	−1.2 −4.2	—	—	—	146	0	Q_1	9
	−19.4	—	—	—	−191	0.38	Q_2	
$K_5P_3O_{10}$	−1.2	−55	−55	106	161	0	Q_1	10
	−4.0	−51	−51	90	141	0	Q_1	
	−19.5	75	16	−148	−194	0.46	Q_2	

a) Symbols have the same meanings as in Table 1. b) This peak might be ascribed to an impurity. c) This peak might be partly ascribed to an impurity.

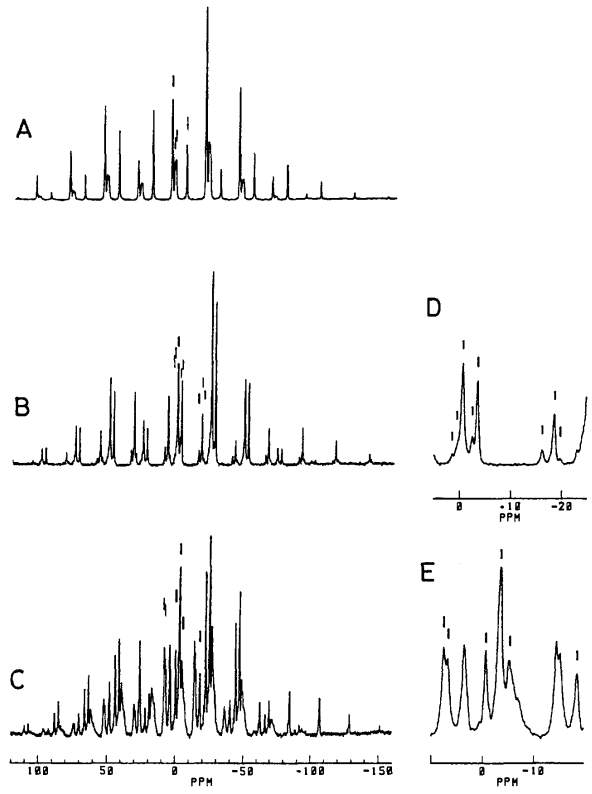

Fig. 5. ^{31}P MAS NMR spectra without ^{1}H dipolar decoupling of (A) $Na_5P_3O_{10}$ (commercial) (B) $K_5P_3O_{10}$ (synthesized), and (C) $K_5P_3O_{10}$ (commercial) measured at ν_0=161.98 MHz. (D) and (E) are expanded plots of the isotropic region of (B) and (C) respectively. Bars on top of the peak indicate the isotropic peaks.

^{1}H dipolar decoupling, the two peaks at 7.6 and 6.8 ppm collapse into one line, at 7.4 ppm, suggesting that the lines are split by the interaction with the ^{1}H spins. The field-dependence measurements demonstrate that the five peaks at 7.4, −0.7, −3.5, −5.3, and −18.6 ppm can be ascribed to inequivalent sites. The magnitudes and signs of the anisotropy suggest that the −18.6 ppm peak can be ascribed to Q_2, and the others, to Q_1. Heat treatment at 200 °C increased the intensities of the 7.4, −3.5, and −5.3 ppm peaks, while the others decreased relatively. This fact and the results on the synthesized sample lead to the following assignments. The −0.7, −3.5, and −18.6 ppm peaks are attributed to the triphosphate anion (Q_1-Q_2-Q_1). The two peaks at −3.5 and −5.3 ppm can be ascribed to Q_1 in the diphosphate anion (Q_1-Q_1), contained as an impurity. The −3.5 ppm peak consists of two components; thus, its intensity is strongest. However, the assignment of the 7.4 ppm peak is still ambiguous.

On the other hand, Grimmer and Haubenreisser[9] have reported the presence of three lines— at −1.2, −4.2, and −19.4 ppm. Duncan and Douglass[10] have reported similar results.

Tetraphosphates (Q_1-Q_2-Q_2-Q_1). Four PO_4 units are linearly linked in tetraphosphates. $Na_6P_4O_{13}$ has two isotropic signals, at 1.5 and −16.4 ppm (Fig. 6A and Table 4), which can be ascribed to Q_1 and Q_2 respectively. The X-ray diffraction results demonstrate that this sample is amorphous. Thus, the broad linewidth is produced by chemical-shift dispersion due to the disorderness in the amorphous material.

Metaphosphates (-Q_2-). In metaphosphates, many PO_4 units are linked by sharing two of the four oxygen atoms to form rings and chains. The spectra of the metaphosphates are shown in Fig. 6, while the shift parameters are summarized in Table 4.

$(NaPO_3)_n$ has an isotropic chemical shift of −19.9 ppm (Fig. 6B); it can be ascribed to the middle-chain PO_4 group (Q_2). A small peak was also observed at −6.2 ppm; it can be ascribed to the end-chain PO_4 group (Q_1). The linewidths are broad because of the amorphousness. Since the chemical-shift dispersion, which is the origin of the linewidth for this sample, is proportional to the static magnetic field (in Hz unit), lower-field measurements are useful in reducing the linewidth if the spinning rate of the sample is constant. The measurements at ν_0=80.76 MHz reveal the presence of the third, small components at about 1 ppm; they might be Q_1. The $(NaPO_3)_6$ sample shows similar results, as is shown in Table 4.

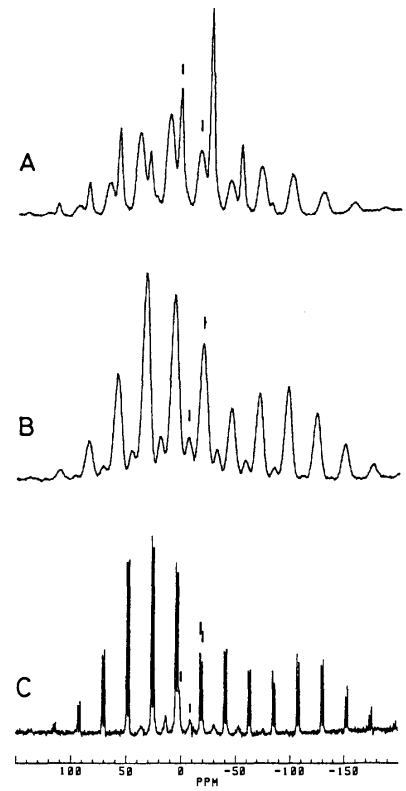

Fig. 6. ^{31}P MAS NMR spectra of (A) $Na_6P_4O_{13}$ and (B) $(NaPO_3)_n$ without ^{1}H dipolar decoupling and (C) $(KPO_3)_n$ with ^{1}H decoupling, measured at ν_0=161.98 MHz. Bars on top of the peak indicate the isotropic peaks.

Table 4. Tetraphosphates (Q_1-Q_2-Q_2-Q_1) and Metaphosphates (-Q_2-)[a]

Compound	δ_i	δ_1	δ_2	δ_3	$\Delta\delta$	η	Q_n	Ref.
	ppm	ppm	ppm	ppm	ppm			
$Na_6P_4O_{13}$	1.5	−47	−47	98	145	0	Q_1	This work
	−16.4	85	18	−152	−204	0.49	Q_2	
$(NaPO_3)_n$	1	—	—	—	NM	NM	Q_1	This work
	−6.2	—	—	—	NM	NM	Q_1	
	−19.9	85	20	−165	−218	0.45	Q_2	
$(NaPO_3)_6$	−6	—	—	—	NM	NM	Q_1	This work
	−19.6	87	19	−165	−218	0.47	Q_2	
$(NaPO_3)_n$	2	−45	−45	95	140	0	Q_1	10
	−19	90	13	−160	−212	0.55	Q_2	
$(NaPO_3)_n$	−15.6, −18.5							
	−19.9, −24.1	—	—	—	NM	NM	Q_2	13
	−26.8							
$(KPO_3)_n$	−17.9	88	33	−174	−235	0.35	Q_2	This work
	−19.8	88	34	−181	−242	0.33	Q_2	
$(KPO_3)_n$	−18.5, −20.7	—	—	—	−237	0.34	Q_2	9
$(KPO_3)_n$	−17.8, −19.8	—	—	—	NM	NM	Q_2	13

a) Symbols have the same meanings as in Table 1.

Duncan and Douglass[10] have reported results similar to ours. Prabhakar et al.[13] have reported five resonance lines— at −15.6, −18.5, −19.9, −24.1, and −26.8 ppm for $(NaPO_3)_n$. The lines were all ascribed to Q_2. Their sample is considered to be crystalline, in contrast to Duncan and Douglass's sample and to ours.

$(KPO_3)_n$ has two isotropic peaks, at −17.9 and −19.8 ppm (Fig. 6C), ascribed to the middle-chain (Q_2) group. The field-dependence experiments demonstrate that these two peaks are produced by two inequivalent sites. The X-ray diffraction study[21] supports the presence of two inequivalent sites. Grimmer and Haubenreisser[9] have reported the values of −18.5 and −20.7 ppm, while Prabhakar et al.[13] have reported the values of −17.8 and −19.8 ppm. Some other peaks were observed which can be ascribed to impurities. The peak at 4.1 ppm interacts with the ^{1}H spins and vanishes after the sample has been heated at 260 °C; it can be ascribed to hydrated species. Three peaks developed in the course of the experiment— at 0.8, −10.4, and −22.6 ppm. They have negligible anisotropy and no interaction with the ^{1}H spins. Heat treatments of the sample could not reduce the intensities of these peaks. From the above observations, they can be ascribed to decomposed species formed by hydrolysis. By analogy with the solution data,[17] the 0.8 ppm peak can be ascribed to Q_0; the −10.4 ppm peak, to Q_1, and the −22.6 ppm peak, to Q_2.

Summary

The ^{31}P chemical shift and its anisotropy in each Q_n species have been discussed previously.[6-13] The present work generally confirms the previous results. An upfield shift in Q_n is observed as n increases. The Q_0 group in M_3PO_4 usually has an isotropic shift-tensor. On the other hand, the Q_1 group usually has an axially-symmetric tensor or an asymmetric factor lower than 0.3. The Q_2 group has a non-axially symmetric tensor with asymmetric factors between 0.3 and 0.6. The magnitudes of the anisotropy, $|\Delta\delta|$, are 100—160 and 170—240 ppm for the Q_1 and Q_2 respectively, while the signs of $\Delta\delta$ are opposite for the two groups.

In the present work, new data on the orthophosphates of Rb and Cs are presented. These orthophosphates have considerably greater magnitudes of anisotropy than the other orthophosphates. Although the data from Li to Cs have been collected, the isotropic chemical shift does not correlate directly with the cation size.

The hydration effects have been carefully examined by means of the ^{1}H decoupling experiment and heat treatment of the materials, accompanied by thermogravimetric analysis. The coexistence of Na_3PO_4 and $Na_3PO_4 \cdot 10H_2O$ demonstrates that the stable hydrate contains 10 H_2O in a quantity not less than 10. Similar phenomena are observed in K_3PO_4 and its hydrate, $K_3PO_4 \cdot 3H_2O$. Hydration causes upfield shifts in Na_3PO_4, K_3PO_4, and $Na_4P_2O_7$, while it causes downfield shifts in Rb_3PO_4 and Cs_3PO_4. Although previous works[9,10] have suggested that two peaks in the spectra of $K_4P_2O_7$ are attributable to its hydrate, our experiment demonstrates that all five peaks can be ascribed to anhydrous $K_4P_2O_7$. In the hydrated compounds, water molecules coordinate to alkali cations, and the phosphate anions interact with the cations indirectly through the water molecules. This situation is similar to that in an aqueous solution; thus, the chemical shifts of the hydrated compounds approach the values in the aqueous solution.

The field-dependence experiment can clearly demonstrate whether the splitting is caused by inequiva-

lent sites or by spin-spin coupling. The splittings in $K_4P_2O_7$ and $(KPO_3)_n$ are caused by inequivalent sites. The doublets in $Na_4P_2O_7$ and its hydrate are also considered to be caused by inequivalent sites, but no experimental evidence was obtained.

Finally, the present work has revealed that some materials contain coexisting phases and/or impurities. The ^1H decoupling experiment, the field-dependence measurements, and the heat treatment of the material can help very much in the confirmation of the impurity, as is demonstrated by the complicated spectra of commercial $K_5P_3O_{10}$.

References

1) E. R. Andrew, *Prog. NMR Spectrosc.*, **8**, 1 (1972).
2) I. J. Lowe, *Phys. Rev. Lett.*, **2**, 285 (1959).
3) C. A. Fyfe, "Solid State NMR for Chemists," C. F. C. Press, Guelph, Canada (1983).
4) E. Lippmaa, M. Magi, A. Samoson, G. Engelhardt, and A.-R. Grimmer, *J. Am. Chem. Soc.*, **102**, 4889 (1980).
5) W. P. Rothwell, J. S. Waugh, and J. P. Yesinowski, *J. Am. Chem. Soc.*, **102**, 2637 (1980).
6) E. R. Andrew, D. J. Bryant, E. M. Cashell, and B. A. Dunell, *Chem. Phys. Lett.*, **77**, 614 (1981).
7) U. Haubenreisser, G. Scheler, and A. -R. Grimmer, *Z. Anorg. Allg. Chem.*, **532**, 157 (1986).
8) N. E. Burlinson, B. A. Dunell, and J. A. Ripmeester, *J. Magn. Reson.*, **67**, 217 (1986).
9) A.-R. Grimmer and U. Haubenreisser, *Chem. Phys. Lett.*, **99**, 487 (1983).
10) T. M. Duncan and D. C. Douglass, *Chem. Phys.*, **87**, 339 (1984).
11) I. L. Mudrakovskii, V. P. Shmachkova, N. S. Kotsarenko, and V. M. Mastikhin, *J. Phys. Chem. Solids*, **47**, 335 (1986).
12) G. L. Turner, K. A. Smith, R. J. Kirkpatrick, and E. Oldfield, *J. Magn. Reson.*, **70**, 408 (1986).
13) S. Prabhakar, K. J. Rao, and C. N. R. Rao, *Chem. Phys. Lett.*, **139**, 96 (1987).
14) "Kagakudaiziten," Kyoritsu (1964).
15) J. Herzfeld and A. E. Berger, *J. Chem. Phys.*, **73**, 6021 (1980).
16) E. Tillmanns and W. H. Baur, *Acta Crystallogr., Sect. B*, **27**, 2124 (1971).
17) "Phosphorus-31 NMR," ed by D. G. Gorenstein, Academic Press (1984), p. 574.
18) K. Y. Leung and C. Calvo, *Can. J. Chem.*, **50**, 2519 (1972).
19) D. M. MacArthur and C. A. Beevers, *Acta Crystallogr.*, **10**, 428 (1957).
20) W. S. McDonald and D. W. J. Cruickshank, *Acta Crystallogr.*, **22**, 43 (1967).
21) V. K. H. Jost and H. J. Schulze, *Acta Crystallogr., Sect. B*, **25**, 1110 (1969).

 © 1989 The Chemical Society of Japan Bull. Chem. Soc. Jpn., 62, 3069—3074 (1989)

The Fluorescence Quenching of Zinc Porphyrins with the ω-[4-(4-Pyridyl)pyridinio]alkyl Group

Kohshin TAKAHASHI,* Tetsuo TERASHIMA, Teruhisa KOMURA, and Hiroto IMANAGA
Department of Chemistry and Chemical Engineering, Faculty of Technology,
Kanazawa University, Kodatsuno, Kanazawa 920
(Received April 10, 1989)

The fluorescence of parent porphyrins in $ZnPC_2bpy^+(n)$, ($PC_2bpy^+(n)$, 5-[*n*-[2-[4-(4-pyridyl)pyridinio]ethoxyl]phenyl]-10,15,20-triphenylporphyrin bromide, n=2,3, and 4), and $ZnPC_8bpy^+(3)$, ($PC_8bpy^+(3)$, 5-[3-[8-[4-(4-pyridyl) pyridinio]octyloxy]phenyl]-10,15,20-triphenylporphyrin bromide), was effectively quenched in non-coordinating solvents, such as *o*-dichlorobenzene and dichloromethane, because the pyridyl group in bpy^+ (ω-[4-(4-pyridyl)pyridinio]alkyl group) was coordinated to zinc in porphyrin. On the other hand, the fluorescence of parent porphyrins in $ZnPC_2bpy^+(3)$, $ZnPC_2bpy^+(4)$, and $ZnPC_8bpy^+$ (3) was partly quenched in such coordinating solvents as *N*,*N*-dimethylformamide and pyridine. However, only the fluorescence of the parent porphyrin in $ZnPC_2bpy^+(2)$ was effectively quenched, even in coordinating solvents. The hydrophobic interaction between the porphyrin ring and bpy^+ in $ZnPC_2bpy^+(2)$ may be considerably large, for bpy^+ in $ZnPC_2bpy^+(2)$ is covalently linked to the ortho position of the phenyl group in ZnTPP, (TPP 5,10,15,20-tetraphenylporphyrin), by a short chain. The emission was effectively quenched by the photoinduced electron transfer from the porphyrin ring to bpy^+, because the axial coordination or the hydrophobic interaction gave bpy^+ access to the porphyrin ring.

A metalloporphyrin covalently bound to an electron acceptor is very interesting as a model of the photoinduced electron transfer that occurs in photosynthetic reaction centers. Furthermore, the study of the photophysical properties of electron acceptor-linked metalloporphyrins is very important in order to produce, in the future, a molecular device for the conversion of solar to chemical and/or electrical energy. The emission properties and the photoinduced electron transfer mechanism have been reported on porphyrins covalently bound to quinone or viologen by a flexible chain.[1-5] An investigation of the photoinduced electron transfer of porphyrins covalently linked to an electron acceptor by a rigid spacer exhibited the importance of distance and orientation between the two reactants.[6-8] The application of an external magnetic field[9,10] and multistep electron transfer[11-14] were examined in order to form a long-lived ion-pair in electron acceptor-linked porphyrins. The photoinduced electron transfer of a porphyrin covalently linked to tetracyanonaphtoquinodimethane[15] or a macrotetracyclic cryptate containing the silver(I) ion[16] was also investigated. Recently, we found the photoinduced electron transfer of a zinc porphyrin with an *N*-methylpyridinio group covalently linked to the meso position in the porphyrin ring.[17]

Blondeel et al.[5] reported that the fluorescence quenching efficiency of a zinc porphyrin covalently linked to bpy^+ by a flexible chain was almost the same as that of a viologen-linked porphyrin, although bpy^+ have a smaller electron affinity than the viologen. In the present paper, we report that the zinc porphyrins (shown in Fig. 1) have different conformations in different solvents because of the axial coordination and the hydrophobic interaction between the porphyrin ring and bpy^+, and also that the fluorescence quantum yield is dependent on the conformation.

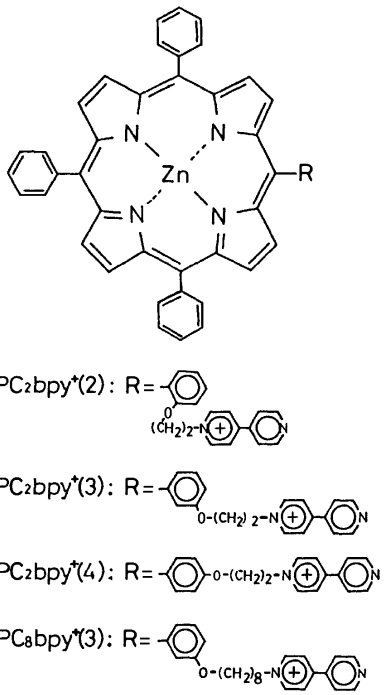

Fig. 1. Structures and abreviations of zinc porphyrins.

Experimental

5-(2-, 3-, and 4-Hydroxyphenyl)-10,15,20-triphenylporphyrins were synthesized and purified by the literature method.[18] The zinc porphyrins were also synthesized by the literature method.[19] The products were purified by column chromatography on alumina. $ZnPC_2Br(n)$, ($PC_2Br(n)$, 5-(*n*-(2-bromoethoxy)phenyl)-10,15,20-triphenylporphyrin, n=2, 3, and 4) and $ZnPC_8Br(3)$, ($PC_8Br(3)$, 5-(3-(8-bromooctyloxy)phenyl)-10,15,20-triphenylporphyrin), were synthesized

and purified by the literature method.[20] $ZnPC_2bpy^+(n)$ and $ZnPC_8bpy^+(3)$ were synthesized by heating a mixture of $ZnPC_2Br(n)$ (or $ZnPC_8Br(3)$) and 4,4'-bipyridine in *N,N*-dimethylformamide (DMF) at 100 °C for 24 hours.[10] The products were purified by column chromatography on silica. Calcd for $C_{56}H_{51}N_6O_7BrZn(ZnPC_2bpy^+(3)\ 6H_2O)$(MW. 1065.34): C, 63.14; H, 4.82; N, 7.89%. Found: C, 63.37; H, 4.26; N, 7.63%. Calcd for $C_{62}H_{55}N_6O_3BrZn(ZnPC_8bpy^+(3)\ 2H_2O)$(MW.1077.44): C, 69.12; H, 4.96; N, 7.80%. Found: C, 68.64; H, 4.84; N, 7.57%. 1-Methyl-4-(4-pyridyl)pyridinium bromide was synthesized and purified by the literature method.[21] Tetraethylammonium perchlorate (Et_4NClO_4) was used after a double recrystallization from water. DMF was distilled twice under reduced pressure in a N_2 atmosphere after dehydration, using Molecular Sieves (4A1/16) and barium oxide. The other solvents were used after distillation.

The absorption spectra were recorded on a Hitachi U-3210 spectrophotometer. The emission and excitation spectra were taken on a Shimadzu RF-540 spectrofluorometer equipped with a Hamamatsu Photonics R928 photomultiplier. The spectral response was corrected by the use of the standard solutions.[22,23] The quantum yields of the emissions in air-equilibrated solutions were determined with reference to the yield of ZnTPP in benzene ($\phi_f^{S1}=0.033$[24]), using the optical dilute method.[25] Cyclic voltammetry was performed in a N_2-purged solution, using a Pt disk (diameters; 1 mm) as the working electrode, a Pt wire as the counter electrode, and Ag/0.1 M $AgNO_3$ in acetonitrile as the reference electrode (1 M=1 mol dm^{-3}). Potential control was obtained by using a Hokuto Denko HA-501 potentiostat and a HB-104 function generator. Cyclic voltammograms were recorded on a Yokogawa 3025 X-Y recorder. The half-wave potentials, measured at the scan rate of 50 mV s^{-1}, were the averages of the cathodic and anodic peak potentials.

Results and Discussion

Inter- and Intramolecular Axial Coordination of Zinc Porphyrins Covalently Linked to bpy^+ by a Flexible Chain. $ZnPC_2bpy^+(2)$, $ZnPC_2bpy^+(3)$, and $ZnPC_8bpy^+(3)$ were slightly soluble, while $ZnPC_2bpy^+(4)$ was insoluble, in non-coordinating solvents, such as *o*-dichlorobenzene (*o*-DCB) and CH_2Cl_2. However, the porphyrins were soluble in coordinating solvents, such as DMF and pyridine.

The addition of pyridine to ZnTPP in *o*-DCB gave rise to a red shift of the absorption peak in the B and Q regions because of the formation of a monopyridine complex.[26] On the other hand, in *o*-DCB, the absorption peaks in the B and Q regions of bpy^+-linked zinc porphyrins were observed at longer wavelengths than those of ZnTPP; also, the Soret bands of bpy^+-linked zinc porphyrins exhibited very broad spectra, with very small molar extinction coefficients at the absorption peak, in comparison with the Soret band of ZnTPP. The absorption spectrum of $ZnPC_2bpy^+(3)$ in *o*-DCB exhibited the characteristic Soret splitting. However, when pyridine was added to the *o*-DCB solution, the Soret bands of the bpy^+-linked zinc porphyrins became sharp. The absorption spectra of ZnTPP, $ZnPC_2bpy^+(3)$, and $ZnPC_8bpy^+(3)$ in *o*-DCB and DMF are shown in Fig. 2, while the absorption spectral features of zinc porphyrin derivatives in different solvents are summarized in Table 1. The intensity ratios of the Q(0,0) and Q(1,0) bands (ε (0,0)/ε (1,0)) for ZnTPP were larger in DMF, pyridine, alcohols, acetonitrile, and nitromethane than in CH_2Cl_2 and *o*-DCB. These results suggested that the solvent molecules, such as DMF, pyridine, alcohols, acetonitrile, and nitromethane, were coordinated to zinc in ZnTPP.[27] The spectral profiles of $ZnPC_2Br(n)$ and $ZnPC_8Br(3)$ in all the solvents were similar to that of ZnTPP, but an enhancement of ε (0,0)/ε (1,0) and a red shift of the B and Q bands for bpy^+-linked zinc porphyrins were observed in the non-coordinating solvents, such as *o*-DCB and CH_2Cl_2.

The above results suggest that the pyridyl group in bpy^+-linked zinc porphyrins was coordinated to zinc in the same or another porphyrin. From the Soret splitting of $ZnPC_2bpy^+(3)$ in *o*-DCB, we tentatively proposed a dimer model of $ZnPC_2bpy^+(3)$ in a non-coordinating solvent, as is shown in Fig. 3a. We previously reported that the Soret band of a zinc porphyrin with a pyridyl group consisted of two components in CH_2Cl_2 because of two intermolecular axial coordinations between the pyridyl group and zinc in porphyrin.[28] Furthermore, Tabushi et al. reported that a gable porphyrin exhibited the same Soret splitting; they inferred that the splitting was due

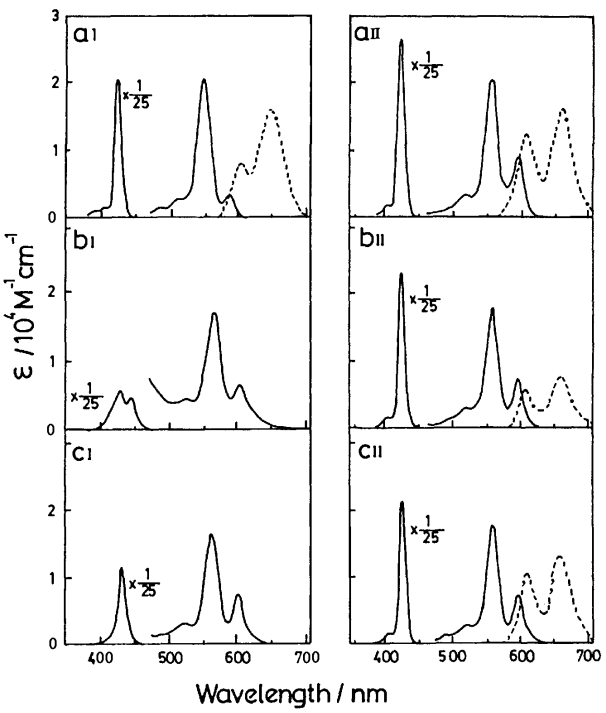

Fig. 2. Absorption (——) and fluorescence (----) spectra of ZnTPP (a), $ZnPC_2bpy^+(3)$ (b) and $ZnPC_8bpy^+(3)$ (c) in *o*-DCB(I) and DMF(II) at room temperature.

Table 1. Absorption Spectral Features of Zinc Porphyrins in Different Solvents at Room Temperature

Solvent	Porphyrin	B(0,0)	Q(1,0)	Q(0,0)	$\varepsilon(0,0)/\varepsilon(1,0)$[a]
		nm			
DMF	ZnTPP	426(66.8)[b]	559(2.08)	599	0.43
	$ZnPC_2bpy^+$ (2)	427(51.0)	560(1.89)	599	0.40
	$ZnPC_2Br$(3)	426	559	599	0.41
	$ZnPC_2bpy^+$ (3)	426(58.0)	559(1.79)	599	0.41
	$ZnPC_2bpy^+$ (4)	426	560	600	0.48
	$ZnPC_8Br$ (3)	426	559	599	0.42
	$ZnPC_8bpy^+$ (3)	426(53.8)	559(1.75)	599	0.42
Pyridine	ZnTPP	431	564	604	0.51
	$ZnPC_2bpy^+$ (3)	431	564	603	0.49
	$ZnPC_8bpy^+$ (3)	431	564	604	0.51
Methanol	ZnTPP	421	556	596	0.36
	$ZnPC_2bpy^+$ (2)	423	558	597	0.36
	$ZnPC_2bpy^+$ (3)	422	556	596	0.34
	$ZnPC_2bpy^+$ (4)	422	557	596	0.40
	$ZnPC_8bpy$ (3)	422	557	596	0.37
1-Propanol	ZnTPP	424	558	597	0.37
	$ZnPC_2bpy^+$ (3)	424	558	597	0.32
	$ZnPC_8bpy^+$ (3)	424	558	598	0.36
Acetonitrile	ZnTPP	422	556	596	0.42
	$ZnPC_2bpy^+$ (3)	422	556	596	0.37
	$ZnPC_8bpy^+$ (3)	424	559	599	0.46
Nitromethane	ZnTPP	422(51.3)	554(1.65)	594	0.35
	$ZnPC_2Br$ (2)	423	554	595	0.31
	$ZnPC_2bpy^+$ (2)	425(45.7)	557(1.87)	599	0.34
	$ZnPC_2Br$ (3)	422	553	594	0.31
	$ZnPC_2bpy^+$ (3)	423(51.3)	555(1.70)	597	0.37
	$ZnPC_2Br$ (4)	423	554	595	0.37
	$ZnPC_2bpy^+$ (4)	423	556	598	0.41
	$ZnPC_8Br$ (3)	422	554	594	0.33
	$ZnPC_8bpy^+$ (3)	425(56.1)	561(1.84)	600	0.50
Dichloromethane	ZnTPP	419(59.6)	548(2.16)	586	0.17
	$ZnPC_2Br$ (3)	420(52.6)	548(1.92)	587	0.17
	$ZnPC_2bpy^+$ (3)	425(22.0)	560(1.39)	601	0.42
	$ZnPC_8Br$ (3)	420	548	586	0.17
	$ZnPC_8bpy^+$ (3)	427(37.0)	560(1.50)	601	0.45
o-DCB	ZnTPP	425(52.1)	550(2.20)	588	0.16
	$ZnPC_2bpy^+$ (2)	438(43.6)	564(1.61)	605	0.43
	$ZnPC_2bpy^+$ (3)	431(15.1) 447(12.5)	565(1.77)	605	0.52
	$ZnPC_8bpy^+$ (3)	431(28.6)	563(1.66)	603	0.46

a) The intensity ratio of the Q(0,0) and Q(1,0) bands. b) The values in parentheses are the molar extinction coefficients ($\varepsilon/10^4$ M^{-1} cm^{-1}).

to the nearly perpendicular orientation between two porphyrin rings, which caused a relatively weak π-π interaction between them.[29] The dimer of $ZnPC_2bpy^+(3)$ in *o*-DCB can be formed by two intermolecular axial coordinations between the pyridyl group and Zn in porphyrin, while the π-π interaction between two porphyrin rings may be relatively weak. The absorption spectra in the Soret region of $ZnPC_2bpy^+(3)$ in *o*-DCB distinctly changed in the range from 25 to 65 °C, although the absorption spectra in the Q region hardly changed at all. Figure 4 shows the temperature-dependence of the absorption spectra in the Soret region of $ZnPC_2bpy^+(3)$ in *o*-DCB. The absorption spectra indicated two isosbestic points—at 417 and 439 nm. The absorbance of the absorption peak at 447 nm decreased with an increase in the temperature, while that of the absorption peak at 431 nm increased. The Soret splitting consequently disappeared at a relatively high temperature. The temperature-dependence of the Soret band was probably attributable to the temperature-dependence of the conformation between the two porphyrin rings.

In nitromethane and acetonitrile, an enhancement of ε (0,0)/ε (1,0) and a red shift of the B and Q bands for $ZnPC_8bpy^+(3)$ were observed, while no spectral change in $ZnPC_2bpy^+(n)$ was observed. The pyridyl group in $ZnPC_8bpy^+(3)$ with a long-flexible chain can be coordinated to zinc in porphyrin, even in nitromethane and acetonitrile, which have a relatively strong power of coordination. Therefore, we tentatively proposed a model of an intramolecular axial coordination for $ZnPC_8bpy^+(3)$ in a non-coordinating

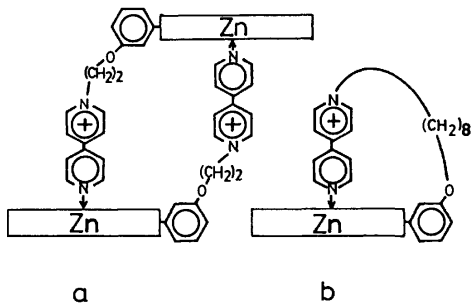

Fig. 3. Typical schematic axial coordination models of $ZnPC_2bpy^+$ (3) (a) and $ZnPC_8bpy^+$ (3) (b). □ Denotes porphyrin ring, and N→Zn coordination between Zn and N(pyridyl group).

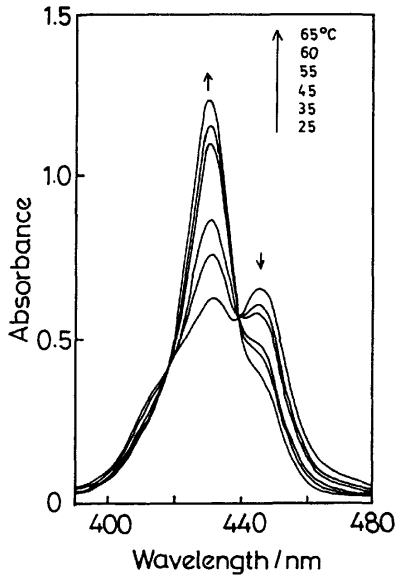

Fig. 4. Temperature-dependence of Soret absorption spectra of 4.1×10^{-6} M $ZnPC_2bpy^+$ (3) in *o*-DCB.

solvent, as is shown in Fig. 3b. Such a model was also supported by the emission properties of $ZnPC_8bpy^+$(3), which will be discussed below.

Since an enhancement of ε (0,0)/ε (1,0) and a red shift of the B and Q bands for $ZnPC_2bpy^+$(2) was observed only in a non-coordinating solvent, such as *o*-DCB, it was inferred that a pyridyl group in $ZnPC_2bpy^+$(2) was also coordinated to zinc in porphyrin only in a non-coordinating solvent. We presumed an intramolecular axial coordination for $ZnPC_2bpy^+$(2) as well as for $ZnPC_8bpy^+$(3) because of the covalent linkage of bpy^+ to the ortho position of the phenyl group in ZnTPP.

Solvent Effects of Fluorescence Properties. When a zinc porphyrin is covalently linked to bpy^+ by a flexible chain, the lowest singlet excited state (S_1) is partly quenched in coordinating solvents, as has been reported by Blondeel et al.[5] On the other hand, the S_1 excited states of parent porphyrins in the bpy^+-linked zinc porphyrins are effectively quenched in non-coordinating solvents; also, only the S_1 excited states of parent porphyrins in $ZnPC_2bpy^+$(2) are effectively quenched, even in coordinating solvents. The S_1 emission spectra of ZnTPP, $ZnPC_2bpy^+$(3), and $ZnPC_8bpy^+$(3) in DMF and *o*-DCB are shown in Fig. 2. Tables 2 and 3 summarize the quantum yields and the relative quantum yields (ϕ/ϕ_0) of S_1 emissions of zinc porphyrins in different solvents, where ϕ and ϕ_0 denote the quantum yields of S_1 emissions of a bpy^+-linked porphyrin and ZnTPP respectively. Since the fluorescence quantum yields of $ZnPC_2Br(n)$ and $ZnPC_8Br$(3) were similar to that of ZnTPP, bpy^+ in bpy^+-linked zinc porphyrins can be said to act as a quencher.

Table 4 summarizes the redox potentials of zinc porphyrin derivatives and Me-bpy^+(1-methyl-4-(4-pyridyl)pyridinium bromide) in DMF. The porphyrin rings in zinc porphyrins were oxidized around 0.4V vs. Ag^+/Ag and were reduced around −1.8 V. The ω-[4-(4-pyridyl)pyridinio]alkyl groups (bpy^+) in bpy^+-linked zinc porphyrins were reduced around −1.3 V. The oxidation potentials in the S_1 excited state ($E(P^+/P_{s1}^*)$), which are estimated from the oxidation potential in the ground state and from the excitation energy from the ground state to the S_1 excited state, are also summarized in Table 4. The photoinduced electron transfer from the porphyrin ring to bpy^+ can occur because the value of $E(P^+/$

Table 2. Fluorescence Quantum Yields[a] of $ZnPC_2bpy^+$ (3) and $ZnPC_8bpy^+$ (3) in Different Solvents at Room Temperature

Solvent	ZnTPP	$ZnPC_2Br$ (3)	$ZnPC_2bpy^+$ (3)	$ZnPC_8Br$ (3)	$ZnPC_8bpy^+$ (3)
DMF	0.031	0.030	0.017(0.55)[b]	0.031	0.027(0.87)
Pyridine	0.036		0.020(0.56)		0.024(0.67)
Methanol	0.027		0.0081(0.30)		0.010(0.37)
1-Propanol	0.032		0.0085(0.27)		0.012(0.38)
Acetonitrile	0.029		0.014(0.48)		0.0051(0.18)
Nitromethane	0.016	0.015	0.0084(0.53)	0.016	0.0017(0.11)
Dichloromethane	0.026	0.026	0.0010(0.038)	0.026	0.0016(0.062)
o-DCB	0.035		0.00018(0.0051)		0.0017(0.049)

a) Excitation at 520 nm. b) The values in parentheses are the relative fluorescence quantum yields (ϕ/ϕ_0), where ϕ and ϕ_0 denote the quantum yields of S_1 emissions of a bpy^+-linked zinc porphyrin and ZnTPP respectively.

Table 3. Fluorescence Quantum Yields[a] of $ZnPC_2bpy^+$ (2), $ZnPC_2bpy^+$ (3), and $ZnPC_2bpy^+$ (4) in Different Solvents at Room Temperature

Solvent	$ZnPC_2bpy^+$ (2)	$ZnPC_2bpy^+$ (3)	$ZnPC_2bpy^+$ (4)
DMF	0.00034(0.011)[b]	0.017(0.55)	0.018(0.58)
Methanol	0.000068(0.0025)	0.0081(0.30)	0.0052(0.19)
Nitromethane[c]	0.00025(0.016)	0.0084(0.53)	0.0079(0.49)
o-DCB	0.00028(0.0080)	0.00018(0.0051)	d

a) Excitation at 520 nm. b) The values in parentheses are the relative fluorescence quantum yields (ϕ/ϕ_0). c) The fluorescence quantum yields of $ZnPC_2Br$(2), $ZnPC_2Br$ (3), and $ZnPC_2Br$ (4) in nitromethane are 0.016, 0.015, and 0.014 respectively. d) $ZnPC_2bpy^+$ (4) is insoluble in *o*-DCB.

Table 4. Half-Wave Potentials and $E(P^+/P_{s1}^*)$[a,b] of Zinc Porphyrins in DMF Solutions Containing 0.1 M Et_4NClO_4 at Room Temperature

Porphyrin	Reduction potential		Oxidation potential	$E(P^+/P_{s1}^*)$
	V			
ZnTPP	−1.75		0.43	−1.61
Me-bpy$^+$[c]		−1.37		
$ZnPC_2bpy^+$ (2)	−1.80	−1.20	0.43	−1.61
$ZnPC_2bpy^+$ (3)	−1.75	−1.27	0.43	−1.61
$ZnPC_2bpy^+$ (4)	−1.78	−1.29	0.41	−1.63
$ZnPC_8bpy^+$ (3)	−1.77	−1.25	0.44	−1.60

a) Measured against Ag/0.1 M $AgNO_3$ in acetonitrile. b) The oxidation potential of the S_1 excited state. c) 1-Methyl-4-(4-pyridyl)pyridinium bromide.

P_{s1}^*.) is more negative than the reduction potential of bpy$^+$.

The S_1 excited states of parent porphyrins in bpy$^+$-linked zinc porphyrins were effectively quenched in non-coordinating solvents, and the very weak fluorescence spectra were almost entirely consistent with the fluorescence spectra of ZnTPP despite the axial coordination of the pyridyl group in bpy$^+$. The excitation spectra of the S_1 emissions of bpy$^+$-linked zinc porphyrins in non-coordinating solvents did not agree with the absorption spectra, but they did agreed with the absorption spectrum of ZnTPP. These results show that the fluorescence of parent porphyrins in bpy$^+$-linked zinc porphyrins was completely quenched when the pyridyl group in bpy$^+$ was coordinated to zinc in porphyrin, and also that the pyridyl group in bpy$^+$ was only slightly dissociated from zinc in porphyrin, even in non-coordinating solvents. Hence, the fluorescence quantum yield of a bpy$^+$-linked zinc porphyrin in a non-coordinating solvent must be an apparent one. The addition of 4,4′-bipyridine to ZnTPP in benzene gave rise to a red shift of the absorption and fluorescence peaks because of the axial coordination of 4,4′-bipyridine to zinc in porphyrin, and caused a slight decrease in the fluorescence quantum yield (0.022 in benzene containing 0.06 M 4,4′-bipyridine). These results suggest that the photoinduced electron transfer from the porphyrin ring to bpy$^+$ effectively occurred, for the axial coordination of the pyridyl group in bpy$^+$ to zinc in porphyrin gave bpy$^+$ access to the porphyrin ring.

Figure 5a shows the Soret absorption spectra of $ZnPC_2bpy^+$(3) in *o*-DCB containing DMF. The absorption spectra indicated two isosbestic points—at 420 and 440 nm. Figure 5b shows the dependence of the value of I/I_0 for $ZnPC_2bpy^+$(3) in *o*-DCB on the concentration of DMF, where I and I_0 denote the fluorescence quantum yields in the presence and in the absence of a coordinating solvent molecule at an excitation wavelength which is an isosbestic point of the absorption spectra respectively. The addition of DMF to the *o*-DCB solution caused a dissociation between the pyridyl group and zinc in the bpy$^+$-linked zinc porphyrin and an increase in the value of I/I_0. Furthermore, when 0.03M pyridine was added to the *o*-DCB solutions, the I/I_0 values for $ZnPC_2bpy^+$(3) and $ZnPC_8bpy^+$(3) were 22 and 14 respectively; also, a red shift of the fluorescence peaks and a change in the intensity ratio of the Q(0,0) and Q(0,1) fluorescence bands were observed. The zinc porphyrins was probably emitted only when the pyridyl group in bpy$^+$ was dissociated from the zinc in porphyrin.

In nitromethane and acetonitrile, the fluorescence quantum yields of $ZnPC_8bpy^+$(3) were considerably smaller than those of $ZnPC_2bpy^+$(3) (Table 2). When 0.03 M pyridine was added to the nitromethane solutions, the value of I/I_0 for $ZnPC_8bpy^+$(3) was 10, although the fluorescence quantum yield of $ZnPC_2bpy^+$(3) hardly changed. These results suggest that, in nitromethane and acetonitrile, the pyridyl group in $ZnPC_8bpy^+$(3) was coordinated to zinc in the same porphyrin as is shown in Fig. 3b, but that the pyridyl group in $ZnPC_2bpy^+$(3) was not.

The fluorescence quantum yields of $ZnPC_2bpy^+$(3)

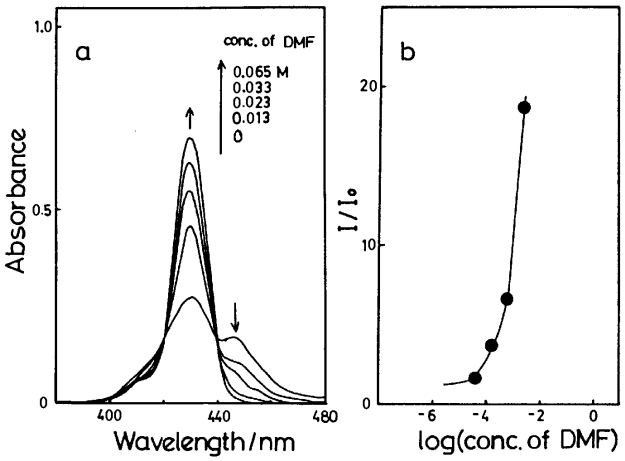

Fig. 5. The dependence of Soret absorption spectra (a) and I/I_0 (b) for 1.7×10^{-6} M $ZnPC_2bpy^+$ (3) in *o*-DCB on the concentration of DMF at room temperature, where I and I_0 denote the fluorescence quantum yields in the presence and the absence of DMF at the excitation wavelength of 420 nm (isosbestic point).

and $ZnPC_8bpy^+$(3) were larger in DMF and pyridine than in *o*-DCB and CH_2Cl_2; also, in DMF and pyridine, the fluorescence quantum yields of $ZnPC_8bpy^+$(3) were larger than those of $ZnPC_2bpy^+$(3) (Table 2). The zinc porphyrins in coordinating solvents probably had a conformation in which the bpy^+ was remote from the porphyrin ring. However, the S_1 excited states of the zinc porphyrins were quenched more effectively in alcohols than in DMF and pyridine (Table 2). The hydrophobic interaction between the porphyrin ring and bpy^+ may be larger in alcohols than in DMF and pyridine. On the other hand, even in coordinating solvents, the fluorescence of the parent porphyrin in $ZnPC_2bpy^+$(2) was effectively quenched (Table 3). The reduction potential of bpy^+ in $ZnPC_2bpy^+$(2) was more positive than those of bpy^+ in other bpy^+-linked zinc porphyrins; also, the reduction potential of the porphyrin ring in $ZnPC_2bpy^+$(2) was more negative (Table 4). The hydrophobic interaction between the porphyrin ring and bpy^+ may be larger in $ZnPC_2bpy^+$(2) than in other zinc porphyrins, for the bpy^+ in $ZnPC_2bpy^+$(2) is covalently linked to the ortho position of the phenyl group in ZnTPP by a short chain; thus, the interaction can easily cause the photoinduced electron transfer.

References

1) I. Tabushi, N. Koga, and M. Yanagita, *Tetrahedron Lett.*, **1979**, 257.

2) J. L. Y. Kong, K. G. Spears, and P. A. Loach, *Photochem. Photobiol.*, **35**, 545 (1982).

3) J. A. Schmidt, A. R.McIntosh, A. C. Weedon, J. R. Bolton, J. C. Connolly, J. K. Hurley, and M. R. Wasielewski, *J. Am. Chem. Soc.*, **110**, 1733 (1988).

4) A. Harriman, G. Porter, and A. Wilowska, *J. Chem. Soc., Faraday Trans. 2*, **80**, 191 (1984).

5) G. Blondeel, D. D. Keukeleire, A. Harriman, and L. R. Milgrom, *Chem. Phys. Lett.*, **118**, 77 (1985).

6) P. Leighton and J. K. M. Sanders, *J. Chem. Soc., Chem. Commun.*, **1984**, 856.

7) M. R. Wasielewski and M. P. Niemczyk, *J. Am. Chem. Soc.*, **106**, 5043 (1984).

8) B. A. Leland, A. D. Joram, P. M. Felder, J. J. Hopfield, A. H. Zewail, and P. B. Dervan, *J. Phys. Chem.*, **89**, 5571 (1985).

9) H. Nakamura, A. Motonaga, T. Ogata, S. Nakao, T. Nagamura, and T. Matsuo, *Chem. Lett.*, **1986**, 1615.

10) T. Saito, Y. Hirata, H. Sato, T. Yoshida, and N. Mataga, *Bull. Chem. Soc. Jpn.*, **61**, 1925 (1988).

11) S. Nishitani, N. Kurata, Y. Sakata S. Misumi, A. Karen, T. Okada, and N. Mataga, *J. Am. Chem. Soc.*, **105**, 7771 (1983).

12) J. L. Sessler, M. R. Johnson, T. Y. Lin, and S. E. Creager, *J. Am. Chem. Soc.*, **110**, 3659 (1988).

13) D. Gust, T. A. Moore, A. L. Moore, L. R. Makings, G. R. Seely, X. Ma, T. T. Trier, and F. Gao, *J. Am. Chem. Soc.*, **110**, 7567 (1988).

14) M. R. Wasielewski, M. P. Niemczyk, W. A. Svec, and E. B. Pewitt, *J. Am. Chem. Soc.*, **107**, 5562 (1985).

15) M. R. Wasielewski, D. G. Johnson, W. A. Svec, K. M. Kersey, and D. W. Minsek, *J. Am. Chem. Soc.*, **110**, 7219 (1988).

16) M. Gubelmann, A. Harriman, J. M. Lehn, and J. L. Sessler, *J. Chem. Soc., Chem. Commun.*, **1988**, 77.

17) K. Takahashi, O. Ohno, Y. Kaizu, and H. Kobayashi, in preparation.

18) R. G. Little, J. A. Anton, P. A. Loach, and J. A. Ibers, *J. Heterocycl. Chem.*, **12**, 343 (1975).

19) A. D. Adler, F. R. Longo, F. Kampas, and J. Kim, *J. Inorg. Nucl. Chem.*, **32**, 2443 (1970).

20) R. G. Little, *J. Heterocycl. Chem.*, **15**, 203 (1978).

21) M. P. Pileni, A. M. Braun, and M. Gratzel, *Photochem. Photobiol.*, **31**, 423 (1980).

22) E. Lippert, W. Nagele, I. Seibold-Blankenstein, V. Staiger, and W. Voss, *Z. Anal. Chem.*, **170**, 1 (1959).

23) W. H. Melhuish, *J. Res. Natl. Bur. Stand. Sect. A*, **76**, 547 (1972).

24) P. G. Seybold and M. Gouterman, *J. Mol. Spectrosc.*, **31**, 1 (1969).

25) J. N. Demas and G. A. Crosby, *J. Phys. Chem.*, **75**, 991 (1971).

26) J. R. Miller and G. D. Dorough, *J. Am. Chem. Soc.*, **74**, 3977 (1952).

27) O. Ohno, Y. Kaizu, and H. Kobayashi, *J. Chem. Phys.*, **82**, 1779 (1985).

28) K. Takahashi, T. Komura, and H. Imanaga, *Bull. Chem. Soc. Jpn.*, **62**, 386 (1989).

29) I. Tabushi, S. Kugimiya, M. G. Kinnaird, and T. Sasaki, *J. Am. Chem. Soc.*, **107**, 4192 (1985).

Fluorescence Studies on the Phase Dependence of Interactions between a Tripeptide, Lys-Trp-Lys, and Dimyristoylphosphatidylserine

Shoji YAMASHITA,* Arthur G. SZABO,† Donald T. KRAJCARSKI,† and Nobuyuki YAMASAKI††
Institute of Biophysics, Faculty of Agriculture, Kyushu University, Hakozaki, Higashiku, Fukuoka 812
†Molecular Biochemistry, National Research Council Canada, Ottawa, Canada, K1AOR6
††Laboratory of Biochemistry, Faculty of Agriculture, Kyushu University, Hakozaki, Higashiku, Fukuoka 812
(Received May 1, 1989)

Interactions of a basic tripeptide, lysyl-tryptophyl-lysine (LTL) with dimyristoylphosphatidylserine (DMPS) were investigated by fluorescence spectroscopy. An interacting LTL-DMPS complex assumes two distinctly different conformations in the lipid bilayer depending on the thermotropic phase of lipid. At temperatures below the gel-liquid crystalline phase-transition temperature (T_c), LTL binds to the polar head groups of DMPS through electrostatic force, and the tryptophan residue is located on the surface of the membrane because of the rigidity of the head groups. Above T_c, it assumes a conformation such that the tryptophan residue slips deeply into the DMPS bilayer. The temperature dependence of the fluorescence quenching by acrylamide supported the penetration of the tryptophan upon the phase transition of DMPS. A fluorescence decay analysis based on the photophysical deactivation mechanism of tryptophan residue has revealed a peculiar interaction of LTL with DMPS in the bilayer.

Recently, much attention has been paid to the peptide-lipid interaction because many small peptides, when brought to interact with membrane systems, exert significant biological effects or display important physiological functions. Investigations of their interactions provide information on the relationship between their structures and functions.[1,2] Fluorescence spectroscopy is endowed with some functions which have been proved useful for such studies. Since only tyrosine and tryptophan residues give efficient fluorescence, they provide a specific intrinsic probe for properties of the peptide-lipid system.

A tripeptide, LTL, has attracted a great deal of interest because of its intrinsic fluorescence due to tryptophan and the positively charged lysine residues which are responsible for electrostatic interactions with the negatively charged head group of phospholipid bilayers. There is evidence that upon LTL's binding with phosphatidylserine, the fluorescence emission spectrum shifted to shorter wavelengths accompanying a marked enhancement in quantum yield, and such a change in fluorescence spectrum has been interpreted as being due to a change in the environment of the indole ring of tryptophan.[3] These results directed us to carry out detailed studies on binding properties of LTL with the phospholipid bilayer. The present paper reports of fluorescence spectroscopic studies on interactions of LTL with DMPS above and below the transition temperature of the phospholipid.

Materials and Methods

LTL and 1,6-diphenylhexatriene (DPH) were purchased from Aldrich Chemicals Co. and purified by recrystallization and sublimation, respectively. DMPS obtained from Avanti Polar Lipid Inc. was used without further purification. The other reagents used throughout the present experiment were of analytical grade.

Unilamellar Vesicles of DMPS. Unilamellar vesicles of DMPS were prepared by the method of Barenholz,[4] and the concentration of DMPS was determined by the method of Bartlett.[5]

Fluorescence Spectra. Fluorescence measurements of LTL and its complex with DMPS vesicles were carried out on a Perkin-Elmer spectrofluorometer MPF-44 equipped with a DCSU-2 microprocessor correction unit. Analog signals were passed into an ADC interfaced to a Commodore minicomputer having a Commodore 2040 disk driver for data storage. For spectroscopic analysis of LTL-DMPS interactions, a small aliquot of DMPS vesicles was added to 2 ml of LTL solution in Tris-acetate buffer at a given pH. This was done in such a manner that the concentration of the remaining LTL is kept constant. Unless otherwise specified, fluorescence was measured with excitation at 280 nm and with 3 nm bandpath. Samples were kept at a constant temperature (±0.5 °C) by circulating water through a thermostated bath.

Fluorescence Decay Analysis. Fluorescence decay measurements were performed by use of the technique of time correlated single photon counting. A synchronously pumped dye laser and a cavity dumper system were employed as the excitation source operating at 825 kHz and with 15 ps pulse width. Detection of emissions was performed on a photomultiplier after their successive passage through a polarizer at the magic angle and a monochromater with 4 nm bandpath. The wavelength dependence of the instrument responce was corrected by using an emission from terphenyl. Data were accumulated in 1024 channels of a multichannel analyzer with a channel width of 21.6 ps, and analyzed by the nonlinear least squares iterative deconvolution method based on the Marquardt algorism. The adequacy of exponential decay fitting was examined by inspection of weighted residual plots and other statistical parameters. The details of the instrumentation and the method of data analysis were described in our previous paper.[6]

Results

Fluorescence Spectra of LTL in the Absence and Presence of DMPS Vesicles. Figure 1 shows fluorescence spectra of free LTL and its complex with DMPS

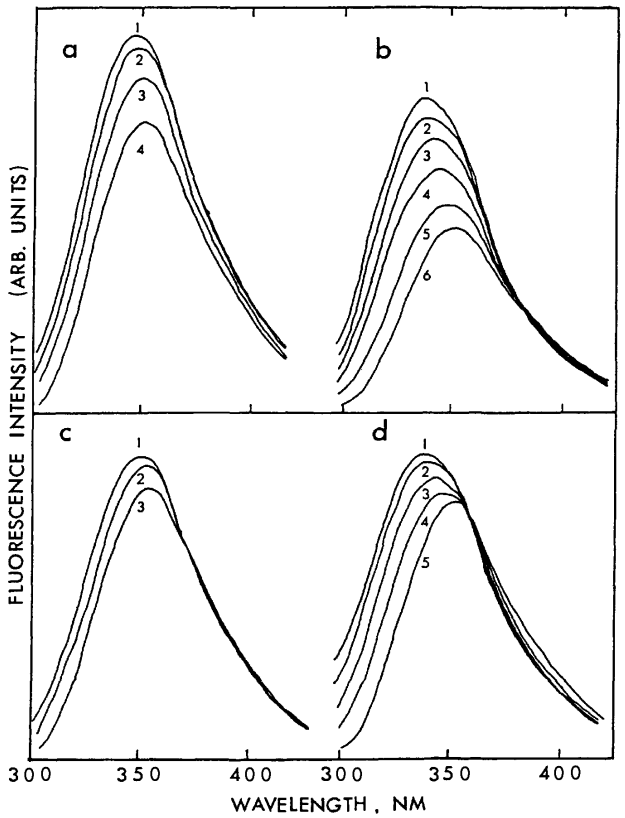

Fig. 1. Fluorescence spectra of LTL in the presence of DMPS vesicles in 20 mM Tris-acetate buffer: LTL concentration, 12.5 μM; (a) pH 5.0; 25 °C; DMPS concentration; 1, 200 μM; 2, 100 μM; 3, 50 μM; 4, 0 μM; (b) pH 5.0; 45 °C; DMPS concentration; 1, 150 μM; 2, 100 μM; 3, 75 μM; 4, 50 μM; 5, 25 μM; 6, 0 μM; (c) pH 7.0; 25 °C; DMPS concentration; 1, 150 μM; 2, 50 μM; 3, 0 μM; (d) pH 7.0; 45 °C; DMPS concentration; 1, 250 μM; 2, 200 μM; 3, 100 μM; 4, 50 μM; 5, 0 μM.

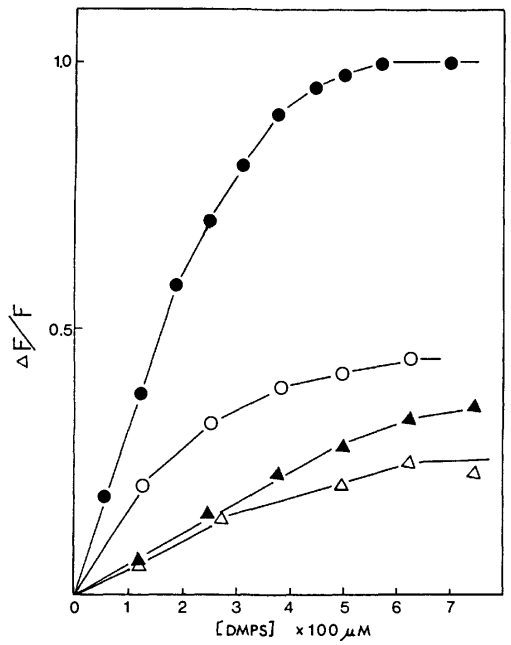

Fig. 2. Relative increase of LTL fluorescence intensity ($\Delta F/F$) on the addition of DMPS: —●—, pH 5.0 at 45 °C; —○—, pH 5.0 at 25 °C; —▲—, pH 7.0 at 45 °C; —△—, pH 7.0 at 25 °C; LTL concentration, 12.5 μM.

at different pHs and temperatures. The fluorescence spectrum of free LTL excited at 280 nm has a maximum at 352 nm. Upon addition of DMPS, the spectrum shifted to shorter wavelengths and the fluorescence intensity increased with increasing concentration of DMPS. From the variation of the fluorescence, titration curves for the binding of LTL to DMPS under various conditions were constructed by plotting $\Delta F/F$ values against the concentration of DMPS, where F is the fluorescence intensity of free LTL and ΔF is the difference in the fluorescence intensities between free and bound LTLs. As shown in Fig. 2, $\Delta F/F$ values increased with increasing concentration of DMPS and reached a plateau for all samples. It is noticeable that the titration curve was varied with pH and temperature. The $\Delta F/F$ values at pH 5.0 were larger than those at pH 7.0, and increased with increasing temperature. Ratios of the maximal fluorescence $\Delta F^{max}/F$ of the LTL-DMPS complex to that of free LTL were obtained at different pHs and temperatures. At pH 5.0 and 26 °C, the $\Delta F^{max}/F$ value was 1.45 and the emission maximum was 348 nm. The emission maximum shifted to 335 nm and the $\Delta F^{max}/F$ value increased to 2.0 with increasing temperature from 26 to 45 °C. Such shift of emission maximum and increase in $\Delta F^{max}/F$ value were also observed when measurement was done at pH 7.0. The maximum shifted from 348 to 340 nm and the $\Delta F^{max}/F$ value increased from 1.30 to 1.40. For better understanding of the nature of the binding of LTL to DMPS vesicles, experiments were done at various temperatures with an LTL-DMPS complex in which the LTL molecule was completely saturated with DMPS vesicles. As shown in Fig. 3, the fluorescence intensity of the LTL-DMPS complex decreased markedly with elevation of temperature from 25 to 36 °C, whereas the emission maximum remained unchanged. On elevation of temperature from 36 to 39 °C, the emission maximum shifted to 335 nm and the fluorescence intensity increased to the same level as at 25 °C. A further elevation of temperaure led to decrease in the fluorescence intensity without any noticeable change in the emission maximum. In the insert of Fig. 3, emission maxima of the LTL-DMPS complex at pHs 5.0 and 7.0 are plotted against temperature, in comparison with similar plots for free LTL. The emission maximum of free LTL remained unchanged when temperature was increased from 25 to 60 °C. Contrary to this, the emission maxima of the LTL-DMPS complex at pHs 5.0 and 7.0 shifted to the shorter wavelength side abruptly at 26 and 36 °C, respectively.

Figure 4 shows the temperature dependence of the

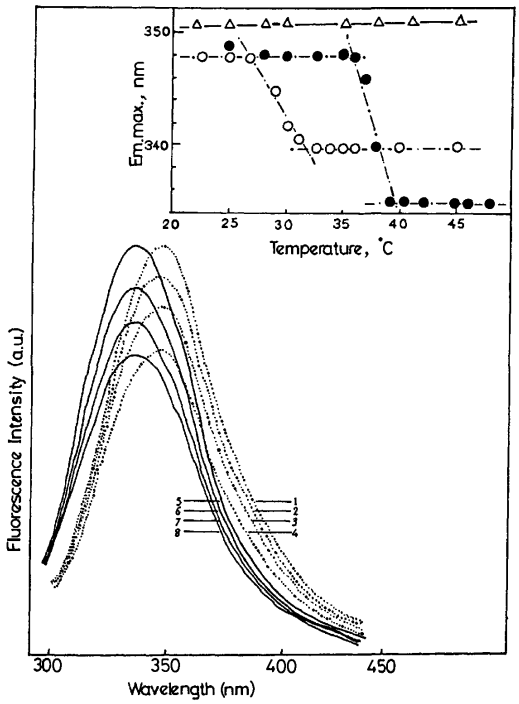

Fig. 3. Temperature dependence of fluorescence spectrum of bound LTL at pH 5.0: 1, 25; 2, 28; 3, 31; 4, 36; 5, 39; 6, 42; 7, 45; 8, 48 °C; Insert, temperature dependence of the fluorescence maximum of LTL; —△—, free LTL at pH 5.0; —○—, bound LTL at pH 7.0; —●—, bound LTL at pH 5.0.

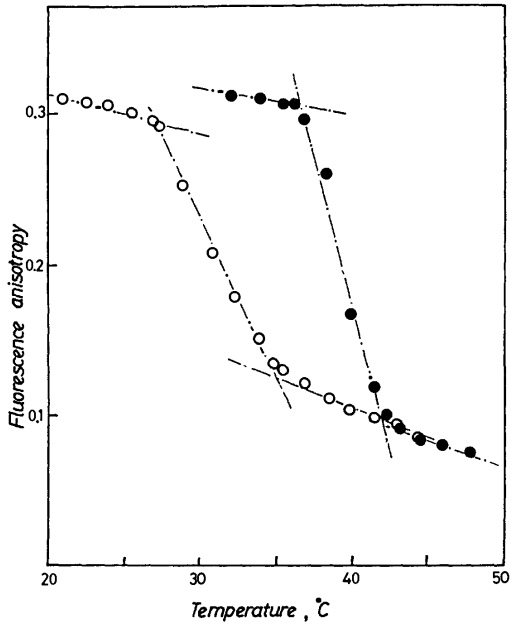

Fig. 4. Fluorescence anisotropy of DPH in DMPS vesicles: —○—, pH 7.0; —●—, pH 5.0; [DMPS]/[DPH]=1000.

fluorescence anisotropy of DPH in DMPS vesicles. When the temperature of gel-liquid crystalline phase transition (T_c) was evaluated from the midpoint of the anisotropy change as shown in Fig. 4, the T_c of DMPS was found to be 39 °C at pH 5.0 and 31 °C at pH 7.0.

Kinetics of Fluorescence Decay. The fluorescence decay kinetics of LTL was analyzed according to the equation

$$F(t)=\sum_j A_j \exp(-t/T_j), \quad (1)$$

where $F(t)$, A_j, and T_j are the fluorescence intensity at t, normalized preexponential factor, and lifetime of the jth component, respectively. The fluorescence decay of LTL in the presence of DMPS vesicles obeys the double exponential kinetics. As shown in Fig. 5, an analysis using the double exponential kinetics has

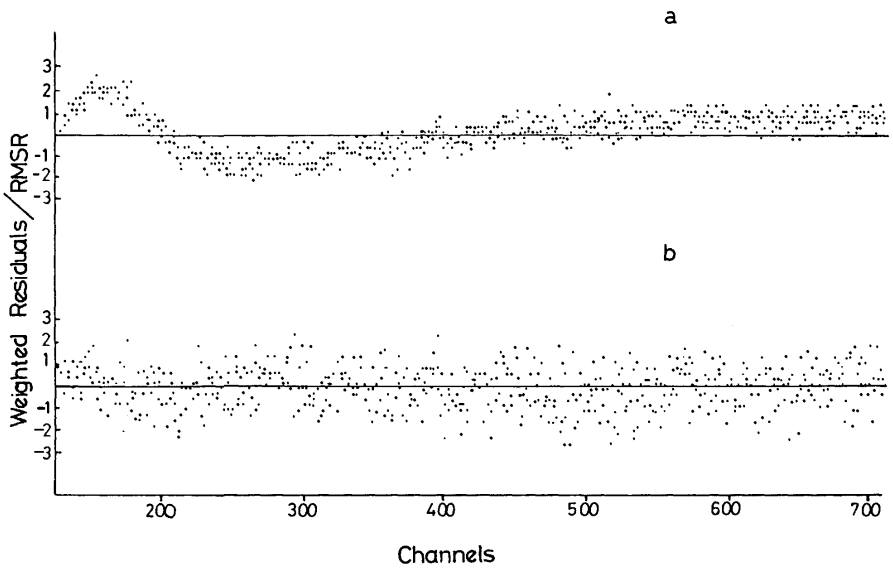

Fig. 5. Plots of weighted residuals after iterative convolution of the fluorescence decay of the bound LTL ([DMPS]/[LTL]=50, 30 °C, pH=5.0) for the best fits: (a) single exponential decay function; (b) double exponential decay function. E_m=335 nm, 22 ps/channel.

Table 1. Kinetic Parameters of the Fluorescence Decay of LTL

	pH	Temp/°C	T_1/ns[a)]	T_2/ns[a)]	A_1	A_2
Buffer	5.0	26	2.24	0.90	0.51	0.51
		40	1.63	0.67	0.47	0.53
DMPS	5.0	26	2.69	0.75	0.69	0.31
		40	2.06	0.60	0.60	0.40
Buffer	7.0	26	2.50	1.20	0.72	0.28
		40	1.90	1.16	0.57	0.43
DMPS	7.0	26	0.56	0.82	0.51	0.49
		40	1.92	0.64	0.45	0.55

a) Standard error=0.02 (for T_1), and 0.03 (for T_2), the weighted root mean square residuals (RMSR) of all measurements are within 1.0±0.1. RMSR=$[1/N\sum_i^C 1/R_{ie}\,(R_{ie}-R_{ic})^2/R_{ie}]^{1/2}$, where N is the number of degrees of freedom, C is the number of channels, and R_{ie} and R_{ic} are, respectively, the experimental and calculated numbers of counts in the ith channel.

revealed that the weighted residuals (RMSR) distribute homogeneously and that the root mean square residuals are nearly 1.0 (panel b), whereas the single exponential analysis gives an extremely heterogeneous distribution of the residuals (panel a). The decay of free LTL also perfectly fits to the double exponential kinetics. The resulting decay parameters are summarized in Table 1. The two preexponential factors (A_1 and A_2) of LTL, whether free or bound, are positive and the emission wavelength dependence of the decay parameters could not be observed over the entire fluorescence spectrum region (310—450 nm). The temperature dependence of the lifetime of free LTL is different from that of the LTL-DMPS complex. When $1/T_1$ and $1/T_2$ of free LTL are plotted against $1/T$, straight lines are obtained as shown in Fig. 6. On the other hand, the lifetime of bound LTL was prolonged temporally at the phase-transition temperature of DMPS vesicles. Although the prolongation of the two lifetimes of bound LTL at pH 7.0 at the phase transition temperature was not so large as at pH 5.0, clear deviation from a linear line is observed with the plots of $\ln[1/T_1, 1/T_2]$ against $1/T$. The fluorescence decays of free and bound LTL can be described in terms of the same type of kinetics (double exponential kinetics). But the decay parameters of free LTL are modified by the binding with DMPS vesicles. A comparison of the lifetime of free LTL with that of bound LTL has revealed that at each temperature in the presence of vesicles the longer lifetime is prolonged, the shorter becoming still shorter. This suggests a peculiar interaction of LTL with DMPS vesicles.

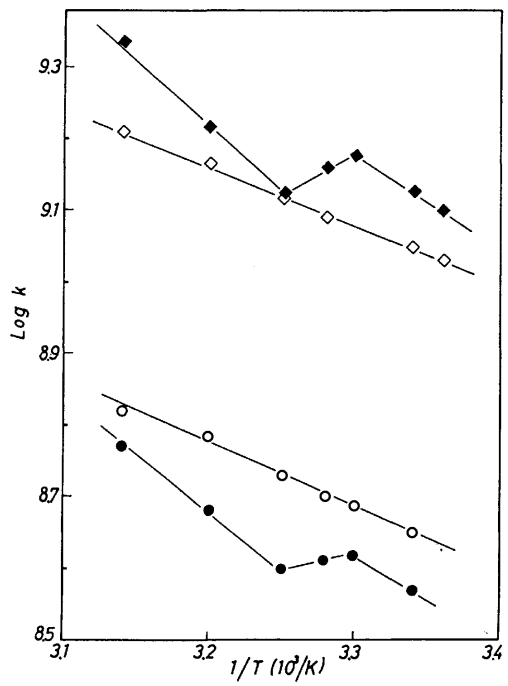

Fig. 6. Temperature dependence of the fluorescence decay constant of LTL at pH 5.0: —◆—, short lived component of bound LTL; —◇—, short lived component of free LTL; —●—, long lived component of bound LTL; —○—, long lived component of free LTL; [DMPS]/[LTL]=50; $k=1/T_1, 1/T_2$.

Solute Quenching of Tryptophan Fluorescence. The fluorescence intensity of bound LTL was measured in the presence of acrylamide, and quenching data were analyzed in accordance with the Stern-Volmer plot based on the equation

$$F_0/F=1+k_qT_{av}[Q] \quad (2)$$

where F_0 and F are the fluorescence intensities in the absence of acrylamide and in its presence at concentration [Q], respectively, k_q is the quenching constant, and T_{av} is the weighted mean lifetime of bound LTL which is defined as $T_{av}=(A_1T_1+A_2T_2)/(A_1+A_2)$. In the plots of F_0/F versus the concentration of acrylamide, straight lines were obtained for all the samples as shown in Fig. 7. In Fig. 8, quenching constants (k_q) are plotted against temperature. Quenching constants of free LTL increase linearly with elevation of temperature. However, reflection points are found at the T_c of DMPS (29 °C at pH 7.0 and 38 °C at pH 5.0) in the plots given for the LTL-DMPS complex, and k_q values increase above the phase transition

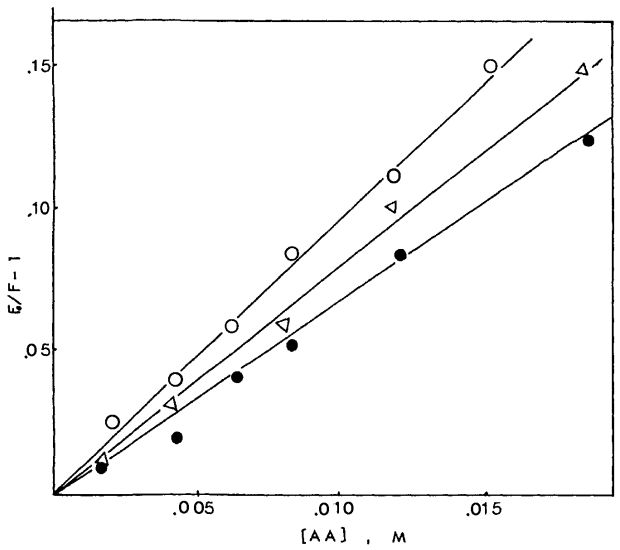

Fig. 7. Stern-Volmer plots for the quenching of the fluorescence of the bound LTL by acrylamide at pH 5.0: —○—, 30 °C; —●—, 40 °C; —△—, 45 °C.

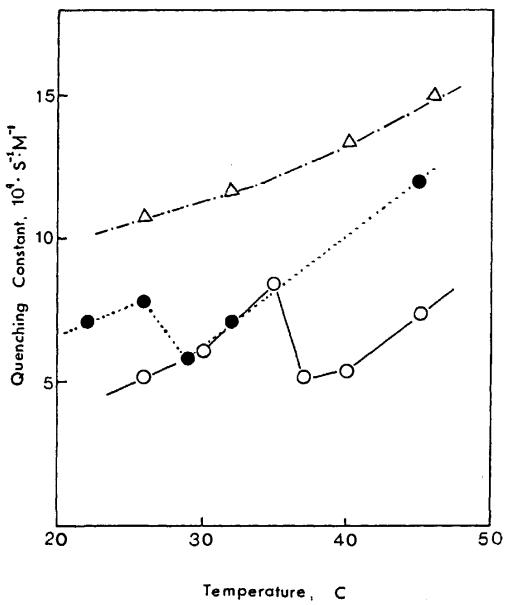

Fig. 8. Temperature dependence of quenching constant for the fluorescence of bound and free LTL: ---△---, free LTL at pH 5.0; —○—, bound LTL at pH 5.0; ---●---, bound LTL at 7.0; [DMPS]/[LTL]=50; Weighted mean lifetimes were used for evaluating the quenching constant (see text).

temperatures.

Discussion

The results presented here provide some insight into the property of the binding of LTL, a tripeptide, to DMPS vesicles. In this work, the intrinsic fluorescence of LTL due to the tryptophan residue was advantageously utilized to analyze the peptide-lipid interaction. As demonstrated here, the binding of LTL to DMPS vesicles induces a shift of the fluorescence emission maximum and change in the fluorescence intensity of LTL (Fig. 1). Such a change in the fluorescence spectrum of LTL can be interpreted as being due to a change in the environment of the tryptophan residue caused by the binding with DMPS vesicles. It is noteworthy that the interaction of LTL with DMPS vesicles, resulting in change in fluorescence spectrum, is greatly influenced by temperature (Fig. 2). Below the phase-transition temperature of DMPS vesicles, the binding of LTL to DMPS induced only a slight shift of emission maximum, whereas large shift of emission maximum was observed above the phase-transition temperature (Fig. 3). Such a difference in the fluorescence spectra of the LTL-DMPS complex observed below and above T_c is attributable to the difference in the behavior of the tryptophan residue in the phospholipid between the gel and liquid crystalline phases. It is postulated that in the temperature range below the T_c of DMPS vesicles, the indole side chain of the tryptophan residue of the peptide would slip into the environment of the acyl chain moiety of DMPS vesicles which is less polar than that in the aqueous medium, but that it would still remain near the head group, i.e., the phosphatidylserine moiety of the DMPS molecule. It is plausible that in the liquid crystalline phase of DMPS vesicles, the packing of the phospholipid is less dense than in the gel phase, which facilitates the penetration of the indole side chain of tryptophan into DMPS vesicles. Such a view is consistent with our previously postulated model in which the gel phase of phospholipid is so tightly packed as to prevent the entry of the indole ring into the acyl moiety of the phospholipid bilayer. NMR studies on lipid-water systems[8,9] have indicated that phosphatidylserine has a rigid head group as compared to phosphatidylcholine and phosphatidylethanolamine, and that the distance of head groups between DMPS molecules in the vesicles is made longer when the phase transition of vesicles occurs. In the solute quenching experiment, the quenching constant for tryptophan fluorescence in the LTL-DMPS complex was reduced at the phase-transition temperature of DMPS vesicles both at pHs 5.0 and 7.0 (Fig. 4). Such a change in the quenching constant as observed at T_c might be explained by change in the distance between head groups in DMPS molecules in vesicles as suggested by NMR measurements.

The phase-transition temperature of DMPS evaluated from the fluorescence anisotropy of DPH is 39 °C at pH 5.0 and 31 °C at pH 7.0 (Fig. 4). These values are in good agreement with those obtained from phase-transition titration curves using spin probe.[10] However, the apparent transition temperatures estimated from the shift of the emission maximum of the LTL-DMPS complex are lower than the T_c values obtained by the fluorescence anisotropy of DPH (the

insert in Fig. 3). The discrepancy of the transition temperatures of DMPS vesicles observed between the two methods may be due to perturbation to the order of the acyl chains in DMPS vesicles caused by the binding with LTL. It has been reported that an electrostatic binding of positively charged molecules to DMPS led to a marked increase in the T_c of phospholipid.[11] In the present case, however, the T_c of DMPS was reduced after DMPS's binding with LTL. There may be differences in modes of binding to phospholipid between LTL and other cationic molecules.

The time resolved fluorescence study also supports the penetration of the tryptophan residue into deeper sites of the membrane on phase transition. The prolongation of the fluorescence lifetime on phase transition is coincident with the solvent polarity dependence of the fluorescence lifetime of indole which is the chromophore of tryptophan residue. The mean lifetime of indole in nonpolar solvent is longer than in aqueous solution, although the radiative lifetime is almost the same.[12]

The double exponential decay kinetics from a single fluorophore arises from the existence of a ground state equilibrium, since the preexponential terms are both positive and their ratio is nearly constant over the entire fluorescence spectrum of LTL. It is confirmed that three rotamers around C_α-C_β of tryptophan residue are responsible for the multiexponential fluorescence decay since they give heterogeneous microenvironments to LTL in association with the decay of the excited singlet state. The indole rings of two rotamers (rotamers I and III) are adjacent to the C_α-carbonyl group and -H or -NH. The other rotamer (rotamer II) has a structure such that the indole is not close to the carbonyl group. C_α-Carbonyl group is an efficient intramolecular quencher in indole derivatives (A. G. Szabo and D. T. Krajcarski, unpublished observation). According Szabo et al.,[12,13] therefore, the longer lived component can be assigned to rotamer II, and rotamers I and III account for the shorter lifetime. The dual fluorescence emission can be rationalized if the quenching efficiences of rotamers I and III are similar to each other or if their interconversion is very rapid. On the basis of the above assignment, the biphasic effect (prolongation of T_1 and shortening of T_2) of the binding on the fluorescence lifetimes of LTL suggests a peculiar interaction between LTL and DMPS. It is clear that the prolongation of T_1 of free LTL by the binding with DMPS is caused by the decrease in polarity of the environment around the indole side chain. The indole side chain of T_2 component also must be under the same conditions. However, clear shortening of T_2 was observed to be caused by the binding with DMPS. This suggests that some quenching interaction which works effectively for rotamer I and III is created by the binding with DMPS. For such specific interaction, we postulate a structural distortion of LTL resulting in the enhancement of the quenching efficiency of C_α carbonyl group. The indole ring could be more accessible to the carbonyl group by the distortion induced by the binding. Since the quenching by the carbonyl group is not involved in the decay channel of rotamer II, the fluorescence lifetime of rotamer II is free from such an effect. Some contribution due to the intermolecular quenching by DMPS should be examined closely. But it seems unreasonable, because the quenching by any groups of DMPS such as carboxyl group is not so efficient as carbonyl group. If DMPS acted as an efficient quencher, we could not observe the increase in the fluorescence quantum yield of LTL with the binding with DMPS as shown in Figs. 1 and 2.

The steady state and time resolved fluorescence studies have consistently described the phase dependence of the interactions between LTL and DMPS vesicles. Further, it has been suggested that structural change of LTL is induced by the binding with the membrane. The present results can give no fine detailed structure of LTL in the membrane. But increase of our knowledge on the photophysics of tryptophan by means of improved instrumentation could contribute to solving the problems we have proposed here.

References

1) L. Massoti, P. Cavatorta, G. Sator, E. Casali, and A. G. Szabo, *Biochim. Biophys. Acta*, **862**, 265 (1986).
2) P. Cavatorta, G. Farrugia, L. Massoti, G. Sator, and A. G. Szabo, *Biochem. Biophys. Res. Commun.*, **141**, 99 (1986).
3) J. Duforcq, J. F. Faucon, R. Maget-Dana, M.P. Pileni, and C. Helene, *Biochim. Biophys. Acta*, **649**, 67 (1981).
4) Y. Barenholz, D. Gibbs, L. Litman, J. Goll, T. E. Tompson, and F. D. Carlson, *Biochemistry*, **16**, 2806 (1977).
5) G. R. Bartlett, *J. Biol. Chem.*, **234**, 466 (1959).
6) M. Zuker, A. G. Szabo, L. Bramall, D. T. Krajcarski, and B. Sellinger, *Rev. Sci. Instrum.*, **56**, 14 (1985).
7) A. G. Szabo and S. Yamashita, *Biophys. J.*, **49**, 149 (1986).
8) J. L. Brownig and J. Seelig, *Biochemistry*, **19**, 1262 (1980).
9) G. Bultz and R. Wohlgemuth, *J. Mem. Biol.*, **58**, 81 (1981).
10) G. Cevec, A. Watts, and D. Marsh, *Biochemistry*, **20**, 4955 (1981).
11) J. M. Boggs, D. D. Wood, and M. A. Moscarello, *Biochemistry*, **20**, 1605 (1981).
12) A. Z. Szabo and D. M. Rayner, *J. Am. Chem. Soc.*, **102**, 554 (1980).
13) S. A. Cocles and A. G. Szabo, *Photochem. Photobiol.*, **34**, 23 (1981).

 © 1989 The Chemical Society of Japan Bull. Chem. Soc. Jpn., 62, 3081—3088 (1989)

The Preparation, Stereochemistry, and Oxidation of 2-Pyridinethiolato Cobalt(III) Complexes, and the Crystal Structure of [Co(2-pyridinethiolato)(en)$_2$](ClO$_4$)$_2$

Masakazu KITA,*,† Kazuaki YAMANARI, and (the late) Yoichi SHIMURA
Department of Chemistry, Faculty of Science, Osaka University, Toyonaka, Osaka 560
(Received January 27, 1989)

A series of mixed complexes $[Co(pyt)_{3-n}(diamine)_n]^{n+}$ (n=0, 1, and 2; pyt=2-pyridinethiolate(1−) and diamine=ethylenediamine, (*R*)-propylenediamine, or 2,2′-bipyridine) have been prepared and characterized by means of their visible and ultraviolet absorption, circular dichroism, and magnetic circular dichroism spectra. In the [Co(pyt)$_3$] or [Co(pyt)$_2$(diamine)]$^+$ complex, only one geometrical isomer, *mer(S)* or *trans(S)* respectively, has been obtained. The [Co(pyt)(en)$_2$](ClO$_4$)$_2$ complex, which was spontaneously resolved, had an orthorhombic space group of $P2_12_12_1$, with a=12.406(1), b=12.754(1), c=11.621(4) Å, V=1838.7(6) Å^3, and Z=4. The refinement of 2276 reflections (Mo $K\alpha$ radiation) led to R=0.049. The Co–N bond trans to the pyt sulfur atom was longer by 0.023(11) Å than the cis one. The novel oxidation product [Co(2-pyridinesulfenato-*N*,*S*)(en)$_2$]$^{2+}$ was photochemically converted into the *N*,*O*-chelated linkage-isomer [Co(2-pyridinesulfenato-*N*,*O*)(en)$_2$]$^{2+}$ in the solid state, accompanied by ring-expansion from a four- to a five-membered chelate ring.

We have long been interested in the synthesis and stereochemistry of cobalt(III)[1] and rhodium(III)[2] complexes containing various kinds of bidentate-*N*,*S* ligands, such as 2-aminoethanethiol (=Haet), L-cysteine, L-cysteine methyl ester, and their oxidation derivatives. We previously prepared only *fac(S)* isomers of the [M(III)(bidentate-*N*,*S*)$_3$] (M=Co(III) and Rh(III)) type complexes. On the other hand, 2-pyridinethiolate(1−)(=pyt), which is an aromatic bidentate-*N*,*S* ligand and which forms a 4-membered chelate ring on coordination, showed a different stereochemical preference, as was reported in our preliminary papers.[3,4]

This paper will describe the preparation and characterization of a series of cobalt(III) complexes containing pyt [Co(pyt)$_{3-n}$(diamine)$_n$]$^{n+}$ (diamine= ethylenediamine(=en), (*R*)-propylenediamine(=R-pn), or 2,2′-bipyridine(=bpy); n=0, 1, or 2) by means of their electronic absorption, circular dichroism (CD), magnetic circular dichroism (MCD), and ^{13}C NMR spectra. In the complexes of [Co(pyt)$_3$] or [Co(pyt)$_2$(diamine)]$^+$, one geometrical isomer, *mer(S)* or *trans(S)* respectively, was obtained. These results are quite different from those obtained from complexes with aliphatic *N*,*S*-ligands. The crystal structure of [Co(pyt)(en)$_2$](ClO$_4$)$_2$ revealed the trans influence (trans lengthening) induced by the pyt sulfur donor atom. The difference in the electronic structures of the pyt and aet complexes is discussed on the basis of the X-ray crystal data. The orange sulfenato complex, which is the oxidation product of [Co(pyt)(en)$_2$](ClO$_4$)$_2$, changed photochemically into a green one in the solid state. These complexes were characterized as novel linkage isomers with a *N*,*S*- and *N*,*O*-chelate as the basis of the X-ray photoelectron spectra (XPS).

† Present address: Department of Chemistry, Faculty of Science, Nagoya University, Chikusa-ku, Nagoya 464-01.

Experimental

Preparation, Separation, and Optical Resolution of 2-Pyridinethiolato Complexes. Most of the complexes were prepared by a redox reaction between di-2-pyridyl disulfide and the cobalt(II) ion.

(1) [Co(pyt)(en)$_2$](ClO$_4$)$_2$: Into a solution of Co(ClO$_4$)$_2$·6H$_2$O) (17.0 g, 0.046 mol) in 30 cm^3 of ethanol we stirred a solution of ethylenediamine (6.0 g, 0.1 mol) in 40 cm^3 of ethanol. To the resulting solution we then immediately added a solution of di-2-pyridyl disulfide (5.0 g, 0.023 mol) in 100 cm^3 of ethanol, after which the mixture was stirred at ca. 50 °C for 2 h. The resulting brown precipitate was filtered and washed with ethanol (100 cm^3) and diethyl ether (100 cm^3). The precipitate was recrystallized by dissolving it in hot water (ca. 70 °C), filtering it, and cooling it to ca. 5 °C. At this stage, the orthorhombic brown crystals of [Co(pyt)(en)$_2$](ClO$_4$)$_2$ obtained were spontaneously resolved, as was confirmed by the CD spectrum of the aqueous solution, which contained one crystal, and by the following X-ray crystallographic data with a chiral space group. The yield was 18.0 g (80%). Found: C, 22.27; H, 4.20; N, 14.41%. Calcd for [Co(pyt)(en)$_2$](ClO$_4$)$_2$=$C_9H_{20}N_5O_8SCl_2Co$: C, 22.14; H, 4.13; N, 14.35%.

For optical resolution, a solution of $K_2[Sb_2\{(R,R)\text{-}C_4H_2O_6\}_2]\cdot 3H_2O$ (1.4 g, 0.002 mol) in 30 cm^3 of water was added to a solution of [Co(pyt)(en)$_2$](ClO$_4$)$_2$ (2.0 g, 0.004 mol) in 30 cm^3 of water. Immediately, crystals of *Λ*[Co(pyt)(en)$_2$][$Sb_2\{(R,R)\text{-}C_4H_2O_6\}_2$]·5H$_2$O which showed a positive CD peak at 588 nm began to deposit, they were filtered off. Ten grams of NaClO$_4$ were then added to the filtrate, and the solution was cooled to induce crystallization. The crystals of *Δ*-[Co(pyt)(en)$_2$](ClO$_4$)$_2$ were collected and recrystallized from hot water. Found for the *Λ*-diastereomer: C, 22.38; H, 3.65; N, 7.61%. Calcd for *Λ*-[Co(pyt)(en)$_2$][$Sb_2\{(R,R)\text{-}C_4H_2O_6\}_2$]·5H$_2$O=$C_{17}H_{34}N_5O_{17}SCoSb_2$: C, 22.32; H, 3.75; N, 7.65%. Found for the *Δ*-complex: C, 22.30; H, 4.13; N, 14.32%. Calcd for *Δ*-[Co(pyt)(en)$_2$](ClO$_4$)$_2$=$C_9H_{20}N_5O_8SCl_2Co$: C, 22.14; H, 4.13; N, 14.35%.

(2) [Co(pyt)$_2$(en)]ClO$_4$: This complex was obtained as a by-product (1.0 g, 5%) from the mother liquor in the above preparation, but was prepared in a higher yield by the following method. Di-2-pyridyl disulfide (1.5 g, 0.0068

mol) was stirred into a solution of $Co(ClO_4)_2 \cdot 6H_2O$ (5.0 g, 0.0135 mol) in 50 cm^3 of ethanol. To this solution we then added a mixed solution of 2-pyridinethiol (1.5 g, 0.0135 mol) and ethylenediamine (1.0 g, 0.0166 mol) in 50 cm^3 of ethanol. After a few minutes, a green precipitate began to deposit. The mixture was stirred at ca. 50 °C for 2 h. The resulting green precipitate was filtered and washed with cold water (below 5 °C) until the washings were no longer brown. The precipitate was then recrystallized from water (ca. 70 °C). Columnar green crystals with a metallic luster were thus collected (4.3 g, 72%). Found: C, 32.98; H, 3.69; N, 12.81%. Calcd for $[Co(pyt)_2(en)]ClO_4=C_{12}H_{16}N_4O_4S_2ClCo$: C, 32.85; H, 3.67; N, 12.77%.

(3) [Co(pyt)$_3$]: This nonelectrolyte complex was effectively prepared by the reaction of freshly prepared CoO(OH) (0.015 mol) with 2-pyridinethiol (5.0 g, 0.045 mol) in 200 cm^3 of ethanol-water (1 : 1). The dark brown orthorhombic crystals of $[Co(pyt)_3]$ (5.0 g, 90%) were collected by filtration and recrystallized by dissolving them in dimethyl silfoxide (DMSO) and by then adding water. The yield was 4.7 g (80%). Found: C, 46.27; H, 3.18; N, 10.92%. Calcd for $[Co(pyt)_3]=C_{15}H_{12}N_3S_3Co$: C, 46.27; H, 3.18; N, 10.79%.

(4) [Co(pyt)$_2$(R-pn)]ClO$_4$: A bis(2-pyridinethiolato) complex containing (*R*)-propylenediamine $[Co(pyt)_2(R\text{-}pn)]ClO_4$ was prepared by the same procedure as that used for $[Co(pyt)_2(en)]ClO_4$ except for the use of R-pn instead of en. A pair of green diastereomers, *Λ*-$[Co(pyt)_2(R\text{-}pn)]ClO_4$ (more soluble in ethanol) and *Δ*-$[Co(pyt)_2(R\text{-}pn)]ClO_4$ (less soluble in ethanol), was obtained. Found for the *Λ*-diastereomer: C, 34.34; H, 4.00; N, 12.17%. Found for the *Δ*-diastereomer: C, 34.74; H, 4.04; N, 12.47%. Calcd for *Λ*- or *Δ*-$[Co(pyt)_2(R\text{-}pn)]ClO_4=C_{13}H_{18}N_4O_4S_2ClCo$: C, 34.48; H, 4.01; N, 12.37%.

(5) [Co(pyt)(bpy)$_2$](ClO$_4$)$_2$: Into a solution of $Co(ClO_4)_2 \cdot 6H_2O$ (7.3 g, 0.020 mol) in 30 cm^3 of water we stirred a solution of 2,2′-bipyridine (6.2 g, 0.040 mol) in 40 cm^3 of hot ethanol. To the solution we then immediately added a solution of di-2-pyridyl disulfide (2.2 g, 0.010 mol) in 100 cm^3 of ethanol, after which the mixture was stirred at ca. 70 °C for 2 h. The resulting brown precipitate was filtered and washed with ethanol (100 cm^3) and diethyl ether (100 cm^3). The precipitate was recrystallized from water (ca. 70 °C). The yield was 12 g (85%). Found: C, 42.22; H, 3.22; N, 9.66%. Calcd for $[Co(pyt)(bpy)_2](ClO_4)_2 \cdot 1.5H_2O=C_{25}H_{23}N_5O_{9.5}SCl_2Co$: C, 42.45; H, 3.28; N, 9.90%.

(6) [Co(pyt)$_2$(bpy)]ClO$_4$: Di-2-pyridyl disulfide (2.0 g, 0.0091 mol) was stirred into a solution of $Co(ClO_4)_2 \cdot 6H_2O$ (7.3 g, 0.020 mol) in 60 cm^3 of water-ethanol (1 : 3). To this solution we then added a mixed solution of 2-pyridinethiol (2.0 g, 0.0182 mol) and 2,2′-bipyridine (4.0 g, 0.0256 mol) in 50 cm^3 of ethanol. The mixture was stirred at ca. 70 °C for 2 h. The resulting brown-green precipitate was filtered and washed with hot water until the washings were no longer brown. The precipitate was recrystallized from methanol. Needle-like yellow-green crystals were collected (5.0 g, 47%). Found: C, 44.85; H, 3.09; N, 10.42%. Calcd for $[Co(pyt)_2(bpy)]ClO_4=C_{20}H_{16}N_4O_4S_2ClCo$: C, 44.91; H, 3.01; N, 10.47%.

Oxidation of [Co(pyt)(en)$_2$](ClO$_4$)$_2$ and Photoisomerization of the Oxidation Product. A solution of 30% aqueous H_2O_2 (10 g) and 60% aqueous $HClO_4$ (10 g) was stirred into a solution of *Δ*-$[Co(pyt)(en)_2](ClO_4)_2$ (5 g) in 50 cm^3 of DMSO below 5 °C to give an orange solution instantly. To the resulting solution we immediately added a mixture of diethyl ether (700 cm^3) and ethanol (300 cm^3). Orange crystals appeared on the inside wall of a beaker in a few minutes; they were filtered. The yield was ca. 1 g. Found: C, 21.44; H, 3.93; N, 13.53%. Calcd for $(-)^{CD}_{507}$-$[Co(pyse)(en)_2](ClO_4)_2=C_9H_{20}N_5O_9SCl_2Co$: C, 21.44; H, 4.00; N, 13.89% (Hpyse=2-pyridinesulfenic acid).

The orange pyse complex immediately turned a green one in the solid state upon exposure to the sun or a fluorescence lamp. The results of an elemental analysis of the photoproduct were identical with the original formula $[Co(pyse)(en)_2](ClO_4)_2$. The DMSO or aqueous solution of the orange complex became dark brownish within several tens minutes, even in the dark. Such a color change in solution was caused probably by redox decomposition and/or solvolysis. However, the green pyse complex was stable in an aqueous or DMSO solution at room temperature.

Measurements. The visible and ultraviolet absorption spectra were measured on a Hitachi 330 spectrophotometer. The CD spectra were recorded on a JASCO MOE-1 spectropolarimeter, and the MCD spectra on the same instrument in 1.5 T magnetic field. The absorption, CD, and MCD measurements were carried out in DMSO and H_2O solutions at the low- and high-energy regions respectively. The XPS data were recorded on a Shimadzu HIPS 70 apparatus. The binding energies relative to the Fermi level were determined by referring to the Na-2s (64.0 eV) and S-$2p_{3/2}$ (169.5 eV) values of Na_2SO_4 mixed with an appropriate amount of each sample. All the measurements were done at room temperature.

X-Ray Study of [Co(pyt)(en)$_2$](ClO$_4$)$_2$. A brown crystal (0.40×0.39×0.33 mm) of the title compound was used for the data collection. Crystal data: orthorhombic, $P2_12_12_1$, a=12.406(1), b=12.754(1), c=11.621(4) Å, and V=1838.7(6) Å^3, D_{calcd}= 1.76, D_{obsd}=1.80 g cm^{-3}, and Z=4. It is very interesting that this complex is spontaneously resolvable, for in the corresponding aet complex the perchlorate forms a conglomerate.[5] The diffraction intensities were measured using a Rigaku four-circle diffractometer, with graphite monochromatized Mo$K\alpha$ radiation (λ=0.71069 Å). μ(Mo$K\alpha$)= 13.80 cm^{-1} and no absorption correction was applied. Within the range of $24° < 2\theta < 55°$, 2276 independent reflections ($I < 3\sigma(I)$) were obtained. All the computations were performed on a HITAC M-200H computer at the Computer Center of the Institute for Molecular Science using the Universal Crystallographic Computation Program System UNICS III.[6] The structure was solved by the usual heavy-atom method. The positions of ten hydrogen atoms were identified in subsequent difference Fourier maps, but the others could not be determined. The positional parameters of the hydrogen atoms, the anisotropic thermal parameters for all the non-hydrogen atoms, and the complete list of $|F_o|$ and $|F_c|$ values are deposited as Document No. 8892 at the Office of the Editor of the Bull. Chem. Soc. Jpn.

Results and Discussion

Characterization and Stereochemistry of 2-Pyridinethiolato Complexes. The electronic strucutre of the Hpyt compound in acidic conditions is considered to be comparable to that of the pyt-*N,S* ligand in a metal complex. In a 0.1 mol dm^{-3} $HClO_4$ solution, the absorption spectrum of the Hpyt compound showed

Table 1. Absorption Spectral Data

Complex/Solvent		σ_{max} (log ε)[a]
Hpyt		
0.1 mol dm^{-3}	$HClO_4$	29.20(3.89), 37.00(4.03)
$[Co(pyt)(en)_2](ClO_4)_2$		
	DMSO	12.66(0.31)^{sh}, 17.00(1.58)^{sh}, 20.20(2.06), 25.00(2.16)^{sh}, 29.85(3.43), 33.90(4.05)
	H_2O	17.00(1.51)^{sh}, 20.35(2.05), 25.11(2.11)^{sh}, 30.50(3.43), 34.48(4.04), 39.22(4.25), 46.51(4.38)
trans(*S*)-$[Co(pyt)_2(en)]ClO_4$		
	DMSO	11.49(0.06), 16.31(2.16), 21.74(2.42)^{sh}, 27.78(3.96), 30.81(4.19)
	H_2O	16.59(2.08), 22.00(2.47)^{sh}, 28.34(3.99), 31.61(4.19), 38.00(4.34), 45.05(4.42), 49.50(4.49)
mer(*S*)-$[Co(pyt)_3]$		
	DMSO	10.00(0.54)^{sh}, 14.93(2.17)^{sh}, 18.00(2.54)^{sh}, 21.00(2.91)^{sh}, 23.53(3.15)^{sh}, 27.40(3.92)^{sh}, 30.77(4.24)^{sh}, 32.79(4.36)^{sh}, 36.36(4.53)
	CH_3OH	18.00(2.50)^{sh}, 21.00(2.85)^{sh}, 23.50(3.15)^{sh}, 27.40(3.87)^{sh}, 31.00(4.25)^{sh}, 33.00(4.30)^{sh}, 36.70(4.54)
trans(*S*)-$[Co(pyt)_2(R\text{-}pn)]ClO_4$		
Λ-diastereomer/DMSO		11.49(0.17)^{sh}, 16.31(2.17), 21.54(2.50)^{sh}, 27.78(3.96) 30.81(4.20)
	H_2O	16.69(2.14), 22.00(2.49)^{sh}, 28.17(3.99), 31.70(2.18), 38.00(4.32), 45.10(4.42), 49.50(4.47)
Λ-diastereomer/DMSO		11.49(0.13)^{sh}, 16.39(2.16), 21.54(2.50)^{sh}, 27.78(3.94), 30.80(4.19)
	H_2O	16.69(2.20), 22.01(2.57)^{sh}, 28.17(3.96), 31.70(4.16), 38.00(4.30), 45.00(4.42)
$[Co(pyt)(bpy)_2](ClO_4)_2$		
	DMSO	12.20(0.36)^{sh}, 16.39(1.52), 20.78(2.10), 25.00(2.34)^{sh}, 33.38(3.45)
Λ-$[Co(pyse\text{-}N,S)(en)_2](ClO_4)_2$		
	DMSO	16.13(1.26)^{sh}, 20.00(2.37)^{sh}, 25.64(3.28), 31.25(3.47)
Λ-$[Co(pyse\text{-}N,O)(en)_2](ClO_4)_2$		
	DMSO	16.53(2.30), 20.00(2.43)^{sh}, 26.30(3.47), 31.25(3.57)
trans(*S*)-$[Co(pyt)_2(bpy)]ClO_4$		
	DMSO	11.49(0.19)^{sh}, 16.39(1.52), 20.78(2.10), 33.38(3.45)

a) Wavenumbers are given in 10^3 cm^{-1} units, and log ε (in parentheses), in mol^{-1} dm^3 cm^{-1}, while sh means a shoulder.

two intense absorption bands, at ca. 27000 and ca. 36000 cm^{-1} (Table 1). The energetically lower and higher bands can be assigned to the π^*(py)$\leftarrow$n(s) and π^*(py)$\leftarrow\pi$(py) transitions respectively (py=pyridine). Such bands can also be expected to appear in the spectra of the pyt complexes.

The absorption, CD, and MCD spectra of $[Co(pyt)(en)_2](ClO_4)_2$ (Fig. 1 and Tables 1, 2, and 3) are quite similar to those of $[Co(aet)(en)_2](ClO_4)_2$[7,8] (aet=2-aminoethanethiolato) in the spin-allowed first d-d transition band region. The shoulder at ca. 17000 cm^{-1} in the CD spectrum (or the positive MCD peak at 17330 cm^{-1}) and the negative CD peak at 19800 cm^{-1} are assigned to the components generated from the $^1E\leftarrow{}^1A_1$ transition in the C_{4v} symmetry on the CoN_5S geometry. These splittings have been ascribed by Houlding et al.[8,9] to the perturbation of the p-like lone pair of the two remaining lone-pairs on the sulfur atom. The positive CD band and the negative MCD one at ca. 22000 cm^{-1} are assigned to the $^1A_2\leftarrow{}^1A_1$ (C_{4v}) transition. The energy peaks at ca. 12000 and 14000 cm^{-1} in the CD and MCD spectra are assigned to the spin-forbidden d-d transition, $^3T_{1g}\leftarrow{}^1A_{1g}$ and $^3T_{2g}\leftarrow{}^1A_{1g}(O_h)$ respectively. The bands at 30000, 35000, and 39000 cm^{-1} in the absorption spectra (in H_2O) can be assigned to π^*(py)$\leftarrow$n(S), σ^*(Co)$\leftarrow\sigma$(S), and π^*(py)$\leftarrow\pi$(py) transitions respectively on the basis of the spectrum-pattern similarity of the Hpyt compound under acidic conditions.

The absorption and MCD spectra of $[Co(pyt)(bpy)_2](ClO_4)_2$ (Tables 1 and 3) are quite similar to those of $[Co(aet)(en)_2](ClO_4)_2$ and $[Co(pyt)(en)_2](ClO_4)_2$ in the spin-allowed first d-d transition region. The positive MCD peak at 15900 cm^{-1} and the negative one at 20400 cm^{-1} of $[Co(pyt)(bpy)_2](ClO_4)_2$ are energetically lower by ca. 1400 and ca. 1900 cm^{-1} respectively, than the corresponding peaks of $[Co(pyt)(en)_2](ClO_4)_2$; tentatively, the difference can be attributed to the destabilization of the Co dπ orbitals by the pi-donor character of bpy ligand.

The absorption and MCD spectra of $[Co(pyt)_2(en)]ClO_4$, and the absortion and CD spectra of *Λ*- and *Δ*-$[Co(pyt)_2(R\text{-}pn)]ClO_4$, are shown in Figs. 2 and 3 respectively. For the former en complex, three geometrical isomers, *C*$_2$-*cis*(*S*), *C*$_1$-*cis*(*S*), and *trans*(*S*), are possible. However, only one green isomer was obtained for $[Co(pyt)_2(en)]^+$, as for $[Co(pyt)_2(R\text{-}pn)]^+$. The bis(pyt) complexes are assigned to a *trans*(*S*) isomer on the basis of the fair agreement of the absorption spectra of the *trans*(S)-$[Co(thiolato)_2(amine)_4]^+$-type complexes[10] in the spin allowed first d-d transition region. The intense transitions, π^*(py)$\leftarrow$n(S) at 28000 cm^{-1} and σ^*(Co)$\leftarrow\sigma$(S) at 32000 cm^{-1}, were considerably red-shifted compared with those of

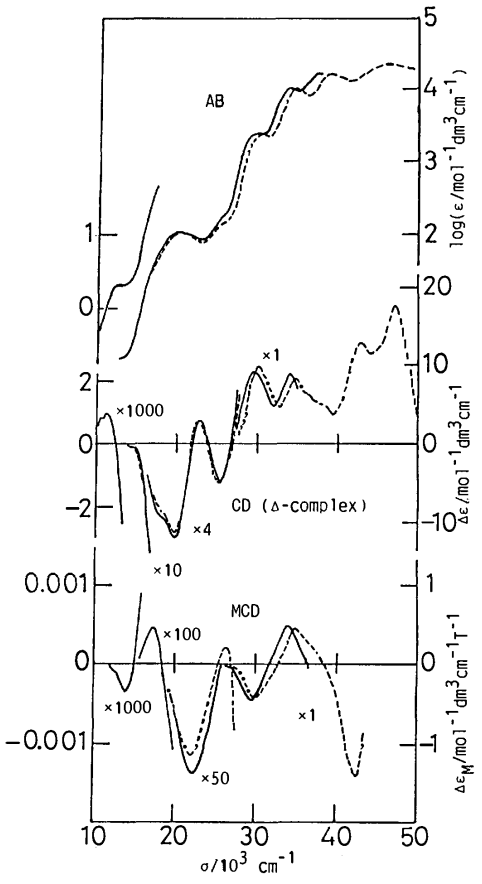

Fig. 1. Absorption, CD (for *Δ*-complex), and MCD spectra of $(Co(pyt)(en)_2](ClO_4)_2$ (—— in DMSO and ----in H_2O).

$[Co(pyt)(en)_2](ClO_4)_2$; tentatively, this may be attributed to the destabilizations of the sulfur nonbonding and sigma-donor orbitals by the mutual 'trans-influence' of the *trans*-*S* donors, whereas the π^*(py)← π(py) transition (38000 cm^{-1}) does not shift.

The absorption and MCD spectra of $[Co(pyt)_2(bpy)]ClO_4$ (Tables 1 and 3) were similar to those of *trans*(*S*)-$[Co(pyt)_2(en)]ClO_4$ in the spin-allowed first d-d transition region. Therefore, the bpy complex is also assigned to the *trans*(*S*) isomer.

Figure 4 shows the absorption and MCD spectra of $[Co(pyt)_3]$. In this complex, only one of the two possible geometrical isomers, *fac*(*S*) and *mer*(*S*), was obtained. This dark brown complex is assigned to a *mer*(*S*) isomer on the basis of the ^{13}C NMR spectrum in the $CDCl_3$ solution, which showed eight resonances; 116.87[b], 125.48[b], 135.45, 135.94, 136.59, 147.10[b], 149.48[b], and 150.41[b] ppm (b=broad), whereas only five signals are expected for the *fac*(*S*) geometry. The splitting pattern of the MCD spectrum in the first d-d transition region (14300, 17900, and 21200 cm^{-1}) also supports this assignment.

The Crystal Structure of $[Co(pyt)(en)_2](ClO_4)_2$. Figure 5 shows the numbering of the title complex ion. The atomic parameters and the bond distances and angles are listed in Tables 4 and 5. The complex has a distorted octahedral structure around Co center. The bite angle of the 4-membered pyt ligand 72.9(2)° is rather narrower than a right angle. The bond length of the Co-N(5) sited trans to pyt's sulfur is 1.993(6) Å, while the average of the Co-N(2) and Co-N(4) sited cis to the sulfur is 1.970(9) Å; that is, the difference is 0.023(11) Å. The trans-influence of the pyt thiolate is less by 0.041(10) Å than that of the aet thiolate in the corresponding complex.[11] The smaller trans influence of the pyt thiolate may be interpreted in terms of the decrease in the orbital interaction between the Co 3d and the sulfur lone pair

Table 2. CD Spectral Data

Complex/Solvent	σ_{ext} ($\Delta\varepsilon$)[a]
Δ-$[Co(pyt)(en)_2](ClO_4)_2$	
DMSO	11.36(+0.004), 18.18(−2.33)[sh], 19.80(−2.95), 22.94(+0.74), 25.32(−1.22), 29.50(+9.13), 33.90(+8.88)
H_2O	18.18(−2.19)[sh], 19.72(−2.83), 22.68(+0.71), 25.19(−1.25), 30.12(+9.96), 34.72(+8.42), 42.92(+12.79), 46.95(+17.61)
trans(*S*)-$[Co(pyt)_2(R\text{-}pn)]ClO_4$	
Δ-diastereomer/DMSO	11.43(+0.013), 16.34(−5.85), 20.00(−1.92), 22.62(+4.46), 27.40(+125.3), 30.30(−28.02)
H_2O	16.61(−5.13), 22.47(+3.58), 28.01(+115.9), 30.86(−31.11), 32.47(−24.16)[sh], 38.31(−27.78), 42.02(+10.57), 45.87(+9.06), 48.08(+10.12)
Λ-diastereomer/DMSO	10.31(−0.009), 16.34(+6.32), 20.20(+1.41), 22.62(−3.37), 27.17(−138.6), 30.30(27.08)[sh], 31.45(+29.45)
H_2O	16.67(+5.59), 19.88(+0.98), 22.47(−2.51), 24.39(+0.72), 27.86(−127.4), 31.06(32.09), 38.76(+32.25), 41.67(−3.99), 43.48(+14.69), 49.50(+7.35)
Δ-$[Co(pyse\text{-}N,S)(en)_2](ClO_4)_2$	
DMSO	10.64(−0.006), 11.36(−0.004), 19.72(−1.05), 25.51(+1.91), 34.84(+3.54)
Δ-$[Co(pyse\text{-}O,N)(en)_2](ClO_4)_2$	
DMSO	10.42(+0.004), 16.58(+2.19), 20.00(+0.23), 23.20(−3.06), 26.81(+1.57), 35.09(−7.13)

a) Wavenumbers are given in 10^3 cm^{-1} units, and $\Delta\varepsilon$ (in parentheses), in $mol^{-1}dm^3cm^{-1}$, while sh means a shoulder.

Table 3. MCD Spectral Data

Complex/Solvent		σ_{ext} ($\Delta\varepsilon_M$)[a]
$[Co(pyt)(en)_2](ClO_4)_2$		
	DMSO	13.89(−0.0003), 17.33(+0.005), 22.32(−0.028), 29.33(−0.458), 33.76(+0.364)
	H_2O	17.24(+0.005), 22.22(−0.023), 26.32(+0.004), 29.94(−0.414), 34.72(+0.449), 42.55(−1.42)
trans(*S*)-$[Co(pyt)_2(en)]ClO_4$		
	DMSO	13.89(−0.00078), 15.87(−0.00084)[sh], 22.22(−0.26), 27.62(−0.430), 32.79(−0.430), 34.48(+0.717), 36.36(−1.698)
	H_2O	21.74(−0.012), 28.17(−0.328), 33.33(−0.282), 35.71(+0.538), 38.46(−1.525), 42.92(+0.852), 45.45(−,1.607)
mer(*S*)-$[Co(pyt)_3]$		
	DMSO	11.36(−0.0006), 12.50(−0.0011), 14.46(+0.010), 17.54(+0.021), 21.19(−0.136), 24.69(+0.042), 27.40(−0.568), 32.05(−1.147), 35.09(−2.144)
	CH_3OH	17.86(+0.017), 21.51(−0.100), 24.69(+0.033), 27.40(−0.447), 32.79(−1.051), 35.71(−2.207), 38.17(+0.063), 41.32(−1.009)
$[Co(pyt)(bpy)_2](ClO_4)_2$		
	DMSO	12.20(+0.0004), 12.66(−0.0006), 15.87(+0.0041), 20.41(−0.032), 28.17(−0.083), 30.21(+0.586), 33.11(−1.861)
	H_2O	28.57(−0.043), 31.06(+0.547), 34.25(−1.122), 38.02(−1.642), 47.62(−1.423)
trans(*S*)-$[Co(pyt)_2(bpy)]ClO_4$		
	DMSO	12.35(−0.0005), 20.83(−0.046), 26.67(−0.277), 28.41(−0.225), 28.99(−0.453), 31.75(−1.534)
	H_2O	30.77(+0.144), 32.26(−0.780), 37.45(−0.990), 40.00(−0.333), 41.67(+0.130), 42.55(−0.459), 44.44(+1.216), 45.45(+0.855), 48.08(−1.306)

a) Wavenumbers are given in 10^3 cm^{-1} units, and $\Delta\varepsilon_M$ (in parentheses), in mol^{-1} dm^3 cm^{-1} T^{-1}, while sh means a shoulder.

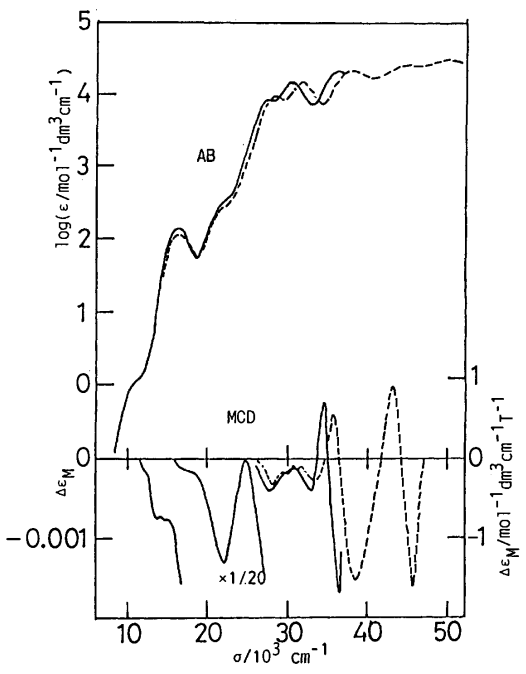

Fig. 2. Absorption and MCD spectra of [Co(pyt)$_2$(en)]ClO_4 in DMSO (——) and in H_2O (----) solutions.

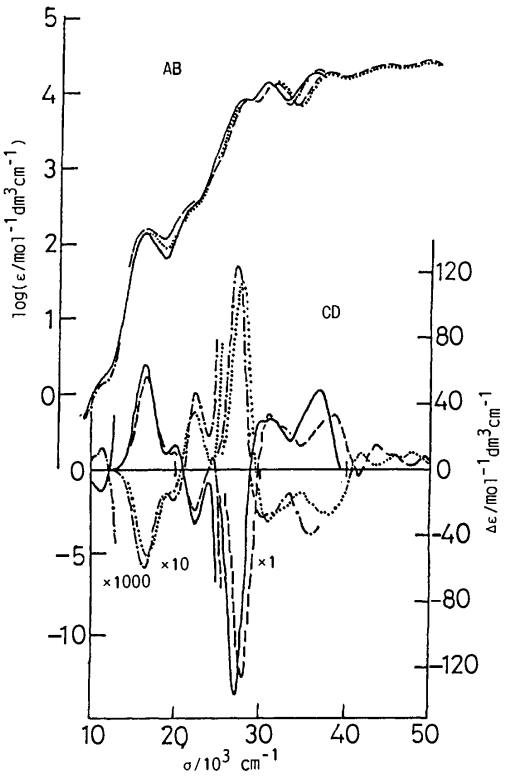

Fig. 3. Absorption and CD spectra of *Λ*-[Co(pyt)$_2$(R-pn)]ClO_4 (—— in DMSO and ---- in H_2O) and *Δ*-[Co(pyt)$_2$(R-pn)]ClO_4 (— · — in DMSO and ····· in H_2O).

orbitals, on the basis of the narrower bite angle (72.9(2)°) compared to the aet one (88.8(2)°).[11] In addition, the resonance structure **b** (anion of 2(1*H*)-pyridinethione) in Fig. 6 contributes to the pyt complex, and the sigma-donor ability of the pyt thiolate becomes weak because of the lesser electron density of the sulfur atom compared to that of the aliphatic thiolato sulfur. This resonance contribution is in good agreement with the facts that the S-C(1) bond distance (1.754(7) Å) is rather shorter than the ali-

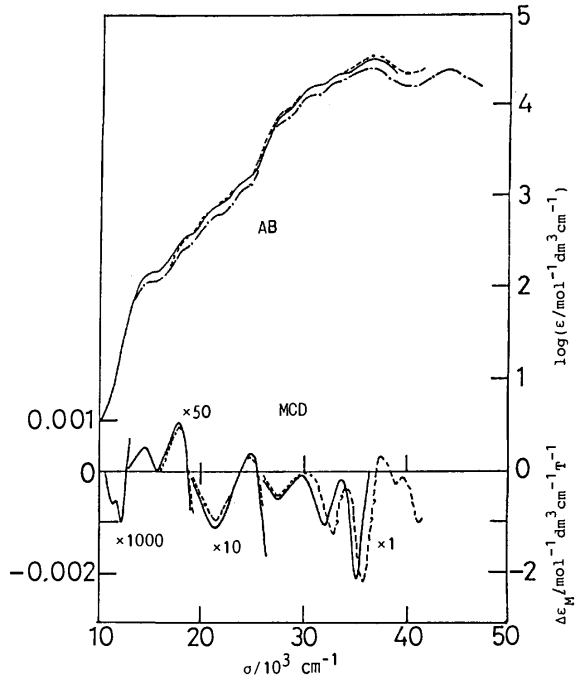

Fig. 4. Absorption and MCD spectra of [Co(pyt)$_3$] (—— in DMSO, ---- in CH_3OH, —·— in $(C_2H_5)_2O$).

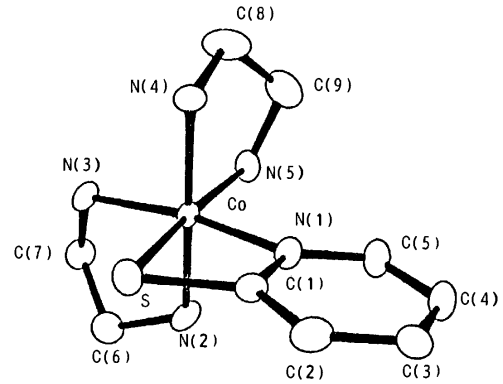

Fig. 5. The perspective view of [Co(pyt)(en)$_2$]-$(ClO_4)_2$.

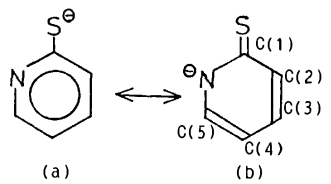

Fig. 6. The resonance structure of the pyt ligand.

phatic S-C one (1.818(8) Å)[11] and that the C(1)-C(2) and C(3)-C(4) bond distances (1.397(10) and 1.405 (14) Å respectively) are considerably longer than the C(2)-C(3) and C(4)-C(5) distances (1.355(12) and 1.362(11) Å respectively). This difference of the trans influence induced by **pyt** and **aet** may be related to the geometrical isomeric preference of the [Co(N-S)$_3$] and [Co(N-S)$_2$(N-N)]$^+$-type complexes. In fact, only the *fac* geometry has been obtained for the aet complexes [Co(aet)$_3$][1] and [Rh(aet)$_3$],[2] whereas only the *mer* geometry has been obtained for the pyt complexes [Co(pyt)$_3$] and [Rh(pyt)$_3$].[12] In the case of [Rh(6-

Table 4. Positional Parameters (×10^4) and Equivalent Temperature Factors (Å^2) of [Co(pyt)(en)$_2$]$(ClO_4)_2$

Atom	x	y	z	B_{eq}
Co	199(1)	36(1)	8525(1)	2.0
S	893(1)	−1309(1)	7464(2)	2.9
Cl(1)	−2844(1)	−2533(1)	8662(2)	3.4
Cl(2)	3429(1)	−3517(1)	5358(2)	3.6
N(1)	1730(4)	−3(5)	8811(5)	2.6
N(2)	−90(5)	−914(5)	9831(5)	3.3
N(3)	−1278(4)	−50(5)	7922(5)	2.7
N(4)	434(4)	1013(5)	7256(6)	3.2
N(5)	−183(5)	1176(5)	9625(6)	3.4
O(11)	4004(7)	−3307(6)	4415(8)	6.1
O(12)	2462(8)	−2922(9)	5612(12)	8.0
O(13)	4152(10)	−3162(15)	6386(12)	10.8
O(14)	3244(11)	−4589(7)	5597(12)	8.6
O(21)	−2192(8)	3655(5)	3717(12)	7.6
O(22)	−2786(19)	2053(15)	4643(18)	12.8
O(23)	−2707(19)	2262(10)	2664(14)	12.5
O(24)	−1117(12)	2262(9)	3851(18)	11.0
C(1)	2032(5)	−840(5)	8193(6)	2.5
C(2)	3111(6)	−1153(7)	8143(7)	3.6
C(3)	3855(6)	−565(9)	8702(7)	4.1
C(4)	3533(6)	321(7)	9333(8)	4.0
C(5)	2469(6)	579(7)	9387(8)	3.6
C(6)	−516(10)	−326(10)	10800(9)	5.6
C(7)	−77(10)	700(10)	10827(8)	5.5
C(8)	−1457(6)	801(6)	7090(7)	3.5
C(9)	−454(7)	934(6)	6418(8)	3.8

Table 5. Selected Bond Distances (l/Å) and Angles (ϕ/°) of [Co(pyt)(en)$_2$]$(ClO_4)_2$

Co-S	2.282(2)	Co-N(1)	1.929(5)
Co-N(2)	1.975(6)	Co-N(3)	1.964(5)
Co-N(4)	1.960(6)	Co-N(5)	1.993(6)
N(1)-C(1)	1.339(9)	S-C(1)	1.754(7)
C(2)-C(3)	1.355(12)	C(1)-C(2)	1.397(10)
C(4)-C(5)	1.362(11)	C(3)-C(4)	1.405(14)
N(2)-C(6)	1.453(13)	C(5)-N(1)	1.358(10)
N(3)-C(8)	1.470(10)	N(5)-C(7)	1.528(12)
C(6)-C(7)	1.417(18)	N(4)-C(9)	1.474(11)
S-Co-N(1)	72.6(2)	C(8)-C(9)	1.479(12)
S-Co-N(3)	96.7(2)	S-Co-N(2)	91.2(2)
S-Co-N(5)	170.0(2)	S-Co-N(4)	90.9(2)
N(1)-Co-N(3)	168.0(2)	N(1)-Co-N(2)	91.8(3)
N(1)-Co-N(5)	98.2(3)	N(1)-Co-N(4)	90.0(2)
N(2)-Co-N(4)	177.6(3)	N(2)-Co-N(3)	94.1(3)
N(3)-Co-N(4)	84.6(2)	N(2)-Co-N(5)	84.9(3)
N(4)-Co-N(5)	93.2(3)	N(3)-Co-N(5)	92.8(3)
Co-N(1)-C(1)	101.8(4)	Co-S-C(1)	77.7(2)
C(1)-N(1)-C(5)	120.7(6)	Co-N(1)-C(5)	137.4(5)
Co-N(3)-C(8)	109.6(4)	Co-N(2)-C(6)	110.2(6)
Co-N(5)-C(7)	106.0(6)	Co-N(4)-C(9)	110.1(5)
C(1)-C(2)-C(3)	118.3(8)	N(1)-C(1)-C(2)	121.2(6)
C(3)-C(4)-C(5)	119.6(8)	C(2)-C(3)-C(4)	120.1(7)
N(2)-C(6)-C(7)	110.8(9)	C(4)-C(5)-N(1)	120.0(8)
N(3)-C(8)-C(9)	107.7(6)	C(6)-C(7)-N(5)	108.3(8)
C(8)-C(9)-N(4)	106.7(7)		

methyl-2-pyridinethiolato)$_3$],[13] only the fac geometry was isolated, but this is due to the steric effect of the 6-methyl groups. Thus, the aet thiolates with a relatively large trans-influence favor the cis disposition toward each other, but the pyt thiolates with a lesser trans influence make a trans disposition possible.

Characterization of the Oxidation Product [Co(pyse-*N,S*)(en)$_2$](ClO$_4$)$_2$ and Its Photoisomerization into [Co(pyse-*N,O*)(en)$_2$](ClO$_4$)$_2$. The H_2O_2 oxidation of the [Co(pyt)(en)$_2$](ClO$_4$)$_2$ in acid media resulted in an orange complex, which was characterized as the sulfenato-*N,S* complex [Co(pyse-*N,S*)(en)$_2$](ClO$_4$)$_2$ on the basis of its elemental analysis and absorption spectrum (Fig. 7). This orange complex changed into a green one photochemically in the solid state. Since the green complex has the same chemical composition, it is reasonable to consider that the linkage isomerization from *N,S*- to *N,O*-bonded is induced by to exposure light. The green complex exhibited a ligand-field transition at 16600 cm^{-1}, as is shown in Fig. 7.[14] Though the ligand-field strength of the oxygen atom of the *O*-bonded sulfenato complex is extraordinarily weak, this may be because of the repulsion between the oxygen and adjacent sulfur lone pairs. The pyse-*S,N* and -*O,N* complexes exhibit a characteristic intense absorption band at ca. 25000 cm^{-1} and ca. 26000 cm^{-1} respectively. All the known *S*-bonded sulfenato complexes showed a similar absorption band at ca. 27000 cm^{-1}. Such an intense band has generally been observed in complexes with the Co-X-Y array, where X and Y are oxygen and/or sulfur atom with lone-pair electrons.[15] The parent complex, [Co(pyt-*S,N*)(en)$_2$]$^{2+}$, did not show such an intense band in the region below 30000 cm^{-1}. On the other hand, both sulfenato complexes showed this intense band, as is consistent with the above strucutre assignments. The optically active complexes, $(-)^{CD}_{500}$-[Co(pyse-*S,N*)(en)$_2$]$^{2+}$ and its linkage isomer $(-)^{CD}_{603}$-[Co(pyse-*O,N*)(en)$_2$]$^{2+}$, are assigned to the *Δ* absolute configuration on the basis of the dominant negative CD sign at 19700 cm^{-1} and at 16600 cm^{-1} respectively in the first d-d band region.

The XPS spectra of the S-2p binding energy region for the orange and green isomers of [Co(pyse)-(en)$_2$](ClO$_4$)$_2$ are shown in Fig. 8. The orange complex exhibited a peak at 166.7 eV, with a shoulder at ca. 164 eV. The green complex showed a peak at 164.3 eV, with a shoulder at ca. 167 eV. These results indicate that the samples used for both measurements are mixtures of two species; that is, the pure orange complex should show a peak at 166.7 eV, and the pure green one, are at 164.3 eV. Since the *N,O*-coordinated pyse must show a lower sulfur binding energy because of the decrease in the partial charge on the sulfur atom as compared with the *N,S*-coordinated pyse, the orange and green isomers can be assigned to the *N,S*- and *N,O*-chelated structures respectively. Thus, the light irradiation of the 4-membered *N,S*-pyse complex caused the linkage isomerization in the solid state to give the *N,O*-chelated complex with the 5-membered ring. In general, the strain energy of a chelate ring is much eliminated in a 5-membered chelate as compared with a 4-membered one. Therefore, the present photoisomerization seems to be energetically favora-

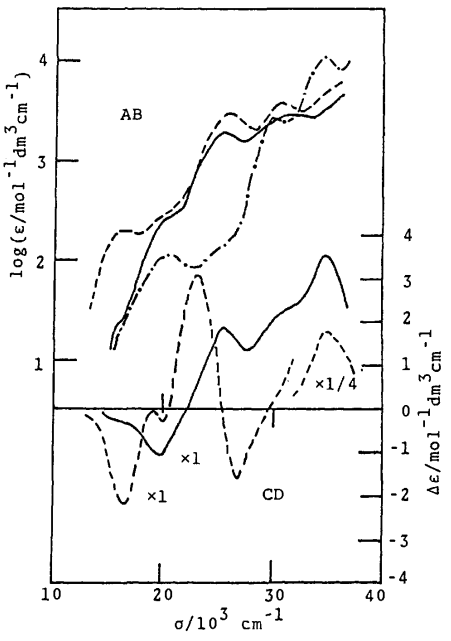

Fig. 7. Absorption and CD spectra of *Δ*-[Co(pyse-*N,S*)(en)$_2$](ClO$_4$)$_2$ (——), *Δ*-(Co(pyse-*N,O*)(en)$_2$]-(ClO$_2$)$_2$ (----), and [Co(pyt)(en)$_2$](ClO$_4$)$_2$ (— · —) in DMSO solution.

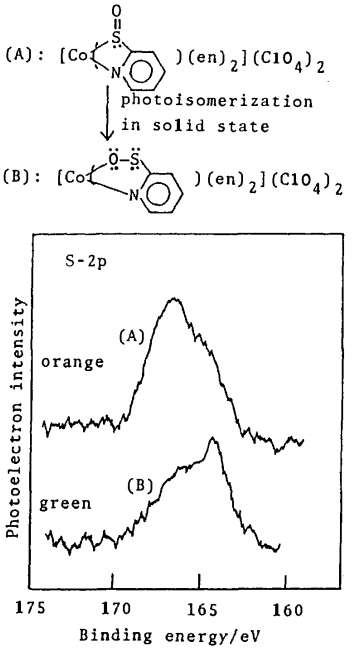

Fig. 8. The XPS spectra of S-2p binding energy region for the orange(A) and green(B) isomers of [Co(pyse)(en)$_2$](ClO$_4$)$_2$.

ble. Photoisomerization has been reported in an aqueous solution of the sulfinato complex [Co(aesi-*N*,*S*)$(en)_2]^{2+}$ (Haesi=2-aminosulfinic acid), though the corresponding sulfenato complex [Co(aese-*N*,*S*)-$(en)_2]^{2+}$ (Haese=2-aminosulfenic acid) did not show any.[8]

References

1) M. Kita, K. Yamanari, and Y. Shimura, *Bull. Chem. Soc. Jpn.*, **55**, 2873 (1982).
2) M. Kita, K. Yamanari, and Y. Shimura, *Bull. Chem. Soc. Jpn.*, **56**, 3272 (1983).
3) M. Kita, K. Yamanari, and Y. Shimura, *Chem. Lett.*, **1983**, 141.
4) M. Kita, K. Yamanari, and Y. Shimura, *Chem. Lett.*, **1984**, 297.
5) K. Yamanari and Y. Shimura, *Bull. Chem. Soc. Jpn.*, **56**, 2283 (1983).
6) T. Sakurai and K. Kobayashi, *Rikagaku Kenkyusho Hokoku*, **55**, 69 (1979).
7) K. Yamanari, J. Hidaka, and Y. Shimura, *Bull. Chem. Soc. Jpn.*, **50**, 2299 (1977).
8) V. H. Houlding, H. Macke, and A. W. Adamson, *Inorg. Chem.*, **20**, 4279 (1981).
9) Y. Shimura, *Bull. Chem. Soc. Jpn.*, **61**, 693 (1988).
10) K. Yamanari, N. Takeshita, T. Komorita, and Y. Shimura, *Chem. Lett.*, **1981**, 861.
11) R. C. Elder, L. R. Florian, R. E. Lake, and A. M. Yacynych, *Inorg. Chem.*, **12**, 2690 (1973).
12) A. J. Deeming, K. I. Hardcastle, M. N. Meah, P. A. Bates, H. M. Dawes, and M. B. Hursthouse, *J. Chem. Soc., Dalton Trans.*, **1988**, 227.
13) A. J. Deeming, M. N. Meah, P. A. Bates, and M. B. Hursthouse, *Inorg. Chim. Acta*, **142**, 37 (1988).
14) The samples used for the absorption and CD measurements are still mixtures of the two isomers as is shown by the XPS spectra in Fig. 8.
15) J. D. Lydon and E. Deutsch, *Inorg. Chem.*, **21**, 3186 (1982).

 © 1989 The Chemical Society of Japan Bull. Chem. Soc. Jpn., 62, 3089—3092 (1989)

Response and Application in Dipolar Aprotic Solvents of Ion-Selective Electrodes Based on Polyacrylamide Modified with Acyclic Poly(oxyethylene) Derivatives

Toshio NAKAMURA,* Hisakazu HIGUCHI, and Kosuke IZUTSU
Department of Chemistry, Faculty of Science, Shinshu University, Asahi, Matsumoto 390
(Received March 16, 1989)

The response of organic polymer membrane electrodes, constructed by coating a platinum disk with polyacrylamide (PAA) coupled to acyclic poly(oxyethylene) derivatives, tetraethylene glycol monododecyl ether (POE4) and hexaethylene glycol monododecyl ether (POE6) was studied in acetonitrile (AN) and *N,N*-dimethylformamide (DMF). The PAA-POE4 electrode showed Nernstian response to the lithium ion in AN and the magnesium and barium ions in DMF, while the PAA-POE6 electrode showed near Nernstian response to the barium ion in DMF. The PAA-POE4 electrode was applied to study the complexation of the lithium ion in AN with DMF. The formation constants, $\beta_1=17$ and $\beta_2=1.2\times10^2$, obtained agreed well with the values obtained previously with an univalent cation sensitive glass electrode. The response of the PAA-POE4 electrode in barium bis(2-ethylhexyl) sulfosuccinate ($Ba(DSS)_2$)-DMF solution has been studied and the results are explained by taking the conductometrically determined association constant ($K_{1A}=5.2\times10^2$) between Ba^{2+} and DSS^- ions.

Some types of ion-selective electrodes have been successfully used in physicochemical as well as in analytical studies of nonaqueous solutions.[1] Recently, we have developed some ion-selective electrodes for use in dipolar aprotic solvents.[2] One of these electrodes was used to study the complexing of the magnesium and barium ions in acetonitrile (AN) with other dipolar aprotic solvent molecules.[3] In the present paper the response and the application of the same type of ion-selective electrodes[2] constructed by coating a platinum disk with polyacrylamide (PAA) coupled to tetraethylene glycol monododecyl ether (POE4) or hexaethylene glycol monododecyl ether (POE6) are reported. The response behavior of the PAA-POE4 and PAA-POE6 electrodes to the lithium, magnesium and barium ions were investigated in several nonaqueous chemical systems. The PAA-POE4 elctrode was used to obtain the successive complex formation constants of the lithium ion in AN with *N,N*-dimethylformamide (DMF) to compare with the values obtained previously with a values obtained previously with a univalent cation sensitive glass electrode.[4] The response behavior of the PAA-POE4 electrode to barium bis(2-ethylhexyl) sulfosuccinate ($Ba(DSS)_2$) in DMF has been studied and the results are explained by taking the conductometrically determined association constant of the compound.

Experimental

Reagents. The sodium bis(2-ethylhexyl)sulfosuccinate was the product of Tokyo Kasei Kogyo Co., Ltd. and the barium bis(2-ethylhexyl) sulfosuccinate, $Ba(DSS)_2$, was prepared and purified according to the method of Kitahara et al.[5] Other reagents and solvents were the same as those in the previous report.[3]

Potentiometric Measurements. Most of the methods of the potentiometric measurements and the electrode construction were the same as those described in the previous report.[3] The responses of the electrodes were tested in the following Cell I,

Ag/10 mM $AgNO_3$+10 mM Et_4NClO_4 (D)//
50 mM Et_4NClO_4(D)//*C* $M(ClO_4)_x$ or $Ba(DSS)_2$+
10 mM Et_4NClO_4 (D)/PAA-POE4 or 6/Pt·····Cell I,

where $M(ClO_4)_x$ was the perchlorate of the cation to be tested (lithium, magnesium, or barium ion), D was AN or DMF, and *C* in mol dm^{-3}. A standard addition method was employed in obtaining calibration curves. Steady state potentials were read to ±0.1 mV. The electrode potentials were not significantly affected by change in the rate of the solution.

Conductivity Measurements. A conductivity meter of Toa Denpa Kogyo, Type CM-40S, equipped with an interval time unit IT-1S and a Yanagimoto conductivity cell, Type C, was used. The conductivity was also monitored simultaneously with a strip chart recorder, Yokogawa Denki type 3056. The $Ba(DSS)_2$-DMF solution of known concentration was added to the conductometric cell (cell constant 0.368_5) with a microburette (Gilmont Instruments, Inc., S1100A and S1200A).

Determination of the Complex Formation Constants. The successive complex formation constants of the lithium ion in AN with DMF were determined by potentiometric measurement in Cell II. The complexing solvent DMF was added to the cell with a microburette, 10 μl in each step, until its volume per cent reached 1%.

Ag/10 mM $AgNO_3$+10 mM Et_4NClO_4(AN)//
50 mM Et_4NClO_4(AN)//0.1 mM$LiClO_4$+
10 mM Et_4NClO_4(AN+DMF)/PAA-POE4/Pt···Cell II.

The potentiometric data were analyzed by the same method as that described in the previous report.[3]

Results

Responses of the Electrodes. The PAA-POE4 and PAA-POE6 electrodes were durable in AN and DMF for at least two weeks. The responses of these electrodes to lithium, magnesium, and barium ions are summarized in Table 1 and Fig. 1. The activity of

Table 1. The Responses of Organic Polymer Membrane Electrodes to Some Metal Ions in Nonaqueous Solvents at 25 °C

Ion	r_c/Å[a]	Solvent	Slope (mV/$pa_{M^{n+}}$)	The activity range of the linear response
			PAA-POE4	
Li^+	0.60	AN	57.4	8×10^{-5}—6×10^{-3}
Mg^{2+}	0.65	DMF	30.4	2×10^{-5}—2×10^{-3}
Ba^{2+}	1.35	DMF	27.3	3×10^{-6}—3×10^{-4}
			PAA-POE6	
Ba^{2+}	1.35	DMF	26.1	1×10^{-5}—4×10^{-4}

a) r_c: Crystallographic ionic radius.

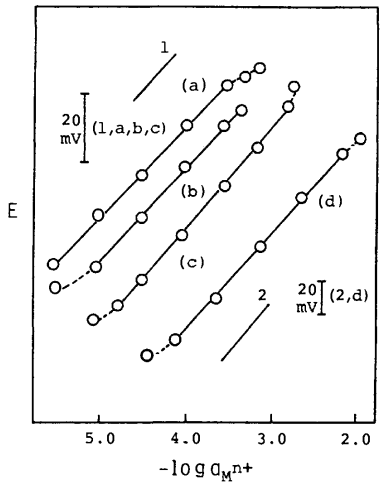

Fig. 1. Calibration curves in nonaqueous solvents at 25 °C. Lines 1 and 2, theoretical slope for bivalent cations (29.6 mV/$pa_{M^{2+}}$) and for univalent cation (59.2 mV/pa_{M^+}), respectively. (a) Ba^{2+} in DMF with PAA-POE4, (b) Ba^{2+} in DMF with PAA-POE6, (c) Mg^{2+} in DMF with PAA-POE4, (d) Li^+ in AN with PAA-POE4.

the metal ion, $a_{M^{x+}}$, was calculated by using the Debye-Hückel second approximation equation as previously described.[6] The results in Table 1 have not been corrected for the change in the liquid junction potential between the sample solution and the salt bridge of Cells I and II, but its effect seems to be small. The PAA-POE4 electrode could respond in a Nernstian way to the activities of the lithium ion in AN between the concentration range 7×10^{-5}—7×10^{-3} M (1M=1 mol dm^{-3}). The electrode could respond in Nernstian ways to the activities of the magnesium and barium ions in DMF between the concentration ranges 5×10^{-5}—1×10^{-2} M and 1×10^{-5}—1×10^{-3} M, respectively. The PAA-POE6 electrode showed near Nernstian response to the activity of the barium ion in DMF between the concentration range 3×10^{-5}—2×10^{-3} M.

Complexing of the Lithium Ion in AN with DMF. The complex formation constants of the lithium ion in AN with DMF were determined by measuring the emf change of Cell II. The relations between the potential change ΔE and the concentration of DMF, [D], and between R_1 and [D] (see Ref. 3) obtained in this experiment are shown in Fig. 2(a) and (b), respectively. Here $R_1 \equiv \{10^{\Delta E/59.16}-1\}/[D]=\beta_1+\beta_2[D]+\beta_3[D]^2+\cdots$. From the intercept and the slope of the straight line, $\beta_1=16$ and $\beta_2=1.5\times10^2$ are obtained (β_1 and β_2; see Ref. 3). The average values obtained in this experi-

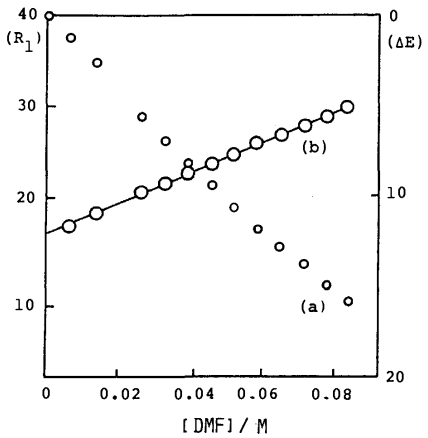

Fig. 2. The relations of ΔE-[DMF] and R_1-[DMF] for Li^+ ion in AN with PAA-POE4 at 25 °C.

Table 2. Complex Formation Constants of Li^+ in AN with DMF

Indicator electrode	Stability constant	
	β_1	$\beta_2(K_2)$
Cation-sensitive glass electrode[a]	16	1.1×10^2(6.9)
PAA-POE4 electrode	17	1.2×10^2(7.0)

a) See Ref. 4.

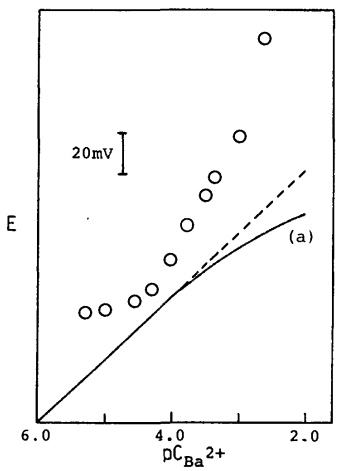

Fig. 3. Calculated potential curve vs. log $C_{Ba^{2+}}$ (curve (a)) and E (○) vs. log $C_{Ba^{2+}}$ relations of $Ba(DSS)_2$ in DMF with PAA-POE4 electrode under the coexistence of 10 mM Et_4NClO_4.

ment are shown in Table 2 with the results obtained previously by the use of an univalent cation-sensitive glass electrode.[4] The agreement between the results obtained with the two electrodes is excellent.

Potentiometric and Conductometric Behavior of $Ba(DSS)_2$ in DMF. (i) Potentiometry: The response of the PAA-POE4 electrode to the amphiphilic substance, $Ba(DSS)_2$, in DMF was measured using Cell I. The result is shown in Fig. 3 and curve (a) shows the calculated potential response to the barium ion in the solution of $Ba(DSS)_2$. The association constant of $Ba(DSS)_2$ in DMF used to elucidate the barium ion activity was obtained by the conductometric measurement shown below. When the concentration of the barium ion in DMF increased, the slope of the E-$pC_{Ba^{2+}}$ relation became steeper. The situation of the potential response of the PAA-POE4 electrode to the barium ion in $Ba(DSS)_2$-DMF solution, in which there was no Et_4NClO_4, was similar to that in Fig. 3 , but the potential change suddenly ceased at the highest concentration of the $Ba(DSS)_2$. **(ii) Conductometry:** The conductometric measurement was carried out to determine the association constant of $Ba(DSS)_2$ in DMF. The equivalent conductivities obtained are shown in Table 3. These values were used to get the association constant of Ba $(DSS)_2$ in DMF using the method of the Modified Fuoss-Edelson.[7] The activity coefficient of Ba^{2+}, y, was calculated using the Debye-Hückel second approximation equation[6] with ion-size parameters, a, of 10 Å and dielectric constant, ε, of 36.71 of DMF. The Modified Fuoss-Edelson plot obtained is shown in Fig. 4. Here the ΔF on the ordinate and the X on the abscissa in Fig. 4 are the same as those in Ref. 7 reported by Doe and Kitagawa. From the intercept and the slope of the straight line in Fig. 4, the limiting equivalent conductivity, Λ_0 of $Ba(DSS)_2$ in DMF and the 1 : 1 association constant between Ba^{2+} and DSS^-, K_{1A}, were obtained to be 54.8 and $5.2_4\times10^2$, respectively. The limiting equivalent conductivity of the barium ion in DMF used for the above calculation was 39.0[8] and that of the DSS^- in DMF was calculated to be 15.8.

Table 3. Equivalent Conductivity of $Ba(DSS)_2$ in DMF at 25 °C

10^4C/mol dm^{-3}	S/cm^2 mol^{-1}
0.6458	53.50
0.9901	52.20
2.248	48.98
4.031	46.99
6.279	44.86
9.091	42.79
12.28	40.96
19.35	37.91

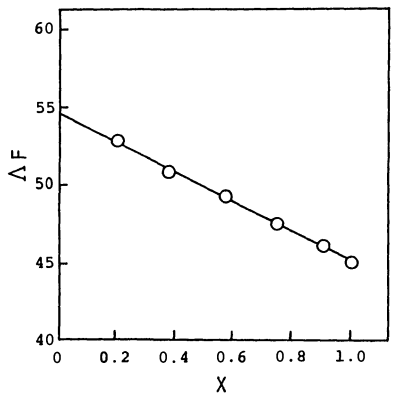

Fig. 4. Modified Fuoss and Edelson plot for $Ba(DSS)_2$ in DMF at 25 °C.

Discussion

The PAA-POE4 electrode can respond to the activities of the lithium ion in AN and the magnesium and barium ions in DMF. The PAA-POE6 electrode may also be used to measure the barium ion activity in DMF.

The PAA-POE4 electrode was used to determine the successive complex formation constants of the lithium ion in AN with DMF and the results agreed well with those obtained previously[4] by the use of an univalent cation-sensitive glass electrode. The glass electrode has been proved to respond in the same way as the amalgam electrode to the variation in solvation energies of the lithium ions.[9] In the previous paper,[3] we also showed that the PAA-POE4 electrode and the barium amalgam electrode could give similar formation constants for the complexation of the barium ion in AN with DMF. These results show that at least in an AN-rich region the electrode can respond thermodynamically to the variation in solvation energies of these ions and can be applied to study the complex formation reaction of alkali and alkaline earth metal ions in AN with other basic aprotic solvents.

In the present study the association constant of the barium ion with DSS^- in the $Ba(DSS)_2$-DMF solution was found to be of the same order of magnitude as that of the barium ion with *p*-toluenesulfonate and more associated than with perchlorate.[8] Using the association constant, the response of the PAA-POE4 electrode in the $Ba(DSS)_2$-DMF solution was estimated theoretically. But, as in Fig. 3, the slope of the potential change was larger than the theoretical one. It may be due to the localization of the barium ion at the PAA-POE4 membrane surface: the hydrophilic sulfonate of the DSS^- seems to be directed to the hydrophilic organic membrane and to concentrate the counter ion, Ba^{2+}, to the vicinity of the membrane. In the absence of Et_4NClO_4 in Fig. 3, the potential suddenly ceased to change at the highest concentration of the $Ba(DSS)_2$ as shown in the Results section. The difference in the electrode responses in the presence and absence of Et_4NClO_4 might be explained by the role of anions. In order to investigate the response mecha-

nism of the PAA-POE4 electrode we prepared a glass filter membrane impregnated with PAA-POE4 and measured the ion transport across the membrane. A conductometric method was used to monitor the ionic transport. From the experiment, we found that the perchlorate ion can enter the membrane freely, while the entrance of the DSS^- into the membrane is fairly limited due to its larger size.[10] The sudden stop of the potential change in the absence of Et_4NClO_4 might be related to the difficulty for DSS^- to enter into the membrane. Probably sufficient anions should be present in the membrane to counterbalance the barium ion necessary for the proper electrode response. Some deficiency of anions would occur in the absence of Et_4NClO_4. In addition to this, it should also be taken into account that surface active substances (DSS^-) may change the property of the electrode surface and may interupt the response of the electrode.

Further studies are now being continued in this laboratory in order to elucidate the mechanism of the potential response at the polymer based ion-selective electrodes.

This work was supported in part by a Grant-in-Aid for Scientific Research from the Ministry of Education, Science and Culture.

References

1) E. Pungor, K. Tóth, P. G. Klatsmányi, and K. Izutsu, *Pure Appl. Chem.*, **55**, 2029 (1983).
2) T. Nakamura and G. A. Rechnitz, *Anal. Chem.*, **57**, 393 (1985); T. Nakamura, K. Ogiwara, K. Izutsu, and G. A. Rechnitz, *Bull. Chem. Soc. Jpn.*, **58**, 3409 (1985).
3) T. Nakamura, H. Higuchi, and K. Izutsu, *Bull. Chem. Soc. Jpn.*, **61**, 1020 (1988).
4) K. Izutsu, T. Nakamura, and K. Iwata, *Anal. Chim. Acta*, **117**, 329 (1980).
5) A. Kitahara, T. Komatsuzawa, and K. Kon-no, Proceedings of 5th International Congress of Surface Active Substances, Vol. 2, Barcelona (1969), p. 135.
6) T. Nakamura, Y. Yumoto, and K. Izutsu, *Bull. Chem. Soc. Jpn.*, **55**, 1850 (1982).
7) H. Doe and T. Kitagawa, *Bull. Chem. Soc. Jpn.*, **58**, 2975 (1985).
8) T. Fuginaga and I. Sakamoto, *J. Electroanal. Chem.*, **73**, 235 (1976).
9) T. Nakamura, *Bull. Chem. Soc. Jpn.*, **48**, 2967 (1975).
10) T. Nakamura, unpublished result.

 © 1989 The Chemical Society of Japan Bull. Chem. Soc. Jpn., 62, 3093—3097 (1989)

The Complexation Equilibria of Mercury(II) Ions with Macromonocyclic 16-Membered Dioxopentamine, 18-Membered Dioxohexamine, and Their Related Compounds

Mutsuo KODAMA* and Eiichi KIMURA†

Department of Chemistry, College of General Education, Hirosaki University, Bunkyo, Hirosaki 036

†Department of Medical Chemistry, Hiroshima University School of Medicine, Kasumi, Hiroshima 734

(Received April 3, 1989)

We have investigated the equilibria of complexation reactions of mercury(II) ions with 16-membered macrocyclic dioxopentamine (dioxo[16]aneN$_5$), 18-membered macrocyclic dioxohexamine (dioxo[18]aneN$_6$), and their related compounds by employing a polarographic method and pH-metric titration. Dioxo[16]aneN$_5$, dioxo[18]aneN$_6$, and other dioxo ligands except dioxotetramines were found to form solely 1 : 1 ratio mercury(II) complexes designated as $HgH_{-1}L^+$ with displacement of one amide proton, while the macrocyclic 16-membered monooxopentamine(monooxo[16]aneN$_5$) forms HgL^{2+} in addition to $HgH_{-1}L^+$. The substitution of amine nitrogen of dioxo[16]aneN$_5$ by the sulfur donor unexpectedly gave no increase in the stability of mercury(II) complex of dioxo ligand, $HgH_{-1}L^+$.

The macrocyclic dioxopolyamines possess novel ligand properties of saturated macrocyclic polyamines blended with oligopeptide features. They can accommodate certain metal ions such as Cu^{2+}, Ni^{2+}, and Co^{2+} in the macrocyclic cavities with simultaneous dissociation of the amide protons to afford 1 : 1 ratio complexes generally designated as $MH_{-1}L^+$ or $MH_{-2}L$.[1-3] However in reactions with Zn^{2+}, Cd^{2+}, and Pb^{2+} they undergo no deprotonation, giving a ML^{2+} complex.[4]

The mercury(II) ion is generally harmful to biological systems and an understanding of its action is of great importance. Its toxic action may be ascribable to the formation of protein complexes, which may block the enzymatic activity or change the conformation and the solubility of proteins. For a more detailed understanding of the toxic effect of mercury(II) ion on living systems, it is necessary to know the nature of the Hg(II)-protein interaction. It is not well known whether the mercury(II) ion can bind to the amide nitrogen atom of the peptide group, promoting the dissociation of the amide proton. In this paper we studied systematically the complexation reactions of mercury(II) ions with macrocyclic dioxopentamine and dioxohexamine using polarographic and pH-metric methods.

Though care should be taken in drawing conclusion about the Hg(II)-protein interaction from studies on low-molecular weight systems, the present equilibrium study on the complexation reactions of Hg(II) ions with macrocyclic dioxopolyamines might shed more light on the properties of Hg(II)-peptide interaction.

Experimental

Reagents. The macromonocyclic 18-membered dioxohexamine L^8 was synthesized as an intermediate to a saturated macrocyclic 18-membered hexamine, [18]aneN$_6$, by employing the method proposed by Tabushi et al.[5] All monooxo and dioxo ligands used in this study (Chart 1) were synthesized according to the reported method.[3]

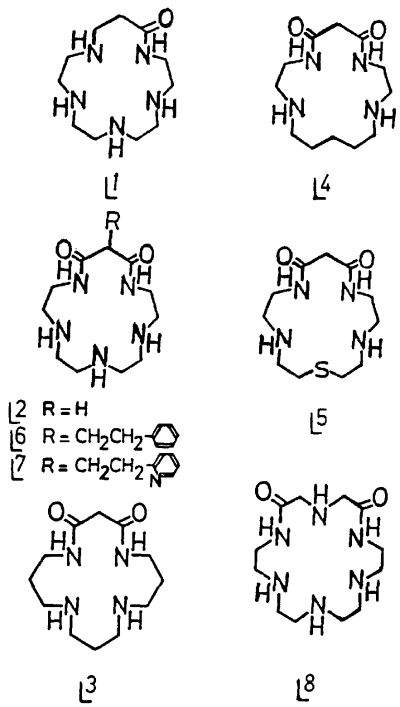

Chart 1.

Polarographic Method. All the polarograms were obtained with a Yanagimoto P-8 pen-recording polarograph or a manual polarograph similar to that of Kolthoff and Lingane.[6] The dropping mercury electrode (DME) had the open-circuit characteristics m=0.928 mg s^{-1} and t_d=4.75 s. in an air-free 0.10 mol·dm^{-3} $NaClO_4$ solution at a column height of 60 cm at 25°C. The polarographic procedures were the same as those applied to the previous mercury(II) complexes of macromonocyclic tetramine[7] and pentamines.[8] In order to maintain the solution pH constant, acetate (5.80>pH>4.00), tris. (8.20>pH>7.00), and borate (10.00>pH>8.20) buffers were used in this study.

Potentiometric Method. Potentiometric (pH-metric) titrations were performed with a Mettler automatic titrator at 25±0.10 °C under a nitrogen or argon atmosphere. The

mixed protonation constants (pK_a's) of the new dioxo ligands, L^3 and L^8, were determined by titrations with 0.100_0 mol·dm^{-3} carbonate-free tetraethylammonium hydroxide (TEAOH) or NaOH solution using a sample solution containing 10^{-3} mol·dm^{-3} ligand with an ionic strength made up to 0.20 mol·dm^{-3} using $NaClO_4$. The pK_a values for L^3 were 9.70 and 8.05, and those for L^8 were 8.70, 7.10, ca.2, and ca.1. The cumulative formation constants for the dioxopentamine and dioxohexamine complexes were also determined by titration with 0.100_0 mol·dm^{-3} TEAOH or NaOH solution of 10^{-3} mol·dm^{-3} equimolar mixture solution of Hg(II) and L^2·3HCl or L^8·4HCl salt. The change in the Na^+ concentration had no effect on the titration curves and polarograms. The values of $-\log[H^+]$ (for calculation of formation constants) were estimated from pH readings at an ionic strength (I)=0.20; $-\log[H^+]$=pH−0.13.

Results and Discussion

In tris.(0.050 mol·dm^{-3}) and borate (0.030 mol·dm^{-3}) buffer solutions all the macromonocyclic monooxopentamine, dioxopentamines, and dioxohexamine studied gave well defined anodic waves at DME. A typical polarogram obtained for the dioxo[16]aneN$_5$ (L^2) at pH=8.36 is shown in Fig. 1. Their polarographic behavior exept for the pH dependence of the half-wave potential were the same as those of the saturated macromonocyclic tetramines[7] and pentamines.[8] The reversible nature of the electrode processes was also confirmed by the ac polarographic method.[7,9]

The half-wave potential, $(E_{1/2})_L$, for the dioxo[16]aneN$_5$ shifted to more negative values on increasing the solution pH according to the relation (1) (Table 1 and Fig. 2), where $(\alpha_H)_L$ is defined as $1+[H^+]/K_3+[H^+]^2/K_3\cdot K_2+[H^+]^3/K_3\cdot K_2\cdot K_1$.[3]

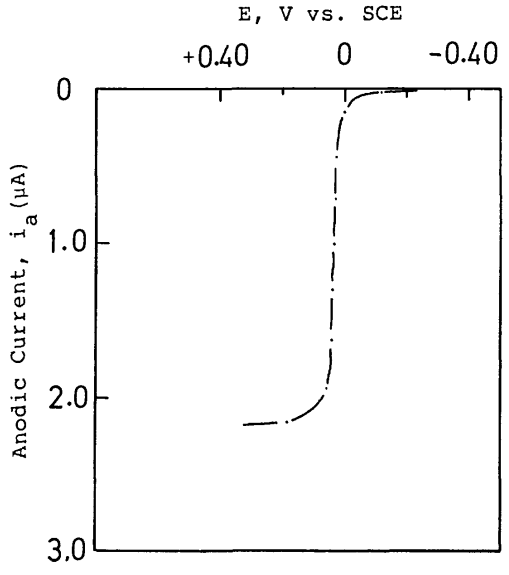

Fig. 1. Anodic dissolution wave at DME due to dioxo[16]aneN$_5$.
[dioxo[16]aneN$_5$]=0.40 mM, borate buffer 0.060 M, pH=8.36, I=0.20 M, 25 °C.

$$\frac{\Delta E_{1/2}}{\Delta\log(\alpha_H)_L\cdot[H^+]} = 30\ \text{mV} \quad (1)$$

The findings evidently indicate that only a 1 : 1 ratio mercury(II)-dioxo[16]aneN$_5$ complex designated as $HgH_{-1}L^+$ is formed in the Eq. 2 with simultaneous dissociation of one amide proton.

$$Hg + H_iL^{i+} \rightleftarrows HgH_{-1}L^+ + (i+1)H^+ \quad (2)$$

The half-wave potential is then expressed as in Eq. 3.

$$(E_{1/2})_L=\varepsilon^0_{Hg}+0.0296[\log f_{Hg}{}^{2+}-\log K_{HgH_{-1}L}+\log(\alpha_H)_L\cdot[H^+]]+0.0296\log(k_L/k_{HgH_{-1}L}) \quad (3)$$

Table 1. Effects of Ligand and Buffer Concentrations and Solution pH on the Half-Wave Potential, $E_{1/2}$.
I=0.20 M, 25 °C

pH	[ligand]$_t$	[buffer]	$E_{1/2}$	$\log(\alpha_H)_L\cdot[H^+]$
	mM	M	V vs. SCE	
7.96[a]	0.40	0.060	+0.0730	-6.18_6
8.36	0.40	0.060	+0.0393	-7.22_7
8.86	0.40	0.060	+0.0092	-8.32_3
9.31	0.40	0.060	−0.0143	-9.07_8
9.82	0.40	0.060	−0.0370	-9.74_1
10.30	0.40	0.060	−0.0533	-10.27_0
8.86	0.40	0.015	+0.0100	
8.86	0.40	0.030	+0.0085	
8.86	0.20	0.060	+0.0096	
8.86	1.20	0.060	+0.0087	

a) Tris. buffer (0.060 M)

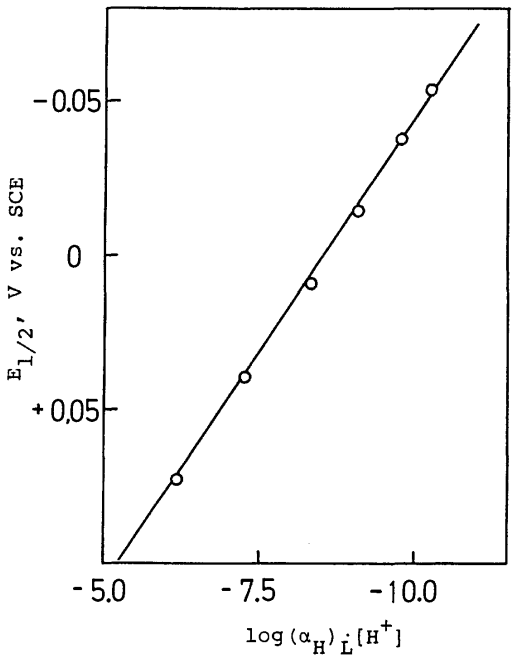

Fig. 2. Plots of half-wave potential, $(E_{1/2})_L$, against $\log(\alpha_H)_L\cdot[H^+]$.
[dioxo[16]aneN$_5$]=0.40 mM, borate buffer 0.060 M, I=0.20 M, 25 °C.

Here, the diffusion current coefficients of the mercury(II)-dioxo[16]aneN$_5$ complex, $k_{HgH_{-1}L'}$ and of the various forms of dioxo[16]aneN$_5$, $k_{L'}$ can be assumed equal for approximation. In Eq. 3, ε^0_{Hg} is the ordinary formal standard potential[10] and a cumulative formation constant, $K_{HgH_{-1}L'}$ is defined as $[HgH_{-1}L^+]\cdot[H^+]/[Hg^{2+}]\cdot[L]$. In a similar way as those applied to the Hg(II)-saturated macrocyclic polyamine complexes,[7,8] the cumulative formation constant can be determined from the $E_{1/2}$ difference from the EDTA (Y^{4-}) system,[11] $\Delta E_{1/2}$, using the Eq. 4. Here, $(\alpha_H)_Y$

$$\log K_{HgH_{-1}L}=\frac{\Delta E_{1/2}}{0.0296}+\log K_{HgY}-\log(\alpha_H)_Y+\log(\alpha_H)_L\cdot[H^+] \quad (4)$$

is the (α_H) value for the EDTA system. With the aid of Eq. 4, $\log K_{HgH_{-1}L}$ value for the Hg(II)-dioxo[16]aneN$_5$ was determined to be 10.14. The reported $K_{HgY}(=[HgY^{2-}]/[Hg^{2+}]\cdot[Y^{4-}])$ and dissociation constants of EDTA (H_4Y^0) at ionic strength I=0.10 mol·dm^{-3} were corrected to I=0.20 mol·dm^{-3} by using the activity coefficients of the ions derived from the Davies relation.[12]

The complexation reactions of dioxo ligands with mercury(II) ions were also studied using the potentiometric method. A typical pH-metric titration curve for the 1.00×10^{-3} mol·dm^{-3} equimolar mixture of mercury(II) ion and dioxo[16]aneN$_5$ ($L^2\cdot3HCl$) is shown in Fig. 3. The complexation reaction occurs in a buffered region of pH 3.0—4.0. The titration data were found to be in best agreement with the concomitant formation of $HgH_{-1}L^+$ (Fig. 4). As was discussed in connection with the reactions of copper(II) ions with macrocyclic dioxotetramine,[13] the following theoretical relation can be expected for the $HgH_{-1}L^+$ formation. β_H in Eq. 5 has the same meaning as those used previously.[3] C_L and α are the

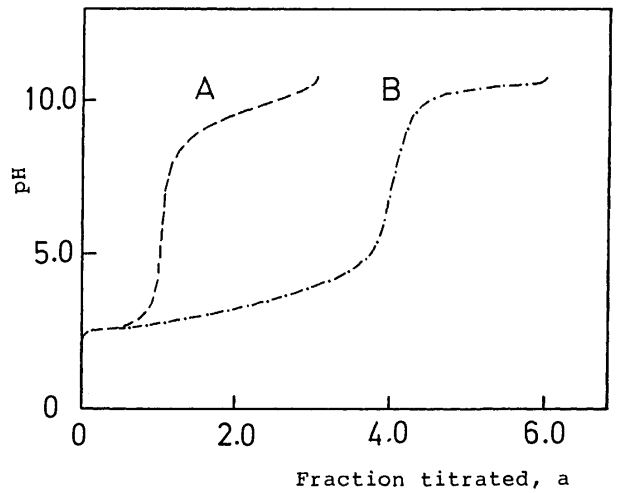

Fig. 3. Titration curves.
I=0.20 M, 25 °C. (A) Dioxo[16]aneN$_5$ 3HCl salt 1.00 mM. (B) Dioxo[16]aneN$_5$ 3HCl salt 1.00 mM+Hg (II) 1.00 mM.

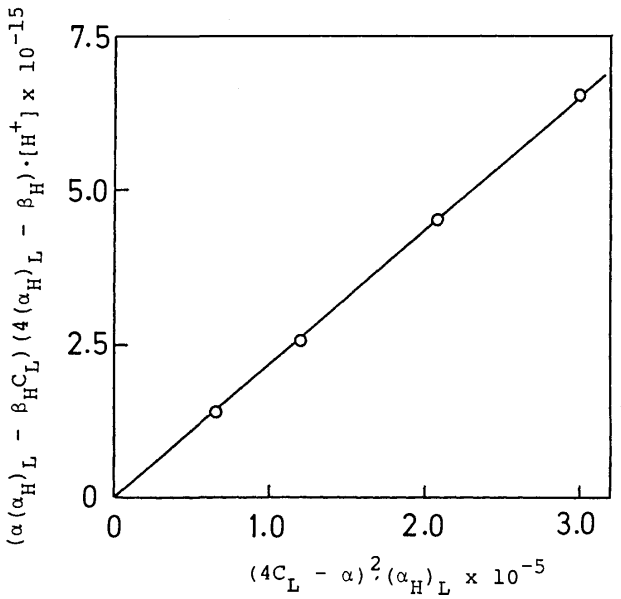

Fig. 4. Plots of $(\alpha(\alpha_H)_L-\beta_H\cdot C_L)\ (4(\alpha_H)_L-\beta_H)\ [H^+]$ against $(4C_L-\alpha)^2\cdot(\alpha_H)_L$.
[dioxo[16]aneN$_5$ 3HCl]=1.00 mM, I=0.20 M, 25 °C.

total concentration of L^2 and $a\cdot C_L+[H^+]$, respectively. Here, a means the fraction titrated. $K_{HgH_{-1}L}$ was determined from the slope of the straight line

$$K_{HgH_{-1}L}(4C_L-\alpha)^2\cdot(\alpha_H)_L=(\alpha\cdot(\alpha_H)_L-\beta_H\cdot C_L)\cdot(4(\alpha_H)_L-\beta_H)\cdot[H^+] \quad (5)$$

in Fig. 4 to be $10^{10.34}$ in a good agreement with that determined polarographically($10^{10.14}$).

Calculations for the simultaneous or separate formation of HgL^{2+} and $HgH_{-2}L^0$ and for the simultaneous formation of HgL^{2+} and $HgH_{-1}L^+$ were also made. However, the equation derived failed to fit the experimental data. Thus we concluded that neither HgL^{2+} nor $HgH_{-2}L^0$ is formed in this buffer region. The pH dependence of $(E_{1/2})_L$ for the anodic wave of dioxo[16]aneN$_5$ and the pH titration curve for the equimolar mixture solution of mercury(II) and dioxo[16]aneN$_5\cdot3HCl$ (shown in Fig. 3) can also be explained in terms of the formation of $HgL(OH)^+$ in which the dioxo[16]aneN$_5$ molecule might coordinate to the Hg(II) ion through its three amino nitrogens. Pure and Schwarzenbach reported that the mercury(II) ion can form a 1:1:1 ratio mixed diethylenetriamine (dien) complex including hydroxide anion, [Hg(dien)(OH)]$^+$.[14] The equilibrium constant (5.0×10^7) reported for the following reaction shows that the Hg(II)-dien complex can exist in the form of

$$[Hg(dien)(OH)]^+ + H^+ \rightleftarrows [Hg(dien)]^{2+}$$

$[Hg(dien)(OH)]^+$ only at pH's higher than 9. Thus, all the above facts lead us to choose the formation of a $HgH_{-1}L^+$ complex in which the amide group of dioxo[16]aneN$_5$ undergoes deprotonation. All the

polarographic and pH-metric behaviors of L^5, L^6, L^7, and L^8 were the same as those of the dioxo[16]aneN$_5$ system. Hence, an identical treatment of the experimental data was applied.

In the case of monooxo[16]aneN$_5$ (L^1) plots of anti-log $(\Delta E_{1/2}/0.0296+\log K_{HgY}-\log(\alpha_H)_Y+\log(\alpha_H)_L]$ against $[H^+]^{-1}$ gave a straight line with an intercept of finite value (Fig. 5). If only the $HgH_{-1}L^+$ complex is formed, the above plots should give a straight line which passes through the origin. Hence, the above linear relationship evidently indicates that under the present experimental conditions the monooxo-[16]aneN$_5$ ligand can form HgL^{2+} as well as $HgH_{-1}L^+$ as in the Reaction 6.

$$Hg+H_iL^{i+} \rightleftarrows \begin{cases} HgL^{2+}+iH^++2e^- \\ HgH_{-1}L^++(i+1)\cdot H^++2e^- \end{cases} \quad (6)$$

Thus the half-wave potential for the above electrode reaction should be given by Eq. 7. The product $K_{HgL}\cdot K^{-H}$ in Eq. 7 corresponds to $K_{HgH_{-1}L}$. From the

$$(E_{1/2})_L=\varepsilon^0_{Hg}+0.0296[\log f_{Hg^{2+}}-\log K_{HgL}\cdot(1+K^{-H}\cdot[H^+]) +\log(\alpha_H)_L+\log(k_L/k_{HgL})] \quad (7)$$

intercept and the slope of the straight line in Fig. 5,

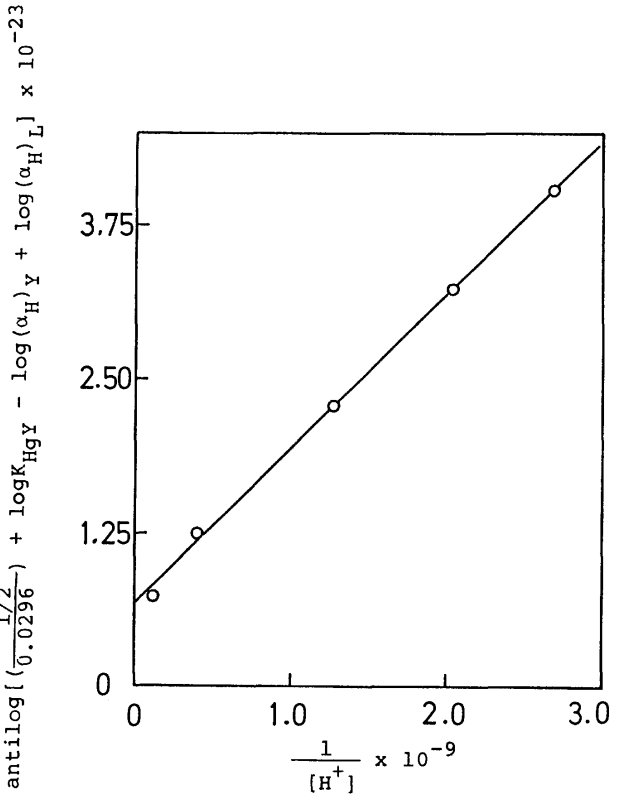

Fig. 5. Plots of antilog $[(\Delta E_{1/2}/0.0296)+\log K_{HgY}-\log(\alpha_H)_Y+\log(\alpha_H)_L]$ against $1/[H^+]$. [monooxo[16]aneN$_5$]=0.40 mM, Tris. or borate buffer 0.060 M, 9.75>pH>8.00, I=0.20 M, 25 °C.

K_{HgL}(=$[HgL^{2+}]/[Hg^{2+}][L]$) and $K_{HgH_{-1}L}$ values were determined to be 6.7×10^{22} and $1.2_6\times10^{14}$ respectively.

At pH's lower than 7.0 the anodic wave due to the uncomplexed dioxo macrocyclic polyamine merges into the mercury oxidation wave (background) completely. For this reason, it is impossible to study the complexation reaction at pH's lower than 7.0 by employing the polarographic technique. Two 16-membered macrocyclic dioxotetramines, L^3 and L^4, gave no anodic wave, suggesting that these dioxotetramines do not form stable mercury(II) complexes under the present experimental conditions.

As shown by the $K_{HgH_{-1}L}$ values in Table 2, $HgH_{-1}L^+$ complex of L^1 is more stable than that of L^2. This may suggest that in the complexation with Hg(II) ion L^1 can afford one more amine nitrogen atom than L^2. The $K_{HgH_{-1}L}$ values also show that the mercury(II) complex of L^8 is less stable than that of L^2. This probably suggests that the 18-membered macrocyclic ring is too large to place firmly nitrogen donors including deprotonated amide nitrogen atom for the stable Hg(II)-nitrogen bond formation. All the above findings may imply that in the macromonocyclic dioxopolyamine system, the presence of more than three amine nitrogen donors and a sufficiently large macrocyclic cavity which fits the mercury(II) ion size are essential for the formation of stable $HgH_{-1}L^+$ complexes.

The dioxo[16]aneN$_5$ system with extra-planar benzyl and pyridyl substituents (L^6 and L^7) also yielded stable $HgH_{-1}L^+$ complexes (Table 2). The appended pyridyl donor stabilizes the mercury(II) complexes of dioxo ligands. The affinity enhancement found may be accounted for by the additional coordination of the pyridyl nitrogen donor to the mercury(II) ion.

Mercury(II) forms strong complexes with thiol groups of proteins.[15] Serum albumin readily reacts with mercury(II) ions, forming the dimer, HgL_2, in which Hg(II) is coordinated to the single thiol group

Table 2. Cumulative Formation Constants, $K_{HgH_{-1}L}$, of Hg(II)-Macrocyclic Dioxopolyamine Complexes

I=0.20 M, 25 °C

Ligand	$\log K^{a)}_{HgH_{-1}L}$	$\log K^{a)}_{HgL}$
monooxo[16]aneN$_5$(L^1)	14.10±0.15	22.82±0.22
dioxo[16]aneN$_5$(L^2)	10.14±0.10 (10.34±0.15)[b)]	—
dioxo[16]aneN$_4$(3,3,3,3)(L^3)	—	—
dioxo[16]aneN$_4$(3,2,5,2)(L^4)	—	—
dioxo[16]aneN$_4$S(L^5)	8.40±0.10	—
benzyl-dioxo[16]aneN$_5$(L^6)	10.03±0.10	—
pyr-dioxo[16]aneN$_5$(L^7)	11.46±0.10	—
dioxo[18]aneN$_6$(L^8)	9.64±0.10 (9.81±0.14)[b)]	—

a) At least three separate experiments were conducted for each system. b) Values determined potentiometrically.

of each protein molecule.[16] The Hg(II)-coordination of this group may also offer an explanation for its action as an enzyme inhibitor. We also studied the reaction of mercury(II) ion with dioxo[16]aneN$_4$S (L^5). As illustrated by the $K_{HgH_{-1}L}$ values in Table 2, the incorporation of a sulfur donor into the dioxo 16-membered macrocyclic frame, contrary to our expectation, gave no increase in the stability of Hg(II)-dioxo ligand complex. This trend was also true for the dioxo-free system.[17] The fact that the mercury(II) complex of dioxo[16]aneN$_4$S is thermodynamically less stable than that of dioxo[16]aneN$_5$ may be explained in terms of failure of the sulfur donor incorporated within the 16-membered cyclic frame to form a stable coordination bond with mercury(II) ion because of the cyclic nature of the ligand and of the larger sulfur donor size.

A typically soft metal ion, Cu(I), is reported to bind to the amide nitrogen atom of the peptide with the simultaneous dissociation of its proton.[18] Since the mercury(II) ion can form stronger complexes with peptides than Cu(I) ions, it is reasonable to believe that the mercury(II) ion may form such complexes with peptides. The present finding concerning the Hg(II)-macrocyclic dioxo ligand interaction lends strong support to the above argument. Though great care is required in drawing conclusion about the metal-protein interaction from the studies on the low-molecular weight system, the macrocyclic dioxo polyamines offer a useful model for the study of the metal-peptide interaction and thus, this is the first paper reporting the possibility of forming a mercury(II)-deprotonated amide nitrogen bond.

References

1) M. Kodama and E. Kimura, *J. Chem. Soc., Dalton Trans.*, **1981**, 694.
2) R. Machida, E. Kimura, and M. Kodama, *Inorg. Chem.*, **22**, 2055 (1983).
3) E. Kimura, R. Machida, and M. Kodama, *J. Am. Chem. Soc.*, **106**, 5497 (1984).
4) Unpublished results.
5) I. Tabushi, H. Okino, and Y. Kuroda, *Tetrahedron Lett.*, **1976**, 4439; H. Kato, Doctoral Thesis, Department of Pharmaceutical Sciences, Kushu University (1977).
6) I. M. Kolthoff and J. J. Lingane, "Polarography," Interscience, New York (1952), Vol. 1, p. 297.
7) M. Kodama and E. Kimura, *J. Chem. Soc., Dalton Trans.*, **1976**, 2335.
8) M. Kodama and E. Kimura, *J. Chem. Soc., Dalton Trans.*, **1978**, 1081.
9) M. Senda, M. Senda, and I. Tachi, *J. Electrochem. Soc., Jpn.*, **27**, 83 (1959).
10) M. Kodama and A. Kimura, *Bull. Chem. Soc. Jpn.*, **40**, 1639 (1967).
11) C. N. Reilley, W. G. Scribner, and C. Temple, *Anal. Chem.*, **28**, 450 (1956).
12) J. N. Butler, "Ionic Equilibrium," Addison-Wesley, Reading, Massachusetts (1964), p. 437.
13) M. Kodama and E. Kimura, *J. Chem. Soc., Dalton Trans.*, **1979**, 325.
14) J. E. Pure and G. Schwarzenbach, *Helv. Chim. Acta*, **53**, 985 (1950).
15) L. G. Sillen and A. E. Martell, "Stability Constants," 2nd ed., Chem. Soc. Spec. Publ. No. 17 (1964); Suppl. No. 1, Chem. Soc. Spec. Publ. No. 25 (1971).
16) W. L. Hughes, Jr., *Cold Spr. Harb. Symposium Quant. Biol.*, **14**, 79 (1950).
17) M. Kodama, T. Koike, N. Hoshiga, R. Machida, and E. Kimura, *J. Chem. Soc., Dalton Trans.*, **1984**, 673.
18) R. Osterberg, *Eur. J. Biochem.*, **13**, 493 (1970).

Association of Some Polynuclear Aromatic Hydrocarbons with Cyclodextrins in Aqueous Medium

Isao SANEMASA,* Tatsuyoshi TAKUMA, and Toshio DEGUCHI
Department of Chemistry, Faculty of Science, Kumamoto University, Kurokami 2-39-1, Kumamoto 860
(Received April 12, 1989)

Complex formation using cyclodextrins (CyDs) as hosts and anthracene, phenanthrene, and naphthacene as guests has been studied in aqueous medium at 25 °C by measuring the guest volatilization rate. The results obtained are compared with those previously determined for benzene and naphthalene. Factors governing the host-guest association are discussed based on the dehydration energy of the guest derived from the Henry's law constant. It was suggested that van der Waals force is the main factor to stabilize the polynuclear aromatic hydrocarbons in the CyD cavity and that the contribution of hydrophobic interaction is less important. The additional van der Waals stabilization does not work fully for naphthacene of the longest molecular axis among the guests studied.

Cyclodextrins (CyDs) consist of glucopyranose units, forming cyclic oligosaccharides with different cavity size: α-, β-, and γ-CyD composed of 6, 7, and 8 units has the cavity diameter, 4.5—6.0, 6.0—8.0, and 8.0—10.0 Å, respectively. The interior of cavity is thought to be of hydrophobic environment, and, in aqueous medium, a wide variety of substances can be included therein as guests, if they are more or less hydrophobic in nature.[1]

In order to elucidate the CyD-guest binding forces and the complex formation process, many investigations have been made using hydrocarbons with polar derivatives.[2-5] In such studies, the use of hydrophobic guest substances without any polar group is desirable, because the presence of polar group in the guest molecule makes the contribution of hydrophobic effect uncertain.

Hydrophobic substances are in general only sparingly soluble in water and, moreover, some are volatile, so that it is difficult to use these solutes as guests. We have recently proposed a method that can be applied to such guests. The method is based on the facts that the guest molecules can be driven out to gaseous phase by introducing an inert gas at a constant flow rate into the aqueous solution and that the volatilization rate of guest decreases with increasing association with the host in aqueous medium. This method is applicable to such a system that the host-guest association rate is rapid compared with the guest volatilization rate. We have applied this method to benzene and alkylbenzenes,[6] and naphthalene and its methyl derivatives.[7] The host-guest spatial fitting was discussed on the basis of their association constants determined.

The present work is concerned with a further application of the method to such guests as anthracene, phenanthrene, and naphthacene. By combining the present results with the previous ones on benzene and naphthalene, we will get a better insight into the inclusion mechanism for polynuclear aromatic hydrocarbons.

Experimental

Materials and Preparation of Sample Solutions. Distilled deionized water was used throughout the experiments. Anthracene (Wako Pure Chemicals Co.), phenanthrene (Kodak Co.), and naphthacene (Tokyo Kasei Co.) as guests and cyclodextrins (α-, β-, and γ-CyD, Nakarai Chemical Co.) as hosts were of analytical reagent grade and used as received. An aqueous stock solution of each guest was prepared by adding an excess of each solid hydrocarbon to water and stirring for at least 24 h in the dark. After standing the mixture for at least 24 h, a portion of the saturated guest solution was transferred to a separatory funnel and the fluorescence of its chloroform extract was measured to determine the guest concentration using the following wavelengths: emission; 383, 367, and 479.1 nm, excitation; 260, 260, and 446.7 nm, for anthracene, phenanthrene, and naphthacene, respectively. Another portion of anthracene or phenanthrene aqueous solution was transferred to a 2.5 ϕ×25 cm cylindrical glass tube. A suitable amount of CyD, which had been dried over phosphorus pentaoxide under vacuum, was weighed and dissolved into the guest solution, and then the solution was diluted to 50

Table 1. The 1 : 1 (Host : Guest) Formation Constants at 25 °C[a]

	Concentration of CyD	Fraction(%) of guest	Formation constant
	10^{-2}mol dm^{-3}	volatilized	dm^3 mol^{-1}
Anthracene			
α-CyD	0.808—4.00	43	40±20
β-CyD	0.151—0.602	18	(2.3±0.2)×10^3
γ-CyD	1.50 —4.50	9	(1.5±0.2)×10^3
Phenanthrene			
α-CyD	1.82 —9.00	47	16±5
β-CyD	0.193—0.934	15	(1.5±0.3)×10^3
γ-CyD	0.800—3.20	8	(7.7±0.1)×10^2
Naphthacene			
β-CyD	0.100	3	3.4×10^3
γ-CyD	0.120	7	1.7×10^3

a) The concentration ranges of guest are, (5.00—17.8)×10^{-8} for anthracene, (5.7—19.1)×10^{-7} for phenanthrene, and (4.6—9.6)×10^{-9} for naphthacene, in mol dm^{-3}.

cm^3 with water. In the case of naphthacene, a 450 cm^3 portion of the guest aqueous solution was transferred to a round-bottom flask of 1 dm^3 capacity and diluted with water to 500 cm^3 after addition of CyD. The host and guest concentration ranges are given in Table 1.

Amberlite XAD-2 resin (Rohm and Hass) of 80—150 mesh size was used as an adsorbent of guest vapor.

Apparatus and Procedures. The apparatus and the experimental procedure were the same as those described in the previous paper.[7] Nitrogen gas was blown at a constant flow rate of 600 $cm^3 min^{-1}$ into the aqueous guest solution placed with or without CyD in the cylindrical glass tube or the round-bottom flask immersed in a bath thermostated at 25.0±0.1 °C. The N_2 gas leaving the sample solution was passed through a glass column of 0.5 ϕ×23 cm filled with XAD resin beads of 8 cm in length and the guest adsorbed on the resin within a fixed time was eluted out with $CHCl_3$ of 4 cm^3, and the amount of guest, ΔQ_ϕ, was determined by fluorescence measurement.

Results

Under the present experimental conditions that host molecules are always excess over guest molecules, the possible host:guest stoichiometric ratios are assumed to be 1 : 1 and 2 : 1. Then, the reactions that should be taken into account are:

$$\mathrm{CyD}+\phi \rightleftarrows \mathrm{CyD}\cdot\phi,\ K_1, \quad (1)$$

$$\mathrm{CyD}\cdot\phi+\mathrm{CyD} \rightleftarrows \mathrm{CyD_2}\cdot\phi,\ K_2, \quad (2)$$

and

$$\phi(\mathrm{aq}) \rightarrow \phi(\mathrm{gas}),\ k, \quad (3)$$

where ϕ refers to a guest molecule, K_1 and K_2 are the corresponding stepwise association constants, and k is the rate constant for the transfer of guest molecules from aqueous to gaseous phase.

We assume that the release of guest molecules at a constant N_2 flow rate is of first-order with respect to the concentration of free species present at any time t in the solution as follows:

$$dQ_\phi V^{-1}/dt = k[\phi], \quad (4)$$

where V is the volume of aqueous solution.

An equation to estimate K_1 and K_2 can be derived using the total concentrations of host (C_{CyD}) and guest (C_ϕ) and the amount of guest released from aqueous solution during the aeration time (Q_ϕ, the sum of ΔQ_ϕ from time 0 to t), in the same way as described in the previous paper.[7]

$$\ln(C_\phi - Q_\phi V^{-1}) = -kt/(1+K_1C_{CyD}+K_1K_2C_{CyD}^2)+\ln C_\phi$$
$$= -k't+\ln C_\phi, \quad (5)$$

where

$$k' = k/(1+K_1C_{CyD}+K_1K_2C_{CyD}^2). \quad (6)$$

Rearrangement of Eq. 6 yields:

$$1/k' = K_1K_2C_{CyD}^2/k + K_1C_{CyD}/k + 1/k. \quad (7)$$

The plots according to Eq. 5 for anthracene-β-CyD are shown in Fig. 1. The plots give straight lines over the aeration time employed; the volatilization rates of guest molecules dealt with in this work are much slower than those previously studied,[6,7] and hence the fraction of the amount of guest released

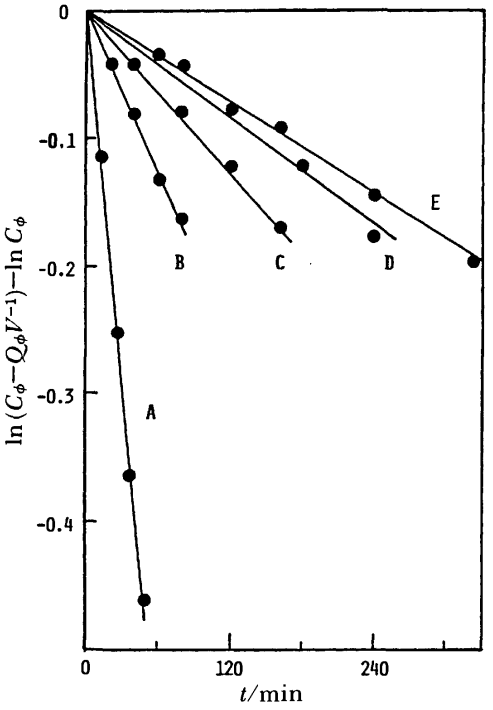

Fig. 1. Anthracene-β-CyD system. The plots of $\ln(C_\phi - Q_\phi V^{-1}) - \ln C_\phi$ vs. t with and without cyclodextrin. $C_{CyD}/10^{-3}$ mol dm^{-3}: (A) 0, (B) 1.51, (C) 3.01, (D) 4.49, (E) 6.02; C_ϕ: (5.00—17.8)×10^{-8} mol dm^{-3}.

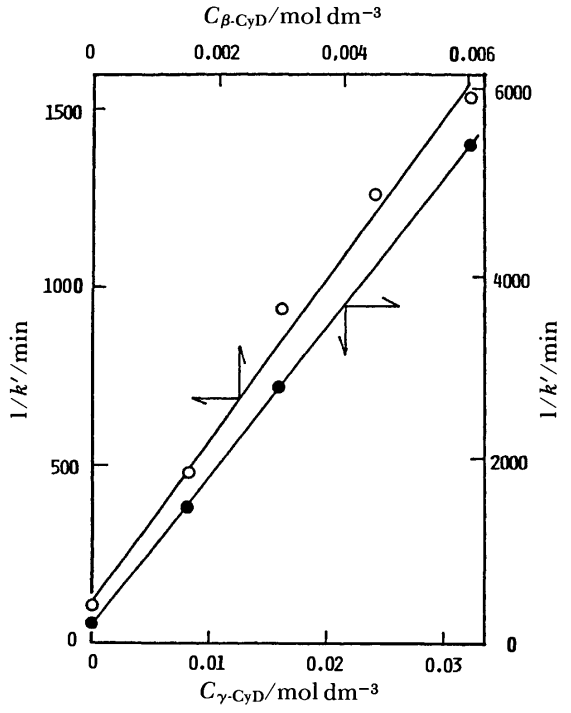

Fig. 2. The plots of $1/k'$ vs. C_{CyD}. Anthracene-β-CyD (○), phenanthrene-γ-CyD (●).

during the aeration is small (see Table 1). This linear relationship verifies the assumption that the volatilization of guest molecules follows a first-order reaction at a constant N_2 flow rate. Slopes of the resulting straight lines, k'(and k), were evaluated using the least-squares method. Typical $1/k'$ vs. C_{CyD} plots are shown in Fig. 2. The plots appeared to be linear for each host-guest combination studied; the K_2 can be neglected. In the case of naphthacene, measurements were made at a constant CyD concentration and the K_1 values were estimated from the average of three (for β-CyD) and two (for γ-CyD) runs. The K_1 values for this guest are, therefore, less reliable. The K_1 values determined in this work are summarized in Table 1. It should be noted that the K_1 values for α-CyD are less reliable because the difference between k and k' is small.

Discussion

Comparison of Association Constants with Literature Values. Vapor pressure,[8] fluorescence,[9-13] UV absorption,[14] and thin-layer chromatographic[15] methods have been used to evaluate CyD association constants with guests relevant to the present study. These are listed in Table 2. Our measurement provides reasonable values for benzene and naphthalene, while, for the other three guests, there is very large disagreement between ours and literature values. These differences probably arise from low solubility of guest substances in water. It is difficult to maintain the guest concentration in water constant owing to the adsorption of guest solute on the walls of glasswares including the cell.[16] Our method is suitable for these guests, because the accurate knowledge of the guest concentration in the aqueous medium is not essential, but what is required is the relative volatilization rate of the guest with and without CyD. While we have no criterion to judge which are more reliable, between ours and literature values, it seems to be helpful to clarify what factors govern the CyD-guest association.

The Inclusion Models. Since the cavity size of α-CyD is relatively small, a benzene ring associates only partly with the host. On the other hand, the other two hosts have sufficiently large cavity to accept linear-condensed benzene-ring compounds. Some water-soluble anthracene derivatives have been demonstrated to be accommodated in γ-CyD as dimer.[17] It seems probable, therefore, that γ-CyD with large internal cavity size includes two anthracene molecules. In this work, however, we have analyzed γ-CyD-anthracene system as a 1 : 1 complex according to the preceding stoichiometric study.[18] We simply postulate that naphthalene, anthracene, phenanthrene, and naphthacene are all axially included in β- and γ-CyD cavities. Inclusion models for anthracene are depicted in Fig. 3.

Factors Governing the Stability of Inclusion Complex. Hydrogen bonding, van der Waals forces, and hydrophobic interaction are generally accepted to be responsible for bonding of guest molecules to CyD

Table 2. Association Constants of 1 : 1 (Host : Guest) Complexation at 25 °C, Comparison with Those in Literatures

Guest-Host	Association constant/dm³ mol⁻¹	
	Our studies	Literature
Benzene-α-CyD	17[6]	31.6[8]
-β-CyD	1.2×10^2[6]	169,[8] 196[9]
-γ-CyD	12[6]	9.1[8]
Naphthalene-α-CyD	83[7]	
-β-CyD	6.3×10^2[7]	685,[10] 730,[11] 850,[12] 186[14]
-γ-CyD	1.3×10^2[7]	
Anthracene-β-CyD	2.3×10^3	420,[14] 32.39[15]
-γ-CyD	1.5×10^3	9.41[15]
Phenanthrene-β-CyD	1.5×10^3	170[13]
Naphthacene-β-CyD	3.4×10^3	221[14]

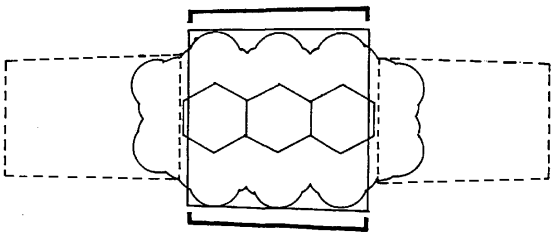

Fig. 3. Anthracene-CyD inclusion model. α-, β-, and γ-cyclodextrin cavities are drawn by dotted, thin solid, and thick solid lines, respectively.

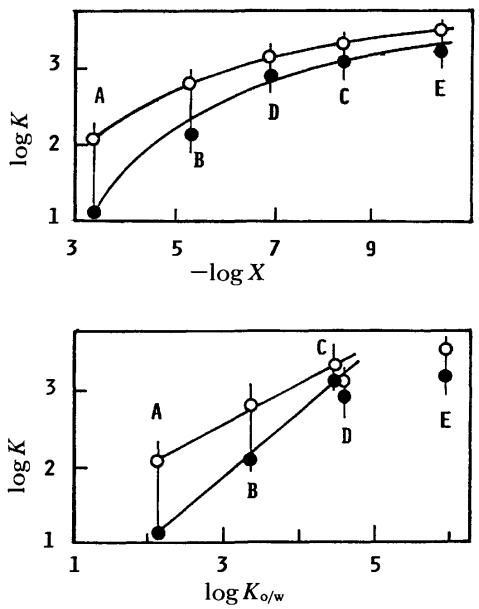

Fig. 4. The dependence of association constant (K) on the mole fraction solubility (X) of guest substance in water (upper), on the partition coefficient ($K_{o/w}$) of guest in 1-octanol/water (lower). Guest: benzene (A), naphthalene (B), anthracene (C), phenanthrene (D), naphthacene (E); β-CyD(○), γ-CyD (●).

cavity. The first one can be excluded in the present case because the guests under consideration have no ability to form hydrogen-bond with CyDs. Hydrophobic interaction has been thought to occur in an aqueous environment between the CyD interior wall and the guest molecule which has lower affinity with water.

It is a problem what should be chosen for an indication of guest hydrophobicity. For some homologous guest series, their solubility in water or their partition coefficient between 1-octanol (or chloroform) and water has been used as a measure of hydrophobicity: logarithmic values vs. $\log K$ plots give fairly good linear relationships.[19-21] Such plots are shown in Fig. 4, from which we can see that the association constant, K, increases with decreasing guest solubility in water or increasing partition coefficient in 1-octanol/water, $K_{o/w}$. A simple interpretation of the phenomena is that the more hydrophobic guest forms the more stable complex with CyD, but we need real reason.

Is a solute with lower solubility in water or larger $K_{o/w}$ value more hydrophobic? The partition coefficient is defined as the ratio of solute concentration in organic solvent to that in water at equilibrium. This coefficient has been measured for a wide variety of chemicals to relate it theoretically to the solute aqueous solubility or to predict the distribution of hydrophobic pollutants in aquatic environments.[22,23] For instance, chemicals with a large partition coefficient are liable to be accumulated into fish body.[24] The partition coefficient is often taken as a measure of the hydrophobic character of a solute,[25] but in a strict sense it is a measure of the relative solubility of the solute in organic solvent and in water, that is, a relative affinity of the solute between surrounding organic and water molecules.

An image of the host-guest association process is that a guest molecule is transferred from water to the hydrophobic environment leaving behind a structured cavity which collapses and redistributes.[26] The free-energy change associated with this process can be easily evaluated, if the hydrophobic environment is substituted for the gaseous phase. Using the Henry's law constant, K_H, $\Delta G_{dehyd}=-RT \ln K_H$. The K_H value is estimated for each guest from its partial vapor pressure and the mole fraction solubility in water at 25 °C. The free-energy change in the 1 : 1 complex formation, $\Delta G_{complex}$ ($=-RT \ln K_1$), is plotted against ΔG_{dehyd} in Fig. 5; a dotted line indicates that $\Delta G_{complex}=\Delta G_{dehyd}$.

For volatile solutes, the most suitable parameter of the hydrophobicity is K_H, a measure of free-energy necessary to carry a solute from aqueous medium to gaseous phase. According to $-\Delta G_{dehyd}$ values, benzene is more hydrophobic than naphthalene, and the latter is more hydrophobic than anthracene. This statement may be strange from the fact that the solubility of naphthalene in water (2.35×10^{-4} M at 25 °C; 1M=1 mol dm^{-3}) is lower two orders of magnitude than that of benzene (2.07×10^{-2} M), and that the solubility of anthracene (2.5×10^{-7} M) is lower three orders of magnitude than that of naphthalene. Such differences in the solubility arise from the difference in the saturated vapor pressure of the solute. The vapor pressure of benzene (1.26×10^{4} Pa at 25 °C) is higher three orders of magnitude than that of naphthalene (10.98 Pa), and the vapor pressure of the latter is higher four orders of magnitude than that of anthracene (8.31×10^{-4} Pa). This is also the case for phenanthrene and anthracene. The former is a little more hydrophobic than the latter in spite of the former aqueous solubility being thirty times larger than the latter.

It can be seen from Fig. 5 that the guests except benzene have considerably larger $-\Delta G_{complex}$ than $-\Delta G_{dehyd}$. If we postulate that a guest molecule is fully embraced in the CyD cavity and that the environment around the guest is a gaseous phase, $-\Delta G_{dehyd}$ for the guest will contribute fully to the $-\Delta G_{complex}$, that is, $-\Delta G_{dehyd}$ estimated from K_H is to be taken as the upper limit of the hydrophobic contribution.

For the guest substances studied here, hydrophobic interaction as a driving force of CyD complexation is not significant, because $-\Delta G_{complex}$ does not increase with $-\Delta G_{dehyd}$. It is van der Waals force that plays the major role to stabilize the complex for the guest of large size. The plots of $\log K$ vs. the total surface area of associating guest are shown in Fig. 6. Nearly

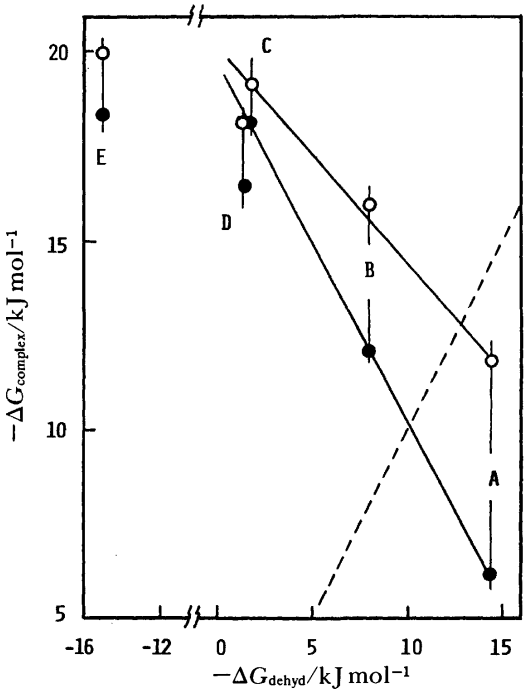

Fig. 5. Free energy changes of CyD-guest complexation and dehydration of guest. Signs and symbols are the same as those shown in Fig. 4.

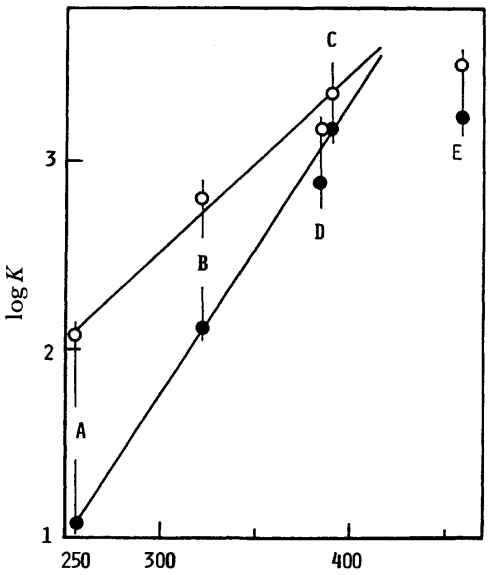

Fig. 6. The dependence of association constant on the surface area of guest molecule. The signs and symbols are the same as those shown in Fig. 4. Values of surface area are taken from Ref. 27.

linear relationships can be seen for β- and γ-CyD except phenanthrene and naphthacene. The increase in the axial length of guest molecule increases the host-guest contact area, leading to the increase in net stabilization. For naphthacene, however, the additional stabilization does not serve to any significant extent, probably because a considerable part of the molecule protrudes out of the CyD cavity. Anthracene and phenanthrene have approximately the same surface area, but the latter forms less stable complexes with CyDs. The reason cannot be fully given at present. Less favorable contact of phenanthrene to the CyD cavity wall may be partially responsible.

The tendency that a guest with the large partition coefficient forms more stable complex with CyD has been observed for guests of homologous series. The tendency is not due to the guest hydrophobicity, but due to the relative strength of guest-water and guest-organic solvent interactions. Intermolecular forces acting between the solute (or guest) and the surrounding solvent molecules (or CyD cavity wall) are similar in its character to each other, that is, the van der Waals forces.

References

1) W. Saenger, *Angew. Chem., Int. Ed. Engl.*, **19**, 344 (1980).
2) H. Schlenk and D. M. Sand, *J. Am. Chem. Soc.*, **83**, 2312 (1961).
3) F. Cramer, W. Saenger, and H.-Ch. Spatz, *J. Am. Chem. Soc.*, **89**, 14 (1967).
4) E. A. Lewis and L. D. Hansen, *J. Chem. Soc., Perkin Trans. 2*, **1973**, 2081.
5) R. I. Gelb. L. M. Schwartz, B. Cardelino, H. S. Fuhrman, R. F. Johnson, and D. A. Laufer, *J. Am. Chem. Soc.*, **103**, 1750 (1981).
6) I. Sanemasa and Y. Akamine, *Bull. Chem. Soc. Jpn.*, **60**, 2059 (1987).
7) M. Fujiki, T. Deguchi, and I. Sanemasa, *Bull. Chem. Soc. Jpn.*, **61**, 1163 (1988).
8) E. E. Tucker and S. D. Christian, *J. Am. Chem. Soc.*, **106**, 1942 (1984).
9) M. Hoshino, M. Imamura, K. Ikehara, and T. Hama, *J. Phys. Chem.*, **85**, 1820 (1981).
10) S. Hamai, *Bull. Chem. Soc. Jpn.*, **55**, 2721 (1982).
11) K. Kano, B. Zhou, M. Sakaguchi, H. Matsumoto, and S. Hashimoto, *Sci. Eng. Rev. Doshisha Univ.*, **25**, 253 (1985).
12) S. Hashimoto and J. K. Thomas, *J. Am. Chem. Soc.*, **107**, 4655 (1985).
13) F. J. Alonso, A. Heredia, and J. C. Marquez, *J. Molec. Struc.*, **143**, 399 (1986).
14) N. Kobayashi, S. Minato, and T. Osa, *Makromol. Chem.*, **184**, 2123 (1983).
15) T. Vo-Dinh and A. Alak, *Appl. Spectrosc.*, **41**, 963 (1987).
16) A. Nakajima, *Spectrochim. Acta, Part A*, **39**, 913 (1983).
17) T. Tamaki, T. Kokubu, and K. Ichimura, *Tetrahedron*, **43**, 1485 (1987).
18) F. Cramer and F. M. Henglein, *Chem. Ber.*, **90**, 2561 (1957).
19) K. A. Connors and D. D. Pendergast, *J. Am. Chem. Soc.*, **106**, 7607 (1984).
20) K. A. Connors, A. Paulson, and D. Toledo-Velasquez, *J. Org. Chem.*, **53**, 2023 (1988).
21) K. Uekama, M. Otagiri, Y. Kanie, S. Tanaka, and K. Ikeda, *Chem. Pharm. Bull.*, **23**, 1421 (1975).
22) S. H. Yalkowsky and S. C. Valvani, *J. Chem. Eng. Data*, **24**, 127 (1979).
23) M. M. Miller, S. P. Wasik, G. -L. Huang, W. -Y. Shiu, and D. Mackay, *Environ. Sci. Technol.*, **19**, 522 (1985).
24) A. Opperhuizen, P. Serné, and J. M. D. Van der Steen, *Environ. Sci. Technol.*, **22**, 286 (1988).
25) F. Gago, J. Alvarez-Builla, J. Elguero, and J. C. Diez-Masa, *Anal. Chem.*, **59**, 921 (1987).
26) I. Tabushi, Y. Kiyosuke, T. Sugimoto, and K. Yamamura, *J. Am. Chem. Soc.*, **100**, 916 (1978).
27) G. L. Amidon and S. T. Anik, *J. Chem. Eng. Data*, **26**, 28 (1981).

 © 1989 The Chemical Society of Japan Bull. Chem. Soc. Jpn., 62, 3103—3108 (1989)

Peptide Synthesis in Aqueous Solution. IV. Preparation and Properties of [*p*-(Benzyloxycarbonyloxy)phenyl]dimethylsulfonium Methyl Sulfate (Z-ODSP), [*p*-(*t*-Butoxycarbonyloxy)phenyl]dimethylsulfonium Methyl Sulfate (Boc-ODSP) and [*p*-(9-Fluorenylmethyloxycarbonyloxy)phenyl]dimethylsulfonium Methyl Sulfate (Fmoc-ODSP) as Water-Soluble *N*-Acylating Reagents†

Ikunori Azuse, Masahiro Tamura, Keisuke Kinomura, Hideo Okai,* Katsushige Kouge,†† Fumio Hamatsu,†† and Tatsuya Koizumi††
Department of Fermentation Technology, Faculty of Engineering, Hiroshima University, Shitami, Saijo-cho, Higashihiroshima 724
††Sanshin Chemical Industrial Co. Ltd., 531, Nagahama, Hirao-cho, Kumage-gun, Yamaguchi 742-11
(Received January 13, 1989)

In order to increase the applications of the water-soluble active ester method, water-soluble acylating reagents, [*p*-(benzyloxycarbonyloxy)phenyl]dimethylsulfonium methyl sulfate, [*p*-(*t*-butoxycarbonyloxy)-phenyl]dimethylsulfonium methyl sulfate and [*p*-(9-fluorenylmethyloxycarbonyloxy)phenyl]dimethyl-sulfonium methyl sulfate, were synthesized from of *p*-hydroxyphenyldimethylsulfonium methyl sulfate. These compounds had high solubility (more than 30%) in water and were found to act as excellent water-soluble acylating reagents for the synthesis of *N*-benzyloxycarbonyl, *N*-*t*-butoxycarbonyl, *N*-9-fluorenylmethyl-oxycarbonyl amino acid derivatives in aqueous solution. They converted dipeptides to *N*-acyl-dipeptides in aqueous media as well as amino acids. In addition, they were found to be efficient reagents for protecting the side chains of lysine, ornithine, and cysteine.

In 1987, we reported that *p*-hydroxyphenyldi-methylsulfonium methyl sulfate (HODSP) was found to be an excellent reagent for peptide synthesis in aqueous solution.[1] We also pointed out that HODSP has a high reactivity, as the same as that of conventional active ester reagents, such as *p*-nitrophenol or *N*-hydroxysuccinimide. By carrying out peptide synthesis in aqueous solution we can strictly control the pH during the reaction. This means that arginine residue, which has a guanide group in the side chain, can be treated while unprotected. By employing the HODSP active ester method, FMRFamide (Phe-Met-Arg-Phe-NH_2), a molluscan neuropeptide from the ganglia of the clam *Macrocallisa nimbosa*,[2] was synthesized.[3] The water-soluble active ester method is an ideal method for both Arg- and Met-containing peptide, such as FMRFamide. The peptide can be prepared without hydrogenation or HF deprotection, which is known to sometime severely damage the peptide during the final step. We prepared several FMRFamide analogs by using this water-soluble active ester method as well as naturally occurring FMRFamide.[4]

After we established peptide synthesis using water-soluble active ester, we then set out to develop new types of water-soluble acylating reagents. We selected three amino protecting groups (benzyl-oxycarbonyl-, *t*-butoxycarbonyl, and 9-fluorenyl-methyloxycarbonyl groups) which are widely used in peptide synthesis; their deprotecting conditions are all different. [*p*-(Benzyloxycarbonyloxy)phenyl]dimethyl-sulfonium methyl sulfate (**1**), [*p*-(*t*-butoxycarbonyloxy)-phenyl]dimethylsulfonium methyl sulfate (**2**), and [*p*-(9-fluorenylmethyloxycarbonyloxy)phenyl]dimethyl-sulfonium methyl sulfate (**3**) were prepared and practically allowed to react with amino acids in aqueous media. Furthermore, we applied these water-soluble acylating reagents to the selective side-chain protection of amino acids (lysine, ornithine, and cysteine). In this paper we discuss the utility and applicability of water-soluble acylating reagents in peptide synthesis.

† This is one part of studies on the water-soluble active ester method for peptide synthesis. The previous studies (part I, II, and III) appeared in this journal. See Refs. 1, 3, and 4.

Results and Discussion

Preparation of [*p*-Benzyloxycarbonyloxy)phenyl]dimethylsulfonium Methyl Sulfate (1), [*p*-(*t*-Butoxycarbonyloxy)phenyl]dimethylsulfonium Methyl Sulfate (2), and [*p*-(9-Fluorenylmethyloxycarbonyloxy)-phenyl]dimethylsulfonium Methyl Sulfate (3). Compounds **1**, **2**, and **3** were all easily synthesized from the reaction of HODSP with benzyloxycarbonyl chloride, di-*t*-butyl dicarbonate, and 9-fluorenylmethyloxy-carbonyl chloride, respectively, in CH_3CN. These compounds were stable and did not undergo decomposition when stored below 10 °C. Compounds **1**, **2**, and **3** were soluble in water (solubility:>30 wt%) and very soluble in DMF, alcohol, CH_3CN, and $CHCl_3$.

Preparation of Benzyloxycarbonyl, *t*-Butoxycarbonyl, 9-Fluorenylmethyloxycarbonyl Amino Acids Derivatives. In order to establish optimal conditions for the reaction between amino acids and **1**, **2**, or **3** in aqueous solution, the effect of five bases (NaOH, Na_2CO_3,

$NaHCO_3$, triethylamine, and pyridine) in acylation of alanine were first studied. It was found that all, except pyridine, promoted the reaction and sodium hydroxide and triethylamine gave the highest yield (83%) of *N*-(benzyloxycarbonyl)-L-alanine.

The reaction rate of **1** and **2** with glycine in aqueous solution at pH 7—10 was measured by HPLC. The rate of **1** and **2** with glycine in several concentrations was also measured. It was found that **1** and **2** gave Z-Gly and Boc-Gly in highest yield when they were treated at a pH concentration greater than 10 and 0.25 M (1 M=1 mol dm^{-3}), respectively. The benzyloxycarbonylation of glycine with **1** (0.25 M) came to completion within 2 h at pH 8. In the case of **2**, the reaction was over within 2 h at pH 10. These results showed that the standard conditions for the reaction involve using triethylamine as a base in aqueous solution at a pH and concentration greater than 10 and 0.25 M, respectively, at room temperature. The yield of *N*-acyl amino acid derivatives, prepared in aqueous solution, are shown in Tables 1, 2, and 3. *N*-Acyl amino acid derivatives were obtained in good yields from **1**, **2**, and **3** only in aqueous media. Even if an aqueous-acetonitrile system was employed for the solvent, the yields of *N*-aryl amino acid derivatives were still good. This result definitely shows that these water-soluble acylating reagents could be used as well as conventional *N*-acylating reagents. It is another merit of water-soluble acylating reagents that the unreacted reagents and HODSP, which forms during the reaction as a by-product, can easily be removed because of their high solubility in water.

We studied a possible side reaction, *N*-methylation, because HODSP has methyl sulfate as a counter anion. We collected some of the reaction mixture of the water-soluble acylating reagent and amino acid, and then carried out the deprotection procedure on that mixture; the resultant mixture was applied to HPLC. No *N*-methyl amino acid was found.

***N*-Acylation of Dipeptides in Aqueous Solution.** The active ester method is generally carried out under mild conditions rather than acid halides, acid anhy-

Table 1. Preparation of Z-Amino Acids in Aqueous Solution[a)]

Z-amino acids	Yield(%)	Mp/°C (lit)	$[\alpha]_D^{25}$ (*c*, solvent) (lit)	Ref.
Ala	83	84—86 (87)	−12.8° (*c* 2.0, AcOH) (−13.9°)	10
Arg(NO_2)	88	130—132 (132—134)	−3.0° (*c* 2.0, MeOH) (−3.5°)	11
Asp	85	115—116 (116)	+7.9° (*c* 7.0, AcOH) (+9.6°)	12
Asn	95	162—163 (165)	+7.3° (*c* 1.6, AcOH) (+7.6°)	13
Glu	82	118—121 (120—121)	−6.8° (*c* 10.0, AcOH) (−7.9°)	14
Gly	90	119—120 (120)	—	12
His	51	165—167 (166—167)	−23.0° (*c* 6.0, 6M HCl) (−25.0°)	15
Ile	85	42—45 (44—46)	+5.9° (*c* 6.0, EtOH) (+6.5°)	16
Leu[b)]	78	149—150 (151.5—152)	−7.3° (*c* 3.05, MeOH) (−7.86°)	17
Met	81	66—67 (68—69)	−14.3° (*c* 2.47, EtOH) (−16.6°)	18
Phe	91	87—89 (88—89)	+5.0° (*c* 2.0, AcOH) (+5.1°)	19
Pro	86	77—80 (77)	−59.0° (*c* 2.0, AcOH) (−60.5°)	19
Ser	85	119—122 (121)	+4.9° (*c* 6.0, AcOH) (+5.6°)	20
Thr	82	97—102 (101—102)	−5.0° (*c* 2.0, AcOH) (−5.6°)	21
Trp	71	123—128 (126)	+2.9° (*c* 1.0, AcOH)	22
Tyr	70	94—98 (101)	+9.7° (*c* 3.0, AcOH) (+11.1°)	12
Val	82	63—66 (66—67)	+0.1° (*c* 10.0, AcOH) (+0.1°)	19
Gly[c)]	88	119—120 (120)		12

a) The reactions were carried out using water as solvent and triethylamine as a base.
b) Dicyclohexylammonium salt. c) This reaction was carried out in water-acetonitrile.

Table 2. Preparation of Boc-Amino Acids in Aqueous Solution[a)]

Boc-amino acids	Yield (%)	Mp/°C (lit)	$[\alpha]_D^{25}$ (c, solvent) (lit)	Ref.
Ala	82	82—84 (83—84)	−1.5° (c 2.0, DMF) (−13.6°)	23
Arg(NO_2)	78	111—113 (111—114)	−4.8° (c 1.0, AcOH) (−6.2°)	24
Asp	75	110—116 (118—119)	−3.0° (c 1.0, DMF) (−3.9°)	25
Asn	70	179—183 (181—182)	−8.2° (c 1.0, AcOH) (−8.96°)	25
Glu	70	108—109 (110—112)	−16.0° (c 1.0, MeOH) (−16.1°)	26
Gly	90	88—89 (88.5—89)	—	26
Ile[b)]	80	47—55 (49—57)	+3.0° (c 2.0, AcOH) (+3.0°)	23
Leu	75	72—74 (70—74)	−27.0° (c 1.0, AcOH) (−27.0°)	27
Met[c)]	77	120—123	−0.99° (c 1.0, AcOH)	
Phe	84	84—87 (85—87)	−3.7° (c 1.0, AcOH) (−4.1°)	28
Pro	75	134—136 (136—137)	−57.2° (c 2.0, AcOH) (−59.5°)	23
Ser[c)]	74	143—144	−0.9° (c 1.0, AcOH)	
Thr[c)]	77	151—152	−3.0° (c 1.0, AcOH)	
Tyr[c)]	70	199—203 (205—208)	−5.5° (c 1.0, AcOH) (−6.3°)	29
Val[c)]	78	139—140 (140.5)	+0.01° (c 1.0, AcOH) (+0.01°)	30

a) The reactions were carried out using water as solvent and triethylamine as a base. b) Hemihydrate. c) Dicyclohexylammonium salt.

Table 3. Preparation of Fmoc-Amino Acids in Aqueous Solution[a)]

Fmoc-amino acids	Yield (%)	Mp/°C (lit)	$[\alpha]_D^{25}$ (c, solvent) (lit)	Ref.
Ala	86	141—143 (143—144)	−19.1° (c 1.0, DMF) (−18.6)	31
β-Ala	82	144—146 (145—147)		32
Gln	78	220—222 (221—223)	−18.4° (c 1.0, DMF) (−17.0°)	31
Gly	94	172—173 (173—174)		31
Leu	76	151—153 (153—154)	−26.1° (c 1.0, DMF) (−24.1°)	31
Met	80	127—131 (129—132)	−29.1° (c 1.0, DMF) (−28.3°)	31
Phe	83	180.5—183 (181—183)	−35.6° (c 1.0, DMF) (−37.6°)	31
Pro	85	112—113 (114—115)	−34.0° (c 1.0, DMF) (−33.4°)	31
Val	75	142—144 (143—144)	−17.0° (c 1.0, DMF) (−16.1°)	31
Gly[b)]	87	172—173 (173—174)		31

a) The reactions were carried out using water as solvent and triethylamine as a base. b) This reaction was carried out in water-acetonitrile.

drides or other condensing reagents. The water-soluble active ester can form an amide linkage under much milder conditions than other active esters. We can control the reactivity of the active ester by changing the pH.

N-Acylation of dipeptides in aqueous solution using **1**, **2**, or **3** were carried out. *N*-Acyl-dipeptides were obtained (Yield; Z-Phe-Gly-OH, 77%; Boc-Leu-

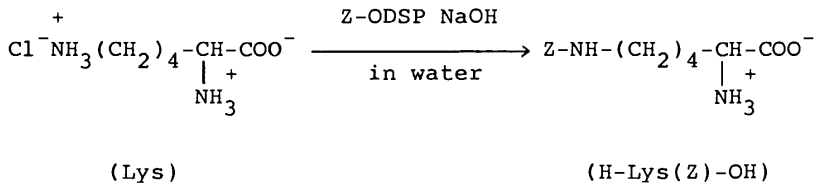

Scheme 1.

Val-OH, 70%; Fmoc-Gly-Gly-OH, 75%) in aqueous solution without any side reaction because the pH of these reaction mixtures was strictly controlled.

Selective Acylation of Amino Groups on the Side Chain of Lysine and Ornithine. The other merit of the reaction in water is that we could presume selective acylation of the amino group of side chains of lysine and ornithine. Compound **1** was allowed to react with lysine by controlling the pH of the reaction mixture automatically. The synthetic route of N^{ε}-(benzyloxycarbonyl)-L-lysine (H-Lys(Z)-OH) is shown in Scheme 1. We studied the yield of H-Lys(Z)-OH and Z-Lys(Z)-OH by changing the pH of the reaction. The amino group on the side chain of lysine was selectively benzyloxycarbonylated and H-Lys(Z)-OH was obtained only during one step by strictly controlling the pH of the reaction mixture. A small amount of Z-Lys(Z)-OH, which was produced at the same time, was easily washed out with ethyl acetate. Lysine was also treated with two equivalents of **1**. We recognized a selective formation of H-Lys(Z)-OH at pH 8 and 9. The highest yield of H-Lys(Z)-OH was obtained at pH 11.5 (63.6%); that condition kept the yield of Z-Lys(Z)-OH, a by-product, below 5.4%. The reaction with Z-OSu (dioxane-water as a solvent), which is a commercial benzyloxycarbonylating reagent, was then studied. A selective aminolysis reaction was not observed since the reaction requires organic solvents and the pH of the reaction mixture can not be accurately controlled.

Ornithine was treated with **1** under the same conditions. The same principle can also be applied to the selective benzyloxycarbonylation of the ω-amino group of ornithine. In the case of the reaction in two equal quantities of **1**, we recognized a selective benzyloxycarbonylation of δ-amino group as well as lysine. Presently, the synthetic route of H-Lys(Z)-(OH) or H-Orn(Z)-OH is first to form a Cu(II) complex of lysine or ornithine; they are then allowed to react with benzyloxycarbonyl chloride.[5-9] The Cu(II) complex is removed by hydrogen sulfide. This procedure requires three steps and decreases the yield of the product. By using of this water-soluble acylating reagent, H-Lys(Z)-OH or H-Orn(Z)-OH can be prepared in one step.

Preparation of *S*-(Benzyloxycarbonyl)-L-cysteine. The mercapto group in cysteine is too reactive to be left unprotected, since it is a stronger nucleophilic group than the amino group and is easily converted to disulfides by air oxidation as well. We investigated the reactivity of the mercapto group of cysteine at various pH's in aqueous media using **1**. *S*-(Benzyloxycarbonyl)-L-cysteine was obtained in one step at pH 6.0 or 6.5 (61%), as well as the case of selective acylation of lysine and ornithine, which have amino groups in their side chains.

We dealt with three typical *N*-protecting groups in peptide synthesis. We also showed that the introduction of those groups using the water-soluble active ester could be carried out successfully. It is clear that the water-soluble active ester method can be applied to other urethane-type amino-protecting groups. Additionally, side-chain-protected amino acids, such as H-Lys(Z)-OH, H-Orn(Z)-OH, and H-Cys(Z)-OH were prepared using the water-soluble active esters very easily. We believe that the water-soluble acylating reagent will also be a powerful tool for the chemical modification of proteins in aqueous solution without causing any conformational changing. We plan to show this elsewhere shortly.

Experimental

All melting points were uncorrected. IR spectra were recorded on a Hitachi 269-30 infrared spectrometer. NMR spectra were measured on a Hitachi R-24B (60 MHz) spectrometer. The chemical shifts are given in δ scale with tetramethylsilane as an internal standard. Amino acid analysis and detection of substances were performed by means of HPLC using JASCO TRI ROTER-V and UNIDEC-100V apparatus.

Synthesis of Z-ODSP(1), Boc-ODSP(2), and Fmoc-ODSP (3). HODSP (13.3 g, 50 mmol) was dissolved in CH_3CN (200 ml), and Et_3N (7.0 ml, 50 mmol) was added to the solution below 5 °C with stirring. After 10 min, Z-Cl, $(Boc)_2O$, or Fmoc-Cl (50 mmol) was added. The reaction mixture was stirred below 5 °C for 2—5 h and then the precipitated triethylammonium chloride or unreacted reagents was removed from the reaction mixture by filtration. The filter cake washed with CH_3CN, and combined filtrates were concentrated in vacuo to give products as crystalline solid, which was readily recrystallized from ethyl acetate.

Z-ODSP (1). Yield 90.0%; mp 78—80 °C. IR data ν_{max}^{KBr} 1760 cm^{-1} (ester C=O). ^1H NMR data (DMSO-d_6); δ=3.30 (s, 6H, $-S^+(CH_3)_2$), 3.42 (s, 3H, $CH_3SO_4^-$), 5.35 (s, 2H, benzyl CH_2), 7.41 (2.5H, C_6H_5), 7.92 (dd, 4H, J_1=31 Hz, J_2=6 Hz, $-O-C_6H_4-S<$). Found: C, 51.42; H, 4.58%. Calcd for $C_{17}H_{20}O_7S_2$: C, 51.51; H, 4.99%.

Boc-ODSP (2). Yield 80.0%; mp 118.5—121 °C. IR data ν_{max}^{KBr} 1760 cm^{-1} (ester C=O). ^1H NMR (DMSO-d_6); δ= 1.50 (s, 9H, *t*-butyl), 3.30 (s, 3H, $CH_3SO_4^-$), 3.40 (s, 6H,

$-S^+-(CH_3)_2$), 7.85 (dd, 4H, J_1=33 Hz, J_2=8 Hz, $-O-C_6H_4-S<$). Found: C, 45.78; H, 6.31%. Calcd for $C_{14}H_{22}O_7S_2$: C, 45.92; H, 6.00%.

Fmoc-ODSP (3). Yield 85.0%; mp 90.5—92 °C. IR data ν_{max}^{KBr} 1760 cm^{-1} ster C=O). ^1H NMR ($CDCl_3$); δ=3.41 (s, 6H, $-S^+(CH_3)_2$), 3.68 (s, 3H, $CH_3SO_4^-$), 4.30 (t, 1H, J=7 Hz, $>CH-CH_2-OCO_2-$), 4.54 (d, 2H, J=7 Hz, $>CH-CH_2-OCO_2-$), 7.24—7.81 (m, 10H, aromatic protons of Fmoc+right peaks of dd of $-O-C_6H_4-S<$), 8.15 (d, 2H, J=11 Hz, left peaks of dd of $-O-C_6H_4-S<$). Found: C, 60.96; H, 5.07%. Calcd for $C_{24}H_{24}O_7S_2$: C, 61.02; H, 5.12%.

***N*-Benzyloxycarbonyl Amino Acids, *N*-*t*-Butoxycarbonyl Amino Acids and *N*-(9-Fluorenylmethyloxycarbonyl) Amino Acids (General Method).** L-Amino acid (10 mmol) and Et_3N (12 mmol) were dissolved in water (10 ml) and Z-ODSP, Boc-ODSP, or Fmoc-ODSP (12 mmol) was added to the solution at room temperature with stirring. After 8—24 h, 1 M HCl or 20% citric acid was added to the solution and the pH of the solution was adjusted to 3.0. In the case of Fmoc-amino acids, water was added to the reaction mixture, then extracted with ether; the aqueous phase was acidified with 1 M HCl. The mixture was extracted with ethyl acetate. The solution was washed with water and then dried over anhydrous sodium sulfate. The filtrate was concentrated in vacuo. The residue was recrystallized from the solvents indicated. Side chain amino acid derivatives were prepared using different procedures.

Synthesis of *N*-Acyl Dipeptides. Z-Phe-Gly-OH. H-Phe-Gly-OH (1.07 g, 3 mmol) was adjusted to 10.0 by 1 M NaOH. Z-ODSP (1.44 g, 3.3 mmol) was added to a stirring solution and the reaction mixture was acidified with 20% citric acid. The mixture was extracted with ethyl acetate. The solution was then washed with water and dried over anhydrous sodium sulfate. The solution was concentrated and crystallized from ether; Yield 77%; mp 158—160 °C [lit, 159—161 °C].[33] Prepared similarly were the following dipeptide derivatives:

Z-Ile-Phe-OH. Yield 72%; mp 174—176 °C [lit, 175—176 °C].[34]

Boc-Leu-Val-OH. Yield 70%; mp 108—110 °C [lit, 109—111 °C].[35]

Fmoc-Gly-Gly-OH. Yield 75%; mp 176—177 °C [lit, 176—177 °C].[32]

Preparation of H-Lys(Z)-OH and H-Orn(Z)-OH. Lys·HCl (1.83 g, 10 mmol) and 2 M NaOH (5 ml) were dissolved in water (50 ml) and the pH of the solution was adjusted to 11.3 by 1 M HCl. Z-ODSP (6.4 g, 16 mmol) was added to a stirring solution below 20 °C, the pH being automatically maintained at the starting pH with 2 M NaOH for 30 min. The precipitate was filtered and washed with water and ethanol. By a similar procedure, H-Orn(Z)-OH (at pH 11.5) was obtained.

H-Lys(Z)-OH. Yield 63.6%; mp 250—253 °C; $[\alpha]_D^{25}$ +16.0° (*c* 1.0, 6 M HCl). Found: C, 59.92; H, 7.12; N, 9.94%. Calcd for $C_{14}H_{20}N_2O_4$: C, 59.98; H, 7.19; N, 9.99%.

H-Orn(Z)-OH. Yield 80%; mp 254—255 °C; $[\alpha]_D^{25}$+17.3° (*c* 0.7, 6 M HCl). Found: C, 58.57; H, 6.84; N, 10.42%. Calcd for $C_{13}H_{18}N_2O_4$: C, 58.63; H, 6.81; N, 10.52%.

Preparation of H-Cys(Z)-OH. Cys·HCl (10 mmol) and Et_3N (1.4 ml) were dissolved in water (50 ml) and pH of the solution was adjusted to 6.0 by 1 M HCl. Z-ODSP (10 mmol) was added to a stirred solution below 20 °C, the pH being automatically maintained at the starting pH with 2 M NaOH for 5 h. The precipitate was filtered and washed with water and ethanol. Yield 61%, mp 162—164 °C, $[\alpha]_D^{25}$—122° (*c* 1.0, DMF). Found: C, 51.72; H, 5.15; N, 5.41%. Calcd for $C_{11}H_{13}NO_4S$: C, 51.75; H, 5.13; N, 5.49%.

Determination of the Rate of Aminolysis. pH Effect: Gly or Val (5 mmol) was dissolved in water (10 ml) and the pH of the solution was adjusted to 7—10 by 2 M HCl. Z-ODSP (**1**, 5 mmol) was added to the solution and the total volume of the solution was increased up to 20 mol by water and stirred. The pH was automatically maintained at the starting pH with 2 M NaOH. At predetermined time intervals, 0.1 ml aliquots of the solution were withdrawn and diluted with 4% citric acid (1 ml) and distilled water (total volume, 100 ml). The consumption of Gly or Val was measured using HPLC (column, AApack Na; eluent, 0.1 M citrate buffer; pH 4.25; 60 °C).

Concentration Effect: Gly or Val (5 mmol) was dissolved in water and the concentration of the solution was adjusted to various concentrations (0.01—1 M). Z-ODSP (**1**, 5 mmol) was added to a solution and stirred. The pH was automatically maintained at the starting pH with 2 M NaOH. At determined time intervals, the same procedures were carried out as described above.

References

1) K. Kouge, T. Koizumi, H. Okai, and T. Kato, *Bull. Chem. Soc. Jpn.*, **60**, 2409 (1987).
2) A. D. Price and J. M. Greenberg, *Science*, **197**, 670 (1977).
3) K. Kouge, H. Soma, Y. Katakai, H. Okai, M. Takemoto, and Y. Muneoka, *Bull. Chem. Soc. Jpn.*, **60**, 4343 (1987).
4) K. Kouge, Y. Katakai, H. Soma, M. Kondo, H. Okai, M. Takemoto, and Y. Nuneoka, *Bull. Chem. Soc. Jpn.*, **60**, 4351 (1987).
5) R. L. M. Synge, *Biochem. J.*, **42**, 99 (1948).
6) B. C. Baras and D. T. Elmore, *J. Chem. Soc.*, **1957**, 3134.
7) A. Neuberger and F. Sanger, *Biochem. J.*, **37**, 515 (1943).
8) A. Kjear and P. O. Larson, *Acta Chim. Scand.*, **15**, 750 (1961).
9) A. Poduska and J. Rudinger, *Collection Crech. Chem. Community*, **24**, 3449 (1959).
10) M. Hunt and V. du Vigneaud, *J. Biol. Chem.*, **18**, 1699 (1965).
11) H. Gibian and E. Schröder, *Ann. Chem.*, **18**, 1699 (1965).
12) M. Bergmann and L. Zervas, *Chem. Ber.*, **56**, 1192 (1932).
13) F. Weygand and K. Hunger, *Chem. Ber.*, **95**, 7 (1962).
14) E. Wunsch and A. Zwick, *Chem. Ber.*, **97**, 2497 (1964).
15) A. Pathonic, A. Berger, and E. Kachalski, *J. Am. Chem. Soc.*, **79**, 6416 (1957).
16) S. Sakakibara and M. Fujino, *Bull. Chem. Soc. Jpn.*, **39**, 947 (1966).
17) E. Klieger, E. Schröder, and H. Gibian, *Ann. Chem.*, **640**, 157 (1961).
18) K. Hoffman, A. Johl, A. E. Furlenmaier, and H. Koppeler, *J. Am. Chem. Soc.*, **79**, 1636 (1957).
19) W. Grassman and E. Wüsch, *Chem. Ber.*, **91**, 462 (1958).

20) J. S. Fruton, *J. Biol. Chem.* **146**, 463 (1942).
21) E. Wunsch and J. Jentsch, *Chem. Ber.*, **97**, 2490 (1964).
22) E. L. Smith, *J. Biol. Chem.*, **175**, 39 (1948).
23) G. W. Anderson and A. C. McGregor, *J. Am. Chem. Soc.*, **79**, 6180 (1957).
24) E. Wunsch and A. Zwick, *Chem. Ber.*, **97**, 3312 (1964).
25) E. Schroder and E. Klieger, *Justus Liebigs Ann. Chem.*, **973**, 208 (1964).
26) E. Schroder and E. Klieger, *Justus Liebigs Ann. Chem.*, **973**, 196 (1964).
27) H. C. Beyerman, C. A. M. Bders-Boonekamp, and H. Maasen van den Brink-Zinnermannova, *Recl. Trav. Chim. Pays-Bas*, **87**, 257 (1968).
28) E. Wünsch and G. Wendlberger, *Chem. Ber.*, **97**, 2504 (1964).
29) T. Nagasawa, Ki Kuroiwa, K. Narita, and Y. Isowa, *Bull. Chem. Soc. Jpn.*, **46**, 1269 (1973).
30) G. R. Pettit, "Synthetic Peptides," van Nostrand Reinhold Company, N. Y. (1971) Vol. 3, p. 35.
31) C. D. Chang, M. Waki, M. Ahmad, J. Meienhofer, E. O. Lundell, and J. D. Haug, *Int. J. Pept. Protein Res.*, **15**, 5966 (1980).
32) L. A. Carpino and G. Y. Han, *J. Org. Chem.*, **37**, 3404 (1972).
33) K. Hoffman, T. A. Thompson, H. Yajima, E. T. Schwartz, and H. Inoue, *J. Am. Chem. Soc.*, **82**, 3715 (1960).
34) F. Weygand, A. Prox, and W. König, *Chem. Ber.*, **99**, 1446 (1966).
35) K. Jost, J. Rudinger, and F. Sorm, *Collect. Czeck. Chem. Commun.*, **28**, 2021 (1963).

 © 1989 The Chemical Society of Japan Bull. Chem. Soc. Jpn., 62, 3109—3113 (1989)

Syntheses and Structures of Indolo[6,7-*g*]indoles, a New Heteroaromatic System[1)]

Yoshinobu NAGAWA,* Midori GOTO, Koichi HONDA, and Hiroshi NAKANISHI
National Chemical Laboratory for Industry, 1-1, Higashi, Tsukuba, Ibaraki 305
(Received March 22, 1989)

Photolysis of 1,1′-(1,8-naphthylene)-bis(1*H*-1,2,3-triazole)s (**1**) in methanol has given new heteroaromatic system compounds, indolo[6,7-*g*]indoles (**2**). The spectral properties of these compounds were studied in comparison with those of the corresponding benz[*g*]indoles (**4**) obtained from the similar photolysis of 1-(1-naphthyl)-1*H*-1,2,3-triazoles (**3**). The ^{1}H NMR and IR spectra of **2** and **4** suggest the existence of a strong intramolecular hydrogen bonding in **2**. The X-ray crystallographic analysis of tetraethyl 1*H*, 10*H*-indolo[6,7-*g*]-indole-2,3,8,9-tetracarboxylate, **2a**, indicates that the molecule has almost twofold rotational symmetry, and the framework is distorted due to the steric overcrowding.

In order to know the properties of peri-substituted naphthalenes with heteroaromatic rings, we have synthesized novel 1,1′-(1,8-naphthylene)-bis(1*H*-1,2,3-triazole)s, which have triazole rings at 1 and 8 positions in the naphthalene ring, and investigated their structure by several spectroscopic analyses.[2)] According to the X-ray diffraction studies of these compounds, the naphthalene ring is considerably distorted owing to the steric repulsion between the two triazole rings.[3)] In addition to these studies, we have investigated photochemical reactions of these compounds. Products based on the interaction between the two triazole rings were expected, but they were not recognized in this reaction. Instead, new heteroaromatic system compounds, indolo[6,7-*g*]indoles, were produced by the denitrogenation from the triazole rings followed by the cyclization with the naphthalene ring.

In this paper, we describe the formation of these compounds by the photolysis of 1,1′-(1,8-naphthylene)-bis(1*H*-1,2,3-triazole)s (**1**) and their structural studies by spectroscopic analyses including X-ray crystallography.

Results and Discussion

Photolysis of Naphthyltriazoles. Irradiation of **1a** in methanol for 15 min afforded tetraethyl 1*H*,10*H*-indolo[6,7-*g*]indole-2,3,8,9-tetracarboxylate (**2a**), which was produced by the elimination of nitrogen molecules from two triazole rings and cyclization toward the naphthalene ring. There are several kinds of indoloindole structures possible depending on the mode of condensation of the two indole rings. Although indolo[3,2-*b*]indole[4)] and indolo[7,6-*g*]-indole[5)] are known, the indolo[6,7-*g*]indole skeleton has not yet been synthesized to our knowledge. A similar reaction was observed on photolysis of the corresponding monotriazoles (**3**). Irradiation of **3a** in methanol for 15 min gave diethyl 1*H*-benz[*g*]indole-2,3-dicarboxylate (**4a**) almost quantitatively. Only a few studies have been investigated about the photochemical reaction of triazoles.[6)] Burgess et al. reported the formation of ketenimine derivatives by the photolysis of 1,4,5-triphenyl-1*H*-1,2,3-triazole.[7)] On the other hand, 1*H*-azirine derivatives were detected by the pyrolysis of triazole rings.[8)] We presumed the formation of similar compounds to the present reaction, but could not detect them to any extent under the experimental conditions. The isopropoxycarbonyl derivatives **2b** and **4b** were also produced by similar photolyses from **1b** and **3b** in excellent yield.

Photolyses of **1** and **3** were followed by HPLC using an ODS column and methanol-water (90 : 10) as an eluent. The starting material (**3a**) disappeared completely after 2 min irradiation, while **1a** required 10 min for the complete decomposition. A similar difference was observed between **1b** and **3b**, indicating that triazolylnaphthalenes (**3**) decompose much faster than disubstituted ones (**1**). The decomposition of the triazole ring in **1** may be restricted by the adjacent triazole ring. As described above, 15 min irradiation of **1a** afforded indolo[6,7-*g*]indole derivatives, **2a**, while irradiation of **1a** for 2 min led to the intermediate diethyl 9-(4,5-diethoxycarbonyl-1*H*-1,2,3-triazol-

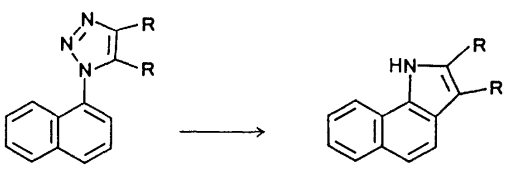

3 → 4

a; R = CO_2Et
b; R = CO_2Pr^i

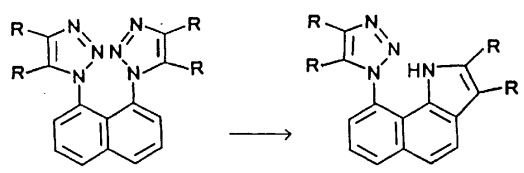

1 → 5

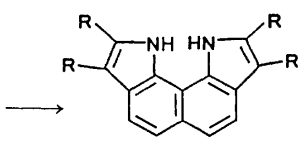

5 → 2

a; R = CO_2Et
b; R = CO_2Pr^i

1-yl)-1*H*-benz[*g*]indole-2,3-dicarboxylate (**5a**), which was isolated from the solution. The amount of **5a** became maximum at 2 min irradiation and thereafter gradually decreased. Finally, **5a** could not detected after 15 min under the reaction condition.

Spectral Properties of Indoles. Spectral properties of **2a—b**, **4a—b**, and **5a—b** are listed in Table 1. In the ^{1}H NMR spectrum, the NH signal of **2a** is ca. δ 0.9 downfield from that of **4a**. This large low field shift is due to the intramolecular hydrogen bonding as well as the anisotropic effect between the two condensed indole rings. The N-H signal of **5a** is observed at ca. δ 2.3 upfield from that of **4a** in the ^{1}H NMR. The reason of this extremely upfield shift is due to the anisotropic effects of the triazole ring. Probably, the triazole ring is perpendicular to the benz[*g*]indole ring because of steric repulsion between the triazole ring and the pyrrole moiety. Then, the triazole ring faces toward the NH proton in short distance, and it makes such a large up-field shift.

In the IR spectrum, the N-H stretching frequency of **2a** is about 100 cm^{-1} lower than that of **4a**, which also suggests the existence of a strong intramolecular hydrogen bonding in **2a**. Since the IR spectra were measured in the very dilute concentration as low as 2 mM (1M=1 mol dm^{-3}), the effect of the intermolecular hydrogen bonding is ruled out for the low frequency shift. Owing to the enlargement of the condensed ring, the longest maximum wavelength band of **2a** shows about 30 nm red shift compared with that of **4a** in the UV spectrum. The spectral relationships observed for **2a**, **4a**, and **5a** as described above are also found in those between **2b**, **4b**, and **5b**. This means the substituted ester groups scarcely affect these spectroscopic properties.

Molecular and Crystal Structure of 2a. The molecular structure of **2a** with the atom numbering is presented by the ORTEP[9] drawing in Fig. 1. The selected bond distances and angles for **2a** are given in

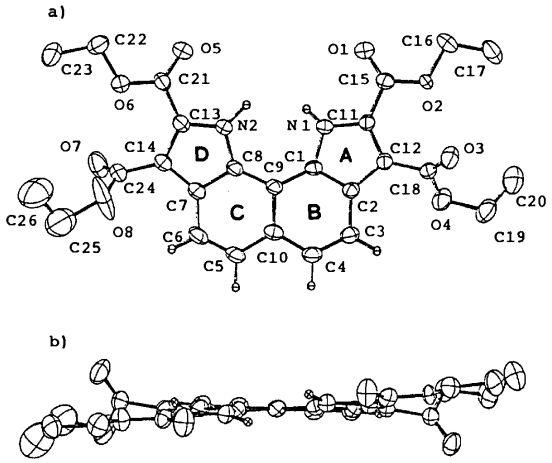

Fig. 1. Molecular structures of **2a**.
Non-hydrogen atoms are expressed as thermal ellipsoids with 40% probability level. Hydrogen atoms in ester groups are omitted for clarity.
(a) Side view. (b) Top view.

Table 1. Spectroscopic Data of Indoles

Product	^{1}H NMR ($CDCl_3$) δ/ppm	IR (CCl_4) ν/cm^{-1}	UV (CH_3OH) λ/nm	MS *m/z* (rel intensity, %)
2a	1.46 (t, *J*=7.1 Hz, 6H), 1.48 (t, *J*=7.1 Hz, 6H), 4.46—4.51 (m, 8H), 7.71 (d, *J*=8.8 Hz, 2H), 8.03 (d, *J*=8.8 Hz, 2H), 11.47 (s, 2H)	3351, 2984, 1730, 1698	376, 361, 278, 247, 208	494(M$^+$, 14) 448(100), 403(16), 376(14), 330(62), 259(16)
2b	1.45 (d, *J*=6.4 Hz, 12H), 1.49 (d, *J*=6.2 Hz, 12H), 5.31—5.42 (m, 4H), 7.74 (d, *J*=8.8 Hz, 2H), 7.99 (d, *J*=8.8 Hz), 11.50 (s, 2H)	3352, 2983, 1727, 1697	376, 315, 257, 216	550(M$^+$, 40), 490(100), 448(90), 405(60), 364(38), 302(42)
4a	1.43 (t, *J*=7.1 Hz, 3H), 1.47 (t, *J*=7.1 Hz, 3H), 4.44—4.52 (m, 4H), 7.50—7.61 (m, 3H), 7.91 (d, *J*=7.5 Hz, 1H), 7.99 (d, *J*=8.9 Hz, 1H), 8.23 (d, *J*=7.9 Hz, 1H), 10.52 (s, 1H),	3448, 2984, 1732, 1697	349, 335, 275, 249, 207	311(M$^+$, 76), 265(96), 193(100), 165(16), 164(14), 138(10)
4b	1.43 (d, *J*=6.2 Hz, 6H), 1.50 (d, *J*=6.2 Hz, 6H), 5.34—5.42 (m, 2H), 7.49—7.59 (m, 3H), 7.90 (d, *J*=7.5 Hz, 1H), 7.94 (d, *J*=9.0 Hz, 1H), 8.24 (d, *J*=7.7 Hz, 1H), 10.57 (s, 1H)	3449, 2980, 1734, 1700	349, 335, 274, 249, 207	339(M$^+$, 70), 297(12), 279(20), 237(100), 193(40), 164(12)
5a	0.83 (t, *J*=7.1 Hz, 3H), 1.40 (t, *J*=7.1 Hz, 3H), 1.43—1.49 (m, 6H), 4.07 (q, *J*=7.1 Hz, 2H), 4.36 (q, *J*=7.1 Hz, 2H), 4.45—4.56 (m, 4H) 7.54 (d, *J*=7.5 Hz, 1H), 7.64 (dd, *J*=8.1, 7.5 Hz, 1H), 7.76 (d, *J*=9.0 Hz, 1H), 8.19 (d, *J*=8.1 Hz, 1H), 8.21 (br, 1H), 8.24 (d, *J*=9.0 Hz, 1H)	3446, 2985, 1746, 1709	352, 335, 278, 253, 210	522(M$^+$, 22), 448(60), 421(28), 376(100), 258(50)
5b	0.78 (br, 6H), 1.37 (d, *J*=6.2 Hz, 6H), 1.45 (d, *J*=6.2 Hz, 12H), 4.88 (m, 1H), 5.22 (m, 1H), 5.34—5.42 (m, 2H), 7.52 (d, *J*=7.4 Hz, 1H), 7.63 (dd, *J*=8.3—7.4 Hz, 1H), 7.75 (d, *J*=9.1 Hz, 1H), 8.19 (d, *J*=8.3 Hz, 1H), 8.22 (br, 1H), 8.23 (d, *J*=9.1 Hz, 1H)	3448, 2983, 1744	351, 335, 278, 253, 209	578(M$^+$, 36), 404(30), 388(40), 362(100), 320(72), 276(54)

Table 2. Selected Bond Lengths and Bond Angles in **2a** with Estimated Standard Deviations in Parentheses

Bond length l/Å				C(6)-C(5)-C(10)	122.8(4)	C(5)-C(6)-C(7)	119.2(5)
C(1)-C(2)	1.417(7)	C(1)-C(9)	1.413(6)	C(6)-C(7)-C(8)	119.4(5)	C(6)-C(7)-C(14)	133.3(4)
C(1)-N(1)	1.374(5)	C(2)-C(3)	1.427(6)	C(8)-C(7)-C(14)	107.4(4)	C(7)-C(8)-C(9)	122.5(4)
C(2)-C(12)	1.417(6)	C(3)-C(4)	1.346(7)	C(7)-C(8)-N(2)	107.2(4)	C(9)-C(8)-N(2)	130.4(4)
C(4)-C(10)	1.436(8)	C(5)-C(6)	1.341(8)	C(1)-C(9)-C(8)	128.3(4)	C(1)-C(9)-C(10)	116.1(4)
C(5)-C(10)	1.419(7)	C(6)-C(7)	1.419(7)	C(8)-C(9)-C(10)	115.6(4)	C(4)-C(10)-C(5)	120.3(4)
C(7)-C(8)	1.413(6)	C(7)-C(14)	1.427(7)	C(4)-C(10)-C(9)	119.5(4)	C(5)-C(10)-C(9)	120.3(4)
C(8)-C(9)	1.418(7)	C(8)-N(2)	1.380(6)	C(12)-C(11)-C(15)	132.2(4)	C(12)-C(11)-N(1)	109.4(4)
C(9)-C(10)	1.438(6)	C(11)-C(12)	1.374(6)	C(15)-C(11)-N(1)	118.2(4)	C(2)-C(12)-C(11)	106.7(4)
C(11)-C(15)	1.471(6)	C(11)-N(1)	1.361(6)	C(2)-C(12)-C(18)	125.6(4)	C(11)-C(12)-C(18)	127.4(4)
C(12)-C(18)	1.474(7)	C(13)-C(14)	1.377(6)	C(14)-C(13)-C(21)	131.4(4)	C(14)-C(13)-N(2)	109.7(4)
C(13)-C(21)	1.475(7)	C(13)-N(2)	1.371(6)	C(21)-C(13)-N(2)	118.7(4)	C(7)-C(14)-C(13)	106.6(4)
C(14)-C(24)	1.470(7)	C(15)-O(1)	1.205(7)	C(7)-C(14)-C(24)	124.6(4)	C(13)-C(14)-C(24)	128.4(4)
C(15)-O(2)	1.324(6)	C(18)-O(3)	1.195(5)	C(11)-C(15)-O(1)	123.1(5)	C(11)-C(15)-O(2)	112.4(4)
C(18)-O(4)	1.340(7)	C(21)-O(5)	1.197(6)	C(1)-C(15)-O(2)	124.4(4)	C(12)-C(18)-O(3)	126.6(5)
C(21)-O(6)	1.324(6)	C(24)-O(7)	1.168(6)	C(12)-C(18)-O(4)	111.4(4)	O(3)-C(18)-O(4)	121.9(5)
C(24)-O(8)	1.307(7)			C(13)-C(21)-O(5)	123.5(5)	C(13)-C(21)-O(6)	111.8(4)
				O(5)-C(21)-O(6)	124.7(5)	C(14)-C(24)-O(7)	126.4(4)
Bond angles ϕ/°				C(14)-C(24)-O(8)	111.9(4)	O(7)-C(24)-O(8)	121.3(5)
C(2)-C(1)-C(9)	122.8(4)	C(2)-C(1)-N(1)	106.3(4)	C(1)-N(1)-C(11)	110.0(4)	C(8)-N(2)-C(13)	109.2(4)
C(9)-C(1)-N(1)	130.9(4)	C(1)-C(2)-C(3)	119.6(4)	C(15)-O(2)-C(16)	116.9(4)	C(18)-O(4)-C(19)	115.8(4)
C(1)-C(2)-C(12)	107.6(4)	C(3)-C(2)-C(12)	132.9(5)	C(21)-O(6)-C(22)	116.9(4)	C(24)-O(8)-C(25)	118.8(5)
C(2)-C(3)-C(4)	118.5(5)	C(3)-C(4)-C(10)	123.4(4)				

Table 2.[10]

The molecule has an approximate twofold rotational symmetry with respect to the C(9)-C(10) bond. The fused angle C(1)-C(9)-C(8), 128.3 (4)°, is fairly large compared with the corresponding angle in naphthalene itself, 121.5°.[11] In a four-ring helicene, benzo[*c*]phenanthrene (**6**), the angle is 124.6°, which is smaller than that in **2a**.[12] These results reflect the

(6)

remarkable steric overcrowding in **2a**.

The dihedral angles between the four rings of **2a** defined in Fig. 1 are listed in Table 3 together with the corresponding data in **6**. The twistings are observed at same intervals from the ring A to the ring D in **2a**. Thus, the dihedral angle of the two pyrrole rings A and D is 9.8 (2)°, while the angle of the corresponding two benzene rings in **6** is 26.5°.[12] These results indicate that the molecule **2a** relieves the steric hindrance by enlargement of the angle C(1)-C(9)-C(8) and by rather small twists in the fused four rings, while the molecule **6** twists largely in order to relieve the steric hindrance. Although the two N-H bonds twist away from each other, the distance between the N-H hydrogen atoms is nearly equal to the sum of the van der Waals radii. The carbonyl groups bonded at the C(11) and C(13) atoms are almost coplanar to the pyrrole rings A and D, respectively, but the carbonyl groups at the C(12) and C(14) twist from the pyrrole ring planes by 55—60°.

The packing modes of molecules in the crystal is shown in Fig. 2. The crystal packing mainly results from intermolecular hydrogen bonds; the shortest

Table 3. Dihedral Angles (°) between the Four Rings of **2a** and **6**[a]

	2a	**6**
Ring A-Ring B	3.6(2)	10.3(2)
Ring B-Ring C	3.3(2)	7.1(2)
Ring C-Ring D	3.2(2)	9.7(2)
Ring A-Ring D	9.8(2)	26.5(2)

a) Calculated with Ref. 12.

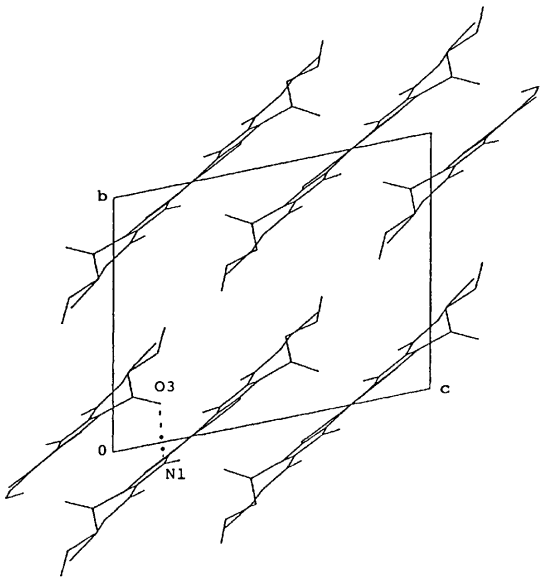

Fig. 2. Crystal structure of **2a**. Projected along the a axis.

intermolecular distance is 3.005(6) Å for N(1)-O(3^{i}) (i=1−x,−y,1−z).

Experimental

Instruments. All melting points were determined on a Mettler FP61 instrument and were uncorrected. ^{1}H NMR spectra were obtained by a JEOL GX-400 spectrometer (399.65 MHz for ^{1}H nuclei) using TMS as an internal standard. IR and UV spectra were measured on a JASCO 5MP and a Shimadzu MPS-2000 spectrometer, respectively. MS spectra were measured with a JEOL JMS-01SG-2 spectrometer at 75 eV of ionization energy. Elemental analyses were performed on a YANACO MT-3 CHN analyzer.

Materials. Compounds **1** and **3** were prepared from 1,8-diazidonaphthalene and 1-azidonaphthalene, respectively, by 1,3-dipolar cycloaddition with acetylene dicarboxylate as previously reported.[2]

Photolyses of 1 and 3. A solution of **1a** (120 mg, 0.22 mmol) in 400 ml of methanol under nitrogen atmosphere was irradiated with a Ushio 450 W high-pressure mercury lamp through a quartz well at 30—35 °C for 15 minutes. Then, the solvent was evaporated, and the residue was chromatographed over silica gel (diethyl ether-hexane as eluent) to give pure **2a**.

2a: pale yellow needles, mp 209—210 °C, 76 mg (70%). Found: C, 63.08; H, 5.39; N, 5.62%. Calcd for $C_{26}H_{26}N_2O_8$: C, 63.15; H, 5.30; N, 5.66%.

Similarly, the photoreactions of **1b**, **3a**, and **3b** (0.22 mmol) in methanol gave **2b**, **4a**, and **4b**, respectively.

2b: pale yellow needles, mp 168—169°C, 72%. Found: C, 65.47; H, 6.16; N, 5.04%. Calcd for $C_{30}H_{34}N_2O_8$: C, 65.44; H, 6.22; N, 5.09%.

4a: colorless needles, mp 133—134 °C, 95%. Found: C, 69.52; H, 5.58; N, 4.53%. Calcd for $C_{18}H_{17}NO_4$: C, 69.44; H, 5.50; N, 4.50%.

4b: colorless needles, mp 116—117 °C, 94%. Found: C, 70.63; H, 6.31; N, 4.19%. Calcd for $C_{20}H_{21}NO_4$: C, 70.78; H, 6.24; N, 4.13%.

Irradiation of **1** for 2 min gave **5** together with the starting material (**1**) and indoloindole, and they were separated with silica-gel chromatography as in case of **2**.

5a: colorless needles, mp 93—94°C, 25%. Found: C, 59.65; H, 4.97; N, 10.65%. Calcd for $C_{26}H_{26}N_4O_8$: C, 59.77; H, 5.02; N, 10.72%.

5b: colorless needles, mp 67—68 °C, 30%. Found: C, 62.33; H, 5.95; N, 9.59%. Calcd for $C_{30}H_{34}N_4O_8$: C, 62.27; H, 5.92; N, 9.68%.

X-Ray Analysis of Compound 2a. Pale yellow needle-like crystals of **2a** were obtained by a slow evaporation of hexane-diethyl ether solution at room temperature. The crystal, approximate dimension of 0.75×0.25×0.10 mm, was used for intensity data measurements.

Crystal data of **2a**; $C_{26}H_{26}N_2O_8$, M=494.5, triclinic, space group $P\bar{1}$, a=9.366(1), b=10.330(1), c=13.052(2) Å, α=101.85(2), β=90.76(2), γ=104.35(4)°, V=1194.6(1) Å^3, D_m=1.39 Mg m^{-3} (by floatation in carbon tetrachloride and hexane), D_c=1.38 Mg m^{-3} for Z=2, μ(Mo$K\alpha$)=0.111 mm^{-1}. The cell dimension and diffraction intensity were measured on a Rigaku AFC-4 four-circle diffractometer with graphite monochromated Mo$K\alpha$ radiation (λ=0.71069 Å) at room temperature. Unit cell dimensions were determined by least-squares fits using 25 reflections in the range $20°<2\theta<30°$. Intensity data were collected by the ω-2θ scan mode at a rate of 2° (2θ)min^{-1}. The scan range was from 2° to 55°. Three standard reflections (202, 022, and 2—20) were measured after every 50 reflections, showing no significant intensity decay throughout the data collection. Totals of 5532 reflections were measured, of which 3111 with $|F_o|>3\sigma|F_o|$ were used. The usual Lorentz and polarization corrections were applied, but no absorption corrections were made. The structure was solved by the direct method using MULTAN78.[13] An E-map using 244 ($|E|>1.2$) revealed all non-hydrogen atoms. Hydrogen atoms in the rings were found from a difference electron density map and those in the ester groups were placed at the calculated positions. The structure was refined by a full-matrix least-squares method, using the UNICS III system.[14] Anisotropic thermal parameters were assumed for the non-hydrogen atoms, and isotropic parameters, for the hydrogen atoms. The final refinement, employing a weighting scheme of $w=(0.011\,|F_o|^2-0.161|F_o|+1.245)^{-1}$, led to R and R_w values of 0.085 and 0.090, respectively. The final atomic parameters are listed in Table 4. Atomic scattering factors were taken from International Tables for X-Ray Crystallog-

Table 4. Fractional Atomic Coordinates (×10^4) and Equivalent Isotropic Thermal Parameters with e.s.d.'s in Parentheses

$B_{eq}=4/3\sum_i\sum_j\beta_{ij}a_ia_j$

Atom	x	y	z	B_{eq}/Å^2
O(1)	7689(4)	1740(4)	976(3)	5.1(1)
O(2)	6801(3)	2620(3)	−248(3)	2.8(1)
O(3)	3868(4)	1546(4)	−1478(3)	4.8(1)
O(4)	2864(4)	3035(4)	−466(3)	5.1(1)
O(5)	6802(4)	−1844(5)	4038(3)	5.6(1)
O(6)	5475(3)	−2676(4)	5277(3)	4.3(1)
O(7)	3055(5)	−1572(5)	6477(3)	6.3(1)
O(8)	1423(8)	−3194(6)	5463(4)	11.9(2)
N(1)	4850(4)	872(4)	1603(3)	3.0(1)
N(2)	4404(4)	−968(4)	3387(3)	3.2(1)
C(1)	3368(4)	599(4)	1765(3)	3.0(1)
C(2)	2704(4)	1106(4)	1003(3)	3.0(1)
C(3)	1167(5)	1048(5)	1013(4)	3.6(1)
C(4)	393(5)	522(5)	1759(4)	3.8(1)
C(5)	141(5)	−561(5)	3295(4)	3.7(1)
C(6)	670(5)	−1088(5)	4030(4)	4.0(1)
C(7)	2156(5)	−1183(4)	4018(3)	3.2(1)
C(8)	3059(4)	−684(4)	3252(3)	3.0(1)
C(9)	2555(4)	−40(4)	2510(3)	2.9(1)
C(10)	1023(4)	−31(5)	2526(3)	3.3(1)
C(11)	5122(5)	1472(4)	766(3)	3.0(1)
C(12)	3822(4)	1613(4)	360(3)	3.0(1)
C(13)	4388(4)	−1570(4)	4231(3)	3.2(1)
C(14)	3030(5)	−1710(4)	4651(3)	3.2(1)
C(15)	6666(5)	1929(5)	510(3)	3.5(1)
C(16)	8286(6)	3137(6)	−551(4)	4.4(2)
C(17)	8169(9)	3969(9)	−1340(6)	6.1(2)
C(18)	3578(5)	2045(4)	−623(3)	3.2(1)
C(19)	2582(8)	3554(8)	−1395(5)	5.9(2)
C(20)	3912(12)	4514(11)	−1616(9)	7.6(3)
C(21)	5691(5)	−2032(5)	4491(3)	3.5(1)
C(22)	6683(7)	−3171(7)	5607(5)	5.0(2)
C(23)	6169(9)	−3907(7)	6464(5)	5.7(2)
C(24)	2577(5)	−2143(5)	5628(4)	3.7(1)
C(25)	518(13)	−3548(14)	6427(9)	9.3(4)
C(26)	1273(20)	−4473(21)	6578(12)	12.0(6)

raphy.[15] All the calculations were carried out on a FACOM M-780 computer at Tsukuba Research Center.

We wish to thank Dr. Nobuhide Wasada and Dr. Akira Nomura, in our Laboratory, for their helpful discussions.

References

1) Preliminary communication; Y. Nagawa, K. Honda, and H. Nakanishi, *J. Chem. Soc., Chem. Commun.*, **1988**, 989.

2) Y. Nagawa, K. Honda, and H. Nakanishi, *Bull. Chem. Soc. Jpn.*, **60**, 2931 (1987).

3) Y. Nagawa, M. Goto, K. Honda, and H. Nakanishi, *Acta Crystallogr., Sect. C*, **42**, 478 (1986); **43**, 147 (1987); Y. Nagawa, M. Goto, K. Honda, and H. Nakanishi, *Bull. Chem. Soc. Jpn.*, **61**, 3553 (1988).

4) G. Heller, *Ber.*, **50**, 1203 (1917).

5) S. A. Samsoniya, M. V. Trapaidze, N. N. Suvorov, and I. M. Gverdtskteli, *Soobshch. Acad. Nauk. Gruz. SSR*, **91**, 361 (1978); *Chem. Abstr.*, **90**, 54860g (1979).

6) H. Wamhoff, "1,2,3-Triazoles and Their Benzo Derivatives," in "Comprehensive Heterocyclic Chemistry," ed by A. R. Katritzky and C. W. Rees, Pergamon Press, Oxford (1984), Vol.5, Part 4a, p. 691.

7) E. M. Burgess, R. Carithers, and L. McCullagh, *J. Am. Chem. Soc.*, **90**, 1923 (1968).

8) T. L. Gilchrist, G. E. Gymer, and C. W. Rees, *J. Chem. Soc., Perkin Trans. 1*, **1975**, 1.

9) C. K. Johnson, "ORTEP II, Report ORNL-5138," Oak Ridge National Laboratory, Tennessee (1976).

10) The lists of observed and calculated structure factors, the atomic parameters for the hydrogen atoms, and the anisotropic thermal parameters for the non-hydrogen atoms are deposited at the Chemical Society of Japan as Document No. 8896.

11) D. W. J. Cruickshank and R. A. Sparks, *Proc. R. Soc. London, Ser. A*, **258**, 270 (1960).

12) F. L. Hirshfeld, S. Sandler, and G. M. J. Schmidt, *J. Chem. Soc.*, **1963**, 2108.

13) P. Main, S. E. Hull, L. Lessinger, G. Germain, J. P. Declercq, and M. M. Woolfson, MULTAN 78, "A System of Computer Programs for the Automatic Solution of Crystal Structures from X-Ray Diffraction Data," University of York, England, and Louvain, Belgium (1978).

14) T. Sakurai and K. Kobayashi, *Rep. Inst. Phys. Chem. Res.*, **55**, 69 (1979).

15) International Tables for X-Ray Crystallography, Vol. IV, Kynoch Press, Birmingham (1974).

Lipid-Protein Interaction in Mixed Monolayers from Phospholipids and Proteins

Tomoyoshi MITA
Department of Natural Science, Osaka Women's University, Daisen-cho, Sakai, Osaka 590
(Received March 29, 1989)

The thermotropic behavior of different proteins with phospholipids in monolayers was investigated by measuring the surface pressure and the surface viscosity. When phospholipids, such as dipalmitoylphosphatidylcholine (DPPC) and dimyristoylphosphatidylcholine (DMPC), were mixed with the hydrophobic proteins, such as hemoglobin and β-casein, below their phase transition temperatures (T_c), a considerable expansion of monolayers was observed. On the other hand, when phospholipids were mixed with the hydrophilic proteins, such as bovine serum albumin (BSA) and lysozyme below T_c, no expansion was observed. When DMPC was mixed with different proteins at T_c or above, all mixtures formed slightly deviated monolayers from ideal mixing, independent of a variety of proteins. This type of behavior suggests that the hydrophobic proteins perturb the structure of boundary lipids near the protein molecule below T_c, while the hydrophobic proteins do not perturb the phospholipid structure below T_c because of their low hydrophobicities. At T_c or above the membrane properties are independent of a variety of proteins, because all lipid hydrocarbon chains cause a disordering, even without proteins. In addition, when DPPC was mixed with a hydrophobic protein, such as hemoglobin, the fluidity of monolayer increased significantly.

The importance of studying mixtures of lipids and proteins in membranes is obvious when one considers the currently accepted fluid mosaic model of membranes.[1] Good knowledge concerning lipid-protein interaction is a key to understanding the structure and function of biological membranes. Intimately related to the above subject is the question how different proteins affect the physical properties of biological membranes, such as membrane fluidity.

From this viewpoint, various theoretical models have been proposed to study the lipid-protein interaction and its effect on the properties of biological membranes.[2-6] A large body of experimental data on the lipid-protein interaction in membranes has also been accumulated during the last two decades by using different experimental techniques; e.g., differential scanning calorimetry (DSC), electron spin resonance (ESR), Raman spectroscopy, deuterium magnetic resonance (^{2}H NMR), fluorescence anisotropy (FA). Chapman et al.[7] have investigated the effect of proteins on the phase behavior of membranes by using DSC and noted that cytochrome C decreases the phase-transition temperature (T_c) of a lipid membrane. On the contrary, Verkleij et al.[8] have reported that the basic myelin protein increases the T_c of a membrane. Papahadjopoulos et al.[9] have reported that a variety of proteins has very different effects on the lipid phase transition from gel to liquid crystalline. In addition, the effect of proteins on lipid order in membranes has been intensively investigated by means of the above-mentioned techniques. That is, the results based on ESR, FA, and Raman spectroscopy indicate that proteins increase the lipid order.[10] On the other hand, ^{2}H NMR indicates that proteins decrease the lipid order.[11] In this way, no consensus has been attained as to whether proteins in biological membranes change the T_c of lipids or not and cause an ordering or disordering of the lipids.

According to the criteria of Papahadjopoulos et al.[9] the physical properties of biological membranes, are characteristic of a hydrophobic interaction between protein and lipid molecules. In addition, Jähnig[12] has demonstrated that the hydrophobic effect of proteins provides the main driving force for insertion into the membrane. Then, many investigators have attempted to define the hydrophobicity of proteins. A fluorescence probe method has been proposed for the evaluation of protein hydrophobicity.[13] However, the above-mentioned hydrophobicity is susceptible to change by the unfolding of proteins, since it reflects the surface hydrophobicity of native proteins. On the other hand, Bigelow[14] has proposed the average hydrophobicity, $H\phi_{ave}$, based on Tanford's Gibbs energy of the transfer of amino acid side chains from an organic environment to an aqueous environment. This index is not influenced by any conformational changes of proteins. In a similar manner, Kyte and Doolittle[15] have proposed the hydropathy index, based upon the probability of being exposed to water from the hydrophobic parts of proteins as well as the Gibbs energy of transfer from water to an organic solvent. The former method for protein hydrophobicity is considerably simpler than the latter. Proteins with high hydrophobicity exhibit higher values of $H\phi_{ave}$ (over 4.6 kJ·res.$^{-1}$).

Previously, the author reported on the thermotropic behavior of different proteins in monolayers.[16] It was observed that the temperature-dependences on the π-A isotherms of hydrophobic proteins, such as hemoglobin ($H\phi_{ave}$=4.65 kJ·res.$^{-1}$) and β-casein ($H\phi_{ave}$= 5.57 kJ·res.$^{-1}$), were fairly different from those of hydrophilic proteins, such as lysozyme ($H\phi_{ave}$=4.06 kJ·res.$^{-1}$) and bovine serum albumin (BSA, $H\phi_{ave}$= 4.35 kJ·res.$^{-1}$), and that hydrophobicity of proteins was an important factor related to the thermal stability of proteins in membranes. Thus, the above-

mentioned confusion may be attributed to differences in the hydrophobicity of proteins.

In order to study the lipid-protein interaction in membranes, the spread monolayer technique is useful, since the orientation of lipid and protein molecules at the air-water interface can be precisely understood by using this technique and the area occupied by each molecule can be determined over a wide limit by careful compression of the monolayers. Then, the interaction of proteins with lipids at the air-water interface has been studied by many workers,[17-21] usually by the technique of injecting protein under preformed lipid monolayers and by measuring the increment of surface pressure during the interaction. However, the above injection technique has serious limitations in that the surface concentration of proteins is not known. Recently, the interaction of lipids with proteins at the air-water interface by spreading the components from a common solvent has been investigated.[22-24]

In this paper, we examined the hydrophobic effect of proteins on the thermotropic behavior of phospholipids, as measured by the miscibility in the mixed monolayers which are obtained by spreading the mixtures dissolved in a common solvent. These results were then discussed concerning the phase behavior of phospholipids. Although the proteins used were not membrane bound but, rather, water soluble, they were chosen because of their well-known amino acid sequences and their three-dimensional structures. The present work also investigated the rheological properties of mixed monolayers from phospholipids and proteins by using a surface viscometer.

Experimental

Reagents. All chemicals were of the highest purity available, used without further purification. Water was distilled once, passed through a mixed ion bed exchanger and redistilled.

Materials. The following high-purity proteins were used in this study from the suppliers: BSA (fatty acid free), bovine hemoglobin (2×crystallized), and bovine β-casein were from Sigma Chemical Co., and lysozyme (6×crystallized) was product of Seikagaku Kogyo Co. The phospholipids dipalmitoylphosphatidylcholine (DPPC) and dimyristoylphosphatidylcholine (DMPC) (Sigma Chemical Co.) used were specified to be 99% pure and were used without further purification.

Surface Pressure. The film balance used for measuring the surface pressure has been described in detail elsewhere.[16] The trough was coated with Teflon and the entire balance was surrounded by a water jacket, providing temperature control within 1 °C. A 50% 1-propanol containing 0.5 mol·dm^{-3} sodium acetate was employed as a spreading solvent for proteins and phospholipids. After the respective proteins and phospholipids were dissolved in the solvent at a concentration of 0.05%, these solutions were stored in a refrigerator and used after about 24 h. For mixed monolayers, the mixtures of lipids and proteins were obtained by an appropriate volumetric mixing of solutions containing each component before application. In the experiments reported below, no buffer was used, in order to prepare a very simple subphase. The water was poured in the trough to a height of 1—2 mm above the rim. The surface of the subphase was cleaned by moving a Teflon barrier from one side of the trough to the other. The cleaning of the surface was repeated until the surface pressure of the subphase did not exceed 0.2 mN·m^{-1}. For the surface pressure-area (π-A) isotherm, these solutions (0.1 cm^3) were then spread onto an area of 897 cm^2. Monolayer spreading was made by a direct application of numerous small drops (≈0.0006 cm^3) of the solution to the surface of the subphase by using a microsyringe (Hamilton Co.), introduced by Ställberg and Teorell.[25] A time interval of 30 min was allowed for the equilibration of the monolayers before it was compressed. The π-A isotherms were obtained by using a compression velocity of 0.0567 m^2·mg^{-1}·min^{-1}.

Surface Viscosity. A Kyowa's surface viscometer (type SVR, Kyowa Surface Science Co.) was used. This apparatus was a rotational torsion surface viscometer of the type described by Karam.[26] The viscometer consisted of a knife-edged bob which hung freely from a torsion wire. A removable dish was placed on a turntable beneath the bob. The radii of the bob and dish were 2.5 and 7.5 cm, respectively. After the knife edge of the bob was placed on the surface of substrate, the monolayer spreading, based upon the recipe for measuring the surface pressure, was made. From the period and damping of the oscillation, the surface viscosity η_s expressed in mN·s·m^{-1} was calculated as follows:

$$\eta_s=\frac{2.303\,I}{2}\left(\frac{\lambda}{T}-\frac{\lambda_w}{T_w}\right)\left(\frac{1}{r_1^2}-\frac{1}{r_2^2}\right), \quad (1)$$

where I is the moment of interia, r_1 and r_2 the respective radii of the bob and dish, λ the (decadic) logarithmic decrement of the oscillation, and T their periodic time when the surface is covered by the monolayers; λ_w and T_w are the respective values for the clean surface.

Each part of all experiments was repeated at least three times and then averaged.

Results

Characteristics of Mixed Monolayers from DPPC and Proteins at an Air-Water Interface. Treatment of data involved adapting the theory of mixing in bulk to a two-dimensional situation. For ideal mixing, monolayers obey the following equation:[27]

$$A_{1,2}=n_1A_1+n_2A_2, \quad (2)$$

where $A_{1,2}$ is the average molecular area in the two-component film, n_1 and n_2 are the respective mole fractions, and A_1 and A_2 are the molecular areas in the two single-component films at the same surface pressure. In case the interaction between two components is detected, Eq. 2 is obeyed.

However, most biological membranes are composed of approximately 50% lipids and 50% proteins by weight,[28] and the molecular weights of proteins are extremely different from those of lipids. Then, Eq. 2

is modified as follows:

$$A_{l,p} = w_l A_l + w_p A_p, \quad (3)$$

where $A_{l,p}$ is the occupied area, expressed in $m^2 \cdot mg^{-1}$, in the mixed monolayer of lipid and protein, w_l and w_p are the respective weight fractions of lipid and protein, and A_l and A_p are the areas ($m^2 \cdot mg^{-1}$) in the lipid and protein monolayers at the same surface pressure.

Figure 1 shows typical π-A isotherms obtained at 25 °C for monolayers of hemoglobin, DPPC, and a mixture (1/1 in weight ratio) of the two spread on water, respectively. The calculated curve shown in Fig. 1 represents the behavior found when the additivity rule in Eq. 3 is obeyed. The result indicates that when DPPC is mixed with hemoglobin below its T_c (T_c=41 °C)[29] an expansion from the calculated curve occurs. Similar measurements were made with DPPC-β-casein, DPPC-BSA, and DPPC-lysozyme mixtures in various weight ratios. Although the deviation from ideal in the area of a mixed monolayer is observed by direct inspection of Fig. 1, a more convenient way of presenting the results of a number of runs on monolayers of the mixtures of different compositions is shown in Figs. 2 and 3. Here, the occupied area of the mixed monolayer at constant surface pressures is plotted as a function of the weight fraction of DPPC in the monolayers. The broken line on these plots represents the behavior found when the additivity rule is obeyed. When DPPC was mixed with such hydrophobic proteins as hemoglobin and β-casein[16] below T_c, an expansion or positive deviation from the additivity line occured. On the other hand, when DPPC was mixed with such hydrophilic proteins as BSA and lysozyme[16] below T_c, little deviation from the additivity line occured.

Phospholipids form a condensed monolayer or a gel phase below T_c and form an expanded monolayer or liquid crystalline phase above T_c.[27] Accordingly, the temperature-dependence upon the lipid-protein interaction in membranes must be investigated. However, the T_c of DPPC is fairly higher than room temperature, and it is difficult to measure the surface pressure near T_c or above, since the surface evaporation of water from subphase occurs appreciably. Then, additional experiments were made by using DMPC (T_c=24 °C[29]).

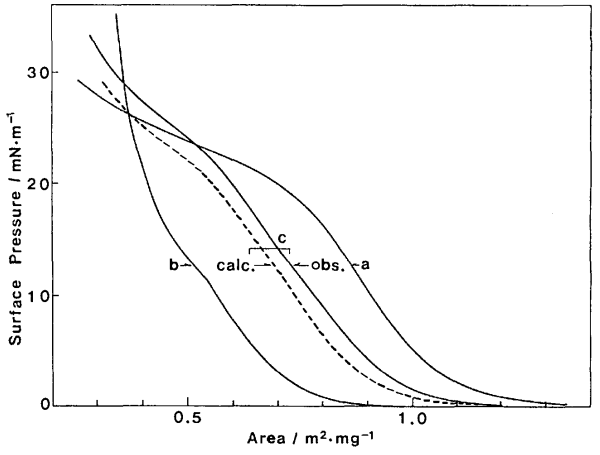

Fig. 1. π-A isotherms for monolayers of hemoglobin, DPPC, and a mixture of the two spread on water at 25 °C. a) hemoglobin, b) DPPC, c) DPPC-hemoglobin (1/1 in weight ratio); ——, experimental; ----, calculated from Eq. 3.

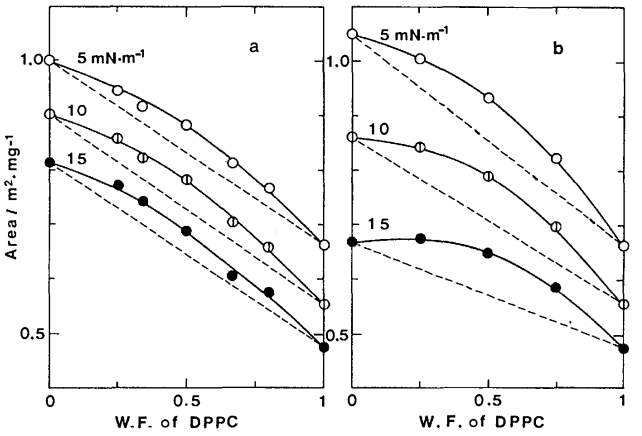

Fig. 2. Plots of mean area of mixed monolayers as a function of weight fractions of DPPC at 25 °C. a) DPPC-hemoglobin, b) DPPC-β-casein.

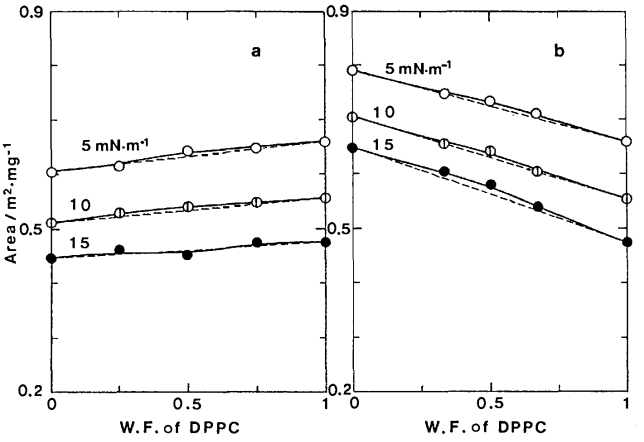

Fig. 3. Plots of mean area of mixed monolayers as a function of weight fractions of DPPC at 25 °C. a) DPPC-lysozyme, b) DPPC-BSA.

Temperature-Dependence of Mixed Monolayers from DMPC and Proteins at an Air-Water Interface. Figures 4 and 5 show plots of the area of mixed monolayers composed of DMPC-hemoglobin and DMPC-β-casein at constant surface pressures as a function of the weight fractions of DMPC in their monolayers at different temperatures, respectively. When DMPC was mixed with hemoglobin below T_c (15 °C), a positive deviation from the additivity rule occured as well as DPPC. On the contrary, when DMPC was mixed with hemoglobin at T_c (24 °C) or

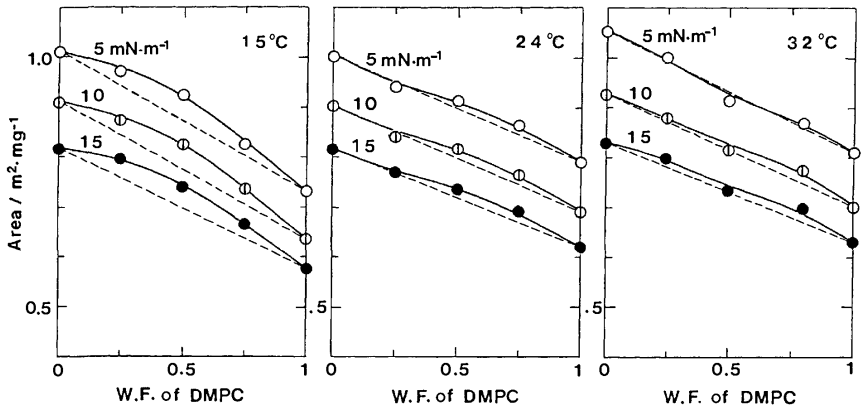

Fig. 4. Plots of mean area of DMPC-hemoglobin monolayer as a function of weight fractions of DMPC at different temperatures.

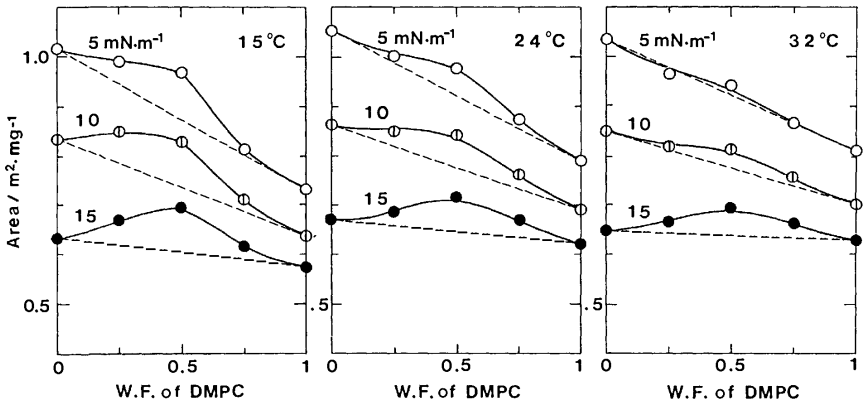

Fig. 5. Plots of mean area of DMPC-β-casein monolayer as a function of weight fractions of DMPC at different temperatures.

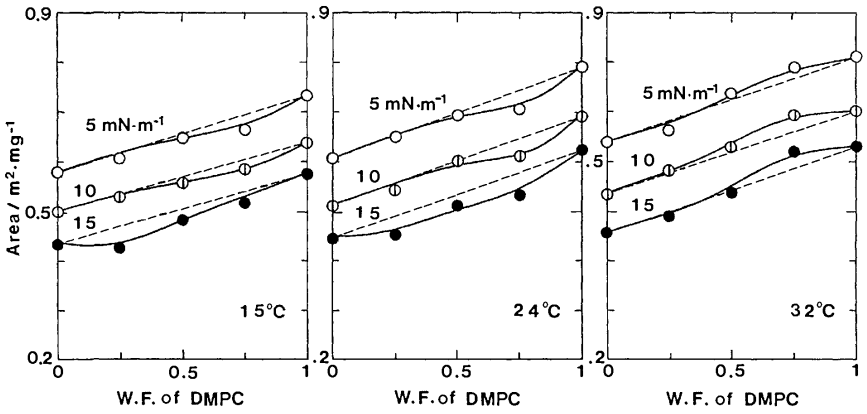

Fig. 6. Plots of mean area of DMPC-lysozyme monolayer as a function of weight fractions of DMPC at different temperatures.

above (32 °C), where DMPC was in a liquid crystalline state, little deviation from the additivity rule occured. When DMPC was mixed with β-casein below T_c, a large expansion from the additivity rule was observed. On the other hand, for the mixed monolayer of DMPC and β-casein, the magnitude of expansion decreased significantly at T_c or above. Figure 6 shows plots of area of the DMPC-lysozyme monolayer at constant surface pressures as a function of the weight fractions of DMPC at different temperatures. Strictly speaking, the DMPC-lysozyme mixture formed a slightly condensed monolayer from the ideal mixing at T_c or below, while the mixture formed a slightly deviated monolayer from the ideal mixing above T_c.

Surface Viscosity of Mixed Monolayers from DPPC and Proteins at an Air-Water Interface. The viscos-

ity, $\eta(c_A,c_B)$, of a solution containing two components, A and B, at concentrations c_A and c_B, is expressed by

$$\eta(c_A,c_B)=\eta_0\{1+([\eta_A]w_A+[\eta_B]w_B)c+s_mc^2+\cdots\}, \quad (4)$$

where $c=c_A+c_B$, $w_A=c_A/c$, $w_B=c_B/c$. η_0 is the solvent viscosity, $[\eta_A]$ and $[\eta_B]$ are the respective intrinsic viscosities of both components in a pure solvent, and s_m is the interaction parameter.[30] If there is no interaction between the two components, the third and following terms in the brace of the right-hand side of Eq. 4 may be ignored. Then, Eq. 4 can be approximated by

$$[\eta_{A,B}]=[\eta_A]w_A+[\eta_B]w_B, \quad (5)$$

where $[\eta_{A,B}]$ is the intrinsic viscosity of the solution containing two components. Accordingly, for ideal mixing without interaction between two components, the surface viscosity of monolayers may obey the additivity rule, as described in Eq. 3, although there are some problems in adapting the theory of mixing in bulk to the two-dimensional situation.

Figure 7 shows the surface viscosity-area (η_s-A) isotherms obtained at 25 °C for monolayers of hemoglobin, DPPC, and the mixtures of the two spread on water. The calculated curve for a mixture (1/1 in weight ratio) shown in Fig. 7 represents the behavior found when the additivity rule is obeyed. For the hemoglobin monolayer, η_s steeply appeared at a higher area than that where π was detectable. On the other hand, for the DPPC monolayer, η_s suddenly appeared at a slightly lower area than which corresponded to the limiting area (0.46 $m^2 \cdot mg^{-1}$). When DPPC was mixed with hemoglobin, a negative deviation from the additivity rule was observed, in contrast to the behavior of π-A isotherm. For example, when DPPC was mixed with hemoglobin at 1/1 in weight ratio, a considerable condensation from the calculated curve was observed. The above-mentioned result indicates that, when DPPC is mixed with hemoglobin below its T_c, η_s of the monolayer decreases by a fair amount. In addition, by using the mixture of DMPC and hemoglobin a measurement of η_s was attempted above T_c. Unfortunately, the measurement was unsuccessful because η_s of pure DMPC in a monolayer was very low.

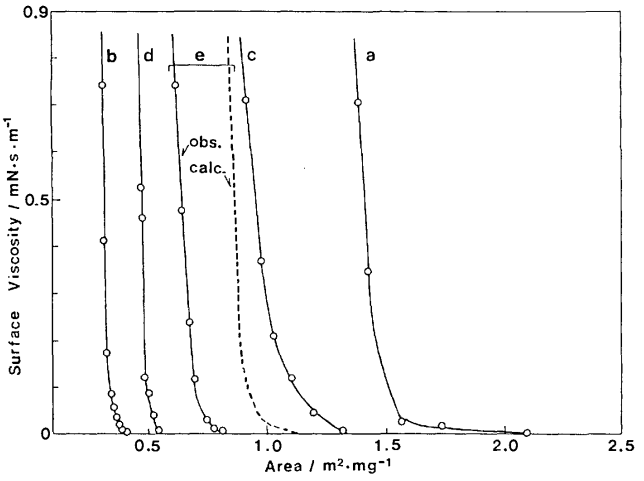

Fig. 7. η_s-A isotherms for monolayers of hemoglobin, DPPC, and mixtures of the two at 25 °C. a) hemoglobin, b) DPPC, c) DPPC-hemoglobin (1/3 in weight ratio), d) DPPC-hemoglobin (3/1), e) DPPC-hemoglobin (1/1); ——, experimental; ----, calculated from Eqs. 3 and 5.

Discussion

Because of the amphipathic nature of protein, the change to an extended conformation in which the protein molecule lowers the Gibbs energy of the system by maximizing contact of nonpolar side chains with the nonpolar phase is understandable. One must, therefore, consider whether the proteins denature irreversibly at the air-water interface or not. When the protein solutions are shaken, the insoluble protein due to the surface denaturation is occasionally seen to separate out. A comparison between the ease of coagulation (irreversible denaturation) by shaking a number of proteins has been carried out by Henson et al.[31] There is a significant difference in the ease of coagulation between the different proteins. Ovalbumin is especially susceptible, and β-lactoglobulin and γ-globulin also coagulate readily at the air-water interface. However, the β-casein, hemoglobin, BSA, and lysozyme, used in this study, are hardly influenced. According to MacRitchie,[32] every protein has a critical surface pressure, π_c, at the air-water interface, and will precipitate once this is exceeded. The coagulation may be observed, therefore, when the spread protein monolayers are compressed above π_c. However, our compression experiment was π_c. In addition, the view that the secondary structure of such proteins as the α-helix is stable at the air-water interface has been reported.[33] Accordingly, it is considered that surface denaturation did not occur during this study.

Biological membranes are sensitive to variation in the environment; for example, temperature essentially modifies such membrane characteristics as the permeability and excitability. Then, most lipids of biological membranes are normally in the liquid crystalline state at physiological temperatures and the lipids have the structure of a bilayer with low viscosity, deformability, and the ability to self-seal.[34] From this viewpoint, the effect of cholesterol on the membrane fluidity has been studied by a number of methods. The picture that emerges from these studies, summarized by Oldfield and Chapman,[35] is that cholesterol somehow fluidizes a lipid that is below the T_c, but rigidifies a lipid above T_c. This effect is called "dual effect."[36] Protein may also exhibit such a behavior as well as cholesterol in biological membranes. It has been found that boundary lipids near a

protein molecule have considerable differences in fluidity and conformation from those of the bulk lipids in the protein-free region and that the boundary lipids of many proteins are more fluid or have more gauche bonds in their hydrocarbon chains than the bulk lipids in the gel phase of the membranes, while the boundary lipids are more rigid or have more trans bonds than the bulk lipids in the liquid crystalline phase.[37-40]

When such phospholipids as DPPC and DMPC were mixed with such hydrophobic proteins as hemoglobin and β-casein below their T_c, a considerable expansion was observed (Figs. 2, 4, and 5), showing the lipid-protein interaction in membranes. On the other hand, when phospholipids were mixed with such hydrophilic proteins as BSA and lysozyme below T_c, no expansion was generally detected (Figs. 3 and 6), showing no interaction between lipids and proteins. Especially, the DMPC-lysozyme mixture formed a slightly condensed monolayer from the ideal mixing below T_c.

Papahajopoulos et al.[9] have extensively studied the effects of different proteins on the thermotropic phase transitions of phospholipid membranes, as detected by DSC and have indicated that ribonuclease leads to an increase in the enthalpy of the transition (ΔH) without any change in T_c, while hemoglobin and gramicidin induce a drastic decrease in ΔH accompanied by either a decrease or no change in T_c. Then, it is considered that a very hydrophilic protein, such as ribonuclease,[16] causes an ordering of the lipid hydrocarbon chains below the T_c of lipids, leading to an increase in ΔH, while such hydrophobic proteins as hemoglobin and gramicidin[14] cause a disordering of the chains below T_c, leading to a decrease in ΔH. In addition, O'Leary[41] has reported that proteins always weaken the intensity of the first-order lipid phase transition (pre-transition), and that they may cause it to broaden, and may induce other continuous transitions above or below it in temperature, depending on the system.

Accordingly, we consider that the hydrophobic proteins lead to an increase in the configurational freedom of lipid hydrocarbon chains, such as trans-gauche conversion,[6,42] due to a hydrophobic effect of proteins with lipid chains, resulting in an expansion of the monolayers composed of lipids and proteins, while that the hydrophilic proteins do not lead any configurational changes because of their low hydrophobicities, exhibiting ideal mixing. Very hydrophilic proteins, such as lysozyme, lead to an increase in the configurational restriction of lipid hydrocarbon chains, due to the electrostatic interaction of the polar head groups with the proteins, inducing the condensation of monolayers. On the other hand, when the phospholipid DMPC was mixed with different proteins near its T_c or above, all mixtures of DMPC-proteins formed little deviated monolayers from the ideal mixing, independent of a variety of proteins (Figs. 4—6). This suggests that the expansion behavior due to the hydrophobic effect does not occur, because all lipids are in the liquid crystalline state near T_c, or above.

The thermotropic behavior of phospholipid molecules in reconstituted glycophorin-containing vesicles has been investigated by means of DSC.[43] Each glycophorin molecule is able to perturb the properties of 80—100 phospholipid molecules, independent of the protein-to-lipid ratio in the membranes, in such a way that these lipid molecules no longer participate in the cooperative gel-to-liquid crystalline phase transition. A value of 15 lipid molecules per protein molecule has also been reported for lipophilin,[44] ten for melittin,[45] and six for gramicidin.[37]

The structural change of proteins owing to lipid-protein interaction in monolayers may be negligibly smaller than that of lipids. Then, the perturbed-to-unperturbed lipid ratios in the mixed monolayers are derived from Eq. 3,

$$A_{l,p} = w_l\{A'_l x + (1-x)A_l\} + w_p A_p, \quad (6)$$

where x is the mole fractions of the perturbed lipids in whole lipids, A'_l and A_l are the respective areas ($m^2 \cdot mg^{-1}$) in the perturbed and unperturbed lipid monolayers, A_p and $A_{l,p}$ are the respective areas in the protein and lipid-protein monolayers at the same surface pressure, and w_l and w_p are the respective weight fractions of lipid and protein. When the phospholipid DPPC is dispersed in excess water, the area per molecule in bilayers is about 4.8 nm^2 below T_c and about 7.0 nm^2 above T_c.[46] A fully-expanded DPPC monolayer above T_c occupies 7.0 $nm^2 \cdot molecule^{-1}$ when π is approximately 20 $mN \cdot m^{-1}$.[27] Since the value of the molecular weight of DPPC is 734, the areas expressed in 4.8 and 7.0 $nm^2 \cdot molecule^{-1}$ correspond to areas of 0.39 and 0.57 $m^2 \cdot mg^{-1}$, respectively. In Fig. 1, when π is 20 $mN \cdot m^{-1}$, hemoglobin and mixture (1/1 in weight ratio) occupy 0.70 and 0.60 $m^2 \cdot mg^{-1}$, respectively. This indicates that about 60% of all lipid molecules are perturbed in the mixed monolayer below T_c (25 °C). Then, it is understandable by the application of the molecular weight (64500) of hemoglobin that each hemoglobin molecule perturbs the properties of 50—60 phospholipid molecules.

Since the molecular weight of hemoglobin is about twice that of glycophorin,[47] and extremely larger than those of lipophilin, melittin, and gramicidin, the value of perturbed lipid molecules per hemoglobin molecule is slightly smaller than those of the integral proteins. This may be attributed not only to a difference in the hydrophobicity between the proteins, but also to a difference in the membrane properties between the monolayer and bilayer. When one considers a two-dimensional lattice of lipid molecules surrounding the protein, each hemoglobin molecule complexes 40—50 phospholipid molecules, independ-

ent of the protein-to-lipid ratio in the monolayer. However, this will be greatly diminished by the phase separation into the protein-rich and protein-free domain below T_c.[21] Then, the perturbation of the phospholipid structure near the hemoglobin molecule, while most pronounced within the annulus of the first neighbor molecules, will extend at least two layers beyond the annulus, coinciding with the result of Marčelja.[2]

Speth and Wunderlich[48] have shown by freeze-etch electron microscopy that, after chilling the cells of protozoan *Tetrahymena pyriformis*, the particles, which are randomly distributed on the outer faces of the fractured alveolar membranes, are largely aggregated, showing a clustering of membrane proteins. This indicates that, when the cells are rapidly cooled, the fluidity of biological membranes is regulated by the phase separation of membrane proteins.[49] The η_s-A isotherms for phospholipid-hemoglobin mixtures showed a considerable condensation below T_c, in contrast to the behavior of π-A isotherms (Fig. 7). Such behavior suggests that, when the phospholipids are mixed with the hydrophobic proteins such as hemoglobin below T_c, the fluidity of the monolayer increases significantly, depending on both the perturbation of lipid hydrocarbon chains and the phase separation of proteins in the monolayers. It is also related to the above-mentioned behavior that hemoglobin drastically increases the permeability of phospholipid vesicles.[50,51]

Finally, we consider the protein distribution is the mixed monolayers from phospholipids and proteins. According to Heckl et al.,[21] the high packing densities in the condensed lipid phases below T_c do not allow for a distribution due to protein penetration, while the low packing densities in the expanded lipid phases above T_c permit a homogeneous distribution of proteins in the monolayers. Accordingly, based on the lattice model of a phospholipid bilayer containing integral protein constructed by Lookman et al.,[52] the model shown in Fig. 8 is being proposed for monolayers composed of phospholipids and different proteins as a function of temperature. The black, open hexagons represent such hydrophobic proteins as hemoglobin and β-casein and such hydrophilic proteins as BSA and lysozyme, respectively. The dots represent perturbed lipids, and the blank areas represent unperturbed lipids. Below T_c the proteins are highly clustered, while at T_c or above they are more uniformly distributed. The hydrophobic proteins perturb the hydrocarbon chains of boundary lipids near the protein molecule below T_c. This perturbation, caused by the protein, extends at least to the second neighbor, leading to an expansion of the monolayers. On the other hand, the hydrophilic proteins do not perturb the phospholipid structure below T_c because of their low hydrophobicities, showing ideal mixing in monolayers. At T_c or above, the membrane properties are independent of a variety of proteins, since all lipid hydrocarbon chains cause a disordering, which results in ideal mixing.

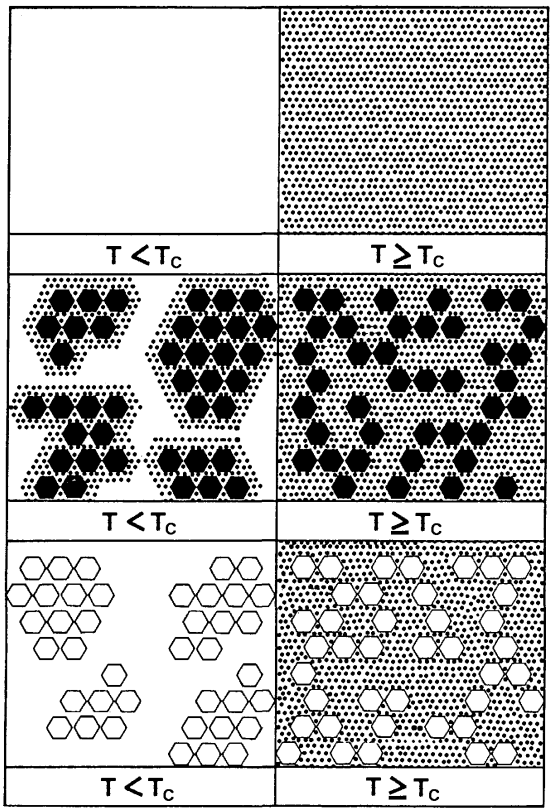

Fig. 8. A model of monolayers composed of phospholipids and different proteins as a function of temperatures, based on the lattice model of proteins and lipids in computer simulation by Lookman et al.[52] The black and open hexagons are the respective hydrophobic and hydrophilic proteins, the dots are perturbed lipids, and the blank areas are unperturbed lipids.

The skillful technical assistance of Misses Junko Hata, Kyoko Morikawa, and Kana Tabata is gratefully acknowledged.

References

1) S. Singer and G. Nicolson, *Science*, **175**, 720 (1972).
2) S. Marčelja, *Biochim. Biophys. Acta*, **455**, 1 (1976).
3) J. C. Owicki, N. W. Springgate, and H. M. McConnell, *Proc. Natl. Acad. Sci. U. S. A.*, **75**, 1616 (1978).
4) J. C. Owicki and H. M. McConnell, *Proc. Natl. Acad. Sci. U. S. A.*, **76**, 4750 (1979).
5) H. L. Scott and S. -L. Cherng, *Biochim. Biophys. Acta*, **510**, 209 (1978).
6) T. Kambara, H. Kohno, N. Sasaki, and K. Gondaira, *J. Phys. Soc. Jpn.*, **53**, 3699 (1984).
7) D. Chapman, J. Urbina, and K. M. Keough, *J. Biol. Chem.*, **249**, 2512 (1974).
8) A. J. Verkleij, B. Dekruyff, P. H. H. Th. Ververgaert, J. F. Tocanne, and L. L. M. Van Deenen, *Biochim. Biophys. Acta*, **339**, 432 (1974).

9) D. Papahadjopoulos, M. Moscarello, E. H. Eylar, and T. Isac, *Biochim. Biophys. Acta*, **401**, 317 (1975).
10) F. Jähnig, H. Vogel, and L. Best, *Biochemistry*, **21**, 6790 (1982).
11) M. Bloom and I. C. P. Smith, "Progress in Protein-Lipid Interactions," ed. by A. Watts and J. J. H. H. De Pont, Elsevier, Amsterdam (1985), Vol. 1, pp. 61—88.
12) F. Jähnig, *Proc. Natl. Acad. Sci. U. S. A.*, **80**, 3691 (1983).
13) A. Kato and S. Nakai, *Biochim. Biophys. Acta*, **624**, 13 (1980).
14) H. F. Bigelow, *J. Theoret. Biol.*, **61**, 187 (1967).
15) K. Kyte and R. F. Doolittle, *J. Mol. Biol.*, **157**, 105 (1982).
16) T. Mita, *Bull. Chem. Soc. Jpn.*, **62**, 2299 (1989).
17) P. J. Quinn and R. M. C. Dawson, *Biochem. J.*, **116**, 671 (1970).
18) J. Peters and P. Fromherz, *Biochim. Biophys. Acta*, **394**, 111 (1975).
19) R. J. Davies and M. N. Jones, *Biochim. Biophys. Acta*, **858**, 135 (1986).
20) M. C. Wilkinson, B. N. Zaba, D. M. Taylor, D. L. Laidman, and T. J. Lewis, *Biochim. Biophys. Acta*, **857**, 189 (1986).
21) W. N. Heckl, B. N. Zaba, and H. Möhwald, *Biochim. Biophys. Acta*, **903**, 166 (1987).
22) D. G. Cornell, *J. Colloid Interface Sci.*, **88**, 536 (1982).
23) D. G. Cornell and R. J. Carroll, *Colloid Surf.*, **6**, 385 (1983).
24) D. G. Cornell and R. J. Carroll, *J. Colloid Interface Sci.*, **108**, 226 (1985).
25) S. Ställberg and T. Teorell, *Trans. Faraday Soc.*, **35**, 1413 (1939).
26) H. J. Karam, *J. Appl. Polym. Sci.*, **18**, 1693 (1974).
27) M. C. Phillips, *Prog. Surf. Memb. Sci.*, **5**, 139 (1972).
28) P. F. Devaux and M. Seigneuret, *Biochim. Biophys. Acta*, **822**, 63 (1985).
29) H. Hinz and J. M. Sturtevant, *J. Biol. Chem.*, **247**, 6071 (1972).
30) D. Staszewska, J. Kovář, and M. Bohdanecký, *Colloid Polym. Sci.*, **258**, 600 (1980).
31) A. F. Henson, J. R. Mitchell, and P. R. Mussellwhite, *J. Colloid Interface Sci.*, **32**, 162 (1970).
32) F. MacRitchie, *Adv. Protein Chem.*, **32**, 283 (1976).
33) T. Takenaka, K. Harada, and M. Matsumoto, *J. Colloid Interface Sci.*, **73**, 569 (1980).
34) R. M. McElhaney, *J. Mol. Biol.*, **84**, 145 (1974).
35) E. Oldfield and D. Chapman, *FEBS Lett.*, **23**, 285 (1972).
36) En-Shinn Wu, K. Jacobson, and D. Papahadjopoulos, *Biochemistry*, **16**, 3936 (1977).
37) D. Chapman, B. A. Cornell, A. W. Eliasz, and A. Perry, *J. Mol. Biol.*, **113**, 517 (1977).
38) P. F. Knowles, A. Watts, and D. Marsh, *Biochemistry*, **18**, 4480 (1979).
39) D. Kimelman, E. S. Tecoma, P. K. Wolber, B. S. Hudson, W. T. Wickner, and R. D. Simoni, *Biochemistry*, **18**, 5874 (1979).
40) M. P. Heyn, R. J. Cherry, and N. A. Dencher, *Biochemistry*, **20**, 840 (1981).
41) T. J. O'Leary, *Biochim. Biophys. Acta*, **731**, 47 (1983).
42) J. R. Abney and J. C. Owicki, "Progress in Protein-Lipid Interactions," ed. by A. Watts and J. J. H. H. De Pont, Elsevier, Amsterdam (1985), Vol. 1, pp. 1—60.
43) E. J. J. Van Zoelen, P. W. M. Van Dijck, B. de Kruijff, A. J. Verkleij, and L. L. M. Van Deenen, *Biochim. Biophys. Acta*, **514**, 9 (1978).
44) D. Papahadjopoulos, W. J. Vail, and M. Moscarello, *J. Membrane Biol.*, **22**, 143 (1975).
45) C. Mollay, *FEBS Lett.*, **64**, 65 (1976).
46) M. C. Phillips and D. Chapman, *Biochim. Biophys. Acta*, **163**, 301 (1968).
47) T. L. Steck, *J. Cell Biol.*, **62**, 1 (1974).
48) V. Speth and F. Wunderlich, *Biochim. Biophys. Acta*, **291**, 621 (1973).
49) B. F. Dickens and G. A. Thompson, Jr., *Biochemistry*, **19**, 5029 (1980).
50) P. Calissano, S. Alema, and G. Rusca, *Biochim. Biophys. Acta*, **255**, 1009 (1972).
51) D. Papahadjopoulos, M. Cowden, and H. Kimelberg, *Biochim. Biophys. Acta*, **330**, 8 (1973).
52) T. Lookman, D. A. Pink, E. W. Grundke, M. J. Zuckermann, and F. de Verteuil, *Biochemistry*, **21**, 5593 (1982).

Photoreactions of Polyhalobenzenes in Benzene. Formation of Terphenyls

Masahiro NAKADA,* Chihiro MIURA, Hideaki NISHIYAMA,† Futoshi HIGASHI,† Toru MORI,† Minoru HIROTA,*,† and Tetsuo ISHII††

Chemical Laboratory, Chiba Institute of Technology, Narashino 275
†Department of Synthetic Chemistry, Faculty of Engineering, Yokohama National University, Hodogaya-ku, Yokohama 240
††Yokohama Research Institute for Environmental Protection, Takigashira, Isogo-ku, Yokohama 235

(Received March 31, 1989)

Polychlorobenzenes, polybromobenzenes, and polychloropolybromobenzenes ($C_6H_{6-n}X_n$) were photolyzed in benzene solutions; the products were analyzed by the GC/MS method. Both dehalogenation and phenylation were shown to take place competitively, producing (poly)halobenzenes bearing one less halogen atom ($C_6H_{7-n}X_{n-1}$) and (poly)halobiphenyls ($C_6H_{6-n}X_{n-1}$-C_6H_5) as the major products. Besides these products, terphenyl was produced by a consecutive phenylation of the halobiphenyl formed. Polychlorobenzenes were shown to form the corresponding terphenyls only when a pathway via 2-chlorobiphenyl is possible; however, polybromobenzenes can produce terphenyls through any of the isomeric bromobiphenyls intermediarily formed. Isomerization through *m*-migration of a chlorine atom was also shown to occur to a considerably lesser extent.

In connection with the photochemical degradation of toxic polyhalobenzenes, several photo-dehalogenation procedures of polyhaloaromatic compounds have been reported.[1-4] Pinhey and Rigby,[5] as well as Ichimura and Mori,[6,7] have independently studied the mechanism of dehalogenation of simple halobenzenes, showing that the initial photochemical process is the fission of the carbon-halogen bond proceeding via a pi-pi* triplet state, of this reaction involved. In contrast to the initial photophysical and photochemical processes involved, the subsequent reactions of the aryl free radicals generated from monohalobenzenes have been extensively studied.[8] The aryl free radical generated by this initial process is assumed to induce several subsequent reactions, such as the abstraction of a hydrogen atom from the solvent, substitution of a hydrogen atom in the solvent molecule, etc. However, relatively few investigations have been reported on the photolytic behavior of polyhalobenzens.[3,4]

We previously examined the photoreactions of polyhalobenzenes in both hexane[9] and acetonitrile,[10] showing that the reactivities of halogen atom in the substrate depend both on its chemical environment and on the nature and number of substituent halogen atoms. It was also shown that a more crowded halogen atom leaves more easily. The photolyses were also dependent on the nature of the solvent, giving isomerized products in solvents which resist hydrogen abstraction.

In this paper, we discuss the photochemical behavior of polyhalobenzenes in benzene solutions, where both dehalogenation and phenylation take place competitively. Special attention is paid to the formation of terphenyls by the consecutive phenylation of the halobiphenyls primarily formed.

Experimental

Materials. The polyhalobenzenes and chlorobiphenyls employed in this research are all known compounds. They were either purchased commercially or prepared by the known methods[11,12] and used after purification by distillation or by column chromatography.

Photoreactions. The photoreactions were carried out using a 32-W (or 20-W) low-pressure mercury arc lamp placed at the center of a concentrically surrounding quartz vessel containing the solution of the reactant polyhalobenzene. They were carried out under a nitrogen atmosphere, unless otherwise noted.

Spectral and Gas Chromatographic Measurements. Gas chromatography/mass spectrometry measurements were carried out on a Hitachi RMU-6L, a Shimadzu LKB-9000-B, or a Shimadzu QP1000 mass spectrometer. Routine gas chromatographic analyses of the products were carried out on a Shimadzu GC-6A or a GC-4B-PTF apparatus equipped with a Silicone SE 30 or an Apiezon L column (3 mm×2 m).

Results and Discussion

General Trends of the Photoreactions. As described in our previous papers,[9,10] the photoreactions were pursued by quantitative GC analyses of the products and the unreacted starting halobenzene. Since our interests were focused on the products in various solvents, only the relative reactivity is presented and discussed. The reaction mixture was sampled at regular intervals and the products were analyzed. The products at halfway conversions of various polyhalobenzenes are given in Table 1.[13]

The reactions in benzene solutions proceeded far more slowly than those in hexane. They are even slower than those in acetonitrile, which is assumed to be a less reactive solvent towards hydrogen abstraction. For example, *o*-dichlorobenzene was photolyzed 26.5-times faster in hexane and 17.6-times faster in acetonitrile when compared with a similar reaction in benzene. The retardation by benzene is quite general in the photolyses in Table 1; it might be ascribable to light absorption by the solvent.

As foreseen from the previous results,[8,14] both dehalogenation and phenylation reactions proceed com-

Table 1. Products by the Photolyses of Polyhalobenzenes[a)]

Reactant	t/h	C/%	Products (Yield/%)
(a) Polychlorobenzenes			
o-$C_6H_4Cl_2$[13)]	40	58.5	2-Cl-BP(42.7), BP(14.0), *o*-TP(1.2)
m-$C_6H_4Cl_2$	40	42.2	3-Cl-BP(40.9), BP(0.8)
p-$C_6H_4Cl_2$	40	26.7	4-Cl-BP(25.8), BP(0.5)
1,2,3-$C_6H_3Cl_3$	40	36.8	2,6-Cl_2-BP(20.6), 6′-Cl-*o*-TP(2.6), 2-Cl-BP(2.2), *o*-TP(1.5), BP(1.4), *m*-Cl_2-B(1.0)
1,2,4-$C_6H_3Cl_3$	40	36.0	2,5-Cl_2-BP(22.3), 3-Cl-BP(2.9), 4-Cl-BP(1.1), *p*-Cl_2-B(0.5)
1,3,5-$C_6H_3Cl_3$	40	33.0	3,5-Cl_2-BP(31.4), *m*-Cl_2-B(0.8)
1,2,3,4-$C_6H_2Cl_4$	40	39.5	2,3,6-Cl_3-BP(21.2), 1,2,4-Cl_3-B(2.7), 4′-Cl-*o*-TP(1.8), 3′,6′-Cl_2-*o*-TP(1.2), 2,5-Cl_2-BP(0.9), BP(0.6)
1,2,3,5-$C_6H_2Cl_4$	40	13.3	2,4,6-Cl_3-BP(6.7), 2,3,5-Cl_3-BP(4.5), 1,3,5-Cl_3-B(2.1)
1,2,4,5-$C_6H_2Cl_4$	40	12.5	2,4,5-Cl_3-BP(8.9), 3,4-Cl_2-BP(1.8), 1,2,4-Cl_3-B(1.8)
(b) Polybromobenzenes			
o-$C_6H_4Br_2$	20	80.7	BP(24.2), 2-Br-BP(16.0), Br-B(12.7), *o*-TP(1.4)
m-$C_6H_4Br_2$	20	62.0	3-Br-BP(36.3), *m*-TP(17.9), Br-B(9.9), BP(7.5)
p-$C_6H_4Br_2$	20	78.0	4-Br-BP(20.0), Br-B(19.6), BP(10.5), *p*-TP(8.8)
p-$C_6D_4Br_2$	15	57.5	4-Br$C_6D_4C_6H_5$(20.3), BP(9.3),[c)] C_6HD_4Br(8.6), *p*-TP-d_4(4.0)
1,2,3-$C_6H_3Br_3$[c)]	24	47.0	2,6-Br_2-BP(14.0), 2,3-Br_2-BP(12.0), *m*-Br_2-B(9.5), 2′-Br-*m*-TP(3.3)
1,2,4-$C_6H_3Br_3$[c)]	24	20.0	3-Br-BP(9.3), *p*-Br_2-B(1.3), 2,5-Br_2-BP(1.0), 4′-Br-*m*-TP(trace)
1,3,5-$C_6H_3Br_3$[c)]	24	30.5	3,5-Br_2-BP(22.0), 5′-Br-*m*-TP(7.2), *m*-Br_2-B(1.0), 1,3,5-Ph_3-B(trace)
1,2,3,4-$C_6H_2Br_4$	20	60.1	4′-Br-*m*-TP(21.1), 1,2,4-Br_3-B(11.7), BP(2.9), 3-Br-BP(1.4), Br_3-BP(23.0)[b)]
1,2,3,5-$C_6H_2Br_4$	20	41.5	3,4,5-Br_3-BP(16.9), 2,4,6-Br_3-BP(16.1), 1,3,5-Br_3-B(4.9), 3,5-Br_2-BP(2.7), BP(0.6), 5′-Br-*m*-TP(trace)
1,2,4,5-$C_6H_2Br_4$	20	44.9	*m*-TP(36.2),[b)] 2,4,5-Br_3-BP(5.6), 3-Br-BP(1.5), 1,2,4-Br_3-B(1.5), 4′-Br-TP(trace), BP(trace)
C_6HBr_5[d)]	20	59.9	4′,6′-Br_2-*m*-TP(35.1), BP(5.1), 1,2,4,5-Br_4-B(19.7), 3-Br-BP(trace)
(c) Polybromochlorobenzenes			
o-C_6H_4BrCl	30	45.4	2-Cl-BP(27.2), BP(16.8), *o*-TP(1.4)
m-C_6H_4BrCl	30	44.7	3-Cl-BP(42.9), BP(1.8)
p-C_6H_4BrCl	30	30.0	4-Cl-BP(28.2), BP(1.2)
2,6-$Cl_2C_6H_3Br$	30	59.2	2,6-Cl_2-BP(42.2), 3′-Cl-*o*-TP(6.7), 2-Cl-BP(3.5), *m*-Cl_2-B(3.4)
2,3-$Cl_2C_6H_3Br$	20	43.1	2,3-Cl_2-BP(28.3), 3-Cl-BP(13.9), 3′-Cl-*o*-TP(1.9)
2,6-$Br_2C_6H_3Cl$	20	82.5	2-Cl-3-Br-BP(28.3), BP(19.2), 3-Br-BP(16.6), 2′-Cl-*m*-TP(16.4), *o*-C_6H_4ClBr(2.0)
2,4-$Cl_2C_6H_3Br$[c)]	22	30.8	2,4-Cl_2-BP(14.0), 4-Cl-BP(10.0), 3-Cl-4-BrBP(4.2), 4′-Cl-*o*-TP(1.6)
2,5-$Cl_2C_6H_3Br$	20	63.0	2,5-Cl_2-BP(44.4), 3-Cl-BP(13.1), 4′-Cl-*o*-TP(4.0)
3,4-$Cl_2C_6H_3Br$	20	33.4	3,4-Cl_2-BP(16.4), *o*-Cl_2-B(8.6), 2-Cl-5-Br-BP(4.1), 4-Cl-BP(1.2)
2,5-$Br_2C_6H_3Cl$	20	37.2	2-Cl-4-Br-BP(17.1), 4-Br-BP(8.2), 3-Cl-4-Br-BP(4.3), *m*-C_6H_4ClBr(2.7), 3-Cl-BP(1.6)
3,5-$Cl_2C_6H_3Br$	20	46.8	3,5-Cl_2-BP(44.5), 3-Cl-BP(1.1), *m*-C_6H_4ClBr(1.1)
3,5-$Br_2C_6H_3Cl$	20	92.4	5′-Cl-*m*-TP(36.1), 3-Cl-BP(30.3), 3-Cl-5-Br-BP(25.2), *m*-C_6H_4ClBr(1.0)

a) Reactions were carried out by using a 32-W low pressure mercury arc lamp under nitrogen atmosphere at ambient temperature (ca. 25 °C). The concentrations of the reactants were 0.10 mol l^{-1} except the runs otherwise remarked. Following abbreviations were used: C=conversion of the reactant, B=benzene, BP=biphenyl, and TP=terphenyl. Yields were calculated with respect to the reactant. b) The overlap of other weaker GC peak(s) is suspected. c) 20-W Lamp was employed for the irradiation. d) 0.04 mol l^{-1}.

petitively. In all runs in Table 1, the phenylation proceeds more predominantly than the dehalogenation when compared with the products of the primary photolysis of the starting polyhalobenzenes. This trend is shown illustratively in the time-conversion curves of Fig. 1. The preference of phenylation becomes more significant in the cases of chlorinated benzenes than in the cases of brominated benzenes. Dihydrobiphenyl derivatives can also be expected to be generated by the disproportionation of the arylcyclohexadienyl radical intermediate (**1**).[15,16)] Actually, they were detected in neither case.

The orientation of the photochemical dechlorination and phenylation in benzene is similar to those observed previously with the reactions in hexane;[9)] i.e., the C-Cl bond scissored by two adjacent(ortho) halogen atoms is cleaved most easily and the one scissored by two hydrogen atoms most difficultly. Thus, the reactivity of the encircled halogen atom increases in the following order:

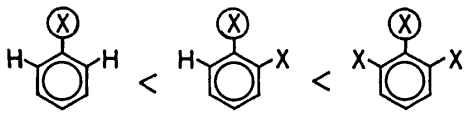

Scheme 1.

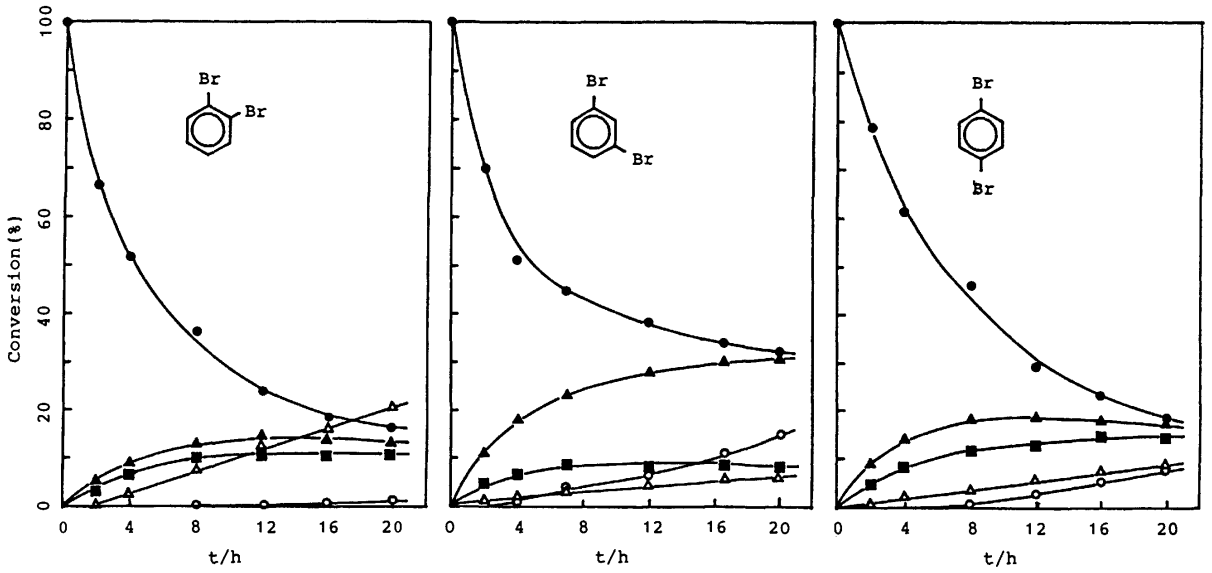

Fig. 1. Time conversion curves for the photolyses of dibromobenzenes (—●—, dibromobenzene (reactant); —▲—, bromobiphenyl; —■—, bromobenzene; —○—, terphenyl; —△—, biphenyl),

This trend is more significant with the photolyses of polychlorobenzenes in benzene solution; the reaction occurs far more preferably on the most crowded C-Cl bond in benzene. Thus, 2,6-dichloro-, 2,5-dichloro-, 2,3,6-trichloro-, and 2,4,6-trichlorobiphenyls were obtained almost exclusively as the phenylated products of the photolyses in benzene of 1,2,3-trichloro-, 1,2,4-trichloro-, 1,2,3,4-tetrachloro-, and 1,2,3,5-tetrachlorobenzenes, respectively.

Corresponding dechlorination products (H in place of C_6H_5) were also found, except for the runs on dichlorobenzenes. These are known as the major products of photolyses in hexane.[9] This fact suggests that the reactions in both solvents proceed via a common haloaryl free-radical intermediate generated by a photolytic cleavage of the encircled chlorine atom in Scheme 2.

Reactant	Major Products	
	in Hexane	in Benzene
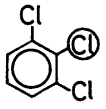	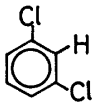	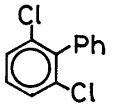
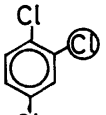	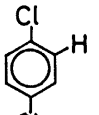	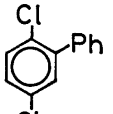
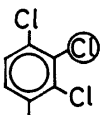	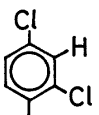	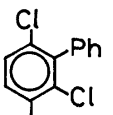
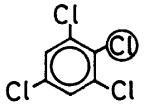	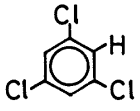	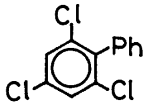

Scheme 2.

In the cases of polybromobenzenes, the reactions proceed less selectively, giving most of the possible phenylated and debrominated products. The distribution of products is not so selective as in the reactions of polychlorobenzenes, on the whole becoming more similar to the reactions in hexane. For example, the photolysis of 1,2,3-tribromobenzene gave comparable amounts of 2,6-dibromobiphenyl (14.0%, a phenylation product), 2,3-dibromobiphenyl (12.0%, the other phenylation product), and *m*-bromobenzene (9.5%, a dehalogenation product). This illustrated that the phenylation does not proceed so regioselectively and is not so overwhelming, as in the photolysis of 1,2,3-trichlorobenzene, which gave 28.3% of 2,6-dichlorobiphenyl and its descents and only 1.0% of *m*-chlorobenzene (all could be derived by the replacement of 2-chlorine atom) without giving detectable amounts of products derived by the replacement of the 1-chlorine atom. Similarly, considerable amounts of *m*-dibromo-, *p*-dibromo-, 1,2,4-tribromo-, 1,3,5-tribromo-, and 1,2,4,5-tetrabromobenzenes were produced as debromination products during the photolyses of 1,2,3-tribromo-, 1,2,4-tribromo-, 1,2,3,4-tetrabromo-, 1,2,3,5-tetrabromo-, and pentabromobenzenes, respectively, in benzene.

In a series of (poly)bromochlorobenzenes, $C_6H_{6-n-m}Br_nCl_m$, bromine is always easier to leave, giving a product formed by the replacement of bromine.

When two different bromine atoms in the same molecule are compared, the reactivity is still governed by the same rule (that the replacement of the most crowded halogen atom takes place most favorably), as is the cases for other polyhalobenzenes. For example, 2-chloro-4-bromobiphenyl, which is produced by the replacement of more crowded bromine atom, is the major photo-product from 2,5-dibromochlorobenzene.

Consecutive Phenylation Forming Terphenyls. As could easily be deduced from the fact that terphenyls were found as the products of the photolyses of dihalobenzenes (Table 1), the primarily produced halobiphenyls were further subjected to subsequent photoreactions producing terphenyl (phenylation) and biphenyl (dehalogenation). Judging from the products of the photolyses of dihalobenzenes, which contain lesser amounts of terphenyls than biphenyl, phenylation should proceed less predominantly than dehalogenation during the photolyses of halobiphenyls. The arylation by the photochemically generated biphenylyl radicals seemed to be dependent both on the nature and the location of the leaving halogen atom. 2-Chlorobiphenyls tend to produce the corresponding *o*-terphenyls far more favorably than 3- and 4-chlorobiphenyls. This trend is considerably different from the photolyses of polyhalobenzenes, which produce phenylated product far more predominantly. As given in Scheme 3, all terphenyls from polychlorobenzenes could be explained by a series of ortho-phenylation (solid arrows) and dehalogenation (broken arrows) reactions. In contrast, the C-Br bonds were shown to behave quite differently from the C-Cl bond. Thus, 3- and 4-bromobiphenyls are inclined to form the corresponding terphenyls more favorably than 2-bromobiphenyls.

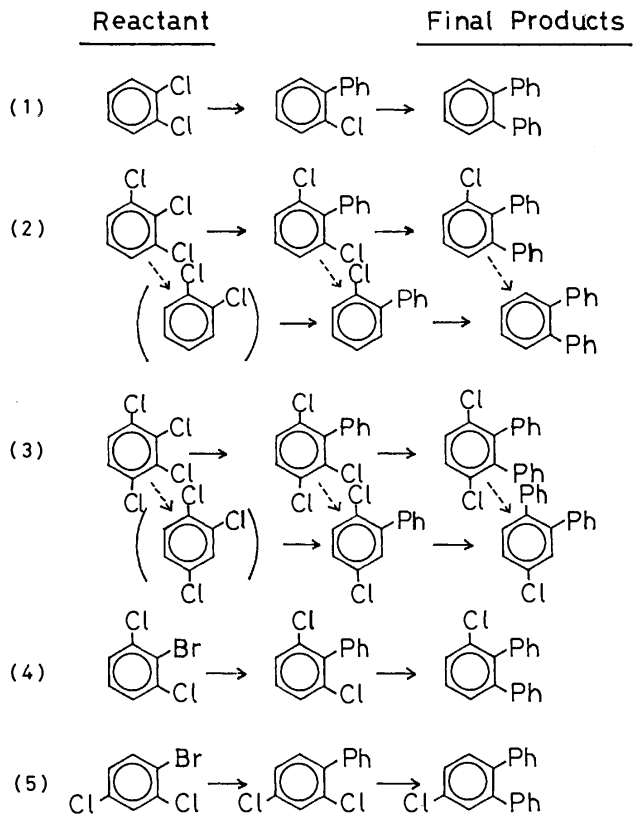

Scheme 3.

In order to confirm the fact that the produced halobiphenyls are subjected to the consecutive photolyses producing terphenyls and biphenyl, the photolyses of chlorobiphenyls were examined in benzene solutions. The photolyses of chlorinated biphenyls had been shown to give dehalogenated products when carried out in solvents susceptible to hydrogen abstraction (alkanes and alcohols).[17,18] Photolysis in benzene has never been reported, however. The reactions of the three isomeric chlorobiphenyls were carrid out under exactly the same conditions as the reactions of dichlorobenzenes in benzene solutions, except for the duration of the reaction. The products and their yields are given in Table 2.

As expected from the results on dichlorobenzenes, 2-chlorobiphenyl photolyzes far faster than the other two isomers, giving biphenyl, *o*-terphenyl, and 4-chlorobiphenyl. *m*- and *p*- Terphenyls were not detected as the products of runs starting from 3- and 4-chlorobiphenyls. In the latter two runs, dechlorination also proceeded much more slowly than the *o*-isomer. The three runs on isomeric chlorobiphenyls (in Table 2) agreed with the assumption that *o*-terphenyl was formed by the successive photolysis of 2-chlorobiphenyl, which is a primary product of the photolysis of *o*-dichlorobenzene. Therefore, the above pathway of the reaction was supported by experiments. In line with the expectation from the results in Table 1, the dechlorination predominates over the phenylation in this series of compound.

The formation of terphenyls from dibromobenzenes can also be assumed to proceed via the concecutive phenylation of bromobiphenyl, which is a primary photoproduct, since the amount of formed terphenyls could be accounted for almost quantitatively from the amounts of bromobiphenyls present in the reaction mixture. To be more concrete, the time-conversion curve (Fig. 1) shows that the amount of the newly produced terphenyl is approximately proportional to the amount of the bromobiphenyl present in the reaction system at the time of measurement.

Isomerization of *o*-Dichlorobenzene and 2-Chlorobiphenyl. We have recently reported the novel

Table 2. Products by the Photolyses of Chlorobiphenyls[a)]

Chlorobiphenyl	*t*/h	*C*/%	Products (Yield/%)
2-$ClC_6H_4C_6H_5$	48	29.8	BP(26.7), *o*-TP(2.4), *p*-ClBP(0.7)
3-$ClC_6H_4C_6H_5$	48	2.3	BP(2.3)
4-$ClC_6H_4C_6H_5$	48	0.3	BP(0.3)

a) See footnotes of Table 1.

photo-rearrangement of a chlorine atom in polychlorobenzenes bearing two or more contiguous halogen atoms on the ring. The meta-migration of the chlorine atom has been shown to take place exclusively, giving, for example, *p*-dichlorobenzene from *o*-dichlorobenzene in acetonitrile.[10] This reaction is very specific; products from ortho- and para-migrations were detected in neither case. The rearrangement seems to compete with the hydrogen abstraction reaction and becomes observable with the photoreactions in solvents resistive to hydrogen-abstraction. The C-H bond of benzene can be expected to be a little less susceptible to hydrogen-abstraction than acetonitrile, since its bond dissociation energy (469 kJ mol^{-1}) is slightly higher than that of acetonitrile (429 kJ mol^{-1}).[20] Thus, the photoproducts from *o*-dichlorobenzene and 2-chlorobiphenyl in benzene were carefully examined in search of the rearranged products.

A small amount (0.7%) of 4-chlorobiphenyl was found in the photoproduct from 2-chlorobiphenyl. Although routine GC analyses gave no evidence of its presence, a trace amount of 4-chlorobiphenyl was also detected by a careful GC/MS examination of the products from the photolysis of *o*-dichlorobenzene. Its yield was estimated to be 0.2%. Rearranged products could not be detected with the runs starting from *m*- and *p*-dichlorobenzenes, even if the products were analyzed by exactly the same conditions using GC/MS.

The authors thank Professor Sachio Fukushi for his advice and encouragement throughout this work. This research was supported partly by the Grant-in-Aid for Scientific Research from the Ministry of Education, Science and Culture to which we are grateful.

References

1) L. Vollner, H. Rohlender, W. Klein, and F. Korte, *GSF-Ber.*, **205**, 71 (1975).
2) L. J. Bailin, B. Herzner, and D. A. Oberacker, *Environ. Sci. Technol.*, **12**, 673 (1978).
3) T. Nishikawa, A. Ninomiya, K. Anda, and S. Nakayama, *Nippon Kagaku Kaishi*, **1982**, 2225; **1973**, 2326.
4) M. Usui, T. Nishiwaki, K. Anda, and M. Hida, *Nippon Kagaku Kaishi*, **1982**, 638.
5) J. T. Pinhey and R. D. G. Rigby, *Tetrahedron Lett.*, **1969**, 1267.
6) T. Ichimura and Y. Mori, *J. Chem. Phys.*, **58**, 288 (1973).
7) T. Ichimura, Y. Mori, H. Shinohara, and N. Nishi, *Chem. Phys. Lett.*, **122**, 51 (1985).
8) T. Matsuura and K. Omura, *Bull. Chem. Soc. Jpn.*, **39**, 944 (1966).
9) M. Nakada, S. Fukushi, H. Nishiyama, K. Okubo, K. Kume, M. Hirota, and T. Ishii, *Bull. Chem. Soc. Jpn.*, **56**, 2447 (1983).
10) K. Morisaki, Y. Miura, K. Abe, M. Hirota, and M. Nakada, *Chem. Lett.*, **1987**, 1589.
11) H. Furuyama and S. Fukushi, *Yuki Gosei Kagaku Kyokaishi*, **29**, 413 (1971).
12) P. E. Fanta, *Synthesis*, **1974**, 9.
13) Three independent runs on *o*-dichlorobenzene gave mixtures of similar composition. All three runs were carried out with 0.1 M benzene solutions at ambient temperature, giving 42.7, 38.0, and 39.5% of 2-chlorobiphenyl, 14.0, 13.6, and 12.9% of biphenyl, and 1.2, 0.9, and 1.0% of *o*-terphenyl, respectively, after 40 h's duration of the irradiation. This enables us to compare the products of different runs and to discuss the relative reactivity.
14) M. Kojima, H. Sakuragi, and K. Tokumaru, *Chem. Lett.*, **1981**, 1539.
15) D. F. DeTar and R. A. J. Long, *J. Am. Chem. Soc.*, **80**, 4742 (1858).
16) M. Eberhardt and E. L. Eliel, *J. Org. Chem.*, **27**, 2289 (1962).
17) L. O. Ruzo, M. J. Zabik, and R. D. Schuetz, *J. Am. Chem. Soc.*, **96**, 3809 (1974).
18) N. J. Bunce, Y. Kumar, L. Ravanal, and S. Safe, *J. Chem. Soc., Perkin Trans. 2*, **1980**, 880.
19) In the case of 2-chlorobiphenyl, phosphorescence spectrum could not been obtained probably because of its photolabile nature.
20) a) "Kagaku Benran" 2nd ed., ed by Chem. Soc. Jpn., Maruzen Publ. Co. 1975, p. 976.

Sulfur Nitrides in Organic Chemistry. 18.[1] Preparation and Reduction of Benzo[1,2-*c*:3,4-*c'*:5,6-*c''*]tris- and Benzo[1,2-*c*:3,4-*c'*]bis[1,2,5]-thiadiazole. A Convenient Route to Benzenehexamine and 1,2,3,4-Benzenetetramine

Shuntaro MATAKA,* Hisao EGUCHI,† Kazufumi TAKAHASHI, Taizo HATTA,† and Masashi TASHIRO
Institute of Advanced Material Study, 86, Kyushu University, 6-1 Kasuga-koh-en, Kasuga-shi, Fukuoka 816
†Department of Molecular Science and Technology, Graduate School of Engineering Sciences, 39, Kyushu University, 6-1 Kasuga-koh-en, Kasuga-shi, Fukuoka 816
(Received April 4, 1989)

Benzotris- (**3**) and benzobis[1,2,5]thiadiazole (**4**) were prepared in a moderate yield, respectively, by the reaction of tetrasulfur tetranitride (**5**) with halocatechols (**6**) and -resorcinols (**7**). The reduction of **3** and **4** with Sn powder in a mixture of concentrated hydrochloric acid and dioxane gave benzenehexamine (**1**) and 1,2,3,4-benzenetetramine (**2a**) and its 5-methyl derivative (**2b**) in good yields, as a stable tri- (**1**·**3HCl**) and dihydrochloride (**2**·**2HCl**), respectively.

Synthesis of benzenehexamine (**1**) was first reported in 1929[2] and some of its derivatives in 1937.[3] It attracted little attention until recently when it has been recognized as a building block for materials having interesting physical properties.[4-8] As to 1,2,3,4-benzenetetramines (**2**), literature survey revealed that 1,2,3,4-benzenetetramine (**2a**)[9] and its 5-methyl derivative (**2b**)[10] were already prepared in 1889 and 1890, respectively. To our best knowledge, subsequently, **2** has not been mentioned, except for LCAO-MO calculations on **2a**.[11]

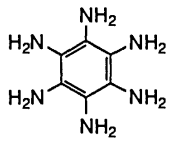

1

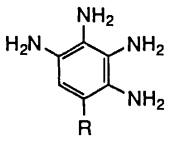

2a: R=H
2b: R=Me

Previously, it was found[12] that benzotris- (**3**) and benzobis[1,2,5]thiadiazole (**4a**), which are synthetic equivalents of **1** and **2a**, respectively, were obtained by the reaction of tetrasulfur tetranitride N_4S_4 (**5**) with alkyl phenyl ether but only in poor yield (Scheme 1). We recently reported[13,14] the reaction of **5** with alkyl- and alkylhalophenols, giving 2,1,3-benzothiadiazoles and the conversion of 4,6-di-*t*-butyl-2,1,3-benzothiadiazole into *o*-phenylenediamine (Scheme 2).

The present paper deals with the convenient preparation of **3** and **4** by the reaction of **5** with benzenediols and benzenetriols such as catechols (**6**), resorcinols (**7**), phloroglucinol (**8a**), and pyrogallol (**8b**) and their reduction to give benzenehexamine (**1**) and 1,2,3,4-benzenetetramine (**2a**) and its 5-methyl derivative (**2b**), respectively.

Results and Discussion

Preparation of 3 and 4. Reactions of **5** with **6**, **7**, and **8** were carried out in refluxing toluene (Schemes 3 and 4). The results are summarized in Tables 1 and 2.

It was found[14,15] that, in the reaction of **5** with phenols, *t*-butyl groups and halogen atoms worked well as a leaving group. In the formation of *t*-butylbenzobis[1,2,5]thiadiazole (**4b**), however, the *t*-butyl group was not effective but bromine atom worked well, giving **4b** in 45% yield. The methyl derivative (**4c**) was prepared in 23% yield from 4-

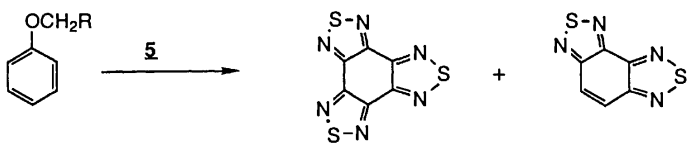

3 **4a**

Scheme 1.

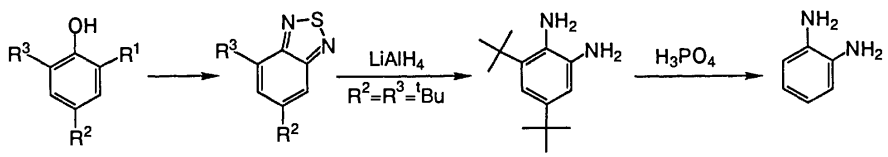

Scheme 2.

bromo-5-methylcatechol (**6e**). Tribromocatechol (**6f**) gave **4d** in a poor yield (8%). Isopropylcatechol (**6g**) gave the expected **4e** in only 6% yield. In reactions with **6e—6g**, a small amount of benzotris[1,2,5]-thiadiazole (**3**) was obtained as a by-product. Interestingly, **3** was the sole product in 32% yield in the reaction with **6h**. Compound **3** is now easily accessible, starting from catechol in only two steps.

In the reactions of **5** with *t*-butylresorcinols, **7a** and **7b**, **4b** was obtained in low yields. Dibromoethylresorcinol (**7c**) gave the expected **4f** in 11% yield, accompanied with 4-(1,2,5-thiadiazol-3-yl)benzobis-[1,2,5]thiadiazole (**4g**). Though **4g** was considered to be formed via **4f**, the reaction of **5** with **4f** did not proceed in refluxing toluene and unchanged **4f** was recovered. The reaction of **5** with polyhaloresorcinols, **7d**, **7e**, **7h**, **7i**, and **7k**, provides a convenient preparative method for halobenzobis[1,2,5]thiadiazoles, **4h** and **4i**. Benzotris[1,2,5]thiadiazole (**3**) was obtained as a by-product in 10—15% yield in these reactions. Only a bromine atom was removed in the reactions with **7h**, **7i**, and **7k**, giving **4i**. Both **4h** and **4i** are inert towards **5** in refluxing toluene. This indicates that **3** was not formed via **4h** and **4i**. The bromo derivative (**4d**) was obtained in a better yield (40%) in the reaction with tribromoresorcinol (**71**) than with tribromocatechol (**6f**) (8%). The reaction with benzenetriols (**8**) gave unsatisfactory results.

Reduction of 3 and 4. The reduction of benzotris-(**3**) and benzobis[1,2,5]thiadiazole (**4**) to benzenehexamine (**1**) and 1,2,3,4-benzenetetramine (**2**) were investigated.

$LiAlH_4$-reduction of **3** and **4** proceeded as evolution of H_2S was observed, but, isolation of unstable **1** and **2** was unsuccessful and tarry materials were formed.

We expected that reduction under acidic conditions might give **1** and **2** as a stable salt. Treatment of **3** with Sn powder in a hot mixture of concentrated hydrochloric acid and dioxane brought about the precipitation of **1-HCl-dioxane** (1/3/0.5) as a white solid during the reaction. This compound gave benzotripyrazine (**9**)[6] in the reaction with benzil (**10**) in 60% yield from **3** (Scheme 5).

When **4b** was treated under the conditions described above, **4b** was consumed, but precipitation of the expected 5-*t*-butyl-1,2,3,4-benzenetetramine dihydrochloride did not occur. Neutralization of the reaction mixture with $NaHCO_3$ afforded dark violet resinous materials. On the other hand, the expected **2b·2HCl** was obtained as white solid in the reduction of **4c**. A bromine atom was eliminated in the reduction of **4d**, and **2b·2HCl** was obtained. A halogen atom was also reductively removed in the reduction of **4h** and **4i**, and both of the compounds gave **2a·2HCl**. Reaction of **2a·2HCl** and **2b·2HCl** with **10** in acetic acid afforded the expected benzodipyrazine **11a** and **11b** (Scheme 6).

In conclusion, benzenehexamine (**1**) and 1,2,3,4-benzenetetramines, (**2a**) and (**2b**), are readily accessible, as stable salts, via the reduction of benzotris- (**3**)

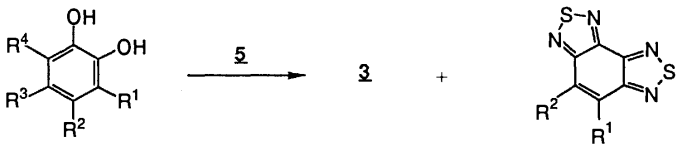

6 4b - 4e

4b: R^1=^{t}Bu, R^2=H, 4c: R^1= Me, R^2=H,
4d: R^1=Me, R^2=Br, 4e: R^1=^{i}Pr, R^2=H

Scheme 3.

Table 1. Reaction[a] of **5** with **6**

Entry	Substrate	R^1	R^2	R^3	R^4	5/Substrate[b]	Products (Yield %)[c]
1	**6a**	H	^{t}Bu	H	H	2/1	**4b** (17)
2	**6b**	H	^{t}Bu	H	^{t}Bu	2/1	**4b** (7)
3	**6c**	H	^{t}Bu	H	Br	2/1	**4b** (45)
4	**6c**	H	^{t}Bu	H	Br	3/1	**4b** (45)
5	**6d**	H	Me	H	H	2/1	—
6	**6e**	H	Me	Br	H	2/1	**3** (1), **4c** (19)
7	**6e**	H	Me	Br	H	3/1	**3** (2), **4c** (23)
8	**6e**	H	Me	Br	H	4/1	**3** (3), **4c** (22)
9	**6f**	Br	Me	Br	Br	3/1	**3** (3), **4d** (8)
10	**6g**	^{i}Pr	H	H	H	2/1	**3** (2), **4e** (6)
11	**6h**	H	Br	Br	H	3/1	**3** (32)
12	**6h**	H	Br	Br	H	4/1	**3** (29)

a) Reaction time; 24 h. b) Molar ratio. c) Yields are calculated upon the substrate.

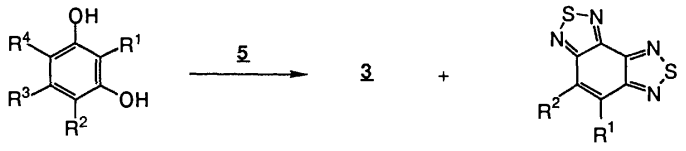

7, 8 — 4b, 4d, 4f - 4i

4f: R^1=Et, R^2=H, 4g: R^1= 1,2,5-thiadiazol-3-yl, R^2=H,
4h: R^1=Br, R^2=H, 4i: R^1=Cl, R^2=H

Scheme 4.

Table 2. Reaction[a] of **5** with **7** and **8**

Entry	Substrate	R^1	R^2	R^3	R^4	5/Substrate[b]	Products (Yield/%)[c]
1	**7a**	H	^{t}Bu	H	^{t}Bu	2/1	**4b** (3)
2	**7b**	Br	^{t}Bu	H	^{t}Bu	2/1	**4b** (15)
3	**7c**	Br	Et	H	Br	2/1	**4f** (11), **4g** (9)
4	**7d**	H	Br	H	Br	3/1	**3** (7), **4h** (30)
5	**7e**	Br	Br	H	Br	2/1	**3** (8), **4h** (32)
6	**7e**	Br	Br	H	Br	3/1	**3** (14), **4h** (36)
7	**7e**	Br	Br	H	Br	6/1	**3** (13), **4h** (37)
8	**7f**	Me	Br	H	Br	2/1	**4h** (3)
9	**7g**	H	Cl	H	H	3/1	**4a** (+),[d] **4i** (3)
10	**7h**	H	Cl	H	Br	3/1	**3** (7), **4i** (35)
11	**7i**	Br	Cl	H	Br	3/1	**3** (14), **4i** (37)
12	**7j**	H	Cl	H	Cl	3/1	**3** (4), **4i** (11)
13	**7k**	Br	Cl	H	Cl	3/1	**3** (15), **4i** (48)
14	**7l**	Br	Br	Me	Br	3/1	**3** (1), **4d** (40)
15	**7m**	Br	CHO	H	Br	3/1	**3** (7)
16	**7n**	I	I	H	I	3/1	—
17	**8a**	Br	Br	OH	Br	3/1	**3** (1)
18	**8b**	OH	H	^{t}Bu	H	3/1	**4b** (5)

a) Reaction time; 24 h. b) Molar ratio. c) Yields are calculated upon the substrate. d) Plus sign means less than 1% yield.

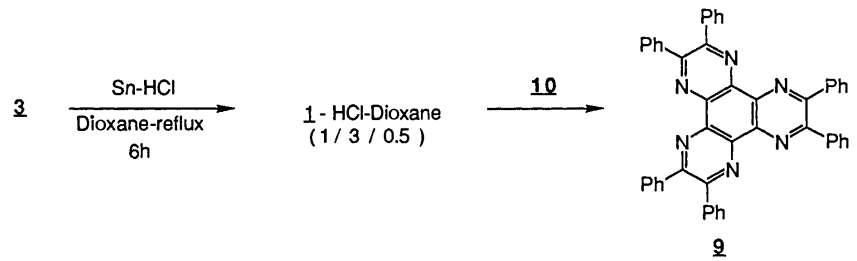

Scheme 5.

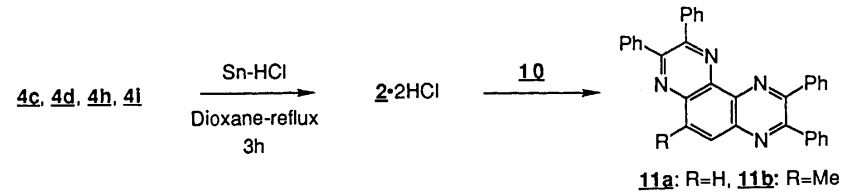

Scheme 6.

and benzobis[1,2,5]thiadiazole (**4**), which are obtainable by the reaction of tetrasulfur tetranitride (**5**) with halobenzenediols, **6** and **7**.

Experimental

General. All melting points were determined on a Yanagimoto micro melting point apparatus and Mitamura-riken MELT-THERMO and are uncorrected. IR spectra were measured on a Nippon-bunko A-102 spectrophotometer as potassium bromide pellets. NMR spectra were recorded on a Nippon Denshi JEOL FT-100 and GSX-270 using TMS as an internal standard in $CDCl_3$. Mass spectra were obtained on a Nippon Denshi JMS-01SG-2 mass spectrometer at 75

eV using a direct inlet system.

Materials. Compounds, **6a**, **6b**, **6d**, **6g**, **7a**, **7g**, **7j**, **7n**, and **8b**, are commercially available and **6f**,[15] **6h**,[16] and **8a**[17] were prepared according to the reported methods. Compounds, **6c**, **6e**, **7b**, **7c**,[18] **7d**,[19] **7e**,[20] **7f**,[21] **7h**,[22] **7i**, **7k**,[22] **7l**,[20] and **7m**, were prepared by the bromination of the corresponding benzenediols with benzyltrimethylammonium tribromide according to Kajigaeshi-Kakinami's procedure[23,24] in the yields as follows. Physical and spectral properties of newly prepared compounds in this study are also given below.

3-Bromo-5-*t*-butylcatechol (6c): Yield 49%; colorless needles (hexane); mp 86—87 °C; IR 3350 cm^{-1}; ^1H NMR δ=1.24 (9H, s), 5.30 (1H, s, D_2O-exchanged), 5.37 (1H, s, D_2O-exchanged), 6.90 (1H, d, J=2.0 Hz), and 6.98 (1H, d, J=2.0 Hz); MS m/z 246 (M^+) and 244 (M^+).

Found: C, 49.04; H, 5.41%. Calcd for $C_{10}H_{13}BrO_2$: C, 49.00; H, 5.35%.

4-Bromo-5-methylcatechol (6e): Yield 68%; colorless needles (cyclohexane); mp 96—98 °C (decomp); IR 3375 cm^{-1}; ^1H NMR δ=2.26 (3H, s), 4.91 (2H, br s, D_2O-exchanged), 6.76 (1H, s), and 7.04 (1H, s); MS m/z 204 (M^+) and 202 (M^+).

Found: C, 41.33; H, 3.69%. Calcd for $C_7H_7BrO_2$:C, 41.41; H, 3.47%.

2-Bromo-4,6-di-*t*-butylresorcinol (7b): Yield 71%; pale yellow prisms (light petroleum); mp 109—111 °C; IR 3540 cm^{-1}; ^1H NMR δ=1.36 (18H, s), 5.35 (2H, s, D_2O-exchanged), and 7.14 (1H, s); MS m/z 302 (M^+) and 300 (M^+).

Found: C, 55.55; H, 7.11%. Calcd for $C_{14}H_{21}BrO_2$: C, 55.82; H, 7.03%.

2,4-Dibromo-6-ethylresorcinol (7c): Yield 76%; mp 69—70 °C (lit,[18] 74 °C).

4,6-Dibromoresorcinol (7d): Yield 71%; mp 112—114 °C (lit,[19] 110—112 °C).

3,4,6-Tribromoresorcinol (7e): Yield 77%; mp 112.5—113.5 °C (lit,[20] 111 °C).

4,6-Dibromo-2-methylresorcinol (7f): Yield 70%; mp 97—99 °C (lit,[21] 102 °C).

4-Bromo-6-chlororesorcinol (7h): Yield 73%; mp 108.5—111 °C (lit,[22] 108.5 °C).

2,4-Dibromo-6-chlororesorcinol (7i): Yield 75%; pale yellow needles (hexane); mp 104—105 °C; IR 3475 cm^{-1}; ^1H NMR δ=5.88 (1H, s, D_2O-exchanged), 5.92 (1H, s, D_2O-exchanged), and 7.45 (1H, s); MS m/z 306 (M^+), 304 (M^+), 302 (M^+), and 300 (M^+).

Found: C, 23.91; H, 1.01%. Calcd for $C_6H_3Br_2ClO_2$: C, 23.84; H, 1.00%.

2-Bromo-4,6-dichlororesorcinol (7k): Yield 75%; mp 101.5—102 °C (lit,[22] 101 °C).

5-Methyl-2,4,6-tribromoresorcinol (7l): Yield 74%; mp 97—99 °C (lit,[20] 98 °C).

2,4-Dibromo-6-formylresorcinol (7m): Yield 76%; colorless needles (chloroform); mp 185—203 °C (decomp); IR 3275 and 1635 cm^{-1}; MS m/z 298 (M^+), 296 (M^+), and 294 (M^+).

Found: C, 28.40; H, 1.50%. Calcd for $C_7H_4Br_2O_3$: C, 28.41; H, 1.36%.

Reaction of N_4S_4 (5) with Benzenediols, 6 and 7, and Benzenetriol 8. Typical procedure. A mixture of **6**, **7**, or **8** (5 mmol) and an appropriate amount of **5** in toluene (40 cm^3) was refluxed for the time shown in Tables 1 and 2. After it was cooled to room temperature, insoluble materials were filtered and extracted with hot CH_2Cl_2. The filtrate and the extract were combined, condensed in vacuo, and chromatographed on silica gel (Wako gel, C-300). After sulfur was eluted with hexane, **4b**, **4d**, **4e**, and **4h** were eluted with benzene, **4c** with $CHCl_3$, and **3**, **4f**, **4g**, and **4i** with CH_2Cl_2. Physical and spectral properties of **4** are as follows.

4-*t*-Butylbenzo[1,2-*c*:3,4-*c'*]bis[1,2,5]thiadiazole (4b): Colorless needles (hexane); mp 128—129.5 °C; ^1H NMR δ=1.63 (9H, s) and 7.86 (1H, s): ^{13}C NMR δ=29.70, 36.57, 118.64, 146.58, 147.58, 148.95, 155.94, and 156.81; MS m/z 250 (M^+).

Found: C, 48.13; H, 4.18; N, 22.14%. Calcd for $C_{10}H_{10}N_4S_2$: C, 47.93; H, 4.03; N, 22.38%.

4-Methylbenzo[1,2-*c*:3,4-*c'*]bis[1,2,5]thiadiazole (4c): Colorless needles (hexane); mp 172—174 °C; ^1H NMR δ=2.78 (3H, d, J=1.5 Hz) and 7.78 (1H, d, J=1.5 Hz); MS m/z 208 (M^+).

Found: C, 40.13; H, 2.11; N, 27.02%. Calcd for $C_7H_4N_4S_2$: C, 40.37; H, 1.93; N, 26.90%.

4-Bromo-5-methylbenzo[1,2-*c*:3,4-*c'*]bis[1,2,5]thiadiazole (4d): Pale yellow prisms (cyclohexane); mp 203—204.5 °C; ^1H NMR δ=2.90 (s, 3H); ^{13}C NMR δ=18.87, 118.71, 134.53, 145.46, 146.80. 154.99, and 157.04; MS m/z 288 (M^+) and 286 (M^+).

Found: C, 29.31; H, 1.35; N, 19.26%. Calcd for $C_7H_3N_4BrS_2$: C, 29.28; H, 1.05; N, 19.51%.

4-Isopropylbenzo[1,2-*c*:3,4-*c'*]bis[1,2,5]thiadiazole (4e): Pale violet needles (methanol-water); mp 95—97 °C; ^1H NMR δ=1.48 (6H, d, J=7.0 Hz), 3.78 (1H, d sept, J=7.0 and 0.8 Hz), and 7.80 (1H, d, J=0.8 Hz); MS m/z 236 (M^+).

Found: C, 45.51; H, 3.54; N, 23.28%. Calcd for $C_9H_8N_4S_2$: C, 45.74; H, 3.40; N, 23.66%.

4-Ethylbenzo[1,2-*c*:3,4-*c'*]bis[1,2,5]thiadiazole (4f): Colorless prisms (methanol); mp 135—136 °C; ^1H NMR δ=1.48 (3H, t, J=7.5 Hz), 3.22 (2H, d, q, J=1.3 and 7.5 Hz), and 7.80 (1H, d, J=1.3 Hz): ^{13}C NMR δ=12.89, 25.42, 119.85, 140.19, 147.54, 148.02, 156.88, and 157.01; MS m/z 222 (M^+).

Found: C, 42.99; H, 2.60; N, 24.98%. Calcd for $C_8H_6N_4S_2$: C, 43.22; H, 2.72; N, 25.21%.

4-(1,2,5-Thiadiazol-3-yl)benzo[1,2-*c*:3,4-*c'*]bis[1,2,5]-thiadiazole (4g): Colorless prisms (carbon tetrachloride); mp 206—208 °C; ^1H NMR δ=8.92 (1H, s), and 9.92 (1H, s); MS m/z 278 (M^+).

Found: C, 34.36; H, 0.60; N, 30.07%. Calcd for $C_8H_2N_6S_3$: C, 34.52; H, 0.72; N, 30.19%.

4-Bromobenzo[1,2-*c*:3,4-*c'*]bis[1,2,5]thiadiazole (4h): Pale orange needles (cyclohexane); mp 177—180 °C; ^1H NMR δ=8.32 (1H, s); ^{13}C NMR δ=118.91, 126.17, 146.54, 147.55, 154.40, and 156.02; MS m/z 274 (M^+) and 272 (M^+).

Found: C, 26.39; H, 0.37; N, 20.51%. Calcd for $C_6HN_4BrS_2$: C, 26.59; H, 0.41; N, 20.44%.

4-Chlorobenzo[1,2-*c*:3,4-*c'*]bis[1,2,5]thiadiazole (4i): Colorless prisms (cyclohexane); mp 167—167.5 °C; ^1H NMR δ=8.15 (1H, s); ^{13}C NMR δ=122.54, 130.33, 147.19, 147.26, 153.60, and 155.56; MS m/z 230 (M^+) and 228 (M^+).

Found: C, 31.61; H, 0.40; N, 24.56%. Calcd for $C_6HN_4ClS_2$: C, 31.51; H, 0.44; N, 24.50%.

Reduction of 3. To a stirred mixture of **3** (252 mg, 1 mmol) and Sn powder (1.54 g, 13 mmol) in degassed dioxane (12 cm^3) at reflux, concentrated hydrochloric acid (6 cm^3) was added dropwise for 6 h. After it was cooled to room temperature, the precipitated solid was filtered, washed with ethanol, and dried at 90 °C under reduced pressure overnight, giving **benzenehexamine trihydrochloride [1-HCl-**

dioxane (1/3/0.5)] (230 mg, 70%) as grey powder: mp 140—165 °C (decomp); MS *m/z* 168 (M^+).

Found: C, 30.22; H, 6.29; N, 26.42%. Calcd for ($C_6H_{15}N_6Cl_3$+C_2H_4O): C, 29.87; H, 5.95; N, 26.13%.

Reduction of 4c. To a mixture of **4c** (208 mg, 1 mmol) and Sn powder (1.19 g, 10 mmol) in degassed dioxane (10 cm^3) under reflux, concentrated hydrochloric acid (4 cm^3) was added dropwise under a nitrogen stream for 3 h. After it was cooled to room temperature, the precipitated solid was filtered. The crude product was dissolved in hot methanol and to the solution, a 5 : 1-mixture of hexane and ethanol was added dropwise to give **5-methyl-1,2,3,4-benzenetetramine dihydrochloride (2b·2HCl)** as white powder (134 mg, 60%): mp 160—170 °C (decomp); MS *m/z* 152 (M^+).

Found: C, 37.05; H, 6.62; N, 24.41%. Calcd for $C_7H_{14}N_4Cl_2$: C, 37.35; H, 6.27; N, 24.89%.

Reduction of 4h. A stirred mixture of **4h** (819 mg, 3 mmol) and Sn powder (3.65 g, 30 mmol) in degassed dioxane (30 cm^3) was treated with concentrated hydrochloric acid (12 cm^3) and worked up as described in the reduction of **4c**, giving **1,2,3,4-benzenetetramine dihydrochloride (2a·2HCl)** (410 mg, 65%) as white powder: mp 170—195 °C (decomp); MS *m/z* 138 (M^+).

Found: C, 34.26; H, 5.70; N, 26.38%. Calcd for $C_6H_{12}N_4Cl_2$: C, 34.14; H, 5.73; N, 26.54%.

Preparation of 9. A mixture of **1·3HCl** [prepared from **3** (252 mg, 1 mmol)] and **10** (1.26 g, 6 mmol) in a 3 : 1-mixture (20 cm^3) of degassed ethanol and degassed acetic acid was refluxed for 11 h under a nitrogen atmosphere. After it was cooled to room temperature, the precipitated solid was filtered and washed with ethanol, giving **1,2,5,6,9,10-hexaphenylbenzo[1,2-*b*:3,4-*b'*:5,6-*b''*]tripyrazine (9)** (417 mg, 60% from **3**): mp 360—361.5 °C (lit,[5] 358 °C).

Preparation of 11a. Crude **2a·2HCl** [obtained from **4h** (550 mg, 2 mmol)] was reacted with **10** (840 mg, 4 mmol) in a mixture of degassed ethanol (15 cm^3) and degassed acetic acid (5 cm^3) at reflux under nitrogen atmosphere for 3 h. The precipitated solid was filtered and recrystallized from a mixture of hexane and chloroform, giving **2,3,6,7-tetraphenylbenzo[1,2-*b*:3,4-*b'*]dipyrazine (11a)** (395 mg, 41% from **4h**) as colorless needles; mp 260—262 °C; ^{1}H NMR δ=7.28—7.40 (12H, m), 7.56—7.74 (8H, m), and 8.34 (2H, s); MS *m/z* 486 (M^+).

Found: C, 84.00; H, 4.53; N, 11.46%. Calcd for $C_{34}H_{22}N_4$: C, 83.93; H, 4.56; N, 11.51%.

From **4i** (460 mg, 2 mmol), **11a** was similarly obtained in 39% overall yield (379 mg).

Preparation of 11b. Crude **2b·2HCl** [obtained by the reduction of **4c** (208 mg, 1 mmol)] was treated with **10** (840 mg, 4 mmol) as described in the preparation of **11a**, giving **5-methyl-2,3,8,9-tetraphenylbenzo[1,2-*b*:3,4-*b'*]dipyrazine (11b)** (114 mg, 23% from **4c**) as colorless prisms (cyclohexane); mp 234—237 °C (lit,[10] 222—225 °C); ^{1}H NMR δ=3.00 (3H, d, *J*=2.5 Hz), 7.32—7.44 (12H, m), 7.57—7.80 (8H, m), and 8.20 (1H, d, *J*=2.5 Hz); MS *m/z* 500 (M^+); (Found: C, 83.86; H, 4.90; N, 10.94%).

Compound **11b** (253 mg) was obtained from **4d** (574 mg, 2 mmol) in total 25% yield.

We are grateful to Professor K. Präfcke of Technische Universität Berlin for providing sample of **9**.

References

1) Part 17. K. Takahashi, H. Eguchi, S. Shiwaku, T. Hatta, E. Kyoya, T. Yonemitsu, S. Mataka, and M. Tashiro, *J. Chem. Soc., Perkin Trans. 1*, **1988**, 1869.

2) B. Fluesheim and E. L. Holmes, *J. Chem. Soc.*, **1929**, 330.

3) H. J. Backer and S. van der Baan, *Recl. Trav. Chim. Pays-Bas. Amsterdam*, **56**, 1175 (1937); Beilsteins Handbuch der Organischen Chemie, **XIII** (E3), 585.

4) R. Breslow, P. Maslak, and J. S. Thomaides, *J. Am. Chem. Soc.*, **106**, 6453 (1984).

5) B. Kohne and K. Praefcke, *Liebigs Ann. Chem.*, **1985**, 522.

6) B. Kohne, K. Praefcke, T. Derz, T. Gondro, and F. Frolow, *Angew. Chem., Int. Ed. Engl.*, **25**, 650 (1986).

7) P. Z. Rogers, *J. Org. Chem.*, **51**, 3904 (1986).

8) B. Kohne and K. Praefcke, *Liebigs Ann. Chem.*, **1987**, 265.

9) R. Nietzki and R. Rosel, *Ber.*, **22**, 1648 (1889).

10) R. Nietzki and L. Schmidt, *Ber.*, **23**, 3216 (1890).

11) D. A. Bochvar, I. V. Stankevich, V. V. Korshak, and A. L. Rusanov, *Dokl. Akad. Nauk SSSR*, **184**, 95 (1969); *Chem. Abstr.*, **70**, 80979 (1969).

12) S. Mataka, K. Takahashi, and M. Tashiro, *J. Heterocycl. Chem.*, **14**, 963 (1977).

13) S. Mataka, K. Takahashi, S. Shiwaku, and M. Tashiro, *J. Chem. Soc., Chem. Commun.*, **1983**, 1136.

14) S. Mataka, K. Takahashi, S. Shiwaku, and M. Tashiro, *J. Chem. Res. (S)*, **1985**, 345; (*M*) 3649.

15) K. Ono and M. Imoto, *Bull. Chem. Soc. Jpn.*, **11**, 127 (1936).

16) M. Kohn, *J. Am. Chem. Soc.*, **73**, 480 (1951).

17) T. Zincke and O. Kegel, *Ber.*, **23**, 1706 (1890).

18) C. M. Brewster and J. C. Harris, *J. Am. Chem. Soc.*, **52**, 4866 (1930).

19) J. Zehenter, *Monatsh. Chem.*, **8**, 296 (1887).

20) R. L. Datta and J. C. Bhoumik, *J. Am. Chem. Soc.*, **43**, 303 (1921).

21) P. R. Digankar and T. S. Gore, *Indian J. Chem.*, **2**, 294 (1964); *Chem. Abstr.*, **61**, 9422f (1964).

22) M. V. Likohoschersstow, *Chem. Zentr. I*, **1934**, 1476.

23) S. Kajigaeshi, T. Kakinami, H. Tokiyama, T. Hirakawa, and T. Okamoto, *Chem. Lett.*, **1987**, 627.

24) S. Kajigaeshi, T. Kakinami, H. Tokiyama, T. Hirakawa, and T. Okamoto, *Bull. Chem. Soc. Jpn.*, **60**, 2667 (1987).

A New and Convenient Synthesis of 1α,25-Dihydroxyvitamin D_2 and Its 24*R*-Epimer

Masahiro Tsuji,* Shinji Yokoyama, and Yoji Tachibana
Research Center, Nisshin Flour Milling, Co., Ltd., Ooimachi, Iruma-gun, Saitama 354
(Received April 8, 1989)

1α, 25-Dihydroxyvitamin D_2 (**1a**) was synthesized by irradiation and subsequent thermal isomerization of (22*E*)-5,7,22-ergostatriene-1α,3β,25-triol (**16a**). The triol **16a** was obtained via 22-oxo-5α,8α-(4-phenyl-3,5-dioxo-1,2,4-triazolidine-1,2-diyl)-23,24-dinor-6-cholene-1α,3β-diyl diacetate (**12**) starting from (22*E*)-5,7,22-ergostatriene-1α,3β-diyl diacetate (**10**), a precursor of 1α-hydroxyvitamin D_2. Introduction of the new side chain with the desired stereochemistry was carried out selectively by the reductive elimination of the β-hydroxy sulfone derived from the C-22 aldehyde (**12**) and an optically active sulfone, prepared via (*S*)-2,3-dimethyl-1,3-butanediol from methyl (*S*)-3-hydroxy-2-methylpropionate. Similarly a C-24 epimer of **1a** was synthesized.

Although the metabolism of vitamin D_2 (ercalciol) has not been extensively investigated as in the case of vitamin D_3 (calciol), it has been shown that vitamin D_2 is hydroxylated at C-25 position in the liver to 25-hydroxyvitamin D_2 (ercalcidiol) and subsequently at the C-1α position in the kidney to 1α,25-dihydroxyvitamin D_2 (ercalcitriol) (**1a**), a most potent metabolite.[1,2] Because it has been reported that 1α-hydroxyvitamin D_2 ((1*S*)-hydroxyercalciol)[3,4] is less toxic than the corresponding 1α-hydroxyvitamin D_3 ((1*S*)-hydroxycalciol), in spite of the almost equal potency of vitamin D activity,[5-7] much attention has been paid to the 1α-hydroxylated vitamin D_2. However, 1α,25-dihydroxyvitamin D_2 (**1a**), an "active form" of vitamin D_2, seems to be more potent than 1α-hydroxyvitamin D_2 for vitamin D activity, because **1a** is thought to elicit its physiological activity after being hydroxylated at C-25 position as described above. These observations prompted us to investigate the synthesis of **1a** and its 24*R*-epimer (**1b**).

DeLuca et al. reported the synthesis of **1a** and/or **1b**[8,9] by the selective hydroxylation at C-1α position of cyclovitamin D derivatives. However, this method

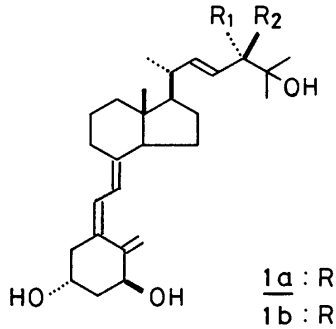

1a : R_1 = Me, R_2 = H
1b : R_1 = H, R_2 = Me

gave 1β-hydroxylated and transvitamin D derivatives as by-products, which were difficult to separate from the 1α-hydroxylated compound. Although Baggiolini et al. reported the synthesis of **1a**,[10] their procedure is complicated.

It is advantageous to use the steroidal block as an intermediate for the preparation of 1α-hydroxylated vitamin D derivatives, because 1α-hydroxylated provitamin D derivatives are easily and selectively converted to the corresponding 1α-hydroxylated vitamin D derivatives.

Previously, we reported the convenient synthesis of (22*E*)-5,7,22-ergostatriene-1α,3β-diyl diacetate (**10**),[11] a precursor of 1α-hydroxyvitamin D_2. To our best knowledge, no one has used this **10** in the synthesis of **1a** and **1b**. The C-22 aldehyde (**12**), available readily from **10**, seemed to be a good key-intermediate for the preparation of **1a** and **1b**. In the present paper we wish to describe a new and convenient synthesis of **1a** and **1b** using **10** as the starting material.

The side-chain fragments, namely optically active sulfones **9a**[12] for **1a** and **9b**[9] for **1b**, were synthesized respectively starting from methyl (*S*)- and (*R*)-3-hydroxy-2-methylpropionate (**2a** and **2b**) as follows (Scheme 1). Although it would be possible to convert **2a** directly to the diol (**5a**) by the Grignard reaction, this method gave a poor yield of **5a** due to its solubility in water. Thus, the hydroxyl group of **2a** was protected as a tetrahydropyranyl (THP) ether[13] to give **3a**.

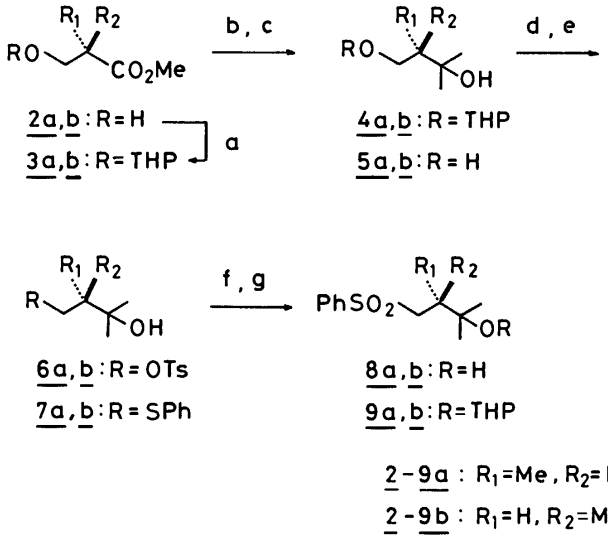

2-**9a** : R_1 = Me, R_2 = H
2-**9b** : R_1 = H, R_2 = Me

Scheme 1. a) DHP, *p*-TsOH; b) MeMgI/Et_2O; c) *p*-TsOH/MeOH; d) *p*-TsCl, Py; e) PhSH, *t*-BuOK/DMF; f) Na_2WO_4-H_2O_2; g) DHP, PPTS.

The Grignard reaction of **3a** using methylmagnesium iodide in ether afforded **4a**, which was subsequently subjected to deprotection of the THP group to provide the diol (**5a**) after distillation in 84% yield from **2a**. Tosylation of the primary hydroxyl group of **5a** in the usual manner afforded the tosylate (**6a**), which was reacted with benzenethiol in the presence of potassium *t*-butoxide in DMF to give the phenyl sulfide (**7a**). Oxidation of **7a** with Na_2WO_4-H_2O_2 yielded the crystalline hydroxy sulfone (**8a**) in 92% yield. Conventional protection of the hydroxyl group of **8a** as a THP ether gave **9a** in 92% yield. Similarly, **2b** was converted to the corresponding sulfone (**9b**) via the hydroxy sulfone (**8b**).

The next task was to construct the (22*E*)-olefin moiety leading to **1a** and **1b** (Scheme 2). The 5,7-diene of (22*E*)-5,7,22-ergostatriene-1α,3β-diyl diacetate (**10**), our starting material, was protected as a Diels-Alder adduct with 4-phenyl-3*H*-1,2,4-triazole-3,5(4*H*)-dione (PTAD)[14] to give **11** in 87% yield. Selective cleavage of the side-chain double bond of **11** was achieved by ozonolysis at −65 °C in 1% pyridine-CH_2Cl_2 solution and successive reductive workup of the resulting ozonide with dimethyl sulfide[14,15] to give the C-22 aldehyde (**12**) after recrystallization in 49% yield. The ^1H NMR spectrum of **12** exhibited only a doublet at δ 9.55 for the aldehyde proton (22-H), while the ^1H NMR spectrum of C(20) epimeric mixture, obtained by treatment of **12** with alumina (grade II—III) in $CHCl_3$,[14] showed a pair of doublets at δ 9.55 and 9.48. This indicates that the aldehyde obtained (**12**) was a single isomer.

Addition of the aldehyde (**12**) to the carbanion generated from the sulfone (**9a**) by butyllithium in THF[16-18] gave the β-hydroxy sulfone (**13a**), which was used in the next step without further purification. Reductive elimination of the β-hydroxy sulfone (**13a**) with sodium amalgam in buffered MeOH (Na_2HPO_4)[16-18] afforded the olefinic product (**14a**) in 32% yield from **12**. This olefination reaction is known to give predominantly or exclusively an (*E*)-olefin.[16-19] Removal of the THP group of **14a** by pyridinium *p*-toluenesulfonate (PPTS) in EtOH afforded the triol (**15a**), which was treated with $LiAlH_4$ in refluxing THF for removal of the triazoledione protective group[14] to give (22*E*)-5,7,22-ergostatriene-1α,3β,25-triol (**16a**) in 54% yield from **14a**.

Irradiation[3,4] of the 5,7-diene-1α,3β,25-triol (**16a**) with a high-pressure mercury lamp using aq. 1.5% KNO_3 solution as a filter gave the previtamin D (**17a**). Thermal-isomerization[3,4] of **17a** in refluxing EtOH and purification by preparative HPLC furnished

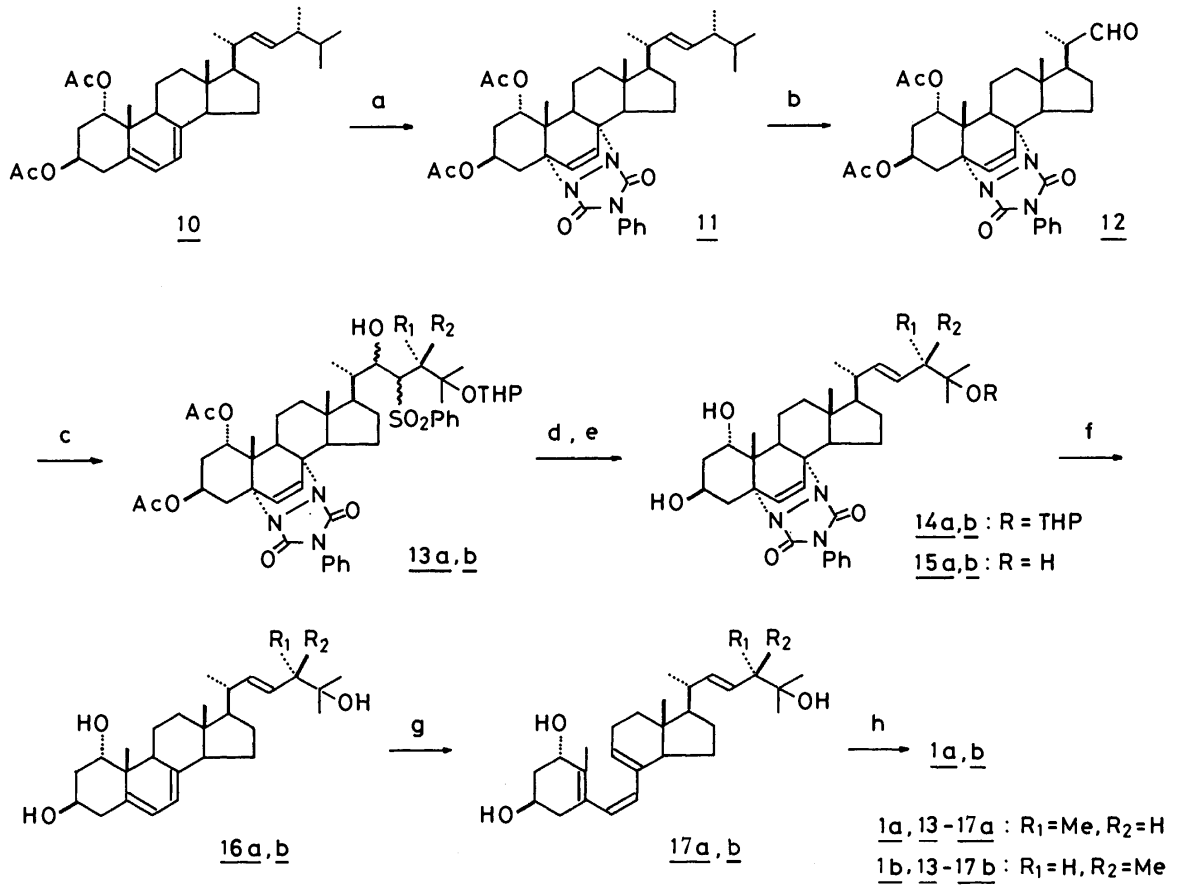

Scheme 2. a) 4-Phenyl-3*H*-1,2,4-triazole-3,5(4*H*)-dione; b) O_3/1% Py-CH_2Cl_2, then Me_2S; c) **9a** or **9b**, *n*-BuLi/THF; d) Na-Hg/MeOH (Na_2HPO_4); e) PPTS/EtOH; f) $LiAlH_4$/THF; g) *hν*; h) reflux/EtOH.

1α,25-dihydroxyvitamin D_2 (**1a**) in 22% yield from **16a**. The physical and spectral data of **1a** were in accord with those reported earlier.[8,10]

Similarly, (24*R*,22*E*)-5,7,22-ergostatriene-1α,3β, 25-triol (**16b**) was prepared from the aldehyde (**12**) and the sulfone (**9b**) in place of **9a** in four steps in 15% yield from **12**. Irradiation of **16b** and purification by preparative HPLC gave the previtamin D (**17b**), which was thermally isomerized to afford the crystalline (24*R*)-1α,25-dihydroxyvitamin D_2 (**1b**) in 12% yield from **16b** after purification by preparative HPLC.

Since (22*E*)-5,7,22-ergostatriene-1α,3β,25-triol is obtainable readily from (22*E*)-5,7,22-ergostatriene-1α,3β-diyl diacetate (**10**), the present study provides an efficient method for the preparation of 1α,25-dihydroxyvitamin D_2. The synthetic method described here will be applicable to other 1α-hydroxylated vitamin D_2 or D_3 derivatives.

Experimental

All the melting points and boiling points are uncorrected. IR spectra were measured on a Jasco IR-810 spectrometer. ^{1}H NMR spectra were recorded with TMS as an internal standard and $CDCl_3$ as a solvent at 200 MHz on a JEOL JNM-FX 200 spectrometer unless otherwise stated. Optical rotations were measured with $CHCl_3$ as a solvent on a Jasco DIP-4 polarimeter or a Jasco DIP-370 polarimeter unless otherwise stated. Mass spectra were recorded on a Hitachi M-80 spectrometer at 70 eV. UV spectra were measured on a Hitachi 320 spectrometer. Merck Kieselgel 60 (Art 7734, 70—230 mesh) or Merck Kieselgel 60 (Art 9385, 230—400 mesh) were used for SiO_2 column chromatography. TLC analyses were performed on a Merck Kieselgel 60 F-254 (Art 5715, 0.25 mm).

(*S*)-2,3-Dimethyl-1,3-butanediol (5a). A solution of methyl (*S*)-3-hydroxy-2-methylpropionate (**2a**) (8.09 g, 68.6 mmol; Sigma Chemical Co.), dihydropyran (8.63 g, 0.10 mol), and *p*-TsOH·H_2O (0.10 g) in dry ether (50 ml) was stirred for 1 h. The mixture was washed with sat. $NaHCO_3$ solution and brine, dried ($MgSO_4$), and concentrated in vacuo to give 13.8 g of crude **3a**. Its IR spectrum was identical with that reported previously.[13] This was employed in the next step without further purification.

A Grignard reagent was prepared from methyl iodide (29.2 g, 0.21 mol) and magnesium (5.00 g, 0.21 mol) in dry ether (30 ml). To this Grignard solution, a solution of crude **3a** (13.8 g) in dry ether (30 ml) was added dropwise for 1 h at a rate sufficient to maintain a gentle reflux. The mixture was stirred for 2 h at reflux temperature. Then to the ice-cooled reaction mixture was carefully added dropwise a cold sat. NH_4Cl solution. The ether layer was separated and the aq. layer was extracted with ether. The combined ether solution was washed with brine, dried ($MgSO_4$), and concentrated in vacuo to give 13.5 g of crude **4a**: IR (film) 3460, 1460, 1390, 1205, 1180, 1125, 1080, 1060, 980 cm^{-1}. This was employed in the next step without further purification.

A solution of crude **4a** (13.5 g) and *p*-TsOH·H_2O (0.65 g, 3.4 mmol) in MeOH (150 ml) was stirred for 1 h at room temperature. The mixture was neutralized with K_2CO_3 and filtered through Celite. After removal of MeOH in vacuo from the filtrate, the residue was dissolved in ether. The ether solution was dried ($MgSO_4$), and concentrated in vacuo. The residue was distilled to give 6.28 g (84% from **2a**) of **5a**: bp 83—85 °C/0.22 mmHg (1 mmHg≈133.322 Pa); n_D^{23} 1.4439; $[\alpha]_D^{23}$+1.7° (*c* 5.12)[lit,[12] $[\alpha]_D^{22}$−2.5° (0.18%, $CHCl_3$)]; IR (film) 3350, 1470, 1385, 1370, 1175, 1160, 1030 cm^{-1}; ^{1}H NMR δ=0.84 (3H, d, *J*=7.1 Hz), 1.18 (3H, s), 1.25 (3H, s), 1.81 (3H, m), 3.70 (1H, m), 3.91 (1H, s), 4.17 (1H, t, *J*=4.6 Hz). Found: *m/z* 118.1000. Calcd for $C_6H_{14}O_2$: M, 118.0994.

(*S*)-3-Hydroxy-2,3-dimethylbutyl *p*-Toluenesulfonate (6a). To a stirred and ice-cooled solution of **5a** (6.00 g, 50.8 mmol) in dry pyridine (24 ml) was added *p*-toluenesulfonyl chloride (11.64 g, 61.1 mmol) and the mixture was stirred for 2 h at that temperature. The mixture was poured into ice water and extracted with ether. The ether solution was washed with water, sat. $CuSO_4$ solution, sat. $NaHCO_3$ solution and brine, dried ($MgSO_4$), and concentrated in vacuo to give 13.5 g of crude **6a**: IR (film) 3450, 1600, 1500, 1470, 1360, 1190, 1175, 1100, 965 cm^{-1}; ^{1}H NMR δ=0.96 (3H, d, *J*=7.1 Hz), 1.12 (3H, s), 1.19 (3H, s), 1.54 (1H, s), 1.80 (1H, m), 2.45 (3H, s), 3.92 (1H, dd, *J*=9.5 and 9.8 Hz), 4.23 (1H, dd, *J*=9.5 and 4.4 Hz), 7.35 (2H, d, *J*=8.3 Hz), 7.80 (2H, d, *J*=8.3 Hz). This was employed in the next step without further purification.

(*R*)-2,3-Dimethyl-4-phenylthio-2-butanol (7a). To a stirred solution of potassium *t*-butoxide (5.89 g, 53.4 mmol) and benzenethiol (5.87 g, 53.4 mmol) in dry DMF (60 ml) was added crude **6a** (13.5 g) and the mixture was stirred for 4 h at room temperature under N_2. The mixture was poured into water and extracted with benzene. The benzene solution was washed with water and brine, dried ($MgSO_4$), and concentrated in vacuo. The residue was chromatographed over SiO_2 (100 g) eluting with hexane-EtOAc (9:1) to give 10.13 g of **7a**: IR (film) 3420, 3060, 1590, 1485, 1440, 1375, 1140, 1095, 1030 cm^{-1}; ^{1}H NMR δ=0.96 (3H, d, *J*=6.8 Hz), 1.18 (3H, s), 1.23 (3H, s), 1.54 (1H, s), 1.80 (1H, m), 2.55 (1H, dd, *J*=10.1 and 12.7 Hz), 3.40 (1H, dd, *J*=10.1 and 2.9 Hz), 7.15—7.48 (5H, m). This was employed in the next step without further purification.

(*R*)-2,3-Dimethyl-4-phenylsulfonyl-2-butanol (8a). WO_3 (55 mg) in water (18 ml) was dissolved by adding 50% NaOH solution to pH 11, the solution was then adjusted to pH 5.6 by adding AcOH. To this solution was added **7a** (10.13 g) in EtOH (10 ml) and then 30% H_2O_2 (3.4 ml). The mixture was stirred for 10 min at 60°C. To the mixture was added 30% H_2O_2 (3.4 ml) and the mixture was stirred for a further 30 min at 75°C. After cooling, $Na_2S_2O_3$ was added to the reaction mixture. The mixture was next extracted with benzene. The benzene solution was washed with water and brine, dried ($MgSO_4$), and concentrated in vacuo. The residue was chromatographed over SiO_2 (200 g) eluting with hexane-EtOAc (9:1—4:1) to give 11.32 g (92% from **5a**) of **8a**, which crystallized on standing. Recrystallization from ether gave **8a** as prisms: mp 68.4—69.1 °C; $[\alpha]_D^{25}$−33.7° (*c* 1.26) [lit,[12] $[\alpha]_D^{22}$−22.4° (0.6%, $CHCl_3$)]; IR (KBr) 3500, 3070, 1585, 1450, 1370, 1300, 1155, 1140, 1110, 1085 cm^{-1}; ^{1}H NMR δ=1.03 (3H, s), 1.12 (3H, d, *J*=6.8 Hz), 1.22 (3H, s), 1.88 (1H, s), 2.15 (1H, m), 2.82 (1H, dd, *J*=13.9 and 9.3 Hz), 3.60 (1H, dd, *J*=13.9 and 2 Hz), 7.53—7.95 (5H, m). Found: C, 59.49; H, 7.48; S, 13.25%. Calcd for $C_{12}H_{18}O_3S$: C, 59.48; H, 7.49; S, 13.23%.

(3*R*)-2,3-Dimethyl-4-phenylsulfonyl-2-butanol THP Ether

(**9a**). A solution of **8a** (5.31 g, 21.9 mmol), dihydropyran (2.76 g, 32.9 mmol) and PPTS (0.55 g, 2.2 mmol) in dry CH_2Cl_2 (60 ml) was stirred for 4 h at room temperature. The mixture was washed with water and brine, dried ($MgSO_4$), and concentrated in vacuo. The residue was chromatographed over SiO_2 (150 g) eluting with hexane-EtOAc (4 : 1) to give 6.58 g (92%) of **9a**: IR (film) 3060, 1585, 1450, 1395, 1305, 1200, 1150, 1110, 1090, 1085, 1025 cm^{-1}; ^1H NMR δ=1.04 and 1.06 (3H, pair of s), 1.13 (3H, m), 1.18 and 1.19 (3H, pair of s), 1.3—1.8 (6H, m), 2.19 (1H, m), 2.88 (1H, m), 3.42 (1H, m), 3.65 (1H, m), 3.82 (1H, m), 4.73 (1H, m), 7.51—7.94 (5H, m).

(*R*)-2,3-Dimethyl-1,3-butanediol (5b). In the same manner as described for **5a**, methyl (*R*)-3-hydroxy-2-methylpropionate (**2b**) (9.28 g, 78.6 mmol; Sigma Chemical Co.) was converted in three steps to 7.61 g (82%) of **5b**: bp 83—84°C/0.25 mmHg; n_D^{23} 1.4437; $[\alpha]_D^{23}$—1.6° (*c* 5.29). Its IR and ^1H NMR spectra were identical with those of **5a**.

(*S*)-2,3-Dimethyl-4-phenylsulfonyl-2-butanol (8b). In the same manner as described for **8a**, **5b** (6.58 g, 55.8 mmol) was converted in three steps to 12.10 g (90%) of **8b**: mp 68.2—69.0°C (from ether, prisms); $[\alpha]_D^{23}$+34.1° (*c* 1.09) [lit,[9]) a thick, colorless oil; $[\alpha]_D^{22}$+27.9° (*c* 1.3, $CHCl_3$)]. Its IR and ^1H NMR spectra were identical with those of **8a**. Found: C, 59.35; H, 7.48; S, 13.29%. Calcd for $C_{12}H_{18}O_3S$: C, 59.48; H, 7.49; S, 13.23%.

(3*S*)-2,3-Dimethyl-4-phenylsulfonyl-2-butanol THP Ether (9b). In the same manner as described for **9a**, **8b** (6.23 g, 25.7 mmol) was converted to 7.89 g (94%) of **9b**. Its IR and ^1H NMR spectra were identical with those of **9a**.

(22*E*)-5α,8α-(4-Phenyl-3,5-dioxo-1,2,4-triazolidine-1,2-diyl)-6,22-ergostadiene-1α,3β-diyl Diacetate (11). To a stirred solution of (22*E*)-5,7,22-ergostatriene-1α,3β-diyl diacetate (**10**) (5.62 g, 11.3 mmol) in $CHCl_3$ (70 ml) was added dropwise a solution of 4-phenyl-3*H*-1,2,4-triazole-3,5(4*H*)-dione (PTAD) (2.26 g, 13 mmol) in acetone (40 ml) at room temperature until a faint pink coloration persisted, and the mixture was concentrated in vacuo. The residue was chromatographed over SiO_2 (80 g) eluting with hexane-EtOAc (2 : 1) to give 6.61 g (87%) of **11** as a foam: $[\alpha]_D^{25}$—139° (*c* 1.09); IR (KBr) 1750, 1700, 1600, 1505, 1395, 1240, 1030 cm^{-1}; ^1H NMR δ=0.79 and 0.82 (6H, each d, *J*=3.7 Hz, 26-H_3 and 27-H_3), 0.84 (3H, s, 18-H_3), 0.89 (3H, d, *J*=6.8 Hz, 28-H_3), 1.02 (3H, d, *J*=6.6 Hz, 21-H_3), 1.06 (3H, s, 19-H_3), 2.01 (3H, s, Ac), 2.03(3H, s, Ac), 3.25 (1H, dd, *J*=13.7 and 5.6 Hz, 9-H), 5.11 (1H, m, 1-H), 5.20 (2H, m, 22-H and 23-H), 5.89 (1H, m, 3-H), 6.33 and 6.45 (2H, ABq, *J*=8.3 Hz, 6-H and 7-H), 7.24—7.51 (5H, m, Ph); MS *m/z* (rel intensity) 671(M^+; 0.3), 496(0.4), 436(8), 376(100), 251(28), 209(23), 155(34).

22-Oxo-5α,8α-(4-phenyl-3,5-dioxo-1,2,4-triazolidine-1,2-diyl)-23,24-dinor-6-cholene-1α,3β-diyl Diacetate (12). Ozone (flow rate 0.07 mmol min^{-1}) was bubbled into a solution of **11** (10.00 g, 14.9 mmol) in 1% pyridine-CH_2Cl_2 (400 ml) with stirring for 4.5 h at −65°C. After the excess ozone was driven out by bubbling Ar, dimethyl sulfide (20 ml) was added dropwise to the mixture at −65°C, and the mixture was stirred for 1 h at −65°C. After the cooling bath was removed, stirring was continued for a further 1 h. The mixture was washed with 2% HCl and brine, dried ($MgSO_4$), and concentrated in vacuo. The residue was chromatographed over SiO_2 (130 g) eluting with hexane-EtOAc (1 : 1) to give 5.99 g of **12.** This was recrystallized from benzene to give 4.40 g (49%) of **12** as needles: mp 191—193°C; $[\alpha]_D^{25}$—131° (*c* 1.06); IR (KBr) 2720, 1740, 1685, 1605, 1505, 1405, 1370, 1250, 1230, 1035 cm^{-1}; ^1H NMR δ=0.87 (3H, s, 18-H_3), 1.07 (3H, s, 19-H_3), 1.14 (3H, d, *J*=6.8 Hz, 21-H_3), 2.01 (3H, s, Ac), 2.04 (3H, s, Ac), 3.26 (1H, dd, *J*=14.2 and 5.4 Hz, 9-H), 5.12 (1H, m, 1-H), 5.88 (1H, m, 3-H), 6.36 and 6.44 (2H, ABq, *J*=8.3 Hz, 6-H and 7-H), 7.26—7.51 (5H, m, Ph), 9.55 (1H, d, *J*=3.4 Hz, 22-H); MS *m/z* (rel intensity) 603(M^+; 0.3), 428(0.3), 368(11), 308(100), 235(20), 177(20), 141(57). Found: C, 67.57; H, 6.84; N, 6.99%. Calcd for $C_{34}H_{41}N_3O_7$: C, 67.64; H, 6.84; N, 6.96%.

(22*E*)-5α,8α-(4-Phenyl-3,5-dioxo-1,2,4-triazolidine-1,2-diyl)-25-tetrahydropyranyloxy-6,22-ergostadiene-1α, 3β-diol (14a). Butyllithium (1.5 mol dm^{-3} in hexane, 3.5 ml, 5.2 mmol) was added to a stirred solution of **9a** (1.70 g, 5.2 mmol) in dry THF (60 ml) at −60—−70°C under Ar. After stirring for 30 min, a solution of **12** (2.40 g, 4.0 mmol) in dry THF (25 ml) was added and the mixture was stirred for 30 min at −60—−70°C. Sat. NH_4Cl solution (1 ml) was added dropwise to the mixture at that temperature, and the mixture was allowed to rise to room temperature. The mixture was poured into sat. NH_4Cl solution and extracted with EtOAc. The EtOAc solution was washed with brine, dried ($MgSO_4$), and concentrated in vacuo to give crude **13a.** This was employed in the next step without further purification.

To a solution of crude **13a** in MeOH saturated with Na_2HPO_4 (330 ml) sodium amalgam (5%, 18.3 g) was added and the mixture was stirred for 15 h at 0°C, followed by a further 3 h at room temperature. The supernatant was concentrated in vacuo, and the residue was poured into water and extracted with EtOAc. The EtOAc solution was washed with brine, dried ($MgSO_4$), and concentrated in vacuo. The residue was chromatographed over SiO_2 (65 g) eluting with hexane-EtOAc (1 : 4) to give 0.87 g (32% from **12**) of **14a** as a crystalline material: IR (KBr) 3420, 1745, 1685, 1600, 1505, 1405, 1315, 1130, 1025, 980 cm^{-1}; ^1H NMR δ=3.48 (1H, m, 6′-H), 3.69 (1H, m, 1-H), 3.95 (1H, m, 6′-H), 4.78 (1H, m, 2′-H), 4.85 (1H, m, 3-H), 5.15—5.42 (2H, m, 22-H and 23-H), 6.18 and 6.34 (2H, ABq, *J*=8.3 Hz, 6-H and 7-H), 7.2—7.4 (5H, m, Ph); MS *m/z* (rel intensity) 512 (M^+—PTAD; 0.3), 428(3), 410(22), 324(3), 251(5), 177(22), 119(28), 85(100), 59(94). This was employed in the next step without further purification.

(22*E*)-5,7,22-Ergostatriene-1α,3β,25-triol (16a). A solution of **14a** (0.84 g, 1.2 mmol) and PPTS (15 mg, 0.06 mmol) in 95% EtOH (6 ml) was stirred for 1 h at 50°C. After removal of EtOH in vacuo from the mixture, the residue was extracted with EtOAc. The EtOAc solution was washed with brine, dried ($MgSO_4$), and concentrated in vacuo to give crude **15a.** This was employed in the next step without further purification. An analytical sample was prepared by recrystallization from ether-EtOH to give **15a** as needles: mp 209—212°C; $[\alpha]_D^{25}$—86.4° (*c* 0.22); IR (KBr) 3530, 3470, 1745, 1680, 1505, 1415, 1150, 1035 cm^{-1}; ^1H NMR δ=0.84 (3H, s, 18-H_3), 0.93 (3H, s, 19-H_3), 0.98 (3H, d, *J*=7.1 Hz, 28-H_3), 1.05 (3H, d, *J*=6.6 Hz, 21-H_3), 1.13 and 1.16 (6H, each s, 26-H_3 and 27-H_3), 1.21 (t, *J*=7.1 Hz, Et_2O), 3.15 (1H, dd, *J*=14 and 7.1 Hz, 9-H), 3.48 (q, *J*=7.1 Hz, Et_2O), 3.85 (1H, m, 1-H), 4.90 (1H, m, 3-H), 6.26 and 6.41 (2H, ABq, *J*=8.3 Hz, 6-H and 7-H), 7.30—7.45 (5H, m, Ph); MS *m/z* (rel intensity) 428(M^+—PTAD; 18), 350(15), 324(25), 251(15), 177(90), 119(100). Found: C, 71.06; H, 8.28; N, 6.81%. Calcd for $C_{36}H_{49}N_3O_5 \cdot 1/4\ Et_2O$: C, 71.41; H, 8.34; N, 6.75%.

A mixture of crude **15a** and $LiAlH_4$ (0.73 g) in dry THF (80 ml) was stirred for 1.5 h at reflux temperature. The excess $LiAlH_4$ was destroyed by the successive addition of water (0.7 ml), 10% NaOH solution (0.7 ml), water (2.1 ml) to the stirred and ice-cooled mixture. The mixture was stirred for a further 30 min at room temperature, dried ($MgSO_4$), and filtered through Celite. The filtrate was concentrated in vacuo to give crude crystalline **16a**. This was recrystallized from EtOH to give 0.28 g (54% from **14a**) of **16a** as needles: mp 222—224 °C; $[\alpha]_D^{25}$−55° (*c* 0.12, MeOH); IR (KBr) 3520, 3350, 1655, 1610, 1465, 1370, 1135, 1070, 975 cm^{-1}; ^1H NMR δ=0.64 (3H, s, 18-H_3), 0.95 (3H, s, 19-H_3), 1.00 (3H, d, *J*=7.1 Hz, 28-H_3), 1.05 (3H, d, *J*=6.8 Hz, 21-H_3), 1.13 and 1.17 (6H, each s, 26-H_3 and 27-H_3), 3.77 (1H, m, 1-H), 4.04 (1H, m, 3-H), 5.35 (3H, m, 7-H, 22-H and 23-H), 5.73 (1H, m, 6-H); MS *m/z* (rel intensity) 428(M^+; 4), 353(2), 312(2), 251(5), 225(5), 145(8), 81(15), 59(100); UV (EtOH) 282nm (ε 11900). Found: C, 77.97; H, 10.40%. Calcd for $C_{28}H_{44}O_3$: C, 78.48; H, 10.35%.

1α,25-Dihydroxyvitamin D_2 (1a). A solution of **16a** (100 mg, 0.23 mmol) in ether–THF (19:1, 1000 ml) was irradiated for 3 min under Ar at water-cooled temperature with a high-pressure mercury lamp (Ushio, UM-452) using 1.5% KNO_3 solution as a filter. The mixture was next concentrated in vacuo. A solution of the residue containing the previtamin D (**17a**) in EtOH (30 ml) was stirred for 1 h at reflux temperature under Ar. The mixture was concentrated in vacuo. The residue was chromatographed on HPLC (Merck, LiChrosorb® Si60 (7 μm), 25×250 mm) eluting with 4% MeOH–CH_2Cl_2 (8.0 ml min^{-1}) to give 22 mg (22% from **16a**) of crystalline **1a**. This was recrystallized from hexane–ether to give **1a** as needles: mp 168—170 °C; $[\alpha]_D^{25}$+48° (*c* 0.07, EtOH) [lit,[10] mp 169—170 °C; $[\alpha]_D^{25}$+47.2° (*c* 0.2, EtOH)]; IR (KBr) 3400, 1640, 1460, 1380, 1370, 1350, 1300, 1265, 1220, 1140, 1055, 975 cm^{-1}; ^1H NMR δ=0.56 (3H, s, 18-H_3), 1.00 (3H, d, *J*=6.8 Hz, 28-H_3), 1.04 (3H, d, *J*=6.8 Hz, 21-H_3), 1.13 and 1.17 (6H, each s, 26-H_3 and 27-H_3), 4.23 (1H, m, 3-H), 4.42 (1H, m, 1-H), 5.00 (1H, narrow m, 19-H), 5.32 (3H, m, 19-H, 22-H and 23-H), 6.01 (1H, d, *J*=10.6 Hz, 7-H), 6.38 (1H, d, *J*=10.6 Hz, 6-H); MS *m/z* (rel intensity) 428(M^+; 5) 410(9), 392(12), 352(6), 269(10), 197(15), 152(23), 134(100); UV (EtOH) 265 nm (ε 16400). Found: *m/z* 428.3271. Calcd for $C_{28}H_{44}O_3$: M, 428.3292.

(24*R*,22*E*)-5α,8α-(4-Phenyl-3,5-dioxo-1,2,4-triazolidine-1,2-diyl)-25-tetrahydropyranyloxy-6,22-ergostadiene-1α,3β-diol (14b). In the same manner as described for **14a**, **12** (1.50 g, 2.5 mmol) and **9b** (1.62 g, 5.0 mmol) was converted in two steps to 0.46 g (27%) of **14b**: IR (KBr) 3430, 1750, 1690, 1605, 1505, 1410, 1310, 1135, 1030, 985 cm^{-1}; ^1H NMR δ=3.50 (1H, m, 6′-H), 3.71 (1H, m, 1-H), 3.90 (1H, m, 6′-H), 4.75 (1H, m, 2′-H), 4.85 (1H, m, 3-H), 5.15—5.40 (2H, m, 22-H and 23-H), 6.19 and 6.35 (2H, ABq, *J*=8.3 Hz, 6-H and 7-H), 7.2—7.4 (5H, m, Ph); MS *m/z* (rel intensity) 428 (M^+−PTAD−DHP; 10), 410 (7), 350 (12), 177 (40), 119 (100).

(24*R*,22*E*)-5α,8α-(4-Phenyl-3,5-dioxo-1,2,4-triazolidine-1,2-diyl)-6,22-ergostadiene-1α,3β,25-triol (15b). This was prepared in the same manner as described for **15a**, and recrystallization from ether–EtOH gave an analytical sample as needles: mp 212—215 °C; $[\alpha]_D^{23}$−95.6° (*c* 0.25); IR (KBr) 3530, 3450, 1745, 1680, 1505, 1420, 1155, 1035 cm^{-1}; ^1H NMR δ=0.83 (3H, s, 18-H_3), 0.92 (3H, s, 19-H_3), 0.98 (3H, d, *J*=7.1 Hz, 28-H_3), 1.04 (3H, d, *J*=6.4 Hz, 21-H_3), 1.12 and 1.15 (6H, each s, 26-H_3 and 27-H_3), 1.21 (t, *J*=7.1 Hz, Et_2O), 3.14 (1H, dd, *J*=13.7 and 4.4 Hz, 9-H), 3.48 (q, *J*=7.1 Hz, Et_2O), 3.83 (1H, m, 1-H), 4.90 (1H, m, 3-H), 5.32 (2H, m, 22-H and 23-H), 6.25 and 6.40 (2H, ABq, *J*=8.1 Hz, 6-H and 7-H), 7.30—7.45 (5H, m, Ph); MS *m/z* (rel intensity) 428 (M^+−PTAD; 22), 350 (16), 324 (48), 251 (20), 177 (75), 119 (100). Found: C, 70.63; H, 8.34; N, 6.62%. Calcd for $C_{36}H_{49}N_3O_5 \cdot 1/4\ Et_2O$: C, 71.41; H, 8.34; N, 6.75%.

(24*R*,22*E*)-5,7,22-Ergostatriene-1α,3β,25-triol (16b). In the same manner as described for **16a**, **14b** (0.87 g, 1.3 mmol) was converted in two steps to 0.31 g (57%) of **16b**: mp 214—217 °C (from EtOH, needles); $[\alpha]_D^{24}$−16.2° (*c* 0.14, MeOH); IR (KBr) 3510, 3360, 1660, 1610, 1465, 1385, 1145, 1075, 970 cm^{-1}; ^1H NMR δ=0.65 (3H, s, 18-H_3), 0.95 (3H, s, 19-H_3), 0.99 (3H, d, *J*=6.8 Hz, 28-H_3), 1.05 (3H, d, *J*=6.8 Hz, 21-H_3), 1.13 and 1.17 (6H, each s, 26-H_3 and 27-H_3), 3.77 (1H, m, 1-H), 4.08 (1H, m, 3-H), 5.35 (3H, m, 7-H, 22-H and 23-H), 5.74 (1H, m, 6-H); MS *m/z* (rel intensity) 428 (M^+; 42), 251 (60), 225 (62), 157 (100), 145 (80); UV (EtOH) 282 nm (ε 11700). Found: C, 78.24; H, 10.37%. Cacld for $C_{28}H_{44}O_3$: C, 78.48; H, 10.35%.

(24*R*)-1α,25-Dihydroxyvitamin D_2 (1b). A solution of **16b** (100 mg, 0.23 mmol) in ether–THF (19:1, 1000 ml) was irradiated for 3 min under Ar at water-cooled temperature with a high pressure mercury lamp (Ushio, UM-452) using 1.5% KNO_3 solution as a filter. The mixture was next concentrated in vacuo. The residue was chromatographed over HPLC (Merck, LiChrosorb® Si60 (7 μm), 25×250 mm) eluting with 5% MeOH–CH_2Cl_2 (8.0 ml min^{-1}) to give 28 mg (28%) of the previtamin D (**17b**): ^1H NMR δ=0.72 (3H, s, 18-H_3), 0.99 (3H, d, *J*=6.8 Hz, 28-H_3), 1.05 (3H, d, *J*=6.6 Hz, 21-H_3), 1.13 and 1.17 (6H, each s, 26-H_3 and 27-H_3), 1.76 (3H, s, 19-H_3), 4.05 (1H, m, 3-H), 4.19 (1H, m, 1-H), 5.31 (2H, m, 22-H and 23-H), 5.51 (1H, m, 9-H), 5.76 and 5.92 (2H, ABq, *J*=12.9 Hz, 6-H and 7-H).

A solution of **17b** (28 mg) in EtOH (15 ml) was stirred for 1 h at reflux temperature. The mixture was concentrated in vacuo. The residue was chromatographed on HPLC (Merck, LiChrosorb® Si60 (7 μm), 25×250 mm) eluting with 5% MeOH–CH_2Cl_2 (7.0 ml min^{-1}) to give 11.8 mg (42%: 12% from **16b**) of **1b**. This was recrystallized from hexane–CH_2Cl_2 to give **1b** as rods: mp 150—152 °C [lit,[9] a colorless oil]; $[\alpha]_D^{23}$+74° (*c* 0.16, EtOH); ^1H NMR δ=0.56 (3H, s, 18-H_3), 0.99 (3H, d, *J*=6.8 Hz, 28-H_3), 1.03 (3H, d, *J*=6.6 Hz, 21-H_3), 1.12 and 1.17 (6H, each s, 26-H_3 and 27-H_3), 4.22 (1H, m, 3-H), 4.42 (1H, m, 1-H), 4.99 (1H, narrow m, 19-H), 5.32 (3H, m, 19-H, 22-H and 23-H), 6.01 (1H, d, *J*=11.2 Hz, 7-H), 6.37 (1H, d, *J*=11.2 Hz, 6-H); MS *m/z* (rel intensity) 428 (M^+; 6), 410 (7), 392 (10), 352 (5), 334 (16), 269 (9), 251 (10), 134 (100), 105 (46); UV (EtOH) 265 nm (ε 16900).

References

1) T. Suda, H. F. DeLuca, H. K. Schnoes, and J. W. Blunt, *Biochemistry*, **8**, 3515 (1969).

2) G. Jones, H. K. Schnoes, and H. F. DeLuca, *Biochemistry*, **14**, 1250 (1975).

3) H.-Y. Lam, H. K. Schnoes, and H. F. DeLuca, *Science*, **186**, 1038 (1974).

4) H.-Y. Lam, H. K. Schnoes, and H. F. DeLuca, *Steroids*, **30**, 2181 (1977).

5) M. F. Holich, E. J. Semmler, H. K. Schnoes, and H. F. DeLuca, *Science*, **180**, 190 (1973).

6) D. H. R. Barton, R. H. Hesse, M. M. Pechet, and E.

Rizzardo, *J. Am. Chem. Soc.*, **95**, 2748 (1973).
7) G. Sjödén, C. Smith, U. Lindgren, and H. F. DeLuca, *Pro. Soc. Exp. Biol. Med.*, **178**, 432 (1985).
8) R. R. Sicinski, Y. Tanaka, H. K. Schnoes, and H. F. DeLuca, *Bioorg. Chem.*, **13**, 158 (1985).
9) A. Kutner, K. L. Perlman, R. R. Sicinski, M. E. Phelps, H. K. Schnoes, and H. F. DeLuca, *Tetrahedron Lett.*, **28**, 6129 (1987); A. Kutner, K. L. Perlman, A. Lago, R. R. Sicinski, H. K. Schnoes, and H. F. DeLuca, *J. Org. Chem.*, **53**, 3450 (1988).
10) E. G. Baggiolini, J. A. Iacobelli, B. M. Hennessy, A. D. Batcho, J. F. Sereno, and M. R. Uskoković, *J. Org. Chem.*, **51**, 3098 (1986).
11) Y. Tachibana, *Bull. Chem. Soc. Jpn.*, **61**, 3915 (1988).
12) S. Yamada, M. Shiraishi, M. Ohmori, and H. Takayama, *Tetrahedron Lett.*, **25**, 3347 (1984).
13) K. Mori, *Tetrahedron*, **39**, 3107 (1983).
14) D. H. R. Barton, T. Shioiri, and D. A. Widdowson, *J. Chem. Soc. C*, **1971**, 1968.
15) D. S. Morris, D. H. Williams, and A. F. Norris, *J. Org. Chem.*, **46**, 3422 (1981).
16) P. J. Kocienski, B. Lythgoe, and S. Ruston, *J. Chem. Soc., Perkin Trans. 1*, **1978**, 829.
17) P. J. Kocienski, B. Lythgoe, and D. A. Roberts, *J. Chem. Soc., Perkin Trans. 1*, **1978**, 843.
18) P. J. Kocienski, B. Lythgoe, S. Ruston, and I. Waterhouse, *J. Chem. Soc., Perkin Trans. 1*, **1980**, 1045.
19) The (*E*)-geometry was finally confirmed by the single-crystal X-ray analysis of **16a**. This will be reported elsewhere.

High-Pressure Aminolysis of Lactones to Hydroxy Amides

Kiyoshi MATSUMOTO,* Shiro HASHIMOTO, Takane UCHIDA,†
Tadashi OKAMOTO,††,# and Shinichi OTANI
Department of Chemistry, College of Liberal Arts and Sciences, Kyoto University, Kyoto 606
†Faculty of Education, Fukui University, Fukui 910
††Institute for Chemical Research, Kyoto University, Uji 611
(Received April 12, 1989)

The preparation of hydroxy amides from a wide variety of lactones and amines has been achieved at 9 kbar and 30 or 65 °C. The yields of hydroxy amides were moderate to excellent. Some limitations were encountered in the reaction of 6-hexanolide; for example, diethylamine gave only a 15% yield of the corresponding amide at 8 kbar and 60 °C. 4-Pentanolide did react with extremely unreactive amines such as 4-nitroaniline and diphenylamine, and the product was a mixture of the hydroxy amide and 3-aminobutyric acid.

Particular attention has been directed to certain hydroxy amides that can serve as novel types of surfactants,[1a] (metal) chelating agents,[1b] liquid crystals,[1c] and protecting groups,[1d] as well as important intermediates for the synthesis of pharmacologically intriguing substances.[1e] Although one of the most convenient and simplest methods for preparing hydroxy amides would consist in the direct nucleophilic ring opening of lactones with amines, this conversion is generally limited either to strained three-membered lactones such as 3-propanolide[2] and 3-butanolide[3] or to relatively highly nucleophilic amines.[4] Specifically, the reactions of 4-substituted 4-butanolides with amines were reported to be sluggish,[5] and 3-butanolide did not react with 4-nitroaniline in refluxing acetonitrile.[3] Since we have previously demonstrated that secondary amines reacted in high yields at moderate temperatures with a variety of nonactivated esters to produce the corresponding acid amides if the reactions were performed under a few kbar,§[6] the same technique was expected to effect aminolysis of lactones by nucleophilic displacement at the carbonyl group.[7,8]

In this paper we wish to report in full detail the preparation of hydroxy amides by the aminolysis of lactones under high pressure.[9] The representative results are summarized in Table 1.

The structures of the amides **3** were confirmed on the basis of their analytical and ^{1}H and ^{13}C NMR spectroscopic data (see Experimental). Neither an inert atmosphere nor dry solvents were required. Alkyl-, aryl-, and aralkylamines **2** react with a wide variety of lactones **1** in moderate to excellent yields at 9 kbar and at room temperature to 65 °C affording the corresponding hydroxy amides **3**. For example, 4-butanolide (**1a**), 4-pentanolide (**1b**), and 5-pentanolide (**1d**) underwent aminolysis with piperidine (**2a**) at 30 °C to give the corresponding hydroxy amides **3aa**, **3ba**, and **3da** in 99, 95, and 96% yields, respectively, whereas no appreciable reaction was observed in refluxing acetonitrile at 1 bar. Similarly, diethylamine (**2b**) reacted smoothly with **1a**, **1b**, and **1d** at 9 kbar and

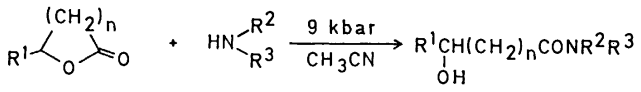

1 2 3

1	n	R^1
a	2	H
b	2	CH_3
c	2	n-C_6H_{13}
d	3	H
e	4	H
f	1	CH_3

2	R^2	R^3
a	-$(CH_2)_5$-	
b	C_2H_5	C_2H_5
c	$C_6H_5CH_2$	H
d	C_6H_5	H
e	p-$NO_2C_6H_4$	H
f	C_6H_5	C_6H_5

Table 1. Reactions of Lactones **1** with Amines **2** at 9 kbar

Product	Reaction conditions		Yield	Mp
	Temp/°C	Time/d	%	θ_m/°C
3aa	30	7	99	Oil
3ab	30	4	100	Oil
3ad	55	5	8	69—70
	65	7	47	
3ba	30	7	95	Oil
3bb	30	4	95	Oil
3bc	30	7	100	Oil
3bd	55	5	19	88—89
	65	7	39	
3ca	30	7	96	Oil
3cb	30	10	93	Oil
3da	30	4	96	Oil
3db	30	4	94	Oil
3dd	55	7	94	67—68
3ea	30	1	40[a]	Oil
	30	4	86[b]	
3eb	55	7	15	Oil
3fe	60	7	40(+60[c])	142—143
	60[d]	7	50(+50[c])	
3ff	60	7	35(+28[e])	98—99
	60[f]	7	8(+8[e])	(99—100)
5a	30	7	87	79—80
5b	30	7	100	Oil
7a	30	7	77	80—90
7b	30	7	88	Oil

a) At 5 kbar for 12 h, **10** (oil) was obtained in 13% yield. b) A 3% yield of **10**. c) The yield of **11e**. d) In THF. e) The yield of **11f**. f) In toluene.

Present address: Ibaraki Research Laboratory, Hitachi Chemical Co., Ltd., Hitachi, Ibaraki 317.

§ 1 bar=10^5 Pa.

30 °C to produce **3ab**, **3bb**, and **3db** in 100, 95, and 94% yield, respectively, while at 5 kbar and 30 °C only a 36% yield of **3bb** was obtained, thus demonstrating a considerable pressure effect in this reaction. It is rather surprising that the reaction of 4-pentanolide (**1b**) with benzylamine (**2c**) took place quantitatively at 9 kbar since some of the original lactone was always recovered even under the vigorous conditions at 1 bar and 190 °C for several days that resulted in much decomposition.[4] Furthermore, **1a** and **1b** did react with aniline (**2d**) at 9 kbar and 65 °C affording **3ad** and **3bd** albeit in moderate yields (47 and 39%). Aniline, with a pK_a of 4.69, is one million times less basic than a typical primary alkylamine and is therefore reported to be inert to **1b** upon heating to 180 °C.[4] 5-Pentanolide (**1d**) was more reactive than 4-butanolide (**1a**), thus 94% yield of the hydroxy amide **3dd** was obtained at 9 kbar and 55 °C.

Other examples of five membered lactones include 4-decanolide (**1c**) and 4,5-dihydro-3-hydroxy-4,4-dimethyl-2(3*H*)-furanone (**4**) that reacted with **2a** and **2b** under similar conditions giving the hydroxy amides **3ca**, **3cb**, **5a**, and **5b**, respectively. The most versatile reagents for the mild aminolysis of esters[10] and lactones[11] are the dialkylaluminum amides. However, the hydrolysis procedure employed in this method often leads to recyclization to the original lactones as exemplified in the reaction of 1(3*H*)-isobenzofuranone (**6**) with diethylaluminum dimethyl amide.[11] This is not the case in the present method;

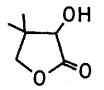

4

$HOCH_2C(CH_3)_2CH(OH)CONR^2R^3$

5a, b

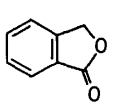

6

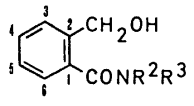

7a, b

for instance, **6** with **2a** at 9 kbar and 30 °C produced the hydroxy amide **7a** in 77% yield.

In contrast to **1a** and **1b**, a bicyclic lactone, 1,2-*O*-isopropylidene-α-D-glucofuranurono-6,3-lactone (**8**) underwent facile aminolysis with **2a** and **2c** at 1 bar and room temperature to give the corresponding amides **9a** and **9c** in 87 and 100% yields, respectively.

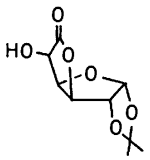

8

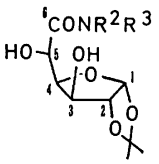

9a, c

This is presumably because of the bicyclic ring strain or the more constrained *cis*-ester structure.[12]

The reaction of 6-hexanolide (**1e**) with the amines was more complicated. For example, **1e** with **2a** at 9

Table 2. Eluents of Chromatography and Elemental Analysis

Compd No	Chromato. Solv.[a]	Found/%			Calcd/%			Formula
		C	H	N	C	H	N	
3aa	E	63.17	10.29	8.16	63.13	10.01	8.18	$C_9H_{17}NO_2$
3ab	E/A(g)	60.03	11.03	8.75	60.35	10.76	8.80	$C_8H_{17}NO_2$
3ad	E/T(7/3)	66.97	7.37	7.72	67.02	7.31	7.82	$C_{10}H_{13}NO_2$
3ba	E	64.40	10.42	7.48	64.83	10.34	7.56	$C_{10}H_{19}NO_2$
3bb	E/A(g)	62.14	11.34	8.09	62.39	11.05	8.09	$C_9H_{19}NO_2$
3bc	E	69.79	8.37	6.77	69.54	8.27	6.76	$C_{12}H_{17}NO_2$
3bd	E/T(7/3)	68.16	7.83	7.35	68.37	7.82	7.25	$C_{11}H_{15}NO_2$
3ca	E/T(7/3)	70.80	11.70	5.68	70.54	11.45	5.48	$C_{15}H_{29}NO_2$
3cb	E/T(7/3)	69.10	12.26	5.80	69.09	12.01	5.76	$C_{14}H_{29}NO_2$
3da	E/A(1/1)	64.73	10.41	7.36	64.83	10.34	7.56	$C_{10}H_{19}NO_2$
3db	E/A(g)	62.01	11.26	7.98	62.39	11.05	8.09	$C_9H_{19}NO_2$
3dd	E/T(7/3)	68.48	7.85	7.25	68.37	7.82	7.25	$C_{11}H_{15}NO_2$
3ea	E/A(g)	66.13	10.87	7.27	66.30	10.62	7.03	$C_{11}H_{21}NO_2$
3eb	E/A(g)	63.87	11.55	7.35	64.13	11.30	7.48	$C_{10}H_{21}NO_2$
3fe	B/E(g)	53.82	5.54	12.36	53.57	5.39	12.49	$C_{10}H_{12}N_2O_4$
3ff	B/E(g)	74.96	6.80	5.43	75.27	6.71	5.49	$C_{16}H_{17}NO_2$
5a	E/T(7/3)	61.39	10.01	6.45	61.37	9.83	6.51	$C_{11}H_{21}NO_3$
5b	E/T(7/3)	58.81	10.69	6.65	59.09	10.41	6.89	$C_{10}H_{21}NO_3$
7a	E/T(7/3)	71.38	7.85	6.37	71.21	7.81	6.39	$C_{13}H_{17}NO_2$
7b	E/T(7/3)	69.28	8.36	6.75	69.54	8.27	6.76	$C_{12}H_{17}NO_2$
10a		64.10	9.93	4.52	64.19	9.76	4.68	$C_{16}H_{29}NO_4$
11e		53.54	5.45	12.39	53.57	5.39	12.49	$C_{10}H_{12}N_2O_4$
11f		75.38	6.74	5.33	75.27	6.71	5.49	$C_{16}H_{17}NO_2$

a) In this column are shown eluents of a column chromatography on silica gel to isolate the product: E=ethyl acetate, A=acetone, B=benzene, T=toluene; and in the parentheses the solvent ratio or g=gradient fashion.

kbar and 30 °C gave an 86% yield of **3ea** along with 6-oxo-6-piperidinohexyl 6-hydroxyhexanoate (**10**, 3%), the formation of which can be explained in terms of acyl-oxygen fission of **1e** with **3ea**. At the lower pressure (5 kbar) and employing the shorter reaction time (12 h), the yield of **10** increased to 13% while that of **3ea** decreased to 40%. Under higher pressure and a longer reaction time, **10** apparently undergoes further aminolysis to give **3ea**. Diethylamine (**2b**) was almost inert to **1e** at 8 kbar and 30 °C. However, the reaction took place at 8 kbar and 60 °C, producing a complex mixture of products from which the amide **3eb** was isolated only in 15% yield.

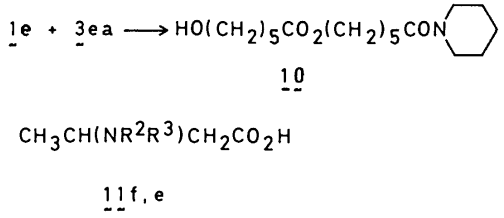

Three-membered lactones, like 3-propanolide and 3-butanolide, readily undergo aminolysis, but presumably because of the effect of ring strain, alkyl-oxygen fission is also observed. The course of the

Table 3. ^{1}H NMR Data of Hydroxy Amides **3**, **5**, **7**, **9**, **10**, and **11**[a]

3aa	1.61 (bs, 6H, $^{3',4',5'}CH_2$), 1.72—2.00 (m, 2H, $^{3}CH_2$), 2.47 (t, J=6.9 Hz, 2H, $^{2}CH_2$), 3.3—3.8 (m, 7H, $^{4,2'6'}CH_2$+OH)
3ab	1.11, 1.19 (each t, J=7.0 Hz, 6H, CH_2CH_3×2), 1.72—2.00 (m, 2H, $^{3}CH_2$), 2.48 (t, J=6.9 Hz, 2H, $^{2}CH_2$), 3.33, 3.34 (each q, J=7.0 Hz, 4H, CH_2CH_3×2), 3.65 (bt, J=5.7 Hz, 2H, $^{4}CH_2$), 4.2 (bs, 1H, OH)
3ad	1.78—2.05 (m, 2H, $^{3}CH_2$), 2.48 (t, J=7.0 Hz, 2H, $^{2}CH_2$), 3.5—3.8 (m, 3H, $^{4}CH_2$+OH), 7.0—7.6 (m, 5H, C_6H_5), 8.38 (bs, 1H, NH)
3ba	1.16 (d, J=5.4 Hz, 3H, $^{5}CH_3$), 1.58 (bs, 6H, $^{3',4',5'}CH_2$), 1.6—1.9 (m, 2H, $^{3}CH_2$), 3.3—3.6 (m, 4H, $^{2',6'}CH_2$), 3.6—4.0 (m, 2H, ^{4}CH+OH)
3bb	1.10, 1.19 (each t, J=7.0 Hz, 6H, CH_2CH_3×2), 1.20 (d, J=6.2 Hz, 3H, $^{5}CH_3$), 1.6—1.9 (m, 2H, $^{3}CH_2$), 2.49 (t, J=7.0 Hz, 2H, $^{2}CH_2$), 3.34, 3.37 (each q, J=7.0 Hz, 4H, CH_2CH_3×2), 3.6—4.2 (m, 2H, ^{4}CH+OH)
3bc	1.12 (d, J=6.3 Hz, 3H, $^{5}CH_3$), 1.5—1.9 (m, 2H $^{3}CH_2$), 2.30 (t, J=7.0 Hz, 2H, $^{2}CH_2$), 3.49 (bs, 1H, OH), 3.6—4.0 (m, 1H, ^{4}CH), 4.32 (d, J=5.7 Hz, 2H, $CH_2C_6H_5$), 6.9 (bs, 1H, NH), 7.1—7.3 (m, 5H, C_6H_5)
3bd	1.19 (d, J=6.2 Hz, 3H, $^{5}CH_3$), 1.6—1.9 (m, 2H, $^{3}CH_2$), 2.49 (t, J=6.9 Hz, 2H, $^{2}CH_2$), 3.43 (bs, 1H, OH), 3.6—4.0 (m, 1H, ^{4}CH), 6.9—7.6 (m, 5H, C_6H_5), 8.35 (bs, 1H, NH)
3ca[b]	0.88 (t, J=7 Hz, 3H, $^{10}CH_3$), 1.3—1.9 (m, 18H, $^{3,5,6,7,8,9,3',4',5'}CH_2$), 2.50 (t, J=7.0 Hz, 2H, $^{2}CH_2$), 3.4—3.6 (m, 6H, ^{4}CH+OH+$^{2',6'}CH_2$)
3cb[b]	0.88 (t, J=7.0 Hz, 3H, $^{10}CH_3$), 1.11, 1.19 (each t, J=7.0 Hz, 6H, CH_2CH_3×2), 1.2—1.5 (m, 10H, $^{5,6,7,8,9}CH_2$), 1.6—2.0 (m, 2H, $^{3}CH_2$), 2.3—2.6 (m, 2H, $^{2}CH_2$), 3.33, 3.36 (each q, J=7.0 Hz, 4H, CH_2CH_3×2), 3.6 (bs, 1H, OH)
3da	1.6 (bs, 10H, $^{3,4,3',4'5'}CH_2$), 2.36 (t, J=7.0 Hz, 2H, $^{2}CH_2$), 3.3—3.8 (m, 7H, $^{5,2',6'}CH_2$+OH)
3db	1.10, 1.18 (each t, J=7.0 Hz, 6H, CH_2CH_3×2), 1.4—1.9 (m, 4H, $^{3,4}CH_2$), 2.35 (bt, J=6.8 Hz, 2H, $^{2}CH_2$), 3.33, 3.36 (each q, J=7.0 Hz, 4H, CH_2CH_3×2), 3.60 (t, J=6 Hz, 2H, $^{5}CH_2$), 3.96 (bs, 1H, OH)
3dd	1.3—1.9 (m, 4H, $^{3,4}CH_2$), 2.33 (bt, J=6.7 Hz, 2H, $^{2}CH_2$), 3.4—3.8 (m, 3H, $^{5}CH_2$+OH), 6.9—7.6 (m, 5H, C_6H_5), 8.58 (bs, 1H, NH)
3ea	1.2—2.0 (m, 12H, $^{3,4,5,3',4',5'}CH_2$), 2.33 (t, J=7.0 Hz, 2H, $^{2}CH_2$), 2.88 (bs, 1H, OH), 3.3—3.8 (m, 6H, $^{5,2',6'}CH_2$)
3eb	1.10, 1.17 (each t, J=7.1 Hz, 6H, CH_2CH_3×2), 1.2—1.9 (m, 6H, $^{3,4,5}CH_2$), 2.31 (t, J=7.2 Hz, 2H, $^{2}CH_2$), 2.48 (bs, 1H, OH), 3.30, 3.37 (each q, J=7.1 Hz, 4H, CH_2CH_3×2), 3.65 (t, J=6 Hz, 2H, $^{6}CH_2$)
3fe[c]	1.19 (d, J=6.2 Hz, 3H, $^{4}CH_3$), 2.46 (d, J=5.8 Hz, 1H, ^{2}CHH), 2.49 (d, J=7.1 Hz, 1H, ^{2}CHH), 4.0—4.4 (m, 1H, ^{3}CH), 4.70 (bd, J=4.6 Hz, 1H, OH), 7.85, 8.15 (ABq, J=9.5 Hz, 4H, C_6H_4), 8.8 (bs, 1H, NH)
3ff	1.0—1.4 (m, 3H, $^{4}CH_3$), 2.0—2.9 (m, 2H, $^{2}CH_2$), 5.32 (bq, J=6 Hz, 1H, ^{3}CH), 4.5—4.9 (m, 1H, OH), 6.8—7.3 (m, 10H, C_6H_5×2)
5a	0.90, 0.96, 1.07, 1.20 (each s, 6H, CH_3×2), 1.4—1.8 (m, 6H, $^{3',4',5'}CH_2$), 2.7—2.9 (m, 2H, $^{2',6'}CHH$), 3.46 (bs, 2H, $^{2',6'}CHH$), 3.3—3.9 (m, 2H, OH×2), 4.01 (d, J=9 Hz, 1H, ^{2}CH), 4.29 (s, 2H, $^{4}CH_2$)
5b	0.94, 0.98 (each s, 6H, CH_3×2), 1.16, 1.22 (each t, J=7.0 Hz, 6H, CH_2CH_3×2), 3.1—4.1 (m, 8H, $^{4}CH_2$+OH×2+CH_2CH_3×2), 4.39 (d, J=9 Hz, 1H, ^{2}CH)
7a	1.3—1.8 (m, 6H, $^{3',4',5'}CH_2$), 2.7—3.8 (m, 4H, $^{2',6'}CH_2$), 4.53 (bs, 2H, CH_2), 5.32 (s, 1H, OH), 7.2—8.0 (m, 4H, C_6H_4)
7b	1.16, 1.36 (each t, J=7.3 Hz, 6H, CH_2CH_3×2), 3.21, 3.57 (each q, J=7.3 Hz, 4H, CH_2CH_3×2), 4.50 (s, 2H, CH_2), 7.6—8.0 (m, 4H, C_6H_4)
9a	1.30, 1.45 (each s, 6H, CH_3×2), 1.6 (bs, 6H, $^{3',4',5'}CH_2$), 3.4—3.8 (m, 6H, $^{2',6'}CH_2$+OH×2), 4.02 (dd, J=8.0, 3.6 Hz, 1H, ^{4}CH), 4.46 (d, J=14.8 Hz, 1H, ^{1}CH), 4.46, 4.71 (ABq, J=8.0 Hz, 2H, $^{2,3}CH$), 5.95 (d, J=3.6 Hz, 1H, ^{5}CH)
9c	1.29, 1.45 (each s, 6H, CH_3×2), 3.6—4.2 (m, 3H, NH+OH×2), 4.2—4.6 (m, 7H, $^{1,2,3,4}CH$+NH+CH_2), 5.92 (d, J=3.6 Hz, 1H, ^{5}CH), 7.1—7.4 (bs, 5H, C_6H_5)
10a	1.2—1.9 (m, 18H, $^{3,4,5,2',3',4',3'',4'',5''}CH_2$), 2.2—2.5 (m, 5H, $^{2,6}CH_2$+OH), 3.3—3.7 (m, 6H, $^{5',2'',6''}CH_2$), 4.07 (bt, J=6 Hz, 2H, $^{1'}CH_2$)
10b	1.10, 1.17 (each t, J=7.2 Hz, 6H, CH_2CH_3×2), 1.1—1.9 (m, 10H, $^{3,4,5,2',3'}CH_2$), 2.2—2.5 (m, 4H, $^{2,4'}CH_2$), 3.30, 3.41 (each q, J=7.2 Hz, 4H, CH_2CH_3×2), 3.63 (bt, J=6 Hz, 2H, $^{3}CH_2$), 4.06 (bt, J=6 Hz, 4H, $^{6,1'}CH_2$)
11e	1.36 (d, J=6.5 Hz, 3H, $^{4}CH_3$), 2.19 (s, 1H, OH), 2.64 (dd, J=5.4, 1.8 Hz, 2H, $^{2}CH_2$), 3.9—4.2 (m, 1H, ^{3}CH), 6.56, 8.06 (ABq, J=9.0 Hz, 4H, C_6H_4), 7.7 (bs, 1H, NH)
11f	1.13 (d, J=6.4 Hz, 3H, $^{4}CH_3$), 2.36 (d, J=5.4 Hz, 2H, $^{2}CH_2$), 3.94 (bs, 1H, OH), 4.0—4.4 (m, 1H, ^{3}CH), 7.1—7.5 (m, 10H, C_6H_5×2)

a) 90 MHz in $CDCl_3$. Superscripts indicate the position of carbons. b) 200 MHz. c) In DMSO-d_6 at 40 °C.

reaction is believed to be sensitive to the reaction conditions.[2,3] The reaction of 3-butanolide (**1f**) with unreactive amines, such as 4-nitroaniline (**2e**) and diphenylamine (**2f**), further demonstrates the utility and generality of the method, since no reaction of **1f** with **2e** at 1 bar in refluxing acetonitrile was

Table 4. ^{13}C NMR Data of Hydroxy Amides **3**, **5**, **7**, **9**, **10**, and **11** in $CDCl_3$

	C=O	$-CH_2-$ and $R^1CH(OH)$	R^2 and/or R^3
3aa	171.3(C-1)	29.9(C-2) 27.6(C-3) 61.4(C-4)	42.4 46.3(C-2′,6′) 25.1 26.0(C-3′,5′) 24.0(C-4′)
3ab	172.0(C-1)	29.4(C-2) 27.5(C-3) 61.1(C-4)	39.6 41.5($\underline{C}H_2$) 12.4 13.6($\underline{C}H_3$)
3ad	172.4(C-1)	34.4(C-2) 28.1(C-3) 61.8(C-4)	137.9(C-1′) 120.2(C-2′,6′) 128.8(C-3′,5′) 124.3(C-4′)
3ba	171.1(C-1)	33.5(C-2) 29.1(C-3) 66.0(C-4) 22.8(C-5)	41.9 46.0(C-2′,6′) 24.8 25.7(C-3′,5′) 23.7(C-4′)
3bb	173.0(C-1)	34.1(C-2) 29.8(C-3) 67.3(C-4) 23.6(C-5)	40.4 42.3($\underline{C}H_2$) 13.0 14.3($\underline{C}H_3$)
3bc	173.9(C-1)	34.3(C-2) 32.7(C-3) 66.8(C-4) 23.1(C-5)	43.1($\underline{C}H_2$) 138.1(C-1′) 127.0(C-4′) 127.3(C-2′,6′) 128.3(C-3′,5′)
3bd	172.6(C-1)	34.2(C-2) 34.0(C-3) 67.3(C-4) 23.5(C-5)	138.0(C-1′) 120.2(C-2′,6′) 128.8(C-3′,5′) 124.2(C-4′)
3ca	171.5(C-1)	37.2(C-2) 31.9(C-3) 70.5(C-4) 31.3(C-5) 29.4 28.9 25.2(C-6,7,8) 22.1(C-9) 13.5(C-10)	42.2 46.2(C-2′,6′) 25.1 26.0(C-3′,5′) 24.0(C-4′)
3cb	172.7(C-1)	37.6(C-2) 32.0(C-3) 71.0(C-4) 31.6(C-5) 29.5 29.1 25.5(C-6,7,8) 22.3(C-9) 14.0(C-10)	40.1 41.9($\underline{C}H_2$) 12.7 13.8($\underline{C}H_3$)
3da	171.0(C-1)	32.3(C-2) 21.0(C-3) 31.6(C-4) 60.9(C-5)	42.0 46.1(C-2′,6′) 24.9 25.9(C-3′,5′) 23.8(C-4′)
3db	172.0(C-1)	32.1(C-2) 21.0(C-3) 31.8(C-4) 61.1(C-5)	39.6 41.6($\underline{C}H_2$) 12.5 13.8($\underline{C}H_3$)
3dd	172.4(C-1)	36.7(C-2) 21.9(C-3) 31.6(C-4) 61.7(C-5)	138.0(C-1′) 120.2(C-2′,6′) 128.7(C-3′,5′) 124.1(C-4′)
3ea	171.2(C-1)	32.9(C-2) 26.2(C-3,4) 32.0(C-5) 61.7(C-5)	42.3 46.4(C-2′,6′) 24.7 25.3(C-3′,5′) 24.2(C-4′)
3eb	172.1(C-1)	32.7(C-2) 25.4 24.8(C-3,4) 32.1(C-5) 61.8(C-6)	39.9 41.8($\underline{C}H_2$) 12.8 14.1($\underline{C}H_3$)
3fe[a]	170.8(C-1)	46.8(C-2) 63.9(C-3) 23.5(C-4)	145.4(C-1′) 118.9(C-2′,6′) 124.9(C-3′,5′) 142.2(C-4′)
3ff	171.0(C-1)	49.6(C-2) 67.2(C-3) 19.6(C-4)	145.7(C-1′) 122.8(C-2′,6′) 129.2(C-3′,5′) 122.0(C-4′)
5a	172.0(C-1)	70.4(C-2) 40.0(C-3) 68.7(C-4) 19.3 21.7($\underline{C}H_3$)	43.3 47.0(C-2′,6′) 25.2 25.9(C-3′,5′) 24.0(C-4′)
5b	173.0(C-1)	71.5(C-2) 40.1(C-3) 68.8(C-4) 19.7 22.3($\underline{C}H_3$)	40.4 42.2($\underline{C}H_2$) 12.7 14.1($\underline{C}H_3$)
7a	169.5	134.7(C-1) 138.3(C-2) 125.4(C-3) 128.8(C-4) 126.7(C-5) 128.5(C-6) 62.2($\underline{C}H_2$)	42.2 48.0(C-2′,6′) 25.2 25.9(C-3′,5′) 23.9(C-4′)
7b	170.5	135.1(C-1) 137.9(C-2) 125.0(C-3) 128.6(C-4) 126.6(C-5) 128.2(C-6) 62.0($\underline{C}H_2$)	38.7 42.8($\underline{C}H_2$) 12.2 13.4($\underline{C}H_3$)
9a	170.7(C-6)	84.4(C-1) 82.4(C-2) 75.0(C-3) 65.0(C-4) 105.2(C-5) 111.6($\underline{C}Me$) 26.0 26.7(CH_3)	43.9 46.6(C-2′,6′) 25.4 26.1(C-3′,5′) 24.3(C-4′)
9c	172.3(C-6)	85.1(C-1) 81.1(C-2) 75.1(C-3) 69.5(C-4) 105.2(C-5) 112.0($\underline{C}Me_2$) 26.2 26.8($\underline{C}H_3$)	43.3($\underline{C}H_2$) 137.6(C-1′) 127.2(C-2′,6′) 128.6(C-3′,5′) 127.4(C-4′)
10a	171.0(C-1)	34.1(C-2) 62.0(C-6) 24.6 24.8 25.2 25.7 28.3 32.1 (C-3,4,5,2′,3′,4′)	64.0(C-1′) 33.0(C-5′) 173.6(C-6′) 42.5 46.5(C-2″,6″) 25.4 26.3(C-3″,5″) 24.3(C-4″)
10b	171.8(C-1)	33.9(C-2) 62.1(C-6) 24.4 24.9 25.4 25.7 27.8 32.2 (C-3,4,5,2′,3′,4′)	63.4(C-1′) 32.7(C-5′) 173.4(C-6′) 39.9 41.2($\underline{C}H_2$) 12.9 14.2($\underline{C}H_3$)
11e	176.8(C-1)	40.3(C-2) 45.3(C-3) 20.1(C-4)	152.3(C-1′) 111.4(C-2′) 126.4(C-3′) 137.6(C-4′)
11f	178.6(C-1)	39.9(C-2) 49.5(C-3) 19.2(C-4)	145.7(C-1′) 122.9(C-2′) 129.3(C-3′) 122.2(C-4′)

a) In DMSO-d_6.

observed and only 0.8% of the amino acid **11f** was formed in the reaction of **1f** with **2f** upon heating at 180—190 °C.[3a] The desired amides **3fe** and **3ff** were obtained in 40 and 35% yields, along with 3-(4-nitrophenylamino)- and 3-(diphenylamino)butyric acids **11e**(60%) and **11f**(28%), respectively. A slight improvement in the yield of **11e** was obtained using tetrahydrofuran as a solvent, whereas the use of more nonpolar solvents, like toluene, in the reaction of **1f** with **2f** retarded the reaction, the product ratio being little improved.

Experimental

General. Melting points are uncorrected. ^{1}H NMR spectra were measured either on a Hitachi R40(90 MHz) or JEOL FX-90Q(90 MHz) or Varian VRX-200(200 MHz) and ^{13}C NMR on a JEOL FX-90Q. The high-pressure instrument employed has been described elsewhere.[7]

High-Pressure Reaction of Lactones 1 with Amines 2. A General Procedure. A mixture of **1** (5 mmol) and **2** (10 mmol) was diluted with acetonitrile in a PTFE (8 cm^3) capsule, which was then stored for a stated time (Table 1) at 9 kbar. After evaporation of the solvent and amine (if volatile), the residue was chromatographed on silica gel, in general using ethyl acetate–acetone (or toluene or benzene) as an eluent in gradient fashion (Table 2). The results of analytical and ^{1}H and ^{13}C NMR spectroscopic data were collected in Tables 2—4.

Reaction of 1,2-*O*-Isopropylidene-α-D-glucofuranurono-6,3-lactone (8) with Piperidine (2a). A mixture of **8** (1 mmol) and **2a** (2 mmol) was stirred in acetonitrile (1 cm^3) at room temperature for 5 h. After evaporation of the solvent and amine, the residue was chromatographed on silica gel. Elution with benzene–ethyl acetate (1:3) gave *N*,*N*-pentamethylene-1,2-*O*-isopropylidene-α-D-glucofuranuronamide (**9a**) in 87% yield: mp 148—149 °C (see Tables 3 and 4). Found: C, 55.84; H, 7.71; N, 4.61%. Calcd for $C_{14}H_{23}NO_6$: C, 55.79; H, 7.71; N, 4.65%.

***N*-Benzyl-1,2-*O*-isopropylidene-α-D-glucofuranuronamide (9c).** The procedure was the same as described above for **9a**. **9c** was obtained quantitatively: mp 130—131 °C (see Tables 3 and 4). Found: C, 59.48; H, 6.47; N, 4.13%. Calcd for $C_{16}H_{21}NO_6$: C, 59.42, H, 6.56; N, 4.33%.

This work was supported by Grant-in-Aid for Developmental Scientific Research from the Ministry of Education, Science and Culture (No. 61840017). The authors express their gratitude to Professor R. M. Acheson for his help in the preparation of this manuscript.

References

1) Examples: a) M. Fieser, L. F. Fieser, E. Toromanoff, Y. Hirata, H. Heymann, M. Tefft, and S. Bhattacharya, *J. Am. Chem. Soc.*, **78**, 2825 (1956); G. R. Newkome, G. R. Baker, M. J. Saunders, P. S. Russo, V. K. Gupta, Z. Yao, J. E. Miller, and K. Bouillion, *J. Chem. Soc., Chem. Commun.*, **1986**, 752; G. R. Newkome, Z. Yao, G. R. Baker, V. K. Gupta, P. S. Russo, and M. J. Saunders, *J. Am. Chem. Soc.*, **108**, 849 (1986); b) S. J. Rodgers, C. Y. Ng, and K. N. Raymond, *J. Am. Chem. Soc.*, **107**, 4094 (1985); T. J. Collins, R. J. Coots, T. T. Furutani, J. T. Keech, G. T. Peake, and B. D. Santarsiero, *J. Am. Chem. Soc.*, **108**, 5333 (1986); c) J. M. Lehn, J. Malthete, and A.-M. Levelut, *J. Chem. Soc., Chem. Commun.*, **1985**, 1794; d) L. F. Tietze, S. Brand, and T. Pfeiffer, *Angew. Chem., Int. Ed. Engl.*, **24**, 784 (1985); e) L. H. Hellberg, C. Beeson, and R. Somannathan, *Tetrahedron Lett.*, **1986**, 3955.

2) T. L. Gresham, J. E. Jansen, F. W. Shaver, R. A. Bankert, and F. T. Fiedorek, *J. Am. Chem. Soc.*, **73**, 3168 (1951); Y. Iwakura, K. Nagakubo, J. Aoki, and A. Yamada, *Nippon Kagaku Zasshi*, **72**, 406 (1951); C. D. Hurd and S. Hayao, *J. Am. Chem. Soc.*, **74**, 5889 (1952).

3) a) Y. Iwakura, K. Nagakubo, J. Aoki, and A. Yamada, *Nippon Kagaku Zasshi*, **75**, 315 (1954); b) A. Sakuma, S. Torii, and I. Yanagisawa, Jpn. Patent, 7313530 (1973).

4) C. D. Lunsford, R. S. Murphey, and E. K. Rose, *J. Org. Chem.*, **22**, 1225 (1957); N. H. Cromwell and K. E. Cook, *J. Am. Chem. Soc.*, **80**, 4573 (1958).

5) J. B. Jones and J. M. Young, *Can. J. Chem.*, **44**, 1059 (1966).

6) K. Matsumoto, S. Hashimoto, and S. Otani, *Angew. Chem., Int. Ed. Engl.*, **25**, 565 (1986).

7) Review for organic synthesis under high pressure: K. Matsumoto, A. Sera, and T. Uchida, *Synthesis*, **1985**, 1; K. Matsumoto and A. Sera, *ibid.*, **1985**, 999.

8) Recent selected examples: M. M. Midland, J. I. McLoughlin, and J. Gabriel, *J. Org. Chem.*, **54**, 159 (1989); L. F. Tietze, T. Hubsch, E. Voss, M. Buback, and W. Trost, *J. Am. Chem. Soc.*, **110**, 4065 (1988); A. Padwa, D. N. Kline, and B. H. Norman, *Tetrahedron Lett.*, **29**, 265 (1988); W. G. Dauben, B. A. Kowalczyk, and D. J. H. Funhoff, *Tetrahedron Lett.*, **29**, 3021 (1988); S. I. Bell and S. M. Weinreb, *ibid.*, **29**, 4233 (1988); R. M. Ortuno, A. Guingant, and J. d'Angelo, *Tetrahedron Lett.*, **29**, 6989 (1988); K. D. Robarge and D. L. Boger, *J. Org. Chem.*, **53**, 3373, 5973 (1988); G. R. Tian, S. Sugiyama, A. Mori, and H. Takeshita, *Bull. Chem. Soc. Jpn.*, **61**, 2393 (1988).

9) For a preliminary communication: K. Matsumoto, S. Hashimoto, T. Okamoto, S. Otani, and J. Hayami, *Chem. Lett.*, **1987**, 803.

10) A. Bash, M. Lipton, and S. M. Weinreb, *Tetrahedron Lett.*, **1977**, 4171; M. F. Lipton, A. Basha, and S. M. Weinreb, *Org. Synth.*, **59**, 49 (1980); J. L. Levin, E. Turos, and S. M. Weinreb, *Synth. Commun.*, **12**, 989 (1982).

11) T. Hirabayashi, K. Ito, S. Sakai, and Y. Ishii, *J. Organomet. Chem.*, **25**, 33 (1970).

12) R. Huisgen and H. Otto, *Tetrahedron*, **6**, 253 (1959).

 © 1989 The Chemical Society of Japan Bull. Chem. Soc. Jpn., 62, 3143—3149 (1989)

The Ullmann Condensation Reaction of Haloanthraquinone Derivatives with Amines in Aprotic Solvents. VI.[1] The Combination of Cu(I) and Hydroxo or Alkoxo Cu(II) as Effective Catalyst System

Sadao Arai, Yoshio Hashimoto, Takamichi Yamagishi, and Mitsuhiko Hida*
Department of Industrial Chemistry, Faculty of Technology, Tokyo Metropolitan University, Fukazawa, Setagaya-ku, Tokyo 158
(Received April 14, 1989)

The reaction rate of the Ullmann condensation reaction of haloanthraquinone with ethylenediamine (EN) by copper(I) halide catalyst decreased along with the formation of inactive Cu(II) species [$Cu(EN)_2X_2$] by one-electron transfer from Cu(I) to haloanthraquinone. However, the combination of Cu(I) and Cu(II) salts, having an OH, OCH_3, or OCOR group, enhanced the reaction rate in the following order: CuCl<CuCl-CuCl(OCH_3)<CuCl-Cu(OCH_3)$_2$<CuCl-Cu(OH)$_2$. In condensation using Cu(OR)$_2$ or CuCl(OCH_3) alone, the Cu(II) species was reduced to Cu(I) to form an active catalyst system [Cu(I)+Cu(II)]. On the other hand, $CuBr_2$ or $CuCl_2$ was not reduced and was ineffective for the reaction. These were confirmed by ESR measurements and the presence of a dehalogenation product. Mixed valence species bridged by the alkoxo or hydroxo group was proposed as an active species.

A wide variety of copper species, such as copper powder, copper(I) oxide, copper(I) halides, and copper(II) salts, has been used for the catalyst of nucleophilic substitution of aryl halides (the Ullmann condensation).[2,3] The choice of the catalyst depends on the structure of aryl halides, nucleophiles, and solvents; however, it is often found that a catalyst that is effective for a certain reaction is ineffective for another reaction system.[3] The mechanism of the Ullmann condensation is further complicated by the fact that a copper species changes its oxidation state during a reaction. For example, a Cu(0) catalyst was changed to the effective Cu(I) species by oxidation with molecular oxygen or some other oxidants.[4] In the case of a Cu(II) catalyst, the reduction of Cu(II) to Cu(I) accelerated the reaction.[4,5]

Although Cu(I) salts were more effective catalysts than Cu(II) salts in the homogeneous Ullmann condensation of haloanthraquinones with amines in aprotic solvents,[6] Cu(II) species formed by a one-electron transfer from Cu(I) to haloanthraquinone under a nitrogen atmosphere played a very important role. The catalytic activity of Cu(I) was enhanced by Cu(II) species produced in condensation with 2-aminoethanol,[6-8] whereas with ethylenediamine (EN)[9] only Cu(I) was active and the reaction rate decreased along with the formation of an ineffective Cu(II) species. On the other hand, the alkoxocopper(II) species enhanced the rate of condensation with EN by a cooperative interaction with the Cu(I) species.[1]

These results prompted us to study a combination of Cu(I) and Cu(II) species in order to explore the more active catalyst system in the Ullmann condensation reaction. In this paper we will report on the results for the catalytic behavior of alkoxo or hydroxo copper(II) as a promoter in the Ullmann condensation reaction of haloanthraquinones with ethylenediamine.

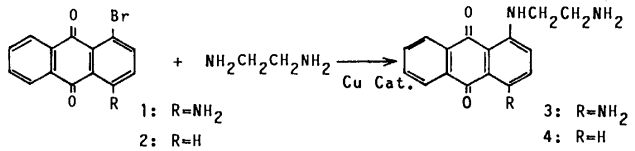

Experimental

Materials. 1-Amino-4-bromoanthraquinone (**1**) and 1-bromoanthraquinone (**2**) were prepared by desulfonation of sodium 1-amino-4-bromoanthraquinone-2-sulfonate with 80% sulfuric acid and by Sandmeyer's bromination of 1-aminoanthraquinone, respectively, as reported previously.[6] Copper(I) bromide and copper(I) chloride were prepared and purified as described in the literature.[10] Commercially available copper(II) bromide and copper(II) chloride (Kanto Chemical Co. Inc., GR grade) were purified according to methods described in the literature.[11] Chloromethoxycopper(II)[12] was prepared by the reaction of copper(I) chloride with molecular oxygen in methanol (Found: Cu. 49.0%). Dimethoxycopper(II)[13] was obtained by the reaction of anhydrous copper(II) chloride with lithium methoxide in methanol (Found: Cu, 50.7%). All other copper salts were commercial materials (Kanto Chemical Co. Inc., GR grade) and used without further purification. All solvents and ethylenediamine were dried and purified by the standard procedure, and stored under a nitrogen atmosphere.

Reaction Procedure. The condensation was initiated by the addition of a solution of copper salt and ethylenediamine in ethanol to the haloanthraquinone solution in THF-ethanol at a regulated temperature. The reaction was carried out under a dry, oxygen-free nitrogen atmosphere. The yield was determined spectrophotometrically as described in our previous papers.[1,6] The debromination product was analyzed by the use of a Shimadzu LC-3A HPLC (column: Unisil C18; mobile phase: methanol-water 4:1) with 1-amino-2-bromoanthraquinone as an internal standard.

Instruments. UV and visible spectra were measured with

a Shimadzu UV-210 spectrometer. ESR spectra were obtained by the use of a JEOL-PE-3X spectrometer, equipped with a 100-kHz field modulation unit.

Results and Discussion

The reaction rate of the condensation of 1-amino-4-bromoanthraquinone (**1**) or 1-bromoanthraquinone (**2**) with ethylenediamine (EN) catalyzed by Cu(I) salt (CuCl or CuBr) decreases along with the formation of an inactive Cu(II) species $[Cu(EN)_2X_2]$ by a one-electron transfer from Cu(I) to haloanthraquinone.[9] However, upon the addition of hydroxo or alkoxo Cu(II) salt the condensation catalyzed by Cu(I) salt was accelerated. As a typical example, Fig. 1 indicates the results of the condensation of **1** with EN using a CuCl-$Cu(OH)_2$ catalyst system. The yield of 1-amino-4-(2-aminoethylamino)anthraquinone (**3**) depended on the molar fraction of $Cu(OH)_2$ to the total copper ([CuCl]+[$Cu(OH)_2$]). An induction period was observed when the copper species was $Cu(OH)_2$ alone.

Copper(II) Species as a Promoter. Figure 2 illustrates plots of the initial rate (V_0) vs. the fraction of Cu(II) to the total copper. In condensation using a CuBr-$CuBr_2$ catalyst system, the initial rate decreased linearly with an increase in the fraction.[1] On the other hand, in catalyst systems containing alkoxo or hydroxo Cu(II) species, the maximum initial rate was observed at a fraction of around 0.3 and the catalytic activity increased in the following order: CuCl-$CuCl(OCH_3)$<CuCl-$Cu(OCH_3)_2$<CuCl-$Cu(OH)_2$. These results clearly show that in condensation using a CuBr-$CuBr_2$ catalyst system, only Cu(I) is effective and the Cu(II) species containing two halide ligands is ineffective. This contrasts to other catalyst systems where the Cu(II) species acts as a promoter.

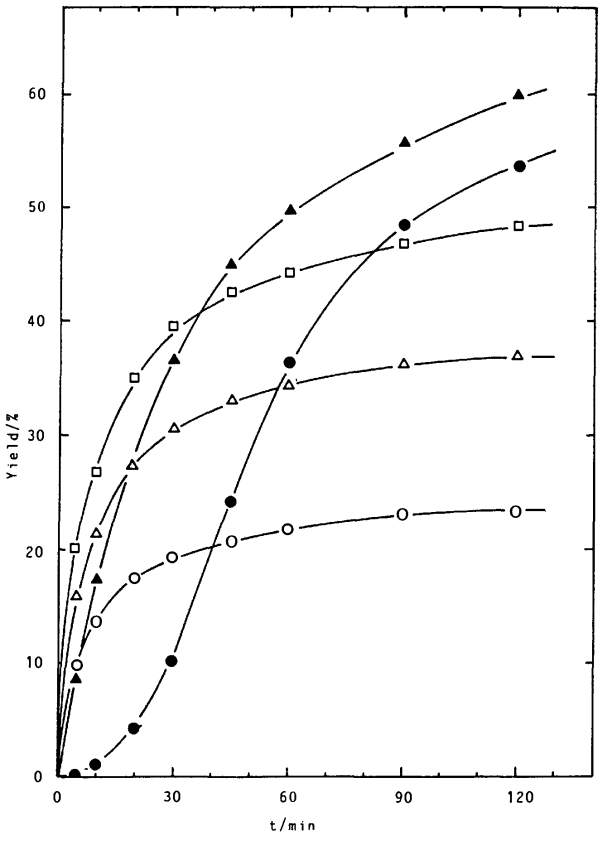

Fig. 1. Time course of the reaction of **1** with EN by CuCl-$Cu(OH)_2$ catalyst system.
$[\mathbf{1}]_0=5.0\times10^{-3}$ mol dm^{-3}, $[EN]_0=0.5$ mol dm^{-3}, $[CuCl+Cu(OH)_2]_0=2.1\times10^{-3}$ mol dm^{-3}, temp 50 °C, solvent THF-EtOH 1 : 1.
○: r ($[Cu(OH)_2]_0/[CuCl+Cu(OH)_2]_0$)=0, △: r=0.164, □: r=0.288, ▲: r=0.755, ●: r=1.0.

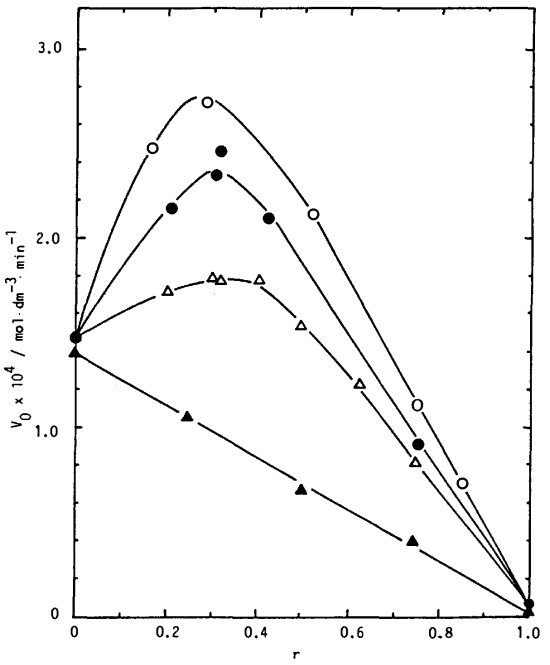

Fig. 2. The dependence of the initial rates, (V_0) on the ratio r ($[Cu(II)]_0/[Cu(I)+Cu(II)]_0$) in the reaction of **1** with EN.
$[\mathbf{1}]_0=5.0\times10^{-3}$ mol dm^{-3}, $[EN]_0=0.5$ mol dm^{-3}, $[Cu(I)+Cu(II)]_0=2.1\times10^{-3}$ mol dm^{-3}, temp 50 °C, solvent THF-EtOH 1 : 1.
○: CuCl-$Cu(OH)_2$, ●: CuCl-$Cu(OMe)_2$, △: CuCl-CuCl(OMe), ▲: CuBr-$CuBr_2$.

The initial rates of the condensation by various kinds of Cu(II) species were compared at a molar ratio of about 0.3 (Table 1). Cu(II) species having an OH, OCH_3, or OCOR group increased the catalytic activity of Cu(I), whereas a Cu(II) species having NO_3, ClO_4, or S, deactivated the condensation. The hyperfine coupling constants (A)[13] of $CuBr_2$ or $CuCl_2$ in a THF-EtOH (1 : 1) solution containing EN were around 80 G, whereas those of the Cu(II) species coordinated by an OY-type ligand (Y=H, R, COR) were around 70 G.

Consequently, the initial rate (V_0) can be expressed as

$$V_0 = k_1[Cu(I)] + k_2[Cu(I)]^m[Cu(II)]^n. \quad (1)$$

Table 1. Initial Rates (V_0)[a] for the Condensation of **1** with EN by Cu catalyst and the Coupling Constants (A) of Cu(II) Species

Catalyst system			V_0	A
Cu(II)	+	Cu(I)	mol·dm^{-3}·min^{-1}	G
$Cu(OH)_2$		CuCl	2.70	69.6
$Cu(OMe)_2$		CuCl	2.33	70.5
CuCl(OMe)		CuCl	1.72	70.4
$Cu(CO_3)\cdot Cu(OH)_2\cdot H_2O$		CuCl	1.69	—
$CuSO_4\cdot 5H_2O$		CuCl	1.33	—
$Cu(AcO)_2\cdot CuO\cdot 6H_2O$		CuCl	1.19	—
$Cu(HCOO)_2\cdot 4H_2O$		CuCl	1.08	70.8
$CuCl_2$		CuCl	1.00	79.7
$CuBr_2$		CuBr	0.92	79.5
$Cu(NO_3)_2\cdot 3H_2O$		CuCl	0.71	69.4
$Cu(ClO_4)_2\cdot 6H_2O$		CuCl	0.55	69.8
CuS		CuCl	0.057	—

a) $[\mathbf{1}]_0=5.0\times10^{-3}$ mol·dm^{-3}, $[EN]_0=0.5$ mol·dm^{-3}, $[Cu(I)+Cu(II)]_0=2.1\times10^{-3}$ mol·dm^{-3}, $[Cu(II)]_0/[Cu(I)+Cu(II)]_0=0.3$, temp 50 °C, solvent THF-EtOH 1 : 1.

If f and v_0 denote the fraction of Cu(I) to the total copper ([Cu(I)]+[Cu(II)]) and the initial rate catalyzed by Cu(I) alone, respectively, Eq. 1 becomes

$$V_0 - fv_0 = k_2[Cu(I)]^m[Cu(II)]^n. \quad (2)$$

Figure 3 shows a plot of V_0-fv_0, which indicates the rate catalyzed by a Cu(I) and Cu(II) couple, against fraction (r) of Cu(II) to total copper. In the CuCl-CuCl(OMe) system, the maximum rate was observed at $r=0.5$, whereas in the CuCl-$Cu(OMe)_2$ and CuCl-$Cu(OH)_2$ systems it appeared at $r=0.3$. Therefore, in a CuCl-CuCl(OMe) catalyst system the ratio of m to n is 1 : 1, whereas in CuCl-$Cu(OH)_2$ and CuCl-$Cu(OMe)_2$ catalyst systems the ratio is 2 : 1. These results suggest that the active species (alkoxo or hydroxo Cu(I)) is formed by the following ligand-exchange reactions:

$$CuCl + CuCl(OMe) \rightarrow CuOMe + CuCl_2$$

and

$$2CuCl + Cu(OR)_2 \rightarrow 2CuOR + CuCl_2.$$

However, the coupling constant (A) of CuCl-$Cu(OH)_2$ (2 : 1) in a THF-EtOH (1 : 1) solution was not 80 G but, rather, 70 G and the ESR spectrum of this system was the same as that of $Cu(OH)_2$-EN. These results exclude the possibility of alkoxo or hydroxo Cu(I) formation by a ligand-exchange reaction. The above results can be explained in terms of the idea that a Cu(II) species having OH or OCH_3 interact with the Cu(I) species to form an oxygen-bridged multi copper species as follows:

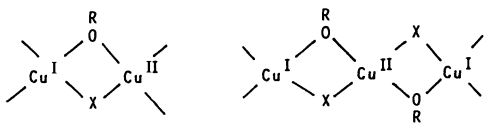

Although we failed to detect the presence of these oxygen-bridged species by ESR measurement, many

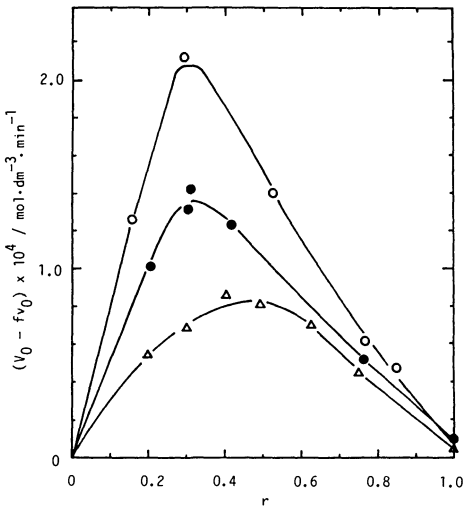

Fig. 3. The dependence of the rate catalyzed by the cooperative Cu(I) and Cu(II) combination on the ratio r ($[Cu(II)]_0/[Cu(I)+Cu(II)]_0$) in the reaction of **1** with EN.
$[\mathbf{1}]_0=5.0\times10^{-3}$ mol dm^{-3}, $[EN]_0=0.5$ mol dm^{-3}, $[Cu(I)+Cu(II)]_0=2.1\times10^{-3}$ mol dm^{-3}, temp 50 °C, solvent THF-EtOH 1 : 1.
○: CuCl-$Cu(OH)_2$, ●: CuCl-$Cu(OMe)_2$, △: CuCl-CuCl(OMe).

examples of alkoxo- or hydroxo-bridged copper species have been reported.[14] On the other hand $CuBr_2$ or $CuCl_2$, which does not form an oxygen-bridged species, is ineffective as a promoter. No reasonable explanation is possible for the deactivation by $Cu(NO_3)_2$, $Cu(ClO_4)_2$.

Change of Oxidation States of Copper Species during the Condensation. Figure 4 shows the results of an ESR measurement of the condensation system (**1**-EN-CuCl). The Cu(II) signal height[15] increased as the condensation proceeded and the coupling constant A remained unchanged at 80 G during the condensation. The ESR spectra of this condensation system were the same as that of a violet solution[16] of $CuBr_2$-EN or $CuCl_2$-EN in THF-EtOH (1 : 1) (A=80 G; Table 1). Therefore, the ineffective Cu(II) species formed during the condensation is considered to be a mononuclear Cu(II) complex: $Cu(EN)_2X_2$.

On the other hand, in the case of CuCl-$Cu(OH)_2$ (2 : 1) catalyst system, which is the most effective one, the formation of the Cu(II) species was much depressed compared to that using the CuCl catalyst system (Fig. 4). However, the coupling constant (70 G) was gradually increased and went up to 77 G after 90 min. This would be due to the coordination of bromide ions accumulated in the solution. These results suggest that a Cu(I)-Cu(II) couple containing an OH group was relatively stable or that a concurrent reduction of Cu(II) to Cu(I) occurred with the oxidation of Cu(I).

In condensation using CuCl-$Cu(OCH_3)_2$ (2 : 1) and CuCl-CuCl(OCH_3) (2 : 1) catalyst systems the time

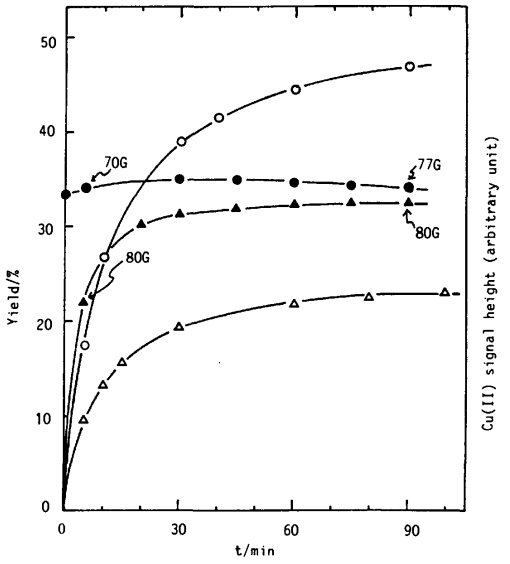

Fig. 4. Time course of the reaction of **1** with EN by Cu catalyst.
$[\mathbf{1}]_0=5.0\times10^{-3}$ mol dm^{-3}, $[EN]_0=0.5$ mol dm^{-3}, $[Cu]_0=2.1\times10^{-3}$ mol dm^{-3}, temp 50 °C, solvent THF-EtOH 1 : 1.
△: Yield of **3** by CuCl catalyst, ○: yield of **3** by CuCl-Cu(OH)$_2$ catalyst (r=0.288), ▲: Cu(II) signal height of the reaction system by CuCl catalyst, ●: Cu(II) signal height of the reaction system by CuCl-Cu(OH)$_2$ catalyst (r=0.288).

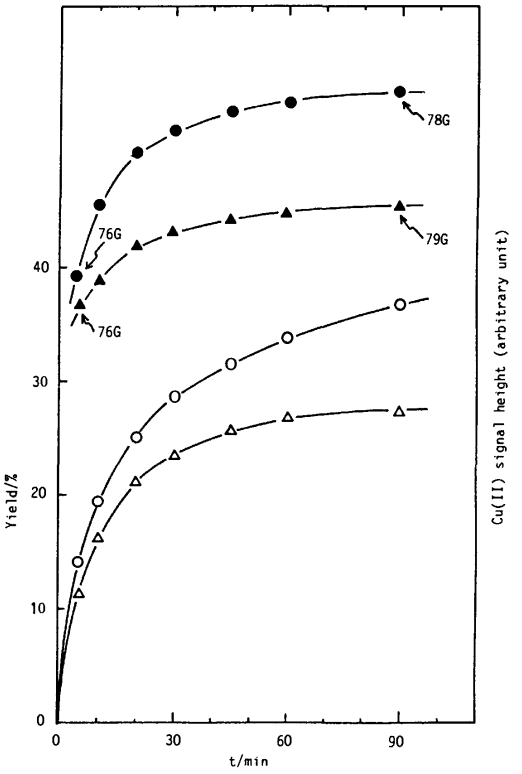

Fig. 5. Time course of the reaction of **1** with EN by Cu catalyst.
$[\mathbf{1}]_0=5.0\times10^{-3}$ mol dm^{-3}, $[EN]_0=0.5$ mol dm^{-3}, $[Cu]_0=2.1\times10^{-3}$ mol dm^{-3}, temp 50 °C, solvent THF-EtOH 1 : 1.
△: Yield of **3** by CuCl-CuCl(OMe) catalyst (r=0.309), ○: yield of **3** by CuCl-Cu(OMe)$_2$ catalyst (r=0.306), ▲: Cu(II) signal height of the reaction system by CuCl-CuCl(OMe) catalyst (r=0.309), ●: Cu(II) signal height of the reaction system by CuCl-Cu(OMe)$_2$ catalyst (r=0.306).

course of the yield of **3** and the coupling constant of Cu(II) (see Fig. 5) lies between those of the CuCl system and CuCl-Cu(OH)$_2$ system.

In condensation using Cu(OH)$_2$, Cu(OMe)$_2$, or CuCl(OMe) alone, which has an induction period, the Cu(II) signal height decreased and then slightly increased as the condensation proceeded (Figs. 6 and 7). It was also observed that the reaction rate tended to decrease along with an increase in the coupling constant. These results show that a part of the Cu(II) species was reduced to the Cu(I) species to form an active catalyst system [Cu(I) + Cu(II)]; then, Cu(I) was oxidized to ineffective Cu(II) by one-electron transfer from Cu(I) to haloanthraquinone and the coupling constant (A) of Cu(II) increased from 70 G to 80 G along with an increase of halide ions in the solution.

The reduction of Cu(II) to the Cu(I) species was also supported by the debromination of **1**. We previously reported that the debromination was caused through a radical anion intermediate, as follows:[8]

$$AQBr + Cu(I) \rightarrow AQBr^{\cdot-} + Cu(II)$$

$$AQBr^{\cdot-} \rightarrow AQH.$$

In fact, Fig. 6 shows that in the case of the **1**-EN-Cu(OH)$_2$ system 1-aminoanthraquinone was formed with an decrease in the Cu(II) signal height. The yields of the aminated product, [1-(2-aminoethylamino)anthraquinone: **4**], and the debrominated product, (anthraquinone) in **2**-EN-Cu(OH)$_2$, were larger than those in **1**-EN-Cu(OH)$_2$. This result corresponds to the fact that the decrease in the Cu(II) signal height was larger in the system of **2**-EN-Cu(OH)$_2$ than in that of **1**-EN-Cu(OH)$_2$ (Fig. 7).

Reduction of Cu(II) to the Cu(I) Species. As described above, the reduction of Cu(II) to the Cu(I) species was clearly observed in a condensation system using Cu(OH)$_2$, Cu(OMe)$_2$, or CuCl(OMe). Figure 6 also shows that in the absence of haloanthraquinone, the Cu(II) signal height was slightly decreased. The catalyst solution [Cu(OH)$_2$-EN] was heated at 50 °C for 110 min and then added to a solution of **1**. In this case the induction period was slightly shortened. These results also indicated that Cu(OH)$_2$ was slightly reduced to the Cu(I) species, even in the absence of haloanthraquinone. Contrary to haloanthraquinones, 1-aminoanthraquinone or anthraquinone did not facilitate a reduction of the Cu(II) species in the system of Cu(OH)$_2$-EN. These results suggest that the Cu(II) species is coordinated by the halogen moiety of haloanthraquinone, and reduced to Cu(I) by a one-electron transfer from EN. This was also sup-

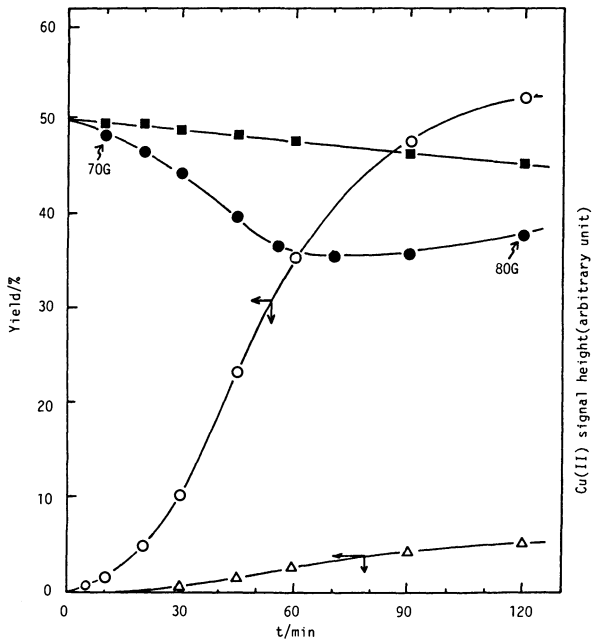

Fig. 6. Time course of the reaction of **1** with EN by $Cu(OH)_2$ catalyst.
$[\mathbf{1}]_0=5.0\times10^{-3}$ mol dm^{-3}, $[EN]_0=0.5$ mol dm^{-3}, $[Cu(OH)_2]_0=2.1\times10^{-3}$ mol dm^{-3}, temp 50 °C, solvent THF-EtOH 1 : 1.
○: **3**, △: 1-aminoanthraquinone, ●: Cu(II) signal height of the reaction system, ■: Cu(II) signal height in the absence of **1**.

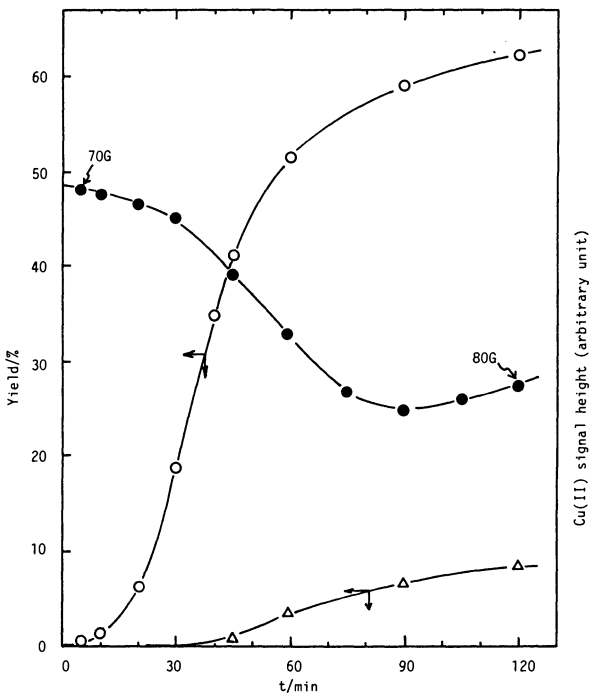

Fig. 7. Time course of the reaction of **2** with EN by $Cu(OH)_2$ catalyst.
$[\mathbf{2}]_0=5.0\times10^{-3}$ mol dm^{-3}, $[EN]_0=0.5$ mol dm^{-3}, $[Cu(OH)_2]_0=2.1\times10^{-3}$ mol dm^{-3}, temp 50 °C, solvent THF-EtOH 1 : 1.
○: **4**, △: anthraquinone, ●: Cu(II) signal height of the reaction system.

ported by the fact that the addition of 1-aminoanthraquinone equimolar to **2** little affected Cu(II) reduction in the system of **2**-EN-$Cu(OH)_2$.

The coupling constants of the catalyst systems containing alkoxo or hydroxo Cu(II) were smaller than that of the $CuCl$-$CuCl_2$ or $CuBr$-$CuBr_2$ system (Table 1). This suggests that the former Cu(II) species has a stronger covalent bond character than that of the latter.[17] On the basis of the reduction potentials of various Cu(II) complexes obtained by polarography, Patterson and Holm[18] reported that mononuclear Cu(II) complexes with a nonplanar structure (e.g., distorted tetrahedron and trigonal bipyramid) were readily reduced to Cu(I), compared with their planar analogs. It has also been reported that binuclear Cu(II) complexes with a planar structure and Cu(II) complexes with a distorted tetrahedral structure were readily reduced to Cu(I) by ascorbic acid, while planar mononuclear Cu(II) complexes were not reduced.[19] Consequently, copper(II) species having a promoter-character in our case has an alkoxo- or hydroxo-bridged structure and would be reduced to Cu(I) by EN. On the other hand, no reduction of Cu(II) to

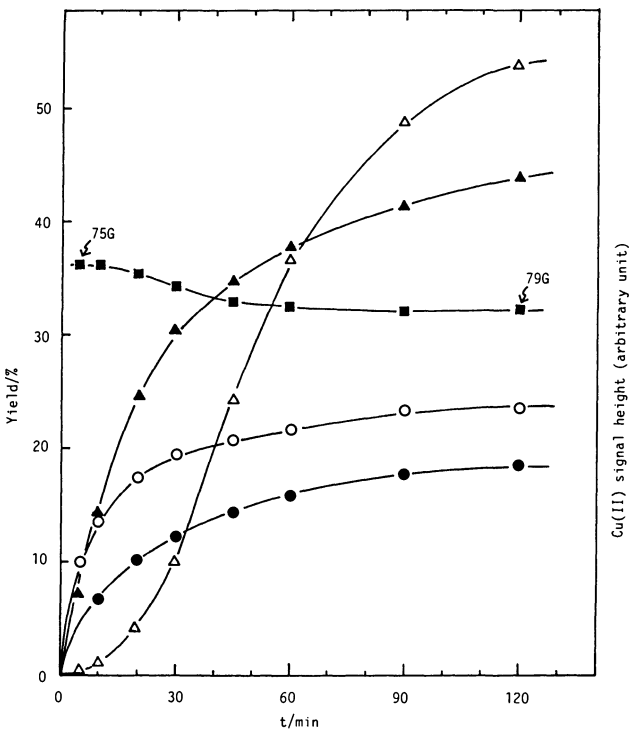

Fig. 8. Time course of the reaction of **1** with EN by Cu catalyst in the presence of glucose.
$[\mathbf{1}]_0=5.0\times10^{-3}$ mol dm^{-3}, $[EN]_0=0.5$ mol dm^{-3}, $[Cu]_0=2.1\times10^{-3}$ mol dm^{-3}, $[glucose]_0=2.27\times10^{-3}$ mol dm^{-3}, temp 50 °C, solvent THF-EtOH 1 : 1.
○: Yield of **3** by CuCl catalyst, ●: yield of **3** by CuCl catalyst in the presence of glucose, △: yield of **3** by $Cu(OH)_2$ catalyst, ▲: yield of **3** by $Cu(OH)_2$ catalyst in the presence of glucose, ■: Cu(II) signal height of the reaction system by $Cu(OH)_2$ in the presence of glucose.

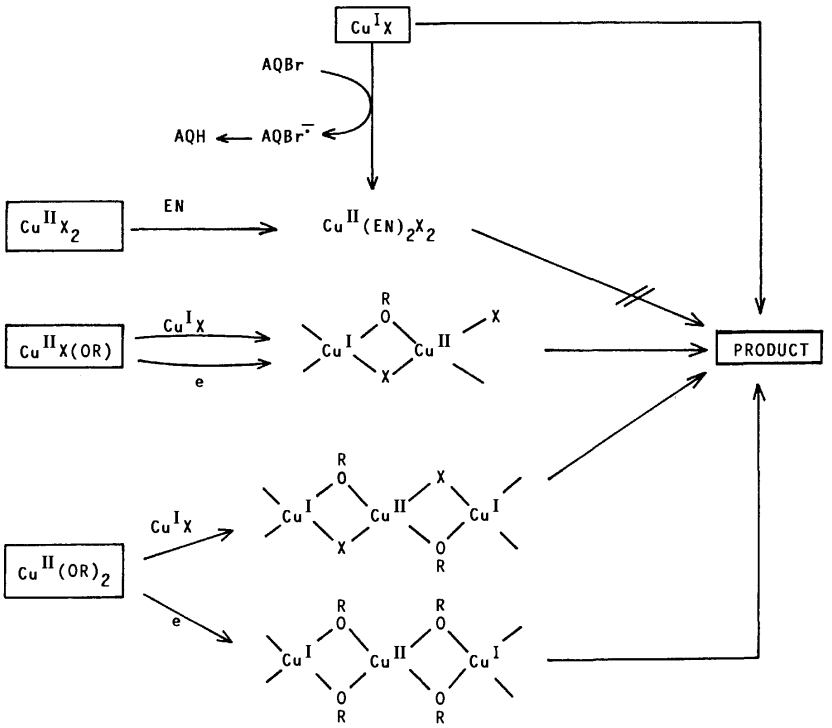

Fig. 9. Reaction pathways.

Cu(I) was observed in the systems using ineffective $Cu(EN)_2X_2$ with a planar structure (A= 80 G).

As Fig. 8 shows, upon the addition of glucose to the condensation system (**1**-EN-$Cu(OH)_2$), little induction period was observed and the Cu(II) signal height decreased very little. Since the coupling constant was observed to be 75 G, even at 4 min, it was concluded that during the first stage of the reaction the Cu(II) species was reduced to active Cu(I) by glucose and then reoxidized to an inactive Cu(II) species. The yield of **3** in **1**-EN-CuCl was decreased upon the addition of glucose. These results suggest that the coordination of glucose to the Cu(I) species interrupts the coordination of haloanthraquinone.

Reaction Pathways. The reaction pathways of the Ullmann condensation using $Cu(OR)_2$ or CuX(OR) are shown in Fig. 9.[20] As discussed above, all of the observed results support the reaction pathways including a Cu(I)···Cu(II) mixed valence complex. Although Cu(I) halide is an active catalyst, the reaction rate decreases along with the formation of inactive $Cu(EN)_2X_2$. The alkoxo- or hydroxo-bridged mixed valence complex would be formed by the reaction between the Cu(I)X and the alkoxo or hydroxo Cu(II) species, or by the reduction of the alkoxo- or hydroxo-bridged Cu(II) species.

References

1) Part V of this series: S. Arai, Y. Hashimoto, N. Takayama, T. Yamagishi, and M. Hida, *Bull. Chem. Soc. Jpn.*, **56**, 238 (1983).

2) J. Lindley, *Tetrahedron*, **40**, 1433 (1984), and references therein.

3) A. J. Paine, *J. Am. Chem. Soc.*, **109**, 1496 (1987).

4) A. C. Williams, R. E. Kinney, and R. F. Bridger, *J. Org. Chem.*, **32**, 2501 (1967).

5) J. A. Connor, D. Dubowski, A. C. Jones, and R. Price, *J. Chem. Soc., Perkin Trans. 1*, **1982**, 1143.

6) S. Arai, T. Yamagishi, S. Ototake, and M. Hida, *Bull. Chem. Soc. Jpn.*, **50**, 547 (1977).

7) S. Arai, M. Hida, T. Yamagishi, and S. Ototake, *Bull. Chem. Soc. Jpn.*, **50**, 2982 (1977).

8) S. Arai, M. Hida, and T. Yamagishi, *Bull. Chem. Soc. Jpn.*, **51**, 277 (1978).

9) S. Arai, A. Tanaka, M. Hida, and T. Yamagishi, *Bull. Chem. Soc. Jpn.*, **52**, 173 (1979).

10) R. N. Keller and H. D. Wycoff, *Inorg. Synth.*, **2**, 1 (1946).

11) H. Finkbeiner, A. S. Hay, H. S. Blanchard, and G. F. Endres, *J. Org. Chem.*, **31**, 549 (1966).

12) C. H. Brubaker, Jr. and M. Wicholas, *J. Inorg. Nucl. Chem.*, **27**, 59 (1965).

13) The coupling constants (A: 1 G = 10^{-4} T were obtained from the spacing of the third and fourth peaks of the Cu(II) signal.

14) H. Okawa, *Kagaku No Ryoiki*, **33**, 11 (1979), D. L. Lewis, K. T. McGregor, W. E. Hatfield, and D. J. Hodgson, *Inorg. Chem.*, **13**, 1013 (1974), C. Arcus, K. P. Firizzani, and S. F. Pavkovic, *J. Inorg. Nucl. Chem.*, **39**, 285 (1977).

15) Cu(II) signal height and an area determined by double integration of ESR signal were directly proportional to Cu(II) concentration in both $CuBr_2$-EN and $Cu(OH)_2$-EN in THF-EtOH (1 : 1) solution.

16) The color of $Cu(EN)_2$ was reported to be violet: Y. Itoh, "Jikken Kagaku Koza," ed by Nippon Kagaku Kai,

Maruzen, Tokyo(1956), Vol. 11, pp. 80—81.
17) B. A. Goodman and J. B. Raynor, "Adv. Inorg. Radiochem." ed by H. J. Emeleus and A. G. Sharpe, Academic, Press, New York (1970), Vol. 13, p. 135.
18) G. S. Patterson and R. H. Holm, *Bioinorg. Chem.*, **4**, 257 (1975).
19) N. Oishi, Y. Nishida, K. Ida, and S. Kida, *Bull. Chem. Soc. Jpn.*, **53**, 2847 (1980).
20) Ethylenediamine ligands are omitted from Fig. 9 for clarity.

Enzymatic Synthesis of Specifically Modified Linear Oligosaccharides from γ-Cyclodextrin Derivatives. Study on Importance of Active Sites of Taka Amylase A[1)]

Kahee FUJITA,* Tsutomu TAHARA,† Toshitaka KOGA,† and Taiji IMOTO††
Faculty of Pharmaceutical Sciences, Fukuyama University, Sanzo, Higashimura-cho, Fukuyama 729-02
†Daiichi College of Pharmaceutical Sciences, Tamagawa, Minami-ku, Fukuoka 815
††Faculty of Pharmaceutical Sciences, Kyushu University, Maidashi, Higashi-ku, Fukuoka 812
(Received May 11, 1989)

Specifically modified linear oligosaccharides were prepared by enzymatic hydrolysis of 6- or 2-*O*-substituted γ-cyclodextrin by Taka amylase A. These results suggest that the importance of the interactions between hydroxyl groups and the subsites (P—V) of Taka amylase A decreases in the following order; for C-6-OH, S>R>T>Q,U and for C-2-OH, R,S>T>Q, U.

Substrate specificity of Taka amylase A[2-8)] has been successfully studied by use of partially *O*-methylated amylose and specifically modified phenyl maltosides in order to obtain information about interaction between the subsites (Fig. 1)[6-8)] of Taka amylase A and substrates.[9-14)] We have reported a novel synthetic method for the preparation of specifically modified linear oligosaccharides by Taka amylase A degradation of α-cyclodextrin (α-CD) or β-cyclodextrin (β-CD) derivatives.[15-21)] This also provided new information about interactions between substrates and the subsites of Taka amylase A. The Taka amylase A-catalyzed hydrolysis of 6-*O*-substituted cyclodextrins (CDs)[16,17,22)] and $6^A,6^X$-*O*-disubstituted (X=B, C, or D) CDs[15-17)] revealed that interaction between subsite S and the C-6-OH was important. Also, the Taka amylase A-catalyzed hydrolysis of 2-*O*-substituted CDs disclosed the importance of interaction between the C-2-OH and subsites R and S.[21)] However, these experiments using the α- or β-CD derivatives can not tell us about the importance of other subsites. The reason is that the slow rate of cleavage of the CD macrocyclic ring does not allow accumulation of intermediate linear oligosaccharides in enough amount to be isolated. However, since γ-cyclodextrin (γ-CD) is hydrolyzed much faster than α- or β-CD by Taka amylase A,[23)] the hydrolysis of γ-CD derivatives can reasonably be expected to give new specifically modified linear oligosaccharides (new intermediates in the enzymatic hydrolysis) which can not be isolated in the hydrolysis of α- or β-CD. Also, this result will provide novel information concerning the importance of the subsites. We describe here Taka amylase A-catalyzed hydrolysis of 6-*O*-tosyl-γ-cyclodextrin (**1**), 6-*O*-(1-naphthylsulfonyl)-γ-cyclodextrin (**2**), 6-*O*-(2-naphthylsulfonyl)-γ-cyclodextrin (**3**), 2-*O*-(1-naphthylsulfonyl)-γ-cyclodextrin (**4**), and 2-*O*-(2-naphthylsulfonyl)-γ-cyclodextrin (**5**).

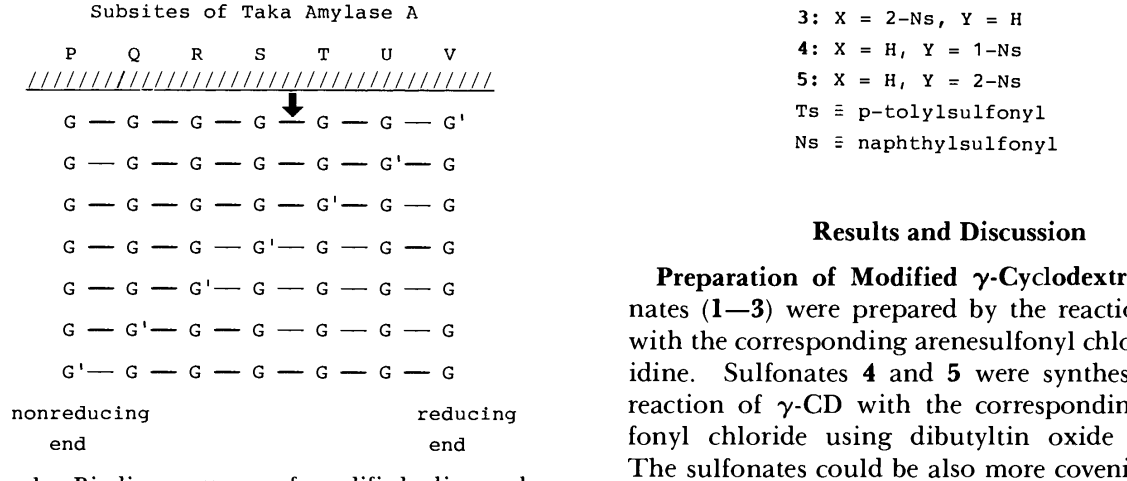

Fig. 1. Binding patterns of modified oligosaccharide to Taka amylase A.
P—V: subsite, G: glucose unit, G': modified glucose unit, ↓: cleavage point of glucosidic bond.

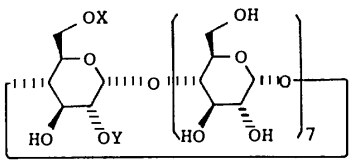

1: X = Ts, Y = H
2: X = 1-Ns, Y = H
3: X = 2-Ns, Y = H
4: X = H, Y = 1-Ns
5: X = H, Y = 2-Ns
Ts ≡ p-tolylsulfonyl
Ns ≡ naphthylsulfonyl

Results and Discussion

Preparation of Modified γ-Cyclodextrins. Sulfonates (**1**—**3**) were prepared by the reaction of γ-CD with the corresponding arenesulfonyl chloride in pyridine. Sulfonates **4** and **5** were synthesized by the reaction of γ-CD with the corresponding arenesulfonyl chloride using dibutyltin oxide in DMF.[24)] The sulfonates could be also more coveniently, however in lower yield, synthesized by the reaction of γ-CD with the corresponding arenesulfonyl chloride in water (see Experimental).

Taka Amylase A-Catalyzed Hydrolysis of the Modified γ-Cyclodextrins. The γ-CD derivatives were hydrolyzed by Taka amylase A to give specifically modified linear oligosaccharides. The reaction conditions, products, and yields are summarized in Table 1.

The modified maltose (**12**) or the modified maltotriose (**17** or **18**) was identified by comparing its high-performance liquid chromatography (HPLC) retention time and its fast atom bombardment mass (FAB MS) spectrum with those of the corresponding authentic compound.[21,22] The other 6′-*O*-(arylsulfonyl)maltoses (**13** and **14**) were converted to *S*-phenyl-6′-thiomaltose[16,17] and then identified similarly. Structures of other linear oligosaccharides were determined as follows. All compounds showed FAB MS spectra and ^{13}C NMR spectra consistent with their structures, whereas the position of sulfonylation in the chain of oligosaccharide was not determined by the spectral data. Sulfonates **6** and **9** were reduced with $NaBH_4$ to give **19** and **20**, respectively, followed by complete acetylation with acetic anhydride in pyridine. The resultant acetates (**21** and **22**) were analyzed by electron impact mass (EI MS) spectra in order to determine the sulfonylation position. The results are shown in Fig. 2. The sulfonate, **10**, or **11**, was converted to the 6″-phenylthio derivative (**23**) which was identified by comparing its HPLC retention time and its FAB MS spectrum to those of an authentic sample prepared from the reaction of **9** with thiophenol.

The sulfonate, **7** or **8**, was converted to the 3,6-anhydro derivative (**24**) by treatment with $Ba(OH)_2$ in water and identified by comparing its HPLC retention time and its FAB MS spectrum to those of the authentic compound which was prepared by the reaction of **6** with aqueous $Ba(OH)_2$. Authentic 3″,6″-anhydromaltotetraose (**24**) was also prepared by Taka-amylolysis of 3,6-anhydro-γ-cyclodextrin.[25,26]

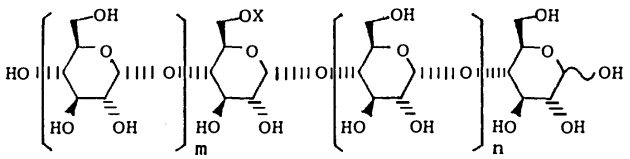

6: m = 1, n = 1, X = Ts
7: m = 1, n = 1, X = 1-Ns
8: m = 1, n = 1, X = 2-Ns
9: m = 0, n = 1, X = Ts
10: m = 0, n = 1, X = 1-Ns
11: m = 0, n = 1, X = 2-Ns
12: m = 0, n = 0, X = Ts
13: m = 0, n = 0, X = 1-Ns
14: m = 0, n = 0, X = 2-Ns
23: m = 0, n = 1, OX = S-C_6H_5

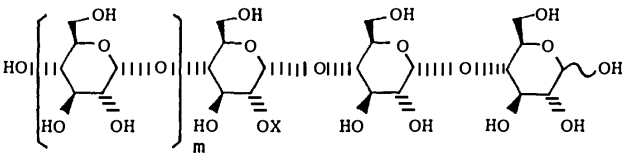

15: m = 1, X = 1-Ns
16: m = 1, X = 2-Ns
17: m = 0, X = 1-Ns
18: m = 0, X = 2-Ns

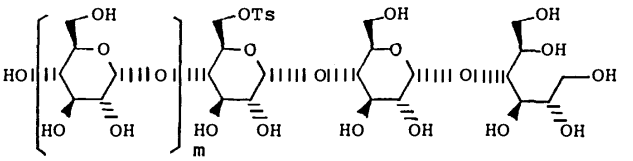

19: m = 1
20: m = 0

On reaction with aqueous $Ba(OH)_2$, the secondary sulfonate, **15** or **16**, gave an epoxide (**25**) which was identified by comparing its HPLC retention time and

Table 1. Taka Amylase A-Catalyzed Hydrolysis of Modified γ-Cyclodextrins[a,b]

CD derivative mg	Reaction temperature	Reaction period	Product
1 (50)	40 °C	3 h	**12** (13.6 mg, 79.5%)
(100)	10 °C	2 h	**6** (17.9 mg, 31.6%)+**9** (19.8 mg, 43.6%)
(100)	10 °C	2 days	**12** (34 mg, 99.4%)
2 (80)	40 °C	4 h	**13** (19.6 mg, 68.6%)
(63)	10 °C	1.5 h	**7** (12.9 mg, 35.5%)+**10** (16 mg, 54.4%)
3 (70)	40 °C	3 h	**14** (24.8 mg, 98.8%)
(200)	10 °C	2 h	**8** (33.2 mg, 28.8%)+**11** (27.2 mg, 29.1%)
(100)	10 °C	2 days	**14** (27.1 mg, 75.7%)
4 (20)	40 °C	3 h	**17** (6.3 mg, 67.7%)
(39.5)	10 °C	2.5 h	**15** (9.8 mg, 43%)+**17** (6.1 mg, 33.2%)
(50)	10 °C	1 day	**17** (15.8 mg, 67.5%)
5 (50)	40 °C	3 h	**18** (19 mg, 81.2%)
(80)	10 °C	1.5 h	**16** (13.2 mg, 28.6%)+**18** (8.8 mg, 23.5%)

a) Solvent, 0.1 mol dm^{-3} acetate buffer (pH 5.5) containing calcium chloride (0.01 mol dm^{-3}).
b) The concentrations of the γ-cyclodextrin derivative and Taka amylase A were each 10 mg/(1 cm^3 of solvent).

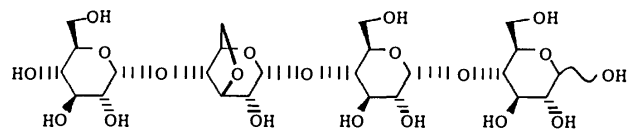

24

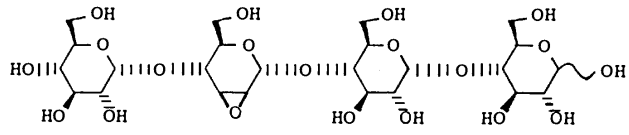

25

its FAB MS spectrum to those of the authentic sample.[21]

α- or β-CD analogues of **1**, **2** or **3** and **4** or **5** gave only G′-G and G′-G-G, respectively, upon Taka amylase A-catalyzed hydrolysis at 40 °C[21] (Hereafter, the following abbreviations are used: G, glucose unit; G′, modified glucose unit.). In an attempt to obtain intermediate linear oligosaccharides, reactions at lower temperature (10 °C or 0 °C) were carried out. However, the reaction rates were too slow to allow accumulation of stable linear oligosaccharide intermediates. The derivatives of γ-CD (**1**—**5**) were enzymatically hydrolyzed much more rapidly than the α- and β-CD analogues at 40 °C, although **1**—**3**, and **4** or **5** gave G′-G and G′-G-G, respectively, at this temperature similarly to the α- and β-CD analogues (Table 1). This suggests the accumulation of intermediates at lower temperature in the case of γ-CD derivatives.

The enzymatic hydrolysis of **1**—**3** at 10 °C afforded a mixture of G′-G-G and G-G′-G-G. Amylolyses of **1**—**3** at 40 °C or at 10 °C for longer reaction period (2 days) gave G′-G exclusively, demonstrating that G′-G-G and G-G′-G-G were the intermediates and that G-G′-G-G was a precursor of G′-G-G which led to G′-G. The enzymatic hydrolysis of **4** and **5** at 10 °C afforded a mixture of G′-G-G and G-G′-G-G. The reactions of **4** and **5** at 40 °C or 10 °C for 1 day gave G′-G-G, showing that G-G′-G-G was an intermediate leading to G′-G-G. Taka amylase A has seven subsites (P—V) in the active site and an oligosaccharide is cleaved between S and T subsites as shown in Fig. 1. The results with **1**—**3** demonstrate that interaction of the C-6-OH with the subsites R and T is important, but that interaction with T is less important than that with R and much less important than that with S. The results with **4** and **5** demonstrate that interaction of the C-2-OH with T is less important than those with R and S. Thus, the order of importance of the subsites is as follows. For C-6-OH, S>R>T>Q,U and for C-2-OH, R, S>T>Q, U. Unfortunately, estimation of importance of the subsites Q, U, P, and V was not possible because the higher oligosaccharides did not accumulate in enough amount to be isolated in this reaction system. It is interesting to note that difference in kind of modification (Ts, 1-Ns or 2-Ns) on the hydroxyl group of saccharide did not influence the kind of product (G′-G, G-G′-G-G, etc.) and that only the position of the modification (2-O or 6-O) determined the kind of product.

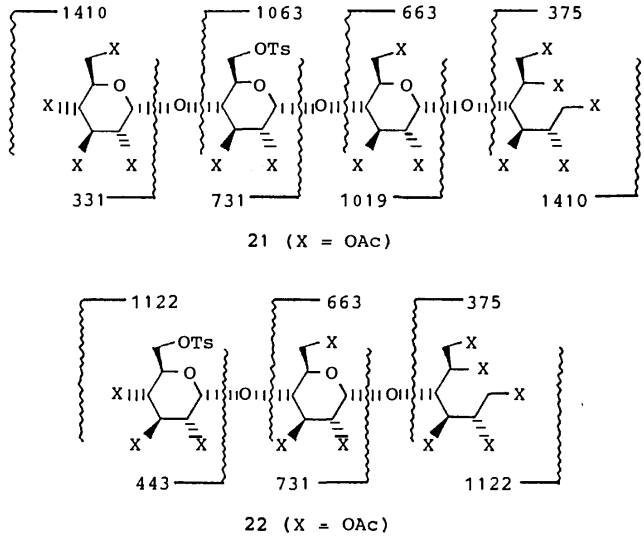

Fig. 2. EI MS spectral fragmentation patterns of **21** and **22**, which also showed correct molecular ions in FD MS spectra.

As mentioned before, the specifically activated (sulfonylated) oligosaccharides **6**—**11**, **15**, and **16** descibed in the present study can not be isolated from the enzymatic hydrolysis of 6- and 2-*O*-arylsulfonyl-α- or β-CDs, even when Taka amylase A was used in an amount equal to that of the CD derivative and/or the reaction was carried out at 5 °C or 10 °C. On the other hand, purely chemical methods for the preparation of these compounds from smaller sugars will need troublesome repeats of activation, protection, and deprotection of hydroxyl groups of the sugars. One-step chemical synthesis of specifically modified linear oligosaccharides from the corresponding linear oligosaccharides is also impossible. This method will require tedious separation of many regioisomeric monosulfonylated oligosaccharides.

Since there does not exist any regiochemical isomer, 2- and 6-*O*-arylsulfonyl-γ-CDs can be easily prepared and easily isolated as a pure material. As shown above, they can be smoothly hydrolyzed to give one or two modified oligosaccharide(s) at 10 °C. Furthermore, the products can be effectively separated by reversed-phase column chromatography. Therefore, the selective chemical modification of γ-CD followed by the Taka amylase A-catalyzed hydrolysis has several advantages for preparation of specifically modified oligosaccharides.

Experimental

General. ^{13}C NMR spectra were determined with a

JEOL FX-90Q spectrometer (22.5 MHz) and a JEOL FX-100 spectrometer (25 MHz). Fast atom bombardment mass spectra (FAB MS), field desorption mass spectra (FD MS), and electron impact mass spectra (EI MS) were recorded with a JEOL JMX DX-300 or DX-303/JMA 5000 data system. Thin-layer chromatography (TLC) was run with precoated silica-gel plates (Merck, Art 5554). Spot detection was carried out by UV light and/or staining with 0.1% 1,3-naphthalenediol in EtOH-H_2O-H_2SO_4 (200:157:43 v/v/v). The solvent for TLC development was n-C_3H_7OH-AcOH-H_2O(7:7:5 v/v/v). A Merck Lobar prepeaked column (LiChroprep RP18 column, 25 mm×310 mm) and/or a Kusano prepacked column ODS (CPO-HS-221-20, 22 mm×100 mm) was used for reversed-phase column chromatography. High-performance liquid chromatography (HPLC) was performed on a Shimadzu LC3A with a Zorbax ODS column (4.6 mm×150 mm, 5 μm, DuPont) or with a TSKgel ODS-120T (4.6 mm×250 mm, 5 μm, TOSOH).

6-*O*-Arylsulfonyl-γ-cyclodextrins (1—3). *p*-Toluenesulfonyl chloride (12 g) was added to a solution of γ-CD (10 g) in pyridine (800 cm^3) and the mixture was stirred for 1 h. After addition of water (10 cm^3), the mixture was concentrated in vacuo and chromatographed on a reversed-phase column with gradient elution from water (1 dm^3) to 50% aqueous ethanol (1 dm^3) to give the monotosylate **1** (3.5 g, 31%). The other arylsulfonates **2** and **3** were similarly prepared and isolated in similar yields.

2-*O*-Arylsulfonyl-γ-cyclodextrins (4 and 5). The titled compound was synthesized by the reaction of γ-CD with the corresponding arenesulfonyl chloride using dibutyltin oxide in DMF following the method of Murakami et al.[24] The compounds **4** and **5** can be more coveniently, however in lower yields, prepared as follows. Powdered arenesulfonyl chloride (3.0 g) was added in one portion to 10 cm^3 of aqueous solution (pH 12.0, adjusted by addition of aqueous NaOH) of γ-CD (2.0 g). The suspension was vigorously stirred at room temperature and the pH of the suspension was allowed to decrease. After the mixture became neutral, it was filtered and chromatographed on a reversed-phase column with gradient elution from water (1 dm^3) to 30% aqueous CH_3CN (1 dm^3) to give **4** (117.0 mg) or **5** (235.2 mg).

4: ^{13}C NMR (25 MHz, Me_2SO-d_6, characteristic nonaromatic absorptions) δ=59.9, 69.0, 72.1, 72.4, 77.2, 80.4, 80.9, 81.1, 96.7, 101.6; FAB MS m/z 1487 ($M+H^+$).

5: ^{13}C NMR (25 MHz, Me_2SO-d_6, characteristic nonaromatic absorptions) δ=59.9, 69.0, 72.2, 72.4, 72.6, 72.8, 77.9, 79.9, 80.0, 80.3, 80.6, 80.9, 97.1, 101.5, 101.7; FAB MS m/z 1487 ($M+H^+$).

Taka Amylase A-Catalyzed Hydrolysis. Commercially available Taka amylase A (α-amylase from Aspergillus oryzae, Type X-A, Sigma) was used. A solution of Taka amylase A and a modified γ-CD (**1—5**) in acetate buffer solution (pH 5.5, 0.2 mol dm^{-3}) containing calcium chloride (0.01 mol dm^{-3}) was kept at 40 °C or 10 °C to give a limited mixture of oligosaccharides as main products. The enzymatic reaction was monitored by silica-gel TLC. Although the reaction at 40 °C gave mainly a single product (**12**, **13**, **14**, **17**, or **18**), a similar reaction for a shorter reaction period at 10 °C afforded mainly two products. After 1% aqueous HCl was added to make the solution acid (pH 2—3) for denaturation of the enzyme, the supernatant obtained by centrifugation of the mixture was filtered, and applied on a reversed-phase column. After elution with water to remove inorganic salts, gradient elution, changing from water to methanol or acetonitrile, was used to give pure products. The reaction conditions and the yields are shown in Table 1.

6: ^{13}C NMR (25 MHz, D_2O, characteristic nonaromatic absorptions) δ=23.5, 62.7, 63.1, 94.8, 98.4, 102.2, 102.6; FAB MS m/z 843 ($M+Na^+$).

7: ^{13}C NMR (25 MHz, D_2O, characteristic nonaromatic absorptions) δ=62.7, 63.1, 98.4, 101.7, 102.0, 102.4; FAB MS m/z 857 ($M+H^+$), 879 ($M+Na^+$).

8: ^{13}C NMR (25 MHz, D_2O, characteristic nonaromatic absorptions) δ=62.7, 63.2, 94.5, 98.4, 102.2, 102.6; FAB MS m/z 857 ($M+H^+$).

9: ^{13}C NMR (25 MHz, D_2O, characteristic nonaromatic absorptions) δ=23.5, 63.2, 94.5, 98.4, 102.2, 102.5; FAB MS m/z 659 ($M+H^+$).

10: ^{13}C NMR (25 MHz, D_2O, characteristic nonaromatic absorptions) δ=63.1, 94.5, 98.4, 102.2, 102.5; FAB MS m/z 695 ($M+H^+$).

11: ^{13}C NMR (25 MHz, D_2O, characteristic nonaromatic absorptions) δ=63.2, 98.4, 102.2, 102.5; FAB MS m/z 695 ($M+H^+$), 717 ($M+Na^+$).

12: ^{13}C NMR (25 MHz, D_2O, characteristic nonaromatic absorptions) δ=23.5, 63.4, 71.6, 72.4, 72.5, 72.9, 73.9, 74.0, 75.3, 75.8, 76.6, 77.2, 78.8, 80.0, 80.2, 94.5, 98.4, 102.2; FAB MS m/z 519 ($M+Na^+$).

13: FAB MS m/z 533 ($M+H^+$).

14: FAB MS m/z 533 ($M+H^+$).

15: ^{13}C NMR (25 MHz, D_2O, characteristic nonaromatic absorptions) δ=62.9, 81.0, 81.3, 81.8, 82.7, 94.7, 96.3, 98.5, 103.0, 103.3; FAB MS m/z 857 ($M+H^+$).

16: ^{13}C NMR (22.5 MHz, D_2O, characteristic nonaromatic absorptions) δ=63.0, 80.6, 80.9, 82.1, 94.5, 97.7, 98.4, 102.9; FAB MS m/z 857 ($M+H^+$).

Treatment of 6″-*O*-(Arylsulfonyl)maltotrioses (9—11) and 6′-*O*-(Arylsulfonyl)maltoses (12—14) with Thiophenol. A mixture of 6″-O-(arylsulfonyl)maltotriose (**9**) (10 mg), thiophenol (0.1 cm^3), and $CsCO_3$ (33 mg) in dry DMF (1 cm^3) was heated at 60 °C for 17 h under nitrogen. After addition of water, the solution was neutralized by addition of dilute HCl, and washed with ether. The mixture was chromatographed on a reversed-phase column with gradient elution of water-CH_3CN to give 7.7 mg (85.0%) of *S*-phenyl-6″-thiomaltotriose (**23**). Similarly, **10** (20 mg) or **11** (20 mg) gave **23** (10.3 mg, 59.9% or 8.1 mg, 47.1%, respectively). Following the procedure described above, **12—14** were converted to the known compound, *S*-phenyl-6′-thiomaltose.

23: FAB MS m/z 597 ($M+H^+$).

Treatment of 6″-*O*-(Arylsulfonyl)maltotetraoses (6—8) with Aqueous Ba(OH)$_2$. A solution of **6** (11.8 mg) in 0.05 mol dm^{-3} $Ba(OH)_2$ (1.2 cm^3) was stirred at room temperature for 5 h, neutralized with 0.05 mol dm^{-3} H_2SO_4 and filtered. The filtrate was chromatographed on a reversed-phase column with eluting with water to give 8.7 mg (93.5%) of 3″,6″-anhydromaltotetraose (**24**) which was identified by comparing its HPLC retention time and its FAB MS spectrum with those of the authentic compound.[25,26] Similarly, **7** (9 mg) or **8** (45.0 mg) gave **24** (4.2 mg, 61.8% or 24.5 mg, 71.8%, respectively).

Treatment of 2″-*O*-(Arylsulfonyl)maltotetraoses (15—16) with Aqueous Ba(OH)$_2$. A solution of **16** (40.6 mg) in 0.05 mol dm^{-3} $Ba(OH)_2$ (4.06 cm^3) was stirred at room temperature for 1 h and neutralized with 0.05 mol dm^{-3} H_2SO_4. After filtration, the filtrate was chromatographed on a

reversed-phase column with elution of water to give 21.3 mg (69.4%) of (2″*S*,3″*S*)-2″,3″-anhydromaltotetraose (**25**) which was identified by comparing its HPLC retention time and its FAB MS spectra with those of the authentic compound.[21] Similarly, **15** (7.6 mg) gave **25** (3.3 mg, 56.9%).

Reduction of 6″-*O*-Tosylmaltotetraose (6) or 6″-*O*-Tosylmaltotriose (9) with $NaBH_4$. A solution of **9** (50 mg) in 1% aqueous $NaBH_4$ (5 cm^3) was kept at 2 °C for 1 h. After neutralization of the solution by addition of dilute HCl, the mixture was chromatographed on a reversed-phase column with gradient elution of aqueous methanol to give **20** (49.9 mg, 99.5%). Similarly, **6** (50 mg) give **19** (44.5 mg, 88.8%).

19: ^{13}C NMR (22.5 MHz, D_2O, characteristic nonaromatic absorptions) δ=23.5, 62.7, 63.1, 64.9, 65.4, 79.4, 80.1, 84.5, 102.2, 102.6, 102.9; FAB MS *m/z* 823 ($M+H^+$), 845 ($M+Na^+$).

20: ^{13}C NMR (22.5 MHz, D_2O, characteristic nonaromatic absorptions) δ=23.6, 63.2, 65.0, 65.5, 80.1, 84.6, 102.5, 103.0; FAB MS *m/z* 661 ($M+H^+$).

Acetylation of 19 or 20. A solution of **20** (10 mg) and acetic anhydride (1 cm^3) in pyridine (1 cm^3) was allowed to stand at room temperature for 48 h and concentrated by evaporation of all volatile materials with a stream of nitrogen. After dry chloroform (1 cm^3) was added to the residue, evaporation was repeated. This procedure was carried out two more times. The crude product was purified by reversed-phase HPLC to give **22** (10.5 mg, 61.8%). Similarly, **19** (10 mg) gave **21** (6.8 mg, 39.5%).

21: MS *m/z* 1433 ($M+Na^+$).

22: FD MS *m/z* 1145 ($M+Na^+$).

We are indebted to Japan Maize Products Co. Ltd. for a generous gift of γ-CD.

References

1) A part of this study has been preliminarily reported: K. Fujita, T. Tahara, T. Imoto, and T. Koga, *Chem. Lett.*, **1988**, 1329.

2) Y. Matsuura, M. Kusunoki, W. Harada, and M. Kakudo, *J. Biochem.*, **95**, 697 (1984).

3) Y. Matsuura, M. Kusunoki, W. Date, S. Harada, S. Bando, N. Tanaka, and M. Kakudo, *J. Biochem.*, **86**, 1773 (1979).

4) Y. Matsuura, M. Kusunoki, W. Harada, N. Tanaka, Y. Iga, N. Yasuoka, H. Toda, K. Narita, and M. Kakudo, *J. Biochem.*, **87**, 1555 (1980).

5) H. Toda, K. Kondo, M. Kakudo, and K. Narita, *Proc. Jpn. Acad. Ser.*, **58B**, 208 (1982).

6) K. Hiromi, *Biochem. Biophys. Res. Commun.*, **40**, 1 (1970).

7) J. A. Thoma, C. Brothers, and J. E. Spradlin, *Biochemistry*, **9**, 1768 (1970).

8) J. A. Thoma, G. V. K. Rao, C. Brothers, J. E. Spradlin, and L. H. Li, *J. Biol. Chem.*, **246**, 5621 (1971).

9) H. Arita, M. Isemura, T. Ikenaka, and Y. Matsushima, *Bull. Chem. Soc. Jpn.*, **43**, 818 (1970).

10) T. Ikenaka, *J. Biochem.*, **54**, 328 (1963).

11) H. Arita, M. Isemura, T. Ikenaka, and Y. Matsushima, *J. Biochem.*, **68**, 91 (1970).

12) H. Arita and Y. Matsushima, *J. Biochem.*, **69**, 409 (1971).

13) H. Arita, T. Ikenaka, and Y. Matsushima, *J. Biochem.*, **69**, 401 (1971).

14) H. Arita and Y. Matsushima, *J. Biochem.*, **68**, 717 (1970).

15) K. Fujita, A. Matsunaga, and T. Imoto, *J. Am. Chem. Soc.*, **106**, 5740 (1984).

16) K. Fujita, A. Matsunaga, and T. Imoto, *Tetrahedron Lett.*, **25**, 5533 (1984).

17) I. Tabushi, T. Nabeshima, K. Fujita, A. Matsunaga, and T. Imoto, *J. Org. Chem.*, **50**, 2638 (1985).

18) K. Fujita, A. Matsunaga, and T. Imoto, *Tetrahedron Lett.*, **26**, 6439 (1985).

19) K. Fujita, S. Nagamura, T. Imoto, T. Tahara, and T. Koga, *J. Am. Chem. Soc.*, **107**, 3233 (1985).

20) K. Fujita, T. Tahara, T. Imoto, and T. Koga, *J. Am. Chem. Soc.*, **108**, 2030 (1986).

21) K. Fujita, T. Tahara, S. Nagamura, T. Imoto, and T. Koga, *J. Org. Chem.*, **52**, 636 (1987).

22) L. D. Melton and K. N. Slessor, *Can. J. Chem.*, **51**, 327 (1973).

23) N. Suetsugu, S. Koyama, K. Takeo, and T. Kuge, *J. Biochem.*, **76**, 57 (1974).

24) T. Murakami, K. Harata, and S. Morimoto, *Tetrahedron Lett.*, **28**, 321 (1987).

25) K. Fujita, H. Yamamura, T. Imoto, and I. Tabushi, *Chem. Lett.*, **1988**, 543.

26) K. Fujita, H. Yamamura, T. Imoto, T. Fujioka, and K. Mihashi, *J. Org. Chem.*, **53**, 1943 (1988).

 © 1989 The Chemical Society of Japan Bull. Chem. Soc. Jpn., 62, 3155—3160 (1989)

Unusual Reactivity of Purinophanes Due to Stereoelectronic Effect[1)]

Yoshiteru SAKATA,* Hiroyuki HIGUCHI, Kazuo DOYAMA, Takayuki HIGASHII, Miho MITSUOKA, and Soichi MISUMI
The Institute of Scientific and Industrial Research, Osaka University, Ibaraki, Osaka 567
(Received May 12, 1989)

Four types of purinophanes (**1**, **2**, **7**, and **10**) where a 6-thiopurine ring is bridged between S^6- and 9-positions or between S^6- and 7-positions were synthesized. Among them (6,9)purinophanes (**1**, **7**, and **10**) showed unusual high reactivity toward nucleophiles ($MeNH_2$, Me_2NH, OH^-) at 6-position to give acyclic compounds. The increased rate constants of these compounds against (6,7)purinophanes **2** and 9-methyl-6-(methylthio)purine could not be explained by molecular strain, neighboring group participation, or some electronic effect due to faced π-systems, but successfully explained by the stereoelectronic effect proposed by Deslongchamps. The rate of the reactions in **1**, **7**, and **10** was increased with an increase in rigidity of the tetrahedral intermediate where lone pairs of two adjacent heteroatoms orient antiperiplanar to the departing group.

The stereoelectronic effect[2)] is recognized as having a major influence on the reactivity of various molecules such as cyclic acetals, esters, amides, and related compounds, all of which contain geminal heteroatoms with nonbonded electron lone pair. The effect, however, has not so far been observed in biologically important nucleic acid bases in spite of their satisfying the structural requirement. Recently, we prepared a series of purinophanes[3)] and pyrimidinopurinophanes[4)] for studying the relationship between hypochromism and stacking geometry of two nucleic acid bases. In the course of the study we observed that **1a**, **b** react with nucleophiles such as alkylamines and hydroxide anion at room temperature to give acyclic compounds such as **3a**, while the isomeric compounds **2a**, **b** did not show such reactivity under

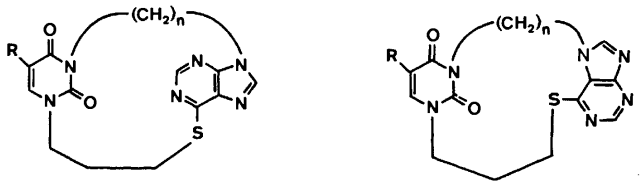

1 **2**

a: R=H, n=3
b: R=H, n=4
c: R=CH_3, n=3
d: R=OCH_3, n=3
e: R=NO_2, n=3

the same conditions. To understand the anomalous behavior of **1a**,**b**, we have prepared various kinds of related compounds and concluded that the stereoelectronic theory provides the best explanation for the unusual reactivity of **1a**,**b**. Here we report the first observation of the stereoelectronic effect in nucleic acid bases.

Results and Discussion

When the electronic spectra of **1a**,**b** were measured in 0.1 M NaOH (1 M=1 mol dm^{-3}), methylamine/H_2O, and dimethylamine/H_2O at room temperature, the spectra changed with time having one or two isosbestic points. A typical example is shown in Fig. 1. Similar behavior was observed for nucleophiles such as RS^-, RNH_2, and R_2NH in ethanol, but not observed for CN^-, I^-, R_3N, and R_4N^+. Figure 1 shows clearly that **1b** underwent some reaction to give single product, which is assumed to be an acyclic compound **3a**. The structure of **3b**, which was derived from **3a**, was determined by the alternative synthesis as summarized in Scheme 1. Thus, the spectral data of the reaction product of **1b** with methylamine, followed with dimethyl sulfate are consistent with those of the coupling product between **4** and **5** (see the Experimental part). Therefore, it is apparent that nucleophiles attack at 6-position of **1a**,**b** to give the product. On the other hand, isomeric pyrimidinopurinophanes **2a**,**b** did not show any spectral change at all under the same conditions as those for **1a**,**b**. First, we assumed that the unusual reactivity originates from strain in the molecules, because cyclophanes frequently show such behavior.[5)] In order to

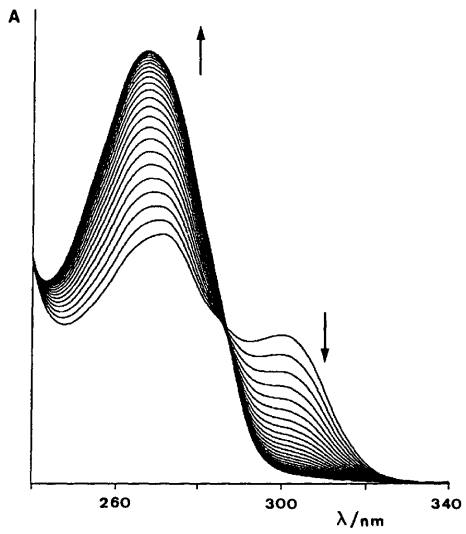

Fig. 1. Spectral change of **1b** at the interval of 30 minutes in the presence of methylamine in ethanol at 25 °C.

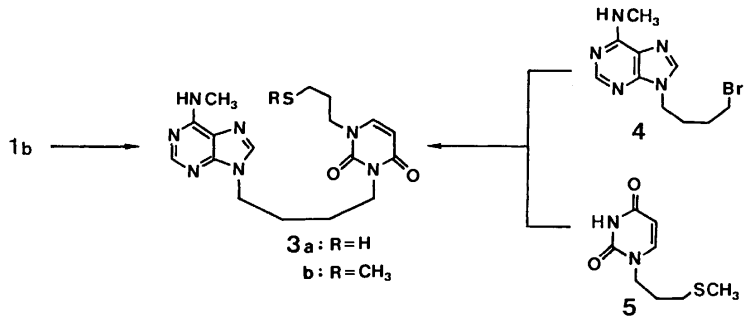

Scheme 1.

Table 1. Bond Lengths and Bond Angles of **1b** and **2a**[a)]

	1b	**2a**		**1b**	**2a**
Bond length (l/Å)			C2-N3-C4	111.6(2)	113.0(3)
N1-C2	1.351(3)	1.341(4)	N3-C4-C5	126.2(2)	123.7(3)
C2-N3	1.332(3)	1.331(4)	N3-C4-N9	127.8(2)	125.8(3)
N3-C4	1.331(2)	1.331(4)	C4-C5-C6	116.4(2)	118.0(2)
C4-C5	1.389(2)	1.404(4)	C4-C5-N7	110.4(2)	105.7(2)
C5-C6	1.382(3)	1.403(4)	C5-C6-N1	119.6(2)	118.2(2)
C5-N7	1.391(2)	1.379(3)	C5-N7-C8	103.2(2)	105.4(2)
N7-C8	1.310(3)	1.365(3)	N7-C8-N9	115.2(2)	114.7(2)
C8-N9	1.358(2)	1.321(4)	C8-N9-C4	105.2(2)	103.6(2)
N9-C4	1.377(2)	1.350(4)	C6-C5-N7	133.2(2)	136.3(2)
C6-S6	1.772(2)	1.765(3)	S6-C6-N1	116.7(1)	120.2(2)
N1′-C2′	1.378(2)	1.375(3)	S6-C6-C5	123.7(1)	121.5(2)
C2′-N3′	1.387(2)	1.384(3)	C6′-N1′-C2′	121.2(2)	121.5(2)
N3′-C4′	1.405(2)	1.404(3)	N1′-C2′-N3′	116.1(2)	116.3(2)
C4′-C5′	1.433(3)	1.429(4)	N1′-C2′-O2′	122.0(2)	121.8(2)
C5′-C6′	1.328(3)	1.340(4)	N3′-C2′-O2′	122.0(2)	121.8(2)
C6′-N1′	1.372(3)	1.373(4)	C2′-N3′-C4′	124.7(2)	124.4(2)
C2′-O2′	1.226(2)	1.220(3)	N3′-C4′-C5′	114.9(2)	115.4(2)
C4′-O4′	1.219(3)	1.227(4)	N3′-C4′-O4′	119.8(2)	120.1(3)
			C5′-C4′-O4′	125.3(2)	124.6(3)
Bond angle (ϕ/°)			C4′-C5′-C6′	120.4(2)	120.3(3)
C6-N1-C2	118.1(2)	118.3(3)	C5′-C6′-N1′	122.7(2)	122.0(3)
N1-C2-N3	127.9(2)	128.5(3)			

a) Values in parentheses are standard deviations.

confirm this point, X-ray analysis[6)] was carried out for **1b** and **2a**. Bond lengths and bond angles of purine and pyrimidine rings in **1b** and **2a** are summarized in Table 1 and the deviations of the ring atoms from the least-squares planes of the two rings are shown in Table 2. From Table 1 it is apparent that there are not so large differences in bond lengths and bond angles between **1b** and **2a**. This is also true when these values are compared with those of 6-(methylthio)purine[9)] and 1,3-dimethyluracil.[10)] The extents of the planality of the purine and pyrimidine rings in **1b** and **2a** are quite similar as shown in Table 2. All of these data clearly show that the reactivity of **1a,b** can not be explained by molecular strain.

The second possible reason for the abnormal reactivity is considered to be the neighboring group participation. As seen from Fig. 2, the carbonyl group at C2′ position in **1b** is located closely to the reaction center: namely, the nonbonded distances in **1b** are

Table 2. Deviation of the Ring Atoms from the Least-Squares Plane

	1b/Å	**2a**/Å
N1	−0.010	−0.019
C2	−0.025	−0.044
N3	0.014	0.017
C4	0.008	0.030
C5	−0.004	0.009
C6	0.033	0.044
N7	−0.019	−0.019
C8	−0.001	−0.033
N9	0.005	0.018
N1′	0.005	0.012
C2′	0.008	−0.020
N3′	−0.021	0.008
C4′	0.020	0.011
C5′	−0.007	−0.019
C6′	−0.005	0.008
O2′	0.032	−0.051
O4′	0.075	0.037

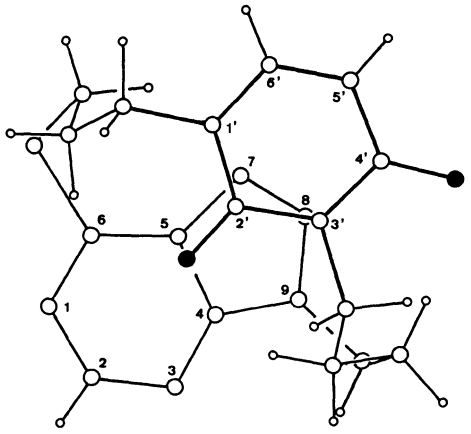

Fig. 2. Views on the least-squares plane defined with a purine ring in **1b**.

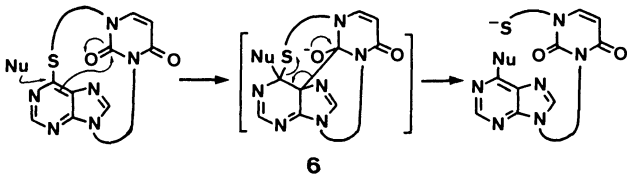

6

Scheme 2.

4.229 Å between C5 and O2′ and 4.058 Å between C5 and C2′. Assuming the C5 participation to C2′, the reaction will proceed via transition state or intermediate **6** as shown in Scheme 2. In order to determine whether such mechanism is correct or not, we prepared **1c—1e**,[4] where an electron-donating or an electron-withdrawing substituent is introduced into the pyrimidine ring so that the reaction rate will more or less be influenced. We also prepared **7**,[4] where the

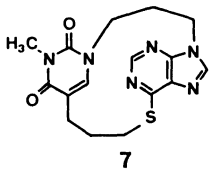

7

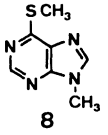

8

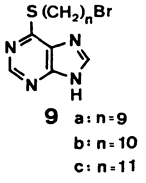

9 a: n=9
b: n=10
c: n=11

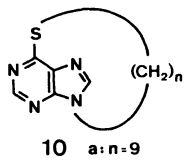

10 a: n=9
b: n=10
c: n=11

11

S6 atom is linked not to N3′ as in the case for **1**, but to C5′. Based on molecular model considerations, **7** has a structure, where the carbonyl group in question is located far apart from the reaction center. On the basis of spectrophotometry, the rate constants of **1**, **7**, and reference compound **8** toward methylamine in ethanol were obtained at 25±1 °C by analyzing the reaction as pseudo-first-order and the results are summarized in Table 3. One can see from the table that there is no essential change among the rate constants of **1b—1e** and **7**. Therefore, it is concluded that the carbonyl group at 2′ position in **1** is not responsible for the unusual reactivity.

The third possibility for the elucidation of the abnormality is some electronic effect due to the transannularly located π-system, that is, pyrimidine ring. To make this point clear, we synthesized **10**, where 6-thiopurine is bridged with a polymethylene chain at the same positions as **1** and **7** and hence there is no possibility of the electoinc effect due to the faced pyrimidine ring. Synthesis of **10a—c** was carried out by the intramolecular cyclization reaction of **9a—c**, which was prepared by the reaction of 6-mercaptopurine and α,ω-dibromoalkane with sodium hydride. The crude product was purified by column chromatography on silica gel and then, recrystallized from chloroform. In ^{1}H NMR spectra methylene protons adjacent to the sulfur atom in **10a—c** show complex multiplets, while the corresponding protons of acyclic compounds **9a—c** appear with the first-order splitting. The other bridge protons of **10a—c** also show complex signals. The result indicates that the purinophanes **10a—c** have more or less rigid structure in solution. The rate constants of **10a—c** thus prepared were determined for the reaction with methylamine in a manner similar to those for **1** and the results are summarized in Table 3. The fact that the values for **10a—c** are similar to those for **1** clearly indicates that the reactivity of **1** is not attributable to the faced pyrimidine ring. Molecular model considerations on **10a—c** revealed that there exists no strain even in **10a** having the shortest bridge among them. This leads to the same conclusion as for **1** that molecular strain does not play an important role for the reactivity of **10a—c**.

The only reasonable explanation for the increased rate constants of **1**, **7**, **10** is, at the present stage, given by the stereoelectronic theory[2] by Deslongchamps. The theory states that in tetrahedral intermediate **11** such reactions are favored for conformations where lone-pair orbitals on two adjacent heteroatoms lie

Table 3. Reaction Rate Constants of **1a—e**, **7**, **8**, and **10a—c** with Monomethylamine in Ethanol at 25±1 °C

Compound	K/s^{-1}M^{-1}
1a	4.4×10^{-3}
1b	4.5×10^{-4}
1c	5.2×10^{-4}
1d	6.2×10^{-4}
1e	5.0×10^{-4}
7	5.5×10^{-4}
8	$<10^{-6}$
10a	2.6×10^{-3}
10b	1.1×10^{-4}
10c	4.6×10^{-5}

antiperiplanar to the bond to the leaving group (X). Theoretical justification for the concept has been given by lowering the energy of transition state by mixing of lone-pair orbitals with the antibonding orbital of the C-X bond. When we apply the theory to the present molecules, the reaction scheme is written as shown in Fig. 3. The tetrahedral intermediate **13a**, which will easily be obtained from **12a**, is expected to give smoothly **14a**, because of its antiperiplanar orientation of the two lone-pair orbitals on the nitrogen atoms and the C-S bond. In the case of (6,7)purinophanes, however, the steric hindrance among R^1, R^2, and R^3 would prevent the formation of tetrahedral intermediate **13b** from **12b** and hence the C-S bond is not cleaved easily. This must be the reason for the higher reactivity of (6,9)-purinophanes than (6,7)-isomers. For the enhancement in reaction rate by the stereoelectronic effect it is requested that the corresponding antiperiplanar conformations have rigid structures.[2c] This is reflected in the order of the rate constants of **10a—c** in Table 1. Thus, the value increases with a decrease of the length of the bridging chain, i.e., **10a>10b>10c**. The quite low reactivity of the reference compound **8** might be also explained by the conformational flexibility of the antiperiplanar structure of the tetrahedral intermediate.

In the present study the unusual reactivity of **1**, **7**, and **10** is well-explained by the stereoelectronic effect and this is the first example for the concept to be successfully applied in the field of purine ring. This suggests that the theory is widely applicable to the elucidation of the reaction course of nucleophilic substitution reactions which occur at various heteroaromatic rings including nucleic acid bases.

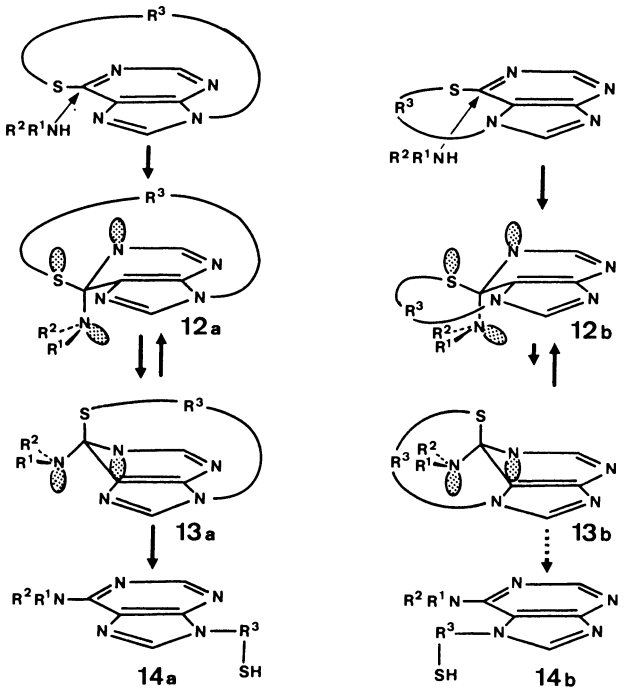

Fig. 3. Reaction course of (6,9)- and (6,7)-purinophanes with alkylamines.

Experimental

Melting points were recorded on a Yanagimoto apparatus and are not corrected. NMR spectra were measured on a JNM PMX-60SI (60 MHz), a JNM FX-100 (100 MHz), and a Brucker WH-360 (360 MHz). Mass spectra were obtained on a Hitachi RMU-7 and UV spectra were measured on a Hitachi 330 and a Hitachi U-3210.

6-(10-Bromodecylthio)purine (9b). To a stirred suspension of 60% NaH (0.17 g, 4.33 mmol) in dry DMSO (5 ml) was added a solution of 6-mercaptopurine[11](0.57 g, 3.78 mmol) and 1,10-dibromodecane (5.17 g, 17.23 mmol) in DMSO (35 ml) at 55 °C in a period of 45 min. Additional stirring was continued for 5 h at 55 °C. After cooling, the mixture was poured onto water and it was extracted with chloroform. The organic layer was washed with sat aq solution of NaCl and dried ($MgSO_4$). The solvent was removed under reduced pressure and the crude product was chromatographed on silica gel with chloroform-acetone (5 : 1) to give 0.22 g (15.7% yield) of **9b**. Recrystallization from chloroform gave pure **9b** as colorless plates, mp 123.0—125.0 °C. ^{1}H NMR ($CDCl_3$, 360 MHz) δ=1.30—1.50 (m, 12, CH_2), 1.76—1.89 (m, 4, CH_2), 3.39—3.44 (m, 5, NH+SCH_2+CH_2Br), 8.32 (s, 1, H8), 8.79 (s, 1, H^2).

Found: C, 48.56; H, 6.11; N, 15.10; S, 8.39; Br, 21.38%. Calcd for $C_{15}H_{23}N_4SBr$: C,48.52; H,6.24; N,15.09; S,8.63; Br,21.52%.

The synthesis of **9a** and **9c** was carried out by the similar method described for **9b**.

9a: 32% yield, mp 96—100 °C. ^{1}H NMR ($CDCl_3$, 360 MHz) δ=1.32—1.48 (m, 10, CH_2), 1.75—1.86 (m, 4, CH_2), 3.38—3.43 (m, 5, NH+SCH_2+CH_2Br), 8.50 (s, 1, H8), 8.80 (s, 1, H2).

9c: 28% yield, mp 101—103 °C. ^{1}H NMR ($CDCl_3$, 360 MHz) δ=1.28—1.52 (m, 14, CH_2), 1.77—1.88 (m, 4, CH_2), 3.35—3.45 (m, 5, NH+SCH_2+CH_2Br), 8.44 (s, 1, H8), 8.83 (s, 1, H2).

1-Thia[11](6,9)purinophane (10b). To a stirred suspension of 60% NaH (0.04 g, 1.02 mmol) in dry DMSO (15 ml) was added dropwise a solution of **9b** (0.37 g, 0.79 mmol) in dry DMSO (25 ml) at 55 °C in a period of 3 h. Additional stirring was continued for 5 h at the same temperature. After cooling, the mixture was poured on cold water and it was extracted with chloroform. The extracts were washed successively with water and sat aq solution of NaCl and dried ($MgSO_4$). Crude product was chromatographed on silica gel with ether to give 18 mg (7.7% yield) of **10b**. Recrystallization from hexane gave pure **10b** as colorless prisms, mp 105.0—107.0 °C. **10b:** MS m/z 290 (M^+). ^{1}H NMR ($CDCl_3$, 360 MHz) δ=0.33—1.22 (m, 12, CH_2), 1.53—2.07 (m, 4, CH_2), 3.28—3.56 (m, 1, SCH_2), 4.02—4.10 (m, 2, SCH_2+NCH_2), 4.59—4.66 (m, 1, NCH_2), 8.06 (s, 1, H8), 8.79 (s, 1, H2).

The synthesis of **10a** and **10c** was carried out in a manner similar to the above.

10a: 8.6% yield, colorless prisms from chloroform, mp 103—104 °C; MS m/z 276 (M^+); ^{1}H NMR ($CDCl_3$, 360 MHz) δ=0.27—1.23 (m, 10, CH_2), 1.49—2.14 (m, 4, CH_2), 3.14—3.49 (m, 1, CH_2), 4.00—4.09 (m, 2, SCH_2+NCH_2), 4.61—4.70 (m, 1, NCH_2), 8.11 (s, 1, H8), 8.73 (s, 1, H2).

10c: 13% yield; colorless prisms from chloroform, mp 99—102 °C; MS *m/z* 304 (M^+); ^{1}H NMR ($CDCl_3$, 360 MHz) δ=0.36—1.35 (m, 14, CH_2), 1.59—2.11 (m, 4, CH_2), 3.26—3.61 (m, 1, SCH_2), 4.06—4.19 (m, 2, SCH_2+NCH_2), 4.60—4.71 (m, 1, NCH_2), 8.09 (s, 1, H8), 8.82 (s, 1, H2).

9-(14-Bromobutyl)-6-(methylamino)purine (4). In a Pyrex ampule were placed 6-(methylthio)purine·$3H_2O$ (1.0 g, 4.2 mmol), H_2O (1 ml), and 40% aq solution of methylamine and the mixture was heated at 130—140 °C for 18 h in the sealed tube. After cooling, the mixture was concentrated to half of its original volume and the residue was kept at 0 °C for 1 h. Yielded precipitates were collected and washed well with water. Crude product was dried by azeotropic distillation with benzene to give 6-(methylamino)-purine·$2H_2O$[11] (590 mg, 81%). Without further purification it was used for the following reaction.

To a stirred suspension of 1,4-dibromobutane (2.0 ml, 16.3 mmol) and K_2CO_3 (1.0 g, 9.0 mmol) in dry DMSO (50 ml) was added dropwise a solution of 6-(methylamino)-purine·$2H_2O$ (590 mg) in dry DMSO (30 ml) in a period of 7.5 h under nitrogen atmosphere. After addition was over, stirring was continued for 11 h. Salts were filtered off and the solvent was removed under reduced pressure. Water (50 ml) was added to the residue and it was extracted with chloroform. The organic layer was washed well with sat aq solution of NaCl and water and dried ($MgSO_4$). Removal of the solvent gave **4** (290 mg, 30% yield) as colorless oil. MS *m/z* 285, 283 (M^+), 204 (M^+−Br); ^{1}H NMR ($CDCl_3$, 60 MHz) δ=2.0 (m, 4, CCH_2CH_2C), 3.2 (d, J=5 Hz, 3, NCH_3), 3.4 (t, 2, CH_2Br), 4.2 (t, 2, CH_2N), 7.0 (br s,. 1,NH), 7.7 (s, 1, H8), 8.4 (s, 1, H2).

1-(3-Methylthiopropyl)uracil (5). A solution of 1-(3-bromopropyl)uracil[12] (300 mg, 1.3 mmol) and thiourea (105 mg, 1.35 mmol) in ethanol (10 ml) was refluxed for 12 h. After removal of ethanol, water (5 ml) was added to the residue and the atmosphere was replaced with N_2. To the mixture was added NaOH (104 mg, 2.6 mmol) and it was heated at 90—100 °C. After cooling, methyl iodide (0.08 ml, 1.3 mmol) was added to the mixture and additional stirring was continued for 1.5 h. To the mixture was added dil HCl and the medium was adjusted to pH around 5 and then, it was extracted with chloroform. The extract was washed with sat aq solution of NaCl and water and dried ($MgSO_4$). After removal of the solvent, the crude product was recrystallized from benzene-hexane to give **5** (50 mg, 19% yield). **5**: colorless crystals, mp 78—79 °C. MS *m/z* 200 (M^+), 186 (M^+−CH_3), 153 (M^+−SMe). ^{1}H NMR ($CDCl_3$, 60 MHz) δ=2.0 (m, 2, CCH_2C), 2.1 (s, 3, SCH_3), 2.2 (m, 2, SCH_2), 3.8 (t, 2, NCH_2), 5.7 (d, 1, H5), 7.2 (d, 1, H6).

6-Methylamino-9-[4-[1,2,3,6-tetrahydro-3-(3-methylthiopropyl)-2,6-dioxo-1-pyrimidinyl]butyl]purine (3b). A suspension of **4** (73 mg, 0.26 mmol), **5** (50 mg, 0.25 mmol), and K_2CO_3 (69 mg, 0.5 mmol) in DMSO (10 ml) was stirred for 12 h at room temperature under nitrogen atmosphere. After usual workup, crude product was purified by preparative-layer chromatography on silica gel with methanol-chloroform (1:15) to give **3b** (54 mg, 54% yield). **3b:** colorless solid from chloroform-ether, mp 53.5—56.0 °C. MS *m/z* 403 (M^+) 388, 357, 356, 342. ^{1}H NMR ($CDCl_3$, 100 MHz) δ=1.40—2.10 (m, 6, CCH_2C), 2.10 (s, 3, SCH_3), 2.52 (t, 2, SCH_2), 3.21 (d, J=5.1 Hz, 3, NCH_3), 3.85 (t, 2, NCH_2), 5.70 (d, J=6.8 Hz 1, H5′), 6.01 (br s, 1, NH), 7.18 (d, J=6.8 Hz, 1, H6′), 7.79 (s, 1, H8), 8.39 (s, 1, H2).

Found: C, 52.96; H, 6.25; N, 24.30%. Calcd for $C_{18}H_{27}N_7SO_2$: C, 53.58; H, 6.25; N, 24.30%.

Synthesis of 3b by the Reaction of 1b with Methylamine Followed by Dimethyl Sulfate. To an ampule was placed **1b** (25 mg, 0.067 mmol) and water (0.5 ml). After replacement of the atmosphere with nitrogen, 40% aq solution of methylamine (0.1 ml, 1.3 mmol) was added to the mixture and it was heated for 1.5 h at 120 °C in the sealed tube. After reaction was over, the ampule was opened and excess methylamine was removed by vigorous bubbling of nitrogen. To the mixture was added NaOH (20 mg, 0.5 mmol) at 0 °C and it was stirred for 10 min at the temperature. To the solution was added dropwise dimethyl sulfate (0.1 mmol) diluted with dioxane. Additional stirring was continued for 2 h at room temperature. After reaction was over, the mixture was extracted with chloroform. The extract was washed well with water and dried ($MgSO_4$). Removal of the solvent gave oily product, which was purified by preparative-layer chromatography on silica gel to give colorless oil (12 mg, 43% yield). **3b:** colorless solid from chloroform-ether, mp 54—56 °C. Spectroscopic data were identical with those of the specimen described above.

Kinetic Studies. Kinetic measurements were carried out on a UV-visible spectrophotometer. The cells were maintained at a constant temperature (25±1 °C) by means of a thermostated cuvette holder. The pseudo-first-order rate constants were determined from the slopes of a $[A_s(t)+A_p(t)-A_\infty]$ vs. time plot, where $A_s(t)$, $A_p(t)$, and A_∞ are absorbance of substrate, product, and final, respectively. Reactions were followed by measuring the rate of decreasing of the 6-(methylthio)purine chromophore at its absorbance maximum (around 304 nm).

This work was supported by Grants-in-Aid for General Scientific Research (Nos. 56470018 and 59470018) from the Ministry of Education, Science and Culture, to Yoshiteru Sakata. He also thanks to Prof. Deslongchamps for helpful discussion.

References

1) Preliminary reports: a) K. Doyama, F. Hama, Y. Sakata, and S. Misumi, *Tetrahedron Lett.*, **24**, 5253 (1983). b) T. Higashii, Y. Sakata, and S. Misumi, *Nucleic Acids Res. Symp. Ser.*, **16**, 125 (1985). c) H. Higuchi, M. Mitsuoka, Y. Sakata, and S. Misumi, *Tetrahedron Lett.*, **26**, 3849 (1985).

2) a) P. Deslongchamps, "Stereoelectronic Effects in Organic Chemistry," Pergamon Press, (1983). b) A. J. Kirby, *Acc. Chem. Res.*, **17**, 305 (1984). c) D. G. Gorenstein, *Chem. Rev.*, **87**, 1047 (1987).

3) F. Seyama, K. Akahori, Y. Sakata, S. Misumi, M. Aida, and C. Nagata, *J. Am. Chem. Soc.*, **110**, 2192 (1988).

4) K. Doyama, T. Higashii, F. Seyama, Y. Sakata, and S. Misumi, *Bull. Chem. Soc. Jpn.*, **61**, 3619 (1988).

5) D. J. Cram and J. M. Cram, *Acc. Chem. Res.*, **4**, 204 (1971); S. Misumi and T. Otsubo, *ibid.*, **11**, 251 (1978).

6) The crystal analysis was carried out[7] using Ni-filtered Cu $K\alpha$ radiation of a full automatic four-circle diffractometer and the structure was solved by a program MULTAN-78[8] and refined by least-squares method. The final R values are 0.038 for **1b** and 0.047 for **2a**.

7) F. Seyama, Y. Sakata, N. Kasai, and S. Misumi, to be published.

8) P. Main, S. E. Hull, L. Lessinger, G. Germained, J. P. Declercq, and M. M. Woolfson, MULTAN-78, University of York (1975).
9) W. J. Cook and C. E. Bugg, *J. Pharm. Sci.*, **64**, 221 (1975).
10) A. Banerjee, J. K. Dattagupta, W. Saenger, and A. Rabczenko, *Acta Crystallogr., Sect. B*, **33**, 90 (1977).
11) G. E. Elion, E. Burgi, and G. H. Hitchings, *J. Am. Chem. Soc.*, **74**, 411 (1952); R. K. Robins, K. Robins, and H. H. Lin, *ibid.*, **79**, 490 (1957).
12) D. T. Browne, J. Eisinger, and N. J. Leonard, *J. Am. Chem. Soc.*, **90**, 7302 (1968).

Intramolecular [2+2] Photocycloaddition. 5.[1] Synthetic Methods toward [2.*n*]-, [3.*n*]-, and [4.*n*]Naphthalenophane Skeletons by Using α,ω-Bis(vinylnaphthyl)alkanes

Jun NISHIMURA,* Motoharu TAKEUCHI, Hideo TAKAHASHI, Eiji UEDA,†
Yasuhiro MATSUDA,† and Akira OKU†
Department of Chemistry, Gunma University, Tenjin-cho, Kiryu 376
†Department of Chemistry, Kyoto Institute of Technology, Matsugasaki, Sakyo-ku, Kyoto 606
(Received May 15, 1989)

[2+2] Photocycloaddition, cationic cyclocodimerization, and reductive ring enlargement were developed for the syntheses of [2.*n*]-, [3.*n*]-, and [4.*n*]naphthalenophanes, respectively, from α,ω-bis(vinylnaphthyl)-alkanes as a single starting material. Using the exclusive syn selectivity of the former two methods, the room required for the intraannular naphthalene-ring rotation in the ring system is determined.

Several naphthalenophanes were already made by 1,6-Hoffman degradation,[2] by solvolysis of appropriate tosylate,[3] by malonate synthesis[4] and tosmic synthesis,[5] and by using dithia intermediates as the most general precursor.[6] Until now *syn*- and *anti*-[2.2](1,4)naphthalenophane,[2] chiral and achiral [2.2](2,6)napthalenophane,[6] [2.2](2,7)naphthalenophane,[7] [2.2](2,6)(2,7)naphthalenophane,[8] [2.2]paracyclo-(1,4)- and (2,6)naphthalenophane,[9] *syn*- and *anti*-[3.3](1,4)naphthalenophane,[4] and chiral and achiral [3.3](2,6)naphthalenophane[10] were reported.

We developed some new methods toward these structurally, physicochemically interesting naphthalenophanes.[11] Here in this paper, we report a photochemical route toward [2.*n*]naphthalenophanes from vinylnaphthalene derivatives and their Birch reduction to [4.*n*] ones together with some application of cationic cyclocodimerization[12] to [3.*n*] skeletons. Moreover we determined the room required for the naphthalene ring rotation after Birch reduction of the conformationally unstable *syn*-naphthalenophane derivatives.

Results

Preparation of Vinylnaphthalenes. Synthetic methods of starting materials are depicted in Chart 1. The standard conditions were already reported for several vinylarene derivatives.[13]

Only the preparation of 2-acetyl-6-bromonaphthalene did not record satisfactory yields. For a large scale preparation, the material should be obtained by other routes than this method which is based on the equilibrium attained in the Friedel-Crafts acylation of 2-bromonaphthalene.[14]

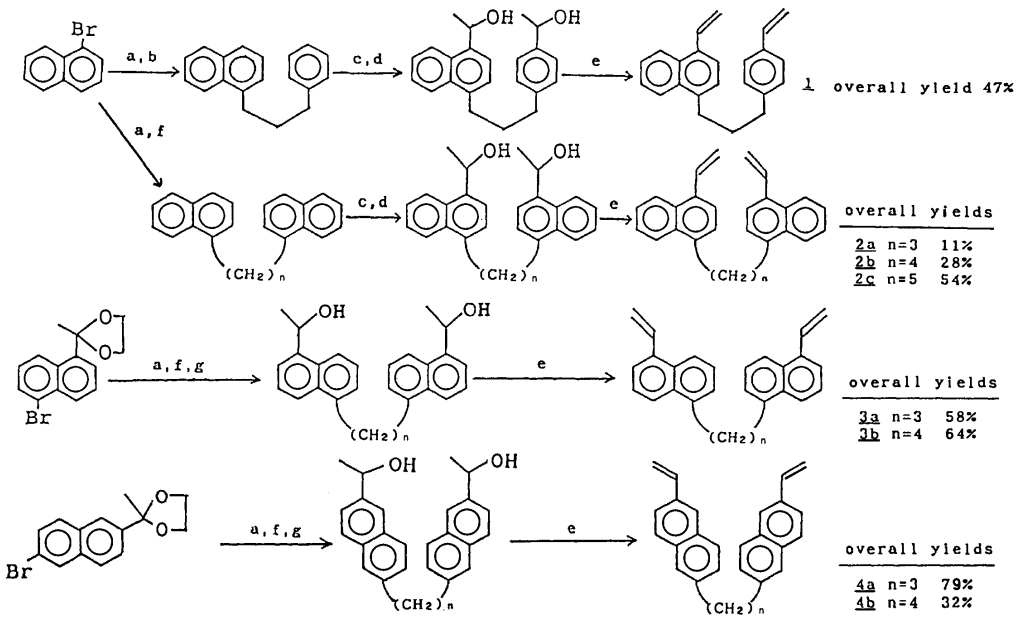

a) Mg/THF. b) Br(CH2)3Ph, CuBr-HMPA. c) CH3COCl, AlCl3/CH2ClCH2Cl.
d) LiAlH4/ether. e) KHSO4/DMSO. f) Br(CH2)nBr, CuBr-HMPA.
g) HCl/DOX-H2O.

Chart 1. Preparation of vinylnaphthalenes.

Synthesis of [2.*n*]Naphthalenophane Derivatives. Intramolecular [2+2] photocycloaddition of vinylnaphthalene derivatives **1—4** successfully gave corresponding naphthalenophanes **5—8** as reported briefly.[11] By this method *syn*-[2.*n*]paracyclo(1,4)-, *syn*-[2.*n*](1,4)-, *syn*-[2.*n*](1,5)-, and [2.*n*](2,6)-naphthalenophanes were prepared. The reaction gives exclusively syn isomer, because the vinyl group has only exo conformation (conformational rigidity of vinyl group[15]) and never attains an endo, exo-divinyl combination for the formation of anti isomer. This selectivity is quite important, because previously reported synthetic methods listed above generally give conformationally stable *anti*-naphthalenophanes exclusively.

Reactions together with their yields are shown in Chart 2. Physical, analytical, and spectroscopic data of products are listed in Tables 1 and 2.

The reaction mixture of olefin **4** showed two HPLC peaks (Cosmosil-C18, MeOH) in the range where naphthalenophanes of this sort should be eluted. These two compounds were isolated from a small portion of the mixture by HPLC for the structural determination, and the major portion was treated by Birch reduction as described below.

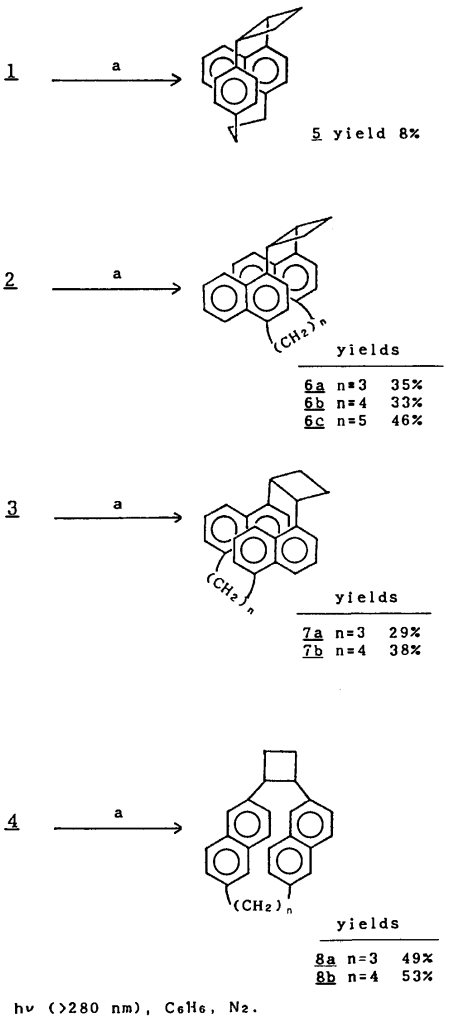

Chart 2. [2+2] Photocycloaddition toward [2.*n*]-naphthalenophanes.

Table 1. Physical and Analytical Data of Novel Naphthalenophanes

Compd[a]	MP θ_m/°C	MS (M+, *m/z*) calcd (found)	Found (%) C	Found (%) H	Calcd (%) C	Calcd (%) H
5	141—142	298.1723(298.1713)	92.63	7.36	92.57	7.43
6a	219—221	348.1879(348.1881)	93.21	6.87	93.06	6.94
6b	220—222	362.2036(362.2041)	92.47	7.40	92.77	7.23
6c	233—234	376.2192(376.2186)	92.42	7.44	92.50	7.50
7a	234—235	348.1879(348.1868)	92.89	7.02	93.06	6.94
7b	233—234	362.2036(362.2028)	92.48	7.28	92.77	7.23
15a[b]	179—181	466.2660(466.2668)				
15b[c]	200—201	480.2819(480.2823)				
16[d]	228—229	466.2660(466.2660)				
17[e]	76—78	466.2660(466.2652)				
18	—[f]	300.1879(300.1876)	91.76	8.07	91.95	8.05
19a	208—209	350.2036(350.2029)	92.51	7.57	92.52	7.48
19b	258—259	364.2192(364.2193)	92.13	7.78	92.26	7.74
19c	110—111	378.2349(378.2343)	91.83	7.91	92.01	7.99
20a	228—230	350.2036(350.2035)				
20b	294—295	364.2192(364.2194)	92.22	8.04	92.26	7.74
21a	230—232		92.27	7.63	92.52	7.48
21b[g]	225—228	364.2192(364.2194)				
22a	235—236		92.38	7.58	92.52	7.48

a) Melting points of new olefins are as follows: **2b**, 139—140; **2c**, 103—104; **3a**, 79—80; **3b**, 104—105; **4a**, 174—175 ; **4b**, 167—168. b) IR absorption of three substituted olefin appears at 813 cm^{-1}. c) IR absorption at 813 cm^{-1}. d) IR absorption at 817 cm^{-1}. e) IR absorption at 815 cm^{-1}. f) Not determined. g) This is a conformationally fluxional compound, so that it contains **22b** as a conformational isomer (see text for details).

Synthesis of [3.*n*]Naphthalenophane Derivatives. One of the synthetic methods for [3.*n*]naphthalenophanes is the cationic cyclocodimerization, although the structures of naphthalenophanes produced are intricate with two substituents at one of their linkages.[12,15] The detailed feature of the reaction has been already discussed with some naphthalenophane derivatives.[15] In this work this cationic cyclization was employed for the synthesis of [3.*n*](1,5)- and [3.*n*](2,6)-skeletons.

Because of the conformational rigidity of the α-vinyl group, only one isomer of 1-methyl-3-(β-methylstyryl)[3.3](1,5)naphthalenophane **15a** was obtained in a reasonable yield from olefin **3a**. The structure was determined by NOESY spectroscopy. A large NOE enhancement (12%) is observed between a peri-hydrogen and allylic hydrogen (H-3).[16] The results clearly indicate that naphthalenophane **15a** is an exo, cis-isomer (See Ref. 16 for the definition of exo, endo-configuration). Syn conformation of **15a** is assigned unequivocally by comparison of the chemical shifts of aromatic proton resonances with those of [3.3](1,4)naphthalenophane derivatives. Accordingly the structure of **15a** is determined as depicted in Chart 3. Since an anti-oriented cation of the reaction

Table 2. ^{1}H NMR Spectroscopic Data of Novel Vinylarenes and Naphthalenophanes[a)]

Compd	Chemical shift δ (intensity, multiplicity, *J* in Hz)
2b	8.14 (2H, m), 8.05 (2H, m), 7.54—7.37 (8H, m), 7.28 (2H, d, 7.6), 5.74 (2H, dd, 17.2 and 1.6), 5.42 (2H, dd, 11.0 and 1.6), 3.10 (4H, m) , 1.88 (4H, m).
2c	8.13 (2H, m), 8.04 (2H, m), 7.52—7.44 (6H, m), 7.46 (2H, dd, 17.2 and 10.8), 7.26 (2H, d, 7.6), 5.74 (2H, dd, 17.2 and 1.7), 5.42 (2H, dd, 10.8 and 1.7), 3.04 (4H, t, 7.7), 1.80 (4H, quint, 7.7), 1.54 (2H, m).
3a	7.99 (2H, d, 7.9), 7.91 (2H, d, 7.9), 7.64—7.30 (10H, m), 5.76 (2H, dd, 17.9 and 1.2), 5.46 (2H, dd, 10.7 and 1.2), 3.20 (4H, t, 7.1), 2.25 (2H, quint, 7.1).
3b	8.04 (2H, dd, 8.4 and 1.5), 8.03 (2H, dd, 8.4 and 1.5), 7.68—7.31 (10H, m), 5.80 (2H, dd, 17.2 and 1.6), 5.50 (2H, dd, 10.8 and 1.6), 3.15 (4H, m) , 1.93 (4H, m).
4a	7.74 (2H, bd, 10.1), 7.72 (2H, bd, 8.4), 7.71 (2H, bs), 7.62 (2H, dd, 10.1 and 1.7), 7.57 (2H, bs), 7.32 (2H, dd, 8.4 and 1.9), 6.87 (2H, dd, 17.5 and 10.8), 5.84 (2H, dd, 17.5 and 1.1), 5.30 (2H, dd, 10.8 and 1.1), 2.83 (4H, t, 7.4), 2.12 (2H, quint, 7.4).
4b	7.75—7.60 (6H, m), 7.59 (2H, dd, 7.8 and 1.6), 7.55 (2H, bs), 7.29 (2H, dd, 8.4 and 1.8), 6.87 (2H, dd, 16.8 and 10.8), 5.84 (2H, dd, 16.8 and 0.8), 5.30 (2H, dd, 10.8 and 0.8), 2.80 (4H, m), 1.78 (4H, m).
5	7.76 (1H, m), 7.68 (1H, m), 7.35 (2H, m), 6.80 (1H, d, 7.3), 6.68 (1H, dd, 7.8 and 1.7), 6.64 (1H, d, 7.3), 6.60 (1H, dd, 7.8 and 1.7), 5.73 (1H, dd, 8.0 and 1.7), 5.30 (1H, dd, 8.0 and 1.7), 4.93 (1H, m), 3.88 (1H, m), 3.54 (1H, m), 2.73 (4H, m), 2.50—2.20 (4H, m), 2.06 (1H, m).
6a	7.45 (2H, m), 7.38 (2H, m), 6.82 (4H, m), 6.74 (4H, t, 6.6), 5.04 (2H, m), 3.59 (2H, dd, 13.6 and 3.8), 2.67 (7H, m), 2.15 (1H, m).
6b	7.67 (2H, m), 7.41 (2H, m), 6.99 (2H, ABq, 7.4), 6.91 (4H, m), 6.83 (2H, ABq, 7.4), 5.09 (2H, m), 3.07 (2H, m), 2.76 (4H, m), 2.34 (2H, m), 1.61 (4H, bs).
6c	7.86 (2H, dd, 7.4 and 2.4), 7.44 (2H, dd, 7.4 and 2.2), 7.13 (2H, d, 7.4), 7.02 (4H, m), 6.85 (2H, d, 7.4), 5.10 (2H, m), 3.27 (2H, dt, 13.6 and 4.2), 2.79 (4H, m), 2.33 (2H, td, 12.8 and 4.2), 1.62 (2H, m), 0.96 (2H, m), 0.55 (2H, m).
7a	7.41 (2H, d, 7.9), 7.33 (2H, d, 8.4), 6.89 (2H, t, 7.9), 6.82 (4H, m), 6.68 (2H, d, 6.8), 5.03 (2H, m), 3.59 (2H, m), 2.74 (7H, m), 2.06 (1H, m).
7b	7.55 (2H, bd, 8.4), 7.33 (2H, bd, 8.0), 6.90 (6H, m), 6.68 (2H, bd, 7.2), 5.06 (2H, m), 3.06 (2H, m), 2.75 (4H, m), 2.30 (2H, m), 1.53 (4H, bs).
15a	6.68—7.70 (17H, m), 6.16 (1H, d, 8.8), 4.60 (1H, m), 3.74 (1H, m), 3.58 (2H, m), 2.88 (3H, m), 2.16—2.57 (3H, m), 2.14 (3H, s), 1.38 (3H, d, 7.4).
15b	7.84 (1H, bd, 8.8), 7.74 (1H, bd, 8.8), 7.39—7.18 (8H, m), 7.11 (1H, dd, 7.2 and 1.1), 6.94 (4H, m), 6.82 (1H, bd, 7.1), 6.73 (1H, bd, 7.1), 6.14 (1H, dd, 8.3 and 1.3), 4.69 (1H, ddd, 11.2, 18.8, and 2.9), 3.87 (1H, m), 3.12 (2H, m), 2.67 (1H, m), 2.39 (3H, m), 2.13 (3H, d, 1.4), 1.81 (4H, m), 1.37 (3H, d, 7.0).
16	7.13—7.37 (9H, m), 7.08 (4H, bs), 6.88 (4H, m), 6.02 (1H, dd, 9.1 and 1.8), 3.79 (1H, ddd, 11.5, 9.1, and 2.8), 3.04 (1H, m), 2.95 (2H, m), 2.83 (2H, m), 2.22 (3H, m), 2.13 (3H, d, 1.8), 1.95 (1H, m), 1.31 (3H, d, 7.0).
17	7.01—7.38 (13H, m), 6.85 (1H, bs), 6.79 (1H, bs), 6.73 (1H, bs), 6.66 (1H, bs), 5.94 (1H, dd, 9.4 and 1.5), 3.73 (1H, ddd, 13.2, 9.4, and 4.0), 2.81 (5H, m), 2.24 (3H, m), 2.15 (3H, d, 1.5), 1.98 (1H, m), 1.33 (3H, d, 7.2).
18	8.04 (2H, m), 7.83 (2H, m), 7.44 (2H, m), 6.79 (2H, bd, 8.2), 6.71 (2H, d, 7.2), 6.62 (2H, bd, 8.2), 6.57 (2H, d, 7.2), 5.82 (2H, bs), 3.59 (1H, m), 3.25 (1H, m), 2.78 (2H, m), 2.58 (2H, m), 2.39 (2H, m), 2.18 (2H, m), 1.95 (2H, m), 1.40 (2H, m).
19a	8.13 (2H, m), 7.85 (2H, m), 7.49 (4H, m), 6.02 (2H, d, 7.2), 5.88 (2H, d, 7.2), 3.55 (2H, m), 3.31 (2H, m), 2.78 (2H, m), 2.50 (2H, m), 2.21 (2H, m), 2.00 (2H, m), 1.41 (2H, m).
19b	7.83 (4H, m), 7.37 (4H, m), 6.29 (4H, bs), 2.78 (8H, bs), 1.81 (8H, bs).
19b[b)]	7.55 (4H, m), 7.08 (4H, m), 5.97 (4H, s), 2.44 (8H, bs), 1.60 (8H, bs).
19c	7.90 (4H, m), 7.37 (4H, m), 6.49 (4H, s), 2.89 (4H, t, 6.0), 2.84 (4H, bs), 1.74 (4H, bs), 1.60 (4H, tt, 10.5 and 6.0), 0.50 (2H, quint, 10.5).
20a	7.57 (2H, bd, 8.2), 7.37 (2H, bd, 8.2), 6.91 (4H, m), 6.84 (2H, bd, 7.6), 6.77 (2H, bd, 7.0), 3.64 (2H, m), 3.12 (2H, m), 2.94 (2H, m), 2.37 (2H, m), 2.23 (2H, m), 1.84 (2H, m), 1.65 (2H, m).
20b	7.46 (4H, bd, 8.6), 6.97 (4H, dd, 8.6 and 7.2), 6.86 (4H, bd, 7.2), 3.15 (4H, m), 2.40 (4H, m), 1.79 (8H, m).
21a	7.20 (2H, bd, 8.1), 7.09 (2H, dd, 8.4 and 2.0), 7.03 (2H, dd, 7.7), 6.83 (4H, bd, 7.8), 6.75 (2H, bs), 2.89 (4H, m), 2.57 (2H, m), 2.32 (6H, m), 1.89 (2H, m).
21b[c)]	7.15 (4H, d, 8.4), 6.91 (4H, bd, 8.4), 6.89 (4H, bs), 2.66 (4H, dd, 12.8 and 4.4), 2.28 (4H, dd, 12.8 and 4.4), 1.96 (4H, m), 1.60 (4H, m).
22a	7.13 (2H, bd, 8.1), 7.10 (2H, bs), 7.04 (2H, bd, 8.4), 6.93 (2H, bs), 6.86 (2H, dd, 8.4 and 1.8), 6.73 (2H, dd, 8.1 and 1.8), 3.03 (2H, m), 2.82 (2H, m), 2.43 (4H, m), 2.29 (4H, m), 1.72 (2H, m).
22b[c)]	7.11 (4H, d, 8.4), 7.02 (4H, bs), 6.79 (4H, bd, 8.4), 2.47 (8H, m), 1.79 (8H, m).

a) Taken in $CDCl_3$. b) In nitrobenzene-d_5. c) NMR data of achiral **21b** and chiral [4.4](2,6)naphthalenophane **22b** were read from the spectrum of the conformer mixture.

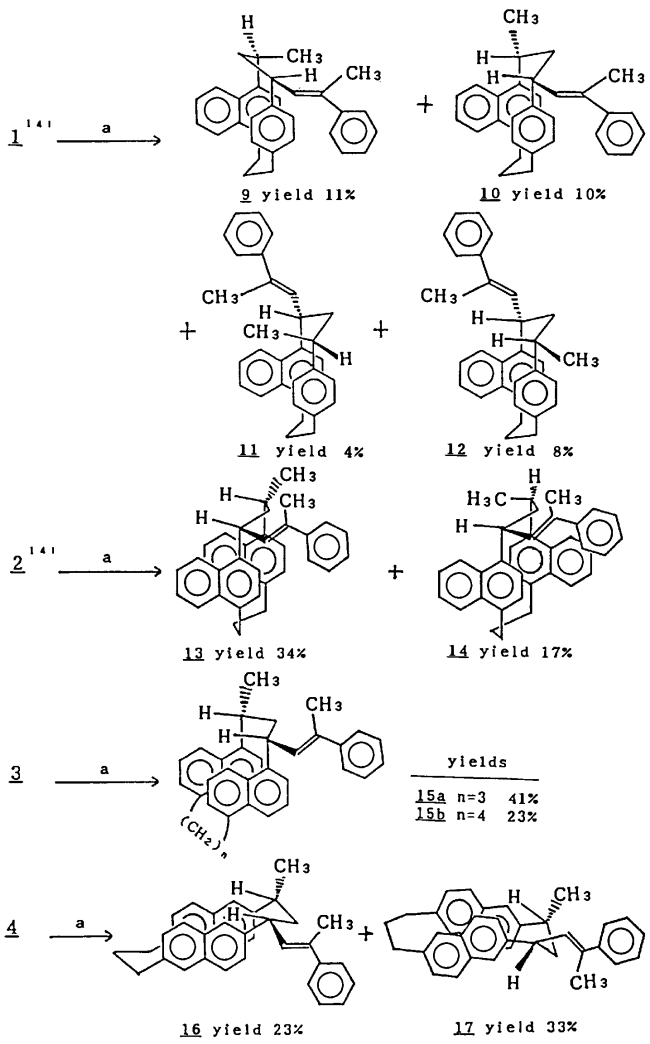

a) 2-phenylpropene, CF_3SO_3H/C_6H_6, 50 °C, 30 min.

Chart 3. Cationic cyclocodimerization toward [3.*n*]-naphthalenophanes.

is sterically unfavorable,[5] only one possible syn-oriented cation with exo-vinyl group affords exo, cis, syn-isomer **15a**, as observed. The structure of **15b** was determined by the same method as above.[16]

From the reaction mixture of olefin **4a** two isomers of 1-methyl-3-(β-methylstyryl)[3.3](2,6)naphthalenophanes (a 1.0:1.4 ratio and total 56% yield) were isolated by HPLC (Develosil-PYE, MeOH). Compared with reported NMR data of chiral and achiral [3.3](2,6)naphthalenophanes,[10] especially underlined chemical shift(s) for peri-hydrogens in Table 2, compound **16** can be concluded as a derivative of the achiral isomer. An NOE experiment indicates that H-1 and one of the peri-hydrogens (22% NOE enhancement), and also H-3 and another peri-hydrogen (14% NOE enhancement), are in vicinity, so that the disubstituted three-carbon bridge is of cis, exo-configuration. Thus the exo, cis, achiral-structure of **16** is concluded as indicated in Chart 3. Compound **17** can be easily concluded to be a derivative of the chiral isomer, as mentioned above.[10] VT-NMR spectra taken in acetone-d_6 from 20 to −90 °C show considerable change at the region of aromatic proton resonance. This change should be the attribute of two conformationally unstable three-carbon linkages, compared with the small change of the aromatic proton peaks of cis-isomer **16**. The fact suggests that **17** has the trans-configuration. The NOE experiment indicates that H-1 and one of the peri-hydrogens are in vicinity (15% NOE enhancement), so that the disubstituted three-carbon bridge must be of exo-configuration. Thus **17** is assigned to the structure depicted in Chart 3. It is interesting that the reaction gave mainly **16** and **17** in an almost equal amount, although eight diastereomers are possible at a random cyclization. This selectivity must be due to the predominant exo-conformation of starting 2-vinylnaphthalene moiety which had already been deduced from the consideration on the chemical shift of methine hydrogen of the 2-vinyl group.[17]

Synthesis of [4.*n*]Naphthalenophane Derivatives. Cyclobutane ring is known to be cleaved regioselectively by electron-transfer reduction like Birch one.[18] The ring cleavage of naphthalenophanes **5—8** becomes ultimately a general synthetic method of [4.*n*]naphthalenophanes which are prepaced only in low yields by other ones reported previously.

Treated under the usual Birch reduction conditions, naphthalenophanes **5—8** gave several over-reduced products. ^{1}H NMR spectroscopic analysis of the products showed olefinic hydrogens which were generated by the reduction of naphthalene rings. In order to obtain desired naphthalenophanes from them, the reduced material were oxidized in decalin with 2,3-dichloro-5,6-dicyano-1,4-benzoquinone (DDQ) at 170 °C. Yields are shown in Chart 4.

The sequence of reactions is depicted in Chart 4. The products were easily isolated by column chromatography (SiO_2, benzene/cyclohexane), purified by recrystallization from hexane, and characterized mainly by ^{1}H NMR spectroscopy. Analytical and spectroscopic data are listed in Tables 1 and 2.

From naphthalenophanes **7**, products **20** were obtained without conformational alteration of naphthalene nuclei, whereas **6** gave conformationally stable *anti*-naphthalenophanes **19** exclusively. Compound **8a** (the chiral/achiral isomer ratio=4.2) gave two isomeric [3.4](2,6)naphthalenophanes **21a** and **22a** (chiral **22a**/achiral **21a** isomer ratio=4.2), which were isolated by HPLC (SiO_2, hexane). These structures were determined by ^{1}H NMR spectroscopy, just as done for compounds **16** and **17**.

Compound **19a** did not change the chemical shift of intraannular hydrogens even at 200 °C. Therefore it is concluded that the naphthalene ring rotation in the ring system needs very high activation energy. On the other hand, compound **19b** showed the coalescence

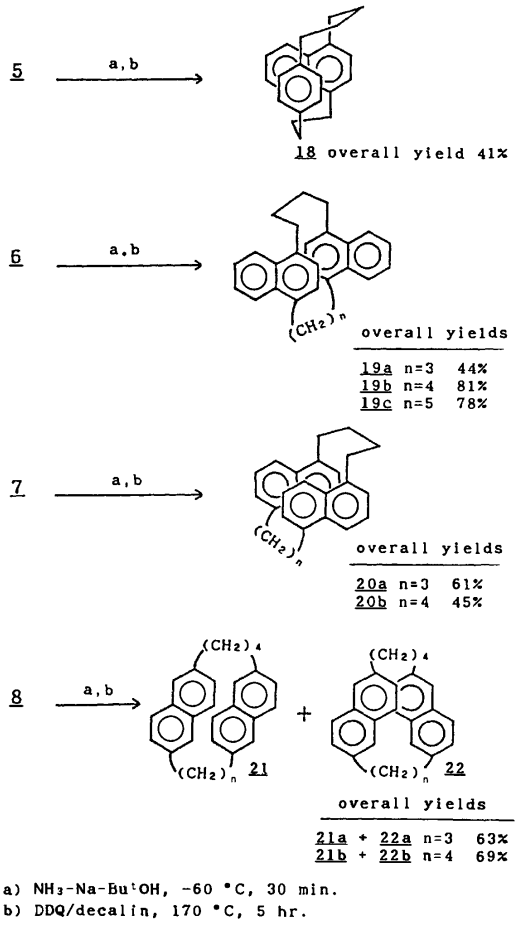

Chart 4. Birch reduction toward [4.*n*]naphthalenophanes.

of intraannular aromatic hydrogens of its syn and anti conformers at 10±5 °C. The rotation barrier at the coalescence temperature is calculated 13 kcal mol^{-1}. Chiral naphthalenophane **22a** was heated at 200 °C for 12 h, but there occurred no isomerization to achiral **21a** by the ring rotation, according to the HPLC analysis. On the other hand, naphthalenophanes **8b** gave conformationally fluxional [4.4](2,6)naphthalenophanes **21b** and **22b**. The conformer ratio (chiral/achiral) at r.t. was 2.4:1. Naphthalenophanes **21b** and **22b** showed the coalescences of aromatic and aliphatic hydrogens at 175±5 °C, and the rotation barrier is calculated 22 kcal mol^{-1}.

Discussion

Among several synthetic methods for structurally interesting naphthalenophanes, the present methods have an advantage; i.e., a single starting material for [2.*n*]-, [3.*n*]-, and [4.*n*]naphthalenophane skeletons. When one needs a large amount of naphthalenophanes, the methods using vinylnaphthalene derivatives will be an unignorable one.

The syn selectivity of the methods mentioned here has a great advantage, because syn isomers are generally conformationally unstable and given as minor products by ordinary methods. By using this advantage of the syn selectivity the room required for the intraannular rotation of naphthalene nuclei was determined. By the enlargement of the ring system from [2.3] to [4.4] one, the (1,5)naphthalenophanes always kept syn conformation under the experimental conditions of −60 °C to 180 °C, because quite a large volume is necessary if the nucleus rotates around the axe through C1 and C5 of naphthalene ring.

Interestingly the (1,4)naphthalenophanes showed the point for the nuclei to start the rotation within [2.3] to [4.5] system. Namely [3.4](1,4)naphthalenophane takes only anti-conformation after the transformation of *cis,exo*-1,2-ethano-*syn*-[2.3]naphthalenophane **6a**, whereas *syn*-[3.3] and [2.4]naphthalenophane take only syn-conformation upto their melting points. The room requirement for the rotation of naphthalene rings is just similar to that previously reported for [*n.m*]paracyclophanes:[19] i.e., activation free energies for [3.4]- and [4.4]paracyclophanes are reported 33 kcal mol^{-1} at 160 °C and 15 kcal mol^{-1} at ca. 15 °C, respectively. From the coalescence temperatures, activation free energies for **19a** and **b** were calculated ≥25 kcal mol^{-1} (≥200 °C) and 13 kcal mol^{-1} (10 °C), respectively.

This is the first report on the naphthalene ring rotation in the skeletons of the (2,6)naphthalenophanes. The ring rotation barrier for [4.4](2,6)naphthalenophane exceeds that of [4.4](1,4)naphthalenophane by 9 kcal mol^{-1}.

Experimental

General. Elemental analyses were done at the Microanalysis Center of Kyoto university. Melting points are not corrected. NMR spectra were recorded on a Varian XL200 FT-NMR spectrometer. IR spectra were taken on a JASCO IR-810 infrared spectrophotometer. Mass spectra were recorded on a Hitachi M-80A mass spectrometer. High performance liquid chromatographic analyses (HPLC) were carried out by using Altex Model 100A and Knauer 64 pumps with a Hitachi wavelength tunable effluent monitor and a Shimadzu SPD-6A UV spectrophotometric detector.

Solvents like benzene, THF, and ether were distilled over sodium diphenylketyl after prolonged reflux. Other commercially available highest-grade reagents were used without further purification. Monomers were prepared conveniently by our methods depicted in Chart 1.[12]

Synthesis of 1,2-Ethano[2.4](1,5)naphthalenophane 7b (General Procedure). A 1-l Pyrex flask equipped with a magnetic stirrer, reflux condenser, and N_2 inlet was placed 4.28 g (11.8 mmol) of 1,4-bis(5-vinyl-1-naphthyl)butane **3b** dissolved in 900 ml of dry benzene under N_2. It was irradiated by a high-pressure mercury lamp (400 W) for 17 h. Then benzene was removed by evaporation. Reaction mixture dissolved in 20 ml of dry THF was transferred to 50-ml two-necked flask equipped with a magnetic stirrer, dropping funnel, and N_2 inlet. A 10 ml of B_2H_6-THF complex (0.1 M) was added to it slowly at r.t. After stirred for 12 h at r.t., THF was removed and products were isolated by column chromatography (SiO_2, hexane). Recrystallization

from benzene–methanol gave 1.41 g (33%) of *cis,exo*-1,2-ethano-*syn*-[2.4](1,5)naphthalenophane.

Synthesis of *cis,exo*-1-Methyl-3-(β-methylstyryl)[3.3](1,5)-naphthalenophane 15a (General Procedure). A 1-l, four-necked round-bottomed flask was equipped with a magnetic stirrer, thermometer, and N_2 inlet was placed 2.36 g (6.78 mmol) of 1,3-bis(5-vinyl-1-naphthyl)propane **3a** and 3.9 ml (36.2 mmol) of 2-phenylpropene which were dissolved in 566 ml of dry benzene under N_2 at 50 °C. Trifluoromethanesulfonic acid (0.01 g, 0.068 mmol) was dissolved in 1 ml of dry benzene and added at once to initiate the reaction under vigorous stirring. After stirred for 30 min, 200 ml of 10% aqueous NaOH was added to stop the reaction. The reaction mixture was washed with 200 ml of water 3 times and dried anhydrous Na_2SO_4. After the reaction mixture was filtered and benzene was removed, products were isolated by column chromatography (SiO_2, benzene–hexane). Recrystallization from benzene–methanol gave 0.73 g (41%) of the title compound as the sole naphthalenophane derivative.

Compound **15** can be isolated by crystallization after the column chromatography. The purity of so-crystallized **15** was usually 95%. Compound **16** and **17** can be separated from each other by MeOH extraction. From the MeOH solution **17** was crystallized and purified up to 90%. From the MeOH-insoluble part **16** was purified up to 95% by recrystallization from EtOH.

Synthesis of *syn*-[4.4](1,5)Naphthalenophane 20b (General Procedure). A 200 ml, three-necked round-bottomed flask equipped with a magnetic stirrer, N_2 inlet, and gas inlet was cooled by Dry Ice–methanol bath at ca. −50 °C. Ammonia gas was introduced into the system. When ca. 100 ml of liquid ammonia was condensed, the gas inlet tube was replaced with a glass stopper. About 1 g of Na was added carefully piece by piece into liquid ammonia and stirred for 10 min. *cis,exo*-1,2-Ethano-*syn*-[2.4](1,5)-naphthalenophane **7b** (500 mg, 1.38 mmol) and 2 ml of *t*-butyl alcohol dissolved in 20 ml of dry THF were added slowly in it, and the mixture was stirred for 30 min. Then the excess Na was consumed by cautious addition of 10 ml of water. The ammonia was allowed to evaporate itself slowly in a hood. Then products were extracted by 20 ml of benzene. The benzene extract was washed with 20 ml of water three times and dried over anhydrous Na_2SO_4. After filtration, benzene was removed, products were isolated by column chromatography (SiO_2, benzene–hexane). The yield was 350 mg. A 50 ml flask equipped with a magnetic stirrer, reflux condenser, and N_2 inlet was placed 200 mg of the Birch reduction products and 300 mg (1.32 mmol) of DDQ were dissolved in 30 ml of decalin under N_2. The reaction mixture was heated with stirring at ca. 180 °C for 12 hours. After removed the decalin, products were isolated by column chromatography on SiO_2 (benzene–hexane). Recrystallization from benzene gave 130 mg (0.036 mmol, a 45% yield) of *syn*-[4.4](1,5)naphthalenophane.

The support of this work through grants from the Ministry of Education, Science and Culture, from Gunma University Foundation for Science and Technology, and from Toray Science Foundation is gratefully acknowledged.

References

1) Part 4 of this series: J. Nishimura, A. Ohbayashi, E. Ueda, and A. Oku, *Chem. Ber.*, **121**, 2025 (1988).

2) a) H. H. Wasserman and P. M. Keehn, *J. Am. Chem. Soc.*, **91**, 2374 (1969); b) N. E. Blank and M. W. Haenel, *Chem. Ber.*, **114**, 1531 (1981).

3) G. W. Brown and F. Sondheimer, *J. Am. Chem. Soc.*, **89**, 7116 (1967).

4) T. Kawabata, T. Shinmyozu, T. Inazu, and T. Yoshino, *Chem. Lett.*, **1979**, 315.

5) K. Kurosawa, M. Suenaga, and T. Inazu, *Tetrahedoron Lett.*, **1982**, 5335.

6) R. S. Grivens, R. J. Olsen, and P. L. Wylie, *J. Org. Chem.*, **44**, 1608 (1979); Hereafter the prefixes, chiral and achiral are used for the configuration of naphthalene rings, even if the products have other asymmetric centers.

7) P. J. Jessup and J. A. Reiss, *Aust. J. Chem.*, **30**, 843 (1977).

8) V. Boekelheide and C. H. Tsai, *Tetrahedron*, **32**, 423 (1976).

9) T. Otsubo, M. Kitasawa, and S. Misumi, *Bull. Chem. Soc. Jpn.*, **52**, 1515 (1979).

10) N. E. Blank and M. W. Haenel, *Tetrahedron Lett.*, **1978**, 1425.

11) J. Nishimura, H. Doi, E. Ueda, A. Ohbayashi, and A. Oku, *J. Am. Chem. Soc.*, **109**, 5293 (1987).

12) J. Nishimura, N. Yamada, Y. Horiuchi, E. Ueda, A. Ohbayashi, and A. Oku, *Bull. Chem. Soc. Jpn.*, **59**, 2035 (1986).

13) R. B. Girdler, P. H. Gore, and J. A. Hoskins. *J. Chem. Soc. C*, **1966**, 518.

14) J. Nishimura, N. Yamada, T. Okuda, Y. Mukai, H. Hashiba, and A. Oku, *J. Org Chem.*, **50**, 836 (1985).

15) J. Nishimura, K. Hashimoto, T. Okuda, H. Hayami, Y. Mukai, and A. Oku, *J. Am. Chem. Soc.*, **105**, 4758 (1983).

16) J. Nishimura, T. Okuda, Y. Mukai, H. Hashiba, and A. Oku, *Tetrahedron Lett.*, **25**, 1495 (1984).

17) a) S. W. Staley, C. K. Dustman, and G. E. Linkowski, *J. Am. Chem. Soc.*, **103**, 1069 (1981). b) K. L. Facchine, S. W. Staley, P. C. M. van Ziji, P. K. Mishra, and A. A. Bothner, *ibid.*, **110**, 4900 (1988).

18) H. Nozaki, R. Noyori, and K. Kawanisi, *Tetrahedron*, **24**, 2183 (1968).

19) D. J. Cram and J. M. Cram, *Acc. Chem. Res.*, **4**, 204 (1971).

 © 1989 The Chemical Society of Japan Bull. Chem. Soc. Jpn., 62, 3167—3170 (1989)

A Synthesis of Unsymmetric Porphyrin Dimers

Kazuhiro MARUYAMA,* Toshi NAGATA, Noboru ONO, and Atsuhiro OSUKA
Department of Chemistry, Faculty of Science, Kyoto University, Kyoto 606
(Received May 18, 1989)

A new synthetic method of porphyrins via bis(hydroxymethyl)dipyrromethanes is described. This new method can be utilized for preparation of several unsymmetric porphyrin dimers.

In recent years, much interest has been focussed on development of conformationally restricted porphyrin dimers as models for photosynthetic reaction center[1] and metalloenzymes such as cytochrome oxidase.[2] Among these, octaalkylporphyrin dimer (**1**) bridged by an aromatic spacer has been shown to be a useful model. The relative geometry of the two porphyrin rings in these compounds is rather restricted because of the steric hindrance between the aromatic spacer and the flanking peripheral alkyl groups.

Symmetric porphyrin dimer **1** is generally prepared by the synthetic routes shown in Scheme 1.[3] However, synthesis of unsymmetric dimers, such as **10a** and **10b**, is not so straightforward as **1**.

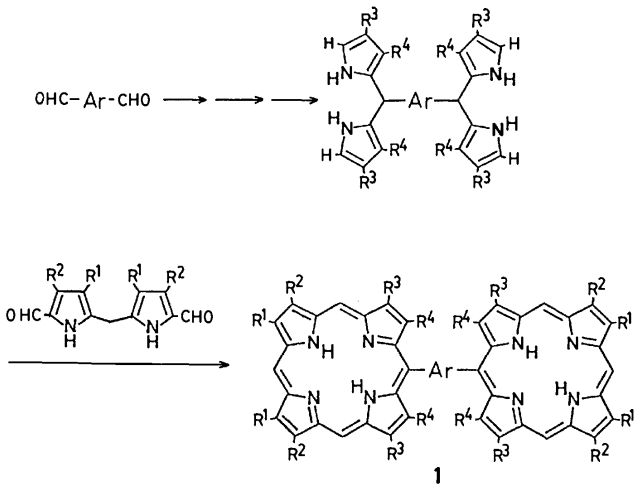

Scheme 1.

We wish to report here a new synthetic method of porphyrins by acid-catalyzed condensation of 5,5′-bis(hydroxymethyl)dipyrromethane and 5,5′-unsubstituted dipyrromethane. Since the conditions are mild enough, this method can be applied for a stepwise synthesis of non-symmetric dimers. It should be noted that this method is an application of the synthesis of octaalkyl- and octaarylporphyrins reported by Ono and Maruyama, in which $LiAlH_4$ treatment of 5-unsubstituted 2-ethoxycarbonylpyrrole followed by acid catalyzed self-condensation is utilized.[4]

Results and Discussion

Dipyrromethane diester **2** was treated with lithium aluminum hydride to give the corresponding diol **3**, which was immediately allowed to react with the 5,5′-unsubstituted dipyrromethane **4** in the presence of acid catalyst. After standing for 1—2 days at room temperature, the reaction mixture was worked up and separated by column chromatography. The desired product **5a** was obtained in a moderate yield. Generally two other porphyrins, **5b** and **5c**, were obtained together with **5a**. These by-products were formed through self-coupling of each dipyrromethane unit. Several cyclization conditions were employed, and the results are summarized in Table 1.

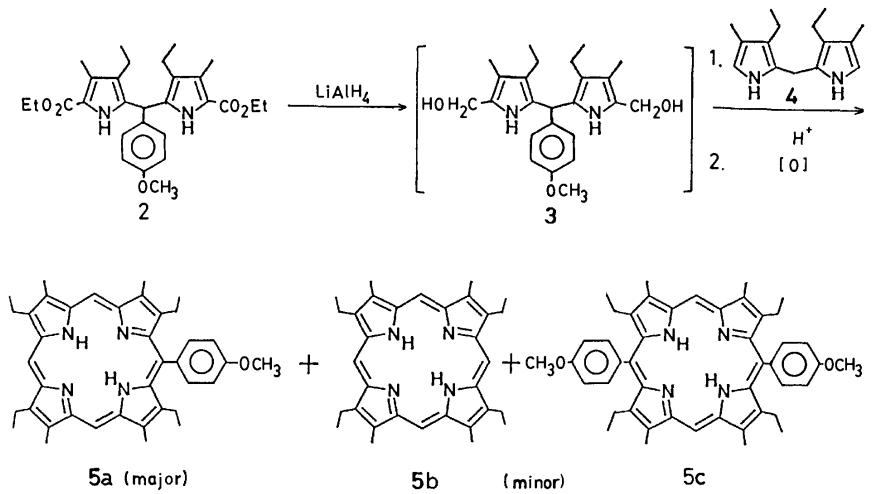

Scheme 2.

In several cases (Runs 1, 2, and 4), "scrambling" of the peripheral alkyl substituents took place during cyclization. This is probably due to acid-catalyzed redistribution reactions of the porphyrinogens (the saturated precursor of porphyrins).[5] When more weakly acidic conditions were employed, no scrambling was observed (Runs 3, 5, and 6). Thus, it was concluded that acetic acid in methanol or silica gel in dichloromethane was the reagent of choice in the reaction of **3** and **4**.

The present method of porphyrin formation was applied for synthesis of unsymmetric porphyrin dimers. Condensation of 1,19-dideoxybiladiene-ac dihydrobromide **6** with isophthalaldehyde gave a porphyrin bearing a formyl group (**7**),[6] which was allowed to react with ethyl 4-ethyl-3-methyl-2-pyrrolecarboxylate to give **8a**. The porphyrin-dipyrromethane **8a** was converted to the zinc complex **8b**, and treated with $LiAlH_4$ to give the corresponding diol **9**, which was allowed to react with **4** in methanol/dichloromethane (pure methanol did not dissolve the porphyrin) in the presence of silica gel. The dimer **10a** was obtained in a moderate yield (9%).

Table 1. Coupling Reaction of **3** and **4**

Run	Catalyst	Solvent	Yield (%) of **5a**[a]
1	$HClO_4$	MeOH	6[b]
2	pTsOH	MeOH	18[b]
3	AcOH	MeOH	15
4	AcOH	CH_2Cl_2	14[c]
5	C-200[d]	CH_2Cl_2	9
6	AcOH	$MeOH/CH_2Cl_2$(1/1)	13

a) Including scrambled products. b) Scrambling. c) Slight scrambling. d) Silica gel (Wako Pure Chemicals).

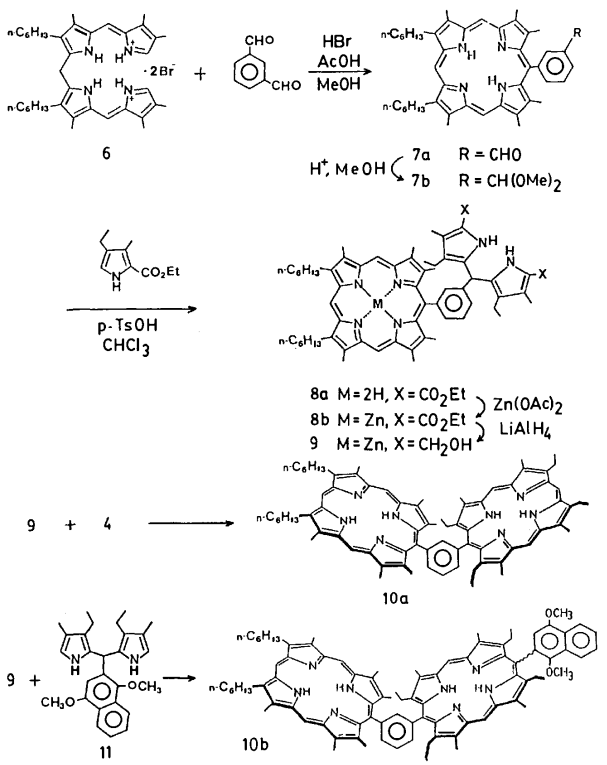

Scheme 3.

Coupling of **9** with dipyrromethane **11** similarly gave an unsymmetric porphyrin dimer **10b** in 0.5% yield. The dimer **10b** can be transformed into a quinone-linked porphyrin dimer, which is a very important model compound in the studies of plant- and bacterial photosynthesis. We are currently preparing other quinone-linked porphyrin dimers with restricted conformation by a similar method as described here, and the photophysical properties of these photosynthetic model systems will be presented in the near future.

Experimental

The instruments were as previously reported.[7] Mass spectra were recorded on a JEOL DX-300 spectrometer using the FAB method; the FAB matrix was $CHCl_3$+trifluoroacetic acid/*m*-nitrobenzyl alcohol (NBA)/glycerol unless otherwise stated. High-resolution mass spectrum was recorded on a JEOL JMS-SX102 spectrometer.

5-(4-Methoxyphenyl)-3,7,13,17-tetraethyl-2,8,12,18-tetramethylporphine (5a). Various conditions were employed (see Table 1), and one typical experiment is described here.

To a suspension of $LiAlH_4$ (40 mg) in 2 ml of anhydrous tetrahydrofuran, a solution of dipyrromethane **2**[8] (100 mg, 0.21 mmol) in tetrahydrofuran (10 ml) was dropwise added (under nitrogen, at room temperature). After 40 minutes, water was carefully added, and the mixture was extracted with dichloromethane (quickly!). The extract was washed with water and dried over sodium sulfate.

The resultant solution (**3**) was diluted with 70 ml of methanol, and bis(3-ethyl-4-methyl-2-pyrrolyl)methane[10] (**4**, 48 mg=0.21 mmol) was added. Acetic acid (15 drops) was added, and the mixture was stirred in the dark under nitrogen for 38 hours (room temperature). Chloranil (50mg) was added, and stirring was continued for 24 hours.

Solvent was evaporated from the reaction mixture, 10% aqueous NaOH was added and the mixture was extracted with dichloromethane. The extract was washed with aqueous NaOH and water, dried (Na_2SO_4), and treated with saturated solution of zinc acetate in methanol (1 ml) for 2 hours at refluxing temperature. The reaction mixture was washed with water, dried, evaporated, and separated by flash column chromatography (CH_2Cl_2). The fractions containing zinc porphyrin were collected, shaken twice with 4M HCl (1 M=1 mol dm^{-3}), neutralized, dried, and evaporated. Separation by flash column chromatography (CH_2Cl_2) gave three porphyrinic fractions. The first fraction was porphyrin **5b**, the second was the desired product **5a**, and the third was bis(*p*-methoxyphenyl)porphyrin **5c**. Yield of **5a**: 19 mg (0.032 mmol, 15%). Mp 290—295 °C. ^{1}H NMR ($CDCl_3$): δ=10.17 (s, 2H, 10,20-H), 9.92 (s, 1H, 15-H), 8.08+7.20 (d+d, 2H+2H, aromatic-H), 4.11 (s, OMe), 4.06 (q, 13,17-Et), 3.64+3.57 (s+s, 6H+6H, Me), 2.82 (q, 4H, 3,7-Et), 1.18+1.17(t+t, 6H+6H, Et), −3.0+−3.2 (br, 1H+1H, NH). UV-vis (CH_2Cl_2): 404, 503, 537, 574 and 624 nm. MS (FAB): *m*/*z* 585 ($M+H^+$).

5-[3-(Dimethoxymethyl)phenyl]-13,17-dihexyl-2,3,7,8,12,18-hexamethylporphine (7b). HBr-catalyzed condensa-

tion[6] of the 1,19-dideoxybiladiene-ac dihydrobromide **6**[11] (286 mg, 0.40 mmol) and isophthalaldehyde (536 mg, 4.0 mmol) gave 5-(3-formylphenyl)-13,17-dihexyl-2,3,7,8,12,18-hexamethylporphine **7a** in 68% yield (185 mg, 0.27 mmol). **7a:** mp 298—301 °C, IR (KBr): 1700 cm^{-1} (C=O). The formylporphyrin **7a** (73mg, 0.11 mmol) was dissolved in chloroform (40 ml). Methanol (10 ml) and *p*-toluenesulfonic acid monohydrate (60 mg) were added, and the resultant mixture was heated under reflux for 5.5 hours. The reaction mixture was cooled, washed with aqueous $NaHCO_3$ and brine, dried, and evaporated. The dimethyl acetal **7b** was obtained in quantitative yield. Mp 271—283 °C. ^1H NMR ($CDCl_3$): δ=10.15 (s, 2H, 10,20-H), 9.95 (s, 1H, 15-H), 5.68 (s, 1H, C<u>H</u>$(OMe)_2$), 4.04 (t, 4H, hex-1), 3.63+3.52+3.49 (s+s+s, 6H+6H+6H, Me and OMe), 2.45 (s, 6H, 3,7-Me), 2.30 (quint, 4H, hex-2), 1.76 (quint, 4H, hex-3), 1.51 (m, hex-4), 1.39 (sext, 4H, hex-5), 0.92 (t, hex-6), −3.15 +−3.30 (s+s, NH); phenyl: 8.18 (s, 1H), 8.01+7.91 (d+d, 1H+1H), 7.75 (t, 1H). UV-vis (CH_2Cl_2): 403, 502, 536, 570, and 623 nm. MS (FAB): *m/z* 713 ($M+H^+$). IR (KBr): no carbonyl. Found: C, 79.28; H, 8.59; N, 7.78%. Calcd for $C_{65}H_{82}O_4N_6$: C, 79.17; H, 8.48; N, 7.76%.

5-(3-[Bis(5-ethoxycarbonyl-3-ethyl-4-methyl-2-pyrrolyl)-methyl]phenyl)-13,17-dihexyl-2,3,7,8,12,18-hexamethylporphine Zinc Complex (8b). The porphyrin dimethyl acetal **7b** (183 mg, 0.26 mmol) and ethyl 4-ethyl-3-methyl-2-pyrrolecarboxylate (183 mg, 1.01 mmol) was dissolved in chloroform (100 ml), *p*-toluenesulfonic acid monohydrate (180 mg, 0.95 mmol) was added, and the resultant mixture was refluxed for 12 hours. The reaction mixture was then cooled, washed with aqueous $NaHCO_3$, and dried over Na_2SO_4. The resultant solution was treated with 10 ml of $Zn(OAc)_2$/MeOH solution (reflux, 2 hours). The reaction mixture was separated by flash column chromatography (benzene). After the unreacted pyrrole and non-porphyrinic by-products were eluted, the porphyrin zinc complex **8b** was eluted by benzene/diethyl ether (v/v=95/5). Yield 246 mg (0.23 mmol, 89%). Mp 140—148 °C. ^1H NMR ($CDCl_3$): δ=10.14 (s, 2H, 10,20-H), 10.03 (s, 1H, 15-H), 4.04 (t, 4H, hex-1), 3.62+3.52 (s+s, 6H+6H, Me), 2.3 (m, 4H, hex-2), 2.46 (s, 6H, 3,7-Me), 1.79 (quint, 4H, hex-3), 1.6 (m, hex-4), 1.41 (m, 4H, hex-5), 0.93 (t, 6H, hex-6); phenyl: 7.99 (d, 1H), 7.95 (s, 1H), 7.73 (t, 1H), 7.50 (d, 1H); pyrrole: 8.44 (s, 2H, NH), 5.83 (s, 1H, $(pyrrolyl)_2C$<u>H</u>-), 4.34 (q, 4H, OC<u>H_2</u>CH_3), 2.41 (m, 4H, C<u>H_2</u>CH_3), 2.31 (s, 6H, Me), 1.39 (t, 6H, OCH_2C<u>H_3</u>), 0.99 (t, 6H, CH_2C<u>H_3</u>). UV-vis (CH_2Cl_2): 407, 537, and 572 nm.

5-[3-(3,7,13,17-Tetraethyl-2,8,12,18-tetramethyl-5-porphinyl)-phenyl]-13,17-dihexyl-2,3,7,8,12,18-hexamethylporphine (10a). The dipyrromethane-porphyrin zinc complex **8b** (66 mg, 0.061 mmol) was treated with $LiAlH_4$ (26 mg) in tetrahydrofuran (10 ml) at 4 °C for 1 hour. The reaction mixture was quenched with aqueous NH_4Cl, and extracted with CH_2Cl_2. The extract was washed with water, dried, and evaporated. The resultant solids were dissolved in 2 ml of CH_2Cl_2, which was added to the solution of dipyrromethane **4** (30 mg) in 10 ml of methanol. Silica gel (C-100, Wako Pure Chemicals) was added (1.0 g), and the mixture was stirred for 3 days (dark, under nitrogen, room temperature). Chloranil (20 mg) was added and the mixture was stirred for 2 hours.

The silica gel was removed by filtration, and the resultant mixture was treated in the similar manner as in the case of **5a**. The dimer **10a** was obtained. Yield 6 mg (0.005 mmol, 9%). Mp>300 °C. ^1H NMR ($CDCl_3$): δ=10.12+10.01 (s+s, 2H+2H, meso), 9.81+9.80 (s+s, 1H+1H, meso), 3.98+3.95 (q+t, 8H, 13,17-Et+hex-1), 3.62+3.57+3.53+3.46+3.6 (4s+m, 28H, 4Me+3,7-C<u>H_2</u>CH_3), 2.97 (s, 6H, Me), 2.20 (quint, 4H, hex-2), 1.80 (t, 6H, Et), 1.67 (quint, hex-3), 1.60 (t, Et), 1.43 (quint, hex-4), 1.31 (sext, hex-5), 0.85 (t, 6H, hex-6), −2.5 to −3.3 (br, 4H, NH); phenyl: 9.38 (d, 1H), 8.58 (d, 1H), 8.23 (t, 1H), 7.83 (s, 1H). UV-vis (CH_2Cl_2): 407, 505, 538, 574, and 626 nm. MS (FAB): *m/z* 1116 ($M+H^+$).

5-(1,4-Dimethoxy-2-naphthyl)-15-[3-(13,17-dihexyl-2,3,7,8,12,18-hexamethyl-5-porphinyl)phenyl]-3,7,13,17-tetraethyl-2,8,12,18-tetramethylporphine (10b). The porphyrin dimer **10b** was prepared by the same method as **10a**, starting from **8b** and 2-[bis(3-ethyl-4-methyl-2-pyrrolyl)methyl]-1,4-dimethoxynaphthalene **11**[1c] (0.5% yield). ^1H NMR ($CDCl_3$):[12] δ=10.14 (s, 2H, meso), 9.97 (s, 2H, meso), 9.75 (s, 1H, meso), 3.97—3.86 (m, 7H, hex-1 and OMe), 3.57—3.42 (5s, 27H, Me and OMe), 2.93 (s, 6H, Me), 2.93—2.50 (4m, 4H, Et), 2.3—2.13 (2m, 4H, hex-2), 1.7—1.6 (2m, hex-3), 1.5—1.2 (m, hex-4 and hex-5), 1.08 (t, Et), 0.81 (t, hex-6), −1.8 (br, NH), −3.1 and −3.2 (br, NH); naphthyl: 8.46+8.1 (m+br, 1H+1H, 6- and 7-H), 7.6 (m, 2H, 5- and 8-H), 7.5 (br, 1H, 3-H); phenyl: 9.3+8.55 (br+br, 1H+1H, 4- and 6-H), 8.17 (t, 1H, 5-H), 7.9 (br, 1H, 2-H). UV-vis (CH_2Cl_2): 404, 505, 537, 575, 624 and 654nm. High resolution mass (FAB, $CHCl_3$+NBA). Found: 1301.806 ($M+H^+$). Calcd for $C_{88}H_{101}O_2N_8$: 1301.805.

References

1) a) Y. Sakata, S. Nishitani, N. Nishimizu, S. Misumi, A. R. McIntosh, J. R. Bolton, Y. Kanda, A. Karen, T. Okada, and N. Mataga, *Tetrahedron Lett.*, **26**, 5207 (1985); b) J. A. Cowan, J. K. M. Sanders, G. S. Beddard, and R. J. Harrison, *J. Chem. Soc., Chem. Commun.*, **1987**, 55; c) J. L. Sessler and M. R. Johnson, *Angew. Chem., Int. Ed. Engl.*, **26**, 678 (1987); d) J. L. Sessler, M. R. Johnson, T.-Y. Lin, and S. E. Creager, *J. Am. Chem. Soc.*, **110**, 3659 (1988).

2) a) J. P. Collman, "Organic Synthesis Today and Tomorrow, 3rd IUPAC," p. 29 and references therein; b) I. Tabushi and T. Sasaki, *Tetrahedron Lett.*, **23**, 1913 (1982); c) I. Tabushi and S. Kugimiya, *J. Am. Chem. Soc.*, **108**, 6926 (1986); d) D. Heiler, G. McLendon, and P. Rogalskyj, *ibid.*, **109**, 604 (1987).

3) a) C. K. Chang and I. Abdalmuhdi, *J. Org. Chem.*, **48**, 5388 (1983); b) C. K. Chang and I. Abdalmuhdi, *Angew. Chem., Int. Ed. Engl.*, **23**, 164 (1984); c) J. L. Sessler, J. Hugdahl, and M. R. Johnson, *J. Org. Chem.*, **51**, 2838 (1986).

4) N. Ono and K. Maruyama, *Chem. Lett.*, **1988**, 1511.

5) K. M. Smith, "Porphyrins and Metalloporphyrins," ed by K. M. Smith, Elsevier, New York (1975), p. 36 and references therein.

6) D. Harris, A. W. Johnson, and R. Gaete-Holmes, *Bioorg. Chem.*, **9**, 63 (1980). No dimeric porphyrins were formed under our reaction conditions (10-fold excess of the dialdehyde).

7) A. Osuka and K. Maruyama, *J. Chem. Res. (S)*, **1987**, 286; *J. Chem. Res. (R)*, **1987**, 2401.

8) The compound **2** was prepared by acid-catalyzed condensation (Ref. 3b) of *p*-anisaldehyde with ethyl 4-ethyl-3-methyl-2-pyrrolecarboxylate (Ref. 9).

9) T. P. Wijesekera, J. B. Paine, III, and D. Dolphin, *J. Org. Chem.*, **50**, 3832 (1985).
10) P. S. Clezy and A. W. Nichol, *Aust. J. Chem.*, **11**, 1835 (1965).
11) A. W. Johnson and I. T. Kay, *J. Chem. Soc.*, **1965**, 1620.
12) Since the compound **10b** was obtained as a mixture of two atropisomers, the ^{1}H NMR spectrum of **10b** was complex and somewhat broadened. The peak assignment was based on the 2D (COSY) ^{1}H NMR spectrum.

 © 1989 The Chemical Society of Japan Bull. Chem. Soc. Jpn., 62, 3171—3176 (1989)

Crystal Structure and Photochemical Behavior of 2,2,4,6-Tetraphenyldihydro-1,3,5-triazine and Its Inclusion Compounds

Yukie MORI, Yuji OHASHI, and Koko MAEDA*
Department of Chemistry, Faculty of Science, Ochanomizu University, Bunkyo-ku, Tokyo 112
(Received February 14, 1989)

Crystal structures of 2,2,4,6-tetraphenyldihydro-1,3,5-triazine (**1**), which shows photocoloration, and its photostable propylamine solvate (**2**) have been determined. The molecular structure of the dihydrotriazine in **1** and **2** showed that it exists in 2,3-dihydro form in the crystals, but the bond distance of N(3)-C(4) was shorter than a normal C-N single bond, indicating that lone-pair electrons on N(3) interact with the π system of C(4)=N(5)-C(6)=N(1). Comparison of crystal structures of **1**, **2**, and other inclusion compounds previously determined revealed that the difference in the photochemical behavior of the crystals is attributable to different hydrogen bonding schemes. Photolysis of **1** in the solid state, which was carried out in connection with the structural investigation of the photocolored species, gave 2,4,6-triphenyl-1,3,5-triazine as a main product.

2,2,4,6-Tetraphenyldihydro-1,3,5-triazine (abbreviated as TPDT) was reported to exhibit photochromism in the solid state by Lottermoser in 1896,[1] but the structure of the colored species is still undetermined. The photochromism is not observed in solutions around room temperature. In 1985 one of the authors revealed that TPDT exists in an equilibrium mixture

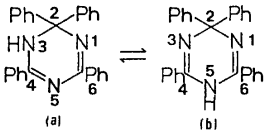

of 2,3-dihydro (a) and 2,5-dihydro (b) forms and the preferred tautomeric form is 2,3-dihydro (a) form both in solutions and in the solid state.[2] Recently we found that TPDT forms 1 : 1 inclusion compounds with various solvent molecules on recrystallization and the inclusion compounds can be classified into two types in terms of their photochemical coloration, that is, photolabile and photostable crystals. In the previous papers[3,4] the crystal structures of photostable ethanol solvate (**3**), 2-propanol solvate (**4**), and photolabile acetone solvate (**5**) were determined and the hydrogen bond between the hydroxyl hydrogen in the solvent molecules and ring nitrogen in TPDT was shown to inhibit the photocoloration. These facts suggested that hydrogen-donating solvents in the inclusion compounds of TPDT inhibit the photocoloration and hydrogen-accepting solvents do not affect the photocoloration. In order to confirm this assumption we have determined the crystal structures of TPDT with no inclusion solvent (**1**), which was recrystallized from toluene-hexane, and its propylamine solvate (**2**) including a different kind of hydrogen-donating solvent from **3** and **4**. Although the red color obtained after irradiation of colorless crystals of **1** gradually faded apparently in the dark, after repeated irradiations and fading processes, TPDT was found to undergo photochemical reactions.

Experimental

Apparatus. Absorption spectra were obtained on a Shimadzu UV-240 spectrophotometer. IR spectra were recorded on a JASCO A-302 IR spectrometer and difference IR spectra were obtained by using a JASCO DP-A330 IR data processor. FT-IR spectra for the reflection method were obtained by a JASCO FT-IR 7000 spectrophotometer. The PA spectrum was measured by Professor Sugitani, University of Tsukuba. The light source was a 500 W xenon lamp (WACOM XD501S), and the light beam was modulated at a frequency of 18 Hz by a chopper. A Nicon P250 spectrometer was used. The output of the microphone was amplified by means of a lock-in amplifier (NF LI-574) and the data were treated with a HP 9816 computer. The correction was carried out by using a PA spectrum of carbon black.

Photolysis of TPDT in the Solid State. The photolysis of **1** or **3** in the solid state was carried out in a KBr pellet [2%(w/w)]. A 100 W high-pressure mercury lamp (Ushio UI-100) was used for the irradiation at room temperature. The progress of the reaction was monitored by difference IR spectra.

General Procedure of Photolysis for Isolation of the Photoproducts in Solutions. All the reactions were performed on solutions (150 cm^3) irradiated by a 400 W high-pressure mercury lamp from outside of a vessel at room temperature under nitrogen. The reactions were monitored by TLC to

Table 1. Crystal Data and Some Experimental Conditions

	1	**2**
Formula	$C_{27}H_{21}N_3$	$C_{27}H_{21}N_3 \cdot C_3H_9N$
F. W.	387.4	446.5
Crystal size /mm	0.5×0.3×0.15	0.3×0.25×0.25
Crystal system	Monoclinic	Monoclinic
Space group	$P2_1/c$	$P2_1/a$
a/Å	12.849(2)	17.164(3)
b/Å	12.783(1)	14.343(2)
c/Å	12.621(1)	10.623(3)
β/°	95.28(1)	98.26(2)
V/Å^3	2064.2(4)	2588.1(9)
Z	4	4
D_x/g cm^{-3}	1.246	1.146
μ/cm^{-1}	4.98	4.58
$F(000)$	816	952
T/K	293	293
$2\theta_{max}$/°	125.0	125.0
scan speed/° min^{-1}	8(2θ)	8(2θ)
scan width/°	1.0+0.15 tan θ	0.8+0.15 tan θ

control the irradiation time. After irradiation was stopped, the solvent was removed under reduced pressure and the resulted residue was chromatographed on a silica gel column with benzene-ethanol as eluent.

Crystal Structure Determination. Colorless plate-like crystals of **1** and **2** were obtained by recrystallization of TPDT from toluene-hexane and propylamine-hexane, respectively. A crystal of **2**, which easily lost the solvent molecule, was sealed in a glass capillary. Cell parameters were refined by least-squares on the basis of 21 and 20 independent 2θ values for **1** and **2**, respectively. Crystal data and some experimental conditions are listed in Table 1. Intensities were measured on a Rigaku AFC-4 diffractometer with graphite-monochromated Cu$K\alpha$ radiation up to $2\theta=125°$, using the ω-2θ scan technique. Background counts were accumulated for 5s before and after each scan. Three standard reflections were monitored for every 50 reflections and no significant variations in intensities were observed. Corrections for the Lorentz and polarization factors were made, but no correction for absorption was applied.

The structure of **1** was solved by the direct method with the program MULTAN 78[5] and refined by the full-matrix least squares with the program SHELX 76.[6] All the hydrogen atoms were found on the difference map. The final refinement was made with the anisotropic temperature factors for non-hydrogen atoms and the isotropic ones for hydrogen atoms. The quantity minimized was $\sum w(|F_o|-|F_c|)^2$ and $w=[\sigma^2(|F_o|)+0.00654\,|F_o|^2]^{-1}$. The final R and R_w values became 0.063 and 0.080 for 2731 observed reflections. No peaks higher than 0.2 e Å^{-3} were found on the final difference map.

The procedure of the structure determination for **2** was similar to that for **1**. The intense reflections with a low 2θ angle (110, 120, and 111) were removed since their F_o values seemed to suffer from extinction. Some of hydrogen atoms were found on the difference map. The others were calculated geometrically and included in further refinements. The atoms of propylamine molecule were disordered between three sets of positions and were refined under the constrained conditions with the usual geometry (C-N 1.47, C-C 1.54 Å, N-C-C 110, C-C-C 109°). The occupancy factors were fixed to 0.33333 for each set, considering from the temperature factors of the disordered atoms. The final refinement was made with the anisotropic temperature factors for non-hydrogen atoms of TPDT molecule and the isotropic ones for hydrogen atoms and the atoms of propylamine. The weighting scheme was $w=[\sigma^2(|F_o|)+0.0097\,|F_o|^2]^{-1}$. The final R and R_w values became 0.095 and 0.117 for 2957 observed reflections. Considerably high R values may be due to the disordered structure of the solvent molecule. No peaks higher than 0.25 e Å^{-3} were found on the final difference map. The atomic scattering factors were taken from the International Tables for X-ray Crystallography.[7] The computation was carried out on HITAC M-680 computer at the Computer Center of the University of Tokyo.

Results and Discussion

Absorption and Photoacoustic (PA) Spectra of the Colored Species of 1. The crystals of **1** and its inclusion compounds showed no absorption longer than 430 nm in the dark. After irradiation for a few minutes, the color of **1**, **5**, and chloroform solvate turned red. The absorption spectrum of **1** obtained by an opal-glass transmission method after irradiation is shown in Fig. 1(a). The absorption spectrum of the crystals of **5** obtained by irradiation in a KBr pellet is shown in Fig. 1(b). Irradiation of the chloroform solvate gave a spectrum similar to that of **5**. The absorption maxima around 510 and 730 nm for the colored species from **1** are considered to be shifted to slightly longer and shorter wavelengths, respectively, by inclusion of solvent molecules.

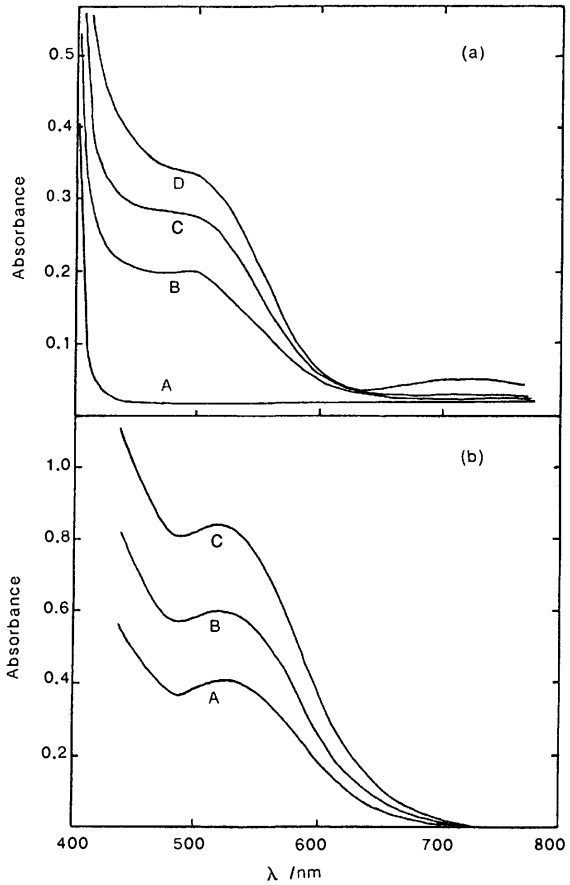

Fig. 1. Variation of absorption spectrum after repeated irradiations. (a) crystal of **1** measured by an opal-glass transmission method (A: before irradiation, B: 1 min, C: 3 min, D: 20 min) (b) acetone solvate (**5**) in a KBr pellet (A: 1 min, B: 4 min, C: 20 min).

The PA spectrum of **1** after 20 min irradiation showed a broad band around 510 nm and a weaker band around 690 nm. The PA spectrum was similar to the absorption spectrum of **1** obtained after 20 min irradiation shown in Fig. 1(a).

Photochemical Reactions of TPDT. Any recognizable differences between IR spectra of colorless and colored crystals of **1** were not obtained under short-time irradiation. After 2 h irradiation, although the red color still remained, a difference IR spectrum showed a number of new bands indicating occurrence

of photochemical reactions. In order to identify the photoproducts, preparative photolysis of **1** was carried out in solutions of benzene or chloroform. On the photolysis of **1** (150 mg) in benzene, the irradiation was stopped after 5 h even **1** still remained, because much longer irradiation afforded dark oily products. In the reaction mixture six products were detected by TLC besides unreacted **1**. Chromatographically two products, 2,4,6-triphenyl-1,3,5-triazine **6** (3 mg) and 2,4,5-triphenylimidazole **7** (5 mg) were isolated and 69 mg of **1** was recovered. Irradiation of **1** in chloroform gave a similar result. After **1** was almost consumed **6** and **7** were isolated in very low yields with a larger amount of dark oily products.

The bands appeared at 1520, 1370, 759, and 690 cm^{-1} in the difference IR spectrum between before and after irradiation of **1** were compared with both of the IR spectrum of the photoproducts **6** and **7**. The bands coinciding with that of **6** indicated the formation of **6** under the solid state photolysis. Although bands assignable to **7** were not found in the difference IR spectrum, after the extraction of the irradiated pellet with benzene **7** was detected by TLC.

In order to obtain the relationship between photocoloration and photoreaction products in the solid state, photolysis of **3** was also carried out. Neither photocoloration nor recognizable differences between IR spectra before and after irradiation (5 h) were found. By extraction of the irradiated pellet with benzene, however, **7** was detected by TLC. The facts indicated that the two types of hydrogen bonds[3] in **3** inhibit both of photocoloration and photoformation of **6**. In connection with the photolysis in the solid state an ethanol solution of **1** (56 mg) was irradiated until **1** was almost consumed. Only one product **7** was detected by TLC and 8 mg of **7** was isolated.

Previously one of the authors reported that irradiation of 2,4,4,6-tetraphenyl-1,4-dihydropyridine (**8**) exhibits photocoloration in deaerated solutions or in the solid state and after a long-time irradiation in solutions 2,3,4,6-tetraphenylpyridine (**10**) was produced. As is shown in Scheme 1 a di-π-methane rearrangement to give 1,3,5,6-tetraphenyl-2-azabicyclo-[3.1.0]hex-3-ene (**9**) has been suggested as the unisolable intermediate.[8]

TPDT has aza-di-π-methane moiety in the molecule, and on the photolysis of **1** occurrence of an aza-di-π-methane rearrangement to give a bicyclic intermediate, 1,3,5,6-tetraphenyl-2,4,6-triazabicyclo[3.1.0]hex-3-ene (**13**), similar to **9** is assumed. Presently carbonyl

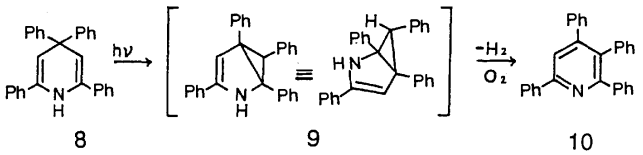

Scheme 1.[8]

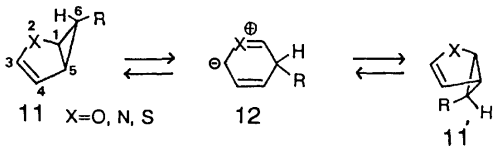

Scheme 2.[10]

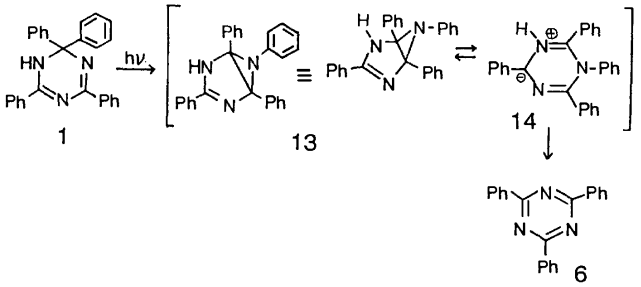

Scheme 3.

ylides and azomethine ylides which are the ring-opening products of oxetane and aziridine, respectively, are attracting considerable interest.[9] Furthermore the 1,5-electrocyclic ring-opening reactions of the bicyclic heterocycles such as homofuran, homopyrrole, and homothiophene are shown to lead to ylide intermediates **12**[10] as is shown in Scheme 2. Photochromic reactions involving these types of ylides or zwitter ions as the colored species have been also reported.[11] As is shown in Scheme 3 as one of the possible candidates of the photocolored species an azomethine ylide type intermediate **14** is postulated, which is formed from **13** by cleavage of the central bond C^1-C^5 in aziridine, as required for the electrocyclic process. IR spectrum of TPDT exhibits two C=N stretching bands at 1610 and 1680 cm^{-1} assignable to 2,3-dihydro- and 2,5-dihydro forms of the dihydrotriazine ring respectively.[2] As the bicyclic intermediate **13** containing an imidazoline ring is produced successfully, appearance of another C=N stretching band around 1650 cm^{-1} is postulated.[12] The difference FT-IR spectrum obtained by the reflection method between before and after irradiation of fine crystals of **1** exhibited a weak band at 1655 cm^{-1}, as it was expected, besides the two characteristic C=N stretching bands in TPDT. This observation supports partially the reaction course shown in Scheme 3. Furthermore, broad bands appeared in the FT-IR spectrum on the range of 2400—3300 cm^{-1} obtained after irradiation suggested involvement of **14** in the photocoloration. It is reasonable to consider that the back reaction from **13** to **1** is not possible and the photochemical color change of **1** is not reversible. Conversion of the colored intermediate **14** into **6** stabilized by its resonance energy is postulated (Scheme 3). The formation of trace amount of **7** can be explained by cleavage of one of the peripheral aziridine bonds C^1-N^6 or C^5-N^6 in **13** followed by intramolecular nucleophilic addition of the nitrogen lone pair to the heterodiene system as is shown in Scheme 4.

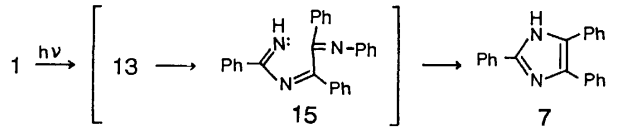

Scheme 4.

Table 2. Final Atomic Coordinates ($\times 10^4$) and Equivalent Thermal Parameters[a] for Non-Hydrogen Atoms of **1**

Atom	x	y	z	B_{eq}/Å^2
N(1)	1802(2)	1547(2)	11724(2)	4.5
C(2)	1819(2)	2418(2)	10969(2)	4.1
N(3)	2620(2)	2212(2)	10238(2)	4.3
C(4)	3532(2)	1779(2)	10627(2)	3.5
N(5)	3629(2)	1319(2)	11559(2)	4.1
C(6)	2695(2)	1121(2)	11994(2)	3.7
C(7)	2746(2)	285(2)	12817(2)	4.1
C(8)	3697(3)	−15(3)	13338(2)	5.4
C(9)	3728(4)	−810(3)	14087(3)	6.8
C(10)	2827(4)	−1321(3)	14294(3)	7.3
C(11)	1895(4)	−1043(3)	13774(3)	6.4
C(12)	1840(3)	−231(2)	13044(2)	5.1
C(13)	4411(2)	1772(2)	9954(2)	3.5
C(14)	4368(2)	2284(3)	8977(2)	4.8
C(15)	5191(3)	2240(3)	8357(3)	5.5
C(16)	6068(2)	1682(3)	8688(3)	4.8
C(17)	6132(2)	1174(2)	9650(3)	4.9
C(18)	5313(2)	1220(2)	10280(2)	4.4
C(19)	782(2)	2482(2)	10275(2)	4.3
C(20)	569(2)	3355(3)	9647(3)	5.2
C(21)	−326(3)	3390(3)	8937(3)	6.4
C(22)	−1004(3)	2559(3)	8864(3)	6.2
C(23)	−804(3)	1702(3)	9488(3)	6.4
C(24)	86(2)	1652(3)	10193(3)	5.3
C(25)	2042(2)	3429(2)	11604(2)	4.2
C(26)	2793(3)	4139(3)	11376(3)	5.6
C(27)	2966(3)	5039(3)	11953(3)	6.7
C(28)	2379(3)	5242(3)	12801(3)	7.1
C(29)	1616(3)	4544(3)	13040(3)	6.4
C(30)	1446(3)	3649(3)	12447(3)	5.3

a) $B_{eq}=\frac{4}{3}\sum_i\sum_j B_{ij}a_ia_j$.

On the photolysis of **3**, in which TPDT molecule connected with solvent molecules alternatively to form a helix structure by two types of hydrogen bonds at N(3)-H and N(5),[3] even if the aza-di-π-methane rearrangement should give the bicyclic intermediate **13** successfully, the following ring-opening process to give **14** should be prohibited by the helical structure. Only small amount of **13** probably transforms into **7** in the same fashion shown in Scheme 4.

Molecular and Crystal Structures. The final atomic coordinates and equivalent isotropic temperature factors for non-hydrogen atoms in **1** and **2** are given in Tables 2 and 3 respectively.** Selected bond distan-

** The lists of the anisotropic temperature factors for non-hydrogen atoms, atomic coordinates and temperature factors for hydrogen atoms, and the observed and calculated structure factors are kept in the Office of the Chemical Society of Japan (Document No. 8899).

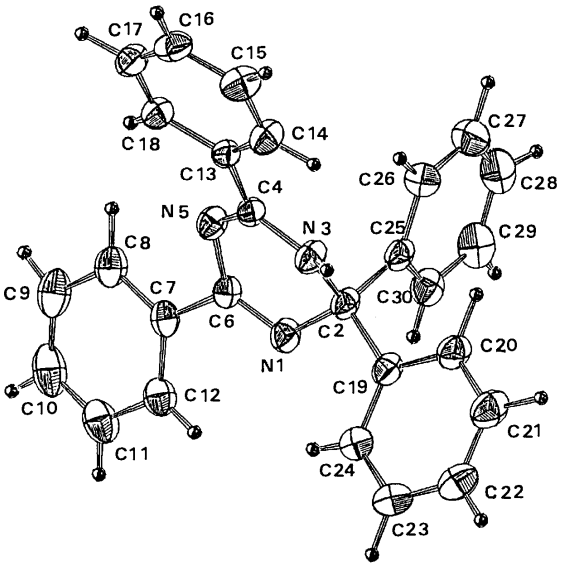

Fig. 2. ORTEP[13] plot of TPDT molecule in **1** with the atom-numbering. The anisotropic ellipsoids for non-hydrogen atoms enclose 30% probability.

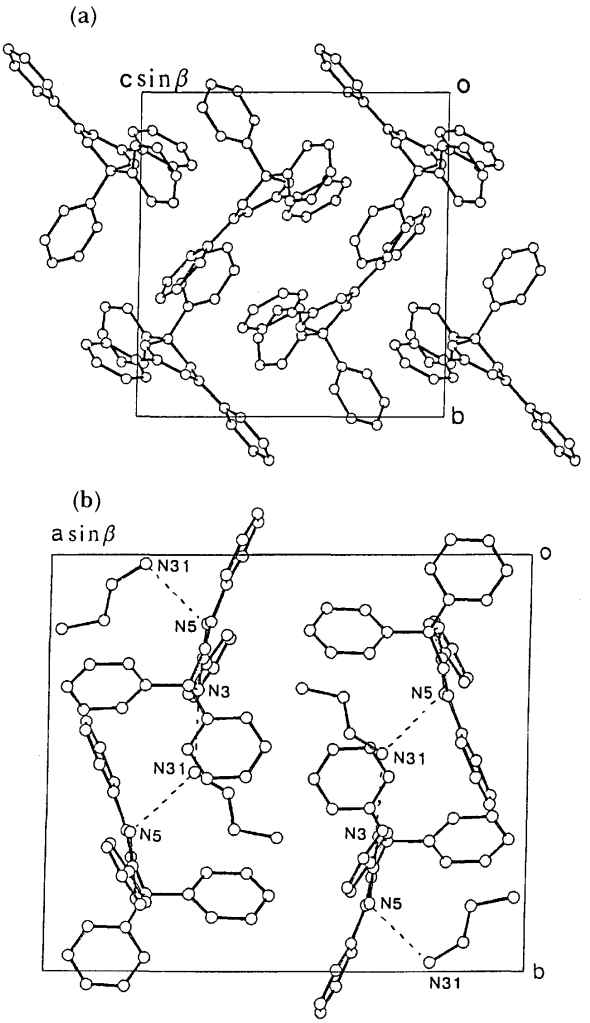

Fig. 3. Crystal structures of **1** and **2**. (a) Viewed along the a axis of **1**. (b) Viewed along the c axis of **2**. The atoms of the solvent molecules with prime or double prime are suppressed for clarity.

Table 3. Final Atomic Coordinates ($\times 10^4$) and Equivalent Thermal Parameters[a] for Non-Hydrogen Atoms of Propylamine Solvate (**5**)[b]

Atom	x	y	z	B[c] or B_{eq}/Å^2	Atom	x	y	z	B[c] or B_{eq}/Å^2
N(1)	1780(2)	2737(2)	12616(3)	4.1	C(22)	4632(3)	1829(4)	13291(5)	6.4
C(2)	2107(2)	1861(3)	12216(3)	4.0	C(23)	4172(3)	2355(4)	13956(5)	6.8
N(3)	1906(2)	1755(2)	10820(3)	4.1	C(24)	3351(3)	2374(3)	13600(4)	5.3
C(4)	1819(2)	2506(3)	10090(3)	4.0	C(25)	1706(3)	1068(3)	12840(3)	4.6
N(5)	1752(2)	3349(2)	10518(3)	4.5	C(26)	2102(3)	331(4)	13456(6)	8.1
C(6)	1676(2)	3390(3)	11798(3)	3.7	C(27)	1693(5)	−362(5)	14001(9)	11.5
C(7)	1376(2)	4308(3)	12192(4)	4.2	C(28)	904(5)	−326(6)	13942(7)	9.7
C(8)	1067(3)	4960(3)	11308(4)	5.7	C(29)	512(4)	385(5)	13360(6)	8.3
C(9)	763(4)	5785(4)	11665(6)	7.8	C(30)	910(3)	1087(4)	12811(4)	5.9
C(10)	777(4)	5991(4)	12922(6)	7.9	N(31)	8047(6)	222(7)	−167(9)	5.1(2)
C(11)	1076(3)	5359(4)	13814(5)	7.1	C(32)	8749(10)	708(14)	524(16)	10.9(6)
C(12)	1387(3)	4528(3)	13468(4)	5.4	C(33)	8893(10)	1580(14)	−254(25)	15.9(9)
C(13)	1749(3)	2385(3)	8674(4)	4.8	C(34)	9772(9)	1786(12)	−204(16)	8.4(4)
C(14)	2105(4)	1665(4)	8130(5)	7.8	N(31′)	8096(7)	375(9)	−498(12)	7.0(3)
C(15)	2001(5)	1608(6)	6777(5)	10.9	C(32′)	8722(12)	583(13)	593(17)	14.4(8)
C(16)	1604(4)	2280(6)	6043(5)	9.3	C(33′)	9038(8)	1576(9)	424(13)	6.4(3)
C(17)	1274(4)	2978(5)	6589(4)	8.3	C(34′)	9415(18)	1573(19)	−816(21)	16.0(9)
C(18)	1341(3)	3066(4)	7898(4)	6.4	N(31″)	8214(7)	153(9)	462(12)	7.4(3)
C(19)	2996(2)	1863(3)	12578(3)	4.0	C(32″)	8806(8)	545(10)	−272(13)	7.1(3)
C(20)	3476(3)	1320(4)	11942(5)	6.4	C(33″)	9138(18)	1500(15)	135(27)	19.1(12)
C(21)	4288(3)	1281(5)	12308(6)	7.6	C(34″)	9740(11)	1737(12)	−781(18)	9.2(5)

a) $B_{eq}=\frac{4}{3}\sum_i\sum_j B_{ij}a_ia_j$. b) All the occupancy factors for the three propylamine molecules, N(31)-C(34), N(31′)-C(34′) and N(31″)-C(34″), are fixed to be 0.33333. c) For the atoms of propylamine isotropic temperature factors are listed instead of B_{eq}.

Table 4. Selected Bond Distances (l/Å) and Angles (ϕ/°) for **1**—**5**

	1	**2**	**3**[a]	**4**[b]	**5**[b]
N(1)-C(2)	1.466(4)	1.464(5)	1.465(3)	1.453(4)	1.460(4)
C(2)-N(3)	1.468(4)	1.481(5)	1.481(3)	1.488(4)	1.474(4)
N(3)-C(4)	1.346(3)	1.323(5)	1.336(3)	1.327(4)	1.329(4)
C(4)-N(5)	1.311(3)	1.303(5)	1.312(3)	1.314(4)	1.299(4)
N(5)-C(6)	1.389(3)	1.386(5)	1.396(3)	1.387(4)	1.393(4)
C(6)-N(1)	1.287(3)	1.273(5)	1.278(3)	1.282(4)	1.274(4)
C(2)-C(19)	1.529(4)	1.519(6)	1.537(4)	1.530(5)	1.535(4)
C(2)-C(25)	1.535(4)	1.529(6)	1.527(4)	1.540(5)	1.544(4)
C(4)-C(13)	1.475(3)	1.501(6)	1.490(4)	1.486(4)	1.489(4)
C(6)-C(7)	1.488(4)	1.495(5)	1.490(4)	1.489(5)	1.493(4)
N(1)-C(2)-N(3)	109.1(2)	109.6(3)	109.2(2)	110.1(2)	110.4(2)
C(2)-N(3)-C(4)	118.7(2)	119.6(3)	119.5(2)	119.4(3)	121.6(3)
N(3)-C(4)-N(5)	121.3(2)	124.0(4)	122.0(2)	123.1(3)	123.0(3)
C(4)-N(5)-C(6)	114.9(2)	114.1(1)	114.6(2)	115.0(3)	114.9(2)
N(5)-C(6)-N(1)	126.9(2)	128.0(4)	127.2(2)	126.4(3)	127.7(3)
C(6)-N(1)-C(2)	115.2(2)	117.1(3)	116.2(2)	117.9(3)	117.8(2)

a) Ref. 3. b) Ref. 4.

ces and angles of **1** and **2** are listed in Table 4, together with those of **3**, **4**, and **5**, and some torsion angles and dihedral angles are in Table 5. Figure 2 shows the molecular structure of TPDT with the atom numbering in the crystal of **1**. For **2** the same numbering scheme is used. The molecular structure of TPDT in **1** and **2** is similar to that in **3**, **4**, or **5**. During the refinements the difference maps showed that a hydrogen atom is bound to N(3), not N(5), that is, TPDT exists in 2,3-dihydro (a) form in both **1** and **2**, as it does in **3**, **4**, or **5**. However, the differences between N(3)-C(4) and C(4)-N(5) were found to be rather small in both **1** and **2**, as was reported for the other three inclusion compounds.[3,4] The bond distance of N(3)-C(4) for the five crystals **1**—**5** (1.323—1.346 Å) is similar to a typical C-N distance of six-membered N-containing aromatic rings. The sums of bond angles around N(3) are 359 and 360° for **1** and **2** respectively, that is, N(3) is planar rather than pyramidal. These results suggest that lone pair electrons on N(3) is effectively conjugated with the π system of C(4)=N(5)-C(6)=N(1). Further inspection of Table 4 reveals that

Table 5. Some Torsion Angles (ϕ/°) and Dihedral Angles (ϕ/°)[a] for **1** and **2**

	1	**2**
N(3)-C(4)-C(13)-C(14)	6.4(4)	−30.2(7)
N(5)-C(6)-C(7)-C(8)	19.8(4)	11.9(6)
N(3)-C(4)-N(5)-C(6)	13.0(3)	−8.0(6)
C(4)-N(5)-C(6)-N(1)	−18.0(4)	11.3(6)
N(5)-C(6)-N(1)-C(2)	−7.8(4)	7.9(6)
[1][a]	53.7(1)	77.4(2)
[2][a]	86.5(1)	78.9(2)
[3][a]	32.2(3)	24.8(4)
[4][a]	12.7(3)	7.7(4)

a) [1]: the dihedral angle between the least-squares plane of N(1), N(3), C(4), and N(6) (plane A) and the least-squares plane of C(19)-C(24). [2]: the dihedral angle between plane A and the least-squares plane of C(25)-C(30). [3]: the dihedral angle between plane A and the plane of N(1), C(2), and N(3). [4]: the dihedral angle between plane A and the plane of C(4), N(5), and C(6).

the bond distance of N(3)-C(4) in **2** is shorter than that in **1**. The corresponding bond distance in **3**, **4**, or **5** is also slightly shorter than that in **1**, suggesting that the hydrogen bond involving N(3) has an effect on N(3)-C(4) bond. The shortening of N(3)-C(4) tends to enlarge N(3)-C(4)-N(5) bond angle in **2**—**5**. The bond distance of C(4)-C(13) in **2** is larger than that in **1**, which may also result from the shortening of N(3)-C(4). No other significant differences in bond distances or angles were observed for the five crystals **1**—**5**. The dihydrotriazine ring in **1** and **2** was found to exist in the boat conformation with the apexes of C(2) and N(5) as was reported in **3**, **4**, or **5**. The torsion angles of N(3)-C(4)-N(5)-C(6) and C(4)-N(5)-C(6)-N(1) in **2** are smaller than the corresponding angles in **1** respectively, indicating that the N(3)-C(4)-N(5)-C(6)-N(1) system in **2** is more planar than that in **1**. The torsion angles of N(5)-C(6)-C(7)-C(8) and N(3)-C(4)-C(13)-C(14) and the dihedral angles between the plane composed of N(1), N(3), C(4), and C(6) and that composed of the phenyl ring C(19)-C(24) or that composed of the ring C(25)-C(30) in **1** and **2** are similar to the corresponding angles in **3**, **4**, or **5**: the two phenyl rings at 4- and 6-positions are nearly coplanar with the dihydrotriazine ring, while the two at 2-position are almost perpendicular to it.

Figure 3 shows the crystal structures of **1** and **2**. In **2** the nitrogen atom of the propylamine is involved in two types of hydrogen bond: N(3)-H(3)···N(31) and N(5)···H-N(31). The distances of N(3)···N(31), N(3)···N(31′), and N(3)···N(31″) are 2.92(1), 3.07(1), and 3.05(1) Å respectively. The distances of N(5)···N(31) [3.18(1) Å], N(5)···N(31′) [3.25(1) Å], and N(5)···N-(31″)[3.31(1) Å] are slightly longer. By these hydrogen bonds TPDT and the solvent molecules are alternately connected to form a ribbon-like structure along the two-fold screw axis, as is shown in Fig. 3(b). This hydrogen bonding scheme was also seen in **3** and **4**, where oxygen atoms of the solvent molecules were involved in the hydrogen bonds. No other short contacts were found between TPDT and the solvent molecules in **2**, which seemed to allow the solvent molecules to take a disordered structure. In **1** there are no unusually short contacts. Thus, comparison of crystal structures of **1**—**5** revealed that the hydrogen bonding scheme constructing the ribbon-like structure is characteristic of **2**, **3**, and **4**, which are photostable. On the other hand in **1** and **5**, which exhibit photocoloration, each TPDT molecule is isolated. It is, therefore, confirmed that the hydrogen bonds observed in **2**, **3**, and **4** inhibit the photocoloration of the crystals.

We thank Professor Yoshinori Sugutani, University of Tsukuba, for the measurement of PA spectrum. We thank Dr. Keiko Takano, Ochanomizu University, for her valuable discussion. This work was supported by a Grant-in-Aid for Scientific Research from Ministry of Education, Science and Culture (No. 63628505).

References

1) A. Lottermoser, *J. Prakt. Chem.*, **54**, 113 (1896).
2) K. Maeda, N. Kihara, and N. Ishimura, *J. Chem. Soc., Perkin Trans. 2*, **1985**, 887.
3) Y. Mori, Y. Ohashi, and K. Maeda, *Acta Crystallogr., Sect. C*, **44**, 704 (1988).
4) Y. Mori, Y. Ohashi, and K. Maeda, *Bull. Chem. Soc. Jpn.*, **61**, 2487 (1988).
5) P. Main, S. E. Hull, L. Lessinger, G. Germain, J.-P. Declercq, and M. M. Woolfson, MULTAN78. A System of Computer Programs for the Automatic Solution of Crystal Structures from X-ray Diffraction Data. Univs. of York, England, and Louvain, Belgium (1978).
6) G. M. Sheldrick, SHELX76. Program for Crystal Structure Determination. Univ. of Cambridge, England (1976).
7) "International Tables for X-Ray Crystallography," Kynoch Press, Birmingham, Vol. IV (1974).
8) J. Shibuya, M. Nabeshima, H. Nagano, and K. Maeda, *J. Chem. Soc., Perkin Trans. 2*, **1988**, 1607.
9) a) R. Huisgen, *Angew. Chem., Int. Ed. Engl.*, **16**, 572 (1977); b) F. Volatron, N. T. Ank, and Y. Jean, *J. Am. Chem. Soc.*, **105**, 2359 (1983); c) D. Feller, E. R. Davidson, and W. T. Borden, *ibid.*, **106**, 2513 (1984) and references cited therein.
10) F. G. Klärner and D. Schroer, *Angew. Chem., Int. Ed. Engl.*, **26**, 1294 (1987).
11) A. M. Trozzolo, T. M. Leslie, A. S. Sarpotdar, R. D. Small, and G. J. Ferraudi, *Pure Appl. Chem.*, **51**, 261 (1979) and references cited therein.
12) D. Dolphin and A. Wick, "Tabulation of Infrared Spectral Data," J. Wiley and Sons, New York (1977), pp.116—122, Imines and Iminium Salts.
13) C. K. Johnson, ORTEP, Report ORNL-3794, Oak Ridge National Laboratory, Tennessee (1965).

 © 1989 The Chemical Society of Japan Bull. Chem. Soc. Jpn., 62, 3177—3181 (1989)

Preparation of Optically Active 1-Aminoalkylphosphonic Acids from Chiral Carbamates and Chiral Ureas

Tatsuo OSHIKAWA* and Mitsuji YAMASHITA
Department of Applied Chemistry, Faculty of Engineering, Shizuoka University, Hamamatsu 432
(Received February 15, 1989)

Optically active 1-aminoalkylphosphonic acids were successfully synthesized from chiral carbamate and urea derivatives which were prepared from such chiral substrates as (−)-menthol, (+)-camphor, and (*R*)-(+)- and (*S*)-(−)-(1-phenylethyl)ureas by the actions of aldehydes and triaryl phosphites. 1-Aminoalkylphosphonic acid derivatives, thus prepared, have an (*R*)-(+)- or (*S*)-(−)-configuration, depending on the chiral source via a retention of the configuration; i.e., (+)-products were prepared from chiral (+)-carbamate and (+)-urea derivatives, and (−)-products from chiral (−)-carbamate and (−)-urea derivatives.

Phosphonodipeptides and phosphonotripeptides possess inhibitory biological activities. Especially, 1-aminoethylphosphonic acid is a well-known substance which inhibits the growth of bacteria by interfering with the biosynthesis of peptidoglycan of the bacteria cell walls.[1]

In general, 1-aminoalkylphosphonic acids were derived by several synthetic methods; addition reactions of Schiff bases with dialkyl phosphonates,[2] Mitsunobu reactions of 1-hydroxyalkylphosphonates with phthalimides,[3] condensation of hydrazines with phosphonoacetic esters,[4] catalytic reduction of dimethylhydrazones of 1-oxoalkylphosphonates,[5] reduction of *t*-butyl diazo(diethoxyphosphoryl)acetate,[6] hydrolyses of diethyl 1-(formylamino)alkylphosphonates,[7] and alkylation of 1-(ethoxycarbonylamino)-1-(ethylthio)methylphosphonate.[8] However, only racemic products were afforded by these reported methods. Optically active 1-aminoalkylphosphonic acids have so far been obtained by the optical resolution of racemic 1-aminoalkylphosphonic acids prepared by peptide synthesis.[1] Successful methods known for the asymmetric syntheses of 1-aminoalkylphosphonic acids are enantioselective addition reactions of dialkyl phosphonates with chiral Shiff bases[9,10] and a reaction of chiral (1-phenylethyl)urea with aldehydes and triethyl phosphite.[11] We now wish to report on the useful application of (−)-menthyl carbamate (**1**), 1,7,7-trimethylspiro[bicyclo[2.2.1]heptane-3,2′-indan]-2-yl carbamate (**2**), and (*R*)-(+)- and (*S*)-(+)-(1-phenylethyl)ureas (**3a** and **3b**) to the asymmetric synthesis of 1-aminoalkylphosphonic acids (**7a—d**) according to Oleksyszyn's methods.[12,13] In a previously published paper[11] no definite reaction mechanism for the formation of optically active 1-aminoalkylphosphonic acids from chiral ureas was discussed; therefore, the present paper deals with the further investigation concerning the reaction mechanism for the formation of chiral 1-aminoalkylphosphonic acids starting from both chiral carbamates and ureas.

Results and Discussion

Chiral carbamates **1** and **2** were synthesized[14] from (−)-menthol and 1,7,7-trimethylspiro[bicyclo[2.2.1]-heptane-3,2′-indan]-2-ol,[15] respectively, in the presence of trifluoroacetic acid and sodium cyanate in benzene. Chiral ureas **3a** and **3b** were synthesized according to the reported method.[11] The reaction of aldehydes **4a—d** with (−)-menthyl carbamate **1** and triaryl phosphite **5** in acetic acid led to **6a—d**, which were hydrolyzed without isolation. Optically active 1-aminoalkylphosphonic acid derivatives **7a—d** given by this methods were levorotatory. (+)-Isomenthyl

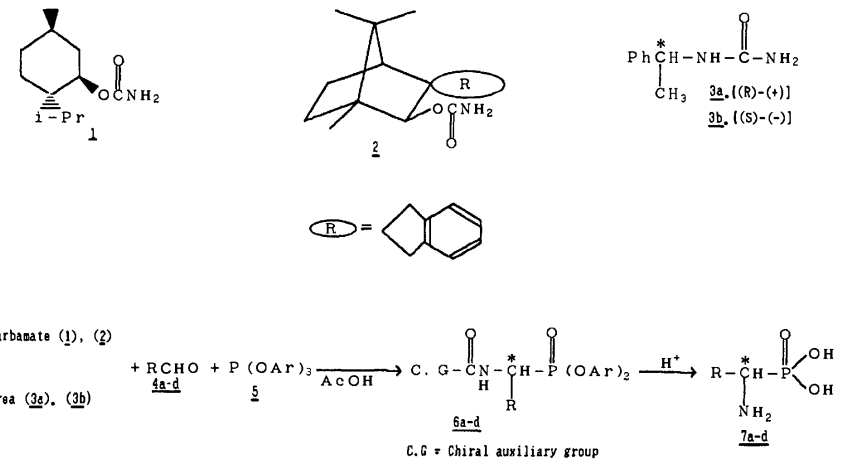

carbamate was then used as the chiral source of this reaction so as to clarify the stereoselectivity. (+)-Isomenthyl carbamate gave phosphonic acid with low optical activity (Table 1).

On the other hand, the reaction with chiral carbamate **2** led to dextrotatory 1-aminoalkylphosphonic acids **7**. Levorotatory 1-aminoalkylphosphonic acids are known to be an (*S*)-configuration, while dextrotatory enantiomers are (*R*)-configuration.[1,16] Therefore, 1-aminoalkylphosphonic acids prepared from (−)-menthyl carbamate (**1**) by the present method must be the (*S*)-enantiomer with a retention of the configuration. The stereoselectivity of 1-aminoalkylphosphonic acid produced by the reaction of (*R*)-(+)- and (*S*)-(−)-(1-phenylethyl)urea (**3a** and **3b**, respectively) led to the same conclusion obtained by a method described in the literature[11] where (*R*)-(+)-urea **3a** produced (*R*)-(+)-1-aminoalkylphosphonic acids and (*S*)-(−)-urea **3b** did (*S*)-(−)-1-aminoalkylphosphonic acids (Table 2). Two plausible reaction mechanisms (routes A and B in Scheme 1) may be proposed, based on the stereoselectivity observed in the present reaction, where (*R*)-(+)-urea **3a** and (*S*)-(−)-urea **3b**, afforded 1-aminoalkylphosphonic acid derivatives having (*R*)-(+)- and (*S*)-(−)-configurations, respectively.

Route A: phosphite attacks intermediate **8** in a similar way as that generated [urylenebis(methylene)]-bisphosphonate.[17] Route B: phosphite attacks enantioselectively the iminium ion.[18] In both routes, triaryl phosphite **5** attacks the carbon atom of aldehydes **4** after formation of carbon-nitrogen bond. In route A, optically active (*R*)-(+)- and (*S*)-(−)-(1-phenylethyl)ureas could attack either the *re* or *si* plane of aldehydes, while (*R*)-(+)-urea **3a** predominantly attacks the *si* plane of the aldehyde, leading to intermediate **8**. The intermediate is expected to be thermodynamically stable owing to hydrogen bonding to form a six-membered ring between the oxygen atom of the carbonyl group and the hydrogen atom of the

Table 1. Preparation of Optically Active 1-Aminoalkylphosphonic Acids **7** from (−)-Menthyl Carbamate (**1**), Aldehydes, and Phosphite **5**

$P(OAr)_3$, **5** Ar	**7a—d** R	1-Aminoalkylphosphonic acids **7a—d**					
		Mp/°C [lit][a]	C.Y./%	$[\alpha]_D^{17}$ observed	$[\alpha]_D$ lit[a]	O.Y./%	Configuration
Ph	**a** Ph	278—279 [278—279]	47	−7.6° (*c* 1.4, 1 M[b] NaOH)	−18°	42.2	(*S*)
				{−0.6° (*c* 1.0, 1 M NaOH)}[c]		(3.3)	(*S*)
Ph	**b** *i*-Pr	277—278 [277—278]	51	−3.6° (*c* 2.0 1 M NaOH)	−10°	36.0	(*S*)
				{racemic form}[c]		—	—
Ph	**c** CH_3	224—225 [223—224]	52	−1.4° (*c* 1.0, 1 M NaOH)	−16.9°	8.3	(*S*)
Ph	**d** CH_3CH_2	265—266 [264—266]	54	−2.6° (*c* 1.0, 1M NaOH)	—	—	(*S*)
o-Methylphenyl	**a** Ph	278—279	45	−5.7° (*c* 1.0, 1 M NaOH)	−18°	31.7	(*S*)
o-Methylphenyl	**b** *i*-Pr	277—278	49	−3.9° (*c* 1.3, 1 M NaOH)	−10°	39.0	(*S*)
o-Methylphenyl	**d** CH_3	224—225	50	−2.3° (*c* 1.0, 1 M NaOH)	−16.9°	13.6	(*S*)

a) Ref. 16. b) 1 M=1 mol dm^{-3}. c) (+)-Isomenthyl carbamate.

Table 2. Preparation of Optically Active 1-Aminoalkylphosphonic Acids **7a—d** from (*R*)-(+)- and (*S*)-(−)-(1-Phenylethyl)urea (**3a, b**), Aldehydes, and Phosphite **5**

Urea **3a, b** Configuration	$P(OAr)_3$, **5** Ar	**7**, R	1-Aminophosphonic acid **7a—d**			
			C.Y.(%)	$[\alpha]_D^{17}$ observed	O.Y.(%)	Configuration
3a (*R*)	Ph	**a** Ph	55	+6.2° (*c* 0.5, 1M NaOH)	34.3	(*R*)
3b (*S*)	Ph	Ph	56	−5.9° (*c* 1.7, 1M NaOH)	32.6	(*S*)
3a (*R*)	Ph	**b** *i*-Pr	60	+1.4° (*c* 1.0, 1M NaOH)	14.0	(*R*)
3b (*S*)	Ph	*i*-Pr	59	−1.3° (*c* 1.0, 1M NaOH)	13.0	(*S*)
3a (*R*)	Ph	**c** CH_3CH_2	65	+3.2° (*c* 1.2, 1M NaOH)	—	(*R*)
3b (*S*)	Ph	CH_3CH_2	65	−3.3° (*c* 1.1, 1M NaOH)	—	(*S*)
3a (*R*)	Ph	**d** CH_3	54	+1.4° (*c* 1.0, 1M NaOH)	8.3	(*R*)
3b (*S*)	Ph	CH_3	56	−1.5° (*c* 1.0, 1M NaOH)	8.9	(*S*)
3a (*R*)	*o*-Methylphenyl	**a** Ph	49	+5.6° (*c* 1.1, 1M NaOH)	30.8	(*R*)
3b (*S*)	*o*-Methylphenyl	Ph	48	−5.5° (*c* 1.0, 1M NaOH)	30.2	(*S*)
3a (*R*)	*o*-Methylphenyl	**d** CH_3	52	+2.3° (*c* 1.1, 1M NaOH)	13.6	(*R*)
3b (*S*)	*o*-Methylphenyl	CH_3	54	−2.2° (*c* 1.0, 1M NaOH)	13.0	(*S*)

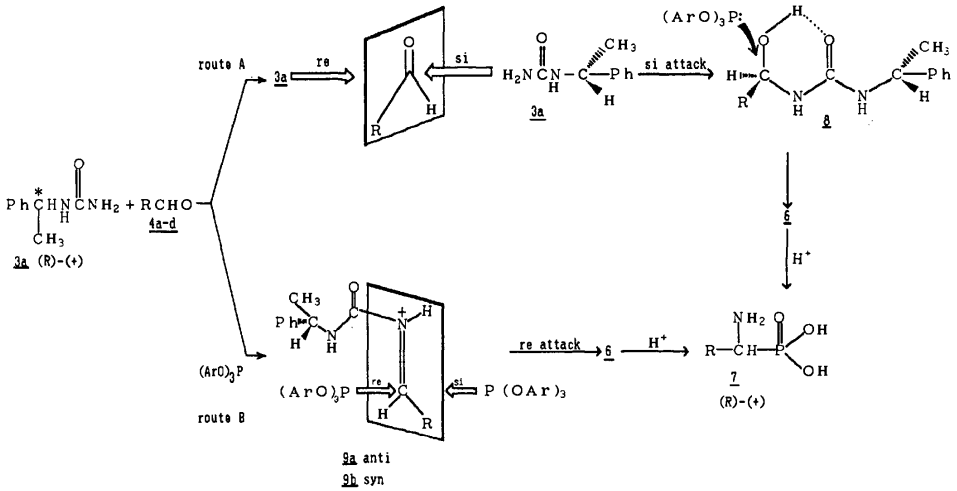

Scheme 1.

Table 3. Preparation of Optically Active 1-Aminoalkylphosphonic Acids **7** from Chiral Carbamate **2**

$P(OAr)_3$ Ar	Produced **7a, b** 7	R	1-Aminoalkylphosphonic acids **7a, b** C.Y.(%)	$[\alpha]_D^{17}$ observed	O.Y. (%)	Configuration
Ph	**a**	Ph	45	+4.6° (*c* 0.8, 1 M NaOH)	25.4	(*R*)
Ph	**b**	CH_3	51	+2.2° (*c* 1.0, 1 M NaOH)	13.0	(*R*)

Table 4. ^1H NMR Data of Optically Active 1-Aminoalkylphosphonic Acids **7a—d**

7a—d[a]	^1HNMR, δ (CF_3CO_2H, TMS)
a	3.11—3.75 (m, 1H, P-CH), 7.00 (s, 5H, Ph)
b	0.80 (s, 3H, CH_3), 0.92 (s, 3H, CH_3), 1.81—2.41 (m, 1H, CH), 2.85—3.59 (m, 1H, P-CH)
c	0.80 (t, J=8.0 Hz, 3H, CH_3), 1.45—2.12 (m, 2H, CH_2), 3.04—3.64 (m, 1H, P-CH)
d	1.39 (dd, J_{HH}=7.8 Hz, J_{PCH}=15.6 Hz, 3H, CH_3), 3.09—3.87 (m, 1H, P-CH)

a) Microanalyses agreed satisfactorily with the calculated values.

hydroxyl group (Scheme 1). An attack of triaryl phosphite on intermediary formed **8** should occur at the same side of the hydroxyl group, since the stereochemistry of the product was retained at the chiral center, i.e., dextrotatory 1-aminoalkylphosphonic acids were derived from (*R*)-(+)-urea **3a**, and levorotatory products from (*S*)-(−)-urea **3b**. Generally, it is known that chiral secondary alcohols add to the formed phosphonium salt at the rate-determining step in an Arbuzov reaction of triaryl phosphite with alkyl halide to produce inverted halides from the chiral alcohol.[19] Alternatively, in route B, the intermediate iminium ion **9** could exist as the syn and anti form, where the anti form **9a** is more stable than *syn*-**9b**. Therefore, triaryl phosphite may approach to *anti*-**9a** from the opposite side of the (*R*)-(+)-(1-phenylethyl) group, acting as the chiral source and, hence, the product should be optically active (*R*)-(+)-1-aminoalkylphosphonic acids. In fact, (*R*)-(+)-1-aminoalkylphosphonic acids were derived from (*R*)-(+)-urea **3a** and (*S*)-(−)-1-aminoalkylphosphonic acids from (*S*)-(−)-urea **3b**. Therefore, route B predominantly proceeds over route A in this reaction. The reaction mechanism via the iminium ion intermediate was further supported by the fact that the 1-aminoalkylphosphonic acids obtained from chiral carbamate **2** retained the (*R*)-configuration (see Table 3 and Scheme 2). If molecule **10** forms such an intermediate as **8**, forming a six-membered ring, **8** should offer such a severe steric hindrance that the chemical yield would be suppressed; however, no such low yield result was obtained. Furthermore, reaction of (−)-menthyl carbamate (**1**) afforded (*S*)-(−)-1-aminoalkylphosphonic acid by Cram's rule.

Tris(*o*-methylphenyl) phosphite showed little effect on the improvement of the optical yield in comparison with triphenyl phosphite, probably because of a remote chiral auxiliary from the reaction center. The optical yield was, nevertheless, improved by using tris(*o*-methylphenyl) phosphite in the case of 1-

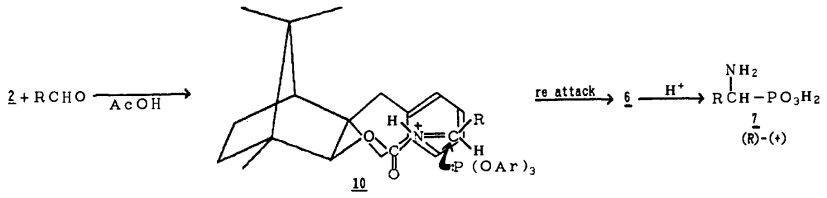

Scheme 2.

aminoethylphosphonic acid (R=CH_3), which is a ubstance which inhibits the growth of bacteria (alafosfaline[1]).

Experimental

Measurements. Melting poits were measured on a Yanagimoto Seisakusho micro melting-point apparatus. ^1H NHR spectra were recorded on a Hitachi R-24B (60 MHz) spectrometer with TMS as an internal standard, and optical rotations were determined with a JASCO DIP-4 digital and Atago Polax polarimeters, and IR spectra on a JASCO A-3 infrared spectrophotometer.

Preparation of Menthyl Carbamate (1); General Procedure: To a stirred mixture of (−)-menthol 7.8 g (50 mmol) and sodium cyanate 6.5 g (100 mmol) in 30 ml of benzene was added slowly 8.0 ml of trifluoroacetic acid at room temperature; the reaction mixture turned cake immediately. The reaction mixture was heavily stirred for 3 h, and then filtrated. A white crystalline mass was washed with benzene (10 ml×3) and water (50 ml×2); obtained crystalline compound **1** was then dried in desiccator under reduced pressure on standing overnight; yield 67%; mp 156—157 °C; IR (cm^{-1}) 3400 (NH_2), 1720 (C=O); $[\alpha]_D^{17}$ −125° (*c* 0.60, $CHCl_3$).

(+)-Isomenthyl carbamate was synthesized by the same method; yield 57%; mp 61—63 °C; $[\alpha]_D^{19}$+23.7° (*c* 1.1, $CHCl_3$).

Preparation of 1,7,7-Trimethylspiro[bicyclo[2.2.1]heptane-3,2′-indan]-2-yl Carbamate (2). A mixture of camphor 4.4 g (28.7 mmol) and sodium amide 2.5 g (63.2 mmol) in anhydrous toluene (30 ml) was heated at 100—105 °C until evaporation of ammonia gas ceased; a mixture of α,α′-dichloro-*o*-xylene 5.0 g (28.7 mmol) and toluene (20 ml) was then slowly added to the solution. The reaction mixture was refluxed for 3 h, cooled to room temperature, and then added into water (20 ml). The product was extracted with benzene (20 ml×2), and the combined organic layer was dried over anhydrous sodium sulfate; the solvent was evaporated in vacuo. The resulting syrupy products were further subjected to reduced pressure in order to remove unreacted camphor. The separation of products by column chromatography on silica gel (eluent; benzene/hexane=4/1, v/v) afforded the syrupy product; 1,7,7-trimethylspiro[bicyclo-[2.2.1]heptane-3,2′-indan]-2-on in 39% yield, ^1H NMR ($CDCl_3$) δ=0.92 (s, 3H, CH_3), 0.96 (s, 3H, CH_3), 1.01 (s, 3H, CH_3), 1.55—2.01 (m, 8H, CH_2×4), 3.11 (t, *J*=6.0 Hz, 1H, CH), 7.04 (s, 4H, C_6H_4). To anhydrous tetrahydrofuran (10 ml) solution of 1,7,7-trimethylspiro[bicyclo[2.2.1]heptane-3,2′-indan]-2-on 1.3 g (5.1 mmol) was added slowly lithium aluminium hydride 0.20 g (5.3 mmol) at room temperature; and the mixture was stirred for 2 h. The reaction was quenched by the addition of diluted hydrochloric acid. The product was extracted with ether (30 ml×3), and the combined organic layer was dried over anhydrous magnesium sulfate; the solvent was then evaporated. The residue was separated by thin-layer chromatography on silica gel (eluent; benzene/hexane= 4/1, v/v) to give the syrupy product, 1,7,7-trimethylspiro[bicyclo[2.2.1]heptane-3,2′-indan]-2-ol,[15] in 95% yield; ^1H NMR ($CDCl_3$) δ=0.98 (s, 6H, CH_3×2), 1.31 (s, 3H, CH_3), 1.55—1.79 (m, 8H, CH_2×4), 2.80 (dd, *J*=15.0 Hz, 1H, CH), 3.38 (br s, 1H, OH), 3.52 (s, 1H, CH), 7.09 (s, 4H, C_6H_4). Carbamate **2** was synthesized by the same procedure as that for carbamate **1**. ^1H NMR ($CDCl_3$) δ=0.90 (s, 3H, CH_3), 0.98 (s, 3H, CH_3), 1.28 (s, 3H, CH_3), 1.61—1.82 (m, 8H, CH_2×4), 3.03—3.18 (m, 2H, CH×2), 4.55 (s, 2H, NH_2), 7.09 (s, 4H, C_6H_4); $[\alpha]_D^{22}$+21.9° (*c* 2.1, EtOH).

Preparation of 1-Aminoalkylphosphonic Acid 7; General Procedure: Mixing of triphenyl phosphite 3.1 g (10 mmol), benzaldehyde 1.6 g (15 mmol), (−)-menthyl carbamate (**1**) 2.0 g (10 mmol), and glacial acetic acid (15 ml) immediately caused a slightly exothermic reaction; the reaction mixture was then stirred for 0.5 h.

The mixture was heated for additional 1 h at 85 °C and hydrolyzed with concentrated hydrochloric acid (15 ml) for 7 h under reflux. The resulting solution was washed with benzene (20 ml×3) in order to remove phenol and menthol; then, the aqueous solution was evaporated in vacuo. The residue was dissolved in methanol (5 ml) and the solution was treated with propylene oxide until pH 6 was reached. The precipitated aminoalkylphosphonic acid **5** was recrystallized from ethanol-water.

References

1) F. R. Atherton, C. H. Hassall, and R. W. Lambert, *J. Med. Chem.*, **29** (1986), and references therein.
2) J. Lukszo and R. Tyka, *Synthesis*, **1976**, 239.
3) D. G. Baraldi, M. Guarnel, F. Moroder, G. P. Pollini, and D. Simoni, *Synthesis*, **1982**, 653.
4) J. R. Chambers and A. F. Isbell, *J. Org. Chem.*, **29**, 832 (1964).
5) Z. H. Kudzin and A. Kotynski, *Synthesis*, **1980**, 1028.
6) C. Shiraki, H. Saito, K. Takahashi, C. Urakawa, and T. Hirata, *Synthesis*, **1988**, 399.
7) J. Rachon, V. Schollkopf, and T. Wintel, *Liebigs Ann. Chem.*, **1981**, 709.
8) W. J. Stec and K. Lesiak, *J. Org. Chem.*, **41**, 3757 (1976).
9) W. F. Gilmore and H. A. McBride, *J. Am. Chem. Soc.*, **94**, 4361 (1972). R. Tyka, *Tetrahedron Lett.*, **1970**, 677.
10) T. Glowiak and W. Sawka-Dobrowolska, *Tetrahedron Lett.*, **1977**, 3965.
11) J. W. Hubber and W. F. Gilmore, *Tetrahedron Lett.*, **1979**, 3049.
12) J. Oleksyszyn and R. Tyka, *Tetrahedron Lett.*, **1977**,

2823.
13) J. Oleksyszyn, L. Subotkowska, and P. Mastslerz, *Synthesis*, **1979**, 985.
14) S. R. Sandler and W. Karo, "Organic Functional Group Preparation," Academic Press, New York (1971), Vol. 2, p. 241.
15) G. Helmchen, A. Selim, D. Dorsch, and I. Taufer, *Tetrahedron Lett.*, **24**, 3213 (1983).
16) R. S. Edmundson, "Dictionary of Organophosphorus Compounds," Chapman and Hall Ltd., London (1988), and references therein.
17) G. H. Birum, *J. Org. Chem.*, **39**, 209 (1974).
18) K. Harada and T. Yoshida, *J. Org. Chem.*, **37**, 4366 (1972).
19) S. R. Landauer and H. N. Ryndon, *J. Chem. Soc.*, **1953**, 2224.

Reactions of Alkenes with Iodine(III) Tris(trifluoroacetate)

Yasuo FUTAMI, Hiroshi NISHINO, and Kazu KUROSAWA*
Department of Chemistry, Faculty of Science, Kumamoto University, Kurokami 2-39-1, Kumamoto 860
(Received May 10, 1989)

The reactions of 1-arylethene, 1,1-diarylethenes, and 1,1-diarylpropenes with iodine(III) tris(trifluoroacetate) gave 1,2-diaryl-1-alkanones, 1-aryl-2-(4-iodophenyl)-1-alkanones, benzoins, benzils, and iodoethenes. A similar reaction of 1,1,4,4-tetraaryl-1,3-butadiene yielded 1,2,4,4-tetraaryl-3-buten-1-one. The reactions of 1,1,5,5-tetraaryl-1,4-pentadienes and 1,1,6,6-tetraaryl-1,5-hexadienes also gave dicarbonyl compounds. The reaction involves aryl migration. The mechanisms and the utility of the reaction for organic synthesis are discussed.

Among the hypervalent iodine compounds, iodine(III) tris(trifluoroacetate) (ITT) has not been well investigated. This is partly because the reagent is extremely unstable towards moisture, although it is readily prepared. However, several interesting reactions of this reagent with alkanes, alkenes, ethers, and ketones have been reported.[1] During our previous investigation of the reaction of aromatic ketones with ITT[2] we found that 1,2-diphenylethanone gave 2-hydroxy-2-(2-iodophenyl)-1-phenylethanone (**5a**) in fairly good yield. This may suggest that iodine could be incorporated into the aromatic ring via an intermediate involving enol form of **5a**. We therefore investigated the reactions of 1,1-diarylethenes, 1,1-diarylpropene, and 1,1,ω,ω-tetraarylalkadienes; however, these gave mainly 1,2-diaryl-1-alkanones and aryl-substituted diketones. It seems to us that such reactions may have a synthetic utility in the preparation of 1,2-diarylethanones and 1,2-diarylpropanones; thus, these reactions were examined by changing the molar ratios of the substrate versus ITT, the substituent in the aromatic ring as well as in olefinic double bond, the reaction temperature, the reaction time, and the solvents.

Results and Discussion

1,1- and 1,2-Diarylethenes. When the reactions of 1,1-diphenylethene (**1a**) with ITT were carried out in various molar ratios at 23 °C for 3 h (Table 1), the products were found to be 1,2-diphenylethanone (**2a**), 1-phenyl-2-(4-iodophenyl)ethanone (**3a**), 2-hydroxy-1,2-diphenylethanone (**4a**), and 2-hydroxy-2-(2-iodophenyl)-1-phenylethanone (**5a**). The best total yield for the products was attained at a molar ratio of 1 : 1 (Table 1, Entry 3). The yield also depended on the temperature: it gave a similar yield at lower temperature, though the major product was **3a** at the reflux temperature (Entry 4). The products distribution changed greatly, depending on the solvent used (Entries 7—12). The reaction in benzene yielded only two products, **2a** and 2-iodo-1,1-diphenylethene (**6a**). In dichloromethane and hexane the reaction gave almost the same products as in the reaction in CCl_4, but in poor yields. In tetrahydrofuran and acetonitrile **6a** was found to be the sole product in poor yield. The reaction was also examined by changing the reaction times (Entries 13—18). It was observed that the maximum yield of **2a** was attained after 1 h, and then the yield gradually decreased, while **3a** slightly increasd.

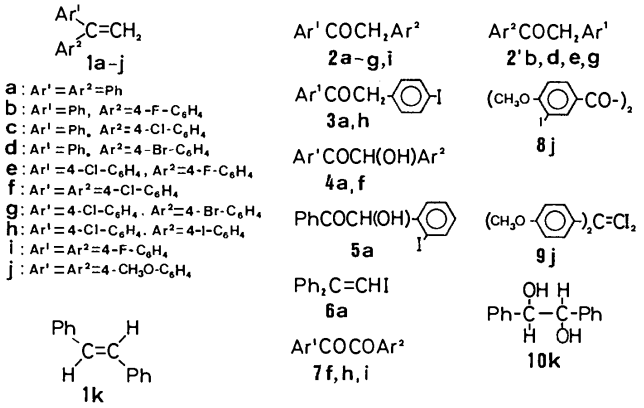

The reactions were examined for 1-(4-fluorophenyl)-1-phenylethene (**1b**), 1-(4-chlorophenyl)-1-phenylethene (**1c**), 1-(4-bromophenyl)-1-phenylethene (**1d**), 1-(4-chlorophenyl)-1-(4-fluorophenyl)ethene (**1e**), 1,1-bis(4-chlorophenyl)ethene (**1f**), 1-(4-bromophenyl)-1-(4-chlorophenyl)ethene (**1g**), 1-(4-chlorophenyl)-1-(4-iodophenyl)ethene (**1h**), 1,1-bis(4-fluorophenyl)ethene (**1i**), and 1,1-bis(4-methoxyphenyl)ethene (**1j**). The results are shown in Table 2.

1,2-Diarylethanone obtained from **1b** was a mixture of 2-(4-fluorophenyl)-1-phenylethanone (**2b**) and 1-(4-fluorophenyl)-2-phenylethanone (**2'b**) with an isomer ratio of 69 : 31, which was determined by measuring the intensities of the signals due to the methylene groups in their ^{1}H NMR spectra with the help of a shift reagent, Eu(fod)$_3$. 1,2-Diarylethanones from **1d**, **1e**, and **1g** were also found to be a mixture of two isomers, the ratios of which were determined in the same way as mentioned above (Table 2). Compounds **1h—j** gave an ethanone (**2i**), ethanediones (**7h**, **i**, **8j**), and a 1,1-diiodoethene (**9i**). The reaction of *trans*-stilbene (**1k**) yielded *erythro*-1,2-diphenyl-1,2-ethanediol (**10k**) (Entry 28).

Arylpropenes. Aryl migration was also observed in the reaction of arylpropenes as in that of 1,1-

Table 1. Reactions of 1,1-Diphenylethene (**1a**) with $I(OCOCF_3)_3$

Entry	Molar ratio[a]	Solvent	Temp	Time	Recovery	Product (yield/%)[b]				
			°C	h	%	**2a**	**3a**	**4a**	**5a**	**6a**
1	1:0.5	CCl_4	23	3	27			12		18
2	1:1	CCl_4	0	3		61	3	4		
3	1:1	CCl_4	23	3		69	13	9	3	
4	1;1	CCl_4	reflux	3			32			
5	1:1.5	CCl_4	23	3			70	5	6	
6	1:2	CCl_4	23	3			39			
7	1:1	CH_2Cl_2	23	3		22	43	3	22	
8	1:1	$CHCl_3$	23	3		39		15		
9	1:1	THF	23	3	32					21
10	1:1	Benzene	23	3	16	53				20
11	1:1	Hexane	23	3		48	29	9		
12	1:1	CH_3CN	23	3	28					18
13	1:1	CCl_4	23	0.25	12			18		10
14	1:1	CCl_4	23	0.5	5	17		15		6
15	1:1	CCl_4	23	1		72	9	10	2	
16	1:1	CCl_4	23	6		69	11	8	2	
17	1:1	CCl_4	23	12		38	44	7	6	
18	1:1	CCl_4	23	18		35	45	5	6	

a) Substrate: $I(OCOCF_3)_3$. b) Yields are based on the substrate added.

Table 2. Reactions of Ethenes, Propenes, and Dienes with $I(OCOCF_3)_3$ at the Molar Ratio of 1 : 1 in CCl_4 at 23 °C for 3 h

Entry	Substrate	Procuct (yield/%)[a]				
		Ethanone	2-Hydroxy-ethanone	Ethanedione	Iodoethene	Ethanediol
19	**1b**	**2b**,**2'b** (63)[b]				
20	**1c**	**2c** (36) **3h** (46)				
21	**1d**	**2d**,**2'd** (64)[c]				
22	**1e**	**2e**,**2'e** (74)[d]				
23	**1f**	**2f** (74)	**4f** (6)	**7f** (19)		
24	**1g**	**2g**,**2'g** (76)[e]				
25	**1h**			**7h** (7)		
26	**1i**	**2i** (24)		**7i** (26)		
27	**1j**			**8j** (5)	**9j** (17)	
28	**1k**					**10k** (23)
29	**11a**	**12a** (39) **13a** (32)				
30	**11b**	**12b** (46)				
31	**11c**	**12c**,**12'c** (79)[f]				
32	**11d**	**12d** (73)				

a) Yields are based on the substrate added. b) **2b**:**2'b**=69:31. c) **2d**:**2'd**=48:52.
d) **2e**:**2'e**=65:35. e) **2g**:**2'g**=50:50. f) **12c**:**12'c**=69:31.

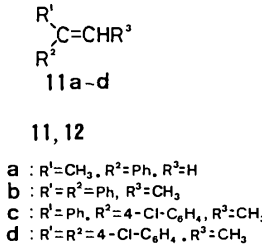

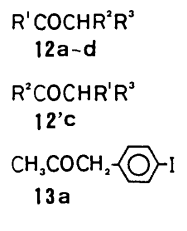

diarylethenes. 2-Phenylpropene (**11a**) gave 1-phenyl-2-propanone (**12a**) and 1-(4-iodophenyl)-2-propanone (**13a**) (Entry 29). 1,1-Diphenylpropene (**11b**), 1-(4-chlorophenyl)-1-phenylpropene (**11c**), and 1,1-bis(4-chlorophenyl)propene (**11d**) yielded the corresponding 1,2-diaryl-1-propanones, (**12b**, **12c**, **12'c**, and **12d**), respectively (Entries 30—32). The isomer ratio was found to be 69 : 31 for **12c** and **12'c**.

1,1,ω,ω-Tetraarylalkadienes. We also studied the reactions of 1,1,ω,ω-tretraarylalkadienes. The reactions of 1,1,4,4-tetraphenyl-1,3-butadiene (**14a**) and 1,1,4,4-tetrakis(4-chlorophenyl)-1,3-butadiene (**14b**) with ITT gave allyl phenyl ketones, i.e. 1,2,4,4-tetraphenyl-3-buten-1-one (**15a**) and 1,2,4,4-tetrakis(4-chlorophenyl)-3-buten-1-one (**15b**). The reactions of 1,1,5,5-tetraphenyl-1,4-pentadiene (**14c**) and 1,1,5,5-tetrakis(4-chlorophenyl)-1,4-pentadiene (**14d**) yielded diketones, i.e. 1,2,4,5-tetraphenyl-1,5-pentanedione (**16c**) and 1,2,4,5-tetrakis(4-chlorophenyl)-1,5-pentanedione (**16d**). Similarly, the reaction of 1,1,6,6-tetraphenyl-1,5-hexadiene (**14e**) and 1,1,6,6-tetrakis(4-

Table 3. Reactions of Dienes (**14a**—f) with ITT at a Molar Ratio of 1 : 1 at 23 °C for 3 h

Entry	Substrate	Product (Yield/%)[a]	
		Aryl ketone	Diketone
32	**14a**	**15a** (37)[b]	
33	**14b**	**15b** (23)	
34	**14c**		**16c** (10)
35	**14d**		**16d** (44)
36	**14e**		**16e** (16)
37	**14f**		**16f** (77)

a) Yields are based on the substrate added. b) Substrate was recovered (60%).

chlorophenyl)-1,5-hexadiene (**14f**) gave 1,2,5,6-tetraphenyl-1,6-hexanedione (**16e**) and 1,2,5,6-tetrakis(4-chlorophenyl)-1,6-hexanedione (**16f**), respectively (Table 3). These diketones (**16c**—**f**) can be a mixture

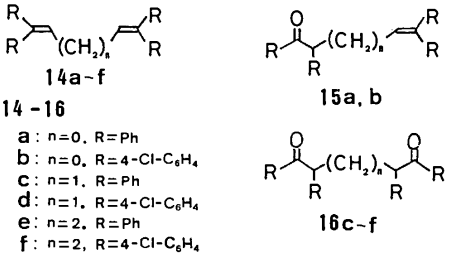

of two diastereoisomers; however, the ^{1}H NMR spectra of these compounds showed that only one of the isomers is produced. The reaction of 1,1,2-triphenylethene with ITT yielded a complex mixture, the products of which could not be characterized.

Reaction Mechanisms. The reaction of alkenes with ITT has been reported by Buddrus,[3] who described that trifluoroacetoxyl groups added to the double bond to form mainly 1,2-glycol bis(trifluoroacetate). The reaction of styrene was briefly mentioned as giving 1,1-bis(trifluoroacetate) as well as 1,2-bis(trifluoroacetate).[4] Our study revealed that 1,1-diaryl-1-alkenes always gives ketones. The reaction mechasnism could be depicted as involving 1,2-aryl shift (**B**→**C**) and the hydrolysis of the reaction intermediate (**C**) upon treatment with aqueous acid (Scheme 1). The ^{1}H NMR (CCl_4) spectrum of the reaction mixture after an hour of stirring showed a singlet at δ=3.83 corresponding to the methylene group in **C**. The IR spectrum (CCl_4) also exhibited a strong absorption at 1802 cm^{-1} due to a trifluoroacetoxyl group. Evidence for an intramolecular rearrangement was obtained when a mixed substrate, **1a** and **1f**, was subjected to a reaction with ITT. The only products that we could find were **2a**, **2f**, and **3a**; there was no crossover product, such as 2-(4-chlorophenyl)-1-phenylethanone and 1-(4-chlorophenyl)-2-phenylethanone.

The substituent in the aromatic ring has a significant effect on the migratory aptitude of the aryl group. As shown in the isomer ratio of **2b**:**2'b**, which is in

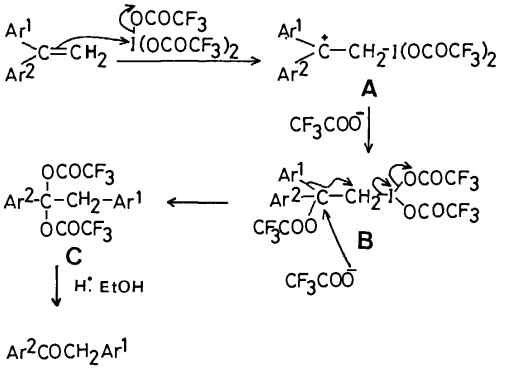

Scheme 1.

favor of **2b**, the 4-fluorophenyl group is more movable than the phenyl group. The phenyl group, on the other hand, is more readily transfered than the 4-bromophenyl and 4-chlorophenyl groups, the latter two being about the same in migratory aptitute. Thus, the order of migratory aptitude is as follows:

$$4\text{-F-}C_6H_4\text{-} > C_6H_5\text{-} > 4\text{-Br-}C_6H_4\text{-} \fallingdotseq 4\text{-Cl-}C_6H_4\text{-}$$

1-Aryl-2-(4-iodophenyl)ethanones (**3a** and **3h**) and 1-(4-iodophenyl)-2-propanone (**13a**) may be formed after a migration of the phenyl group in intermediate **A**. The formation of 2-hydroxyethanone (**5a**) and ethanediones (**7**) has already been discussed in a previous paper.[2]

The formation of iodoethenes, **6a** and **9j**, indicates the electron-donating nature of phenyl and 4-methoxyphenyl groups. These groups stabilize the carbonium ion **A** which is deprotonated and, eventually, affords the iodoethenes (**6a** and **9j**).

In conclusion, the reaction of ITT proved to be useful for the preparation of ethanones and 1,1,ω,ω-tetraarylalkanediones from 1,1-diarylethenes and 1,1,ω,ω-tetraarylalkadienes, respectively. The reaction involves intramolecular aryl migration, confirmed by the absence of the crossover products in the product mixture.

Experimental

Measurements. All ^{1}H NMR spectra were taken in deuteriochloroform or carbon tetrachloride solutions with tetramethylsilane as the internal standard on a JNM-PMX 60 SI spectrometer (60 MHz). The IR spectra were measured in chloroform solutions on a JASCO A-102 IR spectrometer. The mass spectra were obtained with JMS-OISG-2 and JMS-DX-303 HF instruments using a direct-insertion probe at an ionizing voltage of 70 eV. The melting points were determined with a Yanagimoto micromelting point apparatus and were not corrected.

Materials. Arylethenes (**1a**—**j**) arylpropenes (**11a**—**d**) and 1,1,ω,ω-tetraarylalkadienes (**14a**—**f**) were obtained by the dehydration of the corresponding alcohols, which were prepared by a Grignard reaction.[5] **1k** was commercially available from Katayama Chemical Industories. **1g**: Mp 71—72 °C (ethanol); IR ν (cm^{-1}) 1659 (C=C); ^{1}H NMR

($CDCl_3$) δ=5.51 (2H, s, $=CH_2$), 7.03—7.30 (6H, m, ar.H), and 7.34—7.59 (2H, m, H-2′, H-6′). Found: *m/z* 291.9653, Calcd for $C_{14}H_{10}{}^{79}Br^{35}Cl$: M, 291.9655. **1h**: Mp 67 °C (ethanol); IR ν (cm^{-1}) 1660 (C=C); ^1H NMR ($CDCl_3$) δ=5.41 (2H, s, $=CH_2$), 6.89—7.16 (2H, m, H-3′, H-5′), 7.19—7.46 (4H, m, ar.H), and 7.49—7.76 (2H, m, H-2′, H-6′). Found: *m/z* 339.9542, Calcd for $C_{14}H_{10}{}^{35}ClI$: M, 339.9516.

Reactions of Iodine(III) Tris(trifluoroacetate). The general procedure for the reaction of ITT was as follows. To a solution of a substrate (1 or 2 mmol) in a solvent (20 cm^3), iodine(III) tris(trifluoroacetate)[2] (0.5—2 mmol, as shown in Tables 1, 2, and 3), was added under a nitrogen atmosphere. The solution was stirred with undissolved ITT at 23 °C for 3 h. Water (30 cm^3) was added to the reaction mixture and the mixture was stirred again for 1 h. The reaction mixture was then extracted with chloroform and the organic layer was separated and washed with 5% aqueous sodium thiosulfonate solution, and water. The solvent was removed under reduced pressure and the residue was heated with a mixture of ethanol (30 cm^3) and concd hydrochloric acid (0.5 cm^3) at 100 °C for 1 h. The solvent was removed under reduced pressure. The products were separated on TLC with benzene as the developing solvent. The yields on reasonably pure products are summarized in Tables 1,2, and 3. Analytical samples were further purified by recrystallization. The known compounds were identified by comparisons of their spectral data and/or the melting points with those found in the literature.

Reaction Products with ITT. **2a:** Mp 53—54 °C (lit,[6] mp 55—56 °C). Mixture of **2b** and **2′b**: **2b**:**2′b**=69:31; mp 91—92 °C (lit,[7] mp 86 °C for **2b**,lit,[8] mp 11 °C for **2′b**). **2c:** Mp 135 °C (lit,[9] mp 135.5—136.5 °C). Mixture of **2d** and **2d′**:**2d**:**2′d**=48:52; mp 132—133 °C (lit,[10] mp 146—147 °C for **2d**, lit,[11] mp 104—105 °C for **2′d**). Mixture of **2e** and **2e′**: **2e**:**2′e**=65:35; mp 85.5—86.5 °C (ethanol); IR ν(cm^{-1}) 1680 (>C=O); ^1H NMR ($CDCl_3$) δ=4.44 (4H, s, $-CH_2-$, $-CH_2-$), 6.88—7.49 (12H, m, ar.H), and 7.83—8.24 (4H, m, H-2′, H-2′, H-6′, H-6′). Found: *m/z* 248.0397, Calcd for $C_{14}H_{10}{}^{35}ClFO$: M, 248.0404. **2f:** Mp 113—114 °C (lit,[12] mp 112.5—113.5 °C). Mixture of **2g** and **2g′**: **2g**:**2′g**=50:50; mp 123—124 °C (lit,[13] mp 121—121.5 °C for **2g**, lit,[13] mp 106—107 °C for **2′g**). **2i:** Mp 96.5—98 °C (lit,[14] mp 96—97 °C). **3a:** Mp 158—159 °C (ethanol); IR ν(cm^{-1}) 1678 (>C=O); ^1H NMR ($CDCl_3$) δ=4.23 (2H, s, $-CH_2-$), 6.94—7.74 (7H, m, ar. H), and 7.93—8.14 (2H, m, H-2′, H-6′). Found: *m/z* 321.9885. Calcd for $C_{14}H_{11}IO$: M, 321.9945. **3h**: Mp 139—140 °C (ethanol); IR ν (cm^{-1}) 1679 (>C=O); ^1H NMR ($CDCl_3$) δ=4.21 (2H, s, $-CH_2-$), 6.93—7.07 (2H, m, H-3″, H-5″), 7.37—7.51 (2H, m, H-3′, H-5′), 7.60—7.73 (2H, m, H-2″, H-6″), and 7.87—8.01 (2H, m, H-2′, H-6′). Found: *m/z* 355.9479. Calcd for $C_{14}H_{10}O^{35}ClI$: M, 355.9464. **4a**: Mp 133—134 °C (lit,[15] mp 133 °C). **4f:** Mp 87 °C (lit,[16] mp 87—88 °C). **5a:** Mp 114—115 °C (lit,[2] mp 113.2—114.2 °C). **6a:** Liquid (lit,[17] mp 40—41 °C); ^1H NMR ($CDCl_3$) δ=6.91 (1H, s, =CHI), and 7.04—7.47 (10H, m, ar.H). Found: *m/z* 305.9913. Calcd for $C_{14}H_{11}I$: M, 305.9910. **7f:** Mp 198 °C (lit,[18] mp 199 °C). **7h:** Mp 210—211 °C (ethanol); IR ν (cm^{-1}) 1674 (>C=O); ^1H NMR ($CDCl_3$) δ=7.35—7.77 (4H, m, H-3′, H-3″, H-5′, H-5″), and 7.77—8.07 (4H, m, H-2′, H-2″, H-6′, H-6″). Found: *m/z* 369.9283, Calcd for $C_{14}H_8{}^{35}ClIO$: M, 369.9258. **7i:** Mp 118 °C (lit,[19] mp 120—121 °C). **8j:** Mp 218—219 °C (ethanol); IR ν (cm^{-1}) 1660 (>C=O); ^1H NMR ($CDCl_3$) δ=3.96 (6H, s, 2×OCH_3), 6.84 (2H, d, J=8.4 Hz, H-5′, H-5″), 7.93 (2H, dd, J=8.4, 2.0 Hz, H-6′, H-6″), and 8.40 (2H, d, J=2.0 Hz, H-2′, H-2″). Found: *m/z* 521.8837, Calcd for $C_{16}H_{12}I_2O_4$: M, 521.8826. **9j:** Mp 139—140 °C; ^1H NMR ($CDCl_3$) δ=3.76 (6H, s, 2×OCH_3), 6.67—6.95 (4H, m, H-3′, H-3″, H-5′, H-5″), and 7.04—7.31 (4H, m, H-2′, H-2″, H-6′, H-6″). Found: *m/z* 491.9110, Calcd for $C_{16}H_{14}I_2O_2$: M, 491.9084. **10k**: Mp 123—124 °C (lit,[20] mp 119—120 °C). **12a:** Liquid (lit,[21] bp 97—98.5 °C/ 1.73×10^3 Pa). **12b:** Liquid (lit,[22] bp 63—70 °C/ 0.67 Pa). Mixture of **12c** and **12c′**: Liquid; **12c**:**12′c**=69:31; IR ν (cm^{-1}) 1680 (>C=O); ^1H NMR (CCl_4) δ=1.44 (6H, d, J=7.2 Hz, CH_3, CH_3), 4.58 (2H, q, J=7.2 Hz, 2 × >CH-), 6.80—7.65 (14H, m, ar.H), and 7.65—8.05 (4H, m, H-2′, H-2′, H-6′, H-6′). Found: *m/z* 244.0659. Calcd for $C_{15}H_{18}{}^{35}ClO$: M, 244.0655. **12d:** Mp 62.5—63.5 °C (ethanol); IR ν (cm^{-1}) 1682 (>C=O); ^1H NMR (CCl_4) δ=1.45 (3H, d, J=6.6 Hz, CH_3), 4.51 (1H, q, J=6.6 Hz, >CH-), 6.95—7.48 (6H, m, ar.H), and 7.62—7.98 (2H, m, H-2′, H-6′). Found: *m/z* 278.0250. Calcd for $C_{15}H_{12}{}^{35}Cl_2O$: M, 278.0265. **13a**: Liquid (lit,[23] bp 135—136 °C/266 Pa). **15a**: Liquid (lit,[24] mp 91.5—93 °C); IR ν (cm^{-1}) 1678 (>C=O); ^1H NMR ($CDCl_3$) δ=5.30 (1H, d, J=10.2 Hz, -COCH<), 6.66 (1H, d, J=10.2 Hz, =CH-), 6.93—7.55 (18H, m, ar.H), 7.55—7.83 (2H, m, H-2′, H-6′). **15b:** Liquid; IR ν (cm^{-1}) 1680 (>C=O); ^1H NMR (CCl_4) δ=5.15 (1H, d, J=10.2 Hz, -COCH<), 6.55 (1H, d, J=10.2 Hz, =CH-), 6.87—7.48 (14H, m, ar.H), and 7.48—7.77 (2H, m, H-2′, H-6′). Found: *m/z* 510.0083. Calcd for $C_{28}H_{18}{}^{35}Cl_4O$: M, 510.0112. **16c:**[25] Liquid; IR ν (cm^{-1}) 1679 (>C=O); ^1H NMR ($CDCl_3$) δ=2.00—3.12 (2H, m, $-CH_2-$), 4.17—4.74 (2H, m, 2× -COCH<), 6.71—7.57 (16H, m, ar.H), 7.57—8.00 (4H, m, H-2′, H-2′, H-6′, H-6′). **16d:** Mp 164—165 °C (ethanol); IR ν (cm^{-1}) 1679 (>C=O); ^1H NMR (CCl_4) δ=1.97—3.03 (2H, m, $-CH_2-$), 4.13—4.63 (2H, m, 2× -COCH<), 6.87—7.47 (12H, m, ar.H), and 7.53—7.93 (4H, m, H-2′, H-2′, H-6′, H-6′). Found: *m/z* 540.0189. Calcd for $C_{29}H_{20}{}^{35}Cl_4O_2$: M, 540.0217. **16e:**[26] Mp 186—187 °C (ethanol); IR ν (cm^{-1}) 1678 (>C=O); ^1H NMR ($CDCl_3$) δ=1.53—2.40 (4H, m, $-CH_2CH_2-$), 4.27—4.77 (2H, m, 2× -COCH<), 7.10—7.53 (16H, m, ar.H), 7.76—8.03 (4H, m, H-2′, H-2′, H-6′, H-6′); MS *m/z* (rel intensity)=418 (M^+, 6), 296 (75), 117 (100), 105 (100), 91 (48), 77 (60). **16f:** Mp 159—161 °C (ethanol); IR ν (cm^{-1}) 1679 (>C=O); ^1H NMR ($CDCl_3$) δ=1.39—2.36 (4H, m, $-CH_2CH_2-$), 4.12—4.60 (2H, m, 2× COCH<), 6.86—7.43 (12H, m, ar.H), and 7.56—7.88 (4H, m, H-2′, H-6′). Found: *m/z* 554.0388. Calcd for $C_{30}H_{22}{}^{35}Cl_4O_2$: M, 554.0374.

References

1) H. Plettenberg, B. Gosciniak, and J. Buddrus, *Chem. Ber.*, **115**, 2377 (1982). A. S. Marula, E. T. Luu Rang, and G. Ourisson, *Tetrahedron Lett.*, **1977**, 3959. J. Buddrus and H. Plettenberg, *Angew. Chem., Int. Ed. Engl.*, **15**, 436 (1976).

2) N. Fukuyama, H. Nishino, and K. Kurosawa, *Bull. Chem. Soc. Jpn.*, **60**, 4363 (1987).

3) J. Buddrus, *Angew. Chem., Int. Ed. Engl.*, **12**, 163 (1973).

4) J. Buddrus and H. Plettenberg, *Chem. Ber.*, **113**, 1494 (1980).

5) E. W. Garbisch, Jr., *J. Org. Chem.*, **26**, 4165 (1961).

6) C. F. H. Allen and W. E. Barker, *Org. Synth.*, **12**, 16 (1932).

7) A. Fischer, B. A. Grigor, J. Parker, and J. Vaughan, *J. Am. Chem. Soc.*, **83**, 4208 (1968).
8) T. Ando, *Yuki Gosei Kagaku Kyokai Shi*, **17**, 777 (1959); *Chem. Abstr.*, **54**, 4492d (1960).
9) C. R. Hauser and G. F. Morris, *J. Org. Chem.*, **26**, 4740 (1961).
10) R. Hüttel, K. Franke, and H. Martin, *Chem. Ber.*, **93**, 1433 (1960).
11) A. Patchornik and M. A. Kraus, *J. Am. Chem. Soc.*, **92**, 7587 (1970).
12) H. O. House, *J. Am. Chem. Soc.*, **78**, 2298 (1956).
13) K. Ishimura, *Repts. Govt. Ind. Research Inst., Nagoya*, **2**, 197 (1953); *Chem. Abstr.*, **50**, 15477e-f (1956).
14) W. Funasaka, T. Ando, H. Ozaki, and K. Murakami, *Yuki Gosei Kagaku Kyokai Shi*, **17**, 334 (1959); *Chem. Abstr.*, **53**, 17970e (1959).
15) F. L. Benton, Sr. M. C. Voss, and P. A. McCusker, *J. Am. Chem. Soc.*, **83**, 4208 (1961).
16) R. E. Lutz and R. S. Murphey, *J. Am. Chem. Soc.*, **71**, 478 (1949).
17) D. Y. Curtin and E. W. Flynn, *J. Am. Chem. Soc.*, **81**, 4714 (1959).
18) W. Voegtli, H. Muhr, and P. Läuger, *Helv. Chim. Acta*, **37**, 1627 (1954); *Chem. Abstr.*, **49**, 11604f (1955).
19) P. Beak, R. A. Brown, J. Yamamoto, C. C. Chiang, and I. C. Paul, *J. Org. Chem.*, **41**, 3389 (1976).
20) F. D. Greene, *J. Am. Chem. Soc.*, **78**, 2250 (1956).
21) H. G. Walker and C. R. Hauser, *J. Am. Chem. Soc.*, **68**, 1386 (1946).
22) R. A. Barnes and B. R. Juliano, *J. Am. Chem. Soc.*, **81**, 6462 (1959).
23) K. Binovic, S. Vrancea, D. Grandet, J. M. Lebourg, and R. Porquet, *Chim. Ther.*, **1968**, 313; *Chem. Abstr.*, **70**, 87171y (1969).
24) R. E. Lutz, R. G. Bass, and D. W. Boykin, Jr., *J. Org. Chem.*, **29**, 3660 (1964).
25) D. Chakeravarti and N. K. Roy, *J. Indian Chem. Soc.*, **41**, 65 (1964); *Chem. Abstr.*, **60**, 14419d (1964).
26) H. J. Roth and M. H. El Raie, *Arch. Pharm.*, **1972**, 229; *Chem. Abstr.*, **77**, 5298c (1972).

 © 1989 The Chemical Society of Japan Bull. Chem. Soc. Jpn., 62, 3187—3194 (1989)

Perkin-Markovnikov Type Reaction Initiated with Electrogenerated Superoxide Ion

Fumihiro OJIMA and Tetsuo OSA*
Pharmaceutical Institute, Tohoku University, Aobayama, Aoba-ku, Sendai 980
(Received May 12, 1989)

The cyclic condensation of active methylene compounds such as diethyl malonate, dimethyl malonate, ethyl acetoacetate, or acetylacetone and dibromoalkanes such as 1,2-dibromoethane, 1,3-dibromopropane, 1,4-dibromobutane, 1,5-dibromopentane, 1,6-dibromohexane, 1,3-dibromobutane, or 1,4-dibromopentane with electrogenerated superoxide ion was studied electrochemically in *N,N*-dimethylformamide (DMF) using cyclic voltammetry (CV) and controlled potential macro-electrolysis. The CV shows that electrogenerated superoxide ion reacts with both active methylene compounds and dibromoalkanes in the dissolved oxygen medium. Controlled potential macro-electrolysis of the above components generally yielded cycloalkanes as the main products. In comparison, the chemical method using sodium ethoxide was also carried out. Two reaction mechanisms via the proton abstraction of active methylene compounds with electrogenerated superoxide ion and via the nucleophilic attack of the superoxide ion on dibromoalkanes are presented.

Superoxide ion ($O_2^{\cdot-}$) is not only one of the most important activated forms of molecular oxygen in biological systems but also novel activating reagent for organic synthesis,[1-3] and has recently attracted a great deal of attention of biological and organic chemists. Superoxide ion is produced by the electrochemical reduction of oxygen dissolved in non-aqueous solvent such as pyridine, acetonitrile, or *N,N*-dimethylformamide (DMF) at −0.85 V vs. silver-silver chloride (Ag/AgCl) as shown in Eq. 1.

$$O_2 + e^- \rightarrow O_2^{\cdot-} \quad (1)$$

Superoxide ion possesses various reactivities, namely characteristics as a strong base, a nucleophile, an oxidant, a reductant, a free radical, and an electron-transfer agent.[4] In aprotic solvents, superoxide ion acts as an electrogenerated base (EGB),[5] and abstracts a proton of an active methylene group to form a carbanion (EWG-$\bar{C}$H-EWG, EWG: electron-withdrawing group). Electrogenerated superoxide ion has another feature, as a nucleophile;[6] it reacts with alkyl halides to form alkylperoxy radicals (R-OO·), which might be readily reduced further by electrogenerated superoxide ion or by an electron from the electrode to form alkylperoxide ions (R-OO$^-$).

Alkali metal superoxides of potassium and sodium salts are well-known, but their insolubility in the usual organic solvents makes them of little preparative use.[6] Therefore, the reaction of alkali metal superoxides with organic compounds in benzene has been reported by the use of crown ethers in order to solve the problem of their insolubility.[7] On the other hand, the electrochemical method is experimentally more convenient because superoxide ion is continuously generated on the electrode and its solubility is sufficiently high in the presence of the tetraethylammonium cation of supporting electrolyte.[8]

We have investigated the characteristics of the reactivity of electrogenerated superoxide ion toward active methylene compounds and dibromoalkanes, and have reported preliminary results on the reaction of the active methylene compound, such as diethyl malonate, dimethyl malonate, or ethyl acetoacetate and dibromoalkane with electrogenerated superoxide ion.[9] In this paper, we describe in detail the reaction of dibromoalkanes and active methylene compound of acetylacetone as well as malonates and ethyl acetoacetate with electrogenerated superoxide ion in DMF solutions, using cyclic voltammetry and controlled potential macroelectrolysis.

The reaction of this type is well known as Perkin-Markovnikov reaction (Scheme 1).[10,11] The reaction using sodium ethoxide as a base to form an aliphatic ring compound is widely used in organic syntheses. However, the reports on the reaction of this type using electrogenerated superoxide ion as a base, have not previously been published.

After detailed investigation using cyclic voltammetry and macro-electrolysis in DMF, we have concluded that the present reaction system should be considered in terms of the nucleophilic reaction of electrogenerated superoxide ion with dibromoalkanes as frequent as in terms of the proton abstraction of electrogenerated superoxide ion from active methylene compounds. We report here the reaction of active methylene compounds and dibromoalkanes using cyclic

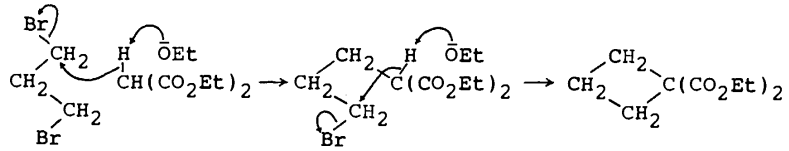

Scheme 1.

voltammetry and macro-electrolysis in DMF, and discuss the results in terms of the basic properties and the nucleophilicity of electrogenerated superoxide ion.

Experimental

Materials. DMF (Guaranteed reagent, Tokyo Kasei) was stored over Molecular Sieves (4A 1/16) for 24 h and then distilled under reduced pressure. Further purification was achieved by passage through a column of activated alumina (ICN Alumina N-Akt. I). Tetraethylammonium perchlorate (TEAP) from Tokyo Kasei (Guaranteed reagent) was dried in vacuo and used as a supporting electrolyte in the electrochemical experiments. The substrates, diethyl malonate (Guaranteed reagent, Nakarai Chemicals), dimethyl malonate (Extra pure reagent, Tokyo Kasei), ethyl acetoacetate (Extra pure reagent, Wako Pure Chemical Industries), and acetylacetone (Guaranteed reagent, Nakarai Chemicals) were purchased commercially and were redistilled. 1,2-Dibromoethane (Extra pure reagent), 1,3-dibromopropane (Extra pure reagent), 1,4-dibromobutane (Guaranteed reagent), 1,5-dibromopentane (Guaranteed reagent), 1,6-dibromohexane (Extra pure reagent), 1,3-dibromobutane (Extra pure reagent), and 1,4-dibromopentane (Extra pure reagent) were also obtained commercially from Tokyo Kasei and were distilled under reduced pressure before use.

Cyclic Voltammety. Cyclic voltammetry was carried out in a DMF solution containing 0.2 M (1 M=1 mol dm^{-3}) TEAP as a supporting electrolyte. A glassy carbon (GC) disk (area ca. 0.71 cm^2) was employed as a working electrode, and a platinum wire was employed as a counter electrode for cyclic voltammetry. The working electrode was polished with a 0.05 μm alumina/water slurry on a felt surface, sonicated in distilled water, throughly washed with acetone, and dried before electrochemical measurements. The cathode potentials were referred to Ag/Ag^+ (0.05 M $AgNO_3$ and 0.1 M TEAP in acetonitrile). Cyclic potential sweeps were generated by a self-made function generator in conjunction with a Hokuto Denko Model HA-305 potentiostat/galvanostat. Cyclic voltammograms were recorded on a Graphtec Model WX1200 X-Y recorder. All electrochemical measurements were carried out at room temperature under a nitrogen atmosphere.

Controlled Potential Macro-Electrolysis. For controlled potential macro-electrolysis, a three compartment cell (H-type cell), in which cathodic and anodic chambers were separated by two fine-porosity sintered-glass frits, was employed with a magnetic stirrer and a reference electrode was put near the cathode. A glassy carbon plate with a surface area of ca. 12.5 cm^2 was used as the cathode, and a platinum plate was used as the anode. An electrolyte solution (0.2 M TEAP) of 60 cm^3 containing two substrates (0.1 M activated methylene compound and 0.1 M dibromoalkane) was placed in the cathodic chamber (25 cm^3), the anodic chamber (25 cm^3), and the middle chamber (10 cm^3). Dry oxygen was bubbled through the cathode. The cathode potential was controlled with a Hokuto Denko Model HA-305 potentiostat/galvanostat. The quantity of electricity passed was measured with a Hokuto Denko Model HF-201 coulomb/amperehour meter. These electrolyses were carried out at room temperature under a nitrogen atmosphere.

Identification of Products and Determination of the Yields. The products of the electrolyses were separated from the catholyte and identified by the following procedure. The catholyte was evaporated in vacuo to remove DMF. The residue was dissolved in water and extracted with diethyl ether. The ether layer was dried over anhydrous sodium sulfate and the ether was removed by distillation under reduced pressure. The resulting liquid was tried to be separated into its components by silica-gel column chromatography using several organic mixed eluents such as hexane–diethyl ether (20 : 1), but could not be well separated.

Authentic samples of the cycloalkanes were prepared by the ordinary chemical preparative method.[12] The procedure was as follows. In a 100-ml three-necked round bottomed flask, equipped with a reflux condenser capped with a calcium chloride tube, a magnetic stirrer, and a 50-ml pressure-equalizing dropping funnel for addition of prepared 0.02 g·atom sodium ethoxide–ethanol solution, were mixed 0.01 mol each of active methylene compound and dibromoalkane. The mixture was heated to 80 °C and vigorously stirred while the sodium ethoxide–ethanol solution was slowly added into the flask over a 1.5 h period. After the addition was finished, the mixture was refluxed, with continued stirring, for an additional 45 min, and then the ethanol was removed by distillation. The reaction mixture was cooled, and 5 ml of cold water was added. After the sodium halides were completely dissolved, the organic layer was separated and the aqueous layer was extracted with three 10 ml portions of diethyl ether. The combined ether extracts were shaken with 5 ml of saturated NaCl solution, dried over anhydrous sodium sulfate, filtered, and concentrated on a rotary evaporator. The identity of the electrochemically prepared cycloalkanes with the respective authentic samples was established by gas chromatography and GC-MS spectroscopy. The main products of electrolyses were detected by using a Shimadzu Model GC-4CM gas chromatograph equipped with 2 m×3 mmϕ column packed with Carbowax 20M, and identified by comparing their retention times with those of authentic samples. Yields of the products were also determined by gas chromatographic analysis. The by-products of electrolyses were identified by using a JEOL Model JMS-DX300 GC-MS spectrograph equipped with 2 m × 3 mmϕ column packed with Silicone OV-101.

Results and Discussion

Cyclic Voltammetry of Active Methylene Compounds and Dibromoalkanes. The cyclic voltammetry of diethyl malonate (**1**), dimethyl malonate (**2**), ethyl acetoacetate (**3**), acetylacetone (**4**), 1,2-dibromoethane (**a**), 1,3-dibromopropane (**b**), 1,4-dibromobutane (c), 1,5-dibromopentane (**d**), 1,6-dibromohexane (**e**), 1,3-dibromobutane (**f**), and 1,4-dibromopentane (**g**) was carried out in a 0.2 M TEAP/DMF solution under a nitrogen atmosphere. All the substrates were reduced at more negative potentials than −2.5 V vs. Ag/Ag^+ as shown in Table 1. The compounds **4**, **c**, **d**, **e**, and **g** exhibited prepeaks (E_p^1) at more positive potentials than the main peaks (E_p^2). The cyclic voltammograms of **1**, **a**, and c are demonstrated in Fig. 1. The reduction peak of **1** could not

Table 1. Reduction Peak Potentials of Substrates

Compound	E_P^1	E_P^2
Diethyl malonate (**1**)		−3.36
Dimethyl malonate (**2**)		−3.33
Ethyl acetoacetate (**3**)		−2.96
Acetylacetone (**4**)	−2.54	−2.97
1,2-Dibromoethane (**a**)		−2.58
1,3-Dibromopropane (**b**)		−2.87
1,4-Dibromobutane (**c**)	(−2.80)	−3.29
1,5-Dibromopentane (**d**)	(−2.80)	−3.31
1,6-Dibromohexane (**e**)	(−2.80)	−3.39
1,3-Dibromobutane (f)		−2.97
1,4-Dibromopentane (g)	(−2.80)	−3.24

E/V vs. Ag/Ag^+, solvent: DMF, supporting electrolyte: TEAP, working electrode: GC, reference electrode: Ag/Ag^+, counter electrode: Pt.

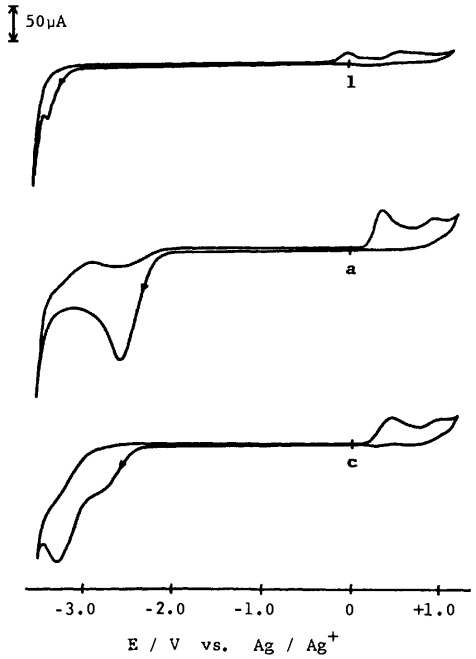

Fig. 1. Cyclic voltammograms of 16 mM **1**, **a**, and **c** in 0.2 M TEAP/DMF at a GC disk electrode. Sweep rate: 0.2 V s^{-1}.

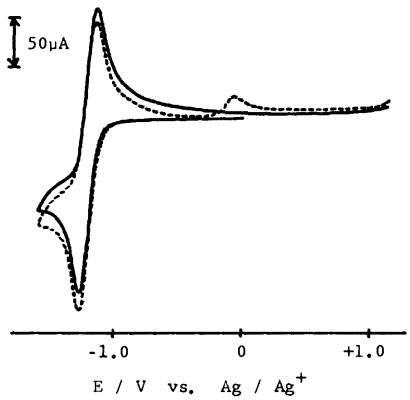

Fig. 2. Cyclic voltammograms of O_2 in the absence (——) and presence (·····) of 2 mM **1**. Sweep rate: 0.1 V s^{-1}.

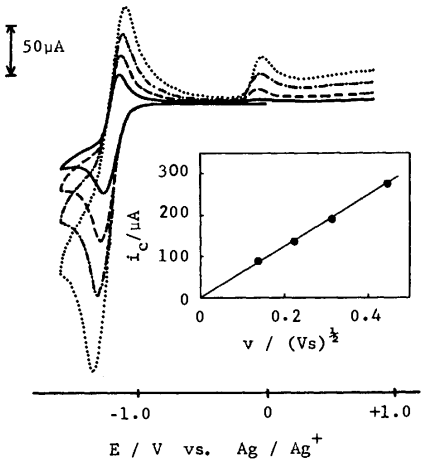

Fig. 3. Cyclic voltammograms of O_2 in the presence of 3 mM **1** at different sweep rates.
——: 0.02 V s^{-1}, ----: 0.05 V s^{-1}, —·—: 0.1 V s^{-1}, ·····: 0.2 V s^{-1}.
Inset. Sweep rate dependence of the cathodic peak current for the reduction of O_2 under 3 mM **1**.

be measured directly because of the deformed CV curve, but the peak potential is estimated to be −3.36 V.

Cyclic Voltammetry of Oxygen in the Presence of Active Methylene Compounds (1—4). As the first reduction potential of oxygen in a 0.2 M TEAP/DMF solution on glassy carbon electrode is −1.28 V, the dissolved oxygen is generally reduced more easily than active methylene compounds. Figure 2 indicates the cyclic voltammograms of saturated oxygen in the absence and presence of **1**. In the absence of **1**, the ratio of the anodic peak current (i_a°) to the cathodic peak current (i_c°) is almost 1.0; that is, the superoxide ion formed in this system is stable. In the presence of 2 mM **1**, the reductive peak current of oxygen at −1.28 V increased and the reoxidation peak current of the superoxide ion at −1.16 V decreased, in comparison with those in the absence of **1**. These results indicate that some of the superoxide ion are consumed by the reaction of **1**. The cathodic peak current of oxygen is linear to the square root of scan speed in the presence of **1** (Inset in Fig. 3). This means that the electrode reaction of oxygen is apparently diffusion-controlled, even if **1** is present in the system. The oxygen reduction behavior in the presence of other active methylene compounds **2**, **3**, and **4** gave similar to those of **1**. But the cyclic voltammograms of oxygen reduction in the case of **3** and **4** gave prepeaks. The prepeaks in the case of **3** is shown in Fig. 4.

The cyclic voltammetry of oxygen in the differrent concentrations of **1** is demonstrated in Fig. 5. Increasing the concentration of **1** resulted in a corresponding increase in the reduction peak current of oxygen. This increase of catalytic current did not continue

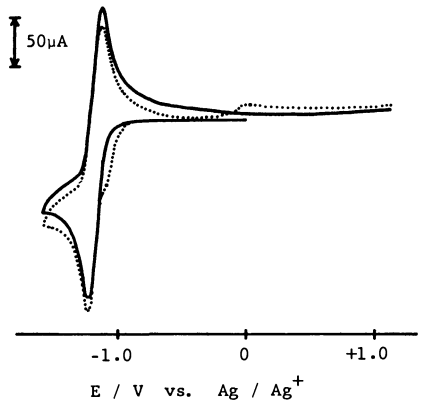

Fig. 4. Cyclic voltammograms of O_2 in the absence (——) and presence (·····) of 2 mM **3**.
Sweep rate: 0.1 V s^{-1}.

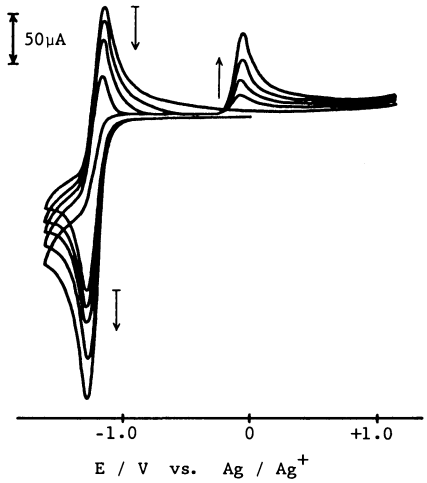

Fig. 5. Cyclic voltammograms of O_2 in the presence of different concentrations (0, 2, 4, 8, and 16 mM) of **1**.
Sweep rate: 0.1 V s^{-1}.

infinitely but reached a saturation at 18 mM **1**. The maximum value of the ratio, i_c/i_c°, is ca. 1.65, where i_c and i_c° are the reduction peak currents of oxygen in the presence and absence of **1**, respectively. These behavior is shown in Fig. 6. Increasing the concentration of **1** also resulted in a corresponding decrease in the reoxidation peak current of the superoxide ion. The peak current ratios, i_a/i_a° are getting smaller with increasing concentrations of **1**, where i_a and i_a° are the reoxidation peak currents of the superoxide ion in the presence and absence of **1**, respectively. These results also support that the electrogenerated superoxide ion is consumed by subsequent chemical reactions during cyclic voltammetry. The new anodic wave at −0.08 V (Fig. 5) is considered to be the oxidation peak characteristics of carbanion ($\overline{C}H(CO_2Et)_2$) at glassy carbon electrode, overlapped with the reoxidation wave of hydroperoxide ion (HO_2^-) formed by the following elementary reactions.

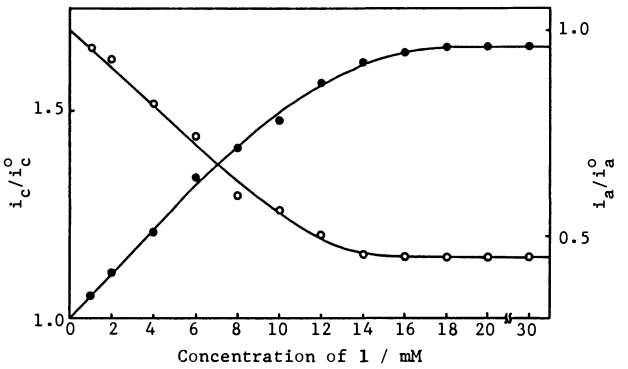

Fig. 6. Dependences of the peak current ratio for the concentration of **1**.
Sweep rate: 0.1 V s^{-1}, ●: i_c/i_c°, ○: i_a/i_a°.

$$O_2 + e^- \rightarrow O_2^{\cdot-} \quad (1)$$

$$\begin{matrix} R_1 \\ \diagdown \\ \quad CH_2 \\ \diagup \\ R_2 \end{matrix} + O_2^{\cdot-} \rightarrow \begin{matrix} R_1 \\ \diagdown \\ \quad \overline{C}H \\ \diagup \\ R_2 \end{matrix} + HO_2^{\cdot} \quad (2)$$

$$HO_2^{\cdot} + e^- \rightarrow HO_2^- \quad (3)$$

R_1, R_2: electron-withdrawing group (EWG)

The new anodic waves agreed with the oxidation peaks observed in the cyclic voltammogram of **1** by the addition of sodium ethoxide and in the cyclic voltammogram of H_2O_2 by the addition of tetraethylammonium hydroxide, respectively.

This oxidation peak current increased with the increasing concentrations of **1**. The increase did not continue infinitely, but reached a saturation in the presence of **1** of more than 18 mM. In the acetylacetone system, three new anodic peaks beside the oxidation peak of the superoxide ion formed appeared as shown in Fig. 7. The first anodic peak at −0.05 V and the second anodic peak at +0.10 V were assigned

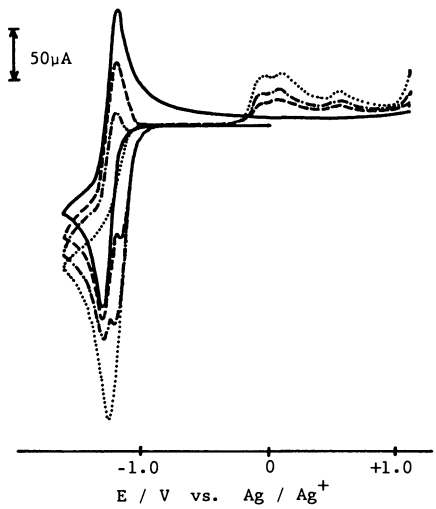

Fig. 7. Cyclic voltammograms of O_2 in the presence of different concentrations of **4**.
Sweep rate: 0.1 V s^{-1}, ——: 0 mM, ----: 4 mM, —·—: 8 mM, ·····: 16 mM.

Table 2. Observed Peak Potentials in the CV of O_2 under **1**—**4**

	Reduction peak potential/V		Reoxidation peak potential/V			
	Prepeak	Oxygen	Superoxide ion	HO_2^-	Carbanion	Unknown
1	—	−1.28	−1.16	−0.08	−0.08	—
2	—	−1.28	−1.16	−0.06	−0.06	—
3	−1.20	−1.28	−1.17	−0.07	+0.00	+0.86
4	−1.18	−1.28	−1.16	−0.05	+0.10	+0.57

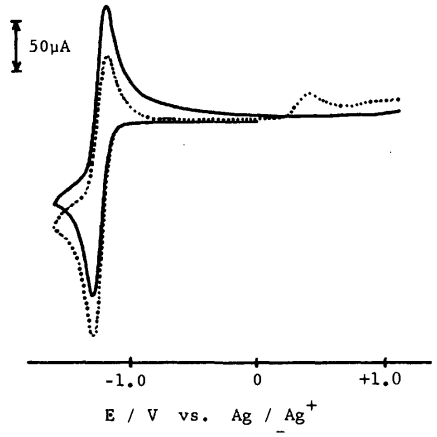

Fig. 8. Cyclic voltammograms of O_2 in the absence (——) and presence (·····) of 2 mM **a**.
Sweep rate: 0.1 V s^{-1}.

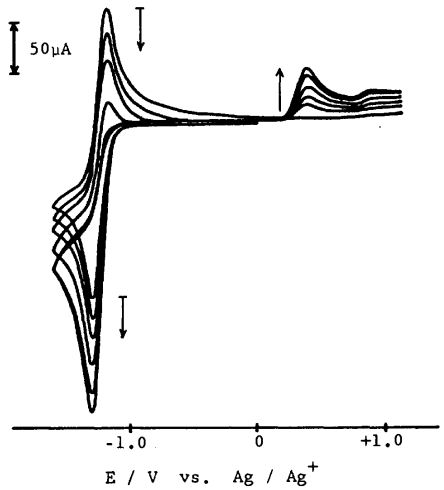

Fig. 9. Cyclic voltammograms of O_2 in the presence of different concentrations (0, 1, 2, 4, 8, and 16 mM) of **a**.
Sweep rate: 0.1 V s^{-1}.

to the oxidation peaks of HO_2^- and $\overline{C}H(COCH_3)_2$, respectively. The second peak was confirmed to appear by the addition of sodium ethoxide. The third anodic peak was not reasonably assigned. The cyclic voltammograms of oxygen in the presence of **2** were very similar to those of **1** and those of **3** were similar to those of **4**. These results are summarized in Table 2.

By comparing the ratio of anodic peak current to cathodic peak current for the oxygen redox system in the presence of 8 mM active methylene compounds, the superoxide ion is found to react with active methylene compounds in the order of **4**(pK_a=9.0)>**3** (10.2)>**2**=**1**(13.5). This order is the same as that of acidity (pK_a) of active methylene compounds as carbon acids.

Cyclic Voltammetry of Oxygen in the Presence of Dibromoalkanes (a—g). As a typical result, the cyclic voltammetry of oygen in the presence of **a** is shown in Fig. 8. This cyclic voltammogram is very similar to that in the presence of **1**. In the presence of 2 mM **2**, the first reduction peak current of oxygen at −1.30 V increased, and the reoxidation peak current of the superoxide ion at −1.18 V decreased, in comparison with those of the saturated oxygen alone. These results indicate a progress of the reaction of superoxide ion with **a**. The cyclic voltammetry of oxygen in the presence of other dibromoalkanes (**b**—**g**) gave similar results to that of **a**.†

† The electrode reaction of oxygen is also apparently diffusion-controlled in the presence of **a**—**g**.

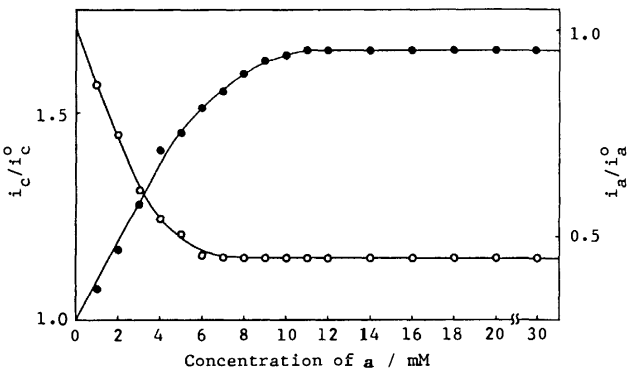

Fig. 10. Dependences of the peak current ratio for the concentration of **a**.
Sweep rate: 0.1 V s^{-1}, ●: i_c/i_c°, ○: i_a/i_a°.

When dichloroalkanes were used in place of dibromoalkanes, no change of cyclic voltammogram in the absence and presence of dichloroalkanes was observed. This means that the superoxide ion is hard to react with dichloroalkanes. On the other hand, when diiodoalkanes were used in place of dibromoalkanes, the superoxide ion reacted with diiodoalkanes to reach a saturation at lower concentrations than dibromoalkanes.

The cyclic voltammetry of oxygen was also carried out in the different concentrations of dibromoalkanes. A typical result containing **a** is shown in Fig. 9.

Table 3. Observed Peak Potentials in the CV of O_2 under a—g

	Reduction peak potential/V		Reoxidation peak potential/V		
	Prepeak	Oxygen	Superoxide ion	Bromide ion	Unknown
a	—	−1.30	−1.18	+0.38	+0.86
b	—	−1.30	−1.18	+0.33	+0.86
c	—	−1.29	−1.18	+0.33	+0.83
d	—	−1.29	−1.18	+0.35	+0.85
e	—	−1.29	−1.18	+0.40	+0.90
f	—	−1.30	−1.19	+0.32	+0.82
g	—	−1.30	−1.19	+0.32	+0.82

Increasing the concentration of **a** resulted in a corresponding increase in the reduction peak current and reached a saturation in the presence of 11 mM **a**. The maximum value of the ratio, i_c/i_c°, is ca. 1.65 and the same as in the presence of active methylene compounds. This behavior is demonstrated in Fig. 10. Two new anodic peaks at +0.38 V and +0.86 V observed in the presence of **a** can be ascribed to the oxidation of bromide ion which was produced by the nucleophilic substitution of the superoxide ion

$$Br(CH_2)_nBr + O_2^{\cdot-} \rightarrow Br(CH_2)_nOO\cdot + Br^- \quad (4)$$

with the dibromoalkane (Fig. 8). These oxidation peak currents also increased with the increasing concentrations of **a** and reached a saturation at the concentration of 11 mM. The cyclic voltammograms of oxygen in the presence of other dibromoalkanes (**b**—**g**) gave similar behavior to that of **a** and are summarized in terms of the potentials in Table 3.

Determination of Simple Rate Constants. In order to clarify each reaction rate of the electrogenerated superoxide ion with a variety of substrates, rate constants have been estimated based on a simple ECE reaction mechanism and the values determined by use of a digital simulation method are listed in Table 4. This is the method which simulates the ratio of enhancement of the cathodic peak current of oxygen reduction in the presence of substrate to that in the absence of substrate. The results indicate that the superoxide ion is more reactive with dibromoalkanes than with active methylene compounds. The rate constants for **3** and **4** could not be obtained accurately in the present simulation method, since the cyclic voltammograms of oxygen showed the prepeaks which might be a very rapid reaction between $O_2^{\cdot-}$ and **3** or **4**.

Table 4. Reaction of Electrogenerated $O_2^{\cdot-}$ with Substrates

Substrate	Rate constant $k^{a)}$/$M^{-1}s^{-1}$
Diethyl malonate (**1**)	1×10^2
Dimethyl malonate (**2**)	1×10^2
Ethyl acetoacetate (**3**)	1×10^2
Acetylacetone (**4**)	1×10^2
1,2-Dibromoethane (**a**)	6×10^2
1,3-Dibromopropane (**b**)	6×10^2
1,4-Dibromobutane (**c**)	5×10^2
1,5-Dibromopentane (**d**)	6×10^2
1,6-Dibromohexane (**e**)	6×10^2
1,3-Dibromobutane (**f**)	6×10^2
1,4-Dibromopentane (**g**)	5×10^2

a) Determined by digital simulation based on the following mechanisms.

(1) $O_2 + e^- \longrightarrow O_2^{\cdot-}$
$O_2^{\cdot-} + RH_2 \longrightarrow RH^- + HO_2^{\cdot}$
$O_2^{\cdot-} + e^- \longrightarrow HO_2^-$
$R = (EWG)_2C$

(2) $O_2 + e^- \longrightarrow O_2^{\cdot-}$
$O_2^{\cdot-} + RBr \longrightarrow ROO^{\cdot} + Br^-$
$ROO^{\cdot} + e^- \longrightarrow ROO^-$
$R = Br(CH_2)_n$

Controlled Potential Macro-Electrolysis. The controlled potential macro-electrolyses of oxygen in the presence of two kinds of substrates, active methylene compounds (**1**—**4**) and dibromoalkanes (**a**—**d**, **f**, and **g**) were carried out at −1.5 V in a 0.2 M TEAP/DMF solution. At −1.5 V, only oxygen was reduced to superoxide ion by one-electron transfer, while both

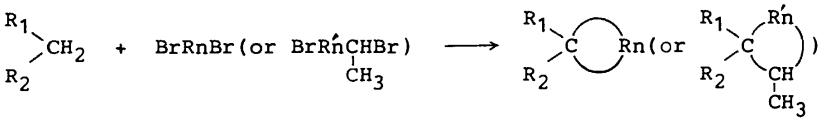

1: $R_1=R_2=CO_2Et$
2: $R_1=R_2=CO_2Mt$
3: $R_1=COCH_3$, $R_2=CO_2Et$
4: $R_1=R_2=COCH_3$

a: $Rn=(CH_2)_2$
b: $Rn=(CH_2)_3$
c: $Rn=(CH_2)_4$
d: $Rn=(CH_2)_5$
e: $Rn=(CH_2)_6$
f: $R'n=(CH_2)_2$
g: $R'n=(CH_3)_3$

5a—d **5f, g**
6a—d **6f, g**
7a—d **7f, g**
8a—d **8f, g**

Scheme 2.

the substrates, active methylene compounds and dibromoalkanes, were not reduced.

The main products were aliphatic cyclic or annulated compounds of one carbon extension comparing to the starting dibromoalkanes (Scheme 2).

Diethyl cycloalkanedicarboxylates (**5a—d**, **f**, and **g**) were produced from diethyl malonate and dibromoalkanes in the presence of electrogenerated superoxide ion, dimethyl cycloalkanedicarboxylates (**6a—d**, **f**, and **g**) from dimethyl malonate and dibromoalkanes, ethyl 1-acetylcycloalkanecarboxylates (**7a—d**, **f**, and **g**) from ethyl acetoacetate and dibromoalkanes, and 1,1-diacetylcycloalkanes (**8a—d**, **f**, and **g**) from acetylacetone and dibromoalkanes, respectively.

The electrolysis results are summarized in Table 5. Numbers in parentheses show the yields of the corresponding products by the ordinary chemical preparative method using sodium ethoxide as a base. The total amount of charge passed was ca. 482.5 C (2 F mol^{-1}). The yields by the electrochemical method and the ordinary chemical method are based on the consumed amount of active methylene compounds. The highest yield of the annulated compounds by the electrochemical method was 90% of **6c**. The yields of **5**, **6**, and **8** by the electrochemical method were higher than those by the chemical method except the case of **5f**. However, the yields of **7** were of the inverse tendency. The yields of the annulated products depended markedly on the methylene length of α,ω-dibromoalkanes, and the yields of stable ring size such as five or six membered ring were generally high. The reason can be explained by the degree of strain, when the ring closure occurs.

In the case of **1** or **2** as active methylene compound, the yields of the annulated products by the electrochemical method decreased in the order of $C_5>C_6>C_4>C_3$, similarly to those observed in the ordinary chemical reaction. In the case of **3**, a somewhat different tendency was observed. For instance, the yields by the electrochemical method decreased in the order of $C_6>C_5>C_4\approx C_3$, whereas the yields by the chemical method was in the order of $C_5>C_4\approx C_6>C_3$.

Table 5. Yields of Annulated Products by Preparative Electrochemical Method

Substrate No.	Product No.	Dibromoalkane a	b	c	d	f	g
1	**5**	49% (28%)	51% (43%)	87% (66%)	82% (50%)	20% (48%)	83% (58%)[a]
2	**6**	52% (4%)	55% (19%)	90% (20%)	81% (21%)	17% (14%)	89% (36%)
3	**7**	28% (20%)	30% (58%)	35% (58%)	56% (67%)	27% (45%)	29% (61%)
4	**8**	19% (3%)	68% (16%)	72% (23%)	58% (25%)	36% (21%)	37% (22%)

a) Numbers in parentheses show the yields of the corresponding products by the chemical preparative method in which 0.01 mol each of active methylene compound and dibromoalkane was reacted with 0.02 g·atom sodium ethoxide in ethanol at 80 °C.

The use of branched dibromoalkanes such as 1,3-dibromobutane (**f**) and 1,4-dibromopentane (**g**) decreased the yields of the annulated products in comparison to those of the same membered ring products formed from α,ω-dibromoalkanes; the yields of **5—8f**, and **7g**, **8g** are lower than those of **5—8c** and **7d**, **8d**, respectively (excluding the cases of **5f**=**5d** and **6f**>**6d**). This trend may be caused by steric hindrance of methyl branch at the carbon substituted.

From the above mentioned results, the following electrochemical reaction mechanism for the system of malonic acid ester and α,ω-dibromoalkane can be presented:

Mechanism 1: Superoxide ion as an EGB

$$O_2 + e^- \rightarrow O_2^{\cdot-} \quad (1)$$

$$\begin{matrix} R_1 \\ \diagdown \\ CH_2 \\ \diagup \\ R_2 \end{matrix} + O_2^{\cdot-} \rightarrow \begin{matrix} R_1 \\ \diagdown \\ \bar{C}H \\ \diagup \\ R_2 \end{matrix} + HO_2^{\cdot} \quad (2)$$

$$HO_2^{\cdot} + e^-(O_2^{\cdot-}) \rightarrow HO_2^- \quad (3)$$

Mechanism 2: Superoxide ion as a nucleophile

$$O_2 + e^- \rightarrow O_2^{\cdot-} \quad (1)$$

$$Br(CH_2)_nBr + O_2^{\cdot-} \rightarrow Br(CH_2)_nOO^{\cdot} + Br^- \quad (4)$$

$$Br(CH_2)_nOO^{\cdot} + e^-(O_2^{\cdot-}) \rightarrow Br(CH_2)_nOO^- \quad (5)$$

$$\longrightarrow Br(CH_2)_nO^- \quad (6)$$

$$\begin{matrix} R_1 \\ \diagdown \\ CH_2 \\ \diagup \\ R_2 \end{matrix} + Br(CH_2)_nOO^- \rightarrow$$

$$\begin{matrix} R_1 \\ \diagdown \\ \bar{C}H \\ \diagup \\ R_2 \end{matrix} + Br(CH_2)_nOOH \quad (7)$$

$$\left(\begin{matrix} R_1 \\ \diagdown \\ CH_2 \\ \diagup \\ R_2 \end{matrix} + Br(CH_2)_nO^- \rightarrow \right.$$

$$\left. \begin{matrix} R_1 \\ \diagdown \\ \bar{C}H \\ \diagup \\ R_2 \end{matrix} + Br(CH_2)_nOH \right) \quad (8)$$

$$\begin{matrix} R_1 \\ \diagdown \\ \bar{C}H \\ \diagup \\ R_2 \end{matrix} + Br(CH_2)_nBr \rightarrow \begin{matrix} R_1 \\ \diagdown \\ C \\ \diagup \\ R_2 \end{matrix} \begin{matrix} H \\ \diagup \\ \\ \diagdown \\ (CH_2)_nBr \end{matrix} + Br^-$$

$$\rightarrow\rightarrow \begin{matrix} R_1 \\ \diagdown \\ C^- \\ \diagup \\ R_2 \end{matrix} \begin{matrix} \\ \diagup \\ \\ \diagdown \\ (CH_2)_nBr \end{matrix} \rightarrow\rightarrow \begin{matrix} R_1 \\ \diagdown \\ C \\ \diagup \\ R_2 \end{matrix} \overset{(CH_2)_n}{\frown} + Br^- \quad (9)$$

R_1, R_2: electron-withdrawing group (EWG)

In mechanism 1, superoxide ion, as an electrogenerated base (EGB), deprotonates an active methylene compound (Eq. 2), and the resulting carbanion reacts with α,ω-dibromoalkane to yield the aliphatic annulated compound (Eq. 9). In mechanism 2, superoxide ion, as a nucleophile, reacts with α,ω-dibromoalkane, and the produced bromoalkylperoxy radical (Eq. 4) is further reduced by superoxide ion or by an electron from the electrode to form bromoalkylperoxide ion

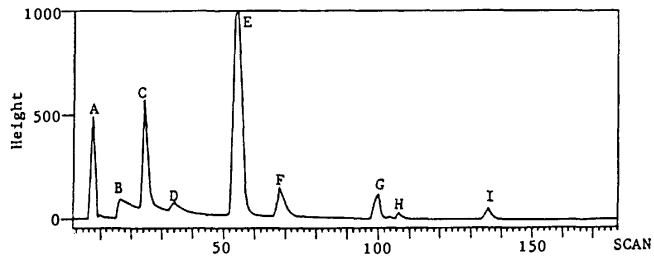

Fig. 11. Typical gas chromatogram of the reaction of $O_2^{\cdot-}$ with **1** and **c**.
A: acetone, B: DMF, C: $CH_2(CO_2Et)_2$,
D: $Br(CH_2)_4Br$,

E: 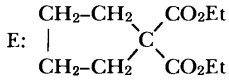 (M^+=215),

F: 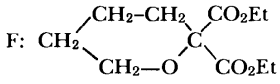 (M^+=231),

G: 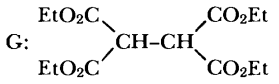 (M^+=319),

H: 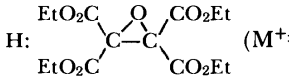 (M^+=333),

I: 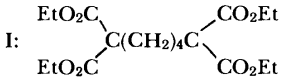 (M^+=375).

(Eq. 5) or bromoalkyloxide ion (Eq. 6). The resulting anions deprotonate, as a base, the active methylene compound (Eqs. 7 and 8), and the produced carbanion reacts with α,ω-dibromoalkane to yield the aliphatic annulated compound as mechanism 1 (Eq. 9). The similar reaction mechanism can be presented in the other cases of branched dibromoalkanes.

In addition to the annulated compounds, cyclic ethers such as tetrahydrofuran and diols such as 1,4-butanediol from **c** were also detected as minor products by the careful gas chromatographic analysis at room temperature, and identified by comparing their retention times with those of authentic samples. Other by-products, mainly some dimers, were detected and assigned using GC-MS spectroscopy. The gas chromatogram in the case of the reaction of $O_2^{\cdot-}$ with **1** and **c** is demonstrated in Fig. 11, and each peak was assigned to the compound shown in the figure, respectively. Most of these by-products were not detected in the products by the ordinary chemical method.

These results indicate that the reaction mechanism for the present electrochemical reaction might be partly different from that for the ordinary chemical reaction. The main difference is that electrogenerated superoxide ion forms intermediates shown in Eqs. 4—6, whereas sodium ethoxide does not form such intermediates. Therefore, the carbanion formation via Eqs. 7 and 8 cannot proceed by the ordinary chemical method.

Conclusion

Perkin-Markovnikov type reaction initiated with electrogenerated superoxide ion was investigated electrochemically using cyclic voltammetry and controlled potential macro-electrolysis. By electrolyses, superoxide ion acted as a base and a nucleophile, and reacted with both the substrates, active methylene compounds and dibromoalkanes, to yield the end products, aliphatic cyclic compounds. This electrochemical method can be applied to synthesize one carbon-extended cyclic compounds from dibromoalkanes.

Besides these compounds as the main products, many by-products, such as dimers and cyclic ethers were detected using GC-MS spectroscopy. The formation reaction of the cyclic ethers is a novel reaction which has never been seen in the usual base-catalyzed reactions. All of these results are based on the dual nature of electrogenerated superoxide ion; i.e., basicity and nucleophilicity, which vary with substrates.

References

1) G. A. Hamilton, "Chemical Models and Mechanisms for Oxygenases in Molecular Mechanisms of Oxygen Activation," ed by O. Hayaishi, Academic Press, New York (1975), p. 405.
2) R. Dietz, M. E. Peover, and P. Rothbaum, *Chem. Ing. Techn.*, **42**, 185 (1975).
3) T. Osa and M. Tezuka, *Denki Kagaku*, **44**, 2 (1976).
4) E. Lee-Ruff, *Chem. Soc. Rev.*, **1977**, 195.
5) M. Sugawara, M. M. Baizer, W. T. Monte, R. D. Little, and U. Hess, *Acta Chem. Scand., Ser. B*, **37**, 509 (1983).
6) R. Dietz, A. E. J. Forno, B. E. Larcombe, and M. E. Peover, *J. Chem. Soc. B*, **1970**, 816.
7) J. S. Valentine and A. B. Curtis, *J. Am. Chem. Soc.*, **97**, 224 (1975).
8) J. W. Peters and C. S. Foote, *J. Am. Chem. Soc.*, **98**, 873 (1976).
9) F. Ojima, T. Matsue, and T. Osa, *Chem. Lett.*, **1987**, 2235.
10) W. H. Perkin, *Ber.*, **16**, 208 (1883).
11) W. Markovnikov and Krestovnikov, *Justus Liebigs Ann. Chem.*, **208**, 333 (1881).
12) R. P. Mariella and R. Raube, *Org. Synth.*, **IV**, 288 (1963).

Studies of the Acidity and Ionic Conductivity of Silica-Supported Heteropoly Compounds. I. The Dehydration of *t*-Butyl Alcohol over Heteropoly Compound Catalysts

Reiji OHTSUKA,* Yoshio MORIOKA, and Jun-ichi KOBAYASHI
Department of Applied Chemistry, Faculty of Engineering, Shizuoka University, Johoku, Hamamatsu 432
(Received February 21, 1989)

The dehydration of *t*-butyl alcohol (TBA) using various heteropoly compound (HPC) catalysts has been studied. Taking the adsorption of water on the surface of the catalyst into consideration, it is presumed that the dehydration of liquid TBA is governed by a Langmuir-Hinshelwood-like mechanism. Also, the change in the catalytic activity with the amount of HPC supported on the silica suggests that TBA is dehydrated through a pseudo-liquid mechanism in which a few layers of the HPC supported take part in the catalytic reaction. The layer thickness, regarded as a pseudo-liquid phase, depends markedly on the kind of HPC supported. For the dehydration of gaseous TBA, on the contrary, the reaction is found to be of the zero-order; it proceeds through in outer-surface mechanism in which only the outer layer of HPC is effective.

Heteropoly compounds (HPC) e.g., 12-molybdophosphoric acid and its salts have been widely used as catalysts for various kinds of reactions since SOHIO catalysts were applied to the oxidation of α,β-unsaturated aldehydes.[1] As may be seen from the latest industrial applications of the hydration of propylene,[2] the selective oxidation of methacrylaldehyde[3] and the oxidative dehydrogenation of isobutyric acid,[4] it is apparent that heteropoly acid (HPA) catalysts are useful for the hydration, dehydration, and dehydrogenation of organic compounds.[5-9]

Some of the HPA catalysts not only behave as strong acids, but also play rôles as oxidizing agents.[10] Also, it has been reported that both surface and inner sites of solid HPC take part in some catalytic reactions, like liquid catalysts. Misono et al. have called this phenomenon the "pseudo-liquid mechanism."[11] For these reasons, there is still much controversy as to the catalytic rôle in the supported HPC for the respective reactions, despite the fact that they are widely used practically.[12] The present paper, therefore, deals with the dehydration of liquid and gaseous *t*-butyl alcohol (TBA):

$$(CH_3)_3C\text{-}OH \rightarrow (CH_3)_2C{=}CH_2 + H_2O \qquad (1)$$

in the presence of the supported HPA on the basis of the activity and the activation energy of the dehydration reaction obtained. HPC prepared by the substitution of other cations, such as sodium, potassium, and ammonium, for the hydrogen ions of HPA will be examined as well, since the control of acid and oxidizing properties is particularly important for catalytic reactions in order to get products with a high yield and selectivity.

Experimental

Preparation of Catalysts. As-received 12-molybdophosphoric acid and 12-tungstophosphoric acid from the Japan New Metals Co., Ltd., were used. The supports used AEROSIL-200, AEROSIL-OX50, AEROSIL-300, and AEROSIL-380 (Aerosil Nippon Co., Ltd.) has surface areas S of about 200, 50, 130, 300, and 380 m^2g^{-1} respectively. Solutions or emulsions of HPC were prepared as follows: Potassium salt emulsions of HPA were prepared by the slow addition of an aqueous potassium carbonate solution into a HPA solution. Sodium and ammonium salt solutions and cesium salt emulsions were obtained by the same procedures. Bismuth oxide salt solutions were prepared by using bismuth carbonate oxide in 0.10 mol dm^{-3} nitric acid. The degree of the substitution of other cations for the hydrogen ion of HPA was defined as the number of hydrogen-ion-substituted n.

The support-free catalysts were as-received HPA themselves or were prepared drying the HPC solutions or the emulsions at 383 K for 24 h, grinding them, and then calcining them at 573 K for 3 h. The supported catalysts were obtained by the following procedure. The support was calcined at 773 K for 3 h and then impregnated with a required amount of the HPC solution. The resulting solution was dried at 383 K for 24 h, ground, and then calcined at 573 K for 3 h. The supported amount of HPC was expressed as m, milimoles of HPC per gram of support; The m varied are the range of 0.05—1.50 mmol/g-supt. The IR spectra confirmed that the catalysts containing bismuth oxide ions were free from nitrate ions. The resulting support-free and supported catalysts will hereafter be abbreviated as H_3PMo-HPA and H_3PMo/SiO_2-200 respectively, where SiO_2-200 stands for AEROSIL-200.

Dehydration of *t*-Butyl Alcohol. The dehydration of liquid TBA in the heterogeneous system using supported catalyst was carried out in a batchwise reactor. The TBA of 0.212 mol (20 cm^3) was pipetted into a 300 cm^3 flask, after which the supported catalyst of 0.15 g was placed in an inner glass ampoule separated from the TBA. They were kept in a preheated oil bath. The TBA was refluxed for more than 1 h at 355.3 K. Afterwards, the ampoule was broken to cause the dehydration of TBA to start. The amount of isobutene (IB) generated as time passed was measured by the use of a gas burette.

The conversion X(liq) was determined as follows:

$$X(\text{liq}) = A/B_0 \times 100 \qquad (2)$$

where A and B_0 stand for the amount of IB generated (mol) and the initial amount of TBA (mol) respectively.

The eluted HPA was determined as follows. The HPA dissolved in the TBA solution was separated from the

dispersed HPA on the support by means of centrifugation. The TBA solution was dried at 383 K for 24 h and then calcined at 573 K for 3 h. The residue was dissolved in a certain volume of water for analysis. An appropriate volume of the sodium hydroxide solution was added to the solution, and then the excess amount of sodium hydroxide was titrated with hydrochloric acid.

The dehydration of TBA in the presence of a support-free H_3PMo solution, in which the H_3PMo has been dissolved in TBA of 20 cm^3, was also examined. The H_3PMo concentration was adjusted to 3.00 mmol dm^{-3}. The amount of H_3PMo present in the solution of 20 cm^3 corresponds to that in 0.40 mmol/g-supt H_3PMo/SiO_2-200 of 0.15 g.

Gas-phase dehydration was performed in a conventional cylindrical continuous-flow-type quartz-reactor, 16 mmϕ× 525 mm, in the temperature range between 413 and 513 K under atmospheric pressure. The catalyst (0.15 g) was mixed with glass beads (5 g) and then placed in the fixed-bed. TBA was fed continuously into the reactor through a preheated tube at the flow rate of 0.158, 0.211, 0.317, and 0.422 mol h^{-1} using a microfeeder. After passing through the reactor, the gas was cooled by a circulation device using circulated ice-cooled water in order to remove the TBA and water. Then the IB generated was assayed by measuring the time taken to obtain 10 cm^3 of IB by the use of a gas burette.

The conversion X(gas) was estimated as:

$$X(\text{gas}) = V/F \times 100 \tag{3}$$

where V is the velocity of IB generated (mol h^{-1}), and F, the velocity of TBA supplied (mol h^{-1}).

Results and Discussion

Kinetics of the Dehydration of Liquid *t*-Butyl Alcohol. Figure 1 shows the representative plots of the conversion X(liq) as a function of the time exiled. The conversion increases markedly with the amount of the supported H_3PMo at the low loadings (less than 0.6 mmol/g-supt), while it increases slightly at higher loadings (Fig. 1(a)). When the hydrogen ions of H_3PMo and H_3PW are replaced by a potassium ion, the catalytic activity decreases with the increase in the number of hydrogen ions substituted n from 1 to 3 (Fig. 1(b)). A similar trend was observed for the replacement of sodium and ammonium ions.

It seems probable that the water evolved during the dehydration of TBA is adsorbed on the surface of HPC. Assuming the formation of the TBA, HPC, TBA·HPC, and H_2O·HPC species, the following Langmuir-Hinshelwood mechanism is obtained:

$$\text{TBA} + \text{HPC} \overset{K_B}{\rightleftarrows} \text{TBA}\cdot\text{HPC} \tag{4}$$

moreover

$$H_2O + \text{HPC} \overset{K_W}{\rightleftarrows} H_2O\cdot\text{HPC} \tag{5}$$

$$\text{TBA}\cdot\text{HPC} \xrightarrow{k_1} \text{IB} + H_2O + \text{HPC} \tag{6}$$

where K_B, and K_W are the equilibrium constants for Eqs. 4 and 5 respectively, and k_1, the rate constant for

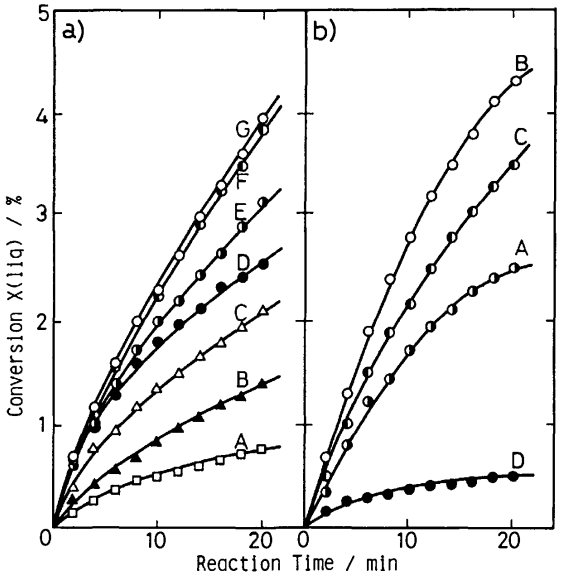

Fig. 1. Plots of the conversion vs. the exciled time for the dehydration of liquid TBA over a) H_3PMo/SiO_2-200 with various loadings of H_3PMo; A: m=0.05, B: m=0.10, C: m=0.20, D: m=0.30, E: m=0.45, F: m=0.60, G: m=0.90 mmol/g-supt H_3PMo/SiO_2-200 and b) 0.10 mmol/g-supt $K_nH_{3-n}PW/SiO_2$-200; A: n=0, B: n=1, C: n=2, D: n=3.

Reaction 6, which will be defined in detail in a later paragraph. Equilibria 4 and 5 lead to these relations:

$$K_B = \frac{[\text{TBA}\cdot\text{HPC}]_s}{[\text{TBA}]\cdot[\text{HPC}]_s} \tag{7}$$

and

$$K_W = \frac{[H_2O\cdot\text{HPC}]_s}{[H_2O]\cdot[\text{HPC}]_s} \tag{8}$$

respectively, where [TBA] and [H_2O] are the equilibrium concentrations of TBA and water (mol dm^{-3}) respectively and where [HPC]$_s$, [TBA·HPC]$_s$, and [H_2O·HPC]$_s$ are the concentrations of HPC, TBA·HPC, and H_2O·HPC at the surface of the catalyst per liter of the HPC-dispersed TBA solution (mol dm^{-3}). If K_B and K_W are big enough, the total concentration of the surface HPC, [HPC]$_{s,t}$ (mol dm^{-3}), should be expressed as:

$$[\text{HPC}]_{s,t} = [\text{TBA}\cdot\text{HPC}]_s + [H_2O\cdot\text{HPC}]_s \tag{9}$$

By combining Eqs. 7, 8, and 9, the following relation is derived:

$$\frac{[\text{TBA}\cdot\text{HPC}]_s}{[\text{HPC}]_{s,t}} = \frac{K_B\cdot[\text{TBA}]}{K_B\cdot[\text{TBA}]+K_W\cdot[H_2O]} \tag{10}$$

On the other hand, the rate of the reaction r (min^{-1}) for Eq. 6 is given by:

$$r = k_1\cdot[\text{TBA}\cdot\text{HPC}]_s, \tag{11}$$

and so the relation:

$$r=\frac{k_1\cdot K_B\cdot[TBA]\cdot[HPC]_{s,t}}{K_B\cdot[TBA]+K_W\cdot[H_2O]} \quad (12a)$$

or

$$\frac{1}{r}=\frac{K_W\cdot[H_2O]}{K_B\cdot k_1\cdot[HPC]_{s,t}\cdot[TBA]}+\frac{1}{k_1\cdot[HPC]_{s,t}} \quad (12b)$$

is worked out. Eq. 12b implies a linear relationship between $1/r$ and $[H_2O]/[TBA]$.

Figure 2 shows the plots of $1/r$ as a function of $[H_2O]/[TBA]$, in which the value of the rate of the reaction for each point was estimated from the data in Fig. 1. It can be seen that this does indeed give a linear relation, implying that the mechanism assumed above is reasonable for the dehydration of liquid TBA with the supported HPC. The same mechanism can also be deduced for the other supported HPCs examined. For this reason, the apparent rate constant k_1' ($=k_1\cdot[HPC]_{s,t}$) and the value of K_W/K_B for the dehydration of liquid TBA with the supported HPC are evaluated from the intercept and the slope of the lines in Fig. 2 respectively.

In the series of molybdophosphates examined, it was observed that the catalysts turned from yellow to blue during the dehydration of TBA, indicating that hexavalent molybdenum is reduced to a pentavalent one. However, the catalysts pre-reduced by hydrogen gas at 373 K did not show any particular catalytic activity. This proves that the dehydration of TBA proceeds via an acid catalytic reaction, not via a redox reaction.

Mechanism of the Dehydration of Liquid *t*-Butyl Alcohol. Figure 3 shows the plots of the apparent rate constant k_1' against the amount of HPC supported on AEROSIL-200. It is noteworthy that, for all the catalysts studied, the apparent rate constant k_1' increases linearly with the amount of HPC loaded, and that it then approaches a limiting value. Also, the activity is in this order: H_3PMo/SiO_2-200<H_3PW/SiO_2-200, while it decreases with the degree of substitution for the hydrogen ion of HPA. The limiting values of the apparent rate constant, k_L, for the respective catalysts are summarized in Table 1.

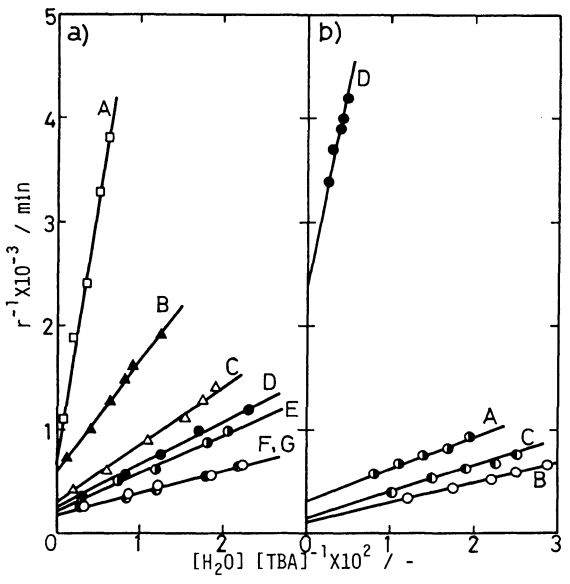

Fig. 2. Kinetics for the dehydration of liquid TBA over a) H_3PMo/SiO_2-200 with various loadings of H_3PMo; A: m=0.05, B: m=0.10, C: m=0.20, D: m=0.30, E: m=0.45, F: m=0.60, G: m=0.90 mmol/g-supt H_3PMo/SiO_2-200 and b) 0.10 mmol/g-supt $K_nH_{3-n}PW/SiO_2$-200; A: n=0, B: n=1, C: n=2, D: n=3.

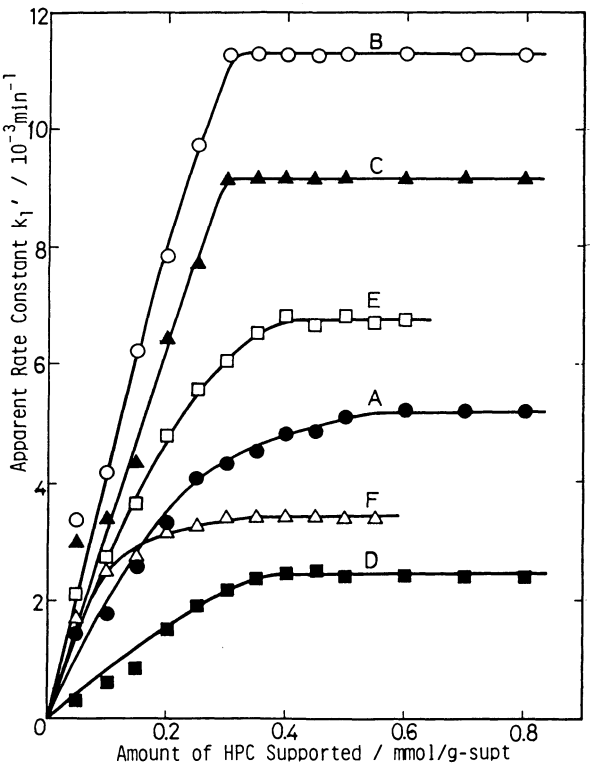

Fig. 3. The plots of the apparent rate constants for the dehydration of liquid TBA k_1' against the amount of HPC supported on silica m; A: H_3PMo/SiO_2-200, B: KH_2PMo/SiO_2-200, C: K_2HPMo/SiO_2-200, D: K_3PMo/SiO_2-200, E: H_3PW/SiO_2-200, F: H_3PMo/SiO_2-130.

Considering the effective cross section per molecule σ of HPC:

$$\sigma=1.09\,(M/L\cdot D)^{2/3} \quad (13)$$

the surface coverage θ is expressed as:

$$\theta=m\cdot\sigma\cdot(L/S)\times10^{-4} \quad (14)$$

where M and D are the molecular weight and the density of HPC respectively, and L, the Avogadro number.

Assuming that HPC molecules adsorb both on the HPC monolayer deposited on the support and on the surface of the support, critical values of m=0.30 or 0.60 can be expected if one or two layers are available respectively. The value of m at the limiting value of the apparent rate constant m_L for H_3PMo/SiO_2-200 in

Table 1. Limiting Activity for the Dehydration of Liquid TBA

HPC[a]	m_L[b] mmol/g-supt	θ_L[c]	$k_L \times 10^3$[d] min^{-1}
H_3PMo	0.55	1.82	5.30
KH_2PMo	0.30	1.01	11.25
K_2HPMo	0.30	1.02	9.15
K_3PMo	0.35	1.20	2.40
Na_3PMo	0.60	1.01	2.00
Cs_3PMo	0.35	1.20	2.25
$(BiO)_3PMo$	0.30	1.22	1.40
H_3PW	0.40	1.79	8.50
K_3PW	0.25	1.15	1.25
$(NH_4)_3PW$	0.25	1.13	1.75

a) The support used is AEROSIL-200 (S=200 $m^2 g^{-1}$). b) m_L means the amount of HPC supported reached at the limiting activity. c) θ_L means the surface coverage given by Eq. 15 at m_L. d) k_L is the limiting activity.

Table 1 agrees well with the latter one. For the other catalysts studied, the values of m_L are in harmony with either critical one.

The number of layers of HPC available for the dehydration of TBA θ_L is, estimated as:

$$\theta_L = m_L/m_1 \quad (15)$$

where m_1 represents the amount of HPC required for the formation of a monolayer on a support. As θ_L=1.82 for H_3PMo/SiO_2-200 is obtained, it is presumed that two layers at the surface of H_3PMo take part in the dehydration of liquid TBA. For the cation-substituted catalyst KH_2PMo/SiO_2-200, on the contrary, the value of θ_L is estimated to be 1.01, implying that only one layer takes part in the catalytic reaction. The difference in the thickness of the pseudo-liquid phase between HPA and its salts may be attributable to the difference in their hydrophilic/hydrophobic properties. Consequently, it is presumed that the dehydration of liquid TBA using the supported HPC proceeds through a pseudo-liquid mechanism.

Effect of Water. Figure 4 shows the plots of the K_W/K_B ratio against the amount of H_3PW and its potassium salts supported on AEROSIL-200. It is apparent that the K_W/K_B ratio decreases with the increase in the number of hydrogen ions substituted n from 1 to 3, this is consistent with the magnitude of the k_1' value. There is no doubt that the anomalously low activity of HPA for the dehydration of TBA compared with those of its salts is attributable to the adsorption of water: the greater the number of hydrogen ions substituted, the more hydrophobic the resulting catalyst is. The cause is the decrease in the affinity of HPC for alcohol. Similar results were also obtained for H_3PMo and its potassium salts (Table 1). It is, therefore, concluded that the hydrophobic/hydrophilic properties of the surface for the supported catalyst are a primary factor affecting their catalytic

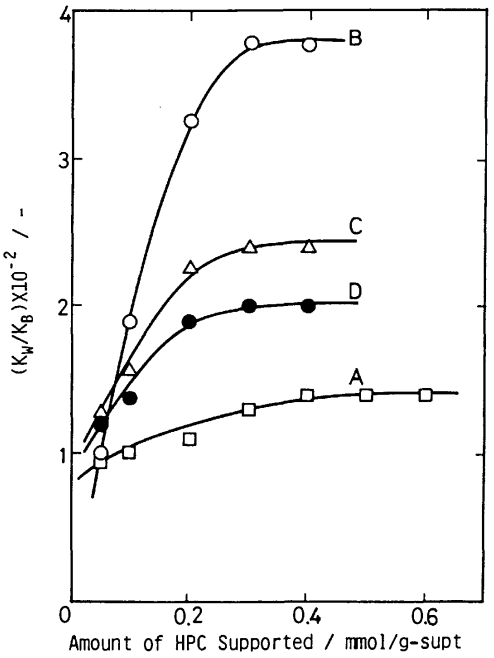

Fig. 4. The plots of K_W/K_B as a function of the amount of $K_nH_{3-n}PW$ supported on AEROSIL-200 m; A: n=0, B: n=1, C: n=2, D: n=3.

activity for the dehydration of liquid TBA.

In Fig. 5, the rate constant k_1 is plotted as a function of the amount of H_3PW and its potassium salts supported on AEROSIL-200. The value of k_1 increases with the HPC loadings until it reaches a maximum at m=0.20; thereafter decreases. At the maximum, θ_L=1, so that the increase in the rate constant at low loadings may be ascribed to the two-dimensional network formation of H_3PW molecules, while the decrease at higher loadings seems due to the stacking effect of HPC molecules on each other. Also, it is presumed that the cluster of HPC in the two-dimensional network works more effectively as a catalyst than does the HPC molecule distributed separately.

Effect of Surface Area of Support. Concerning the surface area of the support, the relative activity of HPC is found to be enhanced as the surface area decreases (Table 2). This may come from the fact that the smaller the surface area is, the easier the two-dimensional network formation of HPC should be.

Comparison of Heterogeneous and Homoeneous Catalysts. The elution of HPA in the heterogeneous system mentioned above has been examined. The kinetics of the dehydration of TBA in the homogeneous systems with the H_3PMo and H_3PW solutions confirms that the reaction proceeds through the same mechanism as does that of the heterogeneous system. H_3PW was found to be more active than H_3PMo, which is the same in the heterogeneous system. A comparison between the heterogeneous and the homogeneous systems indicates that the apparent rate constant of the heterogeneous one is much larger than

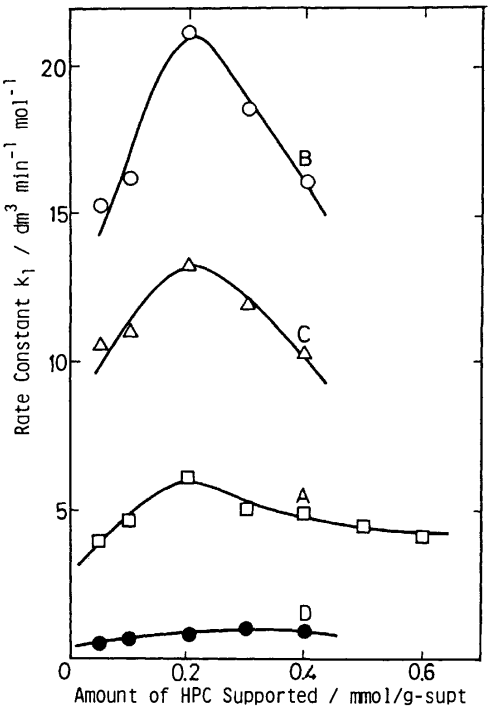

Fig. 5. The plots of rate constant k_1 as a function of the amount of $K_nH_{3-n}PW$ with supported on AEROSIL-200 m; A: n=0, B: n=1, C: n=2, D: n=3.

that of the homogeneous one by a factor of 10. The HPA (6.2, 7.2, and 10.5%) was eluted into the solution in 20 min in the heterogeneous system with H_3PMo, with m=0.20, 0.40, and 0.80 respectively. Hence, under these conditions, the elution of H_3PMo is not considered to affect the activity significantly, especially the initial activity.

Kineties of the Dehydration of Gaseous *t*-Butyl Alcohol. For the dehydration of gaseous TBA, the conversion become constant in 10 min, whatever the catalyst examined. Figure 6 shows plots of the conversion X(gas) as a function of the contact time W/F, in which W denotes the weight of the catalyst (g). There is no doubt that the dehydration of gaseous TBA proceeds through a zero-order reaction.

Assuming the reaction:

$$\text{TBA}\cdot\text{Catalyst} \xrightarrow{k_0} \text{IB} + H_2O + \text{Catalyst} \quad (6')$$

where k_0 is the rate constant for Reaction 6′ per gram of the catalyst (mol g^{-1} h^{-1}), the rate for Reaction 6′ V (mol h^{-1}) is given by:

$$V = k_0\cdot[\text{TBA}\cdot\text{Catalyst}] \quad (16)$$

where [TBA·Catalyst] is the weight of the species TBA·Catalyst (g). If K_B is big enough, and if K_W is small enough to neglect, Eq. 16 should be expressed as:

$$V = k_0\cdot[\text{Catalyst}] = k_0\cdot W \quad (17)$$

where [Catalyst] is the weight of the catalyst (g). By combining Eqs. 2 and 17, the following relation is derived:

$$X(\text{gas}) = k_0\cdot W/F\times 100 \quad (18)$$

The rate constant k_0 was obtained from the slopes given in Fig. 6 at a constant temperature. It is noticeable that the activity of the catalyst was decreased markedly after the feed had been stopped once or when the reaction temperature was raised over 473 K. However, it was re-activated by calcination at 573 K for 3 h. Further investigations of this point are in progress.

Effect of the Amount of HPC Supported for the Gas-Phase Dehydration of *t*-Butyl Alcohol. Figure 7 shows the plot of the rate constant k_0 as a function of the amounts of various HPCs supported on AEROSIL-200. It is obvious that the rate constant k_0 increases with the increase in the amount of HPC supported at the low loadings and is in the order of: $H_3PW \fallingdotseq H_3PMo > KH_2PMo > K_2HPMo > K_3PMo$, in harmony with the increase in the number of hydrogen ions replaced by potassium. For the H_3PMo/SiO_2-200 and H_3PW/SiO_2-200, the values of m_L at the maximum rate constant were 0.25—0.30 (θ_L=0.83—0.99) and 0.20 (θ_L=0.90) respectively. These values are remarkably different from those for the dehydration of liquid TBA, supporting the idea that only the first layer of HPC in contact with reaction gases takes part in the dehydration of gaseous TBA. It is, therefore, concluded that the dehydration proceeds through the outer-surface mechanism.

Table 2. Limiting Activity for the Dehydration of Liquid TBA

Catalyst	m_L[a]	θ_L[b]	$k_L\times10^3$[c]	$k_L/S\times10^5$[d]
	mmol/g-supt		min^{-1}	min^{-1} m^{-2} g
H_3PMo/AEROSIL-OX50[e]	0.15	1.98	3.00	6.00
H_3PMo/AEROSIL-130[f]	0.35	1.78	3.45	2.65
H_3PMo/AEROSIL-200[g]	0.55	1.82	5.30	2.65
H_3PMo/AEROSIL-300[h]	0.75	1.62	7.20	2.40
H_3PMo/AEROSIL-380[i]	1.00	1.74	8.35	2.20

a) m_L means the amount of HPC supported reached at the limiting activity. b) θ_L means the surface coverage given by Eq. 15 at m_L. c) k_L is the limiting activity. d) k_L/S means the relative activity per unit of surface area. d—h) The supports used have the surface areas S of e) 50, f) 130, g) 200, h) 300, and i) 380 m^2 g^{-1}.

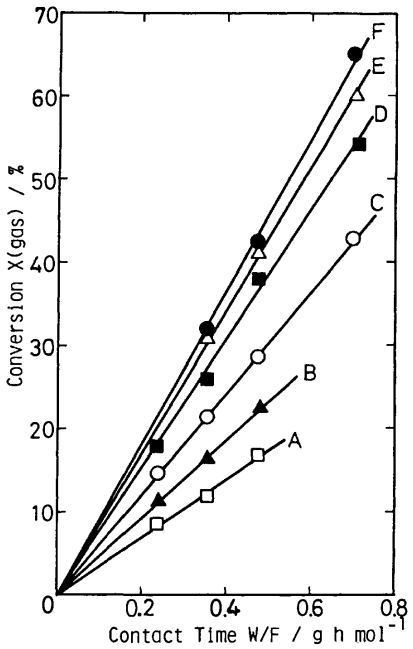

Fig. 6. Kinetics for the dehydration of gaseous TBA over 0.05 mmol/g-supt H_3PMo/SiO_2-200 at various temperature T; A: T=413 K, B: T=433 K, C: T=453 K, D: T=473 K, E: T=493 K, F: T=513 K.

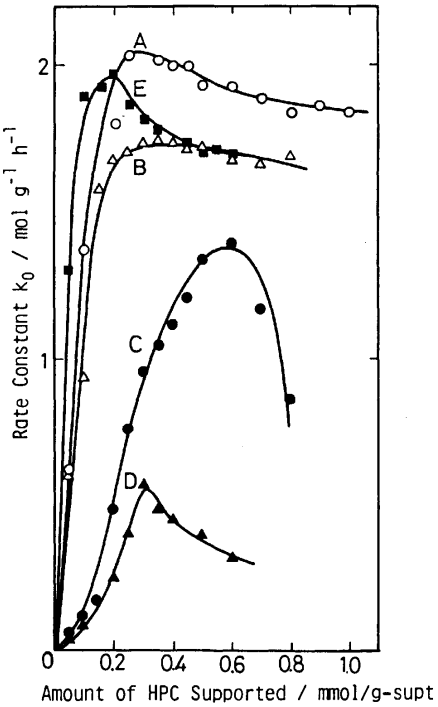

Fig. 7. The plots of the rate constants for the dehydration of gaseous TBA k_0 at 453 K against the amount of HPC supported on AEROSIL-200 m; A: H_3PMo/SiO_2-200, B: KH_2PMo/SiO_2-200, C: K_2HPMo/SiO_2-200, D: K_3PMo/SiO-200, E: H_3PW/SiO_2-200.

At higher loadings of HPC, X-ray diffraction confirmed that they were crystallized. If the diffusion of TBA in the crystal of HPC plays a significantly important rôle in its dehydration rate, the activation energy should depend on the amount of the supported HPC. However, as may be seen in Table 3, the activation energies for the gas-phase dehydration using H_3PMo/SiO_2-200 are independent of the amounts loaded. It is, therefore, presumed that the reaction at the surface is the rate-determining step for the dehydration of gaseous TBA. These results also supported the outer-surface mechanism.

In the dehydration of gaseous TBA using HPA and its potassium salts, the order for the activity with respect to the substitution of hydrogen ions of HPA can reasonable interpreted in terms of the acidity. In the dehydration of liquid TBA, on the contrary, the activity of HPA is not consistent with the order of the acidity. It is conceivable that the extremely low activity of HPA is due to the adsorption of water at the surface of the catalyst.

Concerning the species formed by the replacement of the hydrogen ion by the potassium ion, it has been reported that only one species, $K_3PMo_{12}O_{40}$, is formed, while the $H_3PMo_{12}O_{40}$ species grows epitaxially on its surface.[13] Taking this into consideration, the species with the compositions of K_2HPMo and KH_2PMo are considered to be mixtures of the $H_3PMo_{12}O_{40}$ and $K_3PMo_{12}O_{40}$ species, with K/HPC molar ratios of 2

Table 3. Activation Energy for the Dehydration of Gaseous TBA over HPC Supported on AEROSIL-200

m[a]	Activation energy/kJ mol^{-1}				
mmol/g-supt	H_3PMo[b]	KH_2PMo[b]	K_2HPMo[b]	K_3PMo[b]	H_3PW[b]
0.05	27.2	38.2	39.0	38.2	17.4
0.10	26.6	34.9	35.2	35.8	15.4
0.25	26.8	19.1	20.8	50.7	10.0
0.40	26.2	18.3	18.3	25.7	10.4
0.70	27.0	10.0	17.4	36.6	—
1.00	27.0	—	—	—	—
Free[d]	1.9	—	—	—	—

a) m means the amount of HPC supported on AEROSIL-200. b) The support used is AEROSIL-200 (S=200 m^2 g^{-1}). d) "Free"the support-free H_3PMo-HPA.

and 1 respectively. It can, therefore, be speculated that, at low loadings of HPC, the two species are formed simultaneously on the silica support, while at higher loadings the $H_3PMo_{12}O_{40}$ species is stacked on the $K_3PMo_{12}O_{40}$.

As may be seen from Fig. 7, the values of m_L are 0.30—0.40 (θ_L=1.01—1.34), 0.60 (θ_L=2.04), and 0.30 (θ_L=1.03), for KH_2PMo/SiO_2-200, K_2HPMo/SiO_2-200, and K_3PMo/SiO_2-200 respectively. The dehydration of gaseous TBA with potassium-substituted HPA is thought to proceed through the outer-surface mechanism. If $H_3PMo_{12}O_{40}$ and $K_3PMo_{12}O_{40}$ are distributed homogeneously, the value of θ_L is expected to be approximately unity. Taking the heterogeneous distribution of $H_3PMo_{12}O_{40}$ and $K_3PMo_{12}O_{40}$ (the growth of the $H_3PMo_{12}O_{40}$ species on the surface of the $K_3PMo_{12}O_{40}$ species) into consideration, however, the theoretically estimated values of θ_L are 1.50 and 3.00 for KH_2PMo/SiO_2-200 and K_2HPMo/SiO_2-200 respectively. The experimental results support the latter distribution (Fig. 7).

The activation energies for K_3PMo/SiO_2-200 are about 37 kJ mol^{-1}, regardless of the amount of HPC supported. As may be seen in Table 3, the activation energies for the gas-phase dehydration using partially potassium-substituted HPA decrease with an increase in the amount of HPC supported: at low loading of HPC supported, the activation energy is similar to the value for K_3PMo/SiO_2-200, while at higher loadings of HPC, it is similar to that for H_3PMo/SiO_2-200. It is, therefore, reasonable to speculate that the $H_3PMo_{12}O_{40}$ and $K_3PMo_{12}O_{40}$ species are distributed heterogeneously on the surface of the catalyst.

In conclusion, it is deduced that, for the partially potassium-substituted catalysts, mixtures of $H_3PMo_{12}O_{40}$ and $K_3PMo_{12}O_{40}$ with different mole ratios are formed and that the surfaces of the catalysts are covered with $H_3PMo_{12}O_{40}$ predominantly.

References

1) Standard Oil (Sohio), Jpn. Patent 10308 (1960).
2) K. Urabe, K. Fujita, and Y. Izumi, *Shokubai (Catalyst)*, **22**, 223(1980); Y. Onoue, Y. Mizutani, S. Akiyama, Y. Izumi, and H. Ihara, *ibid.*, **18**, 180 (1976).
3) Mitsubishi Rayon, Jpn. Patent 23013 (1975).
4) M. Otake and T. Onoda, Proc. 7th Int. Congr. Catal., Tokyo, June 1980, B-3.
5) T. Okuhara, A. Kasai, N. Hayakawa, Y. Yoneda, and M. Misono, *J. Catal.*, **83**, 121 (1983).
6) M. Ai, *J. Catal.*, **71**, 88 (1981).
7) M. Akimoto, Y. Tsuchida, K. Sato, and E. Echigoya, *J. Catal.*, **72**, 83 (1981).
8) H. Hayashi and J. B. Moffat, *J. Catal.*, **77**, 473 (1982).
9) Y. Izumi, R. Hasebe, and K. Urabe, *J. Catal.*, **84**, 402 (1983).
10) I.V. Kozhevnikov and K. I. Matveev, *Appl. Catal.*, **5**, 135 (1983).
11) M. Misono, *Catal. Rev.-Sci. Eng.*, **29**, 269 (1987).
12) Y, Izumi and K. Urabe, *Chem. Lett.*, **1981**, 663.
13) J. B. Black, N. J. Clayden, P. L. Gai, J. D. Scott, E. M. Serwicka, and J. B. Goodenough, *J. Catal.*, **106**, 1 (1987).

Selective Preparation of 2,3-Epoxypropanamide and Its Facile Conversion to 2,3-Dihydroxypropanamide with Acidic Resins

Shigeru SUGIYAMA,* Shinji ŌHIGASHI, Ryûichi SAWA, and Hiromu HAYASHI
Department of Chemical Science and Technology, Faculty of Engineering, The University of Tokushima, Minamijosanjima, Tokushima 770
(Received April 18, 1989)

In the equimolar reaction of acrylonitrile with hydrogen peroxide to 2,3-epoxypropanamide (glycidamide), the selectivity and the yield of the epoxide were improved by adding aq. NaOH solution continuously at a constant rate. The conventional literature procedure, by controlled pH from 7.0 to 7.5, resulted in an unfavorable decomposition of hydrogen peroxide. 2,3-Epoxypropanamide could be easily converted to 2,3-dihydroxypropanamide (glyceramide) by a catalytic amount of commercially available acidic resins.

In 1961, Payne and his colleague reported the alkaline epoxidation of acrylonitrile (**1**) with hydrogen peroxide (**2**) to 2,3-epoxypropanamide (**3**), which was hydrated to 2,3-dihydroxypropanamide (**4**) with formic acid.[1] The epoxide (**3**) is a useful intermediate for resins, plant protective and preservative agents, and dyes. An aqueous solution of **4** is equivalent to commercial glyceric acid (65—70% in water). Many articles[2] and patents[3,4] related to the preparation and the properties of **3** have been reported. Payne emphasized that the solution pH should be controlled from 7.3 to 7.5 to obtain **3** in high yield.[1] The succeeding patents[4] also supported his conclusion: that the pH was controlled from 7.0 to 7.5, and improved mainly in the concentration of **2** and the removal of the peroxides. However, an excess of **2** to **1** was sometimes mentioned in those reports,[3,4] where the selectivity of **3** based on **2** must be relatively poor. In the conversion of **3** to **4**, formic acid, which is difficult to remove from the reaction solution, was employed as a catalyst, as mentioned in the literature.[1] If hydration might have occurred with acidic resins, the removal of the acid can be very easy.

Herein, we describe in detail the effect of the pH and the continuous supply of an alkaline solution on the epoxidation of **1** with **2**. The conversion of **3** to **4** with various organic acids and acidic ion-exchange resins is also described.

Experimental

Apparatus and Procedure. Epoxidation of Acrylonitrile (1) to 2,3-Epoxypropanamide (3). To a three-neck, flat-bottom flask equipped with a dropping funnel or a micro-tube pump (MP-101, Tokyo Rika Kikai), a condenser and a standard electrode connected to pH meter (M-5 pH meter, Hitachi-Horiba) were charged with a known amount of *acrylonitrile (1) and hydrogen peroxide (2) (0.2 mol respectively, unless otherwise stated)* in water (total volume of the reaction solution, 100 cm^3) at 35 or 45 °C. The solution was magnetically stirred while a known concentration of aq. NaOH was added through a dropping funnel or a micro-tube pump. After a given reaction period, hydrogen peroxide (**2**) and 2,3-epoxypropanamide (**3**) were analyzed by means of iodometric titration for **2**[5] and titration for oxirane oxygen of **3**,[6] respectively. Furthermore, in order to analyze the other organic species, after the treatment of the reaction solution with 5% palladium carbon to decompose the excess peroxide,[1] and after evaporation of the solution at 50 °C in vacuo, the residue was analyzed with NMR in a DMSO-d_6 solution (Hitachi R-24 spectrometer at 60 MHz); chemical shifts are expressed in the unit δ.

Hydration of 2,3-Epoxypropanamide (3) to 2,3-Dihydroxypropanamide (4). An aqueous solution (30 cm^3) of 18.0 mmol of 2,3-epoxypropanamide (**3**) containing 2.37 mmol of formic acid, acetic acid, carboxylated resin (Amberlite IRC-50, 10 mequiv/g, Rohm and Haas Co.), or sulfonated resin (Amberlyst 15, 4.9 mequiv/g, Rohm and Haas Co.) was allowed to warm at 80 °C. Monitoring of the epoxide (**3**) and 2,3-dihydroxypropanamide (**4**) was carried out with the oxirane titration[6] and the glycol cleavage by periodic acid,[7] respectively.

Materials. Preparation of 2,3-Epoxypropanamide (3). After observing the epoxidation behavior of acrylonitrile (**1**) to 2,3-epoxypropanamide (**3**), the reaction mixture was treated overnight with 5% palladium carbon. After removing the catalyst, the mixture was concentrated at 50 °C in vacuo. To the residue, acetone was added and an insoluble hygroscopic salt was removed by filtration. The solvent was evaporated and the residue was distillated under reduced pressure (bp 90 °C/1.8 mmHg, lit of **3**,[1] 72—73 °/0.2 mmHg 1 mmHg≈133.322 Pa). By using dilute alkali (e.g., 0.2 M NaOH) (1 M=1 mol dm^{-3}) in the epoxidation of acrylonitrile (**1**), acrylamide (**5**) was detected in this fraction; however, upon using 6 M NaOH, the amide (**5**) was not detected with NMR (see Results and Discussion).

2,3-Epoxypropanamide (**3**): ^{1}H NMR (DMSO-d_6) δ= 2.65—3.15 (2H, m), 3.39 (1H, dd, J=5, 3 Hz), and 5.7—7.0 (2H, br m). IR (KBr) 3300, 1660, 1320, 895, and 790 cm^{-1}.

Preparation of 2,3-Dihydroxypropanamide (4). Procedure A. After observing of the hydration behavior of 2,3-epoxypropanamide (**3**) to 2,3-dihydroxypropanamide (**4**) (in the case of the acidic resin, the resin was filtered off), the reaction mixture was evaporated in vacuo at 80 °C. The residue was purified by recrystallization from methanol to give pure diol (**4**).

Procedure B from Glyceric Acid. Commercial glyceric acid (Tokyo Kasei Co., 65—70% in water: the purity was checked by acidmetry; 67.1%; 10.02 g, 63.4 mmol) was dissolved in a mixture of benzene and methanol (1/1 by

volume). Water was removed by azeotropic distillation. Benzene was also removed by azeotrope with methanol.[8] To this solution, 14% boron trifluoride methanol complex (Wako Co., 96 cm^3, 198 mmol) was added and refluxed for 1 h. The solution was then cooled to room temperature and poly(4-vinylpyridine) (Aldrich, 7.6 mequiv/g: 40.03 g, 304 mequiv) was added to the solution in order to remove the Lewis acid. After the solution was stirred for 15 min, the polymer was filtered off and the filtrate was evaporated. The residue was distillated in vacuo to give methyl glycerate (**6**) (5.77 g, 75.7%). To the methanol solution of **6**, NH_3 gas was bubbled until a spot of **6** in TLC (silica gel 60 GF_{254} (Merck); R_f=0.75 with AcOEt) disappeared. The solution was evaporated in vacuo to give 2,3-dihydroxypropanamide (**4**), almost quantitatively. The diol (**4**) was purified with silica-gel column chromatography (Wakogel C-300 (Wako)) with MeOH-AcOEt (1:1) and recrystallization from methanol.

2,3-Dihydroxypropanamide (4): Mp 85—87 °C (lit,[1] 89—90 °C); Found: C, 34.05; H, 6.58; N, 13.11%. Calcd for $C_3H_7NO_3$: C, 34.29; H, 6.71; N, 13.33%. ^{1}H NMR (CD_3OD) δ=3.68 (2H, m), 4.00 (1H, m). IR (KBr) 3200 and 1640 cm^{-1}.

Methyl Glycerate (6): Bp 92—94 °C/2.1 mmHg (lit,[9] 67—69 °C/0.1 mmHg); Found: C, 40.07; H, 6.85%. Calcd for $C_4H_8O_4$: C, 40.00; H 6.71%. ^{1}H NMR (CD_3OD) δ=3.75 (3H,s), 3.76 (2H, d, J=4 Hz), 4.13 (1H, t, J=4 Hz). IR (KBr) 3400 and 1740 cm^{-1}.

Results and Discussion

Epoxidation of 1 to 3. The Effect of pH. Under a weakly alkaline condition, the reaction of α,β-unsaturated nitrile with hydrogen peroxide forms a peroxycarboximidic acid intermediate (**I**) to give epoxyamide (Scheme 1).[1]

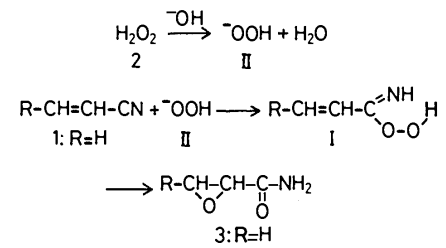

Scheme 1.

In the epoxidation of **1** to **3**, Payne emphasized it was necessary to keep the pH between 7.3 and 7.5 in order to produce **3** in high yield.[1] Indeed, the perhydroxyl anion (**II**) from **2** is generated with alkali.[9] However, an excess of alkali may decompose **2** and polymerize **3**. Thus, the optimum for the yield and selectivity must depend on the concentration of the additive alkaline solution, but not on the pH of the reaction solution.

As shown in Fig. 1, without alkali at 35 °C,[1,10] practically no reaction was observed in the attempted epoxidation. However, according to Payne's procedure, using 1 M NaOH to control the pH from 7.0 to 7.5 at 35 °C,[1] the reaction occurred quickly to give a 38% yield of **3** after 5.2 h, while the selectivity of **3** based on **2** in charge was 45%. In this case, during the initial stage of the reaction, **2** quickly decomposed along with the generation of molecular oxygen. Epoxidation after 2 h was slow due to a lack of **2**. Thus, under this condition, alkali is used both for the generation of **II** from **2** and its decomposition. By controlling pH from 6.0 to 6.5 with 0.5 M NaOH at 35 °C, the consumption of **2** was rather slow and the selectivity of **3** was improved to 63% at 5 h. However, the yield of **3** was scarcely increased (35% at 5 h). These results show that maintaining the pH at an acidic condition can not increase the yield of **3**, while the selectivity can not be improved under a basic condition.

The Effect of Continuous Supply of Aqueous Alkali with Various Concentrations. From the above results, it seemed likely that the yield and the selectivity of **3** might be improved with a continuous addition of an alkaline solution of the appropriate concentration to the reaction solution, instead of the above Payne's procedure. Figure 2 compares the epoxidation behavior for both added 0.2 M and 6 M NaOH at

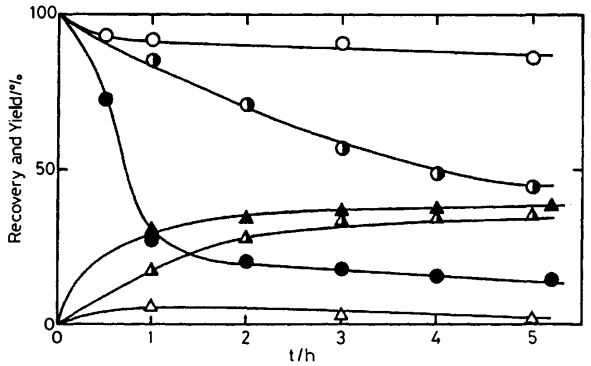

Fig. 1. The effect of pH on the reaction of **1** with **2** at 35 °C.
○: Recovery of **2**. △: Yield of **3**. Open symbols: without alkali. Half-filled symbols: pH at 6.0—6.5. Filled symbols: pH at 7.0—7.5.

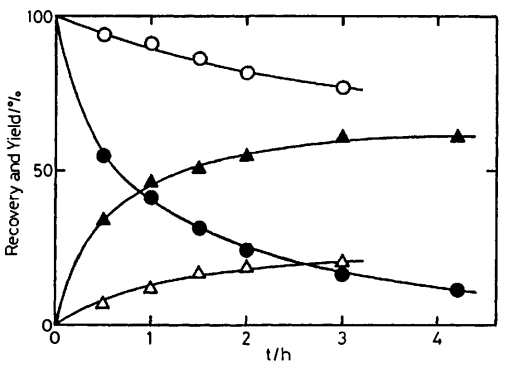

Fig. 2. The effect of concentration of alkali supplying at 1.0 ml h^{-1} on the reaction of **1** with **2** at 45 °C.
○: Recovery of **2**. △: Yield of **3**. Open symbols: addition of 0.2 M NaOH. Filled symbols: addition of 6 M NaOH.

a constant rate of 1.0 ml h^{-1} with a micro-tube pump at 45 °C.[10] In the case of 0.2 M NaOH, the pH was varied between 5.98 and 5.50, and the reaction proceeded very slowly (the yield of **3** was 20% at 3 h), while the selectivity was up to 87% after 3 h. In the case of 6 M NaOH, the pH was varied from 6.34 to 8.51 with the proceeding of the reaction and the yield of **3** increased up to 61% with a relatively poor selectivity of 73% after 3 h. The yield and the selectivity were remarkably improved compared with those of Payne's procedure. During the initial stage, at a reaction time within 1 h, where the concentration of alkali in the reaction solution was low and the pH was less than 6.9, the reaction occurred very quickly with high selectivity. After 1 h, the reaction became slow with lower selectivity and the observed pH was more than 7.0. Therefore, after 1 h, the decomposition of **2** should have occurred prior to epoxidation. Furthermore, in such a strongly alkaline condition (e.g. pH>8), a polymerization of **3** may also be possible (see below).

In Fig. 3, the effects of the concentration of the alkaline solution on the yield of **3**, the conversion of **2**, and the selectivity at 3 h are shown. At a lower concentration (less than 2 M NaOH), the selectivity was relatively good, but the yield was less than 50%. At a higher concentration (more than 3 M NaOH), the yield was better than 50%, but the selectivity was relatively poor. In the present procedure, the yield and the selectivity should depend on both the initial rate of formation of **3** and that of consumption of **2**. As shown in Fig. 4, at a lower concentration (less than 2 M NaOH), the initial rates of formation and consumption overlapped on a single curve to form **3** in high selectivity, while the decrease in the selectivity of **3** was observed at a higher concentration (more than 3 M NaOH) where the rate of consumption of **3** exceeded that of the formation of **2**. The present results show that our improved procedure given above favorably contributes to avoiding the decomposition

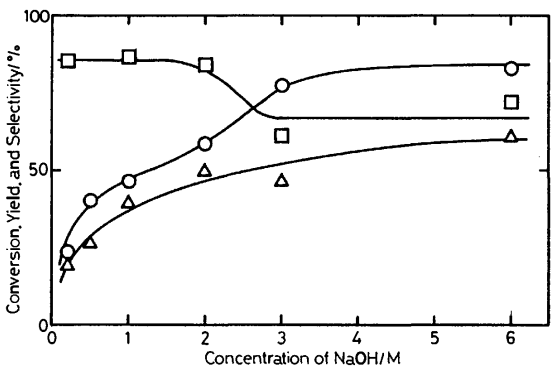

Fig. 3. The behavior of conversion of **2**, yield of **3**, and the selectivity of **3** based on **2** with concentration of alkali in the reaction of **1** with **2** at 45 °C.
○: Conversion of **2**. △: Yield of **3**. □: Selectivity.

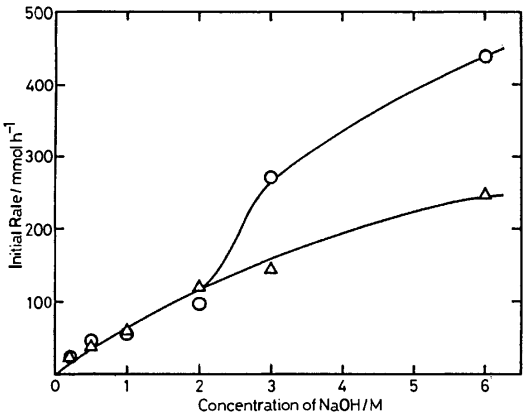

Fig. 4. The effect of concentration of alkali on initial rate of the reaction of **1** with **2** at 45 °C.
○: Initial rate of decomposition of **2**. △: Initial rate of formation of **3**.

of **2** with alkali, and results in increasing both the yield and selectivity of **3**.

The Effect of the Molar Ratio of 1 to 2. According to Payne's procedure,[3] the yield of **3** was affected with a molar ratio of **1** to **2**. This should be related to the decreasing of the selectivity due to the decomposition of **2** with an excess of alkali to maintain the pH. In our procedure, the effect of the alkali must be the most critical factor. We examined the effect of the molar ratio of **1** to **2**. To the solution of a known ratio of **1** and **2** (**1**/**2**=0.1 mol/0.2 mol, 0.2 mol/0.2 mol, or 0.2 mol/0.1 mol, respectively), 0.5 M NaOH was added at 0.9 ml h^{-1}. As shown in Fig. 5, the rate of the forma-

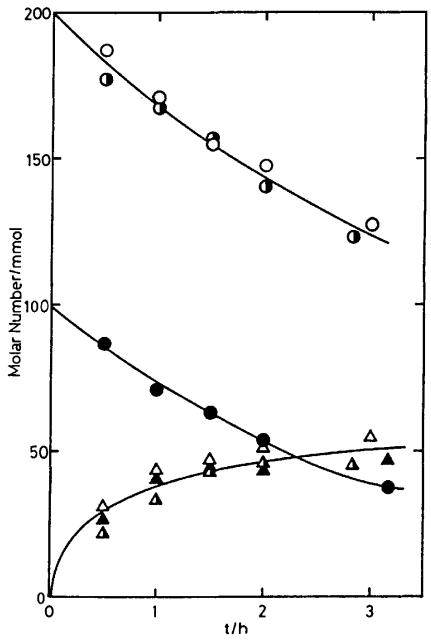

Fig. 5. The effect of molar ratio of **1** and **2** on the reaction of **1** with **2** at 45 °C.
○: Recovered **2**. △: Formed **3**. Open symbols: **1**/**2**=1/1. Half-filled symbols: **1**/**2**=2/1. Filled symbols: **1**/**2**=1/2.

tion of **3** and that of the consumption of **2** are equal in each case. In this case, an excess of alkali did not exist in the reaction mixture and the selective epoxidation to **3** proceeded. It seemed that the rate of formation of **3** and the selectivity were not affected with a molar ratio of **1** and **2** in our procedure.

Formation of 3 via 5. Payne reported that **4** and **5** were given as by-products in the present epoxidation.[1,3] It was apparent that **4** was formed through the hydration of **3**. With our NMR analysis, although the formation of **4** was observed, the reaction mixture had to stand at room temperature for several days. We also detected **5** with NMR in the case of 0.2 M NaOH, where **5** disappeared with time, as shown in Table 1. However, **5** was not detected for a concentration of the alkali higher than 6 M NaOH.

The **5** must be formed by an intermolecular nucleophilic attack of the active intermediate **I** to **1** (Scheme 2).

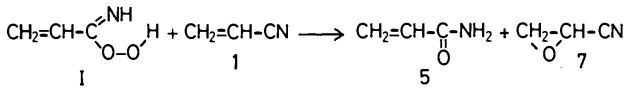

Scheme 2.

2,3-Epoxypropanenitrile (**7**), formed together with **5**, must be reactive to give **3**, successively. The disappearance in 0.2 M NaOH and no formation of **5** in 6 M NaOH could not refer to the oxidation of **5** with **I**. In the oxidation of **5** with **I**, **3** and **5** are formed. Therefore, **5** does not decrease at all with time. Generally,

Table 1. The Behavior of **5** in the Reaction of **1** and **2** with 0.2 M NaOH

t/min	15	45	75	105	150
3/mmol	7	21	23	24	30
5/mmol	8	8	7	3	3

an olefin conjugated with ketons may be oxygenated directly with **2** under the alkaline condition to give an epoxide.[11] In the present case, **5** must be epoxidized directly with **2** to give **3** (Scheme 3).

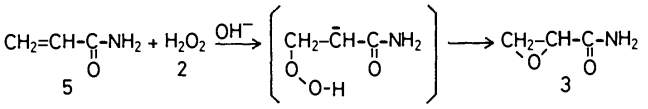

Scheme 3.

In the reaction with 6 M NaOH, the signals for a polymer of **3** or other organic species scarcely appeared in the NMR spectra.

Hydration of 3 to 4. Payne gave **4** by the hydration of **3** with a catalytic amount of formic acid (1/4 equiv) at 75 °C for 5 h (Scheme 4).

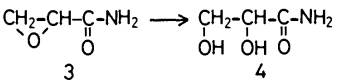

Scheme 4.

A comparison of the hydration at 80 °C with a small amount (ca. 1/10 equiv) of formic acid and acetic acid is shown in Fig. 6.

Obviously, acetic acid was as effective as the stronger acid, formic acid, for the hydration of **3** to afford **4** with the selectivity more than 85%. However, removal of organic acids from the aqueous solution is very difficult to decrease the yield during purification with distillation.[1] By employing acidic resins as a catalyst, the expected product **4** could be separated by simple filtration, and the yield of **4** would be increased. Hydration occurred smoothly on a carboxylated resin (Fig. 6), but it was relatively slow and the selectivity of **4** decreased to less than 74%, presumably due to trapping of the substrate on the resin. In order to increase the yield of **4**, a strongly acidic

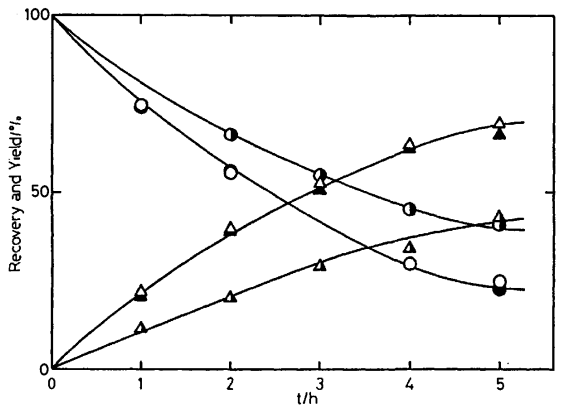

Fig. 6. The comparison of the hydration of **3** to **4** with some acids at 80 °C.
O: Recovery of **3**, Δ: Yield of **4**. Open symbols: formic acid. Filled symbols: acetic acid. Half-filled symols: Amberlite IRC-50.

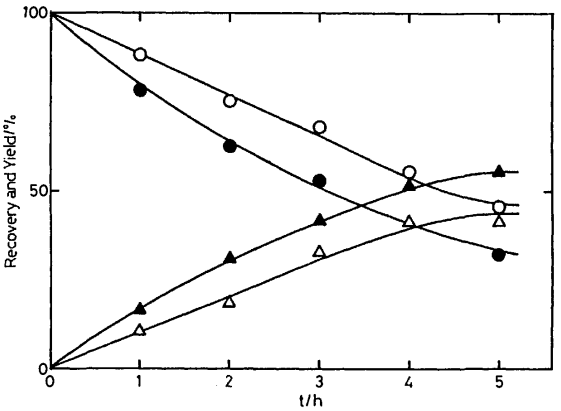

Fig. 7. The comparison of the hydration of **3** to **4** with acidic resins at 80 °C.
O: Recovery of **3**, Δ: Yield of **4**. Open symbols: Amberlite IRC-50. Filled symbols: Amberlyst 15.

sulfonated resin was effectively used (comparable to formic acid, as shown in Fig. 7).

In conclusion, for the preparation of **3** more selectively than the known procedure, a continuous supply of an alkaline solution was a very effective procedure. The hydration of **3** to **4** proceeded smoothly with acidic resins.

References

1) G. B. Payne and P. H. Williams, *J. Org. Chem.*, **26**, 651 (1961).

2) e.g., C. C. Tung and A. J. Speziale, *J. Org. Chem.*, **28**, 2009 (1963): J. Hayashi, S. Sakai, and Y. Ishii, *Kogyo Kagaku Zasshi*, **70**, 198 (1967).

3) G. B. Payne, U. S. Patent 3053857 (1959); *Chem. Abstr.*, **58**, 5521f, (1963).

4) e.g., F. Becke, H. Buckschewski, and B. Sander, Ger. Patent 1154086 (1961); *Chem. Abstr.*, **60**, 2889e (1964): *idem*, Jpn. Patent 6961 (1961); *Chem. Abstr.*, **64**, 11971g (1964).

5) S. Atou, "Bunseki Kagaku," Baifuukan (1967), p. 241.

6) J. L. Jungnickel, E. D. Peters, A. Polgar, and F. T. Weiss, "Organic Analysis," ed by J. Mitchell, Jr., I. M. Kolthoff, E. S. Proskauer, and A. Weissberger, Interscience Publishers, New York (1953), Vol. 1, p. 127.

7) V. C. Mehlenbacher, "Organic Analysis," ed by J. Mitchell, Jr., I. M. Kolthoff, E. S. Proskauer, and A. Weissberger, Interscience Publishers, New York (1953), Vol. 1, p. 41: This quantitative analysis is available to α-glycols, α-hydroxy ketones, α-diketones, and α-oxo aldehydes. But it is not always quantitative; e.g. **4**; 100%,[1)] glyceric acid; 67%, methyl glycerate; 91%, 2,3-dihydroxy-3-phenylpropanoic acid; 100%, tartaric acid; 100%, methyl tartarate; 5%, ethyl tartarate; 1%, oxalic acid; 50%, pyruvic acid; 11%, methyl pyruvate; 0%, pyruvamide; 2%, hydroxy acetone; 62%, diethylene glycol; 1%, and propylene glycol; 100% (reacting with periodic acid for 2 h at room temperature).

8) The ability of BF_3 seemed to be affected with solvent S. Sugiyama, S. Ôhigashi, K. Sato, S. Fukunaga, and H. Hayashi, *Bull. Chem. Soc. Jpn.*, to be published.

9) G. B. Payne, P. H. Deming, and P. H. Williams, *J. Org. Chem.*, **26**, 659 (1961).

10) The reaction was carried out at 45 °C, unless otherwise stated. In Becke's patent (F. Becke and R. Kohlhaupt, Ger. Patent 1568208 (1970); *Chem. Abstr.*, **74**, 3498g (1971)), it was reported that the optimum for the reaction temperature was 45 °C.

11) G. B. Payne, *J. Am. Chem. Soc.*, **81**, 4901 (1959).

 © 1989 The Chemical Society of Japan Bull. Chem. Soc. Jpn., 62, 3207—3210 (1989)

The Effect of Alternative Magnetic Field on the Pigment Ejection from Magnetic Anisotropic Gel Beads

Yasuzo SAKAI, Hidefumi TAGUCHI, and Fujio TAKAHASHI*
Department of Applied Chemistry, Faculty of Engineering, Utsunomiya University,
2753 Ishii-machi, Utsunomiya 321
(Received April 20, 1989)

Magnetic anisotropic gel beads (MA gel beads) were prepared by the gelation of a ferrite suspension in a static magnetic field. MA gel beads were found to oscillate in an alternating magnetic field. This oscillation can possibly reduce the thickness of the diffusion layer on the interface between the gel beads and the surrounding solution, so that the substance can be transferred more quickly across the gel-liquid interface. MA gel beads consisted of alginate gel containing ferrite powder and toluidine blue as a pigment. MA gel beads were loaded into a dual glass tube to make a column bed, which was inserted into a coreless coil which produced the alternating magnetic field. The concentration change of the pigment in the effluent from the column was measured during a lapse in time with repeating off and on the input of the alternating magnetic field. The pigment concentration in the effluent upon exposure to the alternating magnetic field increased to twice the maximum value obtained without a magnetic field. The stronger was the static magnetic field at the time of gelation and the alternating magnetic field, the larger was the increase in pigment concentration in the effluent. Also, the higher was the concentration of ferrite in gel beads, the larger was the increase in pigment concentration in the effluent.

There have been many papers concerning the utilization of gel as a carrier for the immobilization of enzymes or microorganisms.[1-3] A gel carrier is generally useful, but not efficient, if a sufficient amount of substrate can not be supplied to immobilized enzymes or microorganisms in the gel. In this case, the diffusion process of a substrate from the liquid bulk to the gel surface and that of the product from the gel to the liquid might produce the rate-determining steps. The mechanical stirring of gel beads reduces the thickness of the diffusion layer on the interface between the gel and the surrounding liquid, and increases the rate of diffusion. However mechanical stirring can possibly to break the gel beads. Although a fluidized bed was utilized, gel beads were so likely to flow out of the column bed that the flow rate of the effluent might not be sufficiently promoted for stirring.[4]

The stirring method was improved by applying a magnetic field.[4-7] Magnetite containing gel beads which exhibit a magnetic isotropic property (MI gel beads) can be moved due to an applied magnetic force. MI gel beads were reported to spin under a revolving magnetic field.[7] However, some aggregation of the beads was unavoidable in the magnetic field.[8] It seemed that the device for magnetic stirring might be a rather sophisticated instruments.[6,7]

We prepared magnetic anisotropic gel beads (MA gel beads), which exhibited a magnetic dipole like that of a magnet. MA gel beads were expected to oscillate owing to the torque, without migration or aggregation to each other in the alternating magnetic field.

This paper presents the results from a fundamental study concerning the magnetic properties of MA gel beads. Concentration measurements of the pigment diffused from inside the gel into the liquid were carried out for surveying the effects of various conditions, such as the strength of an alternating magnetic field, the concentration of ferrite powder in the gel, the size of the gel beads and the strength of the static magnetic field, in which MA gel beads were prepared.

Experimental

MA gel beads were prepared by the following method: A requisite amount of ferrite powder and 0.1 g of sodium alginate were added into 6.5 mmol dm^{-3} toluidine blue in water to make 10 g (whole weight) and mixed homogeneously (mixture A). Also, a solution of 0.1 mol dm^{-3} $CaCl_2$ in 6.5 mmol dm^{-3} toluidine blue was prepared (solution B). Into a dual beaker (inside diameter: 35 mm), 50 cm^3 of solution B were poured and kept at 25 °C. This dual beaker was placed in the center of the gap between the poles of a permanent magnet (diameter of poles: 75 mm, gap: 55—95 mm) and exposed in a magnetic field of various strengths within the range 500—1900 Oersted. Into solution B, 10 g of mixture A were added (drop by drop) by a syringe to make gel beads. These were allowed to leave over a period of 2 h in the static magnetic field. The shape of the MA gel beads became spheroid, the long axes of which were directed parallel to the flux of the static magnetic field. MI gel beads, the shapes of which were almost spherical, were prepared in the same manner, except that the dual beaker was placed far away from magnet.

Figure 1 shows a schematic diagram of the experimental apparatus. The column (inside diameter: 8 mm) was equipped with a water jacket maintained at 25 °C by circulating water. This column was surrounded with an electromagnetic coil which generated an alternating magnetic field owing to a 50-Hz alternating current. The axis of the alternating magnetic flux was set to be parallel with that of column. The column was filled with 4 cm^3 (real volume) of gel beads, producing a bed height of 9 cm^3. A gauze patch was placed at the bottom of column to hold the MA gel beads. Ten mmol dm^{-3} $CaCl_2$ was fed to the column at a flow rate of 17 $cm^3 min^{-1}$. The effluent out of column was fractionated, and each concentration of the pigment in

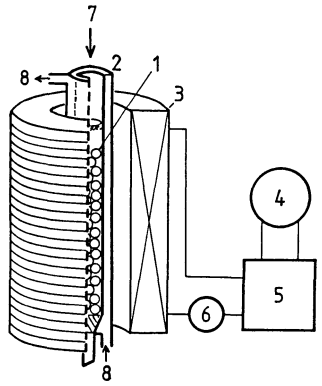

Fig. 1. The schematic diagram of equipment. 1. Gel beads. 2. Column consisted of dual glass tube for water jacket. 3. Coreless coil. 4. Electric power supply (100 V, 50 Hz). 5. Transformer. 6. a.c. ammeter. 7. 10 mmol dm^{-3} $CaCl_2$ (25 °C). 8. Circulating water (25 °C).

the effluent was determined by measuring the absorption with a spectrophotometer (Hitachi model 200-20).

In this paper we use cgs·emu as system of units and a permeability constant of, $\mu_0=1$. Therefore, the magnetic strength, H, was obtained by measuring the density of magnetic flux, B, with a Gauss meter (Yokogawa, type 3251), because $H=B$. Subscripts, s and a of H hereafter express the static and alternating magnetic field, respectively. The deviation of H_a in the column was less than 5%.

The movement of MA gel beads was observed by eye and by slow-motion video-tape.

Results and Discussion

MA Gel Beads and MI Gel Beads. Figure 2 shows photographs of the cross sections of MA and MI gel beads. Ferrite powder in MA gel beads was observed to orient along the direction of the magnetic flux. On the other hand, ferrite powder in MI gel beads dispersed without orientation.

MA gel beads were found to stick to the iron plate, having two points of each bead surface on which the magnetic flux was measured to be 10 Oersted or higher. The movement of an MA gel bead in water was observed in the alternating magnetic field. The bead was observed to leap. This motion was examined with slow-motion video-tape, showing MA gel beads which did not follow the 50-Hz field: At a magnetic strength of 200—500 Oersted, the long axes of the MA gel beads were observed to be at right angles to the magnetic flux, and oscillated at an angle of several to 10 and more degrees. They occasionally rotated to the long axis of the MA gel bead. These results suggest that MA gel beads might possess magnetic poles and a magnetic moment like a magnet.

MI gel beads, on the contrary, exhibited neither magnetic attraction to iron plate in a non-magnetic field nor oscillation under an alternating magnetic field.

The Diffusion Rate of Pigment from MA Gel Beads.

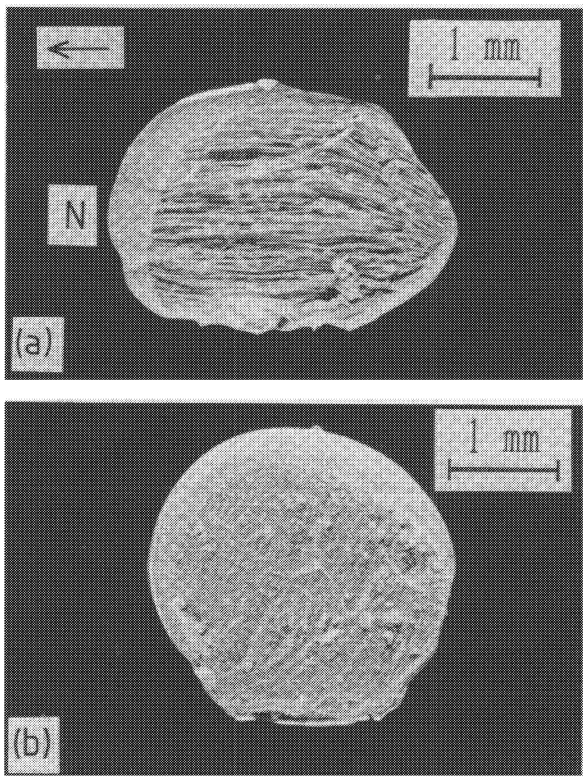

Fig. 2. Photographs on cross sections of an MA gel bead and an MI gel bead. (a): An MA gel bead, which contained 5% ferrite and was prepared in H_s=1600 Oersted. The direction of magnetic flux is shown by an arrow. N and S show north and south as both poles of a bead. (b) An MI gel bead, which contained 5% ferrite and was prepared in H_s<0.5 Oersted.

MA or MI gel beads filling the column were exposed to the alternating magnetic field. The concentration change of toluidine blue as pigment in the effluent was determined. The results are shown in Fig. 3. The concentration of toluidine blue in the effluent gradually decreased with a lapse of time, and increased only when MA gel beads were exposed to the alternating magnetic field. No concentration change of toluidine blue occurred in the case of MI gel beads.

It should be noticed that the surface area of the MA gel beads might not change, since these beads did not transform under a magnetic force in the magnetic field. Meanwhile, the rate of the efflux was kept constant. Therefore, it is reasonable that only the rate change of molecular transfer across the interface between the surface of the gel beads and the liquid bulk may exert to the concentration change of toluidine blue in effluent. The oscillation of MA gel beads may cause a decrease in the thickness of the diffusion layer on the interface between the surface of the gel beads and the liquid bulk, and to increase the concentration of toluidine blue in the effluent.

The Factors Influencing on Efflux of Pigment from MA Gel Beads. The effects of the strength of the

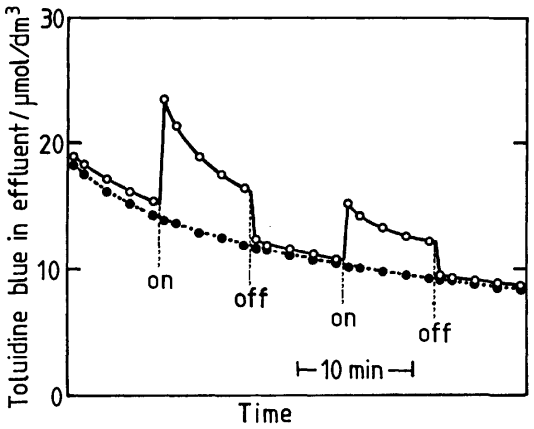

Fig. 3. The concentration change of pigment in effluent by exposing alternating magnetic field off and on. MA gel beads (—○—) prepared in H_s=1600 Oersted and MI gel beads (—●—) prepared in H_s<0.5 Oersted. H_a=600 Oersted. Ferrite concentration in gel beads: 5%. Average diameter of gel beads: 2.7±0.3 mm.

alternating magnetic field (H_a), the concentration of the ferrite powder in the gel, the size of the gel beads and the strength of the static magnetic field (H_s) for producing MA gel beads on the concentration change of the pigment in the effluent were surveyed.

Figures 4, 5, 6, and 7 show the results concerning the concentration change of toluidine blue in the effluent with a time lapse under various conditions. It was found from the inserted figures in Figs. 4—6 that the ΔC_s (the values of subtraction of the toluidine blue concentration before and after exposing magnetic field) are almost proportional to H_a, the size of the gel beads and the concentration of the ferrite powder, respectively. Figure 7 shows that no change appeared below 500 Oersted. It seems that ΔC may be proportional to H_s as a function of the second degree in the region above 500 Oersted in the inserted figure in Fig. 7. These results suggest that the static magnetic field might be the most effective factor concerning the concentration change of the pigment in the effluent.

The magnetic force from both poles in the gap of magnet to ferrite powder inside the gel caused the shape of MA gel beads to be slightly ellipsoidal. This fact was more clearly observed at higher H_s.

The magnetic moment of MA gel beads is produced by the orientation of ferrite powder inside the gel parallel to the direction of the magnetic flux. It seems that the more the NS poles of each ferrite particle of powder are forced to orient parallel to the magnetic flux with elevating H_s, the more the magnetic moment of MA gel beads increases. Also, the magnetic moment may increase with increasing the size of the MA gel beads. The magnetic moment of MA gel beads brings about a torque which is the product of H_a and the magnetic moment of the gel

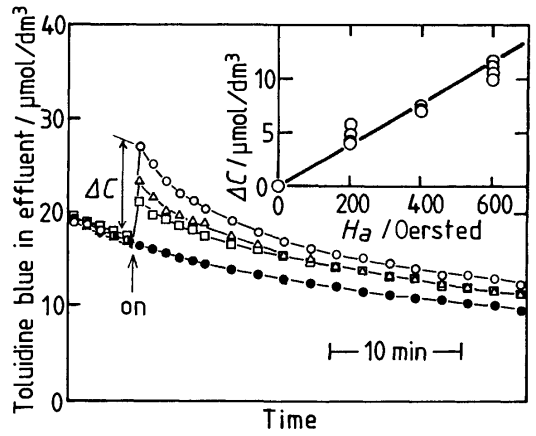

Fig. 4. The relation between ΔC and H_a. H_a=600 (—○—), 400 (—△—), 200 (—□—), and 0 (—●—) Oersted. Other conditions were the same as those in Fig. 3.

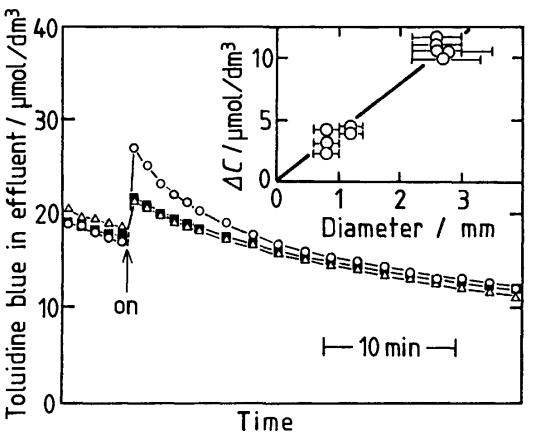

Fig. 5. The relation between ΔC and the size of average diameters of gel beads. Gel beads diameter were 2.6 (—○—), 1.2 (—■—), and 0.8 (—△—) mm. Other conditions were the same as those in Fig. 3.

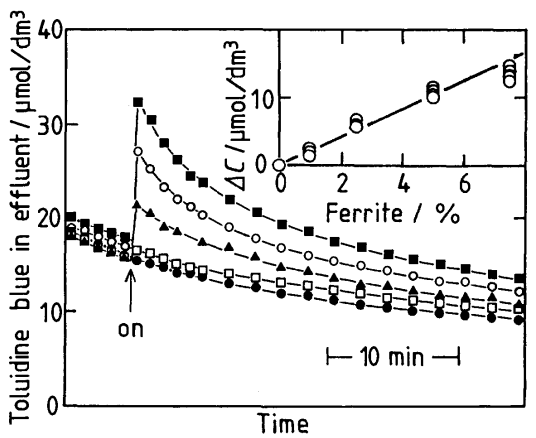

Fig. 6. The relation between ΔC and ferrite concentration in gel. Ferrite concentrations: 7.5 (—■—), 5.0 (—○—), 2.5 (—▲—), 1.0 (—□—), and 0 (—●—) %. Other conditions were the same as those in Fig. 3.

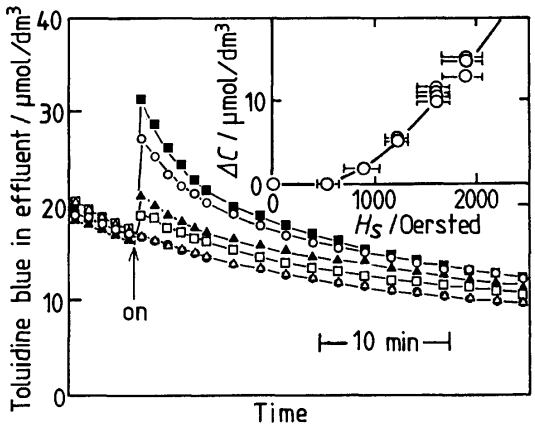

Fig. 7. The relation between ΔC and H_s. H_s=1900 (—■—), 1600 (—○—), 1200 (—▲—), 900 (—□—), 500 (—●—), and 0 (—△—) Oersted. Other conditions were the same as those in Fig. 3.

beads in the magnetic field. MA gel beads oscillate owing to the torque. It is plausible that the diffusion layer on the surface of gel beads reduces the thickness by intensifying the oscillation of MA gel beads. In order to obtain ΔC. H_s has to be pushed up more than 500 Oersted in Fig. 7. This fact indicates the existence of a threshold: The magnitude of the torque must overcome the frictional resistance caused by the thrust of MA gel beads on each other. In this connection, the oscillation can prevent the aggregation of gel beads with each other.

Conclusion

It was demonstrated that MA gel beads prepared in a static magnetic field oscillated due to the torque produced by an alternating magnetic field. The oscillation of MA gel beads promoted the velocity of pigment ejection from the inside gel beads to the liquid bulk, as compared with no alternating magnetic field. This is different from the behavior of MI gel beads in a magnetic field. It is obvious from Figs. 2 and 4—7 that (1) the orientation of magnetite powder in gel in the static magnetic field yields the magnetic moment. (2) the magnitude of the magnetic moment of MA gel beads varies as the concentration of ferrite powder in the gel, the size of MA gel beads and H_s for gelation, and (3) the magnitude of the torque of MA gel beads increases with increasing H_a. We discussed this phenomena in this paper. A theoretical analysis of the relation between the oscillation and the magnetic moment of MA gel beads will be presented in a separate paper.

References

1) H. Tanaka, H. Kurosawa, E. Kokufuta, and I. A. Veliky, *Biotech. Bioeng.*, **26**, 1393 (1984).

2) J. Klein, J. Stock, and K. K. Vorlop, *App. Microbiol. Biotech.*, **18**, 86 (1983).

3) "Koteika Seitai Shokubai," ed by I. Chibata (Immobilized Biocatalysts), Kodansha (1986), pp. 53, 69.

4) E. Sada, S. Katoh, M. Shiozawa, and M. Terashima, *Biotech. Bioeng.*, **25**, 2285 (1983).

5) Tsung-Ting Hu and Jian-Yong Wu, *Chem. Eng. Res. Des.*, **65**, 238 (1987).

6) E. Sada, S. Katoh, and M. Terashima, *Biotech. Bioeng.*, **22**, 243 (1980).

7) E. Sada, S. Katoh, and M. Terashima, *Biotech. Bioeng.*, **23**, 1037 (1981).

8) E. Sada, S. Katoh, M. Shiozawa, and T. Fukui, *Biotech. Bioeng.*, **23**, 2561 (1981).

 © 1989 The Chemical Society of Japan Bull. Chem. Soc. Jpn., 62, 3211—3215 (1989)

The J-Like Structures of Azobenzene-Containing Amphiphiles, $C_{10}AzoC_5N^+Br^-$ and $C_8AzoC_5N^+Br^-$

Kenji OKUYAMA,* Chiyo MIZUGUCHI, Guiqing XU, and Masatsugu SHIMOMURA
Faculty of Technology, Tokyo University of Agriculture and Technology, Koganei, Tokyo 184
(Received March 20, 1989)

Totally synthetic azobenzene-containing amphiphiles $C_{10}AzoC_5N^+Br^-$ and $C_8AzoC_5N^+Br^-$ ($C_{31}H_{50}N_3O_3Br$ and $C_{29}H_{46}N_3O_3Br$ respectively) were crystallized from their solutions by the solvent-evaporation method. Both crystals are triclinic, with the space group of $P\bar{1}$ and $Z=2$. The unit cell dimensions of the former crystal are $a=3.233(5)$, $b=0.854(2)$, $c=0.608(1)$ nm, $\alpha=106.96(8)$, $\beta=86.6(1)$, and $\gamma=88.3(1)°$. Those of the latter crystal are $a=3.0098(6)$, $b=0.8553(2)$, $c=0.6084(1)$ nm, $\alpha=72.99(1)$, $\beta=92.57(2)$, and $\gamma=95.64(2)°$. The crystal structure of $C_{10}AzoC_5N^+Br^-$ was solved by the direct method and refined by the block-diagonal least-squares method: $R=0.082$ for 2927 observed reflections ($2\theta<120°$, Cu $K\alpha$, $\lambda=0.15418$ nm). On the other hand, that of $C_8AzoC_5N^+Br^-$ was refined by the full-matrix least-squares method: $R=0.058$ for 2993 reflections ($2\theta<120°$, Cu $K\alpha$). The molecular and crystal structures of these compounds are quite similar to those of the homologous compounds, $C_{12}AzoC_5N^+Br^-$ and $C_6AzoC_5N^+Br^-$. That is, the $C_nAzoC_5N^+Br^-$ molecules incline about 30° to the bilayer surface to pack in a tail-to-tail fashion. The azobenzene chromophore has a pronounced planarity which makes possible the parallel stacking of adjacent phenyl groups.

Totally synthetic azobenzene-containing amphiphiles with a single alkyl chain, $C_nAzoC_mN^+Br^-$ (Fig. 1), show several types of azobenzene chromophore-aggregation states, depending on the number of carbon atoms in the tail part (n) and the spacer part (m).[1] Different aggregation states of the azobenzene chromophores cause different types of orientation of the transition dipole of the long axis of the chromophore, detectable as a bathochromic or a hypsochromic shift of the absorption spectrum. According to a semi-quantitative application of Kasha's molecular exciton theory,[2] the hypsochromic shift is attributable to the parallel (or side-by-side) orientation of the transition dipole (H-aggregate). This aggregation state was confirmed by an X-ray diffraction study of the cast films of $C_8AzoC_{10}N^+Br^-$.[3] On the other hand, the bathochromic shift is derived from the head-to-tail orientation between adjacent transition dipoles (J-aggregate). This type of aggregation was found in the single crystals, casted films, and the aqueous dispersion of $C_nAzoC_5N^+Br^-$ (n=12, 10, 8, and 6). In the cases of n=12 and 6, their crystal structures were determined in detail by the X-ray single crystal structure analyses and bore out the J-aggregation of azobenzene chromophores at the atomic level.[4,5]

In this paper, the crystal structures of the two compounds (n=10, 8) in the family of $C_nAzoC_5N^+Br^-$ will be determined for the further understanding of the stereochemical characteristics of the J-aggregation.

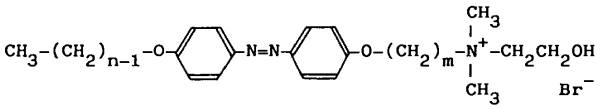

Fig. 1. Chemical formula of azobenzene-containing single chain amphiphiles (abbreviated as $C_nAzoC_5N^+Br^-$).

Experimental and Structure-Determination

Materials. The $C_{10}AzoC_5N^+Br^-$ (15 mg) was dissolved in a boiling solution (18 ml) of water and ethanol (water/ethanol=1/1 by volume ratio). Yellow, plate-like crystals with a thickness of about 0.02 mm were deposited from the solution by the solvent-evaporation method for about a week at room temperature. Single crystals of $C_8AzoC_5N^+Br^-$ were obtained by a similar method using a solution of ethanol and benzene (ethanol/benzene=1/2 by volume ratio).

Table 1. Crystal Data and Details of Experiments and Analyses

Compound	$C_{10}AzoC_5N^+Br^-$	$C_8AzoC_5N^+Br^-$
Formula weight	593.75	564.61
Crystal system	Triclinic	Triclinic
Space group	$P\bar{1}$	$P\bar{1}$
a/nm	3.233(5)	3.0098(6)
b/nm	0.854(2)	0.8553(2)
c/nm	0.608(1)	0.6084(1)
α/°	106.96(8)	72.99(1)
β/°	86.6(1)	92.57(2)
γ/°	88.3(1)	95.64(2)
Cell volume/nm^3	1.601(4)	1.4903(5)
Z	2	2
D_x/g cm^{-3}	1.232	1.263
D_m/g cm^{-3}	1.23	1.26
Radiation	Cu $K\alpha$	Cu $K\alpha$
μ(calcd)/cm^{-1}	17.83	18.50
Crystal size/mm^3	0.5×0.4×0.01	0.5×0.2×0.01
Scan mode	ω	ω
Scan width/° (in ω)	3.4+0.15 tan θ	2.6+0.14 tan θ
Scan speed /° (in ω)min^{-1}	6	8
2θ range/°	2.5—120	2.5—120
No. of observed unique reflections	4498	3356
No. of reflections for R	2927	2993
R	0.082	0.058

X-Ray Work. The lattice parameters and diffraction intensities of $C_{10}AzoC_5N^+Br^-$ were measured on a Rigaku four-circle diffractometer with Ni-filtered Cu $K\alpha$ radiation (λ=0.15418 nm). Those of $C_8AzoC_5N^+Br^-$ were measured on the same type of diffractometer with graphite-monochromatized Cu $K\alpha$ radiation (RASA-5RII). The lattice parameters were refined by the least-squares fit using 31 reflections in the 2θ range of 10—50° for $C_{10}AzoC_5N^+Br^-$ and 25 reflections in the 2θ range of 45—50° for $C_8AzoC_5N^+Br^-$. Crystal data are listed in Table 1. Since the peak profiles of the reflections from the $C_{10}AzoC_5N^+Br^-$ crystal used for data collection were broken into two parts, a considerably wide scan-width was applied. The densities of the crystals were measured by the flotation method in a hexane and tetrachloromethane solution.

Three reference reflections, monitored every 50 reflections, showed no significant intensity-deterioration during the data collection of either sample. Corrections were made for the Lorentz and polarization factors, but not for the absorption and extinction effects. The experimental conditions are summarized in Table 1.

Structure-Determination. The structure of the $C_{10}AzoC_5N^+Br^-$ crystal was solved by the direct method with the MULTAN 78 program,[8] and the atomic parameters were refined by the block-diagonal least-squares method. On the other hand, the direct method with the SAPI 85 program[9] was applied to the structure of the $C_8AzoC_5N^+Br^-$ crystal and the atomic parameters were refined by the full-matrix least-squares method. The quantity minimized in the refinement was $\sum w(|F_o|-|F_c|)^2$, with w=1.0 in the case of $C_{10}AzoC_5N^+Br^-$ and with $w=1/(\sigma^2(F)+(0.01\times F_o)^2)$ in the other case. In the refinement, the reflections with $F_o<3\sigma$ were excluded from the reflection data. After several refinement cycles, the magnitudes of the observed structure factors of ($h00$) reflections were found to be consistently smaller than those of the calculated ones in both crystals. The same phenomenon was observed in the structure analyses of $2C_nN^+2C_1Br^-$ (n=18, 14);[6,7] it is attributable to the absorption effect originating from the very thin plate-like crystal shape and its long lattice constant normal to the plate

Table 2. Fractional Coordinates and Equivalent Isotropic Temperature Factors (B_{eq}) for Non-Hydrogen Atoms of $C_{10}AzoC_5N^+Br^-$ with Estimated Standard Deviations in Parentheses.

$B_{eq}=(4/3)\times\{\beta_{11}a^2+\beta_{22}b^2+\beta_{33}c^2+2(\beta_{12}ab+\beta_{13}ac+\beta_{23}bc)\}$

Atom	x	y	z	$B_{eq}\times10^4$/nm^2
Br	0.92928(4)	0.3923(2)	0.0684(2)	503
O(1)	0.9971(2)	0.1883(8)	−0.3175(11)	464
O(2)	1.1965(2)	−0.4872(8)	−0.5756(11)	461
O(3)	1.3064(2)	−1.6236(8)	−0.0066(12)	530
N(1)	1.0678(2)	0.2073(9)	−0.7063(12)	369
N(2)	1.2383(2)	−1.0046(9)	−0.2324(13)	391
N(3)	1.2649(3)	−1.1077(10)	−0.3492(14)	433
C(1)	0.9928(3)	0.2268(12)	−0.5256(18)	442
C(2)	1.0296(3)	0.3143(10)	−0.5915(15)	366
C(3)	1.1010(4)	0.3204(15)	−0.7352(22)	608
C(4)	1.0589(4)	0.0955(15)	−0.9348(17)	580
C(5)	1.0829(3)	0.1094(11)	−0.5504(15)	343
C(6)	1.1209(3)	−0.0038(12)	−0.6480(16)	380
C(7)	1.1301(3)	−0.1102(12)	−0.4890(17)	409
C(8)	1.1622(3)	−0.2430(11)	−0.5979(16)	378
C(9)	1.1693(3)	−0.3523(11)	−0.4468(16)	389
C(10)	1.2057(3)	−0.6094(12)	−0.4796(16)	390
C(11)	1.1877(3)	−0.6219(12)	−0.2757(17)	435
C(12)	1.2000(3)	−0.7536(12)	−0.1977(17)	435
C(13)	1.2345(3)	−0.7290(12)	−0.6089(16)	398
C(14)	1.2463(3)	−0.8600(12)	−0.5359(16)	417
C(15)	1.2282(3)	−0.8741(11)	−0.3273(17)	387
C(16)	1.2744(3)	−1.2378(11)	−0.2550(16)	385
C(17)	1.2559(3)	−1.2517(11)	−0.0501(16)	379
C(18)	1.2677(3)	−1.3814(12)	0.0272(17)	448
C(19)	1.3034(3)	−1.3553(13)	−0.3793(17)	478
C(20)	1.3156(3)	−1.4876(12)	−0.3049(18)	480
C(21)	1.2970(3)	−1.5013(12)	−0.0997(17)	402
C(22)	1.3362(3)	−1.7533(13)	−0.1280(20)	535
C(23)	1.3392(3)	−1.8637(12)	0.0281(19)	498
C(24)	1.3715(4)	−2.0041(13)	−0.0584(20)	560
C(25)	1.3731(4)	−2.1084(14)	0.1037(22)	617
C(26)	1.4055(4)	−2.2454(14)	0.0377(23)	639
C(27)	1.4063(4)	−2.3512(16)	0.2011(24)	722
C(28)	1.4390(4)	−2.4852(17)	0.1460(27)	780
C(29)	1.4396(5)	−2.5871(18)	0.3123(27)	846
C(30)	1.4721(5)	−2.7232(21)	0.2491(32)	1054
C(31)	1.4729(7)	−2.8218(24)	0.4153(39)	1381

Table 3. Fractional Coordinates and Equivalent Isotropic Temperature Factors (B_{eq}) for Non-Hydrogen Atoms of $C_8AzoC_5N^+Br^-$ with Estimated Standard Deviations in Parentheses.

$B_{eq}=(4/3)\times\{\beta_{11}a^2+\beta_{22}b^2+\beta_{33}c^2+2(\beta_{12}ab+\beta_{13}ac+\beta_{23}bc)\}$

Atom	x	y	z	$B_{eq}\times10^4$/nm^2
Br	1.07584(2)	−0.3539(1)	1.0478(1)	537
O(1)	1.0033(1)	−0.1856(5)	0.6800(7)	516
O(2)	0.7890(1)	0.3791(5)	0.4800(7)	520
O(3)	0.6718(2)	1.4502(5)	1.0845(7)	605
N(1)	0.9276(2)	−0.2435(7)	0.3137(10)	375
N(2)	0.7450(2)	0.8705(6)	0.8354(8)	469
N(3)	0.7157(2)	0.9593(6)	0.7265(9)	479
C(1)	1.0077(2)	−0.2229(8)	0.4711(12)	467
C(2)	0.9687(2)	−0.3280(9)	0.4156(12)	446
C(3)	0.8912(3)	−0.3852(12)	0.2988(20)	821
C(4)	0.9378(3)	−0.1283(10)	0.0802(12)	597
C(5)	0.9111(2)	−0.1546(8)	0.4717(11)	383
C(6)	0.8702(2)	−0.0643(9)	0.3875(11)	453
C(7)	0.8608(2)	0.0371(9)	0.5468(12)	438
C(8)	0.8255(2)	0.1544(8)	0.4460(11)	442
C(9)	0.8188(2)	0.2574(8)	0.6010(11)	430
C(10)	0.7793(2)	0.4955(8)	0.5766(11)	439
C(11)	0.7987(2)	0.5185(8)	0.7787(12)	463
C(12)	0.7860(2)	0.6418(9)	0.8576(12)	506
C(13)	0.7482(2)	0.6001(8)	0.4563(11)	474
C(14)	0.7360(2)	0.7227(8)	0.5350(11)	439
C(15)	0.7549(2)	0.7462(7)	0.7378(11)	409
C(16)	0.7060(2)	1.0836(7)	0.8240(11)	423
C(17)	0.7257(2)	1.1087(8)	1.0243(11)	465
C(18)	0.7131(2)	1.2301(8)	1.1059(12)	492
C(19)	0.6743(2)	1.1867(9)	0.7061(12)	519
C(20)	0.6616(2)	1.3109(9)	0.7867(12)	526
C(21)	0.6815(2)	1.3338(8)	0.9856(11)	474
C(22)	0.6402(3)	1.5627(9)	0.9750(13)	544
C(23)	0.6366(3)	1.6719(10)	1.1296(14)	587
C(24)	0.6019(3)	1.7927(11)	1.0487(15)	665
C(25)	0.5993(3)	1.8996(10)	1.2068(15)	683
C(26)	0.5646(3)	2.0193(11)	1.1373(17)	768
C(27)	0.5625(3)	2.1312(12)	1.2919(20)	769
C(28)	0.5258(3)	2.2421(13)	1.2343(19)	1040
C(29)	0.5212(5)	2.3496(16)	1.3803(28)	1364

surface and from the fairly large absorption coefficient. Therefore, the (h00) reflections with $h<9$ for $C_{10}AzoC_5N^+Br^-$ and those with $h<10$ for $C_8AzoC_5N^+Br^-$ were excluded from the corresponding reflection data set at the final stage of the analyses. The final R values were 0.082 for all the non-hydrogen atoms and for the 46 hydrogen atoms of $C_{10}AzoC_5N^+Br^-$ and 0.058 for all the non-hydrogen atoms and for the 44 hydrogen atoms of $C_8AzoC_5N^+Br^-$. The final atomic parameters for non-hydrogen atoms are given in Tables 2 and 3.[10]

The atomic scattering factors were taken from International Tables for X-Ray Crystallography, Vol. IV.[11] Computations for $C_{10}AzoC_5N^+Br^-$ were done on an ACOS 700S computer at the Crystallographic Research Center, Institute for Protein Research, Osaka University, and on a HITAC M-280H computer at the Computer Center, University of Tokyo, with the help of the UNICS III program.[12] Those for $C_8AzoC_5N^+Br^-$ were done on an A-70 minicomputer with the aid of the CRYSTAN program in the RASA5R-II system (Rigaku Denki).

Results and Discussion

Molecular Conformation of $C_{10}AzoC_5N^+Br^-$ and $C_8AzoC_5N^+Br^-$. The bond distances and angles are shown in Fig. 2, together with their atomic labelling for non-hydrogen atoms. The numbering system of these atoms is the same as those of homologous compounds analyzed previously.[4,5] The average C-C bond distance and C-C-C bond angle in the alkyl spacer and the tail parts are 0.151(3) nm and 113(1)° for $C_{10}AzoC_5N^+Br^-$, and 0.151(2) nm and 113(1)° for $C_8AzoC_5N^+Br^-$. These values are in good agreement with those reported previously for the long hydrocarbon chains of the amphiphilic compounds.[4-7,13,14]

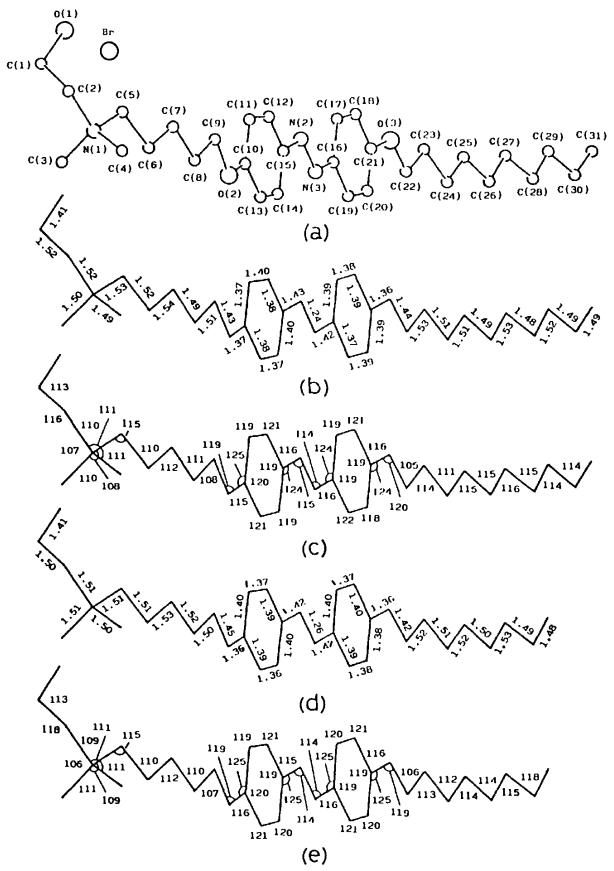

Fig. 2. Atomic labelling (a), bond lengths (1×10/nm) (b), and bond angles (/°) (c) in $C_{10}AzoC_5N^+Br^-$, together with those in $C_8AzoC_5N^+Br^-$ (d) and (e). Maximum estimated standard deviations for bond lengths and angles are 0.003 nm and 1° in $C_{10}AzoC_5N^+Br^-$ and 0.002 nm and 1° in $C_8AzoC_5N^+Br^-$.

The structural similarity of four homologous compounds, $C_nAzoC_5N^+Br^-$ (n=6, 8, 10, 12), clearly appears in the dihedral angles listed in Table 4. The dihedral angles of the four compounds are so similar to each other that the maximum deviation from the average is within 2° in every case. With the exception of the first two, all the dihedral angles have trans conformation. Especially, the planarity of the azobenzene moiety, which depends on the C(12)-C(15)-N(2)-N(3), C(15)-N(2)-N(3)-C(16) and N(2)-N(3)-C(16)-(19) angles, is very remarkable compared with those for other azobenzene-containing compounds, such as *trans*-azobenzene[15] and 4,4′-dimethylazobenzene.[16] The pronounced planarity of the azobenzene moiety must be one of the main features of the J-aggregation state of the $C_nAzoC_5N^+Br^-$ compounds. The alkyl tail part also makes a well-ordered zigzag plane. On the other hand, the zigzag plane in the alkyl spacer part is slightly distorted. This distortion may be ascribed to hydrogen bonds between terminal hydroxyl moieties and bromide anions, to electrostatic interactions between nitrogen cations and bromide anions, and to the existence of

Table 4. Dihedral Angles of $C_nAzoC_5N^+Br^-$

Dihedral angle/°	n=6	n=8	n=10	n=12	Average
O(1) C(1) C(2) N(1)	79	79	80	80	80
C(1) C(2) N(1) C(5)	−55	−56	−58	−57	−57
C(2) N(1) C(5) C(6)	180	179	180	179	180
N(1) C(5) C(6) C(7)	−174	−174	−173	−173	−174
C(5) C(6) C(7) C(8)	169	169	170	170	170
C(6) C(7) C(8) C(9)	−177	−177	−177	−178	−177
C(7) C(8) C(9) O(2)	173	173	173	172	173
C(8) C(9) O(2) C(10)	−176	−176	−176	−175	−176
C(9) O(2) C(10)C(13)	−174	−176	−176	−174	−175
C(12)C(15)N(2) N(3)	−178	−178	−177	−178	−178
C(15)N(2) N(3) C(16)	180	180	−179	180	180
N(2) N(3) C(16)C(19)	179	179	180	179	179
C(18)C(21)O(3) C(22)	180	180	179	180	180
C(21)O(3) C(22)C(23)	180	179	179	179	179
O(3) C(22)C(23)C(24)	−177	−176	−176	−176	−176
C(22)C(23)C(24)C(25)	−178	180	180	180	180
C(23)C(24)C(25)C(26)	−178	−178	−177	−177	−178
C(24)C(25)C(26)C(27)	180	−179	−179	−179	−179
C(25)C(26)C(27)C(28)		−176	−178	−177	−177
C(26)C(27)C(28)C(29)		179	179	179	179
C(27)C(28)C(29)C(30)			179	178	179
C(28)C(29)C(30)C(31)			179	−179	180
C(29)C(30)C(31)C(32)				180	180
C(30)C(31)C(32)C(33)				−179	−179

bulky methyl moieties.

Crystal Structure of $C_{10}AzoC_5N^+Br^-$ and $C_8AzoC_5N^+Br^-$. The packing arrangement viewed along the *c*-axis is shown in Fig. 3 ($C_{10}AzoC_5N^+Br^-$) and Fig. 4 ($C_8AzoC_5N^+Br^-$), together with the short interatomic distances between neighbouring chains and those between a bromide anion and the head portion of the amphiphile. The crystal structure of these two compounds can be seen as an alternation of the hydrophobic and hydrophilic layers stacked in the *a*-direction. Here, the hydrophilic and hydrophobic parts correspond to the bilayer surface and the inner part of the bilayer respectively.

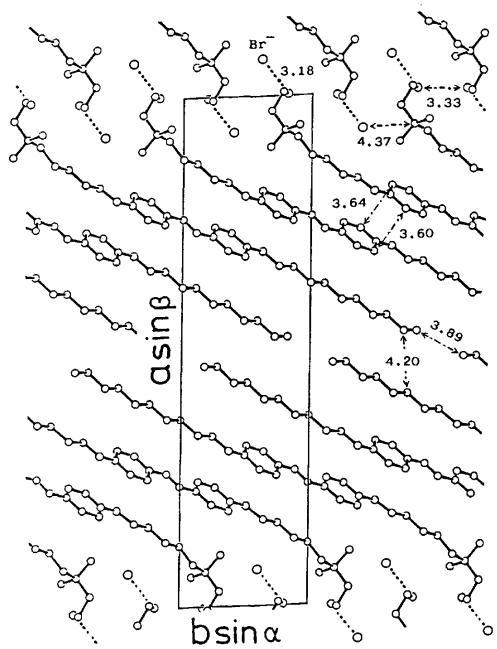

Fig. 3. Packing of $C_{10}AzoC_5N^+Br^-$ projected onto the *c*-plane (ORTEP[17] drawing). Hydrogen bonds between bromide anions and hydroxyl groups are indicated by broken lines. Some short interatomic distances (1×10/nm) are shown.

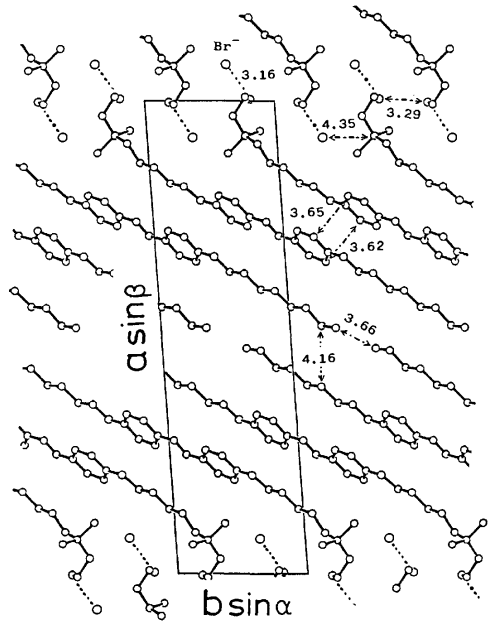

Fig. 4. Packing of $C_8AzoC_5N^+Br^-$ projected onto the *c*-plane.

In the hydrophobic layer, two molecules arranged in a tail-to-tail fashion and related by the inversion symmetry are inclined by about 30° to the layer surface. There is a remarkable tendency for the tail-to-tail distance to decrease along with the number of carbon atoms in the tail part of $C_nAzoC_5N^+Br^-$ compounds. That is, the tail-to-tail distances for n=12, 10, 8 and 6 are 0.391, 0.389, 0.366, and 0.356 nm respectively. This kind of systematic tendency was not found for the intermolecular distances in the other part of the amphiphile, such as the hydrogen-bond distances in the hydrophilic part and interatomic distances between adjacent azobenzene moieties.

In the hydrophilic layer, ammonium cations and bromide anions make a plane parallel to the bilayer surface. Two such planes are contained in one hydrophilic layer. The bromide anion is linked to the hydroxyl group of the adjacent molecule in a different bilayer by a hydrogen bond (0.318 nm in $C_{10}AzoC_5N^+Br^-$ and 0.316 nm in $C_8AzoC_5N^+Br^-$). Through this hydrogen bond, the head groups of amphiphiles in adjacent bilayers interdigitate mutually. In addition to the electrostatic interactions between the cationic ammonium nitrogens and the bromide anions, this interdigitated structure in the hydrophilic layer must contribute to the stabilization of crystals. On the other hand, the hydrophobic alkyl chains and azobenzene moieties are stabilized only by the van der Waals interactions. Therefore, the above tendency for the tail-to-tail distance in the hydrophobic part to decrease is attributable to the increase in the influence of various strong interactions in the hydrophilic part as shortening the tail length in $C_nAzoC_5N^+Br^-$.

The authors wish to express their deep thanks to Professor Yukiteru Katsube at the Crystallographic Research Center, Institute for Protein Research, Osaka University, for the use of the Institute's facilities to analyse one of the specimens.

References

1) M. Shimomura, R. Ando, and T. Kunitake, *Ber. Bunsenges. Phys. Chem.*, **87**, 1134 (1983).

2) E. G. McRae, and M. Kasha, "Physical Processes in Radiation Biology," Academic, New York (1964), p. 23.

3) T. Kunitake, M. Shimomura, T. Kajiyama, A. Harada, K. Okuyama, and M. Takayanagi, *Thin Solid Films*, **121**, L89 (1984).

4) K. Okuyama, H. Watanabe, M. Shimomura, K. Hirabayashi, T. Kunitake, T. Kajiyama, and N. Yasuoka, *Bull. Chem. Soc. Jpn.*, **59**, 3351 (1986).

5) H. Watanabe, K. Okuyama, Y. Ozawa, K. Hirabayashi, M. Shimomura, T. Kunitake, and N. Yasuoka, *Nippon Kagaku Kaishi*, **1987**, 550.

6) K. Okuyama, Y. Soboi, N. lijima, K. Hirabayashi, T. Kunitake, and T. Kajiyama, *Bull. Chem. Soc. Jpn.*, **61**, 1485 (1988).

7) K. Okuyama, N. Iijima, K. Hirabayashi, T. Kunitake, and M. Kusunoki, *Bull. Chem. Soc. Jpn.*, **61**, 2337 (1988).

8) P. Main, S. E. Hull, L. Lessinger, G. Germain, J. P. Declercq, and M. M. Woolfson, MULTAN 78. "A System of Computer Programs for the Automatic Solution of Crystal Structures from X-ray Diffraction Data," Univs. of York, England, and Louvain, Belgium (1978).

9) J. Yao, C. Zheng, J. Qian, F. Han, Y. Gu, and H. Fan, SAPI-85. "A System of Computer Programs for the Automatic Solution of Crystal Structures from X-ray Diffraction Data," Academia Sinica, Beijing, China (1985).

10) Tables of anisotropic thermal parameters, coordinates of hydrogen atoms, and observed and calculated structure factors are deposited as Document No. 8894 at the Office of the Editor of Bull. Chem. Soc. Jpn.

11) International Tables for X-ray Crystallography, Vol.IV, Kynoch Press, Birmingham (1974), p.71.

12) T. Sakurai and K. Kobayashi, *Rep. Inst. Phys. and Chem. Res.*, **55**, 69 (1978).

13) S. Abrahamson, B. Dahlen, and I. Pascher, *Acta Crystallogr., Sect. B*, **33**, 2008 (1977).

14) I. Pascher and S. Sundell, *Chem. Phys. Lipids*, **20**, 175 (1977).

15) J. A. Bouwstra, A. Schouten, and J. Kroon, *Acta Crystallogr., Sect. C*, **39**, 1221 (1983).

16) C. J. Brown, *Acta Crystallogr.*, **21**, 153 (1966).

17) C. K. Johnson, ORTEP II, Report ORNL-5138, Oak Ridge National Laboratory, Tennessee (1976).

Polymorphism and Crystal Structure of Chiral Smectogenic 4′-Heptyloxy-4-biphenylyl *p*-[(*S*)-2-Methylbutyl]benzoate

Kayako HORI* and Yuji OHASHI
Department of Chemistry, Ochanomizu University, Otsuka, Bunkyo-ku, Tokyo 112
(Received March 31, 1989)

Two crystal forms **1** and **2** were found for the title compound. DSC measurements showed that the two crystals transform to different mesophases (Sm* I and Sm* J). Crystal data. 4′-Heptyloxy-4-biphenylyl *p*-[(*S*)-2-methylbutyl]benzoate, **1**, M_r=458.61, $C_{31}H_{38}O_3$, monoclinic, $P2_1$, T=298 K, a=15.065(3), b=45.59(2), c=5.636(1) Å, β=95.51(2)°, V=4109(2) Å^3, Z=6, d_x=1.118 Mg m^{-3}, μ=0.475 mm^{-1}, $F(000)$=1488; **2**, triclinic, $P\bar{1}$, a=13.37(2), b=22.96(2), c=10.213(5) Å, α=105.55(5), β=105.22(6), γ=102.31(9)°, V=2775(5) Å^3, Z=4, d_x=1.102 Mg m^{-3}. The crystal structure of **1** has been determined by single crystal X-ray analysis. Final R was 0.109. The crystal has a distinct layer structure similar to that of a smectic liquid crystal. Two of the three crystallographically independent molecules with extended paraffin chains have parallel arrangement, to which the third molecule with a twisted and highly disordered chain is antiparallel. The paraffin chains of the parallel molecules in a layer have close contacts with each other. Such contacts would enhance the intra-layer interaction which causes the transition to Sm* I.

In the preceding papers,[1,2] we discussed the relationships between mesophase behavior and crystal structures for the two series of chiral smectogenic biphenyl esters. The first series crystals (I-*n*), *p*-pentyloxyphenyl and *p*-heptyloxyphenyl 4′-[(*S*)-2-methylbutyl]biphenyl-4-carboxylates (I-5 and I-7, respectively), transform to a Sm*C followed by a cholesteric, while the second ones (II-*n*), *p*-[(*S*)-2-methylbutyl]phenyl 4′-heptyloxybiphenyl-4-carboxylate and 4′-octyloxybiphenyl-4-carboxylate, (II-7 and II-8, respectively), to a Sm*C and then to a Sm A phase. In the former crystals paraffin chains have close contacts between layers,[1] while in the latter whole molecules including paraffin chains contribute to the lateral molecular overlapping within a layer.[2] Different mesophase behavior related to the different phase sequences was successfully interpreted by the intermolecular interaction revealed in the crystal structures.

In contrast to these two series, the third one, 4′-alkoxy-4-biphenylyl *p*-[(*S*)-2-methylbutyl]benzoates (III-*n*), was reported to have phase sequences highly dependent on the chain length.[3] Since the preceding studies revealed that the different mesophase behavior is closely related to the difference in the packings of paraffin chains in the crystals, the crystal structure analyses of the third series were intended to elucidate the relationships between the mesophase behavior and the chain length. In the course of the crystal structure determination of these compounds, two crystal forms were found for III-7.

This paper describes the polymorphism of III-7 and one of the crystal structures.

Experimental

Compound. 4′-Heptyloxy-4-biphenylol was synthesized in an analogous way to that described previously.[4] 4-[(*S*)-2-Methylbutyl]benzoyl chloride was supplied by Dr. Shungo Sugawara. $[\alpha]_D^{20}$=13.8° (cf. $[\alpha]_D^{20}$=13.1° for the free acid[5]). Esterification and purification were done in the same way as described previously.[5]

Transition temperatures were measured using a Seiko SSC570 DSC and an Olympus POM polarizing microscope equipped with a Mettler FP82.

Crystal Structure Analysis. Transparent long parallelepiped or flat plate-like crystals were separately grown from a methanol-chloroform solution. The unit cell dimensions and space groups determined from oscillation and Weissenberg photographs revealed that they are polymorphs (III-7(**1**) and III-7(**2**), respectively). Accurate cell parameters of III-7(**1**) and III-7(**2**) were determined by a least squares fit for 15 and 20 reflections, respectively, within the range, 22°<2θ<45°, measured on a Rigaku AFC-4 diffractometer with Cu$K\alpha$ radiation (λ=1.54184 Å) monochromated by graphite.

Intensity data of III-7(**1**) were collected on the diffractometer using a crystal of 0.2×0.18×0.15 mm up to 2θ=100°. A 2θ-ω scan mode and scan width of ω=(1.0+0.15tanθ)° were applied. Backgrounds were counted for 5 s at both ends of a scan. Three standard reflections were recorded after every 50 reflections. No significant intensity variations were observed. A total of 4286 reflections were collected at the rate of 4°(2θ) min^{-1}, of which 3378 were treated as significant ($|F_o|>3\sigma(|F_o|)$). The data were corrected for Lorentz and polarization factors but not for absorption. For the III-7(**2**) crystal, unfortunately, sufficient intensity data for the structure analysis have not been obtained probably due to poor crystallinity and large thermal motions.

The structure was determined by applying the program MULTAN78[6] and refined by block-matrix least-squares using SHELX76[7] and subsequently HBLS,[8] since the number of parameters exceeded the limit of SHELX76 at later stages. The quantity minimized was $\sum w(|F_o|-|F_c|)^2$, where $w=(\sigma(F_o)^2+0.004|F_o|^2)^{-1}$. Atomic scattering factors were taken from the International Tables for X-ray Crystallography.[9] In the course of the refinement, several additional peaks of 0.37—0.44 e Å^{-3} were found around the terminal moiety of the twisted paraffin chain, where the atoms had remarkably large temperature factors. These peaks were included as disordered atoms in further refinement. All the non-hydrogen atoms with occupation factors above 0.7 were refined anisotropically. Only 19 hydrogen

atoms found in the difference Fourier maps were included in the refinement, because the number of the reflections was limited due to the large thermal effect. Max. Δ/σ and max. $\Delta\rho$ in the final difference map were 0.46 and 0.30 e Å^{-3}, respectively. Final R and R_w were 0.109 and 0.130. The large R value is due to the large thermal motion and the highly disordered chain.

The final coordinates of non-hydrogen atoms are given in Table 1.[10] Computations were carried out on a HITAC M-680H computer at the Computer Center of the University of Tokyo.

Results and Discussion

Polymorphism. In order to find a relationship

Table 1. Final Atomic Coordinates with Their Estimated Standard Deviations of 4′-Heptyloxy-4-biphenylyl *p*-[(*S*)-2-Methylbutyl]benzoate (III-7(**1**))

Atom	x	y	z	B_{eq}/Å^2[a]	Atom	x	y	z	B_{eq}/Å^2[a]
O(1A)	1.1384(6)	0.9129	1.288(2)	11.7	C(13B)	0.4798(7)	1.0593(3)	0.032(2)	5.2
O(2A)	1.1896(5)	0.9367(2)	0.993(1)	6.4	C(14B)	0.4261(7)	1.0840(3)	0.064(2)	5.3
O(3A)	0.7533(5)	1.0880(2)	0.794(2)	7.5	C(15B)	0.3662(9)	1.0931(3)	−0.124(3)	7.3
C(1A)	0.8100(7)	1.0649(3)	0.819(2)	5.8	C(16B)	0.3130(8)	1.1158(3)	−0.101(2)	6.7
C(2A)	0.8146(7)	1.0440(3)	0.642(2)	6.1	C(17B)	0.3181(8)	1.1323(3)	0.101(2)	6.6
C(3A)	0.8746(8)	1.0218(3)	0.679(2)	6.4	C(18B)	0.3770(8)	1.1250(3)	0.293(2)	7.1
C(4A)	0.9287(7)	1.0216(3)	0.878(2)	4.9	C(19B)	0.4297(8)	1.1005(3)	0.271(2)	6.3
C(5A)	0.9205(7)	1.0430(3)	1.052(2)	6.6	C(21B)	0.2630(9)	1.1574(3)	0.134(3)	7.9
C(6A)	0.8624(7)	1.0646(4)	1.021(2)	7.1	C(22B)	0.3040(13)	1.1853(4)	0.100(4)	12.1
C(7A)	0.9969(6)	0.9985(3)	0.910(2)	4.6	C(23B)	0.2357(18)	1.2110(6)	0.142(5)	17.7
C(8A)	1.0034(8)	0.9776(3)	0.739(2)	6.9	C(24B)	0.2758(20)	1.2399(7)	0.200(7)	20.5
C(9A)	1.0704(9)	0.9562(4)	0.765(2)	7.9	C(25B)	0.3333(17)	1.1887(6)	−0.138(4)	16.2
C(10A)	1.1212(7)	0.9558(3)	0.968(2)	5.7	C(31B)	0.9621(8)	0.8807(3)	0.682(3)	7.1
C(11A)	1.1158(8)	0.9772(3)	1.139(2)	7.1	C(32B)	1.0463(8)	0.8644(3)	0.690(3)	7.7
C(12A)	1.0540(8)	0.9972(3)	1.116(2)	6.7	C(33B)	1.0539(9)	0.8443(3)	0.905(3)	7.8
C(13A)	1.1912(8)	0.9157(3)	1.156(2)	6.5	C(34B)	1.1334(9)	0.8256(4)	0.926(3)	8.2
C(14A)	1.2645(7)	0.8957(3)	1.156(2)	6.0	C(35B)	1.1442(10)	0.8058(4)	1.137(3)	9.4
C(15A)	1.2806(9)	0.8753(4)	1.329(3)	8.5	C(36B)	1.2139(13)	0.7845(5)	1.114(4)	13.5
C(16A)	1.3495(9)	0.8564(4)	1.339(3)	8.2	C(37B)	1.2335(15)	0.7661(6)	1.356(5)	16.8
C(17A)	1.4029(8)	0.8582(3)	1.162(3)	7.4	O(1C)	0.3500(5)	1.0239(2)	−0.669(2)	7.3
C(18A)	1.3893(8)	0.8792(3)	0.989(3)	7.4	O(2C)	0.2922(5)	0.9997(2)	−0.369(2)	6.2
C(19A)	1.3177(8)	0.8973(3)	0.973(2)	6.5	O(3C)	0.7392(5)	0.8521(2)	−0.112(2)	7.7
C(21A)	1.4816(9)	0.8394(4)	1.179(3)	9.1	C(1C)	0.6836(7)	0.8737(3)	−0.135(2)	6.4
C(22A)	1.4643(11)	0.8071(4)	1.117(3)	10.2	C(2C)	0.6337(8)	0.8734(4)	−0.343(3)	8.2
C(23A)	1.5493(14)	0.7914(5)	1.135(5)	13.5	C(3C)	0.5703(7)	0.8948(4)	−0.384(2)	7.4
C(24A)[c]	1.5905(20)	0.7883(7)	1.370(6)	13.1	C(4C)	0.5589(7)	0.9178(3)	−0.219(2)	5.0
C(24A′)[c]	1.5621(58)	0.7697(21)	1.266(17)	16.7(27)[b]	C(5C)	0.6109(8)	0.9170(3)	−0.016(2)	7.2
C(25A)	1.4198(12)	0.8037(4)	0.858(3)	10.8	C(6C)	0.6779(8)	0.8955(3)	0.037(2)	7.0
C(31A)	0.6981(8)	1.0898(3)	0.579(3)	6.9	C(7C)	0.4896(6)	0.9390(2)	−0.277(2)	4.3
C(32A)	0.6487(12)	1.1197(5)	0.594(4)	11.7	C(8C)	0.4346(8)	0.9399(3)	−0.480(2)	6.3
C(33A)	0.6060(13)	1.1219(5)	0.798(4)	12.3	C(9C)	0.3720(7)	0.9595(3)	−0.516(3)	6.4
C(34A)	0.5715(22)	1.1519(7)	0.834(6)	20.0	C(10C)	0.3601(7)	0.9801(3)	−0.337(2)	5.7
C(35A)[c]	0.6150(43)	1.1721(15)	1.071(13)	21.6(24)[b]	C(11C)	0.4147(8)	0.9809(3)	−0.130(2)	5.9
C(35A′)[c]	0.6142(38)	1.1757(14)	0.856(10)	18.6(19)[b]	C(12C)	0.4755(7)	0.9608(3)	−0.099(2)	6.0
C(36A)[c]	0.5746(41)	1.1957(14)	0.966(11)	19.6(22)[b]	C(13C)	0.2943(7)	1.0210(3)	−0.532(2)	5.8
C(36A′)[c]	0.6642(45)	1.1796(16)	1.011(12)	21.9(24)[b]	C(14C)	0.2230(7)	1.0414(2)	−0.518(2)	4.6
C(37A)[c]	0.5951(43)	1.2110(15)	1.188(13)	21.5(24)[b]	C(15C)	0.1683(7)	1.0393(3)	−0.344(2)	5.5
C(37A′)[c]	0.7032(40)	1.2052(14)	1.186(12)	20.1(22)[b]	C(16C)	0.1023(7)	1.0592(3)	−0.347(2)	5.9
O(1B)	0.4813(6)	1.0455(3)	−0.156(2)	8.4	C(17C)	0.0852(7)	1.0800(3)	−0.521(2)	5.5
O(2B)	0.5280(5)	1.0531(2)	0.232(1)	6.0	C(18C)	0.1428(7)	1.0827(3)	−0.705(2)	6.0
O(3B)	0.9543(4)	0.8967(2)	0.465(1)	6.5	C(19C)	0.2131(8)	1.0635(3)	−0.693(2)	6.3
C(1B)	0.8946(7)	0.9171(3)	0.437(2)	5.3	C(21C)	0.0090(8)	1.0996(3)	−0.535(3)	7.2
C(2B)	0.8929(7)	0.9352(3)	0.241(2)	5.2	C(22C)	0.0129(9)	1.1241(3)	−0.358(3)	7.8
C(3B)	0.8340(7)	0.9569(3)	0.194(2)	5.3	C(23C)	−0.0757(10)	1.1378(4)	−0.380(4)	10.2
C(4B)	0.7678(7)	0.9598(3)	0.344(2)	5.0	C(24C)	−0.0767(17)	1.1606(6)	−0.190(5)	17.9
C(5B)	0.7697(7)	0.9429(3)	0.544(2)	5.5	C(25C)	0.0811(11)	1.1475(4)	−0.437(4)	10.8
C(6B)	0.8302(7)	0.9204(3)	0.591(2)	5.5	C(31C)	0.7856(9)	0.8467(3)	0.110(3)	7.9
C(7B)	0.7011(7)	0.9836(3)	0.298(2)	4.7	C(32C)	0.8208(9)	0.8156(4)	0.107(3)	8.4
C(8B)	0.7030(7)	1.0044(3)	0.123(2)	6.0	C(33C)	0.8676(11)	0.8092(4)	0.352(3)	9.7
C(9B)	0.6447(8)	1.0274(3)	0.082(2)	6.2	C(34C)	0.9033(12)	0.7772(4)	0.341(4)	10.8
C(10B)	0.5843(7)	1.0290(3)	0.239(2)	5.4	C(35C)	0.9540(10)	0.7680(4)	0.563(3)	9.8
C(11B)	0.5784(7)	1.0095(3)	0.419(2)	5.6	C(36C)	0.9822(13)	0.7360(4)	0.542(4)	11.9
C(12B)	0.6393(8)	0.9871(3)	0.454(2)	6.1	C(37C)	1.0371(15)	0.7267(5)	0.771(5)	15.4

a) $B_{eq}=(4/3)\sum_{ij}\beta_{ij}(a_i\cdot a_j)$. b) Isotropic temperature factors. c) Occupation factors are fixed to be 0.7 for C(24A), 0.3 for C(24A′), and 0.5 for (35A) to C(37A′).

Table 2. Enthalpies of Transitions (ΔH/kJ mol^{-1})

Transition	III-7a	III-7b
Crystal-mesophase	16.3±0.7	16.8±0.7
Sm*I-Sm*C	2.4±0.2	2.4±0.2
Sm*C-cholesteric	4.7±0.2	4.6±0.1
Cholesteric-isotropic[a)]	1.1±0.1	1.4±0.2

a) Via a blue phase.

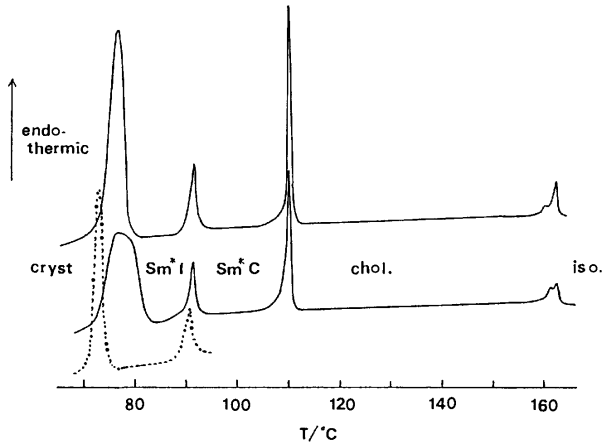

Fig. 1. DSC peaks for the two polymorphs of 4′-heptyloxy-4-biphenylyl *p*-[(*S*)-2-methylbutyl]-benzoate: III-7(**1**) (upper) and III-7(**2**) (lower). A broken line denotes a curve for the solid obtained from a melt. Scan speed was 2° min^{-1}.

between the two polymorphs, DSC measurements were carried out. ΔH values are summarized in Table 2. Transition temperatures of Sm*I-Sm*C and Sm*C-cholesteric were in good agreement with the reported values,[3)] while the cholesteric-isotropic transition temperature was higher (ca.161 °C) than the reported one (154 °C) and a blue phase was observed during the transition.

As shown in Fig. 1, the shapes of the crystal-mesophase transition peaks are remarkably different: a sharp peak for III-7(**1**) and a broad one for III-7(**2**). The former peak is as sharp as the crystal-Sm*C transition peaks of the series I and II and the profile is independent of the heating rate, while the latter has a truncated profile, which is slightly dependent on heating rate. These facts indicate that the former peak corresponds to a single step of transition while the latter is composed of two (or more) steps. Goodby and Leslie reported that the phase sequence of III-7 was crystal-Sm*J-Sm*I-Sm*C-cholesteric-isotropic.[3)] Refering to this, it is interpreted that the sharp peak of III-7(**1**) corresponds to a direct transition to Sm*I, while the broad one of III-7(**2**) to successive transitions, Sm*J-Sm*I-Sm*C, because the Sm*I-Sm*C transition temperature is in good agreement with the reported one. On re-heating, the peak of III-7(**2**) also becomes sharp and ΔH is about 60—70% of the first run, showing that the solid obtained from a melt is much more disordered than the crystalline state obtained from a solution.

Molecular Conformations in the Crystal. All the bond lengths and angles are almost compatible with those found in the mesogens studied previously,[1,2)] as shown in Table 3. All the phenyl rings are planar within the experimental error. Table 4 shows torsion angles. The molecule A has two disordered conformations in the largely twisted chain and the other two molecules B and C have straightly extended paraffin chains. The C(24) atom in the molecule A is also slightly disordered. The molecules B and C have approximately the same structure. Figure 2 shows ORTEP drawings of the molecules A and B with the numbering scheme.

Biphenyl moieties were nearly coplanar in all the molecules. The ester moieties composed of C(10), C(13), C(14), O(1), and O(2) atoms, which are planar within the experimental error, are approximately coplanar with the phenyl rings of C(14)—(19), as is easily expected by considering the conjugation of the double bonds. In the cases of the I and II crystals, they are coplanar with one of the biphenyl rings.

Crystal Packing. Figure 3 shows the crystal structure. In a distinct layer structure parallel to the (010) plane, molecules have two opposite tilt (±45°) alternately from layer to layer.

Molecular arrangement within a layer is quite different from those of the series I and II. The latter two series have antiparallel arrangements of molecular long axes related by a pseudo-inversion (I) or a 2-fold screw axis (II). On the other hand, in the III-7(**1**) crystal the two molecules with the extended paraffin chains have parallel arrangement, to which the third molecule with the twisted chain is antiparallel.

The phenyl rings of adjacent molecules have non-

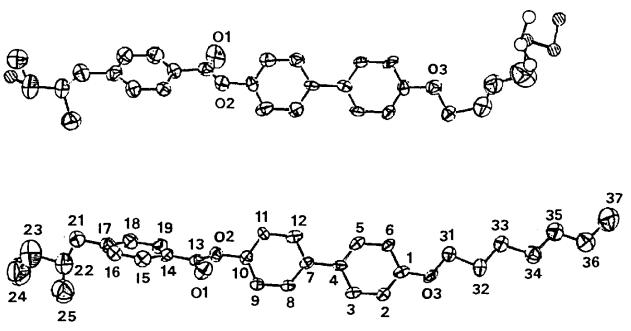

Fig. 2. ORTEP views of the molecules A (upper) and B (lower) in III-7(**1**) with 50% probability thermal ellipsoids. The molecule C has almost the same conformation as the molecule B. The isotropically refined atoms are shown by spheres with an arbitrary diameter. Shadowed atoms indicates the other conformer. All the molecules are numbered in the same way.

Table 3. Bond Lengths (l/Å) and Angles (ϕ/°) of III-7(**1**)[a)]

Atoms	mol. A	mol. B	mol. C	Atoms	mol.A	mol. B	mol. C
Bond length (l/Å)				C(2)-C(1)-C(6)	122(1)	118(1)	122(1)
O(1)-C(13)	1.19(2)	1.24(2)	1.24(2)	C(1)-C(2)-C(3)	118(1)	123(1)	116(1)
O(2)-C(10)	1.40(2)	1.42(2)	1.41(2)	C(2)-C(3)-C(4)	120(1)	119(1)	125(1)
O(2)-C(13)	1.33(2)	1.33(2)	1.34(2)	C(3)-C(4)-C(5)	119(1)	119(1)	115(1)
O(3)-C(1)	1.39(2)	1.34(2)	1.33(2)	C(3)-C(4)-C(7)	120(1)	121(1)	126(1)
O(3)-C(31)	1.43(2)	1.42(2)	1.42(2)	C(5)-C(4)-C(7)	121(1)	120(1)	119(1)
C(1)-C(2)	1.39(2)	1.38(2)	1.40(2)	C(4)-C(5)-C(6)	122(1)	122(1)	123(2)
C(1)-C(6)	1.35(2)	1.42(2)	1.36(2)	C(1)-C(6)-C(5)	119(2)	119(1)	120(2)
C(2)-C(3)	1.40(2)	1.38(2)	1.47(2)	C(4)-C(7)-C(8)	120(1)	120(1)	127(1)
C(3)-C(4)	1.36(2)	1.43(2)	1.36(2)	C(4)-C(7)-C(12)	122(1)	123(1)	118(1)
C(4)-C(5)	1.40(2)	1.37(2)	1.42(2)	C(8)-C(7)-C(12)	118(1)	116(1)	115(1)
C(4)-C(7)	1.52(2)	1.53(2)	1.49(2)	C(7)-C(8)-C(9)	120(1)	121(1)	124(1)
C(5)-C(6)	1.35(2)	1.42(2)	1.41(2)	C(8-C(9)-C(10)	119(2)	119(1)	119(1)
C(7)-C(8)	1.37(2)	1.39(2)	1.38(2)	O(2)-C(10)-C(9)	120(1)	116(1)	120(1)
C(7)-C(12)	1.41(2)	1.37(2)	1.44(2)	O(2)-C(10)-C(11)	118(1)	120(1)	120(1)
C(8)-C(9)	1.45(2)	1.42(2)	1.34(2)	C(9)-C(10)-C(11)	121(1)	123(1)	120(1)
C(9)-C(10)	1.34(2)	1.36(2)	1.40(2)	C(10)-C(11)-C(12)	120(1)	115(1)	119(1)
C(10)-C(11)	1.38(2)	1.38(2)	1.40(2)	C(7)-C(12)-C(11)	122(1)	125(1)	123(1)
C(11)-C(12)	1.35(2)	1.41(2)	1.34(2)	O(1)-C(13)-O(2)	123(1)	124(1)	125(1)
C(13)-C(14)	1.49(2)	1.44(2)	1.48(2)	O(1)-C(13)-C(14)	123(1)	124(1)	125(1)
C(14)-C(15)	1.36(2)	1.42(2)	1.38(2)	O(2)-C(13)-C(14)	114(1)	112(1)	110(1)
C(14)-C(19)	1.40(2)	1.39(2)	1.41(2)	C(13)-C(14)-C(15)	121(1)	121(1)	123(1)
C(15)-C(16)	1.40(2)	1.36(2)	1.39(2)	C(13)-C(14)-C(19)	121(1)	123(1)	117(1)
C(16)-C(17)	1.38(2)	1.36(2)	1.38(2)	C(15)-C(14)-C(19)	118(1)	116(1)	121(1)
C(17)-G(18)	1.37(2)	1.41(2)	1.45(2)	C(14)-C(15)-C(16)	123(2)	123(1)	119(1)
C(17)-C(21)	1.52(2)	1.47(2)	1.51(2)	C(15)-C(16)-C(17)	119(2)	121(1)	124(1)
C(18)-C(19)	1.41(2)	1.41(2)	1.43(2)	C(16)-C(17)-C(18)	119(1)	120(1)	118(1)
C(21)-C(22)	1.54(3)	1.46(3)	1.50(2)	C(16)-C(17)-C(21)	119(1)	123(1)	123(1)
C(22)-G(23)	1.54(3)	1.64(4)	1.55(3)	C(18)-C(17)-C(21)	121(1)	117(1)	119(1)
C(22)-C(25)	1.57(3)	1.47(4)	1.62(3)	C(17)-C(18)-C(19)	122(1)	119(1)	118(1)
C(23)-C(24)	1.43(4)	1.49(5)	1.49(4)	C(14)-C(19)-C(18)	118(1)	122(1)	120(1)
C(31)-C(32)	1.58(3)	1.54(2)	1.52(2)	C(17)-C(21)-C(22)	113(1)	112(1)	115(1)
C(32)-C(33)	1.40(3)	1.52(2)	1.54(2)	C(21)-C(22)-C(23)	107(2)	107(2)	106(1)
C(33)-C(34)	1.50(4)	1.53(2)	1.57(3)	C(21)-C(22)-C(25)	112(2)	114(2)	107(1)
C(34)-C(35)	1.72(8)	1.49(2)	1.49(3)	C(23)-C(22)-C(25)	110(2)	110(2)	111(1)
C(35)-C(36)	1.37(10)	1.50(3)	1.54(3)	C(22)-C(23)-C(24)	116(2)	113(3)	107(2)
C(36)-C(37)	1.44(10)	1.60(4)	1.55(4)	O(3)-C(31)-C(32)	106(1)	106(1)	109(1)
				C(31)-C(32)-C(33)	113(2)	109(1)	108(1)
Bond angle (ϕ/°)				C(32)-C(33)-C(34)	113(2)	114(1)	107(1)
C(10)-O(2)-C(13)	119(1)	120(1)	118(1)	C(33)-C(34)-C(35)	118(3)	116(1)	114(2)
C(1)-O-(3)-C(31)	119(1)	117(1)	121(1)	C(34)-C(35)-C(36)	87(5)	111(2)	110(2)
O(3)-C(1)-C(2)	122(1)	118(1)	123(1)	C(35)-C(36)-C(37)	87(6)	111(2)	110(2)
O(3)-C(1)-C(6)	116(1)	124(1)	115(1)				

a) The bond lengths and angles including the disordered atoms are shown for one of the conformers.

Table 4. Tortion Angles (ϕ/°) of III-7(**1**)

	mol. A	mol. B	mol. C
Phenyl groups			
ring(C1—C6)-ring(C7—12)	3	6	4
ring(C7—C12)-ring(C14—C19)	61	59	61
Phenyl and ester groups			
ring(C7—C12)-ester	68	54	67
ring(C14—C19)-ester	7	5	6
Alkyl chains			
O(3)-C(31)-C(32)-C(33)	57	174	177
C(31)-C(32)-C(33)-C(34)	190	183	180
C(32)-C(33)-C(34)-C(35)	112, 59	181	183
C(33)-C(34)-C(35)-C(36)	192, 63	191	189
C(34)-C(35)-C(36)-C(37)	194, 144	188	182

parallel contacts as found in the former two series. The angles between the mean planes are 60°, on average. The molecular overlapping within a layer is relatively large from an end to the other, as in the case of the series II crystals, although the tilt angle is larger than that in the series II crystals (30°). On the other hand, the packing of the paraffin chains within a layer is different. In the series II crystals paraffin chains have rather loose contacts, while those of the parallel molecules in the III-7(**1**) crystal form sheets composed of close contacts along the c axis, as shown in Fig. 4. This seems to enhance the molecular interaction within a layer, leading to the transition to Sm*I, an intermediately highly ordered smectic with a pseudo-hexagonal arrangement in a layer.[12)]

Intermolecular interaction due to the close contacts

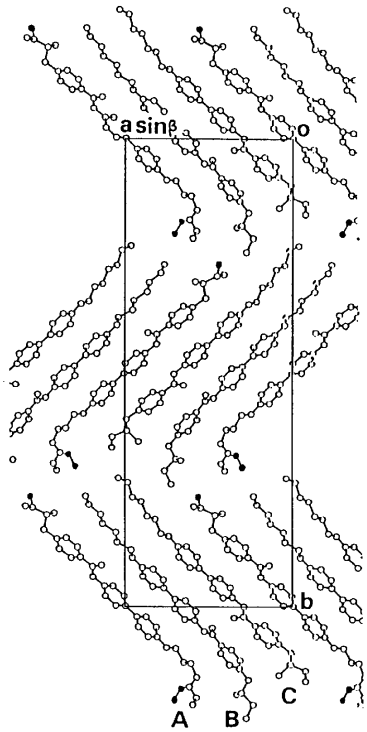

Fig. 3. Crystal structure of III-7(**1**) viewed along the c axis. Filled circles denote disordered atoms.

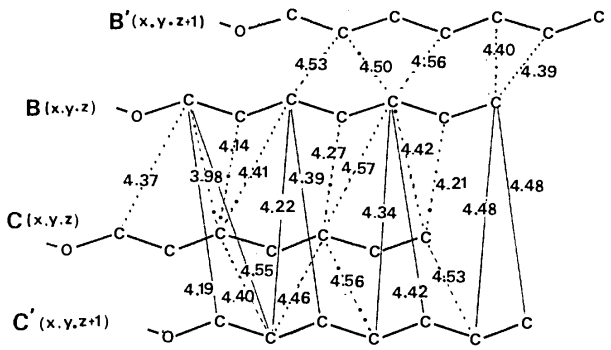

Fig. 4. Inter-chain distances (Å) of III-7(**1**). Only distances less than 4.6 Å are shown. Symmetry codes are shown in parentheses.

between the paraffin chains would largely depend on the chain length. This may be responsible for the different phase sequences depending on the chain length in this series.

The authors express their thanks to Dr. Shungo Sugawara of NTT Ibaraki Electrical Communication Laboratories for supplying the chiral acid chloride and to Professor Atsuko Shimada of this University for supporting the DSC measurement. This work was partially supported by a Grant-in-Aid for Scientific Research No. 60540280 from the Ministry of Education, Science and Culture.

References

1) K. Hori and Y. Ohashi, *Bull. Chem. Soc. Jpn.*, **61**, 3859 (1988).

2) K. Hori, M. Takamatsu, and Y. Ohashi, *Bull. Chem. Soc. Jpn.*, **62**, 1751 (1989).

3) J. W. Goodby and T. M. Leslie, *Mol. Cryst. Liq. Cryst.*, **110**, 175 (1984).

4) E. M. Neubert, L. T. Carlino, R. D'Siodocky, and D. L. Fischel, "Liquid Crystals and Ordered Fluids," ed. by J. F. Johnson and R. S. Porter, Plenum Press, New York (1974), Vol. 2, p. 293.

5) G. W. Gray and D. G. McDonnell, *Mol. Cryst. Liq. Cryst.*, **37**, 189 (1976).

6) P. Main, S. E. Hull, L. Lessinger, G. Germain, J.-P. Declercq, and M. M. Woolfson, MULTAN78. A System of Computor Programs for the Automatic Solution of X-ray Diffraction Data. Univs. of York, England and Louvain, Belgium (1978).

7) G. M. Sheldrick, SHELX76. A Program for Crystal Structure Determination. Univ. of Cambridge (1976).

8) Y. Ohashi, unpublished version of an original program by T. Ashida.

9) "International Tables for X-ray Crystallography," Birmingham, Kynoch Press (1974), Vol. IV.

10) The tables of the anisotropic temperature factors for the non-hydrogen atoms, the atomic parameters for the hydrogen atoms and the F_o–F_c list are deposited as Document No.8897 at the Office of the Editor of the Bulletin of the Chemical Society of Japan.

11) C. Johnson. ORTEP. Report ORNL-3794, Oak Ridge National Laboratory, Tennessee (1965).

12) G. W. Gray and J. W. Goodby, "Smectic Liquid Crystals," Leonard Hill, Glasgow (1984), p. 54.

 © 1989 The Chemical Society of Japan Bull. Chem. Soc. Jpn., 62, 3221—3228 (1989)

Acidity Enhanced Pillared Clay Catalysts. Modification of Exchangeable Sites on Fluor-tetrasilicic Mica by the Fixed Interlayer Cations

Hiroaki SAKURAI, Kazuo URABE,* and Yusuke IZUMI*
Department of Synthetic Chemistry, Faculty of Engineering, Nagoya University, Furo-cho, Chikusa-ku, Nagoya 464
(Received April 12, 1989)

By the use of fluor-tetrasilicic mica (TSM) as a starting material, La^{3+}-modified pillared TSM was prepared by calcining La^{3+}-exchanged TSM followed by Al-pillaring. Nonmodified pillared TSM managed only a 0.1% conversion for toluene alkylation with methanol, but the alkylation activity was greatly enhanced by the modification to give more than a 7% conversion, the activity level of which was roughly comparable to that of the conventional pillared montmorillonite. The effect of modification greatly depended on the calcination temperature at the pretreatment of La^{3+}-exchanged TSM prior to a pillaring operation; the optimum calcination temperature was between 300 and 400 °C. Other multivalent cations with large ionic radii, such as Ce^{3+}, Ca^{2+}, and Sr^{2+}, were also useful as modifiers. On the basis of the results of measurements involving X-ray diffraction, cation-exchange capacity and IR spectra of the adsorbed pyridine, it was concluded that a part of the thermally dehydrated La^{3+} ions lost their exchangeability to be fixed on the cation exchange sites of layers, remained between layers even after Al-pillaring, and took charge of the genesis of acidic sites.

Pillared clays, which function as acid catalysts having good thermal stability and a molecular sieve property, are obtained by the intercalation of aluminum hydroxy cluster cations into the region between the silicate sheets of clay minerals.[1-4] Several kinds of polyoxocations other than Al, e.g., Zr, Cr, Ti, and Fe are also available as guest species, and the clays pillared by these guest species have been extensively studied.[5] In these studies, smectite clay minerals are exclusively employed as host clays: namely, montmorillonite,[2,3] hectorite,[6] fluor-hectorite,[6] laponite,[7,8] beidellite,[9-11] and saponite.[12-14] Through the examination of the acid catalysis of various types of clays, we have recently demonstrated the catalytic efficiency-determining factors in Al-pillared clay catalysts.[13] The factors on host clays include particle size, cation-exchange capacity (CEC) and the position of isomorphous substitution.

Fluor-tetrasilicic mica (TSM) is another interesting material clay, since it has a large CEC and a well-arranged layer structure. The sodium form of TSM, which was first synthesized as $Na(Mg_{5/2})^{oct.}(Si_4)^{tet.}O_{10}F_2$ by Kitajima and Daimon,[15] is known to have a free swelling property and a high cation-exchange ability. Morikawa et al.[16] reported an unusual property of TSM: that it possesses no acidic sites, even in the proton-exchanged form. By employing TSM as a starting material we could prepare an Al-pillared TSM (PTSM).[12,14] Due to its large CEC, TSM could be effectively pillared and the PTSM, thus obtained, showed a pore structure similar to that of pillared montmorillonite (PM); unexpectedly, however, it had few acid sites effective for toluene alkylation with methanol. We thus induced that a principal part in acidity genesis in pillared clays is played not by the pillars as guests but by the sheet silicate itself as a host.[14,17] It is therefore promising to modify not the pillars, but the silicate sheets of pillared clay in order to build up more acidic and active clay catalysts.

There have already been some examples of pillared clays modified through cation exchange. Shabtai et al.[18-20] introduced La^{3+} and Ce^{3+}, Vaughan et al.[21] introduced La^{3+} and Suib et al.[22,23] introduced Cr^{3+} and Fe^{3+}, into pillared montmorillonites or pillared bentonites (montmorillonite is a principal clay mineral of "bentonite" rock). However, the modification effects reported by them on activity improvement for some typical acid-catalyzed reactions remained obscure, because each nonmodified pillared montmorillonite used by them already had a substantial activity by itself. We recently found that the acidity of PTSM can be greatly enhanced when the silicate sheets of pillared TSM are modified by La^{3+} ions.[24,25] After native TSM was exchanged with La^{3+} and calcined at 300—400 °C, successive pillaring by aluminum hydroxy cluster cation was carried out in a mixture of acetone and water. The resulting catalyst gave a much higher catalytic activity for the toluene alkylation with methanol than nonmodified pillared TSM.

In this paper we described the preparative conditions of this La^{3+}-modified pillared TSM to give highly active catalysts in detail, and discuss the mechanism of acid-site generation by La^{3+} modification.

Experimental

Material Clay and Pillaring Agent. Samples of synthetic fluor-tetrasilicic mica were supplied from Topy Ind. and refined by means of the conventional sedimentation technique. The refined TSM contained only trace amounts of impurities, such as α-cristobalite. Reportedly, the composition of this clay by chemical analysis is[26] $Na_{1.00}Mg_{2.63}^{oct.}(Si_{3.94}Al_{0.05}Mg_{0.01})^{tet.}O_{10.19}F_{1.81}$. As a reference clay, refined natural montmorillonite (Kunipia F) was supplied by Kunimine Ind.

An aluminum hydroxy cluster cation solution (OH/Al=2.0) was prepared according to a known method.[2] An aqueous 0.5 M NaOH solution (1 M=1 mol dm^{-3}) was slowly added (100 ml h^{-1}) to a 0.2 M $Al(NO_3)_3$ solution at 60 °C, and the mixture was aged for 2 h at the same temperature. The product solution was stored at room temperature.

Catalyst Preparation. The preparative procedure of various types of metal-modified pillared TSM (M^{n+}-PTSM) is illustrated in Fig. 1. First, metal ion-exchanged TSM (M^{n+}-TSM) was prepared using a metal nitrate solution followed by calcination at 200—500 °C for 3 h (procedure of calc.1). Al-pillaring manipulation was then achieved in a mixture of acetone and water according to the method of Yamanaka et al.[27] The calcined M^{n+}-TSM (1.2 g) was dispersed in a mixed solution of acetone and water (50 ml each) and stirred for 30 min; then, 150 ml of the aluminum hydroxy cluster cation solution (vide supra) was added to the dispersion. After stirring for 12 h, the product was filtered, washed repeatedly with deionized water and air-dried overnight at 60 °C. The M^{n+}-PTSM, thus obtained, was calcined in air (procedure of calc.2) and served as a catalyst. Nonmodified pillared TSM (PTSM) and pillared montmorillonite (PM) were prepared according to a previously reported method.[12,14]

Reaction Procedure and Analysis. Toluene alkylation with methanol and 2-propanol dehydration were both carried out using a conventional continuous-flow system under atmospheric pressure. The liquid products collected in an ice trap were analyzed by GLC using a Bentone 34 and DNP column (4 m) for toluene alkylation and a Porapack S column (1 m) for 2-propanol dehydration, respectively.

Characterization. X-Ray diffraction (XRD) analysis was carried out employing an oriented clay film spread on a glass slide. The nitrogen adsorption on the catalyst was measured at 78 K using constant-volume adsorption equipment; the surface area was calculated according to either the B.E.T. or to the Langmuir equation, depending on the type of adsorption isotherm.

Cation-exchange capacities (CEC) of clay samples were determined based on the amount of the Ca^{2+} which was replaced by Na^{+}[28] in a similar way to the conventional CEC determination.[29] Each clay sample (0.3 g) was diluted with quarts sand and packed in a Pyrex column (18 mm diameter). Aqueous $Ca(CH_3COO)_2$ (0.5 M) was added and the clay was saturated with Ca^{2+} ion. The clay was washed with a 90% EtOH solution and again exchanged to the sodium form with 1.71 M aqueous solution of NaCl. The Ca^{2+} ions leached out were determined by chelatometric titration.

IR spectra were recorded on a JASCO IR-810 spectrophotometer at room temperature. Each wafer sample of clay was mounted in a Pyrex-made IR cell and evacuated for 1 h at 300 °C. After cooling, the background spectrum was recorded, and pyridine was adsorbed at 150 °C. The sample was then treated at a given temperature between 150 and 450 °C in vacuo followed by cooling, and the corresponding spectrum was recorded. Finally, water was adsorbed on the sample at 200 °C, and the sample was evacuated at the same temperature, then the spectrum was recorded to examine the transformation of Lewis into Brønsted acid sites.[30]

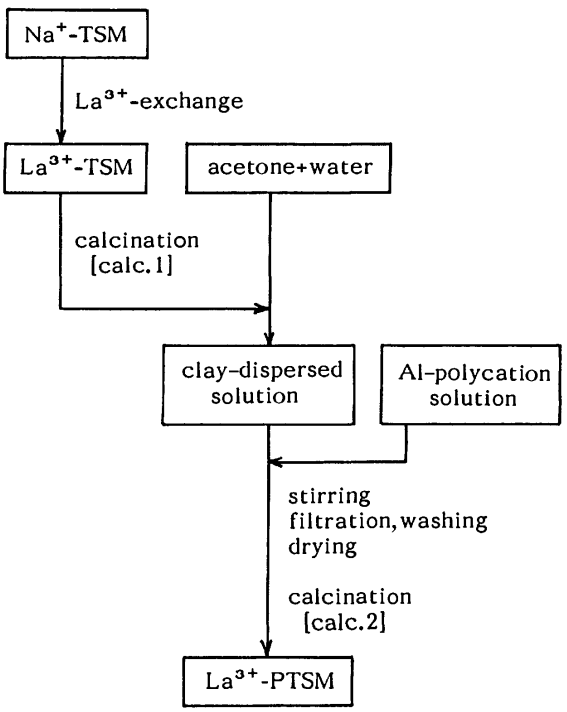

Fig. 1. Preparation procedure of La^{3+}-PTSM.

Results and Discussion

Time Course of Catalytic Activity. The activities for the toluene alkylation with methanol over three kinds of catalysts (La^{3+}-modified pillared TSM (La^{3+}-PTSM), nonmodified pillared TSM (PTSM) and pillared montmorillonite (PM)) are compared in Fig. 2. La^{3+}-PTSM exhibited a high activity by the modification almost comparable to that of the conventional PM, whereas nonmodified PTSM showed only a meager conversion. Owing to carbon deposition, the toluene conversion was rapidly decreased with the

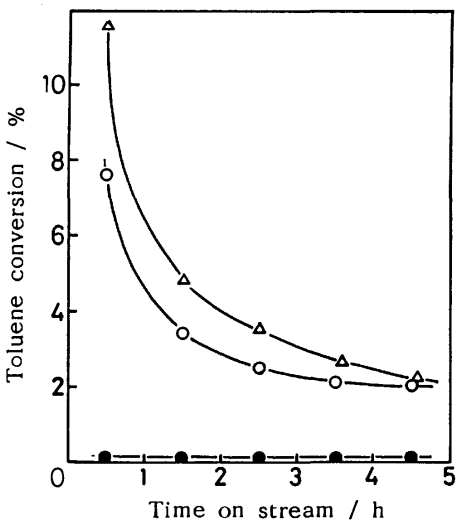

Fig. 2. Time course of catalytic activity for toluene alkylation. Reaction temp 350 °C, W/F=60 g h mol^{-1}, toluene : methanol=2 : 1 (mole ratio), flow rate of N_2 carrier gas 200 ml h^{-1}. (△) PM, (○) La^{3+}-PTSM, (●)PTSM.

time on stream for all catalysts tested. Incidentally, the deactivation rate was somewhat slower for La^{3+}-PTSM than for PM. Taking such deactivation into account, the averaged toluene conversion and xylene selectivity obtained 1 h after the reactant feed was initiated were subsequently taken as standard data to evaluate the catalytic efficiency.

Influence of Modifying Procedure on Catalytic Activity. Table 1 shows the initial conversions of the toluene alkylation by the catalysts obtained through various preparation methods, together with the data of basal spacing and surface area of the catalyst. Over the TSM-based catalysts, xylene was found to be a major product with a selectivity of more than about 80%. The Al-pillared, but nonmodified, catalyst (PTSM; No.1) showed a large surface area (197 $m^2 g^{-1}$) and a basal spacing of 18.4 Å. Considering the layer thickness of the clay itself (9.6 Å), the catalyst has an interlayer spacing (8.8 Å) large enough to accept the reactant organic molecules, though the nonmodified PTSM gave a very low activity. In the case of the La^{3+}-exchanged but nonpillared catalyst (La^{3+}-TSM; No. 2), the interlayer region collapsed (d_{001}=9.7 Å) on heating at 400 °, and the reaction did not proceed. In connection with the La^{3+}-modified and Al-pillared catalyst (La^{3+}-PTSM; Nos. 3—7), the activity varied widely, depending not only on the order of Al-pillaring and La^{3+}-exchange manipulation procedures, but also on the kind of clay-dispersion medium used in Al-pillaring and on the calcination conditions. When La^{3+} was ion-exchanged after Al-pillaring (No.3), the activity improved only slightly (from 0.1% to 0.7% conversion). In this case, La^{3+}-PTSM probably incorporated only a small amount of La^{3+}, because the CEC of once calcined pillared clay is greatly reduced to 10 to 20% of the initial CEC of the parent clay.[10,21] In order to prepare a highly active catalyst, the La^{3+}-exchange procedure prior to the Al-pillaring operation was indispensable. When non-calcined La^{3+}-TSM was pillared, the activity of the resulting La^{3+}-PTSM (No. 4) remained unaltered from that of nonmodified PTSM. On the other hand, when the La^{3+}-TSM was calcined at 400 °C and subsequently pillared in water without acetone (No. 5), the product clay showed a small basal spacing of 9.9 Å, indicating that aluminum hydroxy cluster cations were not intercalated. Thus, only when La^{3+}-TSM was first calcined, followed by Al-pillaring in a mixed medium of acetone and water (No. 6), a very active catalyst was obtained to afford high toluene conversion (3.2%). The best catalyst, which gives a higher toluene conversion (7.6%), was obtained when calc.1 was operated at 300 °C and calc. 2 was omitted (No. 7).

Effect of Calcination Conditions. Since both calc.

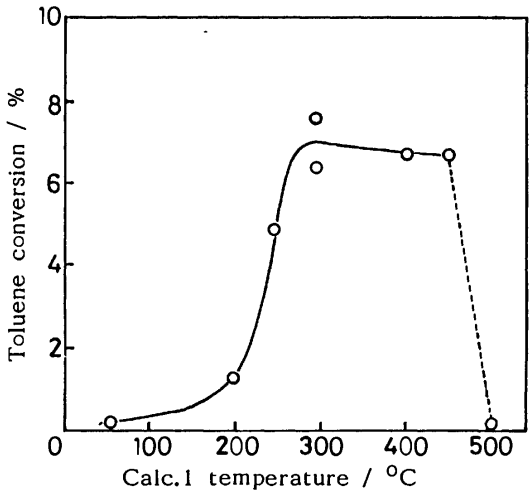

Fig. 3. Effect of the temperature of calc. 1 on toluene aklylation activity of La^{3+}-PTSM. Reaction temp 350 °C, W/F=60 g h mol^{-1}, toluene : methanol=2 : 1 (mole ratio), flow rate of N_2 carrier gas 200 ml h^{-1}.

Table 1. Catalytic Activities[a] of the Catalysts Prepared by Various Methods for Toluene Alkylation by Methanol

No.	Catalyst	Preparation method[b]	Clay dispersion medium[c]	Calcination temp Calc. 1[d] /°C	Calcination temp Calc. 2[e] /°C	d_{001} /Å	Surface area[f] /$m^2 g^{-1}$	Toluene conv. /%	Xylene selec. /%	*p*-Xylene fraction[g] /%
1	PTSM	A	W	—	400	18.4	197[j]	0.11	100	27.1
2	La^{3+}-TSM	B	—	—	400	9.7	—	0.0	—	—
3	La^{3+}-PTSM	C	W	—	400	18.0	—	0.7	100	30.2
4	La^{3+}-PTSM	D	W	h)	400	18.0	—	0.12	100	27.4
5	La^{3+}-PTSM	D	W	400	400	9.9	—	0.0	—	—
6	La^{3+}-PTSM	D	W+A	400	400	17.0	163[j]	3.2	88.7	35.0
7	La^{3+}-PTSM	D	W+A	300	i)	17.7	242[j]	7.6	77.5	40.1
8	PM	A	W	—	400	17.3	228[j]	11.6	73.6	43.2

a) Reaction temp 350 °C, W/F=60 g cat. h mol^{-1} (W=weight of catalyst, F=feed rate of reactants), toluene : methanol=2 : 1 (mole ratio), flow rate of N_2 carrier gas 200 ml h^{-1}, averaged initial activity for 1 h after feeding of reactants. b) A: Al-pillaring only B: La^{3+}-exchange only C: La^{3+}-exchange after pillaring D: Al-pillaring after La^{3+}-exchange. c) Used for Al-pillaring (W: water W+A: mixture of water and acetone). d) Calcined for 3 h. e) Calcined for 4 h. f) Measured after evacuation at 300 °C for 1 h. g) *p*-Isomer fraction among the xylenes produced. h) Dried at 60 °C. i) Pretreated at 350 °C for 1 h under nitrogen gas flow before reaction. j) Langmuir type N_2 adsorption isotherm.

1 and calc. 2 procedures greatly affect the catalytic activity, appropriate calcination conditions were explored. Figure 3 shows the alkylation activities of La^{3+}-PTSM as a function of the temperature of calc. 1. The activity of the catalyst dried at 60 °C as calc. 1 was as low as that of nonmodified PTSM. When the calc. 1 temperature rose to over 200 °C, the activity rapidly increased with a rise in temperature and reached a maximum at 300 °C. The activity was maintained at over 6% conversion until the temperature reached 450 °C, but became almost inactive at 500 °C. This activity loss is due to the unsuccessful formation of a pillared structure of the catalyst (vide infra).

To evaluate the effect of the calc. 2 temperature, 2-propanol dehydration, which proceeds effectively even at a relatively low reaction temperature of 200 °C, was examined. As shown in Fig. 4, 2-propanol conversion rapidly decreased with increasing calcination temperature for both La^{3+}-PTSM and PTSM, but La^{3+}-PTSM exhibited a much higher activity than PTSM at every temperature. La^{3+}-PTSM showed 23% conversion at 300 °C, while PTSM dropped the conversion below 2% at the same temperature. Over either catalyst, the main product was propylene with a selectivity of more than 75%.

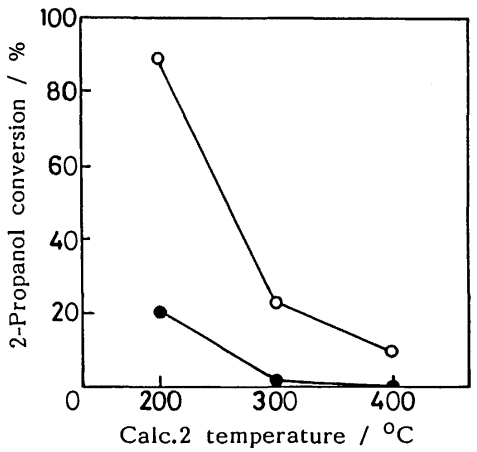

Fig. 4. Effect of the temperature of calc. 2 on 2-propanol dehydration activity. (○) La^{3+}-PTSM and (●) PTSM. Reaction temp 200 °C, W/F=2.1 g h mol^{-1}, flow rate of N_2 carrier gas 600 ml h^{-1}.

Modification by Various Cation Species. The modification of PTSM by various types of cations was performed in the same manner as in the case of La^{3+}-PTSM. As listed in Table 2, the modified pillared catalysts with large basal spacings of more than 17 Å were obtained, except for Al^{3+}-PTSM. These pillared catalysts, whose N_2 adsorption isotherms fitted with the Langmuir equation, showed specific surface areas of more than 160 m^2 g^{-1}. These catalysts have distinct pillared structures in this regard, but displayed different catalytic activities, depending on the modifying cation species used. With respect to monovalent cation Na^+, no differences in terms of both basal spacing and catalytic activity were found between Na^+-PTSM and PTSM (Table 1). With each of the divalent and trivalent cations (Ca^{2+}, Sr^{2+}, Ce^{3+}, and La^{3+}), the catalytic activity was greatly enhanced along with an increase of the *p*-xylene fraction. The highest modification effect was found for La^{3+}-PTSM. On the other hand, Al^{3+}-PTSM showed a "collapsed" basal spacing (9.8 Å) and N_2 adsorption isotherm obeyed the B.E.T. equation. The catalyst, hence, showed only very low activity (not more than 0.1% toluene conversion).

Structure Change of Clay. The structural change of clay in the course of the catalyst preparation process was traced by the use of XRD (Fig. 5). La^{3+}-TSM dried at 60 °C [(a) in Fig. 5(A)] had a double-layer hydrated form (d_{001}=15.8 Å); upon heating to 300 °C, another diffraction peak appeared which corresponds

Table 2. Catalytic Activities[a] of M^{n+}-PTSM for Toluene Alkylation by Methanol

Catalyst	Calcination temp		d_{001} /Å	Surface area[d] /m^2 g^{-1}	Toluene conv. /%	Xylene selec. /%	*p*-Xylene fraction[e] /%
	Calc. 1[b] /°C	Calc. 2[c] /°C					
Na^+-PTSM	300	f)	—	—	0.4	97.1	29.4
Na^+-PTSM	400	400	17.7	—	0.07	85.4	24.1
Al^{3+}-PTSM	300	f)	—	—	0.10	100	27.5
Al^{3+}-PTSM	400	400	9.8	22.0[g]	0.06	100	—
Ce^{3+}-PTSM	300	f)	—	—	2.0	94.9	32.5
Ce^{3+}-PTSM	400	400	17.0	182[h]	1.8	83.6	36.0
Ca^{2+}-PTSM	300	f)	17.3	—	4.9	82.5	34.6
Sr^{2+}-PTSM	300	f)	17.6	—	3.1	89.4	32.0
La^{3+}-PTSM	300	f)	17.7	242[h]	7.6	77.5	40.1
La^{3+}-PTSM	400	400	17.0	163[h]	3.2	88.7	35.0

a) Reaction temp 350 °C, W/F=60 g cat. h mol^{-1} (W=weight of catalyst, F=feed rate of reactants), toluene: methanol=2 : 1 (mole ratio), flow rate of N_2 carrier gas 200 ml h^{-1} averaged initial activity for 1 h after feeding of reactants. b) Calcined for 3 h. c) Calcined for 4 h. d) Measured after evacuation at 300 °C for 1 h. e) *p*-Isomer fraction among the xylenes produced. f) Pretreated at 350 °C for 1 h under nitrogen gas flow before reaction. g) B.E.T. type N_2 adsorption isotherm. h) Langmuir type N_2 adsorption isotherm.

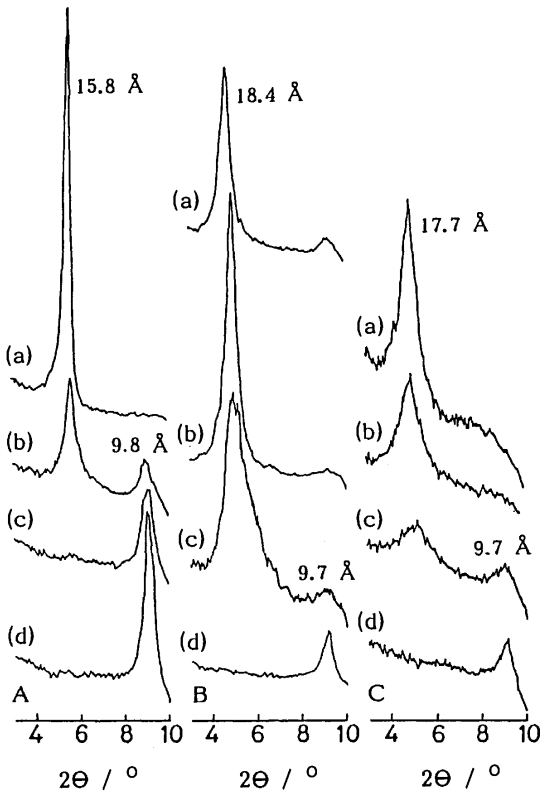

Fig. 5. Change in XRD patterns during the preparation of La^{3+}-PTSM. (A) La^{3+}-TSM after calc. 1, (B) La^{3+}-PTSM after Al-pillaring and drying at 60 °C, (C) after calc. 2 at 400 °C for 4 h. Calcined before Al-pillaring (calc. 1) at 60 °C (a), at 300 °C (b), 400 °C (c), and at 500 °C (d).

to an anhydrous form (d_{001}=9.7 Å) [(b) in Fig. 5(A)]. At 400 °C or above, only this anhydrous form was observed [(c) and (d) in Fig. 5(A)].

Such anhydrous clays could swell no longer in water, and it was impossible to introduce pillars between the layers by the conventional pillaring technique (see Table 1; No. 5). When a mixture of acetone and water was adopted as a clay dispersion medium, the basal spacing of La^{3+}-PTSM expanded to a definite level (17—18 Å) [(a), (b), and (c) in Fig. 5(B)]. When calc.1 was performed at 500 °C, the expansion of basal spacing by pillaring occurred no longer [(d) in Fig. 5(B)]. The low catalytic activity of the La^{3+}-PTSM which underwent heating at 500 °C in calc.1 (vide supra) is ascribed to the lack of an actual pillared structure.

The diffraction peak intensity after calc. 2 at 400 °C also altered, depending upon the calc. 1 temperature. The diffraction peak became weaker with increasing temperature of calc. 1. No collapsed basal spacing after calc. 2 was found, provided the calc.1 temperature remained below 300 °C [(a) and (b) in Fig. 5(C)], indicating a heat-stable pillared structure was obtained.

Thermal Change in CEC of La^{3+}-TSM. Figure 6 shows a change in the CEC of lanthanum-exchanged

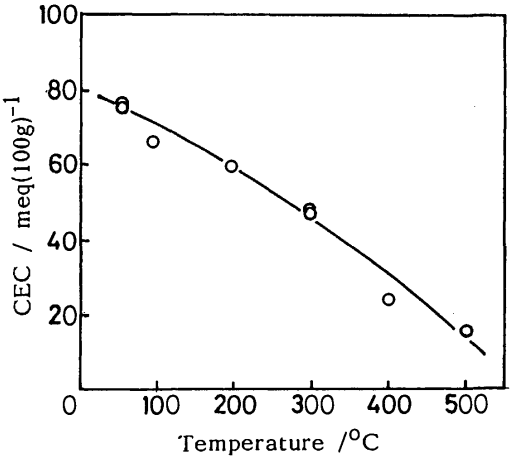

Fig. 6. Cation-exchange capacity of La^{3+}-TSM as a function of temperature of calc. 1.

TSM (La^{3+}-TSM) with the calc.1 temperature. A La^{3+}-TSM sample dried at 60 °C had a CEC of 78 mequiv/100 g-clay. This value is much smaller than the reported CEC of native Na^+-TSM (190 mequiv/100 g)[31] but quite the same as that of Al^{3+}-TSM (78 mequiv/100 g). The discrepancy between the CEC values of Na^+-TSM and Al^{3+}-TSM has been reported to be due to a partial hydrolysis of the Al^{3+} ion.[26] Since the La^{3+} ion[32] is as the easily hydrolyzed as Al^{3+} ion, the small CEC value observed with dried La^{3+}-TSM is not unexpected.

The CEC value of La^{3+}-TSM linearly decreased from 78 to 15 mequiv/100 g with an increase in the temperature of calc.1 from 60 to 500 °C. This means that a part of the La^{3+} ions lost their exchangeability with other metal cations and became fixed between the silicate layers during the course of calcination. In other words, the amount of the fixed La^{3+} must increase with an increase in temperature. Such a reduction of CEC by heating was reported by Mozas et al.[33] in respect of La^{3+}-montmorillonite. Hofmann et al.[34] and Kondo et al.[35-37] also reported that the fixation of exchangeable cations in Ca^{2+}-bentonite occurred upon heating and that the CEC linearly reduced with increasing temperature.

It is well-known that when Li^+-exchanged montmorillonite is heated, small Li^+ ions migrate into the vacant octahedral sites and neutralize the negative charge of montmorillonite, resulting in the reduction of CEC (Hofmann-Klemen effect).[38,39] Since the diameter of La^{3+} (2.34 Å) is larger than that of Li^+ (1.80 Å), such migration of La^{3+} ions into an octahedral vacancy is considered to be unfeasible. Another mechanism must therefore be proposed for the case of La^{3+}-TSM.

Figure 7 shows the oxygen framework of TSM. The oxygen atoms which face an interlayer region (basal oxygens) form a repeated pattern of hexagons, and there is a depression which is called a "hexagonal hole" in the center of this network. When 2:1 type

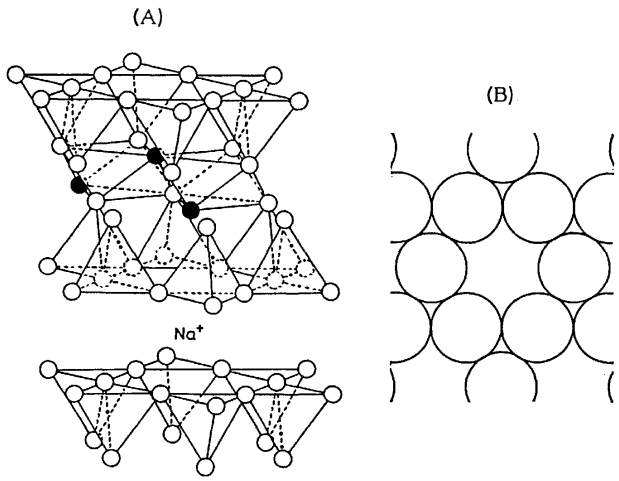

Fig. 7. Structure of fluor-tetrasilicic mica. (A) Layer structure, (○) oxygen, (●) fluorine. Every tetrahedral site is occupied by silicon and octahedral sites are occupied by magnesium or vacancy. (B) Hexagonal network of basal oxygens. "Hexagonal hole" is located in a center.

clay minerals, such as smectites and vermiculites, are heated so as to be converted to anhydrous forms, the interlayer cations are situated more or less within the hexagonal holes.[39] Taking account of the ionic diameter of La^{3+} (2.34 Å) and the fact that the basal spacing of La^{3+}-TSM heated at above 300 °C (9.7 Å) is very close to the layer thickness of TSM (9.6 Å), it seems probable that La ions are almost lodged in the hexagonal holes. The actual form of the fixed La ions in the dehydrated La^{3+}-TSM is not obvious at the present stage. The existence of a species such as $La(OH)^{2+}$, $(La\text{-}O\text{-}La)^{4+}$ or $(La\langle^{O}_{O}\rangle La)^{2+}$ [40-42] has been suggested in the case of La^{3+}-exchanged Y-type zeolite. The bridged species are unlikely to exist in dehydrated La^{3+}-TSM, considering the small size of the hexagonal depression.

Kondo et al. found that the fixation of interlayer cations did occur in Ca^{2+}-bentonite, but not in Na^{+}-bentonite below 500 °C.[35-37] Above this temperature the clay lost its structural OH groups due to thermal dehydroxylation. The ease of the fixation of Ca^{2+} was ascribed to its greater electrostatic force than that of Na^{+} ion acting toward negatively charged surface oxygens.[37] If the La species exists in the form of La^{3+} or $La(OH)^{2+}$, such a nonbridged small-size species is also likely to be easily fixed onto silicate sheets.

Because the La^{3+}-fixed and charge-reduced TSM had a lower swelling ability than the original TSM, the intercalation of large aluminum hydroxy cluster cations into the interlayer spaces became difficult in an aqueous solution, and a pillared clay with an expanded basal spacing was not obtainable. To overcome this situation, the use of a mixture of acetone and water as a clay dispersion medium was effective and indispensable. Such a mixed medium was already reported by Yamanaka and Brindley[27] to be helpful for the Zr-pillaring of charge-reduced montmorillonites which was prepared by applying the Hofmann-Klemen effect described above. The larger dipole moment of the acetone molecule than that of water (water, 1.84×10^{-18} e.s.u.; acetone, 2.71×10^{-18} e.s.u.) must assist in the solvation of the residual exchangeable cations.[43]

Surface Acidity Generated by La-Modification. It has already been ascertained through the temperature-programmed desorption (TPD) of adsorbed NH_3 that the enhancement of the alkylation activity by La^{3+}-modification is attributable to an increased acidity.[25] To examine the characteristics of the acid sites generated by the modification in more detail, the IR spectra of the pyridine adsorbed on both PTSM and La^{3+}-PTSM were analyzed (Fig. 8). After pyridine adsorption at 150 °C followed by evacuation at the same temperature, three apparent absorption peaks of the adsorbed pyridine were observed at 1615, 1490, and 1450 cm^{-1} for La^{3+}-PTSM. The band at 1450 cm^{-1} indicates the presence of coordinatively adsorbed pyridines on the Lewis acid sites and both 1615 and 1490

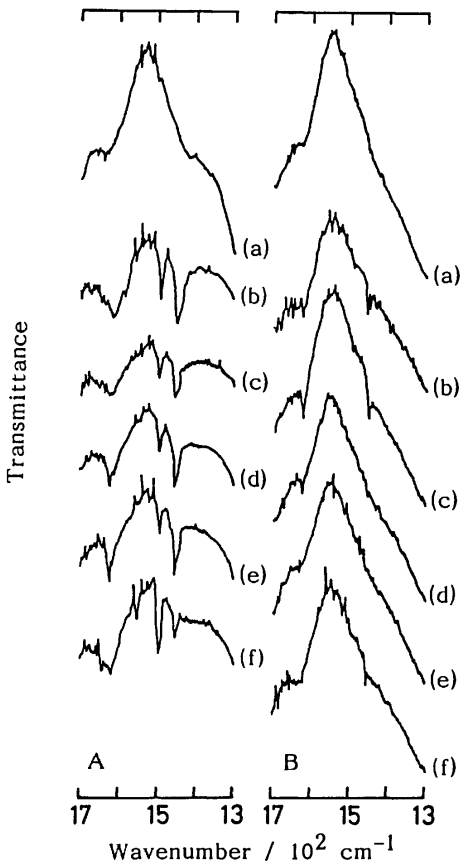

Fig. 8. IR spectra of pyridine adsorbed on La^{3+}-PTSM(A) and PTSM(B). (a) Back ground spectra, (b) after pyridine adsoption followed by evacuation at 150 °C, (c—e) followed by successive evacuation at 250 °C (c), 350 °C (d), and at 450 °C (e), (f) followed by water vapor adsorption and evacuation at 200 °C.

cm^{-1} bands are ascribed to the contribution of the pyridines adsorbed on both the Brønsted acid sites and the Lewis acid sites.[30] The 1490 cm^{-1} band gradually decreased its intensity ratio to the 1450 cm^{-1} band with increasing evacuation temperature up to 450 °C, whereas the intensity of 1450 cm^{-1} band remained nearly constant. This means that La^{3+}-PTSM contains both relatively weak Brønsted acid sites and strong Lewis acid sites. After water adsorption at 200 °C followed by evacuation at the same temperature, the intensity ratio of 1490 cm^{-1} to 1450 cm^{-1} reversed, and a new absorption band appeared at 1550 cm^{-1}. Apparently, some parts of the Lewis acid sites were converted to the Brønsted acid sites by adsorption of water.

For PTSM, the adsorbed pyridine was detected at 1620 and 1455 cm^{-1} after pyridine adsorption followed by evacuation at 150 °C. These bands, however, vanished readily upon evacuation at temperatures higher than 350—450 °C.

These results indicate that the fixed La^{3+} ions which remained between layers after Al-pillaring took charge of the genesis of acidic sites. Probably the fixed La^{3+} ions themselves function as Lewis acid centers; some part of them dissociate water molecules to liberate protons. Multivalent cations, such as La^{3+}, with a high electric field could thus effectively modify PTSM.

Concluding Remarks

Here, we succeeded for the first time in obtaining an acidity-enhanced pillared clay catalyst by making use of a unique phenomenon which occurred over the hexagonal network of a clay tetrahedral array, or the fixation of large interlayer cations, such as La^{3+} ions, onto the hexagonal cavities as cation exchange sites through thermal treatment. Recalling the very weak acidic nature or very low catalytic activity, shown by nonmodified PTSM, we can regard La^{3+}-modified pillared TSM as a well-organized pillared clay which possesses almost all of its acidic sites not on the pillars as guests, but on the walls of silicate sheets as hosts. Studies on the peculiar catalytic performance and microstructure of this modified pillared TSM are in progress through the application to other types of organic reactions and through the analysis by ^{27}Al, ^{29}Si-MAS NMR spectroscopy etc.

We thank the Iwatani Memorial Foundation for financial support of this work.

References

1) G. W. Brindley and R. E. Sempels, *Clay Miner.*, **12**, 229 (1977).
2) D. E. W. Vaughan and R. J. Lussier, "Proc. 5th Int. Zeolite Conf.," ed by L. V. C. Rees, Heyden, London (1980), p. 94.
3) N. Lahav, U. Shani, and J. Shabtai, *Clays Clay Miner.*, **26**, 107 (1978).
4) T. J. Pinnavaia, *Science*, **220**, 365 (1983).
5) *Catalysis Today*, ed by R. Burch, **2**, Nos. 2,3 (1988).
6) J. Shabtai, M. Rosell, and M. Tokartz, *Clays Clay Miner.*, **32**, 99 (1984).
7) T. J. Pinnavaia, M. -S. Tzou, S. D. Landau, and R. H. Raythatha, *J. Mol. Catal.*, **27**, 195 (1984).
8) M. L. Occelli, S. D. Landau, and T. J. Pinnavaia, *J. Catal.*, **90**, 256 (1984).
9) D. Plee, A. Schutz, G. Poncelet, and J. J. Fripiat, "Catalysis by Acids and Bases," ed by B. Imelik et al., Elsevier, Amsterdam (1985), p. 343.
10) G. Poncelet and A. Schutz, "Chemical Reactions in Organic and Inorganic Constrained Systems," ed by R. Setton, D. Reidel Pub., Dordrecht (1986), p. 165.
11) A. Schutz, D. Plee, F. Borg, P. Jacobs, G. Poncelet, and J. J. Fripiat, "Proc. Int. Clay Conf. (Denver)," ed by L. G. Schultz et al., The Clay Minerals Society, Bloomington, Indiana (1987), p. 305.
12) K. Urabe, H. Sakurai, and Y. Izumi, *J. Chem. Soc., Chem. Commun.*, **1986**, 1074.
13) K. Urabe, H. Sakurai, and Y. Izumi, "Proc. 9th Int. Cong. Catal.," ed by M. J. Phillips et al., The Chemical Institute of Canada, Ottawa (1988), Vol.4, p. 1858.
14) H. Sakurai, K. Urabe, and Y. Izumi, *Syokubai (Catalyst)*, **28**, 397 (1986).
15) K. Kitajima and N. Daimon, *Nippon Kagaku Kaishi*, **1975**, 991.
16) Y. Morikawa, K. Takagi, Y. Moro-oka, and T. Ikawa, *J. Chem. Soc., Chem. Commun.*, **1983**, 845.
17) K. Urabe, H. Sakurai, and Y. Izumi, "Abstracts 6th Int. Conf. Surf. Colloid Sci.," (1988), p. 194.
18) J. Shabtai, R. Lazar and A. G. Oblad, "Proc. 7th Int. Cong. Catal.," ed by T. Seiyama et al., Kodansha-Elsevier, Tokyo (1980), p.828.
19) J. Shabtai, F. E. Massoth, M. Tokarz, G. M. Tsai, and J. McCauley, "Proc. 8th Int. Cong. Catal.," Verlag-Chemie, Weinheim (1984), Vol.4, p.735.
20) M. Tokarz and J. Shabtai, *Clays Clay Miner.*, **33**, 89 (1985).
21) D. E. W. Vaughan, R. J. Lussier, and J. S. Magee, US Patent 4271043(1981).
22) K. A. Carrado, S. L. Suib, N. D. Skoularikis, and R. W. Coughlin, *Inorg. Chem.*, **25**, 4217 (1986).
23) N. D. Skoularikis, R. W. Coughlin, A. Kostapapas, K. Carrado, and S. L. Suib, *Appl. Catal.*, **39**, 61 (1988).
24) H. Sakurai, K. Urabe, and Y. Izumi, "Abstracts 6th Int. Conf. Surf. Colloid Sci.," (1988), p.483.
25) H. Sakurai, K. Urabe, and Y. Izumi, *J. Chem. Soc., Chem. Commun.*, **1988**, 1519.
26) S. Goto, K. Sugimori, T. Hayashi, and R. Kondo, *Nendo Kagaku*, **17**, 18 (1977).
27) S. Yamanaka and G. W. Brindley, *Clays Clay Miner.*, **27**, 119 (1979).
28) P. T. Hang and G. W. Brindley, *Clays Clay Miner*, **18**, 203 (1970).
29) C. J. Schollenberger and R. N. Simon, *Soil Sci.*, **59**, 13 (1946).
30) E. P. Parry, *J. Catal.*, **2**, 371 (1963).
31) K. Sugimori, *Nendo Kagaku*, **26**, 127 (1986).
32) B. E. Douglas and D. H. McDaniel, "Concepts and Models of Inorganic Chemistry", 1st ed., Blaisdell (1965),

Chap. 6.
33) T. Mozas, S. Bruque, and A. Rodriguez, *Clay Miner.*, **15**, 421 (1980).
34) U. Hofmann and J. Endell, *Angew. Chem.*, **52**, 708 (1939).
35) S. Suzuki, M. Kondo, and R. Horigome, "Abstracts 21st Annual Meeting of the Clay Science Society of Japan," (1977), p.18.
36) M. Kondo, *Nendo Kagaku*, **21**, 1 (1981).
37) M. Kondo, "Soukan Kagobutsu no Kaihatsu to Ouyou (Development and Application of Intercalation Compounds, in Japanese)," ed by C. Kato et al., CMC Co., Ltd. (1985), p. 149.
38) U. Hofmann and R. Klemen, *Z. Anorg. Allg. Chem.*, **262**, 95 (1950).
39) G. W. Brindley and J. Lemaitre, "Chemistry of Clays and Clay Minerals", ed by A. C. D. Newman, Mineralogical Society (1987), p. 319.
40) P. B. Venuto, L. A. Hamilton, and P. S. Landis, *J. Catal.*, **5**, 484 (1966).
41) J. A. Rabo, C. L. Angell, and V. Schomaker, "Proc. 4th Int. Cong. Catal.," Moscow (1968), p. 96.
42) P. Marynen, A. Maes, and A. Cremers, *Zeolites*, **4**, 287 (1984).
43) G. W. Brindley and G. Ertem, *Clays Clay Miner.*, **19**, 399 (1971).

 © 1989 The Chemical Society of Japan Bull. Chem. Soc. Jpn., 62, 3229—3231 (1989)

The Electronic Spectra of Jet-Cooled Tropolone. Vibrational Assignment for the $\tilde{A}^1B_2$-$\tilde{X}^1A_1$ Transition

Hiroshi Sekiya,* Yusuke Nagashima, and Yukio Nishimura
Institute of Advanced Material Study, and Department of Molecular Science and Technology, Graduate School of Engineering Sciences, Kyushu University, Kasuga-shi, Fukuoka 816
(Received May 22, 1989)

The laser fluorescence excitation spectrum and the single vibronic level fluorescence spectra from the $\tilde{A}^1B_2$ state of tropolone have been measured in a supersonic free jet. Some vibronic bands observed in the region of 270—450 cm^{-1} from the 0_0^0 band have been assigned. A tunneling doublet separation for the ν'_{14} in-plane ring deformation mode has been measured to be 30 cm^{-1}, which is significantly larger than 19 cm^{-1} for that for the zero-point level, suggesting that the average geometry of the ν'_{14} mode deviates significantly from that of the zero-point level.

A tropolone molecule possesses an intramolecular hydrogen bond, and the hydroxyl proton tunnels from one oxygen atom to the other. Spectroscopic studies indicate that tropolone exhibits a double-minimum potential energy function along the proton tunneling coordinate.[1-7] Tunneling doublings have been detected in many vibronic bands in the absorption spectra[1,2,6] and the laser fluorescence excitation spectra.[4,5,7] The separation of tunneling doublings involves information on the interaction between the normal mode and the proton tunneling coordinate. On the other hand, these tunneling doublings make it difficult to assign vibronic bands.

The assignment for the vibronic transitions between the $\tilde{A}^1B_2$ and $\tilde{X}^1A_1$ states has long been a problem. Recently, Alves et al.[6] indicated that some of the complexity in vibrational bands around the 0_0^0 band is due to strong Duschinsky effect[8] involving the two lowest b_1 modes ν_{26} and ν_{25}. Very recently, Redington et al.[7] observed the laser fluorescence excitation spectrum of jet-cooled tropolone, and newly assigned about thirty vibronic bands in the region of 270—450 cm^{-1} from the 0_0^0 band. We have measured single vibronic level fluorescence (SVLF) spectra from about twenty vibronic bands in the $\tilde{A}^1B_2$ state of tropolone in order to confirm the previous assignment, since Redington et al.[7] observed no SVLF spectra. It has been found that previous assignments for vibronic bands involving the ν'_{39} and ν'_{14} modes and $25_0^n26_0^{2n+1}$ (n=1—4) and 26_0^n (n=9—14) progressions are invalid. New assignments have been proposed for some vibronic bands.

Experimental

Experimental apparatus used is essentially the same as that used for the observation of the electronic spectra of 3-isopropyltropolone.[9] Briefly, laser fluorescence excitation spectrum was measured for jet-cooled sample of tropolone in He as a carrier gas. Tropolone was commercially available and used without further purication. The sample was excited by a nitrogen laser pumped dye laser source (Molectron UV22 and DL14P), and total fluorescence was detected with a Hamamatsu R955 photomultiplier and averaged with a boxcar integrator (NF BX-531). SVLF spectra were measured with a 0.75 m monochromator (Spex 1702). The sample was placed in the housing of a pulsed nozzle with an orifice of 0.4 mm diameter and heated to about 70 °C to increase the vapor pressure.

Results and Discussion

In Fig. 1 is shown a typical laser excitation spectrum of tropolone, which is essentially the same as that reported previously.[5,7] The band origin was identified at 27018 cm^{-1}.

Figure 2 shows the SVLF spectrum obtained by the excitation of band ***b*** with $\Delta\nu(\nu-0_0^0)$=293 cm^{-1}, which had been assigned as 39_0^2 by Redington et al.[7] They concluded that the $\Delta\nu$=230.8 cm^{-1} band observed in the absorption spectrum of Alves et al.[6] was $14_0^1 39_1^1$. On the basis of this assignment, $\nu''_{39}(b_1)$ was estimated to be 147 cm^{-1}. However, as is clear from Fig. 2, no $2\nu''_{39}$ band is detected in the SVLF spectrum and dominant bands are combinations of ν''_{25} and ν''_{26}. This suggests that the corresponding upper state involves ν'_{25} and/or ν'_{26}. We have assigned band ***b*** as $25_0^1 26_0^3$ for the reason that $\nu'_{25}+3\nu'_{26}\simeq$289 cm^{-1} is close to 293 cm^{-1}.

Redington et al.[7] had assigned the 295.82 and 326.41 cm^{-1} bands as $39_0^2H_1^1$ and 26_0^{10} respectively. These assignments contradict to the result of SVLF spectra, which are shown in Figs. 3a and 3b. Figure 3a has been obtained by the excitation of band ***c*** at 296 cm^{-1}, which shows a long progression in $\nu''_{14}(a_1)$. This clearly indicates that the corresponding upper state is 14^1. A similar spectrum has been obtained by the excitation of band ***d*** at 326 cm^{-1} as is shown in Fig. 3b, and this band has been assigned to $14_0^1H_1^1$, where H_1^1 designates the high wavenumber tunneling doublet component.[1]

It is worth noting that the separation between 14_0^1 and $14_0^1H_1^1$ (30 cm^{-1}) is much larger than 19 cm^{-1} for the separation between 0_0^0 and H_1^1. Since the tunneling splitting in the zero-point level of the ground state has been estimated to be very small ($\simeq$0.3 cm^{-1})[7] these separations nearly equal to the tunneling doublet splitting in the upper state. The increase in the tunneling splitting for the ν'_{14} mode from that for the

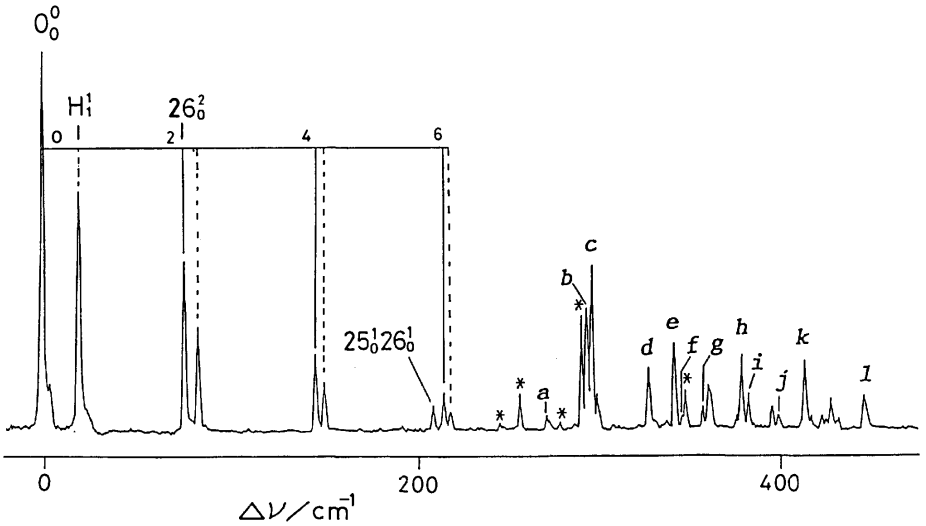

Fig. 1. Laser fluorescence excitation spectrum of tropolone. The stagnation pressure was 0.4 atm. SVLF spectra were measured for bands *a*—*l*. The broken lines indicate high wavenumber tunneling doublet component. The asterisks indicate bands due to the hydrogen-bonded complex between tropolone and water.

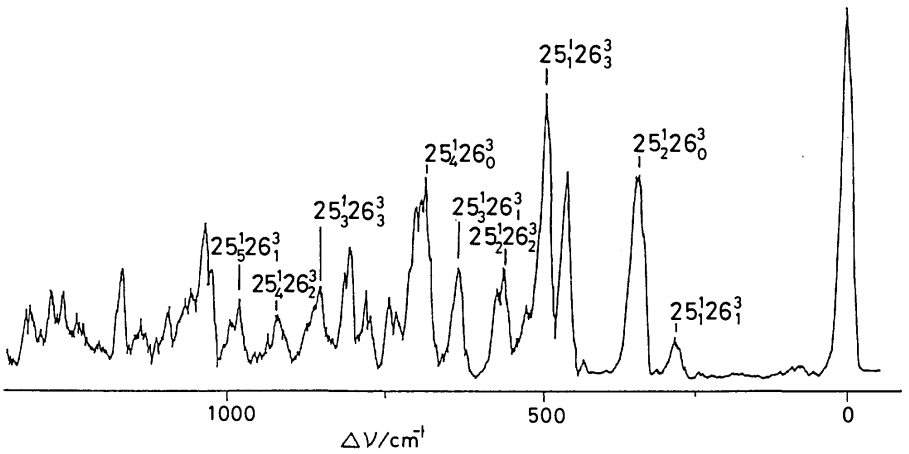

Fig. 2. Part of the SVLF spectrum obtained by the excitation of band *b*.

zero-point level implies that the average geometry of ν'_{14} deviates significantly from that of the zero-point level. From the above result ν'_{14} is considered to be a C-C-O bending in the chelate moiety such that the O···O distance is modulated as suggested by Rossetti et al.[4] rather than a C-C-C bending in the seven-membered ring proposed by Redington and Redington.[3]

The SVLF spectra obtained by the excitation of bands *h* and *i* at 378 and 382 cm^{-1} show one and two quanta of ν''_{14} and various combinations of one and two quanta of ν''_{25} and ν''_{26}, which suggests that the upper state involves both the ν'_{14} and ν'_{26} modes or ν'_{14} and ν'_{25} modes. We have assigned band *h* as $14_0^1 26_0^2$, since the frequency $\nu'_{14}+2\nu'_{26}(\simeq 381\ cm^{-1})$ nearly equals to 378 cm^{-1}. Similarly, band *i* has been assigned as $14_0^1 26_0^2 H_1^1$. These bands had been assigned as 14_0^1 and 26_0^{12}, respectively.[7] A long progression in ν''_{14} was observed in the SVLF spectrum obtained by the excita-

Table 1. Vibrational Assignment of the Fluorescence Excitation Spectrum of Tropolone

Band	$\Delta\nu/cm^{-1}$	Assignment	
		This work	Redington et al.[a]
a	272	26_0^8	26_0^8
b	293	$25_0^1 26_0^3$	39_0^2
c	296	14_0^1	$39_0^2 H_1^1$
d	326	$14_0^1 H_1^1$	26_0^{10}
e	341	25_0^2	25_0^2
f	345	$25_0^2 H_1^1$	$25_0^2 H_1^1$
h	378	$14_0^1 26_0^2$	14_0^1
i	382	$14_0^1 26_0^2 H_1^1$	26_0^{12}
k	414	13_0^1	13_0^1
l	446	$13_0^1 H_1^1$	$13_0^1 H_1^1$

a) From Ref. 7.

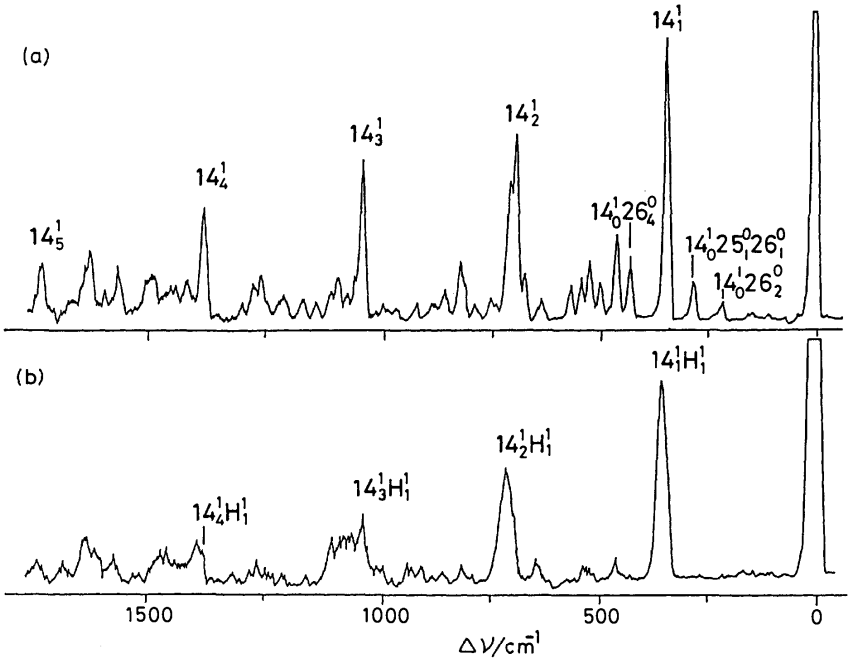

Fig. 3. Part of the SVLF spectra obtained by the excitation of bands *c* (a) and *d* (b).

tion of the $\Delta\nu$=230.8 cm^{-1} band in the absorption spectrum.[6] Since this band is not detected in Fig. 1, the 230.8 cm^{-1} band must be a hot band.

The ν''_{13} fundamental (438 cm^{-1}) has been observed in the SVLF spectra obtained by exciting into bands ***k*** and ***l*** at 415 and 447 cm^{-1}, which suggests that the transitions are from 13^1 and 13^1H^1. Therefore, bands ***k*** and ***l*** should be 13_0^1 and $13_0^1H_1^1$, respectively, which agree with previous assignments.[7]

The 25_0^2 and $25_0^2H_1^1$ bands were identified by Redington et al.[7] at 340.74 and 344.92 cm^{-1}, respectively. The SVLF spectra obtained by the excitation of bands ***e*** and ***f*** at 341 and 345 cm^{-1} show various combinations of one, two, three, and four quanta of ν''_{25} and ν''_{26}. This result is consistent with the previous assignments.[7]

The SVLF spectra obtained by the excitation of bands ***g*** and ***j*** at 355 and 400 cm^{-1} show very low-frequency (65 cm^{-1}) unidentified vibration. Such a low-frequency band was observed in temperature dependent microwave spectrum of tropone.[10] The 65 cm^{-1} vibration would be very low-frequency skeletal wag. The observation of the low-frequency vibration in the ground state suggests that corresponding low-frequency vibration is involved in vibronic bands in the upper state, although bands ***g*** and ***j*** were assigned as 26_0^{11} and $14_0^1H_1^1$, respectively.

In Table 1 are listed the vibronic bands assigned this work together with those assigned by Redington et al.[7] Since the previous assignments of 26_0^{10}, and 26_0^{12}, $25_0^1 26_0^3$ are invalid, the assignments of 26_0^n(n= 9,11,13,14) and $25_0^2 26_0^{n+2}$(n=5,7) are also dubious. Further study is needed to assign these bands.

References

1) A. C. P. Alves and J. M. Hollas, *Mol. Phys.*, **23**, 927 (1972).
2) A. C. P. Alves and J. M. Hollas, *Mol. Phys.*, **25**, 1305 (1973).
3) R. L. Redington and T. E. Redington, *J. Mol. Spectrosc.*, **78**, 229 (1979).
4) R. Rossetti and L. E. Brus, *J. Chem. Phys.*, **73**, 1546 (1980).
5) Y. Tomioka, M. Ito, and N. Mikami, *J. Phys. Chem.*, **87**, 4401 (1983).
6) A. C. P. Alves, J. M. Hollas, H. Musa, and T. Ridley, *J. Mol. Spectrosc.*, **109**, 99 (1985).
7) R. L. Redington, Y. Chen, G. J. Scherer, and R. W. Field, *J. Chem. Phys.*, **88**, 627 (1988).
8) F. Duschinsky, *Acta Physiochim., (USSR)*, **7**, 551 (1937).
9) H. Sekiya, H. Takesue, Z. H. Li, A. Mori, and H. Takeshita, *Chem. Lett.*, **1988**, 1601.
10) R. S. Cresswell, *J. Mol. Spectrosc.*, **51**, 111 (1974).

Entrained Responses of the Current Oscillation of Polymer Gels to Sinusoidal Stimulation

Yoshihito OSADA,* Kayo UMEZAWA, and Aizo YAMAUCHI†
Department of Chemistry, Ibaraki University, Mito 310
†Research Institute for Polymers and Textiles, AIST, MITI, 1-4-4 Higashi Tsukuba 305
(Received June 26, 1989)

The responses of the current oscillation of the water-swollen polymer gels generated by dc current to the sinusoidal stimulation were investigated. The current oscillation was semiquantitatively analyzed by fast Fourier transform and the phase diagram was made up from power spectra. It was found that the entrainment of oscillation occurred in the polymer gels when the frequency of sinusoidal stimulation was closed to that of parent current oscillation. It was also found that the stronger sinusoidal voltage caused the entrainment in wider frequency range.

Recently a variety of spatial- and time-ordered structures (dissipative structure) have been experimentally and theoretically investigated in many nonlinear and nonequilibrium systems. Action potential of nerves occurred by external electrical stimulation is the representative example.[1] In the chemical reaction systems, Belousov-Zhabotinsky reaction whose the reactor concentration changes periodically by means of the autocatalytic process is well-known.[2] More recently, banding pH pattern surrounding the root and the corresponding current pattern was investigated by Toko et al.[3]

The ordered structure is often generated by synchronizing many rhythms consisting the system and this effect is called entrainment. For example, the self-sustained oscillation with a frequency of 145 Hz occurs in the squid giant axon by exchanging seawater for mixture of seawater and 550 mM NaCl solution (1 M=1 mol dm^{-3}). When the external sinusoidal current frequency is closed to 145 Hz, the forced firing frequencies that is the firing frequencies under the sinusoidal current, are entrained to the sinusoidal frequencies.[4] Away from these frequency ranges and in the case of weak sinusoidal current, the amplitude modulation upon the repetitive spikes is only observed. Some chaotic behavior is observed in the forced repetitive spikes when a strong ac is applied.

On the contrary, the artificial oscillating systems consisting of porous polyelectrolyte membranes are the simple artificial model for these oscillative systems observed in biological systems and they were made by Teorell,[5] Kobatake,[6] Seno,[7] Mounier,[8] Shashoua,[9] Katchalsky,[10] and others. For example, Teorell demonstrated that a system consisting of polyelectrolyte membrane, separating two electrolyte solutions of different conductance shows oscillation with a frequency as low as 5×10^{-4} Hz, when a dc flows through the membrane. The oscillatory phenomena was explained as an electroosmotic process causing periodic resistance changes of the membrane. The generation of pulses superimposed on dc was observed by Seno in ion-exchange membranes dipped in an aqueous sodium chloride solution. The phenomenon was associated with the formation of a salt-depletion diffusion layer. Shashoua reported the generation of current oscillations under constant dc electric field in the membranes consisting of polymeric acid-base composite facing each other. In these cases the presence of salt on both sides of the membrane was one of the requirements in order to generate spikes. Katchalsky explained the appearance of these oscillative phenomena as follows: the current flow through the membrane induces salt accumulation in the polymer membranes, which, at a certain concentration, leads to the shrinkage of the membrane and a breakdown region is formed. The excess ions are washed off to reestablish the original state of the membrane.

An electrically activated mechanochemical system made of polyelectrolyte gels was recently reported[11,12] and a variety of electro-mechanical conversion devices were developed.[13-15]

In the course of this study, We found that the repetitive current oscillation occurred in the gel[11,16] when a dc was applied through electrodes and the semiquantitative analyses of the oscillation were made by use of fast Fourier transform (FFT). The Lorentz plot of the current of the gel obtained by plotting each amplitude against the preceding one resulted in a convergent set around a point on the line of slope 1 indicating that the frequency of the repetitive oscillation fluctuates around this peak and any irregular oscillation can be attributed to a quasi-periodic motion. In fact, the Lorentz plot of the gel currents formed a closed line. Different from the membranes described, the oscillation of our gels is not induced neither by change in gradient of the transmembrane concentration of the ions nor by the periodical response of specific chemical reagents like liquids,[17-19] but induced by the amorphous and homogeneously swollen polyelectrolyte gels. The application of constant electric potential, higher than a certain threshold value, is the only requirement for the generation of periodical oscillations.

The purpose of this paper is to report the effects of external sinusoidal voltage upon the current oscillation of the gel. It was found that the entrainment of current oscillation occurs when the frequency of the sinusoidal stimulation become close to that of parent current oscillation and that the stronger sinusoidal voltage caused the entrainment in wider frequency range.

Experimental

Materials. Gel from alginic acid was prepared by immersing a visking tube (diameter 42 mm) containing 1.1% of sodium salt solution of alginic acid in a large amount of 1.0% calcium chloride solution for 2 days. Crosslinked water-swollen gels of poly(methacrylic acid)(PMAA) and poly(2-acrylamido-2-methyl-1-propanesulfonic acid) (PAMPS) were prepared by radical polymerization of 5.0 mol% aqueous solutions of corresponding monomers in the presence of 5×10^{-2} mol% *N,N'*-methylenebis(acrylamide) (MBAA) which was used as a crosslinking agent. In these cases polymerization was carried out at 60 °C under vacuo, and 5×10^{-2} mol% of potassium peroxodisulfate was used as an initiator. The obtained gels were then immersed in water at least for 1 week to remove excess salt. The degree of swelling $DS=(W_s-W_d)/W_d$ was calculated by weighing the weights of dry (W_d) and water-swollen (W_s) gels, respectively.

Method of Measurement. A piece of water-swollen cylindrical polymer gel, 11 mm long and 24 mm in diameter, was placed in a Petri dish containing water of ca 10 mm depth. A pair of platinum wire electrodes 20 mm long and 0.2 mm in diameter were inserted in the gel with a distance of 10 mm and 10 mm in depth. A dc voltage (V_o=5 V) was applied in order to induce the current oscillation through the platinum wire electrodes. A stable current oscillation with a frequency of f_o, was observed after a certain induction period. The sinusoidal voltage, $V_o+V \sin 2\pi f_i xt$ was then applied by the same platinum wire electrodes. In these cases the current supply was delivered to the electrodes from Hokuto 501 potentiometer. The oscillative response of the gel was recorded on a data recorder (Hitachi 561) and the response of the current oscillation to the sinusoidal stimulation (f_i) was analyzed by a personal computer (NEC, model PC 9801 Vm2). The oscillation was simultaneously sampled at intervals 500 ms and in the range of $0.005<f_i<1$ Hz and $0.005<V<2$ V depending on the nature of oscillation and was used for computer analysis.

Measurement of the oscillation was carried out at 25 °C. Water used in these experments had an electric conductivity in the range $1-5\times10^{-7}\ \Omega^{-1}\ cm^{-1}$.

Results and Discussion

Figure 1(A) shows a repetitive curve and its power spectrum of the gel when dc (7 V) was applied to the calcium alginate gel. As reported in the earlier paper[16] the oscillatory current appeared after a certain induction period, and this oscillation occurred undamped for more than several hours and more. There existed a "threshold" value of potential, below which (in this experiment about 3 $V\,cm^{-1}$ or below) practically no oscillation appeared. During the induction period, the undamped oscillations appeared in every crosslinked water-swollen polymeric gel, provided they possess ionized moieties, regardless of strong or weak polyelectrolytes. The power spectrum of this oscillation shows a main peak at the frequency of 0.013 Hz (f_o) with higher harmonics. The magnitude of the main peak was about 9.80% of that of total energy within a range of 0.5 Hz. The maximum amplitude of the current oscillation was about 0.22 mA.

Entrainment by Sinusoidal Voltage. Figure 1 B—D shows the effects of external sinusoidal voltage upon the current oscillations and the power spectra when the ac frequencies (f_i) from 0.005 through 0.03 Hz and amplitude (V) of 2 V were superimposed afterward to the oscillation induced by dc voltage (V_o=5 V). Thus, the electric field by dc+ac does not exceed the value applied by dc. When the ac with the frequency of 0.005 Hz was applied to this oscillating gel, the response of the current oscillation became chaotic as shown in the power spectrum (Fig. 1(B)). The magnitude of this ac was about 0.08 mA and this value was much lower than that induced by dc 5 V. The power spectrum in this case has many peaks but the peak induced by dc (f_o) also remained at 0.013 Hz. The magnitude of f_o is about 0.85% of the total energy and that of frequency of ac (f_i) is about 0.63%. The frequency of the main peak was shifted to 0.15 Hz and magnitude of this peak was about 1.30%.

Figure 1(CI) shows the response of current oscillation and its power spectrum when the ac with a frequency of 0.01 Hz was applied. The power spectrum has a sharp peak at the frequency of 0.01 Hz but there is no peak of f_o this time. The magnitude of this peak is large and comprises about 28.8% of that of total within the range of 0.5 Hz. This suggests the 1:1 entrainment of current oscillation occurred. The response of this current oscillation gradually changed with time. As shown in the spectrum of Fig. 1 (CII); the frequency of main peak changed to that of ac in the course of experiment and after 17 min (1026 s) the entrained frequency changed from 0.01 Hz to 0.02 Hz. This shows that the frequency of the entrained oscillation became twice of that of sinusoidal stimulating oscillation (2 : 1 entrainment).

When the ac of 0.03 Hz was applied to the gel, a complete change of the oscillation was observed as shown in Fig. 1 (D). There is no peak of f_o any more, but only the repetitive oscillation with a frequency of f_i (0.03 Hz) was observed. The magnitude of the peak corresponding to 0.03 Hz was as large as 94% of that of total within a range of 0.5 Hz, clearly showing that the current oscillation induced by dc was completely entrained to the oscillation induced by ac even the magnitude of the latter was much lower. Thus, it was demonstrated that the entrainment of oscillation occurs in the gel when ac with certain frequency is

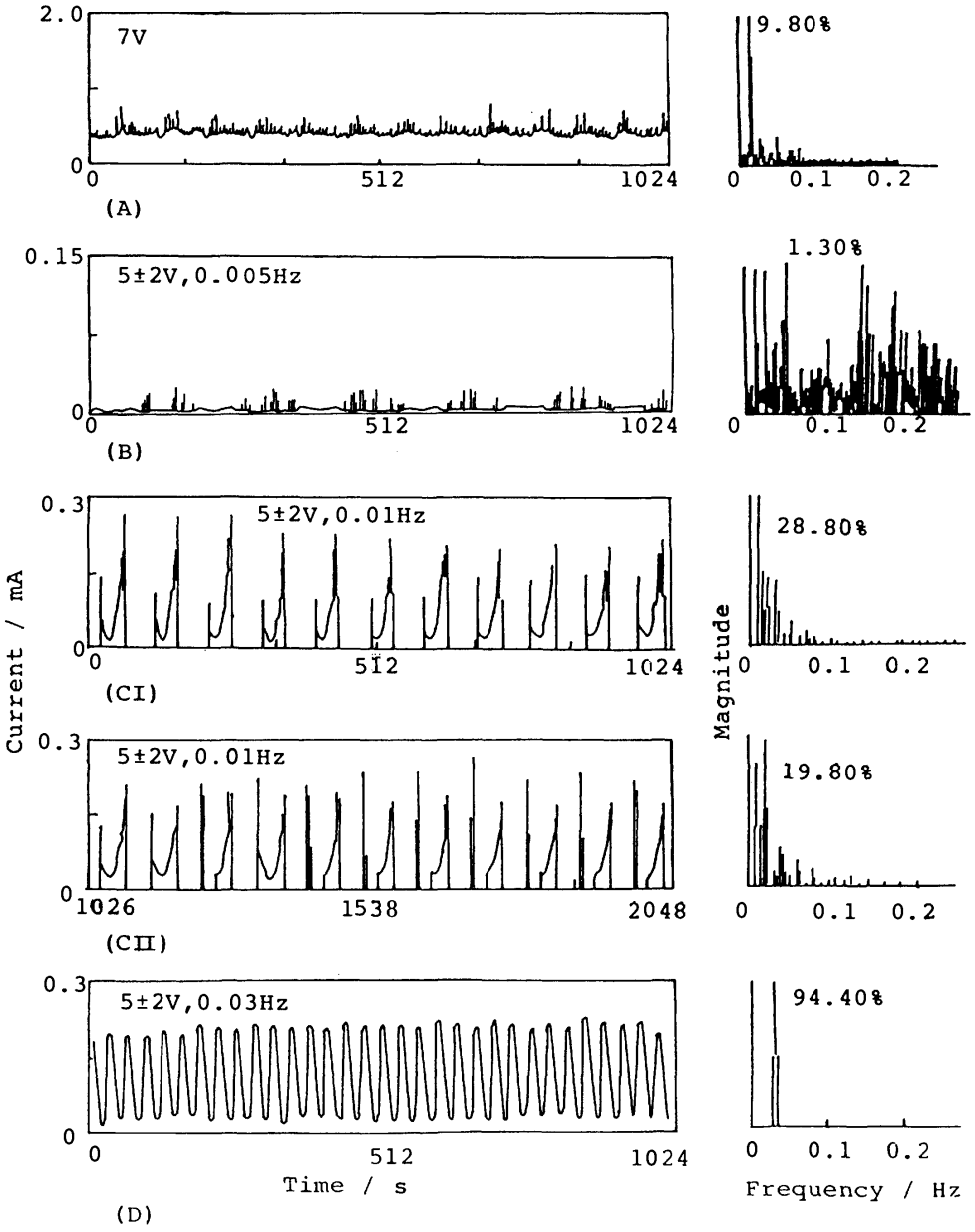

Fig. 1. The effects of frequency of external sinusoidal voltage upon the current oscillation. Gel: calcium alginate, 24 mm in diameter, 11 mm long, DS: 40, electrode distance: 10 mm.
(A) dc: 7 V, (B) dc: 5 V, ac: 0.005 Hz, 2 V, (CI, CII) dc: 5 V, ac: 0.01 Hz, 2 V, (D) dc: 5 V, ac: 0.03 Hz, 2 V. Figures denoted in the power spectra indicate percent magnitude of the main peak of total energy generated within a range from 0 to 0.5 Hz.

imposed, and the phenomena were observed repeatedly for various polymer gels.

Effect of ac Frequency of Sinusoidal Voltage. The dependence of the magnitude of f_o and f_i on the frequency of f_i for various polymer gels is shown in Fig. 2(A—C). In the case of calcium alginate gel (Fig. 2(A)), magnitude of f_o decreased quickly with increasing ac frequency and the oscillation with a frequency of f_o completely disappeared at the value f_i=0.01. This fact indicates that the entrainment of current oscillation was completed at this frequency, and suggests that there exists the threshold ac frequency in this case in order to cause an entrainment.

The entrainment of the oscillation was also observed in other polyelectrolyte gels regardless of weak (PMAA) or strong (PAMPS) polyelectrolyte. The examples are shown in Fig. 2B and 2C, respectively. The threshold frequency in order to induce an complete entrainment was 0.05 Hz for PMAA gel and the magnitude of the peak at 0.05 Hz was 80.5% as shown in Fig. 2B. As shown in Fig. 2B the magnitude of the oscillation corresponding to f_o decreased

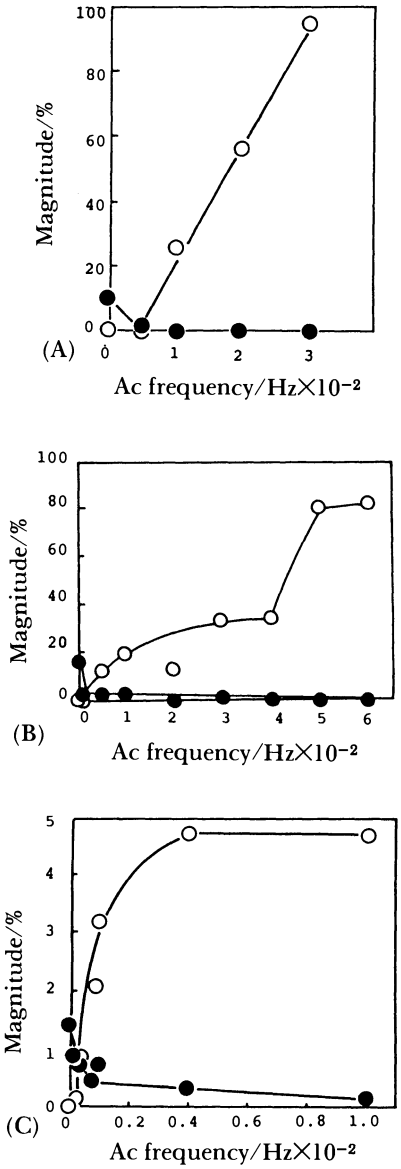

Fig. 2. Dependence of magnitude of f_o(●) and f_i (○) on the frequency of f_i.
Polymer gels: (A) calcium alginate: 26 mm in diameter, 12 mm long, DS: 40, electrode distance: 5 mm, dc: 5 V, ac: 2 V. (B) PMAA: 14 mm in diameter, 10 mm long, dc: 10 V, electrode distance: 7 mm, dc: 5 V, ac: 1 V. (C) PAMPS: 12 mm in diameter, 17 mm long, DS: 50, electrode distance: 7 mm, dc: 5 V, ac: 1 V.

quickly when ac with a frequency (f_i) of 1×10^{-3} Hz was imposed. A gradual decrease of magnitude of f_o was then observed whereas the magnitude of f_i increased rather rapidly. A complete entrainment occurred when f_i was larger than 0.04 Hz. A sudden and steep increase in magnitude of f_i was simultaneously observed.

In the similar manner the magnitude of parent oscillation f_o of PAMPS gel decreased rapidly when ac was imposed (Fig. 2C). However, a complete entrainment was not observed within a range of 1 Hz.

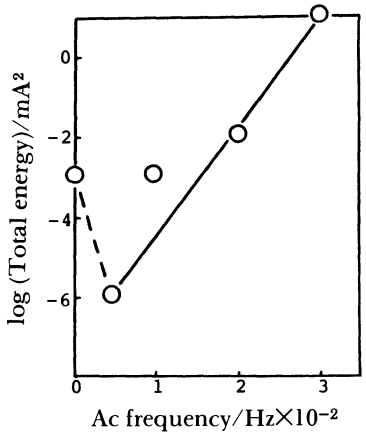

Fig. 3. Dependence of total energy whthin a range from 0 to 0.5 Hz on the frequency of f_i. gel: calcium alginate, 24 mm in diameter, 11 mm long, DS: 40, electrode distance: 10 mm, dc: 5 V, ac: 2 V.

The magnitude of f_i was not large comparing preceding two examples and the value was only 5% or less. Figure 3 shows the dependence of total energy on the ac frequency f_i. Total energy is defined as an integral calculus of the power spectrum within a certain frequency range. It is seen from Fig. 3 that the total energy calculated within 2.5 Hz is extremely low as 10 mA^2 when ac with a frequency of 0.05 Hz was imposed. However, it increased exponentially with increase in ac frequency and the total energy of the oscillation entrained by ac with a frequency of 0.03 Hz, was 10^6 times larger than that entrained by ac 0.005 Hz. We cannot clarify the reason at present, but as reported in the previous paper, PAMPS is a strong polyelectrolyte and exhibits intensive oscillation with many higher harmonics. The different characteristics of entrainment observed in PAMPS gel should be explained with this different nature of the oscillation.

Effect of Amplitude of Sinusoidal Voltage. Complete entrainment could be observed when the frequency of sinusoidal stimulation was kept constant but ac voltage was altered. Figure 4 shows the effects of external sinusoidal voltage upon the current oscillation of calcium alginate gel. Here, the ac frequency (f_i) was kept constant at 0.03 Hz, while amplitude was varied as 0.05, 0.08, 0.13, 0.82, 2.0 V, respectively. Figure 4(A) corresponds to repetitive oscillation curve and its power spectrum of the gel when dc (5 V) was applied. It was found from Fig. 4A that the frequency of the current oscillation induced by dc was about 0.038 Hz and the amplitude of this oscillation was about 0.1 mA.

The current of ac in the gel at 2 V ac was 0.04 mA and this value was less than 50% that of current oscillation induced by dc. Thus, the current oscillation induced by dc is not covered by the ac imposed afterward. When ac voltage (0.03 Hz) as low as 0.05 V

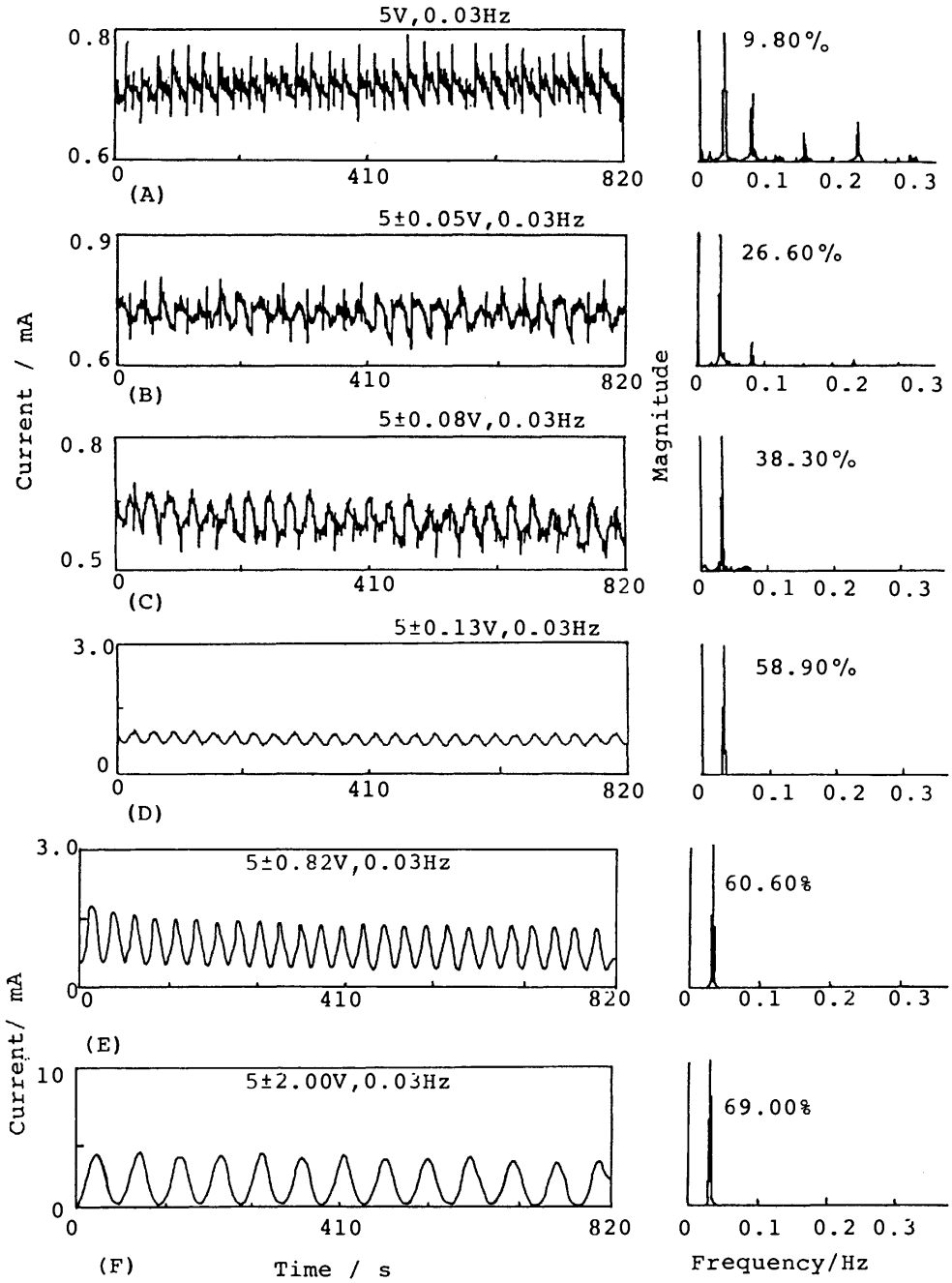

Fig. 4. The effects of amplitude of external sinusoidal voltage upon the current oscillation. Gel: calcium alginate, 26 mm in diameter, 12 mm long, DS: 40, electrode distance: 5 mm.
(A) dc: 5 V, (B) dc: 5 V, ac: 0.05 V, 0.03 Hz, (C) dc: 5 V, ac: 0.08 V, 0.03 Hz. (D) dc: 5 V, ac: 0.13 V, 0.03 Hz, (E) dc: 5 V, ac: 0.82 V, 0.03 Hz, (F) dc: 5 V, ac: 2.00 V, 0.03 Hz. Figures denoted in the power spectra indicate percent magnitude of the main peak of total energy generated within a range from 0 to 2.5 Hz.

or 0.08 V was applied, magnitude of f_o induced by dc decreased from 9.80% to 0.73%. Instead, a new peak corresponding to f_i (0.03 Hz) appeared and this is clearly seen in their power spectra (Fig. 4B and 4C). When the ac amplitude is as high as 0.13 V, the parent oscillation completely disappeared and new ac current having only one peak of f_i was observed (Fig. 4D, 4E, and 4F). Magnitude of this peak is about 58.9%. Further increase in ac voltage up to 0.82 V or 2.0 V (Fig. 4E and 3F) lead to additional increase of magnitude of the oscillation consisting of only one peak of f_i(0.03 Hz). From these results it is seen that the 1 : 1 entrainment of the current oscillation occurs at the amplitude from 0.13 V to 2.0 V and chaotic behavior appears when the ac amplitude is less than 0.13 V. Figure 5 shows the dependences of magnitude of spec-

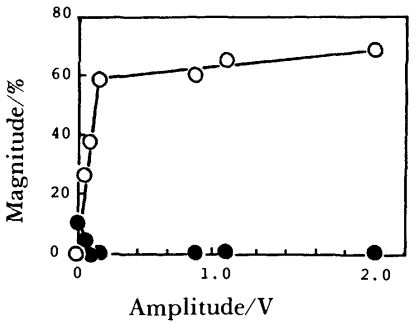

Fig. 5. Dependence of magnitude of f_o and f_i on ac amplitude. gel: calcium alginate, 26 mm in diameter, 12 mm long, DS: 40, electrode distance: 5 mm.

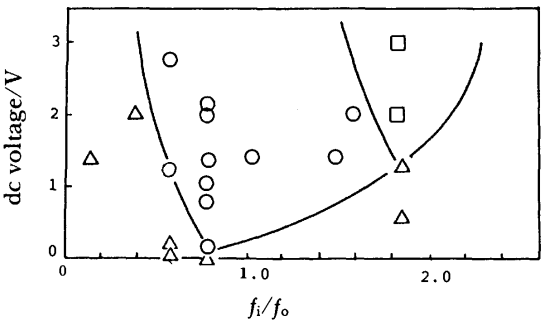

Fig. 6. The phase diagram of the current oscillation under the sinusoidal stimulation. Gel: calcium alginate, 24 mm in diameter, 11 mm long, dc: 40, electrode distance: 10 mm. ○: 1 : 1 entrainment, □: 2 : 1 entrainment, △: chaotic.

tra of f_o and f_i on ac amplitude. The magnitude of the peak at the frequency of 0.038 Hz (f_o) decreased quickly by imposing ac current and disappeared completely at the voltage as low as 0.13 V. Simultaneously, the magnitude of a peak corresponding to 0.03 Hz (f_i) increased until ac voltage becomes 0.13 which then changed almost plateau. It should be noted again that after entrainment only one peak corresponding to 0.03 Hz was seen in the power spectra. Thus, in the similar manner as changed ac frequency (Fig. 2A and 2B), the threshold amplitude of ac was required in order to make an entrainment of current oscillation.

Phase Diagram. The phase diagram of the response of the current oscillation to the sinusoidal stimulation in the case of calcium alginate gel is shown in Fig. 6. When the f_i/f_o is 0.8 or higher, the entrainment of current oscillation was observed in the wide range of dc from 0.1 to 2 V. If the dc voltage is increased, the entraiment occurs in lower f_i/f_o. At higher dc voltage and higher f_i/f_o, a 2 : 1 entrainment preferably occurs. From this figure it is seen that an entrainment of the oscillation induced by dc occurs more easily when the ac frequency was close to that of parent oscillation. It is also seen the stronger sinusoidal voltage cause the entrainment in wider frequency range. Away from these frequency ranges and weak ac amplitude, the chaotic behavior was observed.

Our preliminary hypothesis of the oscillation in the gel is that nonlinear ion transport causes a periodic electrostatic as well as osmotic potential owing to change in charge densities on a local level. One of the experimental evidences is that the pH oscillation occurred in the gel[20] for a prolonged period of time after the electric field was turned off; as reported previously[20] a constant potential was applied to the PAMPS gel for 40 min, thereafter the electrodes were removed, instead a specific micro-pH electrode was inserted. No periodic oscillation or fluctuation of pH appeared for the first 50 min, however, intensive and clear oscillation accompanied with some satellite peaks suddenly appeared.

The obtained results indicate that many ion transport process can be ordered and syncronized by superimposing ac. This fact means that the factors which may cause the nonlinear ion transport have many degree of freedom and are flexible and it is possible to be able to synchronize to external stimulation. To our knowledge, there has been no study on such periodical nature of oscillations in the water-swollen homogeneous gels having no ion gradient and may be of interest in relation to many rhythmic systems and "deterministic chaos".

There has been an increasing interest in the rhythmic systems appeares in the individuals in biology such as oscillation of heart, circadian rhythms, the cellular fussion. Entrainment phenomena observed in the hydrated gel may provide the simplest and suitable model for understanding syncronized rhythmic system in biology.

We are grateful to Dr. Gen Matsumoto (Electrotechnical Laboratory, AIST) for kind advices, useful suggestion to data analysis, and encouragement.

References

1) S. Hagiwara and Y. Oomura, *J. Physiol.*, **8**, 234 (1985).
2) A. N. Zaikin and A. M. Zhabotinsky, *Nature (London)*, **251**, 703 (1974).
3) K. Toko, S. Iriyama, C. Tanaka, K. Yamafuji, and Ke. Yamafuji, *Biophys. Chem.*, **27**, 39 (1987).
4) G. Matsumoto, K. Kim, K. Uehara, and J. Shimada, *J. Phys. Soc. Jpn.*, **49**, 906 (1980).
5) T. Teorell, *J. Gen. Physiol.*, **42**, 831 (1958).
6) K. Kobatake, *Adv. Chem. Phys.*, **29**, 319 (1975).
7) M. Seno, T. Yamabe, *Physiol.*, **36**, 877 (1963).
8) A. M. Monnier, *J. Gen. Physiol.*, **51**, 26 (1968).
9) V. E. Shashoua, *Nature (London)*, **215**, 847 (1967).
10) A. Katchalsky and R. Spangler, *Quart. Rev. Biophys.*, **1**, 127 (1968).
11) Y. Osada and M. Hasebe, *Chem. Lett.*, **1985**, 1285.
12) Y. Osada, *Adv. Polym. Sci.*, **82**, 1 (1987).
13) Y. Osada, M. Hasebe, R. Kishi, and K. Umezawa, 6th

CHEMRAWN Reprints, 622 (1987).
14) Y. Osada and R. Kishi, *J. Polym. Sci., Part C*, **25**, 418 (1987).
15) R. Kishi and Y. Osada, *J. Chem. Soc., Faraday Trans. 1*, **85**, 655 (1989).
16) Y. Osada, K. Umezawa, and A. Yamauchi, *Makromol. Chem.*, **189**, 597 (1988).
17) T. Ishii, Y. Kuroda, T. Omochi, and K. Yoshikawa, *Langmuir*, **2**, 319 (1986).
18) K. Toko, M. Tsukiji, S. Ezaki, and K. Yamafuji, *Biophys. Chem.*, **20**, 39 (1984).
19) I. C. Bassingnana and H. J. Reiss, *Membrane Sci.*, **15**, 27 (1983).
20) K. Umezawa and Y. Osada, *Chem. Lett.*, **1987**, 1795.

Syntheses, Spectroscopic Properties, Crystal Structures, and Antitumor Activities of the Optically Isomeric Mandelate Chelates, Mandelato(*trans*-1,2-diaminocyclohexane)platinum(II)

T. Ken MIYAMOTO,* Kojiro OKUDE, Kazuyuki MAEDA, Hikaru ICHIDA, Yukiyoshi SASAKI, and Tazuko TASHIRO†

Department of Chemistry, Faculty of Science, The University of Tokyo, Hongo, Bunkyo-ku, Tokyo 113
†Cancer Chemotherapy Center, J. C. R., Kami-Ikebukuro, Toshima-ku, Tokyo 170

(Received May 10, 1989)

The four optical isomers of mandelato(*trans*-1,2,-diaminocyclohexane)platinum(II) have been prepared. The CD and NMR spectra of these compounds in solution indicate that the mandelate coordinates to platinum(II) to form a five-membered chelate ring. The X-ray crystal structure analyses of a pair of diastereomers, (*R*)-mandelato[(1*R*,2*R*)-1,2-diaminocyclohexane]platinum(II) and (*S*)-mandelato[(1*R*,2*R*)-1,2-diaminocyclohexane]platinum(II), have confirmed that the skeletal configuration of (*R*)- or (*S*)-mandelic acid is retained during the chelation of platinum(II). As a whole, the structural features of both diastereoisomers are analogous to each other. However, slight differences in hydrogen bonding are noticeable in relation to the solubilities. A preliminary animal test against mice leukemia L1210 was carried out using these compounds. The four isomers show different activities. All these facts together support the conclusion that the chiralities of both ammine (carrier) and mandelate (leaving group) influence the antitumor activities of the platinum agents.

Since the discovery of significant antineoplastic activity of *cis*-dichlorodiammineplatinum(II),[1] this complex has been widely used as an anticancer agent. The drug, however, is highly toxic, especially regarding renal damage. Consequently, a vast number of platinum complexes have been prepared in search of less toxic antitumor agents.

In the process of amelioration, 1,2-diaminocyclohexane (dach) was reported as being a potent ligand (carrier ligand) for antitumor platinum complexes.[2-4] Kidani et al. resolved three isomers of dach and found that the platinum(II) complexes of each isomer have different antitumor activities against mice luekemia L1210.[5] The *trans*-dach complexes were more potent than the *cis*-dach complex. The different activities between the *trans*-dach complexes. i.e., (1*R*,2*R*)- and (1*S*,2*S*)-isomeric complexes, were supposed to be derived from chiral recognitions between the active platinum(II) species and their final targets, DNA bases. This point of view leads to one of the most important subjects in drug design: the chirality of the carrier ligand. Further emphasis should be placed on the fact that the anionic ligands (leaving groups) in the platinum complexes also have considerable influence on antitumor activities,[6,7] and have been supposed to play important roles in drug metabolism. Accordingly, special regard will be paid to not only the chiralities of the carrier ligands, but those of the leaving groups.

Recently, Totani et al. have reported the syntheses of a series of (glycolato-*O*,*O'*)platinum(II) complexes.[8] These complexes have a novel chelate ring in which glycolate is bound to platinum(II) with both carboxylato- and alcoholato-oxygens. By using the optically active mandelate(md) as a leaving group instead of glycolate, a chiral point can be brought about in the vicinity of platinum(II).

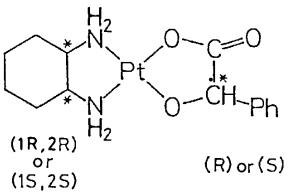

Fig. 1. The proposed structure of [Pt(dach)(md)].

In general, platinum(II) alkoxides are unstable and a limited number of examples are known to date.[9-11] Therefore, alcoholato-platinum(II) bonding stabilized by chelation arouse interest in the study of the structural characteristics. However, even X-ray crystal structure analysis has not so far been applied to the glycolate or mandelate-chelating complexes.

Thus, we have prepared the four optical isomers of platinum(II) complexes with *trans*-dach and md as ligands; i.e., (*R*)- or (*S*)-mandelato[(1*R*,2*R*)- or (1*S*,2*S*)-1,2-diaminocyclohexane]platinum(II) (Fig. 1). Syntheses, X-ray structure analyses and their properties, including the antineoplastic activities, are described here.

Experimental

Materials. From a commercially available mixture of *trans*- and *cis*-diaminocyclohexane an optically pure (1*R*,2*R*)-*trans*- or (1*S*,2*S*)-*trans*-isomer was resolved according to a method described in the literature.[12]

The four nitrate complexes, i.e., dinitrato[(1*R*,2*R*)-1,2-diaminocyclohexane]platinum(II); [Pt(*RR*-dach)$(NO_3)_2$], dinitrato[(1*S*,2*S*)-1,2-diaminocyclohexane]platinum(II); [Pt(*SS*-dach)$(NO_3)_2$], *cis*-dinitratodiammineplatinum(II); [Pt$(NH_3)_2(NO_3)_2$] and *cis*-dinitratodiisopropylamineplatinum(II); [Pt$(ipr)_2(NO_3)_2$], were prepared using a similar method to that of Lippert et al.[13]

The Optical Isomers of Mandelato(*trans*-1,2-diaminocyclohexane)platinum(II): The compound was synthesized

by the modified method from the literature.[8] A 4.61 g (11 mmol) portion of [Pt(*RR*-dach)(NO_3)$_2$] was dissolved in 150 ml of water with heating. The solution was passed through a column packed with the anion exchange resin (Diaion SA10AOH, 160 ml) and a further amount of water was passed through the column. To the combined eluate 1.52 g of (*R*)-mandelic acid (10 mmol) was dissolved. After stirring overnight, the solution was evaporated to dryness. A small amount of water was added and the mixture was stirred at 60 °C. By filtration, a white powder of (*R*)-mandelato[(1*R*,2*R*)-1,2-diaminocyclohexane]platinum(II) monohydrate [Pt(*RR*-dach)(*R*-md)]·H_2O was obtained (3.68 g. 8.0 mmol, 80% yield). A crystal suitable for **X**-ray crystal analysis was obtained by recrystallization from water. In a similar manner, another three optical isomers of mandelato(*trans*-1,2-diaminocyclohexane)platinum(II) were synthesized. Found: [Pt(*RR*-dach)(*R*-md)]·H_2O: C, 35.16; H, 4.65; N, 5.86%; [Pt(*RR*-dach)(*S*-md)]·H_2O: C, 35.37; H, 4.62: N, 5.86%; [Pt(*SS*-dach)(*R*-md)]·H_2O: C, 35.09; H, 4.53; N, 5.81%; [Pt(*SS*-dach)(*S*-md)]·H_2O: C, 35.23; H, 4.62; N, 5.75%. Calcd for $C_{14}H_{22}N_2O_4Pt$: C, 35.22; H, 4.62; N, 5.75%.

(*R*)-Mandelatodiammineplatinum(II) [Pt(NH_3)$_2$(*R*-md)]·1/2H_2O: The complex [Pt(NH_3)$_2$(NO_3)$_2$] (1.05 g, 3.0 mmol) was dissolved in water (150 ml) with heating. The solution was passed through a colunm packed with the anion exchange resin (Dianion SA10AOH, 160 ml) and a further amount of water was passed through the colunm. To the combined eluate 451 mg of (*R*)-mandelic acid (3.0 mmol) was dissolved. After standing overnight the solution was evaporated to ca. 50 ml. The solution turned pale blue after 3 days of standing. After removing the precipitate the solution was cooled to 0 °C overnight. A white crystalline solid containing a small amount of pale blue material was obtained. A blue impurity could not be removed by recrystalization from water. Yield: 23g mg (0.62 mmol, 21%). Found: C, 24.89; H, 3.30; N, 7.21%. Calcd for $C_8H_{13}N_2O_{3.5}Pt$: C, 24.74; H, 3.37; N, 7.21%.

(*S*)-Mandelatodiisopropylamineplatinum(II) [Pt(ipr)$_2$(*S*-md)]: This complex was similarly synthesized as anhydrous salt: Found: C, 36.25; H, 5.25; N, 5.94%. Calcd for $C_{14}H_{24}N_2O_3Pt$: C, 36.28; H, 5.22; N, 6.04%.

Spectroscopy. The CD spectra were recorded with a JASCO-J500A spectrometer. UV-Vis spectra were obtained by the use of a Hitachi 340 spectrometer.

400-MHz ^{1}H NMR spectra were measured for [Pt(*RR*-dach)(*R*-md)] and [Pt(*RR*-dach)(*S*-md)] in D_2O with DSS as an internal standard by the use of a JEOL JNM-GX FT NMR spectrometer. [Pt(*RR*-dach)(*R*-md)]: δ=1.12—1.22 (2H, m, 4- or 5-dach), 1.24—1.33 (2H, m, 4- or 5-dach), 1.55—1.58 (2H, m, 3- or 6-dach), 2.01—2.07 (2H, m, 3- or 6-dach), 2.31—2.35 (2H, m, 1- and 2-dach), 4.931 (1H, s, α-md), 7.39—7.47 (1H, m, *p*-phenyl), 7.44 (2H, d, J=8 Hz, *m*-phenyl), 7.65 (2H, d, J=8 Hz, *o*-phenyl). [Pt(*RR*-dach)(*S*-md)]: δ=1.12—1.21 (2H, m, 4- or 5-dach), 1.22—1.32 (2H, m, 4- or 5-dach), 1.53—1.61 (2H, m, 3- or 6-dach), 2.00—2.05 (2H, m, 3- or 6-dach), 2.20—2.27 (1H, m, 1- or 2-dach), 2.30—2.37 (1H, m, 1- or 2-dach), 4.93 (1H, s, α-md), 7.37—7.49 (1H, m, *p*-phenyl), 7.45 (2H, d, J=7 Hz, *m*-phenyl), 7.72 (2H, d, J=7 Hz, *o*-phenyl).

22.5-MHz ^{13}C NMR spectrum was recorded with a JEOL FX90Q to [Pt(*SS*-dach)(*R*-md)] in DMSO-d_6 with TMS as an internal standard. δ=24.2 (2C, 4- and 5-dach), 31.4 (1C, 3- or 6-dach), 31.9 (1C, 3- or 6-dach), 60.9 (1C, 1- or 2-dach), 61.5 (1C, 1- or 2-dach), 79.7 (1C, α-md), 126.3 (2C, *o*-phenyl), 127.3 (3C, *m*-, and *p*-phenyl), 145.5 (1C, 1-phenyl), 189.4 (1C, C=O).

19.2-MHz ^{195}Pt NMR spectra were measured for [Pt(*RR*-dach)(*R*-md)] (ca. 20 mg cm^{-3}) and [Pt(*RR*-dach)(*S*-md)] (ca. 200 mg cm^{-3}) in DMSO-d_6 with Na_2PtCl_6 in D_2O as an external standerd. (a JEOL FX90Q) [Pt(RR-dach)(S-md)]: δ=−1897. [Pt(*RR*-dach)(*R*-md)]: δ=−1904. A new peak (δ=−2968) had been growing for [Pt(*RR*-dach)(*S*-md)] with time, but no change was observed for [Pt(*RR*-dach)(*R*-md)].

The IR spectra were measured with a Hitachi 260-30. ν(C=O)/cm^{-1} in KBr disk: [Pt(*RR*-dach)(*R*-md)]·H_2O: 1649; [Pt(*RR*-dach)(*S*-md)]·H_2O: 1664; [Pt(NH_3)$_2$(md)]·H_2O: 1622.

Solubility Test. Solubility (mg ml^{-1}) in H_2O (or dmso) at 26 °C: [Pt(*RR*-dach)(*R*-md)]·H_2O: 7.8 (20); [Pt(*RR*-dach)(*S*-md)]·H_2O: 15.3 (>200).

X-Ray Diffraction Measurement and Structure Determination. Among the four optical isomers, a pair of diastereomers, [Pt(*RR*-dach)(*R*-md)]·H_2O and [Pt(*RR*-dach)(*S*-md)]·H_2O, were applied to the **X**-ray crystal structure analysis.

A colorless plate crystal was subjected to an **X**-ray diffraction measurement. The density of the crystal was measured by a flotation method in mixtures of 1,2-dibromoethane and carbon tetrachloride. X-Ray diffraction intensities were collected on a Rigaku AFC-5R goniometer with graphite monochromatized Mo$K\alpha$ (λ=0.71069 Å) radiation (50 kV, 150 mA) at Research Centre for Spectrochemistry, Faculty of Science, The University of Tokyo. The crystal gradually became yellow during exposure to X-rays, but no significant influences was observed regarding the intensities. Data were corrected for both Lorenz and polarization effects. An empirical absorption correction by ψ-scan was applied to both isomers. The positions of the Pt atoms were solved by Mithril,[14] and other atoms were located by successive Fourier and differential syntheses. An absolute configuration was determined by anomalous scattering factors. The enantiomeric structure was rejected because of the larger *R*-factor. H atoms, except crystal water, were located from calculations, but were not refined. Anisotropic thermal parameters were applied for non-hydrogen atoms and isotropic ones for H atoms. The thermal and positional parameters of all non-hydrogen atoms were refined by full-

Table 1. Crystallographic Data of [Pt(dach)(md)]·H_2O Isomers

Isomer	*RR-R*	*RR-S*
Formula	$PtO_4N_2C_{14}H_{22}$	$PtO_4N_2C_{14}H_{22}$
Formula weight	477.43	477.43
Crystal system	Monoclinic	Monoclinic
Space group	$P2_1$	$P2_1$
Z	4	4
a/Å	11.778(2)	11.886(1)
b/Å	10.930(2)	10.623(2)
c/Å	12.217(2)	12.104(1)
β/°	90.71(2)	92.98(1)
V/Å^3	1572.6(9)	1526.3(6)
D_x/g cm^{-3}	2.02	2.08
D_m/g cm^{-3}	1.99	2.06
μ/cm^{-1} (Mo$K\alpha$)	94.05	96.90
F(000)	920	920

Table 2. Measurement Details for [Pt(dach)(md)]·H_2O Isomers

Isomer	*RR-R*	*RR-S*
T/K	300	300
No. of measurements	3996	3895
No. of observations	3053	3219
	($F_o \geqq 3.0\sigma(F_o)$)	($F_o \geqq 3.0\sigma(F_o)$)
No. of variables	378	378
R (wR)	0.042(0.039)	0.042(0.052)
S	1.96	1.39
$(\Delta/\sigma)_{max}$	0.38	0.03
$(\Delta\sigma)_{max}$/e Å^{-3}	2.56	1.54
Crystal dimensions /mm	0.20×0.12×0.05	0.25×0.24×0.15
No. of reflections used in cell dimensions (θ range/°)	22($19<\theta<20$)	24($16<\theta<19$)
Mode	ω-2θ	ω-2θ
Range of measurements (2θ/°)	$4<2\theta<55$	$4<2\theta<55$
Scan rate (° min^{-1} in 2θ)	6	6
Standard reflections (number/interval)	3/100	3/100
Indices	022, 220, 202	1 −30, −1 −3 1, −3 −1 2
Fluctuation(%)	±5.0	±2.0
$h\,k\,l$ range	$-18 \leqq h \leqq 18$	$0 \leqq h \leqq 15$
	$0 \leqq k \leqq 17$	$0 \leqq k \leqq 14$
	$0 \leqq l \leqq 19$	$-16 \leqq l \leqq 16$
Indices used for ψ scan	−2 0 2, −3 0 3, −3 1 5	0 2 −2, 0 4 −4, 0 6 −6
	−5 0 5, −3 1 8, −6 1 8	0 8 −8, 2 9 −8
	−6 1 10	

matrix least squares on F with $W=1/\sigma(F_o)$. All calculations were performed with the TEXSAN[15] program with complex scattering factors from International Tables for X-ray Crystallography[16]and were carried out on DEC Micro Vax II at the Research Centre for Spectrochemistry. Crystallographic data and measurement details are listed in Tables 1 and 2, respectively. The complete F_o—F_c data are deposited as Document No. 8893 at the Office of the Editor of Bull. Chem. Soc. Jpn.

Antitumor Assay in vivo. The antitumor activities of the [Pt(dach)(md)] isomers against mice leukemia L1210 were tested. 10^5 cells/mouse were transplanted i.p. into CDF_1 mice (6 mice/group) and samples were administered i.p. on days 1, 5, and 9. From the mean survival times of treated (T) and control (C) mice, T/C values were calculated as indlcators of activity.

Results and Discussion

Syntheses of the Compounds. By the anion exchange of $[Pt(dach)(NO_3)_2]$, dihydroxo species is supposed to be formed in aqueous solution. The dihydroxo complex was neutralized by the addition of the equivalent mandelic acid. The procedure results in the five-membered chelation of platinum(II) (Scheme 1). The neutralization is a relatively slow process: after overnight standing of the reaction mixture at room temperature, an oily product was only obtained; heating of the aqueous solution at 60 °C for several hours gave a crystalline solid. However, at higher temperature (>80 °C), the solution turned red. This coloring indicated a partial decomposition of platinum(II) alkoxide.

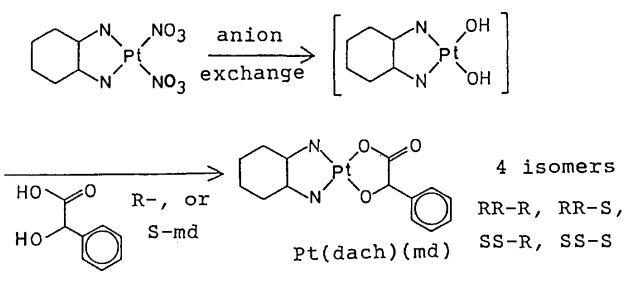

Scheme 1. Synthetic procedure to [Pt(dach)(md)]·H_2O.

In the preparation of $[Pt(NH_3)_2(md)]\cdot 1/2H_2O$ without protection to light, the solution turned blue. The addition of excess mandelic acid to this solution precipitated a blue-black solid. The blue product, which showed IR absorption bands due to mandelate and ammine ligands, was assumed a platinum oligomer, such as a "platinum blue"; however, the structure of this compound has not yet been determined. The formation of the oligomeric species by the use of the bidentate ligands seems to be a relatively familiar phenomenon. For example, the well known oligomers of platinum(II) have bidentate bridging ligands such as uracil, pyridone, pyrrolidone, phosphate;[17-19] in our case mandelate. In the preparation of mandelatoplatinum(II) complexes, the oligomer formation is reduced under shading and at higher pH (with use of excess platinum nitrate).

Table 3. The CD and UV Data

Complex	CD λ_{max}/nm($\Delta\varepsilon$)	UV λ_{max}/nm(ε_{max})
[Pt(*RR*-dach)(*R*-md)]	365(+0.16), 321(+0.19), 253(+2.2), 216(−12)	332(3.8×10^{-3})
[Pt(*RR*-dach)(*S*-md)]	387(−0.09), 326(+0.77), 252(−1.3), 216(+8)	332(4.0×10^{-3})
[Pt(*SS*-dach)(*R*-md)]	386(+0.08), 327(−0.78), 254(+1.2), 216(−11)	332(3.0×10^{-3})
[Pt(*SS*-dach)(*S*-md)]	363(−0.17), 319(−0.21), 254(−2.2), 219(+12)	330(3.7×10^{-3})
[Pt(*RR*-dach)(NO_3)$_2$]	330(+0.40), 246(+1.03)	—
[Pt(*SS*-dach)(NO_3)$_2$]	330(−0.35), 246(−0.95)	—
[Pt(NH_3)$_2$(*R*-md)]	386(+0.11), 336(−0.31), 255(+1.9)	—
[Pt(ipr)$_2$(*S*-md)]	395(−0.11), 340(+0.28), 253(−2.4)	—

Spectroscopic Properties. The CD and UV data are listed in Table 3. The CD spectra of [Pt(*RR*-dach)(*R*-md)] and [Pt(*RR*-dach)(*S*-md)] are inverse to those of their enantiomers, [Pt(*SS*-dach)(*S*-md)] and [Pt(*SS*-dach)(*R*-md)], respectively. On the other hand, the spectra of diastereomers are quite different from each other, indicating a marked influence of the mandelate ligands. The additivity rule due to ligand contributions is generally applied to the CD spectra of coordination compounds. The notable contribution of mandelate is rationalized on the assumption that it is bound to platinum(II) by both carboxylato- and alcholato-oxygens because the chelate configurations have great effects on the CD spectra. If mandelate is linked to the metal via only carboxylato-oxygen, namely in a unidentate fashion, only a vicinal effect could be observed in the CD spectra as a minor contribution. Free mandelic acid has a weak CD at 250 nm or longer wavelength,[20] which is not consistent with the observed strong CD curve. These CD data suggest mandelate chelation in solution.

The CD spectrum of [Pt(dach)(NO_3)$_2$] has two peaks (λ_{max} 330 and 246 nm) assignable to $^1A_{1g}\rightarrow{}^3E_g$ and $^1A_{1g}\rightarrow{}^1E_g$, respectively.[21] Hawkins et al. reported that the octant sign was negative when $^1A_{1g}\rightarrow{}^1E_g$ transition had a positive Cotton effect.[22] In the case of the square planar complexes, the five-membered chelate with λ-gauche conformation has a negative octant sign. The $^1A_{1g}\rightarrow{}^1E_g$ transition of [Pt(*RR*-dach)(NO_3)$_2$] shows a positive Cotton effect and is assumed to have λ-gauche conformation, which is consistent with the (1*R*,2*R*)-configuration of the ligand.

The complex [Pt(NH_3)$_2$(*R*-md)] has four donor atoms (i.e., two nitrogen and two oxygen atoms) in common with [Pt(*RR*-dach)(NO_3)$_2$]. It is therefore expected that the CD spectrum of the former complex may have the $^1A_{1g}\rightarrow{}^1E_g$ transition at similar wavelength as that of the latter complex. A λ_{max} peak at 255 nm, which shows a positive Cotton effect, may be assigned to the $^1A_{1g}\rightarrow{}^1E_g$ transition. In this way we can estimate that the mandelate chelate may have a λ-gauche conformation in aqueous solution. However, this proposal might not be reliable since the mandelate chelate contains a carboxyl group and its symmetry is lower than that of *RR*-dach chelate. In any case, the CD data support the (*R*)-configuration of the mandelate.

The CD spectra of the four isomers, [Pt(dach)(md)] are essentially linear combinations of those of [Pt(dach)(NO_3)$_2$], [Pt(NH_3)$_2$(*R*-md)], and/or [Pt(ipr)$_2$(*S*-md)]. This result suggests again that the configurations of the ligands are retained on the coordination to platlnum(II).

The ^1H NMR spectra were measured for a pair of diastereomers, [Pt(*RR*-dach)(*S*-md)] and [Pt(*RR*-dach)(*R*-md)]. The dach ligand of [Pt(*RR*-dach)(*S*-md)] shows two sets of multiplets due to the methine protons, since these protons become nonequivalent with the coordination of asymmetric mandelate. In the case of [Pt(*RR*-dach)(*R*-md)], such a separation of methine protons is not observed. Both diastereomers also show the mandelate-methine proton as a singlet; unfortunately, though, the coupling with ^{195}Pt, the corroborative evidence,[8] cannot be detected under the influence of too large an HDO signal. Several attempts to reduce the HDO signal (such as a WEFT method, an off-resonance decoupling or the recrystallization from D_2O) have been unsuccessful up to the present. As a whole, the chemical shifts of both diastereomers bear a close resemblance to each other, but only slight differences have been observed on the phenyl proton signals. These differences may be caused by the mandelate conformations.

The ^{13}C NMR spectrum was measured for the soluble isomer, [Pt(*SS*-dach)(*R*-md)] in DMSO-d_6. Since the mandelate ligand is asymmetric, splits of 1,2- and 3,6-dach carbons are observed. On the methine carbons of both dach and mandelate, no satelite peaks have been detected, though the observed signals are somewhat broad.

The ^{195}Pt NMR spectra of both [Pt(*RR*-dach)(*R*-md)] and [Pt(*RR*-dach)(*S*-md)] have a broad peak at ca. −1900 ppm. Usually, the chemical shifts of ^{195}Pt NMR range very widely from compound to compound. The shift differences between the isomers are negligibly small, in due consideration of the concentration difference in solution. The observed shift-values belong to the range characteristic of a type of coordination compound, PtN_2O_2, which consists of the four donor atoms (two nitrogens, two oxygens) and a platinum atom. After 60 days standing in solution, the original compound, [Pt(*RR*-dach)(*S*-

md)], partly changed into another species; a new peak was observed at −2970 ppm. On the other hand, the isomer, [Pt(*RR*-dach)(*R*-md)], did not change at all. The half decay time of the original peak was ca. 25 days. The new species is tentatively assignable to a platinum-dimethyl sulfoxide (DMSO-d_6) complex in which dmso is bound to platinum(II) through an S atom, while mandelate coordinates via only carboxylate-oxygen. A similar reaction between dmso and *cis*-[Pt(NH_3)$_2$$Cl_2$] was reported,[23] but the half decay time of the original peak due to cis-platin is 3 h which is much shorter than that of [Pt(*RR*-dach)(*S*-md)]. From the comparison, it is obvious that the mandelate chelate is relatively stable in solution in spite of the expected instability of platinum alkoxide.

Thus, all CD and NMR results are consistent with the chelate structure of mandelatoplatinum(II) complexes in solution.

The solid state IR spectra of [Pt(*RR*-dach)(*R*-md)]·H_2O and [Pt(*RR*-dach)(*S*-md)]·H_2O are identical to [Pt(*SS*-dach)(*R*-md)]·H_2O, and [Pt(*SS*-dach)(*R*-md)]·H_2O, respectively.

The C=O stretching absorption appears at 1710 cm^{-1} for mandelic acid[24] and at 1582 cm^{-1} for potassium mandelate.[25] The mandelatoplatinum complexes, i.e., the [Pt(dach)(md)]·H_2O isomers and [Pt(NH_3)$_2$-(*R*-md)]·1/2H_2O have the absorption bands between these peaks. As a cosequence of the reduced resonance by coordination, the complexes increase the bond strength of C=O in comparison with that of free mandelate. The spectrum of [Pt(*RR*-dach)(*R*-md)]·H_2O shows the C=O stretching at 1649 cm^{-1} while the band position of [Pt(*RR*-dach)(*S*-md)]·H_2O is 15 cm^{-1} higher. Such a difference between the diastereomers might be caused by the hydrogen-bonding patterns to a carboxyl oxygen.

Structure Description of [Pt(dach)(md)]·H_2O Isomers. The crystal structure of [Pt(*RR*-dach)(*R*-md)]·H_2O is shown in Fig. 2. Two complexes and two water molecules are crystallographically independent.

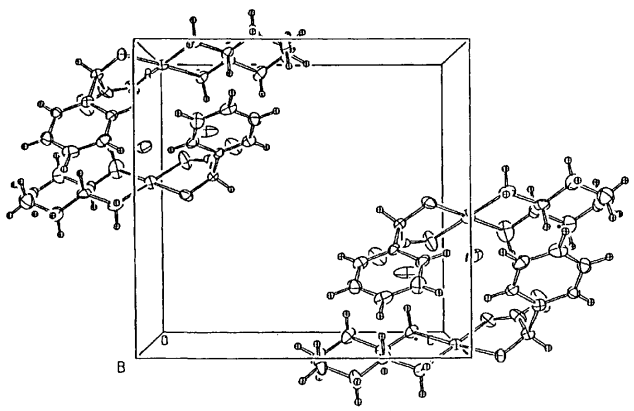

Fig. 2. ORTEP[26] plot of crystal structure of [Pt(*RR*-dach)(*R*-md)]·H_2O. View along b-axis.

These two complexes form a rather discrete cluster; the two independent complexes are related by a pseudo 2-fold axis. Their coordination planes are approximately perpendicular to each other.

The molecular structure of the complex, i.e., crystallographically independent unit of [Pt(*RR*-dach)(*R*-md)]·H_2O, is shown in Fig. 3. The bond lengths and angles are listed in Table 4. Both ligands, namely *RR*-dach and *R*-md, retain their skeletal configurations. The *RR*-dach has a λ-gauche chelate

Table 4. Bond Lengths (Å) and Angles (°) of [Pt(*RR*-dach)(*R*-md)]·H_2O with e.s.d.'s in Parentheses

Bond length (Å)					
Pt1-O1	2.02(1)	Pt1-O2	2.02(1)	Pt1-N1	2.04(1)
Pt1-N2	2.03(2)	Pt2-O11	1.95(1)	Pt2-O12	2.02(1)
Pt2-N11	2.02(2)	Pt2-N12	1.94(2)	O1-C11	1.24(3)
O2-C12	1.43(2)	O3-C11	1.22(2)	O11-C31	1.23(3)
O12-C32	1.41(2)	O13-C31	1.23(2)	N1-C1	1.41(3)
N2-C2	1.49(2)	N11-C21	1.44(3)	N12-C22	1.49(2)
C1-C2	1.53(3)	C1-C6	1.52(3)	C2-C3	1.45(3)
C3-C4	1.51(3)	C4-C5	1.57(4)	C5-C6	1.52(3)
C11-C12	1.53(3)	C12-C13	1.52(2)	C13-C14	1.41(2)
C13-C18	1.36(2)	C14-C15	1.38(2)	C15-C16	1.41(3)
C16-C17	1.40(3)	C17-C18	1.37(3)	C21-C22	1.51(3)
C21-C26	1.53(3)	C22-C23	1.47(3)	C23-C24	1.54(3)
C24-C25	1.47(5)	C25-C26	1.52(3)	C31-C32	1.50(3)
C32-C33	1.53(3)	C33-C34	1.40(2)	C33-C38	1.38(2)
C34-C35	1.37(2)	C35-C36	1.36(3)	C36-C37	1.38(3)
C37-C38	1.38(3)				

Bond angle (°)			
O1-Pt1-O2	83.3(5)	O1-Pt1-N1	95.5(6)
O1-Pt1-N2	178.2(6)	O2-Pt1-N1	178.4(6)
O2-Pt1-N2	97.9(5)	N1-Pt1-N2	82.3(6)
O11-Pt2-O12	82.2(5)	O11-Pt2-N11	98.0(7)
O11-Pt2-N12	178.3(6)	O12-Pt2-N11	178.2(8)
O12-Pt2-N12	99.4(6)	N11-Pt2-N12	80.4(7)
Pt1-O1-C11	114(1)	Pt1-O2-C12	108(1)
Pt2-O11-C31	117(1)	Pt2-O12-C32	109(1)
Pt1-N1-C1	112(1)	Pt1-N2-C2	111(1)
Pt2-N11-C21	111(1)	Pt2-N12-C21	115(1)
N1-C1-C2	112(2)	N1-C1-C6	117(2)
C2-C1-C6	109(2)	N2-C2-C1	106(2)
N2-C2-C3	116(2)	C1-C2-C3	116(2)
C2-C3-C4	111(2)	C3-C4-C5	112(2)
C4-C5-C6	109(2)	C1-C6-C5	113(2)
O1-C11-O3	125(3)	O1-C11-C12	117(2)
O3-C11-C12	118(2)	O2-C12-C11	114(2)
O2-C12-C13	112(2)	C11-C12-C13	108(1)
C12-C13-C14	119(2)	C12-C13-C18	122(2)
C14-C13-C18	119(2)	C13-C14-C15	121(2)
C14-C15-C16	118(2)	C15-C16-C17	120(2)
C16-C17-C18	119(2)	C13-C18-C17	122(2)
N11-C21-C22	107(2)	N11-C21-C26	115(2)
C22-C21-C26	109(2)	N12-C22-C21	101(2)
N12-C22-C23	116(2)	C21-C22-C23	114(2)
C22-C23-C24	110(2)	C23-C24-C25	114(2)
C24-C25-C26	111(2)	C21-C26-C25	112(2)
O11-C31-O13	125(2)	O11-C31-C32	116(2)
O13-C31-C32	119(2)	O12-C32-C31	113(2)
O12-C32-C33	110(2)	C31-C32-C33	112(1)
C32-C33-C34	121(2)	C32-C33-C38	122(2)
C34-C33-C38	117(2)	C33-C34-C35	122(2)
C34-C35-C36	119(2)	C35-C36-C37	120(2)
C36-C37-C38	120(2)	C33-C38-C37	121(2)

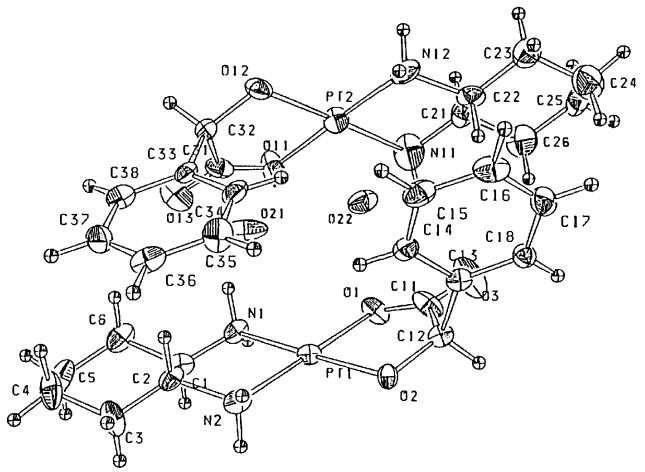

Fig. 3. ORTEP[26] of molecular structure of [Pt(*RR*-dach)(*R*-md)]·H_2O.

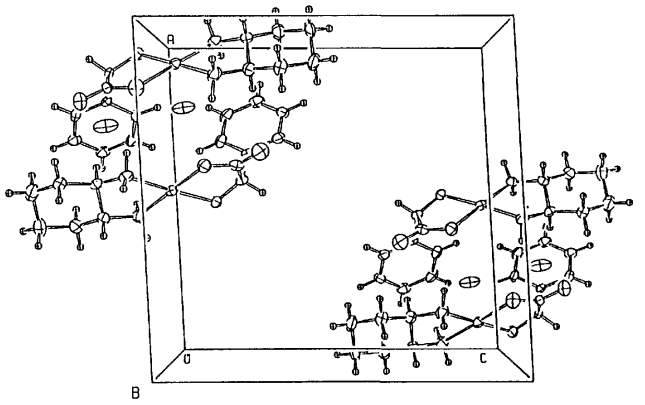

Fig. 4. Crystal structure of [Pt(*RR*-dach)(*S*-md)]·H_2O. View along b-axis.

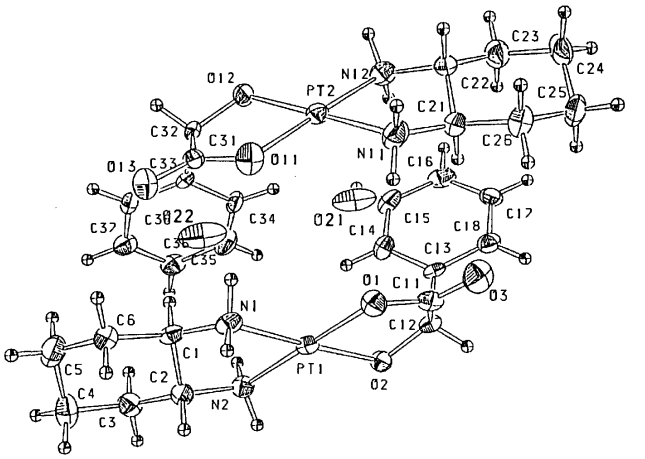

Fig. 5. Molecular structure of [Pt(*RR*-dach)(*S*-md)]·H_2O.

conformation. The mandelate ligand shows bidentate chelation to the platinum atom with carboxylate and alcoholate. Though several mandelate complexes have been reported, their mandelate groups are bound to metals using only carboxylate oxygens.[27,28]

Table 5. Bond Lengths (Å) and Angles (°) of [Pt(*RR*-dach)(*S*-md)]·H_2O with e.s.d.'s in Parentheses

Bond length (Å)					
Pt1-O1	2.01(1)	Pt1-O2	2.02(1)	Pt1-N1	2.04(1)
Pt1-N2	2.04(1)	Pt2-O11	2.00(1)	Pt2-O12	2.02(1)
Pt2-N11	2.03(2)	Pt2-N12	2.01(2)	O1-C11	1.30(2)
O2-C12	1.41(2)	O3-C11	1.20(2)	O11-C31	1.29(2)
O12-C32	1.38(2)	O13-C31	1.21(2)	N1-C1	1.46(2)
N2-C2	1.48(2)	N11-C21	1.48(2)	N12-C22	1.51(2)
C1-C2	1.53(2)	C1-C6	1.53(2)	C2-C3	1.50(3)
C3-C4	1.51(3)	C4-C5	1.56(3)	C5-C6	1.51(3)
C11-C12	1.53(2)	C12-C13	1.51(2)	C13-C14	1.39(2)
C13-C18	1.39(2)	C14-C15	1.38(2)	C15-C16	1.37(3)
C16-C17	1.37(3)	C17-C18	1.37(2)	C21-C22	1.52(2)
C21-C26	1.52(2)	C22-C23	1.47(3)	C23-C24	1.49(3)
C24-C25	1.58(3)	C25-C26	1.52(3)	C31-C32	1.55(3)
C32-C33	1.48(2)	C33-C34	1.41(2)	C33-C38	1.39(2)
C32-C35	1.39(2)	C35-C36	1.36(3)	C36-C37	1.37(2)
C37-C38	1.39(2)				

Bond angle (°)			
O1-Pt1-O2	83.8(5)	O1-Pt1-N1	94.5(5)
O1-Pt1-N2	177.1(6)	O2-Pt1-N1	177.4(5)
O2-Pt1-N2	98.5(5)	N1-Pt1-N2	83.2(6)
O11-Pt2-O12	83.1(5)	O11-Pt2-N11	95.2(6)
O11-Pt2-N12	178.2(6)	O12-Pt2-N11	178.1(6)
O12-Pt2-N12	98.5(6)	N11-Pt2-N12	83.2(6)
Pt1-O1-C11	114(1)	Pt1-O2-C12	109(1)
Pt2-O11-C31	114(1)	Pt2-O12-C32	111(1)
Pt1-N1-C1	109(1)	Pt1-N2-C2	110(1)
Pt2-N11-C21	109(1)	Pt2-N12-C21	111(1)
N1-C1-C2	108(1)	N1-C1-C6	114(1)
C2-C1-C6	110(1)	N2-C2-C1	106(1)
N2-C2-C3	115(1)	C1-C2-C3	111(1)
C2-C3-C4	112(2)	C3-C4-C5	109(2)
C4-C5-C6	112(1)	C1-C6-C5	110(2)
O1-C11-O3	123(2)	O1-C11-C12	115(1)
O3-C11-C12	121(2)	O2-C12-C11	114(1)
O2-C12-C13	113(1)	C11-C12-C13	108(1)
C12-C13-C14	121(1)	C12-C13-C18	121(1)
C14-C13-C18	119(1)	C13-C14-C15	119(2)
C16-C15-C16	121(2)	C15-C16-C17	120(2)
C16-C17-C18	120(2)	C13-C18-C17	121(2)
N11-C21-C22	108(1)	N11-C21-C26	114(2)
C22-C21-C26	111(1)	N12-C22-C21	106(1)
N12-C22-C23	115(2)	C21-C22-C23	113(1)
C22-C23-C24	112(2)	C23-C24-C25	111(1)
C24-C25-C26	110(1)	C21-C26-C25	110(2)
O11-C31-013	122(2)	O11-C31-C32	116(1)
O13-C31-C32	122(2)	O12-C32-C31	112(1)
O12-C32-C33	113(1)	C31-C32-C33	109(1)
C32-C33-C34	121(1)	C32-C33-C38	122(1)
C34-C33-C38	117(1)	C33-C34-C35	120(2)
C34-C35-C36	122(2)	C35-C36-C37	118(2)
C36-C37-C38	121(2)	C33-C38-C37	121(2)

Thus, the complex, [Pt(*RR*-dach)(*R*-md)]·H_2O is the first example of the bidentate chelate formed by a mandelate ligand. This type of five-membered chelate has been proposed to glycolatoplatinum(II) in solution,[8] but the solid state structure is unknown to date. For the first time the crystal structure has been firmly determined in this work. Historically, the platinum alkoxides are believed to be unstable[29] and few examples have been reported so far.[9-11] In the mandelatoplatinum complex, the metal-alkoxide

Table 6. Possible Hydrogen Bonds (Å)[a] with e.s.d.'s in Parentheses

[Pt(*RR*-dach)(*R*-md)]·H_2O							
Atom	Atom	Distance	ADC[b]	Atom	Atom	Distance	ADC
O1	N2	3.20(2)	54702	O2	O21	2.69(2)	55702
O2	N1	3.11(2)	55702	O3	N11	3.12(3)	55501
O11	O21	3.09(2)	55501	O12	O22	2.64(2)	65702
O13	O21	3.06(2)	55501	O21	O22	2.87(3)	55501
O21	N12	2.98(2)	64702	O22	N2	2.87(2)	54702
O22	N11	3.05(2)	55501				
[Pt(*RR*-dach)(*S*-md)]·H_2O							
Atom	Atom	Distance	ADC[b]	Atom	Atom	Distance	ADC
O1	N2	3.19(2)	65502	O2	O22	2.68(2)	64502
O2	N1	3.14(2)	64502	O11	O22	3.10(2)	55501
O12	O21	2.75(2)	74502	O13	O22	3.06(2)	55501
O21	N2	2.86(2)	65502	O21	O22	2.89(3)	55501
O21	N11	2.99(2)	55501	O22	N12	2.96(2)	55501

a) Intermolecular distances between O and N which are shorter than 3.20Å are listed. b) The atom designator code. The 5-digit number is a composite of three one digit numbers and one two digit number: TA(1st)+TB(2nd)+TC(3rd)+SN(4th and 5th). TA, TB, and TC are the lattice translation along cell edges a, b and c, where digit of 5 indicates the origin cell. The SN is symmetry operation.
Symmetry operators: (1) x,y,z. (2) $-x,1/2+y,-z$.

bond may be stabilized by five-membered chelation. The phenyl group of mandelate rises up to the axial direction to the coordination plane. Such a direction possibly resulted from the crystal packing. Consequently, the *R*-md has δ-gauche conformation in the solid state though λ-gauche conformation is suggested in the aqueous solution by the CD spectra.

The crystal and molecular structures of [Pt(*RR*-dach)(*S*-md)]·H_2O are depicted in Figs. 4 and 5, respectively. The bond lengths and angles are listed in Table 5. The structural feature is analogous to that of [Pt(*RR*-dach)(*R*-md)]·H_2O. Two complexes and two water molecules also have crystallographic independence. The configurations of the ligands are retained in comparison with the corresponding free amine or acid. The *RR*-dach ligand has a λ-gauche conformation. The md ligand is bound to the platinum atom to form a five-membered chelate of λ-gauche conformation. The phenyl group rises up to the axial direction to the coordination plane.

Both isomers have a typical square-planar coordination, except for rather small N-Pt-N and O-Pt-O angles due to the five-membered chelation. As a whole, the structural features of both diastereomers (bond lengths and angles) are very similar.

The hydrogen bonds are listed in Table 6. Between the alcoholates and the water molecules, strong hydrogen bonds are formed. The hydrogen-bonding patterns of both isomers have many similarities to each other, though the hydrogen-bond distributions in a pair of diastereomers are slightly different. Fig. 6 shows that only [Pt(*RR*-dach)(*R*-md)]·H_2O has a hydrogen-bond between carboxylate oxygen and amine nitrogen, directly reflecting the configurations of the two diastereomers. Not only the IR spectra,

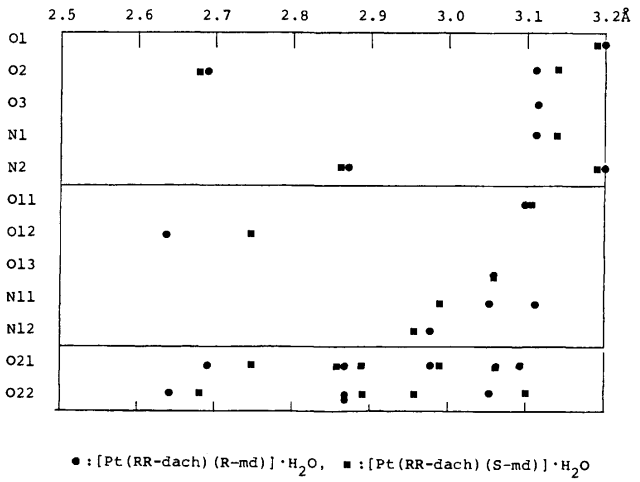

Fig. 6. Hydrogen-bond distributions of two isomers.

but also the solubilities of the diastereomers are practically different from each other. The complex [Pt(*RR*-dach)(*S*-md)]·H_2O is a more soluble isomer in water or dmso (see Experimental). These experimental facts agree well with the above difference in the hydrogen-bond distributions.

Antitumor Activities of [Pt(dach)(md)] Isomers. The results of animal tests against mice luekemia L1210 are listed in Table 7. The complexes show antitumor activities to a certain extent, but not completely. On the other hand, the toxicities are greatly reduced, compared to cis-platin. The four optical isomers exhibit differeences in antitumor activities. Complex [Pt(*RR*-dach)(*R*-md)] is effective over a wide range of dose where its enantiomer, [Pt(*SS*-dach)(*S*-md)], shows no activity. The antitumor activity of [Pt(*RR*-dach)(*S*-md)] is similar to that of [Pt(*SS*-

Table 7. Antitumor Activities against Mice Leukemia L1210

Isomer	T/C (%)					
	Dose (mg/kg)					
	400	200	100	50	25	12.5
RR-R	Toxic	126 P	190 P	162 P	137 P	109
RR-S	138 P	160 P	132 P			
SS-R	126 P	156 P	108			
SS-S	Toxic	124	114			

T/C value over 125 was evaluated as antitumor active and indicated with P.

dach)(*R*-md)], but the toxic dose is different.

These results show that the chiralities of not only the carrier ligands, but that the leaving groups influence the antitumor activities of the complexes. It is also likely that the solubilities of the complexes influence the activities.

References

1) B. Rosenberg, L. Van Camp, J. E. Trosko, and V. H. Mansour, *Nature (London)*, **222**, 385 (1969).

2) M. J. Cleare and J. D. Hoeschele, *Bioinorg. Chem.*, **2**, 187 (1973).

3) T. A. Connors, M. Jones, W. C. J. Ross, T. D. Braddock, A. R. Khokhar, and M. L. Tobe, *Chem. Biol. Interact.*, **5**, 415 (1972).

4) G. R. Gale, E. M. Walker, Jr., L. M. Atkins. A. B. Smith, and S. J. Meischen, *Res. Commun. Chem. Pathol. Pharmacol.*, **7**, 529 (1974).

5) Y. Kidani, M. Noji, and T. Tashiro, *Gann*, **71**, 637 (1980).

6) K. Maeda, T. K. Miyamoto, Y. Sasaki, and T. Tashiro, *Inorg. Chim. Acta*, **153**, 137 (1988).

7) K. Okude, H. Ichida, T. K. Miyamoto, Y. Sasaki, and T. Tashiro, *Chem. Lett.*, **1989**, 119.

8) T. Totani, K. Aono, M. Komura, and Y. Adachi, *Chem. Lett.*, **1986**, 429.

9) L. S. Hollis, A. R. Amunsen, and E. W. Stern, *J. Am. Chem. Soc.*, **107**, 274 (1985).

10) N. W. Alcock, A. W. G. Platt, and P. G. Pringle, *Inorg. Chim. Acta*, **128**, 215 (1987).

11) C. D. Montgomery, N. C. Payne, and C. J. Willis, *Inorg. Chem.*, **26**, 519 (1987).

12) F. Galsbøl, P. Steenbøl, and B. S. Sørensen, *Acta Chem. Scand.*, **26**, 3605 (1972).

13) B. Lippert, C. J. L. Lock, B. Rosenberg, and M. Zvagulis, *Inorg. Chem.*, **16**, 1525 (1977).

14) G. J. Gilmore, Mithril: A Computer Program for the Automatic Solution of Crystal Structure from X-ray Data, Univ. of Glasgow, Scotland (1983).

15) P. N. Swepston, TEXSAN Software, Molecular Structure Coorporation, College Station, Texas, USA (1986).

16) International Tables for X-ray Crystallography Vol. IV., Kynoch Press, Birmingham (Present distributor Kluwer Academic Publishers, Dordrecht.) (1974).

17) E. Lippert, *ACS Symp. Ser.*, **209**, 147 (1983).

18) L. S. Hollis and S. J. Lippard, *J. Am. Chem. Soc.*, **105**, 3494 (1983).

19) T. G. Appleton, R. D. Berry, C. A. Davis, J. R. Hall, and H. A. Kilin, *Inorg. Chem.*, **23**, 3514 (1984).

20) R. Hakansson and S. Gronowitz, *Tetrahedron*, **32**, 2973 (1976).

21) M. Noji, K. Okamoto, Y. Kidani, and T. Tashiro, *J. Med. Chem.*, **24**, 508 (1981).

22) C. J. Hawkins and E. Larsen, *Acta Chem. Scand.*, **19**, 185 (1965).

23) W. I. Sundquist, K. A. Ahmed, L. S. Hollis, and S. J. Lippard, *Inorg. Chem.*, **26**, 1524 (1987).

24) "The Aldrich Library of Infrared Spectra III," ed. by C. J. Pouchert, Aldrich Chemical Company, Milwaukee (1981).

25) "The Sadtler Standard Spectra," Vol. 7, No. 6205.

26) C. K. Johnson. ORTEP II. Report ORNL-5138. Oak Ridge National Laboratory, Tennessee, USA (1976).

27) F. A. Cotton, L. R. Falvello, and C. A. Murillo, *Inorg. Chem.*, **22**, 382 (1983).

28) P. A. Agaskar, F. A. Cotton, L. R. Falvello, and S. Han, *J. Am. Chem. Soc.*, **108**, 1214 (1986).

29) F. R. Hartley, "The Chemistry of Platinum and Palladium," Applied Science Publishers Ltd., London (1973), Chap. 8.

 © 1989 The Chemical Society of Japan Bull. Chem. Soc. Jpn., 62, 3247—3251 (1989)

Synthetic, Spectroscopic and X-Ray Crystallographic Studies of Bivalent Metal Complexes with Amino Acids Having a Thiazolidine Ring. III. The Properties of Bivalent Metal Complexes with Racemic 2-Thiazolidinecarboxylic Acid and the Structure of *trans*-Diaquabis-(2-thiazolidinecarboxylato)zinc(II)

Makoto NAGASE, Yasuhiko YUKAWA,† Yoshie INOMATA,* and Toshio TAKEUCHI
Department of Natural Sciences, Faculty of Science and Technology, Sophia University, 7-1 Kioi-cho, Chiyoda-ku, Tokyo 102
(Received March 4, 1989)

Several complexes with the formula of $ML_2 \cdot 2H_2O$ (HL=racemic 2-thiazolidinecarboxylic acid, S-CH_2-CH_2-NH-CH-COOH, M=Co, Ni, Zn), anhydrous CdL_2 and $CdCl_2(HL)$ were synthesized and characterized by means of their infrared absorption and reflection spectra, magnetic susceptibility, thermal analyses, and powder X-ray patterns. In addition, the crystal structure of $ZnL_2 \cdot 2H_2O$ was also determined. Crystals of this complex are monoclinic, with the space group $P2_1/n$ with a=7.224(1), b=18.246(4), c=5.306(1) Å, and β=104.57(1)° and Z=2. The structure was solved by the heavy atom technique and refined by a block-diagonal least-squares method to a final R value of 0.056 for 1774 unique reflections. The zinc environment consists of two carboxylic oxygen atoms and two thiazolidine nitrogen atoms from two centrosymmetrically related organic ligands in a square-planar arrangement. Two water molecules in the axial positions complete a tetragonal bipyramidal coordination around the metal atom. No sulfur atom is coordinated to the zinc atom. The infrared absorption spectra and the structure of this zinc(II) complex are discussed in comparison with those of zinc(II) complexes with (*S*)-4-thiazolidinecarboxylic acid and racemic 4-thiazolidinecarboxylic acid.

As 4-thiazolidinecarboxylic acid has been reported to induce the restoration of the contact inhibition of tumor cells.[1-3] Tatarowski et al.[4] investigated the NMR and crystallography of zinc(II) complexes with 4-thiazolidinecarboxylic acid and 2-thiazolidinecarboxylic acid. Then we ourselves investigated in detail the coordination behavior of racemic and (*S*)-4-thiazolidinecarboxylic acid toward bivalent metals in the solid state.[5,6] These studies have clearly demonstrated that whether or not the nitrogen atom of the thiazolidine ring coordinates to metal ions depends on the pH of the solution used in the preparation. For complexes which have been prepared in a basic aqueous solution, both a carboxylato oxygen atom and the nitrogen atom bind to metal ions.

In the zinc(II) complex with (*S*)-4-thiazolidinecarboxylic acid prepared at pH<7, the zinc atom is ligated with a carboxylato oxygen atom of a (*S*)-thiazolidinium-4-carboxylate, which has a zwitter ion structure, with two carboxylato oxygen atoms, and with the nitrogen atom of a (*S*)-4-thiazolidinecarboxylate anion and a chlorine atom;[5] in dichlorobis(thiazolidinium-4-carboxylate)zinc(II), the zinc atom seems to be ligated through two chlorine atoms and the carboxylato oxygen atom of the racemic thiazolidinium-4-carboxylate, which has a zwitter ion structure.[6]

In order to discuss the effect of the position of the carboxyl group in thiazolidinecarboxylic acid on the structures of complexes, we have now synthesized it by two methods and characterized bivalent metal complexes with racemic 2-thiazolidinecarboxylic acid. The structure of *trans*-diaquabis(2-thiazolidinecarboxylato)zinc(II) has also been determined. Moreover, we have summarized the coordination behavior of metal complexes with (*S*)-4-thiazolidinecarboxylic and racemic acid as well as with racemic 2-thiazolidinecarboxylic acid.

Experimental

Preparation of Racemic 2-Thiazolidinecarboxylic Acid.[7] An ethanol solution (59.2 g) containing 25% of glyoxylic acid was slowly added to 200 cm^3 of an ethanol solution including 35.5 g (0.31 mol) of cysteamine hydrochloride. This mixed solution was then refluxed for 90 minutes at 80 °C. After the solution had then cooled until room temperature, colorless crystals were precipitated. After these crystals had been separated, they were recrystallized from water and dried in a silica-gel desiccator.

Preparation of Complexes. $CoL_2 \cdot 2H_2O$ was prepared by adding 0.01 mol of fresh cobalt(II) hydroxide to a hot aqueous solution containing 0.02 mol of racemic 2-thiazolidinecarboxylic acid. After the solution had been stirred for an hour in a water bath at 60 °C, the precipitate which formed was filtered, washed with water, and dried in vacuo for six hours at room temperature. $NiL_2 \cdot 2H_2O$, $ZnL_2 \cdot 2H_2O$, and CdL_2 were prepared from the corresponding metal hydroxides by the same procedure as was used for the cobalt(II) complex. The crystal used for the single crystal X-ray analysis was prepared by keeping the saturated aqueous solution for two weeks at room temperature.

$CdCl_2(HL)$ was prepared by adding 0.01 mol of cadmium-

† Present address: Division of Chemistry, General Education Department, Niigata University, 8050 Ikarashi, Ninocho, Niigata 950-21.

(II) chloride to an aqueous solution containing 0.01 mol of this ligand. The mixed solution, after it had been stirred and condensed for an hour at 80 °C, was allowed to stand for two weeks. The crystals thus precipitated were dried in vacuo for six hours at room temperature.

Deuterated complexes were obtained by recrystallization in D_2O.

Physical Measurements. The powder diffuse reflection and infrared absorption spectra, magnetic moments, and thermal analysis were obtained by the methods described in previous papers.[5,6]

Single Crystal X-Ray Analysis. The reflection intensities were collected by the ω-2θ scan technique on a Rigaku AFC-6A automated four-circle X-ray diffractometer with graphite monochromated Mo$K\alpha$ radiation. 1774 reflections with $|F_o|>3\sigma(|F_o|)$ were used for the refinement. The intensities were corrected for the Lorentz and polarization factors: however, no corrections were made for absorption and extinction because $\mu r(<1)$.

All the calculations were carried out on a HITAC M-680H computer at the Computer Center of the University of Tokyo, using the local version of UNICS.[8] The scattering factors were taken from the tables.[9]

The structure was solved by the heavy-atom method and refined by a block-diagonal least-squares method. The positions of the zinc and oxygen atoms were obtained from a three-dimensional Patterson map, while the positions of all the other non-hydrogen atoms were successively located by Fourier syntheses. The positions of the hydrogen atoms were obtained by means of difference-Fourier syntheses. The weighting scheme was $w=1/[\{\sigma(|F_o|)\}^2+(0.02\times|F_o|)^2]$. In the last cycle of the refinement with anisotropic temperature factors for all non-hydrogen atoms, all the parameter shifts were less than one-third of the corresponding standard deviations. The final R value ($R=\sum||F_o|-|F_c||/\sum|F_o|$) was 0.056.

Results and Discussion

The results obtained from the elemental analyses and those of the reflection spectra and magnetic moment calculations are listed in Tables 1 and 2 respectively. These results and the infrared spectra suggest that there are two types of complexes: A and B. The A type is $ML_2\cdot nH_2O$ (M=Co(II), Ni(II), Zn(II), Cd(II), HL=racemic 2-thiazolidinecarboxylic acid n=0, 2). The B type is $CdCl_2$(HL).

The reflection spectra and magnetic moments are similar to those of the corresponding complexes with racemic 4-thiazolidinecarboxylic acid. From these

Table 1. Elemental Analyses of Racemic 2-Thiazolidinecarboxylic Acid (HL) and Its Metal Complexes

Compound	Found (Calcd) /%				
	H	C	N	M	Cl
HL	5.54 (5.30)	35.45 (36.07)	10.52 (10.52)		
$CoL_2\cdot 2H_2O$	4.25 (4.49)	26.93 (26.74)	7.65 (7.80)	16.4 (16.40)	
$NiL_2\cdot 2H_2O$	4.57 (4.49)	27.03 (26.76)	7.87 (7.80)	16.5 (16.35)	
$ZnL_2\cdot 2H_2O$	4.43 (4.41)	26.20 (26.27)	7.48 (7.66)	17.8 (17.88)	
CdL_2	3.24 (3.21)	25.29 (25.50)	7.32 (7.44)	29.1 (29.84)	
$CdCl_2$(HL)	2.38 (2.23)	14.79 (15.18)	4.18 (4.43)	35.6 (35.52)	22.40 (21.67)

Table 2. Magnetic Moments and Powder Diffuse Reflection Spectra of Metal Complexes with Racemic 2-Thiazolidinecarboxylic Acid

	Co(II)	Ni(II)
Magnetic moment μ_{eff}/BM	4.67 (3.87)[a]	3.34 (2.83)[a]
Reflection spectra λ/nm	1050 ($^4T_{2g}\leftarrow{}^4T_{1g}$)	920 ($^3T_{2g}\leftarrow{}^3A_{2g}$)
	535 ($^4A_{2g}\leftarrow{}^4T_{1g}$)	626 ($^3T_{1g}\leftarrow{}^3A_{2g}$)
	450 ($^4T_{1g}(P)\leftarrow{}^4T_{1g}$)	385 ($^1A_{1g}\leftarrow{}^3A_{2g}$)
		356 ($^3T_{1g}(P)\leftarrow{}^3A_{2g}$)

a) Spin-only value.

Table 3. Temperature Range of Decomposition and Mass Loss of Racemic 2-Thiazolidinecarboxylic Acid Complexes

Complex	Temperature range/°C	Thermal reaction	Mass loss/% Observed	Calculated
$CoL_2\cdot 2H_2O$	141—195	Endo	10.7	10.0
	216—426	Exo		
	435—525	Exo	78.6	79.1[a]
$NiL_2\cdot 2H_2O$	159—219	Endo	10.8	10.0
	219—438	Exo		
	447—549	Exo	73.1	79.2[a]
$ZnL_2\cdot 2H_2O$	117—177	Endo	9.4	9.8
	252—516	Exo		
	555—666	Exo	77.1	77.5[a]
CdL_2	249—459	Exo	59.0	61.7[b]
	745—	Exo		65.9[a]
$CdCl_2$(HL)	190		Melt	
	190—265	Exo		
	470—720	Exo		
	790—920	Exo	Sublimated	

a) As metal oxide. b) As metal sulfide.

assignments of the reflection spectra, it seems that the cobalt(II) and nickel(II) complexes have an octahedral configuration, as is suggested by reference to the X-ray analyses for diaqua((*S*)-4-thiazolidinecarboxylato)-zinc(II)[4] and diaqua(2-thiazolidinecarboxylato)-zinc(II) to be discussed below and by the reflection spectra of other complexes.[10-12]

Thermal Analysis. The temperature range and the percentage of the mass loss obtained from the TG and DTA curves are summarized in Table 3. The cobalt(II), nickel(II), and zinc(II) complexes release two molecules of water in the first endothermic reaction. Thereafter these complexes change to the corresponding metal oxides in an exothermic reaction.

The cadmium(II)-A complex gives two exothermic reaction steps with a mass loss. In the first step, the cadmium(II)-A complex becomes cadmium sulfide; then this sulfide seems to change to cadmium oxide in the second step.

For the cadmium(II)-B complex, an endothermic peak is observed at about 190 °C. This peak is assigned to the melt of this complex. After that, the exothermic reaction occurs immediately, with a mass loss, and the complex decomposes to cadmium halide. Finally, after several exothermic reactions with a gradual mass loss, no residual is obtained. In these steps, cadmium halide changes into cadmium oxide, which then sublimes. The same behavior is observed for dichloro(4-hydroxy-L-proline)cadmium(II).[13]

Infrared Absorption Spectra. The infrared spectral data are listed in Table 4. The assignments of the observed frequencies have been made by referring to (*S*)-4-thiazolidinecarboxylic acid, racemic 4-thiazolidinecarboxylic acid, and their metal complexes.[5,6] In the zinc(II) complex, the absorption bands are assigned through comparison with its deuterated compound.

Racemic 2-Thiazolidinecarboxylic Acid: Some bands shift to a lower frequency region on deuteration. They are assigned to the NH_2^+ stretching and bending vibrations. The bands at 1610 cm^{-1} and at 1360 cm^{-1} are assigned to the COO^- antisymmetric and symmetric stretching vibrations respectively. Thus, this ligand has a zwitter ion structure.

Complexes: For the zinc(II) complex, some absorption bands which can be observed in the ligand disappear, while new bands which shift to a lower frequency region on deuteration can be observed. These are assigned to the NH stretching and bending vibrations.

The antisymmetric and symmetric stretching vibrations of the carboxyl group shift to higher frequency regions than those of the free ligand. Therefore, in the zinc(II) complex, each zinc atom is coordinated through a carboxylato oxygen atom and a nitrogen atom of the thiazolidine ring. This fact is confirmed by X-ray analysis.

Since, in the A-type complexes, the C-S stretching vibrations are observed in the same region as for the zinc(II) complex, the sulfur atoms do not seem to be associated with coordination.

The spectra of the cadmium(II)-B complex is different from that of the cadmium(II)-A complex. Some absorption bands due to NH_2^+ vibrations are observed in the same region as those of the free ligand. The antisymmetric and symmetric stretching vibrations of the carboxyl group shift to lower and higher frequency regions respectively than those of the free ligand. The frequency separation between the antisymmetric and symmetric stretching vibrations of the carboxyl group (Δ) is smaller than that of the free ligand.

Deacon and Phillips[14] arrived at the following conclusions on the basis of an examination of the infrared absorption spectra of many acetates and trifluoroacetates with known X-ray crystal structures.[15] Unidentate complexes exhibit Δ values much greater than those of ionic complexes. Chelating (bidentate) complexes exhibit Δ values significantly lower than the ionic values. The Δ values for bridging complexes are close to the ionic values. Therefore, in the cadmium(II)-B complex, two oxygen atoms of the carboxyl group seem to be coordinated with the cadmium atom by either bidentate or bridging types. It has been determined by X-ray analysis that dichloro-(4-hydroxy-L-proline)cadmium(II)[13] and dichloro-(L-proline)cadmium(II) hydrate[16] have bridging carboxyl groups and that dichloro(*N*-methylglycine)-cadmium(II)[17] has a bidentate carboxyl group.

Structure of $ZnL_2 \cdot 2H_2O$. The crystal data are

Table 4. Assignments of Infrared Absorption Spectra of Racemic 2-Thiazolidinecarboxylic Acid (HL) and Its Complexes (cm^{-1})

HL	Co(II)	Ni(II)	Zn(II)	Cd(II)-A	Cd(II)-B	Assignments
	3290	3280	3275	3200		NH str.
3035					3180	NH_2^+ srt.
1610	1614	1612	1613	1582	1596	COO^- asym. str.
1429					1430	NH_2^+ scissors
1360	1374	1380	1378	1407	1380	COO^- sym. str.
1315					1320	NH_2^+ wagging
580	569	576	568	566	583	C-S str.

given in Table 5. The final atomic parameters are listed in Table 6.[18] The bond lengths and bond angles are shown in Tables 7 and 8 respectively. A perspective drawing of the complex, together with the numbering scheme of the non-hydrogen atoms, is shown in Fig. 1. The projection of the unit cell along the b axis is shown in Fig. 2. The zinc atom lies on a center of symmetry and is octahedrally trans-coordinated: two nitrogen atoms of two thiazolidine rings, two oxygen atoms of two carboxyl groups, and two oxygen atoms of two water molecules. In diaquabis((*S*)-4-thiazolidinecarboxylato)zinc(II), however, the zinc atom was octahedrally coordinated by two oxygen and two nitrogen atoms of two ligands and two water molecules in the cis position.[4] The bond distance of Zn-O(w) is longer than that of diaquabis(4-thiazolidinecarboxylato)zinc(II), which

Table 5. Crystal Data of $[ZnL_2(H_2O)_2]$

$ZnC_8H_{16}N_2O_6S_2$	
F. W.	365.76
Monoclinic	
$P2_1/n$	
a/Å	7.224(1)
b/Å	18.246(4)
c/Å	5.306(1)
β/°	104.57(1)
V/Å^3	676.9(2)
Z	2
D_m/g cm^{-3}	1.79
D_x/g cm^{-3}	1.80
λ(Mo $K\alpha$)/Å	0.71073
μ/cm^{-1}	21.7

Table 6. Final Positional Parameters ($\times 10^4$) and Equivalent Isotropic Temperature Factors (B_{eq}/Å^2),[a] for $[ZnL_2(H_2O)_2]$, with the Estimated Standard Deviations in Parentheses[b]

Atom	x	y	z	B_{eq}/Å^2
Zn	0.0(0)	0.0(0)	0.0(0)	2.13
S	3867.4(21)	−1935.0(7)	680.8(29)	5.34
O(W)	1894(3)	673(1)	3064(5)	2.58
O(1)	1941(3)	−71(1)	−2243(5)	2.64
O(2)	4355(4)	−724(2)	−2850(5)	3.43
N(3)	1531(4)	−920(2)	1834(5)	2.07
C(4)	3299(5)	−970(2)	949(6)	2.31
C(5)	528(6)	−1632(2)	1444(9)	3.62
C(6)	2023(7)	−2222(2)	2192(9)	4.00
C(7)	3197(4)	−561(2)	−1594(6)	2.12

a) The equivalent isotropic temperature factors for non-hydrogen atoms were computed using the following expression:

$$B_{eq}=4/3(B_{11}a^2+B_{22}b^2+B_{33}c^2+B_{12}ab\cos\gamma+B_{13}ac\cos\beta+B_{23}bc\cos\alpha).$$

The B_{ij}'s are defined by:

$$\exp[-(h^2B_{11}+k^2B_{22}+l^2B_{33}+klB_{23}+hlB_{13}+hkB_{12})].$$

b) The final atomic parameters of hydrogen atoms have been deposited.[18]

Table 7. Interatomic Distances of $[ZnL_2(H_2O)_2]$, with the Estimated Standard Deviations in Parentheses

Interatomic distance	l/Å	Interatomic distance	l/Å
Zn-O(W)	2.214(2)	S-C(4)	1.822(4)
Zn-O(1)	2.059(3)	S-C(6)	1.797(6)
Zn-N(3)	2.109(3)	N(3)-C(4)	1.470(5)
		N(3)-C(5)	1.475(5)
O(1)-C(7)	1.259(4)	C(4)-C(7)	1.527(5)
O(2)-C(7)	1.230(5)	C(5)-C(6)	1.506(6)

Table 8. Bond Angles of $[ZnL_2(H_2O)_2]$, with the Estimated Standard Deviations in Parentheses

Bond angle	ϕ/°	Bond angle	ϕ/°
O(W)-Zn-O(1)	94.3(1)	S-C(4)-N(3)	108.4(2)
O(W)-Zn-N(3)	87.0(1)	S-C(4)-C(7)	111.4(3)
O(1)-Zn-N(3)	82.1(1)	N(3)-C(4)-C(7)	113.5(3)
C(4)-S-C(6)	92.3(2)	N(3)-C(5)-C(6)	107.3(3)
Zn-O(1)-C(7)	115.8(2)	S-C(6)-C(5)	103.7(3)
Zn-N(3)-C(4)	107.4(2)	O(1)-C(7)-O(2)	124.4(3)
Zn-N(3)-C(5)	117.0(2)	O(1)-C(7)-C(4)	117.4(3)
C(4)-N(3)-C(5)	109.7(3)	O(2)-C(7)-C(4)	118.2(3)

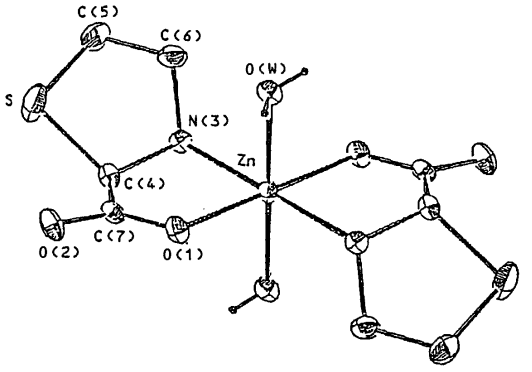

Fig. 1. The perspective drawing of $[ZnL_2(H_2O)_2]$ and the numbering scheme of non-hydrogen atoms.

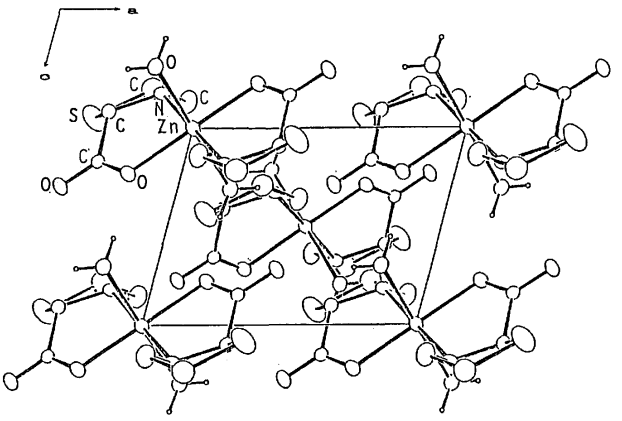

Fig. 2. The molecular packing of $[ZnL_2(H_2O)_2]$ along the b axis.

Table 9. Metal Complexes with Thiazolidinecarboxylic Acids and Coordination Behavior

Type	Metal	(*S*)-4-HL	Racemic-4-HL	Racemic-2-HL
A	Cobalt	CoL_2 (N,O)chelate	$CoL_2 \cdot 2H_2O$ (N,O)chelate	$CoL_2 \cdot 2H_2O$ (N,O)chelate
	Nickel	$NiL_2 \cdot 2H_2O$ (N,O)chelate	$NiL_2 \cdot 2H_2O$ (N,O)chelate	$NiL_2 \cdot 2H_2O$ (N,O)chelate
	Zinc	$ZnL_2 \cdot 2H_2O$ (N,O)chelate	$ZnL_2 \cdot 2H_2O$ (N,O)chelate	$ZnL_2 \cdot 2H_2O$ (N,O)chelate
	Cadmium	CdL_2 (N,O)chelate	CdL_2 (N,O)chelate	CdL_2 (N,O)chelate
B	Zinc	ZnClL(HL) Cl,O,(N,O[a])chelate	$ZnCl_2(HL)_2$ Cl,O	—[b]
	Cadmium	—[b]	—[b]	$CdCl_2(HL)$ Cl,O
		Ref. 5	Ref. 6	This Work

(*S*)-4-HL: (*S*)-4-thiazolidinecarboxylic acid. Racemic-4-HL: racemic 4-thiazolidinecarboxylic acid. Racemic-2-HL: racemic 2-thiazolidinecarboxylic acid. a) Bridging atom. b) Attempts to prepare these complexes in our laboratory were unsuccessful.

was determined by Tatarowski et al.,[4] while the bond distances of Zn-O(1) 2.059(3) and Zn-N(3) 2.109(3) Å are shorter than those of that complex (Zn-O, 2.137(8) and 2.172(8) Å; Zn-N, 2.149(12) and 2.134(12) Å).

The bond angle values of O(1)-Zn-N(3)(82.1(1)°) and O(w)-Zn-O(1)(94.3(1)°) are a little larger than those of diaqua(4-thiazolidinecarboxylato)zinc(II) (78.1(4) and 92.4(4)°). The differences between these and Tatarowski's results are due to the different geometry— that is, cis or trans.

Table 9 summarizes the data for metal complexes with (*S*)-4-thiazolidinecarboxylic acid, racemic 4-thiazolidinecarboxylic acid, and racemic 2-thiazolidinecarboxylic acid, which have been prepared in our laboratory, and the atoms coordinated to the metal atoms.

As for all A-type complexes, the nitrogen atom and an oxygen atom coordinate to the metal ion and form a chelate ring; in some B-type complexes, except for the zinc(II) complex with (*S*)-4-thiazolidinecarboxylic acid, an oxygen atom and chlorine atoms coordinate to the zinc atom. Therefore, in A-type complexes there are no effects of the position of the carboxyl groups in thiazolidinecarboxylic acids on the coordination of the complexes.

The authors wish to express their thanks to Professor Akira Ouchi of the University of Tokyo for the X-ray-intensity data. They would also like to thank Dr. F. S. Howell and Mr. H. Yamaguchi of Sophia University for their helpful advice and for correcting this manuscript.

References

1) M. Gosálvez, *Proc. Am. Assoc. Cancer Res.*, **20**, 17 (1979).

2) M. Gosálvez, L. Pecci, and C. Vivero, *Biochem. Soc. Trans.*, **6**, 659 (1978).

3) A. Burgarolas and M. Gosálvez, *Lancet*, **1**, 68 (1980).

4) T. Tatarowski, M. Kubiak, J. Morawiec, and H. Kozlowski, *Inorg. Chim. Acta*, **93**, L3 (1984).

5) M. Nagase, Y. Yukawa, Y. Inomata, and T. Takeuchi, *Bull. Chem. Soc. Jpn.*, **61**, 775 (1988).

6) M. Nagase, Y. Yukawa, Y. Inomata, and T. Takeuchi, *Inorg. Chim. Acta*, **152**, 211 (1988).

7) T. Shigematsu, K. Yoshida, M. Nakazawa, H. Kasugai, and M. Tsuda, *Jpn. Kokai Tokkyo Koho*, 80 43034 (Cl.C07D277/04); *Chem. Abstr.*, **94**, 103346n (1981).

8) "The Universal Crystallographic Computation Program System (UNICS)," ed. by T. Sakurai, Crystallographic Society of Japan, Tokyo (1967).

9) "International Tables for X-Ray Crystallography," Kynoch Press, Birmingham, U. K. (1974), Vol. IV.

10) R. A. Haines and M. Reimer, *Inorg. Chem.*, **12**, 1482 (1973).

11) Y. Inomata, T. Takeuchi, and T. Moriwaki, *Inorg. Chim. Acta*, **68**, 187 (1983).

12) K. Ueno, "Kireito Kagaku," Vol. 1, Nanko-do, Tokyo (1976), p. 91.

13) Y. Yukawa, Y. Inomata, T. Takeuchi, M. Shimoi, and A. Ouchi, *Bull. Chem. Soc. Jpn.*, **55**, 3135 (1982).

14) G. B. Deacon and R. J. Phillips, *Coord. Chem. Rev.*, **33**, 227 (1980).

15) K. Nakamoto, "Infrared and Raman Spectra of Inorganic and Coordination Compounds," 4th ed, John Wiley and Sons, New York (1986), p. 232.

16) Y. Yukawa, Y. Inomata, and T. Takeuchi, *Bull. Chem. Soc. Jpn.*, **56**, 2125 (1983).

17) J. Yamada, H. Yamaguchi, Y. Inomata, and T. Takeuchi, 56th National Meeting of the Chemical Society of Japan, Tokyo, April 1988. Abstr. 3VA17.

18) The final positional parameters and equivalent isotropic temperature factors of the hydrogen atoms, the final thermal parameters, and the final F_o—F_c table are deposited as Document No. 8895 at the Office of the Editor of the Bulletin of the Chemical Society of Japan.

Facial-Meridional Isomerization of Some Tris-(β-diketonato)ruthenium(III) Complexes

Kyohko KOBAYASHI, Yuichi SATSU, Yoshimasa HOSHINO, Shinji ARAI, Kiyoshi HATAKEYAMA, Akira ENDO, Kunio SHIMIZU, and Gen P. SATÔ*
Department of Chemistry, Faculty of Science and Technology, Sophia University, 7-1 Kioicho, Chiyoda-ku, Tokyo 102
(Received May 31, 1989)

Nine complexes of type $[Ru^{III}(R\text{-}CO\text{-}CH\text{-}CO\text{-}R')_3]$ were examined; only those with R=$-CF_3$ underwent the facial-meridional isomerization in *N,N*-dimethylformamide (DMF) at the reflux temperature. Qualitative examination of the occurrence of isomerization of the complex with R=$-CF_3$ and R'=$-CH_3$ in various solvents supports the presence of solvent-assisted bond-rupture mechanisms. This complex did not isomerize photochemically in acetonitrile. The isomerization of four complexes with R=$-CF_3$ and R'=$-CH_3$, $-C_2H_5$, $-CH(CH_3)_2$, and $-C(CH_3)_3$ in DMF at 70—100 °C followed the reversible first-order kinetics. The equilibrium constants, which were temperature independent, decreased from 4.27 to 1.74 in the order cited above. The enthalpies of activation, ranging from 66.4 kJ mol^{-1} (R'=$-CH(CH_3)_2$) to 96.0 kJ mol^{-1} (R'=$-CH_3$), depended linearly on the atomic bond populations of the Ru-O bonds calculated by means of a modified extended Hückel method.

The facial-meridional isomerization reactions of tris(unsymmetrical β-diketonato)metal chelates have been studied in a number of cases.[1-8] Tris(β-diketonato)ruthenium(III) complexes are known to behave as "slow" complexes in the isomerization and racemization reactions.[4,5] These reactions are believed to proceed through intramolecular, bond-rupture mechanisms. Recently Hoshino et al.[9] reported that the rearrangement reactions between the three geometrical isomers of acetylacetonatobis(4,4,4-trifluoro-1-phenyl-1,3-butanedionato)ruthenium(III) proceeded through certain types of bond-rupture mechanisms.

The rate of the facial-meridional isomerization reaction is largely enhanced by the presence of a trifluoromethyl group at the β-position of the diketone.[4] It is of interest to see how the substituents of the β-diketonato ligands affect the rate of the isomerization.

This report presents qualitative observations on the facial-meridional isomerization reactions of a series of nine tris(substituted acetylacetonato)ruthenium(III) complexes and quantitative kinetic data for four of them.

Experimental

Preparation of Complexes. The complexes studied here are listed in Table 1 together with the ligand names. They will be cited by the numbers given there. The preparation of **1**, **4**, and **6—9** has been described previously.[10] Each of them, except **6** and **7**, was obtained as a mixture of geometri-

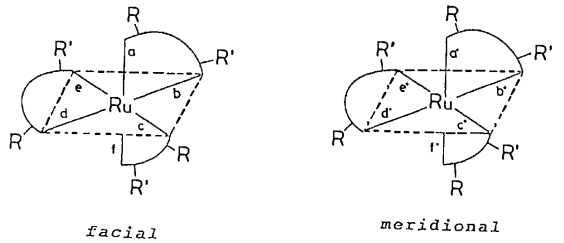

Fig. 1. Geometrical isomers of a tris(unsymmetical β-diketonato)ruthenium complex and their bond designations.

Table 1. Numbers of the Complexes $[Ru^{III}(R\text{-}CO\text{-}CH\text{-}CO\text{-}R')_3]$, Their Reactions, and the Ligand Names

No.	R	R'	Reaction in DMF[a]	Ligand name
1	$-CF_3$	$-CH_3$	i	1,1,1-Trifluoro-2,4-pentanedionato
2[b]	$-CF_3$	$-C_2H_5$	i	1,1,1-Trifluoro-2,4-hexanedionato
3[b]	$-CF_3$	$-CH(CH_3)_2$	i	1,1,1-Trifluoro-5-methyl-2,4-hexanedionato
4	$-CF_3$	$-C(CH_3)_3$	i	1,1,1-Trifluoro-5,5-dimethyl-2,4-hexanedionato
5[b]	$-C_2H_5$	$-CH_3$	n	2,4-Hexanedionato
6[c]	$-CH_3$	$-C(CH_3)_3$	n	5,5-Dimethyl-2,4-hexanedionato
7[c]	$-CF_3$	$-C_4H_3S$	r	4,4,4-Trifluoro-1-(2-thienyl)-1,3-butanedionato
8	$-CF_3$	$-C_4H_3O$	r	4,4,4-Trifluoro-1-(2-furyl)-1,3-butanedionato
9	$-CF_3$	$-C_6H_5$	r	4,4,4-Trifluoro-1-phenyl-1,3-butanedionato

a) Reaction observed when the complex was refluxed in DMF: i, isomerization; n, no isomerization; r, reduction to the Ru^{II} species. b) New compound. c) Only the meridional form was obtained.

cal isomers: the facial and the meridional forms (Fig. 1). The samples of **6** and **7**, however, contained only the meridional forms. The isomeric mixtures of **2**, **3**, and **5** were prepared by means of the "ruthenium blue solution" method.[10] 1,1,1-Trifluoro-2,4-hexanedione and 1,1,1-trifruoro-5-methyl-2,4-hexanedione were prepared according to the method of Reid and Calvin,[11] while 2,4-hexanedione was purchased from Dojindo Laboratories.

Isolation of Isomers. The isomeric mixture of **1**, dissolved in a small volume of benzene, was applied to a column of Merck Kieselgel 60 and developed with a benzene-hexane mixture (volume ratio, 5 : 8). Fractions containing each of the pure isomers were combined, and the solvent was evaporated off. The residue was dissolved in ethanol. Crystals of each isomer were obtained on concentrating the ethanolic solution. The fractions containing incompletely separated isomers were collected and concentrated; the isomers therein were then separated by means of preparative thin-layer chromatography on Merck Kieselgel 60 plate (1 mm thick, 20×20 cm), developing agent being a benzene-hexane mixture (volume ratio, 1 : 1). Separation of the isomers of **2**, **3**, **4**, and **8** was carried out similarly on the silica-gel column with benzene-hexane mixtures (the volume ratios were 1 : 9 for **2** and **3**, 1 : 4 for **4**, and 1 : 1 for **8**). The meridional isomer preceded the facial isomer in every case. In the case of **5**, only partial separation was achieved by means of Kieselgel 60—chloroform preparative thin-layer chromatography: the meridional form was completely separated from the facial isomer, but the latter could not be obtained in pure state. Separation of the isomers of **9** has been described previously.[12] No attempt was made at resolving the optical isomers.

Complexes **2**, **3**, and **5** are new compounds. Their elemental analyses and ^{1}H NMR data are as follows: **2** Found: C, 35.73 (*fac*) and 35.79 (*mer*); H, 2.89 (*fac*) and 2.97% (*mer*). Calcd for $RuC_{18}H_{18}O_6F_9$: C, 35.89; H, 3.01%. **3** Found: C, 39.05 (*fac*) and 38.94 (*mer*); H, 3.70 (*fac*) and 3.65% (*mer*). Calcd for $RuC_{21}H_{24}O_6F_9$: C, 39.14; H, 3.75%. **5** Found (isomeric mixture): C, 48.82; H, 6.21%. Calcd for $RuC_{18}H_{27}O_6$: C, 49.08; H, 6.18%. ^{1}H NMR ($CDCl_3$, room temp): *fac*-**2** δ=−36.1 (3H, s, CH), −4.8 (3H, s, CH_2), −4.3 (3H, s, CH_2), 3.0 (9H, s, CH_3); *mer*-**2** δ=−52.9 (1H, s, CH), −42.9 (1H, s, CH), −26.2 (1H, s, CH), −13.5 (1H, s, CH_2), −12.2 (1H, s, CH_2), −7.7 (1H, s, CH_2), −7.0 (1H, s, CH_2), −2.5 (1H, s, CH_2), −2.0 (1H, s, CH_2), 1.6 (3H, s, CH_3), 1.8 (3H, s, CH_3), 3.2 (3H, s, CH_3); *fac*-**3** δ=−36.4 (3H, s, COCHCO), −2.7 (3H, s, $(CH_3)_2\underline{C}H$), 2.3 (9H, s, CH_3), 3.7 (9H, s, CH_3); *mer*-**3** δ=−51.2 (1H, s, COCHCO), −41.0 (1H, s, COCHCO), −28.4 (1H, s, COCHCO), −7.9 (1H, s, $(CH_3)_2\underline{C}H$), −4.6 (1H, s, $(CH_3)_2\underline{C}H$), −1.8 (1H, s, $(CH_3)_2\underline{C}H$), 0.6 (3H, s, CH_3), 1.0 (3H, s, CH_3), 1.9 (3H, s, CH_3), 2.0 (3H, s, CH_3), 2.4 (3H, s, CH_3), 3.3 (3H, s, CH_3); *fac*-**5** δ=−31.8 (3H, s, CH), −6.4 (9H, s, CH_3CO), −5.3 (3H, s, $CH_3\underline{C}H_2$), −3.3 (3H, s, $CH_3\underline{C}H_2$), 2.6 (9H, s, $\underline{C}H_3CH_2$) (these were obtained from an isomeric mixture by subtracting the peaks of *mer*-**5**); *mer*-**5** δ=−41.7 (1H, s, CH), −31.5 (1H, s, CH), −22.0 (1H, s, CH), −11.4 (3H, s, CH_3CO), −10.0 (1H, s, $CH_3C\underline{H}_2$), −7.9 (1H, s, $CH_3C\underline{H}_2$), −5.6 (3H, s, CH_3CO), −5.0 (1H, s, $CH_3C\underline{H}_2$), −3.7 (1H, s, $CH_3C\underline{H}_2$), −1.1 (3H, s, CH_3CO), −0.3 (1H, s, $CH_3C\underline{H}_2$), 0.7 (1H, s, $CH_3C\underline{H}_2$), 2.3 (3H, s, $C\underline{H}_3CH_2$), 2.5 (3H, s, $C\underline{H}_3CH_2$), 2.6 (3H, s, $C\underline{H}_3CH_2$). Half-wave potentials for one-electron steps in 0.1 mol dm^{-3} $(C_2H_5)_4NClO_4$-acetonitrile vs. Ag|0.1 mol dm^{-3} $AgClO_4$-acetonitrile at 25 °C: *mer*-**2**, −0.48 V (Nernstian reduction) and 1.29 V (quasi-reversible oxidation); *mer*-**3**, −0.50 V (Nernstian reduction) and 1.28 V (quasi-reversible oxidation).

Other Chemicals. *N*,*N*-Dimethylformamide (DMF) was spectral reagent grade (Dojindo Laboratories, Dotite Spectrosol). Acetonitrile (AN) was purified as described previously.[13] Benzene and hexane used in chromatography were chromatographic grade solvents (Wako Pure Chemical Industries, Ltd.), and the other chemicals were of reagent grade.

Apparatus. A Shimadzu Seisakusho Ltd. CHN Analyzer CHN-1A was used for the elemental analyses. UV-vis spectra were measured with a Hitachi Model 200-20 spectrophotometer, and ^{1}H NMR spectra with a JEOL JMN GX270. The light sources for photochemical experiments were a 32 W low-pressure mercury lamp (Riko Kagaku Sangyo, UVL-321LA) and a 250 W high-pressure mercury lamp (Ushio Model UI-501C). High-performance liquid chromatography (HPLC) was carried out by means of a Toyo Soda apparatus consisting of a CCPM solvent delivery system, a UV-8000 spectrophotometric monitor, and a TSK gel ODS-80T$_m$ column (4.6 mm i.d.×150 mm, Toyo Soda).

Measurement of Isomerization Rates. A weighed sample (about 0.025 mmol) of each isolated isomer of **1**—**4** was dissolved in 25 cm^3 of DMF. The solution was transferred into a 30 cm^3 flask containing a magnetic stirrer bar. The flask was immersed in an oil bath (thermostated within ±1 °C) placed on a magnetic stirrer, which was at once put in motion. Small aliquots (ca. 5 mm^3 each) were taken out of the solution at suitable time intervals by means of a microsyringe which had been kept at room temperature, and 4 mm^3 of the aliquot was immediately injected into the HPLC system.

The compositions of the mobile phases used are given in Table 2 together with the retention times. The flow rate was 1 cm^3 min^{-1}. The spectrophotometric monitor was operated at the wave length of the π–π* absorption band[14,15] of each pair of the isomers (Table 2).

The product of the HPLC peak height and the half-peak width was proportional to the amount of the isomer injected. The isomeric concentrations in each aliquot were determined by means of the calibration curves that had been drawn for standard series of mixtures prepared gravimetrically from the isolated samples of the isomers. Statistical tests showed that the main source of error of the HPLC determination was the day-to-day variance. The reproducibility was estimated to be within 4%.

The isomerization of **4** in AN solutions was carried out in a similar way. The mixture was refluxed on an oil bath kept at 90 °C. The reaction temperature was practically the

Table 2. Compositions of the Mobile Phases for HPLC, the Operating Wavelengths (λ), and the Retention Times (t_r) of the Isomers

Complex	Solvent (volume fraction)	λ / nm	t_r/min *fac*	t_r/min *mer*
1	AN(0.7)-H_2O	275	6.8	7.2
2	AN(0.075)-H_2O(0.225)-MeOH	276	8.7	9.2
3	AN(0.9)-H_2O	277	5.0	4.7
4	AN(0.95)-H_2O	277	5.1	4.5

normal boiling point of the solvent (81.6 °C).

Molecular Orbital Calculation. The calculation was based on a modified variety of the extended Hückel method. Computation was carried out on an NEC ACOS-850 at the Computer Center of Sophia University for the facial isomers of **1**—**5** and two representative meridional isomers (**1** and **4**). The details of the procedure and the results are described elsewhere,[15] and only the atomic bond populations for the Ru-O bonds are presented here.

Results

Qualitative Observations. Isomerization of 1 in Various Solvents: The meridional isomer was dissolved in a deoxygenated solvent to ca. 1 mol m^{-3}. The solution was refluxed for ca. 20 h under an argon atmosphere on an oil bath kept at a temperature 5 °C heigher than the normal boiling point of the solvent; it was then examined for the presence of the facial isomer by means of thin-layer chromatography on Merck Kieselgel 60 (developing solvent, hexane-benzene, 5 : 8 by volume).

The results are presented in Table 3. In the first four solvents, neither the facial isomer nor any other product was detected even when the refluxing was prolonged to more than 30 h. In pyridine, the color changed from red to dark green only by allowing the solution to stand overnight at room temperature, indicating that decomposition and/or ligand exchange took place; no facial isomer was detected in the resultant solution. In the other ten solvents, the isomerization occurred more or less rapidly, and the facial isomer was accompanied by some amounts of one or more by-products, which appeared to be ruthenium species produced by partial ligand exchange.

The isomerization of *mer*-**1** did not occur photochemically. Irradiation of its AN solutions under an argon atmosphere with the high-pressure mercury lamp for 9.5 h or with the low-pressure mercury lamp for 25.5 h at room temperatures yielded a small amount of a decomposition product, but no facial isomer was detected. The irradiation of *mer*-**1** in ethanol with the low-pressure mercury lamp did not bring about the isomerization either; instead, *mer*-**1** was reduced to the corresponding ruthenium(II) species, which was completely reoxidized back to the original meridional isomer by atmospheric oxygen. This result agrees with the observation reported by Gordon et al.[4] that no isomerization accompanied the chemical reduction and reoxidation.

Table 3. Some Physical Properties[a] of the Solvents and the Isomerization of *mer*-**1** Therein

Solvent	t_b/°C[b]	ε_r[c]	μ/μ_D[d]	*fac*-**1**[e]
Benzene	80.1	2.27	0	−
Toluene	110.6	2.38	0.31	−
Chloroform	61.2	4.81	1.15	−
Chlorobenzene	131.7	5.62	1.62	−
1,1,2,2-Tetrachlorobenzene	145.1	8.20*	1.71	+
Trifluoroacetic acid	71.8	8.55*	2.28	+
Pyridine	115.3	12.9	2.37	[f]
1-Butanol	117.7	17.5	1.75	+
2-Propanol	82.2	19.9	1.66	+
1-Propanol	97.2	20.5	3.09	+
Ethanol	78.3	24.6	1.66	+
Methanol	64.5	32.7	2.87	+
N,*N*-Dimethylformamide	153.0	36.7	3.24	+
Acetonitrile	81.6	35.9	3.53	+
1,1,1-Trifluoroethanol	74.1	—	—	+

a) From Ref. 19. b) Normal boiling temperature. c) Relative permittivity at 25 °C or at 20 °C (those marked by asterisks). d) Dipole moment; $\mu_D = 3.336\times10^{-30}$ C m. e) +, detected accompanied by by-product(s) after ca. 20 h of refluxing; −, not detected. f) Decomposition and/or ligand exchange.

Isomerization in DMF: The results are indicated in Table 1. Complexes **5** and **6** did not undergo any isomerization in DMF even after being refluxed (ca. 158 °C) for more than 30 h, while **7**, **8**, and **9** were reduced to the corresponding ruthenium(II) species. Complexes **1**, **2**, **3**, and **4** underwent the isomerization when heated in DMF, and their kinetics were studied quantitatively.

Determination of the Rate Constants and Equilibrium Constants. A typical set of isomeric concentration-time curves is shown in Fig. 2. Since preliminary experiments showed that the half-lives of the facial-to-meridional isomerization and its backward reaction

$$\textit{fac}\text{-form} \underset{k_{-1}}{\overset{k_1}{\rightleftharpoons}} \textit{mer}\text{-form} \qquad (1)$$

were independent of the initial concentration, they were treated as essentially reversible, first-order reactions. But the isomerization reactions were accompanied by slow decomposition, as is seen from Fig. 2.

It can be readily shown that Eq. 2 holds if the decomposition is irreversible and follows the first-order rate law with respect to the total concentration of the facial and the meridional isomers:

$$-\ln\{(x-x_e)/(x_0-x_e)\} = (k_1+k_{-1})t. \qquad (2)$$

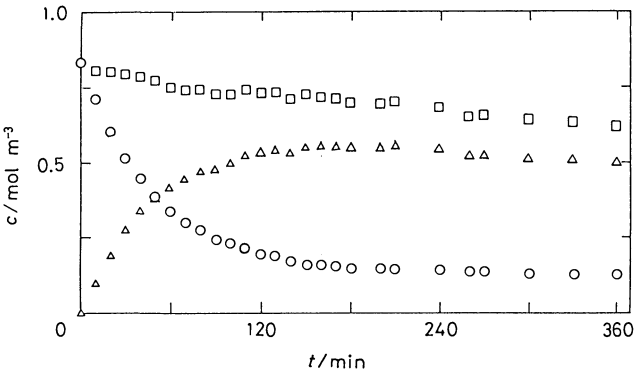

Fig. 2. Concentration-time curves for the reaction of *fac*-**1** in DMF at 90 °C.
○, [*fac*-**1**]; △, [*mer*-**1**]; □, [*fac*-**1**]+[*mer*-**1**].

Here x is the isomeric fraction of the facial isomer at time t as defined by Eq. 3

$$x=[fac]/([fac]+[mer]), \quad (3)$$

where the brackets mean the amount-of-substance concentration at time t of the specified isomer; x_e is its equilibrium value, and x_0 is the initial value of x.

In the present cases, the rates of decomposition were actually proportional to the total concentration of the two isomers with rate constants less than ca. 7% of k_1+k_{-1}.

The present experimental procedure inevitably involved a time lag: it took some time for the temperature of the reaction mixture, T, to reach the bath temperature, T_b. The reaction gradually accelerated during this time lag, and the plot of the left-hand side of Eq. 2 against t became distorted at small times. But beyond a short period (ca. 6 min in the most unfavorable cases), the plot became linear. The values of k_1+k_{-1} were obtained from the slope of the linear portion.

A separate experiment showed that the variation of T followed the Newton's law of heat flow, that is, $dT/dt=a(T_b-T)$ with $a=8.85\times10^{-3}$ s^{-1} for the present experimental arrangement. Digital simulations were carried out on the basis of this value of a and the actual activation energies. Their results reproduced the experimental plots quite well and ascertained that the slope of the linear portion gave exactly the value of k_1+k_{-1}.

The equilibrium constant of reaction (1) is defined by

$$K=[mer]_e/[fac]_e=k_1/k_{-1}=(1-x_e)/x_e. \quad (4)$$

Their values were obtained in the following way, instead of direct measurement of the equilibrium concentrations, in order to avoid possible errors owing to extensive decomposition brought about by prolonged heating and to increase the precision by making use of as many data points as feasible.

Two parallel kinetic runs were carried out: one (run a) was started with a solution of pure facial isomer ($x_0=1$), and the other (run b) with a solution of pure meridional isomer ($x_0=0$). In run a, the fraction of the meridional form at time t_a, $1-x_a$, was determined; in run b, the fraction of the facial form at time t_b, x_b, was determined. Equation 1 shows that

$$1-x_a=(1-x_e)[1-\exp\{-(k_1+k_{-1})t_a\}]$$

and

$$x_b=x_e[1-\exp\{-(k_1+k_{-1})t_b\}],$$

so that

$$(1-x_a)/x_b=f\{(1-x_e)/x_e\}=fK, \quad (5)$$

where

$$f=[1-\exp\{-(k_1+k_{-1})t_a\}]/[1-\exp\{-(k_1+k_{-1})t_b\}].$$

The left-hand side of Eq. 5 would give the K value if t_a could be made exactly equal to t_b. In practice, there was some uncertainty in both t_a and t_b owing to the above-mentioned time lag, and the experimental values of $(1-x_a)/x_b$ at shorter times showed deviating fluctuations. Only the points that gave stable values were used for calculating the mean values of K. The f values of these points were between 0.99 and 1.01 for t_a-t_b up to ±6 min, the largest time lag ever observed.

The equilibrium constants obtained in this way are listed in Table 4. No definite temperature dependence was detectable except for **3**. In the case of **3**, the plot of ln K against T^{-1} was fairly linear, and its linear regression line had a slope which was statistically non-zero at 10% significance level. The slope would give the standard reaction enthalpy value of (3.4±3.2) kJ mol^{-1}. This non-zero slope, however, is very likely to be accidental, in view of the fact that the determinations of the equilibrium constants of this complex (and **2**, too) were difficult owing to relatively poor separation between the chromatographic peaks and the larger extent of the decomposition. It was, therefore, decided that the equilibrium constant was independent of the temperature, and the values for the four temperatures were averaged. In the case of **2**, the value for 373 K was excluded from the average, because its deviation was almost statistically significant at 5% significance level.

The left-hand side of Eq. 2 was calculated with the

Table 4. Equilibrium Constants (K) of Facial-to-Meridional Isomerization Reactions in DMF and Their Forward (k_1) and Backward (k_{-1}) Rate Constants

Complex	T/K	K[a]	k_1+k_{-1}	k_1	k_{-1}
			10^{-5} s^{-1}	10^{-5} s^{-1}	10^{-5} s^{-1}
1	343	4.24	4.83	3.91	0.917
	353	4.32	12.4	10.0	2.35
	363	4.20	32.8	26.6	6.22
	373	4.30	77.2	62.6	14.6
	average	4.27±0.13			
2	343	2.76	6.04	4.41	1.62
	353	2.64	16.1	11.8	4.33
	363	2.75	35.6	26.0	9.57
	(373	2.39)[b]	72.4	52.9	19.5
	average	2.72±0.19			
3	343	2.50	15.4	11.2	4.21
	353	2.68	25.5	18.5	6.97
	363	2.65	51.9	37.7	14.2
	373	2.79	107	77.8	29.2
	average	2.66±0.28			
4	343	1.71	15.3	9.69	5.57
	353	1.74	32.1	20.4	11.7
	363	1.80	74.0	47.0	27.0
	373	1.71	160	102	58.6
	average	1.74±0.10			

a) The uncertainties are 90% confidence limits. b) Not included in the average.

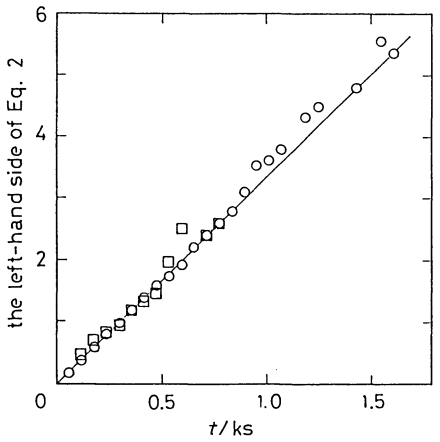

Fig. 3. The left-hand side of Eq. 2 plotted against the reaction time, t, for the reactions of **1** in DMF at 90 °C.
Starting isomer: ○, *fac*-**1**; □, *mer*-**1**.

value of x_e obtained from the K value and plotted against t. The plots were quite linear until the magnitude of the logarithmic term reached ca. 2.5—3 except for the deviations due to the time lag, which were noticeable during the initial period of a few runs with higher bath temperatures. An example is given in Fig. 3 (here the effect of the time lag is barely perceptible). The slopes of the plots were independent of the isomeric form with which the reactions were started. The individual values of k_1 and k_{-1} listed in Table 4 were calculated from the slope and the K value.

Kinetic Parameters. If the equilibrium constant is independent of the temperature, the standard enthalpies of activation of the forward and the backward reactions are the same ($\Delta H^{\neq}$). The $\Delta H^{\neq}$ value and the standard entropies of activation of the forward and backward reactions ($\Delta S_1^{\neq}$ and $\Delta S_{-1}^{\neq}$, respectively) were obtained on the basis of the following equations, by plotting the logarithmic value of $(k_1+k_{-1})/T$ against $1/T$:

$$\ln[\{(k_1+k_{-1})/T\}/\mathrm{s^{-1}\,K^{-1}}]=-\Delta H^{\neq}/RT+A'$$

$$\Delta S_1^{\neq}/R=A'-\ln(k_B h^{-1}/\mathrm{s^{-1}\,K^{-1}})-\ln(1+K^{-1})$$

$$\Delta S_{-1}^{\neq}/R=A'-\ln(k_B\, h^{-1}/\mathrm{s^{-1}\,K^{-1}})+\ln(1+K)$$

Here k_B is the Boltzmann constant and h is the Planck constant.

Table 5. Standard Enthalpies ($\Delta H^{\neq}$) and Entropies ($\Delta S^{\neq}$) of Activation[a]

Comoplex	$\Delta H^{\neq}$/kJ mol^{-1}	$-\Delta S_1^{\neq}/R$[b]	$-\Delta S_{-1}^{\neq}/R$[b]
1	96.0± 3.3	6.1	7.6 ± 1.1
2	85.0± 9.5	9.8	10.8 ± 3.2
3	66.4±14.6	15.5	16.5 ± 4.9
4	81.1± 3.0	10.4	11.0 ± 1.0

a) The uncertainties are 90% confidence limits. b) R is the gas constant, ca. 8.314 J mol^{-1} K^{-1}. Subscripts $_1$ and $_{-1}$ refer to *fac*-to-*mer* and *mer*-to-*fac* reactions, respectively. The uncertainties apply to both $\Delta S^{\neq}$ values.

Table 6. Effect of Electrolytes on (k_1+k^{-1})/ 10^{-5} s^{-1} of the Isomerization of *fac*-**4** in Acetonitrile, at ca. 82 °C

Electrolyte	Concentration/mol dm^{-3} 0.10	0.02	0.01	0
$N(C_2H_5)_4ClO_4$	2.86	2.80	2.78	2.19[a]
$Mg(ClO_4)_2$	2.67	2.66	2.68	
CH_3COOH	3.11	2.92	2.80	

a) The equilibrium constant was 1.83.

The plots were fairly linear. The point for 343 K in the case of **3** appeared to deviate more than the other points did, but the deviation was not statistically significant enough to exclude the point as an outlying one. The values of the kinetic parameters are presented in Table 5.

Effects of Electrolytes. Effects of some electrolytes on the rate of the isomerization of *fac*-**4** were examined by refluxing it in AN instead of DMF, since solubilities of the electrolytes in the latter solvent were insufficient. The reaction temperature was ca. 82 °C. The values of k_1+k_{-1} are listed in Table 6.

Discussion

Effects of Solvents and Electrolytes. The kind of solvent largely influenced the rate of isomerization of *mer*-**1** (Table 3). The isomerization was observed in solvents with higher relative permittivities, except for pyridine, in which the complex was decomposed.

Solvent-assisted bond-rupture mechanisms (e.g., Ref. 2) is compatible with this fact and with the observation that the resultant *fac*-**1** was always accompanied by by-products. An intermediate with a dangling ligand is formed when an Ru-O bond is attacked by solvent molecules. The open end of the dangling ligand may recombine with the central atom either at the original position or at some other position, the latter case leading to the isomerization. The solvent must be a coordinating agent powerful enough to break the Ru-O bond. But it should not be so too much; then the dangling end fails to recombine, and ligand exchange or decomposition predominates, as was the case of the reaction in pyridine, a strong coordinative agent.

The isomerization rate of **1** in AN was not affected by the addition of the free ligand, 1,1,1-trifluoro-2,4-pentanedione, up to 1 mol dm^{-3}; but its addition appeared to reduce the extent of the decomposition. This observation will indicate that the isomerization is a solvent-assisted intramolecular process and the decomposition is ligand-exchange by solvent.

The addition of tetraethylammonium perchlorate and magnesium perchlorate increased the isomerization rate of *fac*-**4** in AN; the addition of acetic acid produced an even larger increase (Table 6). The presence of ions may assist the bond rupture through

the relaxation of the charge separation accompanying the bond rupture. But there seem to be contributions of more specific interaction, since acetic acid is a very weak electrolyte in AN.[16] Their quantitative interpretation is difficult at this stage.

Effects of Substituents. Trifluoromethyl Group: All the complexes for which the facial-meridional isomerization was observed in DMF have trifluoromethyl groups (Table 3). To the authors' knowledge, the ruthenium(III) complexes that so far have been reported to undergo isomeric rearrangement are fluorine substituted β-diketonato complexes, with one exception of tris[(+)-3-acetylcamphorato]ruthenium-(III).[17] Fay et al.[5] reported that no conversion of the optical isomers of tris(acetylacetonato)ruthenium(III) was observed when they were heated in chlorobenzene for 10 h at 165 °C. Complexes **7**, **8**, and **9** would isomerize, were they not reduced when heated in DMF. There is an indication that the equilibrium constants for these three complexes will be almost the same and quite large (see the next subsection). The fact that the facial form of **7** could not be obtained is attributable to experimental difficulty rather than to the absence of isomerization.

The presence of trifluoromethyl group, therefore, appears to be a necessary condition for a β-diketonato ruthenium(III) complex to undergo the facial-meridional isomerization with appreciable rates. The primary reason is that a trifluoromethyl group, being strongly electron-withdrawing, "weakens and lengthens metal-oxygen bonds, thereby facilitating rearrangement."[4] This view is substantiated by a molecular orbital calculation, as will be discussed later.

Equilibrium Constants: Gordon et al.[4] reported that the equilibrium constant of reaction (1) for **1** in 1,1,2,2-tetrachloroethane at 150 °C was 4.9 with $\Delta_rH^\circ=(-4.6\pm2.5)$ kJ mol^{-1} and $\Delta_rS^\circ=(+2.5\pm5.9)$ J mol^{-1} K^{-1}. This equilibrium constant is quite close to the present result in DMF at 70—100 °C (Table 4). On the other hand, Δ_rH° was not detectable in our case. In view of the present experimental errors, a value of $|\Delta_rH^\circ|$ amounting to 2.5 kJ mol^{-1} or more should have been detected.

This discrepancy may be explained in terms of the relative permittivities of the two solvents (Table 3). In each solvent, the major part of the standard affinity of the isomerization will probably be the difference between the solvation Gibbs energies of the facial and the meridional isomers, and these solvation energies will arise mainly from the electrostatic interaction between the polar isomer molecules and the dielectric solvent. By analogy to the ion-dielectric interaction, it is likely that the standard enthalpy of such an interaction will be proportional to $\varepsilon_r^{-1}-T(d\varepsilon_r^{-1}/dT)$. For various common solvents near room temperature, ε_r follows the empirical formula $\varepsilon_r=\varepsilon_r^\circ \exp(-T/\theta)$, where the characteristic temperarue θ usually lies quite near the normal melting point of the solvent (T_{fus}).[18] Then, Δ_rH° will be roughly proportional to the factor $(1-T/T_{fus})/\varepsilon_r$. The value of this factor is −0.18 for the tetrachloroethane (T_{fus}=229.3 K[19]) at 150 °C, and it is −0.03 for DMF (T_{fus}=212.7 K[19]) at 100 °C.

The K values (Table 4) are not very much different from 3, the value expected if the equilibrium is determined solely by the probability. But they show a tendency: K decreases with the increase in the electron donating character of the substituent R′. A fairly straight line is obtained when ln K is plotted against the reversible half-wave potential of the Ru^{III}/Ru^{II} process of the complex (Fig. 4) or against the Hammett constant of R′ (a linear relationship has been established between the reversible half-wave potential and the sum of the Hammett constants of the substituents[13]). This linearity, being based on only four points, cannot be generalized too much. But if its extrapolation is allowed, the K values for complex **7**, **8**, and **9**, whose half-wave potentials were −0.33 V, −0.32 V, and −0.33 V, respectively,[13] will be around 16.

It is difficult to explain this tendency quantitatively. The following is one possibility. Quite likely the entropy of solvation plays a decisive role, since the standard reaction Gibbs energies were essentially entropic. There will be two opposite factors. One is the decrease of entropy caused by the orientation of solvent molecules around the dipolar complex species. This decrease makes the facial form less favorable in terms of entropy, because it always has a larger dipole moment than that of the corresponding meridional form. This effect will play an important role in mildly polar and less structured solvents. The other factor, however, comes into effect in a highly

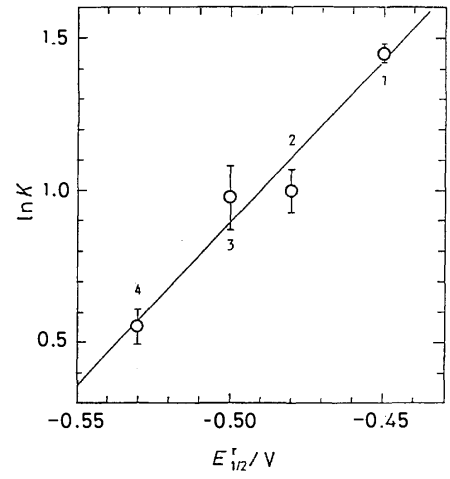

Fig. 4. Correlation between ln K and the revesible half-wave potential of the Ru^{III}/Ru^{II} process in 0.1 mol dm^{-3} $(C_2H_5)_4NClO_4$ in AN at 25 °C vs. Ag|0.1 mol dm^{-3} $AgClO_4$-AN ($E^\circ_{1/2}$).
The error bars represent 90% confidence limits; correlation coefficient=0.9756.

associated or structured solvent like DMF (its entropy of evaporation is 90.0 $J mol^{-1} K^{-1}$ [19]). Then the structure of the solvent will be broken by the presence of strongly dipolar solute molecules and an increase of entropy results, thereby making the facial form more favorable. Even in DMF, the first factor seems to predominate in the case of **1**. But as the substituent R′ becomes more and more strongly electron-donating and bulky, the second factor will overcome the first, and the K value becomes progressively smaller than 3.

Whatever the reason may be, there is an interesting parallelism in the HPLC retention times. With AN-water mixtures of various compositions, the retention time (t_r) of each complex increased with the water content. In a given mixture, the t_r value of *fac*-**1** was smaller than that of *mer*-**1**, indicating that the *fac*-form was more stable in a polar mobile phase. In the cases of **3** and **4**, on the contrary, the order was reversed (Table 2); the *fac*-forms are less stable, in spite of their higher polarity.

Enthalpies of Activation: For the isomerization of **1** in 1,1,2,2-tetrachloroethane at 140.5—174.5 °C,[4] $\Delta H^{\neq}$/kJ mol^{-1} is 138±3.3 (*fac*-to-*mer*) and 118±4.6 (*mer*-to-*fac*). These are a little larger than the present value (Table 5), probably reflecting the smaller dielectric character of the chloroethane. The entropy of activation for the *fac*-to-*mer* reaction, $\Delta S_1^{\neq}/R$=−3.8±1.0, is larger and that for the reverse reaction, $\Delta S_{-1}^{\neq}/R$=−11.5±1.5, is smaller than the corresponding present values.

The enthalpy of activation, showing a minimum at complex **3**, cannot be simply related to the half-wave potential or the Hammett constant, since the latter vary monotonically. But it will be related to the robustness of the Ru-O bonds, if the isomerization proceeds via a solvent-assisted bond-rupture mechanism. One of the measures of bond strength is the atomic bond population,[20] which is believed to be proportional to the bond order. The values obtained by means of a modified extended Hückel method are presented in Table 7. Results of such a calculation

Table 7. Atomic Bond Populations of Ru-O Bonds Calculated by Means of the Modified Extended Hückel MO Method[15]

Ru-O bond[a]	Complex 1	2	3	4	5
fac					
a, c, d	0.244	0.240	0.240	0.241	0.251
b, e, f	0.237	0.234	0.233	0.235	0.250
mer					
a′	0.242			0.239	
b′	0.238			0.236	
c′	0.240			0.238	
d′	0.244			0.241	
e′	0.239			0.238	
f′	0.242			0.238	

a) For the bond designation, see Fig. 1.

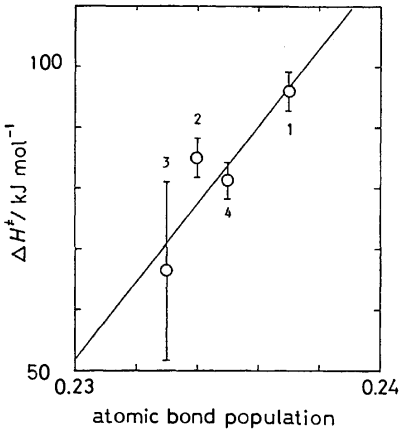

Fig. 5. Correlation between $\Delta H^{\neq}$ and the atomic bond population of the Ru-O bonds b, e, and f. The error bars represent 90% confidence limits; correlation coefficient=0.8985.

are generally not precise. Nevertheless, in these particular instances, where all the compounds are very similar, the values of atomic bond population will correctly reflect the relative robustness of the bond.

The facial isomer has two distinguishable kinds of Ru-O bonds: the atomic bond population of the three Ru-O bonds that are adjacent to the substituents R′ (bonds b, e, and f in Fig. 1) is lower than that of the others in each complex. There is a fairly linear correlation between $\Delta H^{\neq}$ and the atomic bond population of the former Ru-O bonds, as shown in Fig. 5. This may indicate that the isomerization is initiated by the rupture of the least robust Ru-O bond.

The bond rupture mechanisms can be classified according to the idealized geometry of the transition state: trigonal bipyramidal (TBP) or square pyramidal (SP). The rupture of the bonds a′, c′, e′, or f′ is required for the *mer*-to-*fac* conversion to occur through the TBP transition states, whereas the rupture of any bond leads to the *fac*-to-*mer* conversion through both transition states.[2] It is tempting to suggest that the isomerization involved the SP transition states, in view of the result that the least robust bond in the meridional form was the bond b′. Drawing such an inference, however, will be too early because the reaction may involve more than one type of transition state.[2]

The calculated values clearly indicate the weakening effect of trifluoromethyl group.[4] The atomic bond population of *fac*-**5**, 0.250, is very much higher than those of the trifluoromethyl-substituted complexes. If the above linear correlation is extrapolated to this value, $\Delta H^{\neq}$ of **5** will be ca. 180 kJ mol^{-1}. With such a large value of $\Delta H^{\neq}$, k_1+k_{-1} at 100 °C would be of the order of 10^{-15} s^{-1} or less.

The authors are very grateful to Prof. Hiroshi Kobayashi of Kitazato University not only for many valuable suggestions and encouraging discussions,

but also his kindness in providing them with the program of the original Hückel method. They also thank Dr. S. F. Howell, Sophia University, for correcting the manuscript. The elemental analyses were carried out by Mrs. Nakako Tokita and the NMR measurement by Mrs. Hiroko Kin and Mrs. Yukari Suetsugu of the Department of Chemistry, to whom the authors' thanks are due.

References

1) R. C. Fay and T. S. Piper, *Inorg. Chem.*, **3**, 348 (1964).
2) J. G. Gordon, II, and R. H. Holm, *J. Am. Chem. Soc.*, **92**, 5319 (1970).
3) A. Y. Girgis and R. C. Fay, *J. Am. Chem. Soc.*, **92**, 7061 (1970).
4) J. G. Gordon, II, M. J. O'Connor, and R. H. Holm, *Inorg. Chim. Acta*, **5**, 381 (1971).
5) R. C. Fay, A. Y. Girgis, and U. Klabunde, *J. Am. Chem. Soc.*, **92**, 7056 (1970).
6) J. R. Hutchinson, J. G. Gordon, II, and R. H. Holm, *Inorg. Chem.*, **10**, 1004 (1971).
7) C. Kutal and R. E. Sievers, *Inorg. Chem.*, **13**, 897 (1974).
8) K. Saito, *Pure Appl. Chem.*, **38**, 325 (1974).
9) Y. Hoshino, R. Takahashi, K. Shimizu, G. P. Satô, and K. Aoki, *Bull. Chem. Soc. Jpn.*, **62**, 993 (1989).
10) A. Endo, K. Shimizu, G. P. Satô, and M. Mukaida, *Chem. Lett.*, **1984**, 437; A. Endo, M. Kajitani, M. Mukaida, K. Shimizu, and G. P. Satô, *Inorg. Chim. Acta*, **150**, 25 (1988).
11) J. C. Reid and M. Calvin, *J. Am. Chem. Soc.*, **72**, 325 (1950).
12) Y. Hoshino, Y. Yukawa, A. Endo, K. Shimizu, and G. P. Satô, *Chem. Lett.*, **1987**, 845.
13) A. Endo, Y. Hoshino, K. Hirakata, Y. Takeuchi, K. Shimizu, Y. Furushima, H. Ikeuchi, and G. P. Satô, *Bull. Chem. Soc. Jpn.*, **62**, 709 (1989).
14) H. Kobayashi, H. Matsuzawa, Y. Kaizu, and A. Ichida, *Inorg. Chem.*, **26**, 4318 (1987).
15) Y. Satsu, Ph. D. Thesis, Sophia University, Tokyo, 1987.
16) The Chemical Society of Japan, "Kagaku Binran," Maruzen, Tokyo (1984), p.II-343.
17) G. W. Everett, Jr. and R. H. Holm, *J. Am. Chem. Soc.*, **96**, 2087 (1974).
18) R. W. Gurney, "Ionic Processes in Solution," McGraw-Hill, New York, Toronto, London (1953), Chap. 1.
19) J. A. Riddick, W. B. Bunger, and T. K. Sakano, "Organic Solvents, Physical Properties and Methods of Purification," in "Techniques of Chemistry," 4th ed, ed by A. Weissberger, John Wiley & Sons, New York, Chichester, Brisbane, Toronto, Singapore (1986), Vol. II.
20) R. S. Mulliken, *J. Chem. Phys.*, **23**, 1841 (1955).

The Sensitive and Selective Determination of Palladium(II) Based on Ternary-Complex Formation with Phloxine and Thiamine[1)]

Yoshikazu FUJITA, Itsuo MORI,* Minako TOYODA, Yoshihiro NAKAHASHI, Keiji KATO, and Masaki NAKAMURA
Osaka University of Pharmaceutical Sciences, 2-10-65, Kawai, Matsubara-shi, Osaka 580
(Received June 1, 1989)

A sensitive and selective spectrophotometric determination of palladium(II) based on ternary-complex formation with Phloxine and thiamine was established. The apparent molar absorptivity of the proposed method, which does not require an extraction procedure, was 1.02×10^5 dm^3 mol^{-1} cm^{-1} at 565 nm. Only gold(III) in an equimolar ratio of palladium(II) among the metal ion examined interfered. The method was applied to a determination of palladium in palladium carbon and palladium asbestos; the results were in good agreement with those obtained by potassium iodide method, the Michler's thioketone method and ICP-AES. The sensitivity could be further enhanced by about 20 times over that of spectrophotometry and/or fluorimetry by combining it with a membrane filter preconcentration technique. It was suggested that the collection of an aggregate on a membrane filter depends on the molecular size through observing by an scanning electron microscope.

Various determination methods for metal ions based on the ternary-complex formation have been reported[2-4)] for the purpose of enhancing the determination sensitivity, selectivity and so on. Of the ternary-complex system, the ion-association type based on complex formation between a metal ion-organic base cation and the anion of a dyestuff has often used. The organic bases used are limited[3,4)] to such ligands as 1,10-phenanthroline and 2,2′-bipyridyl. Most of these methods are not sufficiently selective and require an extraction step in spite of the high sensitivity.

We have already reported[5-7)] on the determination of organic compounds utilizing a ternary-complex system, {**RML**}, where {**R**}, {**M**}, and {**L**} denote an organic dye, a metal ion and an organic compound, respectively. In previous papers[6,7)] a simple and sensitive determination of {**L**}, such as thiamine and chlorpromazine, was established by using {**RML**} with Eosine, palladium(II) and these {**L**}. In this case only palladium(II) was effective among the various metal ions tested. Thus, it is speculated that a simple, sensitive and selective determination of palladium(II) would be established by selecting suitable {**R**} and/or {**L**}, particularly {**L**}.

We studied the color reactions of palladium(II) based on the formation of a new type of the ternary complex with fluorescein(fl) dyes, palladium(II) and {**L**}; a selective and sensitive determination of palladium(II) was investigated by using Phloxine as {**R**} and thiamine as {**L**}. The proposed method was applied to an assay of palladium in practical samples. In addition, a membrane filter preconcentration technique[8,9)] was also studied for the purpose of enhancing the determination sensitivity. A collection of ternary-complex aggregates on a membrane filter was observed with a scanning electron microscope (SEM).

Experimental

Apparatus. The absorption spectra and absorbance values were measured with a Shimadzu Model 160 recording spectrophotometer using 1.0-cm quartz cells. A Shimadzu Model RF-540 spectrofluorometer with a 1.0-cm quartz cell was used. The pH measurements were made with a Hidachi-Horiba F-7 AD glass electrode pH meter. A Shimadzu Model ICPS-1000V inductively coupled plasma emission spectrometer was used. A Toyo TM 3 membrane filter(made of nitrocellulose, 25 mm diameter, 0.65 μm pore size) and Toyo KGS-25 filter holder were used.

Reagents and Materials. A stock solution (1.0×10^{-2} mol dm^{-3}) and a working solution of palladium(II) were prepared according to a previous report.[7)] All fl derivative solutions were prepared in 1.0×10^{-3} mol dm^{-3} aqueous solutions. 2,4,5,7-Tetrabromo-3′,4′,5′,6′-tetrachloro fl (Phloxine), 2,4,5,7-tetrabromo fl (Eosine), 2,4,5,7-tetraiodo-3′,4′,5′,6′-tetrachloro fl (Rose Bengal), 2,4,5,7-tetraiodo fl (Erythrosine), 4,5-dibromo fl and 4,5-diiodo fl were purchased from Wako Pure Chemical Ind. Ltd., Tokyo Kasei Kogyo Co., Ltd., and Aldrich Chemical Com. Inc., respectively. Fl, 2,4,5,7-tetrachloro fl, 2,7-dichloro fl and 3′,4′,5′,6′-tetrachloro fl were synthesized according to methods described in the literature.[10,11)] A 5.0×10^{-3} mol dm^{-3} thiamine solution was prepared by dissolving thiamine hydrochloride in water. A 1.0% aqueous solution of (2-hydroxypropyl)cellulose (HPC, 6-10 cps) and polyethylene glycol (PEG, 2000) were prepared. A 0.2 mol dm^{-3} sodium acetate-0.2 mol dm^{-3} acetic acid buffer solution was used for pH adjustments. All other reagents and materials were of analytical reagent grade, and deionized water was used.

Standard Procedure for the Spectrophotometry. To a solution containing up to 8 μg of palladium(II) were added 0.3 cm^3 of a 5.0×10^{-3} mol dm^{-3} thiamine solution, 0.5 cm^3 of a 1.0% HPC solution, 3.0 cm^3 of the buffer solution (pH 4.6) and 1.0 cm^3 of a 1.0×10^{-3} mol dm^{-3} Phloxine solution; the solution was diluted to mark with water in a 10-cm^3 volumetric flask. After being kept at room temperature for 20 min, the absorbance of a Phloxine-thiamine-palladium(II) solution (Solution A) was measured at 565 nm against the Phloxine-thiamine (=reagent blank, Solution B) as a reference.

Recommended Procedure for a Membrane Filter Preconcentration. A solution containing up to 0.5 μg of palladium(II) was placed in a 10-cm^3 volumetric flask; to this were added 0.3 cm^3 of a 5.0×10^{-3} mol dm^{-3} thiamine solu-

tion, 0.3 cm^3 of a 1.0 % PEG solution, 3.0 cm^3 of the buffer solution (pH 4.6), and 1.0 cm^3 of a 1.0×10^{-3} mol dm^{-3} Phloxine solution. The mixture was diluted to the mark with water, agitated well, and kept at room temperature for 20 min together with a reagent blank. Both solutions were then filtered through a 0.65-μm pore size membrane filter to collect the aggregates; the filtered substances were then washed with about 20 cm^3 of water. After being dried with a hair-drier, the membrane filter and aggregates were dissolved in 5 cm^3 of dimethyl sulfoxide (DMSO). The absorbance of a DMSO solution containing palladium(II) (Solution A′) was measured at 555 nm against the DMSO solution of a reagent blank (Solution B′). In the case of fluorimetry, the difference in the relative fluoresence intensity between Solutions A′ and B′ at 575 nm emission wavelength with excitation at 520 nm was measured.

Results and Discussion

Choice of Dye {R} and Organic Base {L}. In order to examine the effect of {R} on the color reaction among {R}, {L} and palladium(II), thiamine was selected as {L}. In the absence of a dispersion agent Solution A precipitated gradually; thus, a nonionic surfactant,[9] such as HPC and Methyl Cellulose, was added to Solutions A and B. Of the ten fl derivatives tested, Phloxine, Eosine, Erythrosine, and Rose Bengal were superior to the other {R} in sensitivity. The relationships between the pH change and absorbance by using these four {R} are shown in Fig. 1.

The effect of {L} was examined by combinations of four {R} and various {L} at each optimum pH. Of the various {L} examined (thiamine, papaverine, dibucaine, scopolamine, pilocarpine, pyridoxine, lincomycin, quinine, ergotamine, chlorpromazine, chlorhexidine, acrinol, theophylline, cycloserine, diphenhydramine, sparteine, and spermine), thiamine was the best since it gave the highest sensitivity and stability of the coloration. In addition, compared with the other {R}, thiamine scarcely produced the colored complex with {R}, i.e. the absorbance of Solution B was relatively low. {R} could be arranged in the following order with respect to sensitivity: Phloxine≈Rose Bengal>Erythrosine≈Eosine. Phloxine was superior to Rose Bengal in terms of color contrast between sample and reagent blank solutions, and the purity of reagent. The results are shown in Table 1.

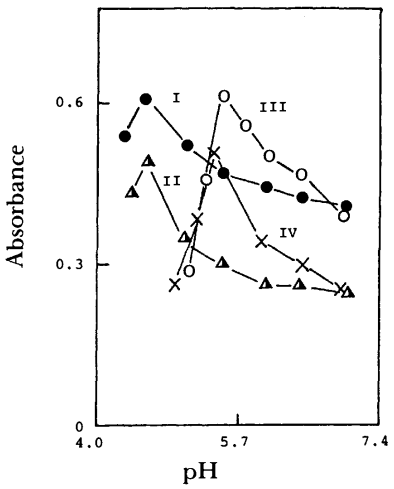

Fig. 1. Effect of pH on the color reaction between palladium(II) and dye-thiamine solution.
Pd(II): 6.0×10^{-6} mol dm^{-3} (4.2 μg/10 cm^3); dye: 1.0×10^{-4} mol dm^{-3}; thiamine: 1.5×10^{-4} mol dm^{-3}; HPC: 0.05%; Reference: Solution B (dye-thiamine solution); dye: I (—●—), Phloxine; II(—▲—), Eosine; III (—○—), Rose Bengal; IV (—×—), Erythrosine.

On the basis of these resutls, Phloxine and thiamine were chosen as {R} and {L}, respectively, for the further experiments.

Optimisation of Conditions. The maximum difference in absorbance between Solutions A and B was at 565 nm. The optimum pH for the color reaction was narrow and was 4.5—4.7. The absorbance of Solution A against Solution B dropped rapidly at both higher and lower pH regions. Hence, 3.0 cm^3 of 0.2 mol dm^{-3} acetate buffer solution (pH 4.6) was used for the pH adjustments. Of various nonionic surfactants tested (HPC, Methyl Cellulose, PEG, poly(*N*-vinylpyrrolidone) and poly(vinyl alcohol)), HPC was the

Table 1. Effect of Organic Bases {L} by Using Four fl Dyes {R}

{L}	{R}, Absorbance at (λ/nm)			
	Phloxine	Eosine	Rose Bengal	Erythrosine
Thiamine	0.610 (565)	0.510 (545)	0.615 (580)	0.502 (560)
Papaverine	0.134[a] (575)	0.153[a] (540)	0.103[a] (565)	0.095[a] (560)
Dibucaine	0.153[a] (575)	0.097[a] (540)	0.102[a] (565)	0.079[a] (560)
Scopolamine	0.089[a] (545)	0.072 (540)	0.096[a] (565)	0.096[a] (535)
Pilocarpine	0.144 (565)	0.079 (540)	0.276 (575)	0.099[a] (535)

Pd(II): 6.0×10^{-6} mol dm^{-3}; {R}: 1.5×10^{-4} mol dm^{-3}; HPC: 0.05%; pH: Phloxine and Eosine—pH 4.5, Rose Bengal and Erythrosine—pH 5.5; Reference: {L}-{R} solution (Solution B).
a) {R-L} complex produced and absorbance of {L}-{R} solution was remarkably high.

best in terms of sensitivity and stability of coloration. A constant absorbance was obtained by the addition of more than 0.1 cm^3 of 1.0% HPC solution to the final volume of 10 cm^3. Since a maximum and almost constant absorbance was obtained upon by the addition of more than 0.2 cm^3 of 5.0×10^{-3} mol dm^{-3} thiamine solution, 0.3 cm^3 was adopted in the final volume of 10 cm^3. Further experiments were carried out with 1.0×10^{-4} mol dm^{-3} Phloxine in the final volume, considering the absorbance of Solution B.

Under standard conditions, the constant absorbance of Solution A at 565 nm against Solution B as a reference was obtained by maintaining it at room temperature for more than 15 min; the absorbance value was almost constant for at least 3 h. Therefore, 20 min of standing time at room temperature was adopted for all measurements.

Calibration Curve. Beer's law held over the range up to 8 μg of palladium(II) in the final volume of 10 cm^3. The apparent molar absorptivity (ε) and the Sandell sensitivity were 1.02×10^5 dm^3 mol^{-1} cm^{-1} and 0.0010 $\mu g\,cm^{-2}$, respectively. This procedure is much more than the methods using potassium iodide[12] (KI, $\varepsilon=1.02\times10^4$) and dithizone[13] ($\varepsilon=3.55\times10^4$), but less sensitive than the methods using Michler's thioketone[14] (MTK, $\varepsilon=3.0\times10^5$) and Rhodamine 6G[15]

Table 2. Effect of Foreign Ions

Ions	Added as	Added ($\mu g/10\ cm^3$)	Added Mole ratio[a)]	Absorbance at 565 nm	Recovery %
—	—	—	—	0.408	100.0
Fe(III)	Alum	4.5×10	20	0.414	101.5
Au(III)	$HAuCl_4$	3.9	1/2	0.477	116.9
Rh(III)	$RhCl_3$	4.1×10^2	100	0.408	100.0
Ir(III)	$IrCl_3$	3.8×10	5	0.385	94.4
Ru(III)	$RuCl_3$	4.0×10	10	0.415	101.8
Sc(III)	$ScCl_3$	3.6×10	20	0.408	100.0
Al(III)	$AlCl_3$	5.4×10	50	0.408	100.0
La(III)	$LaCl_3$	5.6×10^2	100	0.408	100.0
Bi(III)	$Bi(NO_3)_3$	8.4 ×10	10	0.423	103.7
Ti(IV)	$Ti(SO_4)_2$	3.8×10	20	0.402	98.5
Pt(IV)	$PtCl_4$	1.6×10^2	20	0.392	96.1
Zr(IV)	$Zr(NO_3)_4$	1.8×10	5	0.425	104.2
V(V)	NH_4VO_3	2.0×10	10	0.394	96.6
Ta(V)	TaF_5	3.6×10^2	50	0.402	98.5
Mo(VI)	Na_2MoO_4	3.8×10	10	0.392	96.1
Cr(VI)	K_2CrO_4	2.1×10^2	100	0.408	100.0
Re(VII)	$HReO_4$	7.4×10^2	50	0.395	96.8
Os(VIII)	OsO_4	3.8×10	5	0.396	97.1
Cu(II)	$Cu(NO_3)_2$	1.3×10^2	50	0.408	100.0
Co(II)	$Co(NO_3)_2$	1.2×10^2	50	0.408	100.0
Ni(II)	$Ni(NO_3)_2$	1.2×10^2	50	0.408	100.0
Cd(II)	$Cd(NO_3)_2$	4.5×10^2	100	0.408	100.0
Hg(II)	$Hg(NO_3)_2$	1.6×10^2	20	0.432	105.9
Mn(II)	$MnCl_2$	2.2×10^2	100	0.408	100.0
Zn(II)	$ZnCl_2$	2.6×10^2	100	0.408	100.0
Pb(II)	$PbCl_2$	8.3×10^2	100	0.408	100.0
Mg(II)	$MgCl_2$	9.7×10	100	0.408	100.0
Ag(I)	$AgNO_3$	2.2×10^2	20	0.433	106.1
Cl^-	NaCl	3.5×10^2	250	0.408	100.0
Br^-	KBr	8.0×10^2	250	0.385	94.4
I^-	KI	1.0	1/5	0.382	93.6
S^{2-}	Na_2S	1.3×10^{-1}	1/10	0.358	87.7
$S_2O_3^{2-}$	$Na_2S_2O_3$	4.5×10^{-1}	1/10	0.347	85.0
SO_3^{2-}	Na_2SO_3	6.4×10^{-1}	1/5	0.384	94.1
SCN^-	NH_4SCN	5.8×10^{-1}	1/4	0.357	87.5
CN^-	KCN	2.1×10^{-1}	1/5	0.359	88.0
NO_2^-	$NaNO_2$	9.2×10^{-1}	1/2	0.394	99.6
F^-	KF	7.6×10	100	0.408	100.0
PO_4^{3-}	KH_2PO_4	3.8×10^2	100	0.408	100.0
SO_4^{2-}	K_2SO_4	9.6×10^2	250	0.408	100.0
$C_2O_4^{2-}$	$Na_2C_2O_4$	3.5×10	10	0.368	90.2
Tartrate	Sodium tartrate	5.9×10^2	100	0.408	100.0
Citrate	Sodium citrate	7.6×10^2	100	0.408	100.0

Pd(II) taken: 4.2 $\mu g/10\ cm^3$; Phloxine: 1.0×10^{-4} mol dm^{-3}; HPC: 0.05%; pH: 4.6; Reference: Solution B. a) Ion/Pd(II).

(ε=3.0×10^5).

The relative standard deviation (R.S.D.) was 0.84% for ten runs with 4.2 μg of palladium(II).

Interference. Various amounts of foreign metal ions were added to a fixed amount of palladium(II) (4.2 μg). There was no interference under the following conditions: 50- to 100-fold molar ratio of copper(II), cobalt(II), nickel(II), cadmium(II), zinc(II), lead(II), manganese(II), lanthanum(III), chromium(III); 10- to 20-fold molar ratio of titanium(IV), iron(III), mercury(II), scandium(III), rhodium(III), silver(I); equimolar to 2-fold molar ratio of molybdenum(VI), bismuth(III), zirconium(IV), osmium(VIII), iridium(III). Only gold interfered in equimolar ratio of palladium(II). On the other hand, among the anions tested, chloride, sulfate, phosphate, citrate, tartrate, nitrate, and fluoride ions did not interfere in 100- to 250-fold excess over palladium(II). A fairly large error appeared in the presence of some anions belonging to soft bases (sulfide, thiosulfate, nitrite, cyanide, and iodide ions) at a low concentration because of a complex formation between these anions and palladium(II). Interference from gold(III) up to a 2-fold molar ratio of palladium(II) could be overcome by the addition of bromide ion (5.0×10^{-4} mol dm^{-3}) as a masking agent. The interference from iodide, thiosulfate, sulfide, and cyanide ions could be overcome by a preliminary treatment with silver(I), and that from sulfite and nitrite ions with permanganate and hydrogen peroxide. The results are shown in Table 2.

Composition of the Ternary Complex Formed. The palladium(II)-to-thiamine ratio and (palladium/thiamine)-to-Phloxine ratio determined by Job's method of continuous variation were 1:2 and 1:1, respectively. The ternary complex formed may be expressed as $\{Pd^{II}(thiamine)_2\}(Phloxine)$.[7]

Application. The proposed method was applied to the assay of palladium in palladium carbon and palladium asbestos. The palladium in the samples was readily dissolved in aqua regia, the insoluble residue being removed by filtration. The obtained results were in good agreement with those obtained by the KI method, the MTK method and ICP-AES. The recoveries of palladium(II) from each sample were about 98—103%. The results are given in Table 3.

Study for Membrane Filter Preconcentration Technique. A membrane filter preconcentration technique was investigated for the purpose of enhancing the determination sensitivity. Only the use of a surfactant was examined to improve the sensitivity and reproducibility under the same conditions for the standard procedure for spectrophotometry. Only PEG was effective among the various surfactants tested. Several filters of different sorts and pore sizes were examined to collect the ternary-complex aggregates. A nitrocellulose membrane filter was suitable since it readily dissolves in organic solvents. Constant absorbances were obtained over a range of pore size, from 0.2 to 0.65 μm; the absorbances decreased with increasing pore size of the membrane filter. A 0.65 μm pore size was subsequently used because of the higher filtration rate. Of the organic solvents examined, DMSO was the best with respect to the high absorbance and low deviation. The absorption spectra of Solutions A′ and B′ are shown in Fig. 2.

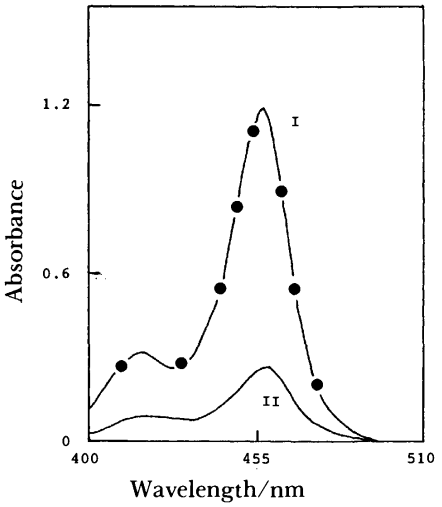

Fig. 2. Absorption spectra of Phloxine-thiamine-palladium(II) DMSO solution (Solution A′) and Phloxine-thiamine DMSO solution (Solution B′) after membrane filter preconcentration technique.
Pd(II): 0.42 μg; Reference: DMSO.
Curve I(—●—), Solution A′; Curve II(——), Solution B′.

Table 3. Determination of Palladium Carbon (Pd-C) and Palladium Asbestos (Pd-A)

Sample	Pd, Amount/%				Recovery test[a] of proposed method	
	Proposed method	KI method	MTK method	ICP-AES	Recovery[b] /%	R.S.D.[c] /%
5% Pd-C	4.75	4.73	4.76	4.70	101.6	1.00
10% Pd-A	9.60	9.71	9.60	9.80	100.1	0.73
20% Pd-A	19.40	19.31	19.32	19.40	102.8	0.70
30% Pd-A	30.54	30.58	30.32	31.00	98.8	0.86

a) Mean of 5 determinations. b) Palladium taken, 2.1 μg/10 ml. c) Relative Standard Deviation.

This procedure is more than 20 times as sensitive as the method employing aqueous medium. Analytical values of 5% palladium carbon and 20% palladium asbestos in Table 3 were 4.60% and 19.20%, respectively.

Furthermore, since Solutions A′ and B′ emitted fluorescence, fluorimetry could be used. The difference in the relative fluorescence intensity between Solutions A′ and B′ at 575 nm of emission wavelength with excitation at 520 nm was measured.

In general, the formation of a ternary-complex results in a quenching of the fluorescence[3] of the dye used. Nevertheless, the fluorescence intensity of Solution A′ was larger than that of Solution B′. The absorption spectrum and the emission spectrum of an independently prepared Phloxine DMSO solution were almost identical to that of Solutions A′ and B′. It is probable that the ternary-complex aggregate collected on a membrane filter dissociates to form at least two components, $\{Pd^{II}(thiamine)_2\}$ and Phloxine. The latter will give a fluorescence and absorption spectrum in a DMSO solution. The reason why the method with a membrane filter preconcentration technique gives an abnormally highly sensitivity ($\varepsilon > 10^6$) is probably that a few Phloxine molecules associate with the ternary complex and a bulky aggregate forms.

The surface of membrane filters was observed with SEM. In the case of depth-type (networks) membrane filters, a little difference was recognized between the sample (photograph(c)) and the reagent blank (photograph(d)), whereas a large difference was observed between the sample (photograph(a)) and the

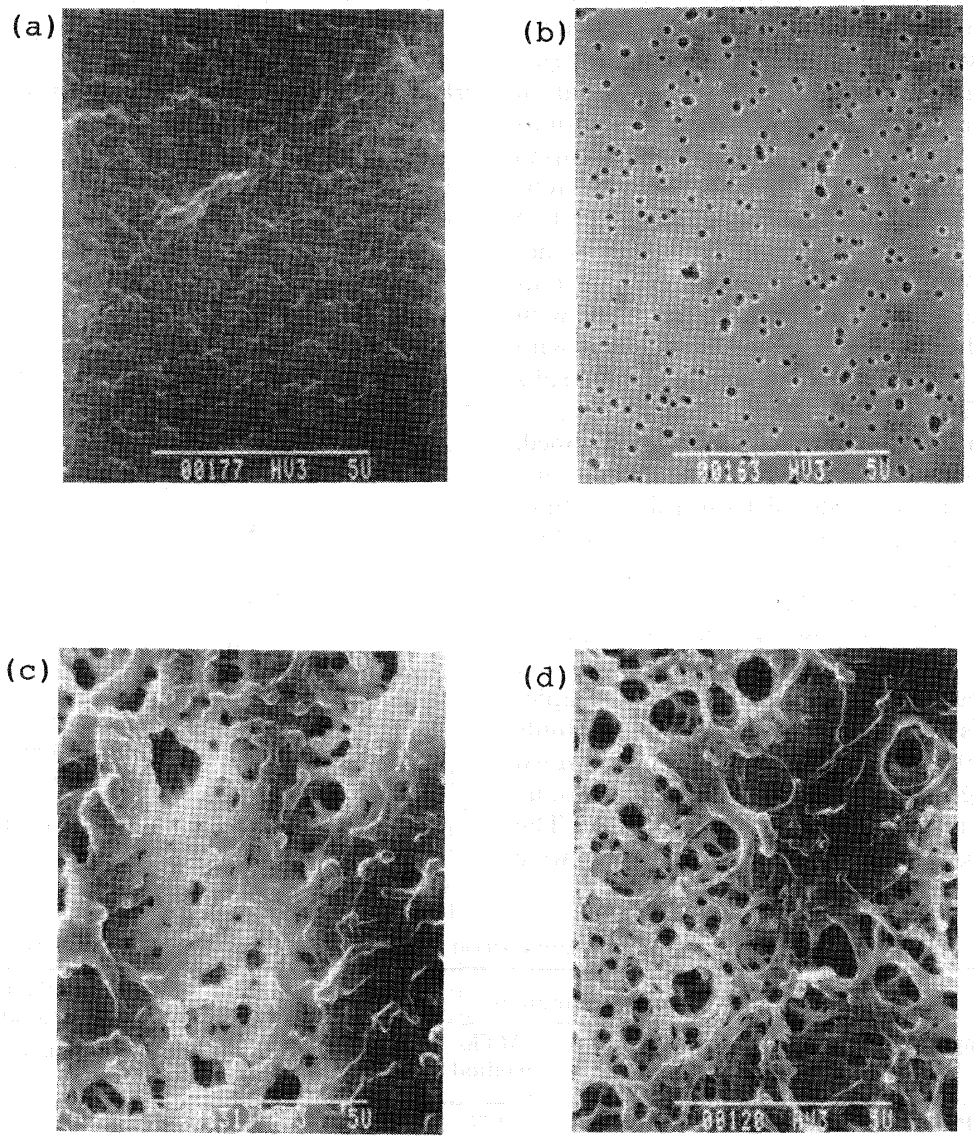

Fig. 3. Scanning electron microscope (SEM) pictures of the aggregates collected on membrane filters.
(a) Sample (Phloxine–thiamine–palladium(II)) on screen-type filter. (b) Reagent blank (Phloxine–thiamine) on screen-type filter. (c) Sample on depth-type filter. (d) Reagent blank on depth-type filter.

reagent blank (photograph(b)) in screen-type (holes) membrane filters. Thus, the collection of aggregate on membrane filters was found to depend not on the adsorptivity but on the molecular size. These photographs are shown in Fig. 3. This point should be studied in greater details.

Conclusion

A simple, sensitive and selective spectrophotometric method of palladium(II) with Phloxine as {**R**} and thiamine as {**L**} was established. The method was applied to the assay of palladium in practical samples, and the analytical results were in good agreement with those obtained by other methods. The sensitivity was enhanced by about 20 times over spectrophotometry and/or fluorimetry (probably by measuring free Phloxine in DMSO) by combining a membrane filter preconcentration technique. It was suggested by observing with SEM that the collection of aggregate on a membrane filter should depend on the molecular size. Though further investigations are necessary for the application of this method to a variety of samples, including the development of the membrane filter preconcentration technique, the proposed method should be useful and convenient for a simple, sensitive determination of palladium(II).

The authors wish to thank Mr. Tsutomu Iwamoto of Osaka University of Pharmaceutical Sciences for SEM photographing of the collection of aggregate on a membrane filter.

References

1) This paper is Part LXXXI of a series entitled "Application of Xanthene Derivatives for Analytical Chemistry". This work was presented at 108th Annual Meetings of Pharmaceutical Society of Japan in Hiroshima, April 1988.
2) A. T. Pilipenko and M. M. Tananaiko, *Talanta*, **21**, 501 (1974).
3) P. R. Haddad, *Talanta*, **24**, 1 (1977).
4) Z. Marczenko,"Separation and Spectrophotometric Determination of Elements," Ellis Horwood Ltd., Chichester (1986).
5) Y. Fujita, I. Mori, S. Kitano, H. Kawabe, and Y. Kamada, *Bull. Chem. Soc. Jpn.*, **57**, 1828 (1984).
6) I. Mori, Y. Fujita, H. Kawabe, and K. Fujita, *Bunseki Kagaku*, **34**, 648 (1985).
7) Y. Fujita, I. Mori, K. Fujita, Y. Nakahashi, and T. Tanaka, *Chem. Pharm. Bull.*, **35**, 5004 (1987).
8) C. Matsubara, Y. Yamamoto, and K. Takamura, *Analyst (London)*, **112**, 1257 (1987).
9) I. Mori, Y. Fujita, H. Kawabe, and K. Fujita, *Chem. Pharm. Bull.*, **34**, 902 (1986).
10) I. Mori, *Yakugaku Zasshi*, **85**, 481 (1965).
11) T. Ohno and I. Mori, *Ann. Proc. Gifu Coll. Pharm.*, **10**, 60 (1960).
12) Z. Marczenko and A. Ramsza, *Chem. Anal. (Warsaw)*, **23**, 23 (1978).
13) J. Minczewski, M. Krasiejko, and Z. Marczenko, *Chem. Anal. (Warsaw)*, **15**, 43 (1970).
14) A. T. Pilipenko, O. P. Ryabushko, and G. S. Matsibura, *Zh. Anal. Khim.*, **35**, 1545 (1980).
15) Z. Marczenko and M. Jarosz, *Talanta*, **28**, 561 (1981).

Formation of (η-Cyclopentadienyl)(1,2-ethylenedithiolato, 1,2-ethylenediselenolato, and 2-selenolatoethylenethiolato-*S*,*Se*)cobalt(III) Complexes in a One-Pot-Reaction of (η-Cyclopentadienyl)(1,5-cyclooctadiene or dicarbonyl)cobalt(I) with Alkyne and a Mixture of S_8 and Se_8

Masatsugu KAJITANI, Ryuji OCHIAI, Kakushi DOHKI, Norikazu KOBAYASHI, Takeo AKIYAMA, and Akira SUGIMORI*
Department of Chemistry, Faculty of Science and Technology, Sophia University, Kioi-cho 7-1, Chiyoda-ku, Tokyo 102
(Received May 19, 1989)

A one-pot-reaction of (η-cyclopentadienyl)(1,5-cyclooctadiene or dicarbonyl)cobalt(I) with alkyne (diphenylacetylene and phenylacetylene) and a mixture of S_8 and Se_8 gives (η-cyclopentadienyl)(2-selenolatoethylenethiolato-*S*,*Se*)cobalt(III) complex in addition to the corresponding dithiolato and diselenolato complexes. When phenylacetylene was used as an alkyne, a (2-phenyl-2-selenolatoethylenethiolato-*S*,*Se*)cobalt(III) complex was formed preferentially rather than the (1-phenyl-2-selenolatothiolato-*S*,*Se*)cobalt(III) complex. The separation of the diselenolato and selenolatothiolato complexes from the dithiolato complex was successfully done by utilizing the difference in how these complexes form adducts with tributylphosphine. The dithiolato complexes have more negative reversible half-wave potentials (for reduction) than the diselenolato complexes; the selenolatothiolato complexes have intermediate half-wave potentials.

Dithiolatometal complexes have unique electronic structures[1] and show several useful functions,[2] such as catalysts for the synthesis of thiophene derivatives[3] and for isomerization of quadricyclane to norbornadiene.[4] Photocatalysis for hydrogen evolution[5] and quenching of singlet oxygen[6] have been reported, along with electron transport[7] and electric conductivity properties.[8] The interest in the chemistry of chalcogen compounds is now expanding to compounds containing selenium and tellurium.

Owing to the development of a new and facile synthetic method for (η-cyclopentadienyl)(1,2-ethylenedithiolato)cobalt(III) complexes in a one-pot-reaction of [Co(cp)(CO)$_2$] or [Co(cp)(cod)] (cod=1,5-cyclooctadiene) with elemental sulfur and alkynes,[3] dithiolatometal complexes of this type with various substituents can be easily synthesized.

This type of reaction has been applied to the synthesis of diselenolatometal complexes.[9] However, this type of reaction has never been examined by using a mixture of elemental sulphur and elemental selenium. In this paper we report that the one-pot-reactions of η-cyclopentadienylcobalt species with alkyne and a mixture of S_8 and Se_8 give (η-cyclopentadienyl)(2-selenolatoethylenethiolato-*S*,*Se*)cobalt(III), in addition to the corresponding dithiolato and diselenolato complexes.[10] Only three reports have appeared on the synthesis of selenolatothiolatometal complexes.[9,11,12] We also discuss the properties of dithiolato, diselenolato, and selenolatothiolato complexes.

Results and Discussion

Formation of Dithiolato, Diselenolato, and Selenolatothiolato Complexes. When a mixture of (η-cyclopentadienyl)(1,5-cyclooctadiene or dicarbonyl)cobalt(I)([Co(cp)(cod)]: **4a** or [Co(cp)(CO)$_2$]: **4b**), diphenylacetylene, elemental sulfur, and elemental selenium is refluxed in xylene, (η-cyclopentadienyl)-(1,2-diphenyl-1,2-ethylenedithiolato)cobalt(III)(**2a**), (η-cyclopentadienyl)(1,2-diphenyl-1,2-ethylenediselenolato)cobalt(III) (**3a**), and (η-cyclopentadienyl)-(1,2-diphenyl-2-selenolatoethylenethiolato-*S*,*Se*)-cobalt(III) (**1a**) are formed.

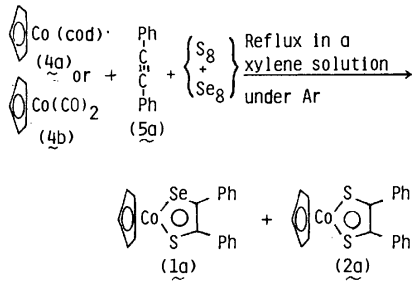

These three complexes could not be separated by ordinary chromatographic methods. However, the separation was successfully carried out by the combination of the adduct formation of these complexes with tributylphosphine and chromatography. Complexes **1a** and **3a** form 1 : 1 adducts with tributylphosphine and are separated from **2a** by means of silica-gel chromatography under Ar (**2a** is eluted more easily than the phosphine-adducts of **1a** and **3a**). The complexes **1a** and **3a** can be easily regenerated from the adducts with tributylphosphine by oxidizing the phosphine on exposure to the air.

When we choose the compositions of S_8 and Se_8 such that **3a** is not formed (for example, under the condition of S : Se=1 : 6), the selenolatothiolato complex, **1a**, can be obtained in pure form.

The yields of **1a**, **2a**, and **3a** determined by the ^{1}H NMR spectroscopy, are shown in Table 1, together with the initial ratios of sulfur and selenium.

Table 1. Yields of Selenolatothiolato (**1a**), Dithiolato (**2a**), and Diselenolato (**3a**) Complexes in the Reaction of [Co(cp)(cod)] (cod=1,5-cyclooctadiene) (**4a**), Diphenylacetylene (**5a**), and a Mixture of S_8 and Se_8

Molar ratio of S_8 and Se_8 to **5a**		Yield of product/%[a]		
S_8	Se_8	**1a**	**2a**	**3a**
2/8	0	—	16	—
0	2/8	—	—	20
2/8	2/8	18	45	0
2/8	8/8	20	30	1
1/8	1/8	17	16	1
1/8	4/8	27	23	6
1/8	6/8	49	23	7
1/20	4/20	21	9	6

a) Yield=(amount of product/amount of **4a** used) ×100.

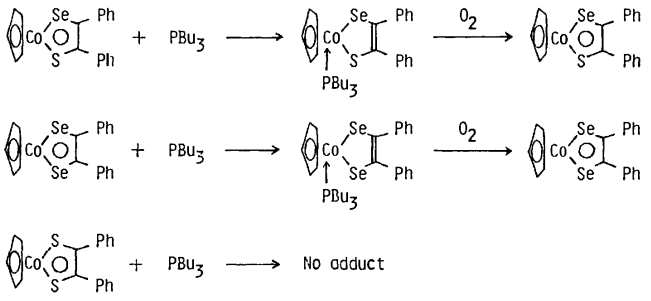

When we used phenylacetylene as an alkyne, we obtained (η-cyclopentadienyl)(2-phenyl-2-selenolatoethylenethiolato-*S*,*Se*)cobalt(III) (**1b**) and (η-cyclopentadienyl)(1-phenyl-2-selenolatoethylenethiolato-*S*,*Se*)cobalt(III) (**1b′**) as the complexes containing both S and Se. In this case, the amount of **1b** was greater than that of **1b′**.

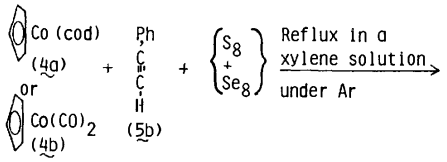

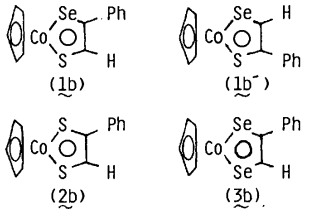

The identification of **1b** and **1b′** was done by the synthesis of **1b′** by the reaction of [Co(cp)I_2CO] and 5-phenyl-1,3-thiaselenole-2-thione in ethanol in the presence of sodium ethoxide. 5-Phenyl-1,3-thiaselenole-2-thione was prepared according to the method of Mayer and Müller.[13]

The dependences of the yields of **1b**, **1b′**, **2b**, and **3b** on the initial ratio of S_8 and Se_8 are shown in Table 2.

The addition of sulfur to the [Co(cp)(cod)]-alkyne-Se_8 system causes remarkable decreases in the yields of the diselenolato complexes. But the addition of selenium to the [Co(cp)(cod)]-diphenylacetylene-S_8 system promotes the formation of the dithiolato complex. In the [Co(cp)$(CO)_2$]-phenylacetylene-S_8 system, the addition of selenium lowers the yield of the dithiolato complex, but the inhibiting effect of selenium on the formation of dithiolato complex is much smaller than that of sulfur on the formation of the diselenolato complex in the reaction of [Co(cp)$(CO)_2$], phenylacetylene, and Se_8.

Table 2. Yields of Selenolatothiolato (**1b** and **1b′**), Dithiolato (**2b**), and Diselenolato (**3b**) Complexes in the Reaction of [Co(cp)$(CO)_2$] (**4b**), Phenylacetylene (**5b**), and a Mixture of S_8 and Se_8

Molar ratio of S_8 and Se_8 to **5b**		Yield of product/%[a]			
S_8	Se_8	**1b**	**1b′**	**2b**	**3b**
2/8	0	—	—	28	—
0	2/8	—	—	—	15
2/8	2/8	15	1.7	13	1.1
1/8	6/8	24	3	8	6
6/8	1/8	Trace	0	35	0

a) Yield=(amount of product/amount of **4b** used) ×100.

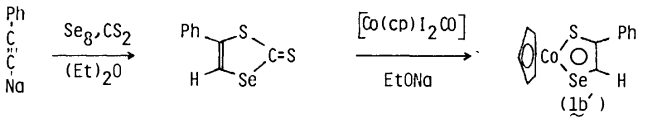

Reaction Mechanism. For the formation of dithiolato, diselenolato, and selenolatothiolato complexes, the intermediacy of "clusters" consisting of η-cyclopentadienylcobalt and chalcogen atoms is presumed. In the absence of alkyne, [Co(cp)(cod)] reacts with a mixture of S_8 and Se_8 (molar ratio of S_8 and Se_8 to **4a** are 1/20 and 1/5 (=4/20), respectively) to give a dark brown solid. The mass spectral analysis of the dark brown solid showed that the solid consists of several S, Se-mixed clusters. A chromatographically separated fraction, which consists of $[Co_4S_2Se_2(cp)_4]$, $[Co_4S_3Se(cp)_4]$, and $[Co_4S_4(cp)_4]$, reacts with **4a** in boiling xylene to afford **1a**, **2a**, and **3a**.

This result indicates that the dithiolato, diselenolato, and selenolatothiolato complexes are formed by the attack of alkyne to the chalcogen atoms of the cluster complexes either in a concerted or in a stepwise process.

One factor in determining the relative amounts of dithiolato, diselenolato, and selenolatothiolato complexes would be the selectivity in the attack of alkyne to the cluster complexes. However, there exists another factor to determine the amounts: the ligand exchange of the primarily formed dichalcogenato complexes. A prolonged heating of a selenolatothiolato complex **1b′** in xylene under reflux (140 °C) brings about the formation of the dithiolato complex

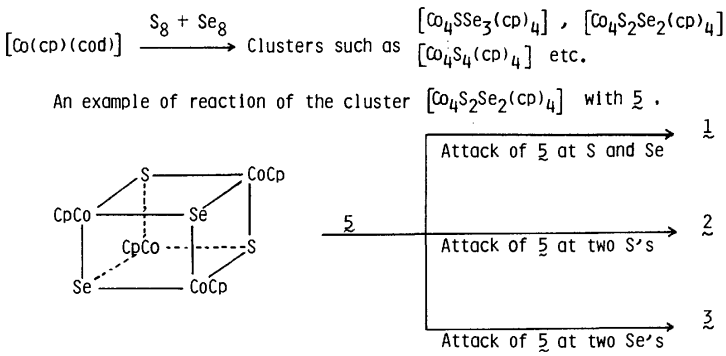

2b. This fact shows the exchange of the chalcogen atoms.

Physical Properties of Dithiolato, Diselenolato, and Selenolatothiolato Complexes. Some important spectroscopic properties as well as the reversible half-wave potentials (for reduction) of the complexes **1**, **2**, and **3** are summarized in Table 3.

The patterns of the electronic spectra of the diselenolatocobalt(III) complexes are similar to those of the dithiolato complexes. Each complex has four absorptions in the UV-vis. region. The absorption maxima of the diselenolatocobalt(III) complexes are situated at wavelengths longer than those of the corresponding dithiolato complexes. The absorption maxima of the selenolatothiolato complexes are located between those of the dithiolato and diselenolato complexes. The weak absorptions around 750—820 and 420—480 nm shift more sensitively dependent on the kinds and number of the chalcogen atoms than the strong absorptions around 600—620 and 290—300 nm.

The reversible half-wave potentials (for reduction) of the diselenolato complexes are higher than those of the corresponding dithiolato complexes: thus the diselenolato complexes are reduced more easily than the dithiolato complexes. The selenolatothiolato complexes have intermediate half-wave potentials between the dithiolato and diselenolato complexes.

The fact that the $E^{r}_{1/2}$ values of the diselenolato complexes are higher than those of the dithiolato complexes suggests that the central cobalt atoms in the diselenolato complexes are charged more positively than those in the dithiolato complexes. There is a contradiction in the values of electronegativities of selenium and sulfur: according to Pauling, the electronegativity of sulfur (2.5) is larger than that of selenium (2.4),[14] while according to Allred-Rochow, the electronegativity of sulfur (2.4) is smaller than that of selenium (2.5).[15] The observed half-wave potentials of diselenolato and dithiolato complexes suggest that the selenium behaves in dichalcogenatometal complexes as a more electronegative element than sulfur does.

The delta value of chemical shifts in ^{1}H NMR spectra for the proton attached to the diselenolene ring in **3b** is larger than that for the proton attached to the dithiolene ring in **2b**. The chemical shifts ascribed to H in selenathiolene rings in **1b** and **1b′** are interme-

Table 3. Spectral Properties and Half-Wave Potentials (for Reduction) of Selenolatothiolato (**1**), Dithiolato (**2**), and Diselenolato (**3**) Complexes

	2a	**1a**	**3a**	**2b**	**1b**	**1b′**	**3b**
^{1}H NMR (δ)							
Cp	5.39	5.37	5.35	5.37	5.36	5.36	5.35
Ring[a]	—	—	—	9.00	9.15	9.74	9.85
^{13}C NMR (δ)							
Cp	79.62	78.80	77.97	79.28	78.42	78.51	77.61
Ring[a]	168.80	165.95	169.14	155.23	158.72	150.62	154.23
		171.93		172.47	169.74	176.60	174.00
UV-vis.							
λ_{max}/nm (ε[b])	750 (770)	772 (970)	812 (1050)	748 (725)	765 (1040)	764 (760)	812 (1060)
	600 (8550)	610 (8730)	612 (8370)	558 (7250)	602 (7450)	601 (5660)	608 (7340)
	424 (1210)	445 (2000)	472 (1980)	424 (1100)	444 (1550)	438 (1410)	471 (1730)
	295 (33500)	299 (35600)	304 (34500)	292 (24000)	298 (27800)	297 (21600)	303 (30000)
Half-wave potential							
$E^{r}_{1/2}$(red)/V	−1.16	−1.12	−1.08	−1.17	−1.13	−1.13	−1.09
Formation of adduct							
with PBu_3	No	Yes	Yes	No	Yes	Yes	Yes

a) Dithiolene, diselenolene, or thioselenolene ring. b) ε/mol^{-1} dm^3 cm^{-1}.

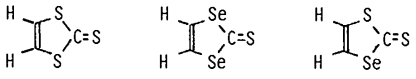

6 7 8

diate. A similar tendency has been reported for 1,3-dichalcogenolene-2-thiones and selones (**6**, **7**, and **8**).[16] (Delta-values of ^{1}H NMR in **6** and **7** are 7.17 and 7.92, respectively. Those in **8** are 7.26 and 7.80.) These facts seem to agree with the results of $E^r_{1/2}$: The more positive selenium attracts electrons more strongly than sulfur does.

The chemical shifts of the ^{1}H and ^{13}C NMR in the cyclopentadienyl ring are influenced much less by the chalcogen atoms than those of H in the dichalcogenolene rings. However, an opposite effect of chalcogen is observed: The signals due to ^{1}H and ^{13}C in the cyclopentadienyl ring in diselenolato complexes appear in higher magnetic field than those in the dithiolato complexes.

The chemical shifts of ^{1}H and ^{13}C NMR in the selenolatothiolato complexes are situated between those of the dithiolato complexes and those of the diselenolato complexes.

Adduct Formation with Tributylphosphine. A remarkable difference in chemical properties among dithiolato, diselenolato, and selenolatothiolato complexes with phenyl group as the substituent is the adduct formation with phosphine. Complexes **1a** and **3a** form 1 : 1 adduct with tributylphosphine, while **2a** does not react with tributylphosphine. A similar difference in the reactivities was observed for **1b**, **1b′**, **2b**, and **3b**. In a separate report,[17] we have described that the adduct formation of dithiolatocobalt complexes with phosphines and phosphites is dependent on the (reversible) half-wave potentials of reduction of the dithiolato complexes: The dithiolato complexes, the $E^r_{1/2}$'s of which are higher than -1.13 V, form an adduct with tributylphosphine. The $E^r_{1/2}$ values of the dithiolato, diselenolato, and selenolatothiolato complexes are accidentally distributed across the critical $E^r_{1/2}$ value. This is the reason why we could separate these complexes by the adduct formation with tributylphosphine.

Experimental

Materials. Commercially available diphenylacetylene, elemental sulfur, and elemental selenium were used as purchased. Phenylacetylene was purified by distillation.

Spectroscopy and Elemental Analysis. NMR spectra were recorded on a JEOL GX-270 instrument and mass spectra on a JEOL JMS-D300 instrument. UV-vis. spectra were measured with a Hitachi spectrometer Model 228. Elemental analysis was carried out with a Perkin-Elmer Model 240 C apparatus.

Reaction of η-Cyclopentadienylcobalt(I) Species, Alkyne, and Elemental Chalcogen. A mixture of [Co(cp)(cod)] or [Co(cp)(CO)$_2$] (ca 1.4 mmol), alkyne (ca 1.7 mmol), and a mixture of S_8 and Se_8 in xylene (25 cm^3) was refluxed for 24 h under an atmosphere of Ar.

Separation and Identification of Products. After the evaporation of the solvent under reduced pressure, the residue was extracted with dichloromethane. The extract was concentrated and the product mixture was submitted to the column chromatography (column, silica gel C-300 made by Wako Pure Chemical Co.; eluent, hexane-dichloromethane). The complexes **1**, **2**, and **3** were eluted together.

In order to obtain pure **1a**, the following procedure was followed. The reaction mixture from the reaction under the condition of S : Se=1 : 6 (the conditions under which only a small amount of **3a** was formed) was preliminarily separated by the procedure described above. The composition of the mixture of **1a**, **2a**, and **3a** was determined by means of ^{1}H NMR. Then, to the mixture under Ar was added tributylphosphine, the amount of which was equal to the sum of the amounts of **1a** and **3a**. Then the mixture was submitted to the column chromatography using a column packed with silica gel C-300. After the elution of **2a** with a mixture of dichloromethane and hexane, the column was exposed to the air and **1a** and **3a** were regenerated by the oxidative elimination of tributylphosphine. By the elution with dichloromethane-hexane, **1a** was obtained in analytically pure form. A similar method was applied to the separation of **1b**, **1b′**, **2b**, and **3b**.

(η-Cyclopentadienyl)(1,2-diphenyl-1,2-ethylenedithiolato)cobalt(III) (2a) was identified by reference to the spectra reported by Bönnemann.[18] Blue crystals; mp 235—238 °C; IR (KBr disk) 3098, 764, 743, and 698 cm^{-1}; ^{1}H NMR ($CDCl_3$) δ=5.39 (5H, s, cp) and 7.12—7.26 (10H, m, Ph); ^{13}C NMR ($CDCl_3$) δ=79.62 (cp), 127.1 (Ph), 127.8m (Ph), 129.0 (Ph), 142.0 (Ph), and 168.8 (dithiolene ring); MS (70 eV) *m/z* (rel intensity) 368 (5, M$^+$), 367 (11, M$^+$), 366 (49, M$^+$), 190 (9), 189 (7), 188 (100), 178 (16), 124 (26), and 59 (7). Found: C, 62.51; H, 3.95%.

(η-Cyclopentadienyl)(1,2-diphenyl-1,2-ethylenediselenolato)cobalt(III) (3a): Green crystals; mp 250—255 °C (lit,[9] mp 237 °C); IR (KBr disk) 3095, 762, 727, and 697 cm^{-1}; ^{1}H NMR ($CDCl_3$) δ=5.35 (5H, s, cp) and 7.10—7.23 (10H, m, Ph); ^{13}C NMR ($CDCl_3$) δ=77.97 (cp), 126.84 (Ph), 127.74 (Ph), 129.22 (Ph), 143.83 (Ph), and 169.14 (diselenolene ring); MS (70 eV) *m/z* (rel intensity) 462 (6, M$^+$), 460 (6, M$^+$), 459 (2, M$^+$), 458 (3, M$^+$), 286 (12), 284 (43), 282 (37), 281 (12), 280 (23), 178 (100), 124 (43), and 59 (7).

Found: C, 49.57; H, 3.26%. Calcd for $C_{19}H_{15}CoSe_2$: C, 49.59; H, 3.29%.

(η-Cyclopentadienyl)(1,2-diphenyl-2-selenolatoethylenethiolato-*S*,*Se*)cobalt(III) (1a): Green crystals; mp 234—236 °C; IR (KBr disk) 3098, 763, 734, and 698 cm^{-1}; ^{1}H NMR ($CDCl_3$) δ=5.37 (5H, s, cp) and 7.10—7.25 (10H, m, Ph); ^{13}C NMR ($CDCl_3$) δ=78.80 (cp), 126.84 (Ph), 127.15 (Ph), 127.78 (Ph), 127.85 (Ph), 128.73 (Ph), 129.56 (Ph), 142.57 (Ph), 143.75 (Ph), 165.95 (thiaselenolene ring), and 171.93 (thiaselenolene ring); MS (70 eV) *m/z* (rel intensity) 416 (8, M$^+$), 415 (7, M$^+$), 414 (32, M$^+$), 412 (16, M$^+$), 411 (6, M$^+$), 410 (6, M$^+$), 238 (22), 237 (8), 236 (100), 234 (49), 233 (17), 232 (19), 178 (57), 124 (55), and 59 (11)

Found: C, 54.87; H, 3.89%. Calcd for $C_{19}H_{15}CoSSe$: C, 55.07; H, 3.62%.

(η-Cyclopentadienyl)(phenyl-1,2-ethylenedithiolato)cobalt(III) (2b) was identified by reference to the spectra

reported by Bönnemann.[18] Blue crystals; mp 85—87 °C; IR (KBr disk) 3098, 757, and 697 cm^{-1}; ^1H NMR ($CDCl_3$) δ=5.37 (5H, s, cp), 7.24—7.80 (5H, m, Ph), and 9.00 (1H, s, H in dithiolene ring); ^{13}C NMR ($CDCl_3$) δ=79.28 (cp), 126.47 (Ph), 127.53 (Ph), 128.62 (Ph), 140.14 (Ph), 155.23 (dithiolene ring attached to H), and 172.47 (dithiolene ring attached to Ph); MS (70 eV) *m/z* (rel intensity) 292 (6, M^+), 291 (10, M^+), 290 (64, M^+), 190 (9), 189 (7), 188 (100), 124 (36), 102 (8), 59 (16).

Found: C, 55.09; H, 3.79%. Calcd for $C_{13}H_{11}CoS_2$: C, 53.79; H, 3.79%.

(η-Cyclopentadienyl)(phenyl-1,2-ethylenediselenolato)-cobalt(III) (3b): Blue crystals; mp 116—118 °C; IR (KBr disk) 3096, 763, 740, and 696 cm^{-1}; ^1H NMR ($CDCl_3$) δ=5.35 (5H, s, cp), 7.29—7.71 (5H, m, Ph), and 9.85 (1H, s, diselenolene ring); ^{13}C NMR ($CDCl_3$) δ=77.61 (cp), 126.96 (Ph), 127.28 (Ph), 128.39 (Ph), 150.70 (Ph), 154.23 (diselenolene ring), 174.00 (diselenolene ring); MS (70 eV) *m/z* (rel intensity) 338 (9, M^+), 386 (29, M^+), 384 (26, M^+), 383 (10, M^+), 382 (15, M^+), 380 (6, M^+), 286 (31), 285 (6), 284 (100), 282 (86), 281 (29), 280 (51), 279 (14), 278 (20), 124 (99), 102 (33), and 59 (18).

Found: C, 40.93; H, 2.84%. Calcd for $C_{13}H_{11}CoSe_2$: C, 40.66; H, 2.87%.

(η-Cyclopentadienyl)(2-phenyl-2-selenolatoethylene-thiolato-*S,Se*)cobalt(III) (1b): Violet crystals; mp 86—88 °C; IR (KBr disk) 3098, 755, and 696 cm^{-1}; ^1H NMR ($CDCl_3$) δ=5.36 (5H, s, cp) and 9.15 (1H, s, thiaselenolene ring); ^{13}C NMR ($CDCl_3$) δ=78.50 (cp), 126.49 (Ph), 127.29 (Ph), 128.70 (Ph), 141.88 (Ph), 158.72 (thiaselenolene ring), and 169.74 (thiaselenolene ring); MS (70 eV) *m/z* (rel intensity) 340 (10, M^+), 339 (7, M^+), 338 (43, M^+), 336 (22, M^+), 335 (8, M^+), 334 (8, M^+), 238 (22), 237 (7), 236 (100), 235 (4), 234 (49), 233 (17), 232 (19), 124 (71), 102 (12), and 59 (22).

Found: C, 45.88; H, 3.22%. Calcd for $C_{13}H_{11}CoSSe$: C, 46.32; H, 3.27%.

(η-Cyclopentadienyl)(2-phenyl-2-selenolatoethylene-thiolato-*S,Se*)cobalt(III) (1b′) was identified by the synthesis in the reaction of [Co(cp)I_2CO] with 5-phenyl-1,3-thiaselenole-2-thione. Violet crystals; mp 98—100 °C; IR (KBr disk) 3096, 764, 746, and 698 cm^{-1}; ^1H NMR ($CDCl_3$) δ=5.36 (5H, s, cp), 9.74 (1H, s, H in the dithiolene ring); ^{13}C NMR ($CDCl_3$) δ=78.51 (cp), 127.06 (Ph), 127.56 (Ph), 128.39 (Ph), 140.74 (Ph), 150.62 (CH in the dithiolene ring), and 176.60 (CPh in the dithiolene ring); MS (70 eV) *m/z* (rel intensity) 340 (11, M^+), 339 (7, M^+), 338 (48, M^+), 336 (24, M^+), 335 (9, M^+), 334 (9, M^+), 238 (22), 237 (7), 236 (100), 235 (4), 234 (49), 233 (16), 232 (19), 124 (80), 102 (17), and 59 (29).

Found: C, 45.72; H, 3.09%. Calcd for $C_{13}H_{11}CoSSe$: C, 46.32; H, 3.27%.

Determination of Yields of Products. The fraction containing **1**, **2**, and **3**, which resulted from the column chromatography of the products, was submitted to the measurement of ^1H NMR in a $CDCl_3$ solution. The contents of **1a**, **2a**, and **3a** from the reaction among diphenylacetylene, [Co(cp)$(CO)_2$], S_8, and Se_8 were calculated from the areas of the ^1H NMR peaks ascribed to cp rings (δ=5.37 for **1a**, δ=5.39 for **2a**, and δ=5.35 for **3a**).

The composition of the mixtures from the reaction among phenylacetylene, [Co(cp)$(CO)_2$], S_8, and Se_8 were calculated from the areas of the ^1H NMR peaks ascribed to the protons in the dithiolene ring (δ=9.15 for **1b**, δ=9.74 for **1b′**, δ=9.00 for **2b**, and δ=9.85 for **3b**).

Formation, Separation, and Identification of Cluster Complexes. A mixture consisting of [Co(cp)(cod)] (4.3 mmol), Se_8 (0.54 mmol), and S_8 (0.54 mmol) in xylene (35 cm^3) was heated under reflux (140 °C) under Ar for 24 h. After the evaporation of the solvent under reduced pressure, the residue was extracted with dichloromethane and the dichloromethane-insoluble substances were removed by filtration. The dichloromethane-soluble substances were separated by column chromatography (column, silica gel C-300 made by Wako Pure Chemical Co.; eluent, dichloromethane–diethyl ether). Black solid was eluted with dichloromethane (3)–diethyl ether (1). The mass-spectral measurement showed it to be a mixture of cluster complexes of [$Co_4S_2Se_2(cp)_4$], [$Co_4S_3Se(cp)_4$], and [$Co_4S_4(cp)_4$] (the mass spectra of the mixture (70 eV): *m/z* (rel intensity) 720 (0.42, M^+ of [$Co_4S_2Se_2(cp)_4$]), 718 (0.36, M^+ of [$Co_4S_2Se_2(cp)_4$]), 674 (1.07, M^+ of [$Co_4S_3Se(cp)_4$]), 672 (3.46, M^+ of [$Co_4S_3Se(cp)_4$]) 670 (1.71, M^+ of [$Co_4S_3Se(cp)_4$]), 626 (2.52, M^+ of [Co_4S_4-$(cp)_4$]), 624 (11.87, M^+ of [$Co_4S_4(cp)_4$], 124 (10.09, Co(cp)), and 66 (100, cpH)).

Reaction of a Mixture of Cluster Complexes with Diphenylacetylene. Diphenylacetylene (30 mg) and the mixture of the cluster complexes (30 mg) described above were reacted in xylene (30 cm^3) under Ar at 140 °C for 24 h. After the reaction, the products were separated in the procedure described above. The yields of **1a** and **2a** are 54 mmol and 46 mmol, respectively. The complex **3a** was formed in a trace amount.

Cyclic Voltammetry. All the electrochemical measurements were carried out in acetonitrile solutions containing 0.1 mol dm^{-3} tetraethylammonium perchlorate at 25 °C with a Yanaco Polarographic Analyzer P-1100. A platinum disk electrode (ϕ=2 mm) served as both a stationary working electrode and a rotating electrode. The potential of the working electrode was measured against a silver-silver ion electrode (Ag| 0.1 mol dm^{-3} $AgClO_4$ in acetonitrile).

The authors are grateful to Professor Kunio Shimizu and Mr. Hirobumi Ushijima for the measurement of cyclic voltammogram.

References

1) Recently, Hoffmann et al. analyzed the structural electronic features by MO method: S. Alvarez, R. Vicente, and R. Hoffmann, *J. Am. Chem. Soc.*, **107**, 6253 (1985).

2) A review: A. Sugimori and M. Kajitani, *Kagaku, Zokan*, **115**, 113 (1988).

3) H. Bönnemann, B. Bogdanovic, W. Brijoux, R. Brinkmann, M. Kajitani, R. Mynott, G. S. Natarajan, and M. G. Y. Samson, "Transition-Metal-Catalyzed Synthesis of Heterocyclic Compounds," in "Catalysis in Organic Reactions," ed by J. R. Kosak, Marcel Dekker (1984), pp. 31—62; M. Kajitani, T. Suetsugu, R. Wakabayashi, A. Igarashi, T. Akiyama, and A. Sugimori, *J. Organomet. Chem.*, **293**, C15 (1985).

4) R. B. King and S. Ikai, *J. Mol. Catal.*, **4**, 361 (1978).

5) R. Henning, W. Schlamann, and H. Kisch, *Angew. Chem.*, **92**, 604 (1980).

6) M. Kajitani, Y. Yoshida, T. Akiyama, and A. Sugimori, *Nippon Kagaku Kaishi*, **1987**, 1464.

7) J. J. Grimaldi and J. M. Lehn, *J. Am. Chem. Soc.*, **101**, 1333 (1979).

8) A. Kokayashi, Y. Sasaki, H. Kobayashi, A. E.

Underhill, and M. M. Ahmad, *J. Chem. Soc., Chem. Commun.*, **1982**, 390.

9) E. J. Miller, S. J. Landon, and T. B. Brill, *Organometallics*, **4**, 533 (1985).

10) We have preliminarily reported that the reaction of [Co(cp)(cod)] diphenylacetylene, and a mixture of S_8 and Se_8. (M. Kajitani, R. Ochiai, N. Kobayashi, T. Akiyama, and A. Sugimori, *Chem. Lett.*, **1987**, 245).

11) E. Fanghanel and H. Poleschner, *Z. Chem.*, **19**, 192 (1979).

12) D. J. Sandman, J. C. Stark, L. A. Acampora, L. A. Samuelson, G. W. Allen, S. Jansen, M. T. Jones, and B. M. Foxman, *Mol. Crtst. Liq. Cryst.*, **107**, 1 (1984).

13) R. Mayer and A. K. Müller, *Z. Chem.*, **4**, 384 (1964).

14) L. Pauling, "The Nature of Chemical Bond," 3rd ed, Cornell University Press, NY (1960), p. 93.

15) A. L. Allred and E. G. Rochow, *J. Inorg. Nucl. Chem.*, **5**, 264 (1958).

16) E. M. Engler and V. V. Patel, *J. Org. Chem.*, **40**, 387 (1975).

17) M. Kajitani, A. Igarashi, T. Aritomo, T. Akiyama, K. Shimizu, A. Sugimori, and H. Bönnemann, *J. Organomet. Chem.*, submitted.

18) H. Bönnemann, private communication.

Physicochemical Studies on Solid Solutions of Calcium Phosphorus Arsenic Hydroxyapatites

P. P. MAHAPATRA,* L. M. MAHAPATRA, and Bagmi MISHRA
Post-Graduate Department of Chemistry, Khallikote College, Berhampur, GM: 760001, India
(Received April 20, 1988)

Samples of arsenic hydroxyapatite and its solid solutions with calcium hydroxyapatite are synthesized in aqueous media. The samples are characterized by X-ray, infrared spectra, the assignments of phosphate, arsenate, and hydroxyl bands are recorded. The possibility of anion migration in the apatite lattice is proposed. Presence of water, adsorbed in nature, is indicated in the TGA and DTA analysis of the samples. The solubility product, K_{sp}, of the samples of arsenic hydroxyapatite $Ca_{10}(AsO_4)_6(OH)_2$, and the solid solutions, $Ca_{10}(PO_4)_{6-x}(AsO_4)_x(OH)_2$, ($x$=1 to 5) are determined considering the formation of ion pairs $[CaHAsO_4]^0$, $[CaHPO_4]^0$, $[Ca(H_2AsO_4)]^+$, and $[Ca(H_2PO_4)]^+$ in solution. The instability of the samples in solution is indicated from the experimental $\Delta G^0_{soln.}$ values.

Arsenic has been recognised as a toxic element, which causes poisoning in vivo.[1,2] It is deposited in bones and bony tissues[3,4] due to the possibility of $P^{5+} \rightarrow As^{5+}$ exchange reaction in the calcium hydroxyapatite, $Ca_{10}(PO_4)_6(OH)_2$, CaPHA of bone.[5] When this exchange reaction in calcium hydroxyapatite is complete, it leads to the formation of arsenic hydroxyapatite, $Ca_{10}(AsO_4)_6(OH)_2$, CaAsHA, isomorphous with $Ca_{10}(PO_4)_6(OH)_2$, CaPHA; while incomplete/partial substitution in it, results in the formation of solid solutions of calcium phosphorus arsenic hydroxyapatite, $Ca_{10}(PO_4)_{6-x}(AsO_4)_x(OH)_2$ (where x is the compositional parameters, ranges from 1 to 5). Though arsenic in naturally occurring phosphatic minerals is well-known[6] and formation of CaAsHA by solid state reaction[7] at high temperature and its characterization is well established, similar studies on CaAsHA and its solid solutions with CaPHA are not available. We, therefore, report here the formation of CaAsHA and calcium phosphorus arsenic hydroxyapatite samples, their characterization by X-ray, IR, and electron microscopy. Since the samples are synthesized in aqueous media at 100 °C, they are likely to carry attendent seats of water molecules with them. The nature of water present in the samples and their thermal stabilities are studied by TGA and DTA methods. The solubility of the samples of the solid solutions are investigated in the pH range 4.0 to 8.0 and their solubility products are reported.

Experimental

The chemicals used in the preparations of the samples were either BDH or E. Merck grade and the solutions are prepared in CO_2 free conductivity water. Calcium nitrate diammonium hydrogen phosphate and disodium hydrogen arsenate were used as desired by the stoichiometry for a sample of the general formula, $Ca_{10}(PO_4)_{6-x}(AsO_4)_x(OH)_2$ for an yield of 15 g. The method used for the preparation was reported earlier.[8] The samples after preparation were centrifuged, washed repeatedly with conductivity water until free from the adsorbed ions. Care was taken to exclude the possibility of incorporation of carbonate during preparation. The samples were dried (12 h) at 110 °C to constant weight and analyzed for Ca, P, and As complexometrically.[9] The X-ray diffraction patterns of the samples were recorded by a Debye-Scherrer powder diffraction instrument using Ni filtered Cu $K\alpha$ radiation. The electron microscopic patterns of acetone-washed samples were obtained using Simens Elminskop I by the method of electromagnetic disperson. The IR spectra of the samples, preheated at 800 °C, were recorded on a Perkin Elmer IR grating instrument. The range covered was from 4000—400 cm^{-1}. The thermal analyses of the samples were made on a Derivatograph (Budapest) which recorded simultaneous photographs of TG, DTA, and DTG of the samples. The samples were heated at a rate of 10° min^{-1} upto 1000 °C in a platinum crucible using Al_2O_3 as reference. The activation energy of dehydration of the samples was obtained by using Freeman and Carrol's equation[10] and also from Arrhenius plot obtained from DTA peaks.

The solubility of the samples was investigated at 35 °C under a constant ionic environment[11] of 0.165 mol dm^{-3} $NaNO_3$ by the method of equilibration. The different concentrations of As_2O_5 in doubly distilled water, for studies in pH range 4.0 to 6.0 and sodium hydroxide for pH 7.10 and 8.0 were used. Equilibration was done in air tight polyethylene thermostated flask containing 200 mg of the samples of particle size 200 μm in 50 ml of the desired solvent. Attainment of saturation was followed kinetically by analyzing in solution calcium, arsenic, and phosphorus content complexometrically.[9] The system attained saturation within ten hours of equilibration.

Calculations

The calculations used in the studies of the solubility are as follows. From the pH of the medium of equilibration and total calcium, arsenic, and phosphorus content, the concentrations of free ionic species XO_4^{3-}, HXO_4^{2-}, and $H_2XO_4^-$ were calculated using Eqs. 1 to 3 (where X=As or P).

$$[XO_4^{3-}] = [X]_{total} \Big/ \left[\frac{(H^+)^3}{K_1K_2K_3} + \frac{(H^+)^2}{K_2K_3} + \frac{(H^+)}{K_3 f_{HAsO_4^{3-}}} + \frac{1}{f_{XO_4^{3-}}}\right] \quad (1)$$

$$[HXO_4^{2-}] = [X]_{total} \Big/ \left[\frac{(H^+)^2}{K_1K_2} + \frac{(H^+)}{K_2 f_{H_2XO_4^-}} + \frac{1}{f_{HXO_4^{2-}}}\right] \quad (2)$$

$$[H_2XO_4^-]=[X]_{total}/\left[\frac{(H^+)}{K_1}+\frac{1}{f_{H_2XO_4^-}}\right] \quad (3)$$

Where K_1, K_2, K_3 are the three dissociation constants of orthoarsenic acid;[12,13] $f_{XO_4^{3-}}$, $f_{HXO_2^{2-}}$, $f_{H_2XO_4^-}$ are the activity coefficients of XO_4^{3-}, HXO_4^{2-}, and $H_2XO_4^-$ respectively. The quantity in the parentheses represented activities. Assuming the activity coefficients unity, approximate ionic strength, μ, was obtained using the equation.

$$\mu=\frac{1}{2}\sum C_iZ_i^2$$

The activity coefficients of the above ionic species of arsenic and phosphorus are obtained by the extended Debye equation.

$$\left(\log f_i=\frac{-A\sqrt{\mu}\,Z_i^2}{1+\sqrt{\mu}}+0.3\mu\right)$$

These were subsequently used and a fresh value of μ was calculated.

Following an iterative procedure, constancy in the value of ionic strength is obtained. The ion activity product, synonymous with the solubility product was calculated using the equation:

$$K_{sp}=[Ca]^{10}[AsO_4^{3-}]^x[PO_4^{3-}]^{6-x}\left[\frac{K_W}{(H^+)}\right]^2 f_2^{10}f_1^{2-}f_{AsO_4^{3-}}^{x}f_{PO_4^{3-}}^{6-x}$$

where f_1 and f_2 stand for activity coefficients of the XO_4 (X=P or As) ions, H^+ and Ca^{2+} ions respectively. The solubility products are redetermined after considering the formation of the ion pairs $Ca(H_2AsO_4)^+$, $(CaHAsO_4)^0$, $Ca(H_2PO_4)^+$, $(CaHPO_4)^0$ in solution. The values of association constants used in the calculations are 8.71×10^{-3}, 0.108×10^{-6} for the arsenate[14,15] and 5.88×10^2, 7.49 for phosphate[16] species respectively. The solubility products of the samples after considering the ion pair formation are determined using the equation:

$$K_{sp}=[Ca-T]^{10}Y_2^{10}[PO_4^{3-}]_{IP}^{6-x}[AsO_4^{3-}]_{IP}^{x}Y_{PO_4^{3-}}^{6-x}Y_{AsO_4^{3-}}^{x}\left[\frac{K_W}{(H^+)}\right]^2$$

where T is the total calcium involved in complex formation: $[PO_4]_{IP}$ and $[AsO_4]_{IP}$ refer to the concentration of the respective species after considering the ion pairs; Y_2, $Y_{PO_4^{3-}}$, and $Y_{ASO_4^{3-}}$, are the activity coefficients of Ca^{2+}, PO_4^{3-}, and AsO_4^{3-} species respectively; and (H^+) in the equation refers to the activity of H^+ ion.

The calculations reported here satisfy the following conditions:

(i) Saturation with respect to the samples.

(ii) Congruent dissolution of the samples.

$$\frac{[Ca]}{([As]-[As]_0)+[P]}-\frac{5}{3}=0 \quad \text{for solid solutions, and}$$

$$\frac{[Ca]}{[As]-[As]_0}-\frac{5}{3}=0 \quad \text{for CaAsHA, and}$$

(iii) Electroneutrality, $E_\pm=Z_iC_i=0$.

where $[As]_0$ is the molar concentration of initial arsenic in As_2O_5, as is the total arsenic in the medium after equilibration and $E_\pm$ is the summation, which includes all the ionic species in the medium.

Results and Discussion

The results of chemical analyses of the samples are given in Table 1. Considering a total of six gram atoms of arsenic and phosphorus in a mole of the sample, chemical formulae are proposed from the analytical data. The [Ca]/[As] and [Ca]/([As]+[P]) gram atom ratio varying is found equal to 1.66±0.01 (Theo. 1.667) indicating the formation of apatite samples.

The X-ray powder diffraction pattern of all samples contained broad and diffused lines due to the colloidal dimensions of the crystals. Consequent upon substitution of a bigger AsO_4^{3-} ion in $Ca_{10}(PO_4)_6(OH)_2$ a dilation of the unit cell with an increase in the lattice parameters a and c (Table 1) resulted. These values when plotted against composition of the samples (Fig. 1) fell on a straight line (Vegard's law) indicating that

Table 1. Results of Chemical Analysis, Lattice Constant of Samples of Calcium Arsenic Hydroxyapatite and Its Solid Solution with Calcium Phosphorus Hydroxyapatite

Sample No.	Wt%			Molecular formula	[Ca]/([P]+[As])	Lattice constants (Å)	
	Ca	P	As			a	c
I	38.52	15.46	5.83	$Ca_{10}(PO_4)_{5.19}(AsO_4)_{0.81}(OH)_2$	1.66	9.47 (±0.01)	7.00 (±0.10)
II	36.58	11.13	14.14	$Ca_{10}(PO_4)_{3.93}(AsO_4)_{2.06}(OH)_2$	1.66	9.65 (±0.01)	7.14 (±0.05)
III	35.39	8.48	19.20	$Ca_{10}(PO_4)_{3.1}(AsO_4)_{2.9}(OH)_2$	1.66	9.76 (±0.02)	7.24 (±0.01)
IV	34.07	5.53	24.86	$Ca_{10}(PO_4)_{2.1}(AsO_4)_{3.9}(OH)_2$	1.66	9.9 (±0.04)	7.30 (±0.02)
V	32.79	2.69	30.31	$Ca_{10}(PO_4)_{1.06}(AsO_4)_{4.94}(OH)_2$	1.66	10.01 (±0.03)	7.45 (±0.03)
VI	31.26	—	35.00	$Ca_{10}(AsO_4)_6(OH)_2$	1.67	10.16 (±0.02	7.50 (±0.01)

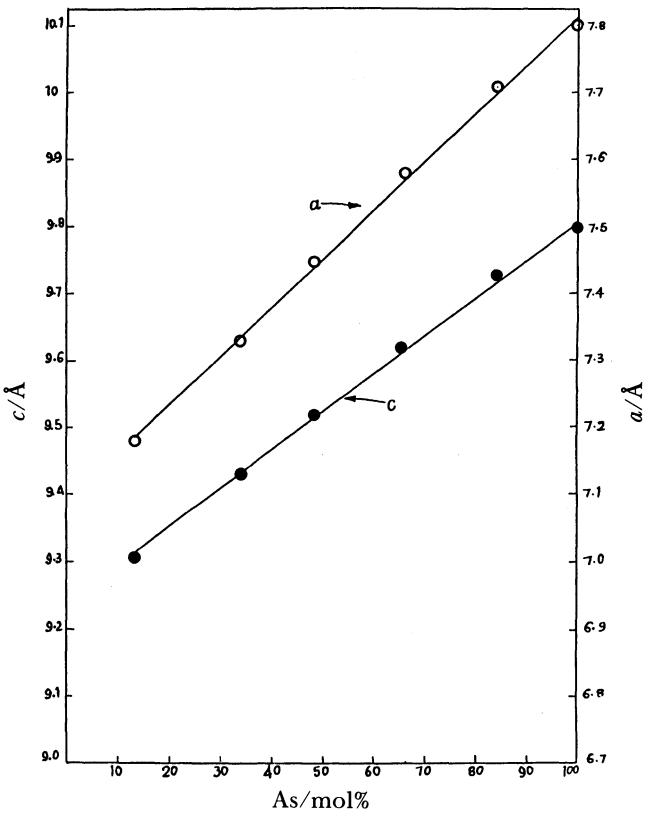

Fig. 1. Dependence of lattice constants a and c on the mole percent arsenic of the samples.

the samples are homogeneous solid solutions.

The electron microscopic patterns of the samples contained distinctly needle shaped crystals characteristic of apatites. The purity of the samples are indicated from the absence of extraneous phases in the microscopic patterns. With increase of AsO_4^{3-} in the samples, the crystals increased in size, the increase along the c-axis, however, is more pronounced than that along the a-axis.

The position in cm^{-1} and the assignments of the IR bands of the samples for x=1 to 5 are given in Table 2. The stretching hydroxyl bands appeared in the spectra of all the samples in the region 3560 to 3539 cm^{-1}. These bands are shifted with respect to the hydroxyl absorption in calcium hydroxide. This is indicated of a hydroxyl lattice interaction[17,18] and strongly suggest that the hydroxyl groups are situated within the three dimensional lattice. In fact, no vibrations at frequency about 3600 cm^{-1}, which are characteristics of hydroxyl group on the surface,[9] have been detected in the spectra.

A decrease of ν_s(OH) with an increase of the proportion of arsenate (AsO_4^{3-}) can be observed in Table 2. In addition, the phosphate vibrations also shifted to lower frequencies. These effects of substitution may be interpreted by considering that the interaction between OH group and the crystal becomes stronger as the arsenate content is increased, besides the effects

Table 2. Positions (cm^{-1}) and Assignments of the Infrared Spectra of $Ca_{10}(AsO_4)_{6-x}(AsO_4)_x(OH)_2$

x=	1	2	3	4	5	Assingment
	3560	3555	3550	3554	3539	ν_s(OH)
	533	533	535	537	539	ν_t(OH)
	965	960	955	950	948	$\nu_1(PO_4)$
	1080	1070	1060	1045	1030	$\nu_3(PO_4)$
	1055	1055	1050	—	—	—
	1044	1044	1035	—	—	—
	465	463	455	450	450	$\nu_2(PO_4)$
	605	605	600	600	600	$\nu_4(PO_4)$
	575	580	575	567	570	
	565	565	565	—	—	—
	870	860	865	860	860	$\nu_3(AsO_4)$
	855	850	855	850	850	
	—	845	841	840	835	
	430	430	420	425	420	$\nu_4(AsO_4)$

of binding energies and atomic masses[20] respectively. The nonappreciable variance of the ν_t(OH) indicates that the relative positions of the OH group with respect to the particular plane varies from one sample to another.

In the spectra of the samples, the ν_1 (As-O) mode cannot be detected, because the force constant of As-O and P-O are quite similar (k for P-O and As-O are 5.66 N cm^{-1} and 5.67 N cm^{-1} respectively) so that ν_1(As-O)/ν_1(P-O)=[μ_m(P-O)/μ_m(As-O)]$^{1/2}$, where μ_m is the reduced mass. In apatites, the ν_1(P-O) appears approximately around 950 cm^{-1}. The ν_1(As-O) appears in the IR region around 850 cm^{-1}, where the intense ν_3 mode of AsO_4 appeared. Therefore, the ν_1(As-O)$\approx$850 cm^{-1} is not observed due to the overlapping of ν_3 AsO_4 vibration in all cases.

The ideal symmetry of the tribasic phosphate ion in the free or undistorted state is tetrahedral i.e. it is a member of the T_d point group. In this ideal symmetry condition, absorptions corresponding to ν_3 and ν_4PO_4 mode should be observed. The appearance of ν_1 and ν_2 modes of phosphate in addition to the ν_3 and ν_4 modes in all cases indicate that T_d symmetry of the phosphate has been lowered to Cs site symmetry[21,22] consequent upon the substitution of the arsenate in CaPHA.

In the IR spectra only one ν_s(OH) at about 3560 cm^{-1} and one ν_t(OH) at about 533 cm^{-1} appeared for all the samples. This indicates that three equivalent anions are situated in the normal plane to the hydroxyl rotation axis of each hydroxyl group. If this were not true, then more than one ν_s(OH) and ν_t(OH) should have resulted. Therefore, in order that this should not happen, the two exchanging anions (PO_4^{3-} and AsO_4) belonging to the unit cell of hydroxyapatite are equivalent and exchange their positions through an interplanar anionic migration, so that each anion site in the phosphorus arsenic hydroxyapatite is occupied by an effective anion, whose characteristics are an average of all the anions present in the unit cell.

In the thermographic analyses in all the samples a

uniform loss in weight was observed upto 800 °C. TG curves (Fig. 2) have no distinct horizontals indicating nonappearance of a new stable phase during the thermal treatment. The possibility of decomposition appears unlikely since it has already been established that stoichiometric apatites decompose[23,24] at about 1200 °C. The total loss in weight may, therefore, be due to adsorbed water. The dehydration process in all cases is only of the type, a hydrate + water vapors is a two component system, where the dissociation pressure is a continuous uniform loss of water on dehydration. In each case an endothermic peak between 170—200 °C was detected. The IR peak at 1620 cm^{-1} in all the unheated samples disappeared after thermal treatment, which confirmed the presence of adsorbed water with the sample.[25] The activation energy of over all dehydration process from the TG

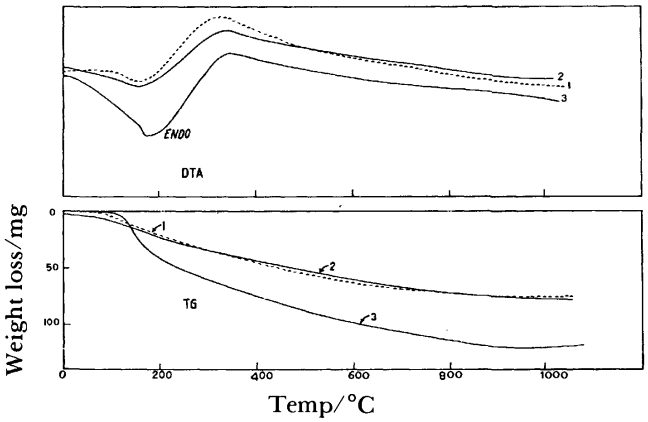

Fig. 2. Thermograms (TGA, DTA) of sample Nos. I, IV, and VI of Table 1.

Table 3. Activation Energies of Arsentic Hydroxyapatite(VI) and Solid Solutions of Calcium Phosphorus Arsenic Hydroxyapatites (Samples I and IV) by Freeman and Carrol's Equation and DTA

Sample No. as in Table 1.	Activation energy	
	Freeman and Carrol	DTA
	kJ mol^{-1}	kJ mol^{-1}
I	67.02	49.37
IV	59.20	48.53
$VI_{(CaAsHA)}$	70.83	72.80

Table 4. Solubility of $Ca_{10}(AsO_4)_6(OH)_2$ and Its Solid Solutions, $Ca_{10}(PO_4)_{6-x}(AsO_4)_x(OH)_2$ at 35 °C in the pH Range 4.0—8.0

Expt. No.	Sample	As_0 ($M\times10^3$ in As_2O_5 soln.)	pH	$C_{Ca}\times10^3$ mol dm^{-3}	$C_{As}\times10^3$ mol dm^{-3}	$C_P\times10^3$ mol dm^{-3}
1	I	0.36	4.0	0.94	0.076	0.47
2		0.11	5.0	0.90	0.07	0.47
3		0.01	6.0	0.86	0.07	0.44
4		—	7.1	0.82	0.065	0.425
5		—	8.0	0.79	0.064	0.414
6	II	0.36	4.0	1.100	0.23	0.45
7		0.11	5.0	1.0	0.21	0.392
8		0.01	6.0	0.98	0.206	0.384
9		—	7.1	0.96	0.202	0.376
10		—	8.0	0.94	0.198	0.368
11	III	0.36	4.0	1.30	0.38	0.40
12		0.11	5.0	1.20	0.37	0.35
13		0.01	6.0	1.10	0.34	0.33
14		—	7.1	1.0	0.30	0.30
15		—	8.0	0.99	0.30	0.30
16	IV	0.36	4.0	1.40	0.48	0.36
17		0.11	5.0	1.24	0.42	0.32
18		0.01	6.0	1.12	0.40	0.27
19		—	7.1	1.02	0.37	0.25
20		—	8.0	1.01	0.36	0.25
21	V	0.36	4.0	1.52	0.71	0.21
22		0.11	5.0	1.26	0.62	0.14
23		0.01	6.0	1.13	0.57	0.11
24		—	7.1	1.06	0.54	0.10
25		—	8.0	1.01	0.50	0.10
26	VI	0.36	4.0	1.70	1.024	—
27		0.11	5.0	1.28	0.88	—
28		0.01	6.0	1.14	0.698	—
29		—	7.1	1.08	0.64	—
30		—	8.0	1.02	0.61	—

Table 5. Electroneutrality $E_{\pm}$ Solubility Product (K'_{sp} and K_{sp}) and Free Energy (ΔG°_{soln}) Calculated from Table 4

Expt. No.	Sample	pH	$E_{\pm}$	K'_{sp} (without ion pair)	K_{sp} (ionpair)	ΔG°_{soin} kJ mol^{-1} deg^{-1} ($-RT \ln K_{sp}$)
1	I	4.0	0.012	6.85×10^{-107}	5.84×10^{-107}	626.38
2		5.0	0.009	6.69×10^{-107}	5.73×10^{-107}	626.43
3		6.0	0.008	6.58×10^{-107}	5.89×10^{-107}	626.36
4		7.1	0.008	5.79×10^{-107}	5.00×10^{-107}	626.78
5		8.0	0.008	4.52×10^{-107}	3.80×10^{-107}	627.47
6	II	4.0	0.010	6.01×10^{-103}	5.57×10^{-103}	602.92
7		5.0	0.010	6.01×10^{-103}	4.99×10^{-103}	603.20
8		6.0	0.010	5.37×10^{-103}	4.56×10^{-103}	603.44
9		7.1	0.009	4.82×10^{-103}	4.04×10^{-103}	603.74
10		8.0	0.009	4.20×10^{-103}	3.60×10^{-103}	604.04
11	III	4.0	0.013	2.92×10^{-100}	2.24×10^{-100}	587.56
12		5.0	0.012	2.75×10^{-100}	2.34×10^{-100}	587.45
13		6.0	0.011	2.51×10^{-100}	2.12×10^{-100}	587.70
14		7.1	0.010	2.54×10^{-100}	2.09×10^{-100}	587.74
15		8.0	0.010	2.54×10^{-100}	2.09×10^{-100}	587.74
16	IV	4.0	0.014	9.79×10^{-98}	8.50×10^{-98}	572.35
17		5.0	0.013	8.94×10^{-98}	8.41×10^{-98}	572.38
18		6.0	0.011	9.06×10^{-98}	8.20×10^{-98}	572.45
19		7.1	0.011	8.68×10^{-98}	7.60×10^{-98}	572.64
20		8.0	0.010	8.59×10^{-98}	8.15×10^{-98}	572.46
21	V	4.0	0.015	6.34×10^{-94}	6.10×10^{-94}	549.62
22		5.0	0.013	7.08×10^{-94}	6.00×10^{-94}	549.66
23		6.0	0.012	6.83×10^{-94}	6.28×10^{-94}	549.54
24		7.1	0.010	5.66×10^{-94}	5.43×10^{-94}	549.92
25		8.0	0.010	5.80×10^{-94}	5.40×10^{-94}	549.93
26	VI	4.0	0.014	3.61×10^{-91}	3.57×10^{-91}	533.30
27		5.0	0.013	3.85×10^{-91}	3.79×10^{-91}	533.15
28		6.0	0.011	3.88×10^{-91}	3.80×10^{-91}	533.14
29		7.1	0.011	5.01×10^{-91}	4.97×10^{-91}	533.45
30		8.0	0.010	5.56×10^{-91}	3.52×10^{-91}	533.34

curves and DTA curves are given in Table 3. The nonuniformity in the values obtained by both the methods is due to difficulty in fixing the base line in DTA curve.

The results of solubility of the samples obtained at a series of pH are summarized in Tables 4 and 5 together with the calculated quantities $E_{\pm}$, K'_{sp}, and ΔG^{0}. Table 5 shows that $E_{\pm}$ is within the anticipated experimental error, indicating no gross error in the analytical figures, calculations, and model used. It is seen from Table 4 that the samples exhibited a stoichiometric dissolution,[25-28] represented by the reaction:

$$Ca_{10}(PO_4)_{6-x}(AsO_4)_x(OH)_2 \rightarrow 10Ca^{2+} + (6\text{-}x)PO_4^{3-} + xAsO_4^{3-} + 2\ OH^-$$

(where x=1—6). The saturation condition is evidenced by the smooth curves obtained in the plots of calcium concentration, versus pH (Fig. 3) for all samples and a reasonable constancy in K_{sp} for the solid solutions. The solubility product (K'_{sp}) without considering the presence of ionpairs and (K_{sp}) after considering ion pairs are given in Table 5. From the K_{sp} values of each solid solution over the entire pH range, the free energy of the solution ΔG^{0}_{soln} have been calculated and are given in Table 5. The investigations indicate that the solubility of solid solutions decreased with increase of OH^- concentration of the medium of dissolution. This observation is understandable from the considerations of alteration in chemical potential[8] of $Ca(OH)_2$, H_3AsO_4, and H_3PO_4 with increase of pH. The solution with increase in OH^- concentration becomes supersaturated and decrease in solubility is therefore resulted.

From the K_{sp} values of the sample given in Table 5 it can be concluded that the solubility of the samples increased with increase in proportion of arsenate. At the first instance, this could reasonably be due to the higher dissociation constant of H_3AsO_4 than H_3PO_4 at a given temperature. This, however, can be substantiated from the possible alteration of lattice energy of the solid solutions consequent upon the replacement of bigger arsenate (1.18 Å) ion in place of phosphate

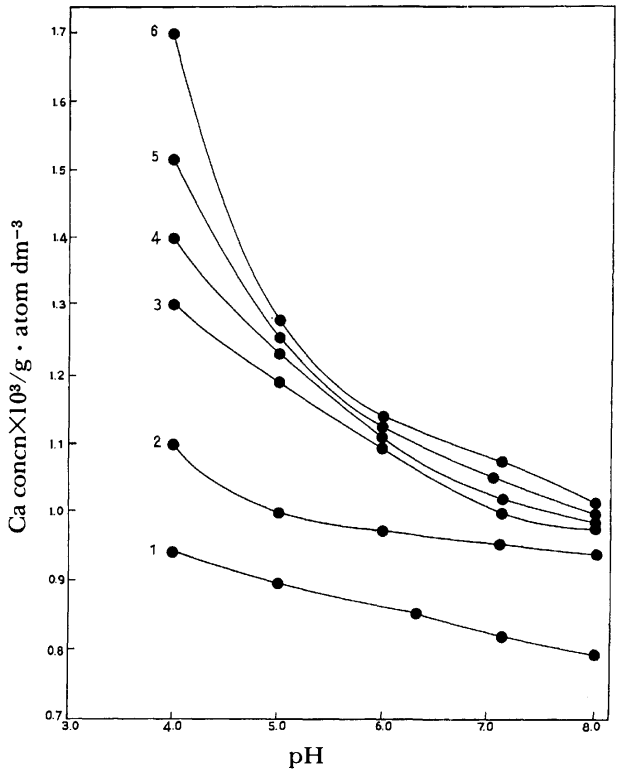

Fig. 3. Solubility equilibria of samples of calcium arsenic phosphorus hydroxyapatite in the pH range 3.0 to 8.0.
(1) Sample No. I, (2) Sample No. II, (3) Sample No. III, (4) Sample No. IV, (5) Sample No. V, (6) Sample No. VI. Sample Nos. indicate the numbers of Table 1.

(1.10 Å) ion in calcium hydroxyapatite. Thus, the loose packing crystalline structure of the solid solution with decreased lattice energy supports the observed increasing solubility trend of the solid solutions with higher proportion of arsenate ions. The decreasing stabilities of the solid solutions is also evidenced from the experimental ΔG^{0}_{soln} values.

The authors thank UGC, New delhi for award of teacher fellowship to LMM.

References

1) C. P. Sitewart and A. Stolman, "Toxicology, Mechanism and Analysis, Method," Academic Press, N. Y. (1960), p. 202.
2) W. B. Deichmann and H. W. Girvade, "Toxicology of Drugs and Chemicals," Academic Press, N. Y. (1969), p. 113.
3) J. M. Arena, "Poisoning," Charles C. Thomas, Springfield (1973).
4) S. N. Tiwari, S. P. Harpalani, and R. C. Sharma, *J. Indian Acad. Forensic Sci.*, **112**, 115 (1976).
5) A. L. Boskey and A. S. Posner, *J. Phys. Chem.*, **85**, 40 (1976).
6) J. W. Meller, "A. Comprehensive Treatise on Inorganic Chemistry and Theoretical Chemistry," Longmans Green & Co., London (1957), Vol. IX.
7) M. Masseys, J. C. Trombey, G. Bonel, and G. Montel, *Bull. Chem. Soc.*, **7**, 2308 (1969).
8) P. P. Mahapatra, L. M. Mahapatra, and B. Misra, *Polyhedron*, **6**, 1049 (1987).
9) P. P. Mohapatra, L. M. Mohapatra, and C. N. Nanda, *Indian J. Chem.*, to be submitted.
10) E. S. Freeman and B. Carrol, *J. Phys. Chem.*, **62**, 112 (1958).
11) V. K. Lamer, *J. Phys. Chem.*, **66**, 1975 (1962).
12) L. G. C. Sillen, A. E. Martell, E. Hogfeldt, and R. H. Smith, *Chem. Soc. Spl. Publ.*, **1971**, 25.
13) A. L. Agafonova and I. L. Agafonv, *Zh. Fiz. Khim.*, **27**, 2237 (1963).
14) P. P. Mohapatra, L. M. Mohapatra, and Bagmi Misra, *Indian J. Chem.*, **25A**, 647 (1986).
15) P. P. Mohapatra, L. M. Mohapatra, and Bagmi Misra, *J. Chem. Industry*, to be submitted.
16) T. M. Gregory, E. C. Moreno, and W. E. Brown, Internat. Assoc. Dental Res., 45th General Meeting, Washington D. C. (1967).
17) P. F. Gonzalez Diaz and A. Hildago, *Spectrochim. Acta, Part A*, **32**, 631 (1976).
18) L. B. Baddichanda and E. E. Berry, *Spectrochim. Acta, Part A*, **22**, 1407 (1966).
19) M. Santos, Ph. D. Thesis, Univ. Conplutense. Md. (1979).
20) R. B. Barnes, R. C. Gore, V. L. Iddel, and V. Z. Williams, "Infrared Spectroscopy," Reinhold, N. Y. (1944).
21) P. Gracia-Fernandez and P. F. Gonzalez Diaz, *Spectrochim. Acta*, **36A**, 1069 (1980).
22) R. Z. LeGeros, G. Bonel, and Beneedegros, *Calcif. Tiss. Res.*, **26**, 111 (1978).
23) E. Hayek and H. Newley, "Inorganic Synthesis," ed by J. Kleinberg, McGraw Hill Book Co. (1963), Vol. VIII, pp. 63—65.
24) T. R. Narayanan Kutty, *Indian J. Chem.*, **8**, 655 (1970).
25) J. S. Clarke, *Can. J. Chem.*, **33**, 11696 (1955).
26) E. C. Moreno, T. M. Gregory, and W. E. Brown, *J. Res. Natl. Bu. Std., Sec. A*, **72**, 773 (1968).
27) R. R. Weir, S. Chieu, and C. A. Black, *Soil Sci.*, **111**, 107 (1971).
28) A. N. Smith, A. S. Posner, and J. P. Quirk, *J. Colloid. Interface Sci.*, **48**, 442 (1974).

Solvent and Reversed Phase Extraction Chromatographic Separation of Molybdenum and Tungsten with Quaternary Ammonium Salt Reagent, Aliquat 336

Nitya Ranjan DAS* and Putul CHATTOPADHYAY
Nuclear Chemistry Division, Saha Institute of Nuclear Physics,
Sector-1, Block-'AF', Bidhannagar, Calcutta-700064, India
(Received August 8, 1988)

A quaternary ammonium salt reagent, Aliquat 336 has effectively been used for radioanalytical separations of molybdenum and tungsten through the techniques of solvent extraction and reversed phase extraction chromatography (RPEC). Studies on solvent extraction revealed that quantitative separations of the elements in a mixture can be achieved by extracting tungsten with ca. 10^{-4} mol dm^{-3} solution of Aliquat 336 in cyclohexane from an aqueous solution of 1 mol dm^{-3} H_3PO_4. The efficiency of separation of the elements which form varieties of metal salts of poly- and heteropolyanion species in aqueous solution is very much dependent on the types of acids as well as on the reagent concentration. In RPEC system, both the elements were found to be quantitatively extracted by an Aliquat 336 impregnated column of Kieselguhr from an alkaline solution containing a hydroxy compound like tartaric acid. The extracted species were subsequently separated by eluting molybdenum and tungsten respectively with HCl solutions of 0.05 mol dm^{-3} and 0.1 mol dm^{-3} concentrations. The purity of the separated species at various stages of their separations was verified by means of gamma-ray spectrometry.

The elements, molybdenum and tungsten, due to lanthanoid contraction, form a critical pair of elements having very close chemical properties. In respect of occurrence, metallurgy and properties of metals, the elements are markedly similar. They exist in varieties of oxidation states and their aqueous chemistry is very complex amongst the transitional elements. Since the formations of varieties of metal complexes, especially poly- and heteropolyanion species are most important feature of the chemistry of both molybdenum and tungsten, it was expected that the high molecular weight amines or the quaternary ammonium salts which are very selective for different elements[1-10] under specific experimental conditions would be very effective in anion-exchange separation of the elements from each other. In this respect, a quaternary ammonium salt reagent, Aliquat 336 ($R_3R'NCl$), has been shown to be a versatile extractant in both solvent and reversed-phase extraction chromatographic (RPEC) separations of metals that are capable of existing as complex anionic species in aqueous solutions.[11-20] Several workers[21] have effectively used the extractant in studying the extraction behaviors of both molybdenum and tungsten in different experimental conditions. Recently, Shabana et al.[22] reported the extraction separation of tungsten in radiochemical purity with Aliquat 336 from rhenium in different acid media. Studies on the extraction chromatographic separation of small quantities of Cr(IV), W(VI), and Mo(VI) in Aliquat 336-HCl system was also reported by Stro'nski.[23] Although Aliquat 336 has been used for extraction separation of molybdenum and tungsten in various systems, no systematic studies on their mutual separation through solvent extraction and RPEC have yet been attempted. The present investigation deals with the development of suitable radioanalytical procedures involving both the extraction techniques for clean separation of molybdenum and tungsten in a mixture using Aliquat 336 as liquid anion exchanger.

Experimental

Reagent. Chemical reagents used were of analytical grade. The extractant, Aliquat 336 (trialkylammonium chloride) of molecular wt. 404.17 was supplied by Aldrich Chemical Co., Inc. USA. The radiotracers, ^{99}Mo(67h), ^{185}W (73d), and ^{187}W (24h), were procured from BARC, Trombay, as sodium molybdate and sodium tungstate respectively in sodium hydroxide solution having high specific activity which were diluted as per requirements.

For gamma-spectrometric study, an ND65 8K channel analyzer connected with a High Purity Germanium detector of 30 cm^3 active volume and with resolution of 2.06 keV at 1.33 MeV was used.

Solvent Extraction Procedure. In solvent extraction separation, 20 ml of aqueous feed containing the tracers ^{99}Mo and ^{185}W or ^{187}W ($<10^{-7}$ mol dm^{-3}) in different acid media was equilibrated with equal volume of Aliquat 336 of desired concentration in different diluents together with 3% (v/v) 1-octanol for a certain period. After disengagement of the liquid phases, radioactivities present in both the phases were rediometrically measured and identified whereby tungsten was found to be preferentially or completely extracted by the organic extractant depending upon the experimental conditions.

Reversed-Phase Extraction Chromatographic Procedure (RPEC). The column material, Kieselguhr, used for reversed-phase extraction chromatographic separation was first hydrophobised with dimethyldichlorosilane and then impregnated with Aliquat 336 following the procedure developed earlier.[24] A packed column (3 cm×0.3 cm) of impregnated Kieselguhr was prepared in a stoppered glass tube. A syringe was inserted through a rubber cork fitted at the top of the glass tube. The flow rate of the eluent

percolated in the column through this syringe was regulated throughout the experiment with a peristaltic pump (LKB 2132 Micro Perpex). Before loading of the radiotracer on the column, it was preconditioned by passing a 8 mol dm^{-3} $LiNO_3$-0.01 mol cm^{-3} HNO_3 solution which made the column more effective in the separation of the elements pair.

In RPEC separation system, small amount of tartaric acid was added to the tracer mixture containing molybdenum and tungsten in alkaline medium and was allowed to extract by the impregnated reagent in the column. After complete extraction, the elements were separated by eluting molybdenum first with a 0.05 mol dm^{-3} HCl solution and then tungsten by a 0.1 mol dm^{-3} HCl solution. A flow rate of 10—12 drops per minute was maintained throughout the experiment. Activities present in different fractions of the effluents were verified and measured by GM counters.

Initially, both solvent extraction and RPEC procedures were tried with individual radiotracers, ^{99}Mo and ^{185}W or ^{187}W, under similar experimental conditions. The purity and extent of separation of the radiotracers at different stages of separation procedures were verified radiometrically.

Discussion

Studies on the solvent extraction behavior of molybdenum and tungsten at tracer scales, in various acid media, namely, HCl, HNO_3, H_2SO_4, and H_3PO_4, with Aliquat 336 as extractant revealed that the extractability of tungsten, in general, is always higher than that of molybdenum whatever be the acidity of the media (Table 1). For both the elements, the extents of extractions follow a decreasing trend with increasing acidity of the aqueous solution but interestingly, it has been found that the differences in the distribution ratio values for the elements at different acidities are very much pronounced in case of orthophosphoric acid.

Extraction studies of molybdenum and tungsten with Aliquat 336 in cyclohexane from phosphoric acid solutions at different acidities, as shown in the Fig. 1, indicate that complete extraction of tungsten free from molybdenum can be achieved at ca. 1 mol dm^{-3} H_3PO_4 concentration below of which partial extraction of molybdenum along with tungsten always takes place. However, at phosphoric acid concentration>1 mol dm^{-3}, although the extraction of molybdenum is very insignificant, extraction of tungsten also follows a decreasing trend. Thus the optimal conditions for extraction of tungsten free from molybdenum is to extract tungsten with a reagent solution of 10^{-4} mol dm^{-3} concentration in cyclohexane from an aqueous phosphoric acid solution of ca. 1 mol dm^{-3} concentration.

The extraction of tungsten from orthophosphoric acid medium at different concentration follows almost similarly with that of molybdenum but with higher degree of extraction (Fig. 1). The insignificant extractibility of molybdenum at higher acidity beyond 1 mol dm^{-3} is attributed to the fact that in this region, it exists mostly in the cationic forms, such as

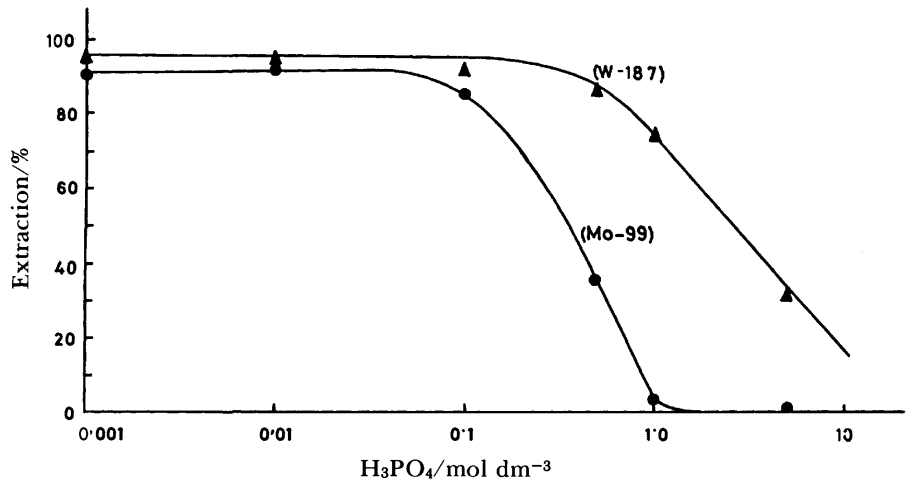

Fig. 1. Extractions of ^{99}Mo and ^{187}W with Aliquat 336 (ca. 10^{-4} mol dm^{-3}) at different concentrations of H_3PO_4.

Table 1. Extraction of Molybdenum and Tungstn from Different Acids at Different Concentrations with 10^{-4} mol dm^{-3} Aliquat 336 in Cyclohexan

Acid concentration/mol dm^{-3}	HCl		HNO_3		H_2SO_4		H_3PO_4	
	Mo/%	W/%	Mo/%	W/%	Mo/%	W/%	Mo/%	W/%
0.01	21.7	33.8	1.1	15.7	4.4	22.7	92.2	94.5
0.10	18.5	31.6	0.4	12.5	2.5	21.8	85.4	90.0
1.00	7.4	9.2	0.3	10.4	0.7	13.5	2.8	75.7
5.00	1.9	2.1	0.1	7.5	0.5	11.5	0.5	35.4

$[MoO_2]^{2+}$, $[MoO(OH)_2]^{2+}$, or $Mo_2O(OH)_8 \cdot 2H_2O^{2+}$ [25] and in very strong acid it is present mainly as $[MoO_2]^{2+}$ [26,27] which are not extractable by the anionic extractant, Aliquat 336. But at comparatively lower acidity, the possibility of formation of heteropoly species like $H_3PMo_{12}O_{40}$ [25] increases resulting in higher extraction of molybdenum by the reagent. Higher extraction of molybdenum with a quaternary ammonium salt at lower acidity as observed by us also corroborates to the findings of Akaiwa et al.[28] who reported that at higher acidity the extracted species, $(R_3R'N)_3PMo_{12}O_{40}$ changes to $(R_3R'N)_2HPMo_{12}O_{40}$ resulting in the decrease of extraction of molybdenum by the reagent. Similarly in strong acid solution the extraction of tungsten is low, but with decreasing acidity, the efficiency of extraction increases appreciably probably due to gradual formation of the heteropoly species like $H_3PW_{12}O_{40} \cdot xH_2O$ and ultimately the existence of varieties of polytungstate anions helps in complete extraction of tungsten by the reagent. The large variation in the distribution ratio values for molybdenum and tungsten which form almost similar types of complex species is perhaps due to the fact that the heteropoly anions of tungsten are in general more stable than those of molybdenum[25] and the existence of varieties of paratungsten anions in solution as well.

Studies on the effect of concentration of Aliquat 336 on the extraction of the elements concerned, as shown in Fig. 2, indicate that the distribution ratio values for molybdenum increase with increasing concentration of the extractant starting from ca. 10^{-4} mol dm^{-3} whereas almost complete extraction of tungsten is possible with the reagent at this concentration other parameters remaining same. Thus to avoid the possibility of contamination due to molybdenum, extraction of tungsten with the reagent of higher concentration is not favored.

The effect of diluents on the extraction behavior of the extractant in extracting the elements was studied with different diluents. Diluents like heptane, cyclohexane, carbon tetrachloride, benzene, and toluene having very close dielectric constant values (1.9—2.38)[29] behave similarly as there is no significant change in D values with change of diluents in the extraction systems. But in case of chloroform which has comparatively a higher dielectric constant value of 5.05, some variations in the D values were observed. It has been reported that the dielectric properties of the diluents effects the extraction efficiency of the extractant and the change in the D values as observed in the study was due to different dielectric constant value of chloroform.

In RPEC system, the extractions of both molybdenum and tungsten by the Aliquat 336 impregnated column in simple sodium hydroxide medium were found to be partial. However, presence of small amount of tartaric acid in alkaline medium containing the tracers, helps in complete extraction of the elements by the reagent in the column. The extracted elements are later separated by eluting molybdenum first and then tungsten with hydrochloric acid solution of 0.05 mol dm^{-3} and 0.1 mol dm^{-3} concentrations respectively (Fig. 3).

In alkaline medium, the oxoanions, MoO_4^{2-} and WO_4^{2-}, with hydroxy compound like tartaric acid form anionic complexes which are found to be totally extracted by the impregnated reagent. Under the experimental conditions, the anionic complexes[30,31]

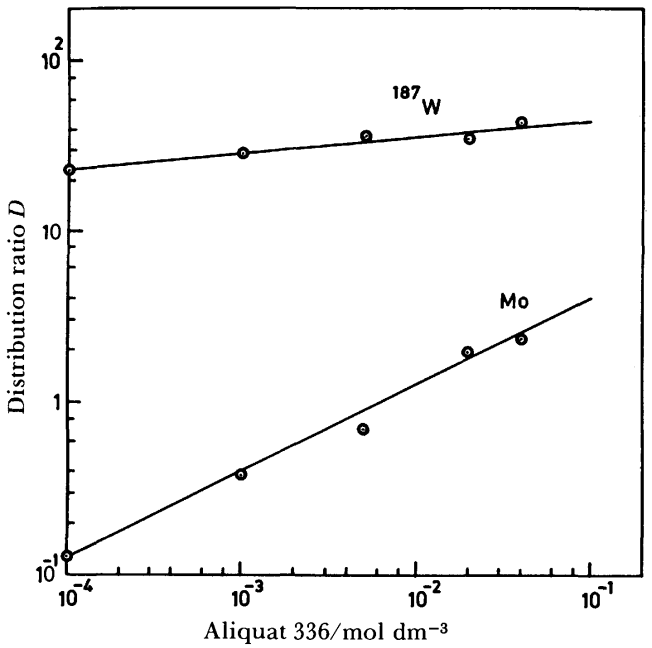

Fig. 2. Extractions of ^{99}Mo and ^{187}W from 1 mol dm^{-3} H_3PO_4 solution with Aliquat 336 solutions of different concentrations.

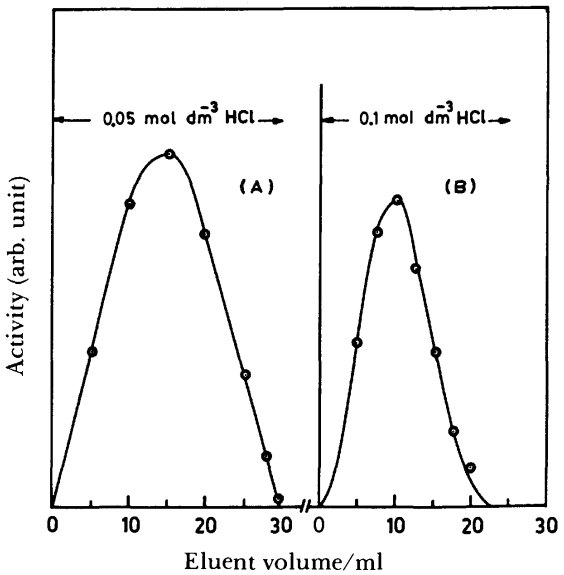

Fig. 3. Elution curves for ^{99}Mo and ^{187}W in RPEC: (A) elution of ^{99}Mo by 0.5 mol dm^{-3} HCl and (B) elution of ^{187}W by 0.1 mol dm^{-3} HCl.

formed by tungsten are comparatively more stable than those of molybdenum and it is expected that tungsten would be bonded more firmly to the reagent than that of molybdenum. Although the nature of anionic species are yet to be ascertained, but the experimental results corroborate the assumptions. For elution of tungsten species which are bonded strongly with the reagent, a solution comparatively of higher acid concentration is required.

Since both the elements in question form varieties of metal anion complexes, more or less of similar types, in different aqueous media, the general reaction responsible for extractions of the elements by the reagent in analogy of our previous investigations,[24,32] may be depicted as:

$$q\mathrm{R_3R'N^+Cl^-_{org}} + \mathrm{MX^{q-}_{aq}} \rightarrow (\mathrm{R_3R'N})_q\mathrm{MX_{org}} + q\mathrm{Cl^-_{aq}}$$

where MX^{q-} is the metal anionic species, $R_3R'N^+Cl^-$ is the quaternary salt having R="capryl" (C_8—C_{10} alkyl) group and R'=methyl group.

For both the techniques, the preliminary measurements of the radioactivities due to the respective isotopes, ^{99}Mo, ^{185}W, or ^{187}W, in different separated media were made by a GM counter. The purity of the separated elements were verified by taking recourse to gamma-ray spectrometry. The presence of molybdenum and tungsten in different phases were characterized by the photopeaks corresponding to the gamma

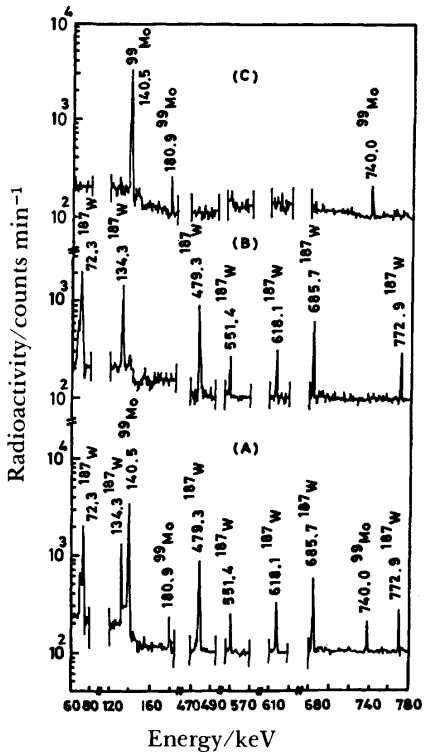

Fig. 4. Gamma-spectra of ^{99}Mo and ^{187}W in solvent extraction system: (A) a mixture of the radiotracers, ^{99}Mo and ^{187}W, (B), organic extractant (ca. 10^{-4} mol dm^{-3} Aliquat 336), and (C) aqueous phase left after extraction of ^{187}W.

energies of 140.5, 180.9, and 740.0 keV due to ^{99}Mo and of 72.3, 134.3, 479.3, 551.4, 618.1, 685.7, and 772.9 keV due to ^{187}W respectively. Typical gamma spectra of a mixture of the radiotracers, ^{99}Mo and ^{187}W and the isotopes in separated phases, as shown in Fig. 4, indicate complete separation of the elements through solvent extraction.

As regards column meterial in RPEC system, Kieselguhr which has been used as inert solid support for the extractant has got the favorable properties of considerable chemical stability, higher absorbing capacity for the extractant and also the resistivity towards any nuclear radiation which is essential in any radiochemical studies.

The extraction profile of the elements under the experimental conditions shows that the methods of solvent extraction and RPEC are almost complementary to each other. The developed procedures are simple and effective in mutual separation of the elements in tracer concentrations. The methods are of considerable importance especially in the field of nuclear technology where the purity of the element is of prime importance.

References

1) H. Green, *Talanta*, **20**, 139 (1973).
2) A. K. De. U. S. Ray and N. Parhi, *J. Indian Chem. Soc.*, **59**, 1334 (1973).
3) H. E. Affsprung and J. Murphy, *Anal. Chim. Acta*, **30**, 501 (1964).
4) T. Ishimori, "Data of Inorganic Solvent Extraction," JAERI, 1047 (1963); 1062 (1964); 1106 (1966).
5) P. L. Artyukhin, E. A. Strartseva, Yu. L. Mitaykin, I. M. Ivanov, L. M. Gindin, and G. G. Glukhov, *Radiokhimiya*, **14**, 150 (1972).
6) A. M. Wilson and O. K. Macfarland, *Anal. Chem.*, **36**, 2488 (1964).
7) T. W. Lee, W. L. Chang, and G. Ting, *Solv. Extr. Ion Exch.*, **2**, 435 (1984).
8) G. M. Vol'dman, A. N. Zelikman, and I. sh. Khutoretskaya, *Izv. Vys. Vcheb. Zaved. SSSR, Ser. Tsvetnaya Metallurgiya*, **2**, 74 (1978).
9) L. S. Zolotareva, I. M. Ivanov, I. G. Yudelevich, G. I. Plotnikova, and L. M. Gindin, *Izv. Sib. Otd. Akad. Nauk SSSR, Ser. Khim. Nauk*, **2**, 92 (1973).
10) I. M. Ivanov, L. S. Zolotareva, I. G. Yudelevich, and L. M. Gindin, *Izv. Sib. Otd. Akak. Nauk SSSR, Ser. Khim. Nauk*, **7**, 90 (1972).
11) C. F. Colman, K. B. Brown, J. G. Moore, and D. J. Course, *Ind. Eng. Chem.*, **50**, 1756 (1958).
12) A. Beck, D. Dyrssen, and S. Ekberg, *Acta Chem. Scand.*, **18**, 1695 (1964).
13) T. Braun and G. Ghersini, "Extraction Chromatography," Elsevier Scientific Publishing Company, Amsterdam (1975).
14) F. L. Moore, *Anal. Chem.*, **41**, 1658 (1969).
15) C. Testa, *Com. Naz. Energ. Nucl., [Rapp, Tec], RT/PROT (Italy)* (65) 33 (1965).
16) E. P. Horwitz, K. A. Orlandini, and C. A. A. Bloomquist, *Inorg. Nucl. Chem. Lett.*, **2**, 87 (1966).

17) J. Van Ooyen, "Solvent Extraction Chemistry," ed by D. Dyrssen, J. O. Liljenzin, and J. Rydberg, North Holland Publ. Co., Amsterdam (1967), p. 485.
18) E. P. Worwitz, C. A. A. Bloomquist, K. A. Orlandini, and D. J. Henderson, *Radiochim. Acta*, **8**, 128 (1967).
19) E. P. Horwitz, L. J. Sauro, and C. A. A. Bloomquist, *J. Inorg. Nucl. Chem.*, **29**, 2033 (1967).
20) E. A. Huff, *J. Chromatogr.*, **27**, 229 (1967).
21) J. Adam and R. Pribil, *Talanta*, **18**, 349 (1971).
22) R. Shabana, S. M. Khalifa, S. Abdalla, and H. F. Aly, *J. Radioanal. Nucl. Chem., Lett.*, **106**, 55 (1986).
23) I. Str'onski, *Radiochem. Radioanal. Lett.*, **1**, 191 (1969).
24) N. R. Das, B. Nandi, and S. N. Bhattacharyya, *J. Radioanal. Chem.*, **62**, 53 (1981).
25) A. F. Trotman-Dickenson (ex. ed.), "Comprehensive Inorganic Chemistry," Pergamon Press, N. Y. (1973), Vol. 5, Chap. 36 and Vol. 4, Chap. 51.
26) B. Nandi, Ph. D. Thesis, University of Calcutta, India.
27) "Progress in Inorganic Chemistry," ed by S. J. Lippard, Interscience Publisher, N. Y. (1977), Vol. 22, p. 35.
28) H. Akaiwa, H. Kawamoto, and T. Takenouchi, *Nippon Kagaku Kaishi*, **1980**, 833.
29) I. S. El-Yamani, M. Y. Farah, and E. N. Abd El-Messich, *J. Radioanal. Chem.*, **45**, 147 (1978).
30) G. F. Lundell, H. H. Bright, and J. I. Hoffman, "Applied Inorganic Analysis," 2nd ed, John Wiley and Sons, Inc., N. Y. (1953), p. 688.
31) N. R. Das and S. N. Bhattacharyya, *Anal. Chim. Acta*, **102**, 221 (1978).
32) N. R. Das and P. Chattopadhyay, *Bull. Chem. Soc. Jpn.*, **61**, 4426 (1988).

 © 1989 The Chemical Society of Japan Bull. Chem. Soc. Jpn., 62, 3283—3290 (1989)

Prototropic Equilibria in Few β-Hydroxy-Substituted 1-Naphthylamines in the Ground and Excited Singlet States

Ranjit S. SARPAL and Sneh K. DOGRA*
Department of Chemistry, Indian Institute of Technology, Kanpur 208016, India
(Received August 18, 1988)

The longest wavelength transition in the absorption spectra of β-hydroxy-substituted 1-naphthylamines is long axis polarised, whereas the fluorescence occurs from the more polar, short axis polarized state. This is based on the spectral characteristics in different solvents. Five different prototropic species are formed in the ground state and six species are obtained in the S_1 state. The ground state precursor for the formation of zwitterion is the monocation. pK_a values for the different prototropic reactions have been calculated in the ground and excited singlet states.

It is now well-established that the amino and hydroxyl groups[1-5] become stronger acids in their first excited singlet states. The monoanion formed by the deprotonation of amino group is generally nonfluorescent,[6-10] with few exceptions.[11,12] Further the proton-induced fluorescence quenching of the free aromatic amine is generally observed before it is protonated to form the monocation.[13-15] Recently, a few exceptions have been observed, where the lifetimes of the aromatic amines are very short and no fluorescence quenching is noticed by the proton,[16,17] even though the charge-transfer state is of lowest energy, a prime condition for the proton-induced fluorescence quench ing. The latter is a common feature during the first protonation of the aromatic diamines[18-20] and in these cases the fluorimetric titrations give rise to the ground state pK_a values for the first prototropic equilibrium. On the other hand, most of the phenoxide ions are nonfluorescent,[21-24] whereas the naphtholate ions are fluorescent.[25-28] Further, the fluorimetric titrations in the former cases yield the ground state pK_a values and this may be due to the shorter lifetime of the conjugate acid-base pairs. In case of naphthols, stretched sigmoid curves are observed, giving rise to both the ground state and excited state pK_a values.

Molecules containing electron-donating and electron-withdrawing groups have been studied extensively.[5] On the other hand, molecules containing electron-donating groups only, have not been investigated in detail and very few such examples are available in literature.[23,24,29-31]

The present study is on the molecules containing electron-donating groups only (i.e. $-NH_2$ and -OH) and the molecules are 2-hydroxy- (1,2 NA), 6-hydroxy- (1,6 NA), and 7-hydroxy-1-naphthylamines (1,7 NA), i.e. hydroxyl group is at the β-position and the amino group is at the α-position. Literature survey has indicated that the above molecules along with 1,3 NA and similar other molecules have been studied by Ellis and Rogers.[32] These workers have predicted the presence of zwitterion for some aminonaphthols in the excited singlet state in the pH range of ca. 4 to 10. The argument given is that the excited singlet state deprotonation constant of 2-naphthol (2 NOH) is 2.8[28] and it is enough to protonate the amino group ($pK_a \approx 4$) to form the zwitterion. But on the other hand, the excited state protonation constant of 1-naphthylamine (1 AN) is (−1.0)[33] and thus it may not be possible to form the phototautomer in the pH range of ca. 4 to 10 in the S_1 state, especially when the phototautomerism is biprotonic in the case of 1,6 NA and 1,7 NA, as the proton migration depends on the environment. The purpose of this study is to resolve this controversy and to find out why the zwitterion has not been observed for 1,7 NA and 1,2 NA. To supplement the above study, 7-methoxy-1-naphthylamine (1,7 MNA) has been prepared. Solvent effects have been studied and pK_a values of the various prototropic reactions have been determined and discussed.

Materials and Method

1-Amino-2-naphthol hydrochloride and 1,7 NA were procured from Aldrich Chemical Company. 1,6 NA was obtained from ICN Pharmaceuticals. 1,6 NA and 1,7 NA were purified from ethanol by repeated crystallization. Neutral 1,2 NA was prepared by titrating its salt with sodium hydrogencarbonate maintaining the pH≈5. 7-Methoxy-1-naphthylamine (1,7 MNA) was prepared from 1,7 NA by the method suggested by Ellis and Rogers.[32]

The purity of these compounds, purification of the solvents, instruments used, and the procedure used for calculating the various parameters are the same as described in our recent papers.[18-20] Pariser-Parr-Pople (PPP)[34,35] method was employed to calculate the transition energies, ground and excited state charge densities at the various centers of the molecules and their monoanions. The program was obtained from QCPE Indiana University, Bloomington, U.S.A. Different parameters required for calculations were taken from the literature.[36] The one center two electron repulsion integrals were calculated by Pariser approximation.[37] Two center electron repulsion integrals were calculated by the Nishimoto-Mataga method.[38] All the configurations obtained by single-electron excitation from occupied molecular orbitals to unoccupied molecular orbitals were considered in calculating all the configurational interaction. The species were assumed to be planar and the rings are taken as regular hexagon. The data regarding the

Table 1. Band Maxima, Oscillator Strength, Direction of Polarization (α), Ground and Excited States Charge Densities at the Nitrogen and Oxygen Centers of Amino and Hydroxyl Groups of Aminonaphthols

Compound	λ_{max} expt. /nm	log ε_{max}	λ_{max} PPP /nm	Osc.St.	α	Charge density			
						Free molecule		Monoanion	
						N	O	N	O
1 AN	324	3.62	312	0.010	359	1.9345	—	—	—
	314	3.70				(1.915)			
	305	3.70	297	0.258	85				
2 NOH	326	3.23	311	0.009	108	—	1.9661	—	—
	312	3.17					(1.953)		
	281	3.56	289	0.213	94				
1,2 NA	335		315	0.024	62	1.9376	1.9686	1.9471	1.7461
						(1.916)	(1.955)	(1.927)	(1.305)
			300	0.228	94				
1,3 NA			314	0.016	298	1.9344	1.9661	1.9347	1.7321
			298	0.237	80	(1.918)	(1.954)	(1.942)	(1.338)
1,6 NA	336	3.55	314	0.014	233	1.9346	1.9693	1.9355	1.733
	299	3.63	298	0.243	90	(1.918)	(1.960)	(1.94)	(1.321)
1,7 NA	334	3.45	315	0.017	125	1.9351	1.9666	1.9377	1.7357
	300	3.62	298	0.24	81	(1.917)	(1.954)	(1.935)	(1.318)
1,7 MNA	330	—	322	0.048	130	1.9358	1.9133	—	—
	316	—	298	0.205	75	(1.920)	(1.820)		
	286								

α is the angle measured counter clock-wise with respect to x-axis.

charge densities on nitrogen and oxygen atoms of $-NH_2$ and -OH/OMe groups of aminonaphthols have been listed in Table 1. The relevant data for 1 AN and 2 NOH are also listed in Table 1 for comparison. The directions of the axes are shown below.

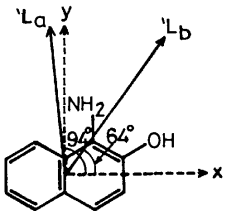

Results and Discussion

Effect of Solvents. Figure 1 depicts the fluorescence spectra of these compounds in different solvents and relevant spectral data are compiled in Tables 2 and 3. Data of Table 2 indicate that the molecular extinction coefficient of each band system decreases with the increase in the wavelength. With the increase in the polarity of solvents, a red shift is noticed in each band system, but in methanol and water, the absorption spectra are blue shifted. On the other hand, a continuous red shift is observed in the fluorescence spectra of these molecules under the similar environments. The fluorescence band maxima of 1,6 NA, 1,7 NA, and 1,7 MNA are nearly at the same wavelength, whereas that of 1,2 NA is slightly red shifted. The above data show that molecules behave as proton donor in polar solvents and proton acceptor in methanol and water in the ground state, whereas proton donor in all the solvents in the first singlet state.

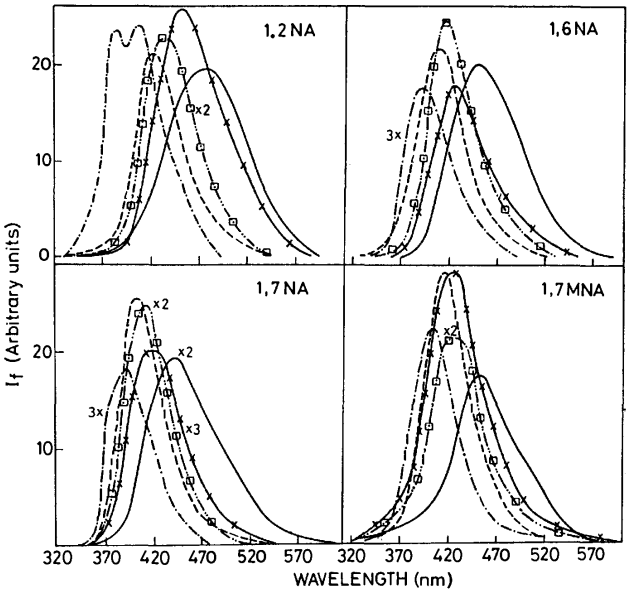

Fig. 1. Fluorescence spectra of 1,2 NA, 1,6 NA, 1,7 NA, 1,7 MNA in different solvents.
λ_{exci}, 1,2 NA and 1,6 NA (337 nm); 1,7 NA (355); 1,7 MNA (330); (—●—) cyclohexane, (------) dioxane, (—□—) acetonitrile, (—×—) methanol, (———) water.

In naphthalene molecule,[39] 312 nm band is weak and long axis polarized ($^1A \rightarrow {}^1L_b$); 286 nm band is moderately strong and short axis polarized ($^1A \rightarrow {}^1L_a$). The longest wavelength band of 1-naphthylamine (1 AN) is broad and a mixture of $^1A \rightarrow {}^1L_a$ and $^1A \rightarrow {}^1L_b$ transitions (322 nm in ethanol),[39] whereas that of 2-

Table 2. Absorption Maxima (nm) and log ε_{max} of Some Aminonaphthols in Different Solvents and Proton Concentration at 298 K

Solvent/Species	1,6 NA		1,7 NA		1,7 MNA	1.2 NA
	λ_{max}	log ε	λ_{max}	log ε	λ_{max}	λ_{max}
Cyclohexane	253		248		244	248
	300		304		284	278
	315		—		—	290
	337		336		333	339
Dioxane	258	(4.44)	253	(4.49)	246	248
	—	—	—	—	282	—
	316	(3.74)	312	(3.76)	—	315
	343	(3.78)	341	(3.69)	334	350
Acetonitrile			251		245	247
			—		282	—
			310		—	312
			339		334	347
Methanol	254	(4.35)	248	(4.39)	243	241
	298	(3.69)	—		282	298
	302	(3.68)	308	(3.68)	—	—
	341	(3.65)	337	(3.60)	331	339
Free aminonaphthol	249	(4.29)	244	(4.34)	240	228
pH 6.5	299	(3.63)	300	(3.62)	286	288
	—		—		316	—
	336	(3.55)	334	(3.45)	330	335
Monoanion	260	(4.38)	248	(4.43)		
pH 12	294	(3.74)	295	(3.76)	—	—
	—		301	(3.74)		
	350	(3.54)	351	(3.52)		
Monocation	267	(3.61)	264	(3.58)	261	268
pH 0	276	(3.69)	274	(3.66)	273	274
	287	(3.59)	285	(3.54)	283	286
	318	(3.27)	320	(3.28)	315	314
	328	(3.33)	331	(3.35)	329	327
Dianion	265		254		268[a]	
H_- 17	296		298			
	—		308		307	
	356		359		344	
Dication	252		250			
H_0 −1	262		261			
	275		275		278	284
	290		285			312
	304		308		314	330
	329		325		334	400

a) Monoanion of MNA.

naphthol (2 NOH) is $^1A \rightarrow {}^1L_b$ (335 nm, ethanol).[36] Further, the resonating effect of the amino group on the spectral transitions is more than that of hydroxyl group. The molecules studied in our work contain the amino group along the shorter axis which will perturb ^1L_a state and the hydroxyl group along the longer axis will primarily affect the ^1L_b state. From the data of Table 2, 340 nm band can be assigned to $^1A \rightarrow {}^1L_b$, whereas 315 nm and 300 nm band to $^1A \rightarrow {}^1L_a$ transitions. This is because: (i) the effect of solvents on ca. 340 nm band is less than that observed on ca. 300 nm band, (ii) the molecular extinction coefficient of 340 nm band is less than that of 300 nm, even though the difference is not so large as observed in naphthalene molecule.[39] The increase in the molecular extinction coefficient of 340 nm band could be partly because of the presence of -OH group and partly due to the mixing of the two transitions, (iii) two peaks around 300 nm band are the vibrational bands of $^1A \rightarrow {}^1L_a$ transition. The vibrational frequency of ca. 1580 cm^{-1} further substantiates our point, as the vibrational frequency associated with $^1A \rightarrow {}^1L_b$ transition[39] is ca. 1000 cm^{-1}, (iv) the above results are further manifested from PPP calculations (Table 1). The agreement between the band maxima, predicted by PPP method and experimental results is not bad. The oscillator strength clearly indicate that the long wavelength band is more forbidden than the short wavelength one. The polarization direction of the second transition is always along the shorter axis (y-axis), indicating that it is ^1L_a one. Whereas the polarization direction of the long wavelength band depends upon the position of the -OH group. Though the direction of this transition does not cor-

Table 3. Fluorescence Maxima (nm) and Fluorescence Quantum Yields of Some Aminonaphthols in Different Solvents and Proton Concentration at 298 K

Solvent/Species	1,6 NA		1,7 NA		1,7 MNA		1,2 NA	
	λ_{max}	(ϕ_f)	λ_{max}	(ϕ_f)	λ_{max}	(ϕ_f)	λ_{max}	(ϕ_f)
Cyclohexane	388	(0.26)	388	(0.14)	400	(0.25)	380, 406	
Dioxane	405	(0.45)	406	(0.55)	410	(0.33)	418	(0.24)
Acetonitrile	413	(0.53)	411	(0.32)	421	(0.21)	432	(0.26)
Methanol	420	(0.33)	416	(0.35)	422	(0.16)	448	—
Free aminonaphthol pH 6.5	443	(0.55)	443	(0.44)	448	(0.104)	470[b]	—
Monoanion pH 12	416	(0.33)	414	(0.47)				—
Dianion H_-16	518	(—)	418		418[a]			—
Zwitterion pH 1	424	(—)	426	(—)	—		428	—
Monocation H_0−1	364	(0.07)	366	(0.09)	366	(0.05)	356[c]	(0.07)
Dication H_0−10	346,363,370		336,353,364		378	(—)	356	

a) Monoanion of MNA. b) pH 4. c) H_0−4.

respond exactly along the longer axis (x-axis), it lies between the x- and y-axes. This indicates that the long wavelength band is influenced by the short wavelength one. This is also reflected by the molecular extinction coefficient, observed for the long wavelength band.

The fluorescence band maxima of each compound is close to that of 1 AN (445 nm, water)[40,41] than to that of 2 NOH (353 nm).[26] Based on the data of Table 3, we speculate that the reversal of ^1L_a and ^1L_b states takes place and ^1L_a becomes the lowest energy singlet state. This can be explained as follows: (i) ^1L_a state is more polar than ^1L_b and its polarity is further increased by the presence of amino group along the shorter axis. (ii) The energy gap between ^1L_a and ^1L_b states is not very large. (iii) Solvatochromic effect observed in case of these compounds resembles more with that of 1 AN[41] than with 2 NOH.[26] (iv) Though the PPP calculations show that the lowest energy state is ^1L_b, these calculations do not take account of solvent interactions and thus the agreement between the results calculated by PPP method and those obtained by fluorescence spectroscopy will not be good. The near consistency of the fluorescence band maxima in all the compounds indicates that the effect of -OH group on the spectral characteristics is same, so long as it is at the β-position of naphthalene moiety. The larger red shift observed in case of 1,2 NA could be either due to the presence of both the groups on the same ring or due to the presence of intramolecular hydrogen bonding.

Effect of Acid Concentration. 1,2 NA decomposes at pH>5, so its spectral characteristics are studied in the H_0/pH range of −10 to 5, whereas those of 1,6 NA, 1,7 NA, and 1,7 MNA have been investigated in the H_0/pH/H_- range of −10 to 17. The absorption and

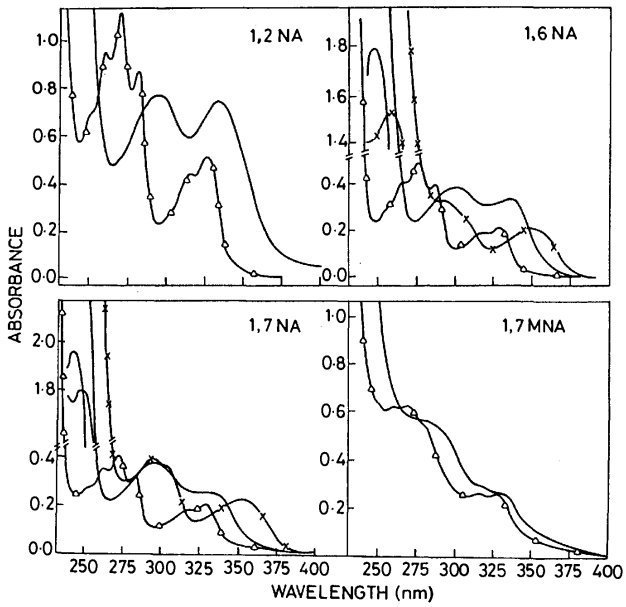

Fig. 2. Absorption spectra of various prototropic species of 1,2 NA, 1,6 NA, 1,7 NA, 1,7 MNA. (——) neutral, (—×—) monoanion, (—△—) monocation.

fluorescence spectra of the various prototropic species are shown in Figs. 2 and 3 respectively. The relevant data have been compiled in Tables 2 and 3. The absorption band maxima of monocation, neutral and monoanion (wherever these exist) of 1,2 NA and 1,7 NA agree with the literature values.[32]

Spectral characteristics accompanying the prototropic dissociation are related to the electron donor properties of the hydroxyl or amino group i.e. dissociation of hydroxyl or amino group will lead to red shift, whereas the protonation reaction will lead to the

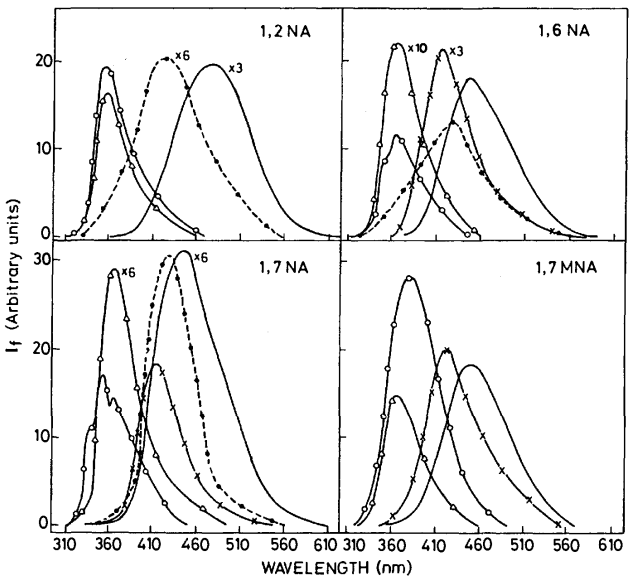

Fig. 3. Fluorescence spectra of various prototropic species of 1,2 NA, 1,6 NA, 1,7 NA, 1,7 MNA. (——) neutral, (—×—) monoanion, (—△—) monocation, (—●—) zwitterion, (—○—) dication.

blue shift in the absorption and fluorescence spectra if $\pi \rightarrow \pi^*$ is the lowest energy transition.

7-Methoxy-1-naphthylamine. Based on above arguments, the molecule exists as a neutral species in the pH/H_- range of 5 to 15. At $H_- > 15$, the species is a monoanion, formed either by the deprotonation of $-NH_2$ group or by one of the C-H bond. Chattopadhyaya and Chowdhury[42] have shown that the absorption spectra of 1 AN and *N,N*-dimethyl-1-naphthylamine are exactly same at $H_- > 15$. The latter compound does not possess the dissociable proton at the amino group. Thus the deprotonation of one of the C-H bond is preferred over the deprotonation of amino group. At pH<4, the species is a monocation. Resemblance of absorption spectrum of this species with that of 2-methoxynaphthalene[15] further confirms this assignment. At $H_0 < -4$, the species is a dication formed by protonating the ring carbon atom of monocation, because protonation of -OH/OMe leads to blue shift.[43-45] Besides this at H_0 −7, the monocation starts decomposing to give a large red shifted absorption spectrum and yellow-colored solution. This is an irreversible reaction and the results obtained are not very accurate in this range of acid concentration.

Prototropic reactions occurring in the S_1 state are exactly same as observed in the S_0 state i.e. dication, $H_0 < -4$; monocation, H_0 −3 to pH 3; neutral, pH 4 to 13 and monoanion, pH>13. The shifts observed in the fluorescence maxima are similar to those observed in the absorption spectra.

The ground state dissociation constant of monocation-free amine was calculated using absorption spectral data and is found to be 3.5. This value agrees with that observed in case of 1 AN. Data of Table 1 also show that the charge density at the nitrogen center of amino group at position 1 is not affected by the presence of methoxyl group at position 7. The equilibrium constants for dication-monocation and free amine-monoanion could not be determined as the formation of dication and monoanion were not complete even at the extreme acid/base conditions.

The pK_a's in the excited singlet state were determined with the help of fluorimetric titrations (Fig. 4). The fluorescence intensities of monoanion and dication were not plotted in Fig. 4 as the intensities for the respective species were quite small. The pK_a* value for the free amine-monoanion equilibrium is thus determined from the decrease in the fluorescence intensity of neutral species, whereas that for dication-monocation is speculated. The spectral data indicate that the C-H bond and amino group become stronger base and acid respectively in the excited singlet state, whereas the fluorimetric titrations have yielded the ground state pK_a values for dication-monocation and monocation-free amine equilibria. The former is consistent with earlier results that the equilibrium for the ring protonation is not established in the S_1 state. The latter result is anomalous in the sense that proton-induced fluorescence quenching is not observed before the amino group is protonated, which is a common feature of this reaction. Recently few exceptions are observed[16,17] and thus it can be concluded that the lifetimes of the conjugate acid-base pair are very short and the prototropic equilibrium is not established in S_1 state. The proton-induced fluorescence quenching of monocation of 1,7 MNA is consistent with earlier results of 2-methoxynaphthalene,[1] with the difference that it is observed at higher acid concentration. This is due to the presence of positive charge on the monocation of 1,7 MNA.

7-Hydroxy-1-naphthylamine. The ground state prototropic species of 1,7 NA, formed in the H_0/pH range −10 to 8 are exactly same as observed for 1,7 MNA, i.e. dication, −10 to −4; monocation, −4 to pH 3; neutral, pH 3 to 8. At pH>8, the species is a

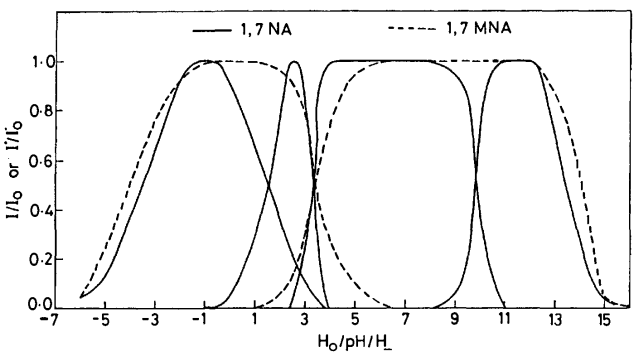

Fig. 4. Fluorimetric titration curves of the various prototropic species of 1,7 NA and 1,7 MNA.

monoanion, formed by deprotonating -OH group. At $H_-<15$, the species is a dianion, obtained by further deprotonating the C-H bond, rather than $-NH_2$ group. This can be explained on the same lines as has been done for the monoanion of 1,7 MNA. The pK_a values for the monocation-free amine and free-amine-monoanion equilibria, determined by using absorption spectral data, are 3.35 and 9.8 respectively. These values are not very different from the protonation constant of 1 AN (3.92) and deprotonation constant of 2 NOH (9.5).[26] As explained for 1,7 MNA, these pK_a's are not affected much by the presence of hydroxyl group or amino group respectively. This is further manifested from the data of Table 1, i.e. formal charge densities at the oxygen atom of -OH group of 1,7 NA and that of 2 NOH are nearly equal. Same is true for the nitrogen atom of amino groups of 1,7 NA and 1 AN.

The prototropic reactions of 1,7 NA occurring in the H_0/pH range of -10 to 0 are the same as observed for 1,7 MNA in S_1 state i.e. dication, -10 to -4; monocation, -4 to pH 0 and proton-induced fluorescence quenching of monocation of 1,7 NA is also observed prior to the formation of dication. This behavior is similar to that of 2 NOH, except that this process is taking place at higher acid concentration and this is due to the presence of positive charge on the 1,7 NA monocation.

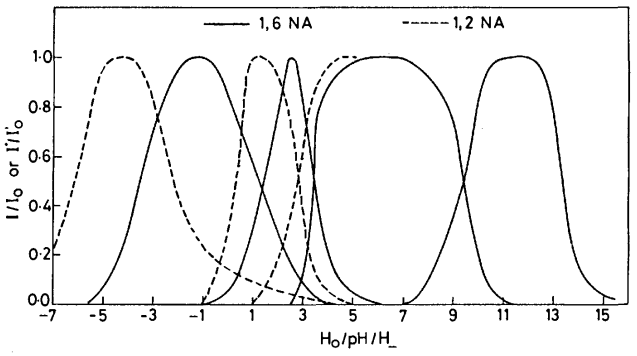

Fig. 5. Fluorimetric titration curves of the various prototropic species of 1,2 NA and 1,6 NA.

In the H_0/pH range -1 to 4 two fluorescence bands were observed. One at 426 nm and the other at 443 nm. The latter one is assigned to a neutral species because this band maximum nearly resembles that of 1,7 MNA, where there is no dissociable -OH group. The former is assigned to a zwitterion, formed by the deprotonation of the -OH group of monocation in the S_1 state. The monocation is the ground state precursor of zwitterion and the above assignment is based on the following results. (i) The fluorescence excitation spectrum of the zwitterion resembles the absorption spectrum of monocation, rather than the neutral molecule. (ii) Had the neutral molecule been the ground state precursor for the zwitterion, the similar results should have been observed at the earlier pH range and the fluorescence spectrum of this species in the pH range of 4 to 0 would have resembled the neutral molecule in nonpolar solvents and that of 1,7 MNA. (iii) The fluorescence spectrum of zwitterion resembles closely the β-naphtholate ion (418).[27] The fluorimetric titration curves in the pH range 4—0 cannot be drawn accurately, as three species are present simultaneously. Assuming that only two species are present in the given range (this assumption is not bad as the fluorescence intensity of monocation is never more than 10% of the fluorescence intensity of zwitterion, where the zwitterion-free-amine species are present) fluorimetric titration curves are drawn (Fig. 4) and the approximate pK_a value is listed on the arrows of Scheme 1. The value cannot be off by more than 10%.

At pH > 9, the 414 nm band is assigned to monoanion formed by the deprotonation of -OH group. The

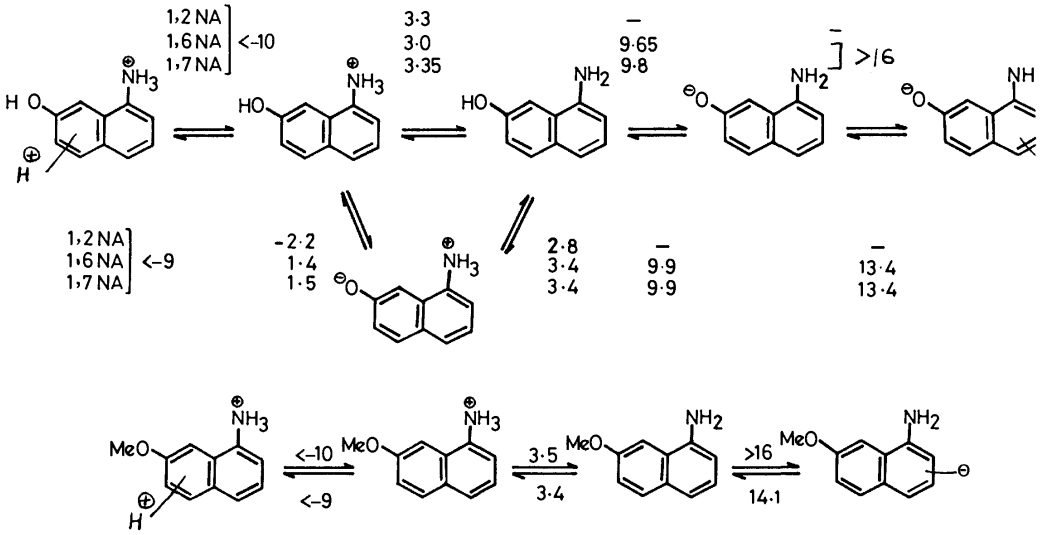

Scheme 1. Scheme representing the various prototropic reactions in the S_0 and S_1 states.

fluorimetric titration curves have given the ground state pK_a value, indicating that free naphthol-monoanion equilibrium is not established in S_1 state. This result is anomalous from that of 2 NOH,[27] in the sense, that extended sigmoid curve is not observed in case of 1,7 NA. It could be due to the shorter lifetimes of the conjugate acid-base pair.

At the extreme basic conditions H_- 16, 418 nm band is assigned to the dianion, formed either by deprotonating the -OH and $-NH_2$ groups or -OH group and the C-H bond. The latter process is preferred because of the following reasons: (i) The monoanion of 1 AN[12] is nonfluorescent and its pK_a* is 12.2, whereas that of 2 AN[12] is fluorescent [λ_{max}(flu)520] with pK_a* 12.3. At H_- 15, 412 nm fluorescence band of 1 AN is assigned to a kind of monoanion (**2** as shown below) by Choudhury and Chattopadhyay,[42] based on their study of 1 AN and 1-(dimethylamino)naphthalene. In general the deprotonation reaction of $-NH_2$ group in S_1 state starts at pH≈11 and is completed by pH≈14, whereas in case of 1,7 NA, this process occurs

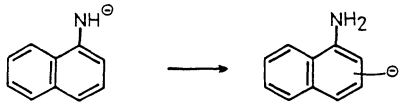

1 **2**

at pH > 14 and the correspondence is observed between the decrease of the fluorescence intensity of monoanion and the increase in that of dianion. (ii) The pK_a* value, determined from Fig. 4, falls in the same region as observed for the ring deprotonation of 1 AN.[12] (iii) Data of Table 1 clearly indicate that the charge density at the nitrogen atom of amino group of monoanion of 1,7 NA is equal to that on the amino group of 1 AN in S_0 state but in S_1 state, the charge density in case of former species is more than that of the latter species. This indicates that the pK_a* for this deprotonation reaction of $-NH_2$ group will increase on excitation as compared to that of 1 AN. (iv) The fluorescence band maximum of dianion of 1,7 NA falls in the same region where the species (**2**) of 1 AN fluorescence.[12] The intensity of 418 nm fluorescence band is weak and pK_a in S_1 state for monoanion-dianion equilibrium is determined from the decrease in the fluorescence intensity of monoanion (Fig. 4).

6-Hydroxy- and 2-Hydroxy-1-naphthylamines. The spectral characteristics of 1,6 NA in H_0/pH/H_- −10 to 16 are exactly similar and the results can be explained in the similar manner, whereas 1,2 NA decomposes at pH > 5.

The Scheme 1 represents the various prototropic reactions occurring in S_0 and S_1 states pK_a* values are depicted on the arrows.

Conclusion

Following conclusions can be drawn from the above study. (i) In absorption spectrum, the long wavelength band is long axis polarized, whereas the fluorescence is observed from ^1L_a state. (ii) The ground state precursor for the formation of zwitterion in the S_1 state is monocation. (iii) At high basic strength, the dianions are formed by the deprotonation of -OH group and one of the C-H bond.

We are thankful to the Department of Science and Technology, New Delhi for the financial support to the project entitled, "Proton Transfer Reactions in the Excited States."

References

1) A. Weller, *Prog. React. Kinet.*, **1**, 189 (1961).
2) E. Vander Donckt, *Prog. React. Kinet.*, **5**, 272 (1970).
3) S. G. Schulman, "Modern Fluorescence Spectroscopy," ed by E. L. Wehry, Plenum Press, Amsterdam (1977).
4) S. G. Schulman, "Fluorescence and Phosphorescence Spectroscopy: Physicochemical Principles and Practice," Pergamon Press, New York (1977).
5) J. F. Ireland and P. A. H. Wyatt, *Adv. Phys. Org. Chem.*, **12**, 132 (1976).
6) A. K. Mishra and S. K. Dogra, *J. Photochem.*, **23**, 163 (1983); *J. Chem. Soc., Perkin Trans. 2*, **1984**, 943.
7) M. Swaminathan and S. K. Dogra, *Can. J. Chem.*, **61**, 1064 (1983); *J. Am. Chem. Soc.*, **105**, 6223 (1983).
8) A. K. Mishra and S. K. Dogra, *Indian J. Chem., Sect. A*, **24**, 364, 815 (1985).
9) A. K. Mishra and S. K. Dogra, *Bull. Chem. Soc. Jpn.*, **58**, 3587 (1985).
10) R. V. Subbarao, M. Krishnamurthy, and S. K. Dogra, *Indian J. Chem., Sect. A*, **25**, 517 (1986) and references listed therein.
11) Th. Forster, *Z. Elektrochem.*, **54**, 531 (1950).
12) A. K. Mishra, M. Swaminathan, and S. K. Dogra, *J. Photochem.*, **28**, 87 (1985).
13) K. Tsutsumi, S. Sekiguchi, and H. Shizuka, *J. Chem. Soc., Faraday Trans. 1*, **78**, 1087 (1982).
14) H. Shizuka, *Acc. Chem. Res.*, **18**, 141 (1985).
15) H. Shizuka and S. Tobita, *J. Am. Chem. Soc.*, **104**, 6919 (1982).
16) H. Shizuka, T. Ogiware, and E. Kimura, *J. Phys. Chem.*, **89**, 4302 (1985).
17) A. K. Mishra and S. K. Dogra, *Indian J. Chem., Sect. A*, **24**, 285 (1985).
18) R. Manoharan and S. K. Dogra, *Bull. Chem. Soc. Jpn.*, **60**, 4409 (1987).
19) R. Manoharan and S. K. Dogra, *Can. J. Chem.*, **65**, 2013 (1987).
20) R. Manoharan and S. K. Dogra, *J. Phys. Chem.*, **92**, 5282 (1988).
21) W. Bortok, P. J. Lucchesi, and N. S. Snider, *J. Am. Chem. Soc.*, **84**, 1842 (1962).
22) P. Phaniraj, M. Krishnamurthy, and S. K. Dogra, *Indian J. Chem., Sect. A*, **25**, 513 (1986) and references listed therein.
23) R. T. Cowgill, *Photochem. Photobiol.*, **13**, 183 (1971).
24) R. S. Sarpal and S. K. Dogra, *J. Photochem.*, **38**, 263 (1987).
25) A. Weller, *Z. Physik Chem. N. F.*, **17**, 224 (1958).
26) N. M. Trieff and B. R. Sundhein, *J. Phys. Chem.*, **69**,

2044 (1965).
27) C. M. Harris and B. K. Sellinger, *J. Phys. Chem.*, **84**, 891 (1980).
28) C. M. Harris and B. K. Sellinger, *J. Phys. Chem.*, **84**, 1366 (1980).
29) R. S. Sarpal and S. K. Dogra, *Indian J. Chem., Sect. A*, in press.
30) J. W. Bridges and R. T. Williams, *Biochem. J.*, **107**, 183 (1968).
31) D. V. S. Jain, F. S. Nandel, and Prem Lata, *Indian J. Chem., Sect. A*, **21**, 559 (1982).
32) D. W. Ellis and L. B. Rogers, *Spectrochim. Acta*, **20**, 1709 (1964).
33) K. Tsutsumi and H. Shizuka, *Chem. Phys. Lett.*, **52**, 485 (1977).
34) R. Pariser and R. G. Parr, *J. Chem. Phys.*, **21**, 467, 767 (1953).
35) J. A. Pople, *Trans. Faraday Soc.*, **49**, 1315 (1953).
36) J. Delbene and H. H. Jaffe, *J. Chem. Phys.*, **48**, 1807, 4050 (1968).
37) R. Pariser, *J. Chem. Phys.*, **21**, 568 (1953).
38) N. Mataga and K. Nishimoto, *Z. Physik. Chem.*, **13**, 140 (1957).
39) H. H. Jaffe and M. Orchin, "Theory and Applications of Ultraviolet Spectroscopy," John Wiley, New York (1962), pp, 301, 304.
40) Th. Forster, *Z. Elekrochem.*, **54**, 531 (1950).
41) S. R. Meech, D. V. O' Connor, and D. Phillips, *J. Chem. Soc., Faraday Trans. 2*, **79**, 1563 (1983).
42) M. Choudhury and N. Chacopadhyay, *J. Photochem.*, **A41**, 337 (1988).
43) M. Krishnamurthy and S. K. Dogra, *Spectrochim. Acta, Part A*, **42**, 93 (1986).
44) H. K. Sinha and S. K. Dogra, *J. Photochem.*, **36**, 149 (1987).
45) H. K. Sinha and S. K. Dogra, *Chem. Phys.*, **102**, 337 (1986).

 © 1989 The Chemical Society of Japan Bull. Chem. Soc. Jpn., 62, 3291—3297 (1989)

Prebiotic Evolution of Oxidoreductases: $[Fe(III)(CN)_5(L)]^{n-}$ Complexes as Models

KAMALUDDIN,* Nath MALA, and W. Deopujari SUSHAMA
Department of Chemistry, University of Roorkee, Roorkee 247667 (U.P.), India
(Received October 31, 1988)

The transition state, where primary ligands like CN^- partially replaced by biomolecules, has been assumed to be interesting from point of view of chemical evolution of oxidoreductase enzymes. Complexes of type $[Fe(III)(CN)_5(L)]^{n-}$ (where n=2, 3 and L=glycine, imidazole, triglycine, and histidine) are proposed as models for peroxidases and catalases. Detailed kinetic investigations of decomposition of hydrogen peroxide catalyzed by $[Fe(III)(CN)_5(L)]^{n-}$ complexes at 40 °C over a wide pH range 6.0—11.0 are discussed. The decomposition reaction is highly pH dependent. In alkaline media, initially L^- is substituted by ^-OH in $[Fe(III)(CN)_5(L)]$; subsequently HOO^- binds to ^-OH through weak intramolecular hydrogen bonding, formation of peroxo complexes has been proposed to be an active intermediate responsible for accelerating the reaction. Decomposition of hydrogen peroxide catalyzed by $[Fe(III)(CN)_5(L)]^{n-}$ complexes conforms to Michaelis Menten type of kinetics.

Peroxidases and catalases are iron containing metalloporphyrins and these enzymes are widely distributed in plants and animals. A common reaction catalyzed by peroxidases is rapid oxidation of organic substrates coupled with decomposition of hydrogen peroxide. Early kinetic investigations on peroxidase-catalyzed decomposition of hydrogen peroxide were interpreted in terms of formation of free radicals.[1-4] The experimental evidences for the partcipation of hydroxyl radicals were also reported.[5-8] While exploring the mechanism of catalytic activity of peroxidases[9,10] intermediates with higher oxidation state of metal were reported.[11] Credit goes to Kremer and Stein,[12,13] who earlier proposed the active species as $[FeO]^{3+}$ for peroxide system containing Fe^{3+}, and to Jones et al. for Fe^{4+} in iron porphyrin systems.[14] From structural and functional point of view, catalases are related to peroxidases. A characteristic reaction of catalases is the rapid catalysis of hydrogen peroxide decomposition with itself.

In recent years, considerable attention has been given on synthesis of metal complexes possessing enzyme-like activity. Peroxidases and catalases are the most extensively studied enzymes which created a lot of interest in the synthesis of model compounds. Metal ions as such or their complexes have been shown to possess enzyme-like activity. Complexes of copper with amino acids, amides, amines, diammines, di- and tripeptides, biurets, heterocyclic compounds,[16,17] some proteins as well as copper complexes of 2,2′-bipyridyl, bis(2,9-dimethyl-1,10-phenanthroline),[18,19] and imidazole[20] have been found to show very high catalytic activity towards decomposition of hydrogen peroxide. Catalytic activity of few iron complexes was also tested towards decomposition of hydrogen peroxide.[21,22] Francis et al.[23] carried out kinetic investigation in detail on [Fe(III) EDTA]-catalyzed decomposition of hydrogen peroxide and proposed hexa coordinated ion viz.

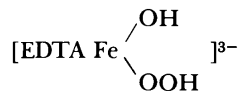

as an active species on the basis of NMR and spectral studies. However, relevance of these models towards chemical evolutionary steps of peroxidases or catalases is very little as these enzymes neither possess copper in their prosthetic group, nor coordination sites of metals in enzymes occupied by ligands like EDTA. It is therefore important to study catalytic behavior of iron(III) complexes with important prebiotic ligands towards decomposition of hydrogen peroxide from the viewpoint of chemical evolution.

In previous papers kinetics of $[Fe(II)(CN)_5(L)]^{n-}$-catalyzed decomposition of hydrogen peroxide were reported.[24,25] In present manuscript we reported the kinetic studies on decomposition of hydrogen peroxide catalyzed by $[Fe(III)(CN)_5(L)]^{n-}$ (where L=glycine, histidine, imidazole, or triglycine; n=2 or 3) from point of view of chemical evolution of peroxidases.

Materials of Methods

Materials. Glycine (B.D.H.), triglycine (Sigma), histidine (Sisco), imidazole (E. Merck), potassium hexacyanoferrate(III) (B.D.H.), sodium pentacyanonitrosylferrate(III) (B.D.H.), and hydrogen peroxide (B.D.H.) were used as supplied and were of Anal R grade. All other chemicals used were of reagent grade.

Preparation of $[Fe(III)(CN)_5(L)]^{n-}$ (Where L=Glycine, Triglycine, Histidine, and Imidazole). Imidazole pentacyanoferrate(III) was prepared by the method of Walters and Spiro.[26] Similar procedure was also adopted for synthesis of triglycine, glycine, and histidine pentacyanoferrate(III) complexes. Sodium (amine)pentacyanoferrate(II) (1.0 g, 3.0 mmol) was dissolved in 6% hydrogen peroxide containing at least five fold excess ligand with constant stirring. Reaction mixture was then kept in dark 45—60 min to allow the formation of $[Fe(III)(CN)_5(L)]^{n-}$ complexes. A few milligrams of activated charcoal was added to the solution to decompose excess of hydrogen peroxide and removed

by filtration. Potassium iodide (8.0 g, 48.0 mmol) was added to the solution and stirred for another 15 min. The complexes were precipitated by adding ethanol and recrystallized from ethanol-water system.

Infrared spectra of complexes of type $[Fe(III)(CN)_5(L)]^{n-}$ are quite similar to those of corresponding analogs of $[Fe(II)(CN)_5(L)]^{n-}$ complexes implying resemblence in the mode of coordination of ligand to metal ion.[24,25] The cyanide stretching frequencies are very sensitive to the oxidation state of central metal ion and generally shifts towards higher wavenumber in case of cyanoferrate(III) complexes. The cyanide stretching frequencies for (amino acid) pentacyanoferrate(III) complexes were obserbed in the range 2070—2100 cm^{-1}, whereas in hexacyanoferrate(III) complexes C≡N was observed around 2100—2200 cm^{-1} region.[27] The weak bands of δFe-CN and νFe-CN were observed respectively in the range 560—595 cm^{-1} and 400—410 cm^{-1} in all Fe(III) complexes. The ν_{asym} COO^- and ν_{sym} COO^- were observed at $1620—1640_m$ cm^{-1} and at $1410—1440_w$ cm^{-1} respectively. When equivalance of CO bond is removed, particularly in case of -COO^- group, the separation in vibrational frequencies was observed.[28] The shift towards higher wavenumber showed the possibility of participation of COO^- group in coordination to metal ion in $[Fe(III)(CN)_5(L)]^{n-}$ complexes (where L=glycine or triglycine). But little or negligible shift for this band in case of histidine complex indicates that the coordination is through nitrogen of imidazole ring, as in case of $[Fe(III)(CN)_5(im)]^{2-}$.[26] Infrared spectral frequencies of all complexes are tabulated in Table 1.

Electronic spectra of all pentacyanoferrate(III) derivatives showed nearly constant bands at 280—290, 350, and 400—410 nm due to transition involving only CN^- ligand and are in agreement with those observed for $[Fe(III)(CN)_6]^{3-}$ by Gale and McCoffery.[29] However, for sodium pentacyanonitrosylferrate(III), Manoharan and Gray[30] observed three peaks at 200 nm, 394 nm, and 495 nm with shoulder peaks at 238, 264, and 363 nm respectively. The absorption spectra of pentacyanoferrate(III) complexes of glycine, triglycine, and imidazole are compared with $[Fe(III)(CN)_5(NH_3)]^{2-}$ and due to the previously reported $[Fe(III)(CN)_5(im)]^{2-}$ and $[Fe(III)(CN)_5(his)]^{2-}$ complexes.[26,31] The absorption bands in UV region at 280—290 nm have been assigned to the CN^- →Fe-$(III)_{d\pi}$ transitions. The absorption bands in visible region 400—410 nm are due to d-d transitions and can be compared with absorption spectra of many other pentacyanoferrate[32] and cobaltates.[33] The visible absorption spectra bands of triglycine pentacyanoferrate(III) and glycine showed very little shift and similarity with the corresponding analogs of iron(II) complexes implies the possibility of coordination through ammine ligand only. The broad charge transfer absorption band at 470—480 nm observed in both imidazole and histidine pentacyanoferrate(III) complexes due to imidazole→Fe(III) transitions thus indicates that the mode of coordination in histidine complex is also through imidazole ring of histidine. The data of electronic spectra are summarized in Table 2.

Rate Measurements. Decomposition of H_2O_2: Test for catalytic activity of iron(III) complexes for decomposition of hydrogen peroxide was studied by monitoring concentration of H_2O_2 at different time intervals. The reaction was initiated by adding known amount of catalyst (1 ml of 0.005 M; 1M=1 mol dm^{-3}) into hydrogen peroxide solution (25 ml of 0.01—0.1M) previously thermostated at 40 °C. Aliquots (2 ml) of reaction mixture were withdrawn each time and titrated against standard sodium thiosulfate in acid medium. The data for $[H_2O_2]$ at corresponding time did not fit a simple rate equation, therefore the initial rate method was used to determine the order of reaction with respect to hydrogen peroxide and catalyst.

Results and Discussion

Catalytic activities of complexes like $[Fe(III)(CN)_5(L)]^{n-}$ towards decomposition of hydrogen peroxide have been studied over a wide pH range 6.0 to 11.0. It was found that decomposition rate of hydrogen peroxide increased sharply till pH 9.18 and thereafter increased slowly (Fig. 1) indicating the participation of only ^-OH in decomposition reaction. An increase in rate of decomposition with increase in pH displayed the possibility of participation of ^-OH and HO_2^- in reaction mechanism. A value of pH 9.18 was found to be most suitable for carrying out all kinetic studies. In alkaline medium, HO_2^- species

Table 1. Characteristic Infrared Spectral Frequencies (cm^{-1}) of $[Fe(III)(CN)_5(L)]^{n-}$ Complexes

Complex	$\nu_{sym}C\equiv N$	δFe-CN	νFe-CN	$\nu_{asym}COO^-$	$\nu_{sys}COO^-$
$K_3[Fe(III)(CN)_5(gly)]$	2090_s	590_w	400_{vw}	1640_m	1430_w
$K_3[Fe(III)(CN)_5(trigly)]$	2080_s	595_{vw}	400_{vw}	1630_m	1425_w
$K_2[Fe(III)(CN)_5(his)]$	2070_s	590_w	410_{vw}	1620_m	1410_w
$K_2[Fe(III)(CN)_5(im)]$	2070_s	560_w	400_{vw}	—	—

s=strong, m=medium, w=week, vw=very weak.

Table 2. Electronic Spectral Bands (nm) of $[Fe(III)(CN)_5(L)]^{n-}$

Complex	Charge transfer band $CN_\pi \rightarrow Fe(III)_{d\pi}$	d-d $^1A_{(1)} \rightarrow {}^1E_{(1)}$	Charge transfer IMH→Fe(III)
$K_3[Fe(III)(CN)_5(gly)]$	283	410	—
$K_3[Fe(III)(CN)_5(trigly)]$	280	405	—
$K_2[Fe(III)(CN)_5(his)]$	290	405	475—480
$K_2[Fe(III)(CN)_5(im)]$	295	407	470—480

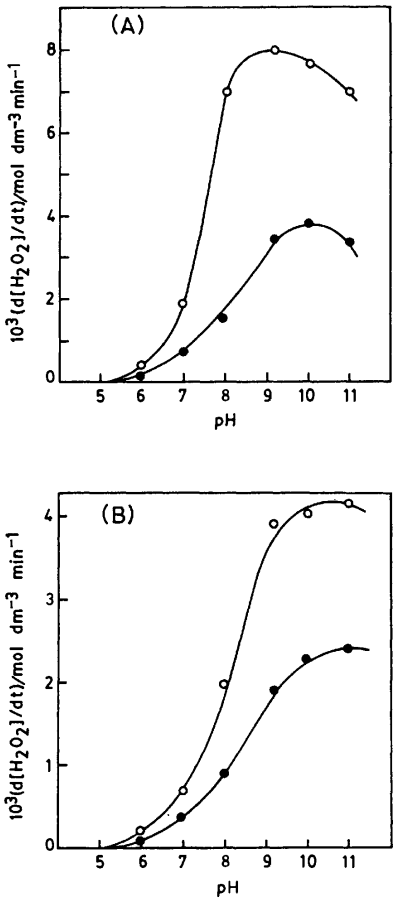

Fig. 1. Hydrogen peroxide decomposition rate as a function of pH. $[H_2O_2]_0=4.5\times10^{-2}$ M; [Catalyst]= 2×10^{-4} M; temp 40±0.1 °C.
(A) ○=$K_3[Fe(CN)_5(gly)]$, ●=$K_2[Fe(CN)_5(his)]$.
(B) ○=$K_2[Fe(CN)_5(im)]$, ●=$K_3[Fe(CN)_5(trigly)]$.

has been proposed by Francis et al.[23] to be most effective species around pH range 9.0—11.0 which easily could form a complex of type

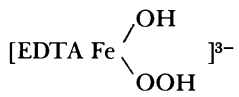

and decomposition of this intermediate complex makes the rate determining step for $[Fe(III)EDTA]^-$-catalyzed decomposition of hydrogen peroxide. In our experiments probability of formation of hepta-coordinated complex like $[Fe(III)(CN)_5(OH)(OOH)]^{4-}$ can not be considered because of high ligand-field stabilization energy of CN^- groups. However, increase in rate with pH may be due to participation of HOO^- species rather than undissociated hydrogen peroxide molecule. Another possibility of replacement of amino acid molecule by ^-OH can also not be ignored at higher pH. It is therefore thought that initially ^-OH is coordinated to metal by replacing weakly-bonded amino acid ligand and subsequently HO_2^- attached to ^-OH group through weak interactions of hydrogen bonding.

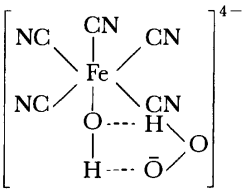

It appears that the function of ^-OH in coordination sphere is simply to facilitate the formation of peroxo complex by weak hydrogen bonding. Sigel[34] compared the catalase like activities of a number of copper(II) chelates and pointed out that the copper polyammine chelate with two free coordination sites show maximum activity while fully coordinated copper(II) complex is inactive. A high catalytic activity was observed for decomposition of H_2O_2 by Mn(II) and Fe(III) chelates of diethylenetriammine when two coordination sites in metal ion were available for inner sphere mechanism as proposed by Wang and Jarinagin.[35,36] In our experiments, the possibility of outer sphere mechanism was completely discarded since $[Fe(III)(CN)_6]^{3-}$ did not show any comparable rate of catalytic activity to $[Fe(III)(CN)_5(L)]^{n-}$ indicating that only inner sphere mechanism for decomposition of hydrogen peroxide is possible. Only one coordination site is available on $[Fe(III)(CN)_5(L)]^{n-}$ complexes for substrate binding that is loosely bonded sixth ligand (L), which can be replaced in presence of substrate, where as in case of hexacyanoferrate(III) CN^- is not easily replaced.

In order to ensure that the catalytic activity observed in decomposition of hydrogen peroxide was only due to (amino acid)pentacyanoferrate(III) derivatives and not because of traces of uncomplexed metal ions, 10% EDTA was added. Addition of EDTA, however, did not change the rate of catalytic activity. Addition of ligands as catalyst was also not effective (Fig. 2).

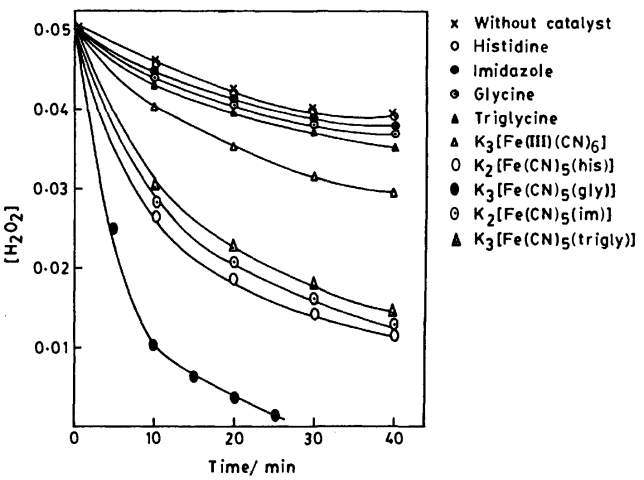

Fig. 2. $[Fe(III)(CN)_5(L)]^{n-}$ catalyzed decomposition of hydrogen peroxide. $[H_2O_2]=5.0\times10^{-2}$ M; [Catalyst]=2×10^{-4} M; pH=9.18; temp=40±0.01 °C.

A tentative mechanism for decomposition of hydrogen peroxide catalyzed by amino acid pentacyanoferrate(III) complexes may be written as follows:

$$H_2O_2 \xrightarrow{K_{H_2O_2}} H^+ + {}^-OOH \quad (1)$$

$$\underset{\mathbf{A}}{[Fe(III)(CN)_5(L)]^{n-}} + {}^-OH \underset{k_2}{\overset{k_1}{\rightleftharpoons}} \underset{\mathbf{B}}{[Fe(III)(CN)_5(OH)]^{3-}} + L^- \quad (2)$$

$$\underset{\mathbf{B}}{[Fe(III)(CN)_5(OH)]^{3-}} + {}^-OOH \underset{k_4}{\overset{k_3}{\rightleftharpoons}} \underset{\mathbf{C}}{[Fe(III)(CN)_5(OH\cdots OOH)]^{4-}} \quad (3)$$

$$[Fe(III)(CN)_5(OH\cdots OOH)]^{4-} \xrightarrow{k_5} \text{Product} \quad (4)$$

The proposed mechanism is somewhat similar to the mechanism proposed by Sigel et al.[18] for decomposition of hydrogen peroxide catalyzed by Cu^{2+} ions and Cu^{2+} complexes of 2,2'-bipyridyl. Applying steady state approximation of **B** and **C** species, the rate of decomposition of hydrogen peroxide may be written as follows:

$$V = \frac{-d[H_2O_2]}{dt} = \frac{k_1 k_5 k_{H_2O_2}[H_2O_2][Fe]_T}{k_1 K_M[H^+] + K_{H_2O_2}[H_2O_2]\left(k_1 + \frac{k_5[H^+]}{k_W}\right)} \quad (5)$$

Also rearranging Eq.5 in Lineweaver-Burk form of equation:

$$\frac{1}{V} = \frac{K_M[H^+]}{k_5 K_{H_2O_2}[H_2O_2][Fe]_T} + \frac{\left(k_1 + \frac{k_5[H^+]}{k_W}\right)}{k_1 k_5 [Fe]_T} \quad (6)$$

where, $K_M = \dfrac{k_4 + k_5}{k_3}$.

Equation 5 clearly indicates that decomposition of hydrogen peroxide follows a first order kinetics with respect to [Catalyst], which is in accord with experimental findings (Fig. 3). The initial rate as function of $[H_2O_2]$ is shown in Fig. 4, where linearity of the curve at lower concentration of H_2O_2 suggests first order dependency at that concentration, whereas at higher concentration the reaction rate becomes constant showing independency on $[H_2O_2]$. The independency of decomposition rate on $[H_2O_2]$ could also be explained from Eq. 5 due to the presence of $[H_2O_2]$ term in the denominator. The most exciting feature of Eq. 5 lies in its nature, being a typical Michaelis-Menten type of kinetics supported by the straight line (Fig. 5), which is obtained on plotting $(d[H_2O_2]/dt)^{-1}$ vs. $[H_2O_2]^{-1}$. Intercept and slope obtained in Fig. 5 should be equal to

$$\frac{k_1 + \frac{k_5[H^+]}{k_W}}{k_1 k_5 [Fe]_T} \quad \text{and} \quad \frac{K_M[H^+]}{k_5 K_{H_2O_2}[Fe]_T}$$

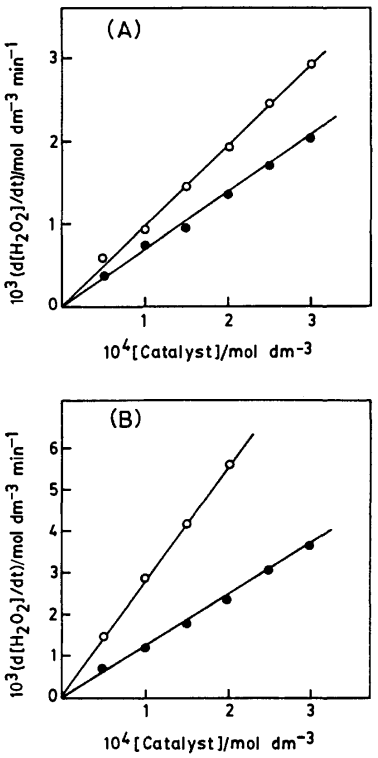

Fig. 3. Hydrogen peroxide decomposition rate as a function of [Catalyst]: $[H_2O_2]_0 = 2.7\times10^{-2}$ M: pH= 9.18; temp=40±0.1 °C.
(A) ○=$K_3[Fe(CN)_5(trigly)]$, ●=$K_2[Fe(CN)_5(im)]$.
(B) ○=$K_3[Fe(CN)_5(gly)]$, ●=$K_2[Fe(CN)_5(his)]$.

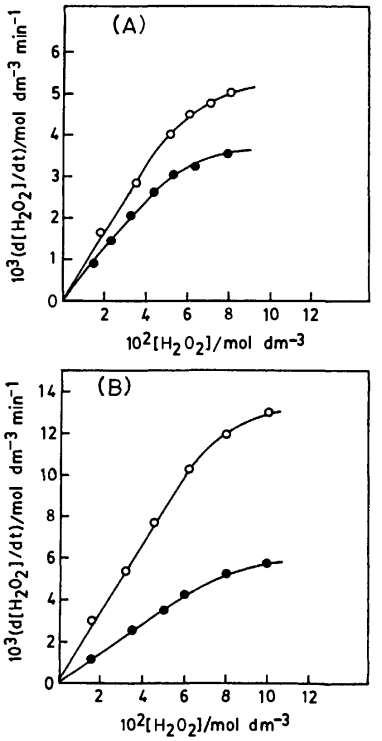

Fig. 4. Hydrogen peroxide decomposition rate as a function of $[H_2O_2]_0$ at pH 9.18; [Catalyst]=2×10^{-4} M; temp=40±0.1 °C.
(A) ○=$K_2[Fe(CN)_5(his)]$, ●=$K_3[Fe(CN)_5(trigly)]$.
(B) ○=$K_3[Fe(CN)_5(gly)]$, ●=$K_2[Fe(CN)_5(im)]$.

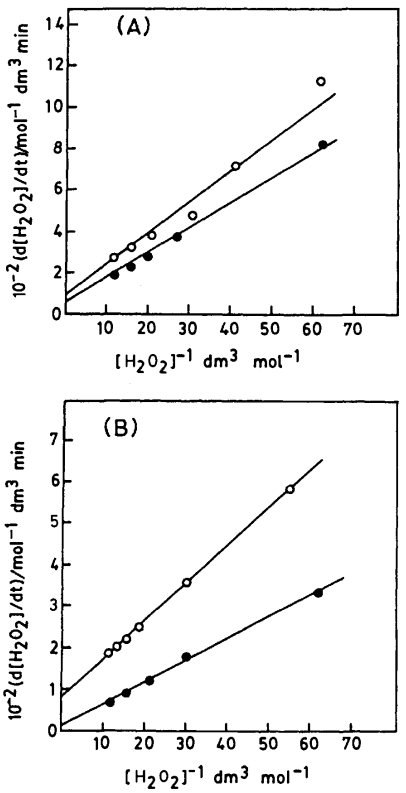

Fig. 5. Lineweaver-Burk plot.
(A) O=$K_3[Fe(CN)_5(trigly)]$, ●=$K_2[Fe(CN)_5(im)]$.
(B) O=$K_2[Fe(CN)_5(his)]$, ●=$K_3[Fe(CN)_5(gly)]$.

respectively as warranted by Eq. 6. On comparing the terms with normal Michaelis-Menten curve,

$$\text{Intercept} = \frac{1}{V'_{max}[Fe]_T}$$

$$\text{where, } \frac{1}{V'_{max}} = \frac{k_1 + k_5[H^+]/k_W}{k_1 k_5}$$

$$\text{and slope} = \frac{K'_M}{k_5[Fe]_T}$$

$$\text{where, } K'_M = \frac{K_M[H^+]}{K_{H_2O_2}}.$$

From the intercept and slope, V'_{max} and K'_M and turnover numbers have been calculated and are tabulated in Table 3.

The proposed mechanism for decomposition of hydrogen peroxide catalyzed by cyano complexes of iron(III) and their derivatives is similar to the catalyzed decomposition of hydrogen peroxide in many ways. Peroxidase and catalase are iron-containing enzymes in which iron(III) is strongly bonded to porphyrin ring, the fifth ligand is imidazole and the sixth ligand is loosely bonded water or cyanide ion. It has been assumed that the peroxidase operates by the exchange of the ligand at the sixth position[37] with peroxide. In our proposed model, five CN^- are tightly bonded to iron(III) and decomposition of H_2O_2 proceeds after exchange with loosely bonded sixth ligand which is an amino acid or peptide.

Cyano complexes of transition metal have a special evolutionary significance to the biological systems.[38] Appearance of biomolecules on earth replaced primary ligands and thereby catalytic activity of the metal complexes increased towards biological processes. The effect of transition where primary ligands were replaced by secondary ligands on biological reactions has been considered to be decisive from evolutionary point of view and therefore, efforts were made to trace out the possible evolutionary path for iron-containing oxidoreductase enzymes. $[Fe(II)(CN)_5(L)]^{n-}$[24,25] and $[Fe(III)(CN)_5(L)]^{n-}$ complexes found to be well-suited models for peroxidases and catalases and these complexes showed remarkable increase in catalytic activity towards decomposition of hydrogen peroxide when one of the cyanide ligands is substituted by biomolecules. Catalytic activity or turnover number of amino acid pentacyanoferrate(III) towards decomposition of hydrogen peroxide does not indicate any dramatic change in catalytic rate when compared with their corresponding analogs amino acid pentacyanoferrate(II) complexes.[24,25] Thus it can be safely concluded that perhaps at later stages of evolution of metalloenzymes, oxidation state of metal played vital role in determining catalytic activity of enzymes and not at very early stages of chemical evolution.

The proposed model for evolution of iron-containing enzymes is not contradictory to the one proposed by Calvin.[39] The only difference lies in the fact that in present studies we have considered much more early stages of proenzymes.

Table 3. Kinetic Constants for Decomposition of Hydrogen Peroxide Catalyzed by $[Fe(III)(CN)_5(L)]^{n-}$

Catalyst	V'_{max}[a]	Turnover number[b]	K'_M[c]
	M min^{-1}	min^{-1}	M
$K_3[Fe(III)(CN)_5(gly)]$	0.100	500.0	0.533
$K_3[Fe(III)(CN)_5(trigly)]$	0.011	55.55	0.178
$K_2[Fe(III)(CN)_5(im)]$	0.018	91.00	0.121
$K_2[Fe(III)(CN)_5(his)]$	0.0125	62.50	0.117

Reaction conditions: Catalyst=2.0×10^{-4} mol dm^{-3}, pH=9.18, temp=40.0±1 °C, a) $V'_{max}=k_1k_5/[k_1+k_5[H^+]/k_w]$. b) Turnover number=$V'_{max}/[Fe]_T$. c) $K'_M=K_M[H^+]/K_{H_2O_2}$.

Appendix

$$H_2O_2 \xrightarrow{K_{H_2O_2}} HOO^- + H^+ \quad (1)$$

$$\underset{\mathbf{A}}{[Fe(III)(CN)_5(L)]^{n-}} + {}^-OH \underset{k_2}{\overset{k_1}{\rightleftharpoons}} \underset{\mathbf{B}}{[Fe(III)(CN)_5(OH)]^{n-}} + L^- \quad (2)$$

$$\underset{\mathbf{B}}{[Fe(III)(CN)_5(OH)]^{n-}} + HOO^- \underset{k_4}{\overset{k_3}{\rightleftharpoons}} \underset{\mathbf{C}}{[Fe(III)(CN)_5(OH\cdots OOH)]^{(n+1)-}} \quad (3)$$

$$\underset{\mathbf{C}}{[Fe(III)(CN)_5(OH\cdots OOH)]^{(n+1)-}} \xrightarrow{k_5} \text{Product} \quad (4)$$

$$\text{Reaction rate} = V = \frac{-d[H_2O_2]}{dt} = k_5[\mathbf{C}]. \quad (5)$$

Assuming steady state to [C], we get,

$$k_3[\mathbf{B}][HO_2^-] = k_4[\mathbf{C}] + k_5[\mathbf{C}]$$

$$[\mathbf{C}] = \frac{k_3[\mathbf{B}][HO_2^-]}{k_4 + k_5}. \quad (6)$$

Assuming steady state to [B], we get

$$k_1[\mathbf{A}][{}^-OH] + k_4[\mathbf{C}] = k_2[\mathbf{B}][L^-] + k_3[\mathbf{B}][HO_2^-]$$

but from Eq. 6,

$$[\mathbf{C}](k_4 + k_5) = k_3[\mathbf{B}][HO_2^-]$$

$$k_1[\mathbf{A}][{}^-OH] + k_4[\mathbf{C}] = k_2[\mathbf{B}][L^-] + k_4[\mathbf{C}] + k_5[\mathbf{C}]$$

$$[\mathbf{C}] = \frac{k_1[\mathbf{A}][{}^-OH] - k_2[\mathbf{B}][L^-]}{k_5}. \quad (7)$$

Equating Eqs. 6 and 7, we get

$$\frac{k_3k_5[\mathbf{B}][HO_2^-]}{k_4 + k_5} = k_1[\mathbf{A}][{}^-OH] - k_2[\mathbf{B}][L^-]$$

$$[\mathbf{B}][k_3k_5[HO_2^-] + k_2[L^-](k_4 + k_5)] = k_1(k_4 + k_5)[\mathbf{A}][{}^-OH]$$

$$[\mathbf{B}] = \frac{k_1(k_4+k_5)[\mathbf{A}][{}^-OH]}{k_3k_5[HO_2^-]+k_2[L^-](k_4+k_5)}. \quad (8)$$

Putting [B] from Eq. 8 in Eq. 6, we get

$$[\mathbf{C}] = \frac{k_1k_3[\mathbf{A}][HO_2^-][{}^-OH]}{k_3k_5[HO_2^-]+k_2[L^-](k_4+k_5)}. \quad (9)$$

Putting the value [C] from Eq. 9 in Eq. 5, we get

$$V = \frac{-d[H_2O_2]}{dt} = \frac{k_1k_3k_5[\mathbf{A}][HO_2^-][{}^-OH]}{k_3k_5[HO_2^-] + k_2[L^-](k_4+k_5)} \quad (10)$$

$$\text{or} \quad V = \frac{k_1k_5[\mathbf{A}][HO_2^-][{}^-OH]}{k_5[HO_2^-] + k_2K_M[L^-]}$$

$$\text{where,} \quad K_M = \frac{k_4 + k_5}{k_3}.$$

Also, if $[Fe]_T$ represent the total concentration of iron(III) containing species participating in the reaction, we can write

$$[Fe]_T = [\mathbf{A}] + [\mathbf{B}] + [\mathbf{C}]$$

$$= [\mathbf{A}] + \frac{k_1(k_4+k_5)[\mathbf{A}][{}^-OH]}{k_3k_5[HO_2^-] + k_2[L^-](k_4 + k_5)} + \frac{k_1k_3[\mathbf{A}][HO_2^-][{}^-OH]}{k_3k_5[HO_2^-] + k_2[L^-](k_4 + k_5)}$$

$$[\mathbf{A}] = \frac{[Fe]_T[k_3k_5[HO_2^-] + k_2[L^-](k_4 + k_5)]}{k_3k_5[HO_2^-] + k_2[L^-](k_4 + k_5) + k_1(k_4 + k_5)[{}^-OH] + k_1k_3[HO_2^-][{}^-OH]}.$$

In the denominator of the above equation, assuming $k_2[L^-](k_4+k_5)$ is very small compared to other terms, hence neglected

$$[\mathbf{A}] = \frac{[Fe]_T[k_3k_5[HO_2^-] + k_2[L^-](k_4 + k_5)]}{k_3k_5[HO_2^-] + k_1(k_4+k_5)[{}^-OH] + k_1k_3[HO_2^-][{}^-OH]}.$$

Putting the value of [A] from above equation in Eq. 10, we get

$$V = \frac{k_1k_5[Fe]_T[HO_2^-][{}^-OH]}{k_5[HO_2^-] + k_1K_M[{}^-OH] + k_1[HO_2^-][{}^-OH]}$$

$$= \frac{k_1k_5K_{H_2O_2}[H_2O_2][{}^-OH][Fe]_T}{[H^+]\left[k_5\frac{K_{H_2O_2}[H_2O_2]}{[H^+]} + k_1K_M[{}^-OH] + k_1\frac{K_{H_2O_2}[{}^-OH][H_2O_2]}{[H^+]}\right]}$$

$$= \frac{k_1k_5K_{H_2O_2}[H_2O_2]\,[Fe]_T}{[H^+]\left[k_5\frac{K_{H_2O_2}[H_2O_2]}{[H^+][{}^-OH]} + k_1K_M + k_1\frac{K_{H_2O_2}[H_2O_2]}{[H^+]}\right]}$$

$$= \frac{k_1k_5K_{H_2O_2}[H_2O_2]\,[Fe]_T}{k_5\frac{K_{H_2O_2}}{k_W}[H_2O_2][H^+] + k_1K_M[H^+] + k_1K_{H_2O_2}[H_2O_2]}$$

$$V = \frac{k_1k_5K_{H_2O_2}[H_2O_2][Fe]_T}{k_1K_M[H^+] + K_{H_2O_2}[H_2O_2]\left(k_1 + \frac{k_5}{k_W}[H^+]\right)}.$$

References

1) C. Walling, *Acc. Chem. Res.*, **8**, 125 (1975).
2) W. G. Barb, J. H. Baxendale, P. George, and K. R. Hargrave, *Trans. Faraday Soc.*, **47**, 591 (1951).
3) S. Fallab, *Angew. Chem., Int. Ed. Engl.*, **6**, 496 (1967).
4) D. M. Jerina and J. W. Daley, "Oxidases and Related Redox Systems," Univ. Press, Baltimore, Maryland (1973), Vol. 1, p. 143.
5) W. Kern and R. C. Shulz, *Makromol. Chem.*, **13**, 210 (1954).
6) T. Shiga, *J. Phys. Chem.*, **69**, 3805 (1965).
7) W. T. Dixon and R. O. C. Norman, *Nature (London)*, **196**, 891 (1962).
8) R. O. C. Norman and P. R. West, *J. Chem. Soc. B*, **1969**, 389.
9) B. Chance, *Acta Chem. Scand.*, **1**, 236 (1947).
10) B. Chance, D. S. Greenstein, and F. J. W. Roughton,

Acta Biochem. Biophys., **37**, 301 (1952).
11) J. M. Pratt, "Techniques and Topic in Bioinorganic Chemistry," ed by C. A. McAuliffe, McMillan London and Basingstoke (1975), p. 109.
12) M. L. Kremer, *Trans. Faraday Soc.*, **58**, 302 (1962).
13) M. L. Kremer and G. Stein, *Trans. Faraday Soc.*, **55**, 959 (1959).
14) P. Jones, "Oxidase and Related Redox Systems," Univ. Press, Baltimore (1973), p. 333.
15) P. Jones, D. Mantle, D. M. Davis, and H. C. Kelly, *Biochemistry*, **16**, 3974 (1977).
16) L. A. Nikolaev, *Vestinik Moskov, Univ.*, **3(10)** 169 (1948).
17) L. A. Nikolaev, *J. Chem. Phys.*, **51**, 757 (1954).
18) H. Sigel, K. Wyss, B. E. Fisher, and S. Brijs, *Inorg. Chem.*, **18**, 1354 (1979).
19) G. Davis, R. Higgon, and P. J. Loase, *Inorg. Chem.*, **15**, 700 (1976).
20) V. S. Sharma and J. Schubert, *J. Am. Chem. Soc.*, **91**, 6291 (1969).
21) C. Walling, M. Kurz, and H. J. Schugar, *Inorg. Chem.*, **9**, 931 (1970).
22) R. E. Heikkiila, "Proc. Int. Conf. Superoxide Dismutase," (1983), Vol. 1, p. 282.
23) K. C. Francis, C. Cummins, and J. Oakes, *J. Chem. Soc., Dalton Trans.*, **1985**, 493.
24) Kamaluddin, M. N. and W. D. Sushama, *Origin of Life*, **17**, 59 (1986).
25) Kamaluddin, M. N. and W. D. Sushama, *Origin of Life and Evolving Biosphere*, in press.
26) M. A. Walters and T. G. Spiro, *Inorg. Chem.*, **22**, 4L14 (1983).
27) E. F. G. Herington and W. Kynaston, *J. Chem. Soc.*, **1955**, 3555.
28) K. Nakamoto, "Infrared Spectra of Inorganic Coordination Compounds," Wiley Interscience, New York (1970), p. 233.
29) R. Gale and A. J. McCoffery, *J. Chem. Soc., Dalton Trans.*, **1973**, 1344.
30) P. T. Manoharan and H. B. Gray, *J. Am. Chem. Soc.*, **85**, 2922 (1963).
31) R. E. Shephered, *J. Am. Chem. Soc.*, **98**, 3329 (1976).
32) H. E. Toma, F. Giesbrecht, J. M. Malm, and E. Fluke, *Inorg. Chim. Acta*, **14**, 11 (1975).
33) V. M. Miskowsky and H. B. Gray, *Inorg. Chem.*, **14**, 401 (1975).
34) H. Sigel, *Angew. Chem., Int. Ed. Engl.*, **8**, 167 (1969).
35) J. H. Wang, *J. Am. Chem. Soc.*, **77**, 4715 (1955).
36) R. C. Jarinagin and J. H. Wang, *J. Am. Chem. Soc.*, **80**, 6477 (1958).
37) B. C. Saunders, "Inorganic Biochemistry," ed by G. L. Eichhom, Academic Press, New York (1973), Vol. 2, p. 991.
38) M. T. Beck, "Metal Ions in Biological Systems," ed by H. Sigel, Marcel Dekker, New York (1978), Vol. 7, p. 1.
39) M. Calvin, *Science*, **130**, 1170 (1959).

Application of Flory Theory to Mixtures of Molten Tetrahydrates of Calcium and Cadmium Nitrates

Nurul ISLAM* and Girija MAHESHWARI
Department of Chemistry, Aligarh Muslim University, Aligarh 202002, India
(Received November 17, 1988)

The Flory theory has successfully been employed to predict the excess volume, viscosity of mixtures, surface tension, and the ultrasonic velocities of mixtures of molten tetrahydrates of calcium and cadmium nitrates. The agreement in the computed and the experimental values has been good. The excess volume as well as the excess adiabatic compressibility suggest maximum solute-solvent interactions at ca. 0.55 mole fraction of Cd^{2+}.

Even though the Flory theory[1,2] was meant to explain the behavior of nonpolar liquids and their mixtures, it was adequately employed to evaluate[1-5] the reduced and the characteristic thermodynamic parameters of polar liquids as well. These parameters, in turn, were employed to evaluate the excess volume, the excess thermodynamic properties, the viscosity of mixtures, the excess viscosity of mixing, the surface tension,[4,5,9,11-13] and the ultrasonic velocity of low melting salts.

In view of the interdependence/correlation of these properties with the intermolecular interactions, they were employed to highlight the solute-solvent interactions. For this purpose, molten tetrahydrates of calcium and cadmium nitrates as well as their mixtures were chosen.

Experimental

Commercial tetrahydrates of calcium and cadmium nitrates (BDH, E. Mercks) were recrystallized. The water of crystallization was determined by the method of comparison of their measured densities with those of the reported values.[14,15]

The density and viscosity measurements were made using a pycnometer (±0.03%) and a Cannon-Ubbelohde viscometer[16] (± 0.3%) in an ultrathermostat (type u-10) of ±0.01 °C thermal stability. The surface tension was measured with a stalagmometer for the purpose of comparison with the predicted values. The ultrasonic velocity (within ± 0.15%) was measured using an ultrasonic interferometer (NPL patent, Mittal's M 77).

Results and Discussion

The Excess Volume. The reduced and the characteristic thermodynamic variables ($\tilde{V}$, $\tilde{T}$ and V^*, T^*, P^*) of Flory theory[1-3] obtained essentially from the density data are employed for the evaluation of excess/reduced volume, $\tilde{V}^E$ using the relevant relations given elsewhere. The computed values of the excess

Table 1. Experimental and Computed Values of Excess Volume (V^E/ml·mol^{-1}) of Molten $Ca(NO_3)_2 \cdot 4.31\ H_2O$-$Cd(NO_3)_2 \cdot 4.34\ H_2O$ System

Mole fraction of Cd^{2+}		T/K=303.15	308.15	313.15	318.15	323.15	328.15	333.15
0.063	1[a]	−0.1258	−0.1408	−0.1550	−0.1692	−0.1834	−0.1976	−0.2118
	2	−0.1261	−0.1414	−0.1563	−0.1702	−0.1843	−0.1996	−0.2142
0.119	1	−0.2506	−0.2736	−0.2966	−0.3196	−0.3426	−0.3656	−0.3886
	2	−0.2519	−0.2708	−0.2915	−0.3161	−0.3403	−0.3658	−0.3910
0.168	1	−0.3548	−0.3864	−0.4181	−0.4497	−0.4814	−0.5130	−0.5447
	2	−0.3550	−0.3829	−0.4116	−0.4450	−0.4781	−0.5118	−0.5462
0.221	1	−0.4688	−0.5062	−0.5434	−0.5806	−0.6178	−0.6550	−0.6922
	2	−0.4706	−0.5037	−0.5385	−0.5769	−0.6149	−0.6551	−0.6948
0.300	1	−0.6877	−0.7165	−0.7453	−0.7741	−0.8029	−0.8317	−0.8605
	2	−0.6875	−0.7118	−0.7378	−0.7682	−0.7970	−0.8288	−0.8610
0.323	1	−0.7395	−0.7676	−0.7957	−0.8238	−0.8519	−0.8800	−0.9081
	2	−0.7394	−0.7636	−0.7886	−0.8178	−0.8465	−0.8783	−0.9085
0.362	1	−0.8397	−0.8661	−0.8924	−0.9188	−0.9451	−0.9715	−0.9979
	2	−0.8413	−0.8631	−0.8866	−0.9143	−0.9404	−0.9700	−0.9989
0.432	1	−1.0090	−1.0249	−1.0408	−1.0567	−1.0726	−1.0885	−1.1044
	2	−1.0100	−1.0217	−1.0350	−1.0514	−1.0670	−1.0869	−1.1058
0.554	1	−1.1801	−1.1932	−1.2063	−1.2194	−1.2325	−1.2455	−1.2587
	2	−1.1813	−1.1910	−1.2011	−1.2142	−1.2261	−1.2436	−1.2610
0.599	1	−1.1881	−1.2023	−1.2164	−1.2306	−1.2447	−1.2589	−1.2730
	2	−1.1899	−1.1994	−1.2114	−1.2251	−1.2386	−1.2573	−1.2746
0.677	1	−1.1497	−1.1684	−1.1870	−1.2057	−1.2243	−1.2430	−1.2616
	2	−1.1496	−1.1634	−1.1794	−1.1982	−1.2146	−1.2387	−1.2615
0.739	1	−1.1003	−1.1134	−1.1265	−1.1396	−1.1527	−1.1658	−1.1789
	2	−1.1004	−1.1097	−1.1192	−1.1323	−1.1439	−1.1619	−1.1794

a) 1. Experimental values of V^E. 2. Computed values of V^E.

Table 2. Comparison of Experimental and Computed Viscosity ($\eta \times 10$/N s m^{-2}) of Molten $Ca(NO_3)_2 \cdot 4.31\ H_2O$-$Cd(NO_3)_2 \cdot 4.34\ H_2O$ System

Mole fraction of Cd^{2+}	T/K=	303.15	308.15	313.15	318.15	323.15	328.15	333.15
0.000	1[a]	1.389	1.064	0.827	0.649	0.521	0.427	0.360
0.063	1	1.370	1.043	0.812	0.640	0.520	0.420	0.334
	2	1.322	0.997	0.799	0.632	0.510	0.422	0.356
0.119	1	1.291	1.003	0.790	0.630	0.509	0.440	0.363
	2	1.255	0.978	0.773	0.616	0.499	0.416	0.352
0.168	1	1.249	0.971	0.771	0.617	0.500	0.421	0.360
	2	1.214	0.952	0.758	0.607	0.493	0.414	0.351
0.221	1	1.201	0.949	0.751	0.611	0.501	0.421	0.356
	2	1.180	0.931	0.745	0.600	0.487	0.411	0.348
0.300	1	1.181	0.941	0.751	0.601	0.491	0.420	0.356
	2	1.170	0.922	0.736	0.590	0.478	0.403	0.339
0.323	1	1.171	0.938	0.749	0.600	0.485	0.417	0.351
	2	1.168	0.920	0.735	0.588	0.477	0.402	0.338
0.362	1	1.167	0.921	0.737	0.591	0.475	0.400	0.332
	2	1.166	0.918	0.732	0.585	0.473	0.398	0.332
0.432	1	1.165	0.917	0.733	0.589	0.482	0.408	0.340
	2	1.164	0.916	0.729	0.581	0.469	0.394	0.329
0.554	1	1.162	0.926	0.732	0.591	0.470	0.400	0.330
	2	1.126	0.888	0.708	0.565	0.456	0.383	0.320
0.599	1	1.131	0.890	0.714	0.563	0.461	0.390	0.320
	2	1.092	0.863	0.689	0.551	0.446	0.375	0.313
0.677	1	1.070	0.853	0.677	0.561	0.452	0.380	0.314
	2	1.019	0.810	0.650	0.522	0.424	0.358	0.300
0.739	1	1.021	0.830	0.661	0.534	0.440	0.367	0.311
	2	0.967	0.769	0.616	0.495	0.403	0.340	0.285
1.000	1	0.588	0.476	0.385	0.315	0.261	0.220	0.188

a) 1. Experimental values of η. 2. Computed values of η.

volume agree well with those obtained experimentally ($V^E = V - \sum_i x_i V_i$) (Table 1). The minimum value of V^E corresponds to 0.55—0.599 mole fraction of Cd^{2+} at every temperature of measurement within the range, 303.15 to 333.15 K.

The Viscosity of Mixture. The viscosities of binary mixtures have been obtained using the equation,[7-9]

$$\ln \eta_{min} = -\frac{\Delta G_m}{RT} + \frac{1}{\tilde{V}-1} - \sum_i \frac{x_i}{\tilde{V}_i - 1} + \sum_i x_i \ln \eta_i ,$$

in which

$$\Delta G_m = \sum_i x_i P_i^* V_i^* \left[\left(\frac{1}{\tilde{V}_i} + \frac{1}{\tilde{V}} \right) + 3\tilde{T}_i \ln \left(\frac{\tilde{V}_i^{1/3} - 1}{\tilde{V}^{1/3} - 1} \right) \right] + x_1 V_1^* \theta_2 x_{12} V .$$

An examination of Table 2 reveals a reasonably good agreement between the experimental and the computed values of viscosity. The viscosity has been found to decrease with an increase in the mole fraction of Cd^{2+} as well as with temperature.

The Excess Adiabatic Compressibility. The excess adiabatic compressibility $\beta_S^E (= \beta_S - \sum_i x_i \beta_{Si})$ of molten Ca^{2+}-Cd^{2+} mixtures has been found to be negative, which suggests the presence of strong associative interactions between the solvent and the solute molecules. However, β_S^E is not affected significantly with temperature. The value of β_S^E shows variations with composition, as apparent from Fig. 1 in which the presence of minima at 0.554 mole fraction of Cd^{2+} indicates maximum interaction at this composition.

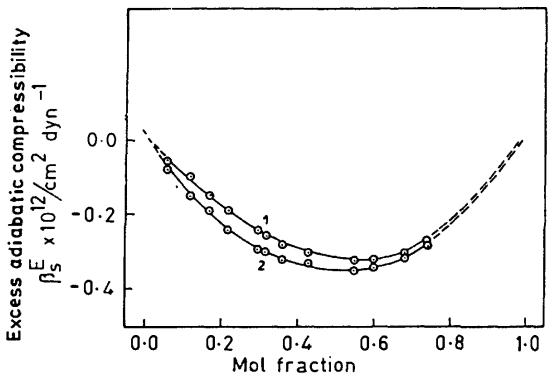

Fig. 1. Plot of excess adiabatic compressibility vs. [solute] for $Ca(NO_3)_2 \cdot 4.31H_2O$-$Cd(NO_3)_2 \cdot 4.34H_2O$ system at 1; 303.15 K and 2; 333.15 K.

It is noteworthy that the excess volume of mixing and the excess adiabatic compressibility factor, both of them suggest the maximum solvent-solute interaction at ca. 0.55 mole fraction of Cd^{2+}.

The Surface Tension. The agreement between the predicted values of surface tension, σ obtainable essentially from the Flory theory[4,5,10,12] with those obtained experimentally has been reasonably good even though σ was measured using the stalagmometer. An examination of Table 3 reveals that unlike the pure $Cd(NO_3)_2 \cdot 4H_2O$ Auerbach relation does not seem to apply to Ca^{2+}-Cd^{2+} system in which Ca^{2+} may appar-

Table 3. Experimental and Computed Values of Surface Tension (σ/dyn cm^{-1}) of Molten $Ca(NO_3)_2 \cdot 4.31\ H_2O$-$Cd(NO_3)_2 \cdot 4.34\ H_2O$ System

Mole fraction of Cd^{2+}	T/K=303.15	308.15	313.15	318.15	323.15	328.15	333.15
0.000	1[a)]	95.41	94.68	94.01	93.28	92.71	91.87	91.21
	2	94.42	93.98	93.70	93.01	92.68	91.29	91.27
	3	74.48	77.82	77.02	76.30	75.51	74.83	74.12
0.063	1	95.66	94.87	94.22	93.50	92.82	92.10	91.35
	2	94.64	94.19	93.89	93.21	92.92	91.57	91.55
	3	79.85	79.12	78.33	77.61	76.87	76.09	75.38
0.119	1	95.88	95.17	94.36	93.65	92.90	92.20	91.50
	2	94.77	94.29	94.01	93.34	93.08	92.56	91.72
	3	81.04	80.36	79.57	78.82	78.07	77.27	76.55
0.168	1	96.15	95.34	94.64	93.85	93.13	92.40	91.62
	2	94.71	94.27	93.94	93.27	93.04	92.51	91.70
	3	82.20	81.45	80.65	79.88	79.09	78.30	77.56
0.221	1	96.51	95.70	94.84	94.16	93.28	92.53	91.72
	2	94.74	94.28	93.95	93.26	93.05	91.79	91.71
	3	83.38	82.60	81.81	81.00	80.20	79.41	78.64
0.300	1	96.90	96.00	95.25	94.40	93.62	92.41	92.01
	2	95.40	94.89	94.46	93.75	93.10	92.88	92.09
	3	85.19	84.26	83.54	82.72	81.87	81.08	80.24
0.323	1	97.14	96.30	95.40	94.56	93.73	92.90	92.14
	2	95.15	94.99	94.55	93.83	93.15	92.95	92.15
	3	85.71	84.76	84.03	83.20	82.35	81.56	80.7
0.362	1	97.36	96.50	95.58	94.83	93.98	93.16	92.24
	2	95.71	95.16	94.69	93.95	93.72	93.03	92.24
	3	86.61	85.76	84.88	84.03	83.16	82.35	81.48
0.432	1	97.87	97.01	96.00	95.20	94.20	93.41	92.50
	2	96.39	95.79	95.24	94.45	94.20	93.44	92.64
	3	88.21	87.34	86.43	85.53	84.65	83.77	82.88
0.554	1	98.86	97.82	96.97	95.90	95.01	94.04	93.03
	2	97.13	96.45	95.79	94.95	94.72	93.83	93.06
	3	91.02	90.05	89.09	88.58	87.18	86.24	85.30
0.599	1	99.27	98.30	97.20	96.30	95.21	94.32	93.30
	2	97.52	96.84	96.17	95.33	95.10	93.85	93.44
	3	92.03	91.04	90.05	89.08	88.11	87.15	86.19
0.677	1	100.03	98.90	97.95	96.76	95.83	94.70	93.70
	2	97.84	97.14	96.43	95.59	95.37	94.44	93.70
	3	93.78	92.77	91.74	90.71	89.69	88.67	86.69
0.739	1	100.60	99.55	98.37	97.35	96.20	95.20	94.80
	2	99.06	98.32	97.56	96.68	96.47	95.47	94.73
	3	95.09	94.02	92.97	91.91	91.03	89.83	88.79
1.000	1	103.50	102.16	100.80	99.55	98.60	96.90	95.50
	2	100.26	99.42	98.49	97.54	97.36	96.17	95.47
	3	100.10	98.95	97.79	96.63	95.47	94.32	93.18

a) 1. Experimental values of σ. 2. Computed values of σ using Flory theory. 3. Computed values of σ using Auerbach relation.

Table 4. Experimental and Computed Ultrasonic Velocity (U/m$\cdot$s^{-1}) in Molten $Ca(NO_3)_2 \cdot 4.31\ H_2O$-$Cd(NO_3)_2 \cdot 4.34\ H_2O$ System

Mole fraction of Cd^{2+}	T/K=303.15	308.15	313.15	318.15	323.15	328.15	333.15
0.000	1[a)]	1738.11	1730.11	1721.61	1713.50	1704.21	1696.71	1688.51
	5	1965.99	1962.85	1961.99	1955.33	1953.75	1937.12	1939.89
0.063	1	1736.60	1728.20	1719.81	1711.40	1703.01	1694.60	1686.21
	2	1738.06	1730.54	1721.25	1721.98	1703.58	1695.87	1687.51
	3	1734.44	1726.99	1717.74	1709.52	1700.17	1692.52	1684.21
	4	1739.62	1732.22	1723.30	1714.86	1705.72	1698.19	1690.03
	5	1951.00	1947.94	1946.94	1940.66	1939.70	1923.99	1926.84
0.119	1	1735.11	1727.32	1718.83	1710.35	1701.87	1693.38	1684.91
	2	1738.03	1730.31	1720.31	1712.51	1703.03	1695.13	1686.62
	3	1731.62	1724.02	1714.72	1706.39	1696.99	1689.21	1680.79
	4	1741.12	1733.62	1724.69	1716.22	1707.08	1699.46	1691.25
	5	1931.94	1928.60	1927.98	1921.94	1921.58	1917.62	1909.13
0.168	1	1735.01	1726.51	1717.91	1709.31	1700.71	1692.11	1683.51
	2	1738.01	1730.11	1720.66	1712.11	1702.55	1694.48	1685.84

Table 4. (Continued)

Mole fraction of Cd^{2+}		T/K=303.15	308.15	313.15	318.15	323.15	328.15	333.15
	3	1729.43	1721.71	1712.36	1703.94	1694.48	1686.58	1678.07
	4	1742.38	1734.81	1725.89	1717.41	1708.27	1700.58	1692.33
	5	1912.95	1910.14	1908.88	1902.91	1902.99	1898.88	1890.98
0.221	1	1734.50	1725.82	1717.13	1708.45	1699.77	1691.08	1682.40
	2	1737.97	1729.89	1720.37	1711.66	1702.03	1693.81	1685.02
	3	1727.46	1719.59	1710.19	1701.65	1692.15	1684.10	1675.49
	4	1743.75	1736.05	1727.10	1718.54	1709.38	1701.58	1693.24
	5	1894.35	1891.40	1890.10	1884.02	1884.32	1870.44	1872.48
0.300	1	1733.61	1724.75	1715.91	1707.05	1698.21	1689.35	1680.50
	2	1737.97	1729.56	1719.92	1711.00	1701.25	1692.75	1683.77
	3	1727.46	1717.01	1707.52	1698.81	1689.21	1680.95	1672.17
	4	1743.75	1738.31	1729.09	1720.22	1710.82	1702.63	1692.98
	5	1871.47	1867.92	1865.48	1859.25	1853.84	1854.13	1847.27
0.323	1	1733.40	1724.51	1715.60	1706.71	1697.81	1688.91	1680.01
	2	1737.91	1729.47	1719.81	1710.81	1701.03	1692.45	1683.41
	3	1724.57	1716.41	1706.89	1698.13	1688.50	1680.18	1671.35
	4	1747.03	1738.84	1729.57	1720.63	1711.19	1702.92	1694.18
	5	1861.70	1862.65	1859.94	1853.59	1847.66	1848.06	1840.48
0.362	1	1733.31	1724.28	1715.27	1706.25	1697.23	1688.22	1679.21
	2	1737.88	1729.31	1719.58	1710.49	1700.65	1691.95	1682.81
	3	1723.81	1715.53	1705.97	1697.12	1687.45	1679.01	1670.11
	4	1748.24	1739.88	1730.52	1721.46	1711.92	1703.49	1694.62
	5	1854.88	1850.76	1847.65	1841.06	1841.04	1834.98	1827.63
0.432	1	1733.00	1723.84	1714.67	1705.51	1696.34	1687.18	1678.01
	2	1737.83	1729.03	1719.20	1709.92	1699.97	1691.04	1681.72
	3	1722.91	1714.41	1704.75	1695.73	1685.97	1677.33	1668.25
	4	1750.27	1741.53	1731.91	1722.54	1712.75	1703.95	1694.78
	5	1840.95	1836.27	1832.27	1825.09	1824.85	1817.99	1810.63
0.554	1	1733.10	1723.51	1714.01	1704.51	1695.50	1685.50	1676.00
	2	1737.76	1728.53	1718.32	1708.92	1698.86	1689.46	1679.84
	3	1722.72	1713.81	1703.99	1694.66	1684.72	1675.69	1666.31
	4	1752.29	1743.07	1733.19	1723.48	1713.45	1704.20	1694.67
	5	1809.72	1804.21	1798.91	1790.32	1791.37	1783.07	1776.18
0.599	1	1733.10	1723.51	1713.90	1704.31	1694.70	1685.11	1675.50
	2	1737.74	1728.35	1718.29	1708.55	1698.36	1688.88	1679.14
	3	1723.11	1714.04	1704.15	1694.69	1684.68	1675.50	1666.01
	4	1752.35	1742.98	1733.23	1723.23	1713.14	1703.76	1694.12
	5	1801.40	1795.97	1790.57	1783.08	1783.11	1770.40	1768.19
0.677	1	1733.71	1723.85	1714.00	1704.15	1694.30	1684.45	1674.60
	2	1737.69	1728.03	1717.85	1707.91	1697.61	1687.87	1677.93
	3	1724.37	1715.00	1704.99	1695.31	1685.17	1675.71	1665.99
	4	1751.80	1742.22	1732.20	1722.26	1712.10	1702.52	1692.73
	5	1779.07	1773.55	1767.86	1760.49	1760.76	1752.26	1746.06
0.739	1	1734.30	1724.28	1714.27	1704.25	1696.23	1684.22	1674.20
	2	1737.66	1727.78	1717.51	1707.41	1697.02	1687.08	1676.98
	3	1725.88	1716.28	1706.16	1696.28	1686.04	1676.35	1666.45
	4	1751.14	1741.27	1731.08	1720.94	1710.62	1700.78	1690.77
	5	1782.25	1776.43	1770.33	1762.71	1763.22	1754.07	1748.04
1.000	1	1737.50	1726.74	1716.10	1705.31	1694.54	1683.77	1673.01
	5	1739.11	1732.33	1724.40	1716.23	1717.07	1705.93	1700.57

a) 1. Experimental U. 2. Computed U using.[18,21] 3. Computed U using.[19,22] 4. Computed U using.[20,23] 5. Computed U using Flory theory.

ently be responsible for offsetting the agreement between the computed and the experimental values. Also, the agreement between the two values is much better at higher temperatures compared to those at lower ones. The σ values of $Ca(NO_3)_2 \cdot 4.3H_2O$ and $Ca(NO_3)_2 \cdot 4.1H_2O$ are, respectively, 1.1% and 0.32% lower when compared with that of $Ca(NO_3)_2 \cdot 4H_2O$.[17] Such a difference seems to have been caused by the difference in the water of hydration which seems to be responsible for decreasing the corresponding cohesive forces.

The Ultrasonic Velocity. The computed values of ultrasonic velocity based on the relation,[11]

$$U = \left\{ \left[(kT^*P^{*2})^{1/3} \left(M\tilde{V}^{-5/3} - \frac{\tilde{V}^{1/3}-1}{\tilde{V}^2} \ln \frac{V^{1/3}-0.5}{V^{1/3}-1} \right) \right] / \rho \times 6.3 \times 10^{-4} \right\}^{2/3}$$

on comparison with the experimental values reveal that the agreement between the two values is better in the case of pure component of Cd^{2+}. Nevertheless, an excellent agreement between the computed values obtained using essentially Nomoto,[18] Van Dael et al.,[19] and Schaaff's collision factor theory[20] and the experimental values of ultrasonic velocities may be seen from Table 4.

The authors wish to express their gratitude to Professor M. S. Ahmad, Chairman of the Department for the necessary facilities and one of them (GM) also thanks the UGC for the Junior Research Fellowship.

References

1) P. J. Flory, *J. Am. Chem. Soc.*, **87**, 1833 (1965).
2) A. Abe and P. J. Flory, *J. Am. Chem. Soc.*, **87**, 1838 (1965).
3) L. A. K. Stavely, W. I. Lupmann, and K. R. Hart, *Trans. Faraday Soc.*, **51**, 823 (1955).
4) J. D. Pandey, B. R. Chaturvedi, and N. Pant, *Acoustics Letter*, **4**, 128 (1981); *Chemica Scripta*, **18**, 221 (1981).
5) J. D. Pandey and U. Gupta, *J. Phys. Chem.*, **86**, 5234 (1982).
6) J. D. Pandey and Alec. D. M. David, *J. Phys. Chem.*, **85**, 3151 (1981).
7) C. Jambon and G. Delmas, *Can. J. Chem.*, **55**, 1360 (1977).
8) R. K. Nigam and P. P. Singh, *Trans. Faraday Soc.*, **65**, 950 (1969).
9) J. K. Holzahaver and W. T. Zeigler, *J. Phys. Chem.*, **79**, 590 (1975).
10) J. D. Pandey, B. R. Chaturvedi, and R. P. Pandey, *J. Phys. Chem.*, **85**, 1750 (1981).
11) N. Auerbach, *Experientia*, **4**, 473 (1948).
12) D. Patterson and A. K. Rastogi, *J. Phys. Chem.*, **74**, 1067 (1970).
13) I. Prigogine, "The Molecular Theory of Solutions," North Holland Pub. Co., Amsterdam (1957).
14) W. W. Eving and R. J. Mikovsky, *J. Am. Chem. Soc.*, **72**, 1390 (1950).
15) W. W. Eving and C. H. Herty, *J. Phys. Chem.*, **57**, 2451 (1953).
16) M. R. Canon, R. E. Manning, and J. D. Bell, *Analyst Chem.*, **32**, 355 (1960).
17) E. Sada, S. Kotoh, and H.C. Damle, *J. Chem. Eng. Data*, **29**, 117 (1984).
18) O. Nomoto, *J. Phys. Soc. Jpn.*, **13**, 1528 (1968).
19) W. Van Dael and E. Vangeel, Proc. 1st Int. Conf. Cal. Therm. Warsaw, p. 555 (1969).
20) W. Schaaffs, *Z. Phys.*, **114**, 150 (1974); **115**, 69 (1940); Molecularakusstic, Ch. **XI** and **XII** Springer, Berlin (1963).
21) S. V. Subrahmanyan and T. Bhimsenachar, *J. Phys. Soc. Jpn.*, **17**, 1447 (1961).
22) M. J. Bladma and D. Weddington, *J. Phys. Chem.*, **74**, 2569 (1970).
23) R. Nutsch-Kuhnkies, *Acustica*, **15**, 383 (1968).

 © 1989 The Chemical Society of Japan Bull. Chem. Soc. Jpn., 62, 3303—3310 (1989)

Kinetics and Mechanism of Oxidation of Amino Acids by Dichloramine T

B. Thimme Gowda* and P. Jagan Mohana Rao
Department of Post-Graduate Studies and Research in Chemistry, Mangalore University, Mangalagangothri 574 199, Mangalore, India
(Received December 6, 1988)

Kinetics of oxidations of several amino acids (alanine, leucine, aspargine, glutamine, and proline) by *N,N*-dichloro-*p*-toluenesulfonamide (generally known as dichloramine-T) have been studied in 1 : 1 (v/v) water-methanol medium in the presence of perchloric acid. The oxidations of alanine and leucine showed second order kinetics in [oxidant], first order in [amino acid] and inverse fractional order in [H^+] over the entire range of [$HClO_4$](0.0005—0.10 mol dm^{-3}) used. But the kinetics of oxidations of aspargine, glutamine, and proline were [H^+] dependent. The rate dependence in [oxidant] was second and first orders in [H^+] ranges 0.0005—0.005 mol dm^{-3} and 0.005—0.10 mol dm^{-3}, respectively. The kinetics in [amino acid] for these oxidations were also different. Variation in ionic strength of the medium or addition of the reduced product of the oxidant had no or negligible effects on the rates of reactions. Decrease in dielectric constant of the medium by increasing the methanol composition of the solvent decreased the rate in all the cases. Activation parameters have been computed from the Arrhenius plots. Plausible mechanisms consistent with the observed kinetics have been discussed.

Although extensive studies have been reported on the kinetics and mechanisms of oxidation of a variety of substrates by *N*-halosulfonamides like *N*-chloro- and *N*-bromobenzene- or toluenesulfonamides,[1-8] studies by *N,N*-dihalosulfonamides have recently been initiated in our laboratories.[7-9]

As a part of these investigations, we report herein the kinetics of oxidation of several amino acids by *N,N*-dichloro-*p*-toluenesulfonamide in 1 : 1 (v/v) water-methanol medium in the presence of perchloric acid. The amino acids studied are alanine, leucine, aspargine, glutamine, and proline.

Materials and Methods

N,N-Dichloro-*p*-toluenesulfonamide, abbreviated as dichloramine-T (DCT) was prepared by the method of Jacob and Nair.[10] The stock solution (ca. 0.05 mol dm^{-3}) of the oxidant in pure methanol was prepared and standardised by iodometric method and preserved in amber colored bottles. Chromatographically pure amino acids: alanine (Ala), leucine (Leu), aspargine (Asn), glutamine (Gln), and proline (Pro) (Sisco Research Laboratories, India) were further assayed by the standard methods reported elsewhere.[11] Aqueous stock solution (0.1 mol dm^{-3}) of the amino acids (S) were prepared in doubly distilled water. Preliminary investigations of the reactions showed that the variations in ionic strength of the medium had no significant effect on the rates of all the oxidations. All other reagents used were of accepted grades of purity.

Kinetic Measurements: Kinetic studies were made in glass stoppered pyrex boiling tubes under pseudo-first-order or pseudo-second-order conditions with [S]≫[DCT]. The reactions were initiated by the quick addition of measured amounts of oxidant solution (0.0005—0.005 mol dm^{-3}), thermostated at a desired temperature, to solutions containing required amounts of amino acid (0.005—0.10 mol dm^{-3}), perchloric acid (0.0005—0.10 mol dm^{-3}), methanol, and water (to maintain 1 : 1 (v/v) water-methanol composition), equilibrated at the same temperature. The progress of the reactions was monitored for two half-lives by iodometric estimation of unreacted oxidant at regular time intervals. The pseudo-first-order or pseudo-second-order rate constants (k_{obs}) were calculated by the graphical methods and the values were reproducible within ±4% error.

Stoichiometry and Product Analysis

The stoichiometries of DCT-amino acid reactions are determined in 1 : 1 (v/v) water-methanol medium in the presence of varying concentrations of perchloric acid (0.0005—0.10 mol dm^{-3}) by equilibrating varying ratios of [DCT]$_0$ to [S]$_0$ at room temperature for different intervals of time. The products were found to be CO_2, ammonia, and the corresponding aldehyde by standard tests.[12,13] *p*-Toluenesulfonamide, the reduced product of DCT, was detected by paper chromatography. The observed stoichiometries may be represented by Eqs. 1 and 2.

$$2RCH(NH_2)COOH + ArSO_2NCl_2 + 2H_2O \longrightarrow 2RCHO + 2CO_2 + 2NH_4^+ + 2Cl^- + ArSO_2NH_2 \quad (1)$$

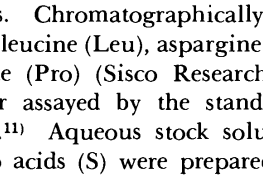

$$+ ArSO_2NCl_2 + 2H_2O \longrightarrow 2H_2C{=}CHCH_2CHO + 2CO_2 + 2NH_4^+ + 2Cl^- + ArSO_2NH_2 \quad (2)$$

where R=CH_3(Ala), $(CH_3)_2CHCH_2$(Leu), $H_2N(CO)CH_2CH_2$(Gln), $H_2N(CO)CH_2$(Asn).

Results

The kinetics of oxidations of Ala, Leu, Asn, Gln, and Pro by DCT in 1 : 1 (v/v) water-methanol medium were studied under varying conditions: [DCT] (0.0005—0.005 mol dm^{-3}), [S] (0.005—0.10 mol dm^{-3}), and [$HClO_4$] (0.0005—0.10 mol dm^{-3}). The results are shown in Tables 1—4 and Figs. 1—6. The kinetics of oxidations were [H^+] dependent. The order in [oxidant] was two and one in the acid ranges 0.0005—0.005 mol dm^{-3} and 0.005—0.10 mol dm^{-3}, respectively, for the oxidations of Asn, Gln,

Table 1. Pseudo-Second-Order Rate Constants (k_{obs}) for the Oxidation of Amino Acids (S) by *N,N*-Dichloro-*p*-toluenesulfonamide (Dicloramine-T, DCT) in 1 : 1 (v/v) Water-Methanol Medium in the Presence of Perchloric Acid at 303 K (Ala and Leu) and 293 K (Asn, Gln, and Pro)

10^3[DCT]$_0$	10^2[S]$_0$		10^2[$HClO_4$]		$10k_{obs}$/dm^3 mol^{-1}s^{-1}				
mol dm^{-3}	mol dm^{-3}		mol dm^{-3}		Ala	Leu	Asn	Gln	Pro
Effect of varying [DCT]$_0$									
0.5	2.0	(5.0)	1.0	(0.10)	2.1	1.5	12.9	20.6	7.5
1.0	2.0	(5.0)	1.0	(0.10)	1.9	1.6	12.9	20.9	7.6
2.0	2.0	(5.0)	1.0	(0.10)	1.9	1.6	12.3	19.9	7.5
4.0	2.0	(5.0)	1.0	(0.10)	1.9	1.6	—	—	—
5.0	2.0	(5.0)	1.0	(0.10)	—	—	12.7	19.3	7.6
Effect of varying [S]$_0$									
1.0	0.5		1.0	(0.10)	0.35	0.36	1.8	2.6	0.8
1.0	1.0		1.0	(0.10)	0.82	0.79	3.1	4.4	1.8
1.0	2.0		1.0	(0.10)	1.9	1.6	5.8	9.4	3.3
1.0	3.0		1.0	(0.10)	2.7	2.2	—	—	—
1.0	5.0		1.0	(0.10)	4.4	4.5	12.9	20.9	7.6
Effect of varying [$HClO_4$]									
1.0	2.0	(5.0)	0.05		6.0	7.3	22.2	41.0	15.2
1.0	2.0	(5.0)	0.10		5.2	5.3	12.9	20.9	7.6
1.0	2.0	(5.0)	0.20		3.9	3.3	6.4	9.8	3.8
1.0	2.0	(5.0)	0.30		—	—	4.9	6.9	2.6
1.0	2.0	(5.0)	0.50		3.3	2.3	—	—	—
1.0	2.0	(5.0)	1.0		1.9	1.6	—	—	—
1.0	2.0	(5.0)	2.0		1.4	1.3	—	—	—
1.0	2.0	(5.0)	5.0		1.1	0.7	—	—	—
1.0	2.0	(5.0)	10.0		0.7	0.5	—	—	—

Values in parentheses are for Asn, Gln, and Pro.

Table 2. Pseudo-First-Order Rate Constants (k_{obs}) for the Oxidation of Amino Acids (S) by *N,N*-Dichloro-*p*-toluenesulfonamide (Dichloramine-T, DCT) in 1 : 1 (v/v) Water-Methanol Medium in the Presence of Perchloric Acid at 303 K

10^3[DCT]$_0$	10^2[S]$_0$	10^2[$HClO_4$]	10^4k_{obs}/s^{-1}		
mol dm^{-3}	mol dm^{-3}	mol dm^{-3}	Asn	Gln	Pro
Effect of varying [DCT]$_0$					
0.5	5.0	1.0	5.8	7.5	3.3
1.0	5.0	1.0	5.4	7.2	3.2
2.0	5.0	1.0	5.4	7.2	3.2
3.0	5.0	1.0	5.4	7.3	3.2
4.0	5.0	1.0	—	—	—
Effect of varying [S]					
1.0	1.0	1.0	—	—	—
1.0	2.0	1.0	1.3	1.9	0.7
1.0	3.0	1.0	2.6	3.4	—
1.0	4.0	1.0	—	—	2.4
1.0	5.0	1.0	5.4	7.2	3.2
1.0	7.0	1.0	8.9	10.1	6.4
1.0	10.0	1.0	13.4	15.8	9.7
Effect of varying [$HClO_4$]					
1.0	5.0	0.2	—	—	—
1.0	5.0	0.5	10.0	17.7	4.8
1.0	5.0	1.0	5.4	7.2	3.2
1.0	5.0	2.0	4.8	4.3	1.4
1.0	5.0	5.0	2.2	2.8	—
1.0	5.0	10.0	—	—	0.51

and Pro. The dependence in [S] for these oxidations was also different (Table 4). But the oxidations of Ala and Leu showed second-order dependence in [oxidant], first order in [S] and inverse fractional order in [H^+] over the entire range of [$HClO_4$](0.0005—0.10 mol dm^{-3}).

(i) Pseudo-Second-Order Kinetics: At fixed [S]$_0$ and [$HClO_4$], the plots of 1/[DCT] versus time were linear at least for two-half lives (Figs. 1 and 2). The pseudo-second-order rate constants (k_{obs}), computed from the plots, were unaffected by changes in [DCT]$_0$ (Table 1), establishing second-order kinetics in [DCT] for the oxidations of Ala and Leu over the entire acid range studied and for Asn, Gln, and Pro in the acid range 0.0005—0.005 mol dm^{-3}. At constant [DCT]$_0$ and [$HClO_4$], the rates increased with increase in [S]$_0$ (Table 1) and the plots of log k_{obs} versus log[S]$_0$ were linear with varying slopes (Table 4), showing nearly first-order to first-order kinetics in [S]. The rates decreased with increase in [$HClO_4$], at fixed [DCT]$_0$ and [S]$_0$, with inverse fractional order to inverse first-order dependences in [H^+]. Variation in ionic strength of the medium or addition of the reduced product of the oxidant, *p*-toluenesulfonamide (TSA), had negligible effects on the rates of oxidations. But the decrease in dielectric constant of the medium by increasing the methanol composition of the solvent

Table 3. Effect of Varying Dielectric Constant of the Reaction Medium and Addition of the Reaction Product, *p*-Toluenesulfonamide (TSA) on the Rates of Oxidations of Amino Acids by *N,N*-Dichloro-*p*-toluenesulfonamide (DCT) in 1 : 1 (v/v) Water-Methanol Medium

% MeOH	$10K_{obs}$[a,b]/dm^{3}mol^{-1}s^{-1}					10^4k_{obs}[c]/s^{-1}		
	Ala	Leu	Asn	Gln	Pro	Asn	Gln	Pro
40	4.6	3.2	19.0	28.8	17.0	7.0	12.6	5.6
45	2.9	2.3	—	—	—	—	—	—
50	1.9	1.6	12.9	19.9	7.5	5.4	7.2	3.2
60	0.8	0.9	8.9	13.4	5.0	3.9	4.8	2.0
10^3[TSA] (mol dm^{-3})								
0	1.9	1.6	12.9	19.9		5.4	7.2	3.2
1.0	1.9	1.6	11.8	18.8		—	—	—
2.0	1.9	1.6	—	—		—	—	—
3.0	1.9	1.6	12.0	19.6		5.3	7.2	3.3
4.0	—	—	—	—		5.4	7.0	3.3

a) 10^3[DCT]$_0$=50[S]$_0$=10^2[HClO$_4$]=1.0 mol dm^{-3}, temp 303 K for Ala and Leu. b) 10^3[DCT]$_0$= 20[S]$_0$=10^3[HClO$_4$]=1.0 mol dm^{-3}, temp 293 K for Asn, Gln, and Pro under pseudo-second-order conditions. c) 10^3[DCT]$_0$=20[S]$_0$=10^2[HClO$_4$]=1.0 mol dm^{-3}, temp 303 K for Asn, Gln, and Pro under pseudo-first-order conditions.

Table 4. Kinetic and Activation Parameters for the Oxidation of Amino Acids by *N,N*-Dichloro-*p*-toluenesulfonamide (DCT) in 1 : 1 (v/v) Water-Methanol Medium in the Presence of Perchloric Acid

Orders observed	Ala	Leu	[HClO$_4$]=0.0005—0.005 mol dm^{-3}			[HClO$_4$]=0.005—0.10 mol dm^{-3}		
			Asn	Gln	Pro	Asn	Gln	Pro
[DCT]	2.0	2.0	2.0	2.0	2.0	1.0	1.0	1.0
[S]	1.0	1.0	0.94	0.98	0.91	1.57	1.65	1.59
[H$^+$]	−0.41	−0.52	−0.85	−1.0	−0.96	−0.66	−0.60	−0.75
Activation parameters								
log A	3.93	4.48	6.28	7.13	9.69	6.47	8.59	5.70
E_a/kJ mol^{-1}	27.0	30.6	35.4	38.4	55.1	56.5	68.1	53.3
$\Delta H^{\neq}$/kJ mol^{-1}	23.7	28.0	31.7	38.3	52.4	55.1	65.1	52.1
$\Delta S^{\neq}$/J K^{-1}	−180.6	−167.9	−134.9	−107.7	−68.4	−125.6	−87.5	−139.9
$\Delta G^{\neq}$/kJ mol^{-1}	78.5	78.9	71.2	69.8	72.5	93.2	91.6	94.5

decreased the rates of oxidations for all the amino acids. The plots of log k_{obs} versus % methanol (by volume) were linear with negative slopes (Fig. 6). The rates were measured at different temperatures (293—313 K) and the activation parameters computed from the Arrhenius plots (Table 4).

(ii) Pseudo-First-Order Kinetics: Oxidations of Asn, Gln, and Pro in the acid range $\geq$0.005 mol dm^{-3} showed pseudo-first-order kinetics in [oxidant]. At fixed [DCT]$_0$ and [S]$_0$, the plots of log[DCT] versus time were linear for at least two-half lives (Fig. 3) and the pseudo-first-order rate constants calculated from the plots were insensitive to the variations in [DCT]$_0$, showing first-order kinetics in [DCT]. The rates increased with increase in [S]$_0$ and the plots of log k_{obs} versus log[S]$_0$ were linear with varying slopes, indicating varying kinetic orders in [S] (Table 4). At constant [DCT]$_0$ and [S]$_0$ the rates decreased with increase in [HClO$_4$] with inverse fractional order dependences in [H$^+$] for oxidations of all the amino acids. Variations in ionic strength of the medium or the addition of *p*-toluenesulfonamide had no effect on the rates. Decrease in dielectric constant of the medium by increasing the methanol composition of the solvent decreased the rates even under these conditions (Table 3). The plots of log k_{obs} versus % methanol (by volume) were also linear with negative slopes (Fig. 6). The rates of oxidations were also measured at different temperatures (283—313 K) and activation parameters were computed from the plots of log k_{obs} versus $1/T$ and log (k_{obs}/T) versus $1/T$ (Table 4).

Discussion

(i) Pseudo-Second-Order Kinetics in [DCT]: The kinetics of second order in [DCT], nearly first-order in [S] and inverse fractional order in [H$^+$] observed for the oxidations of Ala, Leu, Asn, Gln, and Pro may be explained by a mechanism shown in Scheme 1.

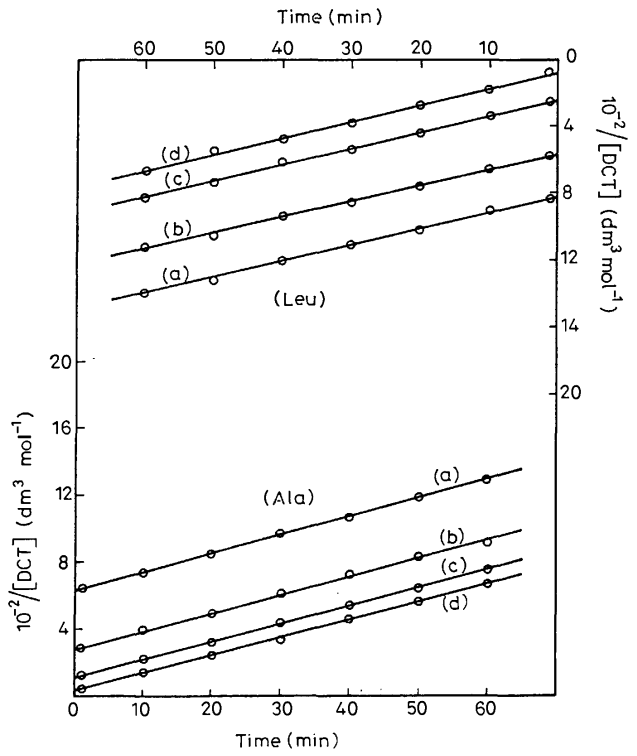

Fig. 1. Plots of 1/[DCT] versus time (Ala and Leu)
$10^2[S]_0$=2.0 mol dm^{-3}, $10^2[HClO_4]$=1.0 mol dm^{-3}, temp 303 K.
$10^3[DCT]_0$(mol dm^{-3}): 0.5(a), 1.0(b), 2.0(c), 4.0(d).

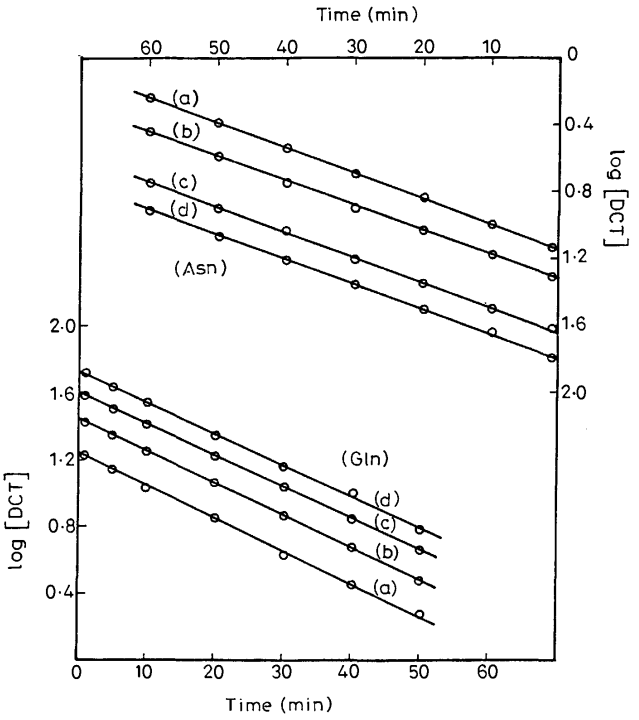

Fig. 3. Plots of log [DCT] versus time (Asn and Gln)
$10^2[S]_0$=5.0 mol dm^{-3}, $10^2[HClO_4]$=1.0 mol dm^{-3}, temp 303 K.
$10^3[DCT]_0$(mol dm^{-3}): 0.5(a), 1.0(b), 2.0(c), 3.0(d).

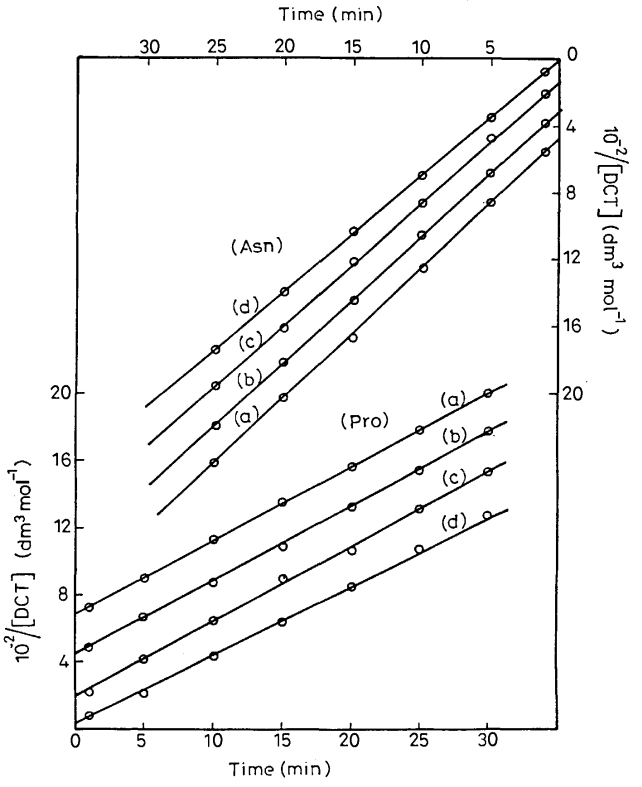

Fig. 2. Plots of 1/[DCT] versus time (Asn and Pro)
$10^2[S]_0$=5.0 mol dm^{-3}, $10^3[HClO_4]$=1.0 mol dm^{-3}, temp 293 K.
$10^3[DCT]_0$(mol dm^{-3}): 0.5(a), 1.0(b), 2.0(c), 5.0(d).

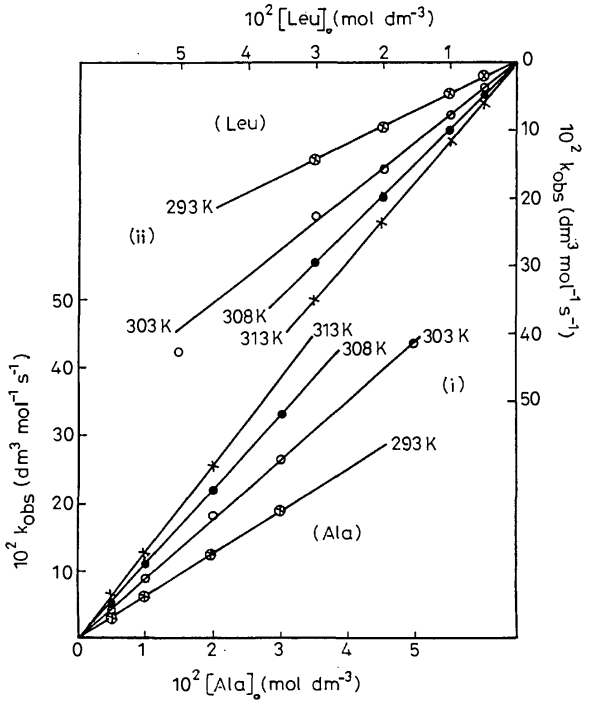

Fig. 4. Plots of (i) k_{obs} versus $[Ala]_0$ and (ii) k_{obs} versus $[Leu]_0$.
$10^3[DCT]_0$=$10^2[HClO_4]$=1.0 mol dm^{-3}.

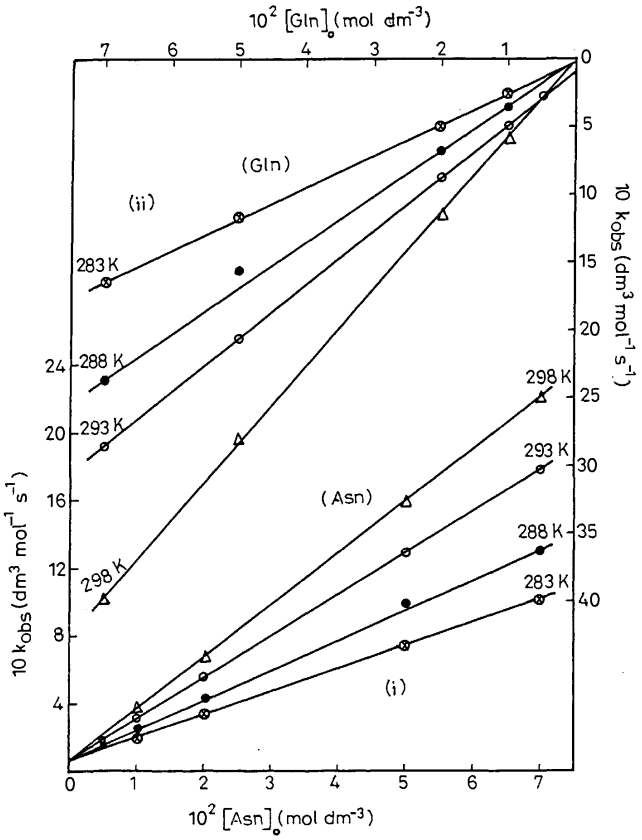

Fig. 5. Plots of (i) k_{obs} versus $[Asn]_0$ and (ii) k_{obs} versus $[Gln]_0$.
$10^3[DCT]_0=10^3[HClO_4]=1.0$ mol dm^{-3}.

$$SH^+ \underset{}{\overset{K_1}{\rightleftharpoons}} S + H^+ \qquad \text{(fast)}$$

$$ArSO_2NCl_2 + S \underset{k_{-2}}{\overset{k_2}{\rightleftharpoons}} \text{Intermediate} \qquad \text{(fast)}$$
(DCT) (X)

$$ArSO_2NCl_2 + X \xrightarrow{k_3} \text{Products} \qquad \text{(slow)}$$

where SH^+: Protonated amino acid

Scheme 1.

Applying the steady state approximation to the intermediate X, we have

$$[X] = \frac{k_2[ArSO_2NCl_2]_0\,[S]}{k_{-2}+k_3[ArSO_2NCl_2]+k_2[S]} \qquad (3)$$

where $[ArSO_2NCl_2]=[ArSO_2NCl_2]_0-[X]$ and $[S]_0\approx[S]$. Since k_3 is small and $[S]\gg[ArSO_2NCl_2]$, $k_3[ArSO_2NCl_2]$ is negligibly small compared with other terms in the denominator, then Eq. 3 becomes,

$$[X]=\frac{k_2[ArSO_2NCl_2]_0[S]}{k_{-2}+k_2[S]}=\frac{K_2[DCT]_0[S]}{1+K_2[S]} \qquad (4)$$

where $K_2=k_2/k_{-2}$.
The rate of the reaction is then given by Eq. 5

$$-\frac{d[DCT]}{dt} = k_3[DCT]\,[X] = \frac{K_2k_3[DCT]_0[DCT][S]}{1+K_2[S]}. \qquad (5)$$

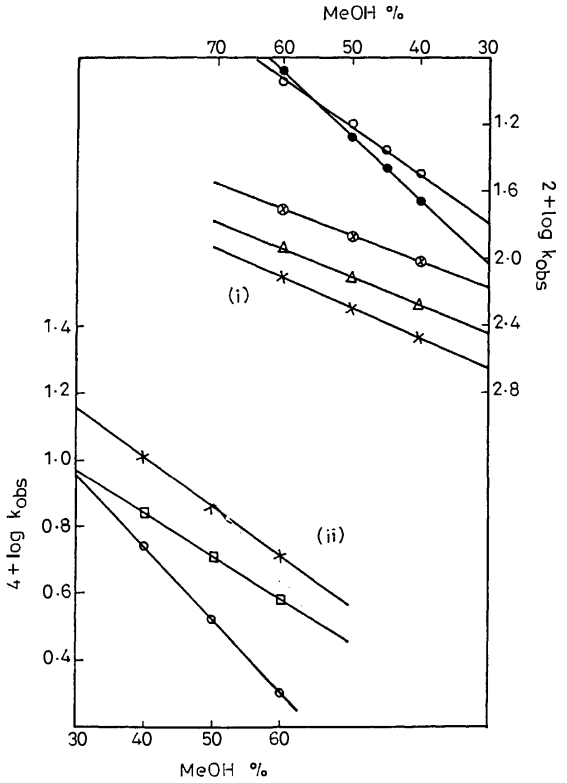

Fig. 6. Plot of log k_{obs} versus % MeOH
(i) Pseudo-second-order rate constants
$10^3[DCT]_0=50[S]_0=10^2[HClO_4]=1.0$ mol dm^{-3}, temp 303 K (Ala and Leu).
$10^3[DCT]_0=20[S]_0=10^3[HClO_4]=1.0$ mol dm^{-3}, temp 293 K (Asn, Gln, and Pro).
● Ala, ○ Leu, △ Asn, × Gln, ○ Pro.
(ii) Pseudo-first-order rate constants
$10^3[DCT]_0=[S]_0=10^2[HClO_4]=1.0$ mol dm^{-3}, temp 303 K.
□ Asn, ×Gln, ○ Pro.

If we now make further assumption that $[DCT]_0\times[DCT]\approx[DCT]^2$ then the rate law (5) becomes

$$-\frac{d[DCT]}{dt} = \frac{K_2k_3[DCT]^2[S]}{1+K_2[S]}, \qquad (6)$$

rearranging Eq. 6, we have Eq. 7

$$-\frac{1}{[DCT]^2}\frac{d[DCT]}{dt} = \frac{K_2k_3[S]}{1+K_2[S]}. \qquad (7)$$

But LHS of Eq. 7 may be written as

$$-\frac{1}{[DCT]^2}\frac{d[DCT]}{dt} = \frac{d\{1/[DCT]\}}{dt} = k_{obs}$$

hence Eq. 7 becomes Eq. 8

$$k_{obs} = \frac{K_2k_3[S]}{1+K_2[S]}. \qquad (8)$$

We also have

$$[S]=K_1[SH^+]/[H^+]. \qquad (9)$$

Therefore Eq. 8 takes the form

$$k_{obs} = \frac{K_1K_2k_3[SH^+]}{[H^+]+K_1K_2[SH^+]} . \quad (10)$$

If K_2 is small, the rate law (8) will take the form

$$k_{obs}=K_2k_3[S]=K_1K_2k_3[SH^+]/[H^+]. \quad (11)$$

The plots of k_{obs} versus [S] (amino acid) gave straight lines passing through the origin with most of the amino acids (Figs. 4 and 5), in conformity with the rate law (11).

The rate laws (Eqs. 10 and 11) explain the observed inverse fractional to nearly inverse first-order in $[H^+]$. The plots of either k_{obs} versus $1/[H^+]$ or $1/k_{obs}$ versus $[H^+]$ were non-linear in most cases (figure not shown).

(ii) Pseudo-First-Order Kinetics in [DCT]: The observed kinetic data (Table 4) for the oxidations of Asn, Gln, and Pro may be accounted for by a mechanism shown in Scheme 2 (modified Scheme 1).

$$SH^+ \overset{K_1}{\rightleftharpoons} S + H^+ \quad \text{(fast)}$$

$$\underset{(DCT)}{ArSO_2NCl_2} + S \underset{k_{-4}}{\overset{k_4}{\rightleftharpoons}} \underset{(Y)}{\text{Intermediate}} \quad \text{(fast)}$$

$$Y + S \xrightarrow{k_5} \text{Products} \quad \text{(slow)}$$

Scheme 2.

Application of the steady state approximation to the intermediate Y, through a procedure similar to the previous one, we have

$$[Y] = \frac{k_4[ArSO_2NCl_2]_0[S]}{k_{-4}+k_5[S]+k_4[S]} \quad (12)$$

or

$$[Y] = \frac{K_4[DCT]_0[S]}{1+K_4[S]} \quad (13)$$

as $k_5[S](k_5$ is very small) in the denominator is negligible compared to other terms and $K_4=k_4/k_{-4}$.

The rate of reaction is then given by Eq. 14

$$-\frac{d[DCT]}{dt} = k_5[Y][S] = \frac{K_4k_5[DCT]_0[S]^2}{1+K_4[S]} \quad (14)$$

or

$$k_{obs} \approx \frac{-1}{[DCT]_0}\frac{d[DCT]}{dt} \approx \frac{K_4k_5[S]^2}{1+K_4[S]} , \quad (15)$$

introducing Eq. 9 into Eq. 15 we have

$$k_{obs} = \frac{K_1^2K_4k_5[SH^+]^2}{[H^+]\{[H^+]+K_1K_4[SH^+]\}} . \quad (16)$$

Thus the rate laws (15) and (16) explain the kinetic data for the oxidations of Asn, Gln, and Pro.

A typical detailed mechanism of oxidation of amino acids is shown in Scheme 3.

Similarly monochlorosulfonamide and HOCl formed further react with amino acids in fast steps to give products.

$$RCH(NH_3^+)COO^- + ArSO_2NHCl + H_2O \xrightarrow[\text{(fast)}]{}$$

$$RCHO + ArSO_2NH_2 + CO_2 + NH_4^+ + Cl^-$$

Table 5. Pseudo-First-Order Rate Constants (k_{obs}) for the Oxidation of Amino Acids (S) by *N*-Chloro-*N*-sodio-*p*-toluenesulfonamide (Chloramine-T, CAT) in 1 : 1 (v/v) Water–Methanol Medium in the Presence of Perchloric Acid at 303 K

$10^3[CAT]_0$	$10^2[S]_0$	$10^3[HClO_4]$	$10^4k_{obs}/s^{-1}$		
mol dm^{-3}	mol dm^{-3}	mol dm^{-3}	Ala	Leu	Asn
Effect of varying $[CAT]_0$					
0.5	2.0	5.0(2.0)	6.5	5.7	3.9
1.0	2.0	5.0(2.0)	6.5	5.9	4.0
2.0	2.0	5.0(2.0)	6.4	6.3	4.0
Effect of varying $[S]_0$					
1.0	0.5	5.0(2.0)	2.3	1.8	—
1.0	1.0	5.0(2.0)	3.8	3.2	1.8
1.0	2.0	5.0(2.0)	6.5	5.9	4.0
1.0	3.0	5.0(2.0)	9.0	8.8	6.1
1.0	4.0	5.0(2.0)	—	—	8.1
1.0	5.0	5.0(2.0)	13.0	12.1	10.6
1.0	10.0	5.0(2.0)	16.4	—	—
Effect of varying $[HClO_4]$					
1.0	2.0	0.1	17.2	—	—
1.0	2.0	0.2	17.2	—	—
1.0	2.0	0.5	17.2	29.6	52.8
1.0	2.0	1.0	17.3	27.5	2.3
1.0	2.0	2.0	10.7	19.3	4.0
1.0	2.0	5.0	6.5	5.9	5.8
1.0	2.0	10.0	3.5	2.9	—
1.0	2.0	20.0	1.3	—	—

Values in the parentheses are for aspargine.

Table 6. Pseudo-Second-Order Rate Constants (k_{obs}) for the Oxidation of Amino Acids (S) by HOCl in the Presence of Perchloric Acid at 303 K

10^3[HOCl]$_0$	10^2[S]$_0$	10^2[$HClO_4$]	$10k_{obs}$/dm^3 mol^{-1} s^{-1}		
mol dm^{-3}	mol dm^{-3}	mol dm^{-3}	Ala	Val	Phe
Effect of varying [HOCl]$_0$					
0.5	2.0	5.0	9.9	9.8	10.3
1.0	2.0	5.0	10.3	10.1	10.7
2.0	2.0	5.0	10.1	10.1	10.5
4.0	2.0	5.0	10.2	10.3	10.5
5.0	2.0	5.0	10.0	10.5	10.8
Effect of varying [S]$_0$					
2.0	0.5	5.0	10.1	10.2	10.5
2.0	1.0	5.0	10.5	10.0	10.7
2.0	2.0	5.0	10.1	10.1	10.5
2.0	4.0	5.0	9.9	10.3	10.5
2.0	5.0	5.0	10.1	10.1	10.7
Effect of varying [$HClO_4$]					
2.0	2.0	1.0	5.0	6.7	5.1
2.0	2.0	2.0	6.9	7.9	7.0
2.0	2.0	5.0	10.1	10.1	10.5
2.0	2.0	10.0	14.1	12.6	14.7
2.0	2.0	20.0	19.4	15.4	20.3

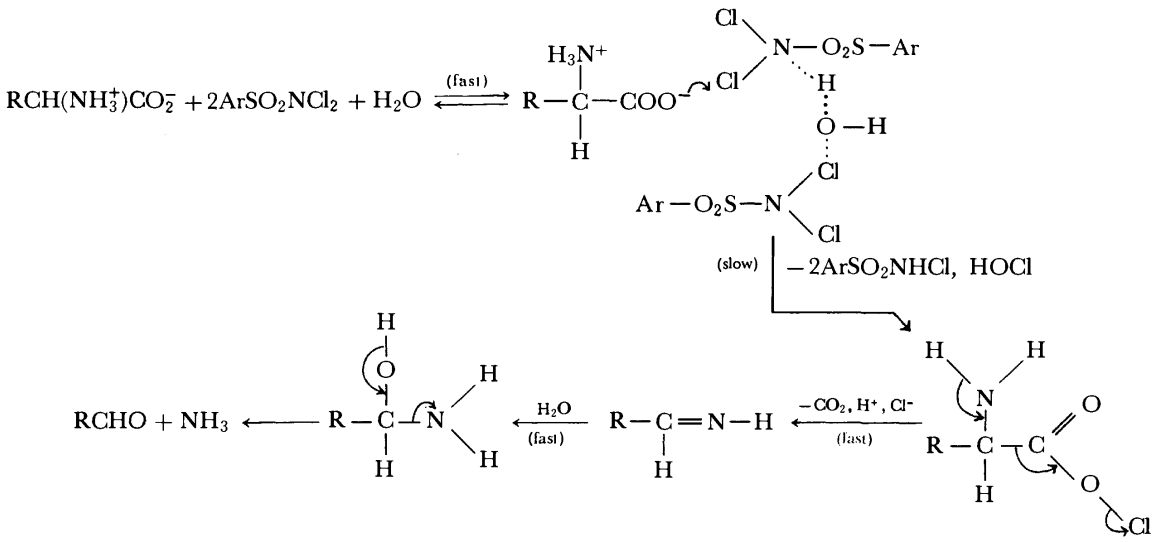

Scheme 3. Where R=CH_3 (Ala), $(CH_3)_2CHCH_2$ (Leu), $H_2N(CO)CH_2$ (Asn), and $H_2N(CO)CH_2CH_2$ (Gln).

$$RCH(NH_3^+)COO^- + HOCl \xrightarrow[(fast)]{} RCHO + CO_2 + NH_4^+ + Cl^-$$

This is supported by investigations with *N*-chloro-*N*-sodio-*p*-toluenesulfonamide (Chloramine-T, $ArSO_2NHCl$) and HOCl under identical conditions (Tables 5 and 6). The rates with these species showed first-order kinetics in [oxidant] and varying orders in [S] and [H^+]. The rates for these oxidations are much higher than those for dichloramine-T oxidations.

Aspargine and glutamine are the amides of acidic amino acids, aspartic and glutamic acids, respectively. Proline is a cyclic amino acid. It is evident from the kinetic data that the kinetic behavior of these amino acids is different from that of simple amino acids (alanine and leucine). The former exhibit different kinetic orders in [DCT] and [S] depending upon [H^+] of the reaction medium, whereas the latter (simple amino acids) show same kinetics over the entire range of [H^+]. This difference in behavior is obvious from the comparison of pK_a values of the amino acids. Asparagine, glutamine, and proline have relatively large values for dissociation constants (Table 7) (smaller pK_a's) and hence are more susceptible to change in [H^+] than the simple amino acids. Hence it is not quite unexpected that they show different kinetic behavior at different [H^+](Table 4).

The observed negligible effect of added reduced product of the oxidant, TSA, and of varying ionic strength of the medium on the rates of oxidations are in agreement with the proposed mechanisms. The latter are also supported by the moderate values of the activation parameters (Table 4).

The observed dielectric effect on the rates of oxida-

Table 7. Ionization Constants and pH Values at the Isoelectric Points of Amino Acids at 25 °C

Amino acid	pK_1	pK_2	pH_i
Alanine	2.34	9.69	6.01
Leucine	2.36	9.60	5.98
Aspargine	2.02	8.80	5.41
Glutamine	2.17	9.13	5.65
Proline	2.00	10.60	6.30

Isoelectric point (or IP): This is the pH at which the maximum number of amino acid molecules are present as zwitter ions, $pH_i=(pK_1+pK_2)/2$.

tions (Table 3), is in conformity with Amis-Jaffee equation for dipolar molecule-dipolar molecule interaction.[14,15]

$$\log k_D = \log k_\infty - \frac{2\mu_1\mu_2}{2.303\, k_B T r^3 D} \quad (17)$$

Where k_D and k_∞ are the rate constants in media of dielectric constant D and ∞, respectively, k_B is the Boltzmann constant, μ_1 and μ_2 are the permanent moments on the dipoles, r is the distance of approach for the dipoles, and T *is* the absolute temperature.

The plots of $\log k_{obs}$ versus $1/D$ were linear (Fig. 6) with negative slopes in accordance with Eq. 17.

References

1) M. M. Campbell and G. Johnson, *Chem. Rev.*, **78**, 65 (1978) and references therein.

2) B. T. Gowda and D. S. Mahadevappa, *J. Chem. Soc., Perkin Trans. 2*, **1983**, 323 and references therein.

3) K. K. Banerji, B. Jayaram, and D. S. Mahadevappa, *J. Sci. Ind. Res.*, **46**, 65 (1987) and references therein.

4) B. T. Gowda and J. I. Bhat, *Indian J. Chem., Sect. A*, **25**, 1129, 1149 (1986); **26**, 215 (1987); *React. Kinet. Catal. Lett.*, **31**, 461 (1986); *Proc. Indian Acad. Sci.*, **100**, 285 (1988); *Int. J. Chem. Kinet.*, **21** (1989).

5) B. T. Gowda and R. V. Rao, *Oxid. Commun.*, **10**, 31 (1987); **11**, 45, 145 (1988); *Indian J. Chem., Sect. A*, **24**, 1021 (1985); **25**, 578, 908 (1986); **27**, 34, 39 (1988).

6) B. T. Gowda and B. S. Sherigara, *Indian J. Chem., Sect. A*, **25**, 960 (1986); *Oxid. Commun.*, **9**, 165 (1986).

7) B. T. Gowda and J. I. Bhat, *Tetrahedron*, **43**, 2119, (1987).

8) B. T. Gowda and R. V. Rao, *J. Chem. Soc., Perkin Trans. 2*, **1988**, 355.

9) B. T. Gowda and B. S. Sherigara, *Int. J. Chem. Kinet.*, **21**, 31 (1989); *Indian J. Chem., Sect. A*, **28**, 120 (1989); *Proc. Indian Acad. Sci. (Chem. Sci.)*, **101**, 155 (1989).

10) T. J. Jacob and C. G. R. Nair, *Talanta*, **19**, 347 (1972).

11) A. I. Vogel, "Quantitative Organic Analysis," Longman and Green, London (1958).

12) F. Feigl, "Spot Tests in Inorganic Analysis," Elsevier, Amsterdam (1958).

13) "Vogel's Text book of Macro and Semimicro Qualitative Inorganic Analysis," ed by G. Svehla, Orient Longman, New Delhi (1982).

14) E. S. Amis, "Solvent Effects on Reaction Rates and Mechanisms," Academic Press, New York (1966).

15) P. Zuman and R. C. Patel, "Techniques in Organic Reaction Kinetics," Wiley, New York (1984).

 © 1989 The Chemical Society of Japan Bull. Chem. Soc. Jpn., 62, 3311—3314 (1989)

Concentrated Mixtures of 1:1 Electrolytes: Densities and Excess Volumes of Aqueous KBr with KCl and NaBr

Anil KUMAR
Department of Sugar Chemistry, Deccan Sugar Institute, Manjari (Bk), Poona 412307, India
(Received December 9, 1988)

Densities of aqueous KCl-KBr and NaBr-KBr mixtures are reported from the ionic strengths 0.5 to 4 mol kg^{-1} of water. The results are analyzed in the light of Pitzer theory of specific interactions. The deviations of experimental quantities from the Young rule (excess volumes) are discussed in terms of interactions between the ions of like charges. The excess volumes showed weak dependence on temperature.

In recent years there has been upsurge in interest in the thermodynamic properties of aqueous concentrated electrolyte mixtures. This upsurge has most probably been caused due to the development of ion-interactions or specific interactions approach of Pitzer,[1,2] which describes various thermodynamic properties like osmotic, activity coefficients, and enthalpies of both pure and mixed electrolyte solutions of high concentrations.[3] However, the understanding of volume properties of concentrated aqueous mixed electrolytes is still very poor, as evidenced by little amount of work in this direction,[4-9] where the studies were carried out in diluted solutions.

The present article describes the densities and apparent molal volumes of mixtures of aqueous KBr with KCl, and with NaBr up to the constant ionic strength of 4 mol kg^{-1} of water. The results are analyzed with the help of Pitzer theory.[1,2] The ion-ion interactions are also discussed in relation to the excess volumes of mixing. Besides detailed study at 298.15 K, the article also discusses the temperature dependence of the excess volumes.

Materials and Methods

KBr, KCl, and NaBr were Baker analyzed and were crystallized twice before preparing solutions on molality basis in deionized water. The concentrations of the solutions were determined by volumetric analysis. The mixtures of different compositions were prepared by mixing appropriate amounts of stock solutions as $y_B=m_B/I$, and remembering that $y_A+y_B=1$. y corresponds to ionic strength fraction, and B refers to KBr. The symbols m and I are molality and ionic strength, respectively.

The experimental density differences, Δd, were measured using a Paar vibrating tube densimeter. The difference between density of solution, d, and of pure water, d_0, is called the density difference, Δd. The densimeter was calibrated using the densities of pure water[10] and of aqueous NaCl solutions.[11] The temperature of thermostat bath was maintained constant to ±0.005 K, and the Δd values were accurate to within 3×10^{-6} g cm^{-3}.

Data Treatment

The Pitzer theory is based on the evaluation of three adjustable parameters from constituent pure electrolytes and then using them in the ionic equations of mixtures. The estimation of ionic property in mixture primarily is based on the cation-anion pair interactions. Subsequently, the corrections arising out of two like charged ion interactions (binary) and three-ion interactions are treated as difference parameters. The volumetric equations of Pitzer as derived from the pressure dependence of the equations applicable to activity coefficients are summarized below. The details of the Pitzer equations are given elsewhere.[12]

Apparent molal volume, ϕ_V, of a single electrolyte is related to its molality, m, as

$$\phi_V = \phi_V^\circ + \nu|Z_M Z_X|\frac{A_V}{2b}\ln(1+bI^{1/2}) + 2\nu_M\nu_X RT[mB_{MX}^V + m^2(\nu_M\nu_X)^{1/2}C_{MX}^V] \quad (1)$$

where

$$B_{MX}^V = \left(\frac{\partial\beta^{(0)}}{\partial P}\right)_T + \left(\frac{\partial\beta^{(1)}}{\partial P}\right)_T (2/\alpha^2 I)[1-(1+\alpha I^{1/2})\exp(-\alpha I^{1/2})] \quad (2)$$

and

$$C_{MX}^V = (\partial C^\phi/\partial P)/2. \quad (3)$$

In these equations $I=1/2\sum_i m_i Z_i^2$, $\nu=\nu_M+\nu_X$, $R=83.1441$ cm^3 bar mol^{-1} K^{-1}, $\alpha=2$ and $b=1.2$, A_V is the Pitzer-Debye-Hückel slope having value of 1.874 cm^3 kg$^{1/2}$ mol$^{-3/2}$ at 298.15 K. ϕ_V° is the partial molal volume of an electrolyte at infinite dilution. $(\partial\beta^{(0)}/\partial P)_T$, $(\partial\beta^{(1)}/\partial P)_T$, and $(\partial C^\phi/\partial P)_T$ are the virial coefficients in the Pitzer equations.

Rogers and Pitzer[13] have suggested that the term $(\partial\beta^{(1)}/\partial P)_T$ could be neglected, as it is not possible to obtain it accurately from volumetric results. Thus, the omission of $(\partial\beta^{(1)}/\partial P)_T$ from Eq. 2 yields into a very simple expression as Eq. 1 with two unknown parameters as $(\partial\beta^{(0)}/\partial P)_T$ and $(\partial C^\phi/\partial P)_T$.

The apparent molal volume of an ion in the mixture, ϕ_{Vi}^* (considering cation-anion pairwise interactions only) is given by

$$\phi_{Vi}^* = \phi_{Vi}^\circ + \frac{Z_i A}{2b}\ln(1+bI^{1/2})RT\sum_j B_{ij}m_j + \frac{RT}{2|Z_i|^{1/2}}\sum_j C_{ij}m_j^2|Z_j|^{1/2} \quad (4)$$

where the summations over j are over ions of opposite charge.

ϕ^*_{Vi} then yields the apparent molal volume of an electrolyte in mixture, ϕ_{VJ}, as

$$\phi_{VJ}=\sum_i \nu_i \phi^*_{Vi} \quad (5)$$

which in turn calculates theoretical mean apparent molal volumes ϕ^*_{Vth} by

$$\phi^*_{Vth}=\sum_J m_J \phi_{VJ}/\sum m_J. \quad (6)$$

Theoretical density, d_{th}, of the mixture is obtained from

$$d_{th}=(1000+\sum_J m_J M_J/(1000/d_0)+\sum_J m_J \phi_{VJ} \quad (7)$$

where M_J is molecular weight of an electrolyte.

The experimental densities, d_{exp}, may be converted to experimental mean apparent molal volumes ϕ^*_{Vexp} by the relationship

$$\phi^*_{Vexp}=\frac{1000(d_0-d_{exp})}{\sum_J m_J d_{exp} d}+\frac{\sum_J m_J M_J}{d_{exp}\sum_J m_J}. \quad (8)$$

Equation 4 does not include the interactions due to the ions of like charge. These interactions i.e. Na^+ and K^+; Cl^--Br^- designated by θ^V_{ik} (i, k are ions with like charges) can be evaluated in the form of difference parameter as:

$$\theta^V_{ik}=(\phi^*_{Vexp}-\phi^*_{Vth})\,(m_i+m_k)/2RT\,m_i\,m_k. \quad (9)$$

It may be noted that Eq. 9 is consistent with Eq. 17 of reference by Pitzer and Kim,[2] who described the mixing therms θ_{ik} for osmotic and activity coefficients of aqueous mixed electrolytes.

An additional term $RT\sum_k \theta^V_{ik} m_k$ may be appended to Eq. 4 in order to obtain ϕ^*_{Vi} with both the cation-anion pair and cation-cation or anion-anion pair interactions as

$$\phi^*_{Vi,corr}=\text{R. H. S. of Eq. 4}+RT\sum_k \theta^V_{ik} m_K. \quad (10)$$

Results and Discussion

Table 1 lists the experimental density differences for both KCl-KBr and NaBr-KBr as a function of y_{KBr} at constant ionic strengths of 0.5, 1, 2, 3, and 4 mol kg^{-1} of water. The values of ϕ^*_{Vexp} can readily be obtained from Eq. 8. The density values for pure constituent electrolytes, i.e. KCl, KBr, and NaBr were in excellent agreement with recent literature.[14-18]

In order to employ the virial coefficients equation of Pitzer, it is essential to obtain the $(\partial\beta^{(0)}/\partial P)_T$, $(\partial\beta^{(1)}/\partial P)_T$, and $(\partial C^\phi/\partial P)_T$ parameters of pure electrolytes from Eqs. 1 to 3. The $(\partial\beta^{(0)}/\partial P)_T$ and $(\partial C^\phi/\partial P)_T$ terms for KCl, KBr, and NaBr were taken from our earlier work[19,20] or calculated from the coefficients cited therein. The values of pure electrolyte parameters are listed in Table 2. The use of these parameters

Table 1. Experimental Relative Densities of Aqueous KCl-KBr and NaBr-KBr at 298.15 K

y_B	$\Delta d\times10^3$/g cm^{-3}	y_B	$\Delta d\times10^3$/g cm^{-3}
KCl-KBr		NaBr-KBr	
I=0.5		I=0.5	
0	22.73	0	33.53
1.1432	25.37	0.1988	39.06
0.2957	28.19	0.4021	39.59
0.4119	30.33	0.5012	39.85
0.5594	33.05	0.6119	40.14
0.6937	35.52	0.8095	40.67
0.8231	37.91	1	41.17
1	41.16		
I=1		I=1	
0	44.28	0	75.72
0.1533	49.83	0.2043	76.66
0.3139	55.64	0.4122	76.68
0.4638	61.07	0.5099	78.12
0.5982	65.92	0.6065	78.58
0.7492	71.38	0.8033	79.50
0.8925	76.55	1	80.43
1	80.43		
I=2		I=2	
0	84.46	0	146.20
0.1123	92.28	0.2055	147.75
0.2194	99.72	0.4079	149.27
0.3452	108.45	0.5005	149.97
0.4298	114.32	0.6663	151.22
0.5389	121.88	0.8065	152.28
0.6721	131.10	1	153.75
0.7690	137.79		
0.8992	146.78		
1	153.74		
I=3		I=3	
0	121.28	0	212.27
0.1243	133.77	0.1992	214.06
0.2395	145.34	0.4040	215.89
0.3701	158.44	0.4998	216.74
0.4695	168.39	0.6045	217.68
0.5921	180.64	0.8013	219.45
0.7119	192.58	1	221.23
0.8399	205.31		
0.9342	214.69		
1	221.23		
I=4		I=4	
0	155.14	0	274.39
0.0981	167.83	0.2022	276.18
0.1952	180.36	0.4045	277.98
0.2666	189.56	0.5017	278.84
0.3531	200.69	0.6061	279.78
0.4555	213.86	0.7998	281.52
0.5521	226.26	1	283.33
0.6661	240.81		
0.8444	263.53		
1	283.33		

Table 2. Pitzer Coefficients for Pure Electrolytes for Correlating ϕ_V and Molality

Electrolyte	ϕ^0_V / cm^3 mol^{-1}	$(\partial\beta^{(0)}/\partial P)$ $\times10^6$	$(\partial C^\phi/\partial P)T$ $\times10^7$	Standard deviation σ/cm^3 mol^{-1}
KCl	27.11	11.82	−11.61	0.01
KBr	33.84	11.45	−14.33	0.01
NaBr	23.52	8.70	−8.70	0.01

in Eqs. 4 to 7 yields the calculated ϕ^*_{Vth} and d_{th} of the mixtures. It is interesting to note that these calculations are manifestation of a simple Young's rule,[21] where the mixture properties are computed from the properties of the individual ions at the same ionic strength. The results of calculations are shown in Table 3 in terms of average deviations of fits, indicating systematic negative deviations for Δd values as demonstrated for example at the highest ionic strength I=4 mol kg^{-1} for both the systems in Fig. 1. In view of these deviations, the interactions between like charged ions were taken into account with the use of Eq. 10, where the θ^V_{ik} values (Table 4) were obtained from Eq. 9. The results of calculations are shown in Table 3. Figure 1 also depicts the results for both the systems at I=4 mol kg^{-1} with the use of θ^V_{ik} terms. An examination of Table 3 indicates a remarkable improvement in the fits, and, also the systematic deviations are removed. In general, the average deviations for KCl-KBr and NaBr-KBr are reduced to 7 and 5 ppm respectively with the use of θ^V_{ik}.

Very recently, Patwardhan and Kumar[22,23] have derived a simple equation from the concept of reduced inoic activity coefficient for estimating densities of concentrated mixed electrolyte solutions. The equation is

$$d=\sum_J(1000\,y_J+m_J M_J)/\sum_J(1000\,y_J+m_J M_J/d^0_J). \quad (11)$$

Table 3. Average Deviations, δ, from Experimental Data as Obtained by Pitzer Equations without (Also by Equation of Patwardhan and Kumar) and with Mixing Term, θ^V_{ik} at 298.15 K

I	$-\delta$/ppm			
mol kg^{-1}	KCl-KBr		MaBr-KBr	
	Without θ^V_{ik}	With θ^V_{ik}	Without θ^V_{ik}	With θ^V_{ik}
0.5	3	2	3	2
1	28	5	10	3
2	89	7	29	6
3	185	9	56	7
4	294	11	85	9

Table 4. Binary Mixing Terms of Pitzer (θ^V_{ik}) and Friedman (v^0) Equations at 298.15 K

I	$\theta^V_{ik}\times10^6$	v^0
	i=Cl$^-$, k=Br$^-$	
0.5	1.94	0.096
1	2.74	0.136
2	2.44	0.121
3	2.16	0.107
4	1.84	0.091
	i=Na$^+$, k=K$^+$	
0.5	0.97	0.048
1	0.81	0.040
2	0.71	0.035
3	0.61	0.030
4	0.52	0.026

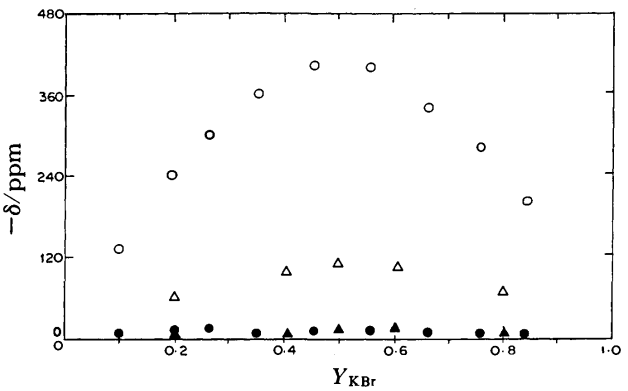

Fig. 1. Deviaition of experimental density data from calculated ones by Pitzer Equations without and with θ^V_{ik} values for KCl-KBr and NaBr-KBr at I=4 and T=298.15 K; KCl-KBr ○ without ● with; NaBr-KBr △ without ▲ with.

In this equation, d^0_J is density of constituent Jth electrolyte at the ionic strength of the mixture. Their equation neglects any interactions due to like charged ions and, thus, is again equivalent to Young's rule.[21] The results, hence, listed in Table 3 without the θ^V_{ik} are also applicable to Eq. 11.

The excess volumes of mixing, ΔV_m, for these mixtures can be obtained as

$$\Delta V_m=\phi^*_{V\,exp}\,m_J-\sum_J m_J\,\phi''_{VJ} \quad (12)$$

where ϕ''_{VJ} is apparent molal volume of Jth electrolyte at the ionic strength of mixture. The ΔV_m values can be fitted to the Friedman equation.[24]

$$\Delta V_m=y_B(1-y_B)I^2[v^0+v^1(1-2y_B)] \quad (13)$$

where v^0 and v^1 are the Friedman parameters indicating binary (ik) and ternary (ijk) interactions, respectively. The use of Eq. 13 fitted, the ΔV_m with good accuracy and v^1 values were found negligible. The values of v^0 values as a function of I can conveniently be represented as

$$v^0=15.3\times10^{-2}-15.0\times10^{-3}I\,(\text{for KCl-KBr}) \quad (14)$$

and

$$v^0=4.5\times10^{-2}-4.75\times10^{-3}I\,(\text{for NaBr-KBr}). \quad (15)$$

One should note that data of I=0.5 are not included in the fit, as the error becomes significantly large at lower ionic strengths.

Wood and Smith[25] reported the heats of mixing data up to I=1 for these mixtures, and fitted the data to analogous equation of Friedman in order to obtain RTh_0 and RTh$_1$ as we did to Eq. 13. Negligible RTh_1 values from their study support our negligible v^1 values for both the systems. A study of their data shows that h_0 value is approximately ten times higher in the case of aq. NaBr-KBr than that of aq. KCl-KBr. The present study on volume indicates the relationships inversed by three times. The former effect is

Table 5. Temperature Dependence of v^0 Values for Aqueous KCl-KBr and NaBr-KBr Systems at Low and High Ionic Strengths

I	Temperature	
mol kg^{-1}	278.15 K	318.15 K
	KCl-KBr	
1	0.131	0.144
4	0.084	0.100
	NaBr-KBr	
1	0.036	0..046
4	0.022	0.032

obtained from the temperature dependence of activity coefficients, while the latter from pressure dependence.

Friedman[24,26,27] using Mayer's ionic cluster expansion method estimated the excess properties of mixing of aqueous mixed electrolytes with a common ion. The equations incorporated the primitive model consisting of hard spheres in a continuous dielectric. According to him, the interaction terms RTg_0 and RTh_0 for excess free energy and enthalpy of mixing, respectively, are finite for common ion mixtures even at infinite dilution. The values of intercepts in Eqs. 14 and 15 confirm Friedman's results of calculations for excess volumes of mixing too. One clearly notes the absence of high order limiting law[28] in the symmetric mixtures like these under study. A survey of v_0 values for both the mixtures indicates a slow variation of v_0 with I or total molality. Thus, v_0 values arising out of like-charged ion-interactions are more important than v^1 which is an indication of ternary interaction. This observation is confirmed both by enthalpy of mixing data of Wood and Smith[25] and by the present work on volumes.

The binary mixing term of Pitzer, θ^V_{ik} could be correlated with v^0 term of Friedman using Eqs. 9, 12, and 13 to give

$$\theta^V_{ik}=v^0/2RT. \quad (16)$$

It is natural that θ^V_{ik} will have same ionic strength dependence.

Since the ΔV_m values at 298.15 K showed maxima at $y_B=0.5$, we conducted one experiment each for $I=1$ and 4 mol kg^{-1} for both the systems at 278.15 and 318.15 K in order to obtain temperature dependence of ΔV_m. Table 5 lists the results in terms of v^0, which indicate poor temperature dependence in both the cases. The values of $\partial v^0/\partial T$ for aqueous KCl-KBr and aqueous NaBr-KBr were found to be 3.6×10^{-4} and 2.5×10^{-4}, respectively in the temperature range of 278.15 to 318.15 K. In view of this, we deferred conducting further experimentations at other intermediate ionic strengths and temperatures.

To summarize, the densities of concentrated aqueous mixed electrolytes can be estimated with accuracy with the Pitzer theory of specific interactions, provided both the interactions (cation-anion and cation-cation or anion-anion) are explicitly considered. Ternary interactions are negligible throughout, although they could be significant in many other systems. In near future, we shall present complete description of the symmetric and asymmetric mixtures, for which we are collecting experimental data. Also, the experimental data, for the treatment of which, ternary interaction term is required, will be presented.

References

1) K. S. Pitzer, *J. Phys. Chem.*, **77**, 268 (1973).
2) K. S. Pitzer and J. J. Kim, *J. Am. Chem. Soc.*, **96**, 5701 (1974).
3) K. S. Pitzer, "Thermodynamics of Aqueous Electrolytes at Various Temperatures, Pressures and Compositions," Thermodynamics of Aqueous Systems with Industrial Applications, ed. by S. A. Newman, ACS 133, Washington, DC (1980), Chap. 13.
4) S. Lee, "The Apparent and Partial Molal Volumes of Electrolytes in Water and in Aqueous Sodium Chloride Solutions, Ph. D. dissertation, Yale University, USA (1966).
5) H. Wirth, *J. Am. Chem. Soc.*, **59**, 2549 (1937).
6) H. Wirth, *J. Am. Chem. Soc.*, **62**, 1128 (1940).
7) H. Wirth and A. Losurdo, *J. Chem. Eng. Data*, **13**, 102 (1968).
8) H. Wirth, *J. Chem. Eng. Data*, **13**, 226 (1968).
9) F. J. Millero, *Geochim. Cosmochin. Acta*, **41**, 215 (1977).
10) G. S. Kell, *J. Chem. Eng. Data*, **20**, 97 (1975).
11) A. Losurdo, E. M. Alzola, and F. J. Millero, *J. Chem. Thermodyn.*, **14**, 649 (1982).
12) A. Kumar and G. Atkinson, *J. Phys. Chem.*, **87**, 5504 (1983).
13) P. S. Z. Rogers and K. S. Pitzer, *J. Phys. Chem. Ref. Data*, **11**, 15 (1982).
14) F. Vaslow, *J. Phys. Chem.*, **70**, 2286 (1966).
15) F. T. Gucker, C. L. Chernik, and P. Roy-Chowdhary, *Proc. Natl. Acad. Sci.*, **55**, 12 (1966).
16) T. Isono, *J. Chem. Eng. Data*, **29**, 45 (1984).
17) L. A. Romankiw and I-Ming Chou, *J. Chem. Eng. Data*, **28**, 300 (1983).
18) J. A. Gates and R. H. Wood, *J. Chem. Eng. Data*, **30**, 44 (1985).
19) A. Kumar, *J. Chem. Eng. Data*, **32**, 106 (1987).
20) A. Kumar, *J. Chem. Eng. Data*, **32**, 109 (1987).
21) T. F. Young, *Rec. Chem. Prog.*, **12**, 81 (1951).
22) V. S. Patwardhan and A. Kumar, *AIChE J.*, **32**, 1419 (1986).
23) V. S. Patwardhan and A. Kumar, *AIChE J.*, **32**, 1429 (1986).
24) H. L. Friedman, "Ionic Solution Theory," Interscience, New York (1962).
25) R. H. Wood and R. W. Smith, *J. Phys. Chem*, **69**, 2974 (1965).
26) H. L. Friedman, *J. Chem. Phys.*, **32**, 1134 (1960).
27) H. L. Friedman, *J. Chem. Phys.*, **32**, 1351 (1960).
28) V. K. La Mer, T. H. Gronwell, and L. J. Greiff, *J. Phys. Chem.*, **35**, 2245 (1931).

 © 1989 The Chemical Society of Japan Bull. Chem. Soc. Jpn., 62, 3315—3319 (1989)

Solvent Effect on Hydrogen Bonding Interaction between 5,6,7,8-Tetrahydro-2-naphthol in the Ground and Excited States and Triethylamine

T. K. PAL, G. K. MALLIK, T. GANGULY, and S. B. BANERJEE*
Department of Spectroscopy, Indian Association for the Cultivation of Science, Jadavpur, Calcutta-700032, India
(Received December 12, 1988)

In the ground state 5,6,7,8-tetrahydro-2-naphthol (ThOH) forms with triethylamine (TEA) simple hydrogen bond, hydrogen-bonded ion pair or solvent-separated ion pair complex depending on the polarity of solvents. Fluorescence emission of ThOH is quenched by TEA in all solvents. The quenching rate constant k_q is large in weakly polar solvents than in highly polar solvents and there is no evidence of formation of solvent-separated ion pair in latter solvents. It is suggested that restricted electron delocalization in excited ThOH molecule lowers the tendency of deprotonation of the OH group. The likely pathway of energy depletion is through intermediate singlet contact CT exciplex of the type A^-D^+ between ThOH and TEA.

Hydrogen-bonding interactions between an acid A-H and a base B can be of different types depending on the polarity of the solvents in which the systems are studied and may lead to simple hydrogen-bond, hydrogen-bonded ion pair or solvent-separated ion pair complex. The present paper concerns absorption and fluorescence spectra of ThOH, a bicyclic molecule of biological interest specially in hormone biology, measured in solvents of different dielectric constant (ε_0) in the presence of TEA as the hydrogen-bond acceptor. In the ThOH molecule the π-electrons extend over one ring and the other alicyclic like ring of the molecule has a flexible distorted half-chair structure like cyclohexane. In a previous communication[1] some changes in the π-electronic absorption spectrum of ThOH and other similar molecules due to hydrogen-bonding with TEA were described. It was also reported that fluorescence of some bicyclic tetrahydronaphthols and amines is quenched by hydrogen-bonding molecules like TEA.[1-3] Hydrogen-bonding properties of molecules are generally different in the ground and excited states. The absorption and emission spectra of ThOH have been measured in the same set of solvents. One of the main objectives is to elucidate dependence of hydrogen-bonding interaction between ThOH in the ground and excited states and TEA on solvent polarity and the nature of the complexes that might be formed. Possible reaction schemes in the ground and excited states and kinetics of energy depletion have been examined.

Experimental

5,6,7,8-Tetrahydro-2-naphthol (ThOH) (Aldrich, 98% pure) was sublimed under reduced pressure before use. TEA (Fluka, AG) was distilled at atmospheric pressure. Spectroscopic grade solvents hexane, ethanol (EtOH), methanol (MeOH), dichloromethane (DCM), tetrahydrofuran (THF), *N,N*-dimethylformamide (DMF), acetonitrile (ACN) supplied by E. Merck, W. Germany were used as received. TEA and all the solvents were tested carefully for any possible interfering emission when excited at 280 nm.

The concentration of ThOH was about 2.25×10^{-4} mol dm^{-3} for both absorption and emission experiments. In ternary mixtures, the concentration of TEA in different solvents varied from 0.1 to 1 mol dm^{-3} for absorption and from 10^{-3} to 0.1 mol dm^{-3} for emission study. The excitation wavelength was 280 nm.

The absorption spectra were recorded with a Shimadzu UV-VIS spectrophotometer model 210A and the emission spectra with a Perkin-Elmer model MPF 44A fluorescence spectrophotometer attached with corrected spectra unit.

Fluorescence decay measurements were made using a time-correlated single photon-counting fluorimeter (model 199, Edinburge Instruments, U. K). The excitation source was a coaxial H_2 flash lamp giving an instrumental response function of about 1.2 ns full width at half-maximum (FWHM) at 30 kHz repetition rate. The excitation and emission wavelengths were 280 nm and 305 nm, respectively. Count versus channel number was recorded separately and fluorescence lifetime was calculated by fitting single exponential function with the experimental data and the computation was done using HCL PC Computer model BUSYBEE PC/XT.

Results and Discussion

Hydrogen-Bonding and Absorption Spectral Changes. The π-electronic absorption spectrum of ThOH in 260—310 nm region has been measured at 300 K in different nonpolar and polar protic and aprotic solvents without and with added amounts of TEA. Figure 1 shows that when TEA is added to the solution of ThOH in hexane (dielectric constant $\varepsilon_0\approx1.89$ at 300 K) the absorption spectrum undergoes a small shift towards the longer wavelength. An isosbestic point is also noted at 290 nm in the absorption spectrum (Fig. 1). TEA does not produce any change in the absorption spectrum of an analogous molecule 6-methoxy-1,2,3,4-tetrahydronaphthalene which is unlikely to have hydrogen-bonding interaction with TEA in hexane. Addition of excess amount of TEA to the tetrahydronaphthol-hexane system does not yield any band on the long wavelength side characteristic of charge transfer or ion pair formation. All this indicates that in hexane medium hydrogen-bonding

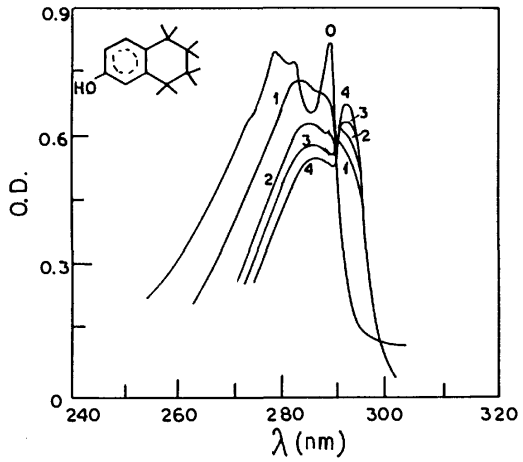

Fig. 1. Ultraviolet absorption curves for ThOH in hexane (2.23×10^{-4} mol dm^{-3}) at 300 K. Concentration (mol dm^{-3}) of TEA: (0) 0; (1) 0.10; (2) 0.67; (3) 0.83; (4) 1.0.

between ThOH and TEA is weak and a simple hydrogen-bonded complex is formed. The simple hydrogen-bonded equilibrium may be expressed as

$$\underset{C_f}{\mathrm{ThOH}}+\underset{C_A}{\mathrm{NR_3}} \overset{K_1}{\rightleftharpoons} \underset{C_b}{\mathrm{ThOH\cdots NR_3}} \qquad (1)$$

where R stands for C_2H_5.

The equilibrium constant K_1 is given by

$$K_1 = C_b/C_fC_A$$

where C_f, C_A, and C_b represent concentrations of free ThOH, TEA, and the hydrogen-bonded species respectively.

When ThOH is dissolved in polar protic solvents EtOH or MeOH or in polar aprotic solvent tetrahydrofuran (THF) the absorption bands of the molecule shift towards the red with respect to the bands observed in hexane solution. When TEA is added to the binary mixture of ThOH-alcohol or ThOH-THF, no further shift is observed. Apparently ThOH becomes engaged in hydrogen-bonding with EtOH, MeOH, or THF and when TEA is added, direct hydrogen-bonding between TEA and ThOH does not take place.

In dichloromethane (DCM) which has a relatively high dielectric constant ($\varepsilon_0 \approx 9.80$ at 300 K) compared to hexane, the tetrahydronaphthol-TEA system yields two absorption maxima at 289 and 325 nm which may be assigned to simple hydrogen-bonded species and hydrogen-bonded ion pair, respectively (Fig. 2, Table 1). This implies establishment of a tautomeric equilibrium between simple hydrogen-bonded complex and the hydrogen-bonded ion pair and the following equilibria may be assumed

$$\mathrm{ThOH}+\mathrm{NR_3} \overset{K_1}{\rightleftharpoons} \mathrm{ThOH\cdots NR_3}$$

$$\underset{C_{HB}}{\mathrm{ThOH\cdots NR_3}} \overset{K_2}{\rightleftharpoons} \underset{C_{HBIP}}{\mathrm{ThO^-\cdots NH^+R_3}} \qquad (2)$$

where K_2 is given by C_{HBIP}/C_{HB}. Here C_{HB} and C_{HBIP} stand for concentration of simple hydrogen-bonded complex and hydrogen-bonded ion pair complex

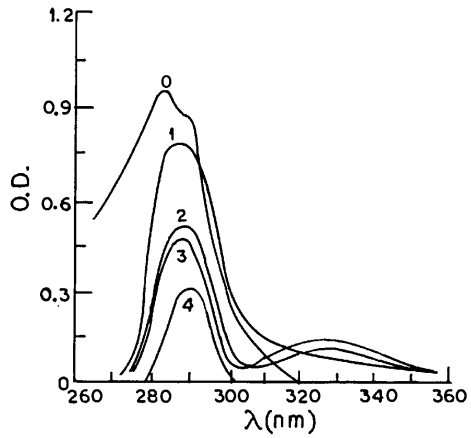

Fig. 2. Ultraviolet absorption curves for ThOH in DCM (2.25×10^{-4} mol dm^{-3}) at 300 K. Concentration (mol dm^{-3}) of TEA: (0) 0; (1) 0.23; (2) 0.67; (3) 0.83; (4) 1.0.

Table 1. Position of Absorption Maxima, λ_{max} in nm

Solvent	ε_0[a)]	ThOH	ThOH···NR$_3$	ThO$^-$···HN$^+$R$_3$	ThO$^-$(solv.)N$^+$HR$_3$
Hexane	1.89	287	292	—	—
		280	286	—	—
THF	7.58	291	—	—	—
		283	—	—	—
DCM	9.08	290	—	—	—
		283	289	325	—
EtOH	24.55	289	—	—	—
		283	—	—	—
MeOH	32.70	289	—	—	—
		283	—	—	—
DMF	36.70	290	—	—	—
		283	—	—	340
ACN	37.50	289	—	—	340
		283	—	—	—

a) Values given at 300 K.

respectively. Baba et al.[3] made similar observation in the case of *p*-nitrophenol-TEA in DCM. The peak at 289 nm in DCM represents absorption by ThOH, hydrogen-bonded with TEA. The corresponding peak due to free molecule before the addition of TEA is at 283 nm (Fig. 2, Table 1). When concentration of TEA is sufficiently high (≈1 mol dm^{-3}) the longer wavelength band at 325 nm assigned to hydrogen-bonded ion pair disappears and only the 289 nm band due to simple hydrogen-bonded species persists (Fig. 2). Therefore, at large concentration of TEA, the tautomeric equilibria shown by Eq. 2 are disturbed. The equilibrium under these conditions is weighted in favor of the simple hydrogen-bonded complex. Evidently when a large amount of TEA, which has a comparatively low dielectric constant (ε_0≈2.24), is present in the mixture containing DCM and TEA, the effective dielectric constant is lowered and the situation tends to be the case of solution of low dielectric constant in which only simple hydrogen-bonded complex is formed.

When TEA is gradually added to solution of ThOH in highly polar aprotic solvents *N*,*N*-dimethylformamide (DMF) (ε_0≈36.7) and acetonitrile (ACN) (ε_0≈37.0), a single broad structureless band (Fig. 3) appears at 340 nm (Table 1) in place of the 325 nm band due to hydrogen-bonded ion pair observed in DCM. At the same time, intensity of the absorption band due to free molecules diminishes (Fig. 3). It is seen from Fig. 3 that naphtholate ion in aqueous solution absorbs near the same wavelength and therefore the 340 nm band may be attributed to absorption by deprotonated naphtholate ion ThO$^-$ in the ground state. The presence of isosbestic point in the spectrum (Fig. 3) indicates a chemical equilibrium which

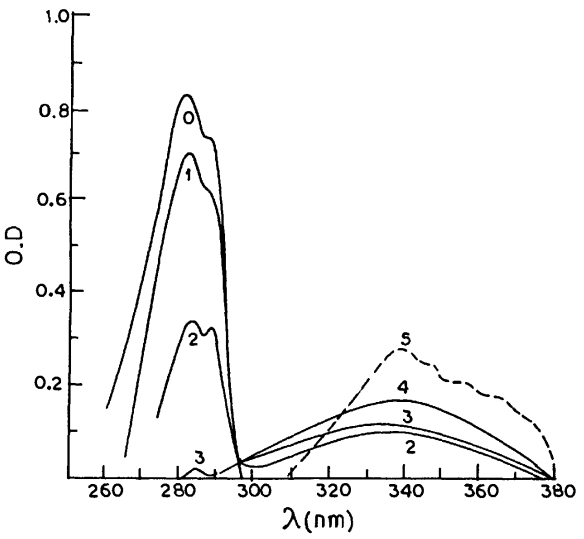

Fig. 3. Ultraviolet absorption curves for ThOH in ACN (2.31×10^{-4} mol dm^{-3}) at 300 K. Concentration (mol dm^{-3}) of TEA: (0) 0; (1) 0.10; (2) 0.67; (3) 0.83; (4) 1.0. Dotted curve (5): spectrum of tetrahydronaphtholate ion (ThO$^-$) in aqueous solution.

may be expressed as

$$\mathrm{ThOH}+\mathrm{NR_3} \overset{K_3}{\rightleftharpoons} \mathrm{ThO^-(solv.)N^+HR_3} \qquad (3)$$

which assumes formation of solvent-separated ion pair by transfer of proton. The ions are separated by one or more solvent molecules and are linked electrostatically.

Hydrogen-Bonding and Fluorescence Spectral Changes. To sum up, absorption measurements demonstrate different types of interaction between ThOH in the ground state and TEA in different solvents depending on the dielectric constants of solvents. It would be interesting to investigate the nature of interaction between excited ThOH and TEA in the same solvents as were employed in absorption study. The fluorescence spectra of ThOH at 300 K are given in Fig. 4(a) and Fig. 4(b). It is seen that in the solvents hexane (ε_0≈1.89 at 300 K), THF (ε_0≈7.58 at 300 K), DCM (ε_0≈9.08 at 300 K), DMF (ε_0≈36.7 at 300 K), and ACN (ε_0≈37.5 at 300 K), fluorescence emission of ThOH is reduced remarkably in the presence of very small amount of TEA (concentration≈ 10^{-3}—10^{-2} mol dm^{-3}), but the shape and position of the bands are unchanged (Figs. 4(a) and (b)).

The absorption spectral changes described above, require comparatively large concentration of TEA (0.1 mol dm^{-3}). So, for very low TEA concentration, ranging from 10^{-3} to 10^{-2} mol dm^{-3}, used in fluorescence measurements, static quenching or innerfilter effect may be neglected and the dynamic quenching rate constant k_q may be determined from simple Stern-Volmer equation

$$f_0/f = 1 + K_{sv}[\mathrm{Q}] \qquad (4)$$

where $K_{sv}=k_q\tau_0$, τ_0 being the fluorescence decay time in absence of TEA. Plots of f_0/f versus [Q] in different solvents are found to be linear and the computed k_q's are given in Table 2. It is seen that the dynamic fluorescence quenching rate constant k_q measured in hexane is larger than the rate constants measured in more polar solvents THF, DMF, and ACN (Table 2). In DCM, k_q is slightly higher than in hexane. In this solvent, external heavy atom perturbation is likely to contribute to deactivation of the excited singlet state of ThOH. In alcoholic solvents, on addition of TEA (Fig. 4(c)), the fluorescence of ThOH is not quenched and this indicates that the nonbonding lone-pair electrons on the nitrogen atom of TEA form hydrogen-bonding of R-OH···N type with alcohols and charge transfer in ThOH-TEA system is retarded. The solvent dependence of quenching constant k_q is not very regular. But it is found to be generally high in solvents of low polarity than in solvents of high polarity (Table 2). This negates existence of solvent-separated ion pair complex in the excited state, similar to the one formed in the ground state, even in highly polar solvent like ACN. Plainly, hydrogen-bonding

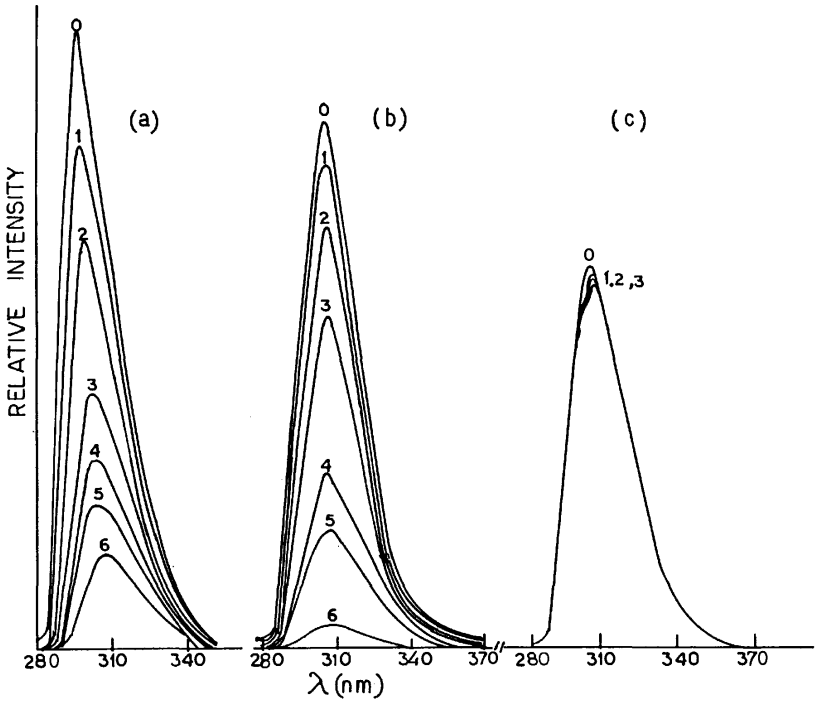

Fig. 4. (a) Fluorescence spectra of ThOH in hexane (2.23×10^{-4} mol dm^{-3}) at 300 K (excitation wavelength: 280 nm). Concentration (mol dm^{-3}) of TEA in (0) 0; (1) 3.17×10^{-3}; (2) 9.51×10^{-3}; (3) 1.90×10^{-2}; (4) 3.17×10^{-2}; (5) 4.76×10^{-2}; (6) 9.52×10^{-2}.
(b) Fluorescence spectra of ThOH in ACN (2.31×10^{-4} mol dm^{-3}) at 300 K (excitation wavelength: 280 nm). Concentration (mol dm^{-3}) of TEA in (0) 0; (1) 1.60×10^{-2}; (2) 3.20×10^{-2}; (3) 6.40×10^{-2}; (4) 1.28×10^{-1}; (5) 1.92×10^{-1}; (6) 9.52×10^{-1}.
(c) Fluorescence spectra of ThOH in EtOH (2.25×10^{-4} mol dm^{-3}) at 300 K (excitation wavelength: 280 nm). Concentration (mol dm^{-3}) of TEA in (0) 0; (1) 1.60×10^{-2}; (2) 6.40×10^{-2}; (3) 1.92×10^{-1}.

Table 2. Bimolecular Fluorescence Quenching Rate Constant (k_q) in Solvents of Varing ε_0 Values for ThOH-TEA System at 300 K

Solvent	ε_0	τ_0/ns	K_{sv}/dm^3 mol^{-1}	k_q/dm^3 mol^{-1} s^{-1}
Hexane	1.89	4.19	69.32	1.65×10^{10}
THF	7.58	5.46	8.55	1.56×10^{9}
DCM	9.08	2.00	35.29	1.76×10^{10}
EtOH	24.55		No quenching	
MeOH	32.70		No quenching	
DMF	36.70	6.83	3.18	4.65×10^{8}
ACN	37.00	4.54	9.20	2.02×10^{9}

properties of ThOH are different in the ground and excited states. The deactivation of the excited ThOH molecule may be through formation of hydrogen-bonded ion pair or contact CT exciplex and the equilibrium may be represented by

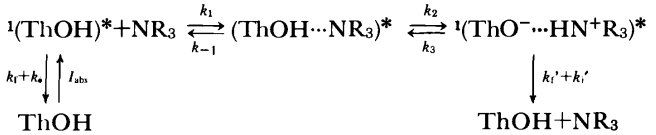

Scheme 1.

The energy gap between the CT state ^{1}(ThO$^-$···NH$^+$R$_3$)* and the ground state of ThOH may be small enough to favor internal conversion[5] and fast non-radiative decay as pictured in Scheme 1. It is interesting to note that in the ground state, 2-naphthol, in which the π-electrons extend over both the rings, reportedly[6,7] enters into simple hydrogen-bonding with TEA in nonpolar solvents. In polar solvents bonding between TEA and unexcited 2-naphthol is supposed to be hindered[6] due to large solvation of both the acceptor and donor molecules. On the other hand, due to interaction between TEA and excited 2-naphthol in polar solvents, formation of solvent-separated ion pair complex equlibrium state from which fluorescence transition occurred was reported.[6]

Therefore hydrogen-bonding behaviors of 2-naphthol and the bicyclic tetrahydronaphthol are different, particularly in the excited state. This difference in behavior may be attributed to the lessening of electron delocalization due to the saturation of one of the rings of the bicyclic system of ThOH and consequent lowering of the number of π-bonds. The outcome of low electron delocalization is that tendency of deprotonation of OH group of ThOH decreases.

Apparently this restriction of electron delocalization is specially important in the excited state of ThOH because as has been noted above, there is no indication of solvent-separated ion pair formation in polar solvents.

We wish to thank Mrs. Jaya Mukherjee and Dr. S. C. Bera of Physical Chemistry Department, Jadavpur University for the fluorescence lifetime measurments. We acknowledge useful conversation with Dr. S. P. Ghosh of Inorganic Chemistry Department of IACS.

References

1) K. Chatterjee, S. Laha, S. Chakravorti, T. Ganguly, and S. B. Banerjee, *Chem. Phys. Lett.*, **100**, 88 (1983).
2) K. Chatterjee, S. Laha, S. Chakravorti, T. Ganguly, and S. B. Banerjee, *J. Chem. Soc., Perkin Trans. 2*, **1986**, 79.
3) H. Baba, A. Matsuyama, and H. Kokubun, *Spectrochim. Acta, Part A*, **25**, 1709 (1969).
4) K. Chatterjee, S. Laha, S. Chakravorti, T. Ganguly, and S. B. Banerjee, *Can. J. Chem.*, **62**, 1369 (1984).
5) M. M. Martin, N. Ikeda, T. Okada, and N. Mataga, *J. Phys. Chem.*, **86**, 4148 (1982).
6) N. Mataga and Y. Kaifu, *Mol. Phys.*, **7**, 137 (1963).
7) P. B. Bisht, G. C. Joshi, H. B. Tripathi, and D. D. Pant, *Chem. Phys. Lett.*, **142**, 291 (1987).

Kinetics and Mechanism of the Reduction of Dodecatungstocobaltate(III) by Iminodiacetate, Nitrilotriacetate, and Ethylenediaminetetraacetate. A Comparative Study of the Reactivity of Different Amine-*N*-carboxylates

Swapan K. SAHA, Prabir BHATTACHARYA, Mahammad ALI, and Pradyot BANERJEE*
Department of Inorganic Chemistry, Indian Association for the Cultivation of Science, Jadavpur, Calcutta 700032, India
(Received October 19, 1988)

The kinetics of reduction of dodecatungstocobaltate(III) by iminodiacetate (IDA), nitrilotriacetate (NTA), and ethylenediaminetetraacetate (EDTA) have been studied in aqueous solution at 50 °C, 30 °C, and 15 °C respectively. In general, the reactivity of the amine-*N*-carboxylates is in the order EDTA > NTA > IDA. All the anionic species have been found to undergo oxidation via both a spontaneous and an alkali metal ion-catalyzed pathway, while molecular form of the acids are oxidized only via spontaneous pathway. The rate of oxidation is given by a general expression $k_{ox}=k^{\circ}+k[M^+]^n$ where $k_{ox}=k_{obs}/2[L]_T$ ($[L]_T$=total concentration of a particular amine-*N*-carboxylate) and n may have values 1 or 2 depending on the nature of M^+. The terms k° and k account for the rate constants of the spontaneous and catalyzed paths respectively. A general trend $K^+ > Na^+ > Li^+$ for the catalyzed path has been observed for the oxidation of these amine-*N*-carboxylates. Reactivities of different species present in the experimental pH range have been evaluated by carrying out experiment at different pH and using these data in appropriate rate expressions. The reactivities (50 °C) of Hida$^-$ are $k^{\circ}=4.70\times10^{-5}$ dm^3 mol^{-1} s^{-1} and $k_1=3.44\times10^{-4}$ dm^6 mol^{-2} s^{-1} for the spontaneous and Na^+ catalyzed paths respectively. For NTA oxidation (30 °C), rates are k°_{10}(H_3nta)$=1.11\times10^{-3}$ dm^3 mol^{-1} s^{-1}, k°_{11}(H_2nta$^-$, spontaneous)$=7.00\times10^{-3}$ dm^3 mol^{-1} s^{-1}, k_{11}(H_2nta$^-$, Na^+ catalyzed)$=3.50\times10^{-2}$ dm^6 mol^{-2} s^{-1}, k°_{12}(Hnta^{2-}, spontaneous)$=7.20\times10^{-3}$ dm^3 mol^{-1} s^{-1}, k_{12}(Hnta^{2-}, Na^+ catalyzed)$=4.01\times10^{-2}$ dm^6 mol^{-2} s^{-1}. The corresponding reactivities (15 °C) for EDTA oxidation are k°_{20}(H_4edta, spontaneous)$=6.80\times10^{-3}$ dm^3 mol^{-1} s^{-1}, k°_{21}(H_3edta$^-$, spontaneous)$=4.80\times10^{-2}$ dm^3 mol^{-1} s^{-1}, k_{21}(H_3edta$^-$, Na^+catalyzed)$=0.48$ dm^9 mol^{-3} s^{-1}, k°_{22}(H_2edta^{2-}, spontaneous)$=0.21$ dm^3 mol^{-1} s^{-1}, k_{22}(H_2edta^{2-}, Na^+ catalyzed)$=1.70$ dm^6 mol^{-2} s^{-1}, k°_{23}(Hedta^{3-}, spontaneous)$=1.71$ dm^3 mol^{-1} s^{-1}, k_{23}(Hedta^{3-}, Na^+ catalyzed)$=30.00$ dm^6 mol^{-2} s^{-1}. A plausible mechanism considering an outer-sphere association between the complex and reductant has been suggested where the alkali metal ions are assumed to act as a bridge between the reactants.

The fascinating redox property of the cage molecule, dodecatungstocobaltate(III) has been considered by several groups[1-9] in the past. In recent years, we have shown that alkali metal ions play significant role in the electron-transfer reactions between this heteropolyanion and a series of carboxylates e.g., formate,[10] oxalate,[11] malonate,[12] and citrate.[13]

We now report here another family of carboxylates e.g., iminodiacetate, nitrilotriacetate, and ethylenediaminetetraacetate that give promise of a similarly rich redox chemistry. Previous studies on the oxidation reactions of some of the amine-*N*-carboxylates by cerium(IV) have been carried out[14] at high acidity where the unique species present was in the molecular form. We have paid a particular attention to explore the reactivity of the individual amine-*N*-carboxylate species present under varying pH and obtain a possible relationship in the light of their behavior toward cation catalysis phenomenon leading to the redox process.

Experimental

Materials and Reagents. Potassium salts of dodecatungstocobaltate(III), $[CoW_{12}O_{40}]^{5-}$ and dodecatungstocobaltate(II) $[CoW_{12}O_{40}]^{6-}$, hereafter designated as $Co^{III}W$ and $Co^{II}W$ respectively, have been prepared, characterized and standardised in the same way as reported earlier.[2,15] Doubly recrystallized disodium salt of iminodiacetic acid, Na_2ida (Fluka AG), nitrilotriacetic acid, H_3nta (Fluka AG), and disodium salt of ethylenediaminetetraacetic acid, Na_2H_2edta (BDH AnalaR) have been used to prepare stock solutions.[16] Cation variation studies have been performed using doubly recrystallized sodium perchlorate, sodium nitrate, sodium sulfate, potassium nitrate, and lithium perchlorate. The pH adjustment has been done with the respective acids (perchloric, nitric, and sulfuric) and carbonate free alkali solutions (sodium, potassium, or lithium hydroxide). All solutions have been prepared using doubly distilled water.

Kinetic Studies. A Pye-Unicam SP8-150 spectrophotometer, equipped with a thermostated cell compartment has been used to monitor the reactions by observing the decrease in absorbance at the absorption maximum 388 nm of $Co^{III}W$ ($\varepsilon_{max}=1155\pm5$ dm^3 mol^{-1} cm^{-1}).[2] Identical kinetic results have been obtained when experiments are carried out at 625 nm, the absorption maximum of $Co^{II}W$.[2] Dissolved oxygen has not shown any observable kinetic effect. pH measurements are done with a Systronics (model 335, India) digital pH meter. Temperature has been controlled using a Haake F3 thermostat.

Polymerization Studies. The generation of free radicals during the course of reaction has been tested by the polymerization of acrylonitrile.[10-13] In three separate vials solutions of IDA, NTA, and EDTA (ca. 0.1 mol dm^{-3}) are taken, and the pH of these solutions are adjusted to 4.45, 3.50, and 4.50 respectively. These solutions are then degassed with dinitrogen and acrylonitrile (5 ml 20% v/v) is added to each reaction mixture at room temperature. When the degassed solution of the complex (ca. 2×10^{-4} mol dm^{-3}) is added to

these reaction mixtures, a heavy precipitate appears almost immediately for the EDTA containing mixture and after about 5—10 minutes for NTA and IDA containing solutions. No polymerization of the monomer is observed when acrylonitrile is added separately to solutions of the complex and amine-*N*-carboxylates. This suggests that the reaction proceeds via the generation of free radicals in solution.

Stoichiometry and Reaction Products. To determine the stoichiometry of the reactions, the amine-*N*-carboxylates have been mixed with a large excess of $Co^{III}W$, and then kept under the reaction conditions, ($(1-5)\times10^{-4}$ mol dm^{-3} $HClO_4$, $[Na^+]=1.0$ mol dm^{-3}) for several days. In the oxidation of iminodiacetic acid, one mole of IDA was consumed per two moles of the $Co^{III}W$ complex after ca. two weeks of the reaction. The organic products which have been identified by paper electrophoresis are glycine and formaldehyde. For NTA oxidation, the same stoichiometry 2:1 is obtained, and the organic products are iminodiacetic acid and formaldehyde. In the case of EDTA oxidation, time dependent stoichiometry is obtained which becomes constant at a complex:reductant ratio of 16:1. Analysis of the products of a 1:1 mixture of complex: EDTA shows the presence of a mixture of ethylenediaminediacetic acid (EDDA), formaldehyde and unreacted EDTA. Carbon dioxide has been detected as one of the oxidation products for all the acids. For EDTA oxidation, following the first decarboxylation, several paths for further oxidation are available. These consecutive and concurrent reactions are expected to yield the observed time dependent stoichiometry. The stoichiometric reactions may therefore be depicted as follows

$$2\,Co^{III}W+HN(CH_2COOH)_2 \longrightarrow 2\,Co^{II}W+\text{other products} \quad (1)$$

$$2\,Co^{III}W+N(CH_2COOH)_3 \longrightarrow 2\,Co^{II}W+\text{other products} \quad (2)$$

$$16\,Co^{III}W+(HOOCCH_2)_2NCH_2CH_2N(CH_2COOH)_2 \longrightarrow 16\,Co^{II}W+\text{other products.} \quad (3)$$

A similar time dependent stoichiometry for EDTA oxidation by Ce(IV) has been observed by Hanna et al.[14] However, the elementary process requires two moles of $Co^{III}W$ per mole of amine-*N*-carboxylate represented by a generalized Scheme 1.

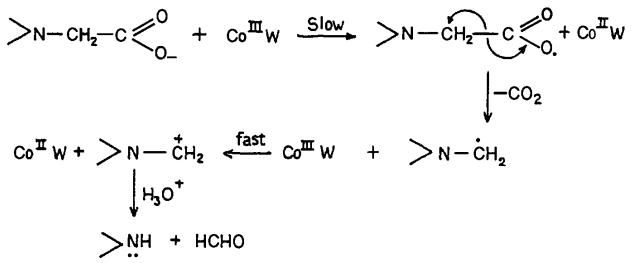

Scheme 1.

Results and Discussions

General Kinetic Features of the Reactions. The kinetics of the oxidation of amine-*N*-polycarboxylates by $Co^{III}W$ has been studied in the pH range 0.05—5.45 at varying alkali metal ion concentrations which have been used as supporting electrolyte. The spectral changes observed during the reactions of $Co^{III}W$ with different carboxylates give a clear isosbestic point near 510 nm in each case. This indicates the absence of appreciable amounts of reaction intermediates. Under pseudo-first-order conditions with excess reductant, the plots of $-\log(A_t-A_\infty)$ vs. time (t), where A_t and A_∞ are the absorbances at times t and infinity respectively, show excellent linearity upto ca. 80—90% of the reactions. Linearity of a plot of k_s vs. $[\text{reductant}]_T$ (where k_s includes the stoiochiometric factor 2 and is defined by $k_s=k_{obs}/2$) holds good at any point in the pH range experimented for the individual amine-*N*-polycarboxylates suggesting a first-order dependence of rate on $[\text{reductant}]_T$. The k_s values for the reduction of $Co^{III}W$ by IDA, NTA, and EDTA are shown in Table 1.

Effect of Specific Ions on Reaction Rates. Reactions between two similarly charged ions are usually found to be catalyzed by a third substance bearing an opposite charge.[17-19] In the reactions of $Co^{III}W$ with the deprotonated forms of the amine-*N*-polycarboxylates, rate acceleration by alkali metal ions have been noticed. Both the change in nature and concentration of supporting electrolytes have considerable effect on the rates. The individual effects of K^+, Na^+, and Li^+ ($=M^+$) on the reaction rate were investigated. In each case, a positive intercept is obtained on the rate axis, and the rate of oxidation is given by the following expression

$$k_{ox}=k^\circ+k[M^+]^n \quad (4)$$

where $k_{ox}=k_s/[L]_T$ ($[L]_T$=total concentration of a particular amine-*N*-polycarboxylate) and n may have values 1 or 2 depending on the nature of M^+. The terms k° and k account for the rate constants of the spontaneous and catalyzed paths respectively. In the cases of IDA, NTA, and EDTA oxidations, a second-order dependence on $[Li^+]$ is obtained. When $[H_3edta]^-$ is the reacting species, the order with respect to $[Na^+]$ is also 2. Dependence on $[K^+]$ is always first-order, and the cation catalytic order[20] is $K^+>Na^+>Li^+$. The kinetic data are presented in Table 2. Equations 5—7 quantitatively describe all of these salt effect results, considering that constant ionic strength was not maintained. The intrinsic effect of ionic strength alone on the reaction was, however, verified by using a mixture of $MClO_4$ (or MNO_3) and M_2SO_4 whereby the total $[M^+]$ was kept constant but ionic strength varied. The results show that the effect of ionic strength on rates for the present system is negligibly small.

To ensure further that the rate enhancement is caused by catalysis and not an ionic strength effect, the rate parameters obtained for $[M^+]$ variation has been subjected to the Bronsted-Bjerrum-Christiansen relationship (Eq. 5) from which $\log k_0'$ defined by Eq. 6[21] has been calculated by using a value of +5 for Z_AZ_B

Table 1. Values of k_s[a] for the Reduction of $Co^{III}W$ by Iminodiacetate, Nitrilotriacetate, and Ethylenediaminetetraacetate

$[IDA]_T$	$10^5 \times k_s$[b]	$10^2 \times [NTA]_T$	$10^4 \times k_s$[c]	$10^2 \times [EDTA]_T$	$10^4 \times k_s$[d]
mol dm^{-3}	s^{-1}	mol dm^{-3}	s^{-1}	mol dm^{-3}	s^{-1}
0.02	1.25	0.40	2.00	0.20	0.48
0.04	1.75	0.70	3.42	0.40	1.06
0.06	2.90	1.00	4.51	0.60	1.71
0.08	3.60	1.20	5.23	0.80	2.25
0.10	4.30	1.60	7.41	1.00	2.58
0.20	8.45				
0.30	12.10				

a) In all cases, the k_s values are reproducible by ±3%, $[Co^{III}W]$=0.0002 mol dm^{-3}. b) pH=4.45, temp=50 °C, $[Na^+]$=1.00 mol dm^{-3}. c) pH=3.90, temp=30 °C, $[Na^+]$=0.90 mol dm^{-3}. d) pH=1.10, temp=15 °C, $[Na^+]$=0.40 mol dm^{-3}.

Table 2. Variation of Alkali Metal Ions for the Reaction of Iminodiacetate, Nitrilotriacetate, and Ethylenediaminetetraacetate with $Co^{III}W$. $[Co^{III}W]$=0.0002 mol dm^{-3}

Medium	$[M^+]$	$10^4 \times k_s$[a]	$10^4 \times k_s$[b]	$10^3 \times k_s$[c]
	mol dm^{-3}	s^{-1}	s^{-1}	s^{-1}
$LiClO_4$	0.20	0.23		
	0.30		1.07	1.30
	0.50	0.62		
	0.60		2.01	2.41
	0.80	1.20	3.33	3.37
	1.00	1.70	4.65	5.14
	1.20	2.46	6.42	7.22
	1.60	4.20		
$NaClO_4$	0.20	0.21		2.22
	0.30		1.85	
	0.40			3.15
	0.50	0.42		
	0.60		3.12	4.69
	0.80	0.65		6.27
	0.90		4.51	
	1.00	0.84		7.41
	1.20	1.00	5.62	
	1.50		6.45	
	1.60	1.20		
	2.00	1.42		
Na_2SO_4	0.60		3.14	4.80
	1.00	0.86		7.55
	1.20	1.00	5.65	
KNO_3	0.20	0.33	2.06	2.62
	0.40		3.53	4.38
	0.50	0.77		
	0.60		5.30	6.01
	0.80	1.04	6.47	7.67
	1.00	1.26	7.54	8.43
	1.20	1.46		
	1.60	1.81		
	2.00	2.40		

a) pH=4.45, temp=50 °C, $[IDA]_T$=0.20 mol dm^{-3}. b) pH=3.90, temp=30 °C, $[NTA]_T$=0.01 mol dm^{-3}. c) pH=4.50, temp=15 °C, $[EDTA]_T$=0.003 mol dm^{-3}.

and a theoretical value[22] of −0.504 for the constant A.

$$\log k_{ox} = \log k_0 + 2AZ_AZ_B \frac{\sqrt{I}}{1+\sqrt{I}} + BI \qquad (5)$$

$$\log k_0' = \log k_{ox} - 2AZ_AZ_B \frac{\sqrt{I}}{1+\sqrt{I}} \qquad (6)$$

Combining these two equations, we get

$$\log k_0' = \log k_0 + BI. \qquad (7)$$

Judging from a simple electrostatic approach, based on the Bronsted-Christiansen-Scatchard equation (Eq. 7),[23] all points should fall on straight line very close together, because the coefficient B should depend mainly on the nature of the ions of opposite signs to that of the reactants.[24] Although this relation has been verified for several reactions, for the present system the plot of $\log k_0'$ vs. I deviates from linearity for each of the cations experimented (Fig. 1). Inter-

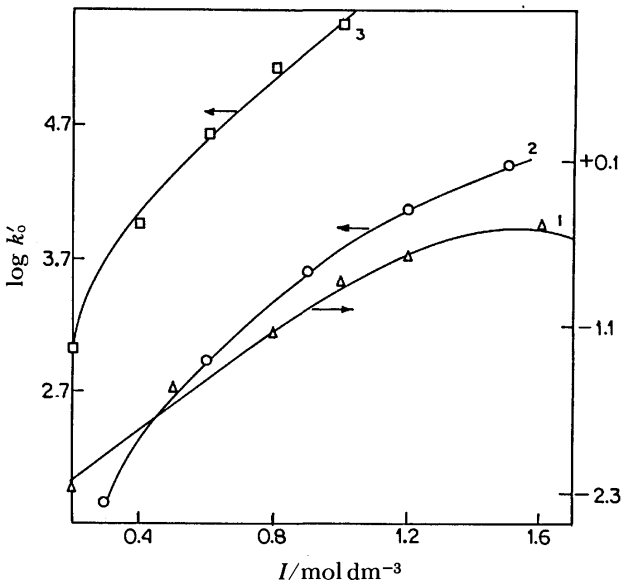

Fig. 1. A plot of $\log k_0'$/vs. I (calculated from $[Na^+]$ variation data for the reactions of $Co^{III}W$ with 1) iminodiacetate at pH 4.45, $[IDA]_T$=0.20 mol dm^{-3} and temperature 50 °C, 2) nitrilotriacetate at pH 3.90, $[NTA]_T$=0.01 mol dm^{-3} and temperature 30 °C, and 3) ethylenediaminetetraacetate at pH 4.50, $[EDTA]_T$=0.003 mol dm^{-3} and temperature 15 °C.

pretation of such deviation obviously requires some specific catalytic intervention by M^+, possibly through a combination of reduction of anion-anion repulsion and facilitation of actual electron transfer through a superexchange type process.[25,26]

The foregoing discussions lead us to believe that the reactions of $Co^{III}W$ with the amine-*N*-polycarboxylates take place in two pathways—a spontaneous and an alkali metal ion catalyzed path. Considering the fact that the heteropolyanion under study is a substitution inert species, the sequence of reactions may be described by assuming an outer-sphere association between the reactants. In general, the mechanism may be depicted as follows

$$Co^{III}W^{5-}+H_nA \rightleftarrows Co^{III}W^{5-},H_nA \xrightarrow{k^\circ} Co^{II}W^{6-}+\text{free readical}_1. \quad (8)$$

The above equation describes the reactions of molecular species of the acids (H_nA). For the anionic forms, the spontaneous path would be the same as in above, and the catalyzed path would incorporate M^+ in the rate-determining step as follows[27]

$$Co^{III}W^{5-}+H_{n-m}A^{m-} \rightleftarrows Co^{III}W^{5-},\ H_{n-m}A^{m-} \xrightarrow{k} Co^{II}W^{6-}+\text{free radical}_2 \quad (9)$$

$$Co^{III}W^{5-}+M^+ +H_{n-m}A^{m-} \rightleftarrows Co^{III}W^{5-}\cdots M^+\cdots H_{n-m}A^{m-} \xrightarrow{k} Co^{II}W^{6-}+\text{free radical}_2. \quad (10)$$

The second order dependence on $[M^+]$ may be explained by incorporating another M^+ in the transition state, i.e., the transition state may be a doubly bridged species of the types

$$MCo^{III}W^{4-} \ldots M^+ \ldots H_{n-m}A^{m-} \quad \text{or} \quad Co^{III}W^{5-}\begin{matrix} M^+ \\ H_{n-m}A^{m-} \\ M^+ \end{matrix}.$$

(A) (B)

A recent vibration spectral study[28] of ionic association has suggested the formation of (B) type of species of mixed aggregates between lithium thiocyanate and lithium halides in nonaqueous solvents.

Reactivities of Different Amine-*N*-polycarboxylate Species. Determination of reactivities of different reacting species present in a reaction mixture is one of the major criteria for the elucidation and interpretation of kinetic data. So an attempt has been made to identify the possible reactants under given conditions and to determine their reactivities. For all the acids and their anions, plots of k_s vs. [reductant]$_T$ where the subscript T denotes the total concentration of any particular amine-*N*-polycarboxylate give straight lines passing through the origin ensuing a first-order dependence of the rate on the reductant concentrations. The rate parameters corresponding to the oxidation of molecular forms of the acids have thus been determined directly from the slope of the plot of k_s vs. [reductant]$_T$ at pH 0.05 for NTA and at pH 0.50 for EDTA. Since the reactions with the anionic amine-*N*-polycarboxylates are catalyzed by alkali metal ions, the rate parameters corresponding to the spontaneous and catalyzed paths have been evaluated by considering the dissociation constants of the acids and identifying the reaction species in solution. For the oxidation of iminodiacetate, though the spontaneous (k°) and catalyzed (k) paths have been evaluated from a plot of $k_{ox}(=k_s/[\text{reductant}])$ vs. $[Na^+]$, the reactivity of the molecular form could not be determined, owing to its extremely slow reaction and poor solubility in water. However, for nitrilotriacetate oxidation, H_3nta is reasonably soluble in aqueous medium and its reactivity (k°_{10}) has been determined by plotting k_s vs. [H_3nta] at pH 0.05. Since the pK_1, pK_2, and pK_3 values of H_3nta are 1.70, 2.40, and 9.67 respectively,[29] rate parameters (k°_{12} and k_{12}) corresponding to the oxidation of $[Hnta]^{2-}$ have been obtained by plotting the values of $k_s/[Hnta^{2-}]$ vs. $[Na^+]$ at pH 3.90±0.02. To determine the reactivity of the monoanionic species (H_2nta^-), a set of experiments have been carried out at pH 1.05±0.02 (where the reacting species are H_3nta and H_2nta^-) varying $[Na^+]$. Utilizing these k_{obs} values, k°_{10} and K_1 (the first acid dissociation constant of H_3nta), the reactivities of the catalyzed (k_{11}) and spontaneous (k°_{11}) paths of $[H_2nta]^-$ have been evaluated from the slope and intercept of the plot of left hand side (LHS) vs. $[Na^+]$ (Fig. 2) in Eq. 11,

$$\frac{k_s(K_1+[H^+])-L_T[H^+]k^\circ_{10}}{K_1L_T} = k^\circ_{11}+k_{11}[Na^+] \quad (11)$$

where L_T denotes the total amount of nitrilotriacetate added. The values of the rate parameters are shown in Table 3.

A similar approach has been followed to evaluate the reactivities of the EDTA. A series of kinetic experiments were carried out at constant $[Co^{III}W]=2\times10^{-4}$ mol dm^{-3}, $[EDTA]_T=(2-3)\times10^{-3}$ mol dm^{-3} but at varying pH and $[Na^+]$. (i) At pH 0.50, kinetic studies have been carried out by varying $[EDTA]_T$ with $[Co^{III}W]=2\times10^{-4}$ mol dm^{-3}. From the slope of k_s vs. $[EDTA]_T$ plot, we can get k°_{20}, the reactivity of H_4edta. (ii) At pH 1.10±0.02 kinetic studies have been carried out by varying $[Na^+]$ at constant $[EDTA]_T=2\times10^{-3}$ mol dm^{-3} and $[Co^{III}W]=2\times10^{-4}$ mol dm^{-3}. It is to be noted here that the acid dissociation constants of H_4edta are given by pK_1'=1.99, pK_2'=2.67, pK_3'=6.16, and pK_4'=10.26 respectively,[30] and at pH 1.10, the species taking part in the reaction are H_4edta (k°_{20}) and $[H_3edta]^-$ (k°_{21} and k_{21}). Utilizing the k_s values at pH 1.10, K_1' and k°_{20}, we can evaluate the values of k°_{21} and k_{21} from the slope and intercept of the plot of LHS vs. $[Na^+]^2$ of Eq. 12

$$\frac{k_s(K_1'+[H^+])-L_T[H^+]k^\circ_{20}}{K_1'L_T} = k^\circ_{21}+k_{21}[Na^+]^2 \quad (12)$$

The evaluated parameters are shown in Table 3. (iii) At pH 4.50 ± 0.02, a set of kinetic experiments has

Table 3. Kinetic Data for the Reaction of $Co^{III}W$ with Iminodiacetate, Nitrilotriacetate, and Ethylenediaminetetraacetate at Varying $[Na^+]$ under Different pH

	IDA	NTA			EDTA			
pH	4.45	0.05	1.05	3.90	0.50	1.10	4.50	5.45
$[Na^+]$/ mol dm^3	10^4k_s/ [IDA]/ dm^3 mol^{-1} s^{-1}	10^3k_s/ [NTA]/ dm^3 mol^{-1} s^{-1}	10^2k_s/ [NTA]/ dm^3 mol^{-1} s^{-1}	10^2k_s/ [NTA]/ dm^3 mol^{-1} s^{-1}	10^2k_s/ [EDTA]/ dm^3 mol^{-1} s^{-1}	10^2k_s/ [EDTA]/ dm^3 mol^{-1} s^{-1}	k_s/ [EDTA]/ dm^3 mol^{-1} s^{-1}	$10k_s$/ [EDTA]/ dm^3 mol^{-1} s^{-1}
0.10								1.16
0.20	1.03	1.09				1.20	0.74	1.69
0.30			0.43	1.83	0.71			2.22
0.40						2.42	1.05	2.96
0.50	2.11	1.11			0.69			3.69
0.60			0.56	3.12		3.90	1.56	
0.80	3.25	1.13			0.67	5.36	2.09	
0.90			0.84	4.51		6.34		
1.00	4.22						2.47	
1.20	4.98	1.09	1.01	5.62	0.65			
1.50		1.13	1.06	6.45				
1.60	6.00							
2.00	7.10							

k°=4.70×10^{-5} dm^{3}mol^{-1}s^{-1}
k_1=3.44×10^{-4} dm^{6}mol^{-2}s^{-1}

k°_{10}=1.11×10^{-3}dm^{3}mol^{-1}s^{-1}
k°_{11}=7.00×10^{-3}dm^{3}mol^{-1}s^{-1}
k_{11}=3.50×10^{-2}dm^{6}mol^{-2}s^{-1}
k°_{12}=7.20×10^{-3}dm^{3}mol^{-1}s^{-1}
k_{12}=4.01×10^{-2}dm^{6}mol^{-2}s^{-1}

k°_{20}=6.80×10^{-3} dm^{3}mol^{-1}s^{-1};
k_{21}=0.48 dm^{9}mol^{-3}s^{-1};
k_{22}=1.70 dm^{6}mol^{-2}s^{-1};
k_{23}=30.00 dm^{6}mol^{-2}s^{-1}

k°_{21}=4.80×10^{-2} dm^{3}mol^{-1}s^{-1}
k°_{22}=0.21 dm^{3}mol^{-1}s^{-1}
k°_{23}=1.71 dm^{3}mol^{-1}s^{-1}

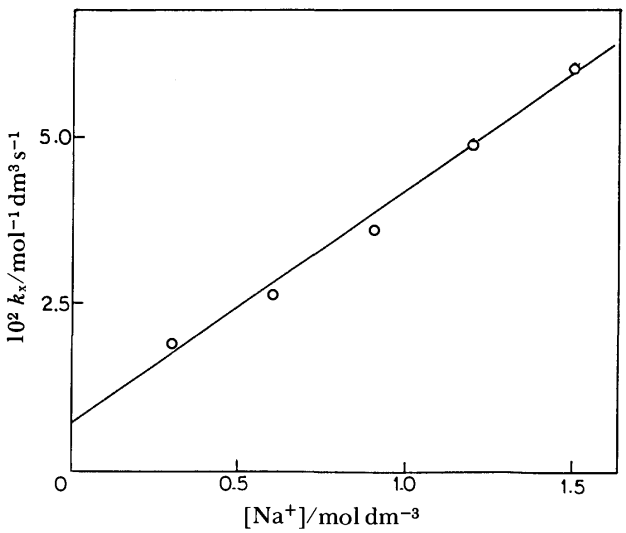

Fig. 2. Representative plot for the evaluation of k°_{11} and k_{11} for H_2nta^- oxidation at pH 1.05±0.02. The ordinate k_x represents the LHS of Eq. 11.

been carried out by varying $[Na^+]$ at a constant $[EDTA]_T$=3×10^{-3} mol dm^{-3} and $[Co^{III}W]$=2×10^{-4} mol dm^{-3}. Considering the second and third acid dissociation constants of H_4edta, the reaction mixture consists of largely $[H_2edta]^{2-}$ species. A plot of k_{ox} vs. $[Na^+]$ gives a straight line from which we can extract a pair of kinetic parameters k°_{22} and k_{22}. We consider these as apparent values since a little amount of $[Hedta]^{3-}$ is also present at this pH. (iv) By varying $[Na^+]$=0.10—0.50 mol dm^{-3}, the rates of the reduction have been followed at $[Co^{III}W]$=2×10^{-4} mol dm^{-3} having $[EDTA]_T$=2×10^{-3} mol dm^{-3} at pH 5.45±0.02. The apparent values of k°_{22} and k_{22} were substituted to the rate equation (Eq.13) to get again a set of apparent k°_{23} and k_{23} values, the uncatalyzed and catalyzed rates for the species $[Hedta]^{3-}$, from a plot of LHS of Eq. 13 vs. $[Na^+]$,

$$\frac{k_s(K_3' + [H^+]) - L_T[H^+](k_{22} + k_{22}[Na^+])}{K_3' L_T} = k^\circ_{23} + k_{23}[Na^+] \quad (13)$$

where L_T denotes the total concentration of EDTA. For the refinement of k°_{22} and k_{22}, the apparent k°_{23} and k_{23} values from Eq. 13 were substituted to the rearranged form Eq. 14 of Eq. 13 but now with the k_s values at pH 4.50.

$$\frac{k_s(K_3' + [H^+]) - K_3' L_T(k^\circ_{23} + k_{23}[Na^+])}{L_T[H^+]} = k^\circ_{22} + k_{22}[Na^+] \quad (14)$$

A new set of k°_{23} and k_{23} can now be generated from Eq. 13 utilizing refined k°_{22} and k_{22} values. The refined parameters obtained by this procedure are listed in Table 3 and the representative plots are shown in Figs. 3(a) and 3(b).

pH-Rate Profiles and the Generalized Rate Equations for NTA and EDTA Oxidations. A general pH variation study has been carried out for both the NTA and EDTA oxidations, and an attempt has been made to match the experimental data with the calculated rate parameters. For this purpose generalized rate expressions have been derived (given by Eqs. 15 and 16) based on the respective reaction schemes (Schemes 2 and 3).

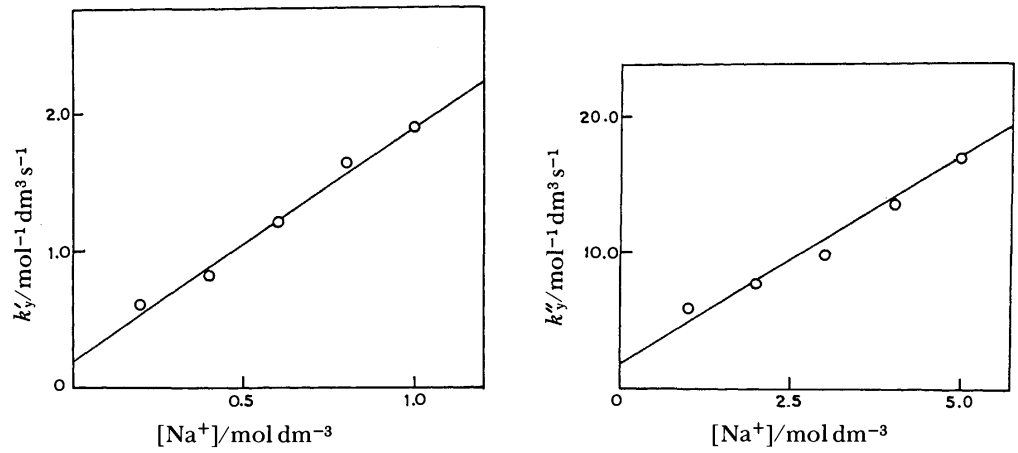

Fig. 3. Representative plots for the evaluation of (a) k°_{22} and k_{22} (refined parameters as presented in Table 3) for H_2edta^{2-} oxidation at pH 4.50±0.02. k'_y represents the LHS of Eq. 14. (b) k°_{23} and k_{23} (refined parameters as presented in Table 3) for $Hedta^{3-}$ oxidation. k''_y denotes the LHS of Eq. 13.

$$k_s = L_T \frac{k^{\circ}_{10}[H^+]^2 + K_1[H^+](k^{\circ}_{11} + k_{11}[Na^+]) + K_1K_2(k^{\circ}_{12} + k_{12}[Na^+])}{[H^+]^2 + K_1[H^+] + K_1K_2} \quad (15)$$

$$Co^{III}W^{5-} + H_3nta \xrightarrow{k^{\circ}_{10}} Co^{II}W^{6-}$$

$$Co^{III}W^{5-} + H_2nta^- \xrightarrow{k^{\circ}_{11}} Co^{II}W^{6-}$$

$$Co^{III}W^{5-} + Na^+ + H_2nta^- \xrightarrow{k_{11}} Co^{II}W^{6-} + Na^+$$

$$Co^{III}W^{5-} + Hnta^{2-} \xrightarrow{k^{\circ}_{12}} Co^{II}W^{6-}$$

$$Co^{III}W^{5-} + Na^+ + Hnta^{2-} \xrightarrow{k_{12}} Co^{II}W^{6-} + Na^+$$

Scheme 2.

and

$$k_s = L_T \frac{k^{\circ}_{20}[H^+]^3 + K'_1[H^+]^2(k^{\circ}_{21} + k_{21}[Na^+]^2) + K'_1K'_2[H^+] + K'_1K'_2K'_3(k^{\circ}_{22} + k_{22}[Na^+])(k^{\circ}_{23} + k_{23}[Na^+])}{[H^+]^3 + K'_1[H^+]^2 + K'_1K'_2[H^+] + K'_1K'_2K'_3} \quad (16)$$

$$Co^{III}W^{5-} + H_4edta \xrightarrow{k_{20}} Co^{II}W^{6-}$$

$$Co^{III}W^{5-} + H_3edta^- \xrightarrow{k^{\circ}_{21}} Co^{II}W^{6-}$$

$$Co^{III}W^{5-} + Na^+ + H_3edta^- \xrightarrow{k_{21}} Co^{II}W^{6-} + Na^+$$

$$Co^{III}W^{5-} + H_2edta^{2-} \xrightarrow{k^{\circ}_{22}} Co^{II}W^{6-}$$

$$Co^{III}W^{5-} + Na^+ + H_2edta^{2-} \xrightarrow{k_{22}} Co^{II}W^{6-} + Na^+$$

$$Co^{III}W^{5-} + Hedta^{3-} \xrightarrow{k^{\circ}_{23}} Co^{II}W^{6-}$$

$$Co^{III}W^{5-} + Na^+ + Hedta^{3-} \xrightarrow{k_{23}} Co^{II}W^{6-} + Na^+$$

Scheme 3.

All the reaction sequences generate respective amine-*N*-polycarboxylate free radicals as stated earlier.

With the help of the various rate parameters included in Table 3, the k_s values at different pH have been calculated. An excellent agreement between the theoretical and experimental values has been obtained (Figs. 4 and 5) and thus the mechanistic formulations are supported strongly.

The pH-rate profile in Fig. 4 for NTA oxidation shows that the rate of reaction increases with increase in pH of the solution at the first phase. It is due to the increase in $[H_2nta^-]$, which has a higher reactivity than H_3nta. Rate saturation starts at pH≈2.80 where $[Hnta]^{2-}$ starts to prevail and no inflexion in the profile is noted below this pH indicating very close reactivities of $[H_2nta]^-$ and $[Hnta]^{2-}$. This is also reflected in the evaluated rate parameters (Table 3). In the case of EDTA, an examination of the pH-rate profile in Fig. 5 reveals that the increase in rate at the first phase is attributable to the increase in $[H_3edta]^-$ reactivity and to a lesser extent by $[H_2edta]^{2-}$ species,

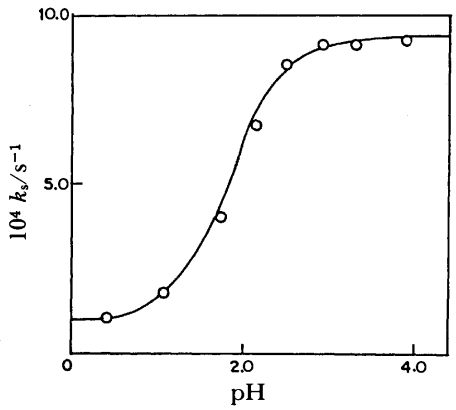

Fig. 4. pH variation results for the reaction of $Co^{III}W$ with nta at $[NTA]_T$=0.02 mol dm^{-3}, $[Na^+]$= 1.00 mol dm^{-3} and temperature=30 °C. Bold line represents the theoretical graph and the experimental values are shown by points O.

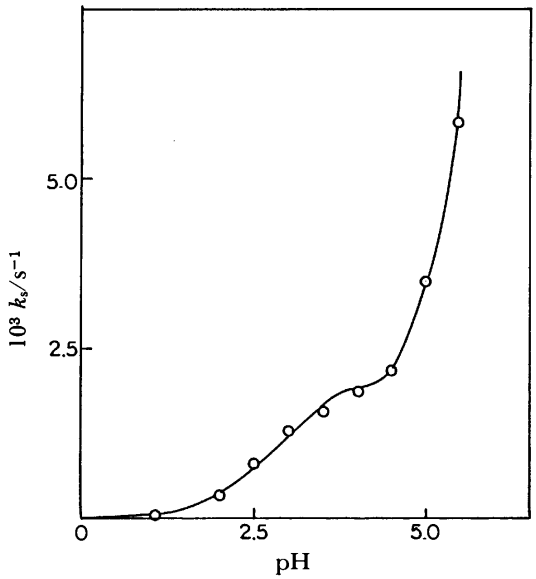

Fig. 5. pH variation results for the reaction of $Co^{III}W$ with edta at $[EDTA]_T=0.002$ mol dm^{-3}, $[Na^+]=0.40$ mol dm^{-3} and temperature=15 °C. The solid line represents the theoretical graph and the experimental values are given by points.

since the pK_1' and pK_2' values are close enough. This trend is followed upto pH≈4.0 where the rate saturation due to both $[H_3edta]^-$ and $[H_2edta]^{2-}$ occurs. This is manifested by a little inflexion in the profile at pH ca. 4.0—4.5. The rate increases sharply beyond pH 4.50, and obviously due to the increased reactivity of $[Hedta]^{3-}$ (Table 3). Since the complex is stable in the pH range 0.0—5.5, kinetic experiments had to be carried out in this range only.

Conclusion

The present study thus provides a systematic approach to the oxidation of amine-*N*-polycarboxylates by $Co^{III}W$. Previous studies on these acids[31-33] have been made in strong acid solutions mainly characterizing a particular species as the reductant. However, in spite of the complications arising out from the overlapping pK values, we could experimentally design and evaluate the different reactivities of various reacting species present in the reaction mixture within our experimental pH range. A comparison of the reactivities of these amine-*N*-polycarboxylates shows a general trend EDTA>NTA>IDA. It has been experimentally recognized that glycine is inert towards $Co^{III}W$. Thus it may be concluded that the increase in number of carboxylate functions for the amino acids increases the reactivities of the molecules i.e., the reducing power. The reactivities of different species for the individual acids have also shown some interesting feature. For EDTA, the trend is $H_4edta<H_3edta^-<H_2edta^{2-}<Hedta^{3-}$. However, for NTA oxidation it is $H_3nta<H_2nta^-\approx Hnta^{2-}$. The above sequences are also true for the catalyzed paths.

The cation catalytic order $K^+>Na^+>Li^+$ obtained in this study is similar to our previous studies[10,11,13] and may be explained by considering the aquated cationic sizes which falls in the order $K^+<Na^+<Li^+$. Thus K^+ will be more effective than Na^+ or Li^+ in bringing the two negatively charged reacting ions together. The absence of catalysis in the oxidation of molecular species is reasonable since the reductant does not carry any charge. But the observation that less effective Li^+ shows a second-order dependence is rather difficult to explain. The greater tendency of the smaller cations to associate with a negatively-charged species[34] is the likely cause for this. Also the second-order dependence on $[Na^+]$ for H_3edta^- in contrast to those observed for H_2edta^{2-} and $Hedta^{3-}$ oxidations seems interesting. Such type of anomaly was encountered in our earlier study in the redox interactions of this heteropolyanion with oxalate.[11] A proper justification of this phenomenon seems difficult because of several factors like size and charge of the reactants, their polarizability as also the size and polarizability of the various cations are associated. An apparent explanation may be put forward by considering the charges of the reactants. As shown in Eqs. 9 and 10, the proposed mechanism involves a cation bridged activated complex where both the complex and the reductant share the alkali metal ion in the transition state. It may be assumed that H_2edta^{2-} and $Hedta^{3-}$ can compete for the Na^+ in the ion pair by virtue of their greater negative charge and utilize it to act as a bridging metal ion in the transition state. Hence the first-order dependence of rate on $[Na^+]$ prevails for these two species. For H_3edta^-, the mononegative charge may not be sufficient to compete for Na^+ in the ion pair. The bridge formation is facilitated by the incorporation of another Na^+ in the ion pair i.e., by reducing the effective charge on the complex, and it results in a second-order dependence on $[Na^+]$.[35]

References

1) P. G. Rasmussen and C. H. Brubaker, *Inorg. Chem.*, **3**, 977 (1964).
2) Z. Amjad, J. Brodovitch, and A. McAuley, *Can. J. Chem.*, **55**, 3581 (1977).
3) G. A. Ayoko and M. A. Olatunji, *Polyhedron*, **2**, 577 (1983).
4) G. A. Ayoko and M. A. Olatunji, *Inorg. Chim. Acta*, **80**, L15 (1983).
5) M. A. Olatunji and G. A. Ayoko, *Polyhedron*, **3**, 191 (1984).
6) G. A. Ayoko and M. A. Olatunji, *Indian J. Chem., Sect. A*, **23**, 769 (1984).
7) G. A. Ayoko and M. A. Olatunji, *Transition Met. Chem.*, **10**, 218 (1985).
8) M. A. Olatunji and G. A. Ayoko, *Bull.de-la Soc. Chim. De France*, **5**, 705 (1985).
9) L. Eberson, *J. Am. Chem. Soc.*, **105**, 3192 (1983).

10) S. K. Saha, M. C. Ghosh, and P. Banerjee, *Inorg. Chim. Acta*, **126**, 29 (1986).
11) S. K. Saha, M. C. Ghosh, and P. Banerjee, *J. Chem. Soc., Dalton Trans.*, **1986**, 1301.
12) S. K. Saha, M. C. Ghosh, and P. Banerjee, Proc. 4th Int. Conf. on the Mechanism of Reactions in Solution, University of Kent, Canterbury (1986), p. 18.
13) S. K. Saha, M. C. Ghosh, and P. Banerjee, *Int. J. Chem. Kinet.*, **20**, 699 (1988).
14) S. B. Hanna, W. R. Carroll, S. A. Attiga, and W. H. Webb, *Z. Naturforsch*, **30B**, 409 (1975).
15) L. C. W. Baker and T. P. McCutcheon, *J. Am. Chem. Soc.*, **78**, 4503 (1956).
16) Although these formulations have been strictly followed when describing the actual species involved in preset pH conditions, designations such as IDA, NTA, and EDTA have also been used in a general way to describe a particular amine-*N*-polycarboxylate without any emphasis to the actual species.
17) Y. A. Majid and K. E. Howlett, *J. Chem. Soc. A*, **1968**, 679.
18) Y. Sulfab, M. S. Al-Obadie, and N. Al-Salem, *Z. Phys. Chem.*, **94**, 77 (1975).
19) R. J. Champion, C. F. Deck, P. King, and A. C. Wahl, *Inorg. Chem.*, **6**, 672 (1967).
20) Though the order $K^+>Na^+>Li^+$ does not hold good for ida oxidation at high $[Li^+]$, at very low $[Li^+]$ where a first-order plot prevails, the above order is valid.
21) E. A. Guggenheim and J. E. Prue, Physicochemical Calculations (Russian Translation), *Izd. Inostr. Lit., Moscow*, **1963**, 450.
22) R. A. Robinson and R. H. Stokes, "Electrolyte Solutions," Butterworths, London (1970), p. 468.
23) E. S. Amis, "Kinetics of Chemical Change in Solution," Macmillan, New York (1949), p. 71.
24) E. A. Guggenheim and L. A. Wigeman, *Proc. R. Soc. London, Ser. A*, **203**, 17 (1950).
25) A. Indelli, G. Nollan, Jr., and E. S. Amis, *J. Am. Chem. Soc.*, **82**, 3233, 3237 (1960).
26) A. Indelli, *Israel J. Chem.*, **9**, 301 (1971).
27) Since the mechanism has been described in a generalized way, the different type of free radicals produced are indicated by their suffixes. It is assumed that free radicals are produced by -COO-H fission in case of molecular species and for the anionic species, it comes from the negative charge of $-COO^-$.
28) P. Goralski and M. Chabanel, *Inorg. Chem.*, **26**, 2169 (1987).
29) G. Anderegg, *Helv. Chim. Acta*, **50**, 2333 (1967).
30) G. Schwarzenbach, R. Gut, and G. Anderegg, *Helv. Chim. Acta*, **37**, 937 (1954).
31) G. N. Rao, *Indian J. Chem.*, **8**, 328 (1970).
32) E. Mentasti, E. Pelizzetti, and G. Saini, *J. Chem. Soc., Dalton Trans.*, **1974**, 1944.
33) R. Varadarajan and M. A. Hossain, *Indian J. Chem., Sect. A*, **18**, 46 (1979).
34) D. M. Druskovich and D. L. Kepert, *J. Chem. Soc., Dalton Trans.*, **1975**, 947.
35) A referee has commented that a higher order dependence on $[Na^+]$ is plausible for electrostatically more favorable species (e.g., H_2edta^{2-} and $Hedta^{3-}$). This is not unlikely, though we could not find such phenomenon even at $[Na^+]\leq 0.50$ mol dm^{-3} with [EDTA]=0.002 mol dm^{-3}. Beyond this $[Na^+]$, experiments could not be carried out by conventional spectrophotometric method owing to rapidity of the reaction.

Synthetic and Spectroscopic Studies of Xanthato-Bridged Heterobimetallic Complexes Containing Diamagnetic and Paramagnetic Metal Ions

Nanhai SINGH,* Nand Kishore SINGH, and Chetna KAW
Chemistry Department, Banaras Hindu University, Varanasi-221005, India
(Received November 8, 1988)

A series of heterobimetallic complexes of the form M[M′(Etxant)$_3$] and M[M′(Etxant)$_3$]$_2$ have been prepared by the reaction of K[M′(Etxant)$_3$] [M′=Ni(II), Cd(II), or Pb(II)] and metal nitrate or sulfate [M=Co(II), Ni(II), Cd(II), Tl(I), Pb(II), or Ag(I), Etxant=ethylxanthate]. These complexes have been characterized by elemental analysis, molecular weight, molar conductance, magnetic susceptibility, (^{1}H, ^{13}C) NMR, electronic, and infrared spectral studies. Magnetic moment and electronic spectral data indicate square planar geometry around Co(II) or Ni(II), except Tl[Ni(Etxant)$_3$] in which Ni(II) is octahedrally coordinated. NMR spectra of M[M′(Etxant)$_3$]$_2$ clearly indicate the presence of two different ethylxanthate moieties, one attached to the diamagnetic Ni(II), Cd(II), or Pb(II) and the other to the paramagnetic Co(II) centre. Electrical conductance values indicate their nonelectrolytic behavior. Interaction of heterobimetallic complexes with different solvent have been studied and solvent characteristics (donor number, dielectric constant, EB (electrovalent) and CB (covalent) parameters) have been related to the structural properties of the complexes. On the basis of these studies, monomeric structure for M[M′(Etxant)$_3$]$_2$ and polymeric structure for M[M′(Etxant)$_3$] have been suggested.

The synthesis and study of heterobimetallic complexes have been the subject of active research over the past few years. The interest in heterobinuclear transition metal complexes has risen sharply in recent years for several reasons.[1-8] The combination of an electron-deficient and an electron-rich metal in a single complex presents the possibility of Lewis acid activation of a substrate molecule bound to the electron rich metal center. This type of cooperative heterobimetallic activation holds potential for applications in catalysis. Heterobinuclear complexes have been used as models for the active sites of many enzyme systems.[9] In addition to enzyme modeling, heteronuclear complexes are of interest in evaluating the factors that contribute to magnetic exchange.[10] Formation of heterobinuclear complexes with bridging ligands as precursor complex is of extreme importance in electron-transfer reaction[11,12] via inner sphere mechanism. Binary and ternary complexes[13,14] of xanthate ion have been extensively studied. Ample work has been done on heterobimetallic complexes of ambidentate ligands, such as SCN^-, $SeCN^-$ etc., involving different donor atoms of these ligands in bridging the two different metal ions. Despite this intensive interest, scarce of work[15,16] has been done on heterobimetallic complexes of dithioligands where two identical sulfur donor atoms are involved in bridging the two different metal ions. We wish to report our investigation on heterobimetallic xanthates of the form M[M′(Etxant)$_3$] and M[M′(Etxant)$_3$]$_2$ containing both univalent and bivalent as well as diamagnetic and paramagnetic metal ions.

Experimental

Material and Methods: All the chemicals used in the preparative work were BDH (AR) or equivalent grades. The solvents were freshly distilled and where necessary dried before use. Potassium ethylxanthate used in the preparative work was prepared by standard literature procedure.[17]

Preparation of the Complexes M[M′(Etxant)$_3$] and M[M′(Etxant)$_3$]$_2$. K[M′(Etxant)$_3$] required for the synthesis of M[M′(Etxant)$_3$] or M[M′(Exant)$_3$]$_2$ [M′=Ni(II), Pb(II), or Cd(II)] was prepared in situ by mixing 25 cm^3 aqueous solution of (2 mmol) potassium ethylxanthate (0.32 g) and (2 mmol) solution/suspension of Ni(Etxant)$_2$ (0.602 g), Cd(Etxant)$_2$ (0.70 g) or Pb(Etxant)$_2$ (0.90 g), in 50 cm^3 acetone/ethanol, following the reported methods.[18,19] M′(Etxant)$_2$ used in the synthesis were prepared by known methods.[13] To the above K[M′(Etxant)$_3$] solution 25 cm^3 (2 mmol/1 mmol) $AgNO_3$ (0.34 g), Tl_2SO_4 (0.50 g), $Pb(NO_3)_2$ (0.33 g), $Co(NO_3)_2 \cdot 6H_2O$ (0.29 g), or $Ni(NO_3)_2 \cdot 6H_2O$ (0.29 g) dissolved in 80:20 water-acetone/water-ethanol (v/v) was gradually added with constant stirring. All the heterobimetallic complexes which precipitated as fine crystalline material were filtered, washed with acetone-water/ethanol-water 50:50 (v/v) mixture and finally with ether, and dried in vacuum. Our attempts to synthesize similar compounds with Cu(II), Fe(II), and Mn(II) were not successful.

Analysis and Physical Measurements: All the complexes were analyzed for their metal contents following standard literature procedures.[20] Sulfur was estimated as barium sulfate. Carbon and hydrogen were determined microanalytically on a Perkin-Elmer 240C model microanalyzer.

The molecular weight of soluble complexes was determined cryoscopically in benzene. The experimental details pertaining to the measurements of electrical conductance, room temperature magnetic susceptibility, recording of electronic and infrared spectra as Nujol mull were the same as described earlier.[16] The absorption spectra of soluble complexes were obtained in $CHCl_3$, THF, DMSO, and pyridine. The infrared spectra were recorded on Perkin-Elmer 783 spectrophotometer. ^{1}H and ^{13}C NMR spectra of the complexes were recorded in $CDCl_3$ while that of potassium ethylxanthate in DMSO-d_6 using TMS as internal reference. The relevant analytical and physicochemical data are give in Tables 1, 2, and 3.

Results and Discussion

The analytical data show the formation of the heterobimetallic xanthates of general formulae M[M′(Etxant)$_3$] or M[M′(Etxant)$_3$]$_2$. The compounds are formed according to the following equations.

[1] M′(Etxant)$_2$+KEtxant ⟶ K[M′(Etxant)$_3$]

[2] K[M′(Etxant)$_2$]+MNO_3/M_2SO_4 ⟶ M[M′(Etxant)$_3$]$_2$+KNO_3/K_2SO_4

Table 1. Analytical Data, Magnetic Moment, Molecular Weight and Molar Conductance of Heterobimetallic Xanthates

Complex	Color	Decomp temp/°C	Found (Calcd)/%					μ_{eff}/ B.M.	Molecular weight	S cm^2 mol^{-1} in nitrobenzene
			M′	M	C	H	S			
Ag[Ni(Etxant)$_3$]	Yellowish green	144	10.89 (11.09)	20.65 (20.37)	20.50 (20.38)	2.90 (2.83)	36.02 (36.24)	dia.	—	—
Tl[Ni(Etxant)$_3$]	Sky blue	>250	8.96 (9.37)	32.03 (32.63)	17.40 (17.25)	2.45 (2.39)	29.75 (30.66)	2.90	—	—
Pb[Ni(Etxant)$_3$]$_2$	Dark brown	114	11.61 (11.18)	19.98 (19.73)	20.62 (20.57)	2.95 (2.85)	36.06 (36.57)	dia.	1010.00 (1050.62)	4.95
Co[Ni(Etxant)$_3$]$_2$	Dark brown	110	12.86 (13.01)	6.62 (6.52)	23.98 (23.94)	3.25 (3.32)	41.82 (42.56)	2.94	870.50 (902.35)	1.40
Ni[Pb(Etxant)$_3$]$_2$	Brown	116	34.27 (34.56)	4.34 (4.89)	18.35 (18.02)	2.58 (2.50)	31.58 (32.04)	dia.	1122.40 (1199.11)	3.19
Co[Pb(Etxant)$_3$]$_2$	Green	113	34.22 (34.46)	4.53 (4.91)	18.40 (18.02)	2.65 (2.50)	31.86 (32.02)	2.95	1125.40 (1199.33)	1.10
Ag[Pb(Etxant)$_3$]	Yellow	116	29.36 (30.56)	15.55 (15.92)	15.75 (15.93)	2.40 (2.21)	28.01 (28.32)	—	—	—
Tl[Pb(Etxant)$_3$]	White	>250	26.48 (26.76)	25.93 (26.38)	13.80 (13.94)	2.02 (1.93)	23.95 (24.79)	—	—	—
Ag[Cd(Etxant)$_3$]	Yellow	129	18.85 (19.27)	18.03 (18.51)	18.65 (18.51)	2.68 (2.57)	32.06 (32.92)	—	—	—
Co[Cd(Etxant)$_3$]$_2$	Green	158	21.96 (22.25)	5.62 (5.84)	21.55 (21.44)	3.02 (2.97)	37.98 (38.07)	2.88	970.00 (1009.73)	1.76
Pb[Cd(Etxant)$_3$]$_2$	Light yellow	125	19.02 (19.41)	17.88 (17.89)	18.70 (18.66)	2.65 (2.59)	32.89 (33.16)	—	1095.50 (1158.00)	2.42

Table 2. Electronic Spectral Bands and Their Assignments in Heterobimetallic Complexes

Complex	Medium	B and Maxima[a]/cm^{-1}		Assignment
Ti[Ni(Etxant)$_3$]	Nujol	8700,	14080—15400, 26300	$^3A_{2g}\rightarrow{}^3T_{2g}(F),\rightarrow{}^3T_{1g}(F),\rightarrow{}^3T_{1g}(P)$
Ag[Ni(Etxant)$_3$]	Nujol		14800, 21000, 25000	$^1A_{1g}\rightarrow{}^1B_{1g},\rightarrow{}^1A_{2g}$
Pb[Ni(Etxant)$_3$]$_2$	Nujol		16000, 20600, 23800	$^1A_{1g}\rightarrow{}^1B_{1g},\rightarrow{}^2A_{2g}$
	$CHCl_3$		15380(400), 20600(475)	
	THF		15800(350), 20800(400)	
	DMSO	9350(85),	14810(140)	$^3A_{2g}\rightarrow{}^3T_{2g}(F),\rightarrow{}^3T_{1g}(F)$
	Pyridine	10310(85),	15870(130)	$^3A_{2g}\rightarrow{}^3T_{2g}(F),\rightarrow{}^3T_{1g}(F)$
Ni[Pb(Etxant)$_3$]$_2$	Nujol		16000, 20600, 23800	$^1A_{1g}\rightarrow{}^1B_{1g},\rightarrow{}^1A_{2g}$
	$CHCl_3$		15380(330), 20800(224)	
	THF		15870(360), 20830(232)	
	DMSO	9400(80),	15000(120)	$^3A_{2g}\rightarrow{}^3T_{2g}(F),\rightarrow{}^3T_{1g}(F)$
	Pyridine	10600(100),	16100(150)	$^3A_{2g}\rightarrow{}^3T_{2g}(F),\rightarrow{}^3T_{1g}(F)$
Co[Pb(Etxant)$_3$]$_2$	Nujol	6500,	11000, 15800, 20600	$^2A_{1g}\rightarrow{}^2E'_g,\rightarrow{}^2E_{2g}$
	$CHCl_3$		11760(55), 15870(390), 20830(500)	
	THF		11760(45), 15870(390), 20830(500)	
	DMSO		11760(60), 16000(385), 20830(540)	
	Pyridine		11750(60), 16000(550), 20580(640)	
Co[Cd(Etxant)$_3$]$_2$	Nujol	6300,	10800, 1600, 20400	$^2A_{1g}\rightarrow{}^2E'_g,\rightarrow{}^2E_g$
	$CHCl_3$		11700(50), 15800(360), 20800(450)	
	THF		11700(45), 15800(350), 20800(430)	
	DMSO		11750(50), 16100(320), 20750(500)	
	Pyridine		11760(55), 15870(310), 20830(420)	
Co[Ni(Etxant)$_3$]$_2$	Nujol	6000,	11700, 15000—16100, 20600, 24000	$^2A_{1g}\rightarrow{}^2E'_g,\rightarrow{}^2E_g$
	$CHCl_3$		12050(75), 15750(350), 20830(400)	
	THF		12120(50), 15750(315), 20830(435)	
	DMSO	9300(120)	15150(220), 21050(300)	
	Pyridine	10200(100)	15870(190), 20830(185)	

a) Molar absorption coefficients are given in parentheses.

Table 3. Selected Infrared Spectral Bands and (^{1}H, ^{13}C) NMR Chemical Shifts of the Complexes

Complex	IR bands/cm^{-1}			^{1}H NMR (δ/ppm)		^{13}C NMR (δ/ppm)	
	ν(C-O)	ν(C⋯S)	ν(M-S)	$-\underline{C}H_3$	$-O\underline{C}H_2$	$-\underline{C}H_3$	$-O\underline{C}H_2$
Co[Cd(Etxant)$_3$]$_2$	1255(m,b)	1030(m)	395(m) 290(w)	1.57t	4.57(5)	13.81	67.07 68.50
Co[Ni(Etxant)$_3$]$_2$	1260(m)	1030(m)	390(m) 380(w)	1.48q	4.57(6)	13.81	67.07 68.48
Co[Pb(Etxant)$_3$]$_2$	1260(m)	1030(m)	390(w) 270(m,b)	1.48t	4.62(5)	13.81	67.07 69.18
Pb[Ni(Etxant)$_3$]$_2$	1260(m)	1020(s)	380(m) 280(w)	1.48t	4.57q	13.81	68.80
Ni[Pb(Etxant)$_3$]$_2$	1250(m)	1025(s)	380(m) 290(w)	1.48t	4.57q	13.81	68.80
Pb[Cd(Etxant)$_3$]$_2$	1210(m,b)	1020(m)	290(w) 275(w)	1.57t	4.57q	13.81	67.07
Tl[Ni(Etxant)$_3$]	1170(m)	1020(w)	395(s) 260(m)	—	—	—	—
Ag[Ni(Etxant)$_3$]	1260(m,b)	1020(s)	380(m) 270(w)	—	—	—	—
Ag[Pb(Etxant)$_3$]	1220(s)	1020(s)	270(w) 260(w)	—	—	—	—
Tl[Pb(Etxant)$_3$]	1200(m,s)	1030(s)	270(w) 265(w)	—	—	—	—
Ag[Cd(Etxant)$_3$]	1220(s)	1020(s)	270(w) 265(w)	—	—	—	—

[3] $2K[M'(Etxant)_3]+M(NO_3)_2 \longrightarrow M[M'(Etxant)_3]_2+2KNO_3$

M′=Ni(II), Pb(II), Cd(II)

M=Ag(I), Tl(I), Ni(II), Co(II), Pb(II).

All the complexes are insoluble in water and common organic solvents, such as ethanol, methanol, acetone, but M[M′(Etxant)$_3$]$_2$ are considerably soluble in chloroform and benzene. M[M′(Etxant)$_3$] are only moderately soluble in nitrobenzene. Poor solubility of M[M′(Etxant)$_3$] indicates their polymeric nature. Electrical conductance value 1.10—4.95 S cm^2 mol^{-1} in 10^{-3} nitrobenzene solution indicate their nonionic nature.[21] The observed molecular weight for M[M′(Etxant)$_3$]$_2$ is well in the range of their monomeric formulation.

Magnetic and Spectroscopic (Electronic, Infrared, ^{1}H and ^{13}C NMR) Studies: The diamagnetism of Ag[Ni(Etxant)$_3$], Pb[Ni(Etxant)$_3$]$_2$, and Ni[Pb(Etxant)$_3$]$_2$ indicate square planar geometry around Ni(II).

Three bands are observed in the visible spectral region of these compounds in 14800—16000 (ν_1), 20600—21000(ν_2), and 23800—25000 cm^{-1} (ν_3) regions which are well in the range reported for square-planar Ni(II) xanthate.[22] The first two bands in each case may be assigned to $^1A_{1g}\rightarrow{}^1B_{1g}$ and $^1A_{1g}\rightarrow{}^1A_{2g}$ transitions[23] respectively in D_{4h} symmetry around Ni(II). The single electron parameter Δ_1 for these complexes have been calculated following the method of Gray and Ballhausen[24] as modified by Shupack,[25] assuming $F_2=10F_4=800$ cm^{-1} in the equation $\Delta_1=35F_4+\nu_1$. The Δ_1 values thus obtained for the above Ni(II) complexes are almost of the same magnitude as for a number of square-planar Ni(II) complexes of dithioligands[26,27] such as dithiocarbamate, isomaleonitrile dithiolate, and trithiocarbonate.

The magnetic moment of 2.90 BM and the presence of electronic spectral bands at 8700; 14080, 15400 (doublet), and 26300 cm^{-1} suggest octahedral coordination around Ni(II) in Tl[Ni(Etxant)$_3$]. These bands may be assigned to $^3A_{2g}\rightarrow{}^3T_{2g}$, $^3A_{2g}\rightarrow{}^3T_{1g}$, and $^3A_{2g}\rightarrow{}^3T_{1g}$(P) transitions[28] respectively. Splitting in ν_2 band is observed because the D_q/B value is nearly unity which is mainly due to mechanism of spin-orbit coupling where spin-forbidden transition has stolen intensity from spin-allowed transition. The μ_{eff} values (2.88—2.95 BM) for Co[Pb(Etxant)$_3$]$_2$, Co[Cd(Etxant)$_3$]$_2$, and Co[Ni(Etxant)$_3$]$_2$ and electronic spectral bands observed in the region 6000—6500, 10800—11000, 15900—16000, and 20400—20600 cm^{-1} suggest square-planar geometry around Co(II). The magnetic moments are almost temperature independent down to 90 K ruling out any possibility of antiferromagnetic interaction in these complexes. The first and third bands are assigned to $^2A_{1g}\rightarrow{}^2E'_g$ and $^2A_{1g}\rightarrow{}^2E_{2g}$ transitions respectively.[29,30] As suggested by Nishida and Kida,[30] the most characteristic band at ca. 11000 cm^{-1} for square-planar Co(II) complexes may be taken as equal to 15B which gives the value of B=720 cm^{-1}. Appearance of a broad band between 14880—16100 cm^{-1} and an additional band at 24000 cm^{-1} in Co[Ni(Etxant)$_3$]$_2$ similar to other heterobimetallic complexes of Ni(II) in the present series suggests square-planar geometry around Ni(II).

The bands occurring in the infrared spectra of M[M′(Etxant)$_3$] and M[M′(Etxant)$_3$]$_2$ in 1200—1260

cm^{-1} and 1020—1030 cm^{-1} regions are consistently assigned to ν(C-O) and ν(C=S) modes respectively,[13,16,19] which are characteristic of the C_2H_5-O-CS_2^- group. ν(C-O) is observed at a lower frequency (ca. 1170 cm^{-1}) in Tl[Ni(Etxant)$_3$]. This marked negative shift in ν(C-O) is probably due to octahedral geometry around nickel(II) as observed[18] with other octahedral complexes. The occurrence of a single band for ν(C⋯S) and its position indicate uninegative bidentate behavior of xanthate ion[31] in the above complexes.

In all the complexes, the bands occurring below 400 cm^{-1} have been tentatively assigned[18,32] to ν(M-S) modes, the lower one may be due to Ag-S, Tl-S, Pb-S and the higher one due to Co-S or Ni-S stretching modes respectively.

The purity and composition of the complexes have been confirmed by ^{1}H and ^{13}C NMR spectral studies. Proton NMR spectrum of potassium ethylxanthate yields a triplet at δ 1.32 and a quartet at δ 4.33 due to -CH_3 and -OCH_2 protons respectively. The spectra of M[M′(Etxant)$_3$]$_2$ [M=Ni(II), Pb(II); M′=Ni(II), Pb(II), Cd(II)], where both metal centers are diamagnetic show a triplet at δ 1.48—1.57 and a quartet at δ 4.57—4.62 (Fig. 1), in the intensity ratio of 3 : 2 for -CH_3 and -OCH_2 protons respectively. The downfield shifts observed for these protons as compared to the ionic potassium ethylxanthate clearly indicate the deshielding of ethoxyl protons in these complexes. For paramagnetic compounds, Co[Ni(Etxant)$_3$]$_2$, Co[Pb(Etxant)$_3$]$_2$, and Co[Cd(Etxant)$_3$]$_2$, the number of peaks (Fig. 1) for -OCH_2 protons are 5 or 6. The increased number of peaks may be due to the mixing of -OCH_2 protons attached to the paramagnetic Co(II) and the diamagnetic Ni(II), Cd(II), or Pb(II) in the heterobimetallic compounds.

^{13}C NMR spectra of the diamagnetic complexes give two signals at δ 13.8 and 67.1—68.6 for -CH_3 and -CH_2 carbons which are comparable to those reported for $Me_2AuS_2COC_2H_5$[33] in which ethylxanthate group is bidentate. However, the spectra of paramagnetic compounds (Fig. 2) show splitting in the peak appearing at δ ca. 67 due to -OCH_2 carbon indicating the presence of two different types of ethoxylcarbon arising from the influence of the unpaired electron of Co(II). But such splitting is absent in case of diamagnetic compounds.

These observations clearly indicate the presence of two different ethylxanthate moieties, one of which attached to the diamagnetic Ni(II), Pb(II), or Cd(II) and the other to the paramagnetic Co(II) center.

Effect of Solvents on the Complexes: While describing their bonding and structure on the basis of various physicochemical studies, it was considered worthwhile to see the effect of solvents on the complexes. Accordingly, they have been treated with a number of solvent and their electronic spectra studied. The effect of solvents on Co(II) and Ni(II) heterobimetallic complexes have been related to their donor numbers, dielectric constant and CB (covalent) and EB (electrovalent) parameters. The results of absorption maxima given in Table 2 show the following:

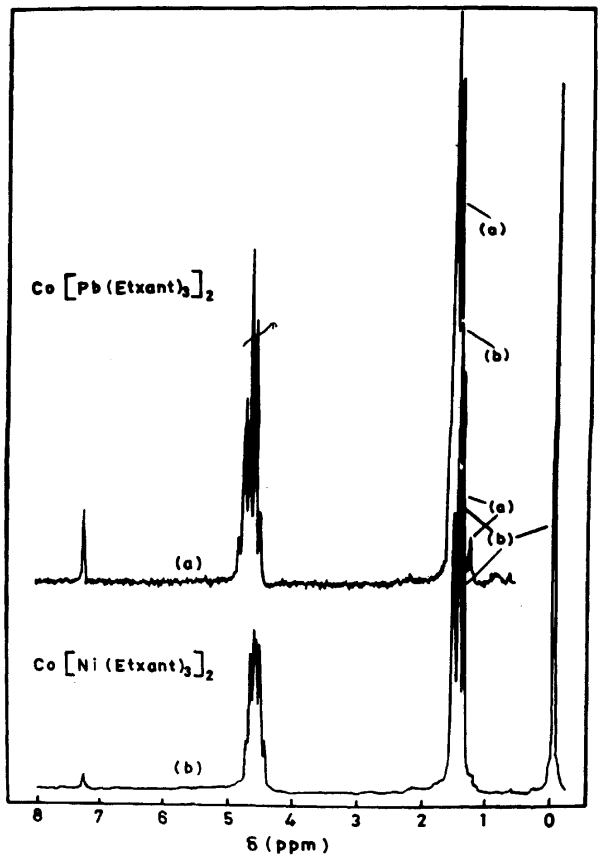

Fig. 1. ^{1}H NMR spectrum in $CDCl_3$.

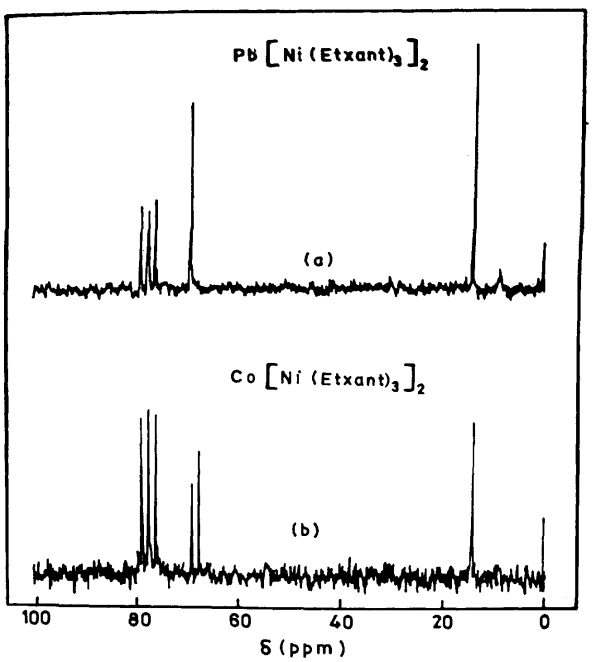

Fig. 2. ^{13}C NMR spectrum in $CDCl_3$.

(1) The complexes Pb[Ni(Etxant)$_3$]$_2$, Ni[Pb(Etxant)$_3$]$_2$, and Co[Ni(Etxant)$_3$]$_2$ are fairly soluble in solvents, such as DMSO and pyridine, having donor number (29.8—33.1) and dielectric constant (12.3—45.0) with a change in color due to coordination of the solvent molecules. The positions of their band maxima and molar absorption coefficient at maximum (Table 2) in DMSO and pyridine clearly indicate that these solvents are coordinated to NiS_4 chromophore bringing octahedral stereochemistry around Ni(II). Co[Pb(Etxant)$_3$]$_2$ and Co[Cd(Etxant)$_3$]$_2$ are also highly soluble in the above solvents. The wavenumbers of their absorption maximum are indicative of square planar geometry around Co(II) ruling out any possibility of solvent coordination to Co(II).

(2) All the above complexes are also soluble in THF with donor number (20.0) and dielectric constant (7.3) but, as indicated by their band maxima, it does not coordinate to either Co(II) or Ni(II).

(3) The absorption maxima of the above complexes recorded in nonpolar solvents like chloroform and benzene with donor number (0.1) and dielectric constant (2.3—4.8) indicate their noncoordinating behavior.

(4) Solvents like ethanol, methanol, acetone, acetonitrile, and water having donor number (14.0—20.0) and dielectric constant (20.7—81.7) neither dissolve nor coordinate but on boiling they decompose M[M′(Etxant)$_3$] because of the disruption of -S-C-S- bridge in their polymeric structure.

Based on chemical composition and physicochemical studies, dimeric structure (**1**) and polymeric structures (**2** and **3**) are proposed for the complexes subject to final confirmation by single crystal X-ray analysis. The arrangement of xanthate group around Ag(I) is nonlinear possibly due to d-electron contribution to the expected linear sp-hybridization scheme as observed when sulfur is the donor atom.[34,35] Zn(II), Cd(II), and Pb(II) presumably possess their preferential tetrahedral geometry as in the case of simple xanthate complexes.[36]

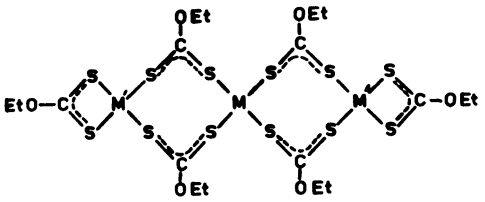

1. M [M′(Etxant)$_3$]$_2$

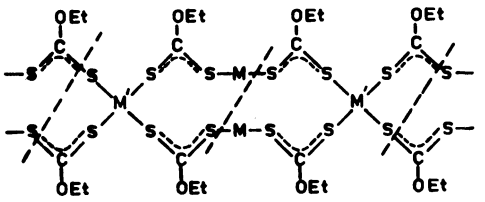

2. M[M′(Etxant)$_3$]

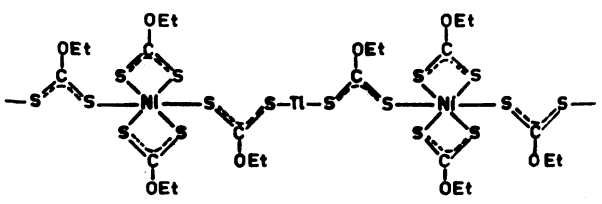

3. Tl[Ni(Etxant)$_3$]

Conclusion

On the basis of the foregoing studies, following conclusions are drawn regarding the present series of complexes:

(1) On the basis of the solubility and molecular weight determination, the complexes are categorised in two classes, viz., monomeric M[M′(Etxant)$_3$]$_2$ and polymeric M[M′(Etxant)$_3$].

(2) Borderline metal ions Ni(II), Co(II), Pb(II), when present together in a complex, form monomeric xanthato-bridged complex, M[M′(Etxant)$_3$]$_2$ with soft sulfur donor atoms of the xanthate moiety. However, if one of the metal ions is soft and the other is soft or borderline, e.g. Ni(II), Ag(I); Ni(II), Tl(I); Ag(I), Pb(II); Tl(I), Pb(II), polymeric bridged complexes are formed.

(3) The low-spin planar geometry of Co(II) and Ni(II) are stabilized in their heterobimetallic complexes except in Tl[Ni(Etxant)$_3$].

(4) As observed by absorption maxima and molar absorption coefficient data, solvents like pyridine and DMSO having higher donor number[37] and CB parameter (2.85—6.40)[38] show coordinating ability towards M[Ni(Etxant)$_3$]$_2$ and Ni[Pb(Etxant)$_3$]$_2$.

(5) Infrared spectral studies invariably indicate uninegative bidentate behavior of xanthate group.

(6) NMR data clearly indicate two types of ethylxanthate in the paramagnetic complexes.

The authors thank the Head of the Department of Chemistry for providing the necessary laboratory facilities. One of the authors (C.K.) is also thankful to C. S. I. R. for financial support.

References

1) G. S. White and D. W. Stephan, *Inorg. Chem.*, **24**, 1499 (1985).
2) C. P. Gasey, R. E. Palermo, and A. L. Rheingold, *J. Am. Chem. Soc.*, **108**, 549 (1986).
3) S. J. Naito, *J. Chem. Soc., Chem. Commun.*, **1985**, 1212.
4) D. H. Berry, J. E. Bercaw, A. J. Jircitano, and K. B. Mertes, *J. Am. Chem. Soc.*, **104**, 4712 (1982).
5) C. J. Ruffing and T. B. Rauchfuss, *Organometallics*, **4**, 524 (1985).
6) I. E. Maxwell, *Adv. Catal.*, **30**, 1 (1981).
7) T. A. Wark and D. W. Stephan, *Inorg. Chem.*, **26**, 363

(1987).
8) A. B. Greg and E. Sinn, *Inorg. Chem.*, **26**, 1529 (1987).
9) W.M. Davis, J. C. Dewan, and S. J. Lippard, *Inorg. Chem.*, **20**, 2928 (1981).
10) E. Sinn, "In Biochemical Inorganic Copper Chemistry," ed by K. D. Karlin and J. Zubieta, Adenine, Guilderland, NY (1985) and references therein.
11) J. P. Costes, J. F. Serra, F. Dahan, and J. P. Laurent, *Inorg. Chem.*, **25**, 2790 (1986).
12) a) H. Taube, "Electron Transfer Reactions of Complex Ions in Solutions," Academic Press (1970); b) A. Haim, *Acc. Chem. Rev.*, **8**, 264 (1975).
13) D. Coucouvanis, *Prog. Inorg. Chem.*, **11**, 233 (1970); **26**, 301 (1979).
14) P. P. Singh, *Coord. Chem. Rev.*, **32**, 33 (1980).
15) M. L. Caffery and D. Coucouvanis, *J. Inorg. Nucl. Chem.*, **37**, 2081 (1975).
16) R. C. Aggarwal, N. Singh, and S. Singh, *Indian J. Chem., Sect. A*, **21**, 268 (1982).
17) S. R. Rao, "Xanthates and Related Compounds," Marcel Dekker, New York (1971).
18) M. R. Hunt, A. G. Kruger, L. Smith, and G. Winter, *Aust. J. Chem.*, **24**, 53 (1971).
19) D. Coucouvanis and J. P. Fackler, Jr., *Inorg. Chem.*, **6**, 2047 (1967).
20) A. I. Vogel, "A Textbook of Quantitative Inorganic Analysis," 3rd ed., Longmans, London (1961).
21) W. J. Geary, *Coord. Chem. Rev.*, **7**, 81 (1971).
22) C.K. Jorgensen, *J. Inorg. Nucl. Chem.*, **24**, 1571 (1962).
23) Y. Nishida and S. Kida, *Bull. Chem. Soc. Jpn.*, **43**, 3814 (1970).
24) H. B. Gray and C. J. Ballhausen, *J. Am. Chem. Soc.*, **85**, 260 (1963).
25) S. I. Shupack, E. Billig, R. J. H. Clark, R. Williams, and H. B. Gray, *J. Am. Chem. Soc.*, **86**, 4595 (1964).
26) R. L. Carlin, "Transition Metal Chemistry," **1**, 227 (1965).
27) A. Pignedoli and G. Peyronel, *Z. Anorg. Allg. Chem.*, **70**, 427 (1976).
28) A. B. P. Lever, "Inorganic Electronic Spectroscopy," 2nd ed., Elsevier, New York (1984), pp. 507—509.
29) F. L. Urbach, R. D. Bereman, J. A. Topich, M. Hariharan, and B. J. Kalbacher, *J. Am. Chem. Soc.*, **96**, 5063 (1974).
30) Y. Nishida and S. Kida, *Inorg. Nucl. Chem. Lett.*, **7**, 325 (1971); *Coord. Chem. Rev.*, **27**, 275 (1979); Y. Nishida, K. Hayashida, A. Sumita, and S. Kida, *Inorg. Chim. Acta Lett.* **31**, 19 (1978).
31) D. C. Bradley and M. H. Gitlitz, *J. Chem. Soc. A*, **1969**, 1152.
32) G. W. Watt and B. J. McCormick, *Spectrochim. Acta*, **21**, 553 (1965).
33) C. Paparizos and J. P. Fackler, Jr., *Inorg. Chem.*, **19**, 2886 (1980).
34) D. Harker, *J. Chem. Phys.*, **4**, 381 (1936).
35) I. Lindquist, *Acta Crystallogr.*, **10**, 29 (1957).
36) C. Chieh and K. Monihan, *Acta Crystallogr., Sect. B*, **36**, 1367 (1980).
37) V. Gutmann, *Chimia*, **31**, (1977). "The Donor-acceptor Approach to Molecular Interaction" Plenum, New York (1978), pp. 4—16.
38) R. S. Drago, G. C. Vogel, and T. E. Needham, *J. Am. Chem. Soc.*, **93**, 6014 (1971).

Correlation of ^{13}C Shifts with Substituent Parameters in 3,4-Diphenyl-1,2,5-oxadiazole 2-Oxides Substituted at the Para-Positions of Either or Both Phenyl Rings[1)]

S. N. Balasubrahmanyam,* N. Rajendran, and D. K. Singh
Department of Organic Chemistry, Indian Institute of Science, Bangalore 560012, India
(Received November 16, 1988)

C-1′, C-1″, C-3, and C-4 ^{13}C shifts in 3,4-di(4′-or/and 4″-X)phenyl-1,2,5-oxadiazole 2-oxides (3,4-diarylfurazan 2-oxides; three series: X=NMe_2, OMe, Me, Cl, H, and NO_2) were correlated vs. seven different divided substituent parameter sets. Results have implied that i) the C-3–C-4 bond does not transmit mesomeric effects efficiently; ii) no effects can be specifically attributed to the possibility that the C-3 aryl maintains a higher dihedral angle with respect to the furoxan ring than the C-4 aryl; iii) there appears to be a directionality to the propagation of localized π-polarization due to lesser ability of C=N(O)→O to convey effects compared with C=N(O); and, iv) the furazan *N*-oxide ring, being generally an electron acceptor, transmits substituent effects nonlinearly.

Correlation of ^{13}C shifts with nonresonance and resonance effects of substituents in the two series of furazan 2-oxides, **1** and **2**, was attempted with a view to examine the consequences of known or expected presence in them of the following features:

a) There is delocalization of charge from the *N*-oxide oxygen towards C-3,[2)] a fact made use of in assigning ^{13}C shifts in the two series.[3)]

b) Transmission of polar effects are different in series **1** and **2** (contrast with polar transmission in the disubstituted series **3** could be instructive).

c) In the solution phases of systems **1** and **2**, the 4-substituted phenyl, vicinal to *N*-oxide in the former, maintains, on the average, a higher dihedral angle (θ) with the furazan ring than the similarly substituted phenyl, distant to *N*-oxide, in the latter; a parallel difference may persist between the two 4-substituted phenyls in series **3**.

Assignment of chemical shifts to C-1′, C-1″, C-3, and C-4 in the three series **1**—**3** has been described;[3)] in Table 1 are gathered the shifts of these carbons relative to those of corresponding carbons in 3,4-diphenylfurazan 2-oxide **3e**. The nature of correlation at these four centers in the three series was expected to provide information sufficient for the proposed assessments. The available substitution, however, fell short of the minimal basis requirement[4)] in three respects. A carbonyl acceptor or even a CF_3 group could not be

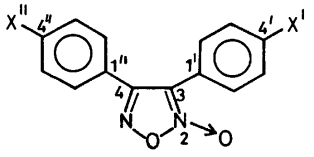

1: X′ = Substituent; X″ = H
2: X′ = H; X″ = Substituent
3: X′ = X″ = Substituent

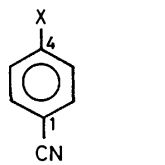

4

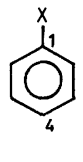

5

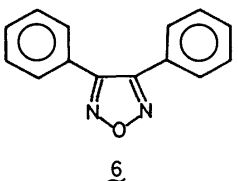

6

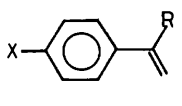

7a: R = H
b: R = Me
c: R = t Bu

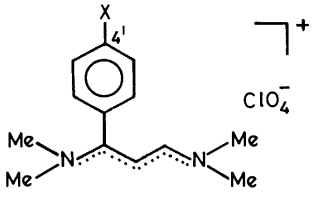

8
(X = OMe, Me, Cl, H, NO_2)

(**1**–**5**, **7**: X, X′, X″ = NMe_2, OMe, Me, Cl, H, NO_2)

Table 1. Chemical Shifts (δ/ppm) of C-1′, C-1″, C-3, and C-4 in the Furazan 2-Oxide Series **1**, **2**, and **3** Relative to Corresponding Carbons in 3,4-Diphenylfurazan 2-Oxide **3e**[a)]

		C-1′			C-1″		
		1	**2**	**3**	**1**	**2**	**3**
a	$-NMe_2$	−14.48	—	−13.49	0.59	(−13.68)[b)]	−12.53
b	−OMe	−8.51	−0.06	−8.10	0.30	−7.78	−7.39
c	−Me	−3.44	−0.22	−3.07	0.16	−2.91	−2.56
d	−Cl	−1.93	−0.63	−2.07	0.20	−1.52	−1.65
e	−H[c)]	→	123.60	←	→	126.98	←
f	$-NO_2$	(5.10)[b)]	−1.21	5.24	−0.74	5.89	5.15

		C-3			C-4		
		1	**2**	**3**	**1**	**2**	**3**
a	$-NMe_2$	0.24	—	0.40	0.12	—	0.28
b	−OMe	−0.04	−0.40	−0.25	−0.06	0.31	−0.25
c	−Me	−0.13	0.13	−0.10	0.00	0.00	−0.09
d	−Cl	−1.00	−0.51	−1.17	−0.19	−1.02	−1.17
e	−H[c)]	→	114.40	←	→	156.28	←
f	$-NO_2$	−1.42	−0.60	−1.09	−0.27	−1.86	−1.46

a) Adapted from Ref. 2; conditions of measurement have been detailed in this reference. b) Value obtained by extrapolation; see text. c) Shifts (δ/ppm; ex TMS) in 3,4-diphenylfurazan 2-oxide **3e**.

included because of difficulties encountered during attempted synthesis. The 4″-NMe_2 system **2a**, for the presence of which ^1H NMR evidence was available, was not formed in quantity sufficient for its ^{13}C lines to be discernible in the spectrum of its mixture with the 4′-isomer **1a**; the mixture could not be separated.[3] The line corresponding to C-1′ was obscured by other lines in the ^1H-decoupled ^{13}C spectrum of the 4′-NO_2 system **1f**. Moreover, the range of variation in chemical shift attending change in substitution was quite small at certain centers, giving room to uncertainty in correlative significance corresponding to error in measurement of small chemical shift changes. There was, however, a possibility that effects of these shortcomings could be compensated to an extent if correlation were tested vs. several different divided substituent parameter sets. The expectation was that any overall trends or consistencies seen could provide means to consider apparent correlations as significant. It has turned out that differences among the correlation coefficients are real, even based on small changes in chemical shift.

A standard statistics library routine, which included in its output certain indices of correlation (correlation coefficient r and the F-test of variance[5]), was used for carrying out the two-variable regression analyses. Data on the seven divided substituent parameter sets against which correlations were tested are listed in Table 2. Calculations, initially carried out with C-1′ and C-1″ shifts in series **3** showed good to very good correlation vs. all sets of Table 2 except set 3 (this set, developed[4] for electron-rich centers, could be inappropriate to C-1′ and C-1″ in furazan 2-oxides of type **3** which may be expected to be electron-deficient; see later discussion). Polar and resonance coefficients from the remaining sets were not dissimilar to those

Table 2. Substituent Parameter Sets Employed in the Present Paper in the Correlation of ^{13}C Shifts in Various Series

Substituent	σ_I	σ_R°	σ_R^{BA}	σ_R^-	σ_R^+
NMe_2	0.06	−0.52	−0.83	−0.34	−1.75
OMe	0.27	−0.45	−0.61	−0.45	−1.02
Me	−0.04	−0.11	−0.11	−0.11	−0.25
Cl	0.46	−0.23	−0.23	−0.23	−0.36
H	0.00	0.00	0.00	0.00	0.00
NO_2	0.65	0.15	0.15	0.46	0.15

Substituent	$\mathscr{F}$	$\mathscr{R}$	F_n	R_n	σ^*	σ^r
NMe_2	−0.097	−0.568	0.69	−3.81	0.82	−1.41
OMe	0.413	−0.500	0.54	−1.68	0.52	−0.94
Me	−0.052	−0.141	−0.01	−0.41	−0.10	−0.42
Cl	0.69	−0.161	0.72	−0.24	1.05	0.00
H	0.00	0.00	0.00	0.00	0.00	0.00
NO_2	1.109	0.155	1.00	1.00	1.40	0.89

Designation numbers of substituent parameter sets and references:
1. σ_I, σ_R°;[6] 2. σ_I, σ_R^{BA};[6] 3. σ_I, σ_R^-;[6]
4. σ_I, σ_R^+;[6] 5. $\mathscr{F}$, $\mathscr{R}$;[7] 6. F_n, R_n;[8]
7. σ^*, σ^r.[9]

found, with the same sets, for C-1 and C-4, respectively, of para-substituted benzonitriles **4** and monosubstituted benzenes **5** with the same six substituents as in series **3** (cf. C-1′, C-1″ data in Table 3C with data in Table 4AB). Therefore, seeing small changes in coefficients as reflecting real differences in transmission of effects, when the three series **1**, **2**, and **3** are compared, appeared justified. However, in the next correlation, attempted with C-1′ shifts in series **1** without a value for the NO_2 substituted system **1f**, the coefficients were found to diverge from those found for the "complete model series" of benzonitriles, monosubstituted benzenes or series **3** even though the quality of correlation had not deteriorated. Such a result could have flowed from any or all of the following reasons: i) the number of variables was too small and correlation (regression) coefficients are unstable to dropping any of them, especially the extreme ones, pertinent to NO_2 and NMe_2; ii) NO_2 was the only representative of groups that cause a positive shift (deshielding with respect to the H-system) at resonance-intensive centers; iii) numbers pertinent to NO_2 are not good in any of the parameter sets (or somewhat better in some than in others); iv) nonlinear effects underlie changes in the regression coefficients, etc. In a possible partial test, correlations were carried out with the "model series" dropping values pertinent to NO_2 and NMe_2, one at a time. Results gathered in Table 5 show that the wide divergences from coefficients obtained with the "complete set," found when NO_2 values are dropped, are not seen when NMe_2 values are dropped, pointing to the possible importance of nonlinear effects. In any case, these results were taken as strong indication that the same set of extreme substituents (i.e. NMe_2 and NO_2) should be taken if one wished to compare correlation in different series, such as the three series of furazan 2-oxides in the present instance.

A plot of C-1′ shifts in series **1** against C-1″ shifts in series **2** for the four substituents common to the two series (OMe, Me, Cl, and H) was found to be linear (Fig. 1; curve E) and it seemed valid to obtain the unavailable values (C-1′ shift in system **1f** and C-1″ shift in system **2a**) by extrapolation. Correlation parameters obtained by including these shift values form part of the listings in Tables 3A—3C. As regards the remaining centers, C-1′, C-3, and C-4 in series **2**, recalculations were carried out for the comparable centers in series **1** and **3**, omitting the NMe_2 values, and the resulting correlations are listed in Tables 6A—6C. Assessments that follow are predicated on effects perceived on both of these bases:

i) Polar coefficients in series **2** seem significantly higher than in series **1** if centers C-1′, C-1″, C-3, and C-4 of series **2** are compared, in order, with C-1″, C-1′, C-4, and C-3 of series **1**.

ii) Polar coefficients at C-3 and C-4 of series **3** are similar to those at centers corresponding, respectively,

Table 3. Coefficients and Indices of Correlation of ^{13}C Shifts in the Furazan 2-Oxide Series **1**, **2**, and **3**

Carbon site	Substituent parameter set no.[a]	I[b]	R[b]	r[b]	F[b]
A. Series **1**					
C-1′[c]	1	5.65	23.22	0.978	33.4
	2	5.63	16.39	0.996	192.6
	3	3.42	16.54	0.855	4.1
	4	5.52	8.56	0.993	118.4
	5	2.78	21.25	0.987	59.5
	6	1.54	4.01	0.987	57.3
	7	−2.06	8.85	0.998	444.5
C-1″	1	−0.92	−1.19	0.998	330.6
	2	−0.92	−0.82	0.997	280.6
	3	−0.77	−0.91	0.952	14.8
	4	−0.93	−0.41	0.984	45.0
	5	−0.51	−1.00	0.999	1721.4
	6	−0.49	−0.25	0.990	73.3
	7	−0.16	−0.52	0.996	199.7
C-3	1	−1.93	−1.00	0.973	26.9
	2	−1.93	−0.71	0.977	32.7
	3	−1.81	−0.76	0.958	16.8
	4	−1.94	−0.35	0.969	23.7
	5	−1.11	−0.74	0.969	23.7
	6	−1.11	−0.31	0.981	37.6
	7	−0.58	−0.58	0.969	23.2
C-4	1	−0.43	−0.18	0.963	19.4
	2	−0.42	−0.14	0.979	33.9
	3	−0.43	−0.10	0.931	9.8
	4	−0.41	−0.08	0.988	64.2
	5	−0.26	−0.12	0.980	36.9
	6	−0.21	−0.07	0.972	26.2
	7	−0.10	−0.12	0.911	7.3
B. Series **2**[d]					
C-1″	1	6.27	22.57	0.982	41.8
	2	6.28	15.88	0.997	297.3
	3	4.01	16.25	0.869	4.6
	4	6.19	8.27	0.992	102.9
	5	3.21	20.44	0.989	70.5
	6	2.03	3.94	0.988	61.1
	7	−1.68	8.66	0.997	290.3
C. Series **3**					
C-1′	1	5.32	22.30	0.984	47.2
	2	5.35	15.63	0.997	272.3
	3	3.01	16.19	0.871	4.7
	4	5.28	8.11	0.990	76.5
	5	2.62	20.33	0.990	77.3
	6	1.58	3.80	0.984	44.6
	7	−1.90	8.42	0.999	540.7
C-1″	1	5.17	20.86	0.984	45.1
	2	5.19	14.65	0.998	382.9
	3	3.04	15.09	0.869	4.7
	4	5.12	7.61	0.991	88.7
	5	2.58	18.98	0.990	74.6
	6	1.56	3.58	0.986	51.6
	7	−1.73	7.90	0.998	402.3
C-3	1	−1.82	−0.58	0.913	7.5
	2	−1.77	−0.53	0.933	10.2
	3	−1.90	−0.17	0.887	5.6
	4	−1.74	−0.31	0.945	12.6
	5	−1.07	−0.39	0.926	9.1
	6	−0.90	−0.28	0.922	8.6
	7	−0.46	−0.48	0.870	4.7
C-4	1	−2.28	−0.65	0.979	34.8
	2	−2.26	−0.50	0.986	52.6
	3	−2.27	−0.37	0.965	20.3
	4	−2.25	−0.27	0.987	59.2
	5	−1.33	−0.37	0.977	32.2
	6	−1.26	−0.29	0.978	33.1
	7	−0.69	−0.53	0.950	14.1

a) Refer to Table 2. b) I: Polar or nonresonance coefficient; R: resonance coefficient; r: coefficient of correlation; F: F-test of variance. c) Correlation includes C-1′ shift in the NO_2 system **1f** obtained by extrapolation. d) Correlation includes C-1″ shift in the NMe_2 system **2a** obtained by extrapolation; correlation at the other centers, C-1′, C-3, and C-4, not including shifts pertinent to the NMe_2 system, are given in Table 6.

in series **1** and **2** i.e. C-3 in series **1** and C-4 in series **2**.

iii) The polar coefficient at C-1″ of series **2** is higher than either at C-1′ of series **1** or at C-1′ or C-1″ of series **3**.

iv) The resonance coefficient at C-1′ of series **1** is higher than at C-1″ of series **2**.

v) Consistent with this is the resonance coefficient at C-1′ being higher than at C-1″ within series **3**.

vi) There appears to be little or no transmission of resonance information along C-3–C-4 in any of the systems.

Resonance Effects. Taking resonance effects first, it is seen that effects comparable to those at β-centers in 4-substituted styrenes[4,11] are not present at C-4 in series **1**, at C-3 in series **2** or at C-3 or C-4 in series **3**. This indicated near total lack of mesomeric communication between C-3 and C-4. Furazan 2-oxides are, presumably, not unlike other 5-membered heteroaromatics in having π-character highly localized[12] between centers 2—3 and 4—5. This proposition as well as that the C-3 and C-4 para-substituted phenyls maintain different θ's was open to test by way of observations on the nature of changes in correlation of ^{15}N shifts in the three series. But constrained resources prevented procurement of enough ^{15}N enriched hydroxylamine hydrochloride to enable preparation[3] of ^{15}N enriched samples of the furazan *N*-oxides in amounts needed to measure required shifts accurately.

X-Ray crystallographic evidence has not decided the question whether the 3-phenyl normally maintains a higher θ than the 4-phenyl in 3,4-diphenylfurazan 2-oxide (**3e**) since it disclosed[12] considerable disorder in the crystalline phase of **3e**: the two phenyls exchange their respective θ's of ca. 59 and 17° in about 16% of the molecules. Clearly, intracrystalline forces play a major role here since it had been reported earlier[13] that the equivalent phenyl groups in 3,4-diphenylfurazan (**6**) are rotated out of coplanarity with the

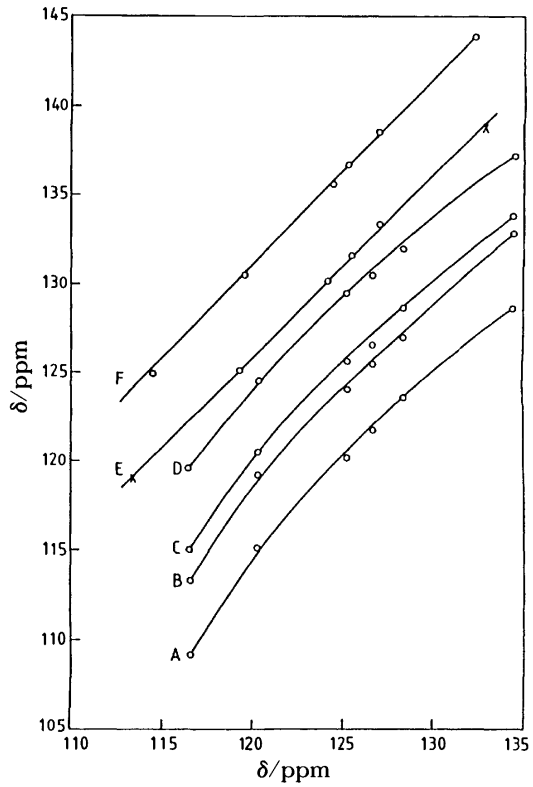

Fig. 1. Plots of ^{13}C shifts of C-1′ in series **1** (A), C-1″ in series **2** (B) and C-1′ and C-1″ in series **3** (C and D, respectively) vs. C-4 shifts in monosubstituted benzenes for the series of substituents NMe_2, OMe, Me, Cl, H, and NO_2. Plots E and F are, respectively, C-1′ shifts in series **1** vs. C-1″ shifts in series **2** and C-1′ shifts vs. C-1″ shifts in series **3**. Points obtained by extrapolation (see text) are indicated by crosses in plot E. For clarity, plots have been displaced along the ordinate as follows: A and B 0, C and D +5, E +10 and F +15 δ (ppm) units while the values on the abscissa apply to all plots.

Table 4. Coefficients and Indices of Correlation of C-1 Shifts in 4-Substituted Benzonitriles[a] **4** and C-4 Shifts in Monosubstituted Benzenes[a] **5**

Substituent parameter set no.[a]	*I*	*R*	*r*	*F*[b]
A. Benzonitriles **4**				
1	6.47	24.43	0.977	32.5
2	6.44	17.28	0.996	232.2
3	4.16	17.34	0.855	4.1
4	6.31	9.04	0.995	155.9
5	3.34	22.24	0.986	56.2
6	1.87	4.28	0.990	76.4
7	−2.05	9.38	0.997	251.3
B. Benzenes **5**				
1	6.06	20.93	0.995	185.3
2	6.21	14.40	0.994	140.6
3	3.49	15.93	0.913	7.6
4	6.25	7.34	0.976	30.6
5	3.04	18.88	0.996	215.2
6	2.58	3.55	0.970	24.1
7	−1.01	7.88	0.997	245.4

a) Chemical shifts reported in Ref. 10. b) Refer to Table 2. c) See footnote b of Table 3.

Table 5. Coefficients and Indices of Correlation of C-1′ and C-1″ Shifts in Furazan 2-Oxides **3**, C-1 Shifts in 4-Substituted Benzonitriles **4**, and C-4 Shifts in Monosubstituted Benzenes **5** on Omitting, in Turn, NO_2 and NMe_2 Shift Values

Substituent parameter set no.[a]	*I*	*R*	*r*	*F*[b]
A. C-1′ in furazan 2-oxides **3** without NO_2[c]				
1	9.39	25.73	0.993	74.3
2	5.34	15.62	0.995	101.0
3	14.25	31.75	0.910	4.8
4	2.28	7.64	0.996	141.2
5	3.48	21.11	0.986	35.2
6	−0.82	3.27	0.986	35.0
7	−2.14	8.18	0.998	266.0
B. C-1″ in furazan 2-oxides **3** without NO_2[c]				
1	9.07	24.16	0.992	68.3
2	5.27	14.70	0.996	143.6
3	13.60	29.73	0.907	4.7
4	2.39	7.19	0.997	233.2
5	3.43	19.77	0.986	34.5
6	−0.61	3.11	0.988	43.4
7	−1.96	7.71	0.997	178.5
C. C-1 in benzonitriles **4** without *p*-nitrobenzonitrile **4f**				
1	11.96	29.04	0.991	55.1
2	7.40	17.68	0.995	108.9
3	17.33	35.57	0.902	4.4
4	3.94	8.67	0.998	311.3
5	4.79	23.58	0.984	31.6
6	−0.07	3.85	0.990	54.6
7	−2.03	9.40	0.994	96.1
D. C-1 in benzonitriles **4** without *p*-(dimethylamino)-benzonitrile **4a**				
1	5.66	20.31	0.994	78.4
2	6.23	16.06	0.996	152.1
3	1.64	14.24	0.963	13.1
4	6.49	10.20	0.996	128.8
5	2.73	19.20	0.999	877.0
6	0.97	5.26	0.995	119.4
7	−1.40	8.51	0.999	694.8
E. C-4 in benzenes **5** without nitrobenzene **5f**				
1	8.02	22.59	0.997	232.3
2	4.45	13.65	0.994	91.7
3	12.52	28.43	0.932	6.7
4	1.77	6.64	0.990	50.8
5	2.80	18.66	0.993	70.2
6	−0.70	2.82	0.974	18.9
7	−1.70	7.22	0.999	3579.1
F. C-4 in benzenes **5** without *N*,*N*-dimethylaniline **5a**				
1	5.77	19.53	0.998	298.6
2	6.36	15.26	0.993	66.1
3	1.82	13.88	0.979	23.0
4	6.61	9.65	0.988	41.2
5	2.91	18.61	0.995	106.5
6	1.24	4.98	0.989	45.8
7	−1.17	8.10	0.994	94.2

a) Refer to Table 2. b) See footnote b of Table 3. c) Correlation at C-1′and C-1″, omitting shifts in NMe_2 system **3a**, are given Table 6.

furazan ring to similarly different extents (61 and 19°). Still, it was considered possible that, because of *N*-oxide oxygen-3-phenyl ortho-hydrogen crowding, the

Table 6. Coefficients and Indices of Correlation of ^{13}C Shifts in Furazan 2-Oxide Series **1**, **2**, and **3** Omitting NMe_2

Carbon site	Substituent parameter set no.[a]	I	R	r	F[b]
A. Series **1**					
C-1′	1	4.92	19.54	0.991	54.0
	2	5.47	15.45	0.993	80.1
	3	1.07	13.65	0.958	11.1
	4	5.72	9.84	0.995	107.9
	5	2.29	18.56	0.998	317.6
	6	0.58	5.04	0.993	76.2
	7	−1.61	8.23	0.999	1478.8
C-1″	1	−0.91	−1.14	0.997	189.0
	2	−0.94	−0.90	0.999	1218.6
	3	−0.68	−0.80	0.983	29.3
	4	−0.95	−0.57	0.998	225.8
	5	−0.52	−1.03	0.999	6593.7
	6	−0.43	−0.32	0.999	687.2
	7	−0.19	−0.47	0.997	200.7
C-3	1	−1.94	−1.03	0.966	14.0
	2	−1.96	−0.90	0.977	21.2
	3	−1.75	−0.70	0.956	10.7
	4	−1.97	−0.56	0.976	20.4
	5	−1.14	−0.92	0.968	15.3
	6	−1.07	−0.35	0.977	21.5
	7	−0.70	−0.41	0.975	19.3
C-4	1	−0.40	−0.07	0.992	61.6
	2	−0.41	−0.07	0.994	88.0
	3	−0.40	−0.05	0.989	48.7
	4	−0.41	−0.04	0.994	89.6
	5	−0.25	−0.05	0.989	44.4
	6	−0.25	−0.04	0.992	68.4
	7	−0.20	−0.03	0.996	124.9
B. Series **2**					
C-1′	1	−1.35	−0.93	0.961	12.1
	2	−1.38	−0.76	0.967	14.5
	3	−1.16	−0.68	0.960	11.9
	4	−1.39	−0.46	0.959	11.5
	5	−0.81	−0.79	0.963	12.8
	6	−0.74	−0.28	0.969	15.8
	7	−0.45	−0.36	0.952	9.9
C-1″	1	5.60	19.16	0.996	123.7
	2	6.15	15.10	0.996	132.1
	3	1.77	13.49	0.970	16.0
	4	6.40	9.57	0.994	84.4
	5	2.76	18.00	0.999	382.4
	6	1.11	4.94	0.995	90.6
	7	−1.20	8.00	0.998	274.9
C-3	1	−0.77	−0.33	0.910	4.8
	2	−0.77	−0.31	0.926	6.1
	3	−0.72	−0.20	0.897	4.1
	4	−0.78	−0.20	0.927	6.1
	5	−0.45	−0.32	0.911	4.9
	6	−0.43	−0.13	0.926	6.0
	7	−0.29	−0.14	0.928	6.3
C-4	1	−2.34	−1.95	0.975	19.1
	2	−2.38	−1.62	0.988	40.5
	3	−1.97	−1.32	0.959	11.5
	4	−2.41	−1.02	0.987	38.4
	5	−1.35	−1.78	0.981	25.6
	6	−1.21	−0.59	0.988	43.2
	7	−0.70	−0.80	0.984	30.1
C. Series **3**					
C-1′	1	4.71	19.24	0.996	111.8
	2	5.26	15.14	0.995	93.0
	3	0.87	13.55	0.968	15.1
	4	5.51	9.60	0.992	69.4
	5	3.53	18.40	0.997	172.8
	6	0.54	4.92	0.993	67.7
	7	−1.62	8.04	0.998	279.9
C-1″	1	4.58	17.89	0.996	129.5
	2	5.09	14.10	0.997	157.6
	3	1.00	12.61	0.969	15.7
	4	5.32	8.93	0.994	83.7
	5	3.47	17.11	0.998	232.0
	6	0.63	4.59	0.995	96.8
	7	−1.41	7.47	0.998	245.3
C-3	1	−1.73	−0.12	0.919	5.4
	2	−1.72	−0.21	0.924	5.8
	3	−1.76	0.02	0.917	5.3
	4	−1.72	−0.15	0.926	6.0
	5	−1.02	−0.15	0.903	4.4
	6	−1.03	−0.14	0.914	5.1
	7	−0.77	−0.06	0.941	7.7
C-4	1	−2.25	−0.48	0.977	21.2
	2	−2.25	−0.45	0.982	27.6
	3	−2.19	−0.27	0.972	17.3
	4	−2.26	−0.30	0.984	31.1
	5	−1.34	−0.41	0.971	16.6
	6	−1.33	−0.23	0.977	21.5
	7	−0.94	−0.19	0.990	48.8

a) Refer to Table 2. b) See footnote b of Table 3.

C-3 aryl would maintain, on the average, a higher θ than C-4 aryl in the solution phases of systems **1**—**3**. Centers C-1′ and C-1″ can then be compared with C-1 centers in 4-substituted α-*t*-butylstyrenes (**7c**) and 4-substituted styrenes (**7a**), respectively. In these styrenes, increase in resonance transmission to C-1 on proceeding from **7a** to **7c** (Table 7) has been attributed to the isolation of the resonance effect at C-1 as θ increases;[11] there is also a small increase in polar transmission to C-1.[11] Resonance transmission to C-1′ in series **1** and **3** is higher than to C-1″ in series **2** and that to C-1′ is higher than to C-1″ in series **3**, both by about the same extent as it is higher at C-1 in **7c** than in **7a**. This can be taken as indicating that the C-3 aryl maintains a higher θ than the C-4 aryl. Higher polar transmission to C-1″ in series **2**, where the substituted phenyl is expected to have *lower* θ than the one in series **1**, is, however, contrary to the situation in the styrenes. This does not detract from the case for higher θ on the part of the C-3 aryl since special circumstances govern polar transmission in furazan 2-oxides, as is hoped to be shown.

It is instructive to compare series **2** with the 2-substituted diazapentadienium (aminopropenimi-

Table 7. Coefficients and Indices of Correlation of C-1 Shifts in 4-Substituted -H, -Me, and -*t*-Bu Styrenes **7a—c**[a]

Substituent parameter set no.[b]	*I*	*R*	*r*	*F*[c]
A. Styrenes **7a**				
1	5.42	19.58	0.996	167.4
2	5.55	13.49	0.996	185.7
3	3.05	14.84	0.910	7.2
4	6.24	9.68	0.991	82.8
5	2.70	17.70	0.997	225.9
6	2.23	3.31	0.971	25.3
7	−1.05	7.34	0.997	276.1
B. α-Methylstyrenes **7b**				
1	5.80	20.35	0.994	137.9
2	5.92	14.05	0.996	215.3
3	3.38	15.34	0.906	6.9
4	6.64	10.08	0.991	87.0
5	2.90	18.41	0.997	242.2
6	2.37	3.46	0.974	27.3
7	−1.06	7.67	0.998	383.3
C. α-*t*-Butylstyrenes **7c**				
1	6.24	20.74	0.998	369.0
2	6.42	14.19	0.994	118.0
3	3.59	16.00	0.924	8.7
4	7.11	10.25	0.993	104.1
5	3.12	18.70	0.998	336.9
6	2.84	3.51	0.966	20.9
7	−0.77	7.79	0.996	197.9

a) Correlations based on C-1 chemical shifts reported[11] for the 4-X-styrenes **7a—c** with X=NMe_2, OMe, Me, Cl, H, and NO_2. b) Refer to Table 2. c) See footnote b of Table 3.

Table 8. Coefficients and Indices of Correlation of C-1 and C-1′ Shifts in the Aminopropeniminium salts **8**[a]

Carbon site	Substituent parameter set no.[b]	*I*	*R*	*r*	*F*[c]
C-1	1	−3.29	−1.94	0.995	140.3
	2	−3.35	−1.59	0.998	463.6
	3	−2.95	−1.35	0.987	56.7
	4	−3.38	−1.02	0.999	984.0
	5	−1.95	−1.80	0.995	148.7
	6	−1.14	−0.78	0.999	1388.0
	7	−1.16	−0.75	0.992	960.7
C-1′	1	5.62	19.12	0.993	101.0
	2	6.32	15.36	0.997	216.3
	3	2.01	13.80	0.974	21.9
	4	6.68	9.82	0.996	175.0
	5	2.82	17.73	0.995	141.5
	6	1.35	5.18	0.997	265.7
	7	−1.14	8.27	0.999	508.4

a) Correlations based on chemical shifts reported[14] for C-1 and C-1′ in series **8** for the set: X=OMe, Me, Cl, H, CN, and NO_2. b) Refer to Table 2. c) See footnote b of Table 3.

nium) salts **8** for which correlations at C-1 and C-1′ vs. the seven parameter sets are given in Table 8 (^{13}C shifts reported in Ref. 14 were used). The resemblances that both polar and resonance transmissions at C-1′ in series **8** bear to those at C-1″ in series **2** (Table 6B) are striking. Persuasive arguments were advanced[14] as demonstrating that the 4-substituted phenyl stays at right angles to the diazapentadienium plane in series **8**. Resemblances in correlation noted now show that the C-4 aryl should be taken as maintaining a high dihedral angle (ca. 90°) with the furazan oxide ring in series **2**. This contradicts arguments advanced earlier as showing that the C-4 aryl maintains *lower* θ than the one at C-3 in series **1** or **3**. Contradiction is resolved only if it is regarded that effects in series **2** and systems **8** have different bases. The lesser magnitude of the resonance coefficient at C-1″ in series **2** compared with that at C-1′ in series **1** as well as maintenance of a similar difference between C-1″ and C-1′ in series **3** could derive from a difference in onward transmission of mesomeric information. Such a difference could arise due either to the steric effect discussed above or to a directionality in the transmission of effects in furazan 2-oxides in the manner about to be described. In systems **8**, on the other hand, opposing effects could be operative at C-1′: decrease in the resonance coefficient at C-1′, caused by the side chain retaining positive charge, is counteracted by increase due to the mesomeric effect being isolated at the same center. Similarity of the coefficient at C-1′ in series **8** to that at C-1″ in series **2** is, then, only coincidental.

Polar (Nonresonance) Effects. Observations noted under i)—iii), earlier, imply a directionality to the

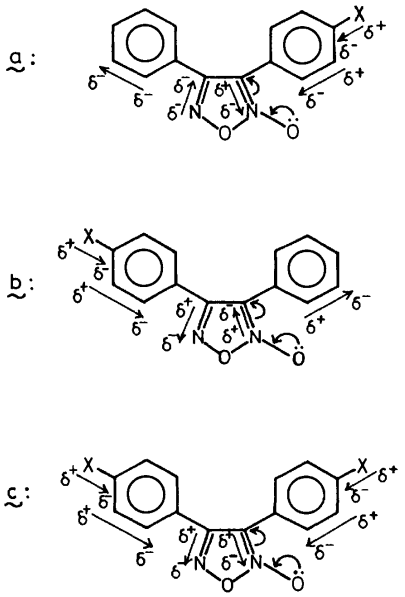

Fig. 2. Structural representations illustrative of conveyance of localized π-polarization (straight arrows) by an electron-repeller substituent X in the furazan 2-oxide series **1** (a), **2** (b), and **3** (c). The resident (mesomeric) delocalization from *N*-oxide oxygen to C-3 (curved arrows) may attenuate the ability of C-3-N-2(O)→O to convey polarization, either way, compared with C-4-N-5(O).

transmission of polar effects. Directionality can appear if the *p*-substituted phenyl maintains different θ's in series **1** and series **2** and induces *extended* π-polarization[4] to different extents at the 4-substituted styrene β-centers', C-4 in series **1** and at C-3 in series **2**. However, such cannot be the case since the sign of polarization at both centers is negative while that of extended polarization is positive[4] (whether extended polarization is active in systems like **1**, **2**, or **3**, involving nitrogen atoms as styrene β-centers, remains to be tested).

It is known that placing a conjugative group at the β-center of a styrene can change the magnitude of the 'reverse' polar effect at the α-center. In 4-substituted chalcones, for example, the effect is a substantial increase in the magnitude of the polar coefficient at C-α (I=−4.0).[4] The effect seen in series **1** and **2** is no way comparable since the value of the polar coefficient at C-3 in series **1** is lower than and that at C-4 in series **2** just about the same as at C-α in 4-substituted styrenes **7** (I=−2.4;[4] cf. relevant entries in Tables 6A and 6B); furazan 2-oxides cannot, therefore, be regarded as β-azastyrenes with a conjugative substituent at the β-atom (nitrogen).

Directionality of the type seen can derive from a difference in the behavior of C-4-N-5(O) and C-3-N-2(O)→O moieties, which constitute the furazan 2-oxide system, in transmitting a second type of polarization viz. *localized* π-polarization:[4] greater polarizability of the former can lead to greater localized effect at C-4 in series **2** or, lesser polarizability of the latter to lesser effect at C-3 in series **1** (see Fig. 2 and Tables 6A and 6B). This consideration is directly applicable to series **3** if the 'right' and 'left' sides of these systems are considered as resembling series **1** and **2**, respectively. However, the effect transmitted onward to C-3 in series **2** is greater than that transmitted onward to C-4 in series **1**. The difference could be only an apparent one since what is conveyed (inefficiently) by C-3-N-2(O)→O in series **2** is an effect that could be larger than that conveyed (efficiently) by C-4-N-5(O) in series **1**. Lesser ability of the C-3-N-2(O)→O moiety to convey localized polarization effects may derive from an intervention by the resident (mesomeric) delocalization from the *N*-oxide oxygen to C-3 (Fig. 2; curved arrows).

Evidence of 'directionality' to the transmission of polar effects is seen in the isomeric phenylfurazan 2-oxides **9a** and **9b** in which the varying substituent is

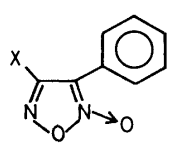

9a

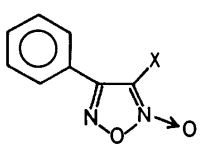

9b

(X = NMe_2, NH_2, Me, SPh, Ph, Cl, H, NO_2)

Table 9. Coefficients and Indices of Correlation of C-1′ Shifts in 3-Phenyl-4-X-furazan 2-Oxides **9a** and C-1″ Shifts in 3-X-4-phenylfurazan 2-Oxides **9b**[a]

Carbon site	Substituent parameter set no.[c]	I	R	r	F[d]
A. Series **9a**					
C-1′[b]	1	−4.17	−2.96	0.994	77.3
	2	−4.21	−2.00	0.996	139.3
	3	−3.87	−2.14	0.962	12.4
	4	−4.27	−0.99	0.996	126.4
	5	−2.46	−2.09	0.996	133.2
	6	−2.29	−0.78	0.995	108.7
	7	−1.01	−1.68	0.997	168.6
B. Series **9b**					
C-1″[b]	1	−3.35	−1.32	0.992	59.7
	2	−3.38	−0.86	0.990	51.7
	3	−3.18	−1.01	0.981	25.8
	4	−3.41	−0.42	0.990	49.1
	5	−2.03	−0.59	0.988	42.6
	6	−1.92	−0.47	0.989	46.0
	7	−0.99	−0.99	0.996	128.6

a) Correlations based on chemical shifts reported[15] for C-1′ in series **9a** and C-1″ in series **9b** for the set: X=NMe_2, NH_2, Me, Ph, SPh, Cl, H, and NO_2. b) This numbering conforms with that in furazan 2-oxides **1**, **2**, or **3**. c) Refer to Table 2. d) See footnote b of Table 3.

directly on the furazan oxide ring[15] (cf. polar coefficients at C-1′ in **9a** with those at C-1″ in **9b**; Table 9).

An interesting further observation is that *'ipso'* centers of the phenyl groups, C-1″ in series **1** and C-1′ in series **2**, exhibit polar coefficients of higher magnitude than centers nearer the sites of substitution, C-4 in series **1** and C-3 in series **2**, to which they are respectively bonded. A reason could be that phenyl groups are more easily polarized (as a whole, by the localized mechanism) than C-3-C-4 bonds in furazan 2-oxide rings, to which only a minor degree of double-bond character can be attributed ("30%" according to Ref. 12).

Nonlinear Effects. Plots of C-1′ shifts in series **1** (Fig. 1; curve A), C-1″ shifts in series **2** (curve B) and C-1′ and C-1″ shifts in series **3** (curves C and D) vs. C-4 shifts in monosubstituted benzenes with the same set of substituents are depicted in Fig. 1 (with shifts referred to TMS=0 ppm). These plots show distinct curvature in comparison with a plot either of C-1′ shifts in series **1** vs. C-1″ shifts in series **2** (curve E) or of C-1′ shifts vs. C-1″ shifts in series **3** (curve F). The gradual transition from higher to lower slope as the substituent changes from electron donor to electron acceptor contrasts with clear bilinearity exhibited by a plot of C-1 shifts in para-substituted nitrobenzenes vs. C-4 shifts in monosubstituted benzenes (Fig. 1 of Ref. 10). The contrast may be taken as evidence that the furazan 2-oxide system responds in nonabrupt manner and only reluctantly to change from electron release to electron withdrawal. The sense of the change indicates that furazan 2-oxide systems are electron accep-

tors. It remained to be tested whether a C-4 substituent is depleted of electron density to a greater extent than one at C-3 on the account that delocalization from *N*-oxide oxygen enhances electron density at C-3 considerably. A symptom of the difference between the two locations is that C-3 shifts are about 40 ppm lower than C-4 shifts in all furazan 2-oxides[3] (Table 1). An effect is also apparently conveyed (σ-inductively?) to C-1′ and C-1″ of the para-substituted phenyls: C-1′ carbons in series **1** are shifted upfield of C-1″ carbons in series **2** about 4 ppm,[3] as seen from Fig. 1 curves A and B (cf. curves C and D pertinent to series **3**).

Tests of nonlinear transmission of effects were possible:

a) The dual substituent parameter-nonlinear resonance (DSP-NLR) treatment[10] offered one possibility and was applied to C-1′ and C-1″ shifts in series **3** for each member of which measured shifts were available for the two centers. The values of the "electron demand parameter", ε, obtained by applying iterative procedure to Eq.1:

$$\Delta\delta = \sigma_I\rho_I + \sigma_R^0\rho_R/(1-\varepsilon\sigma_R^0), \quad (1)$$

were −0.44 and −0.49, respectively. While the negative signs confirmed that both centers are depleted of electron density, the difference in magnitude indicated that the C-3 substituent is less affected than the C-4 substituent, as expected. The electropositivity at C-3 of the furazan 2-oxide system, which can be considered as a net effect, is still within the range set by CF_3 ($\varepsilon=-0.42$) and COMe ($\varepsilon=-0.49$).[10]

b) It was thought possible to obtain independent check on certain of these aspects by comparing the $|B|/|r^*|$ ratio at C-1′ in series **1** and at C-1″ in series **2** with those at corresponding centers in series **3**. The ratio, which has been interpreted[9] as a measure of 'polarization' of a phenyl by such 'π-substituents' as CO_2H, CO_2R, or OH, can be obtained by carrying out regression analysis employing the three-parameter equation[9] (Eq. 2):

$$\Delta\delta = \rho^*\sigma^* + r^*\sigma^r + B \quad (2)$$

where B is a 'free' parameter used in conjunction with set 7. Since at least six values of the dependent variable were required in a three-parameter treatment, C-1′ shift pertinent to system **1f** and C-1″ shift pertinent to system **2a**, both obtained by extrapolation as described earlier, had to be included in the calculations. Results gathered in Table 10, which show greater $|B|/|r^*|$ ratio at C-1″ than at C-1′, allow the interpretation that the furazan 2-oxide system exerts greater influence through C-4 than through C-3. This accords with the following two, not mutually exclusive, possibilities:

i) A para-substituted phenyl at C-4 can exchange mesomeric information with the C-4–N-5 bond of the furazan 2-oxide system more effectively than can a similar group at C-3 with the C-3–N-2 bond because the former can maintain lower θ on the average (cf. earlier comparisons with para-substituted styrenes).

ii) Electron release from the *N*-oxide oxygen towards C-3 attenuates passage of mesomeric information to and from the para-substituted phenyl at C-3, regardless of its conformation with respect to the furazan 2-oxide ring.

A way to disentangle one possibility from the other is not apparent at this time but possibility ii) appears to have greater weightage.

It is noteworthy that the three-parameter treatment also shows higher polar effect at C-1′ (in series **1**) than at C-1″ (in series **2**). This is consistent with the proposition that higher electron density in the phenyl or para-substituted phenyl placed at C-3 makes for greater ease of its polarization through nonresonance mechanisms, a proposition considered earlier in connection with polarization being higher at centers farther from the point of substitution than those nearer.

A Recent Suggestion. Recently, a view has been projected[16] that the concept that resonance effects *complement* polar effects, underlying all efforts hitherto undertaken to separate polar from resonance effects "cleanly", could be seriously flawed. The observation that composite plots of electron-releasing and electron-withdrawing effects vs. any measurable property are bilinear must be seen as resulting from an abrupt major electronic rearrangement within a benzene ring when a π-donor substituent is replaced by a π-acceptor substituent, a rearrangement that must, naturally, affect transmission of polar effects. All hitherto employed dual parameter analyses which do not take into account this deep-seated coupling between polar and resonance effects must be regarded as misdirected. The earlier concept should be replaced by one that sees polar effects as *modified* by resonance.

Without taking a stand on this question, one can take the position that directionality to the conveyance of effects in substituted furazan 2-oxides, originating in the manner just discussed, could be a manifestation of the coupling between polar and resonance effects, since polar transmission seems to be considerably affected by delocalization from the *N*-oxide oxygen towards C-3, really a "resonance" effect. It is neces-

Table 10. Results of the Three-Parameter Correlation (Eq. 2) of C-1′ Shifts in Series **1**, C-1″ Shifts in Series **2** and C-1′ and C-1″ Shifts in Series **3**

Carbon center	ρ^*	r^*	B	r	F	$\lvert B\rvert/\lvert r^*\rvert$
C-1′ in **1**	−2.22	8.92	0.34	0.998	213.3	0.038
C-1″ in **2**	−2.06	8.83	0.84	0.998	184.6	0.095
C-1′ in **3**	−2.10	8.51	0.45	0.999	290.4	0.053
C-1″ in **3**	−2.08	8.06	0.77	0.999	311.6	0.096

sary to point out, however, that the directionality has surfaced in spite of the use of parameter sets developed by authors working in light of the earlier concept.

References

1) Abstracted in part from the Ph. D. thesis (Indian Institute of Science; 1986) of N. Rajendran (present address: GTN Arts College, Dindukkal, Tamil Nadu 624004, India).

2) F. A. L. Anet and I. Yavari, *Org. Magn. Reson.*, **8**, 158 (1976).

3) S. N. Balasubrahmanyam and N. Rajendran, *Indian J. Chem., Sect. B*, **27**, 793 (1988).

4) D. J. Craik and R. T. C. Brownlee, "Substituent effects on chemical shifts in the side chains of aromatic systems," Chap. 1 in "Progress in Physical Organic Chemistry," ed by R. W. Taft, Wiley/Interscience, New York (1983), Vol. 14, pp. 1—73; basic information pertinent to the present paper is to be found in this review.

5) A. M. Neville and J. B. Kennedy, "Basic Statistical Methods for Engineers and Scientists," International Textbook Company, Pennsylvania (1964), Chap. 14, pp. 208—234; the ratio SD/RMS [= *f*; see S. Ehrenson, *J. Org. Chem.*, **44**, 1793 (1979)], that has been recommended[4,6,10] as a measure of quality of correlation, was not calculated.

6) S. Ehrenson, R. T. C. Brownlee, and R. W. Taft, "A Generalized Treatment of Substituent Effects in Benzene Series," Chap. 1 in "Progress in Physical Organic Chemistry" Vol. 10, ed by A. Streitwieser and R. W. Taft, Wiley/Interscience, New York (1973), pp. 1—80.

7) C. G. Swain and E. C. Lupton, *J. Am. Chem. Soc.*, **90**, 4328 (1968); also, C. Hansch, A. Leo, S. H. Unger, K. H. Kim, D. Nikaitani, and E. J. Lien, *J. Med. Chem.*, **16**, 1207 (1973).

8) C. G. Swain, S. H. Unger, N. R. Rosenquist, and M. S. Swain, *J. Am. Chem. Soc.*, **105**, 492 (1983); see C. G. Swain, *J. Org. Chem.*, **49**, 2005 (1984) and three immediately preceeding papers in this issue.

9) I. B. Afanas'ev, *J. Chem. Soc., Perkin Trans. 2*, **1984**, 1589.

10) J. Bromilow, R. T. C. Brownlee, D. J. Craik, M. Sadek, and R. W. Taft, *J. Org. Chem.*, **45**, 2429 (1980).

11) G. K. Hamer, I. R. Peat, and W. F. Reynolds, *Can. J. Chem.*, **51**, 897, 915 (1973).

12) A. K. Sillitoe and M. M. Harding, *Acta Crystallogr., Sect. B*, **34**, 2021 (1978); pertinent bond lengths in system **3e** are indicative: N-2-C-3 1.312, C-3-C-4 1.411, and C-4-N-5 1.316 Å.

13) M. Mellini and S. Merlino, *Acta Crystallogr., Sect. B*, **32**, 1079 (1976).

14) S. N. Balasubrahmanyam and I. M. Mallick, *Org. Magn. Reson.*, **19**, 160 (1982).

15) R. Calvino, R. Fruttero, A. Gasco, V. Mortarini, and S. Aime, *J. Heterocycl. Chem.*, **19**, 427 (1982).

16) G. F. Fadhil and M. Godfrey, *J. Chem. Soc., Perkin Trans. 2*, **1988**, 133.

 © 1989 The Chemical Society of Japan Bull. Chem. Soc. Jpn., 62, 3343—3348 (1989)

Oxidation of Indigo Carmine by *N*-Haloarenesulfonamidates: A Kinetic Study

PUTTASWAMY, Dandinasivara Siddalingaiah MAHADEVAPPA,* and Kanchugarakoppal Subbegowda RANGAPPA
Department of Studies in Chemistry, University of Mysore, Manasagangothri, Mysore-570006, India
(Received December 20, 1988)

Kinetics of oxidation of indigo carmine (IC) by sodium *N*-haloarenesulfonamidates (RNXNa, where R=$CH_3C_6H_4SO_2$- or $C_6H_5SO_2$- and X=Cl or Br) chloramine T (CAT), bromamine T (BAT), chloramine B (CAB), and bromamine B (BAB) in alkaline buffer (pH 9—11) has been followed spectrophotometrically at λ_{max}=610 nm. Rate law, $-d[IC]/dt=k[OX]_0[IC]_0[OH^-]^x$ where $x<1$, is obeyed. The reaction products, benzenesulfonamide and toluenesulfonamide retard the rate. Sulfonated anthranilic acid formed was quantitatively determined. Variation of ionic strength or dielectric constant of medium and addition of halide ions have no effect on the reaction. A two pathway mechanism is proposed in which the hypohalous acid (HOX) and the anion of *N*-haloamine RNX^- interact with the substrate in rate limiting steps. The rate increases in the order: BAT>BAB>CAT>CAB, which is attributed to the difference in electrophilicities of halogen cations Br^+ and Cl^+ involved in the oxidation process and the ease with which these species are formed in reactions.

Considerable attention has centered around the chemistry of *N*-haloarenesulfonamidates because of their diverse properties to act as halonium cations, hypohalites and *N*-anions which behave both as bases and nucleophiles. The subject has been reviewed by Campbell and Johnson[1] and more recently by Banerji et al.[2] The prominent members of this class of compounds are chloramine T (p-$CH_3C_6H_4SO_2NClNa\cdot 3H_2O$ or CAT) and chloramine B ($C_6H_5SO_2NClNa\cdot 1.5H_2O$ or CAB) and analytical and kinetic aspects of their reactions have been extensively studied.

Indigo carmine (IC) is employed as a redox indicator in analytical chemistry. The *N*-haloarenesulfonamides have been used for estimating this compound[3] in solution but very few kinetic studies of this indole derivative are reported in literature.[4,5] The present paper is the first report discussing the spectrophotometric kinetics of oxidation of indigo carmine by chloramine T, chloramine B, bromamine T, and bromamine B in alkaline buffer (pH 9—11) with a view to elucidate the mechanism of oxidation of the dye in solution and also to assess the relative rates of oxidation of the substrate by the *N*-haloarenesulfonamidates.

Results

The reaction was first order in $[IC]_0$ as shown by the linear plots of log(absorbance) vs. time under conditions, $[IC]_0 \ll [OX]_0$ ($r>0.9980$; $s\leq 0.03$; Fig. 1). The pseudo-first-order rate constants k' given in Table 1, were found to be independent of $[IC]_0$ confirming the first-order dependence on substrate. The rate increased with increase in $[OX]_0$ and plot of $\log k'$ vs. $\log [OX]_0$ gave a straight line with unit slope ($r>0.9982$; $s\leq 0.01$).

The rate of reaction increased with pH of medium (Table 2). Plots of $\log k'$ vs. pH were linear ($r<0.9859$; $s\leq 0.03$) with fractional slopes. Further, plots of k' vs. $[OH^-]$ were linear with a Y- intercept corresponding to a rate law of the type: rate=$a+b[OH^-]$.

Addition of reaction product, p-toluenesulfonamide (TSA) or benzenesulfonamide (BSA) to reaction mixture retarded the rate (Table 3), in oxidations involving the respective oxidants.

Ionic strength variation (0.2—0.8 mol dm^{-3}) or addition of bromide or chloride ions in the form of NaBr or NaCl (2×10^{-4}—2×10^{-3} mol dm^{-3}) had no effect on reaction. The rate was not significantly altered on varying the dielectric constant of medium by the addition of methanol (5—20% v/v).

The reaction was studied at different temperatures (298—313 K) and from the Arrhenius plots ($r>0.9961$; $s\leq 0.04$) activation parameters were calculated (Table 4).

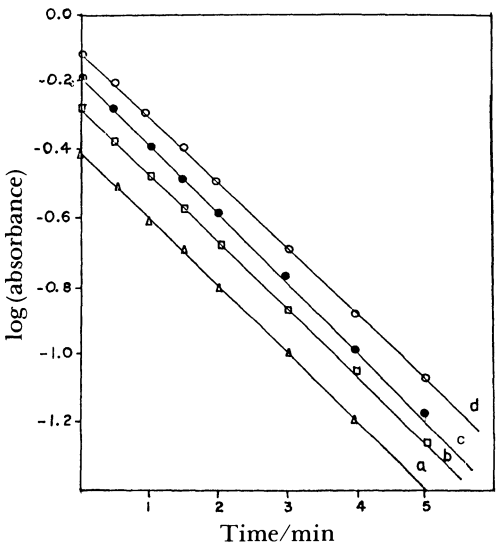

Fig. 1. Typical kinetic plots for the oxidation of indigo carmine by bromamine T at 30 °C.
pH=9.94, $[BAT]_0=5\times10^{-4}$ mol dm^{-3}; μ=0.5 mol dm^{-3}.
a,b,c,d represent different concentrations of indigo carmine (in mol dm^{-3}).
a=4×10^{-5}; b=5×10^{-5}; c=6×10^{-5}; d=7×10^{-5}.

Table 1. Effect of Variation of Reactant Concentrations on the Rate of Reaction at 30 °C
pH=9.94; μ=0.5 mol dm^{-3}

10^4[OX]$_0$ /mol dm^{-3}	10^5[IC]$_0$ /mol dm^{-3}	$10^3k'$/s^{-1}				k'_{BAT}/k'_{CAT}	k'_{BAB}/k'_{CAB}
		BAT	BAB	CAT	CAB		
2.0	5.0	2.86	2.14	0.61	0.38	4.7	5.6
3.0	5.0	4.44	3.26	0.90	0.63	4.9	5.2
4.0	5.0	5.80	4.42	1.21	0.77	4.8	5.7
5.0	5.0	7.54	5.45	1.51	1.04	5.0	5.2
6.0	5.0	8.59	6.50	1.78	1.23	4.8	5.3
7.0	5.0	10.34	7.90	2.10	1.43	4.9	5.5
8.0	5.0	11.69	8.96	2.44	1.57	4.8	5.7
9.0	5.0	13.19	9.85	2.85	1.72	4.6	5.7
5.0	3.0	7.42	5.49	1.53	1.03		
5.0	3.5	7.53	5.41	1.55	1.01		
5.0	4.0	7.67	5.37	1.50	1.07		
5.0	4.5	7.48	5.40	1.54	1.10		
5.0	5.5	7.77	5.50	1.54	1.02		
5.0	6.0	7.58	5.52	1.53	1.05		
5.0	6.5	7.45	5.54	1.48	1.00		
5.0	7.0	7.63	5.47	1.56	1.08		
5.0	7.5	7.62	5.59	1.50	1.04		
5.0	8.0	7.66	5.63	1.44	1.06		
5.0[a)]	5.0[a)]	7.68[a)]	5.64[a)]	1.59[a)]	1.10[a)]		

a) Values refer to reaction in D_2O medium.

Table 2. Effect of Variation of pH on the Rate of Reaction at 30 °C
[OX]$_0$=5×10^{-4} mol dm^{-3}; [IC]$_0$=5×10^{-5} mol dm^{-3}; μ=0.5 mol dm^{-3}

pH	$10^3k'$/s^{-1}			
	BAT	BAB	CAT	CAB
9.24	4.55	3.10	0.57	0.45
9.60	5.62	3.95	0.95	0.70
9.94	7.54	5.45	1.51	1.04
10.20	9.56	7.90	2.20	1.48
10.49	13.25	12.25	3.40	2.35

Table 3. Effect of Reaction Product Sulfonamide on the Rate of Reaction at 30 °C
[OX]$_0$=5×10^{-4} mol dm^{-3}; [IC]$_0$=5×10^{-5} mol dm^{-3}
pH=9.94; μ=0.5mol dm^{-3}

10^4[TSA] or 10^4[BSA] /mol dm^{-3}	$10^3k'$/s^{-1}			
	BAT	BAB	CAT	CAB
5.0	5.47 (5.52)	4.03 (4.79)	1.10 (1.29)	0.77 (0.84)
10.0	4.42 (4.12)	3.26 (2.98)	0.90 (0.84)	0.65 (0.59)
15.0	4.11 (3.65)	2.97 (2.38)	0.80 (0.69)	0.59 (0.50)
18.0	3.95 (3.53)	2.86 (2.21)	0.75 (0.64)	0.56 (0.48)
20.0	3.82 (3.42)	2.78 (2.08)	0.72 (0.61)	0.54 (0.46)

Values in parentheses are obtained from Eq. 7.

Solvent isotope studies in D_2O medium showed that the solvent isotope effect, k'_{H_2O}/k'_{D_2O} is about unity (Table 1).

Addition of reaction mixture to acrylamide in nitrogen atmosphere failed to initiate polymerization of the latter, showing the absence of free radical species.

Table 4. Kinetic and Thermodynamic Parameters for the Oxidation of Indigo Carmine by CAT, CAB, BAT, and BAB

	E_a	$\Delta H^{\neq}$	$\Delta S^{\neq}$	$\Delta G^{\neq}$	log A
	kJ mol^{-1}	kJ mol^{-1}	J K^{-1} mol^{-1}	kJ mol^{-1}	
BAT	36.3	33.8	−174.0	87.0	5.5
BAB	40.9	38.4	−161.8	87.8	6.7
CAT	43.5	40.9	−164.1	91.1	6.4
CAB	53.3	50.7	−134.8	91.9	7.8

Discussion

Investigations of Pryde and Soper,[6] Morris et al.,[7] Bishop and Jennings,[8] and Hardy and Johnston[9] on sodium *N*-haloarenesulfonamidates have shown that similar equilibria exist in acid and alkaline solutions. The following equilibria are noted in acid medium:

$$RNX\,Na \rightleftharpoons RNX^- + Na^+ \quad (1)$$

$$RNX^- + H^+ \rightleftharpoons RNXH \quad (2)$$

$$2\,RNXH \rightleftharpoons RNX_2 + RNH_2 \quad (3)$$

$$RNXH + H_2O \rightleftharpoons RNH_2 + HOX \quad (4)$$

$$HOX \rightleftharpoons H^+ + OX^- \quad (5)$$

Here X=Cl or Br and R=*p*-$CH_3C_6H_4SO_2$- or $C_6H_5SO_2$-.

The free acid RNXH and dihaloamine RNX_2 are present in fairly high concentrations in acid medium. The oxidation potential of haloamine-sulfonamide system is pH dependent[10] and decreases with increase in pH of medium. In alkaline solutions, RNX_2 does not exist, and the predominant species are RNX^-, RNXH, HOX, and OX^- ion. Hardy and Johnston[9] have calculated the concentrations of species present in alkaline BAB solutions. At pH<11, concentra-

tion of OX^- ion is small and it does not make a significant contribution to the oxidation of indigo carmine. Hence RNX^-, RNXH, and HOX are the likely oxidizing agents in alkaline solutions of *N*-haloamines.

In the present investigations, there is a first-order dependence of rate each on $[IC]_0$ and $[OX]_0$. A fractional order dependence on $[OH^-]$ is observed. The rate is retarded by the reaction product, sulfonamide (RNH_2), indicating that it is involved in a preequilibrium. Further a plot of k_{obs} vs. $[OH^-]$ is linear ($r>0.9924$; Fig. 2) with an intercept. Hence, a two pathway mechanism shown in Schemes 1 and 2 can be proposed to account for the experimental observations:

$$RNXH + OH^- \underset{}{\overset{K_1}{\rightleftharpoons}} RNX^- + HOX \quad \text{(i) fast}$$

$$HOX + IC \xrightarrow{k_2} Y \quad \text{(ii) slow}$$

$$Y + 3HOX \xrightarrow{k_3} \text{Products} \quad \text{(iii) fast}$$

Scheme 1.

$$RNX^- + IC \xrightarrow{k_4} Y' \quad \text{(i) slow}$$

$$Y' + 3\,RNX^- \xrightarrow{k_5} \text{Products} \quad \text{(ii) fast}$$

Scheme 2.

The combined rate law from Schemes 1 and 2 can be obtained as in Eq. 6:

$$\text{Rate} = \frac{k_2K_1[OX]_0[OH^-][IC]}{[RNH^-]} + k_4[IC][OX]_0 \quad (6)$$

From Eq. 6

$$k_{obs} = k' = \left[\frac{k_2K_1[OH^-]}{[RNH^-]} + k_4\right][OX]_0. \quad (7)$$

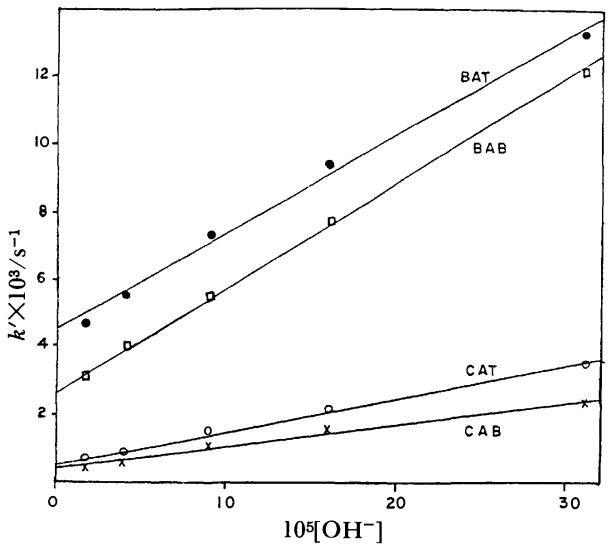

Fig. 2. Plot of k' vs. $[OH^-]$ for the oxidation of IC by *N*-haloamines.
$[OX]_0=5\times10^{-4}$ mol dm^{-3}; $[IC]_0=5\times10^{-5}$ mol dm^{-3}; $\mu=0.5$ mol dm^{-3}; temp: 30 °C.

Table 5. Variation of pH on the Rate of Reaction in Presence of Added Sulfonamide.
$[OX]_0=5\times10^{-4}$ mol dm^{-3}; $[IC]_0-5\times10^{-5}$ mol dm^{-3}; $\mu=0.5$ mol dm^{-3}; $[TSA]_a=[BSA]_a=0.001$ mol dm^{-3}. Temp: 30 °C

pH	$10^3k'/s^{-1}$			
	BAT	BAB	CAT	CAB
9.24	2.78 (3.55)	1.25 (1.85)	0.41 (0.68)	0.35 (0.52)
9.60	3.33 (3.83)	2.02 (2.23)	0.60 (0.74)	0.45 (0.56)
9.94	4.42 (4.41)	3.26 (3.03)	0.90 (0.87)	0.65 (0.64)
10.20	5.28 (5.27)	4.56 (4.23)	1.25 (1.07)	0.82 (0.75)
10.49	7.60 (7.13)	7.50 (6.77)	1.98 (1.49)	1.21 (1.01)

Values in parentheses were calculated from Eq. 7.

To test the validity of Eq. 7 the reaction was studied at different $[OH^-]$ with a constant concentration of added sulfonamide $[RNH_2]_a$ (Table 5). The concentration of RNH^- ion was obtained from the relation,

$$[RNH^-] = \frac{K_s}{K_s + [H^+]}[RNH_2]_a \quad (8)$$

where K_s is the dissociation constant of sulfonamide in aqueous solution (2.88×10^{-11} and 1.55×10^{-11} for TSA and BSA respectively at 30 °C). Plots of k' vs. $[OH^-]$ under these conditions were found to be linear ($r>0.9934$; Fig. 3) and from the slope and intercept, values of k_2K_1 and k_4 are determined:

	BAT	BAB	CAT	CAB
k_4	5.44 (6.68)	2.34 (3.12)	0.76 (1.26)	0.68 (0.98)
k_2K_1	6.42 (4.91)	5.00 (4.05)	2.10 (1.20)	0.69 (0.40)

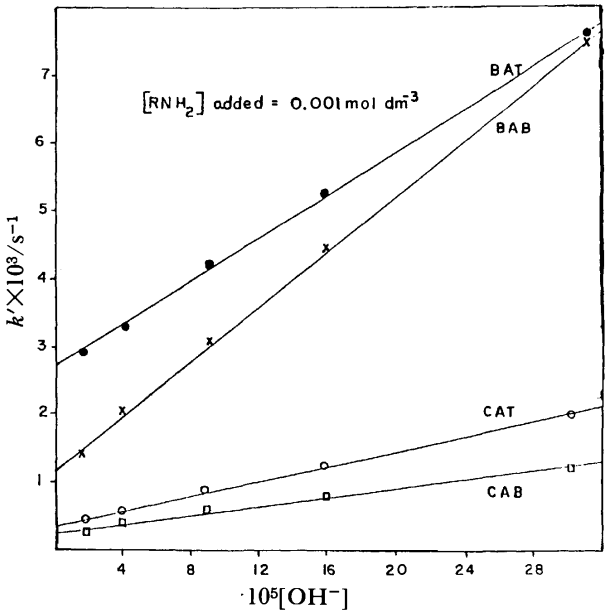

Fig. 3. Plot of k' vs. $[OH^-]$ for the oxidation of IC by *N*-haloamines in presence of added sulfonamide (RNH_2)$_a$.
$[OX]_0=5\times10^{-4}$ mol dm^{-3}; $[IC]_0=5\times10^{-5}$ mol dm^{-3}; $[RNH_2]_a=0.001$ mol dm^{-3}; $\mu=0.5$ mol dm^{-3}; temp: 30 °C.

Values of k_4 and k_2K_1 thus obtained were used to predict the rate constants k' when $[RNH_2]$ was varied in the reaction mixture. The values of k' thus obtained are shown in parenthesis in Table 3. It is seen that there is fair agreement with the experimental values. Further, a plot of k_{obs} vs. $1/[RNH^-]$ (Table 3) at constant $[OH^-]$ and $[OX]_0$ is found to be linear ($r>0.9912$; Fig. 4) and a second set of k_4 and k_2K_1 values could be extracted from these plots, which are shown in parenthesis above. These values of k_4 and k_2K_1 can be employed for predicting the rate constants k' obtained with varying $[OH^-]$ at constant $[RNH_2]=0.001$ mol dm^{-3} (Table 5). The value of k' so obtained are shown in parentheses in Table 5. Thus a fair agreement with the experimental values supports the proposed mechanism for oxidation of IC by the *N*-haloamines.

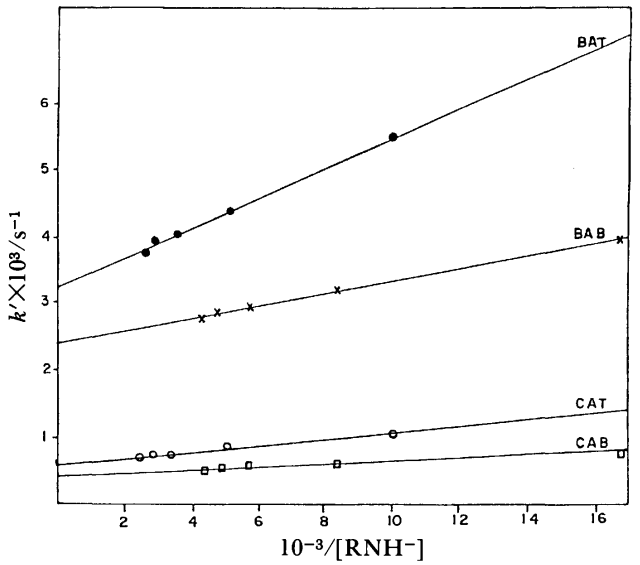

Fig. 4. Plot of k' vs. $1/[RNH^-]$ for the oxidation of IC by *N*-haloamines.
$[OX]_0=5\times10^{-4}$ mol dm^{-3}; $[IC]_0=5\times10^{-5}$ mol dm^{-3}; pH=9.94; $\mu=0.5$ mol dm^{-3}; temp: 30 °C.

A detailed mechanism showing the electron transfer during the oxidation of indigo carmine by the *N*-haloamines is given in Scheme 3. An electrophilic attack by X^+ species of oxidant forms a halohydrin across the C-C double bond in the substrate which subsequently leads to bond rupture. Isatinsulfonate formed undergoes further oxidation to sulfonated anthranilic acid by HOX. A similar scheme can be written for the oxidation of substrate by the anion RNX^-.

The solvent isotope effect[11] shows that the rate is not very much affected in D_2O medium as OH^- ion is involved in an equilibrium (Scheme 1) and only a part of the reaction proceeds through a pH dependent path.

Variation of dielectric constant (D) of medium does not affect the rate. An explanation can be offered in terms of the Born treatment applied by Laidler[12] for a dipole-dipole reaction.

$$\ln k' = \ln k_0 + \frac{3}{8kT}(2/D-1)\left[\frac{\mu_A^2}{r_A^3} + \frac{\mu_B^2}{r_B^3} - \frac{\mu_\pm^2}{r_\pm^3}\right] \quad (9)$$

Here k_0 is the rate constant in a medium of infinite dielectric constant and μ and r refer to the dipole moment and radii of reactants A and B and the activated complex. It is seen from Eq. 9 that rates should be higher in a medium of lower dielectric constant

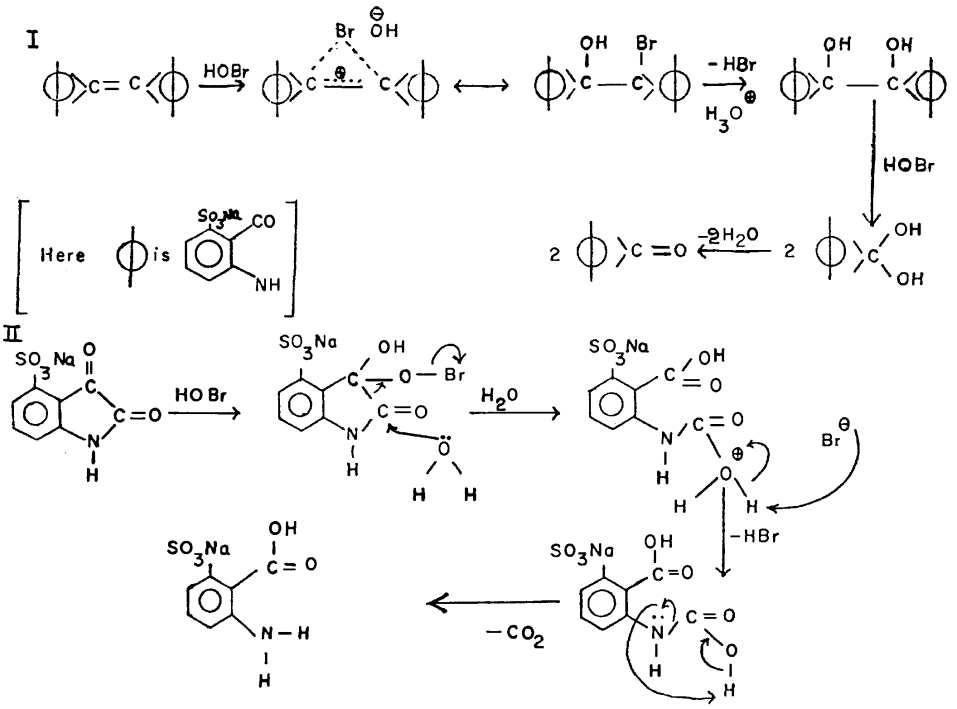

Scheme 3.

when $r^3_{\pm} > r^3_A + r^3_B$ indicating that the extent of charge dispersal in the transition state is different. On the other hand, $r^3_{\pm} \approx r^3_A + r^3_B$ implies the absence of dielectric effect of solvent on rate, as was observed in the present investigations.

The rates are found to be higher with BAB and BAT than the chlorine analogues by a factor of 5 (Table 1), and follow the sequence: BAT>BAB>CAT>CAB. This could be attributed, to the difference in electrophilicities of the halogen cations Br^+ and Cl^+ involved in the oxidation process and is related to the ease with which these species can be formed in reactions. A similar behavior has been noted in the oxidation of dialkylsulfides[13] and conjugated alcohols,[14] by the *N*-haloamines.

Experimental

Chloramine T (Merck) was purified by the method of Morris et al.[7]

Chloramine B was prepared[15] by passing chlorine through benzenesulfonamide dissolved in 4 mol dm^{-3} NaOH over a period of 1 h at 70 °C. The mass obtained was filtered, dried, and recrystallized from water.

Bromamine T was obtained[16] by the partial debromination of dibromamine T (DBT). To a solution containing ca. 20 g of CAT in 400 ml of water, about 4 ml of liquid bromine were added dropwise from a microburette, with constant stirring at room temperature. The dibromamine separated out was filtered under suction, washed thoroughly with water until all the absorbed bromine was completely eliminated and then vacuum dried for 24 h. About 20 g of DBT was dissolved with stirring in ca. 30 ml of 4 mol dm^{-3} NaOH at room temperature and the resultant aqueous solution was cooled in ice. Pale yellow crystals of BAT formed were filtered under suction, washed quickly with the minimum amount of ice cold water, and dried over P_2O_5.

Bromamine B was prepared[17] by the partial debromination of dibromamine B (DBB) which was obtained as follows: Pure chlorine was bubbled through an aqueous solution of CAB (30 g in 560 ml of water) and liquid bromine (6 ml) was added dropwise from a burette with constant stirring. The yellow precipitate of DBB formed was thoroughly washed with water, filtered under suction and dried in a vacuum desiccator. Dibromamine B (31.5 g) was digested in small lots with constant stirring in 50 ml of 4 mol dm^{-3} NaOH. The mass was cooled in ice, filtered under suction and the product dried over anhydrous calcium chloride.

The purity of all oxidants was checked by iodometric assay of the active halogen and by recording their Fourier transform ^{1}H and ^{13}C NMR spectra. Aqueous solutions of compounds were standardized by the iodometric method and preserved in brown bottles to prevent photochemical deterioration.

Aqueous solutions of indigo carmine (Merck) were prepared. Koch-Light (England) benzenesulfonamide and *p*-toluenesulfonamide were used. All other reagents were of Analar grade. Heavy water (99.2%) employed for solvent isotope studies was supplied by the Bhabha Atomic Research Centre, Trombay, India. The ionic strength of system was kept at a high value with a concentrated solution of sodium perchlorate. Standard buffer systems (borax+NaOH)[18] were used. The pK_s values of sulfonamides were determined by emf methods. Regression analysis of experimental data to get the regression coefficient r and s, the standard deviation of points from the regression line were performed on a TDC-316 computer and EC-72 statistical calculator.

Stoichiometry. Varying ratios of oxidant to indigo carmine in presence of buffer (pH 9.94) were equilibrated at 30 °C for 24 h. The unchanged oxidant in the reaction mixture was determined by iodometric titrations. The analysis showed that one mole of IC reacted with four moles of oxidant. The observed stoichiometry is shown by Eq. 10:

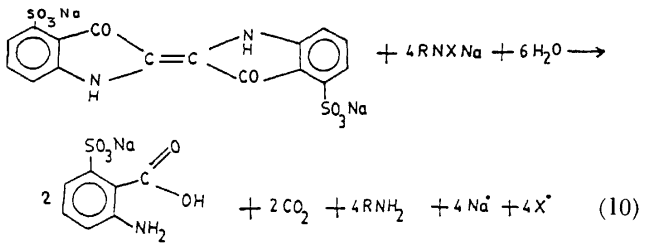

(10)

Here R=*p*-$CH_3C_6H_4SO_2$- for CAT and BAT and $C_6H_5SO_2$- for CAB and BAB; X=Cl or Br.

Product Analysis. *p*-Toluenesulfonamide was detected by paper chromatography. Benzyl alcohol saturated with water was used as the solvent with 0.5% vanillin in 1% HCl solution in ethanol as spray reagent (R_F 0.905). Benzenesulfonamide was identified by TLC using pet. ether-$CHCl_3$-1-butanol (2:2:1 v/v) as the solvent system and iodine as spray reagent (R_f 0.88). The anthranilate was precipitated as its zinc salt.[19] To the reaction mixture calculated volumes of 1 mol dm^{-3} NaOH were added followed by 10 ml of pH 5 buffer and 10 ml of 1% zinc sulfate. The ppt formed was filtered, dried at 105—110 °C and weighed; recovery of $(C_7H_6O_2N)_2$ Zn was 85—90%.

Kinetic Procedure. The kinetic runs were carried out under pseudo-first-order conditions. The course of reaction was followed spectrophotometrically by measuring the absorbance of unreacted indigo carmine at 610 nm using an Elico Model CL 24 spectrophotometer, for three half-lives. Plots of log(absorbance) versus time were linear. The pseudo-first-order rate constants (k') calculated from these plots were reproducible within ±3%.

One of us (PS) acknowledges the award of a Senior Research Fellowship from the Council of Scientific and Industrial Research, New Delhi.

References

1) M. M. Campbell and G. Johnson, *Chem. Rev.*, **78**, 65 (1978).

2) K. K. Banerji, B. Jayaram, and D. S. Mahadevappa, *J. Sci. Ind. Res.*, **46**, 65 (1987).

3) D. S. Mahadevappa, K. S. Rangappa, B. T. Gowda, and N. M. M. Gowda, *Microchem. J.*, **26**, 132 (1981).

4) P. V. Subba Rao, K. V. Subbaiah, and P. S. N. Murty, *React. Kinet. Catal. Lett.*, **10**, 1979; **11**, 79.

5) K. Srinivas, M. Vijayasree, and P. V. Subba Rao, *Indian J. Chem., Sect. A*, **21**, 773 (1982). S. B. Jonnalgadda and R. H. Simoyi, *J. Chem. Soc., Perkin Trans. 2*, **1988**,

1111.

6) B. G. Pryde and F. G. Soper, *J. Chem. Soc.*, **1926**, 1582; **1931**, 1514.

7) J. C. Morris, J. A. Salazar, and M. A. Wineman, *J. Am. Chem. Soc.*, **70**, 2036 (1948).

8) E. Bishop and V. J. Jennings, *Talanta*, **1**, 197 (1958).

9) F. F. Hardy and J. P. Johnston, *J. Chem. Soc., Perkin Trans. 2*, **1973**, 742.

10) A. R. V. Murthy and B. S. Rao, *Proc. Indian Acad. Sci.*, **35**, 69 (1952).

11) "Isotope Effects in Chemical Reactions," ed by C. J. Collins and N. S. Bowman, Van Nostrand-Reinhold, New York (1970), p. 267.

12) K. J. Laidler, "Chemical Kinetics," Tata McGraw Hill, Bombay, Second Edition, p. 227.

13) F. Ruff and A. Kucsman, *J. Chem. Soc., Perkin Trans. 2*, **1975**, 509; **1982**, 1075. *Acta Chim. Acad. Sci. Hung.*, **62**, 437, (1969); **65**, 107 (1970).

14) H. M. K. Naidu, B. Yamuna, and D. S. Mahadevappa, *Indian J. Chem., Sect. A*, **26**, 114 (1987).

15) A. Chrzaszczewska, *Bull. Soc. Sci. Lett. Lodz Cl. III*, **1952**, 3; *Chem. Abstr.*, **49**, 212 (1955).

16) C. G. R. Nair, R. L. Kumari, and P. Indrasenan, *Talanta*, **25**, 525 (1978).

17) M. S. Ahmed and D. S. Mahadevappa, *Talanta*, **27**, 669 (1980).

18) H. T. S. Britton, "Hydrogen Ions-Their Determination and Importance in Pure and Industrial Chemistry," Chapman and Hall, Ltd., London (1955), p. 364.

19) A. I. Vogel, "Quantitative Inorganic Analysis," ELBS and Longman, London (1978), Fourth Edition; p. 427.

 © 1989 The Chemical Society of Japan Bull. Chem. Soc. Jpn., 62, 3349—3354 (1989)

Ortho Effects in Organic Molecules on Electron Impact. 20. Parallel Oxygen Transfers from Nitro Group to Sulfur and Acetylenic Triple Bond in 3-(*o*-Nitrophenylthio)-1-propynes

D.V. RAMANA* and N. V. S. RAMA KRISHNA
Department of Chemistry, Indian Institute of Technology, Madras 600036, India
(Received January 5, 1989)

Oxygen transfers from nitro group to both the sulfur and acetylenic triple bond are noticed in parallel fragmentation pathways during the electron impact induced decompositions of 3-(*o*-nitrophenylthio)-1-propynes. Single oxygen transfer from nitro group to sulfur leads to abundant ions corresponding to *o*-nitrosobenzenesulfinyl cation and $[M-SO]^{+\cdot}$ while a concerted double oxygen transfer to sulfur followed by ejection of SO_2 from the rearranged molecular ion affords intense quinoline radical cation. Further, a single oxygen transfer to acetylenic triple bond, followed by a simple cleavage produces intense fragments corresponding to *o*-nitrosobenzenethiol radical cation at *m/z* 139 and *o*-nitrosophenylthio cation at *m/z* 138. The proposed fragmentation pathways and ion structures are established through high-resolution data, collision-induced dissociation (CID) mass-analyzed ion kinetic energy (MIKE) spectra, B/E linked scan spectra and chemical substitution.

The nitro group in the ortho position is a powerful interacting function in aromatic compounds during mass spectral decompositions. It is capable of transferring oxygens to the double bond,[1-3] heteroatoms[4,5] and activated carbon[6] in the side chain of aromatic ortho-disubstituted compounds. Recently the ortho interaction of nitro group with acetylenic triple bond is described[7] through an oxygen transfer producing abundant aroyl cations in (*o*-nitrophenyl)phenylacetylenes. Sulfur in the form of a thiocarbonyl[8,9] and a sulfide[10,11] is known to interact with the nitro group by accepting one or more oxygen atoms with the subsequent expulsions of SO and SO_2. It is also shown[12] that the oxygen transfer from the nitro group to the acetylenic triple bond is more predominant than to the sulfur when both were present together in the side chain as in (*o*-nitrophenylthio)phenylacetylenes. In the present study the mass spectral decompositions of 3-(*o*-nitrophenylthio)-1-propynes have been undertaken to assess the relative interacting abilities of sulfur and carbon-carbon triple bond to accept oxygens from ortho nitro group under electron impact conditions when a methylene group is inserted between sulfur and acetylenic moiety (Scheme 1).

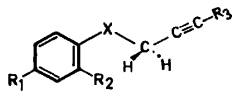

Compd.	X	R_1	R_2	R_3
1.	S	H	NO_2	H
2.	S	NO_2	H	H
3.	S	Cl	NO_2	H
4.	S	H	NO_2	Ph
5.	S	NO_2	H	Ph
6.	SO_2	H	NO_2	H
7.	SO_2	H	NO_2	Ph
8.	O	H	NO_2	H
9.	O	NO_2	H	H

Scheme 1.

Results and Discussion

Evidence for the oxygen transfers from the nitro group to both the sulfur and acetylenic triple bond in parallel pathways is adduced from the mass spectral fragmentations of 3-(*o*-nitrophenylthio)-1-propyne (**1**). The molecular ion rearranges to 'a' after the initial single oxygen transfer from the nitro group to the sulfur (Scheme 2). An α-cleavage with respect to sulfur in 'a' affords 'b' at *m/z* 154 (87). The accurate mass of this fragment, as determined by high-

Table 1. High-Resolution Data

Compound	*m/z*	Observed	Calculated	Elemental composition
1	193	193.0232	193.0214	$C_9H_7NO_2S$
	154	153.9981	153.9979	$C_6H_4NO_2S$
	145	145.0531	145.0527	C_9H_7NO
	139	139.0149	139.0108	C_6H_5NOS
	138	138.0070	138.0030	C_6H_4NOS
	129	129.0524	129.0578	C_9H_7N
	128	128.0445	128.0500	C_9H_6N
	108	108.0042	108.0050	C_6H_4S
	106	106.0312	106.0292	C_6H_4NO
	98	97.9984	97.9843	C_4H_2SO
6	225	225.0077	225.0112	$C_9H_7NO_4S$
	186	185.9876	185.9878	$C_6H_4NO_4S$
	170	169.9916	169.9928	$C_6H_4NO_3S$
8	177	177.0327	177.0426	$C_9H_7NO_3$
	123	123.0239	123.0320	$C_6H_5NO_2$
	122	122.0231	122.0242	$C_6H_4NO_2$

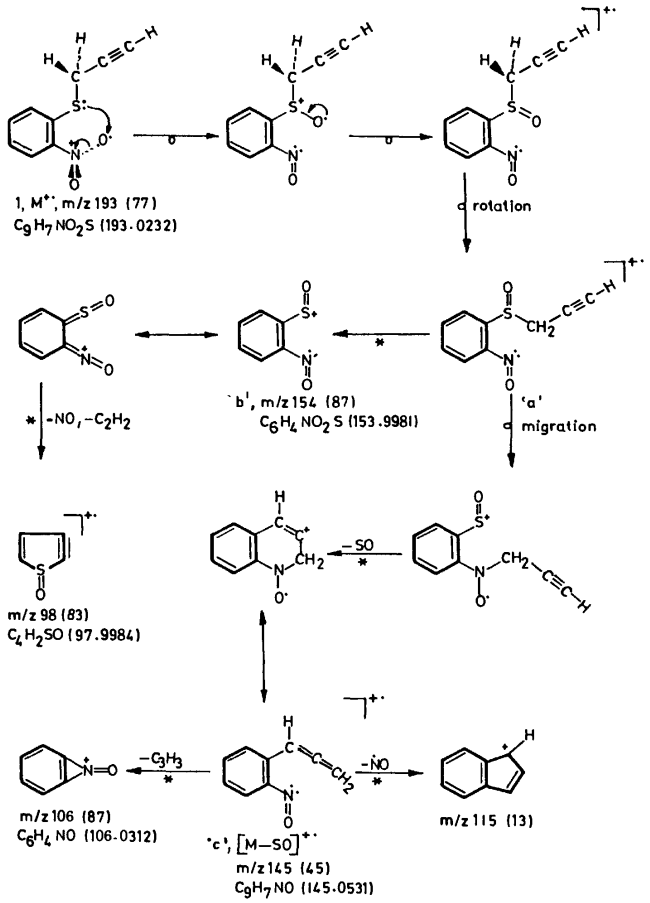

Scheme 2.

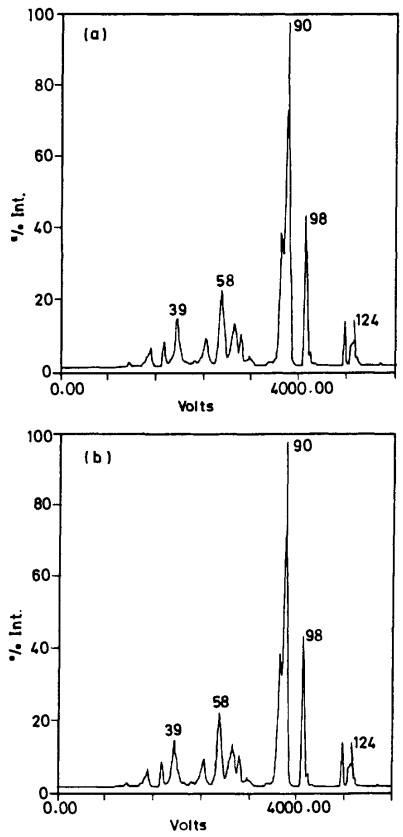

Fig. 1. CID MIKE spectra of ions at (a) *m/z* 154 of compound **1**, (b) *m/z* 154 of bis(*o*-nitrophenyl) disulfide.

Table 2. B/E Linked Scan Spectra

Parent ion	Daughter ions with relative abundances in parentheses
$M^{+\cdot}$, *m/z* 193 of compound **1**	176(5), 163(5), 154(58), 147(3), 145(100), 139(82), 138(78), 129(65), 128(75), 122(34), 96(20).
c, *m/z* 145 of compound **1**	144(100), 115(60), 106(21).
i, *m/z* 139 of compound **1**	138(32), 120(8), 111(40), 106(50), 95(8), 78(36).
$M^{+\cdot}$, *m/z* 225 of compound **6**	186(30), 170(65), 106(100).
$M^{+\cdot}$, *m/z* 177 of compound **8**	160(50), 131(40), 123(80), 122(100).

resolution technique is 153.9981 (Table 1) which corresponds to an elemental composition of $C_6H_4NO_2S$. Furthermore, examination of the B/E linked scan spectrum of $M^{+\cdot}$ of **1** (Table 2) revealed that the ion 'b' at *m/z* 154 is directly formed from the molecular ion. The ion at *m/z* 154 could also arise by a simple α-cleavage with respect to the sulfur in the molecular ion prior to the oxygen transfer. However, such a cleavage can, in principle, occur in the para-isomer (**2**) as well. But the intensity of the ion at *m/z* 154 in the mass spectrum of para-compound (**2**) is insignificant (Table 3). Therefore an ortho interaction is invoked for the formation of this fragment at *m/z* 154. Further the collision-induced dissociation (CID) mass-analyzed ion kinetic energy (MIKE) spectrum of the ion 'b' at *m/z* 154 from **1** is found to be identical (Fig. 1) with that of the ion at *m/z* 154 derived from bis(*o*-nitrophenyl) disulfide (reference compound). Since the fragment at *m/z* 154 in the reference compound is obtained as a result of a simple cleavage, an *o*-nitrosobenzenesulfinyl cation structure can be assigned to it. By the comparative study of the CID MIKE spectra of (Fig. 1) the ion 'b' from **1** and the fragment at *m/z* 154 from the reference compound an *o*-nitrosobenzenesulfinyl cation structure is proposed for the ion 'b' at *m/z* 154 in **1**.

The other characteristic ion resulting from the single oxygen transfer to sulfur in the mass spectrum of **1** is at *m/z* 145(45). Loss of 'SO from the rearranged molecular ion 'a' produces the $[M-SO]^{+\cdot}$ ion 'c' at *m/z* 145 (Scheme 2). The elemental composition C_7H_7NO (145.0531) for 'c' is in good agreement with the proposed elimination of 'SO' from the molecular ion and its direct formation is supported by the B/E linked scan spectrum of $M^{+\cdot}$ of **1** (Table 2). A 1-nitroso-2-(1,2-propadienyl)benzene radical cation structure is proposed for 'c' at *m/z* 145 in **1**, based upon the accurate mass measurements and secondary fragmentations of 'c'.

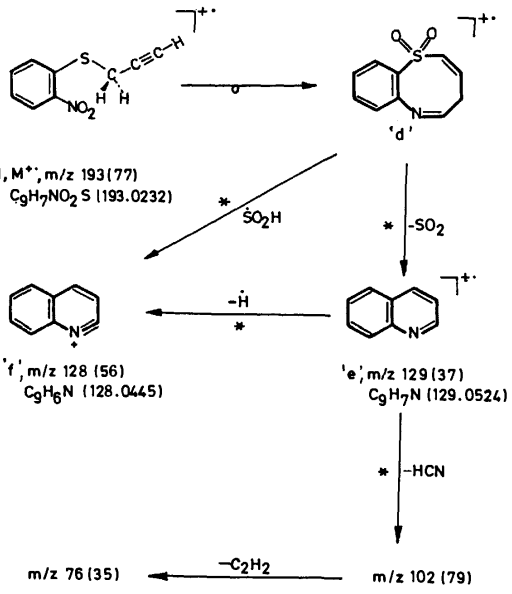

Scheme 3.

The most interesting decomposition mode in the mass spectrum of **1** is the expulsion of SO_2 and SO_2H radical in parallel fragmentation pathways from the molecular ion giving rise to intense ions at *m/z* 129(37) and 128(56), respectively (Scheme 3). The transfer of two oxygens from nitro group to sulfur followed by cyclization leading to the rearranged molecular ion 'd' is envisaged as an intermediate for this process. The rearranged molecular ion 'd' on ejection of SO_2 affords the abundant ion 'e' at *m/z* 129(37) (Scheme 3). Further loss of $\dot{H}$ from 'e' gives rise to an ion 'f' at *m/z* 128 (Scheme 3). The formation of 'f' at *m/z* 128 also takes place through a concerted elimination of SO_2H radical from 'd' as evidenced from the B/E linked scan spectrum of $M^{+\cdot}$ of **1** (Table 2). The elemental compositions C_9H_7N (129.0524) and C_9H_6N (128.0445) for 'e' and 'f' obtained by high-resolution technique, support the proposed elimination of SO_2 and $\dot{S}O_2H$ from the molecular ion for the formation of 'e' and 'f', respectively. Based on these facts a quinoline radical cation structure to 'e' and a dehydroquinolinium cation structure to 'f' are postulated (Scheme 3). Evidence for the proposed quinoline radical cation structure for 'e' is obtained from the observation that the CID MIKE spectra of 'e' from **1** and that of the molecular ion of quinoline, taken as a reference compound, at *m/z* 129 are superimposable (Fig. 3).

Another novel ortho interaction noticed in the mass spectrum of **1** is the formation of fragments initiated by the single oxygen migration from the nitro group to the acetylenic triple bond leading to the rearranged molecular ion 'g' (Scheme 4). An α-cleavage with respect to sulfur in 'g' affords 'h' at *m/z* 138(91) while the ion 'i' at *m/z* 139(61) is derived from a similar cleavage with an α-hydrogen migration. An *o*-nitrosophenylthio cation structure to 'h' and an *o*-

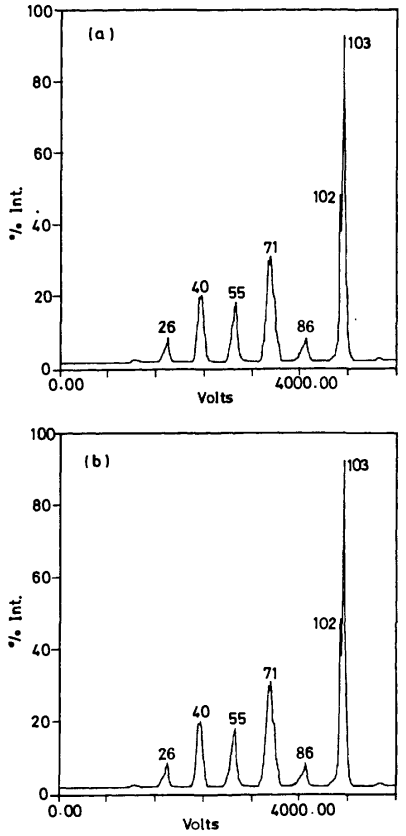

Fig. 2. CID MIKE spectra of ions at (a) *m/z* 129 of compound **1**, (b) $M^{+\cdot}$, *m/z* 129 of quinoline.

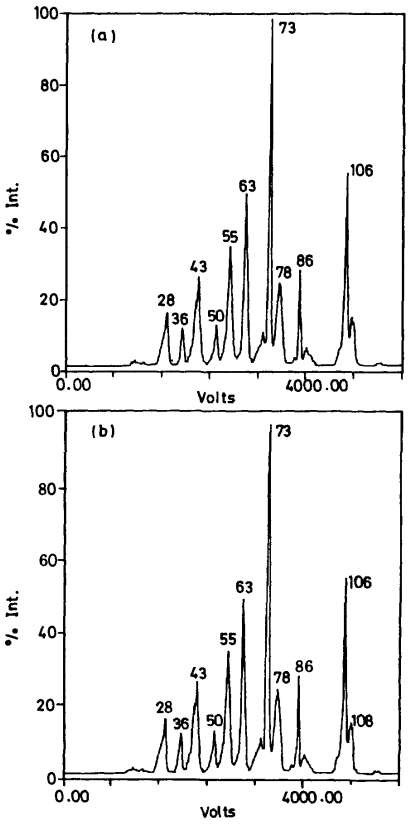

Fig. 3. CID MIKE spectra of ions at (a) *m/z* 138 of compound **1**, (b) *m/z* 138 of bis(*o*-nitrophenyl) disulfide.

nitrosobenzenethiol radical cation structure to 'i' are assigned. The elemental compositions C_6H_4NOS (138.0076) and C_6H_5NOS (139.0149) for 'h' and 'i' respectively, obtained by high-resolution technique agree with the elemental compositions of the structures proposed for the ions 'h' and 'i'. The *o*-nitrosophenylthio cation structure envisaged for 'h' at *m/z* 138 is supported by the fact that the CID MIKE spectrum of 'h' is identical (Fig. 3) with that of the CID MIKE spectrum of the ion *m/z* 138, obtained from bis(*o*-nitrophenyl) disulfide, having *o*-nitrosophenylthio cation structure.[13] The fragmentation pathways described in Scheme 4 are substantiated by B/E linked scan spectra of $M^{+\cdot}$, 'h', and 'i' (Table 2) of compound **1**. All the ions noticed in the mass spectrum of **1** as a result of ortho interaction are also present in the substituted derivative (Compound **3**) with the corresponding shifts in the *m/z* values of the ions (Table 3).

Table 3. Partial Mass Spectra of Compounds **1** to **9**

Compound	*m/z* values with relative abundances in parentheses
1	193(77), 154(87), 147(8), 145(45), 139(61), 138(91), 129(37), 128(56), 108(73), 106(87), 98(83), 96(100).
2	193(60), 176(21), 163(5), 154(3), 147(100), 146(42), 122(9), 96(6).
3	227(30), 188(83), 181(8), 179(16), 173(19), 172(65), 163(6), 162(12), 142(48), 140(55), 132(62), 130(55), 95(100).
4	269(3), 252(6), 221(3), 139(20), 115(100), 105(6).
5	269(12), 115(100), 89(5).
6	225(3), 186(100), 170(37), 107(28), 103(10).
7	301(6), 220(5), 195(9), 186(8), 170(3), 115(100).
8	177(42), 160(8), 131(30), 123(84), 122(100), 106(40), 94(22), 92(42).
9	177(74), 176(40), 160(54), 131(96), 130(100), 103(32).

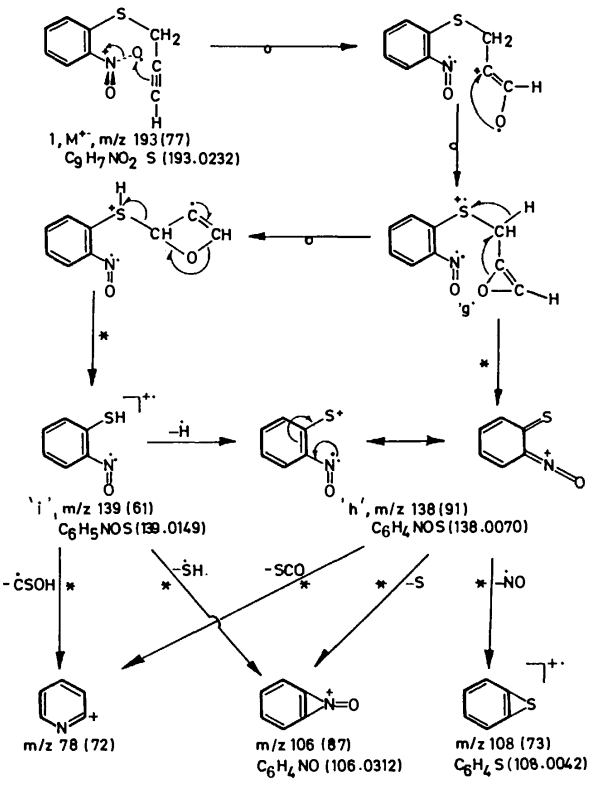

Scheme 4.

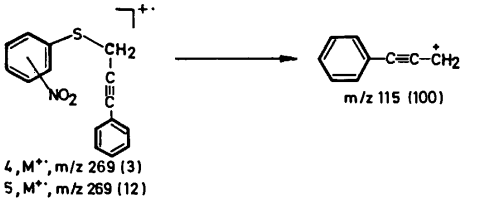

Scheme 5.

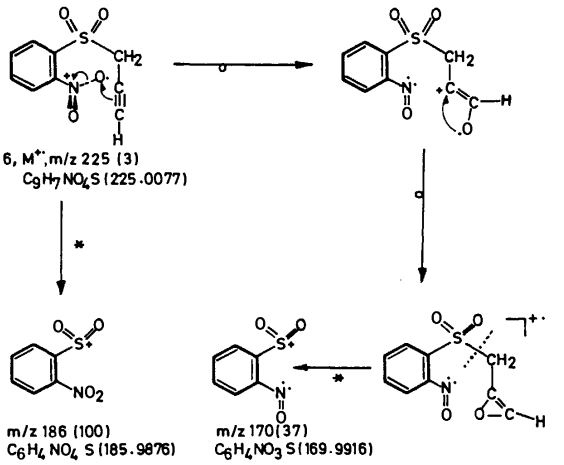

Scheme 6.

When this study is extended to 3-(*o*-nitrophenylthio)-1-phenyl-1-propyne (**4**) and its corresponding para-isomer (**5**), the chief fragment ion observed in the mass spectra of these two compounds is due to simple α-cleavage with respect to sulfur producing the stable 3-phenyl-2-propynyl cation at *m/z* 115 (Scheme 5) (Table 3). However no fragment ions corresponding to oxygen transfers from the nitro group either to sulfur or to the acetylenic triple bond are noticed in the ortho-isomer (**4**).

The mass spectrum of 3-(*o*-nitrophenylsulfonyl)-1-propyne (**6**) is also studied in this work to evaluate the feasibility of ortho interaction of nitro group with the side chain containing acetylenic triple bond and a sulfonyl group. The base peak in the mass spectrum of **6** is due to simple α-cleavage with respect to sulfonyl group producing the ion at *m/z* 186(100) (Scheme 6). Another intense ion observed in the mass spectrum of this compound is due to an oxygen transfer from nitro group to acetylenic triple bond followed by simple cleavage affording the ion at *m/z* 170(37) (Scheme 6). The oxygen analogue of compound **1** i.e., 3-(*o*-nitrophenoxy)-1-propyne (**8**), shows in its mass spectrum, the base peak at *m/z* 122(100) corresponding to oxygen migration from nitro group to acetylenic triple bond followed by simple cleavage

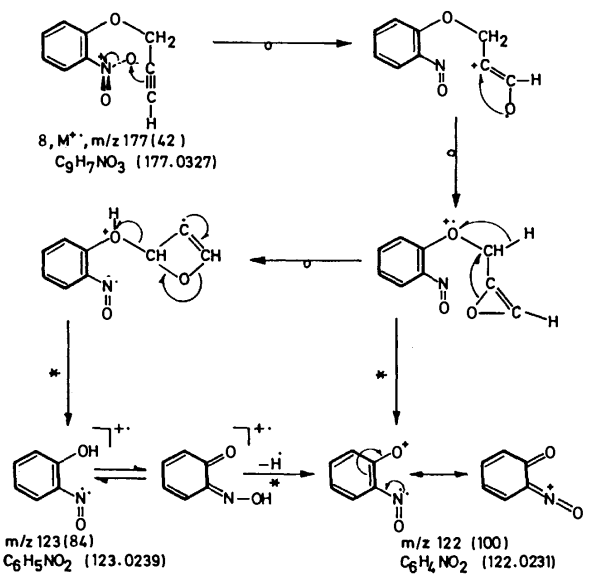

Scheme 7.

(Scheme 7). The same migration process leads to another intense ion at m/z 123(84) by an α-hydrogen transfer followed by simple cleavage from the rearranged molecular ion (Scheme 7). The fragmentation pathways described in Schemes 6 and 7 are substantiated by B/E linked scan spectra (Table 2) and accurate mass measurements (Table 1). It can be noticed from this comparative study of sulfur and oxygen compounds that the ortho interactions of nitro group are noticed with both sulfur and acetylenic triple bond as expected in compound **1** while fragments corresponding to the ortho interaction of the nitro group with the triple bond only are noticed in oxygen analogue (Compound **8**). These fragmentations due to the ortho interactions are of either negligible abundance or totally absent in the corresponding para-isomers (**2** and **9**) (Table 3). In the absence of these ortho interactions, the para-isomers (**2** and **9**) show almost similar fragmentation process (Table 3). The other common fragments observed in **1** and **2** are shown in Scheme 8.

It can be inferred from this study that the oxygen transfers from the nitro group to both sulfur and acetylenic triple bond are equally facile even when a methylene group is interjected between sulfur and acetylenic moiety. It can also be noticed that the carbon-carbon triple bond continues to act as a good oxygen acceptor even when placed one carbon atom away from sulfur. Another interesting aspect observed in this study is that while the sulfur is accepting two oxygens from nitro group, the acetylenic function is able to take only one oxygen, perhaps due to the unfavorable transition states required for the transfer of both the oxygens. Further, it can also be observed that if sulfur already possess oxygens as in the case of sulfone **6**, or if the sulfur is replaced by an oxygen as in the case of ether **8**, the oxygen transfer to the acetylenic triple bond is still noticed.

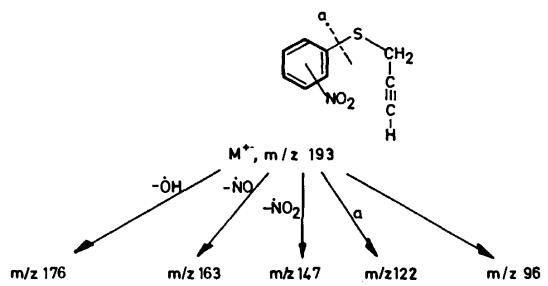

Scheme 8.

Experimental

Compounds **1** to **3** were prepared from the appropriate nitrobenzenethiol and 3-bromo-1-propyne by mechanically stirring for 6 hours in *N,N*-dimethylformamide solvent in the presence of potassium carbonate according to the general procedure reported in the literature.[14] Compounds **4** and **5** were synthesized by the same general procedure using appropriate nitrobenzenethiol and 3-bromo-1-phenyl-1-propyne. The 3-bromo-1-phenyl-1-propyne used in these reactions was prepared from phenylethyne, paraformaldehyde and phosphorus tribromide according to the literature[15] reported procedure. Compounds **6** and **7** were obtained through oxidation of **2** and **4** respectively using hydrogen peroxide in acetic acid at room temperature. Compounds **8** and **9** were prepared from the appropriate nitrophenol and 3-bromo-1-propyne using the same procedure reported for **1** to **3**.

All the compounds studied were recrystallized to constant melting point and their purity was checked by thin-layer chromatography (TLC). The compounds were characterized by nuclear magnetic resonance (^{1}H NMR) and infrared (IR) spectral data. Table 4 gives the yield, melting point (uncorrected), and microanalytical data for the hitherto unreported compounds discussed in this work. The low-resolution mass spectra were taken on a Varian MAT CH-7 and Finnigan MAT 8230 mass spectrometers. The spectra were run at 70 eV or with an emission current of 100 μA. All the compounds were introduced into the mass spectrometer through the direct probe insertion at probe temperatures varying between 30 and 110 °C.

Accurate mass measurements were carried out at a resolution of 7000 (10% valley) with Finnigan MAT 8230 double focussing mass spectrometer using peak-matching technique and PFK was used as reference. The B/E linked scan spectra in the first field free region were investigated with VG micromass 7070-H and Finnigan MAT 8230 mass spec-

Table 4. Characterization Data for Unknown Compounds

Compound	Yield	Mp[a]	Microanalytical data			
			Calcd (%)		Obsd (%)	
	%	°C	C	H	C	H
6	80	163—164	48.00	3.11	47.71	3.31
7	65	115—116	59.80	3.65	59.91	3.92

a) Solvent used for crystallization is benzene-hexane.

trometers. The collision-induced dissociation (CID) mass-analyzed ion kinetic energy (MIKE) spectra were measured using VG analytical ZAB 2F double focussing mass spectrometer with the following conditions: electron energy 70 eV, electron trap current 200 μA, accelerating voltage 6 kV and ion source temperature 200—300 °C. The ions of interest were focussed magnetically into the 2nd FFR and the MIKE spectrum obtained by scanning the ESA voltage. The collision was achieved by introducing 'He' gas into the collision cell of the 2nd FFR at such a rate that the intensity of the main beam was reduced to 50%.

The authors thank Prof. J. H. Beynon and Mr. Dipankar Ghosh, University College of Swansea, Swansea, UK for providing CID MIKE spectra and RRL, Hyderabad, India for few B/E linked scan spectra. Acknowledgements are due to RSIC, IIT, Madras, for high-resolution data. One of us (NVSRK) thanks CSIR, India for a research fellowship.

References

1) J. Seibl and J. Vollmin, *Org. Mass Spectrom.*, **1**, 713 (1968).

2) D. V. Ramana and M. Vairamani, *Org. Mass Spectrom.*, **9**, 1158 (1974).

3) D. Johnston and D. M. Smith, *Org. Mass Spectrom.*, **9**, 789 (1974).

4) H. Schwarz and F. Bohlmann, *Org. Mass Spectrom.*, **9**, 283 (1974).

5) J. Martens, K. Praefcke, and H. Schwarz, *Org. Mass Spectrom.*, **8**, 317 (1973).

6) D. V. Ramana and M. Vairamani, *Org. Mass Spectrom.*, **12**, 166 (1977).

7) D. V. Ramana and N. V. S. Rama Krishna, *Org. Mass Spectrom.*, **24**, 66 (1989).

8) D. V. Ramana and H. F. Grutzmacher, *Org. Mass Spectrom.*, **16**, 227 (1981).

9) D. V. Ramana and S. K. Viswanadham, *Org. Mass Spectrom.*, **18**, 162 (1983).

10) J. Martens, K. Praefcke, and H. Schwarz, *Justus Liebigs Ann. Chem.*, **1975**, 62.

11) S. Pappalardo and M. Di Grazia, *Org. Mass Spectrom.*, **20**, 392 (1985).

12) D. V. Ramana and N. V. S. Rama Krishna, *Org. Mass Spectrom.*, in press.

13) D. N. B. Mallen and J. M. Smith, *Org. Mass Spectrom.*, **14**, 171 (1979).

14) I. Iwai and J. Ide, *Chem. Pharm. Bull.*, **11**, 1042 (1963).

15) Lee I. Smith and Jack S. Swenson, *J. Am. Chem. Soc.*, **79**, 2962 (1957).

 © 1989 The Chemical Society of Japan Bull. Chem. Soc. Jpn., 62, 3355—3358 (1989)

Stopped-Flow Kinetic Investigations of One-Electron Transfer Reactions of Phenothiazines and Their Radical Cations in Aqueous Solution

Lakshmanan VENKATASUBRAMANIAN and Pichai MARUTHAMUTHU*
Department of Energy, University of Madras, A. C. College Campus, Madras 600025, India
(Received March 14, 1989)

The kinetics of one-electron oxidation of the protonated forms of phenothiazines namely, chlorpromazine ($CPZH^+$) and promethazine ($PMZH^+$) with the inorganic peroxides, peroxomonosulfate and peroxodisulfate in aqueous medium, were investigated by stopped flow spectrophotometric technique. The reactions of both the phenothiazines obeyed a total second-order kinetics, first-order each with respect to [phenothiazine] and [peroxide]. Both peroxides generated radical cations from the respective phenothiazines by one-electron transfer. The radical cations, $CPZH^{\cdot 2+}$ and $PMZH^{\cdot 2+}$ were found to oxidize ascorbic acid generating the parent compounds, whereas $CPZH^{\cdot 2+}$ alone was able to react with sulfite, thiosulfate and dithionite to regenerate $CPZH^+$. The kinetics of all these reactions were investigated and discussed.

There is currently a considerable interest focussed on the thermal and photoinduced electron-transfer reactions of phenothiazines and their radical cations. The primary interest in this group of compounds

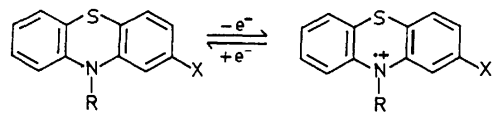

	R	X
Phenothiazine	H	H
Chlorpromazine	$(CH_2)_3$-N$(CH_3)_2$	Cl
Promethazine	$CH_2CH(CH_3)N(CH_3)_2$	H

stems from two aspects: (i) they undergo reversible one-electron redox reaction and (ii) the possible use of phenothiazines as photoredox sensitizers in solar energy conversion systems.[1-3] Furthermore, the diamine derivative of phenothiazine in conjunction with Fe(II) constitutes one of the most studied systems for photogalvanic effects.[4] Phenothiazine drugs have long been used for treatment of psychiatric diseases.[5-8] The effective use of *N*-alkylphenothiazines in psychiatric therapy is attributed to their redox reactivity. The sensitivity of these compounds towards chemical oxidation is well-known and it has been suggested that free-radical cations derived from them may be important intermediates in their potential biochemical action.[9-11]

In the present study, the kinetics of electron-transfer reactions of the protonated forms of phenothiazines (chlorpromazine, $CPZH^+$ and promethazine $PMZH^+$) with peroxosulfur salts, peroxomonosulfate (PMS) and peroxodisulfate (PDS) and the reactions of phenothiazine radical cations ($CPZH^{\cdot 2+}$ and $PMZH^{\cdot 2+}$) with various reducing agents, sulfite, thiosulfate dithionite, and ascorbic acid have been investigated.

Experimental

Chlorpromazine and promethazine were from Fluka (Switzerland). Peroxomonosulfate (Du Pont de Nemours & Co., USA) in the form of a triple salt $2KHSO_5 \cdot KHSO_4 \cdot K_2SO_4$ was used as such. All the other chemicals used were of the research grade available from E. Merck (India). The reaction solutions were prepared with doubly distilled water and were thoroughly deaerated by purified N_2 or Ar. The kinetic experiments were carried out in aqueous medium using stopped-flow technique. The details of the stopped-flow spectrophotometer and the kinetic analysis are given elsewhere.[12] The kinetics of the formation and decay of the radical cations were measured at their respective absorption maxima[13] ($CPZH^{\cdot 2+}$: λ_{max}=510 nm; ε=1.2×10^4 dm^{3}mol^{-1} cm^{-1} and $PMZH^{\cdot 2+}$: λ_{max}=505 nm; ε=9.5×10^3 dm^{3}mol^{-1}cm^{-1}).

Results and Discussion

Because of low solubility of the titled compounds in aqueous medium in neutral and alkaline conditions, the experiments have been limited to solution of pH<7, where the side-chain nitrogen atoms of both the phenothiazines are protonated (pK_a=9.3).[14] Hence the phenothiazines are represented as protonated forms, $CPZH^+$ and $PMZH^+$. The oxidants, peroxomonosulfate and peroxodisulfate were found to oxidize the protonated phenothiazines to their respective radical cations. The radical cations were found to be quite stable for several hours even in the presence of excess concentrations of these oxidants or in the absence of any other reducing agents. The radical cations generated with the stoichiometric amounts of the reactants (phenothiazine : peroxide=1 : 2) were stable for about a week.

All the experiments were carried out under pseudo-first-order conditions, [peroxide]≫[phenothiazine]. The kinetic runs were performed with [PMS] or [PDS]=1.0—5.0×10^{-3} mol dm^{-3} and [$CPZH^+$]=1.0—5.0×10^{-4} mol dm^{-3}; and [PMS]=1.0—5.0×10^{-3} mol dm^{-3}; [PDS]=1.0—5.0×10^{-2} mol dm^{-3}; and [$PMZH^+$]=1.0—5.0×10^{-4} mol dm^{-3}. The plots of log ($A_\infty - A_t$) (where A_∞ is the absorbance at the end of the reaction and A_t is the absorbance at time 't') vs. time for different initial [phenothiazine] were linear with

almost the same slope indicating the first-order dependence of the rate on [phenothiazine]. The pseudo-first-order rate constants for the formation of the radical cation, k_f'/s^{-1} were calculated from the slopes of the above mentioned plots. Variation of the initial [peroxide] at a fixed [phenothiazine] increased the rate and the corresponding plots of k_f' vs. [peroxide] were linear passing through the origin (Figs. 1 and 2) confirming the first-order dependence of the rate on [peroxide]. The overall second-order rate constants for the formation of the radical cation, $k_{2d}/dm^3\,mol^{-1}s^{-1}$ were evaluated from the slopes of the above plots (Table 1). From the observed kinetics the general rate law for the one-electron oxidation of phenothiazines by peroxides may be given as

$$\text{Rate}=\frac{d[CPZH^{\cdot 2+}\text{ or }PMZH^{\cdot 2+}]}{dt}=k_{2f}\,[\text{peroxide}][CPZH^{+}\text{ or }PMZH^{+}]$$

where $k_{2f}/dm^3\,mol^{-1}s^{-1}$ is the overall second-order rate constant for the formation of the radical cation.

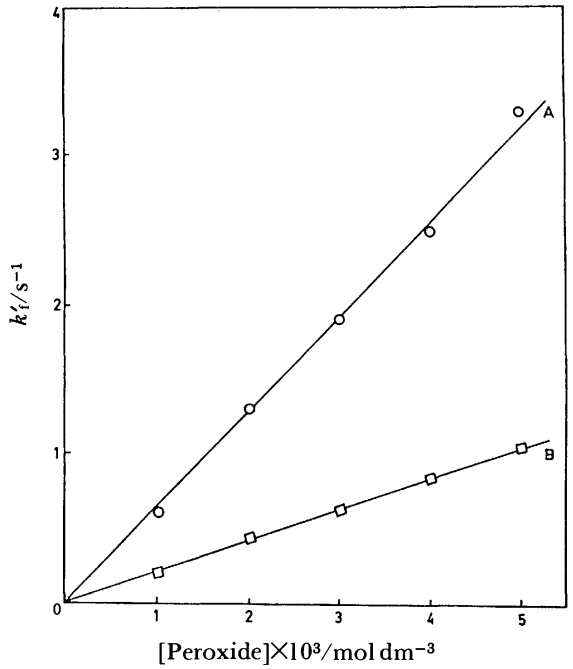

Fig. 1. Formation of $CPZH^{\cdot 2+}$: k_f' vs. [peroxide]
A: PMS; B: PDS.

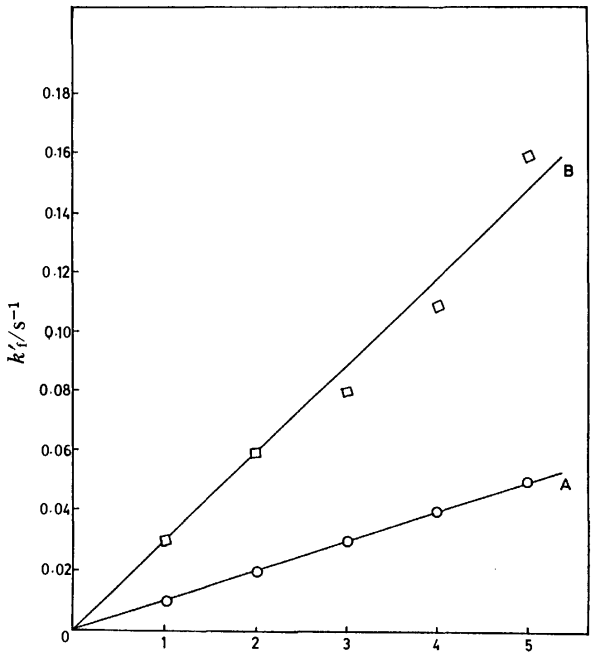

Fig. 2. Formation of $PMZH^{\cdot 2+}$: k_f' vs. [peroxide]
A: PMS; B: PDS.

Table 1. Rate Constants for the One-Electron Transfer Reactions of the Phenothiazines at pH 4.0 and Temp=25 °C

	Oxidizing agent	$k_{2f}/dm^3\,mol^{-1}\,s^{-1}$
$CPZH^+$	PMS	6.4×10^2
	PDS	2.1×10^2
$PMZH^+$	PMS	10.0
	PDS	3.1

It is known that both peroxomonosulfate and peroxodisulfate are potential electron acceptors and are two-electron oxidants. Even though the reactions are carried out at excess concentrations of these oxidants, the formation of only the radical cations and the absence of further reaction of these radical cations indicate that these peroxo salts undergo stepwise two one-electron reduction process, probably with the formation of $SO_4^{\cdot-}$ and $SO_4^{\cdot-}/\dot{O}H$ as the radical intermediates respectively with $S_2O_8^{2-}$ and HSO_5^-. These radical intermediates react fast with the substrates, again generating the respective radical cation.

The following mechanisms may be proposed for the reactions of the peroxides with phenothiazines.
Peroxomonosulfate:

$$CPZH^+/PMZH^+ + HSO_5^- \xrightarrow{\text{slow}} CPZH^{\cdot 2+}/PMZH^{\cdot 2+} + (\dot{O}H + SO_4^{2-})/(OH^- + SO_4^{\cdot-}) \quad (1)$$

$$CPZH^+/PMZH^+ + \dot{O}H/SO_4^{\cdot-} \xrightarrow{\text{fast}} CPZH^{\cdot 2+}/PMZH^{\cdot 2+} + OH^-/SO_4^{2-} \quad (2)$$

Peroxodisulfate:

$$CPZH^+/PMZH^+ + S_2O_8^{2-} \xrightarrow{\text{slow}} CPZH^{\cdot 2+}/PMZH^{\cdot 2+} + SO_4^{\cdot-} + SO_4^{2-} \quad (3)$$

$$CPZH^+/PMZH^+ + SO_4^{\cdot-} \xrightarrow{\text{fast}} CPZH^{\cdot 2+}/PMZH^{\cdot 2+} + SO_4^{2-} \quad (4)$$

From the magnitude of the second-order rate constants (Table 1) it is observed that peroxomonosulfate is ca. 3 times more reactive than peroxodisulfate, albeit, on thermodynamic grounds, peroxomonosulfate is more powerful than peroxodisulfate (E°_{PMS}=1.84 V[15] and E°_{PDS}=2.01 V[16]). The higher reactivity of

PMS over that of PDS has already been observed for the reactions of halide ions[17] and 2,2′-azinobis-(3-ethylbenzothiazole-6-sulfonate)[18] with these peroxides.

Among the phenothiazines investigated, chlorpromazine is found to be more reactive than promethazine. The rate constants measured for the formation of $CPZH^{\cdot 2+}$ and $PMZH^{\cdot 2+}$ by both the peroxides indicate that chlorpromazine reacts ca. 60—70 times faster than promethazine. This difference in reactivities is probably due to the difference in the redox potentials of the phenothiazines (E_{CPZ}=0.78 V and E_{PMZ}=0.86 V).[19]

Reactions of the Radical Cations. The reactions of the radical cations, $CPZH^{\cdot 2+}$ and $PMZH^{\cdot 2+}$ with reducing agents were performed using freshly prepared radical cations by the oxidation of $CPZH^{+}$ and $PMZH^{+}$ with stoichiometric amount of peroxomonosulfate. The radical cations were found to undergo one-electron reduction with ascorbic acid. The reaction of $CPZH^{\cdot 2+}$ with ascorbic acid was very fast and found to occur within the mixing time of the instrument (2 ms) even at a very low concentrations of the reactants ([ascorbic acid]=1×10^{-5} mol dm^{-3} and [$CPZH^{\cdot 2+}$]=1×10^{-6} mol dm^{-3}) and at low pH≤1. However the reactions of $PMZH^{\cdot 2+}$ with ascorbic acid ([ascorbic acid]=1.0—5.0×10^{-5} mol dm^{-3} and [$PMZH^{\cdot 2+}$]=1.0—5.0×10^{-6} mol dm^{-3}) was found to occur at convenient rates measurable by the stopped-flow technique. By pulse-radiolysis technique, Pelizzetti and coworkers[19] have reported the rate constant, k_2($CPZ^{\cdot 2+}$+ascorbic acid)=1.4×10^{9} dm^3 mol^{-1}s^{-1} at pH 5.9. Even though it is expected that decrease of pH will decrease the reactivity of ascorbic acid (AH_2) due to the acid-base equilibrium,[20]

$$AH_2 \underset{pKa}{\overset{4.25}{\rightleftharpoons}} AH^- + H^+ \qquad (5)$$

it is found that even at pH 1, the reaction between ascorbic acid and $CPZH^{\cdot 2+}$ is immeasurably fast to be monitored by the stopped-flow technique. The kinetic investigation of the reaction of $PMZH^{\cdot 2+}$ with ascorbic acid exhibited an overall second-order reaction, first-order each with respect to [ascorbic acid] and [$PMZH^{\cdot 2+}$]. The linear plots of log (absorbance) vs. time and the almost constant slope for different initial [$PMZH^{\cdot 2+}$] indicate the first-order dependence of the rate on [$PMZH^{\cdot 2+}$]. The pseudo-first-order rate constants for the decay of the radical cation, k_d'/s^{-1} were calculated from the slopes of the above plots. Increase in the [ascorbic acid] increased the rate and the plot of k_d' vs. [ascorbic acid] is a straight line passing through the origin confirming the first-order dependence of the rate on [ascorbic acid]. The slope of the above plot gives the second-order decay rate constant, k_{2d}/dm^{3}mol^{-1}s^{-1}. The rate constants for the reaction of $CPZH^{\cdot 2+}$ with the other reducing agents, SO_3^{2-}, $S_2O_3^{2-}$, and $S_2O_4^{2-}$ were also determined (Fig. 3 and Table 2; [$CPZH^{\cdot 2+}$]=1.0—5.0×10^{-4} mol dm^{-3}; [SO_3^{2-}] or [$S_2O_3^{2-}$]=1.0—5.0×10^{-3} mol dm^{-3} and [$S_2O_4^{2-}$]=1.0—5.0×10^{-4} mol dm^{-3}). There was no detectable reaction between these reducing agents with $PMZH^{\cdot 2+}$.

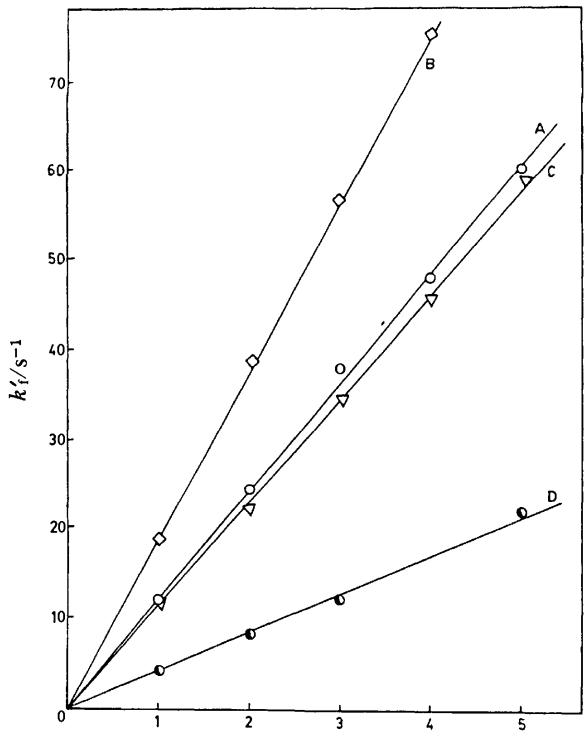

A and B, [RA]$\times10^3$/mol dm^{-3}; C, [RA]$\times10^4$/mol dm^{-3}; D, [RA]$\times10^5$/mol dm^{-3};

Fig. 3. Decay of $CPZH^{\cdot 2+}$ or $PMZH^{\cdot 2+}$: k_d' vs. [reducing agent] A: SO_3^{2-}; B: $S_2O_3^{2-}$; C: $S_2O_4^{2-}$; and D: AH_2.

Table 2. Rate Constants for the One-Electron Transfer Reactions of the Phenothiazine Radical Cations at Temp=25 °C

	Reducing agent	pH	k_{2d}/dm^3 mol^{-1} s^{-1}
$PMZH^{\cdot 2+}$	Ascorbic acid	2.2	4.1×10^5
		5.9	1.3×10^{9} [a]
$CPZH^{\cdot 2+}$	Ascorbic acid	1.0	$>10^6$
		5.9	1.4×10^{9} [a]
	SO_3^{2-}/HSO_3^-	6.0	1.2×10^4
	$S_2O_3^{2-}$	6.0	1.9×10^4
	$S_2O_4^{2-}$	6.0	1.2×10^5

a) Data from Ref. 19.

The mechanism of oxidation of ascorbic acid may be given as

$$PMZH^{\cdot 2+} + AH_2/AH^- \xrightarrow{slow} PMZH^+ + (AH^{\cdot} + H^+)/(A^{\cdot -} + H^+) \qquad (6)$$

$$AH^{\cdot}/A^{\cdot -} \xrightarrow{fast} \text{product} \qquad (7)$$

conforming to the rate law,

$$\text{Rate} = \frac{-d[PMZH^{\cdot 2+}]}{dt} = k_{2d}[PMZH^{\cdot 2+}][\text{reducing agent}].$$

From the magnitudes of the second-order rate constants for the above reaction at two different pH, 2.2 and 5.9, the reactivity of AH^- is found to be ca. 10^3 times higher than that of AH_2.

The proposed rate law and the mechanisms for the reactions of $CPZH^{\cdot 2+}$ with sulfite, thiosulfate and dithionite may be given as,

$$\text{Rate} = \frac{-d[CPZH^{\cdot 2+}]}{dt} = k_{2d}[CPZH^{\cdot 2+}][\text{reducing agent}].$$

$$CPZH^{\cdot 2+} + SO_3^{2-}/HSO_3^- \xrightarrow{\text{slow}} CPZH^+ + SO_3^{\cdot -}/SO_3^{\cdot -} + H^+ \quad (8)$$

$$2SO_3^{\cdot -} \xrightarrow{\text{fast}} S_2O_6^{2-} \quad (9)$$

$$CPZH^{\cdot 2+} + S_2O_n^{2-} \xrightarrow{\text{slow}} CPZH^+ + S_2O_n^{\cdot -} \quad (10)$$
$$(n=3 \text{ and } 4)$$

$$2S_2O_n^{\cdot -} \xrightarrow{\text{fast}} S_4O_6^{2-} + (n-3)O_2. \quad (11)$$

From the magnitudes of the second-order rate constants, the reactivity trend of the reducing agents is in the order, ascorbic acid>dithionite>thiosulfate> sulfite.

In conclusion, chlorpromazine and promethazine are oxidized to the stable radical cations, $CPZH^{\cdot 2+}$ and $PMZH^{\cdot 2+}$ by the inorganic peroxides, peroxomonosulfate and peroxodisulfate. Although these two radical cations individually oxidize ascorbic acid to revert back to the parent compounds, only $CPZH^{\cdot 2+}$ was found to react with the other reducing sulfur compounds, sulfite, thiosulfate, and dithionite.

One of the authors (LV) gratefully acknowledges the Council of Scientific and Industrial Research, New Delhi for the financial support in the form of fellowship.

References

1) S. Alkaitis, G. Beck, and M. Gratzel, *J. Am. Chem. Soc.*, **97**, 5723 (1975).

2) S. Alkaitis, M. Gratzel, and A. Henglein, *Ber. Bunsenges Phys. Chem.*, **79**, 541 (1975).

3) M. Maestri and M. Gratzel, *Ber. Bunsenges Phys. Chem.*, **81**, 504 (1977).

4) K. G. Mathai and E. Rabinowitch, *J. Phys. Chem.*, **66**, 663 (1962). T. Sakata, Y. Suta, J. Tanaka, and H. Tsubomura, *J. Phys. Chem.*, **81**, 537 (1977).

5) "Phenothiazines and Structurally Related Drugs: Advances in Biochemical Pharmacology, Volume 9," ed by I. S. Forrest, C. J. Carn, and E. Usdin, Raven Press, New York (1974).

6) "Phenothiazines and Structurally Related Drugs: Basic and Clinical Studies; Developments in Neurosciences, Volume 7," ed by E. Usdin, H. Eckest, and I. S. Forrest, Elsevier-North Holland, Amsterdam (1980).

7) S. H. Curry, "Biological Effects of Drugs in Relation to this Plasma Concentration," Proceedings of an International Symposium, 1972, ed by D. S. Davies, Univ. Park Press, Baltimore (1973), p. 201.

8) S. H. Curry, "Wenner-Green Centre International Symposium Series 1984," (1976), p. 343.

9) E. Pelizzetti and E. Mentasti, *Inorg. Chem.*, **18**, 583 (1979).

10) T. J. Kemp, P. Moore, and G. R. Quick, *J. Chem. Soc., Perkin Trans. 2*, **1980**, 291.

11) N. A. Klein and D. L. Troppen, *J. Am. Chem. Soc.*, **100**, 4541 (1978).

12) P. Maruthamuthu, L. Venkatasubramanian, and P. Dharmalingam, *Bull. Chem. Soc. Jpn.*, **60**, 1113 (1987).

13) D. Bahneman, K. D. Asmus, and R. L. Willson, *J. Chem. Soc., Perkin Trans. 2*, **1983**, 1661.

14) A. Hulshaff and J. H. Perkin, *Pharm. Acta Helv.*, **51**, 65 (1976).

15) J. S. Price, I. R. Tasker, E. H. Appelman, and P. A. G. O'Hare, *J. Chem. Thermodyn.*, **18**, 923 (1986).

16) D. A. House, *Chem. Rev.*, **62**, 185 (1962).

17) F. Seuo and M. Venturini, *J. Chem. Soc., Dalton Trans.*, **1976**, 1410.

18) L. Venkatasubramanian and P. Maruthamuthu, *Int. J. Chem. Kinet.*, **21**, 399 (1989).

19) E. Pelizzetti, D. Meisel, W. A. Mulac, and P. Neta, *J. Am. Chem. Soc.*, **101**, 6954 (1979).

20) G. Kortum, W. Vogel, and K. Andruesov," Dissociation Constants of Organic Acids in Aqueous Solutions," Butterworths, London (1961).

Photoelectric Effect of Metallophthalocyanine Derivatives

Ryo HIROHASHI,* Toyohide TANAKA, Yoshihiro KOSHIJIMA, and Masafumi KAMIYAMA
Department of Image Science and Engineering, Faculty of Engineering, Chiba University, Yayoi-cho 1-33, Chiba-shi 260
(Received December 16, 1988)

Synopsis. The photoelectric effect of copper phthalocyanine derivatives ($CuPcR_4$) in a dispersed system in polycarbonate (PC) has been investigated with a sandwich-typed cell configuration of Au/$CuPcR_4$ in PC/Ag. When the incident irradiation was directed through the Ag electrode, the photocurrent and photovoltage were observed for all $CuPcR_4$ cells. It has been concluded that the photoelectric characteristics are not missed and that the values of the work functions of all $CuPcR_4$ derivatives are between 4.67 and 4.78 eV.

Metallophthalocyanines (MPc) have been shown to be characteristic of the photoconductivity between visible and infrared irradiation. These materials are used in the field of imaging technology as organic photoconductors[1] or as organic solar cells.[2] The thin films of MPc are prepared by vacuum evaporation,[3] ion sputtering,[4] and a dispersed system in a polymer.[5] We have investigated the photoelectric effect of copper phthalocyanine derivatives ($CuPcR_4$) in a dispersed system in polycarbonate. These $CuPcR_4$ were synthesized by sulfonylation of CuPc or by the Wyler method[6] of trimellitic anhydride with urea.

Experimental

Materials (Specimen). The $CuPcR_4$ derivatives used in the present experiments were synthesized by the methods shown in Fig. 1. The structures of $CuPcR_4$ derivatives are shown in Fig. 2. Though the positions of the substituents in $CuPc(CONH_2)_4$ and $CuPc(COCl)_4$ could be determined in the synthetic processes, the positions of $CuPc(SO_2Cl)_4$ obtained by a substitution reaction of CuPc could not confirmed. Purification of these $CuPcR_4$ derivatives by sublimation at about 600 °C was not successful.

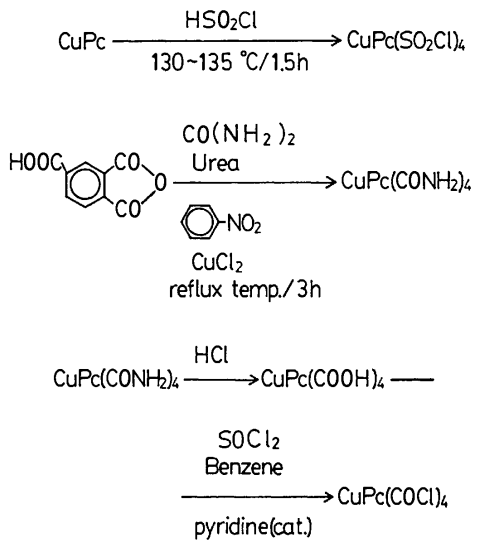

Fig. 1. The synthetic process of CuPc derivatives.

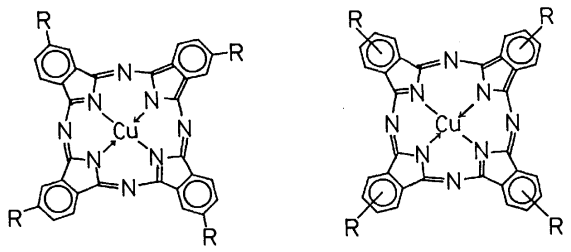

Fig. 2. The molecular structure of CuPc derivatives. The positions of the substituents in $CuPc(COCl)_4$ and $CuPc(CONH_2)_4$ are determined, but $CuPc(SO_2Cl)_4$ is not confirmed.

IR and UV Spectera. The IR spectra from 700 to 800 cm^{-1} of the $CuPcR_4$ derivatives show characteristic absorption at 740 and 790 cm^{-1}; these $CuPcR_4$ derivatives were expected to have a β-type crystalline structure.[7] The IR absorption spectra did not change upon dipping in THF (tetrahydrofuran) for about 24 hours. Since there is no good solvent for these $CuPcR_4$ derivatives, each $CuPcR_4$ derivative was dipped in hot 1-chloronaphthalene for 48 hours. The UV and visible spectral peaks, thus obtained, are shown in Table 1.

Cell Structure. A sandwich-typed cell configuration of Au/$CuPcR_4$ in PC/Ag was used in the experiment; R and PC are substituents and polycarbonate, respectively. The semi-transparent electrode of Au and Ag were coated on the sample by an ion-sputtering method. PC was used as a binder: the $CuPcR_4$ derivatives were blended with PC (weight ratio of 1 to 2) by dispersing for 48 hours with ball-milling by the addition of THF; the resulting product formed into a film by a spin-coating method. The connection between the electrode and lead wire (Ag) was made by the use of an Ag paste (Du Pont).

Measurements. Measurements of the dark current and photocurrent were carried out in a cryostat in vacuum (ca. 10^{-5} Torr; 1 Torr≈133.322 Pa) through the Au or Ag electrode. The apparatus used for the current measurement and spectroscopy were a vibrating reed electrometer (Advantest TR-84M) and a monochromator (Nikon G-250), respectively. Work functions were measured using a low-energy UPS system (Riken Keiki AC-1).

Table 1. Wavelength of Absorption Peaks

	Solution/nm		Dispersed in PC/nm	
CuPc	608	688	650	734
$CuPc(COCl)_4$	628	694	600	710
$CuPc(SO_2Cl)_4$	644	717	605	720
$CuPc(CONH_2)_4$	642	710	632	705

Wavelength of absorption peaks observed on the solution of CuPc derivatives in 1-chloronaphthalene and on the dispersed system in polycarbonate.

Results and Discussion

Dark Current. The applied field dependence of dark current for Au/CuPc$(SO_2Cl)_4$ in PC/Ag cell structure is shown in Fig. 3. The observed non-linearity indicates the presence of a barrier in this device. The highest dark conductivity is obtained in CuPc$(COCl)_4$, followed by CuPc$(SO_2Cl)_4$. The least conductive derivative on the dark state is CuPc-$(CONH_2)_4$. We can note that the dark current is affected by the structure of each molecule.

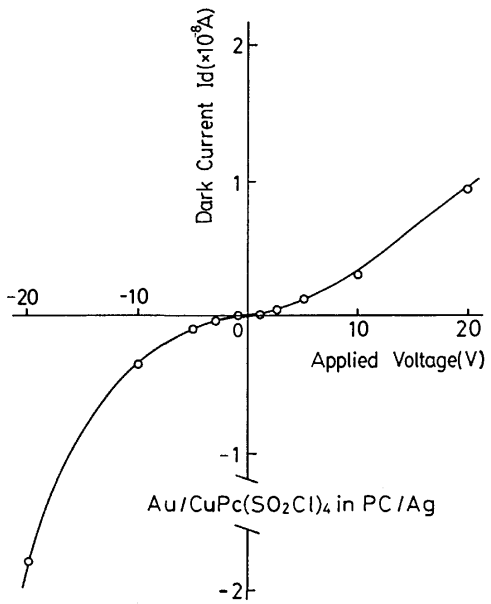

Fig. 3. Applied voltage dependence of dark current for Au/CuPc$(SO_2Cl)_4$ dispersed in PC/Ag cell structure. Applied voltage is measured on the basis of Ag electrode. Thickness of the cell is approximately 10 μm.

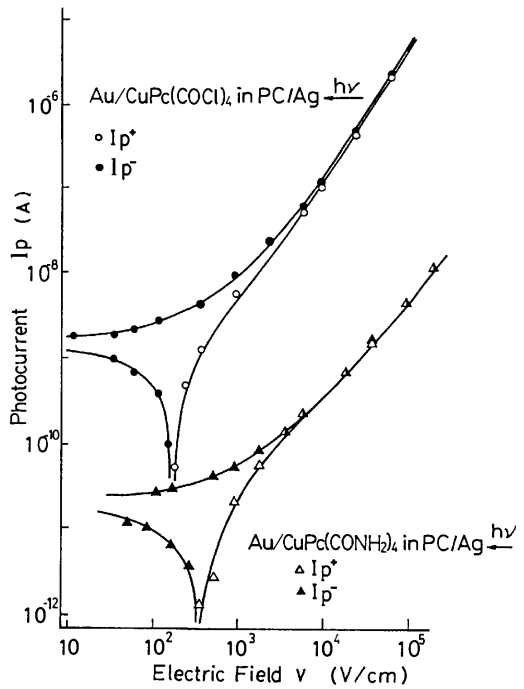

Fig. 4. Applied field dependence of photocurrent for Au/CuPcR$_4$ dispersed in PC/Ag type cells. R is substituent. The signs of I_p^+ and I_p^- represent the polarities of irradiated electrode. The magnitude of photocurrent is the absolute value.

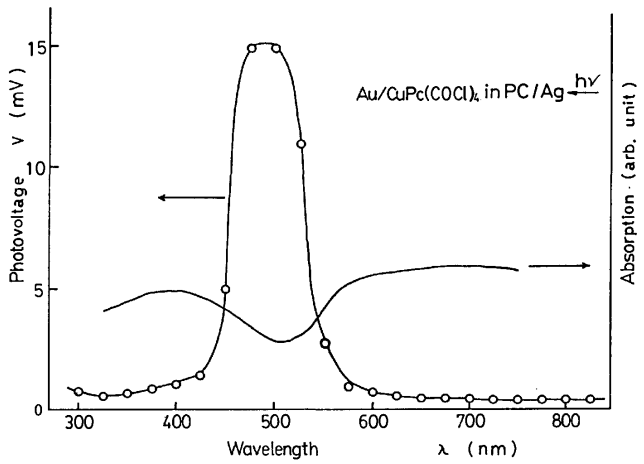

Fig. 5. Action spectrum of photovoltage for Au/CuPc$(COCl)_4$ dispersed in PC/Ag cell, and absorption spectrum of dispersed system (CuPc$(COCl)_4$ in PC. The thickness of the cell is approximately 10 μm. Irradiated electrode is Ag plane.

Photocurrent. The applied field dependences of the photocurrent are shown in Fig. 4. In this figure, the polarity signs of the current were determined by the polarity of the Ag electrode potential. The current and electric field are indicated in absolute value.[8] The photoelectric sensitivity is determined by the ratio of the photocurrent to the dark current (I_p/I_d); these ratios for CuPc$(CONH_2)_4$, CuPc$(SO_2Cl)_4$ and CuPc-$(COCl)_4$ at about 10^3 V cm^{-1} were approximately 14.5, 7.4, and 4.8, respectively. These values may be rather higher than for dispersed systems. The current tends to greatly decrease around 10^2 V cm^{-1} (Fig. 4), indicating that it comes to equilibrium between the applied voltage and photovoltage.

Photovoltage. The photovoltages of CuPc$(CONH_2)_4$, CuPc$(SO_2Cl)_4$, and CuPc$(COCl)_4$ generated by direct irradiation through the Ag electrode with a Xenon lamp, and then followed photocurrent measured by potentiometry, were approximately 200, 110, and 140 mV, respectively. When the Ag electrode is irradiated, the positive polarity of the photovoltage was obtained in all cases. The action spectrum of the photovoltage for Au/CuPc$(COCl)_4$ in PC/Ag cell is shown in Fig. 5. Due to the internal resistance of the voltmeter, the measured photovoltages are smaller than the true values, though the relative forms are not affected. In Fig. 5, the photovoltage peak is obtained in the wavelength region where absorption is the weakest. On the other hand, when the incident irradiation was directed through the Au electrode, a photovoltage was not generated. These result show that the photovoltage is generated not at the Au interface but, rather, only at the Ag interface. Consequently, a Schottky barrier could be formed between the CuPcR$_4$ and Ag interface. The work functions of Au and Ag

are 4.78 and 4.67 eV, and these interfaces form ohmic and Schottky barrier, respectively. Therefore, the values of the work function of the $CuPcR_4$ derivatives are between 4.67 and 4.78 eV.

References

1) R. O. Loutfy, C. K. Hisiao, A. M. Hor, and C. Dipaola-Baranyi, *Photo. Sci. and Eng.*, **29**, 148 (1985).
2) M. Martin, J. J. Andre, and J. Simon, *Nouveal J. Chimie*, **5**, 485 (1981).
3) T. Tanaka and R. Hirohashi, *Electrophotography*, **26**, 240 (1987).
4) S.Miyata, Y. H. Park, Y. Soeda, R. Itoh, and S. Tasaka, *Jpn. J. Appl. Phys.*, **10**, L1632 (1987).
5) N. C. Khe and M. Aizawa, *Nippon Kagaku Kaishi*, **1986**, 393.
6) M. Wyler (ICI), BP 464126 (1936).
7) A. A. Ebert, Jr. and H. B. Gottieb, *J. Am. Chem. Soc.*, **74**, 2806 (1952).
8) T. Tanaka and R. Hirohashi, *Electrophotography*, **25**, 32 (1986).

Interaction of Sodium Dodecyl Sulfate with Pig Serum Low-Density Lipoprotein

Yuki YANO, Toshio TAKAGI,† and Masanobu JANADO*,††
Department of Education, Kogakkan University, Ise-shi 516
†Institute for Protein Research, Osaka University, Suita, Osaka 565
††Department of Food Science, Kyoto Women's University, Kyoto 605
(Received December 20, 1988)

Synopsis. The interaction of sodium dodecyl sulfate (SDS) with the pig serum low-density lipoprotein (LDL) showed a subtle dependence on the SDS concentration. At the SDS concentrations below 0.01%, the binding isotherm conformed to the Langmuir's type, from which the maximum number of the binding site and the intrinsic binding constant were respectively estimated to be 1600 mol mol^{-1} and 6.5×10^3 (mol dm^{-3})$^{-1}$. At the SDS concentrations at or above 0.03%, the LDL structure irreversibly dissociated.

Sodium dodecyl sulfate (SDS), a well-known protein denaturant, has been widely used for various analytical purposes in protein chemistry. The protein denaturation by SDS is believed to involve the hydrophobic binding of SDS and consequent structural unfolding of protein molecules.[1,2] Interaction of SDS with lipoproteins, the micellar complexes of lipid and protein, is expected to be more complex, as both stabilizing and destabilizing effect can be resulted depending on the SDS concentration. The serum lipoproteins in general are quite unstable, readily undergoing irreversible aggregation, particularly after separation, and that often hampers the routine biochemical analyses of the lipoproteins. In this context, elucidation of the SDS-lipoprotein interaction is not only of interest but also profitable in view of possible stabilizing effect of SDS. This communication describes the effects of SDS on the structure of the pig serum low density lipoprotein (LDL) which is known to be closely similar to the human serum LDL in the physicochemical properties.[3]

The pig serum LDL was prepared by ultracentrifugal flotation and, where necessary, separated into two fractions (LDL_1 and LDL_2) by differential flotation.[3] The LDL fractions were exhaustively dialyzed against 0.1 mol dm^{-3} NaCl containing 0.02% EDTA in which most of the measurements were conducted. (For analysis of lithium dodecyl sulfate (LDS)-LDL interaction, 0.1 mol dm^{-3} LiCl was used as the background solution.) The binding data were obtained by the frontal gel chromatography[4] as well as by the equilibrium dialysis at an LDL concentration of 0.1% with the SDS concentration varying from 0.001 to 0.033%. The velocity sedimentation was carried out in a Hitachi model SCP 70H ultracentrifuge equipped with a UV scanner, and gel filtration was performed on a Superose 6 column (1×30 cm, Pharmacia) using an FPLC system (Pharmacia). The SDS-LDL mixtures for the sedimentation and gel filtration experiments were prepared by dializing an appropriate amount of LDL solution (0.1%) against a large volume of SDS solution for 48 hours at 20 °C. Therefore, the SDS concentrations in the mixtures, denoted as [s] in the results, refer to the equilibrium concentrations of free SDS. The distribution curve of the sedimentation coefficient, $g(s)$, was produced from the differential concentration diagram (dc/dx vs. x) according to the equation,[5]

$$g(s)=\frac{1}{c_0}\frac{dc}{dx}\left(\frac{x}{x_m}\right)^2(x\omega^2t),$$

where c_0 is the initial concentration, x the distance from the axis of rotation, x_m the distance to the meniscus, and t and ω the effective centrifugation time and angular velocity, respectively.

Figure 1 shows the binding curve for SDS-LDL in 0.1 mol dm^{-3} NaCl in which the data obtained at two temperatures, 5 ° and 20 °C, were plotted according to the Langmuir's adsorption isotherm in the form,[6]

$$\frac{1}{\theta}=\frac{1}{nk}\cdot\frac{1}{[s]}+\frac{1}{n},$$

where θ is the number of moles of bound SDS per mole of LDL, n the number of the binding site on LDL molecule, K the association constant and [s] the equilibrium concentration of free SDS, respectively. Two prominent features are revealed in Fig. 1: first, at the low concentrations of SDS ([s]<ca. 0.01%) the SDS-LDL binding conforms to the Langmuir's adsorption isotherm giving a linear plot, but it breaks at around [s]=0.01% above which the plot extrapolates to $n=\infty$ and second, the SDS-LDL binding is little affected by temperature. The binding parameters of SDS-LDL at the low SDS concentrations were:

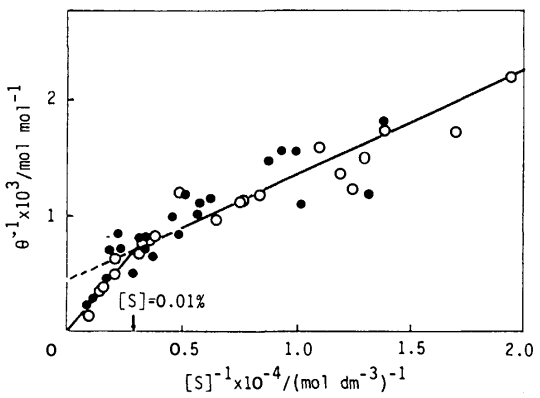

Fig. 1. Binding isotherms for SDS-LDL in 0.1 mol dm^{-3} NaCl at 20 °C (●) and 5 °C (○). θ is the number of moles of bound SDS per mole of LDL and [s] is the equilibrium concentration of free SDS. Concentration of LDL was fixed at 0.1%.

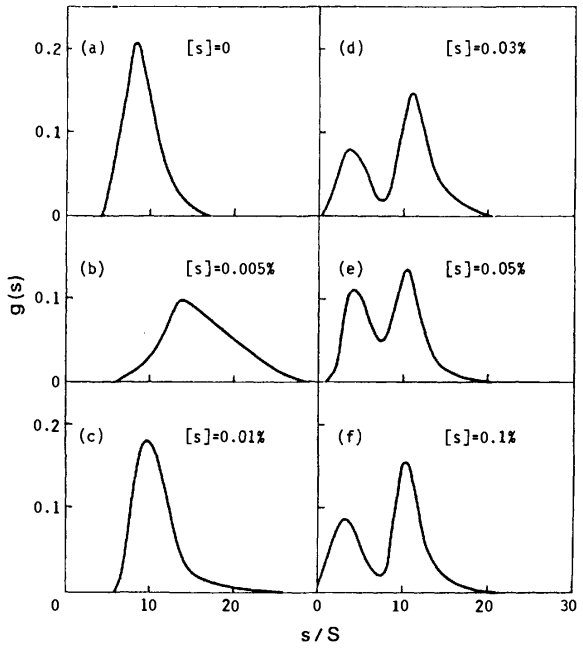

Fig. 2. Effect of SDS concentration on the distribution curve of sedimentation coefficient, $g(s)$, of LDL. [s] refers to the equilibrium concentration of free SDS in the LDL solutions. Concentration of LDL was 0.1%.

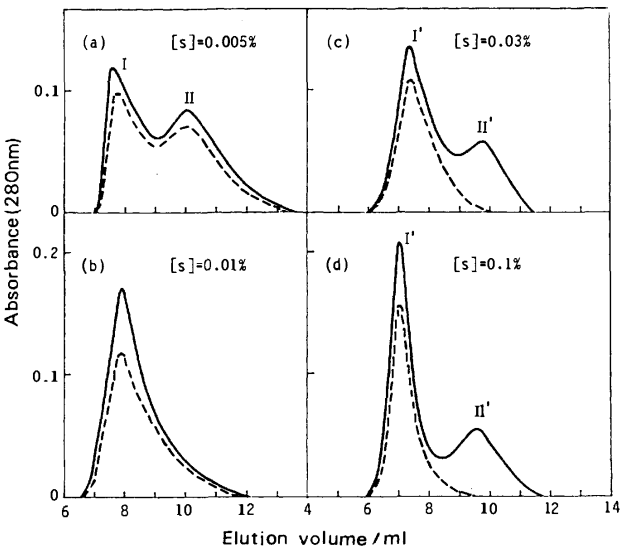

Fig. 3. Effect of SDS concentration on the gel filtration profile of LDL. [s] refers to the equilibrium concentration of free SDS. Gel filtration was performed on a column of Superose 6 (1×30 cm) preequilibrated with the eluent (0.1 mol dm^{-3} NaCl) containing SDS to the concentrations indicated by [s]. The loading concentration of LDL was 0.1%. ——, Absorbance at 280 nm; ----, Lowry's protein.

K=5×10^3 (mol dm^{-3})$^{-1}$ and n=2×10^3 mol mol^{-1}. The binding isotherm for lithium dodecyl sulfate (LDS)-LDL interaction was much similar to that of SDS-LDL interaction yielding n=2×10^3 mol mol^{-1} and K=5×10^3 (mol dm^{-3})$^{-1}$. Figure 2 shows the distribution profiles of the sedimentation coefficient, $g(s)$, of SDS-LDL (0.1%) mixtures with various SDS concentrations. At [s]=0.005% (Fig. 2b), the $g(s)$ curve was notably broad as compared to that at [s]=0 (Fig. 2a), but by increasing [s] to 0.01% it nearly restored the original profile with somewhat increased sedimentation coefficient (Fig. 2c). It is important to note that the broadening and sharpening of the $g(s)$ curves observed at the two concentrations could readily be reversed each other by adjusting [s] by dialysis. Further increases of [s] to above 0.03% caused an irreversible structural dissociation leading to bimodal $g(s)$ curves (Figs. 2d—f).

Figure 3 shows the result of gel filtration obtained for SDS-LDL (0.1%) mixtures with [s] varying from 0.005% to 0.1%. It is to be noted that, due to an LDL-gel interaction, the elution of LDL required the presence of at least 0.005% SDS in the eluent, and hence that the apparent elution volume cannot be directly related to the molecular size. The SDS effect manifested in Figs. 3a and 3b at the low concentrations ([s]<0.01%) was completely reversible, but that observed at the higher concentrations (Figs. 3c and 3d) could not be reversed. The two fractions of Fig. 3a (I and II) both contained protein (the Lowry's protein) and all the lipid components of LDL, i.e., phospholipids, neutral lipids, cholesterol and its ester, and sphingolipids. (The lipid components were identified by thin-layer chromatography after extraction in a chloroform(2)-methanol(1) mixture.) In contrast, as shown in Figs. 3c and 3d, protein was found only in fraction I', although both fractions (I' and II') contained the lipid components.

The present study shows that the mode of the interaction between LDL and SDS depends on the concentration of the latter. At the low SDS concentrations ([s]=0.005—0.01%), the binding isotherm conformed to the Langmuir's type, and the relevant thermodynamic parameters were estimated to be: $\Delta F°$=—5.0 kcal mol^{-1}, $\Delta H°$=0, $\Delta S°$=17 e.u., respectively. The entropic nature of the interaction suggests involvement of the hydrophobic effect. However, even within the narrow range of [s](0.005—0.01%), the state of LDL molecule varies with the SDS concentration: as evident from Fig. 2 (b and c) and Fig. 3 (a and b), at [s]=0.005% LDL reversibly associates to form their oligomers which, upon increasing [s] to 0.01%, dissociates into the monomeric units possessing somewhat greater sedimentation coefficients than the intact LDL. This increment in the sedimentation coefficient may be attributed to the SDS binding. The nature of the reversible association-dissociation of LDL is not clear, but it may be worth to note that a similar behavior was observed for the mixtures of the human serum LDL and dextran sulfate (DS), i.e., aggregation of LDL-DS complexes at low DS/LDL ratios and disaggregation at high DS/LDL ratios.[7,8] The former was attributed to the ionic interactions between LDL-SDS complexes and LDL molecules, and the latter to disruption of the ionic interactions consequent upon an increased binding of DS leading to an increased negative charge density on the LDL molecules. It may tentatively be assumed that a sim-

ilar mechanism operates in the present system.

Upon further increases in [s] to above 0.01%, e.g. 0.03%, the LDL structure appears to irreversibly disintegrate. Breake of the linearity of the binding isotherm at around 0.01% of [s], leading to $n=\infty$ (Fig. 1), may be indicative of a structural dissociation of LDL molecule with subsequent micellar complex formation between SDS and the dissociated LDL fragments. Indeed, this postulate is strongly supported by the sedimentation and gel filtration experiments which revealed that at high SDS concentrations ([s]$\geq$0.03%) LDL irreversibly dissociated into two fragments, an apoprotein containing fraction and a nonprotein fraction (Figs. 2d—2f, 3c, and 3d).

Since there is no additional peak detectable other than the main peak in both sedimentation and gel filtration experiments at [s]=0.01% (Figs. 2c and 2b), one may reasonably conclude that LDL molecules retain their original structures with their hydrophobic surfaces covered by the bound SDS. As expected, SDS of this concentration was found to protect LDL from the disruptive effect of NaSCN,[9] a highly chaotropic salt.

References

1) J. A. Reynolds and C. Tanford, *J. Biol. Chem.*, **245**, 5161 (1970).
2) K. Shirahama, K. Tsujii, and T. Takagi, *J. Biochem.*, **75**, 309 (1974).
3) M. Janado, W. G. Martin, and W. H. Cook, *Can. J. Biochem.*, **44**, 1201 (1966).
4) M. Janado, Y. Yano, H. Nakamori, and T. Nishida, *J. Biochem.*, **86**, 177 (1979).
5) H. K. Schachman, "Ultracentrifugation in Biochemistry," Academic Press, New York (1959), p. 133.
6) I. M. Klotz, F. M. Walker, and R. B. Pivan, *J. Am. Chem. Soc.*, **68**, 1486 (1946).
7) M. Janado and T. Nishida, *J. Lipid Res.*, **6**, 331 (1965).
8) M. Janado and T. Nishida, *Arg. Biol. Chem.*, **36**, 301 (1972).
9) M. Janado, Y. Yano, H. Nishida and T. Nishida, *J. Solution Chem.*, **10**, 839 (1986).

The Preparation and Stereoselectivity of [Cr(L- or D-ala)$_x$(L-leu)$_{3-x}$] and the Possibility of the Optical Resolution of DL-Alanine

Yoshitake YOSHIMURA,* Yuichi KATAOKA, Hirobumi MORIISHI,†
Tetsuo WATANABE,† and Hisaya OKI†
Department of Industrial Chemistry, Fukui National College of Technology, Geshi-cho, Sabae-shi 916
†Department of Chemistry, Faculty of Education, Fukui University, Bunkyo, Fukui-shi 910
(Received September 2, 1988)

Synopsis. *fac*-(+)$_{546}$-[Cr(L-ala)$_2$(L-leu)]·1.5H$_2$O and *fac*-(−)$_{546}$-[Cr(D-ala)$_2$(L-leu)]·1.5H$_2$O were prepared by the method using an ethanol solution, with [Cr(L-leu)$_2$(NCS)(OH$_2$)](leu=leucinato) with L- or D-alanine used as the starting material respectively. Also, *fac*-[Cr(L- or D-ala)(L-leu)$_2$]·2H$_2$O was obtained from the filtrate, the standing temperatures were 5, 25, 40, and 55 °C. The optical purity of *fac*-(Λ)-[Cr(L- or D-ala)(L-leu)$_2$]·2H$_2$O increases with the rise in the standing temperature. In the case of DL-alanine, [Cr(L-ala)$_2$(L-leu)]·1.5H$_2$O and [Cr(D-ala)(L-leu)$_2$]·2H$_2$O were obtained during heating and from the filtrate respectively. By using this procedure, the possibility of the optical resolution of DL-alanine was shown.

We reported previously that tris(amino acidato)chromium(III) complexes which exhibit very high stereoselectivities were obtained by a solid state reaction[2,3] or by use of an ethanol solution.[3] However, no study has been reported concerning the preparation of chromium(III) mixed amino acidato complexes except for that of Watabe et al.[4] It is interesting to study the stereoselectivity in the case of the chromium(III) complexes involving different kinds of amino acid ligands.

We will report here the preparation of some new (mixed amino acidato) chromium(III) complexes containing L-leucine and L- or D-alanine, using [Cr(L-leu)$_2$(NCS)(OH$_2$)] as the starting material. A very high stereoselectivity was also remarked in the cases of the (mixed amino acidato) chromium(III) complexes.

An optical resolution of DL-alanine based on the different reactivities of [Cr(L-leu)$_2$(NCS)(OH$_2$)] to L- and D-alanine is suggested.

Experimental

a) Preparation of the Starting Material, [Cr(L-leu)$_2$(NCS)(OH$_2$)]·H$_2$O. A solution of Reinecke's salt, NH$_4$[Cr(NH$_3$)$_2$(NCS)$_4$]·H$_2$O (2×10^{-2} mol),[5] and L-leucine (6×10^{-2} mol) in 200 cm^3 of H$_2$O was evaporated to dryness in an evaporating dish on a water bath. The residue was washed with 80 cm^3 of H$_2$O. After air-drying, the solid was dissolved in 200 cm^3 of ethanol. After filtration, the filtrate was added to 400 cm^3 of H$_2$O, causing an immediate precipitation of the purple crystals. These crystals were subsequently dried overnight at 55 °C; yield, 21%. Found: C, 37.91; H, 6.72; N, 10.93%. Calcd for CrC$_{13}$H$_{26}$O$_5$N$_3$S: C, 38.39; H, 6.89; N, 10.34%.

b) Preparation of (Mixed Amino Acidato)Chromium(III) Complexes, [Cr(L- or D-ala)$_2$(L-leu)]·1.5H$_2$O and [Cr(L- or D-ala)(L-leu)$_2$]·2H$_2$O. A solution of [Cr(L-leu)$_2$(NCS)(OH$_2$)]·H$_2$O (406 mg: 1×10^{-3} mol) in 50 cm^{-3} of ethanol was added to L-alanine (89 mg: 1×10^{-3} mol). After the addition of 0.5 cm^3 of butylamine, the mixed solution was refluxed for 5 hours at 75 °C. Pink crystals were deposited during the heating. After immediate filtration and washing with ethanol and methanol, [Cr(L-ala)$_2$(L-leu)]·1.5H$_2$O was obtained.

The filtrate was separated into four portions, which were then placed in sealed flasks. They were kept at 5, 25, 40, and 55 °C respectively. The crystals grown in the flasks were filtered after 10 days. In spite of the difference in the standing temperature, only pink crystals of [Cr(L-ala)(L-leu)$_2$]·2H$_2$O were obtained.

By the same method, in the case of D-alanine [Cr(D-ala)$_2$(L-leu)]·1.5H$_2$O was obtained as a purplish pink powder during the heating. From the filtrate, [Cr(D-ala)(L-leu)$_2$]·2H$_2$O was obtained. With the use of DL-alanine [Cr(L-ala)$_2$(L-leu)]·1.5H$_2$O was obtained during the heating and [Cr(D-ala)(L-leu)$_2$]·2H$_2$O was obtained from the filtrate. The yields and elementary analyses are summarized in Table 1.

Measurements. The VIS-UV spectra were measured with a Hitachi 124 spectrophotometer in DMSO. The CD measurements were made with a JASCO-J-500A spectropolarimeter in DMSO.

Table 1. Analytical Data and Yields of [Cr(ala)$_x$(L-leu)$_{3-x}$](10 Days Standing)

Complex		C	H	N	Yield%
CrC$_{12}$H$_{27}$O$_{7.5}$N$_3$	Calcd.	37.37	7.00	10.90	
(1) [Cr(L-ala)$_2$(L-leu)]·1.5H$_2$O[a]	Obsd.	37.42	6.80	10.55	16—22
(2) [Cr(D-ala)$_2$(L-leu)]·1.5H$_2$O[a]	Obsd.	37.85	6.93	10.56	10—15
(3) [Cr(L-ala)$_2$(L-leu)]·1.5H$_2$O[a]	Obsd.	37.74	6.79	10.75	16—22
CrC$_{15}$H$_{32}$O$_8$N$_3$	Calcd.	41.28	7.85	9.63	
(4) [Cr(L-ala)(L-leu)$_2$]·2H$_2$O[b]	Obsd.	41.38	7.87	9.43	8— 9
(5) [Cr(L-ala)(L-leu)$_2$]·2H$_2$O[c]	Obsd.	41.76	7.78	9.60	38—45
(6) [Cr(D-ala)(L-leu)$_2$]·2H$_2$O[b]	Obsd.	41.59	7.83	9.52	8— 9
(7) [Cr(D-ala)(L-leu)$_2$]·2H$_2$O[c]	Obsd.	41.48	7.92	9.33	38—43
(8) [Cr(D-ala)(L-leu)$_2$]·2H$_2$O[b]	Obsd.	41.80	7.67	9.42	7— 9
(9) [Cr(D-ala)(L-leu)$_2$]·2H$_2$O[c]	Obsd.	41.20	7.72	9.88	39—45

x=1 or 2. (1)(4)(5) obtained using L-alanine. (2)(6)(7) obtained using D-alanine. (3)(8)(9) obtained using DL-alanine. a) The reaction product during heating. b) Standing temperature: 5 °C. c) Standing temperature: 55°C.

Table 2. Absorption Maxima and CD Maxima of Mixed Chromium(III) Complexes with L-Leucine and L-, D-, or DL-Alanine (10 Days Standing)

Complex	AB nm (log ε) nm (log ε)	CD nm (Δε) nm (Δε)
(1) [Cr(L-ala)$_2$(L-leu)][a)]	520 (2.15) 393 (2.04)	505 (2.38) 389 (−0.32)
(2) [Cr(L-ala)(L-leu)$_2$][b)]	515 (2.11) 393 (1.98)	495 (−1.25) 385 (0.06)
(3) [Cr(L-ala)(L-leu)$_2$][c)]	515 (2.17) 392 (2.03)	490 (−0.72) 383 (0.06)
(4) [Cr(L-ala)(L-leu)$_2$][d)]	520 (2.16) 390 (2.04)	518 (0.95) 395 (−0.14)
(5) [Cr(L-ala)(L-leu)$_2$][e)]	520 (2.18) 393 (2.05)	505 (1.76) 390 (−0.25)
(6) [Cr(D-ala)$_2$(L-leu)][a)]	517 (2.18) 391 (2.08)	496 (−1.81) 385 (0.43)
(7) [Cr(D-ala)(L-leu)$_2$][b)]	515 (2.10) 394 (1.99)	495 (−1.05) 384 (0.13)
(8) [Cr(D-ala)(L-leu)$_2$][c)]	515 (2.11) 393 (2.02)	493 (−0.65) 383 (0.17)
(9) [Cr(D-ala)(L-leu)$_2$][d)]	519 (2.10) 394 (2.01)	516 (1.05) 394 (−0.28)
(10) [Cr(D-ala)(L-leu)$_2$][e)]	520 (2.15) 394 (2.04)	506 (2.03) 392 (−0.53)
(11) [Cr(L-ala)$_2$(L-leu)][a)]	520 (2.16) 393 (2.03)	505 (2.32) 389 (−0.32)
(12) [Cr(D-ala)(L-leu)$_2$][b)]	515 (2.11) 390 (2.00)	495 (−1.05) 385 (0.13)
(13) [Cr(D-ala)(L-leu)$_2$][c)]	516 (2.12) 391 (1.98)	492 (−0.66) 383 (0.08)
(14) [Cr(D-ala)(L-leu)$_2$][d)]	517 (2.13) 392 (1.99)	515 (1.02) 393 (−0.26)
(15) [Cr(D-ala)(L-leu)$_2$][e)]	520 (2.15) 393 (1.98)	505 (1.95) 390 (−0.42)

(1)—(5) obtained using L-alanine. (6)—(10) obtained using D-alanine. (11)—(15) obtained using DL-alanine. a) The reaction product during heating. b) Standing temperature: 5 °C. c) Standing temperature : 25 °C. d) Standing temperature: 40 °C. e) Standing temperature: 55 °C.

Results and Discussion

The absorption spectral data of the mixed-tris type complexes are listed in Table 2. No splitting of the first band was observed, and the absorption coefficient of the first band is larger than that of the second band. These finding agree well with those of the reported *fac*-tris(amino acidato)chromium(III) complexes,[3] suggesting a *fac*-structure of the present tris type mixed amino acidato complexes.

The CD spectra of (+)$_{546}$-[Cr(L-ala)$_2$(L-leu)] and (−)$_{546}$-[Cr(D-ala)(L-leu)$_2$] in DMSO are shown in Fig. 1, while the numerical data are summarized in Table 2. They are very similar in shape and peak position to those of (+)$_{546}$-and (−)$_{546}$-[Cr(AA)$_3$](AA=amino acidato).[3] Comparing the CD curves of the present complexes with those reported for *Λ*- and *Δ*-[Cr(AA)$_3$], the configuration of the present complexes can be identified as *Λ* for the (+)$_{546}$- and *Δ* for the (−)$_{546}$-isomers.

As is shown in Fig. 1, the Δε values of the major components of the first absorption band of [Cr(L-ala)$_2$(L-leu)] and [Cr(D-ala)(L-leu)$_2$] were +2.38 (505 nm) and −1.81 (495 nm) respectively. We have previously reported that the absolute configuration of [Cr(L-ala)$_3$] was the *Λ*(+) form.[3] On the other hand, the tris complex containing D-alanine, which was prepared according to the literature,[3] is *Δ* form (Δε=−2.41 (495 nm)). Thus, L- and D-alanine favor the *Λ*(+) and the *Δ*(−)-product respectively. From these results, it may be seen that the absolute configuration of the mixed tris-type complexes obtained is dependent on the that of the two alanine molecules coordinated. The reason for this may be the difference in the solubilities of the diastereoisomers, although this is still not clear.

The CD spectra of [Cr(L-ala)(L-leu)$_2$], which was obtained at 5, 25, 40, and 55 °C, are shown in Fig. 2, while the numerical data are summarized in Table 2,

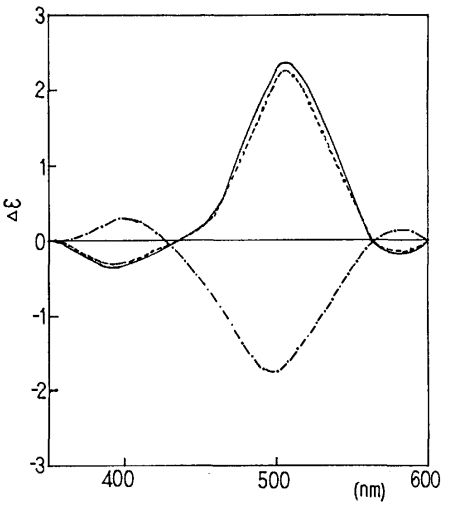

Fig. 1. The CD spectra of *fac*(+)$_{546}$-[Cr(L-ala)$_2$(L-leu)] (——), *fac*(−)$_{546}$-[Cr(D-ala)$_2$(L-leu)] (— · —), and *fac*(+)$_{546}$-[Cr(L-ala)$_2$(L-leu)](Used DL-alanine) (----).

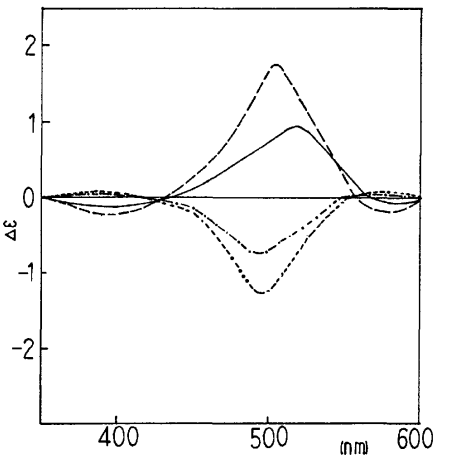

Fig. 2. The CD spectra of [Cr(L-ala)(L-leu)$_2$] obtained at each standing temperature. 55 °C (— —), 40 °C (——), 25 °C (— · —), 5 °C (----).

together with those of [Cr(D-ala)(L-leu)$_2$]. The peak positions and the signs of $\Delta\varepsilon$ of $(-)_{546}$-[Cr(L- or D-ala)(L-leu)$_2$] obtained at 5 °C and of $(+)_{546}$-[Cr(L- or D-ala)(L-leu)$_2$] obtained at 55 °C appear to be similar to those of $(+)_{546}$- and $(-)_{546}$-[Cr(AA)$_3$] respectively. Thus, the configurations of the present complexes can be identified as *Λ* for $(+)_{546}$- and *Δ* for $(-)_{546}$-isomers. On the other hand, the CD data of [Cr(L- or D-ala)(L-leu)$_2$] obtained at 25 °C or 40 °C suggest that the products are mixtures of *Λ*- and *Δ*-isomers. It was found that the ratio of the *Λ*-isomer to the *Δ*-isomer increases with a rise in the standing temperature, irrespective with the difference in the optical isomer of alanine involved.

The preparation of [Cr(L-leu)$_3$] was undertaken according to the present method. The $\Delta\varepsilon$ values of the tris complex obtained at 55 °C and at 5 °C are −0.316 and −0.583 respectively. It may be suggested that the ratio of the *Λ*-isomer to the *Δ*-isomer increases with a rise in the standing temperature. However, the ratio of the increase of the *Λ*-isomer of [Cr(L-leu)$_3$] is smaller than that of [Cr(L-ala)(L-leu)$_2$)]. The solubilities of [Cr(L-leu)$_3$] and [Cr(L-ala)(L-leu)$_2$] obtained at 5 °C and at 55 °C were investigated in an ethanol solution, which was added to KNCS at 5 °C and 55 °C. Nor was [Cr(L-leu)$_3$] dissolved in the solution at each temperature. On the other hand, the $(-)_{546}$-[Cr(L-ala)(L-leu)$_2$] obtained at 5 °C was dissolved at 55 °C, but was not dissolved at 5 °C. The $(+)_{546}$-[Cr(L-ala)(L-leu)$_2$] obtained at 55 °C was slightly dissolved at 55 °C, but was not dissolved at 5 °C. From these results, the stereoselectivity of [Cr(L-ala)(L-leu)$_2$] obtained after standing seems to be brought about by the difference in the solubility of the $(-)_{546}$-isomer, which arises from the difference in the standing temperature.

The characteristic feature of the present method of preparation is that it gives two different types of products.

i) Cr(L- or D-ala)$_2$(L-leu)]. These complexes were obtained during heating, in spite of using the bis-leucinato chromium(III) complexes, [Cr(L-leu)$_2$(NCS)(OH$_2$)], as the starting material.

It should also be noted that the reactions are stereospecific; that is, the $(+)_{546}$- and $(-)_{546}$-isomers were obtained with L- and D-alanine respectively.

ii) [Cr(L- or D-ala)(L-leu)$_2$]. These complexes were obtained from the filtrate. It should be noted that the reactions are also stereospecific and that the optical purity of the product, $(+)_{546}$-[Cr(L- or D-ala)(L-leu)$_2$], increases with a rise in the standing temperature of the filtrate.

The optical resolution of DL-alanine based on the different reactivities of [Cr(L-leu)$_2$(NCS)(OH$_2$)] for L- and D-alanine has been undertaken, the results will be requested in a future report.

The numerical data of the absorption spectra and the CD spectra of the mixed complexes obtained during heating and after standing using DL-alanine are listed in Table 2. The CD curve of the mixed complex obtained during heating is also shown in Fig. 1. A comparison with the CD curves of the mixed complexes obtained using L- and DL-alanine shows that the CD curves and the $\Delta\varepsilon$ values of these complexes are similar to each other. Therefore, in the case of DL-alanine, the mixed complex obtained during heating may be $(+)_{546}$-[Cr(L-ala)$_2$(L-leu)].

In addition, compared with the mixed complexes obtained using D- and DL-alanine, the $\Delta\varepsilon$ values of these complexes obtained after standing are also similar to each other at each temperature. Therefore, in the case of DL-alanine, the mixed complexes which were obtained after standing at each temperature may be [Cr(D-ala)(L-leu)$_2$]. The optical resolution of DL-alanine may be possible through the reaction.

References

1) E. W. Toepfer, W. Mertz, M. M. Polansky, E. E. Roginsky, and W. R. Wolf, *J. Agric. Food Chem.* **25**, 162 (1977).
2) H. Oki, *Bull. Chem. Soc. Jpn.*, **50**, 680 (1977).
3) H. Oki, *J. Sci., Hiroshima Univ. Ser.*, **45**, 447 (1982).
4) M. Watabe, H. Yano, Y. Odaka, and H. Kobayashi, *Inorg. Chem.*, **20**, 3623 (1981).
5) H. D. Dakin, *Org. Synth.*, Vol. 15, 74 (1935).

The Magnetic Properties of Dinuclear Copper(II) 2-Fluoroalkanoates

Shuji EMORI* and Hideki KONDO
Department of Chemistry, Faculty of Science and Engineering, Saga University,
Honjo-machi, Saga 840
(Received March 22, 1989)

Synopsis. Copper(II) pentafluoropropionate and heptafluorobutyrate adducts with 1,4-dioxane, tetrahydropyran, and tetrahydrofuran have been prepared and characterized by means of magnetic-susceptibility and IR-spectroscopy measurements. The variation in their magnetic moments is discussed in terms of the acidity of the parent acid and the hyperconjugative effect of the fluoroalkyl group.

Numerous studies have been carried out to ascertain the factors which determine the magnetic properties of dinuclear copper(II) carboxylates, because they are necessary to understand the mechanism of the spin-exchange coupling. For several series of copper(II) carboxylates, a correlation between the strength of spin-exchange coupling and the acidity of the parent carboxylic acid has been recognized;[1-4] this correlation is supported by molecular orbital calculations.[5,6] However, there are also some exceptions, such as the unusually strong couplings observed for dinuclear copper(II) formates[7] and fluoroacetates,[3,4] which have led many investigators to be critical of such a correlation.[8] They have presumed alternative factors, such as the group polarizability of the carboxylate substituents[9] and the steric hindrance between the substituents and the axial donor ligands.[1] However, these alternative factors have soon been found unjustifiable.[3] In order to investigate the general trend of the magnetic properties of fluoroalkanoates, we have prepared the 1,4-dioxane (dox), tetrahydropyran (THP), and tetrahydrofuran (THF) adducts of copper(II) pentafluoropropionate and heptafluorobutyrate. For the sake of comparison, the corresponding adducts of copper(II) fluoroacetate and difluoroacetate have also been prepared.

The compounds were obtained by standard procedures.[1,10] Their effective magnetic moments (Table 1) were evaluated from the room-temperature molar magnetic susceptibilities (χ_M) using this equation: $\mu_{eff}=2.83\ [(\chi_M-\chi_{dia}-N\alpha)T]^{1/2}$. The appropriate diamagnetic corrections (χ_{dia}) were estimated from the Pascal constants,[11] while the temperature-independent paramagnetic contribution ($N\alpha$) was taken as 60×10^{-6} emu mol^{-1} (1 emu$=4\pi\times10^{-6}$ m^3). For the dioxane adducts of copper(II) difluoroacetate and pentafluoropropionate, the temperature dependence of their magnetic susceptibilities was measured in the temperature range of 80—300 K; it can be represented by the Bleaney-Bowers equation,[12] with parameters of $g=2.17$ and $2J=-314$ cm^{-1} for the difluoroacetate and of $g=2.18$ and $2J=-296$ cm^{-1} for the pentafluoropropionate. The IR spectra of the solid compounds show bands characteristic of bridging carboxylate due to unsymmetric and symmetric carboxyl stretching vibrations.[13] The magnetic and IR spectral data indicate that the present compounds have their "dinuclear tetracarboxylate frameworks."

It has been found that the magnetic moments of dinuclear copper(II) alkanoate adducts with unhindered hard donors, except those of fluoroalkanoate adducts, are determined by these factors: the acidities of the bridging carboxylato and axial donor ligands,[14] the steric strain among the substituents,[14] and the hydrogen bonding between the carboxylato oxygen atoms and the neighboring hydrogen donors.[15] For

Table 1. Analytical Data and Effective Magnetic Moments at 20 °C

Compound		Found(Calcd)/%			μ_{eff}/BM
		Cu	C	H	
$Cu(CF_3CF_2COO)_2\cdot 1/2dox$	(1)	14.69 (14.65)	22.17 (22.16)	0.95 (0.93)	1.41
$Cu(CF_3CF_2COO)_2\cdot THP$	(2)	13.05 (13.36)	22.83 (22.77)	2.15 (2.12)	1.44
$Cu(CF_3CF_2COO)_2\cdot THF$	(3)	13.67 (13.76)	25.95 (26.01)	1.73 (1.75)	1.42
$Cu(CF_3CF_2CF_2COO)_2\cdot 1/2dox$	(4)	11.78 (11.91)	22.58 (22.51)	0.79 (0.76)	1.38
$Cu(CF_3CF_2CF_2COO)_2\cdot THP$	(5)	10.95 (11.04)	27.33 (27.12)	1.76 (1.75)	1.43
$Cu(CF_3CF_2CF_2COO)_2\cdot THF$	(6)	11.28 (11.31)	25.73 (25.66)	1.46 (1.44)	1.46
$Cu(F_2CHCOO)_2\cdot 1/2dox$	(7)	21.11 (21.35)	24.05 (24.21)	2.14 (2.03)	1.36
$Cu(F_2CHCOO)_2\cdot THP$	(8)	18.86 (18.70)	31.89 (31.82)	3.61 (3.56)	1.36
$Cu(FCH_2COO)_2\cdot 1/2dox$	(12)	24.45 (24.28)	27.49 (27.54)	3.27 (3.08)	1.29

example, the room-temperature magnetic moments (BM) for the copper(II) salts of a series of monosubstituted acetic acids can be formulated by the following equation:

$$\mu_{eff}=-0.052(pK_a-0.068pK_a'-4.56+C_{HB})+1.32_7, \quad (1)$$

where pK_a and pK_a' are the acidities of the parent acid and of the conjugate acid of the axial donor ligand respectively, and where C_{HB} is a correction term for the hydrogen bonding in the hydrates and ammonium chloride adducts (the value of $C_{HB}=-0.29$ has been estimated).[15] In order to examine a similar correlation for fluoroalkanoates, the room-temperature magnetic moments of the present compounds, together with the literature data for the hydrates and ammonium choride adducts of copper(II) fluoroalkanoates,[3,4,16] are plotted against the $pK_a-0.068\ pK_a'+C_{HB}$ values in Fig. 1. These points consist of a straight line, with the best least-squares fit yielding:

$$\mu_{eff}=-0.052(pK_a-0.068pK_a'-4.56+C_{HB})+1.18_2. \quad (2)$$

Although the magnetic moments of the corresponding quinoline adducts (1.32 and 1.40 BM at 20 °C for the fluoroacetate[17] and trifluoroacetate[18] respectively) show a similar trend, they are excluded from the plots because the axial coordination of quinoline is affected by the steric hindrance.[19] The variation in the singlet-triplet separation values (e.g., $-2J=384$,[10] 314, and 296 cm^{-1} for the dioxane adducts of copper(II) 2-fluoropropionate, difluoroacetate, and pentafluoropropionate respectively) indicates that the smaller magnetic moment is accompanied by the stronger magnetic interaction between copper(II) ions. Similarly, the carboxyl frequencies (cm^{-1}) for the present compounds, in conformity with Eq. 3, show systematic shifts against the acidities of the carboxylato and axial ligands:

$$\tilde{\nu}_{unsym}=1692-14.9(pK_a-0.068\ pK_a'+C_{HB}). \quad (3)$$

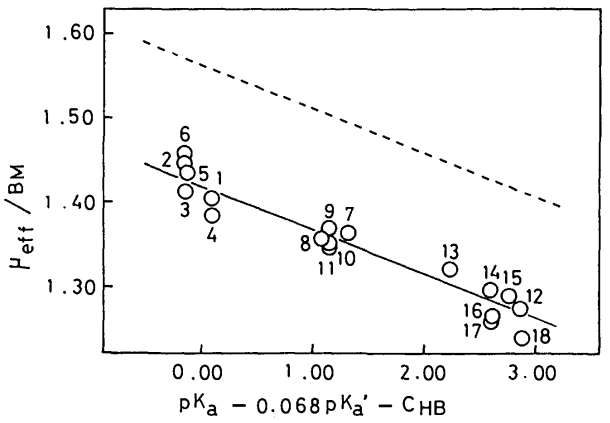

Fig. 1. The magnetic moments at 20 °C plotted against the acidities of the ligands for the copper(II) pentafluoropropionate (**1—3**), hexafluorobutyrate (**4—6**), difluoroacetate (**7—11**), fluoroacetate (**12—17**), and 2-fluoropropionate (**18**) adducts with σ-donor ligands. The broken line represents the linear correlation for copper(II) alkanoates except fluoroalkanoates.

These linear correlations suggest that the influence exerted by the fluoro-substituents is mainly inductive. Nevertheless, the value of the constant term in Eq. 2 (1.18_2 BM) is much smaller than the corresponding values for any other series of alkanoates (e.g., 1.32_7 BM in Eq. 1), indicating the existence of an additional factor affecting their magnetic properties. For the 2-fluoroalkanoates, this effect seems to be independent of the number of fluoro-substituents, for the lines in Fig. 1 are parallel to each other. An inspection of the crystal structures of the copper(II) fluoroacetate[20-22] and trifluoroacetate[8] adducts reveals that they have a fluoro-substituent located closely in the plane of the carboxylato group. This fact seems to indicate that the fluoro-substituent in the plane of the carboxylato group is responsible for this effect.

Previously, we have pointed out that the difference in magnetic moments between copper(II) acetate and copper(II) (substituted acetate)s is attributable to the hyperconjugation of the methyl group of the acetato ligand in addition to the difference in acidities between their parent acids.[14] Similarly, the magnetic moments of fluoroalkanoates must be affected by the hyperconjugation of the fluoroalkyl group.[23] Generally, carboxylic acid may be regarded as a substituted formic acid RCOOH, and the perturbation by a substituent R on the carboxyl group is comprised of changes in both the σ- and π-electron distributions. Since the effect of the change in the σ-electron distribution appears in the acidity change, the residual change in the magnetic moment of dinuclear copper(II) carboxylate may be related to the change in the π-electron distribution:

$$\mu_{eff}=-0.052(pK_a-0.068pK_a'+C_{HB}-3.55)+\Delta\mu_\pi+1.06_9, \quad (4)$$

where $\Delta\mu_\pi$ is a correction term for the perturbation of the π-electron density of the carboxyl group, being obtained as 0.16_8, 0.28_5,[14] 0.30_5,[14] 0.36_3,[14] and 0.35_2[24] BM for the $R=CF_3$, $(CH_3)_3C$, C_2H_5, CH_3, and C_6H_5 substituents respectively. Swain and Lupton have proposed that substituent constants predicting the substituent effects on any kinds of physical properties may be expressed as $fF+rR$,[25] where F and R are field and resonance constants, and where f and r are weight-

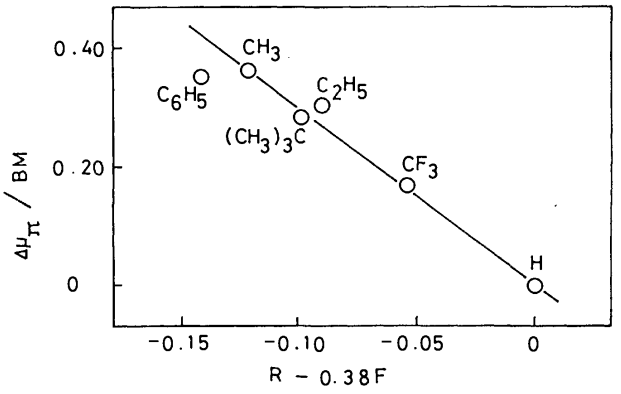

Fig. 2. The correction term for the perturbation on π-electrons in the carboxyl group plotted against the substituent constants $R-0.38F$.

ing factors independent of the particular substituent. The ratio of f to r being chosen as -0.38, the $\Delta\mu_\pi$ values for these substituents are plotted against $R-0.38F$ in Fig. 2. Most data have a linear relation with the slope of -3.0_0 BM, although the plot for the phenyl substituent is a little scattered, perhaps because of the torsion about the C-C bond between the phenyl and carboxyl groups (the dihedral angles are 0.2—27.2°).[26,27] This correlation substantiates the participation of the π-orbitals of the bridging carboxylato in the superexchange pathway. This electron-delocalization mechanism is consistent with the quite large contact shifts observed for the H resonances of copper(II) benzoates[28] and for the ^{13}C resonances of copper(II) butyrate.[29]

References

1) M. Melnik, *Finn. Chem. Lett.*, **1978**, 255.
2) M. Melnik and J. Mrozinski, *Z. Anorg. Allg. Chem.*, **500**, 210 (1983).
3) S. Emori, N. Morishita, and Y. Muto, *Bull. Chem. Soc. Jpn.*, **60**, 1913 (1987).
4) S. Emori, Y. Tohyama, and Y. Muto, *Bull. Chem. Soc. Jpn.*, **60**, 4445 (1987).
5) P. J. Hay, J. C. Thibeaul, and R. Hoffmann, *J. Am. Chem. Soc.*, **97**, 4884 (1975).
6) P. de Loth, P. Cassoux, J. P. Daudey, and J. P. Malriew, *J. Am. Chem. Soc.*, **103**, 4007 (1981).
7) R. J. Doedens, *Prog. Inorg. Chem.*, **21**, 209 (1976).
8) J. A. Moreland and R. J. Doedens, *J. Am. Chem. Soc.*, **97**, 508 (1975).
9) L. C. Porter and R. J. Doedens, *Inorg. Chem.*, **23**, 997 (1984).
10) R. Uggla and M. Melnik, *Acta Chem. Scand.*, **25**, 1790 (1971).
11) G. Foex, "Constants Sélectionées, Diamagnétisme et Paramagnétisme," Masson, Paris (1957).
12) B. Bleaney and K. D. Bowers, *Proc. R. Soc. London, Ser. A.*, **214**, 451 (1952).
13) L. J. Bellamy, "The Infrared Spectra of Complex Molecules," 3rd ed., Chapman and Hall, London (1975).
14) S. Emori, H. Nonaka, N. Ikeda, and Y. Muto, *Bull. Chem. Soc. Jpn.*, **61**, 1812 (1988).
15) S. Emori, H. Kurihara, and Y. Muto, *Bull. Chem. Soc. Jpn.*, **61**, 3317 (1988).
16) K. S. Patel and J. A. Faniran, *J. Inorg. Nucl. Chem.*, **38**, 1001 (1976).
17) Yu. V. Yablokov, L. N. Mosina, Yu. A. Simonov, L. N. Milkova, A. V. Ablov, and V. I. Ivanov, *Zh. Strukt. Khim.*, **19**, 42 (1978).
18) S. F. A. Kettle and A. J. P. Pioli, *J. Chem. Soc. A*, **1968**, 1243.
19) S. Emori, K. Ohishi, H. Kurihara, and Y. Muto, *Bull. Chem. Soc. Jpn.*, **61**, 4439 (1988).
20) Yu. A. Simonov, V. I. Ivanov, A. V. Ablov, T. I. Malinovskii, and L. N. Milkova, *Koord. Khim.*, **1**, 716 (1975).
21) Yu. A. Simonov, A. A. Dvorkii, Yu. V. Yablokov, L. N. Milkova, and A. V. Ablov, *Zh. Strukt. Khim.*, **19**, 175 (1978).
22) K. Smolander, *Inorg. Chim. Acta*, **114**, 1 (1986).
23) J. D. Roberts, R. L. Webb, and E. A. McEihill, *J. Am. Chem. Soc.*, **72**, 408 (1950).
24) Estimated from the data on various copper(II) 3-substituted benzoate adducts with pyridine and quinoline.
25) C. G. Swain and E. C. Lupton, Jr., *J. Am. Chem. Soc.*, **90**, 4328 (1968).
26) A. Bencini, D. Gatteschi, and C. Mealli, *Cryst. Struct. Commun.*, **8**, 305 (1979).
27) B. T. Usubaliev, E. M. Morsumov, F. N. Musaev, G. N. Nadzafov, I. R. Amiraslanov, and H. S. Mamedov, *Koord. Khim.*, **6**, 1091 (1980).
28) R. A. Zelonka and M. C. Baird, *Inorg. Chem.*, **11**, 134 (1972).
29) G. C. Campbell and J. F. Haw, *Inorg. Chem.*, **27**, 3706 (1988).

Synthesis of Ceratiolin, a Constituent of *Ceratiola ericoides*

Heitaro OBARA,* Jun-ichi ONODERA, Katsuhiro YUSA,
Mitsuhiro TSUCHIYA, and Shigeru MATSUBA
Department of Applied Chemistry, Faculty of Engineering,
Yamagata University, Yonezawa 992
(Received April 22, 1989)

Synopsis. Ceratiolin, a constituent of *Ceratiola ericoides* was synthesized by the methylation of 2′,3′,4′,6′-tetrahydroxydihydrochalcone, prepared by the Hoesch reaction of 1,2,3,5-benzenetetrol with 3-phenylpropionitrile. Furthermore, it was proved that ceratiolin easily forms by the oxidation of 2′,4′,6′-trihydroxy-3′,5′-dimethyldihydrochalcone.

Recently, Fischer et al.[1] isolated a new constituent, ceratiolin, from the water-soluble extracts of the fresh leaves of *Ceratiola ericoides*, one of only three genera in the Empetraceae, and proposed the racemic structure **3** for this new compound from its spectral and CD data.

A novel structure of **3** and its characteristic allelopathic property[1,2] have prompted us to attempt the synthesis of **3**.

In this paper, we wish to report on the convenient synthesis of **3** by the di-*C*-methylation of 2′,3′,4′,6′-tetrahydroxydihydrochalcone (**2**). Dihydrochalcone **2** was obtained from 1,2,3,5-benzenetetrol (**1**)[3] and 3-phenylpropionitrile by the Hoesch reaction in 63% yield. Ceratiolin (**3**) was prepared by the methylation of **2** with methyl iodide in the presence of sodium hydride in dimethyl sulfoxide in 48% yield. The structure of synthetic **3** was identified by a comparison of IR, ^{1}H NMR, and ^{13}C NMR spectra with those of a natural sample.

Furthermore, Fischer et al.[1] reported that ceratiolin biogenetically appears to be an oxidative derivative of dihydrochalcone **4**. This speculation was experimentally proved by the formation of **3** through the oxidation of 2′,4′,6′-trihydroxy-3′,5′-dimethyldihydrochalcone (**4**).

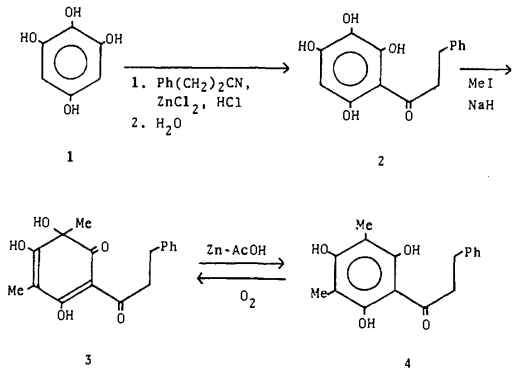

Experimental

All the melting points were uncorrected. The IR and UV spectra were recorded with a Hitachi 100-50 spectrophotometer and Hitachi 215 spectrophotometer, respectively. The ^{1}H NMR and ^{13}C NMR spectra were measured with a Hitachi R-600 spectrometer and a Hitachi R-90H spectrometer, using tetramethylsilane as an internal standard, respectively. The mass spectra were obtained on a Hitachi RMU-6M mass spectrometer.

2′,3′,4′,6′-Tetrahydroxydihydrochalcone (2). To a mixture of 1,2,3,5-benzenetetrol (**1**)[3] (10.0 g), 3-phenylpropionitrile (15.0 g), and anhydrous zinc chloride (3.5 g) in dry ether (100 ml), dry hydrogen chloride gas was passed for 3 h under cooling with an ice-salt bath. The reaction mixture was allowed to stand overnight at 0 °C, and the resulting dark-brown precipitate was heated with water (600 ml) on a water bath for 2 h. The hydrolysis product was extracted with ethyl acetate and chromatographed on a column of silica gel using benzene-ethyl acetate-acetic acid (6:1:1) as an eluent to afford **2** (12.1 g, 63%) as yellow crystals. Mp 138—139 °C (recrystallized from chloroform). MS *m/z* 274 (M^+). IR (KBr) ν 3420, 3030, 1640, 1424, 1200, and 718 cm^{-1}. ^{1}H NMR (DMSO-d_6) δ=2.85—3.48 (4H, m, H_α and H_β), 5.92 (1H, s, 5′-H), 7.26 (5H, s, Ar-H), 11.29 and 12.13 (each 1H, s, OH). Found: C, 65.55, H, 5.04%, Calcd for $C_{15}H_{14}O_5$: C, 65.69, H, 5.14%.

Ceratiolin (3). Into a mixture of **2** (3.0 g) and sodium hydride (0.4 g) in dry dimethyl sulfoxide (60 ml) was added methyl iodide (4.6 g) under cooling with ice-water; the mixture was stirred for 3 h at room temperature. The reaction mixture was poured into cold dilute hydrochloric acid and extracted with ethyl acetate. The organic layer was worked up in the usual manner and the resulting crude product was chromatographed on a column of silica gel (Wakogel C-200) with carbon tetrachloride-ethyl acetate-acetic acid (6:1:1) to give **3** (1.57 g, 48%) as light yellow crystals. Mp 148—149 °C (from benzene) (lit,[1] mp 148—149 °C). MS *m/z* 302 (M^+). ES λ_{max} (MeOH) 227, 326, and 354 nm (log ε=4.46, 4.48, and 4.52). IR (KBr) ν 3450, 1668, 1639, 1578, 1520, 1468, 1285, 1240, 1072, 1056, 1020, and 700 cm^{-1}. ^{1}H NMR ($CDCl_3$) δ=1.50 (3H, s, Me), 1.85 (3H, s, Me), 2.86—3.31 (4H, m, H_α and H_β), 7.26 (5H, s, Ar-H), 18.86 (1H, s, chelated OH). ^{13}C NMR (CD_3OD) δ=7.0 (q), 28.9 (q), 32.4 (t), 41.8 (t), 75.7 (s), 104.0 (s), 105.8 (s), 127.0 (d), 129.2 (d), 142.3 (s), 174.0 (s), 190.6 (s), 197.8 (s), and 201.6 (s).

The synthetic ceratiolin (**3**) was completely identical with a natural specimen. (Natural ceratiolin, although it has a chiral carbon, is optically inactive[1]).

2′,4′,6′-Trihydroxy-3′,5′-dimethyldihydrochalcone (4). A mixed solution of **3** (0.25 g) and activated zinc dust (0.8 g) in acetic acid (10 ml) was refluxed for 10 h. The reaction mixture was filtered and the filtrate was evaporated in vacuo; the residue was recrystallized from benzene to give **4** (0.7 g, 85%) as yellow crystals. Mp 119—120 °C. MS *m/z* 286 (M^+). IR (KBr) ν 3580, 3450, and 1620 cm^{-1}. ^{1}H NMR (DMSO-d_6) δ=2.05 (6H, s), 2.97 and 3.42 (each 2H, m), 7.17 (5H, s), and 10.58 (br. s). Found: C, 71.05, H, 6.23%, Calcd for $C_{17}H_{18}O_4$: C, 71.31, H, 6.34%.

Oxidation of 4 with Air. A mixture of **4** (30 mg) and lead (II) acetate (40 mg) in methanol (0.2 ml) was stirred for 4 h with airing at room temperature. The resulting yellow precipitates were treated with 6 M sulfuric acid (1 M=1 mol dm^{-3}) and extracted with ether. The ether layer was washed with water and dried over anhydrous sodium sulfate and evaporated in vacuo. The residue was chromato-

graphed on a column of silica gel with benzene–ethyl formate–formic acid (15 : 5 : 1) as an eluent to afford pale-yellow crystals (mp 148—149 °C, 9.5 mg, 30%). This compound was completely identical with **3**.

The authors are grateful to Professor N. H. Fischer of Louisiana State University for the identification of our synthetic sample with natural ceratiolin. We also wish to express their thanks Dr. Satoru Kumazawa of the Kureha Chemical Industry Co., Ltd., for the measurement of ^{13}C NMR spectra.

References

1) N. Tanrisever, F. R. Fronczek, N. H. Fischer, and G. B. Williamson, *Phytochemistry*, **26**, 175 (1987).
2) D. Richardson, Ph. D. dissertation, University of South Florida, Tampa, 1987.
3) J. Onodera and H. Obara, *Nippon Kagaku Kaishi*, **1973**, 1808.

Halogenation Using Quaternary Ammonium Polyhalides. XX.[1] Bromination of Phenols with Polymer-Bound Benzyltrimethylammonium Tribromide

Takaaki KAKINAMI,* Hiroyuki SUENAGA, Tadashi YAMAGUCHI, Tsuyoshi OKAMOTO, and Shoji KAJIGAESHI*,†
Department of Industrial Chemistry, Ube Technical College, Tokiwadai, Ube 755
†Department of Industrial Chemistry, Faculty of Engineering, Yamaguchi University, Tokiwadai, Ube 755
(Received May 6, 1989)

Synopsis. Bromo-substituted phenols were obtained quantitatively by passing a solution of phenols in dichloromethane–methanol through a column packed with styrene polymer-bound benzyltrimethylammonium tribromide.

Subsequent to Merrifield's report of the solid-phase peptide synthesis in 1963,[2] a number of functional polymers have been found, and the development of the regeneratable polymers as support is even now an interesting subject regarding organic synthesis. During the course of our investigation on the bromination of aromatic compounds with benzyltrimethylammonium tribromide (BTMA Br_3),[3] we happen to think of the use of polymer-bound BTMA Br_3 (Ⓟ-BTMA Br_3) (**1**) as a brominating agent.

Cacchi et al. have already reported the α-bromination of ketones by the use of a polymeric brominating agent (Amberlyst A 26-Br_3^- form).[4] However, their bromination method was carried out by mixing ketones with the insoluble polymeric agent in a solvent in the usual way. In this paper we wish to report on a facile bromination of phenols by the use of a column packed with **1**.

Results and Discussion

Our polymeric agent **1** (orange red) was readily prepared from AGl-X_2 (**2**) (100—200 mesh, chloride form), which was a commercially available (Bio-Rad Laboratories, USA) anion exchange resin containing a quaternary ammonium group, as shown in Scheme 1:

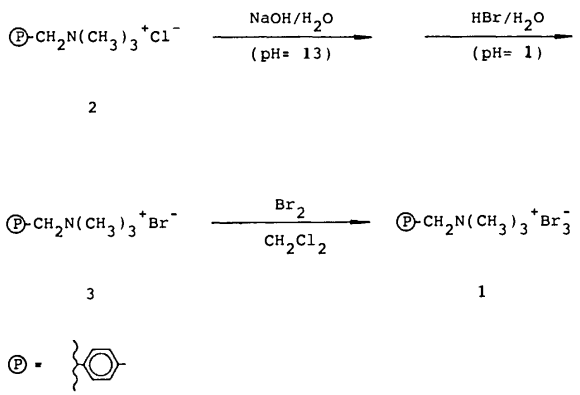

Scheme 1.

Passing a solution of phenols (**4**) in dichloromethane–methanol through a column packed with **1** at room temperature gave bromo-substituted phenols (**5**) in quantitative yields (Scheme 2). As shown in Scheme 2, polymer **1** is transformed into a colorless

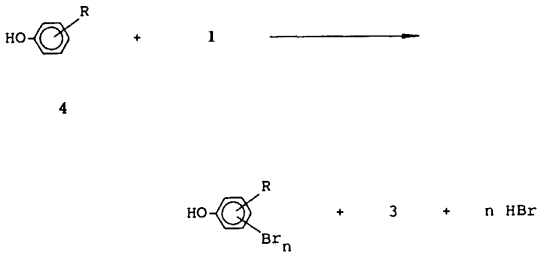

Scheme 2.

Ⓟ-BTMA Br^- (**3**) which can be easily regenerated to the original **1** by passing a solution of bromine in dichloromethane through the column. Still, $CaCO_3$ powder was used for the bromination of phenols bearing electron-attracting groups, because $CaCO_3$ should activate these inactive aromatic ring by the formation of the phenolate ion. The results are summarized in Table 1.

We have already prepared **5** by the reaction of **4** with BTMA Br_3, a soluble reagent in dichloromethane–methanol, at room temperature.[5] However, the procedure using **1** thus provides a facile method of obtaining bromo-substituted products from the corresponding aromatic compounds, owing to the ease of the operation and the capability of regeneration of the reagent. We believe that this method using **1** may be satisfactorily applied for the industrial production of bromo-substituted aromatic compounds.

As a limitation of the procedure, the selective bromination of phenols is difficult since this method cannot be carried out stoichiometrically. Furthermore, attempts at the bromination of a more reactive **4**, such as 4-methoxyphenol, 5-methyl-1,3-benzenediol, 1,3,5-benzenetriol, 1-naphthol, and 2-naphthol, were unsuccessful because these substrates underwent oxidation by **1**.

Experimental

Preparation of Styrene Polymer-Bound BTMA Br_3 (1): To a stirred suspension of AGl-X_2 (**2**) (100 g) in water (300

Table 1. Bromination of Phenols **4** with Ⓟ-BTMA Br_3 (**1**)

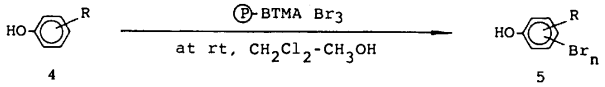

4 5

Substrate (**4**) R		Product (**5**)		Yield[a] %	Mp/°C Found	Mp/°C Reported
H	(**4a**)[b]	2,4,6-Br_3	(**5a**)	97	94—95	95[6]
2-Me	(**4b**)	2,4-Br_2-6-Me	(**5b**)	98	57—58	56.5—57.6[7]
3-Me	(**4c**)	2,4,6-Br_3-3-Me	(**5c**)	99	82—83	81[8]
4-Me	(**4d**)	2,6-Br_2-4-Me	(**5d**)	97	46—47	49[9]
4-t-Bu	(**4e**)	2,6-Br_2-4-*t*-Bu	(**5e**)	99	70—71	70—71[10]
2,3-Me_2	(**4f**)	4,6-Br_2-2,3-Me_2	(**5f**)	96	68—69	67—68[5]
2,5-Me_2	(**4g**)	4,6-Br_2-2,5-Me_2	(**5g**)	99	78—79	79[8]
2,6-Me_2	(**4h**)	4-Br-2,6-Me_2	(**5h**)	99	78	80—81[11]
3,4-Me_2	(**4i**)	2,6-Br_2-3,4-Me_2	(**5i**)	96	39—40	39—40[8]
3,5-Me_2	(**4j**)[c]	2,4-Br_2-3,5-Me_2	(**5j-2**)	91	79—80	72—73[12]
4j		2,4,6-Br_3-3,5-Me_2	(**5j-3**)	97	167—168	166[13]
2-MeO	(**4k**)	4,6-Br_2-2-MeO	(**5k**)	91	66—67	64—65[14]
3-MeO	(**4l**)[c]	4,6-Br_2-3-MeO	(**5l-2**)	94	67—68	73—75[15]
4l	[b]	2,4,6-Br_3-3-MeO	(**5l-3**)	97	106—107	105[15]
2-Cl	(**4m**)[b]	4,6-Br_2-2-Cl	(**5m**)	97	78—79	76[16]
3-Cl	(**4n**)[b]	2,4,6-Br_3-3-Cl	(**5n**)	99	106—107	105—106[17]
4-Cl	(**4o**)[b]	2,6-Br_2-4-Cl	(**5o**)	97	88—89	92[18]
2-Br	(**4p**)[b]	2,4,6-Br_3	(**5a**)	96	93—94	95[6]
3-Br	(**4q**)[b]	2,3,4,6-Br_4	(**5q**)	97	113—114	113[19]
4-Br	(**4r**)[b]	2,4,6-Br_3	(**5a**)	99	92—93	95[6]
3-Me-4-NO_2	(**4s**)[b]	2,6-Br_2-3-Me-4-NO_2	(**5s**)	98	134.5—135	134[20]
4-Me-2-NO_2	(**4t**)[b]	6-Br-4-Me-2-NO_2	(**5t**)	99	68—68.5	68—69[21]
2-NO_2	(**4u**)[b]	4,6-Br_2-2-NO_2	(**5u**)	97	118	118[22]
3-NO_2	(**4v**)[b]	2,4,6-Br_3-3-NO_2	(**5v**)	97	87—88	89—90[23]
4-NO_2	(**4w**)[b]	2,6-Br_2-4-NO_2	(**5w**)	99	143	144[24]
2-COOH	(**4x**)[b]	4,6-Br_2-2-COOH	(**5x**)	98	220	228[25]
2-COOMe	(**4y**)[b]	4,6-Br_2-2-COOMe	(**5y**)	97	147—148	149[26]
2-COOEt	(**4z**)[b]	4,6-Br_2-2-COOEt	(**5z**)	98	101—102	101[26]
4-COOMe	(**4a′**)[b]	2,6-Br_2-4-COOMe	(**5a′**)	95	124.5—125	125[27]
4-COOEt	(**4b′**)[b]	2,6-Br_2-4-COOEt	(**5b′**)	97	108—108.5	108[27]
3-OH	(**4c′**)	2,4,6-Br_3-3-OH	(**5c′**)	95	111—112	111[8]
2-Me-3-OH	(**4d′**)	4,6-Br_2-2-Me-3-OH	(**5d′**)	99	101—102	102[28]

a) Yield of isolated product. b) $CaCO_3$ powder was used. c) This run was done in dichloromethane without methanol.

ml) we added 1-M aqueous sodium hydroxide (1M=1 mol dm^{-3}) at room temperature until the pH of the solution was indicated at about 13. The obtained precipitate was filtered and washed with water until it was neutral; a suspension of the above-mentioned powder in water (300 ml) was made sufficiently acidic (pH=1) with 1-M hydrobromic acid under stirring for 1 h at room temperature. The solid residue was then filtered and washed with water until neutral to give polymer-bound BTMA Br (**3**) as a white polymer; 47.2 g.

A dilute solution of bromine in dichloromethane was slowly added into a stirred suspension of **3** in dichloromethane (300 ml) until the color of bromine in the solution did not fade. The mixture was stirred overnight at room temperature; the obtained solid was filtered, washed with dichloromethane and dried under vacuum at room temperature to give a stable, orange red polymer **1**: yield 61.2 g; mp 210 °C.

2,4,6-Tribromo-3-methylphenol (5c); Typical Procedure: Compound 3-methylphenol (0.54 g, 5 mmol) in dichloromethane (20 ml)–methanol (20 ml) was adsorbed on **1** (50 g) packed in a column. The developing solvent (dichloromethane–methanol (3 : 1)) was passed through the column at a rate of 7 ml/10 min. In this case, the upper part of **1**, which reacted with the substrate, was completely decolorized. The obtained eluate (200 ml) was concentrated and treated with 5% aq solution of $NaHSO_3$ (10 ml); the mixture was then extracted with ether (40 ml×4). The ether solution was dried over $MgSO_4$ and concentrated in vacuo to give **5c** as a colorless crystals; yield 1.70 g (99%); mp 82—83 °C (lit,[8] mp 81 °C).

References

1) Part **XIX** of this series: S. Kajigaeshi, Y. Ueda, S. Fujisaki, and T. Kakinami, *Bull. Chem. Soc. Jpn.*, **62**, 2096 (1989).
2) R. B. Merrifield, *J. Am. Chem. Soc.*, **85**, 2149 (1963).
3) S. Kajigaeshi and T. Kakinami, *Yuki Gosei Kagaku Kyokaishi*, **46**, 986 (1988).
4) S. Cacchi and L. Caglioti, *Synthesis*, **1979**, 64.
5) S. Kajigaeshi, T. Kakinami, H. Tokiyama, T. Hirakawa, and T. Okamoto, *Chem. Lett.*, **1987**, 627.
6) L. Cohn and F. Schultze, *Ber.*, **38**, 3297 (1906).
7) H. A. Iddles, W. H. Miller, and W. H. Powers, *J. Am. Chem. Soc.*, **62**, 71 (1940).
8) R. J. Datta and J. C. Bhoumik, *J. Am. Chem. Soc.*, **43**, 303 (1921).
9) C. Schall and C. Dralle, *Ber.*, **17**, 2532 (1884).

10) E. W. Lewis, *J. Chem. Soc.*, **83**, 330 (1903).
11) S. W. Gleed and A. T. Peters, *J. Chem. Soc.*, **1948**, 209.
12) K. Auwers and E. Borsche, *Ber.*, **48**, 1715 (1915).
13) L. C. Raiford and J. H. Scott, *J. Org. Chem.*, **2**, 213 (1937).
14) N. L. Drake, H. C. Harris, and C. B. Jaeger, Jr., *J. Am. Chem. Soc.*, **70**, 168 (1948).
15) M. Kohn, *J. Am. Chem. Soc.*, **74**, 1601 (1952).
16) L. Garzino, *Ber.*, **25**, ref 121 (1892).
17) M. Kohn and A. Zandman, *Monatsch. Chem.*, **47**, 362 (1926).
18) G. T. Morgan and F. H. Burstall, *J. Chem. Soc.*, **1928**, 3260.
19) H. H. Hodgson and W. H. H. Norris, *J. Chem. Soc.*, **1949**, S 181.
20) R. C. Huston and W. J. Peterson, *J. Am. Chem. Soc.*, **55**, 3879 (1933).
21) L. C. Raiford and C. E. Greider, *J. Am. Chem. Soc.*, **46**, 430 (1924).
22) M. A. Phillips, *J. Chem. Soc.*, **1930**, 2400.
23) R. V. Henley and E. E. Turner, *J. Chem. Soc.*, **1930**, 928.
24) C. O. Obenland, *J. Chem. Educ.*, **41**, 566 (1964).
25) E. Grovenstein, Jr. and U. V. Henderson, Jr., *J. Am. Chem. Soc.*, **78**, 569 (1956).
26) R. Anschutz and A. Robitsek, *Justus Liebigs Ann. Chem.*, **346**, 325 (1906).
27) F. G. Pope and A. S. Wood, *J. Chem. Soc.*, **101**, 1827 (1912).
28) P. R. Dinganker and T. S. Gore, *Indian J. Chem.*, **2**, 294 (1964); *Chem. Abstr.*, **61**, 9422f (1964).

Oxidation Using Quaternary Ammonium Polyhalides. IV.[1] Selective Oxidation of Sulfides to Sulfoxides with Benzyltrimethylammonium Tribromide

Shoji KAJIGAESHI,* Katsuya MURAKAWA, Shizuo FUJISAKI, and Takaaki KAKINAMI†
Department of Industrial Chemistry, Faculty of Engineering,
Yamaguchi University, Tokiwadai, Ube 755
†Department of Industrial Chemistry, Ube Technical College, Tokiwakai, Ube 755
(Received May 19, 1989)

Synopsis. The reaction of sulfides with a stoichiometric amount of benzyltrimethylammonium tribromide and aqueous sodium hydroxide in dichloromethane at room temperature or in 1,2-dichloroethane under reflux gave the corresponding sulfoxides in good yields.

The usual methods of oxidation of sulfides (**1**) to sulfoxides (**2**) were occasionally found to be unsatisfactory. One of the difficulties is the relative ease of further oxidation of **2** to sulfone. However, the selective oxidation of **1** to **2** can be brought about by several reagents. For example, 30% hydrogen peroxide in acetone,[2] chromic acid in pyridine,[3] manganese dioxide in light petroleum,[3] liquid dinitrogen tetroxide under cooling by alcohol-solid carbon dioxide,[4] some organic hydroperoxides in appropriate solvent in sealed tube,[5] and dimethyl sulfoxide under heating at 160—175 °C[6] have been used. For the same purpose, some halogenating agents such as NBS,[7] the addition complex of 1,4-diazabicyclo[2.2.2]octane with bromine,[8] iodine with potassium iodide,[9] *t*-butyl hypochlorite,[10] and sodium bromite[11] are also used.

In connection with our further investigation on the synthetic utility of quaternary ammonium polyhalides, we have found that benzyltrimethylammonium

Table 1. Oxidation of Sulfides (**1**) with BTMA Br_3/NaOH aq

	Substrate **1**	Solvent	Reaction conditions		Product[a] **2**	Yield[b] /%
			Time/h	Temp/°C		
a	$(CH_3CH_2CH_2)_2S$	CH_2Cl_2	1	rt	$(CH_3CH_2CH_2)_2SO$	89
b	$[(CH_3)_2CH]_2S$	CH_2Cl_2	1	rt	$[(CH_3)_2CH]_2SO$	94
c	$[CH_3(CH_2)_3]_2S$	CH_2Cl_2	1	rt	$[CH_3(CH_2)_3]_2SO$	98
d	$[(CH_3)_2CHCH_2]_2S$	CH_2Cl_2	1	rt	$[(CH_3)_2CHCH_2]_2SO$	95
e	$[C_2H_5(CH_3)CH]_2S$	CH_2Cl_2	1	rt	$[C_2H_5(CH_3)CH]_2SO$	76
f	$[(CH_3)_3C]_2S$	CH_2Cl_2	0.2	rt	$[(CH_3)_3C]_2SO$	20[c]
g	$[CH_3(CH_2)_5]_2S$	CH_2Cl_2	1	rt	$[CH_3(CH_2)_5]_2SO$	98
h	$[CH_3(CH_2)_6]_2S$	CH_2Cl_2	1.5	rt	$[CH_3(CH_2)_6]_2SO$	98
i	$[CH_3(CH_2)_7]_2S$	CH_2Cl_2	1	rt	$[CH_3(CH_2)_7]_2SO$	97
j	$[CH_3(CH_2)_{11}]_2S$	CH_2Cl_2	1.2	rt	$[CH_3(CH_2)_{11}]_2SO$	96
k	$[CH_3(CH_2)_{15}]_2S$	CH_2Cl_2	2.5	rt	$[CH_3(CH_2)_{15}]_2SO$	98
l	$[CH_3(CH_2)_{17}]_2S$	CH_2Cl_2	2	rt	$[CH_3(CH_2)_{17}]_2SO$	96
m	$C_2H_5S(CH_2)_2CH_3$	CH_2Cl_2	1	rt	$C_2H_5SO(CH_2)_2CH_3$	85
n	$CH_3(CH_2)_3SC_2H_5$	CH_2Cl_2	1	rt	$CH_3(CH_2)_3SOC_2H_5$	98
o	$CH_3(CH_2)_7SCH_3$	CH_2Cl_2	1.3	rt	$CH_3(CH_2)_7SOCH_3$	98
p	$CH_3(CH_2)_9SCH_3$	CH_2Cl_2	1.5	rt	$CH_3(CH_2)_9SOCH_3$	95
q		CH_2Cl_2	1	rt		66
r	$ClCH_2CH_2SC_2H_5$	CH_2Cl_2	1	rt	$ClCH_2CH_2SOC_2H_5$	47
s	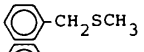	CH_2Cl_2	1	rt	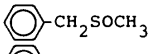	97
t	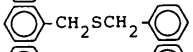	CH_2Cl_2	2	rt	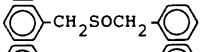	84
u	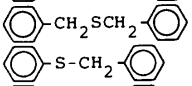	$ClCH_2CH_2Cl$	0.5	Reflux	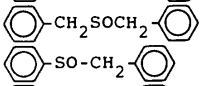	87
v	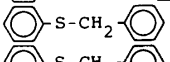	CH_2Cl_2	3	rt	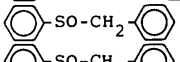	53
w	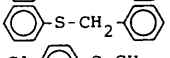	$ClCH_2CH_2Cl$	4	Reflux	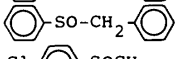	80
x	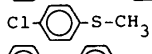	CH_2Cl_2	3	rt	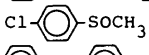	66
y	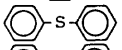	CH_2Cl_2	6	rt	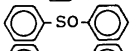	32
z	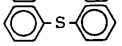	$ClCH_2CH_2Cl$	4	Reflux	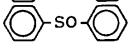	73

a) Products were characterized by comparing ^1H NMR spectra and mp or bp with those of authentic samples or reported data. b) Yield of isolated product. In the cases of run r, v, and y, products **2r**, **2v**, and **2y** were isolated by column chromatography on silica gel. c) Yield was based on its ^1H NMR spectrum.

tribromide (BTMA Br_3) is a useful oxidizing agent. In this paper we wish to report on a selective synthesis of **2** from **1** by the use of BTMA Br_3 in aqueous sodium hydroxide.

Results and Discussion

The reaction of **1** with a calculated amount of BTMA Br_3 and aqueous sodium hydroxide in dichloromethane at room temperature or in 1,2-dichloroethane under reflux gave **2** in good yields. The results are summarized in Table 1, and the reaction scheme can be represented as

$$\underset{\mathbf{1}}{R^1\text{-}S\text{-}R^2} + \text{BTMA } Br_3 + 2\ \text{NaOH} \longrightarrow \underset{\mathbf{2}}{R^1\text{-}S(=O)\text{-}R^2} + \text{BTMA Br} + 2\ \text{NaBr} + H_2O.$$

Aliphatic and aromatic sulfides **1a—z** have readily been oxidized to the corresponding **2a—z.** Our method, using BTMA Br_3, has a merit in that this stable reagent (orange red) can be treated safely and stoichiometrically. Furthermore, the end-point of the reaction can be recognized by decolorization of its initial orange color.

As a limitation of the procedure, attempts at the preparation of an unsaturated **2**, such as allyl phenyl sulfoxide and benzyl styryl sulfoxide, were unsuccessful, since the double bond underwent bromine addition under these conditions.

Experimental

Dihexyl Sulfoxide (2g); Typical Procedure: BTMA Br_3 (4.68 g, 12 mmol) was added to a mixture of dihexyl sulfide (**1g**) (2.02 g, 10 mmol) in dichloromethane (30 ml) and sodium hydroxide (1.1 g, 27.5 mmol) in water (15 ml), and the mixture was stirred at room temperature for 1 h. The orange color of the solution gradually faded and then completely decolorized during the period. To the reaction mixture was added a 20% aq solution of $NaHSO_3$ (10 ml); the organic layer was then separated. The aqueous layer was extracted with dichloromethane (10 ml×2) and the combined solution of dichloromethane was dried over $MgSO_4$ and evaporated in vacuo to give **2g** as colorless crystals; yield 2.14 g (98%); mp 57—58 °C (lit,[12] mp 60 °C).

References

1) Part III of this series: S. Kajigaeshi, H. Kawamukai, and S. Fujisaki, *Bull. Chem. Soc. Jpn.*, **62**, 2585 (1989).
2) R. L. Shriner, H. C. Struck, and W. J. Jorison, *J. Am. Chem. Soc.*, **52**, 2060 (1930).
3) D. Edwards and J. B. Stenlake, *J. Chem. Soc.*, **1954**, 3272.
4) C. C. Addison and J. C. Sheldon, *J. Chem. Soc.*, **1956**, 2705.
5) D. Barnard, *J. Chem. Soc.*, **1956**, 489.
6) S. Searles, Jr. and H. R. Hays, *J. Org. Chem.*, **23**, 2028 (1958).
7) W. Tagaki, K. Kikukawa, K. Ando, and S. Oae, *Chem. Ind. (London)*, **1964**, 1624.
8) S. Oae, Y. Ohnishi, S. Kozuka, and W. Takagaki, *Bull. Chem. Soc. Jpn.*, **39**, 364 (1966).
9) T. Higuchi, I. H. Pitman, and K. H. Gensch, *J. Am. Chem. Soc.*, **88**, 5676 (1966).
10) K. Kikukawa, W. Tagaki, N. Kunieda, and S. Oae, *Bull. Chem. Soc. Jpn.*, **42**, 831 (1969).
11) T. Kageyama, Y. Ueno, and M. Okawara, *Synthesis*, **1983**, 815.
12) D. Jerchel, L. Dippelhofer, and D. Renner, *Chem. Ber.*, **87**, 947 (1954).

Generation and Chemical Fate of 2,2,2-Trifluoro-1-phenylsulfonylethyl Carbanion

Kenji UNEYAMA* and Makoto MOMOTA
Department of Applied Chemistry, Faculty of Engineering, Okayama University, Okayama 700
(Received May 6, 1989)

Synopsis. 2,2,2-Trifluoro-1-phenylsulfonylethyl carbanion generated by the action of LDA in THF-HMPA can be methylated and iodinated, where the tetraethylammonium cation plays an essential role for the stabilization of the carbanion.

The development of reactions at the carbon atom bearing trifluoromethyl group is a subject of interest regarding the preparation of biologically active trifluoromethylated organic compounds.[1] Carbanions bearing the trifluoromethyl group are too reactive to be alkylated and mostly undergo defluorination. Thus, both trifluoroethyl phenyl ether[2] and sulfide[2,3] undergo facile defluorination by the action of LDA. Ishikawa demonstrated an alkylation of dimethyl trifluoromethylmalonate in the presence of a large excess of cesium fluoride where the nucleophilic addition of fluoride anion to the difluoromethylenemalonate occurs, consequently, to maintain a moderate concentration of the carbanion.[4] Recently, Fuchigami and Nakagawa showed an efficient alkylation of dimethyl trifluoromethylmalonate by the aid of electrogenerated base.[5] The alkylation of 2,2,2-trifluoroethyl phenyl sulfide and the subsequent desulfurization of the alkylated products would provide us with a promising process for the preparation of the trifluoromethylated compounds. The phenylsulfonyl group stabilizes any carbanion more effectively than the phenylthio group; there would thus still be a chance to trap 2,2,2-trifluoro-1-phenylsulfonylethyl carbanion **1** by an electrophile. The present note describes a method regarding the alkylation conditions in which the tetraethylammonium cation in THF-HMPA plays an essential role.

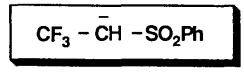

1

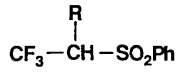

2 ; R = H
3 ; R = CH_3
5 ; R = $CH_2CH{=}CH_2$
6 ; R = I

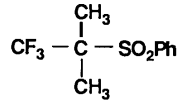

4

Results and Discussion

Both the phenylsulfonyl and trifluoromethyl groups activate the methylene proton of **2** so that even weak bases such as triethylamine, sodium hydroxide, and sodium methoxide can abstract a proton from **2**. However, the carbanion **1** is so unstable that it instantaneously undergoes defluorination rather than nucleophilic substitution. At −70 °C, stronger bases are required for this purpose. At first, LDA was employed in a mixed solvent of THF and HMPA. The carbanion can be trapped with methyl iodide, which must be employed in large excess (tenfold). Under these conditions a mixture of mono- and dimethylated sulfones **3** and **4** was obtained. An increase in methyl iodide resulted in the formation of the dimethylated sulfone **4**, even by the use of one equivalent of LDA (Run 1). This result suggests the existence of the dianion of **2** as an intermediate in an LDA-THF-HMPA system.[6] HMPA is a useful cosolvent for the present methylation. Otherwise, no methylation proceeds and defluorination exclusively occurs in THF where the lithium cation tightly associates with the electron lobe of the carbanion **1** and induces an intramolecular defluorination, as suggested.[7] The reaction temperature is also critical. At a higher temperature the total yields of **3** and **4** become lower (Run 3), suggesting that defluorination is faster than methylation under the reaction conditions.

Then, the effect of a base and the counter cation of diisopropylamide was examined so as to realize an exclusive monomethylation. Hard bases, such as butyllithium and ethylmagnesium bromide, failed in methylation (Runs 5 and 6). Lithium hexamethyldisilazide, potassium *t*-butoxide, and sodium methoxide gave a mixture of **3** and **4**. In contrast, replacing the lithium of LDA with tetraethylammonium leads to exclusive monomethylation (Run 10). Fuchigami and Nonaka demonstrated that a pyrrolidone anion with tetraethylammonium promoted the alkylation of

Table 1. Methylation of 2,2,2-Trifluoroethyl Phenyl Sulfone **2**[a]

Run	Base (equiv)	Additive (equiv)	Temp °C	Yield/% 3	4	Recovery/% 2
1	LDA (1)	—	−70	38	10	40
2	LDA (3)	—	−70	0	69	0
3	LDA (3)	—	−30	11	1	0
4	LiN $(SiMe_3)_2$	—	−70	36	27	0
5	*n*-BuLi	—	−70	0	0	0
6	EtMgBr	—	−70	0	0	0
7	*t*-BuOK	—	−30	29	17	0
8	LDA (1)	TEAC(1)[b]	−70	35	0	52
9	LDA (2)	TEAC(2)[b]	−70	61	0	23
10	LDA (3)	TEAC(3)[b]	−70	80	0	0

a) THF : HMPA=1 : 0.9 (v/v), CH_3I (10eq). b) Tetraethylammonium chloride.

Table 2. Reaction of **1** with Some Electrophiles[a)]

Electrophile	Yield/%
CH_3I	80
CH_3CH_2I	0
CH_2=CH-CH_2I	12
$PhCH_2Br$	0
I_2	82

a) THF : HMPA=1 : 0.9 (v/v), LDA (3 equiv), TEAC (3 equiv), −70 °C.

dimethyl trifluoromethylmalonate.[5)] It is well-known that tetraalkylammonium salts affect the electroreductive carbon-carbon bond formation in an aprotic solvent, although the effect has not yet been clearly explained.[8)] The dianion of **2** would abstract a proton from tetraethylammonium leading to the monoanion **1**.

The monomethylation conditions were applied to the other electrophiles (Table 2). Allyl iodide gave the allylated sulfone in a poor yield (12%). Neither ethyl iodide nor benzyl bromide can trap the carbanion **1** under the present reaction conditions. Interestingly, the reaction of **1** with iodine provides the desired iodinated sulfone **6** as crystals in 82% yield, rather than the oxidative dimer of **1**.[9)]

Experimental

Materials and Measurements: All of the solvents were distilled and stored under nitrogen. The ^{1}H NMR spectra were recorded at 500 MHz by using a Varian VXR-500 spectrometer with tetramethylsilane as the internal standard in $CDCl_3$. The IR spectra were recorded on a Hitachi 270-30 spectrometer.

1,1-Dimethyl-2,2,2-trifluoroethyl Phenyl Sulfone (4): To a solution of **2** (112 mg, 0.5 mmol) and methyl iodide (0.4 ml, 5 mmol) in THF (1 ml) and HMPA (0.9 ml) was added dropwise the LDA solution (1.5 mmol), and the mixture was stirred at −70 °C. After 10 min, the reaction mixture was neutralized with saturated NH_4Cl aq and 10% HCl aq, then extracted with ether/hexane (1 : 1). The extract was washed with water, dried over Na_2SO_4, and then evaporated in vacuo. The crude product was chromatographed on silica gel with hexane/AcOEt (10 : 1) as an eluent to yield 87 mg (69%) of **4** as a viscous oil; bp 125—130 °C/399 Pa; IR (neat) 1343, 1145 (SO_2) cm^{-1}; ^{1}H NMR δ=1.54 (s, 6H, CH_3), 7.55—8.00 (m, 5H, Ph). Found: C, 47.46; H, 4.47%. Calcd for $C_{10}H_{11}F_3O_2S$: C, 47.62; H, 4.40%.

1-Methyl-2,2,2-trifluoroethyl Phenyl Sulfone (3): To a suspension of tetraethylammonium chloride (260 mg, 1.6 mmol) in THF (1 ml) was added the LDA solution (1.6 mmol) at −70 °C; the mixture was then stirred at room temperature for 20 min. A supernatant liquid of the suspension was dropped into a solution of **2** (112 mg, 0.5 mmol) and methyl iodide (0.4 ml, 5 mmol) in THF (1 ml)-HMPA (0.9 ml) at −70 °C. After 10 min, the mixture was neutralized with saturated NH_4Cl aq and 10% HCl aq, and then extracted with ether/hexane (1 : 1). The extract was washed with water, dried over Na_2SO_4, and then evaporated in vacuo. The crude product was chromatographed on silica gel with hexane/AcOEt (10 : 1) as an eluent to yield 96 mg (80%) of **3** as a viscous oil; bp 125—130 °C/399 Pa; IR (neat) 1328, 1150 (SO_2) cm^{-1}; ^{1}H NMR δ=1.61 (d, J=7.4 Hz, 3H, CH_3), 3.75 (qq, $J_{H\text{-}H}$=7.4, $J_{H\text{-}F}$=8.5 Hz, 1H, CH), 7.55—8.00 (m, 5H, Ph). Found: C, 45.41; H, 3.69%. Calcd for $C_9H_9F_3O_2S$; C, 45.38; H, 3.81%.

1-Iodo-2,2,2-trifluoroethyl Phenyl Sulfone (6): Yield (82%) as colorless crystals; mp 72—74 °C; IR (Nujol) 1338, 1156 (SO_2) cm^{-1}; ^{1}H NMR δ=5.51 (q, J=7.2 Hz, 1H, CH), 7.45—8.05 (m, 5H, Ph). Found: C, 27.62; H, 1.75%. Calcd for $C_8H_6F_3IO_2S$: C, 27.45; H, 1.73%.

1-Trifluoromethyl-3-butenyl Phenyl Sulfone (5): Yield (12%) as a viscous oil, bp 95—100 °C/133 Pa; IR (neat) 1650 (C=C), 1330, 1150 (SO_2) cm^{-1}; ^{1}H NMR δ=2.62—3.10 (m, 2H, CH_2), 3.63—3.81 (m, 1H, CH). 5.13—5.26 (m, 2H, =CH_2), 5.75—6.00 (m, 1H, =CH), 7.56—8.00 (m, 5H, Ph). Found: C, 49.80; H, 4.11%. Calcd for $C_{11}H_{11}F_3O_2S$; C, 50.00; H, 4.20%.

We are grateful to the CIBA-GEIGY Foundation for the financial support and the SC-NMR laboratory of Okayama University for the 500 MHz-NMR analysis.

References

1) R. Filler and Y. Kobayashi, "Biomedicinal Aspects of Fluorine Chemistry," Kodansha Ltd., Tokyo (1982).
2) T. Nakai, K. Tanaka, and N. Ishikawa, *Chem. Lett.*, **1976**, 1263.
3) T. Nakai, K. Tanaka, H. Setoi, and N. Ishikawa, *Bull. Chem. Soc. Jpn.*, **50**, 3069 (1977).
4) N. Ishikawa and T. Yokozawa, *Bull. Chem. Soc. Jpn.*, **56**, 724 (1983).
5) T. Fuchigami and Y. Nakagawa, *J. Org. Chem.*, **52**, 5276 (1987).
6) N. Bosworth and P. Magnus, *J. Chem. Soc., Perkin Trans. 1*, **1973**, 2319; K. Kondo and D. Tunemoto, *Tetrahedron Lett.*, **17**, 1397 (1975).
7) T. Yokozawa, T. Nakai, and N. Ishikawa, *Tetrahedron Lett.*, **25**, 3987 (1984); **25**, 3991 (1984).
8) T. Shono, S. Kashimura, and K. Ishizaki, *Electrochim. Acta*, **29**, 603 (1984); W. R. Fawcett and A. Lasia, *Can. J. Chem.*, **59**, 3256 (1981).
9) R. G. Charls, *Org. Synth.*, Coll. Vol. IV, 869 (1963); S. B. Baker, T. H. Evans, and H. Hibbert, *J. Am. Chem. Soc.*, **70**, 60 (1948).

Simple and Efficient Synthesis of α-Allenic Alcohols and Their Novel Conversion into 1-Aryl-3-formyloxy-1,3-butadienes

Masahiko IYODA,* Yoshiaki KANAO, Minoru NISHIZAKI, and Masaji ODA
Department of Chemistry, Faculty of Science, Osaka University, Toyonaka, Osaka 560
(Received May 19, 1989)

Synopsis. Reactions of carbonyl compounds with 3-bromo-1-propyne in the presence of $SnCl_2 \cdot 2H_2O$ and $LiI \cdot 3H_2O$ gave α-allenic alcohols in moderate yields together with small amounts of β-acetylenic alcohols. The α-allenic alcohols can be converted into 1-aryl-3-formyloxy-1,3-butadienes, novel 1,3-butadiene derivatives.

In connection with our interest in the synthetic utility of cumulenic compounds,[1] we required a simple method for the preparation of α-allenic alcohols **3**.[2] Although the reactions of carbonyl compounds with 3-halo-1-propynes are known to give α-allenic alcohols **3**,[3,4] the yields were usually low and large amounts of β-acetylenic alcohols **4** were obtained as a major product of these reactions. We report here a very convenient solution of this problem and the synthesis of 1-aryl-3-formyloxy-1,3-butadienes **5** from the α-allenic alcohols **3**.

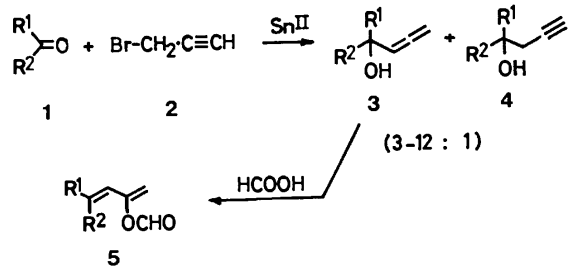

1 2 3 4 5

Scheme 1.

The reactions of **1** with 3-iodo-1-propyne in the presence of anhydrous $SnCl_2$ were reported to give α-allenic alcohols **3**, but considerable amounts of β-acetylenic alcohols **4** were also formed [e.g., the reaction of benzaldehyde with 3-iodo-1-propyne in the presence of $SnCl_2$ gave **3** and **4** in the ratio of 48 : 52 in 98% yield].[3a]

As shown in Table 1, the reaction of carbonyl compounds **1** with 3-bromo-1-propyne (**2**) proceeds smoothly under mild conditions to give α-allenic alcohols **3** as a major product. The hydrates of both $SnCl_2$ and LiI are employed for the reaction without removing water. Thus, benzaldehyde and its derivatives (**1a—h**: R^1=aryl and R^2=H) react with **2** in the presence of $SnCl_2 \cdot 2H_2O$ to give α-allenic alcohols **3a—h** in relatively good yields (Entries 1—9). In the case of 4-methoxybenzaldehyde (**1i**), the yield of a mixture of **3i** and **4i** obtained in the reaction reduced to 40%, owing to the instability of the α-allenic alcohol (**3i**) under the reaction conditions. The reactions of phenylacetaldehyde (**1j**) and butyraldehyde (**1k**) with **2** under similar conditions afforded the corresponding α-allenic alcohols **3j** and **3k** also as a major product (Entries 9 and 10). Furthermore, similar treatment of cyclohexanone (**1l**) with **2** gave the α-allenic alcohol **3l** selectively (Entry 11). Therefore, our method provides a simple and convenient way for the preparation of **3**.

Synthesis of 2-formyloxy-1,3-butadiene (**5**: R^1=R^2=H) was reported five decades ago,[5] and Diels-Alder reaction of this compound was discussed experimentally and theoretically as a typical diene.[6] However, the synthetic methodology for access to 2-formyloxy-1,3-butadiene derivatives is still very limited.

We have found that α-allenic alcohols **3** yield 3-formyloxy-1,3-butadienes (**5**) readily by dissolving **3** in formic acid. Thus, a solution of **3** in ether is added to formic acid at room temperature and the mixture is

Table 1. Reaction of **1** with **2** in the Presence of $SnCl_2 \cdot 2H_2O$ and $LiI \cdot 3H_2O$

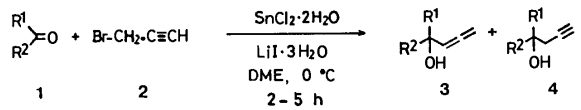

1 2 3 4

Entry	Carbonyl compound 1		R	Yield/% (3/4)	Entry	Carbonyl compound 1		Yield/% (3/4)
1		**1a**	H	92 (3.8/1)[a]	8	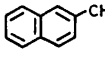	**1h**	89 (4.0/1)[a]
2		**1b**	4-Me	88 (3.3/1)[a]				
3		**1c**	4-Cl	84 (3.1/1)[a]	9	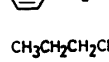	**1j**	91 (3.2/1)[a]
4		**1d**	4-Br	86 (3.3/1)[a]				
5		**1e**	3-OMe	96 (3.5/1)[a]	10	$CH_3CH_2CH_2CHO$	**1k**	67 (4.3/1)[b]
6		**1f**	2-Cl	80 (3.3/1)[a]				
7		**1g**	2-NO_2	77 (4.0/1)[a]	11		**1l**	54 (12/1)[b]

a) Reaction time 2 h. b) Reaction time 5 h.

Table 2. Preparation of 1-Aryl-3-formyloxy-1,3-butadiene (**5**)

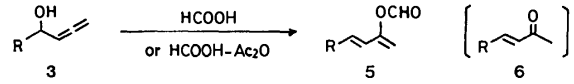

3 5 6

Entry	Starting material 3	X	Product 5	Method[a]	Yield/%
1	**3a**	H	**5a**	A	42
2	**3a**	H	**5a**	B	69
3	**3c**	4-Cl	**5c**	A	55
4	**3c**	4-Cl	**5c**	B	69
5	**3f**	2-Cl	**5f**	A	66
6	**3f**	2-Cl	**5f**	B	63
7	**3b**	4-Me	**5b**	A	27
8	**3b**	4-Me	**5b**	B	49
9	**3h**		**5h**	A	7
10	**3h**		**5h**	B	35

a) Method A: HCOOH, room temperature, 30 min. Method B: HCOOH, Ac_2O, 0 °C, 1 h.

stirred for 30 min (Method A in Table 2). A side reaction of this conversion is the formation of α,β-unsaturated ketones **6** which may be attributable to the competitive addition of water instead of formic acid to the *sp*-carbon of **3**. Therefore, some modification was carried out for the conversion of **3** into **5**. A solution of **3** in ether is added to a solution of formic acid containing acetic anhydride at 0 °C and the mixture is stirred for 1 h at the same temperature (Method B in Table 2). α-Allenic alcohols **3** having electron-withdrawing groups as substituents of aryl rings gave **5** in satisfactory yields by either Method A or B (Entries 1—6). In the case of *p*-tolyl derivative, however, **5b** was obtained in 27% yield by Method A and the yield was improved to 49% by Method B (Entries 7 and 8). A marked difference in yields of **5** was observed for the case involving 2-naphthyl substituent. Thus, the 2-naphthyl-substituted α-allenic alcohol **3h** was converted into the corresponding butadiene **5h** only in 7% yield using Method A, but this conversion was achieved in 35% yield by Method B (Entries 9 and 10).

In conclusion, the 2- or 3-formyloxy-1,3-butadiene derivatives **5** are now readily available through the acid-catalyzed rearrangement of α-allenic alcohols **3**.

Experimental

General. ^1H and ^{13}C NMR spectra were recorded on a Varian XL-100 or JEOL JNM-PMX60Si and JNM-FX90Q instruments, and are reported in δ from tetramethylsilane. IR spectra were observed on a Hitachi EPI-G3 spectrometer. Mass spectral analysis (MS) were performed on a JEOL JMS-O1SG-2 instrument. Melting points were determined on a Mettler FP-2 apparatus and are uncorrected. Column chromatography was carried out with use of Merck silica gel 60, 70—230 mesh, art 7734, or Merck neutral alumina activity II—III, 70—230 mesh.

General Procedure for Table 1. The Reaction of Carbonyl Compound 1 with 3-Bromo-1-propyne (2). To a solution of $SnCl_2{\cdot}2H_2O$ (677 mg, 3 mmol) and $LiI{\cdot}3H_2O$ (752 mg, 4 mmol) in 1,2-dimethoxyethane (DME) (10 ml) were added successively 3-bromo-1-propyne (**2**) (476 mg, 4 mmol) and a solution of carbonyl compound **1** (2 mmol) in DME (5 ml) at 0 °C under argon atmosphere. After the reaction mixture had been stirred at 0 °C for 2—5 h, water (10 ml) was added. Benzene (30 ml) was then added, and the organic layer separated. The aqueous layer was extracted with ether. The combined organic layers were washed successively with aqueous 5% $Na_2S_2O_3$ and saturated NaCl, and dried over $MgSO_4$. After removal of $MgSO_4$, the solution was filtered through a short column of alumina (ca. 20 g) in order to avoid isomerization of **3** to **6**. The filtrate was evaporated and the residue was chromatographed on silica gel with benzene–ether as eluent to give a mixture of α-allenic alcohol **3** and β-acetylenic alcohol **4**. Separation of **3** and **4** can be carried out by column chromatography on silica gel with hexane–ethyl acetate as eluent. α-Allenic alcohols **3** decompose gradually on standing at room temperature, but can be stored at 0 °C in solution using hexane, benzene or carbon tetrachloride as solvent.

1-Phenyl-2,3-butadien-1-ol (3a),[3a—c] **1,2-heptadien-4-ol (3K),**[7] **and 1-(1,2-propadienyl)cyclohexan-1-ol (3l)**[8] were characterized by comparison of the ^1H NMR, IR, and mass spectra with those of literatures.

1-(*p*-Tolyl)-2,3-butadien-1-ol (3b): Colorless oil, IR (neat) 3365 and 1960 cm^{-1}; ^1H NMR ($CDCl_3$) δ=2.16 (br. s, 1H), 2.34 (s, 3H), 4.92 (m, 2H), 5.24 (m, 1H), 5.45 (m, 1H), 7.16 (d, J=7.5 Hz, 2H), and 7.31 (d, J=7.5, 2H); MS m/z 160 (M^+).

1-(4-Chlorophenyl)-2,3-butadien-1-ol (3c): Colorless oil, IR (neat) 3370 and 1955 cm^{-1}; ^1H NMR ($CDCl_3$) δ=2.77 (br. s, 1H), 4.88 (m, 2H), 5.20 (m, 1H), 5.38 (m, 1H), and 7.28 (s, 4H); MS m/z 182 and 180 (M^+).

1-(4-Bromophenyl)-2,3-butadien-1-ol (3d): Colorless oil, IR (neat) 3340 and 1952 cm^{-1}; ^1H NMR ($CDCl_3$) δ=2.39 (br. s, 1H), 4.90 (m, 2H), 5.21 (m, 1H), 5.40 (m, 1H), 7.24 (d, J=8.5, 2H), and 7.41 (d, J=8.5, 2H); MS m/z 226 and 224 (M^+).

1-(3-Methoxyphenyl)-2,3-butadien-1-ol (3e): Colorless oil, IR (neat) 3375 and 1957 cm^{-1}; ^1H NMR ($CDCl_3$) δ=2.19 (br. s, 1H), 3.80 (s, 3H), 4.93 (m, 2H), 5.25 (m, 1H), 5.45 (m, 1H), 6.76—7.05 (m, 3H), and 7.28 (t, J=8.0, 1H); MS m/z 176 (M^+).

1-(2-Chlorophenyl)-2,3-butadien-1-ol (3f): Colorless oil, IR (neat) 3325 and 1958 cm^{-1}; ^1H NMR ($CDCl_3$) δ=2.39 (br. s, 1H), 4.91 (m, 2H), 5.46 (m, 1H), 5.65 (m, 1H), 7.10—7.45 (m, 3H), and 7.58 (m, 1H); MS m/z 182 and 180 (M^+).

1-(2-Nitrophenyl)-2,3-butadien-1-ol (3g): Colorless oil, IR (neat) 3370 and 1952 cm^{-1}; ^1H NMR ($CDCl_3$) δ=2.67 (br. s, 1H), 4.89 (m, 2H), 5.56 (m, 1H), 5.86 (m, 1H), and 7.35—7.97 (m, 4H); MS m/z 191 (M^+).

1-(2-Naphthyl)-2,3-butadien-1-ol (3h): Colorless crystals, mp 47.5—48.0 °C, IR (KBr) 3230 and 1955 cm^{-1}; ^1H NMR ($CDCl_3$) δ=2.35 (br. s, 1H), 4.92 (m, 2H), 5.35—5.62 (m, 2H), 7.39—7.58 (m, 3H), 7.77 (s, 1H), and 7.73—7.93 (m, 3H); MS *m/z* 196 (M^+); Found: C, 85.48; H, 6.14%. Calcd for $C_{14}H_{12}O$: C, 85.68; H, 6.16%.

1-Phenyl-3,4-pentadien-2-ol (3j): Colorless oil, IR (neat) 3350 and 1957 cm^{-1}; ^1H NMR ($CDCl_3$) δ=1.97 (br. s, 1H), 2.85 (d, *J*=6.0, 2H), 4.39 (m, 1H), 4.81 (m, 2H), 5.28 (m, 1H), and 7.11—7.42 (m, 5H); MS *m/z* 160 (M^+).

3b—g and **3j** were not satisfied with their elemental analyses because of their instabity.

General Procedure for the Synthesis of 5 (Table 2). Method A. To 99% formic acid (5 ml) was added a solution of **3** (1 mmol) in ether (2 ml) at room temperature. After stirring at room temperature for 30 min, benzene was added and the resulting solution was evaporated in vacuo (the bath temperature was kept below 30 °C). 1-Aryl-3-formyloxy-1,3-butadienes (**5a—c**, **5f**, and **5h**) were obtained after passing a short column of silica gel (20 g, activity V) at 0 °C using benzene-hexane as eluents. 1-Aryl-3-formyloxy-1,3-butadienes thus obtained are rather unstable and decomposes gradually on standing at room temperature.

Method B. To a solution of acetic anhydride (1 ml) in formic acid (5 ml) was added a solution of **3** (1 mmol) in ether (2 ml) at 0 °C. The solution was stirred at the same temperature for 1 h, and benzene was added. The resulting mixture was evaporated in vacuo below 30 °C, and the evaporations with benzene were repeated until most formic acid and acetic anhydride were removed. After passing through a short column of silica gel (20 g, activity V, 0 °C) with benzene-hexane **5** was obtained in yields summarized in Table 2.

1-Phenyl-3-formyloxy-1,3-butadiene (5a): Colorless oil, decomposed by distillation, IR (neat) 1745, 1645, and 1610 cm^{-1}; ^1H NMR ($CDCl_3$) δ=4.98 (d, *J*=2.0, 1H), 5.12 (d, *J*=2.0, 1H), 6.60 (d, *J*=17.0, 1H), 6.80 (d, *J*=17.0, 1H), 7.26—7.45 (m, 5H), and 8.27 (s, 1H); ^{13}C NMR ($CDCl_3$) δ=105.1 t, 121.8 d, 127.0 d, 128.6 d, 128.7 d, 131.2 d, 135.7 s, 151.8 s, and 159.0 d; MS *m/z* 174 (M^+).

1-(*p*-Tolyl)-3-formyloxy-1,3-butadiene (5b): Colorless oil, IR (neat) 1742, 1642, and 1608 cm^{-1}; ^1H NMR ($CDCl_3$) δ=2.35 (s, 3H), 4.96 (d, *J*=2.0, 1H), 5.09 (d, *J*=2.0, 1H), 6.56 (d, *J*=17.5, 1H), 6.78 (d, *J*=17.5, 1H), 7.15 (d, *J*=8.5, 2H), 7.32 (d, *J*=8.5, 2H), 8.27 (s, 1H); ^{13}C NMR ($CDCl_3$) δ=21.2 q, 104.4 t, 120.8 d, 126.9 d, 129.4 d, 131.1 d, 132.9 s, 138.6 s, 152.0 s, and 159.3 d; MS *m/z* 188 (M^+).

1-(4-Chlorophenyl)-3-formyloxy-1,3-butadiene (5c): Colorless needles, mp 35.5—36.5 °C, IR (KBr) 1725, 1640, and 1608 cm^{-1}; ^1H NMR (acetone-d_6) δ=5.08 (d, *J*=2.0, 1H), 5.25 (d, *J*=2.0, 1H), 6.77 (d, *J*=16.0, 1H), 6.98 (d, *J*=16.0, 1H), 7.38 (d, *J*=8.0, 2H), 7.57 (d, *J*=8.0, 2H), and 8.39 (s, 1H); ^{13}C NMR ($CDCl_3$) δ=105.5 t, 122.4 d, 128.1 d, 128.9 d, 129.3 s, 129.6 d, 134.2 s, 151.5 s, and 158.8 d; MS *m/z* 210 and 208 (M^+).

1-(2-Chlorophenyl)-3-formyloxy-1,3-butadiene (5f): Colorless oil, IR (neat) 1745, 1641, and 1608 cm^{-1}; ^1H NMR ($CDCl_3$) δ=5.05 (d, *J*=2.0, 1H), 5.17 (d, *J*=2.0, 1H), 6.61 (d, *J*=15.0, 1H), 7.14 (d, *J*=15.0, 1H), 7.16—7.60 (m, 4H), and 8.27 (s, 1H); ^{13}C NMR ($CDCl_3$) δ=106.2 t, 124.3 d, 126.7 d, 126.8 d, 127.0 d, 129.3 d, 129.9 s, 133.8 s, 151.4 s, and 158.9 d; MS *m/z* 210 and 208 (M^+).

1-(2-Naphthyl)-3-formyloxy-1,3-butadiene (5h): Colorless plates, mp 57—58 °C, IR (KBr) 1740, 1643, and 1610 cm^{-1}; ^1H NMR (acetone-d_6) δ=5.08 (d, *J*=2.0, 1H), 5.27 (d, *J*=2.0, 1H), 6.92 (d, *J*=16.0, 1H), 7.10 (d, *J*=16.0, 1H), 7.43—7.97 (m, 7H), and 8.44 (s, 1H); ^{13}C NMR (acetone-d_6) δ=106.3 t, 124.1 d, 124.8 d, 127.7 d, 127.8 d, 128.9 d, 129.0 d, 129.4 d, 129.7 d, 131.9 d, 134.7 s, 134.9 s, 135.0 s, 153.6 s, and 160.8 d; MS *m/z* 224 (M^+).

Elemental analyses of **5a—c**, **5f**, and **5h** were not satisfactory because of their instability.

References

1) M. Iyoda, M. Sakaitani, T. Miyazaki, and M. Oda, *Chem. Lett.*, **1984**, 2005; M. Iyoda, S. Tanaka, H. Otani, M. Nose, and M. Oda, *J. Am. Chem. Soc.*, **110**, 8494 (1988), and references cited therein.

2) Reviews: D. J. Pasto, *Tetrahedron*, **40**, 2805 (1984); H. F. Schuster and G. M. Coppola, "Allenes in Organic Synthesis," John Wiley & Sons (1984); M. Huche, *Bull. Soc. Chim. Fr.*, **1975**, 2369.

3) a) T. Mukaiyama and T. Harada, *Chem. Lett.*, **1981**, 621; b) J. Nokami, T. Tamaoka, T. Koguchi, and R. Okawara, *ibid.*, **1984**, 1939; c) G. P. Boldrini, E. Tagliavini, C. Trombini, and A. Umani-Tonchi, *J. Chem. Soc., Chem. Commun.*, **1986**, 685.

4) P. Place, C. Verniere, and J. Gore, *Tetrahedron*, **37**, 1359 (1981); H. Tanaka, T. Hamatani, S. Yamashita, and S. Torii, *Chem. Lett.*, **1986**, 1461, and references cited therein.

5) W. H. Werntz, *J. Am. Chem. Soc.*, **57**, 204 (1935); I. N. Nazarov, G. P. Verkholetova, and L. D. Bergel'son, *Izv. Akad. Nauk SSSR, Otdel. Khim. Nauk*, **1948**, 511; *Chem. Abstr.*, **43**, 2576i (1949).

6) H. Wollweber, "Diels-Alder Reaction," in "Houben-Weyl, Methoden der organischen Chemie," Georg Thieme, Stuttgart (1970), Band 5, Teil lc, pp. 977—1139; S. D. Kahn, C. F. Pau, L. E. Overman, and W. J. Hehre, *J. Am. Chem. Soc.*, **108**, 7381 (1986), and references cited therein.

7) J. S. Cowie, P. D. Landor, and S. R. Landor, *J. Chem. Soc., Perkin Trans. 1*, **1973**, 720.

8) A. Claesson and C. Bogentoft, *Acta Chem. Scand.*, **26**, 2540 (1972).

Aromatic Acetonylation by Using Aryltins with Acetonylium Equivalents under the Palladium Catalysis

Masanori KOSUGI,* Yoshio MIYAJIMA, Hideyuki NAKANISHI, Hiroshi SANO, and Toshihiko MIGITA*
Department of Chemistry, Faculty of Engineering, Gunma University, Kiryu, Gunma 376
(Received May 30, 1989)

Synopsis. Palladium-catalyzed reactions of heteroaromatic tins with 2-ethoxyallyl diethyl phosphate and of nitrophenyltins with 2-methoxymethoxyallyl chloride were found to give the coupling products, which can be hydrolyzed to the corresponding acetonylated aromatics in good yields.

Although a number of methods for aromatic acetonylation were reported so far,[1] there is still in need of an efficient method for aromatics having electron-withdrawing groups or heteroaromatics. Previously, we reported that acetonyltributyltin prepared in situ from methoxytributyltin and isopropenyl acetate reacted with aryl bromide under the palladium catalysis to give the arylacetone in good yield.[2] The reaction, however, was hardly applied to the aryl bromides having electron-withdrawing groups, although recent survey brought some improvements.

On the other hand, we report here an alternative method of preparing acetonyl aromatics, that is, the reaction of aryltins with acetonylium equivalent under the palladium catalysis.

$$Bu_3SnAr + CH_3COCH_2^+ \xrightarrow{[Pd]} ArCH_2COCH_3 + Bu_3Sn^+ \quad (1)$$

Acetonyl halide is the most simple reagent for acetonylium synthon, but is not suitable for the present reaction, because it has a carbonyl group which is reactive toward aryltins. Among the other acetonylium equivalents, 2-methoxyallyl bromide[3] which is labile and 2-trimethylsiloxyallyl halide[4] which is also labile in the presence of palladium complexes are not proper for the present reaction. On the basis of the stability of the compounds and the easiness of their preparation, we chose the following compounds; 2-ethoxyallyl diethyl phosphate,[5] 2-ethoxyallyl acetate,[6] and 2-ethoxyallyl carbonate,[7] 2-methoxymethoxyallyl chloride,[8] and 1-chloromethylvinyl diethyl phosphate.[9] These allylic compounds are converted into π-allyl palladium complexes by the palladium catalyst, and then react with aryltin compounds to give the coupled products.[10] Treatment of the products with aqueous acid would give the expected acetonylated products.

$$Bu_3SnAr + CH_2{=}C(OR)CH_2X \xrightarrow{[Pd]} ArCH_2C(OR){=}CH_2 \xrightarrow{H^+} ArCH_2COCH_3 \quad (2)$$

Palladium-catalyzed reactions of the phenyltributyltin with the various acetonylium equivalents gave the results as shown in the following equations.

$$PhSnBu_3 + CH_2{=}C(OEt)CH_2OPO(OEt)_2 \xrightarrow{[Pd]} PhCH_2C(OEt){=}CH_2 \quad 74\% \quad (3)$$

$$PhSnBu_3 + CH_2{=}C(OEt)CH_2OAc \xrightarrow{[Pd]} PhCH_2C(OEt){=}CH_2 \quad 49\% \quad (4)$$

$$PhSnBu_3 + CH_2{=}C(OEt)CH_2OCO_2Me \xrightarrow{[Pd]} PhCH_2C(OEt){=}CH_2 \quad 17\% \quad (5)$$

$$PhSnBu_3 + CH_2{=}C(OMOM)CH_2Cl \xrightarrow{[Pd]} PhCH_2C(OMOM){=}CH_2 \quad 79\% \quad (6)$$

(OMOM = OCH_2OCH_3)

$$PhSnBu_3 + CH_2{=}C(CH_2Cl)OPO(OEt)_2 \xrightarrow{[Pd]} PhCH_2C[OPO(OEt)_2]{=}CH_2 \quad 58\% \quad (7)$$

2-Methoxymethoxyallyl chloride and 2-ethoxyallyl diethyl phosphate gave the products in good yields.

Palladium-catalyzed reactions of 2-ethoxyallyl diethyl phosphate with nitrophenyltributyltins, pyridyltributyltins, and thienyltributyltins which are chosen as representatives of aromatics having electron-withdrawing group and heteroaromatics, are described in Table 1.

As Table 1 shows, although the yields of *p* and *m*-nitrophenylacetone were rather low, good yields for the reaction of heteroaryltins were obtained. As acetonylpyridines were labile, the coupled products were isolated without hydrolysis.

Results of palladium-catalyzed reactions of 2-methoxymethoxyallyl chloride with aryltributyltins were shown in Table 2.

Good yields of the arylacetones were obtained from the reaction with the *m* and *p*-nitrophenyltin, but moderate yields from the thienyltins. And the reaction with the pyridyltins did not give the product. Thus, suitable reagents for acetonylium synthon are differ-

Table 1. Pd-Catalyzed Reaction of $CH_2{=}C(OEt)$-$CH_2OPO(OEt)_2$ with Aryltins

Ar in Ar-$SnBu_3$	GLC Yield/%, Product	
Ph-	74	$PhCH_2C(OEt){=}CH_2$
p-NO_2-C_6H_4-	56, 48[a]	*p*-$NO_2C_6H_4CH_2COCH_3$
m-NO_2-C_6H_4-	40, 34[a]	*m*-$NO_2C_6H_4CH_2COCH_3$
2-Pyridyl-	60[a]	2-Pyridyl-$CH_2C(OEt){=}CH_2$
3-Pyridyl-	84[a]	3-Pyridyl-$CH_2C(OEt){=}CH_2$
2-Thienyl-	83[a]	2-Thienyl-CH_2COCH_3
3-Thienyl-	72[a]	3-Thienyl-CH_2COCH_3

a) Isolated yield.

Table 2. Pd-Catalyzed Reaction of $CH_2=C(OMOM)-CH_2Cl$[a] with Aryltins

Ar in Ar-$SnBu_3$	Isolated Yield/%, $ArCH_2COCH_3$	
H-C_6H_4-	79[b]	$PhCH_2COCH_3$
m-NO_2-C_6H_4-	71	*m*-$NO_2C_6H_4CH_2COCH_3$
p-NO_2-C_6H_4-	70	*p*-$NO_2C_6H_4CH_2COCH_3$
2-Thienyl-	42	2-Thienyl-CH_2COCH_3
3-Thienyl-	55	3-Thienyl-CH_2COCH_3

a) OMOM=OCH_2OCH_3. b) GLC yield.

ent with the kind of aromatic tin compounds.

There are a number of methods for the conversion of allyl acetate or phosphate into the corresponding allylstannane.[11] If such a conversion could be attained, the same coupling products could be obtained from the 2-alkoxyallylstannane and aryl halide. Unfortunately, many trials for the preparation of the 2-alkoxyallylstannane failed.

However, palladium-catalyzed reaction of a ternary system composed of bromobenzene, hexabutyldistannane, and 2-methoxymethoxyallyl chloride or 2-ethoxyallyl diethyl phosphate gave the expected product in moderate yields, although the reaction with substituted aryl bromides gave the product in lower yields.

$$PhBr+Bu_3SnSnBu_3+CH_2=C(OMOM)CH_2Cl \xrightarrow{[Pd]} PhCH_2C(OMOM)=CH_2 \quad 69\% \quad (8)$$

$$PhBr+Bu_3SnSnBu_3+CH_2=C(OEt)CH_2OPO(OEt)_2 \xrightarrow{[Pd]} PhCH_2C(OEt)=CH_2 \quad 53\% \quad (9)$$

The reaction seems to proceed through the formation of aryltributyltin prepared in situ by the reaction of aryl bromide with hexabutyldistannane under the palladium catalysis,[12] followed by its reaction with acetonylium equivalent under the reaction conditions.

Experimental

Instruments. JASCO Model A-100 for infrared spectra, Varian Associates Model EM-360 for ^1H NMR spectra, JEOL Model JMS-DX302 for mass spectra, JAI Model LC-08 for liquid chromatography, and Ohkura Model for gas chromatography using 10% Silicone SF96 or SE30 on Celite 545 were used.

Materials. 2-Bromothiophene (bp 65—75 °C/15 mmHg; 1 mmHg=133.322 Pa) was prepared by the bromination of thiophene.[13] 3-Bromothiophene (bp 75—77 °C/46 mmHg) was prepared by the bromination of thiophene giving 2,3,5-tribromothiophene (bp 135 °C/16 mmHg), followed by the treatment with zinc in acetic acid.[14] 2-Ethoxyallyl diethyl phosphate,[5] 2-ethoxyallyl acetate,[6] 2-ethoxyallyl carbonate,[7] 2-methoxymethoxyallyl chloride,[8] and 1-chloromethylvinyl diethyl phosphate[9] were prepared according to the method described in the literatures. Phenyltributyltin was prepared by the reaction of phenylmagnesium bromide with tributyltin chloride [prepared from bis(tributyltin) oxide and hydrochloric acid].[15] *m*-, *p*-Nitrophenyltributyltin were prepared by the reaction of the corresponding aryl bromide with hexabutyldistannane in the presence of palladium complexes.[12] 2-, 3-Pyridyl- and 2-,3-thienyltributyltin were prepared by the reaction of the corresponding pyridyl or thienyl bromide with butyllithium, followed by the reaction with tributyltin chloride.[16] Hexabutyldistannane was prepared by the reaction of the tributyltin hydride [prepared from bis(tributyltin) oxide and poly(methylhydrosiloxane)] in the presence of palladium complexes.[17] Tetrakis(triphenylphosphine)palladium,[18] dichlorobis(triphenylphosphine)palladium,[19] and tris(benzylideneacetone)dipalladium,[20] were prepared by the methods described.

Reaction Procedures. In Eqs. 3 and 4, the mixture of aryltin (1.3 mmol), the acetonylating agent (1.0 mmol), and tetrakis(triphenylphosphine)palladium (1 mol%) in HMPA (1 mL) was heated in a sealed tube at 100 °C for 20 h. The product was analyzed by GLC. In Eq. 5, the reaction was carried out at 120 °C. In Eq. 6, at 120 °C and dichlorobis(triphenylphosphine)palladium in THF were used. In Eq. 7, the reaction was carried out at 120 °C by using tris(dibenzylideneacetone)dipalladium (0.5 mol%) plus triphenylphosphine (2 mol%) in HMPA. In Tables 1 and 2, three times of the scale and dichlorobis(triphenylphosphine)palladium in benzene or toluene were used. The reaction mixture was washed with aqueous potassium fluoride, followed by the extraction of organic layer with ether, then dried over anhydrous magnesium sulfate. The product was isolated by Kugelrohr distillation under reduced pressure. It was acetonylated by the use of column chromatogaraphy on silica gel.

Products. 2-Ethoxyallylbenzene, ^1H NMR (CCl_4) δ=1.30 (t, J=7 Hz, 3H), 3.30 (s, 2H), 3.65 (q, J=7 Hz, 2H), 3.70 (bs, 2H), 7.15 (s, 5H). 1-Benzylvinyl diethyl phosphate, ^1H NMR (CCl_4) δ=1.30 (t, J=7 Hz, 6H), 3.50 (s, 2H), 3.95 (q, J=7 Hz, 2H), 4.16 (q, J=7 Hz, 2H), 4.40 (s, 1H), 4.90 (s, 1H), 7.30 (s, 5H). (2-Methoxymethoxyallyl)benzene, ^1H NMR (CCl_4) δ=3.30 (s, 3H), 3.35 (s, 2H), 4.00 (s, 1H), 4.20 (s, 1H), 4.85 (s, 2H), 7.25 (s, 5H). These compounds were hydrolyzed to give phenylacetone. ^1H NMR (CCl_4) δ=2.05 (s, 3H), 3.65 (s, 2H), 7.35 (s, 5H). Its IR spectra were consistent with that of the authentic sample.[21] 3-(2-Ethoxyallyl)-pyridine, ^1H NMR ($CDCl_3$) δ=1.25 (t, J=7 Hz, 3H), 3.40 (s, 2H), 3.80 (q, J=7 Hz, 2H), 3.90 (bs, 2H), 7.1—8.7 (m, 4H). Exact MS, Found: m/z 163.0952, Calcd for $C_{10}H_{13}NO$: M, 163.0997. 2-(2-Ethoxy-2-propenyl)pyridine, ^1H NMR ($CDCl_3$) δ=1.30 (t, J=7 Hz, 3H), 3.60 (s), 3.80 (q, J=7 Hz) 4.00 (s) 6H, 6.9—8.6 (m, 4H). *p*-Nitroacetonylbenzene, ^1H NMR (CCl_4) δ=2.20 (s, 3H), 3.80 (s, 2H), 7.40, 8.25 (ABq, J=10 Hz, 4H). IR (CCl_4) 1715 (C=O), 1515 and 1345(NO_2) cm^{-1}. Exact MS, Found: m/z 179.0549, Calcd for $C_4H_9NO_3$: M, 179.0582. *m*-Nitroacetonylbenzene, ^1H NMR (CCl_4) δ=2.20 (s,3H), 3.80 (s, 2H), 7.5—8.3 (m, 4H). IR (KBr) 1715 (C=O), 1510 and 1340 (NO_2) cm^{-1}. Exact MS, Found: m/z 179.0526, Calcd for $C_4H_9NO_3$: M, 179.0582. *p*-Cyanoacetonylbenzene, ^1H NMR ($CDCl_3$) δ=2.20 (s, 3H), 3.80 (s, 2H), 7.45, 7.80 (ABq, J=10 Hz, 4H). IR (KBr) 2250(CN), 1718 (C=O) cm^{-1}. Exact MS, Found: m/z 159.0668, Calcd for $C_{10}H_9NO$: M, 159.0684. 2-Acetonylthiophene, ^1H NMR ($CDCl_3$) δ=2.20 (s, 3H), 3.90 (s, 2H), 6.8—7.4 (m, 3H). IR (neat) 1710 (C=O) cm^{-1}. Exact MS, Found: m/z 140.0289, Calcd for C_7H_8OS: M, 140.0296. 3-Acetonylthiophene, ^1H NMR ($CDCl_3$) δ=2.20 (s, 3H), 3.65 (s, 2H), 6.8—7.4 (m, 3H). IR (neat) 1720 (C=O) cm^{-1}, Exact MS, Found: m/z 140.0275, Calcd for C_7H_8OS: M, 140.0296.

The gift of bis(tributyltin) oxide by Hokkoh Kagaku Kogyou Co. Ltd. is gratefully acknowledged. The present work was partially supported by a Grant-in-Aid for Special Project Research No. 61225002 from the Ministry of Education, Science and Culture.

References

1) R. A. Rossi and J. F. Bunnett, *J. Org. Chem.*, **38**, 1407 (1973); L. S. Hegedus and R. K. Stiverson, *J. Am. Chem. Soc.*, **96**, 3250 (1974); M. F. Semmelhack, B. P. Chong, R. D. Stauffer, T. D. Rogerson, A. Chong, and R. D. Jones, *ibid.*, **97**, 2507 (1975); M. W. Rathke and A. A. Miland, *ibid.*, **99**, 4833 (1977); J. F. Bunnett and J. E. Sunberg, *J. Org. Chem.*, **41**, 1702 (1976); J. T. Pinhey and B. A. Rowe, *Aust. J. Chem.*, **33**, 113 (1976); C. E. Sacks and P. L. Fuchs, *J. Am. Chem. Soc.*, **97**, 7372 (1975); A. A. Milard and M. W. Rathke, *ibid.*, **97**, 4833 (1975).

2) M. Kosugi, I. Hagiwara, T. Sumiya, and T. Migita, *Bull. Chem. Soc. Jpn.*, **57**, 242 (1984).

3) D. E. Horning, G. Kavadias, and M. Muchowski, *Can. J. Chem.*, **48**, 975 (1970); R. M. Jacobson, R. A. Raths, and J. H. McDonard III, *J. Org. Chem.*, **42**, 2545 (1977).

4) H. Sakurai, A. Shirahata, Y. Araki, and A. Hosomi, *Tetrahedron Lett.*, **21**, 2325 (1980); Y. Ito, H. Aoyama, T. Hirao, A. Mochizuki, and T. Saegusa, *J. Am. Chem. Soc.*, **101**, 494 (1979).

5) M. Kosugi, K. Ohashi, K. Akuzawa, T. Kawazoe, H. Sano, and T. Migita, *Chem. Lett.*, **1987**, 1237.

6) B. M. Trost and E. Keinan, *Tetrahedron Lett.*, **21**, 2591 (1980); B. M. Trost and D. P. Curren, *J. Am. Chem. Soc.*, **102**, 5699 (1980).

7) J. Tsuji, I. Shimizu, I. Minami, and Y. Ohashi, *Tetrahedron Lett.*, **23**, 4089 (1982).

8) X.-P. Gu, N. Nishida, I. Ikeda, and M. Okahara, *J. Org. Chem.*, **52**, 3192 (1987).

9) S. C. Welch, J. M. Assercq, J. P. Loh, and S. A. Glase, *J. Org. Chem.*, **52**, 1440 (1987).

10) F. K. Sheffy and J. K. Stille, *J. Am. Chem. Soc.*, **105**, 7173 (1983).

11) N. A. Bumagin, A. N. Kashin, and I. P. Beletskaya, *Buull. Acd. Sci. USSR*, **33**, 588 (1985); S. Matsubara, K. Wakamatsu, Y. Mrizawa, N. Tsuboniwa, K. Oshima, and H. Nozaki, *Bull. Chem. Soc. Jpn.*, **58**, 1196 (1985); B. M. Trost and J. W. Herndon, *J. Am. Chem. Soc.*, **106**, 6835 (1984); T. Tabuchi, J. Inanaga, and M. Yamaguchi, *Tetrahedron Lett.*, **28**, 215 (1987).

12) M. Kosugi, T. Ohya, and T. Migita, *Bull. Chem. Soc. Jpn.*, **56**, 3855 (1983).

13) "Dictionary of Organic Compounds," fifth ed., Vol. 1, Oxford University Press (1982), p. 883.

14) *Org. Synth.*, Coll. Vol. 5, 149 (1973).

15) W. P. Neumann, "The Organic Chemistry of Tin," John Wiley & Sons, London (1970).

16) P. Jutzi and U. Gilge, *J. Organomet. Chem.*, **246**, 163 (1983); S. Gopinathan, C. Gopinathan, and J. Gupta, *Indian J. Chem.*, **12**, 623 (1974).

17) T. N. Mitchell, *J. Organomet. Chem.*, **304**, 1 (1986).

18) D. R. Coulson, *Inorg. Synth.*, **13**, 121 (1972).

19) J. Chatt and F. G. Mann, *J. Chem. Soc.*, **1939**, 1631.

20) T. Ukai, H. Kawazura, Y. Ishii, J. J. Bonnet, and J. A. Ibers, *J. Organomet. Chem.*, **65**, 253 (1974).

21) "The Aldrich Library of Infrared Spectra," second ed., ed by C. J. Pouchert (1975), 742A.

A Convenient Synthesis of Trifluoromethylated Pyrroles and Porphyrins

Noboru ONO,* Hisayuki KAWAMURA, and Kazuhiro MARUYAMA*
Department of Chemistry, Faculty of Science, Kyoto University, Kyoto 606
(Received June 9, 1989)

Synopsis. 4-Alkyl-3-trifluoromethyl-2-pyrrolecarboxylic acid esters (**2**) were conveniently prepared by the reaction of trifluoromethylated β-nitro acetates (**1**) with ethyl isocyanoacetate. The pyrroles were converted into the corresponding porphyrins via tetramerization of 2-(hydroxymethyl)pyrroles.

Over past several years organofluorine compounds obtained considerable interest due to the enhanced biological activity.[1] A number of fluorine-containing heterocyclic compounds have been prepared so far. As pyrroles are basic components in various biologically active substances such as porphyrins and related compounds, the preparation of trifluoromethylated pyrroles is very important. Recently, Ogoshi and his co-workers have reported the first synthesis of 3-(trifluoromethyl)pyrroles[2] and their conversion into the corresponding porphyrins.[3] These porphyrins are useful probes for clarifying the structure of enzymes and the interaction between substrates and enzymes by use of ^{19}F NMR spectroscopy.[4] The first method to get trifluoromethylpyrroles is based on the Knorr reaction of ethyl trifluoroacetate,[2] and later the method is modified by the reaction of β-trifluoromethyl α,β-unsaturated ketones with *p*-tolylsulfonylmethyl isocyanide.[5] However, much difficulty still exists in the preparation of trifluoromethylpyrroles. In this paper we wish to report a simple and general method to get 4-alkyl-3-trifluromethyl-2-pyrrolecarboxylic acid exters (**2**), which are good precursors to the corresponding porphyrins. Our method is summarized in Scheme 1.

As shown in Scheme 1, the requisite materials to prepare **2** are all readily available and the procedures are very simple.

Reduction of perfluoroacetic acid with $LiAlH_4$ afforded 2,2,2-trifluoro-1,1-ethanediol (bp 105 °C),[6] which was directly converted into nitro alcohols on treatment with nitroalkanes in the presence of DBU. Thus, the tedious procedure for handling perfluoroacetaldehyde (bp −18 °C) is not required. The nitro alcohols were acetylated with acetic anhydride to give the corresponding β-nitro acetates (**1**) in good yields. The reaction of **1** with ethyl isocyanoacetate or *t*-butyl isocyanoacetate in the presence of DBU (2 equiv) gave 4-alkyl-3-trifluoromethyl-2-pyrrolecarboxylic acid (**2**).[7] The results are summarized in Table 1.

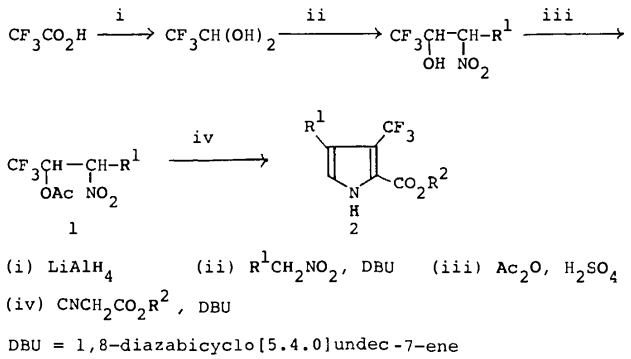

Scheme 1. Preparation of pyrroles (**2**).

Table 1 Preparation of 4-Alkyl-3-trifluoromethyl-2-pyrrolecarboxylic Acid Esters (**2**)

R^1	R^2	**2**, Yield/%
CH_3	C_2H_5	**2a**, 60
CH_3	*t*-C_4H_9	**2b**, 57
C_2H_5	C_2H_5	**2c**, 65
C_2H_5	*t*-C_4H_9	**2d**, 57
$CH_2CH_2CO_2CH_3$	C_2H_5	**2e**, 60

Thus, trifluoromethylated pyrroles are readily prepared starting from CF_3CO_2H and nitroalkanes. Other perfluoroalkylated pyrroles may be also prepared by the similar procedure as shown in Scheme 1 if appropriate perfluoro carboxylic acids are used.

Trifluoromethylpyrroles **2** are less reactive toward electrophiles than the corresponding alkyl derivatives. For example, **2a** reacts with methylal in the presence of *p*-toluenesulfonic acid (*p*-TsOH) to give dipyrromethane **3** in 60% yield. However, it takes about 7 days to complete the reaction, while the corresponding alkyl derivatives react with methylal very quickly under the same conditions.[8]

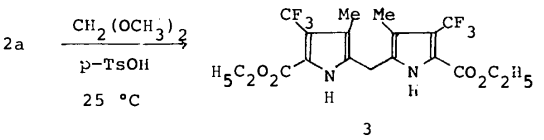

Pyrroles **2** are ideally functionalized for porphyrin synthesis. For example, pyrrole **2a** was converted into porphyrin **4a** via reduction with $LiAlH_4$ followed by treatment with *p*-TsOH and oxidation with chloranil, where type I porphyrin was formed selectively.[8] Other types of porphyrins are prepared via pyrromethanes such as **3**, which is well documented.[9]

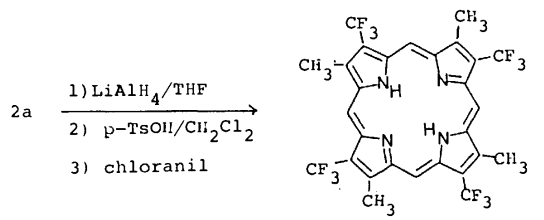

Absorption maxima in electronic spectra and redox potentials of **4a** and Zn complex of **4a** (Zn**4a**) are

Table 2 Absorption Maxima in Electronic Spectra and Redox Potentials of porphyrins

Porphyrins	λ_{max}/nm	Redox potentials[a] E^1/V	E^2/V
4a	407, 504, 539, 580, 635	0.84	1.22
OEP	396, 497, 532, 565, 619	0.60	1.02
Zn**4a**	404, 532, 568	0.78	1.02
ZnOEP	405, 532, 568	0.45	0.79

a) Redox potentials were determined by cyclic voltammetry. Measurements were made on platinum electrode in 0.1 M tetrabutylammonium perchlorate in CH_2Cl_2 at 25 °C. Reversible oxidation was observed, and E^1 and E^2 are the first and second oxidation peak potentials, respectively. Reference is Ag-$AgClO_4$.

compared with those of octaethylporphyrin (OEP) and Zn complex of OEP (ZnOEP). The results are summarized in Table 2. Each absorption maxima of **4a** shows red shift by about 10 nm compared with that of OEP. The redox potentials are dramatically changed by the introduction of the trifluoromethyl group at the β-position. The ring oxidation of **4a** and Zn**4a** occurs at about 200—300 mV higher than for OEP and ZnOEP, respectively.

Experimental

2,2,2-Trifluoro-1,1-ethanediol was prepared according to the procedure of the literature.[6] To a solution of perfluoroacetic acid (0.333 mol) in 300 ml of anhydrous diethyl ether was added slowly a slurry of $LiAlH_4$ (0.19 mol) in 250 ml of anhydrous diethyl ether at −5 °C to 0 °C during 1.5 h. Stirring was continued at −5 °C for 1 h. The reaction mixture was hydrolyzed with 15 ml of water followed by 30 ml of concd H_2SO_4 in 70 ml of water. The ether was decantated, and the solids remaining in the flask were dissolved in 300 ml of water. The aqueous solution was extracted with diethyl ether, and the extracts were combined and dried with anhydrous magnesium sulfate. After the removal of the solvent, the residue was distilled to give 2,2,2-trifluoro-1,1-ethanediol in 70—80% yield, bp 105 °C. This material was used for the next step without further purification.

3-Nitro-1,1,1-trifluoro-2-butanol. A mixture of 2,2,2-trifluoro-1,1-ethanediol (10 g, 0.086 mol), nitroethane (13 g, 0.17 mol), and DBU (2.6 g, 0.12 mol) was stirred at room temperature for 24 h. The resultant solution was poured into 1 M-HCl (100 ml) (1M=1 mol dm^{-3}) and extracted with ethyl acetate. The extracts were washed with water and dried with anhydrous magnesium sulfate. The solvent was removed and the residue was distilled to give the alcohol, 8.7 g (67% yield). Bp 85—87 °C/25 mmHg; 1 mmHg=133.32 Pa. ^{1}H NMR ($CDCl_3$) δ=1.90 (d, 3H), 3.70 (s, 1H), 4.62 (m, 1H), 5.10 (m, 1H). IR (neat) 3400, 1560, 1380, 1260, 1180 cm^{-1}. This compound was acetylated on treatment with acetic anhydride in the presence of H_2SO_4. Yield 90%, bp 57 °C/5 mmHg. ^{1}H NMR ($CDCl_3$) δ=1.75 (d, 3H, J=7 Hz), 2.28 (s, 4H), 4.46—4.84 (m, 1H), 5.85 (m, 1H).

Following nitro alcohols and their acetates were prepared in the same way as described above.

3-Nitro-1,1,1-trifluoro-2-pentanol. Yield 65%, bp 57—58 °C/4 mmHg. ^{1}H NMR ($CDCl_3$) δ=1.02 (t, 3H, J=7 Hz), 2.05 (m, 2H), 3.5 (br s, 1H), 4.45 (m, 1H), 4.75 (m, 1H), IR (neat) 3400, 1560, 1380, 1260, 1180 cm^{-1}. Acetyl Derivative: bp 62 °C/5 mmHg. ^{1}H NMR ($CDCl_3$) δ=1.05 (t, 3H, J=7 Hz), 1.97—2.08 (m, 2H), 2.21 (s, 3H), 4.70—4.83 (m, 1H), 5.75—5.96 (m, 1H).

Methyl 5-Hydroxy-4-nitro-6,6,6-triflurohexanoate. Yield 60%, bp 80 °C/2 mmHg. ^{1}H NMR ($CDCl_3$) δ=2.0—2.2 (m, 4H), 3.4 (br s, 1H), 3.65 (s, 3H), 4.70 (m, 2H), 5.22 (m, 1H). IR (neat) 3400, 1720, 1560, 1380, 1260, 1200 cm^{-1}. Acetyl Derivative: bp 95 °C/2 mmHg.

Preparation of Pyrroles. Ethyl 4-Methyl-3-trifluoromethyl-2-pyrrolecarboxylate (Typical Procedure). To a stirred solution of ethyl isocyanoacetate (2.5 g, 22 mmol) and 2-acetoxy-3-nitro-1,1,1-trifluorobutane (4.0 g, 19 mmol) in tetrahydrofuran (20 ml) was added DBU (5.5 g, 36 mmol) at 0 °C. The resulting mixture was stirred at 25 °C for 12 h. The reaction mixture was poured into water (100 ml) containing 1 M-HCl (10 ml) and extracted with ethyl acetate. The extracts were combined and washed with water. After drying with anhydrous magnesium sulfate and removal of the solvent, the residue was subjected to column chromatography (silica gel/benzene) to give the desired pyrrole (**2a**), 2.5 g (60% yield). Mp 73—75 °C. ^{1}H NMR ($CDCl_3$) δ=1.31 (t, 3H, J=7 Hz), 2.19 (s, 3H), 4.38 (q, 2H, J=7 Hz), 6.65 (d, 1H, J=4 Hz), 9.28 (s, 1H). IR (KBr) 3280, 1670, 1290, 1260, 1140 cm^{-1}. Found: C, 48.97; H, 4.47; N, 6.38; F, 25.60%. Calcd for $C_9H_{10}NO_2F_3$: C, 48.87; H, 4.56; N, 6.33; F, 25.77%.

***t*-Butyl 4-Methyl-3-trifluoromethyl-2-pyrrolecarboxylate (2b).** This pyrrole was prepared by the same procedure as the preparation of **2a**, but *t*-butyl isocyanoacetate was used instead of ethyl isocyanoacetate. Mp 103—105 °C. ^{1}H NMR ($CDCl_3$) δ=1.55 (s, 9H), 2.18 (s, 3H), 6.65 (d, 1H, J=4 Hz), 9.16 (s, 1H). IR (KBr) 3280, 1660, 1290, 1260, 1140 cm^{-1}. Found: C, 53.08; H, 5.60; N, 5.68%. Calcd for $C_{11}H_{14}NO_2F_3$: C, 53.01; H, 5.66; N, 5.62; F, 22.87%. Following pyrroles were prepared by the same procedure.

2c: oil, ^{1}H NMR ($CDCl_3$) δ=1.33 (t, 3H, J=7 Hz), 1.38 (t, 3H, J=7 Hz), 4.32 (q, 2H, J=7 Hz), 6.70 (d, 1H, J=4 Hz), 9.63 (s, 1H). IR (neat) 3300, 1670, 1290, 1260, 1150 cm^{-1}. Found: C, 50.92; H, 5.07; N, 5.67%. Calcd for $C_{12}H_{12}NO_2F_3$: C, 51.06; H, 5.14; N, 5.96%.

2d: mp 93—94 °C. ^{1}H NMR ($CDCl_3$) δ=1.39 (t, 3H, J=7 Hz), 1.59 (s, 9H), 2.63 (q, 2H, J=7 Hz), 6.71 (d, 1H, J=4 Hz), 9.25 (s, 1H). IR (KBr) 3280, 1660, 1290, 1260, 1140 cm^{-1}. Found; C, 54.43; H, 6.07; N, 5.51%. Calcd for $C_{12}H_{16}NO_2F_3$: C, 54.75; H, 6.08; N, 5.31%.

2r: oil ^{1}H NMR ($CDCl_3$) δ=1.32 (t, 3H, J=7 Hz), 2.50—2.72 (m, 4H), 3.72 (s, 3H), 4.26 (q, 2H, J=7 Hz), 6.65 (q, 1H, J=4 Hz), 9.90 (s, 1H). IR (neat) 3300, 1670, 1700, 1290, 1260, 1150 cm^{-1}. Found: C, 49.02; H, 4.72; N, 4.52%. Calcd for $C_{12}H_{14}NO_4F_3$: C, 49.15; H, 4.80; N, 4.78%.

Preparation of Dipyrromethane 3. A mixture of **2a** (0.22 g, 1 mmol), methylal (0.38 g, 5 mmol), and *p*-TsOH (0.1 g) in CH_2Cl_2 (10 ml) was stirred at room temperature for 7 days. The reaction mixture was poured into water, extracted with CH_2Cl_2, and washed with aqueous $NaHCO_3$. The organic layer was dried with anhydrous $MgSO_4$, and the solvent was removed. The residue was subjected to column chromatography (silica gel/CH_2Cl_2) to give **3**, 0.13 g (60% yield). Mp 166—168 °C. ^{1}H NMR ($CDCl_3$) δ=1.31 (t, 3H, J=7 Hz), 2.16 (s, 6H), 3.94 (s, 2H), 4.21 (q, 4H, J=7 Hz), 10.12 (s, 2 H). IR (KBr) 3280, 1680, 1290, 1260, 1140 cm^{-1}. Found: C, 50.15; H, 4.44; N, 6.17%. Calcd for $C_{20}H_{20}N_2O_4F_6$: C, 50.22; H, 4.43; N, 6.16%.

Preparation of Porphyrin 4. To a stirred mixture of $LiAlH_4$ (0.08 g, 2 mmol) in 30 ml of THF was added a solution of **2a** (0.50 g, 2.26 mmol) in 10 ml of THF. The mixture was stirred at 0 °C for 2 h and to the mixture was added 1 ml of ethyl acetate. The reaction mixture was poured into water containing dilute HCl and extracted with CH_2Cl_2. The organic layer was dried with anhydrous $MgSO_4$ and *p*-TsOH (0.1 g) was added to the organic layer

(ca. 100 ml). The resulting solution was stirred at room temperature for 12 h, and then chloranil (0.28 g, 1.1 mmol) was added to the resulting reaction mixture. After stirring at room temperature for 8 h, the reaction mixture was washed with 5%-$NaHCO_3$ and dried with anhydrous Na_2SO_4. The solvent was removed and the residue was subjected to column chromatography (silica gel/$CHCl_3$) to give **4**, 51 mg (14% yield). ^1H NMR ($CDCl_3$) δ=−3.48 (s, 2H, NH), 3.65 (s, 12H, CH_3), 10.40 (s, 4H, meso H). IR (KBr) 1120, 1050 cm^{-1}. Absorption maxima and redox potentials are summarized in Table 2. All these data are in good agreement with those reported by Ogoshi.[3,5]

References

1) T. Fuchikami, *Yuki Gosei Kagaku Kyokai Shi*, **42**, 775 (1984); "Biomedicinal Aspects of Fluorine Chemistry," ed by R. Filler and Y. Kobayashi, Elsevier, New York (1982); R. J. Linderman and M. S. Lonikan, *J. Org. Chem.*, **53**, 6013 (1988); T. Ishihara, Y. Okada, M. Kuroboshi, T. Shinozaki, and T. Ando, *Chem. Lett.*, **1988**, 819 and references therein.

2) H. Ogoshi, M. Homma, K. Yokota, H. Toi, and Y. Yokota, *Tetrahedron Lett.*, **24**, 929 (1983).

3) M. Homma, K. Aoyagi, Y. Aoyama, and H. Ogoshi, *Tetrahedron Lett.*, **24**, 4343 (1983).

4) H. Toi, A. Sudzuki, M. Homma, and H. Ogoshi, *J. Chem. Soc., Chem. Commun.*, **1985**, 1791.

5) K. Aoyagi, H. Toi, Y. Aoyama, and H. Ogoshi, *Chem. Lett.*, **1988**, 1891.

6) D. R. Husted and A. H. Ahlbrecht, *J. Am. Chem. Soc.*, **74**, 5422 (1952).

7) D. H. R. Barton and S. Z. Zard, *J. Chem. Soc., Chem. Commun.*, **1985**, 1098 where simple nitroalkenes are used.

8) N. Ono and K. Maruyama, *Chem. Lett.*, **1988**, 1511.

9) "Porphyrins and Metalloporphyrins," ed by K. M. Smith, Elsevier, Amsterdam (1975).

Synthesis of 2-[1-(Alkoxycarbonyl)alkyl]-3-methylbenzothiazolines and 3-Methyl-2-(2-oxoalkyl)benzothiazolines by the Direct Alkylation of Lithium Enolates with 3-Methylbenzothiazolium Salts

Hidenori CHIKASHITA,* Naoto TAKEGAMI, Yoshiyuki YANASE, and Kazuyoshi ITOH
Department of Applied Chemistry, Faculty of Engineering, Kansai University, Suita, Osaka 564
(Received June 19, 1989)

Synopsis. A variety of lithium enolates derived from esters and ketones could be readily alkylated with 3-methylbenzothiazolium salts to give the novel α-(benzothiazolinyl) esters and ketones, 2-[1-(alkoxycarbonyl)alkyl]-3-methylbenzothiazolines and 3-methyl-2-(2-oxoalkyl)benzothiazolines in good yields, respectively.

1,3-Dithienium tetrafluoroborates,[1] are well-known promising candidates of heterocyclic formyl or acyl cation equivalents. Although, up to now, the introduction of masked formyl and acyl groups at the α-position of carbonyl compounds has been achieved by the reaction of these salts with enol silyl ethers prepared from esters and ketones, a simpler and more direct method with lithium enolates have not been reported yet.[1] We have recently demonstrated that 3-methylbenzothiazolium salts can be used as useful formyl and acyl cation equivalents.[2,3] As an extension of our previous work[2] and as a requirement for the convenient preparation method of α-(benzothiazolinyl) carbonyl compounds in our study of enolate-transfer type aldol reaction,[4] we were interested in examining the direct reaction of lithium enolates with 3-methylbenzothiazolium salts. We now report that lithium enolates **2** and **3** derived from esters and ketones are readily alkylated under mild conditions with 3-methylbenzothiazolium salts **1**, leading to the introduction of the 3-methylbenzothiazoline unit at the α-position of carbonyl compounds.

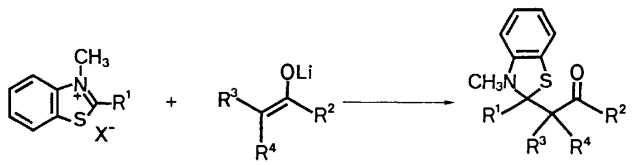

1a : R^1=H , X=I
b : R^1=Ph, X=SO_3F
c : R^1=Me, X=I

2 : R^2=OEt
3 : R^2=alkyl, aryl

4 : R^2=OEt
5 : R^2=alkyl, aryl

The alkylation of ester enolates **2** was carried out by the enolization of esters with lithium diisopropylamide in THF followed by treatment with one equiv of the benzothiazolium salts **1a**—c at −78 °C to room temperature, with the results summarized in Table 1. Under these conditions, 3-methylbenzothiazolium iodide (**1a**), which has a very acidic hydrogen at the 2-position, reacted with a variety of ester enolates **2** without significant abstraction of that hydrogen as a proton[5] to give the corresponding 2-[1-(ethoxycarbonyl)alkyl]benzothiazolines **4a**—**e** in good yields (Entries 1—5). Diastereoselectivity on the reaction of **1a** with the enolates produced from ethyl propionate, ethyl butanoate, and ethyl 3-methylbutanoate was found to be roughly 1 : 1 in each case (Entries 3—5), although the relative stereochemistry of each diastereoisomers has been not clarified. On the other hand, 2-substituted benzothiazolium salts **1b**, c reacted more efficiently with ester enolates to give the corresponding 2,2-disubstituted 3-methylbenzothiazolines in high yields (Entries 6,7).

The alkylation of ketone enolates **3** was similarly and efficiently achieved with benzothiazolium salts **1a**, **b** at 0 °C to room temperature giving the corresponding 2-(2-oxoalkyl)benzothiazolines **5a**—**g** in good

Table 1. Preparation of 2-[1-(Ethoxycarbonyl)alkyl]-3-methylbenzothiazolines **4** by the Reaction of Benzothiazolium Salts **1** with Lithium Enolates **2** from Esters

Entry	Salt **1**	Enolate **2**		Benzothiazoline **4**	Yield/%[a]
		R^3	R^4		
1	**1a**	H	H	**4a**	50
2	**1a**	Me	Me	**4b**	75
3	**1a**	Me	H	**4c**	42[b]
4	**1a**	Et	H	**4d**	48[b]
5	**1a**	*i*-Pr	H	**4e**	67[b]
6	**1b**	H	H	**4f**	87
7	**1c**	Me	Me	**4g**	81

a) Yield of pure product isolated by MPLC. b) Unseparable diastereomeric mixture with the ratio of 55 : 45 (Entry 3), 50 : 50 (Entry 4), and 60 : 40 (Entry 5).

Table 2. Preparation of 3-Methyl-2-(2-oxoalkyl)benzothiazolines **5** by the Reaction of Benzothiazolium Salts **1** with Lithium Enolates **3** from Ketones

Entry	Salt **1**	Enolate **3**			Benzothiazoline **5**	Yield/%[a]
		R^2	R^3	R^4		
1	**1a**	Ph	H	H	**5a**	34
2	**1b**	Ph	H	H	**5b**	71
3	**1b**	Me	H	H	**5c**	34
4	**1b**	*n*-Pr	H	H	**5d**	69
5	**1b**	Ph	Me	H	**5e**	72[b]
6	**1b**	Ph	Et	H	**5f**	55[c]
7	**1b**	$-(CH_2)_4-$		H	**5g**	75[c]

a) Yield of pure product isolated by MPLC. b) Yield of major diastereoisomer (the minor isomer **5e'** was isolated in 3% yield). c) A single diastereoisomer was predominantly obtained.

yields. The results are listed in Table 2. In contrast to the case of ester enolates **2**, the diastereoselectivity on the reaction with ketone enolates **3** was very high, as seen in the results of reactions with the enolates produced from propiophenone, butyrophenone, and cyclohexanone (Entries 5—7). As shown in the successful conversion of the kinetic enolate of 2-pentanone to **5d**, the regiocontrolled introduction of a 3-methylbenzothiazoline unit at the α-position of ketones can be conveniently achieved by the present method (Entry 4).

The present study is the first example of the direct alkylation of lithium enolates with heterocyclic formyl and acyl cation equivalents and provides a useful procedure for introduction of masked formyl and acyl groups at the α-position of carbonyl compounds because of ready and diverse availability of benzothiazolium salts[2,3] and high operational conveniency. The alkylation products can be regarded as selectively protected 1,3-dicarbonyl compounds and potentially useful synthetic intermediates because, for example, the 3-methylbenzothiazoline unit could be, after desired synthetic transformation, hydrolyzed to a carbonyl group as shown in the previous work.[2,3] In addition the another unique functionalities of 3-methylbenzothiazoline ring system increases the value of the present alkylation products in organic synthesis.[4,6]

Experimental

Melting points were recorded on a Yanagimoto micro-melting-point apparatus and are uncorrected. ^{1}H NMR spectra were measured with a JEOL PMX-60 spectrometer at 60 MHz using tetramethylsilane as an internal reference. IR spectra were recorded on a JASCO A-202 spectrophotometer. Silica gel (Merck silica gel 60, 230—400 mesh ASTM) was used for medium-pressure liquid chromatography (MPLC).

Materials. 2,3-Dimethylbenzothiazolium iodide (**1c**) was prepared by methylation of commercially available 2-methylbenzothiazole with iodomethane according to the preparation method reported for 3-methylbenzothiazolium iodide (**1a**).[2] 3-Methyl-2-phenylbenzothiazolium fluorosulfate (**1b**) was prepared by the methylation of 2-phenylbenzothiazole with methyl fluorosulfate according to the preparation method reported for 3-methylbenzothiazolium fluorosulfate.[2]

The Reaction of Benzothiazolium Salts 1 with Lithium Enolates 2 from Esters; General Procedure. To a solution of diisopropylamine (1.21 g, 12 mmol) in THF (20 ml), a 1.6 M hexane solution (1M=1 mol dm^{-3}) of *n*-BuLi (6.9 ml, 11 mmol) was slowly added with stirring at −78 °C and the mixture was then stirred at 0 °C for 10 min. To this mixture, a THF (5 ml) solution of ester (10 mmol) was slowly added at −78 °C and the mixture was then stirred for 50 min. Benzothiazolium salts **1** (10 mmol) was added at −78 °C and the mixture was stirred for 1 h at −78 °C and for 2 h at room temperature. The mixture was quenched by the addition of water and the aqueous mixture was extracted with ether. The extract was dried with $MgSO_4$ and concentrated under reduced pressure. The residue was subjected to MPLC to give pure product **4**. The results are summarized in Table 1. The spectral and physical data of the products **4** are as follows:

4a: pale yellow oil; IR (neat) 1720 cm^{-1} (C=O); ^{1}H NMR ($CDCl_3$) δ=1.16 (t, 3H, *J*=7 Hz), 2.67 (s, 3H), 2.73 (m, 2H), 4.00 (q, 2H, *J*=7 Hz), 5.15 (dd, 1H, *J*=8, 5 Hz), and 6.05—6.87 (m, 4H). Calcd for $C_{12}H_{15}NO_2S$: C, 60.73; H, 6.37; N, 5.90%. Found: C, 60.12; H, 6.46; N, 6.04%.

4b: pale yellow oil; IR (neat) 1720 cm^{-1} (C=O); ^{1}H NMR ($CDCl_3$) δ=1.13 (s, 3H), 1.17 (s, 3H), 1.20 (t, 3H, *J*=7 Hz), 2.82 (s, 3H), 4.04 (q, 2H, *J*=7 Hz), 5.23 (s, 1H), and 6.25—6.90 (m, 4H). Calcd for $C_{14}H_{19}NO_2S$: C, 63.36; H, 7.22; N, 5.28%. Found: C, 62.86; H, 7.30; N, 5.30%.

4c: pale yellow oil (diastereomeric mixture of 55:45 by ^{1}H NMR analysis); IR (neat) 1720 cm^{-1} (C=O); ^{1}H NMR ($CDCl_3$) δ=1.17 (d, 3H, *J*=7 Hz), 1.23 (t, 3H, *J*=7 Hz), 2.74 and 2.82 (each s, 4H), 4.06 and 3.94 (each q, 2H, *J*=7 Hz), 5.13 and 5.29 (each d, 1H, *J*=5 Hz), and 6.10—6.93 (m, 4H). Calcd for $C_{13}H_{17}NO_2S$: C, 62.12; H, 6.82; N, 5.57%. Found: C, 61.86; H, 6.96; N, 5.52%.

4d: pale yellow oil (diastereomeric mixture of 50:50 by ^{1}H NMR analysis); IR (neat) 1710 cm^{-1} (C=O); ^{1}H NMR ($CDCl_3$) δ=0.93 (t, 3H, *J*=7 Hz), 1.20 (t, 3H, *J*=7 Hz), 1.66 (q, 2H, *J*=7 Hz), 2.80 and 2.87 (each s, 4H), 4.05 (m, 2H), 4.97 and 5.08 (each d, 1H, *J*=2, 3 Hz), and 6.23—7.17 (m, 4H). Calcd for $C_{14}H_{19}NO_2S$: C, 63.36; H, 7.22; N, 5.28%. Found: C, 63.31; H, 7.21; N, 5.31%.

4e: pale yellow oil (diastereomeric mixture of 60:40 by ^{1}H NMR analysis); IR (neat) 1720 cm^{-1} (C=O); ^{1}H NMR ($CDCl_3$) δ=0.93 and 0.96 (each d, 6H, *J*=7 Hz), 1.22 (t, 3H, *J*=7 Hz), 2.27 (m, 1H), 2.62 and 2.64 (each d, 1H, *J*=8, 6 Hz), 2.80 and 2.83 (each s, 3H), 3.95 and 4.08 (each q, 2H, *J*=7 Hz), 5.10 and 5.12 (each d, 1H, *J*=8, 6 Hz), and 6.25—7.00 (m, 4H). Calcd for $C_{15}H_{21}NO_2S$: C, 64.48; H, 7.58; N, 5.01%. Found: C, 64.03; H, 7.71; N, 5.06%.

4f: pale yellow oil; IR (neat) 1720 cm^{-1} (C=O); ^{1}H NMR ($CDCl_3$) δ=1.00 (t, 3H, *J*=7 Hz), 2.53 (s, 3H), 3.27 (s, 2H), 3.84 (q, 2H, *J*=7 Hz), and 6.57—7.50 (m, 9H). Calcd for $C_{18}H_{19}NO_2S$: C, 68.98; H, 6.11; N, 4.47%. Found: C, 69.06; H, 6.09; N, 4.50%.

4g: pale yellow oil; IR (neat) 1710 cm^{-1}; ^{1}H NMR ($CDCl_3$) δ=1.19 (t, 3H, *J*=8 Hz), 1.33 (s, 6H), 1.90 (s, 3H), 2.73 (s, 3H), 3.98 (q, 2H, *J*=8 Hz), and 6.00—6.92 (m, 4H). Calcd for $C_{15}H_{21}NO_2S$: C, 64.48; H, 7.58; N, 5.01%. Found: C, 64.16; H, 7.32; N, 4.91%.

The Reaction of Benzothiazolium Salts 1 with Lithium Enolates 3 from Ketones; General Procedure. A THF (5 ml) solution of ketone (10 mmol) was slowly added to a THF solution of LDA (11 mmol) at −78 °C and the mixture was allowed to gradually warm to room temperature. The mixture was stirred for 3 h and then cooled to 0 °C. Benzothiazolium salt **1** (10 mmol) was added to the mixture and the mixture was stirred for 1 h at 0 °C and for 1 h at room temperature. After a similar work-up to the reaction of ester enolates, the crude product was purified by MPLC to give pure product **5**. The results are summarized in Table 2. The spectral and physical data of the products **5** are as follows:

5a: pale yellow oil; IR (neat) 1680 cm^{-1} (C=O); ^{1}H NMR ($CDCl_3$) δ=2.43 (s, 3H), 3.10 (m, 2H), 5.10 (dd, 1H, *J*=8, 6 Hz), and 5.76—7.57 (m, 9H). This compound was unstable at room temperature in air.

5b: pale yellow needles; mp 119—120 °C; IR (KBr) 1680 cm^{-1} (C=O); ^{1}H NMR ($CDCl_3$) δ=2.55 (s, 3H), 3.83 (d, 1H, *J*=16 Hz), 4.33 (d, 1H, *J*=16 Hz), and 6.05—7.83 (m, 14H). Calcd for $C_{22}H_{19}NOS$: C, 76.49; H, 5.54; N, 4.05%. Found: C, 76.42; H, 5.53; N, 3.85%.

5c: pale yellow needles; mp 123—124 °C; IR (KBr) 1700 cm^{-1} (C=O); ^{1}H NMR ($CDCl_3$) δ=2.10 (s, 3H), 2.55 (s, 3H), 3.21 (d, 1H, *J*=11 Hz), 3.47 (d, 1H, *J*=11 Hz), and 6.21—7.52 (m, 9H). Calcd for $C_{17}H_{17}NOS$: C, 72.05; H, 6.05; N, 4.94%. Found: C, 71.91; H, 5.96; N, 4.83%.

5d: pale yellow needles; mp 66—66.7 °C; IR (KBr) 1700

cm^{-1} (C=O); ^1H NMR ($CDCl_3$) δ=0.80 (t, 3H, J=8 Hz), 1.50 (m, 2H), 2.33 (t, 2H, J=6 Hz), 2.50 (s, 3H), 3.28 (d, 1H, J=18 Hz), 3.72 (d, 1H, J=18 Hz), and 6.23—7.70 (m, 9H). Calcd for $C_{19}H_{21}NOS$: C, 73.28; H, 6.80; N, 4.50%. Found: C, 73.09; H, 6.80; N, 4.46%.

5e: pale yellow needles; mp 153—153.5 °C; IR (KBr) 1680 cm^{-1} (C=O); ^1H NMR ($CDCl_3$) δ=1.53 (d, 3H, J=8 Hz), 2.42 (m, 3H), 4.56 (q, 1H, J=8 Hz), and 6.43—7.33 (m, 14H). Calcd for $C_{23}H_{21}NOS$: C, 76.85; H, 5.89; N, 3.90%. Found: C, 76.75; H, 5.98; N, 3.69%.

5e′: pale yellow needles; mp 120.3—121.5 °C; IR (KBr) 1700 cm^{-1} (C=O); ^1H NMR ($CDCl_3$) δ=1.05 (d, 3H, J=6 Hz), 2.55 (s, 3H), 3.85 (q, 1H, J=6 Hz), and 6.31—7.40 (m, 14H). Calcd for $C_{23}H_{21}NOS$: C, 76.85; H, 5.89; N, 3.90%. Found: C, 76.41; H, 6.04; N, 4.55%.

5f: pale yellow needles; mp 150.5—152 °C; IR (KBr) 1680 cm^{-1} (C=O); ^1H NMR ($CDCl_3$) δ=0.96 (t, 3H, J=8 Hz), 2.03 (m, 2H), 2.50 (s, 3H), 4.41 (dd, 1H, J=4, 7 Hz), and 6.23—7.83 (m, 14H). Calcd for $C_{24}H_{23}NOS$: C, 77.17; H, 6.21; N, 3.75%. Found: C, 77.23; H, 6.17; N, 3.42%.

5g: colorless needles; mp 184.2—186 °C; IR (KBr) 1700 cm^{-1} (C=O); ^1H NMR ($CDCl_3$) δ=1.52—2.33 (bm, 9H), 2.40 (s, 3H), and 6.43—7.35 (m, 9H). Calcd for $C_{20}H_{21}NOS$: C, 74.27; H, 6.54; N, 4.33%. Found: C, 74.03; H, 6.49; N, 4.13%.

References

1) I. Stahl, *Chem. Ber.*, **118**, 1798, 3159 (1985); G. Picotin and D. Miginiac, *J. Org. Chem.*, **50**, 1299 (1985) and references cited therein.

2) H. Chikashita, S. Komazawa, N. Ishimoto, K. Inoue, and K. Itoh, *Bull. Chem. Soc. Jpn.*, **62**, 1215 (1989).

3) H. Chikashita, M. Ishibaba, K. Ori, and K. Itoh, *Bull. Chem. Soc. Jpn.*, **61**, 3637 (1988).

4) H. Chikashita, S. Tame, and K. Itoh, *Heterocycles*, **27**, 67 (1988).

5) This proton abstraction from **1a** leads to the formation of the stable ylide, as was described in Refs. 2 and 3. See also: H. Chikashita, M. Ishihara, and K. Itoh, *Heterocycles*, **23**, 2467 (1985).

6) H. Chikashita, Y. Yanase, and K. Itoh, *Chem. Express*, **4**, 393 (1989).

A New Method for the Selective Synthesis of Biphenyl by Dehydrogenative Coupling of Benzene

Masahiro NAKADA, Yu AIMIN, Shigenobu KAWAKAMI,
Shingo IWAKI, and Tatsuaki YAMAGUCHI*
Laboratory of Organic Chemistry, Chiba Institute of Technology,
Tsudanuma, Narashino-shi, Chiba 275
(Received March 13, 1989)

Synopsis. A method has been developed for the direct preparation of biphenyl by the thermal dehydrogenative coupling of benzene in the vapor phase on the surface of heater at 1000—1200 °C. Biphenyl was obtained at a high selectivity of more than 94% over the wide range of benzene conversion (3—77%).

Biphenyl was first reported by Fittig, and then identified by Berthelot as the main product obtained by passing benzene vapor through a hot tube.[1] Since then many methods have been developed for the preparation of this compound.[2-4] Biphenyl is now important as the starting material for heating oil, high aromatic solvent, electric insulating oil and other synthetic use in industry. The modern commercial production process of biphenyl is the thermal dehydrogenation of benzene in a hot tube. In this method, however, the higher is the conversion of benzene, the lower is the biphenyl selectivity due to additional coupling of biphenyl to terphenyls and quaterphenyls. Therefore, the conversion is to be kept below 15% to obtain biphenyl in high selectivity (88—92%).[5] Biphenyl is also obtained as a by-product of benzene production by hydrodealkylation of toluene.[6] A further purification of biphenyl is necessary in this process. A novel method to prepare pure biphenyl in high selectivity and yield will be described in this paper. The characteristic feature of the present method is the temperature gradient system of the reactor heated by a heater from inside. In such a system, the thermal diffusion effect is significant, and the product of the higher molecular weight was separated at the cold wall of the reactor. The highly selective synthesis of ethylene from methane by the thermal diffusion reactor has recently been reported by one of the authors.[7]

Experimental

An electric heater was placed inside of a 1 L three-necked separable flask fitted with a reflux condenser. The heater was made of a nickel chromium steel wire of 0.5 mm in diameter and 25 cm in length made in a spiral. The flask containing 50 g of benzene was heated by a heating mantle under nitrogen. After the boiling of benzene was started, the power of the heater inside was turned on, and the vapor of benzene was contacted with the heater. The surface temperature of the heater was monitored by a radiation pyrometer (Minolta IR-120) and controlled. The reaction mixture was sampled periodically and analyzed by a gas chromatograph (Shimadzu GC-9A).

Results and Discussion

Figure 1 shows the dependence of the benzene conversion on the surface temperature of the heater. The reaction started substantially at 1000 °C. The conversion of benzene increased exponentially with the surface temperature, reaching 77% at 1150 °C. At 1200 °C the color of the benzene vapor near the heater turned brown, suggesting a considerable carbonization. In fact fairly large amount of carbonaceous material deposited on the surface of the nickel chromium steel wire under these conditions. The results are summarized in Table 1 with experimental details. The selectivity of biphenyl remained almost the same 94% over a wide range of benzene conversion. Even at the high conversion of benzene 77.5%, the selectivity of biphenyl was 94.0%. This high selectivity of biphenyl at high conversion of benzene is one of the advantages of this new method over the conventional one, in which benzene vapor is passed through a hot tube heated from outside. In the conventional method, the high selectivity of biphenyl of 90% is obtained only when the one path conversion of benzene is below 15%.

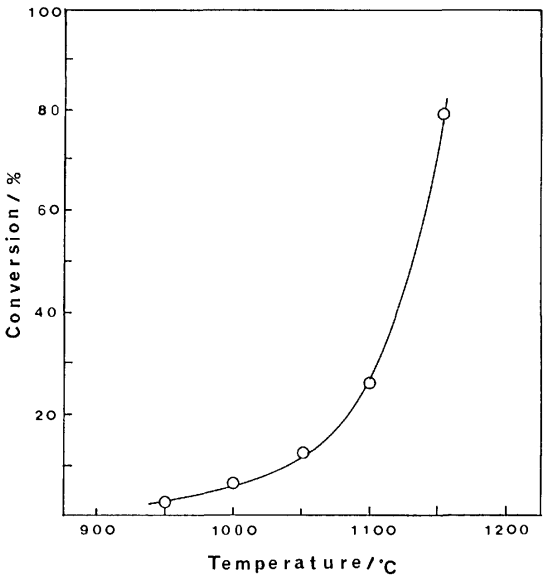

Fig. 1. Dependence of benzene conversion on the surface temperature of the heater (reaction time 6 h).

The phenomenon giving high selectivity of biphenyl may be due to the thermal diffusion effect. The thermal diffusion caused by the temperature gradient between the surface of the heated wire and the cold wall of the reactor effects the produced biphenyl molecule, which is of higher molecular weight than benzene, to leave the heated surface of the heater for the cold wall immediately after its production and

Table 1. Product Distribution of Benzene Coupling

Surface temp.	Reaction time	Benzene conv.	Selectivity[a)]			
			Biphenyl	*o*-Terphenyl	*m*-Terphenyl	*p*-Terphenyl
°C	h	%	%	%	%	%
950	6	1.8	97.0	0.4	1.7	0.9
1000	6	5.7	95.4	0.6	2.6	1.4
1050	6	12.4	94.5	0.8	3.0	1.7
1100	3	8.2	95.3	0.6	2.3	1.5
	6	25.4	94.2	0.8	3.2	1.8
1150	1	3.5	95.4	0.6	2.5	1.5
	2	11.1	94.7	0.7	3.0	1.6
	3	20.6	96.1	0.5	2.2	1.2
	4	31.8	95.4	0.6	2.6	1.4
	5	47.5	95.5	0.6	2.4	1.5
	6	77.5	94.0	0.9	3.3	1.8

a) Values for selectivities were based on the weight of the products.

thus prevents the molecule from further reaction to terphenyls or quaterphenyls.

The authors wish to express their thanks to Professor Emeritus Kozo Hirota of Osaka University for his helpful discussions.

References

1) A. Berthelot, *Justus Liebigs Ann. Chem.*, **142**, 252 (1867).
2) F. Ullmann, *Justus Liebigs Ann. Chem.*, **332**, 48 (1904).
3) M. Gomberg and W. E. Bachmann, *J. Am. Chem. Soc.*, **46**, 2339 (1924).
4) J. H. Gardner and P. Borgstrom, *J. Am. Chem. Soc.*, **51**, 3376 (1929).
5) M. Fujitu and F. Akazawa, Jpn. Patent 38094 (1979).
6) G. Asselin and R. Erickson, *Chem. Eng. Prog.*, **58** (4), 47 (1962).
7) T. Yamaguchi and C. Saito, *Bull. Chem. Soc. Jpn.*, **61**,2649 (1988); T. Yamaguchi, A. Kadota, and C. Saito, *Chem. Lett.*, **1988**, 681.

Selective Lithium Ion Transport through Hollow-Fiber Membrane Containing Easily-Dissociable 14-Crown-4 Derivative

Hidefumi SAKAMOTO, Keiichi KIMURA, Minoru TANAKA, and Toshiyuki SHONO*
Department of Applied Chemistry, Faculty of Engineering,
Osaka University, Yamada-oka, Suita, Osaka 565
(Received March 25, 1989)

Synopsis. A flow-through transport system was fabricated by using a hollow-fiber impregnated with a 14-crown-4 dinitrophenol solution and was found to allow selective Li^+ transport.

Many attempts to transport alkali metal ions through liquid membranes containing crown ether derivatives as ionophores have been widely made in order to attain an effective separation of a certain metal ion from others. In this kind of liquid membrane system, supported liquid membranes[1-3] containing a crown ether solution using a water-immiscible organic solvent (such as diphenyl ether, *o*-nitrophenyl phenyl ether, and *o*-nitrophenyl octyl ether (NPOE)) may be superior in handling to bulk liquid membranes, and may be employed for industrial applications. In the case of using a hollow-fiber as the support for a liquid membrane,[4] separation of a certain metal ion can be carried out under conditions in which the aqueous solutions of the source and receiving phases flow along either or both sides of the membrane phase. Therefore, such a decrease in the metal ion flux with the ion concentration change in the source phase, as is frequently observed in the conventional membrane transport systems, can be prevented. Since the flux in this flow system is kept constant, a large quantity of the desired cation can be separated from the source phase solution continuously. Alternatively, the transport rate of a certain metal ion may be effectively altered with the ion concentration change in the source phase.

We have synthesized several 14-crown-4 derivatives[5] endowed with a lipophilic chain and a nitrophenol moiety and have employed them as ionophores for proton-driven transport of alkali metal ions using a supported liquid membrane.[2] It was found that Li^+ was transported selectively and enriched in the receiving phase on the proton-driven ion transport. Applications of this Li^+-selective membrane transport system to the corresponding flow-through transport system are useful for effective Li^+ recovery from both spring- and seawater and for the construction of pretreatment systems for selective Li^+ analyses.

In this paper we report on the competitive proton-driven transport of alkali metal ions through a hollow-fiber membrane impregnated with a solution of 14-crown-4 dinitrophenol **1**. The effects of the transport conditions on the ion transportability in this hollow-fiber ion-transport system are also described.

Experimental

Competitive transport of alkali metal ions through a hollow-fiber membrane containing 14-crown-4 dinitrophenol **1**, which was prepared according to a previously used procedure,[5] was conducted by using a flow-through transport system (shown schematically in Fig. 1). The inner tube was a hollow fiber (pore size: 0.1 μm, thickness: 0.27 mm, outer diameter: 1.22 mm, inner diameter: 0.68 mm), which was kindly given by Asahi Chemical Industry Co., Ltd. The outer tube was a glass tube (inner diameter: 4.0 mm), both ends of which were joined to the hollow fiber with an epoxy resin adhesive. The hollow fiber was impregnated with a NPOE solution of 14-crown-4 dinitrophenol. Impregnation was performed by slowly flowing a 4×10^{-2} M (1 M=1 mol dm^{-3}) crown ether NPOE solution through the inside of the hollow-fiber membrane. The exposed area in the outer surface of the hollow-fiber membrane was 2.0 cm^2, unless otherwise specified. Aqueous solutions for the source and receiving phases were flowed countercurrently at the inside and outside phases of the hollow-fiber membrane, respectively, at a constant flow rate by using peristaltic pumps. The flow-through transport system was kept at 25 °C by using a thermostated bath during the transport experiment.

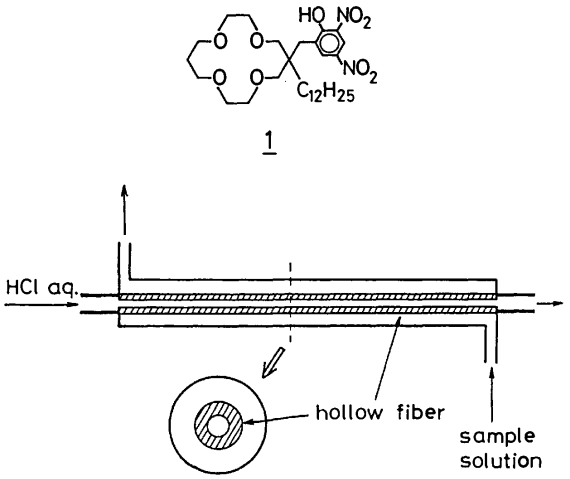

1

Fig. 1. 14-Crown-4 dinitrophenol **1** and schematic diagram of flow-through transport system.

For the proton-driven cation transport, the source (outer) phase contained 1.1×10^{-2} M tetramethylammonium hydroxide (TMAOH) and alkali metal ions, and the receiving (inner) phase did 2.0×10^{-3} M hydrochloric acid. The source phase contained alkali metal chlorides (Li^+, Na^+, K^+, Rb^+, Cs^+) of 1.0×10^{-3} M each for competitive transport. Upon examining the dependence of metal ion (Li^+ and Na^+) concentrations on the Li^+ transportability, the source phase contained Li^+ and Na^+ of appropriate concentrations. In competitive cation transport under conditions in which the temperature was changed from 6 to 45 °C, the source phase of the transport system contained Li^+ and Na^+ of 1.0×10^{-3} M each.

The eluted solution of the receiving phase was collected by a fraction collector every fifteen minutes. The alkali

metal ions in the receiving aqueous phase were determined by flame photometry. Aliquots (1 ml) of the aqueous phase were occasionally taken; then, ten-fold diluted solutions were subjected to ion determination.

Results and Discussion

Competitive Transport of Alkali Metal Ions. Crown ether **1** is endowed with a 14-crown-4 site, which complexes Li^+ selectively, a dinitrophenol moiety as a proton-dissociable anionic site to counterbalance the positive charge of the complexed cation, and a dodecyl group to have the ionophore stay in the membrane phase. This crown ether, the pK_a of which is 4.92 (in 50% dioxane-H_2O), is able to deprotonate under weakly basic conditions and, thereby, to complex Li^+. It was previously shown that effective Li^+-selective transport was attained by using a U-tube equipped with a supported liquid membrane made from a microporous polypropylene film, which was impregnated with a **1**-NPOE solution. That is to say, at the basic interface the dinitrophenol moiety loses a proton; concurrently the crown ether moiety interacts with a lithium ion and forms an electrically-neutral complex. The crown-Li^+ complex diffuses to the acidic interface through the membrane, where it is forced to release the Li^+ by protonation of the anionic site.

The transport profile of alkali metal ions for a flow-through system with a hollow-fiber membrane containing the crown ether NPOE solution is depicted in Fig. 2. It should be noted that cation transport through the membrane is extremely specific to Li^+ and the Li^+ flux appears to level off within 1 h. The other alkali metal ions, even Na^+ which is quite similar to Li^+ in the chemical property, moved through the membrane only at such low transport rates. The Li^+ concentration in the receiving phase was 4.5×10^{-5} M at a flow rate of 0.19 ml min^{-1} (a linear velocity of 52.3 cm min^{-1} in the inner phase of the hollow fiber). The concentration of metal ion in the receiving phase varied inversely as the flow rate of the receiving phase, while the concentration was independent of the flow rate of the source phase. The metal ion transportability was also proportional to the exposed membrane area and, therefore, the length of hollow fiber.

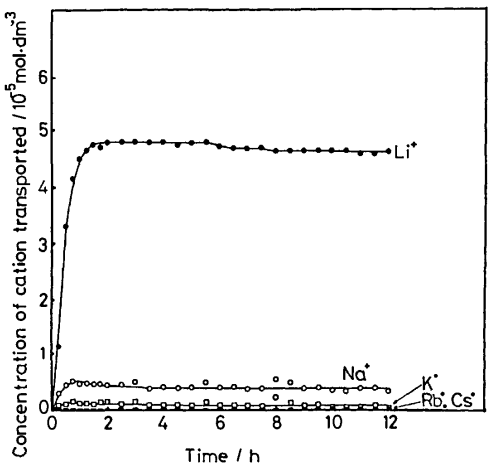

Fig. 2. Competitive proton-driven cation transport of alkali metal ions using flow-through system.

Effects of Transport Conditions. The flux of metal ion transported was directly proportional to the logarithm of the metal ion concentration under conditions in which the Li^+ and Na^+ concentrations in the source phase were varied from 1.0×10^{-5} M to 1.0×10^{-3} M (Fig. 3). The metal ion flux is generally proportional to the cation concentration in the source phase, in the case of a conventional hollow-fiber membrane systems containing ionophores.[6] The difference in the concentration dependence on metal ion flux between this system and conventional hollow-fiber membrane systems has not yet been understood.

The concentration of Na^+ which coexists with Li^+ in the source phase is an important factor governing the Li^+ transportability. Competitive transport of Li^+ and Na^+ through the supported hollow-fiber membrane was carried out by varying the Na^+ concentration in the source phase from 1.0×10^{-3} M to 1.0×10^{-1} M and keeping the Li^+ concentration constant (1.0×10^{-3} M). Increasing the Na^+ concentration enhanced the Na^+ transportability and lowered the Li^+ transportability. It is consequently shown in Table 1 that the selectivity ratio of Li^+ over Na^+ hardly changes.

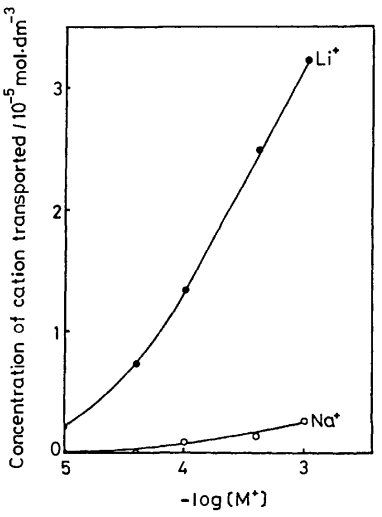

Fig. 3. Effect of cation concentration in source phase on cation transportability.

Table 1. Effect of Na^+ Concentration on Cation Transportability

Cation concentration in source phase (10^{-3}mol dm^{-3})		Concentration of cation transported (10^{-5}mol dm^{-3})		Selectivity ratio
Li^+	Na^+	Li^+	Na^+	Li^+/Na^+
1.0	1.0	3.01	0.10	30
1.0	4.0	2.80	0.32	33
1.0	10.0	2.35	0.83	28
1.0	40.0	1.28	1.98	26
1.0	100.0	0.71	2.62	27

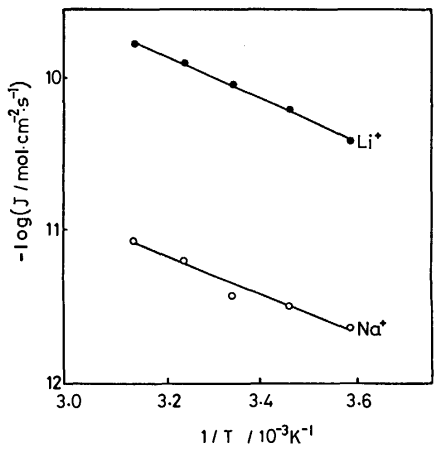

Fig. 4. Arrhenius plots for flux of cation transported.

Permeation coefficients of the metal ions were measured at temperatures ranging from 6 to 45 °C. The Arrhenius plots of Li^+ and Na^+ gave simple straight lines with nearly equal slopes (Fig. 4). If the cation membrane transport were governed only by the cation-crown ether complexation, the transport rates would decrease with a rise in temperature, since the stability of cation-crown ether complexes decreased with temperature.[7,8] It may, therefore, be considered that for a proton-driven cation transport through the hollow-fiber membrane containing **1** the rate-determining step of metal ion transportability is the permeation process of the crown-metal ion complex through the membrane phase.

In conclusion, a hollow-fiber membrane impregnated with a 14-crown-4 dinitrophenol NPOE solution can separate Li^+ efficiently from other alkali metal ions in the flow-through transport system. This supported hollow-fiber membrane was sufficiently stable to permit metal ion transport for 25 h. The present flow-through cation transport system possesses an advantage over a previously-reported batch system in that Li^+ can be separated continuously, although the flow-through system is not superior to the batch system regarding selectivity. Thus, continuity in Li^+ separation seems to allow the present flow-through Li^+ transport system to be applicable to various fields of Li^+ separation and analyses.

We thank Professor Makoto Otomo of Nagoya Institute of Technology for his understanding and support. This work was supported by a Grant-in-Aid for Encouragement of Young Scientists from the Ministry of Education, Science and Culture No. 62790216.

References

1) Y. Yamaguchi, K. Nishimura, and T. Shinbo, *Chem. Lett.*, **1985**, 1549.
2) H. Sakamoto, K. Kimura, and T. Shono, *Anal. Chem.*, **59**, 1513 (1987).
3) H. Sakamoto, K. Kimura, Y. Koseki, and T. Shono, *J. Chem. Soc., Perkin Trans. 2*, **1987**, 1181.
4) H. Yamamoto, Jpn. Kokai Tokkyo Koho JP 62114604 [87114604],(1987); *Chem. Abstr.*, **107**, 80079y (1987).
5) K. Kimura, M. Tanaka, S. Iketani, and T. Shono, *J. Org. Chem.*, **52**, 836 (1987).
6) M. Teramoto and H. Tanimoto, *Sep. Sci. Technol.*, **18**, 871 (1983).
7) C. J. Thoman, *J. Am. Chem. Soc.*, **107**, 1437 (1985).
8) M. Ouchi, Y. Inoue, T. Kanzaki, and T. Hakushi, *J. Org. Chem.*, **49**, 1408 (1984).

Reactivity of $RuCl_3(EPh_3)_2S$ (E=P, As; S=DMSO, DMF, THF, CH_3CHO, CH_3CN, CS_2, $(CH_3)_2CO$) towards 2,4,6-Trichloro-1,3,5,2,4,6-trithiatriazine and Substitution Reactions of $Ru(NS)Cl_3(EPh_3)(E'Ph_3)$(E=P, As; E'=P, As, Sb) with N-Donor Heterocyclic Ligands

Minu GUPTA, Jyoti SETH, and U.C. AGARWALA*
Department of Chemisty, Indian Institute of Technology, Kanpur-208016, India
(Received March 22, 1988)

Synopsis. 2,4,6-Trichloro-1,3,5,2,4,6-trithiatriazine, $N_3S_3Cl_3$, reacts with Ru(III) complexes of the type $RuCl_3(EPH_3)_2S$ to form an intermediate which further reacts with PPh_3, $AsPh_3$, and $SbPh_3$ to form $Ru(NS)Cl_3(EPh_3)_2$ or $Ru(NS)Cl_3(EPh_3)(E'Ph_3)$. Besides, substitution reactions of $Ru(NS)Cl_3(EPh_3)_2$ and $Ru(NS)Cl_3(EPh_3)(E'Ph_3)$ with pyridine, γ-picoline, pyrazine, and pyrazole have been carried out. The compounds were characterized by physicochemical methods.

2,4,6-Trichloro-1,3,5,2,4,6-trithiatriazine, $N_3S_3Cl_3$, is air sensitive and unstable in different solvents. It interacts with metal salts or complexes affording various interesting products containing NS^+, N_2S_2, $N_2S_2^{2-}$, $N_3S_2^{3-}$, $NSCl^{2-}$, NSCl, etc. as coligands.[1-7] The use of $N_3S_3Cl_3$ as a synthetic reagent for thionitrosyl complexes depends upon the reaction conditions and no definite suggestion has yet been made in this direction. The problem is, therefore, still in an embryonic state. Since we are interested in the metal thionitrosyl synthesis, we have chosen ligand-exchange reactions as a possible potential route for their synthesis. This communication reports the reactions of $N_3S_3Cl_3$ with ruthenium complexes having coordinated solvent molecules. Substitution reactions of $Ru(NS)Cl_3(EPh_3)_2$ and $Ru(NS)Cl_3(EPh_3)(E'Ph_3)$ (E=P, As; E'=P, As, Sb) with N-donor heterocyclic bases and their interconversion reactions with $E''Ph_3$ (E''=P, As, Sb) have also been described.

Experimental

All the chemicals used were of Analar or chemically pure grade. Solvents were dried prior to use by the conventional methods. 2,4,6-Trichloro-1,3,5,2,4,6-trithiatriazine and $RuCl_3(EPh_3)_2S$ (E=P, As; S=DMSO, DMF, THF, CS_2, $(CH_3)_2CO$, CH_3CN, CH_3CHO) were prepared by the literature methods.[8,9]

Reactions. (A) Reactions of $N_3S_3Cl_3$ with $RuCl_3(EPh_3)_2S$ (E=P, As; S=DMSO, DMF, THF, CH_3CN, CH_3CHO, CS, $(CH_3)_2CO$). A typical reaction has been carried out as follows. A saturated mint-green solution of trichlorotrithiatriazine in THF (10 ml) was added with stirring to a solution of $RuCl_3(EPh_3)_2S$ (ca. 0.26 mmol) in 40 ml of dichloromethane. The stirring was continued for an hour. A red colored solution was obtained, 50 ml of methanol was added to it, followed by the addition of EPh_3 (ca. 0.06 mmol) whereupon a brown microcrystalline compound was obtained which was separated, washed with methanol, water, methanol, and finally with ether. It was dried under vacuum (yield, ca. 70%). The analytical data corresponded with the formula given in Table 1.

The same compounds $Ru(NS)Cl_3(EPh_3)_2$ were also obtained, though in low yields, using zinc as reducing agent† in place of the EPh_3.

(B) Reactions of $Ru(NS)Cl_3(EPh_3)(E'Ph_3)$(E=P, As; E'=P, As, Sb) with Heterocyclic Bases L (L=Pyridine, γ-Picoline, Pyrazine, Pyrazole). (i) $Ru(NS)Cl_3(EPh_3)(E'Ph_3)$ (ca. 0.14 mmol) in 40 ml of chloroform was refluxed with the heterocyclic base (ca. 0.4 mmol) for a few hours (cf. Table 1) whereby the color of the solution was changed from orange to red-brown. The resulting solution was concentrated to about 10 ml. The addition of petroleum ether (40—60 °C) to the concentrate yielded a compound which was separated. It was recrystallized 2—3 times from benzene/petroleum ether (40—60 °C).

(ii) A solution of $Ru(NS)Cl_3(EPh_3)(E'Ph_3)$ (ca. 0.12 mmol), and base (0.7 mmol) in 40 ml of chloroform was refluxed for a few hours. The resulting solution was concentrated to nearly half its volume, followed by the addition of hexane whereby a compound was precipitated. It was separated, thoroughly washed with benzene, ether and recrystallized several times with dichloromethane/hexane.

The reactions described in section B were also carried out in benzene yielding the same compounds.

Measurements. The measurements on the complexes and the analyses were done as reported elsewhere.[10,11] These data matched extremely well with the formula of the complexes given in Table 1.

Results and Discussion

Reactions of $N_3S_3Cl_3$ with $RuCl_3(EPh_3)_2S$ (E=P, As; S=CH_3CHO, DMSO, DMF, THF, CH_3CN) yielded yellowish brown literature known diamagnetic complexes $Ru(NS)Cl_3(EPh_3)_2$[11] freely soluble in halohydrocarbons. Their purity were tested by TLC and by comparing their physical data (mp, mixed mp, X-ray powder pattern, and other spectral data) with those of the authentic sample. Their identical nature with the authentic samples were further confirmed by (1) their IR spectra which displayed the expected band around 1310 cm^{-1} attributable to terminal $(NS)^+$ group besides the characteristic bands of EPh_3 (E=P, As, Sb) and by (2) ^{31}P NMR data[12] (δ 13.3).

X-Ray powder diffraction data of these substituted complexes were carried out and compared with the powder pattern of $Ru(NS)Cl_3(PPh_3)_2$. Both the compounds were found to be isomorphous. $Ru(NS)Cl_3(PPh_3)_2$ was an octahedral complex with two phosphines trans to each other which was confirmed by the X-ray crystal structure of isomorphous osmium analogue.[13] We assumed that the substituted products

† In the reactions of $RuCl_3(EPh_3)_2S$ (S=DMSO, DMF, CS_2) with $N_3S_3Cl_3$, the solution obtained after stirring and zinc reduction yielded $Ru(NS)Cl_3(EPh_3)_2$ as a precipitate in a very low yield and from the filtrate after its concentration, a black material obtained. The black material was not charaterized.

Table 1. Thionitrosyl Complexes of Ruthenium(II). Characterization Data of Complexes

Sl. No.	Reactant (Procedure)	Ligand	Time for refluxing	Product Color, Mp/°C	IR $\nu(NS)^+$ /cm^{-1}	^{31}P NMR δ/ppm
1.	$RuCl_3(PPh_3)_2S$ (A)	PPh_3	—	$Ru(NS)Cl_3(PPh_3)_2$ B 176	1316	13.3
2.	$RuCl_3(AsPh_3)_2S$ (A)	$AsPh_3$	—	$Ru(NS)Cl_3(AsPh_3)_2$ B >280	1310	—
3.	$RuCl_3(PPh_3)_2S$ (A)	$AsPh_3$	—	$Ru(NS)Cl_3(PPh_3)(AsPh_3)$ B 245—247	1305	13.2
4.	$RuCl_3(AsPh_3)_2S$ (A)	$SbPh_3$	—	$Ru(NS)Cl_3(AsPh_3)(SbPh_3)$ B 220	1300	—
5.	$Ru(NS)Cl_3(AsPh_3)(PPh_3)$[b]	PPh_3[a]	1	$Ru(NS)Cl_3(PPh_3)_2$ B 176	1316	13.3
6.	$Ru(NS)Cl_3(PPh_3)_2$[b]	$AsPh_3$[a]	8	$Ru(NS)Cl_3(PPh_3)(AsPh_3)$ B 245—247	1305	13.2
7.	$Ru(NS)Cl_3(AsPh_3)_2$[b]	PPh_3[a]	2	$Ru(NS)Cl_3(PPh_3)_2$ B 176	1316	13.3
8.	$Ru(NS)Cl_3(AsPh_3)(PPh_3)$[b]	$AsPh_3$[a]	48	$Ru(NS)Cl_3(AsPh_3)_2$ B >280	1310	—
9.	$Ru(NS)Cl_3(AsPh_3)(SbPh_3)$[b]	$AsPh_3$[a]	3	$Ru(NS)Cl_3(AsPh_3)_2$ B >280	1310	—
10.	$Ru(NS)Cl_3(AsPh_3)(SbPh_3)$[b]	PPh_3[a]	1	$Ru(NS)Cl_3(AsPh_3)(PPh_3)$ B 245—247	1305	13.2
11.	$Ru(NS)Cl_3(AsPh_3)(SbPh_3)$[b]	$SbPh_3$[a]	36	Mixture of products	—	
12.	$Ru(NS)Cl_3(PPh_3)_2$[b]	$SbPh_3$[a]	36	Mixture of products	—	
13.	$Ru(NS)Cl_3(PPh_3)_2$ (B, i)	Py	2	$Ru(NS)Cl_3(PPh_3)(Py)$ Y 128	1310	13.0
14.	$Ru(NS)Cl_3(PPh_3)_2$ (B, i)	γ-Pic	2	$Ru(NS)Cl_3(PPh_3)(\gamma\text{-Pic})$ Y 125	1310	—
15.	$Ru(NS)Cl_3(PPh_3)_2$ (B, ii)	Pz	3	$Ru(NS)Cl_3(PPh_3)(Pz)$ B 195	1310	25.5
16.	$Ru(NS)Cl_3(PPh_3)_2$ (B, i)	Pa	3	$Ru(NS)Cl_3(PPh_3)(Pa)$ Y 140	1310	23.3
17.	$Ru(NS)Cl_3(AsPh_3)_2$ (B, i)	Py	3	$Ru(NS)Cl_3(AsPh_3)(Py)$ Y 125—128	1310	—
18.	$Ru(NS)Cl_3(AsPh_3)_2$ (B, i)	γ-Pic	3	$Ru(NS)Cl_3(AsPh_3)(\gamma\text{-Pic})$ Y 125	1310	
19.	$Ru(NS)Cl_3(AsPh_3)_2$ (B, i)	Pz	12	$Ru(NS)Cl_3(AsPh_3)(Pz)$ Y 280	1320	
20.	$Ru(NS)Cl_3(AsPh_3)_2$ (B, ii)	Pa	6	$Ru(NS)Cl_3(AsPh_3)(Pa)$[c] G 175—178	1310	
21.	$Ru(NS)Cl_3(AsPh_3)(SbPh_3)$ (B, ii)	Pa	5	$Ru(NS)Cl_3(SbPh_3)(Pa)$ G 145	1310	
22.	$Ru(NS)Cl_3(AsPh_3)(SbPh_3)$ (B, i)	Py	3	$Ru(NS)Cl_3(AsPh_3)(Py)$ Y 128—130	1310	
23.	$Ru(NS)Cl_3(AsPh_3)(SbPh_3)$ (B, i)	γ-Pic	3	$Ru(NS)Cl_3(AsPh_3)(\gamma\text{-Pic})$ Y 125	1310	
24.	$Ru(NS)Cl_3(AsPh_3)(PPh_3)$ (B, i)	Py	3	$Ru(NS)Cl_3(AsPh_3)(Py)$ Y 128	1310	
25.	$Ru(NS)Cl_3(AsPh_3)(PPh_3)$ (B, i)	γ-Pic	3	$Ru(NS)Cl_3(AsPh_3)(\gamma\text{-Pic})$ Y 125	1310	
26.	$Ru(NS)Cl_3(AsPh_3)(PPh_3)$ (B, i)	Pa	4	$Ru(NS)Cl_3(AsPh_3)(Pa)$ B 175	1310	

B=Brown, Y=Yellow, G=Green, S=DMSO, DMF, THF, CH_3CN, CH_3CHO, $(CH_3)_2CO$, CS_2.
Py=pyridine, γ-Pic=γ-picoline, Pa=pyrazole, Pz=pyrazine.
a) Molar ratio of reactant and ligand=1:5. b) Prepared by known literature method.[11] c) Mass spectra (FD) found.

of these completes were also octahedral in nature.

These reactions appeared to be slightly complicated and perhaps undergo through an intermediate formation. All efforts to isolate the intermediate in the pure solid form were unsuccessful. Although the solutions, obtained after the initial $N_3S_3Cl_3$ reactions with ruthenium complexes yielded a precipitate with light petroleum ether but it became oily on purification through precipitation several times from different solvents. Possibly a coordinatively unsaturated Ru(III) complex is initially formed as an intermediate followed by its reduction with the formation of coordinatively saturated complex by linking with the ligand EPh_3 or $E'Ph_3$.

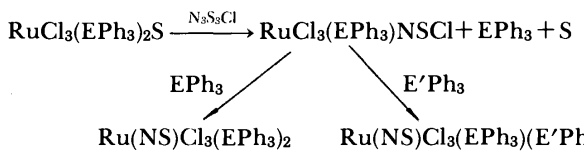

Interconversion reactions of $Ru(NS)Cl_3(EPh_3)_2$ or $Ru(NS)Cl_3(EPh_3)(E'Ph_3)$ with $E''Ph_3$ (E=P, As; E'=P, As, Sb; E''=P, As, Sb) led to the formation of $Ru(NS)Cl_3(EPh_3)(E''Ph_3)$, $Ru(NS)Cl_3(E'Ph_3)(E''Ph_3)$, or $Ru(NS)Cl_3(E''Ph_3)_2$ (cf. Table 1). These complexes exhibited similar analytical, spectral (IR, ^{31}P NMR etc.), chemical, and physical properties as those of the literature known complexes synthesized by photochemical process.[11] It suggested that these complexes are the substitution derivatives of $Ru(NS)Cl_3(EPh_3)_2$.

A chemically interesting feature of these interconversion reactions is the fact that the variation in the substitution reaction rates of $Ru(NS)Cl_3(EPh_3)(E'Ph_3)$ or $Ru(NS)Cl_3(EPh_3)_2$ with $E''Ph_3$ (E''=P, As, Sb) with respect to leaving ligand is in the order $PPh_3<AsPh_3<SbPh_3$. The reaction of $Ru(NS)Cl_3(PPh_3)_2$ with $AsPh_3$ resulted in the formation of $Ru(NS)Cl_3(AsPh_3)_2$ in 48 hours, on the other hand the reverse process, the formation of $Ru(NS)Cl_3(PPh_3)_2$ from $Ru(NS)Cl_3(AsPh_3)_2$ in presence of PPh_3 takes only two hours. $Ru(NS)Cl_3(AsPh_3)(SbPh_3)$ with $SbPh_3$ did not yield $Ru(NS)Cl_3(SbPh_3)_2$ even after a very long refluxing period. The reason for the variations in rates could be due to the differences in the σ-basic and π-acidic characters of the ligands ($PPh_3>AsPh_3>SbPh_3$). The kinetic and the thermodynamic stability of the complexes were in the order $PPh_3>AsPh_3>SbPh_3$ as reported elsewhere.[14] Owing to the weak σ-basic and π-acidic nature of $AsPh_3$ followed by that of $SbPh_3$, the Ru-As and Ru-Sb bonds should be relatively thermodynamically weaker than Ru-PPh_3 bond. Consequently the substitution rate with respect to leaving group should be $PPh_3<AsPh_3<SbPh_3$.

Substitution reactions of $Ru(NS)Cl_3(EPh_3)(E'Ph_3)$ with heterocyclic bases (L) viz. pyridine, γ-picoline, pyrazine, pyrazole led to the formation of $Ru(NS)Cl_3(EPh_3)L$ or $Ru(NS)Cl_3(E'Ph_3)L$. The IR spectra of these complexes exhibited characteristic bands due to vibrational modes of bases besides the bands due to $\nu(NS)^+$ around 1310 cm^{-1} and the characteristic bands of EPh_3. The moderately intense band around 320—290 cm^{-1} was assigned to ν(Ru-Cl).

The substitution reactions of $Ru(NS)Cl_3(EPh_3)(E'Ph_3)$ with bases like 2,2'-bipyridine and 1,10-phenanthroline failed. Inspite the change of solvents and the reaction periods, these reactions led to the formation of a mixture of products. Attempts to separate them were unsuccessful. The presence of different products were confirmed by ^{31}P NMR which displayed a number of bands. Efforts to synthesize bridged compounds with pyrazine were also unsuccessful and only monomers have been obtained.

The substitution of one PPh_3 molecule by heterocyclic base molecule depleted electron density at the ruthenium center through $d\pi$-$d\pi$ back bonding. As a consequence electron density available at ruthenium for $d\pi$-$d\pi$ back bonding towards the remaining PPh_3 molecule is reduced. This results in the reduction of net electron density at phosphorus causing a downfield shift of the ^{31}P NMR band (from δ 13 to δ 25), depending upon the nature of heterocyclic molecule attached to ruthenium. Triphenylphosphine molecules are trans to each other in $Ru(NS)Cl_3(PPh_3)_2$, replacement of one PPh_3 by heterocyclic base will lower the trans effect thereby strengthening the Ru-P bond by sigma bond formation. Thus formation of P→Ru σ bond and weaker Ru→P back bonding will result in the lower electron density at P and will cause the observed downfield shift.

The visible spectra of all the complexes exhibited a rather broad band around 450 nm. Since it is generally believed that (MLCT) transition in ruthenium +2 complexes occur under a broad band around 450—430 nm,[15] a similar band in the electronic spectra of our complexes suggested ruthenium in +2 oxidation state which was also confirmed by magnetic moment (diamagnetic). The electronic spectra of the starting complexes $RuCl_3(EPh_3)_2S$ showed bands in the region 620—350 nm.[16]

In conclusion, all the complexes found to be diamagnetic suggesting ruthenium in +2 oxidation state having (d^6) system.

One of the authors (Ms. Jyoti Seth) thanks C.S.I.R., New Delhi, India for financial support.

References

1) K. K. Pandey, D. K. M. Raju, H. L. Nigam, and U. C. Agarwala, *Ind. Nat. Sc. Acad.*, **48**, 16 (1982).
2) T. Chivers and F. Edelmann, *Polyhedron*, **5**, 1661 (1986).
3) P. F. Kelly and J. D. Woollins, *Polyhedron*, **5**, 607 (1986).
4) J. Hanich, P, Klingelhofer, U. Muller, and K. Dehnicke, *Z. Anorg. Allg. Chem.*, **504**, 13 (1984).
5) K. Volp, W. Willing, U. Muller, and K. Dehnicke, *Z. Naturforsch*, **41b**, 1196 (1986).
6) B. W. S. Kolthammer and P. Legzdins, *J. Am. Chem. Soc.*, **100**, 2247 (1978).
7) U. Kynast, U. Muller, and K. Dehnicke, *Z. Anorg. Allg. Chem.*, **508**, 26 (1984).
8) W. L. Jolly and K. D. Maguire, *Inorg. Synth.*, **9**, 102 (1967).
9) E. S. Switkes, L. Ruiz Ramirez, T. A. Stephenson, and J. Sinclair, *Inorg. Nucl. Chem. Lett.*, **8**, 593 (1972).
10) A. I. Vogel, "A Text book of Quantitative Inorganic Analyses," 4th ed., Longmans-Green, London (1978), p. 491.
11) K. N. Udupa, K. C. Jain, M. I. Khan, and U. C. Agarwala, *Inorg. Chim. Acta*, **74**, 191 (1983).
12) M. B. Hursthouse, N. P. C. Walker, C. P. Warrens, and J. D. Woollins, *J. Chem. Soc., Dalton Trans.*, **1985**, 1043.
13) H. W. Roesky, K. K. Pandey, W. Clegg, M. Noltemeyer, and G. M. Sheldrick, *J. Chem. Soc., Dalton Trans.*, **1984**, 719.
14) G. Booth, *Adv. Inorg. Chem. Radiochem.*, **6**, 1 (1964).
15) C. R. Johnson and R. E. Shepherd, *Inorg. Chem.*, **22**, 2439 (1983).
16) L. R. Ramirez, T. A. Stephenson, and E. S. Swikes, *J. Chem. Soc., Dalton Trans.*, **1973**, 1770.

Extraction and Spectrophotometric Determination of Rhenium(VII) with Thiocyanate and Amides

Neera MISHRA, S. K. SINHA, K. S. PATEL,* and R. K. MISHRA
Department of Chemistry, Ravishankar University, Raipur-492010, M. P., India
(Received October 20, 1988)

Synopsis. A new spectrophotometric method for determining rhenium with thiocyanate and organic reagents such as amides, thioamide and hydrazide over 2.0—6.0 mol dm^{-3} H_2SO_4 is described. The molar absorptivity of the complexes in the organic solvents are (2.57—3.01)×10^4 l mol^{-1} cm^{-1} at absorption maximum. Of these, *N*-phenylacetamide (PAA) has been chosen for detailed studies. The detection limit of the method with PAA is 0.03 μg Re cm^{-3}. The effect of kinds of acids, solvents or reagents and of diverse ions is discussed.

Several spectrophotometric methods for the determination of rhenium have been reported.[1-8] Of these, the classical thiocyanate method is one of the most popular method for the spectrophotometric determination of the metal but it suffers from some experimental difficulties.[1] Thiourea[2] and hexamethylphosphoric triamide[3] were proposed to enhance the selectivity of the classical thiocyanate method, however they require a prolonged heating or extraction and involve the interference of some metals. Oximes were employed as sensitive reagents too but they lack selectivity.[4-6] The sulfur containing reagents like 5,6-diphenyl-3-hydroxy-1,2,4-triazine-3(2*H*)-thione[7] and di-2-pyridyl ketone 2-furyl(thiocarbonyl)-hydrazone[8] were reported for the extraction and spectrophotometric determination of the metal and subject to serious interference from the metal ions. The purpose of this work is to develop a selective and sensitive extraction-spectrophotometric method for rhenium-(VII) with a series of commonly available reagents such as *N*-(alkyl or aryl)acetamides, *N*-(2-pyridyl)-thiobenzamide ($C_6H_5CSNHC_5H_4N$), and *N'*-phenylacetohydrazide ($CH_3CONHC_6H_5$) in presence of thiocyanate ion. Of ten compound reported, the simplest one, *N*-phenylacetamide ($CH_3CONHC_6H_5$) was chosen for detailed studies in the present investigation. The method is applicable over wide acidity range, and removes most of interferences of classical thiocyanate method with improved sensitivity.

Experimental

Reagents. A standard solution of rhenium(VII) was prepared by dissolving (0.5 g) accurately weighed potassium perrhenate in double distilled water. Amides, thioamide, and hydrazide were synthesized as described in the literature.[9] Solutions of amides (1.2—2%) in benzene, and solutions of *N*-(1-naphthyl)acetamide, *N*-(2-pyridyl)thiobenzamide, or *N'*-phenylacetohydrazide (2—3.8%) in chloroform were employed for extraction work. All chemicals and reagents used were of analytical grade (E. Merck). In the case of benzene, all solutions employed were presaturated with benzene.

Procedure. A tin(II) chloride solution (2 cm^3) and 5 cm^3 of 10 mol dm^{-3} H_2SO_4 were added to a perrhenate solution (5—90 μg Re) in a 100-cm^3 separatory funnel, the mixture was reacted with 2 cm^3 potassium thiocyanate solution and diluted to 15 cm^3 with distilled water. The metal complex was extracted with 15 cm^3 benzene solution of the organic reagent for 2 min. The absorbance of the complex was measured at λ_{max} against reagent blank. In the case of *N*-(2-pyridyl)thiobenzamide, *N'*-phenylacetohydrozide, or *N*-(1-naphthyl)acetamide the metal complex was extracted with 15 cm^3 chloroform solution of the reagent and washed with 3×2 cm^3 fresh portions of chloroform. All the dried extract was transferred into a 25-cm^3 volumetric flask and diluted with chloroform to the mark. The absorbance of the complex was measured at λ_{max} against reagent blank.

Results and Discussion

Absorption Spectra. Figure 1 shows the absorption spectra of Re(IV)-SCN^--PAA complex and the reagent blank in benzene. All the complexes of Re(IV) with amides and hydrazide exhibit an absorption maximum around 435 nm while with thiobenzamide at 438 nm. As the reagent shows an absorption at the λ_{max} of the complex, the reagent blank was used as a reference for all measurements.

Choice of Solvents. The extraction of Re(IV)-SCN^- with PAA into various solvents like 1-pentanol, isobutyl methyl ketone, ethyl acetate, chloroform, carbon tetrachloride, benzene, and toluene was performed. The complex was quantitatively extracted in these solvents except carbon tetrachloride (the maximum extraction of the complex require a triple extraction) showing the value of molar absorptivity to be in the range of (2.43—2.70)×10^4 dm^3 mol^{-1} cm^{-1} at λ_{max} 430—435 nm. Of these, benzene was used for further experimental work due to the most sensitive

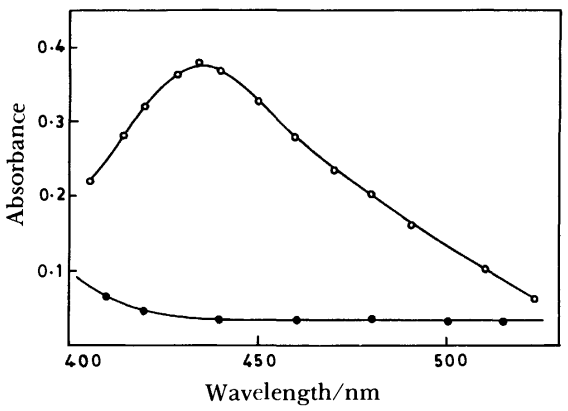

Fig. 1. Absorption spectra of *N*-phenylacetamide (PAA) blank and $[ReO(SCN)_2(PAA)_2]$ in benzene. $[H_2SO_4]$=4 mol dm^{-3}; $[Sn^{2+}]$=0.03 mol dm^{-3}; $[SCN]$=0.26 mol dm^{-3}. (—○—), $[ReO(SCN)_2(PAA)_2]$, $[Re^{7+}]$=1.43×10^{-5} mol dm^{-3}; (—●—) 0.1 mol dm^{-3} PAA in benzene after equilibration.

color reaction in it.

Effect of Acidity. The effect of acids like HCl and H_2SO_4 (10 mol dm^{-3}) on the extraction of Re(IV)-SCN^- with PAA in benzene was studied. With H_2SO_4 in aqueous solution, the rate of extraction was relatively fast and the color intensity of the complex in organic solvent was higher than with HCl. The modified property in hydrochloric acid media is due to further reaction of the thiocyanato or chloro complex species with excess of tin(II) ions.[10] The optimum acidity range was found to be 2.0—6.0 mol dm^{-3} H_2SO_4 with PAA in benzene.

Effect of Reagents and Other Variables. The effect of amount of reagents on the extraction of the metal was examined at 4 mol dm^{-3} H_2SO_4. The reduction of Re(VII) into Re(IV) was made by tin(II) ions and 0.015—0.05 mol dm^{-3} tin(II) ions was adequate for the extraction of the metal. At least 0.15 mol dm^{-3} KSCN and 0.06 mol dm^{-3} PAA (in benzene) were necessary for the maximum color development of the complex in the organic solution, and the addition of more KSCN and PAA up to 0.6 and 0.19 mol dm^{-3}, respectively, caused no adverse effect. The order sequence of addition of reagents was not critical. The variation in volume ratio of the organic to the aqueous phase from 3 : 1 to 3 : 5 did not affect the distribution of the metal. The extract was stable for at least 4 h at room temperature (≈27 °C). The effect of electrolytes i.e. KCl and $(NH_4)_2SO_4$ in extraction of the metal was examined and absorbance of the complex was intact up to 1 mol dm^{-3} KCl or $(NH_4)_2SO_4$.

Stoichiometry of Extraction. The mechanism involved in the reduction of ReO_4^- with tin(II) chloride in the presence of thiocyanate was studied by various workers.[10-12] The formation of $[ReO(SCN)_5]^{2-}$, $[Re(SCN)_6]$, or $[Re(SCN)_6]^-$ has been reported, and the addition of excess Sn^{2+} leads to formation of $[Re(SCN)_6]^{2-}$, exclusively. According to Pavlova[10] the most probable reduced state of rhenium participating in the extraction is Re(IV). In the present investigation, the ratio of variables in the complex was evaluated by plots of logarithm distribution ratio of the metal versus logarithm thiocyanate concentration in the aqueous solution and PAA concentration in the organic solution at equilibrium. Figure 2 shows the slope of these plots to be 1.9 and 2.0, respectively. Since these values are close to 2, the possible reaction mechanism can be written as:

$$ReO^{2+} + n\ SCN^- + n'PAA_o \rightleftarrows [ReO(SCN)_n(PAA)_{n'}]_o$$

For the simplest system, where the metal species in the aqueous phase is ReO^{2+} only and that of the complex is $[Re(SCN)_n(PAA)_{n'}]$ $\log D = \log K + n\log[SCN^-] + n' \log[PAA]_o$.

In present investigation, the value of D (distribution ratio of the metal) was evaluated by spectrophotometric method using the formulae, $D = A/A_{max} - A$. The distribution ratio of PAA in the organic solution is not very high, hence the effective concentration of the amide in the organic phase was determined by following equation.

$$[PAA]_o = \frac{Kd[PAA]_t}{1+Kd}$$

Where, o, Kd, D, K, $[PAA]_o$, $[PAA]_t$, A_{max}, and A represent the organic phase, distribution ratio of the reagent, distribution ratio of the metal, equilibrium or extraction constant, concentration of the reagent in the organic solution at equilibrium, total analytical concentration of the reagent in the organic solvent before equilibrium, maximum absorbance of the complex when the reagent is present in constant excess and absorbance of the complex when the reagent is in equilibrium, respectively.

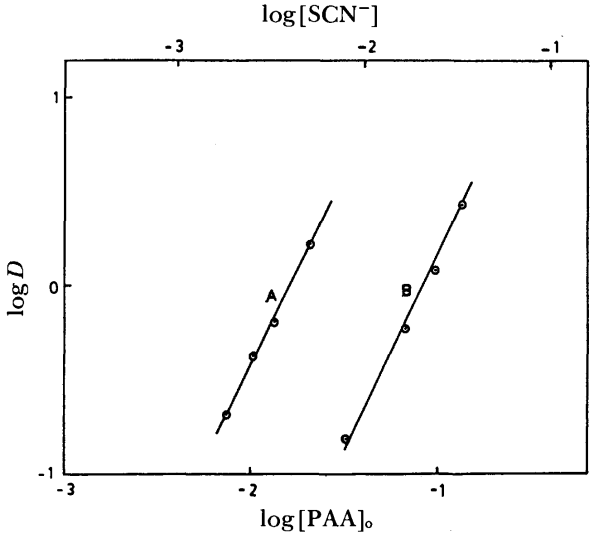

Fig. 2. Determination of the values of the variables in $[ReO(SCN)_n(PAA)_{n'}]$ in benzene. $[H_2SO_4]$=4 mol dm^{-3}; $[Sn^{2+}]$=0.03 mol dm^{-3}; $[Re^{7+}]$=1.43×10^{-5} mol dm^{-3}. (A), log (distribution ratio of the metal) versus $\log[PAA]_o$; $[S\bar{C}N]$=0.26 mol dm^{-3}. (B), log (distribution ratio of the metal) versus log $[S\bar{C}N]$; $[PAA]_o$=0.1 mol dm^{-3}.

Amides, Thioamides, and Hydrazide as Extraction Reagents. In the present investigation, the extraction potentiality of various amides, thioamides, and hydrazide towards Re(IV) in the presence of thiocyanate was examined. In amide series, acetamides derived from aliphatic or aromatic amines (except amines containing electron-withdrawing groups e.g. Cl, OH, etc.) are capable of extracting the metal. Chloroform is an adequate diluent for the extraction of the complex with *N*-(1-naphthyl)acetamide, *N*-(2-pyridyl)thiobenzamide, and *N'*-phenylacetohydrazide. The potentiality of all compounds tested towards Re(IV) are approximately the same, and show the molar absorptivity of (2.57—3.01)×10^4 dm^3 mol^{-1} cm^{-1} at λ_{max} 435—438 nm in the organic solvent. The detection limit of the method is 0.013 μg Re cm^{-3} and it follows Beer's law over 0.5—6.0 μg Re cm^{-3} with PAA in benzene. The relative standard deviation of the method was found to be ±1.4% for 10 measurements each containing 40 μg Re/15 cm^3.

Effect of Diverse Ions. The effect of diverse ions on the determination of 40 μg of Re(VII) was studied with 0.1 mol dm^{-3} PAA in benzene as above. In this method, Nb(V) and Mo(V) seriously interfere in the determination of the metal, and W(VI) is tolerated

only in equal amount. The interference of Mo is removed by prior extraction with 0.1 mol dm^{-3} PAA in benzene from aqueous solution containing 4 mol dm^{-3} H_2SO_4 +0.1 mol dm^{-3} ascorbic acid +0.4 mol dm^{-3} KSCN. The interference of niobium is masked by sodium oxalate (3% solution 3 cm^3). The tolerance limit of various diverse ions (in mg) in the determination of rhenium causing an error less than ±2% is shown in parenthesis as; W (0.04); Pd, Mo (0.1); Cu(0.5); Al, Cr, Co, Zr, F^- (20); U (30); oxalate (40); Zn (75); Cd (100); AsO_4^{3-} (150); tartrate (220); or PO_4^{3-} (250).

We are thankful to Council of Scientific & Industrial Research, New Delhi for partial financial support of this work.

References

1) Z. Marczenko, "Spectrophotometric Determination of Elements," Ellis Horwood, Chichester (1976).
2) C. P. Savariar and T. R. Hariharan, *Mikrochim. Acta*, **I**, 477 (1975).
3) M. Mitra and B. K. Mitra, *Talanta*, **25**, 597 (1978).
4) F. Trusell and R. J. Thompson, *Anal. Chem.*, **36**, 1870 (1964).
5) E. N. Pollock and L. P. Zopatti, *Anal. Chim. Acta*, **32**, 418 (1965).
6) D. Thierig and F. Umland, *Z. Anal. Chem.*, **240**, 19 (1978).
7) A. K. Majumdar and B. Datta, *Anal. Chim. Acta*, **97**, 129 (1978).
8) A. Kettrup, T. Seshadri, and F. Jakobi, *Anal. Chim. Acta*, **115**, 383 (1980).
9) K. S. Patel and K. H. Lieser, *Anal. Chem.*, **58**, 1547 (1986).
10) M. Pavlova, *Zh. Anal. Khim. (English Transl.)*, **25**, 99 (1970).
11) R. A. Bailey, T. W. Michelsen, and W. N. Mills, *J. Inorg. Nucl. Chem.*, **33**, 3206 (1971).
12) A. Davison, A. G. Jones, L. Muller, R. Tatz, and H. S. Trop, *Inorg. Chem.*, **20**, 1160 (1981).

Stereoisomerism and Crystal Structure of (1*R*,2*S*,5*R*)-(+)-4-(Benzoyloxymethylene)-2,6,6-trimethylbicyclo[3.1.1]heptan-3-one {(1*R*,2*S*,5*R*)-(+)-4-(Benzoyloxymethylene)-3-pinanone}

Nasser AZANI, Francis LABRUYERE, Claude METGE, Charles BERTRAND, Jean SOTIROPOULOS,* and Joël JAUD†
Laboratoire de Chimie de Dérivés de Substances Naturelles, Université Paul Sabatier, 118 Route de Narbonne, 31062 Toulouse Cedex, France
†G. I. T. E. R. Laboratoire de Chimie de Coordination du C. N. R. S. Toulouse France, 205 Route de Narbonne, 31077 Toulouse Cedex, France
(Received November 14, 1988)

Synopsis. Conjugated esters from (+)-isopinocamphone, with a terpenic skeleton which is easily epimerizable may theoretically exist as four diastereomers (2*R*,4*E*; 2*R*,4*Z*; 2*S*,4*E*; 2*S*,4*Z*). X-Ray analysis shows that the reaction leads to a single isomer, namely an isopinocamphone derivative (2*S*,4*E*).

The study of some conjugated esters obtained from 3-pinanone [(1*R*,2*R*,5*S*)-(+)-isopinocamphone] showed that their stereochemistry is somewhat complicated. Three points had to be defined:

i) configuration around the double bond (*Z* or *E*)

ii) chirality of the conjugated system due to flexibility of the terpenic cycle (right or left-handed helix) and

iii) configuration of the chiral center C-2 (*R* or *S*).

(+)-Isopinocamphone[1] is indeed a terpenic bicyclic ketone in which the α-carbon atom bearing the methyl group epimerizes easily during reactions in basic media. Many authors showed that at room temperature and in presence of sodium alcoholate,[2] (+)-isopinocamphone leads to a mixture of (1*R*,2*R*,5*S*)-(+)-isopinocamphone (75%) and (1*R*,2*S*,5*S*)-(+)-pinocamphone (25%).

On the other hand, Hirata[3] laid the stress upon the difficulties of structural elucidation due to conformational mobility.

This is why, besides studying NMR spectra and circular dichroism (CD) of these compounds, we called, at last, upon X-ray analysis to achieve structure determination of one of these esters.

Results and Discussion

Synthesis of esters has been performed as follows. The formyl ketone[4] was transformed to ester by acylation in pyridine. The ester has the *E* configuration (presence in the ^{1}H NMR spectrum of a lone signal for the ethylenic proton at about δ 8.3). In the *Z* configuration the signal would appear at higher field. In fact, a comparative study of the ^{1}H NMR spectra of two phenylmethylenepinocamphone[5] and nopinone[6] *Z* and *E* showed for the *Z* isomer an ethylenic proton at δ 6.10 and for the *E* isomer at δ 8.3 due to downfield effect of the two double bonds. This result will be confirmed in this paper by X-ray analysis. Thus, the *E* isomer is formed alone in this reaction. The greater stability of the *E* isomer is consistent with i) the less steric hindrance and ii) the less electric interaction between C=O and C-O dipole in this isomer than in the *Z* one.

Synthesis of the (*Z*)-ester (even as a mixture *Z*/*E*) failed although two attempts were performed: photoisomerization of the (*E*) isomer and acylation at low temperature (−70 °C) of the sodium salt of 4-(hydroxymethylene)isopinocamphone. The latter was obtained by reaction with sodium alcoholate. This technique was successful with similar 2- and 3-bornanone derivatives.[7,8]

Concerning now the configuration of the C-2 chiral center ^{1}H NMR spectra (300 MHz) of the isolated products give some interesting informations.

The *p*-chlorobenzoate revealed in its spectrum the presence of two doublets with the same coupling constant *J*=6.5 Hz at δ 1.20 and 1.30 in a ratio 89/11. Unlike to the *p*-chloro derivative the benzoate and 2,6-dichlorobenzoate purified under the same conditions show a single doublet at δ 1.20 with *J*=6.50 Hz proving the presence of a lone isomer. It was thus interesting to determine precisely the configuration of one of these pure isomers by X-ray analysis.

X-Ray Analysis. A white crystal with approximate dimensions of 0.2×0.25×0.3 mm was used for the data collection. The intensity was measured using a CAD4-ENRAF-NONIUS[9] four circles diffractometer with graphite monochromated Mo*Kα* radiation (λ=0.71073 Å) by means of the ω-2θ scan technique up to 70° in 2θ (scan speed for the pre-scan 10° min^{-1}) at room temperature.

Crystal Data. $C_{18}H_{20}O_3$ crystallizes in orthorhombic system, space group $P2_12_12_1$ with: *a*=10.425(6), *b*=11.049(7), *c*=13.725(7) Å, *V*=1581(3) Å^3 with *Z*=4, *F*(000)=608, d_{cal}=1.19 g cm^{-3}, μ(Mo *Kα*)=0.7 cm^{-1}.

Among the 3889 reflections measured 1509 inde-

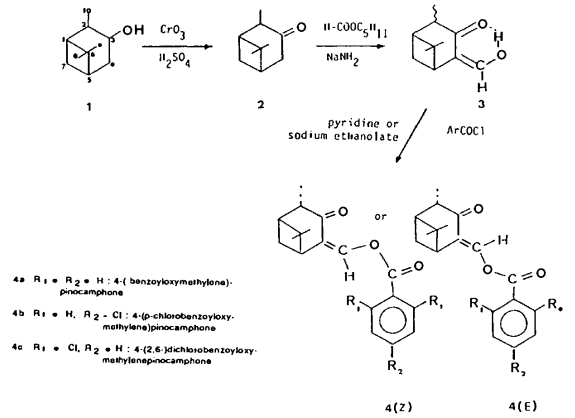

Scheme 1.

pendant reflections with $I>3\sigma(I)$ were used to refine the 190 variable parameters.

The measured intensities were corrected for the Lorentz and polarization factors, no absorption correction was performed according to the small value of the absorption coefficient.

All calculations were performed using a DIGITAL Vax 730 computer, by means of SDP (Structure Determination Package) of ENRAF-NONIUS system. This structure was solved using direct method and refined by full matrix least-squares procedure.

In the last refinement all of the positions and thermal parameters of the nonhydrogen atoms were refined, for the hydrogen atoms their contributions were only introduced but not refined (R=0.055).

The final atomic parameters of the carbon and oxygen atoms are given in Table 1, according with labeling of these atoms shown in Fig. 1.

Analysis shows that the isolated ester obtained from (+)-isopinocamphone is in fact a pinocamphone derivative. Thus, epimerization took place during the reaction. In addition the conjugated system OC-C=C incorporated in the ring is not planar but skewed in the sense of a right-handed helix (torsional angle +11.89°) (Table 2). The skewness in this case is consistent with the sign of the Cotton effect of the $\pi\rightarrow\pi^*$ transition.

However we have to put us in mind of the fact that the CD sign of this transition in conjugated ketones does not reflect always the true chirality of the enone system (many exceptions have been reported[10,11]).

In effect, inspection of Scheme 2 reveals that although the sign of the $\pi\rightarrow\pi^*$ transition in 2-(*p*-chlorobenzylidene) 3-bornanone **6**[12] and 4-(benzoyloxymethylene) 3-pinanone **4** shows the true skewness of the enone system, unfortunately in the case of 3-(*p*-bromobenzylidene) nopinone **5**[13] the CD sign is negative while the conjugated system has a right-handed skewness.

On the other hand, in a similar camphor (bornanone-2) derivative **7**[14] while the enone grouping is planar, the $\pi\rightarrow\pi^*$ transition still has a positive CD.

Table 1. Positional Parameters and Their Estimated Standard Deviations

Atom	x	y	z	B/Å^2
O1	0.3650(3)	1.0026(3)	0.7930(2)	6.96(8)
O2	0.5369(2)	0.8810(3)	0.7821(2)	4.62(6)
O3	0.6395(3)	0.9639(3)	1.0646(2)	6.85(8)
C1	0.9391(4)	0.8509(4)	0.9611(3)	5.6(1)
C2	0.8609(5)	0.9181(4)	1.0381(3)	5.12(9)
C3	0.7204(4)	0.9261(4)	1.0092(3)	4.85(9)
C4	0.6884(4)	0.8861(4)	0.9081(3)	4.29(8)
C5	0.7946(4)	0.8240(4)	0.8543(3)	5.5(1)
C6	0.9190(4)	0.9016(5)	0.8575(3)	6.1(1)
C7	0.8620(5)	0.7374(4)	0.9292(4)	6.7(1)
C8	1.0217(5)	0.8562(7)	0.7862(4)	9.6(2)
C9	0.9031(5)	1.0383(5)	0.8434(4)	7.7(1)
C10	0.8732(6)	0.8618(5)	1.1397(4)	7.3(1)
C11	0.5746(4)	0.9130(4)	0.8748(3)	4.58(9)
C12	0.4249(4)	0.9288(4)	0.7486(3)	4.58(9)
C13	0.3894(4)	0.8798(4)	0.6530(3)	4.50(8)
C14	0.2899(4)	0.9354(5)	0.6026(4)	6.3(1)
C15	0.2543(5)	0.8929(6)	0.5115(4)	7.8(1)
C16	0.3149(5)	0.7949(5)	0.4713(4)	7.3(1)
C17	0.4132(5)	0.7396(5)	0.5200(3)	6.5(1)
C18	0.4513(4)	0.7815(4)	0.6109(3)	5.1(1)

Anisotropically refined atoms are given in the form of the isotropic equivalent displacement parameter defined as: $(4/3)\cdot[a^2\cdot B(1,1)+b^2\cdot B(2,2)+c^2\cdot B(3,3)+ab(\cos\gamma)\cdot B(1,2)+ac(\cos\beta)\cdot B(1,3)+bc(\cos\alpha)\cdot B(2,3)]$

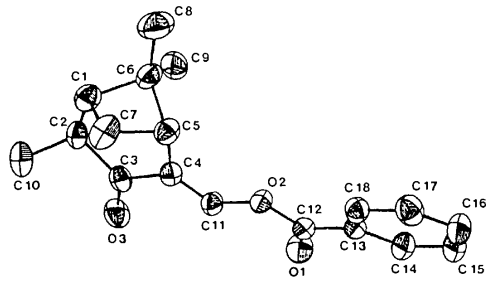

Fig. 1. Perspective view of **4a** and the numbering of the atoms.

Table 2. Torsion Angles

Atom 1	Atom 2	Atom 3	Atom 4	Angle (ϕ/°)
C12	O2	C11	C4	189.89 (0.38)
C11	O2	C12	O1	5.69 (0.58)
C11	O2	C12	C13	185.08 (0.33)
C6	C1	C2	C10	175.77 (0.40)
C7	C1	C2	C3	316.10 (0.47)
C1	C2	C3	O3	171.82 (0.40)
C1	C2	C3	C4	351.01 (0.50)
C10	C2	C3	O3	46.04 (0.54)
C10	C2	C3	C4	225.24 (0.38)
O3	C3	C4	C11	11.89 (0.61)
C2	C3	C4	C11	192.70 (0.37)
C3	C4	C11	O2	179.36 (0.35)
C5	C4	C11	O2	2.48 (0.67)
C4	C5	C7	C1	276.31 (0.38)
O1	C12	C13	C14	10.32 (0.66)
O1	C12	C13	C18	189.97 (0.43)
O2	C12	C13	C14	190.95 (0.37)
O2	C12	C13	C18	10.59 (0.56)
C12	C13	C14	C15	179.22 (0.44)
C12	C13	C18	C17	180.14 (0.42)

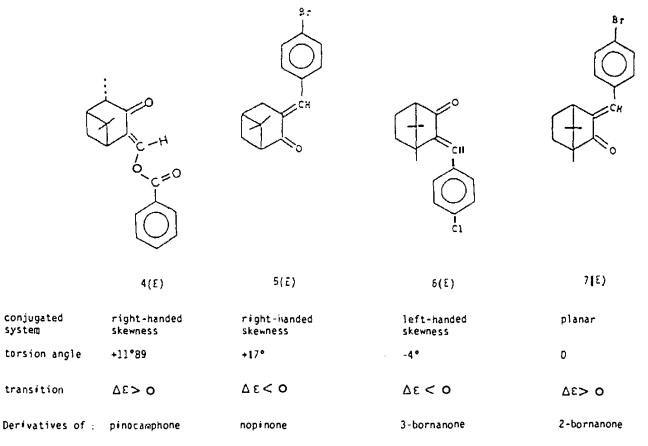

Scheme 2.

These results show undoubtedly that there is no direct correlation between the sign of the CD of the $\pi\rightarrow\pi^*$ transition and the chirality of the conjugated system in enones.

To the best of our knowledge there is yet no satisfactory explanation of these facts.

X-Ray analysis shows also that the aromatic ring is twisted by 10.32° and is no more coplanar with the ester carbonyl group.

At last, the angle between CH_3-10 and the ketone carbonyl group (46°) implies a pseudoequatorial or a pseudoaxial position for this methyl and would explain, in part, the weak values of the CD of the $n\rightarrow\pi^*$ transition.

Experimental

General. Melting points were determined on a oil bath. Values are uncorrected. Rotatory power was measured with a Rudolf type polarimeter and Circular Dichroism with Dichrograph Mark V Jobin-Yvon. IR spectra were recorded on a Perkin-Elmer 1600 FTIR, and NMR spectra on a Bruker AM 300 WB in $CDCl_3$. Shifts are given in parts per million.

The Preparation of (+)-Isopinocamphone (2): (+)-Isopinocamphone [(+)-3-pinanone] was prepared by oxidation with chromium trioxide of (1*R*,2*R*,3*R*,5*S*) (−)-isopinocampheol [mp: 51—53 °C, $[\alpha]_D^{20}$ (*c* 20, ethanol)] by the procedure of Brown et al. (loc. cit.), $[\alpha]_D^{20}=+19°$ (*c* 3, ethanol).

The Preparation of 4-(Hydroxymethylene) Isopinocamphone (3): Formylation of (+)-isopinocamphone has been performed according to the procedure of Bessière-Chrétien et al. (loc. cit.) using sodium amide in the place of sodium ethanolate: yield 75%, $[\alpha]_D^{20}=+52°$ (*c* 3.6, cyclohexane).

The Preparation of Esters of 4-(Benzoyloxymethylene) (4a), 4-(*p*-Chlorobenzoyloxymethylene) (4b), and 4-(2,6-Dichlorobenzoyloxymethylene)pinocamphone (4c). To a stirred solution of **3** (6 g, 0.0209 mol) was added dropwise the acid chloride (6 g, 0.03 mol). A white precipitate is formed. The mixture is kept at room temperature for 12 h, acidified with 100 ml of a 50% hydrochloric acid solution and extracted with ether. The ether solution was washed with a saturated aqueous sodium hydrogencarbonate and water, dried and evaporated. The white residue in recrystallized from cyclohexane: yield 60%.

4a. Mp: 123 °C, $[\alpha]_D^{20}=+112°$, (*c* 3.3, dioxane), IR ($CHCl_3$): C=O ester 1743, C=O terp. 1701, C=C 1629, C-O 1256 and 1149 cm^{-1}; CD (*c* 3.33, dioxane) $\Delta\varepsilon_{333}=+0.85$, (*c* 0.33, dioxane) $\Delta\varepsilon_{270}=+6.1$; ^1H NMR ($CDCl_3$): δ=0.88 (3H, s, C_9H), 1.17 (3H, d, $C_{10}H$, *J*=7.26 Hz), 1.37 (2H, d, C_7H, *J*=10.7 Hz), 1.44 (3H, s, C_8H), 2.01 (1H, m, C_1H, *J*=6.27 and 2.35 Hz), 2.41 (1H, m, C_2H), 2.74 (1H, m, C_7H), 3.25 (1H, t, C_5H, *J*=6.07 Hz), 7.48 (2H, t, *J*=7.8 Hz aromatic protons), 7.62 (1H, dd, *J*=6.19 Hz aromatic protons), 8.07 (2H, m, aromatic protons), 8.37 (1H, s, $C_{11}H$). Found: C, 75.52; H, 7.05; O, 17.43%. Calcd for $C_{18}H_{22}O_3$: C, 75.52; H, 7.69; O, 16.18%.

4b. Mp: 131 °C $[\alpha]_D^{20}=+85.8°$, (*c* 1.3, dioxane), IR ($CHCl_3$): C=O ester 1741, C=O terp. 1701, C=C 1630, C-O 1254 and 1150 cm^{-1}; CD (*c* 1.03, dioxane), $\Delta\varepsilon_{343}=0.52$, (*c* 0.10, dioxane), $\Delta\varepsilon_{266}=5.30$; ^1H NMR ($CDCl_3$): δ=0.88 (3H, s, C_9H), 1.17 (3H, d, $C_{10}H$, *J*=7.2 Hz), 1.37 (2H, d, C_7H, *J*=10.7 Hz), 1.44 (3H, s, C_8H), 2.01 (1H, d, C_1H, *J*=6.22 and 2.39 Hz), 2.63 (1H, m, C_2H), 2.74 (1H, m, C_7H), 3.23 (1H, t, C_5H, *J*=5.90 Hz), 7.47 (2H, t, *J*=7.94 Hz aromatic protons), 8.01 (2H, m, aromatic protons), 8.34 (1H, s, $C_{11}H$). Found: C, 67.11; H, 5.89; O, 14.01; Cl, 12.97%. Calcd for $C_{18}H_{21}O_3Cl$: C, 67.89; H, 6.55; O, 14.97; Cl, 11.07%.

4c. Mp: 108 °C, $[\alpha]_D^{20}=+29°$, (*c* 2.4, dioxane), IR ($CHCl_3$): C=O ester 1763, C=O terp. 1704, C=C 1633, C-O 1249—1154 cm^{-1}; CD (*c* 0.24, dioxane), $\Delta\varepsilon_{345}=+0.42$; (*c* 0.24, dioxane) $\Delta\varepsilon_{258}=+3.90$; ^1H NMR ($CDCl_3$): δ=0.80 (3H, s, C_9H), 1.12 (3H, d, $C_{10}H$, *J*=7.25 Hz), 1.27 (1H, d, C_7H, *J*=10.80 Hz), 1.31 (3H, s, C_8H), 1.93 (1H, m, C_1H, *J*=6.29 and 2.34 Hz), 2.50 (1H, m, C_2H), 2.66 (1H, m, C_7H), 3.25 (1H, t, C_5H, *J*=6.02 Hz), 7.34 (3H, m, aromatic protons), 8.27 (1H, s, $C_{11}H$). Found: C, 61.23; H, 5.12; O, 13.61; Cl, 20.04%. Calcd for $C_{18}H_{20}O_3Cl_2$: C, 61.18; H, 5.13; O, 13.59; Cl, 20.11%.

References

1) H. C. Brown and G. Zweifel, *J. Am. Chem. Soc.*, **83**, 2544 (1961).

2) P. Teisseire, A. Galfre, M. Plattier, and B. Corbier, *Recherches-Paris*, **15**, 78 (1966).

3) F. Hirata, *Bull. Chem. Soc. Jpn.*, **45**, 3458 (1972).

4) Y. Bessière-Chrétien and C. Grison, *Bull. Soc. Chim. Fr.*, **8**, 9, 3103 (1970).

5) N. Azani, to be published.

6) N. El Batouti, A. M. Lamazouère, and J. Sotiropoulos, *J. Chim. Phys.*, **85**, 3, 375 (1988).

7) C. Bouissière, Thèse Doctorat, University Paul Sabatier, Toulouse, France N_o 1434 (1973).

8) F. Labruyère, M. Tricoire, and Ch. Bertrand, *C. R. Acad. Sc. Paris., C*, **282**, 547 (1976).

9) B. A. Frentz Associates, INC, SDP, Structures Determination Package, College Station. Texas 77840 and ENRAF. NONIUS, Deft, Holland (1985).

10) A. W. Burgstahler and R. C. Barkhurst, *J. Am. Chem. Soc.*, **92**, 7601 (1970).

11) J. Sotiropoulos and N. el Batouti, *J. Chim. Phys.*, **81**, 10, 629 (1984).

12) F. Labruyère, Ch. Bertrand, C. Metge, A. Dubourg, R. Roques, J. P. Declercq, and G. Germain, *Acta Crystallogr., Sect. C*, **40**, 277 (1984).

13) R. Roques, J. Sotiropoulos, G. Feuillerat, G. Germain, and J. P. Declercq, *J. Chem. Res. (S)*, **1980**, 370.

14) J. J. Bonnet, Y. Jeannin, and J. Sotiropoulos, *Bull. Soc. Chim. Fr.*, **4b**, 26 (1973).

15) All of the complete calculations (bonds distances and angles, F_o, F_c, *U*, *B*, β) are kept as document No. 8879 at the Office of the Editor of Bull. Chem. Soc. Jpn.

α-Iodination of Ketones and Enol Acetates with Poly[styrene-*co*-(4-vinylpyridinium dichloroiodate(1−))]

Boris ŠKET,* Pavel ZUPET, Marko ZUPAN, and Darko DOLENC
Department of Chemistry and Jožef Stefan Institute, Edvard Kardelj University of Ljubljana, Yugoslavia
(Received December 19, 1988)

Synopsis. Crosslinked poly[styrene-*co*-(4-vinylpyridinium dichloroiodate(1−))] can be used as a very efficient polymeric reagent for α-iodination of ketones, diketones, and corresponding enol acetates.

Halo ketones represent synthetically useful materials and several general methods for their synthesis have been established.[1] In contrast to the chloro and bromo derivatives, α-iodo ketones received much less attention because of their relative instability. Most of the known methods of preparing α-iodo carbonyl compounds proceed from enol derivatives[2-5] or α-bromo ketone,[6] while for the direct iodination of ketones only a few methods have been described using the copper(II) acetate/iodine[7] or mercury(II) chloride/iodine system.[8] On the other hand, the treatment of alkenes with silver chromate and iodine[9] also led to the formation of α-iodo ketones.

Recently, we have found that crosslinked poly[styrene-*co*-(4-vinylpyridinium dichloroiodate(1−))] can be used as a very efficient polymeric reagent for selective electrophilic iodination of activated benzene and naphthalene derivatives,[10] as well as for iodination of heterocyclic systems[10] where electrophilic substitutions can take place.

We now wish to report that our polymeric reagent can be used for the direct α-iodination of ketones and also for iodination of the corresponding enol acetates.

A 5-hour reaction of 1 mmol of acetophenone with 1 g of polymeric reagent in methanol under reflux led to complete conversion of the starting material. ^{1}H NMR spectrum of the crude reaction mixture showed the signal at δ 4.65 corresponding to the α-chloro derivative[11] (Scheme 1).

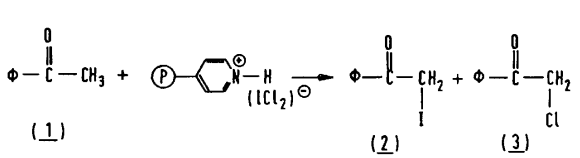

Scheme 1.

When the reaction was carried out in acetic acid solution at 50 °C, besides α-chloroacetophenone, the α-iodo derivative[11] was also formed (Scheme 1). The use of a lower reaction temperature decreased the conversion of the starting material, but increased the formation of iodinated product.

Table 1. The Effect of the Reaction Conditions on the Course of the Reaction with Acetophenone

Solvent	1 /mmol	Polym. reag. /g	T/°C	Relative yields %1	%2	%3
CH_3OH	1	1	Reflux	—	—	100
CH_3COOH	1	1	50 °C	20	27	53
CH_3COOH	1	1	25 °C	25	56	19
CH_2Cl_2	1	1	25 °C	71	16	13

The results presented in the table suggest the initial formation of the iodinated product, while the degree of further substitution of iodine with chlorine depends on the reaction time.

Further, we studied the iodination of cyclic ketones, and 1-indanone, 1-tetralone, and 6,7,8,9-tetrahydro-5*H*-benzocyclohepten-5-one were chosen as substrates. A 4.5-hour reaction of 1 mmol of 1-indanone with 1 g of polymeric reagent in acetic acid solution at 50 °C led to complete conversion of the starting ketone. The mass spectrum and ^{1}H NMR of the product (see Experimental) showed that only iodinated product was obtained. On the basis of the spectroscopic data we concluded that 2-iodo-1-indanone was formed (Scheme 2).

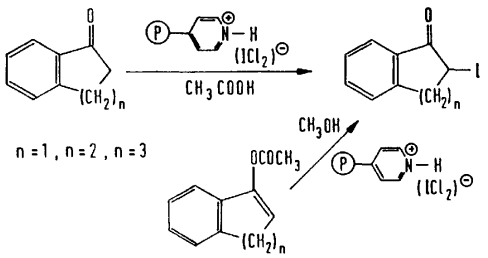

Scheme 2.

In order to determine the influence of the ring size of the cycloketone on the reaction pathway with poly[styrene-*co*-(4-vinylpyridinium dichloroiodate-(1−))], we studied the reaction with 1-tetralone and 6,7,8,9-tetrahydro-5*H*-benzocyclohepten-5-one. The reactions were carried out in methanol at room temperature or at 50 °C, and in both cases complete conversion of the starting material was observed. The product formed in the reaction with 1-tetralone was established to be 2-iodo-1-tetralone[12] by its ^{1}H NMR and mass spectrum. On the basis of the spectroscopic data of the product formed with 6,7,8,9-tetrahydro-5*H*-benzocyclohepten-5-one we concluded that iodination took place at position six and 6-iodo-6,7,8,9-tetrahydro-5*H*-benzocyclohepten-5-one was obtained as the only product.

Further, we studied the reaction of two diketones: 5,5-dimethyl-1,3-cyclohexanedione (dimedone) and 1,3-indandione with the polymeric reagent. A 5-hour reaction of 1 mmol of dimedone and 1 g of polymeric reagent at 50 °C in acetic acid solution gave a mixture with two singlet signals in its ^{1}H NMR spectrum at δ=5.16 and 4.50 with 1 : 2 relative ratio of the integrals. The mass spectrum of the crude reac-

tion mixture, besides other fragmentations, also showed signals at m/z=266 and 174. On the basis of the above mentioned spectroscopic data, we determined that 2-chloro and 2-iodo derivatives were formed in the ratio of 1 : 2. We tried to separate the reaction mixture using several types of chromatographic methods, but we were unsuccessful because of the high instability of 2-halo dimedones.

The reaction of 1,3-indandione with the polymeric reagent under the same reaction conditions led to the formation of only the 2-chloro derivative,[13] as determined by ^{1}H NMR spectroscopy and the mass spectrum. When a lower reaction temperature (25 °C) was used, the conversion of the starting diketone decreased, but besides the 2-chloro derivative, the 2-iodo product was also formed, in the ratio of 65 : 35, respectively. From the results we concluded that initially formation of the iodinated product took place, followed by substitution of iodine by chlorine, which depended on the reaction temperature and reaction time.

As in many known methods for the preparation of α-iodo carbonyl compounds enol derivatives are used as substrates, we decided to study the reactions of poly[styrene-*co*-(4-vinylpyridinium dichloroiodate(1−))] with some enol acetates. A 3.5-hour reaction of 1 mmol of 1-phenylethenyl acetate[14] with 0.5 g of polymeric reagent in methanol at 0 °C gave a crude reaction mixture which, besides a singlet signal at δ=2.6 corresponding to acetophenone, showed two singlet signals in its ^{1}H NMR spectrum at δ=4.4 and 4.7. The signal at the lower field corresponded to the chlorinated product, while the signal at δ=4.4 corresponded to iodinated product (iodinated and chlorinated product were in the ratio of 56 : 44). The formation of acetophenone can be explained by the reaction of the enol acetate with the HCl liberated in small quantity during the course of the reaction. The reaction of 1-cyclohexenyl acetate[14] with the polymeric reagent led to complete conversion of the starting material, 2-iodocyclohexanone[15] being formed as the only product. We also studied the reaction of enol acetates of 1-indanone,[16] 1-tetralone,[17] and 6,7,8,9-tetrahydro-5*H*-benzocyclohepten-5-one.[17] In all cases, α-iodo ketones were formed and the yields of pure products were also satisfactory (Scheme 2).

From the experimental observations we concluded that poly[styrene-*co*-(4-vinylpyridinium dichloroiodate(1−))] can be used as a polymeric reagent for α-iodination of ketones and the corresponding enol acetates.

Experimental

IR spectra were recorded using a Perkin-Elmer 727B instrument, and ^{1}H NMR spectra on a JEOL JNM-PS-100 with Me_4Si as internal reference. Mass spectra were taken on a CEC-21-110 spectrometer. Analytical and preparative TLC were carried out on Merck-PSC-Fertigplatten Kieselgel F 254. Melting points were determined on a Kofler apparatus and are uncorrected.

1-Phenylethenyl acetate,[14] 1-cyclohexenyl acetate,[14] 1*H*-inden-3-yl acetate,[16] 1,2-dihydro-4-naphthyl acetate,[17] and 6,7-dihydro-5*H*-benzocyclohepten-9-yl acetate[17] were prepared by known procedures.

Preparation of Poly[styrene-*co*-(4-vinylpyridinium dichloroiodate(1−))]. a) Thirty-five grams of crosslinked poly(styrene-4-vinylpyridine),[18] containing 42—44% of pyridine rings, was suspended in 150 ml of chloroform, cooled to 0 °C and 50 g of a mixture of HCl-ICl was added. The suspension was stirred at 0 °C for 60 min and at room temperature for a further 30 min. The polymer was filtered off and extracted with chloroform in a Soxhlet apparatus. After drying in vacuo for 24 h, 65 g of polymeric reagent was obtained. Three hours of drying of 1 g of polymer at 100 °C gave 0.93 g of polymeric reagent, containing 30.0% of iodine and 16.6% of chlorine (calculation for poly[styrene-*co*-(4-vinylpyridinium dichloroiodate(1−))] containing 43% of pyridine rings: 29% of iodine and 16.2% of chlorine), which means that the polymeric reagent contained 2.2 mequiv of $(ICl_2)^-$ per gram of resin.

b) Thirty five grams of crosslinked poly(styrene-4-vinylpyridine),[18] containing 42—44% of pyridine rings, was suspended in 150 ml of chloroform, cooled to 0 °C and 30 g of 36% HCl was added. After stirring at 0 °C for 30 minutes, 30 g of ICl was slowly added. The suspension was stirred at 0 °C for another 60 minutes and at room temperature for 30 minutes. The polymer was filtered off, washed with methanol and chloroform, and after drying to constant weight at room temperature 70 g of polymeric reagent was obtained.

General Reaction Procedure: One mmol of substrate was dissolved in the appropriate solvent and a given amount of poly[styrene-*co*-(4-vinylpyridinium dichloroiodate(1−))] was added. The reaction mixture was stirred at a given temperature for a given time, the insoluble beads were filtered off, washed with 10 ml of the reaction solvent, the solvent evaporated in vacuo and the crude reaction mixture analysed by ^{1}H NMR spectroscopy.

Halogenation of Acetophenone: Polymeric reagent: 1 g; solvent: methanol, acetic acid, or CH_2Cl_2, 20 ml. The effect of the solvent and the reaction temperature on the course of the reaction is presented in Table 1. Products were isolated by preparative TLC (SiO_2, CH_2Cl_2 : petroleum ether 1 : 1) and identified on the basis of a comparison of the spectroscopic data with the literature ones.[11]

Iodination of 1-Indanone: Polymeric reagent: 0.5 g; solvent: acetic acid, 20 ml; reaction conditions: 50 °C, 4.5 hours. The crude reaction product was crystallized from ethanol and 193 mg (75%) of 2-iodo-1-indanone were obtained; IR 710, 1260, 1600, 1710 cm^{-1}, ^{1}H NMR (CCl_4) δ=3.45 (1H, dd, $J_{A,B}$=18 Hz, $J_{2,3A}$=3 Hz, H-3A), 3.90 (1H, dd, $J_{A,B}$=18 Hz, $J_{2,3B}$=7.5 Hz, H-3B), 4.92 (1H, dd, $J_{2,3B}$=7.5 Hz, $J_{2,3A}$=3 Hz, H-2), 7.50 (4H, m, aromatic H's), mass spectra m/z (relative intensity): M^+ 258(100), 131(88), 127(23), 103(84), 102(35), 77(61). Found: m/z 257.9550, Calcd for C_9H_7IO: M, 257.9544, mp 68—70 °C (from ethanol).

Iodination of 1-Tetralone: Polymeric reagent: 0.5 g; solvent: methanol, 20 ml; reaction conditions: 25 °C, 5 hours. The crude reaction mixture was crystallized from ethanol and 218 mg (80%) of 2-iodo-1-tetralone[12] were isolated: ^{1}H NMR ($CDCl_3$) δ=2.22 (2H, m, H-4), 3.05 (2H, m, H-3), 5.0 (1H, t, $J_{2,3}$=4.5 Hz, H-2), 7.3 (3H, m, aromatic H's), 8.05 (1H, dd, J=7.5 Hz, 3 Hz, H-8), mass spectra m/z (relative intensity): M^+ 272(77%), 146(17), 145(68), 144(14), 128(17), 127(28), 118(46), 117(86), 116(28), 115(100), 91(40), 90(46), 89(43). Found: m/z 271.9705, Calcd for $C_{10}H_9IO$: M, 271.9700, mp 76—78 °C (lit, 76—77 °C).[12]

Iodination of 6,7,8,9-Tetrahydro-5*H*-benzocyclohepten-5-one: Polymeric reagent: 0.5 g; solvent: methanol, 20 ml: reaction conditions: 50 °C, 5 hours. 257 mg (90%) of oily 6-iodo-6,7,8,9-tetrahydro-5*H*-benzocyclohepten-5-one were obtained: ^{1}H NMR (CCl_4) δ=2.1 (4H, m, H-3, H-4), 3.06

(2H, t, J=6 Hz H-5), 5.25 (1H, t, $J_{2,3A}=J_{2,3B}$=4.5 Hz), 7.45 (4H, m, aromatic H's), mass spectra m/z (relative intensity): M^+ 286(41%), 160(10), 159(29), 132(13), 131(100), 129(20), 128(11), 127(16), 116(11), 115(17), 104(13), 103(14), 91(14), 89(14), 77(20), 63(15), 51(17). Found: m/z 285.9860, Calcd for $C_{11}H_{11}IO$: M, 285.9856.

Halogenation of 5,5-Dimethyl-1,3-cyclohexanedione: Polymeric reagent: 0.5 g; solvent: acetic acid, 20 ml; reaction conditions: 50 °C, 5 hours. On the basis of ^{1}H NMR and mass spectroscopic data we determined that 2-iodo and 2-chloro-5,5-dimethyl-1,3-cyclohexanedione were formed in the ratio of 2 : 1, and we were unable to separate them.

Halogenation of 1,3-Indandione: Polymeric reagent: 1 g; solvent: acetic acid, 20 ml; reaction conditions: 50 °C, 5 hours. The crude product formed was crystallized from ethanol and 150 mg (83%) of 2-chloro-1,3-indandione (mp 112—114 °C, lit,[13] 112—113 °C) were isolated: ^{1}H NMR ($CDCl_3$) δ=4.8 (1H, s, H-2), 8.05 (4H, m, aromatic H's), mass spectra m/z (relative intensity): M^++2 182(31%), M^+ 180(100), 124(26), 104(38), 89(63), 76(45), 50(33). Found: m/z 179.9980, Calcd for $C_9H_5ClO_2$: M, 179.9978.

Halogenation of 1-Phenylethenyl Acetate: Polymeric reagent: 0.5 g; solvent: methanol, 5 ml; reaction conditions: 0 °C, 3 hours. ^{1}H NMR analysis of the crude reaction mixture revealed that 38% of 2-iodoacetophenone, 30% of 2-chloroacetophenone, and 32% of acetophenone were formed, which were isolated by preparative TLC (SiO_2, petroleum ether 40—70 °C: CH_2Cl_2 1 : 1) and identified on the basis of a comparison of their spectroscopic data with the literature ones.[12]

Iodination of 1-Cyclohexenyl Acetate: Polymeric reagent: 0.7 g; solvent: methanol, 5 ml; reaction conditions: 25 °C, 2.5 hours. After purification of the crude product formed by SiO_2 column chromatography (elution by diethyl ether: hexane 1 : 2), 144 mg (64%) of oily 2-iodocyclohexanone[15] was obtained. The spectroscopic data were in agreement with literature.

Iodination of 1*H*-Inden-3-yl Acetate: Polymeric reagent: 0.75 g; solvent: methanol, 5 ml; reaction conditions: 25 °C, 6 hours. The crude product formed was purified by crystallization from ethanol, and 131 mg (52%) of 2-iodo-1-indanone (mp 65—67 °C) were isolated.

Iodination of 1,2-Dihydro-4-naphthyl Acetate: Polymeric reagent: 0.75 g; solvent: methanol, 5 ml; reaction conditions: 25 °C, 6 hours. The crude product formed was purified by crystallization from ethanol, and 205 mg (75%) of 2-iodo-1-tetralone (mp 77—78 °C, lit,[12] 76—78 °C) were isolated. Spectroscopic data were in agreement with those of the authentic sample.

Iodination of 6,7-Dihydro-5*H*-benzocyclohepten-9-yl Acetate: Polymeric reagent: 0.75 g; solvent: metanol, 5 ml; reaction conditions: 25 °C, 6 hours. The crude product formed was purified by SiO_2 column chromatography, and 226 mg (79%) of 6-iodo-6,7,8,9-tetrahydro-5*H*-benzocyclohepten-5-one were obtained. The spectroscopic data were in agreement with those of the authentic sample.

References

1) R. H. Reuss and A. Hassner, *J. Org. Chem.*, **39**, 1785 (1974), and references cited therein.
2) G. M. Rubottom and R. C. Mott, *J. Org. Chem.*, **44**, 1731 (1979).
3) R. C. Cambie, R. C. Hayward, J. L. Jurlina, P. S. Rutledge, and P. D. Woodgate, *J. Chem. Soc., Perkin Trans. 1*, **1978**, 126.
4) C. Djerassi and C. T. Lenk, *J. Am. Chem. Soc.*, **75**, 3493 (1953).
5) C. Djerassi, C. J. Grossman, and G. A. Thomas, *J. Am. Chem. Soc.*, **77**, 3826 (1955).
6) G. Rosenkranz, O. Mancera, J. Gatica, and C. Djerassi, *J. Am. Chem. Soc.*, **72**, 4077 (1950).
7) C. A. Horiuchi and J. Y. Satoh, *Synthesis*, **1981**, 312.
8) J. Barluenga, J. M. Martinez-Gallo, C. Najera, and M. Yus, *Synthesis*, **1986**, 678.
9) G. Cardillo and M. Shimizu, *J. Org. Chem.*, **42**, 4268 (1977).
10) B. Šket and M. Zupan, *J. Org. Chem.*, in press.
11) B. Šket and M. Zupan, *Tetrahedron*, **40**, 2865 (1984).
12) C. L. Stevens, J. J. Beereboom, Jr., and K. G. Rutherford, *J. Am. Chem. Soc.*, **77**, 4592 (1955).
13) Th. Zincke and C. Gerland, *Chem. Ber.*, **21**, 2379 (1888).
14) H. J. Hagemeyer and D. C. Hull, *Ind. Eng. Chem.*, **41**, 2920 (1949).
15) R. D'Ascoli, M. D'Auria, L. Nucciarelli, G. Piancatelli, and A. Scettri, *Tetrahedron Lett.*, **21**, 4521 (1980).
16) E. W. Dehmlow, M. Slopianka, and R. Zeisberg, *Liebigs Ann. Chem.*, **1977**, 1617.
17) P. D. Gardner, *J. Am. Chem. Soc.*, **78**, 3421 (1956).
18) M. Zupan, B. Šket, and Y. Johar, *J. Macromol. Sci. Chem.*, **A17**, 758 (1982).

The Reaction of α,β-Acetylenic Ketones with Aroylhydrazines†

B. Shivarama HOLLA,* K. Venkatramana UDUPA, and K. R. SRIDHAR††
Department of P. G. Studies and Research in Chemistry, Mangalore University, Mangalagangothri 574199 (DK), Mangalore, India
††Department of P. G. Studies and Research in Bio-Sciences, Mangalore University, Mangalagangothri 574199 (DK), Mangalore, India
(Received February 14, 1989)

Synopsis. Reaction of 3-(5-nitro-2-furyl)-1-aryl-2-propyn-1-ones (**1**) with aroylhydrazines (**2**) furnished 1-aroyl-3-(5-nitro-2-furyl)-5-aryl-5-hydroxy-2-pyrazolines (**5**) rather than the expected pyrazoles **3** or **4**. On acid-catalyzed hydrolysis these hydroxypyrazolines are converted into the known 3-(5-nitro-2-furyl)-5-aryl-1*H*-pyrazoles (**6**). The structural elucidation of the products was carried out on the basis of analytical and spectral data. The newly synthesized nitrofuran derivatives are screened for their antibacterial properties against Gram-positive and Gram-negative bacteria. Most of them showed significant activity.

A number of pyrazole derivatives are reported to possess varied biological activities such as analgesic, antiinflammatory, antipyretic, amoebicidic, trichomonacidal, antibacterial, antimicrobial, and hypoglycemic.[1] α,β-Acetylenic ketones belong to a class of activated acetylenes.[2] Sasaki and Yoshioka[3] have prepared isoxazoles, pyrazoles, 1-carbamoylpyrazoles, and pyrimidines containing nitrofuran ring by the reaction of nitrofuryl-substituted α,β-acetylenic ketones with hydroxylamine, hydrazine, semicarbazide, and benzamidine respectively.

Prompted by the varied biological activity of pyrazoles and as a part of our general search for chemotherapeutically important nitrofuran derivatives,[4,5] a project aimed at the synthesis of 1-aroyl-3(or 5)-(5-nitro-2-furyl)-5(or 3)-aryl-1*H*-pyrazoles was undertaken employing the condensation of nitrofuryl-substituted α,β-acetylenic ketones with different aroyl- and (aryloxyacetyl)hydrazines. In all such condensations hydroxypyrazolines (**5**) are obtained rather than the expected pyrazoles **3** or **4**. Synthesis, characterization, degradation and biological activities of such hydroxypyrazolines **5** carrying nitrofuryl substituent are reported in this paper.

Results and Discussion

3-(5-Nitro-2-furyl)-1-aryl-2-propyn-1-ones (**1**) obtained by the dehydrobromination of 2,3-dibromo-1-aryl-3-(5-nitro-2-furyl)-2-propen-1-ones were condensed with the aroylhydrazines and (2-naphthyloxyacetyl)-hydrazine. The condensations were carried out using equimolar reactants in refluxing ethanol. In all the cases hydroxypyrazolines (**5**) were obtained as main products in rather good yields. The structures of the condensation products were established by IR, ^{1}H NMR, mass spectra, and elemental analysis. The hydroxypyrazolines have the structure **5** as shown in Scheme 1.

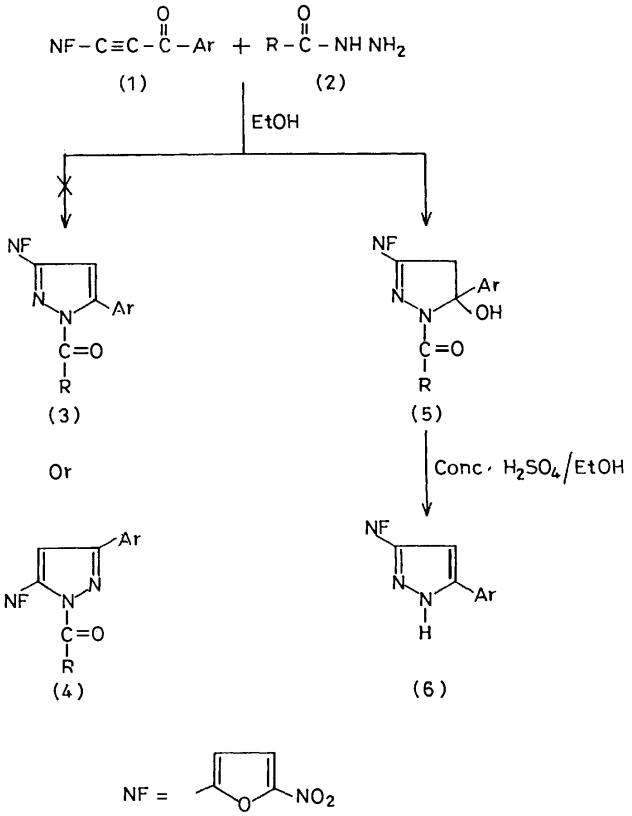

Scheme 1.

The hydroxypyrazoline structure **5** was assigned to these condensation products on the basis of analytical and spectral data and also by conversion of these hydroxypyrazolines **5** into the known pyrazoles **6** by acid hydrolysis. The IR spectra of the most condensation products **5** showed broad bands around 3400 cm^{-1} suggesting the presence of a hydrogen-bonded hydroxyl group. The amide carbonyl absorption was observed around 1650—1690 cm^{-1}. The pyrazoline structure was further confirmed by recording NMR spectra of a few selected compounds. ^{1}H NMR spectrum of the product **5a** showed a doublet of a doublet centred at δ, 8.0 integrating for two protons which is now assigned to the ortho protons of the aroyl moiety. The signals of the other aromatic protons and one β-proton of the nitrofuran ring overlapped with each other and appeared as a multiplet at δ, 7.25—7.65 integrating for nine protons. A sharp doublet (J=4 Hz) integrating for one proton appearing at δ, 7.0 is attributed to furan 3H. The OH signal of the hydroxypyrazoline appeared as a singlet integrating for one proton at δ, 5.3. The signal due to the CH_2 proton at the prochiral carbon atom of the

† Presented at the 24th Annual Convention of Chemists held at Kolhapur, November 23—26, 1987.

Table 1. Characterization Data of 1-Aroyl-3-(5-nitro-2-furyl)-5-aryl-5-hydroxy-1*H*-pyrazolines (**5**) and pyrazoles **6**

Compd. No.	Ar	R	Mp/°C	Yield	Mol. formula	Analysis Found (Calcd)		
						C	H	N
5a	Phenyl	Phenyl	168	70	$C_{20}H_{15}N_3O_5$	63.30 (63.66	4.19 3.98	11.01 11.14)
5b	Phenyl	*p*-Chlorophenyl	135	68	$C_{20}H_{14}ClN_3O_5$	58.05 (58.32	3.28 3.41	10.36 10.21)
5c	Phenyl	*o*-Hydroxyphenyl	208	65	$C_{20}H_{15}N_3O_6$	59.84 (61.07	3.75 3.82	10.48 10.69)
5d	Phenyl	2-Naphthyloxymethyl	231	64	$C_{25}H_{19}N_3O_6$	65.19 (65.65	4.02 4.16	9.33 9.19)
5e	*p*-Tolyl	Phenyl	149	69	$C_{21}H_{17}N_3O_5$	64.13 (64.45	3.99 4.35	10.52 10.74)
5f	*p*-Tolyl	*p*-Chlorophenyl	176	68	$C_{21}H_{16}ClN_3O_5$	59.51 (59.22	3.97 3.76	9.66 9.87)
5g	*p*-Tolyl	*o*-Hydroxyphenyl	164	65	$C_{21}H_{17}N_3O_6$	62.00 (61.92	4.26 4.18	10.14 10.32)
5h	*p*-Tolyl	2-Naphthyloxymethyl	124	66	$C_{26}H_{21}N_3O_6$	66.57 (66.24	4.63 4.46	8.83 8.82)
6a	Phenyl	—	216	60	$C_{13}H_9N_3O_3$	61.32 (61.18	3.68 3.53	16.33 16.47)
6b	*p*-Tolyl	—	227	63	$C_{14}H_{11}N_3O_3$	62.30 (62.45	4.25 4.09	15.39 15.61)

pyrazoline moiety appeared as two doublets centred at δ, 3.45 and 3.76 each integrating for one proton with a geminal coupling of 18 Hz. This coupling is observed in the hydroxypyrazoline due to the non-equivalence of the CH_2 protons at position 4 of the pyrazoline ring. The structure **5** is further confirmed by recording mass spectrum of **5a** which showed a molecular ion peak at m/z 377 corresponding to the molecular formula $C_{20}H_{15}N_3O_5$ thus confirming the assigned structure. A M−18 peak is also observed in the mass spectrum which indicates the loss of water molecule from the molecular ion. Two more peaks at m/z 105 and 77 are also observed in the mass spectrum of **5a** which are attributed to $C_6H_5\overset{+}{C}O$ and $\overset{+}{C_6H_5}$ respectively. The mp, yield, and analytical data of hydroxypyrazolines **5** are summarized in Table 1.

The hydroxypyrazoline structure **5** for these condensation products was further established by converting these pyrazolines to the known (nitrofuryl)pyrazoles.[6] The hydroxypyrazolines underwent smooth dehydration and debenzoylation when refluxed with ethanolic sulfuric acid. The pyrazoles thus formed were identified by their melting point and reference to literature[6] (see Table 1). Attempts to synthesize 1-aroyl-3-(5-nitro-2-furyl)-5-aryl-1*H*-pyrazoles by the dehydration of pyrazolines **5** in acetic anhydride were however unsuccessful.

Antibacterial Activity. All the hydroxypyrazolines (**5**) were screened for their antibacterial activity against S. *aureus*, A. *aerogenes*, E. *coli*, and B. *subtilis* by disc diffusion method as described earlier.[7] The results of such studies are given in Table 2.

Most of the compounds showed moderate to good antibacterial activity against all the four microorganisms tested at 5 $\mu g\,ml^{-1}$ dilution. Compound **5e** showed the highest activity among the compounds tested.

Table 2. Antibacterial Activity of Compounds **5a—h**

Compd. No.	Minimum inhibitory concentration μg/disc (diameter of inhibition in mm)			
	Bs.	*S.au*	*A.aer*	*E.coli*
5a	5 (9.6)	<5 (16.1)	<5 (10.4)	<5 (11.0)
5b	<5 (13.2)	<5 (19.6)	<5 (10.1)	<5 (9.9)
5c	<5 (11.2)	5 (9.8)	5 (9.4)	<5 (13.2)
5d	<5 (13.3)	15 (12.6)	5 (8.3)	5 (9.4)
5e	<5 (13.8)	<5 (14.8)	<5 (10.4)	<5 (10.1)
5f	<5 (12.5)	15 (10.2)	<5 (10.1)	<5 (10.9)
5g	<5 (11.4)	20 (15.1)	5 (8.6)	5 (9.0)
5h	<5 (10.9)	20 (12.1)	<5 (9.9)	5 (8.7)
Nitrofurazone (for comparison)	<5 (12.65)	<5 (14.45)	<5 (10.20)	<5 (11.15)

Experimental

All the melting points are uncorrected. The ^1H NMR spectra in $CDCl_3$ were recorded with a Bruker WH-200 200-MHz NMR spectrometer and the mass spectra with a JEOL JMS D-300 spectrometer. The IR spectra (KBr pellet) were recorded on a Perkin Elmer IR spectrophotometer.

α,β-Acetylenic ketones (**1**) were prepared by the methods reported.[3] Sustituted benzoylhydrazines were prepared from the corresponding carboxylic acids according to literature methods.[8,9]

General Procedure of Synthesizing Hydroxypyrazoline (5a—h). A mixture of appropriate nitrofuryl-substituted α,β-acetylenic ketone (**1**) (10 mmol) and suitably substituted

benzoylhydrazine (**2**) (10 mmol) in absolute ethanol (100 ml) was refluxed on a water bath for 7 h. The solvent was removed under reduced pressure and the residue was triturated with methanol. The residue was collected by filtration, dried and recrystallized from ethanol. Characterization data are given in Table 1.

General Procedure for the Conversion of Pyrazolines (5) into Pyrazoles (6): A solution of hydroxypyrazoline (**5**) (1 mmol) in ethanol (40 ml) was treated with a solution of concentrated sulfuric acid (5 ml) in ethanol (10 ml). The reaction mixture was refluxed for 3 h. The contents were cooled and diluted with water. Yellow precipitate of pyrazoles **6** were collected by filtration and recrystallized from ethanol. Treatment of **5a** as above gave pyrazole (**6a**). Similar treatment of **5g** gave pyrazole **6b**. Characterization data of **6a** and **6b** are also given in Table 1.

We are thankful to RSIC, CDRI, Lucknow for elemental analysis and mass spectra and to CSIR New Delhi for a senior research fellowship to K.V.U. We also thank Dr. K. S. Keshavamurthy, University of Alberta for 200 MHz NMR spectra of some of the samples.

References

1) J. Elguero, "Comprehensive Heterocyclic Chemistry," ed by A. R. Katrizky and C. W. Rees, Pergamon Press, New York (1984), Vol. 5, p. 291.
2) E. Winterfeldt, *Angew. Chem., Int. Ed. Engl.*, **6**, 423 (1967); T. F. Rutledge, "Acetylenes and Allenes," Reinhold, New York (1969), p. 232.
3) T. Sasaki and T. Yoshioka, *Bull. Chem. Soc. Jpn.*, **44**, 803 (1971).
4) B. S. Holla and K. V. Udupa, *Curr. Sci.*, **57**, 79 (1988).
5) B. S. Holla and K. V. Udupa, *J. Indian Chem. Soc.*, **65**, 524 (1988).
6) R. G. Haber and E. Schoenberger, *Israel J. Chem.*, **6**, 631 (1968).
7) B. S. Holla, B. Kalluraya, and K. R. Sridhar, *Curr. Sci.*, **56**, 585 (1987).
8) I. Heilbron and H. M. Bunbury, "Dictionary of Organic Compounds," Vols. 1—5, Eyre and Spottiswoode, London (1953).
9) L. Conti, *Boll. Sci. Fac. Chim. Ind. Bologna*, **22**, 13 (1964); *Chem. Abstr.*, **61**, 4253 (1964).

Electronic Conduction in Solid Nitrobenzene Containing Nitrobenzene Anion Radical and Tetrabutylammonium Perchlorate

Kosaku SUGA,* Hirofumi TAKEMURA, and Masamichi FUJIHIRA
Department of Biomolecular Engineering, Tokyo Institute of Technology, Nagatsuta, Midori-ku, Yokohama 227
(Received March 30, 1989)

The electric conductivities of frozen nitrobenzene containing various amount of tetrabutylammonium perchlorate and nitrobenzene anion radical were measured. The conductivity increased markedly with the concentration of the nitrobenzene anion radical. The mechanism of the electric conduction of the nitrobenzene is discussed and it is concluded that at low concentration of anion radical the increase of the electric conductivity is due to electronic conduction by a hopping mechanism. The rate constant of electron transfer (hopping) between any nearest neighbored sites is about $10^5\ s^{-1}$ at $-15\ °C$, which is smaller by 2 orders than that in hypothetical liquid nitrobenzene at the same temperature.

The ionic conductivity and the diffusion coefficient of an ionic species in a solution are expected to increase by its fast electron exchange reaction with other species in the solution as suggested by Levich, Dahms, and Ruff and Friedrich.[1-3] In our previous paper,[4] we reported that the contribution of the fast electron exchange reaction of the anthracene anion radical with anthracene to its ionic conductivity was successfully detected in a dimethylformamide solution. However, we could not detect such a contribution to the diffusion coefficient of the nitrobenzene anion radical (NB^-) which was undergoing a fast electron exchange reaction with nitrobenzene (NB) as a solvent.[5] In the latter experiment, it was difficult to detect the smaller contribution of the electron exchange reaction to the total conductivity, since the solution contained large amounts of tetraalkylammonium salts as supporting electrolytes.

In this paper, we report the electric conductivity of solid nitrobenzene containing its anion radical and tetrabutylammonium perchlorate (TBAP), and discuss the contribution of the electron exchange reaction between nitrobenzene and its anion radical to the conductivity of the solid, because in such a solid the contribution of the ion migration may be neglected. Furthermore, we discuss the difference between the rate constants of the electron exchange reactions in solution and in the solid state.

Experimental

Reagents. Commercially obtained nitrobenzene was dried with calcium chloride and distilled under reduced pressure in a nitrogen atmosphere. It was then passed through a column packed with activated alumina. Tetrabutylammonium perchlorate was prepared and purified as described in the previous paper.[6]

Preparation of Sample Solutions. Sample solutions of nitrobenzene containing various amounts of its anion radical and TBAP were prepared by electrolysis in an air-tight glass cell filled with nitrogen as described in the previous paper.[5] The concentration of NB^- in the solution was determined by the electric change consumed during the electrolysis.

Measurements of Electric Conductivity. Figure 1 shows the conductivity cell used for measurements in this experiment. Electrodes were made of two platinum disks of 1 cm diameter, which were fixed 3 mm apart from each other with face to face. The temperatures of the samples in the vicinity of the electrodes were measured with a thermister thermometer inserted into the cell as shown in Fig. 1. The sample solution prepared by the electrolysis was transferred to the conductivity cell under nitrogen atmosphere and the cell was cooled in a Dewar-type thermostat filled with liquid air-ethanol refrigerant. The conductivity or resistivity of the cell containing the sample solid was measured with a Mita-Musen Model 12K impedance bridge. The cell constant was determined by measuring the conductivity of a standard KCl solution.

Results and Discussion

Figure 2 shows the temperature dependence of the conductivities (σ) of solid NB containing 0.1 M

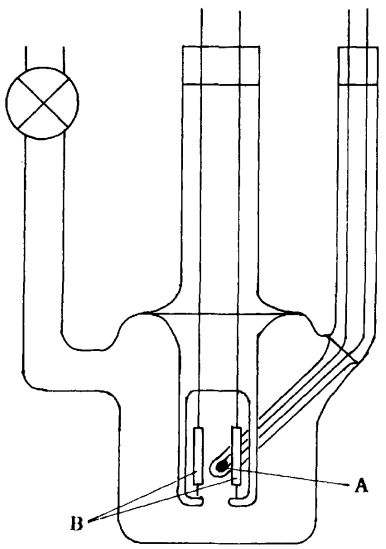

A:Thermister thermometer

B:Platinum disk electrode

Fig. 1. The conductivity cell used in this experiment.

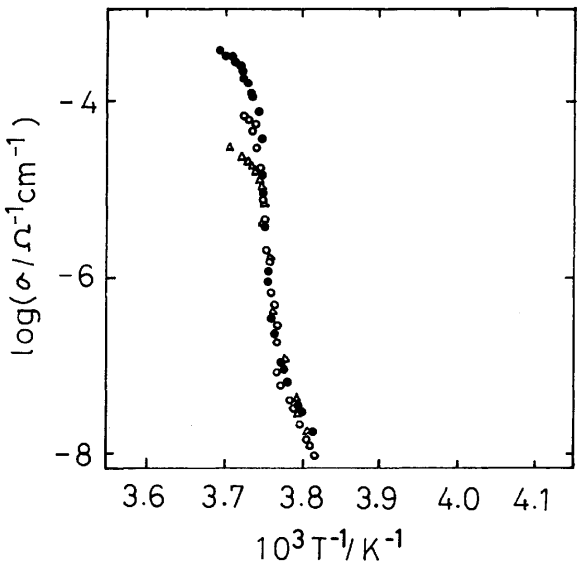

Fig. 2. Temperature dependence of the electric conductivity of NB containing (●) 0.63 M, (○) 0.27 M, (△) 0.10 M TBAP in the absence of NB^-.

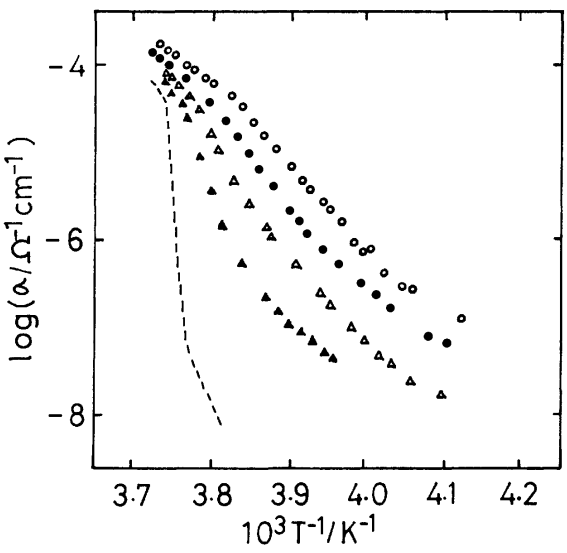

Fig. 3. Temperature dependence of the electric conductivity of NB containing 0.27 M TBAP and (○) 130 mM, (●) 87 mM, (△) 65 mM, and (▲) 43 mM NB^-. Dashed line shows the conductivity at $[NB^-]=0$.

(1 M=1 mol dm^{-3}), 0.27 M and 0.63 M TBAP in the absence of NB^-. In the temperature range used for this experiment, σ decreases rapidly with lowering temperature. Below −6.5 °C the conductivity does not depend on the concentration of TBAP.

Figure 3 shows the temperature dependence of the conductivity of NB cotaining 0.27 M TBAP and various amounts of NB^-. The conductivity increased remarkably with the concentration of NB^- especially at low temperatures. The apparent activation energies for these conductivities determined from the linear part of the curves in this figure are about 170 kJ mol^{-1}. Solid NB samples containing other concentrations of TBAP and various amounts of NB^- showed behavior similar to Fig. 3.

Since the migration of ions is difficult in the solid state, the electric conduction of solid NB containing NB^- may be mainly determined by electronic conduction. In fact, the conductivity of solid NB in the absence of NB^- is much smaller than samples containing NB^-, especially at low temperature.

Electronic conduction in solids is generally classified to two categories, i.e. band conduction and hopping conduction. If the present case is the former, conduction electrons in solid NB are supplied by NB^- and they may be trapped by the electric potential induced by positively charged tetrabutylammonium cations (TBA^+). In other words, the electrons are trapped in the donor levels which are the highest occupied molecular orbitals of NB^- residing in the vicinity of TBA^+. In such a case, the activation energy of σ is mainly determined by the excitation energy of the donor electron to the conduction level. The observed large activation energy of about 170 kJ mol^{-1}, however, can not be explained by a band conduction model, because the excitation energy estimated from the Coulomb interaction energy between NB^- and TBA^+ is not large enough.

If the present case is the latter, the conductivity is represented by the following equation according to Bagley.[7]

$$\sigma = ne^2\delta^2 k_1/k_B T \quad (1)$$

where n, δ, k_1, and k_B denote the number of hopping electrons in unit volume, the jumping distance of hopping electron between two sites, the first-order rate constant of electron hopping and the Boltzmann constant, respectively. Other nomenclature has the usual meaning. This equation has a close relation with the following equation derived by Ruff and Friedrich[3] for the ionic conductivity of ionic species A which is undergoing fast electron exchange with other species B.

$$\lambda_A = \lambda_A^0 + \pi F^2 \delta^2 k_2 c_B/4RT \quad (2)$$

where λ_A, λ_A^0, δ, k_2, and c_B represent the ionic conductivity of A in the presence and absence of B, the electron jumping distance, the second-order rate constant of electron exchange between A and B, and the concentration of B, respectively. The second term of Eq. 2 represents the contribution of the electron exchange to the ionic conductivity of A. The conductivity σ is related to the ionic conductivity λ by the following equation.

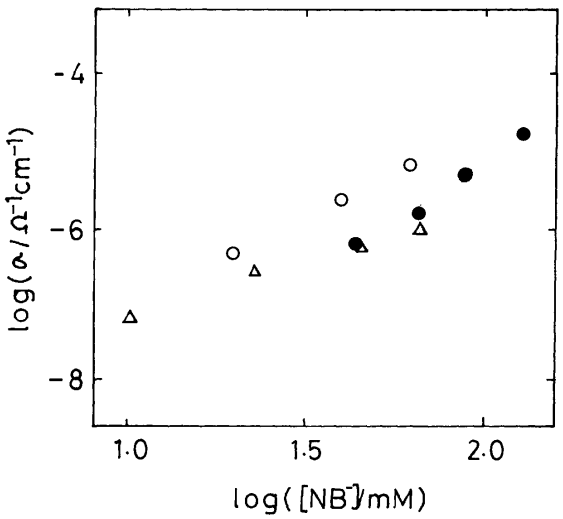

Fig. 4. The electric conductivity, σ vs. the concentration of NB^- plots for NB containing (○) 0.1 M, (●) 0.27 M, and (△) 0.63 M TBAP at −15 °C.

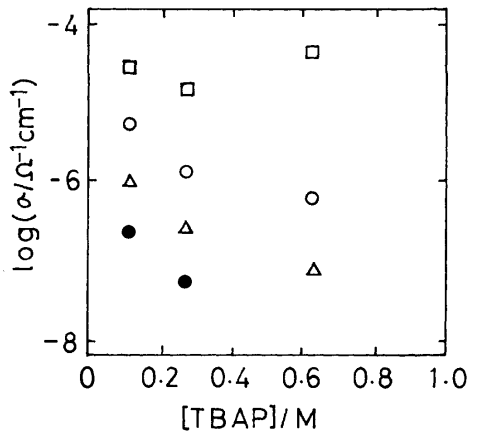

Fig. 5. The electric conductivity, σ vs. the concentration of TBAP plots for NB containing 65 mM NB^- at (□) −10 °C, (○) −15 °C, (△) −20 °C, and (●) −25 °C.

$$\sigma = \sum_i \lambda_i c_i \quad (3)$$

where the summation is taken for all ionic species, i.e. NB^-, TBA^+, and ClO_4^- in this case. Since migration of the ionic species can be neglected in this experiment, we consider only the second term of Eq. 2. In this case, NB^- and NB correspond to A and B, respectively. The following equation, therefore, is derived from Eq. 3.

$$\sigma = \pi F^2 \delta^2 k_2 c_A c_B / 4RT = \pi [NB^-] F^2 \delta^2 k_2 [NB] / 4RT. \quad (4)$$

Considering that $N_A e = F$, $n/N_A = [NB^-]$, $k_2[NB] = k_1$, and $R = N_A k_B$ (N_A: Avogadro's number, F: Faraday's constant), we can obtain Eq. 1 except for the factor $\pi/4$. The difference of this factor is due to the neglect of the electron hopping or jumping directions other than in the direction parallel to the electric field in the derivation of Eq. 1 by Bagley. Coincidence between the Eqs. 1 and 4 shows that hopping conductivity denoted by Eq. 1 is equivalent to the contribution of electron exchange to the ionic conductivity denoted by Eq. 2.

In the case of the hopping conduction, the electron hopping process is the activation process and needs a certain value of activation energy. Such an activation energy is included in the equation which represents the rate constant of electron hopping or electron exchange as follows;

$$\begin{aligned} k_1 &= k_2[NB] = \nu[NB]\exp(-\Delta G^*/RT) \\ &= \nu[NB]\exp(\Delta S^*/R)\exp(-\Delta H^*/RT), \end{aligned} \quad (5)$$

where ν, ΔG^*, ΔS^*, and ΔH^* denote the frequency of electron hopping with zero activation free energy, activation free energy, activation entropy, and activation enthalpy for electron hopping, respectively. Therefore, the fact that the observed conductivity of solid nitrobenzene has a large activation energy does not contradict this hopping mechanism.

If the hopping mechanism can be applied to the solid nitrobenzene in this experiment, Eqs. 1 and 4 show that the conductivity of solid nitrobenzene must be proportional to the number in unit volume or the concentration of NB^-.

Figure 4 shows the plots of $\log(\sigma/\Omega^{-1}\,cm^{-1})$ vs. $\log([NB^-]/mM)$ for NB containing various concentrations of TBAP at −15 °C. It is apparent that the conductivity increases with the concentration of NB^-, although the value of σ at constant $[NB^-]$ and temperature is dependent on the concentration of TBAP as shown in Fig. 5. In these plots, there is fairly good linearity between $\log(\sigma/\Omega^{-1}\,cm^{-1})$ and $\log([NB^-]/mM)$ when the concentration of TBAP is constant. The slope of the plots is about 1 at low concentration of NB^-, while it increases to about 3 at high concentration of NB^-. Although the reason for this is not obvious at the present stage, the conductivity is almost proportional to $[NB^-]$ at low concentration of NB^-. In this concentration range, the rate constant of electron hopping therefore can be determined, if appropriate jumping distance is assumed. If the jumping distance δ is assumed to be 10 Å, the rate constant $k_1 = k_2[NB]$ is estimated to be about $10^5\ s^{-1}$ at −15 °C. The corresponding rate constant in solution is estimated to be about $10^7\ s^{-1}$ at the same temperature by an extrapolation.[5] Such a large difference between the values of k_1 in the solid and in solution can be attributed to the freezing of the molecular motion (orientational and vibrational) in solid NB needed for the formation of activation states of an electron transfer reaction.[8] In particular, near the freezing point of NB at which the measurements were

performed in this experiment, the sudden freezing of molecular motion with the decrease of the temperature may occur.

In the quantum mechanical treatment of electron transfer reactions,[8c] the first-order rate constant for electron transfer at fixed distance is given by the following equation,

$$k_1 = (2\pi/\hbar)H_{AB}^2(FC) \quad (6)$$

where H_{AB} is the matrix element describing the electronic coupling between the electronic states of reactants and products, and the quantity (FC) is the 'Franck-Condon' factor, which is a sum of products of overlap integrals of the vibrational and solvational wave functions of the reactants with those of the products, suitably weighted by Boltzmann factors for the vibrational and solvational energy levels of reactants. With freezing of the sample solution, the orientational vibration of NB^- and NB molecules may be frozen easily and the frequencies of these vibrations may increase remarkably. Consequently, the separation of these vibrational levels increases considerably, the contribution of these vibrations to the value of (FC) can be expected to decrease greatly.

Therefore, the larger activation energy observed in solid NB compared with that observed in solution (about 35 kJ mol^{-1})[5] can also be attributed to the apparent decrease in the value of (FC) as a result of such sudden freezing of molecular motion with the decrease of the temperature.

References

1) V. G. Levich, "Adv. Electrochem. Electrochem. Eng.," ed. by P. Delahay, **4**, 314 (1966).
2) H. Dahms, *J. Phys. Chem.*, **72**, 362 (1968).
3) I. Ruff and V. J. Friedrich, *J. Phys. Chem.*, **75**, 3277 (1971); **76**, 2954 (1972).
4) K. Suga, T. Yorifuji, S. Aoyagui, and T. Saji, *Electrochim. Acta*, **27**, 1259 (1982).
5) K. Suga and S. Aoyagui, *Bull. Chem. Soc. Jpn.*, **60**, 2713 (1987).
6) K. Suga and S. Aoyagui, *Bull. Chem. Soc. Jpn.*, **55**, 358 (1982).
7) B. G. Bagley, *Solid State Commun.*, **8**, 345 (1970).
8) a) R. A. Marcus, *J. Chem. Phys.*, **43**, 679 (1965). b) N. R. Kestner, J. Logan, and J. Jortner, *J. Phys. Chem.*, **78**, 2148 (1974). c) R. A. Marcus and N. Sutin, *Biochim. Biophys. Acta*, **811**, 265 (1985).

 © 1989 The Chemical Society of Japan Bull. Chem. Soc. Jpn., 62, 3417—3420 (1989)

Mesomorphic Properties of Dialkyl *N,N'*-[1,4-Phenylenebis(methylidyne)]-bis[4-aminobenzoates]

Yoshio MATSUNAGA* and Hiroyuki MATSUZAKI
Department of Chemistry, Faculty of Science, Hokkaido University, Sapporo 060
(Received April 26, 1989)

The mesomorphic behavior of fourteen dialkyl *N,N'*-[1,4-phenylenebis(methylidyne)]bis[4-aminobenzoates] has been examined by optical microscopy and differential scanning calorimetry in order to make a comparison with the behavior of *N,N'*-[1,4-phenylenebis(methylidyne)]bis[4-alkylanilines] and to study the effects of branching of the ester alkyl groups. Among the results obtained, the following may be particularly important: (1) the unbranched alkyl ester is generally less polymesomorphic than the corresponding alkyl compound, (2) mesophase(s) is completely eliminated by the 1-methylation, and (3) the 3-methylbutyl, 3-methylpentyl, and 4-methylpentyl esters are more polymesomorphic than the unbranched alkyl esters.

The mesomorphic properties of organic compounds are highly sensitive to changes in chemical structure; therefore, a systematic study of closely related compounds is desirable in order to elucidate the relationship between the structural parameters and the thermal stabilities of various mesophases. This paper presents our work on dialkyl *N,N'*-[1,4-phenylenebis(methylidyne)]bis[4-aminobenzoates] which have the general structure given below (**1**) and are closely related to that of *N,N'*-[1,4-phenylenebis(methylidyne)]-bis[4-alkylaniline] (**2**), well-known for their smectic polymorphism.[1,2] For example, the propyl compound exhibits the smectic H, G, C, and A phases as well as the nematic phase, and the hexyl compound exhibits the smectic G, F, C, and A phases as well as the nematic phase.[2] Therefore, we may be able to find various types of the mesophase in the compounds to be studied. Indeed, Arora et al. have shown that the dibutyl ester exhibits smectic C and A phases as well as the nematic phase.[3] Secondly, we were interested in extending our work on the effects of the branching of the ester alkyl chain on the mesomorphic properties to diesters in which the effects may be more appreciable than in the monoester. The bis(2-methylbutyl) ester has been known to show only the nematic phase, through the work of Coates et al.[4]

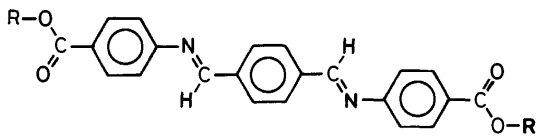

(1)

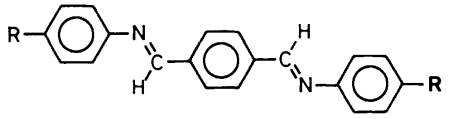

(2)

Experimental

Materials. Alkyl *p*-aminobenzoates were obtained by reactions between *p*-nitrobenzoyl chloride and alcohols, followed by reduction with iron powder and dilute hydrochloric acid, as described by Adams et al., or with zinc dust in 75% aqueous ethanol.[5,6] The Schiff's bases were prepared by condensing terephthalaldehyde with the alkyl *p*-aminobenzoates in boiling ethanol or benzene, employing a small amount of acetic acid as a catalyst.

Measurements. Microscopic observations and calorimetric measurements were made as described in our previous paper.[7] Phase diagrams were determined by the calorimetric curves for binary mixtures in order to identify the smectic phases.

Results and Discussion

The transition temperatures and enthalpy changes are listed in Table 1 for the fourteen esters examined in this work. Here, K, S, N, and I stand for crystalline, smectic, nematic, and isotropic liquid phases, respectively. The seven unbranched alkyl esters are given in section a in this table.

The methyl and ethyl esters are purely nematogenic. Because of the thermal decomposition near the clearing point the enthalpy change in the former ester could not be measured. Both their melting and clearing points are much higher than those of the corresponding alkyl compounds, respectively. The appearance of the smectic H phase in the temperature range from 126 to 150 °C reported by Neubert and Maurer was not supported by Wiegeleben et al.

The propyl ester is transformed into an isotropic liquid at a temperature almost the same as that of the propyl compound (260 °C by Neubert and Maurer and 255 °C by Wiegeleben et al.). The temperature range of the smectic A phase is a little wider than that of the corresponding alkyl compound (26 to 30 °C). The three other smectic phases given by the propyl compound, H, G, and C, are not detectable in this ester.

Thus, the clearing point of the ester is reduced as the

ester alkyl group becomes longer and a profound alternation of the transition temperature is exhibited by higher homologous members. The transformation of the butyl ester from the nematic phase to an isotropic liquid occurs at a lower temperature than the corresponding alkyl compound; namely, 209 versus 235 °C.[1,2] Similarly, the smectic A and C properties are decreased compared with those in the alkyl compound. The difference in their thermal stabilities is in the following order: $S_C > N > S_A$. Therefore, a large depression of the smectic A phase in the hexyl and heptyl esters may explain the absence of nematic properties in these two members. It must be noted that all of the mesophases appearing below the smectic C in the alkyl compounds are eliminated by the change of the terminal substituent from the alkyl to the alkoxycarbonyl group.

Turning now to the branched alkyl esters, the thermal properties are given in section b in Table 1. According to the systematic studies by Gray and Harrison, all of the branched chain esters have lower liquid crystal stabilities than the unbranched chain esters.[8] Especially, the branching methyl group occupying the 1 position greatly reduces the thermal stability and, as the methyl group is moved towards the end of the chain, the transition temperature rises again. In addition to the information given in table, the esters carrying the following alkyl groups were studied: isopropyl, *t*-butyl, 1-methylbutyl, 1,2-dimethylpropyl, 1-methylbutyl, and 1-methylpentyl. No mesophase was found for these esters, indicating that the liquid crystalline behavior in the present series dramatically suffers as the result of a branching methyl substituent on the 1 position in the alkyl chain.

The nonmesomorphic behavior of the neopentyl ester in the present series is in sharp contrast with the observation made for the corresponding ester in the 4-(4-phenylbenzylideneamino)benzoate series.[7] In the latter, the N-I transition temperature of the propyl ester remains at 133 °C by the introduction of a methyl group at the 2 position and is depressed only by 8 °C by the second methyl group. This remarkable discrepancy strongly supports our previous view that the effects of the branching of the alkyl chain on mesomorphic properties greatly vary with the features of the molecular structure.

The N-I transition temperature of the 2-methylpropyl ester is lower by 17 °C than that of the unbranched propyl ester. The smectic A phase observed for the latter compound is lost by the

Table 1. Transition Temperatures (°C) and Enthalpy Changes (kJ mol^{-1}) of Compounds **1**[a]

Alkyl group	K	S_G	S_B	S_C	S_A	N	I
			a. Unbranched				
CH_3	.			243 (53)		.	339 (—) .
CH_2CH_3	.			210 (31)		.	295 (0.21) .
$CH_2CH_2CH_3$	.		153 (39)		.	199 (0.21) .	258 (0.38) .
$CH_2CH_2CH_2CH_3$[b]	.		92 (32)	.	137 (—) .	190 (0.84) .	209 (0.38) .
$CH_2CH_2CH_2CH_2CH_3$	.		100 (34)		.	206 (1.3) .	216 (0.46) .
$CH_2CH_2CH_2CH_2CH_2CH_3$	.		113 (27)	.	148 (—) .		189 (2.9) .
$CH_2CH_2CH_2CH_2CH_2CH_2CH_3$	.		92 (41)	.	140 (—) .		196 (4.5) .
			b. Branched				
$CH_2CH(CH_3)_2$	.			157 (40)		.	241 (0.42) .
$CH_2CH(CH_3)CH_2CH_3$[c]	.			131 (29)		.	183 (0.29) .
$CH_2CH_2CH(CH_3)_2$	.		113 (24)	.	140 (0.33) .	158 (0.33) .	170 (0.29) .
$CH_2CH(CH_3)CH_2CH_2CH_3$	.			115 (39)		.	175 (0.21) .
$CH_2CH_2CH(CH_3)CH_2CH_3$	.	100 (20) .	106 (0.04) .	133 (0.71)	.	145 (0.59) .	147 (0.33) .
$CH_2CH_2CH_2CH(CH_3)_2$	.		109 (56)	.	140 (0.25) .	160 (0.92) .	170 (1.0) .
$CH_2CH(CH_3)CH_2CH_2CH_2CH_3$	.			101 (37)		.	146 (0.25) .

a) The latter quantities are in parentheses. b) 91 (38), 134 (—), 185 (0.88), and 203 °C (0.46) by Arora et al.[3] c) 123 (17) and 184 °C (0.21) by Coates et al.[4]

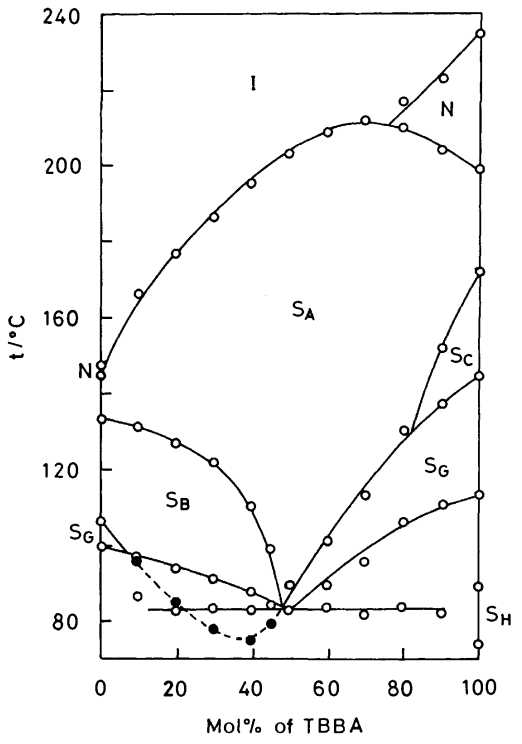

Fig. 1. Phase diagram of the binary system consisting of compound **1** with R=3-methylpentyl and TBBA (compound **2** with R=butyl). The open and shaded circles are transitions observed in the processes of heating and cooling respectively.

introduction of a methyl group at the 2 position.

When the branching methyl group is located at the 2 or 3 position in the butyl ester, the change in the transition temperature is rather unusual. Contrary to what is generally known,[8-11] the 2-methylbutyl ester gives an N–I transition temperature higher by 13 °C than the 3-methylbutyl ester. The latter compound exhibits smectic A and C phases, both of which are characteristic of the butyl ester. While the smectic A behavior is depressed by as much as 32 °C, the smectic C behavior is a little bit promoted by the branching methyl group.

The branching at the 2 or 3 position of the pentyl ester presents very interesting features. The N–I transition temperature of the 2-methylpentyl ester is higher by 28 °C than that of the 3-methylpentyl ester. Although the former ester exhibits only the nematic phase, the latter gives polymesomorphic changes. It must be pointed out that the smectic B phase shown by the 3-methylpentyl ester is not observable for the unbranched pentyl ester. In order to supplement the identification made by the microscopic observation, a phase diagram of the binary system with the butyl compound (TBBA) was prepared.[12] This reference compound is known to exhibit the smectic H, G, C, and A phases and the nematic phase.[2] As is shown in Fig. 1, the eutectic point is found at 50 mol% and 83 °C. Since the smectic A phase is stabilized by mixing, only parts of the N–I transition temperature curve are observable. Nevertheless, it is easily seen that the temperature varies monotonously with the composition. The thermal stabilities of the other smectic phases of TBBA, especially those of the smectic C and H phases, are drastically reduced by the addition of the ester. The intermediate smectic phase in the ester is clearly different from any smectic phase given by the reference compound and was identified to be of the smectic B type by a microscopic observation of the texture. This assignment is in accordance with one of the possible sequences of appearance for three smectic phases.[13] On the other hand, the low-temperature smectic phase is apparently miscible with the smectic G phase of TBBA, even though the smectic B–smectic G transition temperature curve shows a deep minimum.

By a shift of the methyl group from the 3 position to the 4 position, the nematic phase is stabilized by 23 °C and the smectic A phase by 15 °C. The above-mentioned effects of the branching methyl group on the N–I transition temperature of the pentyl ester indicates that the temperature changes alternately in the present series as the branching methyl group moves from the odd to even position in the chain. One may recognize such an alternation, even in the N–I transition temperatures of the methyl-substituted pentyl 4-(4-cyanobenzylideneamino)cinnamates reported by Gray and Harrison;[8] however, it was not detectable in our earlier series of alkyl 4-(4-alkoxybenzylideneamino)benzoates.[10] Thus, the magnitude may markedly depend on the features of the molecular structure. Because of the presence of two alkyl groups, the alternation in the present series may be so large that one cannot miss it. However, monoesters exhibiting similar changes will be provided by the forthcoming papers. The present ester exhibits the smectic C phase, which is not known for the unbranched pentyl ester.

Finally, we add that the 2-methylhexyl ester is purely nematogenic, while the unbranched hexyl ester is purely smectogenic. The appearance of the nematic phase by a partial destruction of the smectic A phase by a branching methyl group has been amply demonstrated in the present author's previous studies.[7,10,11]

References

1) M. E. Neubert and L. J. Maurer, *Mol. Cryst. Liq. Cryst.*, **43**, 313 (1977).

2) A. Wiegeleben, L. Richter, J. Deresch, and D. Demus, *Mol. Cryst. Liq. Cryst.*, **59**, 329 (1980).

3) S. L. Arora, J. L. Fergason, and A. Saupe, *Mol. Cryst. Liq. Cryst.*, **10**, 243 (1970).

4) D. Coates, K. J. Harrison, and G. W. Gray, *Mol. Cryst. Liq. Cryst.*, **22**, 99 (1973).

5) R. A. Adams, E. K. Rideal, W. B. Burnett, R. L. Jenkins, and E. E. Dreger, *J. Am. Chem. Soc.*, **48**, 1758 (1926).
6) W. E. Kuhn, *Org. Synth.*, Coll. Vol. II, 447 (1943).
7) Y. Matsunaga and N. Miyajima, *Mol. Cryst. Liq. Cryst.*, **104**, 353 (1984).
8) G. W. Gray and K. J. Harrison, *Mol. Cryst. Liq. Cryst.*, **13**, 37 (1971).
9) G. W. Gray and S. M. Kelly, *Mol. Cryst. Liq. Cryst.*, **104**, 335 (1984).
10) Y. Matsunaga and N. Miyajima, *Bull. Chem. Soc. Jpn.*, **57**, 1413 (1984).
11) Y. Matsunaga and N. Miyajima, *Mol. Cryst. Liq. Cryst.*, **116**, 207 (1985).
12) As the trivial name, terephthal- or terephthalylidene-bis(*p*-butylaniline) has been widely used, TBBA is the abbreviation in accord with that used in the references.
13) D. Demus, S. Diele, S. Grande, and H. Sackmann, "Advances in Liquid Crystals, Vol. 6," ed by G. H. Brown, Academic Press, New York (1983), p. 11.

 © 1989 The Chemical Society of Japan Bull. Chem. Soc. Jpn., 62, 3421—3425 (1989)

Adsorption of Poly(methyl methacrylate) on Silica Surfaces Having Various Silanol Densities

Kazutoshi KOBAYASHI,* Kazuo ARAKI, and Yoshio IMAMURA
Department of Chemistry, Faculty of Science, Science University of Tokyo, Kagurazaka, Shinjuku-ku, Tokyo 162
(Received May 2, 1989)

The adsorption of poly(methyl methacrylate) (PMMA) on silica surfaces having various silanol densities was studied by ESR and IR spectroscopies. Three silica samples, Nipsil HD, Aerosil 300, and Aerosil R812, which have 8, 2.2, and 0.54 nm^{-2} silanol densities, respectively, were used as the adsorbents. The amount of adsorption, A, the surface coverage, θ, and the fraction of train segments in the polymer, p, were determined. The values of the segment fractions anchoring through the hydrogen bond in all train segments of the adsorbed polymer, f_{HB}, were also estimated. When PMMA adsorbed on Nipsil HD, the polymer adsorbed predominantly by the formation of hydrogen bonds; on the other hand, when PMMA adsorbed on Aerosil 300, the polymer adsorbed through the hydrogen bond in the part of 30—40%. When PMMA adsorbed onto Nipsil HD, the value of p_{ESR} obtained by the ESR method was almost the same as the p_{IR} obtained by the IR method. When PMMA adsorbed onto Aerosil 300, the value of p_{ESR} was 0.47, twice the value of p_{IR}(0.24).

The adsorption of macromolecules is quite different in many respects from that of small molecules. The difference between them arises from the obvious differences in the size and the resultant flexibility of molecures. Among the molecular models proposed for characterizing polymer molecules adsorbed from solution onto a solid surface, the "loop-train-tail" model would be most general and successful. In order to discuss the conformation of an adsorbed polymer molecule, it is very important to estimate the fraction of train segments in the polymer, p. Usually, IR,[1,2] NMR,[3-5] and ESR[6-8] methods are utilized to estimate the value of p.

Fortana and Thomas first developed a technique for a quantitative estimation of the segment fraction attached to the surface sites through the hydrogen bond using IR spectroscopy.[1] They obtained values of p from 0.3 to 0.4 for the adsorbed poly(alkyl methacrylate) on silica in organic solvents. Robb and Smith first employed the ESR method for studies of the adsorption of poly(*N*-vinylpyrrolidone) onto silica, mainly from aqueous solution.[6] They obtained values of p from 0.6 to 0.9. Sakai et al. studies the conformation of adsorbed poly(methyl methacrylate) (PMMA) by the ESR method using three-component spectrum analysis.[7] They discussed the molecular weight dependence upon the polymer adsorption,[8] and also made a direct comparison of the ESR and IR methods using an identical solution-adsorbent system (PMMA-carbon tetrachloride-silica).[9] Based on their experimental results, they pointed out a disagreement in the obtained p values: the ESR method gave much greater values of p than did the IR method. In the present study one of our purposes was to pursue the cause of this disagreement. It was reported that when PMMA adsorbed on a silica surface, the polymer would mainly adsorb by the formation of a hydrogen bond between a carbonyl group of methyl methacrylate and a silanol group of the surface site.[10] Since the IR method evaluates only the segments adsorbed through a hydrogen bond between the carbonyl group and the silanol group, if the segments in PMMA adsorbed except for the hydrogen bond, the value of p would be understimated. In this paper we report on whether the adsorption of PMMA onto a silica adsorbent is caused exclusively by the formation of hydrogen bonds or not. We studied the amount of adsorption (A), the segment fraction of train (p), and the surface coverage (θ), using three kinds of silica surfaces having various silanol densities.

Experimental

Materials. The experimental procedures were basically the same as those described previously.[7,8] Spin-labeled PMMA was prepared by an anionic copolymerization of methyl methacrylate with 4-hydroxy-2,2,6,6-tetramethyl-1-piperidinyloxyl in toluene at 0 °C using a phenylmagnesium bromide catalyst. The polymer was repeatedly fractionated in an acetone-water mixture to give narrow molecular weight distributions. The number-average molecular weight and the $\bar{M}_w/\bar{M}_n$ ratio of the PMMA sample were determined by GPC, calibrated with a standard polystyrene. They were 1.5×10^5 and 1.6, respectively. The spin-concentration of PMMA was approximately one spin per 400 monomer units. Details of the hyperfine coupling- and g-tensor values of the PMMA sample were published in a previous paper.[7]

Three silica-based adsorbents were used (Table 1). Nipsil HD (Nippon Silica Industrial) is a silica of surface area 263 $m^2 g^{-1}$, as determined by N_2 adsorption; it contains a relatively high level of silanol groups, 8 per nm^2. Aerosil 300 (Degussa) is a silica of surface area 303 $m^2 g^{-1}$ with a lower content of silanol groups, 2.2 per nm^2. A sample of surface-

Table 1. Characterization of Silica Sample

Sample name	Specified surface area/$m^2 g^{-1}$	SiOH/nm^2
Nipsil HD	263	8
Aerosil 300	303	2.2
Aerosil R812	245	0.54

modified silica, Aerosil R812 (Degussa), was prepared by treating Aerosil 300 with trimethylchlorosilane; this treatment converts most of the silanols to trimethylsilyl groups. It was reported that the differences of the particle sizes and the specific surface coverage in the used samples do not influence the amount of adsorption, A, and the train segment in polymer, p.[8]

Carbon tetrachloride and benzene used in this work were spectrometric grade.

Techniques of Measurements. The adsorption isotherms of PMMA on the various silica surfaces at 25 °C were measured by ESR spectroscopy, as described previously.[7] Solutions (10 ml) of various polymer concentrations were shaken vigorously with a solid adsorbent (0.1 g) in order to disperse the solid, then tumbled slowly over 24 h to ensure that equilibrium had been reached. The suspensions were then centrifuged and the ESR spectra of the supernatant solution and the adsorbed polymer were recorded. All ESR spectra were recorded with a JEOL JES FE-3X spectrometer.

The surface coverage (fraction of surface silanol groups occupied), θ_{IR}, was determined by the method of Kawaguchi et al., using infrared spectroscopy.[2] The differential IR spectra between the supernatant polymer solution and the silica on which PMMA was adsorbed show two characteristic bands: a band located at 3730 cm^{-1} due to the free silanol groups and another band located at 3420 cm^{-1} due to an interaction between the silanol groups and the carbonyl groups of the adsorbed PMMA. If we know the molar extinction coefficients (L mol^{-1} cm^{-1}) at 3730 and 3420 cm^{-1}, both the number of free silanol groups (S_{3730}) and the number of occupied silanol groups (S_{3420}) can be determined, and the surface coverage, θ_{IR}, can be calculated from the equation

$$\theta_{IR} = S_{3420}/(S_{3420} + S_{3730}). \quad (1)$$

All IR spectra were recorded with JASCO FT-IR 7000 spectrometer. In the case of Aerosil R812, we could not decide on the surface coverage, θ_{IR}, since the absortion of the silanol group was broad and did not shift before and after adsorption. Therefore, instead of θ_{IR}, we determined the surface coverage, θ_{As} (amount of adsorption/amount of maximum adsorption), of Aerosil R812 by using the same procedure as in a previous paper, from data regarding the amount of adsorption.[8]

Analyses of the ESR spectra of the adsorbed polymers were performed using the same procedure described in a previous paper.[7] The ESR line shape observed from the adsorption system was simulated by the summation of three model spectra: a triplet line with a narrowed width showing high mobility, an intermediately broadened line showing a restricted segment motion, and a powder pattern showing rigid immobilization. The spectrum was normalized by the singal intensity obtained from a second integration of the first-derivative spectrum. The amplitude of each model spectrum was determined by a least-squares method on the multiple regression to fit the summation of the three spectra with the observed spectrum. The model spectra were selected to make the correlation coefficient close to unity between the observed spectrum and the summation of the three model spectra. In the three-component analysis, close curve fitting was found in every case.

Results and Discussion

The adsorption isotherms for labeled PMMA from carbon tetrachloride and benzene onto the three kinds of adsorbents are shown in Fig. 1, indicating that the solvent has a strong influence on the affinity of the polymer for the surface. Here, Nipsil HD showed no indication of saturation over the concentration observed. In a benzene solution, relatively small amounts of polymer were required to saturate the surface. In a carbon tetrachloride solution, the adsorption of PMMA was more favored. The difference in the adsorption of PMMA adsorbed from carbon tetrachloride and benzene would be caused by the fact that carbon tetrachloride is a poorer solvent than benzene for PMMA and that benzene has a stronger affinity for a silica surface than does carbon tetrachloride. In both solvents, the adsorption of PMMA decreased with a decrease in the silanol density of the surface (Fig. 1). In the cases of Aerosil 300 and Nipsil HD, the adsorption of PMMA were of a high-affinity type and increased steeply under low equilibrium concentration.

Typical plots of the values of θ_{IR} and θ_{As} against the equilibrium concentration for the PMMA adsorbed on various silica surfaces from carbon tetrachloride solution are displayed in Fig. 2. The values of θ_{IR} increased steeply at a low concentration and reached a

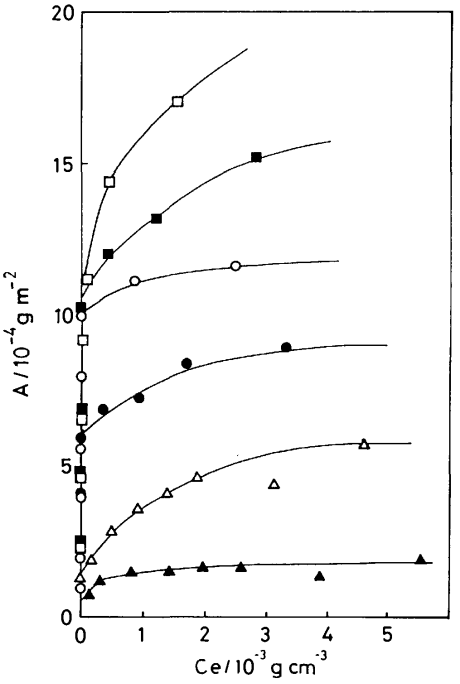

Fig. 1. Adsorption isotherms of PMMA on the three silica samples at 25 °C. □: Nipsil HD in CCl_4, ■: Nipsil HD in C_6H_6, ○: Aerosil 300 in CCl_4, ●: Aerosil 300 in C_6H_6, △: Aerosil R812 in CCl_4, ▲: Aerosil R812 in C_6H_6.

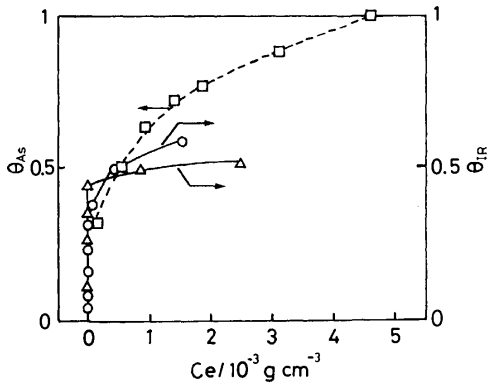

Fig. 2. Plots of the values of θ_{IR} and θ_{AS} against the equilibrium concentration for adsorbed PMMA from CCl_4. O: Nipsil HD, △: Aerosil 300, □: Aerosil R812.

constant value. The values of θ_{As} gradually increased and reached naturally to unity.

When the affinity of the polymer for the surface is relatively weak, the adsorbed polymer molecules are likely to be held rather loosely and have an abundance of loops and tails. When the affinity of the polymer for the surface is strong, the adsorbed chains are held more strongly on the surface. The resulting motionally restricted conformations tend to be relatively flat and to have an abundance of trains. Such conformational differences are apparent in the ESR spectra of the adsorbed labeled PMMA. The spectra of the PMMA adsorbed on the three kinds of silica surfaces from a carbon tetrachloride solution are illustrated in Fig. 3. The ESR spectra of PMMA adsorbed on Nipsil HD and Aerosil 300 are virtually identical and are composites of broad and motionally-nallowed lines, indicating that some of the segments at the surface are located in loops or tails which are relatively free and more mobile. The ESR spectra of PMMA adsorbed on the Aerosil R812 have motionally-nallowed lines, suggesting a loopy conformation.

When PMMA molecules are adsorbed onto an Aerosil 300 silica surface, the segment fractions of train, short loop, and long loop segments against the surface coverage, θ_{IR}, can plotted as in Fig. 4, which shows a decrease in the number of train segments and an increase in the number of long loop segments with an increase in θ_{IR}. At relatively low θ_{IR}, most of the segments were highly localized near the surface. As a result, the adsorbed polymer was flattened and formed a thin adsorbed layer. All of the theoretical treatments predict that a flexible chain polymer molecule would be strongly attracted by a solid surface and would have an appreciably flat structure with a large fraction of train segments, in the case of a high level of the adsorption energy between the segments and the surface. The revealed structures roughly agree with the theoretical predictions.

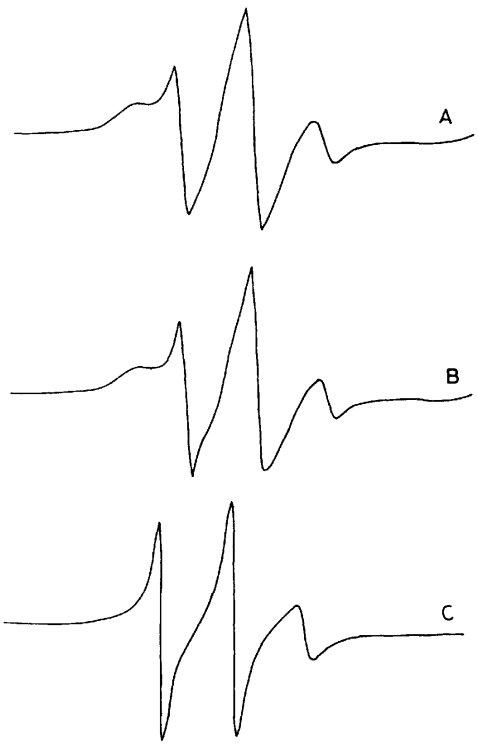

Fig. 3. ESR spectra of the adsorbed PMMA adsorbed on the three silica surfaces. A: Nipsil HD, B: Aerosil 300, C: Aerosil R812.

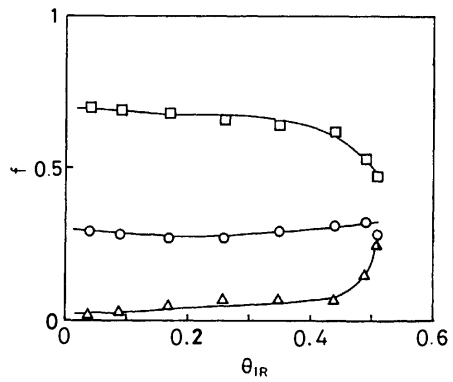

Fig. 4. Plots of the segment fractions, f, of train, short loop, and long loop against the surface coverage, θ_{IR}, for OMMA adsorbed onto the Aerosil 300 silica surface. □: train, O: short loop, ▲: long loop.

The segment fractions of train, short loop, and long loop at the maximum surface coverage are listed in Table 2. In both solvents the fraction of train segments decreased and that of long loop segments increased with a decrease in the silanol densities of the surface. On the three kinds of silica surfaces in benzene, the fraction of train segments is smaller and the fraction of long loop segments is larger than those in carbon tetrachloride. The obtained results in both solvents (Table 2) indicate that when PMMA adsorbs onto Nipsil HD and Aerosil 300, the polymer would

Table 2. Segment Fractions of Adsorbed Polymer

Solvent	Adsorbent	Train	Short loop	Long loop
CCl_4	Nipsil HD	0.50	0.30	0.20
	Aerosil 300	0.47	0.28	0.25
	Aerosil R812	0.12	0.16	0.72
C_6H_6	Nipsil HD	0.48	0.28	0.24
	Aerosil 300	0.41	0.20	0.39
	Aerosil R812	0.11	0.09	0.80

Table 3. Fraction of Hydrogen Bond

Solvent	Adsorbent	A_{train} / $\times 10^{-4}$ g m^{-2}	A'_{train} / $\times 10^{-4}$ g m^{-2}	f_{HB}
CCl_4	Nipsil HD	8.5	7.7	0.91
	Aerosil 300	5.5	1.9	0.34
	Aerosil R812	6.8	—	—
C_6H_6	Nipsil HD	7.3	6.8	0.93
	Aerosil 300	3.6	1.5	0.40
	Aerosil R812	2.0	—	—

have flat conformations; however adsorption onto Aerosil R812 would have a loopy conformation.

The values of the segment fractions anchoring through the hydrogen bond in all train segments of the adsorbed polymer, f_{HB}, are listed in Table 3.

In the table A_{train}(g m^{-2}) indicates the weight of a train segment in terms of the amount of adsorption, and is given by

$$A_{train} = A_s \times p, \tag{2}$$

where A_s is the amount of saturated adsorption. A'_{train}(g m^{-2}) also indicates the weight of segment anchoring through the hydrogen bond in a train segment of a polymer, and is given by

$$A'_{train} = N_{SiOH} \times \theta_{IR} \times M, \tag{3}$$

where N_{SiOH} is the mumber of silanol per unit area and M is the molecular weight of the methyl methacrylate monomer. Consequently, f_{HB} is denoted A'_{train}/A_{train} and is used for the notation of the segment fraction anchoring through the hydrogen bond in all train segments of the adsorbed polymer. As can be seen from the table, when PMMA is adsorbed on Nipsil HD, the polymer adsorbs predominantly by the formation of hydrogen bonds; however, when PMMA is adsorbed on Aerosil 300, the polymer adsorbs through hydrogen bonds in a ratio of 30—40%. The value of f_{HB} of the PMMA adsorbed on Aerosil 300 is similar to the result of Sakai and Imamura,[9] who made a direct comparison of the ESR method with the IR method using an identical solution-solvent system (PMMA-carbon tetrachloride-silica).

When PMMA is adsorbed onto Nipsil HD, f_{HB} is nearly equal to 1. It is then expected that the values of

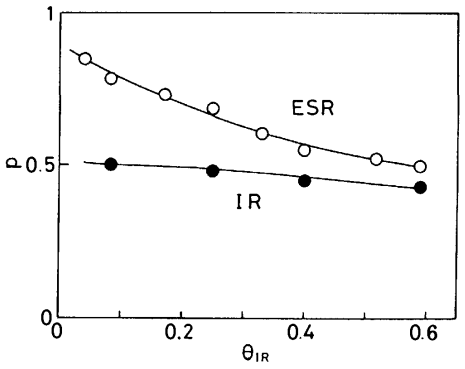

Fig. 5. Plots of the values of p_{ESR} and p_{IR} against the surface coverage, θ_{IR}, for PMMA adsorbed onto Nipsil HD. ○: p_{ESR}, ●: p_{IR}.

p_{ESR} and p_{IR}, obtained by ESR and IR methods, respectively, at the maximum surface coverage, θ_{IR}, are identical. The values of p_{ESR} and p_{IR} in the adsorption onto Nipsil HD, are plotted against the surface coverage, θ_{IR}, in Fig. 5. The values of p_{ESR} and p_{IR} decreased moderately with an increase in θ_{IR}. At a maximum surface coverage, θ_{IR}=0.58, the value of p_{ESR} is almost the same as p_{IR}. This fact is consistent with the result given in Table 3. At a relatively low θ_{IR}, some of the train segments in the polymer adsorb through the hydrogen bond; and the remaining train segments adsorb except for the hydrogen bond. At the maximum surface coverage, most of the train segments in the polymer adsorb through the hydrogen bonds.

When PMMA is adsorbed onto Aerosil 300, f_{HB} is 0.3—0.4; it is expected that the values of p_{ESR} are a much higher level than those of p_{IR}. The values of p_{ESR} and p_{IR} for the PMMA adsorbed onto Aerosil 300 are plotted against the surface coverage, θ_{IR}, in Fig. 6. The values of p_{ESR} and p_{IR} were moderately decreased

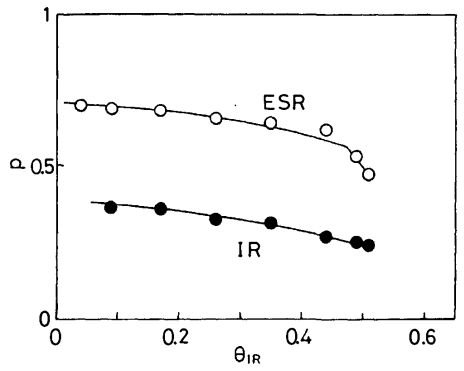

Fig. 6. Plots of the values of p_{ESR} and p_{IR} against the surface coverage, θ_{IR}, for PMMA adsorbed onto Aerosil 300. ○: p_{ESR}, ●: p_{IR}.

with an increase of θ_{IR}. At the maximum surface coverage, $\theta_{IR}=0.51$, the value of p_{ESR} was 0.47. It was twice as the value of p_{IR}, 0.24. This fact is consistent with the result given in Table 3. From the results of Figs. 5 and 6, when Nipsil HD, which has a relatively high level of silanol groups (8 per nm^2) was used as the adsorbent, the value of p_{ESR} was identical with the value of p_{IR}. When Aerosil 300, which has a lower content of the silanol group, 2.2 per nm^2, was used as the adsorbent, the results from the ESR method exhibit a much higher level than those of the IR method.

One possible explanation for the large differences in Figs. 5 and 6, is as follows: some of the train segments in the polymer interact with the silanol groups, while the remaining train segments interact with "non-hydroxylic sites"[11] on the silica surface. The IR method is used to evaluate only the train segments adsorbed through hydrogen bonds between carbonyl groups and silanol groups, whereas the ESR method is used to evaluate the train segments adsorbed through any mechanism. On Nipsil HD, train segments in the adsorbed polymer mainly adsorbed by the formation of hydrogen bonds between carbonyl groups of methyl methacrylate and silanol groups of the surface site; thus, the results obtained from the ESR and IR methods are identical. Since on Aerosil 300, train segments in the adsorbed polymer are anchored with or without hydrogen bonds, the results obtained from the ESR method exhibited a much higher level than those of the IR method.

References

1) B. J. Fontana and J. R. Thomas, *J. Phys. Chem.*, **65**, 480 (1961).
2) M. Kawaguchi, K. Maeda, T. Kato, and A. Takahashi, *Macromolecules*, **17**, 1666 (1984).
3) T. Miyamoto and H. J. Cantow, *Makromol. Chem.*, **43**, 162 (1972).
4) K. G. Barnett, T. Cosgrove, B. Vincent, D. S. Sissons, and M. Cohen-Stuart, *Macromolecules*, **14**, 1018 (1981).
5) T. Cosgrove and K. G. Barnett, *J. Magn. Reson.*, **43**, 15 (1981).
6) I. D. Robb and R. Smith, *Polymer*, **18**, 500 (1977).
7) H. Sakai, T. Fujimori, and Y. Imamura, *Bull. Chem. Soc. Jpn.*, **53**, 3457 (1980).
8) H. Sakai and Y. Imamura, *Bull. Chem. Soc. Jpn.*, **60**, 1261 (1987).
9) H. Sakai and Y. Imamura, *Bull. Chem. Soc. Jpn.*, **53**, 1749 (1980).
10) K. Kalnin'sh, A. N. Krasovskii, B. G. Belen'kii, and G. A. Andreyeva, *Vysokomol. Soedin., Ser. A*, **18**, 2304 (1976).
11) A. N. Sidrov, *Opt. Spektrosk.*, **8**, 806 (1960).

 © 1989 The Chemical Society of Japan Bull. Chem. Soc. Jpn., 62, 3426—3432 (1989) [Vol. 62, No. 11

Thermodynamic Properties of Solution of Nonspherical Molecules Determined from Gas-Liquid Chromatography and Calculated by the Scaled Particle Theory Using the Kihara Potential[1)]

Hideaki FUJIWARA,* Ikuji OHTAKU, Rieko MIYAGI, and Yoshio SASAKI
Faculty of Pharmaceutical Sciences, Osaka University, 1-6 Yamadaoka, Suita, Osaka 565
(Received May 6, 1989)

The free energies, enthalpies, and entropies of solution have been determined for nonspherical molecules by gas-liquid chromatography and the data are discussed on the basis of a simple theory of solution, the scaled particle treatment. The solutes used are normal alkanes from pentane to decane and the solvents used are 10,11-dihydro-5*H*-dibenzo[*a*,*d*]cyclohepten-5-one (DDCO), 9-heptadecanone (HPDN), and squalane. Some basic equations are derived for the nonspherical molecules by regarding the alkane solutes, HPDN and squalane as spherocylinders and DDCO as a disk and by incorporating the Kihara potential in estimating the nonspherical interactions. The enthalpies and entropies observed can be reproduced fairly well by assigning appropriate values of the sizes and potential constants for the solutes as well as for the solvents. However, these two properties tend to cancel each other in yielding the free energies, and the free energies are not reproduced so well as the enthalpies and entropies separately are. The presence of long alkyl chains in HPDN and squalane needs be allowed for better prediction of the entropies and, especially, the free energies. The present method of calculation is also applied to a spherical solute of tetramethyltin in the solvents of HPDN and DDCO with reasonable results. In this way, a relatively simple treatment of the scaled particle theory and the Kihara potential is shown to be fruitful in discussing the thermodynamic properties of solution for nonspherical molecules.

Thermodynamic properties of solution such as the changes in free energy, enthalpy, and entropy accompanying dissolution of a solute from gas phase to liquid phase are key parameters in the studies of partition coefficients and solubilities.[2)] In dealing with these properties, the scaled particle theory has disclosed an important role of cavity formation when transferring a solute from gas to liquid.[3)] Pierotti has shown successful calculations of the solubility properties of gases by applying the scaled particle theory to obtain the cavity term and by combining the Lennard-Jones potential to obtain the solute-solvent interaction terms.[3a)] A merit of the scaled particle treatment is its simplicity with moderate fitness to the experimental results. However, Abraham and Nasehzadeh[4)] reported that a version of the scaled particle treatment yields reasonable values of the free energy of solution ΔG_s^0 for nonpolar solutes in nonaqueous solvents but not for those in water, and that it yields also reasonable values of the entropy of solution ΔS_s^0 for nonpolar solutes in water but not for those in nonaqueous solvents. Hitherto, the scaled particle theory has been developed and applied almost always by assuming both solute and solvent as spheres. The effects of nonspherical shape have also been discussed and found nontrivial by several investigators with regard to the virial coefficients, the excess volumes, the Gibbs free energies and the equations of state.[5a-c)] The scaled particle treatment is also utilized in the perturbation study of solubilities of some simple gases.[5d)]

Recently, the authors have reported that the entropies of solution of several alkanes in nonaqueous solvents measured by the gas-liquid chromatography are interpreted by the scaled particle theory extended to nonspherical molecules.[6)] In the present study we further extend such a treatment to include the enthalpy of solution by using the Kihara potential in estimating the interaction term, and thermodynamic properties of solution are examined with regard to the free energies, enthalpies, and entropies.

Experimental

Gas-Liquid Chromatogaphic Experiments. The gas-liquid chromatographic measurements were made on a Yanagimoto G-1880 gas chromatograph with a TCD cell. A Pyrex glass column with i.d. 3.4 mm and length 2 m was used after a treatment with dichlorodimethylsilane. The solutes used were normal alkanes from pentane to decane. The stationary phases used were 10,11-dihydro-5*H*-dibenzo-[*a*,*d*]cyclohepten-5-one (DDCO), 9-heptadecanone (HPDN), and squalane (2,6,10,15,19,23-hexamethyltetracosane) which were coated on 60/80 mesh Chromosorb W DMCS to an amount of 25 wt%. The column temperature was set at five temperatures between 50 °C and 90 °C for the two solvents, DDCO and HPDN, and between 66 °C and 140 °C for squalane, and monitored with a copper-constantan thermocouple. The retention time was measured 5 times at each temperature and averaged. Such measurements were repeated 3 times for the solvent DDCO and 2 times for that HPDN. The solvent coated lost its quantity slightly during the measurement of retention time. This weight loss was less than 1% and was taken into account in the data treatment.

Materials. The solvents HPDN and DDCO from commercial sources were distilled under reduced pressure. The coating was achieved by using distilled dichloromethane as a diluent. The solutes, normal alkanes from pentane to decane, tetramethyltin, and squalane, all from commercial sources, were used without further purification.

Results

The enthalpies, entropies and free energies of solution were measured by gas-liquid chromatography, which is reported to produce reliable values[7] comparable to a calorimetric method.[8] The solvents DDCO, squalane and HPDN were selected as stationary phases suitable for the GLC measurements. The standard states are selected as 1 atm in gas phase and 1 mole fraction in liquid phase, and so the relationships used for the determination of the thermodynamic properties are:[7,9]

$$V_g^0 = [(t_r - t_a)jF/w](273.15/T) \quad (1)$$

$$K = (W_M/273.15R)V_g^0 \quad (2)$$

$$\ln K = -\Delta H_s^0/RT + \Delta S_s^0/R. \quad (3)$$

In these equations, the meanings of symbols are: V_g^0= specific retention volume, K=partition coefficient, t_r=retention time of sample, t_a=retention time of a reference (air), j=correction factor for the pressure, F=flow rate of the carrier gas (He), w=weight of solvent in the column, T=absolute temperature, W_M=molecular weight of solvent, and R=the gas constant. From the measurement of retention times, V_g^0 is obtained (Eq. 1), which is converted to K through Eq. 2. And then, the plots of ln K vs. $1/T$ afford the values of ΔH_s^0 and ΔS_s^0 (Eq. 3). The plots of ln K vs. $1/T$ are linear successfully as indicated by the correlation coefficients larger than 0.999. The observed thermodynamic properties of solution are listed

Table 1. Thermodynamic Properties of Solution for the Alkanes Dissolved in DDCO[a]

Solute	Experimental			Calculated			
	ΔG_s^0	$-\Delta H_s^0$	$-T\Delta S_s^0$	ΔG_s^0	$-\Delta H_s^0$	$-T\Delta S_s^0$	$G_{int}=H_{int}$
Pentane	4.5±3.3	24.5±1.9	29.0±1.4	0.3	27.2	27.5	−50.1
Hexane	1.6±1.5	28.5±0.9	30.1±0.6	−1.1	30.1	29.0	−56.3
Heptane	−1.4±1.8	32.4±1.1	31.0±0.7	−2.6	33.0	30.4	−62.5
Octane	−6.9±1.0	38.3±0.6	31.4±0.4	−3.8	35.7	31.9	−68.5
Nonane	−8.1±0.6	40.5±0.2	32.4±0.4	−5.3	38.6	33.3	−74.7
Decane	−8.9±0.4	42.3±0.2	33.4±0.2	−6.6	41.4	34.8	−80.9

a) All values are given in the unit of kJ mol^{-1} and at 298.15 K.

Table 2. Thermodynamic Properties of Solution for the Alkanes Dissolved in HPDN[a]

Solute	Experimental			Calculated			
	ΔG_s^0	$-\Delta H_s^0$	$-T\Delta S_s^0$	$\Delta G_s^{0b)}$	$-\Delta H_s^0$	$-T\Delta S_s^{0c)}$	$G_{int}=H_{int}$
Pentane	0.3±0.7	23.8±0.4	24.1±0.3	−7.3(−2.0)	27.7	20.4(25.7)	−42.0
Hexane	−2.8±0.9	29.4±0.4	26.6±0.5	−9.4(−3.9)	30.6	21.2(26.7)	−47.0
Heptane	−5.7±1.1	33.0±0.6	27.3±0.5	−11.5(−5.8)	33.5	22.0(27.7)	−52.0
Octane	−8.4±0.6	37.2±0.3	28.8±0.3	−13.3(−7.4)	36.1	22.8(28.7)	−56.7
Nonane	−11.2±1.5	41.4±0.8	30.2±0.7	−15.4(−9.3)	39.0	23.6(29.7)	−61.7
Decane	−14.0±0.4	46.2±0.2	32.2±0.2	−17.4(−11.1)	41.8	24.4(30.7)	−66.6

a) All values are given in the unit of kJ mol^{-1} and at 298.15 K. b) In parentheses listed are the free energies estimated according to an equation $\Delta G_s^0=\Delta H_s^0-T(1.26\Delta S_s^0)$ (see text). c) In parentheses listed are the entropies corrected (see text).

Table 3. Thermodynamic Properties of Solution of Alkanes Dissolved in Squalane[a]

Solute	Experimental			Calculated			
	ΔG_s^0	$-\Delta H_s^0$	$-T\Delta S_s^0$	$\Delta G_s^{0b)}$	$-\Delta H_s^0$	$-T\Delta S_s^{0c)}$	$G_{int}=H_{int}$
Pentane	−1.6±0.7	25.4±0.4	23.8±0.3	−11.5(−3.1)	28.6	17.1(25.5)	−38.5
Hexane	−4.7±0.7	31.5±0.4	26.8±0.3	−13.9(−5.3)	31.6	17.7(26.3)	−43.0
Heptane	−7.5±0.5	34.6±0.3	27.1±0.2	−16.4(−7.5)	34.6	18.2(27.1)	−47.5
Octane	−10.2±0.4	38.2±0.2	28.0±0.2	−18.5(−9.4)	37.3	18.8(27.9)	−51.8
Nonane	−12.8±0.5	41.8±0.3	29.0±0.2	−20.9(−11.4)	40.2	19.3(28.8)	−56.1
Decane	−15.5±0.7	45.7±0.4	30.2±0.3	−2.32(−13.5)	43.1	19.9(29.6)	−60.5

a) The units of ΔG_s^0, ΔH_s^0, and $T\Delta S_s^0$, are all in kJ mol^{-1}. ΔG_s^0 and $T\Delta S_s^0$ are calculated at 298.15 K. Molecular parameters of the solvent used are: a=1.88 Å, l=28.98 Å, and $U_{0,B}/k$=4285 K. When a and $U_{0,B}$ are changed as : a=2.08 Å and $U_{0,B}/k$=4744 K, the values of ΔH_s^0 change to −29.1, −31.9, −34.7, −37.2, −39.9, and −42.5 from pentane to decane, and those of $-T\Delta S_s^0$ change to 16.2, 16.7, 17.1, 17.5, 17.9, and 18.3 from pentane to decane, respectively. b) In parentheses listed are the values estimated from: $\Delta G_s^0=\Delta H_s^0-T(1.49\Delta S_s^0)$ (see text). c) In parentheses listed are the entropies corrected (see text).

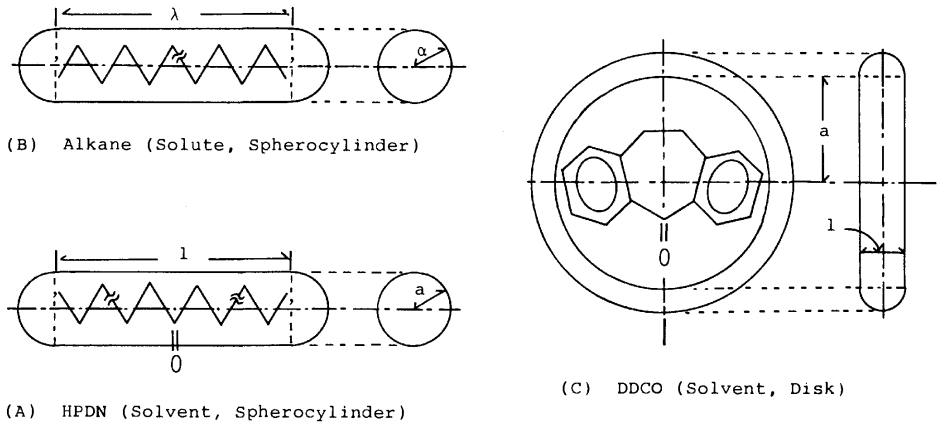

Fig. 1. The nonspherical models of the solute and solvent. The designation of a and l in DDCO needs be corrected as above in the Figure of Ref. 6a.

in Tables 1 to 3. All of these values change linearly with the number of carbons in the alkane solutes. Experimental values of ΔH_s^0 and $T\Delta S_s^0$ are both negative and their absolute values increases with the number of carbons in normal alkanes, and hence they are in a compensation relation. ΔG_s^0 decreases with the carbon number, indicating a relative importance of the enthalpy term.

Discussion

The entropy of solution ΔS_s^0 of nonspherical molecules can be better interpreted by a scaled particle treatment with reasonable molecular sizes when and only when nonspherical shapes are taken into account in the calculation, as already reported in the preliminary report.[6] However, when such a treatment is applied to obtain the cavity term of the enthalpy of solution, positive values are obtained, indicating a necessity of a solute-solvent interaction term to make the enthalpies negative. The authors adopted here the Kihara potential[10] to estimate the interaction term for nonspherical molecules, and derived equations of the thermodynamic properties of solution for spherocylinder and disk shaped molecules (see Appendix).

The solvents HPDN and squalane and the solutes alkanes are approximated as spherocylinders, and the solvent DDCO is approximated as a disk (Fig. 1). The entropy of solution is interpreted reasonably by such models of solute and solvent as discussed in the preliminary report.[6] To calculate the enthalpy of solution ΔH_s^0, the potential constants and the molecular sizes are needed for the normal alkanes as well as for the solvents. The molecular sizes have been determined so as to reproduce the entropy of solution ΔS_s^0 (Table 1 in Ref. 6a) with reasonable precision, and the potential constants are available for several normal alkanes[10a,11] from the data of virial coefficients. The potential constants for nonane and decane are currently unavailable but can be obtained by the extraporation of the data for other normal alkanes. The potential constants of the two solvents are determined by a trial and error method so that they minimize the square sum of the difference between the observed and calculated enthalpies of solution (Fig. 2). Standard deviations between the experimental and recalculated enthalpies are relatively small, supporting a usefulness of the simple model used here. Thermodynamic properties of solution obtained in the experiment and in the calculation are summarized in Tables 1 to 3 for the DDCO, HPDN, and squalane solvents, respective-

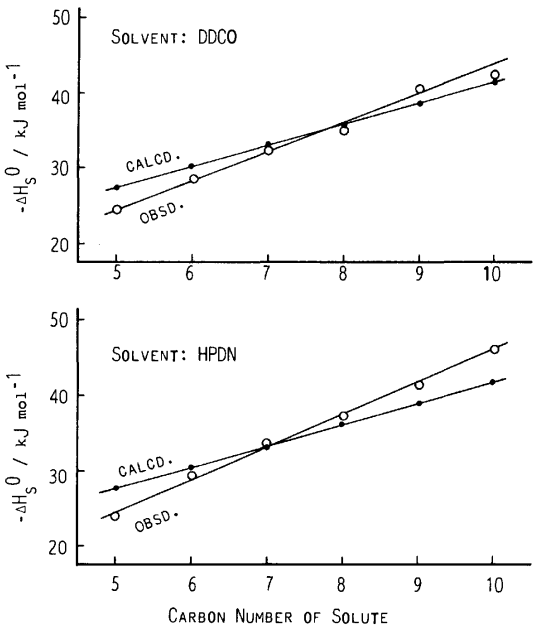

Fig. 2. Comparison of the enthalpies calculated and observed for the normal alkanes in HPDN (lower plots) and DDCO (upper plots). Potential constants of the solvents are $U_{0,B}/k$=3669 K (HPDN) and $U_{0,B}/k$=4080 K (DDCO).

Table 4. Thermodynamic Properties of Solution of Tetramethyltin Dissolved in the Solvents of DDCO and HPDN[a]

Solvent	Experimental			Calculated				
	ΔG_s^0	$-\Delta H_s^0$	$-T\Delta S_s^0$	$\Delta G_s^{0b)}$	$-\Delta H_s^0$	$-T\Delta S_s^{0c)}$	α	$U_{0,B}/k$
DDCO	1.1±0.1	28.1±0.1	29.2±0.14	10.5	17.8	28.3	3.07 Å	400 K
				0.2	28.1	28.3	3.07 Å	495 K
				10.4	18.6	29.0	3.18 Å	400 K
				0.9	28.1	29.0	3.18 Å	482 K
HPDN	−3.9±0.1	30.8±0.1	26.9±0.1	0.02(5.4)	20.7	20.7(26.1)	3.07 Å	400 K
				−7.4(−2.0)	28.1	20.7(26.1)	3.07 Å	481 K
				0.5(5.0)	21.6	21.1(26.6)	3.18 Å	400 K
				−7.0(−1.5)	28.1	21.1(26.6)	3.18 Å	467 K

a) All values are given in the unit of kJ mol^{-1} and at 298.15 K. b, c) See footnotes b and c in Table 2. The same factor of 1.26 is used here.

ly. The enthalpies and entropies of solution calculated fit well with the experimental ones in DDCO (Table 1). However, these two parameters tend to cancel each other in yielding the free energy as already described in the Results section. The errors in estimating the free energies, therefore, become relatively large after such cancellation. Quite a similar trend is seen in the system of HPDN (Table 2). In this case deviations in the entropies are relatively large between the experiment and the calculation. This may be related to some extent to the presence of long alkyl chain. To investigate further an effect of long alkyl chain, squalane is tested as a stationary phase (Table 3). Squalane molecule is regarded to be in a stretched zigzag conformation and approximated by a spherocylinder, for which the length l is estimated to be 28.98 Å, i.e., 23×1.26 Å, and the radius a is set equal to 1.88 Å (the compactness factor y=0.38). This radius is tested with a little larger values, considering several methyl group branches from the normal alkane chain. A relatively good fit is obtained when a is smaller than 2.08 Å (Table 3). The calculated values of ΔS_s^0 become smaller by ca. 7% and larger by ca. 40% when a is changed from 2.08 Å (y=0.46) to 1.88 Å (y=0.38) and 2.28 Å (y=0.56), respectively. Therefore, the entropies of solution observed for the normal alkanes in squalane are said to be reproduced by the calculation to an extent of about 65—70%. This percentage certainly drops from the value of 80% observed in the HPDN solvent having a shorter length of chain. That is, the reproducibility of the entropy of solution decreases much more by the presence of longer alkyl chain in the solvent molecule. This is probably because the flexibility of the long alkyl chain is not taken into account in the present model. An improvement of the model by incorporating this molecular flexibility is not a simple task. But when the correction is assumed to be proportional to the entropies calculated by neglecting the flexibility, the correction factor is determinable so that the corrected entropies fit better with the experimental ones for all of the alkane solutes treated here. Such corrections are included in Tables 2 and 3 (see footnotes b and c). The enthalpies observed in squalane are best fitted by setting $U_{0,B}/k$=4744 K (S.D.=2.4 kJ mol^{-1}) and $U_{0,B}/k$=4285 K (S.D.=2.0 kJ mol^{-1}) when a is set to 2.08 Å and 1.88 Å, respectively. These values of U_0 are higher than that for octane (1150) reflecting the increased molar volume.

To investigate further the applicability of our model, tetramethyltin is tested as a sphere solute (Table 4). The GLC experiment was done once and the errors were estimated from the linear plot of ln K vs. $1/T$. The spherical molecule of tetramethyltin can be included in a spherocylindrical model with vanishing length (λ=0). Note that we have assumed a line with a definite length for the core of spherocylinder, and hence the Kihara function becomes equivalent to the Lennard-Jones one in case of spheres.[12] The standard values of the molecular radius and the potential constant are known to be σ (diameter)=6.13 Å and ε/k=400 K.[4] Several model calculations are compared with the experimental results in Table 4. In the DDCO system ΔH_s^0 and ΔS_s^0 are reproduced best by a calculation using the parameters for DDCO above obtained and the values of α=3.18 Å and $U_{0,B}/k$=482 K for tetramethyltin. The latter value is slightly larger than the average of reported values, 400 K.[4] However, the potential constant reported is relatively large in nonpolar solvents,[13] and hence the value reached in the present study may be accepted as reasonable. In the HPDN system about 80% of ΔS_s^0 is reproduced by the calculation (Table 4). This percentage is the same with that observed[6] for the normal alkane solutes in the same solvent. ΔH_s^0 is seen to be reproduced well by the potential constant quite similar to the above DDCO system.

Conclusion

The main purpose of this study is to examine if thermodynamic properties of solution determined by the GLC method, which has been accepted to yield reliable values of these properties, are reproduced well

by relatively simple modifications of the scaled particle theory and the Kihara potential when nonspherical shapes of molecules are taken into account. The entropies of solution observed are explained almost fully by the cavity term derived from the scaled particle theory, indicating negligible contribution from the interaction term. In the HPDN solvent, however, a flexibility in its long alkyl chain seems to affect the entropies, and some correction factor is necessary for the improved reproducibility of the entropies and free energies of solution.

The enthalpies of solution observed are well reproduced by the calculation when reasonable values are assigned to the potential constants of the solvents. The calculation indicates that the interaction term is dominant for the enthalpies, whereas the cavity term contributes positively (unstably) to the total energy. For the precise estimation of the free energies of solution, much precise estimation of the enthalpy and entropy terms is needed since these two parameters tend to cancel each other in yielding the free energy.

In conclusion, the scaled particle theory is evidenced to be applicable in calculating the thermodynamic properties of solution for nonspherical molecules when nonspherical shapes are taken into account and nonspherical interactions are included through the Kihara potential in the calculation.

Appendix

Equations of the Thermodynamic Properties of Solution for Nonspherical Molecules Derived Basing on the Scaled Particle Theory Incorporated with the Kihara Potential. The free energy of solution ΔG_s^0 is divided into three terms of a cavity formation, solute-solvent interactions, and a correction for the standard states in gas and liquid phases:[3b]

$$\Delta G_s^0 = G_{cav} + G_{int} + RT \ln (RT/V_1) \quad (4)$$

where V_1 means the solvent molar volume and the gas constant R is expressed as 0.08206 atm·l(K·mol)$^{-1}$. Similarly, the enthalpy ΔH_s^0 and entropy ΔS_s^0 of solution are divided as follows:[3,4]

$$\Delta H_s^0 = H_{cav} + H_{int} + \alpha_p RT^2 - RT \quad (5)$$

$$\Delta S_s^0 = S_{cav} + S_{int} + \alpha_p RT - R - R \ln (RT/V_1) \quad (6)$$

G_{cav} in Eq. 4 includes terms of PV work and surface energy. The PV work is expressed as $W=P<V_{A+B}>$, where V_{A+B} is the volume excluded by the center of molecule B surrounding a solute A and $<>$ means a statistical average for the relative orientation of the two molecules. A following equation is reached for $<V_{A+B}>$,[10] where S is the surface area and M is

$$<V_{A+B}> = V_A + V_B + (S_A M_B + S_B M_A)/4\pi \quad (7)$$

the measure which is defined as the mean curvature integrated over the whole surface of the convex molecule.[10] The three fundamental values V, S, and M are derived for a few convex bodies and listed in Table 5. On the other hand, the surface energy is expressed by a differential equation $dW=\gamma dS$, where γ is the surface tension. Here the surface tension is considered to be dependent on the curvature of a surface,

$$\gamma/\gamma_0 = 1 - 2\delta_0 C = 1 - \delta_0(1/R_1 + 1/R_2) \quad (8)$$

where γ_0 is the surface tension for a flat plane and δ_0 the distance corresponding to the plane interface, and where C is the curvature which is equal to $1/R_1+1/R_2$, R_1, and R_2 being the principal radii of curvature.[14]

The free energy term of solute-solvent interactions is obtained as follows. To take into account nonspherical shape of molecules we adopted the Kihara potential[10] for intermolecular interactions.[15] The Kihara potential assumes a core in each molecule and energy of interaction is expressed as a function of the closest distance ρ between the cores of the two interacting molecules:

$$U(\sigma) = U_0[(\sigma_0/\sigma)^{12} - 2(\sigma_0/\sigma)^6] \quad (9)$$

Here, σ_0 and $-U_0$ are the closest core distance and energy, respectively, under the most stable interaction. In the present study we assume for simplicity that a core possesses a vanishing thickness and a molecule is made up of a surface located at a constant distance ρ_0 from the core (Fig. 3). Equation 9 is also adopted here for the potential, where $\sigma_0=\rho_{0,A}+\rho_{0,B}$, $\sigma=\sigma_0+\rho$, and $U_0=(U_{0,A}\cdot U_{0,B})^{1/2}$ are assumed between the interacting molecules of A and B. Therefore, the most stable interaction is reached when surfaces of the two molecules come into contact ($\rho=0$), ρ being the closest distance between the surfaces of the two molecules (Fig. 3). The interaction energy E_{int} is approximated to be equal to the free energy of interaction and is expressed as follows:

Table 5. The Three Fundamental Measures V, S, and M of Convex Bodies

	Sphere	Spherocylinder	Disk
V	$4\pi\alpha^3/3$	$\pi(4\alpha^3/3+\alpha^2\lambda)$	$\pi(\alpha^2\lambda+\alpha\lambda^2/4+\lambda^3/6)$
S	$4\pi\alpha^2$	$2\pi(2\alpha^2+\alpha\lambda)$	$\pi(2\alpha^2+\pi\alpha\lambda+\lambda^2)$
M	$4\pi\alpha$	$\pi(4\alpha+\lambda)$	$\pi(\pi\alpha+2\lambda)$

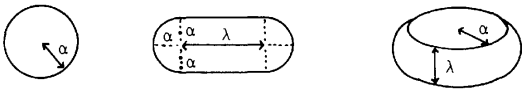

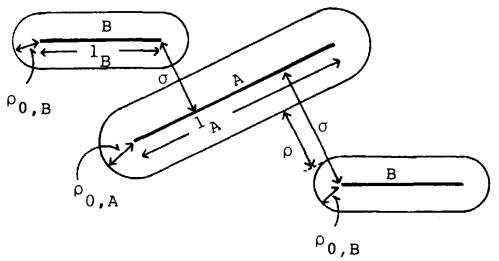

Fig. 3. A model for the Kihara potential of the interacting spherocylindrical molecules of solute (A) and solvent (B). —: Core of the molecule. See text for further details.

$$G_{inl} \simeq E_{int} = <N\int_{vol} U(\sigma)\cdot dg\cdot d\tau> \quad (10)$$

where N means the Avogadro Number, dg is the number density d multiplied by the radial distribution function g, and $d\tau$ is the volume element equal to $S_{A+B+\rho}\cdot d\rho$, $S_{A+B+\rho}$ being the surface area when solute A is surrounded by solvent B separated by a distance of ρ. The symbol "vol" means the integration over the whole system, but the region with positive interaction energies is excluded in practice.[3b] When $g=1$ is assumed over the region of integration, Eq. 10 turns out to be Eq. 11 since ρ is independent of the mutual orientation of the two interacting molecules.

$$G_{int} \simeq E_{int} = Nd\int_{vol} U(\sigma)<S_{A+B+\rho}>d\rho \quad (11)$$

The statistically averaged surface area $<S_{A+B+\rho}>$ is substituted as follows by using Eq. 7 for $<V_{A+B+\rho}>$:

$$\begin{aligned}<S_{A+B+\rho}> &= d<V_{A+B+\rho}>/d\rho \\ &= S_A + S_B + M_A M_B/2\pi + 2(M_A+M_B)\rho + 4\pi\rho^2. \quad (12)\end{aligned}$$

When dg is independent of temperature, $G_{int}=H_{int}$ and $S_{int}=0$ hold, and hence,

$$\begin{aligned}G_{inl} = H_{inl} &= Nd\int_{2^{-1/6}-1}^{\infty} U_0[\{\sigma_0/(\sigma_0+\rho)\}^{12} - 2\{\sigma_0/(\sigma_0+\rho)\}^6]\cdot \\ &\quad \{S_A + S_B + M_A M_B/2\pi + 2(M_A+M_B)\rho + 4\pi\rho^2\}d\rho \\ &= -NdU_0[17(\rho_{0,A}+\rho_{0,B})\{S_A + S_B + M_A M_B/2\pi\}/55 + \\ &\quad 2(\rho_{0,A}+\rho_{0,B})^2(M_A+M_B)/11 + 128\pi(\rho_{0,A}+\rho_{0,B})^3/495 \quad (13)\end{aligned}$$

As described above, ΔG_s^0, ΔH_s^0, and ΔS_s^0 are calculated when molecular shapes and sizes of solute (A) and solvent (B) are known as well as the potential constants $U_{0,A}$ and $U_{0,B}$ and the surface tension of solvent γ_0. Usually the surface tension appears only implicitly in the scaled particle treatment. That is, the form of G_{cav} is determined by considering its dependency on the size parameters of solute.[3a,5c] This process follows to that reported for a spherocylindrical solute in a spherocylindrical solvent.[5c] Equations of the thermodynamic properties related to the cavity formation are listed below which are reached in the present study for a few systems of nonspherical solute in nonspherical solvent. A more advanced theory of solutions, Percus-Yevick theory, predicts that a correction term is necessary in the intuitive Pierotti's expressions when intermolecular interactions are taken into account.[16-18] Such a correction term is now studied to apply to the nonspherical cases together with the terms of induced and dipolar interactions.

i) Spherocylindrical solute in spherocylindrical solvent:

$$\begin{aligned}G_{cav} &= RT\{-\ln(1-y) + \pi d(2a^2+al)(2\alpha+\lambda/2)/(1-y) + \\ &\quad \pi d(4a+l)(\alpha^2+\alpha\lambda/2)/(1-y) + [\pi d(2a^2+al)/ \\ &\quad (1-y)]^2(2\alpha^2+\alpha\lambda)\} + NP\pi(\alpha^2\lambda + 4\alpha^3/3)\end{aligned}$$

$$\begin{aligned}H_{cav} &= \{y + \pi d(2a^2+al)(2\alpha+\lambda/2)/(1-y) + \pi d(4a+l)\cdot \\ &\quad (\alpha^2+\alpha\lambda/2)/(1-y) + [\pi d(2a^2+al)/(1-y)]^2\cdot \\ &\quad (\alpha^2+\alpha\lambda/2)\}\alpha_p RT^2/(1-y) + NP\pi(\alpha^2\lambda + 4\alpha^3/3)\end{aligned}$$

$$\begin{aligned}S_{cav} &= R\{\ln(1-y) + y\alpha_p T/(1-y) + \pi d(2a^2+al)(2\alpha+\lambda/2)\cdot \\ &\quad [\alpha_p T/(1-y) - 1]/(1-y) + \pi d(4a+l)(\alpha^2+\alpha\lambda/2)\cdot \\ &\quad [\alpha_p T/(1-y) - 1]/(1-y) + [\pi d(2a^2+al)/(1-y)]^2\cdot \\ &\quad (2\alpha^2+\alpha\lambda)[2\alpha_p T/(1-y) - 1]\} \\ &\quad y = \pi a^2(4a/3 + l)d\end{aligned}$$

ii) Spherocylindrical solute in disk-like solvent:

$$\begin{aligned}G_{cav} &= RT\{-\ln(1-y) + \pi d(2a^2+\pi al+l^2)(\alpha+\lambda/4)/(1-y) \\ &\quad + \pi d(\pi a + 2l)(\alpha^2+\alpha\lambda/2)/(1-y) + [\pi d(2a^2+\pi al \\ &\quad + l^2)/(1-y)]^2(\alpha^2/2 + \alpha\lambda/4)\} + NP\pi(\alpha^2\lambda + 4\alpha^3/3)\end{aligned}$$

$$\begin{aligned}H_{cav} &= \{y + \pi d(2a^2+\pi al+l^2)(\alpha+\lambda/4)/(1-y) + \pi d(\pi a \\ &\quad + 2l)(\alpha^2+\alpha\lambda/2)/(1-y) + [\pi d(2a^2+\pi al+l^2)/ \\ &\quad (1-y)]^2(\alpha^2+\alpha\lambda/2)\}\alpha_p RT^2/(1-y) + \\ &\quad NP\pi(\alpha^2\lambda + 4\alpha^3/3)\end{aligned}$$

$$\begin{aligned}S_{cav} &= R\{\ln(1-y) + y\alpha_p T/(1-y) + \pi d(2a^2+\pi al+l^2)\cdot \\ &\quad (\alpha+\lambda/4)[\alpha_p T/(1-y) - 1]/(1-y) + \pi d(\pi a + 2l)\cdot \\ &\quad (\alpha^2+\alpha\lambda/2)[\alpha_p T/(1-y) - 1]/(1-y) + [\pi d(2a^2 + \\ &\quad \pi al + l^2)/(1-y)]^2(\alpha^2/2 + \alpha\lambda/4)[2\alpha_p T/(1-y) - 1]\} \\ &\quad y = \pi(a^2 l + \pi al^2/4 + l^3/6)d\end{aligned}$$

iii) Disk-like solute in disk-like solvent:

$$\begin{aligned}G_{cav} &= RT\{-\ln(1-y) + \pi d(2a^2+\pi al+l^2)(\pi\alpha/4+\lambda/2)/ \\ &\quad (1-y) + \pi d(\pi a + 2l)(\alpha^2/2 + \pi\alpha\lambda/4 + \lambda^2/4)/(1-y) \\ &\quad + [\pi d(a^2 + \pi al/2 + l^2/2)/(1-y)]^2(\pi^2\alpha^2/8 + \pi\alpha\lambda/2 \\ &\quad + \lambda^2/2)\} + NP\pi(\alpha^2\lambda + \alpha\lambda^2/4 + \lambda^3/6)\end{aligned}$$

$$\begin{aligned}H_{cav} &= \{y + \pi d(2a^2+\pi al+l^2)(\pi\alpha/4+\lambda/2)/(1-y) + \pi d(\pi a \\ &\quad + 2l)(\alpha^2/2 + \pi\alpha\lambda/4 + \lambda^2/4)/(1-y) + [\pi d(a^2 + \pi al/2 \\ &\quad + l^2/2)/(1-y)]^2(\pi^2\alpha^2/4 + \pi\alpha\lambda + \lambda^2)\}\alpha_p RT^2/(1-y) \\ &\quad + NP\pi(\alpha^2\lambda + \alpha\lambda^2/4 + \lambda^3/6)\end{aligned}$$

$$\begin{aligned}S_{cav} &= R\{\ln(1-y) + y\alpha_p T/(1-y) + \pi d(a^2 + \pi al/2 + l^2/2)\cdot \\ &\quad (\pi\alpha/2+\lambda)[\alpha_p T/(1-y) - 1]/(1-y) + \pi d(\pi a/2 + l)\cdot \\ &\quad (\alpha^2 + \pi\alpha\lambda/2 + \lambda^2/2)[\alpha_p T/(1-y) - 1]/(1-y) + \\ &\quad [\pi d(a^2 + \pi al/2 + l^2/2)/(1-y)]^2(\pi^2\alpha^2/8 + \pi\alpha\lambda/ \\ &\quad 2 + \lambda^2/2)[2\alpha_p T/(1-y) - 1]\} \\ &\quad y = \pi(a^2 l + \pi al^2/4 + l^3/6)d\end{aligned}$$

References

1) Part 2 in the series "Experimental and Theoretical Studies on the Solubility Properties." For part 1 see Ref. 6a.

2) M. J. Kamlet, R. M. Doherty, M. H. Abraham, Y. Marcus, and R. W. Taft, *J. Am. Chem. Soc.*, **92**, 5244 (1988) and references cited therein.

3) a) H. Reiss, *Adv. Chem. Phys.*, **9**, 1 (1966). b) R. A. Pierotti, *Chem. Rev.*, **76**, 717 (1976).

4) M. H. Abraham and A. Nasehzadeh, *J. Chem. Soc., Faraday Trans. 1*, **77**, 321 (1981).

5) a) R. M. Gibbons, *Mol. Phys.*, **17**, 81 (1969) and **18**, 809 (1969). b) K. M. Timling, *J. Chem. Phys.*, **61**, 465 (1974). c) M. A. Cotter and D. E. Martire, *J. Chem. Phys.*, **52**, 1902 and 1909 (1970), and **53**, 4500 (1970) and references cited in these reports. d) T. Boublik and B. C.-Y. Lu, *J. Phys. Chem.*, **82**, 2801 (1978).

6) a) H. Fujiwara, R. Miyagi, I. Ohtaku, and Y. Sasaki, *Chem. Lett.*, **1988**, 1389. b) H. Fujiwara, I. Ohtaku, T. Takagi, S. Murata, and Y. Sasaki, *Bull. Chem. Soc. Jpn.*, **61**, 1853 (1988).

7) E. F. Meyer, *J. Chem. Educ.*, **50**, 191 (1973).

8) E. F. Meyer and F. A. Baiocchi, *J. Chem. Thermodyn.*, **10**, 823 (1978).
9) "Saishin Gas-Chromatography," ed. by W. Funasaka and N. Ikegawa, Hirokawa, Tokyo (1965), Vol. 1, Chap. 2.
10) a) T. Kihara, "Bunshi-kan-ryoku," Iwanami, Tokyo (1976). b) T. Kihara, *Adv. Chem. Phys.*, **5**, 147 (1963).
11) J. F. Connoly and G. A. Kandalic, *J. Phys. Fluids*, **3**, 463 (1960).
12) Note that the Kihara potential constant U_0 is usually larger than the Lennard-Jones one ε for the same molecule.
13) C. L. De Ligny and N. G. Van der Veen, *Recl. Trav. Chim. Pays-Bas*, **90**, 984 (1971).
14) F. P. Buff, *J. Chem. Phys.*, **19**, 1591 (1951) and **23**, 419 (1955).
15) The Kihara potential resembles to the Lennard-Jones one, but the latter is designed only for shpheres.
16) R. O. Neff and D. A. McQuarrie, *J. Phys. Chem.*, **77**, 413 (1973).
17) Y. Yoshimura and M. Nakahara, *Bull. Chem. Soc. Jpn.*, **61**, 1887 (1988).
18) The authors are grateful to a referee for pointing out this problem.

 © 1989 The Chemical Society of Japan Bull. Chem. Soc. Jpn., 62, 3433—3436 (1989)

Photodecomposition of Kraft Lignin Catalyzed by Titanium Dioxide

Koichi KOBAYAKAWA,* Yuichi SATO, Shigeo NAKAMURA, and Akira FUJISHIMA†
Department of Applied Chemistry, Faculty of Engineering, Kanagawa University,
Rokkakubashi, Kanagawa-ku, Yokohama 221
†Department of Synthetic Chemistry, Faculty of Engineering, The University of Tokyo,
Hongo, Bunkyo-ku, Tokyo 113
(Received May 11, 1989)

The photocatalytic reaction of kraft lignin at titanium dioxide photocatalyst was investigated. Kraft lignin was completely decomposed into carbon dioxide and water through dehydrodimers of phenol derivatives constituting kraft lignin, methanol and organic acids such as oxalic and formic acids. Aromatic compounds such as vanillin could not be recovered due to their tendency to dehydrodimerization and the strong oxidizing power of the photo-generated holes by the action of which the dehydrodimers were completely decomposed into carbon dioxide and water. The production of methane, ethane, and ethylene was much smaller than that in the decomposition with hydroxyl radicals in homogeneous solution.

The photo-generated holes at semiconductor powders suspended in solution generally have strong oxidizing power. For example, irradiated titanium dioxide can catalytically decompose substances, which cannot be completely decomposed by activated sludge processes, into inorganic substances like carbon dioxide and water entirely.[1-10]

Lignin and its degradation products cannot be completely decomposed by such sludge processes[11,12] and are the source of chemical oxygen demand (COD) of waste water from pulp and paper mills.[11] Even though the COD value of the discharged water is less than the value regulated by Japanese law,[11] the remaining lignin and its degradation products give an unfavorable impression of the discharged water owing to their brown color.[11] In case the activated sludge process is repeated, the brown color will become lighter. However, this process is expensive so that an inexpensive alternative method is desirable.

Strong oxidants were required for the decomposition of lignin and its degradation products.[12-14] It was reported that hydroxyl radicals produced by the reaction of hydrogen peroxide with UV light or ferric ions (Fenton's reagent) can decompose kraft lignin into carbon dioxide and hydrocarbon gases such as methane and ethane.[13] The decomposition by semiconductor photocatalysts is another possibility due to their strong oxidizing power of the generated holes. This paper describes the catalytic photodecomposition of kraft lignin on TiO_2 photocatalyst.

While kraft lignin can be decomposed into inorganic substances, formation of many useful intermediates such as vanillin and vanillic acid can be expected as are recovered in the electrochemical oxidation of lignin.[15-17] Therefore, in addition to the measurement of the COD value and the absorbance of the irradiated solution, we also identified and determined in detail possible intermediates.

Experimental

The aqueous test solution was 0.02 wt% in kraft lignin (alkali lignin derived from softwoods, Tokyo Kasei Kogyo). Rutile type TiO_2 powder (Furuuchi Chemical, 99.9%, 300 mesh) was used as photocatalyst. This powder showed comparatively high photocatalytic activity for the decomposition of kraft lignin among commercially available TiO_2 powders.[18]

For the examination of the changes of COD, the color of solution and the products in the solution, irradiation was carried out in open system, that is, 0.500 g of TiO_2 powder and 20 cm^3 of air-saturated test solution were placed in a 50 cm^3 beaker and stirred magnetically under the irradiation of a 500 W high-pressure mercury lamp. The solutions were cooled with ice to prevent evaporation of the products. After irradiation for a predetermined time, the photocatalyst was centrifugated off and the filtrate was analyzed. Absorption spectra were measured using a spectrophotometer, and the COD values were calculated according to the JIS K0102 method. The degradation products were identified and determined by high-performance liquid chromatography (HPLC), gas chromatography (GC) and chemical analysis. The experimental conditions of HPLC and GC were as follows. For HPLC, packing material was ODS-silica (Hitachi Kasei, 3056); the column was 4 mm I.D.×150 mm long; the eluent, aqueous acetonitrile solution (15 v/v%) of 0.05% phosphoric acid; the flow rate of eluent, 1.0 $cm^3\ min^{-1}$; the detector, UV (254 nm). For GC, the packing materials, PEG 20M (Shimarite F) and Unisole F-200; the column, 3.2 mm I.D.×2 m long (glass tube); the carrier gas, nitrogen; the detector, FID.

For the determination of the gaseous products irradiation was carried out in a closed system containing 70 cm^3 of the test solution and 1.5 g of TiO_2 powder under oxygen atmosphere. The gaseous products were identified and determined by a GC equipped with a column of active carbon packing and FID detector.

Results and Discussion

Changes of the Properties of the Test Solution with Reaction Time. The optical absorption spectrum of the test solution under nitrogen atmosphere did not change after irradiation for 8 h as shown by the curve b in Fig. 1. On the contrary, in the presence of dissolved oxygen, the brown color of the test solution became lighter with irradiation and disappeared after 8 h as

shown by the curves c and d in Fig. 1. From this result, oxygen was necessary to scavenge the photo-generated electrons. The curve a in Fig. 2 shows the change of the absorbance at 280 nm as a function of irradiation time. This absorption originated predominantly from benzenoid compounds. Therefore, the curve a shows that they decreases almost linearly with irradiation time and disappears after 7 h.

The COD value, shown as the curve b in Fig. 2, also decreases with reaction time. After 7 h of irradiation, COD becomes almost zero suggesting that organic compounds are no more present in the solution. The irradiation time dependence of pH is also given in Fig. 2 (curve c). The pH of the test solution, initially slightly basic, is lowered with the decomposition of kraft lignin. It reaches the lowest value after 4 h and then increases again to neutral. Carbonic acid was identified by the production of CO_2 upon addition of hydrochloric acid to the white precipitate, obtained by adding barium chloride to the filtrate. Oxalic acids was also identified by chemical analysis. The accumulation of oxalic acids, which is stronger than carbonic, will make the solution acidic and its perfect decomposition to carbonic acid will increase the pH of the test solution.

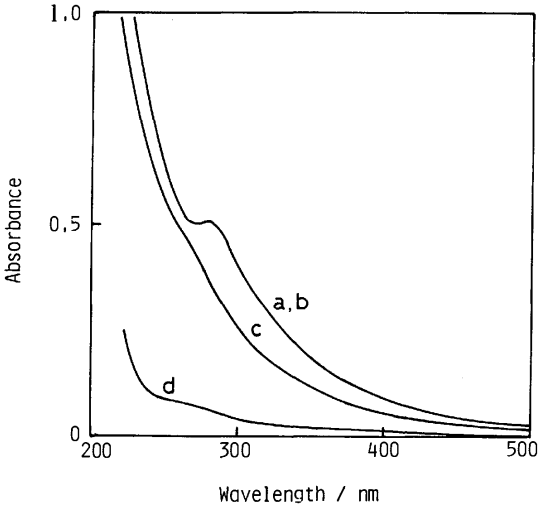

Fig. 1. Absorption spectra of the solution of kraft lignin. a: before irradiation (diluted 10 times, 20 ppm), b: after 8 h of irradiation under nitrogen atmosphere (diluted 10 times), c: after 6 h of irradiation, d: after 8 h of irradiation.

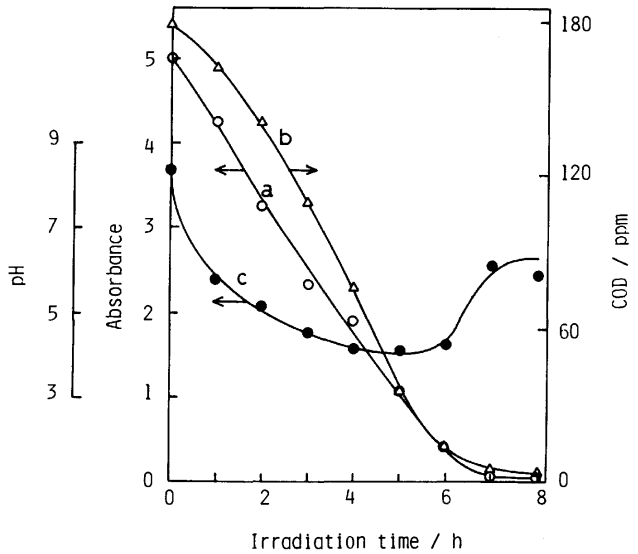

Fig. 2. Changes of the absorbance at 280 nm (a), COD (b), and pH (c) with irradiation time.

Products. Dehydrodimers: Prior to the determination of the degradation products, the separation performance of HPLC was confirmed. Under the conditions used, a number of phenol derivatives, which were expected as the degradation products from kraft lignin, were separated satisfactorily. Their retention times (t_R) were longer than two minutes. The larger the number of hydroxyl or carboxyl group in molecule, the shorter the retention time.

Figure 3 shows the HPLC chromatograms of the test solution before and after 3 h of photocatalytic reaction. Seven peaks are observed in the chromatogram of the starting solution (chromatogram a). Five peaks with retention times longer than 2 minutes were assigned to derivatives of phenol, such as catechol (t_R=4.0 min) and vanillin (t_R=6.7 min), by comparison with the retention time of the authentic compounds. As the degradation of kraft lignin proceeds, the heights of

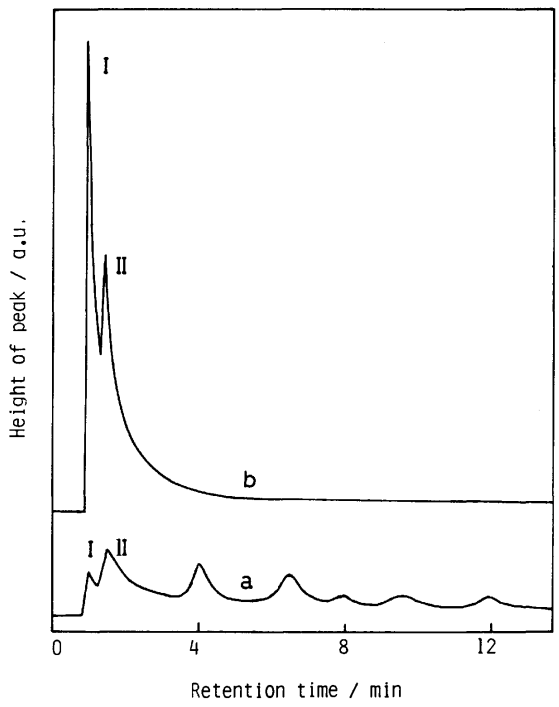

Fig. 3. HPLC chromatograms of the solution of kraft lignin. a: before irradiation, b: after 3 h of irradiation.

peaks longer than 2 minutes decrease, and after 3 h of irradiation they disappear as shown by the chromatogram b in Fig. 3. However, up to 4 h of irradiation two peaks denoted by I (t_R=1.0 min) and II (t_R=1.5 min) increased and then decreased with irradiation time as shown in Fig. 4. The substances corresponding to peaks I and II were thought to be dehydrodimers of the phenol derivatives constituting kraft lignin from following experimental results.

(i) Kraft lignin may be degraded by successive breaking from the terminal of the polymer, almost all of which are phenolic compounds. They are known to be dehydro-dimerized by electrochemical oxidation.[19-21] Therefore, the phenol derivatives liberated from lignin polymer may be also dimerized by the TiO_2 photocatalyzed oxidation.

For the lack of authentic smaples, dehydrodimers of some phenol derivatives were prepared by electrochemical oxidation and their retention times were measured. Protocatechuic acid (3,4-dihydroxybenzoic acid) gave two oxidation products, possibly dehydrodimers, which had the same retention times as peaks I and II. Vanillic acid (4-hydroxy-3-methoxybenzoic acid) gave one prodcut which had the same retention time as peak I and demethoxylated, hydroxylated vanillic acid, that is, protocatechuic acid. The difference in the number of the dehydrodimers produced from above two compounds is attributed the different structure of these compounds. That is, the dimerization of phenol derivatives takes place at the *o*- and *p*-positions to hydroxyl group,[19] so the formation of two types and one type of dimer was expected from protocatechuic and vanillic acid, respectively.

(ii) The t_R (1.5 min) of oxalic acid is identical with that of peak II. However, its peak height was only one half of that of peak II on the chromatogram a in Fig. 3, so that, oxalic acid was not the main product corresponding to peak II.

There is no peak which originates from kraft lignin itself in the chromatogram a in Fig. 3. Alkali lignin becomes insoluble in the acidic eluent, and the insoluble polymers cannot pass through the layer of packing material in the column. This is supported by the observation that a brown substance remained on the top of packing material.

In addition to the dehydrodimers of phenol derivatives, methanol, ethanol, formaldehyde, and oxalic acid were detected as intermediates in solution.

Methanol and Ethanol: The curve a in Fig. 5 shows the relation between the concentration of methanol and the irradiation time. Methanol is produced immediately after irradiation. Its concentration reaches a maximum value after one hour, remains at this value for 2 h and then decreases. Methanol may be formed from methoxy groups. This is confirmed by a catalytic photo-oxidation of vanillic acid and the identification of methanol in the reaction products.

The formation of ethanol was observed after 4 to 4.5 h of irradiation, as shown by the curve b in Fig. 5. This period was thought to be corresponding to the stage of the rapid decomposition of accumulated dimers as shown in Fig. 4.

Formaldehyde: Formaldehyde cannot be distinguished by the colorimetric method from acetaldehyde.[22] However, the production of methanol is larger than that of ethanol as shown in Fig. 5, so that the aldehyde formed is considered mostly to be formaldehyde. The concentration of formaldehyde changes with irradiation time as shown in the curve c of Fig. 5. Formaldehyde is started to be produced immediately after methanol formation. The maximum concentration of formaldehyde is observed when the concentration of methanol has considerably decreased.

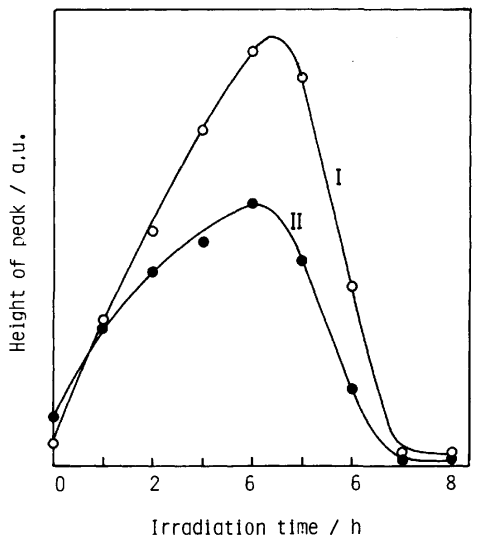

Fig. 4. Changes of the peak heights I and II of HPLC chromatograms as a function of irradiation time.

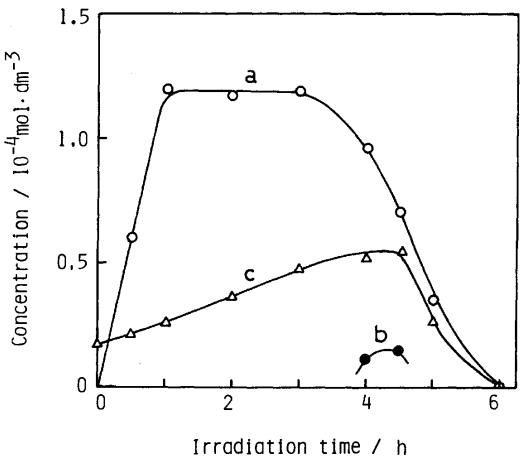

Fig. 5. Changes of the concentration of intermediates with irradiation time. a: methanol, b: ethanol, c: formaldehyde.

Formic Acid: Formic acid was not detected by GC. However, the production of methanol, formaldehyde, and CO_2 suggests the formation of formic acid.

Oxalic Acid: Oxalic acid was detected by glycolic acid formation method[23] and indole method.[24] It might be produced by the decomposition of benzene ring since it was produced by the photocatalytic decomposition of muconic acid (2,4-hexadiendioic acid),[18] the intermediate of benzene ring decomposition.

Gaseous Products: Trace amounts of methane and ethylene were detected. Both yields are about one molecule per twenty thousands of constituents of kraft lignin and are very small compared to those in the decomposition of kraft lignin by hydroxyl radicals.[13]

Decomposition of Kraft Lignin on the TiO_2 Photocatalyst. It was reported that hydroxyl radical, produced by the reaction of hydroxyl group on the photocatalyst surface or water molecule with photo-generated hole, take part in the photocatalytic reactions.[25] However, in the reaction under investigation, the participation of hydroxyl radical is thought to be small for the following reasons.

(i) The photocatalytic oxidation of benzene, phenol, and catechol proceeds by photo-generated holes.[10]

(ii) Large amount of methane, ethane, and ethylene are produced from the decomposition of lignin by Fenton's reagent which produces hydroxyl radicals,[13] whereas very small amounts of these compounds are formed by the TiO_2 catalyzed photoreaction.

(iii) Aromatic phenol compounds are not dimerized by hydroxyl radicals[26,27] whereas they are dimerized by TiO_2 photocatalyst.

So, the photocatalytic decomposition of kraft lignin on TiO_2 proceeds most likely via photo-generated holes.

Conclusion

Following conclusions were obtained.

(1) Kraft lignin is decomposed into inorganic compounds such as carbon dioxide and water by the action of the photo-generated holes.

(2) Aromatic compounds such as vanillin can not be recovered because they are predominantly dehydrodimerized and then decomposed by TiO_2 photocatalyst.

(3) The production of gaseous hydrocarbon products such as methane and ethane is less than that obtained in the decomposition by hydroxyl radicals in homogeneous solution.

The authors thank Dr. Takeo Yamabe, former Professor of Kanagawa University, for his helpful advice in the HPLC analysis, Kazunobu Ishikawa (Tokushu Uchusen Kogyo) for valuable contributions to the experiments and Professor Horst Kisch of Universität Erlangen-Nürnberg for valuable discussions.

References

1) A. L. Prunden and D. F. Ollis, *J. Catal.*, **82**, 404 (1983).
2) C. Y. Hsiao, C. L. Lee, and D. F. Ollis, *J. Catal.*, **82**, 418 (1983).
3) M. Barbeni, E. Pramauro, E. Pelizzetti, E. Borgallero, M. Gratzel, and E. Serpone, *Nouv. J. Chim.*, **8**, 547 (1984).
4) H. Kawaguchi, *Environ. Technol. Lett.*, **5**, 471 (1984).
5) K. Okamoto, Y. Yamamoto, H. Tanaka, M. Tanaka, and A. Itaya, *Bull. Chem. Soc. Jpn.*, **58**, 2015 (1985).
6) K. Okamoto, Y. Yamamoto, H. Tanaka, and A. Itaya, *Bull. Chem. Soc. Jpn.*, **58**, 2023 (1985).
7) I. Izumi, *Denki Kagaku*, **53**, 178 (1985).
8) H. Hidaka, H. Kubota, M. Grätzel, N. Serpone, and E. Pelizzetti, *Nouv. J. Chim.*, **9**, 67 (1985).
9) H. Hidaka, H. Kubota, M. Grätzel, E. Pelizzetti, and N. Serpone, *J. Photochem.*, **35**, 219 (1986).
10) K. Hashimoto, T. Kawai, and T. Sakata, *J. Phys. Chem.*, **88**, 4083 (1984).
11) M. Suzuki, *Sangyo Kogai*, **14**, 562 (1978).
12) K. Tatsumi, N. Takahashi, and K. Murayama, *Kogai*, **22**, 189 (1987).
13) K. Tatsumi, H. Araki, and M. Terashima, *Mokuzai Gakkaishi*, **26**, 327 (1980).
14) K. Tatsumi and M. Terashima, *Mokuzai Gakkaishi*, **27**, 210 (1981).
15) H. L. Chun and M. M. Baizer, "The Electrochemistry of Biomass and derived Materials," American Chemical Society (1985), p. 243.
16) A. Yoshiyama, T. Nonaka, T. C. Chou, and H. J. Tien, *Mokuzai Gakkaishi*, **34**, 155 (1988).
17) A. Yoshiyama, T. Nonaka, H. Kawakami, T. C. Chou, and H. J. Tien, *Mokuzai Gakkaishi*, **34**, 275 (1988).
18) K. Kobayakawa, T. Katsumata, H. Nagashima, Y. Sato, S. Nakamura, and A. Fujishima, *Nippon Kagaku Kaishi*, **1988**, 1175.
19) S. Torii, "Yuki Denkai Gosei," Kodansha (1981), p. 123.
20) F. Fichter, *Trans. Electrochem. Soc.*, **45**, 75 (1924).
21) F. J. Vermillion, Jr. and I. A. Pearl, *J. Electrochem. Soc.*, **111**, 1392 (1964).
22) T. Nash, *Biochem. J.*, **55**, 416 (1953).
23) F. D. Snell, "Colorimetric Methods of Analysis," D. Van Nostrand (1953), Vol. 3, p. 379.
24) J. Bergerman and J. S. Elliot, *Anal. Chem.*, **27**, 1014 (1955).
25) C. D. Jaeger and A. J. Bard, *J. Phys. Chem.*, **83**, 314 (1979).
26) K. Tatsumi and N. Terashima, *Mokuzai Gakkaishi*, **29**, 530 (1983).
27) K. Tatsumi and N. Terashima, *Mokuzai Gakkaishi*, **30**, 580 (1984).

 © 1989 The Chemical Society of Japan Bull. Chem. Soc. Jpn., 62, 3437—3441 (1989)

The Conformational Interconversion of 1,3-Diamine Chelate: Tetracyano(1,3-propanediamine)ferrate(III)

Yoshitaka KURODA, Masafumi GOTO,* and Tomoya SAKAI
Faculty of Pharmaceutical Sciences, Nagoya City University, Mizuho-ku, Nagoya 467
(Received February 22, 1989)

The activation parameters for the chair-to-chair interconversion of the six-membered chelate ring of $[Fe^{III}(CN)_4(1,3\text{-propanediamine})]^-$ have been determined from a line-shape analysis of the ^1H NMR spectra of the paramagnetic complex by taking advantage of the large differences in the chemical shift: $\Delta H^{\neq}=32.2\pm4.6$ kJ mol^{-1}, $\Delta S^{\neq}=31.2\pm28.6$ J mol^{-1} K^{-1}, and $\Delta G^{\neq}_{298}=22.9\pm3.9$ kJ mol^{-1}. The $\Delta H^{\neq}$ and $\Delta S^{\neq}$ values are larger by 7.5 kJ mol^{-1} and 31 J mol^{-1} K^{-1} than those of the corresponding 1,2-ethanediamine chelate, $[Fe^{III}(CN)_4(1,2\text{-ethanediamine})]^-$, respectively. The kinetic data supported the transition state with a half-boat conformation.

Five- and six-membered chelate rings are formed by the coordination of multidentate ligands to transition metal ions.[1,2] Five-membered chelates are known to take either δ or λ *gauche* conformations, while for six-membered ones, chair, skew-boat, and boat forms are possible.[1-4] These chelate rings rapidly change their conformations among such conformers at the ambient temperature.[2-8]

The stereochemistry of the chelate ring of 1,3-propanediamine has been the subject of many studies.[1-4] The most populated conformers are both chair forms, but the interconversion between them has been considered to occur through skew-boat forms as intermediates.[1-4]

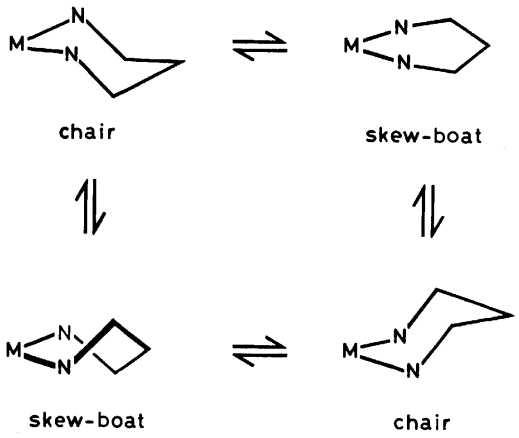

The determination of the rate constant for the conformational interconversion would be desirable for understanding the stereochemistry of metal complexes. We have developed a method of determining the rate constants for paramagnetic compounds by means of NMR spectroscopy; an application to the five-membered chelate ring has been reported in a previous paper.[6]

There have been few reports on the dynamics of the conformational change of six-membered chelate rings except for $[Mo^0(CO)_4(tmtn)]$ (tmtn=*N,N,N',N'*-tetramethyl-1,3-propanediamine), the activation free energy of which has been estimated as $\Delta G^{\neq}_{178}<34$ kJ mol^{-1} for the chair-to-chair interconversion, based on the broadening of $^{13}CH_3$ NMR line-shape at 178 K.[9] Tetracyano(1,3-diamine)ferrate(III) complexes show well-resolved and strongly orientation-dependent ^1H and ^{13}C NMR spectra.[4] These characteristics are suitable for line-shape analysis. We have now applied the method to the chair-to-chair interconversion of the six-membered chelate ring of tetracyano(1,3-propanediamine)ferrate(III).

Experimental

Materials. Tetracyano(1,3-diamine)ferrate(III) complexes, $H[Fe^{III}(CN)_4(tn)]\cdot2H_2O\cdot(CH_3)_2CHOH$ and $H[Fe^{III}(CN)_4(meso\text{-ptn})]\cdot2H_2O\cdot3/4(C_2H_5OH)$ (tn=1,3-propanediamine and *meso*-ptn=(2*R*,4*S*)-2,4-pentanediamine), were prepared as has been reported previously.[4]

NMR Measurements. The measurements were carried out as has been reported previously[6] with a JEOL FX-100 spectrometer at 183—323 K. The positive chemical shifts indicate downfield shifts from sodium 3-(trimethylsilyl)-propionate-2,2,3,3-d_4 (TSP).

Calculation of the Line-Width and the Interconversion Rate Constant. The line-width and the interconversion rate were calculated by using two least-squares programs, SALS[10] and MULTI,[11] on the NEAC ACOS 850 apparatus of the computing center of this university.

Results

Variable-Temperature ^1H NMR Spectra. The 100-MHz ^1H NMR spectra of $[Fe^{III}(CN)_4(tn)]^-$ (tn=1,3-propanediamine) at 8 different temperatures are reproduced in Fig. 1. The temperature range was limited to 183—323 K by the boiling and freezing points of the solvent (CD_3OD containing 0.25% DCl).[6] Two resonances with an area ratio of 2:1 were observed between 183 and 323 K. The upfield signal showed a small temperature dependence, while the downfield signal showed a significant downfield shift, with the decrease in the temperature. These spectra show that the predominant species are the chair forms, which rapidly interconvert on the NMR time scale.

The 100-MHz ^1H NMR spectra of $[Fe^{III}(CN)_4(meso\text{-ptn})]^-$ (*meso*-ptn=(2*R*,4*S*)-2,4-pentanediamine) at 8 different temperatures are reproduced in Fig. 2. Apart from the signals of the solvent impurities (H_2O and

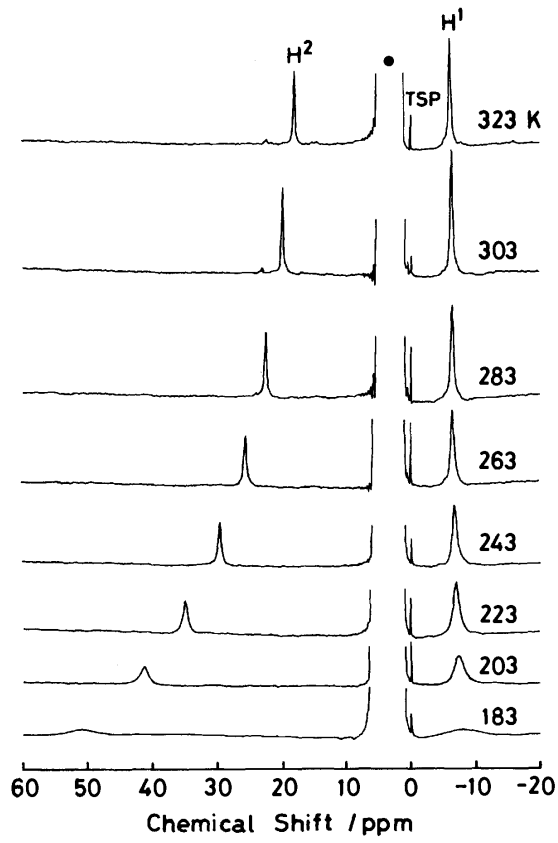

Fig. 1. Temperature-dependent ^{1}H NMR spectra of $[Fe^{III}(CN)_4(tn)]^-$ in CD_3OD containing 0.25% DCl. A dot (●) indicates signals of the solvent impurities (H_2O and CH_3OH) and $(CH_3)_2CHOH$ included in the sample.

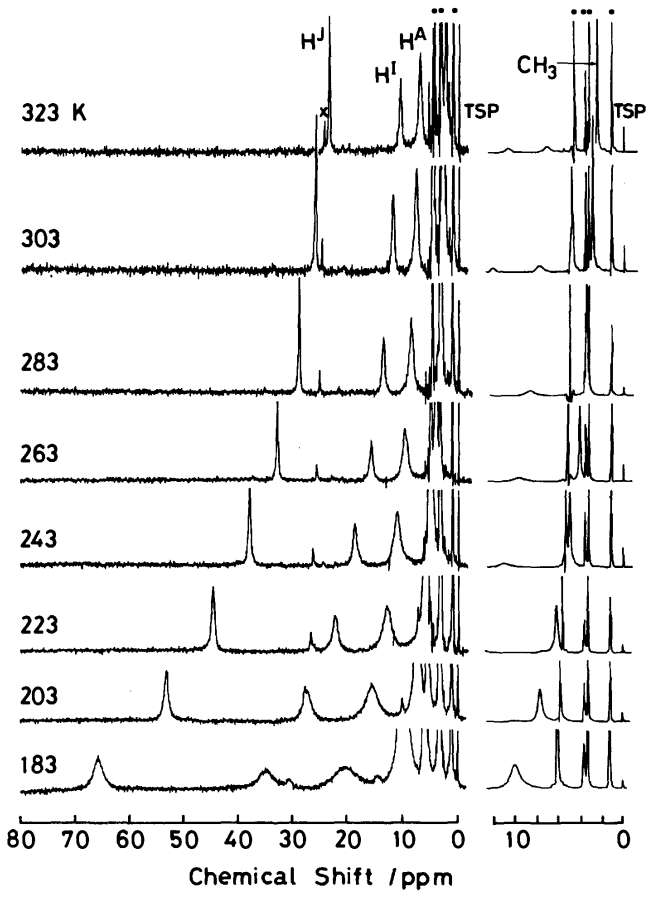

Fig. 2. Temperature-dependent ^{1}H NMR spectra of $[Fe^{III}(CN)_4(meso\text{-ptn})]^-$ in CD_3OD containing 0.25% DCl. A dot (●) indicates signals of the solvent impurities (H_2O and CH_3OH) and ethanol included in the sample. The x-shaped mark denotes a noise which appeared at the central frequency of the irradiation pulses.

CH_3OH) and ethanol included in the sample, four paramagnetically shifted resonances were observed. These resonances moved downfield with the decrease in the temperature. The x mark in Fig. 2 denotes a noise which appeared at the central frequency of the irradiation pulses. These spectral changes show that the conformational interconversion can be regarded as occurring between the two chair forms which are shown below, along with the numbering for the ^{1}H and ^{13}C nuclei:

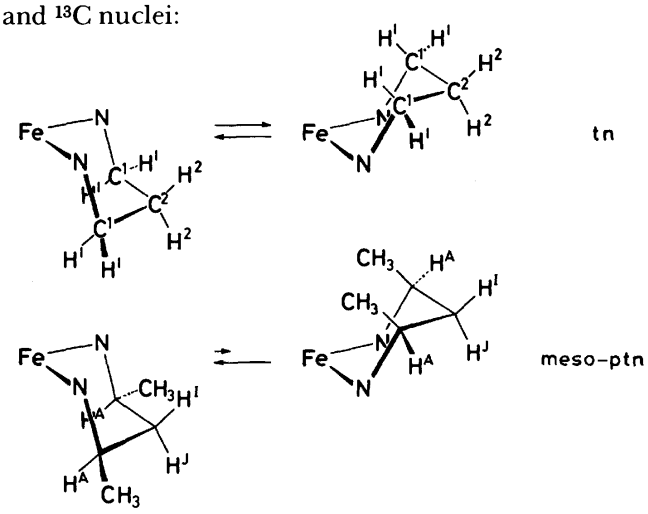

The signal assignments for these complexes have been described in a previous paper.[4] The large difference in chamical shift between the H^I and H^J of the *meso*-ptn chelate shows that the conformation is fixed to the chair form with two equatorial methyl groups.[4] The alteration of the tn chelate between the two chair forms is supported by the observation that the chemical shift of H^2 was almost the same as the mean of the H^I and H^J shifts of the *meso*-ptn chelate.

The plots of the chemical shift vs. T^{-1} showed that the dependence of each ^{1}H shift of the tn and *meso*-ptn complexes on the temperature was not represented by a straight line but by a concave line. This non-Curie law behavior is caused by the participation of both the Fermi contact and pseudocontact mechanisms for this class of complexes. Although the separation of the H^1 or H^2 signal into two peaks, corresponding to the axial and equatorial protons in a frozen conformation, could not be attained even at 183 K, the broadening of these signals, e.g., the half-line-width at the half-height of 236 Hz at 183 K relative to 20 Hz at 303 K for

the H^2 signal, were large enough to obtain the rate constant of the interconversion by means of line-shape analysis. The decrease in the temperature made all signals of the *meso*-ptn chelate broad according to the reduction in the spin-relaxation times. However, the further signal broadening for the tn chelate is caused by an additional factor, i.e., the exchange of resonance sites between the two chair forms.

The rate of the conformational interconversion can be calculated if we can estimate the chemical shifts and line-widths intrinsic to a fixed chair conformer of the tn chelate. In this work, the calculation of the rate for the tn chelate was carried out on the assumption that the H^I and H^J values of the *meso*-ptn chelate are magnetically equivalent to the axial (H^{ax}) and equatorial (H^{eq}) H^2 values of the tn chelate fixed in a chair conformation.

The "one-way" rate constants for the interconversion, k, were calculated from the line-shapes of the H^2 peaks at 183—213 K using the Gutowsky-McCall-Slichter equation[12] according to the method reported previously.[6] The intrisic chemical shifts (ν_{ax} and ν_{eq}) and transverse relaxation times (T_{2ax} and T_{2eq}) expected for the tn chelate fixed in a chair conformation at each temperature were estimated from Eqs. 2 and 5 of Ref. 6, which represent the difference in chemical shift between H^I and H^J (Δ) and the half-line-widths at their half-height (W). The k values at 183, 193, 203, and 213 K were obtained as follows: 1.0×10^5, 4.0×10^5, 8.2×10^5, and 2.5×10^6 s^{-1}. If we assume errors as much as 10% for both Δ and W, the ranges of k were estimated to be $(0.68—1.5)\times10^5$, $(2.0—6.5)\times10^5$, $(0.32—1.6)\times10^6$, and $(1.2—5.7)\times10^6$ s^{-1} at 183, 193, 203, and 213 K respectively. The k values above 213 K could not be determined with sufficient accuracy, since the extent of line-broadening was not large enough.

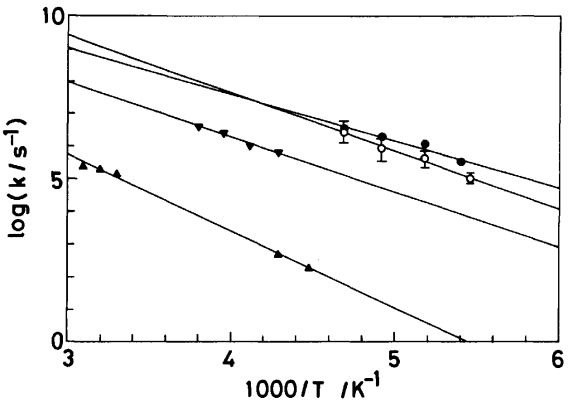

Fig. 3. Arrhenius plots for the conformational interconversion of the chelate ring of $[Fe^{III}(CN)_4(diamine)]^-$ in CD_3OD-DCl: diamine=tn (○), en (●), *meso*-bn (▼), and *cis*-chxn (▲). The I-shaped marks indicate the maximum and minimum of the inversion rate constants.

The activation parameters were calculated from the Eyring equation:[13]

$$k = \kappa(k_B T/h)[\exp(-\Delta H^{\neq}/RT)][\exp(\Delta S^{\neq}/R)]$$

where k_B is the Boltzmann constant and κ is the transmission coefficient, which was set as unity. The $\Delta H^{\neq}$ and $\Delta S^{\neq}$ values were obtained by a least-squares linear regression analysis of $-R\ln(kh/k_BT)$ on T^{-1}: they are summarized in Table 1, along with those obtained for the 1,2-diamine chelates.[6] The Arrhenius plots are shown in Fig. 3.

The errors in the activation parameters are primarily derived from the estimated values of the intrinsic ν_{ax}, ν_{eq}, T_{2ax}, and T_{2eq}. The experimental errors in the temperature (±1 K) and the chemical shift were much smaller than the estimated errors.

Discussion

There are three types of conformations of six-membered chelate rings: chair, skew-boat, and boat.[2,3] The chair form is the most stable conformation, as has been confirmed by X-ray diffraction analysis,[1] NMR spectroscopy,[7,8] and force-field calculation.[14—16] The conformation of the six-membered chelate ring of $[Fe^{III}(CN)_4(meso\text{-ptn})]^-$ is fixed in a chair form, with two equatorial methyl groups at 183—323 K, as has been described in the preceding section. The time-averaged H^2 shift of $[Fe^{III}(CN)_4(tn)]^-$ was nearly equal to the mean of the H^I and H^J shifts of the *meso*-ptn chelate between 183 and 323 K. Therefore, the six-membered chelate ring of the tn complex rapidly alternates between two chair forms, and the population of skew-boat conformers is small in contrast to the chelate ring formed by (2*R*,4*R*)-2,4-pentanediamine,[4] which showed a population of skew-boat and chair conformers of 80:20.[4]

In a previous paper,[6] we have reported that the five-membered chelate rings of tetracyano(1,2-diamine)-

Table 1. Activation Parameters for Conformational Interconversion of $[Fe^{III}(CN)_4(diamine)]^-$ in CD_3OD-DCl

Diamine	$\Delta H^{\neq}$/kJ mol^{-1}	$\Delta S^{\neq}$/J mol^{-1} K^{-1}	$\Delta G^{\neq}_{298}$/kJ mol^{-1}
tn	32.2±4.6	31.2±28.6	22.9±3.9
en[a]	24.7±4.5	0.0±27.0	24.7±3.6
meso-bn[a]	30.1±3.9	−2.9±19.1	31.0±1.8
cis-chxn[a]	42.7±2.0	−7.7± 8.4	45.0±0.5

a) Ref. 6.

ferrate(III) (1,2-diamine=1,2-ethanediamine (en), (2*R*,3*S*)-2,3-butanediamine (*meso*-bn), and *cis*-(1*R*,2*S*)-1,2-cyclohexanediamine (*cis*-chxn)) alternate between δ and λ conformers through an envelope structure as the transition state. Their activation parameters are collected in Table 1. Figure 3 and Table 1 show that the rate of the interconversion of the tn chelate is slower than that of the en chelate below 240 K, but at 298 K the former becomes faster than those of the en as well as *meso*-bn and *cis*-chxn chelates. This difference between the 1,2- and 1,3-diamine chelates is attributable to: (1) the $\Delta H^{\neq}$ of the tn chelate, which is larger by 7.5 kJ mol^{-1} than that of the en chelate,[6] and (2) the positive $\Delta S^{\neq}$ value of the tn chelate, in contrast to a zero or small negative $\Delta S^{\neq}$ value for the 1,2-diamine chelates.[6] The transition state for the tn chelate is, hence, more endothermic than that for the en chelate.

Gollogly and Hawkins have reported the results of energy-minimization calculations for octahedral transition metal-1,3-diamine complexes with a metal-nitrogen bond length of 200 pm.[14] The minimum energy pathway between two chair forms involves a transition state with a conformation where one C^1 is out of the coordination plane, while the other C^1 and C^2 lie on the plane. This pathway has the skew-boat conformation as an intermediate, and the $\Delta H^{\neq}$ value for this pathway is ca. 32 kJ mol^{-1}. A $\Delta H^{\neq}$ value larger than 42 kJ mol^{-1} has been obtained for two other pathways which pass successively through a symmetrical boat conformation and a transition state with the N-C^1-C^2-C^1-N or C^1-N-M-N-C^1 fragment coplanar.[9]

The $\Delta H^{\neq}$ value for the tn chelate was obtained as 32.2 kJ mol^{-1}; this value is in close agreement with the value estimated by Gollogly and Hawkins.[14] The tn chelate is, therefore, expected to change its conformation through the pathway predicted by Gollogly and Hawkins.[14]

According to the force-field calculation by Gollogly et al.,[14,17] the N-C-C angle of the five-membered chelate is larger by 3° in the envelope structure than in the *gauche* form. In the half-boat structure of the six-membered chelate, the angles of M-N-C^1 and N-C^1-C^2 have been reported to be 125.7 and 119.5° respectively, i.e., an increase of more than 7.5° compared with the chair form.[14] The increment in $\Delta H^{\neq}$ observed for the six-membered chelate is attributable to the increase in such angle and torsional strains.

The activation free energy for [$Mo^0(CO)_4$(tmtn)] has been estimated as $\Delta G^{\neq}_{178} < 34$ kJ mol^{-1} from the linewidth of the $^{13}CH_3$ signal at 178 K.[9] The $\Delta G^{\neq}_{178}$ for the tn chelate is evaluated as 26.6 kJ mol^{-1} from the data in Table 1, so that the increment in $\Delta H^{\neq}$ due to the four methyl groups of the tmtn is estimated to be less than 7.4 kJ mol^{-1}, which is almost half of the 14.7 kJ mol^{-1} [6] observed between [$Fe^{III}(CN)_4$(en)]$^-$ and [$Cr^0(CO)_4$(tmen)] (tmen=*N*,*N*,*N*′,*N*′-tetramethyl-1,2-ethanediamine). The difference between 1,2- and 1,3-diamine chelates can be explained by the repulsive interaction of the *N*-methyl groups if tmtn and tmen take half-boat and envelope conformations as transition states respectively. Since the distances between the *N*-methyl groups and the adjacent CH's for both tmtn and tmen are shorter in the transition state than in the ground state, the transition state can be expected to have a larger repulsion energy than the ground state. This difference causes the increase in $\Delta H^{\neq}$ for both diamine chelates. On the other hand, the repulsions between the *N*-methyl groups and other ligands and between the two pseudoaxial *N*-methyl groups are expected to be larger in the ground state than in the transition state in the case of tmtn, but the opposite situation is expected for tmen. Consequently, the $\Delta H^{\neq}$ for 1,2-diamine chelate increases further, but the increase of $\Delta H^{\neq}$ for 1,3-diamine chelate is reduced.

The $\Delta H^{\neq}$ value for the chair-to-chair interconversion of cyclohexane have been reported as 43.1—48.1 kJ mol^{-1}.[18-20] The $\Delta H^{\neq}$ value for the six-membered chelate ring of the tn complex is smaller by 11—16 kJ mol^{-1} than that for cyclohexane, though the former has nonbonded interactions between the ring protons and the apical ligands which are absent in the latter.

Cyclohexane is believed to have a half-chair conformation in the transition state of the conformational interconversion.[21] Wiberg and Boyd,[22] in reporting the results of their force-field calculation for cyclohexane, say that the half-chair conformation is higher in energy by 2.5 kJ mol^{-1} than the half-boat form. This difference has been attributed to the torsional and angle strains arising from the difference in the number of carbon atoms coplanar in the transition state.[22,23]

X-Ray diffraction analysis for [$Co(tn)_3$]$Cl_3 \cdot H_2O$ has revealed a chair conformation of the tn chelate with the following angles: Co-N-C^1, 122.0°; N-C^1-C^2, 112.4°; C^1-C^2-C^1, 113.6°.[24] The transition state for the six-membered chelate, which is expected to have a structure with the N-Fe-N-C^1-C^2 fragment coplanar, corresponds to the half-boat form of cyclohexane. The six-membered chelate ring will be flattened more easily than cyclohexane with the C-C-C angle of 109.5°, since the angles in the former are closer to the angle of ca. 120° required for the transition state. This feature seems to reduce the $\Delta H^{\neq}$ value for the six-membered chelate by ca. 10 kJ mol^{-1} relative to that for cyclohexane.

References

1) Y. Saito, "Absolute Stereochemistry of Chelate Complexes," in "Topics in Stereochemistry," ed by E. L. Eliel and N. L. Allinger, John Wiley & Sons, New York (1978), Vol. 10, pp. 95—174.

2) D. A. Buckingham and A. M. Sargeson, "Conformational Analysis and Steric Effects in Metal Chelates," in "Topics in Stereochemistry," ed by N. L. Allinger and E. L. Eliel,

Wiley-Interscience, New York (1971), Vol. 6, pp. 219—277.
3) C. J. Hawkins and J. A. Palmer, *Coord. Chem. Rev.*, **44**, 1—60 (1982).
4) M. Goto, H. Nakayabu, H. Ito, H. Tsubamoto, K. Nakabayashi, Y. Kuroda, and T. Sakai, *Inorg. Chem.*, **25**, 1684 (1986).
5) Y. Kuroda, M. Goto, and T. Sakai, *Bull. Chem. Soc. Jpn.*, **60**, 3917 (1987).
6) Y. Kuroda, N. Tanaka, M. Goto, and T. Sakai, *Inorg. Chem.*, **28**, 997 (1989).
7) J. E. Sarneski and C. N. Reilley, *Inorg. Chem.*, **13**, 977 (1974).
8) T. G. Appleton and J. R. Hall, *Inorg. Chem.*, **9**, 1807 (1970); **10**, 1717 (1971).
9) C. J. Hawkins, R. M. Peachey, and C. L. Szoredi, *Aust. J. Chem.*, **31**, 973 (1978).
10) T. Nakagawa and Y. Koyanagi, "Statistical Analysis with Least-squares Fitting (SALS)," University of Tokyo, Tokyo (1979).
11) K. Yamaoka, Y. Tanigawara, T. Nakagawa, and T. Uno, *J. Pharmacobio-Dyn.*, **4**, 879 (1981).
12) H. S. Gutowsky, D. W. McCall, and C. P. Slichter, *J. Chem. Phys.*, **21**, 279 (1953); H. M. McConnell, *J. Chem. Phys.*, **28**, 430 (1958).
13) H. Eyring, *J. Chem. Phys.*, **3**, 107 (1935).
14) J. R. Gollogly and C. J. Hawkins, *Inorg. Chem.*, **11**, 156 (1972).
15) L. J. DeHayes and D. H. Busch, *Inorg. Chem.*, **12**, 1505 (1973).
16) S. R. Niketić and F. Woldbye, *Acta Chem. Scand.*, **27**, 3811 (1973).
17) J. R. Gollogly, C. J. Hawkins, and J. K. Beattie, *Inorg. Chem.*, **10**, 317 (1971).
18) F. A. L. Anet and A. J. R. Bourne, *J. Am. Chem. Soc.*, **89**, 760 (1967).
19) D. Höfner, S. A. Lesko, and G. Binsch, *Org. Magn. Reson.*, **11**, 179 (1978).
20) R. Poupko and Z. Luz, *J. Chem. Phys.*, **75**, 1675 (1981).
21) R. T. Morison and R. N. Boyd, "Organic Chemistry," Allyn and Bacon, Boston (1983), p. 178.
22) K. B. Wiberg and R. H. Boyd, *J. Am. Chem. Soc.*, **94**, 8426 (1972).
23) J. B. Hendrickson, *J. Am. Chem. Soc.*, **83**, 4537 (1961).
24) R. Nagao, F. Marumo, and Y. Saito, *Acta Crystallogr., Sect. B*, **29**, 2438 (1973).

Formation of Hydrotalcite-Acrylate Intercalation Compounds and Their Heat-Treated Products

Masahito TANAKA, In Yong PARK, Kazuyuki KURODA, and Chuzo KATO*
Department of Applied Chemistry, Waseda University, Ohkubo-3, Shinjuku-ku, Tokyo 169
(Received March 29, 1989)

Hydrotalcite-like compounds (HT), layered double hydroxides with a few kinds of interlayer anions (X=CO_3^{2-}, Cl^-, and NO_3^-) were allowed to react with acrylate anions in order to prepare a novel inorganic-organic interstratified layered material by anion exchange. When HT-CO_3 was used the anion exchange reaction did not occur. When HT-NO_3 was employed the reaction proceeded to form a HT-acrylate intercalation compound. The formation of the intercalation compound from HT-Cl was observed only under a reaction condition using a concentrated acrylate solution. When the intercalation compound was heated at 80 °C with the addition of an initiator, the interlayer acrylate anions were polymerized to form a HT-polyacrylate intercalation compound.

Hydrotalcite-like compounds (abbreviated HT) are layered double hydroxides, expressed as $[Mg_{1-x}Al_x(OH)_2]^{x+}[A_{x/n}^{n-}\cdot mH_2O]^{x-}$, where A^{n-} is an exchangeable anion, and $0.2 \leqq x \leqq 0.33$.[1,2] A part of Mg in the brucite layer $[Mg(OH)_2]$ is replaced with Al, and the positively charged layers are compensated with interlayer anions. The metals in the layers are not limited to Mg and Al, since many divalent and trivalent metals are employed to form different types of layered double hydroxides.[3] Interlayer anions and water occupy the interlayer space. Since these interlayer anions are exchangeable, hydrotalcite-like compounds have been investigated from the viewpoint of an inorganic anion exchanger. Regarding the selectivity of the interlayer inorganic anions, the high selectivity of anions with higher valency and smaller size has been reported.[4]

In general, HT does not exhibit a swelling property. The layer charge density is also relatively higher than those of intercalating layered oxide materials, such as smectite clay. Accordingly, there have been only several reports on exchange with organic anions in HT. Dicarboxylic acids (Zn^{2+}-Al^{3+} hydroxide),[5] D,L-histidines (Mg^{2+}-Al^{3+}),[6] acetic acid (Ni^{2+}-Fe^{3+} (Co^{3+})),[7] and alkyl sulfates (Zn^{2+}-Cr^{3+}),[8] (Mg^{2+}-Al^{3+})[9] have been investigated so far.

In the present study, as a course of our study on the intercalation chemistry of hydrotalcite, the acrylate anion was selected as the guest anion and the possibility of an anion exchange was examined, since the acrylate anion is small in size and polymerizable. Thus, the interlayer polymerization of acrylate anions by thermal treatment was also investigated.

Experimental

Materials. The HT used in this study was a CO_3-exchanged type (Kyowaad 500 manufactured by Kyowa Chemical Industry Co.). The ratio of aluminum in the total metals (x=Al/(Mg+Al)) was 0.25. The XRD, IR, and thermoanalytical data coincided with the previous results.[4]

The Cl- and NO_3-exchanged types were prepared by the following procedure. HT-CO_3 (5 g) and sodium chloride (ca. 20 g) were mixed with decarbonated water to make a suspension (200 ml) by stirring. The suspension was stirred under a nitrogen flow and 2 M hydrochloric acid (1 M= 1 mol dm^{-3}) was added into the reaction mixture and the pH was maintained at 4.2—4.5 for 10 min. The mixture was centrifuged and washed with decarbonated water twice. The end of the washing was checked by ion chromatography. The ion-exchanged product was dried under reduced pressure at room temperature. The XRD, IR, and thermal analyses of the products showed the same results as the previous data of the HT-Cl.[4] HT-NO_3[10] was prepared with sodium nitrate and 2 M nitric acid instead of sodium chloride and hydrochloric acid, respectively. The other procedure was the same as that for the preparation of HT-Cl.

The ion exchange capacities of both HT-Cl and HT-NO_3 were ca. 270 mequiv/100 g HT, which was ca. 90% of the calculated values based on the chemical formulae of the fully exchanged HT-Cl and HT-NO_3. This finding suggested that a part of interlayer carbonate anions was not exchanged with Cl^- or NO_3^-. Commercially available acrylic acid (Tokyo Kasei Co.) was used without further purification.

Ion Exchange with Acrylate Anions. The amount of acrylate anions used in the anion exchange was calculated on the basis of the anion exchange capacity of hydrotalcite. The amounts were 3, 5, 7, 10, 20, and 50 times the anion exchange capacity when HT-NO_3 was used. The amounts of 5, 10, and 50 times the capacity were selected for experiments with HT-CO_3 and HT-Cl. A given amount of acrylic acid was dissolved in water and the pH of the solution was adjusted to be 7 with a NaOH aq. solution to form acrylate anions; the total volume of the final solution was 400 ml. Thus, the concentrations of acrylate anions were varied from 0.10 to 1.69 mol dm^{-3} for HT-NO_3, and from 0.17 to 1.69 mol dm^{-3} for HT-CO_3 and HT-Cl. When HT-Cl was employed, an exchange reaction using a highly concentrated acrylate solution (6.75 mol dm^{-3}, the total volume was 100 ml, the amount of acrylate anions was 50-times the ion exchange capacity of HT, pH 7) was also performed.

HT (5 g each) was added into these solutions and the reaction mixtures were stirred for 1 week at room temperature. When a shorter reaction time, e.g. 5 days, was attempted, the unreacted HT partly remained. After centrifugation, the products were washed with decarbonated water. The completion of the washing was checked by CHN analyses of the products. After a few repetitions of washing,

the carbon contents reached a constant value. After washing, the products were dried under reduced pressure at room temperature and analyzed. All of the anion-exchange experiments were performed under a nitrogen atmosphere.

Polymerization. The HT-acrylate intercalation compounds were heat-treated at 80 °C for 1 day after the addition of potassium peroxodisulfate (an initiator for polymerization) into the undried products followed by homogeneous mixing.

Analyses. X-Ray powder diffraction patterns were obtained with a Rigaku Rad-IB diffractometer using Ni-filtered Cu $K\alpha$ radiation. IR analyses were performed with a Perkin-Elmer FT-IR 1640 using a KBr disk technique. DTA curves were recorded on a Shimadzu DT-20 thermal analyzer at a heating rate of 10 °C min^{-1} under an air atmosphere. TG curves were recorded on a Shimadzu DT-40 apparatus.

Results and Discussion

Hydrotalcite-Acrylate Intercalation Compound. The formation of intercalation compounds was primarily judged by the variation in the X-ray diffraction patterns. The ratio of the intercalation compound to unreacted HT was roughly estimated by the peak intensities of their (003) diffraction lines. When HT-NO_3 was used as the starting material, the reaction with acrylate solutions of lower concentrations yielded the intercalation compound at a very low ratio with a large amount of unreacted HT. With the increase in the concentration, the formation of the intercalation compound became pronounced. The intercalation compound obtained from the highest concentration formed a single phase and the reproducibility was highest. Therefore, the compound obtained from the acrylate solution (1.69 M) was employed for the following analyses.

Figure 1 shows the X-ray powder diffraction patterns of the reaction products obtained from HT-NO_3. In the profile of the HT-acrylate reaction product (Fig. 1(b)), the diffraction peak due to (003), which corresponded to the basal spacing, shifted to a lower 2θ angle at 6.4° (d=13.8 Å). Correspondingly, the peaks due to (006) and (009) shifted to lower angles in a similar manner.

The IR spectra of HT-NO_3, sodium acrylate, and the reaction product are shown in Fig. 2. In the spectrum of the HT-acrylate reaction product (Fig. 2(c)), the absorption peak due to nitrate anions at 1380 cm^{-1} (ν_3) almost disappeared, whereas peaks due to acrylate anions at 1640 cm^{-1} ($\nu_{C=C}$), 1560 cm^{-1} (ν_{asCOO^-}), and 1450 cm^{-1} (ν_{sCOO^-})[11,12] appeared. A slight deformation in the peak profile at 1360 cm^{-1} (δ_{C-H}) can be explained by considering that the small peak due to carbonate anions ($\nu_{CO_3^{2-}}$) overlapped. As described in Experimental, carbonate anions partly remained in the original HT-NO_3. However,

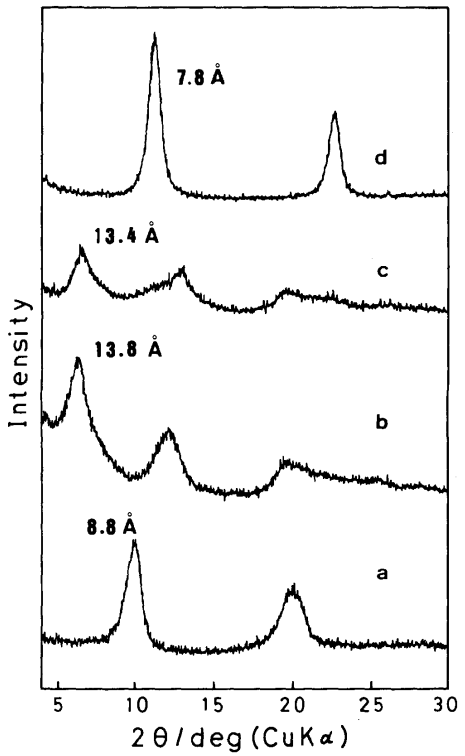

Fig. 1. X-Ray powder diffraction patterns of a) HT-NO_3, b) HT-acrylate intercalation compound, c) HT-polyacrylate intercalation compound, and d) CO_3 re-exchanged HT.

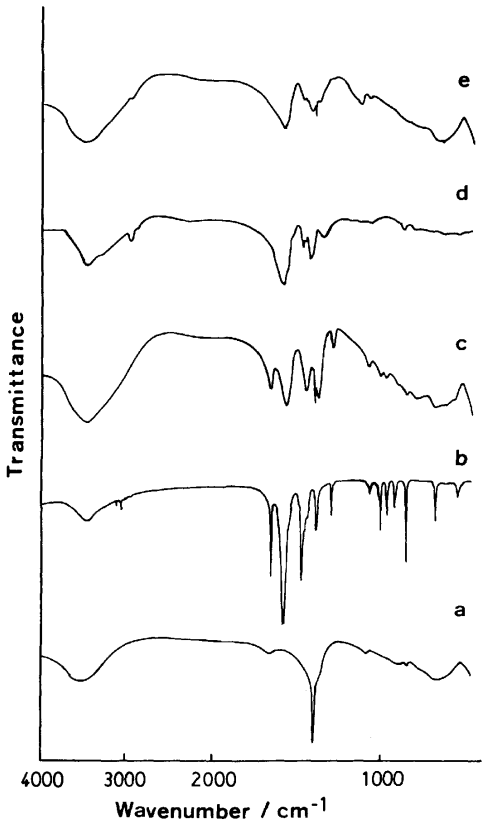

Fig. 2. Infrared spectra of a) HT-NO_3, b) sodium acrylate, c) HT-acrylate intercalation compound, d) sodium polyacrylate, and e) HT-polyacrylate intercalation compound.

carbonate anions must have been partly intercalated during the procedure of ion exchange or washing, since these anions have the highest selectivity in HT.[4]

Part of the product was re-exchanged with carbonate anions by being immersed in a sodium carbonate aqueous solution (2 M) for one day. The XRD result of the re-exchanged product is shown in Fig. 1(d). The peaks shifted to higher angles and showed the characteristic pattern of HT-CO_3. The IR spectrum of the product also showed the presence of carbonate anions along with a disappearance of acrylate anions. From these results, it can be concluded that the reaction can be treated as an interlayer anion exchange and that the double hydroxide layer was retained.

The Mg and Al contents (Mg/Al=0.74/0.26) analyzed by ICP, carbon contents (8.8%) determined by CHN analysis, and the amount of the interlayer water ($0.33H_2O$) calculated from the thermogravimetric curve led to the following chemical formula of the HT-acrylate intercalation compound: $[Mg_{0.74}Al_{0.26}(OH)_2](Ac)_{0.18}(CO_3)_{0.04}\cdot 0.33H_2O$, where Ac represents the acrylate anion. The amounts of acrylate anions and CO_3^{2-} could not be determined separately by TG curves because their weight losses overlapped each other. Therefore, the amounts was deduced from the relationship among the anion exchange capacity, total carbon contents, and the charges of acrylates and carbonates.

When HT-CO_3 was employed as the starting material, the XRD results did not show any variation in their profiles, indicating no reactions. Since the basal spacing of HT is dependent on the size of unhydrated interlayer anions,[4] the increase in the basal spacing should have been detected if acrylate anions were intercalated. The IR results also showed no absorption peaks due to acrylate anions. From these findings, an anion exchange did not take place in a system using HT-CO_3.

When HT-Cl was used, the HT-acrylate intercalation compound was partly obtained only in the case when a highly concentrated acrylate solution was used. The basal spacing of the intercalation compound showed the same value of 13.8 Å. Based on the intensities of (003) diffraction lines of HT-acrylate and HT-Cl, the ratio of the HT-acrylate to the unreacted HT-Cl was roughly estimated to be 3 : 1. In all other cases, however, the intercalation compounds could not be prepared. Therefore, the reactivity of HT-Cl was much lower than that of HT-NO_3.

From these results, the kind of interlayer anions in the starting materials greatly affected the formation of HT-acrylate intercalation compounds. The reason why only HT-NO_3 has a high intercalating ability may be explained by the following two points: the difference in selectivity (or stability) of the interlayer anions and the difference in the interlayer spacings. Regarding the former factor, it has been known[4] that the selectivity decreases in the order

$$CO_3^{2-} \gg Cl^- > NO_3^-.$$

With regard to the latter point, the interlayer distances of both HT-Cl and HT-CO_3 are ca. 3 Å, while that of HT-NO_3 is ca. 4 Å. On the other hand, the thickness of the acrylate anion, which takes a planar geometry, is 2.8 Å. If acrylate anions are intercalated in a flat arrangement during the initial stage of intercalation, it is preferable to use HT-NO_3 due to its larger interlayer thickness. Consequently, it is supposed that acrylate anions can be intercalated more easily. For both of these reasons, HT-NO_3 was most successful for the inclusion of acrylate anions.

Hydrotalcite-Polyacrylate Intercalation Compound. Figure 1(c) shows the XRD data of the polymerized product. The IR spectrum of the product is shown in Fig. 2(e). In the XRD data, the d_{003} value became slightly smaller (d=13.4 Å) than that for a monomer-intercalated substance. Although the peak intensities were weakened, the layer structure was retained. The IR spectrum showed the main characteristic bands due to polyacrylate anions.[13,14] In particular, the absorption peak arising from $\nu_{C=C}$ at 1640 cm^{-1} disappeared and the total profile was similar to that of sodium

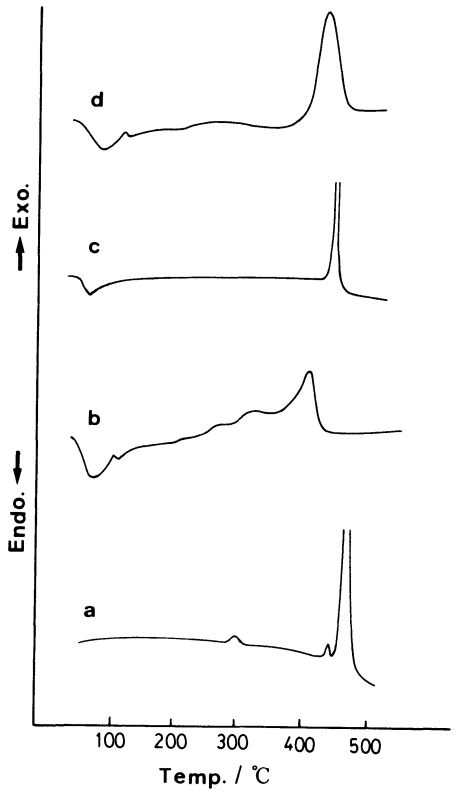

Fig. 3. DTA curves of a) sodium acrylate, b) HT-acrylate intercalation compound, c) sodium polyacrylate, and d) HT-polyacrylate intercalation compound.

polyacrylate, indicating a polymerization of acrylate anions in the interlayer space.

The DTA curves of the intercalation compounds before and after polymerization, sodium acrylate, and sodium polyacrylate are shown in Fig. 3. The DTA curve of sodium acrylate showed exothermic peaks due to polymerization at 280—290 °C and oxidative decomposition starting at 430—440 °C.[15] The reason why decomposition occurred at a comparatively higher temperature may be attributed to the formation of a thermally stable polymer with three-dimensionality which was prepared by bulk polymerization. The DTA curve of sodium polyacrylate did not show an exothermic peak due to polymerization but, rather, exhibited a similar sharp exothermic peak due to its oxidative decomposition.

The complex DTA curve was observed in the HT-acrylate intercalation compound. The several exothermic peaks overlapped and the first started at 250 °C. The XRD data of the heat-treated product at 250 °C for 1 h showed a decrease in the basal spacing to ca. 9 Å. The IR spectrum of the heat-treated product also showed a drastic decrease in the absorption peaks due to acrylate anions. Therefore, the oxidative decomposition of the HT-acrylate intercalation compound proceeded at much lower temperatures than that of the polymerized intercalation compound.

The DTA curve of the HT-polyacrylate intercalation compound was similar to that of sodium polyacrylate. The XRD result of the heat-treated product of the intercalation compound at 250 °C showed the retention of the same basal spacing as the HT-polyacrylate intercalation compound. The IR spectrum of the heat-treated product also showed absorption peaks due to polyacrylate anions. Thus, the difference in the thermal behavior of the intercalation compounds before and after polymerization was confirmed.

From these results we can conclude that acrylate anions were polymerized in the interlayer region of hydrotalcite. The difference in the thermal behavior between HT-acrylate and HT-polyacrylate intercalation compounds was observed, which was attributed to the formation of interlayer polymers.

One of the authors (K. K.) thanks the Yazaki Memorial Foundation for financial support. Waseda University also supported us as a Project Study in Science and Engineering Research Laboratory.

References

1) R. Allmann, *Acta Crystallogr., Sect. B*, **24**, 972 (1968).
2) S. Miyata, *Clays Clay Miner.*, **28**, 50 (1980).
3) W. T. Reichle, *Solid State Ionics*, **22**, 135 (1986).
4) S. Miyata, *Clays Clay Miner.*, **31**, 305 (1983).
5) S. Miyata and T. Kumura, *Chem. Lett.*, **1973**, 843.
6) T. Ikeda, H. Amoh, and T. Yasunaga, *J. Am. Chem. Soc.*, **106**, 5772 (1984).
7) A. Mendiboure and R. Schöllhorn, *Rev. Chim. Miner.*, **23**, 819 (1986).
8) H. Kopka, K. Beneke, and G. Lagaly, *J. Colloid Interface Sci.*, **123**, 427 (1988).
9) Y. Sugahara, N. Yokoyama, K. Kuroda, and C. Kato, *Ceram. Int.*, **14**, 163 (1988).
10) S. Miyata, *Clays Clay Miner.*, **23**, 369 (1975).
11) W. R. Feairheller Jr. and J. E. Katon, *Spectrochim. Acta, Part A*, **23**, 2225 (1967).
12) J. Umemura and S. Hayashi, *Bull. Inst. Chem. Res., Kyoto Univ.*, **52** (4), 585 (1974).
13) J. C. Leyte, L. H. Zuiderweg, and H. J. Vledder, *Spectrochim. Acta, Part A*, **23**, 1397 (1967).
14) S. Crisp, H. J. Prosser, and A. D. Wilson, *J. Mater. Sci.*, **11**, 36 (1976).
15) W. Balcerowiak, J. Hetper, J. Beres, and J. Olkowska, *J. Therm. Anal.*, **11**, 101 (1977).

 © 1989 The Chemical Society of Japan Bull. Chem. Soc. Jpn., 62, 3446—3450 (1989) [Vol. 62, No. 11

Interfacial Adsorption of Iron(II)-4,7-Diphenyl-1,10-phenanthroline Complex in Ion-Association Extraction Systems

Hitoshi WATARAI* and Yoko SHIBUYA
Department of Chemistry, Faculty of Education, Akita University, Akita 010
(Received April 6, 1989)

The interfacial adsorptivity of an iron(II)-4,7-diphenyl-1,10-phenanthroline (DPP) complex in chloroform/aqueous salt solution systems was investigated by means of a high-speed stirring method and interfacial tension measurements. The interfacial spectra observed in the stirred system suggested that the adsorbed species at the interface is the tris-DPP complex. A minor effect of the anion concentration on the adsorptivity suggested that the tris-complex adsorbed as an ion-pair in a 0.1 M anion concentration. The interfacial adsorption of the ion-pair under stirring was analyzed by the Langmuir isotherm. The adsorptivity increased, depending on the counter ions, in the order $ClO_4^- < CCl_3COO^- \simeq Br^- < Cl^- < SO_4^{2-}$, i.e. the order of increasing hydration energies of these anions.

Interfacial phenomena in solvent extraction processes have recently become an attractive subject in both fields of fundamental solvent extraction chemistry[1] and practical solvent extraction technology.[2]

Many studies have been reported concerning the solvent extraction mechanisms of ion-association extraction equilibria. The reactions in the ion-association extraction systems are usually thought to occur in two bulk phases, and the influence of the interface which exists between two liquid phases is completely ignored. Therefore, the extraction constants in the ion-association extraction equilibria are usually represented by using the ion-pair formation constants in bulk phases and the distribution constant of the ion-pair.

In our recent studies, some observations suggested a significant role of the interface in ion-association extraction processes. For example, methyl or phenyl derivatives of 1,10-phenanthroline adsorbed at the interface of chloroform/aqueous dilute hydrochloric acid, more abundantly at lower pH.[3] A tris(1,10-phenanthroline)iron(II) complex, which did not adsorb at the air/water interface,[4] showed the characteristic interfacial adsorptivity, depending on the kinds of organic solvents.[5] The distribution equilibrium of 4,7-diphenyl-1,10-phenanthroline under stirring was affected by the addition of zinc(II) or copper(II) ion, probably because of the interfacial adsorption of a metal complex of the ligand.[6] These findings required extensive investigations concerning the interfacial adsorption of the metal complexes, including 1,10-phenanthroline or its derivatives, in order to clarify the role of the interface in the ion-association extraction mechanism.

In the present study the interfacial adsorptivity of an iron(II) complex with 4,7-diphenyl-1,10-phenanthroline (abbreviated as DPP or L) was investigated in both static and highly agitated chloroform/aqueous electrolyte solution systems. Here, the adsorption isotherm and the effect of counter anions on the adsorptivity are discussed.

Experimental

Chemicals. DPP, Wako G. R., was used as purchased. A stock solution of iron(II) was prepared by dissolving recrystallized iron(II) chloride in dilute hydrochloric acid with hydroxylamine hydrochloride or iron(II) sulfate in dilute sulfuric acid with ascorbic acid. A solution of iron(II)-DPP complex in chloroform was prepared by a batch extraction method in a glass-stoppered centrifuge tube or by extraction in a high-speed stirring apparatus in advance. Sodium salts of perchlorate, bromide, trichloroacetate, chloride, and sulfate (all G. R. grade reagents) were used for the preparation of the aqueous electrolyte solutions. Chloroform (Wako G. R.) was washed three times with water prior to use. Water was purified by means of a Millipore Milli-QII system. Other chemicals used in the present study were of analytical reagent grade.

Interfacial Tension. Interfacial tensions, γ, were measured by means of a drop-volume method at 25±0.1 °C. The apparatus used in this study was the same as described previously.[5] The liquid-liquid systems used for the measurements were prepared by shaking 10 ml of 3×10^{-6}—3×10^{-3} M DPP (1 M=1 mol dm^{-3}) in chloroform and 10 ml of 1×10^{-3} M or 5×10^{-3} M Fe^{2+} in 0.1 M aqueous salt solution for 30—60 min in order to attain extraction equilibrium. The concentrations of $[Fe(DPP)_3]^{2+}$ in the organic phase were determined photometrically. The volume of a detached aqueous drop from a glass capillary was measured with precision to 0.1 μl by the use of Gilmont digital micrometer-syringe. The interfacial tension was calculated by the equation reported by Lando and Oakley.[7] The densities of the aqueous phases required for the calculations of γ were determined in the present study by using a pycnometer.

Stirring Experiment. Interfacial adsorption under stirring was observed at 25±0.1 °C by means of a high-speed stirring apparatus (described in detail elsewhere[3]). Fifty ml of iron(II)-DPP complex in chloroform and an equal volume of aqueous solution containing iron(II) ($<10^{-3}$ M) and 0.1 M sodium salt, which attained extraction equilibrium, was agitated by stirring at a stirring rate of 4700 rpm. The stirring caused a reversible decrease in the organic phase absorbance. From the decrement of the absorbance at the wavelength where the ion-pair showed a maximum absorbance, the interfacial amount of the complex was calculated. The effect of pH on the interfacial amount is not significant

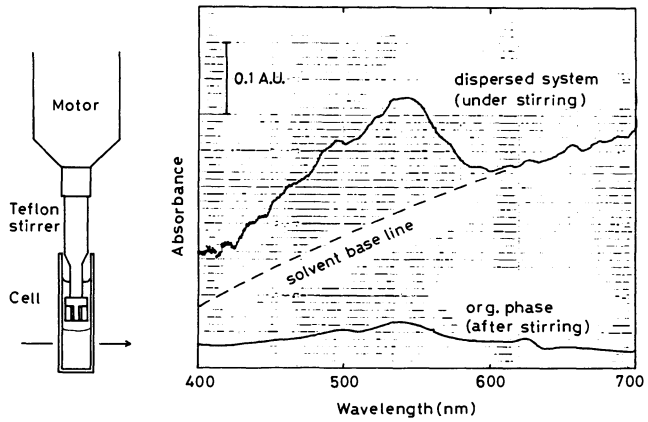

Fig. 1. Left; method for the measurements of interfacial spectra under stirring. Right; an example of the interfacial spectra, $[Fe^{2+}]_{init}=1.0\times10^{-3}$ M, $[DPP]_{o,init}=3.0\times10^{-3}$ M, and $[Na_2SO_4]=0.05$ M, 3500 rpm.

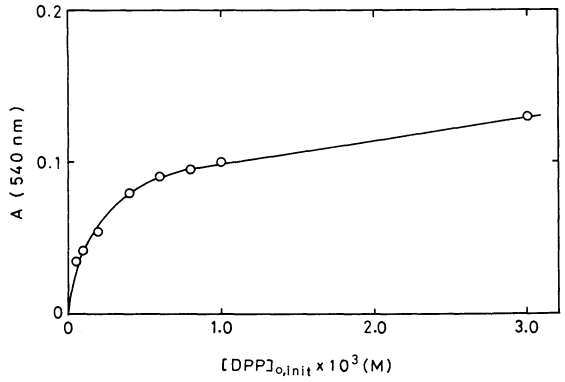

Fig. 2. Effect of DPP concentration on the interfacial spectra; $[Fe^{2+}]_{init}=1.0\times10^{-3}$ M, $[Na_2SO_4]=0.05$ M, 3500 rpm.

over a pH range of 3.5—5.5.

Spectral Measurement. Direct measurements of the absorption spectra of the interfacially adsorbed species were attempted by using the method shown in Fig. 1. In a 1 cm optical cell mounted in a cell compartment of a Jasco Uvidec 430 spectrophotometer, a 1.5 ml chloroform solution of DPP was stirred with an equal volume of aqueous solution of iron(II) and sodium sulfate or sodium chloride by a small Teflon stirrer at the rate of 3500 rpm. The spectra of the dispersed system was recorded while maintaining stirring. The spectra of the solvent blank under stirring and that of the organic phase after stirring were also measured.

Extraction Experiment. The extractability of the ion-pair was observed in four-anion systems by a batch method. Five ml of DPP in chloroform and an equal volume of an aqueous phase containing iron(II) and 0.1 M sodium salt was shaken by a mechanical shaker for 30 min in a thermostated room at 25±1 °C. After centrifugation, the concentration of the ion-pair in the organic phase was determined photometrically. The distribution ratio of iron(II) was obtained under various concentrations of iron(II) and DPP.

Results and Discussion

Interfacial Spectra of the Stirred System. When 6.0×10^{-5}—3.0×10^{-3} M DPP in chloroform was stirred with 1.0×10^{-3} M iron(II) in a 0.05 M sodium sulfate solution, there was no appreciable extraction of the red iron(II) complex in the organic phase after stirring; nor was there an appreciable amount of it formed in the aqueous phase. However, only during stirring of the two-phase system did a reddish color appear on the dispersed mixture. A typical example of the absorption spectrum of the dispersed mixture of a $CHCl_3$/Na_2SO_4 solution system is shown in Fig. 1. The net absorbance of the spectrum under stirring is obviously larger than that after stirring. Since there was no colored species in the bulk aqueous phase, the spectrum observed under stirring was attributable to an interfacial species, which was produced only at the interface. From the shape of the spectrum (maximum at 540 nm), the interfacial species was assigned to the tris-DPP complex, $[Fe(DPP)_3]^{2+}$. The net absorbance at 540 nm under stirring was increased with DPP concentration, as shown in Fig. 2. The plots showed a saturation curve which suggested that the observation was characteristically an interfacial phenomena. In a chloride system, a stirred mixture of 2.0×10^{-4} M DPP in chloroform and 1.0×10^{-3} M iron(II) in a 0.1 M NaCl solution at 3500 rpm gave 0.190 as the difference between absorbances at 537 nm and 600 nm, while the organic phase after stirring gave 0.325 as the corresponding absorbance difference; the aqueous phase showed no color. If there is no formation of the complex at the interface during stirring, the absorbance difference under stirring is equal to half of the absorbance difference of the organic phase after stirring. The experimental result (that 0.190 is larger than 0.325/2=0.1625) strongly suggested the contribution of an extra formation of $[Fe(DPP)_3]^{2+}$ at the interface.

Interfacial Adsorption Isotherm. A typical example of the effect of stirring on the extraction equilibria is shown in Fig. 3 for the cases of trichloroacetate systems. The initiation of stirring of a two-phase system which had already attained an extraction equilibrium caused a decrease in the organic phase absorbance of the ion-pair $[Fe(DPP)_3]X_2$ (X denotes an anion) until it reached a new equilibrium under stirring. When the stirring was stopped, the absorbance was restored to that before stirring, as shown in Fig. 3.

From the absorbance before or after stirring (A) and that under stirring (A'), the absorbance decrement ($\Delta A=A-A'$) was calculated. The values of ΔA depended on the ion-pair concentration in the organic phase as well as on the anion concentration in the aqueous phase. The ion-pair concentration dependence is shown as plots of ΔA against A' for a four-

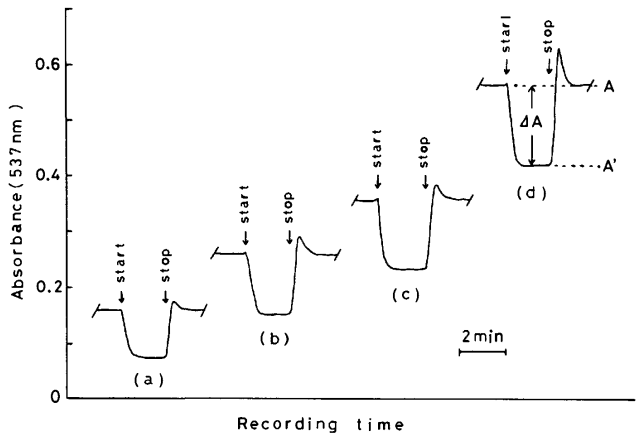

Fig. 3. A typical example of the stirring effect (4700 rpm) on the organic phase absorbance; $[Fe^{2+}]_{init}=1.0\times10^{-3}$ M, $[DPP]_{o,init}=3.57\times10^{-5}$ M (a), 5.03×10^{-5} M (b), 6.48×10^{-5} M (c), and 9.35×10^{-5} M (d).

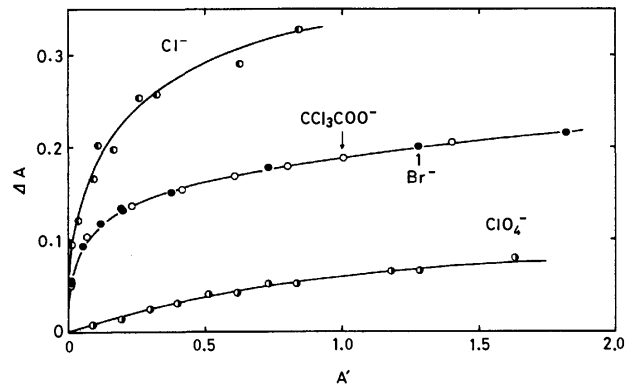

Fig. 4. Adsorption isotherm of $[Fe(DPP)_3]X_2$ under stirring; anion (X) concentration in aqueous phase is 0.1 M in all cases.

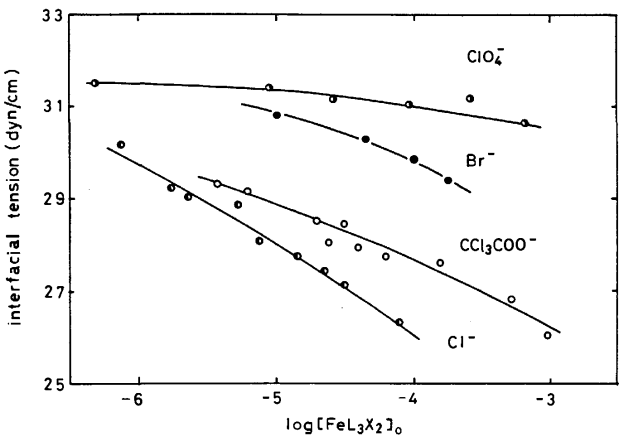

Fig. 5. Lowering of the interfacial tension as a function of the organic phase concentration of $[Fe(DPP)_3]X_2$ in the ion-association equilibria; anion (X) concentration in aqueous phase is 0.1 M.

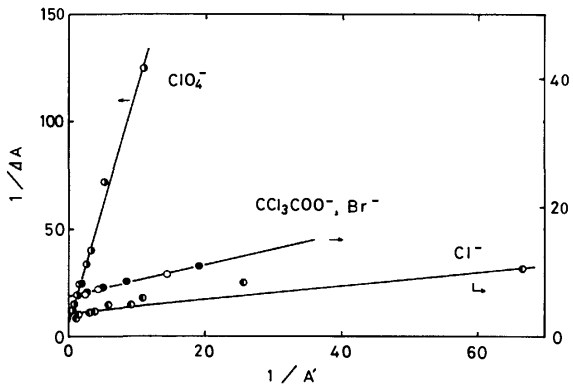

Fig. 6. Langmuir plot for the interfacial adsorption of $[Fe(DPP)_3]X_2$ under stirring.

anion systems in Fig. 4. The value of ΔA was largest in a chloride system and smallest in a perchlorate system, when compared at a given A'. If the observed stirring effects were responsible for the interfacial adsorption of the iron(II)-DPP complex, the interfacial tension in those systems must also be changed with the concentration of the ion-pair in the organic phase. The interfacial tension of the chloroform/aqueous phase system was indeed lowered with an increase in the concentration of the ion-pair in organic phase, depending on the anions (Fig. 5). The order of the lowering in the interfacial tension was found from Fig. 5 to be perchlorate<bromide<trichloroacetate< chloride, which can be understood as the order in the effect of anions on the adsorptivity of the ion-pair. It must be noticed, however, that the interfacial tension lowering in a trichloroacetate system includes the contribution of the adsorption of the anion, itself.

The above results suggest an interfacial adsorption of the complex; thus, the results of stirring were analyzed as follows. The mass balance equation of the tris-complex, FeL_3^{2+} under stirring is represented by

$$[FeL_3^{2+}]_{o,init}V_o = [FeL_3^{2+}]_oV_o + [FeL_3^{2+}]_iA_i, \quad (1)$$

where subscripts o, i, and init refer to the organic phase, interface, and initial concentration, respectively. V_o refers to the volume of the organic phase (l) and A_i to the total interfacial area (cm^2). The interfacial concentration was assumed to obey the Langmuir isotherm,

$$[FeL_3^{2+}]_i = \frac{aK'[FeL_3^{2+}]_o}{a + K'[FeL_3^{2+}]_o} \quad (2)$$

where a refers to the saturated interfacial concentration (mol cm^{-2}) and K' to the adsorption constant (l cm^{-2}) defined by $K'=[FeL_3^{2+}]_i/[FeL_3^{2+}]_o$ at infinitly diluted concentration of FeL_3^{2+}. From Eqs. 1 and 2, the relation between ΔA and A' can be derived as

$$\frac{1}{\Delta A} = \left(\frac{1}{a} + \frac{\varepsilon}{K'A'}\right)\frac{V_o}{\varepsilon A_i}, \quad (3)$$

where ε is the molar absorptivity of the ion-pair in the organic phase. Based on Eq. 3, $1/\Delta A$ was plotted against $1/A'$ for the four-anion systems (Fig. 6). The

Table 1. Interfacial Adsorption of $[FeL_3]X_2$ in the Stirred Chloroform/Aqueous Phase Systems at 25 °C

Anion (0.1 M)	$\varepsilon\times10^4$ (λ_{max})	$\log K_{ex}$*[a]	$aA_i\times10^7$[b]	$K'A_i$
			mol	l
ClO_4^-	2.14 (534 nm)	14.7	4.26±1.40	(4.52±0.14)×10^{-3}
CCl_3COO^-	1.99 (537 nm)	14.2	4.13±0.19	(2.03±0.30)×10^{-1}
Br^-	2.05 (573 nm)	13.4	3.90±0.10	(2.07±0.14)×10^{-1}
Cl^-	1.58 (537 nm)	10.6	8.82±0.60	(4.73±0.32)×10^{-1}

a) Conditional extraction constant, $K_{ex}^*=[FeL_3X_2]_o/[Fe^{2+}][L]_o^3$ estimated when $[X^-]=0.1$ M, where L=DPP.
b) Using $a=2.5\times10^{-11}$ mol cm^{-2} obtained from Fig. 5, A_i is estimated as 2.3×10^4 cm^2.

linear relations in Fig. 6 strongly support the interfacial adsorption mechanism for the stirring effect. From the slopes and the intercepts of the plots in this figure, parameters aA_i and $K'A_i$ were obtained (Table 1).

Effect of Anions on the Interfacial Adsorption. The saturated interfacial amount of the complex, aA_i (Table 1), shows an order of 10^{-7} mol irrespective of the anions, while the values of $K'A_i$ obviously depend on the anions: largest in chloride ion and smallest in perchlorate ion. The results of the interfacial spectra and the stirring effect showed that the effect of the anions on the adsorptivity increased in the order $ClO_4^-<CCl_3COO^-\simeq Br^-<Cl^-<SO_4^{2-}$, essencially corresponding to the same order in the hydration energies of the anions.[8] This order was reversed concerning the effect of anions on the conditional extraction constants, K_{ex}*, of the ion-pair, as listed in Table 1. Similar results were reported in the interfacial adsorption of tridodecylmethylammonium and trioctylmethylammonium salts in *o*-xylene/2 M aqueous acid systems, in which the adsorptivity increased in the order $ClO_4^-<CH_3COO^-<NO_3^-<Cl^-$.[9] As opposed to this, the interfacial adsorptivity of tetrabutylammonium halides increased in the order $Cl^-<Br^-<I^-$.[10] From these results, it can be concluded that when the cation which adsorbs at the interface is highly hydrophobic and the interfacial adsorption takes place from the organic phase side, as in the present case of $[Fe(DPP)_3]^{2+}$, the cation is more adsorbable when a counter anion is more hydrophilic and less extractable. On the other hand, when the cation which adsorbs is soluble in water and its interfacial adsorption occurs from the aqueous phase side, as in the case of tetrabutylammonium ion, interfacial adsorption is more favorable in a less hydrophilic and more extractable anion system.

It is important to know whether $[Fe(DPP)_3]^{2+}$ exists at the interface as an ion-pair or a free cation. Figure 7 shows the effect of the concentrations of ClO_4^- and Cl^- on both ΔA and A. In the ClO_4^- system, the ion-pair concentration in the organic phase (shown by A) was not affected by the anion concentration, while the interfacial amount (shown by ΔA) slightly decreased with an increase in the ClO_4^- concentration. In the Cl^- system, although the ion-pair concentration

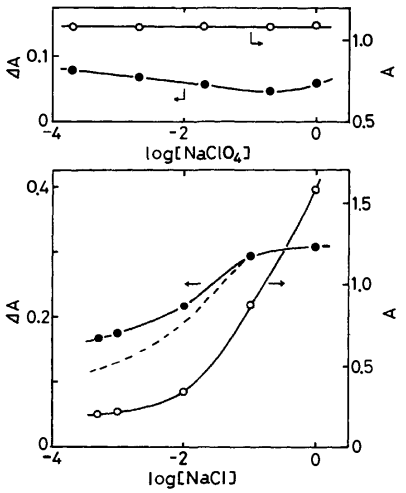

Fig. 7. Effect of the salt concentrations on ΔA and A; upper figure, $[Fe(DPP)_3X_2]_{o,init}=3.0\times10^{-5}$ M, lower figure, $[Fe^{2+}]_{init}=1.0\times10^{-3}$ M, $[DPP]_{o,init}=3.3\times10^{-4}$ M. Dotted line shows hypothetical ΔA when A is the plotted one in [NaCl]=0.1 M.

steeply increased with an increase in the Cl^- concentration, the interfacial amount gradually increased with an increase of the Cl^- concentration and became almost constant around $[Cl^-]=0.1$ M.

A comparison between the change in ΔA observed by varying the NaCl concentration and that observed by varying the $[Fe(DPP)_3]^{2+}$ concentration at [NaCl]= 0.1 M under the same values of A (Fig. 7) indicated that the values of ΔA slightly increased at lower concentrations of Cl^- than 0.1 M. From these results it is supposed that the effect of the anion concentration on the adsorbed amount is not ascribable to an ion-pair formation at the interface but, rather, to the extraction equilibrium between bulk phases. Hence, the interfacial species in 0.1 M anion concentrations is probably the ion-pair.

In conclusion, interfacial adsorption in the ion-association extraction equilibria of a tris-DPP iron(II) complex was clarified and the extent of the contribution was found to be more remarkable in systems of a more dilute complex concentration (as shown by the observation of Langmuir isotherm) and in less extractable anions. These results strongly suggest that the extraction reaction in this system takes place at the

interface, opposite to the usual assumption that the extraction mechanism comprises ion-pair formation in the aqueous phase and a distribution of the ion-pair between two-phases. The role of the interface in the extraction mechanism will be further clarified by kinetic studies which are now in progress.

The authors thank Miss Naoko Sasaki for measurements of the interfacial spectra. This study was supported by a Grant-in-Aid for General Scientific Research from the Ministry of Education, Science and Culture (No. 6140034).

References

1) H. Freiser, *Bull. Chem. Soc. Jpn.*, **61**, 39 (1988).
2) V. V. Tarasov and G. A. Yagodin, *Ion Exch. Solv. Extr.*, **10**, 141 (1988).
3) H. Watarai, *J. Phys. Chem.*, **89**, 384 (1985).
4) S. Ozeki, S. Tachiyashiki, S. Ikeda, and Y. Yamatera, *J. Colloid Interface Sci.*, **91**, 439 (1983).
5) H. Watarai, Y. Horii, and M. Fujishima, *Bull. Chem. Soc. Jpn.*, **61**, 1159 (1988).
6) H. Watarai, *Talanta*, **32** (8B), 817 (1985).
7) J. L. Lando and H. T. Oakley, *J. Colloid Interface Sci.*, **25**, 526 (1967).
8) D. R. Rosseinsky, *Chem. Rev.*, **65**, 467 (1965); V. P. Vasil'ev, E. K. Zolotasev, A. F. Kapustinskii, K. P. Mishchenko, E. A. Podgornaya, and K. B. Yatsimirskii, *Zh. Fiz. Chim.*, **34**, 1763 (1960).
9) G. F. Vandegrift, S. M. Lewey, G. R. Dyrkacz, and E. P. Horwitz, *J. Inorg. Nucl. Chem.*, **42**, 127 (1980).
10) K. Tamaki, *Bull. Chem. Soc. Jpn.*, **40**, 38 (1967).

 © 1989 The Chemical Society of Japan Bull. Chem. Soc. Jpn., 62, 3451—3456 (1989)

Chromatographic Separation of Rare Earth Pairs by a Chelating Resin Having Bis(carboxymethyl)amino Groups

Masatoshi KANESATO,* Toshiro YOKOYAMA, and Toshishige M. SUZUKI
Government Industrial Research Institute, Tohoku, 4-2-1, Nigatake, Miyagino-ku, Sendai 983
(Received April 6, 1989)

Adsorption properties of rare earth elements toward a cross-linked polystyrene resin having bis(carboxymethyl)amino groups (CMA) have been studied. The selectivity sequence of the resin for a series of rare earth metals was in good accordance with that of the corresponding stability constants of diethylenetriamine-*N,N,N',N'',N''*-pentaacetic acid (DTPA) complexes. The chromatographic separation of La(III)/Pr(III), Nd(III)/Sm(III), and Y(III)/Gd(III) has been carried out by use of the present resin. The chromatographic conditions were empirically evaluated in terms of resolution (R_s), with varying column length, pH of the eluent, the flow rate and the column temperature.

Ion exchange chromatography has significantly contributed to the separation of rare earth elements.[1-4] In the conventional separation process, a cation-exchange resin and an aqueous solution of chelating reagent are employed as a stationary phase and a selective mobile phase, respectively.

Complexane-type reagents such as ethylenediamine-*N,N,N',N'*-tetraacetic acid (EDTA),[1] *N'*-(2-hydroxyethyl)ethylenediamine-*N,N,N'*-triacetic acid (HEDTA)[5,6] and DTPA[7] are widely used as the selective reagent in a mobile phase due to their high separation factors for adjacent rare earths. However the solubilities for their protonated forms and the rare earth complexes are sometimes remarkably low. Therefore undesirable precipitation tends to take place during the column operations.[8,9] On the contrary, when we use a highly selective resin as a stationary phase, a simple buffer solution can be used as an eluent in place of valuable chelating reagents. In addition, the difficulty of extracting the rare earths as simple salts from the stable chelate compounds will be eliminated.

It has already been pointed out that selective resins including chelating resins[10,11] and reagent-impregnated resins[12] are effective for the separation of rare earth elements in the chromatographic systems. Takeda et al.,[11] demonstrated the chromatographic separation of several pairs of rare earths using polystyrene resins having functional groups structurally similar to EDTA and DTPA. Prior to experimentation, they have optimized the chromatographic conditions by computer simulation based on newly introduced thermodynamic parameters.

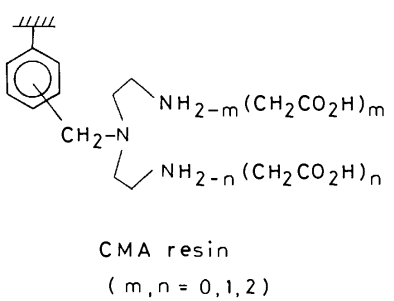

CMA resin
(m, n = 0, 1, 2)

Fig. 1. Cross-linked polystyrene resin having bis(carboxymethyl)amino groups.

We have developed the cross-linked polystyrene beads (macroreticular type) in which diethylenetriamine is linked uniquely through the secondary nitrogen.[13] Upon carboxymethylation of the aminated resin, we have obtained the chelating resin having bis(carboxymethyl)amino moieties (Fig. 1).[13,14] In this paper we have examined the adsorption selectivity of the CMA resin for a series of rare earth metals by measuring the distribution coefficient. The separation efficiency of the present resin has been evaluated by the separation factor derived from the distribution coefficients of the respective metal pairs. The mutual separation of several pairs of metals has also been carried out chromatographically under the optimum experimental conditions.

Experimental

Materials. A rare earth chloride solution was prepared by dissolving the corresponding oxide (99.9%, Japan Yttrium Co., Ltd.) in analytical grade hydrochloric acid. Other reagents were of analytical grade and were used without further purification. Chloromethylated polystyrene beads (Cl, 17.1%, 60—100 mesh) were kindly donated by Mitsubishi Chemical Co., Ltd. The resin matrix was a macroreticular (MR) type styrene-10%-divinylbenzene copolymer with the surface area and mean pore diameter, 7.3 $m^2 g^{-1}$ and 720 Å, respectively.

Preparation of the Chelating Resin. The CMA resin was prepared by *N*-carboxymethylation of the dien-resin[13] in which diethylenetriamine (dien) is linked to the polystyrene resin uniquely through the imino nitrogen. Nitrogen analysis indicated that the CMA resin contains 1.65 mmol of the functional group per gram resin.[14]

Determination of the Adsorption Capacity. A batchwise technique was employed to determine the equilibrium adsorption capacity (amount of metal ion sorbed on one gram of dry resin) with the metal ion always being in excess over the ligand content. Typically, 500 mg of the dry resin (H^+ form) was added to 100 cm^3 of metal ion solution (0.025 mol dm^{-3}) of various pH. After shaking 2 days at 25 °C the equilibrium pH and the amount of metal ion remaining in the solution were determined. The capacity of

the resin was calculated by the change in the metal concentration observed. The resin beads were packed in a glass column and washed thoroughly with water. The sorbed metal ion was liberated from the resin beads by elution with 20 cm^3 of 2 mol dm^{-3} hydrochloric acid and the metal ion in the eluent was analyzed. In most cases, a satisfactory material balance was observed between the metal ion liberated from the resin and that which remained in the solution.

Distribution Coefficients. The equilibrium distribution coefficient of the metal ion was determined under a batchwise procedure. A 500 mg batch of dry resin was immersed in 100 cm^3 of metal ion solution (0.001 mol dm^{-3}). The pH was adjusted with acetate buffer in the pH range 3.0—5.0, with hydrochloric acid below 3.0. After shaking 7 days at 25 °C, the equilibrium pH and the amount of metal ion remained in the solution were determined. The results are expressed as the distribution coefficient, K_d=amount of metal sorbed in one gram of the resin/amount of metal remaining in 1 cm^3 of the solution.

Column Separation of Metal Ion Mixture. A typical procedure is as follows; the resin beads were swollen with water and poured onto a glass column (ϕ 10 mm). An aqueous solution containing two kinds of rare earths of equal molar concentration was prepared. The pH of the solution was adjusted to 3.0 with 1 mol dm^{-3} glycine buffer. The metal ion solution was supplied to the column at a constant flow rate (0.25—1.00 cm^3 min^{-1}), and the sorbed metal ions were then eluted with a buffer solution (1 mol dm^{-3} glycine) of the pH ranging 0.8—2.0. The effluent was fractionated into 10 cm^3 portions and the amount of metal ion was determined.

Metal Analysis. The metal ion concentration was determined by a SEIKO ICP-atomic emission spectrometer, model SPS-1200A.

Results and Discussion

Equilibrium Adsorption Capacity. The capacity-pH profiles for La(III), Pr(III), and Sm(III) are given in Fig. 2. A similar trend was observed for other rare earth metals. The adsorption capacity apparently depends on the pH of the solution due to the competing protonation and complexation reactions of the functional group. The maximum capacity is approximately 1.4 mmol g^{-1} at pH higher than 4.9 irrespective of the metal ions examined. This value is close to the estimated ligand content (1.65 mmol g^{-1}). Hence the functional group in the CMA resin appeared to form 1:1 complexes with these metal ions in a similar manner to those of the EDTA complexes. The adsorbed metal ions can be quantitatively released from the resin on treatment with 2 mol dm^{-3} hydrochloric acid for regeneration.

Distribution Coefficients. Distribution coefficients of the CMA resin for several rare earth metal ions were examined as a function of pH and the results are given in Fig. 3. The reaction of the CMA resin with a metal ions can be expressed as follows;

$$M^{n+} + RH_m \overset{K}{\rightleftharpoons} RH_{m-n}M + nH^+ \quad (1)$$

where R and M denote the resin group and the metal, respectively. The equilibrium constant of the above reaction should be given by

$$K = \frac{[RH_{m-n}M][H^+]^n}{[M^{n+}][RH_m]} \quad (2)$$

The distribution coefficient (K_d) of the metal ion between the resin phase and the aqueous phase is defined by

$$K_d = \frac{[RH_{m-n}M]}{[M^{n+}]} \quad (3)$$

From Eqs. 2 and 3, the following relationship can be obtained.

$$\log K_d = \log K + \log [RH_m] + n\mathrm{pH} \quad (4)$$

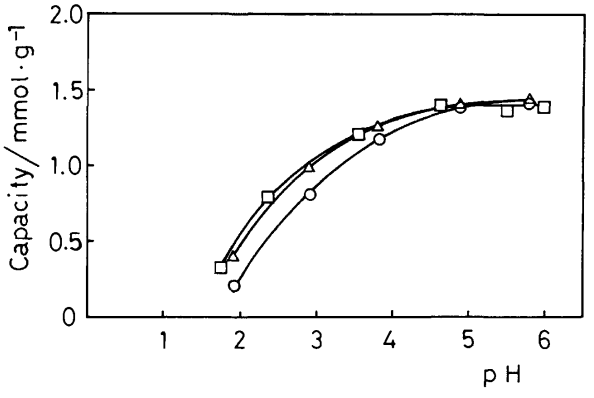

Fig. 2. Equilibrium adsorption capacity of the CMA resin for La(○), Pr(△), and Sm(□) as a function of pH (25 °C).

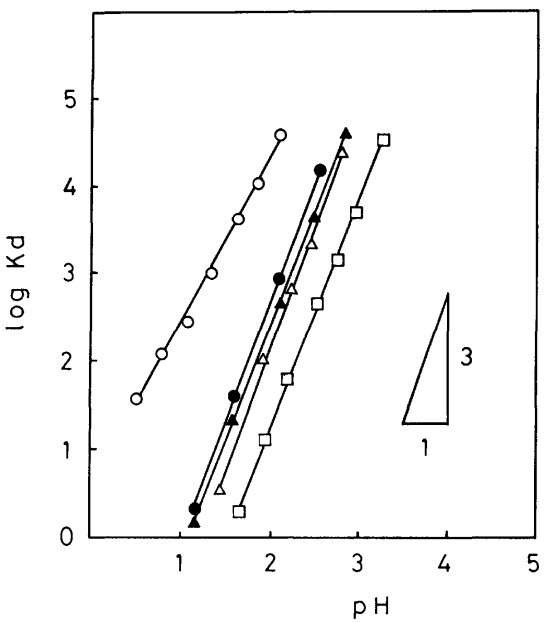

Fig. 3. log K_d of the CMA resin for several rare earth metal ions as a function of pH (25 °C). Sc(○), Y(△), La(□), Eu(●), and Yb(▲).

Equation 4 predicts that the plot of log K_d against pH gives a straight line of slope n under the condition where the amount of functional group is much larger than that of the metal ion. The slopes of the linear plots for the fourteen rare earth elements except Sc(III) were in the range from 2.7 to 3.0, which indicates that the adsorption of a rare earth metal ion is accompanied by the release of three protons. The slope for the Sc(III), 2.0, was smaller than that for other rare earth elements. In this case, some reaction mechanism other than those expressed in Eq. 1 may be involved.

Figure 4 shows the log K_d values at pH 1.6 for fifteen rare earth elements. The distribution coefficient apparently increased with decreasing ionic radius for the light rare earths (La—Sm), reached a maximum and then gradually decreased toward the heavy rare earths. Scandium, having the smallest ionic radius showed the highest affinity to the resin whereas yttrium occurred in the light rare earths. These trends are in good accordance with the stability constant sequence of the corresponding DTPA complexes where the gradual decrease in stability constant takes place for the heavy rare earths.[15] Therefore the selectivity of the resin can be attributed to the nature of a functional group which is structurally similar to DTPA.

Column Separation. The selectivity profile of the CMA resin (Fig. 4) suggests the possibility for mutual separation of light rare earths as well as Y from Sm—Dy. The separation efficiency of a metal ion pair is evaluated by the separation factor expressed by the ratio of distribution coefficients of individual metal ions 1 and 2.

$$S = K_{d1}/K_{d2} \quad (5)$$

In the present study, we chose the following pairs of rare earth metals, La(III)/Pr(III), Nd(III)/Sm(III), and Y(III)/Gd(III) for the chromatographic separation. The separation factors of the above three metal pairs calculated from the K_d values at pH 1.6 are 7.9, 2.3, and 3.0, respectively. Among them, the Nd/Sm pair seems to be most difficult to separate. The chromatographic separation was empirically characterized in terms of the resolution (R_s) of the species 1 and 2.

$$R_s = 2(t_{R2} - t_{R1})/(w_1 + w_2) \quad (6)$$

where t_{R1} and t_{R2} denote the retention time of the species 1 and 2, and w_1 and w_2 denote the band widths of 1 and 2, respectively.

Figure 5 shows the effect of pH of the eluent on the R_s for the separation of the three pairs of metal ions. It is said that the pH of the eluent is an important factor which affects the chromatographic separation.[16,17] The variation in R_s values with pH was not remarkable in the given pH range studied. When the pH is too low, the separation was unfavorable due to the small difference in the retention time, whereas the elution at higher pH lead to a significant band broadening. Therefore the most favorable pH for the separation of La(III)/Pr(III), Nd(III)/Sm(III), and Y(III)/Gd(III) were around 1.6, 1.2, and 1.2, respectively. In the present study we used 1 mol dm^{-3} glycine buffer as an eluent to keep the pH constant.

The effect of column length was examined for the separation of La(III)/Pr(III) (Fig. 5). Better resolution was attained with an increased column length, and a

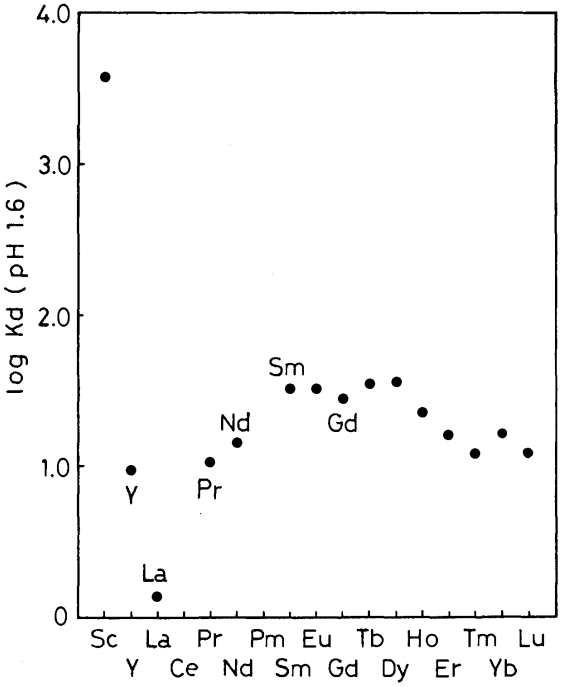

Fig. 4. Intercepts of the log K_d vs. pH plots at pH 1.6 for fifteen rare earth elements.

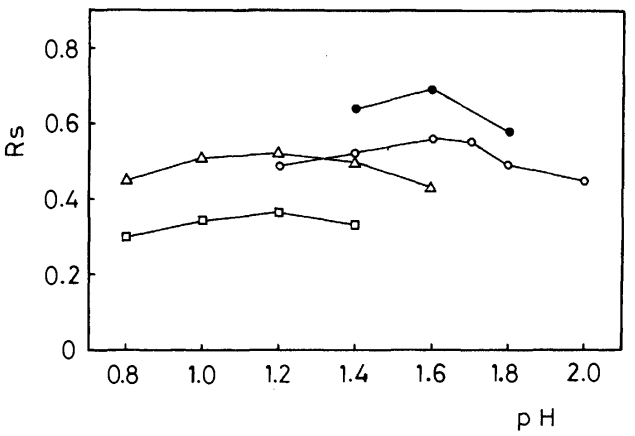

Fig. 5. Effect of pH of the eluent and the column length on the R_s for the separation of three pairs of metal ions. Column temperature: 25 °C. Flow rate: 0.5 cm^3 min^{-1}. ○: La/Pr, ϕ 1.0×14 cm, ●: La/Pr, ϕ 1.0×27 cm, △: Y/Gd, ϕ 1.0×14 cm, □: Nd/Sm, ϕ 1.0×14 cm.

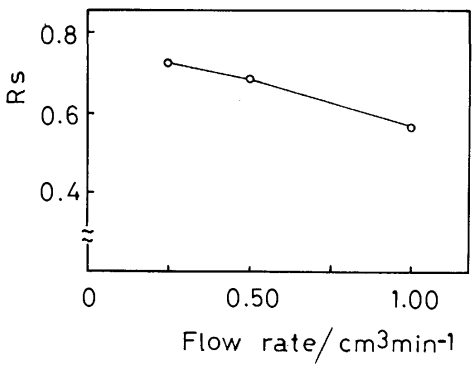

Fig. 6. Effect of the flow rate of the eluent on the R_s for the separation of La/Pr. Column temperature: 25 °C. Column size: ϕ 1.0×27 cm. The pH of the eluent: pH 1.6.

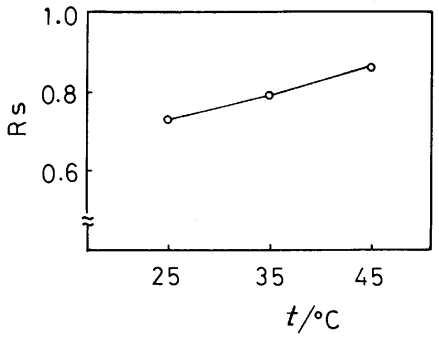

Fig. 7. Effect of the column temperature on the R_s for the separation of La/Pr. Column size: ϕ 1.0×27 cm. The pH of the eluent: pH 1.6. Flow rate: 0.25 cm^3 min^{-1}.

reduced flow rate (Fig. 6). An apparent improvement has also been attained by raising the column temperature from 25 to 45 °C (Fig. 7). The effect of temperature on the chromatographic separation may be attributed to two reasons. One is the increase of the separation factor. We have observed the increase of the retention times for La(III) and Pr(III) with increasing of the column temperature; the t_R values at 45 °C were about 1.20 and 1.24 times those at 25 °C for La(III) and Pr(III), respectively, leading to a better resolution. The second reason is the increase of the number of theoretical plates (N),[18] the N values of Pr(III) evaluated from the chromatograms were 61, 65, and 68 at 25, 35, and 45 °C, respectively. In the present study, all the column operations were carried out below 45 °C for practical reasons.

Figure 8 shows the chromatogram of the La(III)/Pr(III) pair at the optimized column condition. The degree of overlap of two peaks is less than 5% and the R_s value was found to be 0.86. Generally a separation is said to be "good" when R_s is >1.[19] For the separation of rare earth on a small scale, there are some reports in which R_s becomes larger than 1.[20,21] Considering the amount of metal ion in such as 1.2 mmol, the value 0.86 may be fairly good (Fig. 8).

It is interesting to consider a scale-up of these systems for productive purpose. Traditional ion-exchange systems where a chelating reagent is contained in the mobile phase essentially involve a restriction of solubility of the eluent. For example, the concentration of EDTA solution commonly used as an eluent is restricted due to the only moderate solubilities of the protonated EDTA or metal-EDTA com-

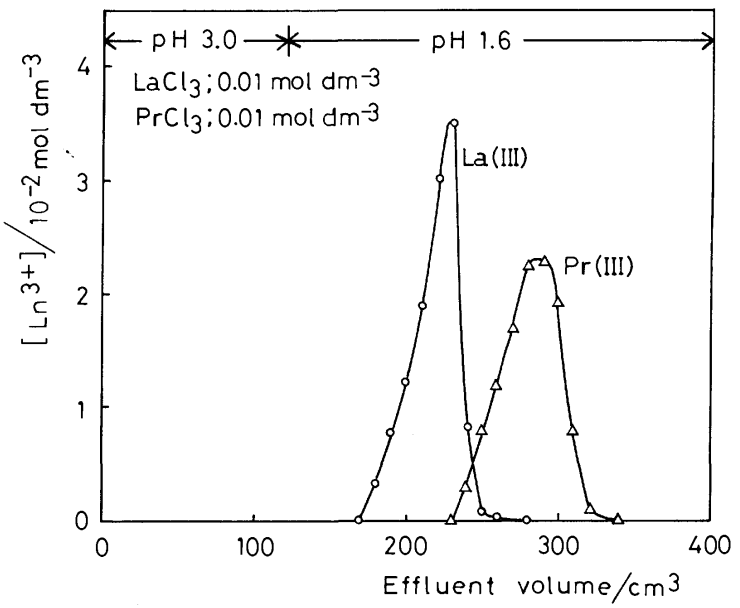

Fig. 8. Separation of La/Pr with the CMA resin. Column size: ϕ 1.0×27 cm. The pH of the eluent: pH 1.6. Flow rate: 0.25 cm^3 min^{-1}. Column temperature: 45 °C. Amount of the each metal ion: 1.2 mmol.

pounds. However, a chelating reagent is not always necessary in the present system, and hence the trouble due to precipitation during column operation can be eliminated. Figures 9, 10, and 11 show the separation chromatograms of the three pairs of metals. The amount of each metal ion is 10 mmol in all cases. The degree of overlapping of the two peaks for the separation of La(III)/Pr(III), Y(III)/Gd(III), and Nd(III)/Sm(III) were 1.1, 2.7, and 19.6%, respectively. In Fig. 9, about 95% of the loaded La(III) was collected in the fractions from 400 to 590 cm^3 of the eluate with the contamination by Pr(III) being less than 0.01%. In this experiment, the band ratio of ion-exchange zone to the metal loaded zone in the column is approximately 3 to 4 (0.75). Thus, highly purified La(III) was obtained in a reasonable yield in spite of the low band ratio. The maximum concentrations in the fractionated eluates are 8.5×10^{-2}, 4.8×10^{-2}, 9.4×10^{-2}, 5.2×10^{-2}, 8.0×10^{-2}, and 4.3×10^{-2} mol dm^{-3} for La(III), Pr(III), Y(III), Gd(III), Nd(III), and Sm(III), respectively.

A favorable separation has been realized under appreciably high loading using the CMA resin as the column stationary phase. In addition this system has advantages over the traditional ion-exchange systems where the chelating reagents are essentially required as the mobile phase. Thus, elution with only a buffer

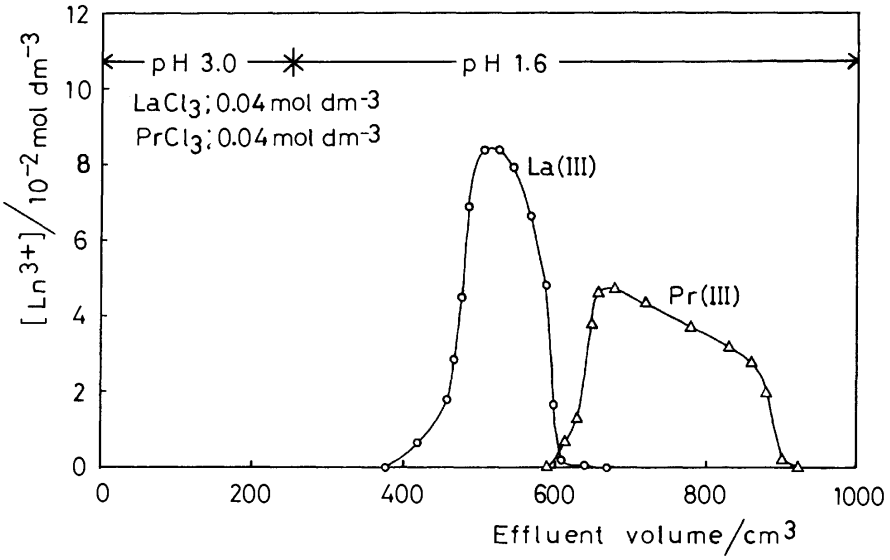

Fig. 9. Separation of La/Pr with the CMA resin. Column size: ϕ 1.0×95 cm. The pH of the eluent: pH 1.6. Flow rate: 0.25 cm^3 min^{-1}. Column temperature: 45°C. Amount of the each metal ion: 10.0 mmol.

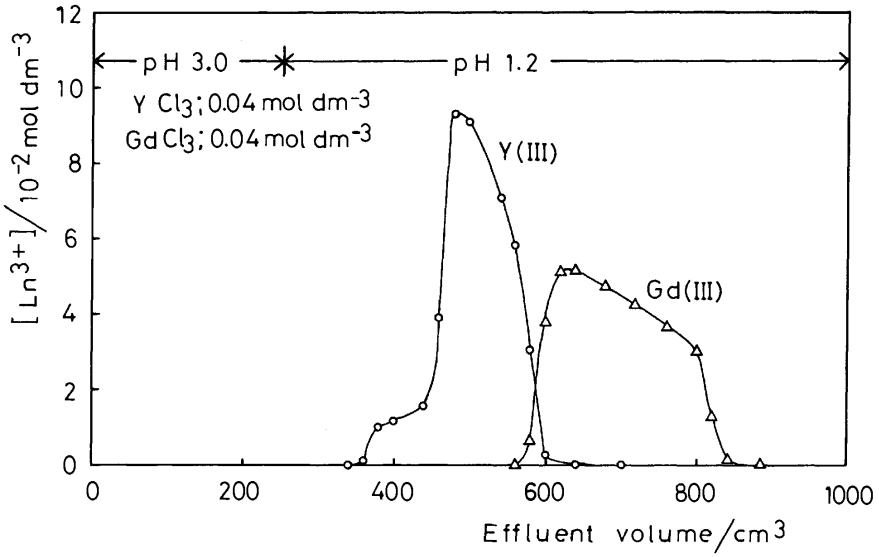

Fig. 10. Separation of Y/Gd with the CMA resin. The pH of the eluent: pH 1.2. Other conditions are the same as those given in Fig. 9.

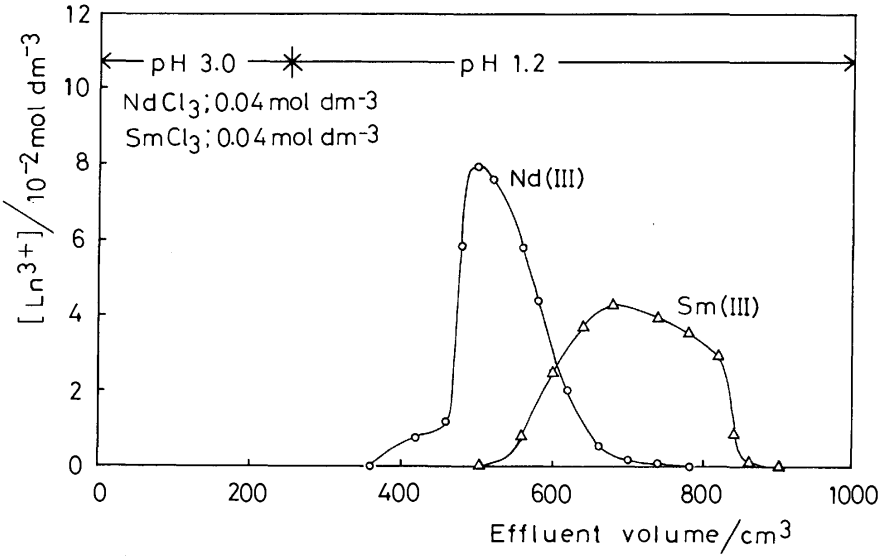

Fig. 11. Separation of Nd/Sm with the CMA resin. Conditions are the same as those given in Fig. 10.

solution may simplify the isolation procedure of metals from the eluates either by evaporation or precipitation as the oxalate or carbonate.

References

1) J. E. Powell and F. H. Spedding, *Trans. Met. Soc. AIME*, **215**, 457 (1959).
2) F. H. Spedding, J. E. Powell, and E. J. Wheelwright, *J. Am. Chem. Soc.*, **76**, 612 (1954).
3) F. H. Spedding, J. E. Powell, and E. J. Wheelwright, *J. Am. Chem. Soc.*, **76**, 2557 (1954).
4) Zenzi Hagiwara, *J. Phys. Chem.*, **73**, 3102 (1969).
5) F. H. Spedding, J. E. Powell, and E. J. Wheelwright, *J. Am. Chem. Soc.*, **78**, 34 (1956).
6) J. R. Morton and D. B. James, *J. Inorg. Nucl. Chem.*, **29**, 2997 (1967).
7) R. D. Hansen and Stanley Chaberek, Dow Chemical Co., unpublished data.
8) J. K. Marsh, *J. Chem. Soc.*, **1957**, 978.
9) R. Oomathi and T. Goto, *Kagaku To Kogyo*, **37**, 86 (1984).
10) J. N. Mathur and P. K. Khopkar, *Solvent Extraction and Ion Exchange*, **3**, 753 (1985).
11) K. Takeda, M. Akiyama, F. Kawakami, and M. Sasaki, *Bull. Chem. Soc. Jpn.*, **59**, 2225 (1986).
12) Y. Wakui, H. Matsunaga, and T. M. Suzuki, *Anal. Sci.*, **4**, 325 (1988).
13) T. M. Suzuki and T. Yokoyama, *Polyhedron*, **3**, 939 (1984).
14) T. M. Suzuki, T. Yokoyama, H. Matsunaga, and T. Kimura, *Bull. Chem. Soc. Jpn.*, **59**, 865 (1986).
15) R. Harder and S. Chaberek, *J. Inorg. Nucl. Chem.*, **11**, 197 (1959).
16) D. Ishii, A. Hirose, and Y. Iwasaki, *J. Radioanal. Chem.*, **46**, 41 (1978).
17) G. Zhao, S. Luo, S. Yao, and S. Yu, *Bunseki Kagaku*, **31**, 62 (1982).
18) Y. Takata and Y. Arikawa, *Bunseki Kagaku*, **24**, 762 (1975).
19) D. O. Campbell, *J. Inorg. Nucl. Chem.*, **35**, 3911 (1973).
20) N. R. Larsen and W. B. Pedersen, *J. Radioanal. Chem.*, **45**, 135 (1978).
21) T. Yamabe and T. Hayashi, *J. Chromatogr.*, **76**, 213 (1973).

 © 1989 The Chemical Society of Japan Bull. Chem. Soc. Jpn., 62, 3457—3463 (1989)

Synthetic Inorganic Ion-Exchange Materials. LI. Synthesis, Characterization, and Thermal Decomposition of Cubic Ammonium Molybdate

Abdul Jabbar KHAN, Masamichi TSUJI, and Mitsuo ABE*
Department of Chemistry, Faculty of Science, Tokyo Institute of Technology,
2-12-1 Ookayama, Meguro-ku, Tokyo 152
(Received April 27, 1989)

A crystalline cubic ammonium molybdate (CAM) was synthesized by the reaction of hexaammonium heptamolybdate and HNO_3 at 60 °C. The X-ray diffraction pattern showed a body-centered cubic structure with crystal lattice of 12.94±0.005 Å. Ammonia free molybdic acid was not obtained even at high acid concentration. CAM contains both exchangeable and structural ammonium ions. On the basis of chemical and thermal analyses and amount of exchangeable H^+, the empirical formula of the H^+ form of CAM referred to $[H_{0.68}(NH_4)_2]O_{1.34}\cdot 14.16MoO_3\cdot 6.92H_2O$. CAM was found to be stable at relatively high acid concentration and temperature, and was suitable for column operations by grading to the desired mesh size.

The oxides and hydrous oxides of molybdenum have been known since 1826.[1] This field got a real interest after Carpenie.[2] Preparation and structure of various molybdenum oxides, hydrates or ammonium molybdates have been studied by different authors. According to Jander et al.[3] the polycondensation of tri, hexa, 12, and 24 molybdates takes place at low pH. A significant number of authors have investigated the polymerization reaction through different analytical means.[2,4-14] A general review for normal ($M_2Mo_3O_{12}$), poly ($M_2Mo_nO_{3n+3}$), and basic ($n<3$) molybdates has been reported by Gleitzer.[15] Ma[16] and Kiss et al.[17] have reported the formation of different Mo(VI) oxide hydrates with ill-defined composition, through the thermal decomposition of ammonium heptamolybdate tetrahydrate. According to Tytko et al.[18] the aqueous chemistry of polymolybdates is very complex. The acid concentration controls the protonation to mono and dibasic species of MoO_4^{2-} present in basic solutions.

Hydrous Mo(VI) oxide or isopolymolybdates have been the subject of research of a significant number of workers. Even though Abe[19] has reported some ion-exchange behavior of $MoO_3\cdot nH_2O$, further investigations were still required to study the optimum conditions or rate of reaction for the synthesis of such compounds. In addition the formation of a product with definite composition by the reaction of hexaammonium heptamolybdate and nitric acid has not been known with certainty. Moreover the definite ion exchange behavior of these materials has not been reported prior to our study.

The present investigations were therefore carried out to describe the systematic synthesis, characterization, thermal decomposition, and some ion-exchange properties of crystalline cubic ammonium molybdate (CAM) as an ion exchanger.

Experimental

Synthesis of CAM. The optimum conditions and reagent specifications for the synthesis of the final product were set up through consideration of starting material and its concentration, $[H^+]/[Mo(VI)]$ mole ratios, aging time and temperature. The apparent rate of reaction for the product formation was determined for a series of samples with different mole ratios. The yields (%) of different products were calculated from the change in molybdenum concentration in the supernatant solutions with respect to the aging time. The Mo concentration was determined by Inductively Coupled Plasma (ICP) spectrometer, model SPS-7000, Seiko Instruments Inc. (Japan). The final synthesis of CAM was carried out as follows.

A 0.2 M (M=mol dm^{-3}) (as Mo-concn) solution of hexaammonium heptamolybdate was added slowly to an equal volume of 0.2 M HNO_3 solution with constant stirring. The mixed solution was kept at 60 °C for three days and then cooled at room temperature. A yellow product was filtered under suction and washed with deionized water till pH>2 and dried in air at room temperature.

H-CAM. CAM (100—200 mesh) was conditioned with 0.5 M HNO_3 in a column till no ammonium ion was detected in effluent, followed by washing with deionized water till pH>2 and was dried in air. The product was again sieved and rewashed to remove the adherent tiny particles. H-CAM thus obtained was finally dried in air and then over silica gel.

A-CAM. The NH_4^+ form of CAM was obtained by successive batch equilibration of H-CAM with 0.1 M NH_4NO_3 solution.

Chemical Composition. The chemical composition of H-CAM was determined by the chemical and thermal analyses. A known quantity (0.1 g) of the sample was dissolved in an adequate volume of 0.1 M NaOH solution. The total ammonia was then determined by Nessler's method spectrophotometrically at 400 nm using a double beam spectrophotometer, model UV-150-02, Shimadzu Co. (Japan). The total molybdenum content of H-CAM was determined gravimetrically by lead(II) acetate precipitation following the Japan Industrial Standards method No. K-8905.

Thermal Analysis. The Rigaku Denki Thermoflex, model 8001, was employed for thermogravimetry (TG) and differential thermal analysis (DTA) at a heating rate of 10 °C min^{-1} using α-Al_2O_3 as a reference material. The ammonia evolved during the thermal decomposition of H-CAM in N_2 gas atmosphere and collected in 0.05 M H_2SO_4

was also determined spectrophotometrically by Nessler's method.

X-Ray Diffraction, IR Spectra, and Electron Microscopy. X-Ray diffractions were carried out with JEOL JDX-7E X-ray diffractometer, Rigaku Denki Co. (Japan), model CN-5320 A-1/CN-2155 D-5 and Philips Automated powder diffractometer model PW-1700, using Ni-filtered Cu $K\alpha$ radiations. The crystal structure was deduced by SANDMAN computer programs.[20-22] The IR spectra were measured by KBr disk method on a JASCO IR spectrometer, model DS-701 G. The JEOL scanning microscope, model JSM-T220, was incorporated for the study of crystal morphology and growth.

Reagents. Hexaammonium heptamolybdate tetrahydrate (Wako Pure Chemical Ind., Ltd. Japan) was used without further purifications. All other reagents used were also of analytical grade.

Results and Discussion

Synthesis. No precipitation was observed even at reasonably long keeping of the mixed solutions at room temperature. Fast precipitation at elevated temperatures (>80 °C) resulted in the reduction of the apparent crystal size. In order to decide the optimum conditions for synthesis, the rate of reaction was studied at different mole ratios of $[H^+]/[Mo(VI)]$ at 60 °C. The prereaction specification of the reactants is given in Table 1 along with yields of the samples in percent. The time dependence of yield in Fig. 1 is shown for the samples A—E. The crystal formation was slower with an increase in the $[H^+]/[Mo(VI)]$ mole ratio greater than unity. Yield of the products decreased with the increase in acid concentration (samples C—E or Q—S), whereas at very low acid concentration (sample A) it resulted in a composite product formation which required maximum aging time at 60 °C. Hence the acid concentration affected both the yield and the composition of CAM.

Table 1. The Specification of Reactants and Yield (%) of Products

Sample	Concn in mixed soln		Mole ratio	Yield
	[Mo(VI)]/M	$[H^+]$/M	$[H^+]/[Mo(VI)]$	%
A	0.11	0.055	0.5	46
B	0.11	0.11	1.0	99
C	0.11	0.55	5.0	86
D	0.11	0.88	8.0	51
E	0.11	1.10	10.0	51
N	0.06	0.03	0.5	0
P	0.06	0.06	1.0	98
Q	0.06	0.30	5.0	88
R	0.06	0.48	8.0	76
S	0.06	0.60	10.0	60

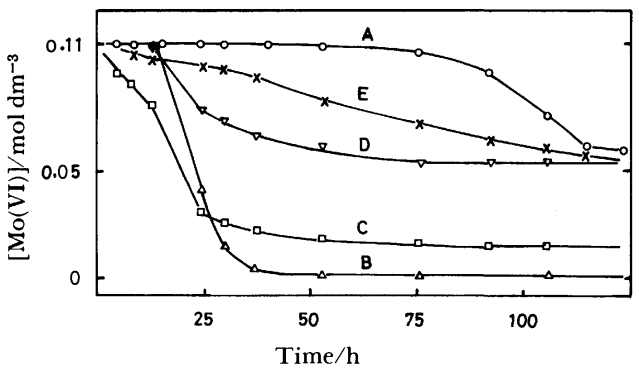

Fig. 1. Change in the concentration of Mo(VI) at different mole ratios of $H^+/Mo(VI)$. Aging temp: 60 ±0.5 °C; initial [Mo(VI)]: 0.11 mol dm^{-3}; mole ratio: 0.5(A), 1.0(B), 5.0(C), 8.0(D), and 10.0(E).

The maximum yield was observed at the mole ratio of 1.0 upto aging time of 72 h irrespective of the HNO_3 concentration. A similar trend was also observed for those of samples P—S. Sample B, due to maximum yield and reasonable rate of formation, was considered for the bulk preparation and subjected to further investigations. In the case of lower concentration of HNO_3, no product was observed in sample N upto the same aging time as for sample A.

Scanning Electron Microscopy (SEM) and X-Ray Diffraction. The SEM photograph of the crystals (Fig. 2) showed the hexagonal crystal shape of CAM arising from the wall of the beaker like cluster of flowers and the crystals were quite large (100—200 μm) in size. Almost the same X-ray diffraction patterns were observed for all samples (B—E or P—S) studied (Fig. 3), except sample A which showed a mixture of CAM and unknown materials in the JCPDS files. The crystal system of the samples was indexed to the body centered cubic structure of space group I43m (Td^3) with a lattice constant (a_0) of 12.94±0.005 Å (Table 2). The H-CAM and A-CAM also showed the same a_0 value within the experimental error.

Thermal Analyses. The TG and DTA curves of CAM and A-CAM (Fig. 4) indicated a broad endothermic peak around 150—160 °C due to loss of H_2O, a small exothermic peak at around 300 °C due to loss of exchangeable NH_4^+ and a strong exothermic peak at around 430 °C due to loss of structural ammonia and water. The small exothermic peak at around 300 °C vanished in the DTA curve of H-CAM (Fig. 5) due to absence of exchangeable NH_4^+. However, a distinct rise in the DTA curve at around 310 °C ending in a sharp exothermic peak at around 430 °C indicates the existence of structural ammonia with different bonding strength. The fractions of ammonia evolved during thermal decomposition of H-CAM was collected with respect to each rise in heating temperature and analyzed (Fig. 6). The evolution profile was in accordance with the weight loss vs. temperature shown by the TG curve (Fig. 5). However the collected ammonia was 33.1% of the total ammonia (1.54%) in H-CAM. Obviously a considerable amount of NO_x was formed due to the oxidation of NH_3, even though the N_2 gas atmosphere was incorporated. It can be estimated that the evolved ammonia at 310—430 °C is

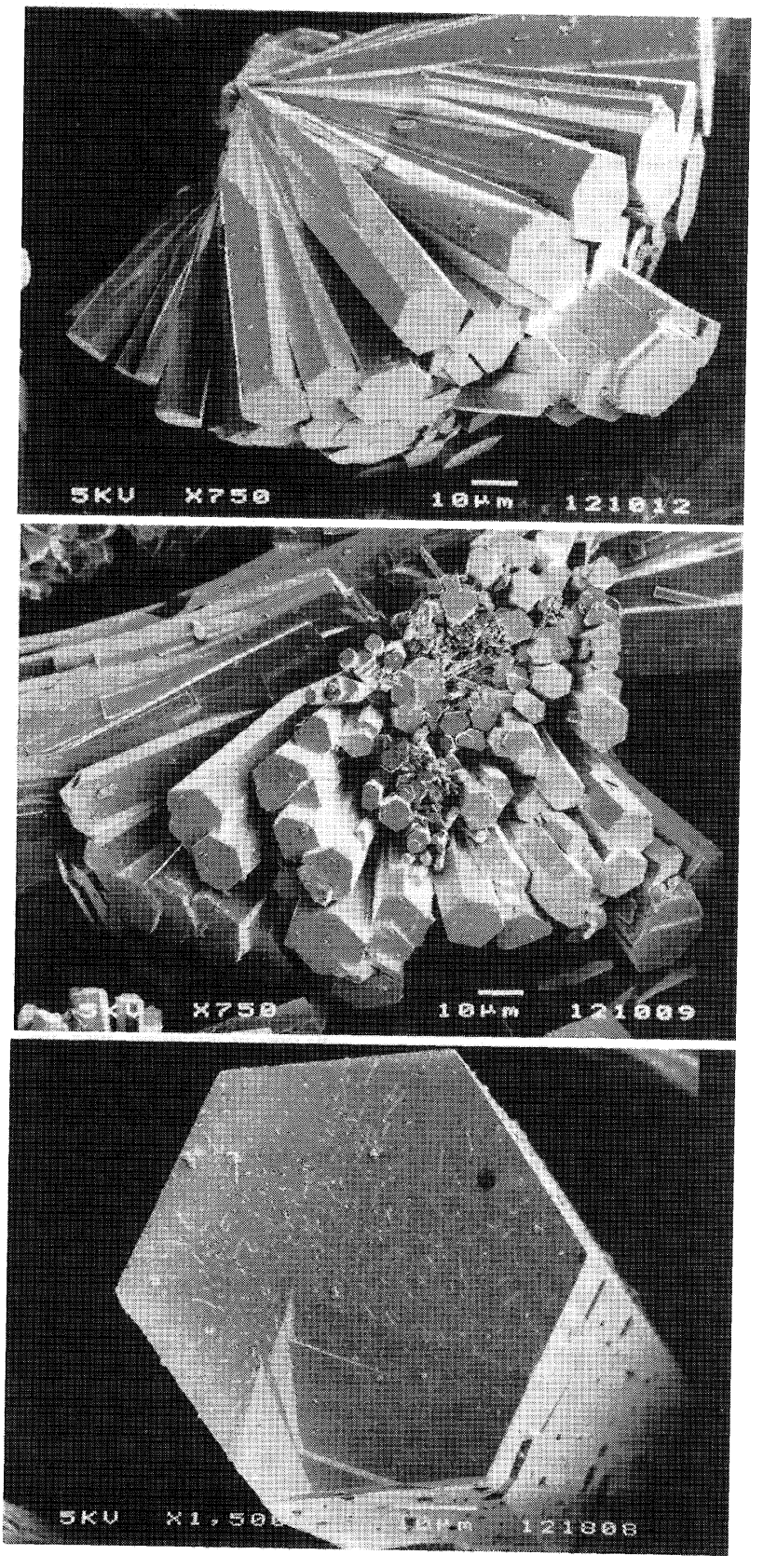

Fig. 2. SEM photograph indicating crystal growth of CAM.

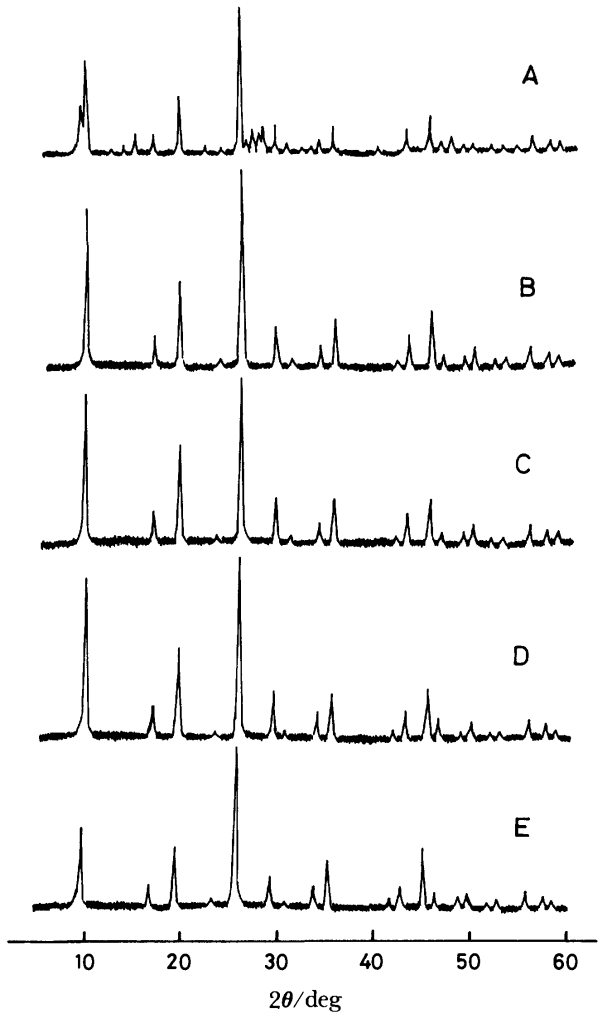

Fig. 3. The X-ray diffraction patterns of the samples A—E, synthesized at different H^+/Mo(VI) mole ratios; X-ray: Cu $K\alpha$.

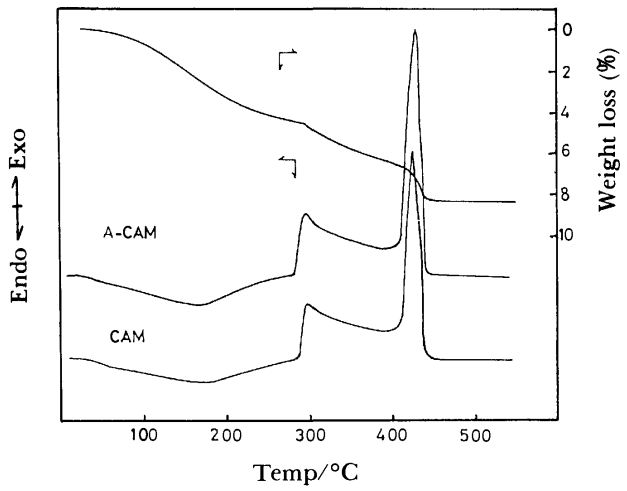

Fig. 4. The TG and DTA curves of CAM and A-CAM. Sample Wt: 0.1010 g; heating rate 10 °C min^{-1}; heating atmosphere: air.

Table 2. The X-Ray Diffraction Data of H-CAM (a_0=12.94±0.005 Å)

d_{obs} Å	I/I_0 %	d_{cal} Å	hkl
9.1573	78.29	9.1500	110
5.2851	14.16	5.2827	211
4.5785	29.09	4.5750	220
3.4542	0.36	3.4584	321 (K_β)
3.4586	100.00	3.4584	321
3.0475	8.24	3.0500	411,330
2.8922	0.96	2.8934	420
2.6412	8.91	2.6413	422
2.5374	14.90	2.5378	510,431
2.2894	0.27	2.2875	440
2.1566	1.73	2.1566	600,442
2.0992	14.41	2.0991	611,532
1.9971	16.38	1.9967	541
1.9500	5.12	1.9508	622
1.8652	1.81	1.8677	444
1.8308	4.05	1.8300	710,543
1.7609	1.60	1.7609	721,633,552
1.7292	2.53	1.7292	642
1.6420	5.69	1.6433	732,651
1.5926	8.20	1.5928	455
1.5688	4.21	1.5692	802
1.5243	0.24	1.5250	660
1.5043	3.18	1.5042	743
1.4656	0.74	1.4652	752
1.4117	0.58	1.4118	842
1.3954	4.08	1.3954	921,556
1.3637	3.63	1.3640	903

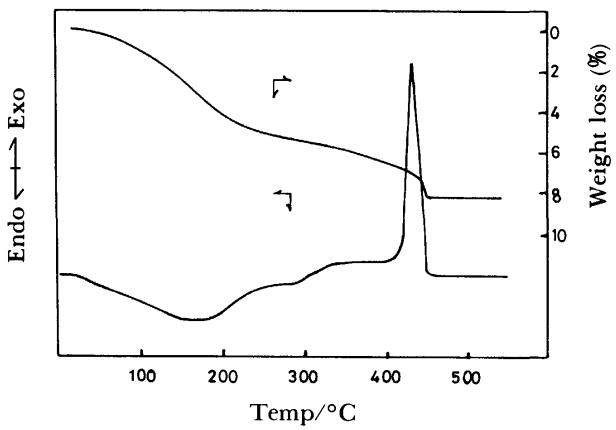

Fig. 5. The TG and DTA curves of H-CAM. Sample Wt: 0.1010 g; heating atmosphere: air; heating rate: 10 °C min^{-1}.

98.7% of the total ammonia, if the evolved ammonia at around 100 °C did not oxidized to NO_x. The powder X-ray diffraction patterns of H-CAM heated upto 300 °C (Fig. 7) showed no change in crystal structure. A little change was indicated upto 400 °C and a mixed X-ray diffraction of H-CAM and orthorhombic MoO_3 was observed. The observed lattice constant was found to be 12.976±0.005 Å. A complete crystal transformation to orthorhombic MoO_3[23] was observed at 660 °C. The little change in structure upto

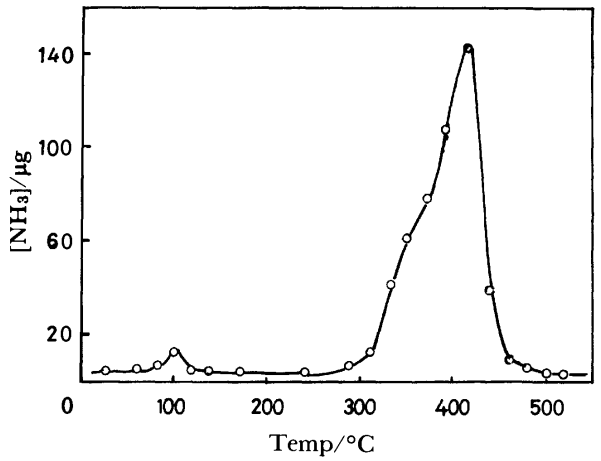

Fig. 6. The ammonia evolved during the thermal decomposition of H-CAM vs. heating temperature. H-CAM: 0.1031 g; heating rate: 10 °C min^{-1}; heating atmosphere: N_2 gas.

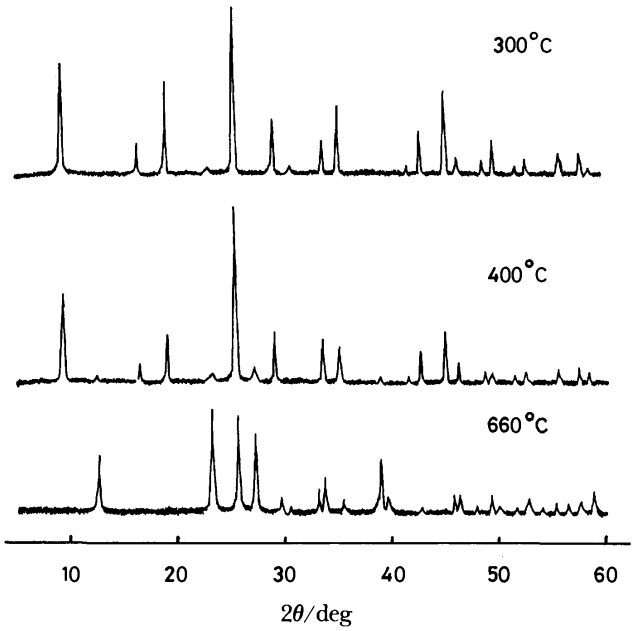

Fig. 7. The X-ray diffraction patterns of the heated samples.

400 °C also supports the evolution of a fraction of structural ammonia and water.

IR Spectroscopy. The IR spectrum of H-CAM (Fig. 8) shows a broad absorption band at 3400 cm^{-1} indicating the ν HOH stretching vibration for water. The absorption at 1600 cm^{-1} is the deformation vibration δ HOH.[24] The absorption bands around 3120 and 1400 cm^{-1} indicate the presence of NH_4^+ [25] as ν_3 and ν_4 stretching vibrations respectively.[28] Since no difference in the IR spectra of CAM and H-CAM was observed in this absorption region, the bands cannot be differentiated as for exchangeable and structural ammonia. The

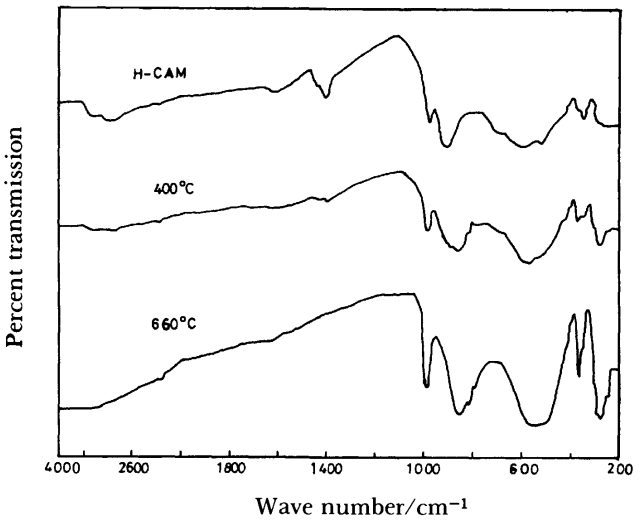

Fig. 8. The IR spectra of H-CAM and heated sample.

Table 3. The Exchange Capacity of H-CAM for NH_4^+

	NH_4^+ uptaken (mequiv g^{-1})	H^+ released (mequiv g^{-1})
1st. Equilibration	0.25_2	0.25_7
2nd. Equilibration	0.03_5	0.05_7
sum	0.28_7	0.31_4

shoulders at 2900 and 1430 cm^{-1} can be assigned to the deformation mode of vibration of NH_4^+. The absorption at 2900 cm^{-1} indicates the combination band of ν_2 and ν_4.[26] The absorption peaks at 3120 and 1400 cm^{-1} diminished at 400 °C and vanished in the IR spectra of heated samples after the exothermic peak at 430 °C. These results supported the scheme of thermal decomposition mentioned above. The strong absorption between 900—1000 cm^{-1} shows the Mo-O stretching vibrations.[27] The weak absorption at 800—900 cm^{-1} in H-CAM can be explained as O-Mo-O stretching vibrations containing ν(O-O) peroxo O_2 vibrations. These absorption bands split into three when oxygen quantity is greater,[28] which can be observed in the IR-spectra of the samples heated at 400 and 660 °C, where H-CAM change to MoO_3 at 660 °C. According to Nakamura et al.[29] the absorption between 500—600 cm^{-1} are due to the M-O-M stretching vibrations. These are the resultant of $\nu(O_2)$ and $\nu_{a,s}$(Mo) complexed together. The absorptions between 200—400 cm^{-1} in H-CAM indicate the Mo-Mo stretching vibrations[30] which become stronger in the heated samples.

Ion-Exchange Capacity for NH_4^+. The NH_4^+/H^+ ion-exchange reaction on H-CAM was carried out by batch experiment using 0.1 M NH_4NO_3 solution. A 1.0 g of exchanger was equilibrated by two successive addition with each 10 cm^3 of the above solution (Table 3). The amount of liberated H^+ from H-CAM was

equivalent to NH_4^+ uptake in the first equilibration. However slightly higher $[H^+]$ was observed in the supernatant solution than the amount of NH_4^+ uptaken by H-CAM due to the hydrolysis in the 2nd equilibration. The ion-exchange capacity for NH_4^+ was found to be 0.31 mequiv g^{-1} of H-CAM.

The acidification of hexaammonium heptamolybdate (aqueous solution) did not result into ammonia free molybdic acid even with 7.5 M HNO_3 or HCl solutions. The positive test for ammonia contents in commercially available so-called molybdic acids proves the authenticity of our observations, though the quantity of ammonia varies from product to product depending on the maker. As a matter of fact even a small content of NH_4^+ cannot be ignored from the ion exchange point of study and the empirical composition of the material. Therefore the products reported by different authors[11,25,31-34] as $MoO_3 \cdot H_2O$ or H_2MoO_4 prepared from aqueous solutions of ammonium heptamolybdate seem to be misleading.

The chemical formulae of H-CAM and A-CAM deduced from the chemical and thermal analysis and ion-exchange capacity, can be represented as $[H_{0.68}(NH_4)_2]O_{1.34} \cdot 14.16MoO_3 \cdot 6.92H_2O$ and $[(NH_4)_{0.68}(NH_4)_2]O_{1.34} \cdot 14.16MoO_3 \cdot 5.26H_2O$ respectively. The empirical formula of the CAM is $[(NH_4)_{0.78}(NH_4)_2]O_{1.39} \cdot 14.16MoO_3 \cdot 6.08H_2O$. The presence of 0.10% higher exchangeable NH_4^+ in CAM than that of A-CAM was due to the greater ammonia concentration in the mother liquor (supernatant solution). The amount of ammonia (1.54%) in H-CAM is independent of the preparation method and cannot be removed by washing even with 1 M HNO_3 solution. The results indicated that the amount of water in H-CAM varies slightly. However, the amount of ammonia evolved upto 100 °C (Fig. 6) was only 0.0226% of total ammonia and the weight loss at around 310 to 450 °C was due to evolution of structural ammonia and water. Kiss et al.[17] have reported the possible presence of $[Mo_{14}O_{43}]^{2-}$ polyanions by heating the ammonium heptamolybdate hydrate at 260 °C called as New Phase-1 $(NH_4)_2O \cdot 14MoO_3 \cdot 3.3H_2O$. They assumed the composition of the precipitate obtained from aqueous solutions to be the same as new phase-1. However for lack of information about the exchangeable NH_4^+ and NO_x formation during thermal decomposition, the calculated composition of their reported material seems to be deceptive.

The thermal decomposition reaction of H-CAM can be written as follows,

$$[H_{0.68}(NH_4)_2]O_{1.34} \cdot 14.16MoO_3 \cdot 6.92H_2O \quad \text{(H-CAM)}$$
$$\xrightarrow{100-300\,^\circ C} [H_{0.68}(NH_4)_2]O_{1.34} \cdot 14.16MoO_3 + 6.92H_2O(\uparrow)$$
$$\xrightarrow{300-450\,^\circ C} 14.16MoO_3 + 2NH_3(\uparrow) + 1.34H_2O(\uparrow).$$

Conclusion

Crystalline cubic ammonium molybdate (CAM) can be prepared by the reaction of HNO_3 and hexaammonium heptamolybdate under controlled temperature conditions and reagents specifications. The chemical and thermal analyses and the amount of exchangeable H^+ indicated the composition of H-CAM as $[H_{0.68}(NH_4)_2]O_{1.34} \cdot 14.16MoO_3 \cdot 6.92H_2O$. The CAM is suitable for grading to a desired mesh size to be used for column chromatography. A reversible exchange NH_4^+/H^+ reaction would find a new application field as an ion exchanger and a catalyst.

References

1) J. J. Berzelius, *Pogg.*, **6**, 381 (1826).
2) G. Carpenie, *Bull. Soc. Chim. Fr.*, **1947**, 484.
3) G. Jander, K. Jahn, and W. Henkeshoven, *Z. Anorg. Allg. Chem.*, **194**, 383 (1930).
4) H. Braekken, *Z. Kristallogr.*, **78**, 484 (1931).
5) G. Anderson and A. Magneli, *Acta Chem. Scand.*, **4**, 793 (1950).
6) A. Magneli, *Acta Chem. Scand.*, **2**, 501, 861 (1948).
7) P. Cannon, *J. Inorg. Nucl. Chem.*, **9**, 252 (1959); **11**, 124 (1959).
8) J. B. Goehring and S. Y. Tyree, Abstract 7th International Conference on Coord. Chem., Stockholms, p. 172 (1962).
9) Y. Doucet and S. Bugnon, *J. Chim. Phys.*, **54**, 155 (1957).
10) J. Bye, *Ann. Chim.*, **20**, 463 (1945).
11) I. Lindquvist, *Acta Chem. Scand.*, **4**, 650 (1950); **5**, 568 (1951); **10**, 1362 (1956).
12) M. K. Cooper and J. E. Salmon, *J. Chem. Soc.*, **1962**, 2009.
13) J. Avestone, E. W. Anacker, and J. S. Johnson, *Inorg. Chem.*, **5**, 735 (1964).
14) T. Ozeki, H. Kihara, and S. Hikime, *Anal. Chem.*, **59**, 945 (1987).
15) C. Gleitzer, *J. Less-Common Met.*, **51**, 215 (1977).
16) E. Ma, *Bull. Chem. Soc. Jpn.*, **37**, 171, 648 (1964).
17) A. B. Kiss, P. Gado, I. Asztalos, and A. J. Hegedus, *Acta Chim. Acad. Sci. Hung.*, **66**, 235 (1970).
18) K. H. Tytko and O. Glemser, *Adv. Inorg. Chem. Radiochem.*, **19**, 239 (1976).
19) M. Abe, "Inorganic Ion Exchange Materials," ed. by A. Clearfield, CRC Press, Boca Raton, FL., (1982), p. 190.
20) T. Ito, "X-Ray Studies on Polymorphism," Maruzen Publishing Co., Tokyo (1950).
21) J. W. Visser, *J. Appl. Crystallogr.*, **2**, 89 (1969).
22) W. N. Schreiner, C. Surdukowski, and R. Jenkins, *J. Appl. Crystallogr.*, **15**, 513, 524 (1982).
23) Nat. Bur. Stand. (U.S.) Monogr., **20**, 118 (1984).
24) F. A. Miller and C. H. Wilkins, *Anal. Chem.*, **24**, 1253 (1952).
25) N. Sotani, *Bull. Chem. Soc. Jpn.*, **48**, 6, 1820 (1975).
26) R. C. Plumb and D. F. Hornig, *J. Chem. Phys.*, **23**, 947 (1955); W. Vedder and D. F. Hornig, *ibid.*, **35**, 1560 (1961).
27) A. B. P. Lever, G. A. Ozin, and H. B. Gray, *Inorg. Chem.*, **19**, 1823 (1980).

28) K. Nakamoto, "Infrared and Raman Spect. Inorg. Compd.," 3rd ed., John Wiley & Sons, (1978), pp. 297—298.
29) A. Nakamura, Y. Tatsuno, M. Yamamoto, and S. Otsuka, *J. Am. Chem. Soc.*, **93**, 23, 6052 (1971).
30) V. R. Mattes, *Z. Anorg. Allg. Chem.*, **B357**, 30 (1968).
31) Gmelins Handbuch Anorg. Chem., Syst. No. 53, 119 (1935).
32) A. Rosenheim, *Z. Anorg. Chem.*, **50**, 320 (1950).
33) F. A. Cotton and G. Wilkinson, "Adv. Inorg. Chem.," 4th ed., Interscience, N. Y. (1980), p. 850, and references therein.
34) "Dickenson Comprehensive Inorg. Chem.," ed by J. C. Bailer, H. J. Emelens, S. R. Nyholm, and A. F. Trotman, (1973), Vol. 3, p. 735.

 © 1989 The Chemical Society of Japan Bull. Chem. Soc. Jpn., 62, 3464—3468 (1989) [Vol. 62, No. 11

Metal Complexes of Peptides. IV. Cobalt(III) Complexes with β-Alanyl-L-histidine (Carnosine) Functioning as a Quadridentate Ligand

Tomoharu AMA,* Hiroshi KAWAGUCHI, Masato UCHIJIMA, Norio KOINE,† and Takaji YASUI
Department of Chemistry, Faculty of Science, Kochi University, Akebono-cho, Kochi 780
†Department of Industrial Chemistry, Faculty of Engineering,
Ehime University, Bunkyo-cho, Matsuyama 790
(Received May 11, 1989)

Three cobalt(III) complexes containing β-alanyl-L-histidine (or carnosine: H_2car), $[Co(car)(L)]^+$ (L=en) and $[Co(car)(L)]^-$ (L=ox^{2-} or CO_3^{2-}), were newly prepared and characterized on the basis of their ^{13}C NMR, UV and visible absorption, and circular dichroism spectra. In these complexes, the carnosine coordinates to a cobalt(III) ion as a quadridentate ligand in a meridional form with respect to the peptide chain. In the pH range of 0—6, these complexes exhibited the visible absorption spectral changes with pH. These changes are attributed to the protonation on the oxygen in β-alanyl moiety of the coordinating carnosine and the pK_a values of $[Co(car)(en)]^+$ and $[Co(car)(ox)]^-$ were estimated as ca. 1.5. The spectral behaviors of the present complexes were compared with that of $[Co(Hcar)(en)(OH_2)]^{2+}$, in which the carnosine functions as a terdentate ligand.

Some studies on the cobalt(III) complexes containing peptides have been reported.[1-16] However, there are few studies on the cobalt(III) complexes of β-alanyl-L-histidine (or carnosine: H_2car), in spite that the complexes are important compounds in a biological sense. Only one coordination mode is reported for the carnosine-cobalt(III) complex,[1] in which the carnosine functions as a terdentate with the uncoordinated amino group. However, it is expected that the carnosine also functions as a quadridentate in a cobalt(III) complex, as found in a chromium(III) complex by Murdoch et al.[17] This expection led us to the experiments to prepare some cobalt(III) complexes containing a quadridentate carnosine under different synthetic conditions from those reported for the terdentate carnosine complex.[1] In the present paper, we will describe the preparation of new carnosine-cobalt(III) complexes and discuss their structures and properties on the basis of the ^{13}C NMR, UV and visible absorption, and CD spectral data.

Experimental

Preparation of Complexes. [Co(car)(en)]Cl (Complex 1): Carnosine (0.1 g) was dissolved in 40 cm^3 of water, and the pH of the solution was adjusted to 9.0 with 1 mol dm^{-3} KOH. To this solution, $K[Co(en)(CO_3)_2]\cdot H_2O$ (1.3 g)[18] was added with stirring. After stirring at 70 °C for 16 h, the solution was cooled to room temperature and then filtered. The filtrate was charged on an SP-Sephadex column (K^+ form) and flushed with water to remove a violet-brown band which was elutable with water, and then developed with 0.2 mol dm^{-3} KCl. A red orange band appeared on the development, a violet-brown band remaining on the top of the column. The red orange band was transferred to another SP-Sephadex column and then repeatedly developed with 0.2 mol dm^{-3} KCl using a micropump. After the red orange band separated into pink and orange bands, an eluant from the orange band was collected and concentrated to small volume with a vacuum evaporator. To the concentrated solution, a large amount of methanol was added in order to make deposit KCl, and then the solution was filtered. The filtrate was evaporated under reduced pressure to a few milliliters, again. The concentrated solution was loaded on a Sephadex G-10 column to eliminate KCl and eluted with water. The eluate from the orange band was concentrated to a small volume. A crude complex was obtained by adding methanol to the concentrate. It was recrystallized from water by addition of methanol (Complex 1; yield: 100 mg). Found: C, 31.44; H, 5.58; N, 20.21%. Calcd for $[Co(car)(en)]Cl\cdot 2H_2O$= $C_{11}H_{24}N_6O_5ClCo$: C, 31.93; H, 5.85; N, 20.31%.

Na[Co(car)(ox)] (Complex 2): Carnosine (0.5 g) was dissolved in 40 cm^3 of water. After the pH of the solution was adjusted to 8.5 with 2 mol dm^{-3} KOH, $K_3[Co(ox)_3]\cdot 3H_2O$ (0.96 g)[19] was added to the solution with constant stirring. The temperature of the solution was kept 40 °C for 10 h. The solution was cooled to room temperature, and then insoluble materials were filtered off. The filtrate was charged on a QAE-Sephadex column (Cl^- form, 4 cm×50 cm). After a violet-brown band elutable with water was eluted out with 1 dm^3 of water, the adsorbed band was developed with 0.1 mol dm^{-3} KCl. A violet band was appeared on the development, a green band remaining on the top of the column. The eluate from the violet band was concentrated to a few milliliters by using a vacuum evaporator and then KCl which deposited was filtered off. To the filtrate, methanol was added to deposit excess of KCl. The solution was filtered and a crude complex (K[Co(car)(ox)]) was precipitated by addition of acetone to the filtrate. The solution obtained by dissolving the crude complex in a small amount of water was treated with an SP-Sephadex column (Na^+ form; eluent: water) to convert the potassium salt to the sodium salt. After the eluate was concentrated, ethanol, saturated with $NaClO_4$, was added to the concentrated solution. A crude complex of Na[Co(car)(ox)] thus deposited was recrystallized from water by addition of ethanol containing $NaClO_4$ (Complex **2**; yeild: 350 mg). Found: C, 23.28; H, 3.22; N, 9.96%. Calcd for $Na[Co(car)(ox)]\cdot NaClO_4\cdot 3H_2O$=$C_{11}H_{18}N_4ClNa_2O_{14}Co$: C, 23.15; H, 3.18; N, 9.82%.

K[Co(car)(CO_3)] (Complex 3): Carnosine (0.5 g) was dissolved in 40 cm^3 of water and $Na_3[Co(CO_3)_3]\cdot 3H_2O$ (0.8 g)[20] was added to the solution. The solution was stirred at 45—50 °C for 24 h. After being cooled to room temperature, the solution was filtered and the filtrate was charged on a QAE-Sephadex (Cl^- form) column. The column was swept with 1 dm^3 of water to remove the violet-brown band which was

elutable with water. The adsorbed band was developed with 0.1 mol dm^{-3} KCl. A violet band appeared on the development, a brown band remaining on the top of the column. The eluate from the violet band was concentrated to a few milliliters by using a vacuum evaporator and then methanol was added to the concentrated solution. White precipitates (KCl) were filtered off. The filtrate was again evaporated almost to dryness and then the residue was dissolved in a few milliliters of water. The solution was treated with a Sephadex G-10 column in order to remove KCl. The crude complex, which was obtained from the violet eluate by addition of ethanol, were recrystallized from water by addition of ethanol (Complex **3**; yield: 250 mg). Found: C, 31.35; H, 4.23; N, 12.85%. Calcd for $K[Co(car)(CO_3)]\cdot 0.5C_2H_5OH\cdot 2H_2O=C_{11}H_{17}N_4O_{7.5}KCo$: C, 31.21; H, 4.05; N, 13.25%.

$[Co(Hcar)(en)(OH_2)]Cl_2\cdot H_2O$ (Complex 4): This complex was prepared by the method described in a previous paper.[1]

Absorption Spectral Changes with pH. In Lower pH Region: 5 cm^3 of the solution containing complex **1** (0.2004 g, 4.8×10^{-4} mol dm^{-3}) in 50 cm^3 of water was placed in a measuring flask (10 cm^3), and then a prescribed volume of 2 mol dm^{-3} HCl solution was added to it. The volume of the acidic solution was adjusted to 10 cm^3 with water. By the same procedure, seven solutions with different pH's (0.1—6.0) were prepared. Absorption spectrum and pH of the each solution were recorded at room temperature. In the same manner as above, the absorption spectral changes with pH's were examined for Complexes **2** and **4**.

In Higher pH Region: The spectral changes in the range of pH 5—10 were examined by the method similar to that described above, except for using 1 mol dm^{-3} NaOH instead of 2 mol dm^{-3} HCl.

Measurements. The absorption and CD spectra were measured by a HITACHI 557 spectrophotometer and a JASCO J-22 spectropolarimeter, respectively. The ^{13}C NMR spectra were recorded on a HITACHI R-90H spectrometer. The chemical shifts in ^{13}C NMR were measured relative to internal dioxane (δ=67.40).

Results and Discussion

^{13}C NMR Spectra. The ^{13}C NMR measurements at various pH provide useful information on the coordination modes of ligand. Figure 1 shows the ^{13}C NMR shift patterns of carnosine and its complexes, together with those of the related complexes. The numbering of all carbons in carnosine and their signal assignments adopted those described in the report of Viola et al.[21] (Fig. 1).

As Fig. 1 shows, the ^{13}C chemical shifts of the free carnosine vary with pH of the solution. The C_5 resonance peak of free carnosine in a pH 5 solution locates at more down-field than that in a 1 M DCl solution. This down-field shift arises from deprotonation on the carboxyl group. The C_7 and C_9 peaks of free carnosine at pH 9 shift to more down-field than those at pH 5, and the C_1 and C_2 peaks of free carnosine at pH 12 shift to more down-field than those at pH 9. The down-field shifts for the former and

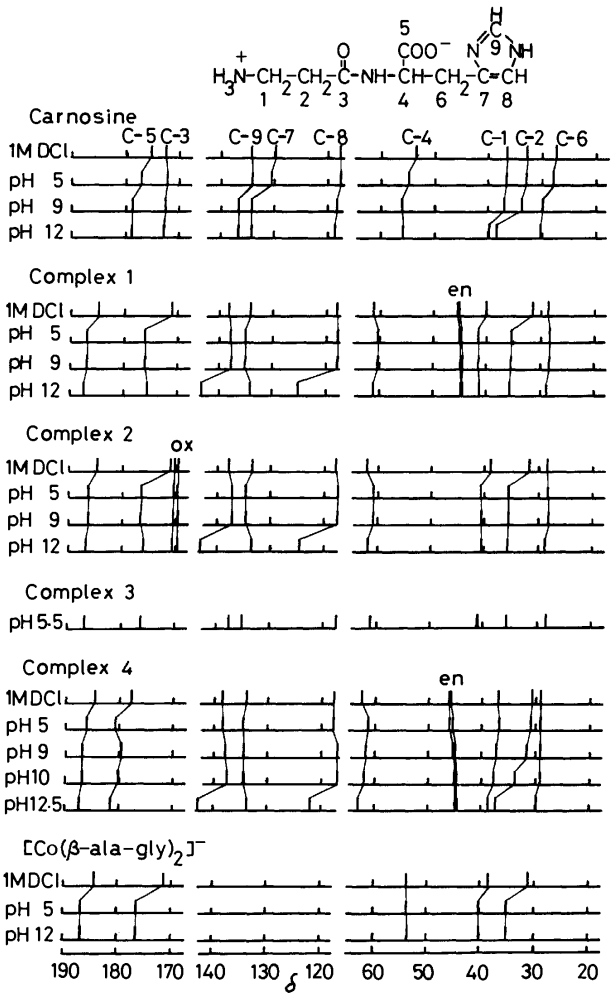

Fig. 1. ^{13}C NMR spectral patterns of carnosine and cobalt(III) complexes at various pH.

latter are related to deprotonations on the imidazole NH and on the amino groups, respectively.

The C_5 resonance peaks of the present complexes at pH 5—7 are observed in more down-field region than that of free carnosine at pH 5. These down-field shifts results from the coordination of the carboxyl groups to cobalt(III). Such down-field shifts due to the coordination of the carboxyl groups to cobalt(III) are also well recognized for the amino acidato and aliphatic acidato complexes.[22]

The ^{13}C chemical shifts of the carnosine-carbons in the present Complexes **1**, **2**, and **3** coincide well with each other for their neutral solutions, suggesting that the coordination mode of carnosine is the same in these complexes. In addition, the ^{13}C chemical shifts of the C_1, C_2, C_3, and C_5 carbons in Complexes **1**, **2**, and **3** are almost equal to those of the corresponding carbons of the terdentate β-ala-gly in $[Co(\beta\text{-ala-gly})_2]^-$. These results suggest that the coordination mode of carnosine in the present complexes is similar to that of β-ala-gly in $[Co(\beta\text{-ala-gly})_2]^-$ with respect to the peptide chain. The C_7 and C_9 resonance peaks of

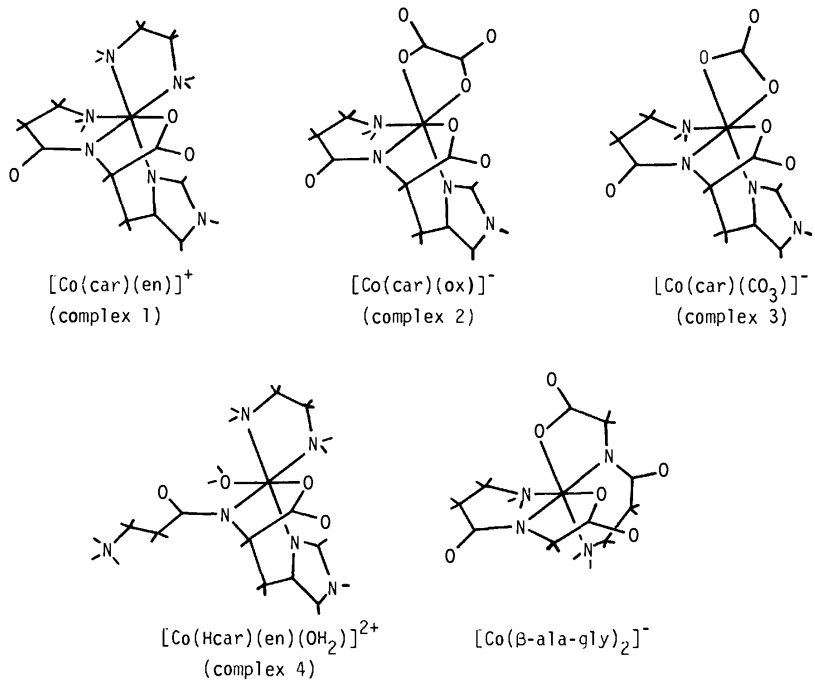

Fig. 2. Structures of the cobalt(III) complexes containing carnosine.

Complexes **1**, **2**, and **3** at pH 5 (or 5.5) are observed at more down-field than those of free carnosine at pH 5. These down-field shifts show that the coordination of imidazole moiety to cobalt(III) occurs. Consequently, the structures shown in Fig. 2 are proposed for Complexes **1**, **2**, and **3**. In these complexes, the marked up-field shifts of C_3 and C_2 at low pH (1 M DCl) are attributed to protonation on the oxygen in β-alanyl moiety of the coordinating carnosine,[23] and the down-field shifts of C_8 and C_9 at high pH (pH 12) are attributed to deprotonation of NH on the coordinating imidazole moiety.

Absorption and Circular Dichroism Spectra. The absorption and CD spectra of the newly prepared carnosine complexes are shown in Fig. 3, together with those of Complex **4** reported in our previous study.[1] The absorption spectral behaviors of complexes **2** and **3** resemble to each other, indicating that these complexes have the same chromophore of the *fac*-$[Co(N)_3(O)_3]$ type[24] and the same coordination mode of carnosine, that is, carnosine coordinate to Co(III) as quadridentate with carboxyl O, amino N, amide N, and imidazole N. The replacement of oxalato in Complex **2** with ethylenediamine gives Complex **1**, whose first absorption band shifts to higher energy side than that of Complex **2**. Moreover, the first absorption band of Complex **1** has characteristics of the $[Co(N)_5(O)]$ type chromophore.[24] These results based on the absorption spectra coincide with the assignment based on the ^{13}C NMR mentioned in the previous section.

While the band splitting in the first absorption band of Complex **1**, **2**, or **3** is not obvious, that of Complex **4** is obvious. This spectral pattern of Complex **4** is characteristic to the *trans*(*O*)-$[Co(N)_4(O)_2]$ type chromophore.[24] This result is consistent with the structure

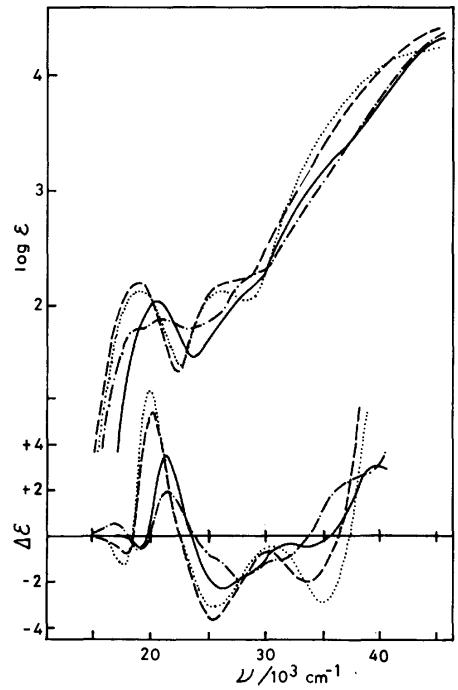

Fig. 3. Absorption and CD spectra of the complexes. $[Co(car)(en)]^+$ (Complex **1**) (——), $[Co(car)(ox)]^-$ (Complex **2**) (———), $[Co(car)(CO_3)]^-$ (Complex **3**) (·····), and $[Co(Hcar)(en)(OH_2)]^{2+}$ (Complex **4**) (—·—·—). (The ε and $\Delta\varepsilon$ values are given in $mol^{-1}\,dm^3\,cm^{-1}$).

determined by means of X-ray crystal analysis.[1]

The CD behaviors of Complexes **2** and **3** quite resemble each other. Both the complexes show two CD peaks with opposite signs in the first absorption band region (a weak (−) sign at lower energy side and an intense peak with (+) sign at higher energy side) and a (−) CD peak in the second band region. Similar spectral pattern also appears in Complex **1**. This similarlity in CD pattern suggests that these complexes have the same absolute configuration (Fig. 2). The CD pattern of Complex **4**, however, is different from those of Complexes **1**, **2**, and **3**, that is, three CD peaks ((+), (−), and (+) signs from lower energy side) appear in the first absorption band region. Such difference in CD patterns is attributed to difference in the coordination modes of carnosine.

Spectral Change with pH. The absorption spectral changes with pH were observed for the present complexes. Figure 4(A) shows the spectral change of Complex **1** in the range of pH 0.53—5.84. The isosbestic points appear at 463 and 426 nm. These spectral changes result from the protonation on the oxygen in the β-alanyl moiety of the coordinating carnosine.[23] The pK_a value estimated from the spectral change is 1.46. Analogous spectral change in an acidic solution (pH range: 1.12—6.19) was also observed for Complex **2**, with four isosbestic points at 523, 448, 335, and 350 nm. The pK_a value was estimated as 1.78. These pK_a values (1.46 and 1.78) are larger than 0.75 for [Co(mida)(L-ala-gly)]$^-$ (mida=*N*-methyl iminodiacetato), but smaller than 2.56 for [Co(mida)(β-ala-gly)]$^-$.[3]

The spectral change of Complex **4** in the range of pH 0.13—5.12 provided three isosbestic points at 565, 389, and 366 nm. The pK_a value estimated is 0.51 and smaller than those of Complexes **1** and **2**. This small value results from that the coordination mode of carnosine in Complex **4** (terdentate with uncoordinated amino moiety) is different from that in Complex **1** or **2** (quadridentate). The X-ray crystal data of Complex **4** imply that hydrogen bond is present between β-alanyl O$^-$ in carnosine and coordinating H_2O. This hydrogen bond makes it difficult for another proton to attach to β-alanyl O$^-$, and lowers the pK_a value of Complex **4**. In addition, the hydrogen bond makes the amino group on the β-alanine moiety keep away from the cobalt center and stabilizes the unique structure containing cis-peptide bond[25] (C_2 and C_4 carbons are in cis position with respect to C_3–N bond) (Figs. 1 and 2).

Complex **4** shows marked absorption spectral change in the range of pH 5.27—9.10, as shown in Fig. 5 (the spectral curve at pH 10.03 coincides with that at pH 9.10 in the range 600—320 nm). However, ^{13}C chemical shifts of Complex **4** at pH 9 are nearly equal to those at pH 5. These results indicate that no deprotonation occurs on the carnosine ligand at pH 9.10 (that is, no deprotonation occurs on either amino or imino group at this pH) but deprotonation occurs on coordinating H_2O to give a hydroxo complex. The pK_a value estimated from the spectral changes is 7.87.

In Complex **4** the absorption spectral curve at pH 9.10 coincides with that at pH 10.03 in the range 600—320 nm, as mentioned above. However, the ^{13}C resonance peaks of the β-alanine moiety in carnosine at pH 9 shift to more down-field than those at pH 10.

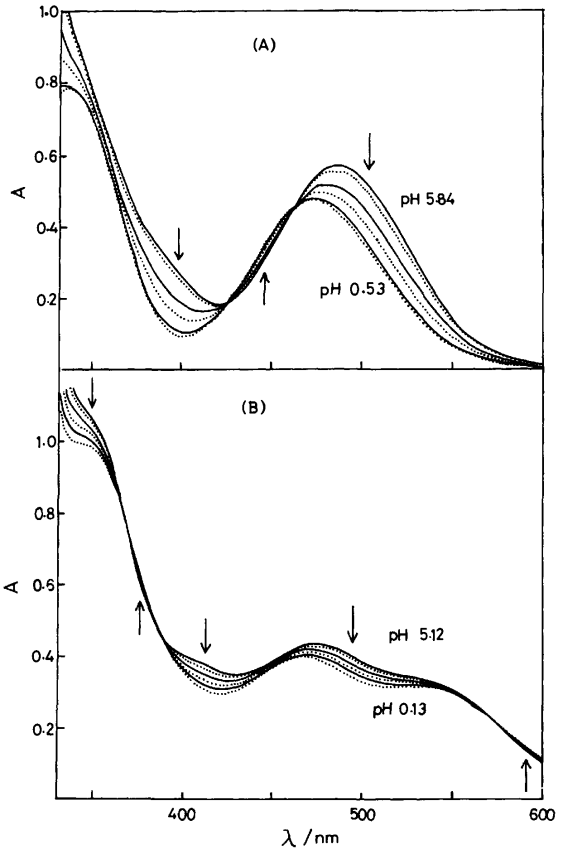

Fig. 4. Absorption spectral changes of the complexes with pH in acidic region. (A) Complex **1** (pH=5.84, 2.29, 1.60, 1.27, 0.79, and 0.53). (B) Complex **4** (pH=5.12, 0.78, 0.55, 0.40, 0.30, and 0.13).

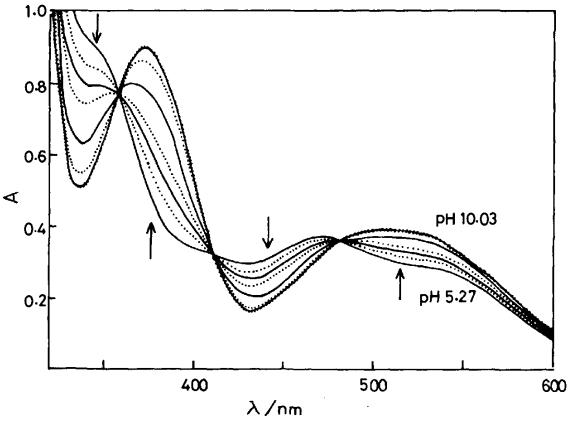

Fig. 5. Absorption spectral change of Complex **4** with pH in basic region. (pH=5.27, 7.20, 7.56, 7.87, 8.35, 8.99, 9.10, and 10.03).

This down-field shift is attributed to the deprotonation on $-NH_3^+$ of the β-alanyl moiety. The C_7 and C_9 resonance peaks of Complex **4** at pH 12.5 locate at more down-field than those at pH 10. The down-field shifts are attributed to the deprotonation of NH in the imidazole moiety. It is noteworthy that the basic solution of Complex **4** (containing carnosine as terdentate with uncoordinated $-NH_3^+$ moiety) does not produce easily Complex **1** (containing carnosine as quadridentate); replacement of the coordinating hydroxy ligand by the uncoordinating amino group does not occur easily. This results from that the cis-peptide bond in Complex **4** is stabilized by the hydrogen bond described above and that the structural conversion from cis- to trans-peptide is not easy at room temperature.

References

1) K. Okamoto, T. Yasui, H. Kawaguchi, T. Ama, and J. Hidaka, *Chem. Lett.*, **1988**, 335.

2) H. Kawaguchi, K. Maeda, T. Ama, and T. Yasui, *Chem. Lett.*, **1979**, 1105.

3) H. Kawaguchi, M. Kanekiyo, T. Ama, and T. Yasui, *Bull. Chem. Soc. Jpn.*, **53**, 3208 (1980).

4) T. Yasui, H. Kawaguchi, and T. Ama, *Bull. Chem. Soc. Jpn.*, **54**, 2918 (1981).

5) H. Kawaguchi, M. Ishii, T. Ama, and T. Yasui, *Bull. Chem. Soc. Jpn.*, **55**, 3750 (1982).

6) J. P. Collman and E. Kimura, *J. Am. Chem. Soc.*, **89**, 6096 (1967).

7) E. Kimura, S. Young, and J. P. Collman, *Inorg. Chem.*, **9**, 1183 (1970).

8) R. D. Gillard and D. A. Phipps, *J. Chem. Soc. A*, **1971**, 1074.

9) Y. Wu and D. H. Busch, *J. Am. Chem. Soc.*, **94**, 4115 (1972).

10) A. R. Manyak, C. B. Murphy, and A. E. Martell, *Arch. Biochem. Biophys.*, **59**, 373 (1955).

11) E. J. Evans, J. E. Grice, C. Hawkins, and M. Heard, *Inorg. Chem.*, **19**, 3496 (1980).

12) E. Evans, C. J. Hawkins, J. Rodgers, and M. R. Snow, *Inorg. Chem.*, **22**, 34 (1983).

13) C. J. Hawkins and J. Martin, *Inorg. Chem.*, **25**, 2146 (1986).

14) L. R. Solujć, R. Herak, B. Prelesnik, and M. B. Ćelap, *Inorg. Chem.*, **24**, 32 (1985).

15) D. A. Buckingham and C. R. Clark, *Inorg. Chem.*, **25**, 3478 (1986).

16) N. Mensi and S. S. Ishida, *Inorg. Chem.*, **25**, 147 (1986).

17) C. M. Murdoch, M. K. Cooper, T. W. Hambley, W. N. Hunter, and H. C. Freeman, *J. Chem. Soc., Chem. Commun.*, **1986**, 1329.

18) M. Shibata, *Nippon Kagaku Zasshi*, **87**, 771 (1966).

19) J. C. Bailar, Jr. and E. M. Jones, *Inorg. Synth.*, **1**, 37 (1939).

20) H. F. Bauer and W. C. Dinkard, *Inorg. Synth.*, **8**, 202 (1966).

21) R. E. Viola, C. R. Hartzell, and J. J. Villafrance, *J. Inorg. Biochem.*, **10**, 281 (1979).

22) T. Ama, H. Kawaguchi, and T. Yasui, *Bull. Chem. Soc. Jpn.*, **54**, 448 (1981).

23) L. V. Boas, C. A. Evans, R. D. Gillard, P. R. Mitchell, and D. A. Phipps, *J. Chem. Soc., Dalton Trans.*, **1979**, 582.

24) N. Matsuoka, J. Hidaka, and Y. Shimura, *Bull. Chem. Soc. Jpn.*, **40**, 1868 (1967).

25) G. N. Ramachandran and V. Sasisekharan, *Adv. Prot. Chem.*, **23**, 283 (1968).

 © 1989 The Chemical Society of Japan Bull. Chem. Soc. Jpn., 62, 3469—3474 (1989)

Tetrakis[3-(diethylamino)propyl]- and Tetrakis[3-(diethylmethylammonio)-propyl]phthalocyanines: The First Amphiphilic Phthalocyanines

Nagao KOBAYASHI,* Fumihiro OJIMA, Tetsuo OSA,* Steve VIGH,† and Clifford C. LEZNOFF*,†
Pharmaceutical Institute, Tohoku University, Aobayama, Sendai 980
†Department of Chemistry, York University, 4700 Keele Street, North York, Ontario, Canada M3J 1P3
(Received June 23, 1989)

The first amphiphilic cobalt (**III**) and copper phthalocyanines (**V**) have been prepared and are characterized by UV-absorption and magnetic circular dichroism (MCD) spectra in water and organic solvents and in their mixtures. These phthalocyanines exist as dimers in water and as monomers in some organic solvents. Monomer-dimer equilibrium was affected by solvent polarity (or hydrophobicity); with lower cosolvent polarity favoring formation of monomers. Cyclic voltammetry suggests that **III** adsorbed onto glassy carbon (GC) from an aqueous or acetonitrile (AN) solution in monomeric, irrespective of its state in solution. The $Co^{II/I}$ redox potential of **III** shifts anodically by adsorption onto GC, and this shift is larger when adsorbed from an AN solution than from an aqueous solution. Electroreduction of oxygen occurs at more positive potential at **III**-adsorbed GC in plain solution than at bare GC in **III**-dissolved solution.

Phthalocyanines (Pcs) are a remarkably versatile and robust class of compounds.[1] However, the solubility of the unsubstituted parent molecules is notoriously low, so that the introduction of bulky or long alkyl chains is generally required to increase their solubility in organic solvents.[2] Phthalocyanines containing sulfonyl,[3] carboxyl,[4] and amino groups[5] are, on the other band, water soluble. Phthalocyanines which dissolve in water at all pH values have not been reported to date, although a brief report on compound **I** and its zinc derivatives for use in photodynamic therapy of cancer appeared recently.[6] In view of such considerations, we report here the first example of amphiphilic phthalocyanines, i.e. the cobalt **III** and copper **V** complexes of **I**. These dissolve not only in water at all pH values, but also in many of the common organic solvents such as chloroform, acetone, alcohols, and benzenes. As will be shown below, they are compounds which can bridge the chemistry of phthalocyanines in water and organic solvents.

Experimental

Measurements. Matheson high-purity argon or high-purity nitrogen has passed through concentrated sulfuric acid (H_2SO_4) and preheated copper filings was used to maintain inert atmosphere conditions. Oxygen was purified by passage through concentrated H_2SO_4. Infrared spectra were recorded on a Pye Unicam SP 1000 infrared spectophotometer using KBr discs. Fast-atom-bombardment (FAB) spectra were obtained with a Kratos MS-50 tripic analyzer mass spectrometer equipped with a FAB ion source of standard Kratos design and an Ion Tech atom gun. The number in parentheses after the indicated ion shows the percentage of the base peak represented by that ion. Absorption spectra were collected on a Hewlett Packard HP8451A Diode Array spectrophotometer or on a Shimadzu UV-250 spectrophotometer. In the experiments in the mixed solvent system, the following procedures were adopted in order to minimize concentration differences among each of the samples. Initially, a concentrated phthalocyanine solution was prepared in acetonitrile. From this solution, a fixed small amount was transferred into a 1 cm cuvette using a microsyringe, and the solvent evaporated. To this cuvette was added 3 cm^3 of a mixed solvent of desired composition ratio, and the spectra were recorded. MCD spectra were run on a Jasco J-500 spectropolarimeter equipped with a Jasco electromagnet to produce longitudinal magnetic fields up to 1.1 T. Each measurement was made with both parallel and antiparallel fields.

Cyclic voltammetric (CV) sweeps were generated by an NF circuit design block FG-100 AD function generator in conjunction with a potentiostat which was built by methods recorded in the literature.[7] A glassy carbon (GC) (area 0.070 cm^2), a saturated calomel electrode (SCE), and a platinum foil were used, respectively, as a working electrode, a reference electrode, and a counter electrode. The GC was polished on one side to a bright surface with fine emery paper and alumina powder (final polish with 0.05 μm particle size, Buehler) immediately prior to use.

Materials. *o*-Dichlorobenzene (DCB) (Aldrich, Gold Label), acetonitrile (AN) (Wako, spectrograde), dioxane, 2-butoxyethanol, and 2-propanol (Nakarai, Guaranteed reagents) were used as supplied. Measurements at pH 1 or 7 were performed in 0.05 M H_2SO_4 or 0.1 M phosphate buffer (1 M=1 mol dm^{-3}), respectively. The GC electrode was purchased from Tokai Carbon Ltd.

2,9,16,23-Tetrakis[3-(diethylamino)propyl]phthalocyaninatocobalt(II), (II). To a solution of 108 mg (0.11 mmol) of **I**[6] in 10 ml toluene/2-methoxyethanol (1:1 v/v), was added 150 mg (1.15 mmol) of anhydrous cobalt dichloride. The solution was stirred at 120 °C (reflux) under argon for 20 h. The crude reaction mixture was applied directly to a short (10 cm×1 cm) basic alumina column (act 3) and eluted with toluene/2-methoxyethanol (3:1 v/v). Evaporation of the solvent gave **II** as a dark blue shining solid, 110 mg (96.5% yield); mp >300 °C. IR (KBr) 2980, 2800, 1610, 1520, 1340, 1100, 750 cm^{-1}. MS, *m/z* 1025 (M^++1, 75), 1024 (M^+, 57), 995(18), 968(15), 924(20). Analysis was performed on the quaternized methyl iodide salt (**III**).

2,9,16,23-Tetrakis[3-(diethylmethylammonio)propyl]-phthalocyaninatocobalt(II) Tetraiodide, (III). To a solution of 75 mg (0.073 mmol) of **II** in 10 ml toluene was added 0.5 ml (8 mmol) of methyl iodide. This solution was stirred for 20 h at room temperature. The observed blue precipitate

was filtered and washed with ether. The yield of the blue powdery solid (**III**) was 94.3 mg (81% yield). Found: C, 48.20; H, 5.39; N, 10.85; Co, 3.60%. Calcd for $C_{64}H_{88}N_{12}CoI_4$: C, 48.28; H, 5.57; N, 10.56; Co, 3.70%. Mp >300 °C. IR (KBr) 2960, 1610, 1520, 1460, 1330, 1100, 820, and 760 cm^{-1}.

2,9,16,23-Tetrakis[3-(diethylamino)propyl]phthalocyaninatocopper(II), (IV). To a solution of 76 mg (0.07 mmol) of **I**[3] in 10 ml of a toluene/2-methoxyethanol (1:1 v/v) mixture was added 150 mg (0.83 mmol) of anhydrous copper(II) acetate. The solution was stirred at 120 °C reflux under an argon atmosphere for 20 h. The crude reaction mixture was applied directly to a short basic alumina (Act 3) column (10×1 cm) and eluted with toluene/2-methoxyethanol (3:1 v/v). Evaporation of the solvent gave **IV** as a dark blue shining solid; 78 mg (96% yield). Mp >300 °C. IR (KBr) 2980, 2800, 1610, 1520, 1330, 1100, 830, and 750 cm^{-1}. MS, *m/z* 1030(10), 1029(M^++1, 15), 1028(M^+, 8), and 927(5). Analysis was performed on the quaternized methyl iodide salt (**V**).

2,9,16,23-Tetrakis[3-(diethylmethylammonio)propyl]-phthalocyaninatocopper(II) Tetraiodide, (V). To a solution of 35 mg (0.034 mmol) of **IV** in 10 ml of toluene was added 0.5 ml (8 mmol) of methyl iodide. This solution was stirred for 20 h at room temperature. The observed blue precipitate was filtered and washed with ether. The yield of blue powdery solid (**V**), after drying, was 40 mg (74% yield). Found: C, 47.80; H, 5.50; N, 10.94; Cu, 3.66%. Calcd for $C_{64}H_{88}N_{12}CuI_4$: C, 48.14; H, 5.55; N, 10.53; Cu, 3.98%. Mp >300 °C. IR (KBr) 2960, 1610, 1450, 1410, 1330, 1170, 1090, and 750 cm^{-1}.

UV data of **II**—**V** in several solvents are summarized in Table 1.

Results and Discussion

Experiments were designed to illustrate the amphiphilic properties of the compounds.

(i) UV-Absorption and MCD Spectroscopy. Figures 1 and 2 show absorption and MCD spectra of **III** and **V**, respectively, in water, AN and in their mixtures. Their absorption spectra in AN are characteristic of monomeric phthalocyanines.[7] When trace amounts of water were admixed, the spectra changed only in the region higher in energy than 270 nm probably as a result of coordination of water molecule to cobalt or copper. When the water content in the solvent exceeded 50% in each case, the whole spectrum started to change as shown by arrows with sets of isosbestic

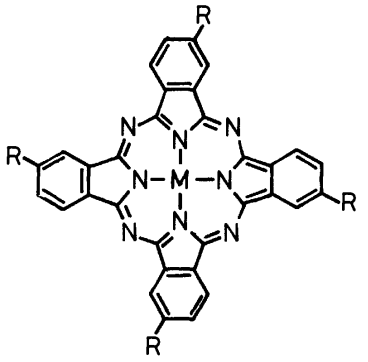

(**I**) R=$(Et)_2N(CH_2)_3$-, M=H_2
(**II**) R=$(Et)_2N(CH_2)_3$-, M=Co
(**III**) R=$(Et)_2\overset{\oplus}{N}Me(CH_2)_3$-$\overset{\ominus}{I}$, M=Co
(**IV**) R=$(Et)_2N(CH_2)_3$-, M=Cu
(**V**) R=$(Et)_2\overset{\oplus}{N}Me(CH_2)_3$-$\overset{\ominus}{I}$, M=Cu

Table 1. Absorption Spectra of Phthalocyanines (Pcs) (**II**—**V**) in Some Solvents

Pc	Solvent	λ(max)/nm (ε in log)			
II	DCB[a]	672(5.16)	650(4.63)	610(4.48)	332(4.76)
		292(4.47)			
III	H_2O[b]	670(4.77)	626(4.82)	320(4.82)	292(4.88)
		226(5.14)			
	AN[c]	660(5.26)	598(4.61)	326(4.98)	287(4.86)
		244(5.10)			
IV	DCB[a]	682(5.14)	658(4.60)	650(4.52)	616(4.53)
		346(4.70)	292(4.18)		
V	H_2O[b]	670(4.57)	630(4.75)	334(4.73)	225(5.01)
	AN[c]	670(5.24)	607(4.39)	338(4.84)	245(4.89)

a) DCB; *o*-dichlorobenzene. b) Data in water were collected at 4.665×10^{-6} M for **III** and 5.216×10^{-6} M for **V**. c) AN; acetonitrile.

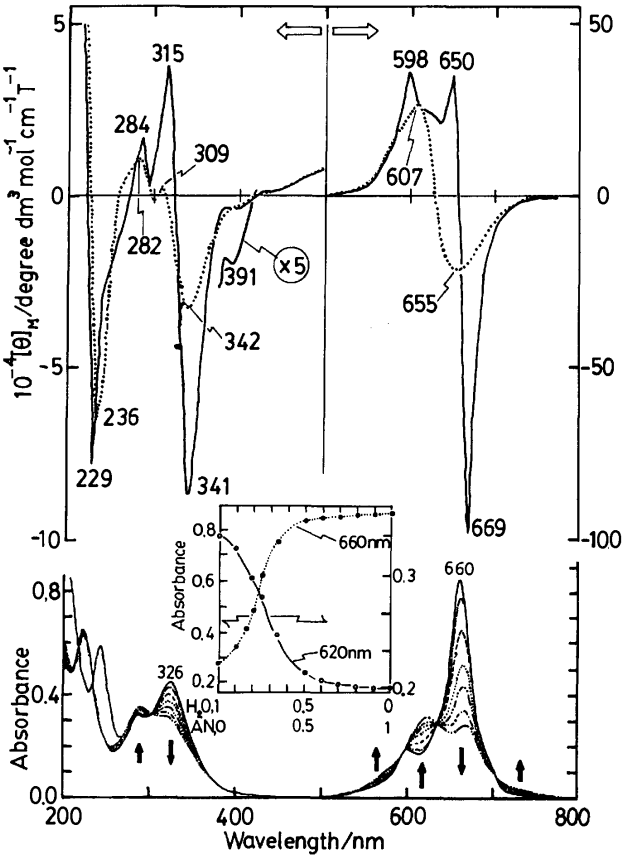

Fig. 1. Absorption (bottom) and MCD (top) spectra of **III** in acetonitrile (solid line), water (dotted line) and in their mixtures. Concentration=4.665×10^{-6} M. Cell path length=10 mm. Magnetic field=1.09 T. The inset shows the absorbance at 660 and 620 nm in acetonitrile-water mixtures.

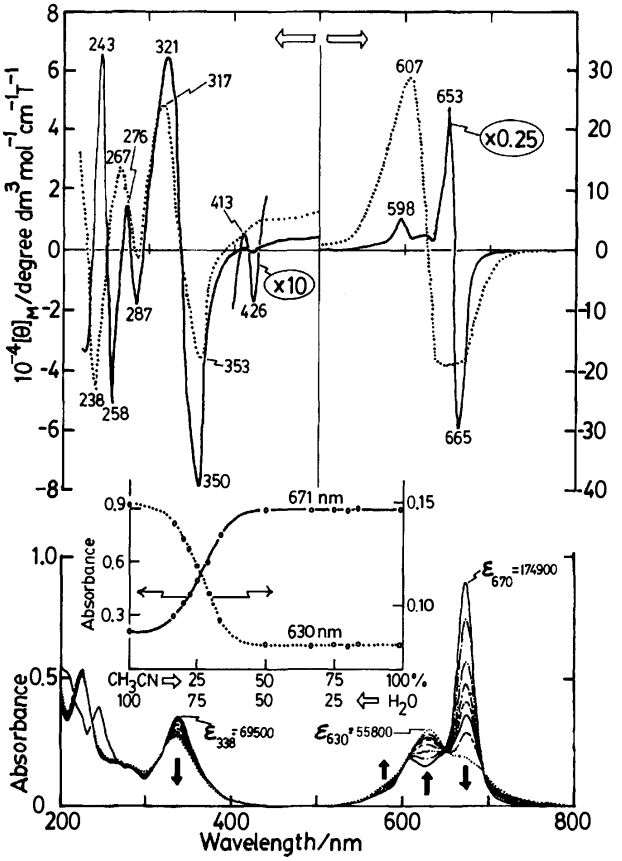

Fig. 2. Absorption (bottom) and MCD spectra (top) of **V** in acetonitrile (solid line), water (dotted line) and in their mixtures. Concentration=5.146×10^{-6} M. Cell path length=10 mm. Magnetic field=1.09 T. The inset shows the absorbance at 671 and 630 nm in acetonitrile-water mixtures.

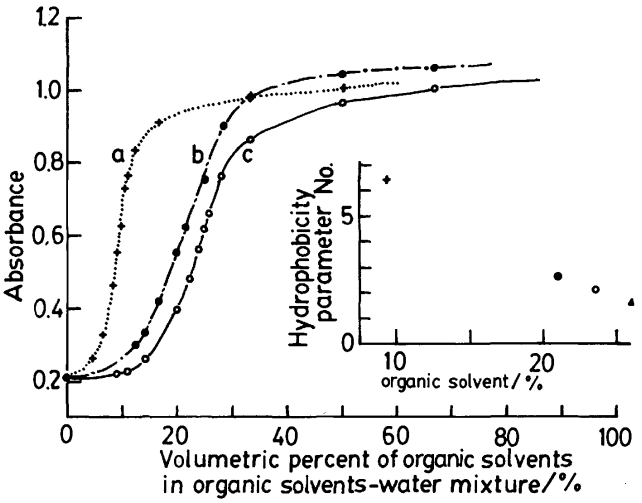

Fig. 3. Absorbance of the Q band of **V** in (a) 2-butoxyethanol-water, (b) dioxane-water, and (c) 2-propanol-water mixtures. Concentration=5.216×10^{-6} M. The inset shows the relationship between the hydrophobicity parameter and the organic solvent percent in organic solvent-water mixtures where 50% of the monomers have formed dimers. These data were obtained from lines a—c and the inset in Fig. 2.

points, and finally in pure water the spectra shown by the dotted lines were recorded. Although shapes of the spectra in pure water can be classified into those of aggregated phthalocyanines,[7] these are thought to be the spectra of dimeric species, since clear isosbestic points at several positions were observed in each case. The blue shift of the Soret and Q bands observed accompanying the change of solvent from AN to water suggests that the phthalocyanine dimers in water are in a card-pack arrangement.[7-9] This type of aggregation has been formed for tetrasulfonated phthalocyanine in water.[9] It is conceivable that, by the increase of polarity of solvent, the more hydrophobic phthalocyanine moieties approach each other (thereby forming dimers). As can be seen from the inflection points of the two curves in the inset, 50% of the monomeric phthalocyanines have dimerized when the AN:water ratio attains 23:77 (v/v) for **III** or 26.5:73.5 (v/v) for **V**.[10] In order to obtain further information on the state of **III** and **V** in water, the ESR spectrum of **V** was recorded in water. A 3.0×10^{-4} M solution gave an ESR singal at g=2.056 at 77 K, but little hyperfine structure which is observed clearly in monomeric species[7,11] appeared. Thus, **III** and **V** may exist as somewhat cofacial but slipped and/or staggered type dimers in water.

The MCD spectra of **III** and **V** in both water and AN are typical of phthalocyanines, in that Faraday *A*-terms appeared corresponding to the main absorption maxima.[12] However, though hardly detectable in the absorption spectra, a small but explicit Faraday *A*-term which indicates another degenerate excited state was discerned in the spectrum in AN at around 375—400 nm for **III** and 410—430 nm for **V**. The presence of this *A* term was only recently discovered for the first time for ZnPc[13] by MCD spectroscopy and assigned as a transition to the B state. So far the band at around 300—360 nm has generally been considered to be the B band.[14] However, if we follow the so-called "Four-Orbital Model" by Gouterman,[14,15] the band at 671, ca. 387, and 338 nm of **III** and 659, 420, 341, 282, and 250 nm of **V** in AN can be assigned as transitions to Q, B, N, L, and C states, respectively, in this order.[16] The possibility of a charge-transfer (CT) transition may not be ruled out completely; however, this possibility appears to be small, because an iron phthalocyanine[17] also reveals Faraday *A*-term type MCD signals in the same wavelength region (395—430[17] nm), irrespective of the different central metals. Especially, in the case of copper phthalocyanines, the CT band is not expected theoretically except in the near infrared region.[18]

The monomer-dimer transformatins of **V** were studied further in various organic-water solvent mixtures (Fig. 3). Three organic solvents which mix

with water in a wide ratio and have a range of hydrophobicity were selected. These were 2-propanol, dioxane, and 2-butoxyethanol, and have polarity parameters of 2.2, 2.6, and 6.4, respectively[19] (the larger the value, the higher the hydrophobicity). From this figure and the inset, it is found that the higher the hydrophobicity of the organic solvents used, the smaller the organic solvent:water ratio which is required for monomer to dimer transformation. Thus, the hydrophobicity (or polarity) of the solvent does affect the monomer-dimer equilibrium.

(ii) Electrochemistry of III in the Presence or Absence of Oxygen in Water. Cobalt phthalocyanines and porphyrins have been employed as catalysts for the electroreduction of oxygen in systems where the catalysts were homogeneously dissolved[20] in solution or adsorbed[21] onto working electrodes. Although there appears to be a general agreement that mononuclear cobalt complexes promote the O_2 reduction process by two electrons to give H_2O_2, almost no comparison has been made on the catalytic behavior between catalyst-dissolved and -adsorbed systems. The change of solvent on adsorption may also affect catalytic activity, but adsorption of catalysts onto electrodes has always been carried out in a single solvent. No study on the effect of varying the solvent has been reported previously. Since **III** is an amphiphilic cobalt phthalocyanine, we can perform O_2 electroreduction experiments under various conditions and can compare the results mutually.

The adsorption of **III** onto a GC electrode was examined from both 10^{-4} M AN and 10^{-4} M 0.1 M phosphate buffer (pH 7.0) solutions. The electrode was dipped in these solutions for a fixed time, taken out and dried in air, and transferred to a blank solution of 0.05 M H_2SO_4 or 0.1 M phosphate buffer (pH 7.0). The adsorption was saturated within ca. 30 s both in AN and aqueous solutions. Cyclic voltammograms at this prepared electrode are shown in Fig. 4 as curves a and a′ (pH 7, under nitrogen). Clear $Co^{II/I}$ redox couples whose peak currents have a linear relationship with the sweep rate (line b and b′) appeared at ca. −0.3 V vs. SCE, and the amount of the adsorbed catalyst, as deduced from the charge under the area (0.085 μC, i.e. 1.2 μC cm^{-2}) is approximately the same in both cases. The redox couple at the modified GC prepared in aqueous solution appears at a slightly (ca. 30 mV) negative potential than that prepared in AN. The relatively symmetrical redox patterns suggest the absence of significant interaction among the adsorbed species,[22] and imply that although **III** exists as a dimer in water (Fig. 1), the dimer structure may not be retained when it is immobilized onto GC by adsorption.

Figure 4, curves c and c′ are cyclic voltammetric curves at these modified electrodes in the presence of oxygen. Oxygen is reduced catalytically[23] at a much more positive potential than the $Co^{II/I}$ redox couple in curve a or a′, but there is no difference in the peak height between the two types of modified electrodes even over a sweep range of 20 to 200 mV s^{-1}. The peak height was linearly proportional to the square root of the sweep rate (lines d and d′), confirming a diffusion limited process, and to O_2 concentration (line e and e′). The difference in the potentials of O_2 reduction peaks of the two electrodes increases to ca. 50 mV compared with 30 mV for the $Co^{II/I}$ redox couple (curves a and a′). Oxygen reduction at the modified electrode in AN occurs at more anodic potentials than that at the electrode prepared in water. Thus the electrode modified in AN may be slightly better from the standpoint of the O_2 reduction potential.

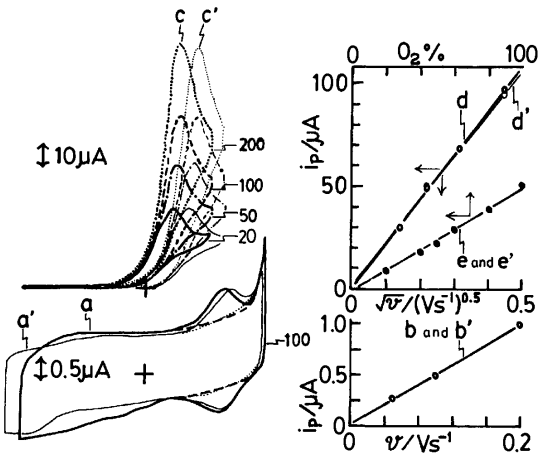

Fig. 4. Cyclic voltammograms at **III**-adsorbed GC electrodes (area, 0.070 cm^2) in water of pH 7.0. Adsorption was carried out either in 10^{-4} M acetonitrile solutions (bolder curves and lines, denoted by alphabet without prime) or in 10^{-4} M aqueous solutions (finer curves and lines denoted by alphabet with prime) for 10 min. Numbers on curves indicate scan rate in mV s^{-1}. Curve a and a′, responses in deaerated solution, and curves c and c′, in O_2-saturated solution. Line b and b′ indicates relationship between peak currents in curve a or a′ (ca. −0.31 or ca. −0.33 V) and scan rate. Lines d and d′ show relationship between peak currents in curves c or c′ and the square root of scan rate, and line e and e′ demonstrates catalytic O_2 reduction peak current vs. O_2 concentration relationship obtained at a sweep rate of 50 mV s^{-1}.

Potentials for the $Co^{II/I}$ couple and O_2 reduction peak at the modified electrodes at pH 1 are summarized together with the data at pH 7 in Table 2. As for other cobalt phthalocyanine systems,[24] the $Co^{II/I}$ redox potentials of **III** at pH 1 lie at much more anodic potentials than at pH 7, but the O_2 reduction potentials at pH 1 do not greatly shift from those at pH 7 and are equal to $Co^{II/I}$ redox potentials of **III** at pH 1. Since the $Co^{II/I}$ and O_2 potentials are similar for the catalyst-adsorbed system at pH 1, the O_2 reduction process can be explained by an electrochemical (EC)

Table 2. Some Potentials at Modified- or Bare Glassy Carbon Electrode

	Electrode with adsorbed **III** from 10^{-4} M AN solution		Electrode with adsorbed **III** from 10^{-4} M 0.1 M phosphate buffer		**III**-dissolved system	
	pH 1	pH 7	pH 1	pH 7	pH 1	pH 7
$Co^{II/I}$potential/V[a]	−0.12	−0.31	−0.15	−0.33	−0.43	−0.38
O_2 reduction Potential/V	−0.12	−0.12	−0.15	−0.17	−0.17	−0.22

a) Defined as (cathodic peak potential+anodic peak potential)/2.

catalytic regeneration mechanism (Eqs. 1 and 2).

$$Co^{II}Pc + e \longrightarrow Co^{I}Pc \quad E' \tag{1}$$

$$Co^{I}Pc + 0.5O_2 + H^+ \longrightarrow Co^{II}Pc + 0.5H_2O_2 \tag{2}$$

where Pc stands for the phthalocyaninato dianion. The mechanism at the catalyst-adsorbed system at pH 7, on the other band, may be different, since the potential difference between the $Co^{II/I}$ redox couple and O_2 reduction is very large (ca. 200 mV[25]). A reaction mechanism such as a CE (chemical step followed by electron transfer) mechanism (Eqs. 3 and 4) might be considered.[24b]

$$Co^{II}Pc + O_2 \longrightarrow Co^{II}PcO_2 \tag{3}$$

$$Co^{II}PcO_2 + 2e + 2H^+ \longrightarrow Co^{II}Pc + H_2O_2 \tag{4}$$

Some responses in the catalyst-dissolved system in aqueous solution at pH 1 are displayed in Fig. 5. In deaerated solutions, the bare GC electrode detected aggregated[22] electroactive species (curves a and b). When O_2 was admitted, the amount of catalytic O_2 reduction current (curve c), which is proportional to the square root of scan rate (curve d), is approximately the same as that in the catalyst-adsorbed systems, and its potential is much more positive than the $Co^{II/I}$ redox couple. Results at the catalyst-dissolved system at pH 7 are similar to those at pH 1 (Table 2). Since the potential difference between the $Co^{II/I}$ redox couple and O_2 reduction is large, it appears difficult to expalin the mechanism as an EC process which has frequently been adopted for O_2 reduction in catalyst-dissolved systems in the past.[20,26] The reduction mechanisms may be affected by pH value, by the kind of solvents used for adsorption of catalysts and so on. However, we can extract at least the following information based on the data in Table 2 and the above mentioned experimental observations. i) The O_2 reduction potential at GC electrode modified in AN is slightly (20—50 mV) more positive than that prepared in water. ii) The $Co^{II/I}$ redox couple shifts anodically by adsorption onto electrodes, by about 300 mV at pH 1 and 50—70 mV at pH 7. iii) O_2 reduction occurs at more positive potential in the catalyst-adsorbed system than in the catalyst-dissolved system by ca. 20—100 mV. iv) Both monomeric and aggregated forms of the catalyst have catalytic activity toward O_2 electroreduction.

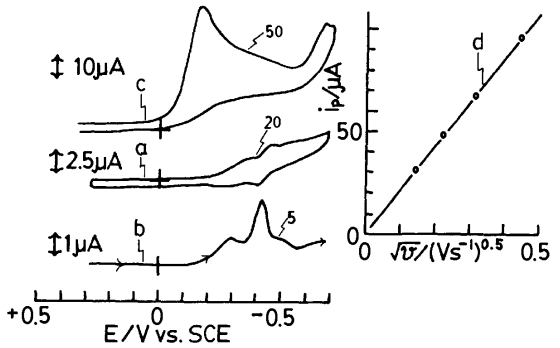

Fig. 5. Cyclic- and differential pulse voltammetric responses at bare GC electrodes in 0.05 M H_2SO_4 solution containing 0.5 mM of **III**. Curves a and b, in deaerated solution, and curve c in O_2-saturated solution. Line d shows the relationship between peak currents in curve c and the square root of the scan rate. Numbers on curves indicate scan rate in mV s^{-1}.

In trying to elucidate reasons for the above observations, and especially iii), we attempted scanning electron microscopy and surface enhanced Raman scattering spectroscopy. However, the amount of adsorbed catalyst was too small for the former spectroscopy and the GC surface was too dark for the latter spectroscopy.

In conclusion, although we cannot yet give a rationale for all the newly observed phenomena, the preparation of amphiphilic phthalocyanines has enabled us to connect and compare phthalocyanine chemistry in organic solvents and in water, which has not previously been possible. Thus, monomer-dimer transformation of phthalocyanines in water-organic solvent mixtures was found to depend on the polarity of organic solvents used. And, although no clear rationale could be given, electroreduction of oxygen at modified electrode was found to be affected not only by the pH value of solution but also by the solvents used for adsorption of catalysts.

We thank Dr. W. A. Nevin for critically reading this manuscript.

References

1) A. B. P. Lever, *Adv. Chem. Radiochem.*, **7**, 27 (1965); F. H. Moser and A. L. Thomas, "The Phthalocyanines," CRC Press, New York, Florida (1983).

2) G. Pawlowski and M. Hanack, *Synthesis*, **1987**, 287; T. W. Hall, S. Greenberg, C. R. McArthur, B. Khouw, and C. C. Leznoff, *Nouv. J. Chim.*, **6**, 653 (1982); H. Shirai, K. Hanabusa, M. Kitamura, E. Masuda, O. Hirabaru, and N. Hojo, *Makromol. Chem.*, **185**, 2537 (1984); D. Wohrle and G. Krawczyk, *Polym. Bull.*, **15**, 193 (1986).

3) J. H. Weber and D. H. Busch, *Inorg. Chem.*, **4**, 469 (1965).

4) D. R. Boston and J. C. Bailor, Jr., *Inorg. Chem.*, **11**, 1578 (1972); N. Kobayashi, H. Shirai, and N. Hojo, *J. Chem. Soc., Dalton Trans.*, **1984**, 2107.

5) V. M. Derkacheva, N. I. Bundina, N. G. Mekhryakova, O. L. Kaliya, T. Yu. Gulinat, and E. A. Luk'yanets, *Russ. J. Inorg. Chem. Engl. Ed.*, **26**, 911 (1981).

6) C. C. Leznoff, S. Vigh, P. I. Svirskaya, S. Greenberg, D. M. Drew, E. Ben-Hur, and I. Rosenthal, *Photochem. Photobiol.*, **49**, 279 (1989).

7) N. Kobayashi and A. B. P. Lever, *J. Am. Chem. Soc.*, **109**, 7433 (1987) and some references therein.

8) A. R. Monahan, J. A. Brado, and A. F. DeLuka, *J. Phys. Chem.*, **76**, 446 (1972); J. H. Sharp and M. Lardon, *ibid.*, **72**, 3230 (1968).

9) S. E. Sheppard and A. L. Geddes, *J. Am. Chem. Soc.*, **66**, 1995 (1944); Z. A. Schelly, R. D. Farina, and E. M. Eyring, *J. Phys. Chem.*, **74**, 617 (1970).

10) Thus, **V** forms a dimer more easily than **III**, since it requires a lower amount of dimer-forming solvent (water). Since there are no structural differences between **III** and **V**, this furhter indicates that copper(II) has a higher tendency toward dimerization than cobalt(II).

11) R. Neiman and D. Kivelson, *J. Chem. Phys.*, **35**, 156 (1961); C. M. Gusy, J. B. Raynor, and M. C. R. Simons, *J. Chem. Soc. A*, **1961**, 2299; S. S. Eaton, K. M. More, B. M. Sawant, and G. R. Eaton, *J. Am. Chem. Soc.*, **105**, 6560 (1983); M. Chikira, H. Yokoi, and T. Isobe, *Bull. Chem. Soc. Jpn.*, **47**, 2208 (1974).

12) P. J. Stephens, *Ann. Rev. Phys. Chem.*, **25**, 201 (1974).

13) T. Nyokong, Z. Gasyna, and M. J. Stillman, *Inorg. Chem.*, **26**, 1087 (1987).

14) M. Gouterman, "The Porphyrins," ed. by D. Dolphin, Vol. III, Chap. 1, Academic Press, New York, London (1978).

15) M. Gouterman, *J. Chem. Phys.*, **30**, 1139 (1959).

16) A. J. McHugh, M. Gouterman, and C. Weiss, *Theor. Chim. Acta*, **24**, 346 (1972).

17) N. Kobayashi, M. Koshiyama, Y. Ishikawa, T. Osa, H. Shirai, and N. Hojo, *Chem. Lett.*, **1984**, 1633.

18) A. B. P. Lever, S. R. Pickens, P. C. Minor, S. Licoccia, B. S. Ramaswamy, and K. Magnell, *J. Am. Chem. Soc.*, **103**, 6805 (1981).

19) J. R. Haak and J. B. F. N. Engburts, *Recl. Trav. Chim. Pays-Bas*, **105**, 307 (1986); K. Dimroth, C. Reichardt, T. Siepman, and F. Bohlman, *Justus Liebigs Ann. Chem.*, **661**, 1 (1963).

20) a) T. Kuwana and A. Bettelheim, *Anal. Chem.*, **51**, 2257 (1979); b) T. Kuwana and P. A. Forschey, *Inorg. Chem.*, **20**, 693 (1981); **22**, 699 (1983); c) T. Kuwana, P. A. Forschey, N. Kobayashi, and T. Osa, *Adv. Chem. Ser.*, **No. 201**, 601 (1982); d) N. Kobayashi, M. Fujihira, T. Matsue, and T. Osa, *J. Electroanal. Chem.*, **103**, 427 (1979); e) N. Kobayashi, M. Fujihira, T. Osa, and T. Kuwana, *Bull. Chem. Soc. Jpn.*, **53**, 2195 (1980); f) N. Kobayashi and T. Osa, *J. Electroanal. Chem.*, **157**, 269 (1983); g) N. Kobayashi, M. Koshiyama, T. Osa, and T. Kuwana, *Inorg. Chem.*, **22**, 3608 (1983); h) N. Kobayashi and Y. Nishiyama, *J. Phys. Chem.*, **89**, 1167 (1985).

21) R. Jasinski, *Nature (London)*, **201**, 1212 (1964); H. Jahnke, M. Schonborn, and G. Zimmermann, *Topics in Current Chemistry*, **61**, 133 (1976); M. R. Tarasevish and K. A. Radyushkina, *Russ. Chem. Rev. Eng. Trans.*, **49**, 1498 (1980); F. van den Brink, E. Barendrecht, and W. Visscher, *Recl. Trav. Chim. Pays-Bas*, **99**, 253 (1980); J. A. R. van Veen and J. F. van Baar, *Rev. Inorg. Chem.*, **4**, 293 (1982); D. J. Schiffrin, *Electrochemistry*, **8**, 126 (1983); E. Yeager, *Electrochim. Acta*, **29**, 1527 (1984); *J. Mol. Catal.*, **38**, 5 (1986).

22) M. R. Hempstead, C. C. Leznoff, and A. B. P. Lever, *Can. J. Chem.*, **65**, 2677 (1987).

23) O_2 reduction at bare GC electrode occurs at ca. −0.58 V vs. SCE in water.[20b,c]

24) a) S. Zecevic, B. Simic-Glavaski, E. Yeager, A. B. P. Lever, and P. C. Minor, *J. Electroanal. Chem.*, **196**, 339 (1985); b) P. Janda, N. Kobayashi, H. Lam, P. R. Auburn, C. C. Leznoff, and A. B. P. Lever, *Can. J. Chem.*, **67**, 1109 (1989).

25) C. P. Andrieux, C. Blocman, J. M. Bouchiat-Dumas, F. M'Halla, and J. M. Saveant, *J. Electroanal. Chem.*, **119**, 19 (1980); C. P. Andrieux and J. M. Saveant, *ibid.*, **134**, 163 (1982); **142**, 1 (1982); F. C. Anson, *J. Phys. Chem.*, **84**, 3336 (1980).

26) D. O. R. Parash, F. Broitman, U. Mor, and A. Bettelheim, *J. Chem. Soc., Faraday Trans. 1*, **80**, 1139 (1984).

 © 1989 The Chemical Society of Japan Bull. Chem. Soc. Jpn., 62, 3475—3478 (1989)

Preparation and Spectroscopic Characteristics of Geometrical Isomers of Bis[1,2-bis(dimethylphosphino)ethane]cobalt(III) Complexes with Thiolate Ligands

Takumi KONNO,* Zhi-Ping BAI, Ken-ichi OKAMOTO, and Jinsai HIDAKA
Department of Chemistry, University of Tsukuba, Tsukuba, Ibaraki 305
(Received June 5, 1989)

The thiolato cobalt(III) complexes, $[Co(SR)_2(dmpe)_2]^+$, where R denotes CH_3, C_2H_5, or $CH_2C_6H_5$ and dmpe denotes 1,2-bis(dimethylphosphino)ethane, were newly prepared from *trans*-$[CoCl_2(dmpe)_2]^+$ and monothiolate ligands. The cis and trans isomers were formed for R=CH_3 and $CH_2C_6H_5$, while only the trans isomer was formed for R=C_2H_5. These isomers were assigned on the basis of the ^1H NMR (500 MHz) and absorption spectra in comparison with those of the newly prepared $[Co(SCH_2CH_2S)(dmpe)_2]^+$ complex. The trans isomer showed the sulfur-to-cobalt charge-transfer band at lower energy than that of the cis isomer.

Cobalt(III) complexes with two or three thiolato donor atoms prefer to take the cis(*S*) geometry,[1-3] and no trans isomer has been obtained for $[Co(SR)_2(amine)_4]^+$ (R=CH_3, C_2H_5, $CH_2C_6H_5$, and C_6H_5).[4] On the other hand, chelating diphosphine ligands, such as dmpe (1,2-bis(dimethylphosphino)ethane) and depe (1,2-bis(diethylphosphino)ethane), tend to favor the formation of *trans*-$[CoX_2(diphosphine)_2]^+$ (X=Cl, Br, and I).[5-8] This trend reveals that the trans(*S*) geometry is possibly formed in the $[Co(SR)_2(diphosphine)_2]$-type complex. The present work is concerned with the preparation of $[Co(SR)_2(dmpe)_2]^+$ (R=CH_3, C_2H_5, and $CH_2C_6H_5$), and the trans(*S*) isomers are presented. The isomers obtained were characterized on the basis of the ^1H NMR (500 MHz) and absorption spectra in comparison with those of the newly prepared $[Co(SCH_2CH_2S)(dmpe)_2]^+$. This is the first example of cobalt(III) complexes containing both diphosphine and monothiolate ligands.

Experimental

A) Preparation of Complexes. (1) The starting complex, *trans*-$[CoCl_2(dmpe)_2]ClO_4$, was prepared by the method of Ohishi et al.[6] Found: C, 26.91; H, 6.13%. Calcd for $[CoCl_2(dmpe)_2]ClO_4 \cdot 0.5H_2O = C_{12}H_{33}O_{4.5}Cl_3P_4Co$: C, 26.76; H, 6.18%.

(2) *cis*- and *trans*-$[Co(SCH_3)_2(dmpe)_2]X$ (X=PF_6 and $B(C_6H_5)_4$). To a solution containing 0.1 g of *trans*-$[CoCl_2(dmpe)_2]ClO_4 \cdot 0.5H_2O$ (0.19 mmol) in 20 cm^3 of degassed methanol was added 0.06 g of $NaSCH_3$ (0.86 mmol) in 1 cm^3 of methanol. The mixture was stirred at 50 °C for 30 min under a nitrogen atmosphere, whereupon the solution became deep brown. To this was added 1 g of $NaPF_6$ in 10 cm^3 of water and the solution was allowed to stand in a refrigerator overnight. The resulting brown crystals of *trans*-$[Co(SCH_3)_2(dmpe)_2]PF_6$ (**A-1**) were collected by filtration. The filtrate was kept in a freezer overnight and the resulting **A-1** precipitate was again filtered off. To this filtrate was added 0.1 g of $NaB(C_6H_5)_4$ in 2 cm^3 of methanol. After the mixture was allowed to stand in a refrigerator for 1 h, the resulting greenish-brown precipitate of *cis*-$[Co(SCH_3)_2(dmpe)_2]B(C_6H_5)_4$ (**A-2**) was collected by filtration. The **A-2** isomer was recrystallized from acetone by adding a small amount of $NaB(C_6H_5)_4$ in methanol. **A-1** isomer: Yield: 0.05 g, 45%. Found: C, 28.17; H, 6.47%. Calcd for $[Co(SCH_3)_2(dmpe)_2]PF_6 = C_{14}H_{38}F_6P_5S_2Co$: C, 28.10; H, 6.40%. **A-2** isomer: Yield: 0.03 g, 20%. Found: C, 59.04; H, 7.66%. Calcd for $[Co(SCH_3)_2(dmpe)_2]B(C_6H_5)_4$: C, 59.07; H, 7.57%.

The trans (**A-1**) and cis (**A-2**) isomers of $[Co(SCH_3)_2(dmpe)_2]^+$ were also formed in nearly the same ratio as that observed above, using $[Co(CO_3)(dmpe)_2]ClO_4 \cdot 2.5H_2O \cdot NaClO_4$[9] as the starting complex instead of *trans*-$[CoCl_2(dmpe)_2]ClO_4 \cdot 0.5H_2O$.

(3) *trans*-$[Co(SC_2H_5)_2(dmpe)_2]PF_6$. This complex (**B-1**) was prepared by a method similar to that described above for *trans*-$[Co(SCH_3)_2(dmpe)_2]PF_6$ (**A-1**), using 0.06 cm^3 of neat HSC_2H_5 (0.81 mmol) and 0.3 cm^3 of 1 mol dm^{-3} NaOH (0.30 mmol) instead of $NaSCH_3$. No significant formation of the cis isomer was noticed in this reaction or in a reaction where $[Co(CO_3)(dmpe)_2]ClO_4 \cdot 2.5H_2O \cdot NaClO_4$ was used as the starting complex instead of *trans*-$[CoCl_2(dmpe)_2]ClO_4 \cdot 0.5H_2O$. Yield: 0.04 g, 34%. Found: C, 30.55; H, 6.68%. Calcd for $[Co(SC_2H_5)_2(dmpe)_2]PF_6 = C_{16}H_{42}F_6P_5S_2Co$: C, 30.68; H, 6.76%.

(4) *cis*- and *trans*-$[Co(SCH_2C_6H_5)_2(dmpe)_2]X$ (**X**=ClO_4 and $B(C_6H_5)_4$). The two isomers, trans (**C-1**) and cis (**C-2**), of $[Co(SCH_2C_6H_5)_2(dmpe)_2]^+$ were prepared and separated by a method similar to that described above for $[Co(SCH_3)_2(dmpe)_2]^+$, using 0.1 cm^3 of neat $HSCH_2C_6H_5$ (0.85 mmol) and 0.3 cm^3 of 1 mol dm^{-3} NaOH (0.30 mmol) instead of $NaSCH_3$. The trans (**C-1**) isomer was obtained as the perchlorate salt using a small amount of a saturated $NaClO_4$ solution instead of $NaPF_6$. It was found from the absorption and ^1H NMR (500 MHz) spectral measurements that the tetraphenylborate salt is the cis (**C-2**) isomer containing a small amount of the trans (**C-1**) isomer. **C-1** isomer: Yield: 0.045 g, 34%. Found: C, 44.12; H, 6.72%. Calcd for $[Co(SCH_2C_6H_5)_2(dmpe)_2]ClO_4 = C_{26}H_{46}O_4P_4S_2ClCo$: C, 44.29; H, 6.58%. $B(C_6H_5)_4$ salt: Yield: 0.03 g, 17%. Found: C, 63.98; H, 7.06%. Calcd for $[Co(SCH_2C_6H_5)_2(dmpe)_2]B(C_6H_5)_4 \cdot H_2O = C_{50}H_{64}BP_4S_2Co \cdot H_2O$: C, 63.83; H, 7.07%.

(5) $[Co(SCH_2CH_2S)(dmpe)_2]PF_6$. This complex was prepared by a method similar to that described for $[Co(SCH_3)_2(dmpe)_2]PF_6$, using 0.05 cm^3 of neat $HSCH_2CH_2SH$ (0.60 mmol) and 0.3 cm^3 of 1 mol dm^{-3} NaOH (0.30 mmol) instead of $NaSCH_3$. The reaction was conducted at room temperature for 30 min. Yield: 0.04 g, 35%. Found: C, 28.60; H, 6.02%. Calcd for $[Co(SCH_2CH_2S)(dmpe)_2]PF_6 = C_{14}H_{36}F_6P_5S_2Co$: C, 28.20; H, 6.08%.

B) Measurements. The electronic absorption spectra were recorded in CH_3CN with JASCO UVIDEC-505 and UVIDEC-610 spectrophotometers at ambient temperatures. The 500 MHz ^1H NMR spectra were recorded with a BRUKER-AM-500 NMR spectrometer in CD_3CN at the probe temperature. Tetramethylsilane (TMS) was used at the internal reference.

Results and Discussion

Two geometrical isomers, cis and trans, are possible for $[Co(SR)_2(dmpe)_2]^+$ (R=CH_3, C_2H_5, and $CH_2C_6H_5$), while only one isomer having the cis(*S*) configuration is possible for $[Co(SCH_2CH_2S)(dmpe)_2]^+$ (Fig. 1). In the 500 MHz ^1H NMR spectrum (Fig. 2), $[Co(SCH_2CH_2S)(dmpe)_2]^+$ exhibits characteristic P-methyl signals in the region of δ 1.4—1.6 (from TMS). That is, four sets of signals due to the eight P-CH_3 groups in the complex are observed (Fig. 2a), reflecting the C_2 symmetry of the complex. A quite similar ^1H NMR spectral pattern is observed for the **A-2** isomer of $[Co(SCH_3)_2(dmpe)_2]^+$, though two signals due to the two S-CH_3 groups appear (δ 1.589 and 1.594) besides four sets of signals due to the eight P-CH_3 groups in the region of δ 1.4—1.6 (Fig. 2b). On the other hand, the **A-1** isomer of $[Co(SCH_3)_2(dmpe)_2]^+$ shows one set of P-methyl signals which appears as a quintet at δ 1.629 (J=2.2 Hz) and one singlet S-methyl signal at δ 1.304 (Fig. 2c). The starting *trans*-$[CoCl_2(dmpe)_2]^+$ complex also gave one set of quintet P-methyl signals at δ 1.572 (J=2.4 Hz). These ^1H NMR spectral behavior indicate that the **A-1** and **A-2** isomers are *trans*- and *cis*-$[Co(SCH_3)_2(dmpe)_2]^+$, respectively. The ^1H NMR spectral behavior of the **B-1** isomer of $[Co(SC_2H_5)_2(dmpe)_2]^+$ and the **C-1** isomer of $[Co(SCH_2C_6H_5)_2(dmpe)_2]^+$ are similar to that of *trans*-$[Co(SCH_3)_2(dmpe)_2]^+$ (**A-1**), showing one set of quintet signals due to the eight P-CH_3 groups in the complex (δ 1.623 (J=2.2 Hz) for **B-1** and δ 1.718 (J=2.1 Hz) for **C-1**). Furthermore, the **B-1** isomer shows one set of triplet signals (δ 1.061, J=7.3 Hz) and one set of quartet signals (δ 1.718, J=7.3 Hz) due to the two SC_2H_5 groups, and the **C-1** isomer shows one singlet signal due to the two S-CH_2- groups at δ 2.931. Accordingly, the **B-1** and **C-1** isomers can be assigned to the trans(*S*) configuration. In the ^1H NMR spectrum of the tetraphenylborate salt of $[Co(SCH_2C_6H_5)_2(dmpe)_2]^+$, four sets of P-methyl signals are observed (centered at δ 1.486, 1.566, 1.629, and 1.775) as in the case of *cis*-$[Co(SCH_3)_2(dmpe)_2]^+$ (**A-2**), in addition to one set of quintet P-methyl signals which corresponds to the signals arising from *trans*-$[Co(SCH_2C_6H_5)_2(dmpe)_2]^+$ (**C-1**). The ^1H NMR spectrum suggests that the tetraphenylborate salt is the cis isomer containing a small amount of the trans one. This is supported by the fact that absorption spectral behavior of this salt agrees with that of *cis*-$[Co(SCH_3)_2(dmpe)_2]^+$ (Fig. 3).

As shown in Fig. 3 and Table 1, the absorption spectrum of *cis*-$[Co(SCH_3)_2(dmpe)_2]^+$ is quite similar to that of $[Co(SCH_2CH_2S)(dmpe)_2]^+$ in the whole

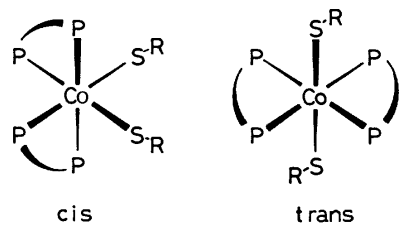

Fig. 1. Two geometrical isomers of $[Co(SR)_2(dmpe)_2]^+$.

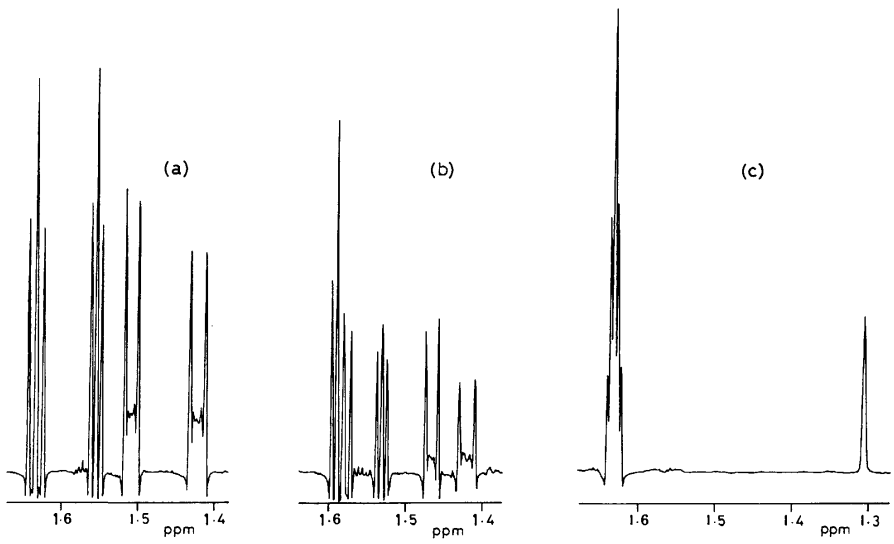

Fig. 2. ^1H NMR (500 MHz) spectra of $[Co(SCH_2CH_2S)(dmpe)_2]^+$ (a), *cis*-$[Co(SCH_3)_2(dmpe)_2]^+$ (b), and *trans*-$[Co(SCH_3)_2(dmpe)_2]^+$ (c) in CD_3CN (TMS reference).

Table 1. Absorption Spectral Data of the Complexes in CH_3CN

Complex	$\sigma/10^3\,cm^{-1}$ ($\log \varepsilon/mol^{-1}\,dm^3\,cm^{-1}$)				
$[Co(SCH_2CH_2S)(dmpe)_2]^+$	19.4(2.7sh)	22.12(3.02)	28.9(3.4sh)	33.17(4.16)	43.48(4.25)
cis-$[Co(SCH_3)_2(dmpe)_2]^+$	17.50(2.61)	21.7(3.0sh)	26.32(3.38)	32.15(4.16)	42.55(4.50)
trans-$[Co(SCH_3)_2(dmpe)_2]^+$	18.73(2.39)	28.53(4.05)	41.15(4.26)		
trans-$[Co(SC_2H_5)_2(dmpe)_2]^+$	18.87(2.35)	28.65(4.06)	41.32(4.26)		
trans-$[Co(SCH_2C_6H_5)_2(dmpe)_2]^+$	17.91(2.48)	28.01(4.36)	42.7(4.4sh)		

sh denotes a shoulder.

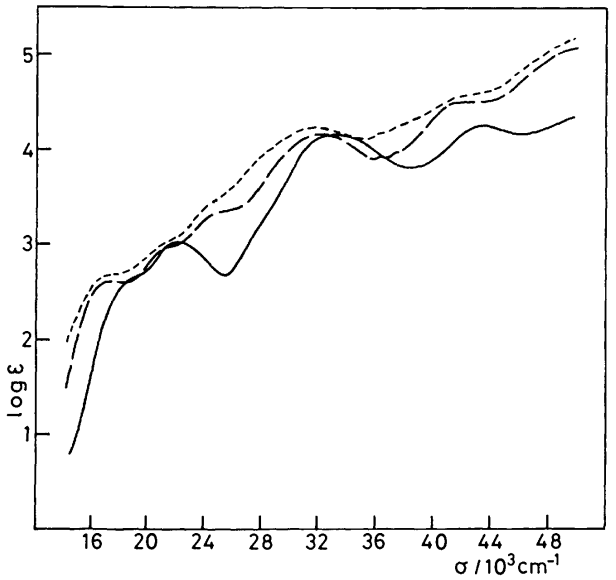

Fig. 3. Absorption spectra of $[Co(SCH_2CH_2S)(dmpe)_2]^+$ (——), *cis*-$[Co(SCH_3)_2(dmpe)_2]^+$ (———), and $[Co(SCH_2C_6H_5)_2(dmpe)_2]^+$ (-----) in CH_3CN.

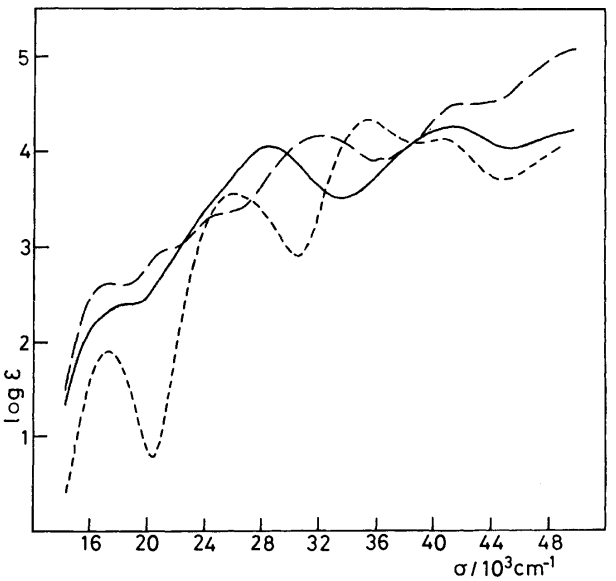

Fig. 4. Absorption spectra of *trans*-$[Co(SCH_3)_2(dmpe)_2]^+$ (——), *cis*-$[Co(SCH_3)_2(dmpe)_2]^+$ (———), and *trans*-$[CoCl_2(dmpe)_2]^+$ (-----) in CH_3CN.

region, though the absorption components of the former complex shift to a somewhat lower energy than those of the latter. On the other hand, the absorption spectral behavior of *trans*-$[Co(SCH_3)_2(dmpe)_2]^+$ differs significantly from those of $[Co(SCH_2CH_2S)(dmpe)_2]^+$ and *cis*-$[Co(SCH_3)_2(dmpe)_2]^+$, especially in the near-UV region (Fig. 4). Namely, the trans SCH_3 isomer exhibits an intense absorption band at 28.53×10^3 cm^{-1}, while the cis SCH_3 isomer exhibits a broad intense band at 32.15×10^3 cm^{-1}. The corresponding broad intense band of $[Co(SCH_2CH_2S)(dmpe)_2]^+$ appears at 33.17×10^3 cm^{-1} (Fig. 3). Quite similar intense absorption bands, which have been assigned to the S-to-Co charge-transfer (SCCT) bands, were observed for the trans(*S*) and cis(*S*) isomers of [Co(quadridentate-SNNS)(diamine)]$^+$:[10] a sharp band at ca. 30×10^3 cm^{-1} for the trans(*S*) isomer and a broad band at ca. 34×10^3 cm^{-1} for the cis(*S*) isomer. For the present $[Co(thiolato)_2(diphosphine)_2]^+$-type complexes, it may be considered that the coordinated diphosphine ligand contributes to the absorption spectral behavior in this region. As shown in Fig. 4, however, *trans*-$[CoCl_2(dmpe)_2]^+$ exhibits an intense band at 35.46×10^3 cm^{-1}, which has been assigned as arising from the P-to-Co charge-transfer (PCCT) transition.[8] Taking this fact into consideration, it is probable that the intense bands for the present isomers are due to the SCCT transition rather than to the PCCT transition. In order to confirm the absorption spectral behavior of the trans and cis isomers, $[Co(SC_2H_5)_2(dmpe)_2]^+$ and $[Co(SCH_2C_6H_5)_2(dmpe)_2]^+$ were also newly prepared. The absorption spectra of the trans SC_2H_5 and $SCH_2C_6H_5$ isomers coincide well with that of *trans*-$[Co(SCH_3)_2(dmpe)_2]^+$ over the whole region (Fig. 5 and Table 1), showing the SCCT band at ca. 28.5×10^3 cm^{-1}. The tetraphenylborate salt of $[Co(SCH_2C_6H_5)_2(dmpe)_2]^+$, which is the cis isomer containing a small amount of the trans one (vide supra), gives a broad SCCT band at ca. 32×10^3 cm^{-1} (Fig. 3), as in the case of *cis*-$[Co(SCH_3)_2(dmpe)_2]^+$. Thus, it is also valid for the present dmpe complexes that the cis(*S*)- and trans(*S*)-type isomers are discriminated on the basis of the relative position of the SCCT bands.[10-13] The cis and trans isomers of $[Co(SCH_3)_2(dmpe)_2]^+$ also show noticeable absorption spectral difference in the visible region (Fig. 4 and Table 1). It has been reported that the cis(*S*) and trans(*S*) isomers of [Co(quadridentate-SNNS)(diamine)]$^+$ can be assigned by the splitting pattern of the first d-d absorption bands.[10] However, it is difficult for the

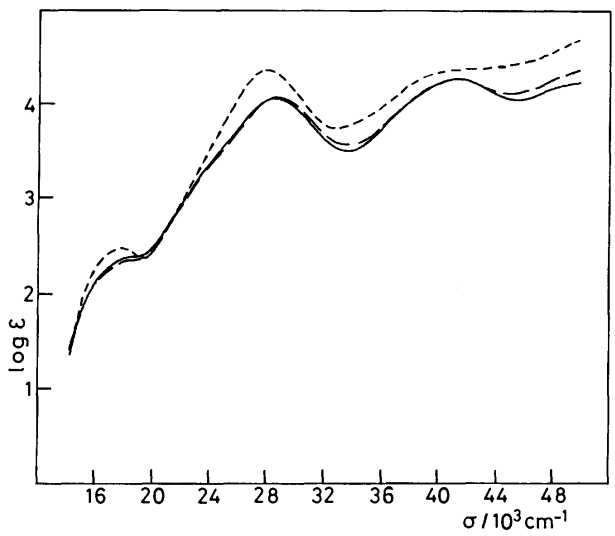

Fig. 5. Absorption spectra of *trans*-$[Co(SCH_3)_2(dmpe)_2]^+$ (——), *trans*-$[Co(SC_2H_5)_2(dmpe)_2]^+$ (— — —), and *trans*-$[Co(SCH_2C_6H_5)_2(dmpe)_2]^+$ (-----) in CH_3CN.

present dmpe complexes to assign the two isomers on the basis of the absorption spectral difference in the visible region.

In this study, a direct treatment of *trans*-$[CoCl_2(dmpe)_2]^+$ with monothiolate ligands produced the $[Co(SR)_2(dmpe)_2]^+$ (R=CH_3, C_2H_5, and $CH_2C_6H_5$) complexes. The trans isomer was formed for all three complexes, while the cis isomer was formed for two complexes (R=CH_3 and $CH_2C_6H_5$). Furthermore, each of the two cis isomers was formed in small amount compared with the corresponding trans isomer. A quite similar preparative result was also obtained by a method in which $[Co(CO_3)(dmpe)_2]^+$ was used as the starting complex instead of *trans*-$[CoCl_2(dmpe)_2]^+$. These results are in contrast to the cis(*S*) selective formation as found in [Co(L-cysteinato-*N*,*S*)$_3$]$^{3-}$,[1,2] [Co(D-penicillaminato-*N*,*O*,*S*)$_2$]$^-$,[3] and $[Co(SR)_2(amine)_4]^+$ (R=CH_3, C_2H_5, $CH_2C_6H_5$, and C_6H_5),[4] and indicate that the trans(*S*) geometry is dominant for $[Co(SR)_2(dmpe)_2]^+$ complexes. Namely, the dmpe ligand functions dominantly in forming *trans*-$[Co(SR)_2(dmpe)_2]^+$. It has been reported that the *cis*-$[CoX_2(dmpe)_2]^+$ (X=Cl, Br, and I) complexes isomerized to the trans isomer and the isomerization reaction was accelerated by ultraviolet light.[8] In contrast to *cis*-$[CoX_2(dmpe)_2]^+$, the present cis and trans isomers of $[Co(SR)_2(dmpe)_2]^+$ in solution are fairly stable in the dark; the intensities of their SCCT bands in CH_3CN or CH_3CN–H_2O (4:1) decreased slightly with time at room temperature (ca. 1.5% in 60 min). No isomerization occurred for the present isomers, even when the solution was exposed to ultraviolet light, though decomposition was promoted. These facts suggest that the cis(*S*) preference of the thiolate ligand prevents the isomerization to the trans(*S*) isomer.

References

1) R. D. Gillard and R. Maskill, *Chem. Commun.*, **1968**, 160.

2) M. Kita, K. Yamanari, and Y. Shimura, *Bull. Chem. Soc. Jpn.*, **55**, 2873 (1982).

3) K. Okamoto, K. Wakayama, H. Einaga, S. Yamada, and J. Hidaka, *Bull. Chem. Soc. Jpn.*, **56**, 165 (1983).

4) H. Umehara, K. Okamoto, and J. Hidaka, presented at the 35th Symposium on the Coordination Chemistry of Japan, Hiroshima, 1985, Abstract No. 2A19; T. Konno, H. Umehara, K. Okamoto, and J. Hidaka, to be submitted.

5) C. E. Wymore and J. C. Bailar, Jr., *J. Inorg. Nucl. Chem.*, **14**, 42 (1960).

6) T. Ohishi, K. Kashiwabara, and J. Fujita, *Chem. Lett.*, **1981**, 1371.

7) H. C. Jewiss, W. Levason, and M. Webster, *Inorg. Chem.*, **25**, 1997 (1986).

8) T. Ohishi, K. Kashiwabara, and J. Fujita, *Bull. Chem. Soc. Jpn.*, **60**, 575 (1987).

9) T. Ohishi, K. Kashiwabara, J. Fujita, S. Ohba, T. Ishii, and Y. Saito, *Bull. Chem. Soc. Jpn.*, **59**, 385 (1986). Found: C, 22.59; H, 5.30%. Calcd for $[Co(CO_3)(dmpe)_2]ClO_4 \cdot 2.5H_2O \cdot NaClO_4 = C_{13}H_{37}O_{13.5}NaP_4Cl_2Co$: C, 22.75; H, 5.44%.

10) K. Yamanari, N. Takeshita, and Y. Shimura, *Bull. Chem. Soc. Jpn.*, **57**, 1227 (1984).

11) J. Hidaka, S. Yamada, and Y. Shimura, *Chem. Lett.*, **1974**, 1487.

12) K. Akamatsu, J. Hidaka, and Y. Shimura, *Bull. Chem. Soc. Jpn.*, **50**, 533 (1977).

13) T. Konno, K. Okamoto, and J. Hidaka, *Bull. Chem. Soc. Jpn.*, **56**, 2631 (1983).

 © 1989 The Chemical Society of Japan Bull. Chem. Soc. Jpn., 62, 3479—3487 (1989)

Photoinduced Intramolecular Cyclization Reaction of 3-Substituted 2-Alkenoyl-1,4-benzoquinones

Hidetoshi IWAMOTO
Department of Chemistry, Faculty of Science, Shimane University, Nishikawatsu-cho, Matsue 690
(Received January 20, 1989)

Irradiation of 3-alkoxy-2-alkenoyl-1,4-benzoquinones in solution gave tricyclic compounds (5*H*-pyrano-[4,3,2-*de*][1,3]benzodioxin derivatives) and 3-alkylthio-2-alkenoyl-1,4-benzoquinones gave similar products (5*H*-pyrano[4,3,2-*de*][3,1]benzoxathiin derivatives). Each reaction initiates via γ-hydrogen abstraction by photoexcited quinone to produce diradical intermediates which intramolecularly cyclize to give the products.

Such isoprenoid 1,4-quinones as plastoquinone, ubiquinone, and menaquinone have been well known to play important roles in nature,[1] e.g. in processes such as electron transport and oxidative phosphorylation. The photochemical reactions of related quinone compounds, therefore, have been extensively investigated under several conditions.[2] For example, irradiation of isoprenoid 1,4-quinones under aerobic conditions gives trioxane and hydroperoxide, but that of the quinones under anaerobic conditions gives dihydrobenzofuran, chromene, or dimer.[2] Chlorobiumquinone,[3] which is an alkenoyl-1,4-quinone with both an olefinic double bond and a carbonyl group in the side chain, was isolated from a natural source. An investigation of the photochemical reactions of 2-alkenoyl-1,4-benzoquinones **1** is, therefore, of interest from both biological and photochemical points of view.

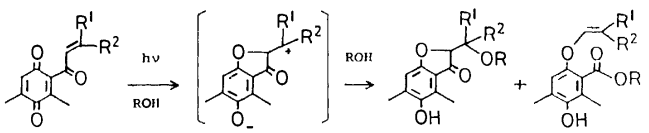

1 **2** **3** **4** (1)

It has been reported that irradiation of alkenoyl quinones **1** in benzene under aerobic conditions affords relatively stable cyclic peroxides.[4] Recently, we reported the photochemical reaction of **1** in alcohols under anaerobic conditions to give two isomeric adducts (**3** and **4**)[5] via a zwitterionic intermediate **2** (Eq. 1). Afterwards, we preliminarily reported that 2-alkenoyl-3-alkoxy-1,4-benzoquinones (**5G**) reacted photochemically to give intramolecular cyclization products, 5*H*-pyrano[4,3,2-*de*][1,3]benzodioxin derivatives (**7G**),[6] via γ-hydrogen abstraction (Eq. 2). The photoinduced γ-hydrogen abstraction of alkoxyquinones[7] or the intramolecular cyclization reaction of 2-alkenyl-3-alkoxy-1,4-quinone,[8] and the intermolecular photochemical reaction of alkoxyquinones with olefins[9] have been extensively investigated so far.

In this paper, we describe the photochemical reaction of alkoxybenzoquinones **5G** and 2-alkenoyl-3-alkylthio-1,4-benzoquinones (**5S**) which are noticeably different from that of other alkoxyquinones; the quinones **5G** gave intramolecularly cyclized products **7G**, and **5S** gave similar cyclization products, 5*H*-pyrano[4,3,2-*de*][3,1]benzoxathiin derivatives (**7S**), in high yields together with minor products, 9*H*-[1,3]oxathiolo[4,5-*f*][1]-benzopyran-9-one derivatives (**8S**)[10] (Eq. 2).

Results and Discussion

Photochemical Reaction of 5G in Acetonitrile. When a solution of 3-methoxy-5-methyl-2-(α-methylcinnamoyl)-1,4-benzoquinone (**5Ga**) in acetonitrile (0.01 mol dm^{-3}) was irradiated with light at wavelengths longer than 410 nm under a nitrogen atmosphere for 3 h, an intramolecularly cyclized product, 4,8-dimethyl-5-phenyl-5*H*-pyrano[4,3,2-*de*][1,3]benzodioxin-9-ol (**7Ga**), was obtained as the major product in 50% yield. The structure of **7Ga** was elucidated by its spectral data and chemical transformation, as reported in a previous paper.[6] Similarly, other alkoxyquinones **5Gb—f** reacted under the same conditions to give **7Gb—f** in reasonable yields. All of the products **7Gb—f**, except **7Gd**, were mixtures of diastereoisomers. In the case of **7Gb**, the diastereoisomers were separated by TLC into each isomer after acetylation.

On the other hand, in the cases of the reaction of **5Gd** and **5Ge**, other minor products, **8Gd** and **8Ge**,[11] were respectively obtained, even though in low yields. The results are summarized in Table 1. The relative

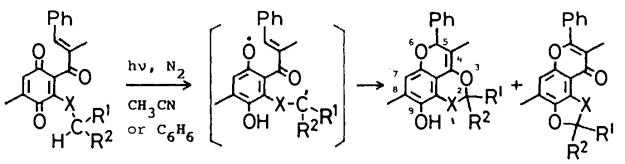

5G (X=O) **6G** **7G** **8G**
5S (X=S) **6S** **7S** **8S**

a: $R^1=R^2=H$; b: $R^1=H$, $R^2=Me$; c: $R^1=H$, $R^2=Et$; d: $R^1=R^2=Me$; e: $R^1=Me$, $R^2=Et$; f: $R^1=H$, $R^2=Ph$ (2)

Table 1. Photochemical Reaction of 5[a]

Quinone	Substituents		Yields of products/%[b]	
	R^1	R^2	**7**	**8**
5Ga	H	H	50[c]	0
5Gb	H	Me	75	0
5Gc	H	Et	81	0
5Gd	Me	Me	77	5
5Ge	Me	Et	72	8
5Gf	H	Ph	81	0
5Sb	H	Me	75	15
5Sc	H	Et	70	17
5Sd	Me	Me	80	7
5Se	Me	Et	89	7
5Sf	H	Ph	66	24
5Sg	$XCHR^1R^2$=SBu^t		0[d]	0[d]

a) Acetonitrile was used for **5G** and benzene was used for **5S**. b) Isolated yields based on the quinone used. Hydroquinones of **5S** were obtained as another minor products. The recovered quinones were mostly under 10 per cent for **5G** and were nothing for **5S**. c) **5Ga** was recovered in a 31% yield. d) **5Sg** was almost recovered.

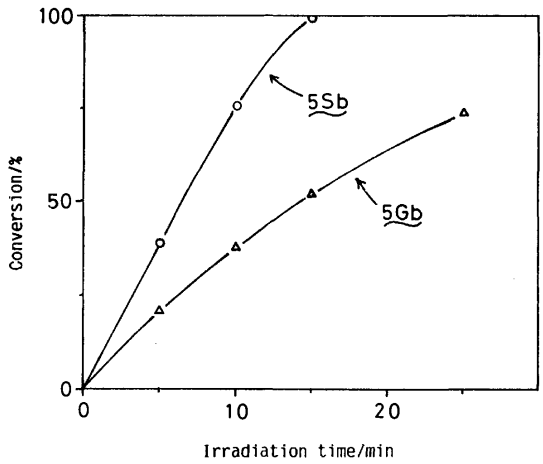

Fig. 1. Comparison of the photoreactivity of **5Gb** and **5Sb**. These reactions were carried out in $CDCl_3$ (ca. 0.026 mol dm^{-3}) and the conversion of quinones was determined by the use of ^{1}H NMR spectrometer.

reactivity of **5Ga**, **b**, and **d** having methoxyl, ethoxyl, and isopropoxyl groups increases in this order by 1:2:3.[6]

From these results, as depicted in Eq. 2, the reaction could proceed through γ-hydrogen abstraction by excited quinone carbonyl. Probably the resulting diradical **6G** intramolecularly attacks the carbonyl oxygen in the alkenoyl side chain, and finally cyclizes to give **7G**. This sort of bicyclo-cyclization reaction initiated by γ-hydrogen abstraction is quite novel.

Photochemical Reaction of 5S in Benzene. Irradiation of 3-isopropylthio-5-methyl-2-(α-methylcinnamoyl)-1,4-benzoquinone (**5Sd**) in benzene for 1.5 h under the same conditions as described in the reaction of **5G** gave two cyclization products, 2,2,4,8-tetramethyl-5-phenyl-5*H*-pyrano[4,3,2-*de*][3,1]benzoxathiin-9-ol (**7Sd**, 80%) and 2,2,4,8-tetramethyl-7-phenyl-9*H*-[1,3]oxathiolo[4,5-*f*][1]benzopyran-9-one (**8Sd**, 7%).[10] The structure of **7Sd** was elucidated by its spectral data. The ^{1}H NMR data of **7Sd** showed similar signal patterns to that of **7Gd**; for instance, **7Sd** showed four singlet peaks at δ 1.60, 1.64, 1.78, and 2.10 due to four methyl groups, three singlet peaks at δ 4.52, 5.57, and 6.24 due to hydroxyl, methine, and aromatic protons, and one singlet peak at δ 7.27 due to a phenyl group. The structure of **7Sd** was further confirmed by chemical derivations with chloroacetic acid to 2,2,4,8-tetramethyl-7-phenyl-7,8-dihydro[1,3]-oxathiolo[4,5-*f*][1]benzopyran-9-one (**9**, 63%) and by

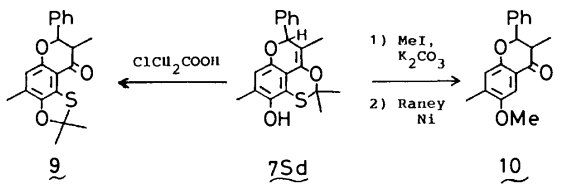

9 **7Sd** **10** (3)

the oxidation of **7Sd** with chloranil to give a stable product **8Sd**.[10] Moreover, the desulfurization[12] of methylated **7Sd** with Raney nickel gave 6-methoxy-3,7-dimethyl-2-phenyl-4-chromanone (**10**, 42%) (Eq. 3).

Similarly, other alkylthioquinones **5Sd—f** reacted to afford **7Sb—f** in good yields together with minor products **8Sd—f** (Table 1). Product **8S** was independently prepared from **7S** by oxidation with chloranil or 2,3-dichloro-5,6-dicyano-1,4-benzoquinone (DDQ).[10]

Thus, the photochemical reaction of alkylthioquinones **5S** in benzene solution was similar to that of alkoxyquinones **5G**. However, the photochemical reaction of **5Sb** was more effective than that of **5Gb**, as shown in Fig. 1.

Irradiation of 3-*t*-butylthio-5-methyl-2-(α-methylcinnamoyl)-1,4-benzoquinone (**5Sg**) for 3 h under the same conditions, however, gave no products and most of **5Sg** was recovered. Therefore, the present reaction proceeds via γ-hydrogen abstraction from the alkylthio group. As expected, the quantum yield of the disappearance of isopropylthioquinone (**5Sd**, Φ=0.50) is larger than that of ethylthioquinone (**5Sb**, Φ=0.30).

Photochemical Reaction of 11G and 11S. Irradiation of an acetonitrile solution of 2-cinnamoyl-3-methoxy-5-methyl-1,4-benzoquinone (**11Ga**), which has no α-methyl group in the alkenoyl side chain, afforded a mixture of 8-methyl-5-phenyl-5*H*-pyrano-[4,3,2-*de*][1,3]benzodioxin-9-ol (**13Ga**, 24%) and 2-cinnamoyl-3-methoxy-5-methylhydroquinone (**15Ga**, 7%) (Eq. 4). The products were separated by column chromatography after acetylation. The structure of each acetate was determined on the basis of spectral data (see Experimental). Other alkoxyquinones, **11Gb** and **11Gd**, similarly reacted to give a mixture of the corresponding **13G** and **15G**. In the case of the reaction of **11Gd** another minor product **14Gd** was obtained.

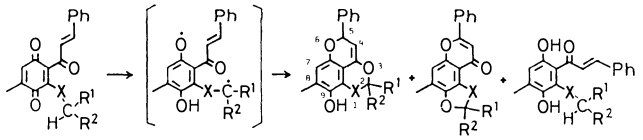

11G (X=O) 12G 13G 14G 15G

11S (X=S) 12S 13S 14S 15S

a: $R^1=R^2=H$; b: $R^1=H$, $R^2=Me$; d: $R^1=R^2=Me$ (4)

Irradiation of a benzene solution of 2-cinnamoyl-3-ethylthio-5-methyl-1,4-benzoquinone (**11Sb**) for 3 h gave a mixture of 2,8-dimethyl-5-phenyl-5*H*-pyrano-[4,3,2-*de*][3,1]benzoxathiin-9-ol (**13Sb**, 31%), 2,4-dimethyl-7-phenyl-9*H*-[1,3]oxathiolo[4,5-*f*][1]benzo-pyran-9-one (**14Sb**, 29%), and hydroquinone (**15Sb**, 12%). After separation by column chromatography their structures were determined on the basis of spectral data. Another quinone **11Sd** similarly reacted to give a mixture of **13Sd**, **14Sd**, and **15Sd**. The yields of the products are summarized in Table 2.

Effect of α-Methyl Group in the Alkenoyl Side Chain. As shown in Tables 1 and 2, the yields of **13** are appreciably less than those of **7**. Thus, the presence of the α-methyl group in the alkenoyl side chain is favorable for a higher yield of **7**. The structural change of alkyl groups in the alkoxyl or alkylthio groups in **11** only slightly affects the yield of product **13**. Therefore, the differences of the yields between **7** and **13** could be ascribed to the presence or absence of the α-methyl group in the alkenoyl side chain. These results may be explained on the basis of the equilibrium of intermediates **17** and **18** or **20** and **21**, as shown in Scheme 1. The ratio of **17**/**18** could be larger than that of **20**/**21** because of a steric hindrance of the methyl group derived from the alkenoyl side chain. This is one reason why the amount of product **7** is greater than that of **13**.

Table 2. Photochemical Reaction of **11**

Quinone	Substituents		Yields of products/%[a]		
	R^1	R^2	**13**	**14**	**15**
11Ga	H	H	24	0	7
11Gb	H	Me	30	0	16
11Gd	Me	Me	28	10	18
11Sb	H	Me	31	29	12
11Sd	Me	Me	58	19	9

a) Isolated yields based on the quinone used. The starting quinones **11Ga**, **b**, and **d** were recovered in 40, 37, and 15% yields, respectively, and **11S** was not recovered.

On the other hand, the hydrogen at the 5-position of products **7** and **13** should be highly activated, since its hydrogen is situated in the benzylic, allylic, and alkoxyl α-position. Actually, product **13** was easily oxidized by quinone **11** to give **14**.[10,13] Contrary to the expectation, the hydrogen at the 5-position of **7S** is resistant[14] to oxidation owing to the bigger steric hindrance from the surrounding methyl group. As a result, product **7** is moderately more stable than **13**.

Photochemical Reaction of 5 in Alcohols. Upon

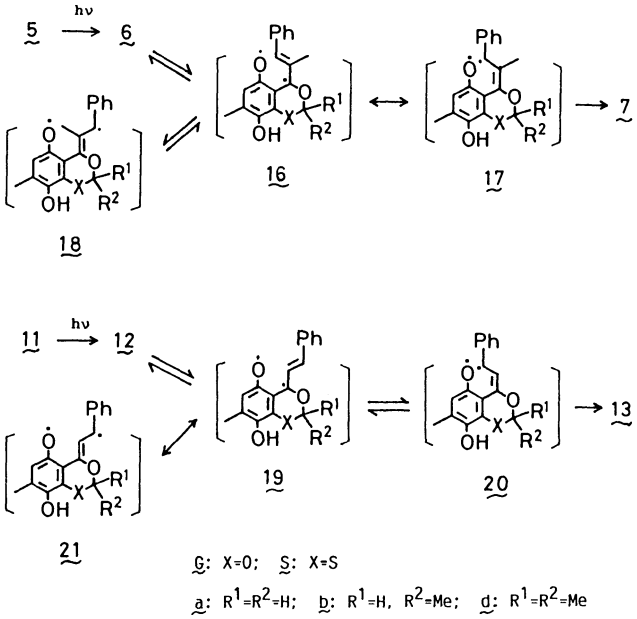

G: X=O; S: X=S

a: $R^1=R^2=H$; b: $R^1=H$, $R^2=Me$; d: $R^1=R^2=Me$

Scheme 1.

Table 3. Photochemical Reaction of **5** in Alcohols

Run	Quinone	Substituents		Solvent	Yields of products/%[a]			
		R^1	R^2		**7**	**8**	**24**	**5H**[b]
1	**5Ga**	H	H	MeOH	43	0	0	10
2	**5Gb**	H	Me	MeOH	32	0	5	21
3				*i*-PrOH	70	0	0	7
4	**5Gd**	Me	Me	MeOH	83	0	0	13
5	**5Sb**	H	Me	MeOH	22	0	50	10
6				EtOH	51	14	15	5
7				*i*-PrOH	82	6	5	3
8				*t*-BuOH	80	8	0	4
9	**5Sd**	Me	Me	MeOH	80	5	0	5

a) Isolated yields based on the quinone used. The other alcohol adducts (type **3** and **4**) and minor unidentified products were obtained. b) **5H** is the hydroquinone of **5**.

irradiation in a methanol solution, the quinones **5** reacted competitively to give cyclization products **7** and/or alcohol adducts (type **3** and **4**, see Eq. 1).[5] As shown in Table 3, all the quinones **5** gave cyclization products **7**. Especially, **5Gd** and **5Sd**, having an isopropoxy or isopropylthio group at the 3-position, gave cyclization products **7Gd** and **7Sd** in high yields (Runs 4 and 9). Thus, the γ-hydrogen abstraction was more preferential than the adduct formation with alcohol.[5]

On the other hand, ethylthioquinone **5Sb** (Run 5) gave another type of methanol adduct **24SbM** (50%, R=Me). The adduct **24SbM** can be afforded by the addition of methanol to the cationic intermediate **22Sb**, which probably forms by an intramolecular electron transfer of **6Sb** followed by a protonation and is stabilized by conjugation with a lone-pair electron of the adjacent sulfur atom, as indicated in **23Sb** (Scheme 2). However, isopropylthioquinone **5Sd** (Run 9) gave no methanol adduct **24SdM**, though the cyclization product **7Sd** was obtained in high yield. This can be explained by a steric hindrance for the addition of methanol to the tertiary cation of intermediate **22Sd** (R^1=R^2=Me). The presence of such a steric hindrance can also be supported by the fact that the formation of the alcohol adduct **24Sb** decreased in turn from methanol to ethyl, isopropyl, and *t*-butyl alcohols (Runs 5—8) and the formation of the cyclization product **7Sb** was increased in this order.

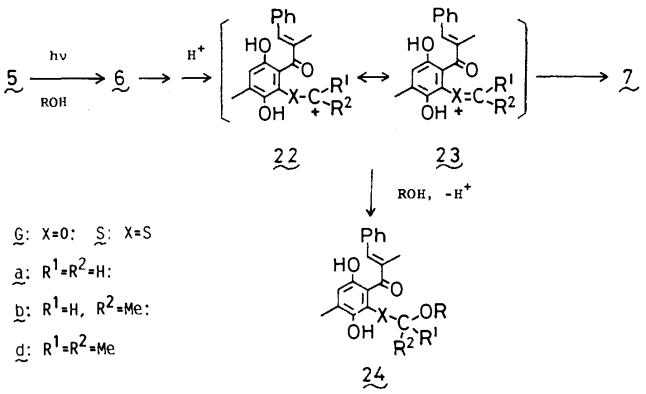

Scheme 2.

In the case of ethoxyquinone **5Gb**, only a small amount of **24Gb** was isolated. It may be suggested that the intermediate **22Gb** is less reactive with alcohols than **22Sb**. On the other hand, since the reaction of **5Gb** in isopropyl alcohol (Run 3) gave **7Gb** in high yield, the absence of the adduct **24Gd** in the reaction of the isopropoxyquinone **5Gd** (Run 4) must also be ascribed to the same reason applied for the case of isopropylthioquinone **5Sd**.

Photochemical Reaction of 11 in Alcohols. The reaction of a methanol solution of **11S**, which has no α-methyl group in the alkenoyl side chain (Table 4, Runs 14 and 15), showed a similar tendency to that of **5S**: The quinones **11S** gave cyclization products **13S**

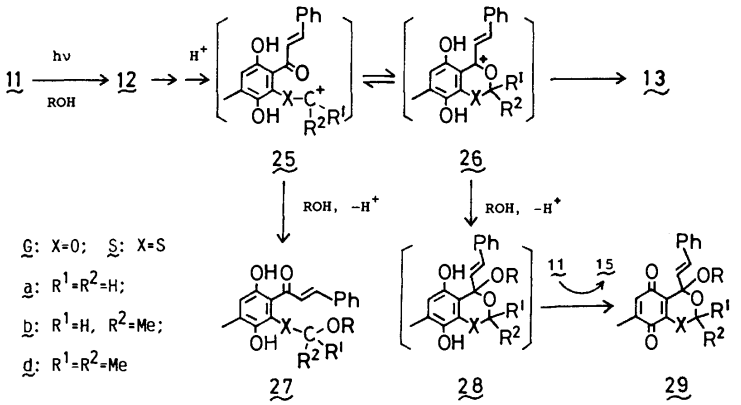

Scheme 3.

Table 4. Photochemical Reaction of **11** in Alcohols

Run	Quinone	Substituents		Solvent	Yields of products/%[a]			
		R^1	R^2		**13**	**27**	**29**	**15**
10	**11Ga**	H	H	MeOH	0	0	16	30
11				*i*-PrOH	9	0	6	16
12	**11Gb**	H	Me	MeOH	0	0	18	32
13	**11Gd**	Me	Me	MeOH	0	0	15	35
14	**11Sb**	H	Me	MeOH	22	22	0	23
15	**11Sd**	Me	Me	MeOH	84	0	0	6

a) Isolated yields based on the quinone used. The other alcohol adducts (type **3** and **4**), **14S**, and other minor products were obtained.

and/or methanol adducts (type **3** and **4**); especially **11Sd**, having an isopropylthio group, afforded **13Sd** in high yield. The ethylthioquinone **11Sb** also gave another methanol adduct **27SbM** (22%, R=Me).

In contrast, the irradiation of alkoxyquinones **11G** in methanol (Table 4, Runs 10, 12, and 13) gave no cyclization product **13G**; however, another methanol adduct **29GM** (R=Me) was obtained in considerable yield. Moreover, no other methanol adduct **27G** was formed.

The structure of **29G** was confirmed by its spectral data and by chemical derivations with zinc-acetic anhydride (see Experimental). As shown in Scheme 4, the adduct **29G** can be formed by the addition of an alcohol to cationic intermediate **26G**, followed by oxidation with the starting quinone **11G**. The reaction of **11Ga** in isopropyl alcohol (Run 11) gave not only the adduct **29GaP** (R=*i*-Pr) but also cyclization product **13Ga**, because the addition of an isopropyl alcohol to **26G** becomes difficult for the steric hindrance.

As described above, the product distribution of **11G** in methanol differed from that of **11S** (Table 4). These differences obviously reflect the relative stability of the cationic intermediates, **25G** and **25S**. Thus, the reaction in alcohols proceeds by an ionic process.

In conclusion, upon the irradiation of alkenoylquinones in acetonitrile or benzene, **5** and **11** readily afforded tricyclic compounds **7** and **13**, respectively. The reaction was initiated by the abstraction of γ-hydrogen; the resulting diradical intramolecularly cyclizes the involved alkenoyl side chain to give **7** or **13**. The presence of an α-methyl group in the alkenoyl side chain affects the yield as well as the stability of product **7**. Upon irradiation in alcohol, the reaction probably proceeds through an ionic process via the cationic intermediates to give the products.

Experimental

The instruments and procedures were as previously reported.[5] 3-Alkoxy-5-methyl-2-(α-methylcinnamoyl)-1,4-benzoquinones (**5G**) were prepared by a modified method of

Table 5. Yields and Physical Data of **5** and **11**

Quinone	Yield %	Mp θ_m/°C	IR(CCl_4) cm^{-1}	^1H NMR(CCl_4) δ(J/Hz)/ppm
5Ga	95	103—104	1670	2.02 (3H, s), 2.10 (3H, s), 3.88 (3H, s), 6.38 (1H, s), 7.12 (1H, s), 7.28 (5H, s).
5Gb	95	78—80	1670	1.26 (3H, t, J=7), 1.99 (3H, s), 2.07 (3H, s), 4.14 (2H, q, J=7), 6.38 (1H, s), 7.12 (1H, s), 7.8 (5H, s).
5Gc[a]	89	74—75	1670	0.89 (3H, t, J=7), 1.62 (2H, m, J=7), 1.98 (3H, s), 2.08 (3H, s), 4.05 (2H, t, J=7), 6.36 (1H, s), 7.19 (1H, s), 7.26 (5H, s).
5Gd	60	103—105	1670	1.21 (6H, d, J=6), 1.99 (3H, s), 2.07 (3H, s), 4.78 (1H, m, J=6), 6.38 (1H, s), 7.08 (1H, s), 7.27 (5H, s).
5Ge[a,b]	55	Oil	1670	0.86 (3H, t, J=7), 1.17 (3H, d, J=6), 1.3—1.8 (2H, m), 2.03 and 2.08 (6H, each s), 4.67 (1H, m, J=6), 6.41 (1H, s), 7.13 (1H, s), 7.31 (5H, s).
5Gf[a,b]	76	101—102	1665	2.01 and 2.07 (6H, each s), 5.23 (2H, s), 6.43 (1H, s), 7.14 (1H, s), 7.25 and 7.32 (10H, each s).
5Sb	88	90—92	1660	1.20 (3H, t, J=7), 2.04 and 2.09 (6H, each s), 2.93 (2H, q, J=7), 6.43 (1H, s), 7.05 (1H, s), 7.28 (5H, s).
5Sc	91	88—90	1665	0.93 (3H, t, J=7), 1.56 (2H, m, J=7), 2.06 and 2.12 (6H, each s), 2.93 (2H, t, J=7), 6.56 (1H, s), 7.18 (1H, s), 7.25—7.50 (5H, m).
5Sd	96	93—95	1660	1.23 (6H, d, J=7), 2.12 and 2.18 (6H, each s), 3.98 (1H, m, J=7), 6.63 (1H, s), 7.20 (1H, s), 7.40 (5H, s).
5Se	97	81—83	1665	0.93 (3H, t, J=7), 1.23 (3H, d, J=7), 1.51 (2H, m, J=7), 2.14 (3H, s), 2.22 (3H, s), 3.85 (1H, q, J=7), 6.69 (1H, s), 7.29 (1H, s), 7.47 (5H, s).
5Sf	83	Oil	1660	1.96 (3H, s), 2.08 (3H, s), 4.21 (2H, s), 6.41 (1H, s), 7.05 (1H, s), 7.12 (5H, s), 7.32 (5H, s).
5Sg	59	128—130	1670	1.37 (9H, s), 2.14 and 2.16 (6H, each s), 6.67 (1H, s), 7.08 (1H, s), 7.40 (5H, bs).
11Ga[c]	87	92—94	1660	2.12 (3H, s), 3.98 (3H, s), 6.57 (1H, bs), 6.92 (1H, d, J=16), 7.3—7.65 (6H, m).
11Gb[c]	85	139—141	1665	1.28 (3H, t, J=7), 2.06 (3H, s), 4.19 (2H, q, J=7), 6.52 (1H, bs), 6.86 (1H, d, J=16), 7.2—7.5 (6H, m).
11Gd	80	Oil	1670	1.21 (6H, d, J=6), 2.00 (3H, s), 4.84 (1H, m, J=6), 6.40 (1H, bs), 6.68 (1H, d, J=16), 7.1—7.6 (6H, m).
11Sb[c]	95	172—174	1655	1.20 (3H, t, J=7), 2.06 (3H, d, J=1.5), 2.96 (2H, q, J=7), 6.52 (1H, q, J=1.5), 6.80 (1H, d, J=17), 7.2—7.6 (6H, m).
11Sd[c]	90	170—172	1660	1.25 (6H, d, J=7), 2.15 (3H, s), 4.00 (1H, m, J=7), 6.69 (1H, s), 6.90 (1H, d, J=17), 7.3—7.7 (6H, m).

a) Reaction conditions: Benzene was used as solvent. b) Reaction conditions: 50 °C. c) $CDCl_3$ was employed for NMR solvent.

Farina and Valderrama[15] from 5-methyl-2-(α-methylcinnamoyl)-1,4-benzoquinone in the following manner. A mixture of 1 mmol of quinone, 1 mmol of $Cu(AcO)_2 \cdot H_2O$,[16] and 50 cm^3 of an alcohol (or added benzene for dissolving) was stirred at 40 °C in the dark overnight under an oxygen atmosphere. After removing the solvent, the residue was purified by column chromatography with benzene as the eluent. All of the obtained quinones **5G** were recrystallized from hexane containing a small amount of benzene to give yellow prisms. 3-Alkoxy-2-cinnamoyl-5-methyl-1,4-benzoquinones (**11G**) were also prepared in the same manner as for **5G** from 2-cinnamoyl-5-methyl-1,4-benzoquinone with the use of 5 mmol of AgOAc instead of $Cu(AcO)_2 \cdot H_2O$. Yields and physical data of **5G** and **11G** are summarized in Table 5.

2-Alkenoyl-3-alkylthio-1,4-benzoquinones, **5S** and **11S**, were also prepared in a similar manner, as follows. A mixture of 2-alkenoyl-1,4-benzoquinone (1 mmol) and thiol (2—10 mmol) in benzene (25 cm^3) was stirred at room temperature overnight under a nitrogen atmosphere. The obtained 2-alkenoyl-3-alkylthiohydroquinone was purified by column chromatography and oxidized with cerium(IV) ammonium nitrate (CAN, 2.5 equiv) at 5 °C for 5 min. The reaction mixture was worked up as usual. All of the resulting quinones were recrystallized from hexane containing a small amount of benzene as orange or reddish orange prisms. The yields and physical properties of quinones **5S** and **11S** are summarized in Table 5.

Photochemical Reaction of 5Ga—f. A solution of **5G** in acetonitrile (30 cm^3, 0.01 mol dm^{-3}) was irradiated with a 300-W halogen lamp through a yellow glass filter (Toshiba L-42; <410 nm cut off) under a nitrogen atmosphere for 3 h. After the solvent was removed under reduced pressure, the resulting oil was chromatographed on a column with benzene as the eluent. The first very pale-yellow eluate was **7G**, the second yellow eluate recovered was **5G**. The third was a mixture of unidentified products. In the cases of **5Gd** and **5Ge**, minor products **8Gd** and **8Ge** were obtained from the third eluate. The yields of the products are summarized in Table 1. Since products **7G** were not stable in air, IR and ^1H NMR data of **7G** are described for acetates which were prepared by the acetylation with acetic anhydride and pyridine. All of products **7G**, except **7Ga** and **d**, were a mixture of diastereoisomers. Only in the case of **7Gb**, could the diastereoisomers be separated into each isomer after acetylation by both recrystallization (from hexane containing small amounts of benzene) and TLC (benzene as developing solvent, Merk, Art. 5715).

9-Acetoxy-4,8-dimethyl-5-phenyl-5*H*-pyrano[4,3,2-*de*][1,3]-benzodioxin (acetate of **7Ga**): colorless prisms, mp 121—122.5 °C; IR ($CHCl_3$) 1760, 1705 (w), and 1195 cm^{-1}; ^1H NMR ($CDCl_3$) δ=1.50 (3H, s), 2.02 (3H, s), 2.26 (3H, s), 5.26 (1H, ABq, *J*=5 Hz), 5.31 (1H, ABq, *J*=5 Hz), 5.74 (1H, s), 6.17 (1H, s), 7.32 (5H, s). Found: C, 71.18; H, 5.64%. Calcd for $C_{20}H_{18}O_5$: C, 71.00; H, 5.36%.

9-Acetoxy-2,4,8-trimethyl-5-phenyl-5*H*-pyrano[4,3,2-*de*]-[1,3]benzodioxin (acetate of **7Gb**) (a mixture of diastereoisomers; ca. 3:1). Major diastereoisomer: oil; IR (CCl_4) 1770, 1705 (w), 1400, 1195 cm^{-1}; ^1H NMR (270 MHz, $CDCl_3$) δ=1.50 (3H, s), 1.64 (3H, d, *J*=5.1 Hz), 2.07 (3H, s), 2.32 (3H, s), 5.34 (1H, q, *J*=5.1 Hz), 5.83 (1H, s), 6.21 (1H, s), 7.3—7.45 (5H, m). Minor diastereoisomer: colorless prisms; mp 150—152 °C; IR (CCl_4) 1770, 1700 (w), 1400, 1195 cm^{-1}; ^1H NMR (270 MHz, $CDCl_3$) δ=1.55 (3H, s), 1.65 (3H, d, *J*=5.1 Hz), 2.05 (3H, s), 2.31 (3H, s), 5.25 (1H, q, *J*=5.1 Hz), 5.76 (1H, s), 6.19 (1H, s), 7.33 (5H, s). Found: C, 71.42; H, 5.69%. Calcd for $C_{21}H_{20}O_5$: C, 71.58; H, 5.72%.

9-Acetoxy-2-ethyl-4,8-dimethyl-5-phenyl-5*H*-pyrano[4,3,2-*de*][1,3]benzodioxin (acetate of **7Gc**) (a mixture of diastereoisomers; 1:1): oil; IR (CCl_4) 1765 and 1190 cm^{-1}; ^1H NMR (270 MHz, $CDCl_3$) δ=1.08 (3H, t, *J*=7.6 Hz), 1.49 and 1.55 (3H, each s), 1.9—2.25 (2H, m), 2.05 and 2.06 (3H, each s), 2.30 (3H, s), 5.03 and 5.12 (1H, each d, *J*=5.3 Hz), 5.75 and 5.83 (1H, each s), 6.18 and 6.20 (1H, each s), 7.3—7.5 (5H, m). Found: *m/z* 366.1444. Calcd for $C_{22}H_{22}O_5$: M, 366.1465.

9-Acetoxy-2,2,4,8-tetramethyl-5-phenyl-5*H*-pyrano[4,3,2-*de*][1,3]benzodioxin (acetate of **7Gd**): colorless prisms, mp 154—155 °C; IR (CCl_4) 1765, 1645, 1190 cm^{-1}; ^1H NMR (CCl_4) δ=1.50, 1.56, and 1.60 (9H, each s), 2.01 (3H, s), 2.25 (3H, s), 5.73 (1H, s), 6.11 (1H, s), 7.32 (5H, s). Found: C, 72.04; H, 5.98%. Calcd for $C_{22}H_{22}O_5$: C, 72.11; H, 6.05%.

9-Acetoxy-2-ethyl-2,4,8-trimethyl-5-phenyl-5*H*-pyrano[4,3,2-*de*][1,3]benzodioxin (acetate of **7Ge**) (a mixture of diastereoisomers; 1:1): oil; IR (CCl_4) 1770, 1645, 1190 cm^{-1}; ^1H NMR (CCl_4) δ=0.98 and 1.01 (3H, each t, *J*=7 Hz), 1.49 and 1.52 (6H, each s), 1.65—2.05 (2H, m, *J*=7 Hz), 2.00 (3H, s), 2.18 (3H, s), 5.70 (1H, s), 6.08 (1H, s), 7.30 (5H, s). Found: *m/z* 380.1623. Calcd for $C_{23}H_{24}O_5$: M, 380.1623.

9-Acetoxy-4,8-dimethyl-2,5-diphenyl-5*H*-pyrano[4,3,2-*de*]-[1,3]benzodioxin (acetate of **7Gf**) (a mixture of diastereoisomers; 2:1): oil; IR (CCl_4) 1760, 1700 (w), 1365, 1190 cm^{-1}; ^1H NMR (CCl_4) δ=1.50 and 1.57 (3H, each s), 2.06 (3H, s), 2.20 (3H, s), 5.70 and 5.81 (1H, each s), 6.10 (1H, s), 6.16 and 6.20 (1H, each s), 7.2—7.7 (10H, m). Found: *m/z* 414.1472. Calcd for $C_{26}H_{22}O_5$: M, 414.1466.

2,2,4,8-Tetramethyl-7-phenyl-9*H*-[1,3]dioxolo[5,4-*f*][1]-benzopyran-9-one (**8Gd**): colorless solid, mp 172—174 °C; IR (CCl_4) 1640, 1460 cm^{-1}; ^1H NMR ($CDCl_3$) δ=1.79 (6H, s), 2.08 (3H, s), 2.28 (3H, s), 6.70 (1H, s), 7.4—7.65 (5H, m). Found: C, 74.66; H, 5.80%. Calcd for $C_{20}H_{18}O_4$: C, 74.52; H, 5.63%.

2-Ethyl-2,4,8-trimethyl-7-phenyl-9*H*-[1,3]dioxolo[5,4-*f*][1]-benzopyran-9-one (**8Ge**): oil; IR (CCl_4) 1635, 1460 cm^{-1}; ^1H NMR (CCl_4) δ=1.07 (3H, t, *J*=7 Hz), 1.70 (3H, s), 2.02 (3H, s), 2.03 (2H, q, *J*=7 Hz), 2.26 (3H, s), 6.61 (1H, s), 7.4—7.7 (5H, m).

Photochemical Reaction of 5Sb—f. A benzene solution of **5S** was irradiated for 1.5 h under the same conditions as for **5G**. After removing the solvent in vacuo, the residue was chromatographed on a column with benzene as the eluent. The first pale-yellow eluate was **7S** and the second yellow eluate was **8S**. The starting quinone **5S** was not recovered. Since products **7S** were unstable, they were methylated with methyl iodide and potassium carbonate in dry acetone in the usual way. In addition, unstable products **7S** were converted to stable **8S** by oxidation[10] and their elemental analyses were measured unless otherwise noted. The yields of products **7S** and **8S** are tabulated in Table 1. IR and ^1H NMR data of **7S** are described for methyl ether, and those of other **8S** were referred to in a preceding paper.[10]

9-Methoxy-2,4,8-trimethyl-5-phenyl-5*H*-pyrano[4,3,2-*de*]-[3,1]benzoxathiin (methyl ether of **7Sb**) (a mixture of diastereoisomers; 5:1): oil; IR (CCl_4) 1680 (w), 1470, and 1210 cm^{-1}; ^1H NMR ($CDCl_3$) δ=1.49 and 1.62 (3H, each s), 1.71 and 1.73 (3H, each, d, *J*=6 Hz), 2.11 and 2.14 (3H, each

s), 3.66 (3H, s), 4.90—5.25 (1H, m, J=6 Hz), 5.51 and 5.64 (1H, each s), 6.17 and 6.22 (1H, each s), 7.15—7.4 (5H, m). Found: m/z 340.1149. Calcd for $C_{20}H_{20}O_3S$: M, 340.1132.

2-Ethyl-9-methoxy-4,8-dimethyl-5-phenyl-5*H*-pyrano[4,3,2-*de*][3,1]benzoxathiin (methyl ether of **7Sc**) (a mixture of diastereoisomers; 3:1): oil; IR (CCl_4) 1675 (w), 1470, 1200 cm^{-1}; ^1H NMR (CCl_4): δ=1.15 (3H, t, J=7 Hz), 1.52 and 1.63 (3H, each s), 1.85—2.3 (2H, m), 2.12 and 2.16 (3H, each s), 3.69 (3H, s), 4.90 and 5.01 (1H, each t, J=6 Hz), 5.58 and 5.70 (1H, each s), 6.23 and 6.28 (1H, each s), 7.37 (5H, s).

9-Methoxy-2,2,4,8-tetramethyl-5-phenyl-5*H*-pyrano[4,3,2-*de*][3,1]benzoxathiin (methyl ether of **7Sd**): oil; IR (CCl_4) 1670 (w), 1470, 1210 cm^{-1}; ^1H NMR (CCl_4) δ=1.56, 1.65, and 1.74 (9H, each s), 2.10 (3H, s), 3.60 (3H, s), 5.57 (1H, s), 6.14 (1H, s), 7.22 (5H, s). Found: m/z 354.1285. Calcd for $C_{21}H_{22}O_3S$: M, 354.1289.

2-Ethyl-9-methoxy-2,4,8-trimethyl-5-phenyl-5*H*-pyrano[4,3,2-*de*][3,1]benzoxathiin (methyl ether of **7Se**) (a mixture of diastereoisomers; 1:1): oil; IR (CCl_4) 1670 (w), 1450, 1395 cm^{-1}; ^1H NMR δ=1.03 and 1.10 (3H, each t, J=7 Hz), 1.58, 1.60, and 1.68 (6H, each s), 1.8—2.4 (2H, m), 2.13 (3H, s), 3.66 (3H, s), 5.65 (1H, s), 6.22 (1H, s), 7.30 (5H, s).

9-Methoxy-4,8-dimethyl-2,5-diphenyl-5*H*-pyrano[4,3,2-*de*]-[3,1]benzoxathiin (methyl ether of **7Sf**) (a mixture of diastereoisomers; 7:3): oil; IR (CCl_4) 1675 (w), 1470, 1400, 1210 cm^{-1}; ^1H NMR (270 MHz, $CDCl_3$) δ=1.55 and 1.68 (3H, each s), 2.16 and 2.20 (3H, each s), 3.76 (3H, s), 5.73 and 5.86 (1H, each s), 6.08 and 6.18 (1H, each s), 6.40 and 6.47 (1H, each s), 7.3—7.8 (10H, m).

2,2,4,8-Tetramethyl-7-phenyl-9*H*-[1,3]oxathiolo[4,5-*f*][1]-benzopyran-9-one (**8Sf**): orange prisms, mp 154—156 °C; IR ($CHCl_3$) 1620, 1430 cm^{-1}; ^1H NMR (CCl_4) δ=2.04 (3H, s), 2.32 (3H, s), 6.88 (1H, s), 7.07 (1H, s), 7.30—7.75 (10H, m). Found: C, 74.60; H, 4.77%. Calcd for $C_{24}H_{18}O_3S$: C, 74.59; H, 4.70%.

Photochemical Reaction of 11Ga—d. The procedures were same as described above for **5G**. The first yellow eluate was a mixture of cyclization product **13G** and hydroquinone **15G**. The yields of **13G** and **15G** were determined by ^1H NMR spectra and the isolation of those was carried out after acetylation in the usual manner. The second orange eluate was recovered **11G** and the third was a mixture of unidentified decomposition products. In the case of **11Gd**, minor product **14Gd** was contained in the third eluate. The yields of the products are summarized in Table 2. The structure of **15G** was identified by oxidation to **11G**.

9-Acetoxy-8-methyl-5-phenyl-5*H*-pyrano[4,3,2-*de*][1,3]-benzodioxin (acetate of **13Ga**): yellow oil; IR (CCl_4) 1765, 1190 cm^{-1}; ^1H NMR (CCl_4) δ=2.08 (3H, s), 2.24 (3H, s), 4.84 (1H, d, J=3.5 Hz), 5.28 (2H, s), 6.00 (1H, d, J=3.5 Hz), 6.21 (1H, s), 7.2—7.4 (5H, m). Found: m/z 324.1020. Calcd for $C_{19}H_{16}O_5$: M, 324.0996.

9-Acetoxy-2,8-dimethyl-5-phenyl-5*H*-pyrano[4,3,2-*de*][1,3]-benzodioxin (acetate of **13Gb**) (a mixture of diastereoisomers; 1:1): yellow oil; IR (CCl_4) 1765, 1190 cm^{-1}; ^1H NMR (CCl_4) δ=1.56 (3H, d, J=5 Hz), 2.01 and 2.04 (3H, each s), 2.20 and 2.25 (3H, each s), 4.72 and 4.78 (1H, each d, J=3 Hz), 5.18 (1H, q, J=5 Hz), 5.85—6.05 (1H, m), 6.14 and 6.18 (1H, each s), 7.1—7.5 (5H, m). Found: m/z 338.1161. Calcd for $C_{20}H_{18}O_5$: M, 338.1153.

9-Acetoxy-2,2,8-trimethyl-5-phenyl-5*H*-pyrano[4,3,2-*de*]-[1,3]benzodioxin (acetate of **13Gd**): yellow oil; IR (CCl_4) 1765, 1200 cm^{-1}; ^1H NMR (CCl_4) δ=1.55 (6H, s), 2.02 (3H, s), 2.18 (3H, s), 4.74 (1H, s, J=3 Hz), 5.95 (1H, d, J=3 Hz), 6.10 (1H, s), 7.1—7.4 (5H, m). Found: m/z 352.1293. Calcd for $C_{21}H_{20}O_5$: M, 352.1308.

2,2,4-Trimethyl-7-phenyl-9*H*-[1,3]dioxolo[5,4-*f*][1]benzopyran-9-one (**14Gd**): pale yellow prisms, mp 168—170 °C; IR (CCl_4) 1650, 1450 cm^{-1}; ^1H NMR (CCl_4) δ=1.74 (6H, s), 2.24 (3H, s), 6.40 (1H, s), 6.65 (1H, s), 7.3—7.5 (3H, m), 7.7—7.9 (2H, m). Found: m/z 308.1019. Calcd for $C_{19}H_{16}O_4$: M, 308.1047.

Photochemical Reaction of 11Sb and d. The procedures were the same as described above for **5S**, except the reaction time was 3 h. The first yellow eluate was a mixture of **13S** and **15S**; their yields were determined by ^1H NMR spectra; separation was achieved after methylation in the usual manner. The second yellow eluate was **14S** and the third was a mixture of unknown decomposition products. Products **13S** were more unstable than **7S**; therefore, elemental analyses of **13S** were achieved with **14S** after oxidation with chloranil. The results are summarized in Table 2. The IR and ^1H NMR data of **13S** are shown for the methyl ether.

9-Methoxy-2,8-dimethyl-5-phenyl-5*H*-pyrano[4,3,2-*de*][3,1]-benzoxathiin (methyl ether of **13Sb**) (a mixture of diastereoisomers; 1:1): oil; IR (CCl_4) 1660 (w), 1470, 1215 cm^{-1}; ^1H NMR (CCl_4) δ=1.65 and 1.67 (3H, each d, J=6 Hz), 2.10 and 2.14 (3H, each s), 3.60 and 3.62 (3H, each s), 4.8—5.1 (2H, m), 5.7—5.9 (1H, m), 6.20 and 6.29 (1H, each s), 7.1—7.4 (5H, m).

9-Methoxy-2,2,8-trimethyl-5-phenyl-5*H*-pyrano[4,3,2-*de*]-[3,1]benzoxathiin (methyl ether of **13Sd**): oil; IR (CCl_4) 1655 (w), 1470, 1210 cm^{-1}; ^1H NMR (CCl_4) δ=1.71 (6H, s), 2.18 (3H, s), 3.68 (3H, s), 5.09 (1H, d, J=4 Hz), 5.97 (1H, d, J=4 Hz), 6.37 (1H, s), 7.25—7.5 (5H, m).

2,4-Dimethyl-7-phenyl-9*H*-[3,1]oxathiolo[4,5-*f*][1]benzopyran-9-one (**14Sb**): yellow needles, mp 175—177 °C; IR ($CHCl_3$) 1630 cm^{-1}; ^1H NMR ($CDCl_3$) δ=1.77 (3H, d, J=6 Hz), 2.28 (3H, s), 6.21 (1H, q, J=6 Hz), 6.65 (1H, s), 6.94 (1H, s), 7.35—7.6 (3H, m), 7.7—7.95 (2H, m). Found: C, 69.46; H, 4.64%. Calcd for $C_{18}H_{14}O_3S$: C, 69.66; H, 4.55%.

2,2,4-Trimethyl-7-phenyl-9*H*-[3,1]oxathiolo[4,5-*f*][1]benzopyran-9-one (**14Sd**): yellow needles, mp 144—146 °C; IR (CCl_4) 1630 cm^{-1}; ^1H NMR (CCl_4) δ=1.85 (6H, s), 2.28 (3H, s), 6.60 (1H, s), 6.94 (1H, s), 7.4—7.6 (3H, m), 7.8—8.0 (2H, m). Found: C, 70.46; H, 5.01%. Calcd for $C_{19}H_{16}O_3S$: C, 70.35; H, 4.97%.

Photochemical Reaction of 5 in Alcohols. The procedures were the same as described above for **5G**, except regarding alcohol. In the reaction of **5Ga** in methanol, the first yellow eluate was a minor unidentified product; the second pale-yellow eluate was **7Ga** (43%); the third was a mixture of type **3** adduct (18%), type **4** adduct (7%), and **15Ga** (10%) which were separated by TLC with benzene as developing solvent after acetylation; and the fourth was a mixture of chromone derivative (3%) and chromamone derivative (8%) which were separated by TLC with chloroform as the developing solvent.

5-Acetoxy-4-methoxy-2-(α-methoxybenzyl)-2,6-dimethylbenzofuran-3(2*H*)-one (acetate of type **3** adduct) (a mixture of diastereoisomers; 3:1): oil; IR (CCl_4) 1770, 1715, 1625, 1195 cm^{-1}; ^1H NMR ($CDCl_3$) δ=1.14 and 1.59 (3H, each s), 2.09, 2.19, 2.22, and 2.31 (6H, each s), 3.06 and 3.29 (3H, each s), 3.87 and 4.12 (3H, each s), 4.40 (1H, s), 6.65 and 6.71

(1H, each s), 7.1—7.5 (5H, m).

Methyl 3-acetoxy-2-methoxy-4-methyl-6-(α-methylstyryloxy)-benzoate (acetate of type **4** adduct) (a mixture of cis-trans isomers; 2:1): oil; IR (CCl_4) 1770, 1735, 1190 cm^{-1}; ^1H NMR ($CDCl_3$) δ=1.95, 2.08, 2.14, and 2.31 (6H, each s), 3.82 and 3.85 (6H, each s), 5.80 and 5.96 (1H, each s), 6.57 and 6.70 (1H, each s), 7.1—7.6 (5H, m).

6-Hydroxy-5-methoxy-2,7-dimethyl-3-phenyl-4*H*-1-benzopyran-4-one: solid; IR ($CHCl_3$) 3500, 1630 cm^{-1}; ^1H NMR ($CDCl_3$) δ=2.22 (3H, s), 2.38 (3H, s), 3.94 (3H, s), 6.09 (1H, s), 7.02 (1H, s), 7.2—7.5 (5H, m).

6-Hydroxy-2,5-dimethoxy-2,7-dimethyl-3-phenyl-4-chromanone (a mixture of diastereoisomers; 1:1): oil; IR ($CHCl_3$) 3525, 1690 cm^{-1}; ^1H NMR ($CDCl_3$) δ=1.36 and 1.39 (3H, each s), 2.26 and 2.30 (3H, each s), 3.18 and 3.22 (3H, each s), 3.75 and 3.84 (3H, each s), 3.65 and 4.03 (1H, each s), 5.76 (1H, bs), 6.60 and 6.67 (1H, each s), 7.22 and 7.31 (5H, each s).

Upon the reaction of **5Gb** and **d** in alcohols, the first yellow eluate was a minor unidentified product, the second pale yellow eluate was **7G**, the third was a mixture of hydroquinone containing the type **3** and **4** adducts, and the fourth was unknown products. In the case of **5Gb** the alcohol adduct **24GbM** (5%, R=Me) was isolated from the fourth eluate, even though in low yield. Since type **3** and **4** adducts yielded only a few per cent, most of them were not separated. The results are summarized in Table 3.

5-Acetoxy-4-ethoxy-2-(α-methoxybenzyl)-2,6-dimethylbenzofuran-3(2*H*)-one (acetate of type **3** adduct): oil; IR (CCl_4) 1770, 1715, 1625, 1195 cm^{-1}; ^1H NMR (270 MHz, $CDCl_3$) δ=1.14 (3H, s) 1.37 (3H, t, *J*=7.1 Hz), 2.22 (3H, s), 2.34 (3H, s), 3.07 (3H, s), 4.03 (2H, dq-like, *J*=7.1 and 2.4 Hz), 4.41 (1H, s), 6.66 (1H, s), 7.35—7.55 (5H, m).

3-(1-Methoxyethoxy)-5-methyl-2-(α-methylcinnamoyl)-hydroquinone diacetate (diacetate of **24GbM**): oil; IR (CCl_4) 1770, 1625, 1365, 1185 cm^{-1}; ^1H NMR (270 MHz, $CDCl_3$) δ=1.30 (3H, d, *J*=5.4 Hz), 2.14, 2.19, 2.22, and 2.34 (12H, each s), 3.28 (3H, s), 5.04 (1H, q, *J*=5.4 Hz), 6.85 (1H, s), 7.2—7.45 (6H, m).

Upon the reaction of **5S** in methanol, the first eluate was **7S**, the second was a minor unidentified prodcut, the third was **8S**, and fourth was a mixture of hydroquinone and **24S** which were separated as acetates after acetylation. However, in the case of **5Sd**, adducts **24Sd** were not isolated. The yields are summarized in Table 3.

Methyl 2-ethylthio-3-methoxy-4-methyl-6-(styryloxy)benzoate (methyl ether of type **4** adduct): oil; IR (CCl_4) 1740 cm^{-1}; ^1H NMR (270 MHz, $CDCl_3$) δ=1.18 (3H, t, *J*=7.3 Hz), 2.30 (3H, s), 2.92 (2H, q, *J*=7.3 Hz), 3.84 (3H, s), 3.93 (3H, s), 6.32 (1H, d, *J*=12.4 Hz), 6.88 (1H, s), 7.03 (1H, d, *J*=12.4 Hz), 7.25—7.40 (5H, m).

3-(1-Methoxyethylthio)-5-methyl-2-(α-methylcinnamoyl)-hydroquinone diacetate (diacetate of **24SbM**: R=Me): colorless prisms, mp 96—97 °C; IR (CCl_4) 1770, 1655, 1365, and 1180 cm^{-1}; ^1H NMR (CCl_4) δ=1.39 (3H, d, *J*=6 Hz), 2.08, 2.15, 2.22, and 2.29 (12H, each s), 3.25 (3H, s), 4.68 (1H, q, *J*=6 Hz), 6.92 (1H, s), 7.01 (1H, s), 7.28 (5H, s). Found: C, 65.37; H, 6.00%. Calcd for $C_{24}H_{26}O_6S$: C, 65.14; H, 5.92%.

3-(1-Ethoxyethylthio)-5-methyl-2-(α-methylcinnamoyl)-hydroquinone diacetate (diacetate of **24SbE**: R=Et): colorless prisms, mp 97—99 °C; IR (CCl_4) 1775, 1660, 1370, and 1180 cm^{-1}; ^1H NMR (270 MHz, $CDCl_3$) δ=11.4 (3H, t, *J*=7.1 Hz), 1.47 (3H, d, *J*=6.1 Hz), 2.14 (3H, s), 2.21 (3H, d, *J*=1.2 Hz), 2.24 (3H, d, *J*=0.5 Hz), 2.34 (3H, s), 3.30—3.45 (1H, m), 3.65—3.80 (1H, m), 4.89 (1H, q, *J*=6.1 Hz), 7.07 (1H, q, *J*=1.2 Hz), 7.09 (1H, q, *J*=0.5 Hz), 7.3—7.4 (5H, m).

3-(1-Isopropoxyethylthio)-5-methyl-2-(α-methylcinnamoyl)-hydroquinone (**24SbP**: R=*i*-Pr): oil; ^1H NMR (270 MHz, $CDCl_3$) δ=1.11 and 1.14 (6H, each d, *J*=6.1 Hz), 1.34 (1H, d, *J*=6.3 Hz), 2.24 (3H, s), 2.30 (3H, s), 3.79 (1H, m, *J*=6.1 Hz), 4.74 (1H, q, *J*=6.3 Hz), 6.66 (1H, bs), 6.81 (1H, s), 6.93 (1H, s), 7.30—7.45 (5H, m), 7.69 (1H, s).

Photochemical Reaction of 11 in Alcohols. The procedures were the same as described above for **5** in alcohol. Upon the reaction of **11G** in methanol, the first yellow eluate was a minor unidentified product, the second was **15G**, the third was **29GM** (R=Me), and the fourth was a mixture of methanol adducts (type **3** and **4**) and the starting quinone. Upon the reaction of **11Ga** in isopropyl alcohol, a mixture of **13Ga**, **29GaP** (R=*i*-Pr), and alcohol adducts (type **3** and **4**) was obtained from the third yellow eluate. The yields of the products were determined by ^1H NMR spectra and the isolation of those was carried out in the usual way after acetylation. The yields of the major products are summarized in Table 4.

4-Methoxy-7-methyl-4-styryl-4*H*-1,3-benzodioxin-5,8-dione (**29GaM**): oil; IR (CCl_4) 1680, 1660, 1610 cm^{-1}; ^1H NMR (270 MHz, $CDCl_3$) δ=2.03 (3H, d, *J*=1.5 Hz), 3.34 (3H, s), 5.41 (1H, d, *J*=5.4 Hz), 5.50 (1H, d, *J*=5.4 Hz), 6.48 (1H, q, *J*=1.5 Hz), 6.71 (1H, d, *J*=16.1 Hz), 7.00 (1H, d, *J*=16.1 Hz), 72.5—7.40 (3H, m), 7.40—7.45 (2H, m); ^{13}C NMR (67.8 MHz, $CDCl_3$) δ=15.2 (q), 49.7 (q), 85.8 (t), 95.6 (s), 121.0 (s), 124.9 (d), 127.1 (d), 128.5 (d), 128.7 (d), 134.0 (d), 134.3 (d), 135.8 (s), 142.6 (s), 151.9 (s), 181.5 (s), 183.9 (s). Found: *m/z* 312.1009. Calcd for $C_{18}H_{16}O_5$: M, 312.0996.

4-Isopropoxy-7-methyl-4-styryl-4*H*-1,3-benzodioxin-5,8-dione (**29GaP**): oil; ^1H NMR (270 MHz, $CDCl_3$) δ=1.18 and 1.26 (6H, each d, *J*=6.1 Hz), 2.01 (3H, d, *J*=1.5 Hz), 4.23 (1H, m, *J*=6.1 Hz), 5.48 and 5.51 (2H, ABq, *J*=5.4 Hz), 6.45 (1H, q, *J*=1.5 Hz), 6.81 (1H, d, *J*=16.1 Hz), 7.01 (1H, d, *J*=16.1 Hz), 7.25—7.45 (5H, m).

4-Methoxy-2,7-dimethyl-4-styryl-4*H*-1,3-benzodioxin-5,8-dione (**29GbM**): oil; IR (CCl_4) 1680, 1660, 1610 cm^{-1}; ^1H NMR (270 MHz, $CDCl_3$) δ=1.75 (3H, d, *J*=5.4 Hz), 2.02 (3H, d, *J*=1.5 Hz), 3.32 (3H, s), 5.52 (1H, q, *J*=5.4 Hz), 6.47 (1H, q, *J*=1.5 Hz), 6.71 (1H, d, *J*=16.1 Hz), 6.97 (1H, d, *J*=16.1 Hz), 7.25—7.45 (5H, m). Found: *m/z* 326.1151. Calcd for $C_{19}H_{18}O_5$: M, 326.1153.

4-Methoxy-2,2,7-trimethyl-4-styryl-4*H*-1,3-benzodioxin-5,8-dione (**29GdM**): oil; ^1H NMR (270 MHz, $CDCl_3$) δ=1.73 (3H, s), 1.81 (3H, s), 2.01 (3H, d, *J*=1.5 Hz), 3.35 (3H, s), 6.47 (1H, q, *J*=1.5 Hz), 6.62 (1H, d, *J*=16.1 Hz), 6.87 (1H, d, *J*=16.1 Hz), 7.25—7.45 (5H, m).

Upon the reaction of **11S** in methanol, the first eluate was type **4** adduct, the second was **13S**, the third was **15S**, and the fourth was a mixture of **14S** and **27S**. However, in the case of **11Sd**, the adducts **27Sd** was not isolated. The yields are summarized in Table 4.

2-Cinnamoyl-3-(1-methoxyethylthio)-5-methylhydroquinone diacetate (diacetate of **27SbM**: R=Me): colorless prisms, mp 127—129 °C; IR (CCl_4) 1770, 1650, 1175 cm^{-1}; ^1H NMR (CCl_4) δ=1.39 (3H, d, *J*=6 Hz), 2.09 (3H, s), 2.24 (3H, s), 2.32 (3H, s), 3.24 (3H, s), 4.67 (1H, q, *J*=6 Hz), 6.80 (1H, d, *J*=16 Hz), 7.02 (1H, s), 7.10 (1H, d, *J*=16 Hz), 7.15—7.6 (5H, m). Found: *m/z* 428.1280. Calcd for $C_{23}H_{24}O_6S$: M, 428.1291.

Reaction of 7Sd in the Presence of Chloroacetic Acid. A benzene solution (5 cm^3) of **7Sd** (0.15 mmol) and chloroacetic acid (ca. 0.5 mmol) in a sealed test tube was stirred at 40 °C for 2 days in the dark. The mixture was chromatographed on silica gel with benzene as the eluent. 2,2,4,8-Tetramethyl-7-phenyl-7,8-dihydro-9*H*-[1,3]oxathiolo[4,5-*f*][1]benzopyran-9-one (**9**, 63%) was obtained from the first yellow eluate. **9** (a mixture of diastereoisomers, ca. 9:2): yellow oil; IR (CCl_4) 2980, 1680, 1620, 1420 cm^{-1}; ^1H NMR (270 MHz, $CDCl_3$) δ=0.98 and 1.00 (3H, each d, J=7.3 and 6.8 Hz), 1.83 (6H, s), 2.20 and 2.23 (3H, each s), 2.80 and 2.96 (1H, each dq, J=7.3 and 2.7 Hz and 12.2 and 6.8 Hz), 4.95 and 5.49 (1H, each d, J=12.2 and 2.7 Hz), 6.46 and 6.58 (1H, each s), 7.40 and 7.42 (5H, each s). Found: *m/z* 340.1112. Calcd for $C_{20}H_{20}O_3S$: M, 340.1132.

Desulfurization of Methylated 7Sd by Raney Nickel. A solution of methylated **7Sd** (0.22 mmol) in 95% ethanol (3 cm^3) was refluxed for 2 h with Raney nickel (ca. 0.5 g). The mixture was filtered, evaporated in vacuo, and the residue was chromatographed on silica gel with benzene as the eluent. 6-Methoxy-3,7-dimethyl-2-phenyl-4-chromanone (**10**, 42%) was obtained as major product from the second eluate. **10**: oil; IR (CCl_4) 1690, 1620, 1470, 1420, 1215 cm^{-1}; ^1H NMR (270 MHz, $CDCl_3$) δ=0.98 (3H, d, J=7.3 Hz), 2.27 (3H, s), 2.77 (1H, dq, J=7.3 and 2.9 Hz), 3.85 (3H, s), 5.52 (1H, d, J=2.9 Hz), 6.92 (1H, s), 7.28 (1H, s), 7.35—7.5 (5H, m). Found: *m/z* 282.1243. Calcd for $C_{18}H_{18}O_3$: M, 282.1254.

Reductive Acetylation of 29GaM with Zinc-Acetic Anhydride. A mixture of **29GaM** (20 mg) and zinc dust (200 mg) in acetic anhydride (2 cm^3) containing two drops of pyridine was stirred at room temperature for 2 h. After removing the zinc, the reaction mixture was worked up in a similar manner to the usual acetylation. The residue was chromatographed on TLC with chloroform as the developing solvent. The first-moved band gave 5,8-diacetoxy-4-methoxy-7-methyl-4-styryl-4*H*-1,3-benzodioxin (diacetate of **28GaM**): 50%; colorless oil; IR (CCl_4) 1770, 1180 cm^{-1}; ^1H NMR (270 MHz, $CDCl_3$) δ=2.17 (3H, d, J=0.5 Hz), 2.27 (3H, s), 2.34 (3H, s), 3.29 (3H, s), 5.26 and 5.29 (2H, ABq, J=5.6 Hz), 6.54 (1H, d, J=15.9 Hz), 6.60 (1H, bd, J=0.5 Hz), 6.87 (1H, d, J=15.9 Hz), 7.25—7.45 (5H, m). Found: *m/z* 398.1395. Calcd for $C_{22}H_{22}O_7$: M, 398.1365.

Quantum Yield Measurement. The quantum yield for consumed quinone **5Sd** was measured by potassium trioxalatoferrate(III) actinometry. A benzene solution of **5Sd** (0.5 mmol dm^{-3}) and a potassium trioxalatoferrate(III) solution (0.15 mol dm^{-3}) were employed. Conversion of the quinone (5—10%) was detected by UV spectrometer and the quantum yield of the disappearance of **5Sd** (Φ=0.50) was calculated in the usual way. The quantum yield of the disappearance of **5Sb** (Φ=0.30) was determined by a comparison with that of **5Sd**.

I am grateful to Professor Kazuhiro Maruyama of Kyoto University for helpful discussions. I also would like to thank Professor Akio Takuwa and Honorary Professor Osamu Soga of Shimane University for helpful advice.

References

1) "Biochemistry of Quinones," ed by R. A. Morton, Academic Press, London and New York (1965).

2) D. Creed, H. Werbin, and E. T. Storm, *J. Am. Chem. Soc.*, **93**, 502 (1971); H. Morimoto, I. Imada, and G. Goto, *Liebigs Ann. Chem.*, **735**, 65 (1970); C. D. Snyder and H. Rapoport, *J. Am. Chem. Soc.*, **91**, 731 (1969); R. M. Wilson, T. F. Walsh, and S. K. Gee, *Tetrahedron Lett.*, **21**, 3459 (1980).

3) R. Powls and E. R. Redfearn, *Biochim. Biophys. Acta*, **172**, 429 (1969); C. D. Snyder, W. E. Bondinell, and H. Rapoport, *J. Org. Chem.*, **36**, 3591 (1971).

4) K. Maruyama, M. Muraoka, and Y. Naruta, *J. Chem. Soc., Chem. Commun.*, **1980**, 1282.

5) K. Maruyama, H. Iwamoto, O. Soga, and A. Takuwa, *Chem. Lett.*, **1984**, 1343; H. Iwamoto, *J. Org. Chem.*, **53**, 1507 (1988).

6) K. Maruyama, H. Iwamoto, O. Soga, A. Takuwa, and A. Osuka, *Chem. Lett.*, **1985**, 1675.

7) J. E. Baldwin and L. E. Brown, *J. Chem. Soc., Chem. Commun.*, **1969**, 167.

8) K. Maruyama, T. Otsuki, and K. Mitsui, *J. Org. Chem.*, **45**, 1424 (1980).

9) T. Otsuki, *Bull. Chem. Soc. Jpn.*, **49**, 2596 (1976).

10) H. Iwamoto, *Chem. Express*, **4**, 185 (1989).

11) The products **8Gd** and **8Ge** were obtained on the purification process of **7Gd** and **7Ge**, respectively. Therefore, **8G** would be formed as an oxidation product of **7G**.

12) S. Cabiddu, G. Cerioni, M. T. Cocco, A. Maccioni, and A. Plumitallo, *J. Heterocycl. Chem.*, **19**, 135 (1982).

13) By the treatment of **13Sd** with **11Sd** in the dark at 35 °C for 3 h, **13Sd** was only recovered in a 10% yield together with the formation of **14Sd** (69%) and **15Sd** (71%).

14) By the treatment of **7Sd** with **5Sd** in the dark at 35 °C for 14 h, **7Sd** was recovered in a 71% yield. Even by the treatment of **7Sd** with chloranil in the dark at 35 °C for 3 h, **7Sd** was recovered in a 40% yield.

15) F. Farina and J. Valderrama, *Synthesis*, **1971**, 315.

16) R. Baltzly and E. Lorz, *J. Am. Chem. Soc.*, **70**, 861 (1948).

 © 1989 The Chemical Society of Japan Bull. Chem. Soc. Jpn., 62, 3488—3491 (1989) [Vol. 62, No. 11

Binding of Modified Guanine Nucleotides to Ribonuclease T_1 as Studied by Absorption Spectroscopy. 8-Aminoguanosine 2′-Phosphate, 8-Methylaminoguanosine 2′-Phosphate, and 8-Dimethylaminoguanosine 2′-Phosphate

Hiroshi YOSHIDA,* Masazumi SUGIYAMA, and Yoshio SHIBAGAKI
Department of Chemistry, Faculty of Science, Tohoku University, Aobayama, Aoba-ku, Sendai 980
(Received May 6, 1989)

The title nucleotides have been synthesized and their binding to ribonuclease T_1 studied by means of absorption spectroscopy. Measurements were made at pH 5.5 and 4.1, where a major portion of the base moiety of the nucleotides was in a neutral form and a cationic form protonated at N7, respectively. At both pH's, difference absorption spectra were induced upon binding of the nucleotides to the enzyme. A comparison of the difference spectra with that for guanosine 2′-phosphate has led to the conclusion that perturbation in the bound nucleotide is the principal cause for the difference spectra. The difference spectra at pH 5.5 and 4.1 were similar, suggesting that the protonation at N7 of the nucleotides can be ruled out as the cause for the difference spectra. The dissociation constants at pH 5.5 and 4.1 of the enzyme–8-aminoguanosine 2′-phosphate complex were of the same magnitude, indicating that both the neutral and the protonated forms bind tightly to the enzyme. However, the cationic form of 8-methylamino- or 8-dimethylaminoguanosine 2′-phosphate has been shown to interact with the enzyme much more loosely than the neutral form.

Ribonuclease (RNase) T_1 is an endoribonuclease that specifically cleaves single-stranded RNA at the 3′ end of guanine nucleotides via 2′:3′-cyclic phosphate intermediates. Specific recognition of the guanine nucleotide is, therefore, a key step in its action mechanism. It can bind monomer guanine nucleotides, among which guanosine 2′-phosphate (**1**) shows the highest affinity.[1] The binding is detected in a number of ways. Absorption spectroscopy is a simple and sensitive method for detection. A difference absorption spectrum is induced upon the binding of a guanine nucleotide to RNase T_1: the spectrum of the RNase T_1–nucleotide complex is not equal to the sum of the component spectra measured separately.[2]

Interpretation of this phenomenon has been controversial. Oshima and Imahori,[3] followed by others,[4,5] have pointed out a gross similarity between the difference spectrum and the acid-induced spectral change of the guanine nucleotide. This led them to propose the hypothesis that the guanine ligand is protonated on N7 upon binding to the enzyme and that this protonation is the cause for the difference spectrum. However, Yoshida and Kanae argued against this hypothesis on the grounds of a spectroscopic study using 8-bromoguanosine 2′-phosphate (**2**).[6] With nucleotide **2**, the acid-induced spectral change was dissimilar to the difference spectrum. However, a possibility can be envisaged that the protonation site of **2** might be different from N7 due to the introduction of a strongly electron-withdrawing group at C8.

In the present study, we have synthesized 8-aminoguanosine 2′-phosphate (**3**), 8-methylaminoguanosine 2′-phosphate (**4**), and 8-dimethylaminoguanosine 2′-phosphate (**5**) and studied their interactions with RNase T_1. The introduction of an electron-donating group at C8 of the guanine base increases the pK_a considerably, thereby allowing a study of the binding properties of a guanine nucleotide protonated at N7. This provides a direct verification of the protonation hypothesis.

Experimental

RNase T_1. This enzyme was purified as described by Kanaya and Uchida[7] and was determined spectrophotometrically using a molar absorbance of 21200 $M^{-1}\,cm^{-1}$ (1 M=1 mol dm^{-3}).[8]

Chemical Syntheses. Nucleotides **3**, **4**, and **5** were synthesized from **2** by the application of published methods for the syntheses of similar, but not identical, compounds shown in parentheses: **3** according to Holmes and Robins (8-aminoguanosine),[9] **4** according to Long et al. (8-methylaminoguanosine)[10] and **5** according to Miller et al. (8-dimethylaminoguanosine 3′:5′-cyclic phosphate).[11] Nucleotide **2** was synthesized essentially according to Yuki and Yoshida.[12] In each synthesis, some modifications were made to the original method in order to improve the performance. Therefore, the whole synthetic procedures will be described. However, the products were identified only on the grounds of the absorption spectra, since the synthetic reactions were the same as the original ones. Generally, the absorption spectra of our products were in good agreement with the reported spectra of the corresponding compounds. The purity of the products was checked by HPLC, which was carried out under the following conditions: chromatograph, Tosoh HLC-803 A; column, TSKgel IEX-540 K 4 mm (i.d.) ×300 mm; eluent, 0.25 or 0.5 M KH_2PO_4; flow rate, 1.0 $cm^3\,min^{-1}$; detection, absorbance at 260 nm. Special attention was paid so that each product was free from its 3′-isomer, a possible by-product of phosphoryl transfer. The nucleotides were determined through quantitation of phosphorus, which was carried out by the method of Fiske and Subbarow.[13]

8-Bromoguanosine 2′-Phosphate (2). To guanosine 2′-

(3′)-phosphate (free acid, 813 mg, 2.23 mmol) dissolved in 4 cm^3 of *N*,*N*-dimethylformamide, was added 0.15 cm^3 of Br_2 in 1 cm^3 of the solvent. The reaction mixture was left standing at room temperature for 15 min, then added dropwise into 6 cm^3 of ice-cold water under stirring. The solution was adjusted to pH ca. 7 with concd aq. ammonia, then poured into 120 cm^3 of ice-cold acetone. The resulting precipitate was collected by centrifugation, washed twice with acetone and once with ether, and dried in vacuo (yield 933 mg). The crude product was purified on a column of DE 52 (HCO_3^- form, 1.8×70 cm) in three portions. One third of the product was dissolved in 10 cm^3 of water and loaded on the column equilibrated with 0.18 M NH_4HCO_3. The column was developed by a linear gradient of 0.18—0.35 M NH_4HCO_3 over 1 dm^3. Nucleotide **2** and its 3′-isomer were separated and recovered by lyophilization: total yield, **2** (1.17 mmol, 57%), the 3′-isomer (0.69 mmol, 34%). Retention time (t_R) in HPLC with 0.5 M KH_2PO_4 as the solvent, **2** (6.0 min), the 3′-isomer (7.25 min).

8-Aminoguanosine 2′-Phosphate (3). Nucleotide **2** (21.4 μmol) was dissolved in 0.5 cm^3 of water containing 6 mm^3 of hydrazine monohydrate. The solution was heated at 95 °C for 26 h in a sealed glass tube, cooled to room temperature, and diluted with 10 cm^3 of water. After being adjusted to pH ca. 7, the solution was loaded on a column of DE 52 (formate form, 1.6×35 cm). After unadsorbed material was washed off with water, the column was developed by a linear gradient of 0—0.1 M formic acid over 0.6 dm^3. The product **3** (7.1 μmol, 33%) was separated from a small amount of the 3′-isomer (1.0 μmol, 5%) and recovered by lyophilization: t_R (0.25 M KH_2PO_4), 4.2 min (the 3′-isomer, 5.0 min); UV (10 mM HCl), 250 (ε 16700), 288 (10600); (H_2O), 255 (16300), 291 (9600); (10 mM NaOH), 258 (14600), ca. 280 (sh, 11800).

8-Methylaminoguanosine 2′-Phosphate (4). Nucleotide **2** (23.2 μmol) was suspended in 0.3 cm^3 of 40 wt% methylamine in methanol; the suspension was heated at 95 °C for 39 h in a sealed glass tube. The work up and the chromatography as described for **3** afforded **4** (15.2 μmol, 66%): t_R (0.25 M KH_2PO_4), 4.1 min; UV (10 mM HCl), 252 (ε 17500), 289 (10200); (H_2O), 259 (16500), 295 (9200); (10 mM NaOH), 261 (15000), ca. 280 (sh, 12550). Only a small amount (<1 μmol) of the 3′-isomer was detected in the chromatography: t_R, 4.9 min.

8-Dimethylaminoguanosine 2′-Phosphate (5). Nucleotide **2** (156 μmol) was suspended in a mixture of anhydrous dimethylamine (2.2 cm^3) and methanol (10 cm^3). The suspension was heated at 120 °C for 5 h in a steel bomb, then evaporated. The residue was dissolved in 10 cm^3 of water and loaded on a column of DE 52 (HCO_3^- form, 1.8×50 cm) equilibrated with 0.05 M NH_4HCO_3. The product **5** (84.6 μmol, 54%) was eluted from the column by a linear gradient of 0.05—0.35 M NH_4HCO_3 over 1 dm^3 and recovered by lyophylization: t_R (0.5 M KH_2PO_4), 4.8 min; UV (10 mM HCl), 264 (ε 17500), ca. 290 (sh, 11100); (H_2O), 262 (16500), ca. 290 (sh, 8700); (10 mM NaOH), 269 (15100).

Measurement of Difference Spectra. This was carried out as described previously[6] in a solvent, 10 mM sodium acetate buffer (pH 5.5 or 4.1) containing 0.1 M NaCl, with a Hitachi 220 A spectrophotometer equipped with a tandem cell holder thermostatted at 25 °C. A typical experiment was run with 2.0 cm^3 of 39.0 μM RNase T_1 and 2.0 cm^3 of 38.2 μM **3** giving rise to a difference absorbance of 0.128 at a maximum wavelength (λ_{max}) of 308 nm in an optical path of 2.0 cm.

Determination of the Dissociation Constant K_d and the Maximum Difference Molar Absorbance $\Delta\varepsilon(\lambda_{max})$ for a RNase T_1–Nucleotide Complex. This was carried out as described previously.[6] A typical run was as follows. To 2.5 cm^3 of 12.2 μM RNase T_1, was added 8.11 mM **3** in 0.2 mm^3 portions up to a total of 13 mm^3. After each addition, the absorbances at 263 nm (a crossover point of the difference spectrum) and 308 nm (λ_{max}) were measured. The data, thus obtained, were processed to give the K_d and $\Delta\varepsilon(\lambda_{max})$.

Results and Discussion

Spectrophotometric Titration of the 8-Substituted Guanine Nucleotides. Guanosine undergoes spectral changes with pH, showing acid dissociation constants (pK_a) of 2.3 and 9.4. Miles et al. have established that the lower dissociation constant (pK_{a1}) corresponds to protonation at N7 and that the higher one (pK_{a2}) corresponds to deprotonation from N1-H. The pK_a's of **3**, **4**, and **5** were examined by spectrophotometric titration. As shown in Table 1, the introduction of an electron-donating group at C8 increased the pK_{a1} considerably and also the pK_{a2} to a lesser extent. These changes are as expected from the protonation and deprotonation sites described above. Therefore, the base moiety of these nucleotides is supposed to be in a cationic form protonated at N7 in a sufficiently acidic solution.

Interaction of the 8-Substituted Guanine Nucleotides with RNase T_1. The difference absorption spectrum induced upon binding of the parent nucleotide **1** to RNase T_1 at pH 5.5 has been shown to have one major trough at 245 nm and one major peak at 290 nm.[2-5] In addition, it has a minor peak at ca. 260 nm and a minor trough at ca. 270 nm in-between. Sato and Egami examined the difference absorbance at 290 nm as a function of pH and found that it remained nearly constant between pH 4 and 5.5, falling off on both acidic and alkaline sides.[2] This suggests that RNase T_1 binds the ligand equally well in a pH range 4—5.5. We studied the binding of **1** to RNase T_1 at pH 4.1 in detail and found that the entire difference spectrum was unchanged from that at pH 5.5. Moreover, the K_d was determined to be 4.0 μM, in good agreement with that (4.6 μM) at pH 5.5. Since the ionization state of the guanine base is the same at pH 5.5 and 4.1, these results indicate that the nucleotide binding property of the enzyme remains the same at these pH's. Having confirmed this fact, we studied the interaction of **3**, **4**, and **5** with RNase T_1 at these pH's.

Table 1. Acid Dissociation Constants of the 8-Substituted Guanine Nucleotides

Nucleotide	pK_{a1}	pK_{a2}
3	4.9	10.4
4	5.0	10.6
5	3.8	10.2

At pH 4.1, these nucleotides are expected to be mainly in the form protonated at N7, due to the elevated pK_{a1}. Therefore, the effect of protonation on the difference spectrum or the binding can be assessed directly.

The base moiety of **3** was calculated from its pK_{a1} to be 80% in the neutral form at pH 5.5 and 86% in the cationic form at pH 4.1. A change in absorption spectrum takes place with the change of ionization state (see UV characteristics shown in the Experimental section). A blue-shift is the main feature accompanying protonation. In spite of this spectral change, the difference spectra induced upon binding of **3** to RNase T_1 were quite similar at pH 5.5 and 4.1 (Fig. 1A). At pH 5.5, two distinct peaks were observed at 270 and 308 nm and two troughs at 248 and 286 nm. At pH 4.1, a slight blue-shift was seen for the shorter wavelength trough and peak. Compared to the difference spectrum for the parent nucleotide **1**, a large red-shift by 18 nm of the longer wavelength peak is noteworthy. This red-shift corresponds almost exactly to the red-shift between 275 and 290 nm of the longer wavelength absorption bands of **1** and **3**, respectively. This suggests that a perturbation of the nucleotide and not a protein chromophore(s) is the principal cause for the difference spectrum. Clearly, the perturbation cannot be protonation of the ligand, since even the protonated nucleotide causes a similar difference spectrum. It should also be noted that the spectral change accompanying the protonation and the difference spectrum are dissimilar. A blue-shift is the characteristic for the former, whereas the latter can be regarded as being due to a red-shift of the absorption bands of the nucleotide.

The K_d for **3** was slightly lower than that for **1** at both pH 5.5 and 4.1 (Table 2). Especially noteworthy is the low K_d, thus the tight binding at pH 4.1, which means that **3** protonated at N7 can bind tightly to the enzyme. This precludes a binding mechanism in which N7 plays an important role as a hydrogen acceptor. The X-ray analysis of the RNase T_1-**1** complex has indicated the probable hydrogen bonds to N7.[14,15] A ^1H NMR study has also proposed hydrogen bond interaction between N7 of the guanine base and a histidine residue in the active site of the enzyme.[16] However, in the tertiary structure determined by the X-ray analysis, the distance between N7 and any of the suggested hydrogen donors is large (>3 Å). Moreover, an ^{15}N NMR study showed no sign of the participation of N7 in the binding.[17] In accordance with these latter observations, our result presents evidence for the dispensability of the hydrogen bond to N7 in the formation of the enzyme-nucleotide complex. In fact,

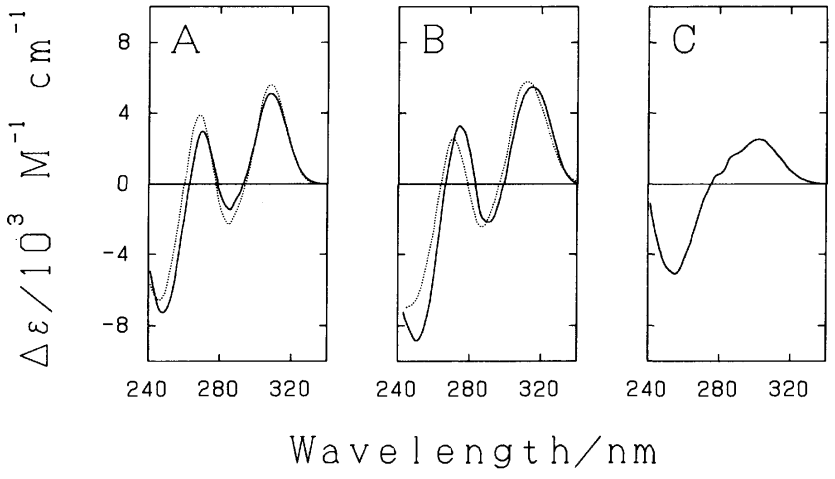

Fig. 1. Difference spectra induced upon binding of the 8-substituted nucleotides to RNase T_1. A: **3**, B: **4**, C: **5**. —: at pH 5.5, ·····: at pH 4.1.

Table 2. Dissociation Constants and Related Parameters for RNase T_1-8-Substituted Guanine Nucleotide Complexes

Nucleotide	pH 5.5			pH 4.1		
	λ_{max}	$\Delta\varepsilon(\lambda_{max})$	K_d	λ_{max}	$\Delta\varepsilon(\lambda_{max})$	K_d
	nm	$10^3\ M^{-1}\ cm^{-1}$	μM	nm	$10^3\ M^{-1}\ cm^{-1}$	μM
3	308	5.1	2.7	308	5.6	1.3
4	315	5.5	26	312	5.8	80
5	302	2.5	15	ca. 302	nd[a)]	nd[a)]

a) Not determined.

Seela et al. have shown that RNase T_1 is able to hydrolyze poly(7-deazaguanylic acid) lacking N7.[18]

The base moiety of **4** is 72% in the neutral form at pH 5.5 and 91% in the cationic form at pH 4.1. As for the difference spectra shown in Fig. 1B, qualitatively the same argument holds as that described for **3**. The major differences are a larger red-shift of the longer wavelength peak to 315 nm and a shift observed between the spectra at pH 5.5 and 4.1 over the entire wavelength region. In spite of the qualitative similarity, an important quantitative difference emerged: the K_d was much higher at pH 4.1 than at pH 5.5 (Table 2). This shows that nucleotide **4** protonated at N7 binds to the enzyme much more loosely than its neutral form. At pH 5.5, the observed K_d is substantially higher for **4** than for **3**. It should be kept in mind, however, that 28% of **4** is still in the cationic form with a large K_d at pH 5.5. The intrinsic K_d for the neutral form of **4** is, therefore, estimated to be much lower than 26 μM actually observed and to be at a level similar to that for **3**. Accordingly, we conclude that the neutral form of **4** binds to the enzyme tightly, whereas the protonated form binds loosely. This is in contrast to the situation for **3**, whereby both forms interact with the enzyme equally well. We have no explanation for this discrepancy at present. However, it is possible that concomitant occurrence of protonation at N7 and a bulky substituent at C8 may seriously hinder the nucleotide from binding to the enzyme.

Nucleotide **5** is almost entirely (98%) in the neutral form at pH 5.5, but only 33% in the cationic form even at pH 4.1. General properties, e.g. absorption spectrum or pK_a, of **5** cannot be simply extrapolated from those of **3** and **4**. Likewise, the difference spectrum induced upon binding of **5** to RNase T_1 at pH 5.5 (Fig. 1C) differed considerably from those for **3** and **4**. The spectrum has only one trough at 255 nm and one peak at 302 nm, both of relatively small magnitude. At pH 5.5, the K_d is several times higher than that for the parent nucleotide **1** (Table 2), but is equivalent to that for the 3′-isomer of **1** (21.3 μM, our own measurement). Accordingly, nucleotide **5** can be regarded to bind to the enzyme still tightly in spite of the bulky dimethylamino group introduced at C8. This shows the considerable freedom of space in the vicinity of C8 of the bound guanine base. Nucleotide **5** can only adopt a syn conformation about the glycosyl bond rotation, because of the bulky substituent at C8.[19] Relatively tight binding of **5** is in accord with the X-ray structure in which the nucleotide bound at the active site of RNase T_1 assumes a syn conformation.[14,15] At pH 4.1, we were unable to determine the K_d for **5** because of the small magnitude of the difference spectrum. However, the attenuation of the difference spectrum suggests that the protonated form of **5** interacts with the enzyme very weakly, like the protonated form of **4**.

In conclusion, the present study shows that a perturbation of the nucleotide base is the main cause for the difference spectrum induced upon its binding to RNase T_1. The contribution of a protein chromophore(s) may be small, if any. Protonation at N7, which used to be assumed to cause the difference spectrum, should be ruled out. It is also clear that the protonation per se does not interfere a nucleotide from binding to the enzyme. This argues against the participation of N7 in the specific binding as a hydrogen acceptor.

References

1) K. Takahashi and S. Moore, "The Enzymes," 3rd ed, ed by P. D. Boyer, Academic Press, New York (1982), Vol. 15, Chap. 13, pp. 435—468.
2) S. Sato and F. Egami, *Biochem. Z.*, **342**, 437 (1965).
3) T. Oshima and K. Imahori, *J. Biochem.*, **69**, 987 (1971).
4) C. Epinatjeff and O. Pongs, *Eur. J. Biochem.*, **26**, 434 (1972).
5) F. G. Walz, Jr. and L. L. Hooverman, *Biochemistry*, **12**, 4846 (1973).
6) H. Yoshida and H. Kanae, *Biochem. Biophys. Res. Commun.*, **114**, 88 (1983).
7) S. Kanaya and T. Uchida, *J. Biochem.*, **89**, 591 (1981).
8) K. Takahashi, *J. Biochem.*, **51**, 95 (1962).
9) R. E. Holmes and R. K. Robins, *J. Am. Chem. Soc.*, **87**, 1772 (1965).
10) R. A. Long, R. K. Robins, and L. B. Townsend, *J. Org. Chem.*, **1967**, 2751.
11) J. P. Miller, K. H. Boswell, K. Muneyama, L. M. Simon, R. K. Robins, and D. A. Shuman, *Biochemistry*, **12**, 5310 (1973).
12) R. Yuki and H. Yoshida, *Biochim. Biophys. Acta*, **246**, 206 (1971).
13) C. H. Fiske and Y. Subbarow, *J. Biol. Chem.*, **66**, 375 (1925).
14) S. Sugio, T. Amisaki, H. Ohishi, and K. Tomita, *J. Biochem.*, **168**, 354 (1988).
15) R. Arni, U. Heinemann, R. Tokuoka, and W. Saenger, *J. Biol. Chem.*, **263**, 15358 (1988).
16) Y. Arata, S. Kimura, H. Matsuo, and K. Narita, *Biochemistry*, **18**, 18 (1979).
17) Y. Kyogoku, M. Watanabe, M. Kainosho, and T. Oshima, *J. Biochem.*, **91**, 675 (1982).
18) F. Seela, Q.-H. Tran-Thi, and D. Franzen, *Biochemistry*, **21**, 4338 (1982).
19) F. Jordan and H. Niv, *Biochim. Biophys. Acta*, **476**, 265 (1977).

Preparation and Properties of Tetrathia[*n*](1,1′)ferrocenophanes with $Pd(BF_4)_2$. The Metal-Metal Interaction Controlled by the Size of the Thiamacrocycles

Masaru SATO* and Sadatoshi AKABORI†
Chemical Analysis Center, Saitama University, Urawa, Saitama 338
†Department of Chemistry, Faculty of Science, Toho University, Funabashi, Chiba 274
(Received May 25, 1989)

1,4,7,10-Tetrathia[10]-, 1,4,8,11-tetrathia[11]-, 1,5,8,12-tetrathia[12]-, and 1,5,9,13-tetrathia[13](1,1′)ferrocenophanes reacted with $(CH_3CN)_4Pd(BF_4)_2$ to give the corresponding 1/1 complexes in good yield. The ^1H NMR spectra of the Pd(II) complexes were not rigid at room temperature, except for the complex of 1,4,7,10-tetrathia[10](1,1′)ferrocenophane. The ^1H and ^{13}C NMR spectra at low temperature showed that the Pd(II) complex of 1,5,9,13-tetrathia[13]ferrocenophane was a single compound, while the other three complexes were a mixture of two isomers. In the electronic spectra of the above series, the low-energy band shifted to the long-wavelength region and increased its absorbance according to the decrease in the size of the thiamacrocycle.

Recently, numerous studies have been reported about heterobimetallic complexes.[1,2] Such complexes have potential applications in homogeneous catalysis. The presence of another metal in close proximity to the catalytically active metal may offer the possibility of a modification of the catalytic activity. Alternatively, interactions between the two proximate metal centers may lead to unique reactivity. Organometallic ligands are the beneficial starting material for preparing heterobimetallic complexes. We previously reported the syntheses of polythia[*n*]ferrocenophanes[3] as such an organometallic ligand, and some their complexes with transition metals.[4-6] In this paper[7] we describe the synthesis and properties of complexes of tetrathia[*n*](1,1′)ferrocenophanes with $Pd(BF_4)_2$, which is known to have a superior catalytic activity.[8]

A solution of 1,4,7,10-tetrathia[10](1,1′)ferrocenophane (**1a**)[4] in acetonitrile was treated with a solution of $(CH_3CN)_4Pd(BF_4)_2$ (**2**), which was prepared from $(CH_3CN)_2PdCl_2$ and 2 equivalent of $AgBF_2$ in acetone,[9] followed by dilution with anhydrous diethyl ether, gave a 1/1 complex (**3a**) as dark-green needles in

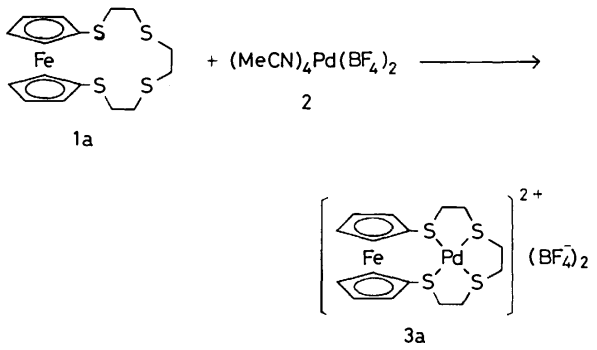

74% yield. In a similar manner, 1,4,8,11-tetrathia[11]- (**1b**), 1,5,8,12-tetrathia[12]- (**1c**), and 1,5,9,13-tetrathia[13](1,1′)ferrocenophanes (**1d**) gave the corresponding 1/1 complexes, **3b**, **3c**, and **3d**, in good yield, respectively. Complex **3b**, alone, contained one equivalent of acetonitrile in the crystal, as shown by elemental analysis. In the IR spectra of these complexes the out-of-plane bending vibration, which was the most diagnostic probe of the oxidation state of ferrocene,[10] was observed at 824, 826, 818, and 818 cm^{-1} for **3a**, **3b**, **3c**, and **3d**, respectively. The frequencies are a little higher than those of the corresponding free ligands **1a—1d**, but considerably lower than those of ferricenium cations (e.g. 846 cm^{-1} in the ferricenium cation of **1d**). These results suggests that the iron atom of a ferrocenyl moiety is somewhat perturbed by the proximate location of the Pd(II) atom. Particularly, in the complexes **3a** and **3b**, there seems to be a significant interaction between two metal atoms. In this connection, the out-of-plane bending vibration in (triphenylphosphine)(1,1′-ferrocenedithiolato-*S*,*S*′,*Fe*)-palladium(II) (**4**), which is confirmed by X-ray analysis to contain a dative Fe-Pd bond,[11] was observed at 830 and 838 cm^{-1}. In the $Pd(BF_4)_2$ complexes of trithia[*n*](1,1′)ferrocenophanes (*n*=7 and 9), this band also appeared at 830 and 844 cm^{-1}, respectively.[7] The differences of the frequencies between the Pd(II) complexes (**3a—3d**) and the corresponding free ligands (**1a—1d**) were 24, 16, 2, and 6 cm^{-1}, respectively. The magnitude of the shifting from the free ligand to the corresponding Pd(II) complex can be assumed to reflect the strength of an interaction between the Pd(II) atom and the Fe atom of a ferrocene nucleus in these complexes, since the coordinating strength of the sulfur atom to the Pd(II) atom seems to be almost the same through the series of the complexes **3a—3d**. Therefore, it will be expected that the largest interaction acts in complex **3a** in a series of complexes, **3a—3d**.

In the ^1H NMR spectrum (CD_3CN, 400 MHz) of **3d**, all signals were broadened at room temperature, indicating the presence of a certain dynamic process.

Table 1. ^{1}H NMR Spectral Data of the Complexes **3a—3d** in the Region of the Cp-Ring Proton Signals (400 MHz, CD_3CN)[a]

Compound	Temp	Isomer	Chemical shifts (δ)[b]
3a	R.T.	Major	5.61 (quasi s, 2H), 5.28 (quasi s, 2H), 4.82 (quasi s, 2H), 4.52 (quasi s, 2H)
		Minor	5.91 (broad s, 2H), 5.61 (quasi s, 4H), 5.82 (quasi s, 2H)
3b	−30 °C	Major	5.67 (quin, 2H), 5.54 (quin, 2H), 4.73 (sex, 2H), 4.27 (sex, 2H)
		Minor	5.58 (quin, 2H), 5.37 (quin, 2H), 4.76 (sex, 2H), 4.39 (sex, 2H)
3c	80 °C		5.14 (s, 4H), 4.65 (s, 4H)
3d	80 °C		5.22 (s, 4H), 4.66 (s, 4H)
	−30 °C		5.20 (broad quin, 4H), 4.75 (sex, 2H), 4.52 (sex, 2H)

a) The methylene proton signals could not surely assigned because of complexation due to the presence of two isomers. b) quin=quintet, sex=sextet.

Table 2. ^{13}C NMR Spectral Data of the Complexes **3a—3d**

Compound	Temp	Isomer	Chemical shifts (δ)
3a	R.T.	Major	86.05,[a] 79.51, 76.17, 75.16, 71.74, 46.29, 43.55, 43.40
		Minor	—,[b] 80.57, 77.10, 75.85, 70.07, 45.63, 43.55, 40.94
3b	−30 °C	Major	83.62,[a] 80.60, 76.10, 75.73, 70.03, 42.71, 42.07, 37.58, 27.18
		Minor	82.28,[a] 80.03, 75.96, 74.67, 70.93, 45.83, 41.59, 37.63, 27.95
3c	−30 °C	Major	79.91, 77.36, 76.77,[a] 75.52, 72.02, 40.05, 38.47, 32.20, 25.68
3d	−30 °C		79.77, 77.53, 75.86, 75.17,[a] 73.12, 38.14, 37.49, 33.06, 25.70, 23.71
	80 °C		79.74, 77.23, 75.84, 75.56,[a] 73.07, 38.39, 37.24, 33.23, 25.82, 23.93

a) This is assigned to be the bridge-head carbon of a ferrocenyl Cp-rings by using the DEPT measurement. b) This signal (which is probably the bridge-head carbon signal) could not be detected.

The static spectrum was obtained at −30 °C, in which the cyclopentadienyl (Cp) ring protons appeared as three pseudosinglests at δ 5.20 (4H), 4.75 (2H), and 4.52 (2H) (The ^{1}H NMR spectral data was summarized in Table 1). The ^{13}C NMR spectrum of **3d** at low temperature similarly showed the presence of a single conformer. That is, the Cp-ring carbons of a ferrocene moiety produced signals at δ 79.77, 77.53, 75.86, 75.17, and 73.12 (The ^{13}C NMR spectral data was summarized in Table 2). The unsymmetric pattern of the ferrocenyl ring observed in the ^{1}H and ^{13}C NMR spectra of **3d** seems to reflect the stepped conformation[12] in which the Fe, Pd(II), and two sulfur atoms connected to the Cp rings are not coplanar, since **3d** has been proved by X-ray analysis to have such a stepped conformation.[13] The metal complexes of ferrocene derivatives containing heteroatoms in the 1,1′-positions can be regarded as an analog of [3](1,1′)ferrocenophanes which involves a bridge reversal process. The bridge reversal energy observed in 1,2,3-trichalcogeno[3](1,1′)ferrocenophanes is ca. 80 kJ mol^{-1}, in solution.[14,15] The proton signals of the Cp-rings of **3d** at δ 4.75 and 4.52 broadened upon warming and coallesced at 42 °C. At 80 °C the Cp-ring protons appeared at δ 5.22 and 4.66 as almost sharp signals, although signals of the methylene protons were still somewhat broad. A similar marked temperature dependence in the ^{1}H and ^{13}C NMR spectra was observed in the $PdCl_2$ complexes of 1,1′-bis(isobutylthio)ferrocenes (**5**),[16] and two independent dynamic processes, sulfur inversion and bridge reversal, were suggested to be involved.[17] In the complex **3d**, the sulfur inversion process seems to be impossible because the four sulfur atoms in the thiamacrocycle coordinate to the Pd(II) atom and, consequently, the methylene groups on the sulfur atoms at the 1,1′-positions are always forced to be in the same direction as that of the Pd(II) atom. Thus, the remarkable dynamic behavior observed in **3d** is probably due to a flipping of the thiamacrocycle moiety coordinated by the Pd(II) atom in which the Pd(II) atom flips from one side of the plane containing the iron atom and two sulfur atoms at the 1,1′-positions to the other. This phenomenon is considered to result from a concurrent occurance of bridge reversal with S-inversion on the sulfur atoms at the 1,1′-positions. From the coalescence temperature (42 °C), $\Delta G^{\ddagger}$=63.2 kJ mol^{-1} was calculated. This value is comparable with that in the complexes of 1,1′-bis(isobutylthio)ferrocene with palladium halides (**5**).[17] This supports the above elucidation, since it was reported that the bridge reversal was fast and the S-inversion was slow in PdX_2 complexes of 1,1′-bis(alkylthio)ferrocenes.[17] The rate

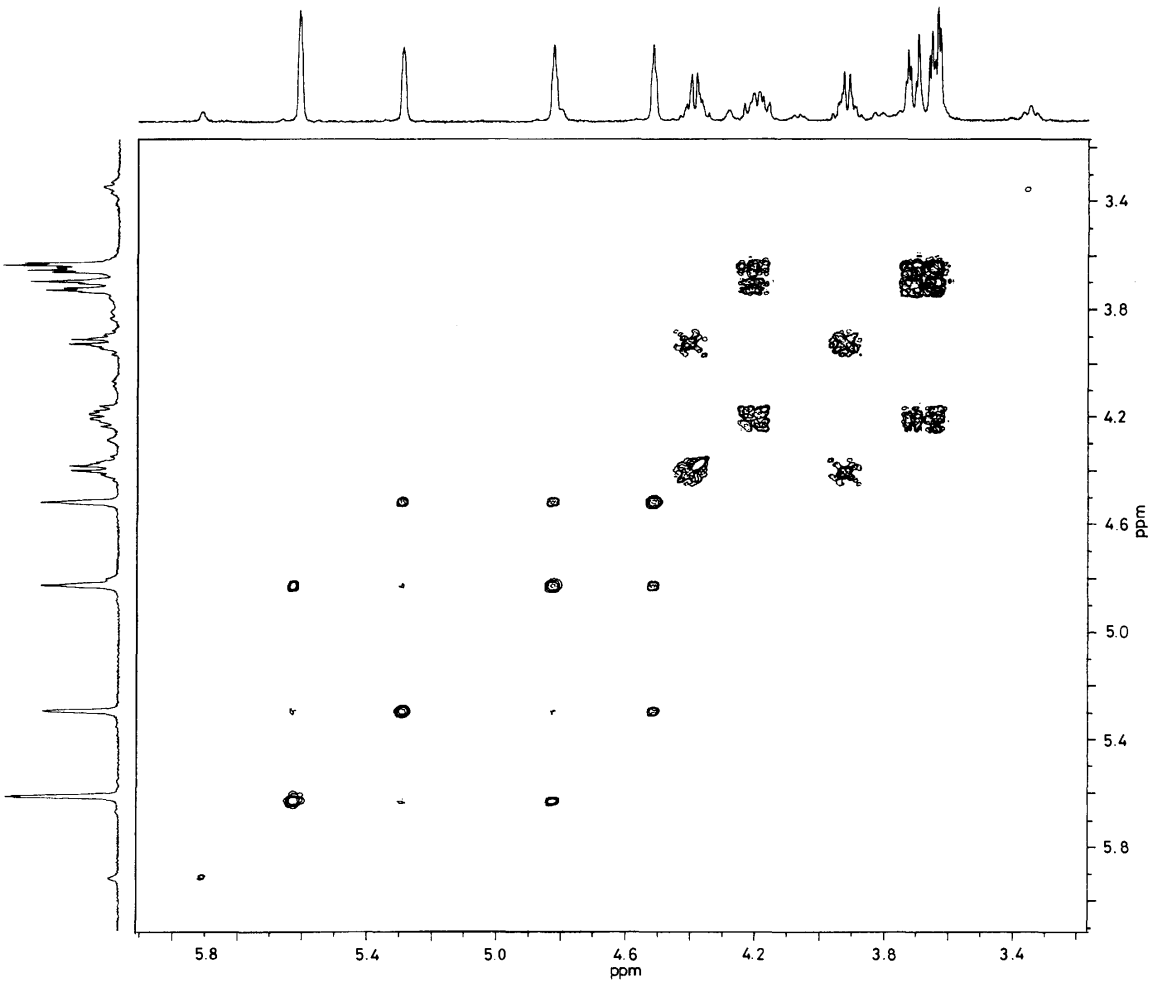

Fig. 1. The H,H-COSY spectrum of the complex **3a**.

of the flipping is, therefore, supposed to be controlled by the rate of S-inversion. The chemical shift of the α- and β-protons of the Cp rings in the ^{1}H NMR spectrum of **3d** is fairly similar to that of **5**.[16] In the latter, the large low-field shift of the α-protons was suggested to be due to a magnetic anisotropy or an inductive effect of the metal halide.[16] A similarity between the complexes **3d** and **5** is also seen in the chemical shift of the ferrocenyl ring carbons in the ^{13}C NMR spectra.

On the other hand, the ^{1}H NMR spectrum of **3a** was static, even at room temperature; moreover, it showed the presence of two isomers in the complex. The isomer ratio of two isomers is established from the integration ratio of the Cp ring proton signals to be about 6:1. In the ^{1}H NMR spectrum of **3a**, the major isomer showed signals of the Cp-ring protons at δ 5.62, 5.29, 4.82, and 4.51. The assignment of these signals to the α- and β-protons of the Cp-rings was successfully performed by the 2D H,H-COSY measurement (Fig. 1). The signals at δ 4.82 and 4.51 correlated intensively with each other and further with the signals at δ 5.62 and 5.29, respectively. This is a clear evidence that the signals at 4.82 and 4.51 can be assigned to the β-protons of the ferrocenyl ring. The remaining signals at 5.62 and 5.29 correspond to the α-protons of the ferrocenyl ring. Thus, the H,H-COSY technique is a more superior method for the assignment of the ferrocenyl ring protons than the *D*-labeling method,[18] if the ring protons are in unsymmetrical circumstances. Here, in order to make a brief explanation, we have tentatively labeled the protons which resonated at δ 5.61, 4.82, 4.52, and 5.28 as H(α), H(β), H(β'), and H(α') atoms, respectively, on the basis of the H,H-COSY experiment. Interestingly, the chemical shifts of the H(α) and H(β) atoms are in a lower field than those of the H(α') and H(β') atoms, especially the signals of the H(α) atom being at a considerably low field (δ 5.61). The difference of the chemical shifts between the H(α) and H(α') atoms ($\Delta\delta$ 0.33 ppm) is fairly large compared with that in **3d**. This is in good agreement with the adoption of the stepped conformation in **3a**. At the same time, the low-field shift of the H(α) signal seems likely to be explained by the anisotropy of the

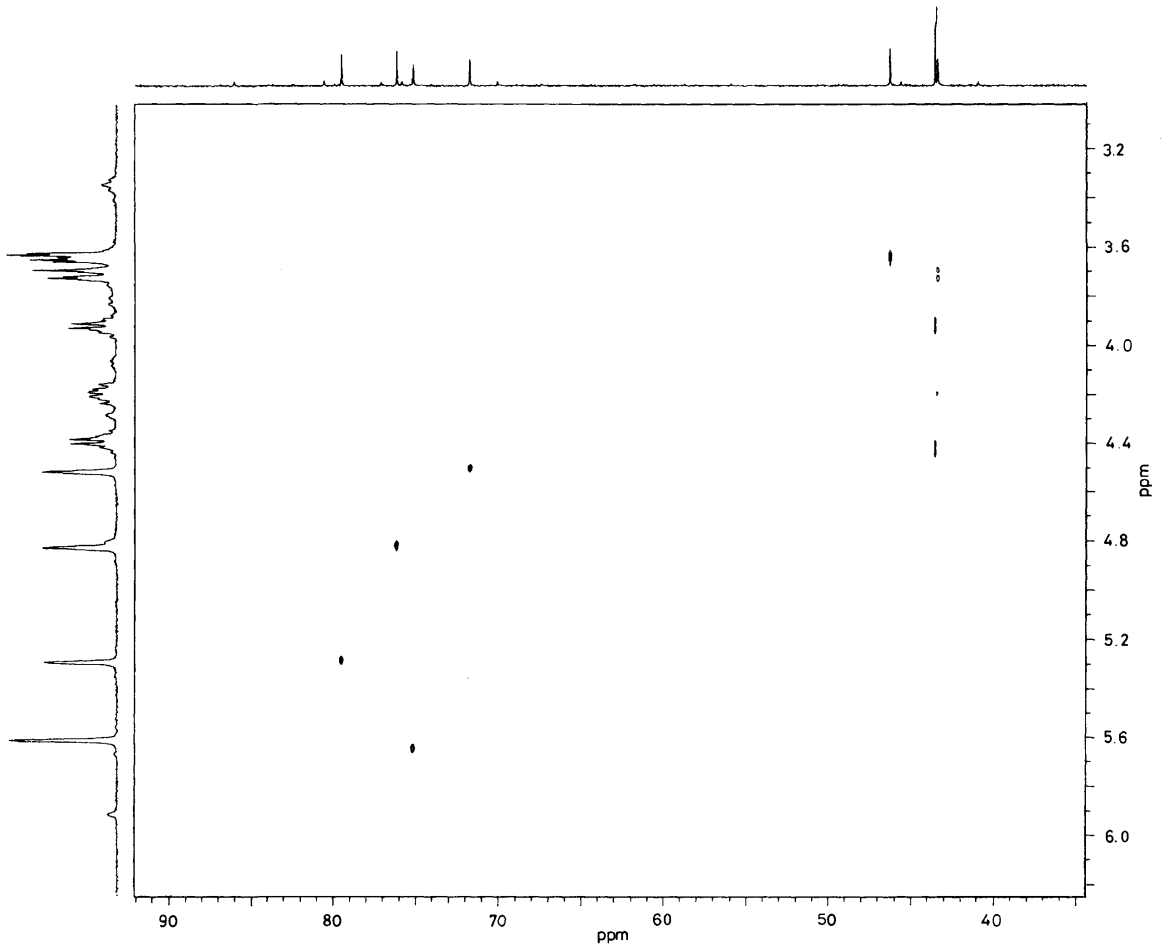

Fig. 2. The C,H-COSY spectrum of the complex **3a**.

lone pair of the sulfur atom connected to the Cp-rings, since the lone pair of the sulfur atom is placed nearly parallel to the H(α) atom on the basis of the molecular model of **3a**. The assignment of the ferrocenyl ring carbons in the major isomer of **3a** was accomplished by the C,H-COSY experiment (Fig. 2). The carbon signals at δ 79.51 and 75.16 correlated to the α-proton signals at δ 5.28 and 5.61, respectively. The carbon signals at δ 76.17 and 71.74 showed good correlation to the β-proton signals at δ 4.82 and 4.52, respectively. Using the labelling described above, the carbon signals at δ 75.16, 76.17, 71.74, and 79.51 were assigned to the C(α), C(β), C(α'), and C(β') atoms, respectively. It is interseting that the lowest field signal in the ^{13}C NMR spectrum of the major isomer of **3a** is the signal of the C(α') atom, while the signals of the H(α) atom appear at lowest field in the ^{1}H NMR spectrum. This may suggest that a certain interaction due to the metal atom incorporated in the thiamacrocycle exerts an influence on the ferrocenyl ring carbons.

The ^{1}H NMR spectra of **3b** and **3c** were broadened at room temperature, similarly to that of **3d**. The static spectrum of **3b** was obtained at 0 °C, and showed the presence of two isomers, as can be seen in the case of complex **3a** (Table 1). The ratio of the major to minor isomers was estimated from the integration ratio of the signals at δ 4.27 and 4.39 to be ca. 2.2 for **3b**. The averaging process of the proton signals in **3b** on warming was very complex because of the presence of two isomers; **3b** gave no completely averaged spectra, even on warming at 80 °C. The dynamic behavior of the ^{1}H NMR spectrum dependent on the temperature was further complicated for complex **3c**. Two pseudo singlets for the Cp-ring protons of **3c** were observed at δ 5.14 and 4.65 at 80 °C. However, even on cooling at −40 °C (limiting low temperature for acetonitrile) no static spectrum was obtained, although the ^{13}C NMR spectrum of **3c** at −40 °C gave a definite spectrum only for the major isomer (Table 2). Judging from the temperature affording the static spectrum and the spectrum at 80 °C, the flipping motion of the thiamacrocycle moiety coordinating the Pd(II) atom increases in the following order: **3a**<**3b**<**3d**$\lesssim$**3c**, the order being in accord with the increase of the ring size in the thiamacrocycle. It is worthy to note that this order is also consistent with that of the decrease of the Fe(II)–Pd(II) interaction obtained from the IR study. Therefore, we feel justified in assuming that the

interaction between the iron atom of the ferrocene moiety and the Pd(II) atom incorporated in the thiamacrocycle may lock the flipping motion of the thiamacrocycle moiety towards the ferrocenyl part in the complexes **3a—3d**. The chemical shift of the bridge-head carbon of ferrocenyl rings of the series **3a—3d** was shifted down-field from δ 75.17 in **3d** to δ 86.05 in **3a** according to the decrease in the size of the thiamacrocycle, although the other ring carbons were little changed. This seems unlikely to be due to a conjugate interaction between the sulfur lone pair and the π-orbital of the ferrocenyl rings, since there was observed no significant difference in the chemical shift between a flexible molecule at 80 °C (δ 75.56) and a fixed molecule at −30 °C (δ 75.17) in **3d**. This down-field shift (described above) probably stems from the change in the coordination mode of a Pd(II) atom to the thiamacrocycle part (vide infra).

It was proven by X-ray analysis[13] that complex **3d** had a stepped conformation and that the Pd(II) atom was located in the center of a square planar consisting of four sulfur atoms of the thiamacrocycle moiety. This is consistent with the ^{1}H and ^{13}C NMR spectra of complex **3d** in solution at −30 °C. On the other hand, the NMR data of complexes **3a—3c** showed the presence of two isomers at low temperature. We suppose that the Pd(II) atom in the complexes can not fit sufficiently in the center of the cavity of the thiamacrocycle moiety, because of the small size of the cavity, contrary to complex **3d**. Consequently, the Pd(II) atoms in the complexes **3a—3c** deviate up or down from the plane of the thiamacrocycle moiety, resulting in two isomers. Although the structure of the major and minor isomers is not decided from the ^{1}H and ^{13}C NMR spectral data, a consideration of the steric hindrance between the Pd(II) atom coordinated to the sulfur atoms in the thiamacrocycle and the α-protons of the ferrocene ring leads to the assignment of the major isomers to a configuration that the Pd(II) atom is deviated to the outer side of the plane of the thiamacrocycle away from the ferrocene moiety (**3B**).

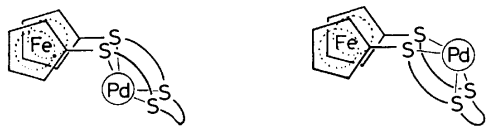

3A 3B

In the minor isomers of **3a—3c**, the decrease of the size of the thiamacrocycle increases the steric hindrance (described above), and at the same time increases the deviation of the Pd(II) atom from the plane consisting of the four sulfur atoms in the thiamacrocycle moiety. The latter change may shrink somewhat the distance between the Pd(II) atom and the iron atom of the ferrocene moiety, and may increase an interaction between both metals (**3A**). This suggestion appears to be supported by the behavior of the electronic spectra.

The electronic spectrum of **3d** showed broad and weak absorption at 572 nm (ε 113), as well as intensive absorptions at 330 sh (15700) and 296 nm (ε 17000). The free ligand **1d** showed an absorption maximum at 443 nm (ε 190), while the $Pd(BF_4)_2$ complex with the open-chain tetrakis(thioether), 2,6,10,14-tetrathiapentadecane, which is considered to have a square-planar coordination, showed no absorption above 370 nm.[9] Furthermore, the Pd(II) complex of 7,16-dimethyl-1,4,10,13-tetrathia-7,16-diazacyclooctadecane, which contains square-planar configuration of the four thioether donor atoms, also showed an absorption only at 373 nm (ε 2175) in the region above 300 nm,[19,20] although weak absorption at 620 nm (ε 55) was observed in bis(1,4,7-trithiacyclononane)palladium(II) tetrafluoroborate, which was confirmed by X-ray analysis to contain a weak interaction between the Pd(II) atom and the apical thioether donor atom.[21,22] We suppose, therefore, that the absorption band at 572 nm observed in complex **3d** may be concerned with an interaction between the iron atom of the ferrocene nucleus and the Pd(II) atom incorporated into the thiamacrocycle moiety. The absorption at 572 nm showed a bathochromic shift and an increase in absorbance according to the decreasing size of the thiamacrocycle in the series **3a—3d**: **3d**, 572 (ε 113) <**3c**, 604 (376) <**3b**, 612 (245) <**3a**, 670 (499). As mentioned above, the distance between the Pd(II) atom incorporated in the thiamacrocycle moiety and the iron atom of the ferrocene ring decrease potentially according to the size of the thiamacrocycle through series **3a—3d**. The observed bathochromic shift, therefore, may be due to an increasing Fe-Pd interaction in the complexes. However, we cannot rule out the possibility that the shift stems from an increasing deviation of the Pd(II) atom from the thiamacrocycle plane because the hole size is insufficient for a good fit.

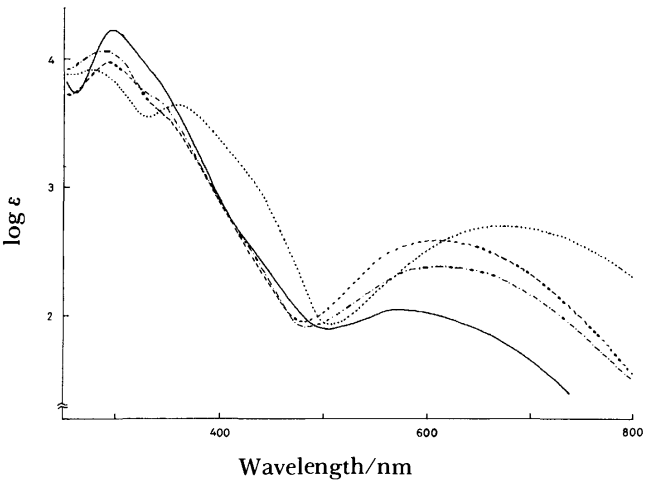

Fig. 3. The electronic spectra of the complex **3a** (·····), **3b** (—·—·), **3c** (----), and **3d** (—).

Finally, we reported the preparation of the $Pd(BF_4)_2$ complexes of 1,5,9-trithia[9]- and 1,4,7-trithia[7](1,1′)-ferrocenophanes.[7,23] In these complexes, a bonding interaction between the Fe atom of the ferrocene nucleus and the Pd(II) atom incorporated into the thiamacrocycle is confirmed by the spectroscopic data. The complexes are rigid, even at high temperature, in contrast with complexes **3b—3d** and showed a greater frequency of out-of-plane bending than that of complexes **3a—3d**. The rigidness of the molecule and the high out-of-plane bending vibration are considered to stem from the presence of the Fe–Pd dative bond in these complexes. From a comparison with these results, it is clear that these is no bonding interaction but, rather, a certain (probably charge-transfer type of) interaction in the present complexes of the tetrathia[*n*](1,1′)ferrocenophanes; the interaction is controlled by the size of the thiamacrocycle moiety.

Experimental

The IR spectra were taken on a Hitachi 270—50 Infrared Spectrometer. The ^1H and ^{13}C NMR spectra were measured on a Bruker AM400 Spectrometer, TMS being chosen as the standard material. The electronic spectra were taken on a Shimadzu UV2100 Spectrometer.

Tetrathia[*n*]ferrocenophanes were prepared as described in a previous paper.[3] Dichlorobis(acetonitrile)palladium-(II) was prepared according to a method from the literature.[9]

(1,4,7,10-Tetrathia[10]ferrocenophane)palladium(II) Tetrafluoroborate (3a). General Procedure. Dichlorobis(acetonitrile)palladium(II) (26 mg, 0.1 mmol) was added to a solution of silver tetrafluoroborate (40 mg, 0.2 mmol) in acetone (5 cm^3). The solution was refluxed for 1 h. The resulting precipitates (AgCl) were filtered off and the filtrate was evaporated under reduced pressure. To a solution of the residue in acetonitrile (2 cm^3) was added a solution of 1,4,7,10-tetrathia[*n*]ferrocenophane (**1a**) (40 mg, 0.1 mmol) in acetonitrile (5 cm^3). The resulting green solution was diluted with anhyd diethyl ether (16 cm^3). The solution was kept overnight in refrigerator. Filtration gave dark green plates, mp ca. 180 °C (decomp). Found: C, 28.71; H, 3.11%. Calcd for $C_{16}H_{20}B_2F_8S_4FePd$: C, 28.41; H, 2.98%.

(1,4,8,11-Tetrathia[11]ferrocenophane)palladium(II) Tetrafluoroborate (3b). Blue black crystals, mp ca. 115 °C (decomp). Found: C, 31.30; H, 3.50; N, 1.95%. Calcd for $C_{17}H_{22}B_2F_8S_4FePd \cdot CH_3CN$: C, 31.20; H, 3.44; N, 1.95%.

(1,5,8,12-Tetrathia[12]ferrocenophane)palladium(II) Tetrafluoroborate (3c). Blue black crystals, mp ca. 195 °C (decomp). Found: C, 30.97; H, 3.45%. Calcd for $C_{18}H_{24}B_2F_8S_4FePd$: C, 30.69; H, 3.43%.

(1,5,9,13-Tetrathia[13]ferrocenophane)palladium(II) Tetrafluoroborate (3d). Blue black needles, mp 250 °C. Found: C, 32.02; H, 3.81%. Calcd for $C_{19}H_{26}B_2F_8S_4FePd$: C, 31.76; H, 3.65%.

References

1) M. I. Bruce, *J. Organomet. Chem.*, **242**, 147 (1983); **283**, 339 (1985).

2) G. L. Geoffroy and D. A. Roberts, "Comprehensive Organometallic Chemistry," ed by G. Wilkinson, F. G. A. Stone, and E. W. Abel, Pergamon Press, Oxford (1982), Chap. 40.

3) M. Sato, H. Watanabe, S. Ebine, and S. Akabori, *Chem. Lett.*, **1982**, 1753: M. Sato, S. Tanaka, S. Ebine, and S. Akabori, *Bull. Chem. Soc. Jpn.*, **57**, 1929 (1984).

4) M. Sato, S. Tanaka, S. Akabori, and Y. Habata, *Bull. Chem. Soc. Jpn.*, **59**, 1515 (1986).

5) M. Sato, K. Suzuki, and S. Akabori, *Bull. Chem. Soc. Jpn.*, **59**, 3611 (1986).

6) M. Sato, S. Akabori, M. Katada, I. Motoyama, and H. Sano, *Chem. Lett.*, **1987**, 1847.

7) A. Preliminary report: M. Sato, K. Suzuki, and S. Akabori, *Chem. Lett.*, **1987**, 2239.

8) L. S. Hegedus, T. A. Mulhern, and H. Asada, *J. Am. Chem. Soc.*, **108**, 6224 (1986).

9) F. R. Hartley, S. G. Murry, and C. A. McAuliffe, *Inorg. Chem.*, **18**, 1394 (1979).

10) J. A. Kramer and D. N. Hendrickson, *Inorg. Chem.*, **19**, 3330 (1980).

11) D. Seyferth, B. W. Hames, T. G. Rucker, M. Cowie, and R. S. Dickson, *Organometallics*, **2**, 472 (1983).

12) J. J. Bishop and A. Davison, *Inorg. Chem.*, **10**, 826 (1971).

13) N. Won, K. Iwai, M. Katada, H. Sano, M. Sato, and S. Akabori, in preparation.

14) A. Davison and J. C. Smart, *J. Organomet. Chem.*, **174**, 321 (1978).

15) E. W. Abel, M. Booth, and K. G. Orrell, *J. Organomet. Chem.*, **208**, 213 (1981).

16) B. McCulloch, D. L. Ward, J. D. Woolins, and C. H. Brubaker, Jr., *Organometallics*, **4**, 1425 (1985).

17) K. G. Orrell, V. Sik, C. H. Brubaker, and B. McCulloch, *J. Organomet. Chem.*, **276**, 267 (1984).

18) D. W. Slocum and C. R. Ernst, *Tetrahedron Lett.*, **1972**, 5217, and the literature therein.

19) G. Reid, A. J. Blake, T. I. Hyde, and M. Schröder, *J. Chem. Soc., Chem. Commun.*, **1988**, 1397.

20) There is also in the literature 22a the description that the $Pd(BF_4)_2$ complex of 1,4,8,11-tetrathiacyclotetradecane shows no absorption near 600 nm.

21) K. Wieghardt, H.-J. Küppers, E. Raabe, and C. Kruger, *Angew. Chem., Int. Ed. Engl.*, **25**, 1101 (1986).

22) a) A. J. Blake, A. J. Holder, T. I. Hyde, Y. V. Roberts, A. J. Lavery, and M. Schröder, *J. Organomet. Chem.*, **323**, 261 (1987): b) A. J. Blake, A. J. Holder, T. I. Hyde, and M. Schröder, *J. Chem. Soc., Chem. Commun.*, **1987**, 987.

23) M. Sato, H. Asano, K. Suzuki, M. Katada, and S. Akabori, *Bull. Chem. Soc. Jpn.*, to be submitted.

 © 1989 The Chemical Society of Japan Bull. Chem. Soc. Jpn., 62, 3498—3507 (1989) [Vol. 62, No. 11

Synthesis and Spectroscopic Investigation of Directly Conjugated Polyyne Porphyrins

Kazuhiro MARUYAMA* and Shigeki KAWABATA
Department of Chemistry, Faculty of Science, Kyoto University, Kyoto 606
(Received May 29, 1989)

A series of conjugated polyyne porphyrin, in which porphyrin macrocycle is directly connected with one end of diarylpolyyne through aromatic ring, has been prepared and their spectroscopic behaviors were investigated. Diarylpolyynes consisting of aryl group and conjugated triple bond system have rigid and linear structure, and the two chromophores are held at a fixed geometry and a determined distance. The UV-vis absorption spectra of these compounds showed strong conjugative interaction, showing broadening of their spectra and slightly red shifted porphyrin Soret bands with increasing the number of acetylenic bond. From their fluorescence excitation spectra energy transfer efficiencies from polyyne moiety to porphyrin moiety were estimated. The energy transfer efficiencies were almost unity regardless of their substituted position, geometry, and orientation.

In the primary process of natural green plant photosynthesis, energy and/or electron donor and acceptor are held at appropriate distance, geometry and orientation and highly effective energy transfer together with charge separation is achieved in these systems. The X-ray analysis of a bacterial photosynthetic reaction center from Rhodopseudomonas viridis[1] clarified an excellent geometrical arrangement of related pigments. Distance, geometry, and orientation have been recognized more importantly to control the efficiency of energy and electron transfer process. In addition, the environment such as polypeptide, residue of amino acid, π-conjugated system, and long-chain hydrocarbon surrounding the prosthetic molecules has a crucial role for electron transport system as the intervening medium. In order to elucidate the meanings of each factor definitely, it is necessary to construct the model systems of rigidly fixed structure, geometry and orientation. In recent years numerous model systems have been investigated by many investigators in different laboratories.[2-15]

We have synthesized a series of directly conjugated polyyne porphyrins, in which porphyrin macrocycle is directly connected with one end of diarylpolyyne through meso-aromatic ring and investigated the interaction between porphyrin and π-conjugated triple bond system. Since diarylpolyynes have rigid and linear structure, two chromophores are held at a fixed geometry. Changing the substituted position of polyyne, three types of polyyne porphyrin have been synthesized. Increasing the number of conjugated triple bond, distance between both ends of diarylpolyyne can be altered systematically.

Gust et al.[7] had already prepared a variety of carotenoporphyrin and investigated the interaction between porphyrin and carotenoid polyenes, which have typical conjugated double bond system. They revealed that the geometry and distance between them much affected the efficiency of energy transfer. Especially, close proximity is the most important factor of efficient energy transfer.

In our case, energy transfer from polyyne to porphyrin had been also observed. However, the efficiency of energy transfer is almost unity regardless of their substituted position, geometry, and orientation. Strong interaction between polyyne and porphyrin through direct conjugation have been observed with electronic absorption spectra. The excitation energy absorbed by polyyne was efficiently transferred to porphyrin and then porphyrin fluoresced. On the other hand, in the polyyne porphyrin systems in which the two chromophores were connected through ester linkage indirectly, energy transfer efficiency was dependent upon substituted position.

In this report, we will describe detailed synthetic methods of a series of polyyne porphyrins together with characterization of synthesized compounds, and strong interaction through conjugation is discussed.

Results and Discussion

Synthesis. The synthetic route of diarylpolyynes is shown in Scheme 1. Ortho (a series), meta (b series), and para (c series) methoxymethoxymethylbenzaldehydes **1** were used as starting materials, respectively. Most of synthetic method of diarylpolyynes were based on a method reported by Armitage et al.[16] and Akiyama et al.,[17] but in some cases their methods were suitably modified.[18,19] Yields in almost all the reactions were satisfactorily high in each series. Methoxymethyl group was a good protective group of the hydroxyl group under these conditions. In these manners, each series of diarylbutadiynes ($\mathbf{Y}_2$), diarylhexatriynes ($\mathbf{Y}_3$), and diaryloctatetraynes ($\mathbf{Y}_4$) were obtained and recrystallized from ethanol. These compounds were characterized by ^{1}H NMR, IR (Table 1), and mass spectroscopy. Diarylhexatriynes and diaryloctatetraynes are heat- and light-sensitive. They gradually polymerize to give insoluble blue and green colored compounds, respectively.

These synthetic diarylpolyynes ($\mathbf{Y}_n$) were converted into polyyne porphyrins ($\mathbf{P}_n$) according to the reaction Scheme 2. Deprotection by acid hydrolysis and oxi-

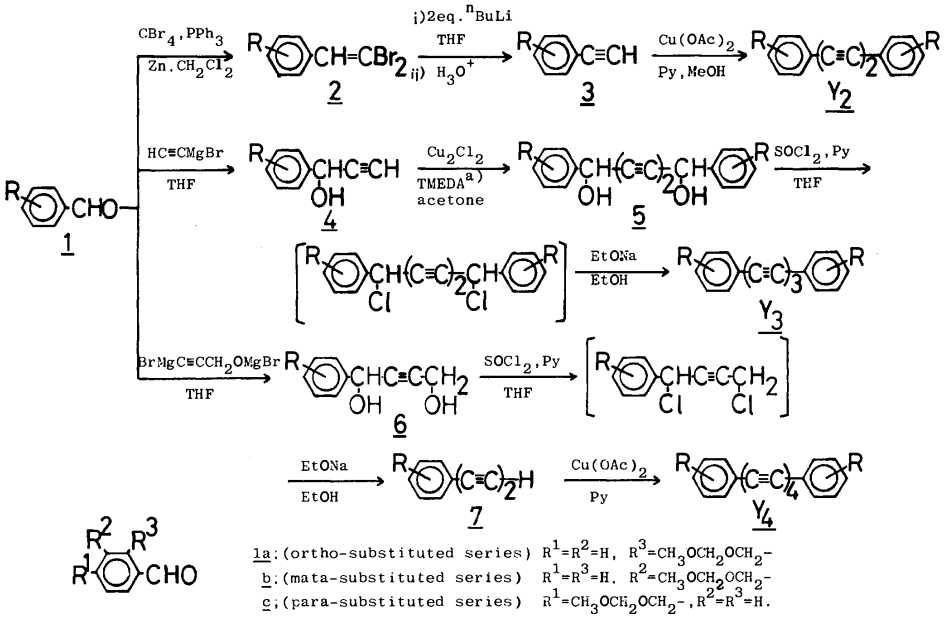

Scheme 1. Synthesis of diarylpolyynes. a) TMEDA: tetramethylethylenediamine.

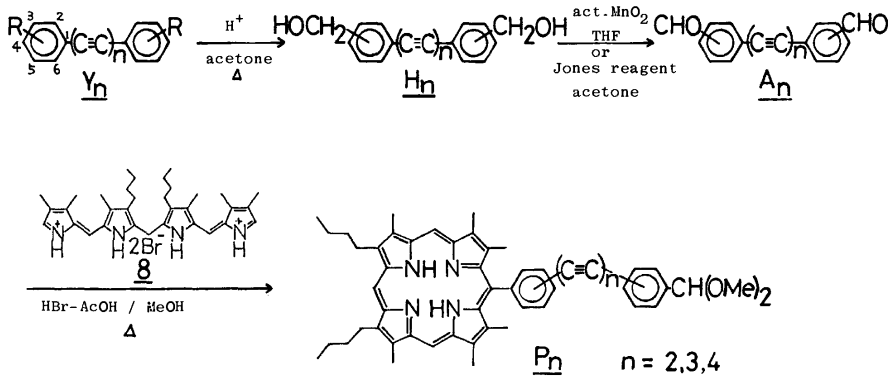

Scheme 2. Synthesis of directly conjugated polyyne porphyrins.

dation with active MnO_2,[20] in some cases with Jones reagent,[21] gave diarylpolyyne dicarbaldehydes ($\mathbf{A}_n$) in satisfactory yields. Melting points, yields, and other spectral data are shown in Table 1. In the dark diarylpolyynes are relatively stable under acidic conditions. The desired conformationally restricted polyyne porphyrins conjugated directly ($\mathbf{P}_n$) could be synthesized by the acid-catalyzed condensation reaction[22] of the corresponding ac-biladiene (**8**)[23] and diarylpolyyne dicarbaldehydes ($\mathbf{A}_n$) in reasonable yields (Table 2). The yields of ortho-substituted polyyne porphyrins were slightly low because of the steric hindrance. Double condensation products of both ends, polyyne porphyrin dimers,[24] could not be produced under these conditions. All these synthesized polyyne porphyrins were recrystallized from dichloromethane-methanol.

Characterization. The structures of directly conjugated polyyne porphyrins are shown in Fig. 1 and melting points, IR, ^{1}H NMR spectral data are shown in Tables 2 and 3. By applying fast-atom-bombardment mass spectrometry to these polyyne porphyrins only characteristic peaks corresponding to the expected $M^+ + nH$ (n=0—4) ions were observed. One end of diarylpolyyne was directly connected with the meso position of porphyrin macrocycle and at the other end aldehyde group was converted into dimethyl acetal group. This dimethyl acetal group was held at fixed geometry toward porphyrin ring, because diarylpolyynes had rigid and linear structure. Especially, in ortho-substituted series its methyl and methine proton were held just on the porphyrin plane and showed upfield shift ($\Delta\delta$=1.2—1.5 ppm) in the ^{1}H NMR spectrum due to the ring current. This upfield shift increases with decreasing the number of acetylenic bond. In para-substituted series dimethyl acetal group

Table 1. Melting Points, Yields of Preparation, ^{1}H NMR Chemical Shift in $CDCl_3$ Solution, and Infrared Spectral Data of Diarylpolyynes

Compd	Mp/°C	Yield/%[a]	Chemical shift δ/ppm								IR/cm^{-1}[e]						
			Aryl					Other protons									
			H2	H6	H3	H5	H4										
								$CH_3OCH_2OCH_2$-				$\nu_{C\equiv C}$					
Y_{2a}	Oil	68	—	7.55	7.50	7.38	7.27	3.46	4.79	4.79	2820—3020	2230,2150	1160	1120	1050	760	
Y_{3a}	60—61	51	—	7.54	7.49	7.40	7.27	3.44	4.77	4.75	2820—2980	2205	1160	1115	1060	760	
Y_{4a}	72—73	15	—	7.55	7.48	7.41	7.27	3.44	4.76	4.74	2890,2940	2210,2160	1155	1110	1055	760	
Y_{2b}	Oil	55	7.51	7.44	—	7.30—7.36		3.41	4.70	4.57	2820—3100	2240,2160	1160	1110	1050	790	690
Y_{3b}	Oil	42	7.54	7.46	—	7.30—7.38		3.40	4.70	4.56	2780—3080	2210	1160	1110	1060	790	690
Y_{4b}	68—72	7	7.54	7.46	—	7.32	7.39	3.40	4.70	4.56	2900,2960	2220	1155	1100	1050	795	700
Y_{2c}	58—60	Quant.	7.62		7.40		—	3.44	4.70	4.60	2800—3000	2145	1170	1120	1070	830	
Y_{3c}	113—114	59	7.57		7.37		—	3.43	4.72	4.62	2760—2960	2200	1150	1110	1050	810	
Y_{4c}	275(decomp)[b]	9	7.52		7.32		—	3.40	4.70	4.59	2950	2210	1150	1115	1050	815	
								-CH_2OH			ν_{O-H}	$\nu_{C\equiv C}$					
H_{2a}	176	70	—	7.55	7.50	7.40	7.28	4.89		1.93	3100—3500	d)	1060		750		
H_{3a}	200—203	Quant.	—	7.55	7.50	7.42	7.25—7.27	4.86		1.88	3160—3500	2210	1050		760		
H_{4a}	193—195	98	—	7.55	7.51	7.42	7.25—7.28	4.86		c)	3090—3480	2220	1050		760		
H_{2b}	149—151	54	7.53	7.45	—	7.31—7.37		4.69		1.67	3100—3480	2140	1050	1020	790	690	
H_{3b}	130	95	7.54	7.46	—	7.33	7.39	4.69		1.68	3100—3400	2210	1050	1020	790	690	
H_{4b}	120—121	90	7.54	7.46	—	7.33	7.40	4.68		1.73	3120—3440	2220	1050		800	690	
H_{2c}	230(decomp)	60	7.52		7.34		—	4.71		c)	3100—3500	2210,2145	1050	1025	820		
H_{3c}	>290	Quant.	7.52		7.34		—	4.72		1.69	3100—3400	2200	1040	1020	820		
H_{4c}	>300	84	7.55		7.40		—	4.66		c)	3100—3400	2205	1050	1015	800		
								CHO			$\nu_{C\equiv C}$	$\nu_{C=O}$					
A_{2a}	171—172	62	—	7.68	7.95	7.52	7.60	10.51			2205	1700 1590	1270	1210	760		
A_{3a}	211—213(decomp)	37	—	7.68	7.95	7.53	7.59	10.45			2205	1705 1590	1270	1200	760		
A_{4a}	180(decomp)	58(87)	—	7.68	7.94	7.52—7.61		10.43			2210	1700 1590	1265	1200	760		
A_{2b}	176—177	57(88)	8.03	7.77	—	7.53	7.89	10.00			d)	1710 1580	1250	1160	800	770	680
A_{3b}	162(decomp)	86	8.03	7.77	—	7.53	7.90	9.99			2220	1710 1580	1205	1170	800	745	680
A_{4b}	180(decomp)	51	8.03	7.77	—	7.53	7.91	9.99			2210	1710 1580	1180	1170	800	725	680
A_{2c}	260—261	36(54)	7.68		7.87		—	10.03			2200	1700 1600	1170		825		
A_{3c}	240(decomp)	40	7.69		7.86		—	10.02			2200	1700 1600	1170		830		
A_{4c}	184(decomp)	96	7.68		7.85		—	10.02			2210	1700 1600	1170		830		

a) In parentheses, yields of Jones oxidation. b) Gradually polymerized at lower temperature. c) Not determined. d) Weak, not determined. e) KBr, but in the cases Y_{2a}, Y_{2b}, and Y_{3b} NaCl.

Table 2. Yields, Melting Points, and Infrared Spectral Data of Polyyne Porphyrins

Compd	Yield/%	Mp/°C	IR/cm^{-1} (KBr)					
$\mathbf{P}_{2a}$	5.8	263—264	2840—3000	a)	1460	1140	1060	770
$\mathbf{P}_{3a}$	1.14	>300	2840—3000	2200	1450	1130	1060	760
$\mathbf{P}_{4a}$	<1	>300	2870—3010	2230	1455	1130	1080	740
$\mathbf{P}_{2b}$	18.5	258	2860—3000	a)	1450	1115	1060	750
$\mathbf{P}_{3b}$	6.1	228—231	2860—3000	2220	1450	1120	1065	750
$\mathbf{P}_{4b}$	6.6	>300	2940	2220	1440	1115	1060	750
$\mathbf{P}_{2c}$	11.5	>300	2820—2950	a)	1440	1110	1060	750
$\mathbf{P}_{3c}$	15.8	>300	2830—2990	2210	1440	1110	1060	750
$\mathbf{P}_{4c}$	16.7	>300	2800—2980	2210	1445	1110	1060	750

a) Weak, not determined.

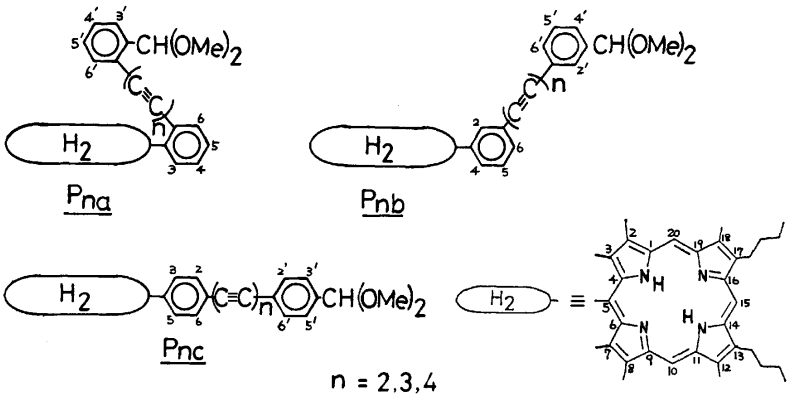

Fig. 1. Directly conjugated polyyne porphyrins.

was so far apart from porphyrin ring that these protons were observed in the lowest field. In the IR spectra a remarkable intensification of the absorption due to $\nu_{C\equiv C}$ with an increase in the number of acetylenic bond was also observed just as in the case of diarylpolyyne.[17] Significant difference, however, was not observed in each substituted series and the number of acetylenic bond. Relatively high melting points and low solubility in organic solvents are similar in ortho- and para-substituted series. Particularly, melting points are low in meta-substituted series.

Absorption and Fluorescence Spectra. The absorption spectra of diarylpolyynes ($\mathbf{Y}_{2c}$—$\mathbf{Y}_{4c}$) and the spectral data of diarylpolyynes ($\mathbf{Y}_n$) are shown in Fig. 2 and Table 4. Diarylpolyynes have vibrational fine structure in their absorption spectra and the novel linear relation between the longest wavelength maxima (λ_{max}) and the number of the acetylenic bond (n) has been found.[25] These synthetic methoxymethoxymethyl-substituted diarylpolyynes have the similar relationship to diphenylpolyyne.[16,25] Absorption maxima and the relationship of each series have not

$$\mathbf{Y}_{na}: \lambda_{max} = 266.0 + 34.0 \times n$$
$$\mathbf{Y}_{nb}: \lambda_{max} = 262.1 + 34.3 \times n$$
$$\mathbf{Y}_{nc}: \lambda_{max} = 266.8 + 33.8 \times n \text{ [26]}$$
$$\text{cf. diphenylpolyyne}: \lambda_{max} = 263.0 + 33.0 \times n \text{ [16,25]}$$

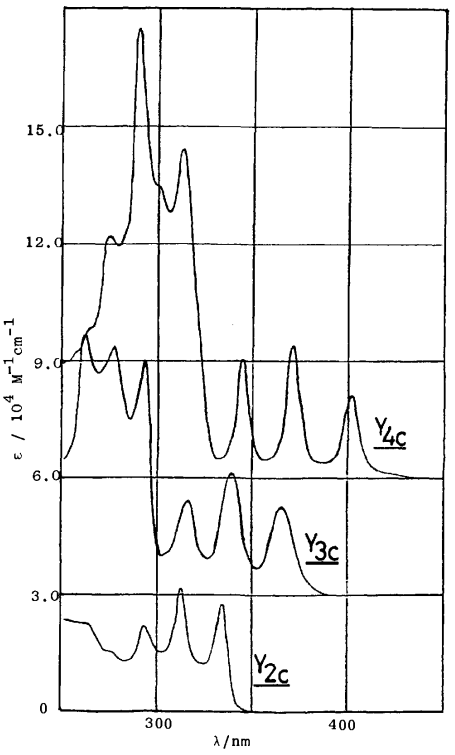

Fig. 2. UV-vis absorption spectra of diarylpolyynes in CH_2Cl_2 solution. Each curve, except for the lowest one, has been displaced upward by 3.0×10^4 ε unit increment from one immediately below it.

Table 3. ^{1}H NMR Chemical Shift of Polyyne Porphyrins in $CDCl_3$ Solution

Compd	Chemical shift δ/ppm																			
	CH_3(pyrrole)			H meso		NH	Meso aryl				Aryl						Dimethyl acetal	
	3,7	2,8	12,18	15	10,20		H2	H6	H3	H5	H4	H2′	H6′	H3′	H5′	H4′	CH	CH_3O
P_{2a}	2.50	3.54	3.61	9.94	10.14	−3.15 −3.32	—	7.97—8.00		7.73	7.80	—	6.75—6.78		6.93—6.99		4.13	1.86
P_{3a}	2.47	3.54	3.62	9.96	10.16	−3.16 −3.31	—	7.93	7.99	7.73	7.79	—	7.02	7.07	7.16	7.30	5.02	2.97
P_{4a}	2.45	3.54	3.63	9.96	10.16	−3.17 −3.31	—	7.94	7.99	7.71—7.81		—	7.43	7.21—7.33		7.12	5.27	3.16
P_{2b}	2.48	3.52	3.63	9.95	10.15	−3.21 −3.34	8.26	7.96	—	7.71	8.07	7.62	7.47	—	7.31	7.43	5.34	3.29
P_{3b}	2.46	3.52	3.62	9.95	10.15	−3.22 −3.35	8.26	7.97	—	7.71	8.09	7.62	7.44 —7.48	—	7.32	7.44 —7.48	5.34	3.29
P_{4b}	2.45	3.52	3.62	9.95	10.15	−3.22 −3.35	8.27	7.98	—	7.72	8.11	7.62	7.47	—	7.32	7.47	5.34	3.29
P_{2c}	2.46	3.52	3.62	9.94	10.14	−3.20 −3.32		7.90		8.03	—		7.62	7.49		—	5.43	3.35
P_{3c}	2.46	3.52	3.62	9.95	10.15	−3.21 −3.33		7.92		8.05	—		7.59	7.46		—	5.42	3.33
P_{4c}	2.45	3.52	3.62	9.95	10.15	−3.21 −3.34		7.92		8.06	—		7.57	7.45		—	5.40	3.32

marked difference. Substitution upon aromatic ring by alkyl group showed little perturbation for the electronic state of diphenylpolyyne. In meta-substituted series (b series), however, slightly blue shift relative to other series was observed.

The absorption curves and electronic spectral data of polyyne porphyrins are shown in Figs. 3 and 4 and Table 5. The absorption spectra in the region above 450 nm were similar to those of reference porphyrin (**9**). Therefore, direct conjugation with polyyne have

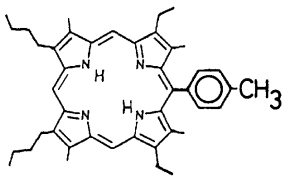

9

little effect upon porphyrin S_1 state. The absorption maxima (λ_{max}) of porphyrin Soret band are slightly red shifted with increasing the number of conjugated acetylenic bond. Especially in para-substituted series (c series) this tendency is remarkable. On the other hand, significant broadening of the vibrational fine structure of diarylpolyyne was observed. Conjugated large porphyrin macrocycle on one end and unsymmetric structure are presumably responsible for these broadening. The absorption maxima were also red shifted. In ortho-substituted series (a series), however, the extinction coefficient of polyyne was greater relative to other series and the vibrational fine structure was somewhat distinguishable. Similar trend was recognized in the case of indirect conjugated compound. Consequently, it is apparent that not only direct conjugation through bond but also close proximity of each component through space have influenced the electronic absorption spectra.

These synthetic directly conjugated polyyne porphyrin have usual fluorescence emission spectra compared to reference porphyrin **9**. Fluorescence emission maxima and total emission intensity were not significantly perturbed by direct conjugation of polyyne. On one hand, it was found that diarylpolyyne could not quench at all the fluorescence of porphyrins in solution. From Table 6 relative emission intensities (I_b/I_a) are different in each series, respectively. Difference in substituted position was presumed to alter the overlap of 0–0 and 0–1 band.

Energy Transfer. Figure 5 shows the uncorrected fluorescence excitation spectra of directly conjugated polyyne porphyrins ($\mathbf{P_4}$). Assuming that the difference between the absorption spectra of polyyne porphyrin and those of reference porphyrin **9** was the excitation energy absorbed by polyyne, energy transfer efficiency from polyyne to porphyrin could be evaluated from the difference between absorption spectra and fluorescence excitation spectra. These values are shown in

Table 4. UV Vis Spectral Data of Diarylpolyynes

Compd	λ_{max}/nm ($\varepsilon/10^3$ M^{-1} cm^{-1})[a]				
Y_{2a}			296.0(23)	313.5(31)	335.0(27)
Y_{2b}			292.0(22)	310.0(31)	331.5(28)
Y_{2c}			294.5(22)	313.0(31)	335.0(27.8)
Y_{3a}	275.0(63)	290.5(52)	317.5(25)	340.0(31)	366.0(21)
Y_{3b}	270.5(62)	287.0(52)	314.5(24)	337.0(31)	363.0(22)
Y_{3c}	277.0(62)	293.5(59)	317.0(23.9)	340.0(31.2)	366.5(21.9)
Y_{4a}	290.5(115)	313.5(82)	346.0(30)	372.5(34)	403.0(21)
Y_{4b}	288.5(121)	310.5(88)	344.0(31)	370.0(34)	400.0(20)
Y_{4c}	290.0(115)	314.0(85.9)	346.0(30.0)	372.0(34.2)	402.5(22.4)

a) 1 M=1 mol dm^{-3}.

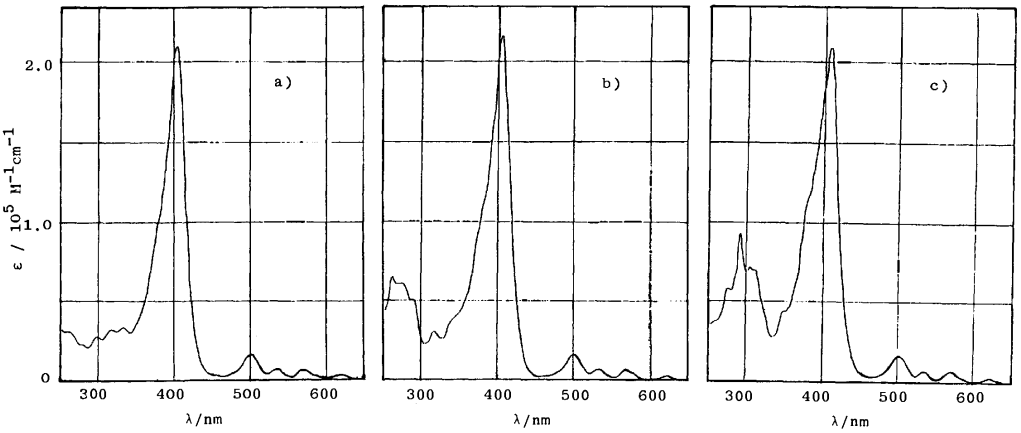

Fig. 3. UV-vis absorption spectra of directly conjugated polyyne porphyrins. a) P_{2c}, b) P_{3c}, c) P_{4c}.

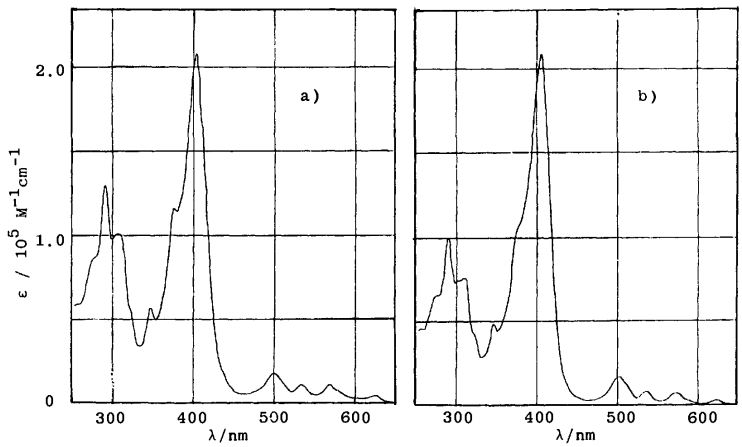

Fig. 4. UV-vis absorption spectra of directly conjugated polyyne porphyrins. a) P_{4a}, b) P_{4b}.

Table 7. Although a little error originating from correction of the fluorescence excitation spectra could not be excluded, energy transfer efficiencies were estimated to be almost unity. Substituted position, distance, and orientation did not affect energy transfer efficiency. Considering the facts that energy transfer had not been observed in a mixed dichloromethane solution of diarylpolyyne and porphyrin and that diarylpolyyne did not fluoresce, this energy transfer mechanism might be intramolecular singlet-singlet energy transfer or internal conversion from polyyne to porphyrin S_1 state through direct conjugation.

For comparison, indirectly conjugated polyyne porphyrins with ester linkage were synthesized (Fig.

Table 5. UV Vis Absorption Spectral Data of Directly Conjugated Polyyne Porphyrins

Compd	λ_{max}/nm (log[ε/M^{-1} cm^{-1}])							
9				403.0(5.32)	502(4.25)	535(3.90)	570(3.87)	623(3.39)
$\mathbf{P_{2a}}$		318(4.6)	337(4.7)	405.7(5.3)	502(4.3)	537(4.0)	572(3.9)	625(3.6)
$\mathbf{P_{2b}}$		313(4.6)	332(4.6)	403.7(5.3)	502(4.3)	537(3.9)	572(3.9)	625(3.5)
$\mathbf{P_{2c}}$		317(4.5)	334(4.5)	404.3(5.3)	502(4.3)	536(3.9)	572(3.9)	624(3.4)
$\mathbf{P_{3a}}$	262(4.9)	319(4.6)	344(4.7)	406.4(5.3)	502(4.3)	537(4.0)	573(3.9)	624(3.6)
$\mathbf{P_{3b}}$	260(4.9)	316(4.5)	340(4.7)	404.6(5.3)	502(4.3)	537(3.9)	571(3.9)	623(3.3)
$\mathbf{P_{3c}}$	263(4.8)	318(4.5)	sh.[a]	405.4(5.3)	502(4.3)	537(3.9)	571(3.9)	624(3.4)
$\mathbf{P_{4a}}$	291(5.1)	348(4.7)	375(5.0)	405.0(5.3)	502(4.3)	537(4.0)	571(4.0)	625(3.6)
$\mathbf{P_{4b}}$	289(5.0)	345(4.7)	sh.	405.9(5.3)	502(4.3)	537(3.9)	571(3.9)	624(3.5)
$\mathbf{P_{4c}}$	291(5.0)	sh.	sh.	407.0(5.3)	503(4.3)	536(3.9)	570(3.9)	624(3.4)

a) sh.; shoulder,

Table 6. Fluorescence Emission Spectral Data of Directly Conjugated Polyyne Porphyrins

Compd	$\lambda_{Em\ max}$/nm a; Q (0-0)	b; Q (0-1)	I_b/I_a
9	625	689	0.72
$\mathbf{P_{2a}}$	626	692	0.53
$\mathbf{P_{2b}}$	625	691	0.64
$\mathbf{P_{2c}}$	625	692	0.70
$\mathbf{P_{3a}}$	625	691	0.53
$\mathbf{P_{3b}}$	624	691	0.61
$\mathbf{P_{3c}}$	624	691	0.72
$\mathbf{P_{4a}}$	625	692	0.54
$\mathbf{P_{4b}}$	625	691	0.62
$\mathbf{P_{4c}}$	625	690	0.72

Table 7. Energy Transfer Efficiency of Directly Conjugated Polyyne Porphyrins

Porphyrins	Energy transfer efficiency
$\mathbf{P_{2a}}$	1.04±0.15
$\mathbf{P_{2b}}$	1.01±0.07
$\mathbf{P_{2c}}$	1.06±0.11
$\mathbf{P_{3a}}$	0.99±0.10
$\mathbf{P_{3b}}$	0.97±0.10
$\mathbf{P_{3c}}$	1.12±0.14
$\mathbf{P_{4a}}$	1.08±0.20
$\mathbf{P_{4b}}$	1.11±0.22
$\mathbf{P_{4c}}$	1.11±0.11

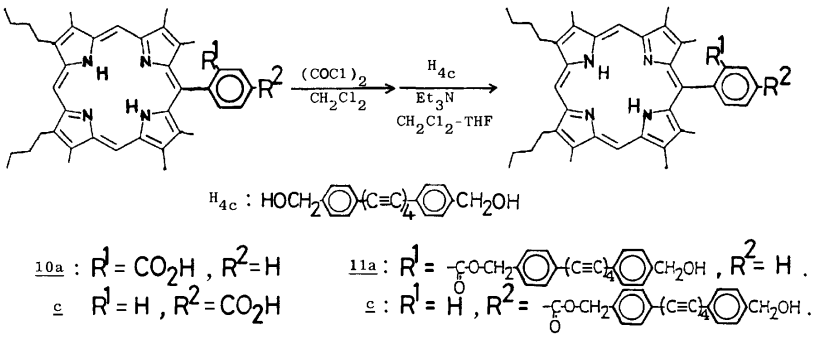

Fig. 6. Indirectly conjugated polyyne porphyrins.

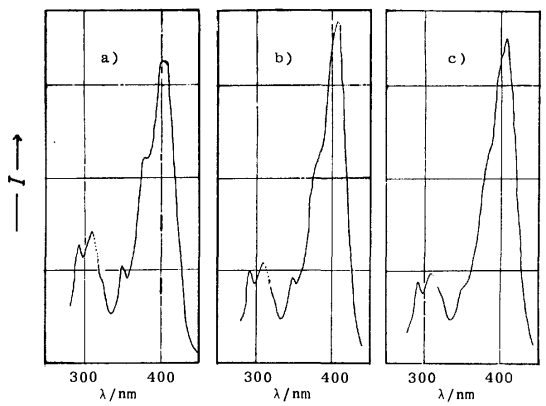

Fig. 5. Fluorescence excitation spectra of directly conjugated polyyne porphyrins. a) $\mathbf{P_{4a}}$, b) $\mathbf{P_{4b}}$, c) $\mathbf{P_{4c}}$. Em. 625 nm, solvent; CH_2Cl_2.

6). The UV-vis absorption spectra and the fluorescence excitation spectra of **11a** and **11c** are shown in Figs. 7 and 8. The absorption spectra of indirectly conjugated polyyne porphyrins are approximately identical to the sum of those of the two components, indicating absence of interaction between them. Energy transfer efficiencies from polyyne moiety to porphyrin moiety calculated similarly as described above are shown in Table 8. Characteristic in these porphyrins is that distance and orientation play a crucial role in energy transfer process. That is, close proximity of the concerned chromophores is quite important for the effective energy transfer. In the mixture of each component, however, energy transfer was not observed and energy transfer efficiency was concentration-independent. Therefore, in this case

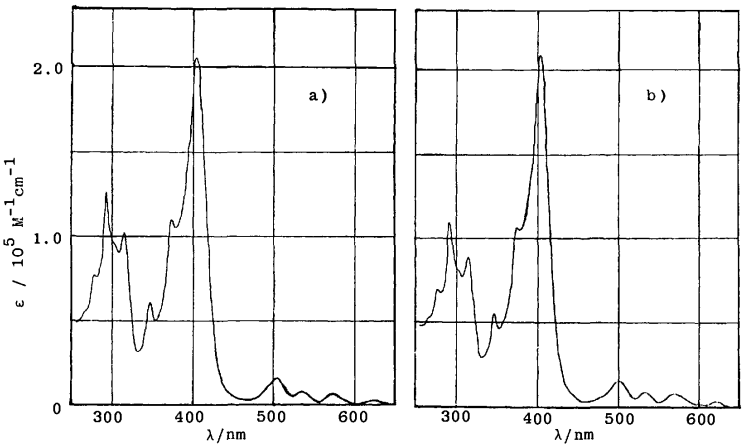

Fig. 7. UV-vis absorption spectra of indirectly conjugated polyyne porphyrins. a) **11a**, b) **11c**. Solvent; CH_2Cl_2.

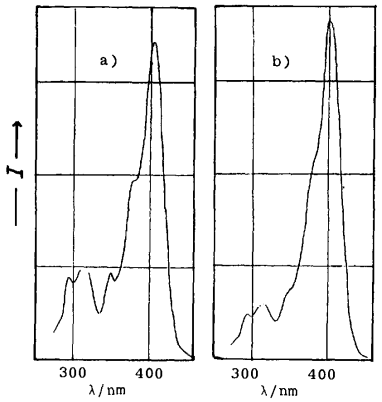

Fig. 8. Fluorescence excitation spectra of indirectly conjugated polyyne porphyrins. a) **11a**, b) **11c**. Em. 625 nm, solvent; CH_2Cl_2.

Table 8. Energy Transfer Efficiency of Indirectly Conjugated Polyyne Porphyrins

Porphyrins	Energy transfer efficiency
11a	0.81±0.16
11c	0.57±0.22

intramolecular singlet–singlet energy transfer had occurred.

Recently, Kobayashi et al. investigated the absorption spectra of diphenylpolyyne in detail.[27] Excited state of diphenylpolyyne has charge-transfer character, from polyyne to aromatic ring or the opposite direction. Two perpendicular π-conjugated systems interact significantly. As in our case one aromatic ring was directly conjugated with large porphyrin macrocycle system, charge-transfer character was presumed to be eminent. In unsymmetric long linear π-conjugated system, vectorial charge-transfer character might play a role of molecular wire from one end to the other.

Experimental

All melting points were measured with a Yanagimoto micro melting point apparatus and uncorrected. The ^{1}H NMR spectra were recorded on 400 MHz JEOL JNM-GX-400 and 100 MHz JEOL-PS-100 instruments, with tetramethylsilane as an internal reference. Infrared spectra were measured with a JASCO IRA-1 spectrometer. Mass spectra were recorded with a JEOL DX-300 spectrometer. UV-vis spectra were measured with Shimadzu UV-3000 and UV-160 spectrometer. Fluorescence spectra were taken on a Shimadzu RF-502A spectrofluorometer. Dichloromethane was freshly distilled and passed through alumina column. The elemental analysis were performed at the Microanalysis Center of Kyoto University.

Preparation of the Polyyne Porphyrins. Melting points, ^{1}H NMR spectral data in $CDCl_3$ solution, and IR spectral data are given in Tables 1—3. Measurement of mass spectra gave satisfactory values. Synthetic methods of nine kinds of compounds (H_{2a-4c}, A_{2a-4c}, P_{2a-4c}) were similar.

Synthesis of Diarylpolyynediols (H_{2a-4c}). To a solution of the corresponding diarylpolyyne (Y_n) (3 mmol) in 30 ml of acetone was added a 12 ml of 6 mol dm^{-3} HCl solution, and resulting solution was refluxed for 2—4 h under nitrogen in the dark. After cooling, the mixture was extracted with tetrahydrofuran–ether, washed with aqueous $NaHCO_3$ solution, and dried over Na_2SO_4. After evaporation and recrystallization from tetrahydrofuran–hexane, corresponding diols were obtained.

Synthesis of Diarylpolyyne Dicarbaldehydes (A_{2a-4c}).
Method A. To a solution of the corresponding diarylpolyynediol (H_n) (1 mmol) in 30—60 ml of tetrahydrofuran was added a 3.0 g of active MnO_2,[20] and resulting solution was stirred overnight at room temperature in the dark. Manganese oxide was filtered off, and the residue obtained from the filtrate by evaporation of the solvent was purified by chromatography over silica gel, using benzene as an eluent with gradual addition of $CHCl_3$.

Method B (Jones Oxidation).[21] One mmol of diarylpolyynediol (H_n) were dissolved in acetone (150—200 ml). To an ice-cooled solution 2 mol dm^{-3} Jones reagent was added dropwise until an orange tint persisted in the reaction

mixture. Then, isopropyl alcohol was added dropwise to destroy excess Jones reagent, as indicated by the reappearance of a deep green color. After removal of the solvent in vacuo and aqueous treatment, the mixture was extracted with tetrahydrofuran-ether and dried over Na_2SO_4. The solvent was evaporated and the solid was purified by chromatography as described above.

Synthesis of Directly Conjugated Polyyne Porphyrins (P_{2a-4c}). A quarter mmol of diarylpolyyne dicarbaldehyde (A_n) and 0.25 mmol of ac-biladiene (**8**) were dissolved in 40 ml of dry methanol with stirring. Anhydrous 25% HBr-acetic acid solution was added and the mixture was refluxed for 2—5 d under nitrogen in the dark. After cooling, the mixture was poured into water and extracted with $CHCl_3$, and dried over Na_2SO_4. After evaporation, the residue was purified by flash-column chromatography, with an eluent CH_2Cl_2. The second fraction was collected and evaporated in vacuo. Recrystallization from CH_2Cl_2-MeOH gave the desired corresponding polyyne porphyrin conjugated directly.

Synthesis of Indirectly Conjugated Polyyne Porphyrin (11a). 28 mg of porphyrin monoacid **10a** was dissolved in 5 ml of CH_2Cl_2. To this solution 0.1 ml of oxalyl dichloride was added, and the mixture was stirred for 8 h at room temperature in the dark. The excess oxalyl dichloride and CH_2Cl_2 were removed in vacuo quickly, then residue, porphyrin acid chloride, was dissolved in dry CH_2Cl_2 (5 ml) again under N_2. This was added to a solution of diarylpolyynediol (H_{4c}) (12.4 mg) and triethylamine (0.01 ml) in 3 ml of THF, and stirred overnight at room temperature in the dark. The reaction mixture was poured into water, then extracted with $CHCl_3$, washed with aqueous $NaHCO_3$ solution, and dried over Na_2SO_4. The solvent was evaporated and the residue was purified with column chromatography on silica gel, using $CHCl_3$ as an eluent. The second colored fraction gave **11a**: ^{1}H NMR ($CDCl_3$) δ=−3.28 (2H, s, NH), 1.17 (6H, t, ^{n}Bu-Me), 1.79—1.85 (4H, m, ^{n}Bu), 2.30—2.40 (4H, m, ^{n}Bu), 2.32 (6H, s, 3,7-Me), 3.44 (6H, s, 2,8-Me), 3.66 (6H, s, 12,18-Me), 4.03—4.13 (4H, m, ^{n}Bu), 4.54 (2H, d, polyyne close phenyl), 4.71 (2H, s, C$\underline{H}_2$OH), 4.83 (2H, d, polyyne close phenyl), 7.35 (2H, d, polyyne far phenyl), 7.58 (2H, d, polyyne far phenyl), 7.81—7.91 (2H, m, meso-phenyl), 7.99 (1H, d, meso-phenyl), 8.35 (1H, d, meso-phenyl), 9.99 (1H, s, H15), and 10.09 (2H, s, H10,20).

Synthesis of Indirectly Conjugated Polyyne Porphyrin (11c). This was synthesized by the same method as described for the synthesis **11a**: ^{1}H NMR ($CDCl_3$) δ=−3.33 (1H, s, NH), −3.20 (1H, s, NH), 1.12 (6H, t, ^{n}Bu-Me), 1.71—1.81 (4H, m, ^{n}Bu), 2.23—2.31 (4H, m, ^{n}Bu), 2.41 (6H, s, 3,7-Me), 3.51 (6H, s, 2,8-Me), 3.62 (6H, s, 12,18-Me), 4.03 (4H, t, ^{n}Bu), 4.70 (2H, s, C$\underline{H}_2$OH), 7.33 (2H, d, polyyne far phenyl), 7.53 (2H, d, polyyne far phenyl), 7.59 (2H, d, polyyne close phenyl), 7.65 (2H, d, polyyne close phenyl), 8.17 (2H, d, meso-phenyl), 8.44 (2H, d, meso-phenyl), 9.93 (1H, s, H15), and 10.15 (2H, s, H10,20).

References

1) J. Deisenhofer, O. Epp, K. Miki, R. Huber, and H. Michel, *J. Mol. Biol.*, **180**, 385 (1984).

2) J. R. Miller, L. T. Calcaterra, and G. L. Closs, *J. Am. Chem. Soc.*, **106**, 3047 (1984); G. L. Closs, L. T. Calcaterra, N. J. Green, K. W. Penfield, and J. R. Miller, *J. Phys. Chem.*, **90**, 3673 (1986); G. L. Closs and J. R. Miller, *Science*, **240**, 440 (1988); G. L. Closs, P. Piotrowiak, J. M. MacInnis, and G. R. Fleming, *J. Am. Chem. Soc.*, **110**, 2652 (1988).

3) J. A. Schmidt, A. Siemiarczuk, A. C. Weedon, and J. R. Bolton, *J. Am. Chem. Soc.*, **107**, 6112 (1985); J. A. Schmidt, A. R. McIntosh, A. C. Weedon, J. R. Bolton, J. S. Connolly, J. K. Hurley, and M. R. Wasielewski, *ibid.*, **110**, 1733 (1988).

4) A. D. Joran, B. A. Leland, G. G. Geller, J. J. Hopfield, and P. B. Dervan, *J. Am. Chem. Soc.*, **106**, 6090 (1984); B. A. Leland, A. D. Joran, P. M. Felker, J. J. Hopfield, A. H. Zewail, and P. B. Dervan, *J. Phys. Chem.*, **89**, 5571 (1985).

5) M. R. Wasielewski and M. P. Niemczyk, *J. Am. Chem. Soc.*, **106**, 5043 (1984); M. R. Wasielewski, M. P. Niemczyk, W. A. Svec, and E. B. Pewitt, *ibid.*, **107**, 1080 (1985); M. R. Wasielewski, M. P. Niemczyk, W. A. Svec, and E. B. Pewitt, *ibid.*, **107**, 5562 (1985).

6) M. N. Paddon-Row, E. Cotsaris, and H. K. Patney, *Tetrahedron*, **42**, 1779 (1986); H. Oevering, M. N. Paddon-Row, M. Heppener, A. M. Oliver, E. Cotsaris, J. W. Verhoeven, and N. S. Hush, *J. Am. Chem. Soc.*, **109**, 3258 (1987); K. W. Penfield, J. R. Miller, M. N. Paddon-Row, E. Cotsaris, A. M. Oliver, and N. S. Hush, *ibid.*, **109**, 5061 (1987).

7) G. Dirks, A. L. Moore, T. A. Moore, and D. Gust, *Photochem. Photobiol.*, **32**, 277 (1980); A. L. Moore, G. Dirks, D. Gust, and T. A. Moore, *ibid.*, **32**, 691 (1980); P. A. Liddell, G. A. Nemeth, W. R. Lehman, A. M. Joy, A. L. Moore, R. V. Bensasson, T. A. Moore, and D. Gust, *ibid.*, **36**, 641 (1982); D. Gust, T. A. Moore, R. V. Bensasson, P. Mathis, E. J. Land, C. Chachaty, A. L. Moore, P. A. Liddell, and G. A. Nemeth, *J. Am. Chem. Soc.*, **107**, 3631 (1985); D. Gust, T. A. Moore, L. R. Makings, P. A. Liddell, G. A. Nemeth, and A. L. Moore, *ibid.*, **108**, 8028 (1986); D. Gust, T. A. Moore, P. A. Liddell, G. A. Nemeth, L. R. Makings, A. L. Moore, D. Barrett, P. J. Pessiki, R. V. Bensasson, M. Rougee, C. Chachaty, F. C. DeSchryver, M. V. der Auweraer, A. R. Holzwarth, and J. S. Connolly, *ibid.*, **109**, 846 (1987); D. Gust, T. A. Moore, A. L. Moore, L. R. Makings, G. R. Seely, X. Ma, T. T. Trier, and F. Gao, *ibid.*, **110**, 7567 (1988).

8) D. N. Beratan, *J. Am. Chem. Soc.*, **108**, 4321 (1986).

9) S. S. Isied and A. Vassilian, *J. Am. Chem. Soc.*, **106**, 1726 (1984); S. S. Isied and A. Vassilian, *ibid.*, **106**, 1732 (1984).

10) S. Larsson, *J. Chem. Soc., Faraday Trans. 2*, **79**, 1375 (1983).

11) H. Heitele and M. E. Michel-Beyerle, *J. Am. Chem. Soc.*, **107**, 8286 (1985); H. Heitele, M. E. Michel-Beyerle, and P. Finckh, *Chem. Phys. Lett.*, **134**, 273 (1987); H. Heitele, M. E. Michel-Beyerle, and P. Finckh, *ibid.*, **138**, 237 (1987).

12) F. Effenberger, H. Schlosser, P. Bauerle, S. Maier, H. Port, and H. C. Wolf, *Angew. Chem., Int. Ed. Engl.*, **27**, 281 (1988).

13) D. Heiler, G. McLendon, and P. Rogalskyj, *J. Am. Chem. Soc.*, **109**, 604 (1987).

14) J. L. Sessler and M. R. Johnson, *Angew. Chem., Int. Ed. Engl.*, **26**, 678 (1987); J. L. Sessler, M. R. Johnson, T.-Y. Liu, and S. E. Creager, *J. Am. Chem. Soc.*, **110**, 3659 (1988).

15) A. Osuka and K. Maruyama, *Chem. Lett.*, **1987**, 825; A. Osuka, H. Tomita, and K. Maruyama, *ibid.*, **1988**, 1205; A. Osuka, K. Maruyama, I. Yamazaki, and N. Tamai, *J. Chem. Soc., Chem. Commun.*, **1988**, 1243; A. Osuka and K.

Maruyama, *J. Am. Chem. Soc.*, **110**, 4454 (1988).
16) J. B. Armitage, N. Entwistle, E. R. H. Jones, and M. C. Whiting, *J. Chem. Soc.*, **1954**, 147.
17) S. Akiyama and M. Nakagawa, *Bull. Chem. Soc. Jpn.*, **40**, 340 (1967); K. Nakasuji, S. Akiyama, K. Akashi, and M. Nakagawa, *ibid.*, **43**, 3567 (1970); K. Nakasuji, S. Akiyama, and M. Nakagawa, *ibid.*, **45**, 883 (1972).
18) A. S. Hay, *J. Org. Chem.*, **27**, 3320 (1962).
19) E. J. Corey and P. L. Fuchs, *Tetrahedron Lett.*, **1972**, 3769.
20) J. Attenburrow, A. F. B. Cameron, J. H. Chapman, R. M. Evans, B. A. Hems, A. B. A. Jansen, and T. Walker, *J. Chem. Soc.*, **1952**, 1094.
21) K. E. Harding, L. M. May, and K. F. Dick, *J. Org. Chem.*, **40**, 1664 (1975).
22) D. Harris, A. W. Johnson, and R. Gaete-Holmes, *Bioorg. Chem.*, **9**, 63 (1980).
23) A. W. Johnson and I. T. Kay, *J. Chem. Soc.*, **1965**, 1620.
24) Directly conjugated polyyne porphyrin dimers have been synthesized successfully by other synthetic method. The detailed synthetic methods and characterization of polyyne porphyrin dimers will be reported elsewhere.
25) S. Akiyama, K. Nakasuji, K. Akashi, and M. Nakagawa, *Tetrahedron Lett.*, **1968**, 1121; K. Nishimoto, R. Fujishiro, S. Akiyama, and M. Nakagawa, *Bull. Chem. Soc. Jpn.*, **39**, 2320 (1966).
26) For n=2—6, the empirical formula: λ_{max}=268.4+32.4×n was obtained.
27) M. Kobayashi, T. Hoshi, J. Okubo, H. Hiratsuka, T. Harazono, M. Nakagawa, and Y. Tanizaki, *Bull. Chem. Soc. Jpn.*, **57**, 2905 (1984); T. Hoshi, J. Okubo, M. Kobayashi, and Y. Tanizaki, *J. Am. Chem. Soc.*, **108**, 3867 (1986).

 © 1989 The Chemical Society of Japan Bull. Chem. Soc. Jpn., 62, 3508—3512 (1989) [Vol. 62, No. 11

Effects of Solvent and Temperature on the 1,4-Asymmetric Induction in the Diastereoselective Hydrogenation of Dehydrodipeptides

Satoru IKEDA,* Takamichi YAMAGISHI,* Motowo YAMAGUCHI, and Mitsuhiko HIDA
Department of Industrial Chemistry, Faculty of Technology, Tokyo Metropolitan University, Fukasawa, Setagaya-ku, Tokyo 158
(Received June 6, 1989)

A study of the effets of solvent and temperature on the stereoselectivity of asymmetric hydrogenation of dehydrodipeptides has been made with Rh(I)-(DPP-AE) catalyst, in which an electrostatic interaction is possible between the dimethylamino group of the ligand and the carboxyl group of the substrate. The highest stereoselectivity was attained in the MeOH-water solvent, while aprotic solvents such as DMF and THF gave comparatively low selectivity and reactivity. With increasing the temperature from −40 °C to 80 °C in alcoholic solvent, the stereoselectivity increased to reach a maximum at 20—40 °C, then decreased. The effects of solvent and temperature on the stereoselectivity were discussed.

The asymmetric hydrogenation of olefinic compounds with Rh(I)-diphoshine catalysts has been widely studied and high enantio- or diastereoselectivity was obtained, especially in the case of the hydrogenation of α-dehydroamino acid derivatives.[1] The stereocontrol in these systems is caused by a large steric repulsion between substrate and chiral ligand coordinated to rhodium.[2] On the other hand, enzymes efficiently use attractive forces such as electrostatic interaction, hydrogen bonding, and van der Waals interaction in addition to simple steric repulsion in their highly stereoselective reactions.[3] Incorporation of such attractive interactions to a catalytic system will enhance stereoselectivity in the asymmetric reactions.

Previously, we have reported the application of Rh(I)–achiral diphosphine [2-[2-(dimethylamino)ethyl]-1,3-propanediyl]bis[diphenylphosphine] (DPP-AE(**1**)) system to the hydrogenation of dehydrodipeptides, where the dimethylamino group of the ligand was expected to interact electrostatically with carboxyl group of the substrate (Scheme 1).[4] The detailed examination showed that the presence of both amino group of the ligand and free carboxyl group of the substrate is essential for high stereoselectivity. The Rh(I)-**1** system showed highly selective 1,4-asymmetric induction for the hydrogenation of *N*-acetyl or *N*-benzyloxycarbonyl dehydrodipeptides. For example, the diastereomeric excess was 94% for the hydrogenation of Ac-ΔPhe-(*S*)-Phe-OH, and 92% for Z-ΔPhe-(*S*)-Val-OH, with the selectivity of (*S*,*S*). In the asymmetric reactions, solvent and/or temperature largely affects the stereoselectivity and the reactivity.[5] In this paper we describe the effects of solvent and temperature on the hydrogenation of dehydrodipeptides using this Rh(I)-DPP-AE system, to confirm the contribution of the electrostatic interaction and to establish the optimum conditions for obtaining high stereoselectivity.

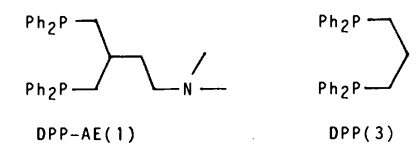

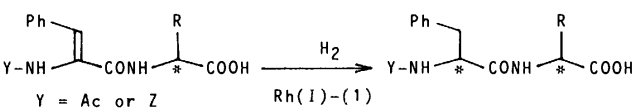

Scheme 1.

Results and Discussion

Solvent Effect. The Rh(I)-DPP-AE catalyst system achieved a high stereoselective 1,4-asymmetric induction and afforded a predominant diastereomer with a (*S*,*S*)- or (*R*,*R*)-configuration corresponding to that of the chiral center in the substrate. The hydrogenation of *N*-acetyldehydrophenylalanylamino acids (Ac-ΔPhe-AA-OH (**2**); where AA is a chiral amino acid residue) gave higher stereoselectivities with an increase in polarity of alcoholic solvents (MeOH>EtOH>*i*-PrOH).[4] Therefore addition of water to methanol was expected to raise the stereoselectivity for the hydrogenation of dehydrodipeptides. As was expected, the selectivity of the reaction of **2a** or **2c** increased with an addition of proper amount of water to methanol, although the degree of increase was a little (96% diastereomeric excess for **2a** and 91% d.e. for **2c**) (Table 1). An excessive addition of water, however, lowered both the reactivity and stereoselectivity. Substrate **2a** having a highly hydrophobic amino acid residue afforded 71% d.e. in the 1:1 methanol-water. On the other hand, **2b** gave 77% d.e. even in the 19:1

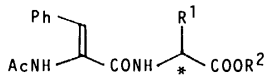

Ac-dehydrodipeptides(2)
2a Ac-ΔPhe-(S)-Phe-OH; R^1 = $PhCH_2$, R^2 = H
2b Ac-ΔPhe-(S)-Ala-OH; R^1 = CH_3, R^2 = H
2c Ac-ΔPhe-(R)-Leu-OH; R^1 = $(CH_3)_2CHCH_2$, R^2 = H
2d Ac-ΔPhe-(S)-Ala-OMe; R^1 = CH_3, R^2 = CH_3

Table 1. Asymmetric Hydrogenation of Dehydrodipeptides with Rh(I)-DPP-AE System in Aqueous Methanol Solution

Solvent system	%d.e.[a] (time/h)		
	Dehydrodipeptide		
	2a	**2b**	**2c**
$MeOH/H_2O$			
10:0	94(0.5)	88(0.8)	87(1.5)
19:1		77(2)	
9:1		72(12)	91(1)
8:2		—(12)[b]	82(18)
7:3	96(0.5)		—(36)[c]
1:1	71(48)[d]		

The reaction was carried out at 20 °C under atmospheric hydrogen pressure. Dehydrodipeptide : **1** : Rh= 50 : 1.1 : 1. The conversion is 100% unless otherwise noted. The configuration of the predominant product was (*S,S*) for **2a** and **2b**, (*R,R*) for **2c**. a) Diastereomeric excess. b) Conversion was ca. 10%. c) Conversion was 55%. d) Conversion 88%.

methanol-water solution and the reaction was too slow in 8:2 methanol-water solution to determine the diastereoselectivity. Addition of excess water would prevent the electrostatic interaction between substrate and ligand, and also decrease the solubility of the substrates and hydrogen gas in the solvent.

The stereoselectivity and reactivity of **2b** and **2c** in aprotic solvents were rather lower than those in protic solvents (Table 2). The reaction of **2b** required 12 hours in DMF to complete and 20 hours in THF, while the reaction completed within 1 hour in methanol. These results indicated clearly that protic and polar solvent is necessary to obtain good selectivity and reactivity by this Rh(I)-DPP-AE catalyst system for dehydrodipeptides, although large increase of solvent polarity by addition of excess water would lower the selectivity because of the reduction of electrostatic interaction. This solvent effect is in contrast to the hydrogenation of acetamidocinnamic acid with Rh(I)-(*R*)-PheNOP system, which gave high selectivities in DMF or THF and the lowest in MeOH.[5b] On the other hand, the Rh(I)-BPPFA ((*S*)-1-[(*R*)-1,2-bis(diphenylphosphino)ferrocenyl]-*N,N*-dimethylethylamine) having a dimethylamino moiety showed a similar solvent dependence in the hydrogenation of acetamidocinnamic acid derivatives to that of the present Rh(I)-DPP-AE system: Rh(I)-BPPFA gave high selectivity in aqueous methanol rather than in methanol.[5c]

The high stereoselectivity in polar and protic solvents suggests that both proton-donating and proton-accepting characters of solvent affect the selectivity. A proton donor can convert amino group to ammonium cation and a proton acceptor can convert the carboxyl group to carboxylate anion. These ionizations are more feasible in polar solvents such as alcohol or mixture of alcohol-water than in less polar

Table 2. Asymmetric Hydrogenation of Dehydrodipeptides with Rh(I)-DPP-AE in Aprotic Solvents

Dehydrodipeptide	Solvent	Time/h	%d.e.
2b	THF	20	74 (*S,S*)
	DMF	12	65
	MeOH	0.8	88
	THF/H_2O[a]	12	78
2c	THF	3 days	68 (*R,R*)
	EtOH/THF[b]	0.5	86
	EtOH	4	78

The reaction was carried out under atmospheric hydrogen pressure at 20 °C for alcoholic solvents, at 25 °C for others. Dehydrodipeptide : **1** : Rh=50 : 1.1 : 1. Conversion was 100% in all cases. a) The THF : H_2O= 9 : 1. b) The EtOH : THF=9 : 1.

solvents. Here alcohols and water act as proton donor as well as proton acceptor, while THF acts only as proton acceptor. The hydrogenation of **2c** in EtOH-THF and **2b** in THF-H_2O afforded higher diastereoselectivity than in EtOH or THF respectively. These were ascribed to the better combination of proton-donating and proton-accepting solvents. It was concluded that the polarity and the proportion of the proton donor and proton acceptor characters of the solvents are important to affect the ionization of the amino and the carboxyl groups and the electrostatic interaction between them. In the present systems, MeOH-H_2O mixed solvent is the best.

We reported that addition of triethylamine to Rh(I)-DPP-AE system lowered the stereoselectivity.[4] The hydrogenation of **2a** with Rh(I)-DPP-AE in MeOH gave 94%d.e. and addition of amine in 10 molar ratio to the rhodium diminished the selectivity to 66% d.e. On the basis of the above consideration, the influence of addition of amine on selectivity was examined over the amine/Rh ratios from 0 to 50 at 20 °C (Fig. 1), since amine is supposed to be a good proton acceptor to favor the ionization of carboxyl group and to prevent the protonation of dimethylamino group. In the case of Rh(I)-DPP (**3**) system without the electrostatic interaction between ligand and substrate, a maximum selectivity was observed at the amine ratio of 10 to rhodium, and addition of 50 fold amine to rhodium reduced the diastereomeric excess to 22%. The increasing in the diastereoselectivity may be explained as an enhancement of the steric recognition of the substrate by catalyst through the axial coordination of the carboxylate unit formed by addition of amine. It was reported that addition of a small amount of amine increased the stereoselectivity in the hydrogenation of acetamidocinnamic acid or itaconic acid with the Rh(I)-diphosphine catalyst.[6] The Rh(I)-DPP-AE system showed a different behavior from the Rh(I)-DPP catalyst system. Increasing the amount of amine up to 10 molar to the rhodium caused the decrease of the stereoselectivity from 94% to about 60% d.e. By further addition of amine, however,

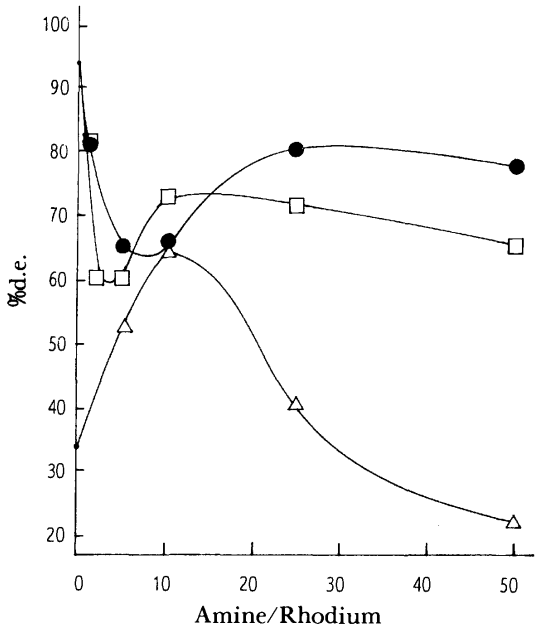

Fig. 1. The influence of amine on stereoselectivity of the hydrogenation of **2b** ●: DPP-AE–triethylamine, □: DPP-AE–*N*-methylmorpholine, △: DPP–triethylamine.

the selectivity turned to increase to reach a maximum (80% d.e. for triethylamine, 72% d.e. for *N*-methylmorpholine) at about 25 molar amine to the rhodium. The initial fall of selectivity was explained by the obstruction of the efficient electrostatic interaction between ligand (**1**) and substrate (**2a**) by the addition of amine. The formed triethylammonium cation will interact with carboxylate anion of the substrate in competition with the ammonium cation unit in the ligand, and suppress the interaction between ligand and substrate. The presence of relatively large amount of amine afforded a high stereoselectivity (80% d.e.), probably by the efficient axial coordination of the carboxylate anion of the substrate, but could not substitute the role of the amino group in DPP-AE catalyst which gave 94% d.e.

Temperature Effect. Generally, the stereoselectivity decreased simply with the elevation of the temperature for the hydrogenation of acetamidocinnamic acid derivatives using Rh(I) catalysts.[5a-d] The reversed trends were reported for some catalytic systems using DIPAMP (1,2-bis[(*o*-methoxyphenyl)phenylphosphino]-ethane) or DIOXOP (4-diphenylphosphino-2-diphenylphosphinomethyl-1,3-dioxolane).[6b,7] We examined the temperature effect of the Rh(I)–DPP-AE system on the hydrogenation of **2b** in MeOH, EtOH, and *i*-PrOH, in the temperature range from −40 °C to 80 °C (Fig. 2). Each plot of the selectivities against temperature showed a curve with a maximum. The optimal temperature shifted to the lower temperature with an increase in the polarity of solvent. EtOH and MeOH gave the maximum around ambient temperature, while *i*-PrOH shifted the maximum to higher temperature. The Arrhenius plot of the (*S,S*)/(*R,S*) ratio apparently showed the presence of at least two predominant active species. Assuming those two species we estimated the difference of activation enthalpies ($\Delta\Delta H^{\neq}$) and entropies ($\Delta\Delta S^{\neq}$) of the reaction in EtOH. The one catalyst species seems to operate at lower temperatures between −40 °C and 20 °C, and has the activation parameters, 16 kJ mol^{-1} of $\Delta\Delta H^{\neq}$ and 74 J deg^{-1} mol^{-1} of $\Delta\Delta S^{\neq}$. The another species seems to operate at higher temperatures between 20 °C and 80 °C, and has −3.9 kJ mol^{-1} of $\Delta\Delta H^{\neq}$ and 8.1 J deg^{-1} mol^{-1} of $\Delta\Delta S^{\neq}$. These activation parameters suggest that the enthalpy term of the former catalyst species selects (*R,S*) isomer, while its entropy term selects (*S,S*) isomer. On the other hand both enthalpy and entropy terms of the latter species select (*S,S*) isomer. The contribution of the entropy term to the stereocontrol of this Rh(I)–DPP-AE catalytic system at lower temperatures is large compared with that of chiral Rh(I) catalyst systems.[8] This fact suggests that the mode of coordination of substrate to catalyst affects largely the control of stereoselectivity. The electrostatic interaction provides an additional recognition point of substrate by catalyst and this interaction plays an important role to determine the mode of coordination at least in the lower temperature range and cause a large contribution of the entropy term to the stereocontrol. This temperature effect is rather similar to the temperature dependence of the heterogeneous systems, hydrogenolytic transamination between α-keto ester and chiral amine with $Pd(OH)_2$ on carbon.[5f] Temperature effects in EtOH were also examined for the hydrogenation of **2b** with DPP and of **2d** (methyl ester of **2b**) with DPP-AE (Fig. 3). Both systems have a similar steric circumstance to that of DPP-AE–**2b** system, but the electrostatic interaction cannot operate in these systems. Both showed stereoselectivities of about 50% d.e. between −40 °C

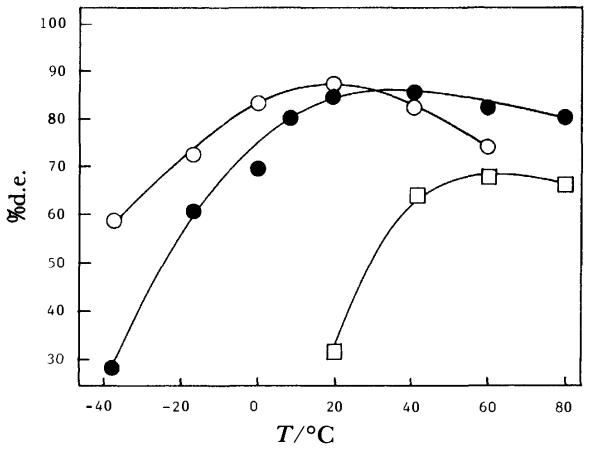

Fig. 2. The temperature dependence of the hydrogenation of **2b** with Rh(I)–DPP-AE system ○: MeOH; ●: EtOH, □: *i*-PrOH.

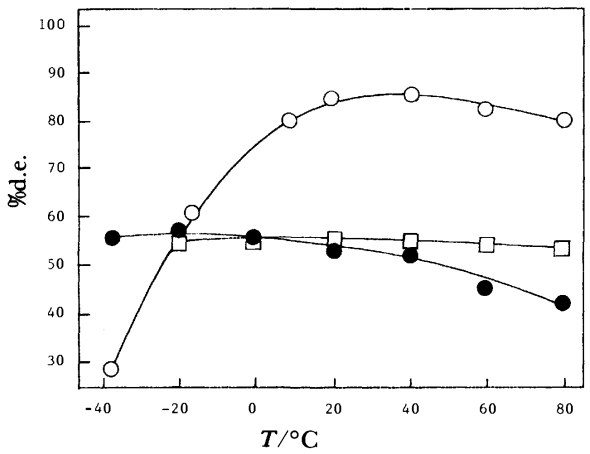

Fig. 3. The temperature dependence of the asymmetric induction in MeOH ○: DPP-AE-**2b**, □: DPP-AE-**2d**,●: DPP-**2b**.

and 80 °C. The $\Delta\Delta S^{\neq}$ was 0.85 J deg^{-1} mol^{-1} (−20 to 80 °C) for DPP-**2b** system, and 13 J deg^{-1} mol^{-1} (−20 to 20 °C), 7.4 J deg^{-1} mol^{-1} (20 to 80 °C) for DPP-AE-**2d** system. The absolute values of $\Delta\Delta S^{\neq}$ of these systems were smaller than that of DPP-AE-**2b** systems. At lower temperature the diastereoselectivity of these two systems are higher than that of DPP-AE system. This suggests that the electrostatic interaction works to increase (*R*,*S*) selectivity by lowering the temperature, although the predominant diastereomer is still (*S*,*S*).

We observed that the Rh(I)-DPP-AE (**1**) system gives the optimum conditions at ambient temperature in MeOH or MeOH-water mixed solvents in which the efficient electrostatic interaction is possible between ligand and substrate for hydrogenation of dehydrodipeptides. This catalytic system achieves highly stereoselective 1,4-asymmetric induction more than 90% d.e. regardless of the chiral amino acid residue in the dehydrodipeptides. Thus this method is useful for synthesis of chiral linear dipeptides.[9]

Experimental

Instrument. ^{1}H NMR spectra were recorded on a Hitachi R-24 or JEOL FX-90Q spectrometer in $CDCl_3$ using tetramethylsilane as an internal standard.

Chemicals and Solvents. DPP-AE (**1**) was prepared in four steps starting from diethyl malonate and 2-chloro-*N*,*N*-dimethylethylamine.[5] DPP (**3**) was prepared from 1,3-dichloropropane and lithium diphenylphosphide. Dehydrodipeptides (**2a**—**2c**) were prepared from the azlactone of acetamidocinnamic acid[10] and corresponding chiral amino acid according to the method by Bergmann et al.[11] Dehydrodipeptide ester (**2d**) was obtained by the reaction of **2b** with MeOH-HCl. Alcohols were dried by refluxing over magnesium (MeOH and EtOH) or sodium (*i*-PrOH) and distilled under nitrogen. Tetrahydrofuran, triethylamine and *N*-methylmorpholine were dried over sodium and distilled, and DMF was dried over Molecular Sieves 4A and distilled. All solvents and amines were stored under nitrogen. NMR shift reagent, Eu(fod)$_3$, was used as purchased. $[Rh(nbd)_2]^+BF_4^-$ (nbd=norbornadiene) was used as the rhodium precursor.

Method of Hydrogenation. All hydrogenations were carried out under atmospheric hydrogen pressure. The catalyst was prepared in situ from the ligand and rhodium precursor. To this catalyst solution in a reaction vessel was added the substrate, and the mixture was stirred for 1 hour under nitrogen. The reaction vessel was immersed in a temperature-regulated bath and hydrogen was introduced. The reaction was monitored by the absorption of H_2 using a gas burette for the reaction above 0 °C. In the case of the reaction under −20 °C, the stopcock of the vessel was closed after introduction of hydrogen and stirring was continued for 1 to 3 days. After the reaction, the catalyst was removed with cation-exchange resin, Dowex 50, and the product was converted to its methyl ester in MeOH-HCl.

Determination of Diastereomeric Excess. ^{1}H NMR spectra of the methyl ester were measured in the presence of Eu(fod)$_3$. Two singlets of diastereotopic methyl protons in the methyl ester shifted in different degrees and the diastereomeric excess was determined based on the area of each signal.

A part of this work was financially supported by a Grant-in-Aid for Scientific Research No. 61470089 from the Ministry of Education, Science and Culture and by a Grant-in-Aid for Special Research Project of Tokyo Metropolitan University.

References

1) K. E. Koenig, "Asymmetric Synthesis," ed by J. D. Morrison, Academic Press, New York (1985), Vol. 5, p. 71; H. Brunner, "Topics in Stereochemistry," ed by E. L. Eliel and S. H. Wilen, John Wiley & Sons, New York (1988), Vol. 18, p. 129.

2) B. Bosnich and M. D. Fryzuk, "Topics in Stereochemistry," ed by N. L. Allinger and E. L. Eliel, John Wiley & Sons, New York (1981), Vol. 12, p. 121.

3) M. I. Page, "The Chemistry of Enzyme Action," Elsevier, Amsterdam (1984); A. L. Allinger, "Principles of Biochemistry," Worth, New York (1982).

4) T. Yamagishi, S. Ikeda, M. Yatagai, M. Yamaguchi, and M. Hida, *J. Chem. Soc., Perkin Trans. 1*, **1988**, 1787.

5) a) R. Selke and H. Pracejus, *J. Mol. Catal.*, **37**, 213 (1986); b) V. A. Pavlov, E. I. Klabunovskii, Yu. T. Struchkov, A. A. Voloboev, and A. I. Yanovsky, *ibid.*, **44**, 217 (1988); c) J. Bakos, I. Tòth, B. Heil, and L. Markò, *J. Organomet. Chem.*, **279**, 23 (1985); d) D. P. Riley and R. E. Shumate, *J. Org. Chem.*, **45**, 5187 (1980); e) T. Hayashi, T. Mise, S. Mitachi, K. Yamamoto, and M. Kumada, *Tetrahedron Lett.*, **1976**, 1133; f) K. Harada and T. Yoshida, *J. Org. Chem.*, **37**, 4366 (1972). In this catalytic system it was indicated that the adsorption of carbonyl group in ester moiety on palladium, in addition to that of CN double bond, is important for steric control.

6) a) I. Ojima, T. Kogure, and N. Yoda, *J. Org. Chem.*, **45**, 4728 (1980); b) D. Sinou, *Tetrahedron Lett.*, **22**, 2987 (1981).

7) C. R. Landis and J. Halpern, *J. Am. Chem. Soc.*, **109**, 1746 (1987).

8) The calculated activation parameters of some Rh(I)

catalytic systems from reported temperature dependence are listed below.

Ligand	Substrate	$\Delta\Delta S^{\neq}$ $\Delta\Delta H^{\neq}$	Temp range/°C	Ref.
(*R*)-Prophos	Bz-ΔPhe-OH	−3.53, −8.17	10—80	5d
(*S,S*)-BDPP	Ac-ΔPhe-OH	−9.2 , −12	−20—70	5c
DIOXOP	Ac-ΔPhe-OH	53 , 15	0—100	6b
(*R,R*)-DIOP	Ac-ΔPhe-OH	−16 , −11	25—100	6b

9) The hydrogenation of dehydrodipeptides on heterogeneous catalyst, such as Pd/C, gave usually low to moderate diastereoselectivities: K. Harada, "Asymmetric Synthesis," ed by J. D. Morrison, Academic Press, New York (1985), Vol. 5, p. 349; M. Nakayama, G. Maeda, T. Kaneko, and H. Katsura, *Bull. Chem. Soc. Jpn.*, **44**, 1150 (1971); D. Meyer, J. C. Poulin, and H. B. Kagan, *J. Org. Chem.*, **45**, 4680 (1980).

10) A. H. Blatt, *Org. Synth.*, Coll. Vol. 2, 1 (1943).

11) D. G. Doherty, J. E. Tietzman, and M. Bergmann, *J. Biol. Chem.*, **147**, 617 (1943).

 © 1989 The Chemical Society of Japan Bull. Chem. Soc. Jpn., 62, 3513—3517 (1989)

Synthesis of 1,5-Bifunctionalized Optically Active 3-Pentanol as a Reversible Chiral Building Block. Asymmetric Reduction of 4-(1,3-Dithian-2-yl)-3-oxobutanoates with Fermenting Bakers' Yeast

Hidenori CHIKASHITA,* Kazuhiko OHKAWA, and Kazuyoshi ITOH
Department of Applied Chemistry, Faculty of Engineering, Kansai University, Suita, Osaka 564
(Received June 12, 1989)

Bakers' yeast reduction of a homologous series of 4-(1,3-dithian-2-yl)-3-oxobutanoates to the corresponding chiral 4-(1,3-dithian-2-yl)-3-hydroxybutanoates was investigated. A shift in enantiomeric excess, stereochemistry, and chemical yield of the reduction product was observed as the size of the ester alkoxyl group was changed. The kind of bakers' yeast (raw or dry) and reaction conditions also affected the optical purity and chemical yield of the product. These studies showed that the reduction of methyl 4-(1,3-dithian-2-yl)-3-oxobutanoate with the raw yeast in the absence of additives was most efficient, giving methyl (*S*)-4-(1,3-dithian-2-yl)-3-hydroxybutanoate with 77% ee in 37% yield.

The synthetic utility of microorganisms and enzymes as organic reagents has recently been demonstrated by their numerous applications to the synthesis of valuable chiral building blocks of high optical purity.[1] Among these bioorganic transformations, the synthesis of optically active and symmetrically functionalized secondary alcohol such as 1,5-bifunctionalized 3-pentanol, symbolized as **1**, is of importance and has received significant attention in recent years.[2,3] Recent studies in this field have made it possible to obtain this type of bifunctional chiral alcohol with varying degree of enantiomeric selectivity.[2,3] We considered, however, that (*S*)- or (*R*)-4-(1,3-dithian-2-yl)-3-hydroxybutanoate **3** could be an excellent candidate as such type of chiral building block for the synthesis of a variety of natural products (e.g., polyoxygenated compounds) because not only for its ease of functional convertibility but its utility as two configurational antipodes (reversible) by synthetic chemical distinguishing between the potentially equivalent two (dithianyl and ester) functional groups. We now wish to report the synthesis of a novel 1,5-bifunctional 3-pentanol **3** as a reversible chiral building block by employing the asymmetric reduction of 4-(1,3-dithian-2-yl)-3-oxobutanoates **2** with fermenting bakers' yeast (*Saccharomyces Cerevisiae*).

1

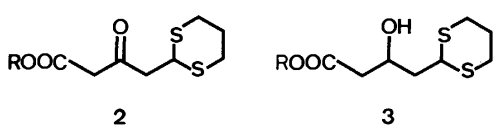

2 3

a : R = CH_3
b : R = C_2H_5
c : R = n-C_8H_{17}
d : R = K

Results and Discussion

Methyl and ethyl esters **2a,b** were prepared by alkylation of dienol silyl ethers **4a,b** of the corresponding 3-oxobutanoates with 1,3-dithienium tetrafluoroborate. Octyl ester **2c** was obtained by the ester-exchange reaction of **2a** with 1-octanol in the presence of *p*-toluenesulfonic acid (*p*-TsOH). Potassium carboxylate **2d** was prepared by the hydrolysis of **2a** in ethanol with 1 M KOH (1 M=1 mol dm^{-3}) and used directly for the subsequent yeast reduction. The reduction of a homologous series of 1,3-dithianyl-3-oxobutanoates **2a—d** with raw bakers' yeast under standard conditions provided the corresponding β-hydroxy esters **3a—c** together with optically pure (*S*)-1-(1,3-dithian-2-yl)-2-propanol (**5**). The latter compound was produced by the yeast reduction of the initially formed decarboxylation product **6**.[4] The results are summarized in Table 1. Optical purity of the β-hydroxy esters obtained was determined by 400 MHz ^1H NMR analyses of the respective (+)-α-methoxy-α-(trifluoromethyl)phenylacetic acid ((+)-MTPA) ester derivatives **7a—c** and the (+)-MTPA esters of the respective racemic form as references obtained by the reduction of **2a,c** with $Zn(BH_4)_2$ and of **2b** with $NaBH_4$.[5]

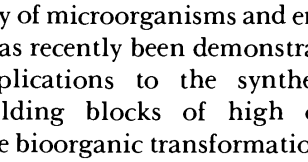

4a : R = CH_3
b : R = C_2H_5

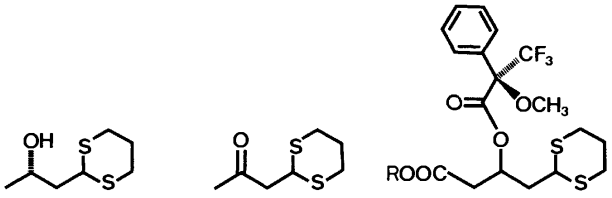

5 6 7

As shown in Table 1, a shift in the enantiomeric

Table 1. Reduction of 4-(1,3-Dithian-2-yl)-3-oxobutanoates **2** with Raw Bakers' Yeast under Standard Conditions[a]

Entry	Substrate	Time/day	Product yields/%[b]		ee of **3**/%[d]	Absolute config.[d]
			3	**5**[c]		
1	**2a**	7	16	26	74	*S*
2	**2b**	10	14	13	50	*S*
3	**2c**	10	15	21	14	*R*
4	**2d**	3	3[e]	8	86	*S*

a) The reaction conditions were described in the Experimental section. b) Yields of pure products separated by MPLC. c) In all cases, the optical purity was determined to be >98% ee. d) See text. e) Isolated as the corresponding methyl ester after work-up with diazomethane.

excess and stereochemistry of the product **3** were observed as a function of the size of the ester alkoxyl group transformed. Methyl and ethyl esters **2a,b** were reduced by bakers' yeast to (*S*)-**3a,b** preferentially in 74% and 50% ee, respectively (Entries 1,2). On the other hand, the yeast reduction of potassium salt **2d** also gave (*S*)-**3a** after work-up with diazomethane with the highest optical purity (86% ee), but the chemical yield was too low to be synthetically useful (Entry 4). However, the reduction of octyl ester **2c** preferentially formed (*R*)-**3c** in 14% ee (Entry 3). Recently, Zhou et al. have closely examined the Prelog rule, which has been used to predict the stereochemistry of yeast reductions of acyclic ketones, on the yeast reduction of 4-chloro-3-oxobutanoates.[6] They showed that the esters having a very small alkoxyl group and a very large one were reduced to the (*S*)- and (*R*)-isomer, respectively, and the ee-value consecutively dropped as the size of the ester alkoxyl group draw near to medium. Our results on stereoselectivity and trend toward the ee-value shift are explicable based on the Prelog rule in analogy to the results of Zhou et al. However, the enantiomeric excess in the reduction of methyl ester **2a** was higher than that (ca. 65% ee) of methyl 4-chloro-3-oxopropanoate while the reduction of octyl ester **2c** showed lower stereoselectivity than that (ca. 97% ee) of octyl 4-chloro-3-oxopropanoate. Since the stereochemical course and enantioselectivity of the bakers' yeast reduction of β-keto esters should be mainly determined by the relative balance in steric bulk derived from the carbonyl substituents, the aforementioned fact is most likely due to the relative bulkiness of the dithianyl moiety when compared with the chloromethyl moiety (i.e., the relatively small difference in size between the dithianyl and ester moieties in **2**).

The absolute configuration of the hydroxy esters obtained in the present bakers' yeast reduction was determined by transforming **3a** into known lactone **11** as follows. Hydrolysis of the dithioacetal group of compound **8** obtained by the silylation of the β-hydroxy ester **3a** with *t*-butyldiphenylsilyl chloride (TBDPS-Cl) and imidazole in DMF provided the aldehyde **9**. The aldehyde **9** was reduced to **10** with $Zn(BH_4)_2$ in ether and the subsequent lactonization of **10** with *p*-TsOH in benzene gave the 3-hydroxyvalerolactone derivative **11**, $[\alpha]_D^{24}$ +7.0° (*c* 0.26, $CHCl_3$). Since the specific rotation of (*R*)-**11** with 80% ee is previously reported in the literature to be $[\alpha]_D$ +9.2° (*c* 7.7, $CHCl_3$),[3] the absolute configuration of the major isomer of **3a** was thus established to be *S*. The absolute configurations of **3b** and **3c** were determined by a similar comparison of $[\alpha]_D$ after respective conversion into the corresponding methyl ester by the ester-exchange reaction with *p*-TsOH in benzene.

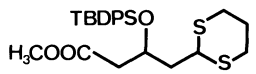

8

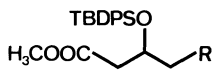

9 : R = CHO
10 : R = CH_2OH

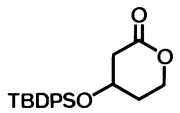

11

It is indicated from recent results appeared in the literature that the optical purity of the yeast reduction of β-keto esters depends on substrate concentration, the kind of commercially available forms of bakers' yeast (raw cake or dried granules), and the concentration of sugars.[7] Thus, we evaluated these effects on the reduction of **2a**, with an aim of possible improvement in the chemical yield and optical purity of **3a**. The results are summarized in Table 2. When dry yeast was used in place of raw yeast under the standard conditions, the enantiomeric excess dropped from 74% to 61% (Entry 4). However, considerable improvement in both chemical yield and optical purity could be achieved by the reduction using raw yeast without sugar, giving **3a** in 37% yield with 77% ee (Entry 2). The reduction without additives under low substrate concentration did not further influence the ee-value of **3a** in spite of the significant improvement in decarboxylation of **2a** (Entry 3). Accordingly, the

Table 2. Bakers' Yeast Reduction of **2a** under Several Conditions

Entry	Reaction conditions[a,b]			Chemical yield/%[e]		ee of **3a**/%[f]
	Yeast	Initial concn of **2a**	Additives[c]	**3a**	**5**	
1	Raw	7.7×10^{-2} M	S/N/M	16	26	74
2	Raw	7.7×10^{-2} M	None	37	45	77
3	Raw	3.8×10^{-2} M	None	28	7	78
4	Dry[d]	7.7×10^{-2} M	S/N/M	31	27	61

a) All the reactions were carried out with the 1-mmol scale of the substrate **2a** according to the standard procedure (see Experimental section). b) Reaction time: 7 days for Entry 1; 5 days for Entries 2 and 3; 4 days for Entry 4. c) S=sucrose, N=$Na_4P_2O_7$, M=$MgSO_4$. d) Half amount of raw yeast was used. e) Yields of pure products separated by MPLC. f) In all cases, absolute configuration of the major product was determined to be S.

useful chiral building block, methyl (*S*)-4-(1,3-dithian-2-yl)-3-hydroxybutanoates **3a**, is now available in 37% chemical yield and in 77% optical purity.

Experimental

Melting points were recorded on a Yanagimoto micro melting point apparatus and are uncorrected. Optical rotations were determined with a Union Digital PM-101 polarimeter. IR spectra were obtained on a Perkin Elmer Model 1660 FT-IR spectrophotometer. ^{1}H NMR spectra were measured with a JEOL JNM-GX400 spectrometer at 400 MHz with tetramethylsilane as an internal reference. Silica gel (Merck silica gel 60, 230—400 mesh ASTM) was used for medium-pressure liquid chromatography (MPLC). Analytical and preparative TLC were carried out on Merck precoated silica gel plates (Merck silica gel 60 F_{254}).

Materials. Raw bakers' yeast (Oriental Yeast Co.) and Dry granular yeast (Oriental Yeast Co.) were commercially available. 1,3-Bis(trimethylsiloxy)-1-methoxy-1,3-butadiene (**4a**) and 1,3-bis(trimethylsiloxy)-1-ethoxy-1,3-butadiene (**4b**) were prepared according to reported methods.[8] 1,3-Dithienium tetrafluoroborate was prepared according to the method of Corey et al.[9] Zinc borohydride was prepared from sodium borohydride and zinc chloride as a 0.3 M ethereal solution.[10] The other reagents were supplied as high grade commercial products and used without further purification.

Methyl 4-(1,3-Dithian-2-yl)-3-oxobutanoate (2a). A solution of 1,3-dithienium tetrafluoroborate (9.02 g, 44 mmol) in dry nitromethane (93 ml) was cooled to −40 °C under nitrogen and a solution of dienol silyl ether **4a** (26 g, 100 mmol) in dry dichloromethane (93 ml) was then added dropwise. After stirring for 30 min at −40 °C, the mixture was allowed to slowly warm to room temperature and the stirring was continued for 19 h under nitrogen. 2 M HCl (20 ml) was added to the mixture and the solution was stirred for 30 min. The aqueous mixture was extracted with ether and the extract was washed with saturated aqueous $NaHCO_3$ solution and water. The organic layer was dried with $MgSO_4$ and concentrated under reduced pressure to give crude crystalline product. Recrystallization from methanol afforded pure **2a** as colorless needles (8.06 g, 78%); mp 70—70.2 °C; IR (KBr) 2976, 2956, 2904, 1737, 1714, 1434, 1416, 1404, 1356, 1321, 1275, 1247, 1196, 1172, 1132, 1116, 1085, 1046, 1016, 1000, 966, 910, and 576 cm^{-1}; ^{1}H NMR ($CDCl_3$) δ=1.88 (m, 1H), 2.11 (m, 1H), 2.88 (m, 4H), 2.98 (d, 2H, J=6.8 Hz), 3.51 (s, 2H), 3.75 (s, 3H), and 4.49 (t, 1H, J=6.8 Hz). Calcd for $C_9H_{14}O_3S_2$: C, 46.13; H, 6.02%. Found: C, 46.75; H, 5.92%.

Ethyl 4-(1,3-Dithian-2-yl)-3-oxobutanoate (2b). Dienol silyl ether **4b** (11.5 g, 41.9 mmol) was reacted with 1,3-dithienium tetrafluoroborate (4.15 g, 20.2 mmol) by a method similar to the preparation of **2a**. Recrystallization of the crude product from ethanol afforded pure **2b** as colorless needles (3.22 g, 64%); mp 71.6—72 °C; IR (KBr) 2978, 1724, 1470, 1438, 1411, 1358, 1316, 1279, 1189, 1171, 1131, 1115, 1085, 1029, 1004, 947, 931, 908, 872, 809, 669, 654, 632, and 575 cm^{-1}; ^{1}H NMR ($CDCl_3$) δ=1.29 (t, 3H, J=7.1 Hz), 1.88 (m, 1H), 2.11 (m, 1H), 2.88 (m, 4H), 2.98 (d, 2H, J=6.8 Hz), 3.49 (s, 2H), 4.21 (q, 2H, J=7.1 Hz), and 4.50 (t, 1H, J=6.8 Hz). Calcd for $C_{10}H_{16}O_3S_2$: C, 48.36; H, 6.49%. Found: C, 48.44; H, 6.51%.

Octyl 4-(1,3-Dithian-2-yl)-3-oxobutanoate (2c). A mixture of **2a** (3.81 g, 16.2 mmol), 1-octanol (30 ml), and *p*-TsOH monohydrate (310 mg, 1.62 mmol) in benzene (60 ml) was refluxed for 20 h. The mixture was cooled to room temperature and washed with saturated aqueous $NaHCO_3$ solution and water and then dried with $MgSO_4$. After evaporation of benzene under reduced pressure, most of remained 1-octanol was removed by vacuum distillation. MPLC purification (benzene-ethyl acetate 25:1 v/v) of the residue gave pure **2c** as a colorless heavy oil (4.15 g, 77%); IR (KBr) 2931, 1744, 1716, 1474, 1456, 1438, 1408, 1394, 1357, 1319, 1271, 1189, 1175, 1132, 1116, 1085, 1045, 1025, 991, 966, 913, 812, 722, 633, and 577 cm^{-1}; ^{1}H NMR ($CDCl_3$) δ=0.89 (t, 3H, J=7.1 Hz), 1.28 (br, 10H), 1.71 (m, 2H), 1.95 (m, 1H), 2.06 (m, 1H), 2.78 (ddd, 2H, J=14.2, 9.8, 2.9 Hz), 2.94 (ddd, 2H, J=14.2, 6.8, 2.9 Hz), 3.36 (d, 2H, J=7.8 Hz), 3.69 (s, 2H), 3.76 (t, 2H, J=6.4 Hz), and 4.32 (t, 1H, J=7.8 Hz). Calcd for $C_{16}H_{28}O_3S_2$: C, 57.79; H, 8.49%. Found: C, 57.89; H, 8.44%.

Bakers' Yeast Reduction of 4-(1,3-Dithian-2-yl)-3-oxobutanoates; Representative Method. Raw bakers' yeast (112 g) was dispersed in a solution of sucrose (22.9 g), $Na_4P_2O_7$ (11.2 g), and $MgSO_4$ (250 mg) in distilled water (335 ml), and the mixture was then stirred for 30 min at 25 °C. To the fermenting mixture was added the β-keto ester **2** (25.6 mmol) and stirred at the same temperature for 7 days (an additional bakers' yeast (56 g), sucrose (11.5 g), $Na_4P_2O_7$ (5.6 g), $MgSO_4$ (125 mg), and distilled water (167 ml) were supplied every day). Ethyl acetate (634 ml) was added to the reaction mixture and the mixture was stirred for 16 h. After filtration through a Celite pad, the filtrate was extracted with ethyl acetate and the extract was dried with $MgSO_4$. The solvent was removed by evaporation under reduced pressure and the residue was diluted with dichloromethane. The solution was filtered through a silica-gel pad (Wakogel

C-300) and evaporated under reduced pressure. Purification of the residue by MPLC (**3a**, hexane-ethyl acetate 5:3 v/v; **3b** and **3c**, benzene-ethyl acetate 10:1 v/v) gave pure β-hydroxy ester **3** as a colorless oil. Spectroscopic and analytical data of the reduction products **3** are as follows:

3a: $[\alpha]_D^{25}$ +1.0° (*c* 1.56, $CHCl_3$) (74% ee); IR (neat) 3460, 2949, 2902, 2850, 1729, 1437, 1372, 1277, 1197, 1075, 1046, 1020, 910, 872, 849, 774, 715, and 665 cm^{-1}; ^1H NMR ($CDCl_3$) δ=1.79—2.00 (m, 3H), 2.13 (m, 1H), 2.47 (dd, 1H, *J*=16.6, 8.4 Hz), 2.54 (dd, 1H, *J*=16.6, 3.7 Hz), 2.87 (m, 4H), 3.14 (d, 1H, *J*=3.9 Hz), 3.72 (s, 3H), 4.29 (dd, 1H, *J*=9.6, 4.6 Hz), and 4.35 (m, 1H). Calcd for $C_9H_{16}O_3S_2$: C, 45.74; H, 6.82%. Found: C, 45.63; H, 6.89%.

3b: $[\alpha]_D^{33}$ +2.6° (*c* 2.83, $CHCl_3$) (50% ee); IR (neat) 3418, 2903, 1732, 1464, 1424, 1374, 1277, 1186, 1074, 1023, 943, 909, 874, 848, 773, and 665 cm^{-1}; ^1H NMR ($CDCl_3$) δ=1.28 (t, 3H, *J*=7.1 Hz), 1.79—2.00 (m, 3H), 2.13 (m, 1H), 2.45 (dd, 1H, *J*=16.6, 8.5 Hz), 2.52 (dd, 1H, *J*=16.6, 3.7 Hz), 2.88 (m, 4H), 3.21 (d, 1H, *J*=3.9 Hz), 4.18 (q, 2H, *J*=7.1 Hz), 4.30 (dd, 1H, *J*=9.8, 4.6 Hz), and 4.34 (m, 1H). Calcd for $C_{10}H_{18}O_3S_2$: C, 47.97; H, 7.25%. Found: C, 47.95; H, 7.36%.

3c: $[\alpha]_D^{22}$ +0.19° (*c* 2.11, $CHCl_3$) (14% ee); IR (neat) 3452, 2926, 2854, 1729, 1466, 1423, 1345, 1276, 1247, 1182, 1073, 1018, 910, 872, 853, 774, 723, and 666 cm^{-1}; ^1H NMR ($CDCl_3$) δ=0.88 (t, 3H, *J*=7.1 Hz), 1.28 (br, 10H), 1.63 (m, 2H), 1.79—2.00 (m, 3H), 2.13 (m, 1H), 2.45 (dd, 1H, *J*=16.6, 8.5 Hz), 2.53 (dd, 1H, *J*=16.6, 3.7 Hz), 2.89 (m, 4H), 3.18 (d, 1H, *J*=4.2 Hz), 4.11 (t, 2H, *J*=6.8 Hz), 4.30 (dd, 1H, *J*=9.8, 4.6 Hz), and 4.34 (m, 1H). Calcd for $C_{16}H_{30}O_3S_2$: C, 57.45; H, 9.04%. Found: C, 57.28; H, 8.97%.

Methyl (*S*)-3-(*t*-Butyldiphenylsiloxy)-4-(1,3-dithian-2-yl)-butanoate (8). To a stirred solution of **3a** (1.01 g, 4.2 mmol) in dry DMF (4.6 ml) was added TBDPS-Cl (1.70 g, 6.2 mmol) and imidazole (0.85 g, 12.4 mmol) at room temperature. After stirring for 2 h at room temperature, the solvent was removed in vacuo. The residue was extracted with ethyl acetate (30 ml) and 5% aqueous oxalic acid solution (8 ml×3). The organic layer was then successively washed with 5% aqueous oxalic acid solution (15 ml), saturated aqueous $NaHCO_3$ solution (15 ml), and water (15 ml). The solution was dried with $MgSO_4$ and evaporated under reduced pressure to give almost TLC-pure product. MPLC purification (benzene-ethyl acetate 25:1 v/v) of the crude product afforded pure **8** as a colorless oil (2.02 g, 99%); $[\alpha]_D^{24}$ −6.9° (*c* 2.28, $CHCl_3$); IR (neat) 3070, 3048, 3014, 2998, 2931, 2896, 2856, 1738, 1472, 1462, 1427, 1390, 1362, 1276, 1197, 1157, 1111, 998, 940, 858, 822, 741, 704, and 610 cm^{-1}; ^1H NMR ($CDCl_3$) δ=1.05 (s, 9H), 1.78 (m, 1H), 1.97 (m, 3H), 2.50 (dd, 2H, *J*=6.0, 2.2 Hz), 2.67 (m, 4H), 3.52 (s, 3H), 3.94 (dd, 1H, *J*=8.4, 6.1 Hz), 4.43 (m, 1H), 7.40 (m, 6H), and 7.69 (m, 4H).

Methyl (*R*)-3-(*t*-Butyldiphenylsiloxy)-5-oxopentanoate (9). To a solution of **8** (1.01 g, 2.13 mmol) in acetonitrile (11 ml) and water (0.38 ml) was added iodomethane (1.59 g, 11.2 mmol) and K_2CO_3 (196 mg, 1.41 mmol). The mixture was refluxed for 3 h and the solvent was then removed by evaporation under reduced pressure. The residue was extracted with dichloromethane and the extract was dried with $MgSO_4$. The residue obtained by evaporation of the solvent under reduced pressure was purified by MPLC (hexane-ethyl acetate 4:1 v/v) to give pure **9** as a pale yellow oil (231 mg, 28%); $[\alpha]_D^{19}$ −1.7° (*c* 2.56, $CHCl_3$); IR (neat) 3073, 2932, 2859, 1742, 1714, 1473, 1428, 1363, 1308, 1160, 1112, 786, 702, 668, 612, 518, and 512 cm^{-1}; ^1H NMR ($CDCl_3$) δ=1.03 (s, 9H), 2.62 (m, 4H), 3.57 (s, 3H), 4.62 (m, 1H), 7.42 (m, 6H), 7.66 (m, 4H), and 9.62 (t, 1H, *J*=2.2 Hz).

Methyl (*R*)-3-(*t*-Butyldiphenylsiloxy)-5-hydroxypentanoate (10). To an ethereal solution of $Zn(BH_4)_2$ (0.3 M, 6.9 ml) cooled to 0 °C was added dropwise a solution of **9** (310 mg, 0.84 mmol) in dry ether (7 ml) with stirring under nitrogen and stirring was then continued for 2 h at 0 °C. After the addition of water (6 ml), the aqueous mixture was filtered and extracted with ether. The organic layer was dried with $MgSO_4$ and concentrated under reduced pressure to give crude product. MPLC purification (benzene-ethyl acetate 4:1 v/v) afforded pure **10** as a colorless oil (160 mg, 49%); $[\alpha]_D^{23}$ −1.7° (*c* 0.92, $CHCl_3$); IR (neat) 2959, 2931, 2858, 1738, 1472, 1428, 1391, 1362, 1309, 1261, 1221, 1164, 1112, 1084, 1027, 1008, 998, 927, 823, 703, and 613 cm^{-1}; ^1H NMR ($CDCl_3$) δ=1.05 (s, 9H), 1.66 (brs, 1H), 1.76 (m, 2H), 2.54 (d, 2H, *J*=6.3 Hz), 3.53 (s, 3H), 3.63 (m, 2H), 4.37 (m, 1H), 7.40 (m, 6H), and 7.69 (m, 4H).

(*R*)-3-(*t*-Butyldiphenylsiloxy)-5-pentanolide (11). A mixture of **8** (144 mg, 0.37 mmol) and *p*-TsOH monohydrate (7 mg, 0.037 mmol) in benzene (3.4 ml) was refluxed for 1 h. After cooling to room temperature, saturated aqueous $NaHCO_3$ solution (10 ml) was added to the mixture and the aqueous mixture was then extracted with benzene. The organic layer was dried with $MgSO_4$ and concentrated under reduced pressure to give crude product. MPLC purification (benzene-ethyl acetate 4:1 v/v) afforded pure **11** as a colorless oil (57 mg, 44%): $[\alpha]_D^{24}$ +7.0° (*c* 0.26, $CHCl_3$) (lit,[3] $[\alpha]_D$ +9.2° (*c* 7.69, $CHCl_3$)); IR (neat) 3461, 3071, 3049, 2932, 2856, 1731, 1589, 1567, 1472, 1427, 1391, 1361, 1261, 1223, 1161, 1114, 928, 864, 822, 742, 701, and 610 cm^{-1}; ^1H NMR ($CDCl_3$) δ=1.07 (s, 9H), 1.84 (m, 2H), 2.58 (d, 2H, *J*=4.9 Hz), 4.22 (m, 2H), 4.62 (ddd, 1H, *J*=11.4, 8.8, 4.2 Hz), 7.42 (m, 6H), and 7.63 (m, 4H).

H. C. thanks the Ministry of Education, Japan, for financial support by a Grant-in-Aid for the Scientific Research (No. 63750820).

References

1) For reviews, see: C. J. Sih and J. P. Rosaza, "Applications of Biochemical Systems in Organic Chemistry," John Wiley & Sons, New York, N. Y. (1976), Part 1; K. Mori and T. Sugai, *Yuki Gosei Kagaku Kyokai Shi*, **41**, 1044 (1983); C. J. Sih and C. S. Chen, *Angew. Chem., Int. Ed. Engl.*, **23**, 570 (1984); G. M. Whitesides and C. H. Wong, *ibid.*, **24**, 617 (1985); J. B. Jones, *Tetrahedron*, **42**, 3351 (1986); T. Fujisawa, T. Sato, and T. Itoh, *Yuki Gosei Kagaku Kyokai Shi*, **44**, 519 (1986); H. Ohta, *ibid.*, **46**, 726 (1988).

2) D. W. Brooks and J. T. Palmer, *Tetrahedron Lett.*, **24**, 3059 (1983); D. W. Brooks, N. C. Lee, and R. Peevey, *ibid.*, **25**, 4623 (1984); A. S. Gopalan and C. J. Sih, *ibid.*, **25**, 5235 (1984); F. Moriuchi, H. Muroi, and H. Aibe, *Chem. Lett.*, **1987**, 1141; R. Roy and A. W. Rey, *Tetrahedron Lett.*, **28**, 4935 (1987); E. Baader, W. Bartmann, G. Beck, A. Bergmann, H. W. Fehlhaber, H. Jendralla, K. Kesseler, R. Saric, H. Schussler, V. Teetz, M. Weber, and G. Wess, *ibid.*, **29**, 2563 (1988); F. Bennett and D. W. Knight, *ibid.*, **29**, 4865 (1988).

3) D. W. Brooks, R. P. Kellogg, and C. S. Cooper, *J. Org. Chem.*, **52**, 192 (1987).

4) The bakers' yeast reduction of the dithianyl ketone **6** to **5** and its application to natural product synthesis have been already reported: D. Ghiringhelli, *Tetrahedron Lett.*, **24**, 287 (1983); H, Chikashita, E. Kittaka, Y. Kimura, and K. Itoh, *Bull. Chem. Soc. Jpn.*, **62**, 833 (1989).

5) J. A. Dale and H. S. Mosher, *J. Am. Chem. Soc.*, **95**, 512 (1973).

6) B. Zhou, A. S. Gopalan, F. VanMiddlesworth, W. R. Shieh, and C. J. Sih, *J. Am. Chem. Soc.*, **105**, 5925 (1983). A similar examination has been reported for the yeast reduction of β-keto esters: M. Hirama, M. Shimizu, and M. Iwashita, *J. Chem. Soc., Chem. Commun.*, **1983**, 599.

7) For example see: K. Nakamura, K. Inoue, K. Ushio, S. Oka, and A. Ohno, *J. Org. Chem.*, **53**, 2589 (1988); K. Nakamura, Y. Kawai, S. Oka, and A. Ohno, *Bull. Chem. Soc. Jpn.*, **62**, 875 (1989).

8) S. Danishefsky and T. Kitahara, *J. Am. Chem. Soc.*, **96**, 7807 (1974); P. Brownbridge, T. H. Chan, M. A. Brook, and G. J. Kang, *Can. J. Chem.*, **61**, 688 (1983).

9) E. J. Corey and S. W. Walinsky, *J. Am. Chem. Soc.*, **94**, 8932 (1972).

10) W. J. Gensler, F. Johnson, and A. D. B. Sloan, *J. Am. Chem. Soc.*, **82**, 6074 (1960).

Preparation of 3(2*H*)-Furanones from 2-Propynyl Alcohol, CO, and Phenyl Halides under CO_2 Atmosphere Catalyzed by Transition Metal Complexes

Yoshio INOUE,* Kunihiro OHUCHI, I-Fang YEN, and Shin IMAIZUMI
Department of Engineering Science, Faculty of Engineering, Tohoku University, Aramaki, Aoba-ku, Sendai 980
(Received May 27, 1989)

The novel synthetic method for 2,2-dimethyl-5-phenyl-3(2*H*)-furanone (bullatenone) from 2-methyl-3-butyn-2-ol, CO, and phenyl halides in the presence of a catalytic amount of transition metal complexes under the influence of CO_2 has been described. It was revealed that there was the intermediate formation of an acetylenic ketone from the acetylenic alcohol, CO, and the phenyl halide followed by the formation of a cyclic carbonate from the acetylenic ketone and CO_2 which underwent the decarboxylative transformation into the 3(2*H*)-furanone quantitatively.

In recent years, considerable interest has been paid for the fixation of carbon dioxide (CO_2) from the points of the recycle of carbon resources and the environment.[1)]

During the course of our studies directed at the effective utilization of CO_2, we have explored that 2-methyl-3-butyn-2-ol (**1**) reacts with carbon monoxide (CO) and phenyl halides in the presence of a catalytic amount of transition metal complexes to afford 2,2-dimethyl-5-phenyl-3(2*H*)-furanone (**2a**) under the influence of CO_2.[2)]

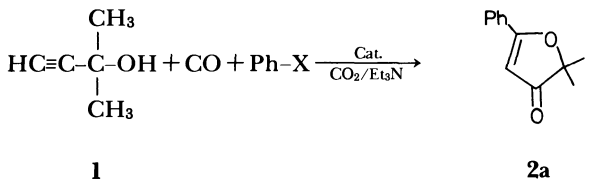

1 **2a**

The product **2a** is called bullatenone, which occurs in the essential oil of Myrtus bullata, a shrub endemic to New Zealand.[3)] The 3(2*H*)-furanone ring is contained in many naturally occurring compounds characterized by important biological activity as antitumor agents (eremantholides, geiparvarin) or aroma constituents.[4)]

It appears that the straightforward production of the furanone from the starting materials is difficult. Furthermore the role of CO_2 on this reaction is not distinct, partly because it does not enter into the stoichiometry. In this paper we describe the elucidation of the reaction pathway as well as the scope of this new method for the synthesis of 3(2*H*)-furanones.

Results and Discussion

Various Group 8, 9, and 10 transition metal–triphenylphosphine complexes were active as the catalyst for the formation of the furanone **2a** from the acetylenic alcohol **1**, CO, and iodobenzene in triethylamine under the influence of CO_2 as shown in Table 1. Yields, in general, were moderate to reasonable except in the case of [$RhCl(PPh_3)_3$], where the yield was only modest. In the present reaction triethylamine functions as a base as well as a solvent. The employment of Na_2CO_3 or K_2CO_3 as the base resulted in the marked decrease in the yield. The effect of CO_2 was significant since the yield of **2a** dropped considerably and oily products came out when the reaction was performed under CO atmosphere.

Table 1. Effect of Catalyst on the Synthesis of **2a**[a)]

Catalyst	Solvent	Base	Yield of **2a**[b)]/%
$FeCl_2(PPh_3)_2$	NEt_3	—	62 (21)
$CoCl_2(PPh_3)_2$	NEt_3	—	61 (29)
$CoCl_2(PPh_3)_2$	CH_3CN	K_2CO_3	15
$NiCl_2(PPh_3)_2$	NEt_3	—	57 (36)
$RuCl_2(PPh_3)_3$	NEt_3	—	52 (19)
$RhCl(PPh_3)_3$	NEt_3	—	18 (3)
$PdCl_2(PPh_3)_2$	NEt_3	—	48 (38)
$PdCl_2(PPh_3)_2$	DMF	Na_2CO_3	18
$PdCl_2(PPh_3)_2$	CH_3CN	K_2CO_3	20
$PdCl_2(PPh_3)_2$	CH_3CN	Li_2CO_3	Trace
$PdCl_2(PPh_3)_2$	CH_3CN	Et_3N	69
$Pd(PPh_3)_3$	NEt_3	—	79 (26)
$Pd(PPh_3)_3$	Toluene	Na_2CO_3	0
$Pd(PPh_3)_4$	NEt_3	—	45 (40)
$Pd(PPh_3)_4$	CH_3CN	K_2CO_3	8
$PtCl_2(PPh_3)_2$	NEt_3	—	45 (23)
$Pt(PPh_3)_4$	NEt_3	—	64 (35)

a) **1** 10 mmol, PhI 10 mmol, CO 10 atm, CO_2 10 atm, catalyst 0.2 mmol, solvent 10 cm^3, base 15 mmol; 100 °C, 8 h. b) GLC yield. The figures in the parentheses represent the yields of the reactions performed under CO atmosphere.

In order to elucidate the reaction pathway as well as the role of CO_2, the reaction was performed at 100 °C under CO atmosphere using [$PdCl_2(PPh_3)_2$] as the catalyst. With a shorter reaction time rather than the standard 8 h reaction, an acetylenic ketone, 4-hydroxy-4-methyl-1-phenyl-2-pentyn-1-one (**3**) was formed as the major product. As shown in Fig. 1, the acetylenic ketone **3** occurred at the early stage and decreased gradually, while the furanone **2a** was generated slowly and almost linearly. The acetylenic ketone appears to be an intermediate for the furanone formation. Apparently, however, not all the acetylenic ketone **3** produced was converted into **2a**. This observation is

consistent with the production of the oily substance (vide supra).

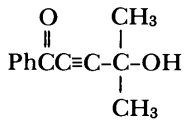

3

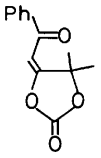

4

On the other hand (*E*)-4-benzoylmethylene-5,5-dimethyl-1,3-dioxolan-2-one (**4**) was produced at the early stage of the reaction in the presence of both CO and CO_2 with $[PdCl_2(PPh_3)_2]$ as the catalyst (Fig. 2). The formation of the acetylenic ketone **3** was not observed in this case. It seems interesting that both CO and CO_2 are incorporated in one molecule. The cyclic carbonate **4** decreased fairly rapidly with efficient formation of the furanone **2a** under the reaction conditions. Consequently the carbonate **4** seems to be another intermediate. This was confirmed actually as follows. The carbonate **4** was subjected to the thermal degradation at 100 °C for 1 h in the presence of 2 molar % of $[Pd(PPh_3)_4]$ under either CO or CO_2 atmosphere. This process led to 73 and 75% conversion of **4** into the furanone **2a**, respectively. The degradation of **4** at 150 °C for 20 min led to the complete conversion into the furanone **2a** after the quantitative evolution of CO_2.

The relationship between **3** and **4** must be elucidated in the next place. This was made clear by reacting **3** with CO_2 at 70 °C for 1 h in triethylamine in the absence of the catalyst. This procedure gave **4** in 68% isolated yield. The cyclization proceeded even in benzene at the sacrifice of the yield (100 °C, 8 h; 21%).

Thus the following pathway is established for the palladium system.

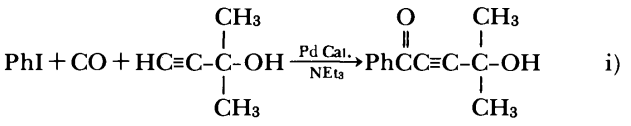

i)

1 3

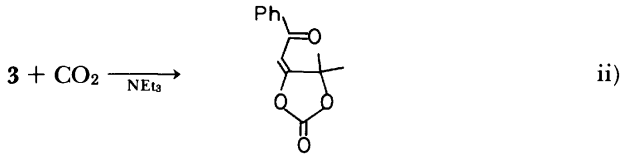

ii)

4

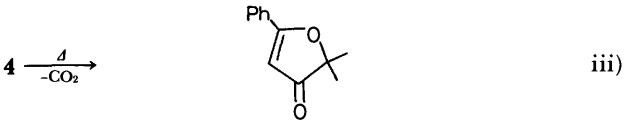

iii)

2a

The initial step i) is the formation of the acetylenic ketone **3** from iodobenzene, CO, and 2-methyl-3-butyn-2-ol (**1**). This type of the reaction has been documentated by Tanaka et al.[5] The reaction has been recognized to involve the oxidative addition of a phenyl halide to a low valent metal complex followed by the insertion of CO into the resulting metal-aryl bond to give the aroyl intermediate which is in turn cloven by the attack of an acetylenic molecule to afford the acetylenic ketone. The subsequent step ii) is the triethylamine-assisted intramolecular cycloaddition of the monocarbonate ($PhC(O)C{\equiv}CC(CH_3)_2OC(O)OH$) generated intermediarily from the acetylenic ketone **3** and CO_2 giving the cyclic carbonate **4**.[6] Addition of oxygen-containing nucleophiles to aryl ethynyl ketones has been demonstrated to proceed in a syn fashion.[7] The present cyclization reaction corresponds to the intramolecular version predicting the (*E*)-stereochemistry around the double bond in **4**. The final step iii) was the decarboxylative conversion of **4** into the furanone **2a**. The (*E*)-stereochemistry permits the ready conversion.

There is an apprehension that different pathways might be accomodated in the distinct systems. It seems difficult to elucidate the reaction pathway of every catalytically active system because of the diversity of

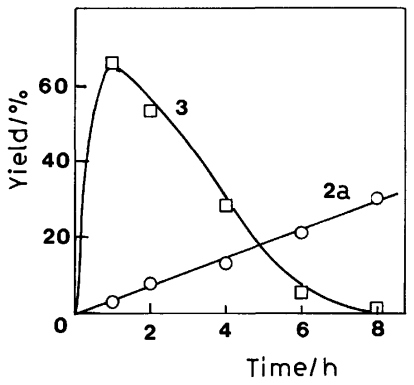

Fig. 1. Reaction of **1** with PhI under CO atmosphere with a $[PdCl_2(PPh_3)_2]$ catalyst.

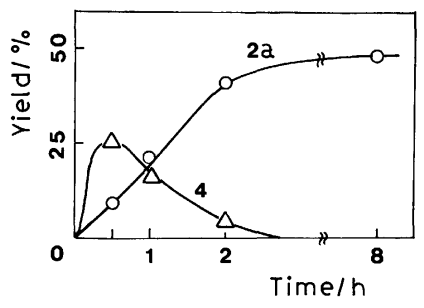

Fig. 2. Reaction of **1** with PhI under CO and CO_2 atmosphere with a $[PdCl_2(PPh_3)_2]$ catalyst.

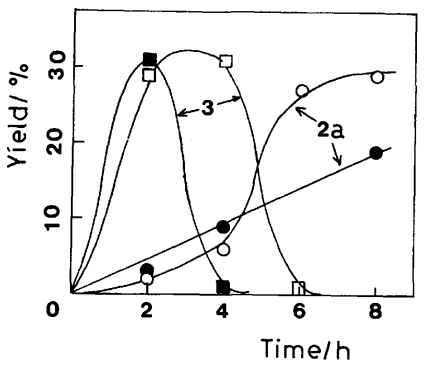

Fig. 3. Reaction of **1** with PhI under CO atmosphere with a $[CoCl_2(PPh_3)_2]$ (□ and ○) or a $[RuCl_2(PPh_3)_3]$ (■ and ●) catalyst.

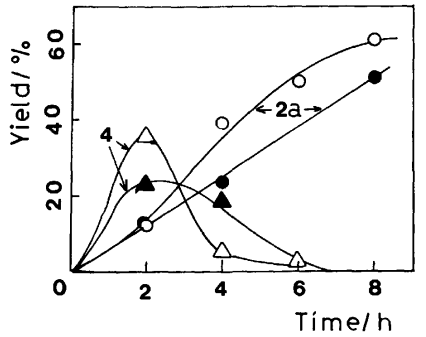

Fig. 4. Reaction of **1** with PhI under CO and CO_2 atmosphere with a $[CoCl_2(PPh_3)_2]$ (△ and ○) or a $[RuCl_2(PPh_3)_3]$ (▲ and ●) catalyst.

metal catalysts. We selected $[RuCl_2(PPh_3)_3]$ and $[CoCl_2(PPh_3)_2]$ as the representative of the Group 8 and 9 metal triad, respectively. The results are shown in Figs. 3 and 4. The same intermediates as the palladium system, **3** and **4**, as well as the similar trends of the reactions were observed. Thus it is evident that the same mechanism is operative at least in these systems, too.

The 3(2*H*)-furanone **2a** occurred even under the atmosphere of CO (Table 1). On careful examination of the products obtained from the reactions performed under CO atmosphere, we found that the cyclic carbonate **4**, albeit in a very small amount, was present in the reaction mixture (by IR; 1855, 1830 cm^{-1}). This indicates the presence of CO_2 in the system. One possible origin is the CO_2 in the air which might be dissolved in triethylamine used as the solvent. To confirm this, the triethylamine distilled under N_2 was subjected to the reaction. However the scope was almost the same under the standard reaction conditions with a $[PdCl_2(PPh_3)_2]$ catalyst. Another one is the water-gas shift reaction, which is known to be catalyzed by transition metal complexes.[8]

$$CO + H_2O \rightleftharpoons CO_2 + H_2$$
$$(\text{or } CO + H_2O + MX_2 \longrightarrow CO_2 + 2HX + M)$$

Table 2. Synthesis of 3(2*H*)-Furanone **2** from Organic Halide (R-X), CO, and **1**[a]

R	X	Yield of **2**[b]/%
C_6H_5-	Br	**2a** (35)
C_6H_5-	I	**2a** (48)
p-$CH_3C_6H_4$-	I	**2b** 46
p-ClC_6H_4-	Br	**2c** 68
(*E*)-PhCH=CH-	Br	**2d** 41
1-Naphthyl	Br	**2e** 45
CH_2=$CHCH_2$-	OAc	**2f** 9[c]

a) **1** 10 mmol, organic halide 10 mmol, CO 10 atm, CO_2 10 atm, $[PdCl_2(PPh_3)_2]$ 0.2 mmol, NEt_3 10 cm^3; 100 °C, 8 h. b) Isolated yield. The figures in the parentheses represent the GLC yield. c) The product was the 1-propenyl derivative.

Consequently eventual water may cause the generation of a trace amount of CO_2. Since the CO_2 produced in this way would work catalytically, a considerable amount of the furanone **2a** could be produced via the steps i), ii), and iii). Thus the reaction under CO atmosphere (10 atm) at 100 °C for 8 h with $[PdCl_2(PPh_3)_2]$ as the catalyst afforded **2a** in 30% yield when care was taken to reduce the eventual water from the chemicals employed by adding appropriate desiccants. With a $[CoCl_2(PPh_3)_2]$ catalyst, the yield of **2a** decreased to 8% with concomitant formation of **3** in 38% yield, supporting the above conjecture.

In order to expand the initial scope of our investigation, several aryl and alkenyl halides were submitted to the reaction. The substrates listed in Table 2 afforded the corresponding furanones in moderate yields with $[PdCl_2(PPh_3)_2]$ as the catalyst. In addition to aryl halides, allyl acetate took part in the reaction yielding the 1-propenyl derivative in a modest yield. *o*-$IC_6H_4NO_2$, *o*-$BrC_6H_4CH_3$, *p*-BrC_6H_4Br, *p*-BrC_6H_4OH, *p*-BrC_6H_4CHO, 2-bromopyridine, and cinnamyl acetate did not afford the corresponding furanones although several of them were consumed. The major difficulty of these compounds in producing the furanone seems to lie in the step i), i.e., acetylenic ketone formation.[5] However further study on the effects of substituents has not been undertaken.

All attempts to utilize 2-propynyl alcohol or 3-butyn-2-ol in place of 2-methyl-3-butyn-2-ol (**1**), for the elaboration of the 3(2*H*)-furanones not disubstituted in the 2-position proved fruitless unfortunately. In conclusion, the present reaction offers a new and facile method for the synthesis of certain simple 3(2*H*)-furanones, e.g., bullatenone. The main feature is the employment of easily available starting materials.

Experimental

Melting points are uncorrected. ^1H and ^{13}C NMR spectra were recorded in chloroform-*d* with JEOL FX-60Q spectrometer with tetramethylsilane as an internal standard. IR and MS spectra were recorded on a JASCO A-3 and JEOL

JMS D-300 spectrometer, respectively. Gas and liquid chromatography was performed on a Hitachi 263-30 gas chromatograph.

Materials. CO and CO_2 gases were used without further purification. Organic halides, 2-propynyl alcohols, and solvents were used as received. In certain cases, $MgSO_4$ (for iodobenzene and **1**) and KOH (for triethylamine) were used as desiccants. Transition metal complexes were synthesized according to the standard methods.

Synthesis of the Furanone 2. The synthesis of 2,2-dimethyl-5-phenyl-3(2*H*)-furanone (**2a**) is typical. Into a 50 cm^3 stainless steel autoclave, 2-methyl-3-butyn-2-ol (**1**; 10 mmol), iodobenzene (10 mmol), triethylamine (10 cm^3), and $[PdCl_2(PPh_3)_2]$ (0.2 mmol) were charged. Then the air in the autoclave was evacuated by a water aspirator. After CO (10 atm) and CO_2 (10 atm) were introduced, the mixture was agitated at 100 °C for 8 h. GLC analysis (DEGS, 2 m, 190 °C) showed the formation of **2a** in 48% yield. Kugelrohr distillation (150 °C/2 mmHg) followed by recrystallization from hexane gave an analytical sample; (1 mmHg=133.322 Pa). Mp 66.5—67.5 °C (lit,[3] 67.5—68.5 °C). The IR,[9] ^1H NMR,[9] ^{13}C NMR,[10] and mass[11] spectra were consistent with those reported in the literatures. Found: C, 76.33; H, 6.44%. Calcd for $C_{12}H_{12}O_2$: C, 76.57; H, 6.43%.

2,2-Dimethyl-5-(*p*-tolyl)-3(2*H*)-furanone (2b): Prepared from *p*-iodotoluene and isolated by Kugelrohr distillation (125—135 °C/0.2 mmHg). Recrystallization from hexane gave an analytical sample. Mp 65.2—66.4 °C. Found: C, 77.49; H, 7.05%. Calcd for $C_{13}H_{14}O_2$: C, 77.20; H, 6.98%. IR ($CDCl_3$) 1690, 1595, 1180 cm^{-1}. ^1H NMR δ=1.47 (s, 6H), 2.40 (s, 3H), 5.87 (s, 1H), 7.20 (d, J=8 Hz, 2H), 7.70 (d, J=8 Hz, 2H).

5-(*p*-Chlorophenyl)-2,2-dimethyl-3(2*H*)-furanone (2c): Prepared from *p*-bromochlorobenzene and isolated by sublimation under reduced pressure (140—150 °C/1 mmHg). Recrystallization from toluene gave an analytical sample. Mp 218 °C. Found: C, 64.32; H, 5.09; Cl, 16.13%. Calcd for $C_{12}H_{11}ClO_2$: C, 64.73; H, 4.94; Cl, 15.94%. IR (KBr) 1680, 1600, 1325, 1100, 765 cm^{-1}. ^1H NMR δ=1.50 (s, 6H), 5.96 (s, 1H), 7.40 (d, J=9.6 Hz, 2H), 7.75 (d, J=9.6 Hz, 2H).

(*E*)-2,2-Dimethyl-5-styryl-3(2*H*)-furanone (2d): Prepared from β-bromostyrene and isolated by Kugelrohr distillation (130—150 °C/3 mmHg) followed by column chromatography on silica gel (chloroform). Mp 75.0—76.1 °C. Found: C, 78.92; H, 6.78%. Calcd for $C_{14}H_{14}O_2$: C, 78.48; H, 6.59%. IR (KBr) 1690, 1630, 1580, 1560, 1380, 1185, 995, 760, 700 cm^{-1}. ^1H NMR δ=1.24 (s, 6H), 5.56 (s, 1H), 6.80 (d, J=16.8 Hz, 1H), 7.20—7.70 (m, 6H).

2,2-Dimethyl-5-(1-naphthyl)-3(2*H*)-furanone (2e): Prepared from 1-bromonaphthalene and isolated by column chromatography on silica gel (chloroform). Mp 130.1—131.3 °C. Found: C, 80.75; H, 5.60%. Calcd for $C_{16}H_{14}O_2$: C, 80.65; H, 5.92%. IR (KBr) 1690, 1570, 1180, 810, 780 cm^{-1}. ^1H NMR δ=1.58 (s, 6H), 5.97 (s, 1H), 7.40—8.40 (m, 7H).

(*E*)-2,2-Dimethyl-5-(1-propenyl)-3(2*H*)-furanone (2f): Prepared from allyl acetate and isolated by column chromatography on silica gel (chloroform). Liquid. Bp 75—85 °C/0.3 mmHg. IR (neat) 1700, 1650, 1390, 1185, 980, 760 cm^{-1}. ^1H NMR δ=1.40 (s, 6H), 1.97 (d, J=7 Hz, 3H), 5.40 (s, 1H), 6.23 (d, J=16 Hz, 1H), 6.83 (dp, J=16 Hz, 7 Hz, 1H).

The Reaction in the Absence of CO_2. The reaction was performed in the absence of CO_2 according to the standard procedure for, for example, 0.5 h with $[PdCl_2(PPh_3)_2]$ as the catalyst. GLC analysis (DEGS, 2 m, 190 °C) showed the formation of 4-hydroxy-4-methyl-1-phenyl-2-pentyn-1-one (**3**) in 66% yield together with the furanone **2a** in 3% yield. The acetylenic ketone **3** was isolated by distillation under reduced pressure. Bp 135—137 °C/2 mmHg. IR (neat) 3400, 2200, 1640, 1270, 1175, 960, 700 cm^{-1}. ^1H NMR δ=1.64 (s, 6H), 2.90 (s, 1H), 7.20—7.60 (m, 3H), 8.00—8.15 (m, 2H).

Short Time Reaction in the Presence of CO and CO_2. When the reaction was discontinued in short time, (*E*)-4-benzoylmethylene-5,5-dimethyl-1,3-dioxolan-2-one (**4**) was obtained together with the furanone **2a** as shown in Fig. 2. The cyclic carbonate **4** was isolated by column chromatography on silica gel eluting with chloroform. This compound was converted completely into the furanone **2a** during the GLC measurement (DEGS, 190 °C). Mp 106—107 °C. IR (KBr) 1855, 1830, 1675, 1620, 1270, 1150, 995 cm^{-1}. ^1H NMR δ=1.87 (s, 6H), 6.80 (s, 1H), 7.20—8.00 (m, 5H). ^{13}C NMR δ=24.0, 88.8, 99.6, 128.0, 128.7, 133.3, 138.0, 149.8, 167.1, 188.1. The reactions in the presence or absence of CO_2 with the other catalysts, for example $[CoCl_2(PPh_3)_2]$ and $[RuCl_2(PPh_3)_3]$, were performed in the similar manner as above.

Synthesis of the Cyclic Carbonate 4 from the Acetylenic Ketone 3 and CO_2. **3** (5 mmol) and triethylamine (5 cm^3) were placed in an autoclave. After the introduction of CO_2 (10 atm), the autoclave was heated at 70 °C for 1 h. Column chromatography of the reaction mixture on silica gel (hexane/ethyl acetate=5) gave the cyclic carbonate **4** in 68% yield. On the other hand the reaction of **3** (5 mmol) with CO_2 (10 atm) in benzene (5 cm^3) at 100 °C for 8 h gave **4** in 21% yield.

Decarboxylative Conversion of the Cyclic Carbonate 4 into the Furanone 2a. Into an autoclave, **4** (105 mg, 0.45 mmol), $[Pd(PPh_3)_4]$ (2 molar%), and trietylamine (5 cm^3) were placed. After CO (10 atm) was introduced, the autoclave was heated at 100 °C for 1 h. This procedure gave the furanone **2a** in 73% yield. The degradation of **4** under CO_2 atmosphere (10 atm) led to the formation of **2a** in 75% yield under the similar conditions. The degradation at 150 °C was performed as follows. Into a 50 cm^3 round bottomed flask connected with a gas buret, **4** (218 mg, 0.938 mmol) was placed and heated at about 150 °C for 20 min in an oil bath. The CO_2 gas evolved was 122.1 cm^3 at 22 °C (0.91 mmol, 97%) and the residue weighed was 172 mg (0.936 mmol, 100%). IR analysis confirmed the complete conversion of **4** into the furanone **2a**.

References

1) For a review, see S. Inoue and N. Yamazaki, "Organic and Bio-organic Chemistry of Carbon Dioxide," ed by S. Inoue and N. Yamazaki, Kodansya, Tokyo (1981).

2) Y. Inoue, M. Taniguchi, H. Hashimoto, K. Ohuchi, and S. Imaizumi, *Chem. Lett.*, **1988**, 81.

3) T. Brandt and W. I. Taylor, *J. Chem. Soc.*, **1954**, 3425; W. Parker, R. A. Raphael, and D. I. Wilkinson, *ibid.*, **1958**, 3871.

4) A. Takeda, S. Tsuboi, and T. Sakai, *Chem. Lett.*, **1973**, 425; Y. Takahashi, H. Hagiwara, H. Uda, and H. Kosugi, *Heterocycles*, **15**, 225 (1981); J. E. Baldwin, R. C. Thomas, L. I. Kruse, and L. Silberman, *J. Org. Chem.*, **42**, 3846 (1977); S.

Sebti and A. Foucand, *Tetrahedron*, **42**, 1361 (1986); A. B. Smith, III and P. J. Jerris, *Synth. Commun.*, **8**, 421 (1978).

5) T. Kobayashi and M. Tanaka, *J. Chem. Soc., Chem. Commun.*, **1981**, 333; M. Tanaka, T. Kobayashi, and T. Sakakura, *Nippon Kagaku Kaishi*, **1985**, 537.

6) Metal assisted cyclization of this type has also been reported: H. Laas, A. Nissen, and A. Nurrenbach, *Synthesis*, **1981**, 958; K. Iritani, N. Yanagihara, and K. Utimoto, *J. Org. Chem.*, **51**, 5501 (1986); Y. Sasaki, *Tetrahedron Lett.*, **27**, 1575 (1986); Y. Inoue, J. Ishikawa, M. Taniguchi, and H. Hashimoto, *Bull. Chem. Soc. Jpn.*, **60**, 1204 (1987).

7) V. K. Tripathi, P. S. Venkataramani, and G. Mehta, *J. Chem. Soc., Perkin Trans. 1*, **1979**, 36.

8) D. J. Darenbourg, M. B. Fischer, R. E. Schmidt, Jr., and B. J. Baldwin, *J. Am. Chem. Soc.*, **103**, 1297 (1981).

9) A. B. Smith, III, P. A. Levenberg, P. J. Jerris, R. M. Scarborough, Jr., and P. M. Wovkulich, *J. Am. Chem. Soc.*, **103**, 1501 (1981); R. E. Rosenkranz, K. Allner, R. Good, W. V. Philipsborn, and C. H. Eugster, *Helv. Chim. Acta*, **46**, 1259 (1963).

10) P. S. Mariano and M. Peters, *Tetrahedron Lett.*, **1974**, 2607.

11) L. H. Briggs and G. W. White, *J. Chem. Soc. C*, **1971**, 3077.

Facile Preparation of Optically Active Bicyclo[3.3.1]nonane-2,6-diol and 3,3,7,7-Tetramethylbicyclo[3.3.1]nonane-2,6-diol by Enzyme-Catalyzed Hydrolysis, and Enantiomer Recognition Behavior of Crown Ethers and Podands Having These Diols as a Chiral Subunit[1)]

Koichiro NAEMURA,* Takahisa MATSUMURA, Masanori KOMATSU, Yoshiki HIROSE, and Hiroaki CHIKAMATSU
Department of Chemistry, Faculty of Engineering Science, Osaka University, Toyonaka, Osaka 560
(Received June 22, 1989)

Hydrolysis of 2,6-diacetoxybicyclo[3.3.1]nonane (**5**) using lipase from Candida *cylindracea* gave (+)-(1*S*,2*R*,5*S*,6*R*)-6-acetoxybicyclo[3.3.1]nonan-2-ol (**4**) with 81% e.e. and (−)-(1*R*,2*S*,5*R*,6*S*)-**5** with 95% e.e., and pig liver esterase-catalyzed hydrolysis of 2,6-diacetoxy-3,3,7,7-tetramethylbicyclo[3.3.1]nonane (**9**) afforded (−)-(1*S*,2*R*,5*S*,6*R*)-3,3,7,7-tetramethylbicyclo[3.3.1]nonane-2,6-diol (**7**) with 96% e.e. and (+)-(1*R*,2*S*,5*R*,6*S*)-**9** with 86% e.e. By lithium aluminum hydride reduction, (+)-**4** and (−)-**5** were converted to (+)-bicyclo[3.3.1]nonane-2,6-diol (**3**) and (−)-**3** with high optical purity, respectively, and (+)-**7** was obtained from (+)-**9**. Using these optically active diols **3** and **7** as a chiral subunit, optically active crown ethers and podands were prepared and their enantiomer recognition behavior was evaluated by the enantiomer differential transport of (±)-1,2-diphenylethylamine and methyl ester of (±)-phenylglycin hydrochloride through bulk liquid membrane.

Since Cram reported the syntheses of a variety of optically active crown ethers incorporating [1,1′-binaphthalene]-2,2′-diol with C_2-symmetry as a chiral subunit,[2)] various kind of C_2-diols have been incorporated into crown ethers as a chiral subunit.[3)] Recently, we have also reported the syntheses and chiral recognition behaviors of the chiral crown ethers having C_2-5,6,11,12-tetrahydro-6,12-methanodibenzo[*a*,*e*]cyclooctene-5,11-diol[4)] and C_2-7,8,15,16-tetrahydro-7,15-methanodinaphtho[1,2-*a*:1′,2′-*e*]cyclooctene-8,16-diol[5)] as a chiral subunit. These diols possess the bicyclo[3.3.1]nonane-2,6-diol moiety as a common structural feature. These recent results prompted us to examine the chiral recognition properties of crown ethers having the bicyclo[3.3.1]nonane derivatives containing no aromatic moiety as a chiral subunit, and we chose bicyclo[3.3.1]nonane-2,6-diol (**3**) and 3,3,7,7-tetramethylbicyclo[3.3.1]nonane-2,6-diol (**7**) as a chiral building block.

Utilization of enzymes in organic synthesis to prepare chiral compounds of synthetic value is well documented.[6)] Especially, hydrolytic enzymes useful for the preparation of optically active alcohols are attractive in this regard because they operate without requiring expensive coenzymes. We have also investigated the enantioselective reaction mediated by enzyme.[7)] Our continuing interest on biocatalysts in organic synthesis led us to resolve the C_2-diols, the chiral building block, by enzyme-catalyzed kinetic resolution. In this paper we wish to report pig liver esterase (PLE)- and lipase from Candida *cylindracea* (CCL)-catalyzed enantiomerically selective hydrolyses of racemic 2,6-diacetoxybicyclo[3.3.1]nonane (**5**) and 2,6-diacetoxy-3,3,7,7-tetramethylbicyclo[3.3.1]nonane (**9**), and to report syntheses and chiral recognition behavior of crown ethers incorporating bicyclo[3.3.1]nonane-2,6-diol (**3**) and 3,3,7,7-tetramethylbicyclo[3.3.1]nonane-2,6-diol (**7**) as a chiral subunit.

Results and Discussion

Bicyclo[3.3.1]nonane-2,6-diol (**3**) is a chiral molecule of C_2-symmetry, and an introduction of methyl groups, an additional steric barrier, into this skeleton provides 3,3,7,7-tetramethylbicyclo[3.3.1]nonane-2,6-diol (**7**) which has also C_2-symmetry.

Treatment of **1** with excess of methyl iodide and potassium *t*-butoxide in *t*-butyl alcohol gave **2** in 70% yield. Reduction of **2** with lithium aluminum hydride yielded a 95:5 mixture of diastereomers, recrystallization of which from hexane–ether provided **7**, and the minor isomer was not isolated. Treatment of **7** with acetic anhydride and pyridine gave **9**. The C_2-endo,endo-configuration of **9** was unambiguously confirmed by its ^{1}H NMR spectrum which exhibited two singlet signals at δ=0.99 and 1.04 due to the exo- and endo-methyl groups, a singlet signal at δ=2.05 due to the $-OCOCH_3$ protons, and a doublet signal at δ=4.78 (J=6.4 Hz) due to the protons on the carbon bearing the hydroxyl group.

Enzyme-Catalyzed Hydrolyses of Diacetates. PLE- and CCL-catalyzed hydrolysis of **5** and **9** were performed in 0.1 M (1 M=1 mol dm^{-3}) phosphate buffer solution at pH 8.0 and pH 7.4, respectively. In every cases, the reaction processes were monitored by GLC and the reactions were terminated at, or closs to, 50%-of-hydrolysis point. The product was extracted with chloroform and purified by column chromatography. The results are summarized in Table 1.

In the case of hydrolysis of (±)-**5**, CCL-catalyzed hydrolysis gave (+)-**4** and (−)-**5** with 81% and 95% e.e., respectively. By lithium aluminum hydride reduction, (+)-**4** and (−)-**5** were converted into (+)-**3** and (−)-**3**, respectively. Since **3** is a crystalline solid, its optical purity was further enriched by recrystallization from

Table 1. Enantioselective Hydrolysis of Racemic Substrates

Entry	Substrate	Enzyme	Time/h	Product (% yield)	e.e./%
1	(±)-**5**	PLE	5.5	(+)-(1*S*,2*R*,5*S*,6*R*)-**4** (47)	30
				(−)-(1*R*,2*S*,5*R*,6*S*)-**5** (43)	31
2	(±)-**5**	CCL	24	(+)-(1*S*,2*R*,5*S*,6*R*)-**4** (36)	81
				(−)-(1*R*,2*S*,5*R*,6*S*)-**5** (46)	95
3	(±)-**9**	PLE	22	(−)-(1*S*,2*R*,5*S*,6*R*)-**7** (43)	96
				(+)-(1*R*,2*S*,5*R*,6*S*)-**9** (46)	86
4	(±)-**9**	CCL	71	(−)-(1*S*,2*R*,5*S*,6*R*)-**7** (5)	66
				(−)-(1*S*,2*R*,5*S*,6*R*)-**8** (40)	55
				(+)-(1*R*,2*S*,5*R*,6*S*)-**9** (40)	53

ethyl acetate and the both enantiomers of **3** with >98% e.e. were obtained. On the basis of the absolute configuration of (+)-(1*S*,2*R*,5*S*,6*R*)-**3**,[8] the chemical correlations described above revealed unambiguously the absolute configurations of the acetates **4** and **5** as illustrated in their structural formulas. The maximum rotation of (−)-**3** ($[\alpha]_{D\,max.}$ −59.8°) permitted to calculate the e.e. values of acetates **4** and **5**. PLE-catalyzed hydrolysis of (±)-**5** proceeded smoothly to give (+)-**4** and (−)-**5**, but the enantiomer selectivity of this hydrolysis is poor.

It has been described that **3** was resolved via diastereomeric camphanic acid ester,[8] but the chemical method is rather troublesome. The CCL-catalyzed kinetic resolution of **3** was more facile than the chemical method, and provided both enantiomers with high optical purity.

PLE-catalyzed hydrolysis of (±)-**9** gave (−)-**7** with 96% e.e. and (+)-**9** with 86% e.e. The latter was transformed to (+)-**7** by lithium aluminum hydride reduction. CCL-catalyzed hydrolysis of (±)-**9** gave (−)-**8** and (+)-**9** together with a small amount of (−)-**7**, but their optical purities were too low to be synthetically useful as a chiral building block. Reduction of (−)-**8** with lithium aluminum hydride gave (−)-**7**. The determination of absolute configurations of **2** and **7** was straightforward. Treatment of (+)-(1*S*,5*S*)-**1**[8] with methyl iodide gave (+)-(1*R*,5*R*)-**2**, which was converted into (+)-**7**. The chemical correlation assigned the 1*R*,2*S*,5*R*,6*S*-configuration to (+)-**7**. The optically active diol (−)-**7**, prepared by PLE-catalyzed hydrolysis, was converted into the optically active benzoate **10** whose e.e. value was determined to be 96% by HPLC-analysis. On the basis of the e.e. value of **7**, those of the acetates **8** and **9** were confirmed. As described above, PLE-catalyzed hydrolysis of **9** provided a facile method for the preparation of the optically active both enantiomers of **7**.

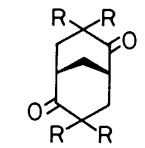

(−)-1 R = H
(−)-2 R = CH_3

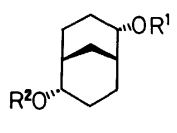

(−)-3 $R^1 = R^2$ = H
(−)-4 R^1 = CCH_3 R^2 = H
(−)-5 $R^1 = R^2$ = CCH_3
(−)-6 R^1 = H R^2 = CH_2Ph

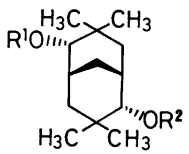

(+)-7 $R^1 = R^2$ = H
(+)-8 R^1 = CCH_3 R^2 = H
(+)-9 $R^1 = R^2$ = CCH_3
10 $R^1 = R^2$ = C

Preparation of Crown Ethers and Podands. Next our task was the preparation of crown ethers and podands using these optically active diols **3** and **7** as a chiral subunit. One of the ethylene glycol units of 18-crown-6 was replaced by the chiral diols (−)-**3** and (+)-**7** to give the crown ethers (−)-**11** and (+)-**12**,

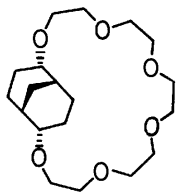

(−)-11

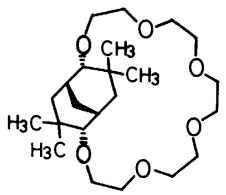

(+)-12

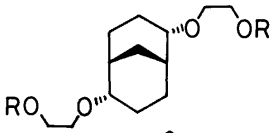

13 R =
(−)-14 R = H
(−)-15 R = Ms
(−)-16 R = Ts
(−)-17 R = $CH_2CH_2OCH_3$

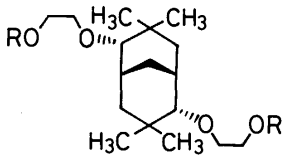

18 R = CH_2OCH_3
(+)-19 R = H
(+)-20 R = Ms
(+)-21 R = $CH_2CH_2OCH_3$

respectively. High dilution condensation of (−)-**3** with pentaethylene glycol bis(*p*-toluenesulfonate) in the presence of sodium hydride in refluxing tetrahydrofuran (THF) provided the crown ether (−)-**11** in 24% yield after chromatography and, similarly, (+)-**12** was prepared from (+)-**7** in 19% yield. The preparation of the crown ethers (−)-**22** and (+)-**23** having two chiral subunits was carried out stepwise. Treatment of (−)-**3** with the *p*-toluenesulfonate of 2-(2-tetrahydropyranyloxy)ethanol and sodium hydride in dimethyl sulfoxide (DMSO) at 40 °C gave **13**, whose protective group was removed with hydrochloric acid and methanol to yield (−)-**14** in 62% yield for two steps. The

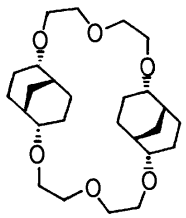

(-)-22

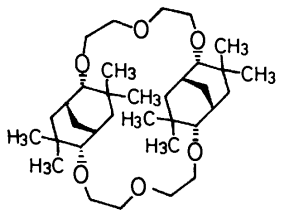

(+)-23

diol (−)-**14** was condensed with (−)-**15**, prepared from (−)-**14** and methanesulfonyl chloride, in the presence of sodium hydride in DMSO at 40 °C to give (−)-**22** in 14% yield. Treatment of (+)-**7** with the *p*-toluenesulfonate of 2-(methoxymethoxy)ethanol and sodium hydride gave **18**, which was transformed to (+)-**19** on treatment with hydrochloric acid and methanol. High dilution condensation of (+)-**19** with (+)-**20**, prepared from (+)-**19**, and sodium hydride in DMSO gave (+)-**23** in 14% yield.

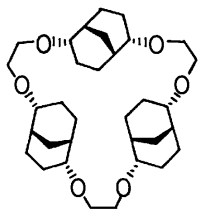

24

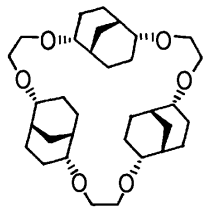

25

Next we attempted to prepare two diastereomeric crown ethers having three chiral subunits.[9] One of them is the crown ether, (*S,S*),(*R,R*),(*S,S*)-isomer **24**, which contains two (2*S*,6*S*)-subunits and a (2*R*,6*R*)-subunit, and the another crown ether, (*R,R*),(*R,R*),(*R,R*)-isomer **25**, contains three chiral subunits, all of which have the same configuration. The key feature of our strategy for construction of these crown ethers **24** and **25** was the preparation of the open-chain polyethers **27** and **30** with the (*S,S*),(*R,R*),(*S,S*) and the (*R,R*),(*R,R*),(*R,R*)-configuration, respectively. The diols (−)-**3** and (+)-**3** were converted into (−)-**6** and (+)-**6**, respectively, with benzyl bromide and sodium hydride in DMSO. Condensation of (+)-**16**, prepared from (+)-**14**, with 2 equiv of (−)-**6** in the presence of sodium hydride in DMSO at 40 °C yielded (−)-**26** with the (*S,S*),(*R,R*),(*S,S*)-configuration in 43% yield. Debenzylation of (−)-**26** with lithium aluminum hydride in THF gave (−)-**27** in 84% yeild, and treatment of (−)-**27** with methyl iodide and sodium hydride yielded (−)-**28** having the methoxyl groups as a terminal group in 76% yield. The another polyether (+)-**29** having three (2*R*,6*R*)-subunits was prepared in 33% yield by condensation of (+)-(2*R*,6*R*)-**16** with 2 equiv of (+)-(2*R*,6*R*)-**6**. Hydrogenolytic debenzylation of (+)-**29** with 10% Pd on carbon and *p*-toluenesulfonic acid under 1 atm of hydrogen gave (+)-**30** in 91% yield, which was also transformed to (+)-**31**. The final step

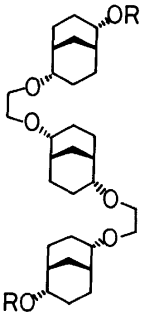

(-)-26 R = CH_2Ph
(-)-27 R = H
(-)-28 R = CH_3

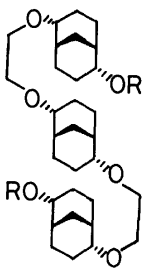

(+)-29 R = CH_2Ph
(+)-30 R = H
(+)-31 R = CH_3

of our strategy was ring closure of the open-chain polyethers (−)-**27** and (+)-**30** by condensation with ethylene glycol bis(methanesulfonate) and sodium hydride. Unfortunately, all attempts to prepare **24** and **25** were failed.

Our final synthetic task was the preparation of the chiral dipodands **17** and **21**. Reaction of (−)-**3** with the *p*-toluenesulfonate of 2-(2-methoxyethoxy)ethanol and sodium hydride in DMSO gave (−)-**17** in 78% yield, and, analogously, (+)-**21** was prepared from (+)-**7** in 90% yield.

Enantiomer Recognition Behavior of Crown Ethers and Podands. The enantiomer recognition behavior of these crown ethers and podands was evaluated by the enantiomer differential transport of (±)-1,2-diphenylethylamine and methyl ester of (±)-phenylglycin hydrochloride through bulk liquid membrane containing the optically active host molecules.[10] The results are given in Table 2.

A few conspicuous features are worth noting. The chiralities of the twisted carbon skeletons of (−)-(1*R*,2*S*,5*R*,6*S*)-subunit **3** and (+)-(1*R*,2*S*,5*R*,6*S*)-subunit **7** are opposite to each other as illustrated in the structures **32** and **33**. However, both (−)-**10** with the

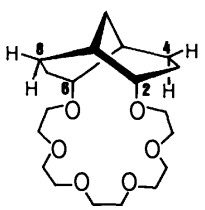

32

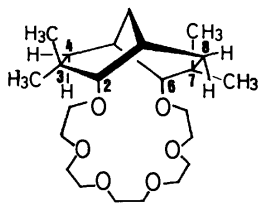

33

(1*R*,2*S*,5*R*,6*S*)-subunit **3** and (+)-**11** with the (1*R*,2*S*,5*R*,6*S*)-subunit **7** transferred preferentially (*S*)-1,2-diphenylethylamine and methyl ester of (*R*)-phenylglycin. The reverse of the selectivity by introduction of the methyl groups into the chiral subunit are rationalized by assuming that, in the case of (−)-**10**, two endo-hydrogen atoms at C-4 and C-8 of the subunit act as a 'chiral steric barrier' and, in the case of (+)-**12**, two endo-methyl groups at C-3 and C-7 are more bulky

Table 2. Differential Transport of Enantiomeric Molecules through Bulk Liquid Membrane Containing Chiral Crown Ethers and Chiral Open-Chain Polyethers

Entry	Host	Guest[a]	Time/h	Transport/%	Configuration of dominant enantiomer	Optical purity/%
1	(−)-**11**	a	2.5	10.7	*S*	21
2	(−)-**11**	b	25	9.9	*R*	20
3	(+)-**12**	a	3.0	10.8	*S*	24
4	(+)-**12**	b	26	10.1	*R*	8
5	(−)-**22**	a	4.8	10.1	*S*	24
6	(−)-**22**	b	74	10.0	*R*	13
7	(+)-**23**	a	8.0	9.9	*S*	26
8	(+)-**23**	b		0[b]		—
9	(−)-**17**	a	5.0	10.4	*S*	26
10	(−)-**17**	b	10(days)	6.7	*R*	4
11	(+)-**21**	a	9.8	10.1	*R*	16
12	(+)-**21**	b	15(days)	4.4	*S*	4
13	(−)-**26**	a	9.4	10.0	*S*	27
14	(−)-**26**	b		0		—
15	(+)-**29**	a	6.2	10.0	*S*	15
16	(+)-**29**	b		0		—
17	(−)-**28**	a	9.8	9.9	*S*	14
18	(−)-**28**	b		0		—
19	(+)-**31**	a	7.4	10.0	*S*	7
20	(+)-**31**	b		0		—

a) a: (±)-1,2-Diphenylethylamine hydrochloride b: Methyl ester of (±)-phenylglycin hydrochloride. b) After 10 days, a significant transport of the guest molecule was not observed.

steric barrier than the endo-hydrogen atoms at C-4 and C-8 as illustrated in **32** and **33**. Introduction of the second chiral subunit into (−)-**11** and (+)-**12** produced little change in the enantiomer selectivity. The results appear to suggest that the cavities of (−)-**22** and (+)-**23**, 24-crown-6 analogue, are so large that the both chiral barriers hardly participate simultaneously in interacting on the guest molecule located in the cavity.

Recently, we examined the enantiomer recognition behavior of the chiral dipodands, and reported that, among the dipodands examined, the dipodand having the 1,4,7-trioxaoctyl groups as a side chain showed the highest enantiomer selectivity and the value was nearly equal to that of crown ether.[11] The enantiomer selectivities of dipodands (−)-**17** and (+)-**21**, both of which have two 1,4,7-trioxaoctyl groups as a side chain, were also comparable to these of crown ethers (−)-**11** and (+)-**12**. The open-chain polyethers (−)-**26** and (−)-**28** with the alternate configuration showed higher enantiomer selectivity toward 1,2-diphenylethylamine than the polyethers (+)-**29** and (+)-**31** having three subunits of the same configuration.

As described above, the parent compound, bicyclo[3.3.1]nonane-2,6-diol itself is certainly effective as a chiral subunit of a crown ether, but the enantiomer selectivity of the crown ether having this subunit is lower than those of the crown ethers containing bicyclo[3.3.1]nonane-2,6-diol derivatives with aromatic moieties as an additional bulky steric barrier.

Experimental

All melting and boiling points are uncorrected. Infrared spectral data were taken on a Hitachi 260-10 spectrophotometer, and ^{1}H NMR spectra were obtained from a JNM-MH-100. Chemical shifts are reported in parts per million (δ) down field from tetramethylsilane. Optical rotations were measured with a JASCO DIP-140 automatic polarimeter. Mass spectra were taken with a JEOL-DX-303 HF spectrometer. Elemental analyses were determined on a Yanagimoto CHN-Coder, Type II.

3,3,7,7-Tetramethylbicyclo[3.3.1]nonane-2,6-dione (2). A solution of **1**[8] (1.71 g, 11.2 mmol) was added to a solution of potassium *t*-butoxide (19.0 g, 0.170 mol) in absolute 2-methyl-2-propanol (200 mL) and then the mixture was stirred for 1.5 h at room temperature. After methyl iodide (19.2 g, 0.135 mol) was dropwise added to the reaction mixture, the resulting mixture was stirred for 1.5 h at room temperature and for an additional 14 h at reflux. The solid precipitated was removed by filtration and the filtrate was concentrated in vacuo. The residue was acidified with 5% hydrochloric acid and extracted with chloroform. The extract was washed with saturated aqueous solution of sodium hydrogencarbonate and water and dried ($MgSO_4$). After the solvent was removed in vacuo, the residue was chromatographed on alumina (hexane/benzene 2/1 v/v eluent) to give **2** (1.63 g, 70% yield) as a solid, recrystallization of which from hexane provided the sample for the analysis, mp 43—45 °C; IR (KBr) 1715, 1700 cm^{-1}; ^{1}H NMR ($CDCl_3$) δ=1.05 (6H, s), 1.20 (6H, s), 2.01 (4H, d, J=5.2 Hz), 2.30 (2H, t, J=2.0 Hz), 2.77 (2H, m). Found: C, 74.71; H, 9.70%. Calcd for $C_{13}H_{20}O_2$: C, 74.96; H, 9.68%.

3,3,7,7-Tetramethylbicyclo[3.3.1]nonane-2,6-diol (7). A solution of **2** (1.16 g, 5.57 mmol) in dry ether (100 mL) was slowly added to a suspension of lithium aluminum hydride (600 mg, 15.8 mmol) in dry ether (100 mL) and then the mixture was heated for 13 h at reflux. After the reaction mixture was cooled in an ice bath, 10% hydrochloric acid was

added to the mixture and the resulting mixture was stirred for 1 h. The inorganic solid was removed by filtration and the solid was continuously extracted using Soxhlet-extraction apparatus. The ethereal solutions were combined and concentrated to give a solid, which was a 95:5 mixture of diastereomers (1.09 g). Recrystallization of the mixture from hexane–ether provided **7** (930 mg, 79% yield), mp 117.5—119 °C; IR (KBr) 3390, 1045 cm^{-1}; ^1H NMR ($CDCl_3$) δ=1.05 (6H, s), 1.10 (6H, s), 1.70 (2H, s), 3.65 (2H, d, J=6.4 Hz), 1.2—2.5 (8H, m). Found: C, 73.35; H, 11.10%. Calcd for $C_{13}H_{24}O_2$: C, 73.53; H, 11.39%.

2,6-Diacetoxy-3,3,7,7-tetramethylbicyclo[3.3.1]nonane (9). To a solution of **7** (15.0 g, 70.7 mmol) in dry pyridine (150 mL) was slowly added acetic anhydride (100 g, 0.980 mol) with ice cooling and then the mixture was stirred for 48 h at room temperature. After the reaction mixture was poured onto ice, the mixture was acidified with hydrochloric acid and extracted with ether. The extract was washed with saturated aqueous solution of sodium hydrogencarbonate and water and dried ($MgSO_4$). After removal of the solvent, the residue was chromatographed on alumina (hexane/benzene 4/1 v/v) to give an oily product, which was distilled to provide **9** (18.5 g, 88% yield); bp 160—165 °C (8 mmHg) (1 mmHg=133.322 Pa); IR (neat film) 1740, 1240 cm^{-1}; ^1H NMR ($CDCl_3$) δ=0.99 (6H, s), 1.04 (6H, s), 2.05 (6H, s), 4.78 (2H, d, J=7.0 Hz), 1.4—2.1 (8H, m). Found: C, 68.55; H, 9.46%. Calcd for $C_{17}H_{28}O_4$: C, 68.89; H, 9.52%.

PLE-Catalyzed Hydrolysis of 2,6-Diacetoxybicyclo[3.3.1]nonane (5). To a solution of (±)-**5** (250 mg, 1.04 mmol) in 0.1 M phospate buffer (400 mL, pH 8.0) was added PLE (Boehringer Mannheim Gmbh Co. 104698 100 Units/mg) (460 μL), and the mixture was stirred for 5.5 h at 30 °C. The mixture was extracted with chloroform and the extract was washed with water and dried ($MgSO_4$). After removal of the solvent, the residue was chromatographed on silica gel. The fractions eluted with chloroform gave (−)-**5** (108 mg, 43% yield) as an oil and the subsequent fractions eluted with the same solvent gave (+)-**4** (97 mg, 47% yield) as an oil.

(+)-**4**; $[\alpha]_D^{23}$ +16.6° (*c* 0.802, $CHCl_3$).

(−)-**5**; $[\alpha]_D^{24}$ −23.0° (*c* 1.24, $CHCl_3$).

CCL-Catalyzed Hydrolysis of 2,6-Diacetoxybicyclo[3.3.1]nonane (5). To a solution of (±)-**5** (500 mg, 2.08 mmol) in 0.1 M phosphate buffer (600 mL, pH 7.4) was added Lipase VII (CCL, Sigma 600—700 Units/mg) (500 mg) and the mixture was stirred for 24 h at 30 °C. The mixture was extracted with chloroform and the extract was washed with water and dried ($MgSO_4$). After removal of the solvent, the residue was chromatographed on silica gel. The fractions eluted with benzene–ether (8/2 v/v) gave (−)-**5** (230 mg, 46%) as an oil and the subsequent fractions eluted with the same solvent gave (+)-**4** (148 mg, 36% yield) as an oil.

(+)-**4**; $[\alpha]_D^{23}$ +45.2° (*c* 1.04, $CHCl_3$); IR (neat film) 3400, 1715, 1240 cm^{-1}.

(−)-**5**; $[\alpha]_D^{24}$ −70.7° (*c* 1.05, $CHCl_3$).

PLE-Catalyzed Hydrolysis of 2,6-Diacetoxy-3,3,7,7-tetramethylbicyclo[3.3.1]nonane (9). By using the same procedure described for the hydrolysis of (±)-**5**, (±)-**9** (500 mg, 1.69 mmol) was hydrolyzed with PLE (300 μL) in 0.1 M phosphate buffer (300 mL, pH 8.0). The chromatography on alumina gave (+)-**9** (230 mg, 46% yield) as an oil and (−)-**7** (155 mg, 43% yield) as a solid.

(−)-**7**; $[\alpha]_D^{24}$ −87.5° (*c* 1.26, $CHCl_3$); mp 144—145 °C.

(+)-**9**; $[\alpha]_D^{25}$ +97.0° (*c* 1.05, $CHCl_3$).

CCL-Catalyzed Hydrolysis of 2,6-Diacetoxy-3,3,7,7-tetramethylbicyclo[3.3.1]nonane (9). By using the same procedure described for the hydrolysis of (±)-**5**, (±)-**9** (250 mg, 0.843 mmol) was hydrolyzed with CCL (750 mg) in 0.1 M phosphate buffer (380 mL, pH 7.4). The chromatography on alumina gave (+)-**9** (100 mg, 40% yield) as an oil, (−)-**8** (86 mg, 40% yield) as a solid, and (−)-**7** (9 mg, 5% yield) as a solid.

(−)-**7**; $[\alpha]_D^{20}$ −60.7° (*c* 0.450, $CHCl_3$).

(−)-**8**; $[\alpha]_D^{22}$ −47.7° (*c* 1.01, $CHCl_3$); IR (KBr) 3450, 1710, 1260 cm^{-1}.

(+)-**9**; $[\alpha]_D^{20}$ +59.3° (*c* 1.91, $CHCl_3$).

(−)-(1*R*,2*S*,5*R*,6*S*)-Bicyclo[3.3.1]nonane-2,6-diol (3). To a suspension of lithium aluminum hydride (1.76 g, 46.4 mol) in dry ether (100 mL) was dropwise added a solution of (−)-**5**; $[\alpha]_D$ −70.7° (2.23 g, 9.28 mmol) in dry ether (100 mL) and then the mixture was heated for 10 h at reflux. To the reaction mixture was added a small amount of ethyl acetate and 10% hydrochloric acid with ice cooling, and the resulting mixture was stirred for 1 h at room temperature. The inorganic solid was filtered off and the solid was continuously extracted with ether using Soxhlet extraction apparatus. The etheral solutions were combined and dried ($MgSO_4$). Removal of the solvent gave **3** (1.15 g, 79% yield); $[\alpha]_D^{24}$ −56.8° (*c* 1.17, ethanol), which was recrystallized from ethyl acetate to yield the specimene; $[\alpha]_D^{25}$ −59.4° (*c* 1.02, ethanol); mp 214.5—215 °C. Found: C, 68.98; H, 10.29%. Calcd for $C_9H_{16}O_2$: C, 69.19; H, 10.32%.

(+)-(1*S*,2*R*,5*S*,6*R*)-Bicyclo[3.3.1]nonane-2,6-diol (3). By using the same procedure described above, (+)-**4**; $[\alpha]_D$ +45.2° (1.61 g, 8.13 mmol) was converted into **3** (1.08 g, 85% yield); $[\alpha]_D^{25}$ +48.5° (*c* 0.773, ethanol), which was recrystallized from ethyl acetate to yield the specimen; mp 214—215 °C; $[\alpha]_D^{26}$ +59.0° (*c* 0.770, ethanol). Found: C, 69.01; H, 10.28%. Calcd for $C_9H_{16}O_2$: C, 69.19; H, 10.32%.

Oxidation of (−)-(1*R*,2*S*,5*R*,6*S*)-Bicyclo[3.3.1]nonane-2,6-diol (3). An excess of Jones' reagent[12] was added to a chilled solution of (−)-**3**; $[\alpha]_D$ −56.4° (*c* 0.378, EtOH) (312 mg, 2.00 mmol), prepared according to Gerlach's procedure,[8] in acetone (8 mL). After stirring for 2 h with ice cooling, sodium bisulfite was added to the reaction mixture. Usual workup followed by chromatography on silica gel (ether) gave (−)-**1**; $[\alpha]_D^{25}$ −206.8° (*c* 1.01, 1,4-dioxane) (94.3% e.e.) (lit,[8] $[\alpha]_{D\,max.}$ −219.2°) (200 mg, 65% yield) as a white solid.

(+)-(1*R*,2*S*,5*R*,6*S*)-3,3,7,7-Tetramethylbicyclo[3.3.1]nonane-2,6-diol (7). By using the same procedure described for the reduction of (−)-**5**, (+)-**9**; $[\alpha]_D$ +97.0° (900 mg, 3.04 mmol) was converted into (+)-**7**; $[\alpha]_D^{25}$ +79.1° (*c* 0.953, $CHCl_3$) (610 mg, 95% yield), which was recrystallized from ether–hexane to provide the specimen; mp 143—144 °C; $[\alpha]_D^{25}$ +91.4° (*c* 1.11, $CHCl_3$). Its spectral data agreed with those of (±)-**7**.

(+)-(1*R*,5*R*)-3,3,7,7-Tetramethylbicyclo[3.3.1]nonane-2,6-dione (2). By using the same procedure described for the preparation of (±)-**2**, (+)-**1**;[8] $[\alpha]_D$ +187.0° (1.71 g, 11.2 mmol) was converted into (+)-**2** (1.25 g, 53% yield); mp 36—38 °C, $[\alpha]_D^{20}$ +100.4° (*c* 0.980, $CHCl_3$). The IR and ^1H NMR spectra are identical with those of (±)-**2**.

Lithium Aluminum Hydride Reduction of (+)-(1*R*,5*R*)-3,3,7,7-Tetramethylbicyclo[3.3.1]nonane-2,6-dione (2). By

using the same procedure described for the preparation of (±)-**7**, (+)-**2**; $[\alpha]_D$ +100.4° (1.16 g, 5.57 mmol) was converted into (+)-**7** (610 mg, 52% yield); mp 141—143 °C, $[\alpha]_D^{24}$ +70.7° (*c* 0.950, $CHCl_3$). The IR and ^1H NMR spectra are identical with those of (±)-**7**.

2,6-Bis(3,5-dichlorobenzoyloxy)-3,3,7,7-tetramethylbicyclo-[3.3.1]nonane (10). To a solution of (±)-**7** (18 mg, 0.085 mmol) in pyridine (2 mL) was added 3,5-dichlorobenzoyl chloride (540 mg, 2.58 mmol) with ice cooling and then the mixture was stirred overnight at room temperature. After addition of ice water to the reaction mixture, the mixture was acidified with 10% hydrochloric acid and then extracted with ether. The extract was washed with saturated aqueous solution of sodium hydrogencarbonate and water and dried ($MgSO_4$). After removal of the solvent, the oily residue was purified by a preparative thin layer chromatography (silica gel, benzene/ether 1/1 v/v) to yield **10** (34 mg, 72% yield) as a white solid; IR (KBr) 1720, 1580, 1270, 810, 780 cm^{-1}. Found: C, 57.76; H, 5.02; Cl, 25.29%. Calcd for $C_{27}H_{28}O_4Cl_4$: C, 58.08; H, 5.06; Cl, 25.40%.

By the same procedure descrived above, (−)-**7**; $[\alpha]_D$ −87.5° was converted into the optically active benzoate, whose e.e. value was determined to be 96% by HPLC-analysis. HPLC-analysis was carried out on Simadzu LC-6A using a chiral column (250×4.6 mm) packed with cellulose tris(3,5-dimethylphenylcarbamate) on silica gel[13] (hexane/2-propanol, 99/1 0.4 mL min^{-1}).

(−)-(1*R*,4*S*,21*S*,24*R*)-5,8,11,14,17,20-Hexaoxatricyclo[19.4.0.0^{4,24}]pentaicosane (11). A suspension of sodium hydride (177 mg, 7.38 mmol) in dry tetrahydrofuran (THF) (80 mL) was gently refluxed and to the boiling mixture a solution of (−)-**3** (327 mg, 2.10 mmol) and pentaethylene glycol bis(*p*-toluenesulfonate) (1.14 g, 2.10 mmol) in dry THF (200 mL) was added dropwise over a period of 12 h in nitrogen atmosphere. The mixture was heated for an additional 50 h at reflux. After the mixture was cooled in an ice bath, a small amount of water was added to the chilled mixture. The solvent was removed in vacuo and the residue was extracted with dichloromethane. The extract was washed with dilute hydrochloric acid, saturated aqueous solution of sodium hydrogencarbonate, and water and dried ($MgSO_4$). After removal of the solvent, the residue was chromatographed on alumina (benzene/chloroform 1/1 v/v) to give **11** (180 mg, 24% yield) as a colorless oil; $[\alpha]_D^{20}$ −33.1° (*c* 0.730, $CHCl_3$); IR (neat film) 1110 cm^{-1}; ^1H NMR ($CDCl_3$) δ=1.3—2.2 (12H, m), 3.5—3.8 (20H, m), 4.0—4.2 (2H, m); MS *m/z* 358 (M^+). Found: C, 63.11; H, 9.49%. Calcd for $C_{19}H_{34}O_6$: C, 63.66; H, 9.56%.

(+)-(1*R*,4*S*,21*S*,24*R*)-3,3,22,22-Tetramethyl-5,8,11,14,17,20-hexaoxatricyclo[19.4.0.0^{4,24}]pentaicosane (12). By using the same procedure described above, reaction of (+)-**7** (425 mg, 2.00 mmol) with pentaethylene glycol bis(*p*-toluenesulfonate) (1.08 g, 2.00 mmol) and sodium hydride (168 mg, 7.00 mmol) in dry THF. The crude product was chromatographed on alumina (benzene/chloroform 1/1 v/v) to give **12** (386 mg, 19% yield) as a colorless oil.

12; $[\alpha]_D^{22}$ +53.2° (*c* 0.470, $CHCl_3$); IR (neat film) 1100 cm^{-1}; ^1H NMR ($CDCl_3$) δ=0.97 (6H, s), 1.03 (6H, s), 1.67 (6H, s), 1.2—2.3 (8H, m), 3.14 (2H, d, *J*=6.6 Hz), 3.5—3.8 (20H, m); MS *m/z* 414 (M^+). Found: C, 63.86; H, 10.05%. Cacld for $C_{23}H_{42}O_6$: C, 66.63; H, 10.21%.

(−)-(1*R*,2*S*,5*R*,6*S*)-2,6-Bis(2-hydroxyethoxy)bicyclo[3.3.1]-nonane (14). To a suspension of sodium hydride (888 mg, 37.0 mmol) in dry dimethyl sulfoxide (DMSO) (30 mL) was added a solution of (−)-**3** (1.45 g, 9.28 mmol) in dry DMSO (30 mL) and then the mixture was heated at 35 °C for 6 h under nitrogen atmosphere. A solution of the *p*-toluenesulfonate of 2-(2-tetrahydropyranyloxy)ethanol (11.2 g, 37.3 mmol) in dry DMSO (50 mL) was added to the reaction mixture and the resulting mixture was stirred for 15 h at 35 °C. After an ice water (100 mL) was added to the reaction mixture, it was extracted with ether. The extract was washed with water, dried ($MgSO_4$), and concentrated in vacuo. The residue was chromatographed on silica gel (hexane/ether 1/1 v/v) to give **13** as a pale yellow oil, which was dissolved in methanol (50 mL). Three drops of hydrochloric acid was added to the solution and the resulting mixture was stirred for 12 h at room temperature. After sodium carbonate (1.00 g) was added to the reaction mixture, the mixture was stirred for 30 min. The solid was removed by filtration and the filtrate was concentrated in vacuo to give an oily residue, which was extracted with chloroform. The extract was washed with water and dried ($MgSO_4$). After removal of the solvent, the residue was chromatographed on silica gel (ether/methanol 96/4 v/v) to yield **14** (1.40 g, 62% yield) as a white solid; $[\alpha]_D^{23}$ −60.1° (*c* 1.03, $CHCl_3$); IR (neat film) 3420, 1100, 1090, 1060 cm^{-1}. Found: C, 63.32; H, 9.71%. Calcd for $C_{13}H_{24}O_4$: C, 63.90; H, 9.90%.

(−)-(1*R*,2*S*,5*R*,6*S*)-2,6-Bis(2-mesyloxyethoxy)bicyclo[3.3.1]-nonane (15). To a mixture of (−)-**14** (1.60 g, 6.55 mmol), triethylamine (6.63 g, 65.5 mmol) and dichloromethane (30 mL) was slowly added a solution of methanesulfonyl chloride (6.00 g, 52.4 mmol) in dichloromethane (20 mL) with ice cooling. After being stirred for 2 h at 0 °C and for an additional 1 h at room temperature, the mixture was poured onto ice and extracted with dichloromethane. The extract was washed with dilute hydrochloric acid, saturated aqueous solution of sodium hydrogencarbonate, and water and dried ($MgSO_4$). After removal of the solvent, the residue was chromatographed on silica gel (hexane/ether 1/9 v/v) to give **15** (2.22 g, 85% yield) as a pale yellow oil, which was used for the next reaction without further purification.

(−)-(1*R*,4*S*,12*S*,15*R*,17*R*,20*S*,28*S*,31*R*)-5,8,11,21,24,27-Hexaoxapentacyclo[26.4.0.0^{4,31}.0^{12,17}.0^{15,20}]dotriacontane (22). To a mixture of sodium hydride (216 mg, 9.00 mmol), potassium tetrafluoroborate (100 mg, 0.794 mmol), and dry DMSO (150 mL) was slowly added a mixture of (−)-**14** (550 mg, 2.25 mmol) and (−)-**15** (901 mg, 2.25 mmol) in dry DMSO (15 mL) over a period of 10 h at 40 °C, and then the resulting mixture was heated for an additional 60 h at this temperature under nitrogen atmosphere. After a small amount of ice water was added to the reaction mixture, the solvent was removed in vacuo and the residue was extracted with ether. The extract was washed with water and dried ($MgSO_4$). After removal of the solvent, the residue was chromatographed on silica gel (hexane/ether 4/6 v/v) to yield **22** (140 mg, 14% yield) as a white solid; mp 56—58 °C; $[\alpha]_D^{25}$ −20.0° (*c* 1.01, $CHCl_3$); IR (KBr) 1100 cm^{-1}; ^1H NMR ($CDCl_3$) δ=1.08—2.40 (24H, m), 3.16—3.76 (20H, m); MS *m/z* 452 (M^+). Found: C, 68.44; H, 9.81%. Calcd for $C_{26}H_{44}O_6$: C, 68.99; H, 9.80%.

(+)-(1*R*,2*S*,5*R*,6*S*)-2,6-Bis(2-hydroxyethoxy)-3,3,7,7-tetramethylbicyclo[3.3.1]nonane (19). By the similar procedure described for the preparation of **14**, reaction of (+)-**7** (2.07 g,

9.75 mmol) with the *p*-toluenesulfonate of 2-(methoxymethoxy)ethanol (14.0 g, 53.8 mmol) and sodium hydride (1.17 g, 48.8 mmol) in dry DMSO was carried out. The crude product was chromatographed on silica gel (hexane/ether 1/1 v/v) to give **18** (3.3 g) as an oil. Treatment of **18** (3.3 g) with methanol and hydrochloric acid followed by chromatography on silica gel gave **19** (2.21 g, 76% overall yield) as a colorless oil; $[\alpha]_D^{25}$ +99.4° (*c* 1.19, $CHCl_3$); IR (neat film) 3350, 1110 cm^{-1}; ^1H NMR ($CDCl_3$) δ=1.00 (6H, s), 1.06 (6H, s), 1.2—1.9 (6H, m), 2.15 (2H, s), 2.30 (2H, br s), 3.18 (2H, d, *J*=9.0 Hz), 3.28—3.76 (8H, m). Found: C, 67.35; H, 10.70%. Calcd for $C_{17}H_{32}O_4$: C, 67.96; H, 10.74%.

(+)-(1*R*,2*S*,5*R*,6*S*)-2,6-Bis(2-mesyloxyethoxy)-3,3,7,7-tetramethylbicyclo[3.3.1]nonane (20). By using the same procedure described for the preparation of **14**, (+)-**19** (800 mg, 2.66 mmol) was reacted with methanesulfonyl chloride (2.44 g, 21.3 mmol) and triethylamine (2.69 g, 26.6 mmol) in dichloromethane. The crude product was chromatographed on silica gel (hexane/ether 3/7 v/v) to yield **20** (1.19 g, 98% yield), which was recrystallized from hexane to give the specimen; mp 46—47 °C; $[\alpha]_D^{24}$ +71.0° (*c* 1.00, $CHCl_3$); IR (KBr) 3025, 1350, 1180 cm^{-1}; ^1H NMR ($CDCl_3$) δ=0.93 (6H, s), 1.07 (6H, s), 1.1—1.9 (8H, m), 2.32 (2H, br s), 3.03 (6H, s), 3.18 (2H, d, *J*=9.0 Hz), 3.66 (2H, m), 4.32 (4H, t, *J*=5.2 Hz). Found: C, 49.65; H, 7.73; S, 13.88%. Calcd for $C_{19}H_{36}O_8S_2$: C, 50.00; H, 7.95; S, 14.05%.

(+)-(1*R*,4*S*,12*S*,15*R*,17*R*,20*S*,28*S*,31*R*)-3,3,13,13,19,19,29,29-Octamethyl-5,8,11,21,24,27-hexaoxapentacyclo[26.4.0.0^{4,31}.0^{12,17}.0^{15,20}]dotriacontane (23). By using the same procedure described for the preparation of **22**, condensation of (+)-**19** (550 mg, 1.83 mmol) with (+)-**20** (835 mg, 1.83 mmol) and sodium hydride (180 mg, 7.50 mmol) in the presence of potassium tetrafluoroborate (100 mg, 0.794 mmol) was carried out in dry DMSO. The product was chromatographed on silica gel (hexane/ether 1/1 v/v) to give **23** (140 mg, 14% yield) as a colorless oil; $[\alpha]_D^{25}$ +104.4° (*c* 1.15, $CHCl_3$); IR (neat film) 1100 cm^{-1}; ^1H NMR ($CDCl_3$) δ=0.98 (12H, s), 1.05 (12H, s), 1.1—2.0 (12H, m), 2.28 (4H, br s), 3.14 (4H, d, *J*=9.0 Hz), 3.28—3.80 (16H, m); MS *m/z* 564 (M^+). Found: C, 67.20; H, 10.13%. Calcd for $C_{34}H_{60}O_6$: C, 72.30; H, 10.71%.

(−)-(1*R*,2*S*,5*R*,6*S*)-6-Benzyloxybicyclo[3.3.1]nonan-2-ol (6). To a suspension of sodium hydride (413 mg, 17.2 mmol) in dry DMSO (30 mL) was added a solution of (−)-**3** (1.90 g, 12.1 mmol) in dry DMSO (20 mL) and then the mixture was heated at 35 °C for 6 h. To the reaction mixture was added a solution of benzyl bromide (2.50 g, 14.6 mmol) in dry DMSO (30 mL) and the resulting mixture was stirred for 15 h at room temperature. After an ice water (50 mL) was added to the reaction mixture, the mixture was extracted with ether. The extract was washed with water, dried ($MgSO_4$), and concentrated in vacuo. The residue was chromatographed on silica gel (benzene/ether 1/1 v/v) to give **6** (1.21 g, 41% yield) as a solid; mp 59—61 °C; $[\alpha]_D^{25}$ −60.1° (*c* 1.02, $CHCl_3$); IR (KBr) 3090, 3060, 3020, 740, 700 cm^{-1}; ^1H NMR ($CDCl_3$) δ=1.2—2.2 (13H, m), 3.4—3.9 (2H, m), 4.47 (1H, d, *J*=10.8 Hz), 4.55 (1H, d, *J*=10.8 Hz), 7.2—7.4 (5H, m). Found: C, 77.55; H, 8.97%. Calcd for $C_{16}H_{22}O_2$: C, 78.01; H, 9.00%.

(+)-(1*S*,2*R*,5*S*,6*R*)-2,6-Bis(2-tosyloxyethoxy)bicyclo[3.3.1]nonane (16). To a solution of (+)-**14**; $[\alpha]_D$ +59.1° (1.05 g, 4.30 mmol), prepared from (+)-**3** by the same procedure described for the preparation of (−)-**14**, in pyridine (30 mL) was added *p*-toluenesulfonyl chloride (3.28 g, 17.2 mmol) with ice cooling and then the mixture was stirred for 2 h at the same temperature. After the reaction mixture was poured onto ice, the resulting mixture was acidified with hydrochloric acid and extracted with benzene. The extract was washed with diluted hydrochloric acid, saturated aqueous solution of sodium hydrogencarbonate, and water, and dried ($MgSO_4$). After removal of the solvent, the residue was chromatographed on silica gel (benzene/ether 9/1 v/v) to give **16** (1.58 g, 67% yield) as an oil; $[\alpha]_D^{26}$ +28.9° (*c* 0.950, $CHCl_3$); ^1H NMR ($CDCl_3$) δ=1.0—2.0 (12H, m), 2.44 (6H, s), 3.36 (2H, m), 3.58 (4H, t, *J*=4.8 Hz), 4.14 (4H, t, *J*=4.8 Hz), 7.29 (4H, d, *J*=8.0 Hz), 7.76 (4H, d, *J*=8.0 Hz). Found: C, 58.21; H, 6.50; S, 11.56%. Calcd for $C_{27}H_{36}O_8S_2$: C, 58.68; H, 6.57; S, 11.60%.

(−)-(1*S*,2*R*,5*S*,6*R*)-2,6-Bis{2-[(1*R*,2*S*,5*R*,6*S*)-6-benzyloxybicyclo[3.3.1]non-2-yloxy]ethoxy}bicyclo[3.3.1]nonane (26). To a suspension of sodium hydride (156 mg, 6.50 mmol) in dry DMSO (40 mL) was added a solution of (−)-**6** (1.00 g, 4.06 mmol) in dry DMSO (30 mL) and then the mixture was heated at 30 °C for 6 h. After the mixture was cooled in an ice bath, a solution of (+)-**16** (895 mg, 1.62 mmol) in dry DMSO (40 mL) was added to the chilled mixture. The resulting mixture was heated at 35 °C for 40 h under nitrogen atmosphere. The reaction mixture was poured into ice water and extracted with ether. The extract was washed with water, dried ($MgSO_4$), and concentrated in vacuo. The residue was chromatographed on silica gel (benzene/ether 9/1 v/v) to yield (−)-**26** (488 mg, 43% yield); mp 119—120 °C; $[\alpha]_D^{25}$ −30.3° (*c* 1.01 $CHCl_3$); IR (KBr) 3060, 3030, 1110, 740, 700 cm^{-1}; ^1H NMR ($CDCl_3$) δ=1.2—2.2 (36H, m), 3.3—3.7 (14H, m), 4.47 (2H, d, *J*=10.8 Hz), 4.55 (2H, d, *J*=10.8 Hz), 7.2—7.4 (10H, m). Found: C, 76.88; H, 9.10%. Calcd for $C_{45}H_{64}O_6$: C, 77.10; H, 9.20%.

(−)-(1*S*,2*R*,5*S*,6*R*)-2,6-Bis{2-[(1*R*,2*S*,5*R*,6*S*)-6-hydroxybicyclo[3.3.1]non-2-yloxy]ethoxy}bicyclo[3.3.1]nonane (27). To a solution of (−)-**26** (400 mg, 0.571 mmol) in dry THF (100 mL) was added lithium aluminum hydride (1.75 g, 46.1 mmol) in a small portions and then the resulting mixture was heated for 14 h at reflux. After water (10 mL) was added to the reaction mixture with ice cooling, the mixture was stirred for 2 h. The inorganic solid was removed by filtration and the solid was continuously extracted with ether using Soxhlet extraction apparatus. The organic solutions were combined, washed with water, dried ($MgSO_4$), and concentrated in vacuo. The residue was chromatographed on silica gel (ether) to yield **27** (250 mg, 84% yield) as a solid; mp 67.5—69 °C; $[\alpha]_D^{26}$ −10.8° (*c* 1.49, $CHCl_3$); IR (KBr) 3360, 2920, 2850, 1100 cm^{-1}. Found: C, 70.15; H, 9.85%. Calcd for $C_{31}H_{52}O_6$: C, 71.50; H, 10.07%.

(−)-(1*S*,2*R*,5*S*,6*R*)-2,6-Bis{2-[(1*R*,2*S*,5*R*,6*S*)-6-methoxybicyclo[3.3.1]non-2-yloxy]ethoxy}bicyclo[3.3.1]nonane (28). To a suspension of sodium hydride (55 mg, 2.3 mmol) in dry DMSO (20 mL) was added a solution of (−)-**27** (150 mg, 0.288 mmol) in dry DMSO (40 mL) and the mixture was heated at 35 °C for 4 h. After the mixture was cooled in an ice bath, a solution of methyl iodide (500 mg, 3.52 mmol) in dry DMSO (30 mL) was added to the chilled mixture. The resulting mixture was heated at 35 °C for 14 h and poured into ice water. The mixture was extracted with ether. The extract was washed with water, dried ($MgSO_4$), and concentrated in vacuo. The residue was chromatographed

on silica gel (benzene/ether 8/2 v/v) to yield (−)-**28** (120 mg, 76% yield); mp 71—73 °C; $[\alpha]_D^{20}$ −21.5° (*c* 1.08, $CHCl_3$); IR (KBr) 1110 cm^{-1}; ^1H NMR ($CDCl_3$) δ=1.2—2.1 (36H, m), 3.32 (6H, s), 3.2—3.7 (14H, m); MS *m/z* 548 (M^+).

(+)-(1*S*,2*R*,5*S*,6*R*)-2,6-Bis{2-[(1*S*,2*R*,5*S*,6*R*)-6-benzyloxybicyclo[3.3.1]non-2-yloxy]ethoxy}bicyclo[3.3.1]nonane (29). By using the same procedure described for the preparation of **26**, (+)-**29** (260 mg, 33% yield) was prepared by condensation of (+)-**6**; $[\alpha]_D$ +59.7° (700 mg, 2.84 mmol), prepared from (+)-**3**, with (+)-**16** (620 mg, 1.12 mmol) and sodium hydride (108 mg, 4.50 mmol). (+)-**29**; a colorless oil; $[\alpha]_D^{20}$ +78.7° (*c* 0.995, $CHCl_3$); IR (neat film) 1100, 740, 700 cm^{-1}; ^1H NMR ($CDCl_3$) δ=1.2—2.2 (36H, m), 3.4—3.7 (12H, m), 4.46 (2H, d, *J*=10.8 Hz), 4.54 (2H, d, *J*=10.8 Hz), 7.2—7.4 (10H, m). Found: C, 76.80; H, 9.20%. Calcd for $C_{45}H_{64}O_6$: C, 77.10; H, 9.20%.

(+)-(1*S*,2*R*,5*S*,6*R*)-2,6-Bis{2-[(1*S*,2*R*,5*S*,6*R*)-6-hydroxybicyclo[3.3.1]non-2-yloxy]ethoxy}bicyclo[3.3.1]nonane (30). A mixture of (+)-**29** (115 mg, 0.164 mmol), *p*-toluenesulfonic acid monohydrate (10 mg), 10% Pd on carbon (100 mg), and 1,4-dioxane (20 mL) was shaken at 1 atm of hydrogen at room temperature. After hydrogen uptake had ceased, the catalyst was removed by filtration. To the filtrate was added sodium carbonate (200 mg), and the resulting mixture was stirred for 1 h. The solid was removed by filtration and the filtrate was concentrated in vacuo. The residue was extracted with chloroform and the extract was washed with water, dried ($MgSO_4$), and concentrated in vacuo. The resulting oil was chromatographed on silica gel (ether) to give (+)-**30** (78 mg, 91% yield) as a colorless oil; $[\alpha]_D^{20}$ +60.6° (*c* 0.929, $CHCl_3$); IR (neat film) 3370, 1100 cm^{-1}; MS *m/z* 520 (M^+).

(+)-(1*S*,2*R*,5*S*,6*R*)-2,6-Bis{2-[(1*S*,2*R*,5*S*,6*R*)-6-methoxybicyclo[3.3.1]non-2-yloxy]ethoxy}bicyclo[3.3.1]nonane (31). By using the same procedure described for the preparation of **28**, (+)-**31** (68 mg, 86% yield) was prepared from (+)-**30** (75 mg, 0.14 mmol) with sodium hydride (28 mg, 1.2 mmol) and methyl iodide (250 mg, 1.78 mmol).

(+)-**31**; a colorless oil; $[\alpha]_D^{22}$ +70.3° (*c* 0.968, $CHCl_3$); IR (neat film) 1100 cm^{-1}; ^1H NMR ($CDCl_3$) δ=1.2—2.1 (36H, m), 3.32 (6H, s), 2.9—3.6 (14H, m); MS *m/z* 548 (M^+).

(−)-(1*R*,2*S*,5*R*,6*S*)-2,6-Bis(1,4,7-trioxaoctyl)bicyclo[3.3.1]nonane (17). To a suspension of sodium hydride (93 mg, 3.9 mmol) in dry DMSO (30 mL) was added a solution of (−)-**3** (100 mg, 0.640 mmol) in dry DMSO (20 mL), and then the resulting mixture was heated at 35 °C for 6 h. After the mixture was cooled in an ice bath, a solution of the *p*-toluenesulfonate of 2-(2-methoxyethoxy)ethanol (1.06 g, 3.87 mmol) in dry DMSO (30 mL) was added to the chilled mixture. After being heated at 35 °C for 15 h, the reaction mixture was poured into ice water and extracted with ether. The extract was washed with water, dried ($MgSO_4$), and concentrated in vacuo. The residual oil was chromatographed on silica gel (benzene/ether 1/1 v/v) to yield **17** (180 mg, 78% yield) as a colorless oil; $[\alpha]_D^{22}$ −56.7° (*c* 0.905, $CHCl_3$); IR (neat film) 1140, 1100 cm^{-1}; ^1H NMR ($CDCl_3$) δ=1.2—2.1 (12H, m), 3.36 (6H, s), 3.4—3.7 (18H, m); MS *m/z* 360 (M^+).

(+)-(1*R*,2*S*,5*R*,6*S*)-2,6-Bis(1,4,7-trioxaoctyl)-3,3,7,7-tetramethylbicyclo[3.3.1]nonane (21). By using the same procedure described for the preparation of **17**, (+)-**21** (440 mg, 90% yield) as an oil was prepared from (+)-**7** (250 mg, 1.17 mmol) and the *p*-toluenesulfonate of 2-(2-methoxyethoxy)ethanol (1.94 g, 7.13 mmol); $[\alpha]_D^{20}$ +84.4° (*c* 0.950, $CHCl_3$); IR (neat film) 1140, 1100 cm^{-1}; ^1H NMR ($CDCl_3$) δ=0.96 (6H, s), 1.04 (6H, s), 1.1—1.9 (6H, m), 2.26 (2H, br s), 3.13 (2H, d, *J*=9.0 Hz), 3.36 (6H, s), 3.4—3.7 (16H, m); MS *m/z* 416 (M^+).

Enantiomer Differential Transport. Enantiomer differential transport was carried out in an apparatus which consisted of an outer cylindrical glass vessel (24.5 mm inner diameter) and a central glass tube (15.5 mm inner diameter). The chloroform solution of the optically active host molecule (5.0×10^{-3} M) separated the inner aqueous phase (0.1 M hydrochloric acid) and the outer aqueous phase (0.08 M hydrochloric acid) containing $LiPF_6$ (0.4 M) and the racemic guest molecule (8.0×10^{-2} M). The chloroform layer was gently stirred at a constant speed (60 rpm) at 20—25 °C. Transport was monitored by ultraviolet spectrum and enantiomer excess of the guest molecule transported was monitored by circular dichroism.

References

1) A preliminary communication: K. Naemura, T. Matsumura, M. Komatsu, Y. Hirose, and H. Chikamatsu, *J. Chem. Soc., Chem. Commun.*, **1988**, 239.

2) E. P. Kyba, K. Koga, L. R. Sousa, M. G. Siegel, and D. J. Cram, *J. Am. Chem. Soc.*, **95**, 2692 (1973).

3) G. W. Gokel and S. H. Korzeniowski, "Macrocyclic Polyethers Syntheses," Springer-Verlag, Berlin, Heiderberg, and New York (1982).

4) K. Naemura, R. Fukunaga, and M. Yamanaka, *J. Chem. Soc., Chem. Commun.*, **1985**, 1561.

5) K. Naemura and R. Fukunaga, *Chem. Lett.*, **1985**, 1651.

6) M. A. Findeis and G. M. Whitesides, *Annu. Rep. Med. Chem.*, **19**, 263 (1984); G. M. Whitesides and C.-H. Wong, *Angew. Chem., Int. Ed. Engl.*, **24**, 617 (1985); R. Porter and S. Clark, "Enzymes in Organic Synthesis," Pitman, London (1985); J. Tramper, H. C. van der Plas, and P. Linko, "Biocatalysts in Organic Syntheses," Elsevier, Amsterdam, Oxford, New York, Tokyo (1985); M. P. Schneider, "Enzymes as Catalysts in Organic Synthesis," Reidel, Dordrecht (1986); J. B. Jones, *Tetrahedron*, **42**, 3351 (1986) and references cited therein.

7) M. Nakazaki, H. Chikamatsu, K. Naemura, and M. Asao, *J. Org. Chem.*, **45**, 4432 (1980); K. Naemura, T. Fujii, and H. Chikamatsu, *Chem. Lett.*, **1986**, 923; K. Naemura, N. Takahashi, and H. Chikamatsu, *ibid.*, **1988**, 1717.

8) H. Gerlach, *Helv. Chim. Acta*, **61**, 2773 (1978); G. Hoffmann and R. Wiartalla, *Tetrahedron Lett.*, **23**, 3887 (1982).

9) F. de Jong, M. G. Siegel, and D. J. Cram, *J. Chem. Soc., Chem. Commun.*, **1975**, 551.

10) H. L. Rosano, J. H. Schulman, and J. B. Weisbuch, *Ann. N. Y. Acad. Sci.*, **92**, 457 (1961); B. Pressman, E. J. Harris, W. S. Jagger, and J. H. Johnson, *Proc. Natl. Acad. Sci. U.S.A.*, **58**, 1949 (1967).

11) K. Naemura, R. Fukunaga, M. Komatsu, M. Yamanaka, and H. Chikamatsu, *Bull. Chem. Soc. Jpn.*, **62**, 83 (1989).

12) J. Meinwald, J. Crandall, and W. H. Hymans, *Org. Synth.*, Coll. Vol. V, 866 (1973).

13) Y. Okamoto, M. Kawashima, and K. Hatada, *J. Chromatogr.*, **363**, 173 (1986).

A Practical Optical Resolution of (Arylsulfinyl)acetones and Its Application to the Synthesis of 2-(Arylsulfinyl)cycloalkanones

Katsuyuki OGURA,* Michio ISHIDA,† Hiroshi TOMORI, and Makoto FUJITA
Department of Synthetic Chemistry, Faculty of Engineering, Chiba University, 1-33 Yayoicho, Chiba 260
†Graduate School of Science and Technology, Chiba University, 1-33 Yayoicho, Chiba 260
(Received July 1, 1989)

Racemic (arylsulfinyl)acetones (**1**) were efficiently resolved by formation of their oxazolidine derivatives with (*R*)- or (*S*)-2-amino-2-phenylethanol followed by chromatography on Florisil-MgO and the subsequent hydrolysis to give (*S*)- or (*R*)-**1**, respectively. Further, derivation of **1** to optically active 2-(*p*-tolylsulfinyl)-cyclohexanone and 2-(*p*-tolylsulfinyl)-4-cycloheptenone is described.

Optically active α-(arylsulfinyl) ketones have proved to be one of the most valuable chiral building blocks for asymmetric syntheses of alcohols,[1] α-hydroxy aldehydes,[2] β-hydroxy ketones,[3] epoxides,[4] γ-substituted γ-lactones,[5] and 4-aryl-3-(*p*-methoxyphenylsulfonyl)-1,4-dihydropyridines,[6] and 3-substituted cycloalkanones.[7] In spite of their potential utilities, these asymmetric syntheses seem to be limited in practical use, mainly due to a multistep preparation of the optically active α-(arylsulfinyl) ketones: Acylation of (*R*)-(methyl *p*-tolyl sulfoxide), obtainable from the reaction of methylmagnesium iodide with *l*-menthyl *p*-toluenesulfinate, has been employed frequently.[1a-d,8] Alternatively, the direct reaction of *l*-menthyl *p*-toluenesulfinate with the enolate ion of a ketone was also reported.[9] Since *l*-menthyl *p*-toluenesulfinate must be synthesized by the reaction of *p*-toluenesulfinyl chloride and *l*-menthyl alcohol followed by repeating recrystallization and epimerization,[10] both of these methods are too tedious to be practical.

For preparing many kinds of optically active α-(arylsulfinyl) ketones, our attention was paid to the utilization of chiral (arylsulfinyl)acetones (**1**) as a versatile intermediate, because the monoanion and dianion of racemic **1** were known to react with various electrophiles to afford a variety of α-(arylsulfinyl) ketones.[11]

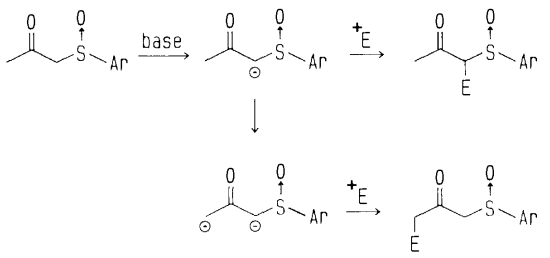

Scheme 1.

Here we wish to disclose a practical method for optical resolution of (arylsulfinyl)acetones (**1**), which is achieved by easy formation of an oxazolidine (**3** or **4**) from **1** and (*R*)- or (*S*)-2-amino-2-phenylethanol (**2**), followed by column chromatography on Florisil-MgO. In order to demonstrate the usefulness of

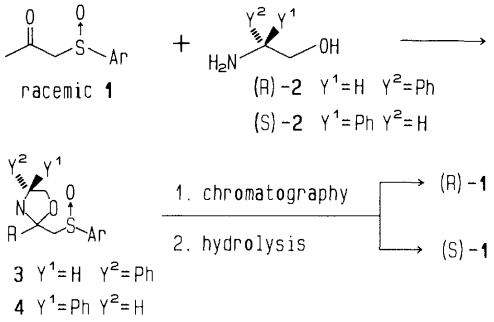

Scheme 2.

optically active **1a**, we further investigated the reaction conditions for deriving **1a** into (R_S)-(*p*-tolylsulfinyl)-cyclohexanone and (S_S)-2-(*p*-tolylsulfinyl)-4-cycloheptenone, the result of which is also described in the present article.

Results and Discussion

Optical Resolution of (Arylsulfinyl)acetones. At first, we found that racemic (*p*-tolylsulfinyl)acetone (**1a**) afforded an oxazolidine derivative (**3a**) by simply stirring **1a** and (*R*)-**2** in ethanol or dichloromethane at room temperature. Thus, an ethanolic solution (3 ml) of racemic (*p*-tolylsulfinyl)acetone (**1a**) (1.0 mmol) and (*R*)-**2** (1.1 mmol) was stirred for 24 h at room temperature. After removal of the solvent under a reduced pressure, the ^{1}H NMR analysis of the residue showed quantitative formation of an oxazolidine (**3a**), which consisted of four diastereomers in the ratio of ca. 2:2:1:1.[12] Without any purification, the crude oxazolidine (**3a**) was subjected to column chromatography (φ 18 mm×290 mm) using benzene–ethyl acetate (9:1) as an eluent. As an adsorbent, we chose 70-fold excess (to **3a** in weight) of Florisil-MgO (70:30, 82:18, and 100:0),[13] prepared by mechanical mixing and subsequent calcination at 200 °C for 2 h. Since **3a** underwent partial hydrolysis during elution, all of the fractions contained **1a** along with **3a**. It was shown by the HPLC analysis that the earlier fractions consisted mainly of **1a** and, as the chromatography proceeded, the content of **3a** increased. The mixture of **1a** and **3a**

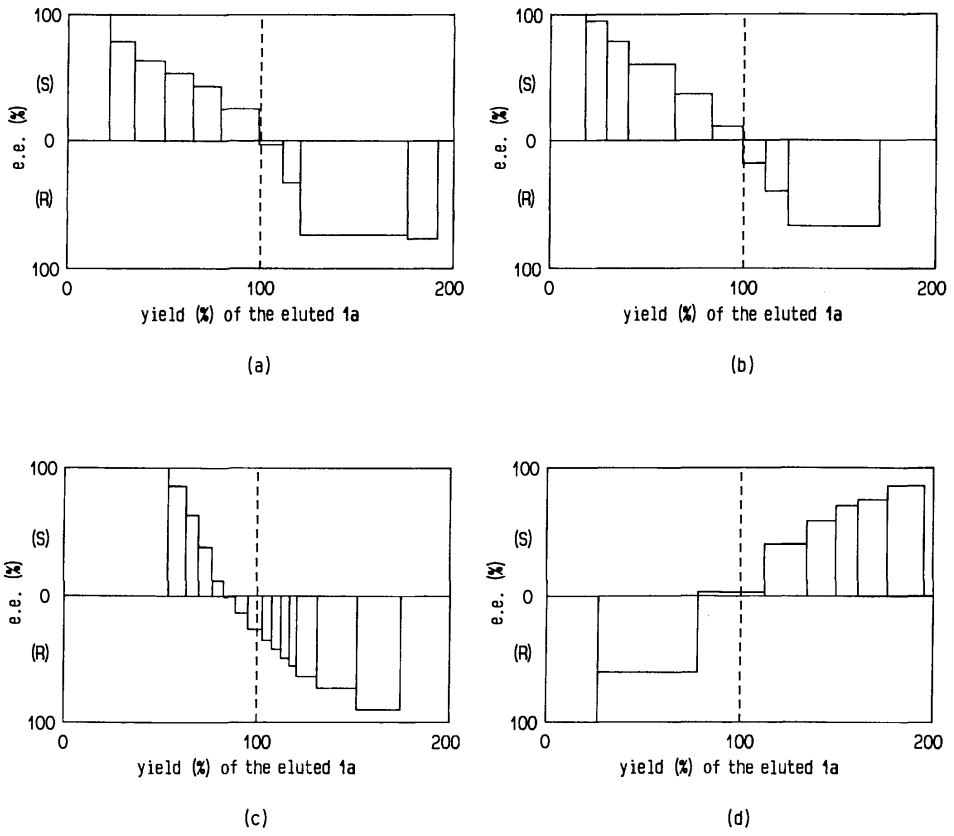

Fig. 1. Chromatography of the oxazolidines: (a) **3a** on Florisil; (b) **3a** on Florisil–MgO (82:18); (c) **3a** on Florisil–MgO (70:30); (d) the oxazolidine derived from **1a** and (*S*)-2-amino-3-methyl-1-butanol on Florisil–MgO (70:30).

in each fraction was treated with silica gel to hydrolyze the involved **3a** to **1a**. This procedure made it possible to isolate **1a** as a sole product. The enantiomeric excess (e.e.) of **1a** of each fraction was determined by HPLC using a column with a chiral stationary phase (Daisel Chiral-cell OB). The results are summarized in Fig. 1, where the ordinate exhibits the e.e. value and the abscissa does integration of the yield of **1a** in each fraction, based on its one enantiomer. Hereafter, the yields of (*R*)- and (*S*)-**1** based on a half of the amount of the used racemic **1** are utilized. Among the adsorbents examined herein, a 70:30 mixture of Florisil and MgO gave the best result: All the fractions containing (*S*)-**1a** with >99% e.e. were combined and concentrated. The yield of (*S*)-**1a** with >99% e.e. amounted to 54%. A parallel experiment using (*S*)-**2** instead of (*R*)-**2** gave (*R*)-**1a** with >99% e.e. in a comparable yield. The present technique can be suitably applied to a large-scale resolution of **1a**. Thus, the oxazolidine (**4a**), produced from **1a** (10 mmol) and (*S*)-**2** (12 mmol), was eluted through the column (ϕ 45 mm×300 mm) packed with 250 g of Florisil–MgO (70:30) by the use of benzene–ethyl acetate (6:1) as an eluent. Hydrolysis of the fractions containing **1a** with a high enantiomeric excess gave (*R*)-**1a** of >99% e.e. in 48% yield together with (*R*)-**1a** (11% yield) of 98% e.e. It should be noted that the column could be regenerated for reuse by washing with methanol and then with benzene.

The separation mechanism of the present system seems to be quite different from that of the usual chromatography. During elution, the oxazolidine (**3a** or **4a**) is partially hydrolyzed to form **1a**, which is less polar than the oxazolidine and, consequently, is more preferably eluted. Therefore, preferential elution of (*S*)-**1a** on chromatography of **3a** derived from (*R*)-**2** might suggest that the (S_s)-isomers of **3a** is more susceptive to hydrolysis than the (R_s)-isomers.

(*R*)-2-Amino-1-butanol and (*S*)-2-amino-3-methyl-1-butanol also reacted with **1a** to produce the corresponding oxazolidines, but the subsequent chromatography on Florisil–MgO (70:30) resulted in less effective resolution: when (*S*)-2-amino-3-methyl-1-butanol was utilized almost optically pure (*R*)-**1a** (>99% e.e.) was obtained in 27% yield. In the case of (*R*)-2-amino-1-butanol, **1a** was not isolated in an optically pure form. Further, we utilized (*R*)-1-phenylethylamine (**5**) instead of **2**. In the reaction of **5** with **1a**, formation of an imine (**6**) and an enamine (**7**) was observed by the ^{1}H NMR analysis of a crude product. Chromatography of the crude product on Florisil–MgO (70:30) using benzene–ethyl acetate

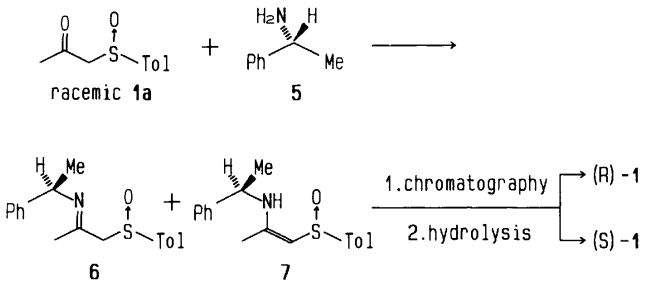

Scheme 3.

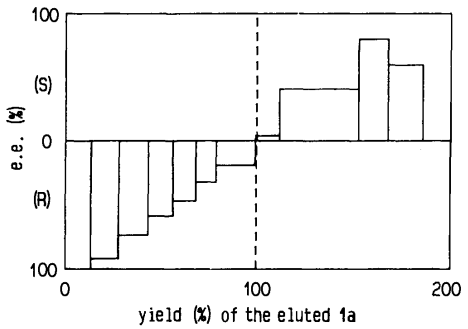

Fig. 2. Chromatography of a mixture of **6** and **7** on Florisil-MgO (70:30).

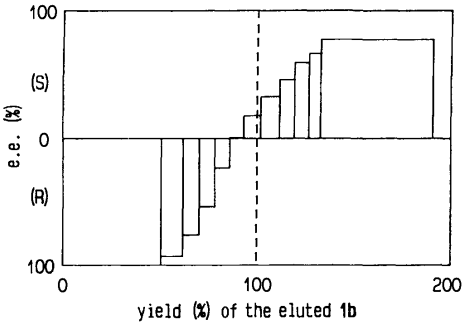

Fig. 3. Chromatography of **4b** on Florisil-MgO (70:30).

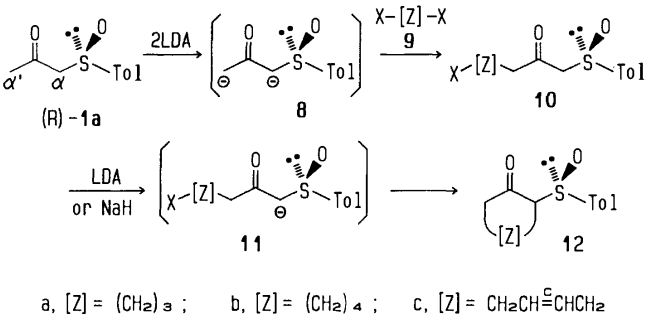

Scheme 4.

(9:1) gave **1a** with >99% e.e. in 13% yield.

In conclusion, chromatography of the oxazolidine (**3a** or **4a**) on Florisil-MgO (70:30) has proved to be most efficient for the optical resolution of **1a**. Recently, (*R*)-(*p*-methoxyphenylsulfinyl)acetone (**1b**) was found to be a good precursor of (*S*)-4-(*m*-chlorophenyl)-3-(*p*-methoxyphenylsulfonyl)-1,4-dihydropyridine, a potent cardiovascular drug.[6] We applied the present technique to an optical resolution of racemic (*p*-methoxyphenylsulfinyl)acetone (**1b**). Like **1a**, **1b** reacted with (*S*)-**2** to quantitatively form the corresponding oxazolidine (**4b**), which was subjected to column chromatography on Florisil-MgO (70:30) using benzene-ethyl acetate (9:1). At the initial stage, we obtained pure (*R*)-**1b** with >99% e.e. in 51% yield (Fig. 3): mp 75.5—77.0 °C (lit,[6] mp 56—58 °C); $[\alpha]_D^{21}$ +231° (*c* 0.75, MeOH) (lit,[6] $[\alpha]_D$ +168°).

Derivation of (*R*$_s$)-2-(*p*-Tolylsulfinyl)cycloalkanones from 1a. Since optically active **1a** are now in hand, their conversion into useful chiral compounds are particularly of interest. As well-known, successive treatment of racemic α-(phenylsulfinyl) ketones with sodium hydride and butyllithium gives the corresponding dianion, which reacts with various electrophiles to give α′-substituted products.[1f,11,14] By applying this chemistry of α-(phenylsulfinyl) ketones to the optically active **1**, we investigated a short-step synthesis of (*R*$_s$)-2-(*p*-tolylsulfinyl)cycloalkanones, which are novel precursors of optically active cyclic compounds, as outlined in Scheme 4. This route may be complementary to the conventional way leading to chiral 2-(*p*-tolylsulfinyl)cycloalkanones which are prepared by the reaction of *l*-menthyl *p*-toluenesulfinate with the enolate of a cycloalkanone.[9]

By the use of racemic **1a**, we first tested the possibility of the reaction paths depicted in Scheme 4. Treatment of **1a** with lithium diisopropylamide (LDA) (2.2 mol equiv) in tetrahydrofuran (THF) at −78 °C to room temperature generated the corresponding dianion (**8**).[15] After addition of excess amount (3 mol equiv) of 1,ω-dihaloalkane (**9**), the resulting mixture was stirred for 10—30 min to give an α′-substituted product (**10**). Reaction of the dianion (**8**) with **9a** (X=Br), **9a** (X=I), and **9b** (X=I) gave the corresponding **10** in 41%, 49%, and 60% yields, respectively. In contrast, treatment of the dianion (**8**) with 1,2-diiodoethane (**9**, X=I) did not give the corresponding **10**, but 1-iodo-3-(*p*-tolylsulfinyl)propanone (54% yield). Next, intramolecular cyclization of **10** to **12** was examined. LDA (1.1 mol equiv) was added to a 0.04 M# THF solution of **10** at −78 °C, and the resulting mixture was stirred at −15 °C to room temperature. In the case of **10a** (X=I), a smooth cyclization took place at −15 °C for 20 h to give **12a** in 51% yield. The reaction of **10a** (X=Br) was so slow that **12a** was produced in 27% yield even after stirring at room temperature for 10 h. However, cyclization of **10b** (X=I) did not form the expected **12b**, but a de-

1 M=1 mol dm^{-3}.

hydroiodinated product, 1-(*p*-tolylsulfinyl)-6-hepten-2-one. Consequently, the synthetic path depicted in Scheme 4 was shown to be suitable to the preparation of **12a**. Starting from (*R*)-**1a**, we obtained (R_s)-**12a** as a 64:36 mixture of two diastereomers: $[\alpha]_D$ +215° (*c* 0.80, $CHCl_3$).[16]

Further, we found that optically active 2-(*p*-tolylsulfinyl)-4-cycloheptenone (**12c**), which seems to be a good synthetic precursor of optically active cycloheptanone derivatives, was synthesized according to the reaction path of Scheme 4: Treatment of the dianion (**8**), generated from (*S*)-**1a**, with *cis*-1,4-dichloro-2-butene (**9c**) in THF at −78 °C for 30 min gave 7-chloro-1-(*p*-tolylsulfinyl)-5-hepten-2-one (**10c**) in 72% yield. Sodium hydride (2 equiv) was added to a THF solution of the thus-obtained **10c** under ice-cooling, and the reaction mixture was stirred at room temperature for 2 h. By the usual workup and subsequent chromatography on silica gel, (S_s)-**12c** was obtained in 74% yield as a 52:48 mixture of two diastereomers.

Thus, (*R*)- or (*S*)-**1a** was shown to provide a new and novel method for preparing optically active 2-(*p*-tolylsulfinyl)cyclohexanone (**12a**) and 2-(*p*-tolylsulfinyl)-4-cycloheptenone (**12c**).

Experimental

Melting points were determined on a hot-stage microscope apparatus (Yanagimoto) and are uncorrected. ^{1}H NMR spectra were obtained on Hitachi R-600 (60 MHz), JEOL JNM-GSX 270 (270 MHz), and JEOL JNM-GSX 500 (500 MHz) spectrometers. Infrared spectra were determined with a JASCO A-200 spectrometer. Optical rotations were measured on a JASCO polarimeter. The adsorbent for chromatography of the oxazolidines (**3** or **4**) was prepared by mechanically mixing Florisil (Wako; 100—200 mesh) and MgO (Merck Art. 5866) followed by being dried in a microwave oven (30 min) and then in an oven (200 °C/2 h). (*R*)-**2** and (*S*)-**2** were prepared by reduction of (*R*)-phenylglycine (Tokyo Kasei) and (*S*)-phenylglycine (Aldrich), respectively, with lithium aluminium hydride in THF and purified by recrystallization from dichloromethane-hexane. Their enantiomeric excesses were determined to be 100% by measuring ^{1}H NMR of their diacetyl derivatives, which were obtained by acetylation with acetic anhydride and pyridine, in the presence of Eu(hfc)$_3$ (0.4 mol equiv).

Preparation of (Arylsulfinyl)acetone (1). The starting materials, racemic **1a** and **1b**, were obtained by oxidation of the corresponding (arylthio)acetone with sodium periodate in ethanol-water (1:1). **1a**: colorless crystals; mp 44.5—45.5 °C (from hexane-diethyl ether) (lit,[17] mp 44—47 °C). **1b**: colorless crystals; mp 69.5—71.0 °C (from hexane-diethyl ether); ^{1}H NMR ($CDCl_3$) δ=2.23 (3H, s), 3.78 (1H, d, *J*=13.5 Hz), 3.87 (1H, d, *J*=13.5 Hz), 3.86 (3H, s), 7.04 (2H, d, *J*=8.9 Hz), and 7.59 (2H, d, *J*=8.9 Hz); IR (KBr) 1711, 1032, and 1020 (sh) cm^{-1}. Calcd for $C_{10}H_{12}O_3S$: C, 56.60; H, 5.70%. Found: C, 56.65; H, 5.69%.

Optical Resolution of 1. A Typical Procedure. A solution of **1a** (196 mg, 1.0 mmol) and (*R*)-**2** (151 mg, 1.1 mmol) in absolute ethanol (2 ml) was stirred at room temperature for 15 h under an atmosphere of nitrogen. After evaporation, the residue was chromatographed through a column (φ 17.5 mm×290 mm) packed with a 70:30 mixture (70 fold excess in weight) of Florisil (16.1 g) and MgO (6.9 g). A 9:1 mixture of benzene and ethyl acetate was eluted and 80-ml fractions were collected. Finally, ethyl acetate was eluted to completely recover **1a** and **3a**. Each fraction was evaporated in vacuo and the residue was subjected to short-path column chromatography on silica gel using benzene-ethyl acetate (1:1) as an eluent. The result was summarized in Table 1 and Fig. 1c. The fractions 23, 24, and 25 involved the oxazolidine (**3a**), which was hydrolyzed by treatment with silica gel in dichloromethane. The enantiomeric excess (e.e.) was analyzed by HPLC with a chiral stationary phase (Daisel Chiral-cell OB) using 2-propanol-hexane (1:2) as an eluent (flow rate: 0.7 ml min^{-1}). Under these conditions, the retention times of (*S*)-**1a** and (*R*)-**1a** were about 13 min and 17 min, respectively. The obtained (*S*)-**1a** and (*R*)-**1a** were identified by comparison of their physical properties (IR and ^{1}H NMR) with those of racemic **1a**. Specific optical rotations of (*S*)-**1a** and (*R*)-**1a** were $[\alpha]_D^{22}$ −269° (*c* 1.00, acetone) and $[\alpha]_D^{22}$ +269° (*c* 1, acetone) (lit,[18] $[\alpha]_D$ +255.0° (*c* 1.00, acetone)).

Table 1. Chromatography of **3a** on Florisil-MgO (70:30)

Fraction	Eluent[a]	Vol/ml	**1a**/mg	E.e./%
1—11	A	80×11	52.8	100 (*S*)
12	A	80	9.1	86 (*S*)
13	A	80	6.4	63 (*S*)
14	A	80	7.0	38 (*S*)
15	A	80	5.6	12 (*S*)
16	A	80	5.9	1 (*R*)
17	A	80	6.5	14 (*R*)
18	A	80	7.3	27 (*R*)
19	A	80	5.0	36 (*R*)
20	A	80	4.7	43 (*R*)
21	A	80	4.3	50 (*R*)
22	A	80	3.7	56 (*R*)
23	A	250	10.4	64 (*R*)
24	B	80	20.5	73 (*R*)
25	B	200	22.2	90 (*R*)

a) A: PhH-AcOEt (9:1); B: AcOEt.

Except for the use of (*S*)-2-amino-3-methyl-1-butanol (1.1 mmol) and (*R*)-1-phenylethylamine (1.1 mmol) instead of **2** (1.1 mmol), the same procedure was repeated and the results were depicted in Figs. 1d and 2. It was shown by ^{1}H NMR analysis that reaction of **1a** with (*R*)-1-phenylethylamine in ethanol gave a mixture which consisted of **6** and **7** in the ratio of ca. 1:1. The signals at δ=3.6—3.9 which consisted mainly of an AB quartet at 3.67 and 3.76 (*J*=13.0 Hz) and a singlet at δ=3.80 were assigned to those of **6** (mainly two isomers). The olefinic protons of **7** (two isomers) appeared at δ=4.83 (s) and 4.95 (s) in a relative intensity of 7:5.

In a similar manner, (*p*-methoxyphenylsulfinyl)acetone (**1b**) was resolved and the result is depicted in Fig. 3. The (*R*)- and (*S*)-**1b** were identified by comparison of their physical properties (IR and ^{1}H NMR) with those of racemic **1b**. Pure (*R*)-**1b** (>99.5% e.e. by HPLC): colorless crystals;

mp 75.5—77.0 °C (diethyl ether-hexane) (lit,[6] mp 56—58 °C); $[\alpha]_D^{21}$ +231° (*c* 0.75, MeOH) (lit,[6] $[\alpha]_D$ +168° (MeOH); no comment on its e.e.).

Reaction of the Dianion (8) with 1,3-Dibromopropane (9a, X=Br). (a) Dianion Formation Using 2 Equiv of LDA: To a solution of **1a** (589 mg, 3.00 mmol) in THF (20 ml), was added a THF solution of LDA, prepared by the action of butyllithium (6.60 mmol/4.26 ml of hexane) and diisopropylamine (1.2 ml, 8.6 mmol) in THF (10 ml), at −78 °C under an atmosphere of nitrogen. The resulting mixture was stirred at the same temperature for 30 min and then at room temperature for 1 h. After the mixture was again cooled to −78 °C, **9a** (X=Br) (0.94 ml, 9.0 mmol) was added and the reaction mixture was stirred at the same temperature for 30 min. The mixture was poured into a saturated aqueous solution (20 ml) of ammonium chloride, followed by extraction with diisopropyl ether (IPE) (20 ml×3). The combined extracts were dried ($MgSO_4$), evaporated, and subjected to column chromatography on silica gel using benzene-ethyl acetate (4:1) as an eluent to give **10a** (X=Br) (390 mg: 41% yield) along with the unchanged **1a** (186 mg). **10a** (X=Br): colorless crystals; mp 107—108 °C (from diethyl ether-hexane); ^{1}H NMR ($CDCl_3$) δ=1.60—1.73 (2H, m), 1.73—1.87 (2H, m), 2.42 (3H, s), 2.50 (1H, dt, *J*=18.5 and 6.9 Hz), 2.55 (1H, dt, *J*=18.5 and 6.6 Hz), 3.36 (2H, t, *J*=6.6 Hz), 3.75 (1H, d, *J*=13.2 Hz), 3.81 (1H, d, *J*=13.2 Hz), 7.34 (2H, d, *J*=7.9 Hz), and 7.52 (2H, d, *J*=7.9 Hz); IR (KBr) 1705 and 1035 cm^{-1}. Calcd for $C_{13}H_{17}BrO_2S$: C, 49.21; H, 5.40%. Found: C, 49.27; H, 5.38%.

(b) Dianion Formation Using NaH and Butyllithium: To a solution of **1a** (498 mg, 2.54 mmol) in THF (20 ml) and hexamethylphosphoric triamide (2 ml), was added NaH (60% dispersion in an oil) (156 mg, 3.90 mmol) under ice-cooling under N_2 atmosphere, and then the resulting mixture was stirred at room temperature for 1 h. After the mixture was cooled to −78 °C, a 1.55 M hexane solution (1.97 ml) of butyllithium (3.05 mmol) was added and the mixture was stirred at room temperature for 1 h. After **9a** (X=Br) (0.94 ml, 9.0 mmol) was added at −78 °C, the reaction mixture was stirred at the same temperature for 1 h. The workup similar to that described in (a) and column chromatography on silica gel gave **10a** (X=Br) (322 mg: 40% yield) along with the unchanged **1a** (63 mg).

In the manner analogous to that described in (a), the reaction of **1a** (316 mg, 1.61 mmol) with **9a** (X=I) (0.56 ml, 4.8 mmol) afforded **10a** (X=I) (246 mg: 42% yield) together with **1a** (105 mg). **10a** (X=I): colorless crystals; mp 101—106 °C (from diethyl ether-hexane); ^{1}H NMR ($CDCl_3$) δ=1.59—1.69 (2H, m), 1.69—1.82 (2H, m), 2.43 (3H, s), 2.49 (1H, dt, *J*=18.5 and 6.9 Hz), 2.51 (1H, dt, *J*=18.5 and 6.9 Hz), 3.13 (2H, t, *J*=6.6 Hz), 3.75 (1H, d, *J*=13.2 Hz), 3.81 (1H, d, *J*=13.2 Hz), 7.35 (2H, d, *J*=7.9 Hz), and 7.53 (2H, d, *J*=7.9 Hz); IR (KBr) 1710 and 1035 cm^{-1}. Calcd for $C_{13}H_{17}IO_2S$: C, 42.86; H, 4.70%. Found: C, 42.89; H, 4.72%.

Similarly, **9b** (X=I) reacted with **1a** to give the corresponding **10b** (X=I) in 60% yield: colorless crystals; mp 73.5—75.0 °C (from diethyl ether-hexane); ^{1}H NMR ($CDCl_3$) δ=1.28—1.42 (2H, m), 1.49—1.63 (2H, m), 1.73—1.85 (2H, m), 2.43 (3H, s), 2.48 (1H, dt, *J*=18.5 and 7.3 Hz), 2.52 (1H, dt, *J*=18.5 and 7.3 Hz), 3.16 (2H, t, *J*=6.9 Hz), 3.75 (1H, d, *J*=13.2 Hz), 3.83 (1H, d, *J*=13.2 Hz), 7.35 (2H, d, *J*=7.9 Hz), and 7.53 (2H, d, *J*=7.9 Hz); IR (KBr) 1705 and 1030 cm^{-1}. Calcd for $C_{14}H_{19}IO_2S$: C, 44.45; H, 5.06%. Found: C, 44.63; H, 5.06%.

Reaction of the Dianion (8) with 1,2-Diiodoethane (9, X=I). To a THF solution (5 ml) of the dianion (**8**) prepared from **1a** (500 mg, 2.55 mmol) and LDA (2.2 equiv), was added a solution of **9** (X=I) (2.22 g, 7.88 mmol) in THF (5 ml) at −78 °C, and the reaction mixture was stirred at the same temperature for 5 min. The mixture was poured into a saturated aqueous solution (20 ml) of ammonium chloride, followed by extraction with IPE (20 ml×1) and dichloromethane (10 ml×4). The combined extracts were washed with 5% aqueous solution of $Na_2S_2O_3$, dried ($MgSO_4$), evaporated, and subjected to column chromatography on silica gel using benzene-ethyl acetate (6:1) as an eluent to give a colorless oil (477 mg) which was too unstable to be completely identified. Its ^{1}H NMR spectrum exhibited the signals which were in accordance with those of 1-iodo-3-(*p*-tolylsulfinyl)-2-propanone: ^{1}H NMR ($CDCl_3$) δ=2.45 (3H, s), 4.00 (1H, d, *J*=13.5 Hz), 4.03 (1H, d, *J*=13.5 Hz), 4.17 (2H, s), 7.39 (2H, d, *J*=9.0 Hz), and 7.55 (2H, d, *J*=9.0 Hz).

Intramolecular Cyclization of 10a (X=I). A Typical Procedure. A THF solution (10 ml) of LDA, prepared from butyllithium (1.26 mmol/0.81 ml of hexane) and diisopropylamine (0.23 ml), was dropwise added to a solution of **10a** (379 mg, 1.04 mmol) in THF (20 ml) at −78 °C under N_2 atmosphere over 5 min. After being stirred at the same temperature for 30 min and then at −15 °C for 20 h, the mixture was poured into a saturated aqueous solution (20 ml) of ammonium chloride, followed by extraction with IPE (15 ml×3). The combined extracts were dried ($MgSO_4$) and evaporated. The oily residue was separated by column chromatography on silica gel using benzene-ethyl acetate (4:1) as an eluent to give **12a** (125 mg: 15% yield) which was shown by HPLC analysis to consist of two diastereomers in the ratio of 6:4. **12a**: colorless crystals; mp 105—115 °C: ^{1}H NMR ($CDCl_3$) δ=1.20—2.10 (6H, broad m), 2.30—2.80 (2H, m), 2.42 (3H, s), 3.00—3.70 (1H, m), 7.30 (2H, d, *J*=9.0 Hz), and 7.51 (2H, d, *J*=9.0 Hz); IR (KBr) 1710 and 1035 cm^{-1}. Calcd for $C_{13}H_{16}O_2S$: C, 66.07; H, 6.82%. Found: C, 66.25; H, 6.83%.

This compound was identified with the product derived from oxidation of 2-(*p*-tolylthio)cyclohexanone[19] with *m*-chloroperbenzoic acid in dichloromethane by comparison of their IR and ^{1}H NMR spectra.

In a similar manner, (R_s)-**12a** was prepared by the cyclization of (R_s)-**10a**: colorless crystals which was shown by HPLC to consist of two diastereomers (64:36); mp 110—118 °C; $[\alpha]_D^{22}$ +215° (*c* 0.80, $CHCl_3$).[16]

Synthesis of (S_s)-12c. To a solution of (*S*)-**1a** (234 mg, 1.19 mmol) in THF (5 ml), was added a THF solution of LDA, prepared by the action of butyllithium (2.86 mmol/1.92 ml of hexane) and diisopropylamine (0.48 ml) in THF (3 ml), at −78 °C under an atmosphere of nitrogen. The resulting mixture was stirred at the same temperature for 30 min and then at room temperature for 1 h. After the mixture was again cooled to −78 °C, **9c** (X=Cl) (464 mg, 2.38 mmol) was added and the reaction mixture was stirred at the same temperature for 30 min. The mixure was poured into a saturated aqueous solution (5 ml) of ammonium chloride, followed by extraction with IPE (5 ml×3). The combined extracts were dried ($MgSO_4$), evaporated, and subjected to column chromatography on silica gel using

benzene-ethyl acetate (1:1) as an eluent to give (*S*)-**10c** (**X**=Cl) (246 mg: 72% yield): colorless crystals; mp 59.5—60.5 °C (from diethyl ether-hexane); $[\alpha]_D^{22}$ −181° (*c* 1.00, $CHCl_3$). The IR and ^1H NMR of this compound was in complete accordance with those of racemic **10c**: colorless crystals; mp 65—66 °C (from diethyl ether-hexane); ^1H NMR ($CDCl_3$) δ=2.10—2.90 (4H, m), 2.42 (3H, s), 4.08 (2H, d, *J*=6.0 Hz), 5.35—5.85 (2H, broad s), 7.35 (2H, d, *J*=8.4 Hz), and 7.57 (2H, d, *J*=8.4 Hz); IR (KBr) 1705 and 1025 cm^{-1}. Calcd for $C_{14}H_{17}O_2ClS$: C, 59.04; H, 6.01%. Found: C, 59.24; H, 6.00%.

To a DMF solution (2 ml) of (*S*)-**10c** (87 mg, 0.31 mmol), was added NaH (60% dispersion in an oil, 15 mg, 0.37 mmol) under ice-cooling, and then the resulting mixture was stirred at room temperature for 2 h. The mixture was poured into a saturated aqueous solution (3 ml) of ammonium chloride and extracted with IPE (5 ml×3). The combined extracts were dried ($MgSO_4$), evaporated, and subjected to column chromatography on silica gel using hexane-ethyl acetate (1:1) as an eluent to give (S_s)-**12c** (56 mg: 74% yield) which was shown by HPLC analysis to consist of two diastereomers in the ratio of 52:48. An analytical sample (its diastereomeric ratio: 72:28) of (S_s)-**12c** was obtained by recrystallization from diethyl ether: colorless crystals; mp 95.5—100.5 °C; $[\alpha]_D^{20}$ −246° (*c* 0.75, $CHCl_3$). The IR and ^1H NMR of this compound was identical to those of racemic **11c**: mp 95—96 °C: ^1H NMR ($CDCl_3$) δ=2.10—3.20 (6H, m), 2.49 (3H, s), 3.72 (1H, dd, *J*=4.8 and 11.4 Hz), 5.28 (2H, broad s), 7.38 (2H, d, *J*=8.4 Hz), and 7.58 (2H, d, *J*=8.4 Hz); IR (KBr) 1705 and 1025 cm^{-1}. Calcd for $C_{14}H_{16}O_2S$: C, 67.71; H, 6.49%. Found: C, 67.74; H, 6.57%.

References

1) a) G. Solladié, C. Greck, G. Demailly, and A. Solladié-Cavallo, *Tetrahedron Lett.*, **23**, 5047 (1982). b) G. Solladié, G. Demailly, and C. Greck, *J. Org. Chem.*, **50**, 1552 (1985). c) G. Solladié, C. Fréchou, and G. Demailly, *Tetrahedron Lett.*, **27**, 2867 (1986). d) G. Solladié, J. Hutt, and C. Fréchou, *ibid.*, **28**, 61 (1987). e) F. Bravo and G. Resnati, *ibid.*, **28**, 4865 (1987). f) T. Fujisawa, A. Fujimura, and T. Sato, *Bull. Chem. Soc. Jpn.*, **61**, 1273 (1988). g) T. Fujisawa, A. Fujimura, and Y. Ukaji, *Chem. Lett.*, **1988**, 1541.

2) a) K. Ogura, M. Fujita, T. Inaba, K. Takahashi, and H. Iida, *Tetrahedron Lett.*, **24**, 503 (1983). b) G. Gianri, E. Narisano, and F. Pero, *J. Chem. Soc., Perkin Trans. 1*, **1984**, 189.

3) F. Schneider and R. Simon, *Synthesis*, **1986**, 582.

4) a) G. Solladié, G. Demailly, and C. Greck, *Tetrahedron Lett.*, **26**, 435 (1985). b) T. Sato, T. Itoh, and T. Fujisawa, *ibid.*, **28**, 5677 (1987).

5) H. Kosugi, H. Konta, and H. Uda, *J. Chem. Soc., Chem. Commun.*, **1985**, 211.

6) R. Davis, J. R. Kern, L. J. Kurz, and J. R. Pfister, *J. Am. Chem. Soc.*, **110**, 7873 (1988).

7) G. H. Posner and C. Switzer, *J. Am. Chem. Soc.*, **108**, 1239 (1986) and the references cited therein.

8) a) P. Bravo, E. Piovosi, and G. Resnati, *Synthesis*, **1986**, 579. b) T. Yamazaki, N. Ishikawa, H. Iwatsubo, and T. Kitazume, *J. Chem. Soc., Chem. Commun.*, **1987**, 1340.

9) a) K. Hiroi and N. Matsuyama, *Chem. Lett.*, **1986**, 65. b) M. C. Carreño, J. L. G. Ruano, and A. Rubio, *Tetrahedron Lett.*, **28**, 4861 (1987).

10) a) H. Phillips, *J. Chem. Soc.*, **127**, 2552 (1927). b) G. Solladié, F. Matloubi-boghadam, C. Luttman, and C. Mioskowski, *Helv. Chim. Acta*, **65**, 1602 (1982).

11) a) P. A. Grieco and C. S. Pogonowski, *J. Org. Chem.*, **39**, 732 (1974). b) I. Kuwajima and H. Iwasawa, *Tetrahedron Lett.*, **1974**, 107.

12) In a separate run, the oxazolidine of optically pure (*R*)- or (*S*)-**1a** with (*R*)-**2** showed two sets of ^1H NMR signals with a relative intensity of ca. 2:1 (see Experimental section).

13) Silica gel is not suitable because it adsorbs the amino part of **3a** too tightly to cause smooth hydrolysis of **3a**. MgO was also shown not to be effective as an adsorbent for separation of **3a**.

14) a) P. A. Grieco, D. Boxler, and C. S. Pogonowski, *J. Chem. Soc.*, **1974**, 497; b) J. Nokami, Y. Kusumoto, K. Jinnai, and M. Kawada, *Chem. Lett.*, **1977**, 715.

15) By the conventional way using sodium hydride and butyllithium as bases in THF,[11] the dianion (**8**) was also generated and subsequent treatment with **9a** (**X**=Br) gave the corresponding **10** in 41% yield (see Experimental section).

16) For a 75:25 diastereomeric mixture of (R_s)-**12a**, its $[\alpha]_D^{20}$ was reported to be +258° (*c* 1, $CHCl_3$).[9b]

17) S. Iriuchijima and G. Tsuchihashi, *Synthesis*, **1975**, 401.

18) L. Banfi, L. Colombo, and C. Gennari, *Synthesis*, **1982**, 829.

19) This compound was obtained by the treatment of an enolate ion of cyclohexanone with di-*p*-tolyl disulfide according to the reaction conditions reported for preparing 2-(phenylthio)cyclohexanone: B. M. Trost, T. N. Salzmann, and K. Hiroi, *J. Am. Chem. Soc.*, **98**, 4887 (1976).

 © 1989 The Chemical Society of Japan Bull. Chem. Soc. Jpn., 62, 3537—3541 (1989)

A Convenient Reductive Removal of Benzylic Hydroxyl and Trimethylsilyloxyl Groups with Me_3SiCl-NaI-MeCN Reagent

Takashi SAKAI,* Kazuyoshi MIYATA, Sadao TSUBOI, Akira TAKEDA, Masanori UTAKA,* and Sigeru TORII
Department of Applied Chemistry, Faculty of Engineering, Okayama University, Tsushima, Okayama 700
(Received February 2, 1989)

Secondary and tertiary hydroxyl groups at benzylic positions were reductively removed by treatment with 6 equivalents of Me_3SiCl-NaI-MeCN reagent in hexane at room temperature. A benzylic trimethylsilyloxyl group was also eliminated by the addition of 2 equivalents of water to the reaction system. The reduction was applied to the syntheses of precursors of such anti-inflammatory agents as ibuprofen, butibufen, naproxen, and related compounds, as well as (±)-*ar*-turmerone, an odorous sesquiterpene.

Recently, attention has been devoted to α-arylalkanoic acids and their derivatives because of their usefulness as nonsteroidal anti-inflammatory agents.[1] For example, ibuprofen (**1a**),[2] butibufen (**1b**),[3] and naproxen (**2**)[4] have been extensively utilized for medical purposes and various synthetic methods for the α-arylalkanoic acid skeleton have been developed.

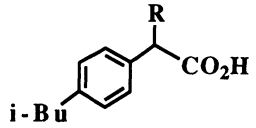

1a R=Me
1b R=Et

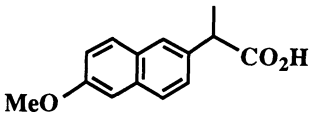

2

One of the straightforward approaches to them relies upon the reductive removal of such benzylic functional groups as $-OP(=O)(OEt)_2$,[2a] -OAc,[2b] $-SO_2Ph$,[2c] -OH,[3] and -SMe.[4] Therein, a convenient reduction method is still sought. It is of interest that a Me_3SiCl-NaI-MeCN reagent has been used for a variety of organic transformations.[5,6] For example, aliphatic alcohols are converted into the corresponding iodides[6,7] and α-ketols are reduced to ketones.[8] We describe here a new potential use of the reagent, in which a benzylic hydroxyl group can be reductively removed.[9] Moreover, a reduction of the benzylic trimethylsiloxyl group was also achieved by the addition of water to the system. The advantages of the present method include the reagent availability and procedural simplicity using mild conditions compared with the reported methods.[10] The synthetic utility of the method has been demonstrated by the syntheses of the precursors of racemic **1a**, **b** and **2** as well as (±)-*ar*-turmerone (**3**),[11a,b] a constituent of the essential oil from Curcuma Longa Linn.[11c]

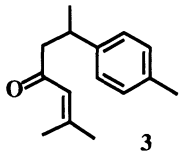

3

Results and Discussion

The reduction of secondary or tertiary benzylic alcohols **4b—p** with the Me_3SiCl-NaI-MeCN reagent gave products **5b—p** in good yields (Scheme 1). The results are summarized in Table 1. Optimun yields were obtained when the reaction was carried out with 6 equivalents of the reagent in hexane at room temperature. A decrease in the reagent ratio to three equivalents against **4a** resulted in a lower yield of **5b** and the partial recovery of **4b**. The obtained products were essentially pure after a simple workup, although cyanohydrins **4j** and **4k** decomposed partially to the corresponding ketones through a reverse cyanohydrin reaction under weakly acidic conditions. The reaction for menthyl ester **4m** required heating and gave a mixture of ester **5m** and its acid.

Furthermore, δ-hydroxy β-keto ester **6** gave β-keto ester **7** in 62% yield and diol **8** was deoxygenated regioselectively, giving alcohol **9** (39% yield) and iodide **10** (7% yield) (Scheme 2). Other functional groups such as aryl, carbonyl, cyano, carboxyl, alkoxycarbonyl, and the β-keto ester moiety were scarcely affected.[12]

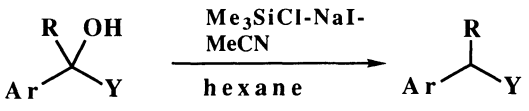

4b-p Y=Alkyl, CO_2R, CN **5b-p**

Scheme 1.

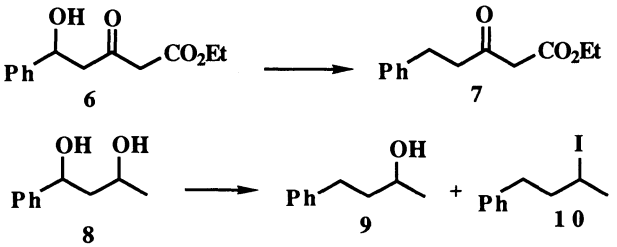

Scheme 2.

Table 1. Reductive Removal of Benzylic Hydroxyl Group Using Me_3SiCl-NaI-MeCN Reagent in Hexane[a,b]

	Alcohol 4			5	
	Ar	R	Y	Yield/%[c]	
4a[d]	Ph	H	H	e)	
4b[d]	Ph	H	Me	**5b**[d]	75
4b[d]	Ph	H	Me	**5b**[d]	57[f]
4c[d]	Ph	H	Et	**5c**[d]	99
4d	Ph	H	Pr	**5d**[d]	75
4e	Ph	H	Bu	**5e**[d]	74
4f	Piperonyl	H	Et	**5f**	57
4g	Ph	H	$-CH_2CO_2Et$	**5g**[d]	91
4h[d]	Ph	Me	Et	**5h**[d]	76
4i	Ph	Me	Pr	**5i**	82
4j	Ph	Me	CN	**5j**[d]	30[g]
4k	*p*-Isobutylphenyl	Me	CN	**5k**	77[h]
4l	*p*-Isobutylphenyl	Me	$-CO_2Et$	**5l**	85[i]
4m[j]	Ph	Me	$-CO_2$menthyl	**5m**	42[k,l]
4n[m]	Ph	Me	$-CH_2CO_2Me$	**5n**	60[i]
4o	*p*-Tolyl	Me	$-CH_2CO_2Et$	**5o**	91
4p	*p*-Tolyl	Me	$-CH_2CO_2H$	**5p**	66

a) Six equivalents of the reagent were used at room temperature for 24 h unless otherwise stated. b) All compounds listed are known. c) Isolated yield by distillation for **5b**—i or preparative TLC for **5j**—p. d) Commercially available. e) Benzyl iodide was obtained (94%). See Refs. 6 and 7. f) Three equivalents of reducing agent. Alcohol **4b** was recovered (12%). g) Acetophenone was produced (60%). h) *p*-Isobutylphenyl methyl ketone was recovered (12%). i) Reaction for 96 h. j) Diastereomeric excess of 22% (^{1}H NMR). k) Reaction for 3 days under reflux. The corresponding carboxylic acid was produced (21%). l) Racemic mixture. m) Enantiomeric excess of 70% (^{1}H NMR, Eu(hfc)$_3$).

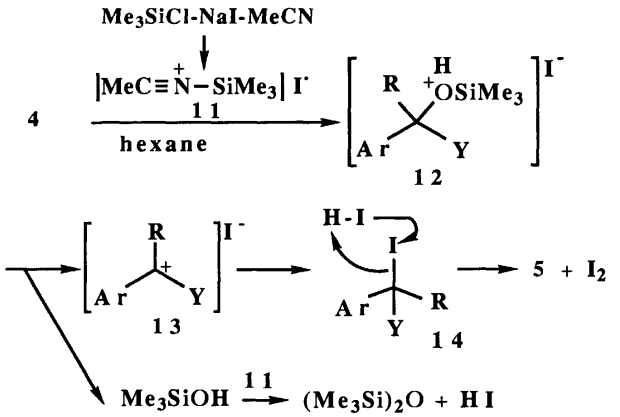

Scheme 3.

Scheme 3 illustrates a possible mechanism for the present reduction, which involves the conversion of the initially formed oxonium ion **12** to intermediate iodide **14**[6] and a subsequent reduction with an in situ generated HI, as discussed previously.[13] The proton for the reduction would, therefore, come from the original hydroxyl group. Optically active alcohols **4m** and **4n** gave racemic products **5m** and **5n**, respectively. Consequently, the present reaction seems to proceed through benzylic cation **13**. The difficulty in the formation of a primary carbonium ion from **4a** would result in the isolation of benzyl iodide.[7]

The above method leaves room for refinement in the case of cyanohydrins **4j** and **4k**. Both their yields and the product selectivity were improved by the use of

Table 2. Reductive Removal of Benzylic Trimethylsilyloxyl Group[a,b]

	16		17	
	Ar	R	Yield/%[c]	
16a	Ph	Me	(**5j**)[d]	74
16b	*p*-Tolyl	Me	**17b**	67
16c	*p*-Isobutylphenyl	Me	(**5k**)[d]	84
16d	*p*-Isobutylphenyl	Et	**17d**	74
16e	*p*-Isobutylphenyl	*i*-Pr	**17e**	82
16f	*p*-*t*-Butylphenyl	*i*-Pr	**17f**	24 (70)[e]
16g	6-Methoxynaphtyl	Me	**17g**	94
16h	2-Thienyl	Me	**17h**	37 (52)[e]

a) Me_3SiCl-NaI-MeCN reagent (6 equivalents) and H_2O (2 equivalents) in hexane for 24 h at room temperature. b) Known compounds except for **16c**—h. c) Isolated yields by preparative TLC. d) See Table 1. e) Overall yield from ketone without isolation of **16f** or **16h**.

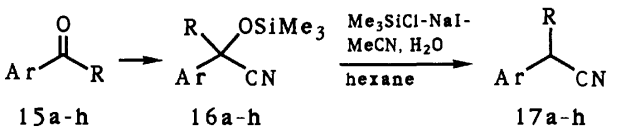

Scheme 4.

α-(trimethylsilyloxy) nitriles **16a** and **16c** (Scheme 4 and Table 2), which gave **5j** and **5k** exclusively. In these cases, the addition of 2 equivalents of water is required as a proton source. Fortunately, nitriles **16** are conveniently prepared from ketones **15**.[14] Reduction using a variety of nitriles, **16b** and **16d**—h,

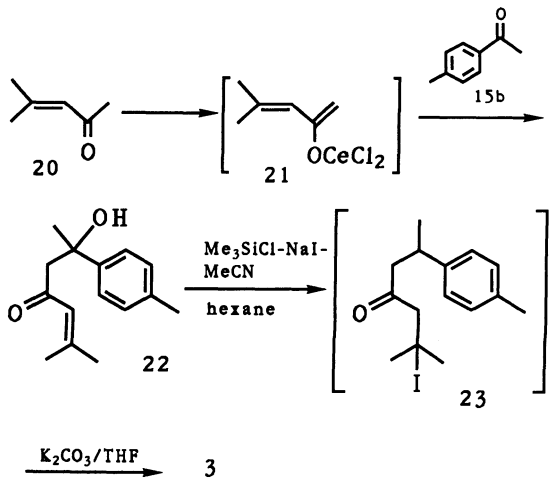

Scheme 5.

afforded **17b** and **17d—h** in acceptable yields, respectively. Nitriles **5k**, **17d**, and **17g** are known to be converted into **1a**, **b** and **2** by alkaline hydrolysis;[3a,10c] other nitriles are also important precursors for anti-inflammatory compounds.

By using this method, a deuterated benzylic compound was conveniently prepared. Thus, the reaction of **16b** in the presence of 2 equivalents of D_2O yielded 2-deuterio-2-*p*-tolylpropiononitrile (**18**) in 56% yield. This result supports the mechanism shown in Scheme 3.

In the case of α-(trimethylsilyloxy) nitriles, decreasing the amount of the reagent made the reaction rather complex. For example, the reaction of **16b** with 3 equivalents of the reagent and 2 equivalents of water in hexane gave a mixture of nitrile **17b** (33% yield), ketone **15b** (26% yield), and 2-*p*-tolylpropanamide (**19**) (26% yield). The reduction may be retarded under the conditions and accompanied by an acidic hydrolysis of the nitrile group or a reverse cyanohydrin reaction.

Finally, the present reaction was applied to an efficient synsthesis of (±)-**3**[11] from mesityl oxide (**20**) and *p*-methylacetophenone (**15b**), as communicated previously[9] (Scheme 5). Cerium enolate **21**[15] was allowed to react with **15b** to give aldol **22** in 54% yield. The reduction of **22** gave a 1:2 mixture of iodide **23** and **3** which, without isolation, was treated with K_2CO_3 in THF to afford **3** in 82% yield from **22**. This method offers one possible straightforward approaches to the synthesis of (±)-**3**.[9,11]

Experimental

General. IR spectra were taken on a JASCO A 102 spectrometer. ^1H NMR spectra (60 MHz) were measured with a JEOL-PMX 60 SI spectrometer. Chemical shifts are reported in value (ppm) down field from Me_4Si and *J* values are given in hertz. Preparative TLC was performed on silica gel (E. Merck, Kiesel gel 60 PF_{254}). Elemental analyses were performed by Eiichiro Amano of this laboratory using a Yanagimoto MT-3 CHN recorder.

Alcohols 4a—p. Compounds **4a—c** and **4h** are commercially available; the others were prepared according to the various methods reported.[16]

Ketones 15a—h. Compounds **15a**, **15b**, and **15h** are commercially available and **15c—g** were prepared by acylation of substituted benzene derivatives ($AlCl_3$, dichloromethane).[17]

General Procedure for Deoxygenation of Benzylic Alcohols 4a—p. To a stirred mixture of Me_3SiCl (1.54 ml, 12 mmol), NaI (1.8 g, 12 mmol), and acetonitrile (0.61 ml, 12 mmol), was added a solution of benzylic alcohol **4a—p** (2 mmol) in hexane (2 ml) at room temperature. The mixture slowly turned dark purple due to liberated iodine. After being stirred for 24 h at room temperature, the reaction was quenched by the addition of water. The organic layer was separated and the aqueous layer was extracted with ether. The combined organic layer was washed with aqueous $Na_2S_2O_3$ and brine, dried over $MgSO_4$, and then concentrated under vacuum. Distillation or preparative TLC (Table 1) of the residual oil gave clean products **5a—p**,[18] whose structures were identified by using IR and ^1H NMR spectra.

Ethyl 3-Oxo-5-phenylpentanoate (7). Crude product from **6**[19] (236 mg, 1 mmol) was purified by preparative TLC (hexane–acetone, 3:1) to give **7**[20] (136 mg, 62% yield): R_f 0.41—0.53; IR (neat) 1745, 1715 cm^{-1}; ^1H NMR (CCl_4) δ=1.20 (3H, t, *J*=7 Hz), 2.83 (4H, m), 3.23 (2H, s), 4.06 (2H, q, *J*=7 Hz), 7.10 (5H, m), 12.15 (trace, br s).

4-Phenyl-2-butanol (9)[21] and 3-Iodo-1-phenylbutane (10).[22] A crude product from diol **8**[23] (166 mg, 1 mmol) was separated by preparative TLC (hexane–acetone, 3:1) to give **9** (R_f 0.24—0.34, 58 mg, 39% yied) and **10** (R_f 0.78—0.90, 23 mg, 7% yield).

General Procedure for the Preparation of α-(Trimethylsilyloxy) Nitriles 16a—h. These reactions were carried out by a modification of Rasmussen's method.[14a] To a stirred suspension of NaCN (735 mg, 15 mmol), Me_3SiCl (1.02 ml, 8 mmol), and ZnI_2 (50 mg) in acetonitrile (2 ml) was added alkyl aryl ketone **15a—h** (5 mmol) at room temperature. The mixture was heated under gentle reflux for 48 h and then made basic by the addition of aqueous $NaHCO_3$; the organic layer was extracted with ether. It was then washed with brine, dried ($MgSO_4$) and concentrated under reduced pressure. The residue was purified by vacuum distillation to give **16a—h** (5 mmol) at room temperature. The mixture was heated under gentle reflux for 48 h and then made basic by the addition of aqueous $NaHCO_3$; the organic layer was extracted with ether. It was then washed with brine, dried ($MgSO_4$) and concentrated under reduced pressure. The residue was purified by vacuum distillation to give **16a—h**. Compound **16a**[14] was identified by a comparison of the spectral data with those reported. Those of **16b—h** are shown below.

2-*p*-Tolyl-2-(trimethylsilyloxy)propiononitrile (16b):[24] bp 140—152 °C (9 mmHg, 1 mmHg=133.322 Pa); IR (neat) 2225 cm^{-1}; ^1H NMR (CCl_4) δ=0.13 (9H, s), 1.76 (3H, s), 2.31 (3H, s), 7.06 (2H, d, *J*=8 Hz), and 7.32 (2H, d, *J*=8 Hz).

2-(*p*-Isobutylphenyl)-2-(trimethylsilyloxy)propiononitrile (16c): bp 115—130 °C (0.2 mmHg); IR (neat) 2230 cm^{-1}; ^1H NMR (CCl_4) δ=0.14 (9H, s), 0.89 (6H, d, *J*=6 Hz), 1.08 (3H, s), 1.5—2.6 (1H, m), 2.46 (2H, d, *J*=8 Hz), 7.05 (2H, d, *J*=9 Hz), and 7.37 (2H, d, *J*=9 Hz). Found: C, 69.71; H, 8.82; N, 5.12%. Calcd for $C_{16}H_{25}NOSi$: C, 69.82; H, 9.09; N, 5.09%.

2-(*p*-Isobutylphenyl)-2-(trimethylsilyloxy)butyronitrile

(**16d**): bp 110—130 °C (0.2 mmHg); IR (neat) 2240 cm^{-1}; ^1H NMR (CCl_4) δ=0.10 (9H, s), 0.89 (6H, d, J=6 Hz), 0.96 (3H, t, J=7 Hz), 1.5—2.2 (3H, m), 2.46 (2H, d, J=7 Hz), 7.03 (2H, d, J=8 Hz), and 7.30 (2H, d, J=8 Hz). Found: C, 70.66; H, 9.37; N, 4.64%. Calcd for $C_{17}H_{27}NOSi$: C, 70.59; H, 9.34; N, 4.84%.

2-(*p*-Isobutylphenyl)-3-methyl-2-(trimethylsilyloxy)butyronitrile (16e): bp 140—155 °C (0.3 mmHg); IR (neat) 2250 cm^{-1}; ^1H NMR (CCl_4) δ=0.14 (9H, s), 0.80—0.36 (12H, m), 1.45—2.35 (2H, m), 2.52 (2H, d, J=7 Hz), and 7.24 (4H, m). Found: C, 71.53; H, 9.59; N, 4.76%. Calcd for $C_{18}H_{29}NOSi$: C, 71.29; H, 9.57; N, 4.62%.

2-(*p*-*t*-Butylphenyl)-3-methyl-2-(trimethylsilyloxy)butyronitrile (16f): bp 105—120 °C (0.3 mmHg); IR (neat) 2350 cm^{-1}; ^1H NMR (CCl_4) δ=0.14 (9H, s), 0.87 (3H, d, J=7 Hz), 1.11 (3H, d, J=7 Hz), 1.38 (9H, s), 1.4—2.7 (2H, m), and 7.35 (4H, s). Found: C, 71.42; H, 9.31; N, 4.50%. Calcd for $C_{18}H_{29}NOSi$: C, 71.29; H, 9.57; N, 4.62%.

2-(6-Methoxy-2-naphthyl)-2-(trimethylsilyloxy)propiononitrile (16g): bp 145—155 °C (0.18 mmHg); IR (neat) 2229 cm^{-1}; ^1H NMR (CCl_4) δ=0.15 (9H, s), 1.85 (3H, s), 3.80 (3H, s), and 7.0—8.0 (5H, m). Found: C, 68.47; H, 6.84; N, 4.55%. Calcd for $C_{12}H_{21}NO_2Si$: C, 68.23; H, 7.02; N, 4.68%.

2-(2-Thienyl)-2-(trimethylsilyloxy)propiononitrile (16h): bp 143—157 °C (15 mmHg); IR (neat) 3125, 3100, 3000, 2250 cm^{-1}; ^1H NMR (CCl_4) δ=0.16 (9H, s), 1.91 (3H, s), 6.78 (1H, m), and 7.16 (2H, m). Found: C, 53.14; H, 6.44; N, 6.13%. Calcd for $C_{10}H_{15}NOSSi$: C, 53.33; H, 6.67; N, 6.22%.

General Procedure for the Reductive Removal of α-Trimethylsilyloxyl Group of 16a—h. Nitriles **16a—h** (0.5 mmol) were added to a mixture of Me_3SiCl (0.38 ml, 3 mmol), NaI (450 mg, 3 mmol), acetonitrile (0.19 ml, 3 mmol), and hexane (1 ml). After the addition of water (18 mg, 1 mmol), the mixture was stirred for 24 h at room temperature. The usual workup, followed by purification with preparative TLC on silica gel (hexane-acetone, 3:1) gave α-aryl nitriles **17a—h**. IR and ^1H NMR data of **17g** were identical with those reported.[25b,c] Those of others, which are not given in the literature, are shown below.

2-*p*-Tolylpropiononitrile (17b):[25a] R_f 0.48—0.60; IR (neat) 2250 cm^{-1}; ^1H NMR (CCl_4) δ=1.53 (3H, d, J=7 Hz), 2.31 (3H, s), 3.64 (1H, q, J=7 Hz), and 7.11 (4H, m).

2-(*p*-Isobutylphenyl)butyronitrile (17d):[25b] R_f 0.61—0.72; IR (neat) 2240 cm^{-1}; ^1H NMR (CCl_4) δ=0.90 (6H, d, J=6 Hz), 1.05 (3H, t, J=7 Hz), 1.5—2.3 (3H, m), 2.46 (2H, d, J=7 Hz), 3.61 (1H, t, J=6 Hz), and 7.10 (4H, m).

2-(*p*-Isobutylphenyl)-3-methylbutyronitrile (17e):[25c] R_f 0.56—0.81; IR (neat) 2250 cm^{-1}; ^1H NMR (CCl_4) δ=0.85—1.28 (12H, m), 1.3—2.7 (2H, m), 2.45 (2H, d, J=7 Hz), 3.54 (1H, d, J=6 Hz), and 7.09 (4H, m).

2-(*p*-*t*-Butylphenyl)-3-methylbutyronitrile (17f):[25d] R_f 0.44—0.60 (hexane-acetone, 5:1); IR (neat) 2250 cm^{-1}; ^1H NMR (CCl_4) δ=0.99 (3H, d, J=7 Hz), 1.03 (3H, d, J=7 Hz), 1.29 (9H, s), 2.10 (1H, m), 3.05 (1H, d, J=6 Hz), and 7.26 (4H, m).

2-(2-Thienyl)propionitrile (17h):[25f] R_f 0.41—0.49; IR (neat) 3130, 3020, 2960, 2260 cm^{-1}; ^1H NMR (CCl_4) δ=1.69 (3H, d, J=7 Hz), 4.09 (1H, q, J=7 Hz), 6.3—7.4 (3H, m).

2-Deuterio-2-*p*-tolylpropiononitrile (18). Nitrile **16b** (233 mg, 1 mmol) was added to a mixture of 6 equivalents of a Me_3SiCl-NaI-MeCN reagent in 1 ml of hexane, and then D_2O (99.6%, 36 mg, 2 mmol) was introduced. The mixture was treated in the usual way, giving **18** (81 mg, 55% yield): IR (neat) 2250 cm^{-1}; ^1H NMR (CCl_4) δ=1.52 (3H, m), 2.29 (3H, s), 3.26 (0.27H, q, J=7 Hz), 7.09 (4H, m); ^{13}C NMR ($CDCl_3$) δ=21.0 (q), 21.3 (q), 30.5 (t from C-D), 30.8 (d, C-H, trace), 121.7 (s), 126.5 (d), 129.7 (d), 134.1 (s), 137.8 (s). The ^1H NMR data indicates the deuterated ratio is 91%.

Reaction of 16b with 3 Equivalents of the Reducing Agent. Crude product from **16b** (233 mg, 1 mmol) was separated by preparative TLC (hexane-acetone 3:1) to give nitrile **17b** (R_f 0.42—0.73, 48 mg, 33% yield), amide **19** (R_f 0.03—0.16, 42 mg, 26% yield), and ketone **15b** (R_f 0.22—0.42, 15.5 mg, 11% yield). Compound **19**: IR (KBr) 3350, 3200, 1660 cm^{-1}; ^1H NMR ($CDCl_3$) δ=1.34 (3H, d, J=7 Hz), 2.26 (3H, s), 3.37 (1H, q, J=7 Hz), 5.80 (1H, br s), 6.97 (4H, m). Found: C, 73.41; H, 7.84; N, 8.64%. Calcd for $C_{10}H_{13}ON$: C, 73.62; H, 7.98; N, 8.59%.

6-Hydroxy-2-methyl-6-*p*-tolyl-2-hepten-4-one (22).[26] To a cooled (−78 °C) solution of LDA (4.4 mmol) [diisopropylamine (0.62 ml, 4.4 mmol) and 1.59 mol dm^{-3} BuLi hexane solution (2.75 ml, 4.4 mmol)] in THF (4 ml) in an acetone-Dry Ice bath, was added dropwise a solution of mesityl oxide (392 mg, 4 mmol) in THF (1 ml). After sitrring for 1 h at −78 °C, a suspension of $CeCl_3$ (1.16 g, 4.7 mmol) in THF (5 ml) was slowly added. The mixture was stirred for 1 h to form a cerium enolate anion. A solution of *p*-methylacetophenone (**15b**) (536 mg, 4 mmol) in THF (1 ml) was then added dropwise through a syringe. Stirring was continued for an additional 3 h at −78 °C. The resulting mixture was poured into water and acidified with 10% HCl. The organic layer was extracted with ether, dried over $MgSO_4$, and then concentrated under reduced pressure. The residue was subjected to vacuum distillation to give **22** (505 mg) as a clean oil: 54% yield; bp 140—150 °C (5 mmHg); IR (neat) 3475, 1675, 1610 cm^{-1}; ^1H NMR (CCl_4) δ=1.37 (3H, s), 1.80 (3H, s), 2.00 (3H, s), 2.24 (3H, s), 2.72 (1H, s), 2.81 (1H, s), 4.41 (1H, brs), 5.81 (1H, m), 6.94 (2H, d, J=8 Hz), and 7.21 (2H, d, J=8 Hz).

(±)-*ar*-Turmerone (3).[11] Compound **22** (101 mg, 0.43 mmol) was treated with Me_3SiCl (0.39 ml, 3 mmol), NaI (450 mg, 3 mmol), acetonitrile (0.15 ml, 3 mmol) in hexane (1 ml) in the usual manner and 116 mg of oily product was obtained. ^1H NMR analysis showed that it was a 1:2 mixture of 2-iodo-2-methyl-6-*p*-tolyl-4-heptanone (**23**)[27] and **3**, which was then stirred with K_2CO_3 (36 mg, 0.26 mmol) in THF (2 ml) for 20 h at room temperature. After the addition of water, the organic layer was extracted with ether, washed with aqueous $Na_2S_2O_3$ and brine, dried over $MgSO_4$, and then concentrated. The residual oil was subjected to vacuum distillation to give **3** (76 mg): 82% yield from **22**; bp 150—160 °C (7 mmHg); IR (neat) 1685, 1620, 1515, 819 cm^{-1}; ^1H NMR (CCl_4) δ=1.31 (3H, d, J=7 Hz), 1.81 (3H, s), 2.05 (3H, s), 2.22 (3H, s), 2.54 (2H, m), 3.15 (1H, m), 5.85 (1H, m), and 6.94 (4H, s). The spectral data are consistent with those reported.[11]

We are grateful to the SC-NMR Laboratory of Okayama University for 500 MHz ^1H NMR and 125 MHz ^{13}C NMR experiments concerning compound **18** using a Varian VXR-500 instrument.

References

1) C. Giordano, G. Castaldi, and F. Uggeri, *Angew. Chem., Int. Ed. Engl.*, **23**, 413 (1984).

2) a) S. Harusawa, S. Nakamura, S. Yagi, T. Kurihara, Y. Hamada, and S. Shioiri, *Synth. Commun.*, **1984**, 1365; b) T. Hiyama, M. Inoue, and K. Saito, *Synthesis*, **1986**, 645; c) H. Suzuki, Q. Yi, J. Inoue, K. Kusume, and T. Ogawa, *Chem. Lett.*, **1987**, 887, and the literatures cited therein.

3) M. Hamada, M. Umeno, S. Kanazawa, Y. Hayakawa, and M. Yajima, Japan Kokai, 7939042 (1979); *Chem. Abstr.*, **91**, p 14057u (1979).

4) a) K. Arai, Y. Ohara, T. Iizumi, and Y. Takakuwa, *Tetrahedron Lett.*, **24**, 1531 (1983); b) T. Ohta, H. Takaya, M. Kitamura, K. Nagai, and R. Noyori, *J. Org. Chem.*, **52**, 3174 (1987).

5) G. A. Olah, S. C. Narang, and B. C. Gupta, R. Malhotra, *J. Org. Chem.*, **44**, 1247 (1979). The reagent is recognized to form a complex **11**.

6) Review: G. A. Olah and S. C. Narang, *Tetrahedron*, **38**, 2225 (1982).

7) M. E. Jung and P. L. Ornstein, *Tetrahedron Lett.*, **1977**, 2659.

8) T.-L. Ho, *Synth. Commun.*, **9**, 665 (1979).

9) T. Sakai, K. Miyata, M. Utaka, and A. Takeda, *Tetrahedron Lett.*, **28**, 3817 (1987).

10) a) P_2I_4: H. Suzuki, H. Tani, H. Kubota, N. Sato, J. Tsuji, and A. Osuka, *Chem. Lett.*, **1983**, 247; b) Me_2SiI_2: W. Ando and M. Ikeno, *Tetrahedron Lett.*, **1979**, 4941; c) $NaBH_4/CF_3CO_2H$: G. W. Gribble, R. M. Leese, and B. E. Evans, *Synthesis*, **1977**, 172; d) Me_3SiH-BF_3: M. G. Adlington, M. Orfanopoulos, and J. L. Fry, *Tetrahedron Lett.*, **1976**, 2955; e) PPh_3-I_2: F. Bohlmann, J. Staffeldt, and W. Skuballa, *Chem. Ber.*, **109**, 1586 (1976); f) M. Hudlicky, "Reduction of Organic Chemistry," Ellis Horwood, West Sussex (1984), p. 79; g) Li/NH_3 (l): G. H. Small, A. E. Minnella, and S. S. Hall, *J. Org. Chem.*, **40**, 3151 (1975); S. D. Lipsky and S. S. Hall, *Org. Synth.*, Coll. Vol. 6, 537 (1988).

11) a) T. Sakai, K. Miyata, M. Ishikawa, and A. Takeda, *Tetrahedron Lett.*, **26**, 4727 (1985); b) T. Sakai, E. Amano, K. Miyata, M. Utaka, and A. Takeda, *Bull. Chem. Soc. Jpn.*, **60**, 1945 (1987); c) S. Gosselin and A. Thuillier, *J. Org. Chem.*, **44**, 2807 (1979), and the literatures cited therein.

12) The present reduction can not be applied to an aliphatic alcohol. Thus, ethyl 2-hydroxy-2-methylpentanoate and ethyl 3-hydroxybutanoate were recovered unchaged and an allylic alcohol, 2-octen-4-ol, gave a complex mixture.

13) T. Sakai, K. Miyata, M. Utaka, and A. Takeda, *Bull. Chem. Soc. Jpn.*, **60**, 1063 (1987).

14) a) J. K. Rasmussen and S. M. Heilmann, *Synthesis*, **1978**, 219; b) K. Sukata, *Bull. Chem. Soc. Jpn.*, **60**, 3820 (1987).

15) T. Imamoto, T. Kusumoto, and M. Yokoyama, *Tetrahedron Lett.*, **24**, 5233 (1983).

16) **4d**: J. -L. Luche and J. -C. Damiano, *J. Am. Chem. Soc.*, **102**, 7926 (1980); **4e**: G. Cahiez and J. F. Normant, *Tetrahedron Lett.*, **1977**, 3383; **4f**: I. V. Micovic, M. Nikolic, M. Bralovic, and K. Popovic, *Glas. Hem. Drus. Beograd*, **46**, 215 (1981); *Chem. Abstr.*, **96**, 52526c (1982); **4g**: K. Maruoka, S. Hashimoto, Y. Kitagawa, H. Yamamoto, and H. Nozaki, *Bull. Chem. Soc. Jpn.*, **53**, 3301 (1980); **4i**: F. C. Moutgomery and W. H. J. Saunders, *J. Org. Chem.*, **41**, 2368 (1976); **4j**: P. G. Gassman and J. J. Talley, *Tetrahedron Lett.*, **1978**, 3773; **4k**: See Ref. 3a; **4l**: See Ref. 3b; **4m**: T. Kaneko, D. L. Turner, M. Newcomb, and D. E. Bergbreiter, *Tetrahedron Lett.*, **1979**, 103; **4n**: E. B. Dongla, D. L. Dull, C. Mioskowski, and G. Solladie, *Tetrahedron Lett.*, **1973**, 4983; **4o**: L.-C. Chao and R. D. Rieke, *J. Org. Chem.*, **40**, 2253 (1975); **4p**: S. Watanabe, T. Fujita, K. Suga, S. Masumura, Y. Hamatani, and K. Miharu, *Yukagaku*, **32**, 389 (1983).

17) **15c**: G. Baddeley and E. Wrench, *J. Chem. Soc.*, **1956**, 4943; **15d**: T. Shioiri, N. Kawai, and M. Ban, Japan Kokai, 79117466 (1979); *Chem. Abstr.*, **92**, p128710y (1980); **15e**: M. Kuchar, B. Brunova, V. Rejholec, Z. Roubal, and O. Nemecek, *Collect. Czeck. Chem. Commun.*, **41**, 633 (1976); **15f**: J. G. Strong, U. S. Patent, 3968168 (1976); *Chem. Abstr.*, **85**, p123578q (1976); **15g**: L. Arsenijevic, V. Arsenijevic, A. Horeau, and J. Jacques, *Org. Synth.*, Coll. Vol. 6, 34 (1988).

18) **5f**: F. R. Hewgill and M. C. Pass, *Aust. J. Chem.*, **38**, 555 (1985); **5i**: A. Stefani, D. Tatone, and P. Pino, *Helv. Chim. Acta*, **59**, 1639 (1976); **5j**: O. H. Oldenziel, D. v. Leusen, and A. M. v. Leusen, *J. Org. Chem.*, **42**, 3114 (1977); **5k**: A. W. Nugents and J. R. Mckinney, *ibid.*, **50**, 5370 (1985); **5l**: K. Fujii, R. Nakao, and T. Yamauchi, *Synthesis*, **1983**, 444; **5m**: J. M.-Solich, I. Rudnicka, and Z. J. J. Jedlinski, *J. Chem. Soc., Perkin Trans. 1*, **1981**, 3034; **5n**: H. O. House and J. M. Umen, *J. Org. Chem.*, **38**, 3893 (1973); **5o**: J. Purman, J. Elliott, A. B. McElroy, and S. J. Warren, *J. Chem. Soc., Perkin Trans. 1*, **1985**, 1237; **5p**: P. A. Grieco and R. S. Finkelhor, *J. Org. Chem.*, **38**, 2245 (1973).

19) T. Izawa and T. Mukaiyama, *Chem. Lett.*, **1975**, 161.

20) E. E. Schweizer and K.-J. Lee, *J. Org. Chem.*, **47**, 2768 (1982).

21) D. A. Jaeger, M. D. Ward, and C. A. Martin, *Tetrahedron*, **40**, 2691 (1984).

22) I. Furukawa, B. Zhou, and S. Hashimoto, *Nippon Kagaku Kaishi*, **1984**, 1208.

23) J. Barluenga, J. Florez, and M. Yus, *J. Chem. Soc., Perkin Trans. 1*, **1983**, 3019.

24) See Ref. 16 for **4j**.

25) a) F. G. Bordwell, A. H. Clemens, D. E. Smith, and J. Begemann, *J. Org. Chem.*, **50**, 1151 (1985); b) T. Kurihara, S. Harusawa, Japan Kokai, 85184085 (1985); *Chem. Abstr.*, **104**, p168192d (1986); M. J. Carretero, L. J. Martin, and A. Ron, *Eur. J. Med. Chem. -Chim. Ther.*, **13**, 77 (1978); c) F. Masuko, H. Yamachika, K. Fujiyoshi, and K. Shiota, Ger. Offen., 2820710 (1978); *Chem. Abstr.*, **90**, p203724v (1979); d) Taisho Pharmaceutical Co., Ltd., Kuraray Co., Ltd., Japan Kokai, 8335162 (1983); *Chem. Abstr.*, **99**, p122060j (1983); e) See Ref. 18 for **5k**: f) Roussel-UCLAF, *Res. Discl.*, **234**, 334 (1983); *Chem. Abstr.*, **100**, 68108e (1984).

26) O. P. Vig, S. D. Sharma, B. R. Soni, and M. L. Sharma, *Indian J. Chem., Sect. B*, **19**, 353 (1980).

27) ^1H NMR (CCl_4) δ=1.17 (d), 1.96 (s), 2.02 (s). 2.22 (s), 2.93 (br s). The product distribution was estimated on the basis of the ^1H NMR spectrum.

Photochemical Hydrogen Abstraction Reactions of 9,10-Dihydro-9,10-*o*-benzenoanthracene-1,4-dione Derivatives with Xanthene: Intramolecular Charge Transfer Quenching

Nobuya KITAGUCHI†

Department of Chemistry, Faculty of Science, Kyoto University, Kitashirakawa, Sakyo-ku, Kyoto 606

(Received April 19, 1989)

Intramolecular charge transfer interaction in triptycene system was investigated. 9,10-Dihydro-9,10-*o*-benzenoanthracene-1,4-dione (triptycenequinone) and its analogs were readily photoreduced with xanthene to give the corresponding hydroquinones and the adducts with two xanthenyl radicals. The chemically induced dynamic nuclear polarization examination and the corresponding thermal reaction proved the adducts to be originated from free radical coupling of xanthenyl radicals and quinones. The quantum yield for disappearance of the quinones depended upon both the substituents and solvents. Kinetic analysis by applying Stern–Volmer plot, using anthracene as a quencher, revealed that the quantum yield of intersystem crossing and the lifetime of the triplet state decreased with increasing electron-donating power of the aromatic rings in triptycenequinones. These solvent and substituent effects suggest that intramolecular charge transfer quenching of both the singlet and the triplet excited states of quinones by neighboring aromatic rings occurs in the triptycenequinone system. Such intramolecular charge transfer interaction would lower the rate constants of hydrogen abstraction reaction from xanthene via the triplet states of triptycenequinone derivatives.

Transannular π–π interaction among neighboring benzene rings in triptycene system is one of the problems of increasing interest in organic chemistry.[1–8] It will be fascinating to investigate a change of such intramolecular interaction caused by introducing benzoquinone moiety into the triptycene system. 9,10-Dihydro-9,10-*o*-benzenoanthracene-1,4-dinoe (triptycenequinone) (**1a**) has one benzoquinone moiety and two benzene rings. Murata has observed the charge transfer (CT) transition for symmetry-forbidden CT interaction in unsubstituted and methyl- or methoxy-substituted triptycenequinones.[6,7] The present author has reported the substituent and solvent effects on the electronic spectra of triptycenequinones **1a—f**.[8] Triptycenequinones show characteristic absorption maxima as a result of intramolecular charge transfer. The substituents on the benzene rings strongly affect the CT bands. Strong electron-donating substituents induce shifts of the absorption maxima to long wavelengths. Calculations by the extended Hückel theory reveal that the charge of aromatic ring is somewhat delocalized to the benzoquinone moiety in the course of HOMO-LUMO excitation.[8] These findings clearly show that intramolecular CT interaction does exist in the singlet excited state of the triptycenequinone system.

On the other hand, benzoquinone derivatives are easily photoreduced with hydrogen donors such as xanthene (**2**) to the corresponding hydroquinones by hydrogen abstraction reactions.[9–14] Some quinones gave 2,3-di(9-xanthenyl)-2,3-dihydro-1,4-naphthoquinone derivatives.[11]

In this paper, the effect of the substituents on the hydrogen abstraction reaction of triptycenequinones with xanthene will be reported to reveal the efficiency of the intramolecular CT quenching of the singlet and triplet excited states of triptycenequinones.

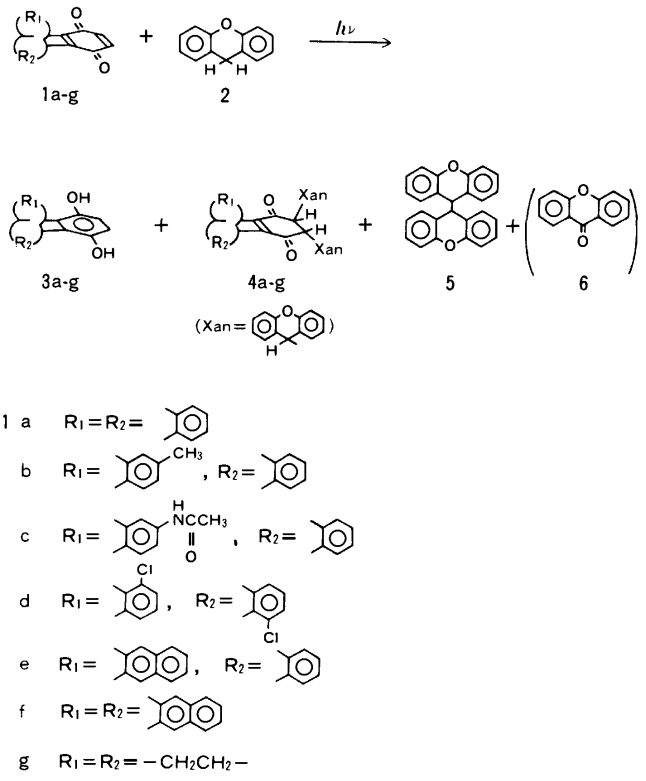

Results and Discussion

Product Analysis. In the photoreactions of tripty-

† Present address: Bio-Science Laboratory, Life Science Research Laboratories, Asahi Chemical Industry Co., Ltd., 2-1 Samejima, Fuji city, Shizuoka 416.

Table 1. Product Yields[a] in Photoinduced Reductions of Triptycenequinones with Xanthene (**2**)

Solvent	Quinone	Hydroquinone **3**	Adduct **4**
		Yield/%	Yield/%
C_6H_6	**1a**	78	17
	1d	75	Trace
	1e	69	23
	1f	93	n.d.[b]
	1g	83	Trace
CH_3CN	**1a**	66	10
	1e	77	n.d.[b]
$(CH_3)_2CO$	**1a**	86	n.d.[b]

a) Yields of isolated products based on the consumed quinones. b) Not detected.

cenequinones **1a**—**f** and 5,6,7,8-tetrahydro-5,8-ethano-1,4-naphthoquinone (**1g**) with xanthene (**2**), all quinones were reduced to the corresponding hydroquinones in high yields. A degassed C_6H_6 solution of **1a** and **2** (molar ratio was 1:2) was irradiated to give the hydroquinone **3a**, the adduct **4a** and 9,9′-bixanthenyl (**5**). The results of various quinones in three solvents are summarized in Table 1. When acetone was used as a solvent, the solution was irradiated at longer wavelengths than 340 nm. In acetonitrile, xanthone (**6**) was also isolated. Triptycensquinones other than those summarized in Table 1 were similarly photoreduced to give only the corresponding hydroquinones.

The structures of the adducts **4** were determined by mass, ^{1}H NMR, UV, and IR spectra. Further, 7.4×10^{-5} mol of the adduct **4a** was oxidized with $KBrO_3$ in acetic acid to give triptycenequinone (**1a**) (6.1×10^{-5} mol) and xanthone (**6**) (1.0×10^{-4} mol). This result confirms that **4a** consists of **1a** and xanthenyl moieties in the ratio of 1:2. Since the ^{1}H NMR spectrum of **4e** shows multiplet-like two doublets at δ=4.16, two xanthenyl groups may be in trans.

Formation of **4a** can be explained in terms of attack of two 9-xanthenyl radicals on **1a** in the ground state. In a thermal coupling experiment, **1a** and 9-xanthenyl radical generated by thermal reaction of **2** and di-*t*-butyl peroxyoxalate gave the adduct **4a** and bixanthenyl (**5**).

$$\mathbf{1a} + \mathbf{2} + (t\text{-BuOOC}\overset{\overset{\displaystyle O}{\|}}{}\!)_2 \xrightarrow[\text{benzene}]{\Delta,\ N_2} \mathbf{4a} + \mathbf{5}$$

On the contrary, the irradiation of **1a** and **5** in benzene gave no adduct **4a** but gave xanthone (**6**) and hydroquinone **3a**.

Chemically Induced Dynamic Nuclear Polarization (CIDNP) Examination of Photoinduced Hydrogen Abstraction Reaction of 1a with 2. In the photoreaction of **1a** with **2**, enhanced ^{1}H NMR signals were observed, although the signals were not so intense compared with those of 1,4-benzoquinone[10,12] or 1,4-naphthoquinone.[10,11] Figures 1 and 2 show the

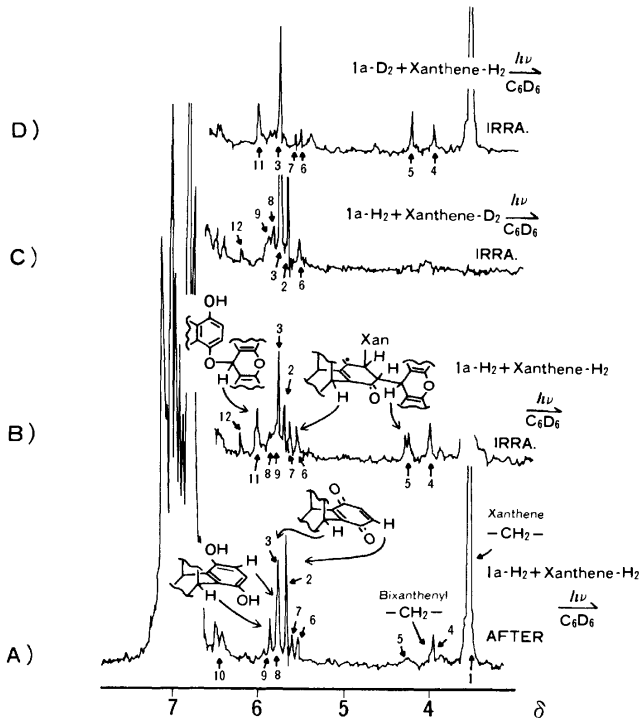

Fig. 1. ^{1}H NMR spectra observed in the photochemical reaction of **1a** with **2** at room temperature (solvent; C_6D_6). A) After irradiation. B) During irradiation. C) During irradiation with xanthene-9,9-d_2 instead of **2**. D) During irradiation with triptycenequinone-2,3-d_2 instead of **1a**.

^{1}H NMR signals observed in the reactions of **1a** with **2** and of **1g** with **2** for comparison. Signal No. 1 was due to the methylene protons of **2**, signals Nos. 2 and 3 due to **1a**, signals Nos. 4 and 10 due to **5**, and signals Nos. 8 and 9 due to the hydroquinone **3a**. By comparison of the spectra given in Fig. 1 A—D, signals Nos. 5, 7, and 11 can be assigned to the methylene protons of xanthenyl groups and signal No. 6 to the bridgehead protons of a triptycenequinone moiety. Signal No. 12 may be due to an unstable intermediate in the reaction of **1a** and the corresponding hydroquinone **3a**, because the similar absorption signal was observed during irradiation of a solution of these two compounds.

The chemical shifts of signals Nos. 5 and 6 were compatible with those of the adduct **4a**. Since these enhanced signals Nos. 5. and 6 were hardly observed at 6 °C and clearly observed at 78 °C (Fig. 2), they may be due to escape products from the solvent-caged initial radical pair. Application of "Kaptein's simple rule",[15] as well as the results of the thermal coupling reaction described in the previous section, also confirms that the precursor of **4a** is a free radical pair (Scheme 1).

In the photoreduction of naphthoquinone derivatives with **2**,[11] the CIDNP examination and the analysis of the structures of isolated products reveal that the quinones give 1:1 adducts, 2-(9-xanthenyl)-

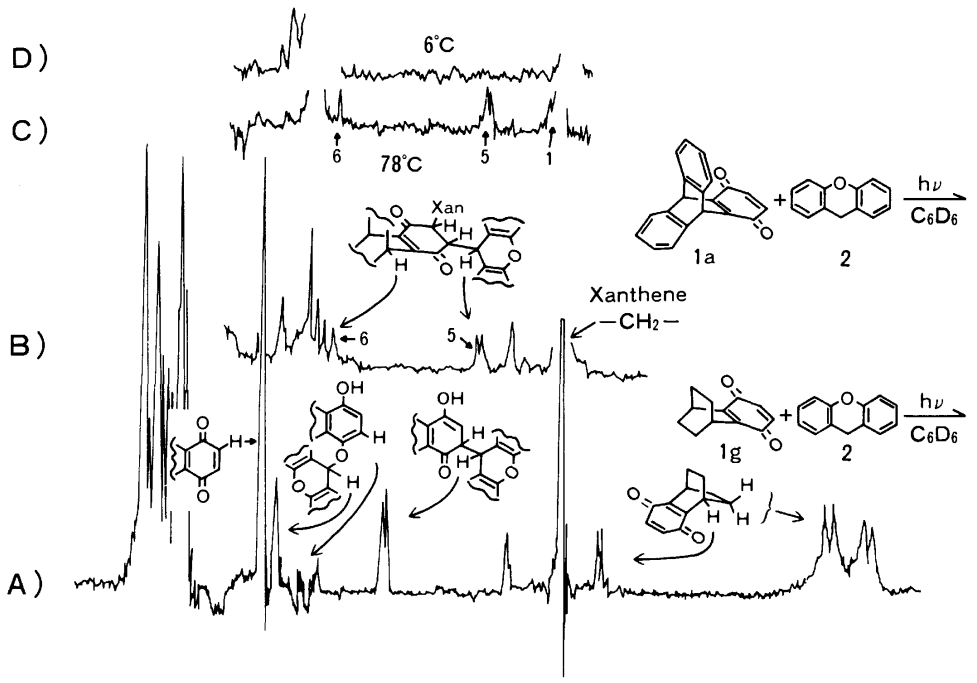

Fig. 2. ^{1}H NMR spectra observed in the photochemical reaction of quinones **1g** or **1a** with **2** during irradiation (solvent; C_6D_6). A) Non-aromatic quinone **1g** was irradiated at room temperature. B—D) Triptycenequinone **1a** was irradiated: B) at room temperature, C) at 78°C, D) at 6°C.

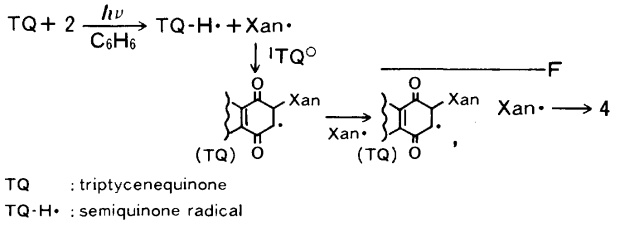

Scheme 1.

2,3-dihydro-1,4-naphthoquinones, as well as 1:2 adducts. In the present study, the non-aromatic derivative **1g** gave CIDNP signals of 1:1 coupling products as shown in Fig. 2. Although triptycenequinone (**1a**) also gave a CIDNP signal which may be assigned to a proton of a 1:1 adduct (Fig. 1B), such 1:1 adduct was not isolated in any photoreactions of triptycenequinone derivatives. Phenoxy type 1:1 adducts may be unstable because of susceptibility to oxidation and steric hindrance between a xanthenyl group and benzene rings of triptycenequinones.

Quantum Yields for Disappearance of Triptycenequinones ($\Phi_{disap.}$). The data of $\Phi_{disap.}$ in the reactions with **2** are summarized in Table 2. The details of the measurement method are described in the experimental section. Electron-donating substituents on benzene ring clearly suppressed the $\Phi_{disap.}$ values in each solvent (**1d**>**1a**>**1b**). Further, the $\Phi_{disap.}$ values of triptycenequinones having electron-donating groups, **1b**, **e**, and **f**, were much smaller in the reactions in polar solvents (acetonitrile and acetone) than in a non-polar solvent (benzene). As previously reported,[8] change of the reduced charge (population change) in the course of HOMO-LUMO excitation, calculated by the extended Hückel theory, can be adopted as a parameter of electron-donating ability. The $\Phi_{disap.}$ values are plotted against the population change of

Table 2. Quantum Yields for Disappearance of Quinones in the Photoreductions with Xanthene (**2**)[a]

Solvent	Quinone[b]	$\Phi_{disap.}$[c]
C_6H_6	**1d**	0.65
	1a	0.35
	1b	0.25
	1c	0.002
	1e	0.50
	1f	0.45
	1g	0.4
CH_3CN	**1d**	0.67
	1a	0.46
	1b	0.12
	1c	0.008
	1e	0.07
	1f	0.04
	1g	0.5
$(CH_3)_2CO$	**1a**	0.21
	1e	0.07
	1f	0.04

a) [**2**]=2.0×10^{-2} mol dm^{-3}. b) [Quinone]=2—5×10^{-3} mol dm^{-3}. c) Measured by means of iron(III) oxalate actinometry.

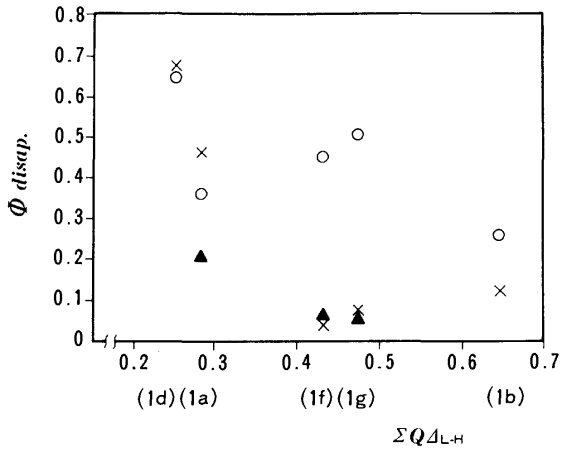

Fig. 3. A plot of $\Phi_{disap.}$ against population change of benzoquinone moiety ($\sum Q\Delta_{L-H}$).[8] Open circle, in benzene; cross, in acetonitrile; closed triangle, in acetone.

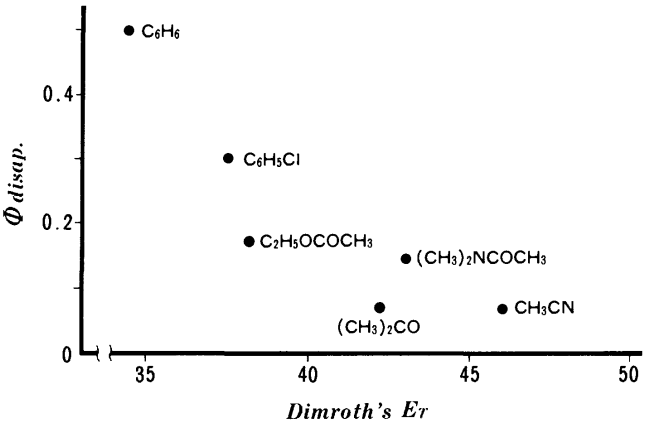

Fig. 4. Effect of solvent polarity on $\Phi_{disap.}$ of **1e**. [**2**]= 2.0×10^{-2} mol dm^{-3}. Dimroth's E_T value of DMF was estimated from its Z value.[8]

benzoquinone moiety ($\sum Q\Delta_{L-H}$) in Fig. 3. The $\Phi_{disap.}$ values obtained in benzene gently decrease with increasing population change $\sum Q\Delta_{L-H}$, while those in more polar solvents, acetonitrile and acetone, steeply decrease to go down to about 0.1 at $\sum Q\Delta_{L-H}$ value of 0.4—0.5. This population-change dependency of $\Phi_{disap.}$ values suggests that CT quenching occurs in the triplet excited state of triptycenequinones.

The $\Phi_{disap.}$ values of **1e** in various solvents clearly showed a decisive effect of solvent polarity. Figure 4 shows that the $\Phi_{disap.}$ values decrease with increasing solvent polarity; Dimroth's E_T values.[16,17] The reason why Kosower's Z-values were not adopted was described previously.[8]

These substituent and solvent effects on the $\Phi_{disap.}$ values suggest that the lowest excited states of triptycenequinones, especially the quinones having electron-donating substituents, may have a strong CT character in polar solvents.

Exceptionally, the $\Phi_{disap.}$ values of **1c** were exceedingly low compared with others (Table 2). Although

Table 3. Quenching of Triplet Excited Triptycenequinone (**1a**) by Anilides in C_6H_6[a]

Quencher	[Quencher] / mol dm^{-3}	$\Phi_{disap.}$
None[b]	—	0.35
Acetanilide[c]	5.4×10^{-3}	0.052
	5.0×10^{-2}	0.022
p-Acetotoluidide[d]	5.0×10^{-3}	0.040
	2.5×10^{-2}	0.015

a) Hydrogen donor was **2**; [**2**]=2.0×10^{-2} mol dm^{-3}. b) [**1a**]=4.0×10^{-3} mol dm^{-3}. c) [**1a**]=4.9×10^{-3} mol dm^{-3}. d) [**1a**]=4.7×10^{-3} mol dm^{-3}.

the Hammett σ^+ constant of acetylamino group (−0.25) is almost identical with that of methyl group (−0.26),[21] the $\Phi_{disap.}$ values of **1c** in both benzene and acetonitrile were less than one-tenth of those of **1b**. This can be explained in terms of quenching of the excited state of quinones by intra- and/or intermolecular electron transfer from lone pair electrons of the nitrogen atom of amino group to carbonyl groups.[18-20] This conception was confirmed by the intermolecular quenching experiment of the photoreduction of **1a** with **2** using acetanilide or acetotoluidide as a quencher. Acetanilide and acetotoluidide strongly decreased the $\Phi_{disap.}$ value of **1a** as shown in Table 3. More effective intramolecular quenching by 3,4-dimethylaniline moiety could suppress the $\Phi_{disap.}$ value of **1c** to about one-tenth of that of intermolecularly-quenched **1a**. A similar substituent effect is observed in the photoreduction of substituted fluorenone.[20] In that case, acetylamino group gives much higher quenching efficiency than ethoxy group (σ^+=−0.78).

Quenching of the Photoreductions of Triptycenequinones. Photoreductions of triptycenequinones with **2** were quenched by anthracene (the energy of the excited singlet state E_S=319.7 kJ mol^{-1}, the energy of the excited triplet state E_T=176.0 in a non-polar solvent), *trans*-stilbene (E_S=394.7, E_T=209.5 in a non-polar solvent), pyrene (E_S=322.2 in a non-polar solvent, E_T=201.5 in a polar solvent)[21], and oxygen. Because quinones were excited with the 450 nm monochromatic light (265.6 kJ mol^{-1}) in the present experiments of quantum yield determination, the quenchers described above could quench the triplet, not singlet, excited states of the quinones. Further, in general, hydrogen abstraction reactions have been considered to occur via the n-π^* triplet excited states.[22] Therefore, the present photoreduction reactions also can be considered to proceed through the n-π^* triplet excited states.

The triplet energy of triptycenequinone was assumed to be similar to the value of 2,3-dimethyl-1,4-benzoquinone (216.2 kJ mol^{-1}).[23] In the following experiments on kinetics, anthracene was used as a suitable quencher because of its E_S and E_T values. Pyrene and *trans*-stilbene were not suitable because

pyrene formed a CT complex with **1a** in the ground state, and the quenching efficiency of *trans*-stilbene was fairly small.

The reaction scheme for the hydrogen abstraction reactions of triptycenquinones can be drawn as described in Scheme 2.

From the thermal coupling experiment and the CIDNP examination described in the previous sections, the excited states of quinones might not directly participate in the formation of the adducts **4**, and the amount of **4** may be negligibly small in the initial step of the reaction. Therefore, formation of the adducts can be excluded from the following kinetic analysis. Based on Scheme 2, a straight line is expected in the Stern–Volmer plot of $\Phi_{disap.}^{-1}$ vs. $[\mathbf{2}]^{-1}$ from the following equation:

$$\Phi_{disap.}^{-1} = \Phi_{i.s.c.}^{-1} + k_d \times \Phi_{i.s.c.}^{-1} \times k_r^{-1} \times [\mathbf{2}]^{-1} \quad (1)$$

where $\Phi_{i.s.c.}$ is the quantum yield of intersystem crossing, k_r is the rate constant of the reaction between the triplet excited triptycenequinones (^{3}TQ*) and **2**, and k_d is the decay rate constant of ^{3}TQ*, that is, the reciprocal of the lifetime τ of ^{3}TQ*.

As another pathway to the hydroquinones **3**, the disproportionation of the semiquinone radicals (TQ–H·) could also be included in the reaction scheme. Based on the scheme containing disproportionation pathway, the intercept in the plot of $\Phi_{disap.}^{-1}$ vs. $[\mathbf{2}]^{-1}$ ($2/\Phi_{i.s.c.}$) cannot be less than two. However, the intercept was found to be less than two in many cases in the present study, suggesting that the contribution of the disproportionation of TQ–H· can be estimated to be small. In such cases, the hydroquinones **3** may be produced mainly by hydrogen abstraction reaction of TQ–H· from **2**.

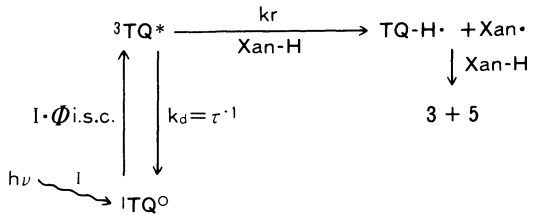

Scheme 2.

In the presence of a quencher (Q) of ^{3}TQ*, Eq. 1 is modified as follows:

$$\Phi_{disap.}^{-1} = \Phi_{i.s.c.}^{-1} + k_d \times \Phi_{i.s.c.}^{-1} \times k_r^{-1} \times [\mathbf{2}]^{-1} + k_q \times \Phi_{i.s.c.}^{-1} \times k_r^{-1} \times [\mathbf{2}]^{-1} \times [Q] \quad (2)$$

where k_q is the quenching rate constant and [Q] is the concentration of the quencher. Based on Eq. 2, a straight line is expected in the Stern–Volmer plot of $\Phi_{disap.}^{-1}$ vs. [Q] at a constant concentration of [**2**].

Stern–Volmer Plots. Benzene (Dimroth's E_T value is 34.5) and acetonitrile (46.0) were adopted as a nonpolar and a polar solvent, respectively. Since the quenching reactions proceed nearly in the diffusion-control, the following rate constants of the quenching reactions were adopted, k_q=5.0×10^9 dm^3 mol^{-1} s^{-1} in benzene and 1.0×10^{10} dm^3 mol^{-1} s^{-1} in acetonitrile.[19,24] All quinones investigated (**1a**, **b**, **d**, **e**, and **g**) gave straight lines in the plots of $\Phi_{disap.}^{-1}$ vs. $[\mathbf{2}]^{-1}$ in both solvents. Since the $\Phi_{disap.}$ values did not depend on the concentration of triptycenequinones (data not shown), intermolecular interaction of triptycenequinones can be neglected at least in the concentrations adopted in these experiments.

The kinetic parameters obtained by Stern–Volmer plots are summarized in Table 4. The $\Phi_{i.s.c.}$ values of the investigated quinones were mostly similar to each other in benzene, but they greatly changed in acetonitrile. The $\Phi_{i.s.c.}$ and τ values obtained in acetonitrile decreased in the order of electron-donating power of the aromatic rings except for the τ value of **1g**. The k_r values of substituted triptycenequinones **1a**, **b**, and **d** in both solvents decreased in the same order as the $\Phi_{i.s.c.}$ and τ values in acetonitrile. These results can be explained by intramolecular CT quenching, that is, by increase of the CT characters of the lowest excited

Table 4. Kinetic Parameters of the Triplet State of Triptycenequinones in the Reactions with Xanthene (**2**)

Solvent	Quinone	$\Phi_{i.s.c.}$	τ / 10^{-7} s	k_r / 10^8 mol^{-1} dm^3 s^{-1}
C_6H_6	**1d**	0.72	5.4	8.0
	1a	0.70	4.2	1.1
	1b	0.74	4.8	0.48
	1e	0.58	11	2.1
	1g[a]	0.83	0.4	4.8
CH_3CN	**1d**	0.67	>20	33
	1a	0.49	16	6.9
	1b	0.16	3.6	5.7
	1e	0.09	1.1	26
	1g	0.7	0.8	17

a) Because **1g** formed CT complex with C_6H_6, **2**, and **5**, the kinetic parameters of **1g** were not so accurate as those of other quinones.

singlet (^{S1}TQ) and triplet (^{T1}TQ) states of the quinones.

As previously reported,[8] increase of electron-donating power of the neighboring aromatic rings enlarges the CT character of ^{S1}TQ, especially in polar solvents. This substituent effect on the $\Phi_{i.s.c.}$ values in acetonitrile (Table 4) can be explained by increase of the CT character, therefore, decrease of the n-π^* character, of ^{S1}TQ. Similarly to the singlet state, the CT character of ^{T1}TQ may increase in the order of electron-donating power of the substituents in **1a**, **b**, and **d**, resulting in decrease of the n-π^* character of ^{T1}TQ to give the low k_r values. Further, the k_r values of the respective quinones were larger in acetonitrile than in benzene. This solvent dependency of the k_r values suggests great contribution of a polar transition state in the reaction with **2**, that is, the exciplex of the triplet excited quinone and **2**. The electron-donating substituents could enlarge electron density in the benzoquinone moiety, resulting in suppression of the formation of the exciplex with the electron-rich hydrogen donor **2**. The large k_r values of **1e** suggest that a naphthalene ring may accelerate such exciplex formation.

The small τ values of the lowest excited triplet state of the quinones having electron-donating substituents, determined by Stern-Volmer plot analysis, can be explained by assuming that the lifetimes of the CT triplet states of triptycenequinones are shorter than those of the n-π^* triplet states, whereas the lifetimes of the CT triplet states of substituted benzophenones, determined by phosphorescence measurement, are longer than those of the n-π^* triplet states.[25]

In benzene, the $\Phi_{i.s.c.}$ and τ values of substituted triptycenequinones (**1a**, **b**, and **d**) were almost identical (Table 4). Since CT levels are higher and n-π^* excited levels are lower in non-polar solvents than in polar solvents, the CT characters of ^{S1}TQ and ^{T1}TQ may decrease in benzene. As a result, the $\Phi_{i.s.c.}$ and τ values would not be affected by the electron-donating power of aromatic rings. The τ value of **1e** with a naphthalene ring, was about twice and that of **1g**, without an aromatic ring, was about one-tenth of those of other triptycenequinones in benzene (Table 4). Therefore, the τ values in benzene seem to depend on somewhat the number of neighboring π electrons (**1e**>**1a**=**1b**=**1d**>**1g**). This can be explained in terms of increasing π-π^* character of ^{T1}TQ. That is, since increase of neighboring π electrons may cause increase of the π-π^* character of ^{T1}TQ and the lifetime of the π-π^* triplet state is reported to be much longer than that of the n-π^* triplet state,[26,27] the τ values of **1e** would be larger and that of **1g** would be smaller than others.

In the case of non-aromatic derivative **1g**, since the lowest excited singlet and triplet states may be n-π^* both in benzene and in acetonitrile, the $\Phi_{i.s.c.}$ and τ values of **1g** showed weaker solvent dependency than those of other quinones.

The CT quenching described above is hard to explain in terms of the energy transfer from the neighboring π-electron systems to benzoquinone moiety, because the triplet energy of the neighboring aromatic ring (benzene, E_T=353.2 kJ mol^{-1}; naphthalene, 255.2)[21] may be too high to quench the triplet excited triptycenequinones (E_T of **1a** is assumed to be about 216.2 kJ mol^{-1} as described in the previous section, and was estimated to be about 200 kJ mol^{-1} by the comparison of the quenching rate constant of **1a** with those of E_T-known compounds, using *trans*-stilbene as a quencher, data not shown).

In conclusion, intramolecular CT quenching may occur both in the singlet and triplet excited states of the triptycenequinone system. Such intramolecular CT interaction may also suppress the exciplex formation between triptycenequinones and an electron-rich hydrogen donor **2**.

Experimental

Apparatus for Measurements. Electronic spectra were taken with a Shimadzu UV-200 spectrometer. ^{1}H NMR and CIDNP spectra were taken with a JEOL PS-100 MHz spectrometer in suitable solvents using TMS as an internal standard. IR spectra were recorded on a JASCO IR-G spectrometer using a KBr disc.

Quinones. **1a—g** were synthesized according to the previous report.[8] **Deuterated Compounds.** 2,3-d_2-Derivative of **1a** was synthesized by Diels-Alder reaction of 1,4-benzoquinone-2,3,5,6-d_4 with anthracene and subsequent oxidation in the same manner as described previously.[8] Xanthene-9,9-d_2 was obtained by the reduction of xanthone (**6**) with $LiAlD_4$.

Photoreductions of the Quinones with 2 on a Large Scale. Deaeration of a reaction solution was undertaken by means of pump-freeze-thaw cycles using a vacuum line covered with black sheets. A degassed solution in a usual glass tube was irradiated with a 300 W high pressure Hg-arc lamp through a water layer 5 cm thick at room temperature, with or without suitable filters. The products, except precipitated hydroquinones, were isolated by column chromatography or by preparative thin-layer chromatography on silica gel. The structure of the hydroquinones were identified after acetylation by comparison of their spectra and melting points with the authentic diacetates. The structure of 9,9'-bixanthenyl was determined by comparison of its spectra and melting point with the authentic sample. Physical properties of the adduct **4a** were as follows. ^{1}H NMR ($CDCl_3$): δ=3.06 (d, J=4 Hz, 2H), 4,21 (d, J=4 Hz, 2H), 5.46 (brs and m like d, 4H), 5.82 (m like d, 2H), 6.5—7.5 (m, 20H). IR (KBr): ν_{CO}=1663 cm^{-1}, $\nu_{C=C-O-C}$=1607, 1578, 1480, 1460, 1240. UV(ethyl acetate): λ_{max}=437 nm (sh, ε=300), 408 (sh, 660), 389 (sh, 920), 341 (1670), 274 (sh, 6800), 265 (sh, 7100). MS m/z=647 (M^+), 646, 466 (M−**X**an), 465, 464, 463, 285 (M−2Xan), 284, 182 (**X**an+1). Molecular weight measured by vapor pressure method; 638±26 (calcd. 646.8). Found: C, 85.21; H, 4.82%. Calcd for $C_{46}H_{30}O_4$: C, 85.43; H, 4.68%. Physical properties of the adduct **4e** were as follows. Mp >195 °C (decomp), 268 °C (melt). ^{1}H NMR ($CDCl_3$):

δ=3.04 (d, J=4 Hz, 2H), 4.13 (d, J=4 Hz, 1H), 4.17 (d, J=4 Hz, 2H), 4.52—4.80 (m, 2H), 5.26—5.50 (m, 2H), 5.45 (s, 2H), 5.65—5.89 (m, 2H), 6.2—7.8 (m, 1H). IR (KBr): ν_{CO}=1660 cm^{-1}, $\nu_{C=C-O-C}$=1605, 1575, 1477, 1458, 1245. MS m/z=515 (M−Xan), 334 (M−2Xan), 181 (Xan). Found: C, 85.91; H, 4.50%. Calcd for $C_{50}H_{32}O_4$: C, 86.19; H, 4.63%.

Quantum Yield Measurement. The $\Phi_{disap.}$ values were measured directly by means of iron(III) oxalate actinometry or indirectly with a merry-go-round as relative quantum yields to a standard solution. A reaction solution in a glass ample was degassed by means of pump-freeze-thaw cycles as described in the previous paragraph and was irradiated at room temperature with the 450 nm monochromatic light (using a 300 W high pressure Hg lamp with one Toshiba KL-45 and two VY-42 filters). A glass ample equipped with a 4 ml cuvette for irradiation and electronic spectra measurements was used in absolute $\Phi_{disap.}$ measurements. The disappearance of quinones was monitored with their visible absorption at more than three points of wavelength. High pressure liquid chromatography (column, μ-porasil Waters; eluent, CH_2Cl_2) was adopted in the case of **1g**.

Stern-Volmer Plot. In the absence of anthracene, the concentration of **2** ([**2**]) was set at several points from 1×10^{-2} to 2×10^{-1} mol dm^{-3} and that of the quinones ([quinone]) were 4×10^{-2} (**1a** in benzene), 3×10^{-3} (**1a** in acetonitrile), 5×10^{-3} (**1b** in both solvents), 3×10^{-3} (**1d** in both solvents), 3×10^{-3} (**1e** in both solvents), 3×10^{-2} mol dm^{-3} (**1g** in both solvents).

In quenching experiments, the concentration of anthracene was set at several suitable points from 0 to 2×10^{-2} mol dm^{-3}. [**2**] was 2×10^{-2} (**1d** in acetonitrile), 5×10^{-2} (**1g** in both solvents), 6.7×10^{-2} mol dm^{-3} (other cases). [Quinone]'s were almost the same as in the anthracene-free experiments.

In all experiments, good straight lines were obtained in the plots of $\Phi_{disap.}$ vs. $[\mathbf{2}]^{-1}$ or vs. [quencher].

The author wishes to express his grateful thanks to Professor Kazuhiro Maruyama for his guidance and invaluable discussions in this work. The author is grateful to Dr. Yasuo Kubo for his helpful suggestions. Thanks are also due to Dr. Tetsuo Otsuki, Dr. Yoshinori Naruta, and Dr. Tatsuhisa Kato for fruitful discussion.

References

1) V. Balaji and K. D. Jordan, *Chem. Phys. Lett.*, **119**, 294 (1985).
2) S. Inagaki, T. Imai, and H. Kawata, *Chem. Lett.*, **1985**, 1191.
3) H. Iwamura and K. Makino, *J. Chem. Soc., Chem. Commun.*, **1978**, 720.
4) E. Lipczynska Kochany and H. Iwamura, *Chem. Lett.*, **1982**, 1075.
5) G. A. Russell and N. K. Suleman, *J. Am. Chem. Soc.*, **103**, 1560 (1981).
6) K. Yamamura, K. Nakasuji, I. Murata, and S. Inagaki, *J. Chem. Soc., Chem. Commun.*, **1982**, 396.
7) I. Murata, *Pure Appl. Chem.*, **55**, 323 (1983).
8) N. Kitaguchi, *Bull. Chem. Soc. Jpn.*, **62**, 800 (1989).
9) K. Maruyama and A. Takuwa, *Bull. Chem. Soc. Jpn.*, **46**, 1529 (1973).
10) K. Maruyama, T. Otsuki, A. Takuwa, and S. Arakawa, *Bull. Chem. Soc. Jpn.*, **46**, 2470 (1973).
11) K. Maruyama and S. Arakawa, *Bull. Chem. Soc. Jpn.*, **47**, 1960 (1974).
12) K. Maruyama, T. Otsuki, and A. Takuwa, *Chem. Lett.*, **1972**, 131.
13) K. Maruyama and A. Takuwa, *Chem. Lett.*, **1972**, 135.
14) K. Maruyama, N. Kitaguchi, and T. Otsuki, *Chem. Lett.*, **1976**, 469.
15) D. Bethell and M. R. Brinkman, *Adv. Phys. Org. Chem.*, **10**, 53 (1972).
16) K. Dimroth, C. Reichardt, T. Siepmann, and F. Bohlmann, *Justus Liebigs Ann. Chem.*, **661**, 1 (1963).
17) K. Dimroth, C. Reichardt, and A. Schweig, *Justus Liebigs Ann. Chem.*, **669**, 95 (1963).
18) P. J. Wagner and B. J. Scheve, *J. Am. Chem. Soc.*, **99**, 1858 (1977).
19) P. J. Wagner, A. E. Kemppainen, and T. Jellink, *J. Am. Chem. Soc.*, **94**, 7512 (1972).
20) S. G. Cohen and G. Parsons, *J. Am. Chem. Soc.*, **92**, 7603 (1970).
21) S. L. Murov, "Handbook of Photochemistry," Marcel Dekker, Inc., New York (1973), Section 1, 2, and 26.
22) For example, N. J. Turro, "Molecular Photochemistry," W. A. Benjamin, Inc., New York (1967), p. 139.
23) A. Kuboyama, *Bull. Chem. Soc. Jpn.*, **35**, 295 (1962).
24) P. J. Wagner and I. Kochevar, *J. Am. Chem. Soc.*, **90**, 2232 (1968).
25) N. C. Yang and R. L. Dusenberg, *J. Am. Chem. Soc.*, **90**, 5899 (1968).
26) S. Lower and M. El-Sayed, *Chem. Revs.*, **66**, 199 (1966).
27) L. Vanquickenborne and S. McGlynn, *J. Chem. Phys.*, **45**, 4755 (1966).

 © 1989 The Chemical Society of Japan Bull. Chem. Soc. Jpn., 62, 3549—3566 (1989)

2-Methoxyethyl Group for Protection of Reducing Hydroxyl Group of Aldose

Shinkiti KOTO,* Naohiko MORISHIMA,† Kazuhiro TAKENAKA, Kumi KANEMITSU, Noriko SHIMOURA, Miyuki KASE, Shizuko KOJIRO, Teiko NAKAMURA, Tomoko KAWASE, and Shonosuke ZEN
School of Pharmaceutical Sciences, Kitasato University, Shirokane, Minato-ku, Tokyo 108
(Received April 21, 1989)

A variety of benzylated 1-OH derivatives, having an acetyl or an allyl group, of D-glucose, D-galactose, D-mannose, D-xylose, L-arabinose, L-fucose, and L-rhamnose, were synthesized from the corresponding protected 2-methoxyethyl glycosides through a brief treatment with $TiCl_4$ in dichloromethane and a subsequent hydrolysis of the intermediary 1-Cl derivatives on a silica-gel column.

Benzyl derivatives of aldose, whose reducing OH group is unprotected, are useful as a precursor of activated glycosyl donors in glycoside synthesis.[1] Under certain conditions,[2] such 1-OH derivatives can perform cross-condensation with alcohols as acceptors to give the corresponding glycosides. Several kinds of protecting groups for the reducing OH group have been proposed for the synthesis of 1-OH derivatives.[3] This report describes the 2-methoxyethyl (ME) group as a novel protecting group for the reducing OH group of aldose (Figs. 1 and 2).

Regeneration of the Reducing OH Group of the Protected 2-Methoxyethyl Glycosides. The isolation of a significant amount (22%) of the 1-OH derivative **4** in a study of rapid (4 s at room temp) anomerization of 2-benzyloxyethyl 2,3,4,6-tetra-*O*-benzyl-β-D-glucopyranoside with $TiCl_4$ in CH_2Cl_2 indicated that such a reaction could be useful in preparing **4** and similar compounds.[4] Later, a facile conversion of the glucoside **3** into the chloride **5** was observed upon its treatment with $TlCl_4$ in CH_2Cl_2 for 5 min at room temp.[5] The reaction mixture containing **5**, thus obtained, was adsorbed on a silica-gel column and eluted afterwards to give the hydrolyzate **4**.[5] The treatment of **3** with a slightly reduced amount (0.7 equiv) of $TiCl_4$ for 5 min at room temp was best for removing the ME group; **4** was obtained in a 66% yield. A longer reaction time and a larger quantity of the reagent diminished the yield of **4**, due to a concurrent formation of debenzylation products. A similar treatment of the α-anomer **8** with 1,2-cis disposition also afforded **4**, but required more reagent (1.0 equiv) to remove the ME group; thus the yield of **4** was low (41%). This procedure was then applied to the other 1,2-trans aldoside derivatives, **35**, **72**, **103**, **127**, **154**, and **181**, to produce the corresponding 1-OH derivatives, **36**, **73**, **104**, **128**, **155**, and **182**, in moderate yields.

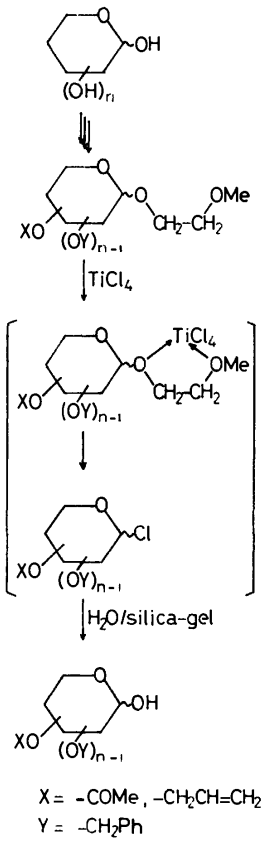

Fig. 1. General scheme.

The benzylated ME glycosides having one acetyl group, **10**, **16**, **23**, **28**, **38**, **49**, **59**, **66**, **75**, **80**, **81**, **98**, **106**, **119**, **129**, **141**, **145**, **156**, **168**, **172**, **183**, **191**, and **200**, and those having one allyl group, **13**, **18**, **25**, **30**, **41**, **51**, **61**, **68**, **78**, **84**, **95**, **100**, **109**, **112**, **121**, **132**, **143**, **147**, **159**, **170**, **174**, **186**, **193**, and **197**, were also converted into the corresponding 1-OH derivatives. The syntheses of the particular 1-OH derivatives, 3-*O*-acetyl-2,4-di-*O*-benzyl-D-xylopyranose[6] and 3-*O*-acetyl-2,4-di-*O*-benzyl-6-deoxy-D-glucopyranose,[7] have been reported before. They may be useful synthones for a linear portion of various oligosaccharides.

Preparation of Protected 2-Methoxyethyl Glycosides. The starting acetylated ME glycoside **33**, the precursor of **35** and **43**, was conveniently prepared from D-galactose (**32**) via a through-process of acetobromination with AcBr in AcOH[8] and a subsequent condensation with 2-methoxyethanol (MEOH) over Ag_2CO_3; the furanoside **34** was separated during chromatography. The fucoside acetate **152** was similarly synthesized from L-fucose (**151**) but L-arabinose (**123**) formed the furanoside **125** seriously;

† Present address: School of Nursing, Kitasato University, Kitasato, Sagamihara 228.

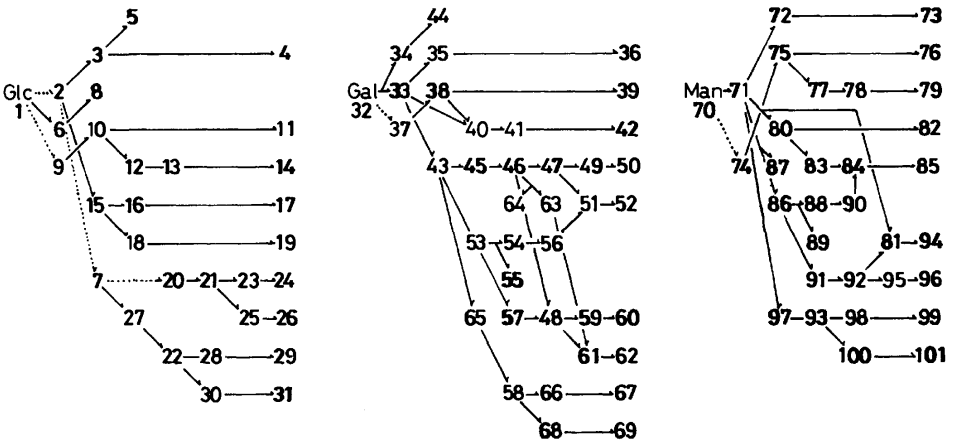

Fig. 2-i. Synthetic diagram.
(Broken arrows show known processes.)

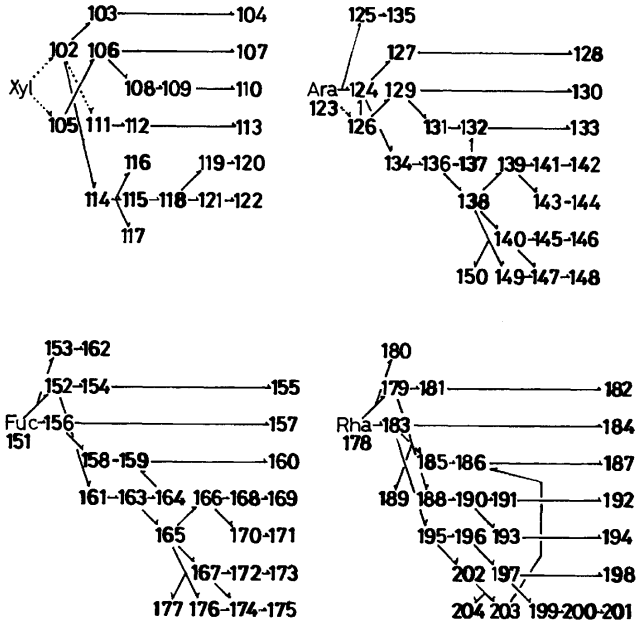

Fig. 2-ii. Synthetic diagram.
(Broken arrows show known processes.)

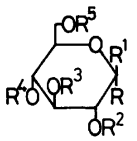

	R	R^1	R^2	R^3	R^4	R^5
1		H,OH	H	H	H	H
2	H	OME	Ac	Ac	Ac	Ac
3	H	OME	Bn	Bn	Bn	Bn
4		H,OH	Bn	Bn	Bn	Bn
5	Cl	H	Bn	Bn	Bn	Bn
6	OME	H	H	H	H	H
7	H	OME	H	H	H	H
8	OME	H	Bn	Bn	Bn	Bn
9	H	OAc	Ac	Ac	Ac	Ac
10	H	OME	Ac	Bn	Bn	Bn
11		H,OH	Ac	Bn	Bn	Bn
12	H	OME	H	Bn	Bn	Bn
13	H	OME	All	Bn	Bn	Bn
14		H,OH	All	Bn	Bn	Bn
15	H	OME	Bn	H	Bn	Bn
16	H	OME	Bn	Ac	Bn	Bn

	R	R^1	R^2	R^3	R^4	R^5
17		H,OH	Bn	Ac	Bn	Bn
18	H	OME	Bn	All	Bn	Bn
19		H,OH	Bn	All	Bn	Bn
20	H	OME	Bn	Bn	H	H
21	H	OME	Bn	Bn	H	Bn
22	H	OME	Bn	Bn	Bn	H
23	H	OME	Bn	Bn	Ac	Bn
24		H,OH	Bn	Bn	Ac	Bn
25	H	OME	Bn	Bn	All	Bn
26		H,OH	Bn	Bn	All	Bn
27	H	OME	H	H	H	Tr
28	H	OME	Bn	Bn	Bn	Ac
29		H,OH	Bn	Bn	Bn	Ac
30	H	OME	Bn	Bn	Bn	All
31		H,OH	Bn	Bn	Bn	All

All = $-CH_2CH=CH_2$ ME = $-CH_2CH_2OMe$
Bn = $-CH_2Ph$ Bd = $=CH(Ph)$
Tr = $-CPh_3$ Ip = $=CMe_2$

CM = chloroform - methanol DME = 1,2-dimethoxyethane
HE = hexane - ethyl acetate DMP = 2,2-dimethoxypropane
TB = toluene - 2-butanone IPE = diisopropyl ether

the pyranoside **124** was eventually synthesized from the acetate **126**[9] via a convenient bromination using AcBr and H_2O in $CHCl_3$.[10] Methanolysis of the acetates **33**, **124**, and **152** afforded the starting ME glycosides, **43**, **134**, and **161**, respectively. The mannoside **71**, on the other hand, was prepared by a direct condensation of D-mannose (**70**) and MEOH in the presence of $MeSO_3H$. The rhamnoside **179** was similarly obtained.

The 2-acetate **10** prepared from the acetate **9** via a rearrangement of a benzylated orthoester[11] was converted into the 2-*O*-allyl ether **13** through deacetylation and allylation. Such a process was used for obtaining the other 2-acetates, **38**, **75**, **106**, **129**, **156**, and **183**, and the corresponding 2-*O*-allyl ethers, **41**, **78**, **109**, **132**, **159**, and **186**. In the case of **151** and **178**, peracetylation prior to the bromination as in the cases of the hexoses could be omitted, both were directly

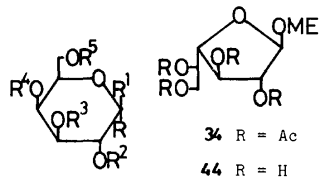

34 R = Ac

44 R = H

	R	R^1	R^2	R^3	R^4	R^5
32	H,OH	H	H	H	H	
33	H	OME	Ac	Ac	Ac	Ac
35	H	OME	Bn	Bn	Bn	Bn
36	H,OH	Bn	Bn	Bn	Bn	
37	H	OAc	Ac	Ac	Ac	Ac
38	H	OME	Ac	Bn	Bn	Bn
39	H,OH	Ac	Bn	Bn	Bn	
40	H	OME	H	Bn	Bn	Bn
41	H	OME	All	Bn	Bn	Bn
42	H,OH	All	Bn	Bn	Bn	
43	H	OME	H	H	H	H
45	H	OME	H	Ip		H
46	H	OME	Bn	H	H	Bn
47	H	OME	Bn	H	Bn	Bn
48	H	OME	Bn	Bn	H	Bn
49	H	OME	Bn	Ac	Bn	Bn
50	H,OH	Bn	Ac	Bn	Bn	
51	H	OME	Bn	All	Bn	Bn

	R	R^1	R^2	R^3	R^4	R^5
52	H,OH	Bn	All	Bn	Bn	
53	H	OME	H	H	Bd	
54	H	OME	H	All	Bd	
55	H	OME	All	H	Bd	
56	H	OME	Bn	All	H	H
57	H	OME	Bn	Bn	H	H
58	H	OME	Bn	Bn	Bn	H
59	H	OME	Bn	Bn	Ac	Bn
60	H,OH	Bn	Bn	Ac	Bn	
61	H	OME	Bn	Bn	All	Bn
62	H,OH	Bn	Bn	All	Bn	
63	H	OME	Bn	H	All	Bn
64	H	OME	Bn	All	H	Bn
65	H	OME	H	H	H	Tr
66	H	OME	Bn	Bn	Bn	Ac
67	H,OH	Bn	Bn	Bn	Ac	
68	H	OME	Bn	Bn	Bn	All
69	H,OH	Bn	Bn	Bn	All	

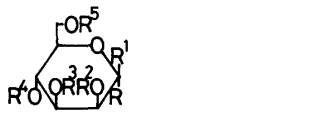

	R	R^1	R^2	R^3	R^4	R^5
70	H,OH	H	H	H	H	
71	OME	H	H	H	H	H
72	OME	H	Bn	Bn	Bn	Bn
73	H,OH	Bn	Bn	Bn	Bn	
74	OAc	H	Ac	Ac	Ac	Ac
75	OME	H	Ac	Bn	Bn	Bn
76	H,OH	Ac	Bn	Bn	Bn	
77	OME	H	H	Bn	Bn	Bn
78	OME	H	All	Bn	Bn	Bn
79	H,OH	All	Bn	Bn	Bn	
80	OME	H	Bn	Ac	Bn	Bn
81	OME	H	Bn	Bn	Ac	Bn
82	H,OH	Bn	Ac	Bn	Bn	
83	OME	H	Bn	H	Bn	Bn
84	OME	H	Bn	All	Bn	Bn
85	H,OH	Bn	All	Bn	Bn	

	R	R^1	R^2	R^3	R^4	R^5
86	OME	H	H	H	Bd	
87	OME	H	Bd		Ac	Ac
88	OME	H	H	All	Bd	
89	OME	H	All	H	Bd	
90	OME	H	Bn	All	H	H
91	OME	H	Bn	Bn	H	H
92	OME	H	Bn	Bn	H	Bn
93	OME	H	Bn	Bn	Bn	H
94	H,OH	Bn	Bn	Ac	Bn	
95	OME	H	Bn	Bn	All	Bn
96	H,OH	Bn	Bn	All	Bn	
97	OME	H	H	H	H	Tr
98	OME	H	Bn	Bn	Bn	Ac
99	H,OH	Bn	Bn	Bn	Ac	
100	OME	H	Bn	Bn	Bn	All
101	H,OH	Bn	Bn	Bn	All	

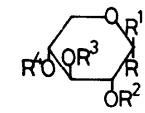

	R	R^1	R^2	R^3	R^4
102	H	OME	Ac	Ac	Ac
103	H	OME	Bn	Bn	Bn
104	H,OH	Bn	Bn	Bn	
105	H	OAc	Ac	Ac	Ac
106	H	OME	Ac	Bn	Bn
107	H,OH	Ac	Bn	Bn	
108	H	OME	H	Bn	Bn
109	H	OME	All	Bn	Bn
110	H,OH	All	Bn	Bn	
111	H	OME	Bn	H	Bn
112	H	OME	Bn	All	Bn

	R	R^1	R^2	R^3	R^4
113	H,OH	Bn	All	Bn	
114	H	OME	H	H	H
115	H	OME	H	H	Tr
116	H	OME	Tr	Ac	Ac
117	H	OME	Ac	Tr	Ac
118	H	OME	Bn	Bn	H
119	H	OME	Bn	Bn	Ac
120	H,OH	Bn	Bn	Ac	
121	H	OME	Bn	Bn	All
122	H,OH	Bn	Bn	All	

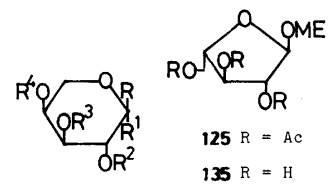

125 R = Ac

135 R = H

	R	R^1	R^2	R^3	R^4
123	H,OH	H	H	H	
124	OME	H	Ac	Ac	Ac
126	OAc	H	Ac	Ac	Ac
127	OME	H	Bn	Bn	Bn
128	H,OH	Bn	Bn	Bn	
129	OME	H	Ac	Bn	Bn
130	H,OH	Ac	Bn	Bn	
131	OME	H	H	Bn	Bn
132	OME	H	All	Bn	Bn
133	H,OH	All	Bn	Bn	
134	OME	H	H	H	H
136	OME	H	H	Ip	
137	OME	H	All	H	H

	R	R^1	R^2	R^3	R^4
138	OME	H	Bn	H	H
139	OME	H	Bn	H	Bn
140	OME	H	Bn	Bn	H
141	OME	H	Bn	Ac	Bn
142	H,OH	Bn	Ac	Bn	
143	OME	H	Bn	All	Bn
144	H,OH	Bn	All	Bn	
145	OME	H	Bn	Bn	Ac
146	H,OH	Bn	Bn	Ac	
147	OME	H	Bn	Bn	All
148	H,OH	Bn	Bn	All	
149	OME	H	Bn	H	All
150	OME	H	Bn	All	H

transformed into the 2-acetates, **156** and **183**, respectively.

Kinetic benzylation of the diol **20**[7] mainly gave the 4-OH compound **21**, the precursor **23** and **25**. A similar method was appled to the diols, **57** and **91**, obtained from the acetals, **53** and **86**, for preparing the 4-OH derivatives, **48** and **92**, which were then changed into the corresponding acetates, **59** and **81**, and the allyl ehers, **61** and **95**.

The 6-OH compound **22** obtained through conventional tritylation of the glucoside **7**[12] was derived into the acetate **28** and the allyl ether **30**. A similar process was applied to **43** and **71** to synthesize the other 6-OH

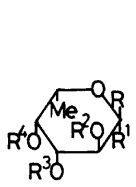

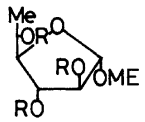

153 R = Ac
162 R = H

	R	R^1	R^2	R^3	R^4
151		H,OH	H	H	H
152	H	OME	Ac	Ac	Ac
154	H	OME	Bn	Bn	Bn
155		H,OH	Bn	Bn	Bn
156	H	OME	Ac	Bn	Bn
157		H,OH	Ac	Bn	Bn
158	H	OME	H	Bn	Bn
159	H	OME	All	Bn	Bn
160		H,OH	All	Bn	Bn
161	H	OME	H	H	H
163	H	OME	H	Ip	
164	H	OME	All	H	H
165	H	OME	Bn	H	H

	R	R^1	R^2	R^3	R^4
166	H	OME	Bn	H	Bn
167	H	OME	Bn	Bn	H
168	H	OME	Bn	Ac	Bn
169		H,OH	Bn	Ac	Bn
170	H	OME	Bn	All	Bn
171		H,OH	Bn	All	Bn
172	H	OME	Bn	Bn	Ac
173		H,OH	Bn	Bn	Ac
174	H	OME	Bn	Bn	All
175		H,OH	Bn	Bn	All
176	H	OME	Bn	H	All
177	H	OME	Bn	All	H

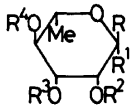

	R	R^1	R^2	R^3	R^4
178		H,OH	H	H	H
179	OME	H	H	H	H
180	H	OME	H	H	H
181	OME	H	Bn	Bn	Bn
182		H,OH	Bn	Bn	Bn
183	OME	H	Ac	Bn	Bn
184		H,OH	Ac	Bn	Bn
185	OME	H	H	Bn	Bn
186	OME	H	All	Bn	Bn
187		H,OH	All	Bn	Bn
188	OME	H	H	Tr	H
189	OME	H	Ac	Ac	Tr
190	OME	H	Bn	H	Bn
191	OME	H	Bn	Ac	Bn

	R	R^1	R^2	R^3	R^4
192		H,OH	Bn	Ac	Bn
193	OME	H	Bn	All	Bn
194		H,OH	Bn	All	Bn
195	OME	H	Ip		H
196	OME	H	H	H	All
197	OME	H	Bn	Bn	All
198		H,OH	Bn	Bn	All
199	OME	H	Bn	Bn	H
200	OME	H	Bn	Bn	Ac
201		H,OH	Bn	Bn	Ac
202	OME	H	H	H	Bn
203	OME	H	All	H	Bn
204	OME	H	H	All	Bn

Table 1. ^{1}H NMR Data (Chemical Shifts (δ) and Coupling Constants (Hz)) of Monoacetate of 2-Methoxyethyl Aldoside Derivatives

Compd	H-1	$J_{1,2}$	H-2	$J_{2,3}$	H-3	$J_{3,4}$	H-4	$J_{4,5}$	H-5	$J_{5,6a}$	$J_{5,6b}$	H-6a	$J_{6a,6b}$	H-6b	OMe	OAc
10	4.56	8	*5.20*	9	3.68	9	—		—			—		—	3.36	1.98
16	4.50	8	3.35	9.5	*5.21*	9.5	3.62	9.5	3.50	2.5	3.5	3.72	10.5	3.70	3.39	1.86
23	4.48	7.5	3.52	9	—	9.5	*4.96*	9.5	—			—		—	3.39	1.84
28	4.46	7.5	3.48	9	—		—		—	1.5	4.5	*4.35*	12	*4.20*	3.39	2.04
38	4.45	8	*5.41*	10	—	3	3.98	0	—			—		—	3.35	2.06
49	4.47	8	3.78	10.5	*4.89*	3	3.95	1	—			—		—	3.37	1.91
59	4.44	7	3.52	10	—	3	*5.58*	1	—			—		—	3.38	2.08
66	4.42	7.5	3.87	10	3.54	2.5	3.79	0	—	6.5	6	*4.23*	11	*4.07*	3.39	1.97
75	4.91	2	*5.46*	3.5	4.04	8.5	—		—			—		—	3.36	2.12
80	4.92	2.5	3.85	4	*5.26*	9	4.04	9	—	4	2	3.79	10	3.70	3.35	1.95
81	4.92	1.5	—		—	10	*5.39*	10	—			—		—	3.36	1.93
98	4.91	2	3.89	3	3.97	9	3.93	10	3.83	4	4	*4.30*	12	*4.32*	3.35	2.06

Table 1. (Continued)

Compd	H-1	$J_{1,2}$	H-2	$J_{2,3}$	H-3	$J_{3,4}$	H-4	$J_{4,5a}$	$J_{4,5b}$	H-5a	$J_{5a,5b}$	H-5b	OMe	OAc
106	4.41	7.5	*4.94*	9.5	3.59	9.5	—	4.5	9	3.99	11	3.26	3.34	1.98
119	4.45	7	3.49	9	3.61	9	*4.91*	5.5	9	4.04	11	3.19	3.39	1.96
129	4.47	5	*5.29*	7.5	3.60	3	3.73	5	2	3.99	12	3.38	3.35	2.05
141	4.47	6	3.79	8	*4.95*	4	3.84	2.5	2	4.02	12.5	3.44	3.38	2.03
145	4.36	7.5	3.68	9.5	3.56	4	*5.28*	2	1.5	4.00	13.5	3.48	3.39	2.15

Compd	H-1	$J_{1,2}$	H-2	$J_{2,3}$	H-3	$J_{3,4}$	H-4	$J_{4,5}$	H-5	$J_{5,6}$	H-6	OMe	OAc
156	4.40	8	*5.36*	10	3.53	3	3.61	1.5	3.49	6.5	1.23	3.34	2.04
168	4.44	7.5	3.77	10.5	*4.87*	3	3.66	1	3.61	6.5	1.22	3.37	1.93
172	4.42	7.5	—	10	3.56	3.5	*5.33*	1	3.65	6.5	1.22	3.38	2.17
183	4.79	2	*5.46*	4	3.99	10	3.46	10	—	6.5	1.35	3.38	2.16
191	4.80	2	3.89	3.5	*5.22*	10	3.62	10	3.80	6	1.33	3.36	1.96
200	4.82	2	3.86	3	3.80	10	*5.22*	10	—	6.5	1.20	3.36	2.02

Table 2. ^{1}H NMR Data (Chemical Shifts (δ) and Coupling Constants (Hz) of Monoacetate of 1-OH Aldose Derivatives

Compd	H-1	$J_{1,2}$	H-2	$J_{2,3}$	H-3	$J_{3,4}$	H-4	$J_{4,5}$	H-5	$J_{5,6a}$	$J_{5,6b}$	H-6a	$J_{6a,6b}$	H-6b	OAc
17α	5.24	4	3.51	10	*5.44*	9.5	—		—			—		—	1.93
17β	4.69	8	3.30	10	*5.21*	9.5	—		—			—		—	1.87
24α	5.20	3.5	—	9.5	3.94	9.5	*5.00*	10	4.10	3.5	5	—		—	1.87
24β	4.72	7.5	—		—	9.5	*4.96*	9.5	—			—		—	1.86
39α	4.57	4	*5.34*	10	3.98	3	—		—	6	6	3.57	9	3.47	2.07
39β	—	8	*5.18*	10	3.57	3	—		—			—		—	2.08
50α	5.31	3.5	4.00	10.5	*5.25*	3	4.03	1	4.29	6.5	6.5	—		—	1.97
50β	4.73	7.5	3.73	10	*4.90*	3	3.95	1	—			—		—	1.92

Table 2. (Continued)

Compd	H-1	$J_{1,2}$	H-2	$J_{2,3}$	H-3	$J_{3,4}$	H-4	$J_{4,5}$	H-5	$J_{5,6a}$	$J_{5,6b}$	H-6a	$J_{6a,6b}$	H-6b	OAc
60α	5.28	4	3.77	10	3.94	3.5	*5.61*	1	4.33	6.5	6.5	—		—	2.06
60β	4.68	7.5	—		—	3	*5.54*	1	3.74	6.5	6.5	—		—	2.09
67α	5.29	4	4.05	10	3.92	3	3.89	1	—			—		—	1.99
67β	4.64	7.5	3.79	9	3.56	3	3.81	1.5	3.61	7	5.5	*4.19*	11	—	1.99
76α	5.22	2	*5.37*	4	4.04	9.5	3.74	10	—			—		—	2.15
76β	—		—		—		—		—			—		—	2.21
82α	5.26	1.5	3.88	3.5	*5.31*	9.5	—	10	4.10	6	3	—		—	1.97
82β	4.77	1.5	3.93	3	*4.97*	10	—	10	3.49	2.5	4.5	—		—	1.95
94α	5.24	2	3.78	3	3.87	10.5	*5.28*	10.5	4.07	7.5	2.5	3.61	10.5	3.48	1.92
94β	—	1.5	3.83	3	—	9	*5.33*	9	—			—		—	1.92
99α	5.25	2	3.82	3	3.99	9	3.95	9	4.03	2	5	*4.39*	12	*4.26*	2.05
99β	—	1.5	3.87	3	3.65	10	3.85	10	3.51	2.5	6	*4.37*	12	*4.24*	2.04

Compd	H-1	$J_{1,2}$	H-2	$J_{2,3}$	H-3	$J_{3,4}$	H-4	$J_{4,5a}$	$J_{4,5b}$	H-5a	$J_{5a,5b}$	H-5b			OAc
107α	5.31	4	*4.80*	10	3.96	9	—			—		—			2.05
107β	—		—		—		—			—		—			2.03
120α	5.10	3	3.52	7.5	3.91	7.5	—			—		—			2.00
120β	—	5.5	3.40	7.5	3.70	7.5	*4.90*	4.5	7.5	4.12	12	3.36			2.00
130α	4.75	3	*5.25*	9	—		—			—		—			2.10
130β	5.40	3	*5.05*	6	—		—	8	4	4.08	11.5	3.63			2.07
142α	4.74	5.5	3.73	8.5	*5.01*	3.5	—	4.5	2	4.02	13	3.50			2.04
142β	5.15	2.5	3.84	8	*5.31*	3.5	—	2.5	5	3.93	12	3.72			2.07
146α	—		—		—		—			—		—			2.12
146β	5.23	4	3.95	9	3.78	4	*5.34*	2	4	4.03	13	3.72			2.13

Table 2. (Continued)

Compd	H-1	$J_{1,2}$	H-2	$J_{2,3}$	H-3	$J_{3,4}$	H-4	$J_{4,5}$	H-5	$J_{5,6}$	H-6	OAc
157α	5.46	4	*5.35*	10.5	3.99	3	3.90	0	4.14	6.5	1.16	2.10
157β	4.49	8	*5.18*	10	3.59	3	3.63	1	3.55	6.5	1.23	2.10
169α	5.29	4	4.01	10.5	*5.24*	3	3.76	1	4.23	6.5	1.17	1.98
169β	—	8	3.72	10.5	*4.88*	3.5	3.69	1	3.66	6.5	1.23	1.94
173α	5.25	4	3.78	10	3.93	3.5	*5.41*	1	4.27	6.5	1.15	2.10
173β	4.12	7.5	3.53	10	3.59	3	*5.34*	1	3.68	6.5	1.22	2.18
184α	5.13	2	*5.39*	3.5	4.01	10	3.45	10	—	6	1.32	2.16
184β	—	1.5	*5.53*	3.5	3.63	9	—		—	6	1.36	2.22
192α	5.16	2	3.89	3.5	*5.26*	10	3.64	10	4.02	6	1.33	1.97
192β	—	1.5	3.95	3	*4.96*	10	3.60	10.5	3.44	6	1.36	1.98
201α	5.20	2	3.81	3	3.85	9.5	*5.23*	9.5	3.96	6.5	1.20	2.03
201β	—		—	3	3.54	10	*5.17*	10	3.40	6.5	1.22	2.05

compounds **58** and **93**, and their derivatives, **66**, **68**, **98**, and **100**.

The diol **46** obtained through isopropylidenation of **43** was selectively benzylated with $PhCH_2Cl$ and KOH in 1,2-dimethoxyethane (DME) to furnish the 3-OH derivative **47**, the precursor of **49** and **51**. Such mild benzylation was useful in the monobenzylation of the diols, **138**, **165**, and **202**, which were derived from the corresponding acetals, **136**, **163**, and **195**, to give **139**, **166**, and **190**, respectively. A similar reaction using allyl bromide instead of $PhCH_2Cl$ worked well in the synthesis of the monoallyl ethers, **63**, **149**, **176**, and **203**, from the correspoinding diols, **46**, **138**, **165**, and **202**. This kinetic allylation was usefully applied to the acetals, **53** and **86**, to synthesize the monoallyl ethers, **54** and **88**, the precursors of **51** and **84**, respectively. The kinetic benzylation using $PhCH_2Cl$ and LiOH[13] for the diols, **138** and **165**, mainly afforded the 4-OH derivatives, **140** and **167**, respectively.

A controlled reaction of the acetate **2** with $PhCH_2Cl$ in the presence of a limited amount of NaOH mainly gave the 3-OH compound **15** (ca. 40%), the precursor of **16** and **18**. A similar reaction of the acetate **33**, but using DME as diluent, afforded the 2-OH derivative **40** (ca. 25%) as the main product. A kinetic benzylation of **71** with $PhCH_2Cl$ and KOH, followed by acetylation and chromatography, mainly furnished the 3-acetate **80** (35%), whereas the use of LiOH instead of KOH brought forth a preferential formation of the 4-acetate **81** (25%).[11]

Tritylation[14] of the xyloside **114** mainly gave the 4-*O*-trityl ether **115** (25%), the precursor of the 4-OH compound **118**, whereas the rhamnoside **179** formed the 3-*O*-substituted glycoside **188** (51%), the precursor of the 3-OH derivative **190**.

The 4-*O*-acetyl derivative **200** was prepared throgh deallylation and reacetylation of the 4-*O*-allyl ether **197**, which was readily obtained from the acetal **195**. The acetals, **136** and **163**, provided alternative routes to the 2-*O*-allyl derivatives, **132** and **159**, respectively.

All the structures of the derivatives of the ME glycosides are to be evident, since the ^1H NMR spectra of the monoacetates were consistently assigned; every proton on the carbon bearing OAc group definitely deshielded (Tables 1 and 2).

Thus, the ME group is considered to be an alternative choice for the protection of the hemiacetal OH group of aldose.[3] In the preparation of various derivarives of the ME glycosides, several kinetic substitutions of the polyols[15] (Fig. 3) were usefully carried out. The ME glycoside derivatives in which one OH group remains unprotected might be of use as

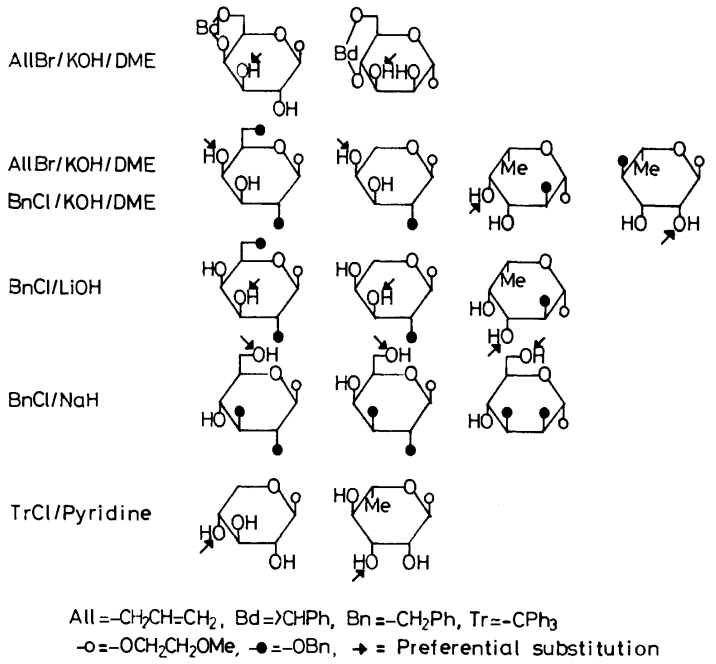

Fig. 3. Kinetic substitution of polyols.

acceptors in oligosaccharide synthesis.

Experimental

The ^{1}H NMR spectra were measured with a Varian VXR-300 spectrometer. The optical rotations were measured at room temp (20—25 °C). The other items were described previously.[16]

The aldoses used were the products of Wako Pure Chemicals Industries, Ltd., whereas the hexose acetates, **9**, **37**, and **74**, were available from Kyowa Pure Chemicals Industries, Ltd.

Synthesis of 1-OH Derivatives. To a stirring solution of a well-dried, protected 2-methoxyethyl aldoside (0.1—2 mmol) in dry CH_2Cl_2 (10 ml mmol^{-1} of substrate) was added $TiCl_4$ (0.7 equiv) at room temp to give a colored (pale yellow to reddish brown) solution. After 5 min, iced H_2O and then toluene were added to the solution. The organic layer was washed well with H_2O and dried over Na_2SO_4 briefly. After evaporation, the residue was adsorbed on a column of silica gel (40 g/g of substrate). After standing overnight, the column was eluted with toluene–2-butanone (TB) system (gradient) to give the corresponding 1-OH derivative. Compounds **4**[17] (66% from **3** and 41% from **8** (1.0 equiv of $TiCl_4$)), **11**[10] (77%), **29**[18] (76%), **36**[17] (74%), **73**[17] (66%), **85**[11] (70%), **96**[11] (67%), and **113**[6] (70%) were identified with the respective compounds prepared before.

2-*O*-Allyl-3,4,6-tri-*O*-benzyl-D-glucopyranose (**14**). 70%, mp 136—137 °C (from diisopropyl ether (IPE)), $[\alpha]_D$ +25° (*c* 0.4, $CHCl_3$) (lit,[19] mp 137—139 °C, $[\alpha]_D$ +25.7° ($CHCl_3$)) (Found: C, 73.37; H, 7.00%).

3-*O*-Acetyl-2,4,6-tri-*O*-benzyl-D-glucopyranose (**17**). 60%, mp 124—126 °C (from IPE), $[\alpha]_D$ +42° (*c* 1.4, $CHCl_3$)

Anal. ($C_{29}H_{32}O_7$) C, H.

3-*O*-Allyl-2,4,6-tri-*O*-benzyl-D-glucopyranose (**19**). 62%, mp 115—116 °C (from IPE), $[\alpha]_D$ +30 ° (*c* 1.0, $CHCl_3$), ^{1}H NMR ($CDCl_3$) δ=3.52 (dd, $J_{1,2}$=3.5 Hz, $J_{2,3}$=10 Hz, H-2α), 3.82 (dd, $J_{3,4}$=9 Hz, H-3α), 5.20 (H-1α), 6.00 (m, allyl).

Anal. ($C_{30}H_{34}O_6$) C, H.

4-*O*-Acetyl-2,3,6-tri-*O*-benzyl-D-glucopyranose (**24**). 63% mp 118—119 °C (from IPE), $[\alpha]_D$ +13 ° (*c* 0.6, $CHCl_3$) (lit,[20] 111—112 °C, $[\alpha]_D$ +9.4° ($CHCl_3$)) (Found: C, 70.66; H, 6.57%).

4-*O*-Allyl-2,3,6-tri-*O*-benzyl-D-glucopyranose (**26**). 62%, mp 108—110 °C (from IPE), $[\alpha]_D$ +35° (*c* 2.0, $CHCl_3$), ^{1}H NMR ($CDCl_3$) δ=3.36 (dd, $J_{1,2}$=7.5 Hz, $J_{2,3}$=9 Hz, H-1β), 3.54 (dd, $J_{1,2}$=3.5 Hz, $J_{2,3}$=9.5 Hz, H-2α), 3.90 (dd, $J_{3,4}$=9 Hz, H-3α), 5.21 (H-1α), 5.81 (m, allyl).

Anal. ($C_{30}H_{34}O_6$) C, H.

6-*O*-Allyl-2,3,4-tri-*O*-benzyl-D-glucopyranose (**31**). 66%, mp 133—135 °C (from IPE), $[\alpha]_D$ +13° (*c* 2.0, $CHCl_3$) (lit,[21] mp 132—134 °C, $[\alpha]_D$ +11.7° ($CHCl_3$)) (Found: C, 73.51; H, 7.01%).

2-*O*-Acetyl-3,4,6-tri-*O*-benzyl-D-galactopyranose (**39**). 56%, $[\alpha]_D$ +43° (*c* 1.7, $CHCl_3$) (lit,[22] $[\alpha]_D$ +45° ($CHCl_3$)) (Found: C, 70.45; H, 6.50%).

2-*O*-Allyl-3,4,6-tri-*O*-benzyl-D-galactopyranose (**42**). 76%, mp 88—90 °C (from hexane), $[\alpha]_D$ +16 ° (*c* 1.5, $CHCl_3$) (lit,[23] mp 90—92 °C, $[\alpha]_D$ +19.4° ($CHCl_3$)), ^{1}H NMR ($CDCl_3$) δ=3.48 (dd, $J_{2,3}$=9 Hz, $J_{3,4}$=2.5 Hz, H-3β), 3.64 (dd, $J_{1,2}$=7 Hz, H-2β), 3.85 (dd, $J_{2,3}$=10 Hz, $J_{3,4}$=3 Hz, H-3α), 3.96 (dd, $J_{1,2}$=4 Hz, H-2α), 4.61 (d, H-1β), 5.36 (d, H-1α), 5.93 (m, allyl) (Found: C, 73.23; H, 7.00%).

3-*O*-Acetyl-2,4,6-tri-*O*-benzyl-D-galactopyranose (**50**). 68%, $[\alpha]_D$ +56° (*c* 3.0, $CHCl_3$).

Anal. ($C_{29}H_{32}O_7$) C, H.

3-*O*-Allyl-2,4,6-tri-*O*-benzyl-D-galactopyranose (**52**). 64%, $[\alpha]_D$ +8° (*c* 2.8, $CHCl_3$), ^{1}H NMR ($CDCl_3$) δ=3.44 (dd, $J_{2,3}$=10 Hz, $J_{3,4}$=3 Hz, H-3β), 3.70 (dd, $J_{1,2}$=8 Hz, $J_{2,3}$=10 Hz, H-2β), 3.80 (dd, $J_{2,3}$=10 Hz, $J_{3,4}$=3 Hz, H-3α), 3.86 (d, $J_{4,5}$=0 Hz, H-4β), 3.93 (dd, $J_{4,5}$=1 Hz, H-4α), 3.98 (dd, $J_{1,2}$=4 Hz, H-2α), 4.10 (m, $J_{5,6a}$=$J_{5,6b}$=6.5 Hz, H-5α), 4.64 (d,

H-1β), 5.25 (d, H-1α).

Anal. ($C_{30}H_{34}O_6$) C, H.

4-*O*-Acetyl-2,3,6-tri-*O*-benzyl-D-galactopyranose (**60**). 53%, $[\alpha]_D$ +26° (*c* 1.5 $CHCl_3$).

Found: C, 70.21; H, 6.54%. Calcd for $C_{29}H_{32}O_7$: C, 70.71; H, 6.55%.

4-*O*-Allyl-2,3,6-tri-*O*-benzyl-D-galactopyranose (**62**). 60%, mp 91—93 °C (from hexane), $[\alpha]_D$ +18° (*c* 1.4, $CHCl_3$) (lit,[24] mp 95—96 °C, $[\alpha]_D$ +19.3° ($CHCl_3$)), ^1H NMR ($CDCl_3$) δ=3.49 (dd, $J_{2,3}$=9.5 Hz, $J_{3,4}$=3 Hz, H-3β), 3.70 (dd, $J_{1,2}$=8 Hz, $J_{2,3}$=9.5 Hz, H-2β), 3.98 (dd, $J_{1,2}$=3.5 Hz, $J_{2,3}$=9.5 Hz, H-2α), 4.64 (d, H-1β), 5.27 (d, H-1α), 5.89 (m, allyl) (Found: C, 73.17; H, 7.00%).

6-*O*-Acetyl-2,3,4-tri-*O*-benzyl-D-galactopyranose (**67**). 43%, mp 81—82 °C, $[\alpha]_D$ +7° (*c* 0.5, $CHCl_3$) (lit,[25] $[\alpha]_D$ +14° ($CHCl_3$)) (Found: C, 70.93; H, 6.89%).

6-*O*-Allyl-2,3,4-tri-*O*-benzyl-D-galactopyranose (**69**). 34%, $[\alpha]_D$ +19° (*c* 0.3, $CHCl_3$), ^1H NMR ($CDCl_3$) δ=3.77 (dd, $J_{1,2}$= 7.5 Hz, $J_{2,3}$=9.5 Hz, H-2β), 3.91 (dd, $J_{2,3}$=10 Hz, $J_{3,4}$=2.5 Hz, H-3α), 3.97 (dd, $J_{4,5}$=1 Hz, H-4α), 4.04 (dd, $J_{1,2}$=3.5 Hz, H-2α), 4.14 (m, $J_{5,6a}$=$J_{5,6b}$=6.5 Hz, H-5α), 4.67 (d, H-1β), 5.29 (d, H-1α), 5.85 (m, allyl).

Found: C, 73.11; H, 6.85%. Calcd for $C_{30}H_{34}O_6$: C, 73.45; H, 6.99%.

2-*O*-Acetyl-3,4,6-tri-*O*-benzyl-D-mannopyranose (**76**). 54%, $[\alpha]_D$ +6° (*c* 1.1, $CHCl_3$) (lit,[26] $[\alpha]_D$ +10.2° ($CHCl_3$)) (Found: C, 70.47; H, 6.56%).

2-*O*-Allyl-3,4,6-tri-*O*-benzyl-D-mannopyranose (**79**). 66%, $[\alpha]_D$ +23° (*c* 0.9, $CHCl_3$), ^1H NMR ($CDCl_3$) δ=3.57 (dd, $J_{2,3}$=3 Hz, $J_{3,4}$=10.5 Hz, H-3β), 3.64 (dd, $J_{5,6b}$=2 Hz, $J_{6a,6b}$= 10.5 Hz, H-6bα), 3.76 (dd, $J_{1,2}$=2 Hz, $J_{2,3}$=3 Hz, H-2α), 3.71 (dd, $J_{5,6a}$=6.5 Hz, H-6aα), 3.78 (dd, $J_{3,4}$=9 Hz, $J_{4,5}$=10 Hz, H-4α), 3.88 (dd, $J_{4,5}$=9 Hz, H-4β), 3.95 (dd, H-3α), 4.33 (m, H-5α), 5.25 (d, H-1α).

Found: C, 72.97; H, 7.10%. Calcd for $C_{30}H_{34}O_6$: C, 73.45; H, 6.99%.

3-*O*-Acetyl-2,4,6-tri-*O*-benzyl-D-mannopyranose (**82**). 70%, $[\alpha]_D$ −8° (*c* 1.0, $CHCl_3$)

Anal. ($C_{29}H_{32}O_7$) C, H.

4-*O*-Acetyl-2,3,6-tri-*O*-benzyl-D-mannopyranose (**94**). 78%, $[\alpha]_D$ +1.3° (*c* 0.5, $CHCl_3$).

Anal. ($C_{29}H_{32}O_7$) C, H.

6-*O*-Acetyl-2,3,4-tri-*O*-benzyl-D-mannopyranose (**99**). 59%, $[\alpha]_D$ +23° (*c* 0.8, $CHCl_3$).

Found: C, 70.24; H, 6.53%. Calcd for $C_{29}H_{32}O_7$: C, 70.71; H, 6.55%.

6-*O*-Allyl-2,3,4-tri-*O*-benzyl-D-mannopyranose (**101**). 74%, $[\alpha]_D$ +20° (*c* 0.5, $CHCl_3$), ^1H NMR ($CDCl_3$) δ=3.44 (m, $J_{4,5}$=10 Hz, $J_{5,6}$=2.5 and 4.5 Hz, H-5β), 3.63 (dd, $J_{2,3}$=2.5 Hz, $J_{3,4}$=10 Hz, H-3β), 3.81 (dd, $J_{1,2}$=2 Hz, $J_{2,3}$=3 Hz, H-2α), 3.86 (t, $J_{3,4}$=$J_{4,5}$=9.5 Hz, H-4α), 3.94 (t, H-4β), 3.98 (dd, H-3α), 5.26 (d, H-1α), 5.90 (m, allyl).

Found: C, 73.01; H, 7.05%. Calcd for $C_{30}H_{34}O_6$: C, 73.45; H, 6.99%.

2,3,4-Tri-*O*-benzyl-D-xylopyranose (**104**). 80%, mp 138—139 °C (from IPE), $[\alpha]_D$ +15° (*c* 2.0, $CHCl_3$) (lit,[27] 130—131 °C, $[\alpha]_D$ +25.1° (CH_2Cl_2)) (Found: C, 74.02; H, 6.74%).

2-*O*-Acetyl-3,4-di-*O*-benzyl-D-xylopyranose (**107**). 51%, $[\alpha]_D$ +30° (*c* 0.8, $CHCl_3$).

Anal. ($C_{21}H_{24}O_6$) C, H.

2-*O*-Allyl-3,4-di-*O*-benzyl-D-xylopyranose (**110**). 71%, mp 56—58 °C, $[\alpha]_D$ +9° (*c* 0.8, $CHCl_3$), ^1H NMR ($CDCl_3$) δ=3.21 (dd, $J_{1,2}$=7.5 Hz, $J_{2,3}$=9 Hz, H-2β), 3.26 (dd, $J_{4,5ax}$=10 Hz, $J_{5eq,5ax}$=11.5 Hz, H-5axβ), 3.42 (dd, $J_{1,2}$=4 Hz, $J_{2,3}$=9 Hz, H-2α), 3.68 (dd, $J_{4,5eq}$=5 Hz, $J_{5eq,5ax}$=11 Hz, H-5eqα), 3.84 (dd, $J_{4,5eq}$=4.5 Hz, H-5eqβ), 5.94 (m, allyl).

Found: C, 71.81; H, 6.99%. Calcd for $C_{22}H_{26}O_5$: C, 71.33; H, 7.07%.

4-*O*-Acetyl-2,3-di-*O*-benzyl-D-xylopyranose (**120**). 78%, $[\alpha]_D$ −4° (*c* 0.7, $CHCl_3$)

Found: C, 67.26; H, 6.48%. Calcd for $C_{21}H_{24}O_6$: C, 67.73; H, 6.50%.

4-*O*-Allyl-2,3-di-*O*-benzyl-D-xylopyranose (**122**). 56%, mp 49—51 °C, $[\alpha]_D$ +6° (*c* 0.6, $CHCl_3$), ^1H NMR ($CDCl_3$) δ=3.25 (dd, $J_{4,5ax}$=10 Hz, $J_{5eq,5ax}$=12 Hz, H-5axβ), 3.30 (dd, $J_{1,2}$=7 Hz, $J_{2,3}$=9 Hz, H-2β), 3.47 (dd, $J_{1,2}$=4 Hz, $J_{2,3}$=9 Hz, H-2α), 3.82 (t, $J_{3,4}$=9 Hz, H-3α), 4.00 (dd, $J_{4,5eq}$=4.5 Hz, H-5eqβ), 4.65 (d, H-1β), 5.12 (d, H-1α), 5.90 (m, allyl).

Anal. ($C_{22}H_{26}O_5$) C, H.

2,3,4-Tri-*O*-benzyl-L-arabinopyranose (**128**). 71%, mp 76—81 °C (from hexane), $[\alpha]_D$ +36° (*c* 1.4, $CHCl_3$) (lit,[28] mp 83—86 °C, $[\alpha]_D$ +51.1° (CH_2Cl_2)) (Found: C, 74.04; H, 6.75%).

2-*O*-Acetyl-3,4-di-*O*-benzyl-L-arabinopyranose (**130**). 48%, $[\alpha]_D$ +60° (*c* 0.3, $CHCl_3$)

Anal. ($C_{21}H_{24}O_6$) C, H.

2-*O*-Allyl-3,4-di-*O*-benzyl-L-arabinopyranose (**133**). 51%, $[\alpha]_D$ +31° (*c* 0.3, $CHCl_3$).

Found: C, 71.80; H, 7.24%. Calcd for $C_{22}H_{26}O_5$: C, 71.33; H, 7.07%.

3-*O*-Acetyl-2,4-di-*O*-benzyl-L-arabinopyranose (**142**). 63%, $[\alpha]_D$ +67° (*c* 0.9, $CHCl_3$).

Anal. ($C_{21}H_{24}O_6$) C, H.

3-*O*-Allyl-2,4-di-*O*-benzyl-L-arbinopyranose (**144**). 60%, $[\alpha]_D$ +24° (*c* 0.8, $CHCl_3$)

Anal. ($C_{22}H_{26}O_5$) C, H.

4-*O*-Acetyl-2,3-di-*O*-benzyl-L-arabinopyranose (**146**). 69%, $[\alpha]_D$ +44° (*c* 0.7, $CHCl_3$).

Anal. ($C_{21}H_{24}O_6$) C, H.

4-*O*-Allyl-2,3-di-*O*-benzyl-L-arabinopyranose (**148**). 51%, $[\alpha]_D$ +21° (*c* 0.6, $CHCl_3$).

Anal. ($C_{22}H_{26}O_5$) C, H.

2,3,4-Tri-*O*-benzyl-L-fucopyranose (**155**). 63%, mp 104—105 °C (from IPE), $[\alpha]_D$ −27° (*c* 0.5, $CHCl_3$) (lit,[29] mp 102—103 °C, $[\alpha]_D$ −26.5° ($CHCl_3$) (Found: C, 74.36; H, 6.91%).

2-*O*-Acetyl-3,4-di-*O*-benzyl-L-fucopyranose (**157**). 37%, $[\alpha]_D$ −31° (*c* 0.6, $CHCl_3$).

Found: C, 68.82; H, 6.92%. Calcd for $C_{22}H_{26}O_6$: C, 68.38; H, 6.78%.

2-*O*-Allyl-3,4-di-*O*-benzyl-L-fucopyranose (**160**). 37%, $[\alpha]_D$ −20° (*c* 0.6, $CHCl_3$), ^1H NMR ($CDCl_3$) δ=1.14 (d, $J_{5,6}$=6.5 Hz, H-6α), 1.18 (d, $J_{5,6}$=6.5 Hz, H-6β), 3.49 (dd, $J_{2,3}$=10 Hz, $J_{3,4}$=3 Hz, H-3β), 3.52 (m, $J_{4,5}$=1 Hz, H-5β), 3.56 (d, $J_{3,4}$= 2.5 Hz, $J_{4,5}$=1 Hz, H-4α), 3.57 (d, H-4β), 3.62 (dd, $J_{1,2}$=7.5 Hz, H-2β), 3.82 (dd, $J_{2,3}$=10 Hz, H-3α), 3.96 (dd, $J_{1,2}$=4 Hz, H-2α), 4.10 (m, H-5α), 4.57 (d, H-1β), 5.40 (d, H-1α).

Found: C, 72.24; H, 7.16%. Calcd for $C_{23}H_{28}O_5$: C, 71,85; H, 7.34%.

3-*O*-Acetyl-2,4-di-*O*-benzyl-L-fucopyranose (**169**). 72%, $[\alpha]_D$ −80° (*c* 0.7, $CHCl_3$).

Anal. ($C_{22}H_{26}O_6$) C, H.

3-*O*-Allyl-2,4-di-*O*-benzyl-L-fucopyranose (**171**). 56%, $[\alpha]_D$ −17° (*c* 0.6, $CHCl_3$), ^1H NMR ($CDCl_3$) δ=1.15 (d, $J_{5,6}$=6.5 Hz, H-6α), 1.21 (d, $J_{5,6}$=6.5 Hz, H-6β), 3.45 (dd, $J_{2,3}$=10 Hz,

$J_{3,4}$=2.5 Hz, H-3β), 3.54 (m, $J_{4,5}$=1 Hz, H-5β), 3.58 (dd, H-4β), 3.66 (dd, $J_{3,4}$=5 Hz, $J_{4,5}$=1 Hz, H-4α), 3.68 (dd, $J_{1,2}$=7.5 Hz, H-2β), 3.79 (dd, $J_{2,3}$=10 Hz, H-3α) 3.98 (dd, $J_{1,2}$=4 Hz, H-2α), 4.11 (m, H-5α), 4.61 (d, H-1β), 5.25 (H-1α), 5.98 (m, allyl).

Anal. ($C_{23}H_{28}O_5$), C, H.

4-*O*-Acetyl-2,3-di-*O*-benzyl-L-fucopyranose (**173**). 70%, $[\alpha]_D$ −57° (*c* 0.9, $CHCl_3$).

Anal. ($C_{22}H_{26}O_6$) C, H.

4-*O*-Allyl-2,3-di-*O*-benzyl-L-fucopyranose (**175**). 32%, $[\alpha]_D$ −27° (*c* 0.6, $CHCl_3$), ^1H NMR ($CDCl_3$) δ=1.22 (d, $J_{5,6}$=6.5 Hz, H-6α), 1.29 (d, $J_{5,6}$=6.5 Hz, H-6β), 3.59 (dd, $J_{3,4}$=3 Hz, $J_{4,5}$=1 Hz, H-4α), 3.84 (dd, $J_{2,3}$=10 Hz, H-3α), 3.97 (dd, $J_{1,2}$=4 Hz, H-2α), 4.11 (m, H-5α), 5.25 (d, H-1α).

Anal. ($C_{23}H_{28}O_5$) C, H.

2,3,4-Tri-*O*-benzyl-L-rhamnopyranose (**182**). 78%, mp 94—95 °C (from IPE), $[\alpha]_D$ −12° (*c* 0.5, $CHCl_3$)(lit,[30] mp 90—92 °C, $[\alpha]_D$ −15.4° ($CHCl_3$)) (Found: C, 74.51; H, 6.94%).

2-*O*-Acetyl-3,4-di-*O*-benzyl-L-rhamnopyranose (**184**). 76%, $[\alpha]_D$ +10° (*c* 0.7, $CHCl_3$).

Anal. ($C_{22}H_{26}O_6$) C, H.

2-*O*-Allyl-3,4-di-*O*-benzyl-L-rhamnopyranose (**187**). 63%, $[\alpha]_D$ −20° (*c* 0.7, $CHCl_3$), ^1H NMR ($CDCl_3$) δ=1.31 (d, $J_{5,6}$=6.5 Hz, H-6α), 1.34 (d, $J_{5,6}$=6.5 Hz, H-6β), 3.36 (m, $J_{4,5}$=10 Hz, H-5β), 3.56 (t, $J_{3,4}$=$J_{4,5}$=10 Hz, H-4α), 3.78 (dd, $J_{1,2}$=2 Hz, $J_{2,3}$=3 Hz, H-2α), 3.91 (dd, H-3α), 5.19 (d, H-1α).

Found: C, 71.46; H, 7.36%. Calcd for $C_{23}H_{28}O_5$: C, 71.85; H, 7.34%.

3-*O*-Acetyl-2,4-di-*O*-benzyl-L-rhamnopyranose (**192**). 79%, $[\alpha]_D$ +20° (*c* 1.0, $CHCl_3$)

Anal. ($C_{22}H_{26}O_6$) C, H.

3-*O*-Allyl-2,4-di-*O*-benzyl-L-rhamnopyranose (**194**). 63%, $[\alpha]_D$ −22° (*c* 1.0, $CHCl_3$), ^1H NMR ($CDCl_3$) δ=1.31 (d, $J_{5,6}$=6.5 Hz, H-6α), 1.34 (d, $J_{5,6}$=6.5 Hz, H-6β), 3.53 (t, $J_{3,4}$=$J_{4,5}$=9.5 Hz, H-4β), 3.58 (t, $J_{3,4}$=$J_{4,5}$=9 Hz, H-4α), 3.85 (dd, $J_{1,2}$=1.5 Hz, $J_{2,3}$=2 Hz, H-2β), 3.92 (m, H-5α).

Found: C, 71.65; H, 6.99%. Calcd for $C_{23}H_{28}O_5$: C, 71.85; H, 7.34%.

4-*O*-Allyl-2,3-di-*O*-benzyl-L-rhamnopyranose (**198**). 72% $[\alpha]_D$ −27° (*c* 0.9, $CHCl_3$), ^1H NMR ($CDCl_3$) δ=1.32 (d, $J_{5,6}$=6.5 Hz, H-6α), 1.34 (d, $J_{5,6}$=6 Hz, H-6β), 3.32 (m, $J_{4,5}$=9 Hz, H-5β), 3.46 (t, $J_{3,4}$=9 Hz, H-4β), 3.50 (t, $J_{3,4}$=$J_{4,5}$=9.5 Hz, H-4α), 3.52 (dd, $J_{2,3}$=2.5 Hz, H-3β), 3.79 (dd, $J_{1,2}$=$J_{2,3}$=3 Hz, H-2α), 3.82 (dd, $J_{1,2}$=1.5 Hz, H-2β), 3.85 (dd, H-3α), 3.91 (m, H-5α), 5.15 (H-1α).

Anal. ($C_{23}H_{28}O_5$) C, H.

4-*O*-Acetyl-2,3-di-*O*-benzyl-L-rhamnopyranose (**201**). 85% $[\alpha]_D$ −13° (*c* 0.9, $CHCl_3$).

Anal. ($C_{22}H_{26}O_6$) C, H.

Formation of the Chloride 5. To a stirring solution of **3** (46 mg) in CH_2Cl_2 (0.77 ml) was added $TiCl_4$ (8.5 µl, 1.0 equiv) at room temp. After 5 min, iced H_2O and toluene were successively added and the organic layer was washed well with H_2O. After a brief treatmetnt with Na_2SO_4, the solution was concentrated up to give a sirup (43 mg) whose ^1H NMR spectrum measured in $CDCl_3$ showed a characteristic doublet of **5** at δ=6.09 ($J_{1,2}$=4 Hz, H-1). TLC indicated that the mixture contained **5** as the dominant product and slower-moving partially debenzylated products.

Synthesis of 2-Methoxyethyl Glycosides and Their Derivatives.

2-Methoxyethyl α-D-glucopyranoside (**6**). A mixture of **1** (200 mg), MEOH (2 ml), and $MeSO_3H$ (200 µl) was heated at 100 °C for 6 h. After neutralizaton with $NaHCO_3$ (0.40 g) and concentration, chromatography with $CHCl_3$-MeOH (CM) system (gradient) gave, after the elution of **7** (14 mg, 5%), **6** (217 mg, 82%), $[\alpha]_D$ +108° (*c* 1.2, H_2O)(lit,[31] $[\alpha]_D$ +94° (H_2O), ^1H NMR (D_2O) δ=3.30 (s, OMe), 3.43 (dd, $J_{1,2}$=4 Hz, $J_{2,3}$=10 Hz, H-2), 4.82 (d, H-1) (Found: C, 45.20; H, 7.82%).

2-Methoxyethyl α-D-Mannopyranoside (**71**). A similar reaction of **70** (10 g) and MEOH (100 ml) containing $MeSO_3H$ (3.0 ml) for 2 h at 100 °C, followed by processing and chromatography (CM system), gave **71** (10.8 g, 82%), $[\alpha]_D$ +29° (*c* 1.4, H_2O), ^1H NMR (D_2O) δ=3.31 (s, OMe), 3.88 (dd, 1H, $J_{1,2}$=1.5 Hz, $J_{2,3}$=3.5 Hz, H-2), 4.80 (d, H-1).

Found: C, 44.76; H, 7.56%. Calcd for $C_9H_{18}O_7$: C, 45.37; H, 7.62%.

2-Methoxyethyl α- and β-L-Rhamnopyranosides (**179** and **180**). A reaction of **178** (monohydrate, 10 g) with MEOH (40 ml) in the presence of H_2SO_4 (0.1 ml) for 3.5 h at 80 °C, followoed by processing and chromatography (CM system), afforded **180** (1.5 g, 12%), $[\alpha]_D$ +29° (*c* 0.3, H_2O), ^1H NMR (D_2O) δ=1.23 (d, $J_{5,6}$=6 Hz, H-6), 3.31 (s, OMe), 3.89 (dd, $J_{2,3}$=3 Hz, $J_{3,4}$=8 Hz, H-3), 3.93 (d, $J_{1,2}$=0 Hz, H-2), 4.58 (s, H-1), and then **179** (7.6 g, 62%), $[\alpha]_D$ −28° (*c* 1.2, H_2O), ^1H NMR (D_2O) δ=1.21 (d, $J_{5,6}$=6.5 Hz, H-6), 3.31 (S, OMe), 3.35 (t, $J_{3,4}$=$J_{4,5}$=10 Hz, H-4), 3.69 (dd, $J_{2,3}$=3.5 Hz, H-3), 3.88 (dd, $J_{1,2}$=1.5 Hz, H-2), 4.72 (d, H-1).

Anal. ($C_9H_{18}O_6$) **179**, C, H. **180**, C, H.

2-Methoxyethyl 2,3,4,6-Tetra-*O*-acetyl-β-D-galactopyranoside (**33**) and 2,3,5,6-Tetra-*O*-acetyl-β-D-galactofuranoside (**34**). To a cold mixture of AcBr (17 ml) and AcOH (11 ml) was added **32** (3.0 g); the suspension was then stirred at 25 °C for 1.5 h. After evaporation and co-evaporation with toluene, the residue was dissolved in cold MEOH (18 ml) and powdery Ag_2CO_3 (7.5 g) was added to the stirring solution. The suspension was stirred in the dark at room temp overnight. After filtration and concentration, the residue was chromatographed (TB system) to afford **34** (0.41 g, 6%), $[\alpha]_D$ −31° (*c* 3.4, $CHCl_3$), ^1H NMR ($CDCl_3$) δ=2.03, 2.05, 2.07, 2.10 (4s, OAc), 3.35 (s, OMe), 4.18 (dd, $J_{5,6b}$=7 Hz, $J_{6a,6b}$=12 Hz, H-6b), 4.25 (dd, $J_{3,4}$=6 Hz, $J_{4,5}$=3.5 Hz, H-4), 4.32 (dd, $J_{5,6a}$=4.5 Hz, H-6a), 4.97 ($J_{2,3}$=2 Hz, H-3), 5.05 (d, $J_{1,2}$=1 Hz, H-1), 5.07 (dd, H-2), 5.34 (m, H-5), and then **33** (3.61 g, 53%), $[\alpha]_D$ −13° (*c* 4.9, $CHCl_3$), ^1H NMR ($CDCl_3$) δ=1.97, 2.04, 2.05, 2.14 (4s, OAc), 3.35 (s, OMe), 4.55 (d, $J_{1,2}$=8 Hz, H-1), 5.01 (dd, $J_{2,3}$=9.5 Hz, $J_{3,4}$=3.5 Hz, H-3), 5.21 (dd, H-2), 5.37 (dd, $J_{4,5}$=1 Hz, H-4).

Found: **33**, C, 50.12; H, 6.52%. **34**, C, 49.75; H, 6.38%. Calcd for $C_{17}H_{26}O_{11}$: C, 50.24; H, 6.45%.

2-Methoxyethyl 2,3,4-Tri-*O*-acetyl-β-L-fucopyranoside (**152**) and 2,3,5-Tri-*O*-acetyl-β-L-fucofuranoside (**153**). To chilled AcBr (4 ml) was added **151** (1 g) and the mixture was stirred for 1 h at 25 °C. After evaporation and co-evaporation with toluene, the bromide was then treated with MEOH (5.5 ml) and Ag_2CO_3 (2.7 g). Processing and chromatography (TB system) furnished **153** (0.20 g, 9%), $[\alpha]_D$ +21° (*c* 0.7, $CHCl_3$), ^1H NMR ($CDCl_3$) δ=1.30 (d, $J_{5,6}$=6.5 Hz, H-6), 2.07, 2.08, 2.09 (3s, OAc), 3.38 (s, OMe), 4.11 (dd, $J_{3,4}$=6.5 Hz, $J_{4,5}$=4 Hz, H-4), 4.99 (dd, $J_{2,3}$=2 Hz, H-3), 5.07 (d, $J_{1,2}$=1 Hz, H-1), 5.09 (dd, H-2), 5.14 (m, H-5), and then **152** (1.59 g, 75%), $[\alpha]_D$ −12° (*c* 2.6, $CHCl_3$), ^1H NMR ($CDCl_3$) δ=1.20 (d, $J_{5,6}$=6.5 Hz, H-6), 1.96, 2.04, 2.15 (3s, OAc), 3.34 (s, OMe), 3.79 (m, $J_{4,5}$=1 Hz, H-5), 4.51 (d, $J_{1,2}$=8 Hz, H-1), 5.00 (dd, $J_{2,3}$=11.5

Hz, $J_{3,4}$=4 Hz, H-3), 5.18 (dd, H-2), 5.21 (dd, H-4).

Anal. ($C_{15}H_{24}O_9$) **152**, C, H. **153**, C. H.

2-Methoxyethyl 2,3,4-Tri-*O*-acetyl-α-L-arabinopyranoside (**124**). To a stirring solution of **126**[9] (0.49 g) in $CHCl_3$ (1.5 ml) was added AcBr (0.61 ml) and then H_2O (0.12 ml) at 0 °C. The mixture was stirred for 0.5 h at room temp. After evaporation and co-evaporation with toluene, the bromide was treated with MEOH (1.5 ml) containing Ag_2CO_3 (0.70 g) overnight, followed by chromatoraphy (TB system) to yield **124** (0.40 g, 78%), $[\alpha]_D$ −21° (*c* 2.8, $CHCl_3$), ^1H NMR ($CDCl_3$) δ=2.01, 2.04, 2.09 (3s, OAc), 3.34 (s, OMe), 3.61 (dd, $J_{4,5b}$=2 Hz, $J_{5a,5b}$=13.5 Hz, H-5b), 4.01 (dd, $J_{4,5a}$=4 Hz, H-5a), 4.48 (d, $J_{1,2}$=7 Hz, H-1), 5.02 (dd, $J_{2,3}$=9.5 Hz, $J_{3,4}$=4 Hz, H-3), 5.18 (dd, H-2), 5.23 (t, H-4).

Anal. ($C_{14}H_{22}O_9$) C, H.

Attempt to prepare **124** directly from **123** (1.0 g) through the procedure described for **152** provided 2-methoxyethyl 2,3,5-tri-*O*-acetyl-α-L-arabinofuranoside (**125**) (0.74 g, 33%), $[\alpha]_D$ −41° (*c* 4.1, $CHCl_3$), ^1H NMR ($CDCl_3$) δ=2.07 (s, 9H, OAc), 3.36 (s, OMe), 4.19 (dd, $J_{4,5b}$=5.5 Hz, $J_{5a,5b}$=10.5 Hz, H-5b), 4.24 (m, $J_{3,4}$=5 Hz, $J_{4,5a}$=2.5 Hz, H-4), 4.40 (dd, H-5a), 4.95 (dd, $J_{2,3}$=1.5 Hz, H-3), 5.06 (d, $J_{1,2}$=0 Hz H-1), 5.11 (d, H-2) (Found: C, 49.97; H, 6.66%) and then **124** (0.79 g, 35%).

2-Methoxyethyl β-D-galactopyranoside (**43**) and β-D-galactofuranoside (**44**). A filtrate obtained after removing the silver salts described for **33**, starting from **32** (3.0 g), was concentrated and redissolved in MeOH (40 ml). The solution was treated with dil NaOMe (7%, 4 ml) overnight. After neutralizatin with AcOH, evaporation and chromatography (CM system) delivered **44** (0.80 g, 12%), $[\alpha]_D$ −41° (*c* 1.4, H_2O), ^1H NMR (D_2O) δ=3.32 (s, OMe), 4.94 (d, $J_{1,2}$=2 Hz, H-1), and then **43** (3.83 g, 58%), $[\alpha]_D$ +4° (*c* 2.1, H_2O) (lit,[32] $[\alpha]_D$ +8.4° (H_2O)), ^1H NMR (D_2O) δ=3.30 (s, OMe), 3.35 (dd, $J_{2,3}$=10 Hz, $J_{3,4}$=3 Hz, H-3), 3.43 (dd, $J_{1,2}$=8 Hz, H-1), 3.82 (d, $J_{4,5}$=0 Hz, H-4), 4.32 (d, H-1).

Found: **43**, C, 42.16; H, 7.55%. **44**, C, 42.19; H, 7.44%. Calcd for $C_9H_{18}O_7 \cdot H_2O$: C, 42.18; H, 7.87%.

2-Methoxyethyl β-L-Fucopyranoside (**161**) and β-L-Fucofuranoside (**162**). A similar deacetylation of a reaction mixture obtained from **151** (5 g) as described for **152**, followed by chromatography (CM system), produced **162** (0.63 g, 9%), $[\alpha]_D$ +63° (*c* 1.0, H_2O), ^1H NMR (D_2O) δ=1.17 (d, $J_{5,6}$=6.5 Hz, H-6), 3.31 (s, OMe), 4.00 (dd, $J_{1,2}$=1.5 Hz, $J_{2,3}$=3 Hz, H-2), 4.93 (d, H-1), and then **161** (5.64 g, 83%), $[\alpha]_D$ +1.2° (*c* 2.2, H_2O), ^1H NMR (D_2O) δ=1.18 (d, $J_{5,6}$=6.5 Hz, H-6), 3.32 (s, OMe), 3.41 (dd, $J_{1,2}$=8 Hz, $J_{2,3}$=10.5 Hz, H-2), 3.56 (dd, $J_{3,4}$=4 Hz, H-3), 4.31 (d, H-1).

Anal. ($C_9H_{18}O_6$) **161**, C, H. **162**, C, H.

2-Methoxyethyl α-L-Arabinopyranoside (**134**). Similarly, a reaction mixture obtained from **126** (1.0 g), followed by chromatography (CM system), gave forth **134** (0.57 g, 87%), $[\alpha]_D$ −8° (*c* 3.8, H_2O), ^1H NMR (D_2O) δ=3.32 (s, OMe), 3.48 (dd, $J_{1,2}$=7.5 Hz, $J_{2,3}$=10 Hz, H-2), 3.84 (dd, $J_{4,5eq}$=2 Hz, $J_{5eq,5ax}$=12 Hz, H-5eq), 4.28 (d, H-1).

Anal. ($C_8H_{16}O_6$) C, H.

An attempt to obtain **134** directly from **123** (12 g) via acetobromination with AcBr (48 ml), 2-methoxyethylation with MEOH (72 ml) and Ag_2CO_2 (36 g), and deacetylation followed by chromatography (CM system), afforded 2-methoxyethyl α-L-arabinofuranoside (**135**) (5.96 g, 36%), $[\alpha]_D$ −39° (*c* 1.2, H_2O), ^1H NMR (D_2O) δ=3.31 (s, OMe), 3.86 (dd, $J_{2,3}$=4 Hz, $J_{3,4}$=6.5 Hz, H-3), 4.02 (dd, $J_{1,2}$=1.5 Hz, H-2), 4.95 (d, H-1) (Found: C, 46.20; H 7.82%), and then **134** (6.4 g, 38%).

2-Methoxyethyl β-D-Xylopyranoside (**114**). Deacetylation of **102**[6] (1.00 g) with dil NaOMe (0.6%), followed by chromatography (CM system), furnished **114** (0.55 g, 88%), $[\alpha]_D$ −45° (*c* 1.8, H_2O) (lit,[33] $[\alpha]_D$ −50.4° (MeOH)), ^1H NMR (D_2O) δ=3.20 (dd, $J_{1,2}$=7.5 Hz, $J_{2,3}$=9 Hz, H-2), 3.23 (dd, $J_{4,5ax}$=9.5 Hz, $J_{5eq,5ax}$=12 Hz, H-5ax), 3.31 (s, OMe), 3.36 (t, $J_{3,4}$=9 Hz, H-3), 3.54 (m, $J_{4,5eq}$=5 Hz, H-4), 3.88 (dd, H-5eq), 4.14 (d, H-1)(Found: C, 45.65; H, 7.86%).

2-Methoxyethyl 2,3,4,6-Tetra-*O*-benzyl-α-D-glucopyranoside (**8**). A mixture of **6** (77 mg), powdered KOH (0.51 g, 7 equiv of OH) and $PhCH_2Cl$ (2.0 ml) was stirred for 2 h at 120 °C, followed by usual processing and chromatography with hexane-ethyl acetate (HE) system (gradient), to yield **8** (170 mg, 88%), $[\alpha]_D$ +23° (*c* 2.4, $CHCl_3$), ^1H NMR ($CDCl_3$) δ=3.37 (s, OMe), 4.82 (d, $J_{1,2}$=4 Hz, H-1).

Anal. ($C_{37}H_{42}O_7$) C, H.

Similar benzylations of **71** and **179** furnished **72** (86%) and **181** (70%), respectively.

2-Methoxyethyl 2,3,4,6-Tetra-*O*-benzyl-α-D-mannopyranoside (**72**). $[\alpha]_D$ +25° (*c* 1.0, $CHCl_3$), ^1H NMR ($CDCl_3$) δ=3.34 (s, OMe), 3.89 (dd, $J_{1,2}$=2 Hz, $J_{2,3}$=2.5 Hz, H-2), 3.94 (dd, $J_{3,4}$=9.5 Hz, H-3), 4.00 (t, $J_{4,5}$=9.5 Hz, H-4), 4.94 (d, H-1).

Anal. ($C_{37}H_{42}O_7$) C, H.

2-Methoxyethyl 2,3,4-Tri-*O*-benzyl-α-L-rhamnopyranoside (**181**). $[\alpha]_D$ −30° (*c* 0.7, $CHCl_3$), ^1H NMR ($CDCl_3$) δ=1.35 (d, $J_{5,6}$=6 Hz, H-6), 3.35 (s, OMe), 3.99 (s, $J_{1,2}$=$J_{2,3}$=0 Hz, H-2), 4.82 (s, H-1).

Found: C, 72.81; H, 7.36%. Calcd for $C_{30}H_{36}O_6$: C, 73.15; H, 7.37%.

2-Methoxyethyl 2,3,4,6-Tetra-*O*-benzyl-β-D-glucopyranoside (**3**). A mixture of **2**[12] (100 mg), crushed KOH (386 mg, 7 equiv OAc), and $PhCH_2Cl$ (1.5 ml) was stirred for 2 h at 120 °C, followed by processing and chromatogrphy (HE system), to yield **3** (86 mg, 58%), mp 68—70 °C, $[\alpha]_D$ +7° (*c* 1.6, $CHCl_3$), ^1H NMR ($CDCl_3$) δ=3.42 (s, OMe), 4.49 (d, $J_{1,2}$=7.5 Hz, H-1).

Anal. ($C_{37}H_{42}O_7$) C, H.

Similar reactions of **33**, **102**,[6] **124**, and **152**, afforded **35** (41%), **103** (78%), **127** (82%), and **154** (80%), respectively.

2-Methoxyethyl 2,3,4,6-Tetra-*O*-benzyl-β-D-galactopyranoside (**35**). $[\alpha]_D$ −6° (*c* 1.8, $CHCl_3$), ^1H NMR ($CDCl_3$) δ=3.37 (s, OMe), 3.52 (dd, $J_{2,3}$=10 Hz, $J_{3,4}$=3 Hz, H-3), 3.84 (dd, $J_{1,2}$=8 Hz, H-2), 3.89 (d, $J_{4,5}$=0 Hz, H-4), 4.40 (d, H-1).

Found: C, 73.67; H, 7.05%. Calcd for $C_{37}H_{42}O_7$: C, 74.22; H, 7.07%.

2-Methoxyethyl 2,3,4-Tri-*O*-benzyl-β-D-xylopyranoside (**103**). $[\alpha]_D$ +10° (*c* 1.3, $CHCl_3$), ^1H NMR ($CDCl_3$) δ=3.21 (dd, $J_{4,5ax}$=10 Hz, $J_{5aq,5ax}$=11.5 Hz, H-5ax), 3.39 (s, OMe), 3.41 (dd, $J_{1,2}$=7.5 Hz, $J_{2,3}$=9.5 Hz, H-2), 3.58 (t, $J_{3,4}$=9.5 Hz, H-3), 3.94 (dd, $J_{4,5eq}$=4.5 Hz, H-5eq), 4.39 (d, H-1).

Found: C, 72.38; H, 4.39%. Calcd for $C_{29}H_{34}O_6$: C, 72.78; H, 7.16%.

2-Methoxyethyl 2,3,4-Tri-*O*-benzyl-α-L-arabinopyranoside (**127**). $[\alpha]_D$ +6° (*c* 1.5, $CHCl_3$), ^1H NMR ($CDCl_3$) δ=3.27 (dd, $J_{4,5ax}$=1.5 Hz, $J_{5eq,5ax}$=13 Hz, H-5ax), 3.39 (s, OMe), 3.52 (dd, $J_{2,3}$=9 Hz, $J_{3,4}$=4 Hz, H-3), 3.84 (dd, $J_{1,2}$=7.5 Hz, H-2), 4.04 (dd, $J_{4,5eq}$=3 Hz, H-5eq), 4.37 (d, H-1).

Anal. ($C_{29}H_{34}O_6$) C, H.

2-Methoxyetheyl 2,3,4-Tri-*O*-benzyl-β-L-fucopyranoside (**154**). $[\alpha]_D$ +7° (*c* 1.6, $CHCl_3$), ^1H NMR ($CDCl_3$) δ=1.19 (d,

$J_{5,6}$=6.5 Hz, H-6), 3.38 (s, OMe), 3.46 (m, $J_{4,5}$=1 Hz, H-5), 3.52 (dd, $J_{2,3}$=10 Hz, $J_{3,4}$=2.5 Hz, H-3), 3.83 (dd, $J_{1,2}$=7.5 Hz, H-2), 4.38 (d, H-1).

Found: C, 72.57; H, 7.36%. Cacld for $C_{30}H_{36}O_6$: C, 73.15; H, 7.37%.

2-Methoxyethyl 3,4-*O*-Isopropylidene-α-L-arabinopyranoside (**136**). To a stirring solution of **134** (2.70 g) in acetone containing 2,2-dimethoxypropane[34] (DMP, 2.5 ml) was added H_2SO_4 (10 μl) at room temp. After 6 h, the solution was treated with $NaHCO_3$ (0.35 g), concentrated, and chromatographed (TB system) to yield **136** (1.80 g, 56%), $[\alpha]_D$ +40° (*c* 2.2, $CHCl_3$), ^1H NMR ($CDCl_3$) δ=1.34, 1.52 (2s, CMe_2), 3.37 (s, OMe), 3.63 (t, $J_{1,2}=J_{2,3}$=7.5 Hz, H-2), 4.06 (dd, $J_{3,4}$=6 Hz, H-3), 4.21 (d, H-1).

Found: C, 52.61; H, 8.19%. Calcd for $C_{11}H_{20}O_6$: C, 53.21; H, 8.12%.

Similar reactions of **161** and **179** afforded **163** (92%) and **195** (84%), respectively.

2-Methoxyethyl 3,4-*O*-Isopropylidene-β-L-fucopyranoside (**163**). $[\alpha]_D$ −30° (*c* 0.9, $CHCl_3$), ^1H NMR ($CDCl_3$) δ=1.35, 1.52 (2s, CMe_2), 1.41 (d, $J_{5,6}$=6.5 Hz, H-6), 3.38 (s, OMe) 3.55 (dd, $J_{1,2}$=8 Hz, $J_{2,3}$=7 Hz, H-2), 3.86 (m, $J_{4,5}$=2 Hz, H-5), 3.99 (dd, $J_{3,4}$=5 Hz, H-4), 4.04 (dd, H-3), 4.19 (d, H-1).

Found: C, 54.52; H, 8.41%. Calcd for $C_{12}H_{22}O_6$: C, 54.95; H, 8.45%.

2-Methoxyethyl 2,3-*O*-Isopropylidene-α-L-rhamnopyranoside (**195**). $[\alpha]_D$ −29° (*c* 0.7, $CHCl_3$), ^1H NMR ($CDCl_3$) δ=1.34, 1.51 (2s, CMe_2), 1.29 (d, $J_{5,6}$=6.5 Hz, H-6), 3.38 (s, OMe), 4.11 (t, $J_{2,3}=J_{3,4}$=6 Hz, H-3), 4.19 (d, $J_{1,2}$=0 Hz, H-2), 4.98 (s, H-1).

Anal. ($C_{12}H_{22}O_6$) C, H.

2-Methoxyethyl 3,4-*O*-Isopropylidene-β-D-galactopyranoside (**45**). To a stirring mixture of **43** (1.87 g), acetone (50 ml), DMP (7 ml) and *N*,*N*-dimethylformamide[35] (4 ml) was added H_2SO_4 (80 μl) at room temp; the mixture was then stirred for 4 h at a reflux temperature. After processing, chromatography (CM system) afforded **45** (1.21 g, 55%), $[\alpha]_D$ −16° (*c* 0.9, $CHCl_3$), ^1H NMR ($CDCl_3$) δ=1.33, 1.50 (2s, CMe_2), 3.38 (s, OMe), 3.56 (dd, $J_{1,2}$=8 Hz, $J_{2,3}$=7 Hz, H-2), 3.82 (dd, $J_{5,6b}$=4 Hz, $J_{6a,6b}$=11 Hz, H-6b), 3.86 (m, $J_{4,5}$=2 Hz, $J_{5,6a}$=6 Hz, H-5), 3.96 (dd, H-6a), 4.08 (dd, $J_{3,4}$=6 Hz, H-3), 4.14 (dd, H-4), 4.22 (d, H-1).

Found: C, 51.42; H, 8.06%. Calcd for $C_{12}H_{22}O_7$: C, 51.79; H, 7.97%.

2-Methoxyethyl 4,6-*O*-Benzylidene-β-D-galactopyranoside (**53**). A mixture of **43** (1.06 g), benzaldehyde (7 ml), and $ZnCl_2$ (0.3 g) was stirred overnight, followed by the usual processing and chromatography (CM system), to furnish **53** (1.03 g, 71%), mp 139—140 °C (from IPE), $[\alpha]_D$ −18° (*c* 0.4, $CHCl_3$), ^1H NMR ($CDCl_3$) δ=3.36 (s, OMe), 3.43 (m, $J_{4,5}$=1 Hz, $J_{5,6eq}$=1.5 Hz, $J_{5,6ax}$=2 Hz, H-5), 3.78 (dd, $J_{1,2}$=8 Hz, $J_{2,3}$=10 Hz, H-2), 4.04 (dd, $J_{6eq,6ax}$=12.5 Hz, H-6ax), 4.16 (dd, $J_{3,4}$=4 Hz, H-4), 4.29 (dd, H-6eq), 4.32 (d, H-1), 5.52 (s, benzylidene).

Found: C, 59.51; H, 6.74%. Calcd for $C_{16}H_{21}O_7$: C, 59.07; H, 6.51%.

2-Methoxyethyl 4,6-*O*-Benzylidene-α-D-mannopyranoside (**86**). A solution of **71** (643 mg) in *N*,*N*-dimethylformamide (13 ml) containing benzaldehyde dimethyl acetal (0.53 ml) was treated with pyridinium tosylate[36] (13 mg) for 6.5 h at 80 °C. Processing and chromatography (CM system) provided **86** (314 mg, 36%), mp 93—95 °C, $[\alpha]_D$ +51° (*c* 0.8, $CHCl_3$), ^1H NMR ($CDCl_3$) δ=3.56 (s, OMe), 4.86 (d, $J_{1,2}$=1 Hz, H-1), 5.58 (s, benzylidene).

Found: C, 58.67; H, 6.77%. Calcd for $C_{16}HO_7$: C, 59.07; H, 6.51%.

After the elution of **86**, another acetal (46 mg, 5%) was obtained. That was acetylated with Ac_2O and pyridine, followed by chromatography (TB system), to yield 2-methoxyethyl 4,6-di-*O*-acetyl-2,3-*O*-benzylidene-α-D-mannopyranoside (**87**), mp 52—53 °C, $[\alpha]_D$ −28° (*c* 0.5, $CHCl_3$), ^1H NMR ($CDCl_3$) δ=2.06, 2.09 (2s, OAc), 3.40 (s, OMe), 3.97 (m, $J_{4,5}$=10.5 Hz, $J_{5,6a}$=5.5 Hz, $J_{5,6b}$=2.5 Hz, H-5), 4.10 (dd, $J_{6a,6b}$=12 Hz, H-6b), 4.24 (dd, H-6a), 4.31 (dd, $J_{1,2}$=1 Hz, $J_{2,3}$=6.5 Hz, H-2), 4.42 (dd, $J_{3,4}$=7 Hz, H-3), 5.12 (dd, H-4), 5.23 (d, H-1), 5.90 (s, benzylidene) (Found: C, 58.60; H, 6.42%).

2-Methoxyethyl 6-*O*-Trityl-β-D-glucopyranoside (**27**). A mixture of **7**[12] (2.40 g), trityl chloride (7.72 g), and pyridine 12 ml) was stirred at 70 °C overnight. The processed mixture was chromatoraphed (CM system) to give forth **27** (2.53 g, 53%), mp 72—73°C (from IPE), $[\alpha]_D$ −32° (*c* 3.3, $CHCl_3$), ^1H NMR ($CDCl_3$) δ=3.35 (s, OMe), 4.02 (m, $J_{4,5}$=11 Hz, $J_{5,6}$=3 and 5 Hz, H-5), 4.31 (d, $J_{1,2}$=8 Hz, H-1),

Anal. ($C_{28}H_{32}O_7$) C, H.

Similar tritylations of **43** and **71** afforded (**65**) (50%) and **97** (61%).

2-Methoxyethyl 6-*O*-Trityl-β-D-galactopyranoside (**65**). $[\alpha]_D$ −29° (*c* 3.0, $CHCl_3$), ^1H NMR ($CDCl_3$) δ=3.32 (s, OMe), 3.65 (dd, $J_{1,2}$=7.5 Hz, $J_{2,3}$=10 Hz, H-2), 4.23 (d, H-1).

Anal. ($C_{28}H_{32}O_7$), C, H.

2-Methoxyethyl 6-*O*-Trityl-α-D-mannopyranoside (**97**). Mp 65—67 °C, $[\alpha]_D$ +11° (*c* 0.9, $CHCl_3$), ^1H NMR ($CDCl_3$) δ=3.37 (s, OMe), 3.94 (dd, $J_{1,2}$=1.5 Hz, $J_{2,3}$=3.5 Hz, H-2), 4.85 (d, H-1).

Found: C, 69.39; H, 6.55%. Calcd for $C_{28}H_{32}O_7$: C, 69.98; H, 6.71%.

2-Methoxyethyl 4-*O*-Trityl-β-D-xylopyranoside (**115**). A mixture of **114** (631 mg), trityl chloride (1.27 g), and pyridine (3 ml) was stirred at 70 °C overnight, followed by processing and chromatography (TB system), to give a mixture of the monotrityl ethers (301 mg) and then **115** (338 mg, 25%), mp 43—45 °C (from hexane containing IPE), $[\alpha]_D$ −58° (*c* 1.1, $CHCl_3$), ^1H NMR ($CDCl_3$) δ=3.32 (s, OMe), 4.66 (d, $J_{1,2}$=4 Hz, H-1).

Anal. ($C_{27}H_{30}O_6$) C, H.

The whole mixture (301 mg) of the faster-moving monotrityl ethers was acetylated with Ac_2O and pyridine, followed by chromatography (TB system), to yield 2-methoxyethyl 3,4-di-*O*-acetyl-2-*O*-trityl-β-D-xylopyranoside (**116**) (77 mg, 5% from **115**), $[\alpha]_D$ −5° (*c* 0.5, $CHCl_3$), ^1H NMR ($CDCl_3$) δ=1.78, 2.11 (2s, OAc), 3.26 (s, OMe), 3.45 (dd, $J_{1,2}$=4.5 Hz, $J_{2,3}$=6.5 Hz, H-2), 3.45 (dd, $J_{4,5b}$=6.5 Hz, $J_{5a,5b}$=12.5 Hz, H-5b), 3.95 (dd, $J_{4,5a}$=4.5 Hz), 4.02 (d, H-1), 4.67 (dd, $J_{3,4}$=6.5 Hz, H-4), 5.25 (t, H-3) (Found: C, 69.62; H, 6.26%), and then 2-methoxyethyl-2,4-di-*O*-acetyl-3-*O*-trityl-β-D-xylopyranoside (**117**) (142 mg, 9%), mp 147—148 °C (from IPE), $[\alpha]_D$ −28° (*c* 1.2, $CHCl_3$), ^1H NMR ($CDCl_3$) δ=1.63, 1.78 (2s, OAc), 3.14 (dd, $J_{4,5b}$=6.5 Hz, $J_{5a,5b}$=12 Hz, H-5b), 3.37 (s, OMe), 4.15 (dd, $J_{4,5a}$=4 Hz, H-5a), 4.34 (dd, $J_{1,2}$=5 Hz, H-1), 4.57 (dd, $J_{3,4}$=6.5 Hz, H-4), 4.87 (dd, $J_{2,3}$=7 Hz, H-2) (Found: C, 70.17; H, 6.42%).

2-Methoxyethyl 3-*O*-Trityl-α-L-rhamnopyranoside (**188**). A similar tritylation of **179** (0.88 g) with trityl chloride (2.2 g)

in pyridine (2.6 ml), followed by chromatography (TB system), produced **188** (0.93 g, 51%), mp 45—47 °C (from hexane containing IPE), $[\alpha]_D$ −48° (*c* 0.7, $CHCl_3$), ^1H NMR ($CDCl_3$) δ=1.26 (d, $J_{5,6}$=6.5 Hz, H-6), 3.31 (s, OMe), 3.07 (dd, $J_{1,2}$=2 Hz, $J_{2,3}$=3 Hz, H-2), 3.79 (dd, $J_{3,4}$=9 Hz, H-3), 4.57 (d, H-1).

Found: C, 72.87; H, 6.83%. Calcd for $C_{28}H_{32}O_6$: C, 72.39; H, 6.94%.

After the elution of **188**, there appeared another trityl ether (0.18 g, 10%), which was acetylated with Ac_2O and pyridine to furnish, after chromatography (TB system), 2-methoxyethyl 2,3-di-*O*-acetyl-4-*O*-trityl-α-L-rhamnopyranoside (**189**), $[\alpha]_D$ −84° (*c* 0.4, $CHCl_3$), ^1H NMR ($CDCl_3$) δ=1.08 (d, $J_{5,6}$=6 Hz, H-6), 1.18, 1.88 (2s, OAc), 3.18 (t, $J_{3,4}=J_{4,5}$=10 Hz, H-4), 3.43 (s, OMe), 4.07 (m, H-5), 4.59 (d, $J_{1,2}$=2 Hz, H-1), 5.22 (dd, $J_{2,3}$=3.5 Hz, H-2), 5.28 (dd, H-3) (Found: C, 70.13; H, 6.74%).

2-Methoxyethyl 2,6-Di-*O*-benzyl-β-D-galactopyranoside (**46**). Amixture of **45** (1.20 g), crushed KOH (3.4 g), and $PhCH_2Cl$ (14 ml) was stirred for 2 h at 120 °C, cooled, and then diluted with toluene. After washing with H_2O thoroughly, the organic layer was concentrated under reduced pressure at 95 °C to give an oily product, which was successively heated in aq AcOH (80%, 20 ml) at 95 °C for 1 h. Concentration and chromatography (TB system) provided **46** (1.36 g, 75%), $[\alpha]_D$ +9° (*c* 3.5, $CHCl_3$), ^1H NMR ($CDCl_3$), δ=3.38 (s, OMe), 3.52 (dd, $J_{1,2}$=7.5 Hz, $J_{2,3}$=9.5 Hz, H-2), 3.60 (dd, $J_{3,4}$=3 Hz, $J_{4,5}$=1 Hz, H-4), 3.99 (dd, H-3), 4.42 (d, H-1).

Anal. ($C_{23}H_{30}O_7$) C, H.

Compounds **53** and **86** were similarly transformed into **57** (84%) and **91** (87%), respectively.

2-Methoxyethyl 2,3-Di-*O*-benzyl-β-D-galactopyranoside (**57**). $[\alpha]_D$ −0.4° (*c* 2.9, $CHCl_3$), ^1H NMR ($CDCl_3$) δ=3.38 (s, OMe), 3.45 (dd, $J_{4,5}$=0 Hz, $J_{5,6a}$=6 Hz, $J_{5,6b}$=5 Hz, H-5), 3.50 (dd, $J_{3,4}$=9 Hz, $J_{3,4}$=3.5 Hz, H-3), 3.68 (dd, $J_{1,2}$=8 Hz, H-2), 3.77 (dd, $J_{6a,6b}$=11.5 Hz, H-6b), 3.94 (dd, H-6a), 3.99 (d, H-4), 4.42 (d, H-1).

Anal. ($C_{23}H_{30}O_7$) C, H.

2-Methoxyethyl 2,3-Di-*O*-benzyl-α-D-mannopyranoside (**91**). $[\alpha]_D$ +22° (*c* 0.9, $CHCl_3$), ^1H NMR ($CDCl_3$) δ=3.36 (s, OMe), 3.74 (dd, $J_{2,3}$=3 Hz, $J_{3,4}$=9.5 Hz, H-3), 3.87 (dd, $J_{1,2}$=1.5 Hz, H-2), 4.04 (t, $J_{4,5}$=9.5 Hz, H-4), 4.90 (d, H-1).

Anal. ($C_{23}H_{30}O_7$) C, H.

2-Methoxyethyl 2-*O*-Benzyl-α-L-arabinopyranoside (**138**). Benzylation of **136** (1.59 g) with $PhCH_2Cl$ (10 ml) and KOH (2.5 g) at 120 °C for 2 H and subsequent processing and chromatography (HE system) afforded a sirup. That was treated with trifluoroacetic acid (TFA, 6 ml) in $CHCl_3$ (20 ml) containing MeOH (20 ml) for 2.5 h at room temp. After quick concentration with an efficient pump at 25 °C and co-evaporation with toluene, chromatography (TB system) afforded **138** (0.86 g, 58%), mp 47—48 °C, $[\alpha]_D$ −13° (*c* 0.9, $CHCl_3$), ^1H NMR ($CDCl_3$) δ=3.37 (s, OMe), 4.60 (d, $J_{1,2}$=4.5 Hz, H-1).

Anal. ($C_{15}H_{22}O_6$) C, H.

Compounds **163** and **195** were similarly converted into **165** (71%) and **202** (88%), respectively.

2-Methoxyethyl 2-*O*-Benzyl-β-L-fucopyranoside (**165**). $[\alpha]_D$ −18° (*c* 1.8, $CHCl_3$), ^1H NMR ($CDCl_3$) δ=1.33 (d, $J_{5,6}$=6.5 Hz, H-6), 3.38 (s, OMe), 3.46 (dd, $J_{1,2}$=7.5 Hz, $J_{2,3}$=9.5 Hz, H-2), 4.38 (d, H-1).

Anal. ($C_{16}H_{24}O_6$) C, H.

2-Methoxyethyl 4-*O*-Benzyl-α-L-rhamnopyranoside (**202**). $[\alpha]_D$ −53° (*c* 0.8, $CHCl_3$), ^1H NMR ($CDCl_3$) δ=1.34 (d, $J_{5,6}$=6.5 Hz, H-6), 3.34 (t, $J_{3,4}=J_{4,5}$=9.5 H, H-4), 3.36 (s, OMe), 3.94 (dd, $J_{2,3}$=3.5 Hz, H-3), 3.98 (dd, $J_{1,2}$=1.5 Hz, H-2), 4.80 (d, H-1).

Anal. ($C_{16}H_{24}O_6$) C, H.

2-Methoxyethyl 3-*O*-Allyl-2-*O*-benzyl-β-D-galactopyranoside (**56**). Benzylation of **54** (380 mg) with $PhCH_2Cl$ (1.6 ml) and KOH (0.41 g) took place for 2 h at 120 °C, followed by a subsequent hydrolysis of the product mixture, processed as described for **46**, with aq AcOH (80%, 15 ml) for 1 h at 95 °C. Chromatography (TB system) gave **56** (295 mg, 77%), $[\alpha]_D$ −0.5° (*c* 3.0, $CHCl_3$), ^1H NMR ($CDCl_3$) δ=3.36 (s, OMe), 3.40 (dd, $J_{2,3}$=9 Hz, $J_{3,4}$=4 Hz, H-3), 3.45 (m, $J_{4,5}$=1 Hz, $J_{5,6a}$= 7 Hz, $J_{5,6b}$=5 Hz, H-5), 3.60 (dd, $J_{1,2}$=7.5 Hz, H-2), 3.79 (dd, $J_{6a,6b}$=11.5 Hz, H-6b), 3.90 (dd, H-6a), 4.40 (d, H-1).

Found: C, 61.55; H, 7.73%. Calcd for $C_{19}H_{28}O_7$: C, 61.94; H, 7.66%.

2-Methoxyethyl 3-*O*-Allyl-2-*O*-benzyl-α-D-mannopyranoside (**90**). A similar process for **88** (332 mg) afforded **90** (271 mg, 81%), $[\alpha]_D$ +18° (*c* 1.1, $CHCl_3$), ^1H NMR ($CDCl_3$) δ=3.36 (s, OMe), 4.90 (d, $J_{1,2}$=1.5 Hz, H-1).

Found: C, 61.38; H, 7.66%. Calcd for $C_{19}H_{28}O_7$: C, 61.94; H, 7.66%.

2-Methoxyethyl 2,3,4-Tri-*O*-benzyl-β-D-glucopyranoside (**22**). A mixture of **27** (2.3 g), $PhCH_2Cl$ (23 ml), and KOH (5.6 g) was stirred for 2 h at 120 °C, processed as described for **46**, and then hydrolyzed with aq AcOH (80%, 40 ml) for 1 h at 95 °C to deliver, after chromatography (TB system), **22** (1.1 g, 45%), mp 63—65 °C (from hexane containing IPE), $[\alpha]_D$ −3° (*c* 5.1, $CHCl_3$), ^1H NMR ($CDCl_3$) δ=3.41 (s, OMe), 3.49 (dd, $J_{1,2}$=7.5 Hz, $J_{2,3}$=9 Hz, H-2), 4.51 (d, H-1).

Anal. ($C_{30}H_{36}O_7$) C, H.

A similar process was applied to **65** and **97** to produce **58** (69%) and **93** (46%), respectively.

2-Methoxyethyl 2,3,4-Tri-*O*-benzyl-β-D-galactopyranoside (**58**). Mp 58—59 °C, $[\alpha]_D$ −22° (*c* 1.0, $CHCl_3$), ^1H NMR ($CDCl_3$) δ=3.38 (s, OMe), 3.54 (dd, $J_{2,3}$=9.5 Hz, $J_{3,4}$=3 Hz, H-3). 3.86 (dd, $J_{1,2}$=8 Hz, H-2), 4.42 (d, H-1).

Anal. ($C_{30}H_{36}O_7$) C, H.

2-Methoxyethyl 2,3,4-Tri-*O*-benzyl-α-D-mannopyranoside (**93**). $[\alpha]_D$ +27° (*c* 1.2, $CHCl_3$), ^1H NMR ($CDCl_3$) δ=3.35 (s, OMe), 3.89 (dd, $J_{1,2}$=2 Hz, $J_{2,3}$=3 Hz, H-2), 3.99 (t, $J_{3,4}=J_{4,5}$= 9.5 Hz, H-4), 4.88 (d, H-1).

Anal. ($C_{30}H_{36}O_7$) C, H.

2-Methoxyethyl 2,3-Di-*O*-benzyl-β-D-xylopyranoside (**118**). Compound **115** (102 mg) was benzylated with $PhCH_2Cl$ (1.4 ml) and KOH (0.36 g) for 2 h at 120 °C. After processing, as described for **46**, the residue was treated with TFA (0.12 ml) in $CHCl_3$ (2 ml) containing MeOH (2 ml) for 1 h at room temp. After removing the volatile substances, as described for **138**, chromatogrphy (TB system) gave **118** (46 mg, 52%), mp 63—64 °C (from hexane), $[\alpha]_D$ −29° (*c* 0.6, $CHCl_3$), ^1H NMR ($CDCl_3$) δ=3.26 (dd, $J_{4,5ax}$=9 Hz, $J_{5eq,5ax}$=11 Hz, H-5ax), 3.38 (s, OMe), 3.45 (dd, $J_{1.2}$=7 Hz, $J_{2,3}$=5 Hz, H-2), 4.00 (dd, $J_{4,5eq}$=4.5 Hz, H-5eq), 4.48 (d, H-1).

Anal. ($C_{22}H_{28}O_6$) C, H.

2-Methoxyethyl 2,4-Di-*O*-benzyl-α-L-rhamnopyranoside (**190**). Compound **188** (510 mg) was converted similarly into **190** (242 mg, 55%), $[\alpha]_D$ −21° (*c* 0.9, $CHCl_3$), ^1H NMR ($CDCl_3$) δ=1.33 (d, $J_{5,6}$=6.5 Hz, H-6), 3.32 (t, $J_{3,4}=J_{4,5}$=9.5 Hz, H-4), 3.36 (s, OMe), 3.96 (m. H-5), 3.79 (dd, $J_{1,2}$=1.5 Hz,

$J_{2,3}$=4 Hz, H-2), 4.86 (d, H-1).

Found: C, 68.10; H, 7.47%. Calcd for $C_{23}H_{30}O_6$: C, 68.64; H, 7.51%.

2-Methoxyethyl 2-*O*-Allyl-α-L-arabinopyranoside (**137**). A mixture of **136** (147 mg), allyl bromide (1.7 ml), and NaH (60%, 0.17 g, 7 equiv of OH) was stirred for 2 h at a reflux temperature. The mixture was cooled, diluted with toluene and treated carefully with H_2O to destroy NaH. The organic layer was washed well with H_2O, concentrated, and then treated with TFA (1 ml) in $CHCl_3$ (3 ml) containing MeOH (3 ml) for 5 h at room temp. After removing the excess reagents, as described for **138**, chromatography (TB system) furnished **137** (91 mg, 62%), $[\alpha]_D$ −32° (*c* 0.6, $CHCl_3$), ^1H NMR ($CDCl_3$) δ=3.38 (s, OMe), 4.59 (d, $J_{1,2}$=4.5 Hz, H-1).

Found: C, 52.65; H, 7.85%. Calcd for $C_{11}H_{20}O_6$: C, 53.21; H, 8.12%.

Compounds **163** and **195** were similarly transformed into **164** (49%) and **196** (85%), respectively.

2-Methoxyethyl 2-*O*-Allyl-β-L-fucopyranoside (**164**). Mp 52—54 °C, (from hexane containing IPE), $[\alpha]_D$ −57° (*c* 1.1, $CHCl_3$), ^1H NMR ($CDCl_3$) δ=1.33 (d, $J_{5,6}$=6.5 Hz, H-6), 3.36 (dd, $J_{2,3}$=10 Hz, $J_{3,4}$=2.5 Hz, H-3), 3.37 (dd, $J_{1,2}$=7.5 Hz, H-2), 3.38 (s, OMe), 3.61 (m, $J_{4,5}$=1 Hz, H-5), 4.32 (d, H-1).

Anal. ($C_{12}H_{22}O_6$) C, H.

2-Methoxyethyl 4-*O*-Allyl-α-L-rhamnopyranoside (**196**). $[\alpha]_D$ −64° (*c*, 0.7. $CHCl_3$), ^1H NMR ($CDCl_3$) δ=1.31 (d, $J_{5,6}$=6.5 Hz, H-6), 3.23 (t, $J_{3,4}$=$_{4,5}$=9.5 Hz, H-4), 3.37 (s, OMe), 3.67 (m, H-5), 3.89 (dd, $J_{2,3}$=4 Hz, H-3), 3.98 (dd, *J*=1.5 Hz, H-2), 4.79 (d, H-1).

Anal. ($C_{12}H_{22}O_6$) C, H.

2-Methoxyethyl 2-*O*-Acetyl-3,4,6-tri-*O*-benzyl-β-D-glucopyranoside (**10**). To a solution of **9** (1.00 g) in $CHCl_3$ (3.0 ml) containing AcBr (1.00 ml) was added H_2O (0.20 ml) at 0 °C; the mixture was then stirred for 1.5 h at 20 °C. After concentration and co-evaporation with toluene at 30 °C in vacuo, the residue was dissolved in chilled $MeNO_2$ (2.4 ml) and 2,6-dimethylpyridine (0.98 ml) and then MEOH (0.61 ml) were added into the solution under stirring. After standing overnight, the solution was diluted with toluene and washed with aq $NaHCO_3$ (5%) thoroughly. The organic layer was concentrated and then stirred in $PhCH_2Cl$ (20 ml) containing KOH (10 g) for 2 h at 120 °C. The mixture was cooled, diluted with toluene and cold H_2O, and then washed well with H_2O. The concentration and subsequent chromatogrphy on alumina (Woelm, 02084), developed with hexane, IPE, and then 2-butanone, afforded an oily benzylated orthoester. That was then treated with $BF_3 \cdot Et_2O$ (12 μl) in CH_2Cl_2 (15 ml) for 5 min at room temp. Processing and chromatography (HE system) gave **10** (0.68 g, 48%), $[\alpha]_D$ +0.8° (*c* 1.0, $CHCl_3$).

Anal. ($C_{32}H_{38}O_8$) C, H.

The acetates **37**, **74**, **105**, and **126** were similarly converted into the 2-acetates **38** (44%), **75** (49%), **106** (50%), and **129** (43%), respectively.

2-Methoxyethyl 2-*O*-Acetyl-3,4,6-tri-*O*-benzyl-β-D-galactopyranoside (**38**). $[\alpha]_D$ +2° (*c* 6.5, $CHCl_3$).

Anal. ($C_{32}H_{38}O_8$) C, H.

2-Methoxyethyl 2-*O*-Acetyl-3,4,6-tri-*O*-benzyl-α-D-mannopyranoside (**75**). $[\alpha]_D$ +27° (*c* 3.8, $CHCl_3$).

Anal. ($C_{32}H_{38}O_8$) C, H.

2-Methoxyethyl 2-*O*-Acetyl-3,4-di-*O*-benzyl-β-D-xylopyranoside (**106**). $[\alpha]_D$ −13° (*c* 5.6, $CHCl_3$).

Anal. ($C_{24}H_{30}O_7$) C, H.

2-Methoxyethyl 2-*O*-Acetyl-3,4-di-*O*-benzyl-α-L-arabinopyranoside (**129**). Mp 60—62 °C (from hexane), $[\alpha]_D$ −9° (*c* 0.9, $CHCl_3$).

Anal. ($C_{24}H_{30}O_7$) C, H.

2-Methoxyethyl 2-*O*-Acetyl-3,4-di-*O*-benzyl-β-L-fucopyranoside (**156**). A mixture of **151** (572 mg) and AcBr (2.9 ml) was stirred for 1 h at 25 °C. After quick concentration and co-evaporation with toluene at 30 °C in vacuo, the residue was dissolved in chilled $MeNO_2$ (3 ml) and the treated with 2,6-dimethylpyridine (2.4 ml) and MEOH (1.5 ml) at room temp overnight. Subsequent processing, benzylation, and rearrangement were carried out as described for **10** to give **156** (383 mg, 25%), mp 84—85 °C (from hexane), $[\alpha]_D$ +1° (*c* 1.1, $CHCl_3$).

Anal. ($C_{25}H_{32}O_7$) C, H.

2-Methoxyethyl 2-*O*-Acetyl-3,4-di-*O*-benzyl-α-L-rhamnopyranoside (**183**). Similarly, **178** (monohydrate, 572 mg) was converted into **183** (645.8 mg, 46%), $[\alpha]_D$ −17° (*c* 5.2, $CHCl_3$).

Anal. ($C_{25}H_{32}O_7$) C, H.

2-Methoxyethyl 3-*O*-Allyl-2,4,6-tri-*O*-benzyl-β-D-galactopyranoside (**51**). Benzylation of **56** (172 mg) with $PhCH_2Cl$ (1.5 ml) and KOH (0.37 g) for 2 h at 120 °C and chromatography (HE system) delivered **51** (208 mg, 81%), $[\alpha]_D$ −14° (*c* 2.3, $CHCl_3$), ^1H NMR ($CDCl_3$) δ=3.40 (s, OMe), 3.46 (dd, $J_{2,3}$=10 Hz, $J_{3,4}$=3 Hz, H-3), 3.82 (dd, $J_{1,2}$=8 Hz, H-2), 3.90 (d, $J_{4,5}$=0 Hz, H-4), 4.43 (d, H-1), 5.98 (m, allyl).

Anal. ($C_{33}H_{40}O_7$) C, H.

The diols **90**, **137**, **164**, and **196** were similarly converted into **84** (78%), **132** (75%), **159** (74%), and **197** (83%), respectively.

2-Methoxyethyl 3-*O*-Allyl-2,4,6-tri-*O*-benzyl-α-D-mannopyranoside (**84**). $[\alpha]_D$ +31° (*c* 1.1, $CHCl_3$), ^1H NMR ($CDCl_3$) δ=3.33 (s, OMe), 4.91 (d, $J_{1,2}$=1.5 Hz, H-1), 5.95 (m, allyl).

Found: C, 71.82; H, 7.33%. Calcd for $C_{33}H_{40}O_7$: C, 72.24; H, 7.35%.

2-Methoxyethyl 2-*O*-Allyl-3,4-di-*O*-benzyl-α-L-arabinopyranoside (**132**). $[\alpha]_D$ −1.2° (*c* 1.4, $CHCl_3$), ^1H NMR ($CDCl_3$) δ=3.25 (dd, $J_{4,5ax}$=1.5 Hz, $J_{5eq,5ax}$=13 Hz, H-5ax), 3.38 (s, OMe), 3.46 (dd, $J_{2,3}$=9 Hz, $J_{3,4}$=3.5 Hz, H-3), 3.70 (dd, $J_{1,2}$=7.5 Hz, H-2), 4.01 (dd, $J_{4,5eq}$=3 Hz, H-5eq), 4.30 (d, H-1), 5.97 (m, allyl).

Anal. ($C_{25}H_{32}O_6$) C, H.

2-Methoxyethyl 2-*O*-Allyl-3,4-di-*O*-benzyl-β-L-fucopyranoside (**159**). $[\alpha]_D$ +24° (*c* 0.7, $CHCl_3$), ^1H NMR ($CDCl_3$) δ=1.15 (d, $J_{5,6}$=6.5 Hz, H-6), 3.37 (s, OMe), 3.43 (m, $J_{4,5}$=1.5 Hz, H-5), 3.45 (dd, $J_{2,3}$=10 Hz, $J_{3,4}$=3.5 Hz, H-3), 3.52 (dd, H-4), 3.68 (dd, $J_{1,2}$=7.5 Hz, H-1), 4.29 (d, H-1), 5.99 (m, allyl).

Anal. ($C_{26}H_{34}O_6$) C, H.

2-Methoxyethyl 4-*O*-Allyl-2,3-di-*O*-benzyl-α-L-rhamnopyranoside (**197**). $[\alpha]_D$ −44° (*c* 1.0, $CHCl_3$), ^1H NMR ($CDCl_3$) δ=1.32 (d, 6.5 Hz, H-6), 3.34 (s, OMe), 3.66 (m, $J_{5,6}$=10 Hz, H-5), 4.79 (d, $J_{1,2}$=1.5 Hz, H-1), 5.94 (m, allyl).

Anal. ($C_{26}H_{34}O_6$) C, H.

2-Methoxyethyl 4-*O*-Allyl-2,3,6-tri-*O*-benzyl-α-D-galactopyranoside (**61**). The monohydroxy compound **63** (163 mg) was stirred in $PhCH_2Cl$ (1.0 ml) containing NaH (60%, 100 mg, 7 equiv) for 2 h at 120 °C. Processing and chromatography (HE system) furnished **61** (148 mg, 76%), $[\alpha]_D$ −2.5° (*c* 0.8, $CHCl_3$), ^1H NMR ($CDCl_3$) δ=3.37 (s, OMe), 3.47 (dd, $J_{2,3}$=10.5 Hz, $J_{3,4}$=3 Hz, H-3), 3.73 (dd, $J_{1,2}$=7.5 Hz, H-1), 3.81

(d, $J_{4,5}$=0 Hz, H-4), 4.39 (d, H-1), 5.90 (m, allyl).

Anal. ($C_{33}H_{40}O_7$) C, H.

Similar benzylations of **149**, **176**, and **203** afforded **147** (79%), **174** (93%), and **186** (85%).

2-Methoxyethyl 4-*O*-Allyl-2,3-di-*O*-benzyl-α-L-arabinopyranoside (**147**). $[\alpha]_D$ +0.8° (*c* 0.5, $CHCl_3$), ^1H NMR ($CDCl_3$) δ=3.29 (dd, $J_{4,5ax}$=1.5 Hz, $J_{5eq,5ax}$=13 Hz, H-5ax), 3.38 (s, OMe), 3.51 (dd, $J_{2,3}$=9 Hz, $J_{3,4}$=4 Hz, H-3), 3.77 (dd, $J_{1,2}$=7 Hz, H-2), 4.16 (d, H-1), 5.95 (m, allyl).

Found: C, 70.29; H, 7.02%. Calcd for $C_{25}H_{32}O_6$: C, 70.07; H, 7.53%.

2-Methoxyethyl 4-*O*-Allyl-2,3-di-*O*-benzyl-α-L-fucopyranoside (**174**). $[\alpha]_D$ +1.4° (*c* 0.5, $CHCl_3$), ^1H NMR ($CDCl_3$) δ=1.28 (d, $J_{5,6}$=6.5 Hz, H-6), 3.37 (dd, OMe), 3.75 (dd, $J_{1,2}$=7.4 Hz, $J_{2,3}$=9 Hz, H-2), 4.36 (d, H-1), 5.95 (m, allyl).

Anal. ($C_{26}H_{34}O_6$) C, H.

2-Methoxyethyl 2-*O*-Allyl-3,4-di-*O*-benzyl-α-L-rhamnopyranoside (**186**). $[\alpha]_D$ −42° (*c* 1.1, $CHCl_3$), ^1H NMR ($CDCl_3$) δ=1.32 (d, $J_{5,6}$=6 Hz, H-6), 3.36 (s, OMe), 3.83 (dd, $J_{1,2}$= 1.5 Hz, $J_{2,3}$=3 Hz, H-2), 3.87 (dd, $J_{3,4}$=9.5 Hz, H-3), 4.80 (d, H-1), 5.94 (m, allyl).

Found: C, 70.25; H, 7.67%. Calcd for $C_{23}H_{34}O_6$: C, 70.56; H, 7.74%.

2-Methoxyethyl 2,4,6-Tri-*O*-benzyl-β-D-glucopyranoside (**15**). To a stirring solution of **2**[12] (2.03 g) in $PhCH_2Cl$ (40 ml) was added crushed NaOH (1.7 g) and the mixture was vigorously stirred for 2.5 h at 100 °C. Processing and chromatography (TB system) gave **3** (0.15 g, 5%) and **15** (1.00 g, 39%), $[\alpha]_D$ +6° (*c* 3.3, $CHCl_3$), ^1H NMR ($CDCl_3$) δ=3.31 (dd, $J_{1,2}$=8 Hz, $J_{2,3}$=9 Hz, H-2), 3.39 (s, OMe), 4.44 (d, H-1).

Anal. ($C_{30}H_{36}O_7$) C, H.

Further elution gave **21** (0.18 mg, 7%) and **12** (0.20 g, 8%).

2-Methoxyethyl 3,4,6-Tri-*O*-benzyl-β-D-galactopyranoside (**40**). A reaction of **33** (180 mg) with $PhCH_2Cl$ (1.8 ml) and crushed KOH (220 mg) in DME (1.8 ml) was conducted under stirring for 2.5 h at 85 °C. The processed mixture of products was chromatographed (TB system) to deliver **35** (34 mg, 13%), **47** (38 mg, 17%), **48** (29 mg, 13%), and then **40** (61 mg, 27%), $[\alpha]_D$ −9° (*c* 3.5, $CHCl_3$), ^1H NMR ($CDCl_3$) δ=3.37 (s, OMe), 3.46 (dd, $J_{2,3}$=10 Hz, $J_{3,4}$=3 Hz, H-3), 3.90 (d, $J_{4,5}$=0 Hz, H-4), 4.00 (dd, $J_{1,2}$=8 Hz, H-2), 4.30 (d, H-1).

Anal. ($C_{30}H_{36}O_7$) C, H.

2-Methoxyethyl 3-*O*-Acetyl-2,4,6-tri-*O*-benzyl- and 4-*O*-Acetyl-2,3,6-tri-*O*-benzyl-α-D-mannopyranosides (**80** and **81**). A mixture of **71** (0.98 g), $PhCH_2Cl$ (19 ml), and crushed KOH (1.08 g) was stirred efficiently for 4 h at 110 °C. Processing and chromatography (TB system) afforded **72** (0.18 g, 7%) and then a mixture of **83** and **92**, which was acetylated with Ac_2O (5 ml) and pyridine (1 ml). After concentration and co-evaporation with toluene, the residue was chromatographed (TB system) to deliver **81** (0.46 g, 20%), $[\alpha]_D$ +19° (*c* 2.6, $CHCl_3$) and then **80** (0.80 g, 35%), $[\alpha]_D$ +11° (*c* 1.4, $CHCl_3$).

Anal. ($C_{32}H_{38}O_8$) **80**, C, H. **81**, C, H.

When benzylation of **71** (2.0 g) was carried out using $PhCH_2Cl$ (40 ml) and LiOH (2.7 g) for 6.5 h at 130 °C, followed by the sequential process described above, to give **81** (1.21 g, 26%), **80** (0.10 g, 2%) were obtained.

2-Methoxyethyl 2,3,6-Tri-*O*-benzyl-β-D-glucopyranoside (**21**). Benzylation of **20**[7] (2.47 g) with $PhCH_2Cl$ (25 ml) and NaH (60%, 0.30 g, 1.3 equiv) under stirring for 1 h at 100 °C and chromatography (TB system) furnished **3** (0.23 g, 7%) and **21** (1.99 g, 66%), $[\alpha]_D$ −18° (*c* 2.3, $CHCl_3$), ^1H NMR ($CDCl_3$) δ=3.39 (s, OMe), 4.47 (d, $J_{1,2}$=7.5 Hz, H-1).

Found: C, 70.34; H, 7.23%. Calcd for $C_{30}H_{34}O_7$: C, 70.84; H, 7.13%.

Further elution gave **22** (0.54 g, 18%).

The diols **57** and **91** were similarly benzylated to afford **48** (77%) and **58** (5%), and **92** (61%) and **93** (7%), respectively.

2-Methxyethyl 2,3,6-Tri-*O*-benzyl-β-D-galactopyranoside (**48**). $[\alpha]_D$ −4° (*c* 1.1, $CHCl_3$), ^1H NMR ($CDCl_3$) δ=3.38 (s, OMe), 3.50 (dd, $J_{2,3}$=9.5 Hz, $J_{3,4}$=4 Hz, H-3), 3.56 (m, $J_{4,5}$=1 Hz, $J_{5,6a}$=$J_{5,6b}$=5.5 Hz, H-5), 3.67 (dd, $J_{1,2}$=7.5 Hz, H-2), 3.72 (dd, $J_{6a,6b}$=10 Hz, H-6b), 3.80 (dd, H-6a), 4.02 (dd, H-4), 4.41 (d, H-1).

Anal. ($C_{30}H_{36}O_7$) C, H.

2-Methoxyethyl 2,3,6-Tri-*O*-benzyl-α-D-mannopyranoside (**92**). $[\alpha]_D$ +1.3° (*c* 1.4, $CHCl_3$), ^1H NMR ($CDCl_3$) δ=3.36 (s, OMe), 3.89 (dd, $J_{1,2}$=2 Hz, $J_{2,3}$=3.5 Hz, H-2), 4.07 (t, $J_{3,4}$=$J_{4,5}$= 10 Hz, H-4), 4.96 (d, H-1).

Found: C, 70.32; H, 7.20%. Calcd for $C_{30}H_{36}O_7$: C, 70.84; H, 7.17%.

2-Methoxyethyl 2,3-Di-*O*-benzyl-α-L-arabinopyranoside (**140**). Benzylation of the diol **138** (150 mg) with $PhCH_2Cl$ (3 ml) and LiOH (60 mg, 5 equiv) for 2 h at 130 °C and chromatography (TB system) delivered **127** (45 mg, 19%), **139** (9 mg, 5%), and then **140** (56 mg, 29%), $[\alpha]_D$ +6° (*c* 1.0) ^1H NMR ($CDCl_3$) δ=3.38 (s, OMe), 3.43 (dd, $J_{4,5ax}$=1.5 Hz, $J_{5eq,5ax}$=13 Hz, H-5ax), 3.54 (dd, $J_{2,3}$=8.5 Hz, $J_{3,4}$=4 Hz, H-3), 3.67 (dd, $J_{1,2}$=7 Hz, H-1), 3.92 (m, $J_{4,5eq}$=3.5 Hz, H-4), 4.00 (dd, H-5eq), 4.37 (d, H-1).

Anal. ($C_{22}H_{28}O_6$) C, H.

The diols **46** (7 equiv of LiOH, 7 h) and **165** (7 equiv of LiOH, 7 h) similarly yielded **47** (20%, the faster-moving) and **48** (32%, the slower-moving), as well as **166** (14%, the faster-moving) and **167** (32%, the slower-moving), respectively.

2-Methoxyethy 2,3-Di-*O*-benzyl-β-L-fucopyranoside (**167**). $[\alpha]_D$ −3° (*c* 0.8, $CHCl_3$), ^1H NMR ($CDCl_3$) δ=1.34 (d, $J_{5,6}$=6.5 Hz, H-6), 3.38 (s, OMe), 3.49 (dd, $J_{2,3}$=9.5 Hz, $J_{3,4}$=2.5 Hz, H-3), 3.52 (m, $J_{4,5}$=1 Hz, H-5), 3.62 (dd, $J_{1,2}$=7.5 Hz, H-2), 4.37 (d, H-1).

Anal. ($C_{23}H_{30}O_6$) C, H.

2-Methoxyethyl 2,4,6-Tri-*O*-benzyl-β-D-galactopyranoside (**47**). A mixture of **46** (188 mg), $PhCH_2Cl$ (1.5 ml), KOH (53 mg, 2.1 equiv), and DME (1.5 ml) was stirred for 1.5 h at 70 °C, followed by processing and chromatography (TB system), to give **35** (42 mg, 16%) and then **47** (131 mg, 57%), $[\alpha]_D$ −1° (*c*1.3, $CHCl_3$), ^1H NMR ($CDCl_3$) δ=3.38 (s, OMe), 3.61 (dd, $J_{1,2}$=7 Hz, $J_{2,3}$=9.5 Hz, H-2), 3.67 (dd, $J_{3,4}$=3 Hz, H-3), 3.87 (d, $J_{4,5}$=0 Hz, H-4), 4.41 (d, H-1).

Found: C, 70.42; H, 7.08%. Calcd for $C_{30}H_{36}O_7$: C, 70.84; H, 7.13%.

Further elution gave **48** (42 mg, 8%).

The diols **138**, **165**, and **202** were similarly benzylated to give **139** (50%) and **140** (22%), and **166** (65%) and **167** (16%), and **190**, (73%, the faster-moving) and **185** (9%, the slower-moving), respectively.

2-Methoxyethyl 2,4-Di-*O*-benzyl-α-L-arabinopyranoside (**139**). Mp 65—66 °C, $[\alpha]_D$ −10° (*c* 0.7, $CHCl_3$), ^1H NMR ($CDCl_3$) δ=3.37 (s, OMe), 3.47 (dd, $J_{4,5b}$=3 Hz, $J_{5a,5b}$=11 Hz, H-5b), 3.63 (dd, $J_{1,2}$=4.5 Hz, $J_{2,3}$=2 Hz, H-2), 3.80 (m, $J_{3,4}$=3 Hz, $J_{4,5a}$=6 Hz, H-4), 3.97 (dd, H-5a), 4.55 (d, H-1).

Anal. ($C_{22}H_{28}O_6$) C, H.

2-Methoxyethyl 2,4-Di-*O*-benzyl-β-L-fucopyranoside (**166**). $[\alpha]_D$ −12° (*c* 0.9, $CHCl_3$), ^1H NMR ($CDCl_3$) δ=1.24 (d, $J_{5,6}$=6.5 Hz, H-6), 3.38 (s, OMe), 4.37 (d, $J_{1,2}$=7.5 Hz, H-1).

Anal. ($C_{23}H_{30}O_6$) C, H.

2-Methoxyethyl 3-*O*-Allyl-2,4,6-tri-*O*-benzyl- and 2-*O*-Allyl-3,4,6-tri-*O*-benzyl-β-D-galactopyranosides (**53** and **55**). A mixture of **53** (1.00 g), allyl bromide (9 ml), KOH (0.28 g, 1.6 equiv), and DME (9 ml) was stirred for 1.5 h at 70 °C. Processing and chromatography (TB system) gave the diallyl ether (0.25 g, 20%) and then **55** (0.25 g, 22%), $[\alpha]_D$ −8° (*c* 4.4, $CHCl_3$), ^1H NMR ($CDCl_3$) δ=3.38 (s, OMe), 3.40 (m, $J_{4,5}$=$J_{5,6a}$=1.5 Hz, $J_{5,6b}$=2 Hz, H-5), 3.51 (dd, $J_{1,2}$=8 Hz, $J_{2,3}$=9.5 Hz, H-2), 3.67 (dd, $J_{3,4}$=4 Hz, H-3), 4.04 (dd, $J_{6a,6b}$=12.5 Hz, H-6b), 4.19 (dd, H-4), 4.29 (dd, H-6a), 4.38 (d, H-1), 5.53 (s, benzylidene).

Further elution afforded **54** (0.52 g, 46%), mp 147—149 °C (from IPE), $[\alpha]_D$ +38° (*c* 0.7, $CHCl_3$), ^1H NMR ($CDCl_3$) δ=3.39 (s, OMe), 3.48 (dd, $J_{2,3}$=10 Hz, $J_{3,4}$=4 Hz, H-3), 3.99 (dd, $J_{1,2}$=8 Hz, H-2), 4.07 (dd, $J_{5,6b}$=2 Hz, $J_{6a,6b}$=12 Hz, H-6b), 4.22 (dd, $J_{5,6a}$=1.5 Hz, H-6a), 4.39 (d, H-1), 5.53 (s, benzylidene).

Found: **54**, C, 61.92; H, 7.07%. **55**, C, 61.93; H, 7.18%. Calcd for $C_{19}H_{25}O_7$: C, 62.45; H, 6.90%.

The diols **46** (3 equiv of KOH, 1 h), **86** (3 equiv of KOH, 2 h), **138** (1.7 equiv of KOH, 45 min), **165** (2 equiv of KOH, 45 min), and **202** (3 equiv of KOH, 1.5 h) were similarly allylated to yield **63** (50%, the faster-moving) and **64** (9%, the slower-moving), **88** (40%, the slower-moving) and **89** (11%, the faster-moving), **149** (56%, the faster-moving) and **150** (21%, the slower-moving), **176** (66%, the faster-moving) and **177** (26%, the slower-moving), as well as **203** (51%, the faster-moving) and **204** (29%, the solwer-moving), respectively.

2-Methoxyethyl 4- and 3-*O*-Allyl-2,6-di-*O*-benzyl-β-D-galactopyranosides (**63** and **64**). **63**, $[\alpha]_D$ −4° (*c* 1.0, $CHCl_3$), ^1H NMR ($CDCl_3$) δ=3.37 (s, OMe), 3.53 (dd, $J_{1,2}$=7.5 Hz, $J_{2,3}$=9.5 Hz, H-2), 4.38 (d, H-1), 5.88 (m, allyl). **64**, $[\alpha]_D$ +7° (*c* 0.7, $CHCl_3$), ^1H NMR ($CDCl_3$) δ=3.38 (s, OMe), 3.40 (dd, $J_{2,3}$=9.5 Hz, $J_{3,4}$=3.5 Hz, H-3), 3.60 (dd, $J_{1,2}$=8 Hz, H-2), 4.40 (d, H-1), 5.93 (m, allyl).

Anal. ($C_{26}H_{34}O_6$) **63**, C, H. **64**, C, H.

2-Methoxyethyl 3- and 2-*O*-Allyl-4,6-*O*-benzylidene-α-D-mannopyranosides (**88** and **89**). **88**, $[\alpha]_D$ +40° (*c* 0.6, $CHCl_3$), ^1H NMR ($CDCl_3$) δ=3.39 (s, OMe), 4.13 (dd, $J_{1,2}$=1.5 Hz, $J_{2,3}$=4 Hz, H-2), 4.20 (t, $J_{3,4}$=$J_{4,5}$=9 Hz, H-4), 4.93 (d, H-1), 5.59 (m, allyl). **89**, $[\alpha]_D$ +23° (*c* 0.9, $CHCl_3$), ^1H NMR ($CDCl_3$) δ=3.40 (s, OMe), 4.92 (d, $J_{1,2}$=1.5 Hz, H-1), 5.57 (s, benzylidene).

Found: **88**, C, 62.42; H, 7.17%. **89**, C, 62.49; H, 7.32%. Calcd for $C_{19}H_{25}O_7$: C, 62.45; H, 6.90%.

2-Methoxyethyl 4- and 3-*O*-Allyl-2-*O*-benzyl-α-L-arabinopyranosides (**149** and **150**). **149**, $[\alpha]_D$ −7° (*c* 0.6, $CHCl_3$), ^1H NMR ($CDCl_3$) δ=3.36 (s, OMe), 3.48 ($J_{4,5b}$=3 Hz, $J_{5a,5b}$=12 Hz, H-5b), 2.61 (dd, $J_{1,2}$=5 Hz, $J_{2,3}$=7 Hz, H-2), 3.73 (dd, $J_{3,4}$=3 Hz, $J_{4,5a}$=6 Hz, H-4), 3.86 (dd, H-3), 3.95 (dd, H-5a), 4.54 (d, H-1), **150**, $[\alpha]_D$ +15° (*c* 0.8, $CHCl_3$), ^1H NMR ($CDCl_3$) δ=3.38 (s, OMe), 3.60 (dd, $J_{1,2}$=7 Hz, $J_{2,3}$=9 Hz, H-2), 4.35 (d, H-1), 5.92 (m, allyl).

Anal. ($C_{18}H_{26}O_6$) **149**, C, H. **150**, C, H.

2-Methoxyethyl 4- and 3-*O*-Allyl-2-*O*-benzyl-β-L-fucopyranosides (**176** and **177**). **176**, $[\alpha]_D$ −13° (*c* 0.6, $CHCl_3$), ^1H NMR ($CDCl_3$) δ=1.30 (d, $J_{5,6}$=6.5 Hz, H-6), 3.37 (s, OMe), 3.55 (m, $J_{4,5}$=1 Hz, H-5), 4.36 (d, $J_{1,2}$=7.5 Hz, H-1), 5.93 (m, allyl). **177**, $[\alpha]_D$ −1.4° (*c* 0.7, $CHCl_3$), ^1H NMR ($CDCl_3$) δ=1.35 (d, $J_{5,6}$=6.5 Hz, H-6), 3.38 (s, OMe), 3.40 (dd, $J_{2,3}$=10 Hz, $J_{3,4}$=4 Hz, H-3), 3.54 (m, $J_{4,5}$=1 Hz, H-5), 3.55 (dd, $J_{1,2}$=7.5 Hz, H-2), 3.76 (dd, H-4), 4.37 (d, H-1), 5.93 (m, allyl).

Anal, ($C_{19}H_{28}O_6$) **176**, C, H. **177**, C, H.

2-Methoxyethyl 2- and 3-*O*-Allyl-4-*O*-benzyl-α-L-rhamnopyranosides (**203** and **204**). **203**, $[\alpha]_D$ −32° (*c* 0.9, $CHCl_3$), ^1H NMR ($CDCl_3$) δ=1.32 (d, $J_{5,6}$=6.5 Hz, H-6), 3.28 (t, $J_{3,4}$=$J_{4,5}$=10 Hz, H-4), 3.37 (s, OMe), 3.68 (m, H-5), 3.70 (dd, $J_{1,2}$=1.5 Hz, $J_{2,3}$=4 Hz, H-2), 3.96 (dd, H-3), 4.84 (d, H-1), 5.93 (m, allyl). **204**, $[\alpha]_D$ −59° (*c* 0.6, $CHCl_3$), ^1H NMR ($CDCl_3$) δ=1.30 (d, $J_{5,6}$=6.5 Hz, H-6), 3.37 (s, OMe), 3.41 (t, $J_{3,4}$=$J_{4,5}$=10 Hz, H-4), 3.72 (m, H-5), 3.75 (dd, $J_{2,3}$=4 Hz, H-3), 4.07 (dd, $J_{1,2}$=1.5 Hz, H-2), 4.84 (d, H-1), 5.95 (m, allyl).

Anal. ($C_{19}H_{28}O_6$) **203**, C, H. **204**, C, H.

The alcohols, **15**, **21**, **22**, **47**, **48**, **58**, **92**, **93**, **118**, **139**, **140**, **166**, **167**, **190**, and **199** were acetylated with excess Ac_2O in pyridine, followed by chromatographical purification (HE system), to yield the corresponding acetates, **16**, **23**, **28**, **49**, **59**, **66**, **81**, **98**, **119**, **141**, **145**, **168**, **172**, **191**, and **200**.

2-Methoxyethyl 3-*O*-Acetyl-2,4,6-tri-*O*-benzyl-β-D-glucopyranoside (**16**). Mp 64—65 °C (from hexane), $[\alpha]_D$ +17° (*c* 1.0, $CHCl_3$).

Anal. ($C_{32}H_{38}O_8$) C, H.

2-Methoxyethyl 4-*O*-Acetyl-2,3,6-tri-*O*-benzyl-β-D-glucopyranoside (**23**). $[\alpha]_D$ −13° (*c* 2.3, $CHCl_3$).

Anal. ($C_{32}H_{38}O_8$) C, H.

2-Methoxyethyl 6-*O*-Acetyl-2,3,4-tri-*O*-benzyl-β-D-glucopyranoside (**28**). Mp 80—81 °C (from hexane), $[\alpha]_D$ −32° (*c* 0.9, $CHCl_3$).

Anal. ($C_{32}H_{38}O_8$) C, H.

2-Methoxyethyl 3-*O*-Acetyl-2,4,6-tri-*O*-benzyl-β-D-galactopyranoside (**49**). $[\alpha]_D$ +29° (*c* 1.0, $CHCl_3$).

Anal. ($C_{32}H_{38}O_8$) C, H.

2-Methoxyethyl 4-*O*-Acetyl-2,3,6-tri-*O*-benzyl-β-D-galactopyranoside (**59**). $[\alpha]_D$ +11° (*c* 2.0, $CHCl_3$).

Anal. ($C_{32}H_{38}O_8$) C, H.

2-Methoxyethyl 6-*O*-Acetyl-2,3,4-tri-*O*-benzyl-β-D-galactopyranoside (**66**). $[\alpha]_D$ −17° (*c* 2.6, $CHCl_3$).

Anal. ($C_{32}H_{38}O_8$) C, H.

2-Methoxyethyl 6-*O*-Acetyl-2,3,4-tri-*O*-benzyl-α-D-mannopyranoside (**98**). $[\alpha]_D$ +30° (*c* 0.9, $CHCl_3$).

Anal. ($C_{32}H_{38}O_8$) C, H.

2-Methoxyethyl 4-*O*-Acetyl-2,3-di-*O*-benzyl-β-D-xylopyranoside (**119**). $[\alpha]_D$ −28° (*c* 0.9, $CHCl_3$).

Anal. ($C_{24}H_{30}O_7$) C, H.

2-Methoxyethyl 3-*O*-Acetyl-2,4-di-*O*-benzyl-α-L-arabinopyranoside (**141**). $[\alpha]_D$ +29° (*c* 0.7, $CHCl_3$).

Anal. ($C_{24}H_{30}O_7$) C, H.

2-Methoxyethyl 4-*O*-Acetyl-2,3-di-*O*-benzyl-α-L-arabinopyranoside (**145**). $[\alpha]_D$ +33° (*c* 0.8, $CHCl_3$).

Found: C, 66.57; H, 7.07%. Calcd for $C_{24}H_{30}O_7$: C, 66.96; H, 7.05%.

2-Methoxyethyl 3-*O*-Acetyl-2,4-di-*O*-benzyl-β-L-fucopyranoside (**168**). $[\alpha]_D$ −41° (*c* 0.6, $CHCl_3$).

Anal. ($C_{25}H_{32}O_7$) C, H.

2-Methoxyethyl 4-*O*-Actyl-2,3-di-*O*-benzyl-β-L-fucopyranoside (**172**). $[\alpha]_D$ −29° (*c* 0.6, $CHCl_3$).

Anal. ($C_{25}H_{32}O_7$) C, H.

2-Methoxyethyl 3-*O*-Acetyl-2,4-di-*O*-benzyl-α-L-rhamonopyranoside (**191**). $[\alpha]_D$ −7° (*c* 0.8, $CHCl_3$).

Anal. ($C_{25}H_{32}O_7$) C, H.

2-Methoxyethyl 4-*O*-Acetyl-2,4-di-*O*-benzyl-α-L-rhamnopyranoside (**200**). $[\alpha]_D$ −39° (*c* 0.5, $CHCl_3$)

Anal. ($C_{25}H_{32}O_7$) C, H.

Deacetylation of **10**, **38**, **75**, **80**, **106**, **129**, **156**, and **183** with dil NaOMe (0.6%) at room temp, followed by chromatography (TB system), furnished the corresponding alcohols, **12**, **40**, **77**, **83**, **108**, **131**, **158**, and **185**.

2-Methoxyethyl 3,4,6-Tri-*O*-benzyl-β-D-glucopyranoside (**12**). $[\alpha]_D$ −6° (*c* 7.4, $CHCl_3$). ^1H NMR ($CDCl_3$) δ=3.40 (s, OMe), 4.32 (d, $J_{1,2}$=7 Hz, H-1).

Anal. ($C_{30}H_{36}O_7$).

2-Methoxyethyl 3,4,6-Tri-*O*-benzyl-α-D-mannopyranoside (**77**). $[\alpha]_D$ +44° (*c* 1.0, $CHCl_3$), ^1H NMR ($CDCl_3$) δ=3.37 (s, OMe), 3.88 (t, $J_{3,4}=J_{4,5}$=8.5 Hz, H-4), 3.95 (dd, $J_{2,3}$=3.5 Hz, H-3), 4.14 (dd, $J_{1,2}$=2 Hz, H-2), 4.97 (d, H-1).

Found: C, 70.29; H, 7.12%. Calcd for $C_{30}H_{36}O_7$: C, 70.84; H, 7.13%.

2-Methoxyethyl 2,4,6-Tri-*O*-benzyl-α-D-mannopyranoside (**83**). $[\alpha]_D$ +16° (*c* 1.1, $CHCl_3$), ^1H NMR ($CDCl_3$) δ=3.35 (s, OMe), 4.99 (d, $J_{1,2}$=1.5 Hz, H-1).

Anal. ($C_{30}H_{36}O_7$) C, H.

2-Methoxyethyl 3,4-Di-*O*-benzyl-β-D-xylopyranoside (**108**). $[\alpha]_D$ −27° (*c* 2.2, $CHCl_3$), ^1H NMR ($CDCl_3$) δ=3.28 (dd, $J_{4,5ax}$=9 Hz, $J_{5eq,5ax}$=12 Hz, H-5ax), 3.39 (s, OMe), 3.98 (dd, $J_{4,5eq}$=4.5 Hz, H-5eq), 4.33 (d, $J_{1,2}$=8 Hz, H-1).

Anal. ($C_{22}H_{28}O_6$) C, H.

2-Methoxyethyl 3,4-Di-*O*-benzyl-α-L-arabinopyranoside (**131**). $[\alpha]_D$ +23° (*c* 0.4, $CHCl_3$), ^1H NMR ($CDCl_3$) δ=3.29 (d, $J_{4,5ax}$=0 Hz, $J_{5eq,5ax}$=13 Hz, H-5ax), 3.39 (s, OMe), 3.41 (dd, $J_{2,3}$=10 Hz, $J_{3,4}$=3 Hz, H-3), 3.69 (dd, $J_{4,5eq}$=2.5 Hz, H-4), 4.00 (dd, $J_{1,2}$=7.5 Hz, H-2), 4.07 (dd, H-5eq), 4.22 (d, H-1).

Anal. ($C_{22}H_{28}O_6$) C, H.

2-Methoxyethyl 3,4-Di-*O*-benzyl-β-L-fucopyranoside (**158**). $[\alpha]_D$ +13° (*c* 0.8, $CHCl_3$), ^1H NMR ($CDCl_3$) δ=1.21 (d, $J_{5,6}$=6.5 Hz, H-6), 3.38 (s, OMe), 3.45 (dd, $J_{2,3}$=10 Hz, $J_{3,4}$=3 Hz, H-3), 3.50 (m, $J_{4,5}$=1.5 Hz, H-5), 3.98 (dd, $J_{1,2}$=7.5 Hz, H-1), 4.26 (d, H-1).

Found: C, 68.25; H, 7.50%. Calcd for $C_{23}H_{30}O_6$: C, 68.64; H, 7.15%.

2-Methoxyethyl 3,4-Di-*O*-benzyl-α-L-rhamnopyranoside (**185**). $[\alpha]_D$ −31° (*c* 1.3, $CHCl_3$), ^1H NMR ($CDCl_3$) δ=1.33 (d, $J_{5,6}$=6 Hz, H-6), 3.38 (s, OMe), 3.47 (t, $J_{3,4}=J_{4,5}$=10 Hz, H-4), 3.89 (dd, $J_{2,3}$=4 Hz, H-3), 4.12 (dd, $J_{1,2}$=1.5 Hz, H-2), 4.86 (d, H-1).

Anal. ($C_{23}H_{30}O_6$) C, H.

2-Methoxyethyl 2,3-Di-*O*-benzyl-α-L-rhamnopyranoside (**199**). The allyl ether **197** (417 mg) was deallylated through the published method,[21] followed by chromatography (TB system), to produce **199** (202 mg, 53%), $[\alpha]_D$ −2° (*c* 1.1, $CHCl_3$), ^1H NMR ($CDCl_3$) δ=1.32 (d, $J_{5,6}$=6 Hz, H-6), 3.37 (s, OMe), 3.88 (dd, $J_{1,2}$=1.5 Hz, $J_{2,3}$=2.5 Hz, H-2), 4 87 (d, H-1).

Anal. ($C_{23}H_{30}O_6$) C, H.

The monohydroxy alcohols **12**, **15**, **21**, **22**, **40**, **47**, **48**, **58**, **77**, **83**, **92**, **93**, **108**, **111**,[6] **118**, **131**, **139**, **140**, **158**, **166**, **167**, **185**, and **190** were allylated by refluxing in neat allyl bromide containing excess NaH, followed by chromatographical purification (HE system), to furnished the corresponding allyl ethers **13**, **18**, **25**, **30**, **41**, **51**, **61**, **68**, **78**, **84**, **95**, **100**, **109**, **112**, **121**, **132**, **143**, **147**, **159**, **170**, **174**, **186**, and **193**.

2-Methoxyethyl 2-*O*-Allyl-3,4,6-tri-*O*-benzyl-β-D-glucopyranoside (**13**). $[\alpha]_D$ −13° (*c* 2.9, $CHCl_3$), ^1H NMR ($CDCl_3$) δ=3.33 (dd, $J_{1,2}$=8 Hz, $J_{2,3}$=9 Hz, H-2), 3.37 (s, OMe), 3.53 (t, $J_{3,4}=J_{4,5}$=9 Hz, H-4), 3.59 (t, H-3), 4.35 (d, H-1), 5.94 (m, allyl).

Anal. ($C_{33}H_{40}O_7$) C, H.

2-Methoxyethyl 3-*O*-Allyl-2,4,6-tri-*O*-benzyl-β-D-glucopyranoside (**18**). Mp 58—59 °C (from hexane), $[\alpha]_D$ +7.3° (*c* 0.4, $CHCl_3$), ^1H NMR ($CDCl_3$) δ=3.39 (s, OMe), 4.40 (d, $J_{1,2}$=7.5 Hz, H-1), 5.96 (m, allyl).

Anal. ($C_{33}H_{40}O_7$) C, H.

2-Methoxyethyl 4-*O*-Allyl-2,3,6-tri-*O*-benzyl-β-D-glucopyranoside (**25**). Mp 118—119 °C (from IPE), $[\alpha]_D$ +20° (*c* 2.8, $CHCl_3$), ^1H NMR ($CDCl_3$) δ=3.39 (s, OMe), 3.44 (dd, $J_{1,2}$=8 Hz, $J_{2,3}$=9 Hz, H-2), 4.44 (d, H-1), 5.82 (m, allyl).

Anal. ($C_{33}H_{40}O_7$) C, H.

2-Methoxyethyl 6-*O*-Allyl-2,3,4-tri-*O*-benzyl-β-D-glucopyranoside (**30**). Mp 59—60 °C (from hexane), $[\alpha]_D$ +2° (*c* 0.3, $CHCl_3$), ^1H NMR ($CDCl_3$) δ=3.39 (s, OMe), 3.46 (m, $J_{4,5}$=9 Hz, $J_{5,6}$=2 and 5 Hz, H-5), 3.49 (dd, $J_{1,2}$=7.5 Hz, $J_{2,3}$=9 Hz, H-2), 3.59 (t, $J_{3,4}$=9 Hz, H-3), 3.68 (t, H-3), 4.45 (d, H-1).

Anal. ($C_{33}H_{40}O_7$) C, H.

2-Methoxyethyl 2-*O*-Allyl-3,4,6-tri-*O*-benzyl-β-D-galactopyranoside (**41**). $[\alpha]_D$ −22° (*c* 1.0, $CHCl_3$), ^1H NMR ($CDCl_3$) δ=3.37 (s, OMe), 3.46 (dd, $J_{2,3}$=10 Hz, $J_{3,4}$=3 Hz, H-3), 3.70 (dd, $J_{1,2}$=7.5 Hz, H-2), 3.86 (d, $J_{4,5}$=0 Hz, H-4), 4.33 (d, H-1), 5.91 (m, allyl).

Anal. ($C_{33}H_{40}O_7$) C, H.

2-Methoxyethyl 6-*O*-Allyl-2,3,4-tri-*O*-benzyl-β-D-galactopyranoside (**68**). $[\alpha]_D$ −1° (*c* 3.5, $CHCl_3$), ^1H NMR ($CDCl_3$) δ=3.37 (s, OMe), 3.84 (dd, $J_{1,2}$=7.5 Hz, $J_{2,3}$=10 Hz, H-2), 4.41 (d, H-1), 5.89 (m, allyl).

Anal. ($C_{33}H_{40}O_7$) C, H.

2-Methoxyethyl 2-*O*-Allyl-3,4,6-tri-*O*-benzyl-α-D-mannopyranoside (**78**). $[\alpha]_D$ +38° (*c* 3.0, $CHCl_3$), ^1H NMR ($CDCl_3$) δ=3.36 (s, OMe), 3.85 (dd, $J_{1,2}$=2 Hz, $J_{2,3}$=1.5 Hz, H-2), 4.92 (d, H-1), 5.94 (m, allyl).

Anal. ($C_{33}H_{40}O_7$) C, H.

2-Methoxyethyl 4-*O*-Allyl-2,3,6-tri-*O*-benzyl-α-D-mannopyranoside (**95**). $[\alpha]_D$ +31° (*c* 1.0, $CHCl_3$), ^1H NMR ($CDCl_3$) δ=3.34 (s, OMe), 4.92 (d, $J_{1,2}$=1.5 Hz, H-1), 5.84 (m, allyl).

Found: C, 71.60; H, 7.47%. Calcd for $C_{33}H_{40}O_7$: C, 72.24; H, 7.45%.

2-Methoxyethyl 6-*O*-Allyl-2,3,4-tri-*O*-benzyl-α-D-mannopyranoside (**100**). $[\alpha]_D$ +27° (*c* 2.2, $CHCl_3$), ^1H NMR ($CDCl_3$) δ=3.34 (s, OMe), 3.88 (dd, $J_{1,2}$=2 Hz, $J_{2,3}$=3 Hz, H-2), 4.92 (d, H-1), 5.93 (m, allyl).

Found: C, 71.84; H, 7.41%. Calcd for $C_{33}H_{40}O_7$: C, 72.24; H, 7.35%.

2-Methoxyethyl 2-*O*-Allyl-3,4-di-*O*-benzyl-β-D-xylopyranoside (**109**). $[\alpha]_D$ −18° (*c* 2.0, $CHCl_3$), ^1H NMR ($CDCl_3$) δ=3.18 (dd, $J_{4,5ax}$=10 Hz, $J_{5eq,5ax}$=11.5 Hz, H-5ax), 3.27 ($J_{1,2}$= 7.5 Hz, $J_{2,3}$=9 Hz, H-2), 3.38 (s, OMe), 3.51 (t, $J_{3,4}$=9 Hz, H-3), 3.91 (dd, $J_{4,5eq}$=5 Hz, H-5eq), 4.31 (d, H-1), 5.95 (m, allyl).

Anal. ($C_{25}H_{32}O_6$) C, H.

2-Methoxyethel 3-*O*-Allyl-2,4-di-*O*-benzyl-β-D-xylopyranoside (**112**). $[\alpha]_D$ −4 ° (*c* 1.5, $CHDCl_3$), ^1H NMR ($CDCl_3$) δ=3.17 (dd, $J_{4,5ax}$=10 Hz, $J_{5eq,5ax}$=11.5 Hz, H-5ax), 3.33 (dd, $J_{1,2}$=7.5 Hz, $J_{2,3}$=9 Hz, H-2), 3.38 (s, OMe), 3.43 (t, $J_{3,4}$=9 Hz, H-3), 3.55 (m, $J_{4,5eq}$=5 Hz, H-4), 3.90 (dd, H-5eq), 4.34 (d, H-1), 5.97 (m, allyl).

Anal. ($C_{25}H_{32}O_6$). C, H.

2-Methoxyethyl 4-*O*-Allyl-2,3-di-*O*-benzyl-β-D-xylopyranoside (**121**). $[\alpha]_D$ +2° (*c* 0.8, $CHCl_3$), ^1H NMR ($CDCl_3$) δ=3.18

(dd, $J_{4,5ax}$=10 Hz, $J_{5eq,5ax}$=11.5 Hz, H-5ax), 3.39 (s, OMe), 4.38 (d, $J_{1,2}$=8 Hz, H-1), 5.89 (m, allyl).

Anal. ($C_{25}H_{32}O_6$) C, H.

2-Methoxyethyl 3-*O*-Allyl-2,4-di-*O*-benzyl-α-L-arabinopyranoside (**143**). $[\alpha]_D$ +11° (*c* 0.7, $CHCl_3$), ^1H NMR ($CDCl_3$) δ=3.39 (dd, $J_{4,5ax}$=1.5 Hz, $J_{5eq,5ax}$=13 Hz, H-5ax), 3.48 (s, OMe), 3.53 (dd, $J_{2,3}$=9.5 Hz, $J_{3,4}$=4 Hz, H-3), 3.87 (dd, $J_{1,2}$=7 Hz, H-2), 4.13 (dd, $J_{4,5eq}$=3 Hz, H-5eq), 4.46 (d, H-1), 6.01 (m, allyl).

Found: C, 69.58; H, 7.49%. Calcd for $C_{25}H_{32}O_6$: C, 70.07; 7.53%.

2-Methoxyethyl 3-*O*-Allyl-2,4-di-*O*-benzyl-β-L-fucopyranoside (**170**). $[\alpha]_D$ +15° (*c* 0.8, $CHCl_3$), ^1H NMR ($CDCl_3$) δ=1.18 (d, $J_{5,6}$=6.5 Hz, H-6), 3.37 (s, OMe), 3.41 (dd, $J_{2,3}$=10 Hz, $J_{3,4}$=3 Hz, H-3), 3.45 (m, $J_{4,5}$=1 Hz, H-5), 3.54 (dd, H-4), 3.75 (dd, $J_{1,2}$=7.5 Hz, H-2), 4.35 (d, H-1), 5.95 (m, allyl).

Found: C, 70.25; H, 7.85%. Calcd for $C_{26}H_{34}O_6$: C, 70.56; H, 7.74%.

2-Methoxyethyl 3-*O*-Allyl-2,4-di-*O*-benzyl-α-L-rhamnopyranoside (**193**). $[\alpha]_D$ −44° (*c* 0.4, $CHCl_3$), ^1H NMR ($CDCl_3$) δ=1.32 (d, $J_{5,6}$=6 Hz, H-6), 3.34 (s, OMe), 3.57 (t, $J_{3,4}$=$J_{4,5}$=10 Hz, H-4), 3.68 (m, H-5), 3.76 (dd, $J_{2,3}$=3.5 Hz, H-3), 3.82 (dd, $J_{1,2}$=2 Hz, H-2), 4.79 (d, H-1), 5.95 (m, allyl).

Found: C, 70.24; H, 7.67%. Calcd for $C_{25}H_{34}O_6$: C, 70.56; H, 7.74%.

References

1) H. Paulsen, "New Synthetic Methodology and Functionally Interesting Compounds", ed by Z. Yoshida, Kodansha, Tokyo (1986), p. 13.

2) G. Grynkiewicz, *Pol. J. Chem.*, **53**, 1571 (1979), A. A. Pavia, J.-M. Rocheville, and S. N. Ung, *Carbohydr. Res.*, **79**, 79 (1980), S. Koto, T. Sato, N, Morishima, and S. Zen, *Bull. Chem. Soc. Jpn.*, **53**, 1761 (1980), W. Szeja, *Synthesis*, **1988**, 223.

3) O. T. Schmidt, T. Auer, and H. Schmadel, *Chem. Ber.*, **93**, 556 (1960), B. R. Barker and H. J. Fletcher, Jr., *J. Org. Chem.*, **26**, 4605 (1961); J. Gigg and R. Gigg, *J. Chem. Soc., C*, **1966**, 82, T. Ogawa and S. Nakabayashi, *Carbohydr. Res.*, **93**, Cl (1981); R. U. Lemieux and H. Driguez, *J. Am. Chem. Soc.*, **97**, 4069 (1975), K. Jansson, S. Ahlfors, T. Frejd, J. Kihlberg, and G. Magnusson, *J. Org. Chem.*, **53**, 5629 (1988), V. Pozsgay, H. J. Jennings, and D. L. Kasper, *J. Carbohydr. Chem.*, **6**, 45 (1987), D. R. Mootoo, V. Date, and B. Fraser-Reid, *J. Am. Chem. Soc.*, **110**, 2662 (1988), J. M. Lacombe, N. Rakotomanomana, and A. A. Pavia, *Carbohydr. Res.*, **181**, 246 (1988).

4) S. Koto, N. Morishima R. Kawahara, K. Ishikawa, and S. Zen, *Bull. Chem. Soc. Jpn.*, **55**, 1092 (1982).

5) N. Morishima, S. Koto, K. Kanemitsu, and S. Zen, *Chem. Lett.*, **1983**, 1189.

6) S. Koto, N. Morishima, K. Takenaka, C. Uchida, and S. Zen, *Bull. Chem. Soc. Jpn.*, **58**, 1464 (1985).

7) S. Koto, N. Morishima, Y. Mori, H. Tanaka, S. Hayashi, Y. Iwai, and S. Zen, *Bull. Chem. Soc. Jpn.*, **60**, 2301 (1987).

8) S. Koto, T. Yoshida, K. Takenaka, and S. Zen, *Bull. Chem. Soc. Jpn.*, **55**, 3667 (1982).

9) C. S. Hudson and J. K. Dale, *J. Am. Chem. Soc.*, **40**, 992 (1918).

10) S. Koto, N. Morishima, H. Sato, Y. Sato, and S. Zen, *Bull. Chem. Soc. Jpn.*, **58**, 120 (1985).

11) S. Koto, K. Takenaka, N. Morishima, A. Sugimoto, and S. Zen, *Bull. Chem. Soc. Jpn.*, **57**, 3603 (1984).

12) B. Helferich and H. H. Hiltmann, *Justus Liebigs Ann. Chem.*, **531**, 160 (1937).

13) N. Morishima, S. Koto, M. Oshima, A. Sugimoto, and S. Zen, *Bull. Chem. Soc. Jpn.*, **56**, 2849 (1983).

14) S. Koto, N. Morishima, T. Yoshida, M. Uchino, and S. Zen, *Bull. Chem. Soc. Jpn.*, **56**, 1171 (1983).

15) A. H. Haines, *Adv. Carbohydr. Chem. Biochem.*, **33**, 11 (1976).

16) S. Koto, N. Morishima, M. Uchino, M. Fukuda, M. Yamazaki, and S. Zen, *Bull. Chem. Soc. Jpn.*, **61**, 3943 (1988).

17) S. Koto, N. Morishima, Y. Miyata, and S. Zen, *Bull. Chem. Soc. Jpn.*, **49**, 2639 (1976).

18) S. Koto, N. Morishima, Y. Kihara, H. Suzuki, S. Kosugi, and S. Zen, *Bull. Chem. Soc. Jpn.*, **56**, 188 (1983).

19) P. A. Gent and R. Gigg, *Carbohydr. Res.*, **49**, 325 (1976).

20) F. Sugawara, H. Nakayama, and T. Ogawa, *Carbohydr. Res.*, **108**, C5 (1982).

21) P. A. Gent and R. Gigg, *J. Chem. Soc., Perkin Trans. 1*, **1974**, 1835.

22) B. Doboszewski and A. Zamojski, *Carbohydr. Res.*, **132**, 29 (1984).

23) P. A. Gent and R. Gigg, *J. Chem. Soc., Perkin Trans. 1*, **1975**, 361.

24) M. A. Nashed and L. Anderson, *Carbohydr. Res.*, **56**, 325 (1977).

25) A. Banaszek, **X**. B. Cornet, and A Zamojski, *Carbohydr. Res.*, **144**, 342 (1985).

26) M. M. Pompipom, *Carbohydr. Res.*, **59**, 311 (1977).

27) S. Tejima, R. K. Ness, R. L. Kaufman, and H. G. Fletcher, Jr., *Carbohydr. Res.*, **7**, 485 (1968).

28) S. Tejima and H. G. Fletcher, Jr., *J. Org. Chem.*, **28**, 2999 (1963).

29) M. Dejter-Juszynski and H. M. Flowers, *Carbohydr. Res.*, **18**, 219 (1971).

30) J. M. J. Fléchet and H. H. Baer, *Carbohydr. Res.*, **42**, 369 (1975).

31) J. Janson and B. Lindberg, *Acta Chem. Scand.*, **13**, 138 (1959).

32) M. E. Jolley, C. P. J, Glaudemans, S. Rudikoff, and M. Potter, *Biochemistry*, **13**, 3179 (1974).

33) C. K. deBruyne and G. van der Groen, *Carbohydr. Res.*, **5**, 95 (1967).

34) P. L. Barili, G. Berti, G. Catelani, F. Colonna, and A. Marra, *Tetrahedron Lett.*, **27**, 2307 (1986).

35) H. Paulsen and M. Paal, *Carbohydr. Res.*, **137**, 39 (1985).

36) J. J. Patroni, R. V. Stick, B. W. Skelton, and A. H. White, *Aust. J. Chem.*, **41**, 91 (1988).

 © 1989 The Chemical Society of Japan Bull. Chem. Soc. Jpn., 62, 3567—3571 (1989)

Reactions of Alkylarenes, Benzyl Alcohols, Sulfides, and Phosphine with Manganese(III) Acetate-Chloride Ions

Yasuo FUTAMI, Hiroshi NISHINO, and Kazu KUROSAWA*
Department of Chemistry, Faculty of Science, Kumamoto University, Kurokami 2-39-1, Kumamoto 860
(Received May 16, 1989)

The reactions of methoxytoluenes and methylnaphthalenes with a manganese(III) acetate-Cl^- complex gave the corresponding aldehydes in 8 to 54% yields. In a similar reaction aromatic compounds having a methylene group were oxidized to the corresponding acetates and ketones. The primary and secondary benzyl alcohols gave aldehydes and ketones, respectively, in good yields. Sulfides and phosphine were oxidized to give oxides by the complex. The reaction of alkylarenes with lower ionization potentials can be explained in terms of an electron-transfer mechanism involving the manganese(III) acetate-Cl^- complex.

Several papers have been published concerning the complex formation and the reaction of manganese(III) acetate in the presence of chloride ions. The reaction of olefins with the complex yielded mainly addition products,[1,2] while α,β-unsaturated carboxylic acids gave addition and chlorine-substituted products accompanied by decarboxylation.[3] α,β-Unsaturated carboxylates also gave addition and chlorine-substituted products.[4] In a previous paper[5] we reported that the reaction of aryl ketones with manganese(III) acetate–lithium chloride gave α-chlorinated ketones in good yields. In the reaction of toluenes with manganese(III) acetate the addition of an equimolar portion of potassium bromide led to an appreciable rate enhancement and gave increased yields of benzyl acetates and benzaldehydes[6] instead of methyl-substituted benzyl acetates, which were the main products in the reaction of manganese(III) acetate alone. However, the reactions were examined only from the mechanistic point of view. This prompted us to investigate the reactions of aromatic compounds having methyl and methylene groups, benzyl alcohols, sulfides and phosphorus compounds with the manganese(III) acetate-Cl^- complex in order to improve the yields of aldehydes, ketones, and oxides. We have examined the reactions of methoxy-substituted toluenes, methylnaphthalenes, diarylmethanes, xanthene, anthrone, methyl phenylacetates, fluorene, benzyl alcohols, diphenyl sulfide, dibenzothiophene, and triphenylphosphine. These compounds were chosen because they may provide a variety of products which reflect the nature of the reaction and that the products can be easily characterized by spectroscopy. The reaction were carried out under various reaction conditions by changing the molar ratio of the substrate, manganese(III) acetate and chloride ions. The effects of changing the source of the chloride ions, and of additives were also examined.

Results

Methoxy-Substituted Toluenes and Methylnaphthalenes. When 4-methoxytoluene (**1a**) was oxidized with the manganese(III) acetate-Cl^- complex in AcOH in a molar ratio of **1a**:Mn(III):LiCl of 1:4:5 at 100 °C, it gave a mixture of 4-methoxybenzyl acetate (**2a**) and 4-methoxybenzaldehyde (**3a**). The reaction

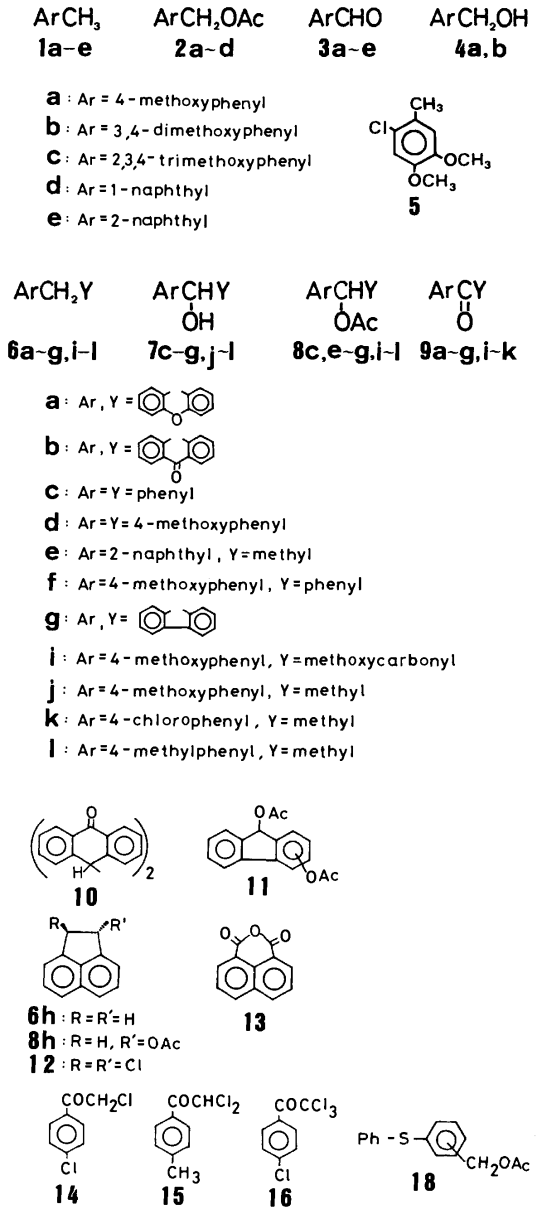

Table 1. Oxidations of Alkylarenes and Methylene Compounds with Mn(III)-Cl^- in AcOH

Entry	Substrate	Molar ratio[a]	Cl^- source	Temp °C	Time h	Recovery %	Product (Yield/%)[b] Acetate	Aldehyde or Ketone	Others
1	**1a**	1:4: 5	LiCl	100	46		**2a**(14)	**3a**(50)	
2	**1a**	1:4:10	LiCl	100	14		**2a**(27)	**3a**(53)	**4a**(9)
3	**1a**	1:4:10	LiCl	Reflux	1		**2a**(31)	**3a**(34)	
4	**1a**	1:4:15	LiCl	100	16		**2a**(18)	**3a**(41)	
5	**1a**	1:4:20	LiCl	100	6		**2a**(12)	**3a**(45)	
6	**1a**	1:4:10[c]	LiCl	100	7		**2a**(60)	**3a**(4)	
7	**1a**	1:4:10[d]	LiCl	100	2.5		**2a**(31)	**3a**(54)	
8	**1a**	1:4:10	KCl	Reflux	2.5		**2a**(66)	**3a**(15)	
9	**1a**	1:4:10	NH_4Cl	Reflux	0.8		**2a**(68)	**3a**(17)	
10	**1a**	1:4:10	$CaCl_2$	Reflux	0.7		**2a**(37)	**3a**(29)	
11	**1a**	1:4:10	NaCl	Reflux	2.5		**2a**(67)	**3a**(10)	
12	**1a**	1:4:10	$ZnCl_2$	Reflux	0.7		**2a**(35)	**3a**(14)	
13	**1b**	1:4:10	LiCl	100	2	6	**2b**(31)	**3b**(17)	**5** (5)
14	**1c**	1:4:10	LiCl	100	3.4		**2c**(34)	**3c**(26)	
15	**1d**	1:4:10	LiCl	100	27		**2d**(35)	**3d**(39)	
16	**1e**	1:4:10	LiCl	100	2			**3e**(8)[e]	
17	**6a**	1:4:10	LiCl	100	3.5	16		**9a**(70)	
18	**6b**	1:4:10	LiCl	100	4			**9b**(56)	**10**(10)
19	**6c**	1:4:10	LiCl	Reflux	4	53	**8c**(12)		
20	**6d**	1:4:10	LiCl	100	4.5			**9d**(61)	**7d**(23)
21	**6g**	1:4:10	LiCl	Reflux	2	25	**8g**(55) **11**(3)		
22	**6h**	1:4:10	LiCl	100	0.5		**8h**(36)		**12**(15) **13**(9)
23	**6i**	1:4:10	LiCl	Reflux	0.8		**8i** (76)	**9i** (11)	

a) Substrate: Mn(III): Cl^-. b) Yields are based on the substrate added. c) Ac_2O (20 cm^3) was added. d) Water (1 cm^3) was added. e) Isolated as a 2,4-DNP.

was conducted at various molar ratios of **1a**:Mn(III): LiCl until all Mn(III) was consumed, and the best yield for **3a** was attained when the molar was 1:4:10 (Table 1, Entry 2). When Ac_2O was added to the reaction medium, the yield of **3a** decreased (Entry 6). The addition of water did not cause any significant change in the yield (Entry 7). It was found that changing the Cl^- source affects the yield of the products in the reaction of **1a** (Entries 8—12). All other salts lowered the yield of **3a**, but increased that of **2a**. In a similar reaction with the manganese(III) acetate-Cl^- complex 3,4-dimethoxytoluene (**1b**) and 2,3,4-trimethoxytoluene (**1c**) gave the corresponding aldehydes (**3b** and **3c**) in poor yields (Entries 13 and 14). In the reaction of **1b** 2-chloro-4,5-dimethoxytoluene (**5**) was obtained in minor quantity. The reaction of 1-methyl- (**1d**) and 2-methylnaphthalene (**1e**) yielded the corresponding (acetoxymethyl)naphthalenes (**2d** and **2e**) and naphthalenecarbaldehydes (**3d** and **3e**).

Methylene Group Flanked by One or Two Aryl Groups. The reaction of xanthene (**6a**), anthrone (**6b**), and bis(4-methoxyphenyl)methane (**6d**) gave the corresponding carbonyl compounds (**9a**, **9b**, and **9d**) in moderate yields (Entries 17, 18, and 20) together with some other products (**7d** and **10**). Diphenylmethane (**6c**) and fluorene (**6g**) did not give ketonic products, but yielded acetates, **8c** and **8g**, respectively (Entries 19 and 21). Acenaphthene (**6h**) gave 1-acetoxyacenaphthene (**8h**), 1,2-dichloroacenaphthene (**12**), and 1,8-naphthalenedicarboxylic anhydride (**13**). The configuration of the chlorine atoms in **12** is determined as a trans, since the melting point and the IR and ^1H NMR spectrum of **12** were identical with those reported.[7]

Benzyl Alcohols. The reaction of 4-methoxybenzyl alcohol (**4a**) with the complex gave a mixture of **2a** and **3a**, the latter being predominant. 3,4-Dimethoxybenzyl alcohol (**4b**) yielded 3,4-dimethoxybenzaldehyde (**3b**) exclusively (Entry 25). Diphenylmethanol (**7c**) yielded a mixture of an acetate (**8c**) and benzophenone (**9c**). The presence of an electron-donating group, such as a methoxyl group in the aromatic ring, slightly increased the yield of the ketone, as shown in the reaction of (4-methoxyphenyl)phenylmethanol (**7f**) (Entry 28). The reaction of **7f** with manganese(III) acetate alone gave **8f** and **9f** in poor yields (Entry 29). The reaction of 1-(4-methoxyphenyl)ethanol (**7j**) yielded an acetate (**8j**) and 4′-methoxyacetophenone (**9j**), the latter being the major product (Entry 31). Similarly, 1-(4-chlorophenyl)ethanol (**7k**) gave an acetate (**8k**), 4′-chloroacetophenone (**9k**), and 2,4′-dichloroacetophenone (**14**). 1-(2-Naphthyl)ethanol (**7e**) yielded an acetate (**8e**) and 2-acetylnaphthalene (**9e**). The chlorination of acetophenones with the Mn(III)-Cl^- complex has already been reported to give α-chlorinated

Table 2. Oxidations of Benzyl Alcohols, Disulfides, and Phosphine with Mn(III)-LiCl in AcOH

Entry	Substrate	Molar ratio[a]	Temp °C	Time h	Recovery %	Product (Yield/%)[b] Acetate	Aldehyde or ketone	Others
24	**4a**	1:3:10	100	0.8		**2a**(6)	**3a**(70)	
25	**4b**	1:3:10	100	1			**3b**(71)	
26	**7c**	1:6:10	Reflux	8		**8c**(33)	**9c**(63)	
27	**7e**	1:3:10	Reflux	0.2	11	**8e**(28)	**9e**(29)	
28	**7f**	1:3:10	Reflux	0.2	21		**9f**(72)	
29	**7f**	1:3: 0	Reflux	9		**8f**(18)	**9f**(12)	
30	**7g**	1:3:10	Reflux	0.8			**9g**(80)	
31	**7j**	1:3:10	Reflux	0.2		**8j**(7)	**9j**(39)	
32	**7k**	1:3:10	Reflux	0.3	43	**8k**(11)	**9k**(18)	**14** (2)
33	**7l**	1:3:10	Reflux	0.3		**8l**(45)		**15** (10)
34	**17a**	1:4:10	Reflux	3	11			**19a**(76)
35	**17a**	1:4: 0	Reflux	7	55	**18**(28)		
36	**17b**	1:4:10	Reflux	6	9			**19b**(21)
37	**20**	1:4:10	Reflux	46				**21** (97)

a) Substrate: Mn(III): LiCl. b) Yields are based on the substrate added.

acetophenones.[5]

Sulfides and Triphenylphosphine. The reaction of diphenyl sulfide (**17a**) with the complex yielded diphenyl sulfoxide (**19a**) in good yield (Entry 34). The reaction of **17a** with manganese(III) acetate in the absence of Cl^- ions gave an acetate (**18**) in 28% yield and a large amount of **16a** was recovered unchanged (Entry 35). Dibenzothiophene (**17b**) afforded dibenzothiophene oxide (**19b**) in 21% yield (Entry 36). The reaction of triphenylphosphine (**20**) gave triphenylphosphine oxide (**21**) in excellent yield (Entry 37).

Discussion

The oxidation of alkylarenes with manganese(III) acetate afforded aldehydes in minor quantities.[8] The addition of alkali halides as catalysts has been reported to improve the yields of carbonyl compounds.[9] However, these reactions were carried out primarily for mechanistic studies using a large excess of the substrate. By contrast, we used a large amount of the manganese(III) acetate–Cl^- complex compared with those in the previous studies.[6,9] Methoxy-substituted toluenes and methylnaphthalenes gave the corresponding aldehydes in 8 to 54% yields, which are better than those reported. When the acetoxymethyl derivative is stable towards Mn(III)-Cl^-, the yields of the aldehydes are not sufficiently high. The oxidation of benzyl alcohols, on the other hand, gave better yields of the aldehydes.

The oxidation of methylene compounds (**6a—d,g**) with the complex gave ketonic compounds in good yields, except for diphenylmethane (**6c**) and fluorene (**6g**). Secondary benzyl alcohols (**7c**, **7f**, and **7g**) also gave the corresponding ketones (**9c**, **9f**, and **9g**). However, the reaction of 1-arylethanols (**7k** and **7l**) gave α-chlorinated ketones (**14** and **15**) along with an aryl methyl ketone (**9k**) and acetates (**8k** and **8l**) and seems to have a less synthetic value.

Gilmore and Mellor[10] have proposed that the potassium bromide-catalyzed oxidation of toluenes using manganese(III) acetate proceeds via radical intermediates. The reaction of norbornene with manganese(III) acetate–$CaCl_2$ gave no rearranged products, suggesting that the radical process is conceivable.[2] However, it is known that the reaction of manganese(III) acetate with aromatic compounds having relatively lower ionization potentials readily takes place via an electron-transfer process.[8] It was found that the reaction of manganese(III) acetate–Cl^- gave a better yield of the aldehyde in the absence of Ac_2O, which normally facilitates a free-radical process; the addition of water has no appreciable effect on the product distribution. We also found that the presence of electron-donating groups in the aromatic rings changes the product distribution in favor of ketonic compounds, as can be seen in the cases of **6a** and **6d**; also, methyl (4-methoxyphenyl)acetate (**6i**) yielded α-acetoxy ester (**8i**) and methyl (4-methoxyphenyl)-glyoxylate (**9i**), while ethyl phenylacetate, which may have a higher ionization potential than **6i**, was totally unreactive.[4] These facts suggest that the reaction of aromatic substrates of lower ionization potentials may proceed via an electron-transfer mechanism (path A in Scheme 1), although the mechanism need not to be operating in all reactions. The benzyl radical (B), once formed, is further oxidized to the benzyl cation (C), as shown in Scheme 1. The benzyl cation (C) is then combined with a chloride ion, acetate ion, and water molecule to give chloro derivatives, acetates, and alcohols, respectively. The substitution of the benzylic chlorine by an acetate ion should be very fast to give the acetate. Although it has been reported that methyl-substituted benzyl acetate is less reactive towards

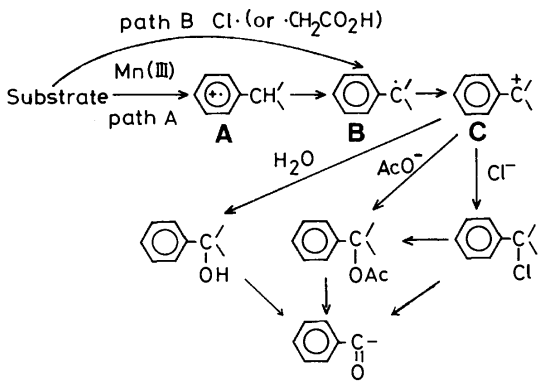

Scheme 1.

manganese(III) acetate than methoxytoluene,[8] the acetates in the reactions can still be oxidized in a similar process to give carbonyl componds. In harmony with the above-mentioned mechanism, 4-methoxybenzyl chloride was readily converted to 4-methoxybenzyl acetate (**2a**, 77%) through a treatment with manganese(II) acetate in AcOH at 100 °C for 50 min; in turn, **2a** was converted to **3a** (45%) by oxidation with the manganese(III) acetate-Cl^- complex at 100 °C in 9 h. A direct oxidation of the benzyl alcohols to the carbonyl compounds is indicated by its faster reaction time (0.8 h at 100 °C) than methyl and methylenes. The route from benzyl chloride to the carbonyl compounds could not be ruled out.

Conclusion

Aldehydes and ketones have been obtained in minor quantities in the reaction of alkylarenes with manganese(III) acetate. We found that when a large excess of the manganese(III) acetate-Cl^- complex is used, the aldehydes and ketones become the major product. Moreover, the primary and secondary benzyl alcohols give the corresponding carbonyl compounds in excellent yields. Sulfoxide and phosphine oxide are also prepared by the reaction of the complex. These reactions can be useful in organic syntheses.

Experimental

Measurements. All of the ^1H NMR spectra (60 MHz) were taken with a Hitachi Perkin-Elmer R-24 and a JMN PMX-60SI NMR spectrometer with tetramethylsilane as the internal standard. The IR spectra were measured in chloroform solutions on a JASCO A-102 IR spectrometer. The mass spectra were obtained on a JMS-O1SG-2 instrument. The melting points were determined with a Yanagimoto micromelting point apparatus and were not corrected.

Materials. Methoxytoluenes (**1a—c**), xanthene (**6a**), diphenylmethanes (**6c** and **6d**), fluorene (**6g**) were obtained from the corresponding aldehydes and ketones by Wolff-Kischner reduction.[11] Methylnaphthalenes (**1d** and **1e**), anthrone (**6b**), acenaphthene (**6h**), and triphenylphosphine (**20**) were commercially available from Wako Pure Chemical Industories. Diphenyl sulfide (**17a**) and dibenzothiophene (**17b**) were purchased from Tokyo Kasei Co., Ltd. Methyl (4-methoxyphenyl)acetate (**6i**) was prepared from the acid by esterification. Primary and secondary alcohols (**4a**, **4b**, **7c**, **7e—g**, and **7j—k**) were prepared by the sodium borohydride reduction[12] of the corresponding aldehydes and ketones.

Reactions of Manganese(III) Acetate in the Presence of Chloride Ions. The typical procedure for the oxidation of manganese(III) acetate in the presence of chloride ions is as follows. To a heated solution of manganese(III) acetate, $[Mn_3O(OAc)_6(OAc)(HOAc)]\cdot 5H_2O$,[13] (3—4 milliequivalents for Mn(III)) and Cl^- (10 mmol) in AcOH a substrate (1 mmol) was added. The mixture was then heated under reflux until the dark-brown color turned opaque white. The reaction mixture was diluted with water (60 cm^3) and then extracted with benzene (30 cm^3) twice. The combined benzene solution was washed with aqueous sodium hydrogencarbonate solution and then evaporated in vacuo. The resulting products were purified on TLC with either benzene or chloroform as the eluting solvent, and recrystallized or distilled. The yields are summarized in Tables 1 and 2. The structures of the products were determined by means of IR, ^1H NMR, and mass spectra. Known compounds were also identified by comparisons of their melting points with those reported in the literature and with authentic samples.

Oxidation Products. 4-Methoxybenzyl Acetate (2a): Liquid. **3,4-Dimethoxybenzyl Acetate (2b)**: Liquid. **2,3,4-Trimethoxybenzyl Acetate (2c)**: Liquid; IR ν (cm^{-1})=1732 (>C=O); ^1H NMR (CCl_4) δ=1.98 (3H, s, OAc), 3.78 (3H, s, OCH_3), 3.87 (3H, s, OCH_3), 3.94 (3H, s, OCH_3), 4.95 (2H, s, $-CH_2-$), 6.52 (1H, d, J=7.8 Hz, H-5), 6.89 (1H, d, J=7.8 Hz, H-6). Found: m/z=240.1001. Calcd for $C_{12}H_{16}O_5$: M, 240.0998. **1-(Acetoxymethyl)naphthalene (2d)**: Liquid. **4-Methoxybenzaldehyde (3a)**: Liquid. **3,4-Dimethoxybenzaldehyde (3b)**: Mp 41—42 °C. **2,3,4-Trimethoxybenzaldehyde (3c)**: Liquid. **1-Naphthalenecarbaldehyde (3d)**: Liquid. **2-Naphthalenecarbaldehyde (3e)**: **2,4-Dinitrophenylhydrazone**, mp 271 °C (lit,[14] mp 270—271 °C). **4-Methoxybenzyl Alcohol (4a)**: Liquid. **6-Chloro-3,4-dimethoxytoluene (5)**:[15] Liquid; ^1H NMR ($CDCl_3$) δ=2.28 (3H, s, CH_3), 3.82 (6H, s, 2×OCH_3), 6.68 (1H, s, H-2), 6.82 (1H, s, H-5). **Bis(4-methoxyphenyl)methanol (7d)**: Mp 71—72 °C (lit,[16] mp 72 °C). **Diphenylmethyl Acetate (8c)**: Liquid (lit,[17] mp 40.5—41.5 °C). **1-(2-Naphthyl)ethyl Acetate (8e)**: Liquid (lit,[18] bp 130 °C/120 Pa). **(4-Methoxyphenyl)phenylmethyl Acetate (8f)**: Liquid (lit,[19] bp 158 °C/119.7 Pa). **9-Fluorenyl Acetate (8g)**: Mp 68—69 °C (lit,[20] mp 68.5—69 °C). **1-Acetoxyacenaphthene (8h)**: Liquid (lit,[21] bp 166—168 °C/665 Pa). **Methyl α-Acetoxy(4-methoxyphenyl)acetate (8i)**: Liquid;[4] IR ν (cm^{-1})=1742 (-COO-); ^1H NMR (CCl_4) δ=2.09 (3H, s, OAc), 3.64 (3H, s, OCH_3), 3.75 (3H, s, OCH_3), 5.79 (1H, s, >CH-), 6.78 (2H, m, H-3′ and H-5′), and 7.29 (2H, m, H-2′ and H-6′). Found: m/z=238.0884. Calcd for $C_{12}H_{14}O_5$: M, 238.0837. **1-(4-Methoxyphenyl)ethyl Acetate (8j)**: Liquid (lit,[18] bp 153—154 °C/3.59×10^3 Pa). **1-(4-Chlorophenyl)ethyl Acetate (8k)**: Liquid (lit,[18] bp 88 °C/146 Pa). **1-(4-Methylphenyl)ethyl Acetate (8l)**: Liquid (lit,[18] 105—106 °C/2.79×10^3 Pa). **9-Xanthenone (9a)**: Mp 172—174 °C. **9,10-Anthraquinone (9b)**: Mp 279—280 °C. **Benzophenone (9c)**: Mp 48 °C. **4,4′-Dimethoxybenzophenone (9d)**: Mp 142—143 °C. **2-Acetylnaphthalene (9e)**: Mp 51—52 °C.

4-Methoxybenzophenone (9f): Mp 58—59 °C. **9-Fluorenone (9g)**: Mp 83—84 °C. **Methyl (4-Methoxyphenyl)glyoxylate (9i)**: Mp 49—50 °C (lit,[22] mp 54 °C); IR ν (cm^{-1})=1675 (>C=O); ^1H NMR ($CDCl_3$) δ=7.94—7.79 (2H, m, H-2′ and H-6′), 6.92—6.77 (2H, m, H-3′ and H-5′), 3.84 (3H, s, OCH_3), 3.82 (3H, s, OCH_3). **4′-Methoxyacetophenone (9j)**: Mp 33—34 °C. **4′-Methylacetophenone (9k)**: Liquid. **10,10′-Bianthrone (10)**: Mp 261—263 °C (lit,[23] mp 235—250 °C). **Diacetoxyfluorene (11)**: Liquid; IR ν (cm^{-1})=1732 (OAc); ^1H NMR ($CDCl_3$) δ=7.70—6.94 (7H, m, arom. H), 6.71 (1H, s, >CH-), 2.29 (3H, s, OAc), 2.16 (3H, s, OAc). Found: m/z=282.0861. Calcd for $C_{17}H_{14}O_4$: M, 282.0892. ***trans*-1,2-Dichloroacenaphthene (12)**: Mp 66 °C (lit,[7] mp 66.5—68 °C). **1,8-Naphthalenedicarboxylic Anhydride (13)**: Mp 267 °C. **2,4′-Dichloroacetophenone (14)**: Mp 99 °C (lit,[24] mp 100—101 °C). **2,2-Dichloro-4′-methylacetophenone (15)**: Liquid (lit,[25] bp 110 °C/1.33×10^3 Pa). **(Acetoxymethyl)-phenyl Phenyl Sulfides (18)**: Isomer ratio 9.8:7.0; Liquid; IR ν (cm^{-1})=1732 (OAc); ^1H NMR ($CDCl_3$) δ=1.91 (3H, s, OAc), 1.97 (3H, s, OAc), 4.94 (2H, s, $-CH_2-$), 5.13 (2H, s, $-CH_2-$), 7.03—7.54 (18H, m, ar. H); MS m/z (rel intensity)=258 (M^+, 100), 215 (23), 197 (79), 137 (42). Found: m/z=258.0687. Calcd for $C_{15}H_{14}O_2S$: M, 258.0715. **Diphenyl Sulfoxide (19a)**: Mp 70 °C (lit,[26] mp 71 °C). **Dibenzothiophene Oxide (19b)**: Mp 183 °C (lit,[27] mp 183.5—184.5 °C). **Triphenylphosphine Oxide (21)**: Mp 152—153 °C (lit,[28] mp 154—155 °C).

4-Methoxybenzyl Acetate (2a) from 4-Methoxybenzyl Chloride. A mixture of 4-methoxybenzyl chloride (1 mmol), manganese(II) acetate tetrahydrate (8 mmol), and lithium chloride (10 mmol) in acetic acid (25 cm^3) was heated at 100 °C for 50 min. After working up in a manner similar to that for the above, 4-methoxybenzyl acetate (**2a**) was obtained in 77% yield.

Oxidation of 4-Methoxybenzyl Acetate (2a) with Manganese(III)-Cl^-. A mixture of 4-methoxybenzyl acetate (**2a**) (1 mmol), manganese(III) acetate (2 mmol), lithium chloride (10 mmol) in acetic acid (25 cm^3) was heated at 100 °C for 9 h. After working up in a manner similar to that mentioned above, the resulting mixture was chromatographed on TLC with chloroform as the eluting solvent to give 4-methoxybenzaldehyde (**3a**) (45%) and *p*-anisic acid (5%) with 4% recovery of **2a**.

We wish to thank Professor Hitoshi Takeshita and Associate Professor Akira Mori of the Research Institute of Industorial Science, Kyushu University for their kind arrangement for measuring mass spectra.

References

1) M. Okano, T. Kinoshita, Y. Muramoto, and T. Aratani, *Nippon Kagaku Kaishi*, **1978**, 578.
2) K. D. Donnely, W. E. Fristad, B. J Gellerman, J. R. Peterson, and B. J. Selle, *Tetrahedron Lett.*, **25**, 607 (1984).
3) H. Yonemura, H. Nishino, and K. Kurosawa, *Bull. Chem. Soc. Jpn.*, **59**, 3153 (1986).
4) H. Yonemura, H. Nishino, and K. Kurosawa, *Bull. Chem. Soc. Jpn.*, **60**, 809 (1987).
5) T. Tsuruta, T. Harada, H. Nishino, and K. Kurosawa, *Bull. Chem. Soc. Jpn.*, **58**, 142 (1985).
6) R. E. van der Ploeg, R. W. de Korte, and E. C. Kooyman, *J. Catal.*, **10**, 52 (1968).
7) S. J. Cristol, F. R. Stermits, and P. S. Ramey, *J. Am. Chem. Soc.*, **78**, 4939 (1956).
8) P. J. Andrulis, Jr., M. J. S. Dewar, R. Dietz, and R. L. Hunt, *J. Am. Chem. Soc.*, **88**, 5473 (1966).
9) A. Chaintreau, G. Adrian, and D. Couturier, *J. Org. Chem.*, **46**, 4562 (1981).
10) J. R. Gilmore and J. M. Mellor, *Chem. Commun.*, **1970**, 507.
11) H. H. Szmant, *Angew. Chem., Int. Ed. Engl.*, **7**, 120 (1968).
12) S. W. Chaikin and W. G. Brown, *J. Am. Chem. Soc.*, **71**, 122 (1949).
13) L. W. Hessel and C. Romers, *Recl. Trav. Chim. Pays-Bas*, **88**, 545 (1969).
14) G. D. Johnson, *J. Am. Chem. Soc.*, **75**, 2720 (1953).
15) J. M. Gess and C. W. Dence, *Tappi*, **1971**, 54; *Chem. Abstr.*, **75**, 78322z (1971).
16) P. D. Bartlett and J. D. McCollum, *J. Am. Chem. Soc.*, **78**, 1441 (1956).
17) B. K. Mores and D. S. Tarbell, *J. Am. Chem. Soc.*, **74**, 416 (1952).
18) R. Taylor, G. G. Smith, and W. H. Wetzel, *J. Am. Chem. Soc.*, **84**, 4817 (1962).
19) C. A. Bunton and T. Hadwick, *J. Chem. Soc.*, **1957**, 3043.
20) G. F. Hennion and B. R. Fleck, *J. Am. Chem. Soc.*, **77**, 3253 (1955).
21) J. Cason, *Org. Synth.*, Coll. Vol. III, 3 (1955).
22) K. Freudenberg, C-L. Chen, and G. Cardinale, *Chem. Ber.*, **95**, 2814 (1962).
23) R. Van Helden and E. C. Kooyman, *Recl. Trav. Chim. Pays-Bas*, **80**, 57 (1961).
24) F. Bergmann, A. Kalmus, and E. Breuer, *J. Am. Chem. Soc.*, **79**, 4178 (1957).
25) S. K. Moitra, A. N. Ganguli, N. N. Chakravarti, and R. N. Adhya, *Tetrahedron Lett.*, **1971**, 199.
26) H. Rheinboldt and E. Giesbrecht, *J. Am. Chem. Soc.*, **68**, 2671 (1946).
27) A. H. Schlesinger and D. T. Mowry, *J. Am. Chem. Soc.*, **73**, 2614 (1951).
28) H. Staudinger and E. Hauser, *Helv. Chim. Acta*, **4**, 861 (1921).

 © 1989 The Chemical Society of Japan Bull. Chem. Soc. Jpn., 62, 3572—3576 (1989) [Vol. 62, No. 11

The β-Sheet Structure-Stabilizing Potential of Twenty Kinds of Amino Acid Residues in Protected Peptides[1)]

Mitsuaki NARITA* and Yoshihisa KOJIMA
Department of Industrial Chemistry, Faculty of Technology, Tokyo University of Agriculture and Technology, Koganei 184
(Received June 14, 1989)

A host-guest approach was devised to investigate the β-sheet structure-stabilizing potential of the 20 common amino acid residues in protected peptides where functional groups in side chains were protected by suitable groups commonly used in peptide synthesis. The potential was evaluated using solvent-titration curves for the disruption of the β-sheet structure of cross-linked polystyrene resin-bound host-guest hexa- and octapeptides in CH_2Cl_2 by HFIP. The β-sheet structure of host-guest hexapeptides, Boc-Val-Ile-X_2-Val-Ile-$NHCH_2$-resins, in which X stands for guest amino acid residues, was disrupted in CH_2Cl_2 by adding increasing amounts of HFIP; the disrupted behaviors were strongly dependent on the nature of guest amino acid residues. A scale for the β-sheet structure-stabilizing potential of the 20 kinds of amino acid residues in CH_2Cl_2 could be derived at 0.25 M of HFIP concentration as follows: Ile, Val ≫ Asn > His(Tos) or His, Gln, Cys(Bzl), Tyr(Bzl) > Phe, Gly, Lys(Z), Arg(Tos), Leu > Thr(Bzl), Ala, Met(O), Glu(OBzl), Trp(CHO) ≫ Ser(Bzl), Asp(OBzl) ≫ Pro. To confirm the scale, their β-sheet structure-stabilizing potential was further examined using host-guest octapeptides, Boc-X_2-Val-Ile-X_2-Val-Ile-$NHCH_2$-resins. The disrupted behaviors of the octapeptides having Gly, Ala, and Thr(Bzl) residues as guests were remarkably different from those of the corresponding hexapeptides; the β-sheet structure-stabilizing potential of the Gly, Ala, and Thr(Bzl) residues became significantly high with an increase in their ratios to host residues. The potential of the Gly, Ala, and Thr(Bzl) residues appears to reflect the ratios of guest amino acid residues to hosts, the repeated sequence, and/or neighbor interactions in the sequence. The significance of the present study in the design of synthetic routes for peptides and proteins is briefly discussed.

One of the most serious obstacles in peptide and protein syntheses is the insolubility of protected peptides in organic solvents, which causes difficulty in successive reactions. In previous papers[2,3)] we proposed a predictive method for the solubility of protected peptides in the highly polar solvents commonly used in peptide synthesis and showed its usefulness for the design of synthetic routes for peptides and proteins. In the method we assumed that the insolubility of protected peptides was caused by a β-sheet aggregation consisting of peptide segments, i.e., sequence units separated by tertiary peptide bonds,[2,4)] as long as or larger than an octa- or nonapeptide sequence and that the β-sheet structure-forming potential of peptide segments was estimated using their average coil conformation $\langle P_c \rangle$ values when a peptide segment is smaller than the critical chain length for the development of a stable helix in the solid state. In the solubility prediction for protected peptides,[2)] the $\langle P_c \rangle$ value was practically not used for a peptide segment but was used for a whole peptide; the adequacy of the above assumption was widely confirmed by the application of the solubility prediction method to various kinds of oligopeptides.[2-8)] Here, the $\langle P_c \rangle$ value of a protected peptide is defined as an arithmetic average of coil conformational parameters, P_c, of the amino acid residues composing the protected peptide. As mentioned in a previous paper,[9)] $\langle P_c \rangle$ values of protected peptides must reflect their β-sheet structure-forming potential because the P_c parameters were determined on the basis of three-dimensional structures of 29 kinds of native globular proteins[2)] and must reflect the nature of the 20 kinds of amino acid residues in native globular proteins. However, it should be emphasized that the P_c parameters are not for the 20 kinds of amino acid residues in protected peptides but for those in native globular proteins. Thus, for the solubility prediction of protected peptides in organic solvents, it is essentially important to evaluate the P_c parameters for the 20 kinds of amino acid residues in protected peptides in organic solvents. Especially, the P_c parameters for amino acid residues having functional groups in side chains should be determined for side chains-protected amino acid residues.

For the solubility prediction of protected peptides, it is also important to evaluate their helix-forming potential when they are at a sufficient peptide chain length for the development of a stable helix in the solid state, since their β-sheet → helix conformational transformation results in a remarkable solubility improvement.[6,10)] In previous papers[9,11,12)] we showed that the average helix and β-sheet conformation values, $\langle P_\alpha \rangle$ and $\langle P_\beta \rangle$, of protected peptides are useful for estimating their potential for the β-sheet → helix transformation with an increasing peptide chain length or with an application of strong shear stress. Again, $\langle P_\alpha \rangle$ and $\langle P_\beta \rangle$ values of protected peptides are defined as arithmetic averages of the helix and β-sheet conformational parameters (P_α and P_β) of the amino acid residues composing them, respectively, which are determined by Chou and Fasman on the basis of three-dimensional structures of 15 kinds of native globular proteins.[13)] It should again be

emphasized that, for the solubility prediction of protected peptides, it is essentially important to evaluate the conformational parameters (P_α and P_β) for the 20 kinds of amino acid residues in protected peptides where functional groups in side chains are protected by suitable groups commonly used in peptide synthesis.

In a recent study[9,14,15] we found that a β-sheet structure of a variety of resin-bound peptides was easily disrupted by adding increasing amounts of HFIP and that the stability of the β-sheet structure was strongly dependent on the amino acid composition of protected peptides. The result suggests that the investigation into the disruption of the β-sheet structure of resin-bound host-guest peptides by HFIP makes it possible to evaluate the β-sheet structure-stabilizing potential of guest amino acid residues in protected peptides. A host-guest approach was introduced by Mutter and coworkers[16] to explore the relationship between the sequence and the secondary structure of protected peptides; it was shown to be useful for the evaluation of the conformational preference of guest amino acid residues in host-guest peptides. Thus, in the present study, the cross-linked polystyrene resin-bound host-guest peptides are designed to be suitable for the evaluation of the β-sheet structure-stabilizing potential of the 20 kinds of guest amino acid residues in protected peptides in CH_2Cl_2. The designed host-guest peptides have a sequence of Boc-Val-Ile-X_2-Val-Ile-$NHCH_2$-resin and Boc-X_2-Val-Ile-X_2-Val-Ile-$NHCH_2$-resin, in which X stands for guest amino acid residues as follows: Ala, Arg(Tos), Asn, Asp(OBzl), Cys(Bzl), Gln, Glu(OBzl), Gly, His(Tos) or His, Ile, Leu, Lys(Z), Met(O), Phe, Ser(Bzl), Thr(Bzl), Trp(CHO), Tyr(Bzl), and Val.

Experimental

Materials. Copoly(styrene-1% divinylbenzene) beads of 200—400 mesh, Bio-Beads S-Xl, were purchased from Bio-Rad Laboratories. The aminomethylation was carried out according to a method described in the literature.[17] The aminomethyl content was 66 μmol g^{-1} of resin. The synthesis of the host-guest peptide resins was performed in CH_2Cl_2 substantially according to the general procedures described previously.[12] For the assembly of host-guest peptides, Boc-Val-Ile-OH and Boc-X-OH were used as carboxyl components and the coupling reactions were carried out using DCC and HOBt as coupling reagents.[18] After a double coupling reaction, the completion of the reaction was checked by a ninhydrin test. When the test was positive, a small amount of HFIP (5 vol% to CH_2Cl_2) was added and the reaction was continued an additional day. When the test was still positive, a triple coupling reaction was performed to force the coupling reaction to completion. A termination reaction using pyridine and acetic anhydride was not performed. Acid hydrolyses of host-guest peptide resins were carried out with propionic acid /12 M HCl (2/1 v/v) (1 M=1 mol dm^{-3}) at 115 °C for 10 days.[19] The amino acid ratios except for Ser, Thr, and Trp residues of acid hydrolysates were in agreement with the calculated values. Acid hydrolyses host-guest peptide resins having Ser(Bzl), Thr(Bzl), and Trp(CHO) residues as guests were examined with propionic acid/3 M TosOH (2/1 v/v) at 115 °C for 10 days;[20] however, they did not proceed sufficiently.

IR Absorption Spectra Measurements. The IR absorption spectra of resin-bound peptides were recorded at room temperature with a JEOL Model JIR-100 FT-IR spectrometer. IR measurements in the swollen state were performed by holding the samples between potassium bromide windows after resin-bound peptides were swollen in CH_2Cl_2 containing a variety of molar concentrations of HFIP.

Results

The host-guest hexa- and octapeptides were prepared by a general procedure[12] and the addition of HFIP in a coupling reaction in CH_2Cl_2 was significantly effective for its completion. The IR absorption spectra of the resin-bound host-guest hexa- and octapeptides swollen in CH_2Cl_2 alone showed strong bands around 3280 cm^{-1} in the amide A region and around 1630 cm^{-1}

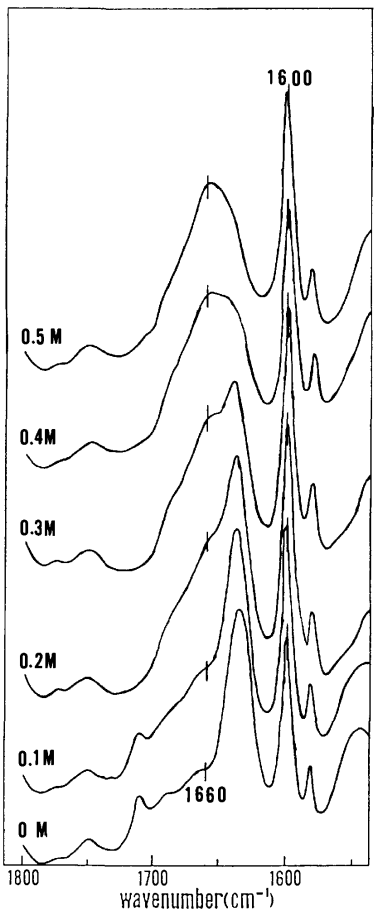

Fig. 1. IR absorption spectra of a resin-bound host-guest hexapeptide (X=Phe) in CH_2Cl_2 containing a variety of molar concentrations of HFIP. The numerals in Fig. 1 indicate molar concentrations of HFIP.

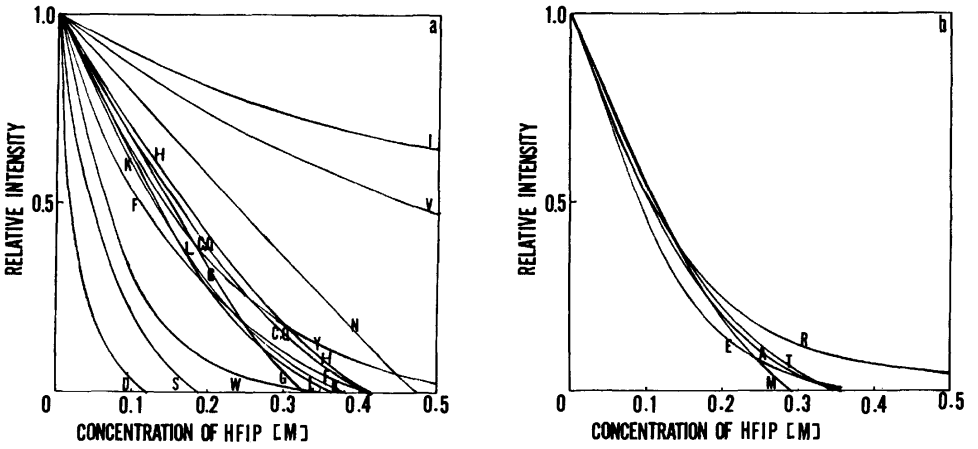

Fig. 2. The solvent-titration curves of resin-bound hexapeptides in CH_2Cl_2 using HFIP as a titrating solvent. A guest amino acid residue for each titration curve is shown in Fig. 2 using a one-letter symbol.[23] a: I=Ile, V=Val, N=Asn, H=His(Tos) or His, C=Cys(Bzl), Q=Gln, Y=Tyr(Bzl), F=Phe, K=Lys(Z), L=Leu, G=Gly, W=Trp(CHO), S=Ser(Bzl), and D=Asp(OBzl) and b: R=Arg(Tos), T=Thr(Bzl), A=Ala, M=Met(O), and E=Glu(OBzl).

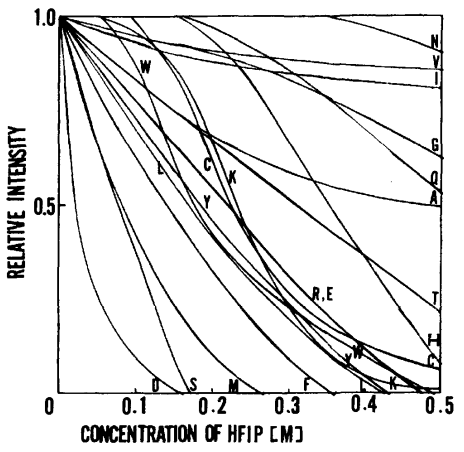

Fig. 3. The solvent-titration curves of resin-bound octapeptides in CH_2Cl_2 using HFIP as a titrating solvent. A guest amino acid residue for each titration curve is shown in Fig. 3 using a one-letter symbol.[23]

in the amide I region, assigned to a β-sheet structure,[12,21] and were accompanied with a weak band around 1660 cm^{-1} (Fig. 1, 0 M), probably assigned to an unordered structure. The disruption of the β-sheet structure by HFIP was investigated using a solvent titration method.[22] It was monitored by a successive decrease in the intensity of the band around 1630 cm^{-1}, together with a successive addition of HFIP. Figure 1 shows the typical IR absorption spectra of resin-bound host-guest hexapeptide (X=Phe) in CH_2Cl_2 containing a variety of molar concentrations of HFIP. The solvent-titration curves of the resin-bound host-guest hexa- and octapeptides in CH_2Cl_2 using HFIP as a titrating solvent are depicted in Figs. 2 and 3, respectively. The relative intensities of the bands around 1630 cm^{-1} shown in Figs. 2 and 3 were obtained using the band at 1603 cm^{-1} due to the aromatic ring of a polystyrene resin support as a standard and were normalized to be 1.0 for each relative intensity in CH_2Cl_2 alone. The relative intensities before the normalization reflected the difference in the intensities of 1660 cm^{-1}-band of host-guest peptide resins and dereased together with an increase in the intensities of the 1660 cm^{-1}-band, indicating the β-sheet structure-forming potential of guest amino acid residues in the resin-bound host-guest peptides. As shown in Figs. 2 and 3, a successive addition of HFIP induced a dramatic decrease in the strong band around 1630 cm^{-1} and an increase in the broad band around 1660 cm^{-1}, indicating that the β-sheet aggregation of the resin-bound hexa- and octapeptides was easily disrupted by increasing the amounts of HFIP.

Discussion

For the evaluation of the β-sheet structure-stabilizing potential of guest amino acid residues in resin-bound host-guest peptides, the completion of a coupling reaction is indispensable at each peptide chain elongation, and the addition of HFIP in a coupling reaction was significantly effective for the quantitative reaction due to the strong β-sheet structure-disrupting potential of HFIP. For the assembly of host-guest peptides, DCC and HOBt were used as coupling reagents. Thus, it is uncertain for the His(Tos) residue to be incorporated in host-guest peptides as a His(Tos) or a His residue since the protecting Tos group for the His residue may be removed by HOBt under the reaction condition.[24] Host-guest peptide resins must also be designed to be

suitable for the evaluation of the β-sheet structure-stabilizing potential of guest amino acid residues. C^{β}-Branched Ile and Val residues are expected to stabilize the β-sheet structure of peptides,[9,13] and the sequence of Ile–X_2–Val resists helix formation due to the repulsion between Ile and Val residues in a helix.[11,14] Thus, host-guest peptides having the sequences of –Val–Ile–X_2–Val–Ile– and –X_2–Val–Ile–X_2–Val–Ile– are suitable for an evaluation of the β-sheet structure-stabilizing potential of guest amino acid residues. In fact, as shown in Fig. 2, the β-sheet structure-disrupted behaviors of resin-bound hexapeptides by HFIP were strongly dependent on the nature of guest amino acid residues. The scale for the β-sheet structure-stabilizing potential of the 20 kinds of guest amino acid residues in hexapeptides can be derived at 0.25 M of the HFIP concentration as follows:

Ile, Val≫Asn>His(Tos) or His, Gln, Cys(Bzl), Tyr(Bzl)>Phe, Gly, Lys(Z), Arg(Tos), Leu>Thr(Bzl), Ala, Met(O), Glu(OBzl), Trp(CHO)≫Ser(Bzl), Asp(OBzl)≫Pro.

The conformational behavior of peptide resins having Pro residues as guests is expected to be different from that of any other one due to the absence of an N–H bond in the Pro residue in peptides;[2,4,15,25] it is obvious that a Pro residue has the lowest β-sheet structure-stabilizing potential in the 20 kinds of amino acid residues. A scale for the β-sheet structure-stabilizing potential of the 20 kinds of guest amino acid residues in octapeptides (Fig. 3) can also be derived at 0.25 M of the HFIP concentration as follows:

Asn, Gln, Val, Ile, Gly, His(Tos) or His≫Ala, Thr(Bzl)≫Glu(OBzl), Arg(Tos), Lys(Z), Cys(Bzl), Tyr(Bzl), Trp(CHO), Leu, Phe≫Met(O), Ser(Bzl), Asp(OBzl)≫Pro.

The disrupted behaviors of the octapeptides having Gly, Ala, and Thr(Bzl) residues as guests are remarkably different from those of the corresponding hexapeptides, and the β-sheet structure-stabilizing potential of the Gly, Ala, and Thr(Bzl) residues becomes significantly high with an increase in their ratios to host residues. The potential appears to reflect the ratios of guest amino acid residues to hosts, the repeated sequence, and/or neighbor interactions in the sequence strongly. The Asn, Gln, and His(Tos) residues in octapeptides also have the same tendency that they stabilize the β-sheet structure of octapeptides.

Here, it is interesting to compare the scale for the β-sheet structure-stabilizing potential of guest amino acid residues in the hexapeptides with the β-sheet structure conformational parameters, P_{β}, obtained by Chou and Fasman,[13] although the media supporting peptide conformations are different from each other (the former, CH_2Cl_2 and the latter, water). The order of the P_{β} parameters is as follows: Met (1.67), Val (1.65), Ile (1.60)≫Cys (1.30), Tyr (1.29), Phe (1.28)>Gln (1.23), Leu (1.22), Thr (1.20), Trp (1.19)≫Ala (0.97), Arg (0.90)>Gly (0.81), Asp (0.80)>Lys (0.74), Ser (0.72), His (0.71), Asn (0.65), Pro (0.62)≫Glu (0.26). For Met(O), Trp(CHO), Arg(Tos), Gly, Lys(Z), His(Tos), Asn, and Glu(OBzl) residues, the former is remarkably different from the latter. Especially, Met(O), Trp(CHO), Arg(Tos), Lys(Z), and Glu(OBzl) residues strongly reflect the influence of their protecting groups and/or media supporting conformations on their β-sheet structure-stabilizing potential. The side-chain protection of Arg, Lys, and Glu residues stabilizes the β-sheet structure of host-guest peptides, while that of Met and Trp residues destabilizes it. Considering the easy disruption of the β-sheet structure of Boc–Val–Gly–Phe–Gly–Leu–Ile–Leu_2–OBzl[26] and Boc–(Val–Gly–Phe–Gly–Leu–Ile–Leu_2)$_n$–Ala–$NHCH_2$–resin (n=1, 2, and 3)[14] by HFIP, the Gly residue in the host-guest hexapeptide appears to reflect the influence of the sequence. It may have a much less stabilizing potential. For Val, Ile, Cys(Bzl), Tyr(Bzl), Phe, Gln, Leu, Thr(Bzl), Ala, Asp(OBzl), and Ser(Bzl) residues, the former is in fair accordance with the latter. As discussed in a previous paper,[9] the P_{β} parameters are assumed to reflect the nature for the β-sheet structure-stabilizing potential of the 20 kinds of corded amino acid residues in native globular proteins. On the other hand, the relative intensities of the 1630 cm^{-1}-band to the 1603 cm^{-1}-band of the host-guest hexapeptides in CH_2Cl_2 alone (data not shown) are assumed to reflect the β-sheet structure-forming potential of the 20 kinds of guest amino acid residues in protected peptides in CH_2Cl_2. A scale for the β-sheet structure-forming potential in the hexapeptides in CH_2Cl_2 alone can be derived: Arg(Tos)>Lys(Z)>Cys(Bzl)>Ile, Val, Leu>Ala, Met(O), Trp(CHO)>Glu(OBzl), Thr(Bzl)>Gly, His(Tos) or His, Phe, Tyr(Bzl)>Gln, Asn>Asp(OBzl), Ser(Bzl). Clearly, the β-sheet structure-forming potential is different from the β-sheet structure-stabilizing potential, and the forming potential of Arg(Tos), Lys(Z), and Cys(Bzl) residues is larger than that of Ile and Val residues.

For the design of synthetic routes for peptides and proteins, an estimation of the β-sheet structure-disrupted behaviors of protected peptides in organic solvents is essentially important since the insolubility of protected peptides due to the β-sheet aggregation causes difficulty in successive reactions. The present study shows that the β-sheet structure-disrupted behaviors of protected peptides are strongly dependent on the nature of amino acid residues composing protected peptides. In previous papers[9,14,15,26] we also demonstrated that the β-sheet structure-disruption by organic solvents is strongly dependent on their electron-acceptor numbers (AN) and electron-donor numbers (DN) and that solvents having large AN or DN values have high potential for the β-sheet structure-disruption. Thus, the scale for the β-sheet

structure-stabilizing potential of the 20 kinds of amino acid residues as well as the β-sheet structure-disrupting potential of solvents is useful for an estimation of the β-sheet structure-disrupted behaviors of protected peptides in organic solvents.

The authors wish to thank Central Glass Co., Ltd., Mitsubishi Kasei Co., Ltd., and Ajinomoto Co., Ltd., for the generous gift of reagents.

References

1) The abbreviations for amino acids are those recommended by the IUPAC-IUB Commission on Biochemical Nomenclature, *J. Biol. Chem.*, **247**, 977 (1972). Amino acid symbols except for Gly denote the L-configuration. Additional abbreviations used are the following: HFIP, 1,1,1,3,3,3-hexafluoro-2-propanol; Boc, *t*-butoxycarbonyl; Tos, *p*-toluenesulfonyl; Bzl, benzyl; Z, benzyloxycarbonyl; OBzl, benzyl ester; CHO, formyl; IR, infrared; DCC, *N,N'*-dicyclohexylcarbodiimide; HOBt, 1*H*-1,2,3,-benzotriazol-1-ol.

2) M. Narita, K. Ishikawa, J.-Y. Chen, and Y. Kim, *Int. J. Peptide Protein Res.*, **24**, 580 (1984).

3) M. Narita, T. Ogura, K. Sato, and S. Honda, *Bull. Chem. Soc. Jpn.*, **59**, 2433 (1986).

4) M. Narita, T. Fukunaga, A. Wakabayashi, K. Ishikawa, and H. Nakano, *Int. J. Peptide Protein Res.*, **23**, 306 (1984).

5) M. Narita, J.-Y. Chen, H. Sato, and Y. Kim, *Bull. Chem. Soc. Jpn.*, **58**, 2494 (1985); M. Narita, M. Doi, T. Nakai, H. Takegahara, *Int. J. Peptide Protein Res.*, **32**, 200 (1988).

6) M. Narita, M. Doi, H. Sugasawa, and K. Ishikawa, *Bull. Chem. Soc. Jpn.*, **58**, 1473 (1985); M. Narita, K. Ishikawa, H. Sugasawa, and M. Doi, *ibid.*, **58**, 1731 (1985).

7) M. Narita, M. Doi, K. Kudo, and Y. Terauchi, *Bull. Chem. Soc. Jpn.*, **59**, 3553 (1986).

8) M. Narita, S. Honda, and H. Umeyama, *Bull. Chem. Soc. Jpn.*, **60**, 4127 (1987).

9) M. Narita, S. Isokawa, S. Honda, H. Umeyama, H. Kakei, and S. Obana, *Bull. Chem. Soc. Jpn.*, **62**, 773 (1989).

10) R. Katakai, *Macromolecules*, **14**, 613 (1981); V. N. R. Pillai and M. Mutter, *Acc. Chem. Res.*, **14**, 122 (1981).

11) M. Narita, M. Doi, and H. Takegahara, *Bull. Chem. Soc. Jpn.*, **60**, 2445 (1987); M. Narita, T. Ogura, K. Sato, and S. Honda, *Bull. Chem. Soc. Jpn.*, **59**, 2439, 2445 (1986).

12) M. Narita, S. Isokawa, Y. Tomotake, and S. Nagasawa, *Polym. J.*, **15**, 25 (1983); M. Narita, Y. Tomotake, S. Isokawa, T. Matsuzawa, and T. Miyauchi, *Macromolecules*, **17**, 1903 (1984).

13) P. Y. Chou and G. D. Fasman, *Biochemistry*, **13**, 211 (1974); P. Y. Chou and G. D. Fasman, *ibid.*, **13**, 222 (1974); P. Y. Chou and G. D. Fasman, *Adv. Enzymology*, **47**, 45 (1978).

14) M. Narita, H. Umeyama, S. Isokawa, S. Honda, C. Sasaki, and H. Kakei, *Bull. Chem. Soc. Jpn.*, **62**, 780 (1989).

15) M. Narita, H. Umeyama, and T. Yoshida, *Bull. Chem. Soc. Jpn.*, **62**, 3577, 3582 (1989).

16) M. Mutter, F. Maser, K.-H. Altmann, C. Toniolo, and G. M. Bonora, *Biopolymers*, **24**, 1057 (1985); M. Mutter and K.-H. Altmann, *Int. J. Peptide Protein Res.*, **26**, 373 (1985).

17) A. R. Mitchell, S. B. H. Kent, M. Engelhard, and R. B. Merrifield, *J. Org. Chem.*, **43**, 2845 (1978).

18) W. König and R. Geiger, *Chem. Ber.*, **103**, 788 (1970).

19) F. C. Westall, J. Scotchler, and A. B. Robinson, *J. Org. Chem.*, **37**, 3363 (1972).

20) T. Y. Liu and Y. H. Chang, *J. Biol. Chem.*, **246**, 2842 (1971).

21) T. Miyazawa and E. R. Blout, *J. Am. Chem. Soc.*, **83**, 712 (1961); T. Miyazawa, "Poly-α-Amino Acids," ed by G. D. Fasman, Marcel Dekker, New York (1967), pp. 69—103.

22) C. Toniolo, G. M. Bonora, M. Mutter, and F. Maser, *J. Chem. Soc., Chem. Commun.*, **1983**, 1298.

23) IUPAC-IUB Commission on Biochemical Nomenclature, *Biochemistry*, **7**, 2703 (1968).

24) T. Fujii and S. Sakakibara, *Bull. Chem. Soc. Jpn.*, **47**, 3146 (1974).

25) M. Narita, S. Isokawa, M. Doi, and R. Wakita, *Bull. Chem. Soc. Jpn.*, **59**, 3547 (1986).

26) M. Narita, S. Honda, and S. Obana, *Bull. Chem. Soc. Jpn.*, **62**, 342 (1989).

 © 1989 The Chemical Society of Japan Bull. Chem. Soc. Jpn., 62, 3577—3581 (1989)

Peptide Segment Separation by Tertiary Peptide Bonds.[1] Synthesis and Conformational Analysis of Cross-Linked Polystyrene Resin-Bound Human Proinsulin C-Peptide Fragments

Mitsuaki NARITA,* Hiroshi UMEYAMA, and Toshihiko YOSHIDA
Department of Industrial Chemistry, Faculty of Technology, Tokyo University of Agriculture and Technology, Koganei 184
(Received June 5, 1989)

In order to clarify the role of tertiary peptide bonds in the conformational development of protected peptides in organic solvents, cross-linked polystyrene resin-bound human proinsulin C-peptide fragments were prepared by a fragment condensation method. For the purpose of clarifying the role of tertiary peptide bonds, it is indispensable to force coupling reactions to completion; the addition of HFIP in coupling reactions in CH_2Cl_2 was significantly effective for their completion when they did not proceed smoothly. The conformational behavior of resin-bound human proinsulin C-peptide fragments in CH_2Cl_2 was successively investigated using IR absorption spectroscopy. Two Pro residues forming tertiary peptide bonds played the role of stopping the development of helix and β-sheet structures in peptides, and the structure of N- and C-termini- and side-chain-protected human proinsulin C-peptide could be regarded as being assembled with peptide segment structures separated by the two Pro residues. When a peptide segment had a high helix-forming potential, a Pro residue in an N-terminal part of the peptide segment promoted its helix formation. β-Sheet structures formed by peptide segments in CH_2Cl_2 were easily disrupted by a strong electron-acceptor solvent of HFIP, suggesting that the β-sheet structure disruption of resin-bound peptides is important in achieving efficient coupling reactions.

In peptide and protein syntheses, sufficient solvation of a peptide chain is indispensable to achieve a coupling reaction quantitatively. As one means to accomplish sufficient solvation, we proposed "peptide segment separation by tertiary peptide bonds."[2] In fact, a tertiary peptide bond at a central position of peptide chains (Fig. 1) helps the sufficient solvation and remarkably improves peptide solubility. On the X–Pro and X–(Z)Y bonds in Fig. 1, X and Y are arbitrary amino acid residues and Z designates a suitable protecting group for the X–Y peptide bond,

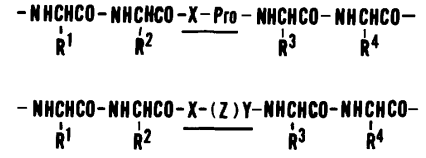

Fig. 1. Insertion of tertiary peptide bonds [X–Pro and X–(Z)Y] into central positions of peptide chains. An explanatory note for X, Y, and Z, see in the text.

which can be removed under certain conditions. Sufficient solvation and solubility improvements have been exactly attributed to the separation and disturbance of a β-sheet structure by rotation, due to a steric hindrance, of the tertiary peptide bond plane.

Here, it is significant to clarify the role of Pro and (Z)Y residues in the conformational development of protected peptides in organic solvents since the conformation of a peptide chain is closely related to sufficient solvation.[3–5] Although the prediction of conformations of protected peptides in organic solvents has been difficult so far, it is important in order to design synthetic routes for peptides and proteins without insolubility problems.[3] A Pro residue is well-recognized as being a strong helix and β-sheet breaker and plays the role in stopping the development of helix and β-sheet structures in native globular proteins.[6,7] Thus, tertiary peptide bonds formed by Pro and (Z)Y residues in protected peptides play the role of separating a peptide structure into various peptide segment structures. Namely, a peptide struc-

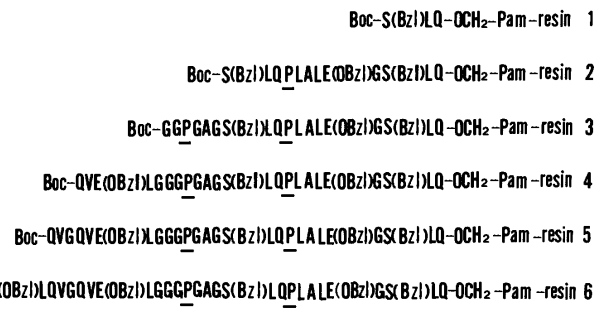

Fig. 2. Resin-bound human proinsulin C-peptide fragments **1**—**6** used in this study.

ture is regarded as being assembled with some of peptide segment structures separated by Pro and (Z)Y residues. We called the role "peptide segment separation by tertiary peptide bonds."[2]

In this study, we prepared resin-bound human proinsulin C-peptide fragments (Fig. 2) and examined their IR absorption spectroscopies in CH_2Cl_2 in order to demonstrate the role of Pro residues in the conformational development of protected peptides in CH_2Cl_2. In connection with efficient coupling reactions in solid-phase peptide synthesis by a fragment condensation procedure, we also investigated the disruption of the β-sheet structure of resin-bound human proinsulin C-peptide fragments in CH_2Cl_2 by the addition of a strong electron-acceptor solvent of HFIP.

Experimental

Materials. Copoly(styrene-1% divinylbenzene) beads of 200—400 mesh, Bio-Beads S-X1, were purchased from Bio-Rad Laboratories. The aminomethylation was carried out according to the method described previously.[8] Human proinsulin C-peptide fragments, Boc-Ser(Bzl)-Leu-Gln-Pro-Leu-Ala-Leu-Glu(OBzl)-Gly-OH, Boc-Gly-Gly-Pro-Gly-Ala-Gly-OH, Boc-Gln-Val-Glu(OBzl)-Leu-Gly-OH, Boc-Gln-Val-Gly-OH, and Boc-Glu(OBzl)-Ala-Glu(OBzl)-Asp(OBzl)-Leu-OH, were prepared before.[9] Boc-Ser(Bzl)-Leu-Gln-*p*-(oxymethyl)phenylacetic acid was obtained by hydrolysis of its trityl ester in a mixture of acetic acid, water, and methanol (5:1:4). The assembly of the peptide fragments was performed in CH_2Cl_2, substantially, according to the general procedures described previously.[10] The coupling reactions were carried out for 1 day using 3 equiv of carboxyl components, DCC, and HOBt, respectively. In the cycle for the peptide chain elongation, no termination reaction using pyridine and acetic anhydride was performed. Each coupling step was tested for completion by a ninhydrin test. When a test was positive after a double coupling reaction, a small amount of HFIP (2 vol% to CH_2Cl_2) was added, and the reaction was continued until the test became negative. Acid hydrolyses of the resin-bound peptides were performed with propionic acid/3 M (1 M=1 mol dm^{-3}) *p*-toluenesulfonic acid[11] (2/1, v/v) at 115 °C for 3 days. Amino acid analyses of the acid hydrolysates showed that the mole ratios of the component amino acid were close to the calculated values (Table 1).

IR Measurements. The IR absorption spectra of resin-bound peptides were recorded at room temperature with a JEOL Model JIR-100 FT-IR spectrometer. IR measurements in the swollen state were performed by holding the samples between potassium bromide windows after resin-bound peptides were swollen in CH_2Cl_2 or in CH_2Cl_2 containing HFIP at 0.1 M.

Results

Syntheses of Cross-Linked Polystyrene Resin-Bound Human Proinsulin C-Peptide. The copoly(styrene-1% divinylbenzene) resin support (Bio-Beads S-X1), used as a starting resin bead, has commonly been used for solid-phase peptide synthesis and the aminomethylated form is expected to have a uniform distribution of aminomethyl groups, based on the reaction mechanism of aminomethylation.[8] The aminomethyl content (76 μmol g^{-1} of resin) was selected in order to obtain rational information regarding the conformational development of peptide chains in the conventional solid-phase method.[12] The carboxyl component peptides were easily soluble in CH_2Cl_2 and were successively coupled with the aminomethylated polystyrene resin in CH_2Cl_2 using DCC and HOBt as coupling reagents.[13] In the preparation of resin-bound peptides **1**—**3**, coulping reactions proceeded smoothly without the addition of HFIP. On the other hand, in the preparation of peptides **4**—**6**, coupling reactions did not proceed smoothly, even at a double coupling reaction, and a ninhydrin test was positive at this stage. The addition of HFIP at this stage[14] was marvelously effective in forcing coupling reactions to completion and a ninhydrin test became negative while the reaction was continued for 24 h.

Conformations of Resin-Bound Human Proinsulin C-Peptide Fragments in CH_2Cl_2. The IR absorption spectra of resin-bound peptides **1**—**6** swollen in CH_2Cl_2 are presented in Fig. 3 in the most significant spectral regions for conformational assignments (3500—3100 cm^{-1}, amide A; 1800—1600 cm^{-1}, amide I). The results indicate the following: (1) resin-bound tripeptide **1** exhibits an unordered structure, characterized by appearance of medium and strong bands at 3425 and 1675 cm^{-1};[10,15] (2) resin-bound dodeca- and octadecapeptides **2** and **3** seem to form a helical structure, assigned by the appearance of medium and strong bands around 3310 and 1660 cm^{-1}, respectively,[10,15] accompanied by a small amount of a β-sheet structure, asigned by the appearance of a weak shoulder band at 1628 cm^{-1};[10,15] and (3) resin-bound tricosa-, hexacosa-, and hentriacontapeptides **4**, **5**, and

Table 1. The Results of Amino Acid Analysis of Resin-Bound Peptides **1**—**6**

Resin-bound peptide	Found (Calcd)							
	Asp	Ser	Glu	Pro	Gly	Ala	Val	Leu
1	—	1.00 (1)	1.00 (1)	—	—	—	—	1.00 (1)
2	—	1.95 (2)	2.85 (3)	0.94 (1)	1.13 (1)	1.13 (1)	—	3.89 (4)
3	—	1.81 (2)	2.89 (3)	2.19 (2)	4.92 (5)	2.19 (2)	—	3.84 (4)
4	—	1.99 (2)	4.89 (5)	2.07 (2)	6.11 (6)	2.14 (2)	0.92 (1)	4.88 (5)
5	—	2.18 (2)	6.44 (6)	2.21 (2)	6.86 (7)	1.89 (2)	1.82 (2)	4.60 (5)
6	1.06 (1)	1.88 (2)	7.86 (8)	2.15 (2)	7.17 (7)	3.24 (3)	1.78 (2)	5.96 (6)

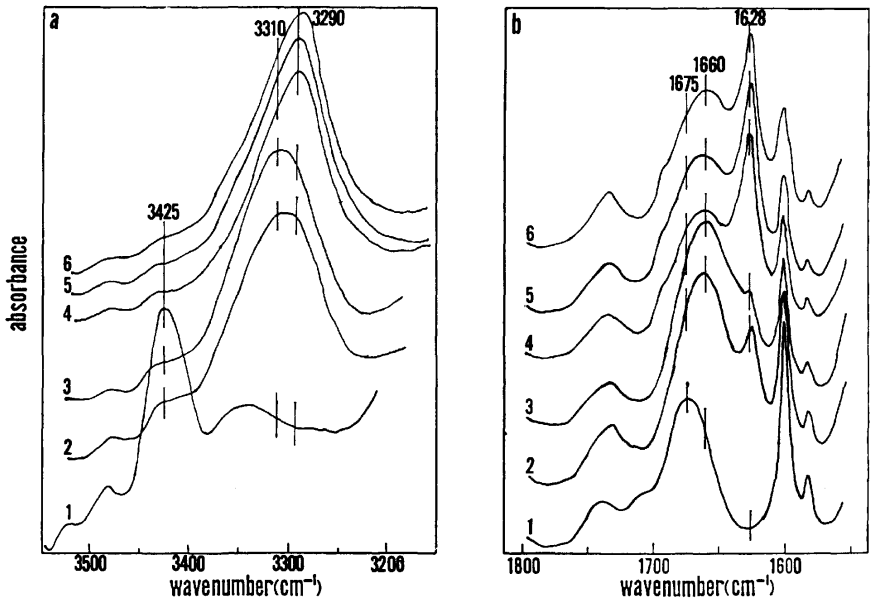

Fig. 3. IR absorption spectra (a) in the amide A and (b) in the amide I regions of resin-bound peptides **1**—**6** swollen in CH_2Cl_2. The absorption band at 1603 cm^{-1} is due to aromatic rings of the polystyrene support.

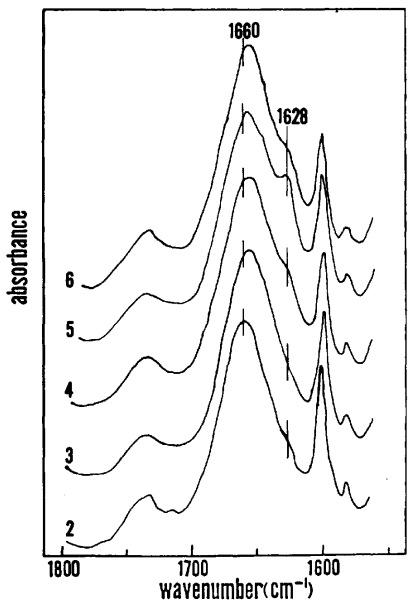

Fig. 4. IR absorption spectra in the amide I region of resin-bound peptides **2**—**6** swollen in CH_2Cl_2 containing HFIP at 0.1 M.

6 appear to have both helical and β-sheet structures, characterized by appearance of bands at 3310, 3290, 1660, and 1628 cm^{-1}, respectively.

In order to elucidate the role of HFIP in efficient coupling reactions in the solid-phase synthesis of human proinsulin C-peptide, conformational analysis of resin-bound peptides **2**—**6** in CH_2Cl_2 containing HFIP at 0.1 M was also performed using IR absorption spectroscopies (Fig. 4). The results showed that the β-sheet structure of resin-bound peptides **2**—**6** was sufficiently disrupted by a strong electron-acceptor solvent of HFIP, even at a low concentration of HFIP.

Discussion

The synthetic results of cross-linked polystyrene resin-bound human proinsulin C-peptide fragments clearly indicated that the addition of HFIP effectively forced coupling reactions in CH_2Cl_2 to completion due to the strong β-sheet structure-disrupting potential of HFIP.[16] Although solid-phase peptide synthesis using a fragment condensation procedure has been expected to be valuable for the synthesis of large peptides and proteins,[17] heterogeneous reaction conditions cause the formation of deletion and truncated sequences, and a drastic decrease in the coupling yields has been a serious obstacle.[18] In previous papers[19] we pointed out that the onset of a β-sheet aggregation by hydrogen bonding among pendant peptide chains brought about an additional cross-linking of the polymer network and that the coupling efficiencies of carboxyl component peptides with pendant peptides were remarkably decreased due to a restriction of their permeability into pendant peptides. The synthetic result, conformational analysis, and β-sheet-structure-disrupted behavior of resin-bound human proinsulin C-peptide fragments clearly indicate that the disruption of their β-sheet structures by the addition of HFIP is effective for the completion of coupling reactions in solid-phase peptide synthesis by a fragment condensation procedure and overcomes the serious obstacle of the drastic decrease in coupling yields.

Conformational analysis of resin-bound peptide **1**—**6** in CH_2Cl_2 also indicates that the concept of "the

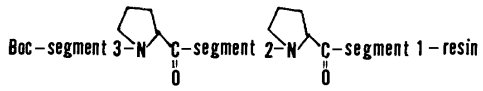

Fig. 5. The separation of human proinsulin C-peptide into three peptide segments by two Pro residues.

peptide segment separation by tertiary peptide bonds" is useful for estimating the conformational development of protected peptides in organic solvents, which is important for designing synthetic routes for peptides and proteins.[3] For example, the conformational behavior of peptides **4**—**6** suggests that the conformations of peptides **4**—**6** can be regarded as being assembled with three peptide segments separated by the two Pro residues (Fig. 5). With respect to conformations of peptides **4**—**6**, most parts of segment 1 and a part of segment 2, namely, Ser(Bzl)-Leu-Gln, are estimated to form a relatively stable helix, and N-terminal segments 3 of peptides **4**—**6** appear to form a relatively stable β-sheet structure although the conformation of segment 2 is not clear. These estimations were actually confirmed by conformational analyses of peptides **2** and **3**. The conformational behavior of resin-bound peptide **2** resembled that of Boc-Ser(Bzl)-Leu-Gln-Pro-Leu-Ala-Leu-Glu(OBzl)-Gly-OPac, which has a helical structure in CH_2Cl_2.[20] In the conformational development of peptide **2**, the Pro residue of resin-bound peptide **2** effectively suppresses the β-sheet formation of the octapeptide segment, Leu-Ala-Leu-Glu(OBzl)-Gly-Ser(Bzl)-Leu-Gln, due to the restriction of the backbone dihedral angles ϕ and ψ of a Pro residue,[4,5,21] and promotes its helix formation due to both the restriction of the backbone dihedral angles ϕ and ψ of a Pro residue[4,5] and the high helix-forming potential of peptide **2**.[20,22] For a prediction of the conformations of protected peptides in organic solvents, we have tentatively used the average helix, β-sheet, and coil conformation values, $<P_\alpha>$, $<P_\beta>$, and $<P_c>$,[3,20,23] which are determined by their amino acid compositions,[6] and demonstrated their validity. Practically, the $<P_\alpha>$ and $<P_\beta>$ values of segment 1 of peptides **2** are 1.06 and 0.92, respectively,[22] indicating the relatively high helix-forming potential of segment 1. The IR absorption spectrum of peptide **3** also shows little contribution of a β-sheet structure, indicating that the Pro residue of Boc-Gly-Gly-Pro-Gly-Ala-Gly- in resin-bound peptide **3** influentially distrurbs the onset of a β-sheet structure by the rotation of the tertiary peptide bond plane (Gly-Pro). A chain elongation of peptide **3** to peptide **4** appears to induce the onset of a β-sheet structure at the N-terminal segment 3 of peptide **4** and a further chain elongation of peptide **4** to peptide **5** seems to develop the β-sheet structure at N-terminal segment 3.[24] On the other hand, the β-sheet structure content of peptide **6** is lower than that of peptide **5**, probably due to the fact that peptide **6** is close to the critical chain length for a stable helix formation in CH_2Cl_2.

Due to the function that a Pro residue stops the development of helix and β-sheet structures in a peptide, conformational development at N-terminal segments 3 of peptides **4**—**6** in CH_2Cl_2 containing HFIP appears to occur regardless of segments 1 and 2. In the mixture, HFIP probably promotes a helical folding and/or a sufficient solvation of each peptide segment, depending on its conformational preference. The conformational development of protected peptides in organic solvents is strongly dependent on the nature of the organic solvents, especially their electron-donating and -accepting properties.[16] Thus, the disruption of the β-sheet structure of resin-bound peptides **2**—**6** by HFIP and by strong electron-donor solvents[22] suggests that the concept of "peptide segment separation by tertiary peptide bonds" is useful for estimating the conformational development of protected peptides in organic solvents having strong electron-donating and -accepting properties.

This work has been supported by a Grant-in-Aid from the Asahi Glass Foundation for Industrial Technology.

References

1) The abbreviations for amino acids are those recommended by the IUPAC-IUB Commission on Biochemical Nomenclature, *J. Biol. Chem.*, **247**, 977 (1972). Amino acid symbols except for Gly denote the L-configuration. Additional abbreviations used are the following: HFIP, 1,1,1,3,3,3-hexafluoro-2-propanol; IR, infrared; Boc, *t*-butoxycarbonyl; Bzl, benzyl; Pam, phenylacetamidomethyl; DCC, dicyclohexylcarbodiimide; HOBt, 1-hydroxy-1*H*-benzotriazole.

2) M. Narita, T. Fukunaga, A. Wakabayashi, K. Ishikawa, and H. Nakano, *Int. J. Pept. Protein Res.*, **23**, 306 (1984).

3) M. Narita, K. Ishikawa, J.-Y. Chen, and Y. Kim, *Int. J. Pept. Protein Res.*, **24**, 580 (1984).

4) C. Toniolo, G. M. Bonora, M. Mutter, and V. N. R. Pillai, *Makromol. Chem.*, **182**, 2007 (1981).

5) M. Narita, S. Isokawa, M. Doi, and R. Wakita, *Bull. Chem. Soc. Jpn.*, **59**, 3547 (1986).

6) P. Y. Chou and G. D. Fasman, *Biochemistry*, **13**, 211 (1974); P. Y. Chou and G. D. Fasman, *ibid.*, **13**, 222 (1974); P. Y. Chou and G. D. Fasman, *Adv. Enzymology*, **47**, 45 (1978).

7) S. Lifson and G. Sander, *Nature (London)*, **282**, 109 (1979).

8) A. R. Mitchell, S. B. H. Kent, M. Engelhard, and R. B. Merrifield, *J. Org. Chem.*, **43**, 2845 (1978).

9) M. Narita, T. Ogura, K. Sato, and S. Honda, *Bull. Chem. Soc. Jpn.*, **59**, 2433 (1986).

10) M. Narita, S. Isokawa, Y. Tomotake, and S. Nagasawa, *Polym. J.*, **15**, 25 (1983).

11) T. Y. Liu and Y. H. Chang, *J. Biol. Chem.*, **246**, 2842 (1971).

12) R. B. Merrifield, *J. Am. Chem. Soc.*, **85**, 2149 (1963).

13) W. König and R. Geiger, *Chem. Ber.*, **103**, 788 (1970).

14) M. Narita and Y. Kojima, *Bull. Chem. Soc. Jpn.*, **62**, 3572 (1989).
15) T. Miyazawa and E. R. Blout, *J. Am. Chem. Soc.*, **83**, 712 (1961); T. Miyazawa, "Poly-α-Amino Acids," ed. by G. D. Fasman, Marcel Dekker, New York (1967), pp. 69—103.
16) M. Narita, S. Honda, and S. Obana, *Bull. Chem. Soc. Jpn.*, **62**, 342 (1989).
17) H. Yajima and S. Funakoshi, *Yuki Gosei Kagaku Kyokaishi*, **43**, 1083 (1985).
18) H. Yajima and Y. Kiso, *Chem. Pharm. Bull.*, **22**, 1087 (1974).
19) M. Narita, S. Isokawa, S. Nagasawa, and T. Ishijima, *Macromolecules*, **20**, 2306 (1987); M. Narita, S. Isokawa, T. Matsuzawa, and T. Miyauchi, *ibid.*, **18**, 1363 (1985).
20) M. Narita, T. Ogura, K. Sato, and S. Honda, *Bull. Chem. Soc. Jpn.*, **59**, 2445 (1986).
21) D. F. De Tar and N. Luthra, *J. Am. Chem. Soc.*, **99**, 1232 (1977); V. Madison, *Biopolymers*, **16**, 2671 (1977); B. V. V. Prasad, H. Balaram, and P. Balaram, *ibid.*, **21**, 1261 (1982).
22) M. Narita, H. Umeyama, and T. Yoshida, *Bull. Chem. Soc. Jpn.*, **62**, 3582 (1989).
23) M. Narita, T. Ogura, K. Sato, and S. Honda, *Bull. Chem. Soc. Jpn.*, **59**, 2439 (1986); M. Narita, M. Doi, and H. Takegahara, *ibid.*, **60**, 2445 (1987); M. Narita, M. Doi, and T. Nakai, *ibid.*, **60**, 3225 (1987); M. Narita, S. Isokawa, S. Honda, H. Umeyama, H. Kakei, and S. Obana, *ibid.*, **62**, 773 (1989).
24) M. Narita, S. Honda, H. Umeyama, and T. Ogura, *Bull. Chem. Soc. Jpn.*, **61**, 1201 (1988).

 © 1989 The Chemical Society of Japan Bull. Chem. Soc. Jpn., 62, 3582—3586 (1989) [Vol. 62, No. 11

The Easy Disruption of the β-Sheet Structure of Resin-Bound Human Proinsulin C-Peptide Fragments by Strong Electron-Donor Solvents[1)]

Mitsuaki NARITA,* Hiroshi UMEYAMA, and Toshihiko YOSHIDA
Department of Industrial Chemistry, Faculty of Technology, Tokyo University of Agriculture and Technology, Koganei 184
(Received June 5, 1989)

The β-sheet structure disruption of cross-linked polystyrene resin-bound human proinsulin C-peptide fragments containing Pro residues at suitable intervals was investigated by a solvent titration method in CH_2Cl_2, mainly using TFE and HMPA as titrating solvents. The easy disruption of the β-sheet structure of resin-bound peptides in CH_2Cl_2 by TFE and HMPA strongly suggested that the concept of "the peptide segment separation by tertiary peptide bonds" was useful for estimating the β-sheet-structure-disrupted behavior and that the β-sheet structure of the protected peptides having high $<P_c>$ values could easily be disrupted in a medium electron-acceptor solvent of CH_2Cl_2 by the addition of a strong electron-donor solvent of HMPA in spite of the electron donor-acceptor interaction between solvents. The present results indicate that effective solvents for solid-phase peptide synthesis by a fragment condensation procedure should be searched by taking the average helix, β-sheet, and coil conformation values, $<P_\alpha>$, $<P_\beta>$, and $<P_c>$, of peptide segments into consideration.

The β-sheet aggregation of protected peptides bound to a cross-linked polystyrene resin in the swollen state is one of the serious obstacles in solid-phase peptide synthesis because it reduces the efficient coupling reactions of the carboxyl component peptides with the pendant amino component peptides due to the restriction of the permeability of carboxyl components into pendant peptides.[2,3)] Thus, an investigation into the β-sheet structure disruption of resin-bound peptides is indispensable to achieve efficient coupling reactions. In previous studies[4,5)] we demonstrated that the β-sheet structure of resin-bound peptides as large as or larger than an octapeptide was disrupted in CH_2Cl_2 only by the addition of a strong electron-acceptor solvent of HFIP and that the disruption was strongly dependent on the electron-donating and -accepting properties[6,7)] of added solvents, peptide chain length, and average helix, β-sheet, and coil conformation values, $<P_\alpha>$, $<P_\beta>$, and $<P_c>$, of peptides. These values are determined on the basis of the three-dimensional structures of native proteins which were resolved by X-ray crystallography;[8,9)] they should be corrected for an estimation of the conformational behavior of protected peptides in organic solvents. Nevertheless, they were useful for the purpose of the estimation of the conformation.[4)] Practically, the β-sheet structure disruption of peptides having a $<P_c>$ value larger than 0.85 and/or a high potential for the β-sheet → helix transformation proceeded smoothly upon adding increasing amounts of HFIP; that of peptides having a low potential for the randomness as well as for the β-sheet → helix transformation did not.

Moreover, we found that the β-sheet structure disruption of cross-linked polystyrene resin-bound peptides was more difficult than that of peptides to be free from a macromolecular protecting group due to the concentrating efficacy of a cross-linked resin.[5)] As a result, the β-sheet structure of resin-bound peptides, which were as large as or larger than an octapeptide and had a $<P_c>$ value lower than 0.90, could not be disrupted by strong electron-acceptor solvents except for HFIP and by strong electron-donor solvents. This result was quite different from that of the corresponding peptides, which were free from a macromolecular protecting group.[7)]

Recently, we also found that the β-sheet structure of resin-bound human proinsulin C-peptide fragments which contained Pro residues at suitable intervals was easily disrupted by the addition of only a slight amount of HFIP, resulting in efficient coupling reactions in solid-phase peptide synthesis by a fragment condensation procedure.[10)] Thus, the investigation into solvents having a high potential for the β-sheet structure disruption of resin-bound peptides is of practical significance for solid-phase peptide synthe-

Boc-S(Bzl)LQPLALE(OBzl)GS(Bzl)LQ-OCH_2-Pam-resin 1

Boc-GGPGAGS(Bzl)LQPLALE(OBzl)GS(Bzl)LQ-OCH_2-Pam-resin 2

Boc-QVE(OBzl)LGGGPGAGS(Bzl)LQPLALE(OBzl)GS(Bzl)LQ-OCH_2-Pam-resin 3

Boc-QVGQVE(OBzl)LGGGPGAGS(Bzl)LQPLALE(OBzl)GS(Bzl)LQ-OCH_2-Pam-resin 4

Boc-E(OBzl)AE(OBzl)D(OBzl)LQVGQVE(OBzl)LGGGPGAGS(Bzl)LQPLALE(OBzl)GS(Bzl)LQ-OCH_2-Pam-resin 5

Fig. 1. Resin-bound peptides **1**—**5** used in this study.

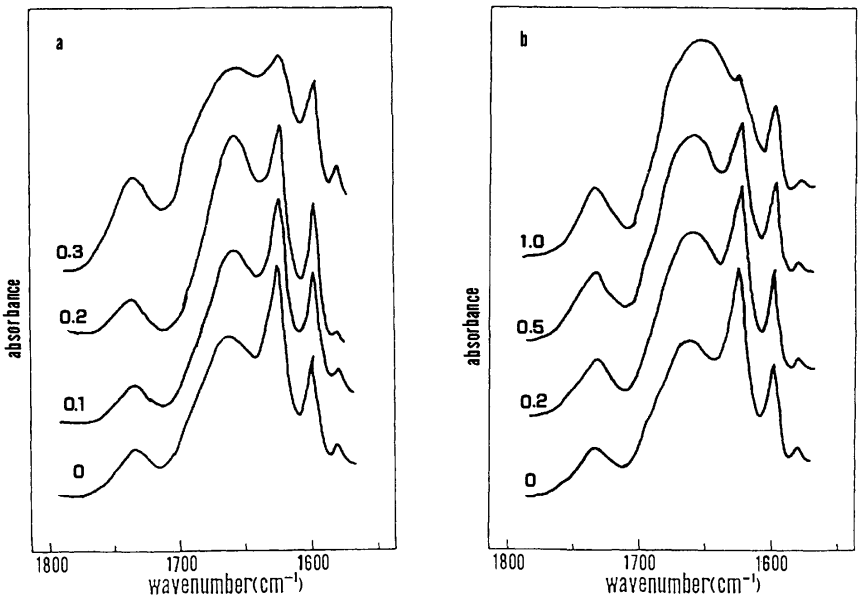

Fig. 2. Tpical IR absorption spectra in the amide I region of resin-bound peptide **4** swollen (a) in a mixture of TFE and CH_2Cl_2 and (b) in a mixture of HMPA and CH_2Cl_2. The numerals in Fig.2 indicate molar concentrations of TFE and HMPA (M).

sis. In the present paper, we report that the β-sheet structure of resin-bound human proinsulin C-peptide segments having $<P_c>$ values larger than 0.98 is marvelously disrupted in CH_2Cl_2, even by the addition of strong electron-donor solvents such as HMPA and DMSO. We also show that the concept of "the peptide segment separation by tertiary peptide bonds"[11] is useful for estimating the β-sheet-structure-disrupted behavior. Resin-bound peptides **1**—**5** used in this study are shown in Fig. 1, where amino acid residues are represented by one-letter symbols.[12]

Experimental

Resin-bound peptides **1**—**5** were prepared in a previous study.[10] The IR absorption spectra of resin-bound peptides **1**—**5** were recorded at room temperature with a JEOL Model JIR-100 FT-IR spectrometer. IR measurements in the swollen state were performed by holding the samples between potassium bromide windows after resin-bound peptides were swollen in CH_2Cl_2 containing TFE, HMPA, DMSO, or MeOH at various concentrations.

Results

The β-sheet structure disruption of cross-linked polystyrene resin-bound peptides **1**—**5** in CH_2Cl_2 was investigated by a solvent-titration method.[13] It was monitored by following a successive decrease in the intensity of the amide I band around 1630 cm^{-1} due to the β-sheet structure together with the successive addition of a titrating solvent. As a representative example, the IR absorption spectra of the resin-bound peptide **4** in CH_2Cl_2 containing TFE or HMPA over a wide range of concentration are presented in Fig. 2. Figures 3 and 4 illustrate the solvent-titration curves of resin-bound peptides **1**—**5** using TFE and HMPA as titrating solvents, respectively. The relative intensities in Figs. 3 and 4 as well as Fig. 5 were obtained using the band at 1603 cm^{-1} due to the aromatic ring of the resin support as a standard and were normalized to 1.0 for each relative intensity in the absence of a titrating solvent. The results indicate that the β-sheet structure of resin-bound peptides **1**—**5** swollen in CH_2Cl_2 is easily disrupted by adding increasing amounts of TFE and HMPA and that the β-sheet structure disruption

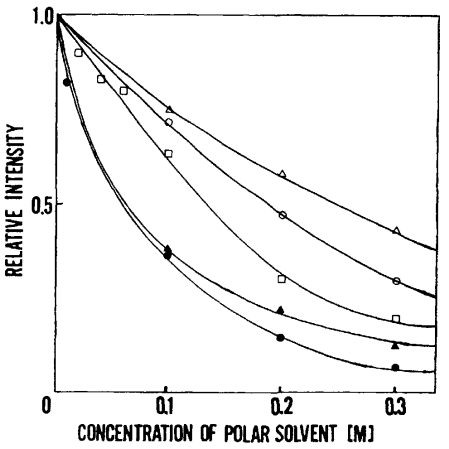

Fig. 3. The solvent-titration curves of resin-bound peptides **1**—**5** in CH_2Cl_2 using TFE as a titrating solvent. Peptide **1**, —▲—; peptide **2**, —●—; peptide **3**, —□—; peptide **4**, —△—; and peptide **5**, —○—.

of peptide **4** is the most difficult in peptides **1**—**5**. In order to elucidate the relationship between the β-sheet structure disruption of peptide **4** and electron-donating and -accepting properties of titrating solvents, the solvent-titration curves of peptide **4** in a medium electron-acceptor solvent of CH_2Cl_2 using strong electron-acceptor solvents of HFIP, TFE, and MeOH and strong electron-donor solvents of HMPA and DMSO as titrating solvents (Fig. 5) were obtained. The solvent-titration curve of peptide **4** in a medium electron-donor solvent of THF using HMPA as a titrating solvent is also shown in Fig. 5.

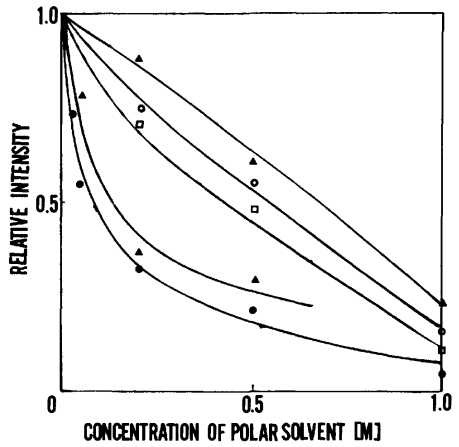

Fig. 4. The solvent-titration curves of resin-bound peptides **1**—**5** in CH_2Cl_2 using HMPA as a titrating solvent. Peptide **1**, —▲—; peptide **2**, —●—; peptide **3**, —□—; peptide **4**, —△—; and peptide **5**, —○—.

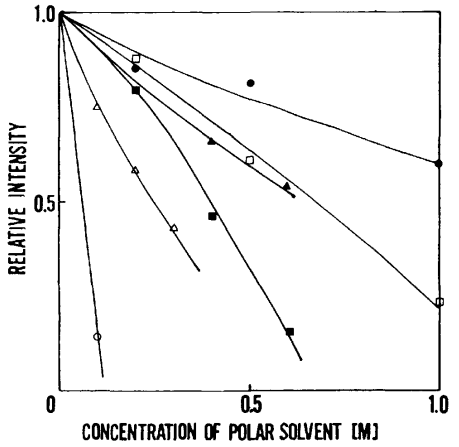

Fig. 5. The solvent-titration curves of resin-bound peptides **4** in CH_2Cl_2 using HFIP, TFE, MeOH, HMPA, and DMSO as titrating solvent. HFIP, —○—; TFE, —△—; MeOH, —▲—; HMPA, —□—; and DMSO, —●—. The solvent-titration curve of peptide **4** in THF using HMPA as a titrating solvent, —■—.

Discussion

Resin-bound peptides **1**—**5** contain Pro residues at suitable intervals, and Pro residues in peptides generally play a role in stopping the development of helix and β-sheet structures. Thus, the structures of resin-bound peptides **1**—**5** could be regarded as being assembled with peptide segment structures separated by Pro residues;[10] we called the role "peptide segment separation by tertiary peptide bonds."[11] In the swollen state in CH_2Cl_2, in fact, most parts of segment 1 (PLALEGSLQ) and a part of segment 2 (PGAGSLQ), namely, Ser(Bzl)-Leu-Gln, were estimated to form a relatively stable helix and N-terminal segment 3 appeared to form a relatively stable β-sheet structure, although the conformation of segment 2 was not clear.[10] Namely, the β-sheet structure of resin-bound peptides **1**—**5** can be regarded as being constructed by peptide segments having short peptide chain lengths. Thus, the β-sheet structure of resin-bound peptides **1**—**5** swollen in CH_2Cl_2 was expected to be disrupted by the addition of a variety of titrating solvents. Practically, it was easily disrupted by a strong electron-acceptor solvent of TFE and a strong electron-donor solvent of HMPA (Figs. 3 and 4), being in marked contrast with that of resin-bound peptides reported previously.[4,5] Especially, the disruption is clearly independent of the chain length of whole peptides, indicating that, for the evaluation of the β-sheet structure disruption of resin-bound peptides containing Pro residues, we should take account of the chain length of peptide segments instead of whole peptides. This is in harmony with the concept that "peptide segment separation by tertiary peptide bonds" is effective for estimating the conformational development of protected peptides in organic solvents.[10]

Resin-bound dodecapeptide **1** has a relatively stable helix in CH_2Cl_2 and is accompanied by a small amount of a β-sheet structure,[10] which is easily disrupted by TFE and HMPA. The disrupted behavior can be regarded as corresponding with that of segment 1. Resin-bound octadecapeptide **2** is assem-

Table 1. The Average Conformational Values, $\langle P_\alpha \rangle$, $\langle P_\beta \rangle$, and $\langle P_c \rangle$ of Peptide Segments

Peptide segment[a]	Number of segment	$\langle P_\alpha \rangle$	$\langle P_\beta \rangle$	$\langle P_c \rangle$
PLALEGSLQ	1	1.06	0.92	0.82
PGAGSLQ	2	0.89	0.86	1.16
QVELGGG	3	0.94	0.96	1.07
QVGQVELGGG	3	0.93	1.03	1.05
EAEDLQVGQVELGGG	3	1.07	0.91	0.98

a) Amino acid residues are represented by one-letter symbols.[12]

bled with segments 1 and 2 and its β-sheet structure is also easily disrupted by TFE and HMPA, since segment 2 has a high $<P_c>$ value (1.16). Especially, the easy disruption of resin-bound peptides **3—5** in CH_2Cl_2 by TFE and HMPA is marvelous and appears to be attributed to the high $<P_c>$ values of segments 3, suggesting that, for the evaluation of the β-sheet structure disruption of resin-bound peptides containing Pro residues, it is pertinent to use the $<P_\alpha>$, $<P_\beta>$, and $<P_c>$ values of peptide segments instead of whole peptides. The $<P_\alpha>$, $<P_\beta>$, and $<P_c>$ values of peptide segments are determined by their amino acid compositions,[8,9] and are summarized in Table 1. The easiness of the β-sheet structure disruption of peptides **3—5** by TFE and HMPA is in the following order: **3**>**5**>**4**. The most easy disruption of the β-sheet sturcture of peptide **3** is explained by both the short chain length and high $<P_c>$ value (1.07) of its segment 3. Segment 3 of peptide **5** also has a high $<P_c>$ value (0.98), and its chain length is close to the critical size for a stable helix formation of cross-linked polystyrene resin-bound peptides in CH_2Cl_2.[14] Furthermore, its $<P_\alpha>$ value (1.07) is larger than its $<P_\beta>$ value (0.91). The easy disruption of the β-sheet structure of segment 3 of peptide **5** is in good agreement with the observation that the β-sheet structure disruption of peptides having a $<P_c>$ value larger than 0.85 and having a high potential for the β-sheet → helix transformation proceeded smoothly upon adding increasing amounts of HFIP.[4] In addition, the easy disruption of the β-sheet structure of peptide **4** in CH_2Cl_2 by TFE, MeOH, HMPA, and DMSO (Fig. 5) clearly indicates that the consideration of $<P_c>$ values of peptide segments is important for a search for effective solvents to be used in solid-phase peptide synthesis.

In a study of the β-sheet structure-disruption of Boc-Val-Gly-Phe-Gly-Leu-Ile-Leu-Leu-Ala-NH-resin in a mixture of a strong electron-donor solvent of HMPA and a medium electron-acceptor solvent of CH_2Cl_2,[5] the electron donor-acceptor interaction between solvents occurred predominantly and the β-sheet structure disruption did not proceed. Thus, the result that the β-sheet structure of resin-bound peptide **4** in CH_2Cl_2 is disrupted by the addition of HMPA and DMSO strongly suggests that the β-sheet structure of resin-bound peptides having high $<P_c>$ values could be disrupted in CH_2Cl_2 even by a strong electron-donor solvent in spite of the electron donor-acceptor interaction between solvents. Contrary to CH_2Cl_2, THF is a medium electron-donor solvent and a weak electron-acceptor solvent.[6] Thus, the electron donor-acceptor interaction between HMPA and THF becomes negligible, and HMPA in THF shows a high potential for the β-sheet structure disruption of resin-bound peptide **4** (Fig. 5). As reported previously,[7] the potential of hydrogen-donor and -acceptor solvents for the β-sheet structure disruption of resin-bound peptide **4** was in the good relationship with their electron-acceptor and -donor numbers (AN and DN), respectively (Fig. 5). The AN values of HFIP, TFE, and MeOH are 88, 59, and 41.3, and the DN values of HMPA and DMSO, 38.8 and 29.8, respectively.[6,7] As AN and DN of titrating solvents are larger, their β-sheet-structure-disrupting potential becomes higher.

In conclusion, the β-sheet-structure-disrupted behavior of resin-bound peptides **1—5** suggests that concept of "peptide segment separation by tertiary peptide bonds" is useful for estimating their β-sheet-structure-disrupted behavior. In solid-phase peptide synthesis by a fragment condensation procedure, the β-sheet structure disruption in CH_2Cl_2 by the addition of HMPA and DMSO is more favorable than that of HFIP and TFE because the latter is nucleophilic and consumes a carboxyl component peptide in a coupling reaction.[15] Thus, the easy disruption of resin-bound peptides **1—5** in CH_2Cl_2 by HMPA is of practical significance for solid-phase peptide synthesis, indicating that effective solvents for solid-phase peptide synthesis should be searched by taking the $<P_\alpha>$, $<P_\beta>$, and $<P_c>$ values of the peptide segments into consideration.

This work has been supported by a Grant-in-Aid from the Asahi Glass Foundation for Industrial Technology.

References

1) The abbreviations for amino acids are those recommended by the IUPAC-IUB Commission on Biochemical Nomenclature, *J. Biol. Chem.*, **247**, 977 (1972). Amino acid symbols denote the L-configuration. Additional abbreviations used are the following: TFE, 2,2,2-trifluoroethanol; HMPA, hexamethylphosphoric triamide; HFIP, 1,1,1,3,3,3-hexafluoro-2-propanol; Boc, *t*-butoxycarbonyl; Bzl, benzyl; Pam, phenylacetamidomethyl; IR, infrared; DMSO, dimethyl sulfoxide; MeOH, methanol; THF, tetrahydrofuran.

2) M. Narita, S. Isokawa, S. Nagasawa, and T. Ishijima, *Macromolecules*, **20**, 2306 (1987).

3) M. Narita, S. Isokawa, T. Matsuzawa, and T. Miyauchi, *Macromolecules*, **18**, 1363 (1985).

4) M. Narita, S. Isokawa, S. Honda, H. Umeyama, H. Kakei, and S. Obana, *Bull. Chem. Soc. Jpn.*, **62**, 773 (1989).

5) M. Narita, H. Umeyama, S. Isokawa, S. Honda, C. Sasaki, and H. Kakei, *Bull. Chem. Soc. Jpn.*, **62**, 780 (1989).

6) V. Gutmann, *Electrochim. Acta*, **21**, 661 (1976); U. Mayer, V. Gutmann, and W. Gerger, *Mh. Chem.*, **106**, 1235 (1975); V. Gutmann, "The Donor-Acceptor Approach to Molecular Interaction," Plenum Press, New York (1978).

7) M. Narita, S. Honda, and S. Obana, *Bull. Chem. Soc. Jpn.*, **62**, 342 (1989).

8) P. Y. Chou and G. D. Fasman, *Biochemistry*, **13**, 211 (1974); P. Y. Chou and G. D. Fasman, *ibid.*, **13**, 222 (1974).

9) M. Narita, K. Ishikawa, J.-Y. Chen, and Y. Kim, *Int. J. Pept. Protein Res.*, **24**, 580 (1984).

10) M. Narita, H. Umeyama, and T. Yoshida, *Bull. Chem.*

Soc. Jpn., **62**, 3577 (1989).
11) M. Narita, T. Fukunaga, A. Wakabayashi, K. Ishikawa, and H. Nakano, *Int. J. Pept. Protein Res.*, **23**, 306 (1984).
12) IUPAC-IUB Commission on Biochemical Nomenclature, *Biochemistry*, **7**, 2703 (1968).
13) C. Toniolo, G. M. Bonora, M. Mutter, and F. Maser, *J. Chem. Soc., Chem. Commun.*, **1983**, 1298.
14) M. Narita, Y. Tomotake, S. Isokawa, T. Matsuzawa, and T. Miyauchi, *Macromolecules*, **17**, 1903 (1984).
15) M. Narita, Y. Kojima, and S. Isokawa, *Bull. Chem. Soc. Jpn.*, **62**, 1976 (1989).

 © 1989 The Chemical Society of Japan Bull. Chem. Soc. Jpn., 62, 3587—3592 (1989)

Lipid-Coating on Polyamide Microcapsules Having Long Alkyl Chains and the Characterization of the Lipid-Coated Surface

Kenji KONO, Shunsaku KIMURA, and Yukio IMANISHI*
Department of Polymer Chemistry, Kyoto University, Yoshida Honmachi, Sakyo-ku, Kyoto 606
(Received June 12, 1989)

Polyamide microcapsules with diameters in the range of 1—5 μm were prepared by interfacial polycondensation between terephthaloyl dichloride and a mixture of L-lysine and piperazine. The carboxyl groups of L-lysine residues involved in the polyamide microcapsules were reacted with alkylamine by using water-soluble carbodiimide as a coupling reagent. The alkylated polyamide microcapsules were incubated with liposome to have the surface of the polyamide microcapsules coated with lipid bilayer membrane. The amount of lipid assemblies adsorbed on the polyamide microcapsules with octyl chains increased up to 1.5 times as much as that on the polyamide microcapsules without octyl chains. The synthetic glycopeptides were introduced to the lipid membrane adsorbed on the surface of the polyamide microcapsules. Interactions of the glycopeptides with the lipid membrane on the polyamide microcapsules and of the glycopeptides in the lipid membrane on the polyamide microcapsules with lectin were investigated.

Liposome has been used as a model membrane in biophysical investigations of cell membrane. Furthermore, liposome can be a biocompatible carrier in drug-delivery systems.[1] However, the vesicular structure of liposome is not very stable and is easily breakable due to osmotic pressure or interactions with plasma proteins in vivo.

Generally, cell membrane is stabilized by skeletal proteins, such as microfilaments, spectrin and actin.[2] Polyamide microcapsules coated with lipid bilayer membrane should mimic the structure of cell membrane lined with proteins. Lipid-coating on capsules having diameters in the range of 1—3 mm has been already reported by Rosenthal and Chang[3] and Okahata et al.[4] It has been also shown that the large polyamide capsule membranes were modified by synthetic glycolipids and the permeation was regulated by lectin addition.[5] They incubated the prepared polyamide microcapsules with a lipid solution in alkane, and transferred them to water. However, this method of lipid-coating is not successfully applied to microcapsules having diameters in the range of 1—5 μm, because the small microcapsules suspended in alkane can not be transferred easily to water due to the low specific gravity. Since microcapsules having diameters in the range of 1—5 μm are a suitable model of the cell and a useful carrier in the drug-delivery system, we tried to synthesize small microcapsules coated with lipid membrane. In combination with biologically active peptides which are associated with lipid bilayer membrane, the lipid-coated microcapsules are expected to act as functional microcapsules.

In the previous report,[6] we have shown that small microcapsules can be coated with lipid bilayer membrane when they were incubated with liposome. However, the surface of poly(terephthaloylpiperazine) microcapsules was not completely coated with lipid bilayer membrane.

In the present investigation, polyamide microcapsules were surface-grafted with long alkyl chains and subjected to lipid-coating. The alkylated polyamide microcapsules are expected to be easily covered with lipid membrane due to the hydrophobic nature of the modified surface.

Experimental

Preparation of Polyamide Microcapsules (Uncoated/Unmodified Polyamide Microcapsules). Polyamide microcapsules were prepared in principally the same method as that reported by Muramatsu and Kondo.[7] An aqueous solution (5 ml) of piperazine (0.13 M; 1 M=1 mol dm^{-3}), L-lysine HCl (0.2 M), and Na_2CO_3 (0.47 M) was added to a $CHCl_3$/cyclohexane (1/3, v/v) solution (100 ml) containing sorbitan trioleate (5 vol%) at 0 °C, and the mixture was stirred for 10 min. To the water-in-oil (W/O) emulsion a $CHCl_3$/cyclohexane (1/3, v/v) solution (100 ml) of terephthaloyl dichloride (12.5 mM) containing sorbitan trioleate (5 vol%) was added, and the mixture was allowed to react for 30 min. The microcapsules prepared were washed succeedingly with cyclohexane (three times), an aqueous solution containing poly(oxyethylene) sorbitan monolaurate (5 vol%), and water. The molecular structure of polyamide is shown in Fig. 1.

Reaction of Polyamide Microcapsules with Alkylamine. An aqueous solution of octylamine or decylamine (0.5 M) was adjusted to pH 4.75 with HCl, and added to a dispersion of the uncoated/unmodified polyamide microcapsules. Condensation reaction of carboxyl groups of microcapsules with alkylamine was carried out by using 1-ethyl-3-(3-dimethylaminopropyl)carbodiimide as a coupling reagent. After standing at room temperature for 12 h, the dispersion was washed several times with water until washing solution became neutral. Although free alkylamines might be adsorbed on polyamide microcapsules, they should be desorbed at the following treatment with the excess amount

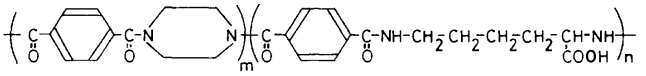

Fig. 1. Chemical structure of uncoated/unmodified polyamide microcapsules.

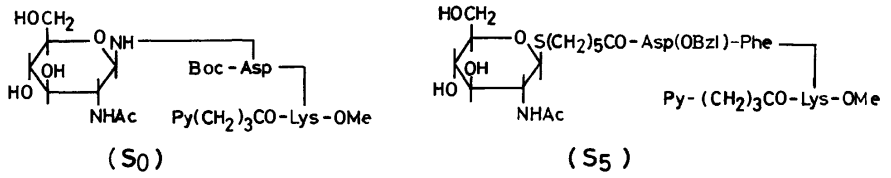

Fig. 2. Structure of synthetic glycopeptides.

of liposome.

Lipid-Coating on Microcapsules. Small unilamellar vesicles (SUV) composed of dimyristoylphosphatidylcholine (DMPC) were prepared by the sonication method. The prepared uncoated/unmodified polyamide microcapsules were incubated with DMPC SUV at 24 °C for 24 h. The dispersion was washed seven times with buffer (4-(2-hydroxyethyl)-1-piperazineethanesulfonic acid (HEPES); 10 mM, NaCl; 0.1 M, pH 7.4) to remove SUV not in use for coating. Other types of microcapsules were also prepared according to the similar procedures.

Synthetic Glycopeptides. The molecular structure of synthesized glycopeptides is shown in Fig. 2. These glycopeptides carry a 1-pyrenyl group in the hydrophobic peptide moiety. The synthetic procedure has been reported previously.[8]

Wheat germ agglutinin (WGA) and lipids were purchased from Sigma. The available agents of the highest grade were used.

Measurements. ζ-Potential of the microcapsules was measured in an aqueous solution buffered with Na_2CO_3/$NaHCO_3$ (pH 10.2, ionic strength 1.8×10^{-4}) using Lazer Zee Meter Model 501 (Ten Kem Inc., New York). The concentration of lipid was determined by colorimetric method using phospholipase D (Diacolor PL, Toyobo, Japan).

The effect of lectin addition on the distribution of glycopeptides in membrane was examined by measuring monomer and excimer emissions of 1-pyrenyl group introduced to the peptide moiety.

Aggregation of polyamide microcapsules upon the addition of lectin was detected by measuring the absorbance at 800 nm.

Fluorescence was measured on an MPF-4 fluorescence spectrophotometer (Hitachi, Japan). 1-Pyrenyl group in the glycopeptides was excited at 345 nm, and monomer and excimer emissions were monitored at 378 and 480 nm, respectively. Absorption spectra were measured on an UVIDEC-1 spectrophotometer (JASCO, Japan).

Results and Discussion

Characterization of the Polyamide Microcapsules. Polyamide microcapsules were prepared by the interfacial polycondensation of terephthaloyl dichloride with L-lysine and piperazine. The size distribution of polyamide microcapsules was examined with a photomicroscope (Fig. 3). The most popular diameter was found to be in the range of 1—2 μm.

The presence of L-lysine as the component of the polyamide microcapsules was confirmed by the existence of free carboxyl groups of L-lysine in microcapsules. That is, ζ-potential of the polyamide microcapsules prepared in the presence of L-lysine was evidently lower than that of poly(terephthaloylpiperazine) microcapsules (Table 1).

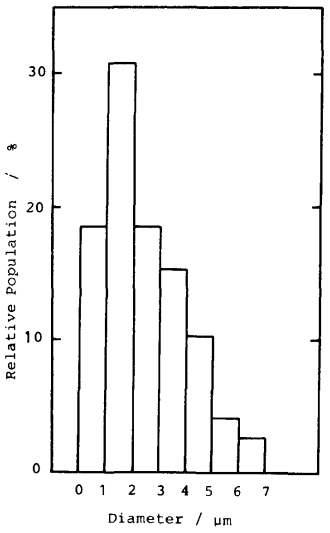

Fig. 3. Size distribution of uncoated/unmodified polyamide microcapsules determined with optical microscope.

Table 1. Zeta-Potential of Polyamide Microcapsules Containing Different Diamine Components

Diamine	Zeta-potential/mV
Piperazine	−20.9±1.6
L-Lysine/piperazine (0.20/0.13 mol/mol)	−42.1±2.0

Potentiometric titration of the polyamide microcapsules revealed that the diamine component of polyamide is composed of 70% of piperazine and 30% of L-lysine units. These values were calculated on the basis of the determination of negative charges on the surface of polyamide microcapsules, in which the contribution from the terminal carboxyl groups was ignored, because it was reported that the interfacial polycondensation of terephthaloyl dichloride and diamines gave polyamides with average molecular weight of about 20000.[9]

The polyamide microcapsules were reacted with

alkylamine to make the surface more hydrophobic. The hydrophobic surface should be favorable for lipid-coating. It was estimated that more than 80% of carboxyl groups of L-lysine units reacted with alkylamine, which was deduced from the titration of the reaction product of poly(terephthaloyllysine) with alkylamine under the same conditions.

Lipid-Coating. The polyamide microcapsules were incubated with DMPC liposome, and washed several times with buffer. It has been reported that lipid molecules not in use for coating are completely removed after seven times of washing, and that the lipid molecules adsorbed on the polyamide microcapsules take a bilayer structure, which was confirmed by the observation of phase transition of membrane by differential scanning calorimetry and measurement of membrane fluidity.[6] The amount of lipid molecules adsorbed on the polyamide microcapsules was determined and is summarized in Table 2. It is clearly shown that the adsorption of lipid molecules on microcapsules is enhanced by the modification of the polyamide microcapsules with alkylamine. The amount of lipid molecules adsorbed on the polyamide microcapsules grafted with octyl chains is 1.5-fold of that on unmodified polyamide microcapsules. Assuming 1.37 g cm^{-3} for the density of polyamide membrane,[10] 13.3 nm for the thickness of polyamide membrane,[10] and 70 $Å^2$ for the area occupied by a DMPC molecule,[11] this amount corresponds to 2.4 bilayers of lipid assemblies. On the other hand, 1.6 bilayers of lipid assemblies were formed on the surface of poly(terephthaloylpiperazine) microcapsules.[6]

Interaction of Glycopeptides with the Polypeptide Microcapsules. The synthetic glycopeptides consist of a hydrophilic glucosamine moiety and a hydrophobic peptide chain. These glycopeptides were shown to be distributed to lipid membrane with the peptide chain buried in the hydrophobic region of lipid membrane.[8] Since the pyrenyl group is connected to the peptide moiety, the interaction of glycopeptides with lipid membrane can be monitored by the fluorescence behavior of the pyrenyl group.

For example, the extent of the distribution of S_0 to lipid membrane can be determined by measuring the quenching rate of pyrenyl fluorescence with acrylamide, because the pyrenyl group is shielded from the aqueous phase upon incorporation into the lipid membrane. S_0 was incubated with various kinds of polyamide microcapsules and the rate of quenching by acrylamide was measured (Table 3). The fluorescence intensity from S_0 was reduced to different extents with the addition of acrylamide in all cases. The fraction of unquenchable S_0 increased in the order of uncoated/unmodified polyamide microcapsules<DMPC-coated/unmodified polyamide microcapsules<DMPC-coated/decyl-grafted polyamide microcapsules<DMPC-coated/octyl-grafted polyamide microcapsules. This order coincides with that of the amount of lipid molecules adsorbed on microcapsules. Therefore, it can be concluded that most of S_0 molecules adsorbed were incorporated into the lipid bilayer membrane formed on the surface of polyamide microcapsules.

The ratio of excimer emission and monomer emission intensities (I_D/I_M) represents the extent of the distribution of glycopeptides in the lipid membrane. Figure 4 shows the dependence of I_D/I_M of S_0 on the temperature in the presence of various kinds of

Table 2. The Amount of Lipid Molecules Adsorbed on Polyamide Microcapsules

Polyamide microcapsule	DMPC adsorbed onto 1 mg microcapsule
Unmodified	280 μg
Octyl-grafted	415 μg
Decyl-grafted	382 μg

Table 3. Quenching of Fluorescence of S_0 Distributed to the Surface of Various Kinds of Polyamide Microcapsules

Polyamide microcapsule	Rate of quenching (%)
Uncoated/unmodified	52.5
DMPC-coated/unmodified	29.9
DMPC-coated/octyl-grafted	22.6
DMPC-coated/decyl-grafted	26.5

[microcapsules]=0.64 mg ml^{-1}. [S_0]=2.2 μM. [acrylamide]=50 mM.

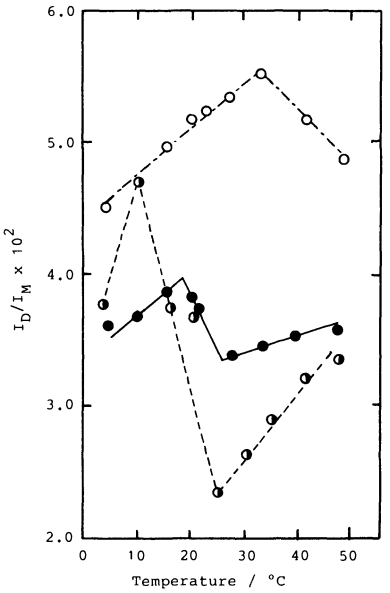

Fig. 4. The temperature dependence of I_D/I_M of S_0 in the presence of uncoated/unmodified polyamide microcapsules (○), DMPC-coated/octyl-grafted polyamide microcapsules (●), and DMPC SUV ([DMPC]= 0.44 mg ml^{-1}) (○). [S_0]=4.3 μM, [microcapsules]= 1.1 mg ml^{-1}.

polyamide microcapsules or DMPC SUV. I_D/I_M of S_0 in the presence of DMPC SUV decreased linearly with descending temperature with a break in the region of the phase-transition temperature of the DMPC bilayer membrane. The monotonous decrease of I_D/I_M should be ascribed to the different temperature dependence of the quantum yields of the excimer and the monomer emission. On the other hand, the abrupt increase of I_D/I_M occurring in the region between 24 and 10 °C can be ascribed to the increasing local concentration of S_0 in the DMPC bilayer membrane due to the phase separation below the phase transition temperature. It is well-known that the phase separation of lipid membrane produces domains of pure lipid molecules in a gel state as well as domains containing high concentrations of solute.[8]

The temperature dependence of I_D/I_M of S_0 in the presence of uncoated/unmodified polyamide microcapsules showed the break at 33 °C. The reason for this phenomenon is two fold. Increasing adsorption of the S_0 to the uncoated/unmodified polyamide microcapsules with descending temperature leads to increasing I_D/I_M in the region of higher temperatures, whilst I_D/I_M by nature decreases with descending temperature as it does in the region of lower temperatures.

In the presence of DMPC-coated/octyl-grafted polyamide microcapsules, the abrupt increase of I_D/I_M of S_0 with descending temperature was observed in the region of the phase transition temperature, indicating that S_0 should be distributed to lipid assemblies, which take the structure of lipid bilayer membrane on the polyamide microcapsules. Although the change observed in the presence of DMPC-coated/octyl-grafted polyamide microcapsules was less marked than that in the presence of DMPC SUV, the former change was more significant than that observed in the presence of DMPC-coated poly(terephthaloylpiperazine) microcapsules.[6] Therefore, the surface of polyamide microcapsules uncoated with lipid membrane can be reduced considerably by grafting octyl groups into microcapsules, resulted in the increase of the amount of lipid assemblies coated on microcapsules.

Interactions of Lectin with Glycopeptides on the Polyamide Microcapsules. The glycopeptide S_5 was used for the investigation on the interaction of lectin and the glycopeptide on the polyamide microcapsules. It has been reported that S_5 in lipid bilayer membrane interacts with lectin without being pulled out of the membrane.[8] WGA is known to possess four binding sites with a high affinity to *N*-acetylglucosamine and to crosslink two glycoproteins embedded in membrane.[12] Interaction of WGA with S_5 on the polyamide microcapsules was investigated by measuring the effect of the lectin addition on I_D/I_M ratio (Fig. 5). I_D/I_M of S_5 increased with the addition of WGA. The relative increase of I_D/I_M was the largest in the presence of DMPC-coated/octyl-grafted polyamide microcapsules, and the second largest in the presence of DMPC liposome. The increase of I_D/I_M with the addition of WGA was not remarkable in the presence of uncoated/unmodified polyamide microcapsules. The interaction of WGA with S_5 on the surface of uncoated/unmodified polyamide microcapsules should have been suppressed by negative charges on the surface of the microcapsules, because the crosslinking of S_5 with the addition of WGA occurred to a higher extent in the presence of uncoated poly(terephthaloylpiperazine) microcapsules.

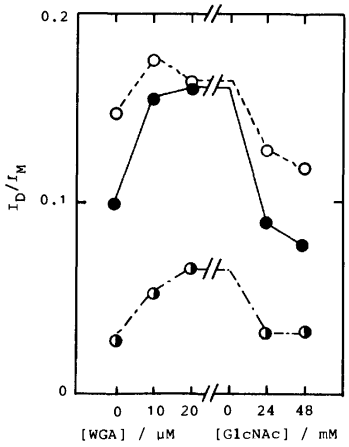

Fig. 5. The change of I_D/I_M of S_5 with the addition of WGA and the dissociation of crosslinked S_5 with the addition of GlcNAc in the presence of uncoated/unmodified polyamide microcapsules (○), DMPC-coated/octyl-grafted polyamide microcapsules (●), and DMPC SUV ([DMPC]=0.44 mg ml^{-1}) (◑). [S_5]=4.5 μM, [microcapsules]=1.1 mg ml^{-1}.

The crosslinking of S_5 molecules by WGA is facilitated on the surface of DMPC-coated/octyl-grafted polyamide microcapsules. The larger change of I_D/I_M in the presence of DMPC-coated/octyl-grafted polyamide microcapsules than that in the presence of DMPC SUV is ascribed to the high local concentration of S_5 on the surface of the polyamide microcapsules. That is, although 2.4 bilayers of lipid membrane are accumulated on DMPC-coated/octyl-grafted polyamide microcapsules, S_5 molecules can not be distributed to the inner bilayers due to the inability of S_5 to permeate through the hydrophobic core of lipid bilayer membrane. Therefore, the concentration of S_5 molecules dispersed in the lipid assembly is higher on the surface of the polyamide microcapsules than that in DMPC SUV for the same total amount of lipid molecules. This explanation is consistent with the higher value of I_D/I_M of S_5 in the presence of DMPC-coated/octyl-grafted polyamide microcapsules than that in the presence of DMPC SUV without the addition of WGA.

The crosslinking of S_5 by WGA was shown to be reversible on the surface of DMPC-coated/octyl-

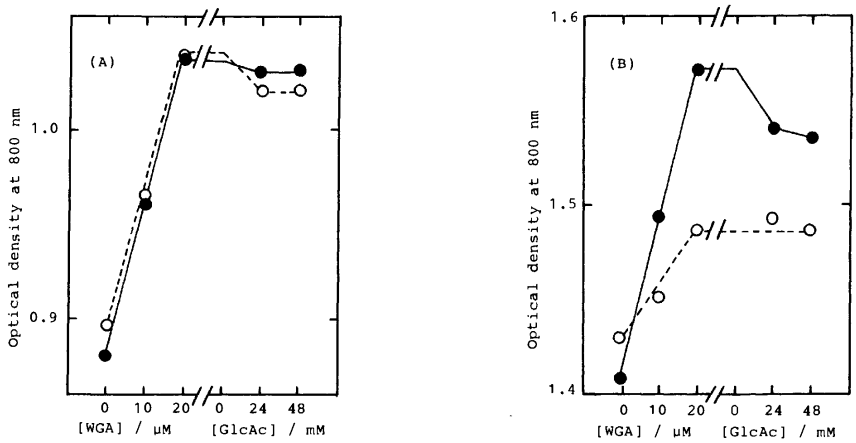

Fig. 6. Aggregation of microcapsules with the addition of WGA and dissociation of the aggregates with the addition of GlCNAc. [microcapsules]=0.64 mg ml^{-1}. [S_5]=0 M (○) and [S_5]=4.5 μM (●). In the presence of (A); uncoated/unmodified microcapsules, and (B), DMPC coated/octyl-grafted polyamide microcapsules.

grafted polyamide microcapsules, since the addition of inhibitor, *N*-acetylglucosamine, restored the original value of I_D/I_M in the absence of WGA.

As shown in Fig. 6A, aggregation of microcapsules was also observed with the addition of WGA, which might have been brought about by crosslinking of microcapsules by WGA. The absorbance of the suspension of uncoated/unmodified polyamide microcapsules increased with the addition of WGA either in the presence or in the absence of S_5. The aggregation of polyamide microcapsules was not dissociated by the addition of *N*-acetylglucose. Therefore, the aggregation should be nonspecific one between WGA and the surfaces of polyamide microcapsules. This type of aggregation was suppressed by coating the microcapsules with lipid membrane, as shown in Fig. 6B. The aggregation of DMPC-coated/octyl-grafted polyamide microcapsules by WGA should occur in the uncoated part of the polyamide microcapsules. The aggregation was enhanced in the presence of S_5 and suppressed partly by the addition of *N*-acetylglucose. Therefore, a part of the aggregation was caused by the specific interaction of WGA with S_5 in lipid membrane on the polyamide microcapsules.

To conclude, it was shown that the surface of polyamide microcapsules having diameters of 1—5 μm can be coated with lipid assemblies, and the efficiency of the lipid coating increased by the introduction of alkyl chains to the surface. The lipid assemblies adsorbed on polyamide microcapsules take the structure of lipid bilayer membrane, and mimics the cellular surface, in which glycopeptides interact with lectin. Therefore, lipid-coated microcapsules provide lipid bilayer membrane stabilized by polyamide microcapsules, and can be utilized as functional microcapsules by modification with biologically active peptides. However, polyamide surface can not be completely covered with lipid membrane. This imperfectness causes some problems in analyzing interactions of glycopeptides in the lipid membrane on the polyamide microcapsules. In addition, the encapsulation of small molecules into the obtained lipid-coated microcapsules will not be possible, which becomes a problem for utilization of microcapsules to the drug-delivery system. Three possibilities are considered for perfect covering the surface with lipid membrane. The first is to introduce more L-lysine residues as a basic component and increase the amount of alkyl chains grafted to the polyamide microcapsules. However, increasing content of L-lysine residues decreases the mechanical strength of the polyamide microcapsules. The second is to use longer alkyl chains to modify the surface. However, the alkylation reaction is very difficult because of the low solubility of long chain alkylamine in water. The third is to use amphiphilic polypeptides to increase the affinity of the polyamide microcapsules to lipid membrane. The last possibility is under investigation.

References

1) G. Gregoriadis, *Nature (London)*, **283**, 814 (1980).
2) S. Lux, *Nature (London)*, **281**, 426 (1979).
3) A. M. Rosenthal and T. M. S. Chang, *J. Membr. Sci.*, **6**, 329 (1980).
4) Y. Okahata, H. J. Lim, G. Nakamura, and S. Hachiya, *J. Am. Chem. Soc.*, **105**, 4855 (1983).
5) Y. Okahata, G. Nakamura, and H. Noguchi, *J. Chem. Soc., Perkin Trans. 2*, **1987**, 1317.
6) K. Kono, S. Kimura, and Y. Imanishi, *J. Membr. Sci.*, in press.
7) N. Muramatsu and T. Kondo, *J. Biomed. Mater. Res.*, **14**, 211 (1980).

8) T. Ohtoyo, M. Shimagaki, K. Otoda, S. Kimura, and Y. Imanishi, *Biochemistry*, **27**, 6458 (1988).
9) V. E. Shashoua and W. M. Eareckson III, *J. Polym. Sci.*, **40**, 343 (1959).
10) K. Takamura, M. Koishi, and T. Kondo, *J. Pharm. Sci.*, **62**, 610 (1973).
11) C. Hung and J. T. Mason, *Proc. Natl. Acad. Sci. U.S.A.*, **75**, 308 (1978).
12) Y. Nagata and M. M. Burger, *J. Biol. Chem.*, **249**, 3116 (1974).

 © 1989 The Chemical Society of Japan Bull. Chem. Soc. Jpn., 62, 3593—3597 (1989)

The Synthesis of Some Dimethylpyranocoumarins and Isopropenyldihydrofuranocoumarins

Seiji YAMAGUCHI,* Ryozo MIYAKAWA, Shinobu YONEZAWA, and Yoshiyuki KAWASE*
Department of Chemistry Faculty of Science, Toyama University,
Gofuku 3190, Toyama 930
(Received June 14, 1989)

Two pyranocoumarins, 7,7-dimethyl-2(7*H*)-benzo[1,2-*b*:4,5-*b'*]dipyranone and 8,8-dimethyl-2(8*H*)-benzo[1,2-*b*:5,4-*b'*]dipyranone, and three dihydrofuranocoumarins, 2-isopropenyl-1,2-dihydro-8-furo[1,2-*f*][1]benzopyranone, 2-isopropenyl-2,3-dihydro-6-furo[1,2-*e*][1]benzopyranone, and 2-isopropenyl-2,3-dihydro-7-furo[2,1-*e*][1]benzopyranone, were synthesized by an effective pyrone-ring formation in corresponding *o*-hydroxybenzaldehyde derivatives. And, 2-[1-(hydroxymethyl)vinyl]-1,2-dihydro-8-furo[1,2-*f*][1]benzopyranone was also synthesized selenium dioxide oxidation.

Natural xanthyletin[1] is a dimethylpyranocoumarin, and natural ammirin,[2] isoangenomalin,[3] angenomalin,[4] masquin,[5] and majurin[6] are isopropenyldihydrofuranocoumarins. In plants, these tricyclic *O*-heteroaromatic compounds may be prepared by prenylations of 7-hydroxycoumarin followed by cyclizations. We have studied the syntheses of 2,2-dimethyl-2*H*-chromenes and 2-isopropenyl-2,3-dihydrobenzofurans. In this paper we describe a new approach to dimethylpyranocoumarins and isopropenyldihydrofuranocoumarins by a pyrone-ring formation in some *o*-hydroxybenzaldehyde derivatives having 2*H*-chromene and dihydrobenzofuran structures.

We have already reported the acylation of 2,2-dimethyl-2*H*-chromenes[7] and 2-isopropenyl-2,3-dihydrobenzofurans,[8] and have obtained some methoxyl aldehydes by their formylations. Two *o*-hydroxybenzaldehyde derivatives having chromene structures, 6-hydroxy-2,2-dimethyl-2*H*-chromen-7-carbaldehyde (**1**) and 7-hydroxy-2,2-dimethyl-2*H*-chromen-6-carbaldehyde (**2**), were prepared from the corresponding methoxy derivatives by demethylation with magnesium iodide etherate. Two *o*-hydroxybenzaldehydes having dihydrobenzofuran structures, 5-hydroxy-2-isopropenyl-2,3-dihydrobenzofuran-6-carbaldehyde (**4**) and 6-hydroxy-2-isopropenyl-2,3-dihydrobenzofuran-5-carbaldehyde (**5**), were also prepared by demethylation of the corresponding methoxy derivatives. However, a similar preparation of 4-hydroxy-2-isopropenyl-2,3-dihydrobenzofuran-5-carbaldehyde (**3**) was not so effective, since in the cyclization of *m*-methoxyphenol with 1,4-dibromo-2-methyl-2-butene, the 4-methoxy derivative was the minor and the 6-methoxy derivative the major; the formylation of the minor 4-methoxy derivative, furthermore, gave a mixture of 5- and 7-formylated products. Thus, **3** was prepared in another procedure. A cyclization of 1,3-cyclohexanedione with 1,4-dibromo-2-methyl-2-butene gave 2-isopropenyl-2,3,6,7-tetrahydro-4(5*H*)-benzofuranone (**11**) in 41% yield. The structure of **11** was confirmed by dehydrogenation to 2-isopropenyl-2,3-dihydro-4-benzofuranol (**12**). The methyl ether of **12** was identical with the sample prepared in cyclization of *m*-methoxyphenol with 1,4-dibromo-2-methyl-2-butene.[8] Condensation of **11** with ethyl formate gave 5-hydroxymethylene-2-isopropenyl-2,3,6,7-tetrahydro-4-(5*H*)-benzofuranone (**13**) in 35% yield, which was easily converted by dehydrogenation with DDQ to the desired *o*-hydroxybenzaldehyde **3** in 87% yield. This isopropenyldihydrobenzofuran **3** showed an ABX signal pattern typical in 2-isopropenyl-2,3-dihydrobenzofurans.

Some methods for pyrone-ring formation in *o*-hydroxybenzaldehydes were reported, but they were not so effective. We tried some new pyrone-ring

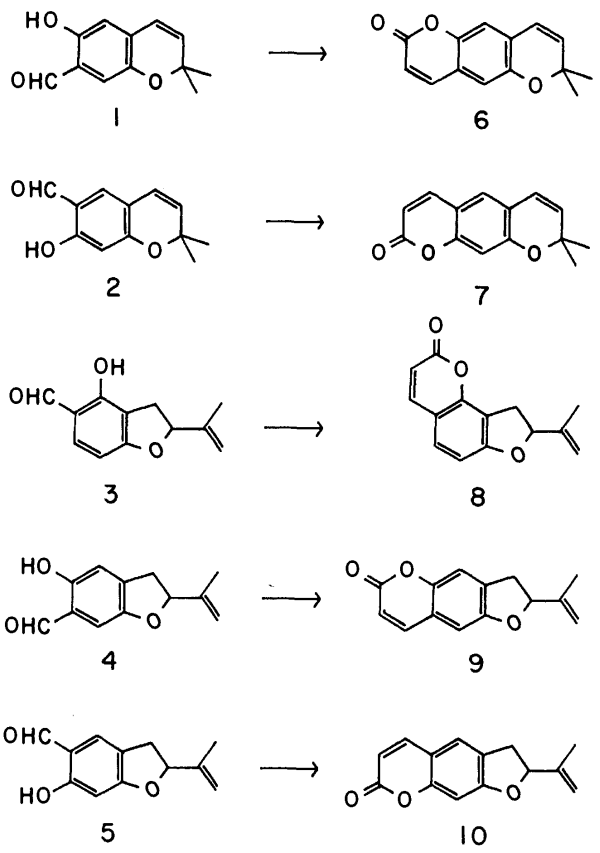

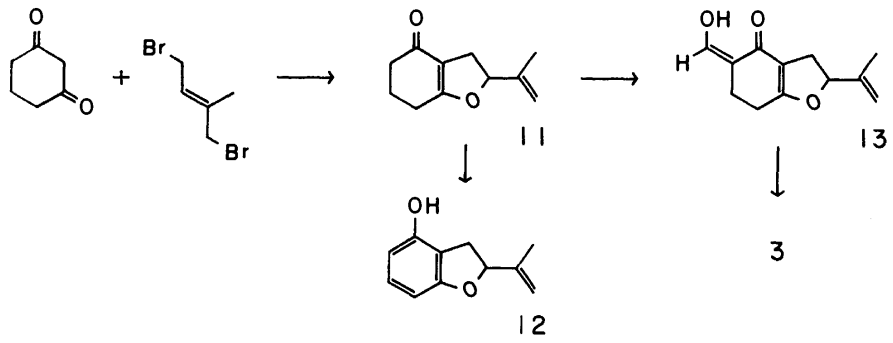

Table 1. The Yields, Some Physical Data, and Elemental Analyses of Dimethylpyranocoumarins and Isopropenyldihydrofurocoumarins

Compound	Yield %	Mp θ_m/°C	IR cm^{-1}	MS (M$^+$)	Elemental analysis[a] C(%)	H(%)
6	64	157—158	1700	228	73.51	5.46
7	49	133—134.5	1720	228	73.46	5.26
8	46	111—113	1735	228	73.96	5.23
9	63	157—158	1710	228	73.45	5.31
10	18[10]	98—98.5	1720	228	73.68	5.30

a) Calcd data for $C_{14}H_{12}O_3$: C, 73.67; H, 5.30%.

Table 2a. NMR Data of Dimethylpyranocoumarins (δ/ppm, J/Hz)

Compound	Me	Olefinic in pyran	Olefinic in pyrone	Aromatic
6	1.4(s)	5.8(d) 6.35(d) J=10	6.3(d) 7.5(d) J=10	6.8(s) 6.9(s)
7	1.4(s)	5.7(d) 6.3(d) J=10	6.2(d) 7.5(d) J=10	6.7(s) 7.0(s)

formation in 2-hydroxy-4-methoxybenzaldehyde, and the corresponding coumarin was obtained in the following three cases: a) heating with acetyl chloride in the presence of DBU at 110—140 °C for 2 h (10%), b) refluxing with *N,N*-dimethylacetamide dimethylacetal in xylene for 30 m (10%), c) refluxing *N,N*-dimethylacetamide dimethylacetal in ether for 6 h (22%). Thus, by pyrone-ring formations with *N,N*-dimethylacetamide dimethylacetal in refluxing ether for 6 h, two chromene derivatives **1,2** were effectively converted to the corresponding pyranocoumarins, 7,7-dimethyl-2(7*H*)-benzo[1,2-*b*:4,5-*b'*]dipyranone (**6**) and 8,8-dimethyl-2(8*H*)-benzo[1,2-*b*:5,4-*b'*]dipyranone (**7**) in 64% and 49% yield. They showed carbonyl absorption at 1700 cm^{-1} (**6**), 1720 cm^{-1} (**7**) in their IR spectra, and new olefinic protons of pyrone-ring at δ 5.8 and 7.5 (**6**), δ 5.7 and 7.5 (**7**) in the ^{1}H NMR spectra. Similar pyrone-ring formations of three dihydrobenzofurans (**3**, **4**, **5**) gave the corresponding furocoumarins, 2-isopropenyl-1,2-dihydro-8-furo[1,2-*f*][1]benzopyranone (**8**), 2-isopropenyl-2,3-dihydro-8-furo[1,2-*e*][1]benzopyranone (**9**), and 2-isopropenyl-2,3-dihydro-7-furo[2,1-*e*][1]benzopyranone (**10**) in 46, 63, and 18%.[9] These furocoumarins showed a carbonyl absorption at 1735 cm^{-1} (**8**), 1710 cm^{-1} (**9**), 1720 cm^{-1} (**10**), and showed the olefinic protons of pyrone-ring at δ 6.2 and 7.6 (**8**), δ 6.3 and 7.6 (**9**), δ 6.2 and 7.6 (**10**). The spectral data of pyrano coumarin **7** were identical with the reported data of natural xanthyletin.[1] Furocoumarins **8**, **10** were also identical with natural majurin,[6] angenomalin,[4] masquin,[5] ammirin,[2] and isoangenomalin,[3] in their spectral data.

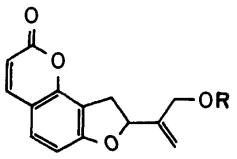

14 a) R = Ac
b) R = H

Another furocoumarin having an oxidized isopropenyl graup (**14b**) was also reported as natural sachalinin[10] and discophoridin.[11] We converted **8** to **14b** by oxidation with selenium dioxide. The oxidation of **8** with selenium dioxide in refluxing acetic anhydride for 7 h gave an acetate, 2-[1-(acetoxymethyl)vinyl]-1,2-dihydro-8-furo[1,2-*f*][1]benzopyranone (**14a**), in 18% yield. This acetate **14a**,

Table 2b. NMR Data of Isopropenyldihydrofurocoumarins
(δ/ppm, J/Hz)

Compound	Me	H_A, H_B, H_X in dihydrofuran				Endo-methylene		Olefinic in pyrone		Aromatic	
8	1.8(s)	3.2(dd)	3.5(dd)	5.5(dd)	J_{AB}=16 J_{AX}= 8 J_{BX}=10	5.0(br.s)	5.1(br.s)	6.2(d)	7.6(d) J=10	6.8(d)	7.3(d) J=8
9	1.8(s)	3.2(dd)	3.4(dd)	5.2(dd)	J_{AB}=16 J_{AX}= 8 J_{BX}=10	4.9(br.s)	5.1(br.s)	6.3(d)	7.6(d) J=9	6.8(s)	7.1(s)
10	1.8(s)	3.1(dd)	3.4(dd)	5.3(dd)	J_{AB}=16 J_{AX}= 8 J_{BX}=10	5.0(br.s)	5.1(br.s)	6.2(d)	7.6(d) J=10	6.7(s)	7.2(s)

showed a new acetoxyl methyl signal at δ 2.0 and a new methylene signal at δ 4.7 in the ^{1}H NMR spectrum. This acetate was easily converted to 2-[1-(hydroxymethyl)vinyl]-1,2-dihydro-8-furo[1,2-*f*][1]benzopyranone (**14b**) in 70% yield by refluxing with 20% potassium hydroxide ethanolic solution for 1 h. This alcohol **14b** showed a hydroxyl absorption at 3400 cm^{-1}, and showed a methylene signal at δ 4.3. The spectral data were identical with those of natural discophoridin.[11]

Experimental

The melting and boiling points were uncorrected (in boiling points: 1 mmHg=133.322 Pa). The IR spectra were measured on a Hitachi 260-50 spectrometer in a liquid film or a KBr disk, and the UV spectra were taken on a Hitachi 220A spectrophotometer in an ethanolic solution. The ^{1}H NMR spectra were recorded on a JEOL PMX-60Si or FX-90Q NMR spectrometer, and the mass spectra were recorded on a JEOL JMS-OISG-2 mass spectrometer.

Preparation of 1 and 2. By a procedure reported in the demethylation of dihydrobenzofurans,[8] 6-hydroxy-2,2-dimethyl-2*H*-chromen-7-carbaldehyde (**1**) and 7-hydroxy-2,2-dimethyl-2*H*-chromen-6-carbaldehyde (**2**) were prepared from the corresponding methoxyl derivatives[7] in 79 and 70% yield. **1**; mp 96.5—98 °C (from hexane). IR (KBr) 1650 cm^{-1}. ^{1}H NMR (CCl_4) δ=1.4 (6H, s), 5.9 (1H, d, J=10 Hz), 6.4 (1H, d, J=10 Hz), 6.6 (1H, s), 7.0 (1H, s), 10.0 (1H, s), 10.8 (1H, s). Found: C, 70.68; H, 5.91%. Calcd for $C_{12}H_{12}O_3$: C, 70.57; H, 5.92%. MS *m/z* 204 (M^+). **2**; mp 97.5—98.5 °C (from hexane). IR (KBr) 1630 cm^{-1}. ^{1}H NMR (CCl_4) δ=1.4 (6H, s), 5.5 (1H, d, J=10 Hz), 6.2 (1H, d, J=10 Hz), 6.2 (1H, s), 7.0 (1H, s), 9.6 (1H, s), 12.9 (1H, s). Found: C, 70.49; H, 5.87%. Calcd for $C_{12}H_{12}O_3$: C, 70.57; H, 5.92%. MS *m/z* 204 (M^+).

Cyclization of 1,3-Cyclohexanedione with 1,4-Dibromo-2-methyl-2-butene. To a solution of 1,3-cyclohexanedione (20.0 g, 179 mmol) and 1,4-dibromo-2-methyl-2-butene (40.3 g, 177 mmol) in dry acetone (250 ml) was added anhydrous potassium carbonate (74.0 g); the mixture was stirred for 8 h under refluxing. After removing the acetone, the mixture was diluted with water and extracted with ether. The ether layer was washed with 5% sodium hydroxide solution and saturated sodium chloride solution, and dried over anhydrous sodium sulfate. After removing the ether, the residue was distilled under reduced pressure. The fractions boiling at 144—156 °C/17 mmHg were re-distilled to give 2-isopropenyl-2,3,6,7-tetrahydro-4(5*H*)-benzofuranone (**11**) as fractions boiling at 145—157 °C 16 mmHg (12.8 g, 41%). **11**; IR (neat) 1630 cm^{-1}. ^{1}H NMR (CCl_4) δ=1.8 (3H, s), 2.0—3.2 (8H, m), 4.9 (1H, broad s), 5.0 (1H, broad s), 5.2 (1H, broad t, J=10 Hz). Found: C, 73.97; H, 7.78%. Calcd for $C_{11}H_{14}O_2$: C, 74.13; H, 7.92%. MS *m/z* 178 (M^+), 163, 150.

Dehydrogenation of 11 to 12. To a solution of **11** (379 mg, 2.13 mmol) in toluene (20 ml) was added 2,3-dichloro-5,6-dicycano-1,4-benzoquinone (DDQ) (490 mg, 2.16 mmol); the mixture was refluxed for 15 h. After removing of the precipitates by filtration, the filtrate was diluted with benzene and then extracted with 5% sodium hydroxide solution. The alkaline solution was acidified with 10% hydrochloric acid and re-extracted with benzene. The benzene layer was washed with saturated sodium chloride

Table 3. The UV Spectral Data of Dimethylpyranocoumarins and Isopropenyldihydrofurocoumarins

Compound	λ_{max}/nm (log ε)
6	248(4.13) 298(4.17) 308sh(4.14) 370(3.95)
7	222.5(4.38) 263(4.29) 300(3.76) 345(4.12)
8	249(3.54) 259(3.58) 325(4.18)
9	229(4.37) 251(3.86) 259(3.85) 281(4.01) 345(3.89)
10	222(4.08) 245(3.65) 256(3.57) 297sh(3.83) 332.5(4.26)
14a	248.5(3.51) 258.5(3.53) 324.5(4.10)
14b	248.5(3.45) 258(3.49) 325(4.15)

solution and dried over anhydrous sodium sulfate. After removing the solvent, the residue was purified on a silica-gel column with benzene eluents to give 2-isopropenyl-2,3-dihydro-4-benzofuranol (**12**)(132 mg, 35%); bp 190—210 °C/15 mmHg (bath temp). IR (neat) 3450 cm^{-1}. ^{1}H NMR (CCl_4) 1.8 (3H, s), 3.0 (1H, dd, J=16 and 8 Hz), 3.2 (1H, dd, J=16 and 9 Hz), 4.9 (1H, broad s), 5.0 (1H, broad s), 5.1 (1H, dd, J=9 and 8 Hz), 5.4 (1H, broad s), 6.2 (1H, d, J=8 Hz), 6.3 (1H, d, J=8 Hz), 6.9 (1H, t, J=8 Hz). MS m/z 176 (M^+), 161. This phenol **12** was labile for its probable partial autooxidation. In the IR spectra, its methyl ether was identical with the sample prepared from *m*-methexyphenol.[8]

Condensation of 11 with Ethyl Formate. To a suspension of sodium hydride (0.43 g, 18 mmol) in dry benzene (50 ml) was added ethyl formate (5.32 g, 71.8 mmol), carefully. Then, 2-isopropenyl-2,3,6,7-tetrahydro-4(5*H*)-benzofuranone (**11**) (3.19 g, 17.0 mmol) was added under refluxing, and the mixture was refluxed for 2 h. After cooling, the mixture was treated with 5% sodium hydroxide solution. The alkaline aqueous layer collected was washed with benzene and acidified with 10% hydrochloric acid, and then re-extracted with ether. The ether layer was washed with a saturated sodium chloride solution and dried over anhydrous sodium sulfate. After removing the ether, the residue was distilled to give 5-hydroxymethylene-2-isopropenyl-2,3,6,7-tetrahydro-4(5*H*)-benzofuranone (**13**) (1.29 g, 35%); bp 140—200 °C/23 mmHg. IR (neat) 1635 cm^{-1}. ^{1}H NMR (CCl_4) δ=1.8 (3H, s), 2.5 (4H, broad s), 2.7 (1H, dd, J=16 and 8 Hz), 2.9 (1H, dd, J=16 and 9 Hz), 4.8 (1H, broad s), 5.0 (1H, broad s), 5.2 (1H, dd, J=9 and 8 Hz), 7.0 (1H, broad s). UV (EtOH) 271 (log ε 4.66), 315 nm (sh). MS m/z 206 (M^+), 191, 178, 163. Found: C, 69.96; H, 6.65%. Calcd for $C_{12}H_{14}O_3$: C, 69.88; H, 6.84%.

Dehydrogenation of 13 to 3. By a procedure described above in dehydrogenation of **11** to **12**, **13** (3.01 g, 14.6 mmol) was dehydrogenated with DDQ (2,3-dichloro-5,6-dicyano-1,4-benzoquinone) (3.31 g, 14.6 mmol) to give a crude phenol, which was purified with a silica-gel column with hexane-ethyl aceteate (1:1) eluents. 4-Hydroxy-2-isopropenyl-2,3-dihydrobenzofuran-5-carbaldehyde (**3**) (2.59 g, 87%); bp 170—180 °C/20 mmHg (bath temp.). IR (neat) 1645 cm^{-1}. ^{1}H NMR (CCl_4) δ=1.8 (3H, s), 3.0 (1H, dd, J=16 and 8 Hz), 3.3 (1H, dd, J=16 and 9 Hz), 4.9 (1H, broad s), 5.1 (1H, broad s), 5.3 (1H, dd, J=9 and 8 Hz), 6.4 (1H, d, J=9 Hz), 7.3 (1H, d, J=9 Hz), 9.7 (1H, s), 11.5 (1H, s). UV (EtOH) 235 (log ε 3.89), 242 (sh), 291 nm (4.25). MS m/z 204 (M^+), 189. Found: C, 70.81; H, 5.99%. Calcd for $C_{12}H_{12}O_3$: C, 70.57; H, 5.92%. The methyl ether derived from **3** by methylation with dimethyl sulfate was identical with the sample from formylation of 2-isopropenyl-4-methoxy-2,3-dihydrobenzofuran.[8]

A New Pyrone-Ring Formation to Coumarin Derivatives. To a solution of *o*-hydroxybenzaldehyde derivatives **1—5** (ca. 5 mmol) in dry ether (20 ml) was added *N*,*N*-dimethylacetamide dimethylacetal (ca. 10 mmol); and the mixture was refluxed for 6 h under stirring. After cooling, the mixture was treated with 10% hydrochloric acid. The ether layer was collected, and the aqueous layer was extracted with chloroform. The organic layer was washed with a saturated sodium hydrogencarbonate solution and dried over anhydrous sodium sulfate. After removing the solvents, the two residues from ether and chloroform layers were combined and purified on a short silica-gel column. Pyronocoumarins **6** and **7** were obtained as the fractions eluted with chloroform and recrystallized from benzene. Dihydrofurocoumarins **8**, **9**, **10** were obtained as the fractions eluted with hexane-ethyl acetate (9:1) and recrystallized from cyclohexane. The yields and the spectral data are summarized in Tables 1, 2, and 3.

Oxidation of 8 to 14a with Selenium Dioxide. To a solution of **8** (0.48 g, 2.1mmol) in acetic anhydride (50 ml) was added selenium dioxide (0.25 g, 2.3 mmol); the mixture was refluxed for 7 h with stirring. After cooling, selenium compounds formed were filtered off, and the excess acetic anhydride was removed under reduced pressure. The residue was diluted with chloroform. The chloroform solution was washed with a saturated sodium hydrogencarbonate solution and a saturated sodium chloride solution, and then dried over anhydrous sodium sulfate. After removing the solvent, the residue was purified on a short silical-gel column. The fractions eluted with hexane-ethyl acetate (8:2) were collected and recrystallized from hexane-ether to give 2-[1-(acetoxymethyl)vinyl]-1,2-dihydro-8-furo[1,2-*f*][1]-benzopyranone (**14a**) (0.10 g, 18%); mp 77.5—78.5 °C. IR (KBr) 1720 cm^{-1}. ^{1}H NMR ($CDCl_3$) δ=2.0 (3H, s), 3.2 (1H, dd, J=16 and 8 Hz), 3.6 (1H, dd, J=16 and 10 Hz), 4.7 (2H, broad s), 5.3 (1H, broad s), 5.4 (1H, broad s), 5.5 (1H, dd, J=10 and 8 Hz), 6.2 (1H, d, J=10 Hz), 6.7 (1H, d, J=8 Hz), 7.4 (1H, d, J=8 Hz), 7.7 (1H, d, J=10 Hz). Found: C, 67.01; H, 4.80%. Calcd for $C_{16}H_{14}O_5$: C, 67.12; H, 4.93%. MS m/z 286 (M^+), 226, 186. As the fractions eluted with hexane-ethyl acetate (95:5), **8** was recovered in 20%.

Hydrolysis of 14a to 14b. To a solution of **14a** (0.32 g, 1.1 mmol) in ethanol (10 ml) was added 20% potassium hydroxide aqueous solution (15 ml); the mixture was refluxed for 1 h with stirring. After cooling, the mixture was diluted with water and extracted with chloroform. The chloroform layer was washed with a saturated sodium chloride solution and dried over anhydrous sodium sulfate. After removing the chloroform, the residue was crystallized from ethanol to give 2-[1-(hydroxymethyl)vinyl]-1,2-dihy-

dro-8-furo[1,2-*f*][1]benzopyranone (**14b**) (0.19 g, 70%); mp 102—103 °C. IR (KBr) 3400, 1720 cm^{-1}. ^1H NMR ($CDCl_3$) δ=2.3 (1H, broad s), 3.3 (1H, dd, J=16 and 8 Hz), 3.5 (1H, dd, J=16 and 10 Hz), 4.3 (2H, broad s), 5.3 (2H, broad s), 5.5 (1H, dd, J=10 and 8 Hz), 6.2 (1H, d, J=9 Hz), 6.7 (1H, d, J=9 Hz), 7.2 (1H, d, J=9 Hz), 7.8 (1H, d, J=9 Hz). Found: C, 68.96; H, 5.04%. Calcd for $C_{14}H_{12}O_4$: C, 68.84; H, 4.95%. MS m/z 248 (M^+), 213, 186.

References

1) W. Steck, *Can. J. Chem.*, **49**, 2297 (1971).
2) T. Kikuchi, T. Yokoi, K. Umemoto, and T. Shingu, *Yakugaku Zasshi*, **94**, 1616 (1974).
3) F. Bohlmann, J. Jacob, and M. Grenz, *Chem. Ber.*, **108**, 433 (1975).
4) F. Bohlmann and H. Franke, *Chem. Ber.*, **104**, 3229 (1971).
5) E. A. Martinez, R. E. Reyes, A. G. Gonzalez, and L. F. Rodriguez, *Ann. Quim.*, **63**, 205 (1967).
6) E. A. Ab-Mustafa, F. K. A. El-Bay, and M. B. E. Fayez, *Tetrahedron Lett.*, **1971**, 1657.
7) S. Yamaguchi, S. Yamamoto, S. Abe, and Y. Kawase, *Bull. Chem. Soc. Jpn.*, **57**, 442 (1984).
8) S. Yamaguchi, A. Miyata, M, Ueno, T. Hase, K. Yamamoto, and Y. Kawase, *Bull. Chem. Soc. Jpn.*, **57**, 617 (1984).
9) S. Yamaguchi, K. Sugiura, R. Fukuoka, K. Okazaki, M. Takeuchi, and Y. Kawase, *Bull. Chem. Soc. Jpn.*, **57**, 3607 (1984).
10) The yield of **10** was improved from 18 to 26% by a longer refluxing (8 h).
11) G. K. Nikonov, *Khim. Prir. Soedin.*, **6**, 623 (1970).
12) W. Bottomley, *Aust. J. Chem.*, **16**, 143 (1963).

Diastereoselective Reduction of α-Keto Amides Having *trans*-2,5-Disubstituted Pyrrolidine as a Chiral Auxiliary

Yasuhiro KAWANAMI,* Izumi FUJITA, Shouko ASAHARA, Tsutomu KATSUKI,† and Masaru YAMAGUCHI†
Department of Chemistry, Faculty of Education, Kagawa University, Takamatsu, Kagawa 760
†Department of Chemistry, Faculty of Science, Kyushu University 33, Higashi-ku, Fukuoka 812
(Received July 11, 1989)

The reduction of α-keto amides derived from (2*R*,5*R*)-*trans*-2,5-bis(methoxymethoxymethyl)pyrrolidine [(*R*)-BMOMP, **1**] with $LiBEt_3H$ or $KBEt_3H$ proceeded with high diastereoselectivity (up to 99% ds) to afford the corresponding α-hydroxy amides in good yields. The additive effect of crown ethers or metallic salts on the stereoselectivity was also examined.

Optically active α-hydroxy acid derivatives are versatile building blocks for the synthesis of natural products[1] and many methods have so far been reported for their preparation.[2] Among them, the diastereoselective reduction of chiral α-keto acid derivatives which bear an appropriate chiral auxiliary, is a conventional approach.[3] However the utility of the reaction has been restricted mainly by its insufficient optical yield. In the course of our investigation on asymmetric reactions using *trans*-2,5-disubstituted pyrrolidine possessed of C_2-axis of symmetry as a chiral auxiliary,[4] we have communicated highly diastereoselective reduction of α-keto amides derived

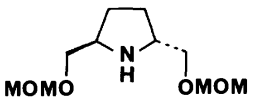

1 (R)-BMOMP

from **1** as illustrated in Scheme 1.[5] The full details of the study is described here.

Results and Discussion

α-Keto amides (**2a** and **2b**) were prepared from (*R*)-BMOMP by *N*-acylation with mixed pivalic benzoylformic or pyruvic anhydride in the presence of 4-dimethylaminopyridine in good yields. Then, the compounds (**2a** and **2b**) were submitted to reduction by metal borohydrides or DIBAL, or to hydrogenation (H_2/Pd-C), where the preferential formation of (*R*)-hydroxy amides (**3a** and **3b**) was observed except for one case. The diastereoselectivity of the reactions was determined by ^1H NMR and/or GLC analysis. The results obtained are summarized in Table 1. Reduction of **2a** (R=Ph) with ordinary metal borohydrides proceeded with moderate diastereoselectivity in a range of 62—77% diastereoselectivity (ds) (Entries 1—3). Reduction with zinc borohydride or DIBAL exhibited very poor diastereoselectivity (Entries 4 and 7), although the former reagent is known to exhibit high erythro-selectivity on the reduction of β-keto esters[6] and amides.[7] The slightly better selectivity was observed in the reduction with tetrabutylammonium borohydride having low ability of chelation (Entry 5). The catalytic hydrogenation also showed a moderate level of selectivity (Entry 6).

We next examined the reduction of **2a** with the bulky trialkylhydroborates which were expected to discern the diastereomerically different environment more effectively and, as expected, it was found that the diastereoselectivity was markedly enhanced up to 96—99% ds, when $LiBEt_3H$ was used in THF or ether at −78 °C (Entries 8 and 9).

On the other hand, the diastereoselectivity in the reduction of pyruvamide (**2b**, R=Me) with borohydrides was generally not so good as that of **2a** (Entries 13—15 and 17),[8] and zinc borohydride reduction of the same substrate showed the opposite sense of diastereoselection (Entry 16). These results suggested that, although α-keto amides (**2a** and **2b**) existed in the form of *s*-trans conformer (**A**) rather than *s*-cis conformer as discussed later (Scheme 2), the relative proportion of **A**

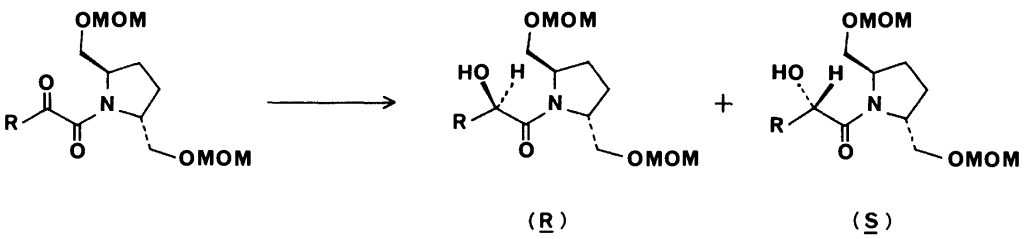

2a R=Ph
2b R=Me
3a R=Ph
3b R=Me

Scheme 1.

Table 1. Asymmetric Reduction of Chiral α-Keto Amides

Entry	Amide	Reducing agent	Solvent	Temp	Yield[a]	Ratio[b,c]
				°C	%	*R* : *S*
1	**2a**	$LiBH_4$	THF	0—rt	64	73:27
2	**2a**	$NaBH_4$	*i*-PrOH	0	87	65:35
3	**2a**	KBH_4	*i*-PrOH[d]	0—r	78	77:23
4	**2a**	$Zn(BH_4)_2$	Et_2O	0	83	52:48
5	**2a**	n-Bu_4NBH_4	CH_2Cl_2	rt	77	78:22
6	**2a**	H_2(Pd-C)	*i*-PrOH	rt	71	78:22
7	**2a**	DIBAL	Et_2O	−78	65	54:46
8	**2a**	$LiBEt_3H$	Et_2O	−78	93[b]	96:4
9	**2a**	$LiBEt_3H$	THF	−78	92	99:1
10	**2a**	$KBEt_3H$	Et_2O	−78	81[b]	86:14
11	**2a**	$KBEt_3H$	THF	−78	83	88:12
12	**2a**	$KB(OPr^i)_3H$	Et_2O	−78	81[b]	64:36
13	**2b**	$LiBH_4$	THF	−78	67	62:38
14	**2b**	$NaBH_4$	*i*-PrOH	0	30	71:29
15	**2b**	KBH_4	*i*-PrOH[d]	0	77	70:30
16	**2b**	$Zn(BH_4)_2$	Et_2O	−78	56	46:54
17	**2b**	$LiBEt_3H$	THF	−78	94	82:18
18	**2b**	$KBEt_3H$	Et_2O	−78	80	83:17
19	**2b**	$KBEt_3H$	THF	−78	83	88:12
20	**2b**	$KB(OPr^i)_3H$	Et_2O	−78	67	87:13
21	**2b**	$KB(OPr^i)_3H$	THF	−78	76[b]	84:16

a) Isolated yield. b) Determined by GLC analysis. c) Configurations of predominant diastereomers of α-hydroxy amides were determined to be 2*R* by the optical rotations of the corresponding hydrolysis products, (*R*)-(−)-mandelic acid and (*R*)-(−)-lactic acid.[9] d) Contained 10% H_2O.

Table 2. The Effect of Crown Ether on the Stereoselectivity[a]

Entry	Reducing agent	Crown ether	Solvent	Yield	Ratio
				%	*R*:*S*
1	$LiBEt_3H$	—	THF	94	82:18
2	$LiBEt_3H$	12-Crown-4	THF	82	87:13
3	$LiBEt_3H$	15-Crown-5	THF	53	85:15
4	$LiBEt_3H$	18-Crown-6	THF	80	80:20
5	$LiBEt_3H$	Kryptofix-211	THF	81	85:15
6	$LiBEt_3H$	Kryptofix-221	THF	89	87:13
7	$KBEt_3H$	—	THF	83	88:12
8	$KBEt_3H$	18-Crown-6	THF	68	88:12
9	$KB(OPr^i)_3H$	—	Et_2O	67	84:16
10	$KB(OPr^i)_3H$	15-Crown-5	Et_2O	83	90:10
11	$KB(OPr^i)_3H$	18-Crown-6	Et_2O	78	90:10
12	$KB(OPr^i)_3H$	18-Crown-6	THF	79	83:17
13	$KB(OPr^i)_3H$	Dibenzo-18-crown-6	Et_2O	69	83:17

a) All reactions were carried out at −78°C using α-keto amide (**2b**) as a substrate.

and **B** was affected by steric bulkiness of α-alkyl group (R) and strongly by the oxygenophilicity of metal ions, and that, especially in the latter case, the equilibrium leaned to **B** due to the chelation of two carbonyl groups to the oxygenophilic zinc ion. Therefore, use of $KBEt_3H$ or $KB(OPr^i)_3H$ bearing less oxygenophilic potassium ion was considered to improve the selectivity and actually higher selectivities (88% and 87% ds) were observed with these reagents (Entries 19 and 20).

In the further attempt to improve the stereoselectivity in the reduction of **2b**, we next examined the additive effect of crown ethers which is expected to capture metal ions and to disturb chelate formation. The results are summarized in Table 2. In the reduction with $LiBEt_3H$, addition of a proper size of 12-crown-4 or kryptofix-221 enhanced the selectivity from 82% ds to 87% ds (Entries 2 and 6). Although the combination of 18-crown-6 and $KBEt_3H$ gave no effect on selectivity, that with $KB(OPr^i)_3H$ further improved the selectivity from 84% ds to 90% ds (Entry 11).

Recently Soai et al. reported that diastereoselectivity in the reduction of benzylformamide derived from (*S*)-proline methyl ester, with $LiBH_4$ was improved up to 93.5% ds by addition of LiBr in the reaction mixture, while reduction of the corresponding isobutylformamide proceeded with diminished stereoselectivity of 79% ds even in the presence of LiBr.[3d] Aiming at the further promotion of the stereoselectivity in the re-

Table 3. The Effect of Metallic Salt on the Stereoselectivity[a]

Entry	Reducing Agent	Additive[b]	Yield	Ratio
			%	*R* : *S*
1	$LiBH_4$	—	67	53:47
2	$LiBH_4$	LiBr	76	63:37
3	$LiBEt_3H$	—	94	82:18
4	$LiBEt_3H$	LiBr	89	84:16
5	$LiBEt_3H$	LiCl	97	88:12
6	$KBEt_3H$	—	83	88:12
7	$KBEt_3H$	LiBr	83	95:5
8	$KBEt_3H$	LiBr[c]	68	93:7
9	$KBEt_3H$	LiCl	65	94:6
10	$KBEt_3H$	$ZnBr_2$	78	76:24
11	$KBEt_3H$	$ZnBr_2$[d]	61	58:42
12	$KBEt_3H$	$MgBr_2$[d]	47	58:42

a) All reactions were carried out in THF at −78 °C using α-keto amide (**2b**). b) Molar ratio; amide: reducing agent: metallic salt=1:1:2. c) Molar ratio; 1:1:1. d) In ether.

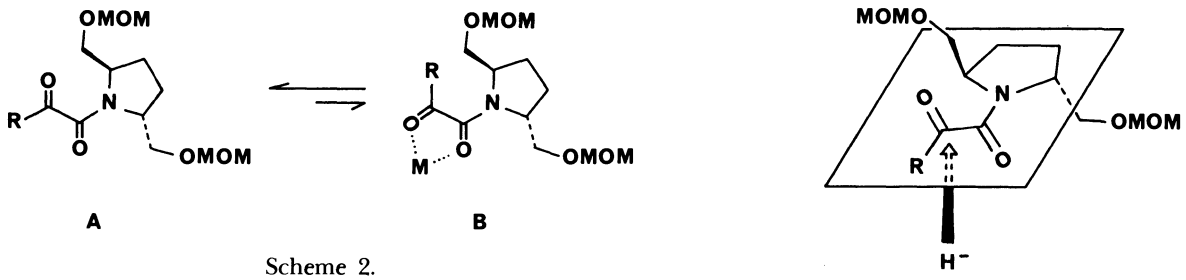

Scheme 2.

duction of **2b**, we also examined the additive effect of the salt. As shown in Table 3, addition of lithium salts increased the selectivity (Entries 2, 4, 5, and 7—9), whereas that of the metal salt such as Mg^{2+} or Zn^{2+}, decrease substantially (Entries 10—12). The optimal result (95% ds) was obtained in the reduction with $KBEt_3H$ in the presence of 2 equiv LiBr (Entry 7).

The hydroxy amide (**3b**) thus obtained was hydrolyzed by refluxing in 1 mol dm^{-3} HCl to give (*R*)-lactic acid without racemization. In the case of **3a** obtained in 99% ds, however, the partial epimerization was observed during hydrolysis, giving (*R*)-mandelic acid of 92% ee.[9]

The exact steric course of the reduction is not clear at present, but preferential formation of (*R*)-α-hydroxy amides and a CPK-model examination suggest as follows. α-Keto amide exists in the equilibrium of two plane conformers (**A** and **B**)[3b] as shown in Scheme 2. The *s*-cis conformer (**B**) is considered to be destabilized by the dipole repulsion of two carbonyl groups and the steric repulsion between α-alkyl group (R) and the amine moiety, and the α-keto amide having a bulky amine component like BMOMP takes *s*-trans conformer preferentially. Another advantage of the use of BMOMP is that the conformational divergence due to the rotation of the bond between the amide carbonyl carbon and nitrogen atoms need not be considered here because of its C_2-symmetry and the planarity of the amide structure. Thus the attack of a hydride anion would occur preferentially from the less hindered side (*si*-face) of α-carbonyl carbon of the predominating *s*-trans conformer to afford the (*R*)-hydroxy amide, as shown in Fig. 1. This seems to hold even for the Pd-catalyzed reduction (Table 1, Entry 6) though *s*-cis conformation has been suggested to catalytic hydrogenation of α-keto amides bearing amine components which are not bulkier than the present pyrrolidine auxiliary.[10]

In summary, we found that highly diastereoselective reduction of α-keto amide could be achieved by using sterically bulky BMOMP as a chiral auxiliary, which weighted the conformational equilibrium of α-keto amide in favor of the *s*-trans conformer, and that addition of crown ethers or lithium salts in the reaction mixture was effective for the further enhancement of the stereoselectivity to a certain extent.

Experimental

Melting points are uncorrected. IR spectra were determined on a Shimadzu IR-435 spectrophotometer and UV spectra on a Shimadzu UV-260 spectrophotometer. ^1H NMR spectra were recorded at 90 MHz with a Hitachi R-90H spectrometer. All NMR spectra were taken in $CDCl_3$ solution with TMS as an internal standard. Optical rotations were determined on a Yanagimoto OR-50 polarimeter. GLC analysis was carried out with a Shimadzu GC-7A chromatograph.

Reactions were carried out under an atmosphere of

nitrogen unless otherwise stated. Tetrahydrofuran (THF) and ether were freshly distilled from sodium benzophenone ketyl before use. Dichloromethane was distilled from calcium hydride. Thin-layer chromatography (TLC) was carried out on Merck glass plates precoated with silica gel 60F-254 (0.25 mm) and column chromatography was performed by using Merck 230—400 mesh silica gel.

(2*R*,5*R*)-*N*-Benzoylcarbonyl-*trans*-2,5-bis(methoxymethoxymethyl)pyrrolidine (2a). Pivaloyl chloride (0.34 ml, 2.78 mmol) was added to a solution of benzoylformic acid (430 mg, 2.78 mmol) and triethylamine (0.39 ml, 2.78 mmol) in dichloromethane (2 ml) at 0 °C and the mixture was stirred for 2 h. (*R*)-BMOMP (152 mg, 0.694 mmol) in dichloromethane (0.5 ml) and 4-dimethylaminopyridine (85.2 mg, 0.694 mmol) were added to the mixture and stirred over night. The reaction mixture was diluted with ether and filtered through Celite. The filtrate was washed with a saturated aqueous $NaHCO_3$ solution and brine successively, and dried over $MgSO_4$. The residue was chromatographed on silica gel (hexane–acetone, 5:1) to give the colorless viscous oil (**2a**, 238 mg, 98%): $[\alpha]_D^{25}$ +165° (*c* 1.07, MeOH); UV (EtOH) 254 nm (ε 54640); IR (neat) 2950, 1678, 1630, 1600, 1428, 1240, 1150, 1110, and 1040 cm^{-1}; ^1H NMR δ=1.53—2.49 (4H, m), 3.04 (3H, s), 3.21—3.32 (2H, m), 3.39 (3H, s), 3.72—3.87 (2H, m), 4.00, 4.15 (2H, ABq, *J*=6.3 Hz), 4.21—4.53 (2H, m), 4.67 (2H, s), 7.30—7.60 (3H, m), 7.95—8.12 (2H, dd, *J*=8.6, 2.0 Hz); Found: C, 61.25; H, 7.40; N, 3.80%. Calcd for $C_{18}H_{25}NO_6$: C, 61.53; H, 7.17; N, 3.99%.

(2*R*,5*R*)-*N*-Acetylcarbonyl-*trans*-2,5-bis(methoxymethoxymethyl)pyrrolidine (2b). Compound **2b** was prepared in a similar manner to that described for **2a**. Yield 77%; $[\alpha]_D^{25}$ +79.7° (*c* 3.314, MeOH); UV (EtOH) 238 nm (ε 2846); IR (neat) 2900, 1710, 1628, 1430, 1210, 1150, 1110, and 1040 cm^{-1}; ^1H NMR δ=1.80—2.24 (4H, m), 2.36 (3H, s), 3.06—3.52 (2H, m), 3.28 (3H, s), 3.33 (3H, s), 3.53—3.81 (2H, m), 4.30 (1H, m), 4.45—4.89 (1H, m), 4.51 (2H, s), 4.58 (2H, s); Found: C, 53.70; H, 8.29; N, 4.54%. Calcd for $C_{13}H_{23}NO_6$: C, 53.97; H, 8.01; N, 4.84%.

General Procedure for Reduction of α-Keto Amide. (2*R*,5*R*)-*N*-[(2*R*)-2-Hydroxy-2-phenylacetyl]-*trans*-2,5-bis-(methoxymethoxymethyl)pyrrolidine (**3a**). A THF solution of $LiBEt_3H$ (1 mol dm^{-3}, 0.23 ml, 0.23 mmol) was added to a solution of the α-keto amide (**2a**, 80 mg, 0.228 mmol) in THF (4.5 ml) at −78 °C. After stirring for 1 h at the same temperature, the reaction mixture was quenched with 5% aqueous H_3PO_4 solution and diluted with ethyl acetate. The organic layer was washed with saturated $NaHCO_3$ solution and brine successively, and dried over $MgSO_4$. An aliquot of the solution was analyzed by GLC (1.5% silicone OV-17 on Chromosorb G, 3 mm×5 m, 210 °C) to give the diastereomeric tatio of 99:1 (34 and 36 min). The solution was concentrated and submitted to preparative TLC on silica gel with hexane–ethyl acetate (1:4) to give the α-hydroxy amide (**3a**) as a colorless oil (74.3 mg, 92%); $[\alpha]_D^{26}$ +5.4° (*c* 1.49, MeOH); IR (neat) 3400, 2900, 1635, 1440, 1370, 1145, 1105, 1030 cm^{-1}; ^1H NMR δ=1.30 (1H, s), 1.56—2.30 (4H, m), 3.28 (3H, s), 3.39 (3H, s), 3.42—3.94 (4H, m), 4.05—4.65 (2H, m), 4.47 (2H, s), 4.63 (2H, s), 5.16 (1H, s), 7.32 (5H, s). 2*S* epimer had the similar spectrum except for δ 5.38 instead of 5.16. Found: C, 60.93; H, 7.92; N, 3.88%. Calcd for $C_{18}H_{27}NO_6$: C, 61.17; H, 7.70; N, 3.96%.

(2*R*,5*R*)-*N*-[(2*R*)-2-Hydroxypropanoyl]-*trans*-2,5-bis(methoxymethoxymethyl)pyrrolidine (3b). A THF solution of $KBEt_3H$ (1 mol dm^{-3}, 0.31 ml, 0.31 mmol) was added to a solution of (**2b**, 90 mg, 0.31 mmol) and lithium bromide (54 mg, 0.62 mmol) in THF (3 ml) at −78 °C and stirred for 1 h. The mixture was quenched with 5% H_3PO_4 solution, diluted with $CHCl_3$–EtOH (3:1), washed with saturated $NaHCO_3$ solution and brine, and dried over $MgSO_4$. Concentration of the solvent and preparative TLC (hexane–ethyl acetate) afforded **3b** (75 mg, 83%) as a colorless oil. GLC analysis showed that the diastereomeric ratio was 95:5 (17 and 19 min, 180 °C). $[\alpha]_D^{25}$ +25.5° (*c* 1.88, MeOH); IR (neat) 3400, 2900, 1635, 1480, 1150, 1110, and 1040 cm^{-1}; ^1H NMR δ=1.31 (3H, d, *J*=6.6 Hz), 1.57 (1H, s), 1.70—2.28 (4H, m), 3.33 (6H, s), 3.38—3.70 (4H, m), 3.95 (1H, m), 4.25 (1H, m), 4.40—4.70 (1H, m), 4.57 (4H, s); Found: C, 53.35; H, 8.93; N, 4.72%. Calcd for $C_{13}H_{25}NO_6$: C, 53.59; H, 8.65; N, 4.81%.

Hydrolysis of (+)-3a to (*R*)-(−)-Mandelic Acid. The amide (**3a**, 37.2 mg, 0.105 mmol) was refluxed in 1 mol dm^{-3} HCl (0.422 ml) for 2 h. The mixture was neutralized with saturated aqueous $NaHCO_3$, washed with dichloromethane, and then adjusted to pH 1 with 2 mol dm^{-3} HCl. The aqueous solution was saturated with sodium chloride, extracted with ethyl acetate, and dried over $MgSO_4$. Evaporation of the solvent gave (−)-mandelic acid (12.8 mg, 80%); $[\alpha]_D^{26}$ −146° (*c* 0.555, H_2O); [lit,[11] $[\alpha]_D$ +158° (H_2O)]. Esterification with diazomethane afforded (−)-methyl mandelate, $[\alpha]_D^{26}$ −167° (*c* 0.48, benzene) [lit,[2d] $[\alpha]_D$ −181.9° (*c* 0.69, benzene)].

Hydrolysis of (+)-3b to (*R*)-(−)-Lactic Acid. A similar treatment of (+)-**3b** (90% de) as described above afforded (*R*)-(−)-lactic acid; $[\alpha]_D^{26}$ −2.0° (*c* 0.76, water). [lit,[12] $[\alpha]_D$ −2.3±0.5° (*c* 3, water)]; lithium salt; $[\alpha]_D^{26}$ +12.7° (*c* 0.315, water). [lit,[13] $[\alpha]_D^{22}$ −14.0° (*c* 3, water)].

References

1) S. Hanessian, "Total Synthesis of Natural Products: The Chiron Approach," Pergamon Press, New York (1983), Chap. 2; A. I. Meyer and R. A. Amos, *J. Am. Chem. Soc.*, **102**, 870 (1980); K. Mori, T. Takigawa, and T. Matsumoto, *Tetrahedron*, **35**, 933 (1982); R. W. Hoffman, W. Helbig, and W. Lander, *Tetrahedron Lett.*, **23**, 3479 (1982).

2) For a recent work, see: a) H. C. Brown, G. G. Pai, and P. K. Jadhav, *J. Am. Chem. Soc.*, **106**, 1531 (1984); b) T. Mukaiyama, K. Tomiori, and T. Oriyama, *Chem. Lett.*, **1985**, 813; c) M. Enomoto, Y. Ito, T. Katsuki, and M. Yamaguchi, *Tetrahedron Lett.*, **26**, 1343 (1985); d) D. A. Evans, M. M. Morrissey, and R. L. Dorow, *J. Am. Chem. Soc.*, **107**, 4346 (1985).

3) J. D. Morrison and H. S. Mosher, "Asymmetric Organic Reactions," Prentice-Hall, Inc., Englewood Cliffs, New Jersy (1972), Chap. 2; b) K. Harada, "Asymmetric Synthesis," ed by J. D. Morrison, Academic Press, Orland (1985); c) K. Tani, E. Tanigawa, Y. Tatsuno, and S. Otsuka, *Chem. Lett.*, **1986**, 737; d) K. Soai, T. Idofs, H. Hasegawa, and M. Ishizaki, *ibid.*, **1986**, 1897.

4) Y. Kawanami, Y. Ito, T. Kitagawa, Y. Taniguchi, T. Katsuki, and M. Yamaguchi, *Tetrahedron Lett.*, **25**, 857 (1984); Y. Ito, T. Katsuki, and M. Yamaguchi, *ibid.*, **25**, 6015 (1984), **26**, 4643 (1985); T. Katsuki and M. Yamaguchi, *ibid.*, **26**, 5807 (1985); T. Hanamoto, T. Katsuki, and M. Yamaguchi, *ibid.*, **27**, 2463 (1986); S. Ikegami, T. Hayama, T. Kastuki, and M. Yamaguchi, *ibid.*, **27**, 3403 (1986); M. Uchikawa, T. Hanamoto, T. Katsuki, and M. Yamaguchi,

ibid., **27**, 4577 (1986); T. Katsuki and M. Yamaguchi, *ibid.*, **28**, 651 (1987); Y. Kawanami, T. Katsuki, and M. Yamaguchi, *Bull. Chem. Soc. Jpn.*, **60**, 4190 (1987).

5) Some results have been preliminarily reported: Y. Kawanami, I. Fujita, Y. Taniguchi, T. Katsuki, and M. Yamaguchi, *Chem. Lett.*, **1987**, 2021.

6) T. Nakata and T. Oishi, *Tetrahedron Lett.*, **21**, 1641 (1980).

7) Y. Ito and M. Yamaguchi, *Tetrahedron Lett.*, **24**, 5385 (1983).

8) The similar results were reported in the reduction of α-keto acid derivatives; from 89% ee (R=Ph) to 48% ee (R=Me), see Ref. 2b; from 72% ee (R=Ph) to 46% ee (R=Me), see Ref. 3c.

9) The hydrolysis of aliphatic α-hydroxy amides derived from BMOMP (1 mol dm^{-3} HCl, reflux) generally proceeds without any detectable epimerization. See Ref. 2c.

10) Harada et al. have discussed the steric course in the catalytic hyrogenation of α-keto amides bearing chiral primary amines, on basis of a cis conformer of α-dicarbonyl moiety locked by chelation to palladium metal. See Ref. 3b.

11) T. Kamanishi and S. Mitsui, *Nippon Kagaku Zasshi*, **86**, 623 (1965).

12) D. B. Hope and M. Walti, *J. Chem. Soc. C*, **1970**, 2427.

13) G. Losse and G. Bachmann, *Chem. Ber.*, **97**, 2671 (1964).

 © 1989 The Chemical Society of Japan Bull. Chem. Soc. Jpn., 62, 3603—3608 (1989)

Substituted Bisphenols as Antioxidants for Autoxidation of Tetralin

Fukiko YAMADA,* Tomihiro NISHIYAMA, Masahiro YAMAMOTO, and Kazunori TANAKA
Department of Applied Chemistry, Faculty of Engineering, Kansai University,
Yamatecho, Suita, Osaka 564
(Received March 16, 1989)

The antioxidative activities of nineteen compounds of seven series of alkylidene- and benzylidenebisphenols were evaluated by means of an oxygen-absorption method at 60 °C for tetralin. The electrochemical oxidation potentials determined using linear-sweep voltammetry and the ^{13}C NMR chemical shifts (δ) of these compounds were obtained. These data were associated with the antioxidative activities. In particular, the activities exhibited by the induction period (min) were found to closely correlate with the ^{13}C chemical shifts of the ipso-carbon of the OH substituent (corr. coeff.=0.991). Very good activities have been observed with a series of 2,2′-alkylidene- and benzylidenebis(4,6-dimethylphenol) derivatives.

In recent studies of benzylphenol derivatives as antioxidants,[1,2] we found that the introduction of a benzyl group to the para- and/or ortho-positions of the hydroxyl group on the benzene ring improved the antioxidative activities of phenols and that these activities increased with a decrease in the ^{13}C NMR chemical shifts (δ) of the ipso-carbon of the OH substituent. Subsequently, on the basis of these facts, we proposed the idea of obtaining a superior antioxidant in each series.[3] Namely, the introduction of a substituent would contribute to providing an upfield shift of the ipso-carbon of the OH substituent, resulting in a superior antioxidant. In our previous paper[2] a series of 4-methoxy-2-benzylphenols was reported as being very good antioxidants. By applying the above-mentioned idea, it was found that 2,2′-ethylidenebis(4-methoxyphenol) has a very good antioxidative activity, superior to those of a series of 4-methoxy-2-benzylphenols.[2,3] Consequently, the present work was directed toward the preparation of several series of substituted bisphenols as antioxidants.

In the present study, the antioxidative activities of nineteen compounds were evaluated by means of an oxgen-absorption method and are discussed in connection with their ^{13}C NMR chemical shifts and electrochemical oxidation data.

Experimental

Measurements. All melting points were uncorrected. ^{13}C NMR spectra were recorded on a Hitachi R-90H FT spectrometer at 22.66 MHz with complete proton decoupling. The spectra were observed as a 1 mmol cm^{-3} solution in $(CD_3)_2CO$. Chemical shifts were referred to internal TMS. GLC analyses were carried out on a Yanagimoto gas chromatograph (model GCG-G 1800-T) using a 1.50-m column packed with Silicone SE-30 (10% wt). Liquid chromatography was carried out on a Shimadzu model LC-6A using Shim-pack CLC-ODS column.

Antioxidants. The bisphenol derivatives studied in this work were as follows; 2,2′-ethylidenebis(4,5-dimethylphenol) (**1**), 2,2′-propylidenebis(4,5-dimethylphenol) (**2**), 2,2′-ethylidenebis(4,6-dimethylphenol) (**3**), 2,2′-propylidenebis(4,6-dimethylphenol) (**4**), 2,2′-isobutylidenebis(4,6-dimethylphenol) (**5**), 2,2′-benzylidenebis(4,6-dimethylphenol) (**6**), 4,4′-ethylidenebis(2,5-dimethylphenol) (**7**), 4,4′-propylidenebis(2,5-dimethylphenol) (**8**), 4,4′-benzylidenebis(2,5-dimethylphenol) (**9**), 4,4′-ethylidenebis(2,6-dimethylphenol) (**10**), 4,4′-propylidenebis(2,6-dimethylphenol) (**11**), 4,4′-benzylidenebis-(2,6-dimethylphenol) (**12**), 4,4′-ethylidenebis(2-isopropyl-5-methylphenol) (**13**), 4,4′-propylidenebis(2-isopropyl-5-methylphenol) (**14**), 4,4′-ethylidenebis(2-*t*-butyl-5-methylphenol) (**15**), 4,4′-propylidenebis(2-*t*-butyl-5-methylphenol) (**16**), 4,4′-isobutylidenebis(2-*t*-butyl-5-methylphenol) (**17**), 4,4′-benzylidenebis(2-*t*-butyl-5-methylphenol) (**18**), and 4,4′-methylenebisphenol (**19**).

Compounds **1**—**18** were prepared by a condensation of the corresponding phenol and aldehyde, respectively, in nitromethane using concd HCl as the catalyst for the desired time at a suitable temperature.[4] The general method for the preparation is as follows. To a well-stirred solution of phenol (0.1—0.2 mol) and aldehyde (0.09—0.18 mol) in nitromethane (50 ml), concd HCl (0.06—0.12 mol) was added dropwise. The reaction mixture was kept at a constant temperature. The progress of the reaction was followed by means of GLC analysis. After being stirred for a suitable length of time, the reaction mixture was cooled, and dichloromethane was added. The mixture was washed with cold water until freed from acidity. The extract was evaporated to give the crystalline product. The product was recrystallized from the hexane–dichloromethane (2:1). The product purified was characterized by chemical shifts in the ^{13}C NMR spectrum. The reaction conditions, results, and the physical properties of the products are summerized in Table 1.

Compoud **19** was commercially available and was purified by recrystallization; mp 157.5—157.8 °C.

Determination of Antioxidative Activity. Measurements of oxygen-absorption rates were performed with an isobaric gas-absorption apparatus under a closed-flow system (2.0± 0.1 L oxygen/h) provided with an electrolyser using 50 cm^3 of tetralin containing an antioxidant (0.001 mol dm^{-3}) and azobis(isobutyronitrile) as the initiator (0.01 mol dm^{-3}). The oxidation temperature was kept at 60±0.1 °C and oxygen absorption was periodically measured in a constant-pressure closed system. Satisfactory and reproducible data were obtained.

The induction period (IP) and the oxidation rates both

Table 1. Conditions, Results, and Physical Properties of the Products **1**—**18**

Compound	Molar ratio [P]/[A]a)	Temp/°C	Time/h	Yield/%	Mp θ_m/°C	Found (%)		Calcd (%)	
						C	H	C	H
1	1.2/1.0	25	8	23.2	143.5—144.3	79.86	8.23	79.96	8.20
2	2.0/1.0	25	7	34.4	139.7—140.5	79.98	8.53	80.24	8.51
3	1.1/1.0	50—60	10	36.0	134.0—134.5	79.68	8.47	79.96	8.20
4	1.1/1.0	70—80	12.5	3.5	130.5—131.2	79.95	8.48	80.24	8.51
5	1.3/1.0	70—80	68.3	11.1	156.3—156.9	80.41	8.86	80.50	8.78
6	1.8/1.0	70—80	17	26.9	108.5—109.0	82.83	7.48	83.09	7.28
7	0.8/1.0	50—60	2	12.2	219.0—219.8	79.77	8.19	79.96	8.20
8	1.3/1.0	45—55	4	18.3	193.5—194.1	80.09	8.53	80.24	8.51
9	1.8/1.0	25	3	15.6	229.0—229.6	82.82	7.29	83.09	7.28
10	1.3/1.0	25	5.2	25.3	140.7—141.0	79.81	8.18	79.96	8.20
11	1.3/1.0	25	86.7	27.1	119.7—120.2	79.95	8.52	80.24	8.51
12	1.3/1.0	60—70	24.5	35.4	162.9—163.4	82.81	7.29	83.09	7.28
13	1.1/1.0	25	1	25.4	178.5—179.4	80.60	9.34	80.94	9.26
14	0.9/1.0	25	4	21.7	203.2—204.1	80.89	9.46	81.13	9.47
15	1.8/1.0	60—70	5	27.5	203.0—203.8	80.98	9.66	81.31	9.67
16	1.8/1.0	80—90	6	17.4	193.7—194.3	81.02	9.86	81.47	9.85
17	1.7/1.0	60—70	4	14.3	236.5—237.0	81.37	10.03	81.62	10.01
18	1.9/1.0	70—80	3	27.4	202.9—203.5	83.32	8.67	83.61	8.71

a) Molar ratio of the corresponding phenol and aldehyde.

Table 2. Carbon-13 Chemical Shifts for Compounds **1**—**19**

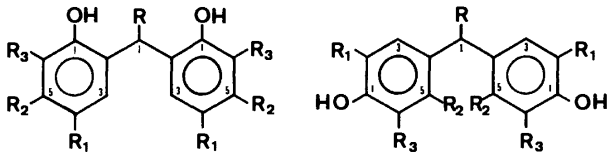

1 and **2**; R_1=R_2=Me
3, **4**, **5**, and **6**; R_1=R_3=Me
7, **8**, and **9**; R_1=R_2=Me
10, **11**, and **12**; R_1=R_3=Me
13 and **14**; R_1=*i*-Pr, R_2=Me
15, **16**, **17**, and **18**; R_1=*t*-Bu, R_2=Me

Compound	Carbon									
	C-1	C-2	C-3	C-4	C-5	C-6	C-7	R_1	R_2	R_3
1	151.9	129.9	127.9	128.6	134.9	117.3	29.4	18.4	18.8	
2	152.4	128.9	128.1	128.8	134.9	117.4	37.7	19.2	19.5	
3	149.8	132.8	125.8	129.5	129.8	124.9	30.8	21.0		16.9
4	150.1	131.6	125.5	129.7	129.5	124.8	38.0	20.8		16.7
5	150.7	131.8	126.3	130.2	129.7	125.4	44.9	21.3		17.3
6	151.0	131.0	128.9	129.0	130.4	125.0	44.9	21.1		17.0
7	153.4	121.5	129.4	136.2	134.3	117.3	36.5	15.9	18.9	
8	153.8	121.9	130.4	135.2	135.1	117.7	44.4	16.7	19.7	
9	153.8	121.3	132.0	134.0	135.1	117.5	49.7	16.0	19.3	
10	151.6	123.9	127.9	138.7			44.1	16.9		16.9
11	151.6	123.9	128.1	137.5			52.7	16.9		16.9
12	151.9	123.9	129.8	136.1			56.2	16.7		16.7
13	152.4	132.3	125.1	136.4	133.9	117.6	37.0	{23.3 27.6	19.1	
14	152.6	132.5	125.8	135.1	134.6	117.8	44.5	{23.5 27.7	19.6	
15	153.6	133.9	125.5	135.5	133.2	118.5	36.7	{30.0 34.9	18.7	
16	153.4	134.0	126.0	134.4	133.1	118.5	44.1	{30.3 35.1	19.2	
17	153.3	134.0	126.4	134.6	133.3	118.3	49.4	{30.4 35.2	19.9	
18	153.9	133.2	126.1	134.7	132.9	118.6	49.8	{30.0 34.9	19.0	
19	155.6	115.4	129.9	133.2			40.0			

during and after the induction period were determined in the usual way.[2,5]

Tetralin was purified by shaking with concd sulfuric acid, dried with sodium, and distilled under an inert atmosphere.

Electrochemical Determination. Linear-sweep voltammograms were recorded for each compound (0.001 mol dm^{-3}) in acetonitrile with $LiClO_4$ (0.1 mol dm^{-3}) as a supporting electrolyte. The counter and working electrodes were made of platinum and the working electrode potential was referred to Ag/AgCl. Potential sweeps were generated by a Hokuto Deko HB-107A function generator in connection with a potentionstat Hokuto Denko HA-104. All the measurements at the scan rate of 200 mV s^{-1} were carried out at 25±0.1 °C using a constant-temperature bath under a nitrogen atmosphere. The acetonitrile was of optically pure grade and was free from water.

Results and Discussion

The ^{13}C NMR Chemical Shifts of Compounds 1—19. The ^{13}C signals in **1—19** were easily assigned using the known chemical shift rules on the parameters[6,7] and the results are given in Table 2. At first glance these shifts are thought to be dependent in the structures of the phenol nuclei with R_{1-3} substituents and various R substituents.

The δ value of C-1 carbon in compound **19** exhibits the lowest downfield shift in comparison with those of the compounds listed in the table. On the contrary, in compounds **3—6**, the C-1 values exhibit higher upfield shifts due to both substituent and steric effects produced by, ortho-, para-methyl, and R substituents.

In our previous study on benzylphenols,[6] it was found that the methylene carbons show signal shifts mainly due to the mesomeric effect of the OH substituent, and that in the case of ortho-substituted benzyl compounds, the methylene carbon signals exhibit upfield due to both mesomeric and steric effects. In this work, C-7 carbons correspond to the methylene carbons of benzylphenols[6] and the δ values of C-7 are influenced by the effects mentioned above. Furthermore, these shifts are greatly affected by each substituent R in the order methyl, ethyl, isopropyl, and phenyl.

Activities of Antioxidants. Data regarding the activities of compounds, **1—19** along with commercially available antioxidants, BHT and BHA, denoted by the induction period (IP), the stoichiometric factor (n), the rates of the oxygen absorption, and the oxidation potential (E_p) are listed in Table 3.

The autoxidation of tetralin at 60 °C was initiated by azobis(isobutyronitrile) (AIBN) and the inhibition by phenol derivatives can be described by the following chain-reaction schemes:[2,9,10]

Initiation:

$$\text{AIBN; RH} \xrightarrow{O_2} RO_2\cdot \quad (1)$$

Propagation:

$$RO_2\cdot + RH \xrightarrow{k_p} ROOH + R\cdot \quad (2)$$

$$R\cdot + O_2 \longrightarrow RO_2\cdot \quad (3)$$

Termination:

$$2RO_2\cdot \xrightarrow{k_t} \text{non-radical products} \quad (4)$$

$$RO_2\cdot + ArOH \xrightarrow{k_{inh}} ROOH + ArO\cdot \quad (5)$$

$$(n-1)RO_2\cdot + ArO\cdot \longrightarrow \text{non-radical products,} \quad (6)$$

where RH denotes tetralin in this work and $RO_2\cdot$ is the peroxyl radical. In the presence of an antioxidant, ArOH, the oxidation chains become shortened, termination 4 is suppressed, and reactions 5 and 6 occur instead of 4. Consequently, the induction period and the rates of inhibited and uninhibited oxidations can be represented by Eqs. 7, 8, and 9, respectively:

$$IP = n[ArOH]/R_i, \quad (7)$$

$$-d[O_2]/dt = k_pR_i[RH]/nk_{inh}[ArOH], \quad (8)$$

and

$$-d[O_2]/dt = k_p(R_i/2k_t)^{1/2}[RH], \quad (9)$$

where R_i is the rate of the chain initiation.

From the above equations, the characterizations of the antioxidative activities can be expressed by three

Table 3. Activities of Antioxidants along with the Oxidation Potentials for Compounds **1—19**

Compound	IP/min	n[a]	$-d[O_2]/dt$[b] mol dm^{-3} min (I)×10^6	(II)×10^4	E_p/V
1	591	4.26	5.1	4.3	1.315
2	555	4.00	4.9	3.1	1.320
3	912	6.57	2.7	5.9	1.260
4	815	5.87	3.6	5.4	1.285
5	768	5.53	3.6	4.6	1.280
6	776	5.59	4.5	4.3	1.300
7	425	3.06	8.9	3.1	1.350
8	382	2.75	8.0	3.0	1.350
9	349	2.51	8.7	2.8	1.355
10	670	4.82	4.5	5.7	1.355
11	650	4.68	6.3	5.2	1.345
12	639	4.60	4.5	4.5	1.350
13	508	3.66	7.1	5.6	1.335
14	502	3.61	7.4	4.6	1.335
15	420	3.02	7.1	3.7	1.360
16	415	2.99	7.1	3.6	1.360
17	378	2.72	8.0	3.3	1.340
18	360	2.59	8.9	3.0	1.350
19	134	0.96	10.7	5.2	1.400
BHT	376	2.67	18.4	7.7	
BHA	408	2.91	8.1	6.1	
Control	22			8.6	

a) The stoichiometries were determined at 60 °C by the induction period method.[5,8] b) The rates of oxygen absorption; (I) for an inhibited autoxidation during IP and (II) for an uninhibited oxidation after IP.

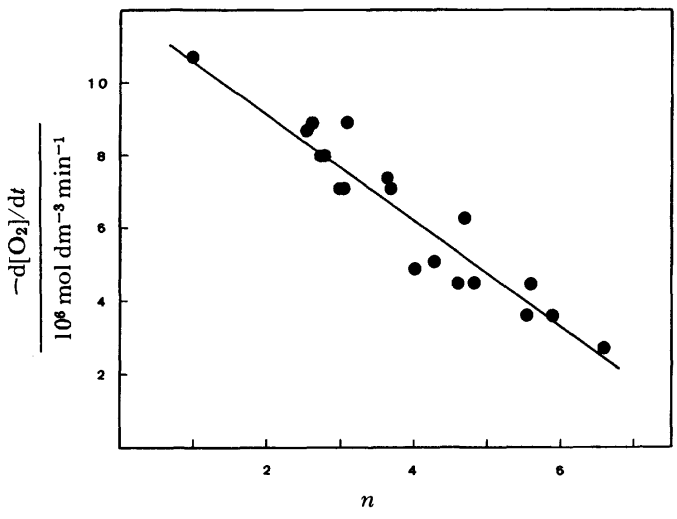

Fig. 1. Plot of n vs. the rate of oxygen absorption.

values: IP, n, and k_{inh}. However, the value of k_{inh} is difficult to obtain experimentally. Consequently, instead of this value the rate of oxygen absorption in Eq. 8 was used.

As can be seen from Table 3, the values are thought to be dependent on the structures of the phenol nuclei with various substitutents at different positions. The IP values increased in the order **3**—**6** (4,6-dimethylphenol)>**10**—**12** (2,6-dimethylphenol)>**1** and **2** (4,5-dimethylphenol)>**13** and **14** (2-isopropyl-5-methylphenol)>**7**—**9** (2,5-dimethylphenol)≧ **15**—**18** (2-*t*-butyl-5-methylphenol)>**19** (phenol). In each series, the compounds with the α-methyl or α-ethyl substituent possessed a longer IP than that of the α-phenyl substituent. Compounds **3**—**6** exhibit a much longer IP and, thus, higher stoichiometric factors, 5.5—6.6 in comparison with those of other compounds.

For oxygen absorption during IP (see (I) in Table 3), relatively lower rates were found in compounds **3**—**5**, while higher rates were observed for **7**—**9** and **17**—**19**. In particular, BHT exhibited the highest rate. According to Eq. 8, the rate varies inversely as the product of n and k_{inh}. In the range around 1 to 6 of n, the data showed an approximately linear relationship, as can be seen in Fig. 1. From this relation, it is thought that the k_{inh} values of compounds **1**—**18** are nearly equal. On the other hand, the rates after IP (see (II) in Table 3) are quite complicated. When all ArOH are consumed by reactions 5 and 6 (up to IP), the rate of autoxidation obeys Eq. 9 and is nearly equal to that of the control test. All of the observed rates are not close to 8.6, but are much lower. This means that the retardation ability persists, even after IP is over, due to some products of the antioxidant.

Correlations of Antioxidative Activities with ^{13}C NMR Chemical Shifts. In order to understand the factors and mechanisms govering the antioxidative activities of compounds **1**—**19**, several attempts were made to plot their IP values and the rates of oxygen absorption against the ipso-carbon chemical shifts of the OH substituets (C-1 shifts in Table 2). The data used in this attempt are listed in Tables 2 and 3.

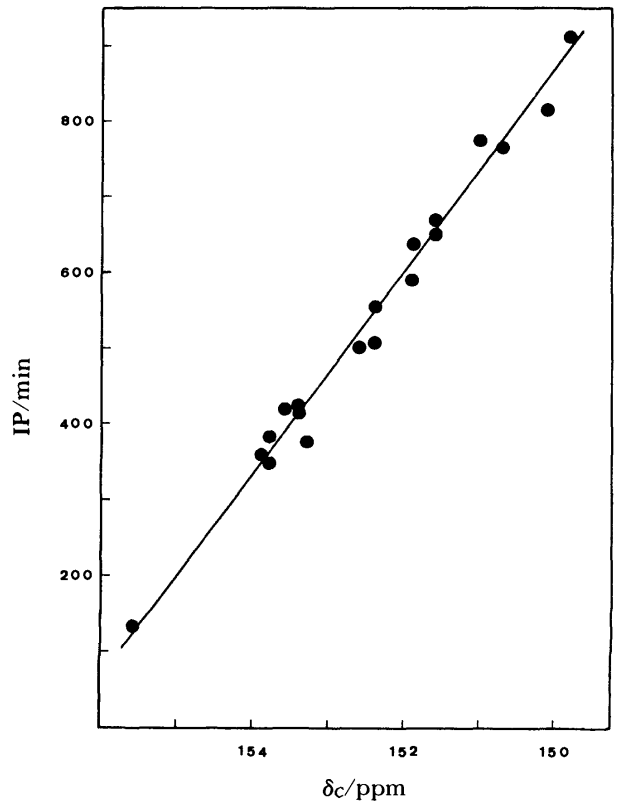

Fig. 2. Plot of IP vs. ^{13}C chemical shift of the ipso-carbon of OH, r=0.991.

Figure 2 shows the relation between the IP values and the ipso-carbon chemical shifts of the OH substituents. The plotted points fall on a straight line. This fact indicates that the IP values increase with a decrease in the chemical shifts, and that the electron density on ipso-carbon of the OH substituent governs the antioxidative activities. In a previous paper[11] we proved that, on the basis of the ^{13}C chemical shifts of *p*-substituted benzylbenzenes, electron transmission through the system by a resonance interaction is the most important factor for the α-carbon. It is, therefore, thought that electron transmission through the ipso-carbon to the oxygen atom in phenols depends mostly upon the resonance contribution. Consequently, the total π-electron density of the oxygen atom may be increased by increasing the electron density of the ipso-carbon atom. This will necessarily decrease the electronegativity of the oxygen atom and make the Coulomb integral of the σ orbital on the oxygen more positive.[12] In the inhibition processes, reactions 5 and 6, the reactivities of phenolic hydrogen and phenoxyl radical are the controlling factors. The reactivity of phenolic hydrogen for an attack of a peroxyl radical, electrophilic radical, is greatly elevated by an increased

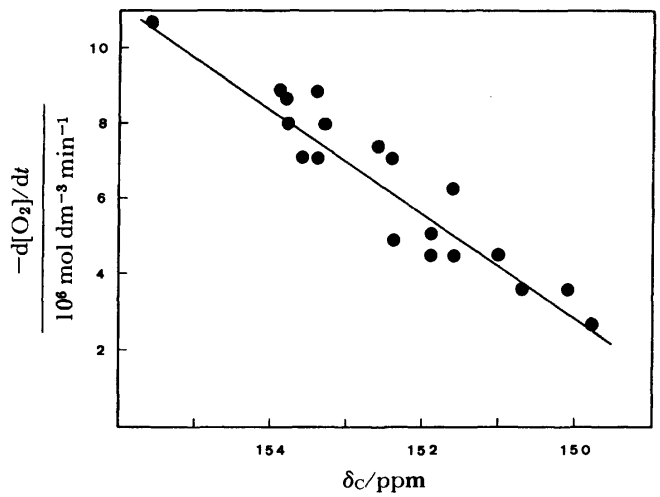

Fig. 3. Plot of the rate of oxygen absorption vs. ^{13}C chemical shift of the ipso-carbon of OH.

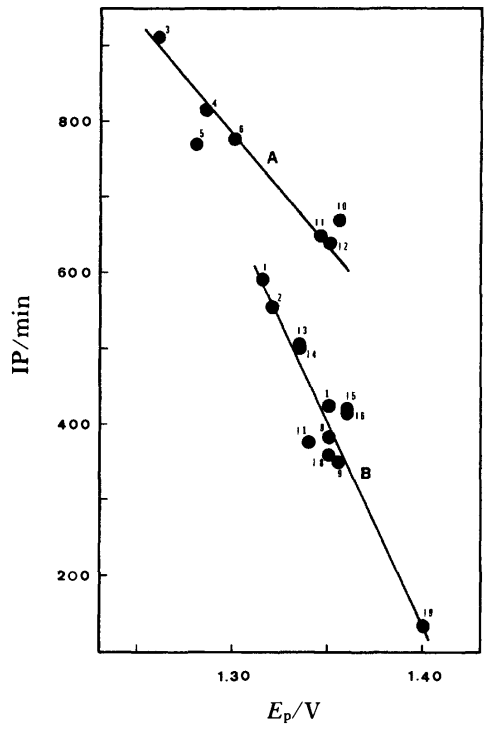

Fig. 4. Plot of IP vs. E_p.

π-electron density on the oxygen. The reactivity of the phenoxyl radical produced can be elevated by the increased π-electron density.

From the reasons mentioned above, the ipso-carbon chemical shifts of the OH substituents may be considered as being reliable and objective indications of the reactivities in the inhibition processes.

Figure 3 also shows a linear relation between the rates of oxygen absorption during IP and the ipso-carbon chemical shifts of the OH substituents. The rates increase with increasing chemical shifts. This indicates that the activity of the antioxidant, which can be expressed by both n and k_{inh} values, is greatly elevated by an increased π-electron density on the phenolic oxygen, as was mentioned above.

Correlations of Antioxidatiove Activities with Oxidation Potentials. As can be seen in Fig. 4, the IP values show two linear relationships, A and B, with the E_p values. Compounds having points plotted on line A have great steric effects on the OH substituent. The other compounds having points plotted on line B have a somewhat weak steric effect (see the structures and ^{13}C NMR data in Table 2). When the oxidation of a molecule is carried out at some potential, the reaction involves an initial electron loss, followed by proton migration. The simplicity of these transfers can be seen by the lower E_p values. In a previous paper[2] we proved that the ease of one-electron and one-proton transfers is greatly increased by an increased electron density at the ipso-carbon of the OH substituent, on the basis of the ^{13}C NMR chemical shifts.

In compounds **7** (on line B) and **10** (on line A), their E_p values are nearly equal (see also Table 3), while the IP values and the ^{13}C chemical shifts (Table 2) of the ipso-carbons of the OH substituents show considerable differences. In ^{13}C NMR data, the steric compression shift due to the substituent can be easily detected. For example, the OH substituent of 4-(α-methylbenzyl)phenol[2] or compound **19** is not sterically crowded. Consequently, their ipso-carbons of the OH substituents exhibit the shifts at δ 156.2[2] and 155.6 (Table 2), respectively. Compound **7**, having one methyl substituent at the ortho-position of the OH substituent, exhibits a shift at δ 153.4, while compound **10**, having two methyl substituents at both ortho-positions of the OH substituent, exhibits a shift at δ 151.6. This shift is 1.8 ppm upfield from that in **7**. Thus, compounds having sterically hindered phenol moieties, such as **3—6** and **10—12**, show very good antioxidative activities.

These facts indicate that in these compounds the electrochemical oxidation in solution and the inhibition reaction for autoxidation under an oxygen atmosphere proceed by a similar mechanism. However, there are some differences in the reaction mechanisms between the initial steps of both oxidations. Consequently, the contribution of the steric effect to the OH substituent appeared to be an important factor.

The present work was supported by a Grant-in-Aid for Scientific Research No. 62550619 from the Ministry of Education, Science and Culture.

References

1) F. Yamada, T. Nishiyama, and Y. Nakai, *J. Am. Oil Chem. Soc.*, **60**, 1651 (1983).

2) F. Yamada, T. Nishiyama, Y. Suzuura, and T. Yamamura, *Bull. Chem. Soc. Jpn.*, **58**, 115 (1985).

3) F. Yamada, T. Nishiyama, and Y. Suzuura, *Chem. Express*, **1**, 319 (1986).

4) F. Yamada, T. Nishiyama, M. Yamamoto, K. Tanaka, S. Sai, and T. Yamamoto, *Chem. Express*, **3**, 495 (1988).

5) C. E. Boozer, G. S. Hammond, C. E. Hamilton, and J. N. Sen, *J. Am. Chem. Soc.*, **77**, 3233 (1955).

6) Y. Nakai and F. Yamada, *Org. Magn. Reson.*, **11** 607 (1978).

7) a) G. C. Levy and G. L. Nelson, "Carbon-13 Nuclear Magnetic Resonance for Organic Chemists," Wiley-Interscience, New York (1972); b) J. B. Stothers, "Carbon-13 NMR Spectroscopy," Academic Press, New York (1972).

8) E. C. Horswill, J. A. Howard, and K. U. Ingold, *Can. J. Chem.*, **44**, 985 (1966).

9) a) Y. Kamiya, "Yuki-sanka-hanno," Gihodo, Tokyo (1973), Chaps. 5 and 13; b) J. A. Howard, "Free Radicals," ed by J. K. Kochi, Wiley, New York (1973), Vol. II, Chap. 12.

10) G. W. Burton and K. U. Ingold, *J. Am. Chem. Soc.*, **103**, 6472 (1981).

11) Y. Nakai, T. Takabayashi, and F. Yamada, *Org. Magn. Reson.*, **13**, 94 (1980).

12) K. Morokuma, H. Kato, and K. Fukui, *Bull. Chem. Soc. Jpn.*, **36**, 541 (1963).

 © 1989 The Chemical Society of Japan Bull. Chem. Soc. Jpn., 62, 3609—3613 (1989)

The Discharge Characteristics of FeOCl in an Aprotic Organic Solvent

Zen-ichiro TAKEHARA,* Kiyoshi KANAMURA, Nobuyuki IMANISHI, and Chen ZHEN
Department of Industrial Chemistry, Faculty of Engineering, Kyoto University,
Yoshida Hommachi, Sakyo-ku, Kyoto 606
(Received March 1, 1989)

The discharge reaction of FeOCl was investigated and the discharge products were identified by XRD and EPMA. Lithium and solvent co-intercalate into FeOCl during the early stage of the discharge, in the low lithium concentration range in the FeOCl solid matrix (Li_xFeOCl, $x<0.6$). Such compounds are stable. However, at higher concentrations of lithium, FeOCl co-intercalated by lithium and solvent gradually decompose to yield α-Fe and other compounds. The results show that three electrons are consumed during the discharge. On the other hand, the discharge curve of FeOCl in propylene carbonate containing 1.0 M $LiBF_4$ indicates only a single charge transfer step. Therefore, the reaction mechanism of FeOCl can be explained by the intercalation of lithium in FeOCl followed by the decomposition of the intercalation compound formed between FeOCl, lithium and the solvent. The structure of FeOCl intercalated by lithium changes during the course of immersion in various solvents. This fact indicates that the solvent can easily intercalate into FeOCl and deintercalate from FeOCl. Such a behavior may arise from a weakening of the interaction between FeOCl layers after lithium intercalation, since the intercalation of lithium into FeOCl influences the chemical bonds in FeOCl. As a result, the interaction between FeOCl layers becomes weaker. Therefore, the intercalation and deintercalation of the solvent can easily take place. The stability of the FeOCl structure after cathodic reduction does not depend only on the concentration of lithium in FeOCl, but also on the kind of solvent.

Layered compounds have been investigated and used as a cathode material for lithium batteries, since lithium ions can be intercalated into their van der Waals gap. The transition metal dichalcogenides, e.g. TiS_2 and MoS_2, are representatives of the most popular layered compounds. On the other hand, some of the transition metal halogenide oxides are also classified as layered compounds. Particularly, iron chloride oxide (FeOCl) has been investigated by some workers in order to be utilized as a cathode material for lithium secondary batteries.[1-3]

In this study, the intercalation of lithium into FeOCl was investigated. The stability of the FeOCl host matrix intercalated with lithium and its structural changes during the course of lithium intercalation are discussed in order to understand the discharge reaction mechanism of FeOCl when in contact with a propylene carbonate electrolyte.

Experimental

FeOCl was prepared by heating on an α-Fe_2O_3 and $FeCl_3$ mixture in a 3:4 mole ratio in sealed and evacuated Pyrex glass tube at 350 °C in an electric furnace for 3 days according to the method of Kikkawa et al.[4] The reaction products were washed fully for 1 day with water to remove excess $FeCl_3$ and washed again with acetone and then dried. The products, thus prepared, were identified by a comparison of the X-ray diffraction (XRD) results of Lind.[5] In this study the prepared FeOCl had the same structure as Lind's with respect to the XRD measurement. Cathode composites were prepared by compressing a mixture of FeOCl, a conducting material (acetylene black), and a binding agent (PTFE) in a weight ratio of 80:15:5. The apparent surface area was 0.785 cm^2. These electrodes were discharged at a constant current in propylene carbonate (PC) containing 1.0 M $LiBF_4$ (1 M=1 mol dm^{-3}). Lithium metal was used as both the reference electrode and the counter electrode. PC was distilled under vacuum. $LiBF_4$ was also dried at 150 °C under vacuum for 2 days. The structural changes of the host matrix along with the discharge process were traced by the XRD method. The samples for X-ray analysis were wrapped with a thin poly(vinylidene dichloride) film in order to avoid any reaction with oxygen and water from the air. Oxygen and water cannot permeate through the thin film during X-ray analysis. The measurement was conducted from $2\theta=70°$ to $2\theta=4°$ at a scan rate of 1° min^{-1}. The iron and chlorine contents of the active materials were analyzed by Electron Probe Micro Analysis (EPMA). All procedures, except for XRD and EPMA, were performed under an argon atmosphere at room temperature.

Results and Discussion

Figure 1 shows the discharge curves of FeOCl at two different current densities in PC containing 1.0 M $LiBF_4$. The discharge curve of FeOCl is different from that of TiS_2. In the case of lithium intercalation into

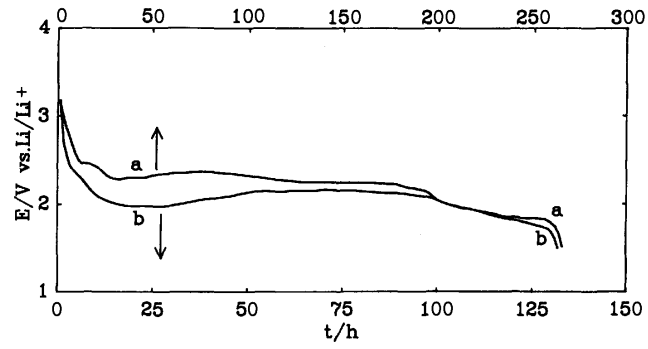

Fig. 1. The discharge curves of FeOCl in PC containing 1.0 M $LiBF_4$ at a constant current of 0.15 mA (a) and 0.3 mA (b).

TiS_2, the S-shaped discharge curve shows a typical simple intercalation of lithium into the host matrix, which takes place during the discharge.[1] For FeOCl, however, the profile of the electrode potential goes through a minimum during the initial period of discharge and then reaches to a potential plateau of about 2 V vs. Li/Li^+. Finally, the electrode potential sharply decreases to more cathodic potentials of about 1.5 V vs. Li/Li^+. Apparently, the discharge reaction may proceed via a single-step charge-transfer reaction.

When lithium intercalates into an interlayer of FeOCl, one electron reaction occurs during the discharge in aprotic solvents containing a lithium salt. Such a reaction can be written as

$$FeOCl + xLi^+ + xe^- \rightarrow Li_xFeOCl\ (0<x<1). \quad (1)$$

The valence of the iron in FeOCl decreases from three to two during the intercalation of lithium. Therefore, the theoretical capacity can be calculated to be 10 mA h from the weight of FeOCl included in the composite of the cathode material (weight of FeOCl=40 mg). The theoretical discharge duration is also calculated to be 33.4 hours (discharge current=0.3 mA). If the discharge was terminated at 1.9 V vs. Li/Li^+, the observed capacity was 30 mA h, which was about three times that of 10 mA h. This means that another reaction takes place in the course of the reduction of FeOCl. The observed capacity corresponds to that expected from the conversion of the iron valence from three to zero.

In order to confirm such a discharge reaction, X-ray diffraction analyses of the discharge products were performed. The X-ray diffraction patterns of FeOCl discharged in PC containing 1.0 M $LiBF_4$ are summarized in Fig. 2. All of the XRD results shown in Fig. 2 were for the stable structures after one week had passed. Figure 2 (a) shows the X-ray diffraction patterns of FeOCl before the discharge. The main peak at $2\theta=11.2°$ corresponds to the van der Waals gap of FeOCl. Figure 3 shows the structure of FeOCl.[5,6] It has a b-axis preferred orientation with an interlayer distance of 7.9 Å. From these patterns, it can be seen that the structure of FeOCl changes during a discharge. During the early stages of a discharge ($Li_{0.2}FeOCl$), its structure is quite different from that before the discharge. However, regarding this point, it must be noted that the stabilization of the structure requires a certain time after intercalation. As shown in Fig. 4, the structure of $Li_{0.2}FeOCl$ changed with the immersion time in PC. From the patterns it can be seen that the structural change was complete after two days. The new peaks in Figs. 2 (b) and (c) correspond to an expanded gap, for which the distance between FeOCl layers is 10.5 Å. Such a large interlayer distance cannot be explained by the intercalation of lithium

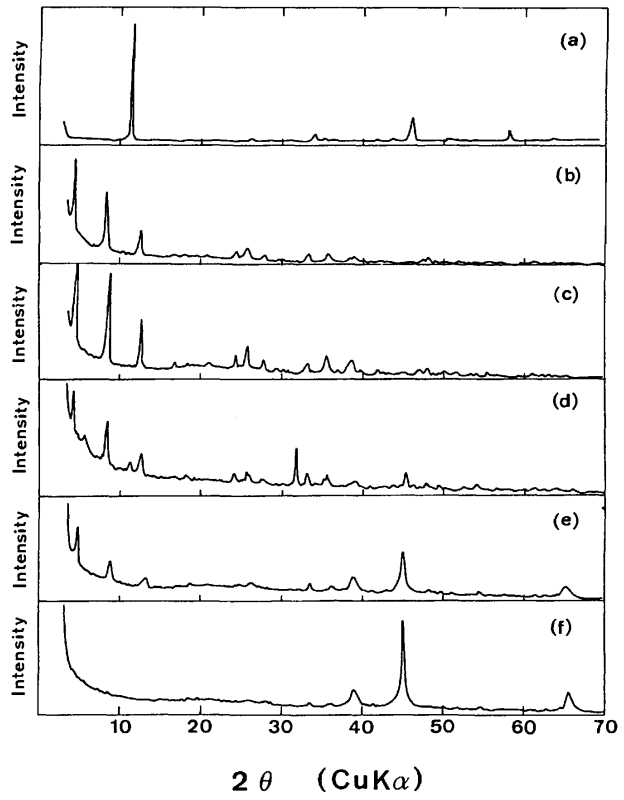

Fig. 2. X-Ray diffraction patterns of FeOCl before and after discharge. Discharge current=0.3 mA. (a) FeOCl, (b) $Li_{0.2}FeOCl$, (c) $Li_{0.6}FeOCl$, (d) LiFeOCl, (e) Li_2FeOCl, (f) Li_3FeOCl, where x in Li_xFeOCl corresponds to the mole ratio of lithium to iron. All the samples had been immersed in PC for one week after discharge.

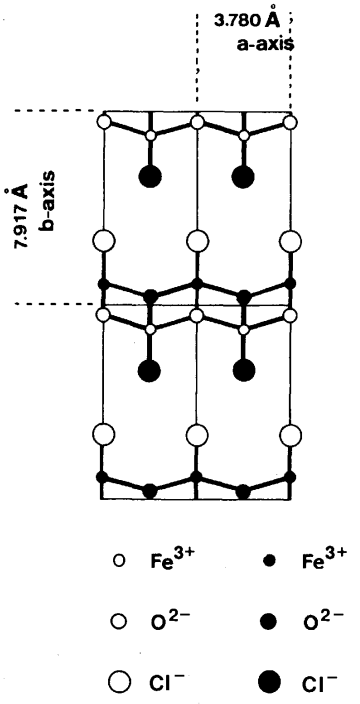

Fig. 3. Schematic illustration of the structure of FeOCl.

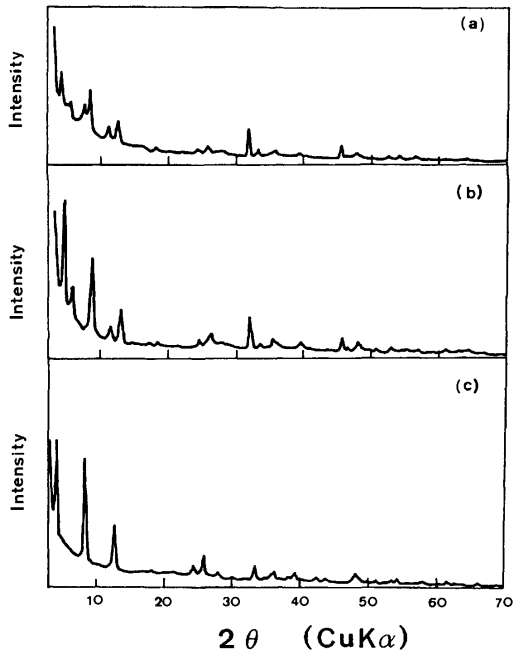

Fig. 4. X-Ray diffraction patterns of $Li_{0.2}FeOCl$ after immersion in PC for one hour (a), seven hours (b), and two days (c).

alone, since lithium is smaller than 1 Å. The large interlayer expansion results from the intercalation of lithium and the solvent. The molecular size of PC is about 5 Å. If PC intercalates into the FeOCl interlayer, the interlayer distance between Fe atoms could expand from 7.9 to 10.5 Å.

The X-ray diffraction pattern of $Li_{0.6}FeOCl$ showed the same peaks as $Li_{0.2}FeOCl$ (Fig. 2), indicating the formation of FeOCl intercalated by lithium and solvent. After sitting for two weeks, such a structure remained unchanged. These results indicate that the intercalation compound of FeOCl with lithium and the solvent is formed during a discharge and is stable in the region from $x=0$ to $x=0.6$, where x corresponds to the ratio of lithium to iron.

Figure 5 shows XRD patterns of $Li_{0.6}FeOCl$ which were discharged in PC and then immersed in various solvents. These XRD patterns were similar, except in the case of acetonitrile (ACN) and dimethoxyethane (DME). From the XRD patterns, no structural change could be observed. However, the peaks slightly shifted to a lower or higher angle. After the immersion in tetrahydrofuran (THF) or dimethylformamide (DMF), the three peaks shifted toward a higher angle. On the other hand, they shifted toward a lower angle after immersion in dimethylsulfoxide (DMSO) or γ-butyrolactone (γ-BL). In this way, the structural change of FeOCl intercalated by lithium was caused by immersion in various solvents. This fact indicates that an exchange of the solvent in the interlayer of FeOCl takes place between PC and the bulk solution, such as

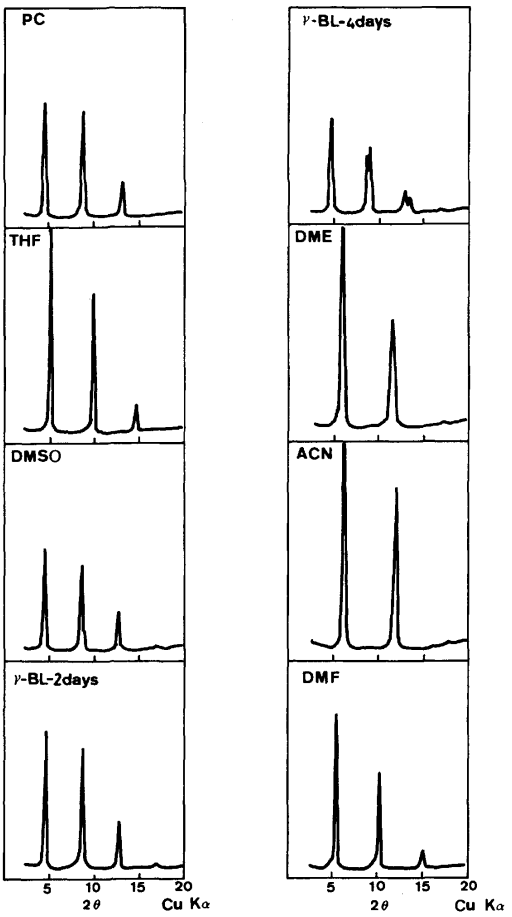

Fig. 5. X-Ray diffraction patterns of $Li_{0.6}FeOCl$ after the immersion in THF, DMSO, γ-BL, DMF, DME, ACN, and PC for two days and γ-BL for four days.

THF, DMSO, γ-BL, and DMF. However, XRD patterns after the immersion in ACN or DME indicated a structural change of $Li_{0.6}FeOCl$. Such a phenomenon can be understood by the strength of the interaction between solvent and FeOCl host matrix. The weak interaction between FeOCl layers may also be the main cause of the solvent exchange. The weak interaction between FeOCl interlayers results in the poor stability of Li intercalated FeOCl.

However, Li_xFeOCl ($x<0.6$) had to be treated carefully, because the stability of these compounds sharply decreased with increased drying time. X-Ray diffraction patterns of Li_xFeOCl ($x<0.6$) changed with the drying time under vacuum, as showed in Fig. 6. When Li_xFeOCl samples were removed from the experimental cell and then kept in an argon dry box for one or two weeks, the structure of the discharged FeOCl changed to an amorphous-like type. It seemed that the solvent being intercalated into the FeOCl deintercalated from the FeOCl interlayer while drying. On the other hand, Li_xFeOCl samples, which were kept in solvent for one or two weeks, were very stable and their X-ray peak positions did not change. From these results, it can be seen that the stability of

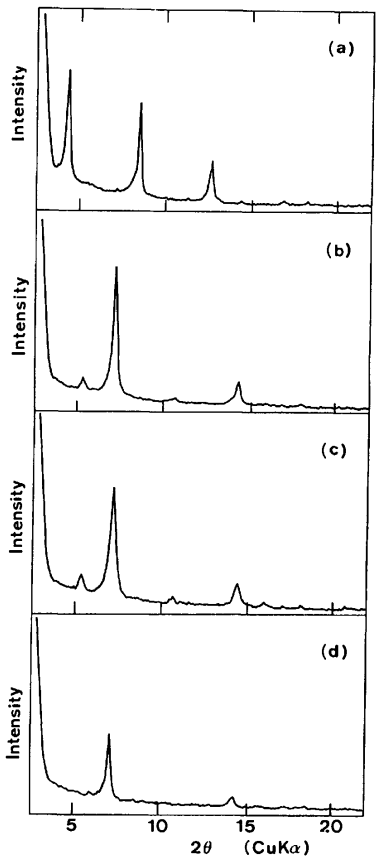

Fig. 6. The structural change of $Li_{0.2}FeOCl$ during drying under vacuum at 80°C for 0 min (a), 25 min (b), 45 min (c), and 65 min (d).

Li_xFeOCl is dependent upon the solvent intercalated into the FeOCl interlayer.

On the contrary, X-ray diffraction patterns of Li_xFeOCl ($x>1$) were very different from those of Li_xFeOCl ($x<0.6$), as shown in Figs. 2 (b), (c), (d), (e), and (f). The main peaks at $2\theta=12.62°$, 8.42°, and 4.24°, decrease when more lithium is inserted into the FeOCl. Moreover, some new peaks appear at $2\theta=45°$ and 66°, and increase with the lithium content. These new peaks in Fig. 2 (f) correspond to those of α-Fe. This tendency increases when more lithium is added. In Li_3FeOCl, X-ray peaks at the lower-angle region disappeared and new peaks increased in intensity and sharpness. Thus, FeOCl was reduced to α-Fe through the intermediate product. Apparently, three electrons are consumed during the discharge reaction of FeOCl. The electron number expected from the results of the X-ray diffraction method was in agreement with that expected from the observed discharge capacity. However, the decomposition of the intercalation compound of FeOCl is a very complex process. The X-ray diffraction pattern of Li_2FeOCl shows that other compounds besides α-Fe are formed during the decomposition. These compounds could not be identified by the XRD method.

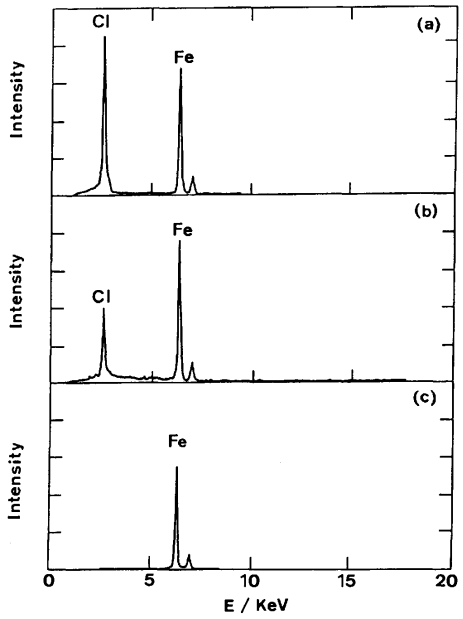

Fig. 7. EPMA results for FeOCl (a), Li_3FeOCl (b), and Li_3FeOCl washed by PC (c).

Elementary analyses of the discharge products of FeOCl were performed by using EPMA. Figure 7 shows the results. Before the discharge, the intensities of the iron and chloride peaks were almost the same, as shown Fig. 7(a). On the other hand, after the three-electron discharge of FeOCl, the chloride peak decreased to about one half that of iron, as shown in Fig. 7 (b). This result indicates that chloride was lost from the FeOCl structure during reduction. This sample was fully washed with PC and again analyzed for chloride. The result is shown in Fig. 7(c). The chloride peak became even smaller, and it was proved that chloride existed as a soluble species (LiCl). Part of the chloride ion remains in the cathode composite as LiCl, since the solubility of LiCl in PC is not very high.

The overall reaction of FeOCl can be assumed to be

$$FeOCl + 3Li^+ + 3e^- \rightarrow \alpha\text{-}Fe + LiCl + Li_2O. \quad (2)$$

However, Li_2O and LiCl were not detected by the XRD method.

Thus, the kinetics of the discharge reaction of FeOCl in an aprotic solvent are not simple. To summarize, as the discharge proceeds, lithium and solvent intercalate into the FeOCl interlayer. As a result, $Li_x(PC)FeOCl$ ($x<0.6$) is formed, which is a stable product in PC. With the proceeding of the discharge reaction, $Li_x(PC)FeOCl$ ($x>0.6$) decomposes to yield α-Fe as the discharge product.

The intercalation compound of FeOCl with lithium was stable in the region of low lithium concentrtion. However, with increasing lithium concentration,

FeOCl decomposes and α-Fe is formed. Such a decomposition permits a three-electron reaction of FeOCl. As a result, the capacity of FeOCl in primary cells is attractive. On the other hand, FeOCl cannot be utilized as the cathode material of a secondary lithium cell, because such a displacement reaction is not reversible. However, if this decomposition reaction could be somehow interrupted, it has the possibility of being utilized in a secondary battery. Further, it is seen that one possible way might be to insert another solvent into the FeOCl gap leading to a stable structure.

References

1) M. Stanley Whittingham, *Prog. Solid St. Chem.*, **12**, 41 (1978).
2) S. Kikkawa, T. Yamamoto, and M. Koizumi, *Yogyo Kyokaishi*, **93**, 311 (1985).
3) H. Meyer, A. Weiss, and J. O. Besenhard, *Mat. Res. Bull.*, **13**, 913 (1978).
4) S. Kikkawa, F. Kanamaru, and M. Koizumi, *Bull. Chem. Soc. Jpn.*, **52**, 963 (1979).
5) M. O. Lind, *Acta Crystallogr., Sect. B*, **26**, 1058 (1970).
6) S. Goldsztaub, *Chem. Rev.*, **198**, 667 (1934).

 © 1989 The Chemical Society of Japan Bull. Chem. Soc. Jpn., 62, 3614—3621 (1989) [Vol. 62, No. 11

Analysis of Isotropic ^1H and ^{13}C NMR Shifts of Low-Spin Fe^{III} Complexes: Tetracyano(1,2-ethanediamine)ferrate(III) and Tetracyano(*N,N'*-dimethyl-1,2-ethanediamine)ferrate(III)

Yoshitaka KURODA,* Masafumi GOTO, and Tomoya SAKAI
Faculty of Pharmaceutical Sciences, Nagoya City University, Mizuho-ku, Nagoya 467
(Received March 31, 1989)

^1H NMR spectra of low-spin d^5 complexes, $[Fe^{III}(CN)_4(en)]^-$ and $[Fe^{III}(CN)_4(s\text{-}Me_2en)]^-$ (en=1,2-ethanediamine, *s*-Me_2en=*N,N'*-dimethyl-1,2-ethanediamine), were measured at 185—323 K. These complexes showed a non-Curie behavior. The spin states of the complexes were determined by an analysis of the *g* values from the ESR spectrum of a polycrystalline sample of $[Fe^{III}(CN)_4(en)]^-$ measured at liquid-helium temperatures. The isotropic shifts for the ^1H and ^{13}C nuclei, δ^{iso}, were separated into Fermi contact shifts, δ^{con}, and dipolar shifts, δ^{dip} and the strong dependence of δ^{iso} on the location of ligand nuclei was found to be due to the different δ^{con} as well as δ^{dip}. A combination of information concerning ESR and NMR enabled the assignment of the *g* values obtained from a polycrystalline sample, i.e. $g_{xx}=3.15$, $g_{yy}=1.99$, and $g_{zz}=0.82$, and determination of spin-orbit coupling constant, $\zeta=160\ cm^{-1}$.

Numerous studies have appeared which applied NMR to investigate the stereochemistry and spin states of paramagnetic complexes, e.g. porphyrins[1] and heme proteins.[2-4] Most of the studies have, however, dealt with the NMR of unsaturated ligands, and little work has been done with saturated compounds coordinated to paramagnetic transition metal ions to investigate the correlations between the NMR shift and stereochemistry.[5]

Tetracyano(1,2-diamine)ferrates, $[Fe(CN)_4(1,2\text{-diamine})]^-$ and $[Fe(CN)_4(1,2\text{-diamine})]^{2-}$, are low-spin complexes with 1,2-diamine as a saturated compound. In a previous paper, we reported that the isotropic ^1H and ^{13}C NMR shifts, δ^{iso}, of the Fe^{III} complexes are strongly dependent on the location of the ligand nuclei and do not follow the Curie law.[6,7]

We have chosen $[Fe^{III}(CN)_4(en)]^-$ and $[Fe^{III}(CN)_4(s\text{-}Me_2en)]^-$ (en=1,2-ethanediamine and *s*-Me_2en=*N,N'*-dimethyl-1,2-ethanediamine) since the five-membered chelate ring formed by en is the simplest one among this class of complexes, and that formed by *s*-Me_2en is practically fixed in either the δ or λ conformation, at least below 323 K.[7] In this paper δ^{iso} for the ^1H and ^{13}C nuclei of the en and *s*-Me_2en complexes[6] were separated into Fermi contact shifts, δ^{con}, and dipolar shifts, δ^{dip}, by using the equations of Kurland and McGarvey.[8,9] Analysis of the ESR spectra of $[Fe^{III}(CN)_4(en)]^-$ at liquid-helium temperatures afforded the information necessary for the separation of δ^{iso} and the clarification of the non-Curie behavior. The distribution of unpaired spin over the chelates is discussed on the basis of the Fermi constants and spin populations in s orbitals for CH, NH, and C nuclei. The present treatment of δ^{iso} is a useful method for assigning the *g* values obtained from ESR measurements of polycrystalline samples, and determining the spin-orbit coupling constant.

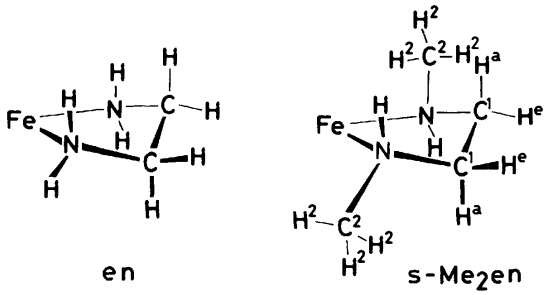

Experimental

Materials. Sodium tetracyano(diamine)ferrate(III) and ferrate(II) (diamine=1,2-ethanediamine (en)[10] and *N,N'*-dimethyl-1,2-ethanediamine (*s*-Me_2en)[11]) and potassium tetracyano(1,2-ethanediamine)cobaltate(III)[12] were prepared as reported previously.

ESR Measurement. The ESR sample was prepared as follows: $Na[Fe^{III}(CN)_4(en)]\cdot 3H_2O$ (0.0010 g) and $K[Co^{III}(CN)_4(en)]\cdot H_2O$ (0.101 g) were dissolved in a solution (precooled at 0 °C) of acetic acid (0.25 cm^3), water (0.25 cm^3), methanol (1.0 cm^3), and ethanol (1.0 cm^3). Ether was added to this solution until it became turbid; the resulting mixture was allowed to stand at −15 °C overnight. Yellow crystals of the Co^{III} complex doped with the Fe^{III} complex were collected on a filter, washed with ether, and dried in vacuo. The obtained crystals were pulverized with an agate mortar and a pestle, placed in an ESR sample tube of 4 mm outer diameter, and sealed in vacuo. The sample was kept at −15 °C while being protected from light until the measurement.

ESR spectra on the polycrystalline sample were recorded with a Varian E-112 spectrometer at X-band frequency at liquid-helium temperatures. The magnetic field was calibrated with 2,2-diphenyl-1-picrylhydrazine (DPPH).

NMR Measurement. ^1H NMR spectra of $[Fe^{III}(CN)_4(diamine)]^-$ in CD_3OD (containing 0.25% DCl) were recorded on a JEOL FX-100 spectrometer at 323—185 K using a sample tube 5 mm in diameter. The concentrations of the complexes were ca. 0.05 mol dm^{-3} in order to prevent the deposition of the complexes below 273 K. Spectra with S/N ratios of ca. 20/1 were obtained by collecting 20—40 transients. Probe temperature were controlled with a JNM-VT-3C temperature-control apparatus and determined based

on the chemical shift difference between the methyl and hydroxyl protons of methanol.[13]

The ^1H and ^{13}C NMR spectra (NH and CH) of $[Fe^{III}(CN)_4(diamine)]^-$ were recorded on a JEOL FX-100 spectrometer at 300 K using a sample tube of 5 mm in diameter and 40—50 mg of the complexes dissolved in pD 2.0 DCl-D_2O (0.3 cm^3). The ^1H and ^{13}C NMR spectra of $[Fe^{II}(CN)_4(diamine)]^{2-}$ were measured in a manner similar to that described above, except that D_2O was used as the solvent.

Sodium 3-(trimethylsilyl)propionate-2,2,3,3-d_4 (TSP; 0.00 ppm) and 1,4-dioxane (67.44 ppm) were used as internal standards for ^1H and ^{13}C NMR measurements, respectively. Positive chemical shifts indicate downfield shifts.

Theoretical

We set the coordinate axes as shown in Fig. 1 for convenience, where the x axis coincides with the twofold axis of C_2 symmetry, and the other two axes are perpendicular to the twofold axis and are involved in the two symmetry planes defined by the donor atoms.

We assume that (1) the delocalization of 3d electrons into ligand orbitals is represented by the "orbital reduction factor",[14,15] k, and (2) there is no mixing of t_{2g} and e_g states. These assumptions lead to sixfold-degenerate t_{2g}^5 spin states in the field of O_h symmetry. The t_{2g}^5 configuration can be treated as being one electron hole in a closed t_{2g}^6 shell (one-hole notation).[15-18]

One-hole notation simplifies the expressions of the six states as follows:

$$|d_{xz}^{\pm}\rangle \equiv -(1/\sqrt{2})(|1^{\pm}\rangle - |-1^{\pm}\rangle),$$
$$|d_{yz}^{\pm}\rangle \equiv (i/\sqrt{2})(|1^{\pm}\rangle + |-1^{\pm}\rangle),$$

and

$$|d_{x^2-y^2}^{\pm}\rangle \equiv (1/\sqrt{2})(|2^{\pm}\rangle + |-2^{\pm}\rangle),$$

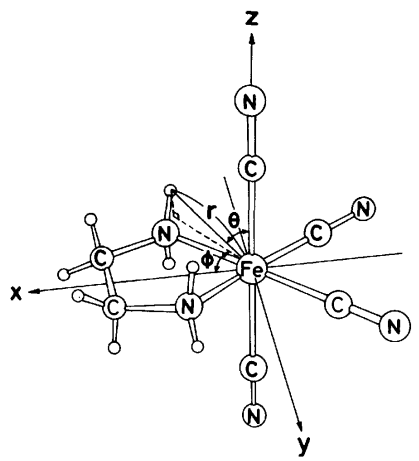

Fig. 1. Schematic representation of the coordinate system for analyzing magnetic resonances of $[Fe^{III}(CN)_4(diamine)]^-$.

where, for example, $|1^+\rangle$ represents a +1/2 spin state with a magnetic quantum number of +1.

ESR. The degeneracy of the t_{2g}^5 configuration is released to generate three Kramers doublets (Eq. 1) by perturbation arising from crystal-field distortions and spin-orbit coupling:

$$|\psi_i^{\pm}\rangle = \pm A_i|d_{xz}^{\mp}\rangle - iB_i|d_{yz}^{\mp}\rangle + C_i|d_{x^2-y^2}^{\pm}\rangle \quad (1)$$
$$i = 1, 2, \text{ and } 3,$$

where i=1 represents the ground doublet.

According to the methods reported by Bohan[19] and Taylor,[20] the eigenvalues of the Kramers doublets, E_i, and the axial and rhombic distortions of the crystal field, U and R, are expressed as follows:

$$E_i/\zeta = -(A_i+B_i+C_i)(1/A_i+1/B_i+1/C_i)/6+1/2, \quad (2)$$
$$U/\zeta = -(A_1+B_1+C_1)(1/A_1+1/B_1-2/C_1)/4, \quad (3)$$

and

$$R/\zeta = -(A_1+B_1+C_1)(1/A_1-1/B_1)/2, \quad (4)$$

where ζ (>0) is the spin-orbit coupling constant.

The principal g values are related to the coefficients of the ground Kramers doublet by the following expressions:[21]

$$g_{xx} = 2(-A_1^2 + B_1^2 + C_1^2 + 2kB_1C_1),$$
$$g_{yy} = 2(A_1^2 - B_1^2 + C_1^2 + 2kA_1C_1), \quad (5)$$

and

$$g_{zz} = -2(A_1^2 + B_1^2 - C_1^2 + 2kA_1B_1),$$

where $A_1^2+B_1^2+C_1^2=1$. For k=1, the coefficients are expressed in terms of the principal g values:

$$A_1 = (g_{yy} - g_{zz})/\sqrt{8(g_{xx} + g_{yy} - g_{zz})},$$
$$B_1 = (g_{xx} - g_{zz})/\sqrt{8(g_{xx} + g_{yy} - g_{zz})}, \quad (6)$$

and

$$C_1 = (g_{xx} + g_{yy})/\sqrt{8(g_{xx} + g_{yy} - g_{zz})},$$

where $g_{xx}+g_{yy}-g_{zz}$ must be positive because Eq. 5 shows

$$g_{xx} + g_{yy} - g_{zz} = 2(A_1 + B_1 + C_1)^2 > 0. \quad (7)$$

The coefficients and eigenvalues for the excited Kramers doublets are obtained by diagonalizing the following perturbation matrix with the U/ζ and R/ζ values calculated from Eqs. 3 and 4:

$$\begin{array}{c} \begin{matrix} |d_{xz}^{\mp}\rangle & -i|d_{yz}^{\mp}\rangle & |d_{x^2-y^2}^{\pm}\rangle \end{matrix} \\ \begin{pmatrix} -U/(3\zeta)-R/(2\zeta) & -1/2 & -1/2 \\ -1/2 & -U/(3\zeta)+R/(2\zeta) & -1/2 \\ -1/2 & -1/2 & (2U)/(3\zeta) \end{pmatrix} \end{array}$$

NMR. The tetracyano(diamine)ferrate(III) com-

plexes are paramagnetic (low-spin),[22] and the corresponding Fe^{II} complexes are diamagnetic.[6] We define isotropic shift, δ^{iso}, for the Fe^{III} complexes as the difference in chemical shift between the Fe^{III}, $\delta_{Fe^{III}}$, and Fe^{II} complexes, $\delta_{Fe^{II}}$: $\delta^{iso}=\delta_{Fe^{III}}-\delta_{Fe^{II}}$. δ^{iso} is composed of three parts,[8,9,23]

$$\delta^{iso} = \delta^{con} + \delta_L^{dip} + \delta_M^{dip}, \quad (8)$$

where δ^{con} is a Fermi contact shift, δ_L^{dip} is a ligand-centered dipolar shift, and δ_M^{dip} is a metal-centered dipolar shift. For ^1H nuclei δ_L^{dip} term is expected to be negligible.

The expressions for δ_M^{dip} and δ^{con} reported by Kurland and McGarvey[8,9] can be rewritten with the symbols used in Eqs. 1 and 2 as follows:

$$\delta_M^{dip}=(10^6/24\pi)[(2\chi_{zz}-\chi_{yy}-\chi_{xx})G_A+3(\chi_{xx}-\chi_{yy})G_B], \quad (9)$$
$$G_A = (3\cos^2\theta - 1)/r^3,\ G_B = \sin^2\theta\cos 2\phi/r^3, \quad (10)$$

$$\chi_{qq}=\mu_0\beta^2[k_BT\sum_{i=1}^{3}\exp(-E_i/k_BT)]^{-1}[\sum_{i=1}^{3}\exp(-E_i/k_BT)\cdot <\mu_q>_{ii}^2-2k_BT\sum_{i=1}^{2}\sum_{j=i+1}^{3}Q_{ij}<\mu_q>_{ij}^2], \quad (11)$$

$$Q_{ij}=[\exp(-E_i/k_BT)-\exp(-E_j/k_BT)][E_i-E_j]^{-1}, \quad (12)$$

$$\delta^{con}=10^6a_N\beta[6k_BT\gamma\hbar\sum_{i=1}^{3}\exp(-E_i/k_BT)]^{-1}\sum_{q=x,y,z}[\sum_{i=1}^{3}\exp(-E_i/k_BT)<\mu_q>_{ii}<s_q>_{ii}-2k_BT\sum_{i=1}^{2}\sum_{j=i+1}^{3}Q_{ij}<\mu_q>_{ij}<s_q>_{ij}], \quad (13)$$

where δ_M^{dip} and δ^{con} are in the unit of ppm, and their positive values indicate downfield shifts. G_A and G_B are geometric factors, and the distance r and angles θ and ϕ are defined as shown in Fig. 1. χ_{qq} ($q=x, y$, and z) is the principal axis component of the susceptibility tensor. μ_0, β, k_B, T, a_N, γ, and $\hbar$ are magnetic permeability of vacuum, the Bohr magneton, the Boltzmann constant, absolute temperature, Fermi contact coupling constant, magnetogyric ratio, and the Planck constant. $<\mu_q>_{ij}$ and $<s_q>_{ij}$ ($q=x, y, z$ and $i, j=1, 2, 3$) are defined as follows:

$$<\mu_x>_{ij} \equiv -A_iA_j + B_iB_j + C_iC_j + k(B_iC_j + B_jC_i),$$
$$<\mu_y>_{ij} \equiv A_iA_j - B_iB_j + C_iC_j + k(C_iA_j + C_jA_i),$$
$$<\mu_z>_{ij} \equiv A_iA_j + B_iB_j - C_iC_j + k(A_iB_j + A_jB_i),$$
$$<s_x>_{ij} \equiv -A_iA_j + B_iB_j + C_iC_j,$$
$$<s_y>_{ij} \equiv A_iA_j - B_iB_j + C_iC_j,$$

and

$$<s_z>_{ij} \equiv A_iA_j + B_iB_j - C_iC_j.$$

Since the three Kramers doublets belong to a single 1/2 spin state, Fermi coupling constants for them, a_N, are represented by a single value in Eq. 13, according to the theory of Kurland and McGarvey.[8,9]

Results and Discussion

Temperature Dependence of ^1H NMR Spectra. It is well-known that the 1,2-diamine coordinated to a metal ion takes λ and δ gauche conformations.[24] The λ and δ forms of the en chelate are enantiomeric and identical in energy and, hence, a conformational

Table 1. Temperature Dependence of the Chemical Shifts, Isotropic, Dipolar, and Fermi Contact Shifts of $[Fe^{III}(CN)_4(1,2\text{-ethanediamine})]^-$

Nucleus	Temp/K	Chemical shift/ppm[a]	δ^{iso}/ppm[a,b] Obsd.	δ^{iso}/ppm[a,b] Calcd.	δ_M^{dip}/ppm[a] Calcd.	δ^{con}/ppm[a] Calcd.
	303	−1.15	−3.65	−4.16	16.21	−20.37
	293	−0.84	−3.34	−3.72	17.36	−21.08
	283	−0.49	−2.99	−3.23	18.61	−21.84
	273	−0.01	−2.51	−2.65	20.00	−22.65
	263	0.44	−2.06	−1.99	21.53	−23.52
	253	1.17	−1.33	−1.22	23.23	−24.45
$C\underline{H}_2$	243	1.87	−0.63	−0.33	25.12	−25.45
	233	3.04	0.54	0.69	27.22	−26.53
	223	3.69	1.19	1.89	29.58	−27.69
	213	5.27	2.77	3.27	32.22	−28.95
	203	6.87	4.37	4.87	35.19	−30.32
	193	9.29	6.79	6.74	38.55	−31.81
	185	12.04	9.54	8.46	41.56	−33.10
$N\underline{H}_2$	300	145	145[c]	145	6.8	138.2
$\underline{C}H_2$	300	251.6[d]	206.4	206.4	38.8	167.4[e]

a) Positive values indicate downfield shifts. b) Isotropic shift is defined as the difference in chemical shift between the Fe^{III} and Fe^{II} complexes. The chemical shifts for $C^1\underline{H}_2$ and $^{13}\underline{C}H_2$ of $[Fe^{II}(CN)_4(1,2\text{-ethanediamine})]^{2-}$ at 300 K were 2.50 and 45.2 ppm, respectively (Ref. 6). c) The chemical shift for $N\underline{H}_2$ of the Fe^{II} 1,2-ethanediamine complex is expected to be a few ppm, although it was not be measured owing to a rapid H-D exchange. The chemical shift observed for the Fe^{III} complex was hence regarded as isotropic shift. d) Ref. 6. e) The value is the sum of δ^{con} and δ_L^{dip}.

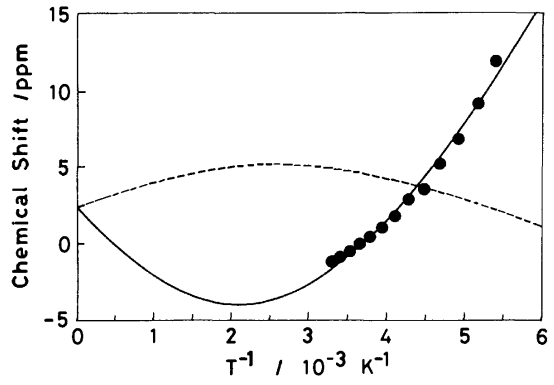

Fig. 2. Temperature dependence of ^1H NMR shift of the methylene protons of $[Fe^{III}(CN)_4(1,2\text{-ethanediamine})]^-$. The observed chemical shift (solid circle) is a time-averaged shift of the axial and equatorial protons due to a rapid conformational interconversion of the chelate between λ and δ gauche forms. Positive values indicate downfield shifts. The solid line shows the best-fitted curve of temperature dependence, and the broken line represents the results obtained from improper assignments of g values. The value at $T^{-1}=0$ represents the chemical shift observed for the diamagnetic Fe^{II} complex, $[Fe^{II}(CN)_4(1,2\text{-ethanediamine})]^{2-}$.

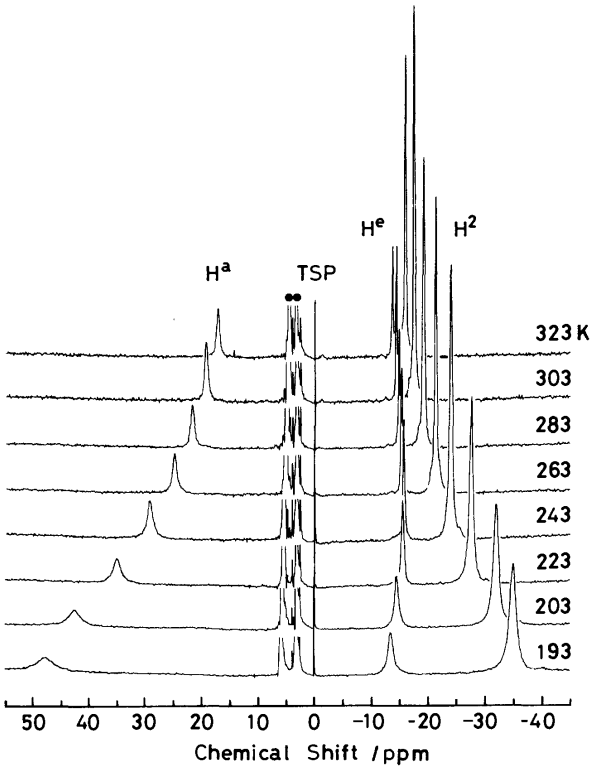

Fig. 3. ^1H NMR spectra of $[Fe^{III}(CN)_4(N,N'\text{-dimethyl-1,2-ethanediamine})]^-$ in CD_3OD containing 0.25% DCl at 323—193 K. A dot (●) indicates a solvent signal.

interconversion between them rapidly occurs on the NMR time scale near room temperature.[6,7] The CH_2 signal of the Fe^{III} complex broadened with a decrease

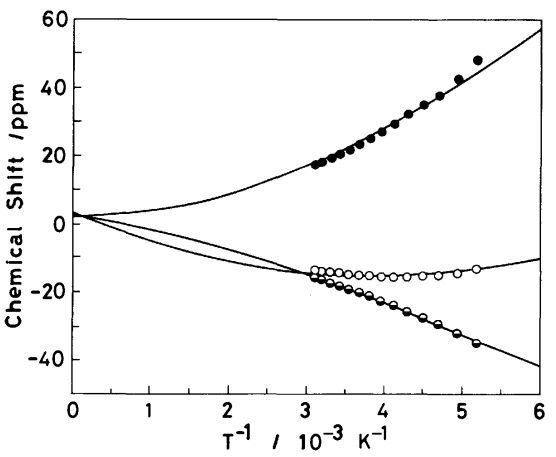

Fig. 4. Temperature dependence of ^1H NMR shifts of $[Fe^{III}(CN)_4(N,N'\text{-dimethyl-1,2-ethanediamine})]^-$. The solid lines are the curves best-fitted to the observed temperature dependence: H^a (●), H^e (○), and H^2 (◒). The values at $T^{-1}=0$ represent the chemical shifts observed for the diamagnetic Fe^{II} complex, $[Fe^{II}(CN)_4(N,N'\text{-dimethyl-1,2-ethanediamine})]^{2-}$.

in temperature, but did not split into two peaks corresponding to the axial and equatorial methylene protons, even at 185 K.[7] The downfield shift of the time-averaged signal accelerated with a decrease in temperature. The observed chemical shifts at 185—303 K are summarized in Table 1 and plotted in Fig. 2.

We reported in a previous paper[6] that a geometric isomerism exists for the Fe^{III} s-Me_2en complex, i.e., racemic and meso forms with respect to the N-methyl groups, and that the isolated complex was a racemic isomer. The five-membered chelate ring of s-Me_2en can be treated as fixed in either a δ or λ gauche conformation; in fact, the axial and equatorial protons (H^a and H^e) appeared as separated peaks at 20.45 and −14.59 ppm, even at room temperature, respectively. The NMR spectra of the racemic isomer measured at 193—323 K are reproduced in Fig. 3. The observed chemical shifts are summarized in Table 2 and plotted in Fig. 4. The decrease in temperature broadened all signals and moved H^a and H^2 signals toward downfield and upfield, respectively. The temperature dependence of H^e is unique: the direction of the variation of the chemical shift reversed at around 243 K. Figures 2 and 4 clearly show the non-Curie behavior of the Fe^{III} complexes.

Chemical Shifts of Amino Protons and Carbon Atoms. Resonances of NH of both the Fe^{III} en and s-Me_2en complexes were observed at 145 ppm at 300 K as a broad peak with a width of 290 and 380 Hz, respectively. The NH signals of the corresponding Fe^{II} complexes could not be observed due to a rapid H-D exchange between the amino protons and the solvent. The ^{13}C shifts of the Fe^{III} and Fe^{II} complexes reported previously[6] are collected together in Tables 1 and 2.

Table 2. Temperature Dependence of the Chemical Shifts, Isotropic, Dipolar, and Fermi Contact Shifts of $[Fe^{III}(CN)_4(N,N'$-dimethyl-1,2-ethanediamine$)]^-$

Nucleus	Temp/K	Chemical shift/ppm[a]	δ^{iso}/ppm[a,b] Obsd.	δ^{iso}/ppm[a,b] Calcd.	δ_M^{dip}/ppm[a] Calcd.	δ^{con}/ppm[a] Calcd.
H^a	323	17.15	15.03	15.80	15.49	0.31
	313	18.02	15.90	16.84	16.52	0.32
	303	19.27	17.15	17.98	17.65	0.33
	293	20.45	18.33	19.24	18.90	0.34
	283	21.79	19.67	20.62	20.26	0.36
	273	23.33	21.21	22.14	21.77	0.37
	263	24.92	22.80	23.82	23.44	0.38
	253	27.10	24.98	25.69	25.29	0.40
	243	29.22	27.10	27.76	27.35	0.41
	233	32.13	30.01	30.07	29.64	0.43
	223	34.99	32.87	32.66	32.21	0.45
	213	37.72	35.60	35.55	35.08	0.47
	203	42.75	40.63	38.82	38.32	0.50
	193	48.05	45.93	42.50	41.98	0.52
H^e	323	−13.64	−16.42	−17.69	12.96	−30.65
	313	−13.95	−16.73	−17.84	13.83	−31.67
	303	−14.30	−17.08	−17.97	14.77	−32.74
	293	−14.59	−17.37	−18.07	15.81	−33.88
	283	−14.86	−17.64	−18.15	16.96	−35.11
	273	−15.12	−17.90	−18.19	18.22	−36.41
	263	−15.33	−18.11	−18.19	19.61	−37.80
	253	−15.54	−18.32	−18.14	21.16	−39.30
	243	−15.65	−18.43	−18.02	22.88	−40.90
	233	−15.65	−18.43	−17.84	24.80	−42.64
	223	−15.54	−18.32	−17.56	26.95	−44.51
	213	−15.27	−18.05	−17.18	29.36	−46.54
	203	−14.51	−17.29	−16.67	32.06	−48.73
	193	−13.33	−16.11	−16.01	35.12	−51.13
H^2	323	−15.86	−18.38	−18.31	−5.64	−12.67
	313	−16.52	−19.04	−19.10	−6.01	−13.09
	303	−17.39	−19.91	−19.95	−6.42	−13.53
	293	−18.24	−20.76	−20.88	−6.88	−14.00
	283	−19.15	−21.67	−21.88	−7.37	−14.51
	273	−20.21	−22.73	−22.97	−7.92	−15.05
	263	−21.27	−23.79	−24.15	−8.53	−15.62
	253	−22.67	−25.19	−25.44	−9.20	−16.24
	243	−24.02	−26.54	−26.85	−9.95	−16.90
	233	−25.82	−28.34	−28.41	−10.79	−17.62
	223	−27.57	−30.09	−30.11	−11.72	−18.39
	213	−29.19	−31.71	−32.00	−12.77	−19.23
	203	−32.04	−34.56	−34.09	−13.95	−20.14
	193	−34.90	−37.42	−36.41	−15.28	−21.13
NH	300	145	145[c]	145	9.9	135.1
C^1	300	301.1[d]	246.9	246.9	38.8	208.1[e]
C^2	300	156.1[d]	114.3	114.3	−3.0	117.3[e]

a) Positive values indicate downfield shifts. b) Isotropic shift is defined as the difference in chemical shift between the Fe^{III} and Fe^{II} complexes. The chemical shifts for H^a, H^e, H^2, C^1, and C^2 of $[Fe^{II}(CN)_4(N,N'$-dimethyl-1,2-ethanediamine$)]^{2-}$ at 300 K were 2.12, 2.78, 2.52, 54.2, and 41.8 ppm, respectively (Ref. 6). c) The chemical shift for NH of the Fe^{II} complex is expected to be a few ppm, although it was not be measured owing to a rapid H–D exchange. The chemical shift observed for the Fe^{III} complex was hence regarded as isotropic shift. d) Ref. 6. e) The value is the sum of δ^{con} and δ_L^{dip}.

ESR Spectrum of $[Fe^{III}(CN)_4(en)]^-$. The general expression of δ^{iso} given by Kurland and McGarvey[8,9] suggests that the eigenvalues and eigenfunctions of the excited as well as the ground Kramers doublets associated with the $^2T_{2g}$ term should be determined in order to analyze δ^{iso} which does not obey the Curie law. Since the required quantities are obtained from the analysis of g values, we measured the ESR spectrum of $[Fe^{III}(CN)_4(en)]^-$ shown in Fig. 5 at liquid-helium temperatures, using a polycrystalline sample diluted

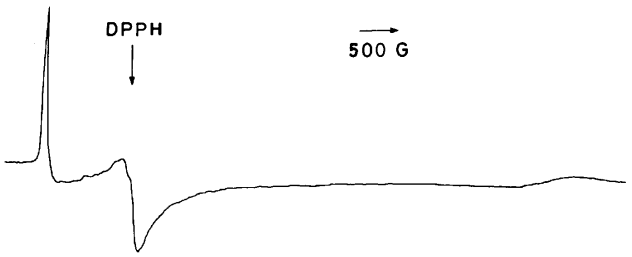

Fig. 5. ESR spectrum of $[Fe^{III}(CN)_4$(1,2-ethanediamine)$]^-$ measured at liquid-helium temperatures. The Fe^{III} complex was magnetically diluted to ca. 1/100 with $K[Co^{III}(CN)_4$(1,2-ethanediamine)].

magnetically to ca. 1/100 with the isostructural Co^{III} complex, $[Co^{III}(CN)_4(en)]^-$. The g values obtained after a correction of the magnetic field with DPPH were 3.15, 1.99, and 0.82.

The following expression of the product $g_{xx}g_{yy}g_{zz}$ is obtained from Eq. 5 with $k=1$:

$$g_{xx}g_{yy}g_{zz} = -8[(A_1 + B_1)^2 - C_1^2][(B_1 + C_1)^2 - A_1^2]\cdot [(C_1 + A_1)^2 - B_1^2].$$

For a complex with a crystal field largly distorted from O_h symmetry, the product is positive. A negative product is obtained for a complex close to O_h symmetry. Since the tetracyano en complex has two kinds of ligands (CN^- and en), which are different in crystal-field strength,[25-27] the complex is expected to have a largely distorted crystal field. The product was, hence, assumed to be positive in an analysis of the g values. To justify this assumption, we measured the Mössbauer spectra of $[Fe^{III}(CN)_4(en)]^-$ at 95—260 K. The temperature dependence of the quadrupole splitting supported $g_{xx}g_{yy}g_{zz}>0$.[28]

The following six sets satisfy Eq. 7 and give a norm close to unity, 0.961: (g_{xx}, g_{yy}, g_{zz})=(3.15, 1.99, 0.82), (1.99, 3.15, 0.82), (3.15, −0.82, −1.99), (−0.82, 3.15, −1.99), (1.99, −0.82, −3.15), and (−0.82, 1.99, −3.15). With the first set, the coefficients for the ground Kramers doublet were calculated from Eq. 6: A_1= 0.2030, B_1=0.4043, and C_1=0.8918. These values were corrected to 0.2108, 0.4141, and 0.8855 by Eq. 5 with k=0.905, respectively. Using the corrected values, we obtained U/ζ=−1.849 and R/ζ=−1.758 from Eqs. 3 and 4. Substitution of the U/ζ and R/ζ values into the perturbation matrix followed by diagonalization gave the following eigenvalues and coefficients for the lowest three Kramers doublets:

Set 1

A_1 = 0.2108, B_1 = 0.4141, C_1 = 0.8855, E_1/ζ = −1.5862,
A_2 = 0.1382, B_2 = 0.8841, C_2 = −0.4464, E_2/ζ = −0.0882,

and

A_3 = −0.9677, B_3 = 0.2165, C_3 = 0.1292, E_3/ζ = 1.6744.

The remaining five g-value sets give the same values of E_i/ζ; the coefficients for each set were obtained by rotating the values of Set 1. For example, Set 2 was obtained from the second set of g values:

Set 2

A_1 = 0.4141, B_1 = 0.2108, C_1 = 0.8855, E_1/ζ = −1.5862,
A_2 = 0.8841, B_2 = 0.1382, C_2 = −0.4464, E_2/ζ = −0.0882,

and

A_3 = 0.2165, B_3 = −0.9677, C_3 = 0.1292, E_3/ζ = 1.6744.

Estimation of Geometric Factors. The geometric factors for the present diamine chelates were calculated from Eq. 10, based on the assumption that the present Fe^{III} complexes have the same configuration of diamine chelate as the Co^{III} complex, *trans*-$[Co^{III}Cl_2(en)_2]Cl\cdot(H_5O_2)^+Cl^-$, the crystal structure of which was analyzed with neutron diffraction by Rozire and Williams.[29] The coordinates of the axial amino protons and the equatorial methyl groups of the Fe^{III} *s*-Me$_2$en complex were estimated, based on an assumption that these nuclei locate at the vertices of tetrahedron with bond lengths of C-H=1.09, N-H= 1.02, and C-N=1.48 Å.

The following values of G_A and G_B were obtained: for the en chelate; H, −1.554, 1.883; N<u>H</u>, −4.355, −1.832; C, −4.275, 3.884×10^{28} m^{-3}, where the former four values are the means of G_A and G_B values for the axial and equatorial protons, and for the *s*-Me$_2$en chelate; H^a, −1.270, 2.346; H^e, −1.838, 1.419; H^2, −0.9783, −1.864; N<u>H</u>, −3.813, −0.9187; C^1, −4.275, 3.884; C^2, −2.735, −2.441×10^{28} m^{-3}. The methyl protons of the *s*-Me$_2$en chelate was assumed to rotate freely.

Analysis of Isotropic Shifts. The observed values of δ^{iso} listed in Tables 1 and 2 were obtained by using the ^1H and ^{13}C chemical shifts for the diamagnetic Fe^{II} complexes, $[Fe^{II}(CN)_4(en)]^{2-}$ and $[Fe^{II}(CN)_4$(*s*-Me$_2$-en)$]^{2-}$, reported previously.[6] Since the chemical shifts for N<u>H</u> of the Fe^{III} complexes were very large, i.e. 145 ppm, and N<u>H</u> shifts of the corresponding Fe^{II} complexes are expected to be at most a few ppm, δ^{iso} of the N<u>H</u>'s was taken as 145 ppm.

The least-squares fitting of Eqs. 8—13 to the δ^{iso} values for C<u>H</u>$_2$ of the en complex yielded ζ=160 cm^{-1} and a_N=−0.69 MHz when Set 1 was used as eigenvalues and eigenvectors. The δ^{iso}, δ_M^{dip}, and δ^{con} estimated by this fitting are shown in the fifth-seventh columns of Table 1. The calculated shifts are compared with the observed shifts in Fig. 2. Set 1 gave the better fit (solid curve), but other sets, e.g. Set 2 gave unsatisfactory results (broken curve). The g values were therefore assigned as follows: g_{xx}=3.15, g_{yy}=1.99, and g_{zz}=0.82.

δ_M^{dip} values for other ^1H and ^{13}C nuclei of the en complex were calculated from Eqs. 9—12 by using Set

1 and ζ=160 cm^{-1}. The difference between the δ_M^{dip} and the observed δ^{iso} values corresponds to δ^{con} for ^{1}H nuclei and $\delta^{con}+\delta_L^{dip}$ for ^{13}C nuclei. These values are collected together in Table 1.

The Fe^{III} *s*-Me$_2$en complex offers an opportunity to investigate the δ^{iso} for H^a and H^e independently, since the complex has a fixed conformation in which both *N*-methyl groups take pseudoequatorial positions (eq-form).[30] The procedure mentioned above was applied to this complex, using Set 1 and ζ=160 cm^{-1}. The calculated results are summarized in Table 2, and the comparison of the observed and calculated shifts is shown in Fig. 4.

The magnitude of the ζ value is considered to be appropriate to the low-spin Fe^{III} complexes for the following reasons. (1) μ_{eff}=2.32 BM[31] at 303 K estimated from ζ=160 cm^{-1} is in good agreement with those observed for a series of tetracyano(1,2-diamine)-ferrate(III) complexes: (*R*)-1,2-propanediamine, 2.3; (1*R*,2*R*)-1,2-cyclopentanediamine, 2.4; (1*R*,2*R*)-1,2-cyclohexanediamine, 2.4 BM.[22] (2) Merrithew et al.[32] employed the spin-orbit coupling constant of ζ=150 cm^{-1} in their Mössbauer study of H[Fe^{III}(CN)$_4$(bpy)] and [Fe^{III}(CN)$_2$(bpy)$_2$]ClO$_4$. (3) We have obtained ζ=150—230 cm^{-1} from the temperature dependence of Mössbauer quadrupole splitting of [Fe^{III}(CN)$_4$(en)]$^-$ at 95—260 K.[28]

Since the application of ζ=160 cm^{-1} to the *s*-Me$_2$en complex gave good agreement between the observed and calculated shifts, as shown in Fig. 4, the variation of ζ is small in this class of Fe^{III} complexes. The combination of Set 1 and ζ=160 cm^{-1} leads to (1) the largest population of the electron hole in $d_{x^2-y^2}$ and (2) the first and the second excited states which are higher in energy by 2.9 and 6.2 kJ mol^{-1} than the ground state, respectively.

Dipolar Shift and Fermi Contact Shift. The δ_M^{dip} for the present Fe^{III} complexes calculated from Set 1 and Eq. 9 (Tables 1 and 2) is zero on the elliptical cone which intersects the *xz* and *yz* planes at 47.3 and 68.9°, respectively. The nuclei inside and outside the cone have negative and positive δ_M^{dip}, respectively. Since the methyl protons of the *s*-Me$_2$en chelate locate inside the cone and the other atoms are outside, δ_M^{dip} is negative for the former and positive for other atoms. The δ_M^{dip} for the methyl carbon is almost zero because this atom exists near the cone.

Subtracting δ_M^{dip} from δ^{iso} gave δ^{con} for each ^{1}H nucleus (Tables 1 and 2). The δ^{con} for H^a is near zero, i.e. $\delta^{iso}\simeq\delta_M^{dip}$. But H^e has large negative δ^{con}, i.e. upfield shift of 30—50 ppm at 193—323 K. H^a and H^e have different δ^{con} values, although they are bound to the same carbon atom.

The δ_M^{dip} for H^e is positive and considerably small in magnitude compared with the negative δ^{con} for H^e. The magnitude of the δ^{iso} for H^e is, hence, reduced and its variation with temperature is small. The characteristics of δ^{iso} for the tetracyanoferrate(III) complexes, e.g. the different sign of δ^{iso} for H^a and H^e and the peculiar temperature dependence of δ^{iso} for H^e, are the results of the different contribution of δ_M^{dip} and δ^{con} for these protons.

The δ_M^{dip} and δ^{con} for H^2 are both upfield shifts, and the δ^{con} of −12.7—−21.1 ppm at 193—323 K is close to the mean of δ^{con}'s for H^a and H^e, i.e. −15.2—−25.3 ppm. This fact suggests that the unpaired spin is transferred to the freely rotating H^2 in a way similar to H^a and H^e.

The large δ^{iso} observed for N<u>H</u> was ascribed to large δ^{con}, ca. 135 ppm, which is larger than at least 4 times that for C<u>H</u>.

For ^{13}C nuclei, δ^{iso} was separated into δ_M^{dip} and $\delta^{con}+\delta_L^{dip}$ (Tables 1 and 2). The carbon atoms constituting the five-membered chelate rings have $\delta^{con}+\delta_L^{dip}$ of 170—210 ppm, and its contribution to the δ^{iso} is over 80%. Since δ_L^{dip} for ^{13}C nucleus is not zero,[8,23] an estimation of δ^{con} for the ^{13}C nucleus requires an elimination of the δ_L^{dip} contribution. A calculation of δ_L^{dip}, however, requires many approximations, as shown in the treatment of ^{13}C NMR shift for [Fe^{III}-(CN)$_6$]$^{3-}$ by Kurland and McGarvey;[8,23] hence, the separation of δ^{con} and δ_L^{dip} may be a problem to settle in future.

Fermi Contact Coupling Constant and Spin Population. The a_N values obtained from the fitting calculation are listed in Table 3. The population of the unpaired spin in the 1s orbital of hydrogen, Q_{1s}, and that in the 2s orbital of carbon, Q_{2s}, were calculated from the a_N by the relations $Q_{1s}=a_N/1420$ and $Q_{2s}=a_N/3110$, where 1420 and 3110 MHz are the Fermi constants calculated for ^{1}H· and ^{13}C· radicals, respectively.[33] The estimated values of Q_{1s} and Q_{2s} are listed in Table 3.

The a_N value for H^e, −1.11 MHz, is similar in magnitude to those for ^{1}H nuclei of unsaturated ligands in low-spin Fe^{III} complexes: −1.08 MHz for ^{1}H nuclei at the position 6 and 6′ of 2,2′-bipyridyl in [Fe^{III}(bpy)$_3$]$^{3+}$, and −1.03 MHz for ^{1}H nuclei at the

Table 3. Fermi Contact Coupling Constants (a_N) and Spin Populations Estimated for [Fe^{III}(CN)$_4$(1,2-ethanediamine)]$^-$ and [Fe^{III}(CN)$_4$(*N*,*N*′-dimethyl-1,2-ethanediamine)]$^-$

Diamine	Nucleus	a_N/MHz	Spin population
en	N<u>H</u>	4.63	0.0033
	H	−0.69	−0.0005
	C	1.42	0.0005
s-Me$_2$en	N<u>H</u>	4.50	0.0032
	H^a	0.01	0.0000
	H^e	−1.11	−0.0008
	H^2	−0.46	−0.0003
	C^1	1.74	0.0006
	C^2	0.98	0.0003

position 2 and 9 of 1,10-phenanthroline in $[Fe^{III}(phen)_3]^{3+}$.[34] The fact that the latter two values are the largest among the a_N values observed for ^1H nuclei within these complexes suggests that σ bonds are not lower in facility of spin propagation than π bonds. The a_N values for ^{13}C nuclei are 1.4—1.7 MHz, though it should be noted that these values were obtained by assuming $\delta_L^{dip}=0$.

Spin population (Table 3) is a better scale for a comparison of the heteronuclear NMR shifts than a_N, since the latter depends on the magnetogyric ratio. The positive spins on NH and C and the negative spins on CH suggest the propagation of spin by polarization effect which results in an alteration in the sign of the spin population with each σ bond.

The transfer of unpaired spin from the Fe^{III} ion to the diamine ligands is considered to occur mainly between the 3d orbitals and the sp^3 hybridized orbitals of the nitrogen atoms by a polarization mechanism.[35] Most of the unpaired spin resides in the $3d_{x^2-y^2}$ orbital, as Set 1 shows; thus, this feature of electronic configuration is expected to result in the predominant population of the unpaired spin near the planes of the chelate rings. The large difference between H^a and H^e can be explained by this anisotropic population.

This work was supported partly by the Joint Studies Program (1980—1981) of the Institute for Molecular Science. We wish to express thanks to Dr. Toshiaki Enoki of Tokyo Institute of Technology for assisting in the measurement of the ESR spectrum. We are grateful to Professor Mitsuo Sato of Teikyo University and Dr. Tetsuo Asaji of Nagoya University for valuable discussions.

References

1) I. Morishima and T. Inubushi, *J. Am. Chem. Soc.*, **100**, 3568 (1978).

2) G. Williams, G. R. Moore, R. Porteous, M. M. Robinson, N. Soffe, and R. J. P. Williams, *J. Mol. Biol.*, **183**, 409 (1985).

3) G. R. Moore, M. M. Robinson, G. Williams, and R. J. P. Williams, *J. Mol. Biol.*, **183**, 429 (1985).

4) G. Williams, N. J. Clayden, G. R. Moore, and R. J. P. Williams, *J. Mol. Biol.*, **183**, 447 (1985).

5) I. Morishima, K. Yoshikawa, and K. Okada, *J. Am. Chem. Soc.*, **98**, 3787 (1976) and the references cited therein.

6) Y. Kuroda, M. Goto, and T. Sakai, *Bull. Chem. Soc. Jpn.*, **60**, 3917 (1987).

7) Y. Kuroda, N. Tanaka, M. Goto, and T. Sakai, *Inorg. Chem.*, **28**, 997 (1989).

8) R. J. Kurland and B. R. McGarvey, *J. Magn. Reson.*, **2**, 286 (1970).

9) J. P. Jesson, "NMR of Paramagnetic Molecules," ed by G. N. La Mar, W. D. Horrocks, Jr., and R. H. Holm, Academic Press, New York (1973), Chap. 1.

10) V. L. Goedken, *J. Chem. Soc., Chem. Commun.*, **1972**, 207.

11) M. Goto and V. L. Goedken, to be published.

12) M. Goto, M. Takeshita, and T. Sakai, *Inorg. Chem.*, **17**, 314 (1978).

13) The probe temperature was calibrated by the use of the calibration chart supplied by JEOL.

14) J. S. Griffith, *Mol. Phys.*, **21**, 135 (1971).

15) B. Bleaney and M. C. M. O'Brien, *Proc. Phys. Soc.*, **B69**, 1216 (1956).

16) J. S. Griffith, *Nature (London)*, **180**, 30 (1957).

17) J. S. Griffith, "The Theory of Transition Metal Ions," Cambridge Univ. Press, Cambridge (1961).

18) M. Kotani, "The Structure and Properties of Biomolecules and Biological Systems," ed by J. Duschene, Interscience, London (1964), pp. 159—181.

19) T. L. Bohan, *J. Magn. Reson.*, **26**, 109 (1977).

20) C. P. S. Taylor, *Biochim. Biophys. Acta*, **491**, 137 (1977).

21) We assume that k is isotropic and constant in order to simplify the analysis, although k is anisotropic for a complex without cubic symmetry and varies with eigenstates.

22) M. Goto, M. Takeshita, and T. Sakai, *Bull. Chem. Soc. Jpn.*, **54**, 2491 (1981).

23) B. R. McGarvey and R. J. Kurland, "NMR of Paramagnetic Molecules," ed by G. N. La Mar, W. D. Horrocks, Jr., and R. H. Holm, Academic Press, New York (1973), Chap. 14.

24) J. Corey and J. C. Bailar, Jr., *J. Am. Chem. Soc.*, **81**, 2620 (1959).

25) H. Yamatera, *Bull. Chem. Soc. Jpn.*, **31**, 95 (1958).

26) G. A. Renovitich, V. A. Baker, Jr., *J. Am. Chem. Soc.*, **90**, 3585 (1968).

27) C. S. Naiman, *J. Chem. Phys.*, **35**, 323 (1961).

28) Y. Kuroda, M. Goto, T. Sakai, M. Takano, and T. Shinjo, to be published.

29) J. Rozire and J. M. Williams, *Inorg. Chem.*, **15**, 1174 (1976).

30) C. J. Hawkins and J. A. Palmer, *Coord. Chem. Rev.*, **44**, 1 (1982). 80—90% population of eq-form has been reported for *N*-methyl-1,2-ethanediamine (Meen) chelates, $[Co^{III}(CN)_4(Meen)]^-$ and $[Co^{III}(NH_3)_4(Meen)]^{3+}$. The Fe^{III} *s*-Me_2en complex is expected to have almost the same or greater population of the eq-form, and we assigned the observed shifts to the eq-form.

31) Molar magnetic susceptibility, χ_M, is related to effective magnetic moment, μ_{eff} (BM), by the equation, $\chi_M=\mu_0 N_A \beta^2 \mu_{eff}^2/(3k_B T)$, where N_A is Avogadro constant. χ_M is related to the average of χ_{xx}, χ_{yy}, and χ_{zz} in Eq. 11: $\chi_M=N_A(\chi_{xx}+\chi_{yy}+\chi_{zz})/3$. $\chi_M=2.79\times10^{-8}$ m^3 and $\mu_{eff}=2.32$ BM at 303 K were estimated from $\zeta=160$ cm^{-1}.

32) P. B. Merrithew, C.-C. Lo, and A. J. Modestino, *Inorg. Chem.*, **14**, 242 (1975).

33) J. R. Morton, J. R. Rowlands, and D. H. Whiffen, *Nat. Phys. Lab. Rep. BPR*, **1962**, 13.

34) R. E. DeSimone and R. S. Drago, *Inorg. Chem.*, **11**, 668 (1972).

35) G. N. La Mar, "NMR of Paramagnetic Molecules," ed by G. N. La Mar, W. D. Horrocks, Jr., and R. H. Holm, Academic Press, New York (1973), Chap. 3.

Kinetic Study on Hydrogenation of Isoquinoline over Supported Ruthenium Catalysts

Hiroshi OKAZAKI,* Mahito SOEDA, Yoshio IKEFUJI,† Ryuji TAMURA,† and Isao MOCHIDA††
R&D Laboratories, Nippon Steel Chemical Co., Tobataku, Kitakyushushi 804
†Technical Part, Iwatani Industrial Gases Corp., Yodogawaku, Osakashi 532
††Research Institute of Advanced Material Study, Kyushu University, Kasugashi 816
(Received May 11, 1989)

The hydrogenation of isoquinoline (**1**) to isomeric decahydroisoquinoline (**4**) via 1,2,3,4-tetrahydroisoquinoline (**2**) or 5,6,7,8-tetrahydroisoquinoline (**3**) was kinetically studied over supported ruthenium catalysts under 50—100 atm hydrogen pressure at 135—170 °C. The results showed that the reaction proceeds mainly via **2** over ruthenium on carbon, and via **2** and **3** competitively over ruthenium on alumina. Such reaction features are explained from the view points of their adsorption and the activation of the molecules on the catalysts based on quantum chemical indices. The acidic nature of alumina support exhibited a preference of nitrogen lone-pair defining the adsorption of substrates, and consequently influencing on the reaction route. The proposed approach distinguished the present catalyst from Raney nickel examined in a previous paper. The noble and base metals may interact differently with the substrate, although both metals are classified as "soft".

In a previous paper,[1] we reported the selective preparation of some useful hydroisoquinolines using several commercial catalysts. Raney nickel (R-Ni) promoted the following consecutive reactions: **1**→**2**→**3**→**4** (cis) →**4** (trans).[2] On the other hand, a preliminary examination of a ruthenium catalyst suggested that **1** was rapidly hydrogenated to the cis- and trans-isomers of **4** via **2** and **3** simultaneously. The isomeric mixture of **4** is a starting material to perfluoro (*N*-methyldecahydroisoquinoline), an oxygen carrier for medical use.[3] Therefore, it is practically important to clarify the kinetics and mechanism of hydrogenation of **1** over ruthenium catalysts to control the product selectivity.

In the present work, the hydrogenation of **1** was studied kinetically in detail using ruthenium on carbon (Ru/C) and on alumina (Ru/Al_2O_3). Such a study may allow discussion on the reaction pathways for the hydrogenation of **1**, and on the adsorption and activation of substrates over ruthenium catalysts, both of which are expected to be entirely different from those over R-Ni. The structural factors of the substrates which influence strongly on their adsorption and activation are discussed by a semiempirical molecular orbital calculation.

Experimental

Materials. Isoquinoline was used after purification of commercial grade material produced from coal tar. Two tetrahydrogenated isomers were separated from the hydrogenated isoquinoline. Both procedures were described in the previous papers.[1,2] No sulfur-containing contaminant was found in all substrates. Ru/C was purchased from Nippon Engelhard Ltd. in dry state. Ru/Al_2O_3 was purchased from Nikki Chemical Co. in wet state (water content is about 50 wt%) and used without drying. Their ruthenium contents were 5 wt% on the dry base.

Hydrogenation Procedure and Analytical Method. 100 g of a starting material was hydrogenated over ruthenium catalyst in a 200 ml-autoclave with stirring at a constant pressure and temperature. The reaction conditions for three starting substrates (**1**, **2**, and **3**) were as follows; temperature range: 135—170 °C, hydrogen pressure range: 50—100 atm, amount of Ru/C or Ru/Al_2O_3 catalysts: 4 wt% in dry state per substrate (see Table 2 for the detailed conditions). The reaction mixture was sampled at appropriate times, and was diluted to 5 ml with methanol. After filtering off the catalyst, the product was analyzed by gas chromatography as described previously.[2] **4** contained two isomers, of which cis/trans ratio ranged from 2 to 4. The compounds other than **1**—**4** were less than 5% in all of the reactions.

Quantum Chemical Calculation. Quantum chemical indices of isoquinoline and its derivatives were obtained by the MNDO-MO[4] calculation using a CRAY X-MP/216 computer.[5] The geometries of all of the molecules were energetically optimized with the flat configuration of aromatic rings.

Results

Kinetic Modeling. Some kinetic models were tested, and the network shown in Fig. 1 and the following Langmuir-Hinshelwood type rate equations[2,6-8] were found to fit with our experimental data. This network contains the isomerization of **2** to **3**, but neither

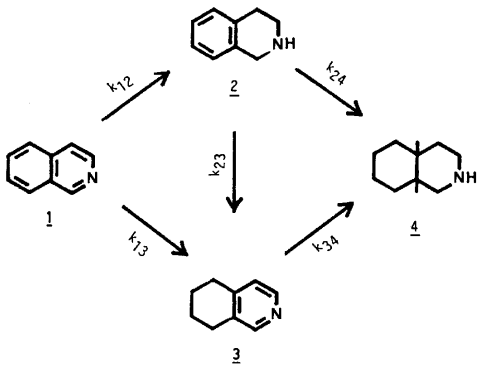

Fig. 1. Simplified reaction network for kinetic analysis.

dehydrogenation nor cis/trans isomerization of **4** was included, because relatively higher hydrogen pressures, lower temperatures, and shorter reaction times were employed in this work.

$$\frac{dC_1}{dt} = \frac{-m(k_{12}+k_{13})K_1C_1}{1+K_1C_1+K_2C_2+K_3C_3+K_4C_4} , \quad (1)$$

$$\frac{dC_2}{dt} = \frac{m[k_{12}K_1C_1-(k_{23}+k_{24})K_2C_2]}{1+K_1C_1+K_2C_2+K_3C_3+K_4C_4} , \quad (2)$$

$$\frac{dC_3}{dt} = \frac{m[k_{13}K_1C_1+k_{23}K_2C_2-k_{34}K_3C_3]}{1+K_1C_1+K_2C_2+K_3C_3+K_4C_4} , \quad (3)$$

and

$$\frac{dC_4}{dt} = \frac{m[k_{24}K_2C_2+k_{34}K_3C_3]}{1+K_1C_1+K_2C_2+K_3C_3+K_4C_4} , \quad (4)$$

where C_i is the concentration of species i (the initial value of isoquinoline, $C_1(t=0)$, was 8.52 mol dm^{-3} under STP conditions), t is the reaction time (h), m is the concentration of catalyst (g dm^{-3}), k_{ij} is the apparent rate constant of reaction $i \rightarrow j$ (the constant is a function of hydrogen pressure), and K_i is the equilibrium adsorption constant of species i. In contrast to the case of the R-Ni catalyst,[2] absolute values of K_i were calculated in this study, because unity in the denominator of Eqs. 1—4 was not neglected on the ruthenium catalysts.

Equilibrium Adsorption Constants and Rate Constants. K_i and k_{ij} in the above equations were determined by a curve fitting procedure. It was assumed that each value of K_i is constant under the present expreimental conditions when the same catalyst is used. The theoretical product distributions were calculated by a numerical analysis containing the Runge-Kutta-Gill routine. The values of K_i and k_{ij} were determined with the degree of agreement between experimental product distributions and the respective theoretical values. First, K_3, K_4, and k_{34} were determined by the Eqs. 3 and 4 and the data obtained from the experiment in which **3** was employed as the starting material. Secondly, K_2, k_{23}, and k_{24}, were determined with the above values of K_3, K_4, and k_{34}, the Eqs. 2—4 and the data obtained from the experiment in which **2** was employed as the starting material. Thirdly, K_1, k_{12}, and k_{13} were determined in a similar manner to the above. Figures 2—7 show some example of the product distributions on the hydrogenation of **1**, **2**, and **3** over Ru/C or Ru/Al_2O_3. The calculated values (solid lines) are in good agreement with the experimental data (dots). Their presisions of simulation were about ±5%. It is noticed during the

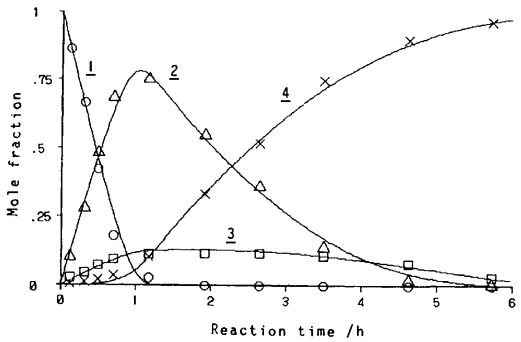

Fig. 2. Product distributions on the hydrogenation of **1** over Ru/C at 150 °C under 100 atm H_2 pressure. **1**: isoquinoline, **2**: 1,2,3,4-tetrahydroisoquinoline. **3**: 5,6,7,8-tetrahydroisoquinoline, **4**: decahydroisoquinoline.

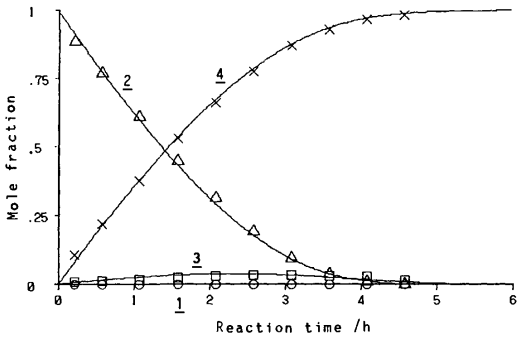

Fig. 3. Product distributions on the hydrogenation of **2** over Ru/C at 145 °C under 100 atm H_2 pressure. See Fig. 2 for the chemical names of symbols.

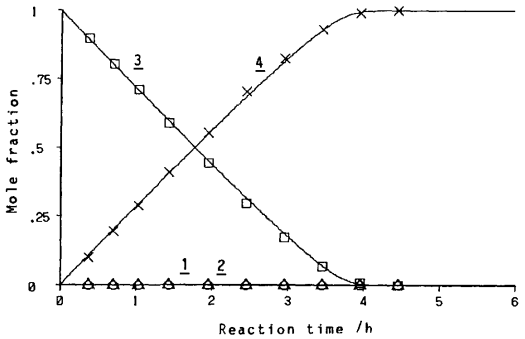

Fig. 4. Product distributions on the hydrogenation of **3** over Ru/C at 170 °C under 100 atm H_2 pressure. See Fig. 2 for the chemical names of symbols.

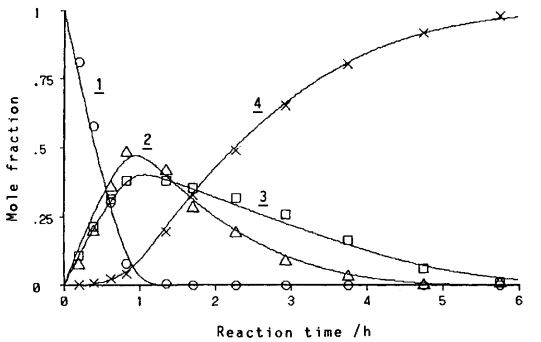

Fig. 5. Product distributions on the hydrogenation of **1** over Ru/Al_2O_3 at 150 °C under 100 atm H_2 pressure. See Fig. 2 for the chemical names of symbols.

hydrogenation of **1** that the composition of **3** over Ru/Al_2O_3 (Fig. 5) was considerably higher than that over Ru/C (Fig. 2).

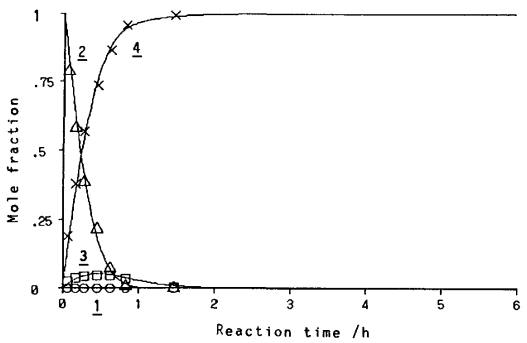

Fig. 6. Product distributions on the hydrogenation of **2** over Ru/Al_2O_3 at 157 °C under 100 atm H_2 pressure. See Fig. 2 for the chemical names of symbols.

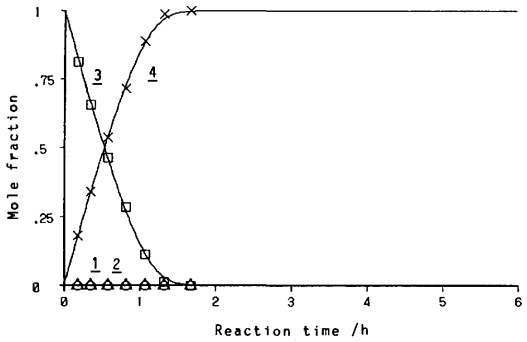

Fig. 7. Product distributions on the hydrogenation of **3** over Ru/Al_2O_3 at 165 °C under 100 atm H_2 pressure. See Fig. 2 for the chemical names of symbols.

Table 1. Equilibrium Adsorption Constants

Catalyst	K_1	K_2	K_3	K_4
	$dm^3\ mol^{-1}$			
Ru/C	35.0	2.3	7.0	0.12
Ru/Al_2O_3	70.0	4.7	14.1	1.8

Table 1 summarizes the values of K_i. The precision of constants K_i was about ±50%. The relative values of K_i/K_1 over the ruthenium catalysts are different from that over R-Ni reported previously.[2] The respective relative values except for K_4/K_1 were much the same over Ru/C and Ru/Al_2O_3.

Table 2 summarizes the values of k_{ij}. The precision of the constants was about ±20%. The value of k_{13} over Ru/Al_2O_3 is much larger than that over Ru/C. Roughly linear relations of the constants against hydrogen pressure were observed at 150 °C over Ru/C as shown in the table.

The effects of temperature on rate constants of all steps over Ru/C under 100 atm of hydrogen pressure are shown in Fig. 8. The apparent activation energy of

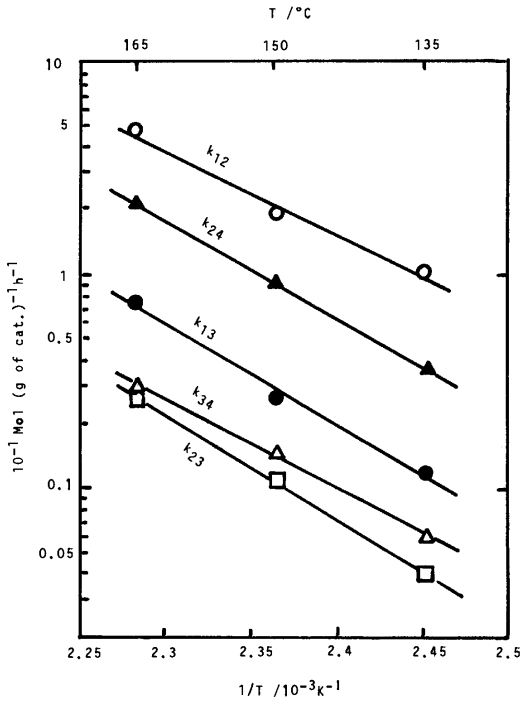

Fig. 8. Arrhenius plot for hydrogenation of isoquinoline over Ru/C under 100 atm H_2 pressure.

Table 2. Rate Constants on Hydrogenation of Isoquinoline and Partial Hydroisoquinolines over Ruthenium Catalysts

Run No.	Cat.[a]	Starting material[b]	Press.	Temp.	k_{12}	k_{13}	k_{23}	k_{24}	k_{34}
			atm	°C	10^{-1} mol (g of cat.)$^{-1}$ h^{-1}				
1	Ru/C	**1**	100	135	1.05	0.12	0.04	0.37	0.06
2		**1**	100	150	1.94	0.27	0.11	0.95	0.15
3		**1**	100	165	4.84	0.76	0.27	2.23	0.31
4		**1**	50	150	1.06	0.16	0.07	0.48	0.07
5		**2**	100	145			0.06	0.77	0.12
6		**3**	100	170					0.56
7	Ru/Al_2O_3	**1**	100	150	1.37	1.06	0.17	1.94	0.33
8		**2**	100	157			0.43	4.65	0.62
9		**3**	100	165					1.94

a) The amount of catalyst is 4wt% on dry base. b) **1**; isoquinoline, **2**; 1,2,3,4-tetrahydroisoquinoline, **3**; 5,6,7,8-tetrahydroisoquinoline.

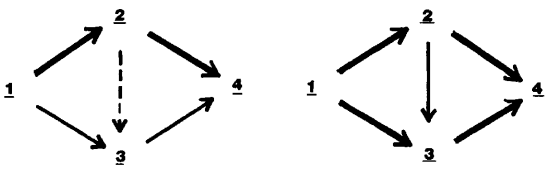

(a) over Ru/C. (b) over Ru/Al_2O_3.

Fig. 9. Reaction pathways on hydrogenation of isoquinoline. (a) over Ru/C, (b) over Ru/Al_2O_3.
➡; major ⟶; minor - - →; rare

step **2**→**4** over Ru/C was calculated to be 20±4 kcal mol^{-1} from the gradients of lines in the figure. It is recognized that the barrier of step **2**→**4** over Ru/C is lower than over R-Ni(about 60 kcal mol^{-1}).[2]

Dominant Reaction Routes. As the result of above analyses, the dominant routes in hydrogenation of **1** to **4** were determined as illustrated in Fig. 9. The reaction proceeds mainly via **2** over Ru/C, and competitively via **2** and **3** over Ru/Al_2O_3. The isomerization of **2** to **3** is very minor and the hydrogenation of **2** to **4** proceeds readily on both ruthenium catalysts in contrast to R-Ni catalyst. The rates of each step except **1**→**2** over Ru/Al_2O_3 are larger than those over Ru/C.

Quantum Chemical Calculation. Table 3 summarizes quantum chemical indices of isoquinoline and its tetrahydrogenated derivatives. Some notable conclusions are as follows: The calculations appear to reproduce the thermodynamic stability of substrates and products. The total energy and energy levels of frontier orbitals indicate that **1** is stabilized by hydrogenation, and that **2** is more stable than **3**. The electronegativity of N-atom localizes more π-electrons in pyridine ring than benzene ring of **1**. The degree of localization is decreased by the hydrogenation of pyridine or benzene ring of **1**. A similar trend of localization is also noted for π-bond orders.

Discussion

The kinetic anlysis of the present study revealed that ruthenium catalysts have some contrast features is the catalytic hydrogenation of isoquinoline to those of R-Ni in the previous studies.[1,2] The catalytic reactions on ruthenium catalysts proceeded in two consecutive routes of **1**→**2**→**4** and **1**→**3**→**4**. The selectivity between the two routes depends upon the supports, carbon or alumina.

Products of **2** and **3** were not further hydrogenated into **4** before almost all of **1** disappeared on the Ru catalysts, while the product retardation indicating stronger adsorption of **2** was observed on R-Ni as previously reported.[2] Such reaction features of the ruthenium catalyst reflect on the equilibrium adsorption constants shown in Table 1. Strong adsorption of **1**, moderate one of **2** and **3** and very weak one of **4** are clearly indicated in the table. In spite of slightly stronger adsorption of **3**, **2** competes with **3** for the active sites for further hydrogenation to **4**, probably due to different concentrations of active sites which reflect on the selectivity.

Such a trend of adsorption strength is completely different from that on R-Ni, which is appreciably related to the pK_a values of the substrates.[1] Although nitrogen heterocyclic compounds such a pyridine and isoquinoline have been widely believed to be vertically adsorbed at their nitrogen lone pair onto the metal surfaces[9,10] as postulated on R-Ni,[2] the aromatic π-electrons can also contribute to the adsorption on metals such as ruthenium which is classified as a "soft" metal.[11] Such π-coordination[12,13] appears to play a major role in defining the trend of adsorption strength on the present noble catalysts.

The equilibrium adsorption constants over the present catalysts will be relevant in first approximation to their number of π-electrons. It is obvious that adsorption of **4** is very weak due to the absence of π-electron. The minor difference betweeen **2** and **3** of the same π-electron number may be ascribed to slightly more localization of π-electron on the nitrogen atom of the substrate **3** according to the quantum chemical calculation. It has been pointed out that the back donation from the metal to the substrate contributes strongly to the adsorption of unsaturated substrate.[14] The energy level of LUMO can be an index for the degree of the back-donation. Substrates **1**, **3**, and **2** show a rising order of energy level of their LUMO as shown in Table 3, corresponding again to the order of their adsorption constants.

Such an adsorption through π-electrons in the aromatic ring defines the adsorption form of **1** to be flat to the surface. The heterocyclic ring which is more reactive as discussed later is preferentially hydrogenated to produce **2**. However, some chance of hydrogenation of benzene ring may also exist to produce **3** especially when the hydrogenation of heterocyclic ring is hindered by some reason. The latter hydrogentation is very difficult on R-Ni, where the substrate seems to be adsorbed vertically at its nitrogen atom in the direction of lone-pair.[2]

The rate constant of the hydrogenation on Ru/C decreased in the order of $k_{12}>k_{24}>k_{34}$. The reactivity of the substrate appears to be related primarily to the π-bond order, which reflects the degree of unsaturation. The highest unsaturation leads to the highest reactivity to hydrogen. The highest value of π-bond order in the substrate **1** is 0.79 and the value is higher than those of **2** and **3**. The energy level of electron donating HOMO may also contribute to the reactivity in such a reaction, the order of substrates **1**, **2**, and **3** corresponds to their reactivity order.

The rate constants k_{12} and k_{13} define the intramolecular selectivity within the substrate **1**. The π-bond

Table 3. Several Quantum Chemical Properties of Isoquinoline and Its Tetrahydrogenated Compounds Calculated by MNDO Method

	Isoquinoline			1,2,3,4-Tetrahydro-			5,6,7,8-Tetrahydro-		
[Total energy[a] and frontier orbital energy/eV]									
	Total	HOMO	LUMO	Total	HOMO	LUMO	Total	HOMO	LUMO
	−1455.86	−8.89	−0.59	−1513.63	−9.34	0.22	−1514.01	−9.66	−0.03
[Total and frontier electron density]									
Atom[b]	Total	HOMO	LUMO	Total	HOMO	LUMO	Total	HOMO	LUMO
1	3.910	0.236	0.377	3.838			3.933	0.431	0.124
2	5.231	0.035	0.099	5.333			5.229	0.003	0.143
3	3.961	0.297	0.170	3.890			3.947	0.473	0.612
4	4.102	0.370	0.337	3.962			4.112	0.400	0.053
5	4.053	0.349	0.343	4.047	0.001	0.000			
6	4.037	0.061	0.164	4.055	0.420	0.482			
7	4.066	0.267	0.151	4.059	0.416	0.399			
8	4.020	0.319	0.358	4.043	0.002	0.009			
9	3.999	0.040	0.000	4.063	0.491	0.486	4.020	0.015	0.326
10	4.108	0.027	0.000	4.079	0.503	0.555	4.137	0.588	0.679
[Total and frontier π-bond orders]									
Bond[b]	Total	HOMO	LUMO	Total	HOMO	LUMO	Total	HOMO	LUMO
1—10	0.471	0.080	0.002				0.638	0.503	−0.290
1—2	0.791	0.091	−0.194				0.675	−0.037	0.133
2—3	0.523	−0.102	0.130				0.658	0.039	−0.295
3—4	0.785	0.332	−0.239				0.658	0.435	−0.179
4—9	0.493	−0.122	−0.006				0.662	0.092	0.131
9—5	0.490	0.118	0.006	0.656	0.021	0.015			
5—6	0.797	0.145	−0.237	0.673	−0.019	−0.015			
6—7	0.515	−0.127	0.157	0.659	0.418	−0.439			
7—8	0.796	0.292	−0.232	0.673	−0.025	0.061			
8—10	0.494	−0.093	−0.002	0.657	0.027	−0.072			
9—10	0.624	0.033	−0.000	0.655	0.497	−0.519	0.663	−0.093	−0.470

a) The sum of electron energy and core repulsion energy. b) The numbering is as follows;

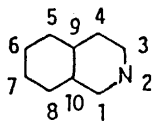

order in HOMO is largest between atoms 3 and 4, probably contributing to the larger reactivity of its pyridine ring, although the largest π-bond orders (total) in the benzene and pyridine rings of substrate **1** are similar. According to the correlations described above, the hydrogenation reaction may be initiated by the addition of hydrogen radical to one of the unsaturated bonds in pyridine ring of **1** over Ru/C, successive hydrogenation being rapid to complete saturation of the ring.

According to the kinetic analyses, the isomerization step of **2**→**3** was very slow in comparison with the rates of major hydrogenation reactions on the ruthenium catalysts. The substrate **2** of which adsorption was not so strong on ruthenium may not find a time to isomerize before its rapid hydrogenation into **4**.

Catalyst supports for ruthenium play some interesting roles in defining the selectivity in the present catalyic hydrogenation even if Ru behaves as a soft metal on both supports. First point is that Ru/Al_2O_3 produced comparable amounts of **2** and **3**, while Ru/C gave **2** preferentially. The presence of Brønsted acids

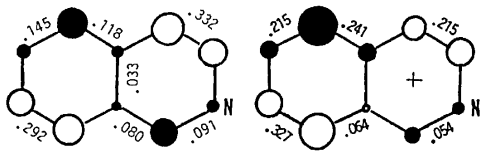

(a) Isoquinoline (b) Isoquinolinium cation

Fig. 10. π-Bond orders in HOMO calculated by MNDO method. (a) Isoquinoline, (b) isoquinolinium cation.

was reported to exclude the hydrogenation of heterocyclic ring of **1**.[15,16] The protonation modifies significantly the reactivity indices of isoquinoline as shown in Fig. 10. The modified regioselectivity against hydrogenation may be explained by the π-bond orders in HOMO of the protonated substrate of **1**. A significant increase of the π-bond order between atoms 7 and 8 and decrease of that between atoms 3 and 4 may cause the change of hydrogenation preference from pyridine to benzene ring. It is therefore

considered that acidity of the catalyst decreases the selectivity of **2** and increases that of **3**, although the contribution of Brønsted acid on the alumina support is not definite and the protonated isoquinoline is a critical model. Much larger equilibrium adsorption constant of highly basic **4** (pK_a=11.0) on Ru/Al_2O_3 than that on Ru/C may also reflect acidic natures of the former support, while the constants for other substrates on the former catalyst were only twice larger than those on the latter catalyst.

The second point is concerned with the rate constants of reactions **2**→**3**, **2**→**4**, and **3**→**4**, which were almost twice larger on the Ru/Al_2O_3 than on Ru/C, while the summed rate constants of **1**→**2** and **1**→**3** reactions were identical. However, the differences on rate constants are not discussed in detail.

The dispersion of ruthenium on the supports will be another important factor affecting the catalytic activity, but it is beyond the scope of the present study.

References

1) H. Okazaki, M. Soeda, K. Onishi, and R. Tamura, *Appl. Catal.*, **41**, 99 (1988).
2) H. Okazaki, M. Soeda, Y. Ikefuji, and R. Tamura, *Appl. Catal.*, **43**, 71 (1988).
3) Y. Naito, Y. Inoue, T. Ono, Y. Arakawa, C. Fukaya, K. Yokoyama, Y. Kobayashi, and K. Yamanouchi, *J. Fluorine Chem.*, **26**, 485 (1984).
4) M. J. Dewar, *J. Am. Chem. Soc.*, **99**, 4899 (1977).
5) The name of program is "MOPAC", Ver. 3.1 (QCPE #516); J. J. P. Stewart, *QCPE Bulletin* **6**, (4), 99(1986), Dept. of Chemistry of Indiana University.
6) J. Sonnemans, J. M. Janus, and P. Mars, *J. Phys. Chem.*, **80**, 2107 (1976).
7) Y. S. Shih and S. S. Yang, *J. Catal.*, **79**, 132 (1983).
8) C. N. Satterfield and S. H. Yang, *Ind. Eng. Chem. Process Des. Dev.*, **23**, 11 (1984).
9) C. E. Calf and J. L. Garnett, *Chem. Commun.*, **1967**, 306.
10) C. G. MacDonald and J. S. Shannon, *Tetrahedron Lett.*, **1964**, 3351.
11) R. G. Pearson, *J. Am. Chem. Soc.*, **85**, 3533 (1963).
12) J. L. Garnett and W. A. Sollich-Baumgartner, *Adv. Catal.*, **16**, 95 (1966).
13) R. R. Fraser and R. N. Renaud, *J. Am. Chem. Soc.*, **88**, 4365 (1966).
14) J. Chatt and L. A. Duncanson, *J. Chem. Soc.*, **1953**, 2939; M. J. S. Dewar, *Bull. Soc. Chim. Fr.*, **18**, C79 (1951).
15) J. Z. Ginos, *J. Org. Chem.*, **40**, 1191 (1975).
16) F. W. Vierhapper and E. L. Eliel, *J. Org. Chem.*, **40**, 2729 (1975).

 © 1989 The Chemical Society of Japan Bull. Chem. Soc. Jpn., 62, 3628—3635 (1989) [Vol. 62, No. 11

Predictions of the Features of the Potential Energy Surfaces from the Diatomic Constants: A Series of Collinear Abstraction Reactions, H+HX (X=F, Cl, Br, I)

Noboru TANAKA
Hachinohe Institute of Technology, Hachinohe 031
(Received May 22, 1989)

A new method, to predict the feature of potential energy surface (PES) from the diatomic constants of reactants molecules, is presented. The PES is calculated by using our proposed semi-empirical method (MT method). Based on MT method, a graphical method is introduced to investigate the relations between the features of the PES and the diatomic constants. Using these relations as guideline, the features of the PES for a series of linear abstraction reactions, H + HX = HH + X with X=F, Cl, Br, and I, are deduced in a simple manner. The PES thus deduced are in good agreement with available experimental and theoretical information.

The knowledge of topological features of potential energy surfaces (PES), such as potential barrier height and location, reaction-path curvature, etc. is of fundamental importance for the theoretical understanding of chemical reaction processes. In recent years, there have been remarkable advances in quantum mechanical computations of PESs by ab initio methods. However, ab initio computations of this kind are complicated, and the results defy simple, intuitive interpretation. In spite of the capability of modern computers, such calculations require a great deal of computer time, and can be carried out only for rather simple systems. For these reasons, methods for semi-empirical estimation of PESs are of considerble value. The early ingenious semi-empirical method of Ering and Polanyi,[1] as later modified by Sato,[2] is widely known as the LEPS method. In the LEPS method, which starts with a quantum mechanical energy expression based on valence bond theory (London's expression),[3] a PES is constructed from diatomic Morse and anti-Morse potential functions, each of which involves three diatomic constants, i.e., the dissociation energy D, range parameter α, and equilibrium internuclear distance R_e. Besides of its simplicity one of the advantages of the LEPS method is that the PES of a three- or four-atomic system can be immediately correlated with the diatomic constants mentioned above. However, this advantage results from the neglect of all overlap and multiple-exchange terms in London's expression. In the past thirty years, other semi-empirical methods have been put forward by various authors: among them, the PK,[4] DIM,[5] and GDIM[6-8] methods are widely known.

In previous papers,[9,10] the present author proposed a new semi-empirical method, herein referred to as the MT method. In the MT method, all overlap and multiple-exchange terms, which were neglected in the London's energy expression, are evaluated; moreover, the connection between the computed PES and the diatomic constants is easily found. In other papers,[11,12] the author, on the basis of this conection, discussed how the PES of a system consisting of three or four hydrogen atoms changes when the hydrogen atoms are replaced by heteroatoms X. In the present paper, which is a sequel of these papers, a graphical method is employed to examine the connection between the PES of the linear H-H-H system and of the linear H-H-H system. The Morse function for the diatomic molecule H-X has D, α, and R_e values which are different from those of H-H. The effects of varying these constants on the features of the PES is closely examined. In addition, by using these results as a guideline, the special cases when X is a halogen atom are considered; the purpose is to deduce the features of the PES for a series of linear abstraction reactions, H+HX=HH+X with X=F, Cl, Br, and I, in a simple manner. Finally, the PES thus deduced are examined by comparing them with available experimental and theoretical information, and the utility of the method is demonstrated.

Theoretical

Remarks on the MT Method: In 1964 Porter and Karplus (PK)[4] proposed a new analytic semi-empirical method for calculating the ground state PES of the H_3 system. They tried to improve the LEPS method by including overlap and multiple-exchange terms in the energy expression and showed a practical way of computing these terms. The present author's MT method differs from the PK method in the evaluation of the multiple-exchange terms; furthermore, the MT method has been generalized to n-electron, n-atom systems in the following respects.

Based on the nonionic valence bond theory,[13] the potential energy E of an n-electron, n-atom system is given by roots of the secular equation:

$$|\boldsymbol{H} - \boldsymbol{M}E| = 0 \tag{1}$$

where $\boldsymbol{H}$ and $\boldsymbol{M}$ are a Hamiltonian matrix and a function of the overlap integrals, respectively. The matrix $\boldsymbol{H}$ can be expressed in terms of multiple-exchange integrals (Λ_p) which are defined as

$$\Lambda_p = \langle \Omega | H | \mathbf{p}\Omega \rangle, \tag{2}$$

where Ω is Hartree product of the atomic orbitals, and P is the permutation operator of electrons.

The multiple-exchange integrals have been classified into three types; one is a transposition type A_p^1; another is a cycle type A_p^2; and the other is a mixed type A_p^3 of A_p^1 and A_p^2.[10] By using the Mulliken approximation,[14] we have shown that first two types A_p^1 and A_p^2 are reduced to diatomic exchange α_i, Coulomb Q_i, and overlap S_i integrals as follows:

$$A_p^1 \simeq (\Pi S_i^2)[Q + \Sigma(\alpha_i/S_i^2 - Q_i)], \tag{3}$$

$$A_p^2 \simeq (\Pi S_i)[Q + \Sigma(\alpha_i/S_i^2 - Q_i)/2] \tag{4}$$

where $Q=nE_H+\sum_{i=1}^{3n-6} Q_i$, E_H is the energy of an atom. Moreover, the last mixed type A_p^3 was proved to be expressed in terms of A_p^1 and the A_p^2 as

$$A_p^3 = (\Pi S_i^2)(\Pi S_j)[A_p^1/(\Pi S_i^2) + \Sigma(A_p^2/(\Pi S_j) - mQ] \tag{5}$$

where m was the number of the cycle.

As a result, all integrals included in Eq. 1 are reduced to "diatomic components" α_i, Q_i, and S_i. Since the "diatomic components" are a properties of the reactant molecule, the method can be applied to many reaction systems by exchanging the value of "diatomic components". This is the most important characteristic of the MT method, because in other semi-empirical methods the multiple-exchange integrals have been evaluated empirically in more complicated ways[4,15] specific to each system, or simply neglected.[1-3]

The analytical expressions for the "diatomic components" α_i, Q_i, and S_i are well-known. The first two diatomic components, α_i and Q_i are expressed in terms of the Morse and anti-Morse functions as

$$\alpha_i = [({}^1E_i - {}^3E_i) + S_i^2({}^1E_i + {}^3E_i)]/2, \tag{6}$$

$$Q_i = [({}^1E_i + {}^3E_i) + S_i^2({}^1E_I - {}^3E_i)]/2, \tag{7}$$

$${}^1E_i(R_i) = D\{\exp[-2\alpha(R_i - R_e)] - 2\exp[-\alpha(R_i - R_e)]\}, \tag{8}$$

$${}^3E_i(R_i) = \eta\{\exp[-2\beta(R_i - R_e)] + 2\exp[-\beta(R_i - R_e)]\}, \tag{9}$$

where ${}^1E$ and ${}^3E$ are the Morse and anti-Morse functions for the diatomic molecule in the singlet and triplet states, respectively; and η and β are adjustable parameters in ${}^3E_i$, and they may calculated by ab initio methods. The analytical expression for the last "diatomic component" S_i is known to be[4]

$$S_i = (1 + R_i\zeta + R_i^2\zeta^2/3)\exp(-R_i\zeta) \tag{10}$$

where ζ is the orbital exponent of the atomic orbital, and its variation with the interatomic distance R_i can be approximately expressed as

$$\zeta = 1.0 + \kappa\exp(-\lambda R_i). \tag{11}$$

Whereas Porter and Karplus[4] determined the values of the parameters κ and λ in Eq. 11 by using the numerical result of Wang's variational calculation[16] of the hydrogen molecule, the present author proposes that these parameters be used as adjustable parameters as explained below.

It should be noted that the evaluations of potential energy surfaces by the MT method are reduced to calculations of "diatomic components" α_i, Q_i, and S_i, so that they are expressed in analytical functions as in Eqs. 6, 7, and 10. Therefore, potential energy E in Eq. 1 is expressed generally as a function of internuclear distances R as follows:

$$E = F(\chi_i, \tau; R) \tag{12}$$

where χ_i and τ are abbreviation for the diatomic constants of the i-th pair and for the adjustable parameters (η, β, κ, λ), respectively. Equation 12 shows that the PES can be calculated by determining the diatomic constants χ_i of the reactant molecules and adjustable paramethers τ.

Construction of the Standard and Reference PES: To see the effects of heteroatom substitution on a PES mentioned in introduction, we proceed as follows. The PES of the linear H-H-H system is computed by using MT method, and used a standard PES. In the computation, the H-H Morse and anti-Morse functions for the atomic pairs, H_a-H_b, H_b-H_c, and H_a-H_c, are used, where H_a and H_c stands for the end hydrogen atoms and H_b stands for the central one. For the H_2 Morse function, Eq. 8, the following values of the diatomic constants are used:

$$D = 0.1744 \text{ hartree}, \alpha = 1.05 \text{ bohr}^{-1}, R_e = 1.40 \text{ bohr}. \tag{13}$$

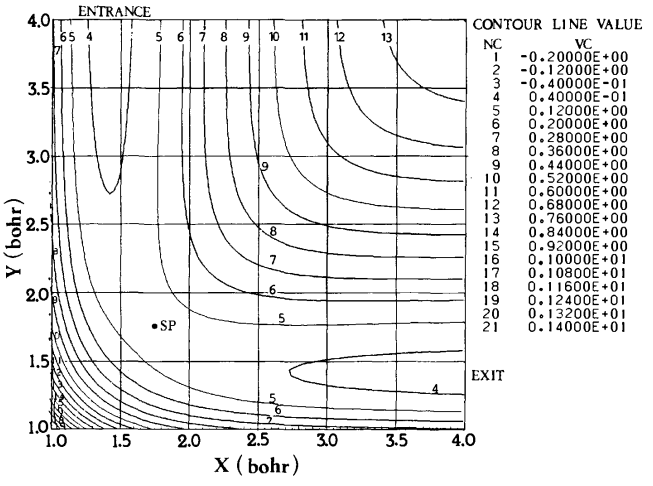

Fig. 1. The standard linear H_3 contour map. The contour intervals are 1/25 of the H_2 dissociation energy. The number and value of each contour line are denoted by NC and VC, respectively.

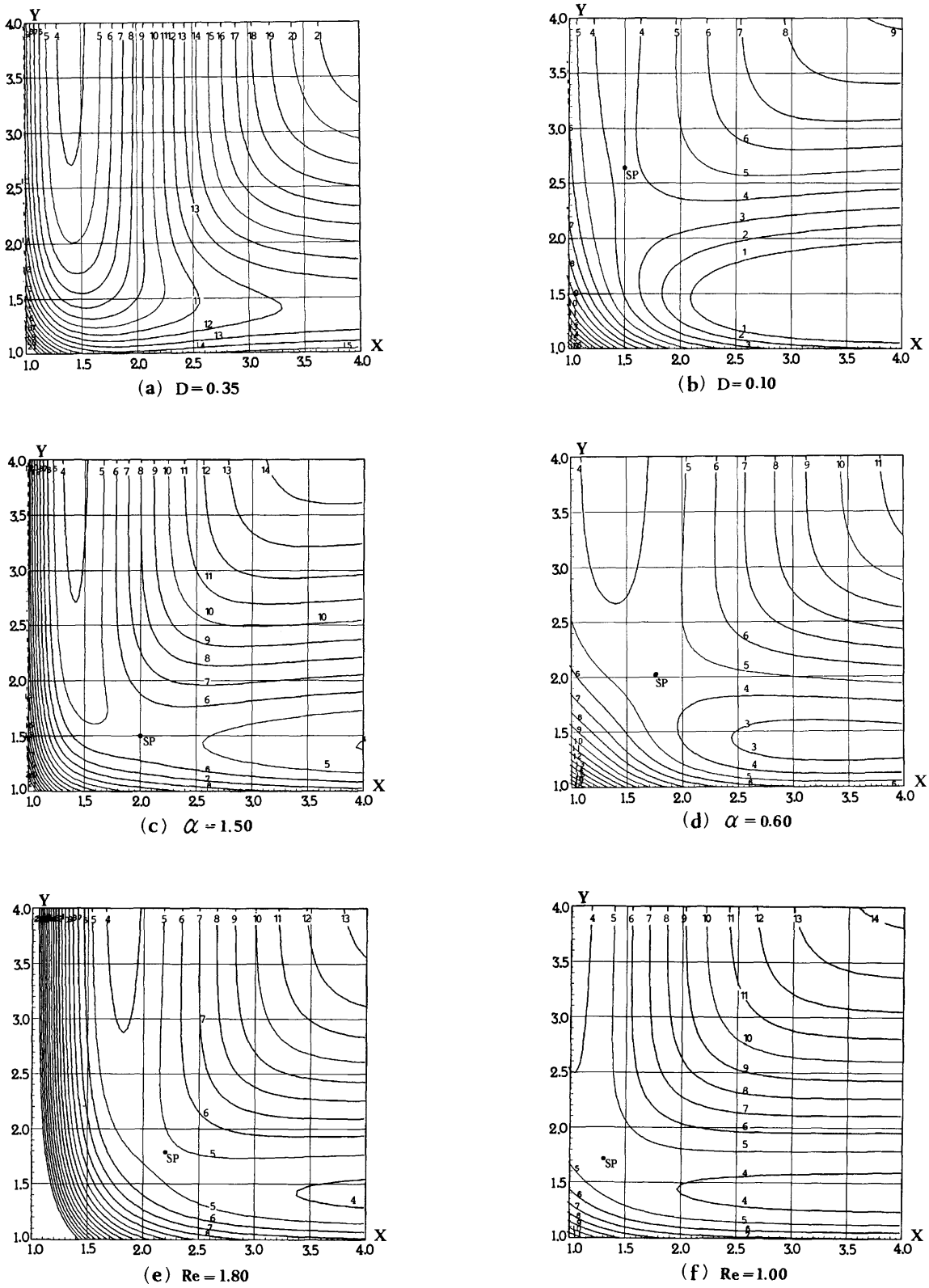

Fig. 2. The contour maps for the linear HHX system with different values of D, α, R_e (see text). The contour intervals are 1/25 of the H_2 dissociation energy. The X-axis and Y-axis show the internuclear distance of H-X and H-H, respectively.

For the H_2 anti-Morse function Eq. 9, the values,

$$\eta = 0.0729 \text{ hertree}, \beta = 1.036 \text{ bohr}^{-1} \quad (14)$$

are employed. The numerical values in Eqs. 13 and 14 have been determined by the results of the precise ab initio calculation for the hydrogen molecule by Kolos and coworkers.[17] For the two adjustable parameters occurring in Eq. 11, the values

$$\kappa = 3.20, \text{ and } \lambda = 1.202 \text{ bohr}^{-1} \quad (15)$$

are chosen to fit the computed H_3 PES at the saddle point and in its vicinity, to the result of Liu's precise ab initio calculation of the H_3 system.[18] All these parameters are given these standard values throughout the following.

The PES so obtained for H_3 is shown in Fig. 1, where the X- and Y-axes represent the H_b-H_c and H_a-H_b distances, respectively. This PES agrees fairly well with the Truhlar-Horowitz PES for linear H_3,[19] which is based on Siegbahn and Liu's precise ab initio calculations[18,20] of the H_3 system.

Now suppose that the end atom H_c is replaced by a heteroatomic X. The PES for this linear H-H-X system is calculated in the same way as the H-H-H PES, except that the H-H Morse functions for H_a-H_c and H_b-H_c in the H-H-H calculation are replaced by the H-X Morse functions, whose D, α, and R_e values are different from those in Eq. 13. To get an idea of how the PES changes by varying these diatomic constants in Eq. 13, six reference contour maps are computed by varying the three constants individually. The results are shown in Figs. 2(a)—(f), where the X- and Y-axes represents the H_b-X and H_a-H_b distances, respectively. The caption of Fig. 2(a), D=0.350 implies that the diatomic constants for H-X are taken to be the same as those for H-H given in Eq. 13, except that D=0.350 hartree is used; also it is assumed that the four parameters in Eqs. 14 and 15 remain unchanged. Captions of similar meaning are attached to Figs. 2(b)—(f). The use of these reference contour maps is described in the next section.

Results and Discussion

Diatomic Constants and the PES of the H-H-X System: Consider the cross section of the PES of the linear H-H-X system by a plane S which is perpendicular to the (X, Y)-plane and parallel to the X-axis. Obviously the cross section continuously approaches the potential curve of the diatomic molecule H-X as the distance between the plane S and the X-axis increases. Owing to this continuity, the features of the entrance valley of the H-H-X PES are immediately deduced from the features of the H-X potential curve.

Interesting points to be noticed as regards Figs. 2(a)—(d) are as follows. We observe in Figs. 2(a) and 2(c) that making D or α greater than the standard values (D=0.1744 or α=1.05) shifts the location of the saddle point to the exit valley side ("late barrier"), and makes the reaction-path curvature larger (a sharper bend of reaction path). Similarly, Figs. 2(b) and 2(d) indicates that making D or α smaller than the standard value shifts the saddle point to the entrance valley side ("early barrier"), and makes the reaction-path curvature smaller.

More quantitative information derived from similar calculations is shown in Tables 1—3 and Figs. 3—7. The trend found in Figs. 2(a) and 2(b) is more evident in Table 1, which indicates how the barrier height E_a, the saddle point location (X_a, Y_a), and the bond extensions ΔR_{HX} and ΔR_{HH} at the saddle point (BESP), change as D is varied. Here ΔR_{HX} and ΔR_{HH} are given by

$$\Delta R_{HX} = X_a - R_e, \Delta R_{HH} = Y_a - R_e,$$

Table 1. The Relations of Dissociation Energy D with Barrier Height E_a, Saddle Point Location (X_a, Y_a), BESP ΔR_{HX}, ΔR_{HH}, and Energy Defect ΔE

D[a]	E_a[b]	(X_a, Y_a)[c]	ΔR_{HX}[c]	ΔR_{HH}[c]	ΔE[b]
0.250	47.25	(6.20, 1.40)	4.80	0.00	47.45
0.220	28.73	(4.20, 1.40)	2.80	0.00	28.61
0.200	17.77	(2.30, 1.50)	0.90	0.10	16.05
0.1744	9.80	(1.74, 1.74)	0.34	0.34	0.00
0.150	6.37	(1.55, 2.05)	0.15	0.65	−15.35
0.100	3.54	(1.50, 2.65)	0.10	1.25	−46.75

a) In units of hartree. b) In units of kcal mol^{-1}. c) In units of bohr.

Table 2. The Relations of Range Parameter α with Barrier Height E_a, Saddle Point Location (X_a, Y_a), and BESP ΔR_{HX}, ΔR_{HH}

α[a]	E_a[b]	(X_a, Y_a)[c]	ΔR_{HX}[c]	ΔR_{HH}[c]
1.50	15.92	(2.00, 1.50)	0.60	0.10
1.20	11.24	(1.80, 1.60)	0.40	0.20
1.05	9.802	(1.74, 1.74)	0.34	0.34
0.80	9.00	(1.70, 1.94)	0.30	0.54
0.60	9.04	(1.74, 2.04)	0.34	6.40

a) In units of bohr^{-1}. b) In units of kcal mol^{-1}. c) In units of bohr.

Table 3. The Relations of Equilibrium Ditance R_e with Barrier Height E_a, Saddle Point Location (X_a, Y_a), and BESP ΔR_{HX}, ΔR_{HH}

R_e[a]	E_a[b]	(X_a, Y_a)[a]	ΔR_{HX}[a]	ΔR_{HH}[a]
3.00	16.48	(3.30, 1.80)	0.30	0.40
2.50	14.67	(2.90, 1.80)	0.40	0.40
2.00	12.65	(2.40, 1.80)	0.40	0.40
1.80	11.82	(2.20, 1.80)	0.40	0.40
1.60	10.98	(2.00, 1.80)	0.40	0.40
1.40	9.80	(1.74, 1.74)	0.34	0.34

a) In units of bohr^{-1}. b) In units of kcal mol^{-1}.

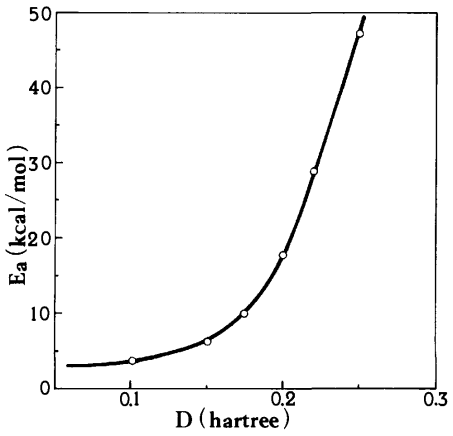

Fig. 3. The relation between the dissociation energy D and the barrier height E_a for the linear HHX system.

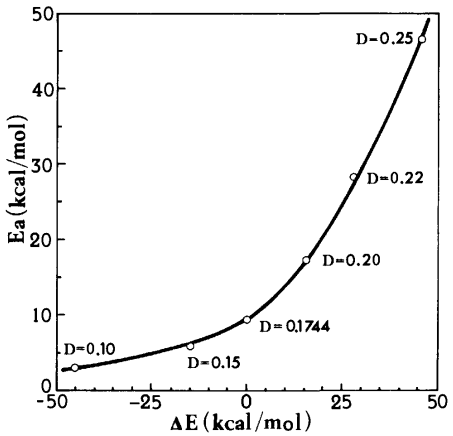

Fig. 4. The relation between the energy defect ΔE and the barrier height E_a for the linear HHX system.

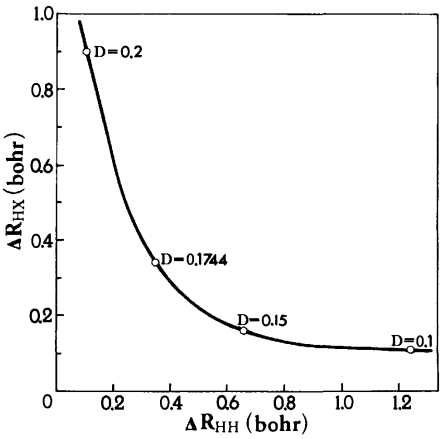

Fig. 5. The relation between the dissociation energy D and the BESP ΔR_{HX}, ΔR_{HH} for the linear HHX system.

where R_e is taken to be 1.40 bohr (the standard value of R_e). The energy defect ΔE of the abstraction reaction is defined as the energy difference,

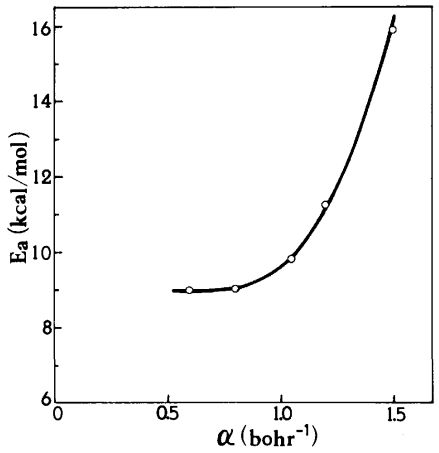

Fig. 6. The relation between range parameter α and barrier height E_a for the linear HHX system.

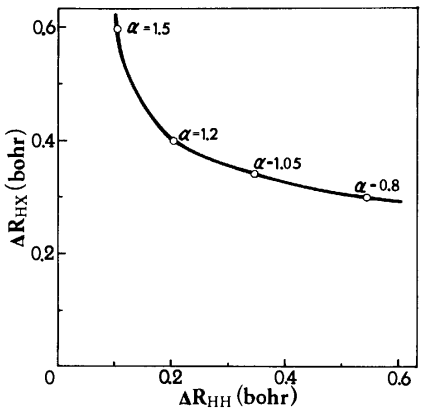

Fig. 7. The relation between the range parameter α and the BESP ΔR_{HX}, ΔR_{HH} for the linear HHX system.

$$\Delta E = E(\text{product}) - E(\text{reactant}). \quad (16)$$

By examining the energy expression of the PK or MT method, it is readily found that

$$E(\text{product}) = -D(\text{H-H}),\ E(\text{reactant}) = -D(\text{H-X}), \quad (17)$$

i.e., ΔE is equal to the difference of the diatomic dissociation energies, D(H-X)−D(H-H). The values of ΔE computed from this relation is also included in Table 1. Table 2 is a table similar to Table 1 but corresponds to Figs. 2(c) and 2(d), and Table 3 corresponds to Figs. 2(e) and 2(f). Also these interesting relations between two sets of quantities presented in Tables 1 and 2 are displayed graphically in Figs. 3—7. For example, Table 2 and Figs. 6 and 7 indicate how the height and location of the barrier change as the range parameter α is varied, provided that the values of the rest of the parameters in Eqs. 13—15 remain the same. In the next section, these relations are used to deduce the features of the PES for a series of linear abstraction reactions, H+HX=

HH+X with X=F, Cl, Br, and I.

PES of the Abstraction Reactions H+HX with X=F, Cl, Br, and I: So far the heteroatom X has not been specified. In this section, we turn to the special case in which X is a halogen atom. This case is of particular interest in relation to the abstraction reaction H+HX=HH+X (X=F, Cl, Br, and I), which are prototypical gaseous elementary reactions and have been the subject of numerous experimental and theoretical investigations.

To proceed in line with the considerations in the preceding section, we need the diatomic constants of the H-X molecules. They are tabulated in Table 4, where theoretical values from ab initio calculations together with some experimental values are given; the former values agree with the latter ones considerably well. We mainly confine our attention to the effect of chaging D(H-X) in the following. Thus, by using the D vs. E_a and the D vs. BESP curves in Figs. 3 and 5 together with the values of D in Table 4, the E_a and BESP for the H-H-X PES are estimated, and the result is tabulated in Table 5, which also includes the values of energy defect ΔE computed by using the relations Eqs. 16 and 17 together with the experimental D values in Table 4.

Table 4. Diatomic Constants of the HX (X=F, C, Br, I) Molecules

	H_2	HF	HCl	HBr	HI
D/hartree					
Ab initio[a]	0.1744	0.2256	0.1701	0.1447	0.1181
Exptl[b]	0.1749	0.2242	0.1714	0.1500	0.1297
α/bohr^{-1}[a]	1.050	1.181	0.989	0.958	0.913
R_e/bohr					
Ab initio[a]	1.401	1.733	2.410	2.684	3.043
Exptl[b]	1.400	1.733	2.410	2.672	3.041

a) Ref. 21. b) Ref. 23.

Table 5. Barrier Height E_a, Energy Defect ΔE and BESP ΔR_{HX}, ΔR_{HH} Obtained from the Present Calculation for the H+HX Abstraction Reactions

	H+H_2	H+HF	H+HCl	H+HBr	H+HI
E_a/kcal mol^{-1}	9.80	32.5	9.3	6.2	4.4
ΔE/kcal mol^{-1}		30.8	−2.2	−15.6	−28.4
ΔR_{HX}/bohr	0.34	1.0	0.3	0.15	0.1
ΔR_{HH}/bohr	0.34	0.1	0.4	0.60	1.0

In recent years, a good knowledge of the PES of the H-H-X systems (X=F, Cl, Br, and I), i.e., those of the abstraction reactions, H+HX=HH+X, has been obtained from ab initio theoretical calculations. Table 6 lists theoretical values relating to the H-H-X PES, calculated by Dunning[21,22] together with experimental values of E_a and ΔE for these abstraction reactions. Comparing Table 5 with Table 6, we find the simple calculations of the present paper lead to results in surprisingly good agreement with those from ab initio calculations. Finally Figs. 8 and 9 are plots similar to Figs. 3 and 5, but are based on the numerical values in Table 6. Again we observe that Figs. 3 and 5 resulting from the present calculation bear a very close resemblance, qualitative and quantitative, to Figs. 8 and 9 obtained from Dunning's ab initio calculation.

Since the early work of Evans and Polanyi,[25] the energetics of the reactions has been discussed by several authors.[26-30] The central point of the arguments may be understood in terms of the relations between the exoergicity and the schematic one-dimensional potential profile of the reaction. Let us start with the case X=I; as pointed out above the molecule HI has the smallest D value in Table 4, i.e., the energy of its bond being broken is smallest. Since D(H-X)<D(H-H), in this case, the reactant valley is shallower than the product valley, and hence $\Delta E<0$ (Table 5); in other words, the abstraction reaction H+HI is exothermic. In this connection the following propensity rules has often been argued: In the case of X=I, where the

Table 6. Theoretical and Experimental Barrier Height E_a, Energy Defect ΔE, Saddle Point Location (X_a, Y_a), and BESP ΔR_{HX}, ΔR_{HH} for the H+HX Abstraction Reactions

	H+H_2	H+HF	H+HCl	H+HBr	H+HI
E_a/kcal mol^{-1}					
Ab initio[a]	9.802	31.4	7.3	3.8	2.3
Exptl[b]		33	4	1.5	0
ΔE/kcal mol^{-1}					
Ab initio[a]		24.9	−5.6	−18.3	−29.6
Exptl[b]		30.8	−2.2	−15.6	−28.3
X_a/bohr[a]	1.757	1.493	1.909	2.381	2.759
Y_a	1.757	2.665	2.702	2.816	3.156
ΔR_{HX}/bohr[a]	0.357	0.932	0.292	0.132	0.113
ΔR_{HH}	0.357	0.093	0.509	0.981	1.359

a) Ref. 21. b) Refs. 22 and 24.

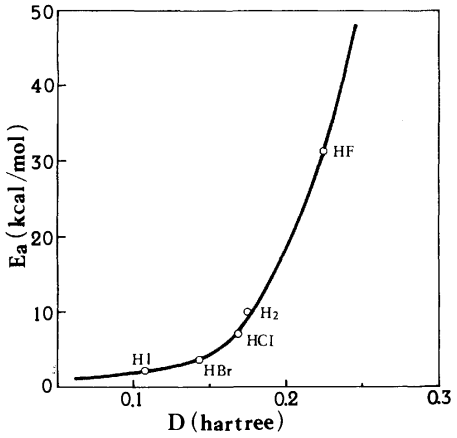

Fig. 8. The relation between the dissociation energy D and the barrier height E_a for the abstraction reactions H+HX (X=F, Cl, Br, I).

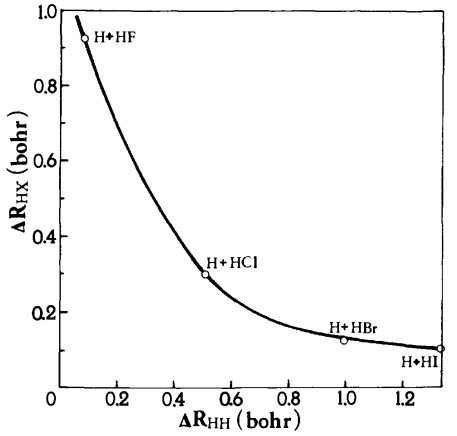

Fig. 9. The BESP ΔR_{HX}, ΔR_{HH} for the abstraction reactions H+HX (X=F, Cl, Br, I).

reactant valley is shallow, the reaction has an "early" potential barrier[31] and the barrier height E_a is rather small, but on going from X=I to X=Br, Cl, and F or, in other words, as the depth of the reactant valley D(H-X) increases, the barrier shifts to the direction of the product valley (shifts towards a "late" position) and the barrier height increases. Although these rules have been suggested by Mok and Polanyi[28] (based on the LEPS and BEBO[26] method), they have been corroborated by Dunning's ab initio calculation (Figs. 8 and 9), and also by the present calculation (Figs. 2, 3, and 5).

Finally, the problem or whether a reaction has an early or late barrier is interesting in connection with reaction dynamics. It has been deduced from molecular dynamics studies that vibrational (translational) energy excitation is effective for enhancing the rate of a reaction having a late (early) barrier.[32] It is interesting to note that the reverse reactions of the above abstraction reaction, i.e., X+HH=HX+H have been found to be enhanced by vibrational excitation when X=Cl, Br, or I, and furthermore the degree of the enhancement has been found to be in the order of Cl<Br<I.[33] This fact is in agreement with the calculated values of BESP given in Tables 5 and 6. (Remember that the PES of the reverse reactions are obtained from those of the abstraction reactions by interchanging the entrance and exit valleys.)

Conclusion

In the present paper, by using a simple semi-empirical method devised by the present author and called the MT method, the PES for the linear H-H-H and H-H-X systems (the standard and reference PES) have been obtained. Referring to these PES, PES and energetics of the abstration reactions, H+HX=HH+X with X=F, Cl, Br, and I, have been discussed. Conclusions arrived at are in good agreement with those from ab initio quantum mechanical calculations. Although the treatment of the present paper is limited to the linear H-H-X system, the applicability of the MT method is wider as shown in previous paper by the author. Therefore, there are possibilities of extending the method of the present paper to treatment of, for example, systems of X-Y-Z type, or systems consisting of four or more atoms. This problem will be discussed in a forthcoming paper.

The author would like to thank Professor Yuusaku Ikegami of Tohoku University for many helpful discussions and for support regarding the present article. The author also wishes to thank Professor Takasi Nakamura of Hokkaido University for reading and improving the manuscript.

References

1) H. Eyring and M. Polanyi, *Naturwissenschaften*, **18**, 914 (1930).
2) S. Sato, *Bull. Chem. Soc. Jpn.*, **28**, 450 (1955); *J. Chem. Phys.*, **23**, 592 (1955).
3) F. London, *Z. Electrochem.*, **35**, 552 (1929).
4) R. N. Porter and M. Karplus, *J. Chem. Phys.*, **40**, 1105 (1964).
5) F. O. Ellison, *J. Am. Chem. Soc.*, **85**, 3540 (1963).
6) A. A. Wu, *Mol. Phys.*, **38**, 843 (1979); **39**, 1287 (1980).
7) C. W. Eaker and L. R. Allard, *J. Chem. Phys.*, **74**, 1821 (1981).
8) M. Baer and I. Last, "Potential Energy Surfaces and Dynamics Calculation," ed by D. G. Truhlar, Plenum Press, New York (1980), p. 519.
9) Noboru Tanaka, *Chem. Phys. Lett.*, **54**, 551 (1978); *Bull. Chem. Soc. Jpn.*, **52**, 3477 (1979).
10) Noboru Tanaka and O. Nomura, *J. Chem. Phys.*, **77**, 1373 (1982).
11) Noboru Tanaka, *Bull. Chem. Soc. Jpn.*, **59**, 3797 (1986).
12) Noboru Tanaka, *Bulletin of H. I. T.*, **7**, 144 (1988).
13) R. McWeeny and B. T. Sutcliffe, "Method of Molecular Quantum Mechanics," Academic Press, New

York (1976).
14) R. S. Mulliken, *J. Chim. Phys.*, **46**, 497 (1949).
15) D. M. Silver and N. J. Brown, *J. Chem. Phys.*, **72**, 3859 (1980).
16) S. C. Wang, *Phys. Rev.*, **31**, 579 (1928); N. Rosen, *Phys. Rev.*, **38**, 2099 (1931).
17) W. Kolos and C. C. J. Roothaan, *Rev. Mod. Phys.*, **32**, 219 (1960); W. Kolos and L. Wolniewicz, *J. Chem. Phys.*, **43**, 2429 (1965).
18) B. Liu, *J. Chem. Phys.*, **58**, 1925 (1973).
19) D. G. Truhlar and C. J. Horowitz, *J. Chem. Phys.*, **68**, 2466 (1978).
20) P. Siegbahn and B. Liu, *J. Chem. Phys.*, **68**, 2459 (1978).
21) T. H. Dunning, Jr., *J. Phys. Chem.*, **88**, 2469 (1984).
22) T. H. Dunning, Jr., L. B. Harding, R. A. Bair, R. A. Eades, and R. L. Shepard, *J. Phys. Chem.*, **90**, 344 (1986).
23) B. Rosen, "Spectroscopic Data Relative to Diatomic Molecules," Pergamon, New York (1970); C. E. Moore, Natl. Bur. Stand. (U.S.) Circ., No. 467, I (1949); II (1952); (III) (1958); G. Herzberg, "Spectra of Diatomic Molecules," Van Nostrand Reinhold, New York (1950).
24) R. N. Porter, L. B. Sims, D. L. Thompson, and L. M. Raff, *J. Chem. Phys.*, **58**, 2855 (1973).
25) M. G. Evans and M. Polanyi, *Trans. Faraday Soc.*, **34**, 11 (1938).
26) H. S. Johnston and C. Parr, *J. Am. Chem. Soc.*, **85**, 2544 (1963).
27) R. A. Marcus, *J. Phys. Chem.*, **72**, 891 (1968).
28) M. H. Mok and J. C. Polanyi, *J. Chem. Phys.*, **51**, 1451 (1969).
29) N. Agmon and R. D. Levine, *Chem. Phys. Lett.*, **52**, 197 (1977).
30) N. Agmon, *J. Chem. Soc., Faraday Trans. 2*, **74**, 388 (1978).
31) In this case we may say that the structure of the activated complex resembles that of the reactant (the Hammond postulates); G. S. Hammond, *J. Am. Chem. Soc.*, **77**, 334 (1955).
32) J. C. Polanyi, *Acc. Chem. Res.*, **5**, 161 (1972).
33) L. B. Sims, L. R. Dosser, and P. S. Wilson, *Chem. Phys. Lett.*, **32**, 150 (1975).

Dielectric Relaxation and Intermolecular Association for Various Secondary and Tertiary Alcohols

Toshiomi SHINOMIYA†
School of Pharmaceutical Sciences, Kitasato University,
Shirokane, Minato-ku, Tokyo 108
(Received May 24, 1989)

The dielectric constants and losses of 2-alkanol (n=4—8), 2-methyl-2-alkanol (n=3—7), six isomeric methylheptanols, and five isomeric nonanols have been measured at the frequencies from 1.35 to 4500 MHz at 15, 25, and 35 °C. The absorption has been resolved into two or three different Debye-like dispersion regions. The first, low-frequency, dispersion region could not be observed for more sterically hindered alcohols, such as several tertiary alcohols. For each alcohol, four concentrations of a linear hydrogen-bonded chain polymer (C_1), a chain dimer and trimer (C_2), a free monomer (C_3), and a nonpolar cyclic polymer (C_R) were evaluated by applying a modified Kirkwood-Fröhlich equation to each dispersion region. The equilibrium between C_1 and C_3 can be considered for more polar alcohols and that between C_R and C_3 for more sterically hindered alcohols. The mechanism of the relaxation process is discussed in terms of observations of the magnitude and relaxation time for the first region. The free energy of activation increases with increasing alkyl chain length, being about 20—23 for the first region, 16—18 for the second region, and 9—12 kJ mol^{-1} for the third region.

The coexistence of two or three dielectric dispersion regions has been found through wide-range measurements of complex dielectric constants for liquid alcohols.[1-4] In a previous paper,[5] we also reported three dispersion regions for pure 1-decanol at 15—40 °C and for cyclohexane and heptane solutions of 1-decanol at 25 °C. We assigned the three dispersion regions to a linear hydrogen-bonded chain polymer, a chain dimer and trimer, and a free monomer. However, no theory can satisfactorily interpret the coexistence of the two or three dispersion regions. The Kirkwood-Fröhlich equation,[6,7] developed on the basis of a single relaxation process, cannot explain a correlation factor that is large or the existence of a nonpolar cyclic polymer which does not contribute to the dispersion. Therefore, we have proposed a modified Kirkwood-Fröhlich equation[8] which could be applied to each dispersion region. These four concentrations, inclusive of a nonpolar cyclic polymer, were evaluated by means of the modified equation and were shown for 1-decanol as a function of temperature and dilution, respectively.[5]

In secondary and tertiary alcohols, dielectric studies have indicated a complex and interesting nature corresponding to a geometric variety of molecules. Dannhauser[4] measured the temperature dependence of the dielectric dispersions for eight isomeric $C_8H_{17}OH$ at low temperatures. A Cole-Cole plot for 3-methyl-3-heptanol shows a small, broad dispersion at 208—189 K. Moriamez et al.[9] also obtained a Cole-Cole plot for 3-ethyl-3-pentanol at room temperature. The small, broad dispersions for tertiary alcohols have been explained by the existence of a ring dimer. The measurement and analysis of the absorption become more difficult at room temperature. There have been almost no reports on detailed analyses of the two or three dispersion regions.

† Present address: 207-52, Shirahata kami-cyo, Kanagawa-ku, Yokohama 221.

We have presently extended the investigation by measuring the dielectric dispersion of various secondary and tertiary alcohols. For these alcohols at room temperature it is interesting to investigate the fact that the dielectric absorption is dependent on the steric interrelation between the hydroxyl group and the terminal methyl and alkyl groups. It was also the purpose of the present work to confirm whether each of the four concentrations, obtained by means of a modified equation, indicates a reasonable behavior or not. The mechanism of the relaxation process is discussed.

Experimental

Purification of Materials. Commercial alcohols were fractionally distilled under reduced pressure at a very high reflux ratio. About 80% of the middle fraction was distilled again by the same method. Two distillation systems were used, as described in a previous paper.[8] The middle portion was dried and finally distilled in a grease-free apparatus under reduced pressure before use.

Apparatus. The dielectric constants and losses were measured by making use of the following three types of apparatus over the frequency range of 1.35—4500 MHz.

In the low-frequency range, a Boonton Radio RX meter (Type 250A) was used for measurements at frequencies of 1.35, 6.3, 17, 30, and 45 MHz. An adaptor (GR 900-QNP) and a T-type adaptor (which is joined to an inductor) were placed between a cell and a terminal of the RX meter's bridge. In the middle-frequency range, measurements at frequencies 60, 80, 100, 150, 200, 250, 300, 400, and 480 MHz were made with a Hewlett-Packard VHF Bridge which comprised a VHF Signal Generator (Model 608C), a VHF Detector (Model 417A), a VHF Bridge (Model 803A), an SWR meter (415E), and a frequency counter. In the high-frequency range, a General Radio Precision Slotted Line (Type 900-LB) was used for measurements at frequencies of 600, 750, 1000, 1400, 2000, 3000, and 4500 MHz. The signal sources were a Modulating Power Supply (Type 1264-B) and a VHF Oscillator (Type 1362), a Modulating Power Supply (Type 1264-B) and a Lockable Oscillator (Type 1218-BV), and a HP Signal Generator (Type 8616A).

In the low- and high-frequency ranges, two dielectric cells were carefully made of a GR Precision Inner-Conductor Rod, an Outer-Conductor Tube, and a GR 900-BT connector. The temperature of the cell was kept constant within ±0.1 °C of the specified values by the circulation of water from a thermostat through a jacket around the cell. The frequencies of the RX meter and VHF Bridge were controlled to be within ±0.01% of the specified values.

The refractive indices were measured by making use of a Pulflich refractometer. The densities and viscosities were measured with a density meter of about 10 cm^3 in volume and with an Ostwald viscometer, respectively.

Results and Discussion

The Cole–Cole plots show that the first dispersion region can be best described by a Debye-like semicircular arc, though it is evident that the experimental data cannot be satisfactorily fitted in the high-frequency region of the absorption. By assuming that the absorption was the sum of several overlapping Debye-like dispersion regions, the data were resolved into two or three different dispersion regions. The limiting high-frequency dielectric constant, ε_3, of the third region contains experimental errors because of a lack of the higher-frequency data of the third region. ε_3, therefore, was assumed to be an average value in all measurements, evaluated using $(\varepsilon_3-1)/(\varepsilon_3+2)=(n_D^2-1)(1+0.19)/(n_D^2+2)$. n_D is the refractive index. The dielectric parameters of two or three dispersion regions were calculated using a least-squares method, as described in a previous paper,[8] and were given for 2-methyl-2-alkanols and isomeric methylheptanols in Table 1, together with the refractive indices, densities, and viscosities. The dielectric parameters were abbreviated for 2-alkanols and isomeric nonanols, since those for the first region were described in a previous paper.[8] We believe that the first dispersion region can be attributed to a linear hydrogen-bonded chain polymer ($n \geqq 4$), the second region to a chain dimer and trimer ($n=2$ and 3), and the third region to a free

Table 1. Dielectric Parameters, Refractive Indices, Densities, and Viscosities of Methyl-Substituted Alkanols

Compound	ε_0	ε_1	ε_2	ε_3	τ_1 / ps	τ_2 / ps	τ_3 / ps	n_D	d / g cm^{-3}	$\eta\times10^3$ / N s m^{-2}
						15 °C				
2-me-2-buta	6.26	3.54	2.97	2.25	481	145	9	1.4075	0.8134	5.55
2-me-2-pent	3.76	3.59	2.79	2.27	1044	191	11	1.4129	0.8112	4.17
2-me-2-hexa	3.32	3.22	2.69	2.29	1438	195	12	1.4204	0.8164	6.00
2-me-2-hept	3.13	3.00	2.58	2.32	1675	191	13	1.4257	0.8196	8.55
7-me-3-hept	5.93	2.95	2.59	2.32	2214	216	15	1.4289	0.8264	10.82
6-me-3-hept	4.74	2.94	2.58	2.33	1448	223	15	1.4291	0.8220	11.87
5-me-3-hept	3.53	2.92	2.56	2.33	1253	235	15	1.4292	0.8285	12.41
4-me-3-hept	—	3.16	2.74	2.34	—	384	15	1.4328	0.8360	11.86
3-me-3-hept	—	2.90	2.65	2.33	—	162	13	1.4306	0.8320	11.10
4-me-4-hept	—	2.78	2.57	2.33	—	138	10	1.4284	0.8276	11.44
						25 °C				
2-me-2-prop	12.53	—	3.14	2.16	518	—	12	1.3849	0.7804	4.52
2-me-2-buta	5.72	3.49	3.00	2.23	239	72	7	1.4026	0.8043	3.48
2-me-2-pent	—	3.83	2.90	2.25	—	149	10	1.4089	0.8033	2.88
2-me-2-hexa	—	3.41	2.77	2.28	—	146	11	1.4162	0.8089	3.97
2-me-2-hept	—	3.20	2.66	2.30	—	151	11	1.4217	0.8120	5.39
7-me-3-hept	5.35	3.21	2.68	2.31	1099	232	15	1.4250	0.8188	6.47
6-me-3-hept	4.60	3.14	2.65	2.30	872	219	14	1.4229	0.8146	6.83
5-me-3-hept	—	3.60	2.80	2.31	—	485	16	1.4254	0.8212	7.29
4-me-3-hept	—	3.28	2.75	2.33	—	196	12	1.4286	0.8283	6.70
3-me-3-hept	—	3.00	2.73	2.32	—	110	11	1.4264	0.8240	6.28
4-me-4-hept	—	2.87	2.64	2.31	—	97	7	1.4243	0.8197	6.27
						35 °C				
2-me-2-prop	10.64	—	3.21	2.14	267	—	10	1.3800	0.7701	2.63
2-me-2-buta	5.41	—	3.32	2.21	—	123	11	1.3979	0.7949	2.32
2-me-2-pent	—	3.89	3.06	2.23	—	106	9	1.4045	0.7947	2.06
2-me-2-hexa	—	3.47	3.04	2.26	—	109	11	1.4118	0.8005	2.76
2-me-2-hept	—	3.29	2.91	2.28	—	121	13	1.4175	0.8040	3.60
7-me-3-hept	—	4.91	2.94	2.30	—	444	15	1.4208	0.8112	4.20
6-me-3-hept	—	4.40	2.89	2.29	—	377	31	1.4188	0.8068	4.37
5-me-3-hept	—	3.69	2.78	2.30	—	243	25	1.4214	0.8137	4.56
4-me-3-hept	—	3.42	2.84	2.31	—	130	13	1.4242	0.8204	4.11
3-me-3-hept	—	3.14	2.89	2.30	—	117	12	1.4218	0.8159	3.89
4-me-4-hept	—	2.98	2.75	2.29	—	74	7	1.4199	0.8117	3.82

monomer (n=1), as described before.[5] The Kirkwood correlation factors were evaluated according to the Kirkwood equation:[6,8,10] g_1=2.38 for the first region, g_2=2.03 as an average value for the second region, and g_3=unity for the third region. Four concentrations, a linear chain polymer (C_1), a chain dimer and trimer (C_2), a free monomer (C_3), and a nonpolar cyclic polymer (C_R), were calculated by means of a modified Kirkwood-Fröhlich equation[8] by making use of these g_i factors and the experimental values of ε_{i-1} and ε_i for the i-th dispersion.

For five 2-alkanols at 25 °C, the Cole-Cole plots are shown in Fig. 1 and the percentages of C_1, C_2, C_3, and C_R against the gross stoichiometric concentration C_0, $C_i \times 100/C_0$, are shown in Fig. 2. The absorption could be resolved into three dispersion regions, except for 2-butanol, as shown by the solid lines in Fig. 1. The magnitude, $\varepsilon_0-\varepsilon_1$, of the first region decreases from 13.44 for 2-butanol to 4.69 for 2-octanol with increasing alkyl chain length. Figure 2 shows that the percentage of C_1 decreases from 71% for 2-butanol to 50% for 2-octanol because of a steric hindrance of the long alkyl group. C_1 decreases linearly with the magnitude. C_2 increases slightly with increasing alkyl chain length, although C_3 decreases, and the sum of C_2 and C_3 almost does not change. Therefore, C_R increases inversely as C_1. The magnitudes of the first region for these 2-alkanols are less than those of normal alcohols[8] having the same number of carbon

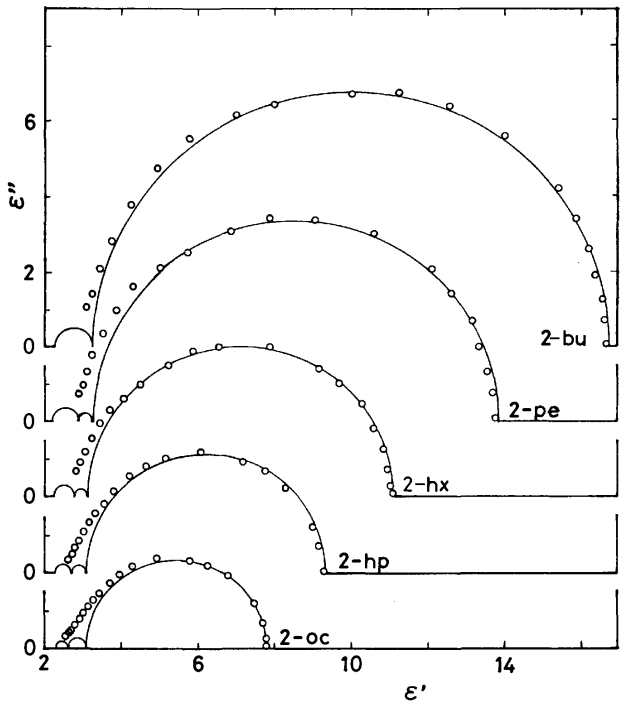

Fig. 1. Cole-Cole plots for 2-alkanol (n=4—8) at 25 °C, together with calculated behavior for the two or three dispersion regions. Butanol, pentanol, hexanol, heptanol, and octanol are abbreviated to bu, pe, hx, hp, and oc, respectively.

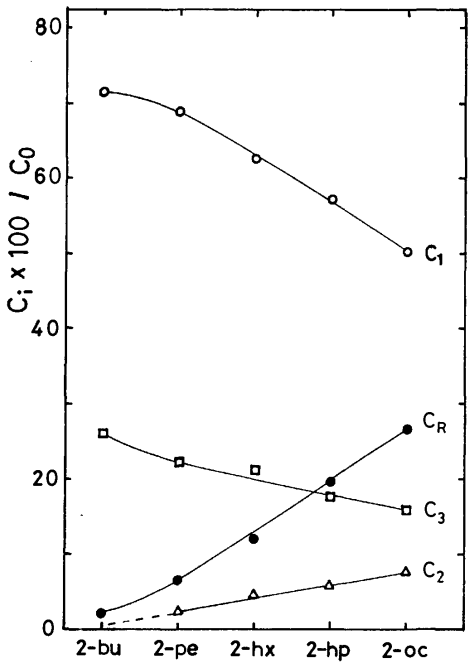

Fig. 2. Percentages of the C_{1-R} at 25 °C as a function of 2-alkanol (n=4—8). Dotted line shows an estimated value.

atoms. It is considered that the formation of a linear hydrogen-bonded chain becomes difficult because of the steric hindrance of the long alkyl group and the terminal methyl group. Figure 2 shows that a linear chain polymer is mainly in equilibrium with a free monomer for 2-butanol and with a nonpolar cyclic polymer for 2-octanol.

For five 2-methyl-2-alkanols at 25 °C, the Cole-Cole plots and the percentages of C_{1-R} are shown in Figs. 3 and 4. The absorption could not be resolved into three dispersion regions for 2-methyl-2-pentanol, 2-methyl-2-hexanol, and 2-methyl-2-heptanol. The magnitude of the first region decreases extremely from 9.39 for 2-methyl-2-propanol to 2.23 for 2-methyl-2-butanol. The percentage of C_1 also decreases from 55 to 15%, as shown in Fig. 4. It is considered for 2-methyl-2-pentanol that the first region comprises both first and second regions, although it could not be resolved into two regions. Separation between the first and second regions becomes difficult, since the magnitude of the first region approaches that of the second one. Moreover, the relaxation frequencies of the Cole-Cole plots in Fig. 3 and an extrapolation (shown as a dotted line) of the C_1 curve in Fig. 4 indicate that the first region vanishes into nothing for 2-methyl-2-hexanol and 2-methyl-2-heptanol. A comparison between Figs. 1 and 3 shows that the tertiary alcohols are more hindered species for intermolecular association. Association into a linear chain polymer becomes unfavorable because of the steric hindrance of the terminal methyl groups. The percentages of C_1, for example, are 69% for 1-octanol, 50% for 2-octanol, and

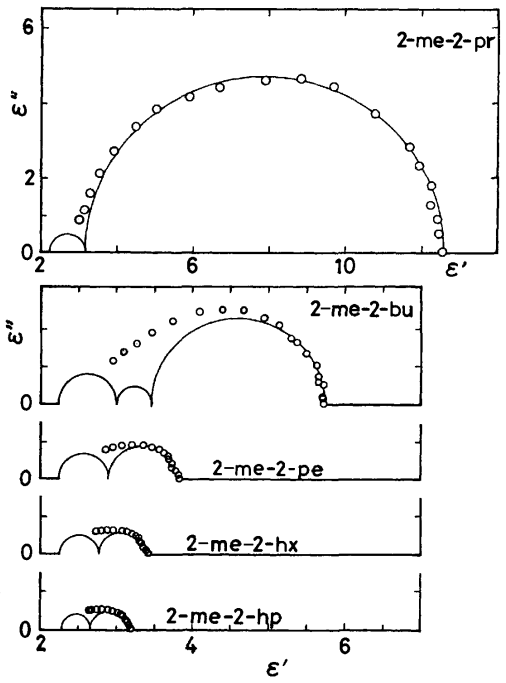

Fig. 3. Cole-Cole plots for 2-methyl-2-alkanol (n= 3—7) at 25 °C, together with calculated behavior. Methyl and propanol are abbreviated to me and pr, respectively.

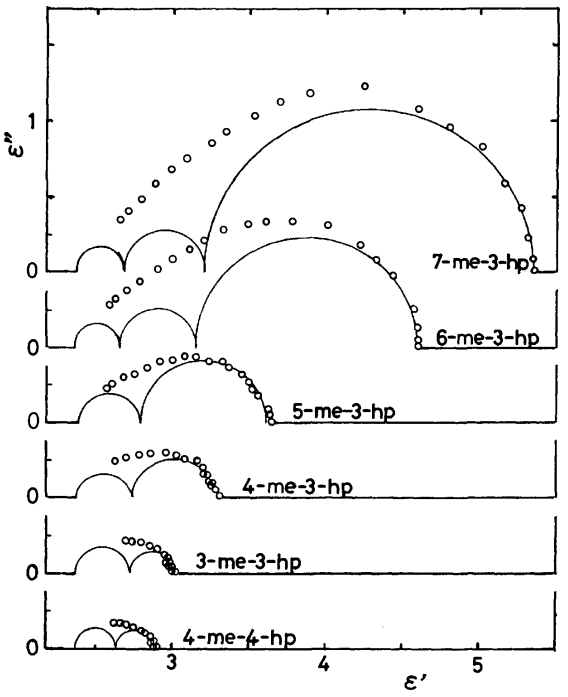

Fig. 5. Cole-Cole plots for isomeric methylheptanols at 25 °C, together with calculated behavior.

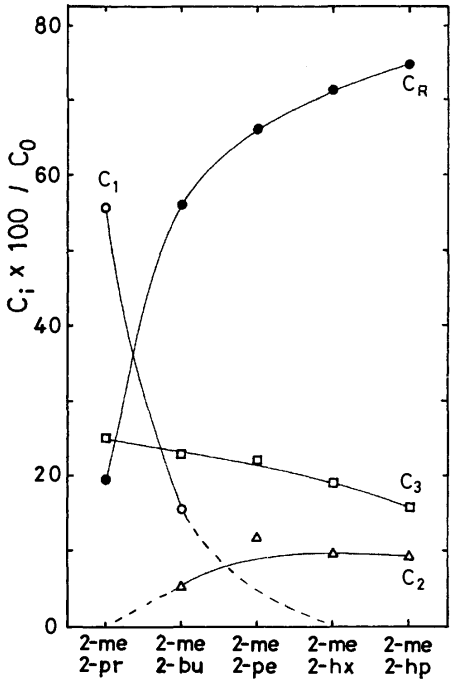

Fig. 4. Percentages of the C_{1-R} at 25 °C as a function of 2-methyl-2-alkanol (n=3—7). Dotted line shows an estimated value.

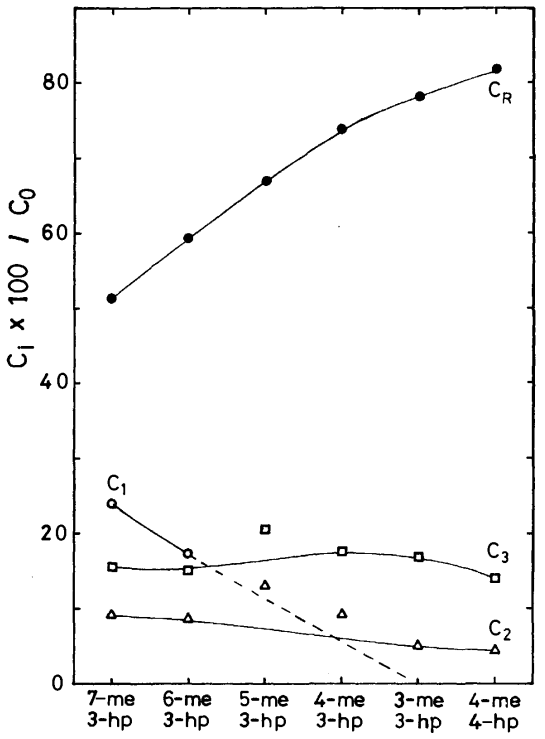

Fig. 6. Percentages of the C_{1-R} at 25 °C as a function of isomeric methylheptanols. Dotted line shows an estimated value.

0% for 2-methyl-2-heptanol at 25 °C. C_1 vanishes into nothing and C_R increases to 74% of the gross concentration for 2-methyl-2-heptanol. Figure 4 shows the equilibrium between a linear chain polymer and a free monomer for 2-methyl-2-propanol and that between a nonpolar cyclic polymer and a free monomer for 2-methyl-2-heptanol.

For six isomeric methylheptanols shown in Figs. 5

and 6 at 25 °C, the absorption could be resolved into three regions for 7-methyl-3-heptanol and 6-methyl-3-heptanol. However, it could not be resolved into three regions for 5-methyl-3-heptanol and 4-methyl-3-heptanol. For both alcohols there was no distinction between the first and second regions. As shown in Fig. 6, therefore, the percentages of C_2 and C_3 become slightly large because of the existence of a small first region. The first region becomes small in magnitude. This indicates that the formation of a linear chain polymer becomes difficult and a nonpolar cyclic polymer is formed as the methyl group approaches the hydroxyl group fixed on the third carbon atom in a molecule. The first region could not be observed in the tertiary alcohols of 2-methyl-2-heptanol (shown in Figs. 3 and 4), 3-methyl-3-heptanol, and 4-methyl-4-heptanol (shown in Figs. 5 and 6). The magnitude of the second region also decreases as both the hydroxyl and the methyl groups approach the center of a molecule. The percentage of C_R is favorable and becomes 74% of the gross concentration for 2-methyl-2-heptanol, 78% for 3-methyl-3-heptanol, and 82% for 4-methyl-4-heptanol. The large value for C_R is one remarkable feature of tertiary alcohols. Figure 6 shows that a nonpolar cyclic polymer is in equilibrium with a linear chain polymer for 7-methyl-3-heptanol and with a free monomer for 3-methyl-3-heptanol.

For five isomeric nonanols at 25 °C, the absorption could be resolved into three dispersion regions, as shown in Figs. 7 and 8. C_1 is large and, accordingly, C_R is small for normal alcohols from propyl through decyl.[8] C_1 decreases rapidly and C_R increases inversely with C_1 as the hydroxyl group approaches the center of a molecule. When the hydroxyl group approaches the center of a molecule (such as 5-nonanol), the formation of a linear chain polymer is hindered by the alkyl groups at both sides of the hydroxyl group. Figure 8 shows that a free monomer is in equilibrium with a linear chain polymer for 1-nonanol and with a nonpolar cyclic polymer for 5-nonanol.

The magnitude of the first region is in proportion to C_1 and becomes small for more hindered alcohols. Both the magnitude and C_1 decrease as the temperature increases.[5] As pure normal alcohol is diluted with a nonpolar solvent[5,11,12] and as the hydroxyl group is more sterically hindered, both the magnitude and C_1 also decrease. Therefore, any decrease in C_1 indicates that the length of a hydrogen-bonded chain shortens, namely, that the number of hydroxyl groups decreases in this polymer. The separation between the first and second regions becomes difficult as the length of a hydrogen-bonded chain approaches that of a chain dimer and trimer. The first region at last vanishes into nothing for the more hindered species (such as several tertiary alcohols), since a long linear chain polymer cannot exist. The hydrogen bond in a long chain polymer is broken by the repulsion between the terminal methyl and the alkyl groups for these more hindered alcohols, although a chain dimer and trimer can be formed. A nonpolar cyclic polymer is stably formed and becomes a preferred species for these alcohols. The second region is due to the chain dimer and trimer and is always small in magnitude. It may, therefore, be considered to be formed as an intermediate.

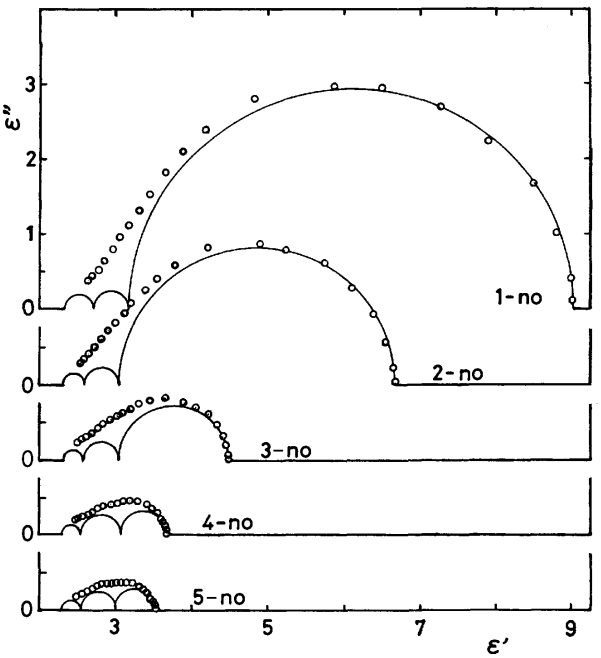

Fig. 7. Cole-Cole plots for isomeric nonanols at 25 °C, together with calculated behavior. Nonanol is abbreviated to no.

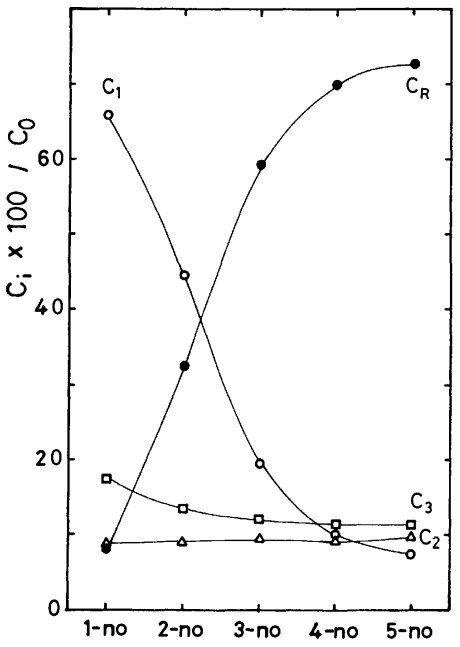

Fig. 8. Percentages of the C_{1-R} at 25 °C as a function of isomeric nonanols.

For the first region of some normal and secondary alcohols (n=3—10),[2,8] the relaxation time (τ_1) becomes long and C_1 decreases with increasing alkyl chain length in a molecule. τ_1 also becomes long with increasing viscosity of the liquid. τ_1 depends on both the alkyl chain length and the viscosity of the liquid. As pointed out by Smyth et al.,[2,13] therefore, it is considered that overall rotation of a molecule is closely associated with the relaxation process. In this work, τ_1 shortens and C_1 decreases for isomeric methylheptanols (in which the alkyl chain length and the viscosity are approximately equal) as the methyl group approaches a hydroxyl group fixed on the third carbon atom in a molecule. For the isomeric nonanols (in which the alkyl chain length and the viscosity also are approximately equal) τ_1 shortens and C_1 also decreases as the hydroxyl group approaches the center of a molecule. These observations show that τ_1 has an immediate association with C_1, namely, that τ_1 becomes shorter with decreasing length of a linear hydrogen-bonded chain. Therefore, τ_1 is considered to be dependent on the alkyl chain length in a molecule, the viscosity of the liquid, and the length of a linear hydrogen-bonded chain. The mechanism of the relaxation process may be envisioned from these relationships, as follows. After one hydrogen bond of a chain-end molecule is broken, the overall rotation of the molecule (which now becomes free) occurs; then, the overall rotation of the next molecule (which is now at the chain end) occurs successively by breaking one hydrogen bond between the molecule and a neighboring molecule. All molecules in this hydrogen-bonded chain are turned over successively. The time of the overall rotation for one molecule depends on the alkyl chain length and the viscosity of the liquid. The magnitude of the dispersion is determined by the concentration of the hydroxyl group in the linear chain polymer. The orientated molecules are rearranged so as to form a linear chain polymer by new hydrogen bondings.

The thermodynamic parameters, the free energy of activation ΔF, the heat of activation ΔH, and the entropy of activation ΔS, were calculated by applying the Eyring's equation[14] to the temperature dependences of the two or three relaxation times τ_{1-3} and the viscosity η. The ΔH and ΔS were calculated from the values at the proper temperatures of 15, 25, and 35 °C in cases where the same dispersion region could not be obtained at all the temperatures investigated. ΔF was obtained at 25 °C. ΔH and ΔS increase with increasing alkyl chain length and also increase for more sterically hindered species. Figure 9 shows that ΔF also increases with increasing alkyl chain length. For isomeric methylheptanols, as shown in Fig. 10, $\Delta F_{\tau 1}$ decreases and approaches $\Delta F_{\tau 2}$ as the methyl group approaches the hydroxyl group. $\Delta F_{\tau 1}$ vanishes into nothing in the vicinity of 3-methyl-3-heptanol, as shown by a dotted line. If the magnitude of the first region would be large for more hindered methylheptanols, the curve of $\Delta F_{\tau 1}$ would be parallel to that of $\Delta F_{\tau 2}$. It is necessary to consider that the thermodynamic parameters should be calculated in terms of the temperature dependence of the same dispersion region for the more hindered alcohols.

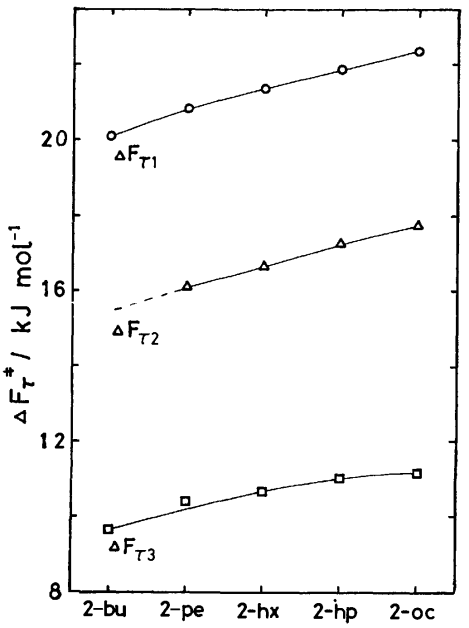

Fig. 9. Free energies of activation as a function of 2-alkanol (n=4—8).

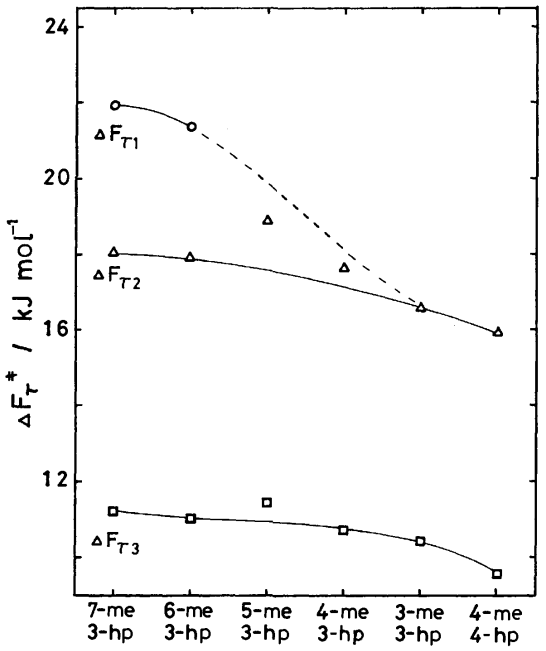

Fig. 10. Free energies of activation as a function of isomeric methylheptanols. Dotted line shows an estimated value.

References

1) A. Lebrun, *Ann. Phys.*, **10**, 16 (1955).

2) S. K. Garg and C. P. Smyth, *J. Phys. Chem.*, **69**, 1294 (1965).
3) R. H. Cole and D. W. Davidson, *J. Chem. Phys.*, **20**, 1389 (1952).
4) W. Dannhauser, *J. Chem. Phys.*, **48**, 1918 (1968).
5) T. Shinomiya, *Bull. Chem. Soc. Jpn.*, **62**, 2258 (1989).
6) G. Oster and J. G. Kirkwood, *J. Chem. Phys.*, **11**, 175 (1943).
7) H. Fröhlich, "Theory of Dielectrics," 2nd ed., Oxford University, New York, N. Y. (1958).
8) T. Shinomiya, *Bull. Chem. Soc. Jpn.*, **62**, 908 (1989).
9) M. Moriamez, L. Raczy, E. Constant, and A. Lebrun, *J. Chim. Phys.*, **61**, 146 (1964).
10) J. G. Kirkwood, *J. Chem. Phys.*, **7**, 911 (1939).
11) H. Komooka, *Bull. Chem. Soc. Jpn.*, **45**, 1696 (1972).
12) M. W. Sagal, *J. Chem. Phys.*, **36**, 2437 (1962).
13) L. Glasser, J. Crossley, and C. P. Smyth, *J. Chem. Phys.*, **57**, 3977 (1972).
14) S. Glasstone, K. J. Laidler, and H. Eyring, "The Theory of Rate Processes," McGraw-Hill Book Company, Inc., New York, N. Y. (1941), Chap. lX.

 © 1989 The Chemical Society of Japan Bull. Chem. Soc. Jpn., 62, 3643—3647 (1989)

Dielectric Behavior and Intermolecular Association for Octanol Isomers. Existence and Transformation of a Nonpolar Cyclic Polymer

Toshiomi SHINOMIYA†
School of Pharmaceutical Sciences, Kitasato University,
Shirokane, Minato-ku, Tokyo 108
(Received May 24, 1989)

The equilibrium dielectric constants of ten isomeric $C_8H_{17}OH$ and binary mixtures of 1-butanol in four isomeric $C_8H_{17}OH$ have been measured at temperatures from 135 to −55 °C. These isomeric $C_8H_{17}OH$ can be grouped roughly into three types, namely, more polar, intermediate, and more sterically hindered alcohols. The dielectric behavior of each of the three types can be explained by equilibrium among a linear hydrogen-bonded chain polymer (**CHAIN**), a free monomer inclusive of a chain dimer and trimer (**MONOMER**), and a nonpolar cyclic polymer (**RING**). As the temperature decreases, **MONOMER** transforms into **CHAIN** for more polar alcohols. Two transformations, **MONOMER** into **RING** at high temperatures and **RING** into **CHAIN** at low temperatures, occur for intermediate alcohols. **MONOMER** transforms into **RING** and **CHAIN** can not be observed for more hindered alcohols. However, a transformation of **RING** into **CHAIN** can be observed by adding 1-butanol to the more hindered alcohols. **CHAIN** is most stable. When formation of **CHAIN** becomes difficult, **RING** can be formed. The transformation is dependent on temperature, molecular geometry, and the amount of 1-butanol in the mixture.

In general, the equilibrium dielectric constants for many compounds increase monotonically with decreasing temperature. However, it is well-known that the dielectric constant for a carboxylic acid decreases conversely with decreasing temperature because of the formation of a nonpolar cyclic dimer. For liquid alcohols, temperature dependence of the dielectric constant indicates a complex and interesting behavior. Dielectric studies have indicated the formation of various hydrogen-bonded species by intermolecular association in pure alcohols and dilute solutions of alcohols. Smyth and Stoops[1] measured the equilibrium dielectric constants for various isomeric $C_8H_{17}OH$ and explained the dielectric complex behavior by molecular orientation. Dannhauser[2] measured the interesting dielectric behavior for 8 isomeric $C_8H_{17}OH$. He analyzed the behavior by the Kirkwood-Fröhlich equation[3,4] and introduced a molecular model which consists of monomers in equilibrium with nonpolar ring dimers and with chain polymers. For various secondary and tertiary alcohols at 15, 25, and 35 °C, we obtained four concentrations, **CHAIN** (C_1), a chain dimer and trimer (C_2), a free monomer (C_3), and **RING** (C_R), by means of a modified Kirkwood-Fröhlich equation.[5,6] An extrapolation of these concentrations to the high- and low-temperature portions was used to explain the complex dielectric behavior for the temperature dependence of the dielectric constant.

The existence of **RING** has been postulated for more sterically hindered alcohols. It is evident that the variable and complex dielectric behavior is attributed to the existence of **RING**. However, there has been little experimental evidence for the existence of **RING** in order not to contribute to the dielectric constant. Therefore, we measured binary mixtures of 1-butanol in some isomeric $C_8H_{17}OH$ to investigate the existence of **RING** and the transformation of **RING** into **CHAIN**.

Experimental

Purification of Materials. Commercial alcohols were fractionally distilled twice, as described in a previous paper.[6]

Apparatus. The equilibrium dielectric constants were measured by making use of a ratio-arm transformer bridge (Ando Electric Co. Type TR-10) at the frequency range of 3—1000 kHz. The cell is a three terminal guarded electrode arrangement of gold-plated brass with Teflon insulation. The cell was made by reference to those reported by Hassion and Cole[7] and Dannhauser and Bahe.[8] The capacitance of the cell is 5.05 pF. The temperature control was maintained within ±0.5 °C.

Results and Discussion

Temperature Dependence of Equilibrium Dielectric Constants (ε_0). Our data shown in Fig. 1 are qualitatively similar to those of eight isomeric $C_8H_{17}OH$ measured by Dannhauser.[2] These isomers have approximately the same dipole moment and the same molecular volume, though the relative positions of the hydroxyl and methyl groups are different. Figure 1, however, shows a variety and complexity of dielectric behavior for these isomeric $C_8H_{17}OH$. This variety and complexity can be attributed to a difference of the hydrogen-bonded species formed by intermolecular association. If it is assumed that all alcohol molecules exist as free monomers, the ε_0 can be calculated from the Kirkwood-Fröhlich equation.[3,4] The behavior of the ε_0 is shown in Fig. 1 as a dotted

† Present address: 207-52, Shirahata kami-cyo, Kanagawa-ku, Yokohama 221.

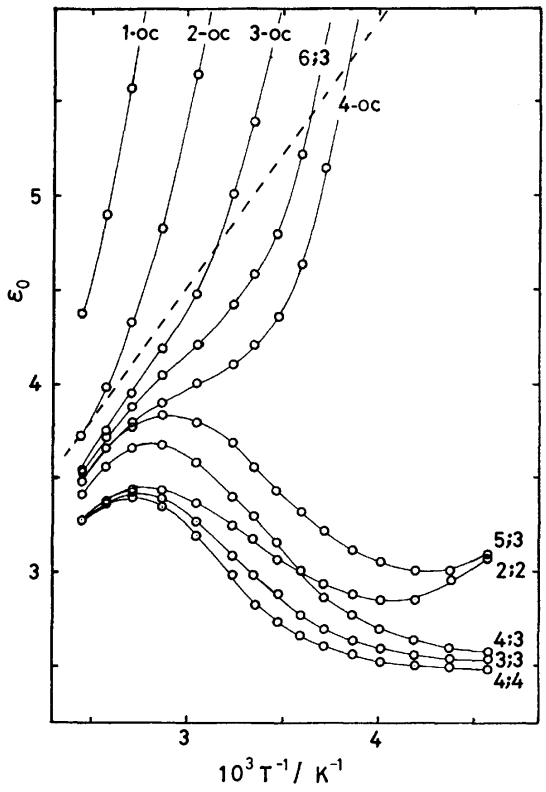

Fig. 1. Equilibrium dielectric constants as a function of reciprocal absolute temperature for ten isomeric $C_8H_{17}OH$. Octanol, 6-methyl-3-heptanol, and 4-methyl-4-heptanol are abbreviated to oc, 6;3, and 4;4, respectively. Dotted line shows a calculated dielectric constant, when all molecules exist as free monomers.

line. In this equation, the limiting high-frequency dielectric constant ($\varepsilon_\infty=\varepsilon_3$) for the third region was evaluated by using $(\varepsilon_\infty-1)/(\varepsilon_\infty+2)=(n_D^2-1)(1+0.19)/(n_D^2+2)$, as described before.[9]

For the isomeric $C_8H_{17}OH$, the behavior of ε_0 can be grouped roughly into three types and explained by estimation of the relative concentrations of the C_{1-R}. A chain dimer and trimer could not be distinguished from a free monomer by the temperature dependence of ε_0. Therefore, **MONOMER** described hereunder includes the existence of a chain dimer and trimer.

The dielectric behavior of the first type is typical of more polar alcohols, such as 1-octanol shown in Fig. 1. The ε_0 is larger than that of the dotted line even at high temperatures and increases linearly with decreasing temperature. This observation indicates that **CHAIN** can be formed at the high temperatures. We established that for 1-octanol at 25 °C the percentages of the C_1, C_3, and C_R are 69, 26, and 5% of the gross concentration, respectively. The C_1 increases and the C_3 decreases because of the transformation of **MONOMER** into **CHAIN**, as the temperature decreases. The ε_0-$1/T$ curve can be explained by an equilibrium between **MONOMER** and **CHAIN**.

The second type consists of intermediate alcohols, such as 4-octanol and 5-methyl-3-heptanol. The ε_0 is smaller than that of the dotted line at high temperatures. Therefore, **RING** can be formed at the high temperatures. For 5-methyl-3-heptanol at 15 °C, the percentages of the C_1, C_3, and C_R are 8, 16, and 76%, respectively. The C_3 decreases and the C_R increases, as the temperature decreases. The C_1 could not be obtained at 25 and 35 °C, since they are small values. The ε_0-$1/T$ curve for 5-methyl-3-heptanol indicates a complex and interesting curve. The ε_0 at first increases with decreasing temperature and becomes a maximum at about 75 °C ($1/T=2.87\times10^{-3}$ K^{-1}) and then decreases conversely with decreasing temperature. Additionally, the ε_0 becomes a minimum at about −40 °C ($1/T=4.29\times10^{-3}$K^{-1}), and increases again with decreases temperature. Therefore, it is necessary to consider the coexistence of **MONOMER**, **RING**, and **CHAIN**, especially, inclusive of two transformations of **MONOMER** into **RING** at high temperatures and of **RING** into **CHAIN** at low temperatures.

The behavior of the third type is typical of more sterically hindered alcohols, such as 3-methyl-3-heptanol and 4-methyl-4-heptanol. The ε_0's for these tertiary alcohols are nearly equal at 135 °C ($1/T=2.45\times10^{-3}$ K^{-1}) and are smaller than that of the dotted line at high temperatures. The ε_0-$1/T$ curve has a maximum at about 80 °C ($1/T=2.83\times10^{-3}$ K^{-1}). The maximum for the tertiary alcohols appears at higher temperature than that for the secondary alcohols, because of the ease of the transformation of **MONOMER** into **RING**. For 3-methyl-3-heptanol at 25 °C, the percentages of the C_1, C_3, and C_R are 0, 22, and 78%, respectively. **CHAIN** can not exist at temperatures between 135 and −55 °C. The C_3 decreases and the C_R increases, as the temperature decreases. The third type shows the equilibrium between **MONOMER** and **RING**.

Binary Mixtures of 1-Butanol in Some Isomeric $C_8H_{17}OH$. When 1-butanol is added to the three types of isomeric $C_8H_{17}OH$, the ε_0-$1/T$ curve for the mixtures differs from that of the pure octanol.

The ε_0-$1/T$ curves for mixtures of 1-butanol in 1-octanol are shown in Fig. 2, together with the dotted line. The ε_0 of pure 1-octanol increases linearly with decreasing temperature, since **CHAIN** can be formed even at high temperatures. The ε_0-$1/T$ curve for the mixture increases in parallel over the temperatures from 135 °C to a freezing point or −55 °C, as 1-butanol is added to 1-octanol. It can be considered that the **CHAIN** formed is composed of both 1-butanol and 1-octanol molecules because the ε_0 increases approximately in proportion to the 1-butanol concentration. Therefore, the first dispersion can be explained by a single relaxation process for binary mixtures of normal alcohols.[10,11]

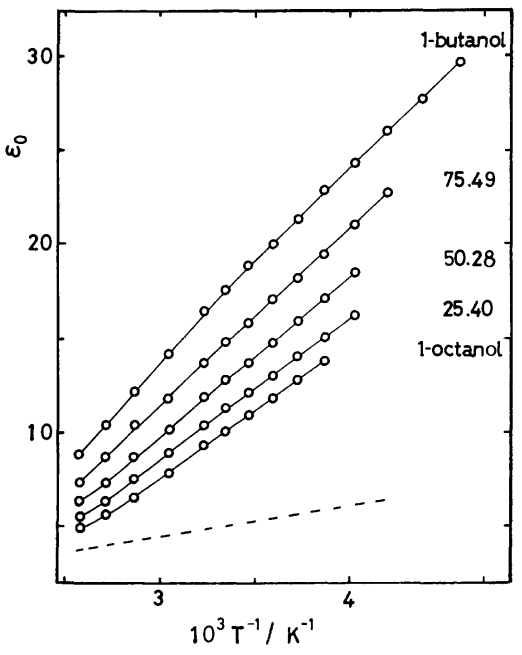

Fig. 2. Equilibrium dielectric constants as a function of reciprocal absolute temperature for the mixtures of 1-butanol in 1-octanol. Number is mol% of 1-butanol.

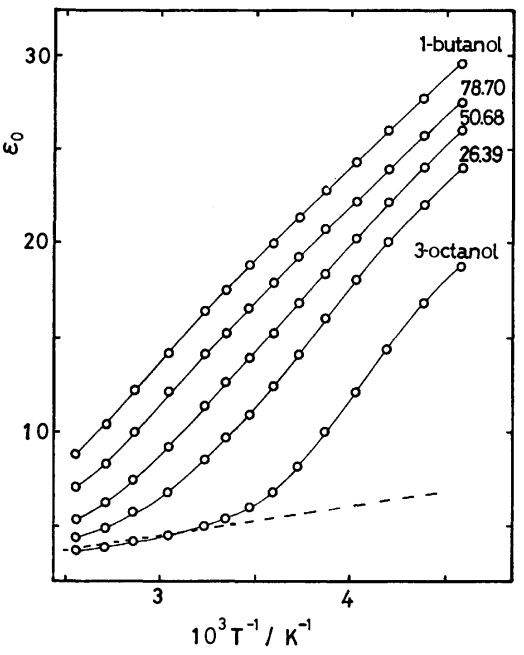

Fig. 3. Equilibrium dielectric constants as a function of reciprocal absolute temperature for the mixtures of 1-butanol in 3-octanol. Number is mol% of 1-butanol.

The ε_0–$1/T$ curves for mixtures of 1-butanol in 3-octanol are shown in Fig. 3. The ε_0 of pure 3-octanol at high temperatures is smaller than that of the dotted line and increases gradually as shown by the dotted line with decreasing temperature. For pure 3-octanol at 25 °C ($1/T$=3.35×10^{-3} K^{-1}), the percentages of the C_R, C_3, and C_1 are 51, 25, and 24%, respectively. The C_R and C_3 decrease and the C_1 increases, as the temperature decreases. Figure 3 shows that **MONOMER** and **RING** coexist at high temperatures and that the transformation of **MONOMER** and **RING** into **CHAIN** occurs, since the ε_0 of pure 3-octanol increases suddenly at about 25 °C. It favors the formation of **CHAIN** at temperatures below about 25 °C. As 1-butanol is added to 3-octanol, the transformation occurs at higher temperatures, namely, at about 25 °C for pure 3-octanol, at about 70 °C ($1/T$=2.91×10^{-3} K^{-1}) for 26 mol% mixture of 1-butanol, and at about 110 °C ($1/T$=2.61×10^{-3} K^{-1}) for 50 mol% mixture of 1-butanol.

The ε_0–$1/T$ curves are shown in Fig. 4 for mixtures of 1-butanol in 4-methyl-4-heptanol and in Fig. 5 for solutions of 1-butanol in heptane in order to emphasize the difference of the dielectric behavior between 4-methyl-4-heptanol and heptane. The ε_0–$1/T$ curve for pure 4-methyl-4-heptanol is similar to that for pure heptane which is a nonpolar solvent. The ε_0 is slightly larger than that of heptane because of the existence of **MONOMER** having a dipole moment. As described above, **CHAIN** can not be formed for pure 4-methyl-4-heptanol over the temperatures from 135 to −55 °C. For 26 mol% mixture of 1-butanol in 4-methyl-4-heptanol, however, the ε_0 at high temperatures increases as indicated by the dotted line with decreasing temperature. It becomes smaller than that of the dotted line over the temperature range of 72—−29 °C and then increases suddenly at about −29 °C ($1/T$=4.10×10^{-3} K^{-1}), although ε_0 of the 25 mol% solution of 1-butanol in heptane hardly changes over the temperature range. This observation can be explained by two transformations of **MONOMER** into **RING** at high temperatures and **MONOMER** and **RING** into **CHAIN** at low temperatures. In a 50 mol% mixture of 1-butanol in 4-methyl-4-heptanol, the transformation of **MONOMER** into **CHAIN** occurs at higher temperatures. The ε_0 of 4-methyl-4-heptanol mixtures is larger than that of heptane solution at the same concentration of 1-butanol and at the same temperature. This difference of ε_0 indicates that the transformation of **RING** into **CHAIN** occurs by the addition of 1-butanol.

At a fixed temperature of −55 °C ($1/T$=4.58×10^{-3} K^{-1}), the ε_0 of the binary mixtures are plotted in Fig. 6 against mol% of 1-butanol. Since the ε_0 of pure 3-octanol is 18.68 at this temperature, almost every molecule exists as **CHAIN** in both pure 3-octanol and mixtures of 1-butanol in 3-octanol. It is noticeable that the ε_0 of the mixtures is larger than that of pure normal alcohols at the same concentration of the hydroxyl group. Figure 6 also shows that the ε_0 is 2.48 for pure 4-methyl-4-heptanol and 2.00 for pure heptane. The difference, 2.48—2.00, suggests the

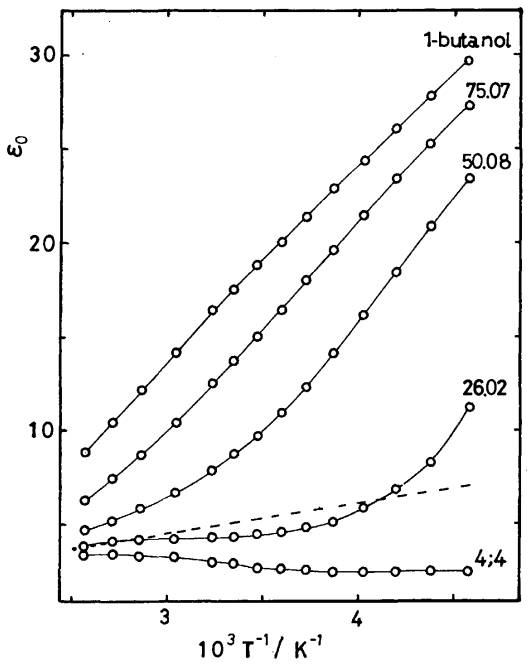

Fig. 4. Equilibrium dielectric constants as a function of reciprocal absolute temperature for the mixtures of 1-butanol in 4-methyl-4-heptanol (4;4). Number is mol% of 1-butanol.

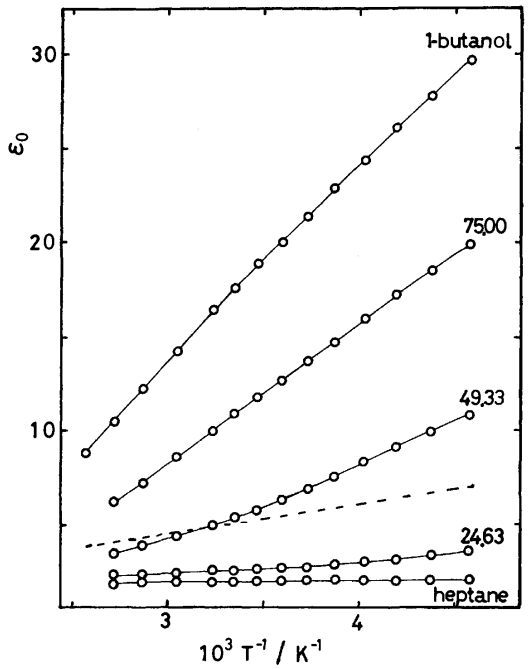

Fig. 5. Equilibrium dielectric constants as a function of reciprocal absolute temperature for the solutions of 1-butanol in heptane. Number is mol% of 1-butanol.

existence of **MONOMER** in pure 4-methyl-4-heptanol. As 1-butanol is added to 4-methyl-4-heptanol, ε_0 increases suddenly at about 30 mol% mixture of 1-butanol. The ε_0 of 50 mol% mixture becomes 23.3

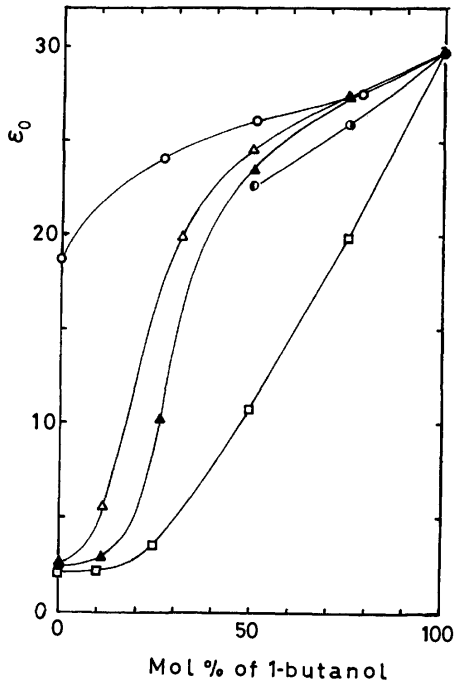

Fig. 6. Equilibrium dielectric constants as a function of mol% of 1-butanol at −55 °C. ○: 1-butanol-3-octanol, △: 1-butanol-4-methyl-3-heptanol, □: 1-butanol-heptane, ▲: 1-butanol-4-methyl-4-heptanol, ◑: pure 1-pentanol, ◐: pure 1-hexanol.

and is larger than 22.5 of pure 1-hexanol having the same concentration of the hydroxyl group, although the ε_0 is 10.9 for 50 mol% solution of 1-butanol in heptane. Therefore, almost every molecule in the 50 mol% mixture is considered to be **CHAIN**, being the same as that in pure normal alcohol. The variation of ε_0, shown in Fig. 6, provides experimental evidence of the existence of **RING**. The mechanism of the transformation of **RING** into **CHAIN** can be envisioned by addition of 1-butanol to some isomeric $C_8H_{17}OH$. For the mixtures of 1-butanol in 4-methyl-4-heptanol at this temperature, for example, **CHAIN** can hardly exist for the 20 mol% mixture which consists of four molecules of 4-methyl-4-heptanol to one of 1-butanol. **CHAIN** can be formed suddenly for 25 and 33 mol% mixtures which are in the molecular ratios of 3:1 and 2:1, respectively. It may be considered that a ring trimer and a ring dimer transform into a chain tetramer and a chain trimer inclusive of one molecule of 1-butanol, respectively. A chain pentamer can not exist because of the repulsion of two alkyl groups of 4-methyl-4-heptanol in both sides of the linear hydrogen-bonded chain. The chain tetramer and chain trimer formed may associate into a chain octamer and chain $3n$-mer, respectively.

References

1) C. P. Smyth and W. N. Stoops, *J. Am. Chem. Soc.*, **51**,

3330 (1929).
2) W. Dannhauser, *J. Chem. Phys.*, **48**, 1911 (1968).
3) G. Oster and J. G. Kirkwood, *J. Chem. Phys.*, **11**, 175 (1943).
4) H. Fröhlich, "Theory of Dielectrics," 2nd ed., Oxford University, New York, N. Y. (1958).
5) T. Shinomiya, *Bull. Chem. Soc. Jpn.*, **62**, 3636 (1989).
6) T. Shinomiya, *Bull. Chem. Soc. Jpn.*, **62**, 908 (1989).
7) F. X. Hassion and R. H. Cole, *J. Chem. Phys.*, **23**, 1756 (1955).
8) W. Dannhauser and L. W. Bahe, *J. Chem. Phys.*, **40**, 3058 (1964).
9) T. Shinomiya, *Bull Chem. Soc. Jpn.*, **62**, 2258 (1989).
10) D. J. Denney and R. H. Cole, *J. Chem. Phys.*, **23**, 1767 (1955).
11) T. Shinomiya, H. Komooka, and H. Okabayashi, 30th National Meeting of the Chemical Society of Japan, April 1974, Abstr., No. 1E39.

 © 1989 The Chemical Society of Japan Bull. Chem. Soc. Jpn., 62, 3648—3654 (1989) [Vol. 62, No. 11

Physicochemical Properties of Eicosane-1,20-bis(trimethylammonium) Dibromide in Aqueous Solution

Masaaki YASUDA, Kenji IKEDA, Kunio ESUMI,* and Kenjiro MEGURO
Department of Applied Chemistry and Institute of Colloid and Interface Science, Science University of Tokyo, Kagurazaka, Shinjuku-ku, Tokyo 162
(Received May 27, 1989)

The physicochemical properties of a cationic α,ω-type(bolaform) surfactant, eicosane-1,20-bis(trimethylammonium) dibromide ($C_{20}Me_6$), were investigated by means of surface tension, electrical conductivity, density, dye solubilization, fluorescence, and light scattering. The results obtained for $C_{20}Me_6$ were compared with those for decyltrimethylammonium bromide ($C_{10}Me_3$). The surface tension measurement suggests that $C_{20}Me_6$ has a folded, "wicket-like" conformation at the air-water interface. The cmc of $C_{20}Me_6$ was smaller than that of $C_{10}Me_3$. The apparent ionization degree of $C_{20}Me_6$ was larger, and the polarity of the micellar Stern layer was higher than that of $C_{10}Me_3$. It was found that the $C_{20}Me_6$ micelle has an aggregation number of about 19, a hydrodynamic radius of 16 Å, and a partial molar volume of 480.49×10^{-3} dm^3 mol^{-1}, suggesting that the micelle is nearly spherical; thus, the main alkyl chain is almost stretched, and the outermost region of the micelle is loose.

The α,ω-type surfactant is different from a "conventional" surfactant since the former has headgroups at each end of the long alkyl chain. This feature can impose a significant constraint on the orientation and the packing of surfactant monomers within a micelle, because both ends of each α,ω-type surfactant monomer must be located on the micellar surface.

There have been several studies of the properties of α,ω-type surfactants in aqueous solution.[1-15] Menger and Wrenn[1] reported that micelles are formed for C_mMe_6 ($m>12$), and concluded that dodecane-1,12-bis(trimethylammonium) dibromide ($C_{12}Me_6$) takes a folded, "wicket-like", conformation at an air-water interface. Johnson et al.[2] confirmed that C_mMe_6 do not form ordinary micelles for $m<10$, indicating that there is considerable bending of the $(CH_2)_m$ chains in aqueous solution and air-water interfaces from measurements of the apparent molar volumes for $m=6$ and 10. In contrast, Zana et al.[4-6,9] found no evidence of conventional micellization for $C_{12}Me_6$ from density, electrical conductivity, and emf measurements, whereas $C_{16}Me_6$ and $C_{22}Me_6$ form micelles. The chemical relaxation studies indicated that $C_{22}Me_6$ monomers diffuse rapidly among the bulk and micellar pseudophases, with a rate similar to that of the conventional surfactant, dodecyltrimethylammonium bromide ($C_{12}Me_3$). Mckenzie et al.[8] estimated the hydrodynamic radii and the ionization degree of $C_{22}Me_6$ using static and dynamic light scattering; they concluded that $C_{22}Me_6$ forms micelles which are similar to those of $C_{12}Me_3$.

On the other hand, Meguro et al.[10-13] have studied the solution properties of anionic α,ω-type surfactants, and concluded that these surfactants also form small and loose aggregates.

The conformational properties of eicosane-1,20-bis(triethylammonium) dibromide ($C_{20}Et_6$) have been investigated by NMR and time-resolved fluorecence quenching.[14-16] It has been concluded that the sufractant chains of $C_{20}Et_6$ adopt a predominantly stretched conformation in micelles. However, the physicochemical properties of α,ω-type surfactants are not fully understood. Still, it is worthwhile studying the properties in the aqueous solution of an α,ω-type surfactant from a comparison of the corresponding conventional surfactants.

In this work we focused the attention on a comparison between the physicochemical property of a cationic α,ω-type surfactant, eicosane-1,20-bis(trimethylammonium) dibromide ($C_{20}Me_6$), and that of a conventional surfactant, decyltrimethylammonium bromide ($C_{10}Me_3$), which has the same head group and an alkyl chain half as long. The comparison was carried out by measuring the surface tension, electrical conductivity, static and dynamic light scattering, steady-state fluorescence quenching, density, and probe solubilization.

Experimental

Materials. The α,ω-type surfactant, $C_{20}Me_6$, was synthesized as follows: 1,20-dibromoeicosane was prepared by the dimerization of 11-bromoundecanoic acid with Kolbe's electrolysis in methanol. A white precipitate was filtered and recrystallized from methanol. The obtained dibromide was converted to $C_{20}Me_6$ according to the procedure.[1] After removing ethanol and trimethylamine, $C_{20}Me_6$ was recrystallized four times from acetone–ethanol mixtures and dried under vacuum for 48 hours. The purity of the product was confirmed to be above 99% by isotachophoresis, elemental analysis, and ^{1}H NMR.

Pyrene was recrystallized four times from ethanol. Orange-OT and Yellow-OB were recrystallized four times from ethanol. Pyrene-3-carbaldehyde and benzoylacetone were used as received. *N*-Hexadecylpyridinium chloride was recrystallized three times from ethanol. Decyltrimethylammonium bromide, $C_{10}Me_3$, was recrystallized three times from acetone. The water used was purified by passing it through a purification system, Milli-Q Reagent Grade Water System, until the specific conductivity of water was below

0.1 μS cm^{-1}.

Measurements. Surface-tension measurements were carried out for various concentrations of $C_{20}Me_6$ in aqueous solutions by using a Wilhelmy-type surface tensiometer (Shimadzu St-1) at 25 °C. The establishment of equilibrium was checked by repeated measurements at 5-minute intervals. The electrical conductivity of $C_{20}Me_6$ solutions was measured by means of an electrical-conductivity meter (Toa Denpa Co. Model CM-30ET) at 25±0.1 °C.

Information about micellar aggregation numbers was obtained by static light-scattering measurements. The scattered intensities were measured at 90° using a light-scattering photometer (DLS-700 (Otsuka electronics Co.)) with an argon laser at 488 nm (13 mW). The average molecular weight of micelles was determined by using the Debye relation. The refractive index increment was measured by a differential refractometer (RM-102 (Otsuka electronics Co.)) at 488 nm. The solutions were previously filtered through a 0.2 μm disposable membrane filter.

The steady-state fluorescence quenching method of Turro and Yekta[17] was carried out by using pyrene as a fluorescence probe and *N*-hexadecylpyridinium chloride as a quencher. In this experiment it was assumed that the probe and the quencher do not migrate from micelle to micelle within the lifetime of pyrene:[18]

$$\ln (I_0/I) = C_q/[\text{micelle}], \quad (1)$$

where C_q is the concentration of the quencher; I_0 and I are the fluorescence intensities in the absence and presence of the quencher. The micellar aggregation number is calculated from

$$N = (C - \text{cmc})/[\text{micelle}]. \quad (2)$$

Dynamic light-scattering measurements were carried out using a sub-micron particle analyzer (4700C (Malvern Co.)) with an argon laser of 488 nm, 5W (Spectra-Physics Co.). The scattering angle was varied from 40 to 140° for a sample with a concentration of 3.0×10^{-2} mol kg^{-1}, and the mean micellar diffusion coefficients for various concentrations were measured at 40°.

The density measurements were carried out by using a ANTON PAAR Model DMA 60 at 25±0.01 °C. The accuracy was ±10^{-5} g dm^{-3}. The apparent molar volume, ϕ, is given by[19]

$$\phi = \frac{M}{d} - \frac{1000(d - d_0)}{m \cdot d \cdot d_0}, \quad (3)$$

where M, m, d, and d_0 are the molar weight of the surfactant, the molality, the density of solution, and the density of water, respectively. The partial molar volume V is related to ϕ by

$$V = \phi + m\left(\frac{\partial \phi}{\partial m}\right)_{T,P,n_0}, \quad (4)$$

where T, P, and n_0 are the temperature, pressure, and mole number of water, respectively. The calculated V is plotted versus the micellized surfactant concentration. The partial molar volume of the micellar species was obtained by extrapolating the plot to the cmc. A similar approach was made for the concentration below the cmc.

The fluorescence spectra of the respective samples were measured by using a fluorescence spectrophotometer (Hitachi 650-10S). The excitation and emission slits were set at 7.5 and 1.0 nm, and the excitation wavelengths of pyrene and pyrene-3-carbaldehyde (PyCHO) were 335 and 356 nm, respectively. The emission spectra were measured in the range 360—520 nm for pyrene and 380—520 nm for PyCHO.

The ultraviolet spectra measurements were carried out using a Hitachi 220A UV spectrophotometer. The concentration of benzoylacetone (BZA) was 1.0×10^{-5} mol dm^{-3}. The absorbances from ketonic- and enolic-form of BZA were measured at 245 and 310 nm.

The procedure of solubilizing power measurements was carried out as follows: after the addition of excess amounts of water-insoluble dyes into the surfactant solution, these mixtures were shaken for 48 hours at 25±0.1 °C. Then, the solutions were centrifuged at 5000 rpm for 10 minutes, and the supernatant liquids obtained were diluted with ethanol. The optical density was measured at the maximal absorption band, and the concentrations of dyes were determined from a calibration of the absorbance versus the dye concentration.

Results and Discussion

Cmc. The cmc values of $C_{20}Me_6$ were found to be 7.5×10^{-3} mol kg^{-1} and 8.2×10^{-3} mol kg^{-1} from surface tension and electrical conductivity measurements, respectively. These cmc values were smaller than that of $C_{10}Me_3$ (6.8×10^{-2} mol dm^{-3}).[20]

Conformation of $C_{20}Me_6$ at Liquid-Air Interface. From the surface-tension values of $C_{20}Me_6$ as a function of the logarithm of the surfactant concentration, the occupying area per molecule at the air-water interface was found to be 78.9 Å^2 using Gibbs adsorption equation:

$$\Gamma = \frac{-1}{nRT} \cdot \left(\frac{\partial \gamma}{\partial \ln C}\right)_T. \quad (5)$$

The value of n was taken as 3 since $C_{20}Me_6$ is regarded as being a 2:1 electrolyte. γ is the surface tension mN m^{-1} and $(\partial\gamma/\partial \ln C)_T$ denotes the maximum slope of γ-log$C$ plots.

$$A = \frac{10^{16}}{N_A \Gamma}, \quad (6)$$

where A is the occupying area per molecule in square angstroms and N_A is Avogadro's number. The value of 78.9 Å^2 for $C_{20}Me_6$ was about twice that of the intrinstic surface area of the trimethylammonium head group (37.9 Å^2)[21] suggesting that $C_{20}Me_6$ has a folded, "wicket-like" conformation at an air-water interface.[1,12]

Ionization Degree. Figure 1 shows the variation of the specific conductivity, κ, with the surfactant concentration. The apparent degree of micelle ionization, α_{ap}, was obtained[9] as the ratio of the slope of these plots above and below the cmc. The α_{ap} value

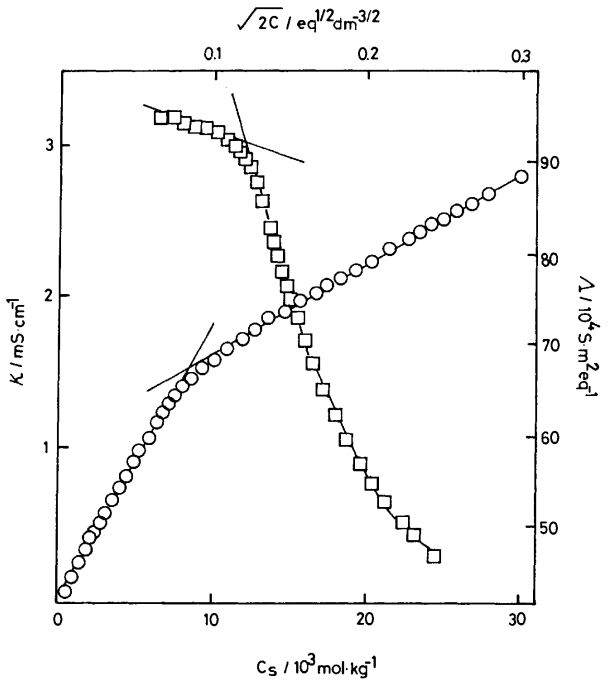

Fig. 1. Variation of specific and equivalent conductivities of $C_{20}Me_6$ with concentration in aqueous solution.

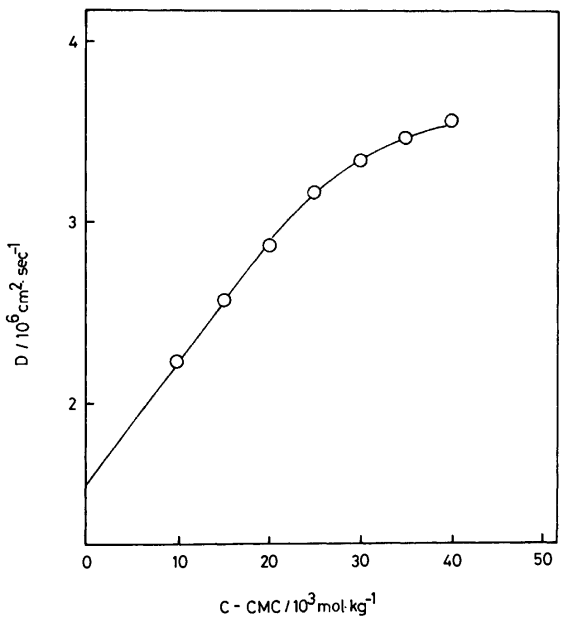

Fig. 2. Mean micellar diffusion coefficients of $C_{20}Me_6$ vs. C—cmc.

of $C_{20}Me_6$ was found to be 0.33, which is somewhat larger than that $C_{10}Me_3$. This α_{ap} value means that the minority of the fixation of the counterion is onto the micelle surface. This high value of $C_{20}Me_6$ indicates that the repulsion force between the two positive charges on trimethylammonium head for $C_{20}Me_6$ is larger than that for $C_{10}Me_3$.

Aggregation Number. From the intercept of the Debye plots at a scattering angle of 90°, the aggregation number of $C_{20}Me_6$ was found to be 18. Similarly, from a good linear relationship between $\ln(I_0/I)$ and C_q, the aggregation number of 19 was obtained by calculating the slope of this plot at the surfactant concentration 3.0×10^{-2} mol kg^{-1}. Thus, the aggregation number of $C_{20}Me_6$ obtained by static light scattering is in good agreement with that obtained by the steady-state fluorescence method. These values are nearly the half that of the aggregation number of $C_{10}Me_3$ (39—41).[22] In other words, the number of head groups per $C_{20}Me_6$ micelle is approximately the same for that of $C_{10}Me_3$ since $C_{20}Me_6$ has two head groups.

Micellar Shape. The shape of $C_{20}Me_6$ was examined by dynamic light scattering.[23,24] The initial slope, Γ, of the decay curve of the field correlation function is defined by the cumulant expansion, and the relationship between Γ and the diffusion coefficient D is generally given by

$$\frac{\Gamma}{q^2} = D_0 + \left(\frac{L^2}{12}\right)\theta f_1(q) + (D_3 - D_1)\left[f_2(q) - \frac{1}{3}\right] + \sum_m D_m a_m(q) \quad (7)$$

The first, second, third, and $\sum$ terms of right side of Eq. 7 are due to contributions of the average translational diffusion, the rotational diffusion, the anisotropy of the translational diffusion, and the motion of bending, respectively. Since the values of Γ/q^2 for each scattering angle are almost constant, terms including q are negligible. Accordingly, the constancy of Γ/q^2 profiles is only derived from the isotropy in the translational diffusion. Thus, this result supports the formation of the spherical micelles for $C_{20}Me_6$ in aqueous solution. The mean micellar diffusion coefficients (D) of $C_{20}Me_6$ are plotted against the surfactant concentration, i.e., C—cmc in Fig. 2. The D value increased with C—cmc due to significant net intermicellar repulsions. This behavior was analyzed according to the following equation:[25,26]

$$D = D_0(1 + KC), \quad (8)$$

where D_0 is the diffusion coefficient in limit of infinite dilution, i.e., extrapolated to the cmc. The radius of the $C_{20}Me_6$ micelle was estimated by using the D_0 value (1.55×10^{-6} cm^2 s^{-1}) and by the Stokes-Einstein equation,

$$D_0 = \frac{kT}{6\pi\eta R_H} \quad (9)$$

where k is Boltzmann's constant, T the absolute temperature, and η the viscosity of the solvent. The hydrodynamic radius value (R_H) of $C_{20}Me_6$ (16 Å) is smaller than that of $C_{10}Me_3$ calculated from reported results.[26] The D versus C—cmc plot for $C_{20}Me_6$ has a

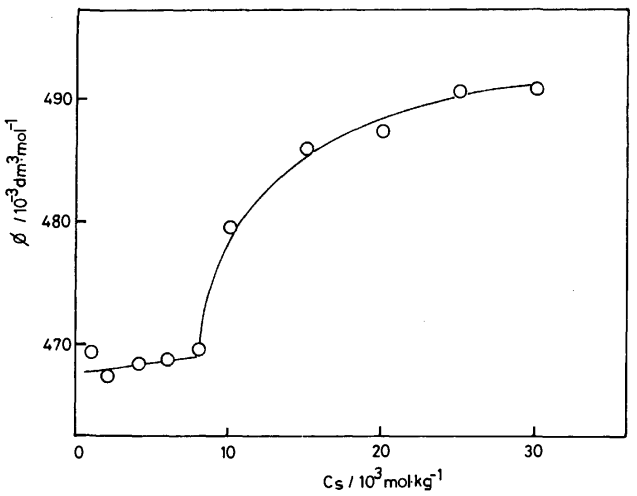

Fig. 3. Apparent molal volume of $C_{20}Me_6$ aqueous solution vs. molality of $C_{20}Me_6$.

larger slope than that for $C_{12}Me_3$.[26] This is attributed to the largeness of the ionization degree for $C_{20}Me_6$.

The partial molar volume derived from the density measurement was used to confirm the conformation of the $C_{20}Me_6$ micelle.[19] The apparent molar volumes, ϕ, are plotted against the molality in Fig. 3. This plot has a clear break, indicating the formation of the micelle of $C_{20}Me_6$. The partial molar volumes below and above the cmc were obtained with the values of 463.91 and 480.49×10^{-3} mol^{-1}, respectively.

In order to estimate the difference in micelles between α,ω-type and conventional surfactants, the surface areas occupied per head group at micelle surface(s) were calculated by some models. For this calculation, the micelle is assumed to be spherical. The superscript of "bola" means α,ω-type surfactants. Three kinds of surface areas are considered for $Br^-(C_{m''}H_{2m''+1})_3N(CH_2)_mN(C_{m''}H_{2m''+1})_3Br^-$:[21,27]

(1) s_0: s_0 is obtained by assuming a micelle radius which is equal to the length of a stretched alkyl chain, plus the length of the head group Δ, corresponding to the charged nitrogen atom and alkyl groups substituting the nitrogen atom:

$$s_0^{bola} = 4\pi[(l_H^{bola} + 2\Delta)/2]^2/2n_0. \quad (10)$$

Here, l_H^{bola} is only due to the methylene $(-CH_2-)_m$ group,

$$l_H^{bola} = 1.265m,[28,29] \quad (11)$$

and

$$\Delta = 0.42m'' + 2.1.[21,27] \quad (12)$$

Equation 12 was obtained by assuming a charged nitrogen atom at the center of a regular tetrahedron having as apexes the three carbon atoms of terminal methyl groups of the three head group alkyl chains.

Table 1. Calculated and Experimental Surface Areas per Head Group

	$C_{20}Me_6$	$C_{10}Me_3$
s_o /Å²	76.1	52.2
s_i /Å²	37.8	37.8
s_H /Å²	84.5	82.7
s_{exp}/Å²	78.0	81.3

(2) s_i: the intrinsic surface area of the head group (s_i) is taken as being that of a circular domain having a radius equal to that of a circle determined by the same three carbon atoms of the terminal methyl groups and corrected for the void space in the packing of these circular domains in a hexagonal lattice,

$$s_1 = 3.46(1.205m'' + 2.1).[2\,21] \quad (13)$$

(3) s_H: s_H is obtained assuming that a micelle radius is equal to the radius of a hydrophobic (oil drop-like) core, plus a length of the head group,[21]

$$s_H^{bola} = 4\pi(r_H + \Delta)^2/2n_0. \quad (14)$$

Zana et al.[4-6] and Broadwater et al.[3] estimated the volume occupied per (CH_2) unit of bolaform alkyl chain for C_mMe_6 (m=6, 10, 16) from density measurements. The value of 15.6×10^{-3} dm^3 mol^{-1} (25.9 Å³) per (CH_2) is adequate for a dispersed monomeric state. The volume per (CH_2) unit in the state of oil drop-like hydrocarbon should be estimated:

$$V^{bola} = 26.9m.[28,29] \quad (15)$$

The radius of the hydrophobic core, r_H, is obtained by $r_H=(3nV^{bola}/4\pi)^{1/3}$ where n is the experimental aggregation number. The calculated values of s_0, s_i, and s_H, are listed in Table 1. In Table 1 the surface areas derived from the partial molar volume, s_{exp}, are also listed. Here, the effect of counter ions on the calculated values of s_0, s_i, and s_H is not taken into consideration. The s_{exp} values for both conventional and α,ω-type surfactants were fairly greater than that of s_i, indicating that the aggregations of both $C_{10}Me_3$ and $C_{20}Me_6$ are controlled by the packing of the surfactant main alkyl chain, not by the head group packing at the micelle surface. For $C_{10}Me_3$, the s_{exp}[30] is comparable to s_H which is derived from an assumption that the moiety of the main alkyl chain is like an oil drop. Accordingly, this result supports the idea that the hydrophobic alkyl chain of $C_{10}Me_3$ takes on an oil drop-like state in the micelle. In contrast with $C_{10}Me_3$, the s_{exp} value of $C_{20}Me_6$ is comparable to that of s_0 rather than s_H. Regarding s_0 it is assumed that the main alkyl chain is stretched, and has a all-trans conformation. It is thereby suggested that the state of the hydrophobic moiety of $C_{20}Me_6$ in the micelles is as follows: the aggregation behavior of

$C_{20}Me_6$ is attributed to the packing of the main alkyl chain. It is likely that the main alkyl chains of $C_{20}Me_6$ do not exist in an oil drop-like moiety, but take on an entangled, predominantly stretched conformation in the micelles.

Polarity of the Micelle. The polarity of the micelle interior was evaluated by the solubilization of two kinds of aromatic compounds, such as pyrene and pyrene-3-carbaldehyde. The intensity ratio of the first emission peak to the third one, i.e., I_1/I_3 of pyrene, is known to be sensitive to the local polarity.[31,32] This value increases upon going from nonpolar to polar solvents. Thus, pyrene can be used as an indicator of the local polarity at the solubilization site in the micelles. In low concentrations, the I_1/I_3 value was over 1.8, indicating that the pyrene monomer is located in water. At around 8.0×10^{-3} mol kg^{-1}, corresponding to the cmc, the I_1/I_3 changed down to about 1.50. This change is attributed to the solubilization of pyrene into the micelles. Since the I_1/I_3 value for $C_{10}Me_3$ is found to be 1.42 at a surfactant concentration (0.2 mol dm^{-3}), it is considered that the pyrene exists in somewhat more polar region in comparison with the conventional surfactant. Therefore, these experimental results suggest either that the interior of the $C_{20}Me_6$ micelles is polar and loose, or that the pyrene in the $C_{20}Me_6$ micelles resides at a more external site than that in the micelles of the conventional surfactant.

The fluorescence of the pyrene-3-carbaldehyde monomer strongly depends on the solvent polarity as well as pyrene.[33] The fluorescence maximum significantly shifts to the region of lower wavelength with increasing solvent polarity, showing a linear relationship with the dielectric constant for a solvent >10.

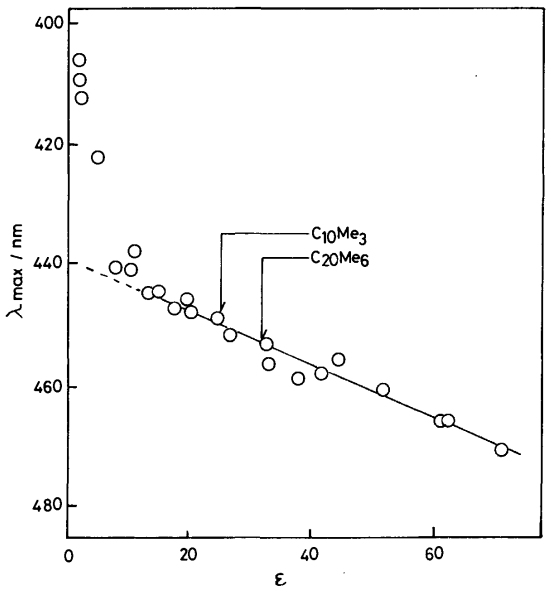

Fig. 4. Relationship between fluorescence maximum of PyCHO and solvent dielectric constant.

Owing to the effect of the solvation in the region of the aldehyde group, PyCHO is considered to be solubilized in the micellar Stern layer.[33] The dielectric constants which denote the polarity are found to be 31.3 for $C_{20}Me_6$ and 25.4 for $C_{10}Me_3$ (Fig. 4). This result indicates that the polarity in the region of the Stern layer of $C_{20}Me_6$ micelles is higher than that of $C_{10}Me_3$

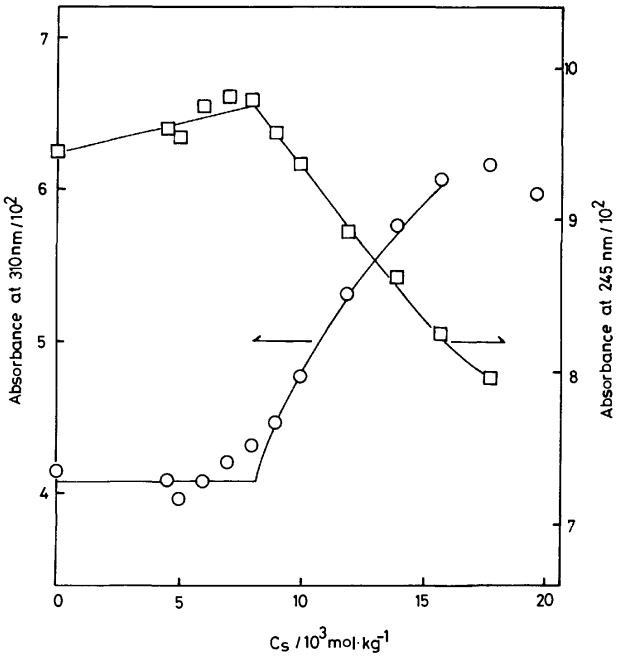

Fig. 5. Change in absorbances of BZA as a function of $C_{20}Me_6$ concentration.

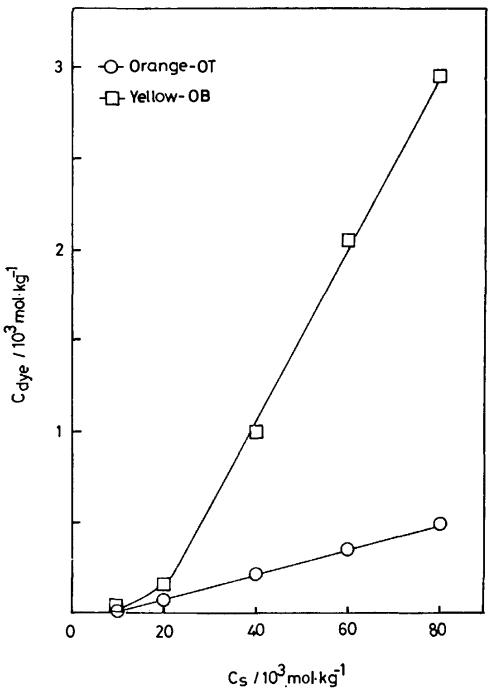

Fig. 6. Molality of Orange-OT solubilized in $C_{20}Me_6$ aqueous solution vs. $C_{20}Me_6$ concentration.

to some degree.

Solubilization of Dyes. It is known[34] that BZA exists in the enolic form in nonpolar media, whereas in the ketonic form in polar media. The change from the ketonic to the enolic form occurs when the polarity of the probe environment decreases. In Fig. 5, the absorbances of the ketonic form decrease, but the absorbances of the enolic form increase above the cmc. The distribution coefficient (α/n) between bulk and micelles is obtained by the following equation:[35]

$$\frac{1}{(C - \mathrm{cmc})} = \frac{(\varepsilon_m - \varepsilon_w)}{(\varepsilon - \varepsilon_w)} \cdot (\alpha/n) - (\alpha/n), \qquad (16)$$

where ε, ε_w, and ε_m are the molar extinction coefficient in the solution, water, and micellar media, respectively. The α/n value obtained was 80, which was somewhat lower than that of $C_{12}Me_3$, dodecyltrimethylammonium bromide (α/n=90).[35]

The molality of Orange-OT solubilized in $C_{20}Me_6$ solutions versus the surfactant concentration is plotted in Fig. 6. Above the cmc, the concentrations of Orange-OT and Yellow-OB increased linearly as the surfactant concentration increased. The solubilizing power (i.e., the number of moles of the solubilized dye per mole of micellized surfactant) was obtained from the slope of the plot. The solubilizing powers were 6.9×10^{-3} and 5.6×10^{-2} moles dye per mole surfactant for Orange-OT and Yellow-OB, respectively. These values of $C_{20}Me_6$ are nearly half that of $C_{10}Me_3$. If the solubilizing power is expressed in moles of solubilized dye per mole of head group, the values of $C_{20}Me_6$ are almost one quarter of those of $C_{10}Me_3$. Further, it has been found that hydrophobic molecules are not easily solubilized into the micelles of $C_{20}Me_6$ in comparison with the corresponding conventional surfactant, $C_{10}Me_3$. Thus, the significant low capacity of the solubilizing power in $C_{20}Me_6$ micelles can be understood on the basis of the conformation of the surfactant chains. The almost stretched conformation of the alkyl chains makes it difficult for hydrophobic compounds to be incorporated into the hydrophobic core of the micelles owing to the inability for the micelles to swell.

Conclusion

The physicochemical properties of $C_{20}Me_6$ in aqueous solution have been studied by measuring the surface tension, electrical conductivity, density, dye solubilization, fluorescence, and light scattering. Further, the properties of $C_{20}Me_6$ are compared with $C_{10}Me_3$.

At the air–water interface, $C_{20}Me_6$ has a folded, "wicket-like" conformation, whereas the micelle is nearly spherical and the main alkyl chain is almost stretched. The apparent ionization degree and the polarity of the micellar Stern layer of $C_{20}Me_6$ are larger than those of $C_{10}Me_3$.

References

1) F. M. Menger and S. Wrenn, *J. Phys. Chem.*, **78**, 1387 (1974).
2) J. R. Johnson and R. Fleming, *J. Phys. Chem.*, **79**, 2327 (1975).
3) T. L. Broadwater and D. F. Evans, *J. Phys. Chem.*, **73**, 164 (1969).
4) S. Yiv, K. M. Kale, and R. Zana, *J. Phys. Chem.*, **80**, 2651 (1976).
5) S. Yiv and R. Zana, *J. Colloid Interface Sci.*, **77**, 449 (1980).
6) R. Zana, S. Yiv, and K. M. Kale, *J. Colloid Interface Sci.*, **77**, 456 (1980).
7) S. K. Abid, S. M. Hamid, and D. C. Sherrigton, *J. Colloid Interface Sci.*, **120**, 245 (1987).
8) D. C. Mckenzie, C. A. Bunton, D. F. Nicoli, and G. Savelli, *J. Phys. Chem.*, **91**, 5709 (1987).
9) R. Zana, Y. Muto, K. Esumi, and K. Meguro, *J. Colloid Interface Sci.*, **123**, 502 (1988).
10) M. Ueno, T. Hokota, T. Mitama, and K. Meguro, *J. Am. Oil Chem. Soc.*, **49**, 250 (1972).
11) M. Ueno, S. Yamamoto, and K. Meguro, *J. Am. Oil Chem. Soc.*, **51**, 373 (1974).
12) K. Meguro, K. Ikeda, A. Otsuji, M. Taya, M. Yasuda, and K. Esumi, *J. Colloid Interface Sci.*, **118**, 372 (1987).
13) K. Ikeda, M. Ishikawa, M. Yasuda, K. Esumi, K. Meguro, W. Binana-Limbele, and R. Zana, *Bull. Chem. Soc. Jpn.*, **62**, 1032 (1989).
14) T. C. Wong, K. Ikeda, K. Meguro, O. Soderman, U. Olsson, and B. Lindman, *J. Phys. Chem.*, **93**, 4861 (1989).
15) K. Ikeda, A. Khan, K. Meguro, and B. Lindman, *J. Colloid Interface Sci.*, in accepted.
16) K. Ikeda, M. Yasuda, M. Ishikawa, K. Esumi, K. Meguro, W. Binana-Limbele, and R. Zana, *Colloid Polym. Sci.*, **267**, 825 (1989).
17) N. Turro and A. Yekta, *J. Am. Chem. Soc.*, **100**, 5951 (1978).
18) S. Atik, M. Nam, and L. Singer, *Chem. Phys. Lett.*, **67**, 75 (1979).
19) M. Drifford, L. Belloni, and M. Dubois, *J. Colloid Interface Sci.*, **118**, 50 (1987).
20) E.A. S. Cavell, *J. Chem. Soc., Faraday Trans. 2*, **80**, 447 (1984).
21) P. Lianos and R. Zana, *J. Colloid Interface Sci.*, **88**, 594 (1982).
22) P. Lianos and R. Zana, *J. Colloid Interface Sci.*, **84**, 100 (1981).
23) M. Corti and V. Degiorgio, "Solution Chemistry of Surfactants," ed by K. L. Mittal, Plenum Press, New York (1979), p. 377.
24) S. J. Candau, "Surfactant Solutions, New Methods of Investigation," ed by R. Zana, M. Dekker, New York, Chap. 3.
25) M. Corti and V. Degiorgio, *J. Phys. Chem.*, **85**, 711 (1981).
26) J. Briggs, R. B. Dorshow, C. A. Bunton, and D. F. Nicoli, *J. Chem. Phys.*, **76**, 775 (1982).
27) R. Zana, *J. Colloid Interface Sci.*, **78**, 330 (1980).
28) C. Tanford, *J. Phys. Chem.*, **76**, 3020 (1972).
29) C. Tanford, *J. Phys. Chem.*, **78**, 2469 (1974).

30) J. M. Corkill, J. F. Goodman, and T. Walker, *Trans. Faraday Soc.*, **63**, 768 (1967).
31) K. Kalyanasundaram and J. K. Thomas, *J. Am. Chem. Soc.*, **99**, 2039 (1977).
32) A. Nakajima, *Bull. Chem. Soc. Jpn.*, **50**, 2473 (1977).
33) K. Kalyanasundaram and J. K. Thomas, *J. Phys. Chem.*, **81**, 2176 (1977).
34) N. Shoji, M. Ueno, and K. Meguro, *J. Am. Oil Chem. Soc.*, **53**, 165 (1976).
35) Y. Miyaka, M. Shigeto, and M. Teramoto, *J. Chem. Soc., Faraday Trans. 1*, **81**, 2941 (1985).

 © 1989 The Chemical Society of Japan Bull. Chem. Soc. Jpn., 62, 3655—3660 (1989)

Preparation of Poly(phenylene sulfide)s: Polymerization of Aromatic Disulfides with Lewis Acids

Kimihisa YAMAMOTO, Shu YOSHIDA, Hiroyuki NISHIDE, and Eishun TSUCHIDA*
Department of Polymer Chemistry, Waseda University, Tokyo 169
(Received July 7, 1989)

Poly(*p*-phenylene sulfide) is prepared through the polymerization of diphenyl disulfide with various Lewis acids, such as $AlCl_3$ and $SbCl_5$. Thiophenol also yield poly(*p*-phenylene sulfide) through its oxidation to diphenyl disulfide in the presence of an oxidizing agent or electrolysis during polymerization. Alkyl-substituted diphenyl disulfides are polymerized with a Lewis acid to efficiently yield alkyl-substituted poly(*p*-phenylene sulfide)s such as poly(2-methyl-, 2,6-dimethyl-, and 2,6-diethylphenylene sulfide)s, with high molecular weight and solubility in common solvents.

Poly(*p*-phenylene sulfide)(PPS) has been increasingly used owing to its excellent chemical, thermal, and mechanical properties.[1-6] A commercially important preparation procedure of PPS involves the polycondensation of 1,4-dichlorobenzene and sodium sulfide in a polar solvent, such as *N*-methylpyrrolidone, at high temperature and pressure.[7-9] Much effort has been consumed in the modification of the synthetic routs for PPS. It has been reported that PPS can also be prepared by the polycondensation of metal *p*-halobenzenethiolate at ca. 350 °C.[10-15] High-temperature conditions are required to increase the reactivity of the monomer in the formation of high-molecular PPS. However, the polycondensation of alkyl-substituted monomers does not provide PPSs with high molecular weight, even at high temperatures. Few papers have reported on the preparation of substituted poly(phenylene sulfide)s.[16,17]

We have reported that diphenyl disulfide as a monomer reacts with Lewis acid to cleave its S-S bond and is easily polymerized to a linear PPS at room temperature and atmospheric pressure.[18-20] In this study, alkyl-substituted diphenyl disulfides were applied for this polymerization in order to prepare the corresponding poly(alkylsubstituted phenylene sulfide)s with high molecular weight. The polymerization behavior of the diphenyl disulfides with Lewis acids and the structure of the formed polymers are described.

Experimental

Materials. Diphenyl disulfide was purified by two recrystallization processes from ethanol-water and dried in vacuo for 1 day at 30 °C, producing a white needles: mp 59 °C. Thiophenol was distilled twice under reduced pressure and stored under nitrogen atmosphere. Bis(2-methylphenyl) disulfide, bis(2-methoxyphenyl) disulfide, bis(2,6-dichlorophenyl) disulfide, bis(4-methylphenyl) disulfide, di(2-naphthyl) disulfide, and dibenzyl disulfide were prepared through the oxidation of the corresponding thiophenols with I_2 in alkaline methanol and used through recrystalized twice before use. Bis(2,6-dimethylphenyl) disulfide and bis(2,6-diethylphenyl) disulfide were prepared by a Leuckart reaction from 2,6-dimethylaniline and 2,6-diethylaniline, as the starting material, respectively.[21] Bis(2,6-dimethoxyphenyl) disulfide was obtained by the oxidation of 2,6-dimethoxythiophenol prepared through the reported method from *m*-dimethoxybenzene.[22] The prepared diphenyl disulfides were recrystallized with analytical purity. Bis(2,6-dimethylphenyl) disulfide: ^{13}C NMR ($CDCl_3$), δ=21 (methyl C); 128, 129, 131, 143 (phenyl C). ^1H NMR ($CDCl_3$), δ=2.2 (methyl 6H); 7.0 (phenyl 3H). IR (KBr, cm^{-1}) 2900, 2960, 3040 (ν_{C-H}); 1460 ($\nu_{C=C}$); 760 (δ_{C-H}). Bis(2,6-diethylphenyl) disulfide: ^{13}C NMR ($CDCl_3$) δ=15, 28 (ethyl C); 126, 130, 134, 150 (phenyl C). ^1H NMR ($CDCl_3$) δ=1.1, 2.8 (ethyl 10H); 7.1 (phenyl 3H). IR (KBr, cm^{-1}), 2960, 3050 (ν_{C-H}); 1460 ($\nu_{C=C}$); 750 (δ_{C-H}). Bis(2-methyl-6-chlorophenyl) disulfide: ^{13}C NMR ($CDCl_3$), δ=22 (methyl C); 128.7, 128.7, 130.3, 134.3, 140.7, 145.2 (phenyl C). IR (KBr, cm^{-1}) 2926, 2962 (ν_{C-H}); 1400, 1500 ($\nu_{C=C}$); 745, 860 (δ_{C-H}). 2,6-Dimethoxythiophenol: white needle-like solid, ^{13}C NMR ($CDCl_3$) δ=57 (methoxy C); 125, 131, 133, 162 (phenyl C). ^1H NMR ($CDCl_3$) δ=6.8 (phenyl 3H); 3.9 (methoxyl 6H); 3.7 (mercapto H). IR (KBr, cm^{-1}) 2960, 3040 (ν_{C-H}); 2592 (ν_{S-H}); 1460 ($\nu_{C=C}$); 740 (δ_{C-H}).

Guaranteed reagents of Lewis acids and oxidizing agents were used without further purification and under a dry nitrogen atmosphere. Dichloromethane, 1,1,2,2-tetrachloroethane, nitromethane, and nitrobenzene as the polymerization solvents were purified by distillation in the usual manner.

Measurements. ^1H NMR and ^{13}C NMR spectra were measured of a 90-MHz JEOL FX-100. IR spectroscopy was carried out on a JAS IR-810 model spectrometer. Mass spectra were measured on a JMS-DX300 model spectrometer at an ionization energy of 20 eV.[23] Melting points were determined on the stage of a microscope at a heating rate of 2 °C min^{-1}. DSC measurements were carried out on a SEIKO thermal analyzed model SSC/500 with a heating rate of 20 °C min^{-1}. The molecular weight of the benzene-soluble part of PPS was measured by vapor pressure osmometry.

Polymerization Method. The typical experiment can be described as follows: 0.1 mol l^{-1} of diphenyl disulfide was dissolved in 50 ml of nitromethane and was poured into 50 ml of nitromethane containing Lewis acid kept at 20 °C under nitrogen atmosphere for 20 h. The reaction mixture color changed to deep black from yellow. After the polymerization, the reaction mixture was poured into 500 ml of methanol with 5% hydrogen chloride to precipitate a polymeric material. The polymer was purified according to the previously reported procedure.[18-20] The purified polymer

was not mixed with Lewis acid metal of more than 200 ppm according to an analysis by inductively coupled plasma emission spectroscopy. Polymerization of thiophenol (0.2 mol l^{-1}) was similarly carried out in the coexistence of an oxidizing agent (0.1 mol l^{-1}).

Electrolysis. A pair of platinum plates (2×5 cm) was placed in the cell with a 1 cm spacing as the working and auxiliary electrodes. The reference electrode was Ag/AgCl. A nitromethane solution of thiophenol (0.1 mol l^{-1}) contained Lewis acid and was kept at 20 °C under a nitrogen atmosphere. The preparative electrolysis was carried out under a controlled potential at 1.5 V with a NIKKO KEISOKU NPGS-301 potentiogarvanostat. The electrolysis was turned off at 5 F mol^{-1}.

Spectroscopic Data of the Formed Polymers. Poly(*p*-phenylene sulfide): Calcd for (C_6H_4S): C, 66.67; H, 3.7; S, 29.63%. Found: C, 66.51; H, 3.81; S, 29.44%. IR(KBr, cm^{-1}) 3025(ν_{C-H}); 1395, 1480, 1580($\nu_{C=C}$); 820(δ_{C-H}); 480, 560, 740, 1015, 1080, 1110. MS (*m/z*) 756, 684, 540, 434. X-Ray diffraction pattern 2θ=19, 21.

Poly(2-methylphenylene sulfide): Calcd for (C_7H_6S): C, 68.85; H, 4.92; S, 26.23%. Found: C, 68.50; H, 4.77; S, 25.92%. IR (KBr, cm^{-1}) 2920, 2950, 2980, 3050 (ν_{C-H}); 1440, 1460, 1580 ($\nu_{C=C}$); 820, 880 (δ_{C-H}); 760, 1050, 1100, 1200, 1380. ^{1}H NMR ($CDCl_3$), δ=2.3 (methyl 3H); 7.1 (phenyl 3H). ^{13}C NMR ($CDCl_3$), δ=21 (methyl C); 127, 130, 131, 134, 136, 141 (phenyl C). NMR signals of methylene proton and carbon were not detected at δ=3.6 and 60, respectively. MS (*m/z*) 612, 490, 368.

Poly(2,6-dimethylphenylene sulfide): Calcd for (C_8H_8S): C, 70.54; H, 5.92; S, 23.54%. Found: C, 70.06; H, 5.97; S, 23.21%. IR and ^{13}C NMR spectra were shown in Figs. 1 and 2. ^{1}H NMR ($CDCl_3$), δ=2.3 (methyl 6H); 7.1 (phenyl 2H). MS (*m/z*) 682, 544, 408.

Poly(2,6-diethylphenylene sulfide): Calcd for ($C_{10}H_{12}S$): C, 73.12; H, 7.36; S, 19.52%. Found: C, 73.05; H, 7.41; S, 19.46%. IR (KBr, cm^{-1}) 2950, 2980, 3050 (ν_{C-H}); 1460, 1560 ($\nu_{C=C}$); 800, 860 (δ_{C-H}); 1020, 1060, 1160, 1320, 1370. ^{1}H NMR ($CDCl_3$), δ=1.25 (methyl 6H); 2.7 (methylene 4H); 7.0 (phenyl 2H). ^{13}C NMR ($CDCl_3$), δ=16 (methyl C); 28 (methylene C); 127, 131, 143, 150 (phenyl C). NMR signals of methylene proton and carbon were not detected at δ=3.6 and 60, respectively. MS (*m/z*) 658, 492.

Poly(2-methoxyphenylene sulfide): Calcd for (C_7H_6SO): C, 60.87; H, 4.35%. Found: C, 60.02; H, 4.62%. IR (KBr, cm^{-1}) 2880 (ν_{C-H}); 1420, 1480, 1580, 1600 ($\nu_{C=C}$); 1180 (ν_{C-O-C}); 840, 880 (δ_{C-H}); 720, 1030, 1070, 1270.

Poly(2,6-dimethoxyphenylene sulfide): Calcd for ($C_8H_8SO_2$): C, 54.14; H, 4.76%. Found: C, 55.23; H, 4.86%. IR (KBr, cm^{-1}) 2870 (ν_{C-H}); 1370, 1470, 1600 ($\nu_{C=C}$); 1180 (ν_{C-O-C}); 820 (δ_{C-H}); 480, 1040, 1210, 1280.

Poly(2-methyl-6-chlorophenylene sulfide): Calcd for (C_7H_5SCl): C, 53.67; H, 3.19%. Found: C, 53.25; H, 3.21%. IR (KBr, cm^{-1}) 2870 (ν_{C-H}); 1440, 1560, 1580 ($\nu_{C=C}$); 820, 860 (δ_{C-H}); 720, 740, 780, 1000, 1100, 1180, 1380. ^{13}C NMR ($CDCl_3$), δ=22.0 (methyl C); 122.8, 128.3, 129.2, 130.4, 137.3, 145.7 (phenyl C).

Poly(thiomethylene phenylene): Calcd for (C_7H_6S): C, 68.85; H, 4.92; S, 26.23%. Found: C, 67.81; H, 5.10; S, 25.98%. IR (KBr, cm^{-1}) 3100 (ν_{C-H}); 1410, 1440, 1450, 1500, 1600 ($\nu_{C=C}$); 810 (δ_{C-H}); 465, 700, 760, 900, 1020, 1080, 1260, 1350.

Poly(naphthylene sulfide): Calcd for ($C_{10}H_6S$): C, 75.95; H, 3.80; S, 20.25%. Found: C, 76.12; H, 3.51: S, 19.34%. IR (KBr, cm^{-1}) 1500, 1550, 1580, 1620 ($\nu_{C=C}$); 820, 870 (δ_{C-H}); 480, 540, 740, 780, 960, 1080, 1120, 1260, 1320, 1350.

Isolation of Thianthrene. The reaction mixture was poured into methanol. The methanol solution was evaporated to dryness after the precipitate was separated out. The product was extracted with chloroform from the residue. The thianthrene formation was confirmed by gass cromatography and ^{13}C NMR spectroscopy. ^{13}C NMR ($CDCl_3$), δ=127.4, 128.6, 135.5. IR (KBr, cm^{-1}) 3050 (ν_{C-H}); 1430, 1550 ($\nu_{C=C}$); 760 (δ_{C-H}); 460, 660, 1250, 1100. MS (*m/z*) 108, 139, 171, 184, 216.

^{13}C NMR Spectrum of the Reaction Mixture. The ^{13}C NMR spectra of disulfides with $SbCl_5$ were measured at −30 °C in double compartment cell probes of which internal and standard sample was CD_3OD/tetramethylsilane. ^{13}C NMR (CH_2Cl_2, phenyl carbon); the reaction mixture of diphenyl disulfide: δ=127.4, 132.8, 135.9, 136.4. Diphenyl disulfide: δ=128.4, 128.8, 130. 9, 138.1. The reaction mixture of bis(2-methylphenyl) disulfide: δ=129.2, 131.4, 131.7, 132.3, 132.9, 140.7. Bis(2-methylphenyl) disulfide: δ=127.9, 128.4, 128.5, 132.0, 136.3, 132.0. The reaction mixture of bis(2,6-dimethylphenyl) disulfide: δ=131.1, 131.4, 134.3, 145.8. Bis(2,6-dimethylphenyl) disulfide: δ=129.6, 131.0, 135.9, 144.9.

Results and Discussion

Polymerization of Diphenyl Disulfides. Diphenyl disulfide was allowed to react with aluminum trichloride at room temperature in nitromethane. The

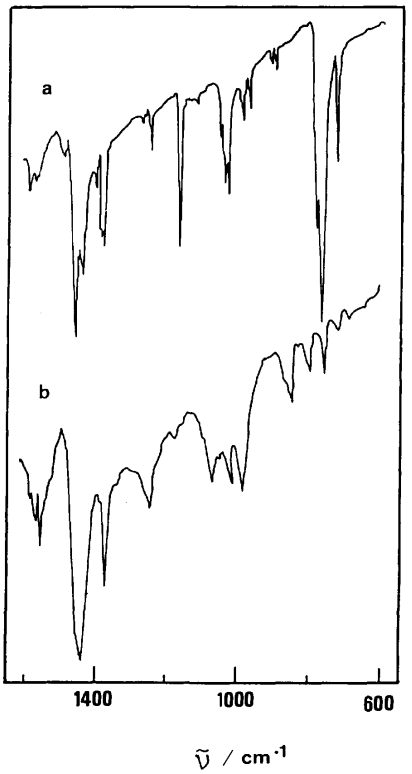

Fig. 1. IR spectra of bis(2,6-dimethylphenyl) disulfide (a) and the formed polymer through the polymerization of bis(2,6-dimethylphenyl) disulfide (*b*).

Table 1. Polymerization[a] of Diphenyl Disulfides with $AlCl_3$

Polymer	Polymer yield	$CHCl_3$-insoluble Mp	$CHCl_3$-soluble Mp	M_n	Lenz's method[b] Mp	M_w	Port's method[c] Mp	M_w
	wt%	°C	°C		°C		°C	
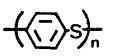	51	213	90	450	250—280	3000	280—285	—
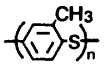	35	240	140	3800	60—120	1550	140—150	5400
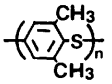	81	245	170	4300	140—180	2500	218	8270
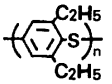	86		195	10000	—	—	—	—

a) 100 h. b) . c) .

polymer was formed as a white powder having an empirical formula C_6H_4S and was soluble in hot *N*-methylpyrrolidone. The spectroscopic data agreed with that of a commercially available product. Polymerization of bis(2-methylphenyl) disulfide with $AlCl_3$ gave a polymer whose IR spectrum and other spectroscopic data agreed with the prepared poly(2-methyl-1,4-phenylene sulfide) by the polycondensation of sodium 4-bromo-2-methylbenzenethiolate.

The absorption bands at 820 and 880 cm^{-1} were attributed to the adjacent 2H of the C–H out-of-plane vibration and to the isolated 1H, respectively, which supports the 1,4-conjugated thiophenylene. Bis(2,6-dimethylphenyl) disulfide was also polymerized to give the polymer. The formed polymer also showed absorption bands at 860 and 820 cm^{-1}, which supported the belief that the polymer does not only contain the 1,4-conjugated thiophenylene structure, but 1,3-conjugated as well (Fig. 1). Bis(2,6-diethylphenyl) disulfide was also polymerized to form a polymer with a molecular weight of 4×10^4—1×10^3. The elemental analysis data of the formed polymer agreed with the calculated values for poly(2,6-diethylphenylene sulfide). The IR spectrum of the polymer supported the structure of poly(2,6-diethylphenylene sulfide). The complete polymerization of bis(2,6-diethylphenyl) disulfide was also indicated by a decrease in the absorption band at 760 cm^{-1} attributed of an adjacent 3H C–H out-of-plane vibration on the monomer. NMR spectra also supported the idea that the formed polymer dose not combine through a thiomethylene moiety but, through a thiophenylene moiety (Fig. 2).

These polymers were quite soluble in chloroform, benzene, *N*-methylpyrrolidone, *N*,*N*-dimethylformamide. The substituent groups on the phenylene ring of PPS greatly increased the solubility of PPS and expanded its application potential. The melting points of polymers were much higher than those of polymers prepared by the conventional polycondensation (Table 1). The substituent alkyl groups drastically increased the solubility of the polymer providing the polymer with a high molecular weight.

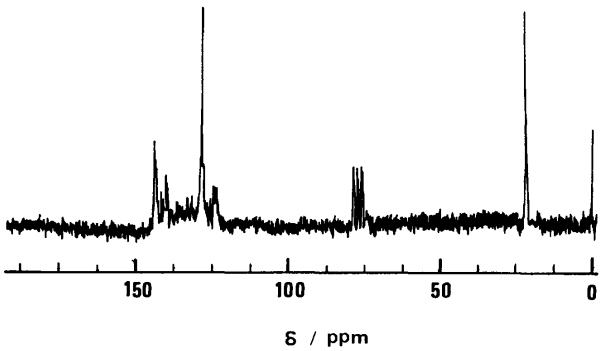

Fig. 2. ^{13}C NMR spectra of the chloroform-soluble part of the formed polymer through the polymerization of bis(2,6-dimethylphenyl) disulfide.

Table 2. Polymerization of Various Aromatic Disulfides with $AlCl_3$

Sulfide monomer[a] R1	R2	R3	Yield wt%	Mp °C
$-OCH_3$	-H	-H	46	270
$-OCH_3$	$-OCH_3$	-H	8	113
$-CH_3$	-Cl	-H	73	214
-Cl	-Cl	-H	0	—
-H	-H	$-CH_3$	0	—
-H	-H	$-C(CH_3)_3$	0	—
Dibenzyl disulfide			89	253
Dinaphthyl disulfide			91	188

a) 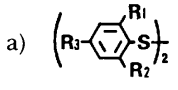 .

Various diphenyl disulfide derivatives such as dibenzyl disulfide, bis(2-methoxyphenyl) disulfide, and di(2-naphthyl) disulfide were also polymerized with aluminum chloride to yield the corresponding

PPS derivatives in high yield (Table 2). Alkylsubsituted PPSs were also efficiently produced by polymerization. Thus, the polymerization route of diphenyl disulfides with Lewis acid is a convenient procedure for the preparation of PPS and poly(aromatic sulfide)s. However, *p*-substituted and bis(2,6-dichlorophenyl) disulfide were not allowed to give the corresponding polymers. Electron-withdrawing substituents and the positions of substituents influenced the polymerization.

Polymerization Mchanism. In previous papers[18,20] we concluded that the sulfonium cation is the active species for the polymerization of diphenyl disulfide, based on ^{13}C NMR and the isolation of the sulfonium cation as a salt. The ^{13}C NMR spectrum of the reaction mixture of bis(2-methylphenyl) disulfide and bis(2,6-dimethylphenyl) disulfide at −30 °C shows signals which were not assigned to the corresponding disulfides and the other sulfides (Experimental section). In this experiment the phenylbis(phenylthio)sulfonium cation was formed with the Lewis acid.

Figure 3 shows polymerization curves for the diphenyl disulfides. The melting point which corresponds to the molecular weight of the polymer, increased after the polymer yield became constant. The formed polymer or oligomer re-reacted with Lewis acid to form PPS. This means that the polymerization proceeds in a stepwise fashion to yield PPS. It is considered that the cation electrophilically reacts with diphenyl disulfide to form the trimer. The polymerization mechanism of diphenyl disulfide is illustrated in Eq. 1. Poly(methyl-substituted phenylene sulfide)s were rapidly formed on the polymerization in comparison with PPS because of the electron-donating substituents. The results also supported the cationic mechanism.

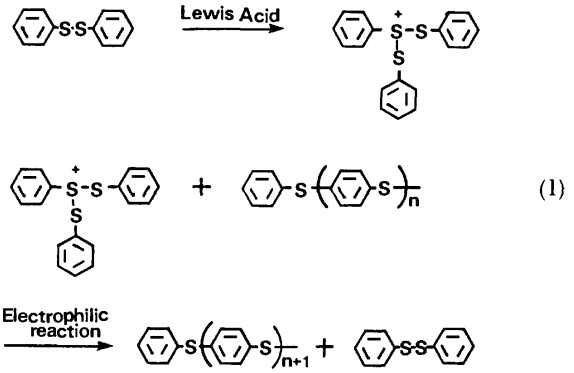

(1)

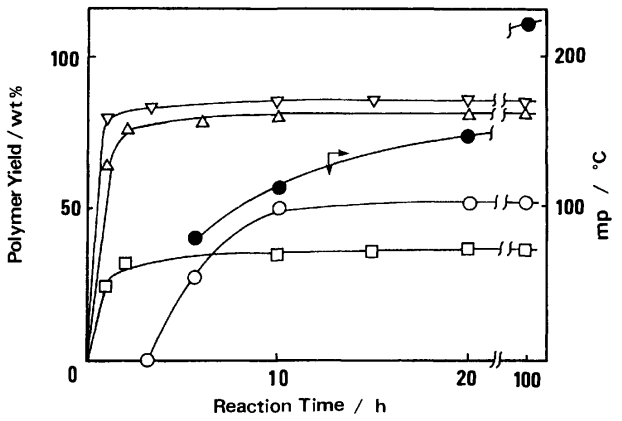

Fig. 3. Polymerization curves of bis(2-methylphenyl) disulfide (□), bis(2,6-dimethylphenyl) disulfide (△), bis(2,6-diethylphenyl) disulfide (▽), and diphenyl disulfide (○); melting point of the formed polymer from diphenyl disulfide (●).

Polymerization with Various Lewis Acids. Polymerization proceeded with various Lewis acids such as $SbCl_5$, $MoCl_5$, and $TiCl_4$, although the PPS yield and/or molecular weight were influenced by Lewis acid and the solvent species (Table 3).

The PPS yield remained at about 50% for the polymerization of diphenyl disulfide, and decreased with an increase in the temperature (Fig. 4). Gaseous mass spectroscopy of the reaction mixture indicated the formation of thianthrene. Thianthrene was isolated and confirmed by the results of NMR and IR spectroscopy (Experimental section). Thianthrene was formed as a by-product during polymerization. In contrast, the polymerization of bis(2,6-substituted phenyl) disulfides gave their polymers with relatively high yield in comparison with those of bis(mono- and unsubstituted phenyl) disulfides (Fig. 4). 2,6-Dialkyl-substituents does not only increased the solubility of the formed polymer, but also strongly suppressed the formation of thianthrene by the side reaction, and gave a polymer with high molecular weight and high yield. These results suggested that the temperature influenced the reaction of diphenyl disulfide with $AlCl_3$. That is, the high temperature resulted in the forma-

Table 3. Polymerization[a] of Diphenyl Disulfide with Lewis Acids

Solvent		$AlCl_3$	$TiCl_4$	$FeCl_3$	$MoCl_5$	$SbCl_5$	$BF_3{\cdot}O(C_2H_5)_2$	$SnCl_4$
$C_6H_5NO_2$	Yield/wt%[b]	31	96	60	29	28	0	0
	Mp/°C	180	183	150	207	194	—	—
CH_3NO_2	Yield/wt%	50	67	93	9	89	59	0
	Mp/°C	135	139	139	108	191	119	—
$(CHCl_2)_2$	Yield/wt%	36	0	42	60	67	0	0
	Mp/°C	124	—	104	115	140	—	—

a) 20 °C, 20 h, [Monomer]=0.1 mol l^{-1}, [Lewis Acid]=0.1 mol l^{-1} ($SbCl_5$, $MoCl_5$, $FeCl_3$), 1.0 mol l^{-1} (other Lewis acids). b) PPS yield.

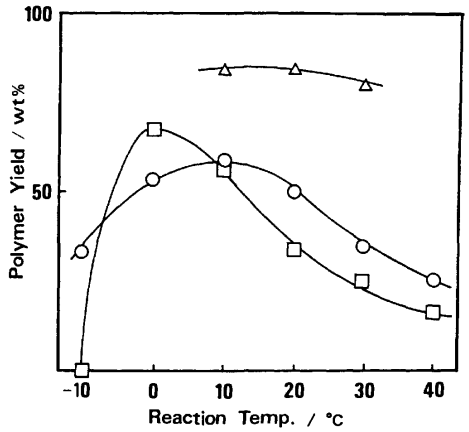

Fig. 4. Effect of the temperature on the polymerization of bis(2-methylphenyl) disulfide (□), bis(2,6-dimethylphenyl) disulfide (△), and diphenyl disulfide (○).

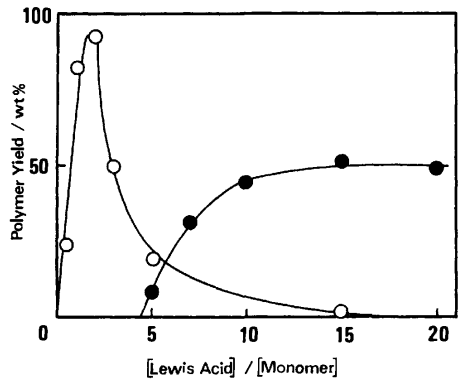

Fig. 5. Effect of the concentration of Lewis acid on the polymerization of diphenyl disulfide. $AlCl_3$ (●), $SbCl_5$ (○).

tion of thianthrene, the result of which was corresponded to the previously reported polymerization.[24-28]

The optimum concentration of $SbCl_5$, $MoCl_5$, and $FeCl_3$ is two times equimolar of diphenyl disulfide in this polymerization. In contrast, $AlCl_3$, $TiCl_4$, and $BF_3 \cdot O(C_2H_5)_2$ required more than ten times equimolar of the monomer for an efficient formation of PPS (Fig. 5). These results support the difference in the initiation mechanism of the polymerization or initiation efficiency, which was based on the difference of the oxidation ability between $AlCl_3$ and $SbCl_5$.[29,30] The melting point of the polymer increased during polymerization with $AlCl_3$ in nitromethane after the polymer yield became constant. This means that the polymerization proceeds in a stepwise manner to grow the polymer. It is considered that an increase in the molecular weight of the polymer caused by an increase in the polymer solubility on the basis of the formation of a polymer complex with $AlCl_3$ in the presence of excess $AlCl_3$.[31]

Polymerization of Thiophenol. It is well-known that thiophenol is quantitatively oxidized to diphenyl disulfide with oxidizing agents.[32,33] The polymerization of thiophenol as a starting material was carried out in the coexistence of an oxidizing agent and $AlCl_3$ to also give PPS (Table 4). This suggests that thiophenol is preferentially oxidized to diphenyl disulfide and polymerized with $AlCl_3$ without any retardation by oxidizing agents. Electrolysis was applied to the oxidation process on the polymerization instead of oxidizing agents. PPS was also precipitated in the electrolysis cell and on the electrode.

Table 4. Polymerization[a] of Thiophenol with Lewis Acid through the Oxidation

Oxidizing agent	Solvent	Polymer yield	Mp
		wt%	°C
I_2	CH_3NO_2	85	142
	$C_6H_5NO_2$	48	192
$CuCl_2$	CH_3NO_2	70	164
	$C_6H_5NO_2$	52	169
Chloramine B[b]	CH_3NO_2	35	178
	$C_6H_5NO_2$	Trace	—
$SOCl_2$	CH_3NO_2	88	189
	$C_6H_5NO_2$	Trace	—
Electrolysis	CH_3NO_2	87	193

a) 20 h. b) $C_6H_5SO_2NNaCl$.

This work was partially supported by a Grant-in-Aid for Scientific Research on Priority Area of "Macromolecular Complexes" from the Ministry of Education, Science and Culture.

References

1) R. T. Howkins, *Macromolecules*, **9**, 189 (1976).
2) G. F. Ehlers, K. R. Fisch, and W. R. Powell, *J. Polym. Sci. Part A-1*, **7**, 2955 (1969).
3) D. G. Brady, *J. Appl. Polym. Sci.*, **36**, 231 (1981).
4) R. L. Elsenbaumer, L. W. Shacklette, J. W. Sowa, and R. H. Baughmam, *Mol. Cryst. Liq. Cryst.*, **83**, 229 (1982).
5) L. W. Shacklette, R. L. Elsenbaumer, R. R. Chance, H. Eckhardt, J. E. Formmer, and R. H. Baughman, *J. Phys. Chem.*, **75**, 1919 (1981).
6) F. Bertinelli, P. C. Bizzarri, C. D. Casa, and S. J. Saltini, *J. Polym. Sci., Polym. Phys. Ed.*, **24**, 2197 (1986).
7) J. T. Edomonds Jr. and H. W. Hill Jr., U.S. Patent, **1967**, 3354129; *Chem. Abstr.*, **68**, 13598 (1968).
8) R. W. Cambell and J. T. Edmonds, U.S. Patent, **1975**, 4038259; *Chem. Abstr.*, **87**, 10285v (1977).
9) M. Koch and W. Heitz, *Makromol. Chem.*, **184**, 779 (1983).
10) R. W. Lenz, C. E. Handlovits, and W. K. Carrington, *J. Polym. Sci.*, **43**, 333 (1959).
11) R. W. Lenz and C. E. Handlovits, *J. Polym. Sci.*, **43**, 167 (1960).
12) R. W. Lenz, C. E. Handlovit, and H. A. Smith, *J. Polym. Sci.*, **58**, 351 (1962).
13) C. E. Handlovit, *Macromol. Synth.*, **3**, 131 (1968—1969).
14) H. A. Smith, C. E. Handlovit, "Phenylene Sulfide Polymers," ASD-TDR 62-322", Part, I II, (1962).

15) A. D. Macallum, *J. Org. Chem.*, **13**, 154 (1949).
16) A. B. Port and R. H. Still, *J. Appl. Polym. Sci.*, **24**, 1145 (1979).
17) S. Tsunawaki and C. C. Price, *J. Polym. Sci., Part A*, **2**, 1511 (1964).
18) E. Tsuchida, K. Yamamoto, H. Nishide, and S. Yoshida, *Macromolecules*, **20**, 2030 (1987).
19) E. Tsuchida, H. Nishide, K. Yamamoto, and S. Yoshida, *Macromolecules*, **20**, 2315 (1987).
20) E. Tsuchida, K. Yamamoto, H. Nishide, S. Yoshida, and M. Jikei, *Macromolecules*, **23**, 1136 (1990).
21) J. R. Cox, Jr., C. L. Gladys, L. Field, and D. E. Pearson, *J. Org. Chem.*, **25**, 1083 (1960).
22) B. M. Trost and L. N. Jungheim, *J. Am. Chem. Soc.*, **102**, 7910 (1980).
23) G. Montaudo, C. Puglish, E. Scamporrino, and Vitalini, *Macromolecules*, **19**, 2157 (1986).
24) M. Wejchan-Judek, E. Pogalond, and A. Zuk, *Polymer*, **22**, 845 (1981).
25) M. Wejchan-Judek and E. Rogal, *Polymer*, **25**, 53 (1984).
26) A. Zuk, M. Wejchan-Judek, and E. Rogal, *Polymer*, **19**, 438 (1978).
27) V. A Sergeyev and V. I. Nedelkin, *J. Polym. Sci., Polym. Chem. Ed.*, **24**, 3153 (1986).
28) J. W. Cleary, *Polym. Sci. Technol.* (Plenum) **1985**, 159.
29) G. A. Olah, "Friedel-Crafts and Related Reaction," Interscience (1964).
30) S. Santini, G. Reichenbach, and V. Mazzucato, *J. Chem. Soc., Perkin Trans. 2*, **1974**, 494.
31) J. E. Frommer, *Acc. Chem. Rev.*, **19**, 2 (1986).
32) F. Magno, G. Bontompelli, and G. Pillon, *J. Electroanal. Chem.*, **30**, 357 (1971).
33) J. T. Wallance and A. Schriesheim, *Tetrahedron*, **21**, 2271 (1965).

 © 1989 The Chemical Society of Japan Bull. Chem. Soc. Jpn., 62, 3661—3665 (1989)

Potential Distribution in a Fluidized Bed Electrode

Tülay Eskikaya
Chemistry Department, Istanbul Technical University, Maslak 80626, Istanbul, Turkey
(Received January 23, 1989)

A study is described on the measurements of potential distribution in the bed and electrolyte of a hydrogen peroxide depolarized fluidized bed electrode consisting of 10 grams of silver coated glass beads in a cell of cyclindrical geometry. The results of potential profiles show that the electrode potentials both in static and fluidized beds were uniform throughout most of the bed. In the latter case, however, the degree of deactivation in the top of the bed is less than for a static bed, which explains current from fluidized bed. The variation of the charge-transfer coefficient along the bed, which is of great importance from the point of the performance of a fluidized bed electrode, is also determined.

In order to understand the functioning of a fluidized bed electrode, the potential distribution in the bed and electrolyte is of great importance. Some work has been done on this line before.[1-8] A direct measurement of electrode potentials was suggested by Backhurst,[1] by means of a pseudo-particle. Hiddleston and Douglas[2,3] recorded bead potentials with respect to the feeder by using a similar probe to that suggested by Backhurst. Mason,[4,5] on the other hand, recorded the frequency of the collisions on the free beads with the pseudo-bead per unit time and the variation in probe potentials as a result of the collisions. A mathematical model for the charge transfer in fluidized bed electrodes was developed by Goodridge et al.[6] Huh[7] also measured the particle and electrolyte potentials and overvoltages in fluidized bed electrodes of two different types. Rojo et al.[8] developed a capacitor model to determine the electric change in fluidized beds on the basis of voltage measurements between a probe and a metallic distributor. Many new contributions by the others, however, are still continuing on the same subject.

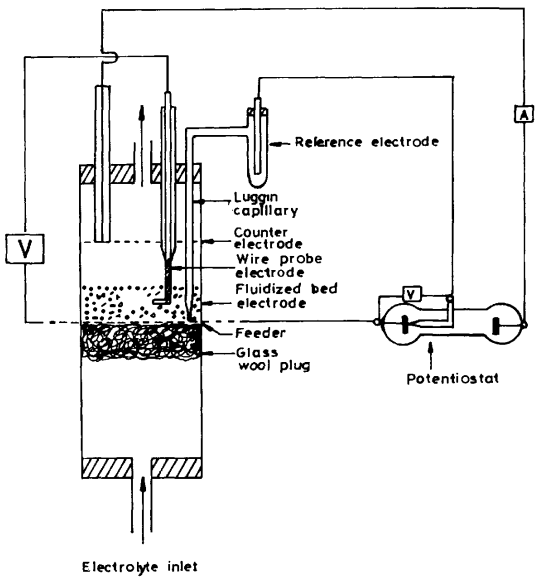

Fig. 1. Experimental cell and potentiostat.

Experimental

Fluidized Bed Material and Catalyst. Potential distribution measurements in the solution and in the bed were studied for a hydrogen peroxide depolarized fluidized bed electrode. The concentrations of the reactant and the electrolyte used during the measurements were 4.1×10^{-2} mol dm^{-3} hydrogen peroxide and 5.0 mol dm^{-3} KOH, respectively.

The body of fluidized beds consisted of "Ballotini" glass beads (mean diameter 600 μm, diameter range 520—690 μm) coated with silver from a solution containing it in the form of ammonia complex and to reduce ammonia complex glucose was used.[9,10] The silver layer acted as both a conducting surface and catalyst. The final mean density of the beads 3.0 g cm^{-3} and the geometric area 33 $cm^2\,g^{-1}$.

Apparatus. The experimental cell system which was used with a potentiostat power supply is shown in Fig. 1. It consisted of two lengths of 2.54 cm dia., Perspex tube joined with an expanded silver coated nickel mesh (strand size 0.00127×0.00127 cm; 772 appertures per cm; mesh 9.8 LWM ×17.7 SWM per cm; free area 60%) stretched between the two sections. A glass wool plug beneath the mesh smoothed the electrolyte flow through the bed. The mesh acted as bed support and electrical contactor to the beads. A nickel mesh counter electrode was situated above the bed. A mercury-mercurly(II) oxide reference electrode was connected to a Luggin capillary, the tip of which was adjacent to the feeder, thus, the feeder potential was controlled.

Other equipments used included an Amel potentiostat capable of giving 10 A at 50 V and a Solartron high impedance voltmeter having a voltage input ranging from ±0.1995 V to 1995 V for measurements of the bed and solution potentials with secondary probes. A Pye cathetometer (accuracy ±0.005 mm) was used to measure bed heights.

Solutions were made up from Analar grade reagents using once-distilled water.

Experimental Procedure. The weight of the bed was 10 g, giving a mean static bed height of 1.16 cm. Fluidizations are quoted as a percentage increase in bed height over the static bed height.

(a) Potential Distribution in the Electrolyte. Potential distribution in the solution within the bed was measured by means of a Luggin capillary which was connected to a mercury-mercury(II) oxide reference electrode. The Luggin capillary was traversed up and down through the bed and at various Luggin capillary positions, solution potentials, ϕ_s,

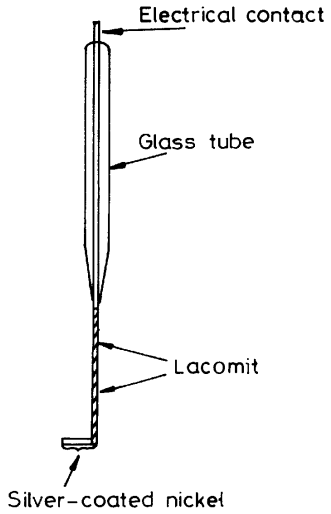

Fig. 2. Wire probe design.

were measured against the feeder.

(b) Potential Distribution in the Bed. For the potential distribution measurements in the bed two different types of probes namely, bead and wire probes were used. The bead probes were prepared by attaching a bead of bed material (600 μm dia. silver plated glass bead) to a nickel wire (0.39 mm dia.) by means of a silver impregnated epoxy resin adhesive (J.M.C. Thermosetting silver cement FSP 49). The wire was insulated from the bed by coating with "Lacomit" varnish. This type of probe was found to be unsatisfactory. A simpler method was adopted, therefore, in which a nickel wire was sealed into a glass road leaving the top end free as electrical contact and the other end of this wire probe, which was bended through 90° providing a horizontal section, acted as pseudo-bead[1,4] (Fig. 2). This pseudo-bead could be made of any area by coating the wire with Lacomit and leaving the correct amount of bare wire projecting. Any oxide film on nickel wire probe was removed by immersing it in dilute hydrochloric acid and then nickel wire was coated with silver in the same way as the plating of the beads. By coupling a Solatron high-impedance voltmeter between the probe and the feeder, it is possible to measure the bead potentials, ϕ_m, which are the potentials detected by the pseudo-bead probe electrode against the feeder electrode.

In order to find the optimum area of the pseudo-bead which would provide the actual potential of beads, potential distribution measurements in the bed were recorded with four different size of wire probes, namely "tip, small, medium and large" having surface areas of silver activated part of 0.477 mm², 1.528 mm², 3.820 mm², and 12.990 mm², respectively.

Results

In Fig. 3 distribution of the solution potential was plotted against x/l, where x is the probe position in the bed relative to the feeder and l is the bed height for 15.0—15.9% fluidized bed at three different applied potentials. As can be seen from the figure the reaction at the feeder surface is insignificant, $\frac{d\phi_s}{dx}=0$ at $x=0$,

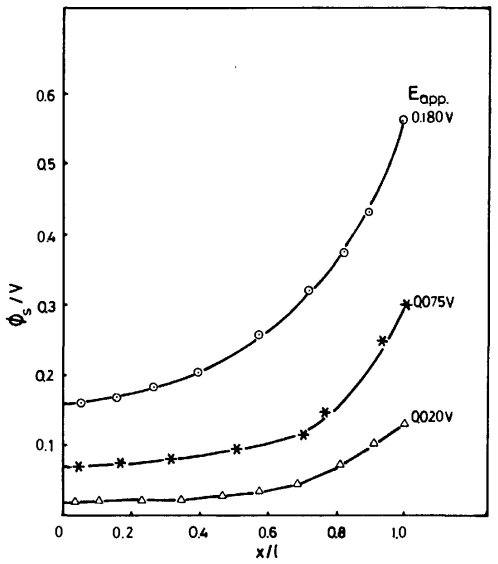

Fig. 3. Potential distribution in solution for a 15% fluidized bed at three different applied potentials.

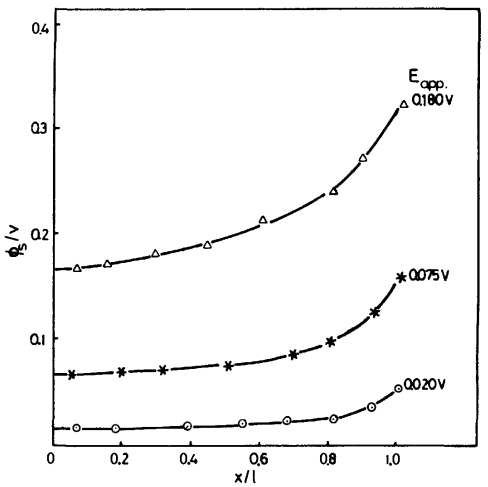

Fig. 4. Potential distribution in solution for the static bed at three different applied potentials.

(where ϕ_s is the solution potential and $x=0$ corresponds to the base of the bed) which satisfies the boundary condition of the following equation developed by Goodridge et al.[6]

$$-\frac{d}{dx}\left(K_s\frac{d\phi_s}{dx}\right)=A_pF(\phi) \quad (1)$$

where A_p is the superficial geometric area of the beads per unit volume of bed in the fluidized state, K_s is the effective specific conductance of the electrolyte in the fluidized bed and $F(\phi)$ is the dependency of current density on, ϕ, electrode potential which is the potential throughout the bed against the feeder.

Figure 4 shows the potential distribution in the solution for the static bed.

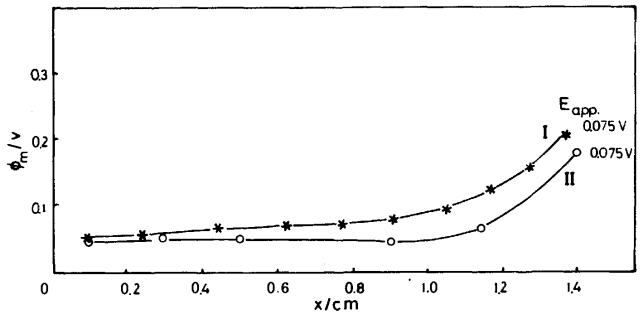

Fig. 5. Potential distribution in a 15% fluidized bed at an applied potential of 0.075 V, large (I) and tip (II) probes.

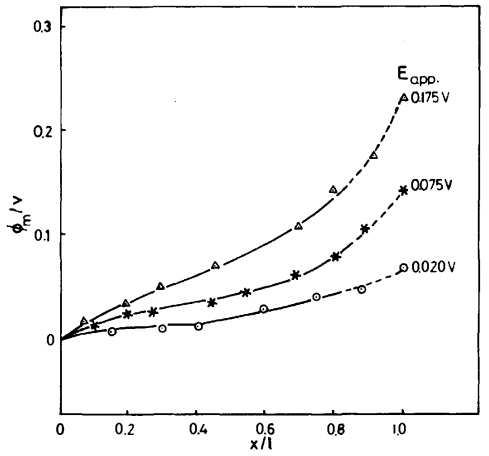

Fig. 6. Potential distribution in a 15% fluidized bed at three different applied potentials, small wire probe.

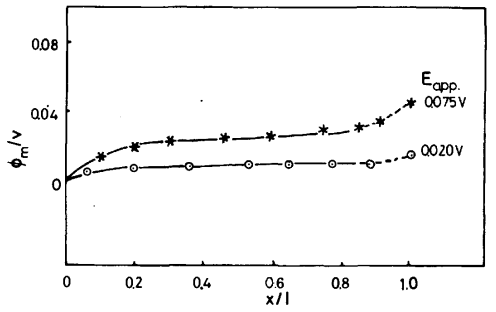

Fig. 7. Potential distribution in the static bed at two different applied potentials, small wire probe.

The potential distribution measurements in the bed taken only with the small and medium probes were quite the same. Figure 5 shows the results for large probes (Curve I) and tip probes (Curve II) for a 15% fluidized bed.

Results of the potential measurements in the bed with four different size of wire probes have shown that the surface area of an adequate probe should not be less than that of the beads, but it should be larger to some extent (the maximum and minimum surface area of the bead used in the experiments were 1.50 mm^2 and 0.85 mm^2 and the active surface area of the small and medium probes were 1.528 mm^2 and 3.82 mm^2, respectively). Since the surface area of the small probe was nearly the same as the beads and the reproducibility of the results recorded with this probe was better than a bead probe, the small probe was used throughout the potential distribution measurements in the bed.

The results recorded by the large probe can be explained by the great influence of the solution on the probe. This probe had an active area of 12.99 mm^2 and the length of the activated part of the probe was 1.35 cm which was more than the half diameter of the bed. There was not enough bead collisions with the probe and its potential was greatly governed by the potential of the solution.

With the tip probes, however, there was a few bed contact with the probe and it was nearly at its rest potential. The deviations observed at the top of the bed was again due to the effect of solution on the probes.

Figure 6 shows the potential distribution of the fluidized beds at three different applied potentials (E_{app}=0.020 V, 0.075 V, and 0.175 V). The dotted line in the figure shows the deviation of the potential at the top of the bed due to the effect of the solution potential on the probe. This could be explained by the assumption that there was not sufficient bead contact on the probe and also 3—4 rows of the beads at the top of the bed were probably not in good contact with the rest of the bed. Comparing the slope of this part of the curve with that of corresponding solution potential curve suggests a 60% solution potential effect on the probe measurement.

Figure 7 shows the potential distribution in the static bed. As can be seen from the figure, after a drop in the potential near to the feeder, the potential distribution in the static bed appeared almost constant through the bed except the slight deviation at the top.

In the operation of a fluidized bed electrode the variation of charge-transfer coefficient (K_m) along the bed has great importance on its performance. In order to observe the general tendency of the variation of charge-transfer coefficient in the fluidized bed, the values of K_m at various points of the bed were calculated using the following equations.[6]

$$I_s = -K_s A\left(\frac{d\phi_s}{dx}\right) \tag{2}$$

$$I_m = -K_m A\left(\frac{d\phi_m}{dx}\right) \tag{3}$$

where I_s is the current flow through the electrolyte, ϕ_s is the solution potential, I_m is the current flow in the bed and A is the area of current flow perpendicular to the direction of flow which is equivalent to the area of the feeder, i.e. 5.06 cm^2.

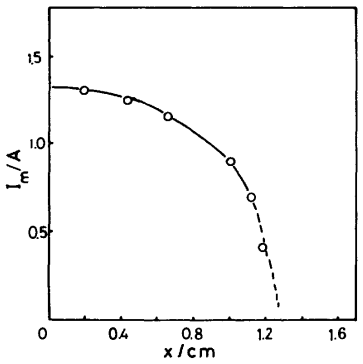

Fig. 8. Variation of current flow along 15% fluidized bed at an applied potential of 0.075 V.

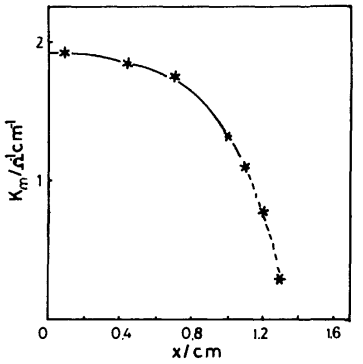

Fig. 9. Variation of charge-transfer coefficient along 15% fluidized bed at an applied potential of 0.075 V.

The current flow through the electrolyte, I_s, was calculated through Eq. 2. The values of $\frac{d\phi_s}{dx}$ were determined from the point slopes of Fig. 3. The effective conductivity of the electrolyte, K_s, which was determined from the Bruggeman relationship, quoted by Goodridge[6] as

$$K_s = \rho \cdot \varepsilon^{3/2} \quad (4)$$

where ε is the bed voidage and ρ is the specific conductivity of the electrolyte. ρ is taken as 0.53 ohm^{-1} cm^{-1} for 5.0 mol dm^{-3} KOH.[11] This equation provides the value of K_s as 0.2247 ohm^{-1} cm^{-1}.

The values of I_s were substracted from the total current values and the values of the current flow in the bed, I_m, were obtained for various points of the bed. The current flow in the bed ceases at the bed boundary so all the current is supported by the solution and at the top of the bed the current flow through the electrolyte should be equal to the total current of the bed. Figure 8 shows the results for a 15% fluidized bed at an applied potential of 0.075 V.

Similary $\frac{d\phi_m}{dx}$ values at various points of the bed can be found from the potential distribution in the bed and since the values of I_m are known, K_m can be obtained from Eq. 3.

Figure 9 shows the variation of charge-transfer coefficient along the bed. The tendency of the curve corresponding to the top of the bed was again represented with a dotted line because of the possibility of the incorrect values of I_m and K_m due to the deviation in the ϕ_m vs. x curve in this region of the bed.

In Fig. 10 the electrode potentials, ϕ, which is $\phi_m - \phi_s$, of a 15% fluidized bed was plotted against x/l at a feeder potential of 0.075 V. From the figure it is shown that the electrode potential is uniform throughout the bed except at the top.

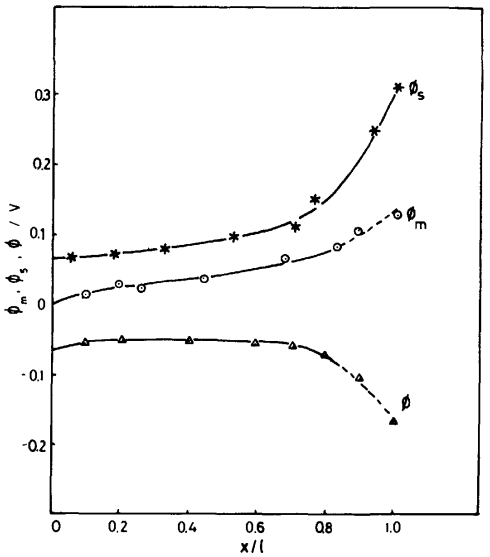

Fig. 10. Potential profiles in a 15% fluidized bed at an applied potential of 0.075 V, electrolyte, ϕ_s; beads, ϕ_m; and electrode potential, ϕ.

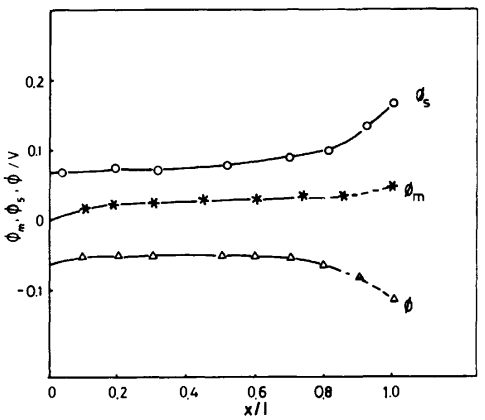

Fig. 11. Potential profiles in the static bed at an applied potential of 0.075 V, electrolyte, ϕ_s; beads, ϕ_m; and electrode potential, ϕ.

Figure 11 shows the electrode potential for the static bed at the feeder potential of 0.075 V.

Discussion

In porous and similar electrodes the physical properties of the electrode material and its porosity may determine the conductivity of electrode. In a fluidized bed electrode, however, the conductivity is not only a function of bed material. For fluidized beds, Goodridge et al.[6] have introduced the concept of the charge-transfer coefficient, K_m, which is not only dependent on the physical properties of bed material but also electrode reaction and hydrodynamic conditions in the bed. The value of K_m and its variation in the bed are of great importance from the point of the performance of a fluidized bed electrode.

The measurements of potential distribution in the bed and electrolyte showed that the electrode potentials both in a static and 15% fluidized beds were uniform throughout most of the bed except at a region corresponding to the top of the bed (Figs. 10 and 11). In the uniform distribution of potential electrode reactions occuring at low current densities, the comparable values of the charge-transfer coefficient and the effective specific conductance of the electrolyte which were 0.2247 $ohm^{-1} cm^{-1}$ and 0.53 $ohm^{-1} cm^{-1}$, respectively, in the present work, might be the important factor.

In comparison of Figs. 10 and 11 shows that the deviation of the fluidized bed curve from the static bed curve seems to indicate that there is more current supported at the top of the bed by the fluidized bed than the static bed.

References

1) J. R. Backhurst, Ph. D. Thesis, Univ. Newcastle (1967).

2) J. N. Hiddleston and A. F. Douglas, *Nature (London)*, **218**, 601 (1968).

3) J. N. Hiddleston and A. F. Douglas, *Electrochim. Acta*, **15**, 431 (1970).

4) R. Mason, Ph. D. Thesis, Univ. Newcastle (1969).

5) T. Berent, R. Mason, and I. Fells, *J. Appl. Chem. Biotechnol.*, **21**, 71 (1971).

6) F. Goodridge, I. Holden, H. D. Murray, and R. E. Plimley, *Trans. Inst. Chem. Eng.*, **491**, 128 (1971).

7) T. Huh, Energy Res. Abstr. 10, Abstr. No. 34287 (1985).

8) V. Rojo, J. Quardiola, and A. Vian, *Chem. Eng. Sci.*, **41**, 2171 (1986).

9) G. A. Dalin, "Encyclopedia of Chemical Technology," Interscience, New York (1954), Vol. 12, p. 443.

10) C. J. Smithells, "Metal Reference Book," Butterworths, London (1967), Vol. 3, p. 1100.

11) J. O'M. Bockris and S. Srinivasan, "Fuel Cells: Their Electrochemistry," McGraw-Hill Book Co., New York (1969).

Theoretical Studies on the Disproportionation of Carbon Monoxide on Nickel Clusters

Arun K. Srivastava,* Isao Kojima,† and Eizo Miyazaki†
Chemistry Department, University of Allahabad, Allahabad, India
†Chemistry Department, Tokyo Institute of Technology, Ookayama, Meguro-ku, Tokyo 152
(Received February 13, 1989)

In the framework of CNDO (Complete neglect of differential overlap method, VOIP (Valence orbital ionization potential) has been evaluated using the method of Anno and Sakai and for exchange integrals Wolfsberg-Helmholtz approximation has been used. With these the problem of parametrization with reference to transition metals becomes rather less troublesome. In its present form the method has been used for studying the disproportionation of carbon monoxide on a nickel cluster having five atoms. A large number of theoretical models were devised, which are based upon various mechanistic possibilities; for each of these, bond energies between different atoms were calculated and plotted against the distance, with an aim of studying the formation and desorption of CO_2. The present studies suggest that this reaction may follow a dissociative path, where in the first step one molecule of CO dissociates, leaving adsorbed carbon and oxygen on the Ni surface, followed by subsequent reaction of this adsorbed oxygen with another molecule of CO from the gas phase or it may follow disproportionation.

At higher temperatures the exposure of crystalline nickel surface to carbon monoxide results in the buildup of carbon. Below 180°C also the buildup of carbon can be brought about by using electrons of sufficiently high energy.[1-4] The adsorption of CO and the subsequent buildup of carbon on the catalyst surface is of great importance since these are the key steps in methanation:

$$3H_2 + CO \rightarrow CH_4 + H_2O$$

and Fischer-Tropsch synthesis. Although Auger data and flash desorption results show 10—20% overlayers of carbide like carbon on the surface following the reaction,[5] but the overall mechanism is not understood very clearly.

The proceeding of a chemical reaction may be described well by the splitting of one and formation of other bonds and consequently the changes in various bond energies may be expected to throw interesting light on the disruption (weakening) and formation of various bonds. The CNDO method as described here may, therefore, be expected to become a good method for studying the course of a reaction mainly because the bond energy is explicity defined in its framework.

Method

The local core matrix elements U_{ii} have been estimated from the atomic data using the following expression.

$$U_{ii} = I_p(i) - (N - 1)\,\gamma_{ss} - M\gamma_{sd} \qquad (1)$$

Where $I_p(i)$ is the valence state ionization potential, N denotes the total number of electrons in the valence s and p orbitals and M represents the number of electrons in the d orbital.

The I_p's have been evaluated by using the method of Anno and Sakai.[6]

The exchange integral H_{ij} was calculated with the Wolfsberg-Helmholtz[7] approximation,

$$H_{ij} = KS_{ij}\,(H_{ii} + H_{ij})/2. \qquad (2)$$

Thus in the present work only K, which is a dimensionless parameter, has been empirically assigned a value of 1.50. The electronic configuration $3d^M4s^2$ or $3d^M4s4p$ was considered for the ground state of the nickel atom. The orbital exponents suggested by Veigele et al.[8] were used for nickel and the Slater values were used for C and O.

The bond energies between atoms A and B were evaluated by the following equation,

$$E_{AB} = \sum_{\gamma}^{A}\sum_{S}^{B}(2P_{rs}\,\beta_{rs} - 1/2P_{rs}^2\,\gamma_{AB}) + (Z_AZ_BR_{AB}^{-1} - P_{AA}V_{AB} - P_{BB}V_{BA} + P_{BB}P_{AA}\gamma_{AB}). \qquad (3)$$

E_{AB} is not identical with the bond energy and in fact represents a simple two-center energy decomposition scheme within the framework of zero differential overlap approximation. In the present communication we use this as a parameter for our theoretical studies. All the terms in Eq. 3 have their usual meaning. The method in the present form has been found to produce satisfactory results[9] on various properties of diatomic molecules of the first transition series and has also been successful in giving valuable information about the mechanism of oxidation of carbon monoxide on nickel clusters.[10] The present method has also been successfully applied to the chemisorption of CO on Ni clusters.[11]

Results and Discussion

At present there are following two main streams in the discussion of mechanism of the carbon deposition on the nickel surface exposed to carbon monoxide at high temperatures and by bombardment with electrons of sufficiently high energy.

1. Dissociative Mechanism: It is claimed that the dissociation of CO is the first step resulting in the formation of Ni-C and Ni-O bonds (2Ni+CO→Ni-C+Ni-O) followed by the CO_2 formation (Ni-O+CO→CO_2).

2. Disproportionation Mechanism: It predicts the reaction between two CO molecules on the surface (2 $CO \rightarrow CO_2(g) + C_{ad}$).

Disproportionation is thermodynamically favorable but there is evidence[13] that the dissociative adsorption is also possible.

For our studies we have visualized three different possibilities for this reaction.

(i) Reaction between two adsorbed CO molecules [Models (1) and (2)].

$$CO_{ad} + CO_{ad} \rightarrow CO_2(g) + C_{ad}.$$

(ii) Reaction between two CO molecules, one of which is in chemisorbed state and the other reacts from the gas phase [Model (6)].

$$CO_{ad} + CO(g) \rightarrow CO_2(g) + C_{ad}.$$

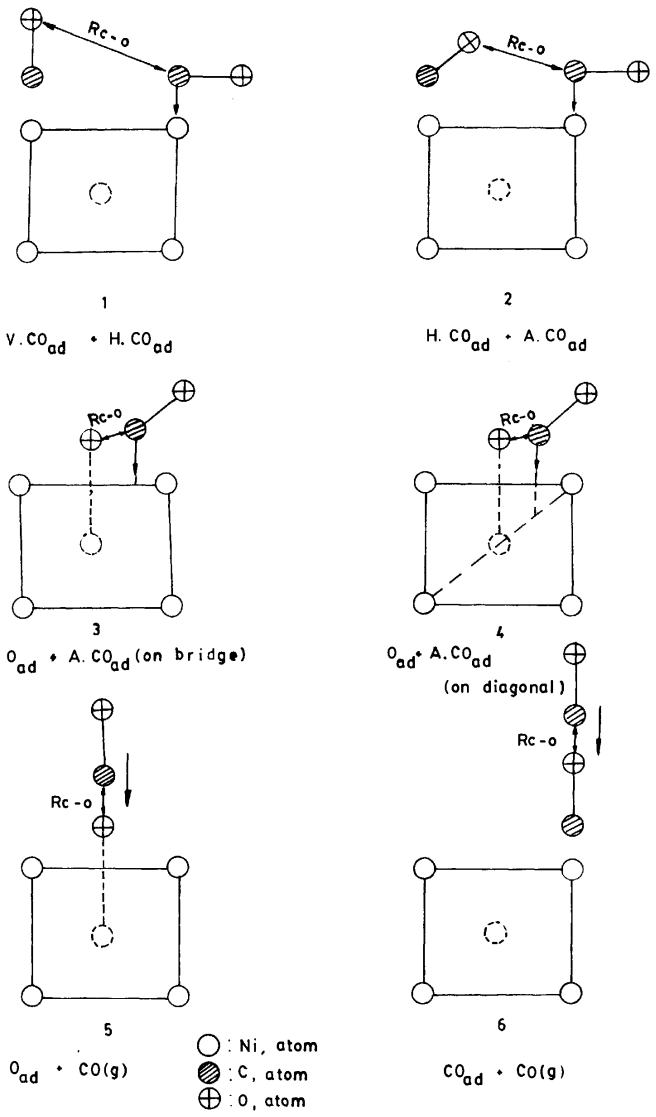

Fig. 1. Models used for studying the disproportionation of carbon monoxide on a 5-atom nickel cluster.

(iii) Dissociation of CO to adsorbed C_{ad} and O_{ad} species followed by a reaction of adsorbed O_{ad} with CO either from the gas phase [Model (5)] or in an adsorbed state [Model (3)] and [Model (4)].

$$CO \rightarrow C_{ad} + O_{ad}.$$

$$O_{ad} + CO(g) \rightarrow CO_2(g) \text{ (Eley-Rideal)}$$

$$O_{ad} + CO_{ad} \rightarrow CO_2(g) \text{ (Langmuir-Hinshelwood)}$$

Based on the above three theoretically possible mechanisms, different models involving Ni_5 cluster were designed (Fig. 1) and in these models horizontal and tilted (30°) forms of adsorbed CO have also been included besides the familiar vertical form. For all these models the energy of interaction E_{int} of a CO molecule to the rest of cluster was calculated by using the following definition.

$$E_{int} = E_t - E_a \qquad (6)$$

Where E_t is the total energy of the system containing all the atoms as shown in each model and E_a is the total energy of the system which has one molecule of CO less than the original model. The bond energy of

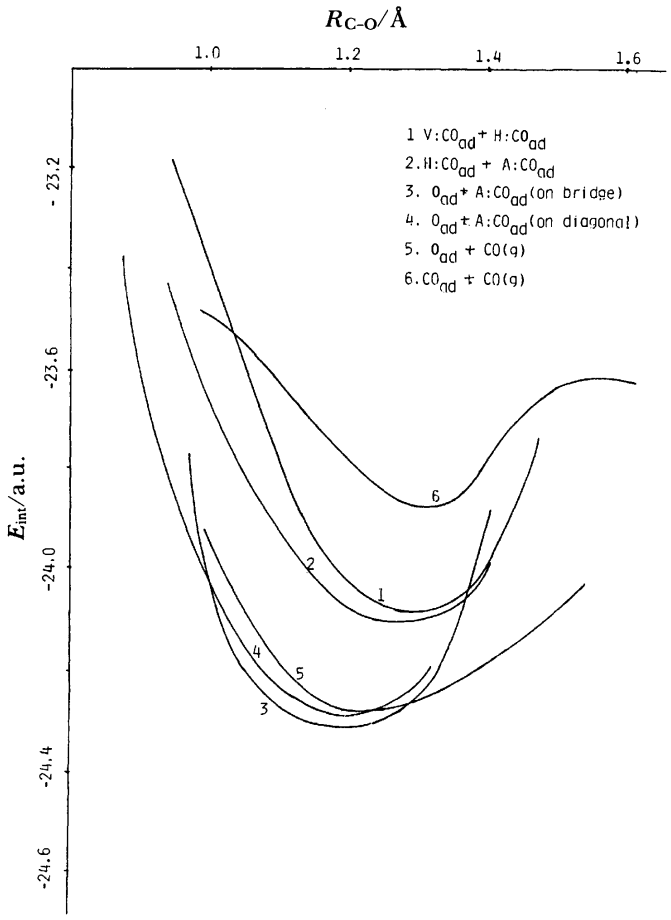

Fig. 2. Plot of E_{int} against $R_{C\text{-}O}$.

CO bond (the new bond which is being formed and is essential for the formation of CO_2) i.e. E_{C-O} as well as sum of the bond energies of all the Ni-C and Ni-O bonds i.e. $\sum E_{Ni-C}+\sum E_{Ni-O}$ have also been calculated. All these energies have been plotted against R_{C-O} i.e. the distance between C and O atoms involved in the new bond formation. The plots of E_{int} and E_{C-O} against R_{C-O} are good indices on the formation on CO_2, and plots of $\sum E_{Ni-O}+\sum E_{Ni-C}$ vs. R_{C-O} may give information regarding the desorption of the CO_2 molecules.

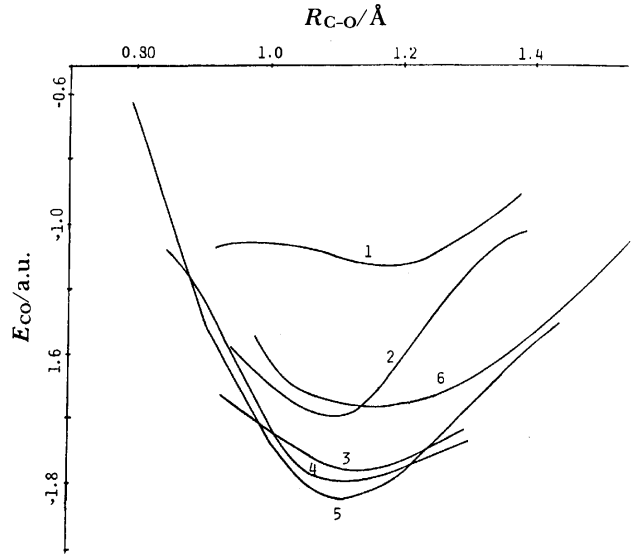

Fig. 3. Plot of E_{C-O} against R_{C-O}.

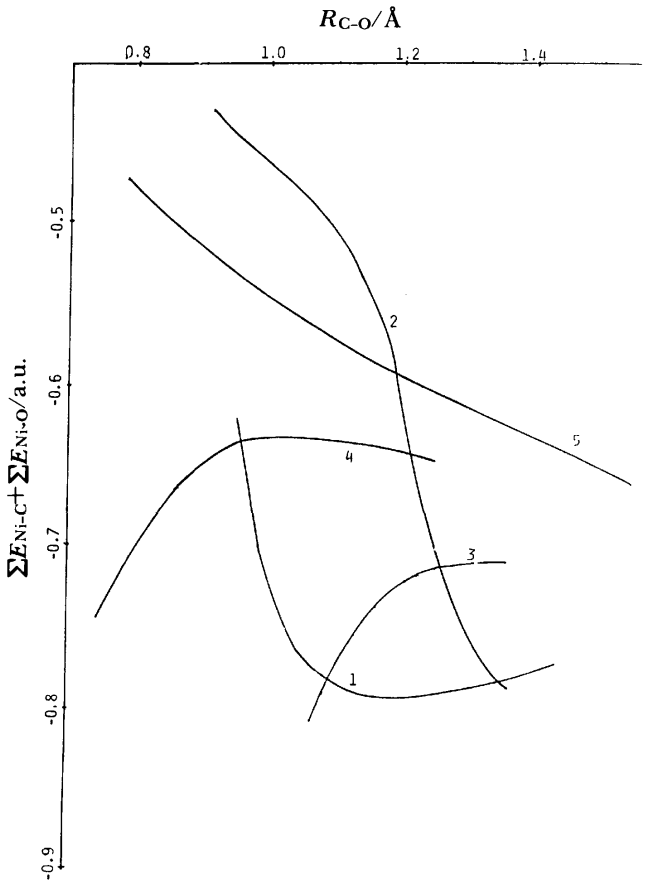

Fig. 4. Plots of $\sum E_{Ni-C}+\sum E_{Ni-O}$ vs. R_{C-O}.

Studies on Ni_5 Cluster: In Fig. 2, the interaction energy E_{int} of CO with the rest of the cluster has been plotted against R_{C-O}, and it seems that models (2), (3), (4), and (5), all of which represent a dissociation path, may be mechanistically more probable.

Figure 3 contains the plots of E_{C-O} vs. R_{C-O} and a comparative study of various curves shows that models (2), (3), (4), and (5) represent a pathway for the reaction which is more favorable for the formation of CO_2.

A study of Fig. 4 which includes plots of $\sum E_{Ni-C}+\sum E_{Ni-O}$ against R_{C-O} reveals that as far as the possibility of desorption of CO_2 is concerned models (2) and (5) may be comparatively better suited.

On the basis of the qualitative studies of Ni_5 it seems that models (2) and (5), representing disproportionation and dissociative path respectively, are the only two suitable paths for the reaction under study.

Conclusion

The qualitative studies presented in this paper on Ni_5 cluster have shown that there are following two plausible mechanisms for this reaction.

1. Disproportionation Mechanism: It has been proposed that the disproportionation reaction occurs between two CO molecules adsorbed on the top of two adjacent Ni atoms. However, our studies are in favor of the scheme with one of these being adsorbed horizontally parallel and the other one tilted at an angle of about 30° to the surface.

$$CO \rightarrow H:CO_{ad} \text{ (Horizontally adsorbed)}$$

$$CO \rightarrow A:CO_{ad} \text{ (Tilted at an angle 30°)}$$

$$H:CO_{ad} + A:CO_{ad} \rightarrow CO_2(g) + C_{ad}$$

The studies of Keim et at.[12] based on ellipsometry and Auger electron spectroscopy suggest disproportionation of the absorbed CO on Ni (100) surface due to bombardment by electrons of very high energy. Our studies presented here suggest that the disproportionation involves a reaction between a horizontally adsorbed CO molecule with a tilted CO molecule adsorbed on an adjacent site (Model 2).

2. Dissociative Mechanism: It is proposed that in the first step the CO molecule dissociates leaving O adsorbed at a four fold symmetrical site, which finally reacts with another molecule of CO from the gas phase to leave adsorbed C and simultaneously form CO_2 which desorbs immediately (Model 5)

$$CO \rightarrow C_{ad} + O_{ad}$$

$$O_{ad} + CO(g) \rightarrow CO_2(g)$$

A dissociative mechanism has also been proposed by Madden and Ertl[4] on the basis of their LEED and AES studies and by Caputi et al.[13] on the basis of their kinetic studies.

One of the authors (AKS) thankfully acknowledges theaward of fellowship by UNESCO and MONBUSHO, Japan. Thanks are also due to Dr. K. Shimokoshi and the staff of Computer Center (American) at Tokyo Institute of Technology for their help in computation.

References

1) G. A. Somorjai, *Surf. Sci.*, **34**, 156 (1973).
2) J. Verhoeven and J. Los, *Surf. Sci.*, **82**, 109 (1979).
3) A. Renouprez, B. Moraweck, M. Dominguez, V. Perrichon, and B. Emelik, *Compt. Rend.*, **C286**, 303 (1979).
4) H. H. Madden and G. L. Ertl, *Surf. Sci.*, **35**, 211 (1973).
5) P. Wentick, B. G. Wood, and H. Wiss, *J. Catal.* **43**, 365 (1976).
6) T. Anno and Y. Sakai, *Theor. Chim. Acta*, **18**, 208 (1970).
7) M. Wolfsberg and C. Helmholtz, *J. Chem. Phys.*, **20**, 837 (1952).
8) W. J. Veigele, D. E. Stevenson, and E. M. Henry, *J. Chem. Phys.*, **50**, 5404 (1969).
9) A. K. Srivastava, Project Report submitted to T. I. T. Japan, 1985.
10) A. K. Srivastava, I. Kojima, and E. Miyazaki, *Bull. Chem. Soc. Jpn.*, **59**, 3375 (1986).
11) A. K. Srivastava, I. Kojima, and E. Miyazaki, *Indian J. Chem., Sect. A*, **25**, 987 (1986).
12) E. G. Keim, F. Labohm, O. L. G. Gizeman, G. A. Bootsma, and J. W. Geus, *Surf. Sci.*, **112**, 52 (1981).
13) L. S. Caputi, R. Rosei, F. Ciccacci, R. Memeo, C. Mariani, and L. Papagno, *J. Catal.*, **83**, 19 (1983).

 © 1989 The Chemical Society of Japan Bull. Chem. Soc. Jpn., 62, 3670—3674 (1989) [Vol. 62, No. 11

Gas-Phase Dehydrogenation of Alkylbenzenes on Rh/$AlPO_4$ Catalysts

Felipa M. BAUTISTA, Juan M. CAMPELO, Angel GARCÍA, Diego LUNA, and José M. MARINAS*
Department of Organic Chemistry, Córdoba University, E-14004 Córdoba, Spain
(Received March 1, 1989)

The nonoxidative dehydrogenation of alkylbenzenes (ethylbenzene, propylbenzene, and isopropylbenzene) has been carried out at 693—853 K on rhodium catalysts at 1 wt% supported on two different types of $AlPO_4$. In similar experimental conditions, the specific catalytic activity of the Rh/$AlPO_4$ catalysts is higher than that obtained previously for Ni/$AlPO_4$ (20 wt%) catalysts. Besides, a linear free energy relationship (LFER) was also obtained, manifesting itself through a "compensation effect" between the $\Delta H^{\neq}$ and $\Delta S^{\neq}$ activation parameters obtained from the Eyring equation (and between $\ln A$ and E_a, from the Arrhenius equation). Furthermore, no extensive metal-support interaction effect was obtained as in the case of Ni/$AlPO_4$ catalysts in spite of exhibiting the same concerted mechanism previously described for the nonoxidative dehydrogenation of alkylbenzenes on supported nickel catalysts.

The dehydrogenation of ethylbenzene to styrene is a very important industrial reaction actually carried out in the vapor phase on iron oxide stabilized with several promotors in the presence of water vapor.[1] However, considerable work has been done in recent years to produce other catalysts such as metallic oxides,[2-4] several oxide salts[5-7] or supported metal catalysts.[8-10] With respect to the latter we studied[11] the nonoxidative dehydrogenation of several alkylbenzenes at 673—823 K on nickel catalysts at 20 wt% supported on Al_2O_3, SiO_2, and two different types of $AlPO_4$ synthesized according to Kearby.[12] Acid and basic sites did not exhibit catalytic activity. However, the acid-basic nature of the supports, through the effects of a strong metal-support interaction were found to play an important part in determining the catalytic activity of the supported nickel catalysts. These metal-support interaction effects were evaluated through several isokinetic parameters obtained from the existence of a linear correlation between the $\Delta H^{\neq}$ and $\Delta S^{\neq}$ activation parameters obtained from the Eyring equation (and between $\ln A$ and E_a, from the Arrhenius equation) known as the compensation effect.

These metal-support interaction effects were previously obtained in the liquid-phase hydrogenation of the olefinic double bond on $AlPO_4$-supported nickel[13-15] and rhodium[16-18] catalysts showing the behavior of $AlPO_4$ as excellent metal supports. In this connection, aluminum phosphates have also been used as supports for platinum[19] and palladium,[20] respectively.

In the present study we investigate the nonoxidative dehydrogenation of some alkylbenzenes (R=Et, *n*-Pr, and *i*-Pr) over rhodium catalysts at 1 wt% supported on the same two $AlPO_4$ supports previously employed as nickel supports[11] which lets us compare the influences of the two metals (rhodium and nickel) since the experimental conditions of this work are also same as those previously used with supported nickel catalysts.[11]

Experimental

Catalysts. Two Rh/$AlPO_4$ catalysts (1 wt% Rh) have been used. The $AlPO_4$ supports (Al/P=1) were obtained by precipitation with ammonia (F) or propylene oxide (P). The supported rhodium catalysts (Rh/$AlPO_4$-F, Rh/$AlPO_4$-P) were prepared by impregnation to incipient wetness with aqueous rhodium chloride solution followed by oven drying (24 h, 390 K) and reduction in flowing hydrogen (200 cm^3 min^{-1}) at 473 K as has been described elsewhere.[21] Besides, metal surface area, S, was, previously, obtained[21] from volume mean diameter, d_v, determined by TEM measurements assuming a spherical geometry of the metal particles (Rh/$AlPO_4$-F: d_v=4.2 nm and S=115 m^2 g_{Rh}^{-1}; Rh/$AlPO_4$-P: d_v=5.4 nm and S=90 m^2 g_{Rh}^{-1}).

The acid-base properties of the catalysts were determined by a spectrophotometric method previously described[22,23] that allows titration of the amount of irreversibly adsorbed benzoic acid (pK_a=4.19) or pyridine (pK_a=5.25) employed as titrant agents of basic and acid sites, respectively. For rhodium catalysts and supports (Rh/$AlPO_4$-F, Rh/$AlPO_4$-P, $AlPO_4$-F, and $AlPO_4$-P) the concentration of basic sites was 156, 152, 200, and 166 mol g^{-1}, and the concentration of acid sites 165, 163, 190, and 227 mol g^{-1}, respectively.

Apparatus and Procedure. The experiments were carried out in a tubular fixed-bed reactor (15×120 mm) with a continuous flow system at atmospheric pressure. The reactor was heated by a tubular electric furnace and the prescribed temperature (693—853 K) was monitored by a thermocouple located in the reactor wall. Isothermal temperatures were measured within an accuracy of ±1 K. The top section of the reactor which functioned as a vaporizer and preheater was packed with glass beads. Fresh catalyst was used in each experiment. The standard pretreatment of the catalyst consisted in heating in a 120 cm^3 min^{-1} nitrogen (99.999%, H_2O<3 ppm) stream for 1 h at the reaction temperature.

The starting materials: ethyl- (EB), propyl- (*n*-PB), and isopropylbenzene (*i*-PB) were supplied by Merck p.a., and purified by distillation under reduced pressure and low temperature. Each substrate was fed at several rates (F in the interval 10—0.1 cm^3 min^{-1}) by means of a microfeeder (Perfusor VI B. Braun), vaporized and passed through the catalyst zone. Nitrogen was used as a carrier gas with a

constant flow of 120 cm^3 min^{-1}.

The liquid products were condensed and analyzed by gas chromatography using 5% polyphenylene oxide on Chromosorb G-AW DMCS 80/100 column. Furthermore, a spectrophotometric analysis of the different samples was made due to the low conversion values obtained (<0.5%) at the higher F values. These experiments are developed at the wavelength of the maximum absorption of the dehydrogenation products in cyclohexane solutions (spectroscopic grade, Merck) and between the concentrations where the Lambert-Beer law fits.

Results and Discussion

The gas chromatographic analysis for all runs indicated that the only reaction products obtained were those corresponding to the dehydrogenation reaction of the alkylbenzenes: styrene, α-, and β-methylstyrene, respectively.

Dehydrogenation reactions were carried out under conditions where the reaction rate, R, was not influenced by diffusion. Thus, the average particle size of the catalysts used (<0.149 mm) determines that the reactions were not influenced by internal diffusion. On the other hand, the representation of R (obtained for 0.4 g of catalyst at several feed rates, F) against F, as shown in Fig. 1a, indicated the absence of external diffusion effects in the present experimental conditions for feed rates over 1.2×10^{-4} mol s^{-1}. According to these results, the bulk of the kinetic runs was performed at a fixed ratio of catalyst mass (0.4 g) and at least three feed rates in the interval $1.2—14\times10^{-4}$ mol s^{-1}, at temperatures between 693—853 K.

In the present experimental conditions the reaction can take place in a negligible extension in the absence of the catalyst, especially at the highest temperatures. Furthermore, identical negligible activities are obtained when the different supports are used as cata-

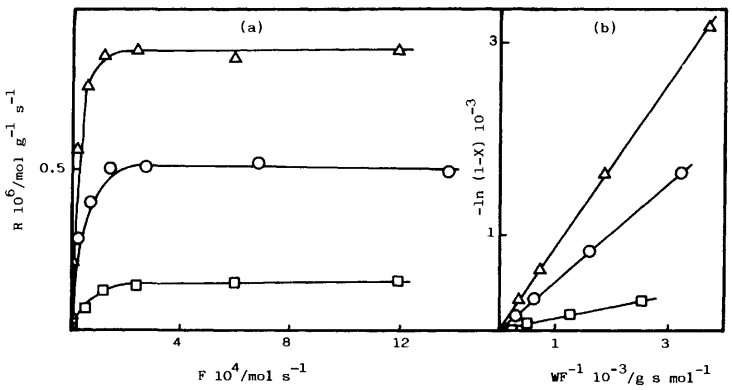

Fig. 1. (a) Dehydrogenation rate, R, of alkylbenzenes on 0.4 g of $Rh/AlPO_4$-F at 723 K as a function of feed rate, F. (b) Least-squares fit of Eq. 1 to the initial conversion data, X, at different residence time, W/F. (○) Ethylbenzene, (□) propylbenzene, (△) isopropylbenzene.

Table 1. Reaction Rate Constants, k (mol g^{-1} s^{-1}) and Specific Reaction Rates, k_S (mol s^{-1} m^{-2}_{Rh}) of Two Catalysts in the Dehydrogenation of Alkylbenzenes Studied at Different Temperatures

Catalyst	T	EB		n-PB		i-PB	
	K	$10^6 k$	$10^6 k_S$	$10^6 k$	$10^6 k_S$	$10^6 k$	$10^6 k_S$
$Rh/AlPO_4$-P	693	0.28	0.31	0.01	0.01	0.16	0.26
	723	0.49	0.55	0.02	0.02	0.45	0.50
	753	0.80	0.89	0.07	0.08	0.72	0.80
	773	1.19	1.32	0.12	0.13	1.10	1.22
	793	1.65	1.83	0.17	0.19	1.50	1.67
	823	2.25	2.50	0.32	0.36	2.37	2.64
	853	3.56	3.96	0.77	0.85	3.63	4.04
$Rh/AlPO_4$-F	693	0.32	0.28	0.07	0.06	0.49	0.50
	723	0.51	0.45	0.12	0.11	0.88	0.76
	753	0.80	0.69	0.25	0.22	1.08	0.94
	773	1.10	0.95	0.38	0.33	1.40	1.22
	793	1.28	1.12	0.45	0.39	2.11	1.83
	823	1.99	1.73	0.75	0.65	3.14	2.73
	853	2.81	2.45	1.21	1.05	4.60	4.00

lysts. Accordingly it may be assumed that the catalytic activity is exclusively developed on the rhodium metal surface, as occurs in nickel catalysts.[11]

The initial conversion data, X (<5%) (defined as the number of moles of dehydrogenated alkylbenzene per mole of alkylbenzene fed) are fitted in a first-order rate equation, Fig. 1b, at residence times lower than 4000 g s mol^{-1}.

$$\ln 1/(1 - X) = k(W/F) \quad (1)$$

The slope of the straight lines yields the value of the reaction rate constant, k (in mol g^{-1} s^{-1}). In Table 1 the k and specific reaction rate constants, k_S (in mol s^{-1} m$^{-2}_{Rh}$) values for the three alkylbenzenes with the two catalysts at each temperature are collected.

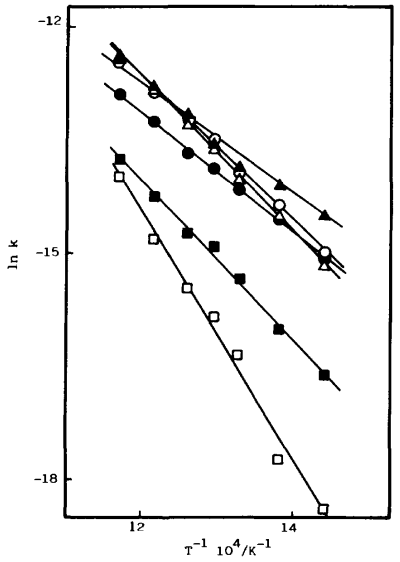

Fig. 2. Arrhenius plots for the dehydrogenation of ethylbenzene: (○) Rh/AlPO$_4$-P, (●) Rh/AlPO$_4$-F; propylbenzene: (□) Rh/AlPO$_4$-P, (■) Rh/AlPO$_4$-F; and isopropylbenzene: (△) Rh/AlPO$_4$-P, (▲) Rh/AlPO$_4$-F.

The results collected in Table 1 show that the catalytic activities of both supported rhodium catalysts are similar so that they do not exhibit a metal-support interaction effect as previously obtained with supported nickel catalysts in the same experimental conditions.[11] With respect to this, we see that specific catalytic activity of rhodium catalysts is clearly higher (between 2 and 3 times) than those obtained with nickel catalysts in the dehydrogenation of EB and *i*-PB. Such differences are not as high in *n*-PB.

The results obtained in the temperature range studied are summarized in Fig. 2 where we can see the evolution of catalytic activity with temperature which lets us apply the Arrhenius equation obtaining the corresponding values of apparent activation energies, E_a, and Arrhenius constants, ln A, collected in Table 2.

Furthermore, the Eyring equation also evaluates the temperature dependence of reaction rate constants in terms of transition state theory by separating enthalpy, $\Delta H^{\neq}$, and entropy, $\Delta S^{\neq}$, components. Their corresponding values, obtained by plotting $\ln(k_S T^{-1})$ against T^{-1} are also shown in Table 2.

We can also see in Fig. 3 how the kinetic parameters $\Delta H^{\neq}$ against $\Delta S^{\neq}$ for rhodium catalysts, in Table 2, and nickel catalysts, previously obtained,[11] fit straight lines for each alkylbenzene. This enthalpy-entropy relationship may be adscribed to the existence of a linear free energy relationship (LFER):

$$\Delta G^{\neq}_{const} = -\theta R \ln K^{\neq} = \Delta H^{\neq} - \theta \Delta S^{\neq} \quad (2)$$

known as the "compensation effect" or "isokinetic relationship" (IKR)[24-26] although the most habitual representation is through the equation

$$\ln A = \ln \alpha + E_a/\theta R \quad (3)$$

where R is the gas constant, θ the isokinetic temperature at which identical values of reaction rate constant $k=\alpha$ are obtained, $K^{\neq}$ the equilibrium

Table 2. Apparent Activation Energies, E_a (kJ mol^{-1}), Arrhenius Constants, ln A (mol s^{-1} m$^{-2}_{Rh}$), Activation Enthalpies, $\Delta H^{\neq}$ (kJ mol^{-1}) and Activation Entropies, $\Delta S^{\neq}$ (J mol^{-1} K^{-1}) with Their Respective Standard Deviations, for the Catalysts and Substrates Studied

Substrate		Rh/AlPO$_4$-P	Rh/AlPO$_4$-F
Ethylbenzene	E_a	78.0±2.0	66.0±1.0
	ln A	−1.4±0.2	−3.6±0.2
	$\Delta H^{\neq}$	71.6±2.0	60.0±1.0
	$\Delta S^{\neq}$	−274.0±2.0	−292.0±2.0
Propylbenzene	E_a	137.0±6.0	87.0±3.0
	ln A	5.0±1.0	−1.4±0.4
	$\Delta H^{\neq}$	131.0±6.0	81.0±3.0
	$\Delta S^{\neq}$	−217.0±2.0	−274.0±3.0
Isopropylbenzene	E_a	84.0±1.0	64.0±4.0
	ln A	−0.5±0.2	−3.5±0.7
	$\Delta H^{\neq}$	78.0±1.0	58.0±4.0
	$\Delta S^{\neq}$	−267.0±2.0	−291.0±6.0

constant of the activated complex and $\Delta G^{\neq}$ the activation free energy. Thus, the values of isokinetic parameters for each substrate (θ, $\ln \alpha$, $K^{\neq}$, and $\Delta G^{\neq}$) are obtained from slopes and intercepts in Eqs. 2 and 3 and collected in Table 3.

Furthermore, if an IKR holds for any set of reactions of the same type exhibiting the same value of $\Delta G^{\neq}$ throughout the experimental temperature range, a single common interaction mechanism can be expected.[24,27,28] In agreement with this and on the basis of the results shown in Fig. 3 and Table 3 we have to conclude that the nonoxidative gas-phase dehydrogenation of alkylbenzenes on $Rh/AlPO_4$ catalysts is carried out through the identical concerted mechanism previously described for $Ni/AlPO_4$ catalysts,[11] developed throughout the reversal of the steps of a classical Horiuti-Polanyi type noncompetitive mechanism,[29] and describing the hydrogenation of an olefinic double bond.

This concerted character can also be accounted for by consideration of the kinetic parameters presented in Table 2. Thus, the negative values of $\Delta S^{\neq}$ indicate that, on going from the ground state to the transition state, an extensive restriction in the degrees of freedom must be considered. This highly ordered transition state is consistent with a reaction mechanism whose slowest step is the stabilization and immobilization of reactant molecules on catalyst active sites. With respect to this, the reaction rate is proportional to the quantity of adsorbed reactant molecules, and the reverse reaction is negligible. Besides, the relatively low $\Delta H^{\neq}$ values appear to be consistent with a concerted evolution in the limiting adsorption step which also must be associated with the low values $\Delta S^{\neq}$.

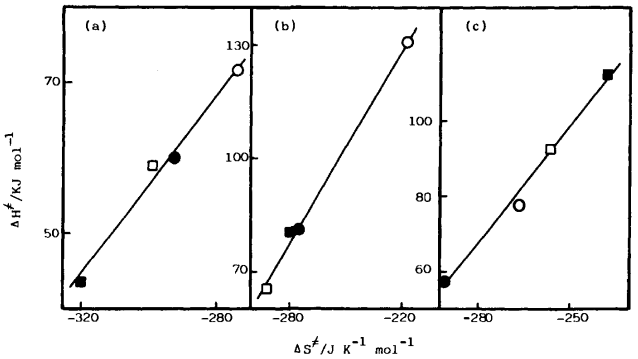

Fig. 3. Compensation effect between $\Delta H^{\neq}$ and $\Delta S^{\neq}$ for (a) ethylbenzene, (b) propylbenzene, and (c) isopropylbenzene with different catalysts: (○) $Rh/AlPO_4$-P; (●) $Rh/AlPO_4$-F; (□) $Ni/AlPO_4$-P; and (■) $Ni/AlPO_4$-F.

In the present mechanism, the active sites on the metal surface are looked on as surface complexes[29-32] with three degrees of coordinative unsaturation where it is possible to absorb two hydrogens and an olefin at the same time in the transition state. The transfer of the two hydrogen atoms from the alkylbenzenes throughout a concerted process, where the interaction with the catalyst removes the symmetry restrictions imposed by the Woodward-Hoffmann rules, leads directly to the olefinic double bond and a hydrogen molecule formation.[33] In agreement with this, Wang et al.[3,34] described the nonoxidative dehydrogenation of ethylbenzene over TiO_2-ZrO_2 catalysts through a concerted two center mechanism, where zirconium ions act like Lewis acid, and titanium ion as a base.

On the other hand, the reaction rate is only determined by the number of active sites present in the reaction. This number is determined not only by the metal surface area (related to the catalyst weight and metal dispersion) but also to the density of active sites on the metal surface, which is closely associated to the metal-support interaction effects. In this way, the higher catalytic activity of $Rh/AlPO_4$ with respect to $Ni/AlPO_4$ catalysts ought to be related to their different behavior in relation to the metal-support interaction effects. Thus, while in supported nickel catalysts the metal deposition induced a strong decrease in the number of acid sites while the number of basic sites remained almost unchanged,[11] in the $Rh/AlPO_4$ catalyst, according to the present results, the metal deposition practically does not induce appreciable changes in either the number of acid sites or basic ones. However, the potential effect of the different metal content ought to be also considered in order to explain this differential behavior between Ni and Rh supported catalysts.

According to Bartholomew et al.[35,36] such metal-support interaction can be attributed to a transfer of electrons between the nickel atoms and the acid sites on the support surface. Possibly due to the higher reduction potential in rhodium atoms, such electron transfer is not developed in $Rh/AlPO_4$ catalysts thus obtaining an enhanced catalytic activity with respect to $Ni/AlPO_4$ catalysts, as also obtained habitually in liquid-phase catalytic hydrogenation of the olefinic double bond.[13,16,17,37] So, here we have an interesting

Table 3. Values of $\ln \alpha$ and θ^a (K) Obtained from the Representation of $\ln A$ againt E_a and Values of θ^b (K), $\Delta G^{\neq}$ (kJ mol^{-1}), and $\ln K^{\neq}$ Obtained from the Representation of $\Delta H^{\neq}$ againt $\Delta S^{\neq}$, Corresponding to Substrates

Substrate	$\ln \alpha$	θ^a	θ^b	$\Delta G^{\neq}_{const}$	$\ln K^{\neq}$
Ethylbenzene	−17.0±1.0	613±67	596±65	235±19	−47±6
Propylbenzene	−13.7±0.6	870±40	867±40	319±11	−44±3
Isopropylbenzene	−10.7±0.8	1038±74	1028±74	355±19	−42±4

difference between the catalytic behavior of Rh and Ni supported catalysts: The former does not exhibit important metal-support interaction effects which could explain in part its excellent catalytic activity. In spite of this, it has not been studied extensively to date as evidenced by the absence of publications during the last few years.

This work was subsidized by a grant for scientific research from the Comisión de Investigación Científica y Técnica (CICYT, Project PA86-0065), Ministerio de Educación y Ciencia, Spain. The authors also acknowledge the grammatical revision of the manuscript carried out by Prof. M. Sullivan.

References

1) P. N. Rylander, "Catalysis Science and Technology," ed by J. R. Anderson and M. Boudart, Springer Chemie, Berlin (1983), Vol. 4, Chap. 1, p. 17.
2) Y. Hirashima, K. Nishiwaki, A. Miyakoshi, H. Tsuiki, A. Ueno, and H. Nakabayashi, *Bull. Chem. Soc. Jpn.*, **61**, 1945 (1988).
3) J. C. Wu, C. S. Chung, C. L. Ay, and I. Wang, *J. Catal.*, **87**, 98 (1984).
4) Y. Murakami, K. Iwayama, H. Uchida, T. Hattori, and T. Tagawa, *Appl. Catal.*, **2**, 67 (1982).
5) G. E. Vrieland, *J. Catal.*, **111**, 1 (1988).
6) A. Schraut, G. Eming, and H. Hofmann, *J. Catal.*, **112**, 221 (1988).
7) K. Brozyna and Z. Dziewiecki, *Appl. Catal.*, **35**, 211 (1987).
8) H. C. Bailey, J. B. Williamson, and C. W. Capp., British Patent 1098697, Sept. 17, 1965.
9) K. Fujimoto and T. Kunugi, *Ind. Eng. Chem., Prod. Res. Dev.*, **20**, 319 (1981).
10) D. Duprez, A. Miloudi, G. Delahay, and R. Maurel, *J. Catal.*, **101**, 56 (1986).
11) F. M. Bautista, J. M. Campelo, A. García, D. Luna, and J. M. Marinas, *J. Catal.*, **107**, 181 (1987).
12) K. Kearby, "Proceedings, 2nd International Congress on Catalysis, Paris, 1960," Technip, Paris (1961), p. 2567.
13) J. M. Campelo, A. García, D. Luna, and J. M. Marinas, *J. Catal.*, **97**, 108 (1986).
14) J. M. Campelo, A. García, J. M. Gutiérrez, D. Luna, and J. M. Marinas, *Appl. Catal.*, **7**, 307 (1983).
15) J. M. Campelo, A. García, D. Luna, and J. M. Marinas, *J. Chem. Soc., Faraday Trans. 1*, **80**, 695 (1984).
16) J. M. Campelo, A. García, D. Luna, and J. M. Marinas, *J. Catal.*, **113**, 172 (1988).
17) J. A. Cabello, J. M. Campelo, A. García, D. Luna, and J. M. Marinas, *J. Catal.*, **94**, 1 (1985).
18) J. A. Cabello, J. M. Campelo, A. García, D. Luna, and J. M. Marinas, *J. Org. Chem.*, **51**, 1786 (1986).
19) M. A. Aramendía, V. Borau, C. Jiménez, J. M. Marinas, and F. Rodero, *Bull. Chem. Soc. Jpn.*, **60**, 3415 (1987).
20) A. Alba, M. A. Aramendía, V. Borau, C. Jiménez, and J. M. Marinas, *J. Catal.*, **98**, 288 (1986).
21) J. M. Campelo, A. García, D. Luna, and J. M. Marinas, *Appl. Catal.*, **10**, 1 (1984).
22) J. M. Campelo, A. García, J. M. Gutiérrez, D. Luna, and J. M. Marinas, *J. Colloid Interface Sci.*, **95**, 544 (1983).
23) J. M. Campelo, A. García, D. Luna, and J. M. Marinas, "Proceedings, 9th Symposium Iberoam. Catal., Lisbon, 1984." Vol. 1, p. 310.
24) W. C. Conner, Jr., *J. Catal.*, **78**, 238 (1982).
25) A. K. Galwey, *J. Catal.*, **84**, 270 (1983).
26) G. C. Bond, *Z. Phys. Chem. N. F.*, **144**, 21 (1985).
27) W. Linert, R. W. Soukup, and R. Schmidt, *Compt. Chem.*, **6**, 47 (1982).
28) A. Galwey and M. Brown, *J. Catal.*, **60**, 335 (1979).
29) M. Ledoux and F. G. Gault, *J. Catal.*, **60**, 15 (1979).
30) R. A. Y. Jones, "Physical and Mechanistic Organic Chemistry," Cambridge, University Press (1984), p. 348.
31) R. L. Augustine and J. F. Van Peppen, *Ann. N.Y. Acad. Sci.*, **172**, 244 (1970).
32) S. Siegel, J. Outland, Jr., and J. Garti, *J. Catal.*, **52**, 102 (1978).
33) R. Ponec, *Collect. Czech. Chem. Commun.*, **51**, 1843 (1986).
34) I. Wang, W. F. Chang, R. J. Shian, J. C. Wu, and C. S. Chung, *J. Catal.*, **83**, 428 (1983).
35) C. H. Bartholomew and R. B. Pannell, *J. Catal.*, **65**, 390 (1980).
36) C. H. Bartholomew, R. B. Pannell, and J. L. Butler, *J. Catal.*, **65**, 335 (1980).
37) J. M. Campelo, A. García, D. Luna, and J. M. Marinas, *Bull. Soc. Chim. Belg.*, **92**, 851 (1983).

 © 1989 The Chemical Society of Japan Bull. Chem. Soc. Jpn., 62, 3675—3678 (1989)

Extraction Spectrophotometric Determination of Bismuth(III) with Iodide and Amidines

Alpana GHOSH, Khageshwar Singh PATEL, and Rajendra Kumar MISHRA*
Department of Chemistry, Ravishankar University, Raipur (M. P.), 492010, India
(Received December 22, 1988)

A new simple and rapid spectrophotometric method for the extraction and determination of bismuth(III) is described. The reaction of *N,N'*-diphenylbenzamidines and its 10 derivatives (HA) with bismuth(III) in presence of iodide have been investigated photometrically in chloroform. The value of molar absorptivity of the complexes with these compounds lies in the range $(0.84—1.35)\times10^4$ l mol^{-1} cm^{-1}. Of these, the most sensitive compound *N*-(2-methylphenyl)-*N'*-phenylbenzamidine hydrochloride (MPPBA) was selected for detailed studies. The detection limit of the method is 0.2 μg Bi cm^{-3}. The elements which are commonly associated with the metal e.g. Cu, Ni, Co, Mn, Cr, Zn, Hg, Ti, Zr, Mo, W, V, Al, Sb, etc. do not interfere. The method has been applied for the determination of the metal to soil and ore.

In earlier communications, amidines were used for the extraction and spectrophotometric determination of Sb(III) and Au(III) as halogeno ternary complexes.[1,2] In this paper, *N,N'*-diphenylbenzamidine and its 10 derivatives are reported for extraction and spectrophotometric determination of microgram amounts of bismuth(III) in the presence of iodide ions. The formation of iodobismuthite complex in the water and in the organic solutions is the absence of amidine were examined at the conditions mentioned in the procedure. The value of molar absorptivity of the complex in the aqueous solution is found to be 8500 l mol^{-1} cm^{-1} at 445 nm and its extraction by polar solvents 1-pentanol, methyl isobutyl ketone, ethyl acetate suffers by unstability of the extract at room temperature. Moreover, the classical iodide method commonly used is complicated because it is applicable in sulfurous acid media and suffers form interferences of metal ions e.g. Sb, Pb, Hg, etc.[3,4] Tetrabutyl ammonium ion[5] and dyes[6—9] were claimed to improve the selectivity of classical iodide method, although they suffers from interference of the metal ions. Thiourea is widely used for spectrophotometric determination of metal in perchloric acid medium. However, it is not sensitive and involves the serious interference of Sb.[3,4] Dithizone is employed for the spectrophotometric determination of metal in alkaline solution using cyanide as masking agent to overcome the interference of heavy metals.[10] Recently mucic acid has been used as a colorimetric reagent for the determination of the metal over pH range 4.0 — 5.0 but it is not sensitive.[11]

The present method remarkably enhances the selectivity and sensitivity of the classical iodide method. The complex is stabilized by amidine in the organic solution unlikely to polar solvents e.g., 1-pentanol, MIBK or ethyl acetate. This method also improves the selectivity of other established methods.

Experimental

Apparatus: A Carl Zeiss "SPEKOL" equipped with 1-cm quartz cells were employed for the absorbance measurements.

Reagents: The standard solution and bismuth(III) was prepared by dissolving a weighed amount of bismuth sulfate in dilute sulfuric acid (0.5 mol dm^{-3}) and standardized volumetrically with EDTA using Pyrocatechol Violet as an indicator.[12] A freshly prepared potassium iodide solution (5% w/v) containing ascorbic acid (1% w/v) was employed. A 0.4% (w/v) solutions of amidines in chloroform was used for all extraction work. All chemicals used were analytical grade and their solutions were prepared in deionized water.

Procedure: Place an aliquot of standard bismuth(III) solution containing 25—450 μg of the metal in a 150-cm^3 separatory funnel. To this add 1 cm^3 of 5% KI solution. Adjust the acidity to the required value with 10 mol dm^{-3} H_2SO_4 and dilute to 10 cm^3 with deionized water. Add 10 cm^3 chloroform solution of the reagent. Shake the content of the funnel vigorously for 2 min and allow the phase to separate. Dry the chloroform extract over anhydrous sodium sulfate in a 50-cm^3 beaker. Wash the aqueous layer with 3×2 cm^3 fresh portions of chloroform. Transfer all the extracts to 25-cm^3 volumetric flask and dilute with chloroform to the mark. Measure it at λ_{max} against reagent blank.

Results and Discussion

Absorption Spectra: The absorption spectra of the ternary complex is chloroform, binary complex in the aqueous solution and that of reagent blank in chloroform are shown in Fig. 1. The maximum absorbance of the ternary and binary complexes lies at 490 nm and 440 nm, respectively. The formation of ternary shows a slight hyperchromic shift and a strong bathochromic shift as shown in Fig. 1. The reagent blank in chloroform shows some absorption at λ_{max} hence it was used as a reference blank for all measurements.

Selection of Extracting Solvents: The influence of various solvents e.g., benzene, toluene, carbon tetrachloride, chloroform, and cyclohexane were examined for the extraction of the complex with *N*-(2-methylphenyl)-*N'*-phenylbenzamidine hydrochloride (MPPBA). The complex is quantitatively extractable into toluene

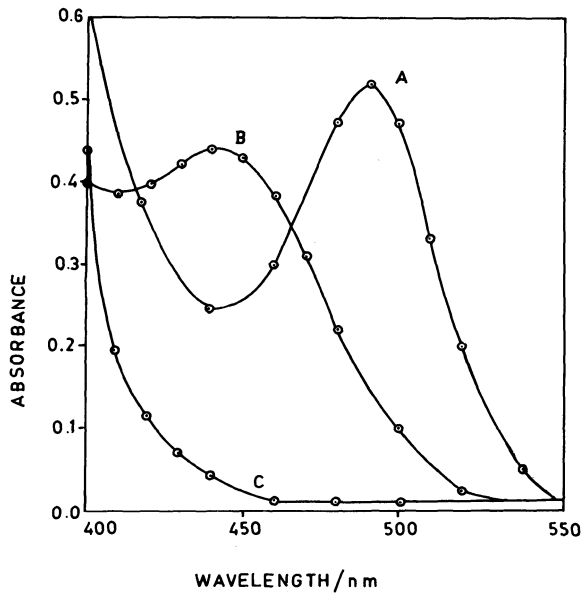

Fig. 1. Absorption spectra of bismuth(III) with iodide in aqueous solution and with iodide and amidine (MPPBA) in chloroform and the reagent blank in chloroform.
(A) $C_{Bi}=3.8\times10^{-5}$ mol dm^{-3}; $C_{KI}=0.03$ mol dm^{-3}; $C_{MPPBA}=0.014$ mol dm^{-3}; $C_{H_2SO_4}=2.0$ mol dm^{-3}. (B) $C_{Bi}=3.8\times10^{-5}$ mol dm^{-3}; $C_{KI}=0.03$ mol dm^{-3}; $C_{H_2SO_4}=2.0$ mol dm^{-3}. (C) $C_{KI}=0.03$ mol dm^{-3}; $C_{H_2SO_4}=2.0$ mol dm^{-3}; $C_{MPPBA}=0.014$ mol dm^{-3}.

and chloroform; whereas partially extracted into aromatic hydrocarbons while no extraction in carbon tetrachloride. The value of molar absorptivity and absorption maximum of the complex in these solvents are: Toluene (λ_{max}-490 nm, ε=13400 l mol^{-1} cm^{-1}), chloroform (λ_{max}-490 nm, ε=13500 l mol^{-1} cm^{-1}). Of these, chloroform is used as a solvent for further extraction work due to high distribution ratio of the reagent in it. Effect of acidity and quantitative extraction of the metal: The effect of acids like sulfuric and hydrochloric acids on the extraction of the metal with iodide and amidines were examined. Hydrochloric acid cannot be used for acidification because of the formation of the chloro complexes which suppress the extraction in the present investigation. Therefore, sulfuric acid has been selected for further extraction work.

The data obtained show that the optimum acidity range for the maximum and constant absorbance of the complex in the organic solution is 0.5—4.0 mol dm^{-3} H_2SO_4. A 100, 200, and 400 μg of Bi(III) is extracted separately as in the procedure. The extract is evaporated, digested with acid treatment and estimated by perchloric acid method. The metal recovered was found to be more than 99%.

Effect of Reagents, Time, Temperature, and Volume of Aqueous Phase: The effect of the concentration of reagents on the extraction of Bi(III) with KI and MPPBA were studied. The extraction is quantitative when the concentration of MPPBA in chloroform is higher than 0.009 mol dm^{-3}. The concentration of potassium iodide should be between 0.0075 to 0.09 mol dm^{-3} in aqueous solution. The function of ascorbic acid added is to prevent the oxidation of iodide as well as to remove any oxidizing materials present in aqueous solution. The order of addition of reagents is not critical. A shaking time of 1 min was sufficient for complete extraction of the metal and further extraction upto 10 min did not cause any adverse effect. The absorbance of the extract was stable for at least 5—6 h at room temperature (25±2 °C). The effect of dilution upon extraction of the metal with MPPBA was examined. The results indicates that the absorbance of the extraction remained unchanged when the volume ratio of organic phase to aqueous phase was 2:1 to 1:10. The reaction temperature of the medium is critical and it should be between 20 and 30 °C. Beyond this temperature the color intensity of the complex decreases.

Optimum Concentration Range, Sensitivity, and Precision of the Method: A linear calibration graph passing through the origin was obtained by the recommended procedure over concentration range 1—18 μg Bi cm^{-1} with MPPBA. The detection limit of the method was determined by taking known microgram amount of the metal in total aqueous phase (5 ml) containing 0.2 ml KI and 1 ml sulfuric acid (10 mol dm^{-3}) and it was shaken with a few drops of chloroform solution of amidine. The experiment was repeated until the orange color of the organic phase has been appeared. The detection limit of the method is 0.2 μg Bi cm^{-3}. The molar absorptivity of the complex obtained by this method is 1.35×10^4 l mol^{-1} cm^{-1}. The relative standard deviation of the method for 10 replicate measurements at 150 μg Bi 10 cm^{-3} was ±1.2%.

Effect of Amidines: The effect of substitution in *N*-phenyl ring of the amidine on the color intensity of the extract was examined (Table 1). The introduction of CH_3 or Cl groups in amido N-ring except 2-CH_3 decrease the color intensity of the complex. The breaking of the conjugation as seen with benzyl and octyl groups greatly suppress the color of the complex. The increase in degree of substitution also causes adverse effect. The position of substituents enhances the color intensity in the order: *p*-<*m*-<*o*-.

Composition of the Complex: Bismuth(III) reacts with iodide in sulfuric acid medium to give colored iodo complex which is extracted as iodo-ternary complex with reagent MPPBA into chloroform. The metal to ligand ratio was determined by plotting log *D* (distribution ratio) versus log *M* molar concentration of the reagents and which give slope of 3.9 and 1.8 for iodide and amidine respectively (Fig. 2). The reaction mechanism can be expressed as following:

Table 1. Spectral Data of Iodobismuth Complex with Various Amidines in Chloroform

	$C_6H_5-C(=N-R')-R-N-H$ R	R′	λ_{max} nm	ε l mol^{-1} cm^{-1}	Sandell's sensitivity μg cm^{-2}
1	C_6H_5	C_6H_5	490	12200	0.017
2	2-$CH_3C_6H_4$	C_6H_5	490	13500	0.015
3	3-$CH_3C_6H_4$	C_6H_5	490	11320	0.021
4	4-$CH_3C_6H_4$	C_6H_5	490	10500	0.020
5	2,5-$(CH_3)_2C_6H_3$	C_6H_5	490	10275	0.020
6	2-ClC_6H_4	C_6H_5	490	10620	0.019
7	3-ClC_6H_4	C_6H_5	490	10450	0.020
8	4-ClC_6H_4	C_6H_5	490	10100	0.020
9	2,5-$(Cl)_2C_6H_3$	C_6H_5	490	8360	0.025
10	$CH_3(CH_2)_7$	C_6H_5	490	9000	0.023
11	$C_6H_5CH_2$	C_6H_5	490	9360	0.022

Table 2. Determination of Bismuth(III) in Complex Materials

Sample No.[a]	Bismuth found (ppm) Present method	Bismuth found (ppm) Thiourea method	Relative standard deviation of the present method[b]
a	37.0	39.0	±1.2%
b	12.5	14.0	±1.1%

a) a: Soil sample obtained from Sonakhan Mines. b: Galena sample obtained from Zawar Mines, Udaipur.
b) Average of six determinations.

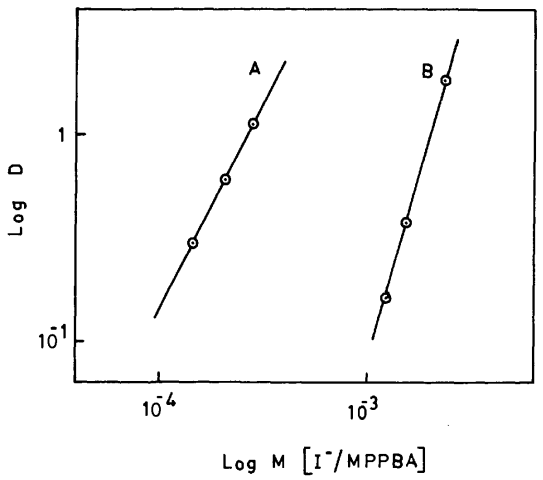

Fig. 2. Determination of composition of the complex in chloroform by curve-fitting method.
C_{Bi}=9.6×10^{-5} mol dm^{-3}; $C_{H_2SO_4}$=2.0 mol dm^{-3}. (A) log D vs. log[MPPBA]; C_{KI}=0.03 mol dm^{-3}. (B) log D vs. log[I$^-$]; C_{MPPBA}=0.014 mol dm^{-3}.

$$Bi^{3+} + 4I^- + H^+ + 2HA_o \rightleftharpoons \{[BiI_4][H(HA)_2]\}_o$$

where subscripts o and HA denote the organic phase and amidine respectively.

Effect of Diverse Ions: The effect of diverse ions in the determination of 175 μg Bi(III) was studied. The complex was extracted as described in the recommended procedure. Interference was considered to occur if the error in the absorbance exceeded ±2%. The tolerance limit of various diverse ions (in mg) are summarized in parentheses as: Cd, Pb (0.7); Ag (1); Sb (3); V, W (4); Hg, Cu, Re (5); Mo, La (30); U (50); Al (70); Ti (80); Th (90); Zr, Cr (100); Be, Mn (120); Zn, Co (200); Ni (300); Br$^-$, $C_2O_4^{2-}$ (50); PO_4^{3-}, Cl$^-$ (80); EDTA (80); NH_2CSNH_2 (50).

Application of the Method: The method has been applied for recovery of the metal to soil and galena samples. A weighed amount of the sample (5 g) is digested with aqua regia (10 cm^3) and dried sample is treated with 5 cm^3 of concentrated hydrochloric acid to remove excess of nitrate ions. It is evaporated upon dryness and then treated with 3—4 cm^3 of concentrated sulfuric acid. The dry residue is then dissolved in water, filter and make up to 50 cm^3 with deionized water. Bi is prior separated by cupferron extraction as described in the literature.[3] The metal content of the sample is determined by standard addition method as described in the procedure. The results indicated that this method is reproducibly applicable to these samples for recovery of the metal.

We are thankful to Ravishankar University for providing fellowship to one of them (A. G.).

References

1) A. Golwelker, K. S. Patel, and R. K. Mishra, *Intern. J. Environ. Anal. Chem.*, **33**, 185 (1988).
2) K. S. Patel and K. H. Lieser, *Anal. Chem.*, **58**, 1547 (1986).
3) E. B. Sandell, "Colorimetric Determination of Traces of Metals," 3rd ed., Interscience, New York (1959).
4) N. M. Lisicki and D. F. Boltz, *Anal. Chem.*, **27**, 1722 (1955).
5) K. Hasebe and M. Taga, *Talanta*, **29**, 1135 (1982).

6) A. Dimitrova and A. Shishov, *Bolg. Akad. Nauk.*, **32**, 1679 (1979); *Chem. Abstr.*, **92**, 190733m (1980).
7) V. E. Poladyan, S. F. Pakhol Chuck, L. M. Avalsovich, and A. M. Andrianov, *Ukr. Knim. Zh.*, **51**, 743 (1985); *Chem. Abstr.*, **103**, 167062d (1985).
8) N. L. Shestidesyataya, P. P. Kish, and A. V. Merenich, *Zh. Anal. Khim.*, **25**, 1547 (1970).
9) Qi-Heng Lu Xu Song and Jin Yao, *K'O Hsuch Tung Pao*, **25**, 302 (1980); *Chem. Abstr.*, **95**, 17501y (1981).
10) H. A. Mottola and E. B. Sandell, *Anal. Chim. Acta*, **25**, 520 (1961).
11) A. Gonzalez, C. Baluja-Santos, and F. Bermejo-Martinez, *Analyst*, **111**, 547 (1986).
12) A. I. Vogel, "A Text book of Quantitative Inorganic Analysis," 3rd ed, Longman, London (1982).

 © 1989 The Chemical Society of Japan Bull. Chem. Soc. Jpn., 62, 3679—3683 (1989)

Extractive Separation and Determination of Lead in Alloys and Environmental Samples

Bhanu RAMAN and V. M. SHINDE*
Analytical Laboratory, Department of Chemistry, Institute of Science,
15, Madam Cama Road, Bombay 400032, India
(Received February 16, 1989)

A method is proposed for the solvent extraction of lead salicylate using triphenylphosphine oxide as an extractant. The optimum extraction conditions were evaluated from a critical study of effects of pH, sodium salicylate concentration and triphenylphosphine oxide concentration. The probable composition of the species has been deduced from log-log plots and the extraction mechanism is suggested. The method has been used to separate lead from commonly associated elements such as copper, nickel, antimony; and also from chromium, iron, and mercury. The method has been further extended to separate and estimate lead in standard alloys, gasoline, and air-borne particulate samples.

The environmental chemistry of lead owes its importance to the pollution caused by autoexhaust emission. The chief source of atmospheric lead is comprised by the variety of antiknock additives in the gasoline which serves the internal combustion engine. Organic lead poisoning is primarily due to the inhalation of the antiknock additive compound viz. tetraethyllead. Lead and its compounds constitute one of the most important industrial health hazards. It is a cumulative poison; hence the toxicity of lead is not immediately felt. It could remain in the bone immobilized for several years. Chronic exposure to lead causes nephritis, scaring, and shrinking of kidney tissues; while, short but intense exposure causes only functional injury. Premature loss of teeth in lead poisoning, is attributed to a demineralization caused by the chemical displacement of the jaw bone calcium by the lead present in the circulatory blood.

In view of the toxic effects of environmental lead, and its compounds, the separation and estimation of lead from the air-borne particulates is desired.

In the various extraction methods available, use has been made of neutral extractants,[1-13] acidic extractants,[14-18] and basic extractants.[19-26] These methods however, have a shortcoming in that, they require a prolonged shaking period,[4,9,13,19] suffer from interference and co-extraction of common cations[9,15] and require high acid concentration for extraction.[19] It is also conspicuous that none of these methods have been applied for the determination of lead in atmospheric air particulate samples.

The proposed method is simple and rapid. It finds a wide range of applications in the separation and determination of lead from a variety of samples.

Experimental

Apparatus and Reagents. A Pye Unicam SP-200 Spectrophotometer and Varian Techron-Model 70 Atomic Absorption Spectrophotometer were used for absorbance measurements. Measurement of pH values was done on a Control Dynamics pH meter.

The stock solution of lead was prepared by dissolving 2.00 g of lead nitrate in 250 ml of distilled water containing 0.5 ml of concentrated nitric acid. The solution was standardized complexometrically[27] using EDTA and test solutions of lower concentration were prepared by suitable dilutions.

A 5% solution of triphenylphosphine oxide (Fluka Grade, mp 156—158 °C) in toluene was used for all extractions.

A 0.1% aqueous solution of 4-(2-pyridylazo)resorcinol was used for spectrophotometric determination of lead.

All other chemincals used were of guaranteed grade and pure, distilled solvents were used throughout the work.

General Extraction Procedure. To an aliquot of solution containing 1 mg of lead, was added 40 mg of sodium salicylate in order to make its concentration of 0.01 M (1 M=1 mol dm^{-3}) in a total volume of 25 ml. The pH of the solution was adjusted to 6.5 with dilute nitric acid and sodium hydroxide solutions. The solution was then transferred to 125 ml separatory funnel and shaken for 90 s with 10 ml of 5% triphenylphoshine oxide in toluene. After separating the two phases, lead was stripped from the organic phase by shaking for 1 min with distilled water (2×10 ml containing 0.5 ml of 0.05 M nitric acid) and estimated complexometrically.[27]

For microgram amounts of lead, the extraction was done using 5 ml of 5% triphenylphosphine oxide solution. The lead was backstripped with distilled water (3×4 ml containing a drop of 0.05 M nitric acid) and estimated spectrophotometrically as follows:

The pH of the aqueous solution was adjusted to 6.5; 1 ml of 0.1% aqueous soltion of PAR was added and diluted to 25 ml. The absorbance of the orange-colored complex was measured at 520 nm[28] against a reagent blank prepared analogously.

Results and Discussion

Extraction Conditions. The extraction of lead was investigated at varying pH (4.0—9.0), salicylate concentration (1.0×10^{-3}—2.0×10^{-2} M) and triphenylphosphine oxide concentration (1—5%). It was observed, that quantitative extraction of lead (in mg amounts) takes place with 10 ml of 5% triphenylphosphine oxide solution from 9.0×10^{-3}—1.0×10^{-2} M sodium salicylate concentration at pH 6.0—6.7. For microgram amounts of lead (25—100 μg) quantita-

Table 1. Optimum Conditions for Extraction of Lead

[Pb]	[Salicylate]/M	Triphenylphosphine oxide (5% in toluene)	pH
1—4 mg	9.0×10^{-3}—1.0×10^{-2}	10 ml	6.0—6.7
25—100 μg	9.0×10^{-3}—1.0×10^{-2}	5 ml	6.0—6.7

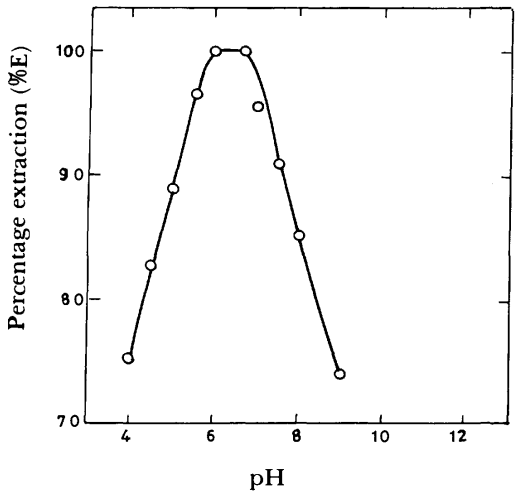

Fig. 1. Extraction behavior of lead salicylate in to triphenylphosphine oxide as a function of pH.
Pb=1 mg; [TPPO]=10 ml of 5% in toluene; [sodium salicylate]=0.01 M; shaking time=90 s.

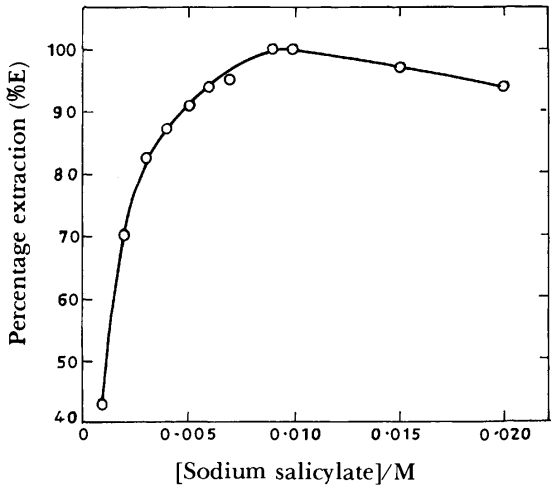

Fig. 2. Extraction behavior of lead salicylate into triphenylphosphine oxide as a function of sodium salicylate concentration.
Pb=1 mg; [TPPO]=10 ml of 5% in toluene; pH=6.5; shaking time=90 s.

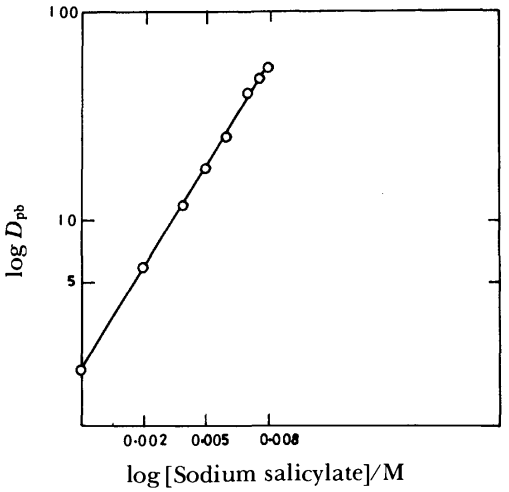

Fig. 3. Distribution ratio of lead(II) as a function of sodium salicylate concentration.
Pb=1 mg; [TPPO]=10 ml of 5% in toluene; pH=6.5; shaking time=90 s.

Table 2. Distribution Ratio of Pb(II) as a Function of Sodium Salicylate Concentration
Pb=1 mg; extractant=10 ml of 5% triphenylphosphine oxide solution in toluene; pH 6.5.

[Sodium salicylate]/M	%E	D
1.0×10^{-3}	43.3	1.91
2.0×10^{-3}	70.2	5.87
3.0×10^{-3}	82.5	11.78
4.0×10^{-3}	87.7	17.77
5.0×10^{-3}	90.9	24.97
6.0×10^{-3}	94.0	39.17
8.0×10^{-3}	95.5	53.05
9.0×10^{-3}—1.0×10^{-2}	100.0	∞

Slope of the plot of log D_{Pb} vs. log C=1.63.

tive extraction of lead is obtained using 5 ml of 5% triphenylphosphine oxide solution. The optimum extraction conditions are reported in Table 1 and illustrated in Figs. 1 and 2.

Nature of Extracted Species. The log-log plots of distribution ratio versus salicylate concentraion, at fixed pH and triphenylphosphine oxide concentration, (Fig. 3 and Table 2) and versus triphenylphosphine oxide concentration, at fixed pH and sodium salicylate concentration (Fig. 4 and Tabel 3) indicate a molar ratio of 1:2 with respect to both salicylate ion and triphenylphosphine oxide. Hence, the probable extracted species is, $Pb(Sal)_2\cdot2TPPO$ where Sal stands for salicylate ion and TPPO stands for triphenylphosphine oxide. Thus, the probable extraction mechanism can be expressed as:

$$Pb(H_2O)_2^{2+} + 2(HOC_6H_4COO)^- + 2TPPO \rightleftharpoons Pb(HOC_6H_4COO)_2\cdot2TPPO + 2H_2O$$

Extracted species

The extraction may be due to the solvation of lead salicylate by triphenylphosphine oxide molecules.

Effect of Foreign Ions. A number of ions were tested for the interference in the extraction of lead. The study showed that for the extraction and photometric estimation of 50 μg of lead, a large number of cations and anions did not interfer (as shown by less than 1% error in analytical recovery of lead). However, ions such as uranium(VI), thorium(IV), and oxalate did offer interference. The results of the study of interfering ions is reported in Table 4.

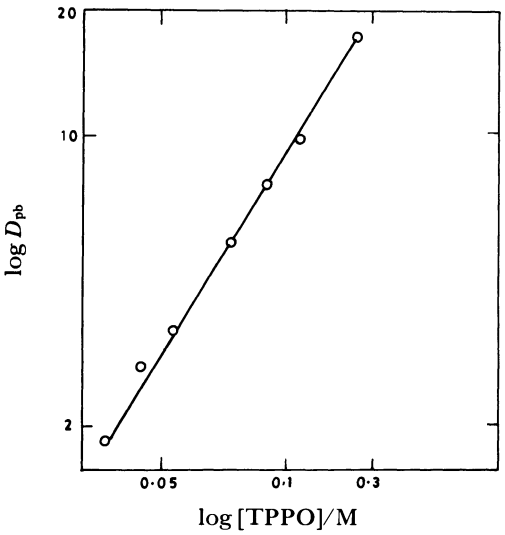

Fig. 4. Distribution ratio of Pb(II) as a function of triphenylphosphine oxide concentration.
Pb=1 mg; [sodium salicylate]=1.0×10^{-2} M; pH=6.5; shaking time=90 s.

Table 3. Distribution Ratio of Pb(II) as a Function of Triphenylphosphine Oxide Concentration
Pb=1 mg; Extractant=10 ml of triphenylphosphine oxide solution in toluene; [Sodium salicylate]=0.01 M; pH=6.5

[TPPO]/%	%E	D
1.0	42.7	1.86
1.25	53.0	2.82
1.5	58.1	3.47
2.0	69.2	5.61
2.5	75.6	7.75
3.0	80.0	10.00
4.0	87.7	17.82
5.0	100.0	∞

Slope of the plot of log D_{Pb} vs. log C=1.7.

Separation of Lead from Chromium(VI), Iron(III), Antimony(III), Copper(II), Nickel(II), and Mercury(II). Ions such as chromium(VI) , iron(III), antimony(III), copper(II), and nickel(II) are not extracted into triphenylphosphine oxide under the optimum extraction conditions of lead. Hence, it is possible to separate lead from these elements in their binary mixtures. The unextracted ions were detemined spectrophotometrically using known methods while lead is estimated spectrophotometrically using PAR as described in the general procedure.

Under the extraction conditions of lead, mercury shows partial extraction. However, by selective stripping of lead with distilled water, which does not backstrip mercury, the two ions can be quantitatively separated from each other. The partially extracted mercury is backstripped with acetate buffer (pH 4.7); combined with the major portion of unextracted mercury and estimated complexometrically.[29]

The recovery of lead and the added ions is ≥99.0%. The results of the separation of binary mixtures is reported in Table 5.

Analytical Applications. 1. Analysis of Alloys. 0.5 g of each of two different standard alloys containing lead, were weighed accurately. Then, 10 ml of concentrated nitric acid was added to each of them and were evaporated to dryness. The residue was taken up with dilute nitric acid (4 M) and the precipitate of metastannic acid was filtered off. The filtrate was diluted to 50 ml and an aliquot of this solution was used for the extraction and estimation of lead using the proposed method.

2. Analysis of Gasoline. 25 ml of Gasoline containing tetraethyllead was evaporated slowly on a water bath (≃80 °C) to remove all the volatile liquids. To the oily residue, 3 ml of concentrated nitric acid was added, slowly, with due care, in order to convert organolead to lead nitrate. This was heated on a water bath for 20 minutes. After cooling, the oily part was removed by extracting it with benzene while the lead

Table 4. Effect of Possible Interfering Ions on the Extraction of 50 μg of Lead(II)[a]

Tolerance limit/μg	Foreign ions
1000	As(III), Sb(III), Ca(II), Fe(III), Cr(VI), Mn(II), Hg(II), Mg(II), F^-, Cl^-, Br^-, NO_3^-, SO_4^{2-}, SCN^-, $S_2O_3^{2-}$
750	Zr(IV), Al(III)
500	Ag(I), Ba(II), Sr(II), Pd(II), Au(III), Te(IV), V(V)
250	Se(IV), ascorbate
100	Ni(II), Co(II), Bi(III)
50	Cu(II), Pt(IV), PO_4^{3-}
Ions not tolerated	U(VI), Th(IV), Oxalate

a) Spectrophotometric estimation.

Table 5. Separation of Pb(II) from Cr(VI), Fe(III), Ni(II), Cu(II), and Hg(II) in Their Synthetic Binary Mixtures

Sr. No.	Composition/μg	Recovery of Pb(II)[a]/%	Relative error/%	Recovery of added ion/%	Relative error/%	Estimation procedure for added ions and their references
1.	Pb(II), 50; Sb(III), 100	99.8	0.2	99.8	0.2	Photometrically with KI (30)
2.	Pb(II), 50; Sb(III), 250	99.9	0.1	99.8	0.2	Photometrically with KI (30)
3.	Pb(II), 50; Cr((VI), 10	99.7	0.3	99.0	1.0	Photometrically with diphenyl carbazide (31)
4.	Pb(II), 50; Cr(VI), 20	99.5	0.5	99.2	0.8	Photometrically with diphenyl carbazide (31)
5.	Pb(II), 50; Fe(III), 50	99.7	0.3	99.3	0.7	Photometrically with 1,10-phenanthroline (30)
6.	Pb(II), 50; Fe(III), 100	99.6	0.4	99.4	0.6	Photometrically with 1,10-phenanthroline (30)
7.	Pb(II), 50; Ni(II), 50	99.2	0.8	99.5	0.5	Photometrically with dimethyl glyoxime (30)
8.	Pb(II), 50; Cu(II), 25	99.5	0.5	99.1	0.9	Photometrically with PAN (32)
9.	Pb(II), 50; Hg(II), 1000	99.1	0.9	99.0	1.0	Complexometrically with EDTA (29)

a) Mean of 6 determinations.

Table 6. Analysis of Lead in Real Samples

Sr. No.	Sample	Lead content (Certified)	Results found by the proposed method	
			Spectrophoto metrically[a]	By AAS
1.	Tin base white metal (179/2)[b]	3.18%	3.10%	3.08%
2.	White metal (8d)[b]	3.26%	3.21%	3.22%
3.	Gasoline	—	5.33 ppm	5.31 ppm
4.	Air-borne particulate samples			
	(a) Tilaknagar area	—	2.36 μg m^3	2.35 μg m^3
	(b) Khar area (I)	—	0.36 μg m^3	0.36 μg m^3
	(c) Khar area (II)	—	0.52 μg m^3	0.52 μg m^3
	(d) Khar area (III)	—	1.03 μg m^3	1.03 μg m^3
	(e) Parel area	—	0.68 μg m^3	0.70 μg m^3

a) Mean of 6 results. b) British Standard Alloys.

nitrate formed in situ was estimated by recommended procedure.

3. Analysis of Air-Borne Particulates. Filter paper strips containing adsorbed lead particles from polluted air samples were supplied by Air Pollution Monitoring and Research Laboratory, Municipal Corporation of Greater Bombey, Khar. The samples belonged to different subrban areas of Bombay such as Parel, Khar, and Tilaknagar. The separation and determination of lead in these glasswool filter papers (containing adsorbed air particulates) were done as follows:

Sample filter paper strips (8 sq cm area) were digested with 10 ml of 50% nitric acid for about 15 minutes. This was then diluted with distilled water to 15 ml volume and filtered to remove the insoluble glasswool filter paper residue and other dust particles. The filtrate was used for the extration and estimation of lead by the proposed method.

The results of the above sample analysis are reported in Table 6. All the samples were also analyzed for comparison of results, using Atomic Absorption Spectrophotometer. The results so obtained were in good agreement with each other.

Our thanks are due to C. S. I. R., New Delhi for financing the project and also to Air Pollution Monitoring and Research Laboratory, Municipal Corporation of Greater Bombay, Khar, for providing the samples.

References

1) T. N. Tweeten and J. W. Knoeck, *Anal. Chem.*, **48**, 64 (1976).

2) B. I. Petrov, M. I Degtev, and V. P. Zhivopestev, *Izv. Vyssh. Uchebn. Zaved., Khim. Khim. Tekhnol.*, **20**, 681 (1977).

3) Y. Akama, H. Naka, T. Nakai, and F. Kawamura, *Bunseki Kgaku*, **27**, 680 (1978).

4) M. V. R. Murti and S. M. Khopkar, *J. Indian Chem. Soc.*, **55**, 735 (1978).

5) I. Yasoo, T. Tsuzuki, and K. Inoue, *Hokkaidoritsu*

Eisei Kenkyushoho, **30**, 98 (1980).
6) A. Atonso, M. Gallego, and M. Valcarcel, *Bunseki Kagaku*, **32**, E-387 (1985).
7) J. Wang, *Huaxe Tongbao*, **7**, 37 (1986).
8) V. V. Mudshingikar and V. M. Shinde, *Indian J. Chem., Sect. A*, **23**, 539 (1984).
9) S. B. Akki and S. M. Khopkar, *Bull. Chem. Soc. Jpn.*, **45**, 167 (1972).
10) A. A. Yadav and S. M. Khopkar, *Talanta*, **18**, 833 (1971).
11) A. Sanz-Medel, D. Blanco Gomis, E. Fuente, and S. Arribas Jimeno, *Talanta*, **31**, 515 (1984)
12) V. V. Yashin, M. B. Korshunov, and M. T. Tolmachova, *Zh. Anal. Khim.*, **40**, 469 (1985).
13) J. W. O'Laughlin and T. P. O'Brion, *Talanta*, **22**, 587 (1975).
14) R. Pietsch, *Anal. Chim. Acta*, **115**, 379 (1980).
15) U. S. Ray, *Indian J. Chem., Sect. A*, **21**, 444 (1982).
16) U. S. Ray, and S. C. Modak, *J. Indian Chem. Soc.*, **61**, 245 (1984).
17) J. Chwastowoska, E. Kosiarska, and G. Maciejko, *Chem. Anal. (Warsaw)*, **22**, 927 (1977).
18) R. Pietsch and P. T. Gilani, *Anal. Chim. Acta*, **75**, 385 (1975).
19) E. Uhlemann, B. Maack, and M. Raab, *Anal. Chim. Acta*, **116**, 403 (1980).
20) S. Werner, *Z. Chem.*, **20**, 383 (1980).
21) T. Suzuki and T. Sotobayashi, *Jpn. Analyst*, **12**, 910 (1964).
22) P. S. Patil and V. M. Shinde, *Sepn. Sci. Technol.*, **14**, 247 (1979).
23) B. Yu. Spivakov, V. I. Lebede, V. M. Shkinus, N. P. Krivenkova, T. S. Plotnikova, I. P. Kharlamev, and Yu. A. Zolotov, *Z. Anelit. Khim.*, **31**, 757 (1976).
24) G. K. de Jong, W. T. Kok, and U. A. T. Brinkman, *J. Chromatogr.*, **135**, 249 (1977).
25) C. W. McDonald, M. M. Mahayni, and M. Konjo, *Sepn. Sci. Technol.*, **135**, 429 (1978).
26) S. P. Rao, R. R. Reddy, and J. Jagdamba, *Acta Cienc. Indica (Ser.) Chem.*, **9**, 235 (1983).
27) A. I. Vogel, "A Text book of Quantitative Inorganic Analysis," 3rd ed, Longmans, London (1961), p. 443.
28) N. M. Malakhova, N. L. Olenovich, and N. I. Kotelnaya, *Zh. Anal. Khim.*, **35**, 475 (1980).
29) F. J. Welcher, "The Analytical Uses of EDTA," ed by D. Van Nostrand, New York (1961), p. 164.
30) Z. Marczenko, "Spectrophotometric Determination of Elements," Wydawnictwa-Nauko-Techniczne and Ellis Harwood Publisher (1976), pp. 127, 311, 372.
31) E. B. Sandell, "Colorimetric Determination of Traces of Metals," 3rd ed, Interscience, New York (1961), p. 397.
32) B. F. Pease and M. B. Williams, *Anal. Chem.*, **31**, 1044 (1959).

 © 1989 The Chemical Society of Japan Bull. Chem. Soc. Jpn., 62, 3684—3690 (1989) [Vol. 62, No. 11

Polar and Dipolar Substituent Effects and Transition State in the Reaction between Substituted Anilines and Nitrosobenzene. An Evaluation of Ortho and Electrostatic Effects

Carla C. SCHMITT, Carlos A. MORITZ, Moacir G. PIZZOLATTI, and Rosendo A. YUNES*
Departamento de Química, Universidade Federal de Santa Catarina, 88049 Florianópolis, SC, Brazil
(Received September 2, 1988)

The rate constants of the hydronium catalyzed attack of substituted anilines on nitrosobenzene, to give azobenzene, exhibit a large dependence on the substituent constant σ^- ($\rho^-=-1.92$). The relatively high value of ρ^- compared to that obtained from the equilibrium of protonation of anilines ($\rho^-=-2.77$) and the solvent effect on the rate constants support the idea that the transition state involves a large amount of nitrogen-nitrogen bond formation and therefore a strong charge development on the nitrogen and oxygen of the amino and nitroso groups, respectively. A good correlation between basicity and nucleophilic reactivity is obtained by the Brönsted equation ($\beta=0.65$, $r=0.988$) for the para and meta dipolar substituents. Aminobenzoates show a significantly higher reactivity than that calculated from the Brönsted line and this is attributed to an electrostatic participation of the carboxylato group. Nevertheless, this effect is somewhat compensated by repulsion between the carboxylato and the negatively charged oxygen of the nitroso group.

The substituent effects of charged and dipolar groups can be used in order to obtain information about the nature of the transition state of organic reactions. Some authors[1] are of the opinion that charged groups cannot be included with the dipolar groups in one general scale of electronic substituent constant, but others[2] list values of substituent constants for charged groups using results obtained mainly by equilibria or physical properties. Rate data are prime sources of information about the substituent effects on the transition state of the reactions but, in spite of this, few studies have been made dealing with the effect of the carboxylato group on reactivity. Capon[3] studied the participation of the carboxylato group in the hydrolysis of 2-bromopropionate, Bordwell and Knipe[4] in the hydrolysis of α-bromophenylacetic acid that follows an S_N1 mechanism with formation of a zwitterionic-like transition state and Anderson and Fife[5] in the hydrolysis of benzaldehyde disalicylacetal.

In this work we have studied the substituent effects, especially of the carboxylato group, in the reaction of substituted anilines with nitrosobenzene in order to i) obtain a better understanding of the transition state structure of the rate determining step and ii) to evaluate the electrostatic participation of the carboxylato group and the ortho effect of the substituents.

The reaction between anilines and nitrosobenzene was previously studied[6-9] and Yunes et al.[9] showed that the mechanism of this reaction is similar to that of the reaction of weakly basic amines with benzaldehydes and other carbonyl substances.[10] Therefore, attack of the amine is rate-determining under acidic conditions and dehydration of an addition intermediate becomes rate-determining in neutral or basic pH.

Experiments were carried out in MeOH 15% wt and acid pH such that the hydronium-catalyzed attack of aniline on nitrosobenzene (k_H) is the rate-determining step (Eq. 1).

$$\mathrm{PhNO + PhNH_2} \overset{\text{slow}}{\underset{k_H}{\rightleftharpoons}} \mathrm{PhN(OH)\overset{+}{N}H_2Ph} \rightleftharpoons \mathrm{PhN(OH)NHPh} \xrightarrow{k_d} \mathrm{PhN{=}NPh + H_2O} \quad (1)$$

The reaction was also studied in different mixed solvents considering that the less polar media could provide better conditions for electrostatic participation of the carboxylato group and could be a simple model for the participation of charged groups in enzyme-catalyzed reactions.

Results

The first-order constant for condensation of aminobenzoic acids with nitrosobenzene in excess of amines in 15% methanol and 85% water by weight, $\mu=0.5$ M (1 M=1 mol dm^{-3}) (KCl), at 25 °C varies linearly with total amine concentration at constant pH. This behavior implies the absence of general acid or base catalysis by the aminobenzoic acids in the concentration range studied. The same result was observed with aniline.[9,10]

The rate law for aminobenzoic acids can be written as:

$$k_{obs} = k_o^{NC}[NC] + k_o^{A}[A] + k_H^{NC}[NC][H^+] + k_H^{A}[A][H^+] \quad (2)$$

where k_o^{NC} is the rate constant of the pH independent reaction of NC. k_o^{A} is the rate constant of the pH independent reaction of A. k_H^{NC} is the rate constant of the hydronium ion-catalyzed reaction of NC. k_H^{A} is the rate constant of the hydronium ion-catalyzed reaction of A. NC and A are the uncharged and anionic species, respectively (Scheme 1).

Rate constants of the pH-independent reaction are negligible in comparison to those for the hydronium-catalyzed reaction (2.5×10^{-4} M^{-2} min^{-1} and 5.1×10^{3} M^{-2} min^{-1} respectively for aniline) and therefore Eq. 1 reduces to:

$$k_{obs} = k_H^{NC}[NC][H^+] + k_H^A[A][H^+] \quad (3)$$

From Eq. 3 and data at different pH the third-order rate constants k_H^{NC} and k_H^A were calculated.

For the other amines the second-order and the third-order rate constants were calculated following methods previously described.[10]

The hydronium ion-catalytic rate constants are collected in Table 1.

In order to evaluate the relation between basicity and nucleophilicity, a Brönsted type relation (4) was used.

$$\log k_H = \beta pK_a + C \quad (4)$$

The parameters determined from the data for compounds **1**, **2**, **4**, **6**, and **7** (Table 1) are β=0.65, C=0.69 and the correlation coefficient r=0.988. The plot is shown in Fig. 1. All the aminobenzoate ions give rate constants larger than those predicted by the Brönsted equation. The largest positive deviation was for the *p*-aminobenzoate ion.

The catalytic rate constants for the hydronium ion-catalyzed reactions of substituted anilines **1**, **2**, **6**, and **7** were plotted logarithmically against the σ substituent constant,[11] yielding a ρ value of −2.08 (r=0.955). If compound **4** is included in the plot a better correlation is obtained with σ^-[12] and ρ^- is −1.92 (r=0.978).

The ratios of the rate constants of the hydronium ion-catalyzed reactions for formation of azobenzene from *o*- and *p*-substituted anilines are collected in Table 2. With the uncharged substituents chloro, methyl, and carboxyl groups the ratio is less than unity, whereas for the carboxylato group the ratio is greater than unity. It is interesting to note that the corresponding ratios for similar reactions of substituted benzaldehydes with a variety of nitrogen nucleophiles, including hydroxylamine, semicarbazide, *p*-toluidine, and phenylhydrazine are considerably greater than unity.[13-17] This result has been attributed to greater electronic delocalization in benzaldehydes brought about by para substituents, as

Table 1. Catalytic Rate Constants for the Hydronium Ion (M^{-2} min^{-1}) for Attack of Substituted Anilines on Nitrosobenzene[a]

	Substituent	pK_a	k_H	log k_H
1	H	4.62[b]	5100	3.70
2	*m*-COOH	3.63[c]	1150	3.06
3	*m*-COO^-	4.64[c]	12500	4.09
4	*p*-COOH	2.39[c]	210	2.32
5	*p*-COO^-	3.73[c]	3900	3.59
6	*p*-CH_3	5.07[b]	11500	4.08
7	*p*-Cl	3.81[b]	980	2.99
8	*o*-COOH	2.40[c]	170	2.23
9	*o*-COO^-	4.76[c]	12300	4.09
10	*o*-CH_3	4.38[b]	1600	3.20
11	*o*-Cl	2.62[b]	100	2.00

a) 15 Wt% methanol-water, at 25 °C and ionic strength 0.5 M (KCl). b) W. P. Jenks and J. Regenstein, "Handbook of Biochemistry," 3rd ed, ed by G. D. Fasman Chem. Rub. Pub., Cleveland (1976). c) Ref. 31.

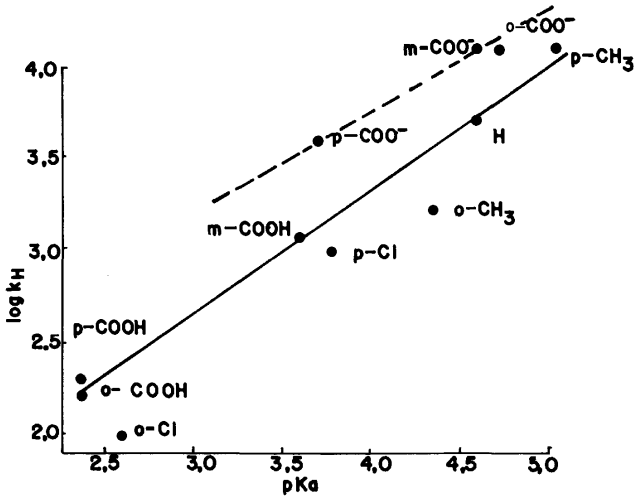

Fig. 1. Logarithms of rate constants of the hydronium ion-catalyzed reaction of nitrosobenzene with anilines in 15 wt% methanol water, 25 °C, ionic strength 0.5 M (KCl) as a function of pK_a of the anilines.

Table 2. Ortho/Para Ratios for the Hydronium-Catalyzed Reaction of Anilines with Nitrosobenzene[a]

Substituent	k_H^{ortho}/k_H^{para}
-CH_3	0.17
-Cl	0.10
-COOH	0.80
-COO^-	3.1

a) In 15 wt% methanol, at 25 °C and ionic strength 0.5 M (KCl).

Table 3. Rate Constants (M^{-2} min^{-1}) of Hydronium Ion-Catalyzed Reactions of Nitrosobenzene with Anilines[a,b]

	EtOH wt%			
	20	35	50[c]	65
k_H	4100	1540	410	250
$k_H^{o\text{-}CH_3}$	1400	600	190	125
$k_H^{p\text{-}CH_3}$	9000	3600	960	550
$k_H/k_H^{p\text{-}CH_3}$	0.45	0.44	0.43	0.45
$k_H/k_H^{o\text{-}CH_3}$	2.93	2.56	2.15	2.00
$k_H^{o\text{-}CH_3}/k_H^{p\text{-}CH_3}$	0.16	0.17	0.19	0.22

a) At 25 °C, in different mixtures of EtOH-H_2O. b) pK_a of anilines from B. Gutbenzahl and E. Grunwald, *J. Am. Chem. Soc.*, **75**, 559 (1953). c) Ref. 7.

Table 4. Rate Constants ($M^{-2}\,min^{-1}$) of Hydronium Ion-Catalyzed Reactions and Charge Effects in Condensation between Aminobenzoic Acids, Aminobenzoates, and Nitrosobenzene[a)]

	CH_3OH wt%	
	15	53
k_H	5100	520
$k_H^{o\text{-}COOH}$	170	35
$k_H^{m\text{-}COOH}$	1150	190
$k_H^{p\text{-}COOH}$	210	40
$k_H^{o\text{-}COO^-}$	12300	70000
$k_H^{m\text{-}COO^-}$	12500	72000
$k_H^{p\text{-}COO^-}$	3900	31500
$k_H^{o\text{-}COO^-}/k_H^{o\text{-}COOH}$	72	2285
$k_H^{m\text{-}COO^-}/k_H^{m\text{-}COOH}$	11	379
$k_H^{p\text{-}COO^-}/k_H^{p\text{-}COOH}$	18	787

a) 15 wt% and 53 wt% methanol, at 25 °C.

compared with ortho substituents.[15,17]

The reaction between *o*-methyl-, *p*-methyl-, and unsubstituted aniline with nitrosobenzene was studied in different mixtures of ethanol-water (Table 3). Increasing the proportion of ethanol decreases the ratio $k_H/k_H^{o\text{-}CH_3}$, but the ratio $k_H/k_H^{p\text{-}CH_3}$ stays practically constant.

Condensation of aniline, aminobenzoic acids, and aminobenzoate ions with nitrosobenzene was studied in 53 wt% of methanol-water (Table 4). The rate constant for the hydronium ion-catalyzed reaction between aniline and nitrosobenzene decreases approximately 10 times when the proportion of methanol is changed from 15 wt% to 53 wt%. With *o*-, *m*-, and *p*-aminobenzoic acids the rate decrease is 4 to 6 fold, and with aminobenzoate ions the rates increase by factors of 6 to 8. Reaction of the *o*-aminobenzoate ion should have a rate constant of $2.5\times10^3\,M^{-2}\,min^{-1}$ in 53 wt% methanol if its response to the change of methanol proportion was similar to that for *o*-aminobenzoic acid, but it has a hydronium-catalytic rate constant of $7.0\times10^4\,M^{-2}\,min^{-1}$ and thus the reaction is 28 times faster. *m*- and *p*-Aminobenzoate ions show similar behavior. The $k_H^{COO^-}/k_H^{COOH}$ ratios are given in Table 4. Correlations of the catalytic constants of hydronium ion for compounds **1**, **2**, **3**, **4**, and **5** (Table 1) using the substituent constants of McDaniel and Brown,[11] in Hammett plots, yield the following values: $\rho=-2.62$ ($r=0.952$) for the reaction in MeOH 15 wt% and $\rho=-4.78$ ($r=0.820$) for the reaction in MeOH 53 wt% (plots are not shown).

Discussion

For aniline protonation in water at 25 °C based on σ^- constants the ρ^- value equals −2.77.[18] This value is considered a measure of the susceptibility of the reaction to substituent effects and is an indication of the complete charge development at the nitrogen atom adjacent to the ring in passing from reagents to products. The correlation with σ^- shows that the conjugation, existing in aniline, between the amino group and the substituents is not present between the ammonio group and the substituents in the anilinium ion. This last assumption is reasonable, theoretically, because the nitrogen on the ammonio group has no unshared electron pair and, being a first-row element, cannot expand its valence shell to accommodate more than eight electrons.

The correlation of nucleophilic reactivity towards the nitroso group, in methanol 15 wt% at 25 °C, and σ^-, gives $\rho^-=-1.92$. Even considering the solvent effect, this value is large, compared with that of aniline protonation in pure water, and is an indication of an extensive charge formation on the nitrogen of the amino group in going from the initial state to the transition state. The good correlation with σ^- shows that there is a clear difference of resonance interaction between the substituents and the reaction center (the amino group) in the initial state and in the transition state. Indeed the delocalization of the unpaired electrons of the amino group in the aniline should be very much reduced in the transition state and consequently the formation of the N-N bond must have proceeded to a considerable extent.

Other piece of evidence about the nature of the transition state is the correlation by the Brönsted equation. The β value for the addition of a proton to aniline, with complete formation of the positive charge, is by definition 1. This value should be smaller for the complete addition of the polarized nitroso group, because it is somewhat less electropositive than the proton. In consideration of this, the value of β obtained 0.65 indicates that the dependence of the reaction on basicity is large. This fact indicates that there should be a large amount of positive charge developed in the attacking nucleophile in the transition state.[10,19] All these results suggest a probable transition state structure that is represented in Eq. 5.

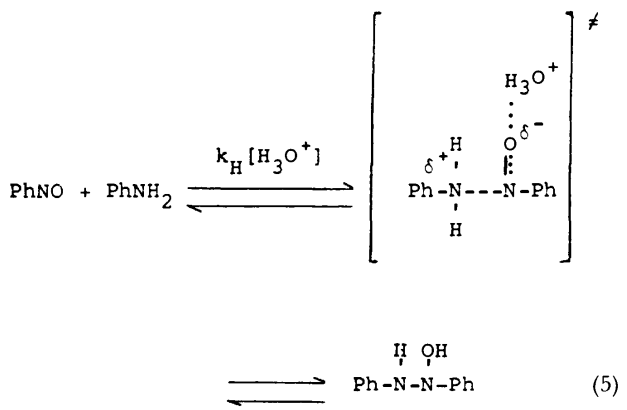

(5)

Considering that the negative charge on the oxygen of the nitroso group is somewhat stabilized by the

catalyst, the strong charge formation on the nitrogen of the amino group would be the main reason for the observed decrease of the catalytic rate constant of aniline and its derivatives with dipolar substituents when the solvent polarity is lowered (Tables 3, 4); under the same conditions, the delocalization of positive charge on the nitrogen of the amino group explains the increase of the rate constants of the attack of water[20] on Schiff bases.

The pK_a of substituted anilines measures the electronic and steric effects of the substituents to protonation of the amino group, however the electron-donating methyl group and the electron-withdrawing chloro atom at the ortho position of aniline give rate constants that fall below the correlation line of the Brönsted plot (Fig. 1) and ortho/para ratios smaller than unity (Table 2). This can be explained by a greater steric effect on the reaction than on the protonation of anilines because the electronic effects of the substituents should be similar in kinetics and equilibria. Wepster[21] has suggested that steric hindrance to solvation of the protonated species is the principal cause of the low basic strength of *o*-alkyl anilines. The reactivity of anilines in different mixtures of ethanol–water (Table 3) suggests that in reaction (5) the steric hindrance to solvation of the transition state is one cause of the smaller experimental value of the catalytic rate constants for ortho-substituted anilines with respect to the value obtained from the Brönsted line. Thus, the $k_H/k_H^{o\text{-}CH_3}$ ratio decreases when the solvating power of the solvent decreases (increasing the ethanol proportion) showing the steric effect of the *o*-methyl group on the transition state solvation. For the *p*-methyl group, where the steric hindrance of transition state solvation is negligible, the $k_H/k_H^{p\text{-}CH_3}$ ratio stays constant. Other steric effects can exist as was indicated by Fujita and Nishioka,[22] in their analysis of ortho effect, but it is evident from the results that they should not be so important to explain the deviation mentioned above. The rate constant of the hydronium ion-catalyzed reaction of *o*-aminobenzoic acid falls on the correlation line of the Brönsted plot. An explanation of this behavior is that there should exist an internal association between the $-\overset{+}{N}H_2$ and the -COOH groups, in the transition state, as is suggested by ^{13}C NMR spectral data[23] of protonated *o*-aminobenzoic acid.

Spectral studies, dipole moment data,[24,25] and kinetic data[15-17] indicate that, when the ortho substituents are in the electrophilic reagent as in the reaction between substituted benzaldehydes and nitrogen nucleophiles,[16,17] steric effects are unimportant. The reaction of *o*-methylnitrosobenzene and aniline gives a hydronium-catalyzed rate constant of 4.8×10^3 $M^{-2}\,min^{-1}$ [26] while the rate constant for the unsubstituted compounds is 5.1×10^3 $M^{-2}\,min^{-1}$; this small decrease should be attributed to electronic effects of the methyl group and indicates that in this case the ortho substituent does not affect significantly the attack of aniline and the solvation of the transition state. This last result can be explained because in the transition state the substituents are sufficiently separated from the charged atoms to affect their stabilization by solvation.

One of the most striking facts of this reaction is that the carboxylato-substituted anilines react faster than predicted by the Brönsted plot (for the anilines with uncharged meta and para substituents) giving a different line with a smaller slope (dashed line in Fig. 1 that was drawn considering the points of *m*- and *p*-aminobenzoates). Bruice and Lapinski[27] have shown that the reactivities of a series of nitrogen nucleophiles toward *p*-nitrophenyl acetate fall on lines of slopes 0.8 but with separate lines for substituted imidazols, pyridines, and anilines. It has also been shown for the reactivities of primary, secondary and tertiary amines toward different substracts.[28] Now it is reported that the reactivities toward nitrosobenzene of the same nucleophile aniline, with charged and uncharged substituents, fall in different lines.

A large number of factors may affect the nucleophilic reactivity of the carboxylato anilines and it is possible that their high reactivity should not depend on a single cause. However, the dramatic increase in the rate constant for these anilines on changing from methanol 15 wt% to methanol 53 wt% indicates an electrostatic participation of the carboxylato group which stabilizes the transition state of the reaction. The participation of electrostatic effect in reactions with charged nucleophiles was demonstrated in different systems.[29] However, in this case, the question is why the electrostatic participation of the carboxylato group is different in kinetics and in equilibria. Basicity of anilines in aqueous solution depends strongly, as the amines in general, on specific solvation of their conjugated acids by hydrogen bonding to the solvent.[21,30] In the transition state of the reaction between anilines and nitrosobenzene there is a smaller adhesion, by hydrogen-bonded structure, of solvent molecules on the charged reaction center surface of the activated complex. Thus, the less polar character of the cavity of low dielectric constant near the reaction center, according to the model of Kirwood-Westheimer,[31] make possible a greater electrostatic effect of the carboxylate group on the transition state.

Considering the arguments discussed above it seems probable that the stabilization of the anilinium positive charge by ion–dipolo interactions with the solvent molecules should be smaller than the corresponding to the positive charge of the activated complex of the reaction between anilines and nitroso-

benzene. As the ortho substituents in aniline should affect more the solvent molecules that interact by ion-dipolo forces than those that interact by hydrogen bonding it is possible to interpret the greater steric effect of *o*-methyl and *o*-chloro substituents to the solvation of the transition state of the reactions than to the solvation of the products of the equilibrium.

The reactivity of the aminobenzoates follows the order of stabilization of the zwitterionic species of aminobenzoic acids: meta>ortho>para, but the order of positive deviation of the values of the experimental catalytic rate constants with respect to the values calculated from the Brönsted lines is: para>meta> ortho (2.9; 2.4; and 1.9 times respectively). In the zwitterions there is a positive charge on the ammonio group but in the proposed structure of the transition state, in addition to the positive charge on the nitrogen of the amino group, there is a negative charge on the oxygen of the nitroso group that, although somewhat stabilized by the catalyst, should cause some repulsive interaction with the carboxylato group. The order of positive deviation corresponds to the distance between the carboxylato and the nitroso groups since the electrostatic repulsion decreases with distance. The strong deviation of the *o*-aminobenzoate, considering the small distance between the two negative groups, can be explained by an intramolecular hydrogen bond between the ortho carboxylato and the positive amino group in the transition state.[23]

The application of the Hammett equation to the hydronium-catalytic rate constants of compounds with polar and dipolar groups (**1**, **2**, **3**, **4**, and **5** of Table 1) using the substituent constants of McDaniel and Brown[11] gives a good correlation for the reaction in MeOH 15 wt% and a bad correlation for the reaction in MeOH 53 wt%. This result can be attributed to the significant increase of the electrostatic effect of pole (carboxylato group) with the change of the solvent and support the observation of Wepster et al.[32] that the variation of σ values of poles is so large, considering the conditions of the reactions, that it probably makes no sense to average σ values of poles.

The principal conclusions drawn from this work are the following:

i) The transition state of the reaction of formation of azobenzenes from nitrosobenzene and aniline when the rate-determining step is the attack of aniline on nitrosobenzene involves a large amount of nitrogen-nitrogen bond formation and consequently a strong charge formation on the nitrogen and on the oxygen of the amino and nitroso group, respectively.

ii) There exists a clear ortho effect, due principally to inhibition of the transition state solvation, in the reaction between nitrosobenzene and *o*-substituted anilines whereas there is none when the reaction is between aniline and *o*-substituted nitrosobenzene.

iii) The substituents and ortho effects, specially of poles, depend significantly on the transition state structure and on the reaction media.

Experimental

Materials: Nitrosobenzene was synthesized according to standard procedures[33] and purified by sublimation. Anilines were redistilled or recrystallized and their solutions were prepared just prior to use.

Kinetic measurements were carried out spectrophotometrically at 25 °C with a Shimadzu 210 A ultraviolet spectrophotometer. Reactions were monitored by observing the appearance of the bands of azobenzene at 435 and 350 nm in solutions containing initial concentrations of 3.33×10^{-4} M and 10^{-1} to 10^{-2} M, or 10^{-2} to 10^{-3} M and 1.6×10^{-5} M, for nitrosobenzene and the anilines respectively. The kinetic studies were performed with nitrogen-degassed solutions. The pH range was between 1 to 5. The error of the obtained rate constants was never higher than 3%, for *p*-carboxylato substituted anilines agreement was within 5%.

Calculations of Concentrations of Anilines: The concentrations of all the aminobenzoic acids and aminobenzoates were calculated considering the equilibria of Scheme 1 and Eqs. 6, 7, and 8 that give the relation between the microscopic constants K_a, K_b, K_c, and K_d and the macroscopic constant K_1 and K_2 given in the literature as acidity constants of the aminobenzoic acids.

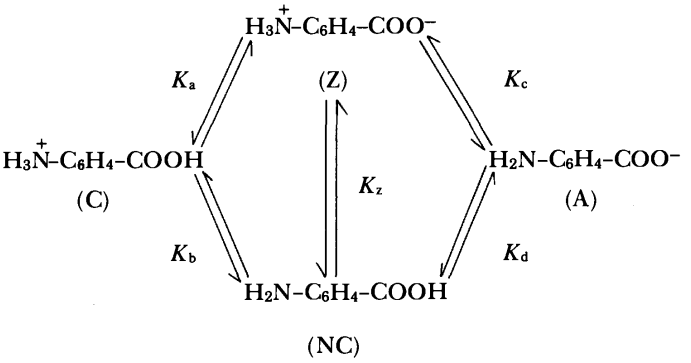

Scheme 1.

$$K_1 = K_a + K_b \tag{6}$$

$$1/K_2 = 1/K_c + 1/K_d \tag{7}$$

$$K_z = K_a/K_b = K_d/K_c \tag{8}$$

The total concentration of aminobenzoic acid is

$$[AMT] = [C] + [NC] + [A] + [Z] \tag{9}$$

and considering the equilibria of Scheme 1, it is possible to obtain Eqs. 10 and 11 that permit calculation of the concentrations of the reactives species NC and A:

$$[NC] = \frac{1}{(1 + K_z)(1 + [H^+]/K_1 + K_2/[H^+])} \cdot [AMT] \tag{10}$$

$$[A] = \frac{1}{1 + [H^+]^2/K_1 \cdot K_2 + [H^+]/K_2} \cdot [AMT] \tag{11}$$

The pK_a values of anilines under the experimental conditions: MeOH 15 wt%, μ=0.5 M [KCl], [anilines] 10^{-1}—10^{-2} M, [nitrosobenzene] 3.33×10^{-4} M were assumed to be the same as in water at zero ionic strength because the opposing effects of a higher ion strength and a change in polarity of the solvent tend to cancel.[34] The values of K_1 and K_2 for aminobenzoic acids[35] given at 20 °C were corrected to 25 °C using the method of Perrin[36] for the values of K_b and K_c.[35] The value of K_z was calculated from Eq. 8.

Reactions of nitrosobenzene (10^{-2} to 10^{-3} M) with *p*-chloro- and *p*-methylaniline (1.66×10^{-5}) were run in MeOH 15 wt%, μ=0.5 M (KCl) using the apparent pK_a's of anilines (see pK_a determinations) to calculate the third-order rate constant. As anilines react in the form of free base the kinetic expression is:

$$v = k_H(PhNO)(An)_l(H^+) \quad (12)$$

where $(An)_l$: aniline as free base concentration. $(An)_l$ can be written as a function of total aniline concentration: $(An)_t$

$$(An)_l = \frac{(An)_t \cdot K_a'}{K_a' + (H^+)} \quad (13)$$

K_a': acid dissociation constant of anilinium ion determined in the same conditions of the reactions.

Combinations of Eqs. 12 and 13 leads to

$$v = k_H \frac{(PhNO)(An)_t(H^+)K_a'}{K_a' + (H^+)} \quad (14)$$

and as the reaction is carried out with a large excess of nitrosobenzene Eq. 14 takes the form that permit us to determine the third-order rate constant: k_H

$$k_{obs} = v/(An)_t = k_H \frac{(PhNO)(H^+)K_a'}{K_a' + (H^+)} \quad (15)$$

The values obtained with this method agree with corresponding values of the first method. The second method was also used in the determination of third-order rate constant in MeOH 53 wt% according to Eq. 16 for aminobenzoic acids. The values of the apparent constant K_1 and K_2 of the aminobenzoic acids were from Mentré[37] and corrected to 25 °C using the above mentioned method (the error introduced is negligible).

$$k_{obs} = k_H^{NC} \frac{[PhNO][H^+]}{(1+K_z)(1+[H^+]/K_1+K_2/[H^+])} + k_H^{A} \frac{[PhNO][H^+]}{1+[H^+]^2/K_1K_2+[H^+]/K_2} \quad (16)$$

The K_z value for *m*-aminobenzoic acid was considered to be 0.1 (calculated from thermodynamic values[35]) and to be negligible for ortho and para aminobenzoic acids.

pK_a Determination: The apparent values of pK_a were determined following the spectrophotometric method of Albert and Serjeant.[36] The apparent pK_a of *p*-chloro- and *p*-methylaniline in methanol 15 wt%, μ=0.5 M, (KCl) 25 °C were 3.71 and 4.99 respectively. The apparent pK_a of aniline in methanol 53 wt% was 3.18.

We thank the Conselho Nacional de Pesquisas (CNPq) and FINEP for financial assistance.

References

1) S. Marriott, W. F. Reynolds, and R. D. Topsom, *J. Org. Chem.*, **50**, 741 (1985) and references therein.
2) a) O. Exner, "Correlation Analysis in Chemistry," ed by N. B. Chapman and J. Shorter, Plenum Press, New York (1978). b) P. J. Vassileva, I. G. Binev, and I. G. Junchnovski, *Spectrochim Acta, Part A*, **39**, 709 (1983) and references therein.
3) B. Capon, *Quart. Rev.*, **18**, 75 (1964).
4) P. G. Bordwell and A. C. Knipe, *J. Org. Chem.*, **35**, 2956 (1970).
5) E. Andersen and T. H. Fife, *Chem. Commun.*, **1970**, 1470.
6) K. Ueno and S. Akiyoshi, *J. Am. Chem. Soc.*, **76**, 3670 (1954).
7) Y. Ogata and Y. Takagi, *J. Am. Chem. Soc.*, **80**, 3591 (1958).
8) R. A. Yunes, A. J. Terenzani, O. D. Andrich, and C. A. Scarabino, *J. Chem. Soc., Perkin Trans. 2*, **1973**, 696.
9) R. A. Yunes, A. J. Terenzani, and L. do Amaral, *J. Am. Chem. Soc.*, **97**, 368 (1975).
10) a) W. P. Jencks, "Catalysis in Chemistry and Enzymology," McGraw-Hill, New York, N.Y. (1969) and references therein. b) W. P. Jencks, *Progr. Phys. Org. Chem.*, **2**, 63 (1964). c) W. P. Jencks, *Chem. Rev.*, **72**, 705 (1972).
11) D. H. McDaniel and H. C. Brown, *J. Org. Chem.*, **23**, 420 (1958).
12) H. H. Jaffé, *Chem. Rev.*, **53**, 191 (1953).
13) G. Vavon and P. Montheard, *Bull. Soc. Chim. Fr.*, **7**, 551 (1940).
14) D. G. Knorre and N. M. Emanuel, *Dokl. Akad. Nauk SSSR*, **91**, 1163 (1953).
15) O. Bloch-Chaudé and C. R. Hebd, *Seances Acad. Sci.*, **259**, 804 (1954).
16) M. P. Bastos and L. do Amaral, *J. Org. Chem.*, **44**, 980 (1970).
17) R. Wolfenden and W. P. Jencks, *J. Am. Chem. Soc.*, **83**, 2763 (1961).
18) C. D. Johnson, "The Hammett Equation," Cambridge Univ. Press, London (1973).
19) W. P. Jencks and M. Gilchrist, *J. Am. Chem. Soc.*, **90**, 2622 (1968).
20) R. M. Pollack and M. Brault, *J. Am. Chem. Soc.*, **98**, 247 (1975).
21) B. M. Wepster, *Recl. Trav. Chim. Pays-Bas*, **76**, 357 (1957).
22) T. Fujita and T. Nishioka, *Progr. Phys. Org. Chem.*, **12**, 49 (1976).
23) G. C. Levy, A. D. Godwin, J. M. Hewitt, and C. Surcliffe, *J. Mag. Res.*, **29**, 553 (1978).
24) E. A. Braude and F. Sondheimer, *J. Chem. Soc.*, **1955**, 3754.
25) J. W. Smith, *J. Chem. Soc.*, **1953**, 109.
26) C. C. Schmitt, M. Pizzolatti, and R. A. Yunes, unpublished results.
27) T. C. Bruice and R. Lapinski, *J. Am. Chem. Soc.*, **80**, 2265 (1958).
28) W. P. Jencks and M. Gilchrist, *J. Am. Chem. Soc.*, **90**,

2622 (1968) and references therein.

29) a) W. P. Jencks and J. Carriuolo, *J. Am. Chem. Soc.*, **82**, 1778 (1960). b) G. Aksnes and J. E. Prue, *J. Chem. Soc.*, **103** (1959).

30) a) R. G. Pearson and D. C. Vogelsong, *J. Am. Chem. Soc.*, **80**, 1038, 1048 (1958). b) H. K. Hall, *ibid.*, **79**, 5441 (1957).

31) F. H. Westheimer and J. G. Kirkwood, *J. Chem. Phys.*, **6**, 513 (1938).

32) a) A. J. Hoefnagel, J. C. Monshouwer, E. C. G. Snorn, and R. M. Wepster, *J. Am. Chem. Soc.*, **95**, 5350 (1973). b) A. J. Hoefnagel and B. M. Wepster, *J. Chem. Soc.*, **1973**, 5357. c) A. J. Hoefnagel, M. A. Hoefnagel, and B. M. Wepster, *J. Org. Chem.*, **43**, 4720 (1978).

33) A. J. Vogel, "Practical Organic Chemistry," 3rd ed, Longsman Green, New York, N.Y. (1956).

34) L. do Amaral and M. P. Bastos, *J. Org. Chem.*, **36**, 3412 (1971).

35) I. Mentré, *Ann. Chim.*, **1973**, 115.

36) A. Albert and E. P. Serjeant, "The Determination of Ionization Constants," 2nd ed, Chapman and Hall, London (1971).

37) I. Mentré, *Ann. Chim.*, **1972**, 333.

 © 1989 The Chemical Society of Japan Bull. Chem. Soc. Jpn., 62, 3691—3696 (1989)

Preparation of Tetraalkylsilanes from Trichloromethylsilane and Trioctylaluminum

Edward T. SABOURIN* and Anatoli ONOPCHENKO
Chevron Research Company, Richmond, California 94802, U.S.A.
(Received October 13, 1988)

The synthesis of methyltrioctylsilane has been achieved in a single-step from commercially available trichloromethylsilane and trioctylaluminum. Co-products resulting from alkyl group redistribution are minimized by addition of sodium or lithium halides. Use of potassium or rubidium halides drastically changes the course of the reaction to produce methyldioctylsilane as the major product.

Silicon derivatives of hydrocarbons have great potential as high-performance lubricants and hydraulic fluids because of their excellent thermal stability. Tetraalkylsilanes with one short chain and three long chains are of particular interest because they exhibit excellent viscosity characteristics over a wide temperature range and have low pour points. Previously, such compounds have been prepared using Grignard or alkyllithium reagents with chlorosilanes,[1,2] or via hydrosilation of 1-alkenes.[3] The Griganard procedure is cumbersome and not suited to large scale production. The hydrosilation procedure is more elegant, but methylsilane, the required starting material, is not available in commercial quantities and would require a difficult reduction step. Therefore, we sought a route based on commercially available starting materials.

Methyltrioctylsilane was selected as the initial target. We considered the reaction of trioctylborane with trichloromethylsilane (Eqs. 1 and 2).

$$6\,RCH{=}CH_2 + B_2H_6 \longrightarrow 2\,(RCH_2CH_2)_3B \quad (1)$$

$$CH_3SiCl_3 + (RCH_2CH_2)_3B \longrightarrow CH_3Si(CH_2CH_2R)_3 + BCl_3 \quad (2)$$

Serveral attempts at this sequence confirmed that step 2 was not feasible as predicted by thermodynamic calculations.[4] We then turned to the reaction of trialkylaluminums with chlorosilanes, a thermodynamically favored process (Eq. 3).[4]

The reaction of trichloromethylsilane with trialkylaluminum compounds is best represented by a series of equilibria (Eq. 4).

$$CH_3SiCl_3 + Al(C_8H_{17})_3 \longrightarrow CH_3Si(C_8H_{17})_3 + AlCl_3 \quad (3)$$

$$CH_3SiCl_3 + R_3Al \rightleftarrows CH_3RSiCl_2 + R_2AlCl \rightleftarrows CH_3R_2SiCl + RAlCl_2 \rightleftarrows CH_3R_3Si + AlCl_3 \quad (4)$$

The reaction of trialkylaluminum compounds with chlorosilanes was first reported by Jenkner who also noted that the addition of one mole of alkali metal chloride per mole of aluminum shifted the equilibrium to the right by formation of metal tetrachloroaluminates.[5] Russell approached the equilibrium from the right by reacting aluminum chloride with tetraalkylsilanes.[6] Hungarian and Russian researchers studied the equilibria starting with alkylaluminum chlorides or sesquichlorides trying to maximize the intermediate products.[7-9] In all the previous studies, only results with methyl or ethyl groups were reported. When methyl and ethyl compounds were used simultaneously, some alkyl-alkyl interchange was noted in addition to the alkyl-chloro exchange.[9]

We now report the results of our use of longer alkylaluminums. The chemistry is much more complex than indicated by Eq. 4. In addition to the intermediates depicted above, the following types of co-products were observed:

1. Products from silicon to silicon alkyl transfer.
2. Products containing silicon-hydrogen bonds.
3. Dimers of the initial alkyl group.
4. Silanes containing alkyl groups derived from dimers.
5. Silanes containing alkyl groups derived from impurities in trioctylaluminum.
6. Products with silicon-oxygen bonds.

Experimental

Chromatographic analyses were performed on a Hewlett-Packard 5880A (FID) instrument using a 25 m, 2% OV-101, fused silica capillary column programmed from 50 to 300 °C at 8 °C min^{-1}. The IR spectra were recorded on a Perkin-Elmer Model 597 spectrometer. GC/MS data were obtained on a Finnigan 4510 system with an electron impact source at 70 eV. Trioctylaluminum (Ethyl Corp.) and alkylchlorosilanes (Aldrich and Petrarch) were used as received.

General Procedure. Reactions were carried out in a thick-walled glass reactor connected to a nitrogen pressure manifold with Fisher-Porter compression fittings. Similar fittings connected a side arm to a wide-bore Hoke valve and a rubber septum. Heat was supplied with a heating mantle and controlled with a West-800 controller. An egg-shaped magnetic stirrer supplied adequate agitation.

The reactor was charged with alkali metal halide and connected to the nitrogen system. The system was purged by pressuring to 30 psig and venting ten times. Trioctylaluminum was added via syringe followed by trichloromethylsilane. Stirring and heating were started. Approximately 25—35

minutes were required to attain temperature. Reaction time was measured as the time at temperature. When the reaction was terminated, the vessel was allowed to cool to room temperature and vented. At this point, the reaction mixture was not pyrophoric. The reactor was disconnected from the nitrogen system and an equal volume of heptane was added. Methanol was added to quench unreacted alkylaluminum and to convert any remaining chlorosilanes to methoxysilanes. The mixture was transferred to a separatory funnel. Water was added to facilitate separation of the layers. The organic layer was dried over magnesium sulfate, filtered, and stripped on a rotary evaporator. The crude product was analyzed by gas chromatography.

Results and Discussion

Physical Aspects of the Reaction. Previous work had been performed in metal autoclaves. Our initial work has employed a thick-walled glass reactor. While the pressure limitations of the glass undoubtedly reduced yields and possibly rates because a significant portion of the volatile trichloromethylsilane remained in the vapor space, the system proved excellent for observing the physical state of the reaction mixture. In a typical run, as the mixture of salt, trichloromethylsilane and trioctylaluminum is heated the following sequence of events occurs:

1. As the boiling points of the volatile components are exceeded the pressure rises and refluxing occurs. The salt remains as a discrete solid until a minimum reaction temperature, characteristic of the particular salt, is attained.
2. At reaction temperature the salt dissolves. The pressure starts to drop.
3. The liquid phase becomes cloudy. If the stirrer is stopped two liquid phases separate rapidly.
4. With time the upper phase diminishes while the lower phase grows.

During this period the pressure remains relatively constant.

5. The upper phase reaches a minimum. The pressure once again begins to drop as the upper phase begins to increase again. When the amount of upper phase stabilizes, the reaction is terminated.
6. Upon cooling, the lower layer solidifies.

Figure 1 gives a graphical representation of this behavior. The relative time periods for the various parts of the sequence vary with reaction temperature and the type and amount of salt employed.

The lower liquid phase obviously is some sort of complex between the salt and the other constituents. It does not appear to be a simple complex of trioctylaluminum and salt, since heating trioctylaluminum and sodium chloride for one hour at 180 °C showed no evidence of dissolution of the salt. Since alkylaluminum chlorides are much stronger Lewis acids than trialkylaluminum and are well-know to form complexes with alkali metal halides,[10] it would appear that initial exchange of alkyl and chloro

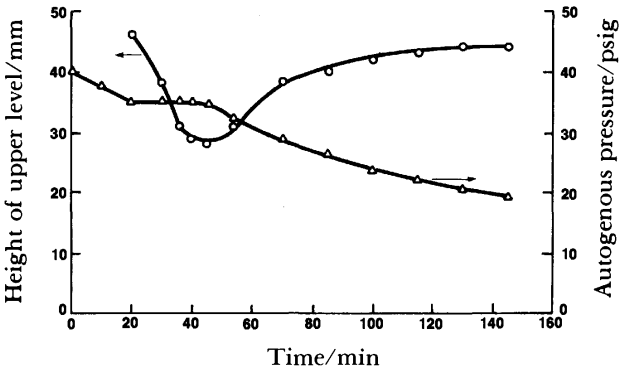

Fig. 1. Profile of autogenous pressure (△) and height (○) of product containing layer with time.

groups are required before the complex can form. The cause of the period of static pressure during the growth of the complex is not understood at this time. If the reaction is terminated at the maximum complex formation (minimum upper layer), the product distribution is similar to that for a typical longer run; but yield is lower.

Effect of Amount of Salt. Runs listed in Table 1 illustrate the effect of the amount of added sodium chloride. Only those reaction products which are severely altered are shown. With no added sodium chloride, extensive transfer of alkyl groups from silicon to silicon occurs. Addition of 0.5 mol of salt per mole of aluminum greatly improves the selectivity to methyltrioctylsilane. Lesser amounts have little effect. Larger amounts show no further improvement. Varying the reaction time between 1 and 6 hours produces no major change in the product distribution. The main effect of sodium chloride appears to be inhibition of alkyl group redistribution rather than shifting the equilibrium as suggested by Jenkner.[5]

Alkyl group redistribution could result from postalkylation equilibrium (Eq. 5).

$$(CH_3)_4Si \rightleftarrows (CH_3)_3(C_8H_{17})Si \rightleftarrows (CH_3)_2(C_8H_{17})_2Si \rightleftarrows CH_3(C_8H_{17})_3Si \rightleftarrows (C_8H_{17})_4Si \quad (5)$$

Alternatively, a prealkylation equilibration of the chlorosilanes could cause the same product distribution (Eq. 6).

$$SiCl_4 \rightleftarrows CH_3SiCl_3 \rightleftarrows (CH_3)_2SiCl_2 \rightleftarrows (CH_3)_3SiCl \rightleftarrows (CH_3)_4Si \quad (6)$$

Aluminum chloride is a known catalyst for the equilibration depicted in Eq. 5.[6] To assess the magnitude of such a reaction, 50 mmol of methyltrioctylsilane and 10 mmol of aluminum chloride were heated to 160 °C for one hour. Gas chromatography revealed that the product contained only 59% of the initial silane. Repetition of the experiment with

Table 1. Effect of Sodium Chloride

Run	Molar ratio[a] TNOA/MTCS/NaCl	Time/h	Yield/mole percent[b] $(CH_3)_3(C_8H_{17})Si$	$(CH_3)_2(C_8H_{17})_2Si$	$CH_3(C_8H_{17})_3Si$	$(C_8H_{17})_4Si$	$CH_3(C_8H_{17})_2SiH$
1	1/0.8/0	6	3.4	8.7	26.1	27.1	—
2	1/0.8/0.25	2	2.6	13.0	33.3	21.3	—
3	1/0.8/0.5	6	—	5.6	63.4	3.9	—
4	1/0.8/1	1	—	3.2	58.5	0.6	0.7
5	1/0.8/1	3	—	3.4	61.3	3.0	2.4

a) TNOA=trioctylaluminum, MTCS=trichloromethylsilane, reaction conditions: 210°C, autogenous pressure, 85 mmol TNOA, 70 mmol MTCS. b) Gas chromatographic yield based on MTCS as limiting reagent.

Table 2. Composition of Vapor Phase

Run	Sample	Timing	Mole percent[a] Isobutene	$(CH_3)_2SiHCl$	CH_3SiHCl_2	$(CH_3)_3SiCl$	CH_3SiCl_3	1-Octene	Other C_8 hydrocarbons
6[b]	1	Upon reaching reaction temp	20.3	—	7.4	2.0	22.7	38.0	9.6
	2	Incipient molten phase	8.2	—	7.7	7.8	26.8	36.8	12.8
	3	Maximum lower phase	11.4	—	6.5	4.9	21.8	44.5	10.9
	4	1 h	12.0	7.6	5.0	6.2	21.3	35.7	12.3
	5	4 h	—	8.8	6.6	5.9	22.1	44.9	11.7
7[c]	1	Upon reaching reaction temp	9.0	—	3.6	1.5	17.7	51.2	17.0
	2	1 h	11.2	—	4.3	2.8	17.1	48.2	16.4
	3	3 h	24.8	—	4.5	—	18.2	3.1	49.4

a) Tentative assignments made by sequentially spiking a sample of 1-octene with the suspected components. $(CH_3)_2SiCl_2$ could not be separated from CH_3SiCl_3 under the conditions employed. b) 100 mmol $(C_8H_{17})_3Al$, 100 mmol NaCl, 89 mmol CH_3SiCl_3, reaction temperature 190°C. c) 50 mmol $(C_8H_{17})_3Al$, 40 mmol CH_3SiCl_3, reaction temperature 190°C.

10 mmol of added sodium chloride gave a product with 76% starting silane. This indicates that sodium chloride is indeed effective in stopping alkyl redistribution. Presumably, in a typical reaction, very little free aluminum chloride ever forms because of prior complexation with the alkali metal salt leading to the direct generation of the inactive tetrachloroaluminate.

To determine if Eq. 6 was of any importance, the composition of the vapor phase of runs with and without sodium chloride was determined by gas chromatography. Table 2 summarizes the results. Some other silicon compounds not present in the feed do form under the reaction conditions. The relative proportions are about the same, with or without sodium chloride, and remain roughly constant throughout the reaction. The isobutene present is derived from impurities in the trioctylaluminum. In the absence of sodium chloride the 1-octene in the vapor phase is gradually isomerized.

These experiments indicate that a small portion of the alkyl redistribution is due to prealkylation equilibria; but, major redistribution is the result of postalkylation equilibria when insufficient sodium chloride is present.

Effect of Type of Salt. While the literature indicated that the alkali metal halides were interchangeable,[5] the obvious importance of the complex to the reaction suggested that different salts should have some effect. The strength of the various alkali metal halides as complexing agents for alkylaluminums increases with the increasing radius of the cation and with the decreasing size of the halide ion.[11] This is usually manifested in a lower temperature of complex formation. If the reaction complex could be formed at lower temperature, the reaction might proceed with greater selectivity.

Based on this premise, reactions were carried out using sodium, potassium, or rubidium chloride with trioctylaluminum and trichloromethylsilane wherein the mixtures were heated at a uniform rate until the salt dissolved. At this point the temperature was stabilized and held. The dissolution temperature and the approximate time from dissolution to separation of the two liquid phases followed the expected trend (Table 3). However, analysis of the products of the potassium and rubidium runs revealed that methyltrioctylsilane was no longer the major product! Infrared showed a strong Si–H absorption at 2120 cm^{-1}. Co-injection with an authentic sample confirmed the major product as methyldioctylsilane.

A series of runs at constant temperature varying both the cation and the halide shows that both affect the product distribution (Table 4). The tendency to form methyldioctylsilane instead of methyltrioctylsilane increases in the sequence Li<Na<K<Rb and in the sequence I<Br<Cl. The fluoride run is somewhat out of line. However, fluoride frequently gives anomalous behavior when compared to the other halides. A decrease in the amount of alkyl redistribution also occurs in the same sequences. Mixtures of two salts gave product distributions intermediate between the individual salts.

Runs with potassium or rubidium chloride produce two to three times as much octene dimers (mainly 2-hexyl-1-decene by GC/MS) as the analogous runs with sodium or lithium chloride. Also, no traces of alkylation by the $C_{16}H_{33}$ group are found when potassium or rubidium salts were present. This suggests that these complexes prefer to expel dimeric molecules as the olefin at some stage of the reaction leaving aluminum hydride residue. Presumably, the hydride is then transferred to silicon in the same manner as an alkyl group. The relatively large loss of octyl groups to dimers probably accounts for larger amounts of partially alkylated silanes rather than inability of potassium to shift the equilibrium.

The relative distribution of the silicon compounds in the vapor phase for potassium runs was similar to that of a sodium run indicating no drastic change in the prealkylation equilibria. Only traces of 1-octene were found. Two closely spaced, unidentified peaks comprised approximately 45% of the vapor phase. Based on gas chromatography retention time, a crude estimate of the molecular weight would be ca. 140—150. Unfortunately, the materials were not stable. No trace could be found after work up.

Reactivity of Silicon-Hydrogen Bonds. The presence of silicon-hydrogen bonds in the vapor phase, even in the sodium chloride runs raised the question of the ability to replace the hydrogen with an alkyl group. Dichloromethylsilane produced predominantly methyltrioctylsilane (Eq. 7).

$$CH_3SiHCl_2 + Al(C_8H_{17})_3 \longrightarrow \underset{43\%}{CH_3(C_8H_{17})_3Si} + \underset{25\%}{CH_3(C_8H_{17})_2SiH} \quad (7)$$

Reaction of hexylsilane under similar conditions

Table 3. Relationship of Type of Salt to Minimum Temperature of Complex Formation[a]

Salt	Dissolution temperature/°C	Time from dissolution to separation of complex/min
NaCl	190—200	5—10
KCl	160—175	15—45
RbCl	140—150	30—60

a) 85 mmol trioctylaluminum, 75 mmol trichloromethylsilane, 85 mmol salt stirred at constant rate with constant heat input until dissolution occurred.

Table 4. Effect of Type of Salt on Product Distribution[a)]

Run	Salt	Selectivity/mole percent					
		$(CH_3)_3(C_8H_{17})Si$	$CH_3(C_8H_{17})_2SiH$	$(CH_3)_2(C_8H_{17})_2Si$	$CH_3(C_8H_{17})_2SiCl$	$CH_3(C_8H_{17})_3Si$	$(C_8H_{17})_4Si$
8	LiCl	0.8	—	8.4	3.8	50.4	7.8
9	LiBr	1.6	—	10.4	7.2	37.6	4.8
10	NaCl	0.9	2.4	3.8	2.1	63.2	2.1
11	NaBr	—	1.0	3.1	3.3	66.7	5.2
12	KF	—	30.3	0.6	7.1	13.9	0.2
13	KCl	—	47.2	0.9	12.2	8.3	0.2
14	KBr	—	18.8	2.0	8.6	47.6	0.6
15	KI	—	13.4	2.2	7.6	54.3	1.8
16	RbCl	—	47.4	2.1	2.1	21.5	0.2

a) Temperature: 180 °C; time: 4 h; mole ratio trioctylaluminum/trichloromethylsilane/salt: 1/1/1.

also produced some alkylation (Eq. 8); but, the reaction of Si–H bond is definitely much slower than the Si–Cl bond. In this case the sodium chloride never changes from its granular state and probably does not enter into the reaction.

$$C_6H_{13}SiH_3 + Al(C_8H_{17})_3 \longrightarrow \underset{31\%}{C_6H_{13}(C_8H_{17})SiH_2} + \underset{20\%}{C_6H_{13}(C_8H_{17})_2SiH} \quad (8)$$

Effect of Impurities in the Feed. The trichloromethylsilane used in this study was chromatographically pure. The vapor phase results indicate that a near steady state concentration of the disproportionation products is achieved very quickly. Since these same disproportionation products are the impurities usually found in technical grade trichloromethylsilane, its use would have no drastic effect.

In the case of trioctylaluminum the effect of impurities is much greater. Since each desired product molecule contains three octyl chains derived from trioctylaluminum, each non-desired alkyl chain can waste up to two octyl chains by its reaction, i.e. one mole percent impurity in the trioctylaluminum produces three mole percent impurities in the product. Preparation of trioctylaluminum is generally accomplished by displacement of isobutylene from triisobutylaluminum with 1-octene. Failure to displace all the isobutyl groups in the preparation of the trioctylaluminum can lead to silanes containing one or more isobutyl substituents. Coinjection with authentic diisobutylmethyloctylsilane and isobutylmethyldioctylsilane confirmed the presence of traces of the former and up to 2% of the latter in a typical run.

Vinylidene impurities present in 1-olefins represent another source of impurity in the trioctylaluminum. In the case of 1-octene this results in the introduction of 2-ethylhexyl substituents. The presence of 2-ethylhexyl-containing silanes was confirmed by independent synthesis and co-injection. Use of longer chain alkylaluminums would exacerbate this problem.

Oxygen Containing Co-Products. In this work any excess of unreacted alkylaluminum was generally quenched with water or methanol. This also hydrolyzes any partially converted chlorosilanes to disiloxanes or methoxysilanes.

References

1) C. Tamborski and C. E. Snyder, Jr., U. S. Patent 4367343 (1983).

2) H. Rosenberg, J. D. Groves, and C. Tamborski, *J. Org. Chem.*, **25**, 243 (1960).

3) A. Onopchenko, E. T. Sabourin, and D. L. Beach, *J. Org. Chem.*, **49**, 3389 (1984).

4) "Comprehensive Organometallic Chemistry," ed by G. Wilkinson, F. G. A. Stone, and E. W. Abel, Pergamon Press, Oxford (1982), Vol. 1, p. 8.

5) a) H. Jenkner, British Patent 825987 (1959); *Chem. Abstr.*, **54**, 10861 g (1960). b) H. Jenkner, U. S. Patent 3103526 (1963).
6) G. A. Russell, *J. Am. Chem. Soc.*, **81**, 4815 (1959).
7) B. Lengyel and T. Szekely, *Z. Anorg. Allg. Chem.*, **287**, 273 (1956).
8) B. Lengyel, T. Szekely, and G. Garzo, *Z. Anorg. Allg. Chem.*, **323**, 65 (1963).
9) L. M. Antypin, V. V. Panomarev, and V. F. Mironov, *Zh. Obshch. Khim.*, **38**, 2580 (1968).
10) T. Mole and E. A. Jeffery, "Organoaluminum Compounds," Elsevier, New York (1972), p. 167.
11) K. Ziegler, R. Köster, H. Lehmkuhl, and K. Reinert, *Justis Liebigs Ann. Chem.*, **629**, 33 (1960).

 © 1989 The Chemical Society of Japan Bull. Chem. Soc. Jpn., 62, 3697—3700 (1989)

Synthesis and Characterization of Some New Organophosphonates and Their Adducts with Some Metal Salts

Ebtsam A. SAAD and Ramadan M. RAMADAN*,†
Chemistry Department, Faculty of Science, Ain Shams University, Cairo, Egypt
(Received November 4, 1988)

The synthesis of the new monobasic organophosphonates $(C_2H_5O)RPO(OH)$, R=benzyl, benzoyl, or butanoyl group, by the hydrolysis of the neutral esters $(C_2H_5O)_2RPO$ is reported. The IR spectra of the new ligands showed that they were existed in solutions as dimers. The p*K*a values in 50% aqueous ethanol found to be 4.46, 3.98, and 3.48 for the benzyl, butanoyl, and benzoyl derivatives, respectively. These values were consistent with the calculated π-electron charge density. Solid complexes of the benzoylphosphonate with Pr, Eu, Er, and Co metal ions as well as the benzyl-Eu complex were isolated. The complex ratios were found to be 1:2 metal to phosphonate dimer. The octahedral arrangements were completed by the presence of a coordinated bidentate NO_3 group. Ionic properties of these complexes were ruled out from conductometric measurements. The IR spectra as well as the calculated π-electron charge density for the benzoyl complexes showed that the preference site for complex formation was from the carbonyl oxygen in contrast with the benzyl one where complexation through the phosphoryl group in addition to the hydroxyl oxygen.

It is well-established that the organophosphorus compounds of the type $(RO)_2PO(OH)$, $(RO)PO(OH)_2$, (RO)R'PO(OH), R'PO(OH)$_2$, and R'HPO(OH), where R and R' are alkyl or aryl group, exist in dimeric forms.[1] These compounds were used as complexing agents for various transition and inner transition metal salts.[2] Neutral alkyl esters of phosphonic acid and phosphoric acid were also used in the formation of adducts with metal salts. However, isolation of crystalline compounds were generally not easily to perform.[3]

Here, we report the preparation of the new monobasic organophosphonates $(C_2H_5O)RPO(OH)$, R=benzyl, benzoyl, and butanoyl group as hydrolyzed products of the neutral esters $(C_2H_5O)_2RPO$. The IR spectra of these ligands and their complexes with some lanthanoid metals are also reported.

Experimental

The infrared spectra of the organophosphonates and their metal adducts were performed on a Perkin-Elmer infrared spectrophotometer Model 1430 with the use of KBr disc technique or in carbon tetrachloride solutions. Liquid film spectra (NaCl cell, 1.0 mm) were also carried out for the liquid ligands.

A Pye-Unicam pH-meter with expandable scale Model 290 Mk2 was used for the potentiometric titrations. It was connected to a Pye-Unicam glass combination electrode and was calibrated by using universal buffers.

The phosphonate ligands $(C_2H_5O)_2RPO$, R=benzyl, benzoyl, and butanoyl group, were purchased from Alfa Products, 99% purity, and were used without further purifications. Praseodymium, europium, erbium, and cobalt nitrates were supplied from British Drug Houses Ltd. Sodium hydroxide was of AnalaR grade. All the solvents used were purified by using the standard methods[4] and stored under nitrogen atmosphere.

Hydrolysis of the neutral phosphonates were carried out by using the following procedure:[5] The phosphonate reagent was mixed with aqueous sodium hydroxide solution in molar ratio of 1:6 (phosphonate:hydroxide). The mixture was stirred at 80 °C for 5 h in a sealed flask under nitrogen. The solution was left to cool and then shaked with benzene several times to remove the formed alcohol and any unhydrolyzed ester. The aqueous layer was separated and acidification with HCl was carried out to isolate the ligand in the acid form which was then extracted in benzene. The organic layer was separated and the acid was recovered by evaporating the benzene and any remaining alcohol by vacuum distillation.

The acid ionization constants of the new ligands were determined by titration of fixed amounts (20 ml) of

Table 1. The Acid Ionization Constants (pK_a's) and the Important Infrared Data of the New Organophosphonate Ligands

Ligand[a]	pK_a values (ethanol-water)		IR data[b] /cm^{-1}		
	50%	25%	$\nu_{OH(bond.)}$	$\nu_{P=O}$	$\nu_{C=O}$
$PhCH_2PO(OH)(OC_2H_5)$	4.46	3.95	2870(m)	1165(m)	—
$C_3H_6COPO(OH)(OC_2H_5)$	3.98	3.72	2880(vs)	1168(s)	1740(s)
$PhCOPO(OH)(OC_2H_5)$	3.48	3.18	2880(vs)	1170(s)	1718(s)

a) $PhCH_2$, benzyl; C_3H_6CO, butanoyl; PhCO, benzoyl. b) Liquid film spectra; m, medium; s, strong; vs, very strong.

† Present address: Chemistry Department, Teachers Junior College, Tabuk, P. O. Box (1144), Saudi Arabia.

Table 2. The Analytical and Important Infrared Data of the New Complexes

Complex[a]	Mp/°C	Elemental analysis[b]				IR data/cm^{-1}[c]			
		%C	%H	%P	%N	$\nu_{OH(bond.)}$	$\nu_{P=O}$	$\nu_{C=O}$	ν_{NO_3}
Co-L_2NO_3	120—121	44.09 (44.32)	4.21 (4.34)	12.81 (12.70)	1.40 (1.44)	2922(vs)	1203(m), 1168(m)	1682(s)	1440(m), 1404(s), 1307(s), 1059(mw), 702(s)
Pr-L_2NO_3	123—125	40.76 (40.89)	3.93 (4.00)	11.79 (11.72)	1.25 (1.32)	2915(vs)	1205(m), 1167(mw)	1680(s)	1438(m), 1402(s), 1305(s), 1057(m), 702(s)
Eu-L_2NO_3	120—122	40.25 (40.46)	3.77 (3.96)	11.52 (11.59)	1.25 (1.31)	2925(vs)	1200(m), 1166(m)	1685(s)	1440(m), 1405(m), 1310(m), 1055(mw), 700(s)
Er-L_2NO_3	122—123	39.65 (39.89)	3.69 (3.91)	11.51 (11.43)	1.21 (1.29)	2900(vs)	1202(m), 1165(m)	1682(s)	1440(m), 1400(s), 1307(s), 1058(m), 705(s)
Eu-$L_2'NO_3$	131—133	42.53 (42.70)	4.78 (4.98)	12.11 (12.23)	1.28 (1.38)	2930(vs)	1175(s), 1100(s)	—	1462(s), 1377(m), 1310(m), 1035(m), 723(m)

a) L=benzoyl phosphonate dimer; L'=benzyl phosphonate dimer. b) Calculated values are given in parentheses. c) CCl_4 solutions; NaCl cell, 1.0 mm; vs=very strong, s=strong, m=medium, mw=moderately weak.

phosphonate solutions in 50 and 25% ethanol-water mixtures with standardized sodium hydroxide solutions at 25 °C. A stream of nitrogen gas was flushed through the solution during the titration. The pK_a values were computed by using the corrected pH values.[6] The results are given in Table 1.

Solid complexes of the benzoyl phosphonate derivative with Co, Pr, Eu, and Er metal nitrates as well as the benzyl phosphonate with europium nitrate were synthesized by mixing equimolar amounts of both reagents with slight excess of the ligand in 50% aqueous ethanol and left to stand at room temperature for 24 h. (The benzyl complex took longer time ca. 40 h with the formation of white amorphous solid). White to pale yellow crystalline needles were isolated, washed with ethanol and left to dry under vacuum. Attempts to prepare the butanoyl analogous were unsuccessful; they decomposed above 0 °C. Elemental analysis were consistent with 1:2 adduct formations. Results for elemental analysis as well as melting points are given in Table 2.

Conductometric measurements were performed on a Griffin conductance bridge Model PJK-301. The conductance of 0.5 g metal complex dissolved in 50 ml of nitrobenzene or methylene chloride solvent was measured at different time intervals at 25 °C.

Results and Discussion

Hydrolysis of the organophosphonate compounds $RPO(OC_2H_5)_2$, R=benzyl, benzoyl, or butanoyl group, by sodium hydroxide solutions led to the formation of the monobasic $RPO(OH)(OC_2H_5)$ derivatives. The infrared spectra of these phosphonate compounds were measured from 4000—600 cm^{-1} in CCl_4 solutions or as a liquid film spectra. All the three compounds showed strong bands in the range of 2880 cm^{-1} (Table 1) which were indicative of the presence of bonded OH groups.[1,5,7] Dilute CCl_4 solutions did not show any stretching frequency due to free OH group. The phosphoryl region showed a lower field shift from the free P=O region as expected for bonding phosphoryl group.[7] Thus, these compounds would have dimeric structures with arrangements, presumably, similar to that proposed previously.[1]

The acid ionization constants of the phosphonate ligands were calculated from potentiometric titrations of known amounts of the phosphonate against standardized sodium hydroxide solutions. The pK_a values, listed in Table 1, clearly show that the acidity increases in the order benzyl<butanoyl<benzoyl derivative. This can be attributed to the effect of the R group on the electron density of the phosphorus atom and consequently on the ionization of the OH moiety. The π-electron densities on the different atoms of the three phosphonates, calculated by the use of simple HMO method,[8] are shown in Scheme 1. The π-electron density on the hydroxyl oxygen is decreased in the order benzyl>butanoyl≈benzoyl. This order is consistent with the order of increasing acidity and accounts for the closest pK_a values of both butanoyl and benzoyl derivatives, 3.98 and 3.48, respectively.

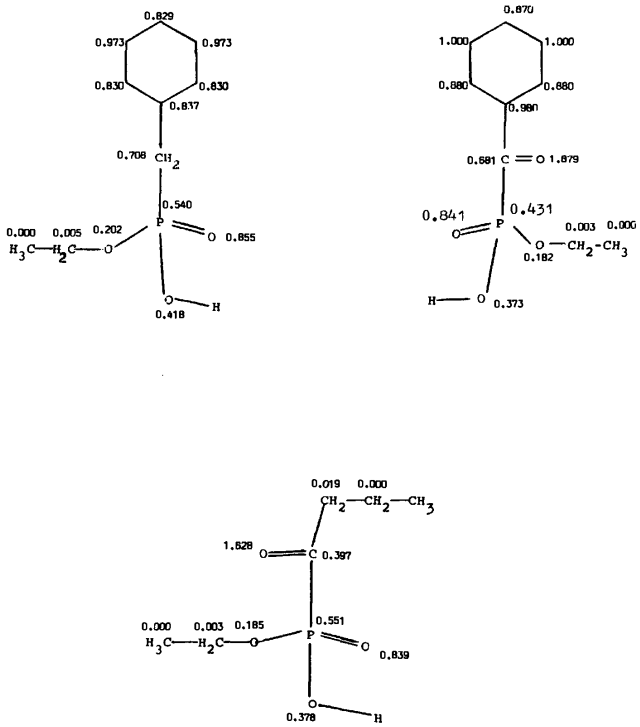

Scheme 1. The π-electron density on the different atoms of the benzyl-, benzoyl-, and butanoylphosphonate derivatives.

Addition of the new phosphonate ligands to solutions of Co(II), Pr(III), Eu(III), and Er(III) nitrates resulted in the formation of the corresponding metal complexes. The pH of the solutions was found to be decreased by time. Attempts to prepare the butanoyl metal complexes were unsuccessful due to their decomposition above 0 °C. The solid complexes were air stable white to pale yellow needle crystals (the benzyl derivative was amorphous solid). The elemental analysis, melting points, and the important IR data of the new complexes are listed in Table 2. The stoichiometry of these complexes were found to be 1:2 metal to phosphonate dimer. The formation of these complexes was accompanied by the release of two protons per one complex as found from solvent extraction and potentiometric analysis of these and other similar complexes.[9]

The infrared sectra of the new complexes in either CCl_4 solutions or in solid state (KBr disc technique) showed that two different types of phosphoryl groups present in the same spectrum. One of them was assigned to the P=O bonded to the OH group (hydrogen bonding) with about the same position as in case of the free ligand. The other has a position dependent on the type of the complex. In case of the benzyl complex, the second phosphoryl group showed lower field shift due to bonding to metal (donation to metal ion was stronger than hydrogen bonding). The interesting facet was the case of the benzoyl complexes. There, the second phosphoryl group showed upfield shift referred to unbonded P=O group, while the carbonyl stretching frequency exhibited a lower field shift. From Scheme 1, one can see that the carbonyl oxygen of the benzoylphosphonate derivative carried higher π-electron density than the phosphoryl oxygen. Thus, it can be concluded that the CO group of this ligand might be involved in the complex formation and donation from its site to the metal ion is predominant rather than from the phosphoryl oxygen. Recall that the synthesis of the benzylphosphonate complex, which has no CO group, took longer time and gave amorphous solid. It is not obvious that why the butanoyl derivative did not form stable complexes. Presumably, the presence of the phenyl group in the benzoyl derivative stabilized the complex formation.

The new complexes were found to be neutral species where a nitrate group was linked to the metal as a bidentate ligand. Effect of nitrate concentration on the extraction of these complexes in hexane revealed the presence of one NO_3 group in the complex sphere.[9] Also, the IR spectra of these complexes showed stretching frequencies attributed to such linkage,[7,10] Table 2. The formation of neutral complexes with the trivelent lanthanoid metal ions is obvious. In case of Co(II) complex it should be ionic. However, conductometric measurements for all cmplexes in nitrobenzene or CH_2Cl_2 solutions gave conductance due to nonelectrolyte materials which ruled out the presence of ionic nitrate. Two possibilities for the Co complex, thus, can be considered. First, the complex is very weak electrolyte where detection of conductance can not be observed. The second possibility is that cobalt in this complex existed with a formal +3 charge presumably due to delocalization of one of its electrons onto the ligand through the carbonyl moiety. The latter assumption does not seem unreasonable; heating the cobalt(II) semiquinone complex (Co_4(3,5-di-*t*-butylsemiquinone)$_8$) with bipyridyl resulted in the formation of the complex (3,5-di-*t*-butylcatecholato)-(3,5-di-*t*-butylsemiquinone)(bipyridyl)cobalt(III). The formation of Co(III) species was confirmed from an X-ray crystal structure determination of the complex.[11] Also, reaction of $Cr(CO)_6$ (zerovalent metal) with 1,2-chrysenequinone gave the semiquinone derivative Cr(chrysenesemiquinone)$_3$ with a formal +3 charge on the metal part.[12]

According to the available data the comlexes may have octahedral arrangements where the metal is linked to two ligands of the phosphonate dimer as well as a bidentate nitrate group. However, as a referee suggested, we can not rule out possibility of formation of rare earth complexes with higher coordination number than six. Here, the ligand dimer could act as a tridentate where it attached to the metal from a phosphoryl and a carbonyl group of one moiety and the OH group of the other moiety with the release of a proton.

The authors thank Prof. J. C. Merlin and Ms. R. Genevieve, Faculty of Science, Claud Bernard, Lyon 1, France, for their assistance in the IR measurements.

References

1) D. F. Peppared, J. R. Ferraro, and G. W. Mason, *J. Inorg. Nucl. Chem.*, **7**, 231 (1958). G. M. Kosolapoff and J. S. Powell, *J. Chem. Soc.*, **1950**, 3535.

2) E. G. Afonin and N. I. Pechurova, *Zh. Neorg. Khim.*, **32**, 1021 (1987); *Chem. Abstr.*, **107**, 108074u. C. M. Mikulski, P. Sanford, N. Harris, R. Rabin, and N. M. Karayannis, *J. Coord. Chem.*, **12**, 187 (1983). C. M. Mikulski, N. Harris, P. Sanford, F. J. Iaconianni, L. L. Pytlewski, and N. M. Karayannis, *J. Inorg. Nucl. Chem.*, **43**, 2753 (1981).

3) N. M. Karayannis, L. L. Pytlewski, and C. Owens, *J. Inorg. Nucl. Chem.*, **42**, 675 (1980). C. M. Mikulski, W. Henry, L. L. Pytlewski, and N. M. Karayannis, *J. Inorg. Nucl. Chem.*, **40**, 769 (1978).

4) J. A. Riddick, and W. B. Bunger, "Organic Solvents," 3rd ed, Wiley, New York (1970).

5) D. F. Peppard, J. R. Ferraro, and G. W. Mason, *J. Inorg. Nucl. Chem.*, **12**, 60 (1959).

6) A. Albert and E. P. Serjeant, "The Determination Of Ionization Constants," 2nd ed, Chapman and Hall, London (1971).

7) R. M. Silverstein, G. C. Bassler, and T. C. Morrill, "Spectrometric Identification of Organic Compounds," 4th ed, Wiley, New York (1981).

8) A. Streitwieser, "Molecular Orbital Theory For Organic Chemists," Wiley, New York (1961).

9) Details of these studies will be published elsewhere.

10) I. S. Ahuja, R. Singh, and C. P. Rai, *J. Mol. Struct.*, **49**, 201 (1978).

11) R. M. Buchanan and C. G. Pierpont, *J. Am. Chem. Soc.*, **102**, 4951 (1980).

12) R. M. Ramadan, W. H. Mahmoud, M. F. El-Shahat, and A. E. Attia, to be submitted for publication.

 © 1989 The Chemical Society of Japan Bull. Chem. Soc. Jpn., 62, 3701—3705 (1989)

Polyazamacrocycles. V. Structure of Isomeric 3,5,7,7,10,12,14,14-Octamethyl-1,4,8,11-tetraazacyclotetradecanes

Ramesh BEMBI,* Sham M. SONDHI, Ashok K. SINGH, Amrit K. JHANJI, Tapashi G. ROY, J. William LOWN,† and R. G. BALL†
Department of Chemistry, University of Roorkee, Roorkee 247667, U.P. India
†Department of Chemistry, University of Alberta, Edmonton, Alberta T6G 2G2, Canada
(Received January 20, 1989)

Reduction of 3,5,7,7,10,12,14,14-octamethyl-1,4,8,11-tetraazacyclotetradeca-4,11-diene (Me8[14]diene) with sodium borohydride yields three diastereomeric Me8[14]anes. These diastereomers can be separated through fractional crystallization from xylene. The structure of these isomers has been established on the bseis of their NMR spectra. The structure of one isomer has been confirmed by X-ray crystallography.

The importance of polyaza macrocycles is now well-documented and needs no elaboration. These macrocycles and their metal complexes present intriguing stereochemical problems. The stereochemistry of Me6[14]anes[1] (**I**), Me6[22]anes[2] (**II**), and Me2[14]-anes[3,4] (**III**), all of which give two isomers, the C-meso and C-rac forms, has been quite comprehensively investigated. No isomers of Me8[14]ane (**IV**) have been isolated, although this macrocycle with four chiral centers is expected to give several isomeric species. However, some reports have indeed appeared on the isomeric nickel(II) complexes of Me8[14]anes.[5] These species have been prepared by the reduction of the nickel(II) complex of 3,10-*C-rac*-Me8[14]diene (**V**). In this paper we report the isolation and characterization of three isomeric 3,10-*C-meso*-Me8[14]anes.

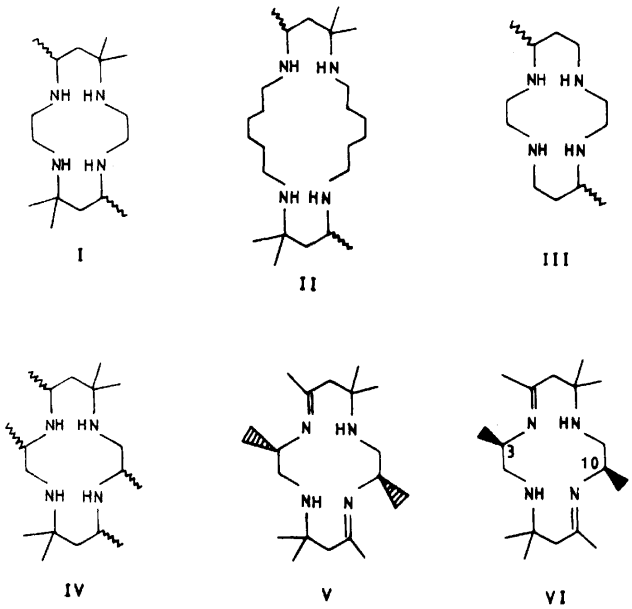

Results and Discussion

Synthesis. 1,2-Propanediamine reacts with acetone to yield Me8[14]diene, an octamethyl derivative of the 14-membered tetraaza macrocycle. The reaction is completely stereospecific and yields Me8[14]diene (**VI**) with the methyls at 3,10 positions in a meso-configuration. This assignment has been confirmed by X-ray studies.[6] The 3,10-*C-rac*-isomer (**V**) cannot be recovered from the mother liquor. The IR spectra of **VI** shows $\nu_{C=N}$ band at 1660 cm^{-1}. This C=N bond can be readily reduced with sodium borohydride to yield the corresponding saturated macrocycles. The infrared spectrum of the product shows no band around 1650 cm^{-1} assignable to $\nu_{C=N}$ and shows a ν_{NH} band at 3200 cm^{-1}. The reduction of **V**, which has a 3*S**,10*R** configuration, generates two new chiral carbons at positions 5 and 12. During the course of reduction, the 3*S**,10*R** configuration is retained. As a consequence, 3,10-*C-meso*-Me8[14]diene (**V**) would give three isomeric 3,10-*C-meso*-Me8[14]anes. These isomers, L_A, L_B, and L_C have been separated by fractional crystallization from xylene. Each isomer gave (i) a single spot on thin-layer chromatograms (TLC) using 80:20% methanol–chloroform mixture as a developing solvent, (ii) a distinct mp, and (iii) showed differences in solubilities in some common solvents like chloroform, methanol, xylene, and trifluoroacetic acid. Isomer L_A showed very low solubility in these solvents except for trifluoroacetic acid.

Structure Assignment. On the basis of the overall macrocyclic structure, some broad conclusions about the expected patterns of the ^1H NMR spectra can be made. The most prominent feature of ^1H NMR spectra of these macrocycles would be that the geminal dimethyl groups would give two singlet signals corresponding to six protons each. The chiral methyl groups should appear as doublets due to coupling with the protons attached to the adjacent carbon. The upfield doublet would be due to an equatorially oriented methyl group, while the downfield doublet would be due to an axially oriented methyl group. The various methylene protons on the macrocyclic ring would appear as multiplets due to complicated coupling patterns. On the other hand, on the basis molecular models, the chiral methyls can be assigned to be equatorial or axial. In each molecular model structure, the ring is placed in a chair form with minimum hydrogen–hydrogen interactions and two adjacent carbons in a gauche conformation. Compar-

ison of the predicted space orientations with the conclusions drawn from ^{1}H NMR spectra, permit assignment of structures to these isomers. A similar method has been successfully used in assigning the isomeric structures of the Co(III) complexes with *C-meso*- and *C-rac*-Me$_2$[14]anes.[7,8]

The 400 MHz ^{1}H NMR spectrum of isomer $\mathbf{L_A}$ (Fig. 1a) shows a sharp methyl singlet at δ 1.6 and an unresolved multiplet at δ 1.7. The singlet at δ 1.6 can be assigned to an equatorial methyl of the gem-dimethyl groups. The other methyl of the gem-dimethyl which is expected to appear at a position downfield in comparison, overlaps with doublets arising from the methyls at C_3, C_5, C_{10}, and C_{12} positions. This type of pattern is suggestive of a completely symmetrical C-meso structure in which C_3, C_5, C_{10}, and C_{12} methyls are all equatorial. This conclusion is based on the fact that a similar assignment has been made for [Ni(tet'a')](ClO$_4$)$_2$[9] (**I**); where the two chiral methyls have an equatorial orientation. It has been concluded that those isomers which show only one methyl singlet for the gem-dimethyl group and an unresolved multiplet, must be meso or racemic diastereomers with all the methyls equatorial. Since in the case of Me$_8$[14]anes, C_3 and C_{10} must have only a meso-configuration by virtue of the method of the synthetic procedure adopted,[6] occurence of a racemic diastereomers is ruled out. Therefore, isomer $\mathbf{L_A}$ is assigned a completely C-meso configuration with the ring lying in a chair form and the four chiral methyls in an equatorial position (**VII**). This requires these centers to be C_3,*S**; C_5,*S**; C_{10},*R**; C_{12},*R**. An X-ray crystal structure determination of the cobalt(III) complexes of $\mathbf{L_A}$ showed complete agreement with the above configuration of the chiral methyls. Details of this work will be published elsewhere.

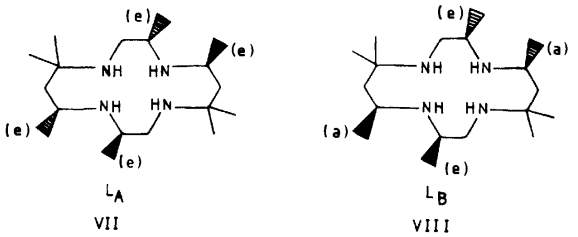

$\mathbf{L_A}$ VII $\mathbf{L_B}$ VIII

Isomer $\mathbf{L_B}$ shows two singlets at δ 1.08 and 1.16 (Fig. 1b) corresponding to 6 protons each that can be assigned to the gem-dimethyl groups. The spectrum also shows two doublets at δ 0.99 and 1.03, each corresponding to 6 protons. This requires that the C_3, C_{10} and C_5, C_{12} methyl groups should be in a pairwise equivalent configuration. The upfield doublet at δ 0.99 can be assigned to equatorial methyls and downfield doublet at δ 1.03 to axial methyls. A diequatorial-diaxial arrangement is possible in the structure in which the C_5, C_{12} methyls occupy a meso-configuration (**VIII**) opposite to that in $\mathbf{L_A}$.

The structure assigned to $\mathbf{L_B}$ on the basis of its ^{1}H NMR spectra is in complete agreement with the one obtained from X-ray crystallographic studies. A perspective view of the molecule is presented in Fig. 2.

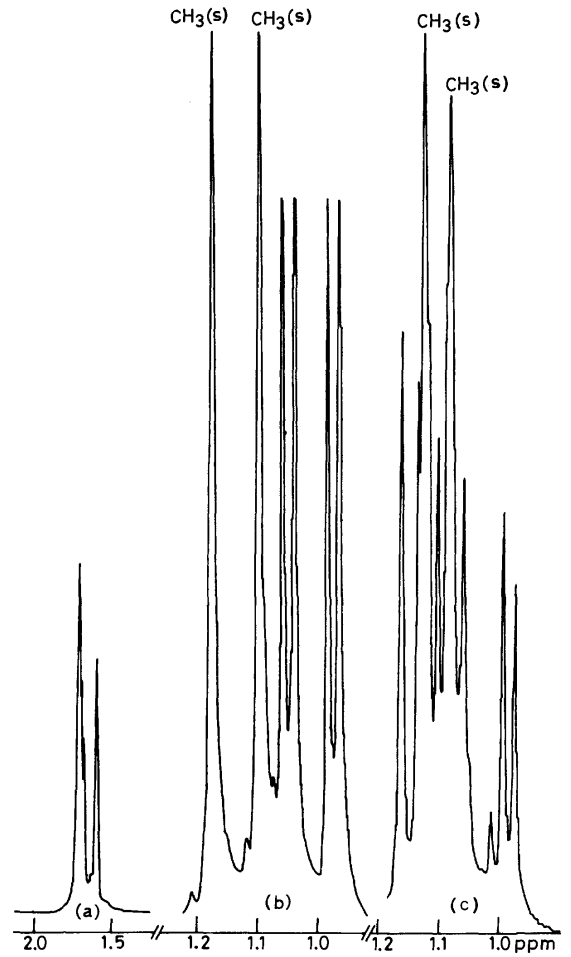

Fig 1. 400 MHz ^{1}H NMR spectrum of $\mathbf{L_A}$ (in CF_3COOH), $\mathbf{L_B}$, and $\mathbf{L_C}$ (both in $CDCl_3$).

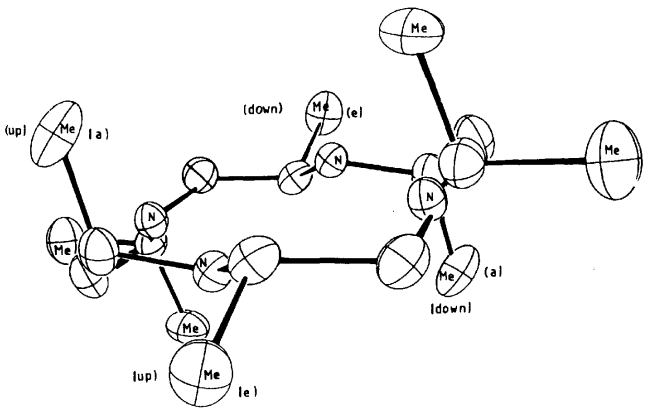

Fig 2. ORTEP perspective view of $\mathbf{L_B}$. Atoms are represented at 50% probability level. Hydrogen atoms have been omitted for clarity.

Included in the unit cell is a water molecule of solvation sitting on a crystallographic two fold center. The molecule is located at an inversion center. This determination shows that the ring lies in a chair form. The bond distances, bond angles, and torsion angles for $\mathbf{L}_B$ are presented in Tables 1—4.

Isomer $\mathbf{L}_C$ shows two singlets at δ 1.07 and 1.11 (Fig. 1c) corresponding to six protons, each assignable to gem-dimethyl groups. The spectrum also shows three doublets at δ 0.99, 1.08, and 1.14 in the ratio of 2:1:1, corresponding to 6, 3, and 3 protons each. The signal at δ 0.99 can be assigned to a pair of equivalent equatorial methyls. The δ 1.08 doublet appears due to an equatorial methyl and the δ 1.14 doublet due to an axial methyl. Such an arrangement is possible if the C_5, C_{12} methyls are in a diequatorial configuration and C_3, C_{10} methyls in an equatorial-axial configuration (IX). The chiral centers then have the forms: C_3,*S**; C_5,*S**; C_{10},*R**; C_{12},*R**. This assignment of the configuration of chiral methyl groups is confirmed by the X-ray structure determination of the Nickel(II) complex of $\mathbf{L}_C$. Details of this work will also be published elsewhere.

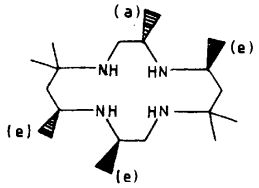

L_C

IX

Table 1. Positional ($\times 10^4$) and Thermal ($\times 10^2$) Parameters

Atom	x	y	z	U/Å^2
O	5000	4967(2)	2500	4.4(1)
N(1)	5395(2)	3746(1)	715(1)	2.53(6)
N(2)	3370(2)	4518(2)	−640(2)	2.63(7)
C(1)	4504(3)	3156(2)	88(2)	3.15(9)
C(2)	4824(3)	2824(2)	−991(3)	4.8(1)
C(3)	3308(3)	3650(2)	−68(2)	3.60(9)
C(4)	2305(2)	5111(2)	−759(2)	3.00(8)
C(5)	1185(3)	4608(2)	−1301(3)	4.8(1)
C(6)	2116(3)	5453(2)	359(3)	4.2(1)
C(7)	2524(2)	5917(2)	−1494(2)	2.96(8)
C(8)	3427(2)	6658(2)	−1040(2)	2.80(8)
C(9)	3466(3)	7393(2)	−1903(3)	4.1(1)

The equivalent isotropic thermal parameter is given by: $U=1/3\Sigma r_i^2$ were r_i are the root-mean-square amplitudes of vibration. Those parameters without an esd were not refined.

Table 2. Bond Distances (Å) of $^1{}_B$

Atom 1	Atom 2	Distance
N(1)	C(1)	1.459 (2)
N(1)	C(8)	1.462 (2)
N(2)	C(3)	1.462 (2)
N(2)	C(4)	1.477 (2)
C(1)	C(2)	1.529 (3)
C(1)	C(3)	1.527 (3)
C(4)	C(5)	1.532 (3)
C(4)	C(6)	1.530 (3)
C(4)	C(7)	1.536 (3)
C(7)	C(8)	1.538 (2)
C(8)	C(9)	1.526 (3)

Numbers in parentheses are estimated standard deviations in the least significant digits.

^{13}C NMR Spectra. ^{13}C NMR spectra gives a separate resonance for each stereochemically distinct carbon atom. Therefore, the method is a sensitive means of characterizing isomers.[10] However, a major problem encountered is that the resonances observed for the methyl carbons cannot be assigned to a particular group on the basis of ^{13}C NMR spectra alone. This is a real limitation on the method for assigning isomeric structures.[11]

The ^{13}C NMR spectra (Figs. 3—5) of the three isomers, $\mathbf{L}_A$, $\mathbf{L}_B$, and $\mathbf{L}_C$ show nine, nine and eighteen resonances respectively. The macrocycles contain

Table 3. Bond Angles (°) of $\mathbf{L}_B$

Atom 1	Atom 2	Atom 3	Angle
C(1)	N(1)	C(3)	116.0 (1)
C(3)	N(2)	C(4)	116.9 (1)
N(1)	C(1)	C(2)	114.6 (2)
N(1)	C(1)	C(3)	108.6 (1)
C(2)	C(1)	C(3)	111.8 (2)
N(2)	C(3)	C(1)	111.0 (1)
N(2)	C(4)	C(5)	112.1 (1)
N(2)	C(4)	C(6)	109.4 (1)
N(2)	C(4)	C(7)	107.4 (1)
C(5)	C(4)	C(6)	109.2 (2)
C(5)	C(4)	C(7)	107.9 (2)
C(6)	C(4)	C(7)	110.7 (2)
C(4)	C(7)	C(8)	118.9 (1)
N(1)	C(8)	C(7)	110.3 (1)
N(1)	C(8)	C(9)	110.5 (2)
C(7)	C(8)	C(9)	109.2 (2)

Numbers in parentheses are estimated standard deviations in the least significant digits.

Table 4. Torsional Angles (°) of $\mathbf{L}_B$

Atom 1	Atom 2	Atom 3	Atom 4	Angle	Atom 1	Atom 2	Atom 3	Atom 4	Angle
C(4)	N(2)	C(3)	C(1)	−174.58 (0.29)	C(2)	C(1)	C(3)	N(2)	−67.86 (1.02)
C(3)	N(2)	C(4)	C(5)	−55.13 (0.41)	N(2)	C(4)	C(7)	C(8)	−71.94 (0.32)
C(3)	N(2)	C(4)	C(6)	66.28 (0.51)	C(5)	C(4)	C(7)	C(8)	167.00 (0.27)
C(3)	N(2)	C(4)	C(7)	−173.47 (0.33)	C(6)	C(4)	C(7)	C(8)	47.50 (0.59)
N(1)	C(1)	C(3)	N(2)	59.60 (0.38)	C(4)	C(7)	C(8)	C(9)	−178.57 (0.81)

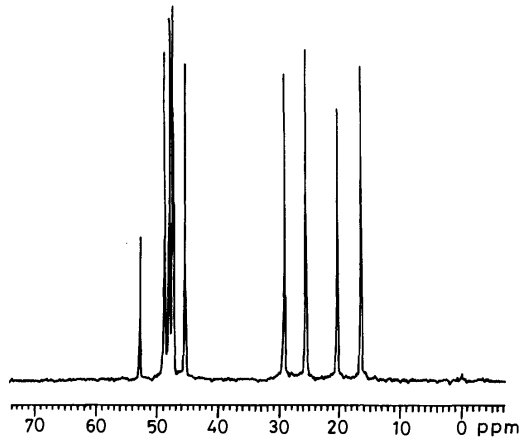

Fig 3. ^{13}C NMR spectrum of L_A (in CF_3COOH).

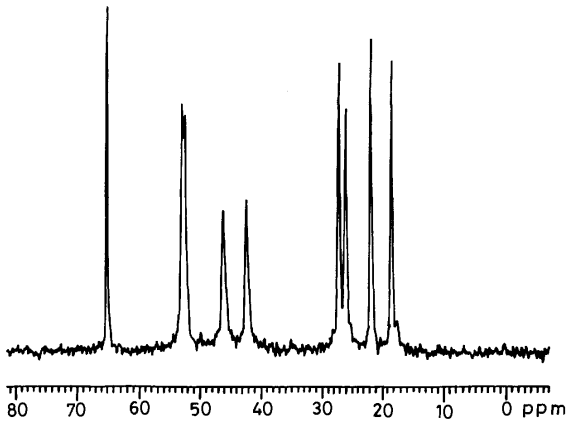

Fig 4. ^{13}C NMR spectrum of L_B (in $CDCl_3$).

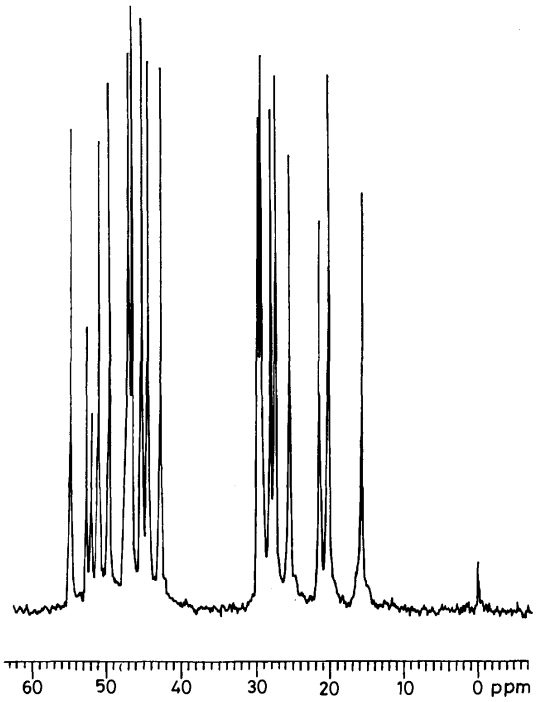

Fig 5. ^{13}C NMR spectrum of L_C (in $CDCl_3$).

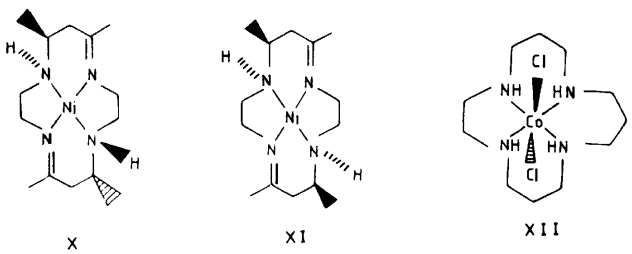

X XI XII

eighteen carbons each. In case of L_A and L_B, only nine peaks are observed due to pairwise equivalence of carbon atoms. This observation is in support of the symmetric 'all equatorial' and 'diaxial-diequatorial' arrangements as has already been assigned on the basis of ^1H NMR spectra. The symmetry of structure L_B has also been confirmed by X-ray crystallography. In contrast, isomer L_C gives eighteen peaks which corresponds to eighteen nonequivalent carbon atoms indicating no symmetry in the molecule.[11-13] The results of ^1H NMR spectra also show that this isomer lacks symmetry. These conclusions are supported by similar observations with Me_4[14]dienes. Two isomeric nickel(II) complexes of Me_4[14]diene (ttcd), *Aα*-$[Ni(ttcd)]^{2+}$ (**X**) and *Bα*-$[Ni(ttcd)]^{2+}$ (**XI**) both containing fourteen carbon atoms show fourteen and seven peaks respectively.[11] Similar observations have been obtained in the case of two isomers[12] of *trans*-$[Co([15]ane)Cl_2]^+$ (**XII**). In another study, the *C-meso*- and *C-rac*-Me_6[22]ane (**II**) are also found to show twelve peaks, equivalent to half the number of total carbon atoms[2] due to the pairwise equivalence of each carbon atom.

In case of ligand L_A and L_B, the first four peaks can be assigned to the eight carbons (pairwise equivalent) of peripheral methyl groups and the next five peaks to the remaining ten carbons (pairwise equivalent) in the ring. On the other hand, the first eight peaks observed in the case of L_C correspond to the eight nonequivalent carbon atoms of peripheral methyl groups and the remaining ten resonances to ten different carbon atoms of the macrocyclic ring. The range of chemical shifts assigned for the peak positions of methyl carbons (δ 15—30) and ring carbons (δ 40—65) is the one which has already been reported for similar type of ligands and for their complexes.[11]

Experimental

Microanalysis, ^{13}C NMR, and the mass spectral measurements were carried out at the University of Stirling, Scotland. 400 MHz ^1H NMR were recorded at the Regional Sophisticated Instrumentation Centre, Central Drug Research institute, Lucknow, India. IR spectra were run on a Beckman IR 20 Spectrophotometer as KBr discs. TLC was performed on 8×2.5 cm glass plates coated with a 0.25—0.5 mm layer of silica gel (BDH, without binder).

Synthesis: 3,10-*C*-*meso*-Me$_8$[14]diene (**VI**) was prepared as described.[6] 10.5 g of 3,10-*C*-*meso*-Me$_8$[14]diene suspended in 400 cm^3 of hot 1:1 water-methanol mixture was reduced by the slow addition of 15 g of sodium borohydride with constant stirring and heated for 2 h on a steam bath. Methanol was then removed on a rotatory evaporator and the pH raised to above 12 with solid NaOH. The solution was again heated on a steam bath for about half an hour and the reduced material extracted several times with chloroform from the hot mixture. The chloroform extracts were dried over anhydrous sodium sulfate and the chloroform stripped off on a rotatory evaporator leaving behind a yellow oily liquid which on cooling gave a white solid. The product of the reduction process consists of a mixture of isomeric 3,10-*C*-*meso*-Me$_8$[14]anes.

50 g of the reduced material obtained above was suspended in 200 cm^3 of xylene and heated on a steam bath for about half an hour at 80—85 °C. The solution was filtered hot and the insoluble white product was washed with hot xylene. The product is Me$_8$[14]aneA (**L$_A$**); yield 9.59 g (19%), mp 350 °C (decomp) (Found: C, 69.2; H, 12.9; N, 17.9%. Calcd for $C_{18}H_{40}N_4$: C, 69.2; H, 12.9; N, 17.9%).

The filtrate from above on standing overnight at room temperature yielded needle shaped crystals of Me$_8$[14]aneB (**L$_B$**). The isomer **L$_B$** was filtered off, washed thoroughly with cold xylene and dried in vacuum. The product was recrystallized from hot ether; yield 19 g (38%), mp 122 °C; (Found: C, 65.7; H, 12.9; N, 17.1%. Calcd for $C_{18}H_{40}N_4 \cdot H_2O$: C, 65.5; H, 12.7; N, 17.0%).

The filtrate after removal of isomer **L$_A$** and isomer **L$_B$** was allowed to stand in the open for several days, when cubic shaped crystals of Me$_8$[14]aneC (**L$_C$**) were deposited. Another crop of isomer **L$_C$** could be collected on standing the mother liquor for another two days. The isomer **L$_C$** was recrystallized from hot ethers; yield 11 g, (22%), mp 85 °C; (Found: C, 69.1; H, 12.9; N, 17.9%. Calcd for $C_{18}H_{40}N_4$: C, 69.2; H, 12.9; N, 17.9%).

The purity of the isomers was checked on thin-layer chromatographic plates of 8 cm×2.5 cm coated with silica gel without any binder. The chromatograms were eluted with 80:20% methanol-chloroform mixture and exposed to iodine vapor. Each isomer gave a single spot on these plates.

The mass spectra of each isomer showed M^+ peak at m/z 312 for $C_{18}H_{40}N$. An additional (M^++1) peak at m/z 313 is observed in case of **L$_B$**.

X-Ray Crystallography.[14] Crystals of **L$_B$** for X-ray crystallography were grown by slow evaporation of its dilute solution in xylene.

Crystal Data. Me$_8$[14]aneB (**L$_B$**), $C_{18}H_{42}N_4O$, M=330.56. Monoclinic, a=11.391(3), b=14.596(4), c=12.481(4) Å, β=99.23(2)°, V=2048(1) Å^3 (by least squares refinement on diffractometer angles for 21 reflections in the range $10<2\theta<32°$), Mo $K\alpha$ radiation, λ=0.71073 Å, space group $C2/c$, Z=4, D_c=1.072 g cm^{-3}. Crystal dimensions: 0.37×0.42×0.26 mm, μ=0.63 cm^{-1}.

Data Collection and Processing. CAD4 automated diffractometer, $\omega/2\theta$ mode with scan width=0.60+0.35 tan θ, speed 10.1 to 1.6 deg min^{-1}, graphite-monochromated Mo $K\alpha$ radiation; 2552 reflections measured, 2431 unique [merging R=0.020] giving 1376 with $I>\sigma(I)$.

Structure Analysis and Refinement.[15] Direct methods program MITHRIL[16] was used. Full matrix least squares refinement on F_o minimising the function where $|F_o|$ and $|F_c|$ are the observed and calculated structure factor amplitudes respectively and the weighting factor is given by $\omega=4F_o^2/\sigma^2(F_o^2)|$. The neutral atom scattering factors were calculated from the analytical expression for the scattering factor curves.[17] The f' and f'' components of anomalous dispersion[18] were included in the calculation for all non-hydrogen atoms.

All hydrogen atoms were included at their idealized calculated positions, assuming C–H 0.95 Å and appropriate sp^2 or sp^3 geometries. The methyl hydrogens were fitted by least squares to peaks observed in a difference Fourier. These atoms were then included in the calculations with fixed, isotropic thermal parameters 1.2 times that of the attached atom and constrained to 'ride' with this atom. The largest shift in any parameter was 0.03 times its estimated standard deviation and the error in an observation of unit weight was 2.71 e.

This work was supported by research grant No. 1 (979)/84-EMR-II from C.S.I.R., New Delhi.

References

1) R. W. Hay and G. A. Lawrence, *J. Chem. Soc., Perkin Trans. 1*, **1975**, 591.
2) R. W. Hay and M. P. Pujari, *Inorg. Chim. Acta*, **99**, 75 (1985).
3) R. A. Kolinski and B. K. Dasziewicz, *Bull. Acad. Pol. Sci.*, **42**, 13 (1969).
4) R. A. Kolinski, *Bull. Acad. Pol. Sci., Ser. Sci. Chim.*, **17**, 13 (1969).
5) T. Ito and D. H. Busch, *J. Am. Chem. Soc.*, **95**, 7528 (1973).
6) N. F. Curtis, D. A. Swann, T. N. Waters, and I. E. Maxwell, *J. Am. Chem. Soc.*, **91**, 4588 (1969).
7) R. W. Hay, R. Bembi, and D. A. House, *J. Chem. Soc., Dalton Trans.*, **1984**, 1921.
8) R. W. Hay, D. A. House, and R. Bembi, *J. Chem. Soc., Dalton Trans.*, **1984**, 1927.
9) L. G. Warner and D. H. Busch, *J. Am. Chem. Soc.*, **91**, 4092 (1969).
10) G. H. Searle, S. F. Lincoln, F. R. Keene, S. G. Teague, and D. G. Rowe, *Aust. J. Chem.*, **30**, 1221 (1977).
11) G. H. Searle, R. W. Hay, and B. Jeragh, *Aust. J. Chem.*, **33**, 1447 (1980).
12) Y. Hung, L. Y. Martin, S. C. Jackels, A. M. Tait, and D. H. Busch, *J. Am. Chem. Soc.*, **99**, 4029 (1977).
13) R. A. Kolinski, B. K. Daszkiewicz, Z. Kubej, and J. Mrozinski, *Inorg. Chim. Acta*, **57**, 269 (1982).
14) The X-ray crystallographic study was carried out by Dr. R. G. Ball. Inquiries regarding the crystallographic results should be directed to him quoting report number SR: 121523-09-86.
15) The complete F_o-F_c data are deposited as Document No. 8891 at the Office of the Editor of Bull. Chem. Soc. Jpn.
16) MITHRIL. A multiple solution direct method program by C. J. Gilmore, Department of Chemistry, University of Glasgow (1984).
17) "International Tables for X-ray Crystallography," Kynoch Press, Birmingham, England (1974), Vol. IV, Table 2. 2B.
18) "International Tables for X-ray Crystallography," Kynoch Press, Birmingham, England (1974), Vol. IV, Table 2. 3. 1.

Induced Circular Dichroism and Molecular Orientations of β-Cyclodextrin Inclusion Complexes with 9,10-Anthraquinone and 9,10-Phenanthrenequinone

Masafumi ATA, Yoshihiro KUBOZONO, Yasunobu SUZUKI, Makoto AOYAGI, and Yasuhiko GONDO*
Department of Chemistry, Faculty of Science, Kyushu University 33, Hakozaki, Higashi-ku, Fukuoka 812
(Received November 19, 1988)

Synopsis. The induced circular dichroism (ICD) spectra of β-cyclodextrin inclusion complexes with 9,10-anthraquinone and 9,10-phenanthrenequinone have been measured, and the electronic structures and molecular orientations of the guests are discussed in terms of the ICD signs and theoretical results.

Cyclodextrins (CDxs) are known as typical hosts in inclusion chemistry. One of the most important spectroscopic benefits brought about by inclusion-complex formation is induced circular dichroism (ICD); since a CDx is composed of several D(+)-glucopyranose units, the Cotton effect is induced on the electronic absorption bands of an achiral guest molecule. On the basis of the coupled oscillator theory, it has been shown that the guest electronic transition polarized perpendicular to the CDx cavity axis exhibits a negative ICD, whereas that polarized parallel exhibits a positive ICD.[1,2] The ICD measurement of CDx-inclusion complexes has been shown to be a very simple and useful tool in the assignment of electronic absorption bands both for neutral molecules[1-5] and for radical ions.[6] In other words, information on the molecular orientation can be gathered from knowledge of the directions of the transition dipole moments in the guest molecule.[4,5] In this report, we will discuss the inclusion orientations and assignment of the electronic absorption spectra of 9,10-anthraquinone (9,10-AQ) and 9,10-phenanthrenequinone (9,10-PhQ) on the basis of the observed ICD signs and the results of the published molecular orbital calculations.[7-9]

Results and Discussion

Figures 1 and 2 show the electronic absorption and ICD spectra of the β-CDx inclusion complexes with 9,10-AQ and 9,10-PhQ respectively in an aqueous solution as observed at room temperature, while Table 1 compares the experimental and theoretical spectral data.[8] Since the nπ* transitions overlap with the ππ* transitions, the precise discussion is restricted to the ππ* transitions; accordingly, the theoretical spectral data cited in Table 1 are concerned solely with the ππ* transitions.

Referring to the molecular orientation of the β-CDx inclusion complex with 1,4-naphthoquinone,[5] the two oxygen atoms of 9,10-AQ are seemingly not fully included in the β-CDx cavity, while one of the benzene moieties can be included. Namely, as is illustrated in Fig. 3, 9,10-AQ is partially included to take an axial orientation with β-CDx; hence, the electronic transitions polarized along the long and short molecular axes should be positive and negative respectively in

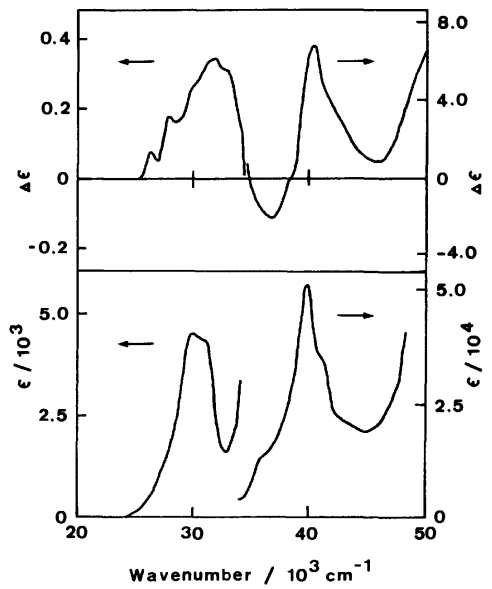

Fig. 1. ICD (upper) and electronic absorption (lower) spectra of β-CDx inclusion complex with 9,10-AQ in aqueous solution observed at room temperature.

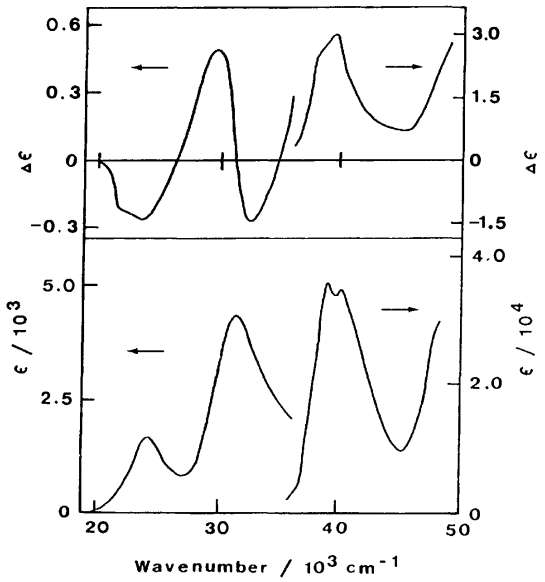

Fig. 2. ICD (upper) and electronic absorption (lower) spectra of β-CDx inclusion complex with 9,10-PhQ in aqueous solution observed at room temperature.

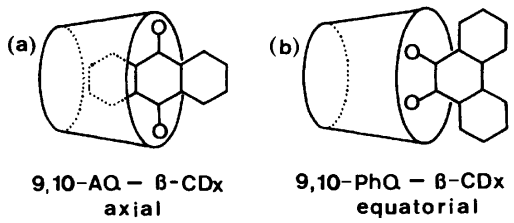

Fig. 3. Probable partial inclusion and molecular orientations in the β-CDx inclusion complexes with 9,10-AQ (a) and 9,10-PhQ (b).

ICD sign. Thus, the absorption bands at 29750 and 39630 cm^{-1} are found to be polarized along the long molecular axis, while the shoulder band at 35900 cm^{-1} is polarized along the short molecular axis. When the axial inclusion is assumed, the theoretical prediction based on the PPP method[8] is in good agreement with the ICD spectrum, as is shown in Table 1, as far as the ππ* transtions are concerned. The absorption bands appearing at 29750, 35900, and 39630 cm^{-1} can be correlated to the ^1L_a, ^1L_b, and ^1B_b bands of anthracene respectively. The structure around 27000 cm^{-1} in the ICD spectrum is due to either the ππ* vibronic or nπ* transition;[7-9] no definite conclusion can be deduced, since the nπ* band overlaps with the ππ* band.[10,11]

Now, let us turn to the β-CDx inclusion complex with 9,10-PhQ. In what follows, we assume that the above-mentioned ICD-sign rule for the guest electronic transitions[1,2] can also be applied when, as is illustrated in Fig. 3(b), a substantial portion of the guest is located outside the CDx cavity. According to the theoretical data in Table 1 obtained on the basis of the PPP method,[8] the first ππ* transition is polarized along the long molecular axis. The second and third transitions are predicted to be polarized differently from each other and to appear around 33000 cm^{-1}; actually, the ICD spectrum in Fig. 2 exhibits two differently polarized transitions in the 28000—35000 cm^{-1} region. The fourth transition is predicted to be short-axis polarized and to be located at 39040 cm^{-1}. If 9,10-PhQ is axially included in β-CDx, the ICD signs should be plus, minus, plus, and minus in order from the low- to the high-energy region; this is in disagreement with the ICD signs shown in Fig. 2. From the correlation between the theoretical and experimental results, the ICD spectrum can be ascribed to such an equatorial inclusion complex as is illustrated in Fig. 3. The minimum and maximum molecular dimensions of a 9,10-PhQ molecule are estimated to be 8.0 and 11.6 Å respectively, inclusive of the van der Waals radii of the hydrogen and oxygen atoms. Thus, in view of the cavity size of β-CDx, 9,10-PhQ is included in β-CDx, not completely but partially, as well as equatorially, with the *o*-benzoquinone moiety located in the cavity; the major binding force between 9,10-PhQ and β-CDx seems to be brought about by intermolecular hydrogen bonding between the carbonyl groups of 9,10-PhQ and the hydroxyl groups of β-CDx. An nπ* transition with out-of-plane polarization must be negative in ICD sign, irrespective of whether the inclusion is axial or

Table 1. ππ* Transition Energies (ΔE), Oscillator Strengths (f), and Polarization (Pol.) of 9,10-AQ and 9,10-PhQ

No.	Theoretical[a]			Experimental	
	$\Delta E/10^3$ cm^{-1}	f	Pol.[b]	$\Delta E/10^3$ cm^{-1}	log ε
		(1) 9,10-AQ			
1	32.83	0.191	L	29.75	3.66
2	33.24	0	Forb.		
3	33.72	0	Forb.		
4	37.59	0.569	S	35.90	4.09
5	42.11	0.935	L	39.63	4.71
6	42.75	0	Forb.		
7	47.03	0	Forb.		
8	47.29	0.192	S		
		(2) 9,10-PhQ			
1	27.67	0.157	L	24.09	3.20
2	32.83	0.054	S	29.85[c]	
3	33.47	0.008	L	32.89[c]	
4	39.04	0.560	S	39.25	5.56
5	40.56	0.660	L		
6	42.51	0.003	S		
7	44.12	0.004	L		
8	48.24	0.001	S		

a) Taken from Ref. 8. b) L, S, and Forb. denote the long-axis polarized, short-axis polarized, and forbidden transitions respectively. c) Determined from the ICD spectrum shown in Fig. 2.

equatorial. The negative shoulder at 21250 cm^{-1} in the ICD spectrum is possibly due to the nπ* transition,[9] but no definite conclustion can be deduced since, just as in the case of 9,10-AQ, the nπ* band overlaps with the ππ* band.[10,11] The theoretical fifth intense transition cannot be identified in the ICD spectrum, probably because it falls outside the spectral range studied.

In conclusion, the ICD spectra of 9,10-AQ and 9,10-PhQ can be ascribed to the axial and equatorial inclusion complexes with β-CDx respectively, as is illustrated in Fig. 3. The respective molecular orientations of the two quinones studied can be interpreted as natural consequences of the intermolecular hydrogen bonding between the quinones and the host.

Experimental

The 9,10-AQ and 9,10-PhQ (Tokyo Kasei, GR) were recrystallized from ethanol (Wako, SSG). The β-CDx (Tokyo Kasei, GR) was recrystallized five times from water and then dried under a vacuum at 80 °C. The deinoized and distilled water was used as a solvent. The electronic absorption and ICD spectra of the β-CDx inclusion complexes were recorded at room temperature, about a day after the sample-preparation, on a Shimadzu MPS 50-L spectrophotometer and on a JASCO J-500C circular dichrograph respectively. A JASCO J-501N data processor was used for the accumulation of the ICD spectra. The concentration of β-CDx was set at 1.5×10^{-2} mol dm^{-3}, while those of the quinones were adjusted so that the maximum absorbances fell in the range of 1.2—1.5.

The authors are indebted to Professor Emeritus Seizo Misumi, Professor Yukito Murakami, and

Professor Tadashi Yonemitsu for providing the facilities for the circular dichroism measurements.

References

1) K. Harata and H. Uedaira, *Bull. Chem. Soc. Jpn.*, **48**, 375 (1975).
2) H. Shimizu, A. Kaito, and H. Hatano, *Bull. Chem. Soc. Jpn.*, **52**, 2678 (1979).
3) H. Yamaguchi, M. Ata, J. W. F. McOmie, J. W. Barton, and H. Baumann, *J. Chem. Soc., Faraday Trans. 2*, **97**, 599 (1983).
4) M. Ata and H. Yamaguchi, *J. Chem. Soc., Chem. Commun.*, **1983**, 3.
5) M. Ata and H. Yamaguchi, *Nippon Kagaku Kaishi*, **1983**, 297.
6) M. Aoyagi, Y. Kubozono, M. Ata, and Y. Gondo, *Chem. Phys. Lett.*, **131**, 201 (1986).
7) G. Olbrich, O. E. Polansky, and M. Zander, *Ber. Bunsenges. Phys. Chem.*, **81**, 692 (1977).
8) H. Hoffmann and G. Rasch, *Z. Phys. Chem. (Leipzig)*, **4**, 689 (1976).
9) A. Kuboyama, Y. Kozima, and J. Maeda, *Bull. Chem. Soc. Jpn.*, **55**, 3635 (1982).
10) H. Hartmann and E. Lorenz, *Z. Naturforsch., A*, **7**, 360 (1952).
11) A. Kuboyama, *Bull. Chem. Soc. Jpn.*, **33**, 1027 (1960).

The Determination of the Poly(oxyethylene) Oligomer Distribution in a Nonionic Surfactant by Means of Thin-Layer Chromatography

Yoshihiro SAITO, Takatoshi SATO,* and Ichiro ANAZAWA†
College of Pharmacy, Nihon University, 7-7-1, Narashinodai, Hunabashi-shi, Chiba 274
†Department of Industrial Chemistry, College of Industrial Technology, Nihon University, 1-2-1, Izumi-cho, Narashino-shi, Chiba 275
(Received April 27, 1989)

Synopsis. The analytical method for determining the distribution of the polymerization degree of the oxyethylene (OE) chain in commercially available poly(oxyethylene) alkyl ether (C_mE_n) was investigated by means of thin-layer chromatography with flame-ionization detection (TLC-FID). It was found that the method of calculating the relative response factors of every OE chain to FID could be determined, and the analysis of the distribution of the polymerization degree of the OE chain in commercially available C_mE_n became possible using the TLC-FID method.

It is known that the distribution as well as the mean length of the oxyethylene (OE) chain in nonionic surfactants greatly affects various surface-chemical characteristics.[1-3] Gas chromatography and high-performance liquid chromatography are now used as general analytical methods for determining the distribution of the polymerization degree of the OE chain.[4-6] Considering the time required for the analysis and the use of a detector, it is difficult to operate every routinely the instruments in order to acquire reproducible data. The present authors have recently reported an advanced separating method of the OE chain using thin-layer chromatography with flame-ionization detection (TLC-FID) as a rapid alternative method.[7] It is necessary to find the relative response factor of each peak to the hydrogen ionization detector (FID) and to correct it in order to determine the real distribution of the polymerization degree of the OE chain from the chromatogram drawn.

The method of calculating the relative response factor of a alkyl ether-type nonionic surfactant to FID and the method of analyzing the distribution of the polymerization degree were investigated in this study. This method should also be applicable for the determination of polyethylene glycol as a by-product in poly(oxyethylene)-type nonionic surfactants.

Experimental

Materials. The poly(oxyethylene) alkyl ether (C_mE_n: $C_mH_{2m+1}O(C_2H_4O)_nH$) with a single chain length and a relatively narrow distribution of OE[8] was obtained from the Nikko Chemicals Co., Ltd. Guaranteed reagents of benzene, ethyl acetate, and acetic acid were used as the developing solvents.

Measurement by TLC-FID. The TLC-FID instrument, the thin-layer rod, and the analytical conditions were the same as those described in a previous report.[7]

Results and Discussion

Calculation of Relative Response Factor. Figure 1 illustrates the relationship between the OE-chain length (n) in C_mE_n with a single-chain length and the peak area (A) in the TLC-FID chromatogram. When the alkyl-chain lengths (m) are the same, the relationship between A per gram and n is linear. The relationship between A and n in each C_mE_n can, therefore, be expressed by the following formula:

$$A = -Pn + b \quad (1)$$

where P is the slope for each straight line in Fig. 1, b is the A of the corresponding higher alcohol, and b is proportional to m, as is shown in Fig. 1. The relationship between P and m in C_mE_n is also linear, as is shown in Fig. 2. This relationship is represented by the following equation:

$$P = 0.095m - 0.50 \quad (2)$$

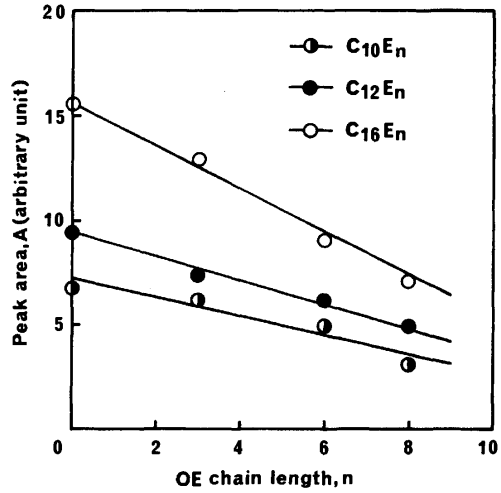

Fig. 1. Relationship between OE chain length in nonionic surfactant and peak area.

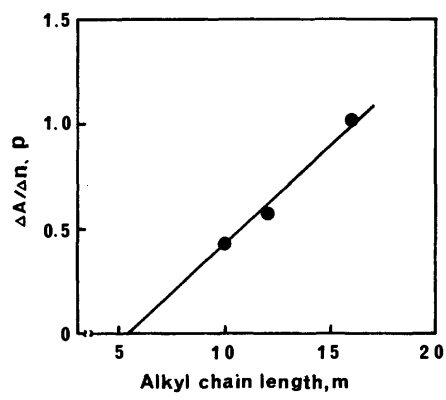

Fig. 2. Plots of P vs. m according to Eq. 2.

Table 1. OE Distribution and Statistical Analysis of Commercially Available $C_{12}E_5$ (n=4)

OE number	Relative response factors	Molar distribution	Weight distribution	SD/X(%)
1	1.00	0.0109	0.0062	13.1
2	1.08	0.0523	0.0354	4.2
3	1.17	0.1552	0.1220	2.2
4	1.28	0.2224	0.1990	1.1
5	1.41	0.2113	0.2120	1.6
6	1.58	0.1525	0.1696	0.7
7	1.78	0.0974	0.1189	2.0
8	2.05	0.0526	0.0699	5.2
9	2.41	0.0305	0.0438	6.3
10	2.92	0.0149	0.0231	9.9

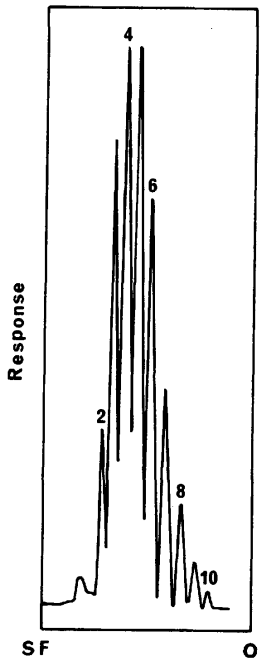

Fig. 3. TLC-FID chromatogram of commercially available $C_{12}E_5$. The peak number corresponds to the number of OE chains. SF: solvent front, O: origin. Mobile phase: 1st development, benzene-ethyl acetate (6/4, vol%), 10 cm; 2nd development, ethyl acetate-acetic acid-water (8/1/1, vol%), 8 cm; gas flow: H_2, 160 mL min^{-1}; air, 2 L min^{-1}; scanning speed: 35 s/scan.

The A value per gram of C_mE_n and the relative response factors of C_mE_n to FID can be calculated from Eqs. 1 and 2. This analytical method is applicable to C_mE_n with m and n values that satisfy $A>0$.

As compared with the previous TLC-FID method,[7] one can calculate the relative response factors of the OE chain for a series of C_mE_n by this method. This method is also widely applicable to the determination of the OE-chain distribution of nonionic surfactants.

Analysis of Chromatogram. Figure 3 shows the TLC-FID chromatogram of commercially available $C_{12}E_5$. Each peak in the chromatogram was identified by using each C_mE_n with a single-chain length. The results indicate that the peaks were detected in the order of the added number of moles of the OE chains. The peaks are satisfactorily separated in the chromatogram. The actual molecular weight distribution was determined using the chromatogram and the relative response factors calculated from Eqs. 1 and 2. The relative response factors are defined as the ratio of the A value per gram of each $C_{12}E_n$ to that of $C_{12}E_1$. All the values were measured relative to $C_{12}E_1$ ($C_{12}E_1$=1.00). The results are shown in Table 1. The table shows that the molecular weight distribution of commercially available $C_{12}E_5$ can be accurately determined. Since the TLC-FID method is a simple, rapid method of analysis requiring no chemical modification, as was stated in the previous report,[7] it is useful for determining the distribution of the OE chain in a poly(oxyethylene)-type nonionic surfactant. In addition, the distribution of the OE chain in any series of C_mE_n can be determined because the relative response factor can be calculated, even for commercially unavailable products,[9] with a single chain. Therefore, the TLC-FID method can be applied to the determination of the OE-chain distribution in other poly(oxyethylene)-type nonionic surfactants by selecting appropriate developing solvents.

References

1) E. H. Crook, D. B. Fordyce, and G. F. Trebbi, *J. Phys. Chem.*, **67**, 1987 (1963).
2) E. H. Crook and D. B. Fordyce, *J. Am. Oil Chem. Soc.*, **41**, 231 (1964).
3) K. W. Dillan, *J. Am. Oil Chem. Soc.*, **62**, 1144 (1985).
4) L. Gildenberg and J. R. Trowbridge, *J. Am. Oil Chem. Soc.*, **42**, 69 (1965).
5) A. Nozawa and T. Ohnuma, *J. Chromatogr.*, **187**, 262 (1982).
6) A. Aserin, M. Frenkel, and N. Garti, *J. Am. Oil Chem. Soc.*, **61**, 805 (1984).
7) T. Sato, Y. Saito, and I. Anazawa, *J. Am. Oil Chem. Soc.*, **65**, 996 (1988).
8) M. Abe, T. Kakihara, H. Uchiyama, and K. Ogino, *Yukagaku*, **37**, 705 (1988).
9) J. D. Mcclure, *J. Am. Oil Chem. Soc.*, **59**, 364 (1982).

Temperature Change of Graphite Surface Due to Electrochemical Intercalation of ClO_4^- Ion

Yasuhisa MAEDA
Materials Science, Toyohashi University of Technology, Tempaku-cho, Toyohashi 440
(Received May 24, 1989)

Synopsis. Anodic intercalation and cathodic deintercalation of ClO_4^- ions were shown to cause exothermic and endothermic changes, respectively, on a graphite surface. This suggests the occurrence of an increase in entropy for the deintercalation process and a decrease for the case of intercalation.

Studies on the syntheses, structure, properties, and applications of graphite intercalation compounds have been actively carried out. There have been several reports concerning electrochemical intercalation on graphite.[1-10] This process is important because it may provide both kinetic and thermodynamic interpretations for intercalation behavior. It has been reported[11-13] that useful information concerning electrochemical reactions may be obtained by the detection of heat due to electrolysis. In the present study in-situ measurements of the temperature changes of graphite surfaces due to electrochemical intercalation were carried out in order to reveal heat behavior during the intercalation process.

Experimental

Measurements of the temperature change were based on the differential thermal method; two thermistors (Takara Industry Co., type: PXK-67) were used, the one of which was attached to the surface of the graphite electrode and the other placed in the bulk of the solution. The temperature difference between them was detected by a bridge (Fuso Seisakusho Co., model: 362A). The solution (volume: 0.1 dm^3) was stirred and N_2 gas bubbled during electrolysis. By circulating thermostated water outside the solution, its temperature was maintained at 20 °C. A graphite sheet (Toyo Tanso Co., size: 12×10×0.5 mm) was used as the working electrode. The counter electrode was a platinum wire, and the reference electrode was an oxidized silver wire galvanostatically (at 1 mA for 10 min) placed in 1 mol dm^{-3} hydrochloric acid. Electrolytic solutions were prepared by the dissolution of anhydrous $LiClO_4$ into distilled propylene carbonate (PC), acetonitrile (AN), and nitromethane (NM). The electrochemical intercalation of ClO_4^- ions was performed by cyclic voltammetry. Simultaneously, the temperature change of the graphite surface was measured during electrolysis.

Results and Discussion

It has been reported[1,2] that anodic oxidation of graphite in organic solutions containing perchlorate causes the intercalation of ClO_4^- ions, as follows:

$$nC + ClO_4^- \rightleftarrows C_n^+ ClO_4^- + e$$

In this case, the reaction on the left represents the cathodic deintercalation of ClO_4^- ions.

Figure 1 shows the cyclic voltammogram (CV) as well as the relation between the temperature change and the electrode potential (ΔT-E) of graphite in a 0.2 mol dm^{-3} $LiClO_4$-PC solution. Regarding the sign of ΔT, the positive and the negative signs represent a rise and a fall in temperature, that is, exothermic and endothermic changes, respectively. Concerning the CV in Fig. 1, the anodic current and the corresponding cathodic current peak were observed. The former indicates the intercalation process of the ClO_4^- ion and the latter its deintercalation. The ΔT-E relation showed a marked increase in temperature with the anodic current; also, the peak of the fall in temperature nearly fit the cathodic peak.

Figure 2 shows the CV and the ΔT-E relation of graphite in a 0.2 mol dm^{-3} $LiClO_4$-AN solution. The anodic current and the corresponding cathodic peak due to the intercalation and deintercalation of ClO_4^- ions, respectively, were observed. The ΔT-E relation showed an increase in temperature with the anodic current; also, the peak of the fall in temperature nearly fit the cathodic peak.

Figure 3 shows the CV and the ΔT-E relation of graphite in a 0.1 mol dm^{-3} $LiClO_4$-NM solution. In this case, a similar rise and a fall in temperature occurred during the processes of intercalation and deintercalation of ClO_4^- ions, respectively, though the fit of the fall in temperature with the cathodic peak

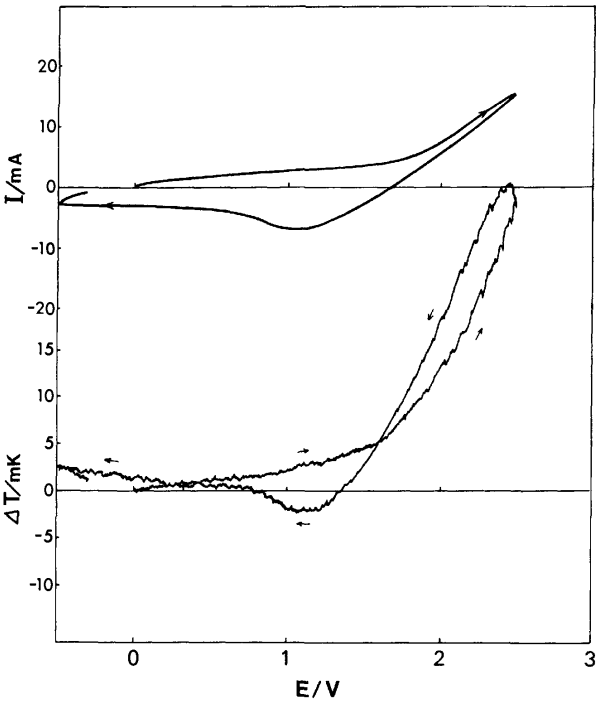

Fig. 1. The CV and the ΔT-E relation of the graphite in a 0.2 mol dm^{-3} $LiClO_4$-PC solution. Scan rate: 10 mV s^{-1}.

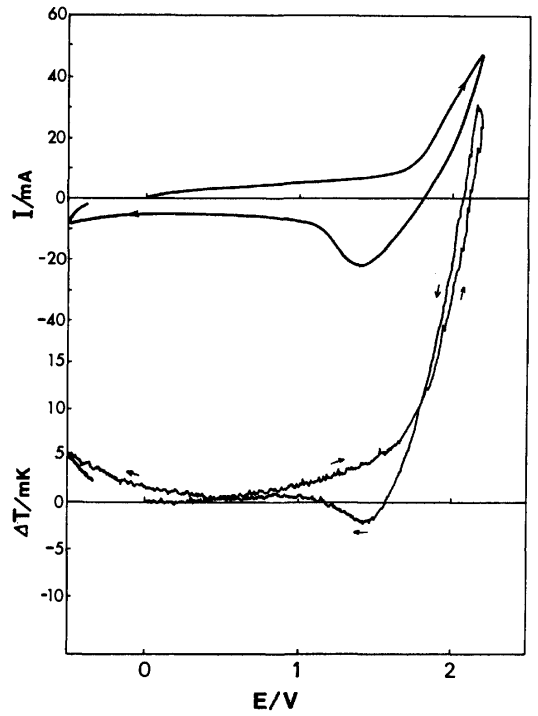

Fig. 2. The CV and the ΔT-E relation of the graphite in a 0.2 mol dm^{-3} $LiClO_4$-AN solution. Scan rate: 10 mV s^{-1}.

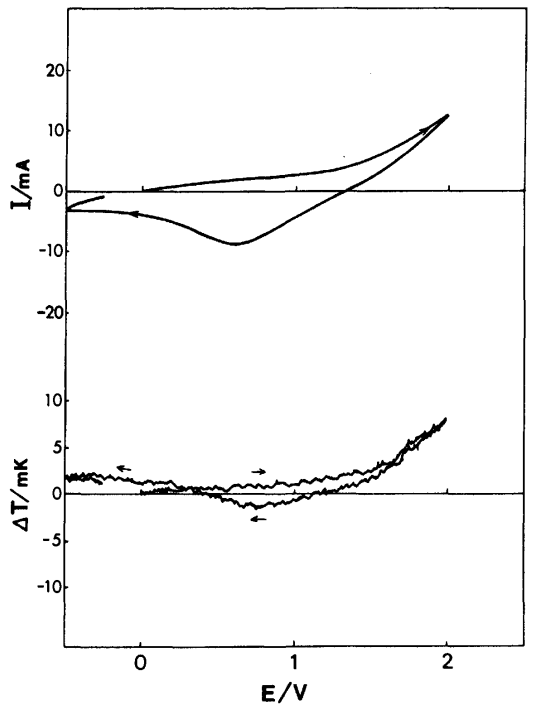

Fig. 3. The CV and the ΔT-E relation of the graphite in a 0.1 mol dm^{-3} $LiClO_4$-NM solution. Scan rate: 10 mV s^{-1}.

was not clear.

At the electrode/electrolyte interphase, the absorbed heat dQ during the electrolysis period dt can be expressed as

$$dQ = \frac{(T\Delta S + Q^*)|I|dt}{nF} - |I|\,\eta\,dt - I^2 R\,dt, \quad (1)$$

where ΔS is the molar entropy change of electrode reaction, Q^* the heat of transfer, I the current, η the overpotential and R the electric resistance. The relation between the temperature change and the absorbed heat at the interphase is given by

$$\Delta T = -K\frac{dQ}{dT}, \quad (2)$$

where K is a positive constant. In Eq. 1, the first term is called the electrochemical Peltier heat. Q^* equals $T\Delta S^*$, where ΔS^* is the molar entropy change of transfer of ions. Since the value of $\Delta S^*/nF$ (except the case of H^+ or OH^- participating) is within +0.08—−0.08 mV deg^{-1} (much smaller than that of $\Delta S/nF$[14]), virtually the first term could be regarded as being the heat due to the entropy change of electrode reaction. The second term represents the heat due to polarization, and the third is the Joule heat. Both the second and third terms are always exothermic, though the first one depends on the sign of ΔS: an increase or decrease in entropy leads to an endothermic or exothermic change, respectively.

The fit of a peak of a fall in temperature with the cathodic peak in Figs. 1 and 2 suggests that the heat in the cathodic process may be mainly due to an entropy change for the deintercalation of ClO_4^- ions in $LiClO_4$-PC and $LiClO_4$-AN solutions. The obscure fit of the fall in temperature with the cathodic peak in an $LiClO_4$-NM solution could be explained by the contribution of not only the first, but also the second and third terms. The endothermic change in the cathodic deintercalation of ClO_4^- ions suggests the occurrence of an increase in entropy and may also lead to a decrease due to intercalation.

It is possible to obtain information concerning the entropy change of the electrode reaction by measuring the temperature-dependence of the electrode potential.[14] The thermal temperature coefficient of the electrode potential $(dE/dT)_{th}$ is expressed as

$$(dE/dT)_{th} = \frac{\Delta S}{nF} + \frac{\Delta S^*}{nF}. \quad (3)$$

Thus, the value of $(dE/dT)_{th}$ for the graphite oxidized anodically in these solutions (that is, after the intercalation of ClO_4^- ions) was checked while changing the temperature of only the graphite electrode. Figures 4 and 5 show the temperature-dependence of the electrode potential of the graphite after anodic oxidation in $LiClO_4$-PC and $LiClO_4$-NM solutions, respectively. In this case, the potential was measured versus a saturated calomel electrode (at room temperature) separated from the compartment of the working electrode by a vessel filled with the electrolyte using a Luggin cappillary and a KCl salt bridge. From the slope of the linear relation by the method of least squares, the values of $(dE/dT)_{th}$ were +1.30 mV deg^{-1} and +3.55 mV deg^{-1} for $LiClO_4$-PC and $LiClO_4$-NM solutions, respectively. Thus, the estimated values of ΔS were +125 J mol^{-1} K^{-1} and +343 J mol^{-1}

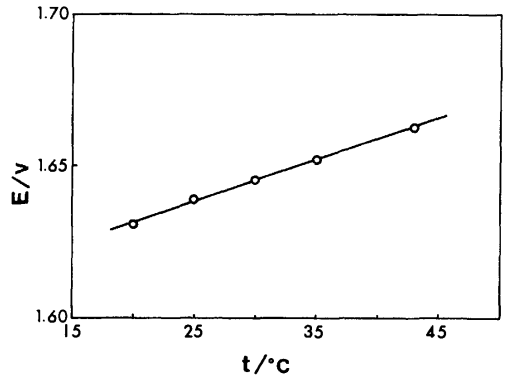

Fig. 4. The temperature-dependence of the electrode potential of the graphite after anodic oxidation (at +2.0 V for 1 h) in a 0.2 mol dm^{-3} $LiClO_4$-PC solution.

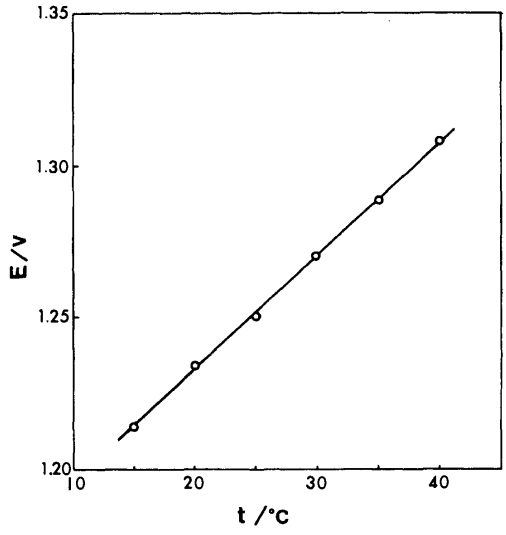

Fig. 5. The temperature-dependence of the electrode potential of the graphite after anodic oxidation (at +2.0 V for 1 h) in a 0.1 mol dm^{-3} $LiClO_4$-NM solution.

K^{-1}, respectively, by supposing that ΔS^* might be negligible. The positive value obtained in $LiClO_4$-PC and $LiClO_4$-NM solutions suggests an increase in entropy due to the deintercalation of ClO_4^- ions. The measurement of $(dE/dT)_{th}$ for graphite oxidized anodically in an $LiClO_4$-AN solution was impossible because of the unstable electrode potential. Nevertheless, also in this case, the occurrence of an increase in entropy could be supported by the thermal result, as mentioned above. This thermal method has the advantage of providing information concerning entropy change directly and promptly by the detection of the heat due to electrolysis.

References

1) J. O. Besenhard and H. P. Fritz, *Z. Naturforsch.*, **26b**, 1225 (1971); **27b**, 1294 (1972).
2) J. O. Besenhard and H. P. Fritz, *J. Electrochem. Soc.*, **119**, 1697 (1972).
3) J. O. Besenhard, *Carbon*, **14**, 111 (1976).
4) J. Simonet and H. Lund, *J. Electroanal. Chem.*, **75**, 719 (1977).
5) T. Ohzuku, Z. Takehara, and S. Yoshizawa, *Denki Kagaku*, **46**, 438 (1978).
6) A. Jobert, Ph. Touzain, and L. Bonnetain, *Carbon*, **19**, 193 (1981).
7) H. Krohn, F. Beck, and H. Junge, *Ber. Bunsenges. Phys. Chem.*, **86**, 704 (1982).
8) Y. Matsuda, M. Morita, and H. Katsuma, *Denki Kagaku*, **51**, 744 (1983).
9) Y. Maeda, Y. Okemoto, and M. Inagaki, *J. Electrochem. Soc.*, **132**, 2369 (1985).
10) Y. Maeda and Ph. Touzain, *Electrochim. Acta*, **33**, 1493 (1988).
11) J. M. Sherfey and A. Brenner, *J. Electrochem. Soc.*, **105**, 665 (1958).
12) J. M. Sherfey, *J. Electrochem Soc.*, **110**, 213 (1963).
13) R. Tamamushi, *J. Electroanal. Chem.*, **45**, 500 (1973), **65**, 263 (1975).
14) A. J. deBethune, T. S. Licht, and N. Swendeman, *J. Electrochem. Soc.*, **106**, 616 (1959).

Studies of Collectors. X. Complexing Ability of Amino Hydroxamic Acid Ligands with Dioxouranium(VI) in Aqueous Solution

Yoshifumi KOIDE,* Masazumi UCHINO, Hideto SHOSENJI, and Kimiho YAMADA
Department of Applied Chemistry, Faculty of Engineering, Kumamoto University, Kurokami, Kumamoto 860
(Received March 27, 1989)

Synopsis. Complexing ability of ligands bearing hydroxyaminocarbonyl group and amino group with UO_2^{2+} in an aqueous solution were examined by the potentiometric method using MINIQUAD program. Stability constants of 2-aminoacetohydroxamic acid complex with UO_2^{2+} are $\log \beta_1=10.45$, $\log \beta_2=18.95$. They are far larger than those of acetohydroxamic acid complexes. The β_1 and β_2 are almost the same as β_1 and β_2 of the acetamide oxime (acetoamidoxime) complexes.

The N^2-hydroxyamidino group in amidoximes, hydroxyaminocarbonyl group in hydroxamic acids, and the pyridyl group are known as affinity groups for uranium.[1,2] The stabilities of the latter two are less than that of the former. A chelating surfactant bearing hydroxyaminocarbonyl group and pyridyl or amino group exerted an excellent flotation-effect for the uranium in seawater.[3] The effect is considered to be caused by the coordination of the amino group to UO_2^{2+}, in addition to the complexation of the hydroxyaminocarbonyl group. However, such a chelate effect was unknown. Moreover, the UO_2^{2+} chelate of *o*-hydroxybenzohydroxamic acid[4] is less stable than the complex of benzohydroxamic acid (B-Hx).[5,6] In this study, the stability constants of the 2-aminoacetohydroxamic acid (A-AHx)-UO_2^{2+} and the *o*-aminobenzohydroxamic acid (B-AHx)-UO_2^{2+} complexes are determined by the potentiometric method and compared with those of acetohydroxamic acid (A-Hx), B-Hx, and acetamide oxime (amidoxime ligand).

Experimental

A-Hx was purchased, and A-AHx, B-Hx, and B-AHx were prepared by the treatment of the corresponding esters (ethyl aminoacetate, ethyl benzoate, and methyl *o*-aminobenzoate) with hydroxylamine.[7] They were refined by recrystallization, and their structures were confirmed by mp, IR (KBr), ^{1}H NMR, and elementary analyses. A-Hx Found: C, 31.86; H, 6.62; N, 18.59%; A-AHx: C, 26.68; H, 7.02; N, 30.95%; B-Hx: C, 61.16; H, 5.04; N, 10.09%; B-AHx: C, 55.17; H, 5.21; N, 18.72%. Standard solutions of HNO_3, UO_2, and NaOH were prepared from 60% HNO_3, $UO_2(NO_3)_2$, and a 50% NaOH solution after removing the Na_2CO_3 precipitate, respectively. Water was deionized by passing through an ion-exchange column and then distilled. Ionic strengths of all the solutions were adjusted to 0.1 M (1 M=1 mol dm^{-3}) with KNO_3.

The equilibrium measurements were carried out with a Recording Auto Titrator (Hiranuma type RAT-11) using a glass electrode (DKK combined type 6155). All titrations were performed at 25.0±0.05 °C under an atmosphere of N_2 in a double-walled titration cell of 100 cm^3 capacity. The potentiometer was calibrated with JIS standard buffer solutions. The pH meter reading, pH_M, was converted into $-\log[H]$ on titrating 4.0×10^{-3} M HCl with 0.01 M NaOH: $-\log[H]=pH_M-0.063$. The apparent ionic product of water, pK'_w, was determined by titrating 0.1 M KNO_3 with 0.01 M NaOH: $pK'_w=pH_M-\log[OH]=13.79$, from which relation the OH^- concentration was calculated. The ligand concentration was adjusted to 4×10^{-3} M in most cases, being twice that of the UO_2^{2+}. The UO_2^{2+} concentration was determined by titration with ethylenediaminetetraacetic acid. The free ligand was first titrated with 0.02 M HNO_3 and then back-titrated with 0.01 M NaOH. In the presence of UO_2^{2+}, the titrations with 0.01 M NaOH were performed by starting from the ligand solutions containing a two-fold excess of acid. For each system two titrations were performed, and each of the titration curves contained more than 50 experimental points.

Results and Discussion

Acid dissociation constants of the amine residue in A-AHx and B-AHx, and stability constants of the UO_2 complexes have not previously been determined.

The dissociation equilibrium of amino hydroxamic acid ligand (HL) may be represented by Eqs. 1 and 2.

$$H_2L^+ \rightleftharpoons HL + H^+ \qquad pK_{a1} \qquad (1)$$

$$HL \rightleftharpoons L^- + H^+ \qquad pK_{a2} \qquad (2)$$

The average number of protons bound to the ligand were calculated in the ligand concentration range of $3.3—4.0\times10^{-3}$ M, and pK_{a1} and pK_{a2} were determined by the calculation using ACBA program.[8]

In the A-AHx system, the pK_{a1} and pK_{a2} were found to be 7.458 and 9.237, respectively. Hydroxyaminocarbonyl group in the A-AHx would dissociate more than that in A-Hx (pK_a 9.328) because of the inductive effect of the electron on the $-NH_3^+$. On the other hand, the absorption of $-NH_3^+$ (HL form: 2550—3100 cm^{-1}) in the IR spectrum dissappeared when A-AHx was treated with two-fold of sodium methoxide, and the absorption of the free amine (L^- form) appeared in 3400—3500 cm^{-1}. Therefore, the pK_{a1} (7.458) and the pK_{a2} (9.237) were assigned to the hydroxyaminocarbonyl group and the amino group, respectively.

Next, the pH titration of A-AHx in the presence of UO_2^{2+} was carried out and the titration curve was obtained over a range of $-\log[H]<6$, above which a precipitate was formed. The stability constant, β_n, was calculated by the MINIQUAD program.[9]

$$UO_2^{2+} + L^- \rightleftharpoons UO_2L^+ \qquad \beta_1 \qquad (3)$$

$$UO_2^{2+} + 2L^- \rightleftharpoons UO_2L_2 \qquad \beta_2 \qquad (4)$$

UO_2^{2+}, with coordination number six, is appreciably hydrolyzed, so that the hydrolyses of UO_2^{2+} were

Table 1. Stability Constants of UO_2^{2+} Complexes[a)]

Ligand	pK_{a1}	pK_{a2}	$\log \beta_1$	$\log \beta_2$	Ref		
					pK_a	$\log \beta_1$	$\log \beta_2$
A-Hx	9.328 (0.006)		8.22 (0.03)	15.30 (0.07)	9.40[13)]		
A-AHx	7.458 (0.005)	9.237 (0.010)	10.45 (0.02)	18.95 (0.04)	7.40[14)]		
B-Hx	8.757 (0.005)		7.49 (0.03)	14.17 (0.07)	8.75[14)]	7.72[5)] 8.71[6)]	16.77[6)]
B-AHx	2.682 (0.010)	8.818 (0.004)	7.82 (0.01)	14.71 (0.02)	9.0[15)]		

a) Conditions: 25 °C, I=0.1 M. Values in parentheses are estimated standard deviations.

considered in the calculation.[10,11)] Thus, stability constants of the 1:1 and 1:2 complexes of A-AHx with UO_2^{2+} were determined to be $\log \beta_1$=10.45 and $\log \beta_2$=18.95. Similar calculations in the A-Hx, B-AHx, and B-Hx systems were carried out, and the pK_a and $\log \beta$ are given in Table 1.

Stability constants of the A-AHx-UO_2^{2+} complex are about 170 (β_1) and 4500 times (β_2) those of the A-Hx complexes. The high stabilities of A-AHx complex were considered to be caused by the chelate effect between the amino group and the hydroxyaminocarbonyl group, that is, in addition to the complexation of the bidentate hydroxyaminocarbonyl group, the six-membered rings of the chelate should increase the stability constant. The strong affinity of the N^2-hydroxyamidino group for UO_2^{2+} is well-known and the stability constants of acetamide oxime-UO_2^{2+} complex were estimated to be $\log \beta_1$=10.6 and $\log \beta_2$=18.8.[12)] Therefore, β_1 and β_2 of the A-AHx complex proved to be almost the same as those of the acetamide oxime-UO_2 complex.

In B-AHx, the pK_{a1} (2.682) and pK_{a2} (8.818) should be assigned to the anilinium ion and the hydroxyaminocarbonyl group respectively, because of the similar resonance to aniline (pK_a 4,65) and nearly the same value to the pK_a of B-Hx. β_1 and β_2 of the B-AHx-UO_2 complex are a little higher than those of the B-Hx-UO_2 complex. The basicity of the amine donor in B-AHx is weak, and the chelates should be seven-membered rings. Therefore, the stability of the B-AHx complex would not become so great.

In the distributions of the UO_2^{2+} complexes, 1:1 and 1:2 species of the A-AHx complex were formed much more than those of the A-Hx complex on the basis of the chelate effect, but the difference of distributions in the B-Hx and B-AHx systems was small.

Thus, it has become apparent that the complexing ability of the amino hydroxamic acid ligand with UO_2^{2+} is greater than that of the hydroxamic acid ligand and is almost the same as that of the amidoxime ligand.

The authors are sincerely grateful to Assistant Professor Akinori Jyo for his help and useful suggestions.

References

1) C. A. Fetscher, U. S. Patent, 3088798 (1963).
2) W. Kern and R. C. Schulz, *Angew. Chem.*, **69**, 153 (1957).
3) Y. Koide, M. Uchino, and K. Yamada, *Bull. Chem. Soc. Jpn.*, **60**, 3477 (1987).
4) N. K. Dutt and T. Seshadri, *J. Inorg. Nucl. Chem.*, **34**, 1291 (1972); stability constant of *o*-hydroxybenzohydroxamic acid-UO_2 complex: $\log \beta_1$=7.71, $\log \beta_2$=14.51; B-Hx $\log \beta_1$=9.03, $\log \beta_2$=17.94.
5) F. Maggio, V. Romano, and R. Cefalu, *J. Inorg. Nucl. Chem.*, **28**, 1979 (1966).
6) F. Baroncelli and G. Grossi, *J. Inorg. Nucl. Chem.*, **27**, 1085 (1965).
7) A. H. Blatt, *Org. Synth.*, Coll. Vol. II, 67 (1943).
8) G. Arena, E. Rizzarelli, S. Sammartano, and C. Rigano, *Talanta*, **26**, 1 (1979).
9) A. Sabatini, A. Vacca, and P. Gans, *Talanta*, **21**, 53 (1974).
10) N. Ogata, N. Inoue, and H. Kakihana, *Nippon Genshiryoku Gakkai Shi*, **13**, 560 (1971); hydrolysis constant $\beta_n=[UO_2(OH)_n^{2-n}]\cdot[H_3O^+]^n/([UO_2^{2+}]\cdot[H_2O]^n)$: $\log \beta_1=-5.0$, $\log \beta_2=-11.2$, $\log \beta_3=-17.1$.
11) P. A. Overvoll and W. Lund, *Anal. Chim. Acta*, **143**, 153 (1982); $\beta_n=[(UO_2)_2(OH)_n^{4-n}]\cdot[H_3O^+]^n/([UO_2^{2+}]^2\cdot[H_2O]^n)$: $\log \beta_1=-4.5$, $\log \beta_2=-5.95$; $\beta_n=[(UO_2)_3(OH)_n^{6-n}]\cdot[H_3O^+]^n/([UO_2^{2+}]^3\cdot[H_2O]^n$: $\log \beta_4=-12.5$, $\log \beta_5=-16.54$.
12) T. Hirotsu, S. Katoh, K. Sugasaka, M. Seno, and T. Itagaki, *J. Chem. Soc., Dalton Trans.*, **1986**, 1611; stability constant of acetamide oxime-UO_2 complex $\beta'_1=[LUO_2^+]\cdot[H^+]/([HL]\cdot[UO_2^{2+}])$, $\beta'_2=[L_2UO_2]\cdot[H^+]^2/([HL]^2\cdot[UO_2^{2+}])$: $\log \beta'_1=-0.97$, $\log \beta'_2=-4.42$, and pK_{a2} was estimated to be 11.6.
13) W. M. Wise and W. W. Brandt, *J. Am. Chem. Soc.*, **77**, 1058 (1955).
14) A. L. Green, G. L. Sainsbury, B. Saville, and M. Stansfield, *J. Chem. Soc.*, **1958**, 1583.
15) M. A. Stolberg and W. A. Mosher, *J. Am. Chem. Soc.*, **79**, 2618 (1957).

Temperature Dependence of Adsorption of Caesium Ions on Crystalline Hydrous Titanium Dioxide Fibers

Hiromichi HAYASHI,* Takashi IWASAKI, Yoshio ONODERA, and Yoshinori FUJIKI†
Government Industrial Research Institute, Tohoku, Sendai 983
†National Institute for Research in Inorganic Materials, Tsukuba 305
(Received June 1, 1989)

Synopsis. The distribution coefficient of caesium ions, K_d, measured as a function of pH at 25—100 °C, decreased with increasing temperature. Enthalpy change of the adsorption of Cs^+ on $H_2Ti_4O_9 \cdot nH_2O$ estimated from the plot of $\log K_d$ vs. T^{-1} in the range of 25—85 °C was −4.6 kcal mol^{-1}. Above 95 °C, K_d values were lower than those extraporated from the plot due to a decrease in the crystallinity of the fibers.

We have worked to develop the techniques to recover caesium ions from geothermal brine and suitable inorganic adsorbents have been investigated by revealing adsorption behavior of caesium ions in hot water.[1] The adsorbents for caesium ions in geothermal brine need selectivity for the ions and hydrothermal stability. It is known that crystalline hydrous titanium dioxide fibers, $H_2Ti_4O_9 \cdot nH_2O$, have high selectivity for caesium ions and that the distribution coefficient for alkali metal ions in weak acid solution at 25 °C increases in the order: Li<Na≪K, Rb<Cs.[2]

The present paper deals with the adsorption of caesium ions on the fibers. The distribution coefficient of caesium ions was measured as a function of pH at 25—100 °C and the enthalpy change was estimated; in addition, X-ray powder diffractometry was done for checking the structural change of fibers.

Experimental

The hydrous titanium dioxide fibers ($H_2Ti_4O_9 \cdot nH_2O$) were prepared by acid treatment of $K_2Ti_4O_9$.[3,4] Adsorption experiments were carried out in batchwise operations in a water bath thermostated at temperatures between 25 and 100 °C.

Glass ampules of 20 cm^3 capacity were used to obtain equilibrium between the solid (0.05 g) and the aqueous solution (10 cm^3) containing caesium ions. The initial concentration of caesium choride was 1 mmol dm^{-3}, and pH was adjusted with hydrochloric acid. The glass ampules were kept in the water bath, and shaken gently at intervals. The reaction time was 7 d, when the equilibrium was sufficiently attained, and then the fibers were separated by a membrane filter with 0.45 μm pores.

The concentration of caesium ions in the aqueous solution was determined by a Hitachi Z-6000 polarized Zeeman atomic absorption spectrophotometer. The pH of the solution was measured by a TOA HM5ES pH meter equipped with GS-5015C pH combination electrode. X-Ray powder patterns were obtained by a Rigaku Denki RAD-IIB diffractometer with Cu $K\alpha$ radiation.

Results and Discussion

The distribution coefficient, K_d, was calculated as

$$K_d = (C_1/\mathrm{g})/(C_2/\mathrm{cm^3}), \quad (1)$$

where C_1 is the amount of adsorbed caesium ions per 1 g of the solid, and C_2 is the concentration of caesium ions per 1 cm^3 of the aqueous solution.

Figure 1 gives the plot of $\log K_d$ vs. pH in aqueous phase for six different temperatures. As the temperature was increased, the $\log K_d$-pH lines shifted downward. The slope of $\log K_d$-pH lines was about +1 except for that at 100 °C. The adsorption of caesium ions on the fibers, therefore, can be represented by an ion-exchange reaction formula:[3]

$$H(s) + Cs^+(aq) = Cs(s) + H^+(aq), \quad (2)$$

where the subscripts "s" and "aq" denote the solid and aqueous phase respectively. The equilibrium constant, K_c, of Eq. 2 is defined as

$$K_c = [Cs(s)][H(aq)]/[Cs(aq)][H(s)]. \quad (3)$$

K_c is rewritten as Eq. 4 using K_d:

$$\log K_c = \log K_d - pH + \text{const.} \quad (4)$$

If the K_d values for different temperatures are compared at identical pH, the enthalpy change of Cs-H ion-exchange reaction can be estimated from $\log K_d$ vs. T^{-1} plot.

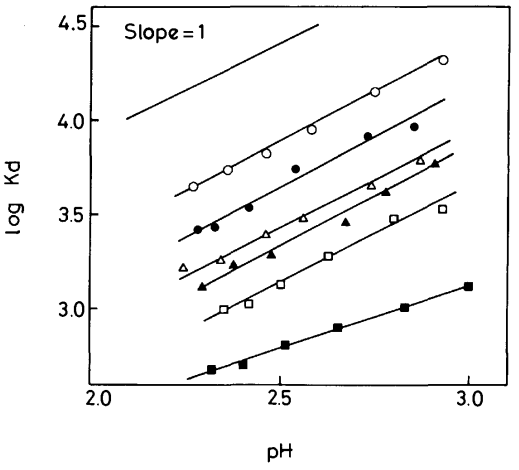

Fig. 1. Distribution coefficients of caesium ions as a function of pH in the aqueous phase at various temperatures. The ion exchanger is 0.05 g of $H_2Ti_4O_9 \cdot nH_2O$. The aqueous solution is 10 cm^3 of hydrochloric acid solution with an initial caesium concentration of 1×10^{-3} mol dm^{-3}. Temperature is (○): 25 °C, (●): 50 °C, (△): 75 °C, (▲): 85 °C, (□): 95 °C, (■): 100 °C.

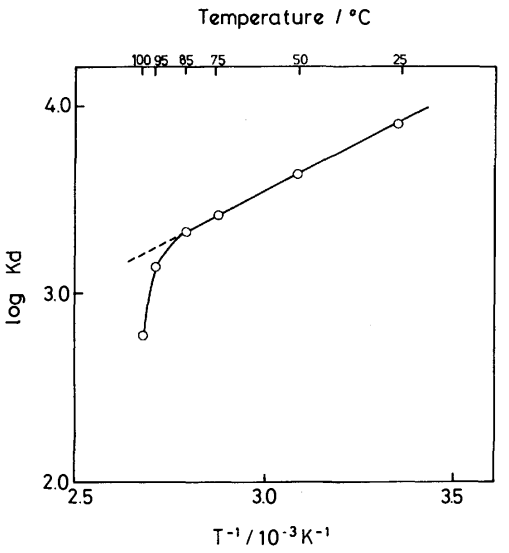

Fig. 2. Distribution coefficients of caesium ions at pH=2.5 in the aqueous phase as a function of temperature.

Figure 2 gives the plot of log K_d vs. T^{-1} at pH 2.5. The log K_d values were on a straight line in the range 25 to 85 °C as expected when enthalpy change (ΔH) is constant. And from the slope of the line, ΔH is obtained by Eq. 5:

$$\Delta H = -2.303\, R\, \mathrm{d}\log K_d/\mathrm{d}\,(1/T), \quad (5)$$

where T is the absolute temperature, and R is the gas constant.[5] The ΔH estimated from Fig. 2 in the range between 25 and 85 °C was −4.6 kcal mol^{-1}. Kraus et al. reported that the enthalpy change of ion exchange reaction between caesium ions and protons on a cation-exchange resin was −3.4 kcal mol^{-1} at 25 °C.[5] Although the enthalpy change values of the both cases are somewhat different, uni-uni valent ion exchange such as proton and caesium ion is supposed to be an exothermic reaction, irrespective of inorganic and organic ion exchangers.[6]

As shown in Fig. 2, K_d values at 95 and 100 °C were lower than those extraporated from the plot. Figure 3 gives the X-ray powder diffraction patterns of the solid treated with caesium solution at temperatures between 50 and 100 °C. The layered structure of the fibers is characterized by very strong (200) reflection with an interplanar spacing, d(200), of ca. 9.1 Å.[7]

The fibers treated at temperatures below 95 °C showed almost similar diffraction patterns to those of the original fibers. This fact indicates that the structure of the fibers remains unchanged below 95 °C. Above 95 °C, however, the fibers converted into the poorly crystallized phase with an interlayer distance smaller than that of the crystalline fibers. This result agrees with that reported by Komatsu et al. in the case of adsorption of cobalt ions.[4] Consequently, the K_d value of caesium ions must be influenced only by the exothermic reaction below 95 °C. Above 95 °C, the

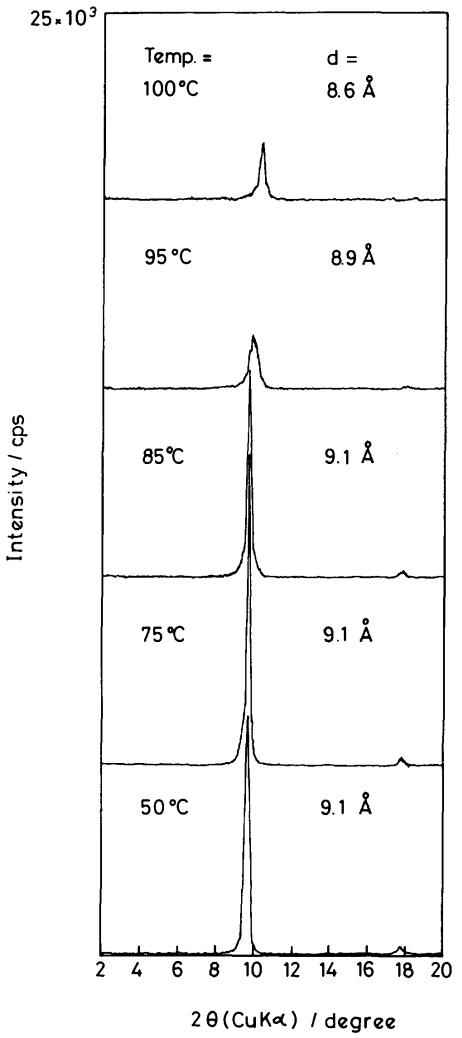

Fig. 3. X-Ray powder diffraction patterns of the solid samples treated with aqueous solutions at various temperatures.

structural change of the fibers causes the decrease of K_d in addition to the temperature effect as an exothermic reaction.

Accordingly, the desired temperature should be below 95 °C when the fibers is utilized for an adsorbent for caesium ions from geothermal brine.

References

1) Y. Onodera, T. Iwasaki, H. Hayashi, and K. Torii, *Nippon Kogyo Kaishi*, **104**, 277 (1988).
2) Y. Komatsu, Y. Fujiki, and T. Sasaki, *Bunseki Kagaku*, **31**, E225 (1982).
3) Y. Fujiki, Y. Komatsu, T. Sasaki, and N. Ohta, *Nippon Kagaku Kaishi*, **1981**, 1656.
4) Y. Komatsu, Y. Fujiki, and T. Sasaki, *Bull. Chem. Soc. Jpn.*, **59**, 49 (1986).
5) K. A. Kraus and R. J. Raridon, *J. Phys. Chem.*, **1959**, 1901.
6) F. Helfflich, "Ion Exchange," McGraw-Hill, New York (1962).
7) T. Sasaki, M. Watanabe, Y. Komatsu, and Y. Fujiki, *Inorg. Chem.*, **24**, 2265 (1985).

Association of Carbon Tetrachloride, Chloroform, and Dichloromethane with Cyclodextrins in Aqueous Medium

Makoto NISHIMURA, Toshio DEGUCHI, and Isao SANEMASA*
Department of Chemistry, Faculty of Science, Kumamoto University, Kurokami 2-39-1, Kumamoto 860
(Received June 14, 1989)

Synopsis. The 1:1 host (cyclodextrin, CyD)-guest (CCl_4, $CHCl_3$, and CH_2Cl_2) association constants at 25 °C have been determined by making use of the volatilization rate of guest from aqueous into gaseous phase. No association was observed between γ-CyD and the three guests and between β-CyD and CH_2Cl_2.

Cyclodextrins (CyDs) are cyclic oligomers forming distinctive cavity; α-, β-, and γ-CyD are composed of 6, 7, and 8 glucoses, respectively. While the outside of the CyD molecule is hydrophilic, the cavity inside is a hydrophobic environment, and various hydrophobic substances in aqueous medium can be included therein as the guest, when they are spatially fitted in the cavity. Owing to this unique property of CyD, much interest has been drawn to its applications such as catalysts in organic syntheses or a modifier in solvent extraction.

Intermediates such as trichloromethyl cation and dichlorocarben derived in situ in CyD with the suitable cavity size from CCl_4 and $CHCl_3$, respectively, play a predominant role in the selective reaction of phenolates.[1] CyDs were also used to modify partition of hydrophobic solutes between organic and aqueous phase.[2,3] In these applications, association constants of CyD with CCl_4, $CHCl_3$, and CH_2Cl_2 in water are essential information to be needed, because the complexation in the aqueous medium plays an important role. On the other hand, when water-insoluble CyD derivatives are used in organic solvent,[4] knowledge of the extent of affinity of the organic solvent molecule with the cavity of parent CyD is required.

A wide variety of guest compounds have been known to be accepted in CyD cavities, but there are no available data concerning carbon tetrachloride, chloroform, and dichloromethane. This is probably due to the lack of suitable methods to detect the free- or associated-guest species in water. UV absorption and fluorescence methods, which are generally used to evaluate the CyD–guest association, cannot be applied to these guests, because they have neither absorption peaks in the ordinary accessible ultraviolet region, nor fluorescence. We have recently proposed a method which can be applied to such guests without any UV absorption and fluorescence.[5] The only requirement is the guest volatility. The guests dealt with in this study are highly volatile and hence ideal objects for our method to be applied.

Experimental

Materials and Preparation of Sample Solutions. Distilled deionized water was used throughout this work. Carbon tetrachloride, chloroform, and dichloromethane (Wako Pure Chemicals Co.) used as guests and cyclodextrins (α-, β-, and γ-CyD, Nakarai Chemical Co.) used as hosts were all of analytical reagent grade and were used as received. An aqueous solution saturated with each guest was prepared by a vapor-circulation method using an apparatus described in the previous paper.[6] The saturated guest concentration was not determined, but taken from the literature.[7] By diluting the saturated aqueous solution with water, each 1.60×10^{-4} M (M≡mol dm^{-3}) solution was prepared. A suitable portion (10 cm^3 for CCl_4 and CH_2Cl_2, 20 cm^3 for $CHCl_3$) was transferred into a 2.5φ×25 cm cylindrical glass tube and diluted with water, with or without addition of CyD aqueous solution, to 50 cm^3 for CCl_4 and CH_2Cl_2 or to 90 cm^3 for $CHCl_3$. CyD aqueous solutions were prepared daily by dissolving suitable amounts of CyD which had been dried over phosphorus pentaoxide under vacuum.

Apparatus and Procedures. Nitrogen gas was blown at a constant flow rate of 15 cm^3 min^{-1} into the aqueous guest solution placed with or without CyD in the cylindrical glass tube immersed in a bath thermostated at 25±0.1 °C. The N_2 gas leaving the sample solution was passed through a collector (a tapered glass tube of 0.5φ×17 cm, packed with Tenax GC resin beads of 60—80 mesh in 10 cm length) for a fixed time. The amount of guest collected at definite time intervals, ΔQ_ϕ, and that collected during a sufficiently long time (1 h in most cases, during which almost all guest molecules were to be driven out of the sample solution), Q_ϕ, were determined by a Shimadzu GC-12A gas chromatograph. An injection port of the chromatograph was connected with a furnace (Shimadzu flush sampler FLS-3) to feed the guest sample; a collector tube was heated to above 200 °C in one min. A SE-30 (60—80 mesh) column of 2 m long was used at 80 ° and a flame ionization detector was used. A Shimadzu Chromatopac C-R6A was used to determine the peak areas.

Results and Discussion

Under the present experimental condition that host molecules are always excessive over guest molecules, the possible host–guest association reactions are:

$$\mathrm{CyD} + \phi \rightleftharpoons \mathrm{CyD}\cdot\phi, \quad K_1, \tag{1}$$

$$\mathrm{CyD}\cdot\phi + \mathrm{CyD} \rightleftharpoons \mathrm{CyD_2}\cdot\phi, \quad K_2, \tag{2}$$

and

$$\phi(\mathrm{aq}) \longrightarrow \phi(\mathrm{gas}), \quad k, \tag{3}$$

where φ refers to a guest molecule, K_1 and K_2 are the corresponding stepwise association constants, and k is the rate constant for the transfer of guest molecules from aqueous to gaseous phase.

We assume that the release of guest molecules at a constant N_2 flow rate is of first-order with respect to the concentration of free species present at any time t in the solution as follows:

$$dQ_\phi V^{-1}/dt = k[\phi], \tag{4}$$

Table 1. The 1:1 (Host:Guest) Formation Constant at 25 °C[a]

	Concentration of CyD	Formation constant
	10^{-2} mol dm^{-3}	dm^3 mol^{-1}
Carbon tetrachloride		
α-CyD	2.07—8.25	42±17
β-CyD	0.414—1.13	150±35
γ-CyD	8.11	b)
Chloroform		
α-CyD	1.11—7.05	42±10
β-CyD	1.07	24[c]
γ-CyD	5.56	b)
Dichloromethane		
α-CyD	2.65—8.32	28±14
β-CyD	1.11	b)
γ-CyD	8.33	b)

a) In the present runs, the concentration of each guest in the aqueous solution before aeration was set at constant, 1.60×10^{-4} mol dm^{-3}. b) The host-guest association was not observed at the given CyD concentration. c) C_{CyD} was not changed, and the formation constant was determined on the assumption of 1:1 association.

where V is the volume of aqueous solution.

An equation to estimate K_1 and K_2 can be derived using the total concentrations of host (C_{CyD}) and guest (C_ϕ) and the total amount of guest released, Q_ϕ (the sum of ΔQ_ϕ from time 0 to t), in the same way as described in the previous paper[5] as follows:

$$\ln(C_\phi - Q_\phi V^{-1}) = -kt/(1 + K_1C_{CyD} + K_1K_2C_{CyD}^2) + \ln C_\phi$$
$$= -k't + \ln C_\phi, \quad (5)$$

where

$$k' = k/(1 + K_1C_{CyD} + K_1K_2C_{CyD}^2). \quad (6)$$

Rearrangement of Eq. 6 yields:

$$1/k' = K_1K_2C_{CyD}^2/k + K_1C_{CyD}/k + 1/k. \quad (7)$$

For each host-guest combination, plots according to Eq. 5 at a constant C_{CyD} gave a similar straight line to that shown in our previous papers.[5] From inclination of the straight line, k' (and k) was determined and plotted according to Eq. 7. The $1/k'$ vs. C_{CyD} plots appeared to be linear, showing that K_2 can be neglected. In the case of $CHCl_3$-β-CyD, the CyD concentration was not changed, and K_1 was estimated on the assumption that this host-guest forms a 1:1 complex. When γ-CyD was used as the host, $1/k'$ values for the three guests were found to be in accordance with $1/k$ within experimental error. It was thus assumed that γ-CyD does not associate with each of guests studied. This is also the case for β-CyD-CH_2Cl_2. The K_1 value evaluated in this work for each combination is given in Table 1.

Molecular sizes of both host and guest being taken into account, the inclusion models are illustrated in Fig. 1; the guest molecule is oriented so that it enters as deeply as possible into the CyD cavity. CCl_4 molecule is only partly included in α-CyD, and a part of $CHCl_3$ molecule protrudes out of the α-CyD cavity, while the CH_2Cl_2 is completely accomodated in the cavity. Contrary to our expectation, however, the association constant of the α-CyD-CH_2Cl_2 complex is rather small. This is probably relevant to the polarity of the guest molecule.

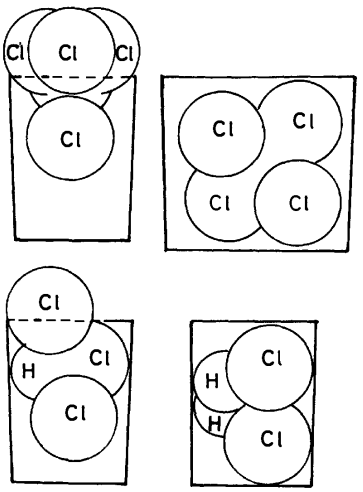

Fig. 1. Inclusion model. The larger cage refers to β-CyD ($CHCl_3$-β-CyD model is omitted).

The guest has to loose surrounding water molecules before it enters the CyD cavity. The free-energy change associated with this process can be estimated from Henry's law constant, K_H, as follows: $\Delta G_{dehyd} = -RT \ln K_H$. Using K_H values reported in the literature,[8] $-\Delta G_{dehyd}$ at 25 °C are evaluated to be 18.4 (CCl_4), 13.2 ($CHCl_3$), and 11.9 kJ mol^{-1} (CH_2Cl_2). The ΔG_{dehyd} is a quantitative measure of guest hydrophobicity: a guest with larger $-\Delta G_{dehyd}$ can be more easily transferred from aqueous into gaseous phase.

CCl_4 molecule is suitably accomodated in the β-CyD cavity. This accounts for larger K value of the β-CyD complex than that of the α-CyD complex. On the other hand, β-CyD is a little large for $CHCl_3$ and too large for CH_2Cl_2 to be fitted in with the cavity. In addition, relatively high polarity of CH_2Cl_2 may also be responsible for unobserved association of this guest with β-CyD. The large cavity of γ-CyD seems to explain the cause of the results that any association between this host and the three guests studied in this work has not been observed.

The association constant of CCl_4 with β-CyD is comparable to that of benzene with β-CyD. Molecular volume of CCl_4 (86.82×10^{-3}) is similar to that of benzene (80.33×10^{-3} nm^3),[9] and benzene also suitably fits with the β-CyD cavity. When we consider that $-\Delta G_{dehyd}$ for CCl_4 is much larger than that of benzene, 14.4 kJ mol^{-1}, a much larger association of CCl_4 with β-CyD will be expected. This may indicate that stabilization such as van der Waals does not work, or even it works, to a lesser extent for CCl_4 than benzene.

It is generally observed that CyDs dissolved in water in relatively high concentrations precipitate upon

shaking with some organic solvents; γ-CyD easily precipitates with chloroform. Some workers believe that this arises from the organic solvent molecule forming stable complexes with CyDs.[2] It is not true because γ-CyD does not form any complex with $CHCl_3$. The precipitation seems to occur through the change in the polarity of aqueous solution caused by organic solvent dissolving in water.

It is now rationalized why the selective syntheses of benzoic acids and benzaldehydes from phenolates using CyDs as catalysts can be performed;[1] α-CyD–dichlorocarben, α- and β-CyDs–chroloform, and β-CyD–carbon tetrachloride are successful combinations but γ-CyD cannot be used for the purpose.

It should be mentioned that the present study does not necessarily exclude the possibility of formation of a CyD complex with more than one guest molecules, because such an association cannot take place under our experimental condition that C_{CyD} is much higher than C_{ϕ}.

References

1) M. Komiyama and H. Hirai, *Bull. Chem. Soc. Jpn.*, **54**, 2053 (1981); *J. Am. Chem. Soc.*, **105**, 2018 (1983); **106**, 174 (1984).

2) L. A. Blyshak, T. M. Rossi, G. Patonay, and I. M. Warner, *Anal. Chem.*, **60**, 2127 (1988).

3) K. Matsunaga, M. Imanaka, T. Ishida, and T. Oda, *Anal. Chem.*, **56**, 1980 (1984); J. Harangi and P. Nánási, *Anal. Chim. Acta*, **156**, 103 (1984).

4) M. Komiyama, H. Yamamoto, and H. Hirai, *Chem. Lett.*, **1984**, 1081; H. Takahashi, Y. Irinatsu, S. Kozuka, and W. Takagi, *Mem. Fac. Eng., Osaka City Univ.*, **26**, 93 (1985).

5) I. Sanemasa and Y. Akamine, *Bull. Chem. Soc. Jpn.*, **60**, 2059 (1987); M. Fujiki, T. Deguchi, and I. Sanemasa, *ibid.*, **61**, 1163 (1988); I. Sanemasa, T. Takuma, and T. Deguchi, *ibid.* **62**, 3098 (1989).

6) I. Sanemasa, M. Araki, T. Deguchi, and H. Nagai, *Bull. Chem. Soc. Jpn.*, **55**, 1054 (1982).

7) M. J. Kamlet, R. M. Doherty, M. H. Abraham, P. W. Carr, R. F. Doherty, and R. W. Taft, *J. Phys. Chem.*, **91**, 1996 (1987).

8) J. M. Gossett, *Environ. Sci. Technol.*, **21**, 202 (1987).

9) R. D. Cramer, III, *J. Am. Chem. Soc.*, **99**, 5408 (1977).

The Reaction of *N*″-Cyanoguanidine with Formaldehyde. IV. The Formation Pathway of 4-Cyanoimino-3-(methoxymethyl)perhydro-1,3,5-oxadiazine

Ryuichi SHIBA,* Miyuki TAKAHASHI, Toichi EBISUNO,† and Michiaki TAKIMOTO†
Department of Applied Science, Faculty of Technology, Tokyo Denki University, Kanda, Chiyoda-ku, Tokyo 101
†Department of Chemistry, Faculty of Science, Toho University, Miyama 2-2-1, Funabashi, Chiba 274
(Received March 17, 1989)

Synopsis. An investigation of reactions involving *N*″-cyanoguanidine (CG) and its methyl derivatives with formaldehyde as well as the consideration of the molecular structures of CG and 4-cyanoimino-3-(methoxymethyl)-perhydro-1,3,5-oxadiazine elucidated the formation pathway of the latter compound from CG: CG → *N*-hydroxymethyl-*N*″-cyanoguanidine → *N*,*N*′-bis(hydroxymethyl)-*N*″-cyanoguanidine → 4-(cyanoimino)perhydro-1,3,5-oxadiazine → 4-cyanoimino-3-(hydroxymethyl)perhydro-1,3,5-oxadiazine → 4-cyanoimino-3-(methoxymethyl)perhydro-1,3,5-oxadiazine.

The maximum number of formaldehyde molecules added to *N*″-cyanoguanidine (CG) can be anticipated to be 4 by analogy with urea, which has an analogous structure to that of CG, and is allowed to react with formaldehyde into 3,5-bis(methoxymethyl)perhydro-1,3,5-oxadiazin-4-one (**1**), tetrakis-substituted urea.[1-3] However, the exhaustive hydroxymethylation of CG with a large excess of formaldehyde provided no tetrakis-substituted CG but, rather, 4-cyanoimino-3-(methoxymethyl)perhydro-1,3,5-oxadiazine (**8**) as the major product.[4]

In our present report we wish to elucidate the reasons why the maximum number of formaldehyde molecules added to CG is not 4, but 3, and to propose a formation pathway for **8**.

Results and Discussion

Two possible molecular structures of CG (**I** and **II**) had previously been proposed.[5-6] A study[7] concerning the IR spectrum of CG suggested that structure **I** is more appropriate than structure **II**. Furthermore, our results concerning the ^{1}H NMR spectrum of CG have revealed that the structure CG is **I** over a wide pH range, including 7—10, since only one signal of the amino proton (δ=6.57 (s, 4H)) was observed. These facts exclude the possibility that the maximum number of formaldehyde molecules may be determined by three hydrogen atoms in the amino and imino groups in the structure of **II**.

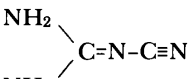

(**I**)

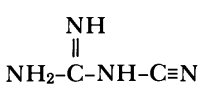

(**II**)

In a previous report,[3] we proposed a new formation pathway of **1** which was derived from urea and formaldehyde via tris(hydroxymethyl)urea and 3-(hydroxymethyl)perhydro-1,3,5-oxadiazin-4-one. The oxadiazine-ring formation may be a rate-determining

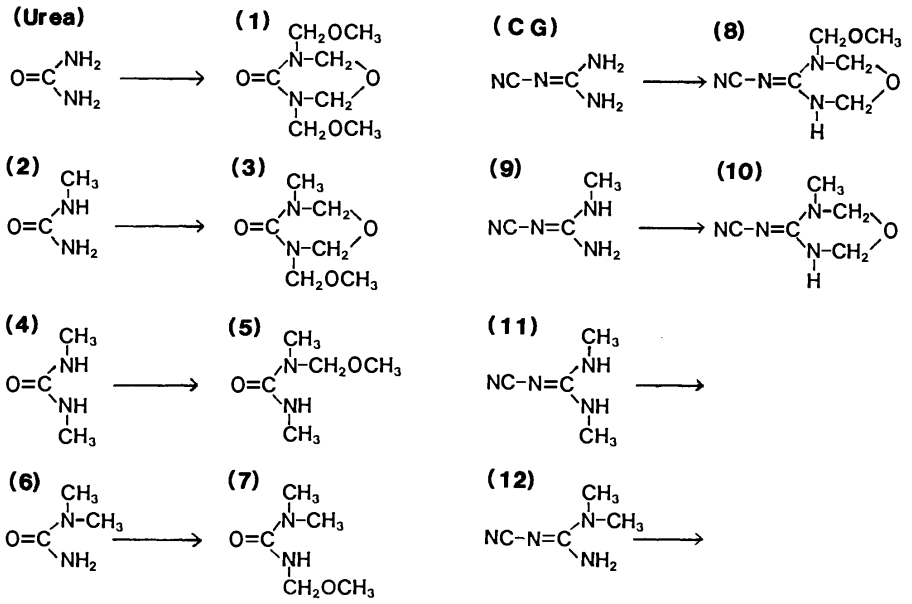

Scheme 1. The reactions of urea or *N*″-cyanoguanidine and its methyl derivatives with formaldehyde. Major products from the reactions of urea or *N*″-cyanoguanidine and its methyl derivatives with formaldehyde are shown and blank spaces represent that starting materials were recovered unchanged.

step in this formation, probably because the steric hindrance of the hydroxymethyl groups interferes with the addition of a fourth formaldehyde molecule to tris(hydroxymethyl)urea.

In order to examine the difference in the reactions of CG with formaldehyde and of urea with formaldehyde, CG and its methyl derivatives were allowed to react with a large excess of formaldehyde. The hydroxymethylated products were etherified by MeOH in order to isolate them. The major products from urea or CG and its methyl derivatives with formaldehyde are shown in Scheme 1 together with their reaction equations. Although the maximum number of formaldehyde molecules added to urea was 4, only one formaldehyde molecule was added to *N,N'*- or *N,N*-dimethylurea (**4** and **6**) into *N*-methoxymethyl-*N,N'*- or *N*-methoxymethyl-*N',N'*-dimethylurea (**5** and **7**). On the other hand, 3-methoxymethyl-5-methylperhydro-1,3,5-oxadiazin-4-one (**3**) was produced from methylurea (**2**) and formaldehyde. These results could be explained by the importance of a steric hindrance; a decrease in the steric hindrance enabled a further addition of formaldehyde molecule to the fourth hydrogen atom in the amino groups.

The reactivity of CG can be understood in terms of a steric hindrance of the cyanoimino group and of a difference in the electron-attracting nature between =O (in urea) and =N-C≡N (in CG). The latter reason may explain why **11** could not react with formaldehyde. However, it may also be explicable in terms of the former reason, since the cyanoimino group in **11** may restrict the movement of the methyl group in the proximal methylamino group; thus, this methyl group may interfere with the addition of a formaldehyde molecule to the other methylamino group. Figure 1 shows the molecular structures of urea, CG and **8**. Four atoms (one oxygen, one carbon, and two nitrogen atoms) in urea lie on the same plane. Each of the six atoms (two carbon and four nitrogen atoms) in CG and **8** lie nearly on the same plane, respectively. The cyanoimino group is located unequivalently in the two amino groups in CG in the crystalline state while the two amino groups in urea are equivalent. The double-bond character of C(1)-N(2), N(2)-C(2), C(2)-N(3), and C(2)-N(4) in CG and **8** can be calculated by using the theoretical single- and double-bond lengths reported by Schomaker and Stevenson[10]: 85, 50, 45, and 59% in CG, and 73, 67, 56, and 60% in **8**, respectively. Therefore, the planary structure of CG can be expected to remain while in solution. Thus, the two amino groups in CG are not equivalent to the addition of a formaldehyde molecule, because of a steric hindrance of the cyanoimino group. This steric

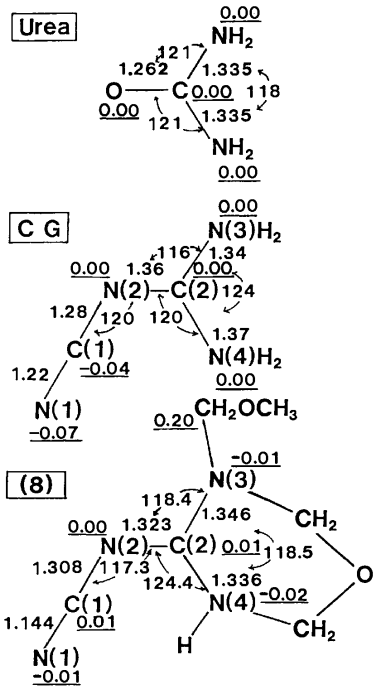

Fig. 1. The molecular structures of urea, *N''*-cyanoguanidine (CG), and 4-cyanoimino-3-(methoxymethyl)perhydro-1,3,5-oxadiazine (**8**) with the selected numbering scheme. Underscored numbers are the heights of Å of the atoms above or below the planes which are composed of four atoms in urea, four atoms (guanidine moiety) in CG and six atoms (*N''*-cyanoguanidine moiety) in **8**, respectively. The signs of ← → represent bond angles and other small numbers represent bond lengths in Å. These data were cited from Vaughan and Donohue's (urea),[8] Hughes' (CG),[6] and our report (**8**).[9]

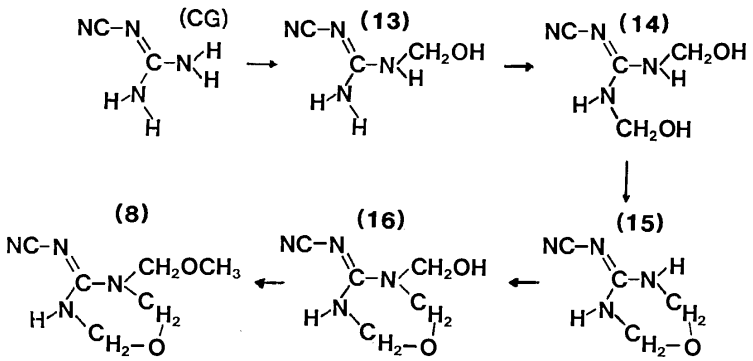

Scheme 2. Proposed formation pathway of 4-cyanoimino-3-(methoxymethyl)perhydro-1,3,5-oxadiazine (**8**).

hindrance is supported by the assembly of the CPK model for CG.

We wish to propose a formation pathway of **8**, shown in Scheme 2. The first addition of a formaldehyde molecule occurs on the most remote hydrogen atom from the cyanoimino group, producing *N*-hydroxymethyl-*N''*-cyanoguanidine (**13**); the second addition of a formaldehyde molecule on the hydrogen atom in a different amino group produces *N,N'*-bis(hydroxymethyl)-*N''*-cyanoguanidine (**14**). The two hydroxymethyl groups condense into an oxadiazine ring by eliminating water to produce 4-(cyanoimino)-perhydro-1,3,5-oxadiazine (**15**); a decrease in the steric hindrance of the hydroxymethyl groups enables a third addition of a formaldehyde molecule on the remote hydrogen atom from the cyanoimino group to produce 4-cyanoimino-3-(methoxymethyl)perhydro-1,3,5-oxadiazine (**16**). Thus, **8** is derived from **16** and MeOH.

Experimental

The Reaction of CG and Its Methyl Derivatives with Formaldehyde. According to the published procedure,[4] **8** was prepared from CG and a large excess of formaldehyde. *N*-Methyl-*N''*-cyanoguanidine (**9**) and *N,N'*- and *N,N*-dimethyl-*N''*-cyanoguanidine (**11** and **12**) were prepared from a mixture of ammonia or methylamine with *N*-cyano-*N'*-methyl-*O*-ethylisourea or *N*-cyano-*N',N'*-dimethyl-*O*-ethylisourea,[11] which was prepared from cyanamide according to a virtually identical procedure described by Suyama and Odo.[12] The methyl derivatives of CG and a large excess of formaldehyde (the feed mole ratio of **9**, **11**, or **12**/formaldehyde=1/5) were mixed and the pH of the solution was adjusted to 9.0. The solution was stirred for 30 min at 95 °C. 4-Cyanoimino-3-methylperhydro-1,3,5-oxadiazine (**10**) was derived from **9** and formaldehyde. However, no products were obtained and the starting materials were recovered unchanged in the reaction of **11** or **12** with formaldehyde.

4-Cyanoimino-3-methylperhydro-1,3,5-oxadiazine (10): Yield: 42%: Mp 121—122 °C (decomp): Found: C, 42.57; H, 5.86; N, 39.82%: Calcd for $C_8H_8N_4O$: C, 42.85; H, 5.75; N, 39.98%: ^{1}H NMR (DMSO-d_6): δ=8.20 (s, 1H, -NH-), 4.79, 4.74 (s, 2H, $-CH_2-$), 2.81 (s, 3H, $-CH_3$).

References

1) H. Kadowaki, *Bull. Chem. Soc. Jpn.*, **11**, 268 (1936).
2) B. Tomita and Y. Hirose, *J. Polym. Sci.*, **14**, 387 (1976).
3) R. Shiba, M. Takahashi, T. Ebisuno, and M. Takimoto, *Bull. Chem. Soc. Jpn.*, **62**, 1930 (1989).
4) M. Takimoto, T. Ebisuno, and R. Shiba, *Bull. Chem. Soc. Jpn.*, **56**, 3319 (1983).
5) E. Bamberger, *Chem. Ber.*, **16**, 1074 (1883).
6) E. W. Hughes, *J. Am. Chem. Soc.*, **62**, 1258 (1940).
7) W. J. Jones and W. J. Orivilla-Thomas, *Trans. Faraday Soc.*, **55**, 193 (1959).
8) P. Vaughan and J. Donohue, *Acta Crystallogr.*, **5**, 530 (1952).
9) T. Ebisuno, M. Takimoto, and R. Shiba, *Bull. Chem. Soc. Jpn.*, **57**, 275 (1984).
10) V. Schomaker and D. P. Stevenson, *J. Am. Chem. Soc.*, **63**, 37 (1941).
11) K. Odo, E. Ichikawa, S. Akira, and J. Fukunaga, *Yuki Gosei Kagaku Kyokai Shi*, **28**, 637 (1970).
12) T. Suyama and K. Odo, *Yuki Gosei Kagaku Kyokai Shi*, **34**, 427 (1976).

[Cycloalkyl(phenylseleno)methylene]triphenylphosphoranes: Synthesis and Reactions of (Phenylseleno)alkenes

Toru MINAMI,* Yasuo UMEZU, Shoji SHIKITA, and Yoshiharu OKADA
Department of Applied Chemistry, Kyushu Institute of Technology, Sensuicho, Tobata, Kitakyushu 804
(Received March 25, 1989)

Synopsis. The Wittig reaction of [cyclopropyl(phenylseleno)methylene]- and [cyclobutyl(phenylseleno)methylene]-triphenylphosphoranes with aldehydes produced (*Z*)- and (*E*)-(1-cyclopropyl-1-phenylseleno)- and (1-cyclobutyl-1-phenylseleno)alkenes in moderate to good yields. The oxidation of the (*E*)-selenoalkenes to the corresponding selenoxides and subsequent thermolysis of the selenoxides led to cyclopropyl- and cyclobutylacetylene derivatives in good yields.

We have recently reported the synthesis of [cycloalkyl(phenylseleno)methyl]triphenylphosphonium salts by the reaction of (cycloalkylmethylene)triphenylphosphoranes with benzeneselenenyl bromide.[1] Although selenenylated phosphonium salts are expected to be useful intermediate reagents, their synthetic utilization has, to our knowledge, been little reported.[1-4] In this paper we report the reaction of [cycloalkyl(phenylseleno)methylene]triphenylphosphoranes derived from the corresponding selenophosphonium salts and base with various aldehydes; we also report on a convenient synthesis of cycloalkylacetylene derivatives from the resulting selenoalkenes.

Results and Discussion

Treatment of a [cyclopropyl(phenylseleno)methyl]-triphenylphosphonium salt **2a** with 1.1 molar equiv of *n*-BuLi at room temperature for 0.5 h in THF, followed by a reaction with benzaldehyde (**4a**) at room temperature for 1 h, gave a 1:1 mixture of (*Z*)- and (*E*)-1-cyclopropyl-2-phenylethene (**5a**) (76%) together with butyl phenyl selenide (75%). This result indicates that the phosphonium salt **2a** underwent facile deselenation with *n*-BuLi to give (cyclopropylmethylene)triphenylphosphorane (**1a**). Replacement of *n*-BuLi by NaH in the same reaction led to a mixture of **5a** (30%) and (*Z*)- and (*E*)-1-cyclopropyl-1-phenylseleno-2-phenylethene (**6a**) (2:3 mixture, 48%), while the reaction using lithium bis(trimethylsilyl)amide [LiN(SiMe$_3$)$_2$] as the base produced a 3:4 mixture of (*Z*)- and (*E*)-**6a** in 70% yield. The Wittig condensation of various aldehydes **4a—d** with the phosphorane **3a**, generated from **2a** and LiN(SiMe$_3$)$_2$, gave mixtures of (*Z*)- and (*E*)-(phenylseleno)alkenes **6b—d** in 26—89% yields (see Table 1). Further treatment of isolated **6d** with **3a** led to a 7:6:1 mixture of (*E,E*)-, (*Z,E*)-, and (*Z,Z*)-*o*-bis[2-cyclopropyl-2-(phenylseleno)ethenyl]benzene (**7**) in 62% yield (Eq. 1). Treatment of **3a** with

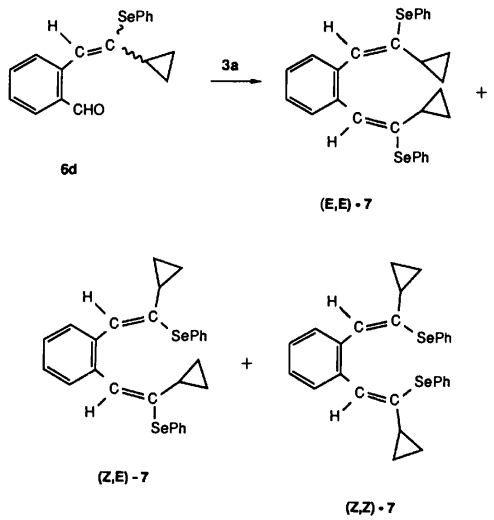

(1)

paraformaldehyde smoothly led to the formation of 1-cyclopropyl-1-(phenylseleno)ethene (**6e**) in 74% yield. The [cyclobutyl(phenylseleno)methyl]triphenylphosphonium salt **2b**,[1] on similar treatment with NaH or LiN(SiMe$_3$)$_2$ and **4a** in THF, afforded a 1:1 mixture of (*Z*)- and (*E*)-1-cyclobutyl-1-phenylseleno-2-phenylethene (**8**) (23 or 54%) along with 1-cyclobutyl-2-

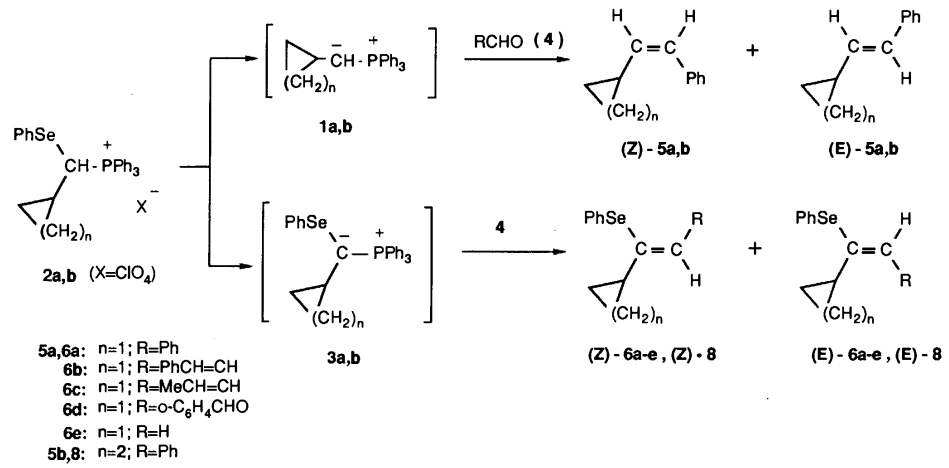

Scheme 1.

Table 1.[a] The Reaction of [Cycloalkyl(phenylseleno)methyl]phosphonium Salts **2a, b** with Aldehydes **4** in the Presence of Base

Entry	Salt **2**	Starting materials **4** (R)	Base	Products (% yield,[b] ratio of $Z:E$[c])	
1	**2a**	**4a** (Ph)	BuLi	**5a** (76, 1:1)	
2	**2a**	**4a** (Ph)	NaH	**5a** (30)	**6a** (48, 2:3)
3	**2a**	**4a** (Ph)	$LiN(SiMe_3)_2$		**6a** (70, 3:4)
4	**2a**	**4b** (PhCH=CH)	$LiN(SiMe_3)_2$		**6b** (89, 2:7)
5	**2a**	**4c** (MeCH=CH)	$LiN(SiMe_3)_2$		**6c** (26, 1:3)
6	**2a**	**4d** (*o*-C_6H_4CHO)	$LiN(SiMe_3)_2$		**6d** (62, 1:1)
7	**2a**	**4e** (H)	$LiN(SiMe_3)_2$		**6e** (74)
8	**2b**	**4a** (Ph)	BuLi	**5b** (70, 3:2)	
9	**2b**	**4a** (Ph)	NaH	**5b** (6)	**8** (23, 1:1)
10	**2b**	**4a** (Ph)	$LiN(SiMe_3)_2$	**5b** (8)	**8** (54, 1:1)

a) Unless othewise indicated, all reactions were carried out using **2** (1 mmol), **4** (1.2 mmol), and base (1.1 equiv) in THF (5 cm^3). b) Isolated yields. c) Based on ^1H and/or ^{13}C NMR spectrum.

phenylethene (**5b**) (Table 1, Entries 9 and 10). This result exhibits that, even using $LiN(SiMe_3)_2$ as well as NaH, the salt **2b** underwent not only deprotonation but deselenation to generate ylides **1b** and **3b**, leading to the products (Scheme 1).

In an attempt to investigate the reactivities of alkenyl selenides, the oxidation of the selenides (**6a, b, 7**, and **8**) with H_2O_2 at room temperature was carried out to produce the corresponding selenoxides (**9a, b, 10**, and **11**) in good yields.

Selenoxides (*E*)-**9a** and (*E*)-**11** were smoothly converted in benzene containing triethylamine at 80 °C for 1 h into cyclopropylethynyl- and cyclobutylethynylbenzenes (**12** and **13**) in 74 and 79% yields. The thermolysis of

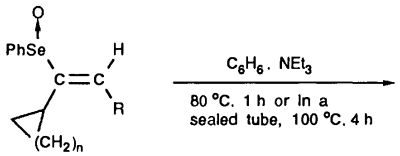

(E)-9a, (E)-11, (1E,3E)-9b

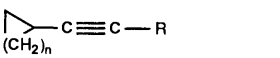

(2)

12, 13, 14

(E)-9a, 12 ; n=1, R=Ph
(E)-11, 13 ; n=2, R=Ph
(1E,3E)-9b, 14 ; n=1, R=CH=CHPh

the selenoxide (1*E*,3*E*)-**9b** under rather vigorous conditions (100 °C, 4 h) gave a mixture of 4-cyclopropyl-1-phenyl-1-buten-4-yne (**14**) (37%) and the reduced product **6b** (40%)[5] (Eq. 2). A similar thermolysis of diselenoxides (*E,E*)-**10** and (*Z,E*)-**10** formed *o*-bis(cyclopropylethynyl)benzene (**15**) and (*Z*)-1-cyclopropylethynyl-2-[2-cyclopropyl-2-(phenylseleninyl)ethenyl]benzene (**16**) in 96% and quantitative yields (Eq. 3).

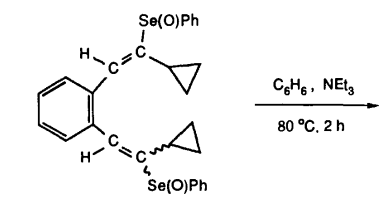

(E,E)-10, (Z,E)-10

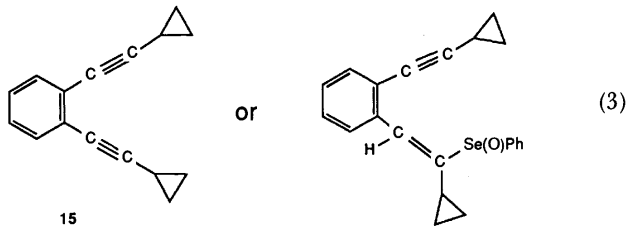

15 16

(3)

Thus, we have found that phosphonium salts **2a, b** can be used as useful intermediate reagents for the synthesis of alkenes and alkynes bearing small-membered cycloalkyl substituents.

Experimental

General. ^1H NMR spectra were obtained on a JEOL JNM-FX-60 spectrometer in $CDCl_3$ operating at 60 MHz with Me_4Si as an internal standard. IR spectra were recorded with a Shimadzu IR-408 instrument. Mass spectra were taken with a JEOL DX-300 spectrometer.

Reaction of 2a, b[1] with *n*-BuLi (or NaH) or $LiN(SiMe_3)_2$ and 4a—e. General Procedure. To solutions of phosphonium ylides, generated in situ from **2a, b** (1 mmol) and *n*-BuLi or $LiN(SiMe_3)_2$ (1.1 mmol) in dry THF (5 cm^3) at 0 °C for 0.5 h or −75 °C for 1 h, was added **4a—e** (1.2 mmol). The mixture was stirred at room temperature for 10 or 12 h. After an aqueous NH_4Cl solution was added to the reaction mixture the mixture was concentrated in vacuo, extracted with CH_2Cl_2, washed with water, and dried over Na_2SO_4. After evaporation of CH_2Cl_2, the residue was chromatographed on preparative TLC (silica gel, Wakogel B-5F, hexane) to give pure samples **5a, b** (or **5a, b** and **6a** or **8**) and butyl phenyl selenide or **6a—e** and **8**. The yields of the products are summarized in Table 1.

1-Cyclopropyl-2-phenylethene (**5a**): yield 0.11 g; IR (neat) 1650, 1600 cm^{-1}; ^1H NMR δ=0.39—0.97 (m, 4H, CH_2), 1.20—2.20 (m, 1H, CH), 5.00 (dd, J=9.67 Hz, 11.43 Hz, 0.5H, cis ***H***C=CPhH), 5.65 (dd, J=8.43 Hz, 15.70 Hz, 0.5H, trans ***H***C=CPhH), 6.31 (d, J=11.43 Hz, 0.5H, cis HC=CPh***H***), 6.43 (d, J=15.70 Hz, 0.5H, trans HC=CPh***H***); Found: *m/z* 144.0987. Calcd for $C_{11}H_{12}$: M, 144.0939.

Butyl phenyl selenide:[6] yield 0.16 g.

1-Cyclobutyl-2-phenylethene (**5b**):[7] yield 0.11 g.

(*Z*)-1-Cyclopropyl-1-phenylseleno-2-phenylethene [(*Z*)-(**6a**)]:[8] yield 58 mg; IR (neat) 1595, 1580 cm^{-1}; ^1H NMR

δ=0.30—1.00 (m, 4H, CH_2), 1.00—1.90 (m, 1H, CH), 6.83 (s, 1H, CH=C); Found: *m/z* 300.0417. Calcd for $C_{17}H_{16}Se$: M, 300.0416.

(*E*)-1-Cyclopropyl-1-phenylseleno-2-phenylethene [(*E*)-(**6a**)]:[8] yield 85 mg; IR (neat) 1595, 1580 cm^{-1}; ^1H NMR δ=0.25—0.69 (m, 4H, CH_2), 1.70—2.30 (m, 1H, CH), 6.89 (s, 1H, CH=C); Found: *m/z* 300.0443. Calcd for $C_{17}H_{16}Se$: M, 300.0416.

(*Z*)-1-Cyclobutyl-1-phenylseleno-2-phenylethene [(*Z*)-(**8**)]:[7,8] yield 35 mg.

(*E*)-1-Cyclobutyl-1-phenylseleno-2-phenylethene [(*E*)-(**8**)]:[7,8] yield 35 mg.

(1*E*,3*Z*)-1-Cyclopropyl-4-phenyl-1-phenylseleno-1,3-butadiene [(1*E*,3*Z*)-(**6b**)]:[7,8] yield 65 mg.

(1*E*,3*E*)-1-Cyclopropyl-4-phenyl-1-phenylseleno-1,3-butadiene [(1*E*,3*E*)-(**6b**)]:[7,8] yield 225 mg.

1-Cyclopropyl-1-phenylseleno-1,3-pentadiene (**6c**):[7] yield 70 mg.

o-[2-Cyclopropyl-2-(phenylseleno)ethenyl]benzaldehyde (**6d**):[7] yield 205 mg.

1-Cyclopropyl-1-phenylselenoethene (**6e**)]:[7] yield 165 mg.

o-Bis[2-cyclopropyl-2-(phenylseleno)ethenyl]benzene (**7**).

The reaction was carried out as described above by using **2a** (0.57 g, 1 mmol) and **6d** (0.38 g, 1.2 mmol) to produce 0.33 g (62%) of a 7:6:1 mixture of (*E,E*)-, (*E,Z*)-, and (*Z,Z*)-**7**.[8] Pure samples of individual (*E,E*)-, (*E,Z*)-, and (*Z,Z*)-**7**, were isolated by preparative TLC (hexane).

(*E,E*)-**7**: IR (neat) 1575 cm^{-1}; ^1H NMR δ=0.54—0.71 (m, 8H, CH_2), 1.59—2.05 (m, 2H, CH), 6.82 (s, 2H, CH=C); MS, *m/z* 522 (M^+).

(*E,Z*)-**7**: IR (neat) 1575 cm^{-1}; ^1H NMR δ=0.53—0.75 (m, 8H, CH_2), 1.25—1.98 (m, 2H, CH), 6.69 (s, 1H, CH=C); 6.75 (s, 1H, CH=C); MS, *m/z* 522 (M^+).

(*Z,Z*)-**7**: IR (neat) 1575 cm^{-1}; ^1H NMR δ=0.54—0.81 (m, 8H, CH_2), 1.36—1.69 (m, 2H, CH), 6.68 (s, 2H, CH=C); MS, *m/z* 522 (M^+).

Oxidation of the Selenides 6a, b, 7, and 8. General Procedure. A solution of selenide (1 mmol) in CH_2Cl_2/H_2O (1/1, 10 cm^3) containing H_2O_2 (5 equiv) was stirred at room temperature for 5 h. The reaction mixture was then extracted with CH_2Cl_2, washed with water, and dried over Na_2SO_4. After evaporation of CH_2Cl_2, the residue was chromatographed on preparative TLC (ethyl acetate) to give selenoxides **9a, b, 10**, and **11**.

(*Z*)-1-Cyclopropyl-1-phenylseleninyl-2-phenylethene [(*Z*)-(**9a**)]: yield 258 mg (82%); IR (neat) 1595, 1575 cm^{-1}; ^1H NMR δ=0.00—1.10 (m, 4H, CH_2), 1.60—2.20 (m, 1H, CH), 6.83 (s, 1H, CH=C), 7.00—7.90 (m, 10H, phenyl H).

(*E*)-1-Cyclopropyl-1-phenylseleninyl-2-phenylethene [(*E*)-(**9a**)]: yield 300 mg (95%); IR (neat) 1595, 1575 cm^{-1}; ^1H NMR δ=0.20—1.80 (m, 5H, CH_2 and CH), 7.0—8.0 (m, 11H, CH=C and phenyl H).

(1*E*,3*E*)-1-Phenyl-4-cyclopropyl-4-phenylseleninyl-1,3-butadiene [(1*E*,3*E*)-(**9b**)]:[7] yield 229 mg (70%).

(*E,E*)-*o*-Bis[2-cyclopropyl-2-(phenylseleninyl)ethenyl]benzene [(*E,E*)-(**10**)]:[7] yield 552 mg (quant).

(*E,Z*)-*o*-Bis[2-cyclopropyl-2-(phenylseleninyl)ethenyl]benzene [(*E,Z*)-(**10**)]:[7] yield 550 mg (quant).

(*Z*)-1-Cyclobutyl-1-phenylseleninyl-2-phenylethene [(*Z*)-(**11**)]:[7] yield 330 mg (quant).

(*E*)-1-Cyclobutyl-1-phenylseleninyl-2-phenylethene [(*E*)-(**11**)]:[7] yield 330 mg (quant).

Thermolysis of the Selenoxides (*E*)-9a, (*E*)-11, (*E,E*)-10, (*E,Z*)-10, or (1*E*,3*E*)-9b. General Procedure. A solution of a selenoxide (1 mmol) in dry benzene (5 cm^3) containing small amounts of triethylamine was heated under reflux for 1 h or at 100 °C for 4 h in a sealed tube. After evaporation of benzene, the residue was chromatographed on preparative TLC (hexane or ethyl acetate) to give an acetylene.

(Cyclopropylethynyl)benzene (**12**): yield 105 mg (74%); IR (neat) 2240 cm^{-1}; ^1H NMR δ-0.50—1.00 (m, 4H, CH_2), 1.00—1.70 (m, 1H, CH); Found: *m/z* 142.0754. Calcd for $C_{11}H_{10}$: M, 142.0782.

(Cyclobutylethynyl)benzene (**13**):[7] yield 123 mg (79%).

o-Bis(cyclopropylethynyl)benzene (**15**):[7] yield 198 mg (96%).

(*Z*)-1-Cyclopropylethynyl-2-[2-cyclopropyl-2-(phenylseleninyl)ethenyl]benzene (**16**):[7] yield 375 mg (quant).

1-Phenyl-4-cyclopropyl-1-buten-4-yne (**14**):[7] yield 62 mg (37%).

References

1) T. Minami, S. Shikita, S. So, M. Nakayama, and I. Yamamoto, *J. Org. Chem.*, **53**, 2937 (1988).

2) G. Saleh, T. Minami, Y. Ohshiro, and T. Agawa, *Chem. Ber.*, **112**, 355 (1979).

3) N. Petragnani, R. Rodrigues, and J. V. Comasseto, *J. Organomet. Chem.*, **114**, 281 (1976).

4) T. Minami, H. Sako, T. Ikehira, T. Hanamoto, and I. Hirao, *J. Org. Chem.*, **48**, 2569 (1983).

5) Thermolysis of the selenoxide (1*E*,3*E*)-**9b** at 80 °C for 2 h gave only the reduced product **6b** in 46% yield.

6) S. Raucher and G. A. Koolpe, *J. Org. Chem.*, **43**, 4252 (1978).

7) The new compounds **5b**, **6b—e**, **8**, **9b**, **10**, **11**, **13**, **14**, **15**, and **16** were fully characterized by the IR, ^1H NMR, and mass spectra, and gave satisfactory high resolution mass spectra.

8) The stereochemistry of each of stereoisomeric vinylselenides **6a—d**, **7**, and **8** were tentatively assigned on the basis of their ^1H and/or ^{13}C NMR spectral data of isolated pure isomers or mixture and chemical properties. Furthermore, their stereostructures were unambiguously confirmed by thermolysis of the corresponding selenoxides.

Synthetic Photochemistry. LII.[1] Substituent Effects of a Bromine Atom on the High-Pressure Cycloaddition between 1-Acetyl-7-bromocyclohepta[*b*]pyrrol-2(1*H*)-one and 2,3-Bis(methoxycarbonyl)-7-oxanorbornadiene and the Photorearrangement of 2-Acetyl-9-bromo-2-azatricyclo-[6.2.2.0^{1,5}]dodeca-4,6,9,11-tetraen-3-one

Guan Rong TIAN,† Akira MORI, and Hitoshi TAKESHITA*
Institute of Advanced Material Study, Kyushu University, 86, Kasuga-koen, Kasuga, Fukuoka 816
(Received March 27, 1989)

Synopsis. A high-pressure cycloaddition reaction of 1-acetyl-7-bromocyclohepta[*b*]pyrrol-2(1*H*)-one and 2,3-bis-(methoxycarbonyl)-7-oxanorbornadiene and a further thermolysis of [4+2] cycloadducts gave 2-acetyl-9-bromo-2-azatricyclo[6.2.2.0^{1,5}]dodeca-4,6,9,11-tetraen-3-one, which was photorearranged to 9-methylenebarbaralane and 5-methylenetricyclo[4.3.0.0^{2,9}]nonadiene derivatives. The product distribution of the photolysis was altered by a bromine atom.

From a comparative point of view of the results of 2,3-bis(methoxycarbonyl)-7-oxabicyclo[2.2.1]heptadiene (**1**) with 2*H*-cyclohepta[*b*]furan-2-ones, we investigated[2] the reaction of **1** with 1-acetylcyclohepta[*b*]-pyrrol-2(1*H*)-one (**2**) in order to observe both [4+2] and [8+2] cycloadducts, the latter of which are of interest in regard to a possible entry to azulene derivatives.[3]

Since the introduction of an electronegative halogen substituent into a seven-membered ring may alter the reaction course, it should be worthwhile carrying out the reaction with an easily available bromo derivative of **2**. Herein, we describe the result for **1** and 1-acetyl-7-bromocyclohepta[*b*]pyrrol-2(1*H*)-one (**3**),[4] disclosing that the heptafulvene structures, formerly proposed by Abe and Takehiro for [8+2] cycloadducts,[5] were shown to be revised. Furthermore, the photorearrangement of 2-acetyl-9-bromo-2-azatricyclo[6.2.2.0^{1,5}]dodeca-4,6,9,11-tetraen-3-one (**4**), the cycloreversed product, gave a different product distribution from that of 2-acetyl-2-azatricyclo[6.2.2.0^{1,5}]dodeca-4,6,9,11-tetraen-3-one (**5**).[2]

When a chlorobenzene solution of **1** and **3** was heated at 120 °C under 3000 bar, six products (**6**—**11**) were isolated. A major product (**6**) was an endo [4+2] cycloadduct from NMR spectral data, whereas product **7** was an exo [4+2] isomer. Product **8** was another endo [4+2] adduct, whose NMR spectrum closely resembled that of the corresponding adduct from **1** and **2**.[2] Product **9** was formally an adduct between **3** and dimethyl butynedioate.

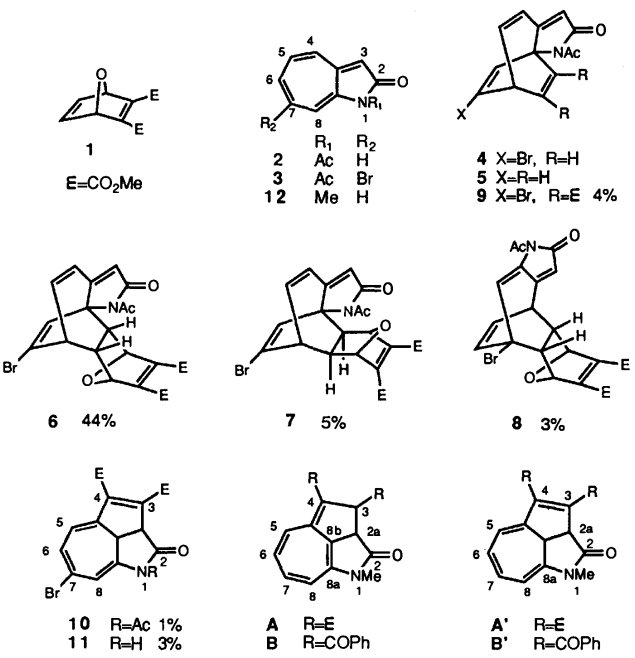

Scheme 1.

The structures of the remaining products (**10** and **11**) were determined as follows: From the rather small values of the coupling constants ($J_{5,6}$=6.6—7.0 Hz for **10** and **11**), the position of a double bond should be located between C_6 and C_7 since the coupling constant across the single bond is smaller than that across the double bond.[6] Therefore, the structures of **10** and **11**

Table 1. NMR Data of **10**, **11** and Related Compounds **A'** and **B'**

	10	**11**	**A'**[a]	**B'**[a]
H_8	7.40 (s)	5.93 (s)	5.66 (d, 6.1)	5.73 (d, 6.1)
H_7	Br	Br	6.65—6.75	6.72 (dd, 9.8, 6.1)
H_6	6.33 (d, 6.6)	6.30 (d, 7.0)	6.4—6.5	6.35—6.45 (m)
H_5	6.99 (d, 6.6)	6.85 (d, 7.0)	6.4—6.5	6.35—6.45 (m)
H_{8b}	3.34 (d, 9.5)	3.35 (d, 8.8)	3.10 (d, 9.2)	3.32 (d, 9.2)
H_{2a}	4.41 (d, 9.5)	4.32 (d, 8.8)	4.32 (d, 9.2)	4.92 (d, 9.2)
MeO	3.88, 3.89	3.86, 3.88	3.86, 3.88	

a) See Ref. 4.

† On leave from Yanbian University, Yanji, Jilin, People's Republic of China.

Table 2. Electronic Spectral Data of **10**, **11**, **A'**, and **B'**[a)]

10	11	A'	B'
225.8 (11700)	234.0 (10100)	228.0 (21200)	227.6 (30600)
266.0 (11500)	274.2 (9400)	270.4 (19000)	258.0 (28400)
323.8 (5300)	400.4 (900)	314.0 (4100 sh)	322.8 (8200 sh)
361.8 (4200)	450.0 (500)	410.8 (3000)	422.0 (3300)
425.0 (240)			

a) Measured in methanol.

were determined as shown in Scheme 1. According to a recent paper regarding the reactions of 1-methylcyclohepta[*b*]pyrrol-2(1*H*)-one (**12**) and acetylenes,[5] heptafulvene structures **A** and **B** have been proposed on the basis of an NMR analysis. However, since their ^{1}H NMR and UV data were very similar to **10** and **11**, except for the appearance of an H_7 proton and up-field shifted neighboring proton signals (Tables 1 and 2[7]), they should be revised to **A'** and **B'**. In the new structures the values of the coupling constants ($J_{6,7}$=9.8 Hz and $J_{7,8}$=6.1 Hz for **B**) are more consistent and the chemical shifts of H_8 around 5.7 are reasonably explained in terms of the electron donation of the nitrogen atom. Furthermore, a small difference in the chemical shift between two methoxy groups and very large difference (over 1 ppm) in the chemical shift of two methine protons are also compatible with the revised structures.

In the reactions of **3** and **1**, the formations of [4+2] adducts were predominated over [8+2] adducts ([4+2]/[8+2]=56/4), while the ratio of [4+2] and [8+2] adducts was 14/16 from **2** and **1**.[2] Thus, the chemical reactivity of **3** toward **1** was different from that of **2**.

The thermal cycloreversion of **6** afforded **4**, the structure of which was elucidated by comparison with spectral data of **5**.[2] The irradiation of **4** with a 400-W high-pressure mercury lamp gave two products (**13** and **14**). The structures of **13** and **14** were determined to be substituted 9-methylenebarbaralane and 5-methylenetricyclo[4.3.0.0^{2,9}]nonadiene derivative by a comparison with the spectral data of **15** and **16**.[2] Among the photoproducts from **4**, a methylenedihydroindene derivative (**17**) was not detected, despite an intensive effort. This was in contrast to the fact that **5** gave a methylenedihydroindene derivative (**18**).

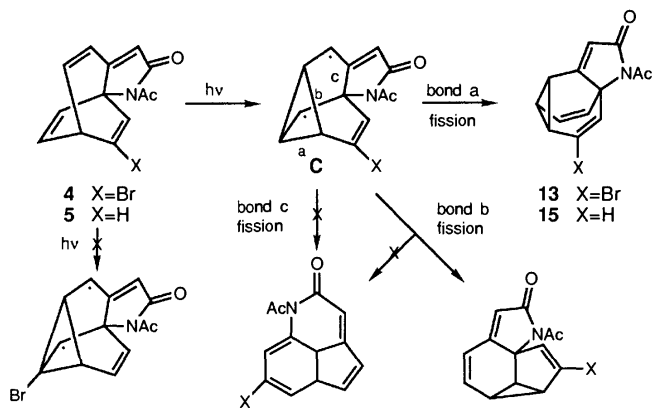

Scheme 2.

The mechanism of the photorearrangement of **4** was considered to be similar to that of **5**.[2] There are two bridging sites between the extended enone and an etheno bridge in **4**. The structure of **14** indicated that the bridging occurred at the etheno bridge carrying no bromine atom to give the intermediate (**C**). Certainly, the bromine atom prevented sterically the formation of the bridged intermediate (**D**).

On the other hand, an absence of methylenedihydroindene derivative, **17**, in the photorearrangement of **4** suggests that **13** and **14** were products via a triplet state: Namely, it has already been clarified, in the photorearrangement of 2-oxatricyclo[6.2.2.0^{1,5}]dodeca-4,6,9,11-tetraen-3-ones,[8] that methylenedihydroindenes were formed via a singlet excited state, and it was conceivable that the intersystem crossing of the singlet state to the triplet one would be facilitated for the brominated **4**, diminishing the formation of methylenedihydroindene **17**.[9]

Experimental

Cycloaddition Reaction of 1 and 3 under 3000 bar. A chlorobenzene solution (2.5 cm^3) of **1** (320 mg) and **3** (150 mg) was heated at 120 °C under 3000 bar for 20 h. The solvent was evaporated under reduced pressure and the residue was purified via silica-gel column chromatography, which followed by HPLC, to give **6** (98.5 mg, 44%), **7** (12 mg, 5%), **8** (7 mg, 3%), **9** (7 mg, 4%), **10** (2.4 mg, 1%), **11** (5.4 mg, 3%), and recovered **3** (26.3 mg).

6: Colorless crystals, mp 191—193 °C; ^{1}H NMR[10] δ=2.25 (1H, dd, J=8.8, 0.7 Hz), 2.54 (1H, dd, J=8.8, 1.1 Hz), 2.66 (3H, s), 3.63 (1H, dm, J=8.4 Hz), 3.78 (3H, s), 3.81 (3H, s), 5.04 (1H, d, J=1.1 Hz), 5.70 (1H, s), 5.78 (1H, s), 6.31 (1H, d, J=10.3 Hz), 6.49 (1H, dd, J=1.1, 0.7 Hz), and 6.77 (1H, dd, J=10.3, 8.4 Hz); ^{13}C NMR δ=26.6, 47.0, 49.1, 50.5, 52.5 (2C), 72.4, 83.6, 85.4, 118.4, 120.4, 123.3, 127.2, 141.8, 144.6, 146.4, 158.3, 162.6, 162.7, 170.2, and 171.4; IR 1720, 1635, and 1285 cm^{-1}; UV (MeOH) 245.8 (ε 8600) and 285.6 nm (6300).

Found: C, 53.01; H, 3.84; N, 2.75%. Calcd for $C_{21}H_{18}NO_7Br$: C, 52.96; H, 3.81; N, 2.94%.

7: Colorless crystals, mp 223 °C; ^{1}H NMR δ=2.64 (3H, s), 2.80 (1H, dd, J=8.8, 5.8 Hz), 3.68 (1H, d, J=8.8 Hz), 3.76 (3H, s), 3.8 (1H, m), 3.82 (3H, s), 4.57 (1H, d, J=1.1 Hz), 4.86 (1H, d, J=1.1 Hz), 5.88 (1H, s), 6.37 (1H, d, J=1.8 Hz), 6.46 (1H, dd, J=10.3, 8.8 Hz), and 6.55 (1H, dd, J=10.3, 1.8 Hz); ^{13}C NMR δ=25.8, 43.0, 47.2, 47.6, 52.4, 52.6, 72.0, 79.8, 83.3, 119.6, 124.6, 127.5, 131.5, 135.9, 145.5, 145.7, 157.0, 161.7, 162.4, 169.8, and 170.1; IR 1720, 1630, and 1280 cm^{-1}; UV (MeOH) 244.2 (ε 9600) and 283.6 nm (7500).

Found: C, 53.11; H, 3.84; N, 2.87%. Calcd for $C_{21}H_{18}NO_7Br$: C, 52.96; H, 3.81; N, 2.94%.

8: Colorless crystals, mp 183—184 °C; ^{1}H NMR δ=2.47 (1H, d, J=7.7 Hz), 2.55 (3H, s), 3.11 (1H, d, J=7.7 Hz), 3.81 (3H, s), 3.83 (1H, d, J=8.1 Hz), 3.85 (3H, s), 5.12 (1H, d,

J=1.5 Hz), 5.52 (1H, d, J=1.5 Hz), 5.91 (1H, d, J=1.8 Hz), 5.96 (1H, ddm, J=9.2, 8.1 Hz), 6.63 (1H, d, J=9.2 Hz), and 8.00 (1H, d, J=1.8 Hz); ^{13}C NMR δ=26.6, 39.8, 46.0, 52.6 (2C), 57.3, 61.1, 86.5, 86.7, 116.4, 126.4, 132.0, 135.5, 142.0, 144.8, 146.1, 152.1, 162.3, 162.5, 168.0, and 170.8; IR 1715, 1600, and 1305 cm^{-1}; UV (MeOH) 240.2 (ε 9100) and 274.0 nm (8200).

Found: C, 53.07; H, 3.84; N, 2.88%. Calcd for $C_{21}H_{18}NO_7Br$: C, 52.96; H, 3.81; N, 2.94%.

9: Colorless crystals, mp 189 °C; ^{1}H NMR δ=2.56 (3H, s), 3.72 (3H, s), 3.79 (3H, s), 4.43 (1H, dd, J=8.1, 2.2 Hz), 5.92 (1H, s), 6.19 (1H, d, J=10.3 Hz), 6.40 (1H, d, J=2.2 Hz), and 6.66 (1H, dd, J=10.3, 8.1 Hz); ^{13}C NMR δ=24.8, 48.8, 52.7, 53.0, 70.7, 121.0, 122.1 (2C), 122.6, 130.5, 135.3, 136.6, 148.5, 163.5, 164.4, 168.6, and 169.6; IR 1725, 1435, 1370, and 1300 cm^{-1}; UV (MeOH) 234.4 (ε 11900) and 285.7 nm (sh 6100).

Found: m/z 407.0008 (M$^+$ for ^{79}Br) and 409.0049 (M$^+$ for ^{81}Br). Calcd for $C_{17}H_{14}NO_6Br$: 407.0005 (M for ^{79}Br) and 408.9984 (M for ^{81}Br).

10: A colorless oil; IR 1760, 1725, 1610, 1590, and 1220 cm^{-1}.

Found: m/z 406.9999 (M$^+$ for ^{79}Br) and 408.9955 (M$^+$ for ^{81}Br). Calcd for $C_{17}H_{14}NO_6Br$: 407.0002 (M for ^{79}Br) and 408.9992 (M for ^{81}Br).

11: A colorless oil; IR 1720, 1430, and 1280 cm^{-1}.

Found: m/z 364.9904 (M$^+$ for ^{79}Br) and 366.9807 (M$^+$ for ^{81}Br). Calcd for $C_{15}H_{12}NO_5Br$: 364.9900 (M for ^{79}Br) and 366.9877 (M for ^{81}Br).

DDQ-Oxidation of 10. A C_6D_6 solution (0.5 cm^3) of **10** (1.5 mg) and DDQ (3 mg) was heated at 80 °C for 4 h in a NMR tube. The reaction was monitored by the ^{1}H NMR spectra. No change was observed.

Thermal Cycloreversion of 6. A chlorobenzene solution (1 cm^3) of **6** (60 mg) was heated for 24 h at 130 °C. The solvent was evaporated and the residue was chromatographed on a silica-gel column and HPLC to give **4** (24 mg, 65%) and 3,4-bis(methoxycarbonyl)furan (16 mg, 69%).

4: A colorless oil; ^{1}H NMR δ=2.61 (3H, s), 3.94 (1H, tm, J=8.0 Hz), 5.79 (1H, s), 6.05 (1H, d, J=10.3 Hz), 6.25 (1H, dt, J=7.0, 1.1 Hz), 6.37 (1H, d, J=1.1 Hz), 6.52 (1H, dd, J=8.0, 7.0 Hz), and 6.65 (1H, dd, J=10.3, 8.0 Hz); ^{13}C NMR δ=25.1, 48.9, 70.8, 119.1, 120.8, 123.3, 131.1, 131.5, 137.7, 151.2, 169.4, and 169.5; IR 1720, 1700, 1685, and 1290 cm^{-1}; UV (MeOH) 264.2 nm (ε 8200).

Found: m/z 290.9925 (M$^+$ for ^{79}Br) and 292.9824 (M$^+$ for ^{81}Br). Calcd for $C_{13}H_{10}NO_2Br$: 290.9896 (M for ^{79}Br) and 292.9875 (M for ^{81}Br).

Photorearrangement of 4. A $CDCl_3$ solution (0.5 cm^3) of **4** (65 mg) was irradiated with a 400-W high-pressure mercury lamp for 2.5 h. After the evaporation of the solvent, the residue was chromatographed on a silica-gel column and HPLC to give **13** (10 mg, 24%), **14** (5.6 mg, 14%), and recovered **4** (21 mg).

13: A colorless oil, ^{1}H NMR δ=2.57 (3H, s), 2.86 (1H, m), 3.01 (1H, td, J=7.7, 2.2 Hz), 3.13 (1H, dd, J=7.7, 7.0 Hz), 5.76 (1H, s), 5.84 (1H, dd, J=9.2, 6.2 Hz), 6.38 (1H, dd, J=9.2, 0.7 Hz), and 6.56 (1H, d, J=2.2 Hz); ^{13}C NMR δ=21.8, 25.2, 29.9, 37.0, 67.5, 111.3, 114.2, 119.7, 127.7, 129.0, 159.5, 169.1, and 169.7; IR 1730, 1695, 1660, 1380, and 1305 cm^{-1}; UV (MeOH) 274.8 (ε 16900) and 273.6 nm (2400).

Found: m/z 290.9929 (M$^+$ for ^{79}Br) and 292.9824 (M$^+$ for ^{81}Br). Calcd for $C_{13}H_{10}NO_2Br$: 290.9896 (M for ^{79}Br) and 292.9875 (M for ^{81}Br).

14: Colorless crystals, mp 153 °C; ^{1}H NMR δ=2.16 (1H, td, J=7.3, 4.4 Hz), 2.55 (3H, s), 2.81 (1H, ddm, J=7.3, 6.6 Hz), 3.02 (1H, dd, J=7.3, 6.6 Hz), 5.21 (1H, d, J=0.7 Hz), 5.71 (1H, s), 6.24 (1H, dd, J=9.9, 4.4 Hz), and 6.65 (1H, d, J=9.9 Hz); ^{13}C NMR δ=25.4, 26.2, 37.3, 45.8, 73.4, 115.4, 122.6, 123.3, 130.9, 132.7, 159.3, 169.5, and 169.6; IR 1725, 1635, 1600, 1375, and 1305 cm^{-1}; UV (MeOH) 231.6 (ε 9975) and 298.0 nm (4800).

Found: m/z 290.9917 (M$^+$ for ^{79}Br) and 292.9824 (M$^+$ for ^{81}Br). Calcd for $C_{13}H_{10}NO_2Br$: 290.9896 (M for ^{79}Br) and 292.9875 (M for ^{81}Br).

The authors wish to express their thanks to Dr. Noritaka Abe of Yamaguchi University for supplying samples (**A′** and **B′**) to measure UV spectra.

References

1) Part LI. T. Hatsui, C. Nojima, and H. Takeshita, *Bull. Chem. Soc. Jpn.*, **62**, 2932 (1989).

2) G. R. Tian, S. Sugiyama, A. Mori, H. Takeshita, M. Higashi, and H. Yamaguchi, *Bull. Chem. Soc. Jpn.*, **62**, 1567 (1989).

3) K. Takase and M. Yasunami, *Yuki Gosei Kagaku Kyokai Shi*, **39**, 1172 (1981).

4) The preparation of **3** will be included in a separate paper as a part of the study for the restricted rotation in troponoids with a heterocyclic ring. See H. Takeshita, A. Chisaka, and H. Mametsuka, *Bull. Chem. Soc. Jpn.*, **53**, 3373 (1980).

5) N. Abe and T. Takehiro, *Bull. Chem. Soc. Jpn.*, **61**, 1225 (1988).

6) D. J. Bertelli, T. G. Andrews, Jr., and P. O. Crews, *J. Am. Chem. Soc.*, **91**, 5286 (1969).

7) It was true that an introduction of a bromine atom at C_7 made the ^{1}H NMR analysis of these derivatives easier.

8) G. R. Tian, S. Sugiyama, A. Mori, and H. Takeshita, *Bull. Chem. Soc. Jpn.*, **61**, 4397 (1988).

9) A referee suggested that **17** should be formed rather via a bond b fission and the following bond c fission than via a bond c and the following bond b fissions. However, we have no experimental evidence to distinguish them.

10) NMR spectra were measured with JEOL FX 100 Model and GSX 270 H Model spectrometers in a $CDCl_3$ solution.

Photoaffinity Labeling of Pepsin

Hiroo YONEZAWA* and Tetsuya WADA
Department of Chemistry, Faculty of Science, Kagoshima University,
1-Korimoto, Kagoshima 890
(Received May 13, 1989)

Synopsis. Photoaffinity reagents for pepsin [Ala-Gly-Phe(N_3), Gly-Gly-Phe(N_3)-Phe-Gly-OEt, Gly-Gly-Phe-Phe(N_3)-Gly-OEt] were synthesized by a solution method. The pentapeptides were cleaved rapidly at the peptide bond between two aromatic amino acid residues by pepsin. This shows that Phe(N_3) residues of the photoaffinity reagents bind with the S_1 or S_1' site of pepsin. Pepsin was irradiated with photoaffinity reagents and the remaining activity was measured. The pepsin activity was decreased more rapidly in the presence of photoaffinity reagents, compared with that in the absence of photoaffinity reagents. Photoaffinity labeling occured at pH 2.0; however, did not occur at pH 4.0. Photoaffinity labeling of pepsin with ^{3}H-labeled Gly-Gly-Phe(N_3)-Phe-Gly-OEt showed that about 9% of the pepsin bound covalently with the photoaffinity reagent.

The specificity of a protease toward substrates was explained by an interaction between subsites of the protease and substrate side chains. Studies of pepsin specificity have shown that the enzyme has at least five subsites: three toward the NH_2-terminate from the sensitive bond (S_3, S_2, S_1) and two toward the COOH-terminate (S_1', S_2'). The S_1 and S_1' sites of pepsin are obviously the primary determinant of specificity.[1] The S_1 and S_1' sites gave a strong preference for aromatic L-amino acid residures. For example, Z-His-Phe-Phe-OMe is hydrolyzed much more rapidly at the Phe-Phe bond than both Z-His-Leu-Phe-OMe and Z-His-Phe-Leu-OMe.[2] Andreeva et al. suggested that the phenolic rings of substrates occupied two hydrophobic pockets which were formed by hydrophobic amino acid residues.[3] These residues are inert in the usual modification reaction. However, it is possible to modify these residues by the use of photoaffinity labeling.[4] The carbenes and nitrenes which were produced by irradiation are very reactive and nonselective in terms of amino acid residues. A peptide containing *p*-azido-L-phenylalanine [Phe(N_3)] at the position of P_1 or P_1' can bind strongly with pepsin, and it may be a good photoaffinity reagent.

Hollands et al. reported that Gly-Gly-Phe(NO_2)-Phe-Gly-OMe was a good substrate of pepsin.[5] Consequently, a peptide which contains an azido group instead of a nitro group of the substrate [Gly-Gly-Phe(N_3)-Phe-Gly-OEt] may covalently bind with the S_1 site of pepsin by irradiation. Similarly, Gly-Gly-Phe-Phe(N_3)-Gly-OEt may covalently bind with the S_1' site. Furthermore, photoaffinity labeling of chymotrypsin with a reagent of product type was carried out.[6] Therefore, Ala-Gly-Phe(N_3) may act as a photoaffinity reagent. In this paper, we report on the synthesis of these three peptides and the photoaffinity labeling of pepsin with these peptides.

Results and Discussion

The substrate and photoaffinity reagents were synthesized by a solution method. A protected tripeptide, Boc-Ala-Gly-Phe(N_3), was prepared by the coupling of Boc-Ala-Gly and Phe(N_3) via an active ester method.[7] The obtained protected tripeptide was treated with hydrogen chloride in ethyl acetate to cleave the protecting group, and free tripeptide was precipitated from aqueous solution.

On the other hand, *p*-azido-L-phenylalanine containing pentapeptides were synthesized by another process. Z-Gly-Gly and Phe(NO_2)-Phe-Gly-OEt or Phe-Phe(NO_2)-Gly-OEt were coupled and the resulting protected pentapeptide esters were hydrogenated. Then, the obtained pentapeptide esters were converted to the corresponding azido compounds by treatment with sodium nitrite and sodium azide. The ^{3}H-labeled Gly-Gly-Phe(N_3)-Phe-Gly-OEt was synthesized by the same procedure. The crude pentapeptides were applied to droplet countercurrent chromatography to give pure peptides. The obtained photoaffinity reagents were employed for enzymatic experiments.

As shown in Fig. 1, these two photoaffinity reagents were cleaved at the same rate as that of the substrate. It is well-known that pepsin cleaves the peptide bond between two aromatic amino acid residues. It is clear that Phe(N_3) residues of the photoaffinity reagents bind with the S_1 or S_1' site of pepsin.

When pepsin was irradiated in the presence of the photoaffinity reagents, the pepsin activity decreased more rapidly than in the absence of the reagents (Fig. 2). The difference in the remaining activities of both cases was small, within 5 minutes. Then, the pepsin activity was decreased enormously after irradiation for 15 minutes, even in the absence of photoaffinity reagents. It was concluded that the appropriate

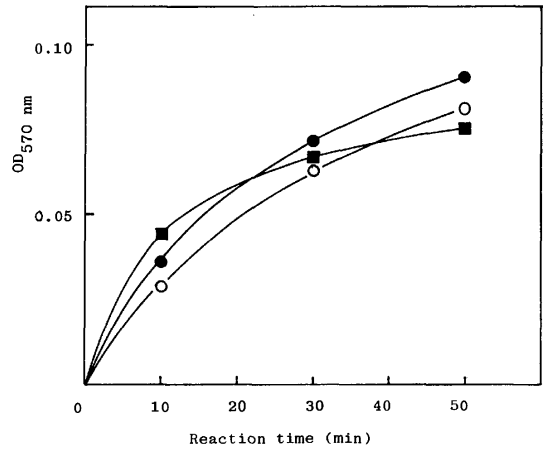

Fig. 1. Hydrolysis of photoaffinity reagents. (○) Gly-Gly-Phe(NO_2)-Phe-Gly-OEt; (●) Gly-Gly-Phe(N_3)-Phe-Gly-OEt; (■) Gly-Gly-Phe-Phe(N_3)-Gly-OEt.

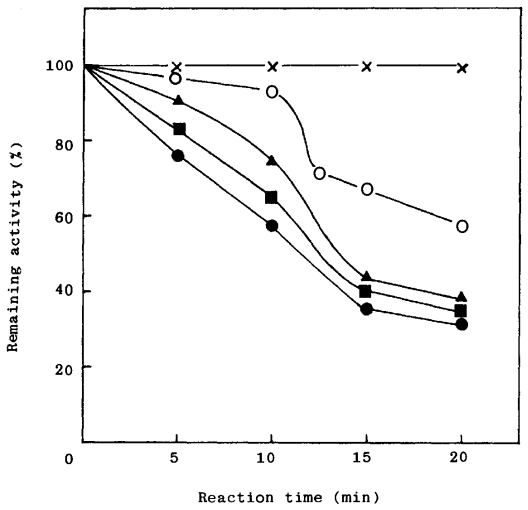

Fig. 2. Effect of irradiation time on photoaffinity labeling. (×) in dark; (○) absence of photoaffinity reagent; (▲) Ala-Gly-Phe(N_3); (■) Gly-Gly-Phe-Phe(N_3)-Gly-OEt; (●) Gly-Gly-Phe(N_3)-Phe-Gly-OEt.

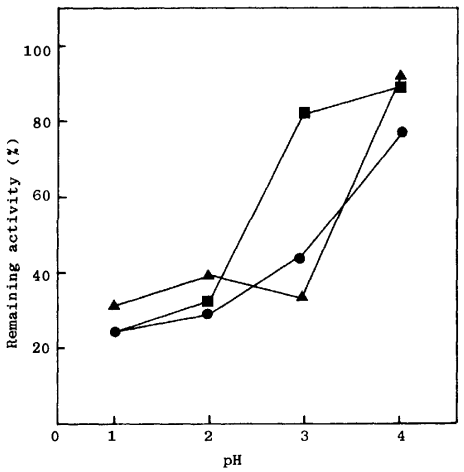

Fig. 3. Effect of pH of solution on photoaffinity labeling. (▲) Ala-Gly-Phe(N_3); (■) Gly-Gly-Phe-Phe(N_3)-Gly-OEt; (●) Gly-Gly-Phe(N_3)-Phe-Gly-OEt.

irradiation time should be 10 minutes. At this time, the remaining pepsin activities were as follows: 93% (absence of the photoaffinity reagent), 68% [Ala-Gly-Phe(N_3)], 65% [Gly-Gly-Phe-Phe(N_3)-Gly-OEt], 60% [Gly-Gly-Phe(N_3)-Phe-Gly-OEt].

The effect of pH on photoaffinity labeling was determined. As shown in Fig. 3, all photoaffinity reagents did not act at pH 4.0. Photoaffinity reagets which contained the azido group at the P_1 acted at pH 3.0; however, the reagent which contained an azido group at the P_1' did not act at this pH.

Then, pepsin was irradiated with a ^{3}H-labeled photoaffinity reagent and the incorporated radioactivity was measured. In this experiment, the measurement was made at concentrations of 0.05 mM of pepsin and 1 mM of the photoaffinity reagent (1 M=1 mol dm^{-3}). The amount of radioactivity incorporated into 4.75×10^{-8} mol of pepsin was 5820 dpm, which corresponded to 4.2×10^{-9} mol of the photoaffinity reagent. Consequently, about 9% of the pepsin was labeled upon irradiation. At this time, the remaining pepsin activities were 89 and 68%, respectively, in the absence and presence of the photoaffinity reagent. The decreased pepsin activity was larger than the amount of incorporated photoaffinity reagent.

Gennari et al. reported the photooxidation of chymotrypsin by *N*-acetyl-3-nitrotyrosine.[8] The possibility of a photooxidation reaction of pepsin with Phe(N_3) residues is not ruled out in these procedures. However, when pepsin was irradiated with 2 mM of Phe(N_3), the remaining activity was equal in the absence of Phe(N_3), indicating that a nonspecific photooxidation reaction did not occur. It may be possible to identify the amino acid residues which form S_1 and S_1' sites of pepsin by photoaffinity labeling.

Experimental

Boc-Ala-Gly-Phe(N_3) (I). This was prepared from Phe(N_3) (410 mg, 2 mmol) and Boc-Ala-Gly-OSu (690 mg, 2 mmol) using the usual procedure. The product was recrystallized from methanol-ether-petroleum ether; yield, 710 mg, (82%); mp 127—128 °C; $[\alpha]_D^{25}$ +18.0° (*c* 1, MeOH); Found: C, 52.35; H, 6.29; N, 19.48%. Calcd for $C_{19}H_{26}O_6N_6$: C, 52.52; H, 6.03; N, 19.35%.

Ala-Gly-Phe(N_3) (II). The **I** (434 mg, 1 mmol) was dissolved in 1.5 M HCl in ethyl acetate (5 ml) at 0 °C. The solution was stirred for 30 min at 0 °C and the resulting crystals were collected and washed with a mixed solvent of ethyl acetate and ether (1 : 1 v/v). The crystals were dissolved in cold water (5 ml) and the free tripeptide was separated by the addition of pyridine to pH 7. The resulting crystals were filtered and washed with a small amount of cold water; yield, 170 mg, (51%); mp 215 °C; $[\alpha]_D^{25}$ +38.9° (*c* 1, 0.1 M HCl); Found: C, 50.24; H, 5.46; N, 25.19%. Calcd for $C_{14}H_{18}O_4N_6$: C, 50.29; H, 5.43; N, 25.14%.

Boc-Phe-Gly-OEt (III). This was prepared from Boc-Phe (5.30 g, 20 mmol), and Gly-OEt·HCl (2.80 g, 20 mmol) by the 1-ethoxycarbonyl-2-ethoxy-1,2-dihydroquinoline (EEDQ) method. The product was recrystallized from ethyl acetate-petroleum ether; yield, 6.31 g, (90%); mp 88—89 °C; $[\alpha]_D^{25}$ −6.0° (*c* 1, MeOH).

Boc-Phe(NO_2)-Phe-Gly-OEt (IV). The **III** (3.50 g, 10 mmol) was dissolved in 1M HCl in acetic acid (50 ml). After 1 h at room temperature, the solution was evaporated and treated with ether. The obtained crystals were coupled with Boc-Phe(NO_2) (3.10 g, 10 mmol), as described above. Recrystallization from DMF-ether gave 4.20 g, (77%); mp 207—209 °C; $[\alpha]_D^{25}$ −14.0° (*c* 1, DMF); Found: C, 60.01; H, 6.17; N, 10.41%. Calcd for $C_{27}H_{34}O_8N_4$: C, 59.77; H, 6.32; N, 10.33%.

Z-Gly-Gly-Phe(NO_2)-Phe-Gly-OEt (V). This was prepared from Z-Gly-Gly (1.06 g, 4 mmol) and Phe(NO_2)-Phe-Gly-OEt·HCl (1.92 g, 4 mmol) by EEDQ method. The product was recrystallized from DMF-ether; yield, 2.38 g, (86%); mp 187—190 °C; $[\alpha]_D^{25}$ −15.1° (*c* 1, DMF); Found: C, 59.34; H, 5.38; N, 12.01%. Calcd for $C_{34}H_{38}O_{10}N_6$: C, 59.12; H, 5.55; N, 12.17%.

Gly-Gly-Phe(NH_2)-Phe-Gly-OEt·2HCl (VI). The **V** (2.76 g, 4 mmol) was suspended in a mixed solvent of H_2O-acetic acid-methanol (30 ml), and concd HCl (0.7 ml) was added. The **V** was hydrogenated in the presence of palladium black at room temperature. After 24 h, the

catalyst was filtered off, and the filtrate was evaporated in vacuo. The resulting crystals were collected with the aid of acetone; yield, 1.97 g, (82%); mp 219—221 °C; $[\alpha]_D^{25}$ −7.1° (*c* 1, 0.1 M HCl); Found: C, 50.33; H, 6.42; N, 13.51%. Calcd for $C_{26}H_{34}O_6N_6 \cdot 2HCl \cdot H_2O$: C, 50.57; H, 6.20; N, 13.61%.

Gly-Gly-Phe(N_3)-Phe-Gly-OEt·HCl (VII). To a solution of **VI** (1.07 g, 1.78 mmol) in 2 M HCl (1.78 ml), was added a solution of 2 M $NaNO_2$ (0.89 ml, 1.78 mmol) at 0 °C and stirred for 1 h at 0 °C. To the solution was added a solution of 2 M NaN_3 (0.89 ml, 1.78 mmol); the reaction solution was then stirred for 1 h at 0 °C. To the solution was added NaCl until saturated; resulting precipitate was then filtered and dried. The resulting crude **VII** (250 mg) was purified by droplet countercurrent chromatography,[9] using the mixed solvent of cyclohexane-1-butanol-acetic acid-water (1:4:2:5 v/v); the upper phase of the mixture was used as a moving phase. Fractions containing **VII** were collected and evaporated. The precipitate was collected with the aid of ether; yield, 170 mg, (16%); mp 204—205 °C; $[\alpha]_D^{25}$ −31.0° (*c* 1, DMF); Found: C, 51.41; H, 5.85; N, 18.50%. Calcd for $C_{26}H_{32}O_6N_8 \cdot HCl \cdot H_2O$: C, 51.44; H, 5.81; N, 18.46%.

Gly-Gly-Phe-Phe(NH_2)-Gly-OEt·2HCl (VIII). This was prepared from Z-Gly-Gly-Phe-Phe(NO_2)-Gly-OEt (4.14 g, 6 mmol), as described for the preparation of **VI**; yield, 3.18 g, (88%); mp 241—242 °C; $[\alpha]_D^{25}$ −11.2° (*c* 1, 0.1 M HCl); Found: C, 50.71; H, 6.34; N, 13.48%. Calcd for $C_{26}H_{34}O_6N_6 \cdot 2HCl \cdot H_2O$: C, 50.57; H, 6.20; N, 13.61%.

Gly-Gly-Phe-Phe(N_3)-Gly-OEt·HCl (IX). The **VIII** (1.00 g, 1.67 mmol) was converted to the corresponding azido compound according to the same manner described above and recrystallized from a mixed solvent of 1-butanol-acetic acid-pyridine-ethanol (4:2:2:1 v/v)-acetone; yield, 760 mg, (77%); mp 208—209 °C; $[\alpha]_D^{25}$ −46.6° (*c* 1, DMF); Found: C, 48.61; H, 6.09; N, 17.44%. Calcd for $C_{26}H_{32}O_6N_8 \cdot HCl \cdot 3H_2O$: C, 48.56; H, 6.11; N, 17.42%.

Gly-Gly-^{3}H-Phe(N_3)-Phe-Gly-OEt·HCl (X). This compound was prepared by the mentioned reaction sequence, starting with 230 mg (1.1 mmol, 0.6 mCi) of ^{3}H-labeled *p*-nitro-L-phenylalanine. The obtained crude product was purified by droplet countercurrent chromatography; yield, 210 mg. The specific radioactivity was 2298 dpm μg^{-1}.

Enzymatic Study. The substrate used was Gly-Gly-Phe(NO_2)-Phe-Gly-OEt·HCl. The cleavage of the substrate was measured at 37 °C, and 0.1 M sodium citrate buffer (pH 4.16) was used to control the pH. Fifty μl of pepsin solution (0.06 mM) was added to 10 ml of the substrate solution (0.25 mM) and the increase in absorbance at 310 nm was measured.[10] The kinetic constant of the substrate was K_m=0.83 mM, k_{cat}=5.5 s^{-1}.

Hydrolysis of VII and IX with Pepsin. Fifty μl of pepsin solution (0.06 mM, pH 4.16) was added to the substrate (**VII** or **IX**) solution (0.5 mM, 10 ml) and incubated at 37 °C. At selected intervals, 0.1 ml of the reaction mixture was taken out and the rate of the cleavage was determined by the ninhydrin method.[11]

Effect of Irradiation Time on Photoaffinity Labeling. Pepsin and photoaffinity reagents were dissolved in a 0.1 M sodium citrate buffer (pH 2.0). A mixture of 0.5 ml of a pepsin solution (0.06 mM) and 0.5 ml of the photoaffinity reagent solution (2 mM) was incubated for 10 min at room temperature and cooled in an ice-bath for 5 min. The solution was irradiated with a Toshiba mercury lamp H400-P at a distance of 60 cm at 0 °C. At selected intervals, 0.1 ml of the solution was taken out and the remaining activity was measured.

Effect of pH of Solution on Photoaffinity Labeling. Mixtures of 0.5 ml of a pepsin solution (0.06 mM) and 0.5 ml of the photoaffinity reagents solution (2 mM) of various pH were irradiated for 15 min at 0 °C under the same conditions described above and the remaining activity was measured.

Photoaffinity Labeling with X. A mixture of 0.5 ml of a pepsin solution (0.1 mM, pH 2.0) and 0.5 ml of a **X** solution (2 mM, pH 2.0) was irradiated for 10 min at 0 °C under the same conditions described above. To the solution, 2 M TCA (1 ml) was added and allowed to stand for 20 min. The reaction mixture (1.9 ml) was filtered with a glass fiber filter, Whatman GF/B and the filter was washed twice with 1 M TCA (1 ml) and ethanol (1 ml). The filter was dried and the radioactivity measured.

References

1) J. S. Fruton, "Acid Proteases," ed. by J. Tang, (1977), p. 131.
2) G. E. Trout and J. S. Fruton, *Biochem.*, **8**, 4183 (1969).
3) N. S. Andreeva, A. S. Zdanov, A. E. Gustchina, and A. A. Fedorov, *J. Biol. Chem.*, **259**, 11353 (1984).
4) H. Bayley and J. R. Knowles, "Methods in Enzymolgy," (1977). Vol. XLVI, p. 69.
5) K. Medzihradszky, I. M. Voynick, H. Medzihradszky-Schweiger, and J. S. Fruton, *Biochem.*, **9**, 1154 (1970).
6) E. Escher and R. Schwyzer, *FEBS Lett.* **46**, 347 (1974).
7) E. Escher and R. Schwyzer, *Helv. Chim. Acta*, **58**, 1465 (1975).
8) G. Gennari, G. Jori, G. Galiazyo, and E. Scoffon, *J. Am. Chem. Soc.*, **92**, 4140 (1970).
9) H. Yonezawa, M. Kaneda, N. Tominaga, S. Higashi, and N. Izumiya, *J. Biochem.*, **90**, 1081 (1981).
10) K. Inoue and J. S. Fruton, *Biochem.*, **6**, 1765 (1967).
11) S. Moor and W. H. Stein, *J. Biol. Chem.*, **176**, 367 (1948).

Abbreviations: Phe(N_3), *p*-azido-L-phenylalanine; -OSu, *N*-hydroxysuccinimide ester; EEDQ, 1-ethoxycarbonyl-2-ethoxyl-1,2-dihydroquinoline.

Cis/Trans Isomerization of Perinaphthothioindigo Dye Adsorbed on Silica Gel

Koushi FUKUNISHI,* Masaya KOBAYASHI, Akihiro MORIMOTO, Masaki KUWABARA, Hiroki YAMANAKA, and Mototeru NOMURA
Department of Chemistry and Materials Technology, Kyoto Institute of Technology, Matsugasaki, Sakyo-ku, Kyoto 606
(Received May 19, 1989)

Synopsis. The photoinduced and thermal cis/trans isomerization of the title compound adsorbed on silica gel has been studied by the immersion method. The cis/trans photoisomerization of the adsorbed state can be reversibly induced by irradiation. Thermal isomerization of the cis-to trans-isomer proceeds very fast on the surface. The results are compared with those obtained in solution.

Although the reversible cis/trans isomerization of olefins is a well-known phenomenon, it is limited for the studies in liquid phase as well as in polymer matrix. More recently, interest has increased in the photochemical reactions of organic molecules which are imposed by adsorption on the surface such as silica gel or alumina.[1-3] Organic molecules often change their spectroscopic and photochemical properties when adsorbed and immobilized on surfaces of solids. Breuer and Jacob studied the photoisomerization of thioindigo adsorbed on alumina by photoacoustic spectroscopy and showed that while the trans-to-cis isomerization can be induced by irradiation, the cis-isomer cannot be back converted.[2] The reverse change for thioindigo adsorbed on silica gel was reported by Mostoslavskii and Nazariko; while the cis-isomer can isomerize to the trans-isomer on irradiation, the photoconversion of the trans- to cis-isomer does not occur.[3]

We describe here the photochemical study and thermal kinetics of the perinaphthothioindigo dye (PNTI) adsorbed on silica gel by the immersion method. There is a growing interest in the field of application of writing and erasing of information with visible light.[4] This application requires that the photochromic process is reversible on the solid surface.

Experimental

General Methods. UV spectra were obtained by using a Hitachi UV-340 spectrometer and an Ohtsuka Denshi MCPD (multichannel photodiode array detector) spectrometer. The solvents used in measuring spectra were spectroanalytically pure cyclohexane, benzene, and chloroform. Nitrobenzene was distilled twice under reduced pressure before use. PNTI (bis[perinaphtothiopyran-(2)]-indigo, HRMS Calcd for $C_{24}H_{12}O_2S_2$: M, 808.4043, Found: m/z 808.4029.) was prepared by intramolecular Friedel-Crafts acylation of α-naphthalenethioacetic acid, followed by oxidative dimerization.[5] Silica gel for thin-layer chromatography (Silica gel 70 Plate-Wako/glass plate) was employed and activated by heating in an oven at 120 °C for at least 3 hours. In some cases, silica gel was treated in the oven of 650—700 °C in order to decrease the silanol group on silica gel, although the reduced amount of the group was not determined. Silica gel/glass plate(s) prepared by adsorbing PNTI in a $CHCl_3$ solution onto nonhydrated silica gel and suspending the glass plate(s) in cyclohexane, was utilized for optical studies. Light scattering in this heterogenious system was minimized by the refractive indices of the solvent and silica gel. The large-pore silica gel employed is characterized by its supplier as having a surface of 450 $m^2 g^{-1}$, and a surface density of 5 equivalents of SiOH group/nm^2. PNTI was adsorbed in the concentration of $1-10\times10^{-6}$ mol g^{-1} of silica gel.

Determination of Quantum Yield Ratios of Cis/Trans Photoisomerization of PNTI in Solvents. The apparatus used consisted of an optical bench with light source (150 W tungusten-helogen lamp), filters (KL-54 and Toshiba L-42 filters, and a cold filter CF-A) and sample holders to permit simultaneous irradiation of two samples. The samples were in 1-cm quartz cell and the $\phi_{t\to c}/\phi_{c\to t}$ ratios were determined from cis:trans ratios of photostationary state on irradiation of 540 nm by using the following equation, [cis]/[trans]= $(\phi_{t\to c}/\phi_{c\to t})(\varepsilon_t/\varepsilon_c)$.

Determination of Quantum Yields of Cis/Trans Photoisomerization of PNTI in Solvents and on Silica Gel. The apparatus used was the same as that for the quantum yield ratios determination, with exception of the filter system, where KL-63, Toshiba L-42, CF-A, and a reduced filter ND-40 for the trans-to-cis isomerization and KL-51, L-42, CF-A, and ND-40 for the cis-to-trans isomerization were used. The silica gel/glass plate(s) was perpendicularly placed in 1-cm quartz cell. The qauntum yields of the cis/trans photoconversion were measured relative to the Reinecke's salt (aqueous $KCr(NH_3)_2(NCS)_4$) actinometer.[6] As the photoisomerization of PNTI adsorbed on silica gel accompanied a relatively fast thermal cis-to-trans isomerization, corrections of the thermal reaction during irradiation were made. The results are shown in Table 1.

Kinetics for Thermal Cis-to-Trans Isomerization of PNTI. The cis isomer of PNTI in solvents and on silica gel was prepared from the corresponding trans isomer by irradiation of filtered light (λ>620 nm). The thermal isomerization of the cis-isomer was followed spectrometrically by monitoring the increase in absorption of the trans isomer. Plots of $-\ln(A_\infty-A_t)/(A_\infty-A_0)$ vs. time were almost linear. The rate constants, k, were obtained from the straight portion whose correlation factors were more than 0.99. The results are shown in Table 2.

Results and Discussion

Solution of PNTI dissolved in organic solvent was violet blue. The color of PNTI adsorbed on silica gel was similar to that in solution. Table 1 shows that the color derives from an intense band ($\varepsilon_{\lambda_{max}}$=20740 $M^{-1} cm^{-1}$ in benzene; 1 M=1 mol dm^{-3}) with λ_{max} 615—635 nm. A π-π^* assignment for the band is reasonable in view of its intensity and the red shift with increasing solvent polarity. The absorption in longer wavelength was observed on silica gel as well as in nitrobenzene.[7] Exposure of *trans*-PNTI solution to visible light of >600 nm revealed a pink-red color, which was

Table 1. Spectral Shifts of PNTI and Quantum Yields for Trans/Cis Photoisomerization

	λ_{max}/nm trans (log ε)	λ_{max}/nm cis (log ε)	Isosbestic point/nm	$\phi_{t\to c}$ (630 nm)	$\phi_{c\to t}$ (510 nm)	$\phi_{t\to c}/\phi_{c\to t}$[a] (540 nm)
Cyclohexane	615 (—)	491 (—)	524	—	—	—
Benzene	621 (4.32)	502 (4.19)	536	0.023	0.058	0.20
Chloroform	624 (4.34)	510 (4.16)	545	0.005	0.035	0.17
Nitrobenzene	631 (4.32)	514 (4.17)	547	0.020	0.017	0.91
Silica gel	635 (4.32)	534 (—)	571	0.0020	0.0023	—
Silica gel[b]	644—661 (—)	540 (—)	575	0.0011	0.0046	—

a) Ratios were determined from photostationary states. b) Silica gel was dried at 700 °C.

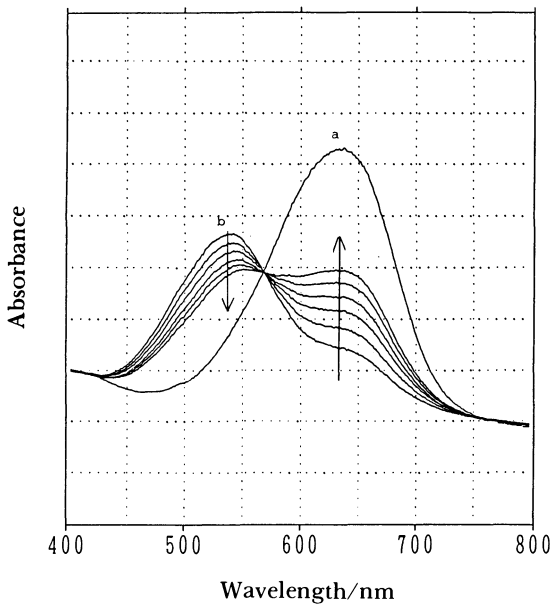

Fig. 1. Absorption spectra of PNTI adsorbed on silica gel/cyclohexane; (a) *trans*-PNTI, (b) *cis*-PNTI. The thermal cis-to-trans isomerization is shown by the arrow.

assigned to *cis*-PNTI. The electronic spectral changes resulted in about 120 nm blue shift, affording the cis-isomer of the intense visible transition ($\varepsilon_{\lambda_{max}}$=8370) with an isosbestic point at 536 nm in benzene. The extent of red shift of the cis-isomer by increasing solvent polarity was higher in compared to that of the trans-isomer. The reverse cis-to-trans photoisomerization was possible with visible light of 510 nm. Such photochromic phenomena were also observed on silica gel dipped in cyclohexane solvent. When immersed in cyclohexane, essentially all of PNTI was adsorbed on silica gel, as evidenced by the absence of PNTI absorption band of the supernatant liquid or the filtered solution. Figure 1 depicts such changes in the cis/trans isomerization on silica gel. If the sample of spectrum (a) was irradiated with light of >600 nm, spectrum (b) was obtained. Similarly, irradiation of the sample (b) with light of 510 nm easily converted into curve (a) with an isosbestic point at 571 nm.

Each of the trans- and the cis-isomer in solution or on silica gel was effectively converted into the another isomer on irradiation with 630 nm and 510 nm light, respectively. Exposure to 540 nm light (i.e., near isosbestic point) brought about the photostationary state containing the mixture of two isomers. Quantum yields ($\phi_{t\to c}$ and $\phi_{c\to t}$) and their ratios ($\phi_{t\to c}/\phi_{c\to t}$) of the isomerization were determined on the direct irradiation of 630 nm, 510 nm, and 540 nm, respectively. Quantum yields in solution and on silica gel were rather small. The ratios of quantum yields, $\phi_{t\to c}/\phi_{c\to t}$, in benzene and nitrobenzene were estimated to be 0.2 and 0.9, respectively, suggesting that the ratio depends upon the polarity of solvent used. Such a polar contribution should be reflected in surface photochemistry of dyes. The ratio on silica gel seems to have the similar propensity to that in nitrobenzene because of high polarity of silica gel. However, the present experiment shows that quantum efficiencies of PNTI on silica gel are less than those in solvents. This lowering of quantum efficiencies might imply the presence of some constraints upon the molecule motions of PNTI adsorbed on silica gel or the formation of a hydrogen-bonding between the carbonyl oxygen of PNTI and a silanol group at the excited state.

The thermodynamically less stable cis-isomer is thermally or catalytically converted to the trans-isomer. This thermal cis-to-trans isomerization of PNTI in the dark proceeded at lower rates ($t_{1/2}$=ca. 30 h at 30 °C) in three solvents examined, whereas the thermal isomerization on silica gel occurred quite rapidly ($t_{1/2}$=ca. 0.3 h at 18.5 °C). The surface of silica gel is characterized by the presence of silanol groups, siloxane bridges, and accompanying water molecules, and often bears an acidic property. Present marked increase in the isomerization rate may be due to the acidic ability of silica gel used[8] and this catalytic isomerization will be explained by a protonation of α,β-unsaturated carbonyl groups.[9] Since silanol groups change into siloxane groups on heating at high temperature, the thermal isomerization of PNTI adsorbed on heat-treated silica gel was expected to retard relative to that on untreated one. The thermal isomerization on silica gel was reduced with the decrease in the silanol groups, though the variable amount was not so large as shown in Table 2. Thus, silanol groups on silica gel may not only exert as active sites of adsorption but also promote the thermal cis-to-trans isomerization

Since the dehydration of the silanol groups leads to the raise of the hydrophobic property and/or to the reduction in acidity, the spectroscopic and photochemical properties of PNTI adsorbed are changeable.

Table 2. Rate Constants of Thermal Cis-to-Trans Isomerization of PNTI

	(°C)	$k\times10^4/s^{-1}$	$t_{1/2}$/h
Benzene	30	0.0614	31.3
Chloroform	30	0.0629	30.6
Nitrobenzene	30	0.0666	28.9
Silica gel	18.5	6.09	0.31
Silica gel[a)]	18.5	2.7—4.8	0.71—0.40

a) Silica gel was dried at 700°C.

In fact, the cis/trans photoisomerization and the thermal cis-to-trans isomerization of PNTI on silica gel were influenced, as stated above. However, the λ_{max} value for the trans-isomer on the absorbent reached to around 660 nm, depending upon the heat-treated conditions of silica gel, as the surface became more hydrophobic. This may be explained by an assumption that the thermal treatment of silica gel may result in the change of the adsorption mode, from the unimolecular to the multimolecular adsorption or the solid-like state,[10] which leads to the additional red shift in the absorption spectra of PNTI on silica gel.

Our results on PNTI are somewhat different from those on thioindigo adsorbed on silica gel obtained by other authors.[3] No trans-to-cis photoisomerization of thioindigo adsorbed is observed. This may result in the effective cancellation of the trans-to-cis photoisomerization by the thermal back-reaction during irradiation.

In conclusion, reversible cis/trans photoisomerization of PNTI on silica gel surface is possible, even though with poor quantum efficiencies. The dark reversion rate is makedly accelerated by silica gel, the effect being changed by variable amounts of silanol groups.

References

1) P. de Mayo, A. Safarzaheh-Amiri, and S. K. Wong, *Can. J. Chem.*, **62**, 1001 (1984); M. M. Abdel-Malik and P. de Mayo, *ibid.*, **62**, 1275 (1984); R. F. Childs, B. Duffey, and A. Mika-Gibala, *J. Org. Chem.*, **49**, 4352 (1984); H. Gusten, G. Heinrich, and H. J. Ache, *J. Photochem.*, **28**, 309 (1985); R. Farwaha, P. de Mayo, J. H. Schauble, and Y. C. Toong, *J. Org. Chem.*, **50**, 245 (1985); V. Dave, R. Farwaha, P. de Mayo, and J. B. Stothers, *Can. J. Chem.*, **63**, 2401 (1985).

2) H. D. Breuer and H. Jacob, *Chem. Phys. Lett.*, **73**, 172 (1980); H. D. Breuer, H. Jacob, and G. Gunster, *Appl. Opt.*, **21**, 41 (1982).

3) M. A. Mostoslavskii and V. E. Nazar'ko, *Zh. Priskl. Khim.*, **59**, 1377 (1986); *Chem. Abstr.*, **106**, 83779s (1987).

4) T. Takahashi, Y. Taniguchi, K. Umetani, H. Yokoshi, M. Hashimoto, and T. Kano, *Jpn. J. Appl. Phys.*, **24**, 173 (1985).

5) J. H-Mason and F. G. Mann, *J. Chem. Soc.*, **1942**, 404.

6) E. E. Wegner and A. W. Adamson, *J. Am. Chem. Soc.*, **88**, 394 (1966).

7) D. Fassler, M. Raddatz and D. Bazold, *Z. Chem.*, **24**, 411.

8) The pK_a value of silica gel used was determined to be in the range of 4.8 and 3.3 by a combination of methyl red and methyl yellow with butylamine.

9) W. I. Gilbert, J. Turkevich, and E. S. Wallis, *J. Org. Chem.*, **3**, 611 (1939).

10) G. S. Egerton and G. Galil, *J. Soc. Dyers Colour.*, **78**, 167 (1962).

Chiral Aryl Grignard Reagents-Generation and Reactions with Carbonyl Compounds

Makoto KAINO, Kazuaki ISHIHARA, and Hisashi YAMAMOTO*
Department of Applied Chemistry, Faculty of Engineering,
Nagoya University, Chikusa, Nagoya 464-01
(Received May 19, 1989)

Synopsis. Chiral aryl Grignard reagents are generated in situ from homochiral 2-halobenzaldehyde acetal, *t*-butyllithium, and magnesium bromide. These reagents react with aromatic aldehydes to moderate diastereoselectivities.

The homochiral acetal method plays an increasingly important role in asymmetric synthesis.[1] We have shown that the Lewis acid catalyzed coupling of homochiral acetals with various nucleophilic organometallic reagents proceeds in a highly diastereoselective manner, ultimately providing a route for generating chiral secondary alcohols in high chemical and optical yields.[2,3] Especially six-membered ring acetals derived from (2*R*,4*R*) or (2*S*,4*S*)-2,4-pentanediols react with excellent diastereoselectivities to give products from which the chiral auxiliary is easily removed.[3] Asymmetric induction produced by the acetal derived from (2*R*,4*R*)-2,4-pentanediol is ascribed to a stereospecific coordination of the Lewis acid to one of the acetal oxygens.

As part of a program aimed at exploring a scope and limitations of homochiral acetal methodology, we now report diastereoselective addition of Grignard reagents which have an adjacent homochiral acetal group.

Results and Discussion

Homochiral aryl Grignard reagent **2** was readily prepared as shown in Scheme 1: Acetalization of 2-bromobenzaldehyde with (−)-(2*R*,4*R*)-2,4-pentanediol, lithiation with *t*-butyllithium, and finally transmetallation with magnesium bromide. The reactions of the Grignard reagent **2** with various carbonyl compounds were carried out in toluene-ether at −78 °C. Some of our results are listed in Table 1. Using an aromatic carbonyl compound as the electrophile, the Grignard reagent **2** gave high diastereoselectivity providing the predominant product **3a** (Entries 1, 4, and 5). The less stereoselectivity, on the other hand, was obtained in the reactions with the other organometallic reagents (Entries 2, 3, and 10) and the reactions with aliphatic aldehydes (Entries 6 and 8).

Evidence for the stereochemical course of the process depicted in Scheme 1 was obtained by the transformation shown in Scheme 2. The product **3a** (R^1=Ph, R^2=H; 88% de) in Entry 1 was converted into phenyl-*o*-tolylmethanol (**6**) whose stereochemistries were already established.[4] Thus, hydrolysis of **3a** with *p*-toluenesulfonic acid afforded hemiacetal **4**, which was further converted to hydrazone **5** by hydrazine. Treatment of **5** by potassium *t*-butoxide gave the compound **6** ($[\alpha]_D^{23}$ =−0.53°, *c* 1.0, benzene) having the *S*-configuration.[4] The stereochemistries of the major product **3a** of the other cases were tentatively assigned from mechanistic analogy.

Table 1. Grignard Reaction via Homochiral Acetal

Entry	Substrate	R^1COR^2 R^1	R^2	Yield(%)	Ratio **3a**:**3b**
1	**1**	Ph	H	91	94 : 6
2[a]				73	72 : 28
3[b]				50	60 : 40
4		*p*-$CF_3C_6H_4$	H	72	89 : 11
5		Ph	Me	34	83 : 17
6		*t*-Bu	H	85	82 : 18
7		PhCH=CH	H	66	74 : 26
8		*c*-Hex	H	69	65 : 35
9	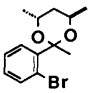	Ph	H	47	82 : 18
10[b]				50	73 : 27

a) $Ti(O\text{-}i\text{-}Pr)_4$ was used instead of $MgBr_2$. b) R^1COR^2 was added after lithiation.

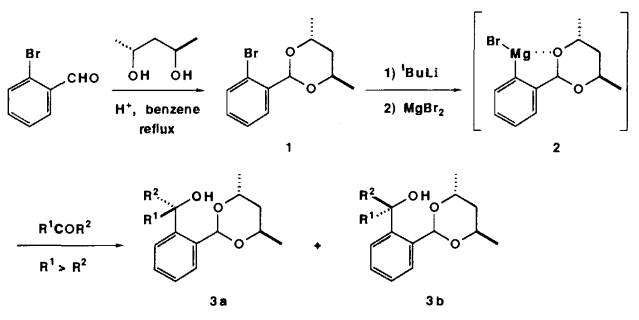

Scheme 1.

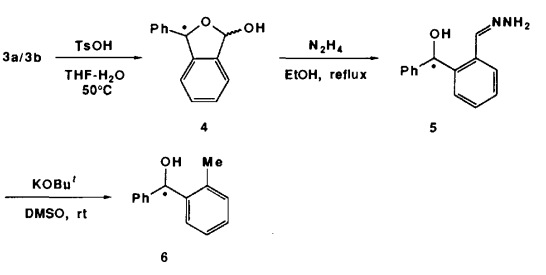

Scheme 2.

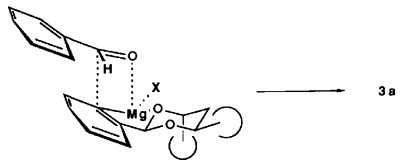

Fig. 1.

Although the detailed stereochemical course is not ascertained, the formation of **3a** as predominant products may be reasonably explained by the attack of the Grignard reagents from *re*-face side in the structure of organometallic reagent on the *re*-face of the carbonyl compounds as shown in Fig. 1. Namely, the magnesium metal is intramolecularly fixed by a stereospecific coordination to one of the acetal oxygen atoms leading to the formation of the five-membered ring structure. Then electrophiles approach to the less hindered side of the magnesium reagent as in the figure.

The study described above illustrates the suitability of optically active alcohols. One obvious advantage of our methodology is that product **3a** could be further transformed into other new chiral compounds by a diastereoselective cleavage of the remaining homochiral acetal group.

Experimental

The IR spectra were determined on a Hitachi 260-10 spectrometer. The ^{1}H NMR spectra were recorded on a Varian Gemini-200 spectrometer, using TMS (tetramethylsilane) as an internal standard. Splitting patterns are indicated as s, singlet; d, doublet; t, triplet; q, quartet; m, multiplet; br, broad. The microanalyses were performed at the Institute of Applied Organic Chemistry, Faculty of Engineering, Nagoya University. Analytical gas-liquid phase chromatography (GLC) was performed on Gaskuro Kogyo model 370 instruments with a flameionization detector and a capillary column of PEG-HT (0.25×25000 mm) using nitrogen as the carrier gas. Ether and tetrahydrofuran (THF) were distilled from benzophenone ketyl. Toluene and benzene were dried over sodium metal. All experiments were carried out under an argon atmosphere. Purification of the product was carried out by column chromatography on silica gel Fuji-Davison BW-300. (−)-(2*R*,4*R*)-2,4-pentanediol was purchased from Wako Pure Chemical Industries Ltd. and used after checking the optical purity; $[\alpha]_D^{23} = -41.2°$ (*c* 9.99, chloroform). Unless otherwise noted, other chemicals were purchased from commercial suppliers and used without further purification.

General Method for Preparation of Homochiral Acetals. The mixture of corresponding aldehyde or ketone (10.0 mmol), *p*-toluenesulfonic acid (10 mg) and (−)-(2*R*,4*R*)-2,4-pentanediol (1,14 g, 11.0 mmol) in 10 ml of benzene was refluxed with continuous azeotropic removal of water for 2 h. The resulting mixture was poured into saturated sodium hydrogen carbonate and the product was extracted twice with hexane. The organic layers were dried over magnesium sulfate and concentrated in vacuo. Purification of the crude oil by column chromatography on silica gel (hexane/ethyl acetate as eluent) afforded the corresponding acetal. The physical data of acetals are listed below.

(4*R*,6*R*)-2-(2-Bromophenyl)-4,6-dimethyl-1,3-dioxane (1): Quantitative yield; IR (CCl_4) 2986, 1366, 1148, 1129, 996 cm^{-1}; ^{1}H NMR ($CDCl_3$) δ=1.31 (d, J=6.2 Hz, 3H, C(equatorial)-H$_3$), 1.40—1.52 (m, 1H, H(equatorial)CH), 1.55 (d, J=6.8 Hz, 3H, C(axial)H$_3$), 1.92—2.10 (m, 1H, H(axial)CH), 4.24 (dqd, J=2.4, 5.9, 11.8 Hz), 1H, OCH(axial)CH$_3$), 4.48 (m, 1H, OCH(equatorial)CH$_3$), 6.13 (s, 1H, O$_2$CH), 7.19 (ddd, 1H, J=1.8, 7.6, 7.6 Hz, ArH), 7.35 (ddd, 1H, J=1.3, 7.7, 7.7 Hz, ArH), 7.53 (dd, 1H, J=1.3, 7.7 Hz, ArH), 7.74 (dd, 1H, J=1.8, 7.7 Hz, ArH). Anal. ($C_{12}H_{15}O_2Br$) C, H.

(4*R*,6*R*)-2-(2-Bromophenyl)-2,4,6-trimethyl-1,3-dioxane: Quantitative yield; IR (neat) 3000, 2950, 2375, 2350, 1460, 1440, 1385, 1378, 1275, 1245, 1185, 1175, 1130, 1030, 970, 765 cm^{-1}; ^{1}H NMR ($CDCl_3$) δ=1.26 (d, J=2.6 Hz, 3H, C(equatorial)-H$_3$), 1.29 (d, J=2.6 Hz, 3H, C(axial)H$_3$), 1.46—1.67 (m, 2H, CH$_2$), 1.70 (s, 3H, O$_2$CCH$_3$), 3.55—3.72 (m, 1H, OCH(axial)-CH$_3$), 4.12—4.29 (m, 1H, OCH(equatorial)CH$_3$), 7.14 (ddd, J=1.8, 7.6, 7.6 Hz, 1H, ArH), 7.32 (ddd, J=1.4, 7.6, 7.6 Hz, 1H, ArH), 7.61 (dd, J=1.4, 7.8 Hz, 1H, ArH), 7.81 (dd, J=1.8, 7.8 Hz, 1H, ArH). Anal. ($C_{13}H_{17}O_2Br$) C, H.

General Procedure for the Grignard Type Coupling of the Homochiral Acetal. To a solution of the acetal (0.5 mmol) in toluene (3 ml) was added *t*-butyllithium (0.26 ml, 0.6 mmol, 2.32 mol dm^{-3} in pentane solution) at −78 °C and the resulting yellow solution was stirred at 0 °C for 30 min. After cooling to −78 °C, a solution of magnesium bromide (1.0 mmol) in ether (3 ml) (prepared in another flask from magnesium turnings (29.2 mg, 1.2 mmol) and 1,2-dibromoethane (0.0862 ml, 1.0 mmol) at room temperature for 30 min) was added at −78 °C, and after 30 min, the corresponding aldehyde (0.5 mmol) was added at the same temperature. The mixture was sirred at −78 °C for 30 min, poured into aqueous ammonium chloride, extracted with ether, and dried over magnesium sulfate. Evaporation of solvents and purification of the residue by column chromatography on silica gel (hexane/ethyl acetate as eluent) gave the corresponding hydroxy acetals (**3a** and **3b**). The diastereomeric ratio of the adducts was determined by ^{1}H NMR. The physical properties and analytical data of the adducts obtained are listed below.

(4*R*,6*R*)-4,6-Dimethyl-2-[2-(α-hydroxybenzyl)phenyl]-1,3-dioxane (**3**, Entries 1, 2, and 3): IR (CCl_4) 3461 (OH), 2999, 2956, 1453, 1381, 1156, 1134, 1106, 1036, 1019, 996, 763, 696 cm^{-1}; ^{1}H NMR ($CDCl_3$) δ=1.30 (d, J=6.2 Hz, 3H, C(equatorial)H$_3$), 1.47 (d, J=7.0 Hz, 3H, C(axial)H$_3$), 1.97—2.12 (m, 1H, H(axial)CH), 1.33—1.43 (m, 1H, H(equatorial)CH), 3.72 (d, J=3.5 Hz, 1H, OH (**3a** isomer)), 3.95 (d, J=4.8 Hz, 1H, OH (**3b** isomer)), 4.21 (dqd, J=2.2, 6.2, 12.2 Hz, 1H, OCH(axial)-CH$_3$), 4.48—4.60 (m, 1H, OCH(equatorial)CH$_3$), 5.92 (s, 1H, O$_2$CH (**3b** isomer)), 6.08 (s, 1H, O$_2$CH (**3a** isomer)), 6.34 (d, J=4.8 Hz, 1H, CHOH (**3b** isomer)), 6.43 (d, J=3.5 Hz, 1H, CHOH (**3a** isomer)), 7.10—7.65 (m, 9H, ArH). Anal. ($C_{19}H_{22}O_3$) C, H.

(4*R*,6*R*)-4,6-Dimethyl-2-[2-(4-trifluoromethyl-α-hydroxybenzyl)phenyl]-1,3-dioxane (**3**, Entry 4): IR (neat) 3400 (OH), 2975, 2930, 2880, 1615, 1455, 1410, 1375, 1320, 1140, 1020, 925, 860, 810, 758 cm^{-1}; ^{1}H NMR ($CDCl_3$) δ=1.27 (d, J=6.0 Hz, 3H, C(equatorial)H$_3$), 1.47 (d, J=7.2 Hz, 3H, C(axial)H$_3$), 1.39—1.53 (m, 1H, H(equatorial)CH), 1.95—2.10 (m, 1H, H(axial)CH), 3.91 (d, J=3.7 Hz, 1H, OH (**3a** isomer)), 3.93 (d, J=2.6 Hz, 1H, OH (**3b** isomer)), 4.13—4.28 (m, 1H, OCH(axial)CH$_3$), 4.44—4.57 (m, 1H, OCH(equatorial)-CH$_3$), 5.92 (s, 1H, O$_2$CH (**3b** isomer)), 6.05 (s, 1H, O$_2$CH (**3a** isomer)), 6.44 (d, J=3.7 Hz, 1H, CHOH (**3b** isomer)), 6.51 (d, J=2.6 Hz, 1H, CHOH (**3a** isomer)), 6.97—7.65 (m, 8H, ArH). Anal. ($C_{20}H_{21}O_3F_3$) C, H.

(4*R*,6*R*)-4,6-Dimethyl-2-[2-(1-hydroxy-1-phenylethyl)phenyl]-1,3-dioxane (**3**, Entry 5): IR (neat) 3423, 2993, 2943, 1443, 1373, 1155, 1135, 1036, 985, 925, 758, 700 cm^{-1}; ^{1}H NMR ($CDCl_3$) δ=1.08 (d, J=8.0 Hz, 3H, C(equatorial)H$_3$), 1.28 (d,

J=8.0 Hz, 3H, C(axial)H_3), 1.25—1.5 (m, 1H, H(equatorial)-CH), 1.75—2.0 (m, 1H, H(axial)CH), 3.46—3.66 (m, 1H, OCH(axial)CH_3), 4.24—4.41 (m, 1H, OCH(equatorial)CH_3), 5.31 (s, 1H, O_2CH (**3b** isomer)), 5.61 (s, 1H, O_2CH (**3a** isomer)), 6.79—8.4 (m, 9H, ArH). Anal. ($C_{20}H_{24}O_3$) C, H.

(4*R*,6*R*)-4,6-Dimethyl-2-[2-(1-hydroxy-2,2-dimethylpropyl)-phenyl]-1,3-dioxane (**3**, Entry 6): IR (neat) 3450, 2970, 2950, 2880, 1372, 1125, 1031, 983, 753 cm^{-1}; ^1H NMR ($CDCl_3$) δ=0.97 (s, 9H, *t*-Bu), 1.25 (d, J=6.2 Hz, 3H, C(equatorial)H_3), 1.46 (d, J=7.0 Hz, C(axial)H_3), 1.39—1.51 (m, 1H, H(axial)CH), 1.92—2.08 (m, H(equatorial)CH), 2.16 (d, J=2.6 Hz, 1H, OH (**3a** isomer)), 2.27 (d, J=2.0 Hz, 1H, OH (**3b** isomer)), 4.16 (dqd, J=2.2, 6,2, 12.4 Hz, OCH(axial)CH_3), 4.40—4.54 (m, 1H, OCH(equatorial)CH_3), 4.83—4.86 (m, 1H, CHOH), 6.22 (s, 1H, O_2CH), 7.26—7.75 (m, 4H, ArH). Anal. ($C_{17}H_{16}O_3$), C, H.

(4*R*,6*R*)-4,6-Dimethyl-2-[2-(1-hydroxy-3-phenyl-2-propenyl)-phenyl]-1,3-dioxane (**3**, Entry 7): IR (neat) 3450, 3040, 2980, 2945, 2880, 1500, 1450, 1408, 1380, 1159, 1135, 1108, 1041, 990, 928, 760, 699 cm^{-1}; ^1H NMR ($CDCl_3$) δ=1.30 (d, J=6.0 Hz, C(equatorial)H_3), 1.43—1.58 (m, 1H, H(equatorial)CH), 1.52 (d, J=6.8 Hz, 3H, C(axial)H_3), 1.98—2.14 (m, 1H, H(axial)CH), 3.58 (d, J=3.0 Hz, 1H, OH (**3a** isomer)), 3.66 (d, J=3.4 Hz, OH (**3b** isomer)), 4.26 (dqd, J=2.6, 6.0, 12.0 Hz, OCH(axial)-CH_3), 4.53 (m, 1H, OCH(equatorial)CH_3), 5.94—5.99 (m, 1H, CHOH), 6.15 (s, 1H, O_2CH), 6.52 (dd, J=4.6, 16.0 Hz, CH=CHPh), 6.88 (dd, J=1.7 Hz, 16.0 Hz, CH=CHPh), 7.21—7.63 (m, 9H, ArH). Anal. ($C_{21}H_{24}O_3$) C, H.

(4*R*,6*R*)-4,6-Dimethyl-2-[2-(cyclohexylhydroxymethyl)phenyl]-1,3-dioxane (**3**, Entry 8): IR (neat) 3443, 2973, 2918, 2700, 1440, 1373, 1148, 1125, 1100, 1033, 980, 918, 753 cm^{-1}; ^1H NMR ($CDCl_3$) δ=1.28 (d, J=6.0 Hz, 3H, C(equatorial)H_3), 1.49 (d, J=6.8 Hz, 3H, C(axial)H_3), 1.92—2.08 (m, 1H, H(axial)CH), 0.89—2.18 (m, 12H, C_6H_{11} and H(equatorial)CH), 2.49—2.54 (m, 1H, OH), 4.20 (dqd, J=2.1, 6.0, 12.0 Hz, 1H, OCH(axial)CH_3), 4.40—4.54 (m, 1H, OCH(equatorial)CH_3), 4.72 (dd, J=2.6, 8.0 Hz, 1H, CHOH (**3b** isomer)), 4.80 (dd, J=2.6, 8.2 Hz, CHOH (**3a** isomer)), 6.08 (s, 1H, O_2CH (**3a** isomer)), 6.12 (s, 1H, O_2CH (**3b** isomer)), 7.24—7.67 (m, 4H, ArH). Anal. ($C_{19}H_{28}O_3$) C, H.

(4*R*,6*R*)-2,4,6-Trimethyl-2-[2-(α-hydroxybenzyl)phenyl]-1,3-dioxane (**3, Entries 9 and 10**): IR (neat) 3500, 2980, 2948, 1450, 1382, 1248, 1178, 1162, 1121, 1039, 1019, 962, 921, 765, 739, 700 cm^{-1}; ^1H NMR ($CDCl_3$) δ=1.25—1.30 (m, 6H, 2CHCH_3), 1.52—1.82 (m, 2H, CH_2), 1.78 (s, 3H, O_2CCH_3), 3.70—3.81 (m, 1H, OCH(axial)CH_3), 4.02 (d, 1H, J=4.0 Hz, OH), 4.21—4.32 (m, 1H, OCH(equatorial)CH_3), 6.40 (d, J=3.8 Hz, 1H, CHOH (**3a** isomer)), 6.61 (d, J=5.0 Hz, 1H, CHOH (**3b** isomer)), 6.98—7.66 (m, 9H, ArH). Anal. ($C_{20}H_{24}O_3$) C, H.

Procedure for the Conversion of 3a/3b to 6. The mixture of **3a**/**3b** (94:6, 1.24 g, 4.2 mmol), *p*-toluenesulfonic acid (200 mg), water (15 ml), and THF (15 ml) was stirred at 50 °C for 5 h. Then the mixture was poured into saturated sodium hydrogen carbonate aqueous solution and extracted with ether. The combined extracts were dried over magnesium sulfate, filtered, and evaporated. Column chromatography (gradient elution, hexane/ethyl acetate, 5:2) gave **4** as a colorless oil (0.863 g, 98% yield).

To a solution of **4** (0.863 g, 4.1 mmol) prepared as detailed above in ethanol was added hydrazine monohydrate (0.971 ml, 20 mmol) at room temperature. After warming to 50—70 °C, the mixture was stirred at the same temperature for 8 h. After cooling to room temperature, the resulting solution was concentrated in vacuo. Column chromatography (gradient elution, Et_2O) gave **5** as a colorless oil (0.731 g, 79% yield).

To a rapidly stirred mixture of sublimed potassium *t*-butoxide and anhydrous dimethyl sulfoxide (20 ml) was added a solution of **5** in anhydrous dimethyl sulfoxide (20 ml) in very small portions over 1 h period. The solution turned deep green. Stirring was continued for 30 min. It was worked up with water and extracted with dichloromethane. The organic layer was washed with water, dried, and concentrated in vacuo. Column chromatography (gradient elution, benzene) gave **6** (455 mg, 71% yield).

3-Phenyl-2-oxaindan-1-ol (**4**): ^1H NMR ($CDCl_3$) δ=3.51 and 3.57 (d, J=7.4 Hz, 1H, OH), 6.13 (s, 1H, CHPh (trans isomer)), 6.36 (d, J=1.7 Hz, 1H, CHPh (cis isomer)), 6.61 (d, J=7.4 Hz, 1H, CHO_2 (trans isomer)), 6.72 (dd, J=1.7, 7.4 Hz, 1H, CHO_2), 7.05—7.53 (m, 9H, ArH).

2-(α-hydroxybenzyl)benzaldehyde Hydrazone (**5**): ^1H NMR ($CDCl_3$) δ=5.49 (br, 3H, NH_2 and OH), 5.99 (s, 1H, PhCH), 7.10—7.44 (m, 9H, ArH), 7.82 (s, 1H, CH=N).

Phenyl-*o*-tolylmethanol (**6**): ^1H NMR ($CDCl_3$) δ=2.30 (d, J=5.0 Hz, 1H, OH), 2.25 (s, 3H, CH_3), 6.00 (d, J=5.0 Hz, 1H, CHOH), 7.12—7.55 (m, 9H, ArH). The %ee of this compound ($[\alpha]_D^{23}$=−0.53°, *c* 1.0, benzene), determined from ^1H NMR by a shift reagent Eu(hfc)$_3$, was 72%.

References

1) D. Seebach, R. Imwinkelried, and T. Weber, "Modern Synthetic Methods 1986, Vol. 4," ed by R. Scheffold, Springer-Verlag Berlin Heidelberg (1986), pp. 191—216.

2) J. Fujiwara, Y. Fukutani, M. Hasegawa, K. Maruoka, and H. Yamamoto, *J. Am. Chem. Soc.*, **106**, 5004 (1984).

3) A. Mori, J. Fujiwara, K. Maruoka, and H. Yamamoto, *Tetrahedron Lett.*, **24**, 4581 (1983); A. Mori, J. Fujiwara, K. Maruoka, and H. Yamamoto, *J. Organomet. Chem.*, **285**, 83 (1983); K. Ishihara, A. Mori, I. Arai, and H. Yamamoto, *Tetrahedron Lett.*, **27**, 983 (1986); A. Mori, K. Ishihara, and H. Yamamoto, *ibid.*, **27**, 987 (1986); A. Mori, K. Ishihara, I. Arai, and H. Yamamoto, *Tetrahedron*, **43**, 755 (1987).

4) (*R*)-(+)-Phenyl-*o*-tolylmethanol, 85% ee, was reported to give $[\alpha]_D^{25}$=+0.38° (*c* 1.0, benzene): D. Seebach, A. K. Beck, S. Roggo, and A. Wonnacott, *Chem. Ber.*, **118**, 3673 (1985).

Electrogenerated Acid-Catalyzed Michael Reaction of Enol Silyl Ethers and Ketene Silyl Acetals to α,β-Unsaturated Carbonyl Compounds

Tsutomu INOKUCHI, Yuji KUROKAWA, Masahiko KUSUMOTO, Shinichi TANIGAWA, Sadahito TAKAGISHI, and Sigeru TORII*

Department of Applied Chemistry, Faculty of Engineering, Okayama University, Okayama 700

(Received June 5, 1989)

Synopsis. 1,5-Dicarbonyl compounds and their enol silyl ethers were prepared by the reaction of α,β-unsaturated ketones and enol silyl ethers or ketene silyl acetals by using an electrogenerated acid (EG acid) as a catalyst. Similar reaction of 1-trimethylsiloxy-1,3-butadiene with enones produced six-membered adducts as the result of a double-Michael process.

The conjugate-addition of basic enolates to α,β-unsaturated carbonyl compounds (i.e. the Michael reaction) is an important tactics for the preparation of 1,5-dicarbonyl compounds.[1] Recently, the reaction has been greatly improved by using enol silyl ethers as an equivalent of enolates in the presence of a stoichiometric amount of Lewis acids such as $TiCl_4$, $Ti(OC_3H_7\text{-}i)_4$, and $SnCl_4$ (the Mukaiyama-Michael reaction),[2] which may suppress side-reactions, e.g. self-condensation, proton transfer, 1,2-addition, and so on. Cesium fluoride (CsF) can catalyze 1,4-addition of enol silyl ethers in a heterogeneous medium.[3] Besides these reagents, homogeneous catalysts such as tris(dimethylamino)sulfonium difluorotrimethylsiliconate (TAS-F)[4] and a number of triphenylmethyl (trityl) salts[5] have currently been developed in order to achieve the 1,4-addition stereoselectively, giving rise to the adducts as a form of enol silyl ethers.

In the preceding paper, we reported the electrogenerated acid (EG acid)-catalyzed aldol reactions, cyanations, allylations, and hydride additions of organosilicon compounds.[6] In continuation of our study on EG acid-catalyzed carbon-carbon bond making reactions, we describe here the EG acid-catalyzed Michael reaction of α,β-unsaturated kenones with enol silyl ethers or ketene silyl acetals and their stereochemical product distributions.

Procedures employed in the EG acid-catalyzed Michael reaction are as follows: (1) The method A is based on the concurrent electrolysis of enol silyl ethers and enones in a CH_2Cl_2–$LiClO_4$–Bu_4NClO_4–(Pt) system.[6] (2) The method B is relied on the treatment with the pre-generated EG acid in an MeCN–$LiClO_4$–Bu_4NClO_4–(Pt) system.[7] (3) The method C is the reaction catalyzed by the electrochemically prepared trityl perchlorate. Prior to the present study, we have found that trityl perchlorate ($TrClO_4$) can be easily provided by the electrooxidation of phenylthiotriphenylmethane in an MeCN–$LiClO_4$–Bu_4NClO_4–(Pt) system in a divided cell.[8]

The reaction of 2-cyclohexenone (**1**) and 1-*t*-butyldimethylsiloxy-1-phenylpropene (**2a**)[9] was examined with EG acids of methods A—C and the results are shown in Table 1. In each case, the reaction proceeded smoothly at −78 °C to give the corresponding 1,4-adducts **3** in good yields. The enol silyl moiety of **3** was subjected to hydrolysis with 10% hydrochloric acid in MeOH–H_2O (1:10 v/v) to give the corresponding 1,5-diketones **4a**, **b**. The anti/syn (threo/erythro)[10] stereochemistry of **4a**, **b** was assigned according to the data reported[5] and then the diastereomeric ratios were estimated by peak areas at δ 1.16, 1.17 and 1.19, 1.21 in ^1H NMR (500 MHz) spectra (Scheme 1). The anti/syn (threo/erythro) ratios of the 1,5-diketones **4a**, **b** are in the range of 76—77:24—23 and these results are virtually same with that[5] obtained with the chemically prepared trityl perchlorate.[11] Similarly, the 1,4-addition of 1-phenyl-1-trimethylsiloxypropene (**2b**)[9] to the enone **1** was attempted with the EG acid (method A) in dichloromethane, giving the corresponding adducts **4a**, **b**, after the hydrolysis of silyl group, in 80% yield with a threo/erythro ratio of 71:29 (Entry 5). In addition to these acid-catalysts, we

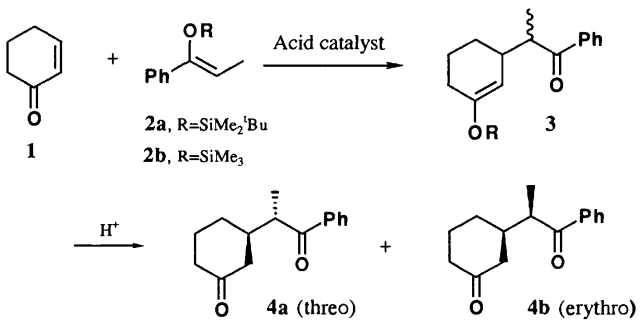

Scheme 1.

Table 1. Michael Reaction of **1** and **2a** to **3**

Entry	Method	Temp(°C)/min	Yield of **3**/%	Threo/Erythro[a]
1	A	−78/30	90	77/23
2	B	−78/20	94	76/24
3	C	−78/90	90	77/23
4	D	−78/90	81	62/38
5[b]	A	−78/60	80	71/29

a) Determined by ^1H NMR (500 MHz). b) Trimethylsilyl ether **2b** was used in place of **2a**.

Table 2. The Reaction of Enones with Enol Silyl Ethers or Ketene Silyl Acetals

Entry	Enones	Enol silyl ethers	Electricity F mol^{-1}	Temp °C	Yield of adducts %	(Isomer ratio)[a]
1			0.05	0	88	
2			0.05	−78	87	(>98/2)
3			0.10	−78	94	
4		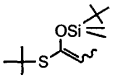	0.10	−78	94	(55/45)
5			0.15	−78	88	

a) Determined by ^{1}H NMR (500 MHz) after hydrolysis to dicarbonyl compounds.

examined triphenylsilyl perchlorate (Ph_3SiClO_4)[12] as an acid-catalyst for the reaction of **1** and **2a** in dichloromethane [method D] and threo/erythro ratio of which has changed to 62:38 [Entry 4] as compared with that obtained by acid-catalysts of Methods A—C.

Among the three different electrochemical procedures, the method A was used for the 1,4-addition of a variety of enones with enol silyl ethers or ketene silyl acetals (Table 2). The reaction of 1-phenyl-2-buten-1-one and enol silyl ether **2a** gave the threo adduct preferentially (Entry 2)[13] in good accordance with the reported trityl cation-catalyzed reaction.[5] Enol silyl ether derived from ethyl acetate and *S*-*t*-butyl thiopropionate added to 2-cyclohexenone (**1**), smoothly.

The reactions of enones **6** with 2-trimethylsiloxy-1,3-butadiene (**5**) as a nucleophile, giving the corresponding six-membered adducts **7** in 51—81% yields by a double-Michael process, were attempted in a CH_2Cl_2–$TrClO_4$ system.[5d,14] Apparently, $TrClO_4$ prepared from stable precursors, e.g. phenylthiotriphenylmethane and lithium perchlorate, by electrolysis can be used for Michael reactions as an effective catalyst as that chemically prepared.

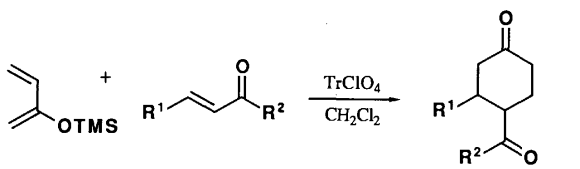

3 **6a**, R^1=Ph, R^2= Me; **6b**, R^1= Me, R^2= Ph

7a 81% (62%)[5d] **7b** 51% (68%)

Experimental

IR spectra were taken on a JASCO FT-IR-5000 spectrometer. NMR spectra were recorded in $CDCl_3$ on a Varian VXR-500 spectrometer.

General Procedure for the Reaction of Enol Silyl Ether with α,β-Unsaturated Ketones (Method A). Into the electrolysis vessel[6] were added $LiClO_4$ (17 mg, 0.15 mmol) and Bu_4NClO_4 (17.1 mg, 0.05 mmol) and the resulting mixture was dried at about 100 °C under vacuum for 1 h and then purged with argon. To this mixture was added a solution of 1-*t*-butyldimethylsiloxy-1-phenylpropene (**2a**, 149 mg, 0.6 mmol) and cyclohexenone (**1**, 48 mg, 0.5 mmol) in CH_2Cl_2 (3 ml). The entire mixture was electrolyzed under a constant current of 6.7 mA cm^{-2} (applied voltage: 10—15 V) at −78 °C. The progress of the reaction was monitored by TLC and the reaction was quenched with Et_3N (3 drops) when the starting **1** has completely disappeared (it took about 30 min and 0.2 F (1F=96480 C)mol^{-1} of electricity has been passed). The volatiles were removed on a rotary evaporator and the residue was purified by column chromatography (SiO_2, hexane–AcOEt 20:1) to give 155 mg (90%) of **3a**: bp 117 °C/0.02 Torr (1 Torr≈133.322 Pa); IR (neat) 3040, 1680 (C=O), 1660 (C=C), 1595, 1575, 1445, 1365, 1250, 1200, 1175, 980, 910, 835, and 780 cm^{-1}; ^{1}H NMR (500 MHz) δ=0.13, 0.14 (s, 6, $SiMe_2$), 0.85, 0.92 (s, 9, $SiCMe_3$), 1.14, 1.16 (d, *J*=7 Hz, 3, CH_3), 1.18—1.30 (m, 1, CH_2), 1.50—1.80 (m, 3, CH_2), 1.90—2.04 (m, 2, CH_2), 2.64 (m, 1, CH), 3.40 (m, 1, PhCH), 4.87 (brs, 1, OC=CH), 7.44—7.48, 7.54—7.57, and 7.93—7.95 (m, 5, PhH).

Hydrolysis of Enol Silyl Ether. To a solution of **3a** (34 mg, 0.1 mmol) in a mixed solution of MeOH (1 ml) and H_2O (10 ml) was added 10% HCl (2 drops). The mixture was stirred at room temperature for 1.5 h and extracted with AcOEt. Washing with brine and concentration followed by column chromatography (SiO_2, hexane–AcOEt) gave 21 mg (91%) of **4a**, **b**: bp 94—95 °C/0.4 Torr; IR (neat) 3066, 1713 (C=O), and 1682 (C=O) cm^{-1}; ^{1}H NMR (500 MHz) δ=1.17, 1.20 (d, *J*=7 Hz, 3, CH_3), 1.43 (m, 1), 1.58—1.68 (m, 1), 1.83—1.91 (m, 1), 1.98—2.06 (m, 1), 2.13 (m, 1), 2.20—2.31 (m, 2), 2.38—2.44 (m, 1), 2.49 (m, 1), 3.47 (m, 1, COCH), 7.42 (m, 1, PhH), 7.57 (m, 1, PhH), and 7.93 (m, 2, PhH).

Preparation of Trityl Perchlorate from Phenylthiotriphenylmethane. A Typical Procedure. Into the anodic compartment of a divided cell separated by a Nafion 324 diaphragm was added a solution of phenylthiotriphenylmethane (176 mg, 0.5 mmol), $LiClO_4$ (110 mg, 1.0 mmol), and Bu_4NClO_4 (340 mg, 1.0 mmol) in MeCN (7 ml). The mixture was electrolyzed at a constant current at 20 mA (applied voltage; 10—20 V) with platinum electrodes (1.5 cm^2) at room temperature. When the electrolysis was initiated, yellow color has appeared in the anolyte. The progress of the

reaction was monitored by TLC and the anolyte was transferred to a Schlenk tube when the sulfide was completely consumed (it took about 150 min and 1.87 F mol^{-1} of electricity has been passed). The mixture was concentrated under vacuum at ca. 0.1 Torr at 0 °C and yellow solids left were dissolved in CH_2Cl_2 (5 ml). A 1.0 ml portion of this solution was used for the following Michael reactions.

Michael Reaction by Using Electrochemically Prepared Trityl Perchlorate. To a solution of **2a** (298 mg, 1.2 mmol) and **1** (96 mg, 1.0 mmol) in CH_2Cl_2 (3 ml) was added a solution of the above trityl perchlorate (1.0 ml) at −78 °C and stirring was continued for 30 min. The mixture was treated with Et_3N (0.5 ml), concentrated under vacuum, and purified by column chromatography (SiO_2, hexane–AcOEt) to give 310 mg (90%) of the adducts **3a**.

Reaction of 1a and 2a by Triphenylsilyl Perchlorate. A solution of **2a** (149 mg, 0.6 mmol) and **1** (48 mg, 0.6 mmol) in CH_2Cl_2 (3 ml) was treated with a 0.2 M Ph_3SiClO_4[11] (1 M=1 mol dm^{-3}) in CH_2Cl_2 (0.3 ml) at −78 °C. After being stirred for 1.5 h at −78 °C, the reaction was quenched with Et_3N (0.3 ml). Concentration under vacuum followed by purification of the residue by column chromatography on SiO_2 (hexane–AcOEt) gave 156 mg (81%) of the adducts **3a** and 12 mg (11%) of the unprotected **4a, b**.

Spectral data of 1,5-dicarbonyl compounds derived from the Michael adducts in Table 2 are as follows.

1,3-Diphenyl-1,5-hexanedione; IR (neat) 1710 (C=O) and 1680 (C=O) cm^{-1}; ^1H NMR (500 MHz) δ=2.00 (s, 3, $COCH_3$), 2.81—2.96 (m, 2, $COCH_2$), 3.26—3.38 (m, 2, $COCH_2$), 3.89 (m, 1, CH), 7.18—7.21, 7.25—7.30, 7.42—7.45, 7.53—7.56, and 7.91—7.92 (m, 10, PhH).

2,3-Dimethyl-1,5-diphenyl-1,5-pentanedione: IR (neat) 3094 and 1682 (C=O) 692 cm^{-1}; ^1H NMR (500 MHz) δ=1.07 (d, J=6.5 Hz, 3, CH_3), 1.23 (d, J=7 Hz, 3, CH_3), 2.70 (m, 1, CH), 2.74 (d, d, J=16, 9.5 Hz, 1, CH_2CO), 3.59—3.65 (m, 1, COCH), 7.39—7.56, and 7.86—7.96 (m, 10, PhH).

Ethyl (3-Oxocyclohexyl)acetate: IR (neat) 1730 (C=O) and 1710 (C=O) cm^{-1}; ^1H NMR (500 MHz) δ=1.25 (t, J=7 Hz, 3, CH_3), 1.41 (m, 1), 1.71 (m, 1), 1.94 (m, 1), 2.02—2.12 (m, 2), 2.21—2.35 (m, 4), 2.38, 2.45 (m, 2, $COCH_2$), and 4.13 (q, 2, OCH_2).

***S-t*-Butyl 2-(3-Oxocyclohexyl)thiopropionate:** IR (neat) 1710 (C=O) and 1670 (COS) cm^{-1}; ^1H NMR (500 MHz) δ=1.09, 1.13 (d, J=7 Hz, 3, CH_3), 1.29—1.42 (m, 1), 1.428, 1.436 (s, 9, $C(CH_3)_3$), 1.55—1.64 (m, 1), 1.90 (m, 1), 1.98—2.08 (m, 2), 2.14 (m, 1), 2.17—2.26 (m, 1), 2.35 (m, 1), and 2.38—2.44 (m, 2).

Ethyl 5-Oxohexanoate: IR (neat) 1730 (COO) and 1710 (C=O) cm^{-1}; ^1H NMR (500 MHz) δ=1.15 (t, J=7 Hz, 3, CH_3), 1.78 (quintet, 2, J=7 Hz, 2, CH_2), 2.04 (s, 3, $COCH_3$), 2.21 (t, J=7 Hz, 2, $COCH_2$), and 2.40 (t, J=7 Hz, 2, $COCH_2$).

Double-Michael Reaction of 2-Trimethylsiloxy-1,3-butadiene (5). To a solution of **5** (284 mg, 2.0 mmol) and the enone **6a** (R^1=Ph, R^2=Me, 146 mg, 1.0 mmol) in CH_2Cl_2 (3 ml) was added a solution of the electrochemically prepared $TrClO_4$ (1.0 ml) in the manner as above at −78 °C. After stirring at −78 °C for 4 h, the mixture was poured into aqueous saturated NH_4Cl and extracted with AcOEt. Usual workup and purification by column chromatography (SiO_2, hexane–AcOEt) gave 174 mg (81%) of 4-acetyl-3-phenylcyclohexanone (**7a**) as solids: mp 63—65 °C (hexane–AcOEt); IR (KBr) 1711 (C=O), 1603 (C=C), and 1584 cm^{-1}; ^1H NMR (500 MHz) δ=1.88 (s, 3, CH_3CO), 1.90—1.98 (m, 1, CH_2), 2.17—2.23 (m, 1, CH_2), 2.45—2.53 (m, 1, CH_2CO), 2.56 (m, 1, CH_2CO), 2.60—2.64 (m, 2, CH_2CO), 3.17 (m, 1, CH), 3.26 (m, 1, CH), and 7.20—7.34 (m, 5, PhH).

4-Benzoyl-3-methylcyclohexanone (7b): mp 58—59 °C (hexane–AcOEt); IR (KBr) 1711 (C=O), 1676, and 1599 (C=C) cm^{-1}; ^1H NMR (500 MHz) δ=0.98 (d, J=6.5 Hz, 3, CH_3), 1.87—1.95 (m, 1, CH), 2.17—2.22 (m, 2, CH_2), 2.38—2.57 (m, 4, CH_2CO), 3.45—3.50 (m, 1, CHCO), 7.50—7.53 (m, 2, PhH), 7.61 (m, 1, PhH), and 7.94—8.01 (m, 2, PhH).

The present work was partially supported by a Grant-in-Aid for Scientific Research on Priority Areas (Advanced Molecular Conversions, No. 01607001) from the Ministry of Education, Science and Culture. We are grateful to the SC-NMR laboratory of Okayama University for experiments with a Varian VXR-500 instrument.

References

1) E. D. Bergmann, D. Ginsburg, and R. Pappo, "Organic Reactions," Vol. 10, p. 179 (1959); H. O. House, "Modern Synthetic Reactions," 2 nd ed, W. A. Benjamin, Menlo Park, California (1972), p. 595.

2) K. Narasaka, K. Soai, and T. Mukaiyama, *Chem. Lett.*, **1974**, 1223; K. Narasaka, K. Soai, and T. Mukaiyama, *Bull. Chem. Soc. Jpn.*, **49**, 779 (1976); K. Saigo, M. Osaki, and T. Mukaiyama, *Chem. Lett.*, **1976**, 163; C. H. Heathcock, M. H. Norman, and D. E. Uehling, *J. Am. Chem. Soc.*, **107**, 2797 (1985).

3) J. Boyer, R. J. P. Corriu, R. Perz, and C. Reye, *Tetrahedron*, **39**, 117 (1983).

4) T. V. RajanBabu, *J. Org. Chem.*, **49**, 2083 (1984).

5) a) S. Kobayashi, M. Murakami, and T. Mukaiyama, *Chem. Lett.*, **1985**, 953; b) T. Mukaiyama, M. Tamura, and S. Kobayashi, *ibid.*, **1986**, 1017; c) T. Mukaiyama, M. Tamura, and S. Kobayashi, *ibid.*, **1986**, 1817; d) T. Mukaiyama, S. Sagawa, and S. Kobayashi, *ibid.*, **1986**, 1821; e) T. Mukaiyama, M. Tamura, and S. Kobayashi, *ibid.*, **1987**, 743.

6) S. Torii, T. Inokuchi, S. Takagishi, H. Horike, H. Kuroda, and K. Uneyama, *Bull. Chem. Soc. Jpn.*, **60**, 2173 (1987).

7) T. Inokuchi, S. Takagishi, K. Ogawa, Y. Kurokawa, and S. Torii, *Chem. Lett.*, **1988**, 1347.

8) Preparation and characterization of trityl salt by the electrolysis will be reported in detail.

9) Enol silyl ethers were prepared by the reaction of the parent ketones or esters with LDA followed by trapping of the enolates with trialkylsilyl chlorides. The compounds **2a** and **2b** were assigned to be more than 99% (*Z*)-isomers, respectively, by ^1H NMR (500 MHz).[15]

10) a) R. Noyori, I. Nishida, and J. Sakata, *J. Am. Chem. Soc.*, **105**, 1598 (1983). b) M. A. Brook, *J. Chem. Educ.*, **64**, 218 (1987).

11) H. J. Dauben, Jr., L. R. Honnen, and K. M. Harmon, *J. Org. Chem.*, **25**, 1442 (1960).

12) G. K. S. Prakash, S. Keyaniyan, R. Aniszfeld, L. Heiliger, G. A. Olah, R. C. Stevens, H.-K. Choi, and R. Bau, *J. Am. Chem. Soc.*, **109**, 5123 (1987).

13) No appreciable amount of stereoisomer has been observed in its ^1H NMR spectra (500 MHz) and stereochemical purity of product was estimated to be more than 98%.

14) M. Ihara and K. Fukumoto, *Yuki Gosei Kagaku Kyokai Shi*, **44**, 96 (1986).

15) P. Brownbridge, *Synthesis*, **1983**, 1.

A Facile Synthesis of 4-Hydroxy- and 4-Aminoindoles through Corresponding Indolines

Hideo TANAKA, Yasuo MURAKAMI, Takao AIZAWA, and Sigeru TORII*
Department of Applied Chemistry, Faculty of Engineering,
Okayama University, Tsushima Naka, Okayama 700
(Received June 29, 1989)

Synopsis. 2-(2,6-Diaminophenyl)ethanol can be conducted to 4-hydroxyindoline under heating in aqueous 70% phosphoric acid, and to 4-aminoindoline under heating in aqueous 30% sulfuric acid. Both 4-hydroxy- and 4-aminoindoles were obtained by dehydrogenation of the indolines under refluxing in 1,4-dimethylbenzene over palladium on charcoal.

Indoles bearing an oxygen or nitrogen atom at the 4-position have been of interest for many years because of their potent and diverse therapeutical activities.[1] 4-Amino- and 4-hydroxyindoles (**5** and **6**) are used as versatile intermediates in the synthesis of therapeutical compounds. Most of electrophilic substitution reactions of indoles take place at the 4 and 7-positions and only the tactics reaching the desired 4-substituted indoles **5** and **6** have been required.[2,3] 4-Hydroxyindole (**6**) has been synthesized from 6-benzyloxy-2-nitrotoluene by one-carbon homologation with *N,N*-dimethylformamide dimethyl acetal and subsequent hydrogenative cyclization.[3d,e] 2,6-Dinitrotoluene (**1**) has also been used for the preparation of 4-hydroxyindole (**6**) via 4-aminoindole (**5**).[3f] In the practical sense, however, these procedures are not necessarily satisfactory, suffering insufficient overall yields and/or the use of the expensive chemicals. Herein, we describe a short-cut route to 4-amino- and 4-hydroxyindoles (**5** and **6**) from 2,6-dinitrotoluene (**1**), which involves 1) one-carbon homologation of **1** with formaldehyde followed by the hydrogenation (**2a**→**2b**) and 2) subsequent cyclization, giving the indoline **3**, or a one-pot cyclization-hydroxylation reaction, affording the indoline **4** (Scheme 1).

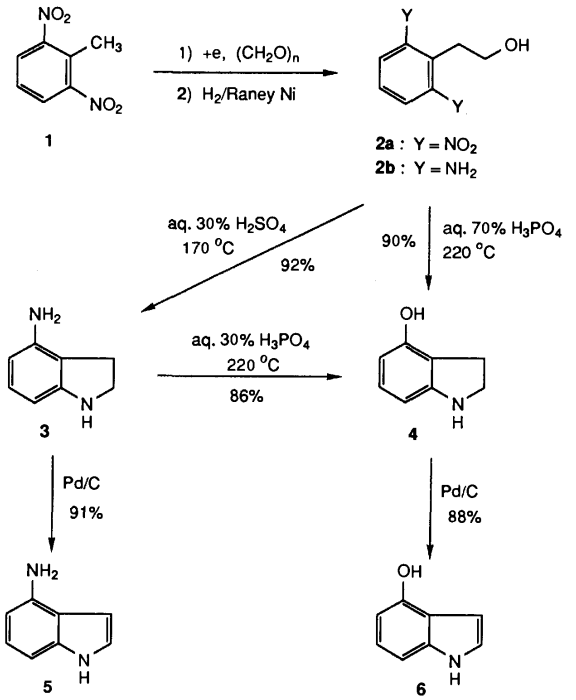

Scheme 1.

One-carbon homologation of 2,6-dinitrotoluene (**1**) with paraformaldehyde was successfully performed by the action of an electrochemically generated base (EG base). In the previous paper,[4] we have disclosed an EG base-induced hydroxymethylation of the side chain of 2-nitrotoluene with paraformaldehyde. The smooth extension of the method to **1** was verified by obtaining 2-(2,6-dinitrophenyl)ethanol (**2a**) in 94% yield after passage of a catalytic amount of electricity (0.06 F mol^{-1}) in a DMF–Et_4NOTs–$(CH_2O)_n$ system. Hydrogenation of **2a** over Raney Ni catalyst gave 2-(2,6-diaminophenyl)ethanol (**2b**) in 86% yield.

The conversion of **2b** into the 4-amino- and 4-hydroxyindolines (**3** and **4**) was performed by heating with proper acids, respectively (Scheme 1). The dehydrogenative cyclization of **2b** to **3** was achieved by heating in a sealed tube with an aqueous 30% sulfuric acid at 170 °C, affording 4-aminoindoline (**3**) in 92% yield. A similar result was obtained by heating of **2b** in an aqueous 1% phosphoric acid at 220 °C (86% yield).

The hydrolysis of the amino moiety of **3** was, at first, carried out by the conventional diazotization-hydrolysis reaction with sodium nitrate in aqueous 60% sulfuric acid (Method A). The satisfactory yields (>77%) were only achieved under high dilution conditions (<1%). When the concentration of **3** rose up to 3%, the yield of **4** decreased to less than 65%. Consequently, we turned our attention to the hydrolysis of 4-aminoindoline (**3**) to 4-hydroxyindoline (**4**) by heating with acids (Method B). The results obtained with various acids are shown in Table 1. Among the

Table 1. Effect of Acid in the Hydrolysis of 4-Aminoindoline (**3**) to 4-Hydroxyindoline (**4**)[a]

Entry	Acid	Yield of **4**	Recovered **3**
		%[b]	%[b]
1	H_3PO_4	86	3
2	H_2SO_4	23	72
3	HCl	30	60
4	H_3BO_4	7	70
5	NaH_2PO_4	Trace	72
6	$NaHSO_3$	—[c]	—
7	None	—	93

a) Carried out with **3** (2.2 mmol) in aqueous 30% acids (6 g) at 220 °C for 24 h. b) Isolated yields. c) A complex mixture of decomposition products was formed.

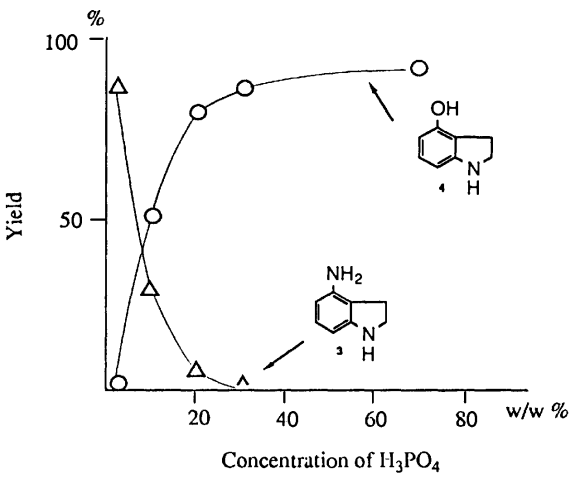

Fig. 1. Effect of concentration of H_3PO_4 on the conversion of 2-(2,6-diaminophenyl)ethanol (**2b**) into 4-amino and 4-hydroxyindolines (**3** and **4**). All experiments were carried out with **2b** (2 mmol) in aqueous H_3PO_4 (6 g) at 220 °C for 24 h.

acids, aqueous 30% phosphoric acid is the best choice, affording the desired product **4** in 86% yield (Entry 1), while sulfuric acid, hydrochloric acid, and boric acid are less effective (Entries 2—4). Sodium dihydrogenphosphate and sodium hydrogensulfite are not feasible for the present purpose (Entries 4 and 5).

As mentioned above, aqueous phosphoric acid is effective both for cyclization of **2b** into 4-aminoindoline (**3**) and for hydrolysis of **3** into 4-hydroxyindoline **4**. This finding, in turn, spurred us to examine a one-pot transformation of 2-(2,6-diaminophenyl)-ethanol (**2b**) into 4-hydroxyindoline (**4**) by heating with an aqueous 1—70% phosphoric acid at 220 °C. As illustrated in Fig. 1, the distribution of the products **3** and **4** was highly dependent on the concentration of phosphoric acid. In fact, the exclusive conversion to **4** was attained with aqueous 70% phosphoric acid.

The 4-substituted indolines **3** and **4** can be readily converted to the corresponding indoles **5** (91%) and **6** (88%) by heating to reflux in *p*-xylene over palladium on charcoal.[5,6] As an alternative route to **6**, hydrolysis of **5** was also attempted under the same conditions as for the hydrolysis of **3**, but all the trials resulted in the formation of a complex mixture.

In conclusion, the preparation of 4-amino- and 4-hydroxyindoles (**5** and **6**) from 2,6-dinitrotoluene (**1**) has been achieved in satisfactory overall yields (64—67%). Further transformation of **5** and **6** into the useful therapeutical compounds are in progress.

Experimental

IR spectra were recorded on a JASCO IRA-1 grating spectrometer and ^1H NMR spectra were measured at 60 MHz with a Hitachi R-24 spectrometer. Chemical shifts are expressed in parts per million downfield from Me_4Si as an internal reference. Melting points are uncorrected. Column chromatography was carried out on Wako gel C-200 (silica gel) with hexane–EtOAc as an eluent.

2-(2,6-Dinitrophenyl)ethanol (2a): Into both anode and cathode compartments of an H-shaped divided cell[4] was placed a DMF solution of Et_4NOTs (420 mg/8 ml each). To the cathode compartment were added 2,6-dinitrotoluene (**1**) (1.04 g, 5.7 mmol) and $(CH_2O)_n$ (220 mg, 7.3 mmol on the basis of formaldehyde). The mixture was electrolyzed under a constant current of 3.3 mA cm^{-2} at room temperature for 50 min (0.06 F mol^{-1}). The catholytes were poured into aqueous 5% HCl and extracted with EtOAc. The extracts were washed with brine, dried (Na_2SO_4), and concentrated in vacuo. The residue was chromatographed to afford **2a**[5b] (1.14 g, 94%): mp 69—71 °C; ^1H NMR ($CDCl_3$) δ=2.05 (1H, s, OH), 3.27 (2H, t, J=6 Hz, $ArCH_2$), 3.90 (2H, t, J=6 Hz, CH_2O), 7.35—8.05 (3H, m, ArH); IR ($CHCl_3$) 3600, 3010, 2885, 1540, 1365, 1050, 910, 705 cm^{-1}.

2-(2,6-Diaminophenyl)ethanol (2b): To a stirred suspension of Raney Ni (W-2, 12.5 g) in MeOH (80 ml) was added at 55—65 °C a solution of 2-(2,6-dinitrophenyl)ethanol (**2a**) (40 g, 0.19 mol) in methanol (180 ml) over a period of 2 h under H_2 atmosphere (5—9 atm). After stirring for additional 2 h, the catalysts were removed by filtration and washed with methanol. The filtrate and washings were combined and concentrated in vacuo. The residue was recrystallized from ethanol to give **2b**[7] (24.7 g, 86%): mp 109—110 °C; ^1H NMR (acetone-d_6) δ=2.63 (2H, t, J=6 Hz, $ArCH_2$), 3.65 (2H, t, J=6 Hz, CH_2O), 4.03 (5H, br s, NH_2, OH), 5.9—6.7 (3H, m, ArH); IR (Nujol) 3370, 3200, 1595, 1463, 1050, 858, 733 cm^{-1}.

4-Aminoindoline (3): 2-(2,6-Diaminophenyl)ethanol (**2b**) (300 mg, 1.97 mmol) and 30% aqueous sulfuric acid (6 g) were charged to a sealed tube and heated at 170 °C for 24 h. The acidic solution was neutralized with aqueous 40% NaOH and extracted with EtOAc. The extracts were washed with brine, dried (Na_2SO_4), and concentrated in vacuo. The residue was chromatographed to give **3**[5b] (245 mg, 92%): mp 44—45 °C; ^1H NMR ($CDCl_3$) δ=2.79 (2H, t, J=8 Hz, $ArCH_2$), 3.1—3.7 (5H, m, CH_2N, NH, NH_2, CH_2N), 5.95 (1H, d, J=8 Hz, ArH), 6.0 (1H, d, J=8 Hz, ArH), 6.7 (1H, t, J=8 Hz, ArH); IR (CH_2Cl_2) 3360, 1633, 1500, 1485, 1315, 1065 cm^{-1}.

4-Hydroxyindoline (4): Method A. To a solution of 4-aminoindoline (**3**) (112 mg, 0.83 mmol) in 70% aqueous H_2SO_4 (11 g) was added 4% aqueous $NaNO_2$ (1.5 ml, 1.0 equiv) at 0—10 °C over a period of 1 h. After stirring at 0—5 °C for 10 h, sulfamic acid (10 mg) was added. The stirring was continued at room temperature for 1 h and at 65—75 °C for additional 4 h. The acidic solution was neutralized with 10% aqueous 40% NaOH and extracted with EtOAc. The extracts were washed with brine, dried (Na_2SO_4) and concentrated in vacuo. The residue was chromatographed to give **4** (86 mg, 77%): mp 139—140 °C (lit,[2c] mp 147 °C).

Method B: 4-Aminoindoline (**3**) (300 mg, 2.24 mmol) and 30% aqueous phosphoric acid (3 g) were charged to a sealed tube. The mixture was heated at 220 °C for 24 h and then cooled to room temperature. The acidic solution was neutralized with aqueous 40% NaOH, extracted with EtOAc. The extracts were washed with brine, dried (Na_2SO_4), and concentrated in vacuo. The residue was chromatographed to afford **4** (260 mg, 86%), whose IR and ^1H NMR spectra are identical with those of **4** obtained above.

Direct Conversion of 2-(2,6-Diaminophenyl)ethanol (2b) to 4-Hydroxyindoline (4): A mixture of 2-(2,6-diaminophenyl)ethanol (**2b**) (300 mg, 1.97 mmol) and 70% aqueous phosphoric acid (3 g) was charged to a sealed tube and heated at 220 °C for 24 h. The mixture was worked up in a similar manner to that described above to give **4** (240 mg, 90%), whose IR and ^1H NMR spectra are identical with those of **4** obtained above.

4-Hydroxyindole (5): A mixture of 4-hydroxyindoline (**4**)

(68 mg, 0.51 mmol) and 10% Pd/C (10 mg), in *o*-xylene (10 ml) was heated to reflux for 2.3 h under N_2 atmosphere. Usual workup of the mixture afforded **5** (59 mg, 88%): mp 98—98.6 °C (lit,[3b] 96—98 °C); ^{1}H NMR (acetone-d_6) δ= 6.3—7.2 (5H, m, ArH, CH=CHN), 8.1 (1H, s, OH), 9.8 (1H, br s, NH); IR (CH_2Cl_2) 3550, 3435, 1590, 1500, 1450, 1355, 1075, 690 cm^{-1}.

4-Aminoindole (6): A mixture of 4-aminoindoline (**3**) (70 mg, 0.52 mmol) and 10% Pd/C (10 mg) in *p*-xylene (2.0 ml) was heated to reflux for 3 h under N_2 atmosphere. Usual workup of the mixture afforded **6** (63 mg, 91%): mp 104—105 °C (lit,[3d] mp 106—108 °C); ^{1}H NMR ($CDCl_3$) δ=3.76 (2H, br s, NH_2), 6.17—7.06 (5H, m, ArH, C=CH–N, ArCH=C), 7.95 (1H, br s, NH); IR (CH_2Cl_2) 3440, 3350, 1618, 1587, 1500, 1405, 1364 cm^{-1}.

References

1) For review: R. J. Sundberg, "Chemistry of Indoles," Academic Press, New York (1970); R. T. Brown, J. A. Joule, and P. G. Sammes, "Comprehensive Organic Chemistry," ed by D. H. R. Barton and W. D. Ollis, Pergamon Press, Oxford (1979), Vol. 4, p. 411; J. E. Saxton, "Indoles," Wiley-Interscience, New York (1983), Part IV.

2) The radical hydroxylation of indoles with hydrogen peroxide, affording a mixture of 4-, 5-, 6-, and 7-hydroxyindoles has been reported: a) J. Gartz, *Pharmazie*, **40**, 356 (1985); b) C. Berrier, J. C. Jacquesy, and M. P. Jouannetaud, and A. Renoux, *Tetrahedron Lett.*, **27**, 4565 (1986); c) *idem*, *New J. Chem.*, **11**, 605 (1987).

3) a) A. Stoll, F. Troxler, J. Peyer, and A. Hofmann, *Helv. Chim. Acta*, **38**, 1452 (1955); b) D. B. Repke, W. J. Ferguson, and D. K. Bates, *J. Heterocycl. Chem.*, **14**, 71 (1977); c) S. Torii, K. Uneyama, T. Onishi, Y. Fujita, M. Ishiguro, and T. Nishida, *Chem. Lett.*, **1980**, 1603; d) L. I. Kruse, *Heterocycles*, **16**, 1119 (1981); e) M. Somei, S. Inoue, S. Tokutake, F. Yamada, and C. Kaneko, *Chem. Pharm. Bull.*, **29**, 726 (1981); f) M. Somei and M. Tsuchiya, *ibid.*, **29**, 3145 (1981); g) R. D. Clark and D. B. Repke, *Heterocycles*, **22**, 195 (1984); h) M. Matsumoto and N. Watanabe, *ibid.*, **22**, 2313 (1984); i) M. Matsumoto, Y. Ishida, and N. Watanabe, *ibid.*, **23**, 165 (1985); j) A. D. Batcho and W. Leimgruber, *Org. Synth.*, **63**, 214 (1985); k) M. E. Krolski, A. F. Renaldo, D. E. Rudisill, and J. K. Stille, *J. Org. Chem.*, **53**, 1170 (1988); and references cited therein.

4) S. Torii, Y. Murakami, H. Tanaka, and K. Okamoto, *J. Org. Chem.*, **51**, 3143 (1986).

5) a) R. R. Hunt and R. L. Rickard, *J. Chem. Soc. C*, **1966**, 344; b) J. Bakke, *Acta Chem. Scand., Ser. B*, **28**, 134 (1974).

6) Direct transformation of 2-(6-halo-2-aminophenyl)-ethanols into 4-haloindoles has been performed by heating with ruthenium catalysts: T. Tsuji, K. T. Huh, Y. Yokohama, and Y. Watanabe, *J. Chem. Soc., Chem. Commun.*, **1986**, 1575.

7) S. T. Rashevskaya, E. S. Kashcheeva, and E. I. Mostoslavskaya, *Zh. Obshch, Khim.*, **33**, 3998 (1963); *Chem. Abstr.*, **60**, 9178e (1964).

Application of Improved Free-Energy Parameters of RNA Stability to Codon-Anticodon Interactions

Naoki SUGIMOTO* and Muneo SASAKI
Department of Chemistry, Faculty of Science, Konan University,
8-9-1 Okamoto, Higashinada-ku, Kobe 658
(Received June 5, 1989)

Synopsis. Free-energy parameters of the RNA duplex stability have been applied in order to investigate the complex between codon oligomers and anticodon loops in transfer RNA. The results suggested that the very large stability of the complex might be due to the stacking interactions of adjacent bases on the codon-anticodon helix and an additional hydrogen-bond formation of the core helix as well as a conformational change of the nucleic acid.

Even at present an interaction between a codon in the messenger RNA and an anticodon in a transfer RNA (tRNA), which is of central importance in the transfer of genetic information from DNA to proteins, still remains a mystery. It has often been found that the codon-anticodon complexes are more stable than found or predicted for two complementary trinucleotides.[1-3] The possible reason for the large stability of the complex was suggested to be the contribution of a base-pair formation between the 5′ adjacent codon base and the 3′ adjacent anticodon base on the helix.[4] However, this explanation can not be applied to complexes containing terminal mismatches or unpaired nucleotides (dangling ends).

Recently, improved thermodynamic parameters for RNA duplex stability[5-9] have been reported by using a nearest-neighbor model.[2] The improvements have permitted the parameters to provide breakthroughs in difficult structure predictions of tRNAs,[10] ribosomal RNAs,[10] a self-splicing intervening sequence,[11] and intermediate complexes of ribozymes.[12,13] In the present study we have applied the improved free-energy parameters of RNA stability to the interaction between codon oligomers and anticodon loops of tRNAs in order to determine the origin of the very large stability of the complexes.

Methods

The measured free-energy changes, ΔG_m, for the formation of codon-anticodon complexes were obtained from the observed association constants, K, for the binding of codon oligonucleotides to $tRNA^{Phe}$ [3,4,14] and $tRNA^{fMet}$ [15] at 273 K:

$$\Delta G_m = -RT\ln K, \quad (1)$$

where R is the gas constant and T is equal to 273 K. The values of ΔG_m for UUCA binding to the CmU-GmAAYA (m, 2′-*O*-methyl ribose; Y, a hypermodified base in $tRNA^{Phe}$) site of dodecamer[4] was also obtained by the same method.

The measured free-energy increments, $\Delta\Delta G_m$, for dangling ends of codon oligonucleotides were obtained by subtracting ΔG_m for codon trinucleotides from ΔG_m for codon tetranucleotides. For example, the value of $\Delta\Delta G_m$ for the AUGA codon oligomer binding to CmU-CAUAA (anticodon loop of $tRNA^{fMet}$) was calculated as being;

$$\Delta\Delta G_m = \Delta G_m(\mathrm{AUGA}) - \Delta G_m(\mathrm{AUG}) = (-21.7) - (-16.3) = -5.4\ \mathrm{kJ\ mol^{-1}},$$

where ΔG_m(AUGA) and ΔG_m(AUG) were the measured free-energy changes for the formation of codon-anticodon complexes of AUGA and AUG with CmUCAU AA, respectively.

The calculated free-energy changes, ΔG_c, for the formation of codon-anticodon complexes were obtained from nearest-neighbor thermodynamic parameters:[5-9]

$$\Delta G_c = \Delta H_c - T\,\Delta S_c, \quad (2)$$

where ΔH_c and ΔS_c are the enthalpy and entropy changes, respectively, and T is the temperature. For example, the value of ΔG_c for an AUG codon oligomer binding to CmUCAUAA (anticodon loop of $tRNA^{fMet}$) was calculated as follows: The calculated entropy change of a core helix formation for $\overrightarrow{\mathrm{CAU}}/\overleftarrow{\mathrm{GUA}}$ was

$$\Delta S_c(\mathrm{core}) = \Delta S_c(\mathrm{initi}) + \Delta S_c(\overrightarrow{\mathrm{CA}}/\overleftarrow{\mathrm{GU}}) + \Delta S_c(\overrightarrow{\mathrm{AU}}/\overleftarrow{\mathrm{UA}}) = (-45) + (-116) + (-65) = -226\ \mathrm{J\ K^{-1}\ mol^{-1}},$$

where ΔS_c(initi) was the entropy change for a helix initiation associated with the formation of the first base pair in the duplex,[6] $\Delta S_c(\overrightarrow{\mathrm{CA}}/\overleftarrow{\mathrm{GU}})$ and $\Delta S_c(\overrightarrow{\mathrm{AU}}/\overleftarrow{\mathrm{UA}})$ were the propagation entropy changes during the formation of each subsequent base pair;[5] the arrows point from the 5′ to the 3′ direction. Similarly, ΔH_c(core)=−67.8 kJ mol^{-1}. Therefore, according to Eq. 2, ΔG_c(core) at 273 K was −6.1 kJ mol^{-1} for the core helix formation. Since the core helix had two dangling bases of 5′U and 3′A in the anticodon loop, $\Delta G_c(\overrightarrow{\mathrm{UC}}/\underline{\mathrm{G}})$ and $\Delta G_c(\overrightarrow{\mathrm{A}}/\overleftarrow{\mathrm{AU}})$ (−0.4 and −2.9 kJ mol^{-1},[7] respectively) had to be added to ΔG_c(core) in order to obtain the total free-energy change, ΔG_c. Consequently, ΔG_c at 273 K was −9.4 kJ mol^{-1} for AUG binding to the anticodon loop of $tRNA^{fMet}$.

Note that in the ΔG_c calculation for a codon binding to the anticodon of $tRNA^{Phe}$ or the CmUGmAAYA site of the dodecamer, two assumptions were used: One was that the stabilization energy of 2′-*O*-methyl ribose was equal to that of the unmodified ribose, and the other was that a dangling Y base which was the hypermodified base in $tRNA^{Phe}$ had the same stabilization energy as the dangling purine base, since the nearest-neighbor energy parameters for the dangling Y

base were not available. These assumptions were reasonable, since they had been applied to the prediction of secondary structures of tRNAs, and the most probable structure, determined by the calculation, was almost consistent with that from phylogenetic data.[10,11]

The calculated free-energy increments, $\Delta\Delta G_c$, by stacking the dangling bases of the codon oligonucleotides were obtained from the literature.[6-9] The values of $\Delta\Delta G_c$ by the fourth base-pair formation between the dangling bases of the codon oligomer and the anticodon loop (shown in parentheses in Table 1) were calculated by the same method for ΔG_c described above. For example, the complex between AUGA and CmUCAUAA had the possibility of an additional A-U base-pair formation on the G-C base pair. The free-energy increment, $\Delta\Delta G_c$, for this fourth base pair was

$$\begin{aligned}\Delta\Delta G_c &= \Delta H(\overrightarrow{GA}/\underleftarrow{CU}) - T\,\Delta S(\overrightarrow{GA}/\underleftarrow{CU}) \\ &= (-55.7) - (273) \times (-148 \times 10^{-3}) \\ &= -15.3\ \text{kJ mol}^{-1},\end{aligned}$$

where $\Delta H(\overrightarrow{GA}/\underleftarrow{CU})$ and $\Delta S(\overrightarrow{GA}/\underleftarrow{CU})$ were the enthalpy- and entropy-changes for forming the A-U base pair on the G-C base pair.

Results and Discussion

The measured free-energy changes, ΔG_m, and the calculated free-energy changes, ΔG_c, for the formation of codon-anticodon complexes are listed in Table 1. The values of $\Delta\Delta G_c$ (the differences between the calculated free-energy changes of helix formation of the tetranucleotide with anticodon and the calculated free-energy changes of helix formation of the trinucleotide with anticodon) are also listed in Table 1 along with the values of $\Delta\Delta G_m$.

In Table 1, the values of $\Delta\Delta G_c$ in parentheses are quite different from those of $\Delta\Delta G_m$, not only for UUCA binding to $tRNA^{Phe}$ but also for AUGA, UAUG, and GUGA binding to $tRNA^{fMet}$ which can form the fourth base pair. This result suggests that there is either the very weak or no hydrogen-bond formation. It has been shown that hydrogen bonding and stacking compete in a base pair.[16] Stacking interactions are more favorable when hydrogen-bonding interactions are less favorable. Therefore, stacking of dangling nucleotides might contribute to the large stability of the codon-anticodon complex.

Within a few kilojouls per mole (that is, within estimated errors) these $\Delta\Delta G_m$ are equal to the $\Delta\Delta G_c$ calculated by the assumption that the adjacent bases on a codon-anticodon core helix do not make a base pair but, rather, are stacking. The good correspondence between $\Delta\Delta G_c$ and $\Delta\Delta G_m$ is also found in the cases of the other 3′ and 5′ end bases of codon oligomers which can not form the fourth Watson-Crick base-pairs with the anticodon loops. These results show that an adjacent base on a codon-anticodon core helix stabilizes the helix by the stacking interaction, though this stabilization is not sufficiently large to provide a good explanation for the very large stability of the codon-anticodon complex. Therefore, the larger stability of ΔG_m than ΔG_c might come from an unusual base-pair formation of the codon-anticodon core helix.

Because the free-energy change for a codon-anticodon helix initiation is positive, the large stability of ΔG_m

Table 1. The Measured and Calculated Free-Energy Changes of the Complex Formation between Codon Oligomers and Anticodon Loops in the tRNA in Solution

Anticodon loop	Codon oligonucleotide	ΔG_m[a]	ΔG_c[b]	$\Delta\Delta G_m$	$\Delta\Delta G_c$[c]
		kJ mol^{-1}	kJ mol^{-1}	kJ mol^{-1}	kJ mol^{-1}
CmUGmAAYA	UUC	−17.2	−12.6		
($tRNA^{Phe}$)	UUCA	−26.8		−9.6	7.1
					(−13.0)
CmUGmAAYA	UUU	−13.4	−7.1		
($tRNA^{Phe}$)	UUUU	−13.0		0.4	−0.4
	UUUU	−13.0		0.4	−0.8
CmUCAUAA	AUG	−16.3	−9.4		
($tRNA^{fMet}$)	AUGA	−21.7		−5.4	4.4
					(−15.3)
	AUGU	−16.3		0	−2.3
	AUGC	−15.5		0.8	−1.5
	UAUG	−15.9		0.4	−0.6
					(−8.6)
CmUCAUAA	GUG	−16.3	−9.4		
($tRNA^{fMet}$)	GUGA	−20.9		−4.5	−4.4
					(−15.3)
CmUGmAAYA	UUCA	−25.5	−25.9		
(Dodecamer)					

a) From the data of the observed binding constants in Refs. 3, 4, 14, and 15. Estimated errors in ΔG_m are within ± 10%. b) Estimated errors in ΔG_c are within ± 5%. c) The values in parentheses were calculated according to the assumption that the dangling bases of the codon oligomer and the anticodon loop were able to make the fourth base-pair.

for helix formation is mainly due to the formation of Watson-Crick base pairs and a G-U base pair. However, as shown in Table 1, the measured stability of ΔG_m is significantly larger than the calculated stability of ΔG_c, which was obtained by the free-energy value of not only the base pairs, but also the stacking interaction of the adjacent bases in a codon oligomer. The differences in the stability between ΔG_m and ΔG_c are -4.6, -6.3, -6.9, and -6.9 kJ mol^{-1} for UUC and UUU binding to $tRNA^{Phe}$ and for AUG and GUG binding to $tRNA^{fMet}$, respectively. The value for each binding suggests a possible explanation for the large stability of the complex: An additional hydrogen bond contributes to the stability of a codon-anticodon helix, since it is known that the addition of a hydrogen bond for terminal and interior base pairs in RNA oligomers changes the free energy for duplex formation by -4 to -7 kJ mol^{-1} [16] and, especially, the value of -7 kJ mol^{-1} is consistent with the free energy increment recently predicted for a hydrogen bond formation between base pairs in the absence of competing stacking interactions.[17] Furthermore, the stability of ΔG_m for UUCA binding to dodecamer is well predicted by the calculated free-energy change, ΔG_c, which does not contain the stability by an additional hydrogen-bond formation. Therefore, the results and the fact that the dodecamer can not form a loop suggest that the additional hydrogen bond on the codon-anticodon helix might come from the other base in an anticodon loop of tRNA as well as a conformational change of the nucleic acid during the formation of the complex.

References

1) S. R. Jaskunas, C. R. Cantor, and I. Tinoco, Jr., *Biochemistry*, **7**, 3164 (1968).

2) P. N. Borer, B. Dengler, I. Tinoco, Jr., and O. C. Uhlenbeck, *J. Mol. Biol.*, **86**, 843 (1974).

3) K. Yoon, D. H. Turner, and I. Tinoco, Jr., *J. Mol. Biol.*, **99**, 507 (1975).

4) K. Yoon, D. H. Turner, I. Tinoco, Jr., F. von der Haar, and F. Cramer, *Nucleic Acids Res.*, **3**, 2233 (1976).

5) N. Sugimoto, R. Kierzek, S. M. Freier, and D. H. Turner, *Biochemistry*, **25**, 5755 (1986).

6) S. M. Freier, R. Kierzek, J. A. Jaeger, N. Sugimoto, M. H. Caruthers, T. Neilson, and D. H. Turner, *Proc. Natl. Acad. Sci. U.S.A.*, **83**, 9373 (1986).

7) N. Sugimoto, R. Kierzek, and D. H. Turner, *Biochemistry*, **26**, 4554 (1987).

8) N. Sugimoto, R. Kierzek, and D. H. Turner, *Biochemistry*, **26**, 4559 (1987).

9) N. Sugimoto, D. H. Turner, T. Sugano, and M. Sasaki, *Mem. Konan Univ., Sci. Series*, **35**, 103 (1988).

10) D. H. Turner, N. Sugimoto, J. A. Jaeger, C. E. Longfellow, S. M. Freier, and R. Kierzek, *Cold Spring Harbor Symp., Qual. Biol.*, **52**, 123 (1987).

11) D. H. Turner, N. Sugimoto, and S. M. Freier, *Ann. Rev. Biophys. Biophys. Chem.*, **17**, 167 (1988).

12) N. Sugimoto, R. Kierzek, and D. H. Turner, *Biochemistry*, **27**, 6384 (1988).

13) A. J. Zaug, C. A. Crosshams, and T. R. Cech, *Biochemistry*, **27**, 8924 (1988).

14) J. Eisinger, B. Fener, and T. Yamane, *Nature New Biology*, **231**, 126 (1971).

15) O. C. Uhlenbeck, J. Baller, and P. Doty, *Nature (London)*, **225**, 508 (1970).

16) D. H. Turner, N. Sugimoto, R. Kierzek, and S. D. Dreiker, *J. Am. Chem. Soc.*, **109**, 3783 (1987).

17) D. H. Turner, N. Sugimoto, S. D. Dreiker, S. M. Freier, and R. Kierzek, "Structure and Expression from Protein to Ribosomes," ed by R. H. Sarma and M. H. Sarma, Adenine Press, New York (1988), p. 249.

Oxidation Using Quaternary Ammonium Polyhalides. V.[1] Selective Oxidation of Benzyl Alcohols by the Use of Benzyltrimethylammonium Tribromide

Tsuyoshi OKAMOTO,* Takeshi UESUGI, Takaaki KAKINAMI, Tomohisa UTSUNOMIYA, and Shoji KAJIGAESHI†,*
Department of Industrial Chemistry, Ube Technical College, Tokiwadai, Ube 755
†Department of Industrial Chemistry, Faculty of Engineering, Yamaguchi University, Tokiwadai, Ube 755
(Received June 10, 1989)

Synopsis. The reaction of several substituted benzyl alcohols with 1 equiv of benzyltrimethylammonium tribromide (BTMA Br_3) in carbon tetrachloride under basic or neutral conditions gave the corresponding benzaldehydes, and with 2 equiv of BTMA Br_3 in aqueous alkaline solution and subsequent acid hydrolysis gave the corresponding benzoic acids, respectively, in satisfactory yields.

Benzyltrimethylammonium tribromide (BTMA Br_3) has recently been introduced as a useful brominating agent by us.[2] During the course of our further investigation on the synthetic utility of BTMA Br_3, we have found that this reagent is also an effective oxidizing agent.[3] In this paper we wish to report on the selective oxidation of several benzyl alcohols **1** to the corresponding benzaldehydes **2** or benzoic acids **3** by the use of BTMA Br_3.

Results and Discussion

Although a variety of substituted **1** has been

Table 1. Oxidation of Benzyl Alcohols **1** to Benzaldehydes **2** and Benzoic Acids **3** with BTMA Br_3

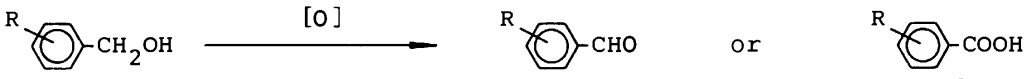

1 **2** **3**

1	R	Molar ratio		Reaction conditions		Product		Isolated yield
		BTMA Br_3/1	NaOH/1	Temp/°C	Time/h	2	3	
1a	H	1	—[a]	70	24	**2a**	—	83
		2	8	rt	6	—	**3a**	98
1b	2-Me	1	3	rt	24	**2b**	—	50[b]
		2	8	rt	22	—	**3b**	90
1c	4-Me	1	3	rt	24	**2c**	—	**53**[b]
		2	8	rt	6	—	**3c**	96
1d	4-isoPr	1	3	rt	24	**2d**	—	—[c]
		2	8	rt	24	—	**3d**	50
1e	4-OMe	1	3	rt	15	**2e**	—	75
		2	8	rt	6	—	**3e**	96
1f	2,5-di-OMe	1	3	rt	24	**2f**	—	58[b]
		2	8	rt	20	—	**3f**	69
1g	3,4-di-OMe	1	3	rt	24	**2g**	—	84
		2	8	rt	17	—	**3g**	77
1h	3,4-OCH_2O-	1	3	rt	17	**2h**	—	76
		2	8	rt	20	—	**3h**	99
1i	2-Cl	1	—[d]	rt	3	**2i**	—	51[e]
		2	8	rt	20	—	**3i**	87
1j	3-Cl	1	—[d]	70	22	**2j**	—	60
		2	8	70	17	—	**3j**	94
1k	4-Cl	1	—[a]	rt	24	**2k**	—	54[e]
		2	8	rt	6	—	**3k**	94
1l	4-Br	1	—[d]	70	22	**2l**	—	63
		2	8	rt	8	—	**3l**	95
1m	2-NO_2	1	—[d]	70	33	**2m**	—	31[e]
		2	8	rt	19	—	**3m**	99
1n	3-NO_2	1	—[a]	70	34	**2n**	—	97
		2	8	rt	19	—	**3n**	94
1o	4-NO_2	1	—[a]	70	27	**2o**	—	87
		2	8	70	15	—	**3o**	98

a) The reaction was done in water without using alkali. b) The desired **2** was separated from the starting material by column chromatography on alumina, and a small amount of the corresponding sodium benzoate was found in the resulting alkaline solutions as by-product. c) A mixtures of **1d** and **2d**, which was not separated by column chromatography on alumina, was obtained. d) The reaction was done in aq Na_2HPO_4 solution (molar ratio: Na_2HPO_4/**1**=2). e) Considerable amount of the starting material was recovered because of its relatively poor reactivity.

converted into the corresponding **2** by means of a number of oxidizing agents,[4] we have found that BTMA Br_3 is also a convenient reagent to oxidize **1** into **2**. That is, the reaction of **1** with 1-equiv of BTMA Br_3 in carbon tetrachloride in the presence of an aqueous alkaline solution, an aqueous solution of Na_2HPO_4, or water, at room temperature or at 70 °C gave **2** in satisfactory yields. The results are summarized in Table 1.

It should also be mentioned that primary alcohols can be oxidized to carboxylic acids by many strong oxidizing agent including chromic acid, permanganate, and nitric acid. However, a few oxidizing agents[5] have been used for the direct conversion of **1** to **3**. We have also found that BTMA Br_3 can be used as a reagent for the oxidation of **1** to **3**. That is, the reaction of **1** with 2-equiv of BTMA Br_3 in an aqueous alkaline solution at room temperature or at 70 °C afforded **3** in good yields. The results are summarized in Table 1.

These reactions, which occurred under basic conditions, can be represented by the following equations:

$$\underset{\mathbf{1}}{\text{Ar-CH}_2\text{OH}} + \text{BTMA Br}_3 + 2\text{NaOH} \longrightarrow \underset{\mathbf{2}}{\text{Ar-CHO}} + \text{BTMA Br} + 2\text{NaBr} + 2\text{H}_2\text{O} \quad (1)$$

$$\mathbf{1} + 2\text{BTMA Br}_3 + 5\text{NaOH} \longrightarrow \underset{\xrightarrow{\text{H}_3\text{O}^+}\ \underset{\mathbf{3}}{\text{Ar-COOH}}}{\text{Ar-COONa}} + 2\text{BTMA Br} + 4\text{NaBr} + 4\text{H}_2\text{O} \quad (2)$$

We assumed that the active species for the oxidation is sodium hypobromite or hypobromous acid, which may be produced from the reaction of BTMA Br_3 with aqueous sodium hydroxide or water, respectively.

As shown in Eqs. 1 and 2, oxidation products **2** or **3** can be obtained selectively from **1** by the use of a stoichiometric amount of BTMA Br_3. However, in these oxidation reactions of **1** (particulary active **1** such as methoxy-substituted benzyl alcohols (e.q., **1e**, **1f**, and **1g**)), an excess amount of alkali was required in order to avoid any aromatic bromination of **1**. Furthermore, the oxidation of **1** (which substituted an electron-attracting group) to **2** required more severe reaction conditions.

We emphasize that the above-mentioned procedure for the oxidation of **1** affording **2** or **3** should be a useful method owing to its simplicity, good yield of the product, and excellent selectivity.

Experimental

All products were characterized by comparing their ^1H NMR spectra and mp or bp with those of authentic samples or reported data.

Oxidation of 4-Methoxybenzyl Alcohol (1e) to 4-Methoxybenzaldehyde (2e); Typical Procedure: A solution of BTMA Br_3 (2.05 g, 5.25 mmol) and sodium hydroxide (0.60 g, 15 mmol) in water (25 ml) was added dropwise into a solution of **1e** (0.69 g, 5 mmol) in carbon tetrachloride (25 ml). The mixture was stirred at room temperature for 15 h until the initial yellow color faded. To the mixture was added 5% aq solution of $NaHSO_3$ (5 ml). Then, the carbon tetrachloride layer was separated and the water layer extracted with dichloromethane (30 ml×3). The organic layer was dried over $MgSO_4$, filtered, and evaporated under reduced pressure to give **2e** as a colorless liquid; yield 0.51 g (75%); bp 243—244 °C/760 mmHg (lit,[6] bp 248 °C/760 mmHg; 1 mmHg≈133.322 Pa).

Oxidation of 3-Chlorobenzyl Alcohol (1j) to 3-Chlorobenzoic Acid (3j); Typical Procedure: Compound **1j** (0.71 g, 5 mmol) was added into a solution of BTMA Br_3 (4.09 g, 10.5 mmol) and sodium hydroxide (1.60 g, 40 mmol) in water (30 ml). The mixture was stirred at 70 °C for 17 h until the initial yellow color faded. To the mixture was added a 5% aq solution of $NaHSO_3$ (5 ml); the mixture was then acidified sufficiently with 6M-HCl. The solution was extracted with ether (40 ml×4) and the ether layer was dried over $MgSO_4$, filtered, and evaporated under reduced pressure to give **3j** as a colorless crystals; yield 0.73 g (94%); mp 156—157 °C (lit,[7] mp 156—157 °C).

References

1) Part IV of this series: S. Kajigaeshi, K. Murakawa, S. Fujisaki, and T. Kakinami, *Bull. Chem. Soc. Jpn.*, **62**, 3376 (1989).

2) S. Kajigaeshi and T. Kakinami, *Yuki Gosei Kagaku Kyokaishi*, **46**, 986 (1988); and references therein.

3) For example: a) S. Kajigaeshi, K. Asano, S. Fujisaki, T. Kakinami, and T. Okamoto, *Chem. Lett.*, **1989**, 463. b) S. Kajigaeshi, T. Kakinami, T. Yamaguchi, T. Uesugi, and T. Okamoto, *Chem. Express*, **4**, 177 (1989). c) S. Kajigaeshi, K. Murakawa, S. Fujisaki, and T. Kakinami, *Bull. Chem. Soc. Jpn.*, **62**, 3376 (1989). d) S. Kajigaeshi, K. Murakawa, K. Asano, S. Fujisaki, and T. Kakinami, *J. Chem. Soc., Perkin Trans. 1*, **1989**, 1702.

4) For example: a) R. E. Partch, *Tetrahedron Lett.*, **1964**, 3071. b) R. C. Cookson, I. D. R. Stevens, and C. T. Watts, *Chem. Commun.*, **1966**, 744. c) J.-M. Lalancette, G. Rollin, and P. Dumas, *Can. J. Chem.*, **50**, 3058 (1972). d) E. J. Corey and C. U. Kim, *Tetrahedron Lett.*, **1973**, 919.

5) a) W. R. Brasen and C. R. Hauser, *J. Org. Chem.*, **18**, 806 (1953). b) K. Nakagawa, R. Konaka, and T. Nakata, *J. Org. Chem.*, **27**, 1597 (1962). c) D. G. Lee, D. T. Hall, and J. H. Cleland, *Can. J. Chem.*, **50**, 3741 (1972).

6) E. L. Niedzielski and F. F. Nord, *J. Am. Chem. Soc.*, **63**, 1462 (1941).

7) W. S. Emerson, V. E. Lucas, and R. A. Heimsch, *J. Am. Chem. Soc.*, **71**, 1742 (1949).

Myeloperoxidase Catalyzed Bromination of Nucleic Acid Bases and Related Compounds

Toshio ITAHARA* and Naoko IDE
Institute of Chemistry, College of Liberal Arts, Kagoshima University, Korimoto, Kagoshima 890
(Received June 17, 1989)

Synopsis. Oxidation of cytosine, uracil, adenine, cytidine, and 2′-deoxycytidine by myeloperoxidase in the presence of hydrogen peroxide and potassium bromide in sodium acetate buffer solution at pH 5.0 resulted in bromination of the substrates. A comparison of bromination of 1,3-dimethyluracil catalyzed by peroxidases such as myeloperoxidase, lactoperoxidase, chloroperoxidase, and horseradish peroxidase was also studied.

Myeloperoxidase (MPO) plays an important role for disinfection with H_2O_2 and halide ions in phagolysosome.[1] On the other hand, mutation[2] and carcinogenesis[3] are known to be caused by human phagocytes. Furthermore, halogenated nucleic acid bases and their deoxyribonucleosides such as 5-bromouracil (**2b**)[4] and 5-bromo-2′-deoxyuridine[5] have mutagenic activities. Therefore, MPO catalyzed halogenation of nucleic acids is of interest. Odajima[6] first reported the incorporation of chlorine into RNA and adenine (**3a**) by MPO in the presence of H_2O_2 and NaCl. However, structures of the chlorinated products were not thoroughly determined.[6] As part of the investigation of the enzymatic and non-enzymatic oxidation of nucleic acid bases,[7] MPO catalyzed halogenation of nucleic acid bases was studied.[8]

MPO catalyzed halogenation of nucleic acid bases was carried out in sodium acetate buffer solution at pH 5.0.[6] While oxidation of cytosine (**1a**), uracil (**2a**), and **3a** with H_2O_2 and NaCl in the presence of MPO gave only a trace amount of product, a similar treatment with KBr instead of NaCl gave brominated products in moderate yields. The results are shown in Table 1. Table 1 shows that the yields of brominated products from **1a**, **2a**, and **3a** decrease in that order. On the other hand, no reaction occurred when thymine was similarly treated. The reaction of guanine was not attempted because it was only slightly soluble in the buffer solution. Treatment of cytidine (**4a**) and 2′-deoxycytidine (**5a**) with H_2O_2 and KBr in the presence of MPO also gave 5-bromocytidine (**4b**) and 5-bromo-2′-deoxycytidine (**5b**), respectively. The compounds **1a**, **2a**, **3a**, **4a**, and **5a** were unreactive to H_2O_2 and KBr in the absence of MPO under similar conditions.

In an attempt to further elucidate the MPO catalyzed oxidation, a comparison of oxidation of 1,3-dimethyluracil (**6a**) by MPO, lactoperoxidase (LPO), chloroperoxidase (CPO), and horseradish peroxidase (HPO)

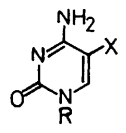

1a : R = H, X = H
1b : R = H, X = Br
4a : R = β-D-ribofuranosyl
X = H
4b : R = β-D-ribofuranosyl
X = Br
5a : R = 2-deoxy-β-D-ribofuranosyl
X = H
5b : R = 2-deoxy-β-D-ribofuranosyl
X = Br

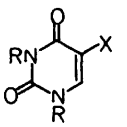

2a : R = H, X = H
2b : R = H, X = Br
6a : R = Me, X = H
6b : R = Me, X = Br

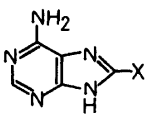

3a : X = H
3b : X = Br

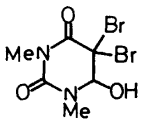

7

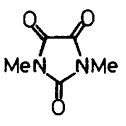

8

Table 1. Peroxidase Catalyzed Bromination of Nucleic Acid Bases and the Related Compounds[a]

Substrate	Peroxidase	KBr	H_2O_2	Temp	Products (Isolated yield/%[b])
		mmol	mmol	°C	
1a	MPO (200 U)	2	2	25—27	**1b**(22)[c]
2a	MPO (200 U)	2	2	25—27	**2b**(4)[c]
3a	MPO (200 U)	2	2	25—27	**3b**(0.9)[c]
4a	MPO (200 U)	4	1	35—38	**4b**(4)[c]
5a	MPO (200 U)	4	1	35—38	**5b**(5)[c]
6a	MPO (200 U)	2	2	25—27	**6a**(88), **6b**(6)
6a	LPO (400 U)	2	2	25—27	**6a**(88), **6b**(4)
6a	CPO (250 U)	2	2	25—27	**6a**(61), **6b**(16), **7**(6), **8**(8)

a) Reaction conditions: substrate (1 mmol), for 1 h reaction. b) Yield based on substrate used. c) Yield of the recovered substrate was not determined.

was investigated. As shown in Table 1, MPO and LPO catalyzed reactions of **6a** yielded 5-bromo-1,3-dimethyluracil (**6b**) whereas CPO catalyzed oxidation gave not only **6b** but also 5,5-dibromo-6-hydroxy-1,3-dimethyl-5,6-dihydrouracil (**7**) and 1,3-dimethylparabanic acid (**8**). However, almost no reaction occurred when **6a** was similarly treated with HPO.

Although many reports concerning halogenation of nucleic acid bases and nucleosides have been published,[9] it was found that **1a**, **2a**, **3a**, **4a**, and **5a** were reacted with H_2O_2 and KBr in the presence of MPO to yield the corresponding brominated products. The results are of interest in connection with the mechanism of mutation caused by phagocytes.

Experimental

MPO from human leukocytes (200 U/vial) was purchased from The Green Cross Corporation (Osaka). LPO from bovine milk and CPO from Caldariomyces fumago were purchased from Sigma Chemical Co. (St. Leuis, USA).

MPO Catalyzed Bromination of Nucleic Acid Bases 1a, 2a, and 3a. A solution of nucleic acid base (1 mmol), MPO (200 U), and KBr (2 mmol) in 0.2 mol dm^{-3} sodium acetate buffer solution at pH 5.0 (110 ml) was stirred. The reaction was initiated by addition of H_2O_2 and incubated at 25—27 °C. Hydrogen peroxide (0.4 mmol) in the sodium acetate buffer solution (2 ml) was added into the solution at 10 min intervals. After 60 min, catalase was added to remove any remaining H_2O_2. The reaction mixture was evaporated to give a white solid mass. The residue was extracted with a large amount of methanol. Droplet countercurrent chromatography (Tokyo Rikakikai, DCC-300-G2) was used for separation of the extract. The separation with $CHCl_3$–MeOH–H_2O (5:5:3) by descending method resulted in the isolation of the brominated products. The isolation of **1a**, **2a**, and **3a** was not attempted. The structures of the brominated products were confirmed by comparison of ^1H NMR spectra (JEOL PMX60A spectrometer) and thin-layer chromatography (TLC) (E. Merck, Silica gel 60 sheet F_{254}) with the authentic samples obtained commercially.

Bromination of 4a and 5a. A solution of **4a** and **5a** (1 mmol), MPO (200 U), and KBr (4 mmol) in the sodium acetate buffer solution described before (110 ml) was stirred at 35—38 °C. The reaction was started by adding H_2O_2 (0.5 mmol) in the buffer solution (5 ml). After 30 min, H_2O_2 (0.5 mmol) in the buffer solution (5 ml) was further added into the solution containing MPO. After 60 min, catalase was added. The reaction mixture was evaporated and extracted with a large amount of methanol. The extract was evaporated and chromatographed on silica gel using a mixture of $CHCl_3$ and MeOH (8:2) to yield the brominated products. The products **4b** and **5b** were further purified by liquid chromatography with low pressure pump (Fuji-gel packed column RQ-2 ODS silica gel 24 mmϕ×360 mm, mobile phase: a mixture of water and acetonitrile (10:1), detected at 250 nm). The structures of the products were confirmed by comparison of ^1H NMR spectra and TLC with the authentic samples obtained commercially. The isolation of **4a** and **5a** was not attempted.

Peroxidase Catalyzed Oxidation of 6a. Reaction of **6a** with H_2O_2 and KBr in the presence of MPO was carried out according to the manner described for the MPO catalyzed bromination of **1a**, **2a**, and **3a**. Under similar conditions, LPO catalyzed bromination in 0.25 mol dm^{-3} potassium phosphate buffer solution at pH 6.0 and CPO catalyzed oxidation in 0.25 mol dm^{-3} potassium phosphate buffer solution at pH 3.0 of **6a** were achieved. The reaction mixture was evaporated and extracted with a large amount of $CHCl_3$. The extract was evaporated and chromatographed on silica-gel TLC (Wako Pure Chemical, Wakogel B-5F) using ethyl acetate or a mixture of ethyl acetate and hexane (2:1, v/v) to give **6a**, **6b**, **7**, and **8**. The structures of **6b**,[10] **7**,[10] and **8**[11] were confirmed by comparison of ^1H NMR spectra and TLC with the samples prepared according to the published procedures.

References

1) S. J. Klebanoff, *J. Bacteriol.*, **95**, 2131 (1968).
2) S. A. Weitzman and T. P. Stossel, *Science*, **212**, 546 (1981).
3) S. A. Weitzman, A. B. Weitberg, E. P. Clark, and T. P. Stossel, *Science*, **227**, 1213 (1985).
4) I. Pietrzyowska, *Mut. Res.*, **19**, 1 (1973).
5) T. C. Tsu and C. E. Somers, *Proc. Natl. Acad. Sci. U.S.A.*, **47**, 396 (1961).
6) T. Odajima, *Shika Kiso Igakkai Zasshi*, **22**, 502 (1980).
7) T. Itahara and N. Ide, *Chem. Lett.*, **1987**, 2311.
8) A part of the results has been preliminarily presented: T. Itahara and N. Ide, International Conference on Medical, Biochemical, and Chemical Aspects of Free Radicals, Kyoto, Apr. 9-13, 1988, PI-2-10.
9) E. K. Ryu and M. MacCoss, *J. Org. Chem.*, **46**, 2819 (1981) and references therein.
10) S. Y. Wang, *J. Org. Chem.*, **24**, 11 (1959).
11) T. Itahara, Y. Fujii, and M. Tada, *J. Org. Chem.*, **53**, 3421 (1988).

A Convenient Synthesis of Naphtho[1,2-*b*]furans

Wen-Bing KANG, Takashi SEKIYA, Takeshi TORU, and Yoshio UENO*
Department of Applied Chemistry, Nagoya Institute of Technology, Nagoya 466
(Received July 10, 1989)

Synopsis. Acid-catalyzed reductive cyclization of 2-alkyl-substituted 3-ethylthio- and 3-phenylthio-1,4-naphthoquinones gave naphtho[1,2-*b*]furans in high yields.

We have been interested in developing new methods for synthesis of naphthoquinone derivatives. Recently we found that 2-phenylthio- and 2-ethylthio-1,4-naphthoquinones (**1a** and **1b**) could be alkylated with lithium enolates[1,2] or pyridinium ylides[2] to give 2-(2-oxoalkyl)-3-phenylthio- and -3-ethylthio-1,4-naphthoquinones **2** in high yields, respectively, and that these alkylated 1,4-naphthoquinones **2** were cyclized successfully to naphtho[2,3-*b*]furan-4,9-dione derivatives. We have further studied on the synthesis of naphtho[1,2-*b*]furans by starting from 3-alkylated 2-thio-substituted 1,4-naphthoquinones **2**. Several naphtho[1,2-*b*]furan derivatives have interesting biological activities such as spasmolytic, local anesthetic,[3] and bactericidal activities.[4] The naphtho[1,2-*b*]furan moiety has also been used as synthetic intermediates for biologically interesting heterocycles.[5] We report here a new synthesis of naphtho[1,2-*b*]furan derivatives from 2-(2-oxoalkyl)-3-phenylthio- and -3-ethylthio-1,4-naphthoquinones **2**.

Treatment of 2-phenacyl-3-phenylthio-1,4-naphthoquinone **2a** (R^1=R^2=Ph)[2] with tin(II) chloride in the presence of hydrochloric acid in acetic acid at room temperature gave 2-phenyl-4-(phenylthio)naphtho[1,2-*b*]furan-5-ol **3a** in 78% yield. Transformation of 2-(2-oxoalkyl)-3-phenylthio-1,4-naphthoquinone **2b**—**2j** (R^1=Ph, R^2=aryl, alkyl) also afforded naphtho[1,2-*b*]furan derivatives **3b**—**3j** in 70—91% yields. The reaction of 1,4-naphthoquinone **2k** or **2l** having an ethylthio substituent also proceeded smoothly to give naphtho[1,2-*b*]furans **3k**—**3l** in 88—95% yields. All reactions of **2**, except **2i**, was carried out at room temperature during a peried of 10 to 60 min, while the reaction of **2i** (R^1=Ph, R^2=2-naphthyl) took 2.5 h at 40 °C. The structures of all these compounds were supported by spectral data and microanalyses. The results as well as the physical and analytical data of the products were summarized in Table 1.

The reasonable mechanism of this reaction may be as follows: the alkylated 1,4-naphthoquinones **2** are reduced by the action of tin(II) chloride and hydrochloric acid[6] to give 1,4-naphthalenediol **4** which is cyclized by acid catalysis to dihydronaphtho[1,2-*b*]-furans **5**. Dehydration of **5** affords substituted naphtho[1,2-*b*]furans **3**.

In summary, the reductive cyclization reaction of 3-alkylated 2-thio-1,4-naphthoquinones, conveniently obtainable from the alkylation of 2-thio-1,4-naphthoquinones,[1,2] gives a general method for the synthesis of various naphtho[1,2-*b*]furan compounds. A further study on the bioactivities[7] of these substivituted naphtho[1,2-*b*]furans and application of this reaction is currently in progress in our laboratory.

Experimental

Mps were recorded on a Yanaco micro melting point apparatus and are uncorrected. IR spectra were measured as KBr discs on a JASCO A-102 spectrometer. NMR spectra were determined with a Varian XL-200 spectrometer in deuteriochloroform with TMS as internal standard.

General Procedure for the Preparation of Naphtho[1,2-*b*]furans 3. To a suspension of thio-substituted 1,4-naphthoquinone **2** (0.5 mmol) in acetic acid (10 ml) was added a solution of tin(II) chloride dihydrate (2 mmol) in concentrated hydrochloric acid (4 ml). The reaction mixture was stirred for the time listed in Table 1, and then poured into water and extracted with toluene. The organic layer was washed successively with sodium hydrogencarbonate solution and water, and then dried over anhydrous sodium sulfate. After evaporation of solvent the residue was purified by column chromatography on silica gel using toluene as an eluent to afford **3**. All the compounds except **3l**, obtained as an oil, were recrystallized from methanol.

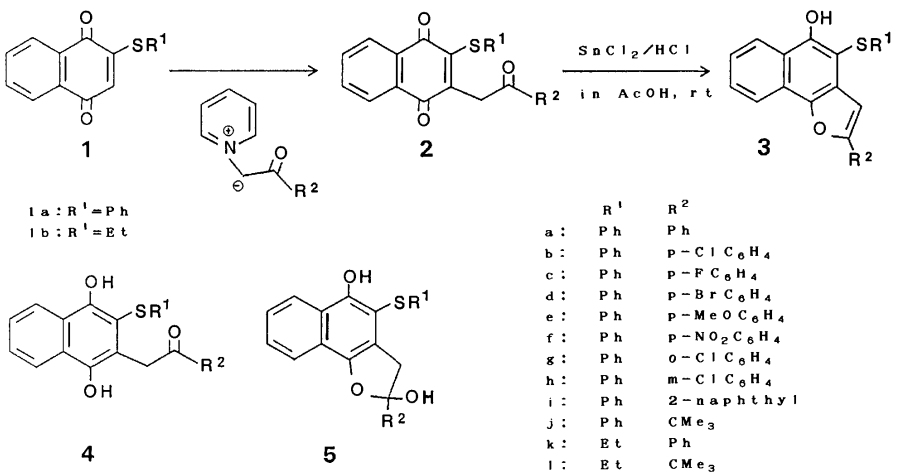

	R^1	R^2
a:	Ph	Ph
b:	Ph	p-ClC_6H_4
c:	Ph	p-FC_6H_4
d:	Ph	p-BrC_6H_4
e:	Ph	p-$MeOC_6H_4$
f:	Ph	p-$NO_2C_6H_4$
g:	Ph	o-ClC_6H_4
h:	Ph	m-ClC_6H_4
i:	Ph	2-naphthyl
j:	Ph	CMe_3
k:	Et	Ph
l:	Et	CMe_3

Table 1. Preparation of Naphtho[1,2-*b*]furans **3**[a]

Quinone **2**	Reaction time/min	Product **3**	Yield %	Physical and analytical data of **3**			
				Mp °C	IR (cm^{-1}) (KBr)	^1H NMR δ/ppm ($CDCl_3$)	Anal.[b] (C, H)
2a	10	**3a**	78	170—171	3415, 3040, 1622, 1568	6.98 (1H, OH), 7.04—7.18 (8H), 7.20 (1H, 3-H), 7.51 (1H, 8-H), 7.67 (1H, 7-H), 7.78—7.88 (2H), 8.32 (2H, 6-H and 9-H)	$C_{24}H_{16}O_2S$
2b	40	**3b**	82	175—176	3400, 3040, 1625, 1572	7.07 (1H, OH), 7.09—7.31 (6H, 3-H and Ph), 7.41 (2H), 7.55 (1H, 8-H), 7.70 (1H, 7-H), 7.77—7.89 (2H), 8.35 (2H, 6-H and 9-H)	$C_{24}H_{15}O_2SCl$
2c	20	**3c**	82	149.5—150.5	3355, 3040, 1570	7.05 (1H, OH), 7.10—7.34 (8H), 7.59 (1H, 8-H), 7.75 (1H, 7-H), 7.86—7.95 (2H), 8.40 (2H, 6-H and 9-H)	$C_{24}H_{15}O_2SF$
2d	15	**3d**	88	192—193	3395, 1595	7.09—7.27 (6H, OH and Ph), 7.30 (1H, 3-H), 7.52—7.67 (3H), 7.68—7.82 (3H), 8.37 (2H, 6-H and 9-H)	$C_{24}H_{15}O_2SBr$
2e	45	**3e**	91	145.5—146.5	3380, 3030, 1605, 1565	3.38 (3H, CH_3), 6.98 (1H, OH), 7.00 (2H), 7.10—7.34 (6H, 3-H and Ph), 7.54 (1H, 8-H), 7.72 (1H, 7-H), 7.84 (2H), 8.37 (2H, 6-H and 9-H)	$C_{25}H_{18}O_3S$
2f	20	**3f**	70	207—208	3375, 1590, 1500	7.13—7.36 (7H, 3-H, OH, and Ph), 7.64 (1H, 8-H), 7.78 (1H, 7-H), 8.02 (2H), 8.10—8.30 (4H)	$C_{24}H_{15}NO_4S$
2g	60	**3g**	91	124—125	3385, 3050	7.10—7.65 (11H), 7.72 (1H, 7-H), 8.14 (1H), 8.38 (2H, 6-H and 9-H)	$C_{24}H_{15}O_2SCl$
2h	60	**3h**	75	149—150	3390, 3035, 1568, 1466	7.10—7.27 (6H, OH and Ph), 7.29 (1H, 3-H), 7.32—7.46 (2H), 7.58 (1H, 8-H), 7.74 (2H, 7-H), 7.89 (1H), 8.35—8.44 (2H, 6-H and 9-H)	$C_{24}H_{15}O_2SCl$
2i	210[c]	**3i**	76	191—192	3400, 3035, 1620	7.11—7.33 (6H), 7.43—7.66 (3H), 7.73 (1H, 7-H), 7.80—7.99 (5H), 8.35—8.47 (3H)	$C_{28}H_{18}O_2S$
2j	15	**3j**	85	130.5—131	3420, 2960, 1624, 1575	1.40 (9H, $3CH_3$), 6.47 (1H, OH), 7.06—7.30 (6H, 3-H and Ph), 7.51 (1H, 8-H), 7.68 (1H, 7-H), 8.27 (1H, 9-H), 8.36 (1H, 6-H)	$C_{22}H_{20}O_2S$
2k	10	**3k**	95	94.5—96	3360, 3050, 2920, 1572	1.25 (3H, CH_3), 2.84 (2H, CH_2), 7.25 (1H, OH), 7.32 (1H, 3-H), 7.35—7.58 (4H), 7.66 (1H, 7-H), 7.96 (2H), 8.33 (2H, 6-H and 9-H)	$C_{20}H_{16}O_2S$
2l	10	**3l**	88	Oil	3380, 3050, 2955, 1572	1.23 (3H, CH_3), 1.45 (9H, $3CH_3$), 2.81 (2H, CH_2), 6.59 (1H, OH), 7.28 (1H, 3-H), 7.48 (1H, 8-H), 7.62 (1H, 7-H), 8.22 (1H, 9-H), 8.31 (1H, 6-H)	$C_{18}H_{20}O_2S$

a) All reactions except that of **2i** were carried out at room temperature. b) Microanalyses for all compounds were satisfactorily done in ±0.3% of calculated values. c) This reaction was carried out at 40°C.

References

1) W. B. Kang, S. Nan'ya, T. Toru, and Y. Ueno, *Chem. Lett.*, **1988**, 1415;

2) W. B. Kang, T. Sekiya, T. Toru, and Y. Ueno, *J. Chem. Soc., Perkin Trans. 1*, in press.

3) A. A. Stolyarchuk, T. I. Mukhanova, N. I. Ivanova, and V. V. Danil'chuk, *Fiziol. Akt. Veshchesstva*, **20**, 16 (1988).

4) C. Bilger, P. Demerseman, J. P. Buisson, R. Royer, P. Gayral, and J. Fourniat, *Eur. J. Med. Chem.*, **22**, 213 (1987).

5) H. Takahata, A. Anazawa, K. Moriyama, and T. Yamazaki, *J. Chem. Soc., Perkin Trans. 1*, **1987**, 1501; H. Takahata, A. Anazawa, K. Moriyama, and T. Yamazaki, *Chem. Lett.*, **1986**, 5; L. Capuano and P. Moersdorf, *Liebigs Ann. Chem.*, **1982**, 2178; H. E. Hoegberg, *J. Chem. Soc., Perkin Trans. 1*, **1979**, 2517.

6) D. B. Bruce and R. H. Thomoson, *J. Am. Chem. Soc.*, **76**, 1429 (1954).

7) A preliminary test for **3f** against HeLa cells was carried at the Research Center of Sankyo Company and the IC_{50} of **3f** was found to be 8.8 μg ml^{-1}.

Efficient Reduction of Triphenylmethanol to Triphenylmethane by 9,10-Dihydro-10-methylacridine in the Presence of Perchloric Acid

Masashi ISHIKAWA,† Shunichi FUKUZUMI,* Tatsushi GOTO, and Toshio TANAKA††
Department of Applied Chemistry, Faculty of Engineering, Osaka University, Suita, Osaka 565
(Received July 17, 1989)

Synopsis. Reduction of triphenylmethanol (Ph_3COH) to triphenylmethane by an NADH model compound, 9,10-dihydro-10-methylacridine ($AcrH_2$), proceeds very efficiently in the presence of perchloric acid ($HClO_4$) in acetonitrile at 298 K via hydride transfer from $AcrH_2$ to triphenylmethyl cation (Ph_3C^+) which is formed by the dehydration of Ph_3COH with $HClO_4$. Mechanisms of hydride transfer reactions from NADH model compounds to Ph_3C^+ are also discussed.

Acid-stable analogues of dihydronicotinamide adenine dinucleotide (NADH) have been employed as effective reductants in reductions of various carbonyl compounds[1-3] and imines[4] in the presence of acid. It has recently been reported that aryl alcohols can also be reduced by acid-stable NADH model compounds in the presence of acid.[5] However, concentrated acid or high temperature (e.g., refluxing acetonitrile) has so far been required for the reactions to undergo smoothly.[5]

This study reports that very facile reduction of triphenylmethanol occurs by using an acid-stable NADH analogue, 9,10-dihydro-10-methylacridine in the presence of slightly excess concentration of perchloric acid ($HClO_4$) to $AcrH_2$ in acetonitrile at 298 K to yield triphenylmethane. The kinetic investigations have been performed using a stopped-flow technique in order to discuss mechanisms of the facile reduction of triphenylmethanol by $AcrH_2$ as well as those of the hydride transfer reactions from NADH model compounds to triphenylmethyl cation which is prepared independently by the dehydration of triphenylmethanol with $HClO_4$.

Experimental

Preparation of 9,10-dihydro-10-methylacridine ($AcrH_2$) and 1-benzyl-1,4-dihydronicotinamide (BNAH) was described elsewhere.[6] Triphenylmethyl perchlorate ($Ph_3C^+ClO_4^-$) was prepared by the literature method.[7] Triphenylmethanol (Ph_3COH) and $HClO_4$ (70%) were obtained commercially. Acetonitrile (MeCN) used as a solvent was purified and dried by the standard procedure.[8]

The reactions in the absence and presence of oxygen in CD_3CN were monitored using a Japan Electron Optics JNM-PS-100 ^1H NMR spectrometer. Kinetic measurements were performed using a Union RA-103 stopped flow spectrophotometer. Rates of the reduction of Ph_3COH by $AcrH_2$ in deaerated MeCN at 298 K were followed by the increase in absorbance due to 10-methylacridinium ion ($AcrH^+$) in the visible region (λ_{max}=358 nm, ε=1.80×10^4 dm^3 mol^{-1} cm^{-1}). Rates of the dehydration of Ph_3COH with $HClO_4$ in deaerated MeCN at 298 K were determined by the increase in absorbance at λ_{max}=405, 433 nm due to Ph_3C^+. Rates of the hydride transfer from $AcrH_2$ and BNAH to Ph_3C^+ were also followed by the increase and decrease in absorbance at λ_{max}=358 and 350 nm due to $AcrH^+$ and BNAH under 4 atm of oxygen (or nitrogen), respectively. All the kinetic measurements were carried out under pseudo-first-order conditions where the concentrations of substrates were maintained at more than 10-fold excess of $AcrH_2$ or BNAH. Pseudo-first-order rate constants were determined by the least-square curve fit using a Union System 77 microcomputer. Second-order rate constants were calculated from the slope of the pseudo-first-order rate constants vs. the concentrations of substrates by the least-squares analysis.

Results and Discussion

Reduction of Ph_3COH by $AcrH_2$ in the Presence of $HClO_4$. Upon mixing $AcrH_2$ with Ph_3COH in the presence of $HClO_4$ in MeCN at 298 K, facile reduction of Ph_3COH by $AcrH_2$ occurs to yield $AcrH^+$ and triphenylmethane (Ph_3CH), Eq. 1. The products were

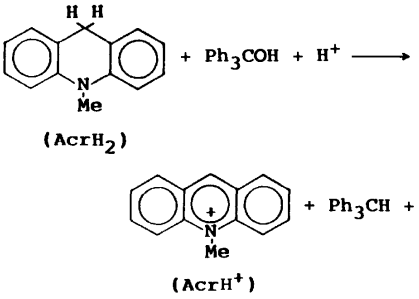

(1)

identified by the ^1H NMR and the electronic spectra. The rates obey the second-order kinetics, showing the first-order dependence on each reactant concentration. The observed second-order rate constants k_{obs} increase with an increase in the $HClO_4$ concentration to reach a maximum value at [$HClO_4$] ca. 1×10^{-3} mol dm^{-3}, and then decrease in the higher concentration region as shown in Fig. 1. Such a decrease of k_{obs} in the higher concenration region of $HClO_4$ may be ascribed to the protonation of $AcrH_2$ by $HClO_4$ to form $AcrH_3^+$ (Eq. 2), since $AcrH_3^+$ is known to be much weaker

$$AcrH_2 + H^+ \rightleftharpoons AcrH_3^+ \quad (2)$$

reductant than $AcrH_2$.[2,3] Thus, the reduction of Ph_3COH by $AcrH_2$ is not catalyzed by $HClO_4$. In such a case, the reduction may proceed via the rate-determining hydride transfer reaction from $AcrH_2$ to Ph_3C^+ (Eq. 3) which is formed by the dehydration of Ph_3COH with $HClO_4$ (Eq. 4). In order to confirm this point, the kinetics of both reactions (Eqs. 3 and 4) have been examined independently.

† Present address: Laboratory of Organic Chemistry, Osaka Women's University, Sakai, Osaka 590.

†† Present address: Department of Applied Physics and Chemistry, Fukui Institute of Technology, Gakuen, Fukui 910.

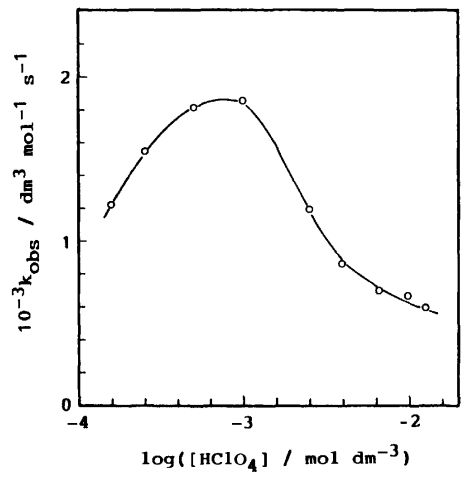

Fig. 1. Dependence of the observed second-order rate constant (k_{obs}) vs. [$HClO_4$] for the reduction of Ph_3COH by $AcrH_2$ in the presence of $HClO_4$ in deaerated MeCN at 298 K.

$$AcrH_2 + Ph_3C^+ \longrightarrow AcrH^+ + Ph_3CH \quad (3)$$

$$Ph_3COH + H^+ \longrightarrow Ph_3C^+ + H_2O \quad (4)$$

Rates of both reactions (Eqs. 3 and 4) also obey the second-order kinetics. The observed second-order rate constant of hydride transfer from $AcrH_2$ to Ph_3C^+ (Eq. 4) is determined as 1.7×10^3 dm^3 mol^{-1} s^{-1}. On the other hand, the observed second-order rate constant of the dehydration of Ph_3COH with $HClO_4$ (Eq. 4) is determined as 8.0×10^4 dm^3 mol^{-1} s^{-1} which is much larger than the k_{obs} value of the hydride transfer reaction (Eq. 3). Thus, the dehydration of Ph_3COH with $HClO_4$ to form Ph_3C^+ occurs firstly and then the rate-determining hydride transfer from $AcrH_2$ to Ph_3C^+ takes place to yield $AcrH^+$ and Ph_3CH. In fact, the maximum k_{obs} value (1.8×10^3 dm^3 mol^{-1} s^{-1}) of the reduction of Ph_3COH by $AcrH_2$ at [$HClO_4$]=ca. 10^{-3} mol dm^{-3} (Fig. 1) is nearly equal to the k_{obs} value (1.7×10^3 dm^3 mol^{-1} s^{-1}) of hydride transfer from $AcrH_2$ to Ph_3C^+.

Mechanisms of Hydride Transfer from NADH Model Compounds to Ph_3C^+. With respect to mechanisms of hydride abstraction of Ph_3C^+, it has recently established that hydride transfer from a tungsten-dimethyl complex [$Cp_2W(CH_3)_2$] (Cp=η-C_5H_5) to Ph_3C^+ consists of two-step processes; the exothermic electron transfer from [$Cp_2W(CH_3)_2$] to Ph_3C^+ occurs firstly as indicated by the more negative oxidation potential of [$Cp_2W(CH_3)_2$] (−0.1 V)[9] than the reduction potential of Ph_3C^+ (0.29 V),[10] and the subsequent hydrogen-atom transfer from [$Cp_2W(CH_3)_2$]$^+$ to $Ph_3C\cdot$ occurs to yield Ph_3CH.[11] Evidence for such initial electron transfer has been obtained also for hydride transfer from rhenium-alkyl complexes to Ph_3C^+, although the electron transfer in this case is endothermic.[12] The intermediate radical $Ph_3C\cdot$ formed by the endothermic electron transfer has been successfully trapped by oxygen when the rate of overall hydride transfer is accelerated by the presence of oxygen. Since one-electron oxidation potentials of rhenium-alkyl complexes (e.g., 0.48 V vs. SCE)[12] are rather close to those of NADH model compounds [e.g., 0.57 V vs. SCE for 1-benzyl-1,4-dihydronicotinamide (BNAH)],[6] the hydride transfer from BNAH to Ph_3C^+ may also proceed via initial electron transfer from BNAH to Ph_3C^+, followed by hydrogen transfer from $BNAH^{+\cdot}$ to $Ph_3C\cdot$ to yield BNA^+ and Ph_3CH as shown in Scheme 1.

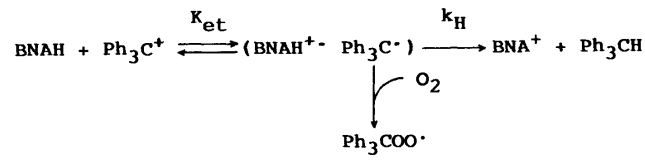

Scheme 1.

In order to examine the contribution of such an electron-transfer process, the second-order rate constants k_{obs} of hydride transfer from BNAH to Ph_3C^+-ClO_4^- in the absence and presence of oxygen were determined under 4 atm of nitrogen and oxygen, respectively. The k_{obs} values are listed in Table 1, together with the reported k_{obs} values of a rhenium-alkyl complex, [$CpRe(NO)(PPh_3)(CH_2Ph)$].[12] The k_{obs} value of $AcrH_2$ in the presence of oxygen (4 atm) was also determined and the k_{obs} values in the absence and presence of oxygen are also listed in Table 1. In the case of the rhenium-benzyl complex, the k_{obs} value in the presence of air becomes more than 10-fold larger as compared with the value in the absence of oxygen (Table 1). In the case of NADH model compounds (BNAH and $AcrH_2$), however, no acceleration of the rate constant is observed in the presence of oxygen even at 4 atm. It has been confirmed that no oxygen is incorporated into the product, either. Such difference in the effect of oxygen on the reactions of the rhenium-benzyl complex and NADH model compounds may be ascribed to the difference in the reactivities of hydrogen transfer processes of the resulting radical cations formed by the initial electron transfer. According to Scheme 1, the observed overall rate constant consists of the electron transfer equilibrium constant K_{et} of formation of the radical pair and the rate constant of hydrogen transfer k_H as shown in Eq. 5, when the hydrogen transfer is assumed to be the

$$k_{obs} = k_H K_{et} \quad (5)$$

rate-determining step. The K_{et} values can be evaluated from the one-electron oxidation potentials E^0_{ox} of reductants and the one-electron reduction potential E^0_{red} of Ph_3C^+ using Eq. 6. Then, the k_H values can be evaluated from the values of k_{obs}, E^0_{ox}, and E^0_{red} using

$$\log K_{et} = -F(E^0_{ox} - E^0_{red})/(2.3RT) \quad (6)$$

Eqs. 5 and 6. The k_H values thus determined are also listed in Table 1.

The second-order rate constant of the radical trap of $Ph_3C\cdot$ with oxygen is known to be close to the diffusion-limited value, 5×10^8 dm^3 mol^{-1} s^{-1}.[12] In

Table 1. Observed Second-Order Rate Constants k_{obs} of Hydride Transfer Reactions from Reductants (a Rhenium-Alkyl Complex and NADH Model Compounds) to Ph_3C^+ in the Absence and Presence of Oxygen in MeCN at 298 K, the One-Electron Oxidation Potentials E^0_{ox} of Reductants, and the Rate Constants k_H of Hydrogen Transfer from the Radical Cations of Reductants to $Ph_3C\cdot$

Reductant	k_{obs}[a]	E^0_{ox} vs. SCE	k_H
	$dm^3\ mol^{-1}\ s^{-1}$	V	s^{-1}
$PhCH_2$-(Re)[b]	2.3×10[c] (2.4×10^2)[c]	0.48[c]	8.2×10^5
BNAH	8.9×10^4 (8.9×10^4)	0.57[d]	1.3×10^{10}
$AcrH_2$	1.7×10^3 (1.7×10^3)	0.80[d]	7.3×10^{11}

a) The values in parentheses are those determined in the presence of oxygen (4 atm unless otherwise noted). b) [CpRe(NO)(PPh_3)(CH_2Ph)]. c) Determined in CH_2Cl_2 at 208 K. The value in parenthesis is determined in aerated MeCN. The data are taken from Ref. 12. d) Taken from Ref. 6.

such a case, 1×10^{-3} mol dm^{-3} oxygen may be sufficient for the oxygen trap to compete with the intramolecular hydrogen transfer process of the rhenium-benzyl complex, resulting in the increase of the overall reaction rate. In contrast, the k_H values of NADH model compounds (Table 1) are too large for the oxygen trap to compete with the hydrogen transfer process, resulting in no effect of oxygen on the observed rate constant k_{obs} of the overall hydride transfer reactions. In the case of BNAH, the rate constant k_{et} of the forward electron transfer from BNAH to Ph_3C^+ is estimated from the E^0_{ox} and E^0_{red} values using Eq. 7. The estimated value 1.9×10^6 dm^3

$$k_{et} = Z\exp[-F(E^0_{ox} - E^0_{red})/(RT)] \quad (7)$$

$mol^{-1}\ s^{-1}$ is larger than the observed overall rate constant 8.9×10^4 $dm^3\ mol^{-1}\ s^{-1}$. Thus, it is concluded that the hydrogen transfer process (k_H) is the rate determining step following the electron-transfer equilibrium (Scheme 1). In the case of a weaker reductant $AcrH_2$, however, the k_H value becomes close to the frequency factor ($h/kT=6\times10^{12}\ s^{-1}$) and thus, the electron transfer may occur concertedly with the hydrogen transfer. In such a case, the differentiation between electron-hydrogen transfers and one-step hydride transfer becomes dubious and these two mechanisms should be reconciled into single unified one.

References

1) A. Ohno, Y. Ishikawa, S. Ushida, and S. Oka, *Tetrahedron Lett.*, **23**, 3185 (1982); S. Shinkai, H. Hamada, Y. Kusano, and O. Manabe, *J. Chem. Soc., Perkin Trans. 2*, **1979**, 699; S. Shinkai, H. Hamada, and O. Manabe, *Tetrahedron Lett.*, **1979**, 1397; A. Awano and W. Tagaki, *Bull. Chem. Soc. Jpn.*, **59**, 3117 (1986).

2) S. Fukuzumi, M. Ishikawa, and T. Tanaka, *J. Chem. Soc., Chem. Commun.*, **1985**, 1069; *Tetrahedron*, **42**, 1021 (1986); *Chem. Lett.*, **1989**, 1227.

3) S. Fukuzumi, M. Chiba, and T. Tanaka, *Chem. Lett.*, **1989**, 31; S. Fukuzumi, S. Mochizuki, and T. Tanaka, *J. Am. Chem. Soc.*, **111**, 1497 (1989).

4) S. Singh and V. K. Sharma, *Tetrahedron Lett.*, **1979**, 2733; S. Singh, V. K. Sharma, S. Gill, and R. I. K. Sahota, *J. Chem. Soc., Perkin Trans. 1*, **1985**, 437.

5) S. Singh, S. Nagrath, and M. Chanana, *J. Chem. Soc., Chem. Commun.*, **1986**, 282; S. Singh, S. Gill, V. K. Sharma, and S. Nagrath, *J. Chem. Soc., Perkin Trans. 1*, **1986**, 1273.

6) S. Fukuzumi, S. Koumitsu, K. Hironaka, and T. Tanaka, *J. Am. Chem. Soc.*, **109**, 305 (1987).

7) H. J. Dauben, Jr., L. R. Honnen, and K. M. Harmon, *J. Org. Chem.*, **25**, 1442 (1960).

8) D. D. Perrin, W. L. F. Armarego, and D. R. Perrin, "Purification of Laboratory Chemicals," Pergamon Press, New York (1966).

9) M. F. Asaro, S. R. Cooper, and N. J. Cooper, *J. Am. Chem. Soc.*, **108**, 5187 (1986).

10) R. Breslow, W. Bahary, and W. Reinmuth, *J. Am. Chem. Soc.*, **83**, 1763 (1961).

11) J. C. Hayes and N. J. Cooper, *J. Am. Chem. Soc.*, **104**, 5570 (1982).

12) G. S. Bodner, J. A. Gladysz, M. F. Nielsen, and V. D. Parker, *J. Am. Chem. Soc.*, **109**, 1757 (1987).

Reaction Behavior of Propylene Oxide in Various Solvents in the Presence of Boron Trifluoride

Shigeru SUGIYAMA,* Shinji ÔHIGASHI, Kiyozumi SATO,
Sadao FUKUNAGA, and Hiromu HAYASHI
Department of Chemical Science and Technology, Faculty of Engineering,
The University of Tokushima, Minamijosanjima, Tokushima 770
(Received May 26, 1989)

Synopsis. The reaction behavior of propylene oxide with boron trifluoride was affected remarkably by solvent. In dioxane, the isomerization to propionaldehyde proceeded smoothly and selectively, while the reaction behavior in heptane, benzene, and tetrahydrofuran was quite different from that in dioxane.

Since Heusser et al. reported the use of boron trifluoride (BF_3) for the isomerization of substituted ethylene oxides,[1] BF_3 has been used widely as a Lewis acid in organic synthesis.[2] In the reaction of propylene oxide, boron trifluoride etherate ($BF_3 \cdot OEt_2$) was used as a polymerization catalyst but has not been reported as an isomerization catalyst.[3] Generally, $BF_3 \cdot OEt_2$ equilibrates in the exchange reactions with cyclic[4] and acyclic[5] ethers, while it dissociates to BF_3 and ether in CH_2Cl_2 to some extent.[6] It is hence expected that the acid strength of BF_3 may be adjusted by selection of solvent. In connection with our studies on epxides,[7,8] we observed an interesting solvent effect in the isomerization of propylene oxide (**1**) to propionaldehyde (**2**) and acetone (**3**) with $BF_3 \cdot OEt_2$. In heptane and benzene, polymerization of **1** occurred as expected, but the reaction behavior was greatly dependent on each solvent. In tetrahydrofuran (THF), the copolymerization of **1** and THF was observed as reported in the literature.[9,10] However, the isomerization to **2** proceeded smoothly and selectively in dioxane. To the best of our knowledge, such a behavior has not been previously described. The findings will be described herein.

Experimental

To a reaction solution (25 cm^3) of **1** (0.5 M)(1 M=1 mol dm^{-3}), a known amount of $BF_3 \cdot OEt_2$ was added and stirred magnetically at room temperature. The progress of the reaction was monitored with a Hitachi 163 model gas chromatograph (3 mmϕ×3 m stainless steel column: 15% PEG 4000 on Uniport B at 70 °C). After a given time, the reaction solution was treated with poly(4-vinylpyridine) (Aldrich; 7.6 mequiv g^{-1}) in order to remove the catalyst and filtered off. The filtrate was evaporated in vacuo at 50 °C until the weight of the residue became constant. In the reaction in THF, the reaction solution was directly analyzed by an IR spectrum . Solvents (Special Grade of Wako Co.), $BF_3 \cdot OEt_2$ (Tokyo Kasei Co.), and **1** (Tokyo Kasei Co.) were used without further purifications. No isomers were found in the commercial **1** gas chromatographically. The IR spectra of the polymers and the reaction solution were recorded as liquid film inserted between NaCl plates. A Shimadzu IR-400 spectrophotometer was used.

Results and Discussion

Solvent Effect. Figure 1 illustrates the solvent

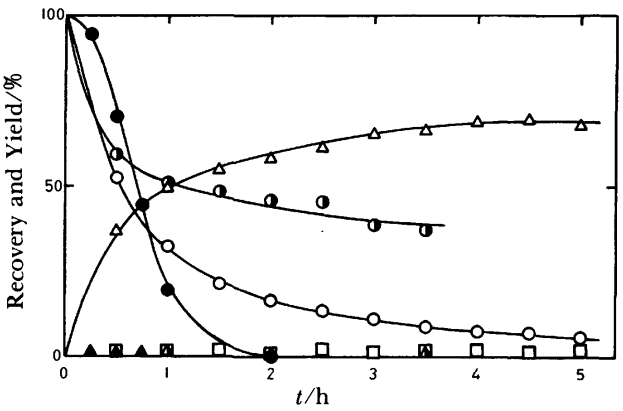

Fig. 1. Reaction behaviors of **1** with $BF_3 \cdot OEt_2$ in various solvents. ○: Recovery of **1**, △: yield of **2**, □: yield of **3**. Open symbols: in dioxane, half-filled symbols: in benzene, filled symbols: in THF.

Table 1. Relative Acid Strength of $BF_3 \cdot OEt_2$ in Various Solvents

Indicator[a]	A	B	C	Ref.
Acid range	Dilute HCl	56—75% H_2SO_4	77—94% H_2SO_4	
Sample				
Concd H_2SO_4	○	○	○	
$BF_3 \cdot OEt_2$	○	○	×	
$BF_3 \cdot OEt_2$/Et_2O	○	×	×	
$BF_3 \cdot OEt_2$/Dioxane	○	×	×	
$BF_3 \cdot OEt_2$/THF	○	×	×	
$BF_3 \cdot OEt_2$/Heptane[b]	○	×	×	Heptane Layer
	○	○	×	Etherate Layer
$BF_3 \cdot OEt_2$/Benzene	○	○	×	

○: Color change identical with that caused by concd H_2SO_4. a) A; 4-(Phenylazo)diphenylamine, B; benzylideneacetophenone, C; anthraquinone. b) Insoluble.

effect on the reaction behavior of **1** with a catalytic amount of $BF_3 \cdot OEt_2$ (30 mg, 0.21 mmol). In heptane, $BF_3 \cdot OEt_2$ did not dissolve completely but form fine oily drops. Immediately after the catalyst was added to a heptane solution of **1**, a brown oil separated and **1** was not detected in the reaction solution.

As shows in Fig. 1, **1** was consumed slowly in benzene during the reaction, but the isomers were scarcely formed. The product was identified as poly(propylene oxide) (PPO) by its IR spectrum,[3] which was in agreement with the spectrum of the product obtained in heptane [IR ν: 3400, 2850, 1440, 1380, and 1080 cm^{-1}]. In THF, a reverse S-type curve was observed and remarkable constriction of the volume (ca. 2 cm^3) of the reaction medium (25 cm^3) occured to give a viscous solution. The IR spectrum of the reaction solution indicated absorption due to alkyl ethers, overlapped with that of THF, and the absence of **1** [IR ν: 2850, 1450, 1360, 1060, and 900 cm^{-1}]. In the present case, copolymerization of **1** and THF by $BF_3 \cdot OEt_2$ proceeded.[9,10] In contrast, the isomerization of **1** to **2** proceeded smoothly and selectively in dioxane. In order to explain the present results, one should consider and an actual acid strength of $BF_3 \cdot OEt_2$ in each solvent. Table 1 lists the relative acid strength of $BF_3 \cdot OEt_2$ in each solvent (1:2 by mole ratio) estimated by Hammett indicators.[11]

In the case of oxygen-containing solvents, the acid strength of $BF_3 \cdot OEt_2$ was decreased due to equilibrated trapping of free BF_3 from the etherate by the solvent. In benzene, the acid strength of $BF_3 \cdot OEt_2$ was high, because benzene interacts only weakly with $BF_3 \cdot OEt_2$. In heptane, a high acid strength must be held due to the low solubility of the etherate and the lack of Lewis basicity of the solvent. The polymerizatin of **1** therefore must need a relatively high acid strength as is shown in heptane and benzene solvents. The decrease in the reactivity of the polymerization in benzene is probably caused by a weak electron-donating character of benzene to decrease the acid strength of $BF_3 \cdot OEt_2$. In cyclic ether solvents, different reaction behavior was observed, although the acid strength of each, estimated by Hammett indicators, was almost the same. It is known that the order of Lewis basicity of ether is as follows.[12]

THF>dioxane>propylene oxide>diethyl ether>epichlorohydrin

BF_3-catalyzed copolymerization between ethers with different basicities such as THF-**1**[9,10] and THF-epichlorohydrin[10] has been reported. However, in the present study, the isomerization of **1** instead of copolymerization predominated in the presence of $BF_3 \cdot OEt_2$ in dioxane whose basicity is similar to that of **1**. BF_3-catalyzed reactions seem to be remarkably affected by the Lewis basicities of the substrate and the solvent. In the isomerization of **1** to **2**, dioxane was found to be an effective solvent presumably due to the appropriate Lewis acidity arising from the exchange reactions between $BF_3 \cdot OEt_2$, **1**, and dioxane. One may expect that an active species in the BF_3-catalyzed reaction is a neutral oxonium salt as shown in the reaction of $BF_3 \cdot OEt_2$, diethyl ether, and epichlorohydrin to give triethyloxonium tetrafluoroborate.[13,14] However, the participation of such a species was not described in the reports about BF_3-catalyzed alkylation of benzene with ethers and alcohols,[15] BF_3-catalyzed polymerization of cyclic ethers,[9,10] and BF_3-catalyzed isomerization of epoxides in benzene and ether.[16] Our results can also be explained by an action of BF_3 as described above. So we conclude that the present reaction of **1** in each solvent proceeds with BF_3.

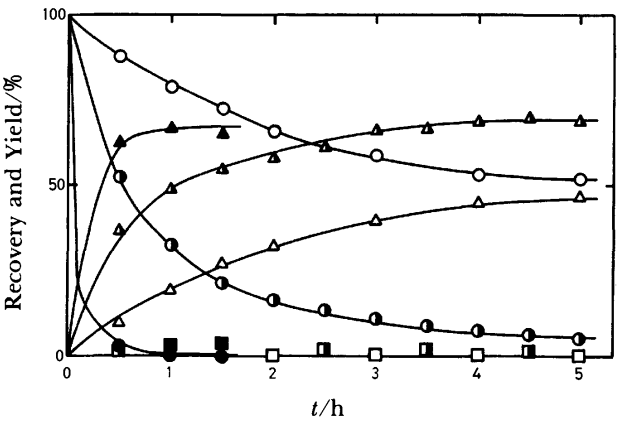

Fig. 2. Isomerization of **1** with $BF_3 \cdot OEt_2$ in dioxane. ○: Recovery of **1**, △: yield of **2**, □: yield of **3**. Open symbols: 0.12 mmol of $BF_3 \cdot OEt_2$, half-filled symbols: 0.21 mmol of $BF_3 \cdot OEt_2$, filled symbols: 0.85 mmol of $BF_3 \cdot OEt_2$.

Effect of Catalyst Amount. The isomerization behavior of **1** to **2** and **3** with different amounts of catalyst are shown in Fig. 2.

In each case, a major product was **2**. The results are reasonable and cosistent with a previous report.[17] On addition of 0.12 mmol of $BF_3 \cdot OEt_2$, the isomerization proceeded almost quantitatively, while the yield of **2** was 46% at 5 h. On addition of 0.21 mmol of the catalyst, the isomerization occurred more rapidly to give 68% yield within 5 h, but the selectivity was relatively poor, because of the polymerization of **1**. After 2 h, about 8% of **1** was isolated as PPO. In the case of 0.85 mmol, the substrate **1** disappeared completely within 30 min to yield 66% of **2**. The final yields of **2** were almost the same whenever 0.21 or 0.85 mmol of the catalyst was used. The addition of an excess of the catalyst in order to increase the yield of **2** thereby led to the polymerization of **1**, resulting in decrease in the selectivity without increase in the yield of **2**. In order to examine the possibility of the copolymerization of **1** and dioxane, the reaction of **1** (101 mmol) and dioxane (203 mmol) with $BF_3 \cdot OEt_2$ (0.21 mmol) was carried out. In this case, only PPO was obtained and no copolymerization occurred.

In conclusion, for the isomerization of **1** to **2**, dioxane was the most favorable solvent. On increasing the amounts of catalyst, the simultaneous polymerization of **1** occured to decrease the selectivity of **2**.

References

1) H. Heusser, K. Eichenberger, P. Kurath, H. R. Dallenbach, and O. Jeger, *Helv. Chem. Acta*, **34**, 2106 (1951).

2) A. P. Marchand, P. Annapurna, and S. P. Reddy, *J. Org. Chem.*, **54**, 187 (1989).
3) Y. Minoura and M. Mitoh, *Makromol. Chem.*, **124**, 241 (1969).
4) A. C. Rutenberg, A. A. Palko, and J. S. Drury, *J. Am. Chem. Soc.*, **85**, 2702 (1963).
5) M. Okada, K. Suyama, and Y. Yamashita, *Kogyo Kagaku Zasshi*, **68**, 1431 (1965).
6) E. Gore and S. S. Danyluk, *J. Phys. Chem.*, **69**, 89 (1965).
7) S. Sugiyama, S. Kubo, and H. Hayashi, *Chem. Express*, **4**, 433 (1989).
8) S. Sugiyama, S. Ôhigashi, R. Sawa, and H. Hayashi, *Bull. Chem. Soc. Jpn.*, **62**, 3202 (1989).
9) L. A. Dickinson, *J, Polym. Sci.*, **58**, 857 (1962).
10) G. V. Korovina, D. D. Novikov, R. A. Barzikina, A. Y. Kuzaev, and S. G. Entelis, *J. Polym. Sci., Part C*, **1968**, 3575.
11) D. L. Hawke and J. Steigman, *Anal. Chem.*, **26**, 1989 (1954).
12) M. Ishimori and T. Tsuruta, *Kogyo Kagaku Zasshi*, **70** 378 (1967).
13) H. Meerwein, G. Hinz, P. Hofmann, E. Kroning, and E. Pfiel, *J. Prakt. Chem.*, [2] **147**, 257 (1937); H. Meerwein, *Org. Synth.*, **46**, 113 (1966).
14) We thank a referee for drawing our attention to this paper.
15) A. Streitwieser, Jr., D. P. Stevenson, and W. D. Schaeffer, *J. Am. Chem. Soc.*, **85**, 1110 (1959).
16) H. O. House, *J. Am. Chem. Soc.*, **77**, 3070 (1955).
17) T. Imanaka, Y. Okamoto, and S. Teranishi, *Bull. Chem. Soc. Jpn.*, **45**, 1353 (1972).

Spectral Studies of Some Coordination Complexes of Pt(II) and Rh(I) with Benzothiazolines

Archana GARG and Jagdish Prasad TANDON*
Department of Chemistry, University of Rajasthan, Jaipur 302004, India
(Received September 12, 1988)

Synopsis. The present paper describes the synthesis and structural features of platinum(II) and rhodium(I) complexes of some benzothiazolines derived by the condensation of various heterocyclic aldehydes viz. 2-pyridinecarbaldehyde, 2-furancarbaldehyde, and 2-thiophenecarbaldehyde. The resulting complexes have been characterized by elemental analyses, conductance measurements and molecular weight determination. The mode of bonding and geometry of these complexes have been suggested on the basis of IR, ^{1}H NMR, electronic spectra, and magnetic studies.

Benzothiazolines derived from the condensation of 2-aminobenzenethiol with the carbonyl compounds constitute an important series of ligands with ONS and NS donor systems.[1] The condensation of 2-mercapto amine with an aldehyde does not normally lead to the isolation of the corresponding Schiff base, but rather to a thiazoline (with a 2-aminobenzenethiol) or a thiazolidine (with a 2-mercaptoalkylamine).[2–5] However, it has been shown that the metal ion acts as a template and favors the formation of the Schiff base rather than the 2,2′-bi(benzothiazoline) form.[6] Later Jadamus et al.[7] reported that even in the absence of metal ion the condensation product of aldehyde and ketone with 2-aminobenzenethiol forms a mixture of benzothiazoline and the Schiff base and an equilibrium may exist between the two as shown below:

where R=

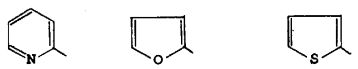

The above equilibrium gets shifted to the right hand side in presence of the metal ion. Singh et al.[8] have studied the reactions of trimethylchlorosilane and dimethylchlorosilane with similar ligands and found that the complexes are five- and six-coordinated. Similarly Tandon et al.[9,10] have studied the reactions of these ligands with transition metals and the geometry of metal complexes have been deduced on the basis of various spectral studies.

Experimental

Preparation of Ligand. Benzothiazolines (HL) were prepared by the condensation of 2-aminobenzenethiol with 2-pyridine-, 2-furan-, and 2-thiophenecarbaldehyde.[11]

Preparation of Complexes. Cyclooctadienyl Complexes of Rhodium [$C_8H_{12}RhL$]: [$C_8H_{12}RhOMe]_2$ was prepared according to the literature method.[12,13] It was then dissolved in ethanol and an ethanolic solution of benzothiazoline in requisite amount was added to it. The solution was refluxed for three hours and cooled. The complex got separated, which was washed repeatedly with cyclohexane and dried in vacuo.

[Pt(HL)$_2$]Cl$_2$: $K_2[PtCl_4]$ was dissolved in a 1:1 mixture of water and ethanol. To this solution, an ethanolic solution of ligand was added and it was then refluxed for about one hour. On cooling, the complex separated out, which was filtered and washed several times with a mixture of water and ethanol and dried in vacuo.

PtL$_2$: The 1:1 water-ethanol solution of $K_2[PtCl_4]$ was mixed with an ethanolic solution of benzothiazoline. Aqueous ammonia was added to the above mixture dropwise until the solution was weakly alkaline. The mixture was refluxed for about two hours and the solid compound was filtered out. It was then washed with the mixture of water and ethanol and dried in vacuo.

Analytical Methods and Physical Measurements. Platinum was estimated gravimetrically[14] and nitrogen by the Kjeldahl's method. Carbon and hydrogen analyses were performed at the microanalytical laboratory of this department. Other measurements were carried out as reported earlier.[11]

Results and Discussion

The 1:1 and 1:2 molar ratio reactions of [$C_8H_{12}RhOMe]_2$ and $K_2[PtCl_4]$ with benzothiazolines in ethanol medium take place as follows:

1. $[C_8H_{12}RhOMe]_2 + 2N\frown SH \longrightarrow 2[C_8H_{12}Rh(N\frown S)_2] + 2MeOH$ **I**

2. $K_2PtCl_4 + 2N\frown SH \longrightarrow [Pt(N\frown SH)_2]Cl_2 + 2KCl$ **II**

3. $K_2PtCl_4 + 2N\frown SH + 2NH_4OH \longrightarrow [Pt(N\frown S)_2] + 2KCl + 2NH_4Cl + 2H_2O$ **III**

All the newly synthesized complexes are colored and monomeric solids. The rhodium complexes are soluble in most of the common organic solvents, whereas complexes of platinum are soluble in *N,N*-dimethylformamide (DMF) and dimethyl sulfoxide (DMSO). The conductanec date of 10^{-3} M solutions (1 M=1 mol dm^{-3}) of complexes at the room temperature show that the complexes of the type **II** are 1:2 electrolytes (200—210 ohm^{-1} mol^{-1} cm^{-2}) and complexes **I** and **III** are nonelectrolytes (15—20 ohm^{-1} mol^{-1} cm^2). All the solids are diamagnetic as expected for the d^8 square planar complexes.

In the solid state IR spectra of benzothiazoline the absence of ν(SH) and appearance of ν(NH) at ca. 1670 cm^{-1} and 3400—3200 cm^{-1} is strong evidence for a ring structure.[15] Further in metal complexes ν(NH)

disappears and in the complexes of type II band due to ν(SH) is observed at ca. 2520 cm^{-1} and which suggests the coordination of sulfur to the metal atom in these complexes.

However, the disappearance of ν(NH) band in the spectra of metal complexes shows its deprotonation and chelation of nitrogen of the ligand to the central metal atom. Further, in the spectra of metal complexes, a strong band around 1580±10 cm^{-1} may be ascribed to the coordinated >C=N group and this very well supports the fact that the resulting complexes are metal azomethine derivatives, as the benzothiazoline ring rearranges to give the azomethine form which in presence of metal ion finally acts as a monobasic bidentate ligand.

Further, in the spectra of rhodium complexes, a sharp band at ca. 1470 cm^{-1} may be due to ν(C=C) of cyclooctadiene moiety, lowered by coordinaton.[16]

To further confirm the bonding pattern in these complexes, proton magnetic resonance spectra of 2-(2-pyridyl)benzothiazoline and it's metal derivatives have been recorded in DMSO-d_6 using TMS as internal reference. The spectrum of 2-(2-pyridyl)benzothiazoline shows the N-H proton signal at δ 4.58 and it disappears in the corresponding metal complexes due to it's deprotonation. The signal due to azomethine proton is observed at δ 8.00 and shifts downfield (δ 8.40) in the spectra of metal complexes, suggesting coordination of azomethine nitrogen to the metal atom. In the spectra of complexes $[Pt(N\frown SH)_2]Cl_2$, the signal appearing at δ 4.85 is due to the SH group.[17] Further, two signals observed at δ 2.5 and 1.6 in the spectrum of rhodium complex may be assigned to the $-CH_2$ group of cyclooctadiene.

In the electronic spectra of platinum(II) complexes, three d-d spin allowed transitions are observed corresponding to the transitions from the three lower lying d levels to the empty $d_{x^2-y^2}$ orbital. The ground state $^1A_{1g}$ and the excited states corresponding to the above transitions are $^1A_{2g}$, $^1B_{1g}$, and ^1E_g, in order of increasing energy. Three different orbital parameters Δ_1, Δ_2, and Δ_3 have been calculated by first using the corelation, $F_2=10F_4=600$ cm^{-1} for the Slator-Condon interelectronic repulsion parameters (F_2 and F_4) and subseuqently the equations suggested by Gray and Ballhausen.[18] The parameters Δ_1, Δ_2, and Δ_3 lie in the

Table 1. Physical Properties and Analysis of Metal Complexes

S.No.	Reactants		Molar ratio	Color and state of compound	Mp/°C	% Analysis (Found/Calcd)			
	Metal compound	Ligand				C	H	N	S
1	$(C_8H_{12}RhOMe)$	Pyridyl BT[a] $(C_{12}H_{10}N_2S)$	1:1	$C_8H_{12}Rh(C_{12}H_9N_2S)$ Dark brown solid	166d	56.4 (56.6)	4.8 (4.9)	6.5 (6.6)	7.2 (7.5)
2	$K_2[PtCl_4]$	Pyridyl BT[a] $(C_{12}H_{10}N_2S)$	1:2	$Pt(C_{12}H_{10}N_2S)_2Cl_2$ Yellow solid	121d	41.0 (41.5)	3.0 (2.9)	8.0 (8.1)	9.1 (9.2)
3	$K_2[PtCl_4]$	Pyridyl BT[a] $(C_{12}H_{10}N_2S)$	1:2	$Pt(C_{12}H_9N_2S)_2$ Yellow solid	211d	46.2 (46.4)	2.8 (2.9)	8.9 (9.0)	10.1 (10.3)
4	$(C_8H_{12}RhOMe)$	Furyl BT[b] $(C_{11}H_9ONS)$	1:1	$C_8H_{12}Rh(C_{11}H_8ONS)$ Brown solid	*	54.9 (55.1)	5.0 (5.1)	3.3 (3.4)	7.6 (7.7)
5	$K_2[PtCl_4]$	Furyl BT[b] $(C_{11}H_9ONS)$	1:2	$Pt(C_{11}H_9ONS)_2Cl_2$ Dark green solid	232d	39.0 (39.3)	2.6 (2.7)	4.0 (4.2)	9.2 (9.5)
6	$K_2[PtCl_4]$	Furyl BT[b] $(C_{11}H_9ONS)$	1:2	$Pt(C_{11}H_8ONS)_2$ Grey solid	54d	43.9 (44.1)	2.8 (2.7)	4.6 (4.7)	10.4 (10.7)
7	$(C_8H_{12}RhOMe)$	Thienyl BT[c] $(C_{11}H_9NS_2)$	1:1	$C_8H_{12}Rh(C_{11}H_8NS_2)$ Black solid	154d	53.0 (53.1)	4.5 (4.7)	3.2 (3.3)	14.7 (14.9)
8	$K_2[PtCl_4]$	Thienyl BT[c] $(C_{11}H_9NS_2)$	1:2	$Pt(C_{11}H_9NS_2)_2Cl_2$ Brown solid	140d	37.5 (37.5)	2.4 (2.5)	3.9 (4.0)	18.0 (18.1)
9	$K_2[PtCl_4]$	Thienyl BT[c] $(C_{11}H_9NS_2)$	1:2	$Pt(C_{11}H_8NS_2)_2$ Green solid	78	41.6 (41.8)	2.5 (2.5)	4.1 (4.4)	19.9 (20.3)

*; stable upto 320°C. d; decompose. a) 2-(2-Pyridyl)benzothiazoline. b) 2-(2-Furyl)benzothiazoline. c) 2-(2-Thienyl)benzothiazoline.

Table 2. Electronic Spectral Data of Pt(II) Complexes

S.No.	Complexes	Spectral bands/cm^{-1}	Transitions	Δ_1	Δ_2	Δ_3
				cm^{-1}		
1.	$[Pt(C_{12}H_{10}N_2S)_2]Cl_2$	20400	$^1A_{1g} \longrightarrow {}^1A_{2g}$			
		24700	$^1A_{1g} \longrightarrow {}^1B_{1g}$	22500	5500	3600
		28600	$^1A_{1g} \longrightarrow {}^1E_g$			
		30000	C.T.			
		31050				
2.	$[Pt(C_{11}H_8ONS)_2]$	20800	$^1A_{1g} \longrightarrow {}^1A_{2g}$			
		25600	$^1A_{1g} \longrightarrow {}^1B_{1g}$	22900	6000	1100
		27000	$^1A_{1g} \longrightarrow {}^1E_g$			

ranges, 22500—22900 cm^{-1}, 5500—6000 cm^{-1}, and 1100—3600 cm^{-1} respectively (Table 2) and which are in close agreement with the values reported earlier for the square planar geometry.[19,20]

In the electronic spectra of rhodium(I) complexes, the d-d transitions generally appear between 20000—30000 cm^{-1}. However, in the present case intense bands appearing at 31000, 34500, and 37000 cm^{-1} may be due to metal to ligand charge transfer transitions.[21]

Thus, on the basis of the above discussions the following structure can be proposed for the different type of complexes:

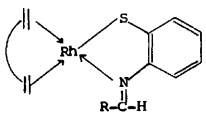

I

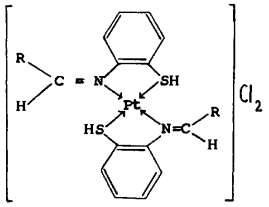

II

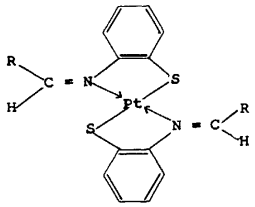

III

References

1) L. F. Lindoy and S. E. Livingstone, *Inorg. Chim. Acta*, **1**, 365 (1967).

2) M. T. Bogert and B. Naiman, *J. Am. Chem. Soc.*, **57**, 1529 (1935).

3) S. Ratnu and H. T. Clarke, *J. Am. Chem. Soc.*, **59**, 200 (1937).

4) F. J. Krepia, V. Mafure, J. J. Finn, J. G. McClamon, and F. Lombardo, *J. Am. Chem. Soc.*, **73**, 1755 (1951).

5) M. C. Thompson and D. H. Busch, *J. Am. Chem. Soc.*, **84**, 1162 (1962).

6) M. C. Thompson and D. H. Busch, *J. Am. Chem. Soc.*, **86**, 213 (1964).

7) H. Jadamus, Q. Fernando, and H. Freiser, *Inorg. Chem.*, **3**, 928 (1964).

8) K. Singh, R. V. Singh, and J. P. Tandon, *Inorg. Chim. Acta*, **151**, 179 (1988).

9) N. Kanoongo, R. V. Singh, and J. P. Tandon, *Synth. React. Inorg. Met-Org. Chem.*, **18** (1988).

10) A. Garg and J. P. Tandon, *Transition Met. Chem.*, **12**, 526 (1987).

11) A. Garg and J. P. Tandon, *Transition Met. Chem.*, **12**, 42 (1987).

12) J. Chatt and L. M. Venanzi, *J. Chem. Soc.*, **1957**, 4735.

13) S. D. Robinson and B. L. Shaw, *J. Chem. Soc.*, **1965**, 4997.

14) A. I. Vogel, "A Text Book of Quantitative Inorganic Analysis," Longmans Green, ELBS, London (1962).

15) R. K. Sharma, R. V. Singh, and J. P. Tandon, *J. Inorg. Nucl. Chem.*, **42**, 1267 (1980).

16) J. A. Ibers and R. G. Snyder, *J. Am. Chem. Soc.*, **84**, 495 (1962).

17) R. M. Silverstein, G. C. Bassler, and T. C. Morrill, "Spectrometric Identification of Organic Compounds," Wiley, New York (1963).

18) H. B. Gray and C. J. Ballhausen, *J. Am. Chem. Soc.*, **85**, 1368 (1963).

19) P. L. Goggin, R. J. Goodfellow, and F. J. S. Reed, *J. Chem. Soc., Dalton Trans.*, **1972**, 1298.

20) S. Chandra, *Synth. React. Inorg. Met.-Org. Chem.*, **13**, 89 (1983).

21) A. B. P. Lever, "Inorganic Electronic Spectroscopy," Elsevier Pub. Company, Amsterdam (1968).

Gravimetric Determination of Nickel with Salicylaldehyde Thiosemicarbazone

S. LALY and Geetha PARAMESWARAN*
Department of Chemistry, University of Calicut, Kerala 673635, India
(Received February 25, 1989)

Synopsis. A study of the use of salicylaldehyde thiosemicarbazone (STSC) in the gravimetric determination of nickel is reported. STSC reacts with Ni(II) in aqueous medium in the pH range 6.5—8.2 to form reddish brown water insoluble complex. The complex can be conveniently filtered at the pump using a G_4 sintered glass crucible and dried at 100—120 °C and weighed as $Ni(C_8H_8N_3OS)_2$. Interference of foreign ions were examined. The influence of concentration, temperature, and pH on the precipitation were studied. The reagent tested in this work was compared with classical 1,2-dioximes[1-3] used in the gravimetric determination of nickel. This method was applied to determine nickel in stainless steel.

The commonly employed organic reagents for the gravimetric determination of nickel were dioximes[1-4] and monoximes.[5-9] Thiosemicarbazones have been used as gravimetric reagent for the estimation of some metal ions.[10-12] In this paper a newly developed gravimetric determination of nickel with salicylaldehyde thiosemicarbazone (STSC) will be described. STSC reacts with Ni(II) in aqueous medium in the pH range 6.5—8.2 to form reddish brown water insoluble complex. The complex is soluble in highly acidic medium, highly alkaline medium, and organic solvents like chloroform, 90—100% ethanol etc. The complex is stable at room temperature for over 24 h. The complex can be conveniently filtered at the pump using a G_4 sintered glass crucible and dried at 100—120 °C and weighed as $Ni(C_8H_8N_3OS)_2$.

The present method is superior to other methods that the pH range is wide and the solubility of the complex in cold and hot water is very low and the complex is partially soluble in rectified spirit or 90—100% ethanol. Its lower conversion factor or high relative molecular masses give appreciably higher sensitivities than classical reagents.

Experimental

Reagents. All chemicals were of reagent grade. Stock solution (0.5%) of STSC in methanol was prepared. The nickel solutions were prepared from nickel chloride and standardized with dimethylglyoxime. 2 mol dm^{-3} sodium acetate solution was prepared.

Synthesis of STSC. Mixture of salicylaldehyde[13] and thiosemicarbazide (1:1 ratio) in 80% ethanol or methanol was refluxed for 2 h. The mixture was cooled and the precipitated STSC was filtered off and dried in a desiccator.

Apparatus. Global digital pH meter, Perkin-Elmer 577 Infrared spectrometer, Gouy-type magnetic balance.

Procedure. An aliquot of Ni(II) solution containing 20 to 40 mg of metal was placed in a 250 ml beaker and was diluted to 100 ml with distilled water. The solution was heated to 70—80 °C and the pH was adjusted to 6.5—8.2 with 2 mol dm^{-3} sodium acetate solution. To this 25—50 ml of 0.5% STSC solution was added with constant stirring and the mixture was heated in a water bath for 30 min. The mixture was allowed to cool and filtered through a weighed G_4 sintered glass crucible. Then it was washed with 40—60% hot methanol solution and finally with distilled water and dried at 110—120 °C. Conversion factor for $Ni(C_8H_8N_3OS)_2$ to Ni is 0.1314.

Results and Discussion

Properties of the Reagents. Salicylaldehyde thiosemicarbazone, was poorly soluble in water but soluble in methanol. Solution in methanol stored at room temperatures was stable for at least 1 month.

Study of Nickel Salicylaldehyde Thiosemicarbazone Complex. Elemental analysis of the nickel complex confirmed the formula $Ni(C_8H_8N_3OS)_2$. A study was made to elucidate the structure. The infrared spectra showed a shift in the C=N stretching vibration bands in relation to the reagent at 1600—1620 cm^{-1} and double bands appeared; on the other hand bands due to the C=S group disappeared and C-S vibration bands showed up. The strong band at 3400 cm^{-1} in the spectrum of the ligand may be due to ν_{-OH}. Since this band is retained almost at the same position, it was an evidence for the nonparticipation of the oxygen atom of the phenolic hydroxyl group in coordination (Fig. 1). A study of the magnetic susceptibility showed that the nickel STSC complex is diamagnetic at 293 K.

From these results it can be concluded that the Ni–STSC complex is square-planar. In general thiosemicarbazones usually react as chelating ligands with transition metal ions by bonding through the sulfur and hydrazine nitrogen atoms.[14]

Determination of Optimum Experimental Conditions for Precipitation. The effect of increasing amounts of reagent was investigated. It was found that for every 10 mg of nickel, 15—20 ml of 0.5% methanolic solution of the reagent sufficed.

Experiments were conducted at various temperatures. Precipitation occurred at room temperature and also at high temperatures. Below 50 °C the solution was found turbid. Therefore precipitation was conveniently conducted above 70 °C.

To determine the optimum pH, complex was precipitated from solutions at different pH, adjusted by

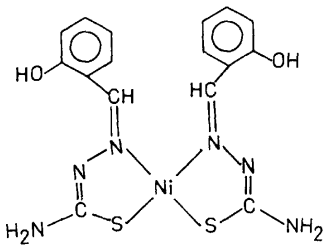

Fig. 1.

Table 1. Effect of Reagent Concentration

Sodium acetate 2 mol dm^{-3} Reagent in ml	Ni=20.09 mg Ni found	Reagent 0.5% Error in mg
5	8.80	−11.29
10	9.20	−10.89
15	10.68	−9.41
20	15.74	−4.35
25	19.67	−0.42
30	20.10	+0.01
35	20.25	+0.16
40	20.55	+0.46

Table 2. Effect of Foreign Ions in the Determination of Ni(II) Using STSC (Ni(II) taken 21.37 mg)

Ions	Tolerance limit in mg
Na^+, K^+, Ag^+, Zn^{2+}, Cl^-, F^-, Br^-, I^-, thiosulfate, thiocyanate, oxalate, tartrate, acetate	100
Pb^{2+}, Hg^{2+}, Cd^{2+}, Mo^{6+}, citrate, phosphate, sulfate nitrate, tetraborate, hydrogen carbonate	50
Mn(II), Bi(III), As(III), Fe(III), Co(II), Th(IV), U(VI)	25
Cu(II), CN^-	10
EDTA	a)

a) Which interfere strongly.

Table 3. Estimation of Metal

Ni(II) added in mg	Ni(II) found in mg	Error in mg	%Error
17.69	17.69	0.00	0
21.37	21.55	+0.18	+0.84
20.09	20.15	+0.06	+0.30
22.41	22.27	−0.14	−0.62
26.53	26.59	+0.06	+0.23
29.24	29.36	+0.12	+0.41

Average of seven determinations.

means of different buffers. The optimum pH was found to be 6.5—8.2.

The influence of various solvents for washing the precipitates was studied. Experiments with different amount of methanol showed that 30—70% methanol water mixture was suitable for washing the precipitate.

Effect of Diverse Ions. Nickel (21.37 mg) was gravimetrically determined in the presence of varying amounts of other cations and anions and the limit of concentration that can be tolerated are given in Table 2.

Composition of the Complex. The amount of precipitate obtained from a known quantity of nickel agreed with the formula $Ni(C_8H_8N_3OS)_2$, which was proved by analysis (Found: C, 42.89; N, 18.58; H, 3.2; S, 13.7%. Calcd: C, 42.98; N, 18.79; H, 3.6; S, 14.3%). The conversion factor is 0.1314. Reproducible results were obtained using varying amounts of nickel as shown in Table 3.

Table 4. Analysis of Stainless Steel

	Ni found using STSC	Ni found using DMG
Sample I	11.29	11.41
Sample II	14.21	14.30
Sample III	29.01	29.21
Sample IV	67.37	67.80

Applications

Determination of Nickel in Stainless Steel. A known weight (1.2 mg) of sample was treated with 50 ml of 12% sulfuric acid and boiled for 1 h nearly to dryness. It was then heated to dryness with 10 ml of concentrated nitric acid, cooled, and added 5 ml concentrated hydrochloric acid. The mixture was boiled, cooled, and made upto 100 ml. Aliquots of this solution (20 ml) was taken, treated with 1:1 ammonia and then filtered through Whatman No. 41 filter paper. The precipitate was dissolved by adding hot hydrochloric acid dropwise and the solution was collected in a beaker, reprecipitated with 50 ml of aqueous ammonia (1:1) and filtered on the same filter paper. The solution was concentrated to 70 ml and nickel was determined with STSC, at pH 7.5 adjusting with sodium acetate solution. The values are given in Table 4.

References

1) V. M. Peshkova and V. M. Savostina, "Analytical Chemistry of Nickel Israel Programme for Scientific

Translations," Jerusalem (1967), p. 53.
2) J. Basset, G. B. Leton, and A. I. Vogel, *Analyst*, **92**, 279 (1967).
3) P. Jain, R. B. Singh, B. S. Garg, and R. P. Singh, *J. Su. Ind. Res.*, **39**, 219 (1980).
4) P. Chattopadhyaya and S. K. Majumdar, *Indian J. Chem., Sect. A*, **26**, 896 (1987).
5) V. V. Balakrishna and N. A. Raju, *J. Indian Chem. Soc.*, **63**, 512 (1986).
6) K. K. Desai and H. B. Naik, *Indian J. Chem., Sect. A*, **25**, 297 (1986).
7) M. Mittal; Lal, Keemti, B.; and S. P. Gupta, *Rev. Port. Quin.*, **25**, 213 (1983).
8) G. K. Jetty, S. Jai, and S. N. Rastogi, *Bangladesh J. Sci. Ind. Res.*, **16**, 134 (1981).
9) Lal, Keemti, B.; Malhotra, and Sita Rani, *Acta Turc.*, **8**, 145 (1980).
10) S. Stankoviansky, J. Carsky, and A. Beno, *Chem. Zvesti*, **23**, 589 (1969).
11) S. S. Guha Sircar and S. Satpathy, *J. Indian Chem. Soc.*, **31**, 450 (1954).
12) Z. Hovorka and Z. Holzbecher, *Bull. Int. Acad. Techeque Sci. Cl. Math. Nat. Med.*, **51**, 43 (1953).
13) A. I. Vogel, "A Text Book of Practical Organic Chemistry," ELBS, Longman (1971), p. 703.
14) J. M. Campbell, *Coord. Chem. Rev.*, **15**, 279 (1975).

Unequivocal Synthesis of the Four *d,l*-Pairs of 3-Substituted 2-Aminonorbornane-2-carboxylic Acids

Alberto AVENOZA, Carlos CATIVIELA,*,† Jose A. MAYORAL,† and Miguel A. ROY
Departamento de Química Orgánica, Colegio Universitario de la Rioja, Logroño, Spain
†Departamento de Química Orgánica, Instituto de Ciencias de los Materiales de Aragón, Universidad de Zaragoza, 50009, Zaragoza, Spain
(Received January 17, 1989)

Synopsis. The Diels-Alder reaction between methyl α-cyanocinnamate and cyclopentadiene, as a key step in the synthesis of 2-amino-3-phenylnorbornane-2-carboxylic acids, is studied. The cycloadducts can be easily separated and converted into the amino acids through simple reactions.

Alicyclic amino acids, such as those with a norbornane skeleton are of interest because of their noticeable biological activities.[1] The parent compounds, 2-aminonorbornane-2-carboxylic acids, can be obtained by Diels-Alder reaction between *N*-acyl-α,β-dehydroalaninates and cyclopentadiene.[2] Nevertheless, the Diels-Alder reaction between cyclopentadiene and *N*-acyl-α,β-dehydrophenylalaninates does not lead to the corresponding amino acids. Furthermore, the reaction of ethyl α-nitrocinnamate with cyclopentadiene followed by catalytic hydrogenation and hydrolysis leads to a mixture of diastereoisomers,[3] so we have directed our attention to the development of a new unequivocal synthesis of the four *d,l*-pairs of the 2-amino-3-phenylnorbornane-2-carboxylic acids (**5**, **8**, **11**, **15**). This synthesis is based on the use of a compound with well-defined stereochemistry and two withdrawing groups which are precursors of both, amino and carboxyl groups as a dienophile, the compound being methyl (*E*)-α-cyanocinnamate[4] (**1**).

Experimental

Table 1 shows the conditions and proportions of the reagents used in the Diels-Alder reaction, together with the results obtained. Figure 1 shows the synthetic route leading to the four amino acids (**5**, **8**, **11**, **15**) and the yields obtained in each step. All products were characterized by elemental analysis and ^{1}H NMR spectra. Microanalyses were carried out on a Perkin-Elmer 240-B analyser. ^{1}H NMR spectra were recorded on a Varian XL-200. Deuterochloroform and D_2O were used as solvents with TMS as the internal standard (the chemical shifts are reported in ppm on the δ scale, coupling constants in Hz).

2a: mp 73—75 °C. Found: C, 76.05; H, 6.08; N, 5.60%: Calcd for $C_{16}H_{15}NO_2$: C, 75.87; H, 5.97; N, 5.53%: ^{1}H NMR ($CDCl_3$): δ=1.91 (1H, dd, *J*=9.6, 2.0), 2.33 (1H, d, *J*=9.6), 3.29 (1H, s), 3.61 (1H, d, *J*=2.0), 3.65 (1H, s), 3.84 (3H, s), 6.06 (1H, dd, *J*=5.6, 2.8), 6.57 (1H, dd, *J*=5.6, 3.2), 7.28—7.42 (5H, m).

2b: mp 88—90 °C. Found: C, 76.10; H, 6,12; N, 5.40%:

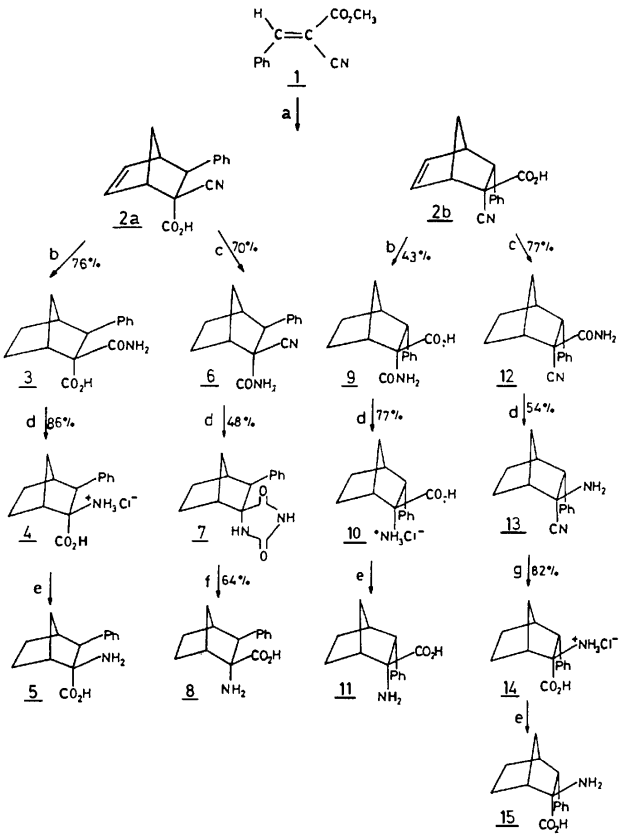

a) i. cyclopentadiene, ii. HO^-/H_2O, iii. iodolactone sep. b) i. H_2O_2/HO^-, ii. H_2(Pd/C). c) i. CH_2N_2/Et_2O, ii. NH_3/MeOH, iii. H_2(Pd/C). d) Br_2/HO^-, Δ. e) Dowex 50W 20—50 mesh, H^+ form. f) $Ba(OH)_2/H_2O/\Delta$. g) 6 M HCl/Δ.

Fig. 1.

Table 1. Diels-Alder Reaction between Methyl (*E*)-α-Cyanocinnamate (**1**) and Cyclopentadiene

Lewis acid	Solvent	Diene/dienophile	*t*/h	*T*/°C	Conversion[a]/%	Ratio[a] of **2a**/**2b** methyl esters
—	1,4-Dioxane	3:1	24	60	83	1.59:1
—	MeOH	3:1	24	60	94	1.60:1
—	H_2O[b]	3:1	7.5	25	100	1.68:1

a) Determined by HPLC. Column: 5 μm Hypersil RMOS (C_8). Eluent: MeOH: H_2O; 60% of MeOH 1 min; gradient 60 to 75% of MeOH 1 min; 75% of MeOH. Flow rate 2 ml min^{-1}. Detection 210 nm $\varepsilon_1:\varepsilon_{2a}:\varepsilon_{2b}$=1.217:1.137:1.00. b) Because of the low solubility a suspension of both diene and dienophile in water was used.

Calcd for $C_{16}H_{15}NO_2$: C, 75.87; H, 5.97; N, 5.53%: ^{1}H NMR ($CDCl_3$): δ=1.72 (1H, d, J=9.2), 1.94 (1H, d, J=9.2), 3.34 (1H, s), 3.52 (1H, s), 3.90 (3H, s), 4.14 (1H, d, J=2.7), 6.50 (1H, dd, J=5.5, 3.2), 6.69 (1H, dd, J=5.5, 3.0), 7.23—7.32 (5H, m).

5: mp>300 °C. Found: C, 72.64; H, 7.33; N, 6.12%: Calcd for $C_{14}H_{17}NO_2$: C, 72.70; H, 7.41; N, 6.06%: ^{1}H NMR (D_2O): δ=1.51—1.58 (5H, m), 1.86 (1H, m), 2.37 (1H, s), 2.65 (1H, s), 3.10 (1H, s), 7.35—7.38 (5H, m).

8: mp>300 °C. Found: C, 72.71; H, 7.49; N, 6.18%: Calcd for $C_{14}H_{17}NO_2$: C, 72.70; H, 7.41; N, 6.06%: ^{1}H NMR (D_2O): δ=1.44—1.74 (5H, m), 2.55 (2H, s), 2.70 (1H, m), 2.84 (1H, s), 7.19—7.23 (5H, m).

11: mp>300 °C. Found: C, 72.80; H, 7.30; N, 6.13%: Calcd for $C_{14}H_{17}NO_2$: C, 72.70; H, 7.41; N, 6.06%: ^{1}H NMR (D_2O): δ=1.39—1.64 (5H, m), 2.01 (1H, m), 2.48 (1H, s), 2.65 (1H, s), 3.53 (1H, d, J=2.0), 7.16—7.29 (5H, m).

15: mp>300 °C. Found: C, 72.85; H, 7.28; N, 6.11%: Calcd for $C_{14}H_{17}NO_2$: C, 72.70; H, 7.41; N, 6.06%: ^{1}H NMR (D_2O): δ=1.43—1.80, (5H, m), 2.39 (1H, m), 2.63 (1H, s), 2.78 (1H, s), 3.20 (1H, d, J=2.0), 7.05—7.34 (5H, m).

Results and Discussion

Table 1 shows the results obtained in the Diels-Alder reaction between cyclopentadiene and methyl (*E*)-α-cyanocinnamate (**1**); as can be seen, high levels of conversion can be achieved under several conditions. Several authors have reported that the use of water greatly increases the rate of Diels-Alder reactions;[5] together with this effect an increase in endo/exo selectivity is sometimes observed. In our case the use of water noticeably increased the reaction rate, but only a small modification in the ratio of cycloadducts (**2a**:**2b**) was obtained.

Cycloadducts **2a** and **2b** were easily separated and converted into the corresponding amino acids by means of simple reactions, but some difficulties stemming from the low reactivity of the groups placed at the endo position, appeared. So when the partial hydrolysis of the cyano group in **2b** was carried out under the conditions used with **2a** (55 °C, 3 days) an equimolecular mixture of **2b** and **9** was obtained, which was treated again under the same conditions to obtain **9** with a total yield of 70% with regard to the initial amount of cycloadduct **2b**.

The Hofmann rearrangement has been the object of several revisions[6] and the results obtained are strongly dependent on the nature of the starting amide. Under the conditions used amide **6** yielded spirohydantoin **7**, probably due to the low intermolecular reactivity of the intermediate isocyanate. The hydrolysis of this spirohydantoin is difficult because position 5 of the hydantoin ring is completely substituted, whereas position 3 is unsubstituted.[7] Hydrolysis was achieved by heating spirohydantoin **7** with aqueous $Ba(OH)_2$ at 140 °C in a closed flask for three days.

Finally the transformation of amino nitrile **13** into amino acid hydrochloride **14** is again made difficult by the low reactivity of the cyano group at the endo position. The transformation was made by heating amino nitrile **13** with 6M HCl (1 M=1 mol dm^{-3}) at 125 °C in a closed flask for fifteen hours.

To sum up, the described synthetic route constitutes a new way to the synthesis of these four amino acids through very simple reactions.

This work was supported by the Comisión Asesora de Investigación Científica y Técnica, project number PB 85-0335.

References

1) H. S. Tager and H. N. Christensen, *J. Am. Chem. Soc.*, **94**, 968 (1972).

2) H. Horikawa, T. Nishitani, T. Iwasaki, Y. Mushika, I. Inoue, and M. Miyoshi, *Tetrahedron Lett.*, **21**, 4101 (1980). M^{a}P. Bueno, C. Cativiela, C. Finol, J. A. Mayoral, and C. Jaime, *Can. J. Chem.*, **65**, 2182 (1987).

3) S. Umezawa, M. Kinoshita, and H. Yanagisawa, *Bull. Chem. Soc. Jpn.*, **40**, 209 (1967).

4) T. Hayashi, *J. Org. Chem.*, **31**, 3253 (1966).

5) D. Rideout and R. Breslow, *J. Am. Chem. Soc.*, **102**, 7817 (1980). R. Breslow, U. Maitra, and D. Rideout, *Tetrahedron Lett.*, **24**, 1901 (1983). R. Breslow and U. Maitra, *ibid.*, **25**, 1239 (1984). S. Larsen and P. Grieco, *J. Am. Chem. Soc.*, **107**, 1768 (1985). P. Grieco, P. Galatsis, and R. Spohn, *Tetrahedron*, **42**, 2847 (1986). A. Lubineau and Y. Quenau, *Tetrahedron Lett.*, **26**, 2653 (1985). H. Schneider and N. Sangwan, *J. Chem. Soc., Chem. Commun.*, **1986**, 1787.

6) For example, E. Wallis and J. Lane, *Org. React.*, **3**, 267 (1957).

7) I. Blagoeva, I. Pojarlieff, and V. Dimitrov, *J. Chem. Soc., Perkin Trans. 2*, **1978**, 887. B. Ivin, G. Rutkovskii, and E. Sochilin, *Zh. Org. Khim.*, **98**, 178 (1983).

Heterocycles Synthesis through Reactions of Nucleophiles with Acrylonitriles. 7. A Novel and Facile One-Step Synthesis of 4*H*-Thiopyrans

Fathy Fahim Abdel-Latif
Chemistry Department, Faculty of Science, El-Minia University, El-Minia, A. R. Egypt
(Received February 10, 1989)

Synopsis. Several new 4*H*-thiopyrans were synthesized via a facile one-step method. Structures and reaction mechanisms are also reported and supported by another synthetic routes.

Thiopyrans and pyrans showed considerable biological activities[1-3] and are important as stabilizers for synthetic resins against heat or light.[4] As a continuation of our previous work for the synthesis of heterocyclic compounds of applied value,[5-8] in this work several new 4*H*-thiopyrans were successfully prepared by a facile one-step method from laboratory available chemicals. Stirring cold ethanolic piperidine solution of equimolar amounts of each of substituted benzaldehyde **Ia—j**, malononitrile, and cyanothioacetamide at room temperature afforded 4*H*-thiopyrans **IIa—j**. The structure of **II** was established for the reaction product based on its analytical and various spectral data (c.f. Experimental). For example, **IIb** showed only one cyano absorption band at 2190 cm^{-1} and one singlet due to the two amino groups at 6.5 ppm in the IR and ^1H NMR spectra respectively. This indicates that the molecule has a plane of symmetry and supports the structure of **IIb**.

Formation of **II** is rationalized in terms of the initial condensation of the aldehyde **I** with malononitrile or cyanothioacetamide affording α-cyanocinnamonitrile **III** or 2-cyano-3-phenyl-2-propenthioamide **IV** respectively followed by the Michael addition of the other active methylene compound to the olefinic bond in **III** or **IV** forming the acyclic intermediate **V** which cyclized under the applied conditions to the thiopyran **II** (Scheme 1).

Structural proof was obtained through another route of synthesis by stirring cold ethanolic piperidine solution of an equimolar amount of **III** with cyanothioacetamide at room temperature and also by stirring ethanolic piperidine solution of **IV** with malononitrile at room temperature (c.f. Scheme 1 and Experimental).

On the other hand, synthesis of 2,6-diamino-3,5-dicyano-4-(2-furyl)-4*H*-thiopyran **IIk** was unsuccessful by using furfural instead of substituted benzaldehyde in this one-step method. While preparation of **IIk** was achieved by stirring ethanolic piperidine solution of α-cyano-β-(2-furyl) acrylonitrile **IIIk** and cyanothioacetamide at room temperature.

Compound **IIk** was also synthesized by another route by refluxing cold ethanolic piperidine solution of an equimolar amounts of 2-cyano-3-(2-furyl)-2-propenethioamide **IVk** and malononitrile at room

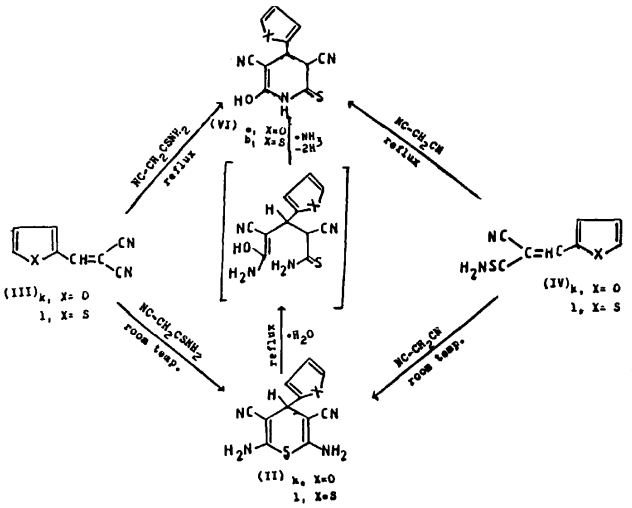

Scheme 2.

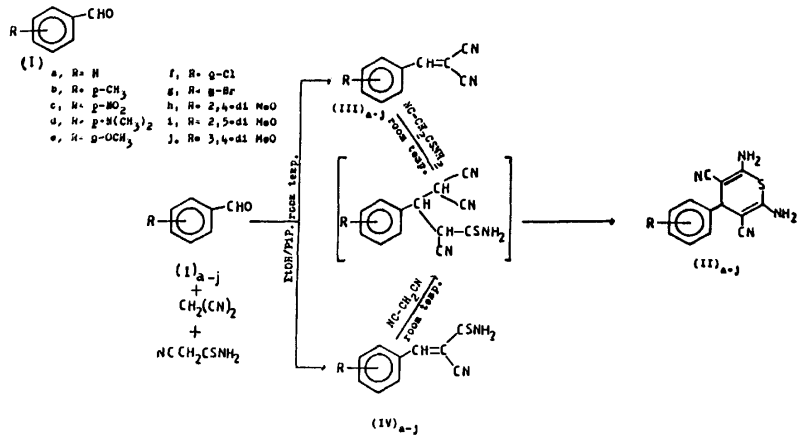

Scheme 1.

temperature (c.f. Scheme 2 and Experimental). In the same mannar, 2,6-diamino-3,5-dicyano-4-(2-thienyl)-4*H*-thiopyrans **III** was synthesized from (**IIIl**) and from **IVl** (c.f. Scheme 2 and Experimental).

In contrast to behavior of both **IIIk,l** toward cyanothioacetamide and/or both **IVk,l** toward malononitrile under the previous conditions, refluxing ethanolic piperidine solution of equimolar amounts of **IIIk,l** and cyanothioacetamide afforded the corresponding 2(1*H*)-pyridinethione derivatives **VIa,b**.

Compounds **VIa,b** were also synthesized by refluxing ethanolic piperidine solution of eqimolar amounts of **IVk,l** and malononitrile.

Formation of **VI** is rationalized in terms of the initial formation of **II** which is the kinetically controlled reaction product followed by its rearrangement via ring opening and recyclization under the applied conditions to the final product (c.f. Scheme 2).

Unequivocal support to the previous mechanism was achieved by synthesis of **VIa,b** by refluxing ethanolic piperidine solution of **IIk,l** (c.f. Scheme 2 and Experimental).

Experimental

All melting points are uncorrected. IR spectra were recorded (KBr) on Shimadzu 408 spectrophotometer. ^{1}H NMR spectra were recorded in DMSO-d_6 on a 90 MHz on a Varian EM-390 spectrometer with Me_4Si as an internal standard and chemical shifts are expressed as δ values. Analytical data were obtained from the microanalytical data unit at Cairo university.

Synthesis of 4*H*-Thiopyrans (II) (General Procedure). Method A: A suspension of equimolar amounts (0.01 mol) of eacn of aromatic aldehyde **Ia—j**, malononitrile, and cyanothioacetamide in ethanol (100 ml) and a catalytic amount of piperidine was stirred at room temperature for 5—6 h. The solid obtained or formed after trituration with water was collected by filtration and crystalized from a proper solvent.

Method B: A suspension of equimolar amounts (0.01 mol) of **IIIa—l** or **IVa—l** was treated with 0.01 mol of cyanothioacetamide or malononitrile and a catalytic amount of piperidine was stirred at room temperature for 3—4 h. The solid product was collected as in method A.

2,6-Diamino-3,5-dicyano-4-phenyl-4*H*-thiopyran (IIa). Colorless crystals (from ethanol), mp 183—184 °C, yield 65%; IR 3460, 3420, 3350, 3210 (NH_2), 2920 (CH stretches), 2200 (CN), and 1635, 1600 cm^{-1} (C=C, δ_{NH_2}). ^{1}H NMR δ=4.2 (s, 1H, thiopyran H-4), 6.5 (s, 4H, 2NH_2), and 7.5 (m, 5H, aromatic protons). Found: C, 61.70; H, 3.80; N, 22.30; S, 12.50%. Calcd for $C_{13}H_{10}N_4S$: C, 61.41; H, 3.93; N, 22.04; S, 12.59%.

2,6-Diamino-3,5-dicyano-4(*p*-tolyl)-4*H*-thiopyran (IIb). Pale yellow crystals (from dil. ethanol), mp 147—149 °C, yield 60%; IR 3470, 3410, 3350, 3210 (NH_2), 2910, 2850 (CH, CH_3 stretches), 2190 (CN), and 1620, 1600 cm^{-1} (C=C, δ_{NH_2}). ^{1}H NMR δ=2.2 (s, 3H, CH_3), 4.1 (s, 1H, thiopyran H-4), 6.5 (s, 4H, 2NH_2), and 7.5 (m, 4H, aromatic protons). Found: C, 62.70; H, 4.40; N, 21.10; S, 11.70%. Calcd for $C_{14}H_{12}N_4S$: C, 62.68; H, 4.47; N, 20.89; S, 11.94%.

2,6-Diamino-3,5-dicyano-4-(*p*-nitrophenyl)-4*H*-thiopyran (IIc). Straw yellow crystals (from dioxane), mp 189 °C, yield 62%; IR 3450, 3410, 3360, 3230 (NH_2), 2920 (CH stretch), 2200 (CN), and 1635, 1610 cm^{-1} (C=C, δ_{NH_2}). ^{1}H NMR δ=4.3 (s, 1H, thiopyran H-4), 6.6 (s, 4H, 2NH_2), and 7.7 (m, 4H, aromatic protons). Found: C, 52.00; H, 2.90; N, 23.40; S, 10.80%. Calcd for $C_{13}H_9N_5O_2S$: C, 52.17; H, 3.01; N, 23.41; S, 10.70%.

2,6-Diamino-3,5-dicyano-4-(*p*-dimethylaminophenyl)-4*H*-thiopyran (IId). Orange crystals (from dioxane), mp 163 °C, yield 85%; IR 3480, 3430, 3320 (NH_2), 2910, 2870 (CH, CH_3 stretches), 2190 (CN), and 1630, 1610 cm^{-1} (C=C, δ_{NH_2}). Found: C, 60.60; H, 5.20; N, 23.70; S, 11.00%. Calcd for $C_{15}H_{15}N_5S$: C, 60.60; H, 5.05; N, 23.57; S, 10.77%.

2,6-Diamino-3,5-dicyano-4-(*o*-methoxyphenyl)-4*H*-thiopyran (IIe). Colorless crystals (from ethanol), mp 180 °C, yield 60%; IR 3400, 3330, 3290 (NH_2), 2950, 2900 (CH, CH_3 stretches), 2210, 2200 (CN), and 1650, 1610 cm^{-1} (C=C, δ_{NH_2}). Found: C, 59.00; H, 4.20; N, 20.00; S, 10.90%. Calcd for $C_{14}H_{12}N_4SO$: C, 59.15; H, 4.22; N, 19.72; S, 11.26%.

2,6-Diamino-3,5-dicyano-4-(*o*-chlorophenyl)-4*H*-thiopyran (IIf). Colorless crystals (from dil. methanol), mp 145—147 °C, yield 50%; IR 3450, 3350, 3250, 3200 (NH_2), 2910, 2800 (CH, stretch), 2200 (CN) and 1625, 1590 cm^{-1} (C=C, δ_{NH_2}). Found: C, 54.10; H, 3.30; N, 19.50; Cl, 12.60; S, 11.10%. Calcd for $C_{13}H_9N_4ClS$: C, 54.07; H, 3.12; N, 19.41; Cl, 12.30; S, 11.09%.

2,6-Diamino-3,5-dicyano-4-(*m*-bromophenyl)-4*H*-thiopyran (IIg). Colorless crystals (from ethanol), mp 189—191 °C, yield 78%; IR 3450, 3350, 3250 (NH_2), 2890, 2850 (CH, stretch), 2200, 2195 (CN) and 1630, 1620, 1600 cm^{-1} (C=C, δ_{NH_2}). Found: C, 47.00; H, 3.00; N, 16.80; Br, 23.70; S, 9.50%. Calcd for $C_{13}H_9N_4BrS$: C, 46.85; H, 2.70; N, 16.81; Br, 24.02; S, 9.61%.

2,6-Diamino-3,5-dicyano-4-(2,4-dimethoxyphenyl)-4*H*-thiopyran (IIh). Pale yellow crystals (from ethanol), mp 159 °C, yield 70%; IR 3450, 3320, 3200 (NH_2), 2910, 2850 (CH, CH_3 stretches), 2200 (CN) and 1635—1620, 1600 cm^{-1} (C=C, δ_{NH_2}). Found: C, 57.10; H, 4.60; N, 18.00; S, 10.30%. Calcd for $C_{15}H_{14}N_4SO_2$: C, 57.32; H, 4.46; N, 17.83; S, 10.19%.

2,6-Diamino-3,5-dicyano-4-(2,5-dimethoxyphenyl)-4*H*-thiopyran (IIi). Colorless crystals (from dil. methanol), mp 152 °C, yield 60%; IR 3450, 3420, 3350, 3200 (NH_2), 2950, 2890, 2850 (CH, CH_3 stretches), 2200, 2192 (CN), and 1630, 1600 cm^{-1} (C=C, δ_{NH_2}). Found: C, 57.20; H, 4.50; N, 17.80; S, 10.10%. Calcd for $C_{15}H_{14}N_4SO_2$: C, 57.32; H, 4.46; N, 17.83; S, 10.19%.

2,6-Diamino-3,5-dicyano-4-(3,4-dimethoxyphenyl)-4*H*-thiopyran (IIj). Yellow crystals (from dil. methanol), mp 140 °C, yield 50%. Found: C, 57.00; H, 4.70; N, 17.60; S, 10.30%. Calcd for $C_{15}H_{14}N_4SO_2$: C, 57.32; H, 4.45; N, 17.83; S, 10.19%.

2,6-Diamino-3,5-dicyano-4-(2-furyl)-4*H*-thiopyran (IIk). Colorless crystals (turns to yellow on standing in light) (from dil. ethanol), mp 170 °C, yield 70% (method B); IR 3400, 3330, 3200 (NH_2), 2900, 2850 (CH stretch), 2185 (CN), and 635—1620 (br), 1605 cm^{-1} (C=C, δ_{NH_2}). ^{1}H NMR δ=3.3 (s, 2H, NH_2), 4.3 (s, 1H, thiopyran H-4), 6.0 (*d*1H, furan H-3), 6.3 (q, 1H, furan H-4), 6.9 (s, 2H, NH_2), and 7.5 (d, 1H, furan H-5). Found: C, 54.40; H, 3.80; N, 23.10; S, 13.30%. Calcd for $C_{11}H_8N_4OS$: C, 64.09; H, 27.00; N, 22.95; S, 13.11%.

2,6-Diamino-3,5-dicyano-4-(2-thienyl)-4*H*-thiopyran (IIl). Gray crystals (from methanol), mp 140 °C, yield 75% (method B), IR 3420, 3320, 3200 (NH_2), 2900, 2850 (CH, stretches), 2190 (CN) and 1635, 1620, 1600 cm^{-1} (C=C, δ_{NH_2}). Found: C, 51.10; H, 2.90; N, 21.40; S, 24.50%. Calcd for $C_{11}H_8N_4S_2$: C, 50.77; H, 3.07; N, 21.53; S, 24.61%.

Synthesis of 2(1*H*)-Pyridinethione (VI) (General Procedure). Method A: To a suspension of an equimolar amount 0.01 mol of **IIIk,l** and/or **IVk,l** in ethanol (50 ml) was added 0.01 mol of cyanothioacetamide and/or malononitrile and catalytic amount of piperidine. The reaction mixture was refluxed for 3 h and then evaporated in vacuo. The residue was triturated with water and acidified with acetic acid. The solid obtained was collected by filtration and recrystallized

from the propar solvent.

Method B: To a solution of **IIk**,l (1.0 g) in ethanol (30 ml) was added 3 drops of piperidine and the reaction mixture was refluxed for 6 h, then left to cool, and then treated as in method A.

3,5-Dicyano-3,4-dihydro-4-(2-furyl)-6-hydroxy-2(1*H*)-pyridinethione (VIa). Red crystals (from ethanol), mp 140 °C, yield 80%, IR, 3450—3100 (br NH, OH), 2900 (CH) 2200 (CN) and br 1670—1630 cm^{-1} (br CO, C=N). ^1H NMR δ=3.1 (s, br, 2H, OH and NH) and 6.5—7.5 (m, 3H, furan 3H). Found: C, 54.50; H, 1.90; N, 17.00; S, 13.40%. Calcd for $C_{11}H_5N_3O_2S$: C, 54.32; H, 2.06; N, 17.28; S, 13.17%.

3,5-Dicyano-3,4-dihydro-4-(2-thienyl)-6-hydroxy-2(1*H*)-pyridinethione (VIb). Yellow crystals (from dil. methanol), mp 190 °C, yield 60%, IR, 3350, 3200 (NH, OH), 2900, 2850 (CH), 2200 (CN) and 11670—1640 (br), 1600 cm^{-1} (CO, C=C). Found: C, 50.80; H; 1.70; N, 16.00; S, 24.40%. Calcd for $C_{11}H_5N_3OS_2$: C, 50.96; H, 1.93, N, 16.22; S 24.71%.

References

1) D. Daniel and R. Rene, *Eur. J. Med. Chem.*, **19**, 477 (1984).

2) M. Sawaki, I. Iwataki, Y. Hirono, H. Ishikawa, A. Wakai, and M. Asada, Japanese Patent **34**, 776 (1978), *Chem. Abstr.*, **89**, 43112 (1978).

3) C. Cyogyszer and V. T. gyara, Belg. Patent 889665 (1981).

4) Rurary Co. Ltd., Jpn. Patent **58**, 219178 (1983).

5) Y. S. Mohamed, A-K. M. N. Gohar, F. F. Abdel-Latif, and M. Z. A. Badr, *Pharmazie*, **40**, H. 5, 312 (1985).

6) A-K. M. N. Gohar, F. F. Abdel-Latif, and M. S. El-Ktatny, *Indian J. Chem., Sect. B*, **29**, 404 (1986).

7) F. F. Abdel-Latif and A-K. M. N. Gohar, *Bull. Soc. Chim. Belg.*, **95**, 211 (1986).

8) F. F. Abdel-Latif, R. M. Shaker, S. A. Mahgoub, and M. Z. A. Badr, *J. Heterocycl. Chem.*, **26**, 769 (1989).

Systematic Enumerations of Highly Symmetric Cage-Shaped Molecules by Unit Subduced Cycle Indices

Shinsaku FUJITA
Research Laboratories, Ashigara, Fuji Photo Film Co., Ltd.,
Minami-Ashigara, Kanagawa-ken 250-01
(Received April 22, 1989)

Cage-shaped hydrocarbons are enumerated, starting from the tetrahedron skeleton ($\mathbf{T}_d$ symmetry). This enumeration stems from an edge strategy in which six edges of the skeleton are substituted by m methylene and n ethylene units. This is accomplished by a new method based on unit subduced cycle indices. This is a versatile methodology for counting cage-shaped hydrocarbons that have a given subsymmetry and an index term, $x^m y^n$, the latter of which corresponds to the molecular formula $C_{4+m+2n}H_{4+2m+4n}$.

Chiral and achiral molecules of high symmetry have been studied both synthetically[1] and theoretically.[2] Two strategies have been applied to the derivation of new compounds of given symmetries. The first is a vertex strategy in which substituents are placed on vertices (nodes) of a parent skeleton.[3] The second (edge strategy) consists of the insertion of methylene or other units into the edges (bonds) of a parent skeleton. In particular, the latter is a versatile methodology used to guide synthetical studies concerning cage-shaped compounds of high symmetry.[4] However, there have emerged no comprehensive studies concerning the following problems: *what symmetries are realized and how many isomers are allowed on the basis of a skeleton of a given symmetry.*

In order to settle the former problem, we now report on the applications of unit subduced cycle indices (USCIs), which are drived by the subduction of coset representations (CRs). In addition, the USCIs are also useful for the latter problem, i.e., an enumeration of isomers with a given symmetry as well as a given molecular formula.

A Set of Equivalent Positions Classified by a Coset Representation. In this paper we choose as an example tetrahedrane (**1**), whose skeleton has $\mathbf{T}_d$ symmetry. The symmetry of the skeleton controls the behavior of its vertices as well as that of its edges. As a result, the vertices and edges are partitioned into several sets of equivalent positions. These sets are called *orbits* according to the terminology of permutation groups.

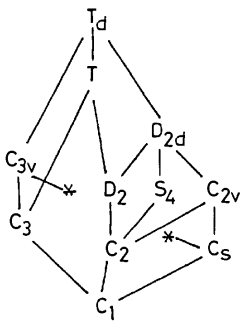

Fig. 1. Subgroup lattice of $\mathbf{T}_d$ group.

Although all of these orbits are subject to the same $\mathbf{T}_d$ symmetry, they behave differently. The characterization of such behaviors is important for a comprehensive understanding of the molecular symmetry.

The behaviors can be specified by coset representations (CRs) (Appendix A). For example, the six edges of the skeleton (**1**) belong to an orbit that is subject to a CR obtained by the corresponding coset decomposition of $\mathbf{T}_d$ by $\mathbf{C}_{2v}$. The CR is denoted by the symbol ($\mathbf{T}_d(/\mathbf{C}_{2v})$) in the present paper.

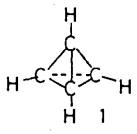

6 bonds (edges) on which $\mathbf{T}_d(/\mathbf{C}_{2v})$ acts,
4 hydrogens (nodes) on which $\mathbf{T}_d(/\mathbf{C}_{3v})$ acts, and
4 carbons (nodes) on which $\mathbf{T}_d(/\mathbf{C}_{3v})$ acts

For the purpose of assigning such a CR to an orbit, we define a set of subgroups (SSG) as a list in which the representative subgroups of a given point group are aligned in ascending order of the orders of the subgroups. Note that the respective representatives are selected in such a way that only one is adopted from every set of conjugate subgroups. For the $\mathbf{T}_d$ group, the SSG is represented by

$$\mathrm{SSG} = \{\mathbf{C}_1, \mathbf{C}_2, \mathbf{C}_s, \mathbf{C}_3, \mathbf{S}_4, \mathbf{D}_2, \mathbf{C}_{2v}, \mathbf{C}_{3v}, \mathbf{D}_{2d}, \mathbf{T}, \mathbf{T}_d\}.$$

The group-subgroup relationship is clarified by the subgroup lattice shown in Fig. 1.

In general, a set of equivalent positions (i.e. an orbit) of a $\mathbf{T}_d$ skeleton is subject to one of the eleven CRs that are associated with the eleven subgroups collected in the SSG. Thus, a set of CRs for $\mathbf{T}_d$ symmetry is obtained as follows:

$$\mathrm{SCR} = \{\mathbf{T}_d(/\mathbf{C}_1), \mathbf{T}_d(/\mathbf{C}_2), \mathbf{T}_d(/\mathbf{C}_s), \mathbf{T}_d(/\mathbf{C}_3), \mathbf{T}_d(/\mathbf{S}_4), \mathbf{T}_d(/\mathbf{D}_2), \mathbf{T}_d(/\mathbf{C}_{2v}), \mathbf{T}_d(/\mathbf{C}_{3v}), \mathbf{T}_d(/\mathbf{D}_{2d}), \mathbf{T}_d(/\mathbf{T}), \mathbf{T}_d(/\mathbf{T}_d)\}.$$

Equivalent positions contained in an orbit are interchangeable with each other, if all of the operations of the $\mathbf{T}_d$ point group are considered. On the other hand, if the operations are restricted to those of a subgroup, several positions of the orbit become fixed. The number of the fixed points is obtained for each of the subgroups collected in the SSG; the number of

fixed points is called a *mark* by Burnside.[5] A row vector which lists these numbers in the same order of the SSG is called a *fixed-point vector* (FPV) in the present paper. The FPV is a clue to the assignment of a CR to an orbit.

A table of marks (Appendix B), which comes from Burnside's textbook,[5] is utilized to determine what CR governs an orbit. The table of marks for the T_d group (Table 1) lists the marks of each CR, the numbers of the fixed points for the operations of the respective subgroups of the SSG. Note that each row of a mark table denotes the FPV of the corresponding CR.

An algorithm for choosing a CR contains the following steps: (1) select a set of equivalent positions (i.e. an orbit), (2) calculate the FPV for each of the orbits, and (3) refer to Table 1 (a mark table) and select the CR in which the row of the table is identical to the FPV. For example, the six edges of the skeleton (**1**) afford the FPV, (62200020000). This is identical to the row of $T_d(/C_{2v})$ in Table 1; therefore, the six positions of **1** are subject to $T_d(/C_{2v})$. Thus, if we consider a given skeleton, the classification of the positions into orbits and their assignment to CRs (steps 1 to 3) are easily acccomplished by inspection. A more mathematical treatment of steps 1 to 3 is given in Appendix B.

Table 1. Mark Table of T_d

i/j	C_1	C_2	C_s	C_3	S_4	D_2	C_{2v}	C_{3v}	D_{2d}	T	T_d
$T_d(/C_1)$	24	0	0	0	0	0	0	0	0	0	0
$T_d(/C_2)$	12	4	0	0	0	0	0	0	0	0	0
$T_d(/C_s)$	12	0	2	0	0	0	0	0	0	0	0
$T_d(/C_3)$	8	0	0	2	0	0	0	0	0	0	0
$T_d(/S_4)$	6	2	0	0	2	0	0	0	0	0	0
$T_d(/D_2)$	6	6	0	0	0	6	0	0	0	0	0
$T_d(/C_{2v})$	6	2	2	0	0	0	2	0	0	0	0
$T_d(/C_{3v})$	4	0	2	1	0	0	0	1	0	0	0
$T_d(/D_{2d})$	3	3	1	0	1	3	1	0	1	0	0
$T_d(/T)$	2	2	0	2	0	2	0	0	0	2	0
$T_d(/T_d)$	1	1	1	1	1	1	1	1	1	1	1

Enumeration of Cage-Shaped Hydrocarbons. Let us consider the insertion of methylene (—●—) or ethylene units (-●-●-) into C-C bonds of the skeleton (**1**). For example, the insertion of six methylenes affords adamantane (**2**).

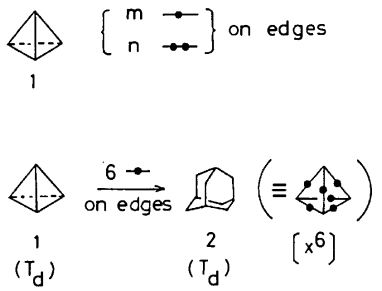

Although the methodology described in the last paragraph has been widely applied to synthetic studies,[4] an important problem still remains unsolved: how many isomers with given molecular formula and symmetry are allowed by this methodology? This problem is ascribed to an edge-coloring problem which enumerates the isomers substituted by three colors onto the six edges of **1** (e.g., one color to no substitution, a second color for *m* of —●— and a third color for *n* of -●-●-). We call this type of formulation and *edge strategy* for producing molecules of a given symmetry.[6]

A solution to the problem requires a table of unit subduced cycle indices (Appendices C and D) and the inverse of a mark table. These are given as Tables 2 and 3 for T_d symmetry.[7]

An algorithm to solve the problem contains the following steps: (1) classify the positions of a skeleton into orbits, (2) find the corresponding CR for each of the orbits, as shown in the last section, (3) read the rows of the obtained CRs from the table of unit subduced cycle indices (USCIs) (e.g., Table 2), (4) construct a subduced cycle index (SCI) from the set of USCIs for each subgroup (Appendix D), (5) introduce a figure inventory into the SCI and expand the result-

Table 2. Unit subduced Cycle Indices for T_d

i/j	C_1	C_2	C_s	C_3	S_4	D_2	C_{2v}	C_{3v}	D_{2d}	T	T_d
$T_d(/C_1)$	s_1^{24}	s_2^{12}	s_2^{12}	s_3^8	s_4^6	s_4^6	s_4^6	s_6^4	s_8^3	s_{12}^2	s_{24}
$T_d(/C_2)$	s_1^{12}	$s_1^4s_2^4$	s_2^6	s_3^4	$s_2^2s_4^2$	s_2^6	$s_2^2s_4^2$	s_6^2	s_4^3	s_6^2	s_{12}
$T_d(/C_s)$	s_1^{12}	s_2^6	$s_1^2s_2^5$	s_3^4	s_4^3	s_4^3	$s_2^2s_4^2$	$s_3^2s_6$	s_4s_8	s_{12}	s_{12}
$T_d(/C_3)$	s_1^8	s_2^4	s_2^4	$s_1^2s_3^2$	s_4^2	s_4^2	s_4^2	s_2s_6	s_8	s_4^2	s_8
$T_d(/S_4)$	s_1^6	$s_1^2s_2^2$	s_2^3	s_2^3	$s_1^2s_4$	s_2^3	s_2s_4	s_6	s_2s_4	s_6	s_6
$T_d(/D_2)$	s_1^6	s_1^6	s_2^3	s_3^2	s_2^3	s_1^6	s_2^3	s_6	s_2^3	s_3^2	s_6
$T_d(/C_{2v})$	s_1^6	$s_1^2s_2^2$	$s_1^2s_2^2$	s_3^2	s_2s_4	s_2^3	$s_1^2s_4$	s_3^2	s_2s_4	s_6	s_6
$T_d(/C_{3v})$	s_1^4	s_2^2	$s_1^2s_2$	s_1s_3	s_4	s_4	s_2^2	s_1s_3	s_4	s_4	s_4
$T_d(/D_{2d})$	s_1^3	s_1^3	s_1s_2	s_3	s_1s_2	s_1^3	s_1s_2	s_3	s_1s_2	s_3	s_3
$T_d(/T)$	s_1^2	s_1^2	s_2	s_1^2	s_2	s_1^2	s_2	s_2	s_2	s_1^2	s_2
$T_d(/T_d)$	s_1	s_1	s_1	s_1	s_1	s_1	s_1	s_1	s_1	s_1	s_1
$\sum_{i=1}^{s}\overline{m}_{ji}$	1/24	1/8	1/4	1/3	1/4	0	0	0	0	0	0

a) The value of each factor is the summation appearing in the rightmost column of Table 3.

Table 3. The Inverse of the Mark of $\mathbf{T_d}$

j/i	$\mathbf{T_d}(/\mathbf{C_1})$	$\mathbf{T_d}(/\mathbf{C_2})$	$\mathbf{T_d}(/\mathbf{C_s})$	$\mathbf{T_d}(/\mathbf{C_3})$	$\mathbf{T_d}(/\mathbf{S_4})$	$\mathbf{T_d}(/\mathbf{D_2})$	$\mathbf{T_d}(/\mathbf{C_{2v}})$	$\mathbf{T_d}(/\mathbf{C_{3v}})$	$\mathbf{T_d}(/\mathbf{D_{2d}})$	$\mathbf{T_d}(/\mathbf{T})$	$\mathbf{T_d}(/\mathbf{T_d})$	$\sum_{i=1}^{s}\overline{m}_{ji}$
$\mathbf{C_1}$	1/24	0	0	0	0	0	0	0	0	0	0	1/24
$\mathbf{C_2}$	−1/8	1/4	0	0	0	0	0	0	0	0	0	1/8
$\mathbf{C_s}$	−1/4	0	1/2	0	0	0	0	0	0	0	0	1/4
$\mathbf{C_3}$	−1/6	0	0	1/2	0	0	0	0	0	0	0	1/3
$\mathbf{S_4}$	0	−1/4	0	0	1/2	0	0	0	0	0	0	1/4
$\mathbf{D_2}$	1/12	−1/4	0	0	0	1/6	0	0	0	0	0	0
$\mathbf{C_{2v}}$	1/4	−1/4	−1/2	0	0	0	1/2	0	0	0	0	0
$\mathbf{C_{3v}}$	1/2	0	−1	−1/2	0	0	0	1	0	0	0	0
$\mathbf{D_{2d}}$	0	1/2	0	0	−1/2	−1/2	−1/2	0	1	0	0	0
$\mathbf{T}$	1/6	0	0	−1/2	0	−1/6	0	0	0	1/2	0	0
$\mathbf{T_d}$	−1/2	0	1	1/2	0	1/2	0	−1	−1	−1/2	1	0

ing equation to give a fixed-point (FP)-counting polynomial for each subgroup (Appendix E), (6) construct a fixed-point matrix (FPM), the each row of which is the FPV for the monomial term of given powers appearing in the polynomials, and (7) multiply the FPM by the inverse of a mark table (e.g., Table 3) to give a matrix, each element of which indicates the number of isomers of a given molecular formula and a given symmetry. The mathematical foundation of these steps is found in Appendices C, D, and E.

The steps listed above are illustrated by using the skeleton (**1**) as an example. The six edges of **1** are subject to $\mathbf{T_d}(/\mathbf{C_{2v}})$. Hence, the $\mathbf{T_d}(/\mathbf{C_{2v}})$ row of Table 2 is selected in order to construct subduced cycle indices (SCIs). A figure inventory is $s_r=1+x^r+y^r$, where x and y are used to count the methylenes and ethylenes, respectively. We then introduce it into the SCIs:

$\mathbf{C}$: $s_1^6=(1+x+y)^6$, (3⁶)
$\mathbf{C_2}$: $s_1^2s_2^2=(1+x+y)^2(1+x^2+y^2)^2$, (3⁴)
$\mathbf{C_s}$: $s_1^2s_2^2=(1+x+y)^2(1+x^2+y^2)^2$, (3⁴)
$\mathbf{C_3}$: $s_3^2=(1+x^3+y^3)^2$, (3²)
$\mathbf{S_4}$: $s_2s_4=(1+x^2+y^2)(1+x^4+y^4)$, (3²)
$\mathbf{D_2}$: $s_2^3=(1+x^2+y^2)^3$, (3³)
$\mathbf{C_{2v}}$: $s_1^2s_4=(1+x+y)^2(1+x^4+y^4)$, (3³)
$\mathbf{C_{3v}}$: $s_3^2=(1+x^3+y^3)^2$, (3²)
$\mathbf{D_{2d}}$: $s_2s_4=(1+x^2+y^2)(1+x^4+y^4)$, (3²)
$\mathbf{T}$: $s_6=1+x^6+y^6$, (3)

and

$\mathbf{T_d}$: $s_6=1+x^6+y^6$. (3)

These equations are expanded to give the corresponding FP-counting polynomials as generating functions. For example, the FPV for x^5y is (62200020000), the coefficients of the terms (x^5y) of the respective polynomials. Multiplication of FPV by the inverse (Table 3) gives an isomer-counting vector (IMV),(00000010000). The vector shows that there is only one isomer which corresponds to homoadamantane (**3**) with x^5y and $\mathbf{C_{2v}}$ symmetry. Similarly, the IMVs for the other x^my^n terms are obtained as shown in Table 4. The x^my^n term is called an *index term*. The resulting isomer is called an x^my^n *isomer*. The intersection of a subsymmetry column and an x^my^n row (Table 4) indicates the number of x^my^n isomers with the subsymmetry.

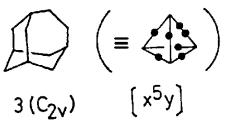

Since the term (x^my^n) indicates the substitution of m of —●— and n of -●-●-, it corresponds to the molecular formula $C_{4+m+2n}H_{4+2m+4n}$.

The total number of isomers is 64, among which 21 belong to chiral subgroups ($\mathbf{C_1}$, $\mathbf{C_2}$, and $\mathbf{D_2}$). Figure 2 depicts $\mathbf{C_2}$ molecules (**4** to **12**), the number of which emerges in the $\mathbf{C_2}$ column of Table 4.

There is only one $\mathbf{D_2}$ molecule which corresponds to the term (x^2y^2), as shown in Table 4. An example of

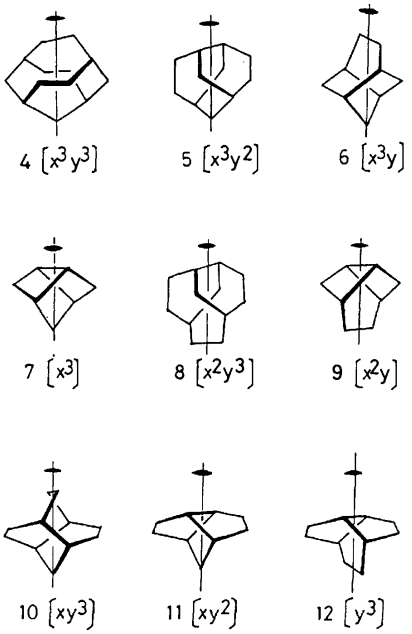

Fig. 2. $\mathbf{C_2}$ Molecules based on a tetrahedron skeleton (**1**).

Table 4. The Numbers of Cage-Shaped Compounds Derived Form the Skeleton (**1**) by an Edge Strategy

Index term	Number of isomers											Total for $x^m y^n$
	C_1	C_2	C_s	C_3	S_4	D_2	C_{2v}	C_{3v}	D_{2d}	T	T_d	
x^6; y^6	0	0	0	0	0	0	0	0	0	0	1	1
x^5y; xy^5	0	0	0	0	0	0	1	0	0	0	0	1
x^5; y^5	0	0	0	0	0	0	1	0	0	0	0	1
x^4y^2; x^2y^4	0	0	1	0	0	0	0	0	1	0	0	2
x^4y; xy^4	1	0	0	0	0	0	1	0	0	0	0	2
x^4; y^4	0	0	1	0	0	0	0	0	1	0	0	2
x^3y^3	0	1	0	0	0	0	0	2	0	0	0	3
x^3y^2; x^2y^3	1	1	2	0	0	0	0	0	0	0	0	4
x^3y; xy^3	1	1	2	0	0	0	0	0	0	0	0	4
x^3; y^3	0	1	0	0	0	0	0	2	0	0	0	3
x^2y^2	2	0	3	0	0	1	0	0	0	0	0	6
x^2y; xy^2	1	1	2	0	0	0	0	0	0	0	0	4
x^2; y^2	0	0	1	0	0	0	0	0	1	0	0	2
xy	1	0	0	0	0	0	1	0	0	0	0	2
x; y	0	0	0	0	0	0	1	0	0	0	0	1
1	0	0	0	0	0	0	0	0	0	0	1	1
Total[a)]	11	9	21	0	0	1	9	6	6	0	1	64

a) The total number is the sum of the numbers in each column over all the index terms. Note that the number of $x^m y^n$ isomers is equal to that of $x^n y^m$.

this type is twistane (**13**), which can be derived by the substitution of 2 methylenes and 2 ethylenes on the edges of the skeleton (**1**) in accordance with the index term. It should be noted that neither C_3 nor **T** molecules can exist. This fact will be discussed later.

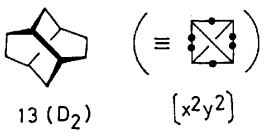

Among the total 64 isomers, there exist 43 achiral isomers (C_s, C_{2v}, C_{3v}, D_{2d}, and T_d). Figure 3 lists all of the D_{2d} molecules, the number of which appears in the D_{2d} column of Table 4. Other achiral isomers can be listed in terms of the index terms. There exist no S_4 isomers, as shown in Table 4. It should be emphasized that the results of Table 4 have been obtained by mathematical manipulation. Hence, they are the probes for verifying manual enumerations, which may sometimes contain duplicated or incomplete counting.

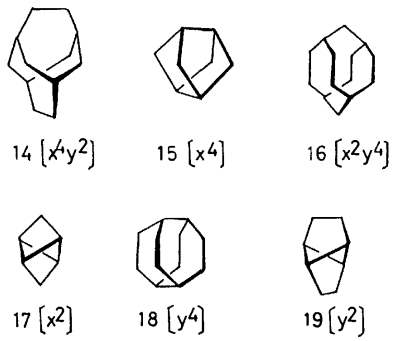

Fig. 3. D_{2d} Molecules based on a tetrahedron skeleton (**1**).

The summation in each column of Table 4 (the bottom) affords the total number of molecules having the corresponding subsymmetry. The number can be obtained by an alternative method (Appendix E). The total number of fixed points concerning each subsymmetry is obtained by introducing $x=y=1$ to the corresponding FP-counting polynomials in order to construct an FPV=(3⁶ 3⁴ 3⁴ 3² 3² 3³ 3³ 3² 3² 3 3), each element of which is the total number. Multiplication of FPV by the inverse (Table 3) affords an IMV=(11 9 21 0 0 1 9 6 6 0 1), the elements of which are identical to those shown in the bottom row of Table 4.

The total number of molecules with the index term ($x^m y^n$) is calculated in the form of a generating function (Appendix E). We use the $T_d(/C_{2v})$ row of Table 2 and the factors collected in the bottom of the same table. We then obtain a cycle index,

$$\mathbf{Z}(\mathbf{T}_d; s_r) = (1/24)s_1^6+(1/8)s_1^2s_2^2+(1/4)s_1^2s_2^2+(1/3)s_3^2+(1/4)s_2s_4$$
$$=(1/24)(s_1^6+9s_1^2s_2^2+8s_3^2+6s_2s_4).$$

The mathematical foundation of this derivation is found in Appendix E. This can be proven to be identical to that obtained alternatively by Pólya's theorem.[8,9] After the introduction of a figure inventory, $s_r=1+x^r+y^r$, into the cycle index, the expansion of the resulting equation provides the following generating function,

$$G(x,y)=\mathbf{Z}(\mathbf{T}_d; 1+x^r+y^r)$$
$$=(1/24)((1+x+y)^6+9(1+x+y)^2(1+x^2+y^2)^2+8(1+s^3+y^3)^2+6(1+x^2+y^2)(1+x^4+y^4))$$
$$=x^6+x^5y+x^5+2x^4y^2+2x^4y+2x^4+3x^3y^3+4x^3y^2+4x^3y+3x^3+\cdots,$$

in which the coefficient of $x^m y^n$ indicates the total number of molecules with $x^m y^n$. These values are identical to those collected in the right-most column of Table 4, which are obtained alternatively by summing up the values in the respective rows.

Selection Rule for Subsymmetries. Table 4 shows that molecules of $\mathbf{C}_3$, $\mathbf{S}_4$, and $\mathbf{T}$ point groups are absent in the above enumeration.[10] Why are these subsymmetries forbidden? This section is devoted to a rationalization of the problem. Note that we consider only achiral substituents.

The existence and nonexistence of molecules having special subgroups can be predicted by examining USCIs. Figure 4 depicts the subgroup lattice of the $\mathbf{T}_d$ point group which contains the USCI of each subgroup in the case of $\mathbf{T}_d(/\mathbf{C}_{2v})$. The USCI indicates the mode of subdivision of the orbit that is subject to $\mathbf{T}_d(/\mathbf{C}_{2v})$. In order to realize a subsymmetry, substituents should occupy the resulting suborbits in accord with the USCI. For example, the USCI (s_3^2) of $\mathbf{C}_{3v}$ is in agreement with the fact that the mode of substitution is A_3B_3 (Fig. 4), where A and B are achiral substituents.

More concretely, let us examine homoadamantane (**3**) of $\mathbf{C}_{2v}$ symmetry that has one ethylene (-●-●-), one methylene (—●—) and four methylenes as respective equivalent positions. This subsitution is in accord with the USCI ($s_1^2 s_4$), which appears in Fig. 4. Further examples are found in Fig. 2, in which each molecule of $\mathbf{C}_2$ symmetry has substituents (—●— and/or -●-●-) in the form of $s_1^2 s_2^2$. Figure 3 depicts various $s_2 s_4$ substitutions that lead to $\mathbf{D}_{2d}$ symmetry.

Since the USCI (s_6) of $\mathbf{T}$ is identical to that of $\mathbf{T}_d$ in the case of $\mathbf{T}_d(/\mathbf{C}_{2v})$, as shown in Fig. 4, the substitution of A_6 onto the suborbit of $\mathbf{T}$ produces no $\mathbf{T}$ but, rather, a superior $\mathbf{T}_d$ molecule. The same reasoning is applicable to $\mathbf{C}_3$ and $\mathbf{S}_4$ cases. Hence, $\mathbf{T}$, $\mathbf{C}_3$, and $\mathbf{S}_4$ subsymmetries are forbidden in case of $\mathbf{T}_d(/\mathbf{C}_{2v})$.

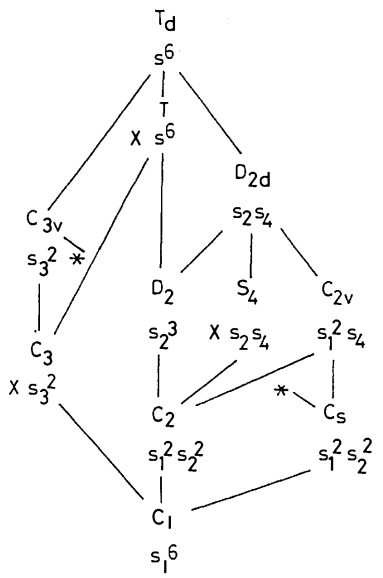

Fig. 4. Allowed and forbidden subsymmetries on the basis of a tetrahedron skeleton (**1**).

In general, because a given skeleton is represented by a set of CRs, a subsymmetry of the skeleton is characterized by a set of USCIs in which the multiplicity of the latter set is identical to that of the former set of CRs. Therefore, if the USCIs of a subgroup are identical to that of any subgroup appearing in an upper level of a subgroup lattice, the former subgroup is forbidden.

Conclusion

Enumerations based on the edge strategy are presented. Thus, a tetrahedrane of $\mathbf{T}_d$ symmetry gives various cage-shaped hydrocarbons of the subsymmetries of $\mathbf{T}_d$ by considering substitution on its edges. The enumerations with respect to subsymmetries and to molecular formulas are accomplished by a novel procedure in which unit subduced cycle indices are utilized. Although we have restricted ourselves to manipulating a tetrahedron skeleton ($\mathbf{T}_d$), we can apply the present method to other $\mathbf{T}_d$ skeletons as well as various skeletons of other symmetries than $\mathbf{T}_d$.

Appendix A. Coset Representations

Let $\mathbf{H}$ be a subgroup of a given finite group $\mathbf{G}$. Then, the elements of $\mathbf{G}$ are partitioned into a set of cosets:

$$\Gamma=\{\mathbf{H}g_1, \mathbf{H}g_2, \cdots, \mathbf{H}g_m\}, \tag{A.1}$$

where g_1 ($=I$), $\cdots$, and g_m are representatives of the cosets. Any element g ($\in \mathbf{G}$) is multiplied onto each coset of Γ to afford

$$\Gamma'=\{\mathbf{H}g_1g, \mathbf{H}g_2g, \cdots, \mathbf{H}g_mg\}. \tag{A.2}$$

The transformation $\Gamma \rightarrow \Gamma'$ is considered to be a permutation represented by

$$\pi_g = \begin{pmatrix} \mathbf{H}g_1, \mathbf{H}g_2, \cdots, \mathbf{H}g_m \\ \mathbf{H}g_1g, \mathbf{H}g_2g, \cdots, \mathbf{H}g_mg \end{pmatrix}, \tag{A.3}$$

which constructs a permutation group homomorphic to the group $\mathbf{G}$. We call this a coset representation (CR) of $\mathbf{G}$ by $\mathbf{H}$, which is denoted as $\mathbf{G}(/\mathbf{H})$. The degree of $\mathbf{G}(/\mathbf{H})$ is $m=|\mathbf{G}|/|\mathbf{H}|$. The coset representation is transitive, so that it has one orbit.

Appendix B. A Table of Marks

Burnside pointed out the importance of a table of marks.[5] Suppose that $\mathbf{G}_i$ ($i=1, 2, \cdots, s$) are an irredundant set of conjugate subgroups of $\mathbf{G}$, where $\mathbf{G}_1=\mathbf{C}_1$ and $\mathbf{G}_s=\mathbf{G}$. We define a set of subgroups as a series of the conjugate subgroups represented by

$$\mathrm{SSG}=\{\mathbf{G}_1, \mathbf{G}_2, \cdots, \mathbf{G}_s\}, \tag{B.1}$$

the elements of which are aligned in the ascending order of $|\mathbf{G}_i|$. The corresponding set of coset representations:

$$\mathrm{SCR}=\{\mathbf{G}(/\mathbf{G}_1), \mathbf{G}(/\mathbf{G}_2), \cdots, \mathbf{G}(/\mathbf{G}_s)\} \tag{B.2}$$

contains all possible transitive representations of the finite group $\mathbf{G}$.

Let the mark of a subgroup **H** in **G** be the number of fixed points of a **G**-set on the action by **H**. When the symbol m_{ij} incidates the mark of subgroup $\mathbf{G}_j$ in $\mathbf{G}(/\mathbf{G}_i)$, we obtain a fixed point vector as

$$\mathrm{FPV}_i=(m_{i1}, m_{i2}, \cdots, m_{is}) \tag{B.3}$$

for each $\mathbf{G}(/\mathbf{G}_i)$. If we collects FPVs for all $\mathbf{G}_j$ (J=1, 2, ···, s) as row vectors, we arrive at a matrix,

$$\mathrm{MT}=(m_{ij})=\begin{pmatrix} m_{11}m_{12}\cdots m_{1s} \\ m_{21}m_{22}\cdots m_{2s} \\ \cdots \\ m_{s1}m_{s2}\cdots m_{ss} \end{pmatrix}, \tag{B.4}$$

which is called a table of marks by Burnside and denoted as a mark table in the present paper.

If a set (Δ) of positions appearing in a given skeleton is a **G**-set in the form of a permutation group ($\mathbf{P}_\mathbf{G}$) acting on the set, it is partitioned into several orbits (i.e. sets of equivalent positions) in accord with

$$\mathbf{P}_\mathbf{G}=\sum_{i=1}^{s}\alpha_i\mathbf{G}(/\mathbf{G}_i), \tag{B.5}$$

where $\mathbf{G}_i$ (i=1, 2, ···, s) belong to the SSG of **G** and $\mathbf{G}(/\mathbf{G}_i)$ are the corresponding coset representations. The multiplicity α_i is obtained by

$$(\mu_1\mu_2\cdots\mu_s)=(\alpha_1\alpha_2\cdots\alpha_s)\mathrm{MT}, \tag{B.6}$$

where $(\mu_1\mu_2\cdots\mu_s)$ is a FPV for the set (Δ) and the $s\times s$ matix is the mark table represented by Eq. B.4. When we define $\bar{m}_{ji}$ as a ji element of an inverse of the mark table (IMT) derived from Eq. B.4, i.e.,

$$\mathrm{IMT}=(\bar{m}_{ji})=\begin{pmatrix} \bar{m}_{11}\bar{m}_{12}\cdots \bar{m}_{1s} \\ \bar{m}_{21}\bar{m}_{22}\cdots \bar{m}_{2s} \\ \cdots \\ \bar{m}_{s1}\bar{m}_{s2}\cdots \bar{m}_{ss} \end{pmatrix}, \tag{B.7}$$

Eq. B.6 is converted to

$$(\alpha_1\alpha_2\cdots\alpha_s)=(\mu_1\mu_2\cdots\mu_s)\mathrm{IMT}. \tag{B.8}$$

Appendix C. Subduced Representations of a Coset Representation

Let us consider a coset representation $\mathbf{G}(/\mathbf{G}_i)$, the element of which homomorphically corresponds to $|\mathbf{G}|$ elements of **G**. Suppose that we restrict the elements of $\mathbf{G}(/\mathbf{G}_i)$ into a set of elements corresponding to a subgroup ($\mathbf{G}_j$). The restricted set is a representation of the subgroup ($\mathbf{G}_j$). This is called a subduced representation (SR) and is denoted by $\mathbf{G}(/\mathbf{G}_i)\downarrow\mathbf{G}_j$ in the present paper. Although $\mathbf{G}(/\mathbf{G}_i)$ is a transitive representation of **G**, the SR, $\mathbf{G}(/\mathbf{G}_i)\downarrow\mathbf{G}_j$, is an intransitive representation of the subgroup $\mathbf{G}_j$. Equation B.5 is applicable to this case and can be transformed into

$$\mathbf{G}(/\mathbf{G}_i)\downarrow\mathbf{G}_j=\sum_{k=1}^{v_j}\beta_k^{(ij)}\mathbf{G}_j(/\mathbf{H}_k^{(j)}), \tag{C.1}$$

wherein $\mathbf{H}_k^{(j)}$ (k=1, 2, ···, v_j) are conjugate subgroups of the group $\mathbf{G}_j$. The multiplicity $\beta_k^{(ij)}$ (k=1, 2, ···, v_j) are obtained by

$$\nu_1=\sum_{k=1}^{v_j}\beta_k^{(ij)}m_{k1}^{(j)}. \tag{C.2}$$

On the basis of this equation, the $k1$ elements, $m_{k1}^{(j)}$, construct a table of marks for the subgroup $\mathbf{G}_j$. It should be noted that each $\beta_k^{(ij)}$ is constant because $\mathbf{G}(/\mathbf{G}_i)$ and $\mathbf{G}_j$ ($/\mathbf{H}_k^{(i)}$) are strictly decided by their components. On the other hand, the term α_i in Eq. B.5 is dependent on **G**-set even if the group **G** is given.

Appendix D. Table of Unit Subduced Cycle Indices and a Subduced Cycle Index

Let us consider $\mathbf{G}_j(/\mathbf{H}_k^{(j)})$ appearing in Eq. C.1. An orbit that is subject to $\mathbf{G}_j(/\mathbf{H}_k^{(j)})$ has a length represented by

$$d_{jk}=|\mathbf{G}_j|/|\mathbf{H}_k^{(j)}|. \tag{D.1}$$

Hence, we can ascribe a variable $s_{d_{jk}}$ to $\mathbf{G}_j(/\mathbf{H}_k^{(j)})$. The variable $s_{d_{jk}}$ is an index representing a behavior of the orbit on which $\mathbf{G}_j(/\mathbf{H}_k^{(j)})$ acts. We then define *a unit subduced cycle index (USCI)* as being

$$\prod_{k=1}^{v_j}(s_{d_{jk}})^{\beta_k^{(ij)}}. \tag{D.2}$$

The USCI corresponds to Eq. C.1 that represents the subdivision provided by $\mathbf{G}(/\mathbf{G}_i)\downarrow\mathbf{G}_j$. A collection of the USCIs over all i and all j as shown in Table 5 is useful to various applications. We call such a table *a table of unit subduced cycle indices (USCIs).*

By using USCIs, we define a *subduced cycle index (USCI)* for a subgroup $\mathbf{G}_j$ as follows:

$$Z(\mathbf{G}_j; s_{d_{jk}})=\prod_{i=1}^{s}\left[\prod_{k=1}^{v_j}(s_{d_{jk}})^{\beta_k^{(ij)}}\right]^{\alpha_i} \tag{D.3}$$

$$=\prod_{k=1}^{v_j}(s_{d_{jk}})^{\sum_{i=1}^{s}\alpha_i\beta_k^{(ij)}} \tag{D.4}$$

(for j=1, 2, ···, s),

where each α_i is the multiplicity of $\mathbf{G}(/\mathbf{G}_i)$ obtained by Eq. B.8.

Appendix E. Enumeration of Isomers with a $\mathbf{G}_i$-Symmetry and a W_θ-Formula

Suppose that a given skeleton of **G** symmetry has $|\Delta|$ positions (vertices or edges) which construct a domain,

$$\Delta=\{\delta_1, \delta_2, \cdots, \delta_{|\Delta|}\}.$$

Consider that m_r figures of X_r selected from a codomain,

$$\mathbf{X}=\{X_1, X_2, \cdots, X_r, \cdots, X_{|\mathbf{X}|}\},$$

occupy the positions of Δ. The resulting isomers have a molecular formula (or a weight) represented by

Table 5. Table of Unit Subduced Cycle Indices

	$\downarrow\mathbf{G}_1$	$\downarrow\mathbf{G}_2$	···	$\downarrow\mathbf{G}_j$	···	$\downarrow\mathbf{G}_s$
$\mathbf{G}(/\mathbf{G}_1)$						
$\mathbf{G}(/\mathbf{G}_2)$				···		
···						
$\mathbf{G}(/\mathbf{G}_i)$		···		$\prod_{k=1}^{v_j}(s_{d_{jk}})^{\beta_k^{(i,j)}}$	···	
···						
$\mathbf{G}(/\mathbf{G}_s)$				···		

$$W_\theta=\prod_{r=1}^{|\mathbf{X}|}X_r^{m_r}, \tag{E.1}$$

wherein the subscript θ runs over all partitions of $m_1+m_2+\cdots+m_r+m_{|\mathbf{X}|}=|\Delta|$. Our objective is an enumeration of isomers with W_θ and of a given subsymmetry. Suppose that the domain Δ, which is originally a **G**-set, is now considered to be a $\mathbf{G}_j$-set. Thus, the domain, which is divided by the action of **G** (Eq. B.5), is further subdivided into suborbits by $\mathbf{G}_j$. The accumulated actions are characterized by the subduced cycle index (SCI) represented by Eqs. D.3 and D.4. Hence, the number ($\rho_{\theta j}$) of $\mathbf{G}_j$-isomers with a W_θ formula is obtained by a generating function,

$$\sum_\theta \rho_{\theta j}W_\theta=Z(\mathbf{G}_j;\ s_{d_{jk}}) \tag{E.2}$$

$$\text{for } j=1, 2, \cdots, s,$$

which is substituted by

$$s_{d_{jk}}=\sum_{r=1}^{|\mathbf{X}|}X_r^{d_{jk}}. \tag{E.3}$$

We call the generating function *a fixed-point-couting polynomial.* Since the number $\rho_{\theta j}$ suffers from duplicated counting, its correction is accomplised by

$$\rho_{\theta j}=\sum_{i=1}^{s}A_{\theta i}m_{ij} \tag{E.4}$$

$$(\text{for } j=1, 2, \cdots, s),$$

where $A_{\theta i}$ is the number of $\mathbf{G}_i$-isomers with W_θ and m_{ji} is the mark defined in Eq. B.4. The θj-elements ($\rho_{\theta j}$) coonstruct a matrix, which is called a *fixed-point matrix (FPM).* Each row of the FPM is an FPV.

Suppose that $X_r=1$ ($r=1, 2, \cdots$, and $|\mathbf{X}|$) are introduced into Eq. E.3. This operation results in the transformation of Eq. 2 into

$$\sum_\theta \rho_{\theta j}=|\mathbf{X}|^{\sum_{i=1}^{s}\alpha_i\beta_{ij}} \tag{E.5}$$

$$(\text{for } j=1, 2, \cdots, s),$$

where

$$\beta_{ij}=\sum_{k=1}^{v_j}\beta_k^{(ij)}. \tag{E.6}$$

The term β_{ij} represents the number of suborbits. The summation of Eq. E.4 over all θ gives

$$\sum_\theta \rho_{\theta j}=\sum_\theta\sum_{i=1}^{s}A_{\theta i}m_{ij}=\sum_{i=1}^{s}(\sum_\theta A_{\theta i})m_{ij} \tag{E.7}$$

$$(\text{for } j=1, 2, \cdots, s).$$

Since the term $A_i=\sum_\theta A_{\theta i}$ is the total number of $\mathbf{G}_i$-isomers, Eqs. E.5 and E.7 provide

$$|\mathbf{X}|^{\sum_{i=1}^{s}\alpha_i\beta_{ij}}=\sum_{i=1}^{s}A_im_{ij} \tag{E.8}$$

$$(\text{for } j=1, 2, \cdots, s).$$

When the symbol ρ_j denotes the number of fixed points on the action of $\mathbf{G}_j$, i.e.

$$\rho_j=|\mathbf{X}|^{\sum_{i=1}^{s}\alpha_i\beta_{ij}} \tag{E.9}$$

Equation E.8 can be rewritten by following matrix representation:

$$(\rho_1\rho_2\cdots\rho_s)=(A_1A_2\cdots A_s)\mathrm{MT}, \tag{E. 10}$$

where MT is a table of marks.

The total number (A_θ) of W_θ-isomers is represented by

$$A_\theta=\sum_{i=1}^{s}A_{\theta i}=\sum_{i=1}^{s}\sum_{j=1}^{s}\rho_{\theta i}\bar{m}_{ji}, \tag{E.11}$$

the latter term of which comes from Eq. E.4. Note that $\bar{m}_{ji}$ is the inverse of a table of marks. Hence, a generating function of A_θ takes the following form:

$$\sum_\theta A_\theta W_\theta=\sum_{j=1}^{s}[(\sum_{i=1}^{s}\bar{m}_{ji})\sum_\theta \rho_{\theta j}W_\theta]. \tag{E.12}$$

Because of Eq. E.2,

$$\sum_\theta A_\theta W_\theta=\sum_{j=1}^{s}[(\sum_{i=1}^{s}\bar{m}_{ji})Z(\mathbf{G}_j;\ s_{d_{jk}})], \tag{E.13}$$

where Eq. E.3 is effective. Equation E.13 can be proved to be identical to that obtained alternatively by Polya's theorem; however, the present formulation is quite different and have some advantages over Pólya's theorem. The term

$$\cdot\sum_{i=1}^{s}\bar{m}_{ji}$$

is the sum of the $\mathbf{G}_j$-row of the inverse of a table of marks. This term is positive if and only if $\mathbf{G}_j$ is a cyclic group. Otherwise, it vanishes to zero. The relationship between the present method and Polya's method will be discussed elsewhere.[9]

References

1) a) M. Nakazaki and K. Naemura, *Yuki Gosei Kagaku Kyokaishi*, **35**, 883 (1977); b) M. Nakazaki, *Top. Stereochem.*, **15**, 199 (1984); c) P. E. Eaton, *Tetrahedron*, **35**, 2189 (1979).

2) a) M. Farina and C. Morandi, *Tetrahedron*, **30**, 1819 (1974); b) V. Prelog and G. Helmchen, *Helv. Chim. Acta*, **55**, 2581 (1972).

3) a) V. Prelog and J. Thix, *Helv. Chim. Acta*, **65**, 2622 (1982); b) S. Fujita, *J. Chem. Educ.*, **63**, 744 (1986).

4) a) G. Helmchen and G. Staiger, *Angew. Chem., Intern. Ed. Engl.*, **16**, 116 (1977); b) M. Nakazaki, K. Naemura and N. Arashiba, *J. Org. Chem.*, **43**, 689 (1978).

5) W. Burnside, "Theory of Groups of Finite Order (2nd Ed.)," Cambridge Univ. Press, Cambridge (1911). For the application of a table of marks, see W. Hässelbarth, *Theor. Chim. Acta*, **67**, 339 (1985); and C. A. Mead, *J. Am. Chem. Soc.*, **109**, 2130 (1987).

6) The present enumeration is not concerned with exact conformations. In other words, it is based on the presumption that a molecule has an average conformation. For example, tricyclo[5.5.2.$2^{4,10}$]hexadecane (y^6) is assigned to T_d symmetry in this paper. If we take account of conformation, we find M- and P-conformers of **T** symmetry, which are determined by their helicity. These conformers can be enumerated by using unit subduced cycle indices *with chirality fittingness* (or with helicity fittingness). We will report this type of enumeration later. See S. Fujita, *Bull. Chem. Soc. Jpn.*, in press and S. Fujita, *J. Math. Chem.*, in press.

7) For further applications, tables of USCIs of other point groups should be prepared. The full lists will be

reported elsewhere. For the proof of the equations appearing in Appendices, see S. Fujita, *Theor. Chim. Acta*, in press.

8) a) G. Pólya, *Acta Math.*, **68**, 145 (1937); b) G. Pólya and R. C. Read, "Combinatorial Enumeration of Groups, Graphs and Chemical Compounds," Springer-Verlag, New York, Berlin, Heidelberg (1987).

9) For the proof, S. Fujita *J. Math. Chem.*, in press.

10) The non-existence of the three subsymmetries was reported in a different context. See Ref. 2b.

 © 1989 The Chemical Society of Japan Bull. Chem. Soc. Jpn., 62, 3779—3782 (1989)

Regioselective Hydrogenation of Unsaturated Alcohol Using Platinum-Alumina Modified with Carboxylic Acid

Hideyuki KUNO,* Kyoko TAKAHASHI, Makoto SHIBAGAKI, and Hajime MATSUSHITA
Life Science Research Laboratory, Japan Tobacco Inc., 6-2 Umegaoka, Midori-ku, Yokohama, Kanagawa 227
(Received May 31, 1989)

Platinum-alumina catalysts modified with carboxylic acid were prepared for the selective hydrogenation of unsaturated alcohols. These catalysts were stable in non-polar solvents. It has been demonstrated that the carbon-carbon double bond which is close to the hydroxyl group is preferentially hydrogenated in the case of several hexenols. This selectivity was applied to the regioselective hydrogenation of geraniol and citronellol was obtained in an 84.5% yield over one of the modified catalyst systems.

It has been difficult to achieve a high regioselective hydrogenation of compounds which had plural unsaturations over a heterogeneous catalyst. It was recently reported that a carbon-carbon double bond far from a hydrophobic site in unsaturated carboxylic acid was more quickly hydrogenated than that near by a hydrophilic site over colloidal palladium or platinum supported on a polymer in a water solution.[1] This selectivity was due to the colloidal micelle. Further, the site-selective epoxidation was also performed over the micelle-type catalyst.[2] On the other hand, highly regioselective reactions, such as esterification,[3,4] were reported to be achieved by using a monomolecular layer which could be prepared on an inorganic solid with carboxylic acid.

In this investigation, the selective hydrogenation of the carbon-carbon double bond was carried out by the application of a monomolecular layer system. The platinum-alumina (Pt/Al_2O_3) catalysts modified with carboxylic acids were prepared and used as catalysts with a monomolecular layer system. The carboxylic acid was presumed to be chemisorbed on an inorganic support as carboxylate anions.[5-8] It was elucidated that the difference in the hydrogenation rates were found in the different positions of the carbon-carbon double bond in unsaturated alcohols. In this paper, we report that the hydroganation rate of the carbon-carbon double bond is dependent on the distance between the double bond and the hydroxyl group in the unsaturated alcohol, and that the regioselective hydrogenation of geraniol is achieved in this catalyst system.

Experimental

Materials. Commercial reagents were used for the reactions without further purification. Five percent platinum on a powdered alumina (Nippon Engelhard Ltd.) was used for the preparation of modified catalysts.

Preparation of Carboxylic Acid-Modified Catalyst (Catalyst A).[2,3] Carboxylic acids (0.1 g) and tridecane or dodecane as an internal standard (0.1 g) were dissolved in 10 cm^3 of *N,N*-dimethylformamide (DMF). A platinum-alumina catalyst (5 w/w% Pt) was immersed in the solution and stirred overnight at room temperature. A catalyst modified with the carboxylic acid was filtered off, washed with a small amount of DMF and dried under reduced pressure. The filtrate was analyzed by gas chromatography (a capillary column OV 101 30 m) in order to determine the adsorbed amount of the carboxylic acid on the catalyst.

Hydrogenation of Hexenols. In a 30-cm^3 round-bottom flask, 10 mg of Catalyst A, or 5 % platinum on alumina (Catalyst B), was suspended in 10 cm^3 of hexane containing 0.1 g of tridecane, and 10 cm^3 of hexane containing *trans*-2-hexen-1-ol (0.1 g or 0.2 g) and/or *trans*-4-hexen-1-ol (0.1 g or 0.2 g) was added with stirring at 0 °C under a hydrogen atmosphere. The reactants and products were analyzed on gas chromatography (a capillary column PEG 20M 30 m). The compounds were assigned and their concentrations were determined using authentic samples and an internal standard.

Hydrogenation of Geraniol. In a 30-cm^3 round-bottom flask, 20 cm^3 of hexane containing tridecane (0.1 g) and geraniol (0.1 g) was stirred with 10 mg of Catalyst A or Catalyst B at 0 °C under a hydrogen atmosphere. The reactants and products were analyzed in a similar manner as described above. The assignment of the products was performed with GC-MS and ^1H NMR spectroscopy.

Results and Discussion

Adsorption of Carboxylic Acid on Alumina. The amounts of several carboxylic acids adsorbed on Pt/Al_2O_3 are listed in Table 1. The amount of myristic acid on Pt/Al_2O_3 was smaller than those of the other carboxylic acids. Monocarboxylic acids were efficiently adsorbed on alumina in comparison with the dicarboxylic acid. The adsorption amounts were not changed when large amounts of carboxylic acids were used in the preparation of the modified catalysts.

Table 1. Amount of Adsorbed Carboxylic Acids on Pt/Al_2O_3

Carboxylic acid	Adsorption amount/mmol g^{-1}
Decanoic acid	0.233
Hexanoic acid	0.240
Myristic acid	0.123
Benzoic acid	0.277
Adipic acid	0.166

Carboxylic acid: 0.1 g, 5% platinum-alumina: 1.0 g, in DMF solution, for overnight at room temperature.

These results showed that an almost saturated amount of the carboxylic acids were adsorbed on Pt/Al_3O_3. Although the prepared Catalyst A was immersed in hexane and stirred under a hydrogen atmosphere overnight, the eliminated carboxylic acid was not detected. Catalyst A was stable in hexane.

Hydrogenation of Some Unsaturated Alcohols. The hydrogenation of *trans*-2-hexen-1-ol and *trans*-4-hexen-1-ol was carried out with catalysts modified by three kinds of carboxylic acids, decanoic acid (Catalyst A-1), hexanoic acid (Catalyst A-2), and myristic acid (Catalyst A-3), and with a non-modified catalyst (Catalyst B). The time-courses of the hydrogenation over Catalyst A-1 are shown in Fig. 1-a. The hydrogenation rate of *trans*-2-hexen-1-ol was higher than that of *trans*-4-hexen-1-ol over Catalyst A-1, while the two hexenols were hydrogenated at similar

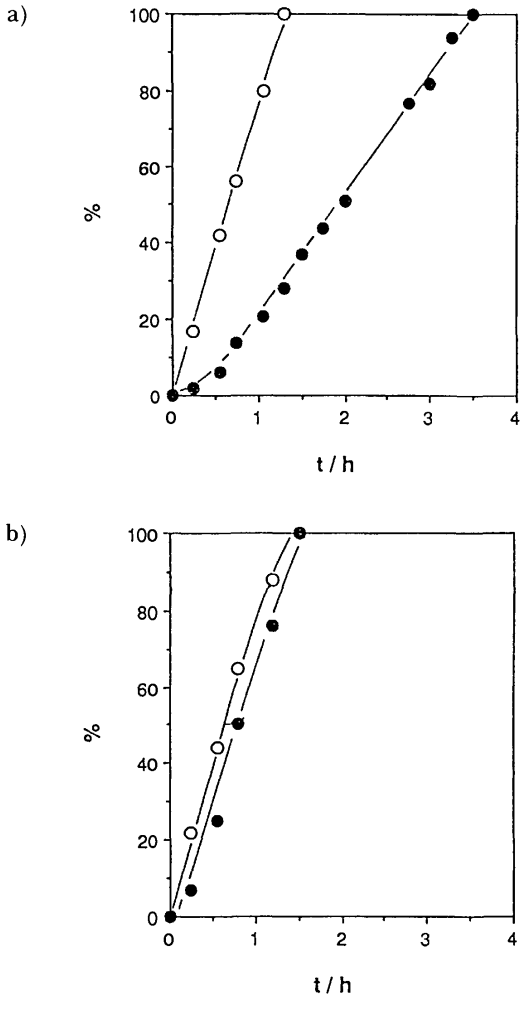

Fig. 1. Hydrogenation of *trans*-2-hexen-1-ol and *trans*-4-hexen-1-ol: a) Catalyst A-1; b) Catalyst B. ○; H_2 uptake in *trans*-2-hexen-1-ol hydrogenation. Conditions: Catalyst: 10 mg, *trans*-2-hexen-1-ol: 0.2 g, tridecane: 0.1 g, hexane: 20 cm^3, reaction temperature: 0 °C. ●; H_2 uptake in *trans*-4-hexen-1-ol hydrogenation. Conditions: Catalyst: 10 mg, *trans*-4-hexen-1-ol: 0.2 g, tridecane: 0.1 g, hexane: 20 cm^3, reaction temperature: 0 °C.

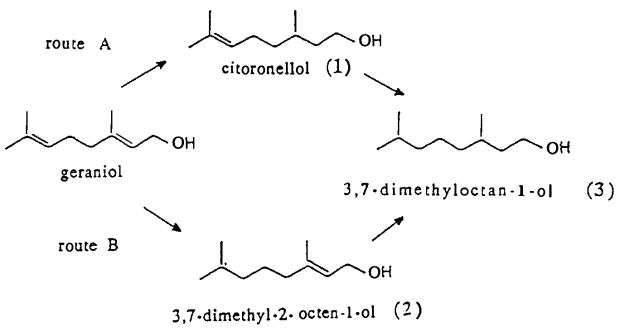

reaction rates over Catalyst B (Fig. 1-b). These results could be explained as follows: in the case of the Catalyst A-1 system, hexenols were adsorbed on the catalyst surface at the hydroxyl group. It was difficult for the carbon-carbon double bond far from the hydroxyl group to approach the active site compared with that of the hydroxyl group nearby because of the long hydrophobic carbon chain of the carboxylic acid which had adsorbed on Pt/Al_2O_3. It is considered that these phenomena are attributable to two effects. One of them is the hydrophilic-hydrophobic effect[9] which is caused by the attached carboxylic acid. Another effect is caused by a steric reguration in the carboxylic acid layer on Pt/Al_22O_3 (matrix effect).[10] Therefore, the hydrogenation of the carbon-carbon double bond near the hydroxyl group was faster than that far from the hydroxyl group. The hydrogenation over Catalyst A-2 or Catalyst A-3 was similar to that over Catalyst A-1. The difference in the rates between *trans*-2-hexen-1-ol and *trans*-4-hexen-1-ol over Catalyst A-1 was largest. It was reasonable that the effect increased with increasing the carbon chain of the adsorbed carboxylic acid; therefore, the matrix effect in Catalyst A-2 was smaller than that in Catalyst A-1. In the case of Catalyst A-3, the matrix effect was lowered because of the small amount of the adsorbed myristic acid.

Competitive hydrogenation of *trans*-2-hexen-1-ol and *trans*-4-hexen-1-ol was carried out on Catalyst A-1, and the results are shown in Fig. 2. Although the hydrogenation rates of the two hexenols were almost the same in the case of the Catalyst B system, *trans*-2-

Table 2. Rate of Hydrogenation for *trans*-2-Hexen-1-ol and *trans*-4-Hexen-1-ol

Catalyst	Initial rate of reaction/mol $g^{-1} h^{-1}$	
	trans-2-Hexen-1-ol	*trans*-4-Hexen-1-ol
Catalyst A-1	3.5×10^{-2}	2.2×10^{-3}
Catalyst A-2	7.0×10^{-2}	8.2×10^{-3}
Catalyst A-3	5.2×10^{-2}	7.9×10^{-3}
Catalyst A-4	4.2×10^{-2}	5.9×10^{-3}
Catalyst A-5	4.5×10^{-2}	5.5×10^{-3}
Catalyst B	7.1×10^{-2}	5.2×10^{-2}

Catalyst: 10 mg, *trans*-2-hexen-1-ol: 0.1 g, *trans*-4-hexen-1-ol: 0.1 g, tridecane: 0.1 g, hexane: 20 cm^3, reaction temperature: 0 °C

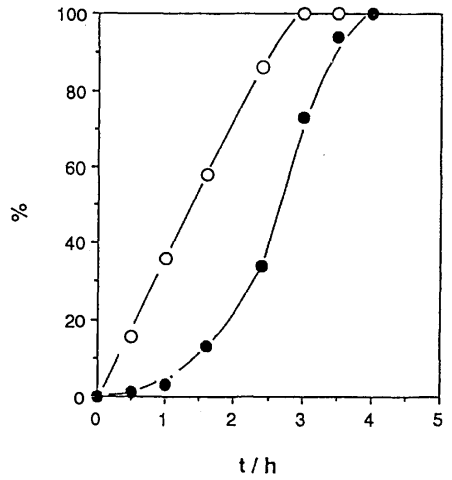

Fig. 2. Hydrogenation of the mixture of *trans*-2-hexen-1-ol and *trans*-4-hexen-1-ol (Catalyst A-1).
Conditions: Catalyst: 10 mg, *trans*-2-hexen-1-ol: 0.1 g, *trans*-4-hexen-1-ol: 0.1 g, tridecane: 0.1 g, hexane: 20 cm^3, reaction temperature: 0 °C.
○; H_2 uptake in *trans*-2-hexen-1-ol hydrogenation.
●; H_2 uptake in *trans*-4-hexen-1-ol hydrogenation.

hexen-1-ol was selectively hydrogenated over Catalyst A-1.

As shown in Table 2, the selective hydrogenation was observed by the use of catalysts modified by hexanoic acid (Catalyst A-2), myristic acid (Catalyst A-3), benzoic acid (Catalyst A-4), and adipic acid (Catalyst A-5). This tendency was independent of the variety of the modified carboxylic acids on Pt/Al_2O_3. Thus, selective hydrogenation could be performed for a mixture of some unsaturated alcohols by a catalyst modified with carboxylic acid.

It was expected that the regioselective hydrogenation of an alcohol possessing a plural of carbon-carbon double bonds could be applied, since a difference in the hydrogenation rates was found in a different position of the carbon-carbon double bond in hexenols. The hydrogenation of geraniol was investigated by catalysis with carboxylic acid-modified catalysts. Since the two double bonds were similar in a steric environment, regioselective hydrogenation could not be achieved over the usual heterogeneous catalyst. In fact, the regioselectivity in the hydrogenation of geraniol was low over Catalyst B, as shown in Fig. 3-b. However, by catalysis with Catalyst A-1, a high regioselective hydrogenation of geraniol was achieved and citronellol was obtained in an 84.5% yield (Fig. 3-a). The catalytic hydrogenation of geraniol proceeds via two kinds of pathways, shown to be routes A and B in the scheme; citronellol (**1**) and 3,7-dimethyl-2-octen-1-ol (**2**) were obtained as intermediates between geraniol and 3,7-dimethyloctan-1-ol (**3**). In the case of hydrogenation over Catalyst B, a slightly regioselective hydrogenation was observed, and **2** was detected during an early stage of the reaction. Furthermore, **3** was rapidly produced. In the

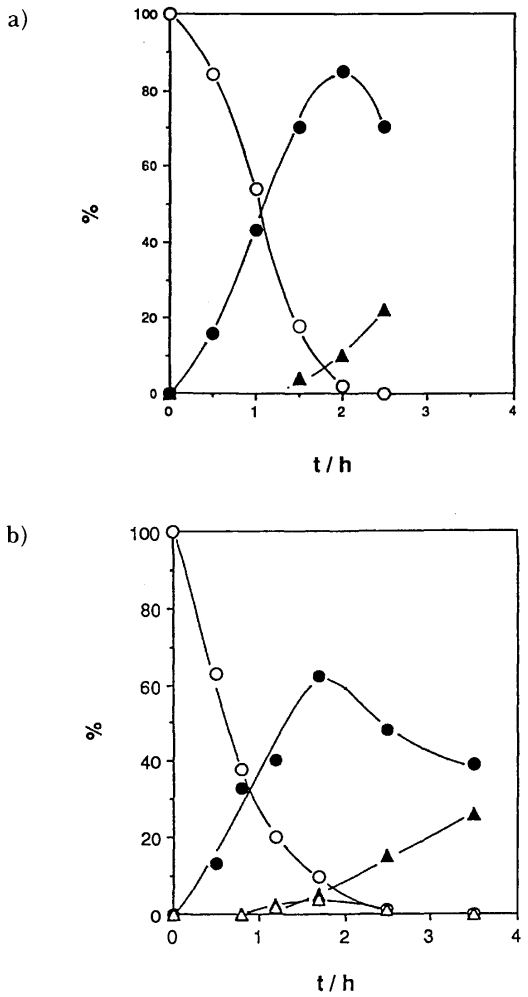

Fig. 3. Hydrogenation of geraniol: a) Catalyst A-1; b) Catalyst B.
Conditions: Catalyst: 10 mg, geraniol: 0.1 g, tridecane: 0.1 g, hexane: 20 cm^3, reaction temperature: 0 °C.
○; Ratio of geraniol. ●; Ratio of citronellol. △; Ratio of 3,7-dimethyl-2-octen-1-ol. ▲; Ratio of 3,7-dimethyloctan-1-ol.

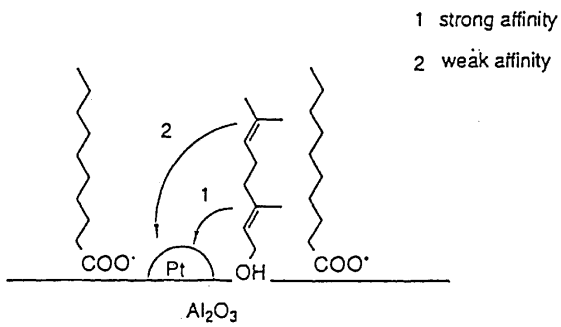

Fig. 4. Reaction model for the hydrogenation of geraniol in Catalyst A system.

hydrogenation on Catalyst A, **2** was never detected and **3** was slowly yielded. As a result, a high regioselectivity was achieved over Catalyst A. By the use of a catalyst modified by other carboxylic acids (for

instance, hexanoic acid, myristic acid, benzoic acid, or adipic acid) high regioselective hydrogenation of geraniol could also be achieved. However, a catalyst modified by decanoic acid was superior in selectivity to the other catalysts.

From these results, the reaction mechanism in the Catalyst A system was assumed to be as follows: by way of the hydroxyl group, as a hydrophilic label, the unsaturated alcohol is attracted in the hydrophilic phase to the surface of alumina and the double bond near the hydroxyl group can more easily approach the platinum by the carboxylic acid layer (Fig. 4). Consequently, the carbon-carbon double bond which was close to the hydroxyl group was easily hydrogenated.

In conclusion, a highly regioselective hydrogenation of the carbon-carbon double bond of the unsaturated alcohol was achieved by carboxylic acid-modified catalysts.

References

1) N. Toshima and T. Takahashi, *Chem. Lett.*, **1988**, 573.

2) J. T. Groves and R. Neumann, *J. Am. Chem. Soc.*, **109**, 5045 (1987).

3) H. Ogawa, T. Chihara, and K. Taya, *J. Am. Chem. Soc.*, **107**, 1365 (1985).

4) H. Ogawa, N. Hiraga, T. Chihara, S. Teratani, and K. Taya, *Bull. Chem. Soc. Jpn.*, **61**, 2383 (1988).

5) S. Hayashi, T. Takenaka, and R. Gotoh, *Nippon Kagaku Zasshi*, **88**, 133 (1967).

6) K. Hirota, K. Fueki, Y. Nakai, and K. Shindo, *Bull. Chem. Soc. Jpn.*, **31**, 780 (1958).

7) Y. Noto, K. Fukuda, T. Onishi, and K. Tamaru, *Trans. Faraday Soc.*, **63**, 2300 (1967).

8) J. T. Hall and P. K. Hansma, *Surf. Sci.*, **77**, 61 (1978).

9) The hydrophilic part in unsaturated alcohol has an affinity for the carboxyl group adsorbed on the surface of Pt/Al_2O_3. On the other hand, the hydrophobic part in the substrate has an affinity for the hydrophobic core in the carboxylic acid. Accordingly, the carbon-carbon double bond near the hydroxyl group can preferentially close to the active site in comparison with the double bond in the hydrophobic part.

10) R. H. Grubbs, L. C. Kroll, and E. M. Sweet, *J. Macromol. Sci. Chem.*, **A7**, 1047 (1973).

 © 1989 The Chemical Society of Japan Bull. Chem. Soc. Jpn., 62, 3783—3789 (1989)

Electrochemical Studies of the Reduction Mechanism of Tetrazolium Salts and Formazans

Kisaburo UMEMOTO
Department of Pure and Applied Sciences, College of Arts and Sciences,
The University of Tokyo, Komaba, Meguro-ku, Tokyo 153
(Received March 24, 1989)

The electrochemical study clarified that ditetrazolium salts are reduced not only to the half-reduced "monoformazans" but also to the fully-reduced "diformazans" at the potential where the first electron is transferred to generate the "tetrazolinyl radical". The key reaction leading to the simultaneous generation of mono- and diformazans was the disproportionation reaction of the tetrazolinyl radicals. The identification of absorption spectra of reaction intermediates was performed at several reaction stages.

Although tetrazolium salts are useful qualitative reagents for the detection of dehydrogenase[1-3] and superoxide radical,[4-7] their use as quantitative reagents has been less successful because of their complex chemistry.[1-4]

For example, Nitro Blue Tetrazolium chloride (NBT)—a tetrazolium salt most widely used for the detection of superoxide radical—is reduced to a blue colored diformazan by a four-electron reaction, and as such, NBT is taken as a four equivalent reagent in the redox reaction. However, when NBT was used as an electron acceptor in organic solvents, the final reaction product contained not only the diformazan but also the half-reduced monoformazan.[8] The reaction of ditetrazolium salts with sodium ascorbate in ethanolic solution also gave a mixture of the mono- and diformazans.[2]

Although ditetrazolium salts are known to exhibit several reaction stages,[1,2,4,10-16] the reaction paths leading to the simultaneous generation of mono- and diformazans are little known. The purpose of the present work is to clarify the reaction paths of the tetrazolium salts and their formazans in order to elucidate the problems encountered in the quantitative use of the tetrazolium salts.

Experimental

The tetrazolium salts†—2,3,5-triphenyltetrazolium chloride (TTC), Neotetrazolium chloride (NT), Blue Tetrazolium chloride (BT), and Nitro Blue Tetrazolium chloride (NBT)—were obtained from Tokyo Kasei and purified by recrystallization from ethanol-diethyl ether mixture. The formazans of TTC, NT, BT, and NBT were prepared by the method of Altman and Butcher.[2] The preparation of tetraethylammonium perchlorate (TEAP) and the purification of dimethyl sulfoxide (DMSO) were carried out by the usual methods.[8]

† NT: 3,3′-[1,1′-biphenyl]-4,4′-diylbis[2,5-diphenyl-2*H*-tetrazolium] dichloride. BT: 3,3′-(3,3′-dimethoxy[1,1′-biphenyl]-4,4′-diyl)bis[2,5-diphenyl-2*H*-tetrazolium] dichloride. NBT: 3,3′-(3,3′-dimethoxy[1,1′-biphenyl]-4,4′-diyl)-bis[2-(4-nitrophenyl)-5-phenyl-2*H*-tetrazolium] dichloride. The molecular structure and the abbreviation of the molecular species are given in Figs. 2, 6, 8, and 10.

The controlled potential electrolysis was carried out by using an H-type cell equipped with a sintered glass separator. The cathode compartment of the cell was made of a standard 1.00 cm spectrophotometric quartz cell, and the absorption spectra of the reaction products were measured by in-situ method.[8] The cathode was a Pt gauge and the anode was a spiral Pt wire. Potentials were all referred to an SCE. The salt bridge connected to the SCE was put in the anode compartment of the cell. Nitrogen gas was bubbled through both compartments in order to deaerate and to agitate the solution during the electrolysis. All experiments were carried out at the room temperature—ca. 20 °C.

Results and Discussion

Reduction of TTC and Its Formazan.[9] The cyclic voltammogram of TTC is given in Fig. 1a. The peak potential separation of the first redox couple (A/A′) is ca. 60 mV, indicating the electrode reaction is a reversible one-electron reaction. Coulometry at −0.8 V, corresponding to the second wave, revealed the overall electrode reaction is a two-electron reaction, and as the result of the electrolysis, a highly red colored solution of formazan anion (TF^-) was obtained as shown in Fig. 2c. From these results, the following stepwise electron transfer reactions are given.

$$TT^+ + e \rightleftarrows TT\cdot \quad (1)$$

$$TT\cdot + e \rightarrow TF^- \quad (2)$$

When the coulometry at −0.55 V, carried out for an attempt to obtain a solution of tetrazolinyl radical (TT·), was brought to completeness, two electrons, contrary to the probable one electron, were found to be transferred per molecule of TTC. The resulted solution gave no ESR signal and gave exactly the same absorption spectrum as that of TF^-. However, when the electrolysis was interrupted half-way, the ESR spectrum of 2,3,5-triphenyl tetrazolinyl radical[10,11,15] was obtained as shown in Fig. 3, irrespective of the electrolysis potential being either −0.55 V or −0.8 V. The same radical was also generated when TTC was added to a solution containing TF^- alone. These results suggest that the following disproportionation reaction of TT· is operating in the solution.

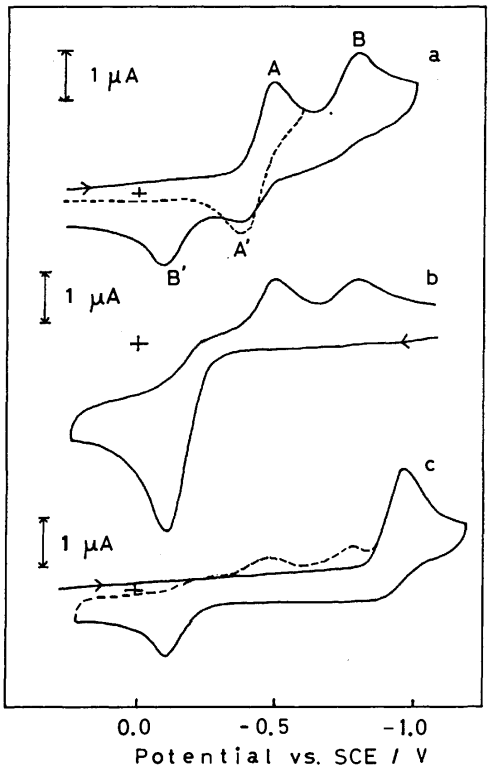

Fig. 1. Cyclic voltammograms of (a) TT^+, (b) TF^- generated by electrochemical reduction of TT^+, and (c) TF. The concentration of depolarizers is 2.5×10^{-4} mol dm^{-3} in DMSO containing 0.1 mol dm^{-3} TEAP. Scan rate: 0.05 V s^{-1}.

$$2\,TT\cdot \rightleftarrows TT^+ + TF^- \quad (3)$$

Although the monitoring of the concentration of TT· or TF^- following the controlled potential electrolysis was unsuccessful because the radical disproportionated rapidly, the disproportionation was appreciable on the cyclic voltammetry. As the half-life of the disproportionation reaction is dependent on the concentration of the radical, the cyclic voltammogram of TT^+ was affected by both the scan rate and the concentration of the depolarizer. In order to determine the rate constant of the disproportionation reaction, a series of cyclic voltammograms were taken by carrying out the potential reversal at −0.6 V, immediately after the first cathodic wave. At sufficiently high scan rate (over 0.2 V s^{-1} for a solution containing 1.0×10^{-3} M of TT^+; 1M=1 mol dm^{-3}) or at sufficiently low concentration of the depolarizer (5×10^{-4} M TT^+ at a scan rate of 0.05 V s^{-1}) only the anodic peak of TT·(A′) was observed. With the increase of the length of the time of the potential hold at −0.6 V as well as with the increase of the concentration of the depolarizer or the decrease of the scan rate, the anodic peak of TF^-(B′) increased in hight with the consumption of the anodic peak of TT·. The rate constant of the disproportionation reaction was estimated to be 2.5×10^2 mol^{-1}s^{-1} by the method of Ohmstead and Nicholson.[17]

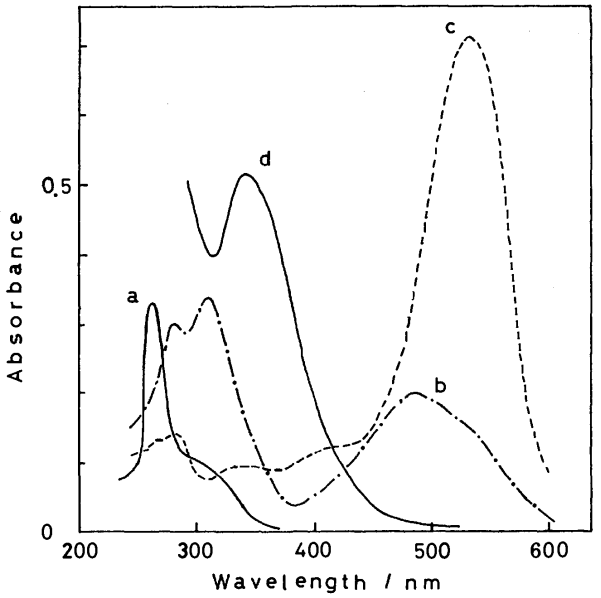

Fig. 2. Absorption spectra of (a) TT^+; 1×10^{-5} mol dm^{-3} in DMSO, (b) TF; 1×10^{-5} mol dm^{-3} in DMSO, (c) TF^- in DMSO generated by electrochemical reduction of TT^+, and (d) TT· generated by the reaction of TF^- with TT^+ in DMSO-benzene mixture (DMSO: benzene=80:20 in volume).

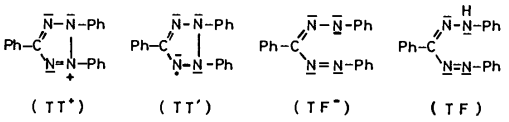

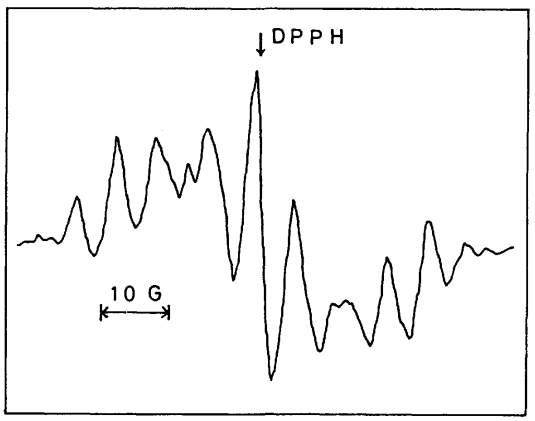

Fig. 3. ESR spectrum of TT· generated by electrochemical reduction of TT^+ in DMSO.

On the absorption spectrum, any band attributable to the radical was not observed. However, when benzene and TTC were added, the color of the solution turned from red to yellow and a new absorption band appeared at 345 nm with the consumption of the absorption band of TF^- as shown in Fig. 2d. The yellow colored solution gave a strong ESR spectrum of TT·. Thus the absorption band at 345 nm was attributed to TT·. This band was gradually substituted by that of TF^- with the increase of the content of DMSO in the DMSO-benzene mixture. The equili-

brium constant of the disproportionation reaction given by Eq. 3 was estimated to be ca. 5×10^2 in pure DMSO.

The cyclic voltammogram of formazan anion TF^-, shown in Fig. 1b, exhibited two cathodic waves at potentials quite close to those of TT^+, indicative of the regeneration of TT^+ by electrochemical oxidation of TF^-. The coulometry of TF^- at +0.2 V revealed the electrode process is a two-electron oxidation, and the original TT^+ was confirmed to be recovered in high efficiency as follows.

$$TF^- - 2e \rightarrow TT^+ \quad (4)$$

The formazan anion TF^- was stable in anhydrous DMSO, but when proton donors—water and acids, such as benzoic acid and acetic acid—were added, TF^- was protonated as follows.

$$TF^- + H^+ \rightarrow TF \quad (5)$$

The cyclic voltammogram of 1,3,5-triphenylformazan (TF) is given in Fig. 1c. The coulometry at −1.0 V revealed TF is reduced to TF^- by a one-electron reaction as follows.

$$TF + e \rightarrow TF^- + H \quad (6)$$

The reaction paths of TTC are summarized in Scheme 1.

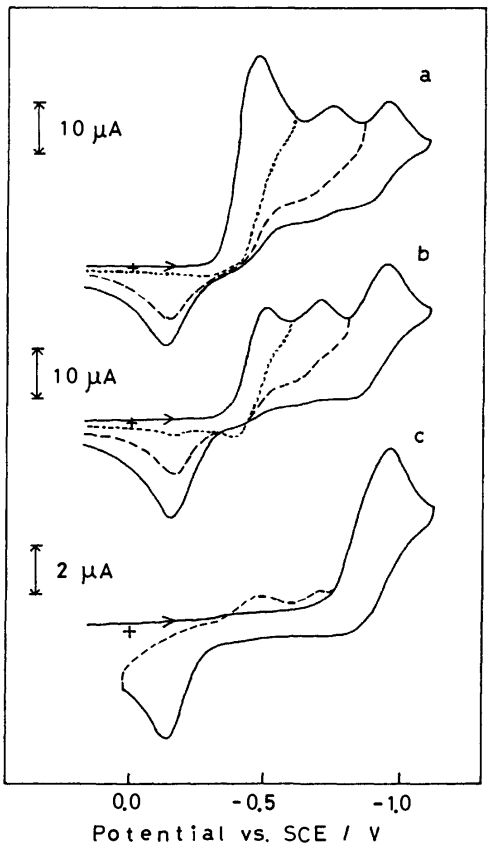

Fig. 4. Cyclic voltammograms of (a) NT^{2+} (1×10^{-3} mol dm^{-3}), (b) $NTMF^+$ (1×10^{-3} mol dm^{-3}), and (c) NTDF (saturated) in DMSO (containing 0.1 mol dm^{-3} TEAP. Scan rate: 0.05 V s^{-1}.

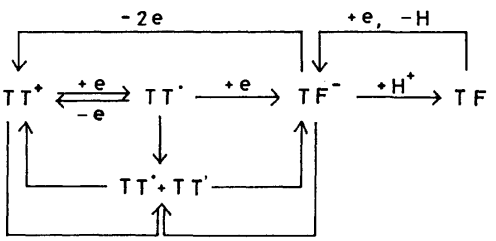

Scheme 1. Reaction paths of TT^+.

Reduction of NT and Its Formazans. Since NT^{2+} is a ditetrazolium ion having a molecular structure composed of two equivalent TT^+, the reaction paths clarified for TT^+ and TF provide the basis for understanding the complicated redox behaviors of NT^{2+} and its formazans. The cyclic voltammograms and absorption spectra of NT^{2+}, NT-monoformazan ($NTMF^+$), and NT-diformazan(NTDF) are given in Figs. 4—6.

As $NTMF^+$ has a molecular structure composed of one teterazolium ring and one formazan moiety, the cyclic voltammogram of $NTMF^+$ revealed the characteristics of both structures. By referring to the cyclic voltammograms of TT^+ and TF, the first and the

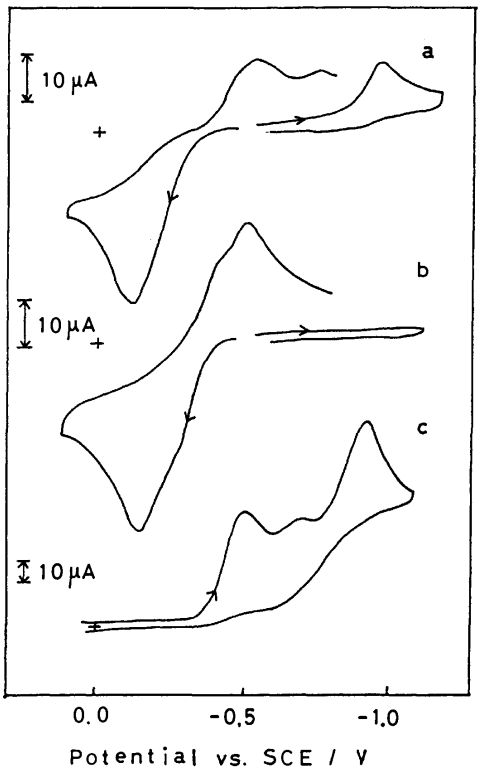

Fig. 5. Cyclic voltammograms of (a) the solution obtained by the exhaustive electrolysis of NT^{2+} at −0.55 V, (b) $NTDF^{2-}$ generated by the reaction of NTDF with tetraethylammonium hydroxide (TEAOH), (c) NT^{2+} in the presence of equimolar amount of acetic acid. The concentration of depolarizers is 1×10^{-3} mol dm^{-3} in DMSO containing 0.1 mol dm^{-3} TEAP. Scan rate: 0.05 V s^{-1}.

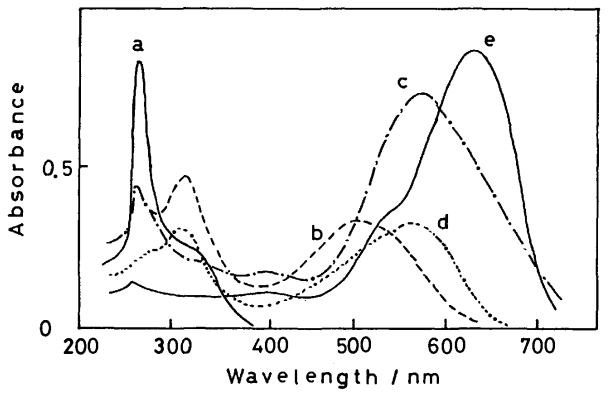

Fig. 6. Absorption spectra of (a) NT^{2+}, (b) $NTMF^+$, (c) NTMF, (d) NTDF, and (e) $NTDF^{2-}$. The concentration is 1.5×10^{-5} mol dm^{-3} in DMSO. The range of absorbance of (d) and (e) is 1/2.

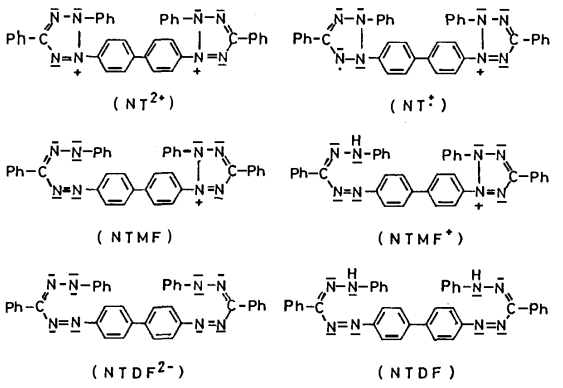

second cathodic waves were attributed to the reduction of the tetrazolium ring. The third wave agreed with the reduction wave of TF.

NTDF exhibited only one cathodic wave at a potential quite close to that of TF, suggesting that there is no or little difference in the potential required for the reduction of any formazan structure in TF, $NTMF^+$, or NTDF. In the presence of base, NTDF dissociated to generate $NTDF^{2-}$, and the cathodic wave of NTDF disappeared as shown in Fig. 5b.

By analogy with $NTMF^+$ the first and the second wave of NT^{2+} were attributed to the reduction of the tetrazolium ring. It is seen that there is no or little difference in the reduction potentials of the mono- and ditetrazolium ions. The observation of the third wave of NT^{2+} indicates the formazan anion of NT is more easily protonated than TF^-. In the presence of proton donor, the formazan peak of NT^{2+} increased in height and the anodic peak of formazan anion disappeared by the protonation reaction as shown in Fig. 5c.

When the coulometry of $NTMF^+$ at -0.55 V, corresponding to the first wave, was completed, overall two electrons were transferred per molecule of $NTMF^+$ as in the case of TT^+. The resulted solution was deep purplish colored. By addition of acids, the solution gave an absorption spectrum of NTDF (λ_{max}=558 nm) as shown in Fig. 6d. These results indicate the reaction paths given by Eqs. 1—5 are exactly working in the reduction of the one-sided tetrazolium moiety of $NTMF^+$ as follows.

$$NTMF^+ + e \rightleftarrows NTMF\cdot \quad (7)$$

$$2\,NTMF\cdot \rightleftarrows NTMF^+ + NTDF^- \quad (8)$$

$$NTDF^- + H^+ \rightarrow NTDF \quad (9)$$

Due to the disproportionation reaction of the tetrazolinyl radical (Eq. 8), the anodic peaks of the cyclic voltammogram of $NTMF^+$ were affected by both the scan rate and the concentration of the depolarizer as in the case of TT^+. The rate constant of the disproportionation reaction was estimated to be 2×10^3 mol^{-1} s^{-1}.

When the constant potential electrolysis of NT^{2+} at -0.55 V was interrupted at the early stage of the electrolysis, the absorption spectrum of NTMF (λ_{max}=570 nm) and an ESR spectrum quite similar to that of TT· were obtained. These species turned to $NTMF^+$ (λ_{max}=500 nm) by addition of acid. These experimental results suggest the reaction paths leading to $NTMF^+$ from NT^{2+} must be the disproportionation reaction of the one-sided tetrazolinyl radical as follows.

$$NT^{2+} + e \rightleftarrows NT^{\ddagger} \quad (10)$$

$$2\,NT^{\ddagger} \rightleftarrows NT^{2+} + NTMF \quad (11)$$

$$NTMF + H^+ \rightarrow NTMF^+ \quad (12)$$

The rate constant of the disproportionation reaction was estimated to be 3×10^3 mol^{-1}s^{-1} by the cyclic voltammetry. As NT^{2+} is a ditetrazolium ion, the generation of a biradical seems to be possible. However, the ESR measurement showed the presence of only one radical species which did not show any line broadening characteristic of the biradical.[15] Such a biradical may be unstable, if existent, since following electron transfer reaction is probable as $NT^{\ddagger}$ must be more stable than NT:.

$$NT^{2+} + 2e \rightarrow NT: \xrightarrow{NT^{2+}} 2\,NT^{\ddagger} \quad (13)$$

When the coulometry of NT^{2+} at the first wave was brought to completeness, the overall reaction was found to be a four-electron reaction. The reaction products were $NTDF^{2-}$ (λ_{max}=626 nm) and its formazans as shown in Fig. 5a. By addition of acid, NTDF (λ=558 nm) was obtained. The generation of diformazan at the first wave suggests the reduction of the residual one-sided tetrazolium ring of NTMF must follow the reactions shown by Eqs. 10 and 11 as follows.

$$NTMF + e \rightleftarrows NTMF^{\cdot-} \quad (14)$$

$$2\,NTMF^{\cdot-} \rightleftarrows NTMF + NTDF^{2-} \quad (15)$$

$$NTDF^{2-} + 2\,H^+ \rightarrow NTDF \quad (16)$$

When NT^{2+} was added into the solution of $NTDF^{2-}$, NTMF was generated. Accordingly, the following disproportionation reaction is also working in the solution.

$$2\,NTMF \rightleftarrows NT^{2+} + NTDF^{2-} \quad (17)$$

As the reduction potential of the one-sided tetrazolium ring of NTMF is almost the same with that of NT^{2+}, the reactions shown by Eqs. 14—17 will occur in parallel with those given by Eqs. 10—13. As the disproportionation reaction given by Eq. 17 is advantageous for the generation of NTMF at high concentration of NT^{2+}, the preferencial generation of monoformazan was observed at the early stage of electrolysis, but the simultaneous generation of both formazans became remarkable on proceeding the electrolysis.

$NTMF^+$ and NTDF gave $NTDF^{2-}$ by the constant potential electrolysis at −1.0 V.

$$NTMF^+ + 3e - H \rightarrow NTDF^{2-} \quad (18)$$

$$NTDF + 2e - 2H \rightarrow NTDF^{2-} \quad (19)$$

As shown above, the complicated reactions of NT^{2+} is considered to be composed of the combination of the fundamental reactions characteristic of the single tetrazolium ion.

Reduction of BT and Its Formazans. BT^{2+} has a molecular structure in which two methoxy groups are introduced into the biphenyl structure of NT^{2+}. The present study was focused on how the fundamental reactions of NT^{2+} are modified by the introduction of methoxy group.

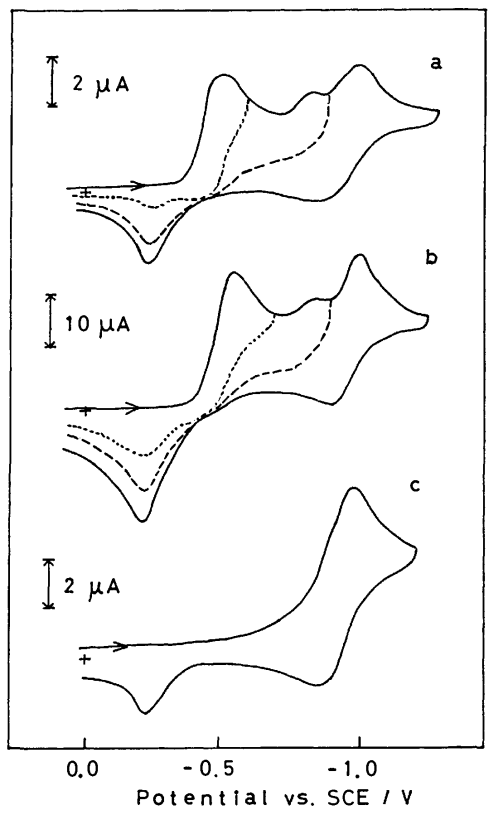

Fig. 7. Cyclic voltammograms of (a) BT^{2+} (saturated -2×10^{-4} mol dm^{-3}), (b) $BTMF^+$ (1×10^{-3} mol dm^{-3}), and (c) BTDF (saturated) in DMSO containing 0.1 mol dm^{-3} TEAP. Scan rate: 0.05 V s^{-1}.

The cyclic voltammograms and the absorption spectra of BT^{2+} and its reaction products are given in Figs. 7 and 8. By referring to the results obtained for NT^{2+}, the first two cathodic waves on the cyclic voltammograms of BT^{2+} and $BTMF^+$ were attributed to the reduction of the tetrazolium ring and the third wave to the reduction of the formazan moiety. The anodic wave was attributed to the oxidation of the formazan anion.

The constant potential electrolysis revealed BT^{2+} is reduced to $BTMF^+$ (λ_{max}=540 nm) by a two-electron reaction and to BTDF (λ_{max}=608 nm) by a four-electron reaction at the first cathodic wave. BTDF was reduced to $BTDF^{2-}$ (λ_{max}=640 nm) at −1.0 V, and $BTDF^{2-}$ reacted with BT^{2+} to give BTMF by a disproportionation reaction analogous to Eq. 17.

From these results, it is likely that the reaction paths of BT^{2+} are exactly analogous to those of NT^{2+} given by Eqs. 7—19, indicative of no effect of the methoxy group.

Reduction of NBT and Its Formazans. The cyclic voltammograms and the absorption spectra of NBT^{2+} and its reduction products are given in Figs. 9 and 10.

As $NBTMF^+$ has one tetrazolium structure and one formazan structure, the cyclic voltammogram of $NBTMF^+$ shown in Fig. 9b is well understood by

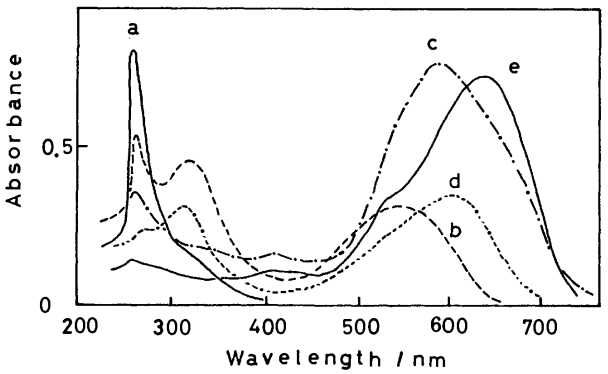

Fig. 8. Absorption spectra of (a) BT^{2+}, (b) $BTMF^+$, (c) BTMF, (d) BTDF, and (e) $BTDF^{2-}$. The concentration is 1.5×10^{-5} mol dm^{-3} in DMSO. The range of absorbance of (d) and (e) is 1/2.

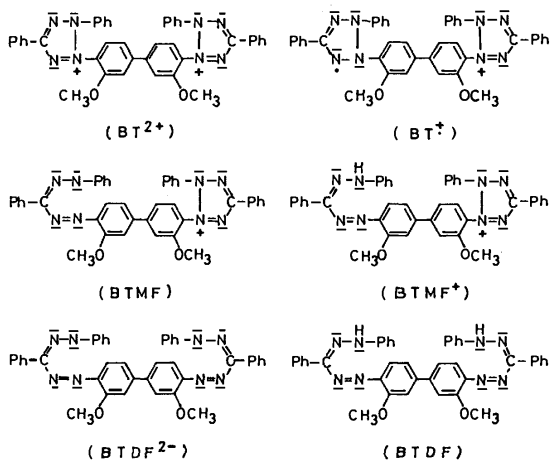

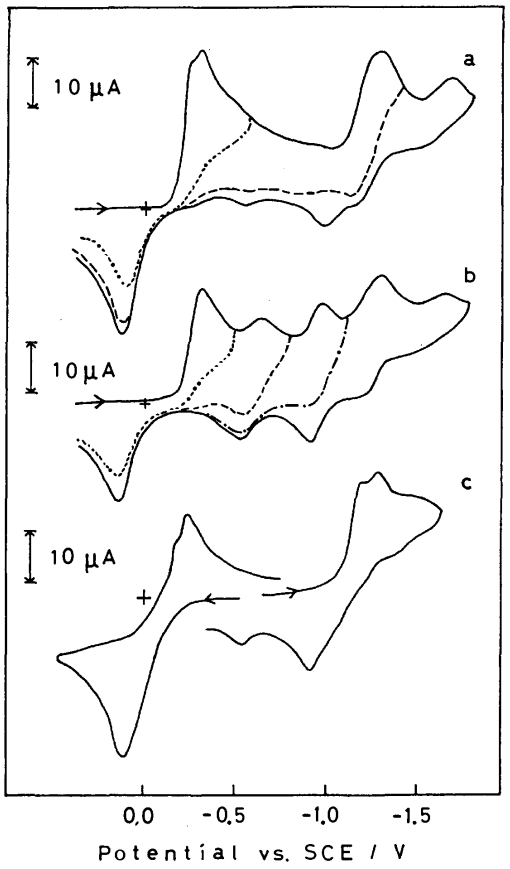

Fig. 9. Cyclic voltammograms of (a) NBT^{2+}, (b) $NBTMF^{+}$, and (c) $NBTDF^{2-}$ generated by the reaction of NBTDF with TEAOH. The concentration of depolarizers is 1×10^{-3} mol dm^{-3} in DMSO containing 0.1 mol dm^{-3} TEAP. Scan rate: 0.05 V s^{-1}.

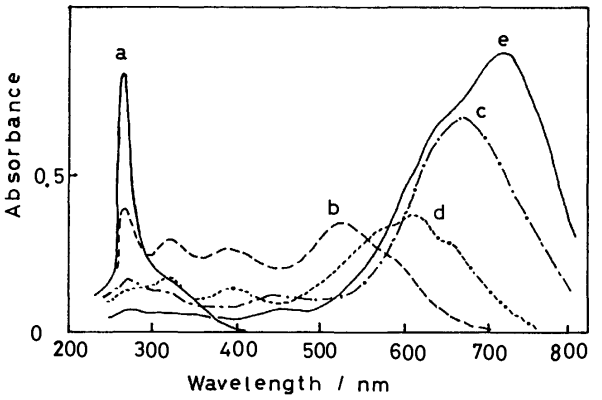

Fig. 10. Absorption spectra of (a) NBT^{2+}, (b) $NBTMF^{+}$, (c) NBTMF, (d) NBTDF, and (e) $NBTDF^{2-}$. The concentration is 1.5×10^{-5} mol dm^{-3} in DMSO. The range of absorbance of (d) and (e) is 1/2.

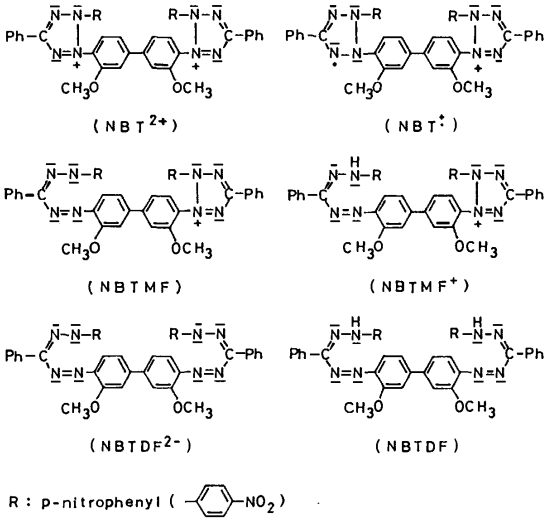

analogy with that of $NTMF^{+}$. The first and the second cathodic waves were characterized to the reduction of the tetrazolium ring, the third wave to the reduction of the formazan structure and the rests to the reduction of the nitro group, since nitrobenzene derivatives gave reduction waves around these potentials.

The coulometry at the first wave revealed that $NBTMF^{+}$ was reduced to $NBTDF^{-}$ (λ_{max}=709 nm) by a two-electron reaction. The reaction paths leading to $NBTDF^{-}$ from $NBTMF^{+}$ are considered to be similar to those of $NTMF^{+}$ shown by Eqs. 7—9. The rate constant of the disproportionation reaction of the tetrazolinyl radical was estimated to be 5×10^{3} mol^{-1} s^{-1} by cyclic voltammetry. The reduction of $NBTMF^{+}$ at the third wave gave $NBTDF^{2-}$ (λ_{max}=724 nm). $NBTDF^{-}$ and $NBTDF^{2-}$ thus generated gave NBTDF (λ_{max}=600 nm) by addition of acid. NBTDF is insoluble not only in DMSO but also in usual organic solvent, such as ethanol, benzene, ether, acetonitrile, and *N,N*-dimethylformamide. However, the DMSO solution of NBTDF appeared to be homogeneous immediately after being shaken with the ultrasonic vibrator, and gave a reproducible absorption spectrum as shown in Fig. 10d. Although the reduction potential of NBTDF could not be determined, the electrolysis of NBTDF was performed at −1.0 V, a potential now specified to be characteristic of the reduction of the formazan structure. Nitrogen purged through the solution for the deaeration secured the continuous contact of NBTDF particle with the Pt mesh electrode. The current density was low, but as the result of the electrolysis, a sky blue solution of $NBTDF^{2-}$ was obtained. $NBTDF^{2-}$ gave a cyclic votammogram as shown in Fig. 9c. The reduction waves at ca. −1.2 V are due to the nitro group. By the electrolysis at +0.2 V, $NBTDF^{2-}$ was oxidized to NBT^{2+}.

The cyclic voltammogram of NBT^{2+} is given in Fig. 9a. By analogy with $NBTMF^{+}$, the first cathodic wave was attributed to the reduction of the tetrazolium ring and the rests to the reduction of the nitro group. The small shoulder at the first wave may discriminate the small difference in the potential of the generation of mono- or ditetrazolinyl radical, but the waves corresponding to the second and the third waves exhibited for NT^{2+} and BT^{2+} were not observed.

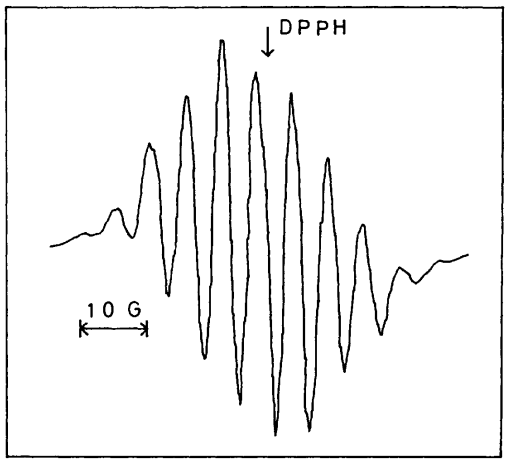

Fig. 11. ESR spectrum of the tetrazolinyl radical generated by electrochemical reduction of NBT^{2+}.

At the early stage of the constant potential electrolysis at −0.4 V, NBT^{2+} gave NBTMF (λ_{max}=680 nm) and a tetrazolinyl radical NBT^{+} which gave an ESR spectrum as shown in Fig. 11. The ESR spectrum with nine line hyperfine structure is characteristic of the tetrazolinyl monoradical, and the biradical of NBT was not evidenced as in the case of NT. The rate constant of the disproportionation reaction of the tetrazolinyl radical was evaluated to be 5×10^3 $mol^{-1}s^{-1}$ by the cyclic voltammetry. By addition of acids, both the ESR spectrum and the absorption spectrum of NBTMF disappeared and the absorption spectrum of $NBTMF^+$ (λ_{max}=530 nm) was obtained.

When the constant potential electrolysis at the first wave was completed, NBT^{2+} was reduced to $NBTDF^{2-}$ by a four-electron reaction. $NBTDF^{2-}$ was stable in anhydrous DMSO and accordingly the cyclic voltammogram of NBT^{2+} did not exhibit any formazan wave. When NBT was added into the solution of $NBTDF^{2-}$, NBTMF was generated by a disproportionation reaction analogous to that shown by Eq. 17.

The reaction scheme shown for NBT^{2+} is exactly understood by reaction paths given by Eqs. 10—19, suggesting no affect of both nitro- and methoxy groups on the fundamental reactions characteristic of the tetrazolium structure.

Summary

Ditetrazolium salts were first reduced to half-reduced monoformazans and successively to fully-reduced diformazans. In both reaction stages, the key reaction leading to the generation of each formazan was the disproportionation reaction of the tetrazolinyl radical generated by one-electron reduction of the tetrazolium structure. As there was almost no difference in the potential required for the generation of tetrazolinyl radical from mono- or ditetrazolium ion, the simultaneous generation of mono- and diformazans appears to be a general feature of the reduction of any ditetrazolium salts. It was only at the early stage of the electrolysis that the half-reduced monoformazan was preferencially generated. In the analytical use of ditetrazolium salts, it was only when the reductant was very weak[2] or the tetrazolium salts existed in vast molar excess over the reductant[4] that the preferential generation of monoformazan secured the quantitative use of the ditetrazolium salts. Otherwise, the separated amount of mono- and diformazan should be determined[3] for the successful application of the tetrazolium method.

The author thanks to Dr. Ryo Hirasawa for his kind permission of using the ESR spectrometer.

References

1) A. W. Nineham, *Chem. Rev.*, **55**, 355 (1955).
2) F. P. Altman and G. R. Butcher, *Histochemie*, **37**, 333 (1973); F. P. Altman, *ibid.*, **38**, 155 (1974).
3) R. G. Butcher and F. P. Altman, *Histochemie*, **37**, 351 (1973).
4) B. H. J. Bielski, G. G. Shiue, and S. Bajuk, *J. Phys. Chem.*, **84**, 830 (1980).
5) I. Saito, T. Matsuura, and K. Inoue, *J. Am. Chem. Soc.*, **105**, 3200 (1983).
6) E. Lee-Ruff, *Chem. Soc. Rev.*, **6**, 195 (1977).
7) F. W. Beyer Jr. and I. Fridovich, *Anal. Biochem.*, **161**, 559 (1987).
8) K. Umemoto and N. Okamura, *Bull. Chem. Soc. Jpn.*, **59**, 3047 (1986).
9) K. Umemoto, *Bull. Chem. Soc. Jpn.*, **58**, 2051 (1985).
10) Y. Deguchi and H. Takagi, *Tetrahedron Lett.*, **1967**, 3179.
11) O. W. Maender and G. C. Russell, *J. Org. Chem.*, **31**, 442 (1966); F. A. Neugebauer and C. A. Russell, *ibid.*, **33**, 2744 (1968).
12) F. A. Neugebauer, *Tetrahedron*, **26**, 4843 (1970).
13) K. M. Dyumaev, G. V. Formin, and Z. K. Kriminskaya, *Khim. Vys. Energ.*, **16**, 558 (1982).
14) Z. K. Kriminskaya, K. M. Dyumaev, L. S. Vischipanova, Yu. V. Ivanov, and A. K. Pikaev, *Khim. Vys. Energ.*, **18**, 40 (1984).
15) N. Azuma, K. Mukai, and K. Ishizu, *Bull. Chem. Soc. Jpn.*, **43**, 3960 (1970).
16) I. Tabakovic, M. Trkovnik, and Z. Gruic, *J. Chem. Soc., Perkin Trans. 2*, **1979**, 166.
17) M. L. Ohmstead and R. S. Nicholson, *Anal. Chem.*, **41**, 862 (1969).

Preparation and Characterization of Rhodium(III) Complexes Containing (2-Aminoethyl)dimethylphosphine (edmp) or 1,2-Bis(dimethylphosphino)ethane (dmpe). Structures of *fac*-$[Rh(edmp)_3]^{3+}$, *trans*(*Cl,Cl*),*cis*(*P,P*)-$[RhCl_2(edmp)_2]^+$, and *trans*-$[RhCl_2(dmpe)_2]^+$

Kim P. SIMONSEN,† Nahomi SUZUKI,†† Masatoshi HAMADA,†† Masaaki KOJIMA, Shigeru OHBA,†† Yoshihiko SAITO,†† and Junnosuke FUJITA*
Department of Chemistry, Faculty of Science, Nagoya University, Chikusa-ku, Nagoya 464-01
††Department of Chemistry, Faculty of Science and Technology, Keio University, 3-14-1, Hiyoshi, Kohoku-ku, Yokohama 223
(Received May 12, 1989)

The *fac*-$[Rh(edmp)_3]^{3+}$ (edmp=(2-aminoethyl)dimethylphosphine), *trans*(*Cl,Cl*),*cis*(*P,P*)-$[RhCl_2(edmp)_2]^+$, and *trans*-$[RhCl_2(dmpe)_2]^+$ (dmpe=1,2-bis(dimethylphosphino)ethane) complexes were prepared and the molecular structures were determined by the single crystal X-ray diffraction method. Crystal data and final R values are: *fac*-$[Rh(edmp)_3]Br_3 \cdot 3H_2O$, orthorhombic, $Pna2_1$, a=26.750(4), b=10.125(1), c=9.592(1) Å, V=2598.2(5) Å^3, Z=4, R=0.039 for 1590 observed unique reflections. *trans*(*Cl,Cl*),*cis*(*P,P*)-$[RhCl_2(edmp)_2]PF_6$, monoclinic, $P2_1/a$, a=18.197(4), b=12.574(2), c=8.615(1) Å, β=96.59(2)°, V=1958.2(6) Å^3, Z=4, R=0.032 for 3379 reflections. *trans*(*Cl,Cl*),*cis*(*P,P*)-$[RhCl_2(edmp)_2]ClO_4$, triclinic, $P\bar{1}$, a=13.122(2), b=17.952(2), c=12.343(2) Å, α=91.65(2), β=102.46(2), γ=80.74(1)°, V=2802.0(7) Å^3, Z=6, R=0.070 for 7513 reflections. *trans*-$[RhCl_2(dmpe)_2]CF_3SO_3$, monoclinic, $P2_1/a$, a=13.166(2), b=24.337(4), c=8.002(2) Å, β=95.95(2)°, V=2550.1(8) Å^3, Z=4, R=0.040 for 3201 reflections. It was found that the shorter the Rh-P bond length, the larger the trans Rh-N bond elongation. The mean Rh-P bond distance in *trans*-$[RhCl_2(dmpe)_2]CF_3SO_3$ (2.337(2) Å) is longer than those in *fac*-$[Rh(edmp)_3]Br_3 \cdot 3H_2O$ (2.283(4) Å) and *trans*(*Cl,Cl*),*cis*(*P,P*)-$[RhCl_2(edmp)_2]PF_6$ (2.252(2) Å). A series of complexes of *trans*(*X,X*),*cis*(*P,P*)-$[RhX_2(edmp)_2]^+$ (X=Cl, Br, I) and *trans*-$[RhX_2(dmpe)_2]^+$ (X=Cl, Br) were also prepared and their absorption spectra were compared with one another and with those of the corresponding cobalt(III) complexes.

In a previous paper,[1] we reported the preparation of trans(*Cl,Cl*),cis(*P,P*) and cis(*Cl,Cl*),trans(*P,P*) isomers of $[RhCl_2(edpp)_2]^+$, where edpp denotes (2-aminoethyl)diphenylphosphine. The X-ray analyses of the complexes revealed the trans influence of P donor atoms on the Rh-N and Rh-P bond lengths. (2-Aminoethyl)dimethylphosphine (edmp) has less bulky substituents on the phosphorus atom than does edpp, and it is interesting to see the steric and electronic effects of the substituent on P on such properties as trans influence.

This paper describes the preparation and X-ray structure analyses of *fac*-$[Rh(edmp)_3]^{3+}$, *trans*-(*Cl,Cl*),*cis*(*P,P*)-$[RhCl_2(edmp)_2]^+$, and the related *trans*-$[RhCl_2(dmpe)_2]^+$ complex. A series of complexes of *trans*(*X,X*),*cis*(*P,P*)-$[RhX_2(edmp)_2]^+$ (X=Cl, Br, I) and *trans*-$[RhX_2(dmpe)_2]^+$ (X=Cl, Br) were also prepared and their absorption spectra were compared with one another and with those of the corresponding cobalt(III) complexes.

Experimental

The edmp[2] and dmpe[3] ligands were prepared according to literature methods, and handled under an atmosphere of nitrogen until they formed air-stable rhodium(III) complexes. Absorption, and ^1H and ^{13}C NMR spectra were recorded on a Hitachi 323 spectrophotometer and a Hitachi R-90H spectrometer, respectively.

Preparation of Complexes. ***fac*-$[Rh(edmp)_3]Cl_3 \cdot 4H_2O$.** A deaerated ethanol solution (10 cm^3) of $RhCl_3 \cdot 3H_2O$ (0.40 g, 1.52 mmol) was heated to reflux. To this solution was added a deaerated ethanol solution (7 cm^3) of edmp (0.74 g, 7 mmol). The mixture was refluxed for 12 h to give a yellow solution together with a white crystalline solid. The mixture was allowed to cool in an ice bath, and the white crystals were collected by filtration. The crude product was dissolved in water (2 cm^3) and filtered. The filtrate was heated and poured into boiling ethanol (25 cm^3). The mixture was allowed to stand at room temperature for a while, and then in a freezer overnight to yield white crystals. They were collected by filtration, washed successively with ethanol and diethyl ether, and air dried. Yield: 0.50 g (55%). Found: C, 24.03; H, 7.19; N, 7.05; Cl, 17.94%. Calcd for $[Rh(edmp)_3]Cl_3 \cdot 4H_2O = C_{12}H_{44}N_3Cl_3O_4P_3Rh$: C, 24.16; H, 7.43; N, 7.04; Cl, 17.82%. Thermogravimetry: loss of weight 127 mg/g sample, i.e. 76.2 g mol^{-1}. Calcd for $[Rh(edmp)_3]Cl_3 \cdot 4H_2O$: 72.1 g mol^{-1}. ^1H NMR (D_2O) δ=1.75—2.05 (18H, four-line multiplet, CH_3), 2.10—2.55 (6H, m, CH_2P), and 2.6—3.5 (6H m, CH_2N). ^{13}C NMR (D_2O) δ=13.6 (six-line multiplet, CH_3), 15.2 (six-line multiplet, CH_3), 34.9 (six-line multiplet, CH_2P), and 42.1 (s, CH_2N). The complex is soluble in water and methanol.

***fac*-$[Rh(edmp)_3]Br_3 \cdot 3H_2O$ (1).** To an aqueous solution (1 cm^3) of *fac*-$[Rh(edmp)_3]Cl_3 \cdot 4H_2O$ (0.10 g, 0.17 mmol) was added a hot aqueous solution (3 cm^3) of NaBr (1.5 g). The solution was allowed to stand overnight for crystallization. The colorless crystals were collected by filtration and washed successively with ice-cold water, ethanol, and di-

† On leave from Chemistry Department I, University of Copenhagen, Universitetsparken 5, DK-2100, Copenhagen φ, Denmark.

ethyl ether and air dried. Yield: 0.10 g (84% based on the chloride). The structure of the complex was determined by X-ray analysis.

***mer*-[RhCl$_3${P(*n*-Bu)$_3$}$_3$].** Attempts to prepare the complex by the published methods[4,5] did not lead to any crystallization of the complex. The complex was prepared by a modified method of Intille.[5] A deaerated ethanol solution (10 cm^3) containing $RhCl_3 \cdot 3H_2O$ (0.94 g, 3.6 mmol) and tributylphosphine (4 cm^3, 16 mmol) was refluxed for 1.5 h to give an orange solution. The solvent was evaporated off under reduced pressure and the residual orange oil was dissolved in hexane (20 cm^3). The solution was then added to water (20 cm^3), and hexane was evaporated slowly (1—2 d) at room temperature. The orange crystals deposited were collected by filtration, washed thoroughly with water and dried in a desiccator over P_4O_{10}. Yield: 2.1 g (72%). Found: C, 52.25; H, 10.11%. Calcd for [RhCl$_3${P(*n*-Bu)$_3$}$_3$]=$C_{36}H_{81}Cl_3P_3Rh$: C, 52.92; H, 10.00%. The ^{1}H NMR spectrum was identical with that reported by Intille.[5]

***trans*(*Cl*,*Cl*),*cis*(*P*,*P*)-[RhCl$_2$(edmp)$_2$]PF$_6$ (2a).** To a deaerated stirred benzene solution (50 cm^3) of *mer*-[RhCl$_3${P(*n*-Bu)$_3$}$_3$] (1.63 g, 2.0 mmol) was added dropwise edmp (0.53 g, 5.0 mmol). The mixture was refluxed for 1 h to give a yellow precipitate. After cooling for a while, the precipitate was collected on a glass filter by filtration, washed with diethyl ether and dried in a desiccator over P_4O_{10}. The product (ca. 0.9 g) was hygroscopic, mixed with ethanol (50 cm^3), and the mixture was filtered to leave a small amount of white crystals on the filter. Yield: 0.04 g. This product was *fac*-[Rh(edmp)$_3$]Cl$_3$. The yellow filtrate was evaporated to nearly dryness under reduced pressure, and the residue was redissolved in water (50 cm^3). The solution was passed through a short column (ϕ1.0 cm×3 cm) of SP-Sephadex C-25 in order to remove highly charged species. The yellow eluate was applied on a column (ϕ2.5 cm×30 cm) of SP-Sephadex C-25. The adsorbed product was eluted with 0.05 mol dm^{-3} NaCl. The eluate containing the fastest-moving yellow main band was collected and evaporated to dryness under reduced pressure. The residue was shaken with ethanol (3×20 cm^3) to extract the complex, the solvent was evaporated to dryness under reduced pressure, and the residue was dissolved in water (10 cm^3). The solution was filtered, heated to 90 °C, and to this solution was added a saturated aqueous solution (4 cm^3) of NH_4PF_6. The mixture was allowed to stand at room temperature for a while, and then in a refrigerator overnight to yield yellow crystals. They were collected by filtration, washed successively with ethanol and diethyl ether, and dried in air. Yield: 0.30 g (28%). Found: C, 18.01; H, 4.63; N, 5.32; Cl, 13.27%. Calcd for [RhCl$_2$(edmp)$_2$]PF$_6$=$C_8H_{24}N_2Cl_2F_6P_3Rh$: C, 18.16; H, 4.57; N, 5.30; Cl, 13.40%. ^{1}H NMR ($C_6D_5NO_2$) δ=1.84—1.97 (12H, filled-in-doublet, CH_3), 2.15—2.6 (4H, m, CH_2P), 3.05—3.8 (4H, m, CH_2N), and 4.2—4.65 (4H, br, NH_2). ^{13}C NMR (CD_3CN) δ=10.9 (filled-in doublet, CH_3), 32.9 (filled-in doublet, CH_2P), and 40.8 (s, CH_2N). The complex is soluble in acetonitrile, dichloromethane, ethanol, and water. Single crystals suitable for X-ray analysis were obtained by slow evaporation of a methanol solution of the complex.

***trans*(*Cl*,*Cl*),*cis*(*P*,*P*)-[RhCl$_2$(edmp)$_2$]ClO$_4$ (2b).** An aqueous solution of *trans*(*Cl*,*Cl*),*cis*(*P*,*P*)-[RhCl$_2$(edmp)$_2$]PF$_6$ (ca. 0.1 g) was applied on a column of SP-Sephadex C-25. The complex was eluted with 0.1 mol dm^{-3} NaCl, and the eluate was evaporated to dryness under reduced pressure. The complex was extracted with ethanol, and the solvent was evaporated. The residue was dissolved in water (5 cm^3) and to this solution was added a hot solution of $LiClO_4$ (2 g) in water (2 cm^3). The mixture was allowed to stand for crystallization. Single crystals for X-ray analysis were obtained by recrystallization from ethanol.

***trans*(*Br*,*Br*),*cis*(*P*,*P*)-[RhBr$_2$(edmp)$_2$]PF$_6$.** This complex was prepared from *trans*(*Cl*,*Cl*),*cis*(*P*,*P*)-[RhCl$_2$(edmp)$_2$]PF$_6$ and KBr. To a hot aqueous solution (12 cm^3) of *trans*(*Cl*,*Cl*),*cis*(*P*,*P*)-[RhCl$_2$(edmp)$_2$]PF$_6$ (0.1 g, 0.19 mmol) was added a large excess of KBr (5 g, 42 mmol), and the mixture was refluxed for 20 h. The solution was evaporated to dryness under reduced pressure, and the residue was shaken with acetonitrile (ca. 60 cm^3) to extract the products until the extracts were colorless. The combined extracts were evaporated to dryness under reduced pressure. The residue was dissolved in water (60 cm^3) and the solution was applied on a column (ϕ2.5 cm ×15 cm) of Sp-Sephadex C-25. By elution with 0.05 mol dm^{-3}KBr, two yellow bands developed, the slower-moving one remaining almost at the top of the column. The eluate containing the faster-moving band was collected and evaporated to dryness under reduced pressure. The residue was extracted repeatedly with acetonitrile, and the solvent was removed under reduced pressure. The residue was dissolved in boiling water (10 cm^3), and to this solution was added a solution of NH_4PF_6 (0.5 g) in water (2 cm^3). The mixture was allowed to stand first at room temperature and then overnight in a refrigerator to yield yellow crystals. They were collected by filtration, washed successively with ice-cold water and diethyl ether, and dried in air. Yield: 0.05 g (43%). Found: C, 15.57; H, 3.89; N, 4.53%. Calcd for [RhBr$_2$(edmp)$_2$]PF$_6$=$C_8H_{24}N_2Br_2F_6P_3Rh$: C, 15.55; H, 3.91; N, 4.53%.

***trans*(*I*,*I*),*cis*(*P*,*P*)-[RhI$_2$(edmp)$_2$]PF$_6$.** This complex was prepared in a similar method to that for the dibromo complex, NaI in ethanol being used instead of KBr and dichloromethane as the extraction solvent. The product was purified by SP-Sephadex C-25 column chromatography (eluent: 0.05 mol dm^{-3} NaI). Yield: 0.06 g (44%, reddish needles). Found: C, 13.49; H, 3.38; N, 3.95%. Calcd for [RhI$_2$(edmp)$_2$]PF$_6$=$C_8H_{24}N_2F_6I_2P_3Rh$: C, 13.50; H, 3.40; N, 3.94%.

***trans*-[RhCl$_2$(dmpe)$_2$]CF$_3$SO$_3$ (3).** To a deaerated, boiling ethanol solution (50 cm^3) of $RhCl_3 \cdot 3H_2O$ (0.54 g, 2.05 mmol) was added dropwise dmpe (0.8 g, 5.3 mmol). The mixture was refluxed for 2 h to give a yellow solution together with a small amount of brownish precipitate. After cooling to room temperature, the mixture was filtered, and the filtrate was evaporated to dryness under reduced pressure. The yellow residue was washed with diethyl ether and was dissolved in water (50 cm^3). The solution was filtered, and the filtrate was applied on a column (ϕ 2.5 cm×30 cm) of SP-Sephadex C-25. The rest of the procedure was the same as that for *trans*(*Cl*,*Cl*),*cis*(*P*,*P*)-[RhCl$_2$(edmp)$_2$]PF$_6$ except that $NaCF_3SO_3 \cdot H_2O$ was used instead of NH_4PF_6 for crystallization. Yield: 0.38 g (30%). Found: C, 24.96; H, 5.23; Cl, 11.46; S, 5.82%. Calcd for [RhCl$_2$(dmpe)$_2$]CF$_3$SO$_3$=$C_{13}H_{32}Cl_2F_3O_3SP_4Rh$: C, 25.06; H, 5.18; Cl, 11.38; S, 5.14%. ^{1}H NMR ($C_6D_5NO_2$) δ=1.65—1.90 (24H, b, CH_3) and 2.0—2.4 (8H, m, CH_2). The complex is soluble in acetonitrile, acetone, ethanol, and methanol, and slightly soluble in water. Yellow needle-like crystals grown from aqueous solution were used for X-ray analysis.

Table 1. Crystal Data, Experimental Conditions, and Refinement Details

	1	**2a**	**2b**	**3**
Chemical formula	$[Rh(PC_4H_{12}N)_3]$-$Br_3 \cdot 3H_2O$	$[RhCl_2(PC_4H_{12}N)_2]$-PF_6	$[RhCl_2(PC_4H_{12}N)_2]$-ClO_4	$[RhCl_2(P_2C_6H_{16})_2]$-CF_3SO_3
Formula weight	712.0	528.8	483.5	623.2
Space group	$Pna2_1$	$P2_1/a$	$P\bar{1}$	$P2_1/a$
D_m and D_x/Mg m^{-3}	1.78(2), 1.82	—,[a] 1.79	1.70(2), 1.72	1.63(2), 1.62
μ (Mo $K\alpha$)/mm^{-1}	5.42	1.79	1.51	1.23
Color of crystals	Colorless	Yellow	Yellow	Yellow
Size of specimen/mm^3	0.36×0.40×0.50	Sphere of 0.45 (5) mm in diameter	0.60×0.43×0.30	0.25×0.25×0.50
Laue group	*mmm*	2/*m*	$\bar{1}$	2/*m*
Range of *h*, *k*, and *l*	$0 \leqq h \leqq 13$ $0 \leqq k \leqq 34$ $0 \leqq l \leqq 12$	$-23 \leqq h \leqq 23$ $0 \leqq k \leqq 16$ $0 \leqq l \leqq 11$	$-17 \leqq h \leqq 17$ $-23 \leqq k \leqq 0$ $-16 \leqq l \leqq 16$	$-17 \leqq h \leqq 17$ $0 \leqq k \leqq 31$ $0 \leqq l \leqq 10$
Systematic absences	*h*0*l*, *h* odd; 0*kl*, *k*+*l* odd	*h*0*l*, *h* odd; 0*k*0, *k* odd		*h*0*l*, *h* odd; 0*k*0, *k* odd
Possible space group	$Pna2_1$ or *Pnam*	$P2_1/a$	*P*1 or $P\bar{1}$	$P2_1/a$
Variation of five standard reflections $\sum(\lvert F_o\rvert/\lvert F_o\rvert_{initial})/5$	0.99—1.01	0.99—1.01	0.99—1.00	1.00—1.01
Number of reflections measured	3172	4794	13283	6269
Number of reflections observed [$\lvert F_o\rvert 3 > \sigma(\lvert F_o\rvert)$]	1591	3607	7775	3411
Transmission factor, *A*	0.121—0.275	0.624—0.628	0.623—0.726	0.718—0.757
Number of unique reflections	1591	3379	7513	3201
Final *R* value	0.039	0.032	0.070	0.040
$(\Delta/\sigma)_{max}$ for nonhydrogen atoms	0.42	0.50	0.27	0.27
$\Delta\sigma$/e Å^{-3}	−0.93, 0.62	−0.57, 0.35	−1.08, 1.84	−0.62, 0.34

a) D_m for **2a** was not measured because almost all of the crystals became opaque gradually in methanol solution and quickly in the air. A transparent part of the crystal was used for X-ray intensity measuerment.

Table 2. Fractional Coordinates (×10^4, ×10^5 for Rh) and Equivalent Thermal Parameters (×10)

Atom	*x*	*y*	*z*	B_{eq}/(Å^2×10)	Atom	*x*	*y*	*z*	B_{eq}/(Å^2×10)
		1			P(2)	1929(1)	1107(1)	1172(1)	33
Rh	13627(3)	76919(8)	0[a]	15	N(1)	−48(2)	3157(3)	531(4)	40
Br(1)	9923(1)	7411(1)	4962(3)	35	N(2)	675(2)	1348(3)	−1301(3)	33
Br(2)	3773(1)	7673(2)	167(2)	45	P	1195(1)	−2780(1)	3560(1)	42
Br(3)	7299(1)	7290(2)	3711(2)	41	F(1)	1291(2)	−3688(3)	2322(4)	83
O(1)	8889(4)	8017(9)	6845(13)	47	F(2)	2044(2)	−2590(5)	3704(5)	127
O(2)	784(5)	5413(14)	3815(16)	76	F(3)	1255(2)	−3634(3)	4911(4)	83
O(3)	7133(4)	4131(12)	4253(20)	84	F(4)	1061(3)	−1892(4)	4686(5)	128
P(1)	514(1)	7809(3)	271(4)	20	F(5)	1090(2)	−1973(2)	2138(4)	70
P(2)	1341(1)	5934(3)	−1483(4)	20	F(6)	343(2)	−3014(4)	3338(5)	96
P(3)	1422(1)	9230(3)	−1731(4)	19	C(1)	367(3)	3997(4)	3049(7)	60
N(1)	1355(4)	9084(10)	1752(12)	24	C(2)	1165(3)	2425(4)	4945(5)	52
N(2)	1457(4)	6206(11)	1587(13)	29	C(3)	1981(3)	3944(4)	3384(5)	49
N(3)	2169(4)	7891(9)	32(16)	24	C(4)	1671(3)	143(4)	−386(5)	43
C(1)	119(5)	8435(14)	−1088(19)	27	C(5)	2823(3)	1654(5)	864(7)	58
C(2)	185(5)	6353(13)	883(19)	31	C(6)	2125(3)	326(4)	2929(5)	52
C(3)	450(6)	9002(13)	1688(15)	29	C(7)A	46(4)	4195(6)	1463(10)	38
C(4)	903(5)	8938(13)	2607(15)	24	C(7)B	−266(5)	3605(9)	1968(12)	49
C(5)	789(5)	5559(14)	−2483(17)	29	C(8)	1313(3)	740(4)	−1779(5)	41
C(6)	1827(6)	5747(13)	−2762(17)	31					
C(7)	1384(6)	4552(12)	−314(14)	22			**2b**		
C(8)	1689(6)	4943(12)	972(17)	28	Rh(A)	98585(7)	64643(5)	37924(7)	28
C(9)	1259(6)	10887(14)	−1266(18)	34	Rh(B)	43698(6)	63560(5)	−19411(6)	23
C(10)	1149(5)	8963(13)	−3441(17)	29	Rh(C)	25069(7)	99641(5)	23582(7)	33
C(11)	2094(5)	9295(14)	−2052(16)	26	Cl(1)A	10509(3)	7591(2)	4292(3)	46
C(12)	2341(5)	9136(14)	−612(16)	26	Cl(2)A	9249(3)	5304(2)	3457(3)	48
					Cl(1)B	5713(2)	5856(2)	−460(2)	39
		2a			Cl(2)B	3051(2)	6766(2)	−3494(2)	43
Rh	9422(1)	21962(2)	8824(3)	23	Cl(1)C	1808(3)	9004(2)	1284(3)	65
Cl(1)	250(1)	940(1)	2078(1)	42	Cl(2)C	3273(3)	10959(2)	3298(3)	54
Cl(2)	1516(1)	3492(1)	−529(1)	38	Cl(3)	4904(2)	3825(2)	−3540(3)	41
P(1)	1167(1)	3121(1)	3129(1)	30	Cl(4)	10751(3)	3181(2)	1711(3)	69

Table 2. (Continued)

Atom	x	y	z	B_{eq}/(Å²×10)	Atom	x	y	z	B_{eq}/(Å²×10)
Cl(5)	6913(4)	10008(3)	1445(4)	83	O(33)	4757(9)	3085(7)	−3434(10)	82
P(1)A	8332(3)	7119(2)	2876(4)	64	O(34)	5444(10)	3875(7)	−4396(10)	92
P(2)A	10726(3)	6276(2)	2398(3)	51	O(41)	11324(15)	3704(11)	2183(15)	153
P(1)B	3369(2)	6888(2)	−767(2)	31	O(42)	10661(20)	2732(15)	2506(22)	233
P(2)B	5208(2)	7325(2)	−2146(2)	29	O(43)	9765(15)	3521(11)	1308(16)	165
P(1)C	1014(3)	10285(2)	2965(3)	48	O(44)	11073(20)	2800(14)	881(71)	220
P(2)C	3405(3)	9154(2)	3713(3)	47	O(51)	6544(14)	9864(10)	2312(15)	142
N(1)A	9200(10)	6564(7)	5243(10)	64	O(52)	6933(14)	9378(10)	748(15)	151
N(2)A	11314(8)	5854(6)	4768(9)	49	O(53)	6316(16)	10614(12)	791(17)	174
N(1)B	3616(7)	5388(5)	−1802(7)	30	O(54)	7740(21)	10305(15)	1792(23)	241
N(2)B	5298(7)	5786(5)	−3053(7)	33					
N(1)C	1728(10)	10764(7)	1034(10)	68			**3**		
N(2)C	3954(10)	9673(7)	1685(10)	64	Rh	21040(3)	12289(2)	−3334(5)	32
C(1)A	7678(14)	7404(10)	4169(10)	82	Cl(1)	1361(1)	758(1)	1811(2)	58
C(2)A	8352(17)	7931(12)	2063(18)	105	Cl(2)	2844(1)	1702(1)	−2474(2)	55
C(3)A	7430(12)	6596(8)	1941(12)	59	P(1)	3715(1)	1115(1)	1144(2)	48
C(4)A	12076(18)	5876(13)	3155(19)	111	P(2)	2082(1)	2048(1)	1196(2)	48
C(5)A	10277(14)	5633(10)	1303(15)	78	P(3)	504(1)	1345(1)	−1845(2)	58
C(6)A	10965(15)	7105(11)	1683(16)	87	P(4)	2151(1)	414(1)	−1869(2)	46
C(7)A	8022(17)	6845(12)	4937(18)	103	C(1)	6400(5)	1222(3)	−3781(9)	65
C(8)A	12046(15)	5490(11)	4114(16)	90	F(1)	6852(4)	1196(2)	−2257(5)	95
C(1)B	2835(10)	6079(7)	−360(10)	43	F(2)	5736(4)	1622(2)	−3822(6)	109
C(2)B	4031(11)	7303(8)	521(12)	54	F(3)	5853(4)	765(2)	−4070(6)	100
C(3)B	2217(11)	7617(8)	−1286(12)	56	S(1)	7273(1)	1309(1)	−5357(2)	59
C(4)B	5898(10)	7008(7)	−3248(10)	42	O(1)	6628(4)	1297(3)	−6870(6)	96
C(5)B	4418(11)	8227(8)	−2623(11)	51	O(2)	7765(5)	1820(3)	−4868(9)	110
C(6)B	6186(11)	7597(8)	−1002(11)	53	O(3)	7932(4)	839(2)	−5086(7)	87
C(7)B	2632(9)	5573(7)	−1385(10)	38	C(2)	3892(7)	1675(4)	2579(14)	131
C(8)B	6240(10)	6135(7)	−3105(10)	41	C(3)	3291(7)	2100(4)	2494(14)	123
C(1)C	165(16)	10929(12)	1815(17)	96	C(4)	382(8)	788(6)	−3245(19)	215
C(2)C	231(12)	9557(9)	3124(13)	65	C(5)	979(7)	366(4)	−3211(13)	125
C(3)C	1043(19)	10829(14)	4249(20)	117	C(6)	4799(5)	1125(4)	−26(11)	99
C(4)C	4727(14)	8967(10)	3421(15)	80	C(7)	3965(6)	510(4)	2425(11)	96
C(5)C	3621(14)	9537(10)	5129(14)	77	C(8)	2022(9)	2682(3)	118(12)	120
C(6)C	2993(12)	8234(9)	3802(13)	61	C(9)	1158(7)	2133(4)	2658(12)	105
C(7)C	655(15)	10952(11)	928(15)	83	C(10)	234(7)	1949(5)	−3068(13)	132
C(8)C	4613(14)	8935(10)	2207(15)	83	C(11)	−589(6)	1347(5)	−679(14)	121
O(31)	3899(8)	4289(6)	−3804(8)	67	C(12)	2216(9)	−229(3)	−759(10)	108
O(32)	5457(8)	4084(6)	−2527(8)	63	C(13)	3105(8)	349(4)	−3291(12)	109

a) This parameter was used to define the origin of the unit cell along z and is listed without e.s.d.

***trans*-[RhBr$_2$(dmpe)$_2$]CF$_3$SO$_3$.** This complex was prepared from trans-[RhCl$_2$(dmpe)$_2$]CF$_3$SO$_3$ and KBr by the same method as that described for *trans*(*Br*,*Br*),*cis*(*P*,*P*)-[RhBr$_2$(edmp)$_2$]$^+$, and isolated as the trifluoromethanesulfonate. Yield: 39%. Found: C, 21.91; H, 4.58%. Calcd for [RhBr$_2$(dmpe)$_2$]CF$_3$SO$_3$=C$_{13}$H$_{32}$Br$_2$F$_3$O$_3$SP$_4$Rh: C, 21.93; H, 4.53%.

Crystal Structure Determination. Experimental conditions and refinement informations are listed in Table 1. For *trans*(*Cl*,*Cl*),*cis*(*P*,*P*)-[RhCl$_2$(edmp)$_2$]$^+$, structure analysis of the PF$_6$ salt (**2a**) was also performed, because the structure of the ClO$_4$ salt (**2b**) could not be determined accurately ($P\bar{1}$, Z=6, R=0.070). Intensities were measured to 2θ=55° using graphite monochromatized Mo$K\alpha$ radiation (λ=0.71073 Å) on a Rigaku four-circle diffractometer AFC-5. The θ-2θ scan technique was employed at a scan rate of 6° min^{-1} in θ. Lattice constants were determined from 14—36 2θ values ($20<2\theta<30$). Absorption corrections were made by the numerical Gauss-integration method[6] for polyhedral crystals and by utilizing the correction factors[7] for a spherical sample. Systematic absences of **1** indicate that the space group is $Pna2_1$ (No. 33) or *Pnam* [acb setting of *Pnma* (No. 62)]. Since Z=4 and the complex cation is chiral, the space group was determined to be $Pna2_1$. The structure was difficult to solve because Rh and all Br atoms nearly lie on the glide plane at y=1/4 or y=3/4 (see Fig. 3). Position of the Rh atom was obtained from E map, and coordinated P and N atoms were located in the weighted Fourier synthesis. The structure of **2a** was solved by the heavy atom method. C(7) atom in the edmp ligand is disordered (see Fig. 5). The population parameters of two possible positions A and B were estimated to be 0.5. All the non-hydrogen atoms were refined anisotropically. The 7 hydrogen atoms among 36 in **1** and 11 among 30 in **2a** were located by the difference synthesis and others were calculated. Before the structure determination of **2a** was carried out, the structure of **2b** had been determined. The positions of the three independent Rh atoms obtained from the E map were confirmed by Patterson function. The other non-hydrogen atoms were located by Fourier syntheses. In order to reduce the number of parameters, C, N, and O atoms were refined isotropically and H atoms were not

included in the refinement. The structure of **3** was solved by Patterson-Fourier method. There exists structural disorder in the dmpe chelate rings (see Fig. 8). The thermal ellipsoids of the carbon atoms in the P-C-C-P moieties were unusually elongated perpendicular to the chelate ring with B_{eq} values 12—22 Å^2, and the five-membered chelate rings were almost flat with unrealistic C-C bond length of 1.30(1) Å. The split atom model was not introduced for this complex, because several possible conformations could be assigned to the five-membered rings and appropriate positions of the methyl groups corresponding to each conformation should be taken into account. Such a procedure would lead to equivocal results. Fortunately, the positions of the P atoms do not seem to be affected severely by the disorder. Complex neutral-atom scattering factors were used.[8] The calculations were carried out on a FACOM M380R computer at Keio University with the computation program system UNICS-III.[9] The function, $\sum w||F_o|-|F_c||^2$ was minimized by block-diagonal least squares. The final atomic parameters are listed in Table 2 and the bond lengths and bond angles within the complex cations in Table 3.[10]

Table 3. Bond Lengths (l/Å) and Bond Angles (ϕ/°)

1

Rh-P(1)	2.288(3)	P(2)-C(7)	1.797(13)
Rh-P(2)	2.279(3)	P(3)-C(9)	1.790(15)
Rh-P(3)	2.282(4)	P(3)-C(10)	1.816(16)
Rh-N(1)	2.193(11)	P(3)-C(11)	1.825(14)
Rh-N(2)	2.155(12)	N(1)-C(4)	1.468(18)
Rh-N(3)	2.166(11)	N(2)-C(8)	1.539(18)
P(1)-C(1)	1.794(17)	N(3)-C(12)	1.477(18)
P(1)-C(2)	1.814(14)	C(3)-C(4)	1.500(21)
P(1)-C(3)	1.826(14)	C(7)-C(8)	1.531(21)
P(2)-C(5)	1.801(15)	C(11)-C(12)	1.540(21)
P(2)-C(6)	1.798(16)		
P(1)-Rh-P(2)	94.9(1)	Rh-P(2)-C(5)	121.2(5)
P(1)-Rh-P(3)	96.7(1)	Rh-P(2)-C(6)	119.3(5)
P(1)-Rh-N(1)	82.6(3)	Rh-P(2)-C(7)	102.5(4)
P(1)-Rh-N(2)	94.1(3)	C(5)-P(2)-C(6)	102.0(7)
P(1)-Rh-N(3)	168.9(3)	C(5)-P(2)-C(7)	102.7(6)
P(2)-Rh-P(3)	94.6(1)	C(6)-P(2)-C(7)	107.3(7)
P(2)-Rh-N(1)	168.4(3)	Rh-P(3)-C(9)	116.2(5)
P(2)-Rh-N(2)	84.2(3)	Rh-P(3)-C(10)	121.9(5)
P(2)-Rh-N(3)	96.1(3)	Rh-P(3)-C(11)	102.5(4)
P(3)-Rh-N(1)	96.9(3)	C(9)-P(3)-C(10)	105.5(7)
P(3)-Rh-N(2)	169.2(3)	C(9)-P(3)-C(11)	104.4(6)
P(3)-Rh-N(3)	83.0(3)	C(10)-P(3)-C(11)	104.4(7)
N(1)-Rh-N(2)	84.8(4)	Rh-N(1)-C(4)	111.8(8)
N(1)-Rh-N(3)	86.5(4)	Rh-N(2)-C(8)	110.9(8)
N(2)-Rh-N(3)	86.5(4)	Rh-N(3)-C(12)	112.6(8)
Rh-P(1)-C(1)	121.3(5)	P(1)-C(3)-C(4)	109.5(10)
Rh-P(1)-C(2)	118.4(5)	N(1)-C(4)-C(3)	109.4(12)
Rh-P(1)-C(3)	102.2(5)	P(2)-C(7)-C(8)	109.6(9)
C(1)-P(1)-C(2)	103.7(7)	N(2)-C(8)-C(7)	108.0(11)
C(1)-P(1)-C(3)	104.6(7)	P(3)-C(11)-C(12)	105.5(10)
C(2)-P(1)-C(3)	104.5(6)	N(3)-C(12)-C(11)	109.3(11)

2a

Rh-Cl(1)	2.3323(13)	N(1)-C(7)A	1.532(9)
Rh-Cl(2)	2.3484(14)	N(2)-C(8)	1.487(7)
Rh-P(1)	2.2547(10)	P-F(1)	1.586(4)
Rh-P(2)	2.2494(17)	P-F(2)	1.554(4)
Rh-N(1)	2.162(4)	P-F(3)	1.578(4)
Rh-N(2)	2.168(3)	P-F(4)	1.517(5)
P(1)-C(1)	1.821(6)	P-F(5)	1.585(3)
P(1)-C(2)	1.793(5)	P-F(6)	1.568(4)
P(1)-C(3)	1.800(6)	C(1)-C(7)A	1.445(10)
P(2)-C(4)	1.829(5)	C(4)-C(8)	1.500(6)
P(2)-C(5)	1.814(6)	N(1)-C(7)B	1.456(11)
P(2)-C(6)	1.805(5)	C(1)-C(7)B	1.480(11)
Cl(1)-Rh-Cl(2)	173.33(5)	C(5)-P(2)-C(6)	103.6(2)
Cl(1)-Rh-P(1)	91.37(4)	Rh-N(1)-C(7)A	111.2(3)
Cl(1)-Rh-P(2)	90.20(5)	Rh-N(2)-C(8)	112.9(3)
Cl(1)-Rh-N(1)	87.50(10)	F(1)-P-F(2)	88.8(2)
Cl(1)-Rh-N(2)	88.37(8)	F(1)-P-F(3)	90.1(2)
Cl(2)-Rh-P(1)	92.23(4)	F(1)-P-F(4)	176.6(2)
Cl(2)-Rh-P(2)	94.77(5)	F(1)-P-F(5)	87.4(2)
Cl(2)-Rh-N(1)	87.29(10)	F(1)-P-F(6)	88.1(2)
Cl(2)-Rh-N(2)	87.76(8)	F(2)-P-F(3)	93.5(2)
P(1)-Rh-P(2)	98.91(5)	F(2)-P-F(4)	93.8(2)
P(1)-Rh-N(1)	84.16(10)	F(2)-P-F(5)	89.6(2)
P(1)-Rh-N(2)	177.20(8)	F(2)-P-F(6)	176.9(2)
P(2)-Rh-N(1)	176.22(11)	F(3)-P-F(4)	91.8(2)
P(2)-Rh-N(2)	83.88(9)	F(3)-P-F(5)	175.9(2)
N(1)-Rh-N(2)	93.04(12)	F(3)-P-F(6)	86.9(2)
Rh-P(1)-C(1)	102.4(2)	F(4)-P-F(5)	90.5(2)
Rh-P(1)-C(2)	118.6(2)	F(4)-P-F(6)	89.2(2)
Rh-P(1)-C(3)	117.8(2)	F(5)-P-F(6)	89.8(2)
C(1)-P(1)-C(2)	104.3(2)	P(1)-C(1)-C(7)A	112.0(5)
C(1)-P(1)-C(3)	107.5(2)	P(2)-C(4)-C(8)	107.9(3)
C(2)-P(1)-C(3)	105.0(2)	N(1)-C(7)A-C(1)	111.0(6)
Rh-P(2)-C(4)	100.8(2)	N(2)-C(8)-C(4)	108.5(4)
Rh-P(2)-C(5)	118.1(2)	Rh-N(1)-C(7)B	113.7(5)
Rh-P(2)-C(6)	120.2(2)	P(1)-C(1)-C(7)B	112.6(5)
C(4)-P(2)-C(5)	107.6(2)	N(1)-C(7)B-C(1)	113.3(7)
C(4)-P(2)-C(6)	105.3(2)		

3

Rh-Cl(1)	2.359(2)	P(2)-C(8)	1.765(8)
Rh-Cl(2)	2.357(2)	P(2)-C(9)	1.785(10)
Rh-P(1)	2.335(1)	P(3)-C(4)	1.755(15)
Rh-P(2)	2.341(2)	P(3)-C(10)	1.781(12)
Rh-P(3)	2.335(1)	P(3)-C(11)	1.794(10)
Rh-P(4)	2.337(2)	P(4)-C(5)	1.790(9)
P(1)-C(2)	1.782(11)	P(4)-C(12)	1.797(8)
P(1)-C(6)	1.786(8)	P(4)-C(13)	1.787(11)
P(1)-C(7)	1.805(10)	C(2)-C(3)	1.300(13)[a]
P(2)-C(3)	1.813(9)	C(4)-C(5)	1.292(16)[a]
Cl(1)-Rh-Cl(2)	179.8(1)	C(6)-P(1)-C(7)	101.5(4)
Cl(1)-Rh-P(1)	89.9(1)	Rh-P(2)-C(3)	107.5(3)
Cl(1)-Rh-P(2)	90.3(1)	Rh-P(2)-C(8)	119.4(3)
Cl(1)-Rh-P(3)	90.9(1)	Rh-P(2)-C(9)	119.2(3)
Cl(1)-Rh-P(4)	90.3(1)	C(3)-P(2)-C(8)	102.2(4)
Cl(2)-Rh-P(1)	90.2(1)	C(3)-P(2)-C(9)	103.5(4)
Cl(2)-Rh-P(2)	89.6(1)	C(8)-P(2)-C(9)	102.7(4)
Cl(2)-Rh-P(3)	89.0(1)	Rh-P(3)-C(4)	104.8(5)
Cl(2)-Rh-P(4)	89.8(1)	Rh-P(3)-C(10)	120.2(4)
P(1)-Rh-P(2)	84.0(1)	Rh-P(3)-C(11)	117.4(3)
P(1)-Rh-P(3)	179.2(1)	C(4)-P(3)-C(10)	106.7(6)
P(1)-Rh-P(4)	95.4(1)	C(4)-P(3)-C(11)	108.0(6)
P(2)-Rh-P(3)	96.2(1)	C(10)-P(3)-C(11)	99.1(5)
P(2)-Rh-P(4)	179.1(1)	Rh-P(4)-C(5)	107.6(3)
P(3)-Rh-P(4)	84.4(1)	Rh-P(4)-C(12)	118.8(3)
Rh-P(1)-C(2)	106.7(3)	Rh-P(4)-C(13)	117.9(4)
Rh-P(1)-C(6)	117.8(3)	C(5)-P(4)-C(12)	103.5(4)
Rh-P(1)-C(7)	119.1(3)	C(5)-P(4)-C(13)	103.4(5)
C(2)-P(1)-C(6)	105.6(4)	C(12)-P(4)-C(13)	103.7(4)
C(2)-P(1)-C(7)	104.7(5)		

a) These short distances are unrealistic (see text).

Results and Discussion

fac-**[Rh(edmp)$_3$]$^{3+}$**. The addition of an excess of edmp to rhodium(III) chloride in ethanol yielded [Rh(edmp)$_3$]Cl$_3$. The complex was also obtained as a by-product in the preparation of [RhCl$_2$(edmp)$_2$]$^+$ from *mer*-[RhCl$_3${P(*n*-Bu)$_3$}$_3$] and edmp in benzene. The geometrical configuration of [Rh(edmp)$_3$]$^{3+}$ is assigned on the basis of the ^{13}C NMR spectrum. The complex in D_2O shows one, one, and two kinds of resonances for the NCH_2, PCH_2, and CH_3 groups, respectively. Thus the complex can be assigned to the fac(C_3) configuration, and the assignment was confirmed by the X-ray structure determination (vide infra). Figure 1 compares the absorption spectrum of *fac*-[Rh(edmp)$_3$]$^{3+}$ with that of *fac*-[Co(edmp)$_3$]$^{3+}$ [2] and the data are given in Table 4. The lowest-energy absorption band at 37300 cm^{-1} of the rhodium(III) complex can be assigned to the first d-d absorption band, $^1A_{1g}\rightarrow{}^1T_{1g}(O_h)$. The band is at higher energy by 13600 cm^{-1} than the corresponding band of the cobalt(III) complex. The ratio of postions ($\tilde{\nu}_{Rh}/\tilde{\nu}_{Co}$) of the first absorption band for the complexes is 1.57. It should be noted that the value is very close to the spectrochemical parameter for rhodium(III), 1.56 given by Shimura (the parameter for cobalt(III) is 1.00).[11] The second d-d absorption band, $^1A_{1g}\rightarrow{}^1T_{2g}(O_h)$ of *fac*-[Rh(edmp)$_3$]$^{3+}$ is hidden by the charge-transfer bands. The strong band at 47400 cm^{-1} may be assigned to the Rh-P charge-transfer transition, since such a strong band is not observed for [Rh(en)$_3$]$^{3+}$ [2] (en=ethylenediamine) in this region.

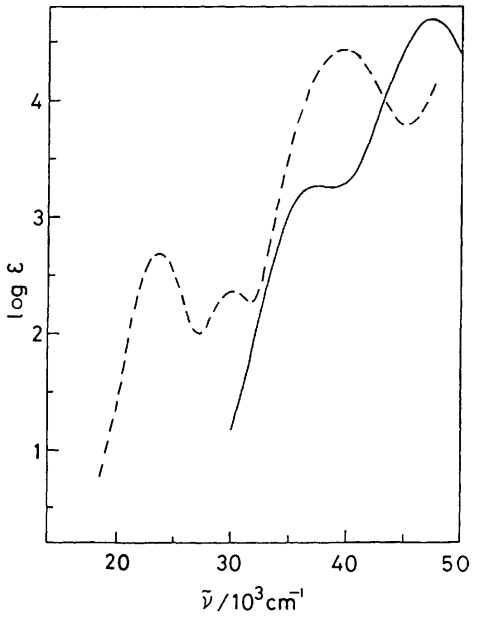

Fig. 1. Absorption spectra of *fac*-[Rh(edmp)$_3$]Cl$_3$·4H$_2$O in water (——) and *fac*-[Co(edmp)$_3$]Br$_3$·3H$_2$O in water (----).

Figure 2 shows a perspective view of the [Rh(edmp)$_3$]$^{3+}$ ion (**1**). The complex has approxi-

Table 4. Absorption Spectral Data[a]

Complex	$\tilde{\nu}/10^3$ cm^{-1} (log ε)
fac-[Rh(edmp)$_3$]Cl$_3$·4H$_2$O	37.3(3.27) 47.4(4.69)
trans(*Cl,Cl*),*cis*(*P,P*)-[RhCl$_2$(edmp)$_2$]PF$_6$	25.5(2.34) 37.7(3.59) 47.0(4.72)
trans(*Br,Br*),*cis*(*P,P*)-[RhBr$_2$(edmp)$_2$]PF$_6$	21(1.4)[b] 24.2(2.32) 33.0(3.36) 42.6(4.62)
trans(*I,I*),*cis*(*P,P*)-[RhI$_2$(edmp)$_2$]PF$_6$	19(1.7)[b] 22.3(2.40) 28.1(3.92) 37.0(4.53) 41(3.9)[b]
trans-[RhCl$_2$(dmpe)$_2$]CF$_3$SO$_3$	25.9(2.42) 32.6(3.78) 43.0(4.61) 46(4.4)[b]
trans-[RhBr$_2$(dmpe)$_2$]CF$_3$SO$_3$	24.5(2.15)[b] 29.8(3.40) 35(3.75)[b] 42.1(4.58)

a) Solvent:CH$_3$OH except for *fac*-[Rh(edmp)$_3$]Cl$_3$·4H$_2$O (H$_2$O). b) Shoulder.

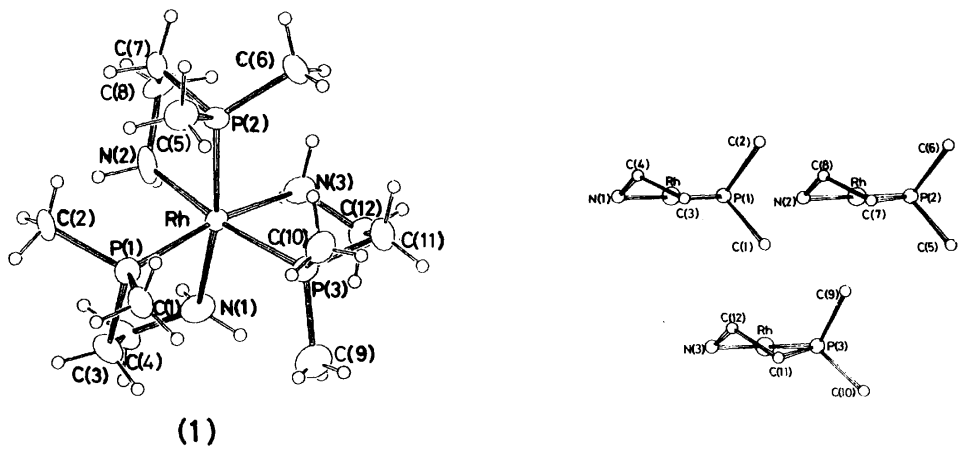

(1)

Fig. 2. A perspective view of *fac*-[Rh(edmp)$_3$]$^{3+}$ (**1**) and edge-on views of the five-membered edmp chelate rings.

mate C_3 symmetry, and the P atoms are arranged in a facial manner as expected from the ^{13}CNMR spectrum. The C-C bonds in the chelate rings are nearly parallel to the pseudo-C_3 axis of the complex ion, and the complex can be designated as the lel_3 isomer. Three methyl groups C(1), C(5), and C(10) are disposed nearly parallel to the pseudo-C_3 axis. The short nonbonded C···C, C···H, and H···H distances among these methyl groups are 3.60(2)—3.70(2), 2.94(14)—3.03(14), and 2.33(17)—2.45(17) Å, respectively. The H···H repulsions are released by adjusting the mutual disposition of C-H bonds in the methyl groups. Such a crowded structure seems to be responsible for a distorted gauche conformation of the two edmp chelate rings (Fig. 2). In *fac*-Λ-$[Co(edmp)_3]^{3+}$, all three chelate rings take a pseudo (distorted) λ-gauche conformation.[2] The Rh-N distance averages 2.171(12) Å, which is significantly longer than that (2.062(7) Å) of $[Rh(en)_3]^{3+}$,[13] and that (2.076(4) Å) of lel_3-$[Rh(chxn)_3]^{3+}$ [14] (chxn=*trans*-1,2-cyclohexanediamine). The elongation of Rh-N distances can be attributed to the strong trans influence of the P donor atoms (vide infra). As seen from Fig. 3, the Br(3) atom lies approximately on the pseudo-C_3 axis of the complex cation of **1** to form three N-H···Br hydrogen bonds. The hydrogen bond distances are listed in Table 5.

Table 5. Intermolecular Hydrogen Bonds (distances in Å)[a]

A···H-B (symmetry code)	A···B	A···H	H-B
1			
Br(3)···H(N1)1-N(1) (iii)	3.441(11)	2.55(14)	0.97(14)
Br(3)···H(N2)1-N(2) (iii)	3.397(12)	2.43(12)	0.99(14)
Br(3)···H(N3)1-N(3) (iii)	3.551(15)	2.61(15)	0.97(15)
O(2)···H(N2)2-N(2) (i)	2.907(19)	2.03(14)	1.01(12)
O(3)···H(N3)2-N(3) (ii)	2.870(16)	1.96(12)	0.97(12)

Symmetry code: (i) x, y, z, (ii) $1-x$, $1-y$, $1/2+z$, (iii) $1/2-x$, $3/2-y$, $1/2+z$.
a) There are no hydrogen bonds in **2a** and **3**.

***trans*(*X*,*X*),*cis*(*P*,*P*)-$[RhX_2(edmp)_2]^+$(X=Cl, Br, I) and *trans*(*X*,*X*)-$[RhX_2(dmpe)_2]^+$(X=Cl, Br).** By reaction of *mer*-$[RhCl_3\{P(n\text{-}Bu)_3\}_3]$ with edmp in benzene, $[RhCl_2(edmp)_2]^+$ was formed. Although five geometrical isomers are possible for $[RhCl_2(edmp)_2]^+$, only one isomer was isolated. No fraction indicative of other isomers was obtained in SP-Sephadex column chromatography. The ^{13}CNMR spectrum of this complex exhibits three kinds of signals, indicating that the complex is either of the two trans(*Cl*,*Cl*) isomers. It should be noted that the P-CH_2 and P-CH_3 signals appear as a filled-in doublet. The appearance of the phosphine α-carbon multiplet in the ^{13}CNMR spectrum of a complex containing two phosphorus donor atoms has been shown to be a function of $^2J_{pp}$.[15,16] A filled-in doublet is expected to appear only for a cis(*P*,*P*) complex. Hence

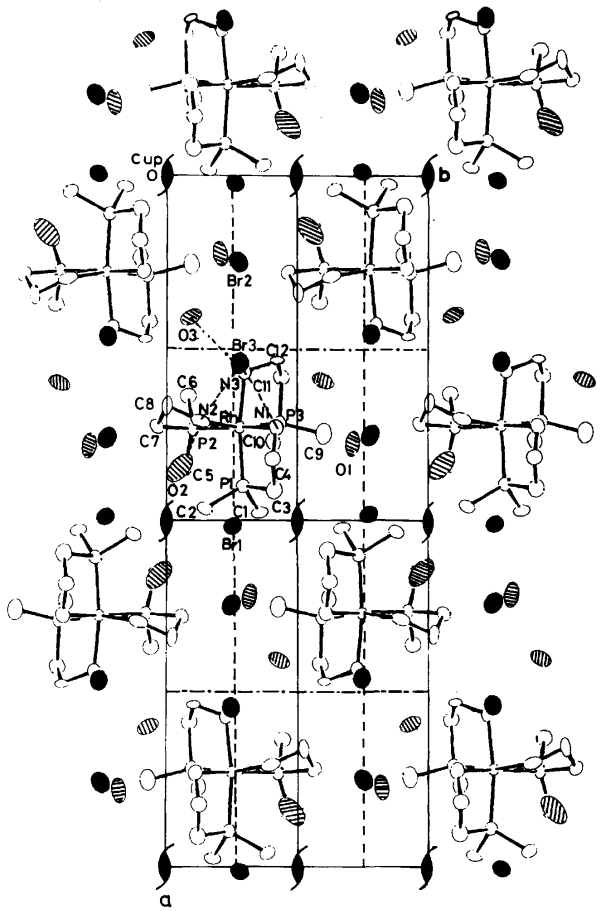

Fig. 3. A projection of the crystal structure of *fac*-$[Rh(edmp)_3]Br_3\cdot 3H_2O$ (**1**) along c. Black and hatched ellipsoids represent Br^- ions and H_2O molecules, respectively.

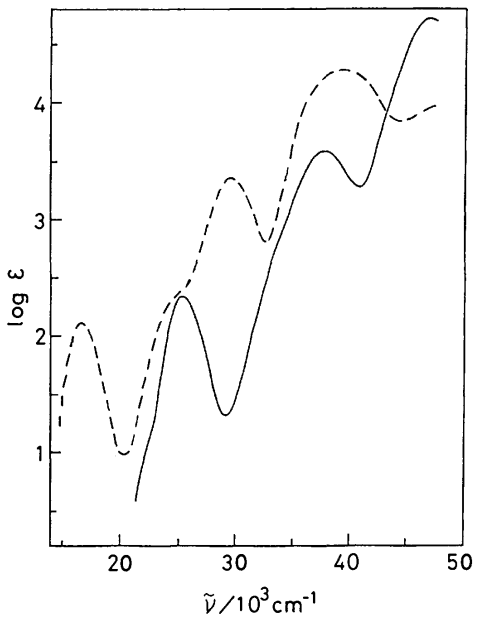

Fig. 4. Absorption spectra of *trans*(*Cl*,*Cl*),*cis*(*P*,*P*)-$[RhCl_2(edmp)_2]PF_6$ in methanol (——) and *trans*-(*Cl*,*Cl*),*cis*(*P*,*P*)-$[CoCl_2(edmp)_2]Cl$ in methanol (----).

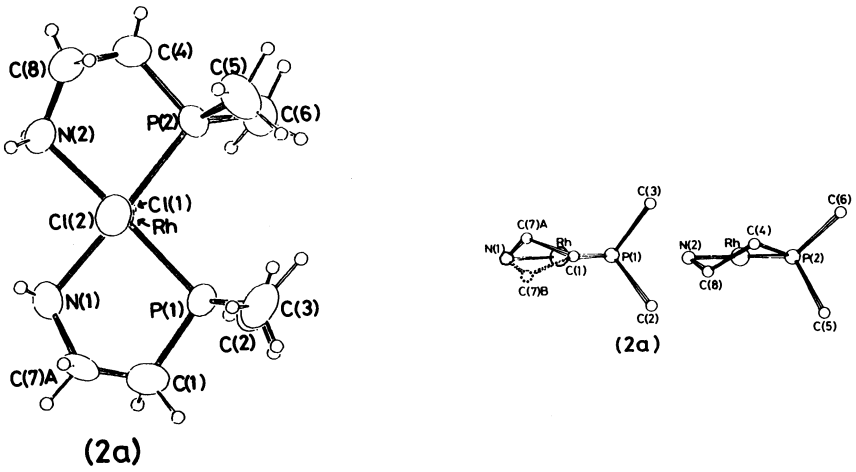

Fig. 5. A perspective view of *trans*(*Cl,Cl*),*cis*(*P,P*)-$[RhCl_2(edmp)_2]^+$ (**2a**) and edge-on views of the five-membered edmp chelate rings.

$[RhCl_2(edmp)_2]^+$ can be assigned to trans(*Cl,Cl*), cis(*P,P*). The same structure was suggested by the absorption spectrum. Figure 4 compares the absorption spectrum of the complex with that of *trans*(*Cl,Cl*),*cis*(*P,P*)-$[CoCl_2(edmp)_2]^+$.[17] Both spectra are quite similar in pattern, although all of the bands of the rhodium(III) complex are shifted by 7500—9500 cm^{-1} toward higher energy compared to the corresponding bands of the cobalt(III) complex. Thus the rhodium(III) complex is suggested to have the trans(*Cl,Cl*),cis(*P,P*) configuration. This assignment was confirmed by the X-ray structure determination (vide infra). The low-energy absorption band at 25500 cm^{-1} of the rhodium(III) complex can be assigned to the split component (I_a) of the first absorption band, $^1A_{1g} \rightarrow {}^1T_{1g}$ (Oh). The I_a component is shifted toward higher energy by a factor of 1.5 on going from the cobalt(III) complex (16600 cm^{-1}) to the rhodium(III) complex (25500 cm^{-1}). The I_b and second absorption bands of the rhodium(III) complex are hidden by the strong charge-tansfer bands.

Figure 5 shows a perspective drawing of the complex cation **2a**. **2a** is the trans(*Cl,Cl*), cis(*P,P*) isomer, and the structure agrees with the assignment based on the ^{13}C NMR and absorption spectra. As illustrated in Fig. 5, one of the edmp chelate rings of **2a** is disordered. In **2b**, three independent complex ions take different conformations, $\delta\delta(\lambda\lambda)$, $\delta\lambda$, or $\delta(\lambda)$ envelope, suggesting flexibility of the edmp chelate rings (Fig. 6). The P(1)-Rh-P(2) angle of 98.91(5)° in **2a** is smaller than 105.4(1)° in *trans*(*Cl,Cl*),*cis*(*P,P*)-$[RhCl_2(edpp)_2]^+$,[1] on account of less bulky substituents on phosphorus atoms. The mean Rh-N bond length in **2a**, 2.165(4) Å is longer than that in *trans*-$[RhCl_2(en)_2]NO_3$ (2.063(2) Å)[18] due to trans influence of the coordinated P atom. In Fig. 7, the M-N bond distance (M=Co or Rh) affected by the trans influence is plotted against the M-P bond distance. The elongation is smaller in the *trans*(*Cl,Cl*),*cis*(*P,P*)-

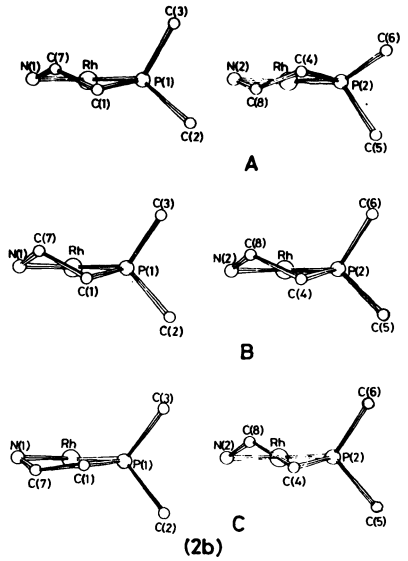

Fig. 6. Edge-on views of the five-membered edmp chelate rings in *trans*(*Cl,Cl*), *cis*(*P,P*)-$[RhCl_2(edmp)_2]$-ClO_4 (**2b**).

$[MCl_2(edpp)_2]^+$ complexes (circular symbols) than those in the others. This trend seems to be due to the longer M-P bond length in the edpp complexes. In general, the shorter the M-P bond length, the larger the M-N bond elongation. The elongations of the Rh-N bond distances (0.07—0.11 Å) by the trans influence are larger than those (0.03—0.07 Å) of the Co-N bond distances. Figure 7 clearly shows that the difference (<0.05 Å) between Rh-P and Co-P bond lengths is much smaller than that (ca. 0.1 Å) between Rh-N and Co-N bond lengths. All these results suggest a stronger affinity of P for Rh^{3+} than for Co^{3+}. The trans influence of P on the Rh-P bond length, the lengthening of mutually trans Rh-P bonds, was observed in the *trans*-$[RhCl_2(dmpe)_2]^+$ complex (**3**). The mean Rh-P bond distance is 2.337(2) Å, which is longer than those in complexes **1** and **2a**, 2.283(4) Å

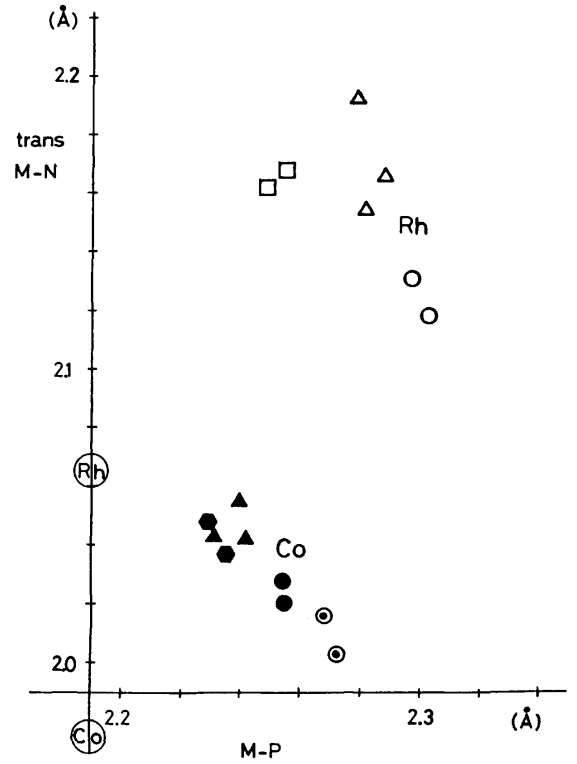

Fig. 7. Plot of the M-N distance (M=Co and Rh) against the trans M-P bond length in Δ=**1**; □=**2a**; ○=*trans*(*Cl*,*Cl*),*cis*(*P*,*P*)-[$RhCl_2$(edpp)$_2$]Cl·$2C_2H_5OH$;[1] ▲=*fac*-[Co(edmp)$_3$]Br_3·$3H_2O$;[2] ●=*trans*(*Cl*,*Cl*),*cis*(*P*,*P*)-[$CoCl_2$(*R*-ebpp)$_2$]ClO_4[17] (*R*-ebpp=(*R*)-(2-aminoethyl)butylphenylphosphine); ●=*trans*(*Cl*,*Cl*),*cis*(*P*,*P*)-[$CoCl_2$(edpp)$_2$]1/2($CoCl_4$);[17] ⊙=*trans*(*NCS*,*NCS*),*cis*(*P*,*P*)-[Co(NCS)$_2$(edpp)$_2$]Br·$3H_2O$·$(CH_3)_2CO$.[25] The circles on the vertical axis indicate bond distances in the $[M(en)_3]^{3+}$ complexes (M=Co[26] and Rh[13]).

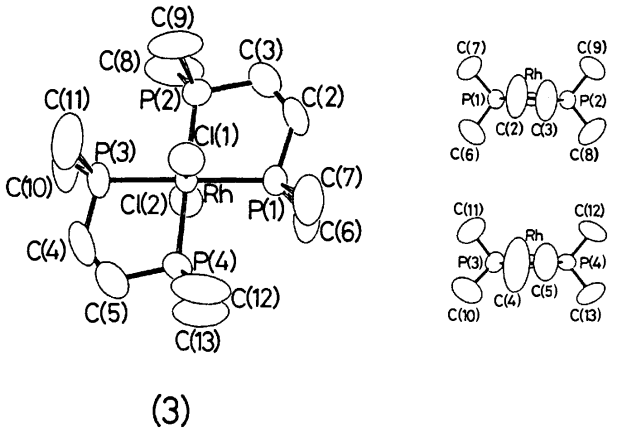

(3)

Fig. 8. A perspective view of *trans*-$[RhCl_2(dmpe)_2]^+$ (**3**) and edge-on views of the five-membered dmpe chelate rings.

and 2.252(2) Å, respectively.

$[RhCl_2(dmpe)_2]^+$ was prepared by refluxing an ethanol solution of $RhCl_3 \cdot 3H_2O$ and dmpe. Butter and Chatt reported that a mixture of the cis and trans

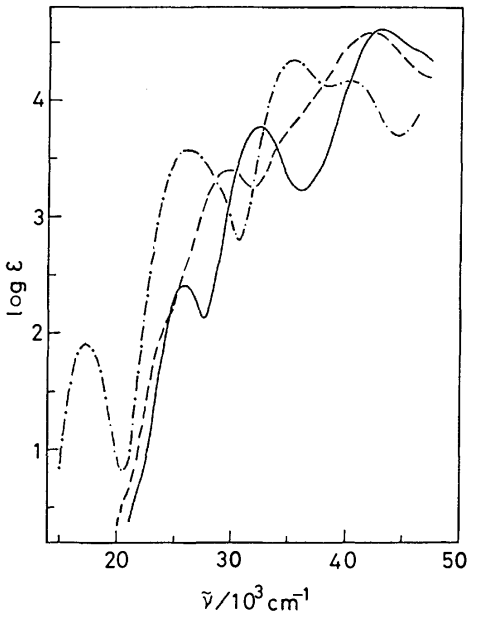

Fig. 9. Absorption spectra of *trans*-$[RhCl_2(dmpe)_2]$-CF_3SO_3 (——), *trans*-$[RhBr_2(dmpe)_2]CF_3SO_3$ (----), and *trans*-$[CoCl_2(dmpe)_2]ClO_4$ (—·—) in methanol.

isomers of this complex was yielded by a similar reaction.[19] We obtained only one isomer, no fraction indicative of the other isomer being obtained in column chromatography. The structure was assigned to the trans isomer on the basis of the ^1H NMR and absortion spectra, and the assignment was confirmed by X-ray analysis (Fig. 8). In the ^1H NMR spectrum, the complex shows a similar spectral pattern to that of *trans*-$[CoCl_2(dmpe)_2]^+$.[20] The ^1H NMR spectral pattern of *cis*-$[CoCl_2(dmpe)_2]^+$ is quite different from that of the trans isomer.[20] The absorption spectral pattern of *trans*-$[RhCl_2(dmpe)_2]^+$ is similar to that of the corresponding cobalt(III) complex; here also the ratio of positions ($\tilde{\nu}_{Rh}/\tilde{\nu}_{Co}$) of the I_a band for the rhodium(III) complex (25900 cm^{-1}) to that for the cobalt(III) complex (17300 cm^{-1})[20] is 1.5 (Fig. 9 and Table 4). The I_a band of *trans*-$[RhCl_2(dmpe)_2]^+$ is at higher energy (25900 cm^{-1}) than that of *trans*(*Cl*,*Cl*),*cis*(*P*,*P*)-$[RhCl_2(edmp)_2]^+$ (25500 cm^{-1}). The trans-dichloro rhodium(III) complexes of en, edpp, and Me_4-en (=*N*,*N*,*N*′,*N*′- tetramethylethylenediamine) show the I_a band at 24600,[21] 24450,[1] and 22000 cm^{-1},[22] respectively. Thus the spectrochemical series for the ligands can be determined as dmpe>edmp>en≧edpp>Me_4-en. The same order has been reported for the trans-dichloro cobalt(III) complexes.[17,20,23] $[RhX_2(edmp)_2]^+$ (X=Br, I) and $[RhBr_2(dmpe)_2]^+$ were prepared by substitution reactions from the trans-dichloro complexes and potassium bromide or sodium iodide. The configurations were retained in the reactions as indicated from the absorption spectra. The absorption spectra of *trans*(*X*,*X*),*cis*(*P*,*P*)-$[RhX_2(edmp)_2]^+$ (X=Cl, Br, I) are

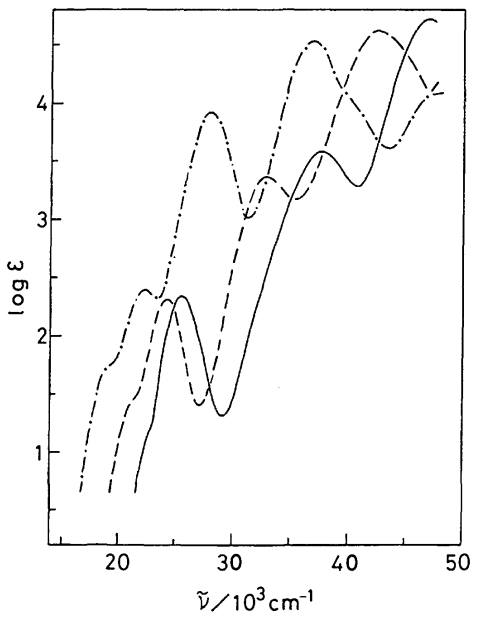

Fig. 10. Absorption spectra of *trans(Cl,Cl),cis(P,P)*-$[RhCl_2(edmp)_2]PF_6$ (——), *trans(Br,Br),cis(P,P)*-$[RhBr_2(edmp)_2]PF_6$ (----), and *trans((I,I),cis(P,P)*-$[RhI_2(edmp)_2]PF_6$ (—·—) in MeOH.

shown in Fig. 10. The spectral patterns of the complexes are similar to one another. In the series, the energy of the I_a component decreases in the order Cl> Br>I. The complexes show a shoulder at the low energy side of the I_a band and the absorption may be assigned to a spin-forbidden transition. The shoulder becomes more pronounced as X proceeds from Cl through Br to I. All of the complexes show two intense charge-transfer bands at energies higher than 28000 cm^{-1}. Both of the charge-transfer bands shift to lower energy in the order X=Cl>Br>I, suggesting that the bands are attributable mainly to the Rh-X charge-transfer transitions. In *trans*-$[CoX_2(dmpe)_2]^+$ (X=Cl, Br, I), the positions of the Co-X charge-transfer transitions change in the same order[20] and in *trans*-$[Co(H_2O)_2(dmpe)_2]^+$ they are missing.[24] Figure 9 shows the absorption spectra of *trans*-$[RhX_2(dmpe)_2]^+$ (X=Cl, Br). The band at 32600 cm^{-1} in the dichloro complex and the band at 29800 cm^{-1} in the dibromo complex are assigned to the Rh-Cl and Rh-Br charge-transfer transitions, respectively. The bands are at lower energy than the corresponding bands in the edmp complexes, and the I_a component of *trans*-$[RhBr_2(dmpe)_2]^+$ is observed as a shoulder by the overlap of the Rh-Br charge-transfer band. The intensity of this Rh-Br charge-transfer band (29800 cm^{-1}, $\log\varepsilon$=3.40) is remarkably smaller than that of the corresponding Rh-Cl charge-transfer band at 32600 cm^{-1} ($\log\varepsilon$=3.78). The same trend is observed in many phosphine and arsine complexes of cobalt(III) and rhodium(III). The origin of the shoulder at ca. 35000 cm^{-1} in the dibromo complex is unknown. The corresponding transition is not observed in the dichloro complex, however, a similar transition is observed in *trans*-$[CoBr_2(dmpe)_2]^+$.[20]

Acknowledgement is made to Japanese Government (Monbusho) for providing generous fellowship support for K. P. S. to work as an exchange student at Nagoya University. We wish to thank Dr. Frode Galsbøl, University of Copenhagen, for helpful discussions and suggestions about our work. The present work was supported by a Grant-in-Aid for Scientific Research No. 61430013 from the Ministry of Education, Science and Culture.

References

1) F. Galsbøl, M. Kojima, T. Ishii, S. Ohba, Y. Saito, and J. Fujita, *Bull. Chem. Soc. Jpn.*, **59**, 1701 (1986).
2) I. Kinoshita, K. Kashiwabara, J. Fujita, K. Matsumoto, and S. Ooi, *Bull. Chem. Soc. Jpn.*, **54**, 2683 (1981).
3) S. A. Butter and J. Chatt, *Inorg. Synth.*, Vol. XIV, 185 (1974).
4) J. Chatt, N. P. Johnson, and B. L. Shaw, *J. Chem. Soc.*, **1964**, 2508.
5) G. M. Intille, *Inorg. Chem.*, **11**, 695 (1972).
6) W. R. Busing and H. A. Levy, *Acta Crystallogr.*, **10**, 180 (1957).
7) C. W. Jr. Dwiggins, *Acta Crystallogr., Sect. A*, **31**, 395 (1975).
8) "International Tables for X-ray Crystallography," Vol. IV, Kynoch Press, Birmingham (1974). (Present Distributor Kluwer Academic Publishers, Dordrecht.)
9) T. Sakurai and K. Kobayashi, *Rikagakukenkyusho Hokoku*, **55**, 69 (1979).
10) Tables of the coordinates of hydrogen atoms, the anisotropic thermal parameters of the non-hydrogen atoms, and observed and calculated structure factors are kept as Document No. 8901 at the Chemical Society of Japan.
11) Y. Shimura, *Bull. Chem. Soc. Jpn.*, **61**, 693 (1988).
12) F. Galsbøl, *Inorg. Synth.*, Vol. XII, 269 (1970).
13) A. Whuler, C. Brouty, P. Spinat, and P. Herpin, *Acta Crystallogr., Sect. B*, **32**, 2238 (1976).
14) H. Miyamae, S. Sato, and Y. Saito, *Acta Crystallogr., Sect. B*, **33**, 3391 (1977).
15) D. A. Redfield, L. W. Cary, and J. H. Nelson, *Inorg. Chem.*, **14**, 50 (1975).
16) P. S. Pregosin and R. W. Kunz, "^{31}P and ^{13}C NMR of Transition Metal Phosphine Complexes," Springer-Verlag, New York (1979), p. 65.
17) I. Kinoshita, Y. Yokota, K. Matsumoto, S. Ooi, K. Kashiwabara, and J. Fujita, *Bull. Chem. Soc. Jpn.*, **56**, 1067 (1983).
18) T. Lynde-Kernell and E. O. Schlemper, *Acta Crystallogr., Sect. C*, **44**, 31 (1988).
19) S. A. Butter and J. Chatt, *J. Chem. Soc. A*, **1970**, 1411.
20) T. Ohishi, K. Kashiwabara, and J. Fujita, *Bull. Chem. Soc. Jpn.*, **60**, 575 (1987).
21) H. Ogino and J. C. Bailar, Jr., *Inorg. Chem.*, **17**, 1118 (1978); S. A. Johnson and F. Basolo, *Inorg. Chem.*, **1**, 925 (1962).
22) G. W. Watt and P. W. Alexander, *J. Am. Chem. Soc.*, **89**, 1814 (1967).

23) M. Atoh, I. Kinoshita, K. Kashiwabara, and J. Fujita, *Bull. Chem. Soc. Jpn.*, **55**, 3179 (1982).
24) T. Ohishi, K. Kashiwabara, and J. Fujita, *Bull. Chem. Soc. Jpn.*, **60**, 583 (1987).
25) M. Atoh, K. Kashiwabara, H. Ito, T. Ito, and J. Fujita, *Bull. Chem. Soc. Jpn.*, **57**, 3139 (1984).
26) M. Iwata, K. Nakatsu, and Y. Saito, *Acta Crystallogr., Sect. B*, **25**, 2562 (1969).

Synthetic Inorganic Ion-Exchange Materials. LII. Ion-Exchange Selectivities of Crystalline Antimonic Acid for Tervalent Metal Ions

Mitsuo ABE,* Masao HIRATA,† and Masamichi TSUJI
Department of Chemistry, Tokyo Institute of Technology, 2-12-1, Ookayama, Meguro-ku, Tokyo 152
(Received May 27, 1989)

The determination of selectivity coefficients for tervalent metal ions/hydrogen ions on cubic crystalline antimonic acid (C-SbA) was carried out for Ga^{3+}, Fe^{3+}, Ce^{3+}, Sm^{3+}, Y^{3+}, Sc^{3+}, and In^{3+} by batch equilibration at 30, 45, and 60 °C in nitric acid media. The selectivity in microamounts showed: $Al^{3+}<Tm^{3+}<Ga^{3+}<Yb^{3+}=Y^{3+}<Er^{3+}<Dy^{3+}<Fe^{3+}<Eu^{3+}<Sm^{3+}<Ce^{3+}<La^{3+}<Sc^{3+}=In^{3+}$. The ion-exchange isotherms of the systems of tervalent metal ions/hydrogen ions have also been studied on C-SbA. The selectivity coefficients in logarithm scale vs. equivalent fraction of metal ions in exchanger showed almost straight line, indicating monofunctional site with steric effect. In order to interpret the selectivity in microamounts of metal ions, hypothetical equilibrium constant was determined by extrapolating to zero loading of metal ions in C-SbA. From these values, the hypothetical thermodynamic data were calculated and evaluated.

During the last two decades much attention has been paid to the development of synthetic inorganic ion exchange materials with higher selectivities and resistance at high temperatures and in intense radiation fields than those of commercial ion-exchange resins.[1-6]

Our works on the systematic studies on adsorption behavior of the hydroxides and hydrous oxides of multivalent metals indicated that "so-called" antimonic acid behaved as an excellent cation exchange material.[7,8] Further studies showed that the antimonic acid can be classified into amorphous, glassy and crystalline materials by different preparative conditions, regardless of starting materials.[9] Recently, monoclinic crystalline antimonic acid was synthesized by treating $LiSbO_3$ with 11 mol dm^{-3} HNO_3 and showed an extremely high selectivity for lithium ion.[10,11] Among them, cubic crystalline antimonic acid (C-SbA) showed excellent ion-exchange properties and an unusual selectivity for various metal ions, compared to strong acid-type cation exchange resins.[13]

The increasing order of selectivity in microamounts shows; $Li^+ \ll K^+ < Cs^+ < Rb^+ \ll Na^+$ for alkali metals,[12-14] and $Mg^{2+} < Ba^{2+} < Ca^{2+} < Sr^{2+}$ for alkaline earth metals.[15,16]

The similar unusual selectivity was observed for bivalent transition metals[17,18] and tervalent metals.[19] It has been known that the selectivity on inorganic ion exchangers strongly depends on the loading of metal ions in the exchangers. An ion-exchange study over various exchange composition may be needed for understanding of their selectivities. However, it is very difficult to study full range of the ion-exchange composition because of incomplete exchange for the limit of steric reason. Moreover, the overall thermodynamic data obtained are not so accurate for those systems, because of long extrapolation from experimental values.

The present paper has been concerned with the interpretation of the selectivity of M^{3+}/H^+ system for "zero loading" of metal ions in C-SbA. From the selectivity coefficient, the hypothetical thermodynamic data may be derived.

Theoretical

The ion exchange process may be represented by the following equation for tervalent metal cation/hydrogen ions system.

$$3\bar{H}^+ + M^{3+} \rightleftarrows \bar{M}^{3+} + 3H^+ \quad (1)$$

where the bar refers to solid phase, and M^{3+} and H^+ are tervalent metal and hydrogen ions.

The thermodynamic equilibrium constant, K, of the above reaction can be defined as

$$K = \frac{m_H^3 \bar{X}_M \gamma_H^3 \bar{f}_M}{m_M \bar{X}_H^3 \gamma_M \bar{f}_H^3} = K_H^M \frac{\bar{f}_M}{\bar{f}_H^3} \quad (2)$$

where K_H^M is defined as the corrected selectivity coefficient. The m_H and m_M are molalities of the cations in solution, γ_H and γ_M are the ionic activity coefficients of H^+ and M^{3+} in solution phase, $\bar{f}_H$ and $\bar{f}_M$ are those in solid phase, and $\bar{X}_H$ and $\bar{X}_M$ are equivalent fractions of H^+ and M^{3+} in the solid phase. The values of the ionic activity coefficient ratio (γ^3_H/γ_M) in solution can be calculated from the following equation.[20]

$$\log(\gamma_H^3/\gamma_M) = 6\frac{S\,I^{1/2}}{1+A\,I^{1/2}} \quad (3)$$

where A and I are the distance of the nearest approach and the ionic strength, and

$$S = 1.8252 \times 10^6 (\rho/\varepsilon^3 T^3)^{1/2}$$

where ρ is the density of water, ε is the dielectric constant of water, and T is the absolute temperature of the system.

The thermodynamic equilibrium constant can be

† Present address: Ooshimizu High School, Fujisawa 251.

evaluated by using a simplified form of the Gaines-Thomas equation,[21] Eq. 4, assuming that the change of water activity in the C-SbA and in the solution is neglected.

$$\ln K = -(Z_M - Z_H) + \int_0^1 \ln K_H^M \, d\bar{X}_M \quad (4)$$

Sometimes, the graph of $\ln K_H^M$ against $\bar{X}_M$, which refers to the Kielland plot,[22] is linear with some inorganic ion exchangers, as follows;

$$\ln K_H^M = 4.606\, C\, \bar{X}_M + (\ln K_H^M)_{\bar{X}_M \to 0} \quad (5)$$

where the term C is called the Kielland coefficient and $4.606C$ is the slope of the line, and $(\ln K_H^M)_{\bar{X}_M \to 0}$ is the value $\ln K_H^M$ when $\bar{X}_M = 0$.

Some investigators have normalized uptakes with the maximum limit of exchange, $(\bar{X}_M)_{max}$, in the case where complete exchange is not obtained. However, this treatment does not allow a comparison between species which are exchanged to different extent.[16,23]

The normalization for C-SbA is based on the assumption that one SbOH group gives one hydrogen ion available for ion exchange. Thus, the theoretical capacity of 5.056 mequiv g^{-1} was used from the experimental formula of $Sb_2O_5 \cdot 4H_2O$.[16]

Experimental

Preparation of C-SbA. The C-SbA was prepared as described previously;[9] the precipitate obtained by hydrolysis of antimony pentachloride solution (1:1) was kept in the mother solution at 40 °C for over 20 d in order to enhance crystallization, and then washed with cold demineralized water until free from chloride ion with an aid of centrifuge (about 10000 rpm). After drying the product was ground and sieved (100—200 mesh size). The collected sample was rewashed with demineralized water in order to obtain clear supernatant solution in the following batch equilibrium experiments.

Distribution Coefficient (K_d). The K_d values were determined by equilibrating C-SbA in hydrogen ion form with a solution containing 1×10^{-4} M (1 M=1 mol dm^{-3}) metal ions and nitric acid at different concentrations. The ratio of volume of the solution to weight of C-SbA was kept in 100 ($cm^3\,g^{-1}$). The K_d values of metal ions were calculated by using following expression;

$$K_d = \frac{\text{amount of metal ions in exchanger}}{\text{amount of metal ions in solution}} \times \frac{\text{cm}^3 \text{ of solution}}{\text{g of exchanger}} \quad (6)$$

Ion-Exchange Equilibria. In the forward reaction, the C-SbA in H^+ form was immersed in a mixed solution of varying ratio of the metal nitrate/nitric acid in a sealed glass tube with intermittent shaking at 30±0.1, 45±0.1, and 60±0.1 °C. The ratio of volume of mixed solution to weight of C-SbA was kept in 100 ($cm^3\,g^{-1}$). The ionic strength in the equilibrium was adjusted to 0.2. The equilibrium concentrations in the solid phase and in aqueous phase were deduced from the change of M^{3+} and H^+ concentration relative to the initial concentration of the solution. The concentration of metal ions in the solutions was determined by spectrophotometric analysis.[24-26] Neutron activation analysis was employed for cross checking the analytical data for Sc, Sm, Eu, and Ce. The emf titration method was employed for determining the H^+ concentration with a standard sodium hydroxide solution.

Results and Discussion

Distribution Coefficient (K_d). Time dependence of adsorption for different metal ions showed that the equilibrium was attained within 20 d for Sc^{3+}, Tm^{3+}, and Eu^{3+}, and about 30 d for Y^{3+} (Fig. 1) The variety of the time dependence from element to element may be due to the rigid structure of C-SbA and rate of the exchange between hydrated water for the element and bulk water molecules in the aqueous solution.

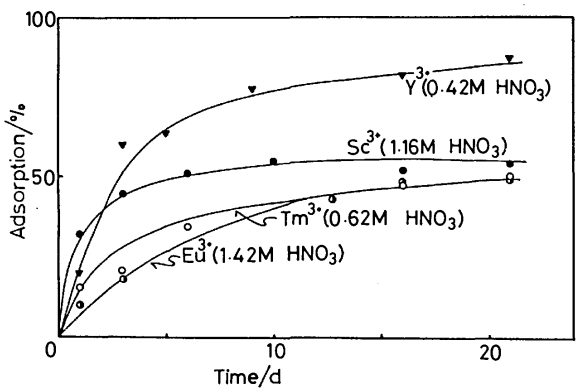

Fig. 1. Time dependence for the adsorption of rare earth ions on C-SbA. Initial concn of metal ions; 1.0×10^{-4} mol dm^{-3}. C-SbA; 0.50 g. Total vol.; 50.0 cm^3. Temp; 30 °C.

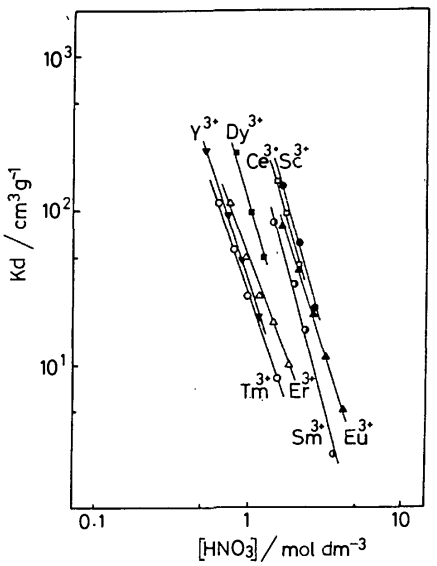

Fig. 2. Logarism K_d values of various metal ions vs. log[HNO_3] on C-SbA. Initial concn of metal ions; 1.0×10^{-4} mol dm^{-3}. C-SbA; 0.20 g. Total vol.; 20.0 cm^3. Temp; 30 °C.

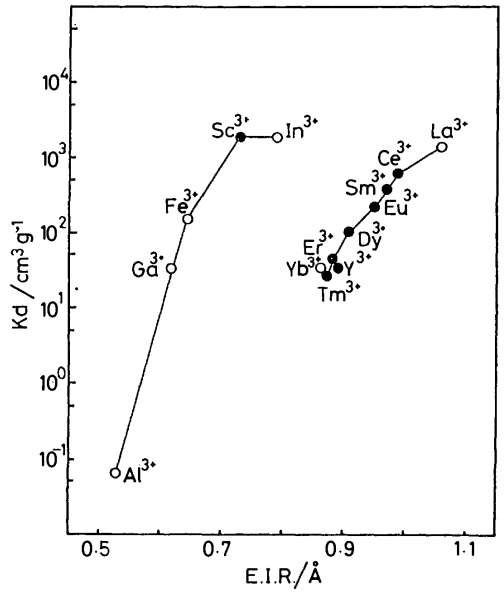

Fig. 3. The K_d of tervalent metal ions as a function of effective ionic radii of metal ions. ●: this work, ○: from Ref. 19.

The log-log plots of K_d vs. [HNO_3] showed that the slopes of dlog K_d/dlog[HNO_3] are about the same as the valency of metal ions studied, indicating the "ideal ion-exchange reaction" (Fig. 2). The equilibrium K_d values in logarithm scale of various tervalent metal ions on C-SbA were plotted against effective ionic radii (EIR)[27] of the metal ion in Fig. 3, after normalizing to a 1 M nitric acid solution. It was difficult to determine the K_d values experimentally higher than 10^3 for detection limit of the spectrophotometric analysis.

The following selectivity series were found for microamounts of tervalent metal ion on C-SbA in nitric acid solution;

$$Al^{3+}<Tm^{3+}<Ga^{3+}=Yb^{3+}<Y^{3+}<Er^{3+}<Dy^{3+}<Fe^{3+}<Eu^{3+}<Sm^{3+}<Ce^{3+}<La^{3+}<Sc^{3+}=In^{3+}$$

Two different selectivity series were found for Al^{3+}, Ga^{3+}, Fe^{3+}, and In^{3+}, and from Tm^{3+} to La^{3+} on C-SbA. The difference in the electron configuration of the ion-exchange cations may be responsible for the results; the latter takes the $s^2p^6f^n$ configuration and the former takes a different configuration. The log K_d values on BIO-RAD AG 50W-X8 increase slightly with increasing EIR[27,28] of exchanging metal ions because of its elastic structure.

Kielland Plot. It has been known that the selectivity on inorganic ion exchangers is much dependent on the concentration of metal ions in the exchanger phase because of their rigid structure mentioned above. It is known that large steric effect may arise in a rigid exchanger which undergoes little swelling or shrinkage, if there is a large difference in the ionic crystal radii of the two exchanging cations.

Among the ion-exchange system of tervalent metal ions/hydrogen ions, Al^{3+}, Ga^{3+}, Fe^{3+}, Sc^{3+}, Y^{3+}, Sm^{3+}, and Ce^{3+}/H^+ were selected in order to interpret the selectivity of tervalent metal ions. The Kielland plot showed fairly good straight line for metal ions/H^+ systems studied (Figs. 4-1 to 4-3). The ln K_H^M values decreased gradually with increasing $\bar{X}_M$, indicating that the steric effect depends on a variety of the exchanging metal ion. The Kielland plots of different tervalent metal ions/H^+ system at 30 °C are summarized in Fig. 4-4. Moving the axis of abscissa from left to right upto $\bar{X}_M$=0.1 in Fig. 4-4, the different selectivity sequences can be found as a function of

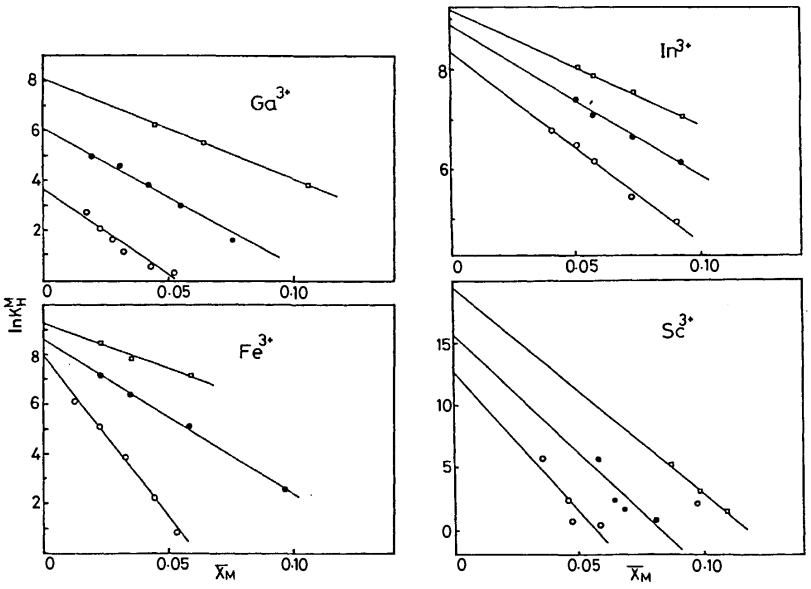

Fig. 4-1. The Kielland plots of Ga^{3+}, Fe^{3+}, In^{3+}, and Sc^{3+}/H^+ exchange systems on C-SbA. Ionic strength: 0.2. Temp, ○: 30, ●: 45, and □: 60 °C.

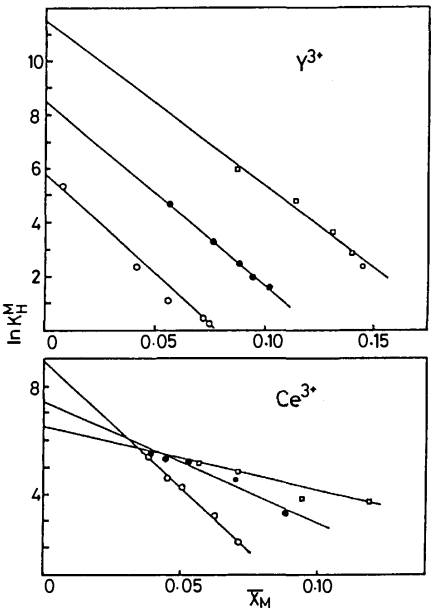

Fig. 4-2. The Kielland plots of Y^{3+} and Ce^{3+}/H^+ exchange systems on C-SbA. Ionic strength: 0.2. Temp, ○: 30, ●: 45, and □: 60 °C.

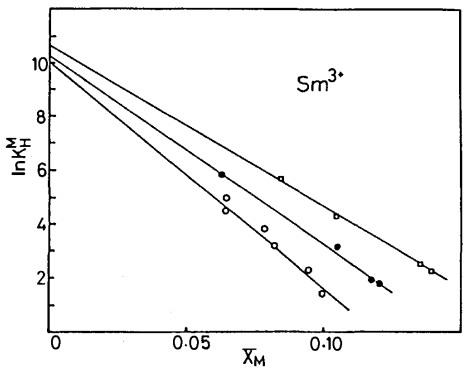

Fig. 4-3. The Kielland plots of Sm^{3+}/H^+ exchange systems on C-SbA. Ionic strength: 0.2. Temp, ○: 30, ●: 45, and □: 60 °C.

$\bar{X}_M$ to increase in the order $Al^{3+}<Ga^{3+}<Y^{3+}<Fe^{3+}<In^{3+}<Ce^{3+}<Sm^{3+}<Sc^{3+}$ for range of $\bar{X}_M=0$ to 0.008, and so on.

In general, when small cations in inorganic ion exchangers are exchanged with large cations in the solution, the ingoing ions are initially preferred and become progressively less preferred with increasing loading. This extent can be evaluated by the comparison of numerical values of Kielland coefficient, i.e., a large negative value of Kielland coefficient indicates a large steric effect.

The C/z, which is referred to equivalent Kielland coefficient,[††] for different exchange systems are plotted as a function of EIR in Fig. 5, other published data[14,16,18] being included. This shows that cations

[††] The Kielland coefficient for multivalent metal ions can be compared to those for alkali metal ions/H^+ system by this procedure.

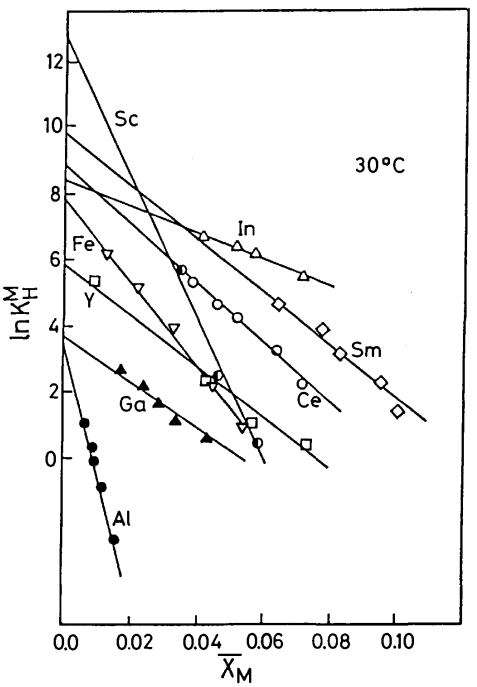

Fig. 4-4. The summarized Kielland plots of tervalent metal ions/H^+ exchange systems on C-SbA at 30 °C. Ionic strength: 0.2

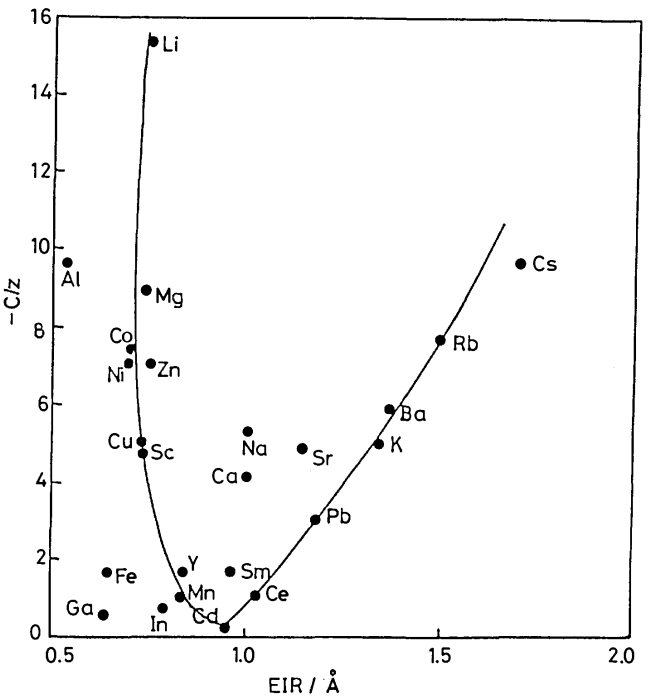

Fig. 5. The equivalent Kielland coefficients of tervalent metal ions/H^+ exchange systems on C-SbA vs. effective ionic radii (EIR) of the metal ions. EIR were taken from Table 1(a) of Shannon and Prewitt.[27]

with an effective ionic radius of about 1.0 Å enter the exchanger with minimum steric hindrance. The C-SbA has a rigid structure in which the change in the

lattice constant is less than 2% for the conversion from the hydrogen form to metal ion form.[14] The small cations, e.g., Li^+, Mg^{2+}, and Al^{3+}, are strongly hydrated in aqueous solution and may be exchanged with keeping their hydration shell. This brings large steric effect in the rigid structure of C-SbA.

The large cations, such as Ba^{2+}, Rb^+, and Cs^+, are less hydrated in the aqueous solution, and can be exchanged with a larger steric effect by increased crystal ionic radii of metal ions. Thus, the minimum steric effect may be interpreted in both contributions.

Hypothetical Thermodynamic Data. The thermodynamic equilibrium constant, K, can be evaluated from Eq. 2 or 4 by assuming that the linear relation between $\ln K_H^M$ vs. $\bar{X}_M$ is valid over the entire range of $\bar{X}_M$ from 0 to 1. However, high accuracy of these values is not obtained for long extrapolation of $\bar{X}_M$ to 1.0. The hypothetical thermodynamic data in infinitesimal concentration were calculated for interpretation of the selectivity of metal ions in microamounts on C-SbA.

The $(\Delta G^\circ)_{\bar{X}_M\to 0}$ is defined as;

$$(\Delta G^\circ)_{\bar{X}_M\to 0} = (-RT/z)\,(\ln K_H^M)_{\bar{X}_M\to 0} \qquad (7)$$

The calculated $(\Delta S^\circ)_{\bar{X}_M\to 0}$ and $(\Delta H^\circ)_{\bar{X}_M\to 0}$ values can be regarded as a constant, because van't Hoff plots, $(\ln K_H^M)_{\bar{X}_M\to 0}$ vs. $1/T$, showed fairly good linearity over the entire range of temperature studied (Fig. 6). The $(\Delta G^\circ)_{\bar{X}_M\to 0}$ values at 298 K were calculated by interpolating or extrapolating the determined $(\Delta G^\circ)_{\bar{X}_M\to 0}$ values to 298 K. The calculated $(\Delta G^\circ)_{\bar{X}_M\to 0}$ values at 298 K were plotted against EIR of the exchanging metal ions (Fig. 7). There appear two maxima which correspond to the selectivity series described above.

The ion-exchange reaction (1) can be separated into the hydration $(-\Delta Y_{hyd})$ and ion-exchange processes (ΔY_{ex}) as follows;

$$1/3\ M^{3+}(aq) + H^+(gas) \rightleftarrows 1/3\ M^{3+}(gas) + H^+(aq) \qquad -Y_{hyd}$$

$$1/3\ M^{3+}(gas) + \bar{H}^+ \rightleftarrows 1/3\ \bar{M}^{3+} + H^+(gas) \qquad \Delta Y_{ex}$$

where the Y represents thermodynamic functions such as G, H, and S. The numerical values of ΔY° contribute to the difference between the thermodynamic function of the ion-exchange (ΔY°_{ex}) and that of hydration (ΔY°_{hyd}) of the cations on the basis of the $\Delta Y^\circ_{hyd}=0$ of the reaction; $H^+(gas)\to H^+(aq)$. The value of ΔY°_{hyd} can be calculated from Rosseinsky's table.[29]

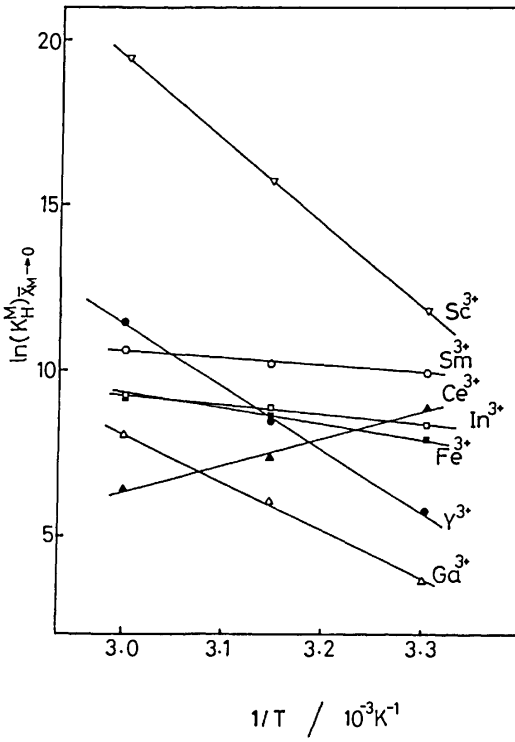

Fig. 6. Van't Hoff plots of $\ln(K_H^M)_{\bar{X}_M\to 0}$ on C-SbA.

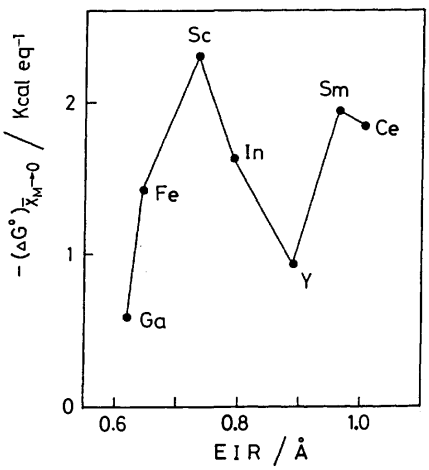

Fig. 7. $-(\Delta G^\circ)_{\bar{X}_M\to 0}$ vs. EIR of metal ions.

Table 1. Hypothetical Thermodynamic Data for Zero Loading of Tervalent Metal Ions in C-SbA

Metal ions	EIR / Å	$(\ln K_H^M)_{\bar{X}_M\to 0}$	C/z	$\Delta G^\circ_{\bar{X}_M\to 0}$ kcal equiv^{-1}	$\Delta H^\circ_{\bar{X}_M\to 0}$ kcal equiv^{-1}	$\Delta S^\circ_{\bar{X}_M\to 0}$ cal deg.$^{-1}$ equiv^{-1}	ΔH°_{hyd} kcal equiv^{-1}	ΔS°_{hyd} cal deg.$^{-1}$ equiv^{-1}	ΔH°_{ex} kcal equiv^{-1}	ΔS°_{ex} cal deg.$^{-1}$ equiv^{-1}
Al^{3+}	0.53	3.5	−28.9							
Ga^{3+}	0.62	3.00	−4.94	−0.592	9.59	34.1	−112.5	−14.7	−102.9	19.4
Fe^{3+}	0.645	7.12	−9.39	−1.41	4.02	18.2	−88.0	−11.2	−83.9$_8$	7.0
Sc^{3+}	0.73	11.6$_5$	−16.4	−2.30	15.0$_4$	58.2	−51.1	−6.2	−36.1	52.0
In^{3+}	0.79	8.22	−2.81	−1.62	1.80	11.5	−66.6	−8.0	−64.8	3.5
Y^{3+}	0.89	4.8	−5.5	−0.947	12.5$_6$	45.2$_9$	−27.4	−4.6	−14.8$_4$	40.7
Sm^{3+}	0.964	9.82	−6.0	−1.94	1.52	11.6	−14.7$_8$	−5.07	−13.2$_6$	6.5
Ce^{3+}	1.034	9.30	−6.72	−1.84	−0.57	4.23	−4.64	−4.59	−5.2	−0.36

The calculated values of ΔY°, ΔY°_{hyd}, and ΔY°_{ex} were summarized on Table 1.

Large numerical values of $(\Delta H^\circ)_{\bar{X}_M \to 0}$ and $(\Delta S^\circ)_{\bar{X}_M \to 0}$ were found on the systems of Sc^{3+} and Y^{3+}/H^+, as compared with those of other systems studied. The ΔS°_{ex} showed all positive value, except Ce^{3+}/H^+ system. An extremely high value was observed on the systems of Sc^{3+} and Y^{3+}/H^+.

If the ΔS° is zero, where the value of ΔS°_{ex} is equal to that of ΔS°_{hyd}, this suggests that the exchanging cation in exchanger has the same hydration structure as that in aqueous solution. The positive value of ΔS°_{ex} may indicate that degree of freedom of metal ion increases in the cavity of C-SbA. Such an increase of ΔS°_{ex} may occur from dehydration of metal ions or net transfer of water molecules from solid phase to aqueous phase. When the less hydrated cations such as Rb^+ and Cs^+ are the ingoing cations, the degree of freedom may increase by the transfer of some water molecules from a C-SbA cage to the aqueous phase.

In order to understand the unusual selectivities on C-SbA, the values of ΔS°_{ex} were plotted against ionic hydration numbers,[30] h^∞_i being taken from ΔS°_{hyd} (Fig. 8).

The h^∞_i calculated from data of hydration entropy contains the primary and secondary hydration shells. The entropy of the hydration of an ion may be written as in Eq. 8.[31]

$$\Delta S^\circ_{hyd} = R \ln(V_f/V_g) + S_A + S_B + S_C \quad (8)$$

where the $R \ln(V_f/V_g)$ term allows for the fact that the free volume (V_f) accessible to the aqueous solution is not the same as that in the gaseous phase (V_g). The term S_A is a contribution for water molecules forming the primary hydration shell, and the term S_C is the Born-model contribution for water outside the primary hydration shell. The term S_B is the contribution from water in the secondary shell. The values of S_B are probably positive (structure breaking effect) for all alkali and alkaline earth metal ions, except Li^+ and Mg^{2+}. Thus the results bring to form the Frank-Wen three zone model.[32] In zone A, water molecules in primary hydration shell are tightly bonded by the strong coulombic field of the ion. Zone B, interposing between zone A and C, is a structure breaking region.

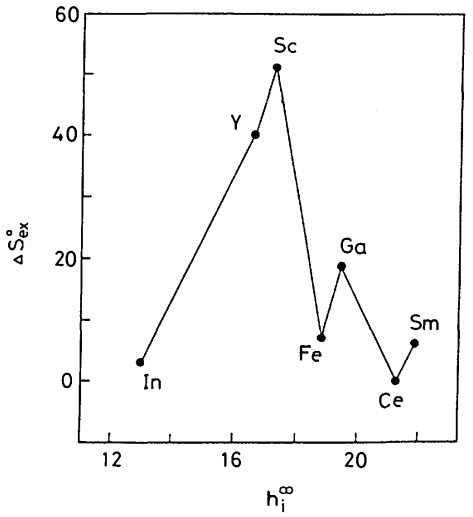

Fig. 8. The correlation between ΔS°_{ex} and hydration number (h^∞_i) for metal ions.

The zone B is less electrostrictive structure than zone A, and is less tetrahedrally coordinated than bulk water in zone C. If there is a contribution of coulombic force to the ion on exchange site enough to break the water structure of the hydration shell, the less hydrated ion can enter the narrow cavity in the exchanger. This may bring an increase in the ΔS°_{ex}. The water molecules of metal ion having small EIR may be tightly bound by the strong coulombic field of the metal ions, such as Mg^{2+}, first-row bivalent transition metal ions and Al^{3+}. It is very interesting in the fact that the electron configuration of Sc^{3+} is essentially the same as that of Y^{3+} and similar numerical value of h^∞_i is given for Sc^{3+} and Y^{3+} in aqueous solution.

When the coulombic force between the ion and the site is not strong enough to break water structure of the primary hydration shell, the small contribution of the ΔS°_{ex} may arise. The large contribution of the ΔS°_{ex} in the Sc^{3+} and Y^{3+}/H^+ systems may be due to both contributions of the net transfer of water molecules from solid phase to the aqueous solution and structure breaking of the water in exchanger.

The larger contribution of ΔS°_{ex} for Sc^{3+}/H^+ system than that of $(\Delta H^\circ)_{\bar{X}_{Sc} \to 0}$ brings a large numerical value of $(\ln K^{Sc}_H)_{\bar{X}_{Sc} \to 0}$, as compared with the system for Y^{3+}/H^+.

References

1) C. B. Amphlett, "Inorganic Ion Exchangers," Elsevier, Amsterdam (1964).
2) V. Veselý and V. Pekárek, *Talanta*, **19**, 219 (1972).
3) V. Pekárek and V. Veselý, *Talanta*, **19**, 1245 (1972).
4) M. Abe, *Bunseki Kagaku*, **23**, 1254 (1974).
5) M. Abe, *Bunseki Kagaku*, **23**, 1561 (1974).
6) "Inorganic Ion Exchange Materials," ed by A. Clearfield, CRC Press, Inc., Boca Raton, Fl., (1982).
7) M. Abe and T. Ito, *Nippon Kagaku Zasshi*, **86**, 817 (1965).
8) M. Abe and T. Ito, *Nippon Kagaku Zasshi*, **86**, 1259 (1965).
9) M. Abe and T. Ito, *Bull. Chem. Soc. Jpn.*, **41**, 333 (1968).
10) R. Chitrakar and M. Abe, *Mater. Res. Bull.*, **23**, 1231 (1988).
11) R. Chitrakar and M. Abe, *Solvent Extr. Ion Exch.*, **7**, 721 (1989).
12) M. Abe and T. Ito, *Bull. Chem. Soc. Jpn.*, **40**, 1013 (1967).
13) M. Abe, *Bull. Chem. Soc. Jpn.*, **42**, 2683 (1969).
14) M. Abe, *J. Inorg. Nucl. Chem.*, **41**, 85 (1979).
15) M. Abe and K. Uno, *Sep. Sci. Technol.*, **14**, 355 (1979).

16) M. Abe and K. Sudoh, *J. Inorg. Nucl. Chem.*, **43**, 2537 (1981).
17) M. Abe and K. Kasai, *Sep. Sci. Technol.*, **14**, 895 (1979).
18) M. Abe and K. Sudoh, *J. Inorg. Nucl. Chem.*, **42**, 1051 (1980).
19) M. Abe, M. Tsuji and M. Kimura, *Bull. Chem. Soc. Jpn.*, **54**, 130 (1981).
20) K. A. Kraus and R. J. Raridon, *J. Phys. Chem.*, **63**, 1901 (1959).
21) G. L. Gaines, Jr. and H. C. Thomas, *J. Chem. Phys.*, **21**, 714 (1953).
22) J. Kielland, *J. Soc. Chem. Ind.*, **54**, 232T (1935).
23) D. W. Breck, "Zeolite Molecular Sieves, Structure, Chemistry and Use," John Wiley & Sons Ltd., New York (1974), p. 532.
24) E. B. Sandell, "Colorimetric Determination of Trace of Metals," Interscience Pub. Inc., New York (1959).
25) F. D. Snell, "Photometric and Fluorometric Methods of Analysis", Wiley Interscience Pub. Inc., New York (1981).
26) R. W. Rinehart, *Anal. Chem.*, **26**, 1820 (1954).
27) R. D. Shannon and C. T. Prewitt, *Acta Crystallogr., Sect. B*, **25**, 925 (1969).
28) F. W. E. Strelow, R. Rethemeyer, and C. J. C. Bothma, *Anal. Chem.*, **37**, 106 (1965).
29) D. R. Rosseinsky, *Chem. Rev.*, **65**, 467 (1965).
30) Y. Marcus, "Ion Solvation," John Wiley and Sons Ltd., New York (1985), table 4.5 in p.79.
31) H. L. Friedman and C. V. Krishnan, "Water; A Comprehensive Treatise," ed. by F. Franks, Plenum Press, New York (1973), Vol. 3, p. 62.
32) H. S. Frank and Wen-Yang Wen, *Discuss. Faraday Soc.*, **24**, 133 (1957).

Thermal Decomposition of Ammonium Copper(II) *cyclo*-Hexaphosphate $Cu_2(NH_4)_2P_6O_{18}\cdot 8.5H_2O$ and Ammonium Calcium *cyclo*-Hexaphosphate $Ca_2(NH_4)_2P_6O_{18}\cdot 7H_2O$

Atsushi TAKENAKA,* Hironobu KOBAYASHI, Katsumi TSUCHIE,
Itaru MOTOOKA,† and Hiroyuki NARIAI
Department of Industrial Chemistry, Yonago National College of Technology,
Otakazuna, Hikona-cho, Yonago, Tottori 683
†Department of Chemistry, Faculty of General Education, Kobe University,
Tsurukabuto, Nada-ku, Kobe 657
(Received June 5, 1989)

Ammonium copper(II) and ammonium calcium *cyclo*-hexaphosphates, $Cu_2(NH_4)_2P_6O_{18}\cdot 8.5H_2O$ and $Ca_2(NH_4)_2P_6O_{18}\cdot 7H_2O$, were prepared by a wet method. TG-DTA, HPLC-FIA, and X-ray diffraction method were used to investigate the thermal decomposition of the *cyclo*-hexaphosphates. The effect of humidity on the pyrolysis was also examined by the use of dry N_2 gas and humid air. $Cu_2(NH_4)_2P_6O_{18}\cdot 8.5H_2O$ was mainly decomposed to oligophosphates by hydrolysis. Parts of the oligophosphates were changed to poly- (n=7—13) and highpolyphosphates through a condensation. The poly- and the highpolyphosphates were more abundant under the dried conditions. Above 280 °C ammonia was liberated. As the crystalline products, $Cu_2P_2O_7$ was identified at 380 °C, and $Cu_2P_4O_{12}$ above 430 °C. $Ca_2(NH_4)_2P_6O_{18}\cdot 7H_2O$ lost almost all its water of crystallization by 177 °C. As ammonia was evolved from 270 to 420 °C, accelerated by humidity, amorphous highpolyphosphates were formed. The formation of the highpolyphosphates was considered to proceed through a radical polymerization, since oligophosphates were scarcely detected in the course of the thermal reaction.

Ammonium calcium *cyclo*-triphosphate and its hydrates have been studied in regard to their formation,[1-4] crystal structures,[5-7] thermal behavior,[5,8] and other properties.[9] Ammonium calcium *cyclo*-tetraphosphate and its hydrate were also investigated mainly in terms of their crystal structures.[10,11] On the other hand, of all the ammonium copper(II) *cyclo*-phosphates, only the *cyclo*-octaphosphate was reported;[12] no ammonium calcium nor ammonium copper(II) *cyclo*-hexaphosphates has been reported in literature.

In the preceding study,[13] the thermal decomposition of ammonium strontium *cyclo*-phosphates was carried out in order to clarify whether a radical polymerization, like the thermal change of ammonium *cyclo*-phosphates to ammonium polyphosphate,[14] took place or not. Finally, it was concluded that the ammonium strontium *cyclo*-phosphates were decomposed to polyphosphates through dehydration-condensation rather than through radical polymerization. Therefore, the dehydration-condensation was supposed to also take place over the course of the thermal decomposition of another ammonium bivalent metal *cyclo*-phosphates.

Several experiments were attempted for the purpose of preparing some ammonium bivalent metal *cyclo*-hexaphosphates, but only the following salts were obtained: Ammonium copper(II) *cyclo*-hexaphosphate $Cu_2(NH_4)_2P_6O_{18}\cdot 8.5H_2O$ and ammonium calcium *cyclo*-hexaphosphate $Ca_2(NH_4)_2P_6O_{18}\cdot 7H_2O$.

The purpose of this series of studies has been to investigate the thermal decomposition of the ammonium bivalent metal *cyclo*-phosphates, especially with regard to the mechanism of the formation of the poly- and/or the highpolyphosphates from the ammonium bivalent metal *cyclo*-phosphates. Since the ammonium copper(II) and the ammonium calcium *cyclo*-hexaphosphates were prepared by wet methods, we studied the thermal decomposition of the two *cyclo*-hexaphosphates in the present work.

The ammonium copper(II) *cyclo*-hexaphosphates were decomposed to oligophosphates through hydrolysis, and polyphosphates generating through the dehydration-condensation of the oligophosphates. However, against our expectation, the ammonium calcium *cyclo*-hexaphosphate was thought to change to the highpolyphosphates via radical polymerization, which was accelerated by the humidity of the atmosphere.

Experimental

The ammonium bivalent metal *cyclo*-hexaphosphates, $Cu_2(NH_4)_2P_6O_{18}\cdot 8.5H_2O$ and $Ca_2(NH_4)_2P_6O_{18}\cdot 7H_2O$, were prepared by wet methods similar to those described in the literature.[13] HPLC-flow injection analyses (HPLC-FIA) for the samples of $Cu_2(NH_4)_2P_6O_{18}\cdot 8.5H_2O$ were carried out after metathesis by the use of a 1% (w/w) sodium sulfide aqueous solution, as reported by Nariai et al.[15] The other analytical procedures were essencially the same as those mentioned in the literature.[13]

$Cu_2(NH_4)_2P_6O_{18}\cdot 8.5H_2O$ was observed to consist only of *cyclo*-hexaphosphate ions. At least 99.9% of the phosphorus atoms were found to be present as *cyclo*-hexaphosphate ions in $Ca_2(NH_4)_2P_6O_{18}\cdot 7H_2O$.

Results and Discussion

Thermal Decomposition of Ammonium Copper(II) *cyclo*-Hexaphosphate $Cu_2(NH_4)_2P_6O_{18}\cdot 8.5H_2O$. Figure

1 shows thermal analyses (TG-DTA) in stationary air and in a stream of dry N_2 gas. Since ammonia was not evolved until 280 °C, the water of crystallization caused a large endothermic peak below 150 °C accompanying a loss in weight.

Figure 2 represents the percentage of phosphorus atoms present as *cyclo*-hexa-, oligo- (n=1—6), and polyphosphates (n=7—13) in the products which were obtained by heating to the temperature indicated by arrows in Fig. 1. Figure 2 shows that the amounts of the oligophosphates were obviously larger under the humid conditions than under the dry conditions—these, humid and dry, conditions were the same as those described in Ref. 13. The oligophosphates were found abundantly even under the dry conditions; thus, $Cu_2(NH_4)_2P_6O_{18}\cdot 8.5H_2O$ was thought to be hydrolyzed mainly by its water of crystallization. The amounts of the polyphosphates were less under the humid conditions, and the highpolyphosphates were not observed at all under the humid conditions. The polyphosphates and highpolyphosphates were formed in largest amounts at 280 °C under the dry conditions. Since the primitive products were the oligophosphates, the poly- and the highpolyphosphates were thought to be produced by dehydration-condensation of the oligophosphates. The smaller amounts of polyphosphates and the absence of the highpolyphosphates under the humid conditions must be attributed to a retardation of the dehydration-condensation, caused by an enhanced partial pressure of the water vapor.

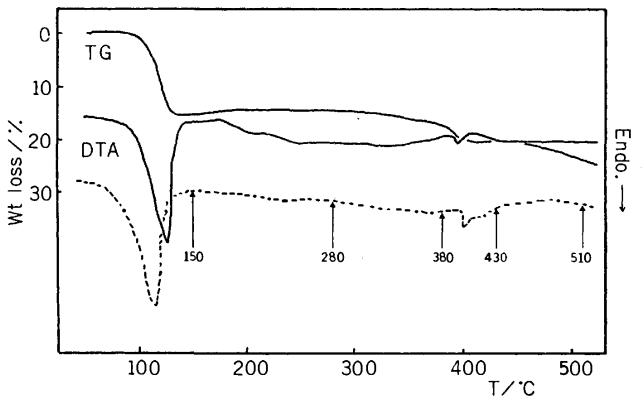

Fig. 1. Thermal analyses of $Cu_2(NH_4)_2P_6O_{18}\cdot 8.5H_2O$ measured in the two different atmospheres. Solid line (——): in stationary air, dotted line (----): DTA in a stream of dry N_2 gas, heating rate: 2.5 K min^{-1}.

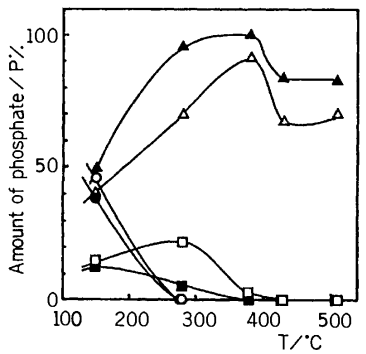

Fig. 2. Amount of phosphates in the decomposition products of $Cu_2(NH_4)_2P_6O_{18}\cdot 8.5H_2O$.
○ and ●: *cyclo*-Hexaphosphate observed under the dried and the humid conditions, respectively; Δ and ▲: oligophosphates (chain length, n=1—6) observed under the dried and the humid conditions, respectively; □ and ■: polyphosphates (n=7—13) under the dried and the humid conditions, respectively.

Since ammonia gradually evolved for temperatures above 280 °C, several reactions, such as a deammoniation and a dehydration (and besides a liberation of diphosphorus pentaoxide), were considered to take place simultaneously. We therefore could not clarify the process of the decomposition. The products obtained by heating until 150 and 280 °C were amorphous, while the X-ray diffraction patterns of the products heated to 380 °C were those of $Cu_2P_2O_7$. Copper(II) *cyclo*-tetraphosphate, $Cu_2P_4O_{12}$, was the only crystalline material at 430 and 510 °C. The oligophosphates fell off from 380 to 430 °C, which was accompanied with a large weight loss. The endothermic peak at 400 °C can probably be attributed to the formation of *cyclo*-tetraphosphate from the oligophosphates, as reported by Thilo and Grunze.[16] Only under the dry conditions was the *cyclo*-triphosphate anion $P_3O_9^{3-}$ detected at 430 °C. Although the phosphorus present as $P_3O_9^{3-}$ was ca. 16%, there were no X-ray diffraction lines except for those of $Cu_2P_4O_{12}$. Therefore, the *cyclo*-triphosphate was considered to be in the form of an amorphous phase.

Thermal Decomposition of Ammonium Calcium *cyclo*-Hexaphosphate $Ca_2(NH_4)_2P_6O_{18}\cdot 7H_2O$. Figure 3 shows thermal analyses in stationary air and in a stream of dry nitrogen gas. Figure 4 represents the

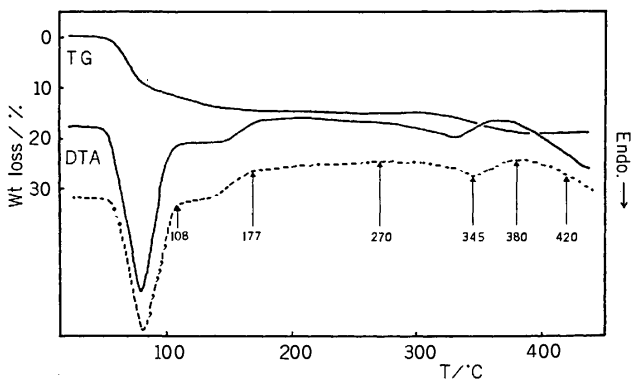

Fig. 3. Thermal analyses of $Ca_2(NH_4)_2P_6O_{18}\cdot 7H_2O$ measured in the two different atmospheres.
Solid line (——): in stationary air, dotted line (----): DTA in a stream of dry N_2 gas, heating rate: 2.5 K min^{-1}.

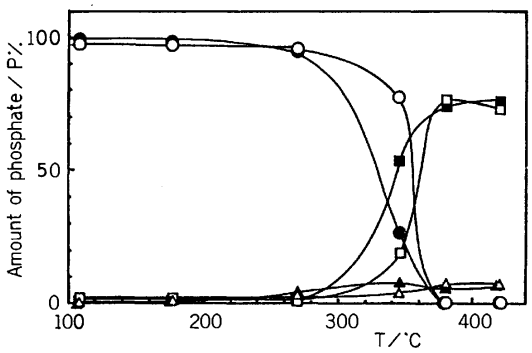

Fig. 4. Amount of phosphates in the decomposition products of $Ca_2(NH_4)_2P_6O_{18}\cdot 7H_2O$.
○ and ●: *cyclo*-Hexaphosphate observed under the dried and the humid conditions, respectively; △ and ▲: oligophosphates (n=1—6) under the dried and the humid conditions, respectively; □ and ■: high-polyphosphates under the dried and the humid conditions, respectively.

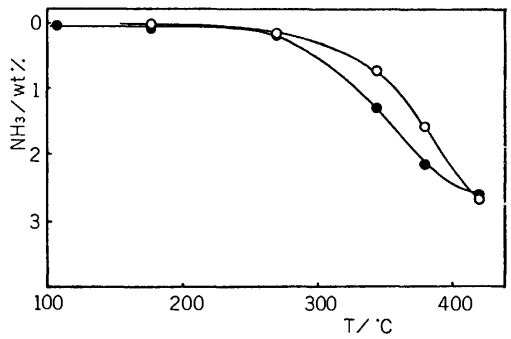

Fig. 5. Amount of ammonia evolved by heating $Ca_2(NH_4)_2P_6O_{18}\cdot 7H_2O$.
○: in the dried atmosphere, ●: in the humid atmosphere.

percentage of phosphorus atoms present as *cyclo*-hexa-, oligo- (n=1—6), and highpolyphosphates, in the products obtained by heating up to the temperature indicated by arrows in Fig. 3.

Ammonia was evolved, as shown in Fig. 5. Until 270 °C, the *cyclo*-hexaphosphate ions were not cleaved and ammonia was hardly evolved. There was little change in weight from 177 to 270 °C. Therefore, the weight loss until 170 °C was attributed to the liberation of the water of crystallization, which caused a series of the endothermic peaks below 177 °C, as expressed by the following equation (Eq. 1):

$$Ca_2(NH_4)_2P_6O_{18}\cdot 7H_2O \rightarrow Ca_2(NH_4)_2P_6O_{18} + 7H_2O. \quad (1)$$

Figure 4 shows that highpolyphosphates were produced more rapidly under the humid conditions than under the dry conditions—these conditions were also the same as those mentioned in Ref. 13— in proportion to the disappearance of a *cyclo*-hexaphosphate. Although the *cyclo*-hexaphosphate was decomposed more rapidly under the humid conditions than under the dry conditions, there were only small amounts of oligophosphates, which are the primitive hydrolytic products of the *cyclo*-hexaphosphate, even under the humid conditions. If the highpolyphosphates were produced by a dehydration-condensation, as in the pyrolysis of $Cu_2(NH_4)_2P_6O_{18}\cdot 8.5H_2O$, they should have been present more abundantly under the dry conditions than under the humid conditions. Therefore, however, the larger amount of the highpolyphosphates under the humid conditions suggests that they were not produced through the dehydration-condensation of the oligophosphates, but through another thermal change.

The TG-curve shows a plateau around 420 °C (Fig. 3). A weight loss of ca. 3.7% from 270 to 420 °C in the dry atmosphere was estimated from the ammonia evolved in this range (ca. 2.6%) and the water remaining at 270 °C in the products (ca. 1.1%). The loss (ca. 3.7%) was close to that actually observed by thermogravimetry (ca. 4.0%); thus, dehydration-condensation was more unlikely as a thermal formation of the highpolyphosphates.

We reported a radical polymerization on the thermal decomposition of ammonium *cyclo*-tetra- and *cyclo*-hexaphosphates.[14] Then, ammonium oligophosphates were yielded little or a little. And it was the "trigger reaction" in the decomposition of the ammonium *cyclo*-phosphates that a small amount of ammonia was liberated.

$Ca_2(NH_4)_2P_6O_{18}$, formed according to Eq. 1, was converted to amorphous highpolyphosphates at between 270 and 420 °C. The conversion was accompanied by a liberation of ammonia (Figs. 4 and 5), as in the case of the pyrolysis of the ammonium *cyclo*-phosphates.[14] The amounts of oligophosphates were small, as shown in Fig. 4, as in the case of the pyrolysis of the ammonium *cyclo*-phosphates.[14] Therefore, it might be concluded that the amorphous highpolyphosphates were produced through a polymerization of the oligophosphate radicals. The thermal change of $Ca_2(NH_4)_2P_6O_{18}$ to the highpolyphosphates can be described according to the following equation (Eq. 2):

$$Ca_2(NH_4)_2P_6O_{18}[\text{crystalline}] \rightarrow 2Ca(NH_4)_{1-x}H_x(PO_3)_3[\text{amorphous}] + 2xNH_3. \quad (2)$$

As shown in Fig. 5, ammonia evolved more abundantly under the humid conditions than under the dry conditions, called the "catalytic effect" of humidity in the literature.[13] The evolution of ammonia caused an endothermic peak at 345 °C (Figs. 3 and 5). The catalytic effect was also shown by a shift in the endothermic peak to a lower temperature by the presence of water vapor.

Figure 3 shows neither an increase in the weight nor a corresponding exothermic peak, resulting from the water-incorporation of oligophosphate radicals, unlike in the pyrolysis of $(NH_4)_4P_4O_{12}$.[14] Perhaps, otherwise, the water molecules supplied by the humid

air might form some weak bondings with the ammonium ions, so accelerating the liberation of ammonia.

It was reported in the literature[13] that ammonium strontium *cyclo*-triphosphate is decomposed to poly- ($n\geq 4$) and oligophosphates ($n=1$—3), e.g., from 250 to 380 °C under humid conditions. Because no observation was made of either an increase in weight nor of a corresponding exothermic peak, we concluded that the formation of the polyphosphates took place through dehydration-condensation. However, some part of the formation must proceed via oligophosphate radicals, especially within the initial temperature range (250—335 °C), since in this range there were hardly any oligophosphates which should appear as the primitive hydrolytic products of the ammonium strontium *cyclo*-triphosphate.

In the thermal decomposition of $Cu_2(NH_4)_2P_6O_{18}\cdot 8.5H_2O$ at higher temperature, a white sublimable material—which was probably diphosphorus pentaoxide—adhered to the inner surface at the outlet of a glass tube placed in a furnace. Although Feldmann reported that ammonium calcium *cyclo*-triphosphate $Ca(NH_4)P_3O_9\cdot aq$ liberated diphosphorus pentaoxide,[8] $Ca_2(NH_4)_2P_6O_{18}\cdot 7H_2O$ did not apparently produce this material under the present conditions.

References

1) D. Z. Serazetdinov, M. Kh. Kim, and A. B. Bekturov, *Vestn. Akad. Nauk Kaz. SSR*, **25**, 56 (1969); *Chem. Abstr.*, **71**, 108537k (1969).

2) A. V. Ekshtelis, D. F. Takezhanova, A. K. Il'yasova, and A. B. Bekturov, *Izv. Akad. Nauk Kaz. SSR, Ser. Khim.*, **22**, 1 (1972); *Chem. Abstr.*, **77**, 147137y (1972).

3) A. V. Ekshtelis and A. K. Il'yasova, *Izv. Akad. Nauk Kaz. SSR, Ser. Khim.*, **24**, 5 (1974); *Chem. Abstr.*, **80**, 115582k (1974).

4) A. Menlibaev, D. Z. Serazetdinov, A. B. Bekturov, and M. Kh. Kim, *Izv. Akad. Nauk Kaz. SSR, Ser. Khim.*, **1980**, 1; *Chem. Abstr.*, **92**, 208212c (1980).

5) R. Masse, J-C Grenier, and A. Durif, *Bull. Soc. Chim. Fr.*, **1968**, 1741; *Chem. Abstr.*, **69**, 48751x (1968).

6) J-C Grenier and R. Masse, *Bull. Soc. Fr. Mineral. Cristallogr.*, **91**, 428 (1968); *Chem. Abstr.*, **70**, 32370g (1969).

7) R. Masse, A. Durif, and J-C Guitel, *Z. Kristallogr., Kristallgeom., Kristallphys., Krystallchem.*, **141**, 113 (1975); *Chem. Abstr.*, **83**, 124460h (1975).

8) W. Feldmann, *Z. Anorg. Allg. Chem.*, **400**, 97 (1973).

9) W. Feldmann and I. Grunze, *Z. Anorg. Allg. Chem.*, **360**, 225 (1968).

10) R. Masse, J-C Grenier, M-T Averbuch-Pouchot, D. Tranqui, and A. Durif, *Bull. Soc. Fr. Mineral. Cristallogr.*, **90**, 158 (1967); *Chem. Abstr.*, **68**, 82107f (1968).

11) I. Torjmann, R. Masse, and J-C Guitel, *Acta Crystallogr., Sect. B*, **32**, 1643 (1976); *Chem. Abstr.*, **85**, 70987f (1976).

12) M. Laught and J-C Guitel, *Z. Kristallogr., Kristallgeom., Krystallphys., Krystallchem.*, **141**, 203 (1975); *Chem. Abstr.*, **83**, 140168z (1975).

13) A. Takenaka, I. Motooka, and H. Nariai, *Bull. Chem. Soc. Jpn.*, **62**, 2819 (1989).

14) A. Takenaka, I. Motooka, and H. Nariai, *Bull. Chem. Soc. Jpn.*, **60**, 4299 (1987).

15) H. Nariai, I. Motooka, Y. Kanaji, and M. Tsuhako, *Bull. Chem. Soc. Jpn.*, **60**, 1337 (1987).

16) E. Thilo and I. Grunze, *Z. Anorg. Allg. Chem.*, **290**, 209 (1957).

Synthesis, Magnetic Property, and Crystal Structure of Imidazolate-Bridged Manganese(III)-Copper(II) Dinuclear Complex

Naohide MATSUMOTO,* Hisashi ŌKAWA, Sigeo KIDA, Takanori OGAWA,† and Akira OHYOSHI†
Department of Chemistry, Faculty of Science, Kyushu University, Hakozaki, Higashi-ku, Fukuoka 812
†Department of Applied Chemistry, Faculty of Engineering, Kumamoto University, Kurokami 2-39-1, Kumamoto 860
(Received June 7, 1989)

The synthesis, crystal structure, and magnetic property of an imidazolate-bridged manganese(III)-copper(II) dinuclear complex [Mn(salen)Cu(A)]BPh_4 are described, where [H_2salen]=*N*,*N*′-disalicylideneethylenediamine, [H_2A]=4-(6-methyl-8-oxo-2,5-diazanonane-1,5,7-trienyl)imidazole, and BPh_4=tetraphenylborate. The X-ray analysis confirmed an imidazolate-bridged manganese(III)-copper(II) dinuclear structure, in which the coordination geometries of the manganese(III) and copper(II) ions are square pyramid and square planar, respectively. The apical position of the manganese(III) ion is occupied by an imidazolate nitrogen N(3) of the [Cu(A)] moiety with the bond distance of Mn-N(3) 2.165(5) Å. As the temperature is lowered, the effective magnetic moment per molecule decreases gradually from 5.17 B.M. at 300.2 K, reaches the minimum value 4.44 B.M. at 24.9 K, and then increases to 4.73 B.M. at 4.2 K, indicating that antiferro- and ferro-magnetic interactions are co-operative in the complex.

The molecular design of hetero-metal polynuclear complexes has been an attractive subject to mimic some biological metal enzymes[1,2] and to develop ferromagnets and ferrimagnets.[3] Imidazolate-bridged hetero-metal dinuclear structure has been found in the active site of bovine erythrocyte superoxide dismutase (BESOD)[1] and has been one of the candidate structures of the active site of the resting form of cytochrome c oxidase.[2] In order to develop structural model compounds of BESOD, Lippard's group[4-8] and other groups[9-14] have synthesized and characterized a number of imidazolate-bridged di- and polynuclear copper(II) complexes. However, only a few examples of imidazolate-bridged hetero-metal complexes have been reported so far.[15-18] Recently we have shown an effective synthetic route to prepare imidazolate-bridged hetero-metal dinuclear complexes with various combinations of metal ions.[19-23] The complexes thus obtained may provide not only structural model compounds of the metal enzymes but also a novel family of hetero-metal complexes which makes it possible to investigate systematically magnetic interaction between magnetic centers with the different electronic configurations. This paper describes the synthesis, magnetic property, and crystal structure of an imidazolate-bridged manganese(III)-copper(II) complex [Mn(salen)Cu(A)]BPh_4, where [H_2salen]=*N*,*N*′-disalicylideneethylenediamine, [H_2A]=4-(6-methyl-8-oxo-2,5-diazanonane-1,5,7-trienyl)imidazole, and BPh_4=tetraphenylborate. The schematic structure of the complex is shown in the drawing.

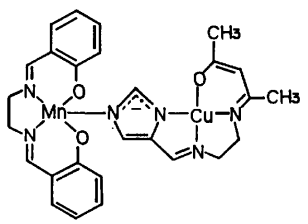

Experimental

Syntheses. Component Compounds. The component compounds [Mn(salen)]BPh_4[24] and [Cu(A)]0.5$CHCl_3$[20] were prepared according to the methods reported earlier.

[Mn(salen)Cu(A)]BPh_4. To a solution of [Mn(salen)]-BPh_4 (500 mg, 1 mmol) in 50 cm^3 of methanol was added a solution of [Cu(A)]0.5$CHCl_3$ (342 mg, 1 mmol) in 50 cm^3 of methanol. The mixture was stirred for 10 min on a hot plate and then filtered. The filtrate was left to stand at room temperature overnight. Red-brown crystals precipitated were collected by suction filtration and dried in air (yield ca. 45%). Attempts for recrystallization were unsuccessful, leading to decomposition of the complex. Calcd for $C_{51}H_{48}N_6BO_3MnCu$: C, 66.42; H, 5.25; N, 9.11; Mn, 5.95; Cu, 6.89%. Found: C, 66.96; H, 5.30; N, 9.05; Mn, 6.06; Cu, 6.92%. Λ_M 83 S mol^{-1} cm^2 (acetonitrile).

Physical Measurements. Elemental analyses (C, H, and N) were performed at the Elemental Analysis Center of Kyushu University. Elemental analyses for Mn and Cu were carried out on a Nippon Jarrel Ash AA 781 atomic absorption and flame emission spectrophotometer. Electrical conductivity was measured on a Denki Kagaku Keiki AOL-10 conductivity meter in ca. 10^{-3} mol dm^{-3} acetonitrile solution. Magnetic susceptibilities were obtained at 4.2—100 K by use of a HOXAN HSM-2000 SQUID magnetometer under the magnetic field of 0.5 T and at 80—300 K by the Faraday balance designed in our laboratory. Data were corrected for magnetization of the sample holder and for the diamagnetism of the component atoms by the use of Pascal's constants. The molar effective magnetic moments were calculated by the equation $\mu_{eff}=2.828(\chi_M T)^{1/2}$.

X-Ray Crystallography. Reflection data were measured on a Rigaku Denki AFC-5 automated four-circle diffractometer with graphite-monochromatized Mo $K\alpha$ radiation at room temperature. Three standard reflections were monitored every 100 reflections and showed no systematic decrease in the intensity. The reflection data were corrected for Lorentz and polarization factors and used in the structure determination. Corrections for absorption and extinction effects were not made. Unit cell parameters were determined by 25 reflections ($20°<2\theta<30°$).

Crystal Data: [Mn(salen)Cu(A)]BPh_4, Formula=$MnCuO_3N_6C_{51}BH_{48}$, F.W.=922.2, triclinic, space group=$P\bar{1}$, crystal dimension 0.2×0.3×0.2 mm, a=14.215(3) Å, b=15.745(3) Å, c=13.944(3) Å, α=121.20(2)°, β=114.28(2)°, γ=58.49(2)°, V=2233.5(1.2) Å^3, μ(Mo$K\alpha$)=7.72 cm^{-1}, d_{calcd}=1.371 g cm^{-3} (Z=2), d_{obsd}=1.36 g cm^{-3} (by floatation method in aqueous KI solution), scan mode θ-2θ, scan speed 6 deg min^{-1}, scan range 2.5°<2θ<45°, scan width (1.2+0.35tanθ)°, octant measured +h, ±k, ±l, no. independent reflections 4698, R=7.32%, R_w=7.29%. the largest residue in the final D-Fourier synthesis 0.8 e Å^{-3}.

The structure was solved by the standard heavy-atom method and refined by the block-diagonal least-squares method, where the function minimized is $\sum w(|F_o|-|F_c|)^2$ and equal weight for all reflections was adopted. The contribution of hydrogen atoms bound to carbon were introduced in the calculated positions. These hydrogen atoms were included in the structure factor calculation but not refined. The atomic scattering factors were taken from literature.[25] All computations were performed on a FACOM M 780 computer at the Computer Center of Kyushu University using the UNICS III program system.[26] The final atomic prameters are given in Table 1. Tables of observed and calculated structure factors, listings of atomic positional and anisotropic thermal parameters, and complete lists of bond lengths and angles with their estimated standard deviations have been deposited as Document No. 8903 at the Office of the Editor of Bull. Chem. Soc. Jpn.

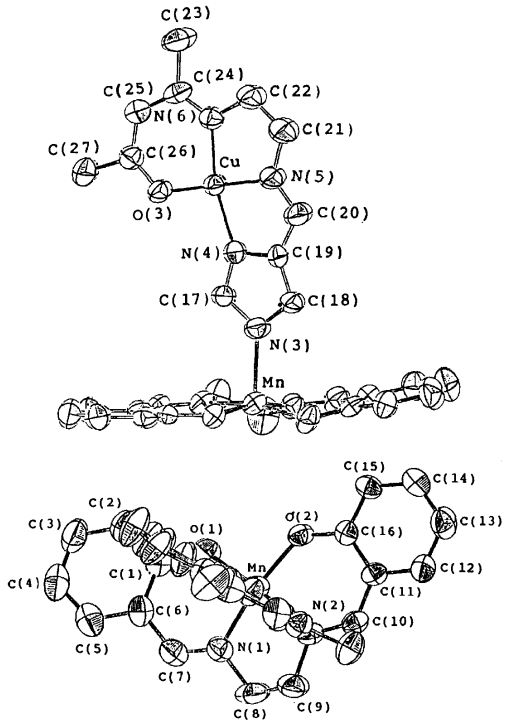

Fig. 1. Molecular structure of the cation [Mn(salen)-Cu(A)]$^+$ with the atom numbering scheme: (1) view projected on the plane of [Cu(A)] part; (2) view projected on the plane of salen ligands.

Table 1. Positional Parameters (×10^4) for [Mn(salen)Cu(A)]BPh_4

Atom	x	y	z	B_{eqv}/Å^2	Atom	x	y	z	B_{eqv}/Å^2
Mn	5995(1)	4008(1)	5644(1)	3.6	C(22)	12415(7)	−924(8)	7474(9)	5.7
O(1)	6439(5)	4354(4)	4839(4)	4.6	C(23)	12607(8)	−2086(8)	8587(9)	6.7
O(2)	5493(4)	3007(4)	4314(4)	3.5	C(24)	11489(7)	−1276(6)	8249(7)	4.6
N(1)	6114(5)	5306(5)	7030(5)	4.0	C(25)	10542(7)	−1135(7)	8525(7)	4.7
N(2)	5209(5)	4020(4)	6544(5)	3.5	C(26)	9465(6)	−393(6)	8360(6)	4.0
C(1)	7142(6)	4837(6)	5275(6)	3.8	C(27)	8557(8)	−402(8)	8644(8)	5.5
C(2)	7715(7)	4691(7)	4564(8)	5.1	B	3024(7)	3025(7)	8250(7)	3.3
C(3)	8428(8)	5189(9)	4961(9)	6.2	C(28)	2267(6)	4345(6)	8745(7)	4.1
C(4)	8600(8)	5875(9)	6098(10)	7.0	C(29)	2087(7)	4958(7)	8184(8)	5.1
C(5)	8040(8)	6040(8)	6828(8)	5.8	C(30)	1447(8)	6060(7)	8508(9)	6.1
C(6)	7322(7)	5527(6)	6446(7)	4.4	C(31)	1017(9)	6583(8)	9482(11)	7.4
C(7)	6726(7)	5774(7)	7237(7)	4.6	C(32)	1174(10)	6055(8)	10106(10)	8.0
C(8)	5409(9)	5700(8)	7823(8)	6.3	C(33)	1797(8)	4920(7)	9705(8)	5.9
C(9)	5313(8)	4789(7)	7739(7)	5.3	C(34)	2474(6)	2430(6)	6924(6)	3.6
C(10)	4683(6)	3421(6)	6193(6)	3.6	C(35)	1522(8)	2934(8)	6254(7)	5.3
C(11)	4590(6)	2607(6)	5065(6)	3.4	C(36)	1134(10)	2354(12)	5101(9)	8.6
C(12)	4048(7)	1979(7)	4848(7)	4.6	C(37)	1741(11)	1251(12)	4630(9)	9.0
C(13)	3946(8)	1165(7)	3792(8)	5.3	C(38)	2624(10)	730(9)	5240(9)	7.4
C(14)	4375(7)	974(7)	2936(7)	4.7	C(39)	2997(7)	1288(7)	6376(7)	4.9
C(15)	4882(6)	1595(6)	3119(6)	3.7	C(40)	3071(7)	2461(6)	8990(6)	3.7
C(16)	5001(6)	2432(6)	4189(6)	3.3	C(41)	2074(8)	2528(8)	9041(8)	5.3
Cu	10047(1)	355(1)	7321(1)	3.5	C(42)	2070(9)	2057(9)	9648(9)	6.9
O(3)	9136(4)	322(4)	7963(4)	4.0	C(43)	3063(9)	1491(8)	10205(8)	6.5
N(3)	7613(5)	2874(5)	6168(5)	4.1	C(44)	4044(9)	1403(7)	10149(7)	5.8
N(4)	8901(5)	1537(5)	6747(5)	3.7	C(45)	4055(7)	1881(6)	9555(7)	4.5
N(5)	11013(5)	416(5)	6719(6)	4.8	C(46)	4308(6)	2848(6)	8352(6)	3.3
N(6)	11418(5)	−746(5)	7727(6)	4.0	C(47)	4759(6)	3597(6)	9267(6)	3.5
C(17)	7826(6)	2199(6)	6625(7)	4.0	C(48)	5866(7)	3456(6)	9452(7)	4.1
C(18)	8623(6)	2620(7)	6001(8)	4.8	C(49)	6581(7)	2559(6)	8737(7)	4.1
C(19)	9415(6)	1786(6)	6347(7)	4.2	C(50)	6165(7)	1813(7)	7821(7)	4.3
C(20)	10584(7)	1160(7)	6349(8)	5.4	C(51)	5062(6)	1949(6)	7630(6)	3.9
C(21)	12184(7)	−362(8)	6791(10)	6.7					

Results and Discussion

The component complex [Cu(A)] plays a key role in producing imidazolate-bridged hetero-metal complexes, because [Cu(A)] functions like a monodentate ligand at the imidazolate nitrogen, coordinating to another metal ion to form an imidazolate-bridged complex. The mixed-metal complex was readily prepared by mixing [Mn(salen)]BPh_4 and [Cu(A)] in methanol. The elemental analysis (C, H, N, Cu, and Mn) was consistent with the formula of [Mn(salen)-Cu(A)]BPh_4. Molar electrical conductance in acetonitrile was 83 S mol^{-1} cm^2 which is consistent with 1:1 electrollyte.

Structural Description. The molecular structure of $[Mn(salen)Cu(A)]^+$ with the atom numbering scheme is shown in Fig. 1. Selected bond distances and bond angles are given in Table 2. The X-ray analysis has confirmed that the complex assumes an imidazolate-bridged manganese(III)-copper(II) dinuclear structure. The coordination geometries of the manganese(III) and copper(II) ions are square pyramid and square planar, respectively. In the square pyramid of the manganese(III) ion, the basal coordination plane is occupied by the N_2O_2 donor set of the salen ligand with the bond distances 1.869(4)—1.985(5) Å and the apical position is occupied by the imidazolate nitrogen atom N(3) of the [Cu(A)] moiety with the bond distance of Mn-N(3) 2.125(5) Å. The bond distance of Mn-N(3) 2.125(5) Å is shorter than those of Mn(III)-apical imidazole nitrogen atom of [Mn(HIm)(salen)]ClO_4 (2.231(4) Å) and [Mn(biim)-(salen)]ClO_4 (2.278(5), 2.283(4) Å), where HIm=imidazole and biim=1,4-di(1-imidazolyl)butane.[24] The manganese(III) ion deviates by 0.23 Å toward the apical position from the basal coordination plane. The [Cu(A)] plane is nearly perpendicular to the [Mn-(salen)] plane and intersects it approximately at the Mn-O(2) and Mn-N(1) bonds, where the dihedral angle between the mean planes of these moieties is 86.8°.

Figure 2 shows a packing view of two crystallographically unique units related by the inversion center. As often seen in the metal complexes with salen, two manganese(III) ions are bridged by two phenoxo oxygen atoms O(1) and O(1)* ($-x$, $-y$, $-z$) of the salen in the out-of-plane fashion, where the distance of Mn-O(1)* is 3.103(5) Å. The bond distance is substan-

Table 2. Bond Distance (Å) and Angles (deg) for [Mn(salen)Cu(A)]BPh_4

Bond distances (Å)				N(1)-Mn-N(3)	95.5(2)	N(2)-Mn-N(3)	94.2(3)
				Mn-O(1)-C(1)	126.2(5)	O(1)-C(1)-C(2)	119.4(6)
(a) Manganese site				O(1)-C(1)-C(6)	122.7(10)	C(2)-C(1)-C(6)	117.7(9)
Mn-Mn*	3.658(2)	Mn-O(1)	1.878(9)	C(1)-C(2)-C(3)	121.9(8)	C(2)-C(3)-C(4)	120.9(14)
Mn-O(1)	3.103(5)	Mn-O(2)	1.869(4)	C(3)-C(4)-C(5)	118.6(13)	C(4)-C(5)-C(6)	121.5(8)
Mn-N(1)	1.985(5)	Mn-N(2)	1.982(9)	C(5)-C(6)-C(1)	119.2(11)	C(5)-C(6)-C(7)	118.6(7)
Mn-N(3)	2.165(5)	O(1)-C(1)	1.327(13)	C(1)-C(6)-C(7)	121.9(10)	C(6)-C(7)-N(1)	125.1(7)
C(1)-C(2)	1.388(18)	C(2)-C(3)	1.367(19)	Mn-N(1)-C(7)	124.9(6)	Mn-N(1)-C(8)	113.0(7)
C(3)-C(4)	1.386(13)	C(4)-C(5)	1.382(22)	C(7)-N(1)-C(8)	121.9(7)	N(1)-C(8)-C(9)	109.1(7)
C(5)-C(6)	1.395(17)	C(6)-C(7)	1.437(17)	C(8)-C(9)-N(2)	110.1(9)	Mn-N(2)-C(9)	112.8(7)
N(1)-C(7)	1.273(16)	N(1)-C(8)	1.471(16)	Mn-N(2)-C(10)	126.8(5)	C(9)-N(2)-C(10)	120.2(9)
C(8)-C(9)	1.453(20)	N(2)-C(9)	1.469(9)	N(2)-C(10)-C(11)	124.5(10)	C(10)-C(11)-C(12)	116.9(9)
N(2)-C(10)	1.281(13)	C(10)-C(11)	1.432(8)	C(10)-C(11)-C(16)	123.1(9)	C(12)-C(11)-C(16)	119.9(6)
C(11)-C(12)	1.400(17)	C(11)-C(16)	1.406(14)	C(11)-C(12)-C(13)	120.3(11)	C(12)-C(13)-C(14)	119.7(12)
C(12)-C(13)	1.376(10)	C(13)-C(14)	1.387(18)	C(14)-C(15)-C(16)	120.7(9)	C(15)-C(16)-O(2)	118.0(9)
C(14)-C(15)	1.366(17)	C(15)-C(16)	1.406(8)	C(15)-C(16)-C(11)	118.2(9)	O(2)-C(16)-C(11)	123.6(6)
O(2)-C(16)	1.317(13)			Mn-O(2)-C(16)	129.5(5)		
(b) Copper site				(b) Copper site			
Cu-O(3)	1.884(8)	Cu-N(4)	2.014(7)	O(3)-Cu-N(4)	99.5(3)	O(3)-Cu-N(6)	96.3(3)
Cu-N(5)	1.941(11)	Cu-N(6)	1.924(5)	N(4)-Cu-N(5)	81.0(3)	N(5)-Cu-N(6)	82.9(3)
N(3)-C(17)	1.355(15)	N(3)-C(18)	1.362(13)	N-N(3)-C(18)	126.4(8)	Mn-N(3)-C(17)	127.7(6)
N(4)-C(17)	1.325(8)	N(4)-C(19)	1.364(16)	C(17)-N(3)-C(18)	105.5(7)	N(4)-C(17)-N(3)	112.2(10)
C(19)-C(18)	1.374(13)	C(19)-C(20)	1.420(10)	C(17)-N(4)-C(19)	105.8(8)	Cu-N(4)-C(17)	144.3(9)
N(5)-C(20)	1.276(16)	N(5)-C(21)	1.463(9)	Cu-N(4)-C(19)	109.7(4)	N(4)-C(19)-C(20)	109.7(4)
C(21)-C(22)	1.450(22)	N(6)-C(22)	1.451(15)	N(4)-C(19)-C(18)	108.5(8)	C(18)-C(19)-C(20)	134.3(13)
N(6)-C(24)	1.309(16)	C(24)-C(23)	1.504(11)	N(3)-C(18)-C(19)	107.8(11)	C(19)-C(20)-N(5)	114.4(12)
C(24)-C(25)	1.426(17)	C(25)-C(26)	1.371(9)	Cu-N(5)-C(20)	117.2(6)	Cu-N(5)-C(21)	116.4(9)
C(26)-C(27)	1.505(19)	O(3)-C(26)	1.293(13)	C(20)-N(5)-C(21)	126.2(11)	N(5)-C(21)-C(22)	110.2(11)
				C(21)-C(22)-N(6)	114.0(7)	Cu-N(6)-C(22)	115.3(7)
Bond angles (deg)				Cu-N(6)-C(24)	120.6(7)	C(22)-N(6)-C(24)	120.6(7)
				N(6)-C(24)-C(23)	120.3(10)	N(6)-C(24)-C(25)	123.3(7)
(a) Manganese site				C(23)-C(24)-C(25)	116.3(7)	C(24)-C(25)-C(26)	125.6(7)
O(1)-Mn-O(2)	93.1(2)	O(1)-Mn-N(1)	90.1(3)	C(25)-C(26)-C(27)	118.2(11)	C(25)-C(26)-O(3)	115.5(6)
O(2)-Mn-N(2)	91.3(2)	N(1)-Mn-N(2)	82.2(3)	C(27)-C(26)-O(3)	126.2(11)	Cu-O(3)-C(26)	123.8(5)
O(1)-Mn-N(3)	99.1(3)	O(2)-Mn-N(3)	97.9(2)				

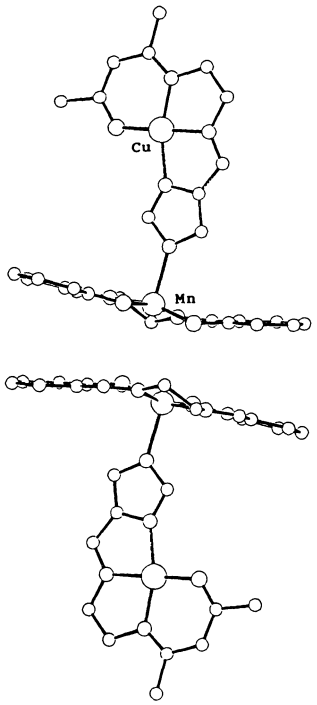

Fig. 2. Arrangement of two cations related by a center of symmetry, showing weak interactions between Mn and O(3)* with out-of-plane fashion.

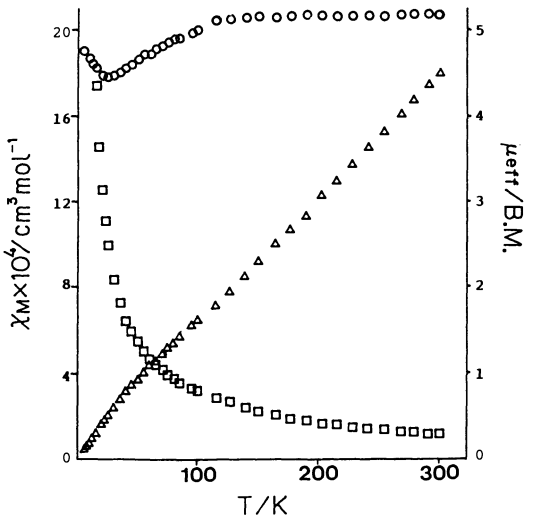

Fig. 3. Temperature dependence of the magnetic susceptibility per molecule (□), the reciprocal magnetic susceptibility per molecule (△), and the effective magnetic moment (○).

cially longer than the corresponding Mn-O bonds of the related manganese(III) complexes [Mn(HIm)(salen)]ClO_4 (2.635(3) Å)[24] and [Mn(hapacen)H_2O]ClO_4(2.305(2) Å),[27] where hapacen denotes the condensation product of acetylacetone, ethylenediamine, and *o*-hydroxyacetophenone with the mole ratio 1 : 1 : 1.

Magnetic Property. The magnetic behavior of the complex is shown in Fig. 3 in the form of the χ_M vs. T, $1/\chi_M$ vs. T, and μ_{eff} vs. T plots, where χ_M denotes the magnetic susceptibility per molecule, μ_{eff} the effective magnetic moment per molecule, and T the absolute temperature. The numerical values of the observed magnetic data are given in the supplementary material.

The effective magnetic moment per molecule at room temperature, 5.17 B.M., is nearly equal to the spin-only value of dinuclear system (5.20 B.M.) assuming no magnetic interaction between high-spin manganese(III) (S_1=2) and copper(II) (S_2=1/2) ions. As the temperature is lowered, the moment decreases gradually from 5.17 B.M. at 300.2 K, reaches the minimum value 4.43 B.M. at 24.9 K, and then increases to 4.73 B.M. at 4.2 K, indicating antiferromagnetic behavior at the higher temperature region and ferromagnetic behavior at the lower temperature region. There are two magnetic interactions which could mainly contribute to this result, i.e., intradinuclear Mn-Cu and interdinuclear Mn-Mn interactions.

First, the magnetic interaction between manganese(III) and copper(II) ions through an imidazolate group is compared with that of the analogous imidazolate-bridged manganese(III)-copper(II) complex [Mn(L)Cu(A)]BPh_4,[22] in which no intermolecular Mn-Mn interaction is feasible because of the completion of six-coordination, where H_2L denotes a quinquedentate ligand 4-methyl-*N*,*N*′-disalicylidene-4-azaheptane-1,7-diamine. The magnetic moment decreases gradually from 5.11 B.M. at 299 K to 3.31 B.M. at 4.3 K through an inflection point 3.86 B.M. at 20 K. In this case the magnetic behavior can be explained by antiferromagnetic coupling between high-spin manganese(III) and copper(II) ions and the zero-field splitting of the spin ground state.

Magnetic interaction between two manganese(III) ions through phenoxo-oxygen atoms similar to the present system[27] can be seen in [Mn(hapacen)H_2O]-ClO_4.[28] Its magnetic moment decreases gradually from 4.84 B.M. at 298 K to 1.70 B.M. at 4.4 K and can be well reproduced by the spin-Hamiltonian $H=-2JS_1S_2$ (S_1=S_2=2) with the parameters of J=−1.68 cm^{-1} and g=2.01.

On the basis of the above facts one could only expect antiferromagnetic interaction for the present complex. At present, we could not yet elucidate the origin of ferromagnetic behavior of the complex and more structural and magnetic data of more complexes are needed to settle the problem.

We thank for the financial support from the Ministry of Education, Science and Culture (No. 63740342).

References

1) J. S. Richardson, K. A. Thomas, B. H. Rubin, and D. C. Richardson, *Proc. Natl. Acad. Sci. U.S.A.*, **72**, 1349 (1975).
2) M. F. Tweedle, L. J. Wilson, L. Garcis-Iriguez, G. T. Babcock, and G. J. Palmer, *J. Biol. Chem.*, **253**, 8065 (1978).

3) O. Kahn, "Structure and Bonding," Springer-Verlag, Berlin, Heidelberg (1987), Vol. 68, pp. 89—167.
4) C. O'Young, J. C. Dewan, H. R. Lilienthal, and S. J. Lippard, *J. Am. Chem. Soc.*, **100**, 7291 (1978).
5) R. N. Katz, G. Kolks, and S. J. Lippard, *Inorg. Chem.*, **19**, 3845 (1980).
6) G. Kolks, C. R. Frihart, P. K. Coughlin, and S. J. Lippard, *Inorg. Chem.*, **20**, 2933 (1981).
7) J. C. Dewan and S. J. Lippard, *Inorg. Chem.*, **19**, 2079 (1980).
8) G. Kolks, S. J. Lippard, J. V. Wasczak, and H. R. Lilienthal, *J. Am. Chem. Soc.*, **104**, 717 (1982).
9) M. Suzuki, H. Kanatomi, H. Koyama, and I. Murase, *Inorg. Chim. Acta*, **L41**, 44 (1980).
10) B. K. S. Lundberg, *Acta Chem. Scand.*, **26**, 3902 (1972).
11) K. Matsumoto, S. Ooi, Y. Nakao, W. Mori, and A. Nakahara, *J. Chem. Soc., Dalton Trans.*, **1981**, 2045.
12) M. G. B. Drew, M. McCann, and S. M. Nelson, *J. Chem. Soc., Dalton Trans.*, **1981**, 1868.
13) C. Benelli, R. K. Bunting, D. Gatteschi, and C. Zanchini, *Inorg. Chem.*, **23**, 3074 (1984).
14) A. Bencini, C. Benelli, D. Gatteschi, and C. Zanchini, *Inorg. Chem.*, **25**, 1748 (1986).
15) S. E. Dessens, C. L. Merrill, R. J. Saxton, R. L. Ilaria, J. W. Lindsey, and L. J. Wilson, *J. Am. Chem. Soc.*, **104**, 4357 (1982).
16) T. Prosperi and A. A. G. Tomlinson, *J. Chem. Soc., Chem. Commun.*, **1979**, 196.
17) R. J. Saxton and L. J. Wilson, *J. Chem. Soc., Chem. Commun.*, **1984**, 359.
18) J. P. Costes, J. F. Serra, F. Dahan, and J. P. Laurent, *Inorg. Chem.*, **25**, 2790 (1986).
19) N. Matsumoto, H. Murakami, T. Akui, J. Honbo, H. Ōkawa, and A. Ohyoshi, *Bull. Chem. Soc. Jpn.*, **59**, 1609 (1986).
20) N. Matsumoto, T. Akui, H. Murakami, J. Kanesaka, A. Ohyoshi, and H. Ōkawa, *J. Chem. Soc., Dalton Trans.*, **1988**, 1021.
21) N. Matsumoto, J. Kanesaka, A. Ohyoshi, M. Nakamura, S. Kohata, and H. Ōkawa, *Bull. Chem. Soc. Jpn.*, **60**, 3056 (1987).
22) N. Matsumoto, Y. Maeda, H. Ōkawa, T. Akui, T. Kawaji, A. Ohyoshi, M. Kodera, H. Ohshio, and S. Kida, *J. Chem. Soc., Dalton Trans.*, **1989**, 943.
23) N. Matsumoto, K. Inoue, H. Ōkawa, and S. Kida, *Chem. Lett.*, **1989**, 1079.
24) N. Matsumoto, N. Takemoto, A. Ohyoshi, and H. Ōkawa, *Bull. Chem. Soc. Jpn.*, **61**, 2984 (1988).
25) "International Tables for X-Ray Crystallography," Kynoch Press, Birmingham (1974), Vol. 4.
26) T. Sakurai and K. Kobayashi, *Rikagaku Kenkyusho Houkoku*, **55**, 69 (1979); S. Kawano, *Rep. Comput. Cent. Kyushu Univ.*, **13**, 39 (1980).
27) N. Matsumoto, Z. J. Zhong, H. Ōkawa, and S. Kida, *Inorg. Chim. Acta*, **160**, 153 (1989).
28) B. J. Kennedy and K. S. Murray, *Inorg. Chem.*, **24**, 1552 (1985).

Cobalt(III) Complexes with Quadridentate Ligands. X.[1] The Preparation and Properties of Isomers of the Salicylaldehydato(quadridentate amine)cobalt(III) Complexes

Eiko TOYOTA and Yoshihisa YAMAMOTO*
Faculty of Pharmaceutical Sciences, Higashi Nippon Gakuen University,
Ishikari-Tobetsu, Hokkaido 061-02
(Received June 10, 1989)

In a recent study, *t*- and *p*-salicylaldehydato[tris(2-aminoethyl)amine]cobalt(III) complexes, *t*- and *p*-[Co(salad)tren]$Cl_2 \cdot H_2O$, and *cis*-β_1- and β_2-*RR,SS*-salicylaldehydato(quadridentate amine)cobalt(III) complexes, *cis*-β_1- and β_2-*RR,SS*-[Co(salad)L]$Cl_2 \cdot nH_2O$ (L: 2,3,2-tet; 3,2,3-tet), have been obtained from a reaction mixture of [$CoCl_2$L]$Cl \cdot nH_2O$ (L: tren; 2,3,2-tet; 3,2,3-tet), Ag_2O, and salicylaldehyde. Two isomers were separated for each complex by SP-Sephadex C-25 column chromatography. The formation ratio of *t*- to *p*-isomers was ca. 1 : 3. The *t*- and *p*-configurations have been established by their absorption and ^{1}H NMR spectra. On the other hand, the formation ratio of cis-β_1 to β_2-*RR,SS*-isomers was ca. 1 : 1 for both L=2,3,2-tet and 3,2,3-tet ligands. Their configurations have been established by their IR, absorption, and NMR spectra. The corresponding cis-α-isomer could not be obtained. Isomerization between *t*- and *p*-isomers or cis-β_1- and β_2-isomers was not observed in water at room temperature. The formation ratio and the absorption spectra of the complexes are different from those of the corresponding salicylato(quadridentate amine)cobalt(III) chloride hydrate, [Co(sal)L]$Cl \cdot nH_2O$ (L: tren; 2,3,2-tet; 3,2,3-tet), previously reported. These differences have been attributed to a carbonyl bond between the carbonyl oxygen of the formyl group and a cobalt atom in the complexes.

Previously, we were concerned with the preparation and properties of isomers of the *cis*-β-salicylaldehydato(triethylenetetramine)cobalt(III) dichloride dihydrate,[2] *cis*-β-[Co(salad)trien]$Cl_2 \cdot 2H_2O$. The corresponding cis-α-isomer has not yet been obtained. The formation of the cis-α-isomer might be due to the configurations of the coordinated quadridentate tetramine ligands and to the coordinate atom of the coordinated organo ligands. We selected two ligands of 3,7-diazanonane-1,9-diamine (abbreviation: 2,3,2-tet) and 4,7-diazadecane-1,10-diamine (abbreviation: 3,2,3-tet) which are relatively strain-free[3,4] compared with trien (2,2,2-tet) ligand from their molecular models. On the other hand, the carbonyl oxygen of the formyl group of the salicylaldehydato (formylphenolato) ligand forms a carbonyl bond to a cobalt atom. This property is different from the carbonyl oxygen of the carboxyl group of salicylato and thiosalicylato (*o*-mercaptobenzoato) ligands. Then, *cis*-α-salicylaldehydatocobalt(III) complexes with 2,3,2-tet and 3,2,3-tet ligands may be obtained. Further, the preparation and properties of octahedral salicylaldehydatocobalt(III) complexes with amine ligands have not been studied, except for *cis*-β-[Co(salad)trien]$Cl_2 \cdot 2H_2O$, because salicylaldehyde reacts with ammine, *N*-alkyl (or *N*-aryl) amine, ethylenediamine, and quadridentate amine, and yields to the corresponding Schiff base ligands.[5-10] Thus, the present paper deals with the preparation and properties of the mixed-ligand cobalt(III) complexes with salicylaldehydato and tris(2-aminoethyl)amine (abbreviation: tren), 2,3,2-tet or 3,2,3-tet ligands as well as with the assignments of the configurations of these complexes.

Experimental

Measurements. The magnetic susceptibilities were measured by Faraday's method using a magnetic balance (Shimadzu) at room temperature. The electric conductivities in aqueous solutions were determined by the use of a conductometric meter, CM-30 (Shimadzu) at room temperature. The IR spectra were recorded in potassium bromide disks with a 270-30 spectrophotometer (Hitachi). The visible absorption spectra were recorded with a Shimadzu UV-210 recording spectrophotometer. The NMR spectra were recorded with an FX90Q apparatus (JEOL) for ^{1}H NMR and an FX-60 apparatus (JEOL) for ^{13}C NMR. The melting points were measured on a MP-500D apparatus (Yanako).

Preparation of Complexes. Dichloro[tris(2-aminoethyl)amine]cobalt(III) Chloride Hydrate, [$CoCl_2$(tren)]$Cl \cdot H_2O$ (1) and *trans*-Dichloro(3,7-diazanonane-1,9-diamine)cobalt(III) Chloride Hydrates, *trans*-[$CoCl_2$(2,3,2-tet)]$Cl \cdot 2.5H_2O$ (2), *trans*-Dichloro(4,7-diazadecane-1,10-diamine)cobalt(III) Chloride Hydrate, *trans*-[$CoCl_2$(3,2,3-tet)]$Cl \cdot H_2O$ (3): Complexes **1** and **2**, **3** were prepared by the methods of Kimura,[11] and Bosnich,[3,12] respectively.

***t*-Salicylaldehydato[tris(2-aminoethyl)amine]cobalt(III) Dichloride Hydrate (4) and *p*-Salicylaldehydato[tris(2-aminoethyl)amine]cobalt(III) Dichloride Hydrate (5):** Complex **1** (5.0 g, 15.17 mmol) was added to moistened fresh Ag_2O, which was made from silver nitrate (5.17 g, 30.43 mmol) and potassium hydroxide (1.71 g, 30.48 mmol). The mixture was stirred for several minutes at room temperature; then, 10 cm^3 of water was added to the mixture. The mixture was stirred for about 30 min at 60 °C, and the precipitated silver chloride was filtered off and washed with a small amount of water. The methanol solution (20 cm^3) of salicylaldehyde (1.85 g, 15.15 mmol) was added, drop by drop, to the reddish-violet filtrate. The solution was stirred at room temperature for 6 h and was then concentrated on a rotary evaporator and dried. Yield: orange complex (a

mixture of **4** and **5**) 3.4 g. The separation of complexes **4** and **5** from the orange complex of 0.5 g was achieved by a column of ion-exchange resin (SP-Sephadex C-25, ϕ2.5×40 cm). On elution with 0.1 mol dm^{-3} NaCl, the effluent of the first orange band (complex **5**, *p*-isomer) and the second red band (complex **4**, *t*-isomer) was collected and concentrated on a rotary evaporator, and the precipitated NaCl was removed by filtration. Complexes **4** and **5** were recrystallized from methanol-ether. Yields: 0.47 g (7.5%) for **4**, 1.36 g (21.6%) for **5**. Found **4**: C, 37.77; H, 6.23; N, 13.76; Cl, 16.85%. **5**: C, 37.30; H, 6.31; N, 13.73; Cl, 17.34%. Calcd for $CoC_{13}H_{25}N_4O_3Cl_2$ (MW 415.20) C, 37.60; H, 6.07; N, 13.50; Cl, 17.08%. Dp: 188—189 °C for **4**, 191—193 °C for **5**. Λ=245 for **4**, 250 S cm^2 mol^{-1} for **5** in water.

***cis*-β-Salicylaldehydato(3,7-diazanonane-1,9-diamine)-cobalt(III) Dichloride Hydrate:** To a mixture of complex **2** (5.0 g, 13.49 mmol) and Ag_2O (26.96 mmol) was added salicylaldehyde (1.64 g, 13.43 mmol) in methanol (20 cm^3) according to the procedure for complexes **4** and **5**. The solution was stirred at room temperature for 20 h and was then concentrated on a rotary evaporator. The concentrated solution was injected onto an alumina column. Upon elution with methanol, the effluent of the first red band was collected and concentrated. Yield: orange complex (a mixture of **6** and **7**) 3.8 g.

***cis*-β_1-Salicylaldehydato(3,7-diazanonane-1,9-diamine)-cobalt(III) Dichloride Dihydrate (6) and *cis*-β_2-Salicylaldehydato(3,7-diazanonane-1,9-diamine)cobalt(III) Dichloride Dihydrate (7):** The separation of complexes **6** and **7** from the orange complex of 0.5 g was achieved by a column of ion-exchange resin (SP-Sephadex C-25, ϕ2.5×70 cm). Upon elution with 0.1 mol dm^{-3} NaCl, the effluents of the upper and lower layers of the orange band were collected and concentrated, respectively. The separated NaCl was removed by filtration. The isolation of complex **6** from the upper layer was achieved by a column of ion-exchange resin by the above method, i.e., the upper layer of orange band was collected again and concentrated. The separated NaCl was removed. Complex **6** was recrystallized from methanol-ether. This procedure was repeated again. The isolation of complex **7** from the lower layer was achieved according to the same procedure for complex **6**. Yields: 0.76 g (12.6%) for **6**, 1.02 g (16.9%) for **7**. Found **6**: C, 37.30; H, 6.41; N, 12.37; Cl, 16.10%. **7**: C, 37.89, H, 6.66; N, 12.25; Cl, 16.08%. Calcd for $CoC_{14}H_{29}N_4O_4Cl_2$ (MW 447.24) C, 37.60; H, 6.54; N, 12.53; Cl, 15.85%. Dp: 201—203 °C for **6**, 206—208 °C for **7**. Λ=225 for **6**, 230 S cm^2 mol^{-1} for **7** in water. IR spectra **6**: 1030, 1045, 1075, 1085 cm^{-1}; 3070, 3100, 3120, 3200 cm^{-1}. **7**: 1030, 1045, 1075, 1085 cm^{-1}; 3060, 3100, 3130, 3200 cm^{-1}.

***cis*-β_1-Salicylaldehydato(4,7-diazadecane-1,10-diamine)-cobalt(III) Dichloride Hydrate (8) and *cis*-β_2-Salicylaldehydato(4,7-diazadecane-1,10-diamine)cobalt(III) Dichloride Hydrate (9):** A mixture of complexes **8** and **9** was prepared from the reaction mixture of complex **3** (5.0 g, 13.98 mmol), flesh Ag_2O (3.4 g, 14.67 mmol), and salicylaldehyde (1.8 g, 14.74 mmol). Complexes **8** and **9** were isolated according to the method for **6** and **7**, and recrystallized from methanol-ether. Yields: 0.93 g (15.0%) for **8**, 1.26 g (20.3%) for **9**. Found **8**: C, 40.86; H, 6.92; N, 12.40; Cl, 16.16%. **9**: C, 40.96; H, 6.40; N, 12.79; Cl, 16.07%. Calcd for $CoC_{15}H_{29}N_4O_3Cl_2$ (MW 443.26) C, 40.64; H, 6.59; N, 12.64; Cl, 16.00%. Dp: 196—198 °C for **8**, 192—194 °C for **9**. Λ=237 for **8**, 233 S cm^2 mol^{-1} for **9** in water. IR spectra **8**: 1035, 1065, 1080, 1090 cm^{-1}; 3070, 3100, 3120, 3170 cm^{-1}. **9**: 1015, 1040, 1060, 1070 cm^{-1}; 3070, 3100, 3130, 3170 cm^{-1}.

Solubility. All complexes were very soluble in water, methanol, and DMSO, and slightly soluble in ethanol but insoluble in common organic solvents, such as ether and acetone.

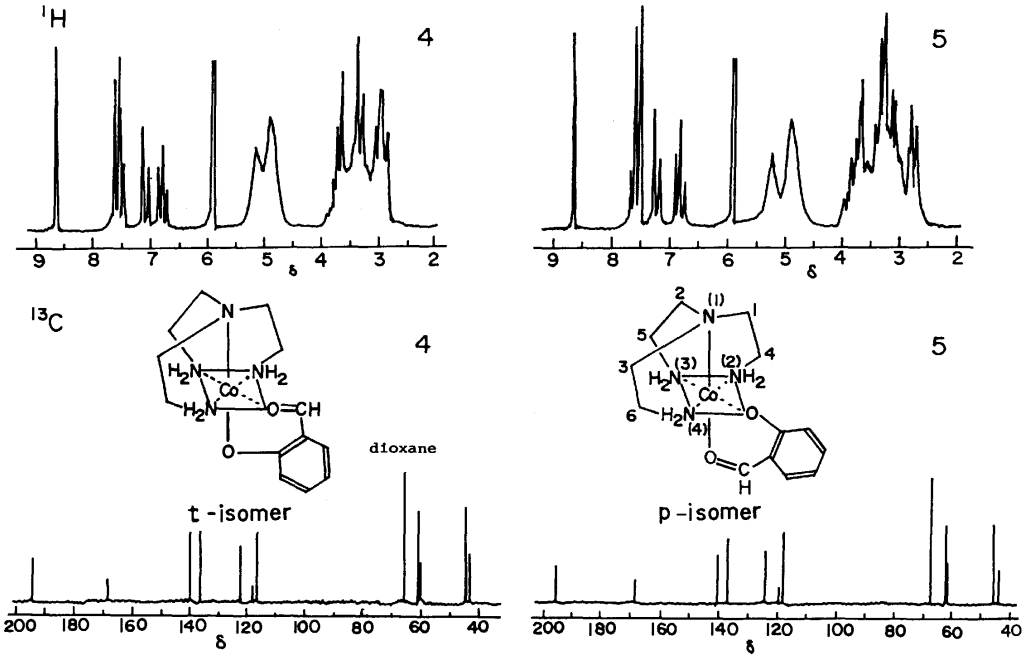

Fig. 1. The *t* and *p* configuration of [Co(salad)tren]$Cl_2 \cdot H_2O$, and ^{1}H and ^{13}C NMR spectra of complexes **4** and **5**.
4: *t*-[Co(salad)tren]$Cl_2 \cdot H_2O$; **5**: *p*-[Co(salad)tren]$Cl_2 \cdot H_2O$. Solvent: ^{1}H NMR, 1.8 mol dm^{-3} D_2SO_4; ^{13}C NMR, D_2O.

Results and Discussion

***t*- and *p*-Salicylaldehydato(tren)cobalt(III) Dichloride Hydrate (*t*: 4, *p*: 5):** Octahedral salicylaldehydato(tren)cobalt(III) complexes exist in two isomeric forms of *t*- and *p*-isomers,[13] as shown in Fig. 1. A mixture of *t*- and *p*-salicylaldehydato(tren)cobalt(III) dichloride hydrate has been obtained from a reaction mixture of $[CoCl_2(tren)]Cl$ (**1**), Ag_2O, and salicylaldehyde. Two geometrical isomers of *t*- (**4**) and *p*- (**5**) of the complex were separated by SP-Sephadex C-25 column chromatography. The formation ratio of **4** to **5** was ca. 1 : 3. The isomerization between **4** and **5** was not observed in water and methanol at room temperature. The electric conductivities for **4** and **5** in aqueous solutions were 245 and 250 $S\,cm^2\,mol^{-1}$, respectively.

The absorption spectra of **4** and **5** were measured in water (Table 1). The absorption bands at around 410 and 500 nm were assigned to a specific absorption band and the first d-d absorption band, respectively.

The ^{13}C NMR spectra of **4** and **5** were measured in D_2O (Fig. 1 and Table 2). Four signals have been observed for the tren ligand and seven signals for the salicylaldehydato ligand. The signals at δ 44.2 and 45.5 for **4** were assigned to the NH_2- side methylene carbons, and those at δ 61.3 and 62.1 were assigned to the -N side methylene carbons.[14] The signals at δ 44.2 and 61.3 were assigned to the C(5) and C(2) carbons, respectively, and those at δ 45.5 and 62.1 were assigned to the C(4), C(6) and C(1), C(3) carbons,[14] respectively. The spectral data of **5** are shown in Table 2.

The ^1H NMR spectra of **4** and **5** were measured in 1.8 mol dm^{-3} D_2SO_4 (Fig. 1). The signals of the NH_2- side and -N side methylene protons, ring and formyl group protons of **4** and **5** were assigned by comparisons with those of *t*- and *p*-salicylato(tren)-

Table 1. ^1H NMR and Absorption Spectra of Complexes **4**—**9** and **17**, **18**

^1H Complex No. (isomer)	$N(CH_2CH_2NH_2)_3$ δ			
	NH_2- side methylene protons	NH_2-+-N side methylene protons	-N side methylene protons	$N(2)H_2$+$N(3)H_2$
4 (*t*)	2.70—3.13(4H)	3.13—3.95(8H)		4.90(4H)
5 (*p*)	2.55—2.86(2H)	2.86—3.45(6H)	3.45—4.00(4H)	4.80(4H)

	$NH_2(CH_2)_xNH(CH_2)_yNH(CH_2)_zNH_2$ δ					
x, *y*, *z* (isomer)	Center methylene protons	NH_2- side methylene protons	NH- side methylene protons	$N(1)H_2$	$N(4)H_2$	N(3)H
6 2,3,2(β_1)	1.77—2.20(2H)	2.20—3.28(12H)		4.32(2H)	5.12(3H)	
7 2,3,2(β_2)	1.75—2.16(2H)	2.16—2.49(3H)	2.49—3.30(9H)	4.35(1H)4.60(1H)	5.12(3H)	
8 3,2,3(β_1)	1.45—2.26(6H)	2.26—3.22(10H)		3.54(1H)4.28(1H)	4.68(2H)	5.20(1H)
9 3,2,3(β_2)	1.42—2.07(4H)	2.07—2.56(6H)	2.56—3.22(6H)	3.61(1H)4.15—4.90(3H)		5.14(1H)
17 2,2,2(β_1)	—	2.42—3.40(12H)		4.40(2H)	4.98(2H)	6.20(1H)
18 2,2,2(β_2)	—	2.35—2.75(3H)	2.75—3.75(9H)	4.30(1H)4.43—4.92(2H)	5.08(1H)	6.15(1H)

^1H Complex No. (isomer)	$N(CH_2CH_2NH_2)_3$ δ	Salicylaldehydato δ		Absorption bands in water λ/nm (ε/$cm^{-1}\,mol^{-1}\,dm^3$)
	$N(4)H_2$	Ring protons	CHO	
4 (*t*)	5.10(2H)	6.7—7.7(4H)	8.65(1H)	415(2050) 500(235)
5 (*p*)	5.20(2H)	6.7—7.7(4H)	8.63(1H)	405(2100) 490(240)

x, *y*, *z* (isomer)	$NH_2(CH_2)_xNH(CH_2)_yNH(CH_2)_zNH_2$ δ	Salicylaldehydato δ		λ/nm (ε/$cm^{-1}\,mol^{-1}\,dm^3$)
	N(2)H [N(2)H+Ring protons]	Ring protons	CHO	
6 2,3,2(β_1)	6.31(1H)	6.6—7.7(4H)	8.54(1H)	412(1900) 500(260)
7 2,3,2(β_2)	6.32(1H)	6.6—7.7(4H)	8.50(1H)	412(1940) 495(240)
8 3,2,3(β_1)	6.23(1H)	6.7—7.8(4H)	8.49(1H)	410(1910) 510(220)
9 3,2,3(β_2)	6.20(1H)	6.6—7.7(4H)	8.60(1H)	410(1980) 505(200)
17 2,2,2(β_1)	[6.5—7.6(5H)]		8.48(1H)	418(2000) 500(292)
18 2,2,2(β_2)	[6.5—7.6(5H)]		8.59(1H)	418(1830) 500(270)

Solvent and standard: 1.8 mol dm^{-3} D_2SO_4, internal DSS (δ=0).

Table 2. ^{13}C NMR Spectra of Complexes **4**—**9**

Complex No.	$N(CH_2CH_2NH_2)_3$ δ				Salicylaldehydato δ						
	C(5)	C(4) C(6)	C(2)	C(1) C(3)	c-1	c-2	c-3	c-4	c-5	c-6	c-7
4	44.2	45.5	61.3	62.1	120.0	169.5	118.3	141.8	124.1	138.1	196.5
5	43.7	45.5	61.8	62.1	119.7	169.3	118.2	141.3	124.5	137.6	197.0

	$NH_2(CH_2)_xNH(CH_2)_yNH(CH_2)_zNH_2$ δ										
	c-5	c-2 c-8	c-1 c-9	c-3 c-7	c-4 c-6						
6	23.7	— —	[43.2 43.8]	[51.2 55.7]	[46.0 48.0]	120.2	170.2	118.2	141.5	124.2	137.7	196.3
7	23.5	— —	[43.3 43.5]	[51.0 55.7]	[45.2 47.2]	120.1	169.6	118.2	141.3	124.4	137.5	196.4
8	—	[21.6 27.1]	[36.5 38.4]	[44.7 48.3]	[48.3 53.4]	120.4	169.3	118.4	141.6	124.4	137.7	196.1
9	—	[21.8 27.0]	[37.4 38.1]	[45.0 47.7]	[48.5 53.5]	120.3	169.3	118.3	141.3	124.2	137.5	196.0

Solvent and standard: D_2O, internal dioxane (δ=67.4).
[ ]: The chemical shifts could not be assigned to the individual methylene carbon.

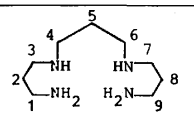

Quadridentate amine

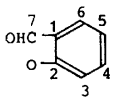

Salicylaldehydato

cobalt(III) chloride hydrate,[14] *t*- and *p*-[Co(sal)-tren]Cl·H_2O (*t*: **10**, *p*: **11**) (Table 1). The amine protons showed two peaks at δ 4.90 and 5.10 for **4** and δ 4.80 and 5.20 for **5** with an intesity ratio of 2:1. The signals at δ 4.90 for **4** and 4.80 for **5** were assigned to $N(2)H_2$ and $N(3)H_2$ protons.[14] Those at δ 5.10 for **4** and at δ 5.20 for **5** were assigned to the $N(4)H_2$ protons.[14]

The chemical shift (δ 4.80) of the proton signal of the NH_2 groups of **5** was at a higher field than that (δ 4.90) of **4**, i.e., the NH_2 group of **5** is considered to be in a position trans to the phenoxyl oxygen of the coordinated salicylaldehydato ligand, which is more electronegative than the formyl oxygen. Also, the methylene proton signals of **5** showed two very sharp peaks[14] in the δ 2.5—2.9 region, but those for **4** did not show the corresponding peaks. In addition, the first absorption band of **4** was at a longer wavelength than that of **5**. These properties of **4** and **5** are in agreement with those of **10** and **11**,[14] respectively. Thus, complexes **4** and **5** have been assigned to *t*- and *p*-isomers, respectively.

The color, melting point, formation ratio, and absorption spectra of **4** and **5** were different from those of **10** and **11**. The color of **4** and **5** was reddish-brown and orange, respectively, but that of **10** and **11** was russet and red, respectively. The melting points (ca. 190 °C) of **4** and **5** were lower than those (ca. 240 °C) of **10** and **11**. The formation ratio of *t*- to *p*-isomers was ca. 1:3 for **4** and **5**, but was ca. 3:1 for **10** and **11**. The specific absorption bands at around 410 nm of **4** and **5** were at longer wavelengths than those at around 330 nm of **10** and **11**, though the first absorption bands at 490—500 nm for **4** and **5** were at a shorter wavelength than those at 515—530 nm for **10** and **11**. These differences are attributed to a carbonyl bond, i.e., the corbonyl oxygen of the formyl group of **4** and **5** is bonded to a cobalt atom, but the carbonyl oxygen of the carboxyl group of **10** and **11** is not bonded to the cobalt atom.

***cis*-β-Salicylaldehydato(2,3,2-tet)cobalt(III) Dichloride Dihydrate (β1: 6, β2: 7) and *cis*-β-Salicylaldehydato-(3,2,3-tet)cobalt(III) Dichloride Hydrate (β1: 8, β2: 9):** Octahedral salicylaldehydato(quadridentate amine)-

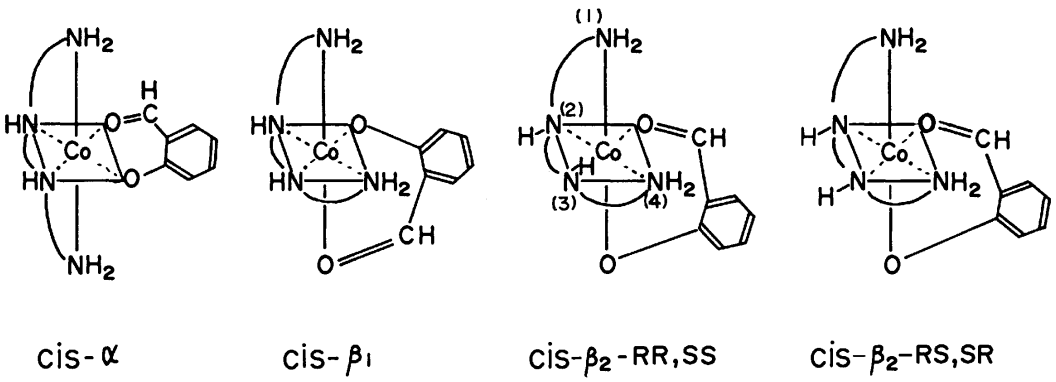

Fig. 2. The cis-α, β1, β2-*RR,SS*, and β2-*RS,SR* configurations of [Co(salad)(quadridentate amine)]cobalt(III) complexes.

cobalt(III) complexes exist in three geometrical isomers of cis-α, cis-β_1, and cis-β_2. The cis-β-isomers exist in two diastereoisomers of *RR,SS* and *RS,SR*, as shown in Fig. 2. *cis*-β-Salicylaldehydato(quadridentate amine)cobalt(III) dichloride hydrate has been obtained from a reaction mixture of *trans*-[$CoCl_2$(2,3,2-tet)]Cl·2.5H_2O (**2**) or *trans*-[$CoCl_2$(3,2,3-tet)]Cl·H_2O (**3**), Ag_2O, and salicylaldehyde. Complexes **6** and **7** or **8** and **9** were separated by SP-Sephadex C-25 column chromatography. Complexes **6—9** are highly hygroscopic. Complexes **8** and **9** were diamagnetic from the magnetic susceptibility. The electric conductivities for **6—9** in aqueous solutions were 225—237 S $cm^2 mol^{-1}$.

The absorption spectra of **6—9** were measured in water, as shown in Table 1. Their absorption bands at around 410 nm and 500 nm were assigned to the specific absorption band and the first absorption band, respectively.

The ^1H and ^{13}C NMR spectra of **6—9** were measured in 1.8 mol dm^{-3} D_2SO_4 and D_2O, respectively. Their center, NH_2- and NH- side methylene protons (and carbons) and salicylaldehydato protons (and carbons) and amine protons were assigned by comparisons with those of *cis*-β-salicylato(quadridentate amine)-cobalt(III) chloride hydrates,[15,16] *cis*-β-[Co(sal)L]Cl·$n H_2O$ (L: trien, β_1: **12**, β_2: **13**; 2,3,2-tet, β_1: **14**, β_2: **15**; 3,2,3-tet, β_2: **16**). Their chemical shifts are shown in Tables 1 and 2. The ^{13}C chemical shifts of the coordinated quadridentate amine ligands were difficult to assign to the individual carbon atoms, but the regions of the chemical shifts of the center, NH_2-, and NH-side methylene carbons were close to those of **12—16**.

The IR spectra of **6—9** showed four absorption bands in the NH_2 twisting region (990—1100 cm^{-1}) and four absorption bands in the NH stretching region (3000—3300 cm^{-1}). The ^{13}C NMR spectra of **6—9** showed 7—8 signals for the quadridentate amine ligand. They indicate that these complexes are assigned to the cis-β-form.[16,17]

A distinction between **6** and **7** was found in the ^1H NMR and absorption spectra. In the ^1H NMR spectra, the methylene proton signals of **6** in the δ 2.2—3.3 region could not be divided into two groups, but those of **7** could be divided into two groups, as shown in Fig. 3. The ε of the first absorption band of **6** was larger than that of **7**, and the band of **6** was at a longer wavelength than that of **7**. These results for **6** and **7** were similar to those of complexes **12**,[15] **14**,[16] and *cis*-β_1-salicylaldehydato(trien)cobalt(III) dichloride dihydrate,[2] *cis*-β_1-[Co(salad)trien]Cl_2·$2H_2O$ (**17**) and complexes **13**,[15] **15**,[16] and *cis*-β_2-[Co(salad)-trien]Cl_2·$2H_2O$ (**18**),[2] respectively. Thus, complexes **6** and **7** were assigned to the cis-β_1 and β_2-isomers, respectively. In complexes **8** and **9**, the ^1H NMR, absorption spectra, and the elution order of the chromatography of **8** and **9** were very close to those of **6**, **17** and **7**, **18**, respectively, i.e., **8** and **9** could be assigned to the cis-β_1 and β_2-isomers, respectively. Next, cis-β-isomer will adopt more stable *RR,SS* configurations; e.g., Buckingham et al. were interested in the stability between the cis-β-*RR,SS* and *RS,SR* configurations of Co(III) complexes with a trien ligand. The *RR,SS* configurations have been shown to be more stable

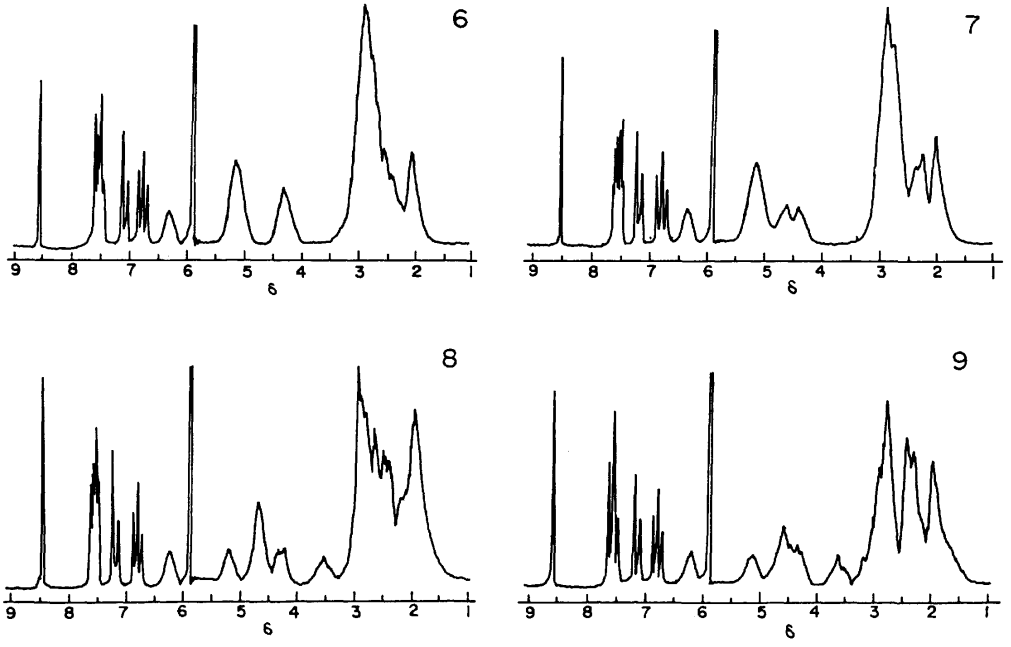

Fig. 3. The ^1H NMR spectra of complexes **6—9** in 1.8 mol dm^{-3} D_2SO_4.
6: *cis*-β_1-*RR,SS*-[Co(salad)2,3,2-tet]Cl_2·$2H_2O$; **7**: *cis*-β_2-*RR,SS*-[Co(salad)2,3,2-tet]-Cl_2·$2H_2O$; **8**: *cis*-β_1-*RR,SS*-[Co(salad)3,2,3-tet]Cl_2·H_2O; **9**: *cis*-β_2-*RR,SS*-[Co(salad)-3,2,3-tet]Cl_2·H_2O.

than the *RS,SR* configurations for a *cis*-β-[CoL_2(trien)]$^{n+}$ (L_2: Cl_2, $(H_2O)_2$, CO_3, gly).[18-20] Also, *cis*-β-[CoL(2,3,2-tet)]$^{n+}$ (L: oxalato, glycinato, alaninato, valinato, and sarcosinato),[21,22] *cis*-β-[Co(ox)(Me_2-2,3,2-tet)]$^+$,[23] and *cis*-β-[CoL(3,2,3-tet)]$^{n+}$ (L: oxalato, acetylacetonato, carbonato)[12,24] have been found to have *RR,SS* configurations by their CD spectra and X-ray diffractions. Thus, we suggest that the structures of **6—9** and **17**, **18** are assigned to the *RR,SS* configurations.

The corresponding cis-α isomer has not been obtained in this study and the corresponding studies.[2,15,16,25] However, *cis*-α-*RR,SS*-[Co(gly)L]$^{2+}$ (gly: $NH_2CH_2COO^-$; L: trien, 3,2,3-tet) has been reported.[22,26] This difference may be due to the coordinate atom of the chelated ligands. Thus, we suggest that the cis-α isomer may be obtained from a reaction mixture of the N-O^- chelate ligand with 2,3,2-tet or 3,2,3-tet ligand.

The color, melting point, and absorption spectra of **6—9** and **17**, **18** were different from those of **12—16**, such as the corresponding tren complexes. Especially, the cis-β_1 of **6**, **8**, and **17** could not be isomerized to the cis-β_2 of **7**, **9**, and **18**, respectively, in water, but the cis-β_1 of **12** and **14** are isomerized to the cis-β_2 of **13** and **15**, respectively,[14] in water at room temperature.

The preparation of the mixed-ligand metal complexes with salicylaldehydato and amine ligands has been difficult, because metal complexes with Schiff base ligands are obtained. In this study, it has been elucidated that the preparation of the mixed-ligand cobalt(III) complexes with salicylaldehydato ligand is dependent upon the reaction temperature. (*N,N'*-Disalicylidene-substituted quadridentate amine)cobalt(III) complexes,[10]

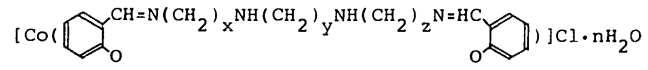

(*x,y,z*: 2,2,2; 2,3,2; 3,2,3; 3,3,3), were prepared from a reaction mixture of $[CoCl_2L]Cl \cdot nH_2O$ (L: quadridentate amine), Ag_2O, and salicylaldehyde in methanol at 50 °C. On the other hand, complexes **6—9**, **17**, and **18** were prepared at room temperature from the same reaction mixture.

References

1) Y. Yamamoto, E. Toyota, and S. Shimokawa, *Bull. Chem. Soc. Jpn.*, **62**, 2717 (1989).
2) Y. Yamamoto, E. Toyota, and S. Tsukuda, *Bull. Chem. Soc. Jpn.*, **58**, 1595 (1985).
3) B. Bosnich, R. D. Gillard, E. D. McKenzie, and G. A. Webb, *J. Chem. Soc. (A)*, **1966**, 1331.
4) M. D. Alexander and H. G. Hamilton, Jr., *Inorg. Chem.*, **8**, 2131 (1969).
5) Y. Yamamoto and E. Toyota, *Bull. Chem. Soc. Jpn.*, **57**, 2650 (1984).
6) B. O. West, *J. Chem. Soc.*, **1960**, 4944.
7) H. Nishikawa, S. Yamada, and R. Tsuchida, *Z. Naturforsch.*, Teil B, 78 (1962).
8) H. Nishikawa and S. Yamada, *Bull. Chem. Soc. Jpn.*, **37**, 1154 (1964).
9) M. Nakamura, H. Ōkawa, T. Inazu, and S. Kida, *Bull. Chem. Soc. Jpn.*, **55**, 2400 (1982).
10) Y. Yamamoto and S. Tsukuda, *Bull. Chem. Soc. Jpn.*, **58**, 1509 (1985).
11) E. Kimura, S. Young, and J. P. Collman, *Inorg. Chem.*, **9**, 1183 (1970).
12) B. Bosnich, J. M. Harrowfield, and H. Boucher, *Inorg. Chem.*, **14**, 815 (1975).
13) The designations *t* and *p* refer to the position of the carboxyl oxygen trans to a tertiary (*t*) or a primary (*p*) amine nitrogen of tren, respectively.
14) E. Toyota, Y. Yamamoto, and Y. Yamamoto, *Bull. Chem. Soc. Jpn.*, **61**, 3175 (1988).
15) Y. Yamamoto and E. Toyota, *Bull. Chem. Soc. Jpn.*, **52**, 2540 (1979).
16) Y. Yamamoto, H. Kudo, and E. Toyota, *Bull. Chem. Soc. Jpn.*, **56**, 1051 (1983).
17) D. A. Buckingham and D. Jones, *Inorg. Chem.*, **4**, 1387 (1965).
18) D. A. Buckingham, P. A. Marzilli, and A. M. Sargeson, *Inorg. Chem.*, **6**, 1032 (1967).
19) D. A. Buckingham, P. J. Cresswell, R. J. Dellaca, M. Dwyer, G. J. Gainsford, L. G. Marzilli, I. E. Maxwell, W. T. Robinson, A. M. Sargeson, and K. R. Turnbull, *J. Am. Chem. Soc.*, **96**, 1713 (1974).
20) D. A. Buckingham, M. Dwyer, G. J. Gainsford, V. Janson Ho, L. G. Marzilli, W. T. Robinson, A. M. Sargeson, and K. R. Turnbull, *Inorg. Chem.*, **14**, 1739 (1975).
21) G. R. Brubaker and D. P. Schaefer, *Inorg. Chem.*, **10**, 968 (1971).
22) G. R. Brubaker and D. P. Schaefer, *Inorg. Chem.*, **10**, 2170 (1971).
23) F. Mizukami, *Bull. Chem. Soc. Jpn.*, **48**, 472 (1975).
24) M. Saburi, C. Hattori, and S. Yoshikawa, *Inorg. Chim. Acta*, **6**, 427 (1972).
25) Y. Yamamoto, K. Yoshii, E. Toyota, and K. Konno, *Bull. Chem. Soc. Jpn.*, **62**, 724 (1989).
26) B. F. Anderson, J. D. Bell, D. A. Buckingham, P. J. Cresswell, G. J. Gainsford, L. G. Marzilli, G. B. Robertson, and A. M. Sargeson, *Inorg. Chem.*, **16**, 3233 (1977).

Gallium Coprecipitation Associated with Magnesium for Preconcentration of Trace Metals in Seawater

Tasuku AKAGI, Keiichiro FUWA,† and Hiroki HARAGUCHI*,††
Department of Chemistry, Faculty of Science, The University of Tokyo, 7-3-1, Hongo, Bunkyo-ku, Tokyo 113
†National Institute for Environmental Studies, 16-2, Tsukuba, Ibaragi 305
††Department of Applied Chemistry, Faculty of Engineering, Nagoya University, Chikusa-ku, Nagoya 464
(Received July 1, 1989)

The coprecipitation of trace metals with gallium has been investigated in detail especially with respects to the role of magnesium ion in saline or seawater. Gallium does not precipitate even at pH 9 when magnesium ion does not exist. The concentration of gallium in the precipitate increased with increasing that of magnesium in solution. The recoveries of trace metals also showed strong dependence on the concentrations of both gallium and magnesium in the aqueous solution.

Since the concentrations of trace metals in seawater are extremely low, preconcentration prior to analysis is necessary to determine these elements by the convenient analytical measurement method. Among a variety of preconcentration techniques for trace metals in seawater, coprecipitation technique has been widely employed.[1-12] Zirconium,[1] Fe,[2,3,6] Bi,[2,3] Co-APDC,[4,7] In,[8] La,[9] and Mg,[5,10,11] have been used as the coprecipitation reagents for preconcentration of analyte metals from seawater and/or brine samples.

The present authors developed a coprecipitation technique using gallium as a coprecipitation reagent[12] for preconcentration of trace metals in seawater in order to determine them simultaneously by inductively coupled plasma atomic emission spectrometry (ICP-AES). In the study, it was found that gallium precipitates between pH 5—6 and above pH 9 in seawater, while it does not precipitate between pH 7—8. Furthermore gallium did not precipitate in the river water even above pH 9. This characteristic features of gallium precipitation is very helpful for the preconcentration of trace metals in seawater because of negligibly small contamination from chemicals required for pH adjustment.

According to the present authors' survey, the reason why gallium does precipitate at pH 9 in seawater has not been investigated yet. In the present study, hence, the precipitate formation of gallium has been examined by using saline water samples with various compositions so as to elucidate the role of gallium coprecipitation in seawater.

Experimental

Apparatus. An ICP-AES spectrophotometer used for metal analysis was Plasma Atomcomp MK II from Jarrell Ash Co. The operating conditions of the ICP-AES instrument are summarized in Table 1. A double-beam spectrophotometer UV-210A (Shimadzu Co., Ltd.) was used to monitor the formation of the precipitates at the wavelength 660 nm, which was the same wavelength as that for convenient turbidity measurement. The length of the sample cell used was 10 cm and the width of the entrance slit was set at 2 mm. A pH meter model Ionalyzer 407A (Orion Research Inc.) was employed to adjust pH of the test solutions.

Chemicals. The chemicals used were of analytical reagent grade. All acids were of extra pure grade purchased from Wako Chemicals Co. The stock solutions for metals were prepared by dissolving the corresponding metals or oxides in the acids. One g of gallium metal (99.99%; Wako Chemicals Co.) was dissolved in 10 ml of (1+1) nitric acid and diluted to 200 ml with water. Sodium hydroxide solution (9 M; 1 M=1 mol dm^{-3}) used for pH adjustment was prepared from its salt (Suprapur; Merck).

Procedures. The test solution (100 ml) was prepared by dissolving the required amount of magnesium chloride (0, 5, 20, 100, 400 mg Mg/100 ml) in pure water. Then different amounts of gallium (0, 0.02, 0.1, 0.5, 2 mg) were added to all the test solutions. After stirring well, pH of all the test solutions was adjusted to 9 by adding sodium hydroxide solution. The precipitate formation was monitored at 660 nm by measuring turbidity. The precipitate was stood for 24 h, and then filtered with a Nuclepore filter. After washing with 3 ml of pure water, the precipitate collected on the filter was dissolved with 2.5 ml of 1 M hydrochloric acid, and diluted exactly to 5 ml with water. The final solution was supplied to the ICP-AES measurement. In the recovery test, analytes (10 μg for each element) were added to the above solutions.

Table 1. Instrumental Components and Operating Conditions

Spectrometer	Jarrell-Ash Plasma Atomcomp MK II
frequency	27.12 MHz
r.f. output power	1.1 kw
coolant gas	argon 15 l min^{-1}
auxiliary gas	argon 0.5 l min^{-1}
carrier gas	argon 1.0 l min^{-1}
observation height	17 mm above work coil
Nebulizer	Cross-flow type
Polychromater	Paschen-Runge type (75 cm focal length)
grating	2400 grooves/mm
reciprocal linear dispersion	0.54 nm/mm at 270 nm
entrance slit width	25 μm
exit slit width	50 μm
Monochromator	Ebert type (50 cm focal length)

Results and Discussion

pH Dependence of Gallium Precipitation. Since gallium is an amphoteric metallic element, it dissolves in aqueous solution at both low and high pH region. The equilibria and their dissociation constants of gallium hydroxide in solution are as follows.[13]

$$Ga(OH)_3(s)=Ga^{3+}+3OH^- \qquad K=5\times10^{-37}$$
$$Ga(OH)_3(s)=GaO_2^-+H^++H_2O \qquad K=10^{-15}$$

The pH dependences of the precipitate formations for the solutions containing gallium and/or magnesium were examined by measuring transmittance at 660 nm. The experimental results are shown in Fig. 1-(a), (b), and (c). As is shown in Fig. 1-(a), gallium formed the precipitate in aqueous solution at the pH range between 4 and 6, which was observed as the slight decrease of the transmittance of the solution. The pH dependence of the precipitate formation of magnesium in aqueous solution, in which the concentration of magnesium is the same as those in natural seawater, i.e., 1300 mg of Mg/l, is shown in Fig. 1-(b). The transmittance of the solution began to decrease markedly from pH 10. At pH 11 the precipitation of magnesium took place so significantly that the transmitted light could be hardly detected.

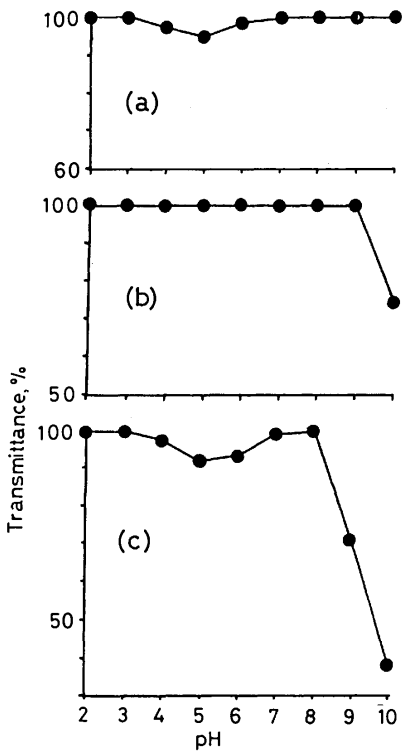

Fig. 1. Precipitation behaviors of gallium and/or magnesium in aqueous solution as a function of pH. Precipitation was monitored as transmittance at 660 nm.
(a); 10 mg of gallium/l, (b); 1300 mg of magnesium/l, (c); 10 mg of gallium/l and 1300 mg of magnesium/l.

The transmittance of the solution containing both gallium (10 mg l^{-1}) and magnesium (1300 mg l^{-1}) at various pH is shown in Fig. 1-(c). Precipitation occurred between pH 4—6 and above pH 9. The precipitation behavior below pH 8 was almost identical to the result obtained for only the gallium solution (see Fig. 1-(a)). On the other hand, above pH 9 the behavior was similar to that of the magnesium solution (Fig. 1-(b)), but the precipitation took place from the lower pH. It should be noted that the mixed solution of magnesium and gallium precipitated at pH 9, where the solution containing only magnesium did not.

pH Dependence of Gallium Precipitation in Seawater Martix Solution. The amounts of seawater-matrix elements (sodium, potassium, calcium, and magnesium) and gallium in the precipitate were analyzed as the pH function, when the gallium coprecipitation was applied to seawater. The compositions of the precipitate were measured by ICP-AES as the relative concentration, where the amount of each element at pH 9 was defined as 1. The experimental results are shown in Fig. 2. In the pH range between 7 and 8, no precipitation took place, and then test was not made. Gallium precipitated almost quantitatively between pH 5 and 6 and above pH 9, as can be seen in Fig. 2. Among the matrix elements in seawater, magnesium and calcium in the precipitate showed a strong dependence on pH around pH 9. The amount of Ca in the precipitate started to increase suddenly above pH 9.3. The amounts of magnesium and gallium in the precipitate at pH 9 were about 5 mg, when 5 mg of gallium is added to 1 l of seawater. They were rather larger than the amounts of calcium, sodium, and potassium in the precipitate (0.05 mg, 0.005 mg, and 0.05 mg, respectively). The strong dependence of the magnesium content in the precipi-

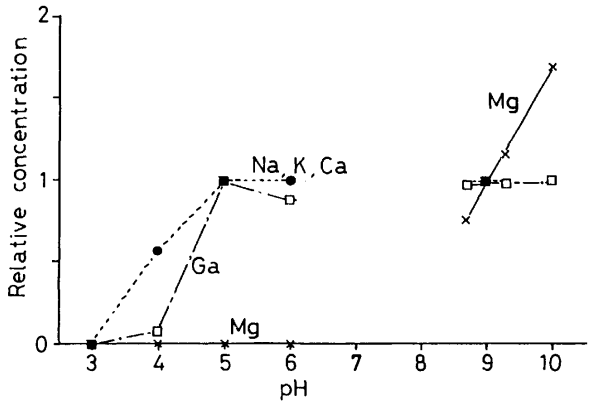

Fig. 2. Concentrations of gallium, alkali and alkaline earth elements in the precipitate at various pH in the case of gallium coprecipitation. Artificial seawater was used. Five mg of gallium was added to 1 l of seawater. The concentrations of all elements at pH 9 are defined as 1.
●: Na, K, Ca, □: Ga, ×: Mg.

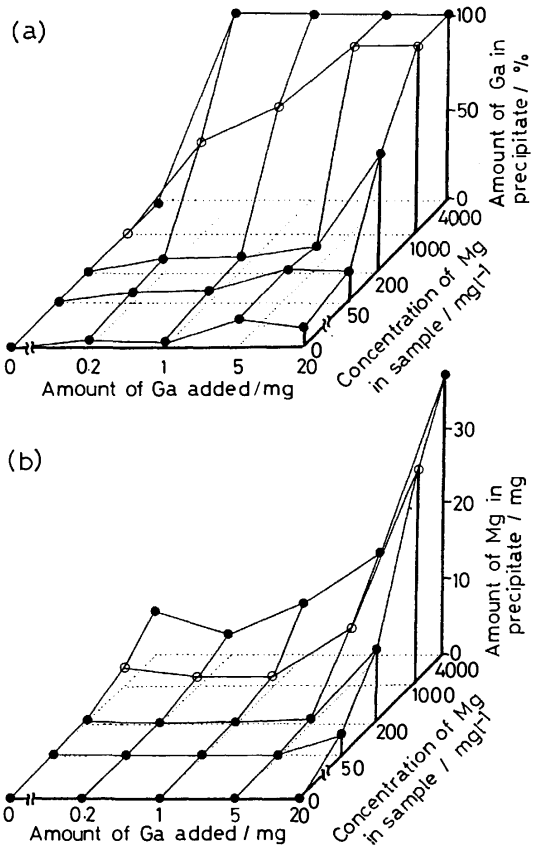

Fig. 3. Dependences of the precipitate compositions on the concentrations of magnesium and gallium at pH 9.0.
(a); amount of gallium in the precipitate (%). (b); amount of magnesium in the precipitate (mg). Open circles indicate the results for the solutions containing magnesium at the seawater level. The experiment was done using 100 ml of test solutions. The values in the figure was converted ones for 1 l of solutions.

tate on pH as well as the precipitate formation of the magnesium and gallium solution (Fig. 1-(c)) suggest the role of Mg in the precipitation of gallium. Therefore, the precipitation behaviors of gallium associated with magnesium in seawater was further investigated at pH 9.

Effect of Amounts of Magnesium and Gallium on Precipitate Formation. The precipitate formation of gallium at pH 9 was investigated using the solutions which contained both gallium and magnesium at various concentrations. The experimental results are shown in Fig. 3. The test solutions were prepared by dissolving required amounts of magnesium chloride in pure water and then different amounts of gallium were added into the solutions, in which the concentrations of magnesium in the test solutions were varied from 0 to 4000 mg l^{-1}, and those of gallium from 0 to 20 mg l^{-1}. The precipitate collected on a filter was dissolved in 1 M HCl solution. The percent recovery of gallium and amount of magnesium in the precipitates are shown in Figs. 3-(a) and -(b), respectively, as the functions of magnesium and gallium concentrations. As is seen in Fig. 3-(a), the percent recovery of gallium in the precipitate showed strong dependence on the concentrations of both gallium and magnesium in the solutions, and it was improved at the higher concentrations of both gallium and magnesium in the solution. When the concentration of magnesium in the sample was 4000 mg l^{-1}, gallium formed completely the precipitate at its concentration larger than 0.2 mg l^{-1}. For the solution containing magnesium at the concentration of seawater level (1000 mg l^{-1}, indicated by open circle in Figs. 3), gallium precipitated quantitatively (100%), when it was added not less than 5 mg l^{-1}. On the other hand, only a few percentage of gallium formed the precipitate when the magnesium concentration was below 50 mg l^{-1}.

Similar dependence was observed for the magnesium precipitation (Fig. 3-(b)). The amount of magnesium in the precipitate increased with the increases of the concentrations of both gallium and magnesium

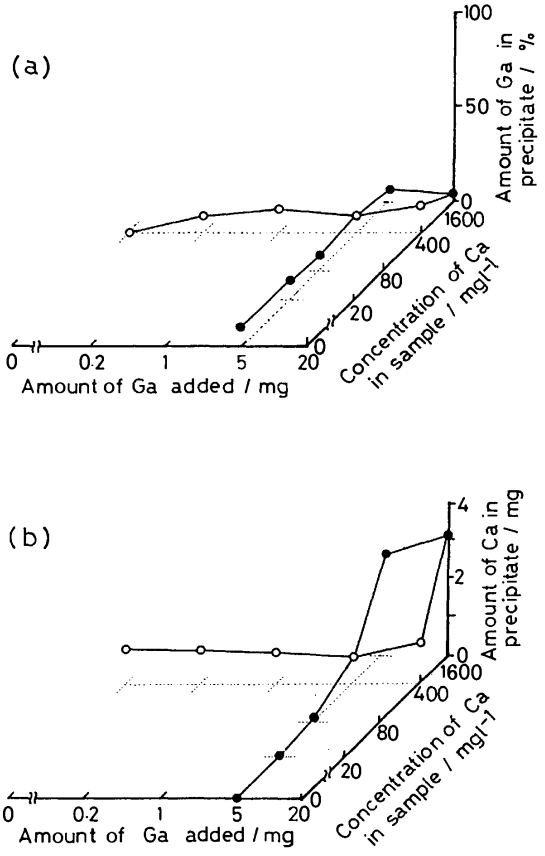

Fig. 4. Dependence of the precipitate compositions on the concentrations of gallium and calcium at pH 9.0.
(a); amount of gallium in the precipitate (%). (b); amount of calcium in the precipitate (mg). Open circles indicate the results for the solutions containing calcium at the seawater level. The experiment was done using 100 ml of test solutions. The values in the figure was converted ones for 1 l of solutions.

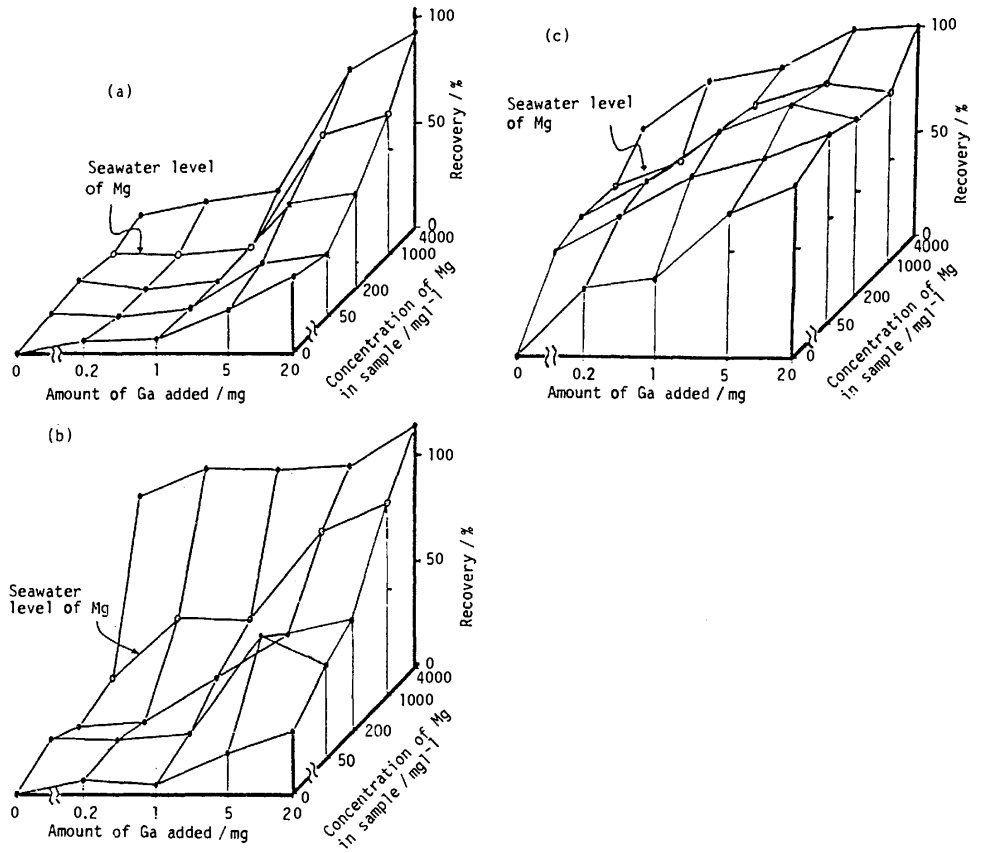

Fig. 5. Recoveries of cadmium (a), manganese (b), and yttrium (c) as the function of both gallium and magnesium concentrations at pH 9.0.
Open circles indicate the results for the solutions containing magnesium at the seawater level.

in solution. However, the amount of magnesium in the precipitate did not show proportionality to neither its concentration nor the added amount of gallium in the solution.

The experimental results described above indicate the interactions between magnesium and gallium in their precipitate formations.

Influence of Calcium on Gallium Precipitation. One l of seawater contains about 400 mg of calcium, which is about one third of magnesium content in seawater. The chemical property of calcium is more similar to that of magnesium than those of any other salts in seawater such as sodium and potassium. Thus, it is worthwhile to examine the influence of calcium on gallium precipitation. Such an influence was tested in the same manner as the case of magnesium. The calcium solutions (0—1600 mg l^{-1}) were prepared by dissolving required amounts of calcium chloride in pure water. The concentations of calcium in the test solutions were 0—4 times as large as that in seawater. The pH of the test solutions was adjusted to 9. The experimental results, the percent recovery of gallium and the amount of calcium in the precipitate, are shown in Figs. 4-(a) and (b), respectively. As can be seen in the figures, the percent recovery of gallium was low and did not depend on the gallium amount added or the concentration of calcium in the sample solution. The amount of calcium in the precipitate showed slight dependence on both of them, but it was much lower than that of magnesium (Fig. 4-(b)). Thus it is concluded that calcium had little cooperation in gallium precipitation.

Influence of Anions on Gallium Precipitation. Although large amount of chloride ion is present in seawater, the behavior of magnesium in its precipitation with gallium was investigated, when magnesium ion coexisted with different anion such as nitrate ion. The experiment was carried out by using magnesium nitrate solution. The results obtained for magnesium nitrate were almost similar to those using magnesium chloride. This experimental result may lead to the conclusion that only magnesium ion is responsible for its interaction with gallium in the gallium precipitation. The present result is due to the existence of Mg as the ionic form in high ionic strength solution, according to the calculation by Berner.[14]

Influence of Gallium and Magnesium Matrices on Recoveries of Heavy Metals. The precipitate in the gallium coprecipitation consists of magnesium as

well as gallium. So far only magnesium hydroxide has been used as a coprecipitation carrier.[10,11] Therefore, not only gallium hydroxide but also magnesium hydroxide are expected to collect heavy metals in solution. Hence the recoveries of analyte elements were investigated in terms of the added amount of gallium and the concentration of magnesium in solution. The original concentration of each analyte metal was 10 $\mu g\,l^{-1}$. The experimental results for Cd, Mn, and Y are shown in Figs. 5-(a), (b), and (c), respectively. As can be seen in the figures, the recoveries of analyte metals were dependent on both of the added amount of gallium and the concentration of magnesium in the test solution, i.e., the recoveries of such metals were improved with the increases of gallium and magnesium. Slight differences in the recovery patterns were, however, observed, depending on the analyte metals examined. The recovery of Mn was influenced by the concentration of magnesium rather than that of gallium (Fig. 5-(b)), while the recovery of Y depended more largely on the concentration of gallium (Fig 5-(c)). Iron showed a similar tendency to Mn, but Cu, Co, and V had the similar trends to Y. The tendencies of Zn, As, and Cr were similar to that of Cd. The results may be explained by the difference in chemical affinities of analyte metals with gallium and/or magnesium hydroxides.

Conclusion

The gallium coprecipitation method can be efficiently used for trace metal preconcentration in seawater in association with magnesium in solution. It has been elucidated that the cooperative interaction between gallium and magnesium is necessary in the efficient precipitate formation. The presence of magnesium ion in sample solution helped the quantitative precipitation of gallium added as a coprecipitation reagent, although very small portion of magnesium (about 0.3%) in seawater was found in the precipitate at pH 9. To coprecipitate analyte elements, both gallium and magnesium play as the coprecipitation carriers, which provides some unique advantages[12] in seawater analysis by ICP-AES.

The present research has been partially supported by the Grant-in-Aid for the Special Scientific Research (Nos. 63108003 and 63602019) from the Ministry of Education, Science and Culture.

References

1) T. Akagi, H. Nojiri, M. Matsui, and H. Haraguchi, *Appl. Spectrosc.*, **39**, 662 (1985).
2) E. Nakayama, H. Tokoro, T. Kuwamoto, and T. Fujinaga, *Nature (London)*, **290**, 768 (1981).
3) E. Nakayama, T. Kuwamoto, H. Tokoro, and T. Fujinaga, *Anal. Chim. Acta*, **131**, 247 (1981).
4) K. Fujiwara, S. Toda, and K. Fuwa, *Bull. Chem. Soc. Jpn.*, **54**, 3209 (1981).
5) D. S. Lee, *Anal. Chem.*, **54**, 1682 (1982).
6) R. S. S. Murthy and D. E. Ryan, *Anal. Chem.*, **55**, 682 (1983).
7) P. C. Cole, J. M. Eckert, and K. L. Williams, *Anal. Chim. Acta*, **153**, 61 (1983).
8) M. Hiraide, T. Ito, M. Baba, H. Kawaguchi, and A. Mizuike, *Anal. Chem.*, **52**, 804 (1980).
9) K. Himeno, K. Yanagisawa, T. Yuki, and Y. Nakamura, *Bunseki Kagaku*, **33**, T44 (1984).
10) A. Andresen and B. Salbu, *Radiochem. Radioanal. Lett.*, **52**, 19 (1982).
11) A. S. Buchanan and P. Hannaker, *Anal. Chem.*, **56**, 1379 (1984).
12) T. Akagi, K. Fuwa, and H. Haraguchi, *Anal. Chim. Acta*, **177**, 139 (1985).
13) F. A. Cotton and G. Wilkinson, "Advanced Inorganic Chemistry," Interscience Publishers, New York (1966), p. 437.
14) R. A. Berner, "Principles of Chemical Sedimentology," McGraw Hill, New York (1971), p. 240.

Synthesis and Characterization of the Pd(II) and Pt(II) Complexes of Trichalcogeno[*n*]ferrocenophanes (*n*=7 and 9). A Dative Fe–Pd or Fe–Pt Bond Formation

Masaru SATO,* Hirofumi ASANO, Kaoru SUZUKI, Motomi KATADA,† and Sadatoshi AKABORI††
Chemical Analysis Center, Saitama University, Urawa, Saitama 338
†Department of Chemistry, Faculty of Science, Tokyo Metropolitan University, Setagayaku, Tokyo 158
††Department of Chemistry, Faculty of Science, Toho University, Funabashi, Chiba 274
(Received May 29, 1989)

1,7-Dithia-4-selena[7]- and 1,9-dithia-5-selena[9](1,1′)ferrocenophanes were prepared. These compounds, as well as 1,4,7-trithia[7]- and 1,5,9-trithia[9](1,1′)ferrocenophanes, were treated with $(CH_3CN)_4Pd(BF_4)_2$ or $(CH_3CN)_4Pt(BF_4)_2$ to give the corresponding 1/1 complexes in good yield. The spectral data of these complexes confirmed that there exsisted a dative Fe–Pd or Fe–Pt bond in these bimetallic complexes.

Much attention has been focused on the heterobimetallic complexes.[1,2] Such species should be capable of generating unique reactivity by virtue of the close proximity of the adjacent metals. The coordination of the nonbonding e_{2g} electrons of the iron atom in ferrocene to vacant orbitals of a transition metal has also become a topic of interest in recent years. Ferrocene derivatives involving heteroatoms in the 1,1′-positions formed 1/1 complexes (**1**) with various metals.[3] However, it was reported that there was no evidence of an interaction between the iron atom of a ferrocene nucleus and the metal coordinated to the hetero atoms.[4,5] In this connection, Seyferth et al. carried out a reaction of 1,2,3-trithia[3](1,1′)ferrocenophane with tetrakis(triphenylphosphine)palladium(0) to obtain (triphenylphosphine)(1,1′-ferrocenedithiolato-*S,S′,Fe*)palladium(II) (**2a**), which was confirmed by X-ray analysis to have a weak dative Fe–Pd bond.[6,7] A similar Pt(II) complex (**2b**) was also reported.[8] In the same year, Sano et al. reported that the stable metal halide adducts (**3**) of [2](1,1′)ferrocenophane were confirmed by Mössbauer spectroscopy to have a strong bonding interaction between the iron atom and metal halides.[9] On the other hand, thiamacrocyclic compounds are of interest in that these form stable complexes with various transition metals and stabilize an unusual valence of the metal.[10] Since we have already prepared various metal complexes of tetrathia-[*n*]- and trithia[*n*]ferrocenophanes,[11,12] these findings have stimulated us to attempt a reaction of trichalcogeno[*n*]ferrocenophanes with a highly acidic $Pd(BF_4)_2$ or $Pt(BF_4)_2$.[13,14]

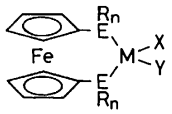

1

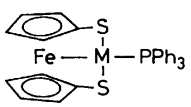

2a : M=Pd
2b : M=Pt

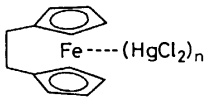

3

Results and Discussion

1,5,9-Trithia[9](1,1′)ferrocenophane (**4**)[12] was allowed to react with $(CH_3CN)_4Pd(BF_4)_2$, which was prepared from the reaction of $(CH_3CN)_2PdCl_2$ and $AgBF_4$,[15] in acetone at ambient temperature. Stable dark-brown fine needles (**5a**) were isolated in good yield, which proved by elemental analysis to be a 1/1 complex. A similar reaction of 1,4,7-trithia[7]-(1,1′)ferrocenophane (**6**)[16] with $(CH_3CN)_4Pd(BF_4)_2$ gave a black 1/1 complex (**7a**) and a green powdery 2/1 complex (**8a**) in 74 and 12% yields, respectively. Complexes **5a** and **7a** contained one equivalent of acetone in the crystals. Upon recrystallization from acetonitrile–diethyl ether, the acetone was replaced by acetonitrile. In order to extend the scope of the reaction, each trithia[*n*]ferrocenophane was treated with $(CH_3CN)_4Pt(BF_4)_2$.[15] Only the reaction of the [9]-ferrocenophane (**4**) with $(CH_3CN)_4Pt(BF_4)_2$ in warm acetonitrile under nitrogen gave a stable 1/1 complex (**5b**) as red needles in good yield.

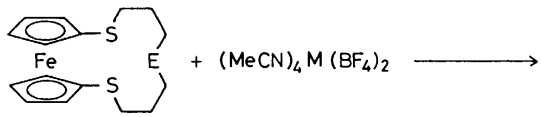

4 : E=S
13 : E=Se

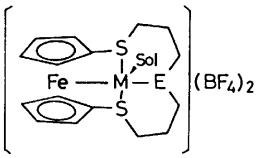

5a : E=S, M=Pd
5b : E=S, M=Pt
15a : E=Se, M=Pd
15b : E=Se, M=Pt

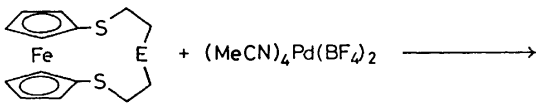

6 : E = S
14 : E = Se

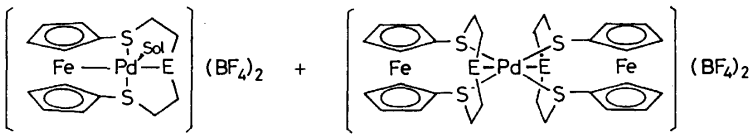

7a : E = S
16a : E = Se

8a : E = S
17a : E = Se

Dithiaselena[*n*](1,1′)ferrocenophanes could not be synthesized by the procedure used for preparing trithia[*n*](1,1′)ferrocenophanes. For example, 1,1′-bis(3-chloropropylthio)ferrocene (**9**) reacted with sodium selenide to give no desirable product. This failure seems to be due to the low nucleophilicity of sodium selenide compared with sodium sulfide. Thus, the chloride (**9**) was converted to 1,1′-bis(3-iodopropylthio)ferrocene (**11**) by treating **9** with sodium iodide in refluxing 2-butanone for 24 h. Similarly, 1,1′-bis(2-iodoethylthio)ferrocene (**12**) was obtained in good yield from 1,1′-bis(2-chloroethylthio)ferrocene (**10**). The reaction of the iodide **11** with an aqueous solution of sodium selenide[17] in refluxing THF under high-dilution conditions gave the desired product, 1,9-dithia-5-selena[9](1,1′)ferrocenophane (**13**), although in low yield. The ring closure of the iodide **11** using a thiourea method proceeded successfully to give a more sufficient yield. Thus, **11** was treated with thiourea in refluxing ethanol under high-dilution conditions, followed by the addition of 10% aqueous sodium hydroxide; then, refluxing continued for 4 h to give **13** in 33% yield along with the dimeric compound, 1,9,20,28-tetrathia-5,24-diselena[9,9](1,1′)ferrocenophane in 25% yield. In a similar fashion, 1,7-dithia-4-selena[7](1,1′)ferrocenophane (**14**) was synthesized as red plates in 25% yield from 1,1′-bis(2-iodoethylthio)ferrocene (**12**).

1,9-Dithia-5-selena[9](1,1′)ferrocenophane (**13**) reacted with $(CH_3CN)_4Pd(BF_4)_2$ in acetone to give a 1/1 complex (**15a**) as dark-green needles in good yield. The reaction of 1,7-dithia-4-selena[7](1,1′)ferrocenophane (**14**) with the same Pd(II) salt gave a 1/1 complex (**16a**) and a 2/1 complex (**17a**) in 54 and 31% yields, respectively. A platinum analog (**15b**) was successfully obtained from a treatment of **13** with $(CH_3CN)_4Pt(BF_4)_2$ in warm acetonitrile, but the reaction of the [7]ferrocenophane **14** with the same Pt(II) salt gave no isolable complex.

The out-of-plane bending vibration found in ferrocene at 815 cm^{-1} moves to 851 cm^{-1} in the ferricenium ion and is thus known to be a diagnostic probe for examining the oxidation state of the iron atom of ferrocene derivatives.[18] The frequencies of the Pd(II) complexes, **5a**, **7a**, **15a**, and **16a** (Table 1), were shifted to a higher wavenumber region than those of the corresponding free ligands and the $PdCl_2$ complexes. For example, the out-of-plane bending vibration of **5a** appeared at 844 cm^{-1}, while that of the corresponding free lignand and the $PdCl_2$ complex absorbed at 806 and 820 cm^{-1}, respectively.[12] Such a large shift of this band in **5a** to high wavenumber region suggests the occurrence of a strong perturbation in the iron atom of a ferrocene nucleus by the Pd(II) atom through the coordinated sulfur atoms and/or a direct Fe-Pd bonding interaction. In this connection, the frequency of the corresponding vibration is observed at 830 and 838 cm^{-1} in the phosphine complex **2a** which is confirmed by X-ray analysis to have a weak dative Fe-Pd bond.[6,7] The platinum complexes, **5b** and **15b**, also exhibited a similar high wavenumber shift of the out-of-plane bending vibration, as shown in Table 1, indicating similar structural features to those in the palladium analogs, **5a** and **15a**. The ring size of the chalcogenomacrocycle moiety in the Pd(II) complexes exerted a significant influence on the out-of-bending vibration. Thus, the frequencies of the [7]ferrocenophane complexes, **7a** and **16a**, were observed at 830 cm^{-1}. The relatively low wavenumber frequency in **7a** and **16a** compared with that in **5a** and **15a** may suggest a weaker bonding

Table 1. Infrared (KBr) and Visible Spectral Data (CH_3CN)

Compound	Out of bending vibration/cm^{-1}	λ_{max} /nm(ε)
4[a]	806	446 (211)
6[a]	810	462 (349)
13	810	448 (215)
14	810	461 (249)
5a	844	620sh (206), 444 (6240)
7a	830	812 (2800), 408 (4300)
15a	842	620sh (274), 448 (8730)
16a	830	772 (2420), 408 (8410)
5b	846	500 (309), 372 (5650)
15b	844	500 (419), 372 (7610)

a) From Ref. 11.

interaction in [7]ferrocenophane complexes than that in [9]ferrocenophane complexes.

The ^{1}H NMR spectrum of **15a** (400 MHz, CD_3CN) showed the ferrocenyl ring protons as narrow sextets at δ 5.95 and 6.09, and narrow quintets at δ 3.43 and 3.93. It has been previously shown that in monosubstituted ferrocenyl ring protons adjacent to the substituent (i.e. α-protons) give a 1:2:2:2:1 multiplet pattern while internal protons (i.e. β-protons) give a 1:1:2:2:1:1 pattern.[19] We therefore assigned the signals at δ 3.43 and 3.93 to the α-ring protons and the signals at δ 5.95 and 6.09 to the β-ring protons. The facts that in the 2D H,H-COSY experiment for **15a** the signals at δ 3.43 and 3.93 correlated strongly with the signals at δ 5.95 and 6.09, respectively, and that the latter signals also correlated strongly with each other, provide conclusive evidence for the assignment described above. It is noteworthy that the α-ring protons in complex **15a** appears at a higher field than those of the corresponding free ligand (δ 4.23) and that the β-ring protons produce signals at a considerably low field. Generally, the α- and β-protons of the ferrocenyl ring in the complexes coordinated to a metal atom through the heteroatoms at the 1,1′-positions shift to a lower field than those of the corresponding free ligand, and the α-protons appear at a lower field than the β-protons.[5,11,12,20] The low-field shift can be elucidated by the magnetic anisotropy or the inductive effect of the metal halide.[5] The large separation between the α- and β-proton signals of the ferrocenyl ring and the reversal of their chemical shifts observed in complex **15a** appear to be elucidated only by a magnetic anisotropy of a metal-metal bond between the iron atom of the ferrocene moiety and the Pd(II) atom incorporated in the chalcogenomacrocycle. A similar phenomenon concerning the ferrocenyl ring protons is also observed in complexes **2a** and **2b** which have dative Fe-Pd and Fe-Pt bonds in the molecule, respectively.[6-8] Complexes **5a**, **5b**, **7a**, **15b**, and **16a** also showed the same spectral features concerning the ferrocenyl ring protons, suggesting that these ferrocenophane complexes also have a structure containing an iron-metal bond. The replacement of one of the sulfur atoms in complex **5a** for a selenium atom (producing complex **15a**) exerts little influence on the spectral features of the ferrocenyl ring protons. In platinum complexes **5b** and **15b**, the chemical shifts of the α- and β-proton signals of a ferrocenyl ring show no significant change compared with those in palladium complexes **5a** and **15a**. These results seem to indicate that the iron-metal bond in the [9]ferrocenophane complexes is little influenced by the kind of central metal or the kind of coordinating heteroatoms.

In the ^{13}C NMR spectrum of palladium complex **15a**, the α-ring carbons of a ferrocenyl ring were observed at δ 71.30 and 71.74 and the β-ring carbons appeared at δ 85.22 and 86.70. The assignment of these signals of the ferrocenyl ring carbon could be successfully performed by the C,H-COSY experiment. It has been reported that the coordination of $PdCl_2$ to 1,1′-bis(isobutylthio)ferrocene brings about a high-field shift of the bridge-head carbon signal (Δ 3.4 ppm), though little increase of the separation between the α- and β-carbon signals of a ferrocenyl ring (Δ 0.8 ppm). On the other hand, complex **15a** showed a similar high-field shift of the bridge-head carbon signal compared to the corresponding free ligand **13** (Δ 4.6 ppm); however, the separation between the α- and β-carbon signals is considerably increased upon complexation with $Pd(BF_4)_2$ (Δ ca. 13 ppm). The latter change is mainly due to the large low-field shift of the β-ring carbon signals of a ferrocenyl ring in complex **15a**. The deshielding of the β-carbons of a ferrocenyl ring appears to be in part responsible for the low-field shift of the β-proton signals in the ^{1}H NMR spectrum of **15a** described above.

Cowie et al. proposed three canonical forms, I—III, in order to represent the bonding in the phosphine complex **2a**, and supposed that the actual structure may have significant contributions from all three resonance forms.[7] The ^{1}H NMR spectra of **5** and **15**

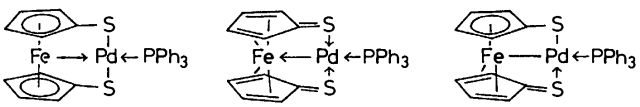

can afford some information concerning the structure of the present complexes. The deshielding of the β-protons compared with the α-protons and the large separation between them found in the ferrocenyl moiety of **5** and **15** are similar to those in the ferrocenylmethylium ions [H(α), δ 4.72; H(β), 6.23].[21,22] In the latter comounds, the contribution of a fulvene structure is considered for the substituted cyclopentadienyl ring, since the X-ray analysis shows that ferrocenyldiphenylmethylium tetrafluoroborate can be described as a fulvenecyclopentadienyl cation.[23] The similarity of the ^{1}H NMR spectral features in **5** and **15** to that in the ferrocenylmethylium ions seems to suggest that the resonance forms corresponding to II and III contributed to the actual structure in complexes **5** and **15** much more than in complex **2a**. As mentioned previously, the ^{13}C NMR spectra of complex **15a** showed a deshielding of the β-carbons in the ferrocenyl ring and large separation between α- and β-carbon signals. Similarly, the low-field shift of the β-carbon signals compared with the α-carbon signals of a ferrocenyl ring [C(α)=Δ 17.6 ppm and C(β)=Δ 27.4 ppm) and the large separation between the α- and β-carbon signals (δ 9.8 ppm) are observed when the carbon chemical shifts in ferrocenylmethylium ions are compared with those in the corresponding alcohols.[24,25] These facts may also support the sugges-

Table 2. The ^{1}H NMR Spectral Data (400 MHz, CD_3CN)

Compound	Ring-H (δ)	Methylene-H(δ)
5a	3.47 (m, 2H, Hα), 4.02 (qu, 2H, Hα), 5.98 (se, 2H, Hβ), 6.12 (se, 2H, Hβ)	2.31 (qu, 2H, H_3), 2.52 (qu, 2H, H_3), 2.86 (dq, 2H, H_2), 3.09 (dq, 2H, H_4), 3.47 (m, 2H, H_2), 3.61 (dq, 2H, H_4)
7a	3.65 (m, 2H, Hα), 4.23 (m, 2H, Hα), 5.29 (m, 2H, Hβ), 5.58 (m, 2H, Hβ),	2.34 (m, 2H, H_2), 3.38 (m, 2H, H_3), 3.62 (m, 4H, H_2 and H_3)
15a	3.43 (qu, 2H, Hα), 3.93 (qu, 2H, Hα), 5.95 (se, 2H, Hβ), 6.09 (se, 2H, Hβ)	2.22 (m, 2H, H_3), 2.67 (m, 2H, H_3), 2.90 (m, 2H, H_2), 3.03 (m, 2H, H_4), 3.54 (m, 2H, H_2), 3.57 (m, 2H, H_4)
16a	3.58 (m, 2H, Hα), 4.10 (m, 2H, Hα), 5.35 (m, 2H, Hβ), 5.63 (m, 2H, Hβ)	2.27 (m, 2H, H_2), 3.45 (m, 2H, H_3), 3.68 (m, 2H, H_3), 4.01 (m, 2H, H_2)
5b	3.66 (s, 2H, Hα), 4.16 (m, 2H, Hα), 5.95 (m, 2H, Hβ), 6.16 (m, 2H, Hβ)	2.41 (m, 2H, H_3), 2.48 (m, 2H, H_3), 3.02 (m, 2H, H_2), 3.31 (m, 2H, H_4), 3.60 (m, 2H, H_2), 3.72 (m, 2H, H_4)
15b	3.64 (m, 2H, Hα), 4.11 (m, 2H, Hα), 5.94 (m, 2H, Hβ), 6.16 (m, 2H, Hβ)	2.48 (m, 4H, H_3), 3.07 (m, 2H, H_2), 3.21 (m, 2H, H_4), 3.68 (m, 4H, H_2 and H_4)

The assignment of **5a**, **5b**, and **15b** was done tentatively according to that of **15a** and the proton signals of **7a** was assigned analogously in **16a**.
qu=quintet, se=sextet, dq=double quartet.

Table 3. The ^{13}C NMR Spectral Data (100 MHz, CD_3CN)

Compond	Ring-C (δ)	Methylene-C (δ)
5a	71.63 (Cα), 72.24 (Cα), 85.01 (C$_b$), 85.65 (Cβ), 87.33 (Cβ)	28.70 (C_3), 34.41 (C_4), 36.86 (C_3)
7a	70.09 (Cα), 72.00 (Cα), 76.36 (C$_b$) 78.66 (Cβ), 79.47 (Cβ)	39.89 (C_3), 41.31 (C_2)
15a	71.30 (Cα), 71.74 (Cα), 82.20 (C$_b$), 85.22 (Cβ), 86.70 (Cβ)	29.86 (C_3), 32.09 (t, J=55.1 Hz,[a] C_4), 35.23 (C_2)
16a	69.88 (Cα), 72.26 (Cα), 75.13 (C$_b$), 79.49 (Cβ), 80.06 (Cβ)	36.26 (t, J=48.5 Hz,[a] C_3), 41.31 (C_2)
5b	70.83 (Cα), 72.65 (t, J=13.0 Hz, Cα), 79.80 (C$_b$), 86.27 (Cβ), 86.98 (Cβ)	28,03 (t, J=86.7 Hz,[b] C_3), 35.45 (t, J=21.1 Hz,[b] C_4), 38.01 (t, J=29.6 Hz,[b] C_2)
15b	70.71 (Cα), 72.34 (t, J=13 Hz, Cα), 77.53 (C$_b$), 86.09 (Cβ), 86.68 (Cβ)	28.87 (t, J=85.1 Hz,[b] C_3), 33.42 (p, J=29.5,[b] and 53.6Hz, [a] C_4), 36.33 (t, J=20.6 Hz,[b] C_2)

The assignment of the signals in **5a** and **5b** was undergone according to those in **15a** and **15b.** The signals in **7a** were assigned analogously in **16a**.
a) ^{13}C-^{77}Se coupling constant. b) ^{13}C-^{195}Pt coupling constant.

tion described above.

The ^{1}H NMR spectra of the [7]ferrocenophane complexes, **7a** and **16a**, showed the same pattern of ring protons in a ferrocenyl moiety with that found in the [9]ferrocenophane complexes, as shown in Table 2. The separation between the α- and β-proton signals is somewhat small compared with that found in the [9]ferrocenophane complexes. This may partly reflect the decrease in the deshielding in the β-carbons of the ferrocenyl ring in complexes **16a**, as seen in the ^{13}C NMR spectrum (Table 3). The β-carbon resonances in **16a** shift by ca. 6 ppm to a higher field than those in **15a**. These facts seem to suggest that there also exsists an Fe-Pd bond in the [7]ferrocenophane complexes, although it is somewhat weak compared with that in the [9]ferrocenophane complexes. A remarkable feature was observed in the region of the methylene protons of the ^{1}H NMR spectra of the [7]ferrocenophane complexes, **7a** and **16a.** One of the protons attached to C(2) resonated at δ 4.01, the position of which is in a 0.47 ppm lower field than the corresponding proton in the [9]ferrocenophane complex, **15a**. The other proton attached to C(2) appeared at δ 2.27, the chemical shift of which is in a 0.63 ppm higher field than the corresponding proton in **15a**. This can probably be explained by the constrained structure of **16a**, in which one of the protons attached to C(2) is greatly imposed to be in the deshielding zone and the other in the shielding zone of ferrocene.[26] In such strained complexes, **7a** and **16a**, the Fe-Pd(II)-S angle can be no longer 180° because of the small ring size of the thiamacrocycle; thus, that the Pd(II) atom cannot assume a regular square-planar coordination. In these complexes, the distinct distortion from a square-planar (probably to a trigonal-bipyramidal coordination as shown in **18**) seems to

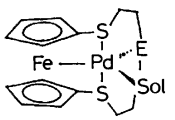

18

occur in terms of a strong coordination of solvent molecules. The weakening of the Fe-Pd bond in the [7]ferrocenophane complexes seems to be probably due to a structural deformation, as mentioned above.

The visible spectrum of the [9]ferrocenophane complex, **5a**, exhibited one strong absorption at 444 nm (ε 6240) and one weak shoulder at 620 nm (ε 206), while the free ligand **4** showed an absorption maximum at 446 nm (ε 211). The square-planer $Pd(BF_4)_2$ complexes of 2,6,10,14-tetrathiapentadecane[15] and 7,16-dimethyl-1,4,10,13-tetrathia-7,16-diazacyclooctadecane[27] showed no absorption above 380 nm.[28] Therefore, either of the two absorptions seems to relate to the Fe-Pd bonding interaction. A similar absorption pattern, as seen in **5a**, was also observed in the phosphine complex, **2a**, which has a dative Fe-Pd bond, although the absorption peaks somewhat shift to a long-wavelength region.[6,7] As shown in Table 1, the replacement of one sulfur atom of trithiamacrocycle in complexes **5** for a selenium atom had no influence on the electronic absorption of the [9]ferrocenophane complexes, while the absorption maxima in the Pt analog **5b** shifted to a short-wavelength compared with those in the Pd analog, **5a** [Δ ca. 70 nm]. A similar blue shift was observed in the phosphine complex, **2b**. The electronic spectra of the [7]ferrocenophane complexes, **7a** and **16a**, were considerably different from those of the [9]ferrocenophane complexes, **5a** and **15a**, respectively. The most remarkable difference was, for example, the appearance of a large and broad band at 812 (ε 2800) in **7a**. A similar band near 800 nm was also observed in the oxidized 1,5,7-trithia[7]ferrocenophane [λ_{max} 850 nm (ε 1150) and 752 nm (ε 955)]. This may suggest that complex **7a** contains a contribution from the ferricenium cation structure, which is generated through an intramolecular redox reaction, as seen in similar copper complexes.[29] However, this is not the fact, since **7a** afforded a clear ^{1}H NMR spectrum. The absorption in the long-wavelength region may be caused by the distorted coordination manner described above.

The Mössbauer spectral data of complexes **5a** and **7a**, along with those of the related complexes, are summarized in Table 4. The QS value of **5a** is similar to that of the corresponding free ligand **4**, while a considerably large QS value was obtained in the $HgCl_2$ adducts (**3**) of [2](1,1′)ferrocenophane.[9] This may suggest that there is no substantial metal-metal bonding interaction between the Fe atom in the ferrocene moiety and the Pd(II) atom coordinated to the thiamacrocycle. However, only a small decrease of the QS value was obtained in the bisthiolate complex **2a**, in which a weak Fe-Pd dative bond was confirmed by X-ray analysis.[6,7] It may also be worth noting that an increased IS value was observed, especially at low temperature, in complexes **2a**, **5a**, and **7a**, in which a metal-metal bonding interaction was assumed. Anyway, at the present stage, no definite conclusion seems to be derived from the Mössbauer parameter.

Table 4. The Mössbauer Spectral Data

Compound	Conditions	IS/mm s^{-1}	QS/mm s^{-1}
4	R.T.	0.43	2.36
4$^+$ BF_4^-	R.T.	0.45	0.72
5a	R.T.	0.49	2.36
	Liq. N_2	0.57	2.39
7a	R.T.	0.50	2.10
2a	R.T.	0.48	1.99
	Liq. N_2	0.53	2.03

Experimental

The melting point was measured by using a differential scanning calorimeter (SEIKO DSC-20). The IR spectra were taken by a Hitachi 750-20 Infrared Spectrometer. The electronic spectra were measured by a Shimadzu UV-2000 Spectrometer. The ^{1}H and ^{13}C NMR spectra were taken by a Bruker AM 400 or GEOL FX-90Q Spectrometer, using TMS as an internal standard.

1,1′-Bis(3-chloropropylthio)ferrocene,[16] 1,1′-bis(2-chloroethylthio)ferrocene,[16] 1,5,9-trithia[9](1,1′)ferrocenophane (**4**),[12] 1,4,7-trithia[7](1,1′)ferrocenophane (**6**),[16] dichlorobis(acetonitrile)palladium(II) and -platinum(II)[15] were prepared according to the literature. Silver(I) tetrafluoroborate and selenourea were commercially available.

(1,5,9-trithia[9](1,1′)ferrocenophane-*S,S′,S″,Fe*)palladium(II) Tetrafluoroborate (5a). To a solution of dichlorobis(acetonitrile)palladium(II) (0.16 g, 0.6 mmol) in dry acetone (15 cm^3) was added silver(I) tetrafluoroborate (0.25 g, 1.3 mmol). The mixture was stirred for 1 h and the resulting silver(I) chloride was filtered off. To the filtrate, 1,5,9-trithia[9](1,1′)ferrocenophane (**4**) (0.22 g, 0.6 mmol) was added and then the solution was stirred for 1 h. The resulting brown crystals were collected by filtration to give the title compound (**5a**) containing one equivalent of acetone as dark-brown needles (0.30 g, 73%), mp 250 °C. Found: C, 32.33; H, 3.72%. Calcd for $C_{16}H_{20}B_2F_8S_3FePd \cdot C_3H_6O$: C, 32.48; H, 3.73%. The complex was recrystallized from acetonitrile–diethyl ether to give **5a** containing one equivalent of acetonitrile as black needles, mp 250 °C. Found: C, 31.64; H, 3.41; N, 1.89%. Calcd for $C_{16}H_{20}B_2F_8S_3FePd \cdot C_2H_3N$: C, 31.54; H, 3.38; N, 2.04%.

(1,4,7-Trithia[7](1,1′)ferrocenophane-*S,S′,S″,Fe*)palladium(II) Tetrafluoroborate (7a). A mixture of dichlorobis(acetonitrile)palladium(II) (0.26 g, 1 mmol) and silver(I) tetrafluoroborate (0.40 g, 2.1 mmol) was stirred for 1 h at room temperature and then filtered to remove the resulting silver(I) chloride. To the filtrate diluted with dry acetone (50 cm^3) was added a solution of 1,4,7-trithia[7](1,1′)-ferrocenophane (**6**) (0.34 g, 1 mmol) in dry acetone (50 cm^3) dropwise for a period of 30 min. The mixture was stirred for 1 h and then filtered. A green powder (55 mg, 12%) of bis(1,4,7-trithia[7](1,1′)ferrocenophane-*S,S′,S″*)palladium(II) tetrafluoroborate (**8a**) was obtained. Mp 250 °C. Found: C, 34.95; H, 3.53%. Calcd for $C_{28}H_{32}B_2F_8S_6Fe_2Pd$: C, 35.30; H, 3.39%. IR (KBr): 3120, 2976, 1418, 946, 900, 888, 824, 538, 528, 504, and 488 cm^{-1}. VIS (CH_3CN): λ_{max} 380sh

and 784 nm (log ε 2.7). ^{1}H NMR (90 MHz, CD_3CN): δ=3.32—3.92 (m, 16H, CH_2S), 4.50 (m, 12H, ring-H), and 4.65 (m, 4H, ring-H). The filtrate was evaporated under reduced pressure and then the residue was dissolved in acetone (5 cm^3). The resulting solution was diluted with dry diethyl ether (2.5 cm^3) and kept in a freezer to give the title complex **7a** containing one equivalent of acetone as fine black needles, mp 250 °C. Found: C, 30.49; H, 3.38%. Calcd for $C_{14}H_{16}B_2F_8S_3FePd\cdot C_3H_6O$: C, 30.27; H, 3.29%.

1,1′-Bis(3-iodopropylthio)ferrocene (11). A mixture of sodium iodide (2.24 g, 14.9 mmol) in methyl ethyl ketone (40 cm^3) was refluxed for 1 h under nitrogen. To the resulting solution was added 1,1′-bis(3-chloropropylthio)ferrocene (2.00 g, 4.96 mmol). The mixture was then refluxed for 8 h under nitrogen and cooled to room temperature. The mixture was filtered and the precipitate was washed with methyl ethyl ketone (20 cm^3). The filtrate and the washing were combined and washed with water (60 cm^3), 5% sodium thiosulfate solution (20 cm^3), 5% sodium hydrogencarbonate (20 cm^3), and water (20 cm^3), and then dried over anhyd $MgSO_4$. The solution was evaporated under reduced pressure and the residue was chromatographed on silica gel by elution of hexane-toluene (2 : 1). The title compound (**11**) was obtained as yellow plates (2.66 g, 91%) after recrystallization from ethanol-hexane, mp 49.5—51.5 °C. Found: C, 32.65; H, 3.44%. Calcd for $C_{16}H_{20}I_2S_2Fe$: C, 32.79; H, 3.44%. MS (75 eV): *m/z* 586 (M^+, 100%). IR (KBr): 3076, 2952, 1448, 1422, 1390, 1318, 1238, 1166, 1022, 900, 824, 724, 572, 528, 512, and 456 cm^{-1}. ^{1}H NMR (90 MHz, $CDCl_3$): δ=1.98 (p, *J*=6.8 Hz, 4H, CH_2), 2.66 (t, *J*=6.8 Hz, 4H, SCH_2), 3.25 (t, *J*=6.8 Hz, 4H, CH_2I), and 4.27 (m, 8H, ring-H).

1,1′-Bis(2-iodoethylthio)ferrocene (12). To a solution of sodium iodide (4.07 g, 27.2 mmol) in methyl ethyl ketone (40 cm^3), prepared as described above, was added 1,1′-bis(2-chloroethylthio)ferrocene (1.50 g, 4.00 mmol). The mixture was refluxed for 16 h under nitrogen. After the reaction had been completed, the resulting yellow crystals were collected by filtration. The filtrate was washed with water (80 cm^3), 10% sodium thiosulfate solution (20 cm), 5% sodium hydrogencarbonate solution (20 cm^3), and water (40 cm^3), and then dried over anhyd $MgSO_4$. After evaporation, the residue was chromatographed on silica gel by elution of hexane-toluene (1 : 1). The title compound (**12**) was obtained as yellow plates (mp 136—139 °C). The yield was 1.62 g (72.6%) in all. Found: C, 30.13; H, 2.89%. Calcd for $C_{14}H_{16}I_2S_2Fe$: C, 30.31; H, 2.90%. MS (75 eV): *m/z* 558 (M^+, 100%). IR (KBr): 3076, 1414, 1162, 896, 816, 726, 566, 504, and 454 cm^{-1}. ^{1}H NMR (90 MHz, $CDCl_3$): δ=2.96 (dd, *J*=6.6 and 1.8 Hz, 4H, SCH_2), 3.20 (dd, *J*=6.6 and 1.8 Hz, 4H, SCH_2), 3.20 (dd, *J*=6.7 and 1.8 Hz, 4H, CH_2I), and 4.30 (m, 8H, ring-H).

1,9-Dithia-5-selena[9](1,1′)ferrocenophane (13). A mixture of 1,1′-bis(3-iodopropylthio)ferrocene (**11**) (1.00 g, 1.7 mmol) and selenourea (0.21 g, 1.7 mmol) in ethanol (50 cm^3) was refluxed under nitrogen for 4 h. To the solution diluted with ethanol (800 cm^3) was added 10% aqueous sodium hydroxide (1.8 cm^3) under refluxing; the solution was then refluxed for 4 h. After evaporation, the residue was dissolved in benzene (100 cm^3). The solution was washed with water (60 cm^3) and dried over anhyd $MgSO_4$. The solution was then condensed under reduced pressure and chromatographed on silica gel by elution of hexane-toluene (2 : 1) to give the title compound (**13**) as red crystals (0.26 g, 37%) after recrystallization from ethanol-hexane, mp 62.0—62.5 °C. Found: C, 47.02; H, 4.94%. Calcd for $C_{16}H_{20}S_2SeFe$: C, 46.73; H, 4.90%. IR (KBr): 3092, 2928, 1418, 1290, 1222, 1158, 1024, 882, 810, 516, and 472 cm^{-1}. ^{1}H NMR (400 MHz, $CDCl_3$): δ=2.16 (p, *J*=6.9 Hz, 4H, CH_2), 2.89 (t, *J*=6.7 Hz, 4H, CH_2Se), 3.09 (t, *J*=7.0 Hz, 4H, CH_2S), and 4.22 (s, 8H, ring-H). ^{13}C NMR (100 MHz, $CDCl_3$): δ=23.30 (t, *J*=62.4 Hz, $SeCH_2$), 30.47 (CH_2), 34.85 (SCH_2), 67.88 (C_β), 71.37 (C_α), and 86.87 (C_b).

1,7-Dithia-4-selena[7](1,1′)ferrocenopahne (14). A mixture of 1,1′-bis(2-iodoethylthio)ferrocene (**12**) (0.10 g, 0.18 mmol) and selenourea (25 mg, 0.20 mmol) in tetrahydrofuran (30 cm^3) was refluxed for 3 h under nitrogen. To the solution diluted with tetrahydrofuran (70 cm^3) was added 10% aqueous sodium hydroxide (1.5 cm^3) under refluxing; the solution was then refluxed for 1 h. After evaporation, the residue was disolved in benzene (50 cm^3). The solution was washed with water (50 cm^3) and dried over anhyd $MgSO_4$. After evaporating the solvent, the residue was chromatographed on silica gel by elution of hexane-toluene (2 : 1) to give the title compound (**14**) as red-orange plates (16 mg, 24%) after recrystallization from hexane-toluene, mp 116.5 °C. Found: C, 44.07; H, 4.27%. Calcd for $C_{14}H_{16}S_2SeFe$: C, 43.88; H, 4.21%. IR (KBr): 3096, 3080, 2916, 1416, 1380, 1260, 1160, 1050, 1022, 890, 846, 810, 526, 504, and 474 cm^{-1}. ^{1}H NMR (400 MHz, $CDCl_3$): δ=3.17 (dd, *J*=7.2 and 6.0 Hz, 4H, CH_2Se), 3.46 (dd, *J*=7.2 and 6.0 Hz, 4H, CH_2S), 4.26 (t, *J*=1.8 Hz, 4H, H_α), and 4.31 (t, *J*=1.8 Hz, 4H, H_β). ^{13}C NMR (100 MHz, $CDCl_3$): δ=24.91 (t, *J*=67.9 Hz, $SeCH_2$), 37.99 (SCH_2), 67.87 (C_β), 71.29 (C_α), and 89.24 (C_b).

(1,9-Dithia-5-selena[9](1,1′)ferrocenopahane-*S,S′,Se,Fe*)-palladium(II) Tetrafluoroborate (15a). A mixture of dichlorobis(acetonitrile)palladium(II) (26 mg, 0.1 mmol) and silver(I) tetrafluoroborate (40 mg, 0.2 mmol) in acetone (2 cm^3) was stirred for 1 h at room temperature and then filtered to remove the resulting silver(I) chloride. To the filtrate was added a solution of 1,9-dithia-5-selena[9]-(1,1′)ferrocenophane (41 mg, 0.1 mmol) in dry acetonitrile (5 cm^3); the solution was then stirred for 1 h at room temperature. The solution was evaporated under reduced pressure and the residue was then dissolved in acetonitrile (5 cm^3). The resulting dark-brown solution was diluted with dry diethyl ether and kept in a freezer overnight to give the title compound (**15a**) containing one equivalent of acetonitrile as black needles, mp 250 °C. Found: C, 29.76; H, 3.24; N, 1.94%. Calcd for $C_{16}H_{20}B_2F_8S_2SePd\cdot C_2H_3N$: C, 29.52; H, 3.16; N, 1.91%.

(1,7-Dithia-7-selena[7](1,1′)ferrocenophane-*S,S′,Se,Fe*)-palladium(II) Tetrafluoroborate (16a). To a solution of palladium(II) tetrafluoroborate [prepared as described above and then diluted with dry acetone (20 cm^3)], a solution of 1,7-dithia-4-selena[7](1,1′)ferrocenophane (38 mg, 0.1 mmol) in dry acetone (10 cm^3) was added dropwise for a period of 10 min. After the solution was stirred for 1 h the resulting crystals were filtered. A green powder (16 mg, 31%) of bis(1,7-dithia-4-selena[7](1,1′)ferrocenophane-*S,S′*)-palladium(II) tetrafluoroborate (**17a**) was obtained. Mp 250 °C. Found: C, 32.37; H, 3.02%. Calcd for $C_{28}H_{32}B_2F_8S_4Se_2Fe_2Pd$: C, 32.13; H, 3.08%. IR (KBr): 3116, 2996, 2944, 1416, 1258, 1084, 926, 886, 830, 528, 486, and 456 cm^{-1}. After the filtrate was evaporated under reduced pressure, the residue was dissolved in dry acetonitrile (5 cm^3). The

resulting solution was diluted with dry diethyl ether (5 cm^3) and kept in a freezer overnight to give the title compound (**16a**) containing one equivalent of acetonitrile as black fine needles, mp 250 °C. Found: C, 27.44; H, 2.74; N, 2.37%. Calcd for $C_{14}H_{16}B_2F_8S_2SeFePd \cdot C_2H_3N$: C, 27.28; H, 2.71; N, 1.98%.

(1,5,9-Trithia[9](1,1′)ferrocenophane-*S,S′,S″,Fe*)-platinum Tetrafluoroborate (5b). A mixture of dichlorobis(acetonitrile)platinum(II) (35 mg, 0.1 mmol) and silver(I) tetrafluoroborate (40 mg, 0.2 mmol) in dry acetonitrile (5 cm^3) was refluxed for 2 h under nitrogen. To the resulting mixture was added a solution of 1,5,9-trithia[9](1,1′)-ferrocenophane (36 mg, 0.1 mmol) in dry acetonitrile (5 cm^3). The mixture was refluxed for 1 h and then filtered to remove silver(I) chloride. The filtrate was evaporated under reduced pressure; then, the residue was dissolved in dry acetone–acetonitrile (4:1 v/v, 5 cm^3). The resulting solution was filtered and the filtrate was diluted with dry diethyl ether (2 cm^3) to give the title compound **5b** as red needles (53 mg, 73%), mp 250 °C. Found: C, 26.42; H, 2.76%. Calcd for $C_{16}H_{20}B_2F_8S_3FePt$: C, 26.21; H, 2.75%.

(1,9-Dithia-5-selena[9](1,1′)ferrocenophane-*S,S′,Se,Fe*)-platinum(II) Tetrafluoroborate (15b). This compound was prepared from 1,9-dithia-5-selena[9](1,1′)ferrocenophane (41 mg, 0.1 mmol) according to the procedure described above. The title compound (**15b**) was obtained as red needles (55 mg, 70%), mp 250 °C. Found: C, 24.27; H, 2.54%. Calcd for $C_{16}H_{20}B_2F_8S_2SeFePt$: C, 24.63; H, 2.58%.

The present work was supported by a Grant-in-Aid for Science Research (No. 63540382) from the Ministry of Education, Science and Calture.

References

1) M. I. Bruce, *J. Organomet. Chem.*, **242**, 147 (1983); **283**, 389 (1985).
2) G. L. Geoffroy and D. A. Roberts, "Comprehensive Organometallic Chemistry," ed by G. Wilkinson, F. G. A. Stone, and E. W. Abel, Pergamon Press, Oxford (1982), Chap. 40.
3) W. R. Cullen and J. D. Woolins, *Coord. Chem. Rev.*, **39**, 1 (1981).
4) G. M. Whitesides, J. F. Gaasch, and E. S. Stedronsky, *J. Am. Chem. Soc.*, **94**, 5258 (1972).
5) B. M. McCulloch, D. L. Ward, J. D. Woolins, and C. H. Brubacker, Jr., *Organometallics*, **4**, 1425 (1985).
6) D. Seyferth, B. W. Hames, T. G. Rucker, M. Cowie, and R. S. Dickson, *Organometallics*, **2**, 472 (1983).
7) M. Cowie and R. S. Dickson, *J. Organomet. Chem.*, **326**, 269 (1987).
8) S. Akabori, T. Kumagai, T. Shirashige, S. Sato, K. Kawazoe, C. Tamura, and M. Sato, *Organometallics*, **6**, 526 (1987).
9) M. Watanabe, H. Ichikawa, I. Motoyama, and H. Sano, *Bull. Chem. Soc. Jpn.*, **56**, 3291 (1983).
10) S. R. Cooper, *Acc. Chem. Res.*, **21**, 141 (1988).
11) M. Sato, S. Tanaka, S. Akabori, and Y. Habata, *Bull. Chem. Soc. Jpn.*, **59**, 1515 (1986).
12) M. Sato, K. Suzuki, and S. Akabori, *Bull. Chem. Soc. Jpn.*, **59**, 3611 (1986).
13) L. S. Hegedus, T. A. Mulhern, and H. Asada, *J. Am. Chem. Soc.*, **108**, 6224 (1986).
14) A preliminary report: M. Sato, K. Suzuki, and S. Akabori, *Chem. Lett.*, **1987**, 1847.
15) F. R. Hartley, S. G. Murray, and C. A. McAukiffe, *Inorg. Chem.*, **18**, 1394 (1979).
16) M. Sato, S. Tanaka, S. Ebine, and S. Akabori, *Bull. Chem. Soc. Jpn.*, **57**, 1929 (1984).
17) M. L. Bird and F. Challenger, *J. Chem. Soc.*, **1942**, 570.
18) J. A. Kramer and D. N. Hendrickson, *Inorg. Chem.*, **19**, 3330 (1980).
19) K. Wieghardt, H.-J. Kuppers, E. Raabe, and C. Kruger, *Angew. Chem., Int. Ed. Engl.*, **25**, 1101 (1986).
20) I. R. Butler, W. R. Cullen, T.-J. Kim, S. J. Rettig, and J. Trotter, *Organometallics*, **4**, 972 (1985).
21) M. Cais, J. J. Dannenberg, A. Eisenstadt, M. I. Levenberg, and J. H. Richards, *Tetrahedron Lett.*, **1966**, 1695.
22) M. Hisatome and K. Yamakawa, *Tetrahedron*, **27**, 2101 (1971).
23) U. Behrens, *J. Organomet. Chem.*, **182**, 89 (1979).
24) S. Braun and W. E. Watts, *J. Organomet. Chem.*, **84**, C33 (1975).
25) S. Braun, T. Abram, and W. E. Watts, *J. Organomet. Chem.*, **97**, 429 (1975).
26) L. N. Mulay and M. E. Fox, *J. Chem. Phys.*, **38**, 760 (1963).
27) G. Reid, A. J. Blake, T. I. Hyde, and M. Schröder, *J. Chem. Soc., Chem. Commun.*, **1988**, 1397.
28) There is the description that the $Pd(BF_4)_2$ complex of 1,4,8,11-tetrathiacyclotetradecane shows no absorption near 600 nm, in the following paper: A. J. Blake, A. J. Holder, T. I. Hyde, Y. V. Roberts, A. J. Lavery, and M. Schröder, *J. Organomet. Chem.*, **323**, 261 (1987).
29) M. Sato, S. Akabori, M. Katada, I. Motoyama, and H. Sano, *Chem. Lett.*, **1987**, 1847.

Study on the Claisen Rearrangement. VI.[1] Catalytic Effect of Alkali Metal Salts on the Claisen Rearrangement of Allyl *o*- or *p*-Hydroxyphenyl Ether

Takatoshi HAYASHI, Yutaka OKADA,* and Takeshi INABA†
Department of Chemistry, Faculty of Science and Engineering, Ritsumeikan University, Kita-ku, Kyoto 603
(Received June 17, 1989)

The Claisen rearrangement of allyl *o*- or *p*-hydroxyphenyl ether is catalyzed by alkali metal salts. The mechanism of the catalytic effect is different from that by Lewis acids such as zinc chloride. It is considered that the hydroxyl group is dissociated into phenoxide ion $-O^-$ with loss of its proton through attack by the anion residue of an alkali metal salt. Thus, the catalytic effect is attributable to a strong electron-releasing effect of phenoxide ion $-O^-$. Furthermore, for the *o*-isomer, an intramolecular repulsion between the phenoxide ion $-O^-$ and the ethereal oxygen operates.

Usually, the Claisen rearrangement is a thermal reaction. However, the rearrangement is accelerated through acid catalysis.[2,3] The authors found an accelerated effect by zinc chloride for the rearrangement of allyl (substituted phenyl) ether (x-APE) and discussed the mechanism.[4] In the transition state of the Claisen rearrangement, the electron density of the ethereal oxygen of allyloxyl group increases.[5] However, in the presence of zinc chloride, the high electron density is reduced by the coordination of the salt to the ethereal oxygen. Therefore, the transition state is stabilized, and the reaction is accelerated.

In this research, alkali metal salts were used as catalysts for the Claisen rearrangement of x-APE. For an methoxy derivative (OCH_3-APE), no catalytic effects by these salts were noticed. However, the rearrangement of hydroxy derivatives (OH-APE) was strongly catalyzed by these salts. The mechanism of this catalytic effect is discussed.

Experimental

Preparation of Materials. The preparation and physical properties of x-APE were reported in the preceding papers.[5,6]

Measurements on the Claisen Rearrangement. The Claisen rearrangement was carried out in a small glass

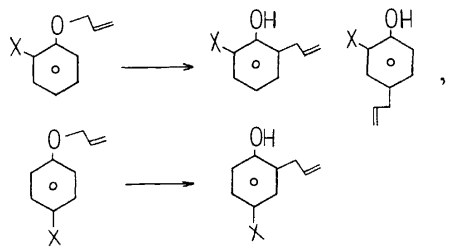

ampoule as described in a previous paper.[7] x-APE and an alkali metal salt were put into an ampoule with a solvent (methanol or water-methanol). The solvent was 20 times and the catalyst (alkali metal salt) was 0.1—0.5 time in mol as much as the x-APE. The ampoule was heated at a constant temperature in an oil bath. After a measured time, the reaction mixture was cooled. The solvent was evaporated from the reaction mixture. The residue was acidified with 10% HCl and extracted with ether. The amounts of the unreacted material and products were determined by GLC. For *o*-x-APE, the conversion amount is defined as the sum of those of *o*- and *p*-rearranged products.

† Present address: Nissha Printing Co., 3 Mibu Hanai-cho, Nakagyo-ku, Kyoto 603.

Results and Discussion

For the Claisen rearrangement of *o*-OH-, *o*-OCH_3-, and *p*-OH-APEs, the catalytic effect by sodium acetate is shown in Fig. 1, where the magnitude of catalytic effect is defined as the difference between the conversion amounts in the presence and absence of the salt. For *o*-OH-APE, the catalytic effect is observed, increasing with a increasing amount of sodium acetate. For *o*-OCH_3-APE, the catalytic effect is quite small. For *p*-OH-APE, the catalytic effect is observed.

The catalytic effect by sodium acetate will be compared with that by zinc chloride.[4] As shown in Fig. 2, for the methoxy derivative, the effect by sodium acetate is much smaller than that by zinc chloride. However, for the *p*-hydroxy derivative, sodium acetate accelerates the reaction by far more than zinc chloride. It may thus be considered that the mechanism of the

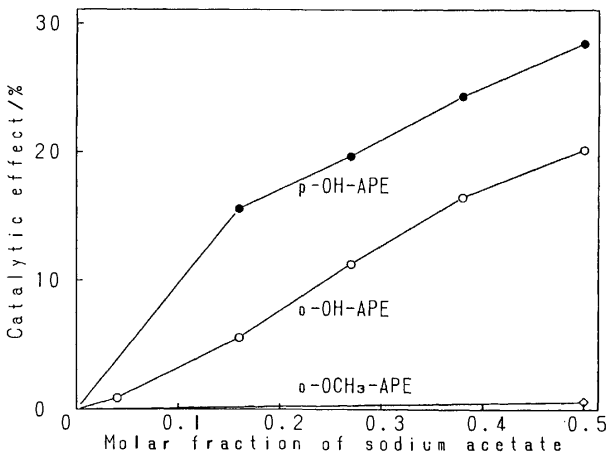

Fig. 1. The catalytic effect of CH_3COONa for the conversion of x-APE (solv.: CH_3OH, reaction time: 1 h, reaction temperature: 145 °C (*o*-isomer), 160 °C (*p*-isomer)).

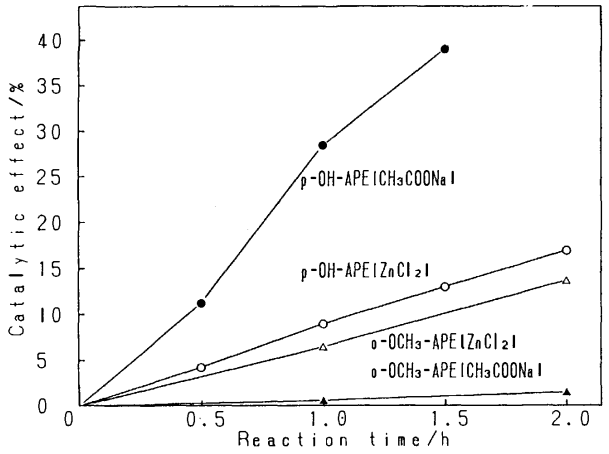

Fig. 2. The catalytic effect of CH_3COONa and $ZnCl_2$ for the conversion of x-APE (solv.: CH_3OH, salt: APE=0.5 : 1, reaction temperature: 145 °C (*o*-isomer), 160 °C (*p*-isomer)).

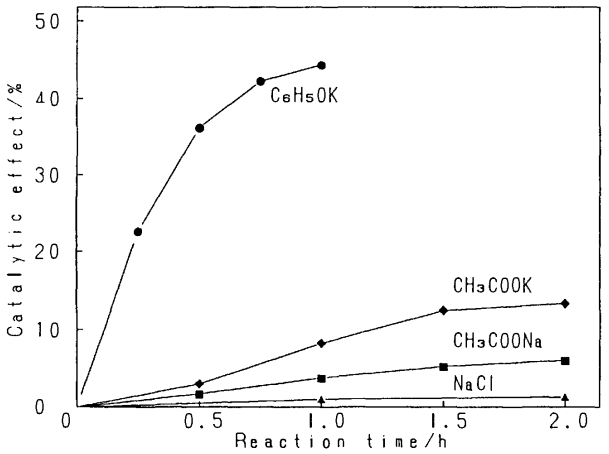

Fig. 3. The catalytic effect of alkali metal salts for the conversion of *o*-OH-APE at 145 °C (solv.: CH_3OH (potassium salt), $CH_3OH : H_2O$=1 : 1 (sodium salt), salt: APE=0.5 : 1).

catalytic effect by sodium acetate is different from that by zinc chloride.

As shown in Fig. 3, the order of the catalytic effects by the alkali metal salts is

phenolate > acetate > chloride.

This order is the same as that of the basicities of the anion residues of the salts.[8] The degree of dissociation of the hydroxyl group of OH-APE is largest in the presence of phenolate and smallest in the presence of chloride:

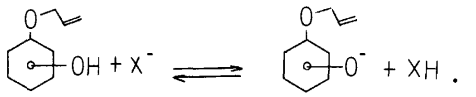

$X^- = C_6H_5O^-, CH_3COO^-, Cl^-$

Table 1. Catalytic Effect of Alkali Metal Salts for the Conversion of *o*-OH-APE at 145 °C (Solv. CH_3OH)[a]

Reaction time/h	Catalytic effect/%		
	CH_3COOLi	CH_3COONa	CH_3COOK
0.5	26.9	10.0	3.0
1.0	43.3	20.2	8.3
1.5	48.8	24.6	12.5

a) CH_3COOM : APE=0.5 : 1.

Table 2. Conversion of *o*-OH-APE in the Presence of Alkali Metal Salts at 145 °C (Solv. CH_3OH)[a,b]

Salt	*o*/%	*p*/%	*p*/*o*	log (*p*/*o*)
None	16.5	9.5	0.58	−0.24
CH_3COOLi	20.8	48.5	2.33	0.37
CH_3COONa	19.4	26.8	1.38	0.14
CH_3COOK	17.3	17.0	0.98	−0.01
C_6H_5OK	18.0	52.4	2.91	0.46

a) Salt : *o*-OH-APE=0.5 : 1. b) Reaction time: 1 h.

For the change in metal ions (Table 1), the order is

Li salt > Na salt > K salt.

In methanol, the degree of solvation of metal ions increases with decreasing ionic radius.[9] This order seems parallel with the stability of the alkali metal ions in methanol. It is in agreement with the order of the degrees of dissociation of the alkali metal salts.

As shown in Table 2, the (para rearranged product)/(ortho rearranged product) value (*p*/*o* ratio) for *o*-OH-APE is increased by the addition of the alkali metal salts. The order of the magnitudes of the *p*/*o* ratios is

phenolate > acetate

and

Li salt > Na salt > K salt.

These orders agree with that of the catalytic effects. As stated in preceding paper,[1] the *p*/*o* ratio is closely

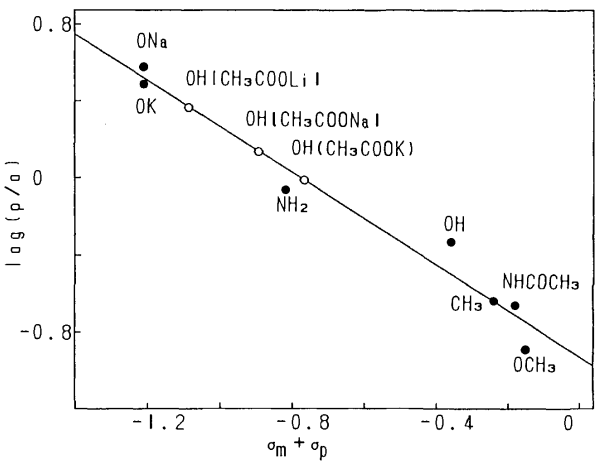

Fig. 4. The relationship between *p*-product to *o*-product (*p*/*o*) in *o*-X-APE and ($\sigma_m+\sigma_p$) (σ_m and σ_p values of -ONa and -OK are used in that of $-O^-$).

related to the value of substituent constant $(\sigma_m+\sigma_p)$.[10,11] A strongly electron-releasing substituent possesses a negative large value of $(\sigma_m+\sigma_p)$. For the rearrangement of an APE possessing such an electron-releasing substituent, the value of p/o ratio is large. As shown in Fig. 4, the value of $(\sigma_m+\sigma_p)$ of hydroxyl group alone is -0.36, and $\log(p/o)$ in the absence of alkali metal salt is -0.33. However, in the presence of the salt, $\log(p/o)$ is -0.01—0.37. This value corresponds to -0.77— -1.09 of $(\sigma_m+\sigma_p)$ (Fig. 4). The electron-releasing ability of hydroxyl group is increased by the addition of alkali metal salt. It seems that the value of $(\sigma_m+\sigma_p)$ of hydroxyl group increased by the addition of alkali metal salt is close to the values of $(\sigma_m+\sigma_p)$ of pheoxide ion ($-O^-$).

Consequently, the mechanism of the catalytic effect by the alkali metal salts may be interpreted as follows. The hydroxyl group of *o*(or *p*)-OH-APE is converted to phenoxide ion $-O^-$ by the anion residue of the salt:

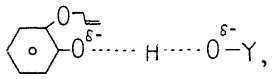

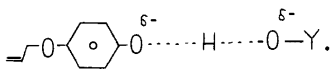

Y = $COCH_3$, C_6H_5

Therefore, in analogy with APEs bearing metal oxide groups,[1] the benzene ring is stabilized by the strong electron-releasing effect of phenoxide ion $-O^-$. (In the transition state, a positive charge is produced on the benzene ring of APE.[7]) In addition to the above effect, for *o*-isomer, another effect is to be considered: an intramolecular repulsion between the phenoxide ion $-O^-$ and the ethereal oxygen of allyloxyl group. By this repulsion, the ground state is unstabilized and the activation energy for the rearrangement decreased.

For *o*-OH-APE, the rearrangement is accelerated by these two effects (the strong electron-releasing effect and the intramolecular repulsion effect). On the other hand, for *p*-isomer, only the strong electron-releasing effect is put into operation. Therefore, it is expected that the catalytic effect for *o*-OH-APE is larger than that for *p*-OH-APE. In fact, the experimental results agree with this assumption (Fig. 5). However, the difference in catalytic effect between *o*- and *p*-OH-APEs is not so large. The reactivity of *o*-OH-APE alone is much higher than that of *p*-OH-APE (Fig. 5) because, in *o*-OH-APE, an intramolecular hydrogen bond is formed between the hydroxyl group and the ethereal oxygen.[6] The negative charge of the ethereal oxygen produced in the transition state is reduced by this hydrogen bond.[6] But by the addition of alkali metal salt, the above intramolecular hydrogen bonding effect for *o*-OH-APE is caused to disappear. It seems that the observed catalytic effect for *o*-OH-APE by alkali metal salt is not so large as to be balanced by the profit and loss.

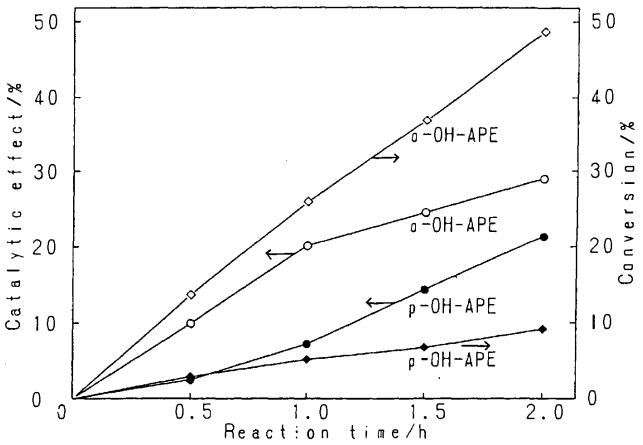

Fig. 5. The conversion and the catalytic effect of CH_3COONa for the conversion of *o*- and *p*-OH-APE at 145 °C (solv.: CH_3OH, salt: APE=0.5 : 1).

References

1) Part V: M. Goto, T. Hayashi, K. Goda, and Y. Okada, *Nippon Kagaku Kaishi*, **1986**, 1096.
2) W. N. White and E. F. Wolfarth, *J. Org. Chem.*, **35**, 2196 (1970).
3) H. L. Goering and R. R. Jacobson, *J. Am. Chem. Soc.*, **80**, 3277 (1958).
4) T. Hayashi and M. Goto, *Nippon Kagaku Kaishi*, **1978**, 1007.
5) T. Hayashi and M. Goto, *Nippon Kagaku Kaishi*, **1977**, 1512.
6) M. Goto and T. Hayashi, *Nippon Kagaku Kaishi*, **1986**, 49.
7) M. Goto and T. Hayashi, *Nippon Kagaku Kaishi*, **1979**, 743.
8) "Kagaku Binran," ed by the Chemical Society of Japan, Maruzen, Tokyo (1984), p. 343.
9) Z. Tokura, "Yobaiwa," Kagaku Dozin, Kyoto (1973), p. 28.
10) W. N. White, D. Gwynn, R. Schlitt, C. Girard, and W. Fife, *J. Am. Chem. Soc.*, **80**, 3271 (1958).
11) H. H. Jaffé, *Chem. Rev.*, **53**, 191 (1953).

The Effect of Sodium Hydroxide on the Stereoselectivity of Hydrogenolytic Asymmetric Transaminations between (*R*)-2-Amino-2-phenylethanol and 2-Keto Acids†

Minoru TAMURA,†† Shozo SHIONO,††† and Kaoru HARADA*
Department of Chemistry, University of Tsukuba, Tsukuba, Ibaraki 305
(Received June 30, 1989)

Hydrogenolytic asymmetric transaminations between (*R*)-2-amino-2-phenylethanol and 2-keto acids were carried out over Pd catalyst in the absence or presence of various amount of sodium hydroxide in water or alcohols. The stereoselectivity of the reaction was significantly influenced by the amount of sodium hydroxide in the reaction mixture. When pyruvic acid was used in water the optical purity of alanine was 22% ee (*R*) and in 1 M (1 M=1 mol dm^{-3}) sodium hydroxide solution it was 62% ee (*S*). When 2-oxobutyric acid was used in ethanol in the absence and presence of sodium hydroxide (1M), the optical yields of 2-aminobutyric acid were 2% ee (*R*) and 81% ee (*S*), respectively. In contrast, the addition of sodium hydroxide had little or no effect on the stereochemistry of the reaction using (*S*)-α-methylbenzylamine as a chiral source in aqueous or ethanolic solution. The substituent, additive, temperature, and solvent effects on the asymmetric reactions were examined in aqueous or ethanolic alkaline solution. Based on these experimental results, a possible explanation for the change in stereoselectivity by using sodium hydroxide is discussed.

There have been many studies on the hydrogenolytic asymmetric transamination between chiral amines or amino acid derivatives and 2-keto acids or their esters, and some of them have been explained by the chelation mechanism.[1-6]

In the previous study,[6] a hydrogenolytic asymmetric transamination between pyruvate and (*R*)-2-amino-2-phenylethanol (**1a**) in organic solvent was carried out. The configuration of the resulting amino acid was (*S*), and its optical purity increased with the decrease of the polarity of the solvent used. Such an effect and also substituent effect on the stereoselectivity were explained by the chelation mechanism.

In the present study, hydrogenolytic asymmetric transaminations between 2-keto acids and **1a** were carried out in aqueous and alcoholic alkaline solutions (Scheme 1). As a result, we found that (*S*)-selectivity increased by the addition of sodium hydroxide. This result could not be explained by the chelation mechanism, because (*S*)-selectivity should be decreased with the increase of the solvent polarity.

Figure 1 shows the results of the preliminary experiments of hydrogenolytic asymmetric transamination between pyruvic acid and **1a** in the mixtures of methanol or ethanol and 1 M of aqueous NaOH (1 M=1 mol dm^{-3}). With the increase of the content of 1 M NaON, the optical purites of the products (52, 57%) decreased and reached a minimum (8,13%) with a 33% content of 1 M NaOH and then increased (61, 62%).

Figure 2 shows the result of the experiments carried out in the mixtures of water and methanol in various ratios at certain alkali concentrations. It was found that the addition of sodium hydroxide increased the optical yeild of the product, while an increase of water content decreased the optical purity. It was therefore concluded that the increase of (*S*)-selectivity in the reaction was mainly due to sodium hydroxide.

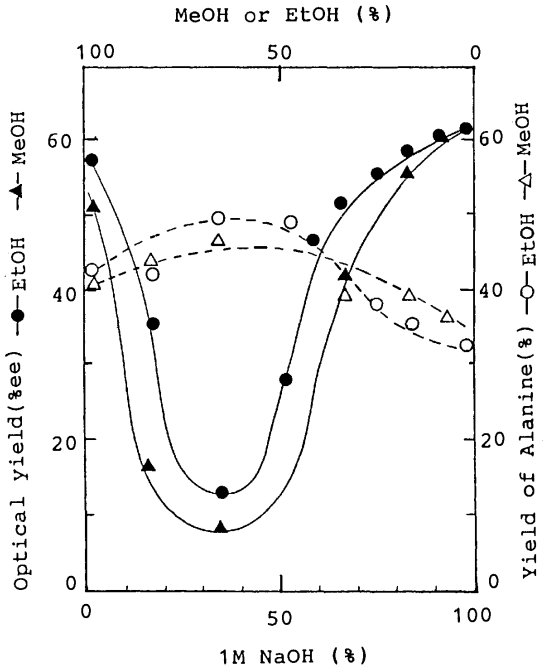

Fig. 1. Asymmetric hydrogenation in a mixture of alcohol and 1M NaOH aq.

Catalytic Hydrogenation in Aqueuous Solution. Asymmetric transaminations between **1a** and pyruvic acid or 2-oxobutyric acid were carried out in aqueous solution containing various amounts of sodium hydroxide (Fig. 3). The optical yield of the products increased considerably by the addition of sodium

† This work is a part of Ph. D. Thesis of M. Tamura (Tsukuba University, 1984).

†† Present address: Department of Biochemistry, Medical College of Oita, Hazama-cho, Oita 879-56.

††† Present address: Research Laboratory, Shionogi Pharmaceutical Co., Osaka.

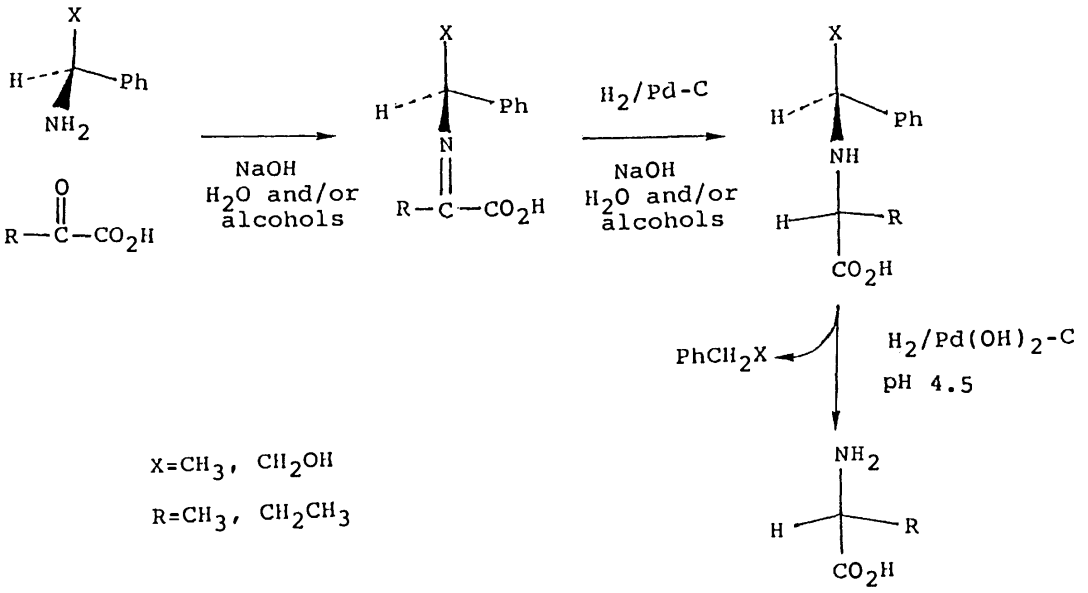

Scheme 1. Hydrogenolytic asymmetric transamination in aqueous and alcoholic alkaline solutions.

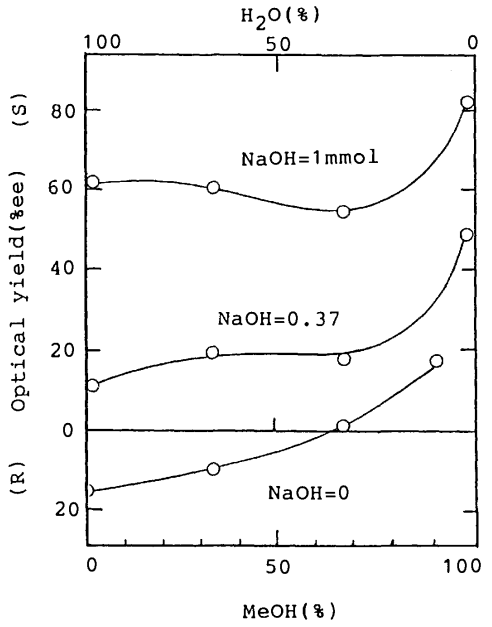

Fig. 2. Asymmetric hydrogenation in a mixture of MeOH and water in the presence of different amount of NaOH.

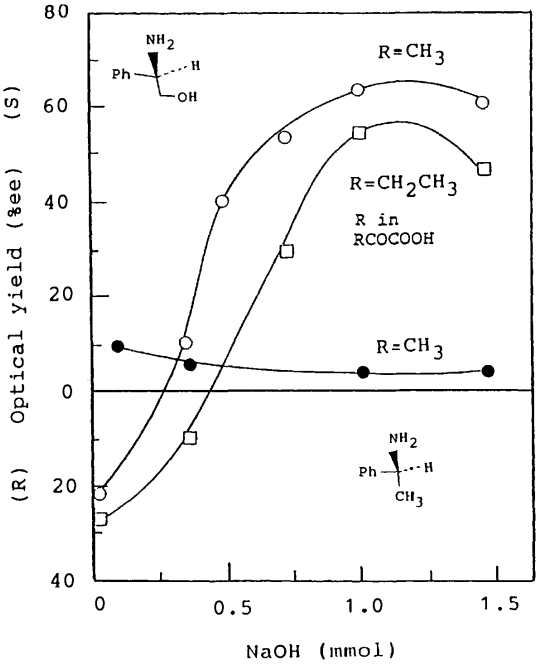

Fig. 3. Effect of NaOH on the optical yield of the asymmetric transamination in aqueous solution.

hydroxide. When the amount of sodium hydroxide was zero or small, (*R*)-product was obtained in excess. With an increase of sodium hydroxide, the configuration of the product inverted from (*R*) to (*S*), and the optical purity of the product increased to 62% ee (alanine) or 54% ee (2-aminobutyric acid) at 1 mmol of sodium hydroxide. By further increasing the amount of sodium hydroxide, the optical yield decreased slightly.

In order to examine whether the hydroxyl group of the chiral source was involved or not in the improvement of the optical yield in alkaline solution, (*S*)-α-methylbenzylamine (**1b**) was used as a chiral source, in which the hydroxymethyl group of **1a** is replaced with a methyl group. The addition of sodium hydroxide had no significant effect on the stereochemistry of the catalytic hydrogenation with **1b** (Table 1, Fig. 3). This result suggested that the hydroxyl group plays an important role in determining the steric course of the reaction in the presence of sodium hydroxide.

Table 2 shows the effect of various additives on the optical purity of the product obtained in aqueous

Table 1. Effect of NaOH on Asymmetric Hydrogenation in Aqueous Solution

R in RCOCOOH	Asymmetric moiety	NaOH (mmol)	Amino acid formed	Chem.y. (%)	Opt.y. (% ee)
R=CH_3	**1a**	0	Ala	41	22 (*R*)
		0[a]		35	33 (*R*)
		0.37		36	11 (*S*)
		0.5		37	40 (*S*)
		0.73		35	54 (*S*)
		1.0		34	62 (*S*)
		1.46		27	61 (*S*)
		1.0[b]		29	61 (*S*)
	1b	0.1	Ala	49	11 (*S*)
		0.37		43	9 (*S*)
		1.0		47	3 (*S*)
R=CH_2CH_3	**1a**	0	But	54	28 (*R*)
		0.37		48	10 (*R*)
		0.73		34	29 (*R*)
		1.0		34	54 (*S*)
		1.46		29	47 (*S*)

a) Pd-C was washed well with water before use. b) The starting mixture was stirred without NaOH, and NaOH was added just before hydrogenation reaction.

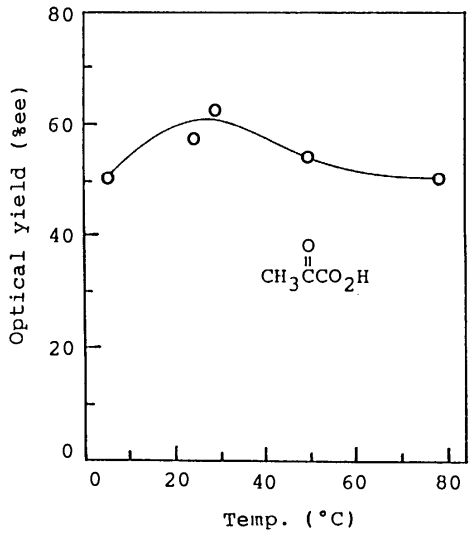

Fig. 4. Temperature effect on the optical yield of asymmetric transamination in aqueous alkaline solution.

solution. When alkali halides or triethylamine were added to the reaction mixture, the (*S*)-product was obtained in a small excess. The effects of potassium hydroxide and lithium hydroxide were similar to that of sodium hydroxide. When NaCl or urea was added together with sodium hydroxide, the optical yield was lower than that with sodium hydroxide alone. These results indicated that the effect of sodium hydroxide on optical yield is mainly caused by hydroxide ion.

The temperature effect was examined by the use of pyruvic acid (Fig. 4). The temperature dependence on the optical yield was not high. This result was apparently different from that with phenylglycine,[4] in which the optical yield decreased with increase of the temperature.

Table 2. Effect of Additives on Asymmetric Hydrogenation in Aqueous Solution[a]

Additives (1 mmol)	Chem.y.[b] (%)	Opt.y.[c] (% ee)	Confign
—	41	14	(*R*)
NaCl	17	2	(*S*)
KBr	19	19	(*S*)
Triethylamine[d]	46	2	(*S*)
Triethylamine	36	11	(*S*)
NaOH	34	62	(*S*)
LiOH	36	55	(*S*)
KOH	37	63	(*S*)
NaOH+NaCl	22	23	(*S*)
NaOH+Urea[d]	24	29	(*S*)

a) The reaction was carried out with **1a** and pyruvic acid. The asymmetric hydrogenation was performed with various additives. b) Chemical yields of alanine were starting from pyruvic acid. c) Optical yields were determined by GLC-method. d) 0.36 mmol of additives were used.

Table 3. Asymmetric Transamination Using Several α-Keto Acids[a] in Aqueous Alkaline Solution

α-keto acids	Amino acids formed	Chem.y. (%)	Opt.y.[b] (% ee)	Confign
CH_3CCO_2H (O)	Ala	38	64	(*S*)
$CH_3CH_2CCO_2H$ (O)	But	29	54	(*S*)
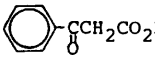	Phe[c]	10	10	(*S*)
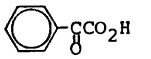	Ph-Gly[c]	18	19	(*R*)

a) Asymmetric hydrogenation was carried out in aqueous alkaline solution (NaOH, 1 mmol). b) Optical yields were determined by GLC-method. c) Trace amount of hexahydrophenylalanine or α-cyclohexylglycine was also formed.

Table 4. Effect of NaOH on the Asymmetric Hydrogenation in Ethanolic Solution

R in RCOCOOH	Asymmetric moiety	NaOH (mmol)	Amino acid formed	Chem.y. (%)	Opt.y.(% ee) GLC-method	DNP-method
$R=CH_3$	**1a**	—[a]	Ala	44	48 (*S*)	
		0.37		43	51 (*S*)[b]	49 (*S*)
		0.73		42	76 (*S*)	
		1.0		40	85 (*S*)[b]	82 (*S*)
		1.5		41	84 (*S*)	
$R=CH_2CH_3$	**1a**	—[a]	But	69	2(*R*)	
		0.37		58	6(*R*)[b]	5 (*R*)
		0.73		38	70(*S*)	
		1.0		35	87(*S*)[b]	87 (*S*)
		1.5		30	82(*S*)	
		1.0[c]		19	81(*S*)	
	1b	0.37	But	40	35 (*R*)	
		0.73		31	28 (*R*)	
		1.1		16	21 (*R*)	

a) Et_3N (1 equiv mol, 0.37 mmol) was added to the reaction mixture. b) These values were the averages of the results from independent experiments. c) The reaction was carried out in the presence of NaOH (1 mmol) and NaCl (0.5 mmol).

The substituent effect was examined by the use of several 2-keto acids in the presence of sodium hydroxide (Table 3). When pyruvic acid, 2-oxobutyric acid, and phenylpyruvic acid were used, the optical purities were 62, 54, and 11% ee (*S*), respectively. When benzoylformic acid was used, the configuration of the product was inverted. The selectivity of (*S*)-product decreased in the order of CH_3->CH_3CH_2->$PhCH_2$->Ph-. This order agreed with the effective bulkiness of R group of 2-keto acids.[5]

Catalytic Hydrogenation in Ethanolic Solution. In order to examine the alkali effect in ethanol, the reaction was performed in ethanol containing various amounts of sodium hydroxide using pyruvic acid and 2-oxobutyric acid (Table 4, Fig. 5). When pyruvic acid was used in the absence of sodium hydroxide (1 equiv mol of triethylamine was used in the reaction), the optical yield of alanine was 48% ee (*S*). With the increase of the amount of sodium hydroxide, the optical purity increased to 85% ee (*S*). When 2-oxobutyric acid was used in the absence of sodium hydroxide, (*R*)-2-aminobutyric acid was favored slightly. Addition of sodium hydroxide resulted in the inversion of configuration of the product, and a sudden increase in the selectivity of (*S*)-configuration was observed. When 1 mmol of sodium hydroxide was used, (*S*)-2-aminobutyric acid was obtained in an optical yield of 87% ee. In the reaction with 2-oxobutyric acid, the chemical yields decreased with increasing amount of sodium hydroxide.

When (*S*)-α-methylbenzylamine was used in the reaction with 2-oxobutyric acid, the configuration of the product was (*R*). The addition of sodium hydroxide had little effect on the optical yield in contrast to the result with **1a**. These results clearly indicate that the hydroxyl group in the substrate is involved in the stereochemistry of the reaction.

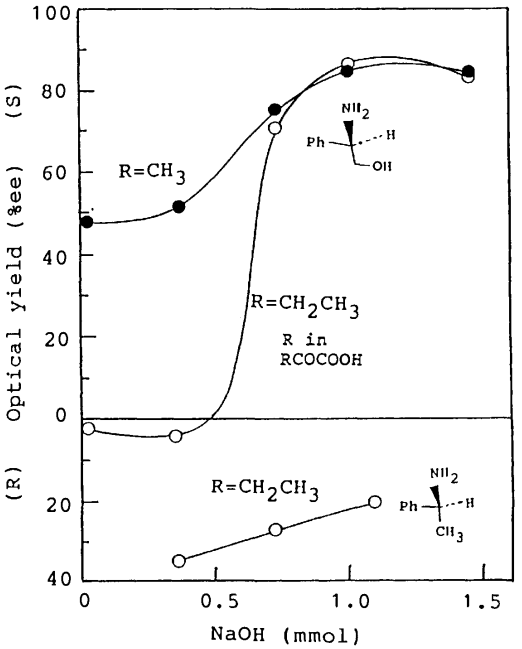

Fig. 5. Effect of NaOH on the optical yield of the asymmetric hydrogenation in ethanolic solution.

In Table 4, the optical yield of the products were further confirmed by DNP method. The optical yields determined by GLC method were in good agreement with those by DNP method.

The effect of substituents in 2-keto acids was examined. The reaction was carried out using several 2-keto acids in the presence of 1 mmol of sodium hydroxide in ethanol. The results are shown in Table 5. When 2-oxobutyric acid was used, the optical yield of the resulting 2-aminobutyric acid was similar to that with pyruvic acid. The selectivity of (*S*)-product was as follows CH_3->C_2H_5->$PhCH_2$->Ph-.

Table 5. Asymmetric Transamination with Several α-Keto Acids in Ethanolic Alkaline Solution[a]

α-Keto acid	Amino acids formed	Chem.y. (%)	Opt.y.[b] (% ee)	Confign
CH_3CCO_2H (O)	Ala	42	85	(*S*)
$CH_3CH_2CCO_2H$ (O)	But	33	86	(*S*)
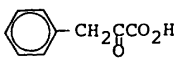	Phe	17	17	(*S*)
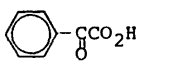	Ph-Gly	21	25	(*R*)

a) The asymmetric hydrogenation was carried out in ethanolic alkaline solution (NaOH, 1 mmol). b) The optical yields were determined by GLC-method.

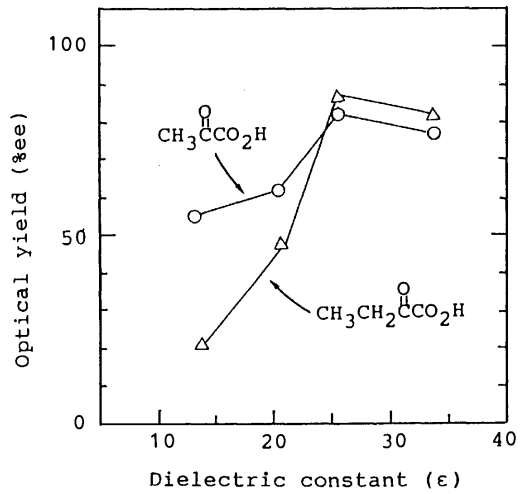

Fig. 6. Effect of solvent on the optical yield of asymmetric hydrogenation in the presence of NaOH.

Table 6. Effect of Triethylamine on the Asymmetric Hydrogenation in Ethanolic Solution

R in RCOCOOH	Et_3N[a] (mmol)	Amino acid formed	Chem.y. (%)	Opt.y. (% ee)
$R=CH_3$	0.37 (1.0)	Ala	44	48 (*S*)
	0.73 (2.0)		40	47 (*S*)
	1.1 (3.0)		38	51 (*S*)
$R=CH_2CH_3$	0.37 (1.0)	But	69	2 (*R*)
	0.73 (2.0)		50	4 (*R*)
	1.1 (3.0)		49	1 (*R*)

a) The values in parentheses were equivalent mol of triethylamine to starting 2-keto acids.

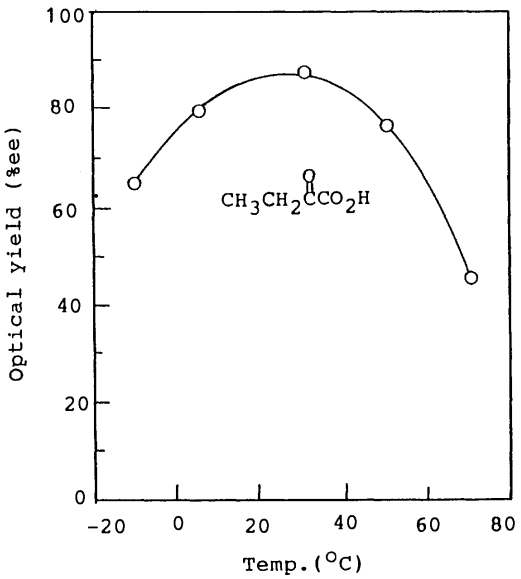

Fig. 7. Temperature effect on the optical yield of the asymmetric hydrogenation in ethanolic alkaline solution.

The solvent effect on the asymmetric transamination in the presence of 1 mmol of sodium hydroxide is shown in Fig. 6. When methanol was used as the solvent, the optical purity of the (*S*)-product was slightly lower than that with ethanol. When isopropyl alcohol or *s*-butyl alcohol was used, the optical yield of the reaction was much lower than that with ethanol. The order of the optical purity with these alcohols is: EtOH>MeOH>*i*-PrOH>*s*-BuOH. And this order was not consistent with the order of the polarity of the solvent.

The temperature effect on the optical yield of the reaction of 2-oxobutyric acid with **1a** is shown in Fig. 7. The plots of the optical yield versus temperature gave a bell-shape profile with a maximum at 30 °C.

In order to examine whether the optical yield was influenced by bases other than sodium hydroxide, the reactions were carried out in the presence of different amounts of triethylamine (Table 6). The change of the amount of triethylamine had no effect on the optical yield with pyruvic acid or 2-oxobutyric acid in the range of 0.37 to 1.1 mmol, although chemical yields decreased with the increase of triethylamine.

Experimental

The amino acid analyses were performed with a Yanagimoto LC-5S and Durrum model 500. The gas chromatographic analyses were carried out with a Hitachi 163 type gas chromatograph. Chirasil-Val glass capillary column was purchased from Applied Science Laboratories, Inc., U.S.A. The specific rotations were measured with a JASCO DIP-181 type polarimeter using a 50 mm cell. (*S*)-Methylbenzylamine (**1b**) was purchased from Aldrich Chemical Co., Inc. and distilled under nitrogen before use (**1b**; $[\alpha]_D$ −42.6, benzene).[7] (*R*)-2-Amino-2-phenylethanol (**1a**) was synthesized from (*R*)-phenylglycine as described previously[6] (**1a**; $[\alpha]_D$ −26.4, benzene). Palladium on charcoal (5% Pd-C) was obtained from Nippon Engelhard, Inc. Palladium hydroxide on charcoal was prepared according to the method of Hiskey and Northrop.[8] Pyruvic acid and 2-oxobutyric acid were distilled before use.

General procedure of the hydrogenolytic asymmetric transamination was as follows: Compound **1a** (50 mg, 0.365 mmol) and 2-keto acid (0.365 mmol) were dissolved in 1 ml of water or alcohol containing a given amount of sodium

hydroxide. The mixture was stirred under nitrogen for 12 h to form corresponding Schiff base. Asymmetric hydrogenation was carried out by using 5% Pd-C (100 mg) at 30 °C under 1 atm of hydrogen for 3 days. The catalyst was removed by filtration and washed with a small volume of 3 M HCl. The solution was evaporated to dryness, and the residue was dissolved in about 3 ml of water. After the pH of the solution was adjusted to 4.5 with sodium hydrogencarbonate, hydrogenolysis was performed with $Pd(OH)_2$ on charcoal (200 mg) at room temperature under 3 atm of hydrogen for 12 h or under 1 atm for 4 days. The catalyst was removed by filtration and washed with a small volume of 3 M HCl. The solution was evaporated to dryness and a small portion of the aqueous solution was applied to an amino acid analyzer to determine the chemical yield of the resulting amino acid. The optical purities of amino acids were determined by gas chromatographic analysis with a chiral column (GLC-method). Some of the values (Table 4) were confirmed by polarimetry after DNP-ylation.

Determination of Optical Purity. i) GLC-method—The synthesized amino acid, not isolated, was esterified by reflux with isopropyl alcohol saturated with HCl gas and then trifluoroacetylated with trifluoroacetic anhydride in dichloromethane. The derivatives were applied to gas chromatograph equipped with Chirasil-Val,[9] (0.3 mm i.d.×25 m). The column temperature was raised from 90 to 150 °C at a rate of 4 °C min^{-1}. The gas chromatographic analysis was repeated three times each and the peaks were integrated with a Hitachi 834-30 chromato-processor.

ii) DNP-method—The dinitrophenylation of amino acids was carried out as described in the earlier paper. The DNP-derivatives of the amino acids were purified with thin layer chromatography. The specific rotations of the purified DNP-amino acids were measured in 1 M NaOH. The following values were used as the specific rotations of optically pure DNP-amino acids; DNP-(*S*)-alanine, $[\alpha]_D$−143.9 (1 M NaOH); DNP-2-aminobutyric acid, $[\alpha]_D$−98.8 (1 M NaOH).[7] When the DNP-method was used for determining the optical yield, the reaction was carried out in ten-fold scale of the standard procedure described above.

Discussion

There have been many studies on the asymmetric transamination, but few dealing with the effect of alkali.[5] Alkali effects on the stereoselectivity have been studied on the hydrogenation of C=C or C=O double bond over Pd,[10–16] although the mechanism of the effect have not been fully clarified. It was also reported that the hydroxide ion has strong affinity to Pd surface,[17] and that hydroxide ion adsorbed on the Pd catalyst.[11]

Based on the experimental results and the examination with molecular model, a possible steric course for the catalytic hydrogenation in the absence or presence of sodium hydroxide are discussed below. Possible mechanism for the hydrogenation in aqueous and alcoholic solutions.

In the absence of sodium hydroxide, the hydroxyl group of the substrate could have low affinity with the catalyst. Under these conditions, the preferred conformation of the substrate on the catalyst in aqueous solution was thought to be **A**, which would lead to (*R*)-configuration (Fig. 8). In the presence of alkali, the hydroxyl group of the substrate could interact with hydroxide ion adsorbed on the catalyst, presumably by the formation of hydrogen bond. Consequently, the prefered conformation in the adsorption step was assumed to be **B**, in which the carboxyl group would be placed away from hydroxymethyl group owing to steric repulsion. (*S*)-Product is expected to form through structure B. This hypothetical mechanism is supported by the fact that the selectivity of the (*S*)-product of the reaction decreased with the increase of the bulkiness of the alkyl group of 2-keto acids

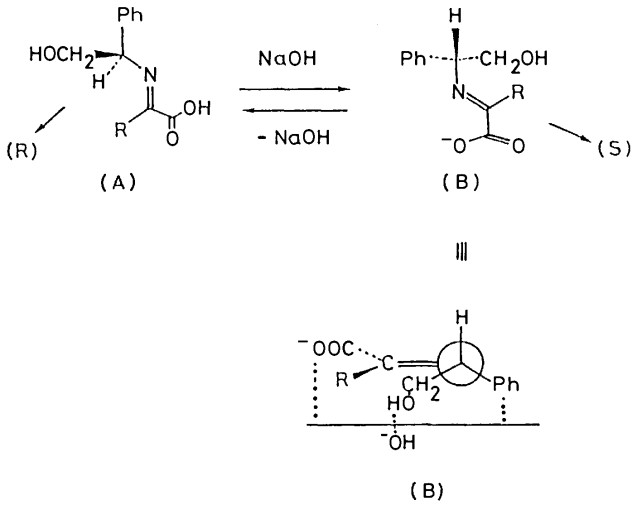

Fig. 8. Possible conformation in the catalytic hydrogenation in aqueous solution in the absence and presence of NaOH.

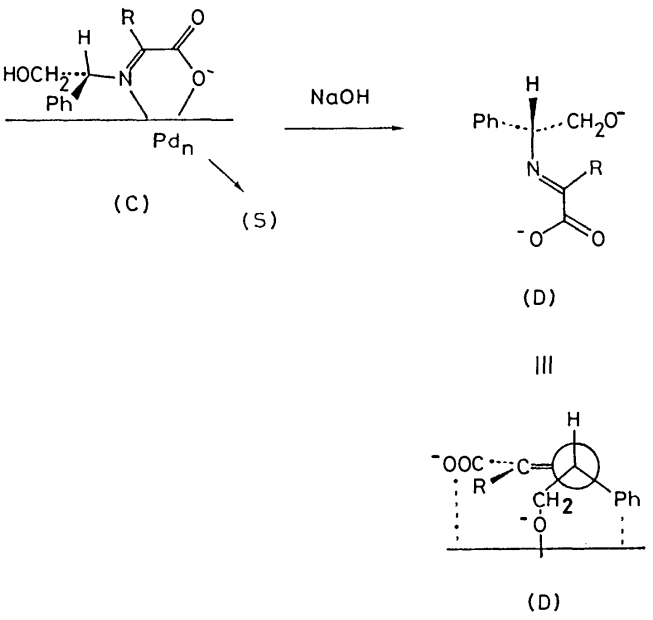

Fig. 9. Possible conformations of the substrate in the absence and presence of NaOH in alcoholic solvent.

(Table 3). The decrease of the optical yield by addition of NaCl together with sodium hydroxide could be caused by the replacement of hydroxide ion with chloride ion on the catalyst surface (Table 2).

When the amount of sodium hydroxide was none or small in alcoholic solution, the experimental results could be interpreted by the chelation mechanism (Fig. 9).[1,2,7] When pyruvic acid was used, conformation **C** was thought to be preferable,[6] which would lead to the (*S*)-product.

In the presence of alkali, the preferred conformation of the substrate was thought to be **D**. This conformation is similar to the conformation **B** except that the proton of hydroxyl group in asymmetric moiety is dissociated and that the distance between the substrate and the catalyst surface is shorter. In this conformation, the carboxyl group is apart from the alkoxide anion by steric and electrostatic repulsion. When 2-oxobutyric acid was used, the relative bulkiness of the R group increase compared with that of pyruvic acid. However, the carboxyl group is thought to be placed away from alkoxide anion as in the conformation **D** owing to the electrostatic repulsion. That may be a reason why the optical yield with 2-oxobutyric acid was similar to that with pyruric acid. When benzoylformic acid was used, the (*R*)-product was preferably obtained. The inversion of the configuration was explained by the dominant steric repulsion between R and alkoxide anion over the electrostatic repulsion between carboxylate and alkoxide anion.

It was also shown that the optical yield was lower in less polar solvent such as *i*-PrOH and *s*-BuOH than that in more polar solvents. This result may be due to the difference of the solvation ability of these alcohols to the alkoxide anion. The stabilization of alkoxide ion by the solvation may not be sufficient in less polar solvents.

The examination of the temperature effect showed that the peak of the optical yield was at around 30 °C. This result might related to the fact that the dissociation is generally accelerated by a rise of the temperature to some extent and decrease at higher temperature.[18]

In summary, it was found that the preferred conformation of the substrate in aqueous or alcoholic solution changed by the modification of the Pd catalyst surface with hydroxide ion. The hydroxyl group of the substrate also played an important role on the adsorbed stage on the catalyst in the hydrogenation process. The alkali concentration effect, additive effect, temperature effect, substituent effect in the hydrogenolytic asymmetric transaminations in both aqueous and alcoholic solutions support the possible mechanism presented for the hydrogenation in the presence of sodium hydroxide.

References

1) K. Harada and Y. Kataoka, *Tetrahedron Lett.*, **1978**, 2103, and the references cited therein.
2) K. Harada, T. Munegumi, and S. Nomoto, *Tetrahedron Lett.*, **22**, 111 (1981).
3) J. D. Morrison and H. S. Mosher, "Asymmetric Organic Reactions," Prentice-Hall, Inc., New Jersey (1971), Chap. 7.
4) D. Valentine, Jr., and J. W. Scott, *Synthesis*, **1978**, 329.
5) S. Mitsui and Y. Imai, *Nippon Kagaku Zasshi*, **87**, 183 (1966).
6) K. Harada and M. Tamura, *Bull. Chem. Soc. Jpn.*, **52**, 1227 (1979).
7) K. Harada and K. Matsumoto, *J. Org. Chem.*, **33**, 4467 (1968).
8) R. G. Hiskey and R. C. Northrop, *Proc. Natl. Acad. Sci. U.S.A.*, **83**, 4798 (1961).
9) H. Fank, G. J. Nicolson, and E. Bayer, *J. Chromatogr.*, **146**, 197 (1978).
10) R. L. Augustine, *J. Org. Chem.*, **23**, 1853 (1958).
11) R. L. Augustine, *J. Org. Chem.*, **28**, 152 (1963).
12) R. L. Augustine, D. C. Migliorini, R. E. Fascante, C. S. Sodano, and M. J. Sisbarro, *J. Org. Chem.*, **34**, 1075 (1969).
13) I. Jardine, R. W. Howsam, and F. J. Mcquillin, *J. Chem. Soc. C*, **1969**, 260.
14) F. J. Mcquillin, W. O. Ord, and P. L. Simpson, *J. Chem. Soc.*, **1963**, 5996.
15) S. Nishimura, M. Shimahara, and M. Shiota, *J. Org. Chem.*, **31**, 2394 (1966).
16) S. Mitsui, H. Saito, Y. Yamashita, M. Kaminaga, and Y. Senda, *Tetrahedron*, **29**, 1531 (1973).
17) A. P. G. Kieboom and F. van Rantwijk "Hydrogenation and Hydrogenolysis in Synthetic Organic Chemistry," Delft University Press (1977) pp. 71 and 133.
18) D. H. Everett and W. F. K. Wynne-Jones, *Trans. Faraday Soc.*, **35**, 1395 (1939).

NAD(P)$^+$-NAD(P)H Models 70. Reduction of Imines with Hantzsch Ester in the Presence of Silica Gel

Masayuki FUJII,* Tetsuo AIDA, Masakuni YOSHIHARA,† and Atsuyoshi OHNO††
Department of Industrial Chemistry, Faculty of Engineering, Kinki University in Kyushu, Iizuka, Fukuoka 820
†Department of Applied Chemistry, Faculty of Science and Engineering, Kinki University, Higashi-Osaka 577
††Institute for Chemical Research, Kyoto University, Uji, Kyoto 611
(Received July 1, 1989)

Imines are reduced into the corresponding amines in high yields by Hantzsch ester in the presence of silica gel. The reduction shows high chemoselectivity and stereoselectivity. Reduction of α,β-unsaturated imines proceeds with high regioselectivity to yield allylic amines (1,2-reduction products).

The reduction of imines is very important in organic synthesis[1] and has been studied intensively, especially in connection with the syntheses of alkaloids[2] and amino acids.[3] Although there has been many investigations contributing to this subject, the procedures generally employed at the present time seem to involve certain problems to be improved. For example, a carbonyl group will be reduced into hydroxyl group by hydride reagents and a carbon-carbon double bond will be saturated by catalytic hydrogenation. These poor chemoselectivities seem to make it difficult to apply these methods to the reduction of such molecules that bear various functional groups along with an imino group.

On the other hand, from the viewpoint of biomimetic reactions of NAD$^+$-coenzymes,[4] reduction of imines[5-11] and iminium salts[12-14] as well as that of carbonyl compounds has been studied intensively. It is shown that reduction of imines with NAD(P)H models is susceptible to acid-catalysis such as proton[5-8] or metal cation.[9-11]

Recently, it was found that diethyl 2,6-dimethyl-1,4-dihydro-3,5-pyridinedicarboxylate (Hantzsch ester, HEH) acted as a mild and selective reducing agent for electron-defficient olefins in the presence of silica gel.[15-19] The HEH-SiO_2 reduction has some unique characteristic features. For example, it shows an excellent chemoselectivity, that is, olefins conjugated with a nitro, a formyl, or a keto group are reduced in quantitative yields whereas those conjugated with an alkoxycarbonyl, or a cyano group are not affected at all.[15-17] It also shows a high regioselectivity in the reduction of conjugated dienones.[18] The reduction proceeds in a manner of 1,4-reduction to afford γ,δ-unsaturated ketones. These features of HEH-SiO_2 reduction system seem to be very attractive for the syntheses of certain natural products that bear various functional groups susceptible to reduction. In fact, the system was applied to the convenient syntheses of some natural products.[19] In the present paper, application of this HEH-SiO_2 system to the reduction of imines is described.

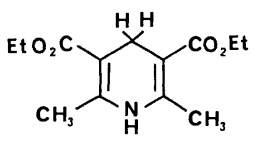

Hantzsch ester, HEH

Results and Discussion

The HEH-SiO_2 system has been proved to be effective for the reduction of imines into the corresponding amines (Scheme 1) as it was in the reductions of certain carbon-carbon double bonds. Table 1 shows that the reduction of *N*-benzylideneaniline (**1a**) with HEH was highly accelerated by silica gel. Without silica gel, the reduction gave **2a** only in 15% yield after 12 h, whereas the reaction completed within 1 h in the presence of silica gel. Solvent effect was so significant and only nonpolar solvents such as hexane or benzene gave satisfactory results. It can be considered that polar solvents retard the adsorption of HEH and imine **1a** onto the silica gel surface. Aluminum oxide (basic or acidic) was also proved to be a good catalyst for the reduction.[20] A variety of imines derived from ketones and aldehydes were also reduced smoothly in high yields as shown in Table 2. It is

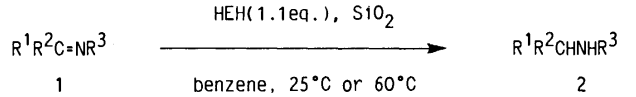

Scheme 1.

Table 1. Reduction of **1a** with HEH-SiO_2 or Al_2O_3[a]

Catalyst[b]	Solvent	Time/h	Yield[c]/%
None	Benzene	12	15
SiO_2	Benzene	1	100
SiO_2	Hexane	1	100
SiO_2	THF	12	17
SiO_2	Acetonitrile	12	51
Al_2O_3 (Merck, basic)	Benzene	1	93
Al_2O_3 (Merck, acidic)	Benzene	1	96

a) Reaction conditions: **1a**, 0.10 mmol; HEH, 0.11 mmol; SiO_2, 100 mg; solvent, 1.0 ml; 25 °C; N_2. b) Dried at 80 °C for several days. c) Determined on GLC analysis.

Table 2. Reduction of Imines with HEH-SiO_2[a)]

1/2	R^1	R^2	R^3	Time/h	Yield[b)]/%
a	Ph	H	Ph	1	86
b	Et	H	Ph	3	78
c	Ph	H	Bu	3	83
d	Et	H	Bu	3	68
e	Ph	CH_3	Ph	3	85
f	Ph	CH_3	Bu	3	64
g	CH_3	CO_2Et	$PhCH_2$	3	58
h	$(CH_3)_2C{=}CH(CH_2)_2CH(CH_3)-$	H	Ph	3	72

a) Reaction temperature: 25 °C for a, b, c, d, h. 60 °C for e, f, g. b) Isolated yield.

notable to find that the reductions of aldimines (**1a—d, h**) completed within 3 h at 25 °C, whereas the reductions of ketimines (**1e—g**) required higher temperature of 60 °C. *N*-(1-Ethoxycarbonylethylidene)benzylamine (**1g**) and *N*-(2,6-dimethyl-5-heptenylidene)aniline (**1h**) was reduced chemoselectively into *N*-benzylalanine ethyl ester and *N*-(2,6-dimethyl-5-heptenyl)aniline (**2h**) respectively. The high chemoselectivity of the HEH-SiO_2 system was further demonstrated by the following competition reactions. Reduction of a mixture of **1a** and 4-phenyl-3-buten-2-one (**3**), or a mixture of **1a** and *N*-(α-methylbenzylidene)aniline (**1e**) was carried out with 1.1 equivalent amounts of HEH at 25 °C. In the former reaction, **1a** was converted into **2a** in 95% yield (on GLC) in 1 h whereas most of **3** remained unchanged. An apparent predominance of **1a** over **1e** was also observed in the latter reaction. The aldimine **1a** was reduced to give **2a** in 86% yield after 1 h while only a trace amount of the ketimine **1e** was converted into **2e** within the same reaction time.

Preparation of α-deuteriated amines and α-deuteriated amino esters can be easily performed with HEH-4,4-d_2 (d>98%) (Scheme 2). Reduction of **1a** and **1g** with HEH-4,4-d_2 indicates that the deuterium atom was regioselectively transferred onto the carbon atom in the imine moiety without any contamination.

Investigation on the regioselectivity of the reduction of α,β-unsaturated imines **1i** and **1j** revealed that the reduction with the HEH-SiO_2 system proceeded in a manner of 1,2-reduction to afford allylic amines **2i** and **2j** (Scheme 3) which is in a flat contrast to the reduction of α,β-unsaturated ketones.[19] In the reduction

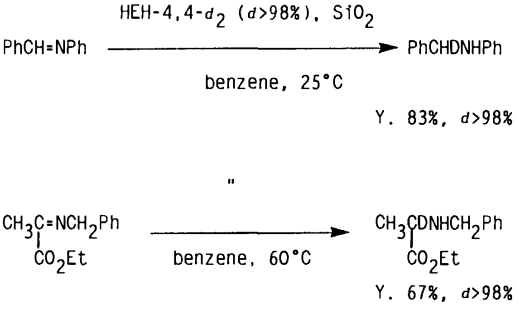

Scheme 2.

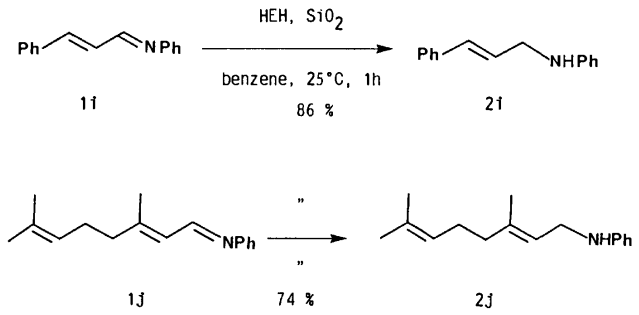

Scheme 3. Regioselectivity in the reductions of α,β-unsaturated imines.

of α,β-unsaturated ketones, it was reported that the 1,4- vs. 1,2-regioselectivity is affected by the reactivity of the reducing agents.[21] In the present system, since the reducing agent is kept unchanged, the difference in the regioselectivity between the α,β-unsaturated imines and ketones may reflect the difference in reactivity of the substrate.

Substituent effect on the stereochemical properties of the present reduction were also examined. As an example of acyclic imines, reduction of (*R*)-*N*-(α-methylbenzylidene)-α-methylbenzylamine (**1k**) was carried out and the product was characterized on ^1H NMR analysis[11] to contain 80% of the (*R*,*R*)-isomer and 20% of the (*S*,*R*)-isomer (Scheme 4). Reductions of methyl-substituted *N*-(cyclohexylidene)benzylamines (**1l—n**) represents the stereoselectivity for the cyclic systems (Table 3). The results revealed that thermodynamically more stable isomer was preferred in each case, which suggests that the reduction under-

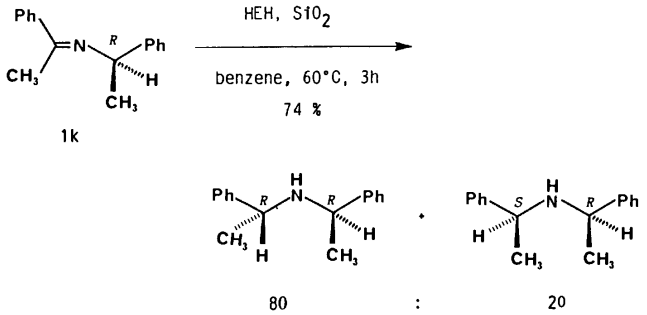

Scheme 4. Stereoselectivity in the reduction of **1k**.

Table 3. Stereoselectivity in the Reductions of *N*-(Methylcyclohexylidene)benzylamines[a]

1/2	Substituent	Yield[b]/%	Cis/Trans[c]
l	2-CH_3	85	18/82
m	3-CH_3	73	72/28
n	4-CH_3	89	4/96

a) Reactions were run in benzene at 60 °C for 3 h. b) Isolated yields. c) Determined on GLC analysis.

goes through the product-like transition state. It is notable that stronger steric effect was observed for methyl substituent at the 4-position than that at the 2 or 3-position.

Applications of the present reduction system to certain natural products are now in progress in our laboratory.

Experimental

Instruments. ^{1}H NMR srectra were measured at 90 MHz with a Hitachi R-90H FT-NMR spectrometer, and at 400 MHz with a JEOL GX400 Fourier Transfer NMR spectrometer. IR spectra were recorded on a JASCO IR-810 infrared spectrophotometer. Gas chromatography analyses were performed on a Shimadzu GC-12A gas chromatograph. GC-Mass spectra were measured with a Hitachi M-80A GC-Mass spectrometer.

Materials. Hantzsch ester (HEH) and its 4,4-dideuteriated analog (HEH-4,4-d_2) were prepared as reported in a previous paper.[22] The deuterium content in HEH-4,4-d_2 was confirmed to be over 98% by 400 MHz ^{1}H NMR analysis. Imines **1a—n** were prepared as described in the literature.[23] Solvents were distilled immediately prior to the use. Silica gel (Nakarai Silica Gel 60, 35—70 mesh) was activated in an oven at 80 °C for a few days and stored in a desiccator. Other chemicals were purchased from Wako Pure Chemicals Industries Ltd. and Nakarai Chemicals Ltd.

Reduction of Imine. A mixture of 1.0 mmol of an imine, 293 mg (1.1 mmol) of HEH, 1.50 g of silica gel and 10 ml of absolute benzene was stirred at 25 °C (**1a**, **1b**, **1c**, **1d**, **1h**, **1i**, **1j**), or at 60 °C (**1e**, **1f**, **1g**, **1k**, **1l**, **1m**, **1n**) under a nitrogen atmosphere for an appropriate reaction time (1—3 h). The silica gel was removed by filtration and the residue was subjected to a column chromatography on silica gel using dichloromethane as an eluent to afford the corresponding amine. Chemical yields were: **2a**, 86%; **2b**, 78%; **2c**, 83%; **2d**, 68%; **2e**, 85%; **2f**, 64%; **2g**, 58%; **2h**, 72%; **2i**, 86%; **2j**, 74%; **2k**, 74%; **2l**, 85%; **2m**, 73%; **2n**, 89%.

***N*-Benzylaniline-α-*d* and *N*-Benzylalanine-2-*d* Ethyl Ester.** Reduction of **1a** and **1g** with HEH-4,4-d_2 was carried out by the same procedure as described above. The analysis of the 400 MHz ^{1}H NMR spectrum revealed that the deuterium was incorporated in the α-position of the product. The deuterium content determined was 98%. Chemical yields were 83% for **2a** and 67% for **2g**.

References

1) H. O. House, "Modern Synthetic Reactions," 2nd ed., W. A. Benjamin Inc., California (1972), pp. 73—77 and 210—213.

2) For example, see K. Yamada, M. Takeda, and T. Iwakuma, *J. Chem. Soc., Perkin Trans. 1*, **1983**, 265, and references cited therein.

3) K. Harada, "Asymmetric Synthesis," Vol. 5, ed by J. D. Morrison, Academic Press Inc., New York (1985), pp. 359—383.

4) For a recent review, see S. Yasui and A. Ohno, *Bioorg. Chem.*, **14**, 70 (1986).

5) S. Shinkai, S. Shiraishi, and T. Kunitake, *Bull. Chem. Soc. Jpn.*, **49**, 3656 (1976).

6) S. Singh, V. K. Sharma, S. Gill, and R. I. K. Sahota, *J. Chem. Soc., Perkin Trans. 1*, **1985**, 437.

7) R. Srinivasan, R. T. Medary, H. F. Fisher, D. J. Norris, and R. Stewart, *J. Am. Chem. Soc.*, **104**, 807 (1982).

8) K. A. Schellenberg, G. W. McLean, H. L. Lipton, and P. S. Lietman, *J. Am. Chem. Soc.*, **89**, 1948 (1967). R. W. Huffman and T. C. Bruice, *ibid.*, **89**, 6243 (1967).

9) K. Nakamura, A. Ohno, and S. Oka, *Tetrahedron Lett.*, **1977**, 4593.

10) L. H. P. Meijer, J. C. G. van Niel, and U. K. Pandit, *Tetrahedron Lett.*, **1978**, 1335.

11) J. C. G. Nan Niel and U. K. Pandit, *Tetrahedron*, **41**, 6005 (1985).

12) S. Shinkai and T. Kunitake, *Chem. Lett.*, **1974**, 1113.

13) U. K. Pandit, F. R. Mas Cabre, R. A. Gase, and M. J. de Nie-Sarink, *J. Chem. Soc., Chem. Commun.*, **1974**, 627.

14) U. K. Pandit, H. van Dam, and J. B. Steevens, *Tetrahedron Lett.*, **1977**, 913.

15) K. Nakamura, M. Fujii, A. Ohno, and S. Oka, *Tetrahedron Lett.*, **25**, 3983 (1984).

16) S. Yasui, M. Fujii, and A. Ohno, *Bull. Chem. Soc. Jpn.*, **60**, 963 (1987).

17) S. Yasui, M. Fujii, and A. Ohno, *Bull. Chem. Soc. Jpn.*, **60**, 4019 (1987).

18) M. Fujii, K. Nakamura, S. Yasui, S. Oka, and A. Ohno, *Bull. Chem. Soc. Jpn.*, **60**, 2423 (1987).

19) M. Fujii, *Bull. Chem. Soc. Jpn.*, **61**, 4029 (1988).

20) Although it was reported that carbonyl compounds were reduced into the corresponding alcohols on alumina surfaces (Woelm W-200, neutral) using 2-propanol as a hydrogen donner [G. H. Posner, A. W. Runquist and M. J. Chapdelaine, *J. Org. Chem.*, **42**, 1202 (1977)], no reduction of imine **1a** was observed under the reaction conditions described therein even after 48 h in the present study.

21) A. Ohno, T. Yasuma, K. Nakamura, and S. Oka, *Bull. Chem. Soc. Jpn.*, **59**, 2905 (1986).

22) A. Singer and S. M. McElvain, *Org. Synth.*, Coll. Vol. II, 214 (1966).

23) S. R. Sandler and W. Karo, "Organic Functional Group Preparations," 2nd ed., Academic Press Inc., New York (1986), Chap. 12, pp. 291—322.

A Cross-Coupling Reaction of Methylsulfinylarene

Shoji WAKABAYASHI,* Takakazu TANAKA, Yukihiro KUBO, Junichi UENISHI, and Shigeru OAE*
Department of Chemistry, Faculty of Science, Okayama University of Science, Ridai-cho, Okayama 700
(Received July 19, 1989)

Cross-coupling product 2-(2-pyridyl)quinolines were obtained in the reaction of 2-(methylsulfinyl)-quinolines and 2-(methylsulfinyl)pyridines with methylmagnesium bromide. Attempts of cross coupling in the reaction of other substrates were unsuccessful.

Earlier, we have reported many ligand coupling reactions of sulfoxides with various types of Grignard reagents.[1] This reaction provides a new carbon-carbon bond formation between α and ipso carbons of arylsulfinyl group or ipso carbon and the Grignard reagent with retention of the configuration.[2] In this coupling reaction which is typically described in Scheme 1, R is usually a benzylic, allylic, aromatic, and azaaromatic group,[1,3] otherwise the reaction becomes messy and gives no desired coupling product.

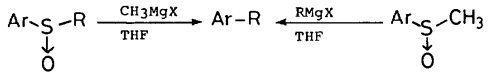

Scheme 1.

When R is methyl or other alkyl group, a dimeric compound is a major product. For example, in the coupling reaction of 2-(methylsulfinyl)pyridine (**1a**) with methylmagnesium bromide, 2,2′-bipyridyl (**2a**) was formed in moderate yields.[4] This is quite a unique reaction because it involves ligand coupling of two azaaromatic groups after initial ligand exchange on the sulfoxide and has promised to be a productive method for preparation of biazaaromatics.[5]

In the extension of these studies, we were interested in cross-coupling reaction between two different azaaromatic sulfoxides, and have found some successful examples. In this article the details are described.

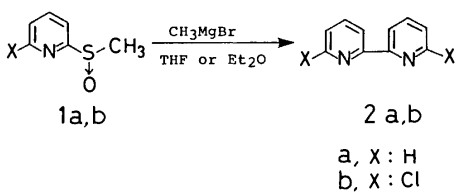

Scheme 2.

Results and Discussion

A mixture of 2-(methylsulfinyl)quinoline (**3a**) and **1a** was treated with methylmagnesium bromide in THF at room temperature. The reaction completed in about 15 min and gave 2-(2-pyridyl)quinoline (**4**) in 57% yield. Homo-coupling product 2,2′-biquinolyl (**8a**) and **2a** were also formed in 42 and 23% yields respectively. Results of the other combination of the reactions between **3a**, **b** and **1a**, **b** are summarized in Table 1, in which the cross coupling products **4—7** were obtained in 20 to 57% yield.

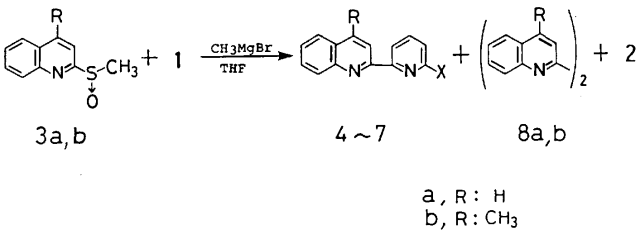

Scheme 3.

Meanwhile, the cross coupling reaction of **1a** and **1b** provides unsymmetric 2,2′-bipyridyl along with symmetric bipyridyls **2a** and **2b**. But somehow the yield of unsymmetric bipyridyl was low, only 16% of 6-chloro-2,2′-bipyridyl (**9**) was obtained. The yields of **2a** and **2b** were 36 and 77% respectively. Reaction of **3a** and **3b** gave three kinds of 2,2′-biquinolyls, thus 4-methyl-2,2′-biquinolyl (**10**), **8a** and **8b**, which were hard to be purified by chromatographic techniques. The product ratios of **10**, **8a**, and **8b** were found to be 6:4:7 approximately determined by ^{1}H NMR spectrum of the mixture.

Table 1. Cross-Coupling Reaction of **3** and **1**

Starting		Sulfoxide R	X	Cross-coupling product (yield/%)		Homo-coupling product (yield/%)			
3a	**1a**	H	H	**4**[a]	(57)	**8a**[b]	(42)	**2a**[c]	(23)
3a	**1b**	H	Cl	**5**	(20)	**8a**	(42)	**2b**[d]	(11)
3b	**1a**	CH_3	H	**6**[e]	(54)	**8b**[f]	(42)	**2a**	(42)
3b	**1b**	CH_3	Cl	**7**	(36)	**8b**	(61)	**2b**	(41)

a) Ref. 6. b) Ref. 7. c) Ref. 8. d) Ref. 9. e) Ref. 10. f) Ref . 11.

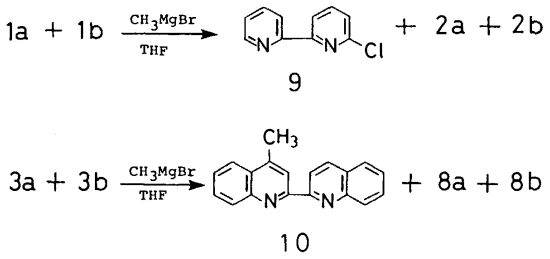

Scheme 4.

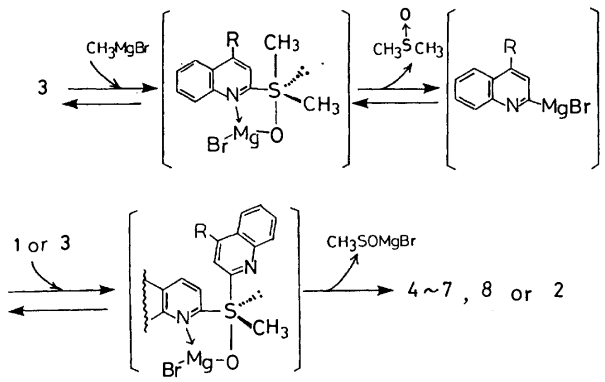

Chart 1.

The mechanism of the reaction has been examined carefully in the cases of 2-(alkylsulfinyl)pyridines and proposed by Oae et al.[4] According to the mechanism, an initial attack of the methylmagenesium bromide on the sulfur atom of **3** forms a σ-sulfurane intermediate followed by dispropotionation to release dimethyl sulfoxide and 2-quinolylmagnesium bromide, which subsequently reacts with another sulfoxide **1** or **3** to promote a normal ligand coupling, and finally affording the cross coupling product **4**—**7** as well as the homo-coupling products **8** and **2**.

The coupling reaction of **3a** with 2-(*t*-butylsulfinyl)-pyridine (**11**) also gave the desired cross couling product **4** in 22% yield along with **8a** in 8% yield but none of **2a** was detected in the reaction mixture.[13] The rest of the starting sulfoxide **11** was recovered in 71% yield. The result would be due to the steric hindrance of the *t*-butylsulfinyl group, thus the rate of formation of the intermediary σ-sulfurane derived from 2-quinolylmagnesium bromide and **11** is anticipated to be considerably slow. The cross coupling reaction obviously competes with the usual ligand coupling reaction as well as other side reactions involving simple ligand exchange or disulfide formation. Thus the reaction is not simple. In fact, no cross couling was observed between **3a** and 1-methylsulfinyl-4-(phenylsulfonyl)benzene (**12**). The major product was 2-methyl-1,2-dihydro-2,2′-biquinolyl (**13**) along with 90% recovery of the other sulfoxide **12**. The compound **13** is known to be produced by treatment of two equivalents of methylmagnesium bromide and **3a**.[5]

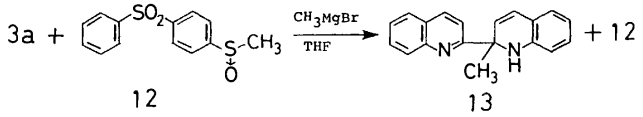

Scheme 5.

Reactions of **3a** with other substrates, 2-(methylsulfinyl)pyrimidine, methylsulfinylbenzene, and their *t*-butylsulfinyl derivatives gave almost similar results in which no cross coupling product was detected among the reaction mixtures. In the reaction of **1a** and **12**, the dimeric compound **2a** was obtained in 89% yield and the sulfoxide **12** was recovered quantitatively.

Experimental

Melting points were determined with Yanaco micromelting point apparatus and were uncorrected. ^{1}H NMR spectra were run on JEOL-GX400 spectrometer in $CDCl_3$ with tetramethylsilane as an internal standard. Chemical shifts are given as σ value. Infrared spectra were obtained with JASCO IR-A spectrometer. Low- and high-resolution mass spectra were taken on JEOL-JMS 303HF spectrometer with a direct inlet method at 70 eV. Only strong and/or structurally important peaks are reported here for IR and MS. Column chromatography was carried out on silica gel (Wako gel 200). THF for the reactions was dried over sodium benzophenone ketyl and freshly distilled just before use. Methylmagnesium bromide was purchased from Kanto Chemical Co. as THF solution.

Typical Procedure of the Cross-Coupling Reaction. To a mixture of sulfoxide (1 mmol) and another sulfoxide (1 mmol) in THF (5 ml) was dropped methylmagnesium bromide (2 ml, 1M solution in THF) at room temperature during a min under Argon atmosphare. The reaction mixture was stirred for 15 min at the same temperature. It was quenched with aq. ammonium chloride (2 ml) and extracted with chloroform (60 ml). The extract was washed with water (4 ml×2) and brine (4 ml), dried over $MgSO_4$ and evaporated under reduced pressure. The residue was purified by column chromatography on silica gel. Characteristic properties of the products are the following.

4: Colorless crystals, mp 98—99 °C (EtOH) (lit,[6] 99 °C); ^{1}H NMR δ=7.36 (1H, td, J=6.4, 1.8 Hz), 7.56 (1H, td, J=7.1, 1.5 Hz), 7.74 (1H, dt, J=7.9, 1.5 Hz), 7.85 (1H, d, J=8.5 Hz), 7.88 (1H, td, J=7.3, 1.9 Hz), 8.19 (1H, d, J=8.7 Hz), 8.29 (1H, d, J=8.2 Hz), 8.56 (1H, d, J=8.2 Hz), 8.66 (1H, dd, J=8.1, 1.1 Hz), 8.75 (1H, ddd, J=4.7, 1.9, 1.1 Hz).

8a: Colorless crystals, mp 193—194 °C (EtOH) (lit,[7] 193—196 °C; ^{1}H NMR δ=7.58 (2H, ddd, J=7.5, 5.0, 1.1 Hz), 7.76 (2H, td, J=8.0, 1.1 Hz), 7.89 (2H, d, J=8.0 Hz), 8.23 (2H, d, J=8.1 Hz), 8.33 (2H, d, J=8.1 Hz), 8.85 (2H, d, J=8.1 Hz).

2a: Colorless crystals, mp 70—73 °C (EtOH) (lit,[8] 69.7 °C); ^{1}H NMR δ=7.31 (2H, ddd, J=7.5, 5.0, 1.3 Hz), 7.82 (2H, td, J=7.7, 1.8 Hz), 8.39 (2H, d, J=8.1 Hz), 8.69 (2H, dd, J=5.0, 0.3 Hz).

5: Colorless crystals, mp 156—158 °C (EtOH); ^{1}H NMR δ=7.57 (1H, td, J=8.1, 1.5 Hz), 7.75 (1H, td, J=8.0, 1.5 Hz), 7.76 (1H, t, J=7.9 Hz), 7.82 (1H, d, J=8.1 Hz), 8.16 (1H, d, J=8.4 Hz), 8.28 (1H, d, J=8.4 Hz), 8.34 (1H, dd, J=7.7, 0.7 Hz), 8.55 (1H, d, J=8.7 Hz), 8.62 (1H, dd, J=7.9, 0.8 Hz); IR($CHCl_3$) 2930, 2850, 1600, 1570, 1550, 1410, 1150, 1140

cm^{-1}; MS *m/z*(rel intensity) 240, 242 (M^+, 67 and 23), 205 (65), 128 (26), 28 (base); Found: C, 69.67; H, 3.78; N, 11.77%. Calcd for $C_{14}H_9N_2Cl$: C, 69.86; H, 3.77; N, 11.64%.

2b: Colorless crystals, mp 216—219 °C (benzene : hexane, 1 : 1) (lit,[9] 218—219 °C); ^1H NMR δ=7.36 (2H, d, J=8.1 Hz), 7.78 (2H, t, δ=7.7 Hz), 8.35 (2H, dd, J=7.7, 0.7 Hz).

6: Colorless crystals, mp 64—66 °C (petr. ether) (lit,[10] 69—70 °C); ^1H NMR δ=2.78 (3H, s), 7.32 (1H, ddd, J=7.3, 4.8, 1.1 Hz), 7.56 (1H, td, J=8.4, 1.4 Hz), 7.72 (1H, td, J=7.7, 1.2 Hz), 7.86 (1H, td, J=7.7, 1.8 Hz), 8.01 (1H, d, J=8.4 Hz), 8.17 (1H, dd, J=8.4, 0.7 Hz), 8.39 (1H, s), 8.63 (1H, dd, J=7.0, 1.0 Hz), 8.73 (1H, dm, J=4.0 Hz).

8b: Colorless crystals, mp 279—280 °C (chloroform) (lit,[11] 280 °C); ^1H NMR δ=2.85 (6H, s), 7.60 (2H, td, J=8.0, 1.1 Hz), 7.76 (2H, td, J=7.7, 1.0 Hz), 8.06 (2H, d, J=8.4 Hz), 8.25 (2H, d, J=8.4 Hz), 8.67 (2H, s).

7: Colorless crystals, mp 110—112 °C (EtOH); ^1H NMR δ=2.80 (3H, s), 7.38 (1H, d, J=7.0 Hz), 7.58 (1H, td, J=7.3, 0.9 Hz), 7.73 (1H, td, J=7.3, 1.5 Hz), 7.82 (1H, t, J=7.7 Hz), 8.03 (1H, dd, J=8.4, 0.7 Hz), 8.15 (1H, d, J=8.4 Hz), 8.39 (1H, s), 8.60 (1H, dd, J=7.7, 0.7 Hz); IR($CHCl_3$) 2960, 2940, 1600, 1585, 1570, 1550, 1440, 1420, 1360, 1160, 1140 cm^{-1}; MS *m/z* (rel intensity) 254, 256 (M^+, base and 31), 219 (65), 112 (14); Found: C, 70.62; H, 4.50; N, 10.69%. Calcd for $C_{15}H_{11}N_2Cl$: C, 70.72; H, 4.32; N, 10.99%.

9: Colorless crystals, mp 59—60 °C (petr. ether) (lit,[12] 60—62 °C); ^1H NMR δ=7.33 (1H, td, J=6.2, 1.1 Hz), 7.34 (1H, dd, J=8.0, 0.7 Hz), 7.77 (1H, t, J=7.7 Hz), 7.82 (1H, td, J=7.9, 1.7 Hz), 8.35 (1H, d, J=7.7 Hz), 8.41 (1H, d, J=7.7 Hz), 8.67 (1H, dm, J=4.4 Hz).

10: ^1H NMR δ=2.85 (3H, s), 7.58 (1H, t, J=8.0 Hz), 7.60 (1H, t, J=8.0 Hz), 7.75 (1H, t, J=8.4 Hz), 7.76 (1H, t, J=8.4 Hz), 7.88 (1H, d, J=8.0 Hz), 8.06 (1H, d, J=8.4 Hz), 8.22 (1H, d, J=8.4 Hz), 8.23 (1H, d, J=8.4 Hz), 8.32 (1H, d, J=8.8 Hz), 8.68 (1H, s), 8.85 (1H, d, J=8.8 Hz).

References

1) S. Oae, *Croat. Chem. Acta*, **59**, 129 (1986); S. Oae, *Phosphorus and Sulfur*, **27**, 13 (1986); S. Oae, T. Kawai, and N. Furukawa, *Tetrahedron Lett.*, **25**, 69 (1984).

2) S. Oae, T. Kawai, and N. Furukawa, *J. Chem. Soc., Perkin Trans. 2*, **1987**, 405; S. Oae, T. Takeda, and S. Wakabayashi, *Tetrahedron Lett.*, **29**, 4445 (1988).

3) S. Wakabayashi, M. Ishida, T. Takeda, and S. Oae, *Tetrahedron Lett.*, **29**, 4441 (1988); T. Kawai, Y. Kodera, N. Furukawa, S. Oae, M. Ishida, T. Takeda, and S. Wakabayashi, *Phosphorus and Sulfur*, **34**, 139 (1987).

4) T. Kawai, N. Furukawa, and S. Oae, *Tetrahedron Lett.*, **25**, 2549 (1984); S. Oae, T. Kawai, and N. Furukawa, *Phosphorus and Sulfur*, **34**, 123 (1987).

5) S. Wakabayashi, Y. Kubo, T. Takeda, J. Uenishi, and S. Oae, *Bull. Chem. Soc. Jpn.*, **62**, 2338 (1989).

6) D. H. Hey and J. M. Williams, *J. Chem. Soc.*, **1950**, 1678.

7) G.M. Badger and W. H. F. Sasse, *J. Chem. Soc.*, **1956**, 616.

8) Merck Index **10**, 3367.

9) S. Ogawa and S. Shiraishi, *J. Chem. Soc., Perkin Trans. 1*, **1980**, 2527.

10) J. Haginiwa, Y. Higuchi, T. Kawashita, and T. Goto, *Yakugaku Zasshi*, **95**, 204 (1975).

11) J. Haginiwa and Y. Higuchi, *Yakugaku Zasshi*, **93**, 144 (1973).

12) D. B. Moran, G. O. Morton, and J. D. Albright, *J. Heterocycl. Chem.*, **23**, 1071 (1986).

13) The compound **3a** is at least 10^3 times more reactive than **1a** in the homolytic dimerization reaction, the details see in Ref. 5.

Preparation of Optically Pure α-Alkyl β-Hydroxy Nitriles by the Bakers' Yeast Reduction

Toshiyuki ITOH,* Tsuneyasu FUKUDA, and Tamotsu FUJISAWA*,†
Department of Chemistry, Faculty of Education, Okayama University, Okayama 700
†Chemistry Department of Resources, Mie University, Tsu, Mie 514
(Received May 13, 1989)

The bakers' yeast reduction of 2-alkyl-3-oxobutyronitrile gave optically pure 2-alkyl-3-hydroxybutyronitriles. Especially 2-phenyl-3-oxobutyronitrile gave only syn diastereomer of 2-phenyl-3-hydroxybutyronitrile in high optical yield.

Nitrogen-functionalyzed optically active secondary alcohol derivatives are sometimes found in biologically active compounds as important moiety for their activity.[1] It is, therefore, required to develop the efficient and convenient methods to supply nitrogen-functionalized alcohol derivatives. Since the bakers' yeast has been recognized as a useful reducing agent for asymmetric reduction of various functionalized ketones to produce optically active secondary alcohols under mild conditions and simple operations.[2] Chemical yield and enantioselectivity in the yeast reduction of various substrates, however, are not always satisfactory i.e. it has sometimes been observed that low enantioselectivity and decomposition of the substrate occured. Although much efforts have been paid for screening microbes which have good ability to reduce various kind of ketones with high enantioselectivity, it is also important to get a knowledge for the functional groups which have a good affinity toward the microbe.[3] We would like to report in this paper that the bakers' yeast reduction of 2-alkyl β-keto nitriles into the corresponding hydroxy nitriles with high enantioselectivity (Scheme 1). Since the cyano group is a functional group widely used as a precursor of both of amino group and carbonyl group,[4] hydroxy nitriles obtained should become wide variety of useful key intermediates in the synthesis of optically active natural products which are involving nitrogen functional group and carbonyl group.

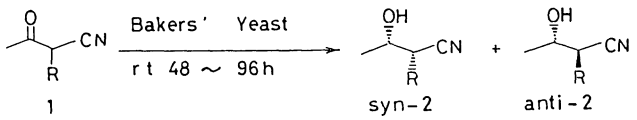

Scheme 1.

Results and Discussion

Several keto nitriles, i.e. 2-methyl- (**1a**), 2-ethyl- (**1b**), 2-butyl- (**1c**), and 2-phenyl-3-oxobutyronitrile (**1d**) were prepared by the reaction of acetyl chloride with α-lithiated nitriles and subjected to the reduction with bakers' yeast. Results of the present microbial reduction of β-keto nitriles are summarized in Table 1.

The products **2** consisted of syn and anti isomers, which could be separated into each of pure diastereomers as 3,5-dinitrobenzoates by silica gel flash column chromatography except for the case of nitrile **2c**. Each of benzoates were converted into (+)-α-methoxy-α-(trifluoromethyl)phenylacetates (MTPA esters) of 2-alkyl-3-hydroxybutyronitriles by treatment with lithium aluminum hydride followed by (+)-MTPA chloride for determination of their enantiomeric excess by ^{1}H NMR and ^{19}F NMR analysis.[5] Completely enantioselective reduction was achieved (Entries 2, 3, and 4), except for the reduction of 2-methyl-3-oxobutyronitrile (Entry 1). To determine the configuration, each of diasteromers of **2b** were converted into the correesponding hydroxy esters. According to ^{1}H NMR analysis of the hydroxy ester,[6] the assignment of diastereomers could be achieved. Consequently it was found that the chemical shift of the methine proton at 2-position of *syn*-**2b** was in lower field than the anti one, in analogy with compounds **2a** and **2c**, the isomers which have higher value of chemical shift of the methine proton were presumed to be the syn isomers. Hence the ratio of each of diastereo-

Table 1. Results of the Bakers' Yeast Reduction of 3-Oxobutyronitriles

Entry	Product	R	Yield/%	syn : anti[a]	$[\alpha]_D$ in EtOH, *c* ca. 1	
					syn-**2**	*anti*-**2**
1	**2a**	CH_3	69	56 : 44	+17.3°(82%ee, 3*S*)[b]	−11.9° (74%ee, 3*S*)[b]
2	**2b**	C_2H_5	46	54 : 46	+ 9.5°(>98%ee, 3*S*)[b]	−18.8° (>98%ee, 3*S*)[b]
3	**2c**	*n*-C_4H_9	43	58 : 42	+14.3°(>98%ee, 3*S*)[b]	—[c]
4	**2d**	Ph	61	>99 : <1	−33.3°(>98%ee, 3*S*)[b]	

a) Determined by ^{1}H NMR analysis. b) The enantiomeric excess was determined by ^{1}H and ^{19}F NMR analyses of (+)-MTPA ester.[5] c) Anti isomer could not be isolated in pure state by the flash column chromatography on silica gel.

mers of yeast reduction products of **2a**, **2b**, and **2c** could be determined by ^{1}H NMR analysis. For the determination of the absolute configuration, anti isomer of 2-ethyl-3-hydroxybutyronitrile (**2b**) was converted into the corresponding hydroxy ester **4**. Comparing the specific rotation of methyl (2*S*,3*R*)-2-ethyl-3-hydroxybutanoate (**5**) which was derived from methyl (3*R*)-3-hydroxybutanoate,[7] the absolute configuration of the starting nitrile *anti*-**2b** was assigned to be 2*R*, 3*S*.

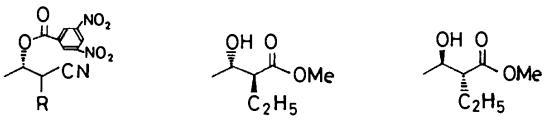

3 4 5

Fig. 1.

Absolute configuration of 3-position of **2a** and **2c** were presumed by the specific rotations and the chemical shift of the methoxyl group of (+)-MTPA esters by comparison with the result in the case of (3*R*)-2-ethyl-3-hydroxybutyronitrile which was assigned by the method above mentioned.

Although the starting material was racemic at C-2 position, only single diastereoisomer was obtained in the case of the reduction of 2-phenyl-3-oxobutyronitrile (**1d**) in optically pure state (Entry 4). To determine the absolute configuration, nitrile **2d** obtained by bakers' yeast reduction was converted into the hydroxy ester **6** by the acid hydrolysis of the cyano group followed by treatment of diazomethane. ^{1}H NMR spectrum of the acetate of **6** agreed completely with that of syn isomer of (±)-**6**.[8] The absolute configuration of nitrile **2d** at C-2 and C-3 position was presumed to be 2*R*, 3*S* on the basis of the sign of the optical rotation of the hydroxy ester **6** with that of (−)-(2*S*, 3*R*)-**7**. This result agreed with a general rule for the enantioselectivity in the bakers' yeast reduction.[9]

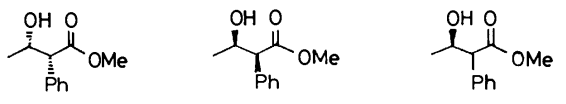

6 7 8

Fig. 2.

This microbial reduction of 3-oxobutyronitriles possesses two outstanding characteristics for the preparation of optically active building blocks for organic synthesis. First, the reduction of 2-phenyl-3-oxobutyronitrile gave a single diastereoisomer of the hydroxy nitrile in optically pure state in good yield. We presumed the reason of this extremely high syn diastereoselectivity of the reduction of 2-phenyl-3-oxobutyronitrile was due to the enhanced enolization of the 3-oxo group[10,11] by the phenyl group. Recently, it has been reported that details of the diastereoselectivity of the bakers' yeast reduction of 2-alkyl-3-oxobutanoate.[12] The keto nitrile **1d** is regarded as equivalent in 2-phenyl-3-oxobutanoate. The bakers' yeast reduction of methyl 2-phenyl-3-oxobutanoate, however, gave a corresponding hydroxy ester in very low yield. In addition, only the reduction of **1d**, the high diastereoselectivity was observed. Other ketones of **1a**, **1b**, and **1c**, however, the bakers' yeast reduction provided good enantioselectivity but poor diastereoselectivity. It is of much interest to compare the results of this microbial reduction of 3-oxobutyronitrile **1** with those of 2-alkyl-3-oxobutanoates[12] in considering the factor which define the stereoselectivity in the enzymatic systems of the yeast. Second, the reduction products involve a cyano group in the molecule. Since the cyano group is a precursor of both of amino group and carbonyl group,[4] hydroxy nitriles **2** obtained in this reaction should become useful building blocks for the synthesis of variety of optically active natural products. As described above, 3-hydroxy esters **9** could be converted from the nitrile **2** easily. And the reduction of **2b** at room temperature for 24 h with 10 mol% of PtO_2 under hydrogen atmosphere[13] provided the amino alcohol **10** in 85% yield. Nitriles react with some nucleophilic reagents under presence of acidic catalyst,[4] both of β-hydroxy ketone **11** and γ-amino alcohol **12** may also be derived from **2** (Scheme 2).

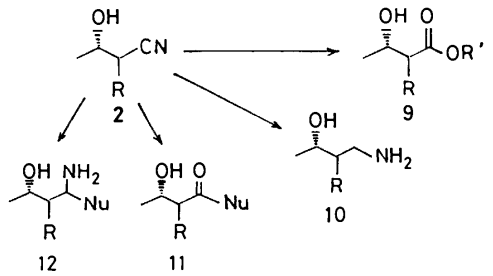

Scheme 2.

It should be emphasized here that the most important thing is to use yeast as a reagent in organic synthesis in designing the substrate to supply the microbial reduction and to modify the substrate which could become a good chiral synthon after reduction. In the present reaction, it has been revealed that the bakers' yeast could play an important role to reduce 3-oxobutyronitriles giving 3-hydroxybutyronitriles with high optical purity.

Experimental

Instruments. NMR spectra were recorded on Varian VXR-200, VXR-500, and JEOL MH-100 spectrometers in $CDCl_3$ with tetramethylsilane (TMS) as an internal reference. Optical rotations were measured with a JASCO DIP-

4 digital polarimeter. IR spectra were recorded on JASCO A-102 spectrometer on KBr disk.

Materials. Solvents and commercially available starting materials were generally used without additional purification unless otherwise indicated. Flash chromatography was done on a column of silica gel (Wako gel C-300). Tetrahydrofuran (THF) and diethyl ether (Et_2O) were freshly distilled from sodium benzophenone ketyl. Pyridine and dichloromethane were refluxed on calcium hydride for 5 h and distilled and stored under argon in the presence of Molecular Sieves 4A.

Preparation of 2-Alkyl-3-oxobutyronitrile (1). To a solution of lithium diisopropylamide (LDA) in 30 mL of THF was added a solution of a nitrile (30 mmol) in 60 mL of THF at −50 °C under argon atmosphere and the solution was stirred for 3 h to produced a white sluggish solution, then THF (15 mL) solution of acetyl chloride (1.178 g, 15 mmol) was added one portion into the sluggish solution at −78 °C. After the addition was complete the mixture was stirred and allowed to warm to 0 °C. The reaction mixture was acidified with 2 M HCl solution, then extracted with ethyl acetate. The organic layer was dried over $MgSO_4$, filtered, and concentrated in vacuo to give the crude product. Purification by silica gel flash chromatography (ethyl acetate/hexane=1 : 20 to 1 : 5) gave 3-oxobutyronitrile **1** in 51 to 80% yields. Chemical yield (%), boiling point (°C/mmHg; 1 mmHg≈133.322 Pa), R_f value on silica gel TLC, ^{1}H NMR spectral data (100 MHz, δ TMS in $CDCl_3$), and IR spectral data of ketones **1** are summarized below.

1a: 60%; 60/75 mmHg by Kugelrohr; 0.4 (AcOEt/hexane=1 : 2); 1.5 (3H, d, J=7.8 Hz), 2.4 (3H, s), and 3.7 (1H, q, J=8.4 Hz) ; 3000, 2950, 2310 (CN), 1725 (C=O), 1480, 1360, and 1170 cm^{-1} (neat).

1b: 58%; 85/75 mmHg by Kugelrohr; 0.4 (AcOEt/hexane=1 : 2); 1.1 (3H, t, J=6.6 Hz), 1.8—2.1 (2H, m) , 2.3 (3H, s), and 3.5 (1H, t, J=7.0 Hz) 2970, 2920, 2870, 2230 (CN), 1720 (C=O), 1360, 1160, and 1010 cm^{-1} (neat).

1c: 51%; 110/25 mmHg by Kugelrohr; 0.5 (AcOEt/hexane=1 : 5); 1.0 (3H, t , J=6.5 Hz) , 1.2—2.2 (6H, m), 2.5 (3H, s) 3.5—3.9 (1H, t, J=4.0 Hz); 2970, 2930, 2250 (CN), 1720 (C=O) cm^{-1} (neat).

1d: 80%; mp 97 °C; 0.5 (AcOEt/hexane=1 : 1); 2.3 (3H, s), 4.8 (1H, s), and 7.6 (5H, s); 3050, 2950, 2200(CN), 1730(C=O), 1360, and 1140 cm^{-1} on KBr disk.

Reduction of 2-Alkyl-3-oxobutyronitrile with Bakers' Yeast. To a stirred solution of 30 g of D-glucose in 200 mL of water was added 25 g of bakers' yeast (Oriental Yeast Co.) and the suspension was stirred for 30 min, then, 20 ml of an ethanol solution of 2-phenyl-3-oxobutyronitrile (**1d**) (0.815 g, 5.12 mmol) was added. The mixture was stirred at room temperature for 48 h, and then the yeast suspension of 25 g of yeast, 30 g of D-glucose in 200 mL of water was added and stirred for an additional 148 h. The mixture was filtered through a Celite pad. The filtrate was saturated with NaCl, and extracted with ethyl acetate. The extracts were concentrated in vacuo and the residue was subjected to silica gel flash column to give the alcohol **2d** (0.502 g, 3.12 mmol, 65%) as a yellow oil. The chemical yield of another alcohols **2** obtained by the same method as above are described as followed. **2a**=69%, **2b**=46%, and **2c**=43%. The ratio of diastereomers was determined by 200 MHz ^{1}H NMR analysis. In the case of the reduction of **1d**, no diastereomer could not be detected in **2d** produced in the yeast reduction using 500 MHz ^{1}H NMR.[14]

Preparation of 3,5-Dinitrobenzoates (3).[15] To a solution of **2** (1.0 mmol), pyridine (1.0 mmol), and 4-dimethylaminopyridine (DMAP)(0.1 mmol) in 2.5 mL of dichloromethane (CH_2Cl_2) solution was added 1.5 mmol of 3,5-dinitrobenzoyl chloride in 1.5 mL of CH_2Cl_2 under argon at 0 °C and stirred for 3 h at room temperature. Some pieces of crashed ice were then added to the reaction mixture, and this mixture was extracted with CH_2Cl_2. The organic layer was dried over $MgSO_4$ and concentrated in vacuo to give a yellow solid. Separation of diastereomers could be performed by silica gel flash column chromatography or silica gel TLC. Chemical yield (%), melting point (°C), R_f value on silica gel TLC, and IR spectral data(KBr disk) are summarized below.

3a: 95%; 70 (syn), 65 (anti); 0.6 (syn) and 0.5 (anti), AcOEt/hexane=1 : 1 after 5 times of development; 3100, 2960, 2240(CN), 1730(CO) , 1550, 1170, 920, 720 cm^{-1}.

3b: 95%; 70 (syn), 92 (anti); 0.6, (syn), 0.45 (anti), AcOEt/hexane=1 : 5, after 4 times of development; 3100, 2960, 2920, 2240(CN) , 1730(CO) , 1550, 1340, 1270, 1170, 920, 720 cm^{-1}.

3c: 87%; 98 (syn); 0.65 (syn), AcOEt/hexane=1 : 5, after 10 times of development; 3150, 2950, 2850, 2230(CN), 1730(CO), 1550, 920 cm^{-1}.

3d: 61%; 115; 0.25, AcOEt/hexane=1 : 3, after 3 times of development; 3110, 2950, 2850, 2230 (CN), 1780 (CO), 1530, 950 cm^{-1}.

Spectral data, each diastereomers of the esters of **3** of ^{1}H HMR (200 MHz, δ, $CDCl_3$, J/Hz), ^{13}C NMR (50 MHz, δ, $CDCl_3$, ppm) are summarized below.

3a(syn): 1.423 (3H, d, J=7.25), 1 579 (3H, d, J=6.40), 3.172 (1H, dq, J_1=4.99, J_2=7.26), 5.245, (1H, dq, J_1=5.05, J_2=6.38), 9.131 (2H, d, J=2.11), 9.236 (1H, t, J=2.12); 14.146, 16.085, 31.143, 72.740, 122.840(CN), 119.259, 129.405, 133.071, 148.612, 161.555.

3a(anti): 1.420 (3H, d, J=6.35), 1.555 (3H, d, J=6.35), 3.025 (1H, dq, J_1=5.42, J_2=7.23), 5.318 (1H, dq, J_1=5.40, J_2=6.30), 9.141 (2H, d, J=2.06), 9.230 (1H, t, J=2.12); 14.366, 17.925, 31.627, 72.925, 122.711(CN), 199.259, 129.043, 133.043, 148.805, 161.555.

3b(syn): 1.128 (3H, t, J=7.40), 1.523 (3H, d, J=6.24), 1.60—1.76 (2H, m), 2.980 (1H, dq, J_1=5.21, J_2=7.54), 5.253 (1H, dq, J_1=5.61, J_2=5.96), 9.097 (2H, d, J=3.00) 9.187 (1H, t, J=2.20); 11.640, 16.588, 22.284, 39.192, 71.699, 118.426, 122.364(CN), 129.451, 133.142, 148.707, 161.578.

3b(anti): 1.156 (3H, t, J=7.20), 1.569 (3H, d, J=6.30), 1.750 (2H, dq, J_1=7.57, J_2=7.30), 2.834 (1H, dt, J_1=5.08, J_2=7.49), 5.386 (1H, dq, J_1=6.15, J_2=5.22), 9.150 (2H, d, J=2.17), 9.244 (1H, t, J=2.14); 11.701, 18.535, 22.478, 39.835, 71.713, 118.422, 122.809(CN), 129.514, 133.185, 148.762, 161.620.

3c(syn): 0.931 (3H, t, J=6.64), 1.581 (3H, d, J=6.41), 1.27—1.50 (2H, m), 1.50—1.75 (4H, m), 3.00—3.13 (1H, m), 5.27 (1H, dq, J_1=6.35, J_2=4.97), 9.133 (2H, d, J=2.12) 9.239 (1H, t, J=2.14); 13.706, 16.487, 22.078, 28.488, 29.251, 37.455, 72.112, 118.663, 122.816(CN), 129.482, 133.176, 148.734, 161.667.

3c(syn+anti mixture): 0.917 (3H, t, J=7.38), 0.935 (3H, t, J=6.64), 1.30—1.50 (2H, m), 1.570 (3H, d, J=6.35), 1.50—1.80 (4H, m), 2.84—2.94 (1H, m), 3.00—3.13 (1H, m), 5.27 (1H, dq, J_1=6.35, J_2=4.97), 5.373 (1H, dq, J=6.35, J_2=6.40), 9.137 (2H, d, J=2.12), 9.153 (2H, d, J=2.13), 9.243 (1H, t, J=2.17); 13.705, 16.487, 18.517, 22.078, 28.473, 28.586, 29.170, 29.243, 37.442, 38.099, 71.916, 72.094, 118.589, 122.775(CN), 129.490,

133.161, 148.726, 161.598. Underlined signals are presumed to be of anti isomer's.

3d(syn): 1.510 (3H, d, J=6.40), 4.407 (1H, d, J=5.20), 7.30—7.50 (5H, m), 9.121 (2H, d, J=2.20), 9.233 (1H, t, J=2.00); 16.059, 43.077, 73.830, 117.309, 122.830(CN), 128.080, 129.121, 129.403, 129.467, 130.819, 133.049, 148.712, 161.681.

Lithium Aluminum Hydride Reduction of 3. To a suspension of 45 mg (1.16 mmol) of lithium aluminum hydride in 1.8 mL of THF at −78°C under argon was added a solution of 144.1 mg (0.469 mmol) of **3b** in 4 mL of THF, and the solution was stirred for 3.5 h. After quench reaction by the addition of wet ether and aqueous solution saturated with Na_2SO_4, the reaction solution was dried by anhydrous K_2CO_3, filtration through a glass filter and evaporation provided a crude oil. Kugelrohr distillation gave **2b** as a colorless oil (47.4 mg, 0.419 mmol, 89%). By the same method other benzoyl esters **3** could be coneverted into the alcohol **2** in 80 to 99% yield. Specific rotation in EtOH at 23°C, boiling point, IR spectral data and elemental analyses of **2** are summarized below.

2a: (syn) +17.3°, c 1.00, (anti) −11.3°, c 0.890; 80°C/1.5 mmHg (Kugelrohr); 3430, 2930, 2240(CN), 1460, 1120 cm^{-1} (neat); Calcd for C_5H_9ON: C, 60.58; H, 9.15; N, 14.13%. Found: C, 60.62; H, 9.29; N, 14.25%

2b: (syn) +9.5°, c 0.820, (anti) −18.8°, c 0.920; 110°C/12 mmHg (Kugelrohr); 3430, 2970, 2870, 2240(CN), 1460, 950 cm^{-1} (neat); Calcd for $C_6H_{11}ON$: C, 63.69; H, 9.80; N, 12.38%. Found: C, 63.41; H, 9.82; N, 12.47%.

2c: (syn) +14.3°, c 0.650; 135°C/2.0 mmHg (Kugelrohr); 3450, 2950, 2930, 2870, 2240(CN), 1470, 1410, 1120 cm^{-1} (neat); Calcd for $C_8H_{155}ON$: C, 68.05; H, 10.71; N, 9.92%. Found: C, 67.87; H, 10.61; N, 10.04%.

2d: (syn) −33.3°, c 0.650; 150°C/2.0 mmHg (Kugelrohr); 3400, 3050, 2950, 2790, 2230(CN), 1480, 730, 680 cm^{-1} (neat); Calcd for $C_{10}H_{11}ON$: C, 74.51; H, 6.88; N, 8.69%. Found: C,74.48; H, 6.80; N, 8.82%.

^1H NMR (200 MHz, $CDCl_3$, δ, J/Hz) and ^{13}C NMR (50 MHz), $CDCl_3$, δ, ppm) spectral data, and ^{19}F NMR (470 MHz, $CDCl_3$, δ, C_6F_6, ppm) spectral data of (+)-MTPA ester are summarized below.

2a(syn): 1.30 (3H, d, J=7.25), 1.34 (3H, d, J=6.29), 1.85 (1H, broad, s, OH), 2.74 (1H, dq, J_1=5.54, J_2=7.21), 3.88 (1H, dq, J_1=6.11, J_2=5.99); 13.717, 20.069, 33.918, 68.574, 121.054; 90.280(p1), 90.310(p2), p1 : p2=8.94 : 91.04, 82%ee.

2a(anti): 1.33 (3H, d, J=6.27), 1.34 (3H, d, J=7.19), 1.947 (1H, d, J=5.60, OH), 2.632 (1H, dq, J_1=4.75, J_2=7.75), 3.87 (1H, dq, J_1=6.16, J_2=5.68); 14.338, 21.209, 34.245, 68.588, 121.231; 90.123(p1), 90.405 (p2), p1 : p2=13.9 : 86.1, 72%ee.

2b(syn): 1.08 (3H, t, J=7.33), 1.33 (3H, d, J=6.24), 1.50—1.70 (2H, m), 2.28 (1H, s, OH), 2.60 (1H, dt, J_1=9.52, J_2=5.67), 3.89 (1H, dq, J_1=6.40, J_2=6.20); 11.755, 20.428, 21.748, 42.172, 67.310, 120.231; 90.224 (single peak), >98%ee.

2b(anti): 1.06 (3H, t, J=7.38), 1.32 (3H, d, J=6.34), 1.58—1.78 (2H, m), 2.28 (1H, s, OH), 2.46 (1H, dq, J_1=4.56, J_2=6.20), 3.82—3.99 (1H, m); 11.721, 21.460, 22.217, 42.366, 67.053, 120.168; 90.256 (single peak), >98%ee.

2c(syn): 0.90 (3H, t, J=6.80), 1.34 (3H, d, J=6.20), 1.18—1.43 (2H, m), 1.48—1.78 (2H, m), 2.03 (1H, broad s, OH), 2.50 (1H, q, J=4.45), 3.89 (1H, dq, J_1=6.34, J_2=6.23); 13.732, 21.576, 22.179, 28.510, 29.400, 40.671, 67.464, 120.179; 90.268 (single peak), >98%ee.

2c(syn+anti mixture): 0.90 (3H, t, J=6.80), 1.325 (3H, d, J=6.29), 1.333 (3H, d, J=6.20), 1.20—1.45 (2H, m), 1.45—1.80 (2H, m), 2.00 (1H, s, OH), 2.46—2.56 (1H, m), 2.60—2.70 (1H, m), 3.82—3.94 (1H, m); 13.732, 13.746, 20.361, 21.566, 21.576, 22.179, 28.043, 28.056, 28.516, 29.410, 40.478, 40.677, 67.442, 67.625, 120.179, 129.427. Underlined signals are presumed to be of anti isomer's.

2d(syn): 1.330 (3H, d, J=6.18), 2.002 (1H, s, OH), 3.911 (1H, d, J=6.24), 4.09 (1H, dq, J_1=6.21, J_2=6.16), 7.20—7.50 (5H, m); 19.842, 46.254, 70.150, 76.933, 128.217, 128.593, 129.154, 132.354; 90.119(single peak), >98%ee.

Methyl (2*R*,3*S*)-2-Ethyl-3-hydroxybutanoate (4). A solution of *anti*-**2b** (49.3 mg, 0.436 mmol) with 5 mL of concd HCl was refluxed for 8 h. After dilution with 10 mL of ethyl acetate, the organic layer was washed with brine, dried, and evaporated to give a colorless oil. The oil was diluted with ether and treated with diazomethane. Purification by silica gel TLC gave **4** as a colorless oil (21.3 mg, 0.146 mmol, 33%).

$[\alpha]_D^{23}$+8.48° (c 0.825, $CHCl_3$); R_f 0.75, AcOEt/hexane=1 : 2; ^1H NMR (100 MHz, δ, $CDCl_3$), 0.9 (3H, t, J=4.4 Hz), 1.2 (3H, d, J=6.0 Hz), 1.3—1.8 (2H, m), 2.2 (1H, q, J=6.4 Hz), 3.0 (OH, s), 3.7 (3H, s), 3.7—4.1 (1H, m); IR (neat), 3430, 2960, 2860, 1730, 1430, 1260, 1200, 1020, and 795 cm^{-1}.

Methyl (2*S*,3*R*)-2-Ethyl-3-hydroxybutanoate (5).[7] To a solution of 6.0 mmol of LDA in 3 mL of THF was added a THF (2.0 mL) solution of 351.4 mg (2.97 mmol) of methyl (3*R*)-3-hydroxybutanoate, $[\alpha]_D^{23}$+43.0° (neat), under argon at −50°C and the solution was stirred for 2 h. Into the resulting orange solution of dianion was added a solution of 1.404 g (19.00 mmol) of ethyl iodide in THF (1.0 mL) and 1.3 mL of HMPA and the mixture was stirred allowed to warm to −25°C for 8 h. After quenching of the reaction by the addition of 2 M HCl, the mixture was extracted with ethyl acetate. The organic layer was dried and evaporated to give a colorless oil. Purification by silica gel TLC gave **5** as a colorless oil in 58% yield (251.3 mg, 1.72 mmol, anti:syn=98.2:1.8). $[\alpha]_D^{23}$ −9.21° (c 1.086, $CHCl_3$); ^1H NMR (100 MHz, δ, $CDCl_3$) 0.9 (3H, t, J=4.4 Hz), 1.2 (3H, d, J=6.4 Hz), 1.3—1.8 (2H, m), 2.2 (1H, q, J=6.4 Hz), 3.0 (1H, broad s, OH), 3.7 (3H, s) 3.7—4.1 (1H, m).

Methyl (2*R*,3*S*)-2-Phenyl-3-hydroxybutanoate (6). The nitrile **2d** (105.5 mg, 0.657 mmol) was converted into the ester **7** (55.6 mg, 0.554 mmol) by the acid hydrolysis of the cyano group followed by the treatment of diazomethane as described above in 65% yield.

$[\alpha]_D^{23}$ +99.8° (c 1.85, $CHCl_3$); R_f 0.6, AcOEt/hexane=1 : 5, after 10 times of development; ^1H NMR (100 MHz, δ, $CDCl_3$) 1.1 (3H, d, J=13.0 Hz), 2.9 (1H, s, OH), 3.4 (1H, d, J=8.4 Hz), 3.6 (3H, s), 4.0—4.5 (1H, m), and 7.2—7.6 (5H, broad s); IR (neat) 3345, 3000, 1740 (C=O), 1240, 1060, 960, 730, and 700 cm^{-1}.

Methyl (±)-2-Phenyl-3-hydroxybutanoate (8).[8,16] To a solution of 10 mmol of LDA in 10 mL of THF was added 1.502 g (10.0 mmol) of methyl 2-phenylacetate at −78°C under argon and the solution was stirred for 1.5 h and was added a solution of 0.44 g (10 mmol) of acetaldehyde in THF (5 mL) at the same temperature and stirred for 1.0 h. After addition of 2 M HCl, the solution was extracted with ether, and the organic layer was dried, evaporated and purification using silica gel flash column chromatography to give *syn*-**8** (0.590 g, 3.04 mmol, 30%) and *anti*-**8** (0.587 g, 3.01 mmol, 30%) as a colorless oil respectively.

syn-**8**: ^1H NMR (100 MHz, δ, $CDCl_3$), 1.1 (3H, d, J=13.0

Hz), 2.9 (1H, s, OH), 3.4 (1H, d, J=8.4 Hz), 3.6 (3H, s), 4.0—4.5 (1H, m), 7.2—7.6 (5H, broad s); IR (neat) 3400, 3000, 1740 (C=O), 1240, 960, and 730 cm^{-1}. *anti*-**8**: ^1H NMR (100 MHz, δ, $CDCl_3$) 1.0 (3H, d, J=6.5 Hz), 3.0 (1H, s, OH), 3.5 (1H, d, J=10.9 Hz), 4.1(3H, s), 4.2—4.5 (1H, m), 7.3—7.5 (5H, m).

Acetate of *syn*-8: ^1H NMR (200 MHz, δ, $CDCl_3$), 1.292 (3H, d, J=6.40 Hz), 1.801 (3H, s, OAc), 3.669 (3H, s, OMe), 3.719 (1H, d, J=8.80 Hz), 5.527 (1H, dq, J_1=8.80 Hz, J_2=6.20 Hz), 7.20—7.30 (5H, m); ^{13}C NMR (50 MHz, δ, $CDCl_3$), 18.650 (4C), 20.831 ($\underline{C}H_3CO$), 52.146 (2C), 56.943 ($COO\underline{C}H_3$), 70.622 (3C), 127.590, 128.429, 128.753, 135.240, 169.954(1C), 171.736 ($CH_3\underline{C}OO$). Acetate of *anti*-**8**: ^1H NMR (200 MHz, δ, $CDCl_3$), 1.048 (3H, d, J=6.20 Hz), 2.042 (3H, s, OAc), 3.666 (3H, s), 3.701 (1H, d, J=10.4 Hz), 5.495 (1H, dq, J_1=10.4 Hz, J_2=6.2 Hz), 7.2—7.3 (5H, m); ^{13}C NMR (50 MHz, δ, $CDCl_3$) 17.673(4C), 21.124, 52.079 (2C), 57.427, 71.785 (3C), 128.070, 128.581, 128.876, 134.782, 180.011 (1C), and 171.974.

Methyl (2*S*,3*R*)-2-Phenyl-3-hydroxybutanoate (7). To a suspension of 91.5 mg (0.387 mmol) of *syn* acetate of **8** in 2.0 mL of 0.1 M phosphate buffer (pH 7.2) was added 46 mg of lipase A6 (from *Aspergillus niger* by Amano Co.), and the suspension was stirred at room temperature for 143 h (30% conversion determined by ^1H NMR). Extraction from the reaction mixture with ethyl acetate and purification by silica gel TLC gave the alcohol **7** as a colorless oil (16.9 mg, 0.087 mmol, 22%).

$[\alpha]_D^{26}$ −97.0° (*c* 1.71, $CHCl_3$), 96%ee determined by the 200 MHz ^1H NMR analysis using chiral shift reagent Eu(hfc)$_3$. When 30 mol% of Eu(hfc)$_3$ was added into the $CDCl_3$ solution of **7**, the methoxy peak at δ 3.70 (s) was split up into two peaks at δ 3.97 and 4.21. According to the ratio of the peak intensity of these two peaks (the low field peak: the high field one=92:2), the absolute configuration at C-3 position of **7** was presumed as 3*R* because this ratio was just the same tendency of the chemical shift of the ester methyl group of 74%ee of methyl (2*R*,3*R*)-2-phenyl-3-hydroxybutanoate,[16] $[\alpha]_D^{23}$ +57.0° (*c* 1.05, $CHCl_3$) in ^1H NMR analysis in the presence of the same chiral shift reagent of 30 mol% of Eu(hfc)$_3$.

We are grateful to professors Masanori UTAKA of Faculty of Engineering at Okayama University and Toshio Sato of Faculty of Science at Tokyo Institute of Technology for their helpful discussions through all of this work. We also thank Mr. Eiichiro Amano of Faculty of Engineering at Okayama University for the elemental analysis.

References

1) For examples, J. D. Morrison, and J. W. Scott, "Asymmetric Synthesis," Academic Press, New York (1984), Vols. 2, 3, and 4; A. Zamojski and G. Grynkiewicz, "The Total Synthesis of Natural Products," John Wiley & Sons (1984), Vol. 6, p. 141.

2) For the reduction of nitrogen functionalized ketones with bakers' yeast, only limited works have been reported: B. S. Deol, D. D. Ridley, and G. W. Simpson, *Aust. J. Chem.*, **29**, 2459 (1976); S. Iriuchijima and M. Ogawa, *Synthesis*, **1982**, 41; B. Banchi, G. Comi, and I. Ventirini, *Gazz. Chem. Ital.*, **114**, 285 (1954); T. Fujisawa, H. Hayashi, and Y. Kishioka, *Chem. Lett.*, **1987**, 129; M. Eberle, M. Egli, and D. Seebach, *Helv. Chim. Acta*, **71**, 1 (1988); K. Nakamura, Y. Inoue, J. Shibahara, S. Oka, and A. Ohno, *Tetrahedron Lett.*, **29**, 4769 (1988).

3) For examples, K. Mori and S. Kuwahara, *Yuki Gosei Kagaku Kyokai Shi*, **46**, 467 (1988); T. Fujisawa, T. Sato, and T. Itoh, *ibid.*, **44**, 519 (1986); T. Oishi and H. Akita, *ibid.*, **41**, 1031 (1983); H. Ohta, *ibid.*, **41**, 1083 (1983); C. J. Sih, and C.-S. Chen, *Angew. Chem., Int. Ed. Engl.*, **23**, 570 (1984); D. Seebach, R. Imwinkelreid, and T. Weber," Modern Synthetic Methods 1986," ed by R. Scheffold, Springer-Verlag, (1986), p. 125, and references sited herein.

4) G. Tennant, "Comprehensive Organic Chemistry," ed by D. Barton and D. Ollis, Pergamon Press (1979), Vol. 2, p. 385.

5) J. A. Dale and H. S. Mosher, *J. Am. Chem. Soc.*, **95**, 512 (1973).

6) H. O. House, D. S. Crumrine, A. Y. Teranishi, and H. D. Olmstead, *J. Am. Chem. Soc.*, **95**, 3310 (1973).

7) G. Fráter, V. Müller, and G. Günter, *Tetrahedron*, **40**, 269 (1984); D. Seebach, H.-F. Chow, R. F. W. Jackson, K. Lawson, M. A. Sutter, S. Thaisirivongs, and J. Zimmermann, *J. Am. Chem. Soc.*, **107**, 5292 (1985).

8) J. Mulzer and G. Bruntrup, *Chem. Ber.*, **115**, 2057 (1982).

9) V. Prelog, *Pure Appl. Chem.*, **9**, 119 (1964).

10) T. Itoh, T. Sato, and T. Fujisawa, *Nippon Kagakukai Shi*, **1987**, 1414; T. Itoh, Y. Yonekawa, T. Sato, and T. Fujisawa, *Tetrahedron Lett.*, **27**, 5405 (1986).

11) By the ^1H NMR analysis, it was found that the rate of deuterium incorporation at 2-position of **1d** was so high that the signal of the methine proton rapidly disappeared when CD_3OD was added in $CDCl_3$ solution of **1d**.

12) K. Nakamura, T. Miyai, A. Nagar, S. Oka, and A. Ohno, *Bull. Chem. Soc. Jpn.*, **62**, 1179 (1989).

13) K. I. Frampton, J. D. Edwards, and H. R. Henze, *J. Am. Chem. Soc.*, **73**, 4432 (1951).

14) A control experiment established a practical limit for the detection of 1% of diastereoisomer of **2a** by the ^1H NMR spectrum of Varian VXR 500 spectrometer.

15) D. W. Brooks, *Tetrahedron Lett.*, **23**, 4991 (1982); E. Hungerbühler, D. Seebach, and D. Wasmuth, *Helv. Chim. Acta*, **64**, 1467 (1981).

16) J. Mulzer and O. Lammer, *Chem. Ber.*, **119**, 2178 (1986).

NMR Determination of Association Constants for Aqueous Calixarene Complexes and Guest Template Effects on the Conformational Freedom[1)]

Seiji SHINKAI,* Koji ARAKI, Tsutomu MATSUDA, and Osamu MANABE§
Department of Organic Synthesis, Faculty of Engineering, Kyushu University, Fukuoka 812
§Department of Industrial Chemistry, Faculty of Engineering, Nagasaki University, Nagasaki 852
(Received March 16, 1989)

The association constants (K) for aqueous complexes with water-soluble p-sulfonatocalix[n]arene ($\mathbf{1}_n$: n=4, 6, and 8) were determined by the NMR method. It was found that $\mathbf{1}_4$ and $\mathbf{1}_6$ form 1 : 1 complexes with guest molecules (trimethylanilinium chloride and 1-adamantyltrimethylammonium chloride), whereas $\mathbf{1}_8$ forms 1 : 2 $\mathbf{1}_8$/guest complexes. The finding supports the view that calixarenes $\mathbf{1}_n$'s are capable of molecular recognition on the basis of the ring size. Examination of the thermodynamic parameters for the association process established that the complexation with $\mathbf{1}_4$ is mainly due to the electrostatic force, whereas that with $\mathbf{1}_6$ and $\mathbf{1}_8$ is mainly due to the hydrophobic force. The coalescence temperatures (T_c's) for calixarene ring inversion were subject to the template effect by these molecules. The activation parameters for the rate of ring inversion were estimated by a computer-assisted spectrum simulation: it was found that the T_c increase, observed in the presence of these guest molecules acting as templates, is caused by the increase in $\Delta H^{\neq}$. These findings provide new insights into the association characteristics of water-soluble calixarenes.

Calixarenes are cyclic oligomers which belong to the class of [$\mathbf{1}_n$]cyclophanes. A variety of calixarenes may now be synthesized in good yields.[2,3)] Since they have a cavity-shaped architecture, they have been expected to be useful as a basic skeleton in the design of new functionalized host molecules.[2-5)] However, unequivocal evidence for the formation of host-guest-type complexes was not found for a long time since the discovery of calixarenes. Conceivably, the difficulty is related to the poor solubility in solvents, particularly, in water. Beginning in 1984, we synthesized and studied p-sulfonatocalixarenes, the first example for water-soluble calixarenes.[6)] Using these water-soluble calixarenes, we found substantial evidence that they can form host-guest-type complexes in an aqueous system.[6-8)]

The next (and probably, most urgent) approach to the design of functionalized host molecules would be to test if the calixarene cavity is capable of molecular recognition in solution. Several groups have reported on the ionophoric properties of calixarenes.[9-12)] In contrast, the study of molecular recognition of organic molecules has been very limited and the question remained unresolved. We report here the NMR method, which is more complicated but applicable to a variety of guest molecules. We have determined the association constants (K), $\Delta H°$, and $\Delta S°$ for the complexation of p-sulfonatocalix[n]arene (n=4, 6, and 8 : $\mathbf{1}_n$) with trimethylanilinium chloride (**2**) and 1-adamantyltrimethylammonium chloride (**3**). During this study we unexpectedly found unequivocal evidence for the formation of the 1 : 2 complexes with $\mathbf{1}_8$.

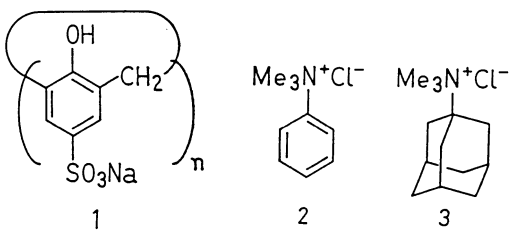

1

2

3

Experimental

The synthesis of $\mathbf{1}_n$ was reported previously.[7)] ^{1}H NMR spectra were measured with a JEOL GX-400 NMR apparatus.

The association constants were estimated from plots of δ_{obs} versus [$\mathbf{1}_n$]/[**2**]. The concentrations of $\mathbf{1}_n$'s were maintained constant while that of **2** was varied. The results were analyzed by the computer-assisted nonlinear least-squares procedure (see Results and Discussion).

The temperature-dependent ^{1}H NMR spectra of $\mathbf{1}_4$ in the absence and the presence of the guest molecules were simulated by the computer-assisted line shape analysis method. In particular, we were concerned with peaks for the ArCH$_2$Ar protons which sensitively reflected the calixarene conformation. Further details are described in Results and Discussion.

Results and Discussion

NMR Determination of Association Constants. Since the present study is related to molecular recognition, the measurements must be carried out below the critical micelle concentration (if any). As reported previously, the critical micelle concentration can be easily detected by ^{1}H NMR or conductance.[7,13)] We confirmed that none of $\mathbf{1}_4$, $\mathbf{1}_6$, and $\mathbf{1}_8$ form the micelle-like aggregate under the experimental conditions.

Figure 1 shows the chemical shift of **2** in the presence of $\mathbf{1}_4$ in D_2O at 25 °C. Clearly, all peaks shift to higher magnetic field with increasing [$\mathbf{1}_4$]/[**2**] ratio. This indicates that **2** interacts with $\mathbf{1}_4$ and undergoes the effect of the ring current of the calixarene benzene components. The fact that the shift width of the four

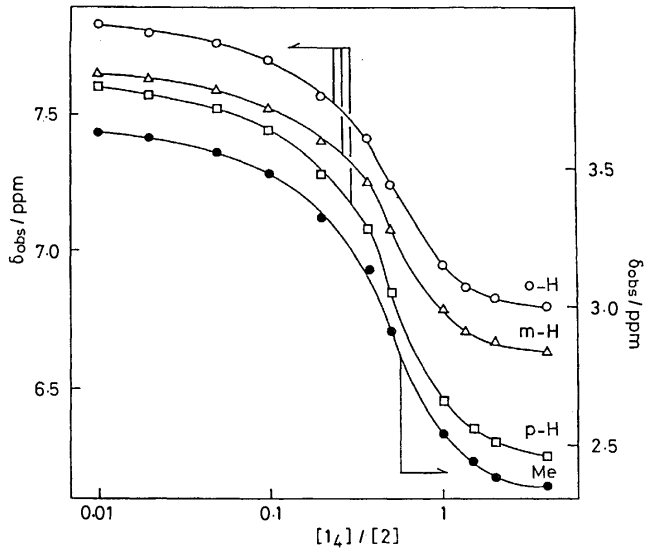

Fig. 1. Plots of δ_{obs} versus $[\mathbf{1}_4]/[\mathbf{2}]$. The concentration of $\mathbf{1}_4$ was maintained constant (1.00 mM) while that of **2** was varied (0.25—100 mM): D_2O, 25 °C, pD 7.3 with 0.1 M phosphate buffer, internal standard DSS.

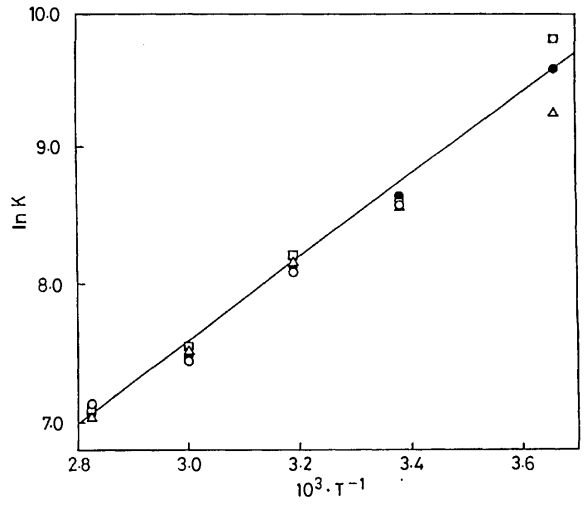

Fig. 2. Plots of $\ln K$ versus T^{-1} for the $\mathbf{1}_4$-**2** system: ○ ortho-H, △ meta-H, □ para-H, ● methyl.

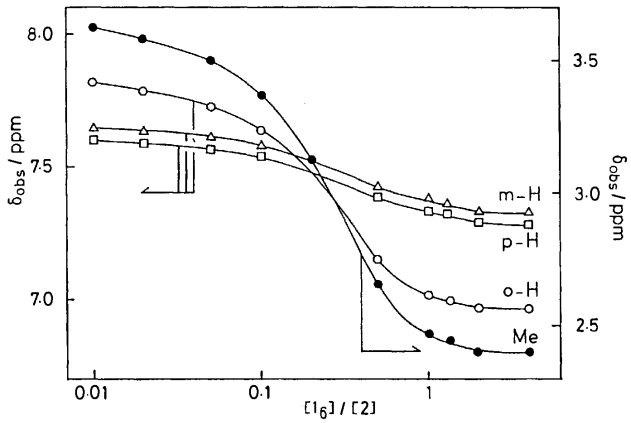

Fig. 3. Plots of δ_{obs} versus $[\mathbf{1}_6]/[\mathbf{2}]$. The measurement conditions are recorded in a caption to Fig. 1.

different protons is similar suggests that the binding of **2** to the $\mathbf{1}_4$ cavity is not specific to give a single complex structure but rather "nonspecific" to give time-averaged, various complexes. It is also seen from Fig. 1 that the change in the chemical shifts is almost saturated at $[\mathbf{1}_4]/[\mathbf{2}]=1.0$, supporting the formation of the 1 : 1 complex. The observed chemical shift (δ_{obs}) appears as an average of the free **2** (δ_{free}) and the complexed **2** ($\delta_{complex}$). Assuming the formation of a 1:1 complex ($\mathbf{1}_n+\mathbf{2} \rightleftarrows \mathbf{1}_n\cdot\mathbf{2}$), δ_{obs} is expressed by Eq. 1.

$$\delta_{obs}=\delta_{free}(([\mathbf{1}_n]_0-[\mathbf{1}_n\cdot\mathbf{2}])/[\mathbf{1}_n]_0)+\delta_{complex}([\mathbf{1}_n\cdot\mathbf{2}]/[\mathbf{1}_n]_0) \quad (1)$$

where $[\mathbf{1}_n]_0$ is the initial concentration of $\mathbf{1}_n$. Thus, this equation is rewritten as Eq. 2.

$$\delta_{obs}=[\mathbf{1}_n]_0+[\mathbf{2}]_0+K^{-1}\pm((([\mathbf{1}_n]_0+[\mathbf{2}]_0+K^{-1})^2 -4[\mathbf{1}_n]_0[\mathbf{2}]_0)^{1/2}(2[\mathbf{2}]_0)^{-1}(\delta_{complex}-\delta_{free})+\delta_{free} \quad (2)$$

where $[\mathbf{2}]_0$ is the initial concentration of **2**. The K value was determined from Eq. 2 by the computer-assisted nonlinear least-squares procedure: $K=5.39\times 10^3$ M^{-1}.** The similar plots of δ_{obs} vs. $[\mathbf{1}_4]/[\mathbf{2}]$ were made at 0, 40, 60, and 80 °C, and the K values were determined at each temperature. As shown in Fig. 2, plots of $\ln K$ vs. T^{-1} shows a good linear relationship with $r=0.99$. This supports the formation of the 1 : 1 complex between $\mathbf{1}_4$ and **2**. The $\Delta H°$ and $\Delta S°$ were determined from the slope ($-\Delta H°/R$) and the intercept ($\Delta S°/R$) by the least-squares procedure: $\Delta H°=-6.2$ kcal mol^{-1} and $\Delta S°=-3.6$ cal mol^{-1}deg^{-1}. From these thermodynamic parameters we calculated the most reliable association constant at 25 °C (Table 1).

The NMR peaks of **2** measured at 25 °C also shifted

Table 1. Association Constants and Thermodynamic Parameters for **2**

Parameter	$\mathbf{1}_4$	$\mathbf{1}_6$	$\mathbf{1}_8$	
			1 : 1	1 : 2
$10^{-2}\cdot K/M^{-1}$ (at 25 °C)	56.0±2.5	5.5±0.4	52.0±0.5	46.0±0.5
$\Delta G°$/kcal mol^{-1} (at 25 °C)	−5.1±0.5	−3.7±0.2	−5.1±0.2	−5.0±0.1
$\Delta H°$/kcal mol^{-1}	−6.2±0.3	−0.25±0.10	0.0±0.10	0.0±0.10
$\Delta S°$/cal mol^{-1} deg^{-1}	−3.6±0.8	11.7±0.3	17.0±0.3	16.7±0.1

** 1 M=1 mol dm^{-3}.

to higher magnetic field with increasing [$\mathbf{1}_6$]/[**2**] ratio and suggest the formation of a 1 : 1 complex (Fig. 3). We repeated the similar measurements at 0, 40, 60, and 80 °C in addition to 25 °C. Plots of $\ln K$ vs. T^{-1} showed a good linear relationship (r=0.99: data not shown here). Thus, we could determine the K and thermodynamic parameters for the 1 : 1 complex with $\mathbf{1}_6$ (Table 1). In contrast, plots for $\mathbf{1}_8$ showed an unusual biphasic dependence (Fig. 4): the NMR peaks of **2** shifted to higher magnetic field at [$\mathbf{1}_8$]/[**2**]<0.5, while the slight downfield shift occurred at [$\mathbf{1}_8$]/[**2**]>0.5. The similar biphasic dependence was also observed at 0, 40, 60, and 80 °C. The new finding that a break point appears at [$\mathbf{1}_8$]/[**2**]=0.5 supports the formation of a 1 : 2 $\mathbf{1}_8$/**2** complex. We thus assumed the following two-step association scheme and estimated K_1 and K_2 independently. The results are summarized in Table 1.

$$\mathbf{1}_8 + 2 \overset{K_1}{\rightleftarrows} \mathbf{1}_8 \cdot 2 \quad (3)$$

$$\mathbf{1}_8 \cdot 2 + 2 \overset{K_2}{\rightleftarrows} \mathbf{1}_8 \cdot (2)_2 \quad (4)$$

We carried out the ^{1}H NMR measurements about **3**, the larger guest molecule at 0, 25, 40, 60, and 80 °C.

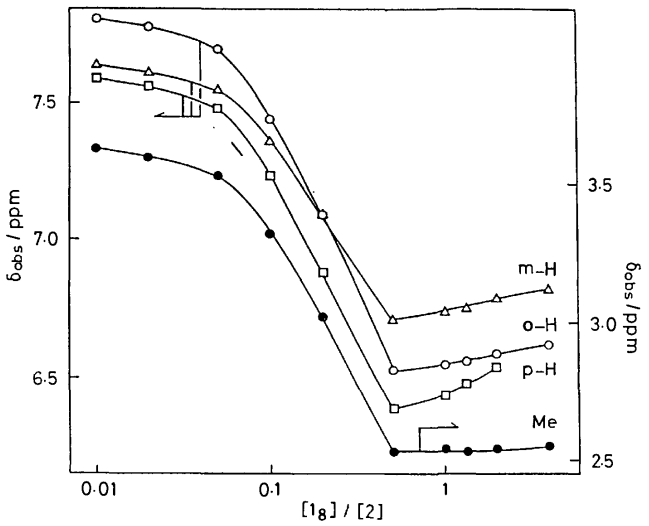

Fig. 4. Plots of δ_{obs} versus [$\mathbf{1}_8$]/[**2**]. The measurement conditions are recorded in a caption to Fig. 1.

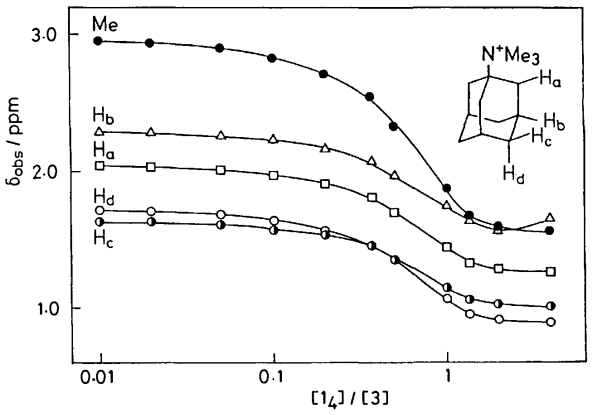

Fig. 5. Plots of δ_{obs} versus [$\mathbf{1}_4$]/[**3**]. The concentration of $\mathbf{1}_4$ was maintained constant (1.00 mM) while that of **3** was varied (0.25—100 mM): D_2O, 25 °C, pD 7.3 with 0.1 M phosphate buffer, internal standard DSS.

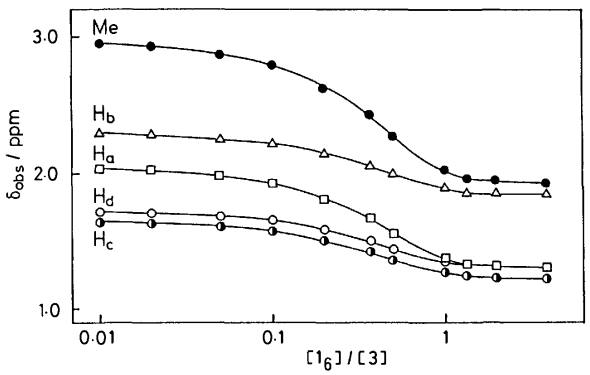

Fig. 6. Plots of δ_{obs} versus [$\mathbf{1}_6$]/[**3**]. The measurement conditions are recorded in a caption to Fig. 5.

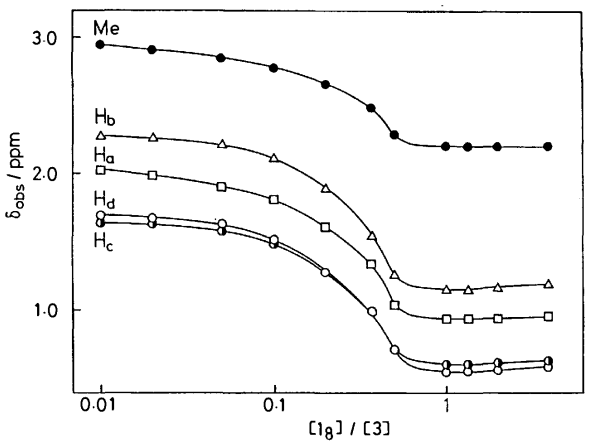

Fig. 7. Plots of δ_{obs} versus [$\mathbf{1}_8$]/[**3**]. The measurement conditions are recorded in a caption to Fig. 5.

Table 2. Association Constants and Thermodynamic Parameters for **3**

Parameter	$\mathbf{1}_4$	$\mathbf{1}_6$	$\mathbf{1}_8$	
			1 : 1	1 : 2
$10^{-3} \cdot K/M^{-1}$ (at 25 °C)	21.0±1.5	1.0±0.3	19.0±0.5	17.0±0.5
$\Delta G°$/kcal mol^{-1} (at 25 °C)	−5.9±0.4	−4.1±0.2	−5.8±0.2	−5.8±0.1
$\Delta H°$/kcal mol^{-1}	−5.7±0.3	−0.15±0.10	0.0±0.10	0.0±0.10
$\Delta S°$/cal mol^{-1} deg^{-1}	0.65±0.6	13.3±0.3	19.6±0.3	19.3±0.2

The results are illustrated in Figs. 5—7. It is seen from these figures that $\mathbf{1}_4$ and $\mathbf{1}_6$ form the 1 : 1 complexes with **3**, whereas $\mathbf{1}_8$ form the 1 : 2 complex indicating that the cavity of $\mathbf{1}_8$ is still big enough to accept two **3** molecules. From the plots of $\ln K$ vs. T^{-1} we determined $\Delta H°$ and $\Delta S°$. The results are summarized in Table 2.

The formation of the 1 : 2 complex with $\mathbf{1}_8$ is primarily attributed to the large ring size. This means that in principle, the "hole-size" selectivity is operative in molecular recognition by water-soluble calixarenes. In this connection, it is interesting to note that among *p*-alkylcalix[*n*]arenes (*n*=4, 6, and 8) only *p*-alkylcalix[8]arene is capable of extracting alkali metal cations in a 1 : 2 calixarene/M^+ ratio.[14] We consider that in addition to the ring size, the ring flexibility plays an important role in the binding of the second guest molecule. It is known that β- and γ-cyclodextrins can include two guest molecules in the cavity.[15-17] In these 1 : 2 complexes K_2 is usually greater than K_1. This situation is observed because the molecular size of the first guest is smaller than the cyclodextrin cavity and the cavity is just filled up by the binding of the second guest. In other words, the cyclodextrin cavity is relatively rigid. In the binding of **2** and **3** to $\mathbf{1}_8$, on the other hand, we observed the relation $K_1 \approx K_2$. The fact that the thermodynamic parameters for K_1 are similar to those for K_2 supports the view that the binding mechanism for K_1 and K_2 is also similar. The results can be reasonably rationalized in terms of the flexibility of $\mathbf{1}_8$ called a "pinched conformation":[2,3] flexible calix[8]arene can "pinch" transannularly to provide two half-cavities. Hence, the first guest is included in the cavity in an induced-fit manner and the circumstance is similar to the remaining half-cavity for the binding of the second guest (Eq. 5). Comparison of Fig. 4 with Fig. 7 manifests, however, that in the $\mathbf{1}_8 \cdot \mathbf{2}$ complex the highest chemical shifts are attained for the 1 : 2 complex (i.e., at $[\mathbf{1}_8]/[\mathbf{2}]=0.5$), whereas in the $\mathbf{1}_8 \cdot \mathbf{3}$ complex the chemical shifts are similar between the 1 : 1 and 1 : 2 complexes (i.e., constant δ_{obs} at $[\mathbf{1}_8]/[\mathbf{3}] \geqq 0.5$). This suggests that two **2** molecules can adopt, although in some probability, a face-to-face orientation, undergoing the anisotropic effect of each benzene π-system.

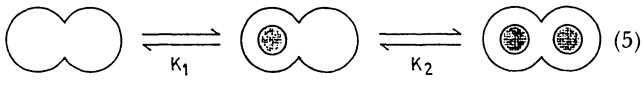

(5)

The *K* value for $\mathbf{1}_4$ is apparently comparable with K_1 and K_2 for $\mathbf{1}_8$. Careful examination of Tables 1 and 2 indicates, however, that the thermodynamic parameters are quite different: the binding to $\mathbf{1}_4$ occurs owing to negative $\Delta H°$, whereas that to $\mathbf{1}_8$ occurs owing to positive $\Delta S°$. The results suggest that the association of $\mathbf{1}_8$ with **2** and **3** is primarily based on hydrophobic interactions, whereas that of $\mathbf{1}_4$ with **2** and **3** is rather supported by electrostatic interactions. What is the origin of this difference? The first difference is that the cavity of calix[4]arene is very rigid and open like a bowl.[2,3] Since hydrophobic interactions are based on stacks between host and guest,[18] it seems fairly difficult for rigid, open $\mathbf{1}_4$ to adopt such an association mode favorable for hydrophobic interactions. The second difference is related to the strong, anionic electrostatic field provided by $\mathbf{1}_4$. We have found that *p*-sulfonatocalixarenes, having anionic sulfonato groups on one side of the calixarene cavity, provide a strong anionic field.[7,19] In particular, *p*-sulfonatocalix[4]arene, having four sulfonato groups on the small cavity showed the strongest electrostatic effect.[19,20] These characteristics of $\mathbf{1}_4$ would lead to the negative $\Delta H°$.

Another interesting point seen from Tables 1 and 2 is that the *K* values for $\mathbf{1}_6$ are generally smaller than those for $\mathbf{1}_4$ and $\mathbf{1}_8$. Examination of the thermodynamic parameters for $\mathbf{1}_6$ reveals that the $\Delta H°$ values are not so negative as those for $\mathbf{1}_4$ while the $\Delta S°$ values are not so positive as those for $\mathbf{1}_8$. Probably, the association with $\mathbf{1}_6$ is an intermediary case between $\mathbf{1}_4$ and $\mathbf{1}_8$ where neither the electrostatic force nor the hydrophobic force operates efficiently.

The *K* values for **3** are greater by a factor of about 5 than those for **2**. When the thermodynamic parameters for **3** are compared with those for **2**, we notice that the *K* values are enhanced owing to the increase in $\Delta S°$. This is well-accounted for by the hydrophobic effect of the adamantyl group.

The complexation geometry of **2** and **3** can be

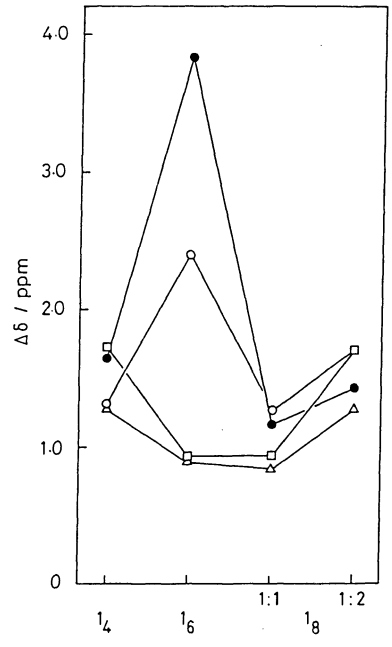

Fig. 8. Shifts of the ^1H NMR peaks of **2** to higher magnetic field. The shift width was calculated for 100%-complexed **2** from the parameters obtained by the nonlinear least-squares procedure (Eq. 2) used for the determination of *K* in Figs. 1, 3, and 4.

presumed from the magnitude of the higher magnetic-field shifts. As shown in Fig. 8, the shift width observed for the $\mathbf{1}_4$ and $\mathbf{1}_8$ complexes is rather similar among all protons, suggesting that **2** is bound in a nonselective manner. In contrast, the *N*-methyl and ortho protons particularly shift to higher magnetic field on the addition of $\mathbf{1}_6$. This suggests that the ammonium moiety, rather than the phenyl moiety, is incorporated into the aromatic cavity of $\mathbf{1}_6$. A similar trend is observed for **3** (Fig. 9). The unusual chemical shifts were also observed by Stauffer and Dougherty[21] for **3** bound to water-soluble cyclophanes. They proposed an ion-dipole interaction between guest N^+ and host π-system. At present, we are not sure if this is the case in our system. Probably, the ion-dipole interaction is hidden in an aqueous system but becomes operative when the hydrophobic interaction between the guest and the host cavity is mismatched. This may be related to the small *K* values for $\mathbf{1}_6$.

Guest Template Effects. What influence does included **2** (or **3**) have on the calixarene conformation? It is known that the temperature-dependent ^{1}H NMR spectrum displays a singlet resonance for the $ArCH_2Ar$ methylene protons at high temperature and a pair of doublets at low temperature. Thus, the coalescence temperature (T_c) appears at intermediary temperature. This behavior has been interpreted in terms of a conformational change from "alternate" to "cone" (Fig. 10).[2,3,22,23] We estimated the influence of added **2** (or **3**) on T_c of $\mathbf{1}_4$ in D_2O. The T_c in the absence of a guest molecule appeared at 9 °C (Table 3). Very interestingly, we found that the T_c values are significantly enhanced in the presence of **2** or **3**. This indicates that these organic guest molecules act as template cations. The Corey-Pauling-Koltun molecular model buildings and the recent X-ray crystallographic studies show that the "cone" conformation provides a cavity-shaped stoma more suitable to guest-binding than the "alternate" conformation.[24-26] The circular dichroism studies also support the view that the conformation of water-soluble calixarenes is fixed to "cone" upon inclusion of guest molecules.[27] Probably, **2** and **3** act as efficient templates not only because of electrostatic interactions between NMe_3^+ and oxide anions but also because of inclusion of a phenyl or adamantyl group into the "cone"-shape hydrophobic cavity of $\mathbf{1}_4$.

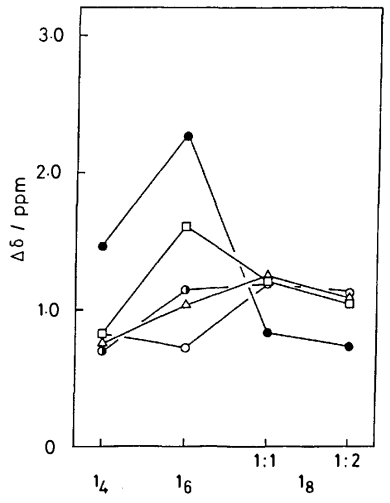

Fig. 9. Shifts of the ^{1}H NMR peaks of **3** to higher magnetic field. The shift width was calculated for 100-complexed **3** from the parameters obtained by the nonlinear least-squares proceduce (Eq. 2) used for the determination of *K* in Figs. 5—7.

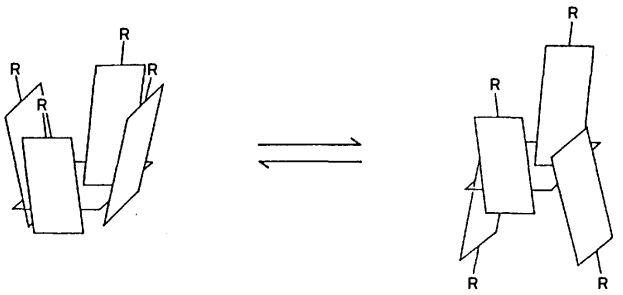

Fig. 10. Schematic illustration of "cone" and "alternate" calix[4]arene.

Table 3. Influence of Guest Molecules on T_c of $\mathbf{1}_4$[a]

Guest (concn/M)	T_c/°C
None	9
2 (0.005)	20
2 (0.010)	43
2 (0.020)	50
2 (2.00)	65
3 (0.005)	25
3 (0.010)	50
3 (0.020)	57

a) pD 8.9 with 0.5 M borate buffer, $[\mathbf{1}_4]=1.10\times10^{-2}$ M.

In order to obtain a further insight into the template effect we applied computer-assisted spectrum simulation (complete line shape analysis)[28] to the temperature-dependent ^{1}H NMR spectra of $\mathbf{1}_4$ in the absence and the presence of these guest molecules. The typical example is shown in Fig. 11: the observed spectral change (*A*) was simulated assuming the lifetime (τ) at each temperature (*B*). Excellent agreement is seen between the observed and the simulated spectra. Plots of $\log k$ (rate constant for the spin exchange τ^{-1}) vs. T^{-1} afforded excellent linear relationships ($r>0.99$), as shown in Fig. 12, from which we obtained $\log A$ and E_a. From these values we calculated $\Delta G^{\ddagger}_{298}$, $\Delta H^{\ddagger}$, and $\Delta S^{\ddagger}$ (Table 4).

As mentioned above, the spectral change has been interpreted in terms of a conformational change from "cone" to "alternate".[2,3,22,23] However, the continuity in the Arrhenius plots indicates that such a conformational transition does not exist. This means that the spectral change is best understood as a consequence of the temperature-dependent rate

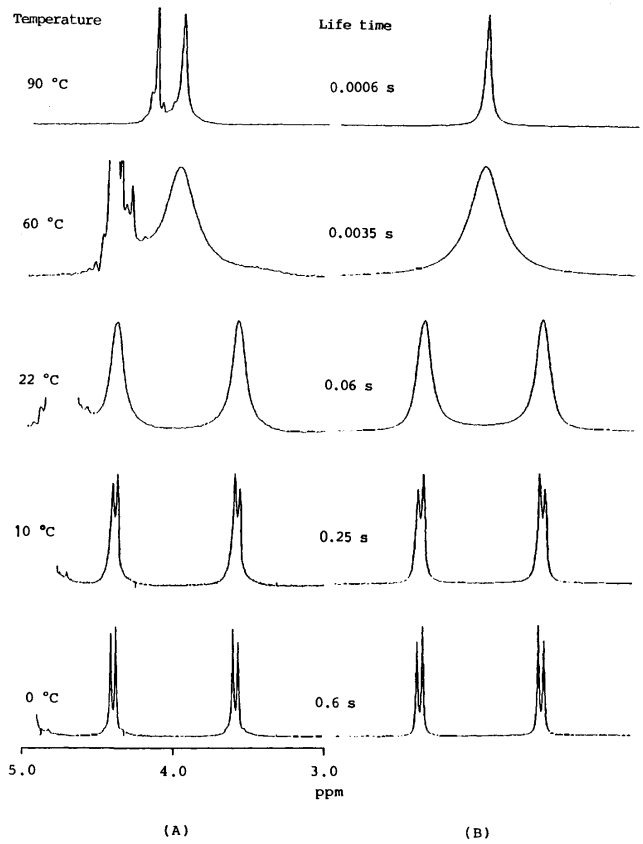

Fig. 11. Observed (A) and simulated spectra (B) of the $ArCH_2Ar$ protons in $\mathbf{1}_4$ (1.00×10^{-2} M) in the presence of **2** (2.00×10^{-2} M).

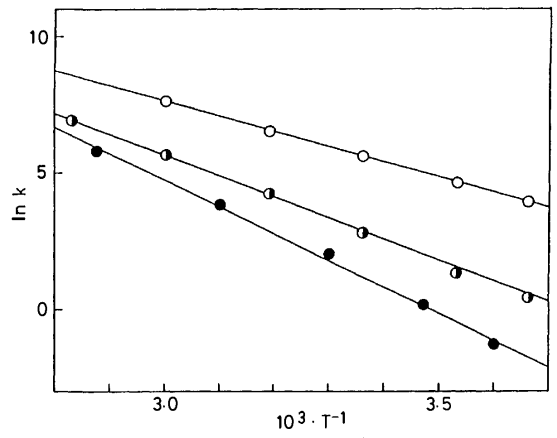

Fig. 12. Arrhenius plots for the rate of $\mathbf{1}_4$ (1.00×10^{-2} M) ring inversion: ○ no guest, ◑ [**2**]=2.00×10^{-2} M, ● [**3**]=2.00×10^{-2} M.

change for ring inversion between "cone" conformations.[29]

Examination of Table 4 represents an interesting view: $\Delta H^{\ddagger}$ and $\Delta S^{\ddagger}$ compensates each other and the $\Delta G^{\ddagger}_{298}$ increase, observed in the presence of **2** or **3**, is caused by the $\Delta H^{\ddagger}$ increase. On the contrary, the $\Delta S^{\ddagger}$ value increases in the presence of these guest molecules, indicating that from a steric viewpoint,

Table 4. Activation Parameters for the Spin Exchange in $\mathbf{1}_4$ (0.010 M)[a]

Guest (concn/M)	$\Delta G^{\ddagger}_{298}$	$\Delta H^{\ddagger}$	$\Delta S^{\ddagger}$
	kcal mol^{-1}	kcal mol^{-1}	cal mol^{-1} deg^{-1}
None	14.1±0.3	10.4±0.1	−12±1.3
2 (0.020 M)[b]	15.7±0.6	14.6±0.3	−1.8±3.0
3 (0.020 M)[c]	16.7±1.4	18.7±0.7	6.7±4.0

a) pD 7.3 with 0.1 M phophate buffer, [$\mathbf{1}_4$]=1.00×10^{-2} M. b) Under the measurement conditions (25 °C) 98.3% of $\mathbf{1}_4$ include **2**. c) Under the measurement conditions (25 °C) 99.5% of $\mathbf{1}_4$ include **3**.

guest inclusion makes the ring inversion easier. In order to attain the ring inversion, the $\mathbf{1}_4$-guest complex should be dissociated once at a transition state. This dissociation process would be reflected by the $\Delta H^{\ddagger}$ increase. On the other hand, it is not easy to elucidate the $\Delta S^{\ddagger}$ increase reasonably. We believe that complexed $\mathbf{1}_4$ is sterically more hindred than vacant $\mathbf{1}_4$, leading to entropic destabilization of the initial state.

Conclusion

The present study demonstrated that the association properties of water-soluble calixarenes are conveniently estimated by the NMR methods. Of particular significance are the unexpected findings that only $\mathbf{1}_8$ can form the 1:2 complexes with organic guest molecules and that these guests serve as efficient templates to fix the calixarene conformation. This suggests that in principle, calixarene cavities are capable of molecular recognition. We believe that in near future calixarenes would become a useful building block to design enzyme mimics in totally synthetic systems.

We are indebted to Professor Hiroki Kondo and Mr. Yuichiro Ohama for measurements of 400 MHz NMR spectra. This research was supported by the Grant-in-Aid from the Ministry of Education.

References

1) Preliminary communication: S. Shinkai, K. Araki, and O. Manabe, *J. Am. Chem. Soc.*, **110**, 7214 (1988).
2) C. D. Gutsche, *Acc. Chem. Res.*, **16**, 161 (1983).
3) C. D. Gutsche, *Top. Curr. Chem.*, **123**, 1 (1984).
4) S. Shinkai, *Pure Appl. Chem.*, **58**, 1523 (1986).
5) S. Shinkai and O. Manabe, *Nippon Kagaku Kaishi*, **1988**, 1917.
6) S. Shinkai, S. Mori, T. Tsubaki, T. Sone, and O. Manabe, *Tetrahedron Lett.*, **25**, 5315 (1984).
7) S. Shinkai, S. Mori, H. Koreishi, T. Tsubaki, and O. Manabe, *J. Am. Chem. Soc.*, **108**, 2409 (1986).
8) Water-soluble calixarenes are also being studies by other groups: C. D. Gutsche and I. Alam, *Tetrahedron*, **44**, 4689 (1988); A. Arduini, A. Pochini, S. Reverberi, and R. Ungaro, *J. Chem. Soc., Chem. Commun.*, **1984**, 981.
9) S. -K. Chang and I. Cho, *J. Chem. Soc., Perkin Trans. 1*, **1986**, 211.

10) M. A. McKervey, E. M. Seward, G. Ferguson, B. Ruhl, and S. J. Harris, *J. Chem. Soc., Chem. Commun.*, **1985**, 388.
11) A. Arduini, A. Pochini, S. Reverberi, and R. Ungaro, *Tetrahedron*, **42**, 2089 (1986).
12) S. Shinkai, S. Edamitsu, T. Arimura, and O. Manabe, *J. Chem. Soc., Chem. Commun.*, **1988**. 1622.
13) S. Shinkai, K. Araki, and O. Manabe, *J. Chem. Soc., Chem. Commun.*, **1988**, 187.
14) S. R. Izatt, R. T. Hawkins, J. J. Christensen, and R. M. Izatt, *J. Am. Chem. Soc.*, **107**, 63 (1985).
15) A. Ueno, K. Takahashi, and T. Osa, *J. Chem. Soc., Chem. Commun.*, **1980**, 921.
16) S. Hamai, *Bull. Chem. Soc. Jpn.*, **55**, 2721 (1982).
17) K. Kano, I. Takenoshita, and T. Ogawa, *Chem. Lett.*, **1982**, 321.
18) C. Tanford, "The Hydrophobic Effect," Wiley Intersci., New York (1973).
19) S. Shinkai, S. Mori, K. Araki, and O. Manabe, *Bull. Chem. Soc. Jpn.*, **60**, 3679 (1987).
20) H. Sato, K. Araki, S. Shinkai, and O. Manabe, *J. Chem. Soc., Perkin Trans. 1*, to be submitted.
21) D. A. Stauffer and D. A. Dougherty, *Tetrahedron Lett.*, **29**, 6039 (1988).
22) C. D. Gutsche and L. J. Bauer, *Tetrahedron Lett.*, **22**, 4763 (1981).
23) G. Happel, B. Mathiasch, and H. Kämmerer, *Makromol. Chem.*, **176**, 3317 (1975).
24) R. Ungaro, A. Pochini, G. D. Andreetti, and P. Domiano, *J. Chem. Soc., Perkin Trans. 2*, **1985**, 197.
25) S. G. Bott, A. W. Coleman, and J. L. Atwood, *J. Am. Chem. Soc.*, **108**, 1709 (1986).
26) S. G. Bott, A. W. Coleman, and J. L. Atwood, *J. Am. Chem. Soc.*, **110**, 610 (1988).
27) S. Shinkai, T. Arimura, H. Satoh, and O. Manabe, *J. Chem. Soc., Chem. Commun.*, **1987**, 1495.
28) J. I. Kaplan and G. Fraenkel, "NMR of Chemically Exchanging Systems," Acacemic Press, New York (1980), p. 71.
29) K. Araki, S. Shinkai, and T. Matsuda, *Chem. Lett.*, **1989**, in press.

Electron Transfer Resulting from Excitation of Contact Charge Transfer Complexes of Some Styrene Derivatives and Oxygen. The Role of Oxygen as an Electron Acceptor

Masanobu KOJIMA,*,† Hirochika SAKURAGI,* and Katsumi TOKUMARU
Department of Chemistry, University of Tsukuba, Tsukuba, Ibaraki 305
†Faculty of Liberal Arts, Shinshu University, Asahi, Matsumoto, Nagano 390
(Received June 7, 1989)

Irradiation of contact charge transfer (CCT) bands (320—370 nm) of 4-methoxystyrene (**1a**) and 4-methylstyrene (**1b**) with molecular oxygen in acetonitrile and benzene resulted in the formation of the corresponding *cis*- and *trans*-1,2-diarylcyclobutanes (**2** and **3**) as well as benzaldehydes (**4**), oxidative cleavage products. In the case of **1b**, 7-methyl-1-(4-tolyl)-1,2,3,4-tetrahydronaphthalene (**5**) and 6-methyl-4-(4-tolyl)-1,2,3,4-tetrahydronaphthalen-1-one (**6**) were also afforded. The formation of these products is reasonably explained by electron transfer in the excited CCT pair followed by addition of the resulting **1** cation radical to ground-state **1** to form a dimer cation radical; its cyclization leads to the dimeric products and trapping of a cyclic dimer cation radical by oxygen affords ketone **6**.

In photochemical reactions, oxygen has often been investigated only as an oxidant. It is well-known that singlet oxygen generated by dye sensitization oxidizes olefins to afford hydroperoxides, endoperoxides, and dioxetanes.[1] In contrast to active studies on singlet oxygen, another role of oxygen as an electron acceptor has attracted little attention.[2]

The formation of contact charge transfer (CCT) complexes between organic compounds and oxygen has been observed.[3] However, their roles in photochemical reactions had not been recognized until a few years ago. Recently, the copolymerization of styrene and its derivatives with oxygen was reported to be initiated by irradiation of the CCT bands between the olefins and oxygen.[4] Also, the excitation of the CCT band between hexamethylbenzene and oxygen in methanol-benzene was shown to produce 2,3,4,5,6-pentamethylbenzyl cations followed by their reaction with methanol to give 1-methoxy-2,3,4,5,6-pentamethylbenzene.[2b] Furthermore, in dye-sensitized photooxygenation of *trans*-stilbene, oxygen was reported to serve as an electron acceptor.[5]

In a previous communication,[6] we demonstrated that the photoexcitation of CCT complexes of 4-methoxy- and 4-methylstyrene with oxygen in acetonitrile induces electron transfer from the styrenes to oxygen to generate cation radicals of the styrenes followed by their addition to the styrenes finally affording dimers of the styrenes.[7] The present paper describes a full account of our work on the photochemical reactions of the olefins resulting from their CCT band excitation.

Results

Formation of CCT Complexes of 4-Methoxy- and 4-Methylstyrene with Oxygen. The longest wavelength end of the absorption band of 4-methoxystyrene (**1a**) lies at 325 nm under argon in acetonitrile or benzene (Fig. 1a). On saturation with oxygen a new absorption band appeared in the range of 320—370 nm in both solvents. Figure 1c shows a difference spectrum of **1a** under argon and oxygen. This band disappeared reversibly on introduction of argon to exclude oxygen, and therefore, is reasonably assigned to a CCT pair of **1a** and oxygen. 4-Methylstyrene (**1b**) exhibited a similar absorption due to its CCT pair with oxygen in the region of 310—370 nm in acetonitrile (Fig. 1e).

On addition of 1,4-dicyanobenzene (DCNB) under nitrogen in acetonitrile, **1a** exhibited a new absorption band in the region of 320—390 nm (Fig. 1f). This band can be assigned to a charge transfer (CT) complex.

Irradiation of 4-Methoxystyrene (1a). Direct irradiation of **1a** under nitrogen in acetonitrile with 254- or 313-nm light afforded head-to-head cycloadducts, *cis*- and *trans*-1,2-bis(4-methoxyphenyl)cyclobutane

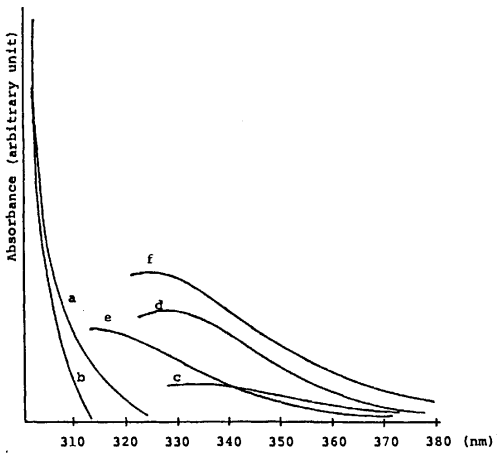

Fig. 1. UV spectra of CCT pairs.
a: **1a** under argon in MeCN. b: **1b** under argon in MeCN. c: **1a** under oxygen in MeCN. d: **1a** under oxygen in PhH. e: **1b** under oxygen in MeCN. f: **1a** in the presence of DCNB in MeCN.

(**2a** and **3a**, respectively, 63—65% yield) in a ratio of ca. 90/10.

Irradiation of **1a** under oxygen in acetonitrile with 366-nm light gave **2a** and **3a** (31%, **2a**/**3a**=5/95) together with 4-methoxybenzaldehyde (**4a**, 32%), an oxidative cleavage product (Scheme 1). However, no reaction products were essentially detected on irradiation under nitrogen. The results on irradiation of **1a** under various conditions are summarized in Table 1.

Irradiation of **1a** at 313 or 366 nm in the presence of DCNB under nitrogen in acetonitrile afforded **3a** predominantly with a small amount of **2a** (**2a**/**3a**=2/98, Runs 11 and 12 in Table 1). On benzophenone-sensitized irradiation (366 nm) under otherwise similar conditions, **1a** gave the dimers in an isomer ratio of **2a**/**3a**=13/87 (Run 10). 4-Methoxybenzaldehyde (**4a**) hardly sensitized the dimerization under 366-nm illumination; however, with 313-nm light **4a** sensitized the dimerization to produce **2a** and **3a** in a ratio of 22/78 (Run 9).

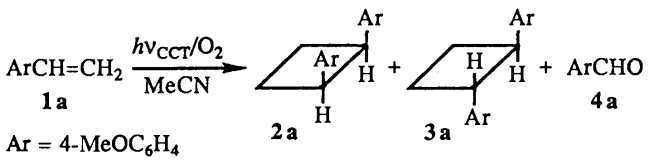

Scheme 1.

Irradiation of 4-Methylstyrene (1b). Irradiation of **1b** in acetonitrile under oxygen with 313-nm light led to the formation of three cyclodimers (20%), *cis*- and *trans*-1,2-bis(4-tolyl)cyclobutane (**2b** and **3b**, respectively, head-to-head cycloadducts) and a tetralin derivative, 7-methyl-1-(4-tolyl)-1,2,3,4-tetrahydronaphthalene (**5**) (isomer ratio, **2b**:**3b**:**5**=58:33:9), and a dimeric ketone, 6-methyl-4-(4-tolyl)-1,2,3,4-tetrahydronaphthalen-1-one (**6**, 20%) together with 4-methylbenzaldehyde (**4b**, 8%) (Scheme 2). On the other hand, the irradiation of **1b** under nitrogen gave cyclodimers **2b**, **3b**, and **5** in a ratio of 83:10:7, but no dimeric ketone **6**.

Irradiation of **1b** at 313 nm in the presence of DCNB under nitrogen in acetonitrile afforded 1-(4-cyanophenyl)-6-methyl-4-(4-tolyl)-1,2,3,4-tetrahydronaphthalene (**7**) as a main product (30%) together with the olefin dimers (5%, **2b**:**3b**:**5**=11:11:78). The results are summarized in Table 2.

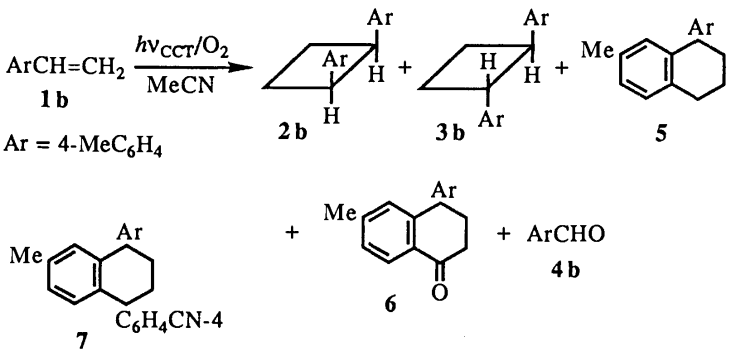

Scheme 2.

Table 1. Photodimerization of 4-Methoxystyrene[a)]

Run	Conditions	$h\nu$[b)] / nm	Conversion/%	Yield/% 2a+3a	Yield/% 4a	Isomer ratio 2a:3a
1)	MeCN, O_2	254	34	56	9	63:37
2)	MeCN, O_2	313	63	47	14	16:84
3)	MeCN, O_2	366	43	31	32	5:95
4)	MeCN, N_2	254	23	65	Trace	90:10
5)	MeCN, N_2	313	26	63	Trace	87:13
6)	MeCN, N_2	366	3	Trace	Trace	—
7)	PhH, O_2	313	37	18	11	80:20
8)	PhH, O_2	366	—	Trace	Trace	—
9)	MeCN, N_2 4-$MeOC_6H_4CHO$[c)]	313	28	75	Trace	22:78
10)	MeCN, N_2 Ph_2CO[d)]	366	12	50	Trace	13:87
11)	MeCN, N_2 DCNB[e)]	313	95	42	—	2:98
12)	MeCN, N_2 DCNB[f)]	366	77	68	—	2:98

a) Olefin concentration, 0.59 mol dm^{-3}. b) Effective excitation wavelength. c) 0.12 mol dm^{-3} d) 0.13 mol dm^{-3}. e) 0.13 mol dm^{-3}. f) 0.08 mol dm^{-3}.

Table 2. Photodimerization of 4-Methylstyrene[a)]

Run	Conditions	$h\nu$[b)] / nm	Conversion/%	Yield/%				Isomer ratio
				2b+3b+5	4b	6	7	2b:3b:5
1)	MeCN, O_2	313	45	14	8	20	—	58:33:9
2)	MeCN, N_2	313	15	42	—	—	—	83:10:7
3)	MeCN, N_2 DCNB[c)]	313	65	45	—	—	30	11:11:78

a) Olefin concentration, 0.63 mol dm^{-3} b) Effective excitation wavelength. c) 0.13 mol dm^{-3}.

Discussion

Photochemical Reactions of 4-Methoxystyrene on CCT Band Excitation. Direct irradiation of 4-methoxystyrene (**1a**) with 254- or 313-nm light in acetonitrile under nitrogen gave cis and trans cyclodimers **2a** and **3a** in a ratio of ca. 90/10. The predominant formation of **2a** indicates that the dimerization proceeds through an excimer with the geometry in which the aromatic rings are overlapped with each other, collapsing mainly into the cis dimer, as previously proposed for the dimerization of styrene[8)] (Scheme 3a).

Excitation of the CCT pair of **1a** and oxygen at 366 nm in the same solvent gave **2a** and **3a** in a contrasted ratio of 5/95 together with 4-methoxybenzaldehyde (**4a**); however, a similar irradiation in benzene gave no dimers. This remarkable solvent effect suggests that the excitation of CCT pair in polar solvents results in electron transfer from the olefin to molecular oxygen to afford the olefin cation radical and superoxide anion. The former either adds to **1a** in the ground state to form a dimer cation radical which is finally converted to the dimer (Scheme 3b) or accepts an electron from the latter to give the original olefin.

Irradiation under oxygen with light of wavelengths shorter than 366 nm tends to decrease the ratio of the trans isomer; 313-nm light resulted in a **2a/3a** isomer ratio of 16/84 and 254-nm light led to a ratio of 63/37. These results can be understood in terms of competitive excitation of the olefin and its CCT pair, leading to the formation of the excimer and cation radical, respectively.

Excitation of the CT band of **1a** and DCNB in acetonitrile also gave cis and trans dimer **2a** and **3a** in a ratio of 2/98 (Scheme 3c) as previously reported by Yamamoto et al.[7a)] This isomer ratio is very similar to that obtained in the CCT pair excitation. Yamamoto proposed a mechanism that excited **1a** interacts with DCNB to give the cation radical of **1a** finally resulting in dimerization of **1a**.[7a)] However, in the present case, the CT band excitation resulted in the dimerization of **1a**, indicating that the CT pair excitation also induces the electron transfer from **1a** to DCNB to generate $\mathbf{1a}^{+\cdot}$ and $DCNB^{-\cdot}$.

On triplet sensitization with benzophenone under nitrogen in acetonitrile, **1a** gave the dimers in an isomer ratio (**2a/3a**=13/87) different from that in the above dimerization under oxygen (Scheme 4). 4-Methoxybenzaldehyde (**4a**) also sensitized (313 nm) the dimerization of **1a** to produce **2a** and **3a** (**2a/3a**=22/78); however, 366-nm irradiation of **4a** did not induce the dimerization. These results rule out a possibility that on irradiation of **1a** under oxygen with 366-nm

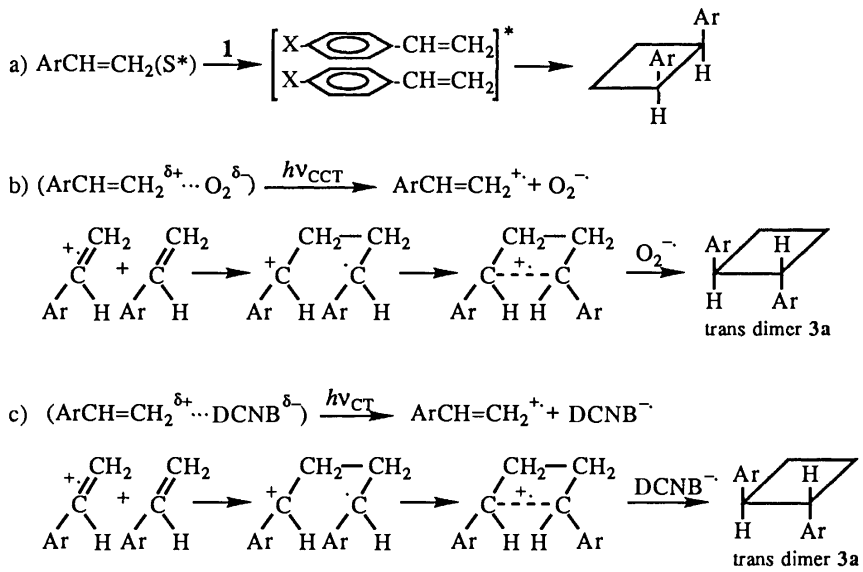

Scheme 3.

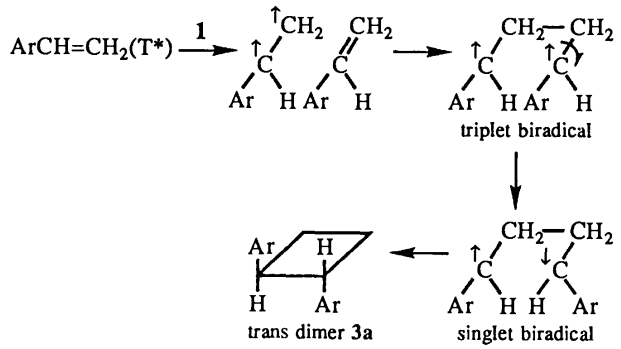

Scheme 4.

light the resulting **4a** would sensitize the reaction.

Photochemical Reaction of 4-Methylstyrene. Excitation of the CCT pair of **1b** and oxygen in acetonitrile gave three cyclodimers (**2b**, **3b**, and **5**) and a dimeric ketone (**6**), and that of the CT pair of **1b** and DCNB afforded 1-(4-cyanophenyl)-6-methyl-4-(4-tolyl)-1,2,3,4-tetrahydronaphthalene (**7**) together with the olefin dimers (**2b**:**3b**:**5**=11:11:78). Ketone **6** and diaryltetralin **7** are products from a tetralin-type dimer cation radical trapped by oxygen species (O_2 or O_2^{-}) and DCNB (neutral molecule or anion radical), respectively, as depicted in Scheme 5, because tetralin-type dimer **5** is reported to be produced only through olefin cation radicals.[7b] In fact, benzophenone-sensitized dimerization of **1b** in benzene gave only cyclodimers **2b** and **3b** (20/80) but no tetralin-type dimer **5**.[7b] Therefore, the production of dimeric ketone **6** indicates that the excitation of the CCT pair of **1b** and oxygen caused dissociation of the excited CCT pair into the **1b** cation radical and superoxide anion.

Arnold et al. reported the trapping of triene intermediates through an ene reaction in photochemical electron-transfer dimerization of 1,1-diphenylethene or cross-cycloaddition of 1,1-diphenylethene with 2-methylpropene in the presence of acrylonitrile or methyl acrylate.[9] However, it should be noted that such quenching products of dimer cation radicals as **6** and **7** have scarcely been reported.

Role of Oxygen as an Electron Acceptor. The free energy change ($\Delta G°$) associated with the electron transfer from excited singlet **1** to molecular oxygen or in the CCT pair is given by Eq. 1,[10] where $E(D^+/D)$ and $E(A/A^-)$ are the oxidation potential of donor (D) and the reduction potential of acceptor (A), respectively. The term $e_o^2/\varepsilon a$ is the coulombic energy (ca. 0.06 eV in MeCN) gained by bringing the two ion radical species to encounter distance a in a solvent of dielectric constant ε, and $E_{0,0}$ is the electronic excitation energy of **1** or the CCT pair.

$$\Delta G°(\text{kcal mol}^{-1}) = 23.06[E(D^+/D) - E(A/A^-) - e_o^2/\varepsilon a] - E_{0,0} \quad (1)$$

The $\Delta G°$ values for electron transfer from excited singlet **1a** to oxygen and in the CCT pairs of **1** with oxygen are estimated to be highly negative as shown in Table 3. These values indicate that the photochemical electron transfer can easily take place as the primary process of the present reactions. Large negative $\Delta G°$ values are also estimated for electron transfer from excited singlet **1a** and **1b** to DCNB (Table 3). Thus, the CCT pairs, on excitation, will undergo electron transfer to generate **1** cation radicals and superoxide anions. The former will either add to **1** in the ground state to give dimer cation radicals or undergo back electron transfer to generate **1** triplets.

The triplet state of **1** might be responsible for the present reaction. The free energy of the pair of ion

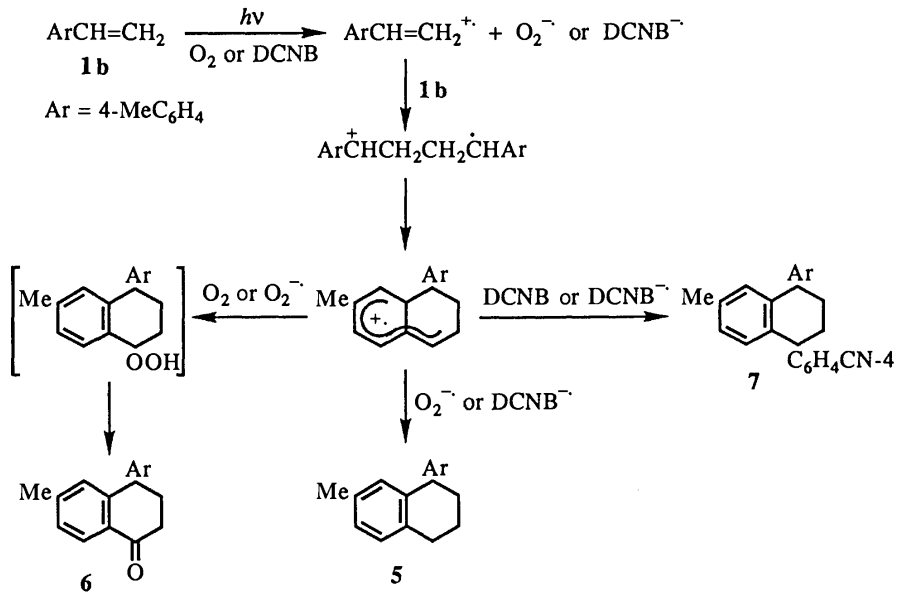

Scheme 5.

Table 3. Free Energy Changes ($\Delta G°$) Associated with Electron Transfer from Excited Singlet 4-Methoxystyrene (**1a**) and 4-Methylstyrene (**1b**) to Oxygen or DCNB

	$E(D^+/D)$	$E(A/A^-)$	$E_{0,0}$	$E_{0,0}$(CCT)[b]	$\Delta G°$
	V[a]	V[a]	kcal mol^{-1}	kcal mol^{-1}	kcal mol^{-1}
1a/O_2	1.15	−1.28	94	78	−39[c] or −23[d]
1a/DCNB		−2.00			−23[c] or −7[d]
1b/O_2	1.38	−1.28	97	78	−39[c] or −18[d]
1b/DCNB		−2.00			−20[c] or −1[d]

a) Vs. Ag/0.1 mol dm^{-3} $AgNO_3$ in MeCN. b) Energies of CCT pairs calculated from the wavelength of their CCT bands. c) Calculated using $E_{0,0}$. d) Calculated using $E_{0,0}$ (CCT).

radicals $\mathbf{1a}^+$ and O_2^- in acetonitrile can be estimated to be 54 kcal mol^{-1} over the ground-state molecules. The singlet excitation energy of **1a** is estimated to be 94 kcal mol^{-1} from its fluorescence spectrum and its triplet excitation energy to be nearly 60 kcal mol^{-1} because styrene has a triplet excitation energy of 62 kcal mol^{-1}.[11] Such estimation enables us to exclude a possibility of production of **1a** triplets through back electron transfer, since this process is endothermic by ca. 6 kcal mol^{-1}. The situation is similar in **1b**.

Therefore, it is reasonable to conclude that on excitation of the CCT pair the resulting olefin cation radical adds to ground-state olefin to give a dimer cation radical to which an electron is reverted from a superoxide anion finally to give the olefin dimer. In the interaction of the cation radical and the olefin molecule to give the dimer cation radical, the aromatic rings substituted in the ethylenic linkage will avoid steric crowding, therefore, to take a trans configuration.

Experimental

^{1}H NMR and ^{13}C NMR spectra were recorded on a JEOL JMN-MN-100 spectrometer and a JEOL FX-100 spectrometer, respectively. Infrared (IR) and UV spectra were obtained on a Hitachi 260-50 spectrophotometer and a Hitachi 200-20 spectrophotometer, respectively. Mass spectra were determined with a Hitachi RMU-6MC mass spectrometer. The oxidation and reduction potentials were determined by means of cyclic voltammetry in acetonitrile using a Ag/Ag^+ (0.1 mol dm^{-3}) electrode as a reference electrode and 0.1 mol dm^{-3} tetraethylammonium perchlorate as a supporting electrolyte. Irradiations were carried out with a 400-W high-pressure mercury lamp (Riko UVL-400HA) or with a 160-W low-pressure mercury lamp (Riko UVL-160LA).

Materials. 4-Methoxystyrene (**1a**) and 4-methylstyrene (**1b**) were prepared by decarboxylation of the corresponding cinnamic acids as described in the literature.[12] Acetonitrile and benzene were guaranteed reagents and distilled before use.

Contact Charge Transfer (CCT) and Charge Transfer (CT) Absorption Spectra of Styrene Derivatives. A solution of **1a** (0.59 mol dm^{-3}) in acetonitrile or benzene or of **1b** (0.61 mol dm^{-3}) in acetonitrile was placed in a sample cell and a reference cell, and a stream of oxygen was passed for several minutes through the solution in the sample cell. Spectra were measured at room temperature. Immediately after a spectrum was recorded, argon was passed through the solution in the sample cell and a spectrum was again measured.

A solution of **1a** (0.59 mol dm^{-3}) and DCNB (50 mg, 0.39 mmol) was prepared immediately before measurement and placed in a sample cell. In a reference cell was placed an acetonitrile solution of **1a** in the same concentration as in a sample cell.

Photochemical Reaction. a) Isolation of Reaction Products. *cis*-1,2-Bis(4-methoxyphenyl)cyclobutane (2a). 4-Methoxystyrene (2 g, 15 mmol) was irradiated in acetonitrile (250 cm^3) with a 160-W low-pressure mercury lamp under a nitrogen stream at room temperature. After 48 h, 4-methoxystyrene was completely consumed as determined by GLPC analysis. Column chromatography of the concentrated reaction mixture on silica gel with hexane as eluent gave an oily product, the structure of which was determined as *cis*-1,2-bis(4-methoxyphenyl)cyclobutane (**2a**) based on the following spectral data. GLPC analysis showed that the product contained the trans isomer (**3a**) (**2a**/**3a**=91/9).

2a: oil; MS: *m/z* 268 (M^+), 240, 225, 134 (M^+/2, 100%), 119; ^{1}H NMR ($CDCl_3$) δ=2.36 (q, 4H, CH_2), 3.64 (s, 6H, OMe), 3.68 (m, 2H, CH), 6.52—6.84 (q, 8H, aromatic H); ^{13}C NMR ($CDCl_3$) δ=157.4 (s), 133.7 (s), 128.8 (d), 113.0 (d), 55.0 (q), 44.5 (d), 24.5 (t).

***trans*-1,2-Bis(4-methoxyphenyl)cyclobutane (3a).**[7a] Irradiation of **1a** (500 mg, 3.7 mmol) in acetonitrile (5 cm^3) under oxygen atmosphere with a 400-W high-pressure mercury lamp through a Pyrex filter for 24 h gave trans dimer **3a** (320 mg, 64%) after separation by chromatography on silica gel with benzene as eluent.

3a: oil; MS: *m/z* 268 (M^+), 266, 240, 225, 160, 134 (M^+/2, 100%) 119; ^{13}C NMR ($CDCl_3$) δ=158.0 (s), 136.8 (s), 127.6 (d), 113.7 (d), 55.2 (q), 47.8 (d), 26.0 (t).

***cis*-1,2-Bis(4-tolyl)cyclobutane (2b).**[7b] 4-Methylstyrene (1.8 g, 15 mmol) was irradiated in acetonitrile (250 cm^3) with a 160-W low-pressure mercury lamp under an argon stream at room temperature for 48 h. The solvent was evaporated in vacuo and the residue was separated by chromatography on silica gel to give **2b** (1 g, 56%) and trace amounts of **3b** and **5**.

2b: oil; MS: *m/z* 236 (M^+), 208, 193, 178, 132, 118 (M^+/2, 100%), 90; ^{13}C NMR ($CDCl_3$) δ=138.6 (s), 134.7 (s), 128.3(d), 127.8 (d), 44.9 (d), 24.6 (t), 21.0 (q).

***trans*-1,2-Bis(4-tolyl)cyclobutane (3b).**[7b] A solution (3 cm^3) of **1b** (216 mg, 1.83 mmol) in acetonitrile was irradiated in the presence of benzophenone (100 mg, 0.55 mmol) in a uranium glass tube with a 400-W high-pressure mercury lamp under argon atmosphere at room temperature to give **2b** and **3b** in a ratio of 30/70 but no tetralin dimer **5**.

3b: MS: *m/z* 236 (M^+), 234, 221, 219, 206, 193, 191, 179, 178, 144, 118 ($M^+/2$, 100%), 105, 90.

1-(4-Tolyl)-7-methyl-1,2,3,4-tetrahydronaphthalene (5).[7b] Oil; MS: *m/z* 236 (M^+), 221, 208, 193, 144 (M^+—4-MeC_6H_4, 100%), 129, 118; ^{13}C NMR ($CDCl_3$) δ=144.5 (s), 139.1 (s), 135.1 (s), 134.8 (s), 134.3 (s), 130.4 (d), 128.7 (d), 128.6 (d), 126.6 (d), 45.0 (d), 33.3 (t), 29.3 (t), 21.0 (t and q).

6-Methyl-4-(4-tolyl)-1,2,3,4-tetrahydronaphthalen-1-one (6). 4-Methylstyrene (1.8 g, 15 mmol) was irradiated in acetonitrile (60 cm^3) under oxygen atmosphere with a 400-W high-pressure mercury lamp through a Pyrex filter at room temperature. After 72 h, **1b** was completely consumed as determined by GLPC analysis and **6** was separated from other dimers (**2b**, **3b**, and **5**) by chromatography on silica gel using benzene as eluent.

6: oil; MS: *m/z* 250 (M^+, 100%), 235, 222, 208; IR (neat): 1670 cm^{-1}, $\nu_{C=O}$; ^1H NMR ($CDCl_3$) δ=2.34 (s, 3H, CH_3), 2.30—2.65 (m, 4H, CH_2CH_2), 4.0—4.25 (m, 1H, CH), 6.7—8.0 (m, 7H, aromatic H); ^{13}C NMR ($CDCl_3$) δ=197.7, 146.4, 144.3, 140.7, 136.2, 130.6, 129.8, 129.2, 128.4, 127.9, 127.2, 44.8, 36.5, 31.9, 21.7, 21.0. The phenylhydrazone of **6**, mp 131—133 °C (decomp); Found: C, 84.73; H, 7.10; N, 8.26%. Calcd for $C_{24}H_{24}N_2$: C, 84.66; H, 7.10; N, 8.22%.

1-(4-Cyanophenyl)-6-methyl-4-(4-tolyl)-1,2,3,4-tetrahydronaphthalene (7). 4-Methylstyrene (1.8 g, 15 mmol) was irradiated in the presence of 1,4-dicyanobenzene (1 g, 8 mmol) in acetonitrile (250 cm^3) with a high-pressure mercury lamp under a nitrogen stream at room temperature. After 44 h, the solvent was evaporated in vacuo and silica-gel chromatography of the residue gave dimers (**3b** and **5**, trace) and **7** (570 mg, 21%) as a 1:1 mixture of cis and trans isomers, the assignment of which was based on ^{13}C NMR spectrum.

7: colorless amorphous; mp 111—112 °C from hexane-methanol; MS: *m/z* 337 (M^+), 245 (100 %), 234, 219, 208; IR (KBr): 2210 cm^{-1}, $\nu_{C\equiv N}$; ^1H NMR ($CDCl_3$) δ=1.6—2.1 (m, 4H, CH_2CH_2), 2.16 and 2.18 (s, 3H, CH_3), 2.30 (s, 3H, CH_3), 3.95—4.35 (m, 2H, 2CH), 6.6—7.55 (m, 11H, aromatic H); ^{13}C NMR ($CDCl_3$) δ=153.3, 153.2, 144.0, 143.9, 139.6, 136.3, 136.1, 135.7, 135.3, 135.2, 132.1, 131.0, 130.7, 129.9, 129.6, 129.0, 128.6, 127.5, 127.3, 119.0, 109.9, 45.7, 45.6, 45.3, 44.8, 30.9, 30.1, 29.7, 21.0. Found: C, 89.03; H, 6.87; N, 4.16%. Calcd for $C_{25}H_{23}N$: C, 88.97; H, 6.87; N, 4.15%.

b) Determination of Product Yields. Irradiations with a High-Pressure Mercury Lamp. A solution (3 cm^3) of 4-methoxystyrene (238 mg, 1.78 mmol) in acetonitrile or benzene was irradiated under oxygen or nitrogen atmosphere in a Pyrex tube or a uranium glass tube with a 400-W high-pressure mercury lamp for 16 h at room temperature. The yields of all products were determined by GLPC analysis on a Hitachi 163 gas chromatograph equipped with a flame ionization detector using 2-m columns of 5% polyethylene glycol 20M and 5% Silicone GE SE-30.

A solution (3 cm^3) of **1b** (216 mg, 1.86 mmol) in acetonitrile was irradiated under oxygen or nitrogen atmosphere in a Pyrex or a uranium glass tube with a 400-W high-pressure mercury lamp at room temperature for 20 h using a merry-go-round apparatus. The yields of the products were determined by GLPC analysis.

A solution (3 cm^3) of **1a** (238 mg, 1.78 mmol) in acetonitrile was irradiated in the presence of **4a** (56 mg, 0.41 mmol) or DCNB (50 mg, 0.39 mmol) in a Pyrex or a uranium glass tube with a high-pressure mercury lamp under nitrogen atmosphere at room temperature. The yields of products were determined by GLPC analysis.

Irradiations with a Low-Pressure Mercury Lamp. A solution (3 cm^3) of **1a** (238 mg, 1.78 mmol) in acetonitrile was irradiated in a quartz tube with a 160-W low-pressure mercury lamp under oxygen or nitrogen atmosphere for 16 h at room temperature. The yields of products were determined by GLPC analysis.

References

1) "Singlet Oxygen," ed by H. H. Wasserman and R. W. Murray, Academic Press, New York (1979).

2) a) R. A. Carruthers, R. A. Crellin, and A. Ledwith, *J. Chem. Soc., Chem. Commun.*, **1969**, 252; b) K. Onodera, H. Sakuragi, and K. Tokumaru, *Tetrahedron Lett.*, **21**, 2831 (1980); c) H. Sakuragi, G. Furusawa, K. Ueno, and K. Tokumaru, *Chem. Lett.*, **1982**, 1213; d) R. Akaba, H. Sakuragi, and K. Tokumaru, *Tetrahedron Lett.*, **25**, 665 (1984); *Chem. Lett.*, **1984**, 1677; e) K. Onodera, G. Furusawa, M. Kojima, M. Tsuchiya, S. Aihara, R. Akaba, H. Sakuragi, and K. Tokumaru, *Tetrahedron*, **41**, 2215 (1985).

3) a) H. Tsubomura and R. S. Mulliken, *J. Am. Chem. Soc.*, **82**, 5966 (1960); b) M. Tamres and R. L. Strong, "Molecular Association," Vol. 2, ed by R. Foster, Academic Press, London (1979), p. 397; c) D. F. Evans, *J. Chem. Soc.*, **1953**, 345; d) V. I. Stenberg, R. D. Olson, C. T. Wang, and N. Kulevsky, *J. Org. Chem.*, **32**, 3227 (1967); e) K. S. Wei and A. H. Adelman, *Tetrahedron Lett.*, **1969**, 3297.

4) a) T. Kodaira, K. Hashimoto, Y. Sakanaka, S. Tanihata, and K. Ikeda, *Bull. Chem. Soc. Jpn.*, **51**, 1487 (1978); b) K. Kanno, M. Hisaoka, H. Sakuragi, and K. Tokumaru, *Bull. Chem. Soc. Jpn.*, **54**, 2330 (1981).

5) J. Eriksen and C. S. Foote, *J. Am. Chem. Soc.*, **102**, 6083 (1980).

6) As a preliminary report, see; M. Kojima, H. Sakuragi, and K. Tokumaru, *Tetrahedron Lett.*, **22**, 2889 (1981).

7) a) M. Yamamoto, T. Asanuma, and Y. Nishijima, *J. Chem. Soc., Chem. Commun.*, **1975**, 53; b) T. Asanuma, M. Yamamoto, and Y. Nishijima, *J. Chem. Soc., Chem. Commun.*, **1975**, 608; c) T. Asanuma, M. Yamamoto, and Y. Nishijima, *J. Chem. Soc., Chem. Commun.*, **1975**, 56; d) Y. Yamamoto, M. Irie, Y. Yamanoto, and K. Hayashi, *J. Chem. Soc., Perkin Trans. 2*, **1979**, 1517; e) S. Farid and S. E. Shealer, *J. Chem. Soc., Chem. Commun.*, **1973**, 677; f) R. A. Neunteufel and D. R. Arnold, *J. Am. Chem. Soc.*, **95**, 4080 (1975).

8) W. G. Brown, *J. Am. Chem. Soc.*, **90**, 1916 (1968).

9) D. R. Arnold, R. M. Borg, and A. Albini, *J. Chem. Soc., Chem. Commun.*, **1981**, 138.

10) D. Rehm and A. Weller, *Isr. J. Chem.*, **8**, 259 (1970).

11) S. L. Murov, "Handbook of Photochemistry," Marcel Dekker, New York (1973), p. 20.

12) R. H. Wiley and N. R. Smith, *Org. Synth.*, Coll. Vol. **4**, 731 (1963).

Synthesis of Bis(deoxyribonucleoside) Phosphoromorpholidate Derivatives for Oligodeoxyribonucleotide Preparation by Use of a Selective Phosphitylating Reagent

Hiroaki OZAKI, Shuhei YAMOTO, Seiichirou MAIKUMA, Kenichi HONDA, and Takeo SHIMIDZU*
Division of Molecular Engineering, Graduate School of Engineering, Kyoto University, Sakyo-ku, Kyoto 606
(Received June 17, 1989)

Sequence-defined bis(deoxyribonucleoside) phosphoromorpholidate derivatives as stable intermediates to prepare oligodeoxyribonucleotides have been synthesized using morpholinodi(1-tetrazolyl)phosphine as a phosphitylating reagent. The general procedure is composed of following steps (in situ); a) a reaction of 5'-O-protected deoxyribonucleoside with morpholinodi(1-tetrazolyl)phosphine (phosphitylation), b) a reaction of the resulting 5'-O-protected deoxyribonucleoside phosphorobisamidite with the second deoxyribonucleoside (coupling), and c) a nonaqueous oxidation with *t*-BuOOH (oxidation). In the coupling step, the 5'-O-protected deoxyribonucleoside phosphorobisamidite was selectively reacted with 5'-OH group of the second deoxyribonucleoside, and therefore, a protection of hydroxyl groups of the second deoxyribonucleoside is not necessary. As the resulting P-N bond in the phosphoramidate linkage after oxidation is stable both in acidic and basic conditions, the morpholino function as a phosphoryl protecting group may have many potential use in the synthetic chemistry of oligonucleotide. A thymidine trimer can be obtained in a high yield by extending the present synthetic method.

Since Letsinger[1] and Caruthers[2] introduced phosphite and phosphoramidite approaches to the synthesis of oligonucleotides, extensive research has been directed toward developments of more promising methodologies by using the efficient phosphitylating reagents.[3,4] Moreover, it is of particular importance to develop a method for a large scale synthesis of sequence-defined oligonucleotides in order to solve many genetic phenomena by physical chemical studies and to use them for new medicines. The purpose of our study has been focused on a rapid and large scale synthesis of sequence-defined oligonucleotides by using the selective phosphitylating reagents. Previously, we have developed tris(azolyl)phosphines as phosphitylating reagents which react selectively with the cis-glycol of ribonucleosides. Based on the selective phosphitylation, homo-oligoribonucleotides can be obtained directly from unprotected ribonucleosides by the chemical polymerization approach.[5,6] A new class of phosphitylating reagents, (dialkylamino)-dichlorophosphine possessing the same selectivity to the ribonucleoside hydroxyl groups, were synthesized and adapted to the solution phase synthesis of oligoribonucleotides having defined sequences.[7]

The next objective of our research is to use the phosphitylating reagent for synthesizing sequence-defined oligodeoxyribonucleotides and their analogs. We have developed the convenient procedure for the synthesis of sequence-defined bis(deoxyribonucleoside) derivatives having phosphoromorpholidate linkage, which contains the following steps (Scheme 1); i) a reaction of 5'-O-protected deoxyribonucleoside with morpholinodi(1-tetrazolyl)phosphine (phosphitylation), ii) a reaction of the resulting 5'-O-protected deoxyribonucleoside phosphorobisamidite with the second deoxyribonucleoside (coupling), and

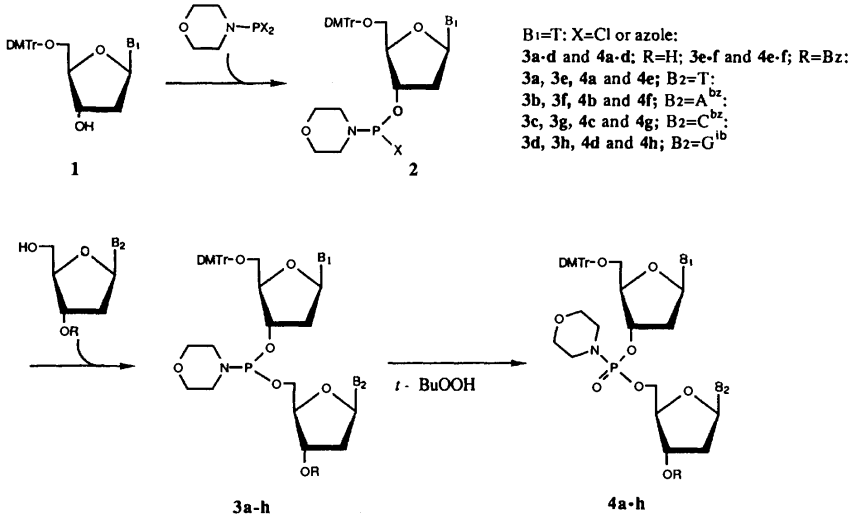

Scheme 1.

iii) a nonaqueous oxidation of resulting phosphoromorpholidite linkage by using *t*-butyl hydroperoxide (*t*-BuOOH) (oxidation).[8,9] In order to demonstrate the possibility of a chain elongation, the synthesis of a trimer was performed by repeating the procedure described above.

Additionally, our present approach may provide a useful method for the preparation of biologically interesting oligonucleotide analogs having phosphoramidate linkages. In the literature, several oligonucleotide analogs having various internucleotide bonds were synthesized and it was shown that they had resistance in cleavage by a variety of nucleases.[10,11] Also, nonionic oligonucleotide analogs having methylphosphonates have been synthesized,[12] and shown to form complexes with complementary DNA or RNA with different stabilities and to exert inhibitory effects on a protein synthesis.[13] The oligodeoxyribonucleotide analogs having phosphoramidate linkages could be also expected to have biochemical and biological effects and the analogs were synthesized by H-phosphonate method.[14] The present synthetic method is a simple and convenient procedure for the synthesis of oligonucleotide analogs having phosphoramidate linkage.

In this paper, we describe the synthesis of the sequence-defined bis(deoxyribonucleoside) phosphoromorpholidate derivatives, as the stable intermediates for the synthesis of oligodeoxyribonucleotides by use of a selective phosphitylating reagent.

Results and Discussion

Phosphitylation of 5′-O-Protected Deoxyribonucleoside (Scheme 2). Several (dialkylamino)dichlorophosphines have been prepared and their reactivity and selectivity have been examined in the reaction with ribonucleosides.[7] Among them, dichloromorpholinophosphine was found to be highly reactive toward the secondary hydroxyl groups of ribonucleosides. We therefore tried to use the reagent for the phosphitylation of 5′-O-protected deoxyribonucleoside. However, it was found that the reaction of 5′-*O*-[bis(4-methoxyphenyl)phenylmethyl]thymidine (5′-*O*-dimethoxytritylthymidine, d-DMTrT) with the phosphitylating reagent is non-selective and gave a considerable amount of an undesired 3′,3′-linked dithymidylate analog, **5**. On the contrary, the use of its azolide instead of the chloride for the phosphitylation improved the selectivity. Results are summarized in Table 1. In case of using monoazolide derivatives as the phosphitylating reagent, a significant amount of side products were still yielded. A good selectivity in the reaction was obtained by using di(triazolide) and di(tetrazolide) derivatives. From the practical point of view, morpholinodi(1-tetrazolyl)-phosphine was found to give the phosphitylated product **2** in a yield of over 80% within 30 min under the present condition.

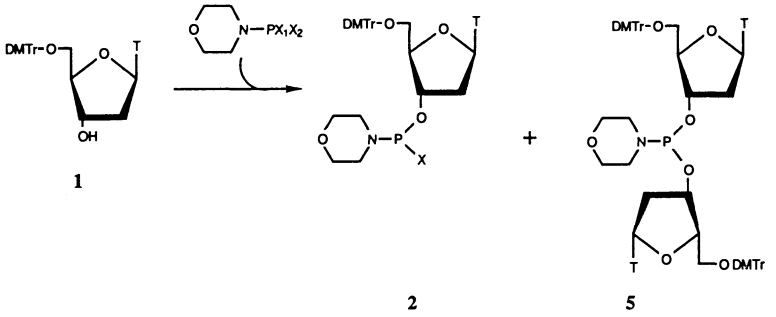

1 2 5

Scheme 2.

Table 1. Selectivity in the Phosphitylation of d-DMTrT with $X_1X_2PN(CH_2CH_2)_2O$

$X_1X_2PN(CH_2CH_2)_2O$		Yield[b]		
X_1[a]	X_2[a]	**1**	**2**	**5**
Im	Cl	30.6	20.4	49.0
Im	Im	92.2	7.8	—
Tri	Cl	35.2	22.9	41.9
Tri	Tri	41.1	58.6	—
Te	Cl	16.9	60.3	22.8
Te	Te	9.3	82.1	8.6

a) Im, imidazolyl; Tri, triazolyl; Te, tetrazolyl. b) d-DMTrT was phosphitylated by $X_1X_2PN(CH_2CH_2)_2O$ in CH_2Cl_2–pyridine at 0 °C under N_2 for 30 min. After the reaction mixture was treated by absolute CH_3OH, TLC analysis was carried out.

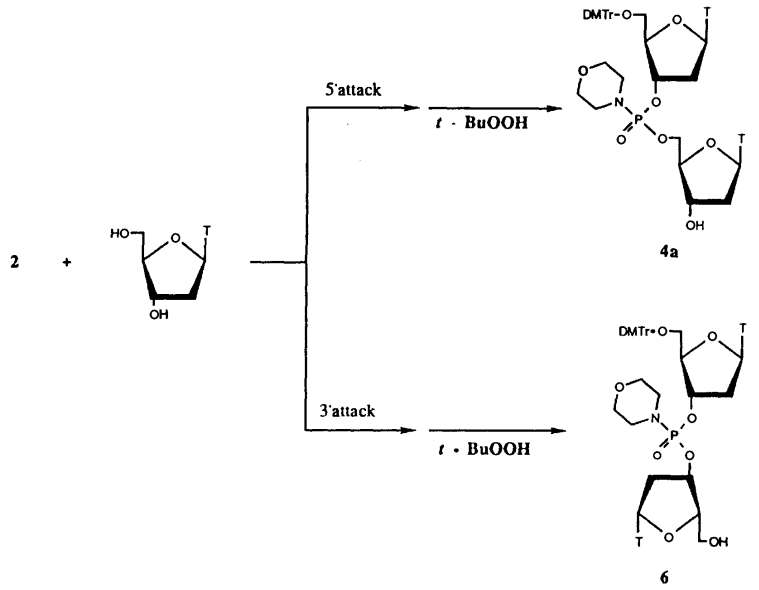

Scheme 3.

Selectivity in the Coupling Reaction (Scheme 3). d-DMTrT phosphorobisamidite **2** (X=tetrazolyl) thus obtained was allowed to react with thymidine. The reaction was completed within 30 min which is indicated by TLC and HPLC. After the in situ oxidation using *t*-BuOOH, 3′-5′ linked dithymidine phosphoromorpholidate **4a** was obtained as a main product together with only a little amount of an undesired 3′-3′ linked product **6** (**4a**/**6**=96.2/3.8). The result clearly indicates that compound **2** reacts predominantly with the 5′-OH of the second deoxyribonucleoside in the coupling reaction. Therefore, this highly selective reaction provides a simple and convenient route to the synthesis of bis(deoxyribonucleoside) derivatives without any protection of 3′-OH of the second deoxyribonucleoside.

Oxidation of Phosphoromorpholidite Linkage. Since an intermediate **3a** having a phosphoromorpholidite linkage is sensitive to atmospheric oxygen and moisture, its isolation by recrystallization or silica-gel column was not successful. Preliminary experiments showed that the in situ oxidation of **3a** with I_2-H_2O and *m*-chloroperbenzoic acid gave a large number of side products. We have solved this problem by using *t*-BuOOH.[8,9] The reaction product was also analyzed by ^{31}P NMR (Fig. 1). ^{31}P NMR shows that after the oxidation of **3a** with 3 M *t*-BuOOH in toluene (1 M=1 mol dm^{-3}) for 10 min at 0 °C, **3a** (138.4 ppm) completely disappeared to give the single peak (7.08 ppm) due to the phosphoromorpholidate derivative **4a**. This result indicated that the phosphoromorpholidite linkage in **3a** was smoothly converted to the corresponding phosphoromorpholidate linkage without any side reactions.

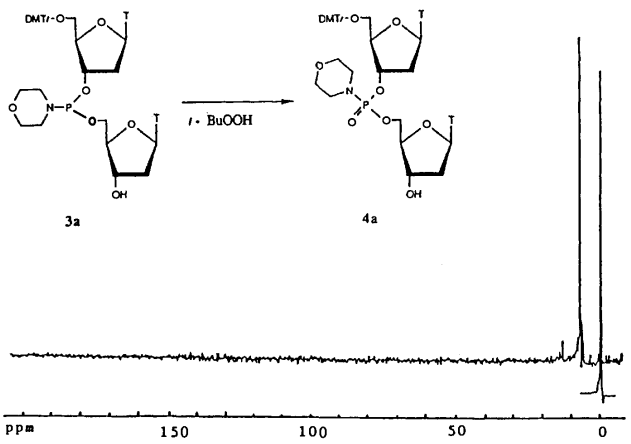

Fig. 1. ^{31}P NMR of bis(deoxyribonucleoside) derivative (**4a**) obtained by use of *t*-BuOOH (in $CDCl_3$, relative to external 85% H_3PO_4).

Effect of (*i*-Pr)$_2$NEt. We examined the effect of ethyldiisopropylamine ((*i*-Pr)$_2$NEt) on coupling reaction. When the synthesis of **4a** was carried out by using (*i*-Pr)$_2$NEt of 2 equiv for the phosphitylating reagent, namely equimolar amounts of hydrochloride released to the system, a lot of unknown products were formed in the reaction (Fig. 2). On the other hand, when it was carried out by using (*i*-Pr)$_2$NEt of 4 equiv for the phosphitylating reagent, unknown products decreased and desired products (**4a**) increased. This result suggests that it is required to trap the released tetrazolium ion by using base in order to conserve the phosphoromorpholidite linkage and to increase efficiency of the coupling reaction.

Synthesis of Bis(deoxyribonucleoside) Phosphoromorpholidate Derivatives (4a—d). The applicability of the synthetic route described above was tested in the syntheses of bis(deoxyribonucleoside) phosphoromorpholidate derivatives having different sequences. The yields and physical chemical data of the obtained

bis(deoxyribonucleoside) phosphoromorpholidate derivatives (**4a—d**) were summarized in Table 2. **4a—d** agreed with 3′-5′ linked bis(deoxyribonucleoside) phosphoromorpholidates derived from **4e—h** (Scheme 1) on HPLC, which were synthesized by use of 3′-O-protected deoxyribonucleosides as the second deoxyribonucleosides in the similar procedure. In the every case, the desired 3′,5′-linked bis(deoxyribonucleoside) phosphoromorpholidate derivatives were obtained with good yields by the convenient method without the protection of the hydroxyl groups of the second deoxyribonucleosides.

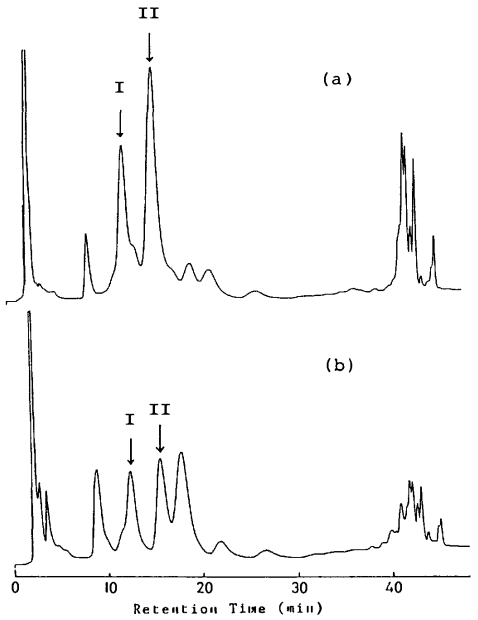

Fig. 2. Effect of $(i\text{-Pr})_2$NEt on dithymidine derivative (**4a**) synthesis. (a) 4 equiv of $(i\text{-Pr})_2$NEt for phosphitylating reagent. (b) 2 equiv of $(i\text{-Pr})_2$NEt for phosphitylating reagent. HPLC condition: column, Cosmosil $5C_{18}$ (4.6 mm i.d. ×150 mm length); eluent, 70—100% CH_3OH gradient in H_2O; flow rate, 1 mL min^{-1}; detect: UV at 254 nm. The peaks of **4a** are indicated by the arrows.

Stability of Phosphoromorpholidates. Table 3 shows the stability of the P-N bond in **4a** under various conditions. The P-N bond was stable in 80% acetic acid, concentrated aq. NH_3, and 0.5 M NaOH. Since the phosphoromorpholidate linkage is stable for acid and alkaline, the fully protected dimer block, **4e**, can be used to elongate the nucleotide chain both toward 3′- and 5′-direction from 3′-free derivatives obtained by alkaline treatment and 5′-free derivatives obtained by acid treatment, respectively. Moreover, it is possible to introduce phosphoramidate at all or any specific sites within oligodeoxyribonucleotides and these molecules are expected to have several interesting biological effect.

Removal of Phosphoryl Protecting Group (Scheme 4). Since hydroxylamine is known to hydrolyze phosphoramidates,[15,16] it appeared a potential deprotection agent for a phosphoramidate link. The P-N bond underwent hydrolysis to phosphodiester by a treatment with hydroxylamine. In the case of treat-

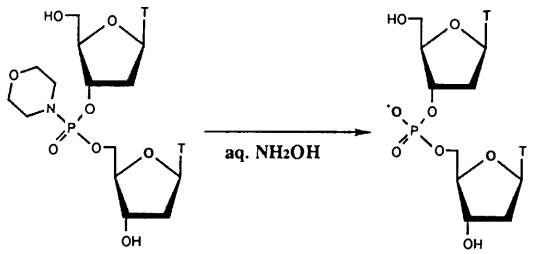

Scheme 4.

Table 3. Stability of Phosphoromorpholidate in **4a** under Several Conditions

Reagent	Solvent	pH	Temp/°C	Time/h
80% AcOH	H_2O	0.4	r.t.	48
Isopentyl nitrite	Py-AcOH(1 : 1)	4.6	r.t.	24
28% NH_3 aq.	H_2O	12.5	r.t.	12
0.5 M NaOH	EtO-H_2O(1 : 1)	13.0	30	29

Table 2. Yields and Physical Chemical Data of Sequence Defined Bis(deoxyribonucleoside) Phosphoromorpholidate Derivatives (**4a—d**)

Compound	Yield[a]	δ-^{31}P[b]	λ_{max}	R_f[c]	T_r[d]	Isomer[e] ratio I/II
	%	ppm	nm		min	
4a	74 67[f]	7.08	266, 235	0.39	11.8 14.5	36/64
4b	62	7.01, 7.08	275, 234	0.42	21.2 25.1	33/67
4c	55	6.98, 7.22	304, 261, 236	0.43, 0.44	30.2 32.7	31/69
4d	70	6.04	261, 237	0.27, 0.28	18.8 22.2	30/70

a) Based on HPLC. b) Relative to external 85% H_3PO_4. c) TLC on silica using $CHCl_3$: CH_3OH (8 : 1, v/v). d) Reversed-phase HPLC on Cosmosil $5C_{18}$ using eluent A. e) Diastereomer. Isomer I was earlier eluted isomer and isomer II was later eluted isomer on the reversed-phase HPLC. Absolute configuration was not assigned. f) Isolated yield.

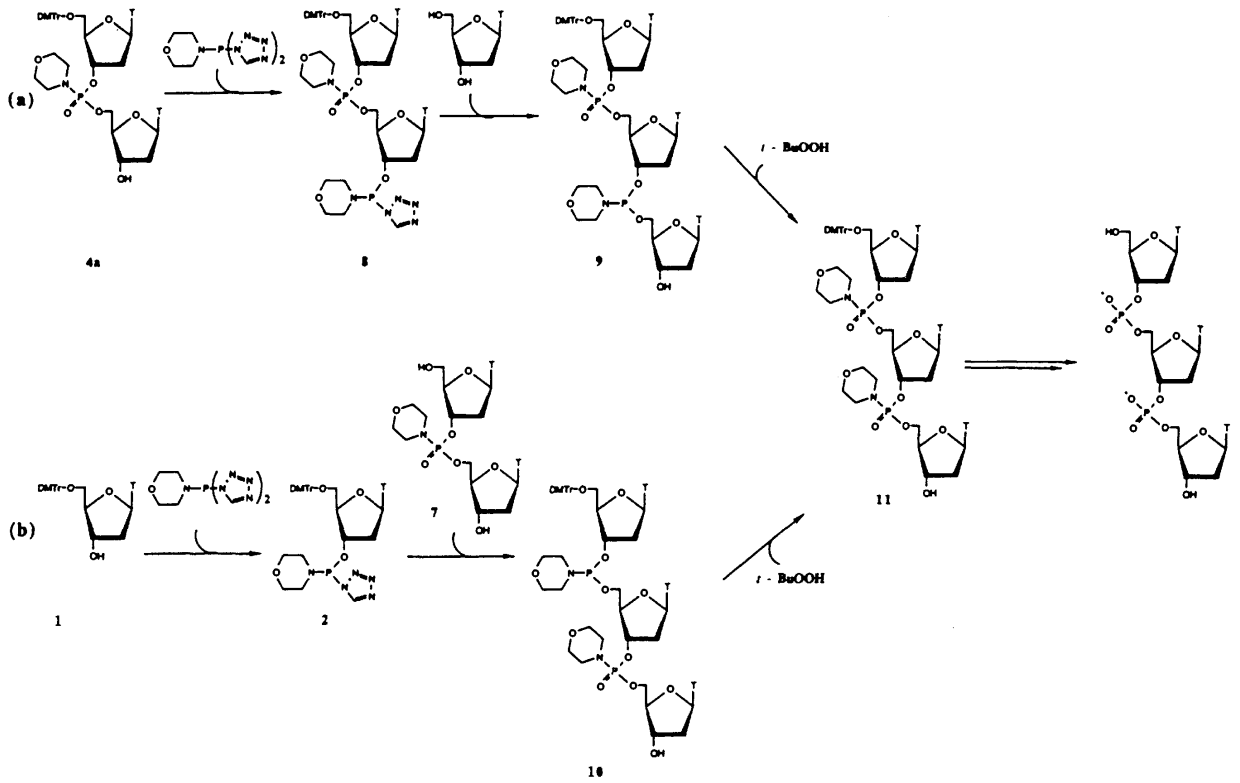

Scheme 5.

ing compound **7** with 4.0 M aqueous hydroxylamine, a small amount of unknown product formed. Compound **7** was treated with 2.0 M aqueous hydroxylamine at 50 °C. Based on HPLC analysis, the reaction resulted in complete deprotection within one week to give thymidylyl(3′-5′)thymidine (d(T-T)). The structure of this product was confirmed by an authentic sample, and a degradation with snake venom phosphodiesterase and spleen phosphodiesterase.

Chain Elongations of Bis(deoxyribonucleoside) Derivatives Both toward 3′- and 5′-Direction. In order to demonstrate chain elongations of bis(deoxyribonucleoside) derivative toward 3′- and 5′-direction, syntheses of $(dT)_3$ derivatives, trimer, were attempted by the coupling of the dithymidine derivatives such as **4a** or **7**, and thymidine or d-DMTrT **1**, respectively. First, the trimer synthesis was carried out in the similar synthetic method of bis(deoxyribonucleoside) phosphoromorpholidate derivatives by use of compound **4a** (3′-OH free derivative) as a starting material and unprotected thymidine as a coupling deoxyribonucleoside (Scheme 5a). After oxidation the total products were analyzed by HPLC. Yield of compound **11** was 77% (based on HPLC). ^{31}P NMR (in $CHCl_3$) δ=6.47 ppm (relative to external 85% H_3PO_4). The structure was confirmed by the following method. The product isolated by HPLC was treated with 80% acetic acid for 30 min at room temperature to remove the 5′-O-protecting group. After the reaction mixture was evaporated, 2.0 M aqueous hydroxylamine was added to the residue, and then the mixture was stirred at 50 °C for one week to remove phosphoryl protecting group. The resulting thymidine trimer $(dT)_3$ was confirmed by an agreement with an authentic sample (Sigma) on HPLC and a degradation method with snake venom phosphodiesterase and spleen phosphodiesterase.

Also, d-DMTrT **1** as a starting material and **7** (3′,5′-OH free dithymidine derivative) as a second deoxyribonucleoside derivative were used (Scheme 5b). The other conditions were similar to those of the above-mentioned trimer synthesis. The structure of the obtained product **11** was confirmed in the similar manner as the identification of **11** obtained above. Yield of compound **11** in this procedure was 67% based on HPLC analysis. This results indicate that chain elongations both toward 3′- and 5′-direction from dithymidine derivatives were carried out with as high yield as dithymidine derivative synthesis (74%, see Table 2).

Conversion of 3e into Phosphorous Triester. The phosphoramidite in **3e** can easily be converted to phosphorous triester by reaction with alcohol (Scheme 6). Accordingly, **3e** was readily converted to **12** by a reaction with methanol, and this intermediate **12** is widely used in phosphite chemistry. This experiment was examined by ^{31}P NMR. The addition of absolute CH_3OH (3.0 equiv) to a solution of **3e** resulted in the complete disappearance of the signal at 138.4 ppm (in $CDCl_3$) and its replacement by two new singlets at 141.7 and 142.0 ppm, which were in agree-

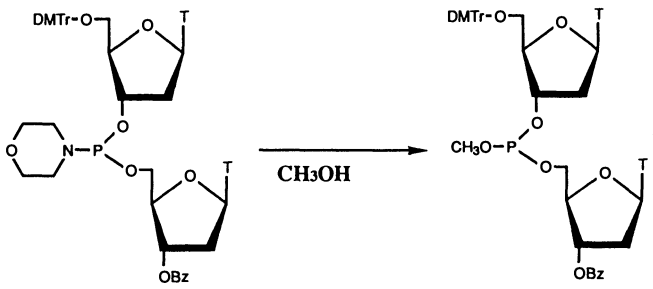

Scheme 6.

ment with the structure of **12**, as expected for two diastereomers. This result suggests that bis(deoxyribonucleoside) phosphoromorpholidite derivatives can be adapted as a key intermediate which can easily be converted to compounds bearing other phosphite linkages by the reaction of nucleophilic reagents.

Conclusion

The present approach using morpholinodi(1-tetrazolyl)phosphine provides a simple and convenient procedure for synthesizing bis(deoxyribonucleoside) derivatives, which does not require any protection of hydroxyl group of the second deoxyribonucleoside. The phosphoromorpholidite linkage can be used as a key intermediate capable of converting to other phosphite compounds and the stability of the P-N bond in the phosphoromorpholidate linkage provides a phosphoryl-protecting group in the oligodeoxyribonucleotide synthesis. In addition, it is expected that the present method to synthesize the bis(deoxyribonucleoside) derivatives having phosphoramidate linkages is applied to the syntheses of several functional oligonucleotide derivatives whose phosphorus is linked with fluorescent, intercalating and cross-linking moiety, through the reaction of nucleoside and phosphorus derivatives bearing those moieties.

Experimental

HPLC was carried out on a Shimadzu LC 6A apparatus using Cosmosil $5C_{18}$ analytical column (4.6 mm i.d. × 150 mm length, Nacalai Tesque Co.). The eluents were 70—100% CH_3OH gradient in water (eluent A) or 8—25% CH_3CN gradient in 0.1 M ammonium acetate solution (eluent B). TLC was carried out on Merck silica-gel plates (No. 5554 for analysis or No. 5717, 13793 for preparative work). Preparative silica-gel column chromatography was performed on Wako gel C-200 (Wako Pure Chemicals Co.). Middle pressure liquid chromatography was carried out on a Yamazen 540-3 apparatus using LC-SORB SP-B-SI preparative column (30 mm i.d. × 300 mm length, Chemco Scientific Co., Ltd.). ^{31}P NMR were recorded on a Hitachi R-900FT NMR (^{31}P 36.43 MHz) or a JEOL JNM-EX90 (^{31}P 36.23 MHz) relative to external 85% H_3PO_4.

Thymidine, deoxyadenosine, deoxycytidine, and deoxyguanosine were supplied from Yamasa Shoyu Co., Ltd. d-DMTrT was synthesized according to published procedures.[17] N^6-benzoyldeoxyadenosine (d-bzA),[18] N^4-benzoyldeoxycytidine (d-bzC),[18] N^2-isobutyryldeoxyguanosine (d-ibG),[18] 3′-*O*-benzoylthymidine (d-TBz),[19] N^6, 3′-*O*-dibenzoyldeoxyadenosine (d-bzA(Bz)),[20] N^4, 3′-*O*-dibenzoyldeoxycytidine (d-bzC(Bz)),[20] and 3′-*O*-benzoyl-N^2-isobutyryldeoxyguanosine (d-ibG(Bz))[20] were also synthesized according to published procedures. These compounds were coevaporated with pyridine prior to use. CH_2Cl_2 was refluxed over CaH_2 and distilled immediately prior to use. Pyridine was refluxed over CaH_2, distilled and stored over 4A Molecular Sieves. Ethyldiisopropylamine ($(i\text{-Pr})_2NEt$) was refluxed over CaH_2, distilled over CaH_2, and then stored over CaH_2. *t*-Butyl hydroperoxide (*t*-BuOOH) in toluene (3 M solution) was purchased from Aldrich Chemicals Co. and stored over 4A Molecular Sieves. Other reagents were used without further purification.

Preparation of Dichloromorpholinophosphine. A solution of morpholine (86.5 mL, 1.0 mol) in 100 mL of dry ether was added dropwise over 2 h to a vigorously stirred solution of phosphorus trichloride (43.6 mL, 0.5 mol) in 300 mL of dry ether at 0 °C. After stirring for 1 h, the amine hydrochloride was removed by filtration and ether was distilled at atmospheric pressure. The residue was distilled from cesium fluoride under reduced pressure and the desired material was isolated in a pure form (Yield: 56.9 g (60.5%), 58.0 °C/1.0 mmHg; 1 mmHg=133.322 Pa). ^{31}P NMR ($CDCl_3$) δ=156.5. Found: C, 25.48; H, 4.33; N, 7.66; P, 16.63; Cl, 37.45%. Calcd for $C_4H_8NOPCl_2$: C, 25.55; H, 4.29; N, 7.45; P, 16.47; Cl, 37.71%.

Preparation of Azolylchloromorpholinophosphine. A solution of azole (0.55 mmol) in CH_2Cl_2-pyridine (1:1 v/v, 1 mL) was added dropwise to dichloromorpholinophosphine (77.5 mL, 0.55 mmol) in CH_2Cl_2 (1 mL) containing (i-Pr)$_2$NEt (0.2 μL) with stirring at 0 °C under N_2 and the solution was stirred for 20 min. These phosphitylating reagents prepared in situ were then used in the phosphitylation of d-DMTrT.

Preparation of Bis(azolyl)morpholinophosphine. A solution of azole (1.1 mmol) in CH_2Cl_2-pyridine (1 : 1 v/v, 1 mL) was added dropwise to dichloromorpholinophosphine (77.5 μL, 0.55 mmol) in CH_2Cl_2 (1 mL) containing (i-Pr)$_2$NEt (0.2 mL) with stirring at 0 °C under N_2 and the solution was stirred for 20 min. These phophitylating reagents prepared in situ were then used in the phosphitylation of d-DMTrT.

Phosphitylation of d-DMTrT. A solution of d-DMTrT (272.5 mg, 0.5 mmol) in CH_2Cl_2 (1.5 mL) was added dropwise over a period of 10 min to azolylchloromorpholinophosphine (0.55 mmol) or bis(azolyl)morpholinophosphine (0.55 mmol) in CH_2Cl_2 (1.0 mL) containing (i-Pr)$_2$NEt (0.2 mL) with stirring at 0 °C under N_2. After the appropriate time intervals, the aliquot of the reaction mixture was treated with absolute CH_3OH. The resulting thymidine phosphoramidite derivatives were analyzed by TLC (on siica gel, CH_2Cl_2-EtOAc-Et_3N, 40/50/10, v/v/v).

General Procedures for the Preparation of Bis(deoxyribonucleoside) Phosphoromorpholidate Derivatives (4a—h). A solution of tetrazole (77.1 mg, 1.1 mmol) in CH_2Cl_2-pyridine (1 : 1 v/v, 1.0 mL) was added dropwise to dichloromorpholinophosphine (77.6 μL, 0.55 mmol) in CH_2Cl_2 (1 mL) containing (i-Pr)$_2$NEt (0.2 mL). After the reaction mixture was stirred at 0 °C for 20 min under N_2, a solution of

d-DMTrT (272.5 mg, 0.5 mmol) in CH_2Cl_2 (1.5 mL) was added dropwise over a period of 10 min to the solution with stirring at 0 °C. After 30 min, the solution was added dropwise to thymidine (243 mg, 1.0 mmol) in CH_2Cl_2–pyridine (1 : 2 v/v, 3 mL) containing (i-Pr)$_2$NEt (0.2 mL) with stirring and the reaction mixture was stirred for an additional 30 min. Further 3 M t-BuOOH in toluene (0.2 mL) was added to the reaction mixture and the solution was stirred for 10 min at 0 °C. The mixture was evaporated and coevaporated with toluene. Analysis of HPLC (in eluent A) revealed two major peaks corresponding to a diastereomeric mixture of compound **4a**. The mixture was applied to a silica-gel column and eluted with $CHCl_3$–CH_3OH (95 : 5 v/v). The appropriate fractions were collected, evaporated, and precipitated with CH_2Cl_2 (5 mL) into hexane (300 mL). The white precipitate was collected by filtration, washed and dried over P_2O_5 in vacuo. Isolated yield of **4a** was 67% (307.2 mg)(for d-DMTrT) and the purity was analyzed by HPLC (>90%). Isomer I, Found: C, 57.06; H, 5.61; N, 7.65%. Calcd for $C_{45}H_{52}O_{14}N_5P$: C, 58.88; H, 5.71; N, 7.63%, mp 137—139 °C. Isomer II, Found: C, 56.91; H, 5.62; N, 7.50%, mp 135—138 °C.

Compound **4b** was prepared by the similar procedure, except that the second deoxyribonucleoside was d-bzA (355.4 mg, 1.0 mmol) in pyridine (3 mL). Yield was 62% (based on HPLC). Isomer I, Found: C, 59.10; H, 5.37; N, 10.25%. Calcd for $C_{52}H_{55}O_{13}N_8P$: C, 60.58; H, 5.38; N, 10.87%, mp 144—148 °C. Isomer II, Found: C, 59.58; H, 5.12; N, 10.67%, mp 142—144 °C.

Compound **4c** was prepared by the similar procedure, except that the second deoxyribonucleoside was d-bzC (331.4 mg, 1.0 mmol) in pyridine (5 mL). Yield was 55% (based on HPLC). Isomer I, Found: C, 59.15; H, 5.26; N, 7.99%. Calcd for $C_{51}H_{55}O_{14}N_6P$: C, 60.83; H, 5.50; N, 8.35%, mp 146—149 °C. Isomer II, Found: C, 59.43; H, 5.41; N, 8.17%, mp 146—147 °C.

Compound **4d** was prepared by the similar procedure, except that the second deoxyribonucleoside was d-ibG (337.3 mg, 1.0 mmol) in pyridine (3 mL). Yield was 70% (based on HPLC). Isomer I, Found: C, 55.29; H, 5.44; N, 10.90%. Calcd for $C_{49}H_{57}O_{14}N_8P$: C, 58.10; H, 5.67; N, 11.06%, mp>159 °C. Isomer II, Found: C, 56.43; H, 5.51; N, 10.41%, mp>155 °C.

Compound **4e** was prepared by the similar procedure, except that the second deoxyribonucleoside was d-Tbz (173.2 mg, 0.5 mmol) in CH_2Cl_2–pyridine (1 : 2 v/v, 3 mL). Yield was 62% (based on HPLC, isomer I/isomer II=33/67). Isomer I, ^{31}P NMR ($CDCl_3$) δ=7.03, UV (CH_3OH): λ_{max} 266 and 231 nm, λ_{min} 250 nm. R_f (on silica gel, $CHCl_3$: CH_3OH=8 : 1)=0.57. Found: C, 59.57; H, 5.42; N, 6.77%. Calcd for $C_{52}H_{56}O_{15}N_5P$: C, 61.11; H, 5.52; N, 6.85%, mp 137—139 °C. Isomer II, ^{31}P NMR ($CDCl_3$) δ=6.96, UV (CH_3OH): λ_{max} 266 and 231 nm, λ_{min} 250 nm, R_f (on silica gel, $CHCl_3$: CH_3OH= 8 : 1)=0.57. Found: C, 59.24; H, 5.46; N, 6.75%, mp 140—141 °C.

Compound **4f** was prepared by the similar procedure, except that the second deoxyribonucleoside was d-bzA(Bz) (229.7 mg, 0.5 mmol) in pyridine (3 mL). Estimated yield from ^{31}P NMR was 72%. ^{31}P NMR ($CHCl_3$) δ=6.87.

Compound **4g** was prepared by the similar procedure, except that the second deoxyribonucleoside was d-bzC(Bz) (217.2 mg, 0.5 mmol) in pyridine (3 mL). Estimated yield from ^{31}P NMR was 64%. ^{31}P NMR($CHCl_3$) δ=6.33.

Compound **4h** was prepared by the similar procedure, except that the second deoxyribonucleoside was d-ibG(Bz) (220.7 mg, 0.5 mmol) in CH_2Cl_2–pyridine (1:2 v/v, 3 mL). Estimated yield from ^{31}P NMR was 41%. ^{31}P NMR ($CHCl_3$) δ=6.06.

Conversion of 4e to 7. Compound **4e** was treated with methanolic ammonia at room temperature overnight and extracted with $CHCl_3$ three times. The organic layer was evaporated to dryness and the residue was treated with 80% acetic acid at room temperature for 30 min. The mixture was evaporated to dryness and freed from acetic acid by three coevaporation with hexane. The residue was dissolved in H_2O and washed with EtOAc three times. Compound **4e** was quantitatively converted into **7** on the basis of HPLC analysis. ^{31}P NMR (H_2O) δ=7.92.

Removal of Phophoryl Protecting Group. Compound **7** was treated with 2.0 M aqueous hydroxylamine (pH 4.75) at 50 °C. Analysis by HPLC in eluent B revealed that **7** was completely converted to d(T-T) in one week. The resulting unprotected d(T-T) was confirmed by a degradation of snake venom phosphodiesterase and spleen phosphodiesterase.

Chain Elongation of Dithymidine Derivative. Route a: (dT)$_3$ derivative was synthesized from compound **4a** as starting material and unprotected thymidine as a coupling deoxyribonucleoside. The synthesis was carried out in the similar procedure as the preparation of bis(deoxyribonucleoside)phosphoromorpholidate derivatives. Yield of compound **11** was 77% (based on HPLC). ^{31}P NMR ($CHCl_3$) δ=6.47 (relative to external 85% H_3PO_4). The structure was confirmed by the following method. The product isolated by HPLC was treated with 80% acetic acid for 30 min at room temperature to remove the 5′-O-protecting group. After the reaction mixture was evaporated, 2.0 M aqueous hydroxylamine was added to the residue, and then the mixture was stirred at 50 °C for one week to remove phosphoryl protecting group. The resulting thymidine trimer (dT)$_3$ was confirmed by an agreement with an authentic sample (Sigma) on HPLC and a degradation method with snake venom phosphodiesterase and spleen phosphodiesterase.

Route b: d-DMTrT **1** as a starting material and compound **7** as a second deoxyribonucleoside derivative were used. The synthetic procedures were similar to those of the synthetic route a. The structure of the obtained product **11** was confirmed in the same manner as the identification of **11** obtained by the above-mentioned synthetic procedure. Yield of compound **11** in this procedure was 67% based on HPLC analysis.

Preparation of 5′-*O*-[Bis(4-methoxyphenyl)phenylmethyl]-3′-thymidine 3′-*O*-Benzoyl-5′-thymidine Methylphosphite (12). The preparation of **3e** was repeated in preparation of **4e**. At the stage before oxidation an absolute CH_3OH was added to the reaction mixture. The mixture was washed with $NaHCO_3$ (5% aq.). The organic layer was dried over Na_2SO_4. Analysis by TLC on silica gel using 10% benzene in EtOAc containing 1% Et_3N revealed two spots (R_f=0.44 and 0.57). The product was dissolved in 1 mL of a mixture of 40% benzene in EtOAc containing 1% Et_3N, applied to a silica-gel column and eluted with 30% benzene in EtOAc containing 1% Et_3N. The appropriate fractions were collected and evaporated to dryness. The residue was taken up in 2 mL $CHCl_3$ and added dropwise to 200 mL hexane at

−20 °C (47.6 mg, 50%). UV ($CHCl_3$): λ_{max} 246 and 268 nm; λ_{min} 252 nm. ^{31}P NMR ($CDCl_3$) δ=141.7 and 142.0. R_f (10% benzene in EtOAc containing 1% Et_3N)=0.44 and 0.57.

We would like to thank Dr. Kazushige Yamana, Himeji Institute of Technology, and Mr. Hiroshi Kawabata, Kyoto University, for NMR measurements and variable suggestions. We wish to thank Dr. Yoshihiro Hayakawa, Nagoya University, for the helpful suggestion with oxidizing agents.

References

1) R. L. Letsinger, J. L. Finnan, G. A. Heavner, and W. B. Lunsford, *J. Am. Chem. Soc.*, **97**, 3278 (1975).
2) M. D. Matteucci and M. H. Caruthers, *J. Am. Chem. Soc.*, **103**, 3185 (1981).
3) R. L. Letsinger, E. P. Groody, N. Lander, and T. Tanaka, *Tetrahedron*, **40**, 137 (1984).
4) A. D. Barone, J.-Y. Tang, and M. H. Caruthers, *Nucleic Acids Res.*, **12**, 4051 (1984).
5) T. Shimidzu, K. Yamana, K. Nakamichi, and A. Murakami, *J. Chem. Soc., Perkin Trans. 1*, **1981**, 2294.
6) T. Shimidzu, K. Yamana, N. Kanda, and S. Maikuma, *Nucleic Acids Res.*, **12**, 3257 (1984).
7) T. Shimidzu, K. Yamana, and S. Maikuma, *Tetrahedron Lett.*, **25**, 4237 (1984).
8) Y. Hayakawa, M. Uchiyama, and R. Noyori, *Tetrahedron Lett.*, **27**, 4191 (1986).
9) A. Jäger and J. Engels, *Tetrahedron Lett.*, **25**, 1437 (1984).
10) M. J. Nemer and K. K. Ogilvie, *Tetrahedron Lett.*, **21**, 4149 (1980).
11) R. L. Letsinger, S. A. Bach, and J. S. Eadie, *Nucleic Acids Res.*, **14**, 3487 (1986).
12) P. S. Miller, J. Yano, E. Yano, C. Carroll, K. Jayaraman, and P. O. P. Ts'O, *Biochemistry*, **18**, 5134 (1979).
13) P. S. Miller, K. B. McParland, K. Jayaraman, and P. O. P. Ts'O, *Biochemistry*, **20**, 1874 (1981).
14) B. C. Froehler, P. Ng, and M. D. Matteucci, *Nucleic Acids Res.*, **16**, 4831 (1988).
15) W. P. Jencks and M. Gilchrist, *J. Am. Chem. Soc.*, **87**, 3199 (1965).
16) R. I. Gumport and I. R. Lehman, *Proc. Natl. Acad. Sci. U.S.A.*, **68**, 2559 (1971).
17) H. Schaller, G. Weimann, B. Lerch, and H. G. Khorana, *J. Am. Chem. Soc.*, **85**, 3821 (1963).
18) G. S. Ti, B. L. Gaffney, and R. A. Jones, *J. Am. Chem. Soc.*, **104**, 1316 (1982).
19) R. Lohrmann and H. G. Khorana, *J. Am. Chem. Soc.*, **86**, 4188 (1964).
20) M. Ikehara and E. Ohtsuka, *Tanpakushitsu Kakusan Kouso*, **26**, 531 (1981).

 © 1989 The Chemical Society of Japan Bull. Chem. Soc. Jpn., 62, 3877—3885 (1989)

Non-Catalyzed Thermal Reactions of Acylquinones with Allylstannanes

Kazuhiro MARUYAMA* and Yoshihiro MATANO
Department of Chemistry, Faculty of Science, Kyoto University, Kitashirakawa, Sakyo-ku, Kyoto 606
(Received June 28, 1989)

Thermal reactions of acylquinones with allylstannanes in benzene afforded several kinds of product after column chromatography on silica gel; acyl allyl quinones, acyl allyl epoxy quinones, cyclopentanoid compounds including stannyl moiety, allyl hydroxy quinones, acyl hydroquinones, and acyl allyl hydroquinones. The main product comprises cyclopentanoid compounds, which are novel [2+3] cyclo adducts with 1,2-migration of trialkylstannyl moiety. Spectroscopic examinations (^{1}H NMR and Vis-UV) enabled us to confirm the reaction pathways that four types of precursors were initially generated via polarized tight pair and inverted to isolated products during purification by column chromatography. Similar reactions in acetonitrile showed a remarkable difference in the reactivity, that is, acyl allyl quinones and the corresponding hydroquinones are obtained, but the [2+3] cyclo adducts are not produced at all. From ^{1}H NMR examination, it was confirmed that three types of precursor are generated via solvent separated ion pairs at the initial stage. The rather strong reactivity of acylquinones towards allylstannanes will be due to electron withdrawing ability of acyl group.

In recent years, organotin chemistry has been dramatically developed.[1] A variety of organotin compounds have been applied as reagents or catalysts in the field of synthetic organic chemistry.[2] Allylstannanes are the best reagents for allylation of electrophilic substrates, but, in general, activation of substrates or transmetallation of reagents by Lewis acid is necessary for smooth and selective allylation.[3] For example, Lewis acid such as BF_3 coordinates to the carbonyl oxygen and enhances the electrophilicity of the substrate.

Electron deficient acylquinones exhibit unique reactivity, and several investigations relating to acylquinones have been reported by different groups.[4-7] We have reported Lewis acid catalyzed thermal reactions of acylquinones with allylstannanes, which are the key step of the total synthesis of antibiotics such as deoxyanthracyclinones[8] and pyranonaphthoquinones.[9] In these reactions, one or two allyl adducts are afforded in high yields. On the other hand, acylquinones react with allylstannanes even in the absence of Lewis acid, owing to both electron withdrawing ability and resonance efficiency.

In this paper, the thermal reactions of acylquinones with allylstannanes in the absence of catalyst will be discussed from products analyses, ^{1}H NMR, and Vis-UV. The characteristic diversity in the reactivity of acylquinones is considered from the steric and electronic nature of the relating reagents and polarity of solvents.

Results

Thermal Reactions of Acetylquinones with Allylstannanes. Thermal reactions of two kinds of acetylquinone (**1a,b**) with allylstannanes (**2a,b**) were investigated by examining the products and spectroscopic (^{1}H NMR and Vis-UV) analyses.

2-Acetyl-1,4-naphthoquinone **1a** (1 mmol) and allyltrimethylstannane **2a** (2 mmol) were dissolved in benzene (25 ml) and allowed to stand for 24 h under argon atmosphere. After treating the reaction mixture by column chromatography on silica gel, six compounds were isolated as the major products 5-acetyl-2*H*-benzo[*h*]chromene-6-ol **3a** (3%), 2-acetyl-3-allyl-1,4-naphthoquinone **4a** (20%), 2-acetyl-3-allyl-2,3-epoxy-2,3-dihydro-1,4-naphthoquinone **5a** (20%), 3a-acetyl-2-trimethylstannyl-2,3,3a,4,9,9a-hexahydro-1*H*-cyclopenta[*b*]naphthalene-4,9-dione **6a** (32%), 3-allyl-2-hydroxy-1,4-naphthoquinone **7a** (3%), and 2-acetyl-1,4-naphthalenediol **8a** (20%) (Scheme 1). The identification of these isolated products was carried

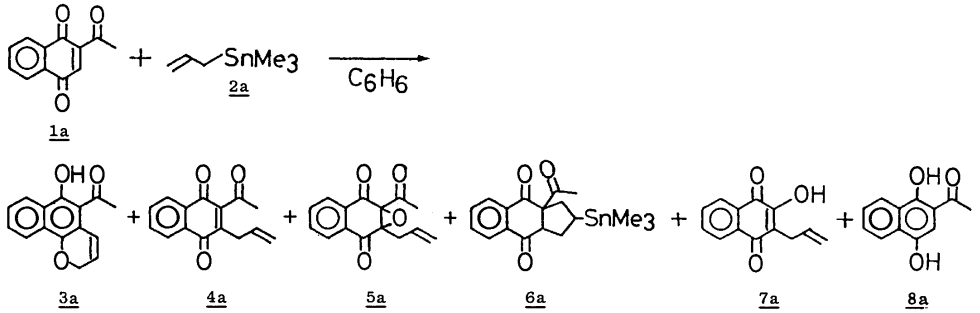

Scheme 1.

out on the basis of ^{1}H NMR, ^{13}C NMR, IR, mass spectroscopy, elementary analysis, and comparison with the authentic samples. Several spectral data which were characteristic of each product are described below. The IR spectrum of **3a** showed characteristic bands due to hydrogen bonded hydroxyl and carbonyl group at 3300 and 1600 cm^{-1}, respectively, and the allyl position methylene signal appeared at δ 4.77 as a doublet in its ^{1}H NMR spectrum. The IR spectrum of **4a** showed absorption bands due to carbonyl group at 1705 and 1665 cm^{-1}, and that of **5a** showed characteristic bands due to carbonyl group at 1710, 1695, and 1680 cm^{-1}. In their ^{1}H NMR spectra, the allyl methylene of **4a** appeared at δ 3.28 as a doublet (J=6 Hz), while that of **5a** showed diastereomeric peaks at δ 2.49 (dd, J=7, 15 Hz) and 3.00 (dd, J=7, 15 Hz). In the mass spectrum of **5a**, the parent peak and the ion peak arising from elimination of acetyl group appeared at m/z 256 (M^+) and 213 (M^+-43). All spectral data of **5a** was consistent with those of the authentic sample synthesized through another route.[6] The IR and ^{13}C NMR spectra of pale yellow compound **6a** showed characteristic bands due to carbonyl group at 1710, 1695, 1680 cm^{-1} and δ 203, 196, 194. Since ^{1}H NMR spectrum of **6a** showed only one peak due to trimethylstannyl group at δ 0.06, only one diastereomer was generated, and cis stereochemistry has been assigned to **6a** based upon analysis of the ^{13}C-^{119}Sn coupling constant.[10] In its mass spectrum, ion peaks arising from elimination of methyl group appeared at m/z 391 and 389 (M^+-15) along with those of tin isotopes ^{120}Sn and ^{118}Sn. Compound **7a** and **8a** were identified by comparison with the authentic samples.[6,11]

Of these isolated products, **3a** and **7a** were generated from **4a** and **5a**, respectively, during the treatment with silica gel. Furthermore, the generation of the cyclopentanoid adduct **6a** is worth mentioning, because it is a [2+3] cycloaddition product resulted via migration of trimethylstannyl moiety. A similar [2+3] cycloaddition reaction of allylstannanes was recently reported by Herndon.[12]

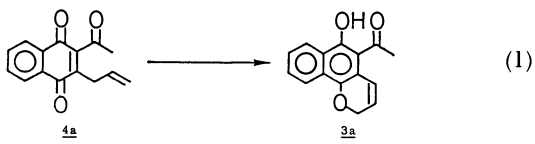

(1)

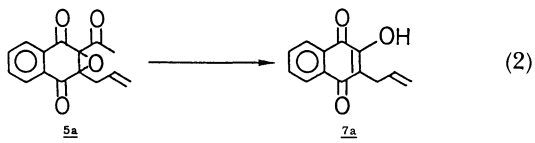

(2)

Although the thermal reaction between **1a** and **2a** in dichloromethane gave the same products as those obtained in benzene in a slightly different distribution, remarkable differences were observed in the reaction in acetonitrile. The color of an acetonitrile solution changed from yellow to dark green soon after mixing **1a** with **2a** and the reaction completed within 30 min. It seems interesting that compounds **3a**, **4a**, **5a**, **7a**, and **8a** were generated but the cyclopentanoid compound **6a** was not obtained at all.

Similarly, thermal reaction of **1b** with **2a** in benzene gave 3a-acetyl-2-trimethylstannyl-2,3,3a,4,7,7a-hexahydrindene-4,7-dione **6b** (23%), 2-acetyl-1,4-benzenediol **8b** (36%), and 2-acetyl-3-allyl-1,4-benzenediol **9b** (27%) as the major products after purification by column chromatography on silica gel (Scheme 2). On the contrary, in acetonitrile, a yellow solution changed to dark green immediately after mixing **1b** with **2a**, and the reaction completed within 10 min. After the usual examination, **8b** (18%) and **9b** (18%) were identified but the cyclopentanoid compound **6b** was not observed at all.

A similar reactivity of **1a,b** in the reaction with allyltributylstannane **2b** was recognized. The results are summarized in Table 1. Compared with other p-quinones such as non-substituted quinones, halogeno quinones, alkyl quinones, alkoxy quinones, and so on, the reactivity of 2-acetyl-1,4-quinones **1a,b** was quite specific in the aspects as follows. First, the reaction proceeds spontaneously without activation of reagents. In general, the reaction of p-benzoquinone with **2** does not proceed without irradiation or catalyst. Second, polarity of solvents strongly affects both the reaction rate and products distribution. Thus, in a nonpolar solvent such as benzene, the reaction proceeded relatively slowly, resulting in the formation of [2+3] cycloadducts **6a,b**. On the other hand, in a polar solvent such as acetonitrile, the reaction proceeded quickly, but **6a,b** were not given.

In order to clarify the reaction pathways, ^{1}H NMR measurement was carried out in the reaction of **1a** with **2a**. When a benzene-d_6 solution containing **1a** (ca. 10^{-2} M; 1 M=1 mol dm^{-3}) and **2a** (ca. 10^{-2} M) was allowed to stand in an NMR sample tube under argon atmosphere, many new peaks emerged stepwisely, but

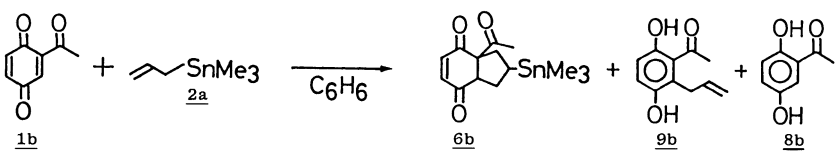

Scheme 2.

Table 1. Thermal Reactions of Acetylquinones (**1**) with Allylstannanes (**2**)

Quinone	Tin	Reaction Conditions		Isolated yields/%							
1a	**2a**	C_6H_6	21h	**3a**(3)	**4a**(20)	**5a**(12)	**6a**(32)	**7a**(3)	**8a**(21)		
1a	**2a**	CH_2Cl_2	20h	**3a**(2)	**4a**(23)	**5a**(12)	**6a**(41)	**7a**(3)	**8a**(3)		
1a	**2a**	CH_3CN	1h	**3a**(1)	**4a**(28)	**5a**(28)		**7a**(4)	**8a**(12)		
1a	**2b**	C_6H_6	20h	**3a**(2)	**4a**(18)	**5a**(10)		**7a**(2)	**8a**(15)		**10a**(35)[a]
1a	**2b**	CH_3CN	1h	**3a**(3)	**4a**(30)	**5a**(22)		**7a**(3)	**8a**(19)		
1b	**2a**	C_6H_6	5h				**6b**(23)		**8b**(36)	**9b**(27)	
1b	**2a**	CH_3CN	10min						**8b**(18)	**9b**(18)	
1b	**2b**	C_6H_6	1.5h						**8b**(10)	**9b**(29)	**10b**(10)[b]

a) **10a**: 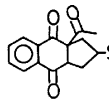 b) **10b**: 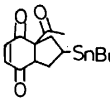

the peaks gradually disappeared due to the starting reagents. After standing for 24 h, trace amounts of **1a**, **2a**, and four main products were observed. Compared with the ^{1}H NMR spectra of the authentic samples and structurally related substrates, these four products were assigned to **6a** (40%), **15a** (40%), **16a** (10%), and **17a** (3%) as shown in Scheme 3. The assignments were accomplished by using (2-deuterioallyl)trimethylstannane **2c** instead of **2a**, but several unidentified peaks remained.[13] To our surprise, the isolated products **3a**, **4a**, **5a**, **7a**, and **8a** were not observed during this measurement. It was thus confirmed that these five isolated products were the resultants of **15a**, **16a**, and **17a**. The ^{1}H NMR spectrum of **15a** showed characteristic bands due to acetyl group and trimethylstannyl group at δ 2.42 (3H, d, J=2 Hz) and 1.12 (9H, s), respectively. In addition, similar resonances arising from the diastereomer of [4+2] cycloadduct **15a** were observed at δ 2.44 (3H, d, J=2 Hz) and 1.13 (9H, s). The relative ratio of diastereomers was estimated to be 6/1 from integral values of each peak at δ 2.42 and 2.44. The ^{1}H NMR spectrum of **17a** showed characteristic singlet peak due to trimethylstannyl group at δ 0.24 (9H, s). However, any attempts to isolate **15a** and **17a** have failed so far. Furthermore, the reaction mixture was passed through a very short silica-gel column after standing for 24 h, and then, all fractions were collected, concentrated, and measured similarly by ^{1}H NMR. Five compounds, **4a** (4%), **5a** (2%), **6a** (38%), **8a** (5%), and **16a** (45%) were observed, but **15a** and **17a** completely disappeared. The quantity of cyclopentanoid compound **6a** was little affected by treating with silica-gel column, but the quantity of **16a** slightly increased.[14] In the presence of Lewis acid such as BF_3, compound **16a** was given as the sole allyl adduct.

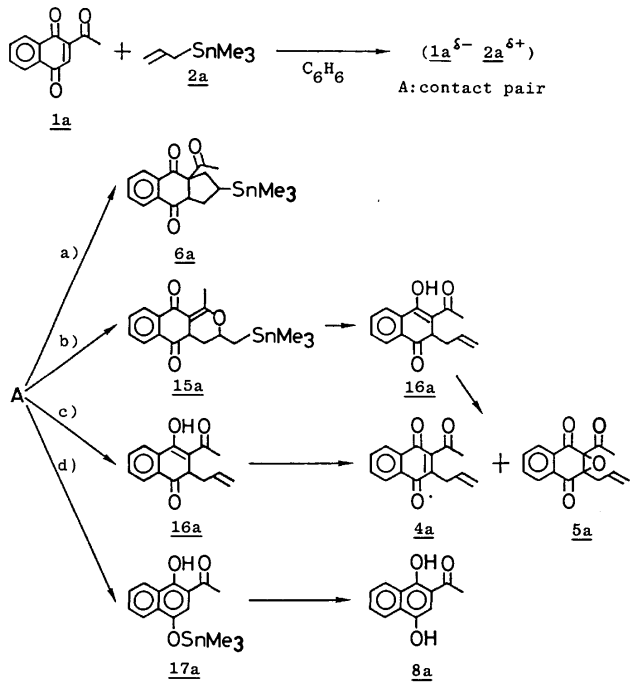

Scheme 3.

(3)

A similar ^{1}H NMR measurement in acetonitrile-d_3 was also undertaken. In this case, the color of a solution changed from yellow to green soon after mixing of **1a** with **2a**. The peak of the 3-position of **1a** broadened instantly and new peaks emerged quickly. The starting acylquinone **1a** was completely consumed within 30 min, and three products, **4a** (10%), **16a** (55%), and **17a** (17%) were observed. The cyclized products, **6a** and **15a**, involving trimethylstannyl moiety were not generated in this case. After treating the reaction mixture with silica gel, **4a** (9%), **5a** (2%), **8a** (15%), and **16a** (50%) were identified (Scheme 4).

Furthermore, we have applied Vis-UV absorption method to follow the reaction of **1a** with **2b** in benzene. Addition of **2b** to a benzene solution of **1a** resulted in a development of absorption bands corre-

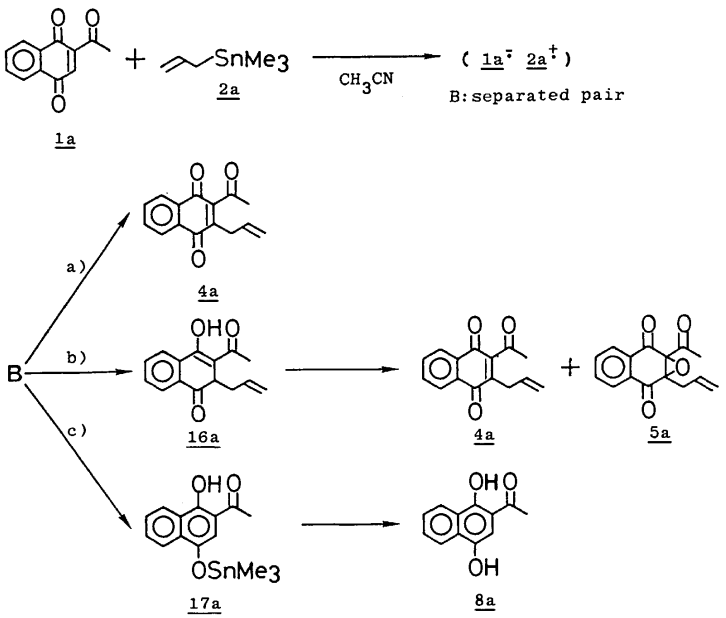

Scheme 4.

sponding to each product with three isosbestic points at 328, 371, and 425 nm, which were not influenced by concentrations of two reagents (Fig. 1). These facts suggest that each product was generated via an identical intermediate. In other words, the rate determining step of the reaction seems to be the formation of the common intermediate.

Thermal Reactions of Related Acylquinones with Allylstannane. The thermal reactions of other acylquinones **1c—f** (1 mmol) with allyltrimethylstannane **2a** (2 mmol) were carried out in benzene (25 ml). By the reaction of 2-propionyl-1,4-naphthoquinone **1c** with **2a**, several kinds of product were given after purification by column chromatography on silica gel and spectroscopically identified; chromene **3c**, allyl quinone **4c**, allyl epoxy quinone **5c**, [2+3] cycloadduct **6c**, allyl hydroxy quinone **7a**, and hydroquinone **8c**. On the other hand, the thermal reactions of 2-pivaloyl-1,4-naphthoquinone **1d** and 2-acetyl-3-methyl-1,4-naphthoquinone **1e** with **2a** did not proceed at all.[15] The reaction of 2-acetyl-8-methoxy-1,4-naphthoquinone **1f**, in which electron donating methoxyl group was introduced to phenyl ring, with **2a** gave allyl quinone **4f**, [2+3] cycloadduct **6f**, and hydroquinone **8f**. The results are summarized in Scheme 5.

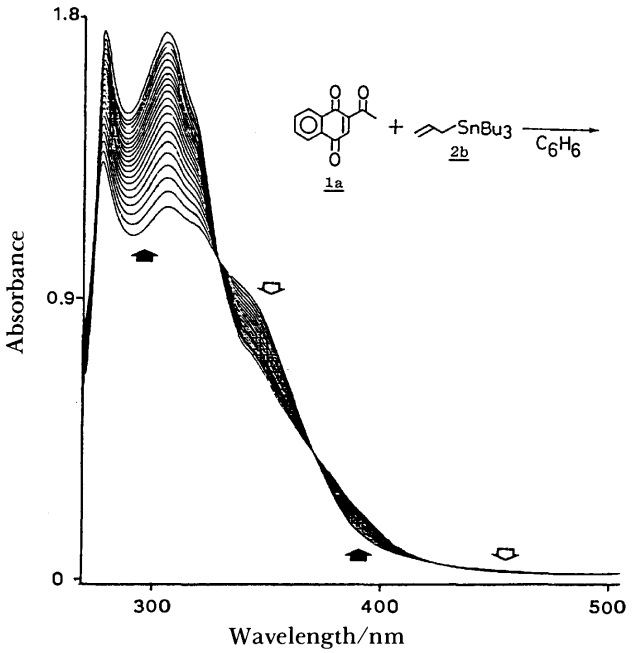

Fig. 1. Absorption spectral change observed during the reaction of **1a** with **2b** in benzene.

Thermal Reactions of Acetylquinones with Methallyl- or Benzylstannanes or Allylsilane. In the thermal reaction of 2-acetyl-1,4-naphthoquinone **1a** with (2-methylallyl)trimethylstannane **2d**, allylated products **11a** and **12a** were obtained as usual, but [2+3] cycloadduct like **6a** was not formed. In the thermal reaction of **1a** with benzyltrimethylstannane **2e** or with allyltrimethylsilane **2f** in benzene, no progress of reactions was recognized. The results are summarized in Scheme 6.

Discussion

The reactivity of acylquinones with allylstannanes was quite specific from two aspects: 1) thermal reaction proceeded spontaneously without activation of reactants and 2) solvent polarity strongly affected the distribution of product ratio. These characteristics seem to derive from both strong oxidizing power and resonance ability of acyl group under anionic state of acylquinones **1**, and from both mild reducing power and probable cleavage of carbon-tin bond under

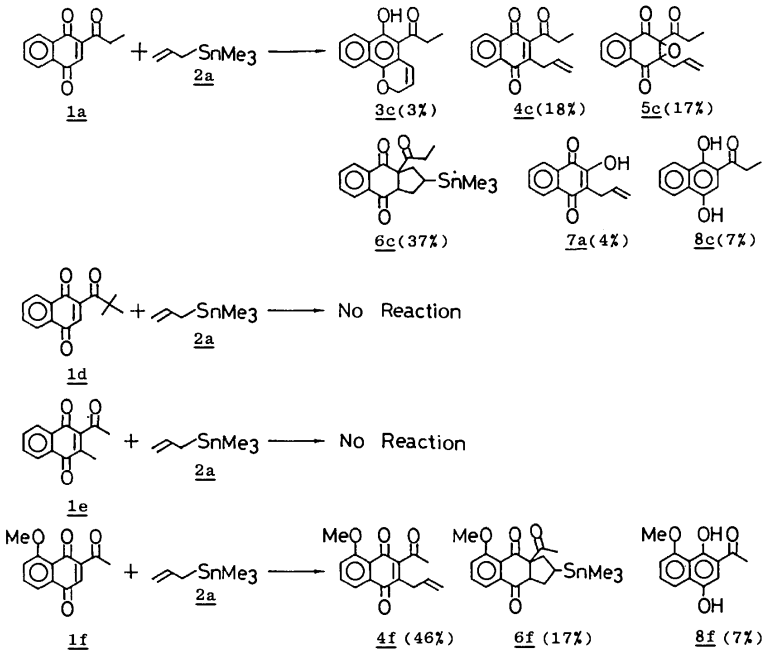

Scheme 5.

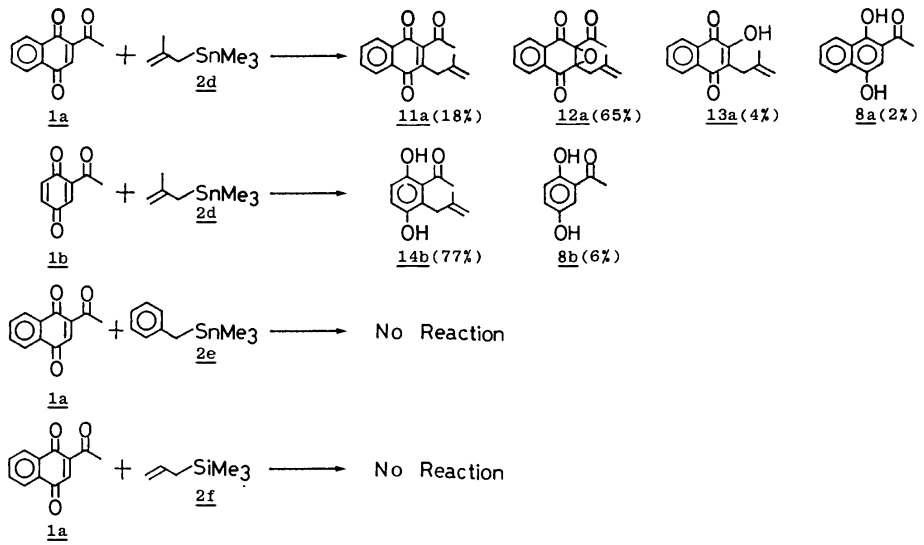

Scheme 6.

cationic state of allylstannanes **2**. During these reactions, acylquinones **1** behave as electron acceptors and allylstannanes **2** behave as electron donors.

Based upon the above results, reaction pathways were proposed as given in Schemes 3 and 4. The reaction between **1a** and **2a** was selected as a representative.

In a nonpolar solvent such as benzene, polarized species are not stabilized by solvent molecules, and the charge transfer can therefore occur only in the case that two species are brought sufficiently close and the polarized two species $\mathbf{1a}^{\delta-}$ and $\mathbf{2a}^{\delta+}$ will be kept in a tightly contacted pair in solvent cage (intermediate pair **A**). In general, the 3-position of $\mathbf{1a}^-$ shows highly electrophilic reactivity toward electron rich reaction center and the negative charge is stabilized by resonance effect of acyl group. The following four pathways a—d) from tight pair **A** will be most reasonable. As for the generation of compound **6a**, since tin stabilizes its cationic β-position by hyperconjugative interaction, [2+3] cycloaddition between $\mathbf{1a}^-$ and $\mathbf{2a}^+$ will occur before C-Sn bond cleavage of $\mathbf{2a}^+$ with 1,2-migration of trimethylstannyl moiety.[16] Similarly to the path a), generation of compound **15a** will proceed by [4+2] cycloaddition before C-Sn bond cleavage of $\mathbf{2a}^+$. In this path, cationic β-carbon of $\mathbf{2a}^+$ will be trapped by resonant acetyl-carbonyl oxygen. Contrary to the cases a) and b), generation of compound **16a** will proceed by allylation of $\mathbf{1a}^-$ at the 3-position with C-Sn bond cleavage of $\mathbf{2a}^+$. The H

atom of hydroxyl group at the 1-position may be released from solvent molecules. As for the compound **17a**, escaped $\mathbf{1a}^-$ from solvent cage will abstract H atom from solvent molecules and remaining anionic oxygen atom may trap trimethylstannyl cation.

Probably, three compounds **15a**, **16a**, and **17a** convert to the corresponding isolated products during the usual working-up process such as silica-gel long column chromatography (Scheme 3). The six membered [4+2] cycloadduct **15a** generated via path b) has enol structure in its skeleton, and converts into **16a** with C-Sn bond cleavage under acidic condition followed by aromatization to 2-acetyl-3-allyl-1,4-naphthalenediol, which will be easily autoxidized to the corresponding quinone **4a** with air or remaining **1a**. Thus, both **15a** and **16a** are the precursors of **4a** and **5a**, and **17a** converts into **8a**.

On the other hand, in a polar solvent such as acetonitrile, polarized species can be stabilized by solvent molecules, and electron transfer will occur even in the case that two reactants are apart somewhat each other. From two facts that the color of the reacting solution turned from yellow to green soon after mixing the reagents and that the 3-position of **1a** broadened instantly in ^{1}H NMR examination, single electron transfer seems to occur from **2a** to **1a**, resulting in the formation of solvent separated loose radical ion pair between $\mathbf{1a}^{\cdot-}$ and $\mathbf{2a}^{\cdot+}$ (intermediate pair **B**). Owing to the high $\sigma_{C\text{-}Sn}$ bond orbital energy and to electropositive character of tin, $\mathbf{2a}^{\cdot+}$ tends to undergo rapid generation of allyl radical and trimethylstannyl cation, so C-C bond formation between $\mathbf{1a}^{\cdot-}$ and allyl radical will occur.[17] Therefore, the cyclized compounds having trimethylstannyl moiety such as **6a** and **15a** will not be obtained under these conditions. The remarkable difference between the reactivity of the reactions in benzene and that in acetonitrile should be ascribed to the difference in the activation energy of formation of the two intermediates **A** and **B**.

The results in the reactions of related acylquinones **1c—f** with **2a** in benzene provided information on steric and electronic effects for the reactivity. Thus, introduction of electron donating methoxyl group to phenyl ring or introduction of methyl group to acetyl group did not affect reactivity as a whole, that is, [2+3] cycloadducts and allylated quinones were obtained as the case of **1a**. On the other hand, introduction of *t*-butyl group as a part of acyl group (**1d**) or introduction of methyl group to the reacting 3-position (**1e**) diminished the reactivity completely. From these results, it is concluded that decreasing oxidizing power of acylquinones can not appreciably reduce the reactivity toward **2a**, but that increasing steric hindrance around the 3-position of acylquinone entirely reduces the reactivity.[18]

Thermal reactions of **1a,b** with methallylstannane **2d** in benzene afforded allylated products, but [2+3] cycloadduct such as **6a** was not obtained at all. This is due to the inductive effect of methyl group which stabilizes the intermediary cationic β-position of $\mathbf{2d}^+$ and the effect of the steric hindrance between methyl group and trimethylstannyl group. The 1,2-migration of the trimethylstannyl moiety was thus suppressed. Thermal reactions of **1a,b** with benzylstannane **2e** or allylsilane **2f** did not proceed at all, due to the lower electron donating ability of **2e** and **2f**.

Experimental

General Remarks. All melting points were determined on a Yanagimoto micro-melting point apparatus and uncorrected. Mass spectra were measured by a JEOL JMS-DX-300 mass spectrometer. ^{1}H NMR spectra were obtained by a JEOL JNM-PX-100 and a JEOL JNM-GX-400 spectrometers. ^{13}C NMR spectra were obtained by a JEOL JNM-GX-400 spectrometer. Chemical shifts were recorded as δ values in parts per million (ppm) from tetramethylsilane as an internal standard. IR spectra were obtained by a JASCO IRA-1 spectrometer for KBr pellets or neat oil on NaCl. The electronic spectra were obtained by a Shimadzu UV-3000 spectrometer. Column chromatography was done on Wakogel C-200 and Merck Kieselgel 60H for flash column chromatography. Elementary analyses were performed by the Microanalytical Laboratory of Kyoto University. Cyclic voltammetry was carried out by a PAR Model 174 with working electrodes of platinum wire.

Starting Materials. Benzene was used after distillation from sodium wire. Acetonitrile and dichloromethane were used after distillation from phosphorus pentaoxide. Benzene-d_6 and acetonitrile-d_3 were commercially available and used after distillation. 2-Acetyl-1,4-naphthoquinone **1a**, 2-acetyl-1,4-benzoquinone **1b**, 2-propionyl-1,4-naphthoquinone **1c**, 2-pivaloyl-1,4-naphthoquinone **1d**, 2-acetyl-3-methyl-1,4-naphthoquinone **1e**, and 2-acetyl-8-methoxy-1,4-naphthoquinone **1f** were synthesized by the previously reported methods.[6,19] All acylquinones were purified by recrystallization and sublimation. Allylic- and benzylstannanes **2a—e** were prepared by the reported methods.[20,21] All tin reagents were purified by distillation. Allyltrimethylsilane **2f** was commercially available and used without further purification.

General Procedures. Acylquinone (1 mmol) and allylstannane (2 mmol) were dissolved in benzene or acetonitrile (25 ml) and allowed to stand for suitable time under argon atmosphere. The reaction mixture was concentrated, subjected to column chromatography on silica gel, and eluted with hexane–ether.

Physical Properties of the Products. 5-Acetyl-2*H*-benzo[*h*]chromene-6-ol (**3a**): Yellow needles from hexane–chloroform; mp 119—123 °C. MS; *m/z* 240 (M^+). Found: C, 74.82; H, 4.82%. Calcd for $C_{15}H_{12}O_3$: C, 74.99; H, 5.03%. IR (KBr); 3300 (OH), 1600 (C=O) cm^{-1}. ^{1}H NMR ($CDCl_3$) δ=2.63 (3H, s), 4.77 (2H, d, *J*=4 Hz), 5.8 (1H, dt, *J*=9, 4 Hz), 6.75 (1H, d, *J*=9 Hz), 7.5—7.7 (2H, m), 8.12 (1H, d, *J*=8 Hz), 8.42 (1H, d, *J*=8 Hz), 13.8 (1H, s).

5-Propionyl-2*H*-benzo[*h*]chromene-6-ol (**3c**): Yellow needles from hexane–ether; mp 69—72 °C. MS; *m/z* 254 (M^+). High resolution MS; Found: *m/z* 254.0944. Calcd for $C_{16}H_{14}O_3$: M, 254.0944. IR (KBr); 3400 (OH), 1605 (C=O) cm^{-1}. ^{1}H NMR ($CDCl_3$); δ=1.25 (3H, t, *J*=7 Hz), 2.94 (2H,

q, J=7 Hz), 4.78 (2H, d, J=4 Hz), 5.88 (1H, dt, J=9, 4 Hz), 6.74 (1H, d, J=9 Hz), 7.5—7.7 (2H, m), 8.11 (1H, d, J=8 Hz), 8.41 (1H, d, J=8 Hz), 13.66 (1H, s).

2-Acetyl-3-allyl-1,4-naphthoquinone (**4a**): Yellow needles from hexane-chloroform; mp 57—59 °C. MS; m/z 240 (M^+). High resolution MS; Found: m/z 240.0789. Calcd for $C_{15}H_{12}O_3$: M, 240.0785. IR (KBr); 1705 (C=O), 1665 (C=O) cm^{-1}. ^1H NMR ($CDCl_3$); δ=2.50 (3H, s), 3.28 (2H, d, J=6 Hz), 5.1—5.3 (2H, m), 5.8—6.0 (1H, m), 7.8—7.9 (2H, m), 8.1—8.3 (2H, m).

2-Propionyl-3-allyl-1,4-naphthoquinone (**4c**): Yellow oil. MS; m/z 254 (M^+). High resolution MS; Found: m/z 254.0937. Calcd for $C_{16}H_{14}O_3$: M, 254.0944. IR (neat); 1705 (C=O), 1660 (C=O) cm^{-1}. ^1H NMR ($CDCl_3$); δ=1.20 (3H, t, J=7 Hz), 2.76 (2H, q, J=7 Hz), 3.25 (2H, d, J=7 Hz), 5.1—5.2 (2H, m), 5.8—5.9 (1H, m), 7.75—7.85 (2H, m), 8.1—8.2 (2H, m).

3-Acetyl-2-allyl-5-methoxy-1,4-naphthoquinone (**4f**): Pale yellow crystals from hexane-ether; mp 127—129 °C. MS; m/z 270 (M^+). Found: C, 70.99; H, 5.10%. Calcd for $C_{16}H_{14}O_4$: C, 71.10; H, 5.22%. IR (KBr); 1705(C=O), 1650 (C=O), 1630 (C=O) cm^{-1}. ^1H NMR ($CDCl_3$); δ=2.47 (3H, s), 3.23 (2H, d, J=7 Hz), 4.01 (3H, s), 5.12 (2H, m), 5.83 (1H, m), 7.2—7.4 (1H, m), 7.6—7.8 (2H, m).

2-Acetyl-3-allyl-2,3-epoxy-2,3-dihydro-1,4-naphthoquinone (**5a**): Pale yellow needles from hexane-chloroform; mp 88—90 °C. MS; m/z 213 (M^+−43). Found: C, 70.23; H, 4.66%. Calcd for $C_{15}H_{12}O_4$: C, 70.31; H, 4.72%. IR (KBr); 1710 (C=O), 1695 (C=O), 1680 (C=O) cm^{-1}. ^1H NMR ($CDCl_3$); δ=2.46 (3H, s), 2.49 (1H, dd, δ=7, 15 Hz), 3.00 (1H, dd, J=7, 15 Hz), 5.19 (2H, m), 5.85 (1H, m), 7.7—7.8 (2H, m), 8.0—8.1 (2H, m).

3-Allyl-2-propionyl-2,3-epoxy-2,3-dihydro-1,4-naphthoquinone (**5c**): Yellow crystals from hexane-ether; mp 53—55 °C. MS; m/z 270 (M^+). High resolution MS; Found: m/z 270.0929. Calcd for $C_{16}H_{14}O_4$: M, 270.0892. IR (neat); 1725 (C=O), 1690 (C=O), 1680 (C=O) cm^{-1}. ^1H NMR ($CDCl_3$); δ=1.16 (3H, t, J=7 Hz), 2.5—2.9 (4H, m), 5.1 (2H, m), 5.85 (1H, m), 7.7—7.9 (2H, m), 8.0—8.1 (2H, m).

3a-Acetyl-2-trimethylstannyl-2,3,3a,4,9,9a-hexahydro-1*H*-cyclopenta[*b*]naphthalene-4,9-dione (**6a**): Pale yellow crystals from hexane-ether; mp 93—95 °C. MS; m/z 391 (M^+−15, ^{120}Sn), 389 (M^+−15, ^{118}Sn). Found: C, 53.27; H, 5.39%. Calcd for $C_{18}H_{22}O_3Sn$: C, 53.37; H, 5.47%. IR (KBr); 1705 (C=O), 1680 (C=O), 1670 (C=O) cm^{-1}. ^1H NMR ($CDCl_3$); δ=0.06 (9H, s), 1.50 (1H, m), 1.92 (1H, t, J=13 Hz), 2.0—2.2 (5H, m), 3.07 (1H, dd, J=8, 13 Hz), 3.62 (1H, dd, J=8, 11 Hz), 7.75—7.85 (2H, m), 8.05—8.15 (2H, m). ^{13}C NMR($CDCl_3$); δ=−11.2, 20.1, 26.6, 34.2, 39.6, 53.8, 77.6, 127.0, 133.8, 134.1, 134.8, 194.5, 196.2, 202.6.

3a-Acetyl-2-trimethylstannyl-2,3,3a,4,7,7a-hexahydrindene-4,7-dione (**6b**): Yellow crystals from hexane-chloroform; mp 45—47 °C. MS; m/z 341 (M^+−15, ^{120}Sn), 339 (M^+−15, ^{118}Sn). Found: C, 47.44; H, 5.64%. Calcd for $C_{14}H_{20}O_3Sn$: C, 47.37; H, 5.68%. IR (neat); 1700 (C=O), 1680 (C=O) cm^{-1}. ^1H NMR ($CDCl_3$); δ=0.03 (9H, s), 1.32 (1H, m), 1.83 (1H, t, J=13 Hz), 2.0—2.2 (5H, m), 2.86 (1H, dd, J=7, 12 Hz), 3.45 (1H, dd, J=6, 10 Hz), 6.63 (1H, d, J=17 Hz), 6.67 (1H, d, J=17 Hz).

3a-Propionyl-2-trimethylstannyl-2,3,3a,4,9,9a-hexahydro-1*H*-cyclopenta[*b*]naphthalene-4,9-dione (**6c**): Pale yellow needles from hexane-ether; mp 59—62 °C. MS; m/z 405 (M^+−15, ^{120}Sn), 403 (M^+−15, ^{118}Sn). Found: C, 54.72; H, 5.78%. Calcd for $C_{19}H_{24}O_3Sn$: C, 54.45; H, 5.77%. IR (KBr); 1710 (C=O), 1680 (C=O) cm^{-1}. ^1H NMR ($CDCl_3$); δ=−0.01 (9H, s), 0.85 (3H, t, J=7 Hz), 1.41 (1H, m), 1.85 (1H, t, J=12 Hz), 2.09 (2H, t, J=10 Hz), 2.46 (2H, q, J=7 Hz), 3.01 (1H, dd, J=7, 13 Hz), 3.54 (1H, dd, J=9, 10 Hz), 7.65 (2H, m), 7.9—8.0 (2H, m).

3a-Acetyl-2-trimethylstannyl-5-methoxy-2,3,3a,4,9,9a-hexahydro-1*H*-cyclopenta[*b*]naphthalene-4,9-dione (**6f**): Pale yellow crystals from hexane-ether; mp 113—115 °C. MS; m/z 421 (M^+−15, ^{120}Sn), 419 (M^+−15, ^{118}Sn). Found: C, 52.48; H, 5.59%. Calcd for $C_{19}H_{24}O_4Sn$: C, 52.45; H, 5.56%. IR (KBr); 1695 (C=O), 1680 (C=O), 1665 (C=O) cm^{-1}. ^1H NMR ($CDCl_3$); δ=0.06 (9H, s), 1.47 (1H, m), 1.75 (1H, t, J=13 Hz), 2.10 (1H, m), 2.16 (3H, s), 2.23 (1H, m), 3.13 (1H, dd, J=7, 13 Hz), 3.71 (1H, dd, J=7, 10 Hz), 3.93 (3H, s), 7.15—7.25 (1H, m), 7.55—7.65 (2H, m).

2-Allyl-3-hydroxy-1,4-naphthoquinone (**7a**): Yellow crystals from hexane-ether; mp 113—116 °C. MS; m/z 214 (M^+). High resolution MS; Found: m/z 214.0626. Calcd for $C_{13}H_{10}O_3$: M, 214.0629. IR (KBr); 3350 (OH), 1655 (C=O), 1640 (C=O) cm^{-1}. ^1H NMR ($CDCl_3$); δ=3.37 (2H, d, J=7 Hz), 5.10 (2H, m), 5.91 (1H, m), 7.35 (1H, s), 7.6—7.8 (2H, m), 8.0—8.2 (2H, m).

2-Acetyl-1,4-naphthalenediol (**8a**): Yellow powders from ethanol; mp 209—210 °C. MS; m/z 202 (M^+). IR (KBr); 3280 (OH), 1600 (C=O) cm^{-1}.

2-Acetyl-1,4-benzenediol (**8b**): Yellow crystals from ethanol; mp 201—203 °C. MS; m/z 152 (M^+). IR (KBr); 3220 (OH), 1600 (C=O) cm^{-1}.

2-Propionyl-1,4-naphthalenediol (**8c**): Yellow crystals from ethanol; mp 182—184 °C. MS; m/z 216 (M^+). High resolution MS; Found: m/z 216.0786. Calcd for $C_{13}H_{12}O_3$: M, 216.0786. IR (KBr); 3360 (OH), 1625 (C=O) cm^{-1}. ^1H NMR ($CDCl_3$); δ=1.28 (3H, t, J=7 Hz), 3.03 (2H, q, J=7 Hz), 4.96 (1H, s), 7.55—7.70 (2H, m), 8.10 (1H, d, J=8 Hz), 8.46 (1H, d, J=8 Hz), 13.70 (1H, s).

2-Acetyl-8-methoxy-1,4-naphthalenediol (**8f**): Yellow crystals from ethanol; mp 153—155 °C. MS; m/z 232 (M^+). High resolution MS; Found: m/z 232.0741. Calcd for $C_{13}H_{12}O_4$: M, 232.0736. IR (KBr); 3500 (OH), 3220 (OH), 1620 (C=O) cm^{-1}. ^1H NMR ($CDCl_3$); δ=2.66 (3H, s), 4.06 (3H, s), 5.21 (1H, s), 6.96 (1H, d, J=7 Hz), 7.10 (1H, s), 7.56 (1H, dd, J=7, 8 Hz), 7.75 (1H, d, J=8 Hz), 13.50 (1H, s).

2-Acetyl-3-allyl-1,4-benzenediol (**9b**): Pale yellow crystals from ethanol; mp 78—80 °C. MS; m/z 192 (M^+). IR (KBr); 3400 (OH), 1670 (C=O) cm^{-1}. ^1H NMR ($CDCl_3$); δ=2.11 (3H, s), 2.93 (2H, d, J=6 Hz), 4.33 (1H, s), 4.5—4.6 (2H, m), 5.5—5.6 (1H, m), 6.2—6.3 (2H, m), 13.80 (1H, s).

3a-Acetyl-2-tributylstannyl-2,3,3a,4,9,9a-hexahydro-1*H*-cyclopenta[*b*]naphthalene-4,9-dione (**10a**): Pale yellow needles from hexane-ether; mp 48—49 °C. MS; m/z 475 (M^+−57, ^{120}Sn), 473 (M^+−57, ^{118}Sn). Found: C, 61.28; H, 7.53%. Calcd for $C_{27}H_{40}O_3Sn$: C, 61.04; H, 7.59%. IR (KBr); 1700 (C=O), 1670 (C=O) cm^{-1}. ^1H NMR($CDCl_3$); δ=0.6—0.8 (15H, m), 1.2—1.4 (6H, m), 1.5—1.6 (7H, m), 1.92 (1H, t, J=13 Hz), 2.1—2.3 (5H, m), 3.12 (1H, dd, J=8, 13 Hz), 3.66 (1H, dd, J=8, 10 Hz), 7.75—7.85 (2H, m), 8.05—8.15 (2H, m). ^{13}C NMR($CDCl_3$); δ=8.2, 13.5, 19.8, 26.5, 27.2, 29.0, 34.5, 40.0, 53.8, 77.7, 127.0, 127.1, 133.7, 134.1, 134.7, 194.3, 196.0, 202.5.

3a-Acetyl-2-tributylstannyl-2,3,3a,4,7,7a-hexahydrindene-4,7-dione (**10b**): Yellow oil. MS; m/z 483 ($M+H^+$, ^{120}Sn), 481 ($M+H^+$, ^{118}Sn). Found: C, 57.12; H, 8.15%. Calcd for

$C_{23}H_{38}O_3Sn$: C, 57.40; H, 7.96%. IR (neat); 1700 (C=O), 1680 (C=O) cm^{-1}. ^1H NMR ($CDCl_3$); δ=0.7—0.9 (15H, m), 1.2—1.4 (6H, m), 1.5—1.6 (7H, m), 1.83 (1H, t, J=13 Hz), 2.1—2.3 (5H, m), 2.86 (1H, dd, J=7, 12 Hz), 3.45 (1H, dd, J=6, 10 Hz), 6.7 (2H, m).

2-Acetyl-3-(2-methylallyl)-1,4-naphthoquinone (**11a**): Yellow needles from hexane-ether; mp 53—55 °C. MS; m/z 254 (M^+). High resolution MS; Found: m/z 254.0948. Calcd for $C_{16}H_{14}O_3$: M, 254.0944. ^1H NMR ($CDCl_3$); δ=1.78 (3H, s), 2.45 (3H, s), 3.26 (2H, s), 4.62 (1H, s), 4.83 (1H, s), 7.75—7.85 (2H, m), 8.05—8.15 (2H, m).

2-Acetyl-3-(2-methylallyl)-2,3-epoxy-2,3-dihydro-1,4-naphthoquinone (**12a**): Pale yellow needles from hexane-ether; mp 72—74 °C. MS; m/z 227(M^+−43). Found: C, 71.02; H, 5.07%. Calcd for $C_{16}H_{14}O_4$: C, 71.10; H, 5.22%. IR (KBr); 1720 (C=O), 1690 (C=O), 1685 (C=O) cm^{-1}. ^1H NMR ($CDCl_3$); δ=1.73 (3H, s), 2.37 (3H, s), 2.54 (1H, d, J=16 Hz), 2.75 (1H, d, J=16 Hz), 4.65 (1H, s), 4.81 (1H, s), 7.7—7.8 (2H, m), 7.9—8.0 (2H, m).

2-Hydroxy-3-(2-methylallyl)-1,4-naphthoquinone (**13a**): Yellow crystals from hexane-ether; mp 116—120 °C. MS; m/z 228 (M^+). High resolution MS; Found: m/z 228.0763. Calcd for $C_{14}H_{12}O_3$: M, 228.0786. IR (KBr); 3360 (OH), 1655 (C=O), 1640 (C=O) cm^{-1}. ^1H NMR ($CDCl_3$); δ=1.80 (3H, s), 3.32 (2H, s), 4.73 (1H, s), 4.78 (1H, s), 7.35 (1H, s), 7.65—7.75 (2H, m), 8.05—8.15 (2H, m).

2-Acetyl-3-(2-methylallyl)-1,4-benzenediol (**14b**): Pale yellow crystals from ethanol; mp 78—80 °C. MS; m/z 206 (M^+). High resolution MS; Found: m/z 206.0943. Calcd for $C_{12}H_{14}O_3$: M, 206.0943. ^1H NMR ($CDCl_3$); δ=1.85 (3H, s), 2.58 (3H, s), 4.59 (1H, s), 4.94 (1H, s), 5.28 (1H, s), 6.76 (1H, d, J=8 Hz), 6.94 (1H, d, J=8 Hz), 10.28 (1H, s).

^1H NMR Measurements. 2-Acetyl-1,4-naphthoquinone **1a** (0.03 mmol) and allyltrimethylstannane **2a** (0.04 mmol) were dissolved in benzene-d_6 (0.5 ml) and allowed to stand for 24 h under argon atmosphere in an NMR sample tube. The ^1H NMR measurements were carried out several times during the reaction. Then, the reaction mixture was poured into silica-gel short column, and all fractions were concentrated, dissolved in benzene-d_6, and measured again.

^1H NMR Spectral Data of Products in Benzene-d_6. Compound **15a** (diastereomer A): δ=1.12 (9H, s), 0.93 (1H, dd, J=7, 12 Hz), 0.97 (1H, dd, J=9, 12 Hz), 2.05 (1H, m), 2.26 (1H, m), 2.42 (3H, d, J=2 Hz), 3.13 (1H, ddq, J=6, 11, 2 Hz), 3.74 (1H, m), 7.0—7.2 (2H, m), 8.03 (1H, d, J=7 Hz), 8.44 (1H, d, J=7 Hz).

Compound **15a** (diastereomer B): δ=1.13 (9H, s), 0.90—0.95 (2H, m), 2.44 (3H, d, J=2 Hz), 3.8 (1H, m). Other peaks overlapped and were unable to be analyzed. The ratio A/B was estimated to be 6/1 from integral values of each peak at δ=2.42 and 2.44. Compound **15a** was not isolated.

Compound **16a**: δ=1.66 (3H, s), 2.00 (1H, m), 2.20 (1H, m), 3.25 (1H, dd, J=5, 7 Hz), 4.6—4.7 (2H, m), 5.3—5.4 (1H, m), 7.0—7.2 (2H, m), 7.84 (1H, d, J=8 Hz), 7.96 (1H, d, J=8 Hz).

Compound **17a**: δ=0.24 (9H, s), 2.25 (3H, s), 6.67 (1H, s), 6.9—7.1 (2H, m), 7.95 (1H, d, J=7 Hz), 8.38 (1H, d, J=7 Hz).

Compound **4a**: δ=2.15 (3H, s), 3.14 (2H, d, J=7 Hz), 4.9—5.1 (2H, m), 5.7—5.9 (1H, m), 7.0—7.1 (2H, m), 7.8—7.9 (2H, m).

Compound **5a**: δ=2.09 (3H, s), 2.41 (1H, dd, J=7, 15 Hz), 2.88 (1H, dd, J=7, 15 Hz), 4.9—5.0 (2H, m), 5.8—5.9 (1H, m), 6.9—7.0 (2H, m), 7.7—7.8 (2H, m).

Compound **6a**: δ=−0.03 (9H, s), 1.26 (1H, m), 1.8—2.1 (6H, m), 2.89 (1H, dd, J=8, 13 Hz), 3.64 (1H, dd, J=8, 10 Hz), 7.0—7.1 (2H, m), 8.02 (1H, d, J=7 Hz), 8.15 (1H, d, J=7 Hz).

Compound **8a**: δ=0.95 (1H, s), 2.25 (3H, s), 6.18 (1H, s), 7.2—7.4 (2H, m), 8.21 (1H, d, J=8 Hz), 8.68 (1H, d, J=8 Hz).

References

1) "Comprehensive Organic Chemistry," ed by G. Wilkinson, Pergamon Press, Oxford (1982).

2) M. Pereyre, J. P. Quintard, and A. Rahm, "Tin in Organic Synthesis," Butterworths, London (1987). Y. Yamamoto, *Aldrichimica Acta*, **20**, 45 (1987). "Organotin Compounds in Organic Synthesis," ed by Y. Yamamoto, *Tetrahedron*, **45**, 909 (1989).

3) A. Schweig and U. Weinder, *J. Organomet. Chem.*, **67**, C4 (1967). Y. Naruta, *J. Am. Chem. Soc.*, **102**, 3774 (1980). Y. Naruta, *J. Org. Chem.*, **45**, 4097 (1980). Y. Yamamoto, *Acc. Chem. Res.*, **20**, 243 (1987). A. Gambaro, V. Peruzzo, and D. Marton, *J. Organomet. Chem.*, **258**, 291 (1987). S. E. Denmark, T. Wilson, and T. M. Willson, *J. Am. Chem. Soc.*, **110**, 984 (1988). M. T. Reetz, M. Hullmann, W. Massa, S. Berger, P. Rademacher, and P. Heymanns, *J. Am. Chem. Soc.*, **108**, 2405 (1986).

4) Y. Miyagi, K. Kitagawa, K. Maruyama, and Y. L. Chow, *Chem. Lett.*, **1978**, 33. K. Maruyama, N. Narita, and Y. Miyagi, *Chem. Lett.*, **1978**, 1033. K. Maruyama and N. Narita, *J. Org. Chem.*, **45**, 1421 (1980).

5) S. Arakawa, *J. Org. Chem.*, **42**, 3800 (1977).

6) G. Read and V. M. Ruiz, *J. Chem. Soc., Perkin Trans. 1*, **1973**, 235. G. Read and V. M. Ruiz, *J. Chem. Soc., Perkin Trans. 1*, **1973**, 368.

7) U. Kucklander, U. H. Wahl, W. Poll, and L. Rickerich, *Chem. Ber.*, **121**, 1841 (1988).

8) Y. Naruta, Y. Nishigaichi, and K. Maruyama, *J. Org. Chem.*, **53**, 1192 (1988).

9) H. Uno, *J. Org. Chem.*, **51**, 350 (1986).

10) The coupling constant between the γ-acyl carbon of **6a** and ^{119}Sn was 42 Hz, which is consistent with the cis orientation. See: H. G. Kuivila, J. L. Considine, R. H. Sarma, and R. J. Mynott, *J. Organomet. Chem.*, **111**, 179 (1976). G. Dumartin, J. P. Quintard, and M. Pereyre, *J. Organomet. Chem.*, **185**, C34 (1980).

11) L. F. Fieser, *J. Am. Chem. Soc.*, **48**, 3201 (1927).

12) J. W. Herndon, *J. Am. Chem. Soc.*, **109**, 3165 (1987).

13) All ^1H NMR yields were determined using dichloromethane as an internal standard.

14) Addition of $BF_3 \cdot OEt_2$ to a dichloromethane solution of **6a** resulted in the formation of 2-acetyl-3-allyl-4-oxo-3,4-dihydro-1-naphthol **16a**, but treatment of **6a** with silica gel didn't give **16a**.

15) After standing for 10 days, starting reagents were completely recovered.

16) T. G. Traylor, H. J. Berwin, J. Jerkunica, and M. L. Hall, *Pure Appl. Chem.*, **30**, 599 (1972).

17) It is well known that single electron oxidation of tetraalkylstannane induces cleavage of C-Sn bond to produce alkyl radical and trialkylstannyl cation. See: S. Fukuzumi, K. Mochida, and J. K. Kochi, *J. Am. Chem. Soc.*, **101**, 5961 (1979). B. W. Walther, F. Williams, W. Lau, and J. K. Kochi, *Organometallics*, **2**, 688 (1983). M. C. R. Symons, *Chem. Soc. Rev.*, **1984**, 393.

18) Reduction potentials of acylquinones were measured in CH_3CN with Et_4NClO_4 as supporting electrolyte vs. Ag/Ag^+ (0.1M). E^{red}(peak) **1a**: −0.79 V. **1b**: −0.69 V. **1c**: −0.84 V. **1d**: −0.96 V. **1f**: −0.92 V.

19) W. W. Prichard, *Org. Synth.*, Coll. Vol. 3, 452. G. C. Amin and N. M. Shah, *Org. Synth.*, **28**, 42 (1948). M. C. Kloetzel, R. P. Dayton, and B. Y. Abadir, *J. Org. Chem.*, **20**, 38 (1955). P. R. Hammond, *J. Chem. Soc.*, **1964**, 471.

20) E. A. Abel and R. J. Rowley, *J. Organomet. Chem.*, **84**, 199 (1975).

21) Y. Naruta, Y, Nishigaichi, and K. Maruyama, *Chem. Lett.*, **1986**, 1857.

Use of Axially Chiral 2′-Methoxy-1,1′-binaphthyl-2-carboxylic Acid as Chiral Derivatizing Agent for Discrimination of Enantiomeric Alcohols and Amines by ^{1}H NMR

Sotaro MIYANO,* Shin-ichi OKADA, Hiroki HOTTA, Masayuki TAKEDA, Takatsugu SUZUKI, Chizuko KABUTO,† and Fujiko YASUHARA††

Department of Biochemistry and Engineering, Faculty of Engineering, Tohoku University, Aramaki-Aoba, Aoba-ku, Sendai 980

†Department of Chemistry, Faculty of Science, Tohoku University, Aramaki-Aoba, Aoba-ku, Sendai 980

††Department of Chemistry, College of General Education, Tohoku University, Kawauchi, Aoba-ku, Sendai 980

(Received July 28, 1989)

Axially chiral 2′-methoxy-1,1′-binaphthyl-2-carboxylic acid (**1**) was effectively utilized as chiral derivatizing agent for discrimination of enantiomeric alcohols and amines by ^{1}H NMR with the aid of Eu(fod)$_3$. Among a pair of the diastereomeric esters or amides prepared from (a*S*)-**1** and an α-chiral alcohol or amine, the methoxyl protons of the (a*S*,*R*)-diastereomer showed the larger lanthanoid-induced downfield shift than those of the (a*S*,*S*)-counterpart. Thus, addition of up to 0.5—1.0 equiv amount of Eu(fod)$_3$ caused base-line separation of those protons, allowing determination of the enantiomeric purities and assignment of the absolute configurations of the enantiomeric alcohols and amines. An X-ray crystallographic analysis of the amide ((a*S*,*S*)-**2**) obtained from (a*S*)-**1** and (*S*)-1-phenylethylamine showed structural resemblance between the amides and esters of **1**. Steric models which explain the NMR behavior of the diastereomeric esters and amides are presented based on X-ray analyses. Also reported are two methods to regenerate free acid **1** from amide **2** to afford axially homochiral **1**.

Recently a variety of chiral derivatizing agents have been developed for determination of absolute configurations and enantiomeric purities of optically active compounds,[1] among which Mosher's α-methoxy-α-trifluoromethylphenylacetic acid (MTPA) has been most widely used for discrimination by NMR.[2] In our previous paper[3] we have reported the optical resolution of 2′-methoxy-1,1′-binaphthyl-2-carboxylic

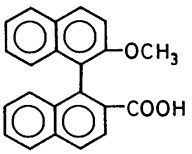

1

acid (**1**) and the use of atropisomeric **1** as highly efficient chiral derivatizing agent for differentiation of enantiomeric alcohols and amines by high-performance liquid chromatography (HPLC). In our continuing efforts to extend the scope and the utility of **1** as a chirality-recognizing element, we have studied ^{1}H NMR behavior of the diastereomeric esters and amides of **1**. Herein we wish to report that the methoxyl group serves as a chiral probe, as the MeO protons of a pair of the diastereomeric esters or amides were nicely separated at 60 MHz by addition of up to 0.5 to 1.0 equiv amount of Eu(fod)$_3$ (tris(6,6,7,7,8,8,8-heptafluoro-2,2-dimethyl-3,5-octanedionato)europium). Also reported are alternative procedures for optical resolution of **1** by fractional crystallization of the diastereomeric *N*-(1-phenylethyl)amides (**2**).

Results and Discussion

^{1}H NMR Study of the Diastereomeric Esters and Amides of (a*S*)-1.[4] The preparation of the samples of

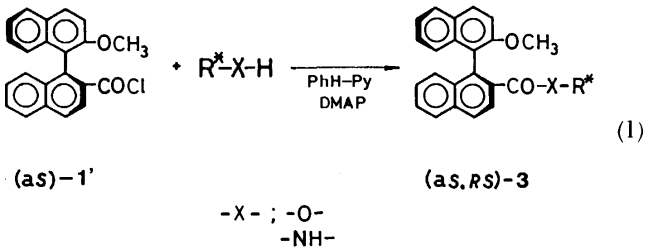

(1)

diastereomeric esters or amides of (a*S*)-**1** from partially active alcohols or amines has been reported in the previous paper unless otherwise noted (Eq. 1).[3] NMR measurements of those samples showed that the shift differences of respective ^{1}H absorptions of a pair of the diastereomers were not always large enough to enable quantitative analysis at 60 MHz (Table 1). However, it was found that the lanthanoid-induced downfield shifts of the MeO signals of the (a*S*,*R*)-diastereomers were consistently larger than those of the corresponding (a*S*,*S*)-isomers, causing base-line separation of those signals by addition of up to 0.5 to 1 equiv amount of Eu(fod)$_3$. Results summarized in Table 1 show that axially chiral **1** is useful as chiral derivatizing agent for discrimination of enantiomeric alcohols and amines not only by HPLC but also by ^{1}H NMR. A potential problem of kinetic resolution by use of **1** has been discussed in the previous paper.[3] Emphasis should be placed on the discrimination of the amide diastereomers (vide infra). As a typical example, Fig. 1 shows the induced shift of the MeO signals of *N*-[(*R*)- and (*S*)-1-methylhexyl]amide of (a*S*)-**1** ((a*S*,*R*)- and (a*S*,*S*)-**4**)) by successive addition of Eu(fod)$_3$. It should be noted that addition of Eu(fod)$_3$ did not apparently cause collapse of the MeO signals; although the lanthanoid-induced shift (LIS) method

Table 1. Chemical Shifts of MeO Protons of the Diastereomers Derived from (aS)-**1** and Enantiomeric Alcohols and Amines[a)]

Run	Substrate	Chemical shift of MeO (δ)			
				Eu(fod)$_3$ added (1 equiv)	
		(a*S*,*R*)	(a*S*,*S*)	(a*S*,*R*)	(a*S*,*S*)
1	Me HO-CH-Ph	3.15	3.19	4.84	4.42
2	Menthol	3.28	3.23	4.70	4.00
3	Borneol	3.27	3.25	4.58	4.37
4	Me HO-CH-Et	3.23	3.22	4.99	4.79
5	Me HO-CH-CHMe$_2$	3.11	3.13	5.18	4.71
6	Me HO-CH-C$_6$H$_{13}$	3.27	3.23	5.07	4.71
7	α-Tetralol	3.09	3.23	5.00	4.82
8	Me H$_2$N-CH-Ph	3.04	3.12	5.47	5.19
9	Me H$_2$N-CH-(1-Naphthyl)	2.86	2.97	4.97	4.56
10	Me H$_2$N-CH-(2-Naphthyl)	3.00	3.09	5.06	4.89
11	Me H$_2$N-CH-Et	3.17	3.19	5.04	4.81
12	Me H$_2$N-CH-C$_5$H$_{11}$	3.19	3.19	5.43	4.99
13	Me H$_2$N-CH-C$_6$H$_{13}$	3.20	3.18	5.91	4.92
14	Bornylamine	3.21	3.20	5.12	4.65
15	Isobornylamine	3.19	3.21	6.11	5.16
16	Me H$_2$N-CH-⬡	3.19	3.19	6.52	5.22
17	CH$_2$Ph H$_2$N-CH-CH$_2$OMe	3.28	3.20	5.00	4.72
18	Me H$_2$N-CH$_2$-CH-Ph	3.10	3.10	6.13	5.50
19	Et H$_2$N-CH$_2$-CH-C$_4$H$_9$	3.21	3.21	5.26	5.13
20	3-(Aminomethyl)pinane	3.21	3.21	5.86	5.36

a) Measured in C_6D_6 using TMS as internal standard at 60 MHz.

has been successfully applied to diastereomeric MTPA esters for discrimination of a wide range of alcohols,[2,5)] it has rarely been used for MTPA amides because of the broadening of the signals by addition of Eu(fod)$_3$.[6)] Table 1 also contains the examples of the discrimination of β-chiral amines[7)] (Runs 18—20).

X-Ray Crystallographic Analysis of (a*S*,*S*)-2. Figure 2 shows an ORTEP drawing of (a*S*,*S*)-**2**. It was shown that the dihedral angle θ between the two naphthalene rings is 97.5°, and that the -CO-NH-CH- atoms are almost on a same plane, the -CO-NH- linkage being *s*-trans conformation and the dihedral angle ϕ of C_1-C_2-C=O being 52.6° as schematically depicted in Fig. 3. The structure is similar to that of (−)-menthyl ester of (a*S*)-**1** except that the plane which contains the ester linkage -CO-O-CH- is almost on the same plane of the relevant naphthalene ring (ϕ=0—10°).[3)] In case of the amide, the deviation of the dihedral angle ϕ from coplanarity with the naphthalene ring seems to be caused by the steric repulsion between the amide proton and the other naphthalene ring (Fig. 3). In any event, these X-ray analyses suggest the structural resemblance between the amides and the esters derived from axially chiral **1**.

Configuration Correlation Models to Explain the Lanthanoid-Induced Shifts. The lanthanoid-induced shifts of the diastereomeric MTPA esters have been rationalized in terms of the steric interactions for the

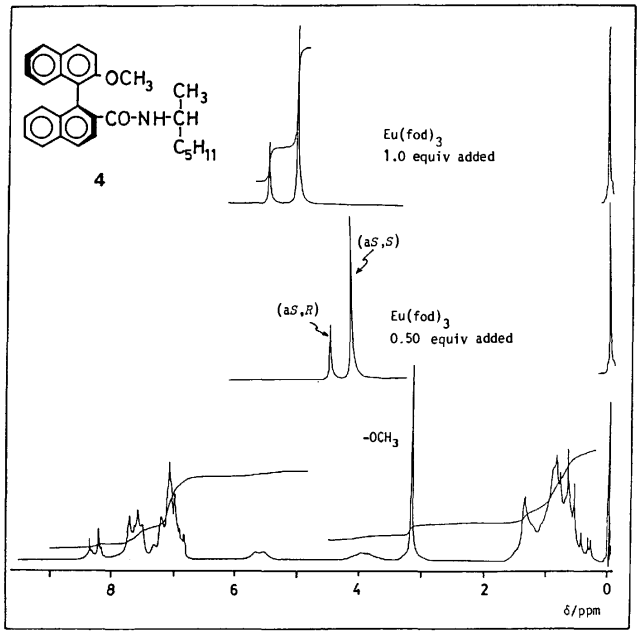

Fig. 1. ^{1}H NMR spectra of a pair of the diastereomeric amides prepared from (*S*)-2-heptanamine (50% ee) and (a*S*)-**1** in the presence or absence of Eu(fod)$_3$.

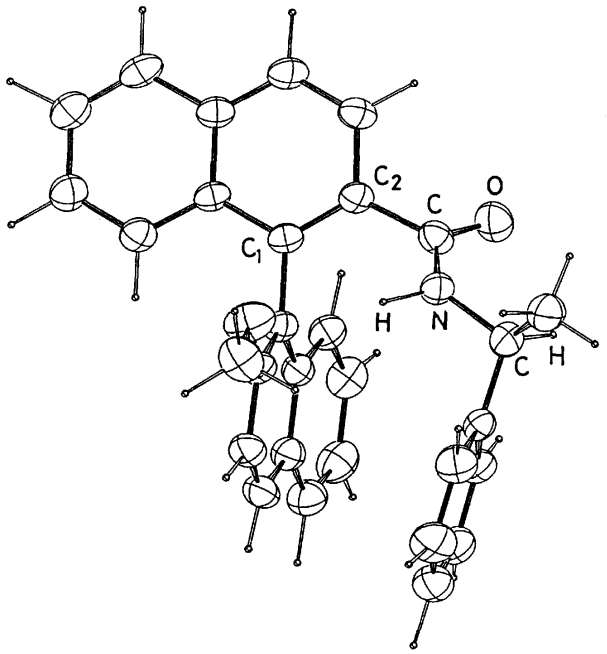

Fig. 2. ORTEP drawing of (a*S*,*S*)-**2**.

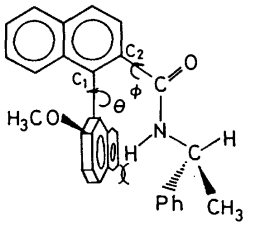

Fig. 3. Schematic view of crystal structure of (a*S*,*S*)-**2**.

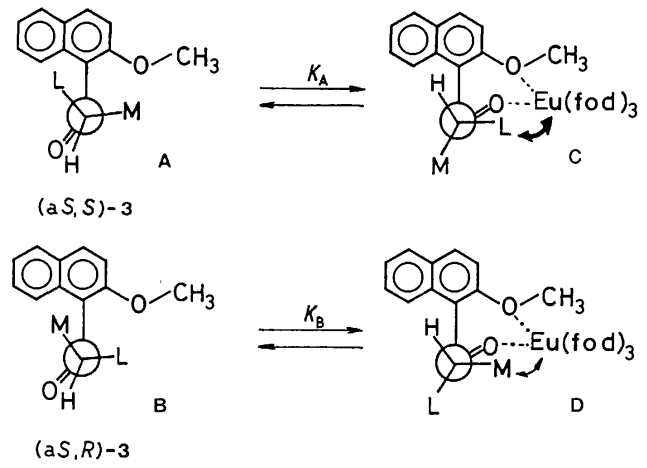

Scheme 1.

complex formation between the esters and Eu(fod)$_3$.[2,5] Application of the models with slight modifications to the diastereomers of α-chiral esters and amides of **1** (**3**) also explains the shift behavior listed in Table 1 (Scheme 1): On the basis that preferred conformations of these diastereomers in solutions are deducible from the X-ray crystallographic analyses as suggested in the previous paper,[3] the conformations of (a*S*,*S*)- and (a*S*,*R*)-**3** are schematically depicted as structures **A** and **B**, respectively, where L and M stand for the largest and the medium substituent on the carbinyl (C-1) carbon of the original alcohol or amine. Structures **C** and **D** represent empirical models of the complexes of **3** with Eu(fod)$_3$, where the esters or amides coordinate to Eu(fod)$_3$ by virtue of the two oxygen atoms from the methoxyl and carbonyl group of the (a*S*)-2′-methoxy-1,1′-binaphthylcarboxylic acid moiety. In the complex **C**, the largest ligand L is arrayed toward the Eu-metal, while in the complex **D** the medium ligand M directs toward the metal-center posing less steric repulsions. Thus, the complexation constant K_A for the formation of **C** may be smaller than that (K_B) for the formation of **D**, inducing the larger downfield shifts of the MeO signals for the (a*S*,*R*)-**3** complexes as are observed. The reasoning could not be applied to 1-methoxy-3-phenyl-2-propanamine (Run 17); the steric bulk of methoxymethyl group is seemingly smaller than that of benzyl group, which does not agree with the priority order of the two groups by the *R* and *S* designation. However, this exceptional behavior of the amine may be

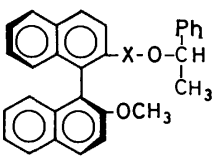

(a*S*,*RS*)-**5** ; -X- = -CO-

(a*S*,*RS*)-**6** ; -X- = -CH$_2$-

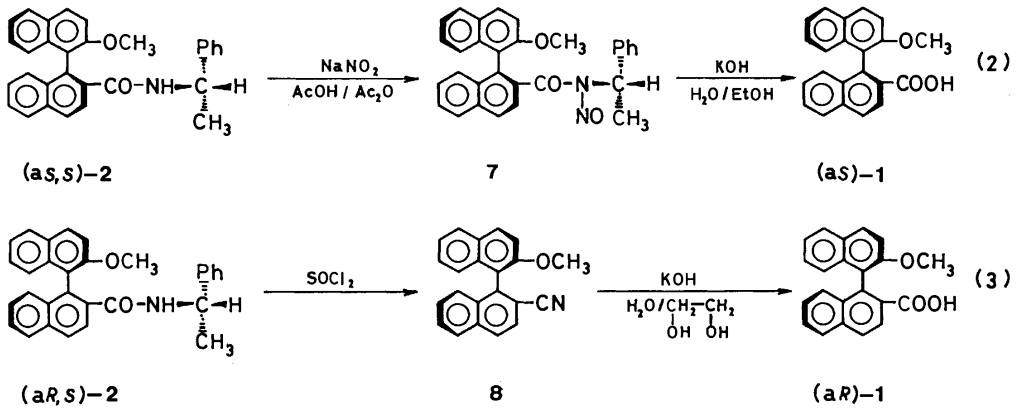

explained by assuming that the 1-methoxyl group of the (a*S*,*S*)-amide effectively competes with the binaphthyl 2′-methoxyl group for the coordination site of Eu (**C**; L=CH_2OMe), thus reducing the magnitude of the lanthanoid-induced shift of the latter MeO protons.

To demonstrate the importance of the coordination to Eu(fod)$_3$ by the carbonyl oxygen as well as the 2′-methoxyl oxygen, the shift behavior of ester diastereomers **5** was compared with that of the ether counterparts **6**. As Table 1 shows, methoxyl groups of diastereomeric **5** are good probes for discrimination of the 1-phenylethyl moiety with the aid of Eu(fod)$_3$. On the other hand, the magnitude of the induced shifts of the MeO protons of (a*S*,*S*)- and (a*S*,*R*)-**6** were not only small but also almost identical on addition of up to 2 equiv amounts of Eu(fod)$_3$ (see Experimental).

Optical Resolution of 1 via *N*-(1-Phenylethyl)-amides. Racemic **1** was converted into the acid chloride (**1′**), which was then treated with (*S*)-1-phenylethylamine to give the mixture of diastereomeric amides ((a*S*,*S*)- and (a*R*,*S*)-**2**)) in quantitative yield. The mixture was crystallized twice from hexane-ethyl acetate to give diastereomerically pure (a*S*,*S*)-**2** as fine cubic crystals in a 55% yield based on one enantiomer present in the racemate; suitable one of the crystals was used for X-ray analysis (vide supra). Subsequent column chromatography of the mother liquor readily afforded (a*R*,*S*)-**2** of 100% diastereomeric excess (de) in a 63% yield as the first eluting component.

The amide bond of **2** was highly resistant to acidic or alkaline hydrolysis,[8] but regeneration of the axially chiral acids was achieved by either of the two routes without racemization. These are, 1) nitrosation to *N*-nitroso amide **7** followed by alkaline hydrolysis (Eq. 2),[9] and 2) conversion into nitrile **8** by treatment with thionyl chloride (the von Brawn reaction)[10] followed by alkaline hydrolysis (Eq. 3).[11] Although **1** can be resolved by column-chromatographic separation of the diastereomeric esters,[3] it should be pointed out that the amide routes disclosed here enable treatment of a larger amount of the diastereomeric mixture because of the crystallization out of one of the diastereomers and better separability of the amides on silica-gel column than that of the ester diastereomers.[12]

Experimental

Instruments and materials were those disclosed previously unless otherwise noted.[3] Partially active (*R*)-2-phenyl-1-propanamine was prepared by referring to a literature procedure;[13] IR (KBr) 3500—3300 (br) and 900—800 (br); $[\alpha]_D$ +8.0° (*c* 1.38, EtOH) (lit,[14] $[\alpha]_D$ max +34.0° (*c* 1.0, EtOH)). Commercial (*S*)-3-(aminomethyl)pinane (HCl salt) and (*S*)-2-ethyl-1-hexanamine (HCl salt) were allowed to react with partially active (a*S*)-**1′** (ca. 50% ee) as before[3] to prepare diastereomeric amide samples for ^{1}H NMR measurements.

NMR Shift Studies. Discrimination of 2-heptanamine enantiomers is representative. Partially active (*S*)-2-heptanamine (prepared to be ca. 50% ee by mixing (*S*)-isomer with the racemate) was treated with (a*S*)-**1′** as before to give a mixture of the diastereomeric amides ((a*S*,*S*)- and (a*S*,*R*)-**4**).[3] A part of the sample (15 mg, 0.035 mmol) was dissolved in ca. 0.40 ml of C_6D_6. ^{1}H NMR spectra of the sample were taken with successive addition of 1 M† solution of Eu(fod)$_3$ in C_6D_6, and the magnitudes of the induced shift of MeO signals were recorded (Fig. 1). The further shifted, smaller MeO signal was readily assigned to (a*S*,*R*)-**4** by comparing the peak areas, and the diasteromeric composition was calculated to be 49.7% de by integrating those MeO signals.

Preparation of (a*S*,*RS*)-6 and Its Shift Study. Diastereomerically pure (−)-menthyl ester of (a*S*)-**1**[3] (0.17 g, 0.36 mmol) was boiled with $LiAlH_4$ (0.30 g) in ether (10 ml) for 3 h. The reaction was worked up as usual, and TLC on silica gel/$CHCl_3$ gave 92 mg of (a*S*)-2-hydroxymethyl-2′-methoxy-1,1′-binaphthyl (**9**) (81%); $[\alpha]_D^{23}$ +75.0° (*c* 1.09, $CHCl_3$) (lit,[15] for (a*R*)-isomer of 96% ee, $[\alpha]_D$−71.4° (*c* 0.15, $CHCl_3$)). To a solution of **9** (90 mg, 0.29 mmol) in acetic acid (15 ml) was added dropwise 0.80 ml of 48% HBr at 80 °C for 30 min, and the mixture was stirred at this temperature for another 30 min. The mixture was diluted with 70 ml of water, and treated as usual. Volatiles were removed in vacuo to give (a*S*)-2-bromomethyl-2′-methoxy-1,1′-binaphthyl (104 mg, 94%), which was dissolved in DMF (5 ml). This was added dropwise to a solution of sodium (*S*)-1-phenylethoxide in 5 ml of DMF (prepared from (*S*)-1-phenylethanol of ca. 30% ee (35 mg, 0.29 mmol) and NaH). The mixture was stirred overnight at ambient temperature,

† 1 M=1 mol dm^{-3}.

and then heated at 80 °C for 10 h. After a usual work-up, (a*S*,*RS*)-**6** enriched in (a*S*,*S*)-isomer was obtained by TLC on silica gel/$CHCl_3$ (70 mg, 61%); ^1H NMR δ=1.20 and 1.25 (3H, d, J=6.9 Hz, C-CH_3), 3.04 and 3.12 (3H, s, O-CH_3), 3.8—4.6 (3H, m, CH and CH_2), and 6.8—8.2 (17H, m, Ar-H).

The methoxyl protons of (a*S*,*R*)-**6** which appeared at δ 3.04 shifted to δ 3.12 and 3.17 on addition of 1 and 2 equiv amounts of Eu(fod)$_3$, respectively. On the other hand, those of (a*S*,*S*)-**6** which appeared at δ 3.12 shifted to δ 3.20 and 3.24 on addition of 1 and 2 equiv Eu(fod)$_3$, respectively.

Preparation and Resolution of 2. To a stirred solution of (*S*)-1-phenylethylamine (12.9 g, 107 mmol) and 4-dimethylaminopyridine (1.25 g) in benzene (250 ml) was added dropwise a solution of acid chloride **1′** (prepared from 16.7 g of (±)-**1** (50.9 mmol)) in benzene (250 ml) under a nitrogen atmosphere at ambient temperature. The mixture was stirred at this temperature for 5 h, and then heated at 60 °C for 3 h. The reaction mixture was diluted with benzene, washed successively with 2 M HCl, 1 M Na_2CO_3, and water, and dried over Na_2SO_4. Evaporation of volatiles under reduced pressure gave 22.8 g of a crude mixture of the diastereomeric amides (104%). HPLC of the mixture on a silica-gel column eluting with hexane-2-propanol (3%) showed two peaks of (a*S*,*R*)- and (a*S*,*S*)-**2** in the ratio of 50.06:49.94 (by absorptions at 254 nm) in the order of increasing retention volume. The mixture was crystallized from hexane-ethyl acetate (8/5) to give 7.85 g of (a*S*,*S*)-**2** of 93% de, and recrystallization of which from the same solvent system afforded 6.08 g of diastereomerically pure (a*S*,*S*)-**2** (55% based on one of the enantiomers of **1**). Concentration of the recrystallization mother liquor gave additional 1.09 g of (a*S*,*S*)-**2** (98.4% de) as crystals, and 0.50 g of (a*S*,*S*)-**2** of 0.8% de was recovered from the filtrate.

The mother liquor of the initial crystallization was concentrated and subjected to column chromatography on silica gel (825 g) eluting with hexane-ethyl acetate with varing the composition of the eluent from 5/1 to 5/3, to give five fractions as follows: (1) 6.86 g (63% yield), (a*R*,*S*), 100% de; (2) 1.32 g, (a*R*,*S*), 86.0% de; (3) 2.16 g, (a*S*,*S*), 12.6% de; (4) 1.24 g, (a*S*,*S*), 65.4% de; (5) 0.14 g, (a*S*,*S*), 93.4% de. Total recovery of optically active **2** amounted to 89% yield based on the starting (±)-**1**.

(a*S*,*S*)-2: mp 161—163 °C; $[\alpha]_D^{23}$ +72.7° (c 1.0, $CHCl_3$); IR (KBr) 3475, 1642, 1510, and 1246 cm^{-1}; ^1H NMR (C_6D_6, TMS) δ=0.89 (3H, d, J=6.7 Hz, CH_3), 3.12 (3H, s, OCH_3), 4.8—5.2 (1H, m, CH), 6.2—6.5 (1H, br, NH), and 6.5—8.4 (12H, m, Ar-H).

(a*R*,*S*)-2: mp 61—65 °C; $[\alpha]_D^{23}$+122.4° (c 1.0, $CHCl_3$); IR (KBr) 3395, 1654, 1505, and 1247 cm^{-1}; ^1H NMR (C_6D_6, TMS) δ=0.67 (3H, d, J=6.7 Hz, CH_3), 3.04 (3H, s, OCH_3), 4.7—5.3 (1H, m, CH), 5.9—6.4 (1H, br, NH), and 6.5—8.4 (12H, m, Ar-H).

Regeneration of 1 from 2. Typical examples are as follows.

Method A: To a stirred mixture of 5.87 g of (a*S*,*S*)-**2** (13.6 mmol) in acetic acid (13.6 ml) and acetic anhydride (68.0 ml) was added portionwise 24.4 g of $NaNO_2$ (0.299 mol) over 5 h at 0 °C, followed by stirring for another 5 h at this temperature. After the mixture was allowed to stand for 20 h at ambient temperature, it was heated at 40 °C for 4 h. The mixture was diluted with water (150 ml), extracted with portions of ether. The combined organic layers were washed with 5% aq Na_2CO_3 and then with water, and dried over Na_2SO_4. Evaporation of volatiles in vacuo left *N*-nitroso amide **7** (5.5 g), which was directly boiled for 3 h in a solution of KOH (30 g) in ethanol (300 ml) and water (30 ml). The mixture was diluted with 0.5 M NaOH (1 dm^{-3}) and extracted with portions of ether. The aqueous layer was made acidic by addition of concd HCl, and precipitated solid was taken into ether and worked up as usual to give 3.40 g of (a*S*)-**1** (76%): $[\alpha]_D^{23}$ −24.6° (c 1.05, THF) (lit,[16] $[\alpha]_D^{25}$ −25.98° (c 1.22, THF)); IR (KBr) 3045 (br), 1685, and 1260 cm^{-1}; ^1H NMR (DMSO-d_6, TMS) δ=3.60 (3H, s, OCH_3), 6.5—8.2 (12H, m, Ar-H), and 12.2 (1H, br, COOH). The sample was more than 99.5% ee as evidenced by HPLC on Pirkle column as methyl ester eluting with hexane-2-propanol (2%).

Method B: A sample of 670 mg of (a*R*,*S*)-**2** (1.55 mmol, >99.5% de) was boiled in ca. 5 ml of thionyl chloride for 3 h. After careful evaporation of excess thionyl chloride, the residue was diluted with ether, washed successively with 2 M NaOH, 2M HCl, and then water, and dried over Na_2SO_4. Trap-to-trap distillation gave a small amount of (*R*)-1-phenylethyl chloride, $[\alpha]_D^{23}$ +1.6° (c 6.84, $CHCl_3$), leaving 2-cyano-2′-methoxy-1,1′-binaphthyl **8** as the residue, IR (KBr) 2300 cm^{-1}. The residue was boiled for 6 h in a solution of KOH (10 g) in 45 ml of a 8:1 mixture of ethylene glycol and water. After the reaction, the mixture was diluted with water and extracted with ether. The aqueous phase was made acidic by addition of concd H_2SO_4. White precipitate was extracted with ether and worked up as usual to give 0.34 g of (a*R*)-**1** (67%), IR (KBr) 1685 cm^{-1}, which was enantiomerically pure as evidenced by HPLC on Pirkle column as above.

Crystal Structure Determination of (a*S*,*S*)-2. A colorless crystal of (a*S*,*S*)-**2** with the dimensions of 0.10×0.20×0.25 mm was used for the data collection on a Rigaku-Denki automated four-circle diffractometer (Rigaku AFC-5R), equipped with a rotating anode (40 kV, 200 mA), using graphite monochromated Cu $K\alpha$ radiation (λ=1.5418 Å). Crystal data are as follows: M.F.=$C_{30}H_{25}NO_2$, M.W.=431.5, orthorhombic space group $P2_12_12_1$, a=10.119(1), b=24.581(3), c=9.250(1) Å, V=2300.8(5) Å^3, Z=4, D_{calcd}=1.25 g cm^{-3}, μ(Cu $K\alpha$)=5.724 cm^{-1}. A total of 1921 reflections within 2θ=126° were collected by the θ-2θ scan mode at a 2θ scan rate of 4° min^{-1}. The structure was solved by the direct method using RANTAN81 program with some modifications.[17] After the block-diagonal least-squares refinement for non-hydrogen atoms with anisotropic temperature factors, hydrogen atoms were almost located from the difference Fourier map, some methyl hydrogen atoms were calculated, and then included in the refinement with isotropic temperature factors. The final R factor was 0.060 (R_w=0.064) for 1781 reflections with $|F_o|>3\sigma(|F_o|)$.

The atomic scattering factors from the International Tables for X-ray Crystallography[18] were used. All the computations were carried out by a ACOS 2000 computer using the applied library program of UNICS III system.[19]

Tables of final atomic coordinates, temperature factors, bond lengths and bond angles, and the F_o—F_c structure factors are kept at the Chemical Society of Japan (Document No.8907).

The authors wish to express their deep gratitude to Professor Emeritus Harukichi Hashimoto, Tohoku

University, and Professor Shozo Yamaguchi, Tohoku Gakuin University, for their encouragement and helpful suggestions throughout this study. This work was partially supported by the Asahi Glass Foundation for Industrial Technology, and a Grant-in-Aid for Scientific Research (No. 62550539) from the Ministry of Education, Science and Culture.

References

1) For a general overview, see: "Asymmetric Synthesis," ed by J. D. Morrison, Academic Press, New York (1983), Vol. 1.

2) S. Yamaguchi, "Asymmetric Synthesis," ed by J. D. Morrison, Academic Press, New York (1983), Vol. 1, p. 125.

3) S. Miyano, S. Okada, H. Hotta, M. Takeda, C. Kabuto, and H. Hashimoto, *Bull. Chem. Soc. Jpn.*, **62**, 1528 (1989).

4) In this paper, axial chirality is denoted by prefix "a" as in a*S* or a*R*.

5) S. Yamaguchi, F. Yasuhara, and K. Kabuto, *Tetrahedron*, **32**, 1363 (1976); K. Kabuto, F. Yasuhara, and S. Yamaguchi, *Tetrahedron Lett.*, **25**, 5801 (1984).

6) Recent examples of NMR-discrimination of amines by derivatization: A. Nabeya and T. Endo, *J. Org. Chem.*, **53**, 3358 (1988); D. Terunuma, M. Kato, M. Kamei, H. Uchida, S. Ueno, and H. Nohira, *Bull. Chem. Soc. Jpn.*, **59**, 3581 (1986); K. Saigo, K. Sekimoto, N. Yonezawa, F. Ishii, and M. Hasegawa, *ibid.*, **58**, 1006 (1985).

7) Herein, "β-chiral" means that an amine or alcohol has the pertinent chiral center at the C-2 position, while "α-chiral" at the C-1 position.

8) F. X. Webster, J. G. Millar, and R. M. Silverstein, *Tetrahedron Lett.*, **27**, 4941 (1986).

9) E. H. White, *J. Am. Chem. Soc.*, **77**, 6008 (1955).

10) W. R. Vaughan and R. D. Carlson, *J. Am. Chem. Soc.*, **84**, 769 (1962).

11) S. Ôi, Y. Matsuzaka, J. Yamashita, and S. Miyano, *Bull. Chem. Soc. Jpn.*, **62**, 956 (1989).

12) Cf., G. Helmchen, G. Nill, D. Flockerzi, W. Schühle, and M. S. K. Youssef, *Angew. Chem., Int. Ed. Engl.*, **18**, 62 (1979), and literatures cited therein.

13) H. Biere, C. Rufer, H. Ahrens, O. Loge, and E. Schröder, *J. Med. Chem.*, **17**, 716 (1974); P. Newman, "Optical Resolution Procedures for Chemical Compounds," Optical Resolution Information Center, Manhattan Collge, Riverdale, New York (1978), Vol. 1, p.142.

14) W. R. Brode and M. S. Raasch, *J. Am. Chem. Soc.*, **64**, 1449 (1942).

15) A. I. Meyers and K. A. Lutomski, *J. Am. Chem. Soc.*, **104**, 879 (1982).

16) J. M. Wilson and D. J. Cram, *J. Org. Chem.*, **49**, 4930 (1984).

17) Y. Jia-xing, *Acta Crystallogr., Sect. A*, **37**, 642 (1981); **39**, 35 (1983).

18) "International Tables for X-ray Crystallography," Kynoch Press, Birmingham (1974), Vol. 4, p. 72.

19) T. Sakurai and K. Kobayashi, *Rep. Inst. Phys. Chem. Res.*, **55**, 69 (1979).

Stereoselective Synthesis of Conjugated 2,4-Alkadienoates via the Palladium-Catalyzed Cross-Coupling of 1-Alkenylboronates with 3-Bromo-2-alkenoates

Teiji YANAGI, Takayuki OH-E, Norio MIYAURA, and Akira SUZUKI*
Department of Applied Chemistry, Faculty of Engineering, Hokkaido University, Sapporo 060
(Received July 28, 1989)

(2*E*,4*E*)-, (2*Z*,4*E*)-, and (2*E*,4*Z*)-2,4-Alkadienoates can be synthesized in high yields by the cross-coupling of ethyl (*E*)-3-bromoacrylate, methyl (*E*)-3-bromo-2-methylpropenoate, ethyl (*Z*)-3-bromocrotonate,1-bromo-2-(ethoxycarbonyl)cyclohexene, and 4-bromocoumarin with 2-[(*E*)-1-alkenyl]-1,3,2-benzodioxaboroles or diisopropyl (*Z*)-1-hexenylboronate in the presence of 3 mol% of $Pd(OAc)_2$, 6 mol% of PPh_3, and 2 equivalents of Na_2CO_3 or K_2CO_3 in alcoholic solvents while retaining the original configuration of the double bonds in β-bromo esters and 1-alkenylboronates. Although the coupling reaction with 1-hexenylboronate with (*Z*)-3-bromoacrylate gave a mixture of ethyl (2*Z*,4*E*)- and (2*E*,4*E*)-nonadienoates in a ratio of 63 : 37, it was found that the use of bis(diphenylphosphino)ferrocene as a ligand of palladium brought about the stereoselective coupling under mild conditions.

2,4-Alkadienoic acid esters are versatile intermediates for a variety of chemical reactions such as Diels-Alder, and are also frequently found in skeletons of natural products. The Wittig or Horner olefin synthesis[1a] provides the most general and flexible approach for the synthesis of stereoisomers of these esters. Conjugated addition of vinylcopper reagents to acetylenic esters also gives a particularly facile route to stereodefined 2,4-dienoates.[1b,c] Although such methods have their own excellence, the scope of these reactions has still been limited to the synthesis of one or two stereoisomers among four, or they have often suffered the disadvantage that an accurate estimate of the stereochemical course of reaction is difficult. Recently, we have reported[2] a stereoselective synthesis of alkadienes and trienes by the palladium-catalyzed cross-coupling reaction of 1-alkenylboronates with 1-halo-1-alkenes. Synthesis of conjugated dienones[3] by the reaction of 1-alkenylboronates with 3-halo-2-alken-1-ones was also demonstrated. In this paper, we describe the development of the reaction for the synthesis of stereodefined 2,4-alkadienoates (**5**, **8**, and **11**)[4] as shown in Eqs. 2—4.

1 2 3

4 5

The cross-coupling reaction of 1-alkenylboron compounds with organic halides proceeds in the presence of a suitable base and palladium catalyst. The organic halides with electron-withdrawing groups such as 3-bromoacrylate are highly susceptible to SN2 displacement at the bromine position with base or saponification of the ester group. For example, the reaction of 2-(1-hexenyl)-1,3,2-benzodioxaborole with 3-bromoacrylate in the presence of 3 mol% of $Pd(PPh_3)_4$ and 2 equivalents of sodium ethoxide, such reaction conditions of which are employed in most cases of the coupling reaction[2] of 1-alkenylborates, lead to extremely fast formation of 3-ethoxyacrylate without any formation of the desired coupling product. Thus, the conditions used for usual haloalkenes can not be applicable for such substrates. Although relatively strong bases such as NaOH or NaOR were required for the coupling of 1-alkenylborates with unfunctionalized haloalkenes, we found that Na_2CO_3 or K_2CO_3 suspended in an alcoholic solvent was effective for the reaction with 3-bromoacrylate. A combination of palladium(II) acetate and two equivalents of triphenylphosphine was recognized to be more effective than $Pd(PPh_3)_4$ commonly used. Thus, we used the conditions using $Pd(OAc)_2$ (3 mol%), PPh_3 (6 mol%), and Na_2CO_3 or K_2CO_3 (2 equivalents) in refluxing methanol or ethanol as a general procedure for the present reaction. The representative results are summarized in Table 1.

(*E*)-1-Alkenylboronates can be most conveniently prepared by hydroboration[5] of alkynes with catecholborane (1,3,2-benzodioxaborole) (Eq. 1). 2-[(*E*)-1-Alkenyl]-1,3,2-benzodioxaboroles derived from terminal and internal alkynes gave 2,4-alkadienoates in good yields by the reaction with (*E*)-3-bromoacrylate, their methylated derivatives, or cyclic α,β- unsaturated β-bromo esters. The dienoates thus obtained were indicated to be (2*E*,4*E*)-isomers by ^1H NMR and GLC analysis, and their isomeric purity is 99% in each case.

We previously reported[2a] that (*Z*)-1-alkenylboronates couple with 1-halo-1-alkenes preserving their *Z*-configuration. (*Z*)-1-Alkenylboronates[6] are readily prepared by the hydroboration of 1-bromo-1-alkynes with dibromoborane-dimethyl sulfide, followed by the reaction with 2-propanol and then with

Table 1. Synthesis of 2,4-Alkadienoate

Run	1-Alkenylboronate (3)		Haloester	Conditions[a]	Product	Yield/%[b]
	R^1=	R^2=				
1	C_6H_{13}	H	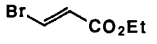	A	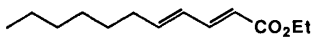	89(>99)
2	$Cl(CH_2)_4$-	H	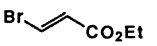	A	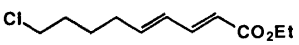	71(>99)
3	C_2H_5	C_2H_5		A	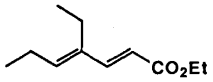	88(>99)
4	C_4H_9	H	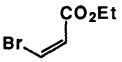	B	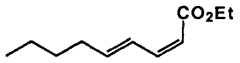	73(>95)
5	C_4H_9	H	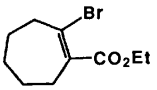	C	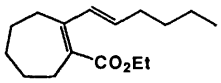	53(>99)
6	C_4H_9	H	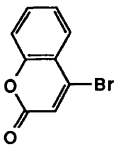	C	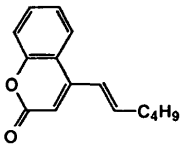	88(>(99)
7	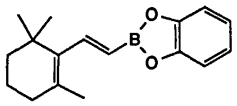		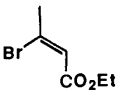	C	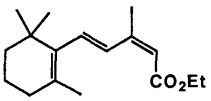	43(>98)
8	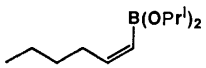		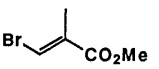	D	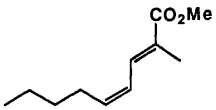	95(>98)

a) The coupling reactions are conducted under the following conditions. A: $Pd(OAc)_2$ (3 mol%), PPh_3 (6 mol%), and Na_2CO_3 (2 equiv) in 75% ethanol at refluxing temperature for 4 h. B: $Pd(OAc)_2$ (3 mol%), DPPF (3 mol%), and K_2CO_3 (2 equiv) in 75% ethanol for 24 h at room temperature. C: $Pd(OAc)_2$ (3 mol%), PPh_3 (6 mol%), and K_2CO_3 (2 equv) in dry ethanol at refluxing temperature for 3—5 h. D: The same conditions with C, except methanol is used in place of ethanol. b) GLC yields are based on the bromoesters employed, and the isomeric purity in each case is shown in the parenthesis.

Table 2. Effect of Catalysts for Cross-Coupling of (*Z*)-3-Bromoacrylate (Eq. 4)

Catalyst[a]	Temp/°C	Time/h	Yield/%	(2*E*,4*E*)/(2*Z*,4*E*)
$Pd(OAc)_2(PPh_3)_2$	Reflux	5	70	37/63
$Pd(OAc)_2$(dppe)	Reflux	5	86	80/20
$Pd(OAc)_2$(dppf)	Reflux	5	86	23/77
$Pd(OAc)_2$(dppf)	50	5	71	19/81
$Pd(OAc)_2$(dppf)	20	24	73	5/95

a) Dppe and dppf are bis(diphenylphosphino)ethane and bis(diphenylphosphino) ferrocene.

potassium hydrotriisopropoxyborate. The above conditions also gave a good result for the reaction of (*Z*)-1-hexenylborate (**6**) to give (2*E*,4*Z*)-isomer (**8**) in a yield of 95% with the isomeric purity of 98% (Eq. 3).

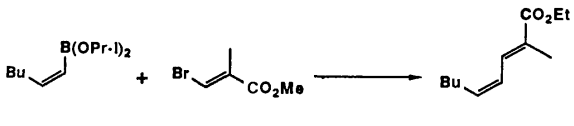

6 7 8 (3)

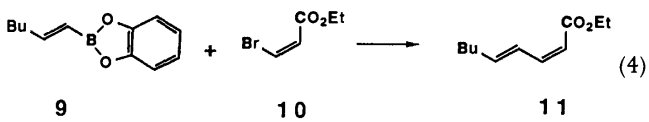

9 10 11 (4)

On the other hand, the reaction between (*E*)-1-hexenylboronate (**9**) and (*Z*)-3-bromoacrylate (**10**) also took place readily. However, 2,4-nonadienoate thus obtained under such conditions was a mixture of (2*Z*,4*E*)- and (2*E*,4*E*)-isomers in a ratio of 63 : 37. Pre-

sumably, isomerization[7] may occur while the boron compound and Pd complex are bound or before the reductive elimination proceeds in the mechanism[2a] of cross-coupling reaction. Bis(diphenylphosphino)-ferrocene (DPPF)[8] is known as a ligand to accelerate the reductive elimination from diorganopalladium complexes, and to minimize the isomerization around the double bond. By using DPPF as a ligand of palladium, the yield in Eq.4 was improved to give 73% yield of ethyl (2*Z*,4*E*)-2,4-nonadienoate and the isomeric ratio of (2*Z*,4*E*):(2*E*,4*E*) to be 95:5 (Table 2). However, such isomerization appears to be highly dependent on the structure of 3-bromo-2-alkenoates since no remarkable isomerization was observed in the reaction of 3-bromocrotonate (Run 7 in Table 1).

There have been some published procedures for the synthesis of α,β-unsaturated esters including conjugated 2,4-alkadienoates from alkynes via hydrometallation, for example, the palladium-catalyzed cross-coupling reaction of ethyl (*E*)- or (*Z*)-3-(tributylstannyl)propenoate[9] with 1-iodo-1-alkenes, and (*E*)-1-alkenylaluminum[10] or zirconium compounds with 3-bromoacrylates. We previously reported that the methoxycarbonylation[11] of 1-alkenylboronates with carbon monoxide and methanol in the presence of palladium catalyst provides a convenient procedure for synthesis of α,β-unsaturated ester, stereoselectively. The present method affords a convenient alternative procedure for the synthesis of the titled compounds.

Experimental

All reactions were carried out under nitrogen atmosphere. 1-Hexyne, 1-octyne, and 2-butyne were commercial products and purified by distillation before use. 6-Chloro-1-hexyne,[12] 1-ethynyl-2,6,6-trimethylcyclohexene,[13] ethyl (*E*)- and (*Z*)-3-bromoacrylates,[14] methyl (*E*)-3-bromo-2-methylpropenoate,[15] and ethyl (*Z*)-3-bromocrotonate[16] were prepared according to the literature procedures. 1,3,2-Benzodioxaborole (cathecolborane) from Aldrich Chemical Co. was used after distillation. 1-Bromo-(2-ethoxycarbonyl)-cycloheptene was prepared by the oxidation[17] of 2-bromo-1-formylcycloheptene[2d] with manganese(IV) oxide in the presence of sodium cyanide, followed by esterification with *N*,*N*-dimethylformamide diethyl acetal.

The ^{1}H NMR spectra were measured with a Hitachi R-90H (90MHz) spectrometer (solvent, $CDCl_3$; TMS as an internal reference). Mass spectra were recorded on a JEOL JMS-D 300 for high resolution analysis and Finnigan ITD 800. GLC analyses were performed with a Hitachi 023 gas chromatograph using a fused silica capillary column (OV-101, 25m).

1-Alkenylboronate (3). Preparations of (*E*)-1-hexenyl-, (*E*)-1-octenyl-, [(*E*)-6-chloro-1-hexenyl]-, and [(*E*)-1-methyl-1-propenyl]-1,3,2-benzodioxaboroles were reported[2a] previously. Hydroboration of 1-ethynyl-2,6,6-trimethylcyclohexene was carried out as follows. A dry 10 ml flask equipped with a septum inlet and a magnetic stirring bar was flushed with nitrogen, and was charged with the enyne (1.48 g, 10 mmol) and dry benzene (2 ml). 1,3,2-Benzodioxaborole (1.2 ml, 10.8 mmol) was added dropwise by a hypodermic syringe. The reaction mixture was stirred for 20 h at 70 °C, and then 0.1 ml of methanol was added at room temperature to destroy the residual hydride. The flask was quickly attached to Kugelrohr and flushed with nitrogen. Distillation under reduced pressure gave the dienylboronate (2.2 g 76%), bp 170 °C/0.55mmHg (1 mmHg= 133.322Pa); ^{1}H NMR ($CDCl_3$) δ=1.10 (s, 6H), 1.4—1.7 (m, 4H), 1.79 (s, 3H), 1.95—2.20 (m, 2H), 5.79 (d, 1H, *J*=18.6 Hz), 6.95—7.25 (m, 4H), and 7.45 (d, 1H, *J*=18.6 Hz).

Standard Procedure for the Synthesis of 2,4-Alkadienoate (Eq. 2). A 200 ml flask equipped with a septum inlet, a reflux condenser and a magnetic stirring bar was flushed with nitrogen. The flask was charged with $Pd(OAc)_2$ (0.067 g, 0.3 mmol), PPh_3 (0.15 g, 0.6 mmol), Na_2CO_3 (2.12g, 20 mmol), and 40 ml of 75% ethanol (Conditions A in Table 1) or K_2CO_3 (2.76 g, 20 mmol) and 40 ml of dry ethanol (Conditions C). Ethyl (*E*)-3-bromoacrylate (1.79 g, 10 mmol) and 2-(1-alkenyl)-1,3,2-benzodioxaborole (11 mmol) were then added by a hypodermic syringe through septum inlet. The reaction mixture was heated gradually to reflux and then to keep reflux for 4 h. The product was extracted with 60 ml of 1:1 benzene–hexane, washed with water, and dried over $MgSO_4$. Analytically pure ester was obtained by chromatography over silica gel or distillation by Kugelrohr. GLC yields using hydrocarbons as internal standards are shown in Table 1.

The dienoates prepared by employing the above procedure are as follows.

Ethyl (2*E*,4*E*)-2,4-Undecadienoate: IR (neat) 1720, 1645, and 1620 cm^{-1}; ^{1}H NMR δ=0.90 (t, 3H, *J*=6.5 Hz), 1.30 (t, 3H, *J*=7.5 Hz), 1.25—1.70 (m, 8H), 2.05—2.30 (m, 2H), 4.13 (q, 2H, *J*=7 Hz), 5.71 (d, 1H, *J*=15 Hz), 6.0—6.4 (m, 2H), and 7.16 (ddd, 1H, *J*=3, 7, and 15 Hz); MS *m*/*z* 210, 165, 153, 125; Found: C, 74.07; H, 10.49%. Calcd for $C_{13}H_{22}O_2$: C, 74.24; H, 10.54%.

Ethyl (2*E*,4*E*)-9-Chloro-2,4-nonadienoate: IR (neat) 1710, 1645, and 1620 cm^{-1}; ^{1}H NMR δ=1.28 (t, 3H, *J*=7.5 Hz), 1.5—2.0 (m, 4H), 2.1—2.4 (m, 2H), 3.51 (t, 2H, *J*=6 Hz), 4.16 (q, 2H, *J*=7 Hz), 5.73 (d, 1H, 16Hz), 6.0—6.4 (m, 2H), and 7.19 (dd, 1H, *J*=10 and 16 Hz); MS *m*/*z* 216, 171, 143, and 125; Found: C, 61.29; H, 7.91%. Calcd for $C_{11}H_{17}O_2Cl$: C, 61.97; H, 7.91%.

Ethyl (2*E*,4*E*)-4-Ethyl-2,4-heptadienoate: IR (neat) 1715 and 1625 cm^{-1}; ^{1}H NMR δ=0.99 (t, 3H, *J*=7 Hz), 1.0 (t, 3H, *J*=7 Hz), 1.23 (t, 3H, *J*=7 Hz), 2.0—2.4 (m, 4H), 4.11 (q, 2H, *J*=7 Hz), 5.71 (d, 1H, *J*=15.5 Hz), 5.77 (t, 1H, *J*=7 Hz), and 7.1 (d, 1H, *J*=15.5 Hz); Found: C, 72.28; H, 9.93%. Calcd for $C_{11}H_{18}O_2$: C, 72.49, H, 9.95%.

1-[(*E*)-1-Hexenyl]-2-(ethoxycarbonyl)cycloheptene: IR (neat) 1715, 1640, and 1595 cm^{-1}; ^{1}H NMR δ=0.895 (t, 3H, *J*=7 Hz), 1.31 (t, 3H, *J*=7 Hz), 1.1—1.9 (m, 10H), 1.9—2.3 (m, 2H), 2.3—2.6 (m, 4H), 4.21 (q, 2H, *J*=7.3 Hz), 5.85 (dt, 1H, *J*=7 and 16 Hz), and 6.75 (d, 1H, *J*=16 Hz); MS *m*/*z* 250, 205, 193, and 165; Found: *m*/*z* 250.1934. Calcd for $C_{16}H_{26}O_2$: M, 250.1933.

4-[(*E*)-1-Hexenyl]coumarin: Mp 67 °C; IR (Nujol) 1720, 1650, and 1610 cm^{-1}; ^{1}H NMR δ=0.96 (t, 3H, *J*=7 Hz), 1.2—1.6 (m, 4H), 2.2—2.5 (m, 2H), 6.41 (s, 1H), 6.43 (dt, 1H, *J*=6 and 21 Hz), 6.73 (d, 1H, *J*=21 Hz), and 7.1—7.9 (m, 4H); MS Found: *m*/*z* 228.1138. Calcd for $C_{15}H_{16}O_2$: M, 228.1151.

Ethyl (2*Z*,4*E*)-5-(2,6,6-Trimethylcyclohexenyl)-3-methylpentadienoate: IR (neat) 1715, 1615, 1230, and 955 cm^{-1};

^{1}H NMR δ=1.07 (s, 6H), 1.27 (t, 3H, J=7.2 Hz), 1.5—2.2 (m, 6H), 1.77 (s, 3H), 2.04 (s, 3H), 4.16 (q, 2H, J=6.8 Hz), 5.64 (s, 1H), 6.58 (d, 1H, J=16.3 Hz), and 7.63 (d, 1H, J=16.3 Hz); MS m/z 262, 246, 217, 189, and 119; Found: m/z 262.1915. Calcd for $C_{17}H_{26}O_2$: M, 262.1933.

Cross-Coupling of (*E*)-1-Hexenyl-1,3,2-benzodioxaborole (9) with Ethyl (*Z*)-3-Bromoacrylate (10) (Eq. 4). A mixture of the catalyst (0.03 mmol), K_2CO_3 (2 mmol), ethyl (*Z*)-3-bromoacrylate (1 mmol), and 2-[(*E*)-1-hexenyl]-1,3,2-benzodioxaborole (1.1 mmol) in 3 ml of 75% ethanol was stirred under the conditions indicated in Table 2. After the reaction was over, the product was extracted with benzene, washed with water and dried over $MgSO_4$. Chromatography over silica gel with hexane-ether gave **11**: IR (neat) 1713, 1640, and 1600 cm^{-1}; ^{1}H NMR δ=0.93 (t, 3H, J=7 Hz), 1.28 (t, 3H, J=7 Hz), 1.2—1.7 (m, 4H), 2.1—2.4 (m, 2H), 4.16 (q, 2H, J=7 Hz), 5.52 (d, 1H, J=11 Hz), 5.99 (dt, 1H, J=7 and 15 Hz), 6.47 (dd, 1H, J=11 and 11 Hz), 7.41 (dd, 1H, J=11 and 15 Hz); MS m/z 182, 153, 137, 125, and 109; Found: C, 71.63; H, 9.69%, Calcd for $C_{11}H_{18}O_2$: C, 72.49; H, 9.95%. The results are summarized in Table 2.

Synthesis of (*Z*)-1-Hexenylboronate (6) and Its Reaction with 7 (Eq. 3). To a solution of diisopropyl (*Z*)-(1-bromo-1-hexenyl)boronate (2.2 mmol) in ether (4 ml) was added 4 ml of a solution of potassium hydrotriisopropoxyborate in THF (0.6M solution, 2.4 mmol) at 0 °C. The reaction mixture was stirred for 15 min at 0 °C, and then for 30 min at room temperature. After evaporation of the solvent under reduced pressure, the residue **6** was dissolved in 8 ml of methanol. $Pd(OAc)_2$ (0.06 mmol), PPh_3 (0.12 mmol), K_2CO_3 (4 mmol), and methyl (*E*)-3-bromo-2-methylpropenoate (2 mmol) were added, and the mixture was refluxed for 5 h. The reaction mixture was diluted with benzene (30 ml), washed with water, and dried over $MgSO_4$. The product was isolated by chromatography over silica gel with benzene/ethyl acetate (20:1). Analysis by GLC revealed the formation of **8** (1.9 mmol, 95%): IR (neat) 1710, 1635, 1605, 1115, and 735 cm^{-1}; ^{1}H NMR δ=0.91 (t, 3H, J=7 Hz), 1.2—1.5 (m, 4H), 1.93 (s, 3H), 2.1—2.4 (m, 2H), 3.76 (s, 3H), 5.75 (dt, 1H, J=7.6 and 11.2 Hz), 6.27 (dd, 1H, J=11.2 and 11.6 Hz), and 7.49 (d, 1H, J=11.6 Hz); MS m/z 182, 151, and 125; Found: m/z 182.1289. Calcd for $C_{11}H_{18}O_2$: M, 182.1297.

References

1) a) P. Kocovsky, F. Turecek, and J. Hajicek, "Synthesis of Natural Products: Problems of Stereoselectivity," Vol. 2, CRC Press, Florida (1986), p. 220; b) G. H. Posner, *Org. React.*, **19**, 1 (1972); c) A. Alexakis, G. Cahiez, and J. F. Normant, *Tetrahedron*, **36**, 1961 (1980).

2) a) N. Miyaura, K. Yamada, H. Suginome, and A. Suzuki, *J. Am. Chem. Soc.*, **107**, 972 (1985); b) N. Miyaura, M. Sato, and A. Suzuki, *Tetrahedron Lett.*, **27**, 3745 (1986); c) M. Sato, N. Miyaura, and A. Suzuki, *Chem. Lett.*, **1986**, 1329; d) N. Miyaura, T. Ishiyama, H. Sasaki, M. Ishikawa, M. Sato, and A. Suzuki, *J. Am. Chem. Soc.*, **111**, 314 (1989).

3) N. Sato, T. Ishiyama, N. Miyaura, and A. Suzuki, *Chem. Lett.*, **1986**, 1329.

4) The coupling reaction of 1-alkenylboronic acids and 3-bromoacrylates was recently reported; M. V. Mavorov, N. A. Urdaneta, and Nguyen Kong Hao, *Bull. Chem. Soc., USSR (Engl. Transl.)*, **36**, 2447 (1987).

5) a) H. C. Brown and S. K. Gupta, *J. Am. Chem. Soc.*, **94**, 4370 (1972); b) H. C. Brown, "Organic Synthesis via Boranes," John Wiley & Sons, New York (1975), p. 64.

6) H. C. Brown and T. Imai, *Organometallics*, **3**, 1392 (1984).

7) A. Schoenberg, I. Bartoletti, and R. F. Heck, *J. Org. Chem.*, **39**, 3318 (1974).

8) T. Hayashi, M. Konishi, Y. Kobori, M. Kumada, T. Higuchi, and K. Hirotu, *J. Am. Chem. Soc.*, **106**, 158 (1984).

9) J. K. Stille and B. L. Groh, *J. Am. Chem. Soc.*, **109**, 813 (1987).

10) S. Baba and E. Negishi, *J. Am. Chem. Soc.*, **98**, 6729 (1976).

11) N. Miyaura and A. Suzuki, *Chem. Lett.*, **1981**, 879.

12) L. Brandma, "Preparative Acetylenic Chemistry," Elsevier, Amsterdam (1971).

13) G. Kobrich, H. Trapp, K. Flory, and W. Drischel, *Ber.*, **99**, 689 (1966).

14) F. Stolz, *Ber.*, **19**, 536 (1886).

15) P. Canbere, *Bull. Soc. Chim. Fr.*, **1964**, 144.

16) R. Vessiere and F. Theron, *Comptes Rendus.*, **260**, 597 (1965).

17) E. J. Corey, *J. Am. Chem. Soc.*, **90**, 5616 (1968).

2,5-Diaryl-1,3,2-dioxaborinanes: A New Series of Liquid Crystals

Hiroshi MATSUBARA, Koji SETO,† Tadasu TAHARA,† and Shigetoshi TAKAHASHI*
The Institute of Scientific and Industrial Research, Osaka University, Mihogaoka, Ibaraki, Osaka 567
†Research & Development Division, Nitto Kasei Co., Ltd., 3 Nishiawaji, Higashiyodogawa, Osaka 533
(Received July 31, 1989)

2,5-Diaryl-1,3,2-dioxaborinane derivatives having various terminal groups were synthesized and found to form mesomorphic phases in a wide temperature range. They provide a new series of liquid-crystalline compounds containing a boron atom in the principal structure.

The majority of liquid-crystalline molecules consist of carbon, oxgen, nitrogen, and hydrogen atoms. Though a few examples containing heteroatoms are known,[1] liquid crystalline materials containing metal atoms are of special interest since they are expected to have unique properties based on the incorporation of metals having special electric and magnetic properties.

In general, organometallic compounds are thermally and chemically unstable, however, 1,3,2-dioxaborinane derivatives are fairly stable and we recently reported a preliminaly result that the compounds having 2,5-disubstituted 1,3,2-dioxaborinane structure **1** form stable nematic and/or smectic mesophases.[2] They are the first examples of thermotropic liquid-crystalline molecules with a boron atom in the principal structure. Boron atoms have vacant p-orbitals and are electron-deficient, hence conjugation between the p-orbital and aromatic π-electron system may be expected for 2-aryl-1,3,2-dioxaborinane derivatives. This conjugation may give a double bond character to the bond between boron atom and aromatic ring, resulting in a rigid core structure favorable to liquid-crystalline materials.

In this paper we report in detail on the synthesis and properities of liquid-crystalline compounds **2** which are constructed by three rings containing the dioxaborinane ring as the principal structure. And we wish to discuss especially the influence of terminal groups on mesomorphic properties, as well as the comparison with other liquid-crystalline materials

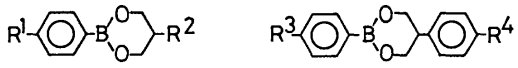

1 2

having the analogous structure.

Results and Discussion

A simple approach to the synthesis of compound **2** has been developed according to Scheme 1. The synthetic intermediate **4** was prepared by the palladium-(0)-catalyzed cross-coupling reaction of ethyl cyanomalonate with aryl halides **3**.[3] The aryl halides were prepared by the halogenation of arenes according to a literature method.[4] Although a small amount of the ortho-substituted isomer was formed as a by-product, a mixture of the isomers was used for the coupling reaction, since the ortho-isomer has a less reactivity and recrystallization gave pure diols **5**.

Boronic acids **6a**—c were obtained by the reaction of Grignard reagents with trimethoxyborane in tetrahydrofuran at temperatures below −60 °C. Boronic acid **6a** was converted to **6d** by oxidation with potassium permanganate in an alkaline solution.[5] *p*-Cyanophenyl derivative **6e** was prepared according to Scheme 2. The intermediate **8** was transformed into **9** by a literature method.[6]

Finally, condensation between **5** and **6** was carried out in a toluene solution and we obtained dioxaborinane derivatives **2** in nearly quantitative yields. Pur-

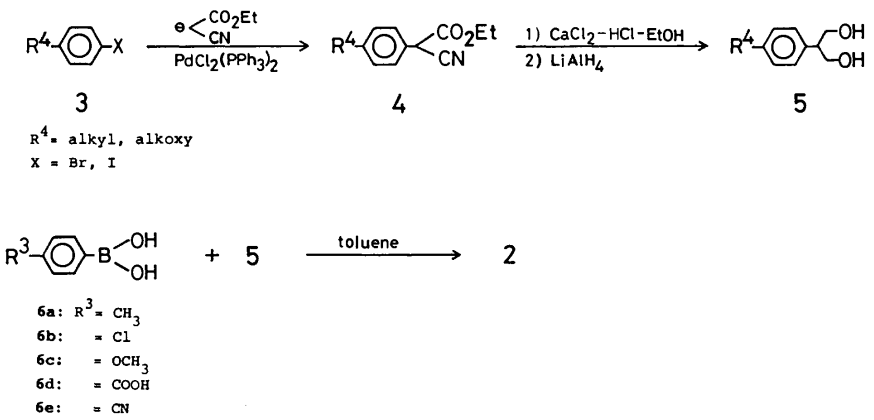

Scheme 1.

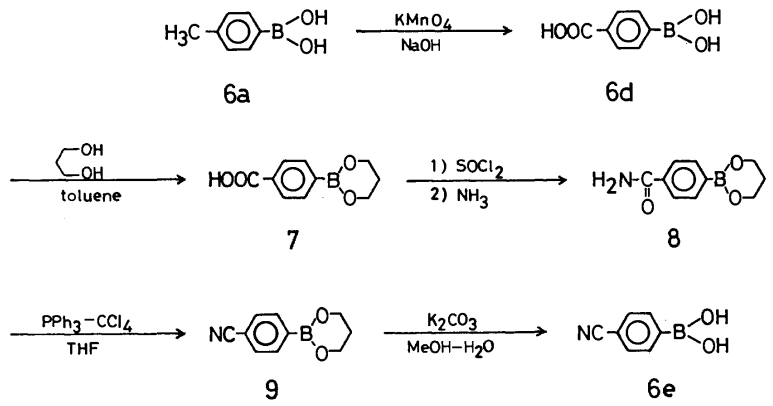

Scheme 2.

ification of **2** was achieved by column chromatography and recrystallization. The structures of compound **2** are consistent with analytical data including mass, IR, and NMR spectra. The present method for the preparation of **2** has a great advantage because their various derivatives are prepared easily by the simple condensation of selected pairs of **5** and **6**. A number of 2,5-disubstituted 1,3,2-dioxaborinanes thus synthesized are listed in Table 1. The table shows that the dioxaborinane derivatives form mesophases with a variety of terminal groups, indicating that the dioxaborinane ring provides a suitable core structure for the formation of liquid crystals.

The terminal groups can promote the formation of mesophases in the following order, -CN>-OMe, -Cl>-Me>-COOMe. The order is almost same as the tendency for organic liquid-crystalline materials shown by Gray et al.[7] Especially, the cyano gruop is a good terminal group for the formation of mesophases. It is known that cyano groups lead molecules to a dimer structure favorable to the formation of liquid crystals.

In order to investigate the influence of alkyl chain length on the formation of mesophases, compounds **2**, (R^3=CN or CH_3O) bearing a variety of alkyl groups (R^4) were synthesized, and the results are summarized in Tables 2 and 3. The compounds having a cyano group at the terminal form a stable nematic phase for various alkyl chains, while those having a methoxyl group exhibit only a monotropic nematic phase. The transition temperatures for the compounds having a cyano group are plotted against the alkyl chain length in Fig. 1. An odd-even effect was observed for the nematic-to-isotropic (N-I) transition temperatures,

Table 1. Transition Temperatures for 2,5-Disubstituted 1,3,2-Dioxaborinanes (**2**)

	R^3	R^4	Transition temperatures (°C)[a]		
			Cryst.	N	Iso
2a	CH_3	OC_4H_9	· 126.4	(124.0)[b]	·
2b	Cl	OC_4H_9	· 145.0	(132.8)[b]	·
2c	OCH_3	OC_4H_9	· 133.9	· 146.6	·
2d	CN	OC_4H_9	· 117.0	· 166.0	·
2e	CO_2CH_3	OC_4H_9	· 156.2	· 158.5	·
2f	CH_3	C_6H_{13}	· 100.0	(83.0)[b]	·
2g	Cl	C_6H_{13}	· 124.8		·
2h	OCH_3	C_6H_{13}	· 103.0	(91.4)[b]	·
2i	CN	C_6H_{13}	· 98.0	· 122.4	·
2j	CO_2CH_3	C_6H_{13}	· 140.5	· 130.3	·

a) N: nematic; Iso: isotropic liquid. b) Monotropic transition.

Table 2. Transition Temperatures for 2-(4-Methoxyphenyl)-5-(4-alkylphenyl)-1,3,2-dioxaborinanes

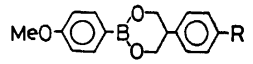

R	Transition temperatures (°C)[a]			
	Cryst.	N		Iso
CH_3	·	147.8	(91.3)[b]	·
CH_3CH_2	·	144.0		·
$CH_3(CH_2)_2$	·	139.6	(91.0)[b]	·
$CH_3(CH_2)_3$	·	109.9	(88.3)[b]	·
$CH_3(CH_2)_4$	·	114.1	(99.7)[b]	·
$CH_3(CH_2)_5$	·	103.0	(91.4)[b]	·
$CH_3(CH_2)_6$	·	108.3	(97.3)[b]	·
$CH_3(CH_2)_7$	·	94.8	(93.3)[b]	·

a) N: nematic; Iso: isotropic liquid. b) Monotropic transition.

Table 3. Transition Temperatures for 2-(4-Cyanophenyl)-5-(4-alkylphenyl)-1,3,2-dioxaborinanes

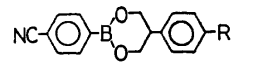

R	Transition temperatures (°C)[a]				
	Cryst.	S_A		N	Iso
CH_3	· 151.9			· 157.2	·
CH_3CH_2	· 121.6			· 136.0	·
$CH_3(CH_2)_2$	· 117.1			· (115.2)[b]	·
$CH_3(CH_2)_3$	· 120.4			· 128.0	·
$CH_3(CH_2)_4$	· 103.0			· 132.7	·
$CH_3(CH_2)_5$	· 98.0			· 122.4	·
$CH_3(CH_2)_6$	· 95.0			· 127.0	·
$CH_3(CH_2)_7$	· 87.3	·	102.0	· 120.6	·

a) S_A smectic A; N: nematic; Iso: isotropic liquid. b) Monotropic transition.

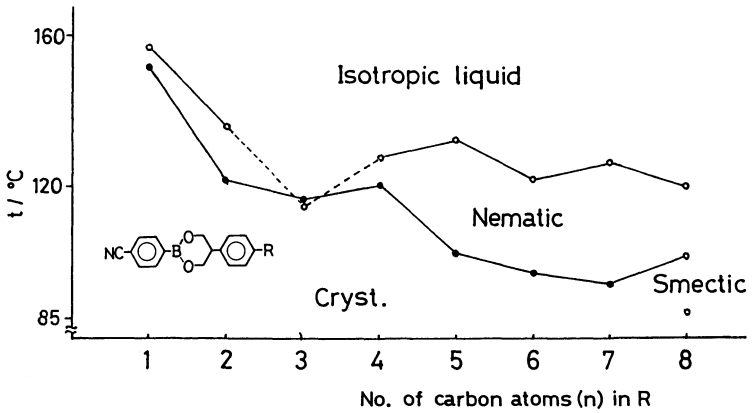

Fig. 1. Plot of transition temperatures against the number of carbon atoms (n) in alkyl chain (R) of the 2-(4-cyanophenyl)-5-(4-alkylphenyl)-1,3,2-dioxaborinanes.

Table 4. Comparison of Liquid-Crystalline Behavior for Tricyclic Compounds

	Transition temperatures (°C)[a]		
	Cryst.	N	Iso
NC-Ph-Ph-Ph-C_5H_{11}	· 130	· 239	·
NC-Ph-H-Ph-C_5H_{11}	· 84	· 154	·
NC-Ph-O,O-Ph-C_5H_{11}	· 110	· 164	·
NC-Ph-B(O,O)-Ph-C_5H_{11}	· 103.0	· 132.7	·

a) N: nematic; Iso: isotropic liquid.

and the longer alkyl groups showed the wider temperature range of mesophases. These facts also agree with the tendency of liquid-crystalline materials reported by Gray et al.[7,8] As described later, the dioxaborinane derivatives show lower N-I transition temperatures than other liquid-crystalline materials having analogous three-ring structures.

The dioxaborinane derivatives have a unique structure containing a metalloid atom, boron, in the principal structure, however, they are fairly stable in air and moisture, and showed similar thermal properties of organic liquid-crystalline materials.

It is known that the structures of rigid core in liquid-crystalline materials give strong influence to their clearing points, that is mesophases-to-isotropic transition temperatures. For examples, displacement of the central benzene ring in a terphenyl system by other six-membered rings such as cyclohexane and dioxane results in lowering the clearing points.[9] The dioxaborinane ring exhibited the same influence and compound **9** showed the lowest clearing point among the compounds summarized in Table 4.

Experimental

Measurements of transition temperatures and observations of mesophases were made using Olympus BH-2 polarising microscope in conjunction with Metler FP52 heating stage and FP5 control unit. ^{1}H NMR spectra were measured for solutions in $CDCl_3$ with tetramethylsilane as internal standard using a Bruker WM-360 spectrometer. IR spectra were recorded with a Hitachi 295 infrared spectrophotometer, and mass spectra were taken on a JEOL JMS06 instrument.

Diethyl 4-Butylphenylmalonate.[3] To a suspension of potassium *t*-butoxide (6.73 g, 60 mmol) in 1,2-dimethoxyethane (50 ml), ethyl cyanoacetate (3.97 g, 35 mmol) was added at room temperature with stirring. After 10 min 4-butylphenyl iodide (**3**, R=C_4H_9, X=I, 7.80 g, 30 mmol) and a catalytic amount of dichlorobis(triphenylphosphine)-palladium (600 mg, 0.85 mmol) were added, and then the mixture was heated at 70 °C for 8 h under nitrogen. After cooling the reaction mixture, 1 M hydrochloric acid was added and the product was extracted with ether. The extract was washed with water and dried over sodium sulfate. After evaporation of ether the residue was purified by chromatography on silica gel using hexane/dichloromethane as eluent. The viscous, oily product was distilled using a Kugelrohr bulb-to-bulb distillation apparatus to give ethyl 4-butylphenylcyanoacetate (as a colorless oil; yield 4.13 g (56%); IR (neat) 2240 (CN), and 1760 cm^{-1} (C=O). The product obtained here was contaminated by a small amount of impurity, but the next procedure for saponification of the cyano group was carried out without further purification of the product. A mixture of the crude cyanoacetate (4.00 g), ethanol (15 ml), concd hydrochloric acid (18.6 ml), calcium chloride (20.1 g), and benzene (6 ml) was stirring at room temperature for 3 h, then heated at 55 °C for 2 h, and finally under reflux for 5 h. After cooling to room temperature, water was added and the product was extracted with benzene. The extract was dried over sodium sulfate, and after concentration the crude product was purified by chromatography on silica gel using dichloromethane as an eluent. The resultant oily product was distilled using a Kugelrohr bulb-to-bulb distillation apparatus, affording diethly 4-butylphenylmalonate as a colorless oil; yield 3.32 g (70%); IR (neat) 1765 and 1750 cm^{-1} (C=O); ^{1}H NMR δ=0.90—2.10 (13H, m, alkyl), 2.50 (2H, t, J=8 Hz, $CH_2C_6H_4$), 4.20 (4H, q, J=7 Hz, CH_2O), 4.57 (1H, s, CH), and 7.27 (m, 4H, Ar).

2-(4-Butylphenyl)-1,3-propanediol (5, R=C_4H_9). To a suspension of lithium aluminum hydride (0.76 g, 20 mmol) in diethyl ether (60 ml), diethyl 4-butylphenylmalonate (2.92 g, 10 mmol) in diethyl ether (10 ml) was added dropwise with stirring at 0 °C. And then the reaction mixture was heated to reflux temperature. After 6 h the mixture was cooled to 0 °C again, and ethyl acetate (5 ml), and 5% sodium hydroxide solution (10 ml) were added successively. After the reaction at room temperature for 10 h, the inorganic salt precipitated was separated by filtration, then the organic layer was separated and the aqueous layer was extracted with ether. The combined ether solution was dried over sodium sulfate. After evaporation of ether, the resultant product was purified by recrystallization from hexane, affording 2-(4-butylphenyl)-1,3-propanediol as white needles; yield 3.32 g (70%); mp 74.5—76.0 °C; IR (Nujol) 3250 cm^{-1} (OH); ^1H NMR δ=0.87—1.59 (7H, m, alkyl), 2.57 (2H, t, J=8 Hz, $C\underline{H}_2C_6H_4$), 3.02 (1H, m, CH), 3.86—3.96 (4H, m, OCH_2), and 7.11 (4H, s, Ar).

***p*-Tolylboronic Acid (6a).** To a solution of trimethoxyborane (20.4 g, 194 mmol) in dry tetrahydrofuran (100 ml), *p*-tolylmagnesium bromide, prepared from *p*-bromotoluene (22.4 g, 131 mmol) and magnesium (3.41g, 140 mmol), was added dropwise at −70 °C. After the Grignard reagent had been added, the reaction mixture was stirred below −60 °C for one hour, and then hydrolyzed with 10% sulfuric acid (70 ml). The inorganic salt formed was filtered off and the tetrahydrofuran layer was separated and then the aqueous layer was extracted with ether. The combined organic layer was washed with water and dried over sodium sulfate. Consentration of the solution gave white crystals, which was washed with hexane and water, affording pure *p*-tolylboronic acid; yield 15.0 g (86%); mp 245—247 °C; IR (Nujol) 3480, 3400 (OH), and 1365 cm^{-1} (BO).

Similarly, *p*-chloro- (**6b**) and *p*-methoxyphenylboronic acid (**6c**) were prepared by starting from *p*-chloro and *p*-methoxyphenyl bromide, respectively.

4-Carboxyphenylboronic Acid (6d).[5] *p*-Tolylboronic acid (6.8 g, 50 mmol) was dissolved in 40 ml of water containing sodium hydroxide (4 g), and then 290 ml of water was added to the solution. Into the agitated mixture a solution of potassium permanganate (16.6 g, 105 mmol) in water (500 ml) was added in the following way. The permanganate solution was devided into eight volumes, and each volume was added in turn every one hour. After all portions of the permanganate solution had been added, the mixture was stirred overnight. Excess of permanganate was destroyed by addition of ethanol (20 ml) at 50 °C, and the manganese dioxide was filtered off. The filtrate was concentrated to about 200 ml below 40 °C, and then acidified carefully with hydrochloric acid. The crystal separated was collected, washed with water, and recrystallized from water; yield 4.82 g (58%); mp 232—234 °C; IR (Nujol) 3500—2500 (OH), 1700 (C=O), and 1355 cm^{-1} (BO).

2-(4-Carboxyphenyl)-1,3,2-dioxaborinane (7). 4-Carboxyphenylboronic acid (4.82 g, 29 mmol) was reacted with 1,3-propanediol (2.23 g, 29 mmol) in toluene (100 ml) under reflux for 2 h. During the reaction the water formed was removed azeotropically using a Dean-Stark apparatus. When the reaction was completed, the mixture was cooled to room temperature and the crystals separated were collected by filtration; yield 5.78 g (92%); mp 211—213 °C; IR (Nujol) 3400—2500 (OH), 1695 (C=O), and 1315 cm^{-1} (BO).

2-(4-Carbamoylphenyl)-1,3,2-dioxaborinane (8). 2-(4-Carboxyphenyl)-1,3,2-dioxaborinane (5.56 g, 24.9 mmol) was reacted with thionyl chloride (12 ml) in the presence of *N,N*-dimethylformamide under reflux for 2 h. Removal of excess thionyl chloride under a reduced pressure afforded the acid chloride, which was used for the next reaction, ammonolysis, without further purification. To a 28% of aqueous ammonia (65 ml), a solution of the acid chloride in tetrahydrofuran (130 ml) was added dropwise at 0 °C, and then stirred at room temperature for 30 min. The solvent and aqueous ammonia were removed by evaporation, and toluene (100 ml) was added to the residue in order to remove water azeotropically. After completion of dehydration, toluene was distilled away, and the resultant residue was extracted with acetone. Concentration of acetone solution gave 2-(4-carbamoylphenyl)-1,3,2-dioxaborinane as pale yellow crystals; yield 2.87 g (52%); mp 204—206 °C; IR (Nujol) 3550, 3100 (NH), 1685 (C=O), 1625, and 1615 cm^{-1} (NH).

4-Cyanophenylboronic Acid (6e).[6] To a solution of triphenylphosphine (7.32 g, 27.9 mmol) in carbon tetrachloride (30 ml), 2-(4-carbamoylphenyl)-1,3,2-dioxaborinane (**8**, 2.87 g, 13.9 mmol) dissolved in tetrahydrofuran (30 ml) was added, and then the mixture was warmed to 50 °C for 20 h. Insoluble solids precipitated were separated, and the filtrate was concentrated. The residue was extracted with warm hexane, and removal of hexane give crude nitrile (**9**), 2.05 g (78%); IR (Nujol) 2220 (CN), and 1310 cm^{-1} (BO).

Finally, the protective group of boronic acid was taken off as follows. A mixture of (**9**) (2.05 g, 10.9 mmol) and potassium carbonate (3.75 g) in water and methanol (10 ml) was stirred at room temperature for 10 h. Insoluble solids were filtered off, and methanol was removed in vacuo. The aqueous alkali solution was cooled and acidified carefully with hydrochloric acid. The crystal separated was collected by filtration and washed with water; yield 1.26 g (78%); mp>300 °C; IR (Nujol) 3550, 3440 (OH), 2220 (CN), and 1345 cm^{-1} (BO).

2,5-Diaryl-1,3,2-dioxaborinanes (2). General Procedure. A mixture of 4-substituted phenylboronic acid (**6**, 0.5 mmol), 2-(4-substituted phenyl)-1,3-propanediol (**5**, 0.5 mmol), and toluene (25 ml) was stirred under reflux for 2 h. During the reaction the water formed removed azeotropically using a Dean-Stark apparatus. When the reaction was completed, toluene was distilled away, and the resultant residue was purified by chromatography on silica gel using dichloromethane as an eluent. Recrystallization from hexane gave the corresponding products (**2**).

2-(4-Methylphenyl)-5-(4-butoxyphenyl)-1,3,2-dioxaborinane (2a). Found: C, 74.08; H, 7.80%. Calcd for $C_{20}H_{26}BO_3$: C, 73.86; H, 8.06%; IR (Nujol) 1315 cm^{-1} (BO); ^1H NMR δ=0.97 (3H, t, J=8 Hz, $CH_2C\underline{H}_3$), 1.45—1.52 (2H, m, $C\underline{H}_2CH_3$), 1.75 (2H, m, $OCH_2C\underline{H}_2$), 2.36 (3H, s, $C\underline{H}_3C_6H_4$), 3.25 (1H, m, CH), 3.95 (2H, t, J=6 Hz, $OC\underline{H}_2CH_2$), 4.14 (2H, dd, J=11 and 11 Hz, $OC\underline{H}_2CH$, ax), 4.24 (2H, dd, J=5 and 11 Hz, $OC\underline{H}_2CH$, eq), 6.88 (2H, d, J=9 Hz, Ar), 7.12 (2H, d, J=9 Hz, Ar), 7.17 (2H, d, J=8 Hz, Ar), and 7.70 (2H, d, J=8 Hz, Ar).

2-(4-Chlorophenyl)-5-(4-butoxyphenyl)-1,3,2-dioxaborinane (2b). Found: C, 66.09; H, 6.53; Cl, 10.10%. Calcd for $C_{19}H_{23}BClO_3$: C, 66.02; H, 6.71; Cl, 10.26%; IR (Nujol) 1315 cm^{-1} (BO); ^1H NMR δ=0.97 (3H, t, J=7 Hz, CH_3), 1.46—1.52 (2H, m, $CH_2C\underline{H}_3$), 1.76 (2H, m, $OCH_2C\underline{H}_2$), 3.25 (1H, m, CH), 3.95 (2H, d, J=6 Hz, $OC\underline{H}_2CH_2$), 4.14 (2H, dd, J=11

and 11 Hz, OCH_2CH, ax), 4.25 (2H, dd, J=5 and 11 Hz, OCH_2CH, eq), 6.89 (2H, d, J=9 Hz, Ar), 7.12 (2H, d, J=9 Hz, Ar), 7.33 (2H, d, J=8 Hz, Ar), and 7.73 (2H, d, J=8 Hz).

2-(4-Methoxyphenyl)-5-(4-butoxyphenyl)-1,3,2-dioxaborinane (2c). Found: C, 70.52; H, 7.42%. Calcd for $C_{20}H_{25}BO_4$: C, 70.61; H, 7.41%; IR (Nujol) 1315 cm^{-1} (BO); ^1H NMR δ=0.93 (3H, t, J=7 Hz, CH_2CH_3), 1.37—1.46 (2H, m, CH_2CH_3), 1.78 (2H, m, OCH_2CH_2), 3.25 (1H, m, CH), 3.83 (3H, s, OCH_3), 3.98 (2H, d, J=6 Hz, OCH_2CH_2), 4.14 (2H, dd, J=11 and 11 Hz, OCH_2CH, ax), 4.24 (2H, dd, J=5 and 11 Hz, OCH_2CH, eq), 6.87 (2H, d, J=9 Hz, Ar), 6.89 (2H, d, J=9 Hz, Ar), 7.12 (2H, d, J=9 Hz, Ar), and 7.75 (2H, d, J=9 Hz); MS, m/z 340 (M^+).

2-(4-Cyanophenyl)-5-(4-butoxyphenyl)-1,3,2-dioxaborinane (2d). Found: C, 71.92; H, 6.62; N, 3.96%. Calcd for $C_{20}H_{22}BNO_3$: C, 71.66; H, 6.62; N, 4.18%; IR (Nujol) 2220 cm^{-1} (CN); ^1H NMR δ=0.93 (3H, t, J=7 Hz, CH_3), 1.17—1.45 (2H, m, CH_2CH_3), 1.74—1.80 (2H, m, OCH_2CH_2), 3.27 (1H, m, CH), 3.94 (2H, d, J=6 Hz, OCH_2CH_2), 4.17 (2H, dd, J=11 and 11 Hz, OCH_2CH, ax), 4.28 (2H, dd, J=5 and 11 Hz, OCH_2CH, eq), 6.89 (2H, d, J=9 Hz, Ar), 7.12 (2H, d, J=9 Hz, Ar), 7.63 (2H, d, J=8 Hz, Ar), and 7.89 (2H, d, J=8 Hz, Ar).

2-(4-Methylphenyl)-5-(4-hexylphenyl)-1,3,2-dioxaborinane (2f). Found: C, 78.39; H, 8.67%. Calcd for $C_{22}H_{29}BO_2$: C, 78.58; H, 8.69%; IR (Nujol) 1310 cm^{-1} (BO); ^1H NMR δ=0.88 (3H, t, J=7 Hz, CH_2CH_3), 1.28—1.36 (6H, m, alkyl), 1.58—1.62 (2H, m, $CH_2CH_2C_6H_4$), 2.37 (3H, s, $CH_3C_6H_4$), 2.59 (2H, t, J=7 Hz, $CH_2C_6H_4$), 3.28 (1H, m, CH), 4.18 (2H, dd, J=10 and 10 Hz, OCH_2CH, ax), 4.27 (2H, dd, J=4 and 10 Hz, OCH_2CH, eq), 7.13 (2H, d, J=9Hz, Ar), 7.17 (2H, d, J=9 Hz, Ar), 7.18 (2H, d, J=8Hz, Ar), and 7.70 (2H, d, J=8 Hz, Ar).

2-(4-Chlorophenyl)-5-(4-hexylphenyl)-1,3,2-dioxaborinane (2g). Found: C, 70.91; H, 7.06; Cl, 9.99%. Calcd for $C_{21}H_{26}BClO_2$: C, 70.71; H, 7.35; Cl, 9.94%; IR (Nujol) 1320 cm^{-1} (BO); ^1H NMR δ=0.88 (3H, t, J=7 Hz, CH_3), 1.30—1.36 (6H, m, alkyl), 1.56—1.62 (2H, m, $CH_2CH_2C_6H_4$), 2.59 (2H, t, J=8 Hz, $CH_2C_6H_4$), 3.28 (1H, m, CH), 4.18 (2H, dd, J=11 and 11 Hz, OCH_2CH, ax), 4.27 (2H, dd, J=5 and 11 Hz, OCH_2CH, eq), 7.12 (2H, d, J=9 Hz, Ar), 7.17 (2H, d, J=9 Hz, Ar), 7.33 (2H, d, J=8 Hz, Ar), and 7.73 (2H, d, J=8 Hz, Ar).

2-(4-Methoxyphenyl)-5-(4-hexylphenyl)-1,3,2-dioxaborinane (2h). Found: C, 75.25; H, 8.16%. Calcd for $C_{22}H_{29}BO_3$: C, 75.00; H, 8.29%; IR (Nujol) 1320 (BO) and 1240 cm^{-1} (Ar-O); ^1H NMR δ=0.88 (3H, t, J=7 Hz, CH_2CH_3), 1.31—1.36 (6H, m, alkyl), 1.56 (2H, m, $CH_2CH_2C_6H_4$), 2.58 (2H, t, J=8 Hz, $CH_2C_6H_4$), 3.27 (1H, m, CH), 3.82 (3H, s, OCH_3), 4.16 (2H, dd, J=11 and 11 Hz, OCH_2CH, ax), 4.26 (2H, dd, J=5 and 11 Hz OCH_2CH, eq), 6.89 (2H, d, J=8 Hz, Ar), 7.12 (2H, d, J=8 Hz, Ar), 7.16 (2H, d, J=8 Hz, Ar), and 7.76 (2H, d, J=8 Hz, Ar); MS, m/z 352 (M^+). Elemental analysis for the derivatives of **2h** are listed in Table 5.

2-(4-Cyanophenyl)-5-(4-hexylphenyl)-1,3,2-dioxaborinane (2i). Found: C, 76.21; H, 7.59; N, 3.92%. Calcd for $C_{22}H_{26}BNO_2$: C, 76.09; H, 7.54; N, 4.03%; IR (Nujol) 2220 (CN) and 1310 cm^{-1} (BO); ^1H NMR δ=0.88 (3H, t, J=7 Hz, CH_3), 1.31 (6H, m, alkyl), 1.60 (2H, m, $CH_2CH_2C_6H_4$), 2.59 (2H, t, J=8 Hz, $CH_2C_6H_4$), 3.29 (1H, m, CH), 4.19 (2H, dd, J=11 and 11 Hz, OCH_2CH, ax), 4.29 (2H, dd, J=5 and 11 Hz, OCH_2CH, eq), 7.12 (2H, d, J=8 Hz, Ar), 7.18 (2H, d, J=8 Hz, Ar), 7.62 (2H, d, J=8 Hz, Ar), and 7.88 (2H, d, J=8 Hz, Ar). Elemental analysis for the derivatives of **2i** are listed in Table 6.

2-[4-(Methoxycarbonyl)phenyl]-5-(4-butoxyphenyl)-1,3,2-dioxaborinane (2e). 2-(4-Carboxyphenyl)-5-(4-butoxyphenyl)-1,3,2-dioxaborinane (177 mg, 0.50 mmol), prepared from 4-carboxyphenylboronic acid (**6d**) and 2-(4-butoxyphenyl)-1,3-propanediol (**5**, R=C_4H_9O), was reacted with methanol (15 ml) in the presence of sulfuric acid (0.3 ml) under reflux for 6 h. After cooling the reaction mixture, excess methanol was removed off, and the residue was purified by chromatography on silica gel using dichloromethane as an eluent. Recrystallization from hexane gave pure product (**2e**); yield 124 mg (67%); Found: C, 68.76; H, 6.71%. Calcd for $C_{21}H_{25}BO_5$: C, 68.49; H, 6.84%; IR (Nujol) 1735 (C=O), 1320 (BO), and 1280 cm^{-1} (COC); ^1H NMR δ=0.97 (3H, t, J=8 Hz, CH_2CH_3), 1.46—1.52 (2H, m, CH_2CH_3), 1.72—1.80 (2H, m, OCH_2CH_2), 3.27 (1H, m, CH), 3.92 (3H, s, CH_3OCO), 3.95 (2H, t, J=7 Hz, $CH_2OC_6H_4$), 4.17 (2H, dd, J=11 and 11 Hz, OCH_2CH, ax), 4.27 (2H, dd, J=5 and 11 Hz, OCH_2CH, eq), 6.89 (2H, d, J=9 Hz, Ar), 7.13 (2H, d, J=9 Hz, Ar), 7.87 (2H, d, J=8 Hz, Ar), and 8.01 (2H,

Table 5. Elemental Analyses for 2-(4-Methoxyphenyl)-5-(4-alkylphenyl)-1,3,2-dioxaborinanes

R	Found (%)		Molecular formula	Calcd (%)	
	C	H		C	H
CH_3	72.46	6.69	$C_{17}H_{19}BO_3$	72.37	6.79
CH_3CH_2	72.93	6.91	$C_{18}H_{21}BO_3$	73.00	7.14
$CH_3(CH_2)_2$	73.61	7.28	$C_{19}H_{23}BO_3$	73.57	7.47
$CH_3(CH_2)_3$	74.37	7.49	$C_{20}H_{25}BO_3$	74.09	7.77
$CH_3(CH_2)_4$	74.87	8.21	$C_{21}H_{27}BO_3$	74.56	8.04
$CH_3(CH_2)_5$	75.26	8.16	$C_{22}H_{29}BO_3$	75.00	8.29
$CH_3(CH_2)_6$	75.58	8.47	$C_{23}H_{31}BO_3$	75.79	8.75
$CH_3(CH_2)_7$	75.55	8.74	$C_{24}H_{33}BO_3$	75.89	8.74

Table 6. Elemental Analyses for 2-(4-Cyanophenyl)-5-(4-alkylphenyl)-1,3,2-dioxaborinanes

R	Found (%)			Molecular formula	Calcd (%)		
	C	H	N		C	H	N
CH_3	73.97	5.59	4.78	$C_{17}H_{16}BNO_2$	73.68	5.82	5.05
CH_3CH_2	74.36	5.95	4.82	$C_{18}H_{18}BNO_2$	74.25	6.23	4.81
$CH_3(CH_2)_2$	74.68	6.36	4.33	$C_{19}H_{20}BNO_2$	74.78	6.61	4.59
$CH_3(CH_2)_3$	75.23	7.05	4.09	$C_{20}H_{22}BNO_2$	75.25	6.95	4.39
$CH_3(CH_2)_4$	76.00	6.93	4.31	$C_{21}H_{24}BNO_2$	75.69	7.25	4.20
$CH_3(CH_2)_5$	76.21	7.59	3.92	$C_{22}H_{26}BNO_2$	76.09	7.54	4.03
$CH_3(CH_2)_6$	76.40	7.51	3.84	$C_{23}H_{28}BNO_2$	76.46	7.81	3.88
$CH_3(CH_2)_7$	76.58	8.17	3.71	$C_{24}H_{30}BNO_2$	76.81	8.06	3.73

d, J=8 Hz, Ar); MS, m/z 368 (M^+).

2-[4-(Methoxycarbonyl)phenyl]-5-(4-hexylphenyl)-1,3,2-dioxaborinane (2j). Found: C, 73.21; H, 7.71%. Calcd for $C_{24}H_{29}BO_4$: C, 73.48; H, 7.45%; IR (Nujol) 1735 (C=O), 1320 (BO), and 1275 cm^{-1} (COC); ^1H NMR δ=0.88 (3H, t, J=7 Hz, $CH_2C\underline{H}_3$), 1.30—1.34 (6H, m, alkyl), 1.58—1.62 (2H, m, $C\underline{H}_2CH_2C_6H_4$), 2.59 (2H, t, J=8 Hz, $C\underline{H}_2C_6H_4$), 3.30 (1H, m, CH), 3.92 (3H, s, CH_3OCO), 4.20 (2H, dd, J=11 and 11 Hz, $OC\underline{H}_2CH$, ax), 4.30 (2H, dd, J=5 and 11 Hz, $OC\underline{H}_2CH$, eq), 7.13 (2H, d, J=9 Hz, Ar), 7.18 (2H, d, J=9 Hz, Ar), 7.88 (2H, d, J=8 Hz, Ar), and 8.02 (2H, d, J=8 Hz, Ar).

We thank the Material Analysis Center, I.S.I.R, Osaka University for spectral measurements and micro-analyses.

References

1) See, for example, H. Kelker and R. Hatz, "Handbook of Liquid Crystals," Verlag Chemie, Weinhein (1980), p. 102; H. Zaschke, A. Isenberg, and H. M. Vorbrodt, "Liquid Crystals and Ordered Fluids," ed. by A. C. Griffin and J. F. Johnson, Plenum Press, New York (1984), Vol. 4, p. 75.

2) K. Seto, S. Takahashi, and T. Tahara, *J. Chem. Soc., Chem. Commun.*, **1985**, 122; *Mol. Cryst. Liq. Cryst., Lett.*, **2**, 197 (1985).

3) M. Uno, K. Seto, and S. Takahashi, *J. Chem. Soc., Chem. Commun.*, **1984**, 932.

4) H. Suzuki, K. Nakamura, and R. Goto, *Bull. Chem. Soc. Jpn.*, **39**, 128 (1966).

5) A. Michaelis and E. Richter, *Justus Liebigs Ann. Chem.*, **315**, 33 (1901).

6) E. Yamato and S. Sasagawa, *Tetrahedron Lett.*, **1970**, 4383.

7) G. W. Gray, "The Molecular Physics of Liquid Crystals," ed. by G. R. Luckhurst and G. W. Gray, Academic Press (1979), pp. 1—29, 263—284.

8) R. Dabrowski and E. Zytynski, *Mol. Cryst. Liq. Cryst.*, **87**, 109 (1982).

9) H. Zascheke, A. Isenberg, and H. M. Vorbrodt, "Liquid Crystals and Ordered Fluids," ed. by A. C. Griffin and J. F. Johnson, Plenum Press, New York (1984), Vol. 4, p. 75.

Splitting of ^{1}H NMR Signal of Long Methylene Chain with Various Terminal Substituent in Aromatic Solvent

Takashi HOSHINO*,† and Yoshio IMAMURA
Department of Chemistry, Faculty of Science, Science University of Tokyo, Kagurazaka, Shinjuku-ku, Tokyo 162
(Received May 6, 1989)

The splitting of the methylene peaks in ^{1}H NMR spectra was studied for alkyl compounds with various substituents in 1-chloronaphthalene solutions. The solvent shifts for the higher field split methylene peak and the α-methylene peak varied with a dependence on the magnitude of the electric group moment of the terminal substituent; those for the lower- and middle-field split methylene peaks and the terminal methyl peak remained constant. It was found that the different behaviors of the solvent shifts of the methylene signals could be ascribed to the origin of the peak splitting observed for long alkyl compounds.

For long-chain alkanes (number of carbons $n_c > 16$) it was known that the methylene ^{1}H NMR peak was observed to split into a doublet in 1-chloronaphthalene.[1] After the discovery for *n*-alkanes, similar phenomena have been observed for long alkyl compounds with a terminal substituent, such as *N*-alkylmaleimides[2] and alkyl 11-maleimidoundecanoates.[3] On the other hand, methylene-peak splittings were observed for the long alkyls of surfactant molecules in water upon the addition of an aromatic solubilizate;[4-9] these phenomena have been discussed regarding the solubilization site of aromatics in surfactant micelles.

The first theoretical investigation of such splittig phenomena of the methylene peak was carried out by Ando and Nishioka.[10-12] They performed a chemical shift calculation and concluded that the splitting of peaks in an aromatic solvent arises from an increase in the number of gauche forms for long-chain hydrocarbons. On the other hand, Winnik et al. concluded that the splitting was due to a solvent effect associated with the chain end, and conclusively rejected the presence of slowly interconverting gauche and trans conformations for long alkyl chains.[13] Furthermore, several papers have been published which discuss the origin of these phenomena.[14,15]

The present authors studied the ^{1}H NMR spectra for the methyl alkanoates of various alkyl lengths in 1-chloronaphthalene and observed that the methylene peak splits into a doublet for a longer alkyl with $n_c \geq 12$ and into a triplet for $n_c \geq 20$.[16] We also studied aqueous dispersed systems of several surfactants of various chain lengths, and found that the methylene peaks of the ^{1}H spectra also split upon the addition of aromatic solubilizates, as similar manner in a homogeneous solution.[17] From those observations of the dependence of the chain length on the methylene ^{1}H NMR spectra for solutions and solubilizated dispersions, we speculated that the origin of the splitting phenomena can be ascribed to a solute-solvent interaction.

In this paper we will describe the relation between the solvent shifts in long alkyl compounds and the electric group dipole moment of their terminal substituent, the assignment of the methylene signal to 3 split peaks and, consequently, the origin of the splitting of the methylene peaks by aromatic solvents.

Experimental

Long-chain compounds with the following substituted groups were applied in this study: $-CH_3$, $-C_6H_5$, $-SH$, $-NH_2$, $-OH$, $-Cl$, $-Br$, $-COOCH_3$, $-NCO$, $-COCl$, $-COC_6H_5$, and $-CN$. These substances consist of long alkyl groups with carbon numbers of n_c=12 or 18. For compounds with a carbonyl function, the carbonyl carbon is included within the carbon number, n_c. The terminal group for nonsubstituted *n*-alkanes (dodecane and octadecane) could be represented by $-CH_3$. All the reagents used in this study were of commercially highest grade.

Samples were prepared in about a 0.5 mol dm^{-3} solution of chloroform-*d* or a mixed solvent of 90 vol% 1-chloronaphthalene/10 vol% benzene-d_6. (The latter benzene-d_6 was used to provide the deuteriumlock signal.)[15] Tetramethylsilane (TMS) was used as an internal standard. ^{1}H NMR spectra were observed using a JEOL FX-100 NMR spectrometer operated at 100 MHz at ambient temperature.

Results and Discussion

For the alkyl compounds with various terminal substituents, splittings of the methylene signal were observed in 1-chloronaphthalene, similar to that found for normal alkanes. For the compounds with the substituents, $-NH_2$, $-OH$, $-COOCH_3$, $-NCO$, $-COCl$, and $-CN$, the methylene signals (excluding of α- and β-methylenes) were observed to split into doublets for compounds of n_c=12 and into triplets for n_c=18. In the other compounds used in this study, i.e. $-CH_3$, $-C_6H_5$, $-SH$, $-Cl$, $-Br$, and $-COC_6H_5$ derivatives, the methylene signals did not split for n_c=12 but, rather, split into a doublet for n_c=18. Generally, the splitting for n_c=12 was observed for compounds with the terminal substituent of a larger electric dipole moment.

† Present address: Material Development Department, 2nd Group, Isuzu Motors Limited, Tutidana, Fujisawa Kanagawa 252.

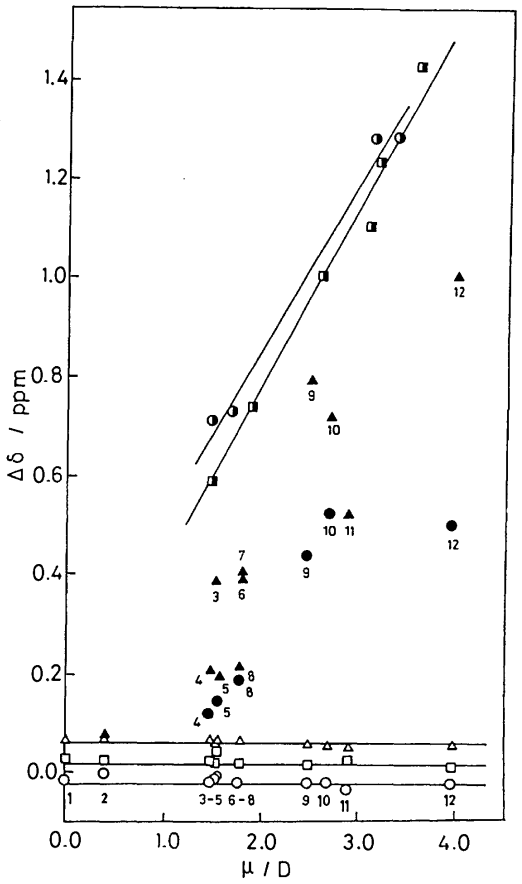

Fig. 1. Plots of the solvent shifts vs. dipole moment, for the compounds of n_c=18. ▲: α-methylene ●: higher △: middle □: lower field methylene ○: terminal methyl ◨,◑: methyl for CH_3-X compounds (Ref. from 18 and 19, respectively).
1: $-CH_3$ 2: $-C_6H_5$ 3: -SH 4: $-NH_2$ 5: -OH 6: -Cl 7: -Br 8: $-COOCH_3$ 9: -NCO 10: -COCl 11: $-COC_6H_5$ 12: -CN.

In Fig. 1 the values of the solvent shifts ($\Delta\delta$= $\delta(CDCl_3)-\delta$(1-chloronaphthalene)) of the signals are plotted against the electric dipole moment of the substituents, where δ are chemical shift of solute relative to TMS in $CDCl_3$ or 1-chloronaphthalene. The absolute magnitudes of these solvent shifts must be interpreted with caution since there were negative solvent shifts relative to the internal TMS standard. The observed solvent shifts are the difference in the specific interaction on the reference and the solute. Thus, the relative magnitude of the solvent shifts and their dependence on the terminal substituents are discussed. For low molecular weight compounds, the aromatic solvent-induced shift (ASIS) has been well studied. For example, ASIS for compounds of CH_3-X in benzene have been known to depend on its dipole moment or the group moment of substituent (X).[18,19] In Fig. 1 ASIS vs. the dipole moment (μ) of the CH_3-X compounds are also plotted. It should be noted that the aromatic and inert solvents used for CH_3-X were not the same as those used in this study.

We now discuss the relative solvent shifts of split methylene signals compared with those of small molecules. For the higher-field split methylene and α-methylene peaks, the solvent shifts depended on the electric dipole moment of the terminal substituent, as in CH_3-X compounds; however, no dependence was found for the other peaks, i.e. lower- and middle-field split methylene peaks and terminal methyl peaks. Thus, the higher-field split-methylene and α-methylene peaks behaved in a similar manner to ASIS for simple compounds, such as CH_3-X. Though the solvent shifts for the lower and middle methyene peaks and the terminal methyl peaks are different from that for CH_3-X regarding behavior, they are not affected by the choice of the terminal substituents.

Similarities in the solvent shifts for compounds of n_c=12 and 18 are as follows. For α-methylene and the higher-field split methylene peaks, solvent shifts depended on μ; for other peaks, however, they were independent. The dependence of the solvent shifts on μ for α- and higher-field methylene peaks did not vary for n_c=12 and n_c=18. In Fig. 2 the solvent shifts for α- and higher-field split methylene peaks of n_c=12 are plotted against those of n_c=18. It can be recognized that the ASIS for these peaks is not affected by the chain length, but is affected by the substituent. Figure 1 shows that the dependence of the solvent shifts on μ for n_c=18 is smaller than those for CH_3-X compounds; data are sometimes scattered. However, this phenomena is interpreted as having the same origin in both cases, i.e. an interaction between aromatics and substituent.

The difference in the splittings at n_c=12 and 18 was that the former splitting was observed to be dependent on the types of terminal substituents; the later splitting, however, into a triplet or doublet was always observed, irrespective of the substituents. (It may be noted that the splitting was observed exceptionally for longer alkyls than n_c=20 for some compounds.)

In the series of methyl alkanoates, the intensity of the higher-field split peak relative to that of lower-field split peak decreased with an increase in the total

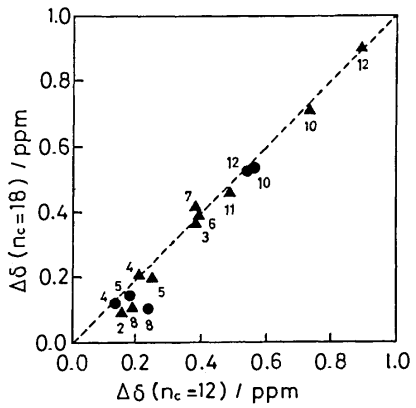

Fig. 2. Plots of ASIS for n_c=18 vs. those for n_c=12. ▲: α-methylene. ●: Higher field methylene. Numbering is same as in Fig. 1.

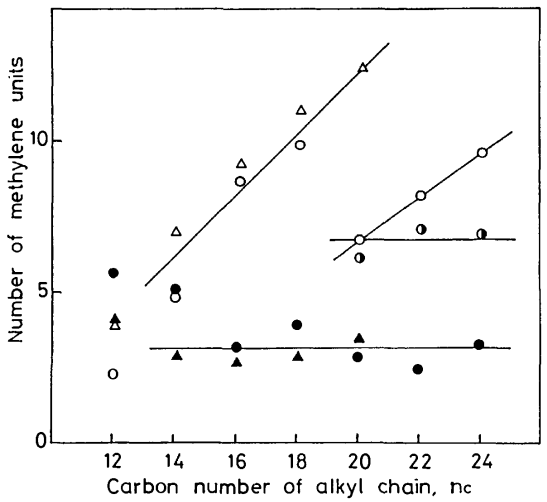

Fig. 3. Plots of methylene units assigned to higher (●), middle (◑) and lower field (○) split peaks vs. carbon numbers of alkyl chain, n_c. ○: in 1-chloronaphthalene, △: in benzene.

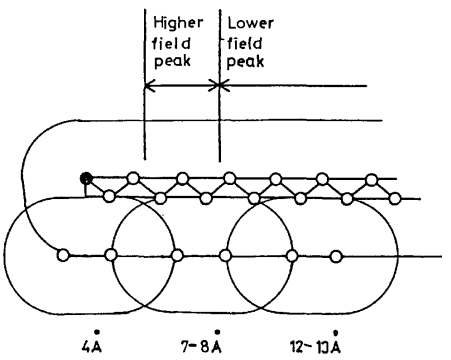

Fig. 4. Model for long alkyl compounds.

chain length. The region of the alkyl chain which experiences the solvent shifts varies with X, and is considered to consist of a definite number of methylene units. Since the solvent shifts for higher-field split peaks behaved in the same manner as those for α-methylene peaks, a definite number of methylene units neighboring the substituent are considered to be shielded by an aromatic solvent. In order to estimate the number of methylene units of the alkyl chain affected by the magnetic anisotropy of the aromatic solvent, the authors tried to assign the methylene signal to three peaks for the series of methyl alkanoates of various chain lengths from an estimation of the intensities of the split signals. The numbers of methylene units estimated for split peaks are plotted against the total carbon numbers of the alkyl chain, n_c, in Fig. 3. The contribution of the higher-field split peaks, which is affected by an aromatic solvent, was about 3 methylene units and almost constant regardless of the chain length. The contribution of the lower-field split peaks increased with n_c. This contribution increased linearly with the carbon numbers of alkyls, n_c, while the contribution of the middle peak was about 7 methylene units and almost constant. Thus, the shielded region by aromatic molecules next to the substituent consists of about 5 methylene units, in which α and β methylenes are included.

Since the behavior of solvent shifts for alkyl compounds with various substituent (X) is similar to that for CH_3-X compounds and the shielded region of alkyl chains consists of a definite number of methylene units, the solvent shifts for such long alkyl compounds can be interpreted as having the same origin as that for small molecules such as CH_3-X compounds. In the ASIS phenomena for small molecules, the association of the solute and the solvent is considered to be favorite in the so-called "solvation sphere". For long alkyl containing molecules, the corresponding solvation sphere would be restricted to local areas of the polar end of the alkyl chain.

Based on the time-averaged cluster model for ASIS,[20,21] the associated states between a long-size solute and a small solvent is considered to involve a variety of orientations of aromatic molecules and their interaction energies. However, some distinct orientations which shield about 5 methylene units are favorite around the polar end of the alkyl chain. These orientations of aromatic molecules are remarkable regarding the first neighbors, just around the polar groups. The aromatic molecules around alkyl chains far from the polar site are randomly oriented around the alkyl methylene units.

The distinct energy difference of the orientation between the first and second neighbors produces a splitting of the methylene signals. In the case of a small energy difference, for example in the substituent of -Cl and -Br, there was observed only a broadening of the methylene signals, but no splitting, was observed.

A schematic representation of the solvent effect for long alkyls is shown in Fig. 4 using Kihara's core model.[22] A distance of 70 to 80 nm from the substituent corresponds to the size of the aromatic molecule in the first neighbors and include approximately 5 methylene units.

In conclusion, observations on the peak splitting of methylene proton signals in terminal substituted alkyl compounds indicated a larger aromatic solvent shift of the terminal end methylenes than the methylene envelopes. These different behaviors of the solvent shifts between the methylenes neighboring of the polar end group and those distant from it in a long alkyl compound are concluded to be the origin of the peak splitting of the methylene signals in long alkyl compounds in aromatic solvents. A schematic molecular model for the aromatic solvent effect on a long alkyl compounds has been proposed as the result of the assignment of split methylene signals for methyl

alkanoates.

References

1) K. J. Liu, *J. Polym. Sci., Part A-2*, **5**, 1209 (1967).
2) J. I. Gonzalez de la Campa, J. M. Barrales-Rienda, and J. Gonzalez Ramos, *Macromolecules*, **10**, 989 (1977).
3) J. I. Gonzalez de la Campa and J. M. Barrales-Rienda, *Polym. J.*, **13**, 679 (1981).
4) C. A. Bunton, M. J. Minch, J. Hidalgo, and L. Sepulveda, *J. Am. Chem. Soc.*, **95**, 3262 (1973).
5) M. Grazel, K. Kalyanasundam, and J. K. Thomas, *J. Am. Chem. Soc.*, **96**, 7869 (1974).
6) J. H. Fendler, E. J. Fendler, G. A. Infante, P.-S. Shih, and L. K. Patterson, *J. Am. Chem. Soc.*, **97**, 89 (1975).
7) S. Miyagishi and M. Nishida, *J. Colloid Interface Sci.*, **73**, 270 (1980).
8) S. Miyagishi and M. Nishida, *J. Colloid Interface Sci.*, **78**, 195 (1980).
9) C. A. Bunton and C. Þ. Cowell, *J. Colloid Interface Sci.*, **122**, 154 (1988).
10) I. Ando and A. Nishioka, *Makromol. Chem.*, **152**, 7 (1972).
11) I. Ando and A. Nishioka, *Makromol. Chem.*, **160**, 145 (1972).
12) I. Ando and A. Nishioka, *Makromol. Chem.*, **171**, 195 (1973).
13) M. A. Winnik, A. Mar, W. F. Reynoldes, Ph. Dais, B. Clin, and B. Caussade, *Macromolecules*, **12**, 257 (1979).
14) I. Ando and Y. Inoue, *Makromol. Chem., Rapid. Commun.*, **4**, 754 (1983).
15) W. F. Reynoldes, M. A. Winnik, and R. G. Enriquez, *Macromolecules*, **19**, 1105 (1986).
16) T. Hoshino and Y. Imamura, *Bull. Chem. Soc. Jpn.*, **61**, 2957 (1988).
17) T. Hoshino and Y. Imamura, to be published.
18) T. L. Brown and K. Stark, *J. Phys. Chem.*, **69**, 2679 (1965).
19) R. S. Armstrong, M. J. Aroney, R. K. Duffin, H. J. Stootman, and R. J. W. Le Fevre, *J. Chem. Soc., Parkin Trans. 2*, **1972**, 1362.
20) T. Matuo, *J. Phys. Chem.*, **72**, 1819 (1968).
21) E. M. Engler and P. Laszlo, *J. Am. Chem. Soc.*, **93**, 1317 (1971).
22) T. Kihara, "Bunshi Kan Ryoku," Iwanami Shoten, Tokyo (1976); "Intermolecular Forces," in "Physical Chemistry. An Advanced Treatise," ed by H. Eyring, W. Jost, and D. Henderson, Academic Press, New York (1970).

Study of Mixed-Valence State in Halogen-Bridged Mixed-Valence Platinum(II,IV) Complexes by Temperature Dependence of Intervalence Charge-Transfer Spectra

Nobuyuki MATSUSHITA,*,† Norimichi KOJIMA, Toshiro BAN, and Ikuji TSUJIKAWA
Department of Chemistry, Faculty of Science, Kyoto University, Kitashirakawa, Sakyo-ku, Kyoto 606
(Received June 7, 1989)

The low-energy absorption edge due to the intervalence charge-transfer (IVCT) transition from Pt^{II} to Pt^{IV} has been investigated at 4.2 K and room temperature in single crystals of $[Pt(en)_2][PtBr_2(en)_2]Y_4$ {Y=ClO_4(PBC), HSO_4(PBHS)}, $[Pt(en)_2][PtI_2(en)_2](HSO_4)_4 \cdot 4H_2O$ (PIHS) and $[Pt(en)_2][PtX_2(en)_2](SO_4)_2 \cdot 6H_2O$ {X=Cl(PCSW), Br(PBSW), I(PISW)}. The IVCT absorption edges in PCSW, PBSW, and PISW shifted to the lower-energy side (i.e. red shift), while those in PBC, PBHS, and PIHS shifted to the higher-energy side (i.e. blue shift) with an increase in temperature. We consider that the thermal effect of the valence fluctuation of the Pt mixed-valence state causes a red shift of the IVCT absorption edge and that the thermal effect of the hydrogen bond between the Pt^{II} complex ion and the Pt^{IV} complex ion causes a blue shift of the IVCT absorption edge. These two effects coexist and compete with each other in one complex. The dominant effect of the two effects determines the direction of the shift of the IVCT absorption edge, namely, the temperature dependence of the Pt mixed-valence state.

In recent years,[1-3] one-dimensional halogen-bridged mixed-valence complexes analogous to Wolffram's Red Salt (WRS) $[Pt(C_2H_5NH_2)_4][PtCl_2(C_2H_5NH_2)_4]Cl_4 \cdot 4H_2O$ have been investigated from the viewpoints of physics and chemistry as a model of one-dimensional mixed-valence compounds. Figure 1 shows the structure of the Pt chain bridged by halogens in these Wolffram's Red Salt Analogues (WRA) mixed-valence complexes. The bridging halogen is not at the middle point between Pt^{II} and Pt^{IV}, but closer to Pt^{IV} than Pt^{II}. The electronic state of Pt is not strictly bivalent or quadrivalent, and approaches that of Pt^{III} by the medium of a charge-transfer interaction between the electronic state of Pt^{II} and that of Pt^{IV}.

The solid state properties in WRS and WRA mixed-valence complexes as a one-dimensional electron system have been investigated both experimentally and theoretically on the basis of the extended Peierls-Hubbard model.[4,5] The dependence of the solid state properties and the mixed-valence state on chemical members of the complexes has been investigated, mainly through substitution of the metal atom and the bridging halogen. Very recently, we reported the investigation on the idea that the influence of the substitution of a counter ion on the mixed-valence state can be interpreted by a hydrogen bond network from a comparison of the optical properties of the sulfate complexes and the hydrogensulfate complexes at 4.2 K.[6] On the other hand, it has been reported that the lattice constants along the Pt chain of $[Pt(NH_3)_4][PtX_2(NH_3)_4](HSO_4)_4$ (X=Cl, Br)[7,8] decrease, while those of $[Pt(NH_3)_4][PtI_2(NH_3)_4](HSO_4)_4 \cdot 2H_2O$[8] and $[Pt(en)_2][PtX_2(en)_2](ClO_4)_4$ (X=Cl, Br, I),[9] where en denotes ethylenediamine, increase with an increase in temperature. These results show that there are two kinds of temperature dependences regarding the Pt-Pt distance: One is that the Pt-Pt distance becomes longer with an increase in temperature; the other is that the Pt-Pt distance becomes shorter with an increase in temperature. This suggests that there are also two kinds of temperature dependences regarding the Pt mixed-valence state. We expect that the temperature dependence of the Pt mixed-valence state is dominated by the constituents of the complexes as the metal ion, the bridging halogen, the in-plane ligand amine and the counter ion. However, the temperature dependence of the mixed-valence state has not yet been investigated in detail. We have investigated the temperature dependence of the optical properties in some WRA mixed-valence complexes in order to clarify the temperature dependence of the mixed-valence state. In this paper we report on the optical properties of single crystals at 4.2 K and at room temperature in $[Pt(en)_2][PtX_2(en)_2](SO_4)_2 \cdot 6H_2O$ {X=Cl(PCSW), Br(PBSW), I(PISW)}, $[Pt(en)_2][PtBr_2(en)_2]Y_4$ {Y=ClO_4(PBC), HSO_4(PBHS)}, $[Pt(en)_2][PtI_2(en)_2](HSO_4)_4 \cdot 4H_2O$ (PIHS). In addition, we also report on the synthesis, structure and the mixed-valence state of a new WRA mixed-valence complex, PCSW. From these experimental results, we discuss the temperature dependence of the Pt mixed-valence state on the basis of the hydrogen bond network.

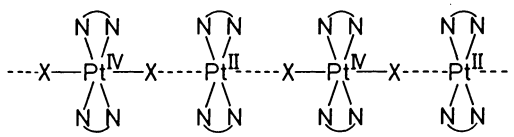

Fig. 1. The Pt chain structure of the halogen-bridged mixed-valence platinum complexes.

† Present address: Department of Chemistry, College of Arts and Sciences, The University of Tokyo, Komaba, Meguro-ku, Tokyo 153.

Experimental

Preparation. The Pt^{II}-Pt^{IV} mixed-valence complexes (PBHS, PIHS, PBSW, PISW) were prepared; these single crystals were obtained according to a previously described method.[6] The PBC was prepared by a procedure of Bekaroglu et al.[10] Single crystals of the low-temperature phase** of PBC were obtained at 13 °C by recrystallization from an aqueous solution. The above-mentioned mixed-valence complexes were identified by elemental analysis and a powder X-ray diffraction method.

$[Pt(en)_2][PtCl_2(en)_2](SO_4)_2 \cdot 6H_2O$ (PCSW): $[PtCl_2(en)_2](HSO_4)_2$ was obtained by the oxidation of $[Pt(en)_2]Cl_2$ with an aqueous hydrogen peroxide solution, and then by the addition of a small amount of hydrochloric acid and an excess of aqueous sulfuric acid to the oxidized platinum complex solution. Its Pt^{IV} complex (1.7 mmol) and $[Pt(en)_2]Cl_2$ (1.7 mmol) were dissolved in water (ca. 100mL). Yellow plate-like single crystals, which show dichroism, were obtained by a slow concentration of this colorless solution. Found: C, 9.63; H, 4.46; N, 11.31; O, 22.44; S, 6.45; Cl,7.06%. Calcd for $C_8H_{44}Cl_2N_8O_{14}Pt_2S_2$: C, 9.61; H, 4.44; N, 11.21; O, 22.41; S, 6.42; Cl, 6.89%.

Elemental analysis was carried out by "The Laboratory for Organic Elemental Microanalysis" of Kyoto University.

Instrumental Measurements. Powder X-ray diffraction patterns were recorded at room temperature (20 °C for PBC) on a Rigaku diffractometer using the θ-2θ scan technique and graphite-monochromated Cu $K\alpha$ radiation (λ=1.5418 Å). It was confirmed that crystals of PBC were the low-temperature phase. The crystals of PBC in the low-temperature phase were used for measurements of the absorption spectra.

The TGA of PCSW was performed on a Rigaku TG DTA 8112S apparatus in the temperature region from room temperature to 200 °C.

The absorption spectra of single crystals were measured at 4.2 K and room temperature with a Jasco CT-100 spectrometer using a tungsten lamp for the light source and a Glan-Taylor prism for polarizing light. A lock-in system working with HTV R376 and R316 photomultipliers and a PbS photoconductive cell was used for detection. The sample measured at 4.2 K was placed in a double glass Dewar's vessel and immersed in liquid helium to cool. The measurement at room temperature was carried out by irradiating the sample with monochromatic light to prevent thermo-damage of the single crystal due to white light.

Results and Discussion

PCSW. TGA shows that the content of the crystallized water (10.8%) calculated from the chemical formula of PCSW corresponds with the weight loss (10.6%, 48—121 °C) on heating. The powder X-ray diffraction pattern shows that PCSW is isomorphous to PBSW and PISW in structure. The lattice constants of PCSW (a=13.74, b=11.54, c=9.19 Å, β=101.7°) was determined by the powder X-ray diffraction pattern of PCSW with index numbers which were numbered by reference to that of PBSW and PISW. To our knowledge, it is the first example that Cl-, Br-, and I-bridged complexes are isomorphous in the WRA mixed-valence complexes whose chemical entities are the same, except for the bridging halogen. Figure 2 shows the absorption spectra of a single crystal of PCSW at 4.2 K. The absorption edge P for the light polarized parallel to the Pt chain axis (***E*//** chain) is the low-energy absorption edge due to the IVCT transition from the d_{z^2} of Pt^{II} to the d_{z^2} of Pt^{IV}. The energy of the IVCT absorption edge of PCSW (22.3×10^3 cm^{-1}) is higher than that of PBSW (17.7×10^3 cm^{-1})[6] and PISW (9.5×10^3 cm^{-1}).[6] The energies of the IVCT absorption edge in complexes comprising a bivalent counter ion are in the order I<Br<Cl, as well as those in complexes comprising a univalent counter ion. The energy of the IVCT absorption edge of PCSW is higher than that of $[Pt(en)_2][PtCl_2(en)_2](ClO_4)_4$ (PCC) (19.1×10^3 cm^{-1})[11] as well as that of PBSW, being higher than that of PBHS (8.4×10^3 cm^{-1})[6] and PBC (7.5×10^3 cm^{-1}). In other words, the energy of the IVCT absorption edge of a complex comprising a bivalent counter ion is higher than that of the complexes comprising a univalent counter ion, also in the chloro-bridged mixed-valence complexes. As previously described in our paper,[6] complexes comprising a univalent counter ion have more hydrogen bonds which link a platinum atom with an adjacent platinum on the same chain by way of the amine and the counter ion than the complexes comprising a bivalent counter ion. This is because the molar ratio of the counter ion for a platinum atom in the former complexes is twice as large as that in the latter complexes. Thus, the bond between a platinum atom and an adjacent platinum atom on the same chain in univalent counter ion complexes is more strongly supported by the hydrogen bond network than that in

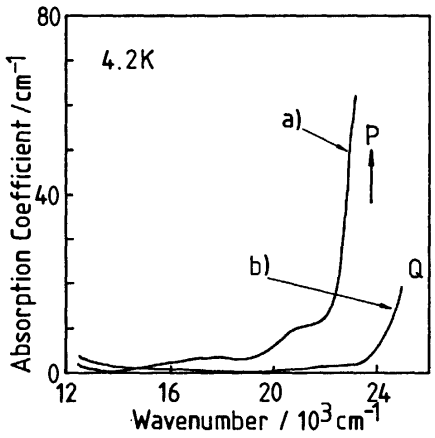

Fig. 2. Single crystal absorption spectra of $[Pt(en)_2][PtCl_2(en)_2](SO_4)_2 \cdot 6H_2O$ (PCSW) at 4.2 K. Curve a) is the spectrum for the light polarized parallel to the Pt chain axis (***E*//**chain). Curve b) is the spectrum for the light polarized perpendicular to the Pt chain axis (***E*⊥**chain).

** The structure phase transition occurs in PBC at ca. 30 °C. The high-temperature phase is orthorhombic and the low-temperature phase is monoclinic.

the bivalent counter ion complexes. Therefore, the result of PCSW and PCC can also be explained by the effect of this hydrogen bond network. The peak energy of the IVCT band obtained by a Kramers-Kronig transformation of the reflection spectra of $[Pt(chxn)_2][PtCl_2(chxn)_2](ClO_4)_4$ (Pt-chxn-Cl-ClO_4) (3.2 eV), where chxn denotes 1,2-cyclohexanediamine, is much higher than that of PCC (2.72 eV),[4] and the crystal color of Pt-chxn-Cl-ClO_4 is the same yellow as that of PCSW. These results show that the mixed-valence state of PCSW is comparable to that of Pt-chxn-Cl-ClO_4. We can explain the change in the mixed-valence state with a change from en to chxn as follows. The distinction between the electronic state of Pt^{II} and that of Pt^{IV} becomes large with a decrease in the effect of the hydrogen bond network, since the C_6H_{10} ring of chxn blocks the formation of the hydrogen bonds between the $-NH_2$ of chxn and the counter ion ClO_4^-. The influence of the substitution from the univalent counter ion as ClO_4^- or HSO_4^- to the bivalent counter ion as SO_4^{2-} on the mixed-valence state is comparable to that of the substitution of the in-plane ligand amine from en to chxn. In other words, this fact is proof that the hydrogen bond between the counter ion and the amine contributes to the mixed-valence state.

Temperature Dependence of the Mixed-Valence State. Figures 3—5 show the IVCT absorption edges for the *E*//chain at 4.2 K and at room temperature in PBC, PBHS, and PIHS, respectively; Table 1 shows those energies. The energies of these IVCT absorption edges at room temperature are higher than those at 4.2 K. Namely, the IVCT absorption edges in PBC, PBHS, and PIHS shifted to the higher-energy side with an increase in temperature. This blue shift is opposite to a broadening of the spectra due to an increase in temperature. Therefore, this result shows that the energy distinction between the electronic state of the Pt^{II} and that of the Pt^{IV} in the mixed-valence state increases with an increase in temperature.

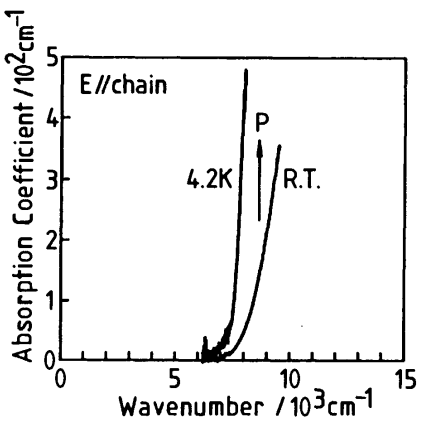

Fig. 3. The IVCT absorption edges of the single crystal of $[Pt(en)_2][PtBr_2(en)_2](ClO_4)_4$ (PBC) for *E*//chain at 4.2 K and room temperature (R.T.).

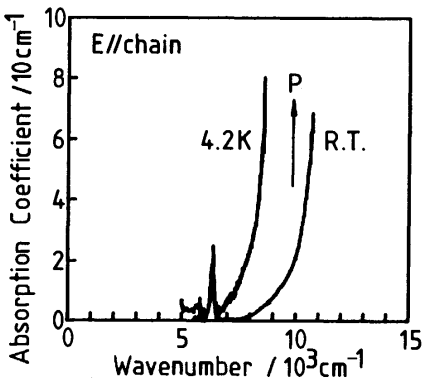

Fig. 4. The IVCT absorption edges of the single crystal of $[Pt(en)_2][PtBr_2(en)_2](HSO_4)_4$ (PBHS) for *E*//chain at 4.2 K and room temperature (R.T.).

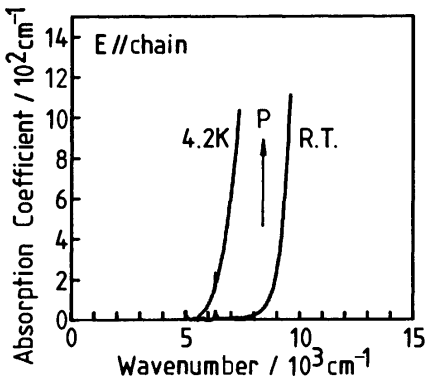

Fig. 5. The IVCT absorption edges of the single crystal of $[Pt(en)_2][PtI_2(en)_2](HSO_4)_4 \cdot 4H_2O$ (PIHS) for *E*//chain at 4.2 K and room temperature (R.T.).

Table 1. The Energy of the IVCT Absorption Edges at 4.2 K and Room Temperature

Complex	Energy/10^3 cm^{-1}	
	4.2 K	Room temp
PBC	7.5	8.3
PBHS	8.4	10.2
PIHS	6.4	9.0
PCSW	22.3	19.8
PBSW	17.7	14.8
PISW	9.5	7.3

Figures 6—8 show the IVCT absorption edges for the *E*//chain at 4.2 K and at room temperature in PCSW, PBSW, and PISW, respectively; Table 1 shows those energies. The energies of these IVCT absorption edges at room temperature are lower than those at 4.2 K. Namely, the IVCT absorption edges in PCSW, PBSW, and PISW shifted to the lower-energy side with an increase in temperature. This result shows that the energy distinction between the electronic state of the Pt^{II} and that of the Pt^{IV} in the mixed-valence state decreases with an increase in temperature, for the following reasons. The lower-energy side shift, i.e. the red shift (2000—3000 cm^{-1}), is much larger than

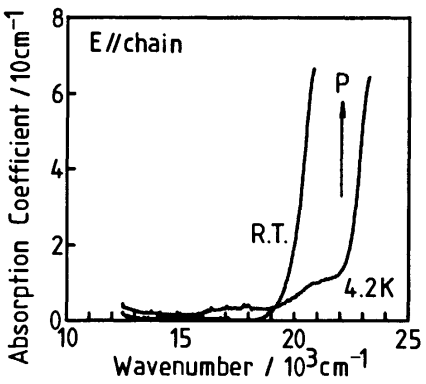

Fig. 6. The IVCT absorption edges of the single crystal of $[Pt(en)_2][PtCl_2(en)_2](SO_4)_2 \cdot 6H_2O$ (PCSW) for *E*//chain at 4.2 K and room temperature (R.T.).

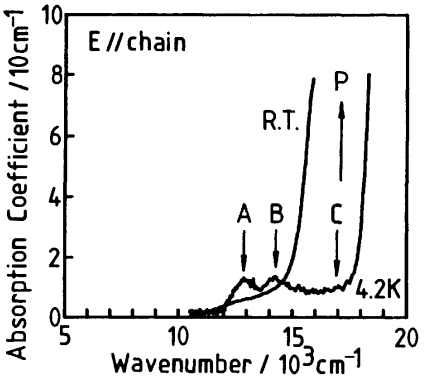

Fig. 7. The IVCT absorption edges of the single crystal of $[Pt(en)_2][PtBr_2(en)_2](SO_4)_2 \cdot 6H_2O$ (PBSW) for *E*//chain at 4.2 K and room temperature (R.T.).

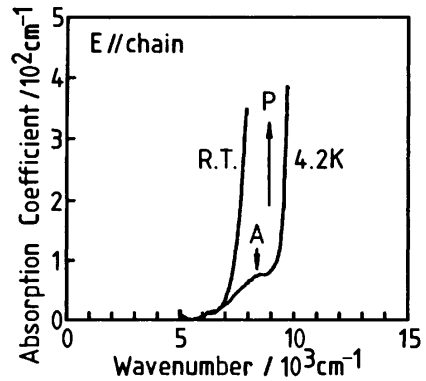

Fig. 8. The IVCT absorption edges of the single crystal of $[Pt(en)_2][PtI_2(en)_2](SO_4)_2 \cdot 6H_2O$ (PISW) for *E*//chain at 4.2 K and room temperature (R.T.).

the temperature broadening of the spectra. Its large red shift cannot be explained by both a broadening of the spectra and an increase in the energy distinction between the electronic state of the Pt^{II} and that of the Pt^{IV}, which was mentioned above. In addition, we have found that the peak energy of the reflection spectra of PBSW at room temperature is lower than that at 77 K.[12] The result of the reflection spectra is consistent with the absorption spectral result of PBSW. Therefore, the result of the red shift of the IVCT absorption edge shows that the energy distinction between the electronic state of Pt^{II} and that of Pt^{IV} in the mixed-valence state decreases with an increase in temperature.

We found that there are two kinds in the temperature dependences of the mixed-valence state from the absorption spectra. These two dependences are consistent with the two types of temperature dependences of the mixed-valence state obtained from the structural result: that there are two kinds in the temperature dependences of the Pt-Pt distance along the Pt chain. To interpret the two types of temperature dependences of the mixed-valence state, we propose two types of thermal effects contributing to the mixed-valence state as follows.

One is an effect that the electronic state of the Pt^{II} and that of the Pt^{IV} approach each other with an increase in temperature. A positional fluctuation of the bridging halogen becomes vigorous by a thermal excitation of the Pt^{IV}-X stretching vibration with an increase in temperature. This fluctuation induces a valence fluctuation of the Pt mixed-valence state by the medium of the electron-phonon coupling, which is one of characteristics of this WRA system. This valence fluctuation becomes vigorous with an increase in temperature, and approaches the electronic state of the Pt^{II} and that of the Pt^{IV} to that of the Pt^{III}, respectively. Consequently, the distinction between the energy level of the d_{z^2} of Pt^{II} and that of Pt^{IV} in the mixed-valence state decreases with an increase in temperature. As a result, this change in the Pt electronic state causes a red shift of the IVCT absorption edge. Equally, the negative thermal expansion coefficient of the lattice constant along the Pt chain axis of $[Pt(NH_3)_4][PtX_2(NH_3)_4](HSO_4)_4$ (X=Cl, Br)[7,8] is theoretically interpreted as the valence fluctuation.[13]

The other is an effect that the electronic state of the Pt^{II} and that of the Pt^{IV} are more distinguishable from each other with an increase in temperature. Positional fluctuations of the hydrogen atom of the in-plane ligand amine and the oxygen atom of the counter ion become vigorous by thermal excitation with an increase in temperature. These fluctuations weaken the link by the hydrogen bond between the Pt^{II} complex ion and the Pt^{IV} complex ion. Consequently, the weak link of the hydrogen bond weakens the intervalence charge-transfer bond between the $Pt^{II}$and the Pt^{IV}. Therefore, the electronic state of the Pt^{II} and that of the Pt^{IV} at higher temperatures become more distinguishable than those at lower temperatures. As a result, this change in the Pt electronic state causes a blue shift of the IVCT absorption edge.

In a comparison between the crystal structure of $[Pt(NH_3)_4][PtBr_2(NH_3)_4](HSO_4)_4$ at 298 K and that at 134 K, the Pt-Pt distance becomes long, and the N(-H)···O distance becomes short with a decrease in

temperature.[8] The change of the Pt-Pt distance is consistent with the red shift, and the change of the N(-H)···O distance is consistent with the blue shift. This result regarding the structure shows that both effects causing the red and blue shifts coexist together and compete with each other in one WRA mixed-valence complex, since changes in both the Pt-Pt distance and the N(-H)···O distance coexist. In addition, from the results concerning the IVCT absorption edge, the dominant effect of the two competing effects determines the direction of the shift of the IVCT absorption edge. In the sulfate complexes, PCSW, PBSW, and PISW, the effect of the valence fluctuation due to the thermal vibration of the bridging halogen (namely, the effect causing the red shift) dominates. In PBC, PBHS, and PIHS, the effect regarding the weakening of the hydrogen bond link due to the thermal vibration (namely, the effect causing the blue shift) dominates. Furthermore, we consider which of the thermal effects (the valence fluctuation or the hydrogen bond) dominates the temperature dependence of the mixed-valence state. This dominance can be explained from the effect of the hydrogen bond network. As mentioned above, the dependence of the energy of the IVCT absorption edges on the substitution of the counter ion and that of the in-plane ligand amine is explained from this effect of the hydrogen bond network. Relatively speaking, the perchlorate and hydrogensulfate complexes comprising the univalent counter ion belong to a system in which the effect of the hydrogen bond network is stronger, while the sulfate complexes comprising the bivalent counter ion belong to a system in which that effect is weaker. This classification is used because the composition ratio of the counter ions for a platinum atom in the former is twice as much as that in the latter.[6] First, in the former system, in which the effect of the hydrogen bond network is stronger, the temperature dependence of the mixed-valence state is dominated by the thermal effect of the hydrogen bond rather than the thermal effect of the valence fluctuation. Therefore, the energy distinction between the electronic state of Pt^{II} and that of Pt^{IV} becomes larger, namely, the IVCT absorption edge shows a blue shift with an increase in temperature. On the other hand, in the latter system, in which the effect of the hydrogen bond network is weaker, the temperature dependence of the mixed-valence state is dominated by the thermal effect of the valence fluctuation rather than the thermal effect of the hydrogen bond. Therefore, the energy distinction between the electronic state of Pt^{II} and that of Pt^{IV} becomes smaller, namely, the IVCT absorption edge shows a red shift with an increase in temperature.

In the above discussion, the mixed-valence state and its temperature dependence in the perchlorate and hydrogensulfate complexes are not only dominated by the direct contribution due to the interaction between the Pt^{II} and the Pt^{IV} through the bridging halogen, but are also dominated by the hydrogen bond between the amine and the counter ion. On the other hand, the mixed-valence state and its temperature dependence in the sulfate complexes are almost dominated by the direct contribution and are little dominated by the hydrogen bond.

To confirm the temperature dependences of the mixed-valence state by the reflection spectra, measurements of the reflection spectra in PBC, PBHS, PIHS, PCSW, and PISW are in progress. To clarify the relation between the temperature dependence of the IVCT spectra and that of the structure, studies of the temperature dependence of the crystal unit cell for PBHS, PIHS, PCSW, PBSW and PISW, and that of the IVCT absorption edges of $[Pt(NH_3)_4][PtX_2(NH_3)_4](HSO_4)_4$ (X=Cl, Br) and $[Pt(NH_3)_4][PtI_2(NH_3)_4](HSO_4)_4 \cdot 2H_2O$ are necessary.

The authors wish to thank Dr. Koshiro Toriumi of I.M.S. and Dr. Masahiro Yamashita of Nagoya University for valuable discussions concerning the crystal structure. We are also indebted to Dr. Naohilo Watanabe of Kyoto University for his kind help and advice concerning data processing computer programs. This study was supported by a Grant-in-Aid for Scientific Research No. 63540485 from the Ministry of Education, Science and Culture.

References

1) H. J. Keller, "Extended Linear Chain Compounds," ed by J. S. Miller, Plenum, New York (1982), p. 357.
2) R. J. H. Clark, "Mixed-Valence Compounds," ed by D. B. Brown, Reidel, Dordrecht (1980), p. 271.
3) K. Nasu, M. Yamashita, T. Mitani, and S. Kurita, *Butsuri*, **41**, 317 (1986).
4) Y. Wada, T. Mitani, M. Yamashita, and T. Koda, *J. Phys. Soc. Jpn.*, **54**, 3143 (1985).
5) K. Nasu, *J. Phys. Soc. Jpn.*, **52**, 3865 (1983); **53**, 302 (1984); **53**, 427 (1984).
6) N. Matsushita, N. Kojima, T. Ban, and I. Tsujikawa, *Bull. Chem. Soc. Jpn.*, **62**, 1785 (1989).
7) M. Tanaka, I. Tsujikawa, K. Toriumi, and T. Ito, *Acta Crystallogr., Sect. B*, **38**, 2793 (1982).
8) M. Tanaka and I. Tsujikawa, *Butsuri*, **41**, 275 (1986).
9) K. Toriumi and M. Yamashita, private communication.
10) O. Bekaroglu, H. Breer, H. Endres, H. J. Keller, and H. Nam-Gung, *Inorg. Chim. Acta*, **21**, 183 (1977).
11) M. Tanaka, S. Kurita, T. Kojima, and Y. Yamada, *Chem. Phys.*, **91**, 257 (1984).
12) N. Matsushita, N. Kojima, N. Watanabe, and T. Ban, in preparation for publication.
13) T. Murao, *Phys. Rev. B*, **35**, 6051 (1987).

 © 1989 The Chemical Society of Japan Bull. Chem. Soc. Jpn., 62, 3911—3918 (1989)

Analysis of Cyclic Voltammograms for Polypyrrole-as-Deposited Pt/poly[tris(4-vinyl-4′-methyl-2,2′-bipyridine)ruthenium(II) perchlorate] Electrodes

Kenji MURAO,* Naoki TANAKA, and Kazuhiro SUZUKI
Advanced Research Laboratory, Hitachi Ltd., Kokubunji, Tokyo 185
(Received July 29, 1989)

Oxidation waves in cyclic voltammograms (CVs) observed during repeated potential cyclings of polypyrrole-as-deposited Pt/poly-1 electrodes (poly-1: poly[tris(4-vinyl-4′-methyl-2,2′-bipyridine)ruthenium-(II) perchlorate]) in 0.1 M TBAP/acetonitrile, that lead to the bilayer (BL) electrochemistry, have been quantitatively analyzed. As the potential cycling is repeated, the CV change occurs, i.e., decrease of the peak current and positive shift of the peak potential. This is shown to be the result of logarithmic decrease in the complementary charge transfer coefficient β in the totally irreversible thin-layer (TITL) electrochemistry. k°_{TL} (standard rate constant for polypyrrole oxidation) and C°_{TL} (initial concentration of the reduced sites in polypyrrole) have been determined to be 5.50×10^{-9} cm mol^{-1} s^{-1} and 3.15×10^{-3} mol cm^{-3}, respectively, by fitting CV data to the theory of the TITL model. The subsequent onset and growth of the CV waves in the higher potential region are explained as being due to progressive partitioning of polypyrrole sites from the TITL mode to the BL mode in which polypyrrole sites are oxidized. The partition coefficient θ, defined as the ratio of polypyrrole sites oxidized in the BL mode to all the polypyrrole sites, has been found to approximately depend on the logarithm of β. In the BL mode, a linear relationship is found between peak current and peak potential. Simulation of the CV waves has been performed based on the theoretical models of TITL and BL electrochemistry, and has revealed that a model assuming separation of polypyrrole sites into the TITL and BL modes prior to each cyclic sweep explains the occurrence of the significantly separated current peaks in both modes. These results are discussed in terms of Electrochemically driven Phase Separation (ECPS), in which the decrease in β is directly related to the separation of the mixed poly-1 and polypyrrole phase.

Fabrication of microstructures with conducting polymers such as polypyrrole[1] has been the subject of recent keen interest because of both their basic importance in solid state physics[2] and potential applications.[3-7] We previously[8] reported on the successful deposition of polypyrrole onto an electrochemically active polymer film, poly-1 (poly[tris(4-vinyl-4′-methyl-2,2′-bipyridine)ruthenium(II) perchlorate]), giving an electrode expressed as Pt/poly-1/polypyrrole. Preparation of the bilayer electrodes consists of the following two steps; 1) electropolymerization of pyrrole at a Pt/poly-1 electrode, 2) repeated potential cyclings between 2+/3+ and 2+/1+ redox potentials of the $[Ru(vbpy)_3]^{2+}$ center (vbpy: 4-vinyl-4′-methyl-2,2′-bipyridine) in 0.1 M TBAP (tetrabutylammonium perchlorate)/acetonitrile (1 M=1 mol dm^{-3}). In step 1), electropolymerization of pyrrole occurs at the platinum substrate as a result of permeation of the monomer molecules throughout the poly-1 layer, as is evidenced by the CVs (cyclic voltammograms) which indicate direct charge exchange between the polypyrrole layer and the platinum substrate.[8] This means that a mixed phase of poly-1 and polypyrrole is formed in this stage. However the subsequent potential sweeps (step 2)) ultimately result in the bilayer electrochemistry in which redox reactions of polypyrrole are totally mediated by the $[Ru(vbpy)_3]^{2+}$ sites in the poly-1 layer. These electrochemical processes contrast with those employed for the preparation of bilayer electrodes based on electro-nonconducting redoxing polymers,[9] although our electrodes finally obtained through the above steps behave essentially in the same way. During step 2), a series of characteristic CV changes have been recorded as shown in Fig. 1

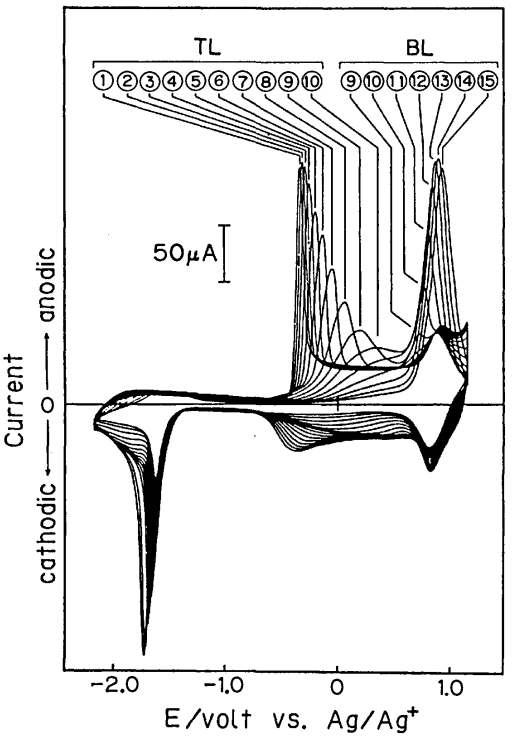

Fig. 1. Cyclic voltammograms of a polypyrrole-as-deposited Pt/poly-1 electrode measured upon repeated potential sweeps in 0.1 M TBAP/acetonitrile. Sweep rate: 0.1 V s^{-1}. (A part of this figure is reproduced from Fig. 2(b) of Ref. 8 with permission.)

(partially reproduced from Fig. 2(b) of Ref. 8). These CVs have aroused our great interest because they seem to represent certain unknown electrochemical processes that involve dynamic changes taking place in the polymer matrix. To account for the electrochemical changes, we proposed Electrochemically driven Phase Separation (ECPS) of the mixed phase from optical studies.[10] Polythiophenes have been found to undergo similar electrochemical processes.[11,12]

We show here that the CVs in Fig.1 represent a gradually developing crossover from a regime essentially described by totally irreversible thin layer electrochemistry[13] (TL regime) to bilayer electrochemistry (BL regime), associated with systematic decrease in β (complementary charge-transfer coefficient, $\equiv 1-\alpha$ where α is the charge-transfer coefficient). This finding not only supports the hypothesis of the ECPS scheme[10,14] but also provides insight into the implications of the charge-transfer coefficient in the electrochemistry of polymer-coated electrodes. The electrochemistry of polymer-coated electrodes has been studied[15-18] in relation to that of chemisorbed systems[19,20] which have the same basis as thin-layer electrochemistry.

Experimental

Materials. Preparation of the monomer precursor of poly-1, $[Ru(vbpy)_3]^{2+}$ $2PF_6^-$ was described in previous papers.[8,10] Acetonitrile was used after distillation. Commercial TBAP was purified by recrystallizing from an EtOH/H_2O 2:3 mixed solvent and was dried in vacuo at 80 °C for 32 h.

Electrochemistry. Platinum disks (3 mm diameter) embedded in glass were used as the working substrates. The surface of the platinum substrates was polished with 1 μm diamond paste. Each working electrode was sonicated three times in freshly distilled acetone, two times in trichloroethylene, two times in distilled water, and then dried at 80 °C. All of the electrochemical experiments were performed under argon-purged conditions. Electropolymerizations and electrochemical measurements were performed in a one-compartment cell with an Ag/Ag^+ quasi-reference electrode which showed 290 mV vs. SCE (saturated calomel electrode) in 0.1 M TBAP/acetonitrile. Potentials are all indicated vs. Ag/Ag^+. Deposition of poly-1 and polypyrrole were described in previous papers.[8,10] Electrochemical experiments were performed on a PAR Model 175 Universal Programmer and a 173 Potentiostat, and were recorded on a YEW 3086 X-Y Recorder.

Results and Discussion

Nature of the Cyclic Voltammograms. Figure 1 depicts the CVs for polypyrrole-as-deposited Pt/poly-1 electrode, recorded during repeated potential sweeps at a sweep rate of 0.1 V s^{-1} in 0.1 M TBAP/acetonitrile. The repeated potential sweeps lead to the bilayer electrochemistry.[8] Just after the break-in,[8] the oxidation waves of polypyrrole show sharp peaks which are not observed for Pt/polypyrrole electrodes. The following potential sweeps (**1—8**) cause shifts in $E_{p,TL}$ (peak potential for polypyrrole oxidation wave in the TL regime) in the positive direction associated with decrease in $i_{p,TL}$ (peak current for polypyrrole oxidation waves). In this stage, all of the polypyrrole sites are oxidized in the TL regime. Subsequently repeated potential sweeps evolve current peaks near the 2+/3+ redox potential of poly-1 (**9,10** in the BL regime), owing to the onset of mediated oxidation of polypyrrole, which increases with further sweeps, eventually leading to the oxidation of all polypyrrole sites in the BL mode.

To prove the nature of the sharp peaks, CVs were measured for a separate electrode (Fig. 2) in a stage approximately corresponding to **1—4** of Fig. 1. These CVs are anomalous in the sense that, although the sharp oxidation peak ③ is a result of direct electron transfer to the electrode, its rereduction ① is

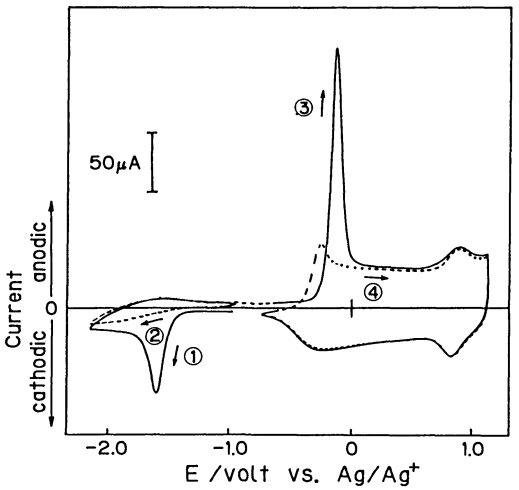

Fig. 2. Cyclic voltammograms of similarly prepared electrode as that of Fig. 1 measured in 0.1 M TBAP/acetonitrile at a sweep rate of 0.1 V s^{-1}. The CVs approximately correspond to the stage of the sweeps **1—4**. Numbers in circles indicate the sequence of the sweeps.

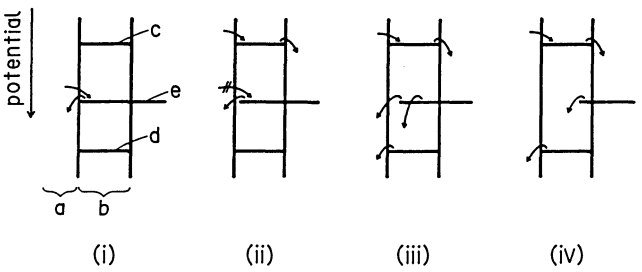

Fig. 3. Representation of possible electron transfer modes inferred on the basis of the electrochemistry depicted in Figs. 1 and 2. a: platinum electrode; b: poly-1 layer; c,d: 2+/1+ and 2+/3+ redox levels of $[Ru(vbpy)_3]^{2+}$ centers in poly-1, respectively; e: redox level of polypyrrole where the extent of phase separation is represented by relative positions of the bar.

mediated by the 2+/1+ redox level of poly-1. This implies that the sharp current peak ③ is due to the totally irreversible oxidation of polypyrrole. The nature of this peak is essentially faradaic because optical changes due to the polypyrrole oxidation are substantiated by the peak.[21]

These points are illustrated in Fig. 3. In the initial stage (i), both oxidation and reduction reactions of polypyrrole occur only through direct charge exchange with the platinum electrode. The above mentioned anomaly is shown in (ii) in which the oxidative and reductive charge transfers are effected asymmetrically. Stage (iii) corresponds to sweeps **9—12**, where both direct and indirect (mediated) oxidation modes of polypyrrole occur in a single sweep, while its rereduction is totally mediated. Stage (iv) represent the finally achieved bilayer electrochemistry corresponding to **13—15**. Hence, the electrochemistry involved in Fig. 1 can be summarized as follows; the current waves denoted by TL in Fig. 1 represent totally irreversible oxidations of polypyrrole. The following repeated potential sweeps increase the portion of polypyrrole sites that is mediatively oxidized by poly-1, eventually leading to the mediated oxidation of the whole polypyrrole sites. This suggests that the TL regime may be analyzed on the basis of the thin layer model for totally irreversible electrode processes.[13]

Analysis of Cyclic Voltammograms Using the Thin Layer Model for Totally Irreversible Electrode Processes (TITL Model). CVs for polypyrrole-as-deposited Pt/poly-1 electrodes were measured in the same way as for Fig. 1, for three separate electrodes, A—C. Coverages of poly-1 (mol cm^{-2}) and charge densities passed during the electropolymerization of pyrrole (mC cm^{-2}) are as follows, respectively; A: 3.45×10^{-9}, 40.0; B: 3.86×10^{-9}, 39.6; C: 2.68×10^{-9}, 41.2. Since the CVs involving polypyrrole include non-faradaic components significantly,[21a,b,22-24] their quantitative analysis of the whole waveforms is not straightforward. Therefore, the following analysis only considers peak currents and peak potentials which are expected to be less affected by non-faradaic contributions as mentioned above. Table 1 lists peak currents and peak potentials for electrodes A—C. Sweep number **1** for each electrode in Table 1 are determined as the sweep by which peak currents in the TL regime reach the initial saturation level after break-in.[8] Subsequent sweep numbers, as indicated in Fig. 1, are given for every consecutive three sweeps.

According to the TITL model,[13] oxidative currents upon a linear potential sweep are given by

$$i_{TL}=n_{TL}FS\,k^{\circ}_{TL}\,C^{\circ}_{TL}\exp\left\{\frac{\beta n_{o,TL}F}{RT}(E-E^{\circ}_{TL})-\frac{SRTk^{\circ}_{TL}}{\beta n_{o,TL}FVr}\exp\left[\frac{\beta n_{o,TL}F}{RT}(E-E^{\circ}_{TL})\right]\right\} \quad (1)$$

n_{TL} : number of electrons per reaction center oxidized
$n_{o,TL}$: number of electrons per reaction center oxidized in the rate-determining step
k°_{TL} : standard rate constant (cm mol^{-1} s^{-1})
C°_{TL} : initial concentration of reduced centers (mol cm^{-3})
F : Faraday constant
R : gas constant
T : absolute temperature of the reaction system
V : volume of the reaction system
S : electrode area
r : sweep rate of electrode potential (V s^{-1})
E°_{TL} : standard electrode potential

By differentiation, peak current, $i_{p,TL}$, and peak potential, $E_{p,TL}$, are obtained.

Table 1. Observed Peak Currents and Peak Potentials

Electrode	Peak No.	i_p[a]		E_p[b]	
		TL	BL	TL	BL
A	1	213		−0.340	
	2	219		−0.318	
	3	215		−0.288	
	4	199		−0.253	
	5	174		−0.200	
	6	153		−0.135	
	7	123		−0.050	
	8	92.8		0.063	
	9	67.5	64.0	0.200	0.718
	10	51.3	102	0.365	0.750
	11		155		0.790
	12		196		0.825
	13		220		0.853
	14		222		0.878
	15		213		0.913
B	1	182		−0.398	
	2	186		−0.375	
	3	187		−0.338	
	4	180		−0.300	
	5	154		−0.263	
	6	126		−0.205	
	7	101		−0.133	
	8	82.5		−0.038	
	9	69.0	60.0	0.050	0.725
	10	60.0	89.0	0.100	0.750
	11	48.5	113	0.220	0.785
	12		130		0.795
	13		151		0.810
	14		165		0.823
	15		170		0.850
C	1	237		−0.325	
	2	241		−0.313	
	3	241		−0.300	
	4	237		−0.275	
	5	227		−0.248	
	6	198		−0.210	
	7	140		−0.155	
	8	90.0		−0.045	
	9	77.0	56.3	0.380	0.733
	10	59.0	88.8	0.208	0.760
	11	47.3	141	0.375	0.800
	12		181		0.825
	13		209		0.850
	14		223		0.875
	15		221		0.905

a) 10^{-6} A. b) V vs. Ag/Ag^{+}.

$$i_{p,TL}=\frac{\beta n_{o,TL}\, n_{TL}\, F^2\, V\, r\, C^\circ_{TL}}{eRT} \quad (2)$$

$$E_{p,TL}=E^\circ_{TL}+\left(\frac{RT}{\beta n_{o,TL}\, F}\right)\ln\left(\frac{\beta n_{o,TL}\, FVr}{SRTk^\circ_{TL}}\right) \quad (3)$$

Since β values for each ($i_{p,TL}$, $E_{p,TL}$) set are not known, direct evaluation of the data in Table 1 with Eqs. 2 and 3 is not practical. By combining Eqs. 2 and 3, $\beta n_{o,TL}$ is eliminated to give

$$f(i_{p,TL})\equiv\frac{n_{TL}\, FVr\, C^\circ_{TL}}{ei_{p,TL}}\ln\frac{ei_{p,TL}}{n_{TL}\, FSC^\circ_{TL}\, k^\circ_{TL}}=(E_{p,TL}-E^\circ_{TL}) \quad (4)$$

An alternative criterion is to see if the sets ($i_{p,TL}$, $E_{p,TL}$) in Table 1 systematically fit in with Eq. 4. Since the exact values of V and C°_{TL} for polypyrrole sites are not available, the (V, k°_{TL}, C°_{TL}, E°_{TL}) set that fits the (i_{TL}, E_{TL}) data was sought. As a result, a linear fit to $f(i_{p,TL})$ vs. $(E-E^\circ_{TL})$, though only for a part in the TL regime, has been found for electrode A as shown in Fig. 4(a), when $V_A=0.636\times10^{-6}$ cm^3, $k^\circ_{TL}=5.50\times10^{-9}$ cm mol^{-1} s^{-1}, $C^\circ_{TL}=3.15\times10^{-3}$ mol cm^{-3}, $E^\circ_{TL}=-0.535$ V and $n_{TL}=n_{o,TL}=1$. Here, each peak current is assumed to include a background current of 5 μA. Owing to the fact that the E°_{TL} (or $E^{\circ\prime}_{TL}$) value cannot be pinpointed

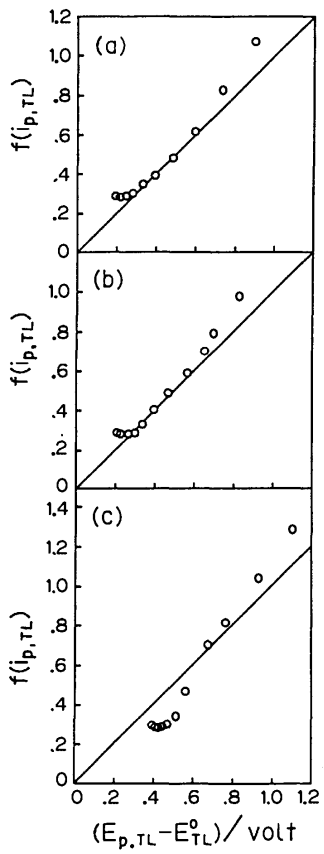

Fig. 4. Plots of $f(i_{p,TL})$ vs. $(E_{p,TL}-E^\circ_{TL})$, according to Eq. 4. $k^\circ_{TL}=5.50\times10^{-9}$ cm mol^{-1}s^{-1}, $C^\circ_{TL}=3.15\times10^{-3}$ mol cm^{-3}. E°_{TL} values: (a) −0.535 V; (b) −0.600 V; (c) −0.720 V. (a)—(c) correspond to electrodes A—C, respectively.

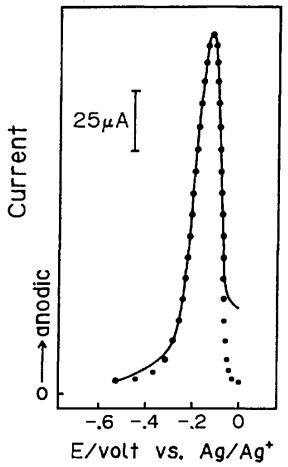

Fig. 5. Fitting of the voltammogram calculated based on Eq. 1 by using the same (V, k°_{TL}, C°_{TL}, E°_{TL}) parameters for electrode A as in Fig. 4(a) (dots). β=0.525. The solid line represents the oxidation wave of the sweep number **6** of electrode A.

in the original CV, the parameter set (V, k°_{TL}, C°_{TL}) that gives similar linearity can exist not uniquely because of the small changes in E°_{TL}. However, it has been found that current waves calculated based on Eq. 1 using the above particular parameter set fit in with the experimental waveforms, as exemplified for electrode A in Fig. 5. Here the same amount of background current, 5 μA, is assumed as in Fig. 4. This result also gives further evidence that the sharp oxidation peaks in the TL regime in Fig. 1 are essentially faradaic.

Furthermore, it has been found that, when V_B and V_C are given by 'normalization' as indicated below, ($i_{p,TL}$, $E_{p,TL}$) sets of the electrodes B and C also show linearity similar to Fig. 4 (a), as shown in Fig. 4(b) and (c), respectively, with precisely the same (k°_{TL}, C°_{TL}) set used in Fig. 4(a). This normalization is based on the $i_{p,TL}$ values of sweep number **1** of each electrode so that $V_B=V_A\times i_{p,TL}(B)/i_{p,TL}(A)$ and $V_C=V_A\times i_{p,TL}(C)/i_{p,TL}(A)$. This normalization is not unreasonable since the peak current is known to be proportional to V (or S for surface systems) in thin layer[13] and chemisorbed[19,20] systems, regardless of their electrochemical reversibility. The fact that precisely the same set of (k°_{TL}, C°_{TL}) fits the ($i_{p,TL}$, $E_{p,TL}$) sets of the separate electrodes with apparently different coverages (A, B, and C) is a strong indication that major portions of the data in Table 1 can be described essentially by the TITL model. Different E°_{TL} values are obtained for the three electrodes by the fitting procedure, i.e., A: −0.535 V; B: −0.600 V; C: −0.720 V. Such differences persist even when different (k°_{TL}, C°_{TL}, E°_{TL}) sets, that give the similar linearity, are used. Since the deviations of the plots from the linearity are larger in Fig. 4(c) than in the other two cases, E°_{TL} values of electrodes A and B seem to be more reliable. In fact, the E°_{TL} values for electrodes A and B are only slightly different from $E^{\circ\prime}$ values of

polypyrrole estimated on the basis of the separations of E_{pa} and E_{pc}.[25,26]

Significant deviations from the linearity are seen in Fig. 4 for both smaller and larger sweep numbers. Although the electrochemical mechanism that governs the initial sweeps is not known, it may be due to some strong interactions between polypyrrole and the electrode substrate. The deviations in larger sweep numbers ($\geq$8), in which BL mode oxidation also occurs, are understood as a result of the reductions in $i_{p,TL}$ due to partial consumption (oxidation) of C°_{TL} in the BL mode. This partitioning of C°_{TL} from the TL to BL mode is further analyzed in the following sections.

Estimation of Complementary Charge Transfer Coefficient. In plotting Fig. 4, all parameters in Eq. 4 are fixed except for β. Hence, the different values of $f(i_{p,TL})$ are assumed to be generated by the changes in β values in Eqs. 2 and 3 for each cyclic sweep. Thus the β values can be obtained from these equations. However, it should be noted that, because of the partitioning of C°_{TL} from the TL to BL modes for sweep numbers larger than **8** as mentioned above, β values obtained from Eq. 2 can be inaccurate. Therefore, β is alternatively estimated, by using experimental $E_{p,TL}$ values and the parameter set used in Fig. 4, based on Eq. 3 in which β is not dependent on C°_{TL}. The result of the calculations are shown in Fig. 6. It is seen from Fig. 6 that β values decrease logarithmically as the sweep number increases, meeting the condition of $0 \leq \beta \leq 1$ for $E_{p,TL}$ values that fit linearly in with Fig. 4. On the other hand, β values obtained for $E_{p,TL}$ values from ($i_{p,TL}$, $E_{p,TL}$) sets, that deviate significantly from the linearity in Fig. 4, deviate from the linearity and/or violate the $\beta \leq 1$ condition.

If one gets 'intact' $i_{p,TL}$ values without TL$\rightarrow$BL partitioning ($i^{\circ}_{p,TL}$) from Eq. 2, by using β values in Fig. 6 and the same (V, C°_{TL}) set in Fig. 4, then one should be able to estimate the deviation of the experimental $i_{p,TL}$ values from the corresponding $i^{\circ}_{p,TL}$. Such calculations for electrodes A—C have shown that the deviation defined by $\delta \equiv (i^{\circ}_{p,TL} - i_{p,TL})/i^{\circ}_{p,TL}$ increases approximately linearly as the sweep number increases from **8** (Fig. 7(a)). δ should be directly related to the partition coefficient θ (defined as the ratio of polypyrrole sites oxidized in the BL mode to all the polypyrrole sites), since $i_{p,TL}$ is proportional to C°_{TL} (Eq. 2). Estimation of δ (and hence θ) as above is possible only for sweep numbers smaller than **12**, because well defined current peaks are detectable only for them. Since $\ln\beta$ is approximately proportional to sweep number (Fig. 6), the results in Fig. 7(a) suggest that δ may be proportional to $\ln\beta$. δ vs. $\ln\beta$ plots in Fig. 7(b) confirms such expectation, where both values are roughly proportional each other. The result in Fig. 7(b) implies that the progress of the crossover, and hence the phase separation of poly-1 and polypyrrole,

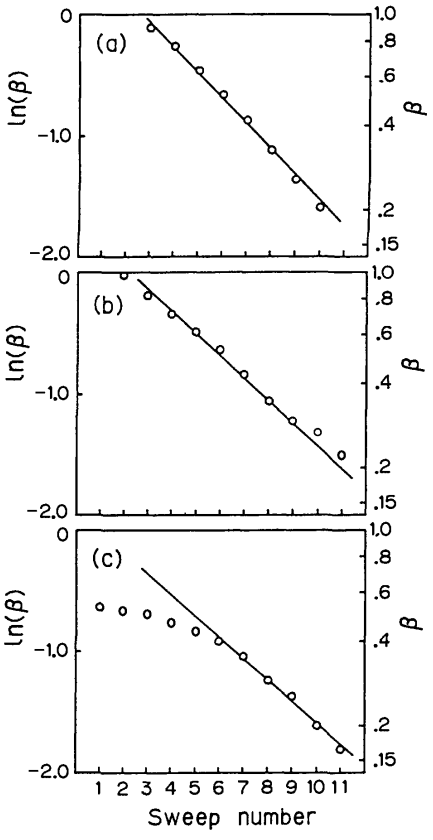

Fig. 6. Plots of ln β vs. the sweep number. β values were obtained based on Eq. 3 using the same parameters as in Fig. 4. β values exceeding unity are neglected. (a)—(c) correspond to electrodes A—C, respectively.

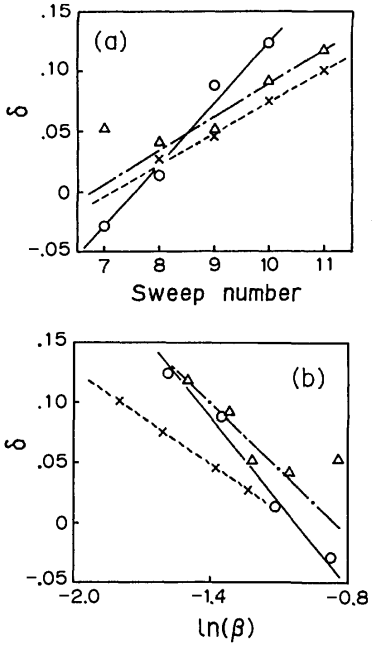

Fig. 7. (a): plot of δ vs. sweep number I; (b): plot of δ vs. ln β (β: complementary charge transfer coefficient). $\delta \equiv (i^{\circ}_{p,TL} - i_{p,TL})/i^{\circ}_{p,TL}$. —O—, —·—△—·—, and ···×··· represent electrode A, B, and C, respectively.

may be expressed as a function of β.

Analysis of the Mediated Oxidation Waves of Polypyrrole (BL Regime). A linear relationship has been found between the peak currents in the BL regime, $i_{p,BL}$, and the peak potentials ($E_{p,BL}-E^{\circ\prime}_{BL}$) ($E^{\circ\prime}_{BL}$: formal oxidation potential of $[Ru(vbpy)_3]^{2+}$ centers of the inner layer, +0.85 V), as shown in Fig. 8, although contributions by the inner layer are neglected here.

A theoretical treatment of bilayer electrochemistry[9b,27] has been presented for a case in which the e^- transfer process across the interface is the rate-determining step and a Nernstian equilibrium is established throughout the inner layer except for the interface layer.

$$i_{BL}=n_{ch,BL}\,FS\,k^{\circ}_{BL}\,\phi^2\{1+\exp[f(E_{init}-E^{\circ\prime}_{BL})]\}^{p} \times\{1+\exp[f(E_{init}+rt-E^{\circ\prime}_{BL})]\}^{-p-1} \times\exp[f(E_{init}+rt-E^{\circ\prime}_{BL})] \quad (5)$$

where

$$p=\frac{k^{\circ}_{BL}\phi^2}{\Gamma^{\circ}_{BL}fr},\quad f=\frac{n_{BL}F}{RT}$$

$n_{ch,BL}$: number of electrons per reaction center oxidized on e^- transfer across the inner layer/outer layer interface

n_{BL}: number of electrons per reaction center oxidized

k°_{BL}: rate constant for e^- transfer across the interface ($cm^2\,mol^{-1}\,s^{-1}$)

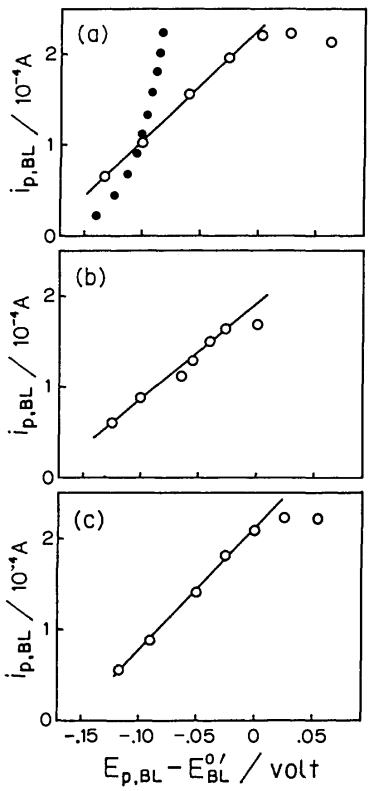

Fig. 8. Plots of $i_{p,BL}$ vs. ($E_{p,BL}-E^{\circ\prime}_{BL}$). Closed circles represent calculated values based on Eqs. 6 and 7. (a)—(c) correspond to electrodes A—C, respectively.

ϕ: coverage that can participate in direct charge transfer across the interface (mol cm^{-2})

E_{init}: potential at which positive potential sweep is initiated

$i_{p,BL}$ for $E_{init}\ll E^{\circ\prime}_{BL}$ are given by differentiating Eq. 5',

$$i_{p,BL}=\frac{n_{BL}\,n_{ch,BL}\,F^2\,S\,r\,\Gamma^{\circ}_{BL}}{RT}\left(1+\frac{1}{p}\right)^{-p-1} \quad (6)$$

$$E_{p,BL}=E^{\circ\prime}_{BL}-\frac{1}{f}\ln p \quad (7)$$

Closed circles in Fig. 8 represent the calculated [$i_{p,BL}$, ($E_{p,BL}-E^{\circ\prime}_{BL}$)] values based on Eqs. 6 and 7, which show no linear relationship. This would imply that assumptions employed in deriving Eqs. 5—7 are not valid in the present case. Inappropriateness of the assumptions have been noted.[27] Plots in Fig. 8 imply how $i_{p,BL}$ and $E_{p,BL}$ change when the coverage of the outer layer (number of polypyrrole sites) is variously changed as a result of increasing partitioning. $i_{p,BL}$ is also found to linearly depends on sweep number. This means that $i_{p,BL}$ and $E_{p,BL}$ may be proportional to C_{BL} or Γ_{BL}, since δ is also approximately proportional to sweep number.[28] These results povide a guideline in obtaining the analytical equations to describe the electrochemistry of the BL mode.[29]

Simulation of Cyclic Voltammograms. Simulation of the CVs in Fig. 1 has been studied on the basis of TITL model accompanying subsequent crossover to the BL mode. The following simulation is based on the assumption that portions of polypyrrole sites contributing to TL and BL mode oxidations are given separately at the beginning of each cyclic sweep (separation model). The change in β upon repeated potential sweeps is formulated according to the result of Fig. 6.

$$\beta=\exp[-0.2\times(I-1)] \qquad I\text{: sweep number} \quad (8)$$

Partition coefficient θ for each sweep is given arbitrarily, since it cannot be known for larger sweep numbers ($12\leq I$). For $12\leq I$, the BL mode oxidation prevails and no current peaks in the TL regime are detectable. Since we have not found analytical formulations that successfully describe the electrochemistry of the BL mode where charge transfer processes within both layers are considered as rate-limiting steps,[27] Eq. 5 is alternatively used to show overall waveforms at the expense of the detailed waveforms in the BL mode. The result is shown in Fig. 9. In spite of such limitations, the waveforms simulate the overall changes including the crossover phenomenon.

An alternative model on the progress of the crossover is possible as follows. The partitioning from TL to BL progresses competitively as a function of the applied potential (parallel progress model or PP model), instead of initial separation of polypyrrole sites into two distinct portions. In the PP model,

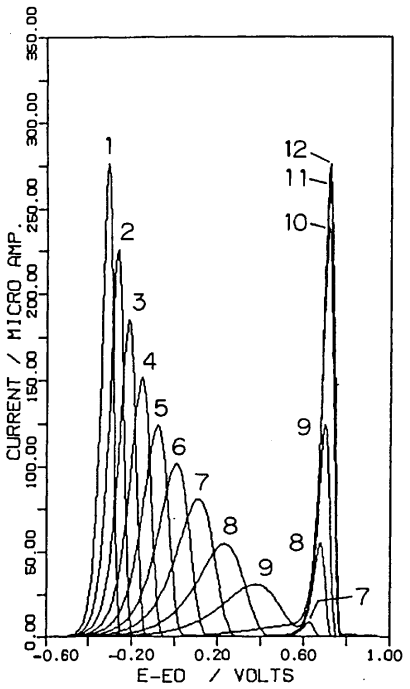

Fig. 9. Cyclic voltammograms generated based on Eqs. 1, 5, and 8, according to the separation model. E°_{TL}=−0.535 V; E°_{BL}=+0.850 V; E_{init}=−0.6 V. The same k°_{TL} (5.50×10^{-9} cm mol^{-1} s^{-1}) and C°_{TL} (3.15×10^{-3} mol cm^{-3}) values are used as in Fig. 4. $n_{TL}=n_{o,TL}=n_{ch,BL}=n_{BL}=1$; $k^{\circ}_{BL}=8.00\times10^{15}$ cm^2 mol^{-1} s^{-1}; $\phi=0.483\times10^{-10}$ mol cm^{-2}. Partition coefficient θ is given as; sweep number I=1—6: 0; I=7: 0.03; I=8: 0.2; I=9: 0.45; I=10: 0.86; I=11: 0.96; I=12: 1.0. β is changed from unity to 0.11.

oxidation of reduced polypyrrole sites proceeds in both modes competitively, according to the different potential dependencies defined by Eqs. 1 and 5. Simulations based on the PP model, however, have proved that this model fails to produce large current peak separations like sweep **9** of Fig. 1 in TL and BL modes in a single sweep. This model also does not produce any deviation of $i_{p,TL}$ from $i^{\circ}_{p,TL}$.

To account for the substantial change in the β value, the following explanation may be possible. The charge carriers in the oxidized state of polypyrrole are bipolarons.[2] The generation and rereduction of bipolarons in polypyrrole occur at different levels, i.e., at valence band edge and at bipolaron level, respectively. Because of this situation, polypyrrole present in the polymer matrix (poly-1) may be subject to such assymetric electrochemistry as in Fig. 2. On the other hand, the progress of phase separation of polypyrrole and poly-1 should change the distance to be moved in the reaction coordinate to achieve the oxidation of polypyrrole. This change in the distance in the reaction coordinate, associated with the above assymetry, would change β significantly.

It should be stressed that the consideration of a simple voltage-loss process in the polypyrrole oxidation cannot explain the systematic changes of the CVs in Fig. 1.

To our knowledge, there has been little preceding work on the relevance of spatial factors in polymer-coated electrodes to the charge transfer coefficient. Essentially the same CV changes have been recorded for poly(3-methylthiophene)- and poly(2,2′-bithiophene)-as-deposited Pt/poly-1 electrodes.[11] If examples of ECPS are found for other redoxing polymers without a capacitive effect, more detailed analyses will be possible, because they would provide precise experimental information on the concentration, electrochemical coverage of reaction centers, $E^{\circ\prime}$ and i_{TL} values. The ECPS scheme may find applications as means for fabricating microstructures using electroactive polymers.

Conclusion

CV changes observed during the electrochemical potential sweeps of polypyrrole-as-deposited Pt/poly-1 electrodes have been found to be essentially described by a thin layer model for totally irreversible electrode processes (TITL model) with a subsequent gradual crossover to bilayer electrochemistry (BL model). Systematic shifts of peak potential associated with the decrease in peak current in the TL mode are ascribed to the result of logarithmic decrease of the complementary charge transfer coefficient β as the sweep number increases. After each cyclic sweep of potential, the system is reset to the initial state, except that smaller β values are given after each cycle. It has been found that the model, which assumes that reduced polypyrrole sites are separated into portions of TL and BL mode oxidations prior to each cyclic potential sweep, well simulate the CV changes of Fig. 1.

The present results shed light on the electrochemical aspect of polymer phase separation. We assume that the decrease in the β value in the present study should be related to the progress of the polymer phase separation.

References

1) a) A. F. Diaz, K. K. Kanazawa, and G. P. Gardini, *J. Chem. Soc., Chem. Commun.*, **1979**, 635; b) K. K. Kanazawa, A. F. Diaz, B. H. Geiss, W. D. Gill, J. F. Kwak, J. A. Logan, J. F. Rabolt, and G. B. Street, *ibid.*, **1979**, 854; c) A. F. Diaz and J. I. Castillo, *ibid.*, **1980**, 397.

2) See for example; A. J. Heeger, *Philos. Trans. R. Soc. London, Ser. A*, **314**, 17 (1985).

3) R. A. Bull, F.-R. Fan, and A. J. Bard, *J. Electrochem. Soc.*, **130**, 1636 (1983).

4) a) H. S. White, G. P. Kittlesen, and M. S. Wrighton, *J. Am. Chem. Soc.*, **106**, 5375 (1984); b) G. P. Kittlesen, H. S. White, and M. S. Wrighton, *ibid.*, **106**, 7389 (1984); c) C.-F. Shu and M. S. Wrighton, *J. Phys. Chem.*, **92**, 5221 (1988).

5) a) P. Burgmayer and R. W. Murray, *J. Am. Chem. Soc.*, **104**, 6139 (1982); b) P. Burgmayer and R. W. Murray, *J.*

Electroanal. Chem., **147**, 339 (1983).
6) T. Skotheim and I. Lundström, *J. Electrochem. Soc.*, **129**, 894 (1982).
7) H. Koezuka and S. Etoh, *J. Appl. Phys.*, **54**, 2511 (1983).
8) K. Murao and K. Suzuki, *J. Chem. Soc., Chem. Commun.*, **1984**, 238.
9) a) H. D. Abruna, P. Denisevich, M. Umana, T. J. Meyer, and R. W. Murray, *J. Am. Chem. Soc.*, **103**, 1 (1981); b) P. Denisevich, K. W. Willman, and R. W. Murray, *ibid.*, **103**, 4727 (1981); c) K. W. Willman and R. W. Murray, *J. Electroanal. Chem.*, **133**, 211 (1982); d) C. R. Leidner, P. Denisevich, K. W. Willman, and R. W. Murray, *ibid.*, **164**, 63 (1984); e) C. R. Leidner and R. W. Murray, *J. Am. Chem. Soc.*, **107**, 551 (1985).
10) K. Murao and K. Suzuki, *J. Electrochem. Soc.*, **135**, 1415 (1988).
11) a) K. Murao and K. Suzuki, *Chem. Lett.*, **1986**, 2101; b) K. Murao and K. Suzuki, *Bull. Chem. Soc. Jpn.*, **60**, 2809 (1987).
12) K. Murao and K. Suzuki, *Solid State Commun.*, **62**, 483 (1987).
13) a) A. T. Hubbard, *J. Electroanal. Chem.*, **22**, 165 (1969); b) A. J. Bard and L. R. Faulkner, "Electrochemical Methods: Fundamentals and Applications," Wiley, New York (1980), pp. 406—413.
14) K. Murao and K. Suzuki, *Appl. Phys. Lett.*, **47**, 724 (1985).
15) a) M. S. Wrighton, R. G. Austin, A. B. Bocarsly, J. M. Bolts, O. Haas, K. D. Legg, L. Nadjo, and M. C. Palazzotto, *J. Electroanal. Chem.*, **87**, 429 (1978); b) M. S. Wrighton, M. C. Palazzotto, A. B. Bocarsly, J. M. Bolts, A. B. Fischer, and L. Nadjo, *J. Am. Chem. Soc.*, **100**, 7264 (1978).
16) a) K. Itaya and A. J. Bard, *Anal. Chem.*, **50**, 1487 (1978); b) A. Merz and A. J. Bard, *J. Am. Chem. Soc.*, **100**, 3222 (1978).
17) a) J. C. Lennox and R. W. Murray, *J. Electroanal. Chem.*, **78**, 395 (1977); b) K. Kuo, P. R. Moses, J. R. Lenhard, D. C. Green, and R. W. Murray, *Anal. Chem.*, **51**, 745 (1979).
18) a) N. Oyama, K. B. Yap, and F. C. Anson, *J. Electroanal. Chem.*, **100**, 233 (1979); b) N. Oyama and F. C. Anson, *J. Electrochem. Soc.*, **127**, 640 (1980); c) K. Shigehara, N. Oyama, and F. C. Anson, *J. Am. Chem. Soc.*, **103**, 2552 (1981).
19) a) E. Laviron, *J. Electroanal. Chem.*, **39**, 1 (1972); b) E. Laviron, *ibid.*, **100**, 263 (1979).
20) R. F. Lane and A. T. Hubbard, *J. Phys. Chem.*, **77**, 1401 (1973).
21) We note close similarity of the waveform to that of the faradaic component; a) J. Tanguy, N. Mermilliod, and M. Hoclet, *Synth. Metals*, **18**, 7 (1987); b) J. Tanguy, N. Mermilliod, and M. Hoclet, *J. Electrochem. Soc.*, **134**, 795 (1987).
22) S. W. Feldberg, *J. Am. Chem. Soc.*, **106**, 4671 (1984).
23) R. A. Bull, F.-R. Fan, and A. J. Bard, *J. Electrochem. Soc.*, **129**, 1009 (1982).
24) S. Kuwabata, H. Yoneyama, and H. Tamura, *Bull. Chem. Soc. Jpn.*, **57**, 2247 (1984).
25) A. F. Diaz, J. I. Castillo, J. A. Logan, and W.-Y. Lee, *J. Electroanal. Chem.*, **129**, 115 (1981).
26) P. G. Pickup and R. A. Osteryoung, *J. Am. Chem. Soc.*, **106**, 2294 (1984).
27) P. G. Pickup, C. R. Leidner, P. Denisevich, and R. W. Murray, *J. Electroanal. Chem.*, **164**, 39 (1984).
28) Since the slope for the plot of δ vs. I (sweep number) in Fig. 7(a) is only about 0.04, extrapolation to sweep number **14** does not yield the 100% crossover. Hence the linearity between δ and I may be established only for small I values.
29) Interestingly, we have observed similar non-linear $i_{p,TL}$ vs. $E_{p,TL}$ relationship as the closed circles of Fig. 8 for Pt/poly-1/polypyrrole electrodes with very small coverages of the inner layer ($\leqq 1.6\times10^{-9}$ mol cm^{-2}). This is probably due to the significantly reduced rate-limiting character of the inner layer.

The Thermotropic Liquid-Crystalline Behavior of Alkylammonium Benzenesulfonates and Related Salts

Masato Ito, Yoshio Matsunaga,* Hiroyuki Matsuzaki, and Saeko Shimojima
Department of Chemistry, Faculty of Science, Hokkaido University, Sapporo 060
(Received June 2, 1989)

Alkylammonium benzene-, pyridine-3-, *p*-toluene-, and *p*-ethylbenzenesulfonates were found to be smectogenic when the cation carries an octyl or longer alkyl group. The thermal stability of the mesophase usually reaches its maximum at the octadecylammonium salt. The temperature range of stable existence is in the following order: pyridine-3-sulfonate > *p*-toluenesulfonate > benzenesulfonate > *p*-ethylbenzenesulfonate, suggesting the presence of a specific interaction between the ammonium ion and the nitrogen atom in the pyridine ring.

Several series of long-chain alkylammonium salts have been known to exhibit liquid-crystalline phases. They include salts containing counter ions as simple as halide ions and also two-dimensional sheets of tetrahalometallate ions.[1-5] In our previous paper, the thermotropic liquid-crystalline properties of alkylammonium alkanesulfonates were described.[6] Because the thermal stability of the mesophase in these salts was considerably affected by the counter ions, we then decided to extend our study of alkylammonium salts employing a wide range of aromatic anions. As will be described below, the picrate ion was found to be of limited use; however, benzenesulfonic acid was discovered to form mesomorphic salts with many long-chain alkylamines. As a large number of derivatives of the latter acid are readily available, we may be able to examine the effects on the mesomorphic behavior of various substituents carried by the aromatic nuclei. This paper will present the results of our work on the benzenesulfonates and three related series of salts.

Experimental

Materials. The benzene-, pyridine-3-, *p*-toluene-, *p*-ethylbenzenesulfonic acids, picric acid, and 2,4-dinitro- and 2,6-dinitrophenols are commercially available. Equimolar amounts of an alkylamine and an acid dissolved in boiling methanol were mixed. The salt thus precipitated was purified by recrystallization until a sharp mesomorphic-isotropic transition was recorded on the calorimetric curve during the processes of heating and cooling at the same temperature. For example, Found: C, 67.27; H, 10.52; N, 3.33; S, 7.59%. Calcd for $C_{18}H_{37}NH_3^+ \cdot C_6H_5SO_3^-$: C, 67.40; H, 10.60; N, 3.28; S, 7.50%.

Measurements. The calorimetric and X-ray diffraction measurements were carried out as described in our previous paper.[6]

Results and Discussion

Many benzene-, pyridine-3-, *p*-toluene-, and *p*-ethylbenzenesulfonates can produce a smectic phase. Table 1 presents their melting and clearing points, the associated enthalpies, and the layer spacings as measured within 10 °C above the melting points. The

Table 1. Transition Temperatures (°C), Enthalpy Changes (kJ mol^{-1}), and Layer Spacings (nm) of Alkylammonium Salts[a]

n[b]	Melting	Clearing	Layer spacing
	Benzenesulfonates		
9	102(32)	—	—
10	98(35)	99(2.9)	2.06
11	89—92(32)	107(2.7)	2.19
12	88—92(33)	114(2.4)	2.31
13	89—92(40)	120(2.3)	2.41
14	91—96(21)	124(2.2)	2.57
15	97(21)	127(2.2)	2.65
16	95(26)	130(2.1)	2.77
17	94—96(62)	130(2.0)	2.90
18	98—100(23)	133(2.0)	3.01
	Pyridine-3-sulfonates		
11	102(46)	—	—
12	97(85)	106(0.6)	2.51
13	103(53)	134(0.8)	2.66
14	96(44)	152(0.9)	2.76
15	100(62)	154(1.0)	2.89
16	99(56)	173(1.0)	3.05
17	105(66)	178(1.0)	3.14
18	103(65)	186(1.0)	3.27
	p-Toluenesulfonates		
8	131(17)	—	—
9	130(18)	127(3.6)	2.07
10	128(19)	129(3.4)	2.19
11	118(14)	133(3.3)	2.30
12	105(14)	137(3.1)	2.44
13	100(16)	140(3.0)	2.54
14	98(17)	144(2.8)	2.65
15	99(19)	145(2.8)	2.78
16	98(21)	146(2.9)	2.86
17	98(22)	146(2.7)	2.94
18	98(23)	144(2.5)	3.01
	p-Ethylbenzenesulfonates		
7	136(17)	—	—
8	129(18)	129(3.4)	—
9	121(18)	125(2.8)	2.01
10	123(21)	120(2.5)	2.16
11	121(19)	119(2.4)	2.28
12	111—114(17)	119(2.6)	2.39
13	104(16)	122(2.7)	2.49
14	101(18)	123(2.7)	2.58
15	101(19)	124(2.6)	2.69
16	101—103(22)	125(2.6)	2.78
17	101(23)	126(2.5)	2.87
18	101(23)	127(2.4)	2.99

a) The second quantities are in parentheses. b) The number of carbon atoms in the alkyl group.

rather broad peak due to melting recorded for several salts, mostly benzenesulfonates, suggests the presence of a solid-solid transition just below the melting point. In these cases, the temperature range estimated by taking into consideration the normal peak width due to melting is presented in the table; the value of enthalpy change is given for the whole peak. Solid-solid transitions well separated from the melting were also recorded quite often, but they are not included in this table.

In Fig. 1, the melting and clearing points of the benzene- and pyridine-3-sulfonates are plotted against the number of carbon atoms (n) in the cation. In this diagram, the upper limit of the temperature range indicated in Table 1 is taken as the melting point. The narrow temperature range of the mesophase found in the decylammonium salt in the former series is widened by the destabilization of the crystalline phase and by the stabilization of the mesophase with an increase in the alkyl chain length. While the melting point ceases to fall soon and then gradually rises (see Curve a), the clearing point continues to rise (see Curve b). In the hexadecyl-, heptadecyl-, and octadecylammonium salts, the mesophase exists over 35 °C. The pyridine-3-sulfonate exhibits a mesophase when the cation carries a dodecyl group. The melting point shows a marked even-odd alternation, but it remains within a range of only a few degrees (see Curve c). The mesophase is rapidly promoted by the increase in the number of carbon atoms in the alkyl group with a marked even-odd alternation, providing an additional check on the purity (see Curve d). The temperature range of the stable existence of the mesophase exceeds 80 °C in the octadecylammonium salt.

As is depicted in Fig. 2, the alkyl group attached to the aromatic nucleus significantly influences the thermal stability of the mesophase. The phase is metastable in nonylammonium p-toluenesulfonate, but it becomes stable in the next homologous member. The melting point is lowered with an increase up to n=14, but thereafter it remains at almost the same temperature (see Curve a). On the other hand, the clearing point is raised to n=17 (see Curve b). The mesophases in the hexadecyl-, heptadecyl-, and octadecylammonium salts are stable over 48 °C. The melting point and clearing point in octylammonium p-ethylbenzenesulfonate are not distinguishable from each other in the process of heating, but the two can easily be separated in the process of cooling. The mesophase is stable in the next member, but again metastable in the following two. The melting point then changes nearly in parallel to that of the p-toluenesulfonate in a slightly higher temperature range (see Curve c). As the clearing point increases only slowly with n (see Curve d), even the widest temperature range of stable existence achieved with the octadecylammonium salt is no more than 26 °C, the narrowest among the four series examined in the present work.

In the benzene-, p-toluene-, and p-ethylbenzenesulfonates, the enthalpy change at the clearing point decreases with the number of carbon atoms in the alkylammonium ion. Such a tendency is in agreement with what we found for the alkanesulfonates studied previously.[6] The value tends to be high in the p-toluenesulfonates. On the other hand, the pyridine-3-sulfonate is transformed into an isotropic

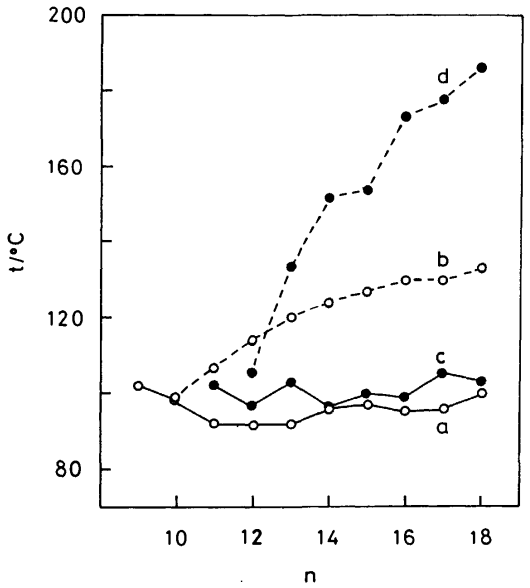

Fig. 1. Plots of transition temperatures against the number of carbon atoms in the alkyl group (n). (a) Melting point, (b) clearing point of alkylammonium benzenesulfonates, (c) melting point, and (d) clearing point of the pyridine-3-sulfonates.

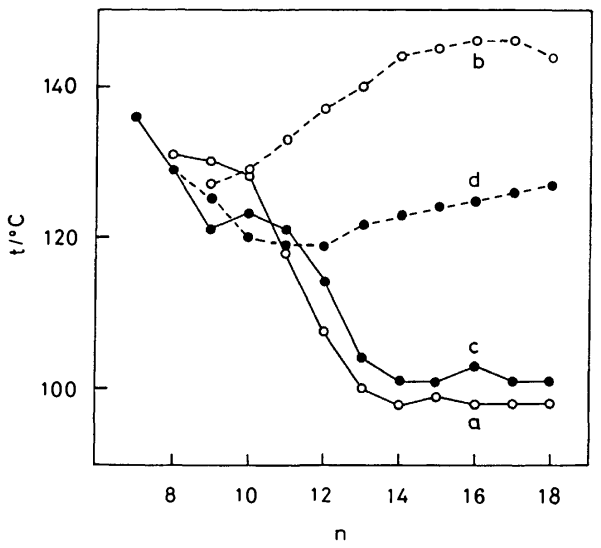

Fig. 2. Plots of transition temperatures against the number of carbon atoms in the alkyl group (n). (a) Melting point, (b) clearing point of alkylammonium p-toluenesulfonates, (c) melting point, and (d) clearing point of the p-ethylbenzenesulfonates.

liquid with a rather small enthalpy change. Besides, the value increases as the homologous series ascends.

In all the salts, the X-ray diffraction pattern recorded for the mesophase consists of a sharp inner peak and a diffuse outer one, indicating that the phase is of the smectic A or C type. The inner peak is accompanied by a weaker one assignable to the second-order reflection. The plot of the layer spacing in the mesophase of the benzenesulfonates against the number of carbon atoms in the cation gives a slope of 0.125 nm per methylene unit, in conformity with the fully-extended configuration of the alkyl group (see Line a in Fig. 3). The same slope is obtained by the plot for the pyridine-3-sulfonates. The latter salts give layer spacings longer by about 0.2 nm than the corresponding benzenesulfonates, even though the two anions are of nearly the same size (see Line b).

When the alkyl group in the cation is relatively short, the layer spacing in the *p*-toluenesulfonate is longer by about 0.1 nm than that of the corresponding benzenesulfonate; however, the deviation from the slope of 0.125 nm per methylene in the higher homologous members is so appreciable that the octadecylammonium salt exhibits essentially the same spacing as that given by the corresponding benzenesulfonate. The spacing shown by the *p*-ethylbenzenesulfonate comes intermediate between the benzene- and *p*-toluenesulfonates and deviates from the slope of 0.125 nm per methylene on ascending the homologous series. The mesophases given in these sulfonates may be concluded to be of the smectic A type on the basis of the observed slope of 0.125 nm per methylene and also the pseudo-isotropic texture, with oily streaks. The lateral spacing is about 0.45 nm for all the series.

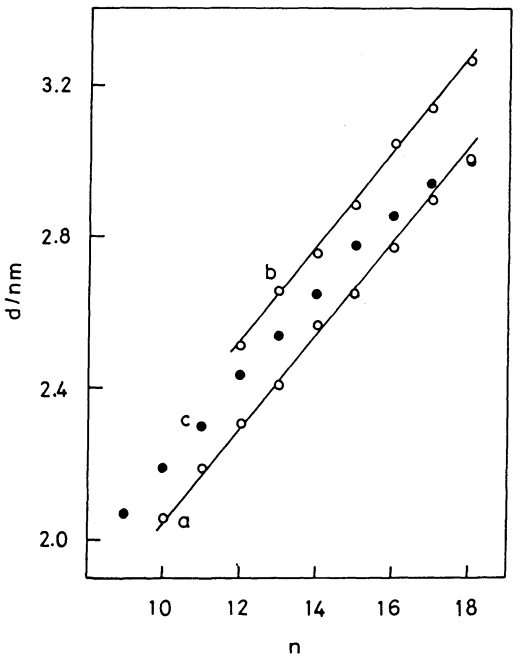

Fig. 3. Plots of layer spacings (d) in mesophases against the number of carbon atoms in the alkyl group (*n*) for alkylammonium benzenesulfonates (a), pyridine-3-sulfonates (b), and *p*-toluenesulfonates (c).

Previously, we showed that the layer spacing measured for the alkylammonium methanesulfonates agrees well with the sum of the lengths of the cation and anion and proposed a structure in which ion-pairs are alternatively oriented so that the long alkyl chains can be interdigitated with each other.[6] Similar models have been employed to represent the mesophases of alkylammonium chlorides by Busico et al., 1-methyl-4-dodecylpyridinium salts by Sudhölter et al., and 1-alkyl-4-methylpyridinium halides by Bazuin et al.[1,7,8]

The octadecylammonium ion in the most extended configuration is estimated to be about 2.60 nm long, employing a van der Waals radius of the methyl group of 0.20 nm, a C-C bond length of 0.154 nm, a C-N bond length of 0.147 nm, a tetrahedral angle, and a thermochemical radius of the ammonium ion of 0.14 nm. The difference between the calculated length of the cation and the spacing in the octadecylammonium benzenesulfonate, 3.01 nm, is no more than 0.41 nm. This value is much shorter than the estimated length of the anion, 0.95 nm, but it is long enough to accommodate the charged head group of the anion. Apparently, the long axis of the rigid anion cannot be in line with the alkylammonium ion orthogonally oriented to the layer plane. The length of the anion may be calculated on the basis of the following data; a van der Waals radius of hydrogen atom in C-H bond of 0.12 nm, a C-H bond length of 0.110 nm, an aromatic C-C bond length of 0.140 nm, a C-S bond length of 0.182 nm, and a thermochemical radius of the sulfate ion of 0.26 nm. The required thermochemical radii were taken from a table compiled by Jenkins and Thakur.[9]

As to the pyridine-3-sulfonates, the longer spacing and also the higher thermal stability of the mesophase relative to that in the benzenesulfonates may imply the presence of a specific interaction between the ammonium ion and the nitrogen atom in the anion. Indeed, the formation of a hydrogen-bonded complex cation between triethylammonium ion and pyridine has been shown by the work of Masri and Wood.[10] Therefore, the side-by-side hydrogen bonding in the sheet of ion-pairs may promote the smectic thermal stability, thus providing additional lateral intermolecular attraction. The layer structure may be destroyed only when the long alky chains are conformationally more disordered—in other words, more liquid-like, as is suggested by the relatively small enthalpy changes at the clearing point.

The fact that the spacing in the *p*-toluenesulfonate is longer by 0.1 nm than that in the corresponding benzenesulfonate may be explained by the difference between the sum of the van der Waals radius of the methyl group and the C-C bond length, 0.35 nm, and

the sum of the van der Waals radius of the hydrogen atom and the C-H bond length, 0.23 nm. The shorter spacing in the *p*-ethylbenzenesulfonates may be an indication that the alkyl group attached to the anion is dissolved into the layer formed by the paraffinic parts of the cations. We have shown that the layer spacing decreases as the alkyl group on the anion becomes longer in the alkanesulfonates and that the spacings in the 1-propanesulfonates are shorter by 0.30 nm than those in the corresponding methanesulfonates.[6]

As the temperature range of the stable existence of the mesophase is wide in the octadecylammonium pyridine-3-sulfonate, we examined the layer spacing as a function of the temperature. The spacing decreases monotonously from 3.27 nm at 110 °C to 3.12 nm at 170 °C, suggesting that the increased conformational disorder gives rise to some decrease in the layer spacing. The deviations in the spacing from the linear relationship observed for the *p*-toluene- and *p*-ethylbenzenesulfonates are within the above-mentioned change caused by the temperature increase and might be ascribed to the extensive conformational disorder of the long paraffinic chains.

Octadecylammonium and heptadecylammonium picrates are smectogenic. While the former solid salt is transformed into a smectic phase at 120 °C with an enthalpy change of 66 kJ mol^{-1}, and then into an isotropic liquid at 135 °C with a change of 0.6 kJ mol^{-1}, the mesophase given by the latter is metastable. When the melt formed at 114 °C with an enthalpy change of 51 kJ mol^{-1} is cooled, a smectic phase appears at 113 °C with 0.4 kJ mol^{-1}. The layer spacing of 3.33 nm found for the octadecylammonium salt is the longest among those recorded in this work, but it is still not long enough to position the long axis of the anion perpendicular to the layer plane. No mesophase was observed with the hexadecylammonium salt which melts at 113 °C. Neither the octadecylammonium 2,4-dinitrophenolate nor the 2,6-dinitrophenolate was found to be mesogenic.

The present work was supported by a Grant-in-Aid for Scientific Research (No. 60470001) from the Ministry of Education, Science and Culture.

References

1) V. Busico, P. Cernicchiaro, P. Corradini, and M. Vacatello, *J. Phys. Chem.*, **87**, 1631 (1983).
2) J. D. Gault, H. A. Gallardo, and H. J. Muller, *Mol. Cryst. Liq. Cryst.*, **130**, 163 (1985).
3) V. Busico, D. Castaldo, and M. Vacatello, *Mol. Cryst. Liq. Cryst.*, **78**, 221 (1981).
4) G. F. Needham, R. D. Willett, and H. F. Franzen, *J. Phys. Chem.*, **88**, 674 (1984).
5) K. J. Schenk and G. Chapuis, *J. Phys. Chem.*, **92**, 7141 (1988).
6) Y. Matsunaga and K. Nishida, *Bull. Chem. Soc. Jpn.*, **61**, 3435 (1988).
7) E. J. R. Sudhölter, J. B. F. N. Engberts, and W. H. de Jeu, *J. Phys. Chem.*, **86**, 1908 (1982).
8) C. G. Bazuin, D. Guillon, A. Skoulios, and J. F. Nicoud, *Liq. Cryst.*, **1**, 181 (1986).
9) H. D. B. Jenkins and K. P. Thakur, *J. Chem. Educ.*, **56**, 576 (1979).
10) F. N. Masri and J. L. Wood, *J. Mol. Struct.*, **14**, 201 (1972).

Laser Flash Photolysis Study of the Magnetic Field Effects on the Biradicals Generated from Aromatic Ketone-Xanthene Bifunctional Chain Molecules

Yoshifumi TANIMOTO,* Masanobu TAKASHIMA, and Michiya ITOH
Faculty of Pharmaceutical Sciences, Kanazawa University, Takara-machi, Kanazawa 920
(Received June 26, 1989)

The external magnetic field effects (MFE) on the biradicals generated from the intramolecular photoreactions of bifunctional chain molecules, α-(xanthone-2-carbonyloxy)-ω-(xanthene-2-carbonyloxy)alkanes (**XO-*n*-XH**, *n*=2—12) and Ar-12-**XH** (Ar=anthraquinone-4-carbonyloxy (AQ), 4-benzoylphenoxy (BP), and 4-acetylphenoxy (AP)) were studied by laser flash photolysis. All biradicals exhibit significant MFE. The simultaneous observation of the effects on the two radicals at the ends of the chain, generated from **XO-12-XH**, AQ-12-**XH**, and BP-12-**XH**, presents unequivocal evidence that the respective two radical centers correlate magnetically each other. The *n* dependence of the effects on biradicals generated from XO-*n*-**XH** indicates that the singlet-triplet degeneracy of the biradical occurs at the chain length of around *n*=6, i.e., the interradical distance of about 15 Å.

In the middle of 1970's, magnetic field effects (MFE) on radical reactions have been successfully interpreted in terms of the radical pair mechanism, in which the triplet (T)-singlet (S) intersystem crossing (isc) of a radical pair, a short-lived intermediate, is affected by a magnetic field.[1] It is speculated that the significant MFE could be observable when the lifetime of a pair is considerably long. In homogenous solution, however, the diffusive separation of the components of a pair competes with isc, leading to the shortening of the lifetime of the pair. These considerations suggest that MFE on bimolecular reactions in homogeneous solutions are rather insignificant, if any. In this regard, such a microheterogeneous solution as a micellar solution is expected to present us an ideal environment for sufficient T-S development of a radical pair. In an aqueous micellar solution, for example, the separation of the component radicals in a radical pair is considerably slow, because of the dimentionality of the micelle, and the microviscosity and polarity in it. Therefore, the isc, which is the magnetic field dependent process, can become the rate-controlling process. Based on the above-mentioned argument, quite a few numbers of research groups have studied MFE on photoreactions in micellar solutions and microemulsions.[2-7] Our main interest has been the MFE on the hydrogen abstraction reaction of aromatic ketones in micellar solutions.[5] Particularly, in order to confirm the mechanism, the MFE have been examined in detail in the hydrogen abstraction reaction of xanthone from xanthene.[5e] Then, new questions arise as for the roles of a micellar cage. a) What is the key factor for the significant effect, though dimentionality, polarity, microviscosity and others are expected to influence the lifetime of a radical pair? b) At what distance between the two radicals does the S-T degeneracy of a pair occur? However, the analysis of the photoreactions in microheterogeneous systems is too complex to answer these questions, since a micellar solution is the statistical ensemble of micelles with different sizes, and since microviscosity and polarity in a micelle depend on location in it.[8]

In order to answer these questions and to elucidate the governing factors in MFE, we have designed the end-to-end photoreactions of bifunctional chain molecules in homogeneous solutions as the intramolecular analogue of the bimolecular reaction of aromatic carbonyls in micellar solutions. First example was the intramolecular photoreaction of *n*-alkyl anthraquinone-2-carboxylates,[9] as the analogue of the reaction of anthraquinone in micellar solution.[5c,d] The hydrogen abstraction reaction of the excited triplet quinone from its methylene side chain generates the biradicals composed of alkyl and semiquinone radicals. It was shown that the S-T degeneracy of the biradicals occurs at the chain length of *n*=12 or so, from the MFE on the reaction yields under the steady-state photolysis. This system was, however, found to be inadequate for the dynamical study of MFE on the biradicals, since the rate-controlling step was not the isc but the generation of biradicals. In the present paper,[10] we report on MFE on the dynamics of the biradicals generated from the intramolecular abstraction reaction of the bifunctional chain molecules composed of the aromatic carbonyls (H acceptor) and xanthene (H donor) moieties, as the analogue of the radical pairs generated from the corresponding reaction in micellar solution.[5]

Experimental

Materials. Xanthone-2-carboxylic acid and xanthene-2-carboxylic acid were prepared with the literature procedure.[11,12] Xanthone-2-carboxylic acid (9.6 g, 0.04 M) in *N*,*N*-dimethylacetamide (DMAc, 130 ml) was slowly added into a hot DMAc solution (40 ml) of 1,12-dibromododecane (39.4 g, 0.12 M) and K_2CO_3 (6.1 g, 0.044 M), and the solution was then stirred at 90 °C for 6 h (1 M=1 mol dm^{-3}). The reaction mixture was treated with water, extracted with chloroform, and purified by chromatography, yielding a

white solid of α-bromo-ω-(xanthone-2-carbonyloxy)dodecane (12.7 g): Mp 78—79 °C. ^{1}H NMR (60 MHz, $CDCl_3$): δ=1.18—2.00 (s, 20H, $-CH_2-$), 3.35 (t, 2H, $-CH_2-Br$), 4.32 (t, 2H, $-CO_2-CH_2-$), 7.10—8.92 (m, 7H, aromatic). IR (KBr): 2920—2850 (methylene), 1720 (aromatic ester), 1663 cm^{-1} (aromatic ketone). Calcd for $C_{26}H_{31}O_4Br$: C, 64.07; H, 6.41%. Found C, 64.26; H, 6.53%. M, 488.

α-Bromo-ω-(xanthone-2-carbonyloxy)dodecane (12.18 g, 0.025 M) was added into a hot DMAc solution (40 ml) of xanthene-2-carboxylic acid (5.99 g, 0.0265 M), and K_2CO_3 (4.14 g, 0.03 M), and the solution was stirred at 90 °C for 8 h. The reaction mixture was treated with water, extracted with chloroform, and purified by chromatography and recrystallization, yielding a white solid of α-(xanthone-2-carbonyloxy)-ω-(xanthene-2-carbonyloxy)dodecane (XO-12-XH, 6.6 g).

Other chain molecules, Ar-*n*-XH (Ar=xanthone-2-carbonyloxy (**XO**, *n*=2—10), anthraquinone-2-carbonyloxy (AQ, *n*=12), 4-benzoylphenoxy (BP, *n*=12), 4-acetylphenoxy (AP, *n*=12)), and 1-(xanthone-2-carbonyloxy)dodecane (**XO**-12) were prepared in an analogous manner. Their melting points are shown in Table 1, and the typical spectral data of chain molecules are given as follows:

XO-12-XH. ^{1}H NMR (60MHz, $CDCl_3$): δ=1.18—2.00 (s, 20H, $-CH_2-$), 4.02 (s, 2H, methylene of XH), 3.97—4.47 (m, 4H, $-CO_2-CH_2-$), 6.87—8.93 (m, 14H, aromatic). IR(KBr): 2910—2830 (methylene), 1725 (aromatic ester), 1673 cm^{-1} (aromatic ketone). Calcd for $C_{40}H_{40}O_7$: C, 75.93; H, 6.37%. Found: C, 75.71; H, 6.34%. M, 632.

AQ-12-XH. ^{1}H NMR($CDCl_3$): δ=1.18—2.00 (s, 20H, $-CH_2-$), 4.02 (s, 2H, methylene of **XH**), 4.2—4.46 (m, 4H, $-CO_2-CH_2-$), 6.83—8.87 (m, 14H, aromatic). IR(KBr): 2910—2840 (methylene), 1730 (ester), 1678 cm^{-1} (ketone). Calcd for $C_{41}H_{40}O_7$: C, 76.37; H, 6.25%. Found: C, 76.42; H, 6.25%. M, 645.

BP-12-XH. ^{1}H NMR ($CDCl_3$): δ=1.18—2.00 (s, 20H, $-CH_2-$), 4.03 (s, 2H, methylene of XH), 3.85—4.37 (m, 4H, $-CO_2-CH_2-$, $-O-CH_2-$), 6.76—7.84 (m, 16H, aromatic). IR(KBr) 2920—2840 (methylene), 1710 (ester), 1640 cm^{-1} (ketone). Calcd for $C_{39}H_{42}O_5$: C, 79.29; H, 7.17%. Found: C, 79.38; H, 7.19%. M, 591.

Table 1. Melting Points of Chain Molecules

Ar-*n*-XH	Mp/°C	Ar-*n*-XH	Mp/°C
XO-2-XH	214—215	XO-10-XH	165—166
XO-3-XH	140—141	XO-12-XH	121—122
XO-4-XH	189—190	AQ-12-XH	135—136
XO-5-XH	156	BP-12-XH	82—83
XO-6-XH	177—178	AP-12-XH	99—100
XO-8-XH	149—150	XO-12	79—80

AP-12-XH. ^{1}H NMR($CDCl_3$): δ=1.18—2.00 (s, 20H, $-CH_2-$), 2.49 (s, 3H, $-CO-CH_3$), 4.02 (s, 2H, methylene of **XH**), 3.83—4.36 (m, 4H, $-O-CH_2-$, CO_2-CH_2-), 6.69—7.95 (m, 11H, aromatic). IR(KBr): 2920—2840 (methylene), 1710 (ester), 1670 cm^{-1} (ketone). Calcd for $C_{34}H_{40}O_5$; C, 77.24; H, 7.63%. Found C, 77.17; H, 7.91%. M, 528.

Spectrograde acetonitrile (AcCN) and benzene were used as received. Concentrations of solutes were ≈10^{-4} M and all solutions were deaerated by freeze-pump-thaw cycles.

Laser Flash Photolysis. Figure 1 shows the experimental setup for a nanosecond laser flash photolysis. A sample cell (10×5 mm) placed between pole pieces of a small

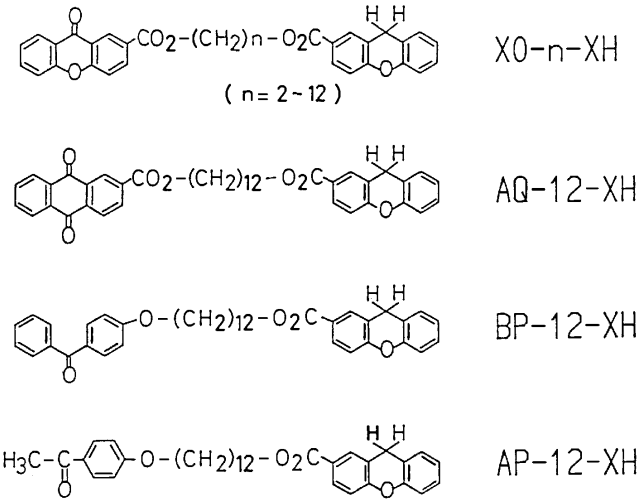

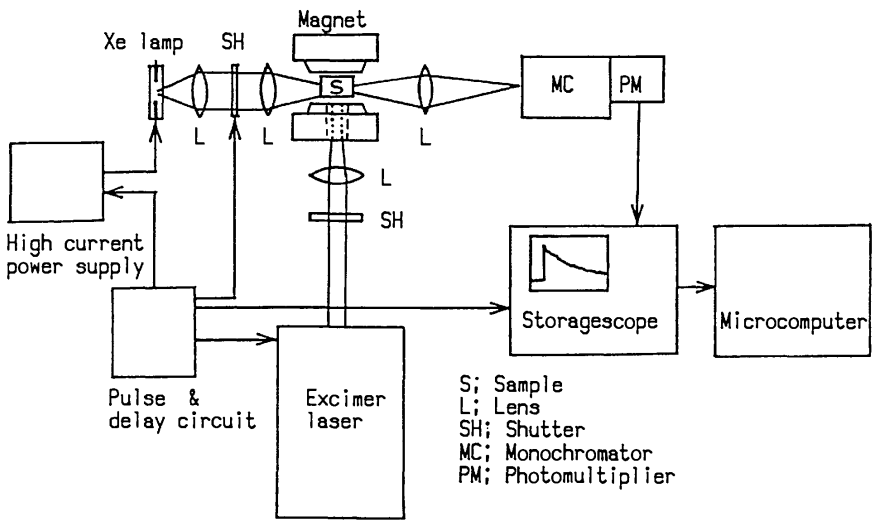

Fig. 1. Experimental setup of a laser flash photolysis apparatus.

electromagnet (Tokin SEE-9, <1 T) was irradiated by a light from an excimer laser (Lambda Physik EMG-50E, 308 nm) or an N_2 laser (Molectron UV-12, 337 nm) through a small hole (10 mm in diameter) on a pole piece. A xenon arc lamp (Ushio UXL-500-O) was used as a probe light source, whose intensity was intensified by applying a pulse of a high electric current (100 A, 3 ms). A laser, a probe light, and a high-speed electric shutter (Copal No. 0) were synchronized with a home-made pulse and delay circuit. The transient signal was detected by a combination of a monochromator (Ritsu NC-10N), a photomultiplier (HTV R-666), and a storagescope (Iwatsu TS-8123), and was fed into a microcomputer (Fujitsu FM-11BS) for analysis. Residual field of an electromagnet was canceled by applying a dc current (<0.3 mT).

In analysis of transient decay curves, the initial decaytime (1/e) was defined as the apparent lifetime (τ), as, in some cases, they deviated slightly from an exponential function.

Calculation of Interradical Distance. The radical-radical distance at the two ends of a methylene chain was calculated at 25 °C for biradicals generated from XO-*n*-XH by the direct enumeration method described in detail in the literature.[13] Here, the radical centers were assumed to be the carbon atoms at 9-position of XO and XH, respectively. The model considered for the methylene chain was the rotational isomeric state model, where all the C-C bonds of the methylene chain were assumed to be one of the three rotational isomers, trans (t), gauche (g^+, 120°), and gauche (g^-, −120°), and the relative orientation of C=O and O-C bonds at the ester was fixed in the trans form. Conformational energies were allotted as 0 cal mol^{-1} for t, 500 cal mol^{-1} for $g^{\pm}$, respectively. For $g^{\pm}g^{\mp}$ sequence, 2000 cal mol^{-1} was added.

Results and Discussion

1. Magnetic Field Effects on the Transient Absorption of Ar-12-XH. XO-12-XH. Figure 2 shows transient absorption spectra of XO-12-XH and XO-12 in acetonitrile. An intense and broad band around 620 nm (τ, 2 μs) of XO-12, having no XH chromophore, is assigned to the triplet-triplet (T-T) absorption of the xanthone (XO) chromophore.[5e,14] Absence of the absorption band of a xanthone ketyl radical around 490 nm[14] indicates that the hydrogen abstraction of the excited triplet XO, ^{3}XO*, from its methylene chain and the solvent is insignificant in the present time scale (<10 μs).

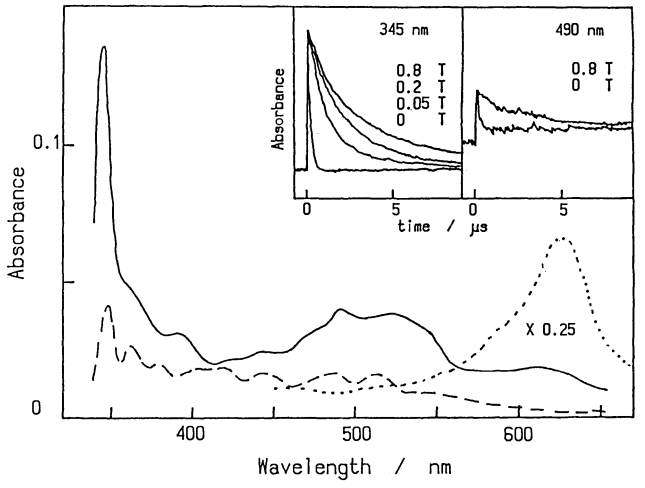

Fig. 2. Transient absorption spectra of XO-12-XH and XO-12 in acetonitrile. —— and ---- are the spectra of XO-12-XH monitored at 0.15 and 0.4 μs delay after laser excitation, respectively. ····· is the spectrum of XO-12 at 0.2 μs delay. Insets are magnetic field effects on the decay curves of transients.

In the spectra of XO-12-XH, a sharp band at 345 nm and a weak one around 500 nm are assigned to the xanthenyl (Ẋ) and xanthone ketyl (ẊOH) radical, respectively, from the comparison with the spectra reported in the literature.[5e,14,15] Since they appear concurrent with the rapid decrease (<10 ns) of the T-T absorption of XO around 620 nm, the hydrogen abstraction of the excited triplet, ^{3}XO*, of XO from the XH chromophore at the other end of the chain, results in the generation of a triplet biradical of Ẋ and ẊOH, ^{3}(ẊOH-12-Ẋ). Intermolecular photoreaction is not involved in the reaction of XO-12-XH in the present time scale, since the generation of a xanthenyl radical is very slow (risetime, 780 ns) in the corresponding intermolecular reaction of xanthone (1.4×10^{-4} M) and xanthene (1.4×10^{-4} M).

The effects of external magnetic fields on the decay curves of Ẋ (345 nm) and ẊOH (490 nm) chromophores are shown in the insets of Fig. 2. Significant MFE were observed in the intramolecular reaction of XO-12-XH, though no appreciable effect was detected in the corresponding intermolecular reaction of xanthone and xanthene. Lifetimes of Ẋ and ẊOH in the ẊOH-12-Ẋ biradicasl are 0.14 and 0.18 μs at zero field, respectively, while they are 3 and 4 μs at 0.8 T, respectively. Small disagreement of the lifetimes determined from the two chromophores may result from the contamination of photoproducts. The simultaneous observation of MFE on the two radicals presents unequivocal evidence that the two radicals at the ends of the chain correlate magnetically each other. These findings are in good agreement with our previous observation that two radicals composing a pair exhibit MFE simultaneously in a micellar cage.[5f]

Furthermore, analogous MFE were observed for the transients of XO-12-XH in benzene solution (Table 2). The lifetime of ẊOH-12-Ẋ in a magnetic field is about two times longer in benzene than in acetonitrile. This might be attributable to the conformational difference and/or the different reactivity of the biradical in the two solvents. Since XO-12-XH is less soluble in acetonitrlie than in benzene, its average conformation in acetonitrile may be rather compact compared with that in benzene. This difference of conformations may somewhat affect the lifetime in magnetic fields. An alternative explanation is the reactivity of the biradical The diffusion-controlled reaction-rate in benzene is considered to be about two times smaller

than in acetonitrile, taking into account of the viscosity of two solvents (acetonitrile (0.345 cp; 1 p=0.1 Pa s) and benzene (0.649 cp)). Thus, in a high field, the lifetime of the biradical may be shorter in acetonitrile than in benzene, if diffusion-controlled bimolecular reactions take place substantially. The polarity of a solvent itself, therefore, does not affect the magnitude of MFE on the neutral biradical significantly.

Other Bifunctional Chain Molecules. Analogous chain molecules, AQ-12-XH, BP-12-XH, and AP-12-XH exhibit similar end-to-end photoreactions. Intramolecular hydrogen abstraction from the methylene chain may not be involved significantly in these reactions in the time scale of the present observation (<10 μs), since intramolecular hydrogen abstraction of alkyl anthraquinone-2-carboxylates and alkyl benzophenone-4-carboxylates is insignificant in that time scale,[9,16] and since the excited triplets of anthraquinone, benzophenone, and acetophenone react readily with xanthene in micellar solution.[5g]

In the transient spectra of AQ-12-XH in benzene (Fig. 3a), absorption bands of Ẋ and anthrasemiquinone radical (ȦQH) appear at 345 and 380 nm, respectively.[5b,17] Here, benzene is used as a solvent on account of solubility. The decay curves of both bands exhibit remarkable MFE as shown in the insets.

In the laser flash photolysis of BP-12-XH in acetonitrile, absorption bands appear around 340 and 530 nm (Fig. 3b). The former band is mostly attributable to the sum of absorptions of Ẋ, benzophenone ketyl radical ḂPH, and T-T absorption of BP.[3a,18] On the other hand, a weak band around 530 nm may be composed of T-T absorption of BP (≈510 nm) and that of ḂPH (≈540 nm), since its peak shifts slightly toward longer wavelengths with time.[3b] Indeed, the transient decay curve monitored at 510 nm is scarcely affected by a magnetic field, as expected. Hydrogen abstraction reaction in BP-12-XH is considered to be slower than XO-12-XH and AQ-12-XH, as the lifetime of the T-T absorption of BP monitored at 510 nm was estimated to be 0.2 μs. Significant MFE were observed on the decay curves at 345 nm (Ẋ and ḂPH) and at 545 nm (ḂPH) as shown in the insets of Fig. 3b, though the accurate determination of the biradical lifetime was difficult due to the interferrence of the T-T band of

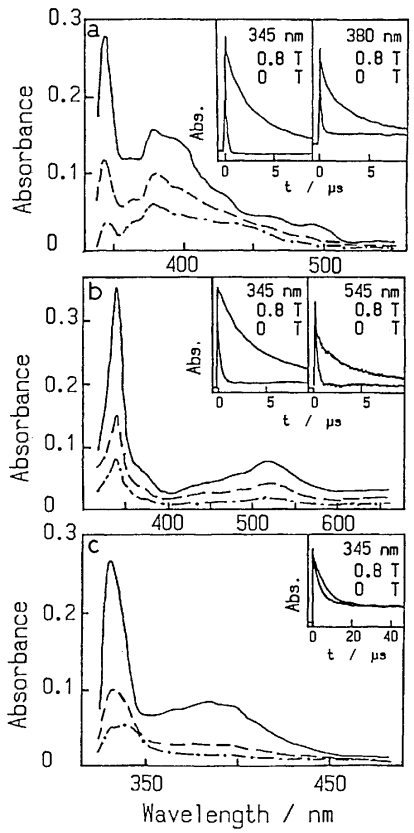

Fig. 3. Transient absorption spectra of bifunctional chain molecules. (a) AQ-12-XH in benzene. Delaytimes are 0.12 (——), 0.5 (----), and 1 μs (—·—). (b) BP-12-XH in acetonitrile. Delaytimes are 0.25 (——), 1 (----), and 5 μs (—·—). (c) AP-12-XH in acetonitrile. Delaytimes are 2 (——), 10 (----), and 20 μs (—·—). Insets in the respective figures are the magnetic field effects on the decay curves of transients.

the BP chromophore in both wavelength region. The lifetime of the biradical determined from the former band, however, seems to be less contaminated by the decay of T-T band, because of high absorption intensities of Ẋ and ḂPH radicals.

In the case of AP-12-XH in acetonitrile (Fig. 3c), the rate of hydrogen abstraction is much slower than that of BP-12-XH. Absorption bands around 320 and 390 nm are mainly assigned to the T-T absorption of

Table 2. Lifetimes of Biradicals[a]

ȦrH-12-Ẋ Solvent	ẊOH-12-Ẋ AcCN	ẊOH-12-Ẋ Benzene	ȦQH-12-Ẋ Benzene	ḂPH-12-Ẋ AcCN	ȦPH-12-Ẋ AcCN
τ(0 T)	0.14 (345 nm)[b]	0.13 (345 nm)	0.14 (345 nm)	0.38[c] (345 nm)	8[c] (345 nm)
μs	0.18 (490 nm)	0.20 (490 nm)	0.17 (380 nm)	0.23[c] (545 nm)	
τ(0.8 T)	3.0 (345 nm)	4.2 (345 nm)	3.0 (345 nm)	5.1 (345 nm)	10[c] (345 nm)
μs	4.0 (490 nm)	4.8 (490 nm)	3.4 (380 nm)	5.7 (545 nm)	

a) Experimental errors are ±20%. b) Wavelength where transient decay curves were monitored. c) Measurements were difficult due to the interference from the T-T absorption. See text.

AP,[19,20] whose lifetime is estimated to be 3.3 μs. On the other hand, a band around 345 nm observed at 20 μs delay may be assigned to Ẋ, generated from the hydrogen abstraction reaction, indicating the generation of the triplet biradical of the acetophenone ketyl radical (ȦPH) and Ẋ, ^{3}(ȦPH-12-Ẋ). Indeed, only small MFE were detected on the decay curve of Ẋ at 345 nm (see inset of Fig. 3c), though no appreciable effect was detected in the decay curves monitored at 320 and 390 nm. The apparent lifetimes of the 345 nm band, presumably the mixture of the absorptions of ^{3}AP* and Ẋ, are approximately 8 μs at zero field and 10 μs at 0.8 T.

Magnetic field effects on the lifetimes of biradicals are summarized in Table 2. Drastic MFE were simultaneously observed on transient absorptions of two chromophores in ẊOH-12-Ẋ, ȦQH-12-Ẋ, and ḂPH-12-Ẋ. The facts present an unequivocal evidence that two radicals at the ends of methylene chain interact magnetically each other. Small disagreement in lifetimes determined from the respective two chromophores may be due to the contamination of the short-lived T-T absorption of the respective precursors and/or the absorption of photoproducts. In the case of ȦPH-12-Ẋ, its dynamics may be chiefly controlled by its slow formation process, and, for this reason, no significant MFE might be detected. Figure 4 shows the magnetic field dependence of the lifetimes of ẊOH-12-Ẋ, ȦQH-12-Ẋ, and ḂPH-12-Ẋ biradicals. Lifetimes are determined from the decay curves of the 345 nm band of Ẋ because of its high absorbance. In all cases, the lifetimes increase suddenly around 0.05 T and gradually in higher fields (>0.1 T). Saturation of the effects seems to occur at higher fields (>0.5 T).

Furthermore, the magnitude of MFE on these biradicals in both polar and nonpolar solvents is comparable with or greater than that observed in the radical pairs generated from the corresponding bimolecular reactions in micellar solution.[5] These facts indicate that the linking of two radicals by a methylene chain, to hinder their separation, is essential for significant MFE. Therefore, from comparison of results on the present biradicals with those on the radical pairs in micellar solution,[5] we can conclude that, in micellar solution, the dimentionality of a micellar cage, keeping the components of a pair in a short distance, is of the primary factor for significant MFE, as assumed so far in MFE on the photoreactions in micellar solutions. It is also likely that the high microviscosity in a micelle as well as the high solubility of hydrophobic radicals in a micellar phase acts all together to elongate lifetime of the pair in it.

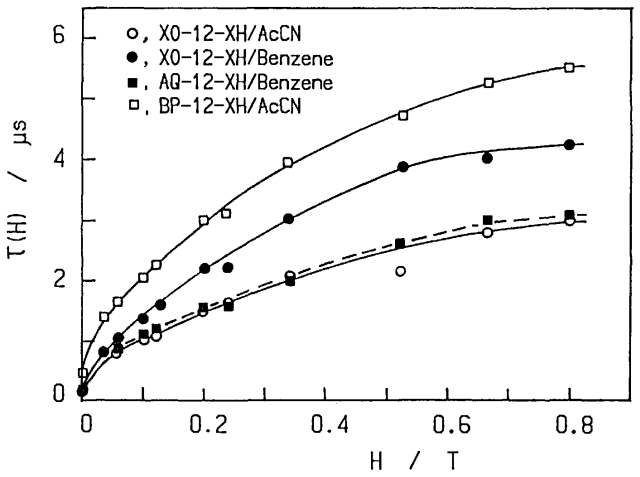

Fig. 4. Magnetic field dependence of the lifetimes of biradicals. Lifetimes were determined from the decay curves at 345 nm.

Reaction Mechanism. All the results mentioned above can be ascribed by the following reaction scheme:

$$\text{Ar-12-XH} \xrightarrow{h\nu} {}^1\text{Ar*-12-XH} \quad (1)$$

$${}^1\text{Ar*-12-XH} \rightarrow {}^3\text{Ar*-12-XH} \quad (2)$$

$${}^3\text{Ar*-12-XH} \rightarrow {}^3(\dot{\text{A}}\text{rH-12-}\dot{\text{X}}) \quad (3)$$

$${}^3(\dot{\text{A}}\text{rH-12-}\dot{\text{X}}) \rightleftarrows {}^1(\dot{\text{A}}\text{rH-12-}\dot{\text{X}}) \quad (4)$$

$${}^1(\dot{\text{A}}\text{rH-12-}\dot{\text{X}}) \rightarrow \text{ArH-12-X} \quad (5)$$

$${}^1(\dot{\text{A}}\text{rH-12-}\dot{\text{X}}) \rightarrow \text{Ar-12-XH} \quad (6)$$

Here, ȦrH is the ketyl or the semiquinone radical generated from aromatic carbonyl, Ar, after the hydrogen abstraction. Upon photoexcitation of Ar in Ar-12-XH, the excited triplet, ^{3}Ar*, of Ar is generated ((1) and (2)). ^{3}Ar* abstracts a hydrogen atom from XH at the other end of the chain to generate the triplet biradical of ȦrH and Ẋ, ^{3}(ȦrH-12-Ẋ). ^{3}(ȦrH-12-Ẋ) deactivates via isc to the singlet biradical, ^{1}(ȦrH-12-Ẋ) (4), from which the product formation (5) and the back reaction (6) may occur. For simplicity, bimolecular reactions such as the reaction between two biradicals are not included in the scheme as the reaction of the triplet biradical, since the concentration of Ar-12-XH is as low as ca. 10^{-4} M. They may be of minor importance in the time scale shorter than 10 μs, though, in the presence of a high magnetic field, they might also take place to some extent.

Now let's consider the mechanism of MFE observed for the present biradicals. The magnetic field effects on a radical pair or a biradical can be interpreted in terms of four mechanisms, i.e., (a) the Δg mechanism, (b) the hyperfine coupling (hfc) mechanism, (c) the relaxation mechanism, and (d) the triplet mechanism.[1,21] In (a), a difference in the electron-spin Larmor frequencies of the two radicals caused by the different electron g values induces the T-S isc of the pair. In (b), a local field generated by nuclear spins (i.e., electron-nuclear hfc) induces the isc, and, in high field, the rates are reduced because of the electronic Zeeman splitting of triplet sublevels (T_+, T_0, and T_-). On the other hand, in (c), electron spin relaxation due to the dipole-dipole anisotropic interaction of an elec-

tron and nuclear spins is affected by the Zeeman splitting of triplet sublevels. Finally, in mechanism (d), spin polarization in an excited triplet precursor is transferred to a radical pair, when the pair formation is fast compared with the relaxation in the excited triplet. Unequal distribution among triplet sublevels in the pair may affect the magnetic field dependence of the lifetime of a radical pair.

Mechanism (a) is not operative in the present magnetic fields (<1T), since the g factors of a xanthenyl radical and a xanthone ketyl radical are the same within experimental error (g=2.0033±0.0005).[22] The hfc-induced isc rate constant k_{isc}(hfc) can be estimated from the effective hfc constants, B_{av}, of radicals in a pair:[23]

$$k_{isc}(\text{hfc})=g\mu B_{av}/\hbar, \quad (7)$$

where μ is the Bohr magneton, and $\hbar$ is the Planck's constant. In mechanism (b), the hfc-induced T-S isc occurs between the energetically degenerated three triplet sublevels and the singlet state at zero field, and the $T_{\pm}$-S isc is quenched in a field much higher than B_{av}, due to the Zeeman splitting of two triplet sublevels. The saturation of the effect appears at a relatively low field (around 0.1 T).

In the case of ẊOH-12-Ẋ, B_{av} is estimated to be 2.5 mT,[24,25] giving k_{isc}(hfc)=10^8 s^{-1} at zero field and 0.3×10^8 s^{-1} at high fields. The observed lifetimes of the biradical are 0.14 μs at zero field and 3 μs at 0.8 T, and the saturation of the effect occurs around 0.8 T, which is much higher than B_{av} (2.5mT). These results indicate that hfc-induced isc is not the rate-determining step at zero field, though one of the three reaction processes (chain dynamics, isc, and cage recombination (product-forming step)) is considered to control the decay rate of the biradical. The chain dynamics may not control it, as the fact that this biradical is formed within a laser pulse width (15—20 ns) confirms the collision of two ends of the chain is a very fast process. The lifetime of ẊOH-12-Ẋ at zero field is, therefore, most probably controlled by the recombination reaction in the singlet state. Furthermore, according to the mechanism (c) the relaxation rate is estimated to be in the order of 10^5—10^6 s^{-1},[26,27] which is compatible with the lifetimes of the present biradical in the higher magnetic fields. On this basis, it is concluded that the lifetime of ẊOH-12-Ẋ is determined by the recombination rate in the singlet at zero field, while in high fields it may be attributable to the relaxation rate, as predicted by the mechanism (c).

The lifetime increases dramatically even in a weak magnetic field (<0.1 T). For example, the lifetimes of this biradical are 0.14 μs (zero field) and 0.77 μs (0.05 T). In low magnetic fields, the hfc-induced isc among non-degenerate spin states may become slower than the cage recombination, and, therefore, the former may be the rate-controlling step at low magnetic fields (<0.1 T). Furthermore, mechanism (d) may be also operative to some extent in addition to the mechanism (c), since the short lifetime of ^{3}XO*-12-XH indicates that the reaction initiates from the spin-polarized triplet state. An analogous argument may hold as for the mechanism in the ȦQH-12-Ẋ biradical. In the case of ḂPH-12-Ẋ and ȦPH-12-Ẋ, however, mechanism (d) may not be involved, since the lifetimes of their precursors seem long enough to attain thermal equilibrium in the excited states.

2. Dependence of the Magnetic Field Effects on Methylene Chain Length of ẊOH-*n*-Ẋ. S-T energy gap of a radical pair or a biradical is considered to be the function of interradical distance, and, therefore, MFE may be affected by the interradical distance. Thus, the influence of the distance between two radical centers on MFE was examined as a function of chain lengths for XO-*n*-XH systems (n=2—12). All bifunctional molecules XO-*n*-XH (n=2—10) exhibit transient spectra similar to that with n=12 in acetonitrile. The magnetic field effect on the lifetimes of these biradicals is shown in Table 3. In the presence of a magnetic field (0.8 T), they increase very remarkably. At zero field, the lifetimes of ẊOH-*n*-Ẋ (n=3—12) are almost independent of the chain length (0.1—0.2 μs), though that of ẊOH-2-Ẋ is considerably long. The facts indicate that the lifetimes of ẊOH-*n*-Ẋ (n=3—12) are likely controlled by the same reaction step, i.e., cage recombination reaction in the singlet state. The lifetime of ẊOH-2-Ẋ may be controlled mainly analogous process to those of other biradicals, since it exhibits considerable MFE. The n dependence of MFE was , therefore, estimated from the lifetime ratio $R=\tau(\text{H})/\tau(0)$ of biradicals, where τ(H) and τ(0) are the lifetimes in the presence and absence of a magnetic field (0.8 T) (Fig. 5). The ratio, R, which may represents the magnitude of the effect, increases with increasing n and reaches a plateau around n=6. The fact implies that the T-S degeneracy of the biradical occurs effectively at the chain length of around n=6. In the case of ẊOH-2-Ẋ, its lifetime (≈1 μs) at zero field is considerably long and the MFE are relatively small compared with those of other biradicals.

Table 3. Lifetimes of Biradicals Generated from XO-*n*-XH in Acetonitrile[a]

n	τ(0 T) / μs	μ(0.8 T) / μs	R[b]
2	0.98	2.7	2.8
3	0.18	0.8	4.4
4	0.22	1.7	7.7
5	0.13	1.1	8.5
6	0.11	1.7	15.5
8	0.16	2.3	14.5
10[c]	0.29	6.0	20.7
12	0.14	3.0	21.4

a) Experimental errors are ±20%. b) Lifetime ratio τ(0.8 T)/τ(0 T). c) Experimental errors are ±30%, because of low solubility.

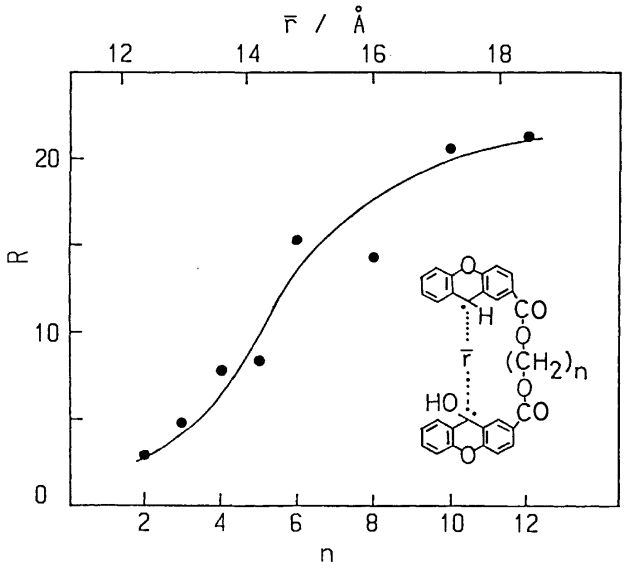

Fig. 5. Methylene chain length n dependence of R of ẊOH-n-Ẋ in acetonitrile. $R=\tau(0.8\,T)/\tau(0\,T)$ is the ratio of the lifetimes τ in the presence and the absence of a magnetic field, 0.8 T. Lifetimes were determined from the decay curves at 345 nm. Top of the figure is the mean distance $\bar{r}$ of two radical centers at the ends of methylene chain. See text.

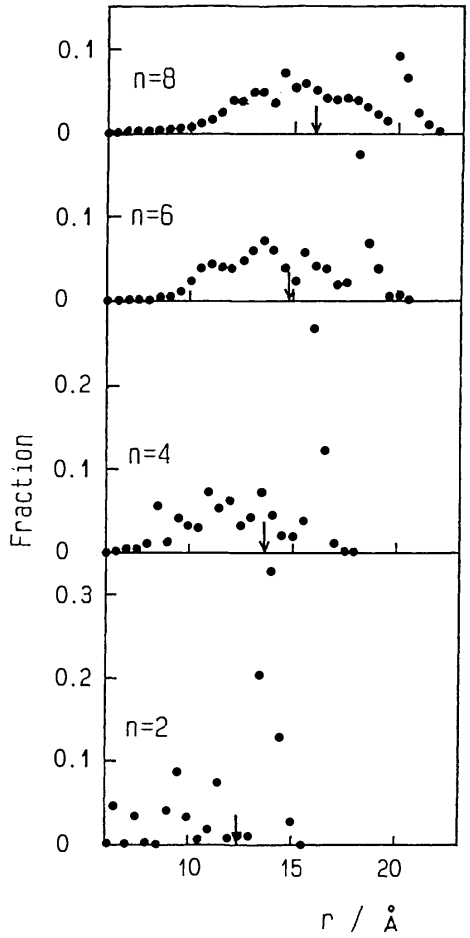

Fig. 6. Typical distribution of the interradical distance r of the ẊOH-n-Ẋ biradicals, the hydroxyl carbon atom of ẊOH and the methylene carbon atom of Ẋ being assumed to be the respective radical centers. Arrows indicate the respective mean interradical distance $\bar{r}$.

In this case, isc may occur among non-degenerate S and T states even at zero field. A steric hindrance and chain dynamics might not be very important, since the generation of this biradical is within the laser pulse width (15—20 ns) as observed for every other molecules.

In order to estimate the distance between the two radical centers at the ends of the chain, we calculated the distribution of interradical distance r and mean interradical distance $\bar{r}$ with the aid of the direct enumeration method, by assuming that the hydroxyl carbon atom of ẊOH and the methylene carbon atom of Ẋ are the respective radical centers. The typical results are shown in Fig. 6. Distribution of interradical distances, especially for short chain molecules, is deviated far from the normal distribution curve. It is mostly because the number of chain conformations are limited due to the fixed conformation of the carboxyl groups in the chain and to the steric hindrance of the bulky aromatic rings. The distance dependence of MFE was, thus, roughly estimated from the mean distance, $\bar{r}$, though it was not a good representative of the ensemble of the conformations. The mean interradical distance for the biradical ẊOH-6-Ẋ, where saturation of MFF occurs, was obtained to be about 15 Å (see Fig. 5). It is most likely that the triplet and singlet states degenerate each other at a mean interradical distance of about 15 Å, and at this distance, therefore, isc in the biradical occurs efficiently. In the case of ẊOH-2-Ẋ, the mean distance was estimated to be as long as about 12 Å, suggesting a very small S-T energy gap. For this reason, MFE might be observed even though the magnitude was relatively small compared with those of longer chain biradicals.

Next, the S-T energy gap ($2J$) of the ẊOH-n-X biradicals was estimated. $2J$ is usually expressed by an exponential function, when it is controlled by the through-space exchange interaction:[28,29]

$$2J=2J_0\exp(-ar). \tag{8}$$

Assuming that $2J_0=1.896\times10^9$ mT and $a=2.136$ Å^{-1}, the $2J$ values were calculated (Table 4). The n dependence of $2J(r)$ values, calculated by weighting the distribution of r, does not reproduce the observed tendency of R shown in Fig. 5. This is attributable to the conformations of biradicals having short interradical distance r, as shown in Fig. 6. Since the exchange energy increases exponentially with decreasing r, averaged energy becomes considerable magnitude, even though fraction of such conformations is quite small. When the mean distance $\bar{r}$ is used for calculation, the trend of $2J(\bar{r})$ fits qualitatively the observed one,

Table 4. Mean Interradical Distance $\bar{r}$ (Å) and Electron Exchange Energy $2J$ (mT) of Biradicals, ẊOH-*n*-Ẋ

n	2	3	4	5	6	7	8
$\bar{r}$	12.4	12.8	13.6	14.3	14.8	15.5	16.1
$2J(r)$[a]	21.8	0.05	0.08	30.7	0.45	30.8	1.1
$2J(\bar{r})$[b]	0.006	0.003	0.001	0.000	0.000	0.000	0.000

a) Averaged over all of $2J(r)$ values for the distribution of r. b) Calculated by using mean distance $\bar{r}$.

though its magnitude is too small to explain the observed results. As was discussed in the CIDNP study of biradicals generated from cyclic ketones,[29] the exponential approximation of $2J$ is incomplete for complex systems like the present ones, since exchange interaction is influenced by mutual orientation of orbitals occupied by unpaired electrons.

Recently, MFE on the dynamics of radical pairs and radical ion pairs (rip) generated from bifunctional chain molecules have been reported. In studies of the MFE on the intramolecular exciplex fluorescence of phenanthrene-$(CH_2)_n$-*N*,*N*-dimethylaniline (n=3—10)[30] and pyrene-$(CH_2)_n$-*N*,*N*-dimethylaniline (n=3—16),[31] the S-T degeneracy of singlet intramolecular rip was reported to occur at the chain length of around n=10. These results are equivalent with the present ones for the triplet biradical, ẊOH-*n*-Ẋ, since they contain two ester groups in the chain. Analogous conclusion on the S-T degeneracy of triplet biradicals were also reported for PhĊH-$(CH_2)_n$-Ċ=O (n=8—10) biradicals[32] and the biradicals generated from α-(4-benzoylphenoxy)-ω-[4-(phenylamino)phenoxy]alkanes (n=2—16).[33] Therefore, it is generally concluded that the S-T degeneracy of biradicals, independent from their spin multiplicity, occurs when the number of chain units becomes larger than 10 or so.

Conclusion

In this paper we have presented a detailed study of MFE on the dynamics of methylene chain linked biradicals. Drastic MFE were observed on the decay of ẊOH-12-Ẋ, ȦQH-12-Ẋ, and ḂPH-12-Ẋ biradicals in both polar and nonpolar solvents. The facts present that the linking of two radicals to hinder their separation is essential for significant effects. These results also suggest that dimentionality of a micellar cage is the key for significant MFE on radical pairs observed previously in micellar solution.

The effects are qualitatively interpreted in terms of the relaxation mechanism, where relaxation in triplet sublevels of biradicals is a rate-controlling step in higher fields. The S-T degeneracy of biradicals, ẊOH-*n*-Ẋ, occurs at the chain length of around n=6, which corresponds to the interradical distance of about 15 Å.

The authors wish to express their thanks to Professor Masahiko Sisido, Kyoto University, for the use of his conformational calculation program, and to Professor Saburo Nagakura and Dr. Ryoichi Nakagaki, Institute for Molecular Science, for several illuminating discussions. This work was supported by the Yamada Science Foundation, the Takeda Science Foundation, and a Grant-in-Aid for Scientific Research from the Ministry of Education, Science and Culture.

References

1) "Spin Polarization and Magnetic Field Effects in Radical Reactions," ed by Yu. N. Molin, Elsevier, Amsterdam (1984).

2) a) N. J. Turro and B. Kraeutler, *J. Am. Chem. Soc.*, **100**, 7432 (1978); b) N. J. Turro and B. Kraeutler, *Acc. Chem. Res.*, **13**, 369 (1980); c) N. J. Turro, *Proc. Natl, Acad. Sci. U.S.A.*, **80**, 609 (1983); d) I. R. Gould, M. B. Zimmt, N. J. Turro, and B. H. Baretz, *J. Am. Chem. Soc.*, **107**, 4607 (1985); e) N. J. Turro, M. B. Zimmt, and I. R. Gould, *J. Phys. Chem.*, **92**, 433 (1988), and references therein.

3) a) Y. Sakaguchi, S. Nagakura, and H. Hayashi, *Chem. Phys. Lett.*, **72**, 420 (1980); b) Y. Sakaguchi, H. Hayashi, and S. Nagakura, *J. Phys. Chem.*, **86**, 3177 (1982); c) Y. Sakaguchi and H. Hayashi, *ibid.*, **88**, 1437 (1984); d) Y. Sakaguchi and H. Hayashi, *Chem. Phys. Lett.*, **106**, 420 (1984); e) H. Hayashi, Y. Sakaguchi, M. Tsunooka, H. Yanagi, and M. Tanaka, *ibid.*, **136**, 436 (1987).

4) a) J. C. Scaiano and E. B. Abuin, *Chem. Phys. Lett.*, **81**, 209 (1981); b) J. C. Scaiano, E. B. Abuin, and L. C. Stewart, *J. Am. Che. Soc.*, **104**, 5673 (1982); c) J. C. Scaiano and D. J. Lougnot, *J. Phys. Chem.*, **88**, 3379 (1984); d) J. C. Scaiano and D. -J. Lougnot, *Chem. Phys. Lett.*, **105**, 535 (1984); e) C. Evans, K. U. Ingold, and J. C. Scaiano, *J. Phys. Chem.*, **92**, 1257 (1988).

5) a) Y. Tanimoto and M. Itoh, *Chem. Phys. Lett.*, **83**, 626 (1981); b) Y. Tanimoto, H. Udagawa, and M. Itoh, *J. Phys. Chem.*, **87**, 724 (1983); c) Y. Tanimoto, H. Udagawa, Y. Katsuda, and M. Itoh, *ibid.*, **87**, 3976 (1983); d) Y. Tanimoto, K. Shimizu, and M. Itoh, *J. Am. Chem. Soc.*, **106**, 7257 (1984); e) Y. Tanimoto, M. Tahashima, and M. Itoh, *J. Phys. Chem.*, **88**, 6053 (1984); f) Y. Tanimoto, M. Takashima, and M. Itoh, *Chem. Lett.*, **1984**, 1981; g) Y. Tanimoto and M. Itoh, "Physical Organic Chemistry 1986," ed by M. Kobayashi, Elsevier, Amsterdam (1987), p. 257.

6) a) W. Schlenker, T. Ulrich, and U. E. Steiner, *Chem. Phys. Lett.*, **103**, 118 (1983); b) T. Ulrich and U. E. Steiner, *ibid.*, **112**, 365 (1984); c) T. Ulrich, U. E. Steiner, and W. Schlenker, *Tetrahedron*, **42**, 6131 (1986).

7) a) M. Okazaki, S. Sakata, R. Konaka, and T. Shiga, *J.*

Am. Chem. Soc., **107**, 7214 (1985); b) M. Okazaki and T. Shiga, *Nature (London)*, **323**, 240 (1986); c) M. Okazaki, S. Sakata, R. Konaka, and T. Shiga, *J. Phys. Chem.*, **91**, 1131 (1987); d) M. Okazaki, S. Sakata, R. Konaka, and T. Shiga, *J. Chem. Phys.*, **86**, 6792 (1987).

8) J. H. Fendler and E. J. Fendler, "Catalysis in Micellar and Macromolecular Systems," Academic Press, New York (1975), Chap. 2.

9) a) Y. Tanimoto, M. Takashima, M. Uehara, M. Itoh, M. Hiramatsu, R. Nakagaki, T. Watanabe, and S. Nagakura, *Chem. Lett.*, **1985**, 15; b) Y. Tanimoto, M. Takashima, M. Uehara, M. Itoh, M. Hiramatsu, R. Nakagaki, T. Watanabe, and S. Nagakura, XIIth International Conference on Photochemistry, Tokyo (1985), Abstr., No. 3P27; c) Y. Tanimoto, M. Uehara, M. Takashima, and M. Itoh, *Bull. Chem. Soc. Jpn.*, **61**, 3121 (1988).

10) A preliminary result has appeared: Y. Tanimoto, M. Takashima, K. Hasegawa, and M. Itoh, *Chem. Phys. Lett.*, **137**, 330 (1987).

11) M. Fckstein, H. Marona, and J. Mazur, *Pol. J. Pharmacol. Pharm.*, **35**, 159 (1983).

12) a) R. D. Hoffsommer, D. Taub, and N. L. Wendler, *Chem. Ind. (London)*, **1964**, 482; b) A. L. Wilds, "Organic Reactions," John Wiley and Sons, New York (1944), **2**, p. 178.

13) M. Sisido, and K. Shimada, *J. Am. Chem. Soc.*, **99**, 7785 (1977).

14) A. Garner and F. Wilkinson, *J. Chem. Soc., Faraday Trans. 2*, **72**, 1010 (1976).

15) H. Masuhara, M. Okuda, and M. Koizumi, *Bull. Chem. Soc. Jpn.*, **41**, 2319 (1968).

16) M. A. Winnik, S. N. Basu, C. K. Lee, and D. S. Saunders, *J. Am. Chem. Soc.*, **98**, 2928 (1976).

17) N. K. Bridge and G. Porter, *Proc. R. Soc. London, Ser. A*, **244**, 259 (1958).

18) T. S. Godfrey, J. W. Hilpern, and G. Porter, *Chem. Phys. Lett.*, **1**, 490 (1967).

19) H. Lutz, E. Breheret, and L. Lindqvist, *J. Phys. Chem.*, **77**, 1758 (1973).

20) A. Beckett, A. D. Osborne, and G. Porter, *Trans. Faraday Soc.*, **60**, 873 (1964).

21) a) S. K. Wong, D. A. Hutchinson, and J. K. S. Wan, *J. Chem. Phys.*, **58**, 985 (1973); b) P. W. Atkins and G. T. Evans, *Chem. Phys. Lett.*, **25**, 108 (1974); c) F. J. Adrian, *J. Chem. Phys.*, **61**, 4875 (1974).

22) M. Terajima and T. Azumi, private communication.

23) a) K. Schulten and P. G. Wolynes, *J. Chem. Phys.*, **68**, 3292 (1978); b) A. Weller, F. Nolting, and H. Staerk, *Chem. Phys. Lett.*, **96**, 24 (1983).

24) a) M. D. Sevilia and G. Vincow, *J. Phys. Chem.*, **72**, 3635 (1968); b) L. Lunazzi, A. Mangini, G. Placucci, and C. Vincenzi, *J. Chem. Soc., Perkin Trans. 1*, **1972**, 2418.

25) a) R. Wilson, *J. Chem. Soc. B*, **1968**, 1581; b) R. S. Davidson, F. A. Younis, and R. Wilson, *J. Chem. Soc., Chem. Commun.*, **1969**, 826.

26) H. Hayashi and S. Nagakura, *Bull. Chem. Soc. Jpn.*, **57**, 322 (1984).

27) R. Kaptein, "Chemically Induced Magnetic Polarization," ed by L. T. Muus, P. W. Atkins, K. A. McLauchlan, and J. B. Pedersen, D. Reidel, Dordrecht (1977), p.1.

28) C. Herring and M. Flicker, *Phys. Rev.*, **134**, A362 (1964).

29) a) F. J. J. de Kanter, J. A. den Hollander, A. H. Huizer, and R. Kaptein, *Mol. Phys.*, **34**, 857 (1977); b) F. J. J. de Kanter, R. Z. Sagdeev, and R. Kaptein, *Chem. Phys. Lett.*, **58**, 334 (1978).

30) a) Y. Tanimoto, N. Okada, M. Itoh, K. Iwai, K. Sugioka, F. Takemura, R. Nakagaki, and S. Nagakura, *Chem. Phys. Lett.*, **136**, 42 (1987); b) Y. Tanimoto, N. Okada, K. Hasegawa, M. Itoh, K. Iwai, K. Sugioka, F. Takemura, R. Nakagaki, and S. Nagakura, *J. Phys. Chem.*, **93**, 3586 (1989).

31) H. Staerk, W. Kuhnle, R. Treichel, and A. Weller, *Chem. Phys. Lett.*, **118**, 19 (1985).

32) M. B. Zimmt, C. Doubleday, Jr. and N. J. Turro, *J. Am. Chem. Soc.*, **107**, 6726 (1985).

33) Y. Tanimoto, N. Okada, and M. Itoh, Symposium on Photochemistry, Tokyo (1988), Abstr. No. IA209.

Optical Resolution of a Co(III) Complex of 2-Hydroxy-1,3-propanediamine-*N,N,N′,N′*-tetraacetic Acid: Crystal Structure of $(+)_{589}$-Strychnine (2-Hydroxy-1,3-propanediamine-*N,N,N′,N′*-tetraacetato)-cobaltate(III) Sesquihydrate, $(+)_{589}$-(STC)-[Co(dhpta)]·1.5H_2O

Mitsunobu SATO* and Shigenobu YANO*,†

The Department of Science and Engineering, National Science Museum, Ueno-Park, Taito-ku, Tokyo 110
†The Department of Chemistry, Faculty of Science, Nara Women's University, Kita-Uoya-Nishimachi, Nara 630

(Received March 13, 1989)

The 2-hydroxy-1,3-propanediamine-*N,N,N′,N′*-tetraacetatocobaltate(III) complex has been optically resolved using strychnine nitrate. The crystal structure of the optically active complex with the resolving agent, $(+)_{589}$-(STC)[Co(dhpta)]·1.5H_2O has been determined from three dimensional X-ray diffraction data. The absolute configuration around the cobalt atom, to which two nitrogen and four oxygen atoms in the ligand are bonded nearly octahedrally, is Δ. The six-membered chelate ring adopts the λ-skew boat conformation. The intermolecular hydrogen bonding between the coordinated oxygen atom of the acetate ring and the protonated nitrogen atom of strychnine, which is one of the asymmetric centers, plays an important role in the diastereomeric discrimination. In contrast, the non-coordinated hydroxyl group in the complex ion does not interact directly with the strychnine molecule. The relationship between the absolute configuration around the cobalt center and the circular dichroism has been examined for the optically active complex ion.

Optical resolution of racemic compounds, which has many empirical aspects, is an important area of chemistry. The optical resolution of the tetragonal Co(III) complex of 2,2′-bipiperidine, which has no net chirality around the central cobalt ion, has been attained by the organic resolving agent ammonium (+)-3-bromocamphor-9-sulfonate in our recent study.[1] By the crystal structure study of the complex having the resolving agent, we reported an indirect type of interaction between the complex cation and the resolving agent anion, implying the importance of the water molecules of crystallization and the asymmetric nitrogen centers caused by coordination,[2] as compared with the known type of direct interaction,[3] in the case of the (+)-3-bromocamphor-9-sulfonate salt. On the other hand, there is little information on the interaction between the anionic complex ion and the organic resolving agent.

Recently, by the preparation of the strychnine salt, the optically active Co(III) complex of 2-hydroxy-1,3-propanediamine-*N,N,N′,N′*-tetraacetic acid (DHPTA) was obtained, in which the carbon atom bonded to the hydroxyl group becomes an asymmetric center by coordination. Strychnine, which has eight asymmetric centers including two asymmetric nitrogen atoms, is a type of alkaloid and can be used as a cationic resolving agent. We report here the preparation and the optical resolution of the cobalt(III) complex of DHPTA, and to our knowledge, the first X-ray structure determination of a Co(III) complex having strychnine as a counter cation. We are interested in this hexadentate ligand, DHPTA, since the existence of the hydroxyl group may afford the opportunities for certain modification, including the tethering of the complex to silica surfaces and polymers.

The X-ray crystal structure study on the complex, (±)-K[Co(dhpta)], has been performed by Kalina et al.,[4] and they indicated that the non-coordinated hydroxyl group significantly interacts with the carboxyl groups in the neighbouring complex ions. Our purpose in undertaking the present X-ray structure determination was fourfold: to determine the absolute configuration around the cobalt center of the $(+)_{589}$-$[Co(dhpta)]^-$ ion, to elucidate the conformation of the six-membered chelate ring involving the *C*-substituted hydroxyl group in the optically active form; to clarify the interaction between the complex anion and the resolving reagent, i.e. the strychnine cation; and to examine relationships between CD curves and absolute configuration at the cobalt center of EDTA-type hexadentate ligands, where EDTA represents ethylenediaminetetraacetic acid.

Experimental

Measurements. The absorption (AB) spectra were recorded on a Shimadzu UV-240 spectrophotometer. The CD spectra were measured with a JASCO J-500A recording spectropolarimeter. These spectra were obtained in water. The ^{13}C NMR spectra were measured on a JEOL GNM JX-400 (400 MHz) spectrometer in D_2O, with dioxane as the internal standard. The optical rotations were measured in a 10 mm tube at 18 °C on a JASCO DIP-360 digital polarimeter.

Materials. All the reagents were of the best commercial grade and were used without further purification.

Preparation of K[Co(dhpta)]·0.5H_2O; 6.0 g of $Na_3[Co(NO_2)_6]$ were dissolved in 30 ml of water. To the solution 5.0 g of 2-hydroxy-1,3-propanediamine-*N,N,N′,N′*-tetraacetic acid were added with stirring. The solution was heated on a water bath at 60 °C until the original orange-yellow color changed to deep purple. During the reaction, a deep purple complex was precipitated from the solution. After cooling to room temperature, the solution was kept in a

refrigerator overnight. The rather insoluble sodium salt of the complex formed was filtered, washed with water, and dried in a desiccator. Yield; 4.90 g. In order to purify the compound, the countercation was changed from sodium to potassium as follows: A large amount of aqueous solution, in which the precipitate was dissolved, was poured onto a cation-exchange resin (Dowex50W-X2, K^+ form) packed in a column. The deep purple eluent from the column, which was flushed with water, was collected and evaporated under reduced pressure to 50 ml. The solution was allowed to stand in a refrigerator for a week, and the crystals formed were collected, washed with cold water, and dried in a desiccator. Found : C, 30.9; H, 3.39; N, 6.54%. Calcd for $C_{11}H_{15}N_2O_{9.5}CoK$: C, 31.1; H, 3.55; N, 6.59%. ^{13}C NMR (D_2O) δ=58.2, 60.6, 64.0, 64.8, 65.7, 69.9, 70.1, 181.2, 181.3, 182.8, and 183.4.

Optical Resolution: Preparation of (+)$_{589}$-(STC)[Co(dhpta)]·1.5H_2O. 1.72 g of K[Co(dhpta)]·0.5H_2O was dissolved in 50 ml of water at 60 °C. To the solution 0.90 g of strychnine nitrate was added as a resolving agent and the solution was warmed at the same temperature until complete dissolution was achieved. After filtration, the solution was kept in a refrigerater for a week. The deep purple prismatic crystals formed were collected, washed with cold water and air-dried. Yield; 0.91 g. The crystals formed after recrystallization in water at 60 °C, gave the same value of the ratio α (589 nm)/ε(absorption coefficient) as that of the crystals before recrystallization. Found: C, 52.0; H, 5.62; N, 7.46%. Calcd for $C_{32}H_{40}N_4O_{12.5}Co$: C, 52.0; H, 5.45; N, 7.58%.

Preparation of (+)$_{589}$-K[Co(dhpta)]·H_2O. (+)$_{589}$-(STC)-[Co(dhpta)]·1.5H_2O was dissolved in water with sonicated stirring. The solution was poured into a column (45×2 cm) containing a cation-exchange resin (Dowex50W-X2, K^+ form). The column was flushed with water to elute the purple complex thoroughly. The eluted solution was collected and evaporated under reduced pressure to 20 ml. Twice this volume of methanol was gradually added to the solution, and then the solution was allowed to stand for overnight at ambient temperature. The resulting crystals were collected and washed with methanol, and dried under reduced pressure. Found: C, 31.5; H, 3.57; N, 6.60%. Calcd for $C_{11}H_{14}N_2O_9CoK$: C, 31.7; H, 3.39; N, 6.73%. $[\alpha]_D$=+874°(in 0.174% aqueous solution). $[M]_D$=+3638°.

Intensity Data Collection. The crystal employed in the data collection was a deep purple prism and bounded by (100), (001), and (010) faces. Crystal size 0.24×0.29×0.17 mm. The diffraction data were measured on a Rigaku AFC-5 diffractometer with graphite monochromatized Mo$K\alpha$ radiation. Unit cell and orientation parameters were determined on the basis of the setting angles of 28 carefully centered reflections (2θ=20—30°). Within the range of 2θ<65°, 3632 independent reflections with $F_o>5[\sigma(F_o)]$ were obtained. Intensities were measured by the ω-2θ scan method. Three check reflections, (3,0,0), (0,4,0), and (0,0,4), were measured every 50 reflections and no significant variation in intensities was found. Lorentz and polarization corrections were applied. An absorption correction was not performed because the absorption coefficient of the compound was low (μ=6.01 cm^{-1}).

Crystal data: Monoclinic, $P2_1$, a=15.536(3) Å, b=11.100(2) Å, c=9.339(2) Å, β=92.86(2)°, and Z=2, D_m=1.55, D_x=1.53 g cm^{-3}.

Solution and Refinement of the Structure. The structure was solved by the heavy-atom method. All the nonhydrogen atoms except for the oxygen atoms of water molecules were located on a difference Fourier map. Subsequent difference Fourier calculations, phased with refined nonhydrogen atoms, gave the coordinates of the oxygen atoms of crystalline water and almost all the hydrogen positions except for those of the water molecules and some in the strychnine residue. Idealized coordinates of the remaining hydrogen atoms of the strychnine molecule were calculated

Table 1. Atomic Parameters for Non-Hydrogen Atoms, with Their Standard Deviations in Parentheses[a)]

Atom	x	y	z	B_{eq}
Co	1119(1)	2500(1)	3914(1)	1.8
O(1)	−86(3)	2837(5)	3851(6)	2.7
O(2)	−1199(4)	3132(8)	2329(8)	5.0
O(3)	1378(4)	4096(5)	3259(6)	2.9
O(4)	2037(5)	4995(7)	1534(8)	5.1
O(5)	1219(4)	2967(5)	5891(6)	2.7
O(6)	745(4)	2455(8)	8012(6)	3.5
O(7)	2311(3)	2159(5)	3962(6)	2.6
O(8)	3267(4)	800(9)	4675(10)	5.7
O(9)	−173(5)	−275(7)	1318(7)	4.3
O1	6674(4)	−4619(7)	9016(9)	5.0
O2	4556(4)	−1945(6)	7258(10)	5.7
OW1	7660(7)	−4816(11)	11596(10)	7.9
OW2	1776(12)	7523(24)	763(29)	10.8
N(1)	995(3)	2132(6)	1892(7)	2.0
N(2)	934(4)	870(6)	4673(6)	2.2
N1	5274(4)	−5101(7)	8464(8)	2.7
N2	2468(4)	−5280(6)	6600(8)	2.7
C(1)	1169(6)	845(8)	1532(9)	2.8
C(2)	620(6)	−117(8)	2200(9)	3.0
C(3)	324(5)	148(8)	3725(9)	2.8
C(4)	99(5)	2489(11)	1382(8)	2.8
C(5)	−446(5)	2858(8)	2584(9)	2.8
C(6)	1640(5)	2919(8)	1241(9)	2.7
C(7)	1684(6)	4102(8)	2079(9)	3.1
C(8)	514(6)	1100(8)	6077(9)	3.0
C(9)	861(5)	2261(7)	6741(8)	2.4
C(10)	1794(5)	284(8)	4907(9)	2.9
C2	4422(7)	−8112(8)	7718(11)	3.5
C(11)	2532(6)	1134(9)	4509(10)	3.3
C2	4422(7)	−8112(8)	7718(11)	3.5
C3	5139(8)	−8850(8)	8113(11)	4.0
C4	5926(7)	−8347(9)	8588(10)	3.7
C5	6036(6)	−7104(9)	8793(11)	3.5
C6	5340(5)	−6389(8)	8382(9)	2.8
C7	4440(4)	−4689(7)	7756(8)	2.0
C8	3885(5)	−5864(7)	7611(9)	2.4
C9	3320(5)	−5918(8)	6217(10)	2.9
C10	3680(6)	−5333(8)	4904(9)	2.9
C11	3911(5)	−4020(8)	5284(8)	2.3
C12	4671(4)	−4066(7)	6370(8)	2.0
C13	5123(5)	−2887(7)	6784(10)	2.8
C14	5732(6)	−3026(9)	8134(12)	3.7
C15	5963(5)	−4324(9)	8560(10)	3.2
C16	3945(7)	−1512(9)	6315(18)	6.5
C17	3124(5)	−2260(10)	6275(13)	4.4
C18	3111(5)	−3382(8)	5805(9)	2.5
C19	2312(5)	−4121(8)	5747(10)	3.1
C20	2501(5)	−5097(9)	8167(11)	3.3
C21	3196(5)	−5930(8)	8768(10)	3.0

a) Positional parameters are multiplied by 10^4.

by assuming a tetrahedral coordination about the carbon atoms with a C-H bond distance of 1.08 Å. All the non-hydrogen atoms were refined anisotropically, and hydrogen atoms were refined isotropically. Refinement was carried out by use of a block-diagonal least-squares procedure. The atomic-scattering factors and the anomalous terms for Co, O, N, and C were taken from Ref. 5. The final indicies were $R=0.063$ and $R'=0.072$, where $R=\sum||F_o|-|F_c||/\sum|F_o|$ and $R'=(\sum w(|F_o|-|F_c|)^2/\sum w|F_o|^{1/2}$; $w=1/[\sigma(F_o)]^2$. The final difference Fourier synthesis still showed peaks at heights up to 0.98 e Å^{-3} around the cobalt atom, and 0.68 e Å^{-3} around an oxygen atom of strychnine, although the electron density did not rise above 0.56 e Å^{-3} elsewhere. The final atomic coordinates along with their standard deviations and thermal parameters of non-hydrogen atoms are incorporated in Table 1. Compilations of the anisotropic thermal parameters for non-hydrogen atoms, atomic parameters for hydrogen atoms and observed and calculated structure factors are available.[6] All the calculations were performed on a HITAC M-680H computer at the Computer Center of the University of Tokyo with Universal Program System UNICS III.[7]

Results and Discussion

Preparation and Optical Resolution. The syntheses of Co(III) complexes coordinated by the hexadentate EDTA type ligands, for instance, ethylenediaminetetrapropionate (EDTP), trimethylenediaminetetraacetate (TNTA), propylenediaminetetraacetate (PDTA) and *trans*-1,2-cyclohexanediaminetetraacetate (CHXNTA) ions, have been well established. In each case, the potassium salt has been prepared in sufficient yield,[8-11] by application of the oxidation reaction from Co^{2+} in the presence of hydrogen peroxide and each ligand. On the other hand, the present complex, $K[Co(dhpta)]\cdot 0.5H_2O$ was synthesized in sufficient yield by the substitution reaction from the starting material $Na_3[Co(NO_2)_6]$, whose cobalt ion is trivalent. In the case of the reaction of ethylenediaminetetraacetic acid disodium salt (Na_2H_2edta) with $Na_3[Co(NO_2)_6]$, it is known that the substitution reaction of the nitro groups occurs incompletely under similar conditions, and the complex, $Na_2[Co(NO_2)(Hedta)]\cdot 2H_2O$ can be obtained in high yield.[12] In contrast, complete substitution was attained in the present case. This result may be related to the less strained ring system of the present complex having the central six-membered chelate ring. This assumption is supported by failure of attempts to prepare a complex in which trimethylenediaminetetraacetate functions as a pentadentate ligand.

The optical resolution of the ethylenediaminetetraacetatocobaltate(III), through its strychnine salt, was first attained by Busch and Bailar.[13] They obtained the active complex of the $(-)_{589}$-form by the fractionation from mixed solvents, because of the extreme solubility of the salt in water. The resolution of the present complex can be effected by strychnine, and the $(+)_{589}$-form of the complex was adequately obtained from water. Spontaneous resolution was reported by Ogino et al., in the case of $[Co(tnta)]^-$,[14] though in the present case no tendency to resolve spontaneously into optical isomers was observed.

Description of the Molecular Structure. Perspective drawings of the complex anion and strychnine cation showing ellipsoids of thermal motion are given in Fig. 1. Interatomic distances and angles are listed in Tables 2 and 3, respectively.

The cobalt atom is surrounded by two nitrogen atoms and four oxygen atoms from the four carboxyl groups at the apices of a slightly distorted octahedron. Each atom of the complex anion is inequivalent, because of the substituted hydroxyl group on the central carbon atom, through which the pseudo two-fold axis exists. This result agrees with the ^{13}C NMR spectrum of the inactive complex ion before resolution, which shows eleven signals for eleven carbon atoms (see Experimental section). The absolute configuration around the cobalt atom is Δ. This config-

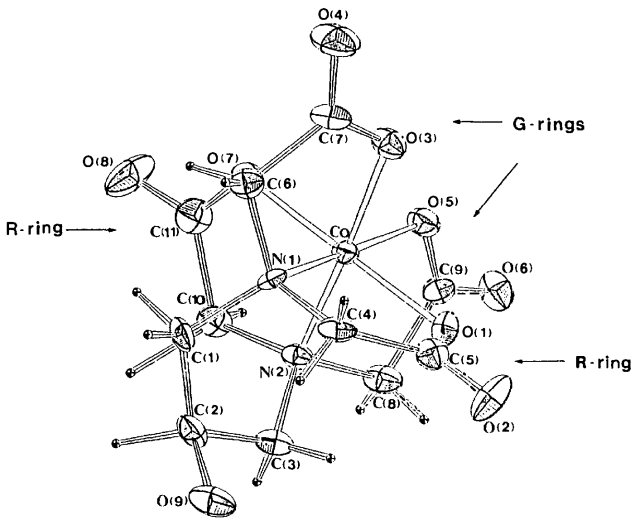

(a)

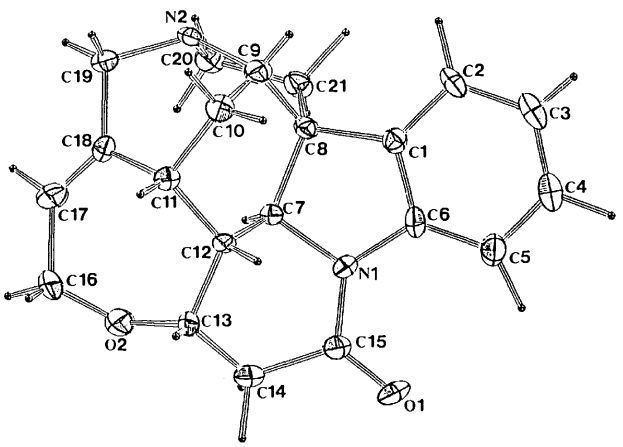

(b)

Fig. 1. Perspective drawings of (a) the complex anion and (b) strychnine cation with their numbering schemes, shown as 50% probability ellipsoids.

uration was determined by reference of the known absolute configuration of the strychnine molecule used in the optical resolution. The central six-membered chelate ring adopts the λ-skew boat conformation, and both of the G- and R-rings have envelope conformations, where G- and R-rings represent the five-membered glycinate chelate rings as shown in Fig. 1.

The average Co-O bond length of the G-ring chelates and that of the R-ring chelates are 1.920(6) and 1.898(5) Å, respectively. Each of them is slightly long compared with the distances in (±)-K[Co(dhpta)] studied by Kalina et al.,[4] the average Co-O (G-ring) and Co-O (R-ring) distances being 1.875(9) and 1.887(9) Å, respectively. Moreover, in the present case, the average distance between cobalt and coordinated oxygen atoms in G-ring chelates is slightly longer than that in R-ring chelates, contrary to the previous correlation observed in (±)-K[Co(dhpta)]. This relation, between the Co-O bond distances of G-rings and those of R-rings, observed in the present complex ion is also found in the other complex ion of EDTA type ligands,[15-17] excent for the previous report.

X-Ray structure studies on EDTA type Co(III) complexes,[4,15-17] have indicated that the structure of the in-plane G-ring forming a girdle around the cobalt atom is more strained than that of the out-of-plane R-ring. The deviations of the atoms from the individual planes are listed in Table 4. Pronounced deviations are observed of the C(6), C(7), C(8), and C(9) atoms, of which the G-ring chelates consist, whereas the displacements of the carbon atoms in the R-rings from the mean planes are not so significant. Each glycinate ring of the present complex ion is less deformed from defined planes than that of the complex ion previously reported,[4] except for one G-ring,

Table 2. Bond Distances (l/Å)[a]

(a) Complex anion			
Co-O(1)	1.906(5)	Co-O(3)	1.923(6)
Co-O(5)	1.917(6)	Co-O(7)	1.889(5)
Co-N(1)	1.933(6)	Co-N(2)	1.969(7)
O(1)-C(5)	1.284(10)	O(2)-C(5)	1.221(10)
O(3)-C(7)	1.222(11)	O(4)-C(7)	1.254(12)
O(5)-C(9)	1.264(10)	O(6)-C(9)	1.229(9)
O(7)-C(11)	1.287(11)	O(8)-C(11)	1.205(11)
O(9)-C(2)	1.458(11)		
N(1)-C(1)	1.494(11)	N(1)-C(4)	1.501(9)
N(1)-C(6)	1.483(10)	N(2)-C(3)	1.497(11)
N(2)-C(8)	1.515(11)	N(2)-C(10)	1.492(11)
C(1)-C(2)	1.520(12)	C(2)-C(3)	1.547(13)
C(4)-C(5)	1.497(12)	C(6)-C(7)	1.528(13)
C(8)-C(9)	1.517(12)	C(10)-C(11)	1.544(13)
(b) Strychnine cation			
O1-C15	1.210(11)	O2-C13	1.451(11)
O2-C16	1.350(16)		
N1-C6	1.436(11)	N1-C7	1.497(9)
N1-C15	1.373(11)	N2-C20	1.476(12)
N2-C9	1.558(11)	N2-C19	1.526(12)
C1-C2	1.400(12)	C1-C6	1.409(11)
C1-C8	1.527(11)	C2-C3	1.417(14)
C3-C4	1.397(15)	C4-C5	1.402(14)
C5-C6	1.380(13)	C7-C8	1.565(11)
C7-C12	1.526(11)	C8-C9	1.535(12)
C8-C21	1.560(12)	C9-C10	1.518(13)
C10-C11	1.538(12)	C11-C12	1.519(10)
C11-C18	1.531(11)	C12-C13	1.526(11)
C13-C14	1.546(13)	C14-C15	1.532(14)
C16-C17	1.520(14)	C17-C18	1.320(14)
C18-C19	1.488(12)	C20-C21	1.509(12)

a) Estimated standard deviations in parentheses.

Table 3. Bond Angles (ϕ/°)[a]

(a) Complex anion			
O(1)-Co-O(3)	91.7(3)	O(1)-Co-O(5)	90.6(2)
O(1)-Co-O(7)	179.5(3)	O(1)-Co-N(1)	87.8(2)
O(1)-Co-N(2)	91.8(3)	O(3)-Co-O(5)	92.8(3)
O(3)-Co-O(7)	88.4(3)	O(3)-Co-N(1)	84.0(3)
O(3)-Co-N(2)	175.7(3)	O(5)-Co-O(7)	89.9(2)
O(5)-Co-N(1)	176.4(3)	O(5)-Co-N(2)	84.7(3)
O(7)-Co-N(1)	91.8(2)	O(7)-Co-N(2)	88.1(3)
N(1)-Co-N(2)	98.5(3)		
Co-O(1)-C(5)	114.5(5)	Co-O(3)-C(7)	112.9(6)
Co-O(5)-C(9)	114.8(5)	Co-O(7)-C(11)	115.4(5)
Co-N(1)-C(1)	114.3(5)	Co-N(1)-C(4)	107.4(4)
Co-N(1)-C(6)	103.8(5)	Co-N(2)-C(3)	112.2(5)
Co-N(2)-C(8)	103.5(5)	Co-N(2)-C(10)	108.0(5)
O(1)-C(5)-O2)	123.6(8)	O(3)-C(7)-O(4)	124.6(9)
O(5)-C(9)-O(6)	126.1(8)	O(7)-C(11)-O(8)	123.8(9)
O(1)-C(5)-C(4)	116.7(7)	O(2)-C(5)-C(4)	119.7(8)
O(3)-C(7)-C(6)	116.6(8)	O(4)-C(7)-C(6)	118.8(8)
O(9)-C(2)-C(1)	109.2(7)	O(9)-C(2)-C(3)	105.2(7)
C(1)-N(1)-C(4)	110.9(7)	C(1)-N(1)-C(6)	109.7(6)
C(4)-N(1)-C(6)	110.4(6)	C(3)-N(2)-C(8)	108.3(6)
C(3)-N(2)-C(10)	112.9(6)	C(8)-N(2)-C(10)	111.6(6)
N(1)-C(1)-C(2)	117.9(7)	N(1)-C(4)-C(5)	112.6(6)
N(1)-C(6)-C(7)	108.1(7)	N(2)-C(3)-C(2)	116.0(7)
N(2)-C(8)-C(9)	109.7(7)	N(2)-C(10)-C(11)	111.6(7)
C(1)-C(2)-C(3)	116.3(7)		
(b) Strychnine cation			
O1-C15-N1	123.2(9)	O1-C15-C14	122.9(9)
C13-O2-C16	118.4(10)	O2-C13-C12	114.6(6)
O2-C13-C14	100.4(8)	O2-C16-C17	112.5(10)
N1-C6-C1	109.3(7)	N1-C6-C5	127.9(8)
N1-C7-C8	104.2(6)	N1-C7-C12	106.1(6)
C6-N1-C7	110.1(6)	C6-N1-C15	124.8(7)
C7-N1-C15	119.5(7)	C9-N2-C19	112.2(6)
C9-N2-C20	107.7(6)	C19-N2-C20	113.4(7)
C2-C1-C6	121.2(8)	C2-C1-C8	128.1(7)
C6-C1-C8	110.3(7)	C1-C2-C3	116.3(9)
C2-C3-C4	121.0(9)	C3-C4-C5	122.4(9)
C4-C5-C6	116.1(8)	C1-C6-C5	122.7(8)
C8-C7-C12	117.2(6)	C1-C8-C7	103.3(6)
C1-C8-C9	116.3(7)	C7-C8-C9	113.3(7)
C1-C8-C21	110.7(7)	C7-C8-C21	112.0(7)
C21-C8-C9	101.7(6)	C8-C9-C10	116.8(7)
C9-C10-C11	108.0(7)	C10-C11-C12	106.7(6)
C10-C11-C18	109.2(7)	C12-C11-C18	114.8(6)
C7-C12-C11	111.9(6)	C7-C12-C13	107.4(7)
C11-C12-C13	118.3(7)	C12-C13-C14	112.1(7)
C13-C14-C15	115.6(8)	C16-C17-C18	121.5(9)
C11-C18-C17	122.9(7)	C11-C18-C19	115.0(7)
C17-C18-C19	122.1(8)	C8-C21-C20	102.5(7)

a) Estimated standard deviations in parentheses.

i.e., the C(8) and C(9) atoms deviate 0.70 and 0.45 Å, respectively from the equatorial plane, the corresponding values being 0.62 and 0.17 Å, respectively.

The other bond distances and angles of the present complex ion are almost comparable with the reported values for (±)-K[Co(dhpta)], except for the relationship described above and of characteristics for the Co(III) complexes of EDTA type ligands. According to the structural study on the Co(III) complexes of EDTA type ligands, which functions as a pentadentate ligand,[18] the relationship mentioned above may be significant, because the coordination site corresponding to one G-ring is substituted by a monodentate ligand in those cases. Easier bond cleavage of Co-O bonds of G-rings than those of R-rings can be interpreted by the correlation.

The structure of the strychnine cation, used as the resolving agent, agrees with the known absolute configurations, and the stereochemistry is almost identical with that previously reported on the molecule and its derivatives.[19]

Description of the Unit Cell and Diastereomeric Discrimination. A perspective drawing of the crystal structure viewed along the b axis is presented in Fig. 2. The unit cell consists of two complex anions, two strychnine counterions, and the four water molecules of crystallization.

Hydrogen bonds of the type O-H···O probably exist between the O(6) atom of the non-coordinated oxygen atom in one G-ring chelate and the O(9) atom of the hydroxyl group in the neighboring complex anion, the O···O distance being 2.75 Å. Such a strong intermolecular hydrogen bond of the same manner was observed in (±)-K[Co(dhpta)]. The O(2) atom of the carboxylato group in one R-ring, which is not coordinated to the cobalt atom, is not only linked to the oxygen OW1 atom of the water but also associated to the other water OW2 atom, by an O-H···O hydrogen bond of distances 2.95 and 3.06 Å respectively. The two water molecules are not connected to any other atoms. In the crystal structures of potassium salts of (+)$_{546}$-[Co(tnta)]$^-$ and (±)-[Co(dhpta)]$^-$, the cationic potassium ions are surrounded through electrostatic attraction by the uncoordinated carboxylate oxygen atoms and also the oxygen atoms of water molecules in defined[15] and nondifined[4] arrangements, respectively. Such a rigid network of electrostatic attraction found in the previous reports, however, among the complex anion, the strychnine, and the water

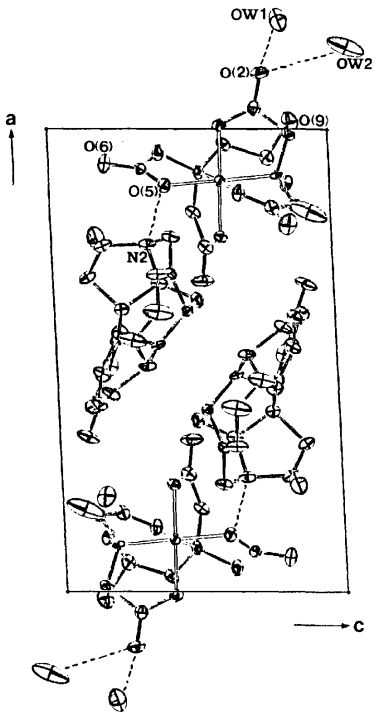

Fig. 2. Perspective drawing of the crystal structure viewed along the b axis. The significant hydrogen bonds among the complex anion, strychnine cation, and water molecules are indicated by the broken line, except for that between O(6) and O(9) atoms.

Table 4 Deviations of the Atoms from Planes

Plane, No.	Atoms defining the plane	Out-of-plane atoms	Distances between out-of-plane atoms, l/Å
1	N(1)	C(1)	−0.54
	Co	C(2)	0.14
	N(2)	C(3)	0.73
2[a]	Co	C(2)	0.13
	O(3)	C(6)	−0.78
	O(5)	C(7)	−0.56
	N(1)	C(8)	0.70
	N(2)	C(9)	0.45
3	Co	C(4)	−0.21
	O(1)	C(5)	−0.18
	N(1)		
4	Co	C(10)	−0.04
	O(7)	C(11)	−0.09
	N(2)		

a) Plane defined by least-square procedure.

molecules can not be observed in the present case.

Significantly the coordinated O(5) atom, of which the same G-ring of the O(6) atom connecting with the O(9) atom of the neighboring complex ion by hydrogen bond consists, is associated with the nitrogen atom N2 of the strychnine cation with an N···O distance of 2.80 Å, by an N-H···O hydrogen bond. It is assumed that a hydrogen atom may be attached to the N(2) atom of the strychnine molecule, though examination of the difference fourier map was unable to reveal a possible hydrogen position near the N2 atom.

The O(2), O(3), and O(4) atoms of the complex ion are near the hydrogen atoms bonded to the carbon atoms of strychnine around the N2 atom, the O···H distances ranging from 2.37 to 2.98 Å, as the result of the hydrogen bond between the O(5) atom of the complex anion and the N2 atom of the strychnine molecule, mentioned above. Moreover, the carbon and hydrogen atoms belonging to the benzene residue of the strychnine interact with the other hydrogen atoms in the hydrophilic sphere of the neighboring strychnine, showing distances from 2.58 to 3.01 Å for C···H intermolecular interaction and from 2.40 to 3.08 Å for H···H interaction, though the self-stacking of the benzene residue of the strychnine molecule can not be observed.

Thus, the close contact by the possible hydrogen bond between the O(5) atom of the complex anion and the N2 atom of the strychnine molecule may play an important role in the diastereomeric discrimination in the present complex, since the N2 atom is one of the asymmetric centers in the strychnine molecule. On the other hand, the O(9) atom of the hydroxyl group bonding to the C(2) carbon atom, which is a resulting asymmetric center by coordination, does not interact directly with the strychnine molecule by an obvious hydrogen bond, though the atom forms the hydrogen bond network together with the O(6) atom in the same G-ring of the O(5) atom. The close contacts between the benzene residue and the atoms in hydrophilic sphere of the neighboring strychnine molecule, described above, probably assist in formation of the diastereomeric compound, i.e., in the optical resolution of the complex.

Absolute Configuration and Circular Dichroism. The AB and CD spectra of the present complex ion $(+)_{589}$-[Co(dhpta)]$^-$ are shown in Fig. 3. Numerical data are summarized in Table 5, along with those of the $(-)_{546}$-[Co(tnta)]$^-$ ion. The shape and positions of AB and CD spectra of the present $(+)_{589}$-form complex are quite similar to those of $(+)_{546}$-[Co(tnta)]$^-$ reported by Ogino et al.[14] X-Ray structure analysis and circular dichroism studies of the series of EDTA type complex, whose CD spectra usually show two Cotton effects of opposite sign in the first absorption region, suggest the following empirical rule: The sign of the CD band in the region can be related to the configuration around the cobalt centers. When they

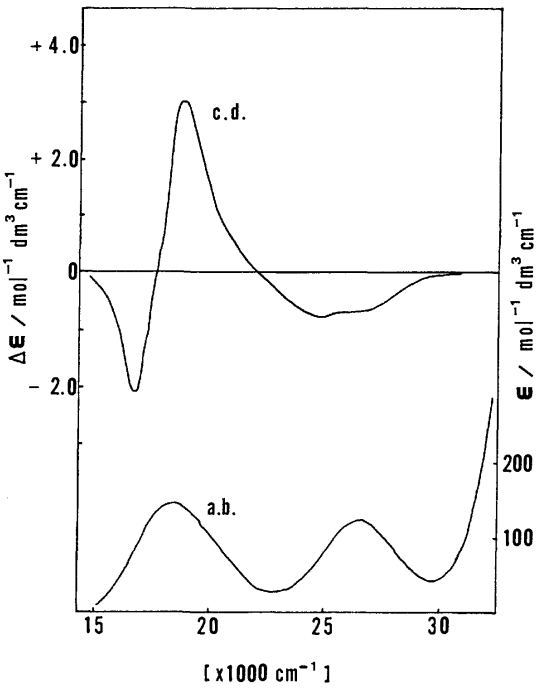

Fig. 3. Absorption and circular dichroism spectra of $(+)_{589}$-Δ-K[Co(dhpta)] in H_2O.

Table 5. Absorption and Circular Dichroism Data for $(+)_{589}$-Δ-K[Co(dhpta)], with Those for $(-)_{546}$-Δ-Na[Co(tnta)]·3H_2O in Parentheses[a)]

Absorption		Circular dichroism	
Peak position, ×1000 cm^{-1}	ε	Peak position, ×1000 cm^{-1}	$\Delta\varepsilon$
18.25 (18.20)	142 (131)	16.72 (17.00)	−2.12 (+1.91)
		18.73 (19.00)	+3.01 (−2.41)
26.46 (26.40)	121 (115)	24.39 (24.60)	−0.80 (+0.69)

a) References 8 and 13.

give a positive and negative Cotton effect respectively from the lower energy band of the first absorption region, they should be assigned to the Δ configuration around the asymmetric cobalt center. In the CD spectrum of $(+)_{589}$-[Co(dhpta)]$^-$, which was derived from the crystals of the present work, a negative and a positive Cotton effect has been observed, from the lower energy band in the region. The absolute configuration of the cobalt atom has been determined as Δ from the present study. Consequently, the empirical rule appears to be applicable to the series of EDTA type complex, even though the hydroxyl group exists in the central chelate ring.

Conclusion

Optical resolution of the 2-hydroxy-1,3-propanediamine-*N*,*N*,*N*′,*N*′-tetraacetatocobaltate(III) complex ion has been accomplished by the organic resolving agent, strychnine. By the X-ray structure study

on the crystal involving the resolving agent, the oxygen atom coordinated to the cobalt ion plays an important role in the diastereomeric discrimination through the O···H-N type of hydrogen bond, though the non-coordinated hydroxyl group does not interact directly with strychnine in the same manner. This fact suggests that the coordinated oxygen atom in the G-ring is an essential site for the discrimination of the form of a compound by the complex and certain modification of the corresponding hydroxyl group may not prevent the optically active complex from functioning as a discriminator. The chemical modification of the hydroxyl group in the complex is now in progress.

The authors are grateful to Dr. Takashi Kodama for collecting the X-ray diffraction data and to Dr. Katsuaki Ishida for measurement of NMR spectra. We also thank Prof. Masanobu Hidai at the usage of available instruments of the University of Tokyo and Dr. Andrew Street for his helpful advice on the manuscript. This research was aided in part by a Grant-in-Aid for scientific research on priority areas (Macromolecule Complexes No. 63612003) from the Ministry of Education, Science and Culture.

References

1) M. Sato, Y. Sato, S. Yano, and S. Yoshikawa, *J. Chem. Soc., Dalton Trans.*, **1985**, 895.

2) M. Sato, Y. Sato, S. Yano, S. Yoshikawa, K. Toriumi, H. Itoh, and T. Itoh, *Inorg. Chem.*, **21**, 2360 (1982).

3) M. Kuramoto, Y. Kushi, and H. Yoneda, *Bull. Chem. Soc. Jpn.*, **51**, 3196 (1978).

4) M. Kalina, F. Pavelcik, and J. Majer, *Collect. Czech. Chem. Commun.*, **43**, 3140 (1978).

5) "International Tables for X-ray Crystallography," Kynoch Press, Birmingham, England (1974), Vol. IV.

6) These numerical data are deposited as Document No. 8906 at the Office of the Editor of Bull. Chem. Soc. Jpn.

7) T. Sakurai and K. Kobayashi, *Rikagaku Kenkyusho Hokoku*, **55**, 69 (1979).

8) F. P. Dwyer, E. Gyarfas, and D. Mellor, *J. Phys. Chem.*, **59**, 296 (1955). *Inorg. Synth.*, Vol. V, p. 186.

9) C. W. Van Saum and B. E. Douglas, *Inorg. Chem.*, **8**, 1145 (1969).

10) F. P. Dwyer and F. L. Garvan, *J. Am. Chem. Soc.*, **81**, 2955 (1959).

11) F. P. Dwyer and F. L. Garvan, *J. Am. Chem. Soc.*, **83**, 2610 (1961).

12) F. P. Dwyer and F. L. Garvan, *J. Am. Chem. Soc.*, **80**, 4480 (1958).

13) D. H. Busch and J. C. Bailar, *J. Am. Chem. Soc.*, **75**, 4574 (1953).

14) H. Ogino, M. Takahashi, and N. Tanaka, *Bull. Chem. Soc. Jpn.*, **43**, 424 (1970).

15) R. Nagao, F. Marumo, and Y. Saito, *Acta Crystallogr., Sect. B*, **28**, 1852 (1972).

16) H. A. Weakliem and J. L. Hoard, *J. Am. Chem. Soc.*, **81**, 549 (1959).

17) M. Kanesaka, K. Okamoto, M. Nomoto, and J. Hidaka, *Bull. Chem. Soc. Jpn.*, **57**, 3111 (1984). K. Okamoto, T. Tsukihara, J. Hidaka, and Y. Shimura, *ibid.*, **51**, 3534 (1978). K. Okamoto, T. Tsukihara, J. Hidaka, and Y. Shimura, *Chem. Lett.*, **1973**, 145.

18) D. J. Radanovic, S. R. Trifunovic, D. E. Bause, C. Maricondi, J. E. Abola, and B. E. Douglas, *Inorg. Chem.*, **26**, 3994 (1987).

19) S. B. B. Glover, R. O. Gould, and M. D. Walkinshaw, *Acta Crystallogr., Sect. A*, **40**; *Sect. C*, **85** (1984). J. H. Robertson and C. A. Beevers, *Acta Crystallogr., Sect. B*, **29**, 2760 (1973).

Linear Tetranuclear Copper(II) Complexes with Bridging Methoxide and a Schiff-Base Ligand: The Preparation and Magnetic Study of the [Cu(salpd-μ-O,O')(μ-L)Cu(μ-CH_3O)$_2$Cu(μ-L)(sapd-μ-O,O')Cu] Complexes (and L=Acetate or Formate Ions) and the Structure Determination of the Complex with L=Acetate

Chōki FUKUHARA,* Kazuhiko TSUNEYOSHI, Kosho KATSURA, Naohide MATSUMOTO,† Sigeo KIDA,† and Masayasu MORI††

Department of Chemistry, College of Science, University of the Ryukyus, Senbaru Nishihara-cho, Okinawa 903-01
†Department of Chemistry, Faculty of Science, Kyushu University, Hakozaki, Higashi-ku, Fukuoka 812
††Department of Chemistry, Faculty of Science, Osaka City University, Sumiyoshi-ku, Osaka 558

(Received June 1, 1989)

The title complexes have been synthesized in quantitative yield from [Cu(salpd)] and copper(II) acetate or copper(II) formate , where H_2salpd represents *N,N'*-disalicylidene-1,3-propanediamine. [Cu(salpd-μ-O,O')-(μ-L)Cu(μ-CH_3O)$_2$Cu(μ-L)(salpd-μ-O,O')Cu] crystallizes in the monoclinic space group $P2_1/n$ with formula=$Cu_4C_{40}H_{44}N_4O_{10}$, F.W.=995.0, a=11.826(2) Å, b=17.192(4) Å, c=9.836(2) Å, β=94.08(2)°, V=1994.8(7) Å^3 and Z=2 (R=3.83%), where L=CH_3COO. The complex forms a centrosymmetric molecule made up of two units of [Cu(salpd-μ-O,O')(μ-CH_3COO)Cu] bound by a pair of methoxo bridges; each terminal copper(II) ion forms four short bonds with N and O atoms of salpd and a slightly longer (2.235(4) Å) axial bond with one of the oxygens of the acetato group, whereas each inner copper(II) ion is also pyramidally coordinated by two methoxo oxygens, one of the acetato oxygens, and one of the bridging salpd oxygens, the distant axial position being occupied (Cu–O=2.323(3) Å) by the remaining bridging salpd oxygen. The magnetic susceptibilities of the complexes in the 86.8—299.0 K range have been analyzed on the basis of a four-spin model for the linear copper(II) complexes, and the values of g and J_{ij}, based on the Heisenberg-type Hamiltonian $H=-2\sum J_{ij}S_i\cdot S_j$, have been estimated as g (average)=2.13, J_{12}=−390 cm^{-1}, J_{13}=67 cm^{-1} and J_{14}=J_{34}=0 cm^{-1} in the complex with acetate bridges, and as g (average)=2.20, J_{12}=−263 cm^{-1}, and J_{13}=39 cm^{-1} and J_{14}=J_{34}=0 cm^{-1} in the complex with formate bridges, where the numbering refers to the 3-1-2-4 arrangement of the Cu^{2+} ions.

Intramolecular exchange interaction in multinuclear transition metal complexes has a long history of research work by an enormous number of investigators, yet there remain many unsettled problems. Although a large number of polynuclear complexes with the antiferromagnetic property have been reported, only a limited number of multinuclear complexes with the ferromagnetic property are known.[1-8] In recent years, the present authors have prepared a series of trinuclear Schiff-base complexes in which the central metal ion is different from the terminal ones in its oxidation state or elemental species.[9,10] In the course of a study of the preparation of trinuclear complexes with Schiff-base copper(II) terminal units, new compounds were obtained and were proved to be novel type of tetranuclear copper(II) complexes in which copper ions are linearly linked with methoxide, phenolate, and acetate ions. In this paper we wish to report on the synthesis, structure, and magnetism of these tetranuclear complexes, [Cu(salpd-μ-O,O')(μ-L)Cu(μ-CH_3O)$_2$Cu(μ-L)(salpd-μ-O,O')Cu]. Here, when L=CH_3COO, and HCOO, the compounds are designated by **1** and **2** respectively. The temperature dependence of the magnetic susceptibility showed that the ferromagnetic and antiferromagnetic interactions operate simultaneously in these complexes.

Experimental

Syntheses: 1. Nitrogen gas was bubbled through a methanol solution (60 cm^3) containing copper(II) acetate monohydrate (0.57g, 0.0029 mol) for 10 min. To this solution we added [Cu(salpd)] (1 g, 0.0029 mol) and then triethylamine (0.58 g, 0.0057 mol). The mixed solution was then stirred at room temperature for ca. 36 h. The light green product thus deposited was collected on a sintered-glass filter and washed with methanol and diethyl ether. The product was dried at 60 °C under reduced pressure for 40 min. Yield, 1.45 g (100%). Found: C, 47.91; H, 4.39; N, 5.63; Cu, 26.00%. Calcd for $Cu_4C_{40}H_{44}N_4O_{10}$: C,48.29; H, 4.46; N, 5.63; Cu, 25.55%.

The Preparation of a Single Crystal of 1. The copper(II) acetate monohydrate (0.11 g, 0.00057 mol) and [Cu(salpd)] (0.2 g, 0.00058 mol) were dissolved in methanol (60 cm^3) by using a shaker. When the dark-green solution was allowed to stand in the dark for 5 days, well-formed dark-green prisms were separated. Found: C, 48.10; H, 4.38; N, 5.55%. Calcd. for $Cu_4C_{40}H_4N_4O_{10}$: C, 48.29; H, 4.46; N, 5.63%.

2. Nitrogen gas was bubbled into a suspension containing copper(II) formate tetrahydrate (0.65 g, 0.0029 mol) in methanol (50 cm^3) for 15 to 20 min at room temperature. In to this suspension we then stirred triethylamine (0.59 g, 0.0058 mol) and subsequently [Cu(salpd)] (1 g, 0.0029 mol). The reaction mixture was stirred further at room temperature for ca. 65 h. The green product thus deposited was treated in the same manner as in the case of Complex **1** described above. Yield, 1.34 g (97.1%). Found: C, 46.82; H, 4.20; N, 5.75; Cu, 25.73%. Calcd for $Cu_4C_{38}H_{41}N_4O_{10}$: C, 46.77; H, 4.23; N, 5.74; Cu, 26.04%.

Physical Measurements. The IR spectra were measured with a Hitachi-Perkin-Elmer 225 grating IR spectrometer on KBr disks. The magnetic susceptiblities were measured

by the Faraday method in the range of 80—300 K using a Cahn 2000 electric balance. The apparatus was calibrated using $Hg[Co(NCS)_4]$. Diamagnetic corrections were carried out using Pascal's constants. The molar effective magnetic moment was calculated by the use of the equation: $\mu_{eff}=2.828\sqrt{X_A \cdot T}$.

X-Ray Crystallography. The diffraction data of a single crystal of **1** were obtained on a Rigaku AFC-5 four-circle diffractometer at the Faculty of Science, Kyushu University, using graphite-monochromatized Mo$K\alpha$ radiation at 24±1 °C. The scan mode was θ-2θ, with the scan speed of 6 min^{-1}, $2\theta_{max}=52°$, the scan width of $(1.0+0.35\tan\theta)°$, and the octant measured as $+h$, $\pm k$, and $\pm l$. The intensities of the monitored standard reflections showed no changes during data collection. The unit cell dimensions and standard deviations were obtained by the least-squares fit of 25 reflections ($20°<2\theta<30°$).

The reflections were corrected for the Lorentz-polarization effect, but not for absorption.

Crystal Data: Formula=$Cu_4C_{40}H_{44}N_4O_{10}$, F.W.=995.0, monoclinic system, space group $P2_1/n$. a=11.826(2) Å, b=17.192(4) Å, c=9.836(2) Å, β=94.08(2)°, and V=1994.8(7) Å^3, D_{calcd}=1.657 g cm^{-3}, Z=2. μ(Mo$K\alpha$)=21.71 cm^{-1}, crystal dimensions 0.4×0.5×0.3 mm, 2999 reflections with $|F_o|>3\sigma(|F_c|)$.

The structure was solved by the heavy atom method and refined by the block-diagonal least-squares method, in which the function minimized was $\sum\omega(|F_o|-|F_c|)^2$; the equal weight of ω=1 was adopted for all the reflections. The hydrogen atoms were located on the difference Fourier map and refined. The positions of the non-hydrogen atoms were refined by the use of anisotropic thermal parameters, while those of the hydrogen atoms were refined by the use of the isotropic thermal parameters, giving R=3.83%, and R_w=4.22%. The final difference Fourier synthesis was featureless, where the heighest peak was 0.4 e Å^{-3}. The atomic parameters of the hydrogen atoms, the thermal parameters of non-hydrogen atoms, and the F_o—F_c tables are deposited as Document No. 8902 at the Office of the Editor of Bull. Chem. Soc. Jpn. The caculations were carried out by the use of the UNICS III computer program system[11] on a FACOM M 780 computer at the Computer Center of Kyushu University. The atomic scattering factors were taken from Ref. 12. The final positional parameters are given in Table 1.

Table 1. Atomic Coordinates for [Cu(salpd-μ-O,O')-(μ-CH_3COO)Cu(μ-CH_3O)$_2$Cu($\mu$$CH_3COO$)-(salpd-$\mu$-$O,O'$)Cu][a]

Atom	X	Y	Z	B_{EQV}/Å^2
Cu(1)	178.2(0.5)	699.2(0.3)	4104.5(0.5)	2.67(1)
Cu(2)	−510.0(0.5)	2409.6(0.3)	3362.5(0.6)	2.90(1)
O(1)	−898.2(2.7)	1333.9(1.6)	2850.7(2.9)	2.95(7)
O(2)	−132.8(3.1)	1904.1(1.7)	5079.9(3.1)	3.46(8)
O(3)	1504.8(2.8)	1029.4(1.9)	3232.6(3.5)	3.68(9)
O(4)	1167.1(3.1)	2236.0(1.9)	2491.6(3.9)	4.18(9)
OM	987.8(2.7)	−124.5(1.7)	5080.6(3.4)	3.43(8)
CM	2063.0(4.5)	−419.1(3.2)	4901.5(5.8)	4.20(14)
N(1)	−1384.6(3.9)	2813.2(2.3)	1723.6(4.7)	4.29(12)
N(2)	−51.5(4.0)	3448.4(2.1)	4110.3(4.5)	4.11(12)
C(1)	−1254.4(4.0)	1069.2(2.6)	1632.9(4.4)	2.96(11)
C(2)	−1251.1(6.8)	287.5(3.2)	1363.7(6.4)	6.60(21)
C(3)	−1610.4(8.0)	−5.8(4.0)	121.4(7.5)	8.51(27)
C(4)	−1974.7(6.5)	466.9(4.1)	−935.2(6.0)	6.34(20)
C(5)	−2024.5(5.2)	1241.3(3.7)	−687.0(5.1)	4.82(16)
C(6)	−1663.6(4.3)	1565.5(2.8)	573.9(4.6)	3.36(12)
C(7)	−1752.8(5.0)	2392.7(3.0)	731.7(5.5)	4.51(14)
C(8)	−1628.0(7.2)	3661.5(3.3)	1598.7(10.0)	8.95(29)
C(9)	−519.5(8.8)	4100.9(4.0)	1895.8(9.0)	9.53(32)
C(10)	−125.1(8.1)	4158.5(3.7)	3265.6(8.4)	8.79(28)
C(11)	414.7(4.6)	3545.6(2.7)	5312.2(5.5)	3.89(13)
C(12)	572.6(4.2)	2992.2(2.7)	6390.4(4.9)	3.34(12)
C(13)	1010.4(5.1)	3263.7(3.4)	7675.2(6.0)	4.83(16)
C(14)	1081.3(6.1)	2795.1(4.1)	8786.9(5.9)	6.01(20)
C(15)	734.6(5.8)	2025.5(4.1)	8663.3(5.9)	5.61(18)
C(16)	338.5(5.0)	1736.1(3.3)	7417.0(5.3)	4.40(15)
C(17)	256.2(4.2)	2203.0(2.7)	6239.9(4.7)	3.18(11)
C(18)	1752.4(4.1)	1642.9(2.7)	2615.6(4.5)	3.10(11)
C(19)	2885.1(4.8)	1645.4(3.4)	2019.2(6.1)	4.58(15)

a) Aomic parameters are multiplied by 10^4. Thermal parameters are given by the equivalent temperature factors.

Results and Discussion

Formation of the Acetate-, Methoxide-, and Phenolate-Bridged Tetranuclear Complex. The formation of the tetranuclear copper(II) complex with methoxo bridges, for example, can be represented by this equation:

$$2\,[Cu(salpd)]+2\,Cu(L)_2+2\,CH_3OH \rightarrow [Cu(salpd\text{-}\mu\text{-}O,O')(\mu\text{-}L)Cu(\mu\text{-}CH_3O)_2Cu(\mu\text{-}L)\text{-}(salpd\text{-}\mu\text{-}O,O')Cu]+2\,LH$$

where L=HCOO or CH_3COO. This reaction, accompanied by methoxide-bridging, takes place even without the addition of a base, although the addition of triethylamine makes the reaction quantitative. However, attempts to obtain the tetranuclear copper(II) complex with bridging ethoxide ions instead of methoxide ions were unsuccessful under similar conditions.

Structure of 1. The molecular structure, with its atomic numbering, is shown in Fig. 1, while the bond lengths and bond angles are given in Table 2. The complex is tetranuclear and has a center of inversion. The zigzag-chain structure of the copper(II) ions in the complex is made up of four units of a square pyramid. Each salpd ligand occupies the four equatorial positions of the terminal copper(II) ion, with the bond distances of 1.963(3)—1.978(5) Å, while the apical position is occupied by one of the oxygens of the acetate ion with the bond distance of 2.235(4) Å. Each basal plane of the inner two copper(II) ions is formed by the two bridging methoxide oxygens (1.917(3) Å, 1.927(3) Å), one of the phenolate oxygens (2.027(3) Å) and one of the acetate oxygens (1.926(3) Å). The apical position is occupied by another phenolate oxygen of salpd (Cu(1)-O(2)=2.323(3) Å). It is noteworthy that one of the oxygen atoms of the bridging acetate ion coordinates to Cu(2) at the apical position, while the other oxygen atom coordinates to Cu(1) at an equatorial position.

The Cu(1), OM, Cu(1′), and OM* atoms make a

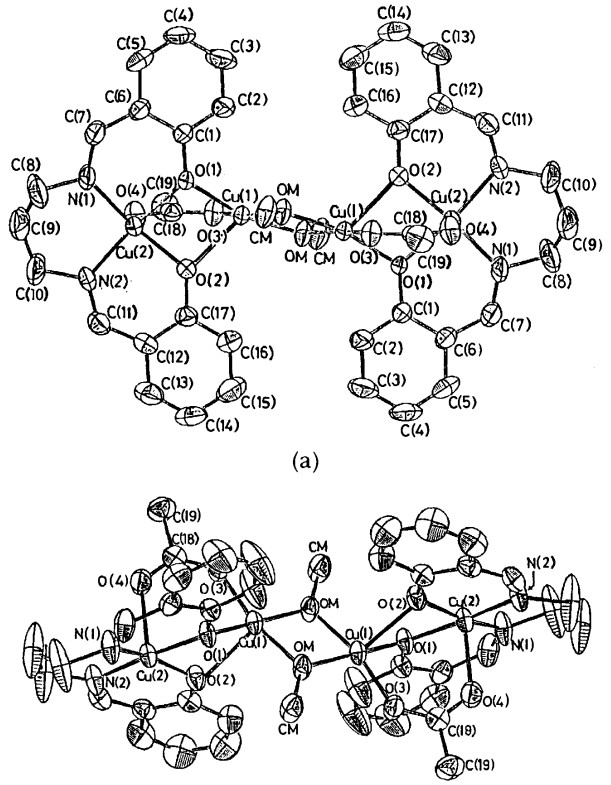

Fig. 1. Molecular structure of [Cu(salpd-μ-O,O′)(μ-CH3COO)Cu(μ-CH3O)2Cu(μ-CH3COO)(salpd-μ-O,O′)Cu] (a) and the side view (b) drawn by ORTEP.[17]

Table 2. Interatomic Distances (l/Å) and Bond Angles (φ/°) of the Coordination Sphere for [Cu(salpd-μ-O,O′)(μ-CH3COO)Cu(μ-CH3O)2Cu(μ-CH3COO)(salpd-μ-O,O′)Cu] with Estimated Standard Deviations in Parentheses

Distance (l/Å)		Angle (φ/°)	
Cu(1)-Cu(1′)	3.027(1)	Cu(1)-OM-Cu(1′)	103.9(2)
Cu(1)-Cu(2)	3.123(1)	Cu(1)-OM-CM	129.1(3)
Cu(1)-OM	1.927(3)	Cu(1′)-OM-CM	123.8(3)
Cu(1)-OM*	1.917(3)	Cu(1)-O(3)-C(18)	133.2(3)
OM-CM	1.392(7)	Cu(2)-O(4)-C(18)	129.4(3)
Cu(1)-O(1)	2.027(3)	O(3)-C(18)-O(4)	126.2(5)
Cu(2)-O(2)	2.323(3)	O(3)-C(18)-C(19)	115.8(4)
Cu(1)-0(3)	1.926(3)	O(4)-C(18)-C(19)	118.0(5)
Cu(2)-O(1)	1.963(3)	O(1)-Cu(1)-O(2)	70.1(1)
Cu(2)-O(2)	1.924(4)	O(1)-Cu(1)-O(3)	93.8(1)
Cu(2)-O(4)	2.235(4)	O(1)-Cu(1)-OM*	95.3(1)
Cu(2)-N(1)	1.978(5)	O(3)-Cu(1)-OM	92.7(1)
Cu(2)-N(2)	1.992(5)	OM-Cu(1)-OM*	76.1(1)
O(3)-C(18)	1.262(6)	O(1)-Cu(2)-O(2)	80.5(2)
O(4)-C(18)	1.234(6)	O(1)-Cu(2)-N(1)	91.2(2)
C(18)-C(19)	1.500(8)	N(1)-Cu(2)-N(2)	95.7(2)
		Cu(1)-O(1)-Cu(2)	103.0(2)
		Cu(1)-O(2)-Cu(2)	94.2(1)

perfect plane, as required by the crystallographic symmetry.

The most prominent feature of the structure is that the basal planes of the inner copper atoms (Cu(1) and Cu(1′)) are nearly perpendicular to those of the terminal copper atoms (Cu(2) and Cu(2′)), the dihedral angle between the mean basal planes of Cu(1) and Cu(2′) being 108.4°. The basal atoms of terminal copper are slightly distorted toward a tetrahedron, the dihedral angle formed by the Cu(2), O(2), N(2), and Cu(2), O(1), N(1) planes being 163.6°. Cu(2) is lifted by 0.11 Å toward the acetate oxyen.

Table 3. IR Data of Tetranuclear Copper(II) Complexes (cm^{-1})

Complex	Skeletal	ν_{C-O}		ν_{M-OCH_3}	
		ν(as)	ν(s)	ν_{C-O}	ν_{M-O}
1	1538vs 1550vs	1578vs	1390vs	1062vs	535s
2	1540vs 1550vs	1590vs	1346vs	1063vs	530s

The skeletal vibration of [Cu(salpd)] is found at 1538 cm^{-1}.

Infrared Spectra. Some frequencies of the selected bands of the complexes are listed in Table 3. The two bands at 1550 and 1540 cm^{-1} may be assigned to the skeletal vibrations related to the phenolic oxygen of the Schiff-base ligand.[13-15] A similar band was observed at 1538 cm^{-1} for the mononuclear complex [Cu(salpd)]. Since it is known that the phenoxide band shifts to a higher frequency when a singly coordinated phenoxide oxygen further coordinates to another metal ion, the band at 1550 cm^{-1} should be assigned to the vibration related to O(1), which strongly binds to both coppers (Cu(1) and Cu(2)), while the lower-frequency band seems to be due to the vibration related O(2), which is only weakly bound to Cu(1).

Magnetic Properties. Figure 2 represents the temperature variation in the magnetic susceptibilities (χ_A) and the magnetic moment (μ_{eff}) of the tetranuclear complexes in the temperature range of 77.4—296.0 K. The magnetic moments gradually decrease with the lowering of the temperature, as is shown in Fig. 2. This suggests that there is antiferromagnetic interaction between copper(II) ions. Hatfield and Inman proposed the interaction Hamiltonian for a four spin model with superexchange interaction to account for the unusual magnetic properties of the complex, [4-(*o*-hydroxyphenylimino)-2-pentanonato]-copper(II), as given below.[16]

$$\boldsymbol{H}=-2J_{12}\mathbf{S}_1\mathbf{S}_2-2J_{13}(\mathbf{S}_1\mathbf{S}_3+\mathbf{S}_2\mathbf{S}_4) -2J_{14}(\mathbf{S}_1\mathbf{S}_4+\mathbf{S}_2\mathbf{S}_3)-2J_{34}\mathbf{S}_3\mathbf{S}_4 \quad (1)$$

Here the numbering both on the exchange integrals J_{ij} and on the spin vectors **S** refers to the 3-1-2-4 arrangement of the Cu(II) ions. The present study has shown that the magnetic susceptibility expression for this sort of system may be given in an explicit form as follows:

$$\chi_A = Ng^2\beta^2/kT \cdot A/B + TIP \quad (2)$$
$$A = 10\exp[(K/2+N)/(kT)] + 2\exp[(K/2-N)/(kT)] + 2\exp[(-K/2+\sqrt{M^2+L^2})/(kT)] + 2\exp[(-K/2-\sqrt{M^2+L^2})/(kT)]$$
$$B = 5\exp[(K/2+N)/(kT)] + 3\exp[(K/2-N)/(kT)] + 3\exp[(-K/2+\sqrt{M^2+L^2})/(kT)] + 3\exp[(-K/2-\sqrt{M^2+L^2})/(kT)] + \exp[(-K/2-N-\sqrt{(K-N)^2+3L^2})/(kT)] + \exp[(-K/2-N+\sqrt{(K-N)^2+3L^2})/(kT)]$$

where $K=J_{12}+J_{34}$, $L=J_{14}-J_{13}$, $M=J_{12}-J_{34}$, and $N=J_{14}+J_{13}$, β is is the Bohr magneton; N, Avogadro's number; k, the Boltzmann constant, and g, the Lande g factor over copper(II) ions. The magnetic susceptibility data were, therefore, fit to Eq. 2 by using the best-fit method, assuming $J_{14}=J_{34}=0$ and $TIP=60\times10^{-6}$ c.g.s. u. per gram-atom copper; the coupling constants J_{12}, and J_{13} were varied systematically until the standard deviation of the value for Lande g factor reached a minimum in the range of 77.4—296.0 K. The calculation yielded g (average)=2.13, $J_{12}=-390$ cm^{-1}, $J_{13}=67$ cm^{-1} in Complex **1**, and g (average)=2.20, $J_{12}=-263$ cm^{-1}, $J_{13}=39$ cm^{-1} in Complex **2**. The solid curves in Fig. 2 represent the theoretical curves of the best fit of the data to Eq. 2 with the parameters specified above. The magnetic coupling constants in both complexes **1** and **2** indicate the existence of a strong antiferromagnetic superexchange interaction between the inner copper pair and a weak ferromagnetic superexchange interaction between the outer adjacent copper pairs.§

During the last two decades structural factors determining spin exchange coupling in dialkoxo-bridged dicopper(II) complexes have been the subject of continuing discussions by many researchers.[18-26] Among the many structural factors, the Cu-O-Cu angle or the coplanarity of the two coordination planes has been pointed out as the major factor by many workers. These two factors are not independent, but are linked to each other so that each factor may be used for the diagnosis of spin-exchange interaction.[26] In view of this, the strong antiferromagnetic interaction between the inner copper pair observed for the present complexes seems quite natural, since the 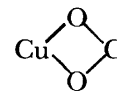 bridging system is perfectly coplanar and the Cu-O-Cu angle (103.6°) is fairly large.[20] As for the outer copper (Cu(1), Cu(2)) pair, the geometry of the bridging system is very complicated, as has been described in the preceding section, so that it is not easy to predict the extent of spin coupling in a straightforward manner. However, in many cases of such bridging systems with a very distorted geometry, as is the present complex, only a weak spin coupling has been reported.[27] Thus, the weak ferromagnetism found in this study is not a surprising result.

Judging from the qualitative similarity of the magnetic parameters, the principal configuration of Complex **2** is likely to be similar to that of **1**.

§ It is possible to obtain a tolerable agreement between the experimental data and the theoretical χ-T curve by using a value from a considerably wide range (±30 cm^{-1}) for J_{13}, with a slight adjustment of the J_{12} value. However, we have confirmed that a much less satisfactory agreement be obtained by using a negative J_{13} value.

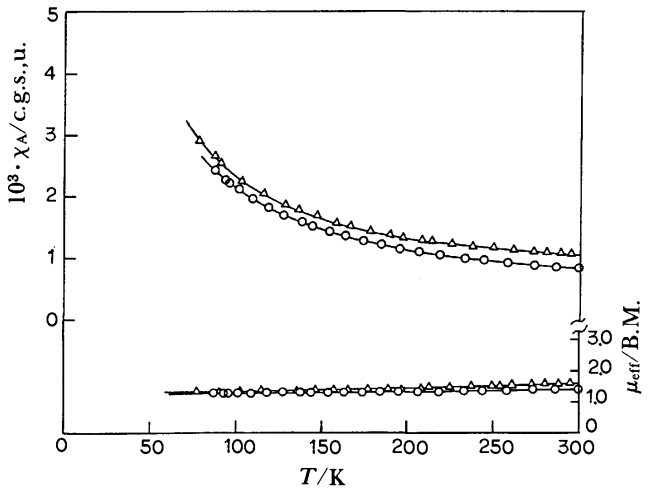

Fig. 2. Temperature variation of the atomic susceptibility (χ_A) and magnetic moment (μ_{eff}) for the tetranuclear complexes: **1** (○) and **2** (△). The solid lines were drawn on the basis of the values of χ_A and μ_{eff} obtained from Eq. 2, when $J_{12}=-390$ cm^{-1}, $J_{23}=67$ cm^{-1}, $J_{14}=J_{34}=0$ cm^{-1}, and $g=2.13$ for complex **1**, and $J_{12}=-263$ cm^{-1}, $J_{13}=39$ cm^{-1}, $J_{14}=J_{34}=0$ cm^{-1}, and $g=2.20$ for complex **2**.

References

1) J. A. Barnes, D. J. Hodgson, and W. E. Hatfield, *Inorg. Chem.*, **11**, 144 (1972).

2) K. T. McGregor, N. T. Watkins, D. L. Lewis, R. F. Drake, D. J. Hodgson, and W. E. Hatfield, *Inorg. Nucl. Chem. Lett.*, **9**, 423 (1973).

3) O. Kahn, P. Tola, J. Galy, and H. Coudanne, *J. Am. Chem. Soc.*, **100**, 3931 (1978).

4) N. Torihara, H. Ōkawa, and S. Kida, *Chem. Lett.*, **1978**, 1969.

5) G. D. Fallon, K. S. Murray, W. Mazurek, and M. J. O'Conner, *Inorg. Chim. Acta*, **96**, L53 (1985).

6) S. G. N. Roundhill, D. M. Roundhill, D. R. Bloomquist, C. Landee, R. D. Willett, D. M. Dooley, and H. B. Gray, *Inorg. Chem.*, **18**, 831 (1979).

7) C. Fukuhara, T. Arakaki, K. Katsura, M. Mori, M. Ando, M. Mikuria, and S. Kida, The 54th Annu. Meeting of Chem. Soc. Jpn., Tokyo, April 1987, Abstr. I, p. 213.

8) U. Geiser, R. M. Gaura, R. D. Willett, and D. X. West, *Inorg. Chem.*, **25**, 4203 (1986).

9) C. Fukuhara, E. Asato, T. Shimoji, K. Katsura, M. Mori, K. Matsumoto, and S. Ooi, *J. Chem. Soc., Dalton Trans.*, **1987**, 1305.

10) C. Fukuhara, K. Tsuneyoshi, K. Katsura, M. Mori, M. Mikuria, and S. Kida, the 38th Symposium on Coordination

Chemistry, (1988), Abstr., p. 533.
11) T. Sakurai and K. Kobayashi, *Rikagaku Kenkyusho Houkoku*, **1979**, 55, 69; S. Kawano, *Rep. Comput. Cent. Kyushu Univ.*, **1980**, 13, 39.
12) "International Tables for X-Ray Crystallography," Kynoch Press, Birmingham (1974), Vol. 4.
13) G. E. Batley and D. P. Graddon, *Aust. J. Chem.*, **20**, 877 (1967).
14) S. J. Gruber, C. M. Harris, and E. Sinn, *J. Inorg. Nucl. Chem.*, **30**, 2723 (1968).
15) T. Tokii, Y. Muto, M. Kato, K. Imai, and H. B. Jonassen, *J. Inorg. Nucl. Chem.*, **35**, 1539 (1973).
16) W. E. Hatfield and G. W. Inman, *Inorg. Chem.*, **8**, 1376 (1969).
17) C. K. Johnson, Report No. ORNL 3794, Oak Ridge National Laboratory, Oak Ridge, Tennessee (1965).
18) D. J. Hodgson, *Prog. Inorg. Chem.*, **19**, 173 (1975); V. H. Crowford, H. W. Richardson, J. R. Wasson, D. J. Hodgson, and W. E. Hatfield, *Inorg. Chem.*, **15**, 2107 (1976).
19) L. Merz and W. Haase, *J. Chem. Soc., Dalton Trans.*, **1980**, 875.
20) K. Nieminen, *Ann. Acad. Sci. Frenn., Ser. A*, 2, **197**, 8 (1983).
21) P. J. Hay, J. C. Thibeault, and R. Hoffmann, *J. Am. Chem. Soc.*, **97**, 4884 (1975).
22) O. Kahn, *Inorg. Chim. Acta*, **62**, 3(1982).
23) A. Bencini and D. Gatteschi, *Inorg. Chim. Acta*, **31**, 11 (1978).
24) R. M. Countryman, W. T. Robinson, and E. Sinn, *Inorg. Chem.*, **13**, 2013 (1974); E. Sinn, *ibid.*, **15**, 358 (1976).
25) M. Mikuriya, K. Toriumi, T. Ito, and S. Kida, *Inorg. Chem.*, **24**, 629 (1985).
26) M. Handa, N. Koga, and S. Kida, *Bull. Chem. Soc. Jpn.*, **61**, 3853 (1988).
27) Y. Nishida, T. Tokii, and Y. Mori, *J. Chem. Soc., Chem. Commun.*, **1988**, 675.

Triethylamine-Mediated Generation of a Synthetic Equivalent of Parent Azomethine Imine by Condensation of Ethyl 3-Benzylcarbazate with Paraformaldehyde

Shuji KANEMASA,* Naoki TOMOSHIGE, Eiji WADA, and Otohiko TSUGE*
Institute of Advanced Material Study, and Department of Molecular Science and Technology, Interdisciplinary Graduate School of Engineering Sciences, Kyushu University, Kasugakoen, Kasuga 816
(Received April 27, 1989)

A synthetic equivalent of parent azomethine imine is accessible by simple heating of ethyl 3-benzylcarbazate with paraformaldehyde under reflux in toluene in the presence of triethylamine, which effectively suppresses the undesired formation of imine dimers. The resulting imines can be trapped with a variety of dipolarophiles.

The cycloaddition of azomethine imine 1,3-dipoles with olefin dipolarophiles offers a short synthetic method for producing pyrazolidine derivatives.[1] The pyrazolidines which have been synthesized by this route are derivatives bearing at least one *N*-substituent.[2] To the best of our knowledge, not only the parent azomethine imine, itself, but also its synthetic equivalent is unknown.

We planned to establish a route leading to a synthetic equivalent of the parent azomethine imine 1,3-dipole. Cycloadditions of this synthetic equivalent with olefins and a subsequent removal of the *N*-substituents would produce *N*-unsubstituted pyrazolidines. Therefore, the cycloadducts would serve as functionalized cyclic hydrazines in heterocyclic synthesis; a reductive cleavage of the nitrogen-nitrogen bond of *N*-unsubstituted pyrazolidines would provide a new synthetic way to functionalized 1,3-diamines.

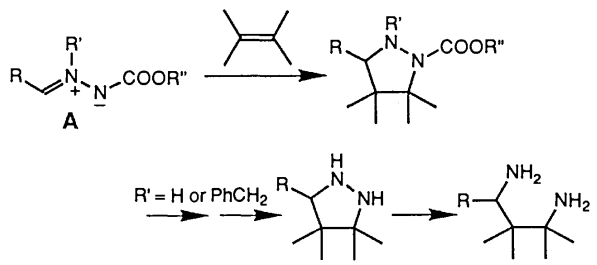

The synthetic equivalent of our choice is azomethine imine **A**, which bears an anion-stabilizing ester group at the terminal nitrogen and the central nitrogen is either unsubstituted or substituted by a removable benzyl group.

In the present work we investigated the condensation of ethyl 3-benzylcarbazate with formaldehyde and its equivalent reactions. It was found that triethylamine could effectively inhibit the formal dimerization of the transient azomethine imine. The generation procedure is simply carried out by heating ethyl 3-benzylcarbazate with paraformaldehyde and triethylamine in toluene in the presence of a dipolarophile.

Results and Discussion

Hydrazones undergo thermal[3] or acid-catalyzed tautomerism[4] generating azomethine imines bearing an unsubstituted nitrogen **A** (R'=H). Ethyl 3-benzylidenecarbazate (**1**) was selected as an imine precursor and its thermal tautomerism was investigated since **1** has an array of functionalities similar to that of the imines of α-amino esters whose thermal tautomerism is known to generate ester-stabilized azomethine ylides.[5]

Heating hydrazone **1** with *N*-(*p*-tolyl)maleimide under reflux in toluene for 72 h gave a single stereoisomer of cycloadduct **2** in 39% yield (Scheme 1). The structure of **2** was assigned as being a 3,3a-cis isomer on the basis of $J_{3\text{-}3a}$=8.8 Hz, indicating the endo-selective cycloaddition of azomethine imine **B**. However, the poor reactivity cancels the advantage of high stereoselectivity. Attempts to trap imine **B** with less reactive olefins, such as methyl acrylate and crotonate (each excess in a sealed tube), were unsuccessful, and attempts to activate hydrazone **1** by the aid of lithium bromide/triethylamine[6] were all in vain. The use of 1-benzylidene-2-(*p*-tolylsulfony)hydrazine, instead of **1**, produced no cycloadducts.

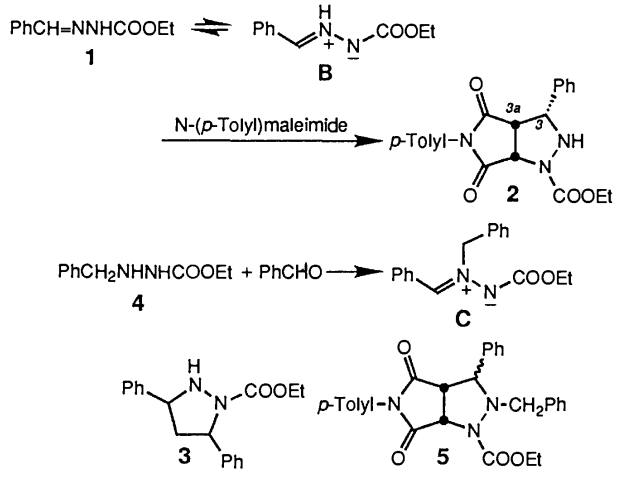

Scheme 1.

Although boron trifluoride etherate[4] showed some catalysis in a hydrazone-azomethine imine tautomerism of **1**, a 5 : 1 stereoisomeric mixture of cycloadduct **3** was obtained only in 38% yield in a reaction with styrene. Similar boron trifluoride-catalyzed reactions with butyl vinyl ether or *N*-(*p*-tolyl)maleimide gave no cycloadducts.

The next generation method employed was the condensation of carbonyl compounds with 1,2-disubstituted hydrazines.[1] For this purpose, hydrazone **1** was reduced with either zinc borohydride or a borane/pyridine complex into ethyl 3-benzylcarbazate (**4**).

Heating **4** with benzaldehyde under reflux in toluene resulted in a quantitative generation of azomethine imine **C**, which was captured by *N*-(*p*-tolyl)maleimide to give a 73:27 mixture of endo and exo isomers of cycloadduct **5** (Scheme 1). Both isomers, which were separated from each other by silica-gel column chromatography by using hexane-ethyl acetate, were assigned on the basis of $J_{3\text{-}3a}$.

In expectation of the generation of a synthetic equivalent of the parent azomethine imine, a reaction of hydrazine **4** with paraformaldehyde was performed under reflux in toluene with a continuous removal of water by the aid of a Dean-Stark trap. The azomethine imine **D** generated was trapped with several olefins such as *N*-(*p*-tolyl)maleimide, dimethyl fumarate, and styrene (Scheme 2). Even when two equimolar amounts of the olefins were employed, the yields of the corresponding cyloadducts **6a,b,d** were low (Table 1, Entries 1, 6, 11). In all these cases, the cycloadducts were accompanied by diethyl 2,5-dibenzylperhydro-1,2,4,5-tetrazine-1,4-dicarboxylate (**7**), the formal dimer of imine **D**, in 15 to 50% yields. Although the yield of **6d** went up to 73% when a large excess of styrene (13 equiv) was used, side-product **7** was still formed in 10% yield (Entry 12).

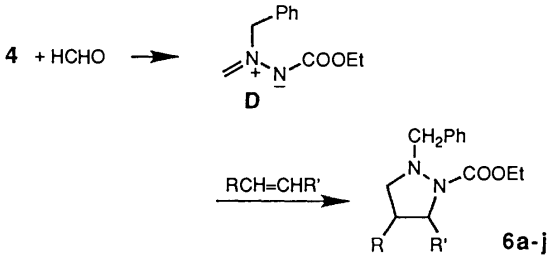

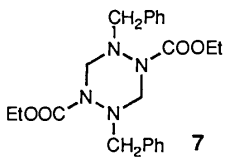

6a: R,R' = CON(*p*-Tolyl)CO (cis)
6b: R = R' = COOMe (trans)
6c: R = R' = COOMe (cis)
6d: R = H, R' = Ph
6e: R,R' = $CH_2C_6H_4$-*o* (cis)
6f: R = H, R' = COOMe
6g: R = COOMe, R' = H
6h: R = Me, R' = COOMe (trans)
6i: R = COOMe, R' = Me (trans)
6j: R = H, R' = OBu-*n*

Scheme 2.

The azomethine imine **D**, thus generated, failed to react with less reactive olefins, such as methyl acrylate and crotonate, dimer **7** being the only product (Entries 23, 25). As anticipated, dimer **7** was formed also in the absence of dipolarophiles. Thus, heating **4** with paraformaldehyde under reflux in toluene produced 24% of **7** after 2 h, and 79% after 42 h. Under these reaction conditions, a thermal cleavage of dimer **7** did not take place, indicating no possibility for the regeneration of azomethine imine **D** by the thermolysis of **7**.

When dipolarophiles are not highly reactive in the simple heating method (Method A), the formation of side-product **7** becomes critical.

Molecular sieves of 4A were used to remove the water formed during the condensation (Method B). Under these conditions, the formation of dimer **7** was significantly suppressed in the reactions with styrene and butyl vinyl ether, so that the relative yields of cycloadducts **6d,j** slightly increased (Entries 13, 28). However, no significant improvement was observed in the reaction with *N*-(*p*-tolyl)maleimide (Entry 2).

The 2-(phenylthiomethyl) derivative of hydrazine **4** is the second precursor of azomethine imine **D** of our choice. Treatment of **4** with aqueous formaldehyde, and then benzenethiol in ethanol at room temperature, gave ethyl 3-benzyl-3-(phenylthiomethyl)carbazate (**8**) in 93% yield (Scheme 3), which is sufficiently stable to be purified by coluumn chromatography over silica gel.

Simple heating of **8** generated azomethine imine **D** which was trapped with electron-deficient activated dipolarophiles, such as *N*-(*p*-tolyl)maleimide and dimethyl maleate, to afford the corresponding cycloadducts **6a,c**. Although the formation of dimer **7** was effectively suppressed during this procedure, the slow generation of imine **D** resulted in the recovery of some starting precursor **8**, even after the lapse of long reaction times (Entries 4, 9). More troublesome, especially in the reaction with *N*-(*p*-tolyl)maleimide as a highly reactive Michael acceptor, was the Michael addition of phenylthiol nucleophile, arising from the elimination of **8**. A considerable amount of *N*-(*p*-tolyl)-2-(phenylthio)succinimide was produced. Poor stereospecificity in the reaction with dimethyl maleate was another disadvantage (Entry 9).

The base-induced azomethine imine generation by treating **8** with sodium hydride, in *N*,*N*-dimethyl-

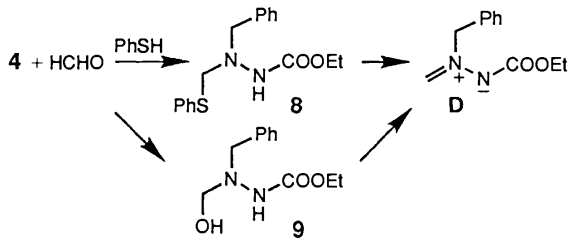

Scheme 3.

Table 1. Cycloaddition of Azomethine Imine **D** with Olefinic Dipolarophiles

Entry	Olefin	Method[a,b]	Solvent	Additive	Time/h	Product (yield/%)[c]			
						6		**7**	Others
1	*N*-(*p*-Tolyl)maleimide	A[d]	Toluene		6	**6a**	41	38	
2	*N*-(*p*-Tolyl)maleimide	B	Toluene		10	**6a**	41	42	
3	*N*-(*p*-Tolyl)maleimide	C	Toluene		50	**6a**	93	0	
4	*N*-(*p*-Tolyl)maleimide	D	THF		45	**6a**	67	0	(15)[e], (23)[f]
5	*N*-(*p*-Tolyl)maleimide	E	Toluene		11	**6a**	61	5	
6	Dimethyl fumarate	A	Toluene		7	**6b**	70	15	
7	Dimethyl fumarate	C	Toluene		50	**6b**	93	0	
8	Dimethyl maleate	A	Toluene		7	**6c**	41	44	
9	Dimethyl maleate	D	Toluene		44	**6c**	19	0	(42)[e], (31)[g]
10	Dimethyl maleate	E	Toluene	AcOH(cat)	20	**6c**	50	23	
11	Styrene	A	Toluene		23	**6d**	34	50	
12	Styrene	A[h]	Toluene		3	**6d**	73	10	
13	Styrene	B	Toluene		23	**6d**	51	34	
14	Styrene	C	Toluene		50	**6d**	88	0	
15	Styrene	D	Xylene		96	**6d**	32	0	(37)[e]
16	Styrene	D	Xylene	AcOH (1 equiv)	50	**6d**	48	0	(24)[e]
17	Styrene	D	Xylene	AcOH (10 equiv)	50	**6d**	18	35	(10)[e]
18	Styrene	E	Xylene	AcOH (cat)	4	**6d**	35	49	
19	Styrene	E	Xylene	CF_3COOH (cat)	4	**6d**	0	92	
20	Styrene	E	Toluene	NEt_3 (1.2 equiv)	24	**6d**	56	8	
21	Styrene	E	Toluene	NEt_3 (3 equiv)	50	**6d**	72	0	
22	Indene	E	Toluene	NEt_3 (3 equiv)	50	**6e**	76	0	
23	Methyl acrylate	A	Toluene		72	**6f, g**	0	85	
24	Methyl acrylate	C	Toluene	NEt_3 (3 equiv)	50	**6f, g**	96[i]	0	
25	Methyl crotonate	A	Toluene		12	**6h, i**	0	60	
26	Methyl crotonate	C	Toluene	NEt_3 (3 equiv)	15	**6h, i**	42[j]	0	(20)[k]
27	Butyl vinyl ether	A	Toluene		21	**6j**	37	10	
28	Butyl vinyl ether	B	Toluene		21	**6j**	58	0	
29	Butyl vinyl ether	C	Toluene	NEt_3 (3 equiv)	50	**6j**	80	0	

a) Unless otherwise referred, all reactions were carried out by heating a mixture of a precursor, paraformaldehyde (1.5—2 equiv), and a dipolarophile (2 equiv) under reflux in the solvent shown above with continiuous removal of water by the aid of a Dean-Stark trap. b) As methods A to E, see experimental section. c) Yield of isolated products based on **4** or **8**. d) One equivalent of the maleimide was used. e) Recovered **8**. f) *N*-(*p*-Tolyl)-2-(phenylthio)succinimide. g) The fumarate adduct **6b**. h) A large excess (13 equiv) of styrene was used. i) **6f**: 50%; **6g**: 46%. j) **6h**: 14%; **6i**: 28%. k) Ethyl 4-benzylperhydro-1,3,4-oxadiazole-3-carboxylate.

formamide (DMF) at 0 °C in the presence of butyl vinyl ether, formed complex mixture of many compounds. It was found, however, that the imine generation was effected by an acid catalysis. Thus, the reaction of **8** with styrene was catalyzed by one equivalent of acetic acid, but the formation of dimer **7** was also facilitated in the presence of a large excess of acetic acid (Entries 15—17).

The reaction of hydrazine **4** with aqueous formaldehyde in ethanol at room temperature and evaporation of all the volatile materials left an unstable liquid which was assigned to be ethyl 3-benzyl-3-(hydroxymethyl)carbazate (**9**) on the basis of the ^1H NMR spectrum. The use of **9** as a precursor of azomethine imine **D** was investigated next.

The generation of azomethine imine **D** by the thermal or acid-catalyzed dehydration of (hydroxymethyl)hydrazine **9** accompanied the formation of significant amounts of dimer **7** (Entries 5, 10, 18), and the use of a strong acid catalyst, such as trifluoroacetic acid, resulted in a quantitative formation of dimer **7** (Entry 19). To our delight, however, triethylamine was found to effectively suppress the formation of dimer **7** (Entries 20—22).

We examined the direct generation route of imine **D** by heating hydrazine **4** with paraformaldehyde in the presence of excess (3 equiv) triethylamine. This procedure (Method C) worked well for a variety of olefinic dipolarophiles to produce the corresponding cycloadducts **6a,b,d,j** in excellent yields (Entries 3, 7, 14, 29). Even with less reactive olefins, such as methyl acrylate and crotonate, imine **D** underwent a smooth cycloaddition to give cycloadducts **6f,g** and **6h,i** (Entries 24, 26).

It is apparent that the condensation of hydrazine **4** with formaldehyde initially forms (hydroxymethyl)-hydrazine **9**, which then eliminates water leading to iminium intermediate **E** (Scheme 4). The direct formation of dimer **7** through the cycloaddition dimerization of azomethine imine **D** is thermally forbidden.[7] The most likely path is the nucleophilic addition of azomethine imine **D** or (hydroxymethyl)hydrazine **9** to the iminium intermediate **E** leading to **F** or **F'**. Either of them undergoes a ready cyclization to give dimer **7**.

In the presence of a weak acid catalyst, the dehydra-

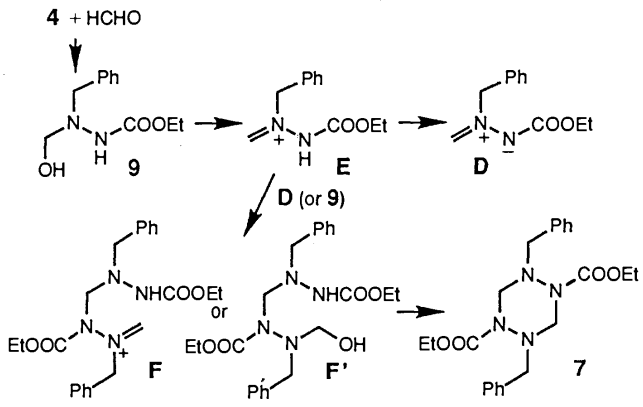

Scheme 4.

tion of **9** is facilitated to accumulate iminium salt **E**. The generation of imine **D** competes with the coupling reaction leading to **F** or **F'**. When the catalyst is strongly acidic, deprotonation of **E** becomes difficult, so that the dimer formation becomes a major path. On the other hand, triethylamine catalyzes the deprotonation stage of **E** leading to azomethine imine **D** while minimizing the opportunity for a coupling reaction.

The removal of both the ester and benzyl substituents from the cycloadducts **6a—j** can be readily performed by acid- or base-catalyzed hydrolysis and catalytic hydrogenation on Pd/C, respectively. The use of the resulting heterocycles in organic synthesis is now under investigation; the results will soon be published elsewhere.

Experimental

General. Melting points were determined on a Yanagimoto melting point apparatus and are uncorrected. IR spectra were taken with JASCO IRA-1 and A-702 spectrometers. ^{1}H and ^{13}C NMR spectra were recorded on JEOL FX-100 (100 MHz for ^{1}H NMR and 25.05 MHz for ^{13}C NMR) and GSX-270 (270 MHz for ^{1}H NMR and 67.94 MHz for ^{13}C NMR) instruments. Chemical shifts are expressed in parts per million downfield from tetramethylsilane as an internal standard. Mass spectra and high-resolution mass spectra (HRMS) were measured with a JEOL-01SG-2 spectrometer at an ionization energy of 70 eV. Elemental analyses were performed on a Hitachi 026 CHN analyzer. For preparative column chromatography, Wakogel C-200, C-300 (Wako), and Silica gel 60 (Merck) were employed. Flash chromatography was carried out on an EYELA EF-10 apparatus using a column (20×180 mm) packed with Silica gel 60 (Merck, size: 0.04—0.063 mm).

Ethyl 3,3a-*cis*-3a,6a-*cis*-4,6-Dioxo-3-phenyl-5-(*p*-tolyl)-perhydropyrrolo[3,4-*c*]pyrazole-1-carboxylate (2): A mixture of **1** (0.191 g, 1 mmol) and *N*-(*p*-tolyl)maleimide (0.15 g, 0.8 mmol) was heated under reflux in toluene (4 ml) for 72 h. The mixture was evaporated in vacuo and the residue was chromatographed on silica gel by using hexane-ethyl acetate (2:1 v/v) to give **2** (0.117 g, 39%): Colorless prisms (diethyl ether-hexane); mp 203—205 °C; IR (KBr) 3210, 1710, 1365, and 1180 cm^{-1}; ^{1}H NMR ($CDCl_3$) δ= 1.36 (3H, t, J=7.2 Hz, COOEt), 2.35 (3H, s, *p*-Me), 3.83 (1H, dd, $J_{3a\text{-}3}$=8.8 and $J_{3a\text{-}6a}$=8.1 Hz, 3a-H), 4.32 (2H, m, COOEt), 4.67 (1H, t, $J_{3\text{-}3a}$= $J_{3a\text{-}NH}$=8.8 Hz, 3-H), 4.98 (1H, br d, J=8.8 Hz, NH), 5.48 (1H, d, $J_{6a\text{-}3a}$=8.1 Hz, 6a-H), and 7.0—7.5 (9H, m, Ar); ^{13}C NMR ($CDCl_3$) δ=14.56 (COOEt), 21.19 (*p*-Me), 52.01 (COOEt), 61.97 (3a-C), 63.37 (6a-C), 66.45 (3-C), 125.41, 127.11, 128.65, 128.81, 129.02, 129.82, 133.37, 138.93 (each Ph), 156.74 (COOEt), 171.89, and 172.94 (each CON). Found: C, 66.66; H, 5.68; N, 10.93%. Calcd for $C_{21}H_{21}N_3O_4$: C, 66.47; H, 5.59; N, 11.08%.

Ethyl 3,5-Diphenyl-1-pyrazolidine-1-carboxylate (3): A solution of **1** (0.191 g, 1 mmol), styrene (0.17 ml, 1.5 mmol), and trifluoroborane etherate (0.16 ml, 1.3 mmol) in dichloromethane (5 ml) was stirred at room temperature for 20 h. The solvent was evaporated in vacuo, and the residue was treated with saturated aqueous sodium hydrogencarbonate; the mixture was then extracted with diethyl ether (25 ml×3). The combined extracts were dried over magnesium sulfate and evaporated in vacuo. The residue was chromatographed on silica gel with hexane-ethyl acetate (5:1 v/v) to give the major stereoisomer of **3** (0.112 g, 38%) which was contaminated by a trace of the minor isomer: Colorless liquid; IR (neat) 3250, 1695, 1325, and 1120 cm^{-1}; ^{1}H NMR ($CDCl_3$) major isomer: δ= 1.2—1.3 (3H, COOEt), 2.46 (1H, dt, J_{gem}=12.8 and $J_{4\text{-}3}$=$J_{4\text{-}5}$=6.6 Hz, one of 4-H), 2.81 (1H, ddd, J_{gem}=12.8, $J_{4\text{-}3}$=8.1, and $J_{4\text{-}5}$=4.4 Hz, the other of 4-H), 4.0—4.3 (2H, m, COOEt), 4.62 (1H, dd, $J_{3\text{-}4}$=6.6 and 4.4 Hz, 3-H), 5.02 (1H, dd, $J_{5\text{-}4}$=8.1 and 6.6 Hz, 5-H), and 7.2—7.5 (10H, m, Ph); minor isomer: δ=2.17, 3.10 (each 1H, m, 4-H), 4.34 (1H, dd, $J_{3\text{-}4}$=10.6 and 5.4 Hz, 3-H), and 5.24 (1H, t, $J_{5\text{-}4}$= 9.2 Hz, 5-H); ^{13}C NMR ($CDCl_3$) major isomer: δ=14.61 (COOEt), 45.41 (4-C), 60.96, 61.52, 61.67 (3-, 5-C, and COOEt), 125.76, 126.32, 127.17, 127.40, 128.58, 139.97, 142.30 (each Ph), and 156.12 (COOEt); minor isomer: δ=45.86, 61.88, 63.48, 63.58, 126.81, 127.12, 127.73, 128.25, 128.66, 128.69, 128.85, 129.05, and 142.30. Other ^{1}H and ^{13}C signals of the minor isomer are overlapping with those of the major isomer.

Ethyl 3,3a-*cis*-2-Benzyl-4,6-dioxo-3-phenyl-5-(*p*-tolyl)perhydropyrrolo[3,4-*c*]pyrazole-1-carboxylate (5): A mixture of **4** (0.04 g, 0.2 mmol), benzaldehyde (0.024 g, 0.2 mmol), and *N*-(*p*-tolyl)maleimide (0.038 g, 0.2 mmol) was heated under reflux in toluene (3 ml) for 24 h, during which time the water formed was removed by the aid of a Dean-Stark trap. The solvent was evaporated in vacuo and the residue was chromatographed on silica gel to give 3,3a-*trans*-**5** (0.025 g, 27%) from the fraction eluted with hexane-ethyl acetate (5:1 v/v) and 3,3a-*cis*-**5** (0.069 g, 73%) with ethyl acetate. 3,3a-*cis*-**5**: Colorless prisms (diethyl ether-hexane); mp 98 °C; IR (KBr) 1720 cm^{-1}; ^{1}H NMR ($CDCl_3$) δ=1.44 (3H, t, J=7.3 Hz, COOEt), 2.26 (3H, s, *p*-Me), 3.72 (1H, t, $J_{3a\text{-}3}$=$J_{3a\text{-}6a}$=8.6 Hz, 3a-H), 4.12, 4.25 (each 1H, d, J_{gem}=12.7 Hz, $PhCH_2$), 4.42 (2H, m, COOEt), 4.76 (1H, d, $J_{6a\text{-}3a}$=8.6 Hz, 6a-H), 5.11 (1H, d, $J_{3\text{-}3a}$=8.6 Hz, 3-H), 6.21, 7.01 (each 2H, d, J=8.3 Hz, Ar), and 7.3—7.4 (10H, m, Ph); MS *m/z* (rel intensity, %) 469 (M^+, 1), 91 (base peak), and 44 (23). Found: C, 71.37; H, 6.06; N, 8.89%. Calcd for $C_{28}H_{27}N_3O_4$: C, 71.61; H, 5.81; N, 8.95%. 3,3a-*trans*-**5**: Colorless prisms (diethyl ether-hexane); mp 203—204 °C; IR (KBr) 1720 cm^{-1}; ^{1}H NMR ($CDCl_3$) δ= 1.28 (3H, t, J=7.1 Hz, COOEt), 2.43 (3H, s, *p*-Me), 3.89 (1H, d, J_{gem}=12.5 Hz, one of $PhCH_2$), 3.96 (1H, dd, $J_{3a\text{-}6a}$=8.6 and $J_{3a\text{-}3}$=1.3 Hz, 3a-H), 4.1—4.4 (3H, m, COOEt and the other of $PhCH_2$), 4.89 (1H,

br s, 3-H), 5.43 (1H, d, $J_{6a\text{-}3a}$=8.6 Hz, 6a-H), and 7.3—7.5 (14H, m, Ar); MS *m/z* (rel intensity, %) 469 (M^+, 28), 278 (29), and 91 (base peak). Found: C, 71.73; H, 5.77; N, 8.93%. Calcd for $C_{28}H_{27}N_3O_4$: C, 71.61; H, 5.81; N, 8.95%.

General Proceudre for Cycloadditions of Azomethine Imine D with Olefinic Dipolarophiles Leading to 6a—j. The following five procedures were employed for the generation of **D** and its cycloaddition: Method A: A mixture of hydrazine **4** (0.194 g, 1 mmol), paraformaldehyde (1.5—2 mmol), and an olefin (2 mmol) was heated under reflux in toluene (3 ml) with a continuous removal of water by the aid of a Dean-Stark trap. Method B: Similar to Method A, except that the mixture was heated together with Molecular Sieves 4A (1 g). Method C: The same as Method A, except that the mixture was heated in the presence of triethylamine (0.3 g, 3 mmol). Method D: (Phenylthiomethyl)hydrazine **8** (0.316 g, 1 mmol) and an olefin (2 mmol) were heated in the solvent shown in Table 1 in the absence or presence of acetic acid. Method E: Hydrazine **4** (0.194 g, 1 mmol) was treated with aqueous formaldehyde in ethanol (4 ml) at room temperature for 1 h. The ethanol was evaporated in vacuo; then the residue was dissolved in water (25 ml), and extracted with dichloromethane (20 ml×2). The combined extracts were dried over magnesium sulfate and evaporated in vacuo. The residue was heated with an olefin (2 mmol) in the absence or presence of a catalyst.

After the reaction had come to completion, the mixture was evaporated in vacuo and the residue was purified by silica-gel chromatography. The eluent used was as follows: **6a**: ethyl acetate; **6b**: hexane-ethyl acetate (3 : 1 v/v); **6c**: hexane-ethyl acetate (5 : 1 v/v); **6d**: hexane-ethyl acetate (3:1 v/v); **6e**: hexane-ethyl acetate (3 : 1 v/v); **6f** and **6g**: hexane-ethyl acetate (2 : 1 v/v); **6h** and **6i**: hexane-ethyl acetate (3 : 1 v/v); **6j**: hexane-ethyl acetate (4 : 1 v/v).

Ethyl 3,3a-*cis*-2-Benzyl-4,6-dioxo-5-(*p*-tolyl)perhydropyrrolo[3,4-*c*]pyrazole-1-carboxylate (6a): Colorless needles (diethyl ether-hexane); mp 143 °C; IR (KBr) 1700, 1380, and 1180 cm^{-1}; ^1H NMR ($CDCl_3$) δ=1.21 (3H, t, J=7.2 Hz, COOEt), 2.41 (3H, s, *p*-Me), 3.35 (1H, dd, J_{gem}=12.8 and $J_{3\text{-}3a}$=8.7 Hz, one of 3-H), 3.64 (1H, br d, J_{gem}=12.8 Hz, the other of 3-H), 3.69 (1H, d, J_{gem}=12.0 Hz, one of $PhCH_2$), 3.77 (1H, dt, $J_{3a\text{-}3}$=$J_{3a\text{-}6a}$=8.7 and $J_{3a\text{-}3}$=1.5 Hz, 3a-H), 4.00 (1H, d, J_{gem}=12.0 Hz, the other of $PhCH_2$), 4.17 (2H, m, COOEt), 5.40 (1H, d, $J_{6a\text{-}3a}$=8.7 Hz, 6a-H), and 7.2—7.4 (9H, m, Ar); ^{13}C NMR ($CDCl_3$) δ=14.34 (COOEt), 21.24 (*p*-Me), 47.57 (COOEt), 54.82 (3-C), 60.39, 62.78, 63.34 (each $PhCH_2$, 3a-, and 6a-C), 125.67, 128.02, 128.52, 129.01, 129.74, 130.08, 136.06, 139.17 (each Ar), 155.99 (COOEt), 173.66, and 176.58 (each CON); MS *m/z* (rel intensity, %) 393 (M^+, 36), 202 (31), and 91 (base peak). Found: C, 67.08; H, 5.90; N, 10.64%. Calcd for $C_{22}H_{23}N_3O_4$: C, 67.15; H, 5.90; N, 10.68%.

Dimethyl 3,4-*trans*-1-Benzyl-2-ethoxycarbonyl-3,4-pyrazolidinedicarboxylate (6b): Colorless liquid; IR (neat) 1730, 1380, 1340, and 1030 cm^{-1}; ^1H NMR ($CDCl_3$) δ=1.18 (3H, t, J=7.1 Hz, COOEt), 3.15 (1H, dd, J_{gem}=11.7 and $J_{5\text{-}4}$=10.6 Hz, one of 5-H), 3.36 (1H, dd, J_{gem}=11.7 and $J_{5\text{-}4}$=7.3 Hz, the other of 5-H), 3.7—3.8 (2H, m, 4-H and one of $PhCH_2$), 3.75, 3.83 (each 3H, s, COOMe), 4.0—4.2 (3H, m, COOEt and the other of $PhCH_2$), 4.96 (1H, $J_{3\text{-}4}$=8.1 Hz, 3-H), and 7.3—7.5 (5H, m, Ph); ^{13}C NMR ($CDCl_3$) δ=14.38, 48.32 (each COOEt), 52,73, 52.90 (each COOMe), 55.79 (5-H), 61,50, 62.19, 62.66 (each $PhCH_2$, 3-, and 4-C), 127,71, 128.38, 129.76, 136.78 (Ph), 154.90 (COOEt), 170.68, and 171.96 (each COOMe); MS *m/z* (rel intensity %) 350 (M^+, 26), 127 (24), 91 (base peak). Found: C, 58.40; H, 6.42; N, 8.05%. Calcd for $C_{17}H_{22}N_2O_6$: C, 58.27; H, 6.34; N, 8.00%.

Dimethyl 3,4-*cis*-1-Benzyl-2-ethoxycarbonyl-3,4-pyrazolidinedicarboxylate (6c): Colorless liquid; IR (neat) 1740, 1680, 1430, 1380, and 1210 cm^{-1}; ^1H NMR ($CDCl_3$) δ=1.26 (3H, t, J=7.0 Hz, COOEt), 3.27 (1H, dd, J_{gem}=11.0 and $J_{5\text{-}4}$=7.0 Hz, one of 5-H), 3.4—3.6 (2H, m, 4-H and the other of 5-H), 3.70, 3.76 (each 3H, s, COOMe), 3.97, 4.07 (each 1H, d, J_{gem}=12.3 Hz, $PhCH_2$), 4.17 (2H, q, J=7.0 Hz, COOEt), 4.85 (1H, d, $J_{3\text{-}4}$=8.8 Hz, 3-H), and 7.3—7.5 (5H, m, Ph); ^{13}C NMR ($CDCl_3$) δ=14.68, 47.01 (each COOEt), 52.71, 53.87 (each COOMe), 61.53, 62.25, 62.44 (each $PhCH_2$, 3-, and 4-C), 127.97, 128.69, 129.93, 137.11 (each Ph), 154.85 (COOEt), 170.16, and 170.31 (each COOMe); MS *m/z* (rel intensity, %) 350 (M^+, 12), 127 (22), 103 (20), 91 (base peak), and 58 (24). Found: C, 58.04; H, 6.33; N, 8.09%. Calcd for $C_{17}H_{22}N_2O_6$: C, 58.27; H, 6.34; N, 8.00%.

Ethyl 2-Benzyl-5-phenyl-1-pyrazolidinecarboxylate (6d): Colorless prisms (diethyl ether); mp 81—83 °C; IR (KBr) 1675, 1410, 1330, and 1130 cm^{-1}; ^1H NMR ($CDCl_3$) δ=1.19 (3H, t, J=7.1 Hz, COOEt), 2.28 (1H, ddt, J_{gem}=13.0, $J_{4\text{-}5}$=8.2, and $J_{4\text{-}3}$=7.5 Hz, one of 4-H), 2.56 (1H, dddd, J_{gem}=13.0, $J_{4\text{-}5}$=8.2, and $J_{4\text{-}3}$=6.0 and 5.0 Hz, the other of 4-H), 3.0—3.1 (2H, m, 3-H), 3.85 (1H, d, J_{gem}=12.1 Hz, one of $PhCH_2$), 4.0—4.2 (2H, m, COOEt), 4.17 (1H, d, J_{gem}=12.1 Hz, the other of $PhCH_2$), 5.08 (1H, t, $J_{5\text{-}4}$=8.2 Hz, 5-H), and 7.2—7.5 (10H, m, Ph); MS *m/z* (rel intensity, %) 310 (M^+, 5) and 91 (base peak). Found: C, 73.44; H, 7.23; N, 9.11%. Calcd for $C_{19}H_{22}N_2O_2$: C, 73.51; H, 7.16; N, 9.03%.

Ethyl 3a,8a-*cis*-2-Benzyl-1,2,3,3a,4,8a-hexahydroindeno-[1,2-*c*]pyrazole-1-carboxylate (6e): Pale yellow liquid; IR (neat) 1700, 1130, and 750 cm^{-1}; ^1H NMR ($CDCl_3$) δ=1.24 (3H, t, J=7.1 Hz, COOEt), 2.9—3.4 (5H, m, 3-, 3a-, and 4-H), 3.58, 3.81 (each 1H, d, J_{gem}=12.1 Hz, $PhCH_2$), 4.1—4.2 (2H, m, COOEt), 5.73 (1H, d, $J_{8b\text{-}3a}$=6.6 Hz, 8b-H), and 7.1—7.7 (9H, m, Ar); MS *m/z* (rel intensity, %) 322 (M^+, 30), 159 (30), 115 (20), and 91 (base peak). HRMS Found: *m/z* 322.1683. Calcd for $C_{20}H_{22}N_2O_2$: M, 322.1680.

Ethyl 2-Benzyl-5-methoxycarbonyl-1-pyrazolidinecarboxylate (6f) and Ethyl 2-Benzyl-4-methoxycarbonyl-1-pyrazolidinecarboxylate (6g): 6f: Colorless liquid; IR (neat) 1740, 1690, 1420, and 1200 cm^{-1}; ^1H NMR ($CDCl_3$) δ=1.18 (3H, t, J=7.1 Hz, COOEt), 2.3—2.5 (2H, m, 4-H), 2.9—3.2 (2H, m, 3-H), 3.73 (1H, d, J_{gem}=11.0 Hz, one of $PhCH_2$), 3.79 (3H, s, COOMe), 4.0—4.2 (3H, COOEt and the other of $PhCH_2$), 4.53 (1H, t, $J_{5\text{-}4}$=8.2 Hz, 5-H), and 7.2—7.5 (5H, m, Ph); ^{13}C NMR ($CDCl_3$) δ=14.43 (COOEt), 29.79 (4-C), 51.89 (3-C), 52.45 (COOMe), 59.91 (COOEt), 61.32, 61.88 (5-C and $PhCH_2$), 127.54, 128.33, 129.80, 137.38 (each Ph), 154.96 (COOEt), and 172.92 (COOMe); MS *m/z* (rel intensity, %) 292 (M^+, 29), 91 (base peak), and 69 (37). Found: C, 61.40; H, 7.13; N, 9.36%. Calcd for $C_{15}H_{20}N_2O_4$: C, 61.62; H, 6.91; N, 9.58%. **6g**: Colorless liquid; IR (neat) 1740, 1690, 1430, and 1210 cm^{-1}; ^1H NMR ($CDCl_3$) δ=1.20 (3H, t, J=7.1 Hz, COOEt), 3.1—3.3 (3H, m, 3-H and one of 5-H), 3.69 (3H, s, COOMe), 3.81 (2H, s, $PhCH_2$), 3.8—4.0 (2H, m, 4-H and the other of 5-H), 4.11 (2H, m, COOEt), and 7.2—7.5 (5H, m, Ph); ^{13}C NMR ($CDCl_3$) δ=14.56 (COOEt), 43.24 (4-C), 47.33 (5-C), 52.25 (COOMe), 55.16 (3-C), 60.98, 61.64 (COOEt and $PhCH_2$), 127.70, 128.36, 129.69, 136.78 (each Ph), 155.29 (COOEt), and 172.64 (COOMe); MS *m/z* (rel intensity, %) 292 (M^+, 45), 219 (28), 201 (21), 129 (48), 97 (21), 91 (base

peak), and 69 (32). HRMS Found: m/z 292.1403. Calcd for $C_{15}H_{20}N_2O_4$: M, 292.1422.

Ethyl 4,5-*trans*-2-Benzyl-5-methoxycarbonyl-4-methyl-1-pyrazolidinecarboxylate (6h) and Ethyl 4,5-*trans*-2-Benzyl-4-methoxycarbonyl-5-methyl-1-pyrazolidinecarboxylate (6i): **6h:** Colorless liquid; IR (neat) 1740, 1690, 1420, and 1030 cm^{-1}; ^1H NMR ($CDCl_3$) δ=1.16 (3H, t, J=7.0 Hz, COOEt), 1.23 (3H, d, J=6.2 Hz, 4-Me), 2.68 (1H, t, $J_{gem}=J_{3\text{-}4}$=11.4 Hz, one of 3-H), 2.8—3.0 (1H, m, 4-H), 3.14 (1H, dd, J_{gem}=11.4 and $J_{3\text{-}4}$=6.2 Hz, the other of 3-H), 3.75 (1H, d, J_{gem}=12.1 Hz, one of $PhCH_2$), 3.83 (3H, s, COOMe), 4.0—4.1 (3H, m, COOEt and 5-H), 4.19 (1H, d, J_{gem}=12.1 Hz, the other of $PhCH_2$), and 7.2—7.5 (5H, m, Ph); ^{13}C NMR ($CDCl_3$) δ=14.40 (COOEt), 15.67 (4-Me), 38.57 (4-C), 52.51 (COOMe), 59.74 (COOEt), 61.80, 61.88 (3-C and $PhCH_2$), 67.14 (5-C), 127.50, 128.30, 129.83, 137.50 (each Ph), 154.98 (COOEt), and 172.94 (COOMe); MS m/z (rel intensity, %) 306 (M^+, 66), 233 (30), 91 (base peak), and 83 (26). Found: C, 62.79; H, 7.52; N, 9.15%. Calcd for $C_{16}H_{22}N_2O_4$: C, 62.72; H, 7.25; N, 9.14%. **6i:** Colorless liquid; IR (neat) 1740, 1690, 1420, and 1030 cm^{-1}; ^1H NMR ($CDCl_3$) δ=1.22 (3H, t, J=7.1 Hz, COOEt), 1.52 (3H, d, $J_{5\text{-}4}$=6.6 Hz, 5-H), 3.1—3.3 (3H, m, 3- and 4-H), 3.70 (3H, s, COOMe), 3.77, 4.00 (each 1H, d, J_{gem}=12.5 Hz, $PhCH_2$), 4.0—4.2 (2H, m, COOEt), 4.2—4.3 (1H, m, 5-H), and 7.2—7.5 (5H, m, Ph); ^{13}C NMR ($CDCl_3$) δ=14.51 (COOEt), 22.22 (5-Me), 50.88 (3-C), 52.24 (COOMe), 54.63 (4-C), 58.53 (COOEt), 61.55, 62.66 ($PhCH_2$ and 5-C), 127.73, 128.38, 129.74, 136.99 (each Ph), 155.80 (COOEt), and 171.74 (COOMe); MS m/z (rel intensity, %) 306 (M^+, 7), 111 (21), 91 (base peak), and 83 (39). HRMS Found: m/z 306.1586. Calcd for $C_{16}H_{22}N_2O_4$: M, 306.1578.

Ethyl 2-Benzyl-5-butoxy-1-pyrazolidinecarboxylate (6j): Colorless liquid; IR (neat) 1690, 1370, 1330, and 1200 cm^{-1}; ^1H NMR ($CDCl_3$) δ=0.94 (3H, t, J=7.3 Hz, n-Bu), 1.22 (3H, t, J=7.1 Hz, COOEt), 1.3—1.5, 1.5—1.7 (each 2H, m, n-Bu), 2.2—2.3 (2H, m, 4-H), 3.0—3.2 (2H, m, 3-H), 3.52 (1H, dt, J_{gem}=9.5 and J=6.6 Hz, one of n-Bu), 3.65 (1H, dt, J_{gem}=9.5 and J=6.6 Hz, the other of n-Bu), 3.80 (1H, d, J_{gem}=12.1 Hz, one of $PhCH_2$), 4.0—4.2 (2H, m, COOEt), 4.27 (1H, d, J_{gem}=12.1 Hz, the other of $PhCH_2$), 5.53 (1H, dd, $J_{5\text{-}4}$=4.8 and 3.7 Hz, 5-H), and 7.2—7.5 (5H, m, Ph); MS m/z (rel intensity, %) 306 (M^+, 46), 233 (22), 143 (22), 91 (base peak), and 87 (23). HRMS Found: m/z 306.1941. Calcd for $C_{17}H_{26}N_2O_3$: M, 306.1942.

Diethyl 2,5-Dibenzylperhydro-1,2,4,5-tetrazine-1,4-dicarboxylate (7): A mixture of **4** (0.205 g, 1.1 mmol) and paraformaldehyde (0.054 g, 1.8 mmol) was heated under reflux in toluene (4 ml) for 42 h. The solvent was evaporated in vacuo and the residue was washed with hexane to give **7** (0.179 g, 79%): Colorless prisms (diethyl ether-hexane); mp 139—140 °C; IR (KBr) 1680, 1420, 1340, 1290, and 1150 cm^{-1}; ^1H NMR ($CDCl_3$) δ=1.26 (6H, t, J=7.0 Hz, COOEt), 4.08 (4H, br s, $PhCH_2$), 4.20 (4H, q, J=7.0 Hz, COOEt), 4.72 (4H, br s, 3- and 6-H), and 7.2—7.6 (10H, m, Ph); ^{13}C NMR ($CDCl_3$) δ=14.51, 55.04 (each COOEt), 56.28 ($PhCH_2$), 62.14 (3- and 6-C), 127.86, 128.35, 129.74, 135.75 (each Ph), and 155.85 (COOEt); MS m/z (rel intensity, %) 412 (M^+, 6), 279 (24), 250 (33), and 91 (base peak). Found: C, 63.80; H, 6.82; N, 13.47%. Calcd for $C_{22}H_{28}N_4O_4$: C, 64.05; H, 6.86; N, 13.58%.

Ethyl 3-Benzyl-3-(phenylthiomethyl) carbazate (8): Hydrazine **4** (0.194 g, 1 mmol) was treated with aqueous formaldehyde (37% solution) in ethanol (3 ml) for 1 h at room temperature. The ethanol was evaporated in vacuo, the residue was dissolved in water (20 ml), and extracted with dichloromethane (25 ml×2). The combined extracts were dried over magnesium sulfate, and evaporated in vacuo; the residue was then heated with benzenethiol (0.11 g, 1 mmol) under reflux in toluene (3 ml) for 1 h. The toluene was evaporated in vacuo and the residue was chromatographed on silica gel with ethyl acetate to give **8** (0.294 g, 83%): Colorless solid (purified by silica-gel column chromatography); mp 65 °C; IR (KBr) 3300, 1690, 1515, and 1240 cm^{-1}; ^1H NMR ($CDCl_3$) δ=1.13 (3H, t, J=7.1 Hz, COOEt), 3.91 (2H, s, $PhCH_2$), 4.01 (2H, q, J=7.1 Hz, COOEt), 4.55 (2H, s, SCH_2), 6.22 (1H, br s, NH), and 7.1—7.5 (10H, m, Ph); ^{13}C NMR ($CDCl_3$) δ=14.58, 59.82 (each COOEt), 61.30 ($PhCH_2$), 64.31 (SCH_2), 127.12, 127.75, 128.43, 129.32, 129.39, 131.44, 136.00, 136.25 (each Ph), and 155.45 (COOEt); MS m/z (rel intensity, %) 207 (M^+ −109, 10), 109 (38), 91 (base peak), and 65 (30). Found: C, 64.46; H, 6.42; N, 8.75%. Calcd for $C_{17}H_{20}N_2O_2S$: C, 64.52; H, 6.38; N, 8..85%.

Ethyl 3-Benzyl-3-(hydroxymethyl)carbazate (9): Hydrazine **4** (0.194 g, 1 mmol) was treated with aqueous formaldehyde (37% solution) in ethanol (3 ml) for 1 h at room temperature. The ethanol was evaporated in vacuo; the residue was then dissolved in water (20 ml), and extracted with dichloromethadcne (25 ml×2). The combined extracts were dried over magnesium sulfate and evaporated in vacuo to give viscous liquid of **9** (0.22 g, 98%) as an unstable compound, for which only IR and ^1H NMR spectra were recorded: IR (neat) 3300, 1700, 1240, and 740 cm^{-1}; ^1H NMR ($CDCl_3$) δ=1.21 (3H, t, J=7.5 Hz, COOEt), 3.91 (2H, s, $PhCH_2$), 4.0—4.3 (3H, m, COOEt and OH), 4.38 (2H, s, CH_2OH), 4.92 (1H, s, OH), and 7.2—7.5 (6H, m, Ph and NH).

References

1) A. Padwa, "1,3-Dipolar Cycloaddition Chemistry," in "General Heterocyclic Chemistry Series," ed by E. C. Taylor and A. Weissberger, John Wiley & Sons, New York, Chichester, Brisbane, Toronto, Singapore (1984), Chap. 7, pp. 733—814.

2) a) W. Oppolzer, *Tetrahedron Lett.*, **1970**, 2199 and 3091; b) W. Oppolzer, *ibid.*, **1972**, 1707; c) J. W. Lown and B. E. Landberg, *Can. J. Chem.*, **53**, 3782 (1975).

3) H. Ogura, K. Kubo, Y. Watanabe, and T. Itoh, *Chem. Pharm. Bull.*, **21**, 2026 (1973); M. K. Saxena, M. N. Gudi, and M. V. George, *Tetrahedron*, **29**, 101 (1973); R. Grigg, J. Kemp, and N. Thompson, *Tetrahedron Lett.*, **1978**, 2827.

4) K. D. Hesse, *Liebigs Ann. Chem.*, **743**, 50 (1971); G, Le Fevre, S. Sinbabdhit, and J. Hamelin, *Tetrahedron*, **35**, 1821 (1979); R. M. Wilson, J. W. Rekers, A. B. Packard, and R. C. Elder, *J. Am. Chem. Soc.*, **102**, 1633 (1980).

5) R. Grigg, *Chem. Soc. Rev.*, **16**, 89 (1987).

6) Imines of α-amino esters were sufficiently activated by the action with lithium bromide and triethylamine (O. Tsuge, S. Kanemasa, and M. Yoshioka, *J. Org. Chem.*, **53**, 1384 (1989)).

7) R. B. Woodward and R. Hoffmann, *Angew. Chem., Int. Ed. Engl.*, **8**, 781 (1969).

Synthesis of 2-Amino-2-deoxy-α-D-altrofuranoside Derivatives from 2,3-*O*-Isopropylidene-D-glyceraldehyde via Bicyclic β-Lactam Intermediates

Masao SHIOZAKI,* Noboru ISHIDA, and Sadao SATO†
New Lead Research Laboratories, Sankyo Co., Ltd., Hiromachi 1-2-58, Shinagawa-ku, Tokyo 140
†Analytical and Metabolic Research Laboratories, Sankyo Co., Ltd.,
Hiromachi 1-2-58, Shinagawa-ku, Tokyo 140
(Received May 10, 1989)

A bicyclic β-lactam (**4**), obtained from 2,3-*O*-isopropylidene-D-glyceraldehyde in 3 steps, was converted to methyl 2-benzamido-2-deoxy-5,6-*O*-isopropylidene-3-*O*-(3-chlorobenzoyl)-α-D-altrofuranoside (**24**) through an additional 8 steps by utilizing the β-lactam nitrogen via the oxidative decarboxylation of diacyl peroxide (**23**). Additionally, it was shown that the bicyclic β-lactam intermediate is a suitable precursor for 2-amino-3-(branched-chain)-2-deoxy-D-furanoside derivatives.

Many effective approaches to the synthesis of amino sugars, which are widely distributed in a variety of glycoconjugates, and which also play many important roles in living bodies, have been developed, and considerable progress has been achieved.[1] However, the synthesis of 2-amino-2-deoxy-D-altrofuranoside derivatives has not been reported, except for the conversion of D-glucose[2] or D-arabinose[3] to 2-amino-2-deoxy-D-altropyranoside analogs. We were interested in developing an alternative approach without using a sugar source, such as D-glucose or D-arabinose, for synthesizing a 2-amino-2-deoxy-D-altrofuranoside derivative. For this purpose, it has been predicted that it is suitable to use the bicyclic β-lactam previously reported[4] to introduce the 2-amino group of 2-amino-2-deoxy-D-altrofuranoside. We thus tried to synthesize a 2-amino-2-deoxy-D-altrofuranoside derivative using this approach and, as a result, could obtain that derivative from 2,3-*O*-isopropylidene-D-glyceraldehyde via bicyclic β-lactam intermediates, even though it was low in total yield. Still, this method via bicyclic 2-azetidinone offers a potential for the syntheses of various stereoisomers of amino sugars by choosing the starting epoxy carboxylic acid, such as **1a** or **1'a**. This method may also provide a route for various stereoisomers of 3-(branched-chain)-2-amino sugars in a stereo-controlled manner. We would like to describe a new procedure for 2-aminoaltrofuranoside analogs.

The treatment of 2,3-*O*-isopropylidene-D-glyceraldehyde[5] in dimethyl sulfoxide (DMSO) with dimethylthetin anion[6] under nitrogen at room temperature for 20 h gave a 2.6:1 mixture of (2*S*,3*R*,4*R*)- and (2*R*,3*S*,4*R*)-2,3-epoxy-4,5-isopropylidenedioxypen-

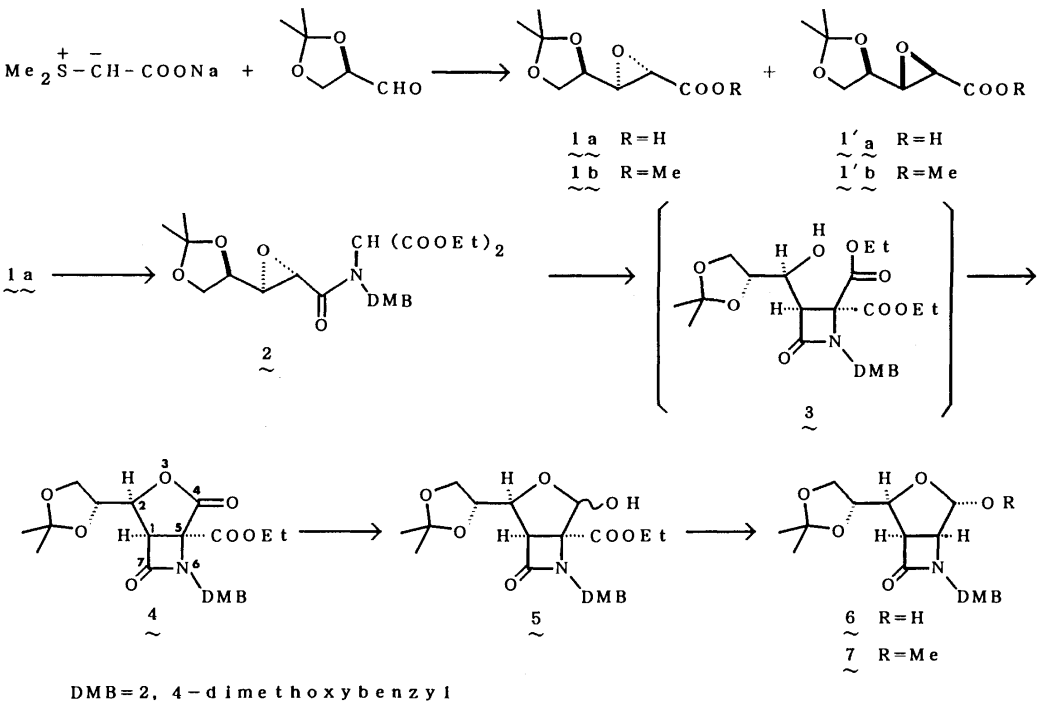

Scheme 1.

tanoic acid, **1a** and **1'a** in 77% yield (Scheme 1). The ratio of this mixture was determined from a separation of the corresponding methyl esters, **1b**[7] (42%) and **1'b** (16%). Saponification of the methyl ester (**1b**) gave acid **1a**, which was identical with an authentic sample.[8]

Treatment of the optically pure acid **1a** and diethyl 2-(*N*-2,4-dimethoxybenzylamino)malonate[9] with dicyclohexylcarbodiimide (DCC) gave the amide **2**. When a mixture of **1a** and **1'a** was used without separation, **2** was obtained in 22% yield from **1** after chromatographic purification. However, a small amount of isomer (an amide resulting from **1'a**) was an occasional contaminate.[10] Then, an azeotropic treatment of **2** in benzene with a catalytic amount of 1,8-diazabicyclo[5.4.0]undec-7-ene (DBU) to remove the ethanol released during the reaction afforded a bicyclic β-lactam **4** via **3**. If the ethanol released was not removed, the reaction did not complete.

The reduction of **4** with sodium borohydride in methanol containing a catalytic amount of silica gel[11] gave an anomeric mixture of hemiacetal **5**. During this reaction, when the methanol solution is not treated quickly, only esterification by methanol occurs to give the corresponding methyl ester quantitatively; thus, **3** is easily obtained by allowing the ethanol solution of **4** to stand together with a catalytic amount of DBU. However, both **3** and the methyl ester are converted into **4** in good yield by an azeotropic removal of the liberated ethanol or methanol using a catalytic amount of DBU in benzene. The conversion of compound **5** to **6** was achieved by saponification of the ester and successive decarboxylation. The anomeric proton of compound **6** was almost a singlet (by D_2O addition) without only coupling with a neighboring proton on the β-lactam ring. Therefore, the configuration of the anomeric position of **6** must be the *S* configuration. This configuration was also confirmed from a series of experiments (**6**→**7**→**8**→**10**→**7**) (Scheme 2). The glycosidation of **6** with methyl iodide and silver oxide[12] in *N*,*N*-dimethylformamide (DMF) gave **7**. The treatment of crude **7** with 2 equivalents of 2 M hydrochloric acid (1 M=1 mol dm^{-3}) in methanol solution at reflux temperature gave a single product **8**. The structure of **8** was confirmed by an analysis (400 MHz ^1H NMR) of compound **9**. No coupling was observed between the anomeric proton and its neighboring proton in compound **9**. Therefore, it has been elucidated by the Karplus equation that the dihedral angle of these two protons should approach 90°, and that they exist in a trans relationship to each other. As a result, the configuration of the anomeric position of **9** is *S*. A treatment of **8** with methylmagnesium bromide[13]

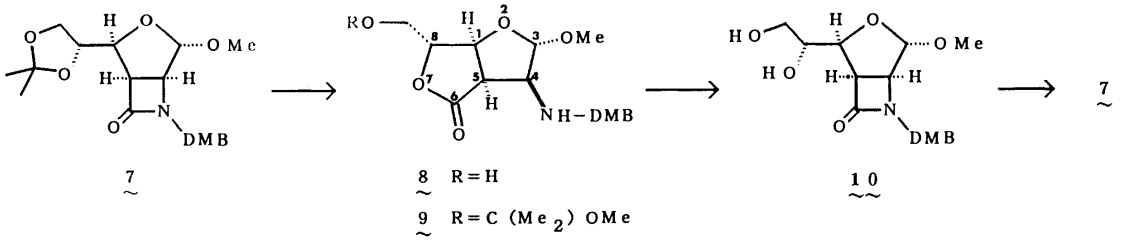

Scheme 2.

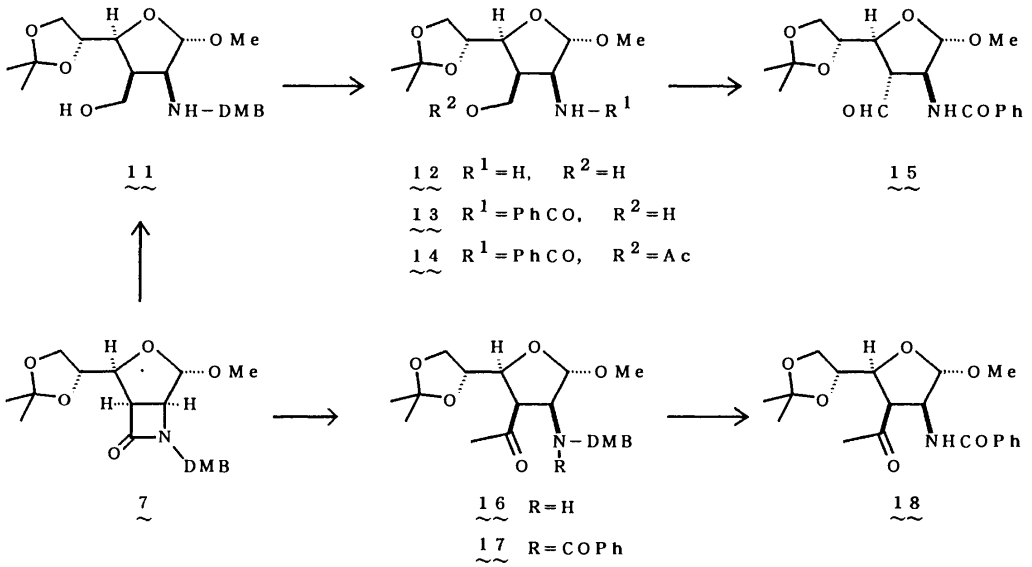

Scheme 3.

gave a β-lactam **10**, which was reprotected with 2,2-dimethoxypropane in DMF containing pyridinium *p*-toluenesulphonate as a catalyst to reproduce **7**. Consequently, the configuration of **7** is (1*R*,2*S*,4*S*,5*S*).

We need to introduce an oxygen atom at the carbon 3 position for the conversion of compound **7** to an altrosamine or mannosamine derivative. At first, we attempted a Baeyer-Villiger oxidation of the C-3 formyl or C-3 acetyl groups to prepare altrosamine and mannosamine analogs.

The C_3-formyl compound **15** was prepared as follows (Scheme 3). The treatment of **7** with lithium aluminum hydride in tetrahydrofuran (THF) at 5 °C gave a C-3 hydroxymethyl compound **11**. Hydrogenolysis of **11** in ethanol by the use of 10% Pd on carbon as a catalyst gave an amino alcohol **12**, which was further converted to a benzamide **13**. Treatment of **13** with pyridinium chlorochromate (PCC)-sodium acetate gave a C_3-formyl compound **15**. The configuration of **15** was elucidated from ^{1}H NMR. Each coupling constant of $J_{1,2}$, $J_{2,3}$, and $J_{3,4}$ was almost zero. This means that the configuration of protons at C_1, C_2, C_3, and C_4 was trans to each other, and that an inversion of the formyl group occurred at C_3.

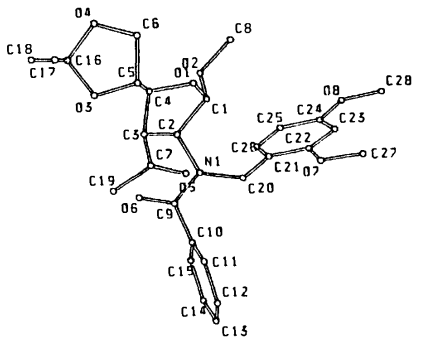

Fig. 1. Molecular structure and atomic numbering of **17**.

The C_3-acetyl compound **18** was prepared as follows. A treatment of **7** with methyllithium gave C_3-acetyl compounds **16**. This type of reaction with *N*,*N*-disubstituted amides or a single β-lactam with alkyllithium[14] is already known. However, this is the first example, as far as we know, for the reaction of β-lactam fused with a furanoside ring with alkyllithium; this reaction provides a new method for the synthesis of 2-amino-2,3-dideoxy-3-acyl-D-furanoside. Benzoylation of **16** with benzoyl chloride and triethylamine gave **17** as a main product. There was a possibility to epimerize the configuration at the C_3-acetyl group of **16** by a strong base (methyllithium) treatment. However, an X-ray crystallographic analysis of the major product **17** showed that the epimerization of the C_3-acetyl group did not occur (Fig. 1). A deprotection of the 2,4-dimethoxybenzyl group of **17** with cerium(IV) ammonium nitrate (CAN)[15] in acetone-water (1 : 1) gave **18**.

Baeyer-Villiger oxidation of both **15** and **18** with 3-chloroperbenzoic acid in chloroform failed to yield altrosamine and mannosamine analogs, respectively. We therefore tried another route to synthesize an altrosamine analog (Scheme 4). Deprotection of the 2,4-dimethoxybenzyl group of **7** with potassium persulphate-potassium hydrogenphosphate[16] in acetonitrile-water at 78 °C under argon afforded **19**. Benzoylation of **19** yielded **20**. Treatment of **20** in methanol containing DBU as a catalyst at reflux temperature gave **21**. The coupling constant between C_2-H and C_3-H of **21** changed to almost zero. This reveals that epimerization occurred at the C_3 position. This ester **21** was saponified with 1 M NaOH in methanol to give **22**, and X-ray crystallographic analysis further con-

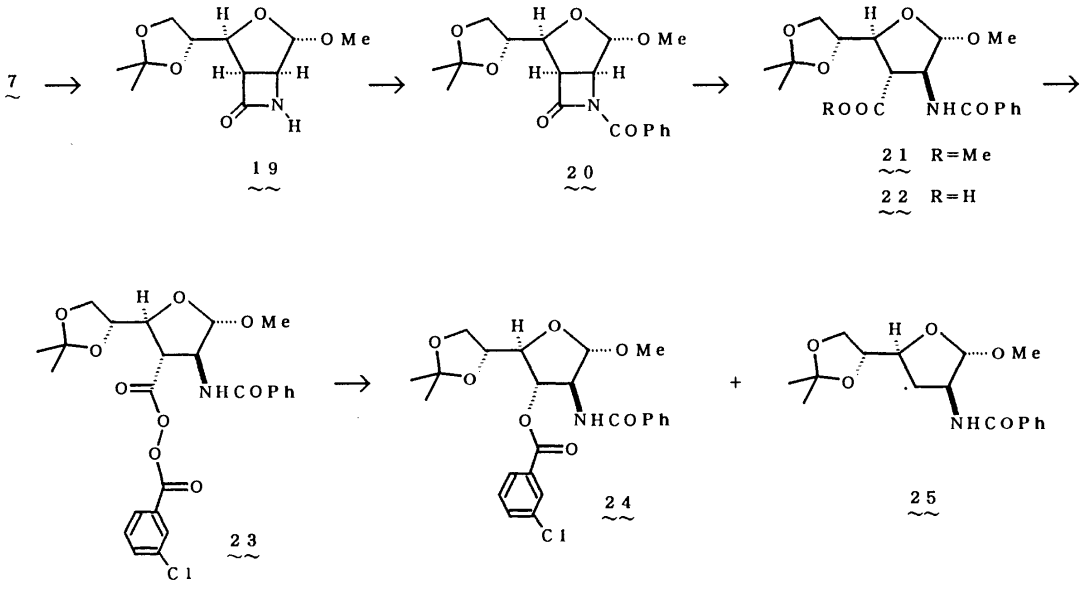

Scheme 4.

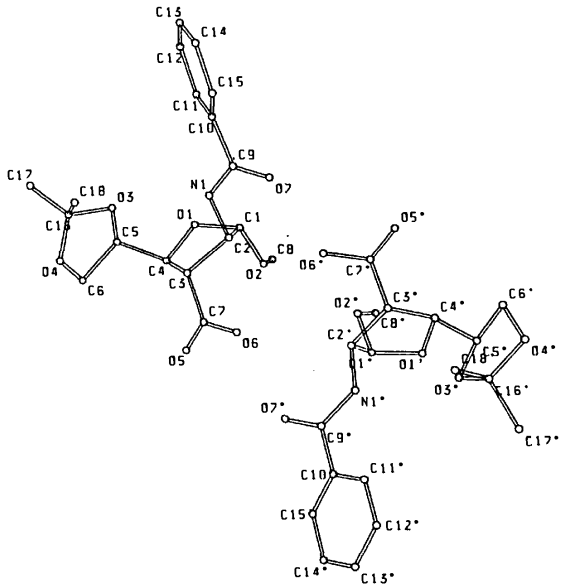

Fig. 2. Molecular structures of the two crystallographically independent molecules in the asymmetric unit, together with the numbering scheme of **22**.

firmed the epimerization (Fig. 2). The reaction of **22** with 3-chloroperbenzoic acid by using DCC as a condensing reagent gave a diacyl peroxide **23**, which was a surprisingly stable compound at room temperature. The obtained **23** was refluxed in octane to give rise to a rearrangent.[17] As a result, an altrosamine analog **24** and a decarboxylated compound **25** were obtained in 32 and 35% yield, respectively. This reaction did not occur in carbon tetrachloride at reflux temperature. The C_3-H chemical shift of **24** shows δ 5.38 shifted from 3.21 of **23**, 3.01 of **22** and 2.91 of **21**, and the coupling constants, $J_{1,2}$, $J_{2,3}$, and $J_{3,4}$, of compound **24** were 0, 0, and 2.2 Hz, respectively. This reveals that an oxygen atom attached directly to the C_3 carbon, and four substituted groups on the tetrahydrofuran ring of **24**, were alternately arranged in a trans relationship.[18] Thus, we could obtain stereoselectively an altrosamine analog **24** from 2,3-*O*-isopropylidene-D-glyceraldehyde via an bicyclic β-lactam intermediate **7** in 12 steps.

Experimental

Melting points were determined on a Yanagimoto micromelting point apparatus and were uncorrected. Optical rotations were obtained by the use of a Perkin-Elmer 241 polarimeter. ^{1}H NMR spectra were recorded using the following spectrometers: at 60 MHz with a Varian T-60, at 270 MHz with a JEOL JNN-270, and at 400 MHz with a JEOL JNN-GX 400. Tetramethylsilane was used as an internal standard (δ value). The IR absorption spectra were determined on a Jasco IR A-2 spectrophotometer. Mass spectra were obtained on a JMS-01SG mass spectrometer. Preparative TLC was performed on silica-gel plates (Merck 60 PF_{245}), and column chromatography was carried out on columns packed with Merck silica-gel 60 (230—400 mesh ASTM) using a slightly increased pressure (1.2 atm) for elution. Elemental analyses were performed by the Analytical Center of the Analytical and Metabolic Research Laboratories, Sankyo Co., Ltd.

A Mixture of (2*S*,3*R*,4*R*)- and (2*R*,3*S*,4*R*)-2,3-Epoxy-4,5-isopropylidenedioxypentanoic Acid, 1a and 1'a. To a solution of dimethylthetin bromide (4.02 g, 20 mmol) in DMSO (20 ml) was added NaH (55% mineral oil dispersion, 2.58 g, 60 mmol) with stirring under nitrogen at 15 °C. The reaction mixture was stirred for 1.5 h at room temperature to produce a suspension of the dimethylthetin anion. To this suspension was added a 2 : 1 mixture of (*R*)-2,2-dimethyl-1,3-dioxolane-4-carbaldehyde and acetic acid (2.14 g, aldehyde=40/3 mmol, acetic acid=20/3 mmol)[5] in DMSO (2 ml) with stirring at ice-cooling temperature. Then, the mixture was stirred for 20 h at room temperature, and poured into ice water (200 ml) with stirring. The mixture was washed twice with ether, and the aqueous layer was acidified with 1 M HCl (50 ml). The whole was then extracted with EtOAc. The organic layer was washed with water and brine, dried over $MgSO_4$, and concentrated in vacuo to give an oily mixture (1.88 g, 77% from the dioxolane) of acids.

Determination of the Ratio, 1a and 1'a. The mixture obtained above was esterified with diazomethane, and the oily mixture was separated to **1b** (42%) and **1'b** (16%) by silica-gel column (**1b** : **1'b**=2.6 : 1). ^{1}H NMR of **1b**: (60 MHz, $CDCl_3$) δ=1.35 (3H, s), 1.44 (3H, s), 3.20—3.35 (1H, m, C_3-H), 3.41 (1H, d, J=2 Hz, C_2-H), 3.79 (3H, s), 3.8—4.3 (3H, m, C_4-H, C_5-H_2). ^{1}H NMR of **1'b**: ($CDCl_3$) δ=1.35 (3H, s), 1.40 (3H, s), 3.20—3.35 (1H, m, C_3-H), 3.47 (1H, d, J=2 Hz, C_2-H), 3.79 (3H, s), 3.8—4.3 (3H, m, C_4-H, C_5-H_2).

(2*S*,3*R*,4*R*)- 2,3-Epoxy-4,5-isopropylidenedioxypentanoic Acid (1a). To a solution of methyl ester **1b** (72 mg, 0.356 mmol) in EtOH (1 ml) was added 0.5 ml of 1 M NaOH. The mixture was allowed to stand at room temperature overnight, diluted with water, and washed with ether. The aqueous layer was acidified with 1 M HCl (0.5 ml), extracted with EtOAc, washed with water and brine, and dried over $MgSO_4$. The concentration of EtOAc gave 57 mg (91%) of **1a**. IR (film): ν_{max} 3600—2500, 1735 cm^{-1}. 60 MHz ^{1}H NMR ($CDCl_3$) δ=1.37 (3H, s), 1.46 (3H, s), 3.31 (1H, m, C_3-H), 3.43 (1H, d, J=1.5 Hz, C_2-H), 3.8—4.3 (3H, m), 8.0 (1H, bs).

Diethyl 2-[*N*-(2,4-Dimethoxybenzyl)-2,3-epoxy-4,5-isopropylidenedioxypentanamido]malonate (2). To a solution of compound **1a** (42 mg, 0.223 mmol) and *N*-bis(ethoxycarbonyl)methyl-*N*-2,4-dimethoxybenzylamine (80 mg, 0.246 mmol) in CH_2Cl_2 (1 ml) was added DCC (50 mg, 0.242 mmol) at room temperature with stirring. After 30 min, the reaction mixture was filtered to remove a precipitate which was washed with a small volume of CH_2Cl_2. The filtrate was purified on a preparative silica-gel TLC plate. Development with cyclohexane: EtOAc (1 : 1) gave 50 mg (45%) of **2** at the R_f=0.36. IR (film): ν_{max} 1750 (shoulder), 1740, 1668, 1610, 1587 cm^{-1}. 60 MHz ^{1}H NMR ($CDCl_3$) δ=1.18 (3H, t, J=7 Hz), 1.20 (3H, t, J=7 Hz), 1.31 (6H, bs, CH_3×2), 3.27 (1H, m, C_3-H), 3.7—4.4 (14H, m, containing two 3H singlets at δ 3.79 and 3.81, respectively), 4.73 (2H, bs, benzyl), 5.17 (1H, s, NCH), 6.37—6.57 (2H, m), 7.13—7.30 (1H, m). MS m/z 495 (M^+), 449, 434, 394, 364, 348, 292, 166, 151, 121, 101. Found: C, 57.89; H, 6.80; N, 2.91%. Calcd for $C_{24}H_{33}NO_{10}$: C, 58.17; H, 6.71; N, 2.83%.

Ethyl (1*R*,2*S*,5*R*)-6-(2,4-Dimethoxybenzyl)-4,7-dioxo-2-[(1*R*)-1,2-isopropylidenedioxyethyl]-3-oxa-6-azabicyclo-[3.2.0]heptane-5-carboxylate (4). a) Benzene (10 ml) was distilled azeotropically to remove H_2O from a solution of **2** (496 mg, 1 mmol) in benzene (50 ml); then, DBU (40 mg) was added to this solution, and the distillation was continued gradually until the end of the liberation of ethanol. After cooling the reaction mixture was diluted with EtOAc, washed with dil. HCl, H_2O, aq. $NaHCO_3$, and brine, dried over $MgSO_4$, filtered, and concentrated in vacuo to give an oily mixture. A chromatographic analysis of the mixture was quickly performed using a silica-gel (20 g) column. Elution with EtOAc–cyclohexane (1 : 1) gave **4** (235 mg, 52%) as a gum, a by-product (58 mg), and **3** (44 mg, 10%). b) The same treatment of **3** as described above gave **4** quantitatively. IR (film): ν_{max} 1770, 1740 (shoulder), 1613, 1590 cm^{-1}. 60 MHz ^1H NMR ($CDCl_3$) δ=1.25 (3H, t, J=7 Hz), 1.36 (3H, s), 1.43 (3H, s), 3.80 (6H, s), 3.9—4.6 (9H, m), 6.3—6.5 (2H, m), 7.15 (1H, d, J=9 Hz). MS m/z 450, 449 (M^+), 434, 348, 217, 193, 192, 151, 121, 101, 91, 43. Found: m/z 449.16834. Calcd for $C_{22}H_{27}NO_9$: M, 449.16854. c) A mixture of **1a** and **1'a**, treated successively as described above, gave a mixture of **4** (23% overall yield) and **i** (cf. Scheme 5),[10] which was separated by silica-gel column.

Diethyl 3-[(1*S*,2*R*)-1-Hydroxy-2,3-isopropylidenedioxypropyl]-2-oxoazetidine-4,4-dicarboxylate (3). A solution of **4** (100 mg) in EtOH (10 ml) containing DBU (2 mg) was stirred at 0 °C for 5 min. The concentration and silica-gel column chromatography as described above gave **3**, quantitatively. IR (film): ν_{max} 3440, 1750, 1613, 1588, 1510 cm^{-1}. 60 MHz ^1H NMR ($CDCl_3$) δ=1.09 (3H, t, J=7 Hz), 1.27 (3H, t, J=7 Hz), 1.39 (3H, s), 1.41 (3H, s), 2.5 (1H, broad, OH), 3.6—4.7 (17H, m, containing 6H singlet at δ 3.78), 6.3—6.5 (2H, m), 7.11 (1H, d, J=9 Hz). Found: C, 58.26; H, 6.50; N, 2.72%. Calcd for $C_{24}H_{33}NO_{10}$: C, 58.17; H, 6.71; N, 2.83%. MS m/z 495 (M^+), 449, 434, 394, 364, 348, 151. Found: m/z 495.20805. Calcd for $C_{24}H_{33}NO_{10}$: M, 495.21035.

A Mixture of Ethyl (1*R*,2*S*,4*R*,5*R*)- and (1*R*,2*S*,4*S*,5*R*)-6-(2,4-Dimethoxybenzyl)-4-hydroxy-2-[(1*R*)-1,2-isopropylidenedioxyethyl]-3-oxa-7-oxo-6-azabicyclo[3.2.0]heptane-5-carboxylate (5). To a solution of compound **4** (3.58 g) in MeOH (80 ml) was added a silica gel powder (50 mg)[10] and then $NaBH_4$ (650 mg) at −40 °C under nitrogen with stirring. After 15 min, the excess $NaBH_4$ was gradually quenched with AcOH (2.5 ml). The reaction mixture was diluted with EtOAc, washed with aq. $NaHCO_3$ and brine, dried over $MgSO_4$, filtered, and concentrated to give a hemiacetal **5**. Purification of crude **5** by silica-gel column chromatography (developed with cyclohexane : EtOAc=1 : 1) gave pure **5** (3.51 g, 98%) as a gummy anomeric mixture. IR (film): ν_{max} 3380, 1760 (shoulder), 1750—1730, 1610, 1588 cm^{-1}. 60 MHz ^1H NMR ($CDCl_3$) δ=1.50 (3H, t, J=7 Hz), 1.37 (3H, s), 1.40 (3H, s), 1.8 (1H, broad, OH), 3.6—4.6 (15H, m, containing 6H singlet at δ 3.80), 5.00 (1H, d, J=3.5 Hz, changed to a singlet on addition of D_2O), 6.3—6.6 (2H, m), 7.15 (1H, d, J=9 Hz). Found: C, 58.95; H, 6.74; N, 3.28%. Calcd for $C_{22}H_{29}NO_9$: C, 58.53; H, 6.47; N, 3.10%. In this reaction, the corresponding methyl ester of **3** was obtained quantitatively on occasion. However, the same treatment of this compound, as described above in the formation of **4** from **3**, regenerated **4** (94%).

(1*R*,2*S*,4*S*,5*S*)-6-(2,4-Dimethoxybenzyl)-4-hydroxy-2-[(1*R*)-1,2-isopropylidenedioxyethyl]-3-oxa-6-azabicyclo-[3.2.0]heptan-7-one (6). A solution of compound **5** (3.87 g) in pyridine (40 ml), water (2 ml) and DBU (400 mg) was refluxed for 45 min, and concentrated in vacuo to give a crude oily mixture for chromatography by silica-gel column. Elution with cyclohexane : EtOAc (1 : 2) gave **6** (2.59 g, 79%), mp 172—173 °C (needles from EtOAc); IR (Nujol): ν_{max} 3320, 1715, 1612, 1590 cm^{-1}. 60 MHz ^1H NMR ($CDCl_3$) δ=1.36 (3H, s), 1.42 (3H, s), 3.10 (1H, d, J=2 Hz, OH, D_2O exchangeable), 3.4—4.6 (14H, m, containing two 3H singlets at δ 3.80 and 3.82), 5.17 (1H, d, J=2 Hz, changed to a singlet on addition of D_2O), 6.3—6.6 (2H, m), 7.12 (1H, d, J=9 Hz). $[\alpha]_D^{24}$ −10.5° (c 1.61, $CHCl_3$). MS m/z 379 (M^+), 364, 321, 279, 250, 193, 166, 151, 121, 101. Found: C, 59.86; H, 6.56; N, 3.72%. Calcd for $C_{19}H_{25}NO_7$: C, 60.14; H, 6.64; N, 3.69%.

(1*R*,2*S*,4*S*,5*S*)-6-(2,4-Dimethoxybenzyl)-2-[(1*R*)-1,2-isopropylidenedioxyethyl]-4-methoxy-3-oxa-6-azabicyclo-[3.2.0]heptan-7-one (7). To a solution of compound **6** (379.4 mg, 1.0 mmol) in DMF (5 ml) and methyl iodide (5 ml) was added Ag_2O (700 mg) with stirring at room temperature. After stirring for 4 h the reaction mixture was diluted with EtOAc, and filtered. The filtrate was washed with water and brine, dried over $MgSO_4$, and concentrated in vacuo to give a crude mixture for chromatography by silica-gel column. Elution with cyclohexane : EtOAc (1 : 1) gave a gummy **7** (340 mg, 86%). MS m/z 393 (M^+), 378 (M^+−15), 362, 335, 264, 193, 151, 121, 101, 43. IR (film): ν_{max} 1748, 1610, 1588 cm^{-1}. 60 MHz ^1H NMR ($CDCl_3$) δ=1.38 (3H, s), 1.43 (3H, s), 3.29 (3H, s), 3.6—4.6 (14H, m, containing 6H singlet at δ 3.83), 4.69 (1H, s, C_1-H), 6.35—6.60 (2H, m), 7.15 (1H, d, J=8.5 Hz).

(1*S*,3*S*,4*S*,5*R*,8*R*)-4-(2,4-Dimethoxybenzylamino)-8-hydroxymethyl-3-methoxy-2,7-dioxabicyclo[3.3.0]octan-6-one (8). A solution of **7** (67 mg) in MeOH (2 ml) and 1 ml of 2 M HCl solution in MeOH was refluxed for 1.5 h and concentrated in vacuo. The residue was dissolved in CH_2Cl_2 (4 ml). $NaHCO_3$ (0.2 g) was added and the mixture was stirred for 30 min. After filtration, the solution was concentrated and the residue was subjected to chromatography by silica-gel column. Elution with EtOAc gave **8** (47 mg, 78%) as a thick oil and an unknown solid (5 mg) having a lower R_f value. IR (film): ν_{max} 3500—3200, 1760 (broad), 1612, 1588 cm^{-1}. 60 MHz ^1H NMR ($CDCl_3$) δ=2.8 (2H, broad, OH and NH, D_2O exchangeable), 3.2—3.6 (5H, m, containing a 3H singlet at δ 3.33), 3.70—3.85 (10H, m), 4.4—4.9 (3H, m, containing a 1H singlet at δ 4.87), 6.3—6.5 (2H, m), 7.11 (1H, d, J=9 Hz). MS m/z 354 (M^++1), 353, 352, 322, 293, 262, 218, 166, 151, 121.

(1*S*,3*S*,4*S*,5*R*,8*R*)-4-(2,4-Dimethoxybenzylamino)-3-methoxy-8-(1-methoxy-1-methylethoxy)methyl-2,7-dioxabicyclo[3.3.0]octan-6-one (9). A solution of **8** (20 mg) in DMF (0.5 ml) and 2,2-dimethoxypropane (1 ml) containing toluene-4-sulfonic acid monohydrate (5 mg) was refluxed for 1.5 h. Concentration and preparative chromatography on a silica-gel plate (developed with cyclohexane–EtOAc=1 : 1) gave 15 mg of **9** (63%) as a gum. IR (film): ν_{max} 1763, 1612, 1588 cm^{-1}. MS m/z 426 (M^++1), 394, 352, 323, 293, 275, 204, 166, 151, 121, 91, 73, 43. 400 MHz ^1H NMR ($CDCl_3$) δ=1.282 (3H, s), 1.299 (3H, s), 1.920 (1H, bs, NH), 3.159 (3H, s), 3.365 (3H, s), 3.365 (1H, dd, J=8—9, 6—7 Hz, C_5-H), 3.469 (1H, dd, J=8.8, 1.0 Hz, C_4-H), 3.520 (1H, dd, J=10.7, 1.9 Hz, C_8-CH), 3.734 (1H, dd, J=10.7, 2.4 Hz, C_8-CH), 3.781 (3H, s), 3.826 (3H, s), 3.700, 3.867 (2H, AB-q, J=13.6

Hz, NCH_2Ar), 4.680 (1H, t, J=1.9—2.4 Hz, C_8-H), 4.715 (1H, d, J=6.8 Hz, C_1-H), 4.896 (1H, s, C_3-H), 6.428 (1H, dd, J=2.4, 8.3 Hz), 6.450 (1H, d, J=2.4 Hz), 7.126 (1H, d, J=8.3 Hz).

(1*R*,2*S*,4*S*,5*S*)-2-[(1*R*)-1,2-Dihydroxyethyl]-6-(2,4-dimethoxybenzyl)-4-methoxy-3-oxa-6-azabicylo[3.2.0]heptan-7-one (10). To a solution of **8** (54 mg, 0.153 mmol) in THF (4 ml) was added 0.6 ml of a 1 M solution of MeMgBr in THF with stirring under nitrogen at −78 °C and then another 1 ml of the same Grignard reagent. After 30 min the reaction mixture was quenched with 1 M HCl (1.6 ml) and extracted with EtOAc. The organic layer was washed with sat. $NaHCO_3$ and brine, dried over $MgSO_4$, and concentrated in vacuo to give an oily mixture, which was subjected to chromatography by silica-gel column. Elution with EtOAc gave recovered **8** (9 mg, 17%) and elution with 10% MeOH in EtOAc gave **10** (36 mg, 67%), which was employed for the next reaction.

(1*R*,2*S*,4*S*,5*S*)-6-(2,4-Dimethoxybenzyl)-2-[(1*R*)-(1,2-isopropylidenedioxyethyl]-4-methoxy-3-oxa-6-azabicyclo-[3.2.0]heptan-7-one (7). A solution of **10** (33 mg) and pyridinium *p*-toluenesulfonate (1 mg) in DMF (0.3 ml) and 2,2-dimethoxypropane (0.6 ml) was stirred for 18 h at room temperature. The reaction mixture was concentrated in vacuo, and subjected to chromatography by silica-gel column. Elution with cyclohexane : EtOAc (1 : 1) gave 34 mg of **7** (92%).

Methyl 2,3-Dideoxy-2-(2,4-dimethoxybenzylamino)-3-hydroxymethyl-5,6-*O*-isopropylidene-α-D-mannofuranoside (11). To a solution of β-lactam **7** (200 mg) in THF (4 ml) was added $LiAlH_4$ (60 mg) at 5 °C with stirring. The reaction mixture was quenched with acetic acid, diluted with EtOAc, washed with sat. $NaHCO_3$ and brine, and dried over $MgSO_4$. After filtration, the solvent was concentrated in vacuo, and the residual oil was subjected to chromatography by silica-gel column. Elution with cyclohexane : EtOAc (1 : 4) gave 178 mg of **11** in 88% yield. 270 MHz ^{1}H NMR ($CDCl_3$) δ=1.35 (3H, s), 1.40 (3H, s), 2.67 (1H, quintuplet, J=6.5 Hz, C_3-H), 3.31 (1H, dd, J=2.6, 6.5 Hz, C_2-H), 3.32 (3H, s, C_1-OMe), 3.72, 3.73 (2H, AB-q, J=12.8 Hz, N-CH_2Ar), 3.80 (3H, s), 3.82 (3H, s), 3.88—4.03 (4H, m), 4.11—4.24 (2H, m), 4.77 (1H, d, J=2.6 Hz, C_1-H), 6.42—6.46 (2H, m), 7.11 (1H, d, J=8.4 Hz). IR (film): ν_{max} 3500—3300, 1610, 1588 cm^{-1}. MS m/z 397 (M^+), 382, 339, 306, 236, 166, 151, 121. Found: m/z 397.20715; Calcd for $C_{20}H_{31}NO_7$: 397.20995.

Methyl 2-Amino-2,3-dideoxy-3-hydroxymethyl-5,6-*O*-isopropylidene-α-D-mannofuranoside (12). A solution of **11** (143 mg) in EtOH (8 ml) was hydrogenolyzed on 10% Pd on charcoal for 5 h with stirring under hydrogen. After filtration, the reaction mixture was concentrated and subjected to chromatography by silica-gel (1.0 g) column. Elution with cyclohexane : ethyl acetate (1 : 1) to remove 2,4-dimethoxytoluene and then with methanol : ethyl acetate (1 : 9) gave 43 mg of **12** (48.3%) as a gum. 270 MHz ^{1}H NMR ($CDCl_3$) δ=1.37 (3H, s), 1.43 (3H, s), 1.90 (3H, bs, D_2O exchangeable, OH and NH_2), 2.68 (1H, quintuplet, J=6.5 Hz, C_3-H), 3.34 (3H, s, C_1-OCH_3), 3.52 (1H, dd, J=1.7, 6.4 Hz, C_2-H), 3.91—4.00 (3H, m), 4.05 (1H, dd, J=7.3, 9.5 Hz), 4.18 (1H, dd, J=6.1, 8.6 Hz), 4.31 (1H, dt, J=9.5, 5.7 Hz), 4.66 (1H, d, J=1.8 Hz, C_1-H). IR (film): ν_{max} 3360 (broad) cm^{-1}.

Methyl 2-Benzamido-2,3-dideoxy-3-hydroxymethyl-5,6-*O*-isopropylidene-α-D-mannofuranoside (13). A mixture of **12** (37 mg), benzoyl chloride (25 mg), and triethylamine (50 mg) in THF (2 ml) was stirred for 15 min at room temperature. Preparative TLC on a silica-gel plate developed with cyclohexane : ethyl acetate (1 : 1) gave **13** (51 mg, 97%) as a gum. IR (film): ν_{max} 3350, 1640 cm^{-1}. 270 MHz ^{1}H NMR ($CDCl_3$) δ=1.37 (3H, s), 1.41 (3H, s), 2.91 (1H, m, C_3-H), 3.40 (3H, s, C_1-OCH_3), 3.51 (1H, dd, J=5.1, 8.8 Hz, D_2O exchangeable, OH), 3.91—4.03 (2H, m, C_3-CH and C_6- or C_5-H), 4.08 (1H, td, J=5.1, 12.8 Hz, changed to dd, J=5.1 and 12.8 Hz in addition of D_2O, C_3-CH), 4.14—4.27 (3H, m, C_4-H, C_6-H and C_5-H or C_6-H), 4.59 (1H, t, J=6.2 Hz, C_2-H), 4.99 (1H, s, C_1-H), 7.42—7.56 (4H, m, containing CONH), 7.78—7.82 (2H, m).

Methyl 3-Acetoxymethyl-2-benzamido-2,3-dideoxy-5,6-*O*-isopropylidene-α-D-mannofuranoside (14). A solution of **13** (29 mg) in 0.6 ml of pyridine : acetic anhydride (2 : 1) was allowed to stand overnight at room temperature. Evaporation in vacuo gave **14** (quantitatively) which was recrystallized from hexane : EtOAc (9 : 1). Mp 120—121 °C (needles). $[\alpha]_D^{24}$ +48.9° (c 1.13, EtOH). IR (film): ν_{max} 3360, 1737, 1640 cm^{-1}. 270 MHz ^{1}H NMR ($CDCl_3$) δ=1.37 (3H, s), 1.41 (3H, s), 2.04 (3H, s, $OCOCH_3$), 3.19 (1H, m, C_3-H), 3.38 (3H, s, OCH_3), 3.86 (1H, dd, J=6.6, 8.4 Hz, C_5-H or C_6-H), 4.13 (1H, dd, J=7.1, 8.6 Hz, C_5-H or C_6-H), 4.28 (1H, dd, J=5.5, 8.4 Hz, C_4-H), 4.34—4.42 (2H, m, C_3-CH and C_5-H or C_6-H), 4.50 (1H, dd, J=8.1, 11.7 Hz, C_3-CH), 4.79 (1H, ddd, J=1.0, 6.4, 8.8 Hz, C_2-H), 4.84 (1H, d, J=1.0 Hz, C_1-H), 7.08 (1H, d, J=8.8 Hz, NH), 7.40—7.54 (3H, m), 7.77—7.80 (2H, m). MS m/z 378 (M^+−15), 362, 345, 333, 304, 292, 232, 173. Found: C, 61.22; H, 7.13; N, 3.59%. Calcd for $C_{20}H_{27}NO_7$: C, 61.05; H, 6.92; N, 3.56%.

Methyl 2-Benzamido-2,3-dideoxy-3-formyl-5,6-*O*-isopropylidene-α-D-altrofuranoside (15). To a solution of **13** (121 mg, 0.344 mmol) in CH_2Cl_2 (10 ml) were added anhydrous CH_3COONa (280 mg) and pyridinium chlorochromate (740 mg, 3.44 mmol) with stirring at room temperature (24 °C). After 15 min, the reaction mixture was passed through a silica gel (20 g) column eluted with EtOAc (200 ml), and the eluant was washed with saturated $NaHCO_3$ and brine. The EtOAc layer was dried over $MgSO_4$ and concentrated in vacuo to give an oily residue which was subjected to chromathography by silica-gel column. Elution with cyclohexane-EtOAc (3 : 2) gave **15** in 92% yield as a gum. IR (film): ν_{max} 1665—1655, 1601, 1579 cm^{-1}. 270 MHz ^{1}H NMR ($CDCl_3$) δ=1.30 (3H, s), 1.40 (3H, s), 2.75 (1H, d, J=2.9 Hz, C_3-H), 3.61 (1H, dd, J=7.0, 8.8 Hz, C_6-H), 4.18 (1H, dd, J=7.7, 8.8 Hz, C_6-H), 4.55 (1H, dd, J=1.5—1.8, 2.9—3.3 Hz, C_4-H), 4.62 (1H, dt, J=1.5, 7.0—7.7 Hz, C_5-H), 4.91 (1H, s, C_1H), 5.13 (1H, d, J=8.8 Hz, C_2-H), 7.40—7.55 (4H, m, olefinic 3H and NH), 7.78—7.82 (2H, m), 9.87 (1H, s, CHO). MS m/z 334 (M^+−15), 328, 260, 248, 228, 213, 199, 189.

Methyl 3-Acetyl-2,3-dideoxy-2-(2,4-dimethoxybenzylamino)-5,6-*O*-isopropylidene-α-D-mannofuranoside (16). To a solution of **7** (393 mg, 1 mmol) in THF (10 ml) was added MeLi (1.5 ml of 1.4 M solution in diethyl ether) in THF (2 ml) at −78 °C under a nitrogen atmosphere with stirring. After 15 min, the reaction mixture was quenched with acetic acid, diluted with EtOAc, washed with sat. $NaHCO_3$ and brine, dried over $MgSO_4$ filtered, and concentrated in vacuo to give an gummy mixture. The mixture was subjected to chromatography by silica-gel column. Elution with cyclohexane : EtOAc (1 : 1) gave 311 mg of **16** (higher R_f value, 76% yield) and 44 mg of unknown product.

16: Found: *m/z* 409.20950. Calcd for $C_{21}H_{31}NO_7$: 409.21010.

Methyl 3-Acetyl-2,3-dideoxy-2-(*N*-2,4-dimethoxybenzylbenzamido)-5,6-*O*-isopropylidene-α-D-mannofuranoside (17). To a solution of **16** (82 mg, 0.2 mmol) in THF (2 ml) was added Et_3N (50 mg) and benzoyl chloride (30 mg, 0.213 mmol) with stirring at room temperature. Preparative TLC on a silica-gel plate (developed with cyclohexane : EtOAc=3 : 2) gave 76 mg (74%) of **17** as a crystalline solid. Mp 143—146 °C (from EtOAc-cyclohexane). $[\alpha]_D^{24}$ +140.0° (*c* 1.21, $CHCl_3$). IR (Nujol): ν_{max} 1705, 1625, 1607, 1588, 1205 cm^{-1}. 400 MHz ^1H NMR ($CDCl_3$) δ=1.304 (3H, s), 1.492 (3H, s), 2.369 (3H, s, $COCH_3$), 2.960 (3H, s, OCH_3), 3.671 (3H, s, 2′-OCH_3), 3.803 (3H, s, 4′-OCH_3), 3.879 (1H, td, *J*=6.5—6.8, 4.0 Hz, C_5-H), 4.090 (2H, m, C_6-H_2), 4.152 (1H, dd, *J*=5.2, 7.0 Hz, C_4-H), 4.356 (1H, broad, C_3-H), 4.507 (2H, s, N-CH_2Ar), 4.945 (1H, dd, *J*=7.5, 3.0 Hz, C_2-H), 5.052 (1H, d, *J*=3.4 Hz, C_1-H), 6.355 (1H, d, *J*=2.4 Hz, $C_{3'}$-H), 6.509 (1H, dd, *J*=8.3, 2.4 Hz, $C_{5'}$-H), 7.115 (1H, d, *J*=8.3 Hz, $C_{6'}$-H), 7.283 (4H, d, *J*=3.9 Hz), 7.300 (1H, m). MS *m/z* 513 (M^+), 495, 481, 436, 408, 350, 322, 270, 188, 151. Found: *m/z* 513.23404. Calcd for $C_{28}H_{35}NO_8$, 513.23616. Found: C, 65.15; H, 6.86; N, 2.76%. Calcd for $C_{28}H_{35}NO_8$: C, 65.48; H, 6.87; N, 2.73%.

Methyl 3-Acetyl-2-benzamido-2,3-dideoxy-5,6-*O*-isopropylidene-α-D-mannofuranoside (18). To a stirred solution of **17** (51 mg, 0.10 mmol) in acetone (1.5 ml) was added a solution of cerium(IV) ammonium nitrate (165 mg, 0.30 mmol) in H_2O (1 ml) at 25 °C. After 15 min, the reaction mixture was diluted with EtOAc and washed with aq. $NaHCO_3$, dried over $MgSO_4$, and concentrated to give a residue which was subjected to chromatography by silica-gel column. Elution with cyclohexane-EtOAc (3 : 2) gave **18** (12 mg, 33%) as a solid. 270 MHz ^1H NMR ($CDCl_3$) δ=1.33 (3H, s), 1.43 (3H, s), 2.35 (3H, s), 3.39 (3H, s), 3.94—3.99 (2H, m), 4.04—4.15 (2H, m), 4.28 (1H, dd, *J*=7.7, 9.2 Hz), 4.69 (1H, dt, *J*=2.2, 6.9 Hz, C_2-H), 5.08 (1H, d, *J*=2.2 Hz, C_1-H), 7.41—7.81 (6H, aromatic 5H and NH). MS *m/z*, 362 (M^+−1), 348 (M^+−15), 332, 227, 199, 167, 122, 105.

(1*R*,2*S*,4*S*,5*S*)-2-[(1*R*)-(1,2-*O*-Isopropylideneethyl]-4-methoxy-3-oxa-6-azabicyclo[3.2.0]heptan-7-one (19). To a solution of **7** (1.3 g, 3.3 mmol) in CH_3CN (70 ml) and H_2O (70 ml), was added $K_2S_2O_8$ (10 g) and K_2HPO_4 (5 g). The mixture was heated at 78 °C for 30 min under an argon atmosphere with stirring. The reaction mixture was concentrated in vacuo, and the residue was extracted with EtOAc. The organic layer was washed with aq. $NaHCO_3$ and brine, dried over $MgSO_4$, and then concentrated to give a residue. The crude material was subjected to chromatography by silica-gel column to give **19** (642 mg, 80%) as a crystalline solid. Mp 166—167 °C. IR (Nujol): ν_{max} 3310, 1750 cm^{-1}; 270 MHz ^1H NMR ($CDCl_3$) δ=1.38 (3H, s), 1.45 (3H, s), 3.36 (3H, s), 3.80—4.08 (4H, m), 4.15 (1H, dd, *J*=6.2, 8.8 Hz), 4.41 (1H, m), 4.89 (1H, s), 5.89 (1H, bs, NH). MS *m/z* 228 (M^+−15), 212, 155, 125, 101.

(1*R*,2*S*,4*S*,5*S*)-6-Benzoyl-2-[(1*R*)-(1,2-*O*-isopropyridene-ethyl]-4-methoxy-3-oxa-6-azabicyclo[3.2.0]heptan-7-one (20). To a solution of **19** (390 mg, 1.6 mmol), Et_3N (1.6 ml), DMAP (30 mg) in CH_2Cl_2 (10 ml) was added a solution of PhCOCl (340 mg, 1.5 equiv, 2.4 mmol) in CH_2Cl_2 (2 ml) with stirring at room temperature. After 1 h, the reaction mixture was diluted with EtOAc, washed with aq. $NaHCO_3$ and brine, dried over $MgSO_4$, and concentrated in vacuo to give a residue which was subjected to chromatography by silica-gel column. Elution with cyclohexane-EtOAc (2 : 1) gave 512 mg of **20** (92%). IR (film): ν_{max} 1795, 1732, 1672, 1601, 1581 cm^{-1}. 60 MHz ^1H NMR ($CDCl_3$) δ=1.38 (3H, s), 1.46 (3H, s), 3.40 (3H, s), 3.7—4.5 (5H, m), 4.57 (1H, d, *J*=4.5 Hz), 5.27 (1H, s), 7.3—7.6 (3H, m), 7.9—8.1 (2H, m). MS *m/z*, 348 (M^++1), 334, 333, 332 (M^+−15), 316.

Methyl 2-Benzamido-2,3-dideoxy-5,6-*O*-isopropylidene-3-methoxycarbonyl-α-D-altrofuranoside (21). A solution of **20** (150 mg) in MeOH containing 10 mg of DBU was refluxed for 30 min. The mixture was concentrated in vacuo to give a residue which was subjected to chromatography by silica-gel column. Elution with cyclohexane-EtOAc (1 : 1) gave 150 mg (90%) of **21** as a viscous gum. IR (film): ν_{max} 3360, 1732, 1662, 1643 cm^{-1}. 270 MHz ^1H NMR ($CDCl_3$) δ=1.32 (3H, s), 1.41 (3H, s), 2.91 (1H, d, *J*=3.7 Hz, C_3-H), 3.32 (3H, s, C_1-OCH_3), 3.70 (1H, dd, *J*=7.0, 8.8 Hz, C_6-H), 3.79 (3H, s, C_3-$COOCH_3$), 4.17 (1H, dd, *J*=7.3, 8.8 Hz, C_6-H), 4.61 (1H, dt, *J*=1.6, 7.3 Hz, C_5-H), 4.75 (1H, dd, *J*=1.7, 3.7 Hz, C_4-H), 4.86 (1H, s, C_1-H), 5.17 (1H, d, *J*=8.8 Hz, C_2-H), 7.33 (1H, d, *J*=8.8 Hz, NH), 7.39—7.51 (3H, m), 7.78—7.82 (2H, m). MS *m/z* 380 (M^++1), 364, 348, 290, 278, 258, 219.

Methyl 2-Benzamido-3-carboxy-2,3-dideoxy-5,6-*O*-isopropylidene-α-D-altrofuranoside (22). A solution of **21** (326 mg, 0.859 mmol) in MeOH (2.6 ml), and aqueous 1 M NaOH (1.03 ml, 1.03 mmol, 1.2 equiv) was refluxed for 30 min. The whole was concentrated in vacuo, acidified with 1 M HCl (1.1 ml), and extracted with EtOAc. The organic layer was washed with H_2O and brine, dried over $MgSO_4$, and concentrated to give 310 mg of an acid **22** (99%) as a crystalline solid. Mp 145—146.5 °C (from EtOAc-hexane). 270 MHz ^1H NMR ($CDCl_3$) δ=1.29 (3H, s), 1.38 (3H, s), 3.01 (1H, dd, *J*=1.3, 4.6 Hz, C_3-H), 3.36 (3H, s, C_1-OCH_3), 3.75 (1H, dd, *J*=7.1, 9.3 Hz, C_6-H), 4.15 (1H, dd, *J*=7.1, 9.3 Hz, C_6-H), 4.58 (1H, dt, *J*=2.1, 7.1 Hz, C_5-H), 4.74 (1H, dd, *J*=2.1, 4.6 Hz, C_4-H), 4.95 (1H, dd, *J*=1.3, 8.1 Hz, C_2-H), 4.97 (1H, s, C_1-H), 7.34 (1H, d, *J*=8.1 Hz, C_2-NH), 7.41—7.57 (3H, m), 7.79—7.82 (2H, m), 9.50 (1H, bs, COOH). $[\alpha]_D^{24}$ −60.0° (*c* 1.06, $CHCl_3$). Found: C, 59.06; H, 6.26; N, 3.74%. Calcd for $C_{18}H_{23}NO_7$: C, 59.17; H, 6.35; N, 3.83%.

Methyl 2-Benzamido-3-(3-chlorobenzoyldioxycarbonyl)-2,3-dideoxy-5,6-*O*-isopropylidene-α-D-altrofuranoside (23). To a solution of **22** (121.8 mg, 1/3 mmol) and 3-chloroperbenzoic acid (80—90%, 75 mg) in CH_2Cl_2 (3 ml) was added DCC (83 mg, 1.2 equiv) at room temperature with stirring. After 15 min, the precipitate was filtered off. The filtrate was concentrated and subjected to chromatography by silica-gel column. Elution with cyclohexane-EtOAc (3 : 2) gave 146 mg of **23** (84%) as a powder. IR (Nujol): ν_{max} 3330, 1800, 1768, 1640, 1602 cm^{-1}. 270 MHz ^1H NMR ($CDCl_3$) δ=1.37 (3H, s), 1.42 (3H, s), 3.21 (1H, dd, *J*=1.1, 4.1 Hz, C_3-H), 3.40 (3H, s), 3.76 (1H, dd, *J*=7.0, 8.8 Hz, C_6-H), 4.20 (1H, dd, *J*=7.3, 8.8 Hz, C_6-H), 4.64 (1H, ddd, *J*=1.8, 4.0, 7.3 Hz, C_5-H), 4.79 (1H, dd, *J*=1.8, 4.0 Hz, C_4-H), 4.98 (1H, s, C_1-H), 5.20 (1H, dd, *J*=1.1, 8.8 Hz, C_2-H), 7.27 (1H, d, *J*=8.8 Hz, C_2-NH), 7.4—8.02 (9H, m). Found: C, 57.47; H, 5.04; N, 2.60; Cl, 7.08%. Calcd for $C_{25}H_{26}NO_9Cl$: C, 57.75; H, 5.04; N, 2.69; Cl, 6.82%.

Methyl 2-Benzamido-3-*O*-(3-chlorobenzoyl)-2-deoxy-5,6-*O*-isopropylidene-α-D-altrofuranoside (24) and Methyl 2-Benzamido-2,3-dideoxy-5,6-*O*-isopropylidene-α-D-altrofuranoside (25) The peroxyester **23** (91 mg) in octane (5 ml) was refluxed for 1 h with stirring. Concentration of the

reaction mixture and preparative TLC on a silica-gel plate (developed with cyclohexane-EtOAc=3:2) gave 27 mg of **24** (32%) as a gum and 20 mg of **25** (36%) as a gum. Physical data of **24**: IR (film): ν_{max} 3350, 1723, 1646 cm^{-1}. 270 MHz ^{1}H NMR ($CDCl_3$) δ=1.40 (3H, s), 1.44 (3H, s), 3.47 (3H, s), 4.04 (1H, t, J=8.1—8.8 Hz, C_6-H), 4.16 (1 H dd, J=6.6, 8.8 Hz, C_6-H), 4.38 (1H, dd, J=1.5, 2.2 Hz, C_4-H), 4.51 (1H, dt, J=1.5, 6.6—8.1 Hz, C_5-H), 4.81 (1H, d, J=8.4 Hz, coupling with NH, C_2-H), 5.04 (1H, s, C_1-H), 5.39 (1H, d, J=2.2 Hz, C_3-H), 7.38 (1H, d, J=8.4 Hz, NH), 7.38—7.58 (5H, m), 7.80—8.04 (4H, m). Found: C, 60.52; H, 5.78; N, 2.96; Cl, 7.64%. Calcd for $C_{24}H_{26}NO_7Cl$: C, 60.58; H, 5.51; N, 2.94; Cl, 7.45%. Found: m/z (M^++1) 476.14390. Calcd for $C_{24}H_{26}NO_7Cl$ (Cl=34.96885): 476.14750. Physical data of **25**: IR (film): ν_{max} 3360, 1650 cm^{-1}. 270 MHz ^{1}H NMR ($CDCl_3$) δ=1.35 (3H, s), 1.43 (3H, s), 1.82 (1H, dd, J=2.9, 13.6 Hz, C_3-βH), 2.52 (1H, ddd, J=8.1, 9.5, 13.6 Hz, C_3-αH), 3.37 (3H, s), 3.52 (1H, t, J=8.4 Hz, C_6-H), 4.14 (1H, dd, J=7.3, 8.4 Hz, C_6-H), 4.32 (1H, ddd, J=1.9, 2.9, 9.5 Hz, C_4-H), 4.54 (1H, dt, J=1.9, 7.3—8.4 Hz, C_5-H), 4.61 (1H, dd, J=8.1, 8.4 Hz, C_2-H), 4.88 (1H, s, C_1-H), 7.38—7.49 (4H, m, aromatic 3H and NH), 7.52—7.80 (2H, m). Found: C, 63.28; H, 7.01; N, 4.07%. Calcd for $C_{17}H_{23}NO_5$: C, 63.53; H, 7.21; N, 4.36%. Found: m/z (M^++1) 322.16809. Calcd for $C_{17}H_{24}NO_5$: 322.16549.

X-Ray Crystallography of 17, 22, and vi. Crystals of dimensions 0.7×0.4×0.4 mm for **17**, 0.5×0.4×0.4 mm for **22**, and 0.4×0.3×0.2 mm for **vi** were used for X-ray crystallography. Lattice constants were determined by least-squares fit of angular settings of 20 reflections within the range $15<\theta<30°$. Intensity data were obtained on a Rigaku AFC-5R diffractometer equipped with graphite-monochromatized Cu $K\alpha$ radiation and using θ-2θ scan technique ($2\theta<128°$). During data collection five standards, measured before every 200 reflections, indicated no systematic variation of intensity with time. Of 2591, 3270, and 1904 independent reflections measured, only 2411, 2689, and 1750 for **17**, **22**, and **vi**, respectively, were considered as observed on the basis of the criterion $F_o>2\sigma(F_o)$. All intensities were corrected for Lorentz and polarization effects, but not for absorption.

Crystal data: **17**, $C_{28}H_{35}NO_8$, M_r=513.4. Orthorhombic, space group $P2_12_12_1$, a=22.449(6), b=16.662(5), c=7.219(2) Å, U=2700.4 Å^3, Z=4, D_c=1.26 g cm^{-3}, μ(Cu $K\alpha$)=8 cm^{-1}.

22, $C_{18}H_{23}NO_7$, M_r=365.4. Monoclinic, space group $P2_1$, a=16.380(3), b=7.438(1), c=15.738(5) Å, β=109.51(2)°, U=1807.3 Å^3, D_c=1.34 g cm^{-3}, μ(Cu $K\alpha$)=9 cm^{-1}.

vi, $C_{19}H_{25}NO_7$, M_r=379.4. Orthorhombic, space group $P2_12_12_1$, a=19.719(5), b=9.682(2), c=10.382(2) Å, U=1982.2 Å^3, D_c=1.27 g cm^{-3}, μ(Cu $K\alpha$)=8 cm^{-1}.

The structures of **17**, **22**, and **vi** were solved by MULTAN84,[19] and refined by the block-diagonal least-squares methods. The positions of the hydrogen atoms were estimated using standard geometry. The final refinements with anisotropic temperature factors for the nonhydrogen atoms and isotropic temperature factors for the hydrogen atoms were lowered R values to 0.080 (R_w=0.069, $w=1/\sigma^2(F_o)$), 0.070 (R_w=0.057, $w=1/\sigma^2(F_o)$), and 0.072 (R_w=0.057, $w=1/\sigma^2(F_o)$) for **17**, **22**, and **vi**, respectively.

The complete F_o—F_c data are deposited as Document No. 8900 at the Office of the Editor of Bull. Chem. Soc. Jpn

We thank Mr. Harumitsu Kuwano for measuring the 400 MHz ^{1}H NMR spectra.

References

1) F. M. Hauser and S. R. Ellenberger, *Chem. Rev.*, **86**, 35 (1986); M. Hirama, *Yuki Gosei Kagaku Kyokaishi*, **45**, 346 (1987).

2) W. H. Myers and G. J. Robertson, *J. Am. Chem. Soc.*, **65**, 8 (1943); R. D. Guthrie and D. Murphy, *J. Chem. Soc.*, **1963**, 5288.

3) M. B. Perry and J. Furdova, *Can. J. Chem.*, **46**, 2859 (1968).

4) M. Shiozaki and N. Ishida, *Chem. Lett.*, **1987**, 1403.

5) E. Baer and H. O. L. Fischer, *Ber.*, **128**, 463 (1939).

6) J. Adams, L. Hoffman, Jr., and B. M. Trost, *J. Org. Chem.*, **35**, 1600 (1970).

7) T. Shono, N. Kise, and T. Suzumoto, *J. Am. Chem. Soc.*, **106**, 259 (1984).

8) M. Murakami and T. Mukaiyama, *Chem. Lett.*, **1982**, 1271.

9) M. Shiozaki, N. Ishida, T. Hiraoka, and H. Yanagisawa, *Tetrahedron Lett.*, **22**, 5205 (1981); M. Shiozaki, N. Ishida, H. Maruyama, and T. Hiraoka, *Tetrahedron*, **39**, 2399 (1983).

10) The stereochemical assignments of compounds, ano-

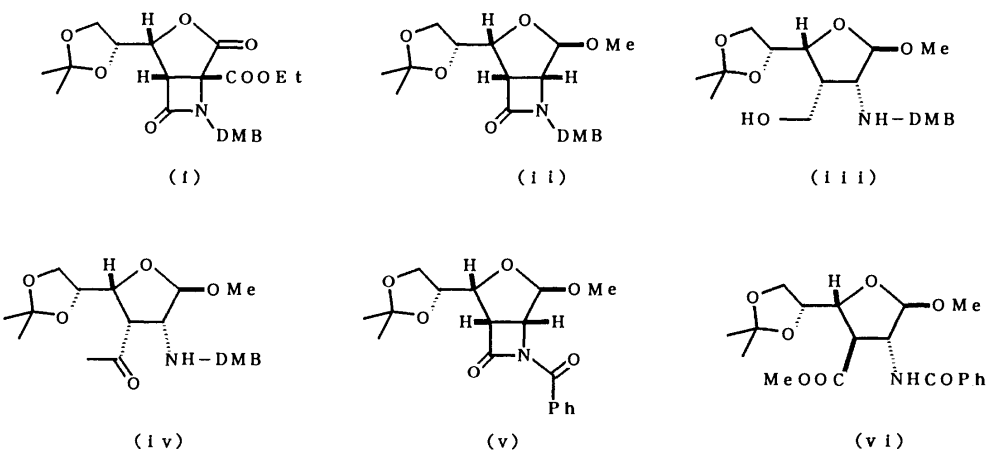

Scheme 5.

mer of **7**, that of **11** and also that of **16** described in "*Chem. Lett.*, **1987**, 1403"[4] must be corrected as ii, iii, and iv, respectively. The chromatographic separation of the mixed fractions should be repeated. If the separation was not sufficient, a small amount of **i** derived from **1'a** contaminates, causing the contamination of iii, iv, or v in latter stages, although fortunately separable by chromatography. (Scheme 5).

iii: 270 MHz ^{1}H NMR, ($CDCl_3$) δ=1.35 (3H, s), 1.40 (3H, s), 2.63—2.68 (1H, m, C_3-H), 3.7—4.2 (15H, m, containing two 3H singlets at δ 3.80 and 3.81), 4.85 (1H, d, J=1.8 Hz, C_1-H), 6.41—6.45 (2H, m), 7.13 (1H, d, J=8.1 Hz). IR (film): ν_{max} 3500—3300, 1612, 1590 cm^{-1}. MS m/z 397 (M^+), 392, 366, 339, 322, 306, 296, 279, 264, 248, 236, 166, 151, 121. Found: m/z 397.20979. Calcd for $C_{20}H_{31}NO_7$: 397.20995.

iv: High resolution MS: Observed, 409.21010. Calcd for $C_{21}H_{31}NO_7$: 409.21010. 270 MHz ^{1}H NMR ($CDCl_3$) δ=1.33 (3H, s), 1.37 (3H, s), 1.73 (1H, broad, NH), 2.25 (3H, s), 2.89 (1H, dd, J=3.8, 6.4 Hz, C_3-H), 3.28 (3H, s), 3.47 (1H, d, J=3.7 Hz, C_2-H), 3.77 (2H, s), 3.80 (3H, s), 3.81 (3H, s), 3.7—3.9 (1H, m), 4.09 (1H, dd, J=6.8, 7.6 Hz), 4.25 (1H, dd, J=5.7, 12.3 Hz), 4.40 (1H, t, J=6.0 Hz), 4.82 (1H, s, C_1-H), 6.42—6.47 (2H, m), 7.19 (1H, d, J=9.2 Hz).

v: 60 MHz ^{1}H NMR ($CDCl_3$) δ=1.39 (3H, s), 1.46 (3H, s), 3.44 (3H, s), 3.5—4.5 (5H, m), 4.56 (1H, d, J=4.5 Hz, C_1-H), 5.31 (1H, s), 7.3—7.6 (3H, m), 7.8—8.1 (2H, m). IR (film): ν_{max} 1795, 1713, 1672, 1601, 1581 cm^{-1}. MS m/z 348 (M^++1), 332 (M^+−15), 316, 125, 105, 101.

vi: Mp 109—111 °C (from cyclohexane). $[\alpha]_D^{24}$ −59.8° (c 0.94, $CHCl_3$). IR (Nujol): ν_{max} 3400, 1732, 1635 cm^{-1}. 270 MHz ^{1}H NMR ($CDCl_3$) δ=1.25 (3H, s), 1.43 (3H, s), 3.02 (1H, d, J=3.6 Hz, C_3-H), 3.32 (3H, s), 3.79 (3H, s), 4.05 (1H, dd, J=8.1, 8.4 Hz, C_6-H), 4.14 (1H, dd, J=6.6, 8.4 Hz, C_6-H), 4.29 (1H, ddd, J=1.3, 6.6, 8.1 Hz, C_5-H), 4.72 (1H, dd, J=1.3, 3.6 Hz, C_4-H), 4.88 (1H, s, C_1-H), 5.10 (1H, d, J=9.2 Hz, C_2-H, coupling with NH), 7.40—7.55 (4H, m, aromatic 3H and NH), 7.77—7.81 (2H, m). Found: C, 60.02; H, 6.60; N, 3.77%. Calcd for $C_{19}H_{25}NO_7$: C, 60.15; H, 6.64; N, 3.67%.

The structure of **vi** derived from **v** was confirmed by **X**-Ray crystallographic analysis. (Fig. 3).

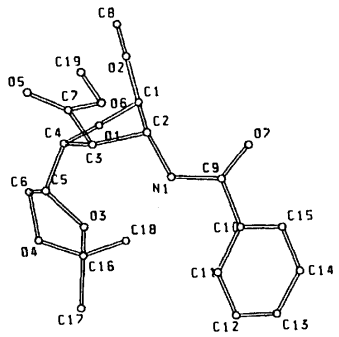

Fig. 3. Molecular structure and atomic numbering of **vi**.

11) Addition of a catalytic amount of silica gel (Silica gel 60, 230—400 mesh, Merck) makes the reduction rate faster.

12) C. S. Hudson and D. H. Brauns, *J. Am. Chem. Soc.*, **38**, 1216 (1916).

13) R. W. Holly and A. W. Holly, *J. Am. Chem. Soc.*, **71**, 2124 (1949).

14) References therein; J. March, "Advanced Organic Chemistry," 3rd ed, p. 435; S. Kano, T. Ebata, and S. Shibuya, *Chem. Pharm. Bull.*, **27**, 2450 (1979).

15) T. Fukuyama, R. K. Frank and C. F. Jewell, Jr., *J. Am. Chem. Soc.*, **102**, 2122 (1980); D. R. Kronethal, C. V. Han, and M. K. Taylor, *J. Org. Chem.*, **47**, 2765 (1982).

16) W. F. Haffman, K. G. Holden, T. F. Buckley, III, J. G. Gleason, and L. Wu, *J. Am. Chem. Soc.*, **99**, 2352 (1977).

17) D. B. Denney and N. Sherman, *J. Org. Chem.*, **30**, 3760 (1965); D. H. Barton, I. H. Coates, and P. G. Sammes, *J. Chem. Soc. Perkin Trans. 1*, **1973**, 599; K. Yamamoto, T. Yoshioka, Y. Kato, N. Shibamoto, K. Okamura, Y. Shimauchi, and T. Ishikura, *J. Antibiotics*, **33**, 796 (1980); S. Oae and K. Fujimori, "The Chemistry of Peroxide," ed by S. Patai, pp. 608—632.

18) J. D. Stevens and H. G. Fletcher, Jr., *J. Org. Chem.*, **33**, 1799 (1968).

19) P. Main, G. Germain, and M. M. Woolfson, (1984), University of York, England, and Louvain, Belgium. MULTAN84 is a system of computer programs for the automatic solution of crystal structures from **X**-ray diffraction data.

Model Compound Studies of Coal Liquefaction with Zinc-Butyl Iodide under Mild Conditions

Yoshiharu YONEYAMA,* Yu AKAKI, and Tsutomu KATO
Department of Industrial Chemistry, Faculty of Engineering, Toyama University, Gofuku, Toyama 930
(Received May 25, 1989)

A number of model compounds having representative coal structures were treated with zinc-butyl iodide under mild conditions. Gas chromatography and gas chromatography/mass spectrometry were used to identify the reaction products. Polynuclear aromatic compounds gave the butyl-substituted and butyl-addition products. In a reaction of anthracene, its aromatic backbone was cleaved. Alkoxynaphthalene and dibenzyl ether were butylated along with cleavage of ether linkage, while diphenyl ether gave only the butyl-substituted products without cleavage. Butylation and cleavage also took place in the reactions of diphenylmethane and bibenzyl. In the cases of substitution reaction, some butyl groups were rearranged to *s*-butyl. Because the formation of the most reaction products is interpreted by a similar mechanism to that of Friedel-Crafts alkylation and the formation of some butyl-addition products of polynuclear aromatic compounds is explained by assuming a radical reaction mechanism, it is suggested that both alkyl cation reaction and alkyl radical reaction occur competitively.

A new coal liquefaction concept has recently been developed: Depolymerization of coal by use of zinc metal and butyl iodide under atmospheric pressure at 130 °C.[1] This method can effectively convert coal to benzene-soluble products under mild conditions. For example, Kairan coal (carbon content, 87.2%) can be solubilized in benzene to the extent of 96.7% by this method. The effectiveness of the zinc-butyl iodide for depolymerization of coals has stimulated a further investigation into the mechanism of the conversion. An advantage of coal conversion study using model compounds is that both the starting materials and products are easily characterized by simple analytical techniques.

In the present study, some polynuclear aromatic compounds, aryl ethers, diphenylmethane, and bibenzyl have been treated with zinc-butyl iodide and the products were analyzed by gas chromatography (GC) and gas chromatography/mass spectrometry.

Experimental

The model compounds used in the present study were commercially available and used without further purification except anthracene which was recrystallized. The butylation reaction was carried out as follows: 11.9 mmol of a model compound, 8 g of zinc metal powder and 30 ml of butyl iodide were placed in a three-necked flask attached with a reflux condenser and a Teflon stirrer. While being agitated, the mixture was heated at 130 °C for 5 h under nitrogen stream in an oil bath. The reaction mixture was cooled to room temperature, and then extracted with benzene or pentane. After removing the solvent the products were analyzed by a Hitachi model 163 gas chromatograph (glass capillary column, 12 m×0.28 mm; SE-52) equipped with a YANACO model S-1000 integrator and by a JEOL model JMN-D3000 GC-MS (25 m×0.25 mm; SE-52).[2,3] Naphthalene and phenanthrene were used as internal standards.

Results and Discussion

The model compounds were selected on the basis of the structural information on coals. From time to time, various structures of coals have been suggested, depending upon the extent of knowledge available at the time; e.g., those suggested by Given,[4,5] Hill and Lyon,[6] Wiser,[7] and Heredy and Wender.[8] As coal has no uniform composition, the most widely

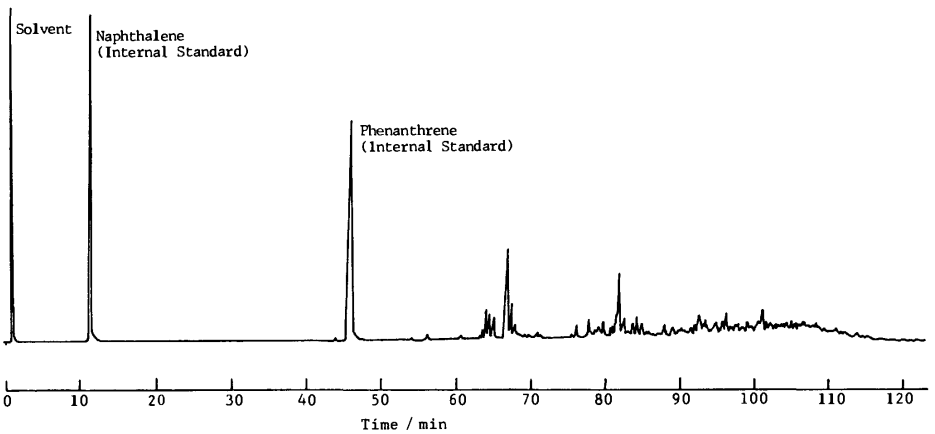

Fig. 1. Gas chromatogram of the products of phenanthrene.

Table 1. Results of the Butylation Reaction of Polynuclear Aromatic Compounds

	Reactant			
	1-Methylnaphthalene	Acenaphthene	Phenanthrene	Anthracene
Conversion/%	80	93	100	100
Product[a)]	Yield of fraction/area %			
BSD of Re	65.4	51.1	42.0	7.3
BAD of Re	15.8	20.4	20.5	43.7
BDAD of Re	1.8	Nil	Nil	0.2
BSD of pentylbenzene	—	—	—	2.6
BSD of dipentylbenzene	—	—	—	1.4
Hexabutylbenzene	—	—	—	3.3

a) BSD: mono and polybutyl-substituted derivatives; Re: reactant compound; BAD: butyl-addition derivatives; BDAD: butyl-diaddition derivatives.

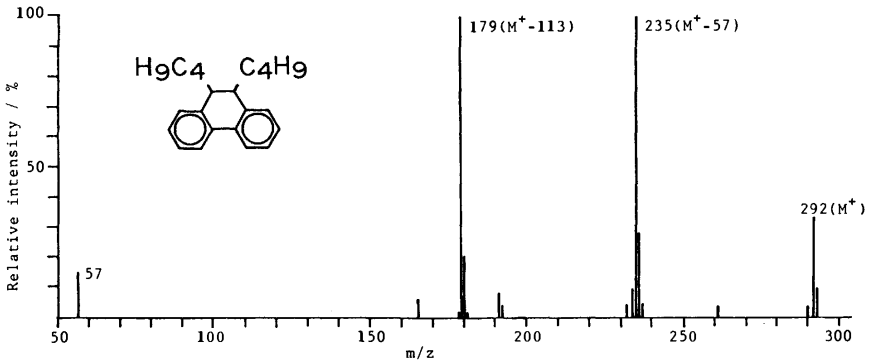

Fig. 2. Mass spectrum of the dibutyl-addition product of phenanthrene.

accepted structural view of bituminous coal contains statistical proportions of groups of fused aromatic and hydroaromatic ring clusters, composed of an average of two to six ring units connected with various aliphatic and ether bridges.

The model compounds selected as polynuclear aromatic compounds for this study are 1-methylnaphthalene, acenaphthene, phenanthrene, and anthracene. Every reaction product contained many components, showing over 200 peaks in each gas chromatogram. Figure 1 shows the gas chromatogram of the product of phenanthrene. Because of small area of each GC peak, the percentage of the components identified was meager: that of 1-methylnaphthalene, acenaphthene, phenanthrene, and anthracene were 83.0, 71.5, 62.5, and 58.5%, respectively. The reaction products and their yields are summarized in Table 1.

The reaction pattern observed with phenanthrene will be discussed first, because it is characteristic of other model compounds. Phenanthrene, when treated by this method, showed the quantitative conversion. The products consist of butyl-substituted derivatives (BSD) and butyl-addition derivatives (BAD)** of phenanthrene.

In our previous paper,[1)] we have reported that no evidence about the formation of butyl-addition products was found in the ^{13}C NMR spectra of the reaction products. However, in the present study, the products included not only the butyl-substituted components but also the butyl-addition components. Stobart and Zaworotko[9)] have shown that polynuclear aromatic compounds (naphthalene, anthracene, and phenanthrene) were hydrogenated, when treated with $AlCl_3$ in hexane and heptane at 20—70 °C. Therefore we considered initially that phenanthrene was hydrogenated, and subsequently butyl-substitution reaction occurred. However it was confirmed that phenanthrene was subjected to butyl-addition reaction. Figure 2 shows the mass spectrum of one of the products of phenanthrene whose molecular mass is 292. The mass spectrum showed the peaks at m/z M^+-57 and M^+-113 which are characteristics of dibutyl-addition compounds.[10)] 9,10-Dibutyl-9,10-dihydrophenanthrene[11)] was assigned to the product, but this product was not stereochemically followed up. Five isomers showing almost the same fragmentation were also observed. Accordingly, it is suggested that the products were formed from the butyl-addition. The use of ^{13}C NMR spectra failed to detect the formation of butyl-addition products, because the amount of these

** Butyl-addition derivatives (BAD) of aromatic compound implies polybutylated derivatives of dihydroaromatic compound.

products was too little to be found. In addition, this butyl-addition products were included also in the reaction products of some other model compounds examined in this study.

1-Methylnaphthalene showed 79.5% conversion. The products were BSD and BAD of 1-methylnaphthalene. Moreover a small amount of the butyldiaddition derivatives (BDAD)*** was also included.

Acenaphthene showed 93.1% conversion. The products were BSD and BAD of acenaphthene. Introducing of alkyl substituents to aromatic rings usually enhances[12] the reactivity of the aromatic compound for alkylation reaction and this is in accord with the fact that the conversion rate of acenaphthene was higher than that of 1-methylnaphthalene.

Anthracene also showed the quantitative conversion, giving BSD, BAD, and BDAD of anthracene. Differing from other three compounds, the products of anthracene included much more BAD than BSD. Furthermore the products included the components breaking the backbone of anthracene; BSD of dipentylbenzene and pentylbenzene, and hexabutylbenzene were 1.4, 2.6, and 3.3%, respectively. The first two compounds probably arose from butyl-addition to the 9 and 10 positions of anthracene, followed by cleavage, and it is suggested that hexabutylbenzene was formed from polybutylation of aromatic fragments which came out in aromatic ring destruction. The attack of the butyl groups at the 9 and 10 positions yields the structure of diphenylmethane type for anthracene and that of biphenyl type for phenanthrene. It is known that the linkage of diphenylmethane can be cleaved easily, but that of biphenyl cannot under various mild liquefaction conditions.[13,14] Therefore it is deduced that the aromatic rings of anthracene break, but those of phenanthrene do not.

As mentioned before, aliphatic linkages play an important role in linking aromatic and hydroaromatic ring clusters in coals. Other model compounds selected for this study include diphenylmethane and bibenzyl. The reaction products of these compounds contained over 100 components. The percentage of products identified in the runs of diphenylmethane and bibenzyl were 81.1 and 80.3%, respectively. Diphenylmethane showed 44.7% conversion. BSD of diphenylmethane was formed in 59.0% yield and the components which cleaves methylene linkage were also included. These were methylbiphenyl (6.2%), its monobutylated derivatives (5.2%), benzyltoluene (9.7%), and its monobutylated derivatives (1.0%). Bibenzyl showed 43.6% conversion, with BSD (69.1%) of bibenzyl, dibenzylated derivatives of bibenzyl (3.4%), their BSD (3.9%), pentylbenzene (2.8%), diphenylmethane (0.6%), and benzyltoluene (0.5%). The products other than BSD of bibenzyl are the compound with cleavage of ethylene linkage. No butyl-addition components were observed in both the reaction products.

Compounds containing aliphatic linkages gave the products with cleaved linkages, though their yields are low. Tuge and Tashiro[15] have reported that easiness of the cleavage of the methylene linkage of diphenylmethane increased with increasing the number of alkyl groups at benzene ring. Since both BSD of diphenylmethane and of bibenzyl in this study have only 1—2 butyl groups, the yields of linkage-cleaved products were low. Because coals themselves include many alkyl substituents on aromatic rings, one would expect that aliphatic linkages in coal structures can be cleaved by this method.

Another important feature of coal involves ether linkages, which are also believed to play an important role in the depolymerization of coal. The model compounds selected for this study include 2-methoxy-, 2-propoxynaphthalene, diphenyl ether, and dibenzyl ether. Every reaction product contained over 100 components. The percentage of the products identified in the reaction of 2-methoxy-, 2-propoxynaphthalene, diphenyl ether, and dibenzyl ether was 86.5, 81.6, 92.2, and 87.2%, respectively. When diphenyl ether was treated under this reaction system, 39.7% conversion was observed, and the products were only BSD (92.2%) of diphenyl ether. No ether linkage-cleaved components were found in the reaction products.

2-Methoxy- and 2-propoxynaphthalene showed 95.4 and 96.2% conversions, respectively. The reaction products of 2-methoxynaphthalene contained its BSD (29.5%) and BAD (23.4%), and similarly BSD (24.1%) and BAD (29.9%) of 2-propoxynaphthalene were found in its reaction products. The reactivity of the substrate did not differ with the alkyl chain length. In the reaction of 2-methoxynaphthalene, ether linkage-cleaved products, BAD (0.3%) of naphthalene, BSD (7.1%), and BAD (26.2%) of butoxynaphthalene were found. Similarly, in the reaction of 2-propoxynaphthalene, BAD (1.0%) of naphthalene, BSD (8.0%), and BAD (18.6%) of butoxynaphthalene were observed. The reaction products of alkoxynaphthalenes included the components which had been subjected to the cleavage of alkyl ether linkages and substituted by butyl groups. Furthermore, by means of a small amount of the components which cleaves the ether O-aromatic carbon linkage, BAD of naphthalene was observed in the reaction of alkoxynaphthalene.

Dibenzyl ether showed the quantitative conversion. All the reaction products were ether linkage-cleaved ones. Most of them were BSD (51.3%) of toluene, pentylbenzene, BSD (28.2%) of benzyltoluene, and its benzylated derivatives (6.3%). Other products were dibutylbenzene (0.5%), diphenylmethane (0.2%), and butyl benzyl ether (0.8%). The yield of the products,

*** Butyl-diaddition derivatives (BDAD) of aromatic compound implies polybutylated derivatives of tetrahydroaromatic compound.

BSD of toluene and pentylbenzene, is shown together, because it is indistinguishable from fragmentation mass spectra whether they are toluene or pentylbenzene derivatives. It is known that alkyl ether linkage is easily cleaved, but aryl ether linkage hardly is.

As described above, it has been found in this reaction system that polynuclear aromatic compounds undergo the butyl-substitution and butyl-addition reactions, and aromatic compounds containing aliphatic linkages and some ether linkages cleave themselves. Therefore, the formation of most reaction products can be interpreted by assuming a similar mechanism to that of Friedel-Crafts reaction.[14,16] However, the formation of butyl-addition products cannot be interpreted. It has been already known that a radical reaction takes place in the early stage of this reaction.[17] The butyl-addition products can be explained by assuming a radical mechanism; butyl radical attacks the nucleus of aromatic compound, and the combination of the resulting radical with another butyl radical yields butyl-addition product.[18] In order to clarify whether this reaction mechanism is radical type or not, the fragmentation of the mass spectra of the products substituted by monobutyl group was analyzed, because butyl radical is not usually rearranged, but butyl cation is likely to be rearranged into *s*-butyl. The mass spectrum of the compound substituted by butyl group shows a peak at m/z M^+-43, whereas that of the compound substituted by *s*-butyl shows a peak at m/z M^+-29.[3] The results obtained on the seven compounds are shown in Table 2. In all the reaction products, a large amount of the components substituted by butyl was contained, but the components substituted by *s*-butyl were also contained. These results do not agree with the rule that rearrangement of the intermediate free radical does not occur.[19] Both of an observation of rearrangement of butyl to *s*-butyl and formation of BSD of polynuclear aromatic compounds can be interpreted by alkyl cation reaction mechanism,[1] whereas formation of BAD in the reaction of polynuclear aromatic compounds can be explained by assuming radical mechanism. Therefore it is suggested that both alkyl-cation and radical reaction occurred competitively in this reaction.

Table 2. Rearrangement of the Butyl Group of the Monobutyl-Substituted Model Compounds

Reactant	Yield of the fraction/area %	
	Butyl	*s*-Butyl
1-Methylnaphthalene	29.6	5.8
Acenaphthene	14.6	1.6
Phenanthrene	15.0	2.6
Anthracene	0.9	Nil
Diphenylmethane	34.0	14.5
Bibenzyl	42.6	15.6
Diphenyl ether	45.7	7.0

In view of the efficiency of this method on coal liquefaction it can be concluded that high benzene extractability of coal can be attained by introducing many butyl groups and the cleavage of the linkages in compounds, such as bibenzyl, diphenylmethane, dibenzyl ether, and alkoxynaphthalene. The reaction product of anthracene includes the components which cleave the aromatic backbone.

References

1) H. Tsukashima, T. Kato, Y. Yoneyama, and Y. Sakai, *Fuel Processing Technology*, **14**, 193 (1986).
2) E. Stenhagen, S. Abrahamson, and F. W. Mclafferty, "Registry of Mass Spectral Data," John Wiley & Sons, New York (1974).
3) S. Sasaki and M. Ohashi, "Shituryo-Supekutoru Ensyu," Nankodo, Tokyo (1971).
4) P. H. Given, *Fuel*, **39**, 147 (1960).
5) P. H. Given, *Fuel*, **40**, 427 (1961).
6) G. R. Hill and L. B. Lyon, *Ind. Eng. Chem.*, **54**, 36 (1962).
7) W. H. Wiser, *Am. Chem. Soc. Div. Fuel Chem. Preprint*, **20**, 122 (1975).
8) I. Wender, L. A. Heredy, M. B. Neuworth, and I. G. C. Dryden, "Chemical Reactions and the Constitution of Coal," in "Chemistry of Coal Utilization," Second Supplementary Volume, Wiley, New York (1981).
9) S. R. Stobart and M. J. Zaworotko, *Fuel*, **64**, 1623 (1985).
10) S. Nakamura, MS Thesis, Toyama University, Toyama, (1983).
11) A. I. Nogaideli, N. I. Tabashidze, and I. I. Abkhazava, *Soobsch. Akad. Nauk. Gruz. SSR*, **55**, 569 (1969).
12) T. W. G. Solomons, "Organic Chemistry," 3rd ed., Jorn Willy & Sons, New York (1984), p. 483.
13) N. D. Tayler and A. T. Bell, *Fuel*, **59**, 499 (1980).
14) G. A. Olah and A. Husain, *Fuel*, **63**, 1427 (1984).
15) O. Tuge and M. Tashiro, *The Coal Tar (Koru Taru)*, **14**, 513 (1962).
16) D. P. Mobley and A. T. Bell, *Fuel*, **58**, 661 (1979).
17) Y. Yamamoto and Y. Raruta, "Yuuki-Kinzoku Kagoubutu," Maruzen, Tokyo (1983), p. 31.
18) N. Inamoto, "Radikaru Hannou," in "Gendai No Yuuki-Kagaku," Hirokawa Publishing Co., Tokyo (1977), p. 313.
19) R. T. Morrison and R. N. Boyd, "Organic Chemistry," 5th ed., Allyn and Bacon, Inc., Boston (1987), p. 114.

Structures of 1,4,13,16-Tetraoxa-7,10-dithia[16](1,1′)ruthenocenophane and Its 1 : 2 $HgCl_2$ Complex

Sadao SATO,*,† Yoichi HABATA, Masaru SATO,†† and Sadatoshi AKABORI*
Department of Chemistry, Faculty of Science, Toho University, Funabasi, Chiba 274
†Analytical and Metabolic Research Laboratories, Sankyo Co., Ltd., Hiromachi, Shinagawa-ku, Tokyo 140
††Chemical Analysis Center, Saitama University, Urawa, Saitama 338
(Received May 30, 1989)

The reaction of 1,1′-bis(6-chloro-1,4-dioxahexyl)ruthenocene with disodium 1,2-ethanedithiolate gave 1,4,13,16-tetraoxa-7,9-dithia[16](1,1′)ruthenocenophane (**5**) in 63% yield. The reaction of **5** with $HgCl_2$ in acetonitrile gave a 1 : 2 complex (**6**) in 47% yield. The crystal structure of complex **6** and its metal free ligand **5** were determined by an X-ray method. Crystal data: **5**, triclinic, a=11.128(2), b=12.720(2), c=10.196(2) Å, α=113.55(1), β=64.13(1), γ=122.01(1)°, U=1074.1 Å^3. $P\bar{1}$, Z=2, D_c=1.54 Mg m^{-3}, μ(Mo $K\alpha$)=9 mm^{-1}. R=0.028. **6**, triclinic, a=16.595(4), b=12.645(3), c=7.401(1) Å, α=104.92(1), β=92.37(1), γ=69.38(2)°, U=1402.4 Å^3, $P\bar{1}$, Z=2, D_c=2.46 Mg m^{-3}, μ(Mo $K\alpha$)=12.2 mm^{-1}, R=0.081. The X-ray analysis of **6** revealed that one Hg atom was bonded to the Ru atom of the ruthenocene nucleus with a distorted trigonal-planar configuration and another Hg atom was bonded to the two sulfur atoms of the macrocycle. This result is completely different from that obtained regarding complex 4,7,10,13-tetraoxa-1,16-dithia[16](1,1′)ruthenocenophane with $HgCl_2$.

It is well-known that mercury forms a very wide range of complexes with thioethers and cyclic thioethers. Mercury halides readily form 1 : 1, 1 : 2, and 2 : 3 complexes with thioethers when the metal and ligands are mixed in aqueous alcoholic solution.[1-4] The 1 : 1 complexes[5] involve essentially linear mercury(II) coordination $[R_2SHgCl]Cl$ (type 1) and the 1 : 2 complexes[5,6] are thought to involve HgX_2 and $[R_2SHgX]X$ units held together by weak chloride bridges (type II), while 2 : 3 complexes[3] appear to be a mixture of 1 : 1 and 1 : 2 complexes. In contrast with the above, the reaction of mercury(II) halide with polyethylene glycols gives complexes of type 1 only.[7-9] Pedersen[10] has reported that mercury(II) chloride does not form a complex with dibenzo-18-crown-6 in methanol. Recently, Kawasaki et al.,[11] however, reported the formation of a mercury(II) chloride complex of dibenzo-18-crown-6 in acetonitrile or toluene. In this complex a linear Cl-Hg-Cl moiety (type 1) was found by X-ray analysis to be held perpendicularly to a quasi-planar ring of O_6. It has also been reported that the reaction of the metallocene with HgX_2 gives various adducts.[12] For example, the complex of ruthenocene with $HgBr_2$ is essentially a simple adduct complicated by the presence of halide bridging. In connection with the above-mentioned viewpoints we have been interested in the complexing manner of the metallocenocrown ethers with $HgCl_2$.

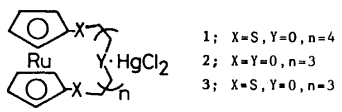

In previous papers,[13,14] we reported on the molecular structures of a 1 : 1 complexes (**1**, **2**, and **3**) of 4,7,10,13-tetraoxa-1,16-dithia[16](1,1′)ruthenocenophane, 1,4,7,10,13-pentaoxa- and 1,13-dioxa-4,7,10-trithia[13](1,1′)ruthenocenophanes with $HgCl_2$. In this paper we report on the molecular structure of a 1 : 2 complex (**6**) of 1,4,13,16-tetraoxa-7,10-dithia[16](1,1′)ruthenocenophane (**5**) with $HgCl_2$ in order to clarify the manner of the complexing.

Syntheses. The following reactions were carried out to obtain complex **6**. The reaction of 1,1′-diacetoxyruthenocene with bis(2-chloroethyl) ether in ethanol in the presence of potassium hydroxide gave **4** in 73% yield. The reaction of **4** with dipotassium 1,2-ethanedithiolate in ethanol gave **5** in 63% yield. A solution of $HgCl_2$ in 1 ml of acetonitrile was added, dropwise, to a solution of 1 ml of acetonitrile containing **5**. The resulting precipitates were filtered and washed with a small amount of acetonitrile to give a 1 : 2 complex (**6**) in 47% yield. In spite of the many attempts to prepare the 1 : 1 complex of **5** with $HgCl_2$ it could not be obtained.

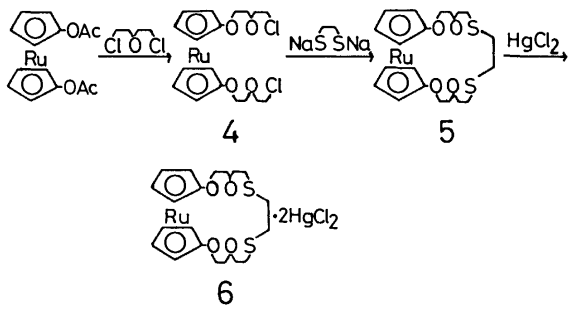

^{1}H NMR spectra of **5** and its mercury(II) complex (**6**) were measured in DMSO-d_6 as the solvent. Upon comparing the ^{1}H NMR spectra of **6** with **5**, the signals of the β-protons of the Cp-rings in **6** were shifted further down field (3.0 ppm) than the α-protons (2.1 ppm). The signals of the methylene protons attached to the sulfur atoms of **6** were also shifted down field (0.05—0.06 ppm), although the change in the chemical shifts of the methylene protons attached to the oxygen atoms was negligible. These results sug-

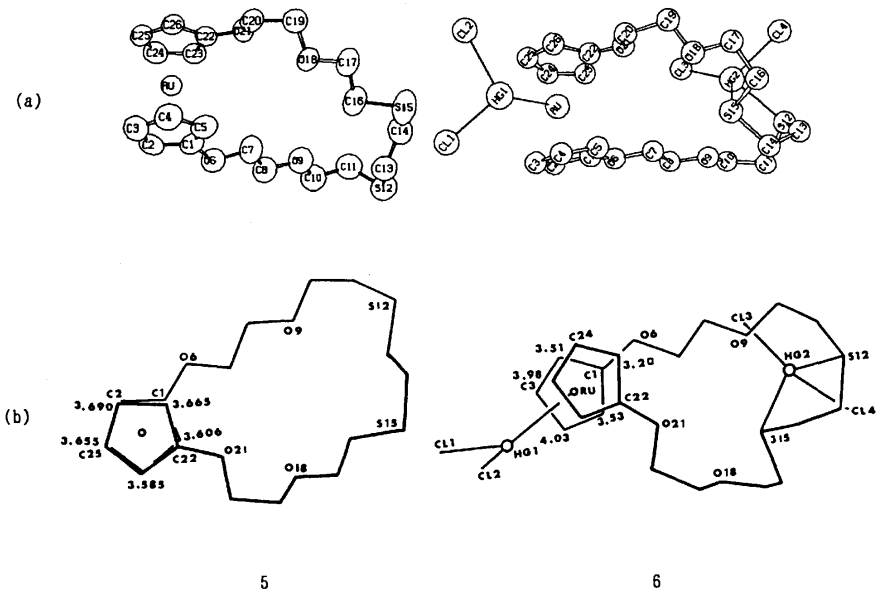

5 6

Fig. 1. ORTEP (Johnson, 1965) drawings of the molecules **5** and **6** with atom numbering scheme. (b) Projections of the molecules on the Cp rings containing the C(1) atom with the C···C distances (The mean standard deviations are 0.005 and 0.04 Å for **5** and **6**, respectively).

Table 1. Fractional Atomic Coordinates ($\times 10^4$) and Thermal Parameters, with Estimated Standard Deviations in Parentheses of **5**

Atom	x	y	z	B_{eq}[a]/Å^2
Ru	2432.1(3)	4457.0(2)	2551.6(3)	3.34
C(1)	1289(3)	2686(3)	1095(3)	4.1
C(2)	1283(3)	3713(3)	866(3)	4.4
C(3)	478(3)	4247(3)	2272(4)	4.7
C(4)	37(3)	3560(3)	3324(4)	4.3
C(5)	544(3)	2582(3)	2607(4)	4.2
O(6)	1845(2)	1888(2)	−80(2)	5.4
C(7)	2206(4)	1138(3)	289(4)	6.0
C(8)	2803(4)	393(3)	−1181(4)	5.8
O(9)	3237(3)	−350(2)	−910(2)	5.8
C(10)	3837(4)	−1066(3)	−2275(4)	6.0
C(11)	4309(4)	−1821(3)	−1942(4)	5.7
S(12)	2862(1)	−3312(1)	−1434(1)	6.1
C(13)	1860(4)	−2847(3)	472(4)	5.2
C(14)	2722(4)	−2440(3)	1536(4)	5.2
O(15)	1755(1)	−2038(1)	3470(1)	6.6
C(16)	1732(4)	−620(3)	3495(4)	5.4
C(17)	2011(4)	353(3)	4900(4)	5.2
O(18)	1971(2)	1423(2)	4831(2)	5.0
C(19)	2519(4)	2524(3)	5923(4)	4.8
C(20)	2656(3)	3627(3)	5585(3)	4.1
O(21)	3792(2)	3849(2)	4214(2)	4.1
C(22)	3919(3)	4727(3)	3655(3)	3.7
C(23)	4722(3)	4855(3)	2157(3)	3.6
C(24)	4706(3)	5906(3)	1995(3)	4.2
C(25)	3876(3)	6407(3)	3380(4)	4.4
C(26)	3360(3)	5676(3)	4432(3)	3.8

a) W.C. Hamilton, *Acta Crystallogr.*, **12**, 609 (1959).

Table 2. Fractional Atomic Coordinates ($\times 10^4$) and Thermal Parameters, with Estimated Standard Deviations in Parentheses of **6**

Atom	x	y	z	B_{eq}[a]/Å^2
Hg(1)	4082.2(7)	−47.0(9)	3352.9(13)	3.63
Hg(2)	1333.1(8)	7795.3(10)	5112.1(15)	5.28
Ru	2747.7(12)	1923.7(16)	3271.4(24)	3.08
Cl(1)	4621(4)	−1943(5)	974(9)	4.5
Cl(2)	4510(4)	−694(5)	6373(8)	4.1
Cl(3)	534(5)	6782(7)	6013(9)	7.0
Cl(4)	1731(5)	9327(6)	7454(9)	6.1
C(1)	2227(15)	2741(20)	894(28)	3.7
C(2)	2216(16)	1580(19)	477(30)	3.9
C(3)	3030(17)	831(20)	348(29)	4.0
C(4)	3623(16)	1444(23)	738(31)	4.6
C(5)	3100(16)	2645(21)	1124(28)	4.2
O(6)	1526(10)	3669(12)	929(22)	4.1
C(7)	1666(17)	4774(21)	1232(36)	5.0
C(8)	833(18)	5591(18)	910(36)	5.0
O(9)	951(11)	6694(12)	1120(22)	4.3
C(10)	182(16)	7607(22)	1055(33)	4.8
C(11)	379(16)	8642(21)	898(33)	4.5
S(12)	833(5)	9295(6)	3001(10)	5.1
C(13)	1912(19)	8989(23)	2259(39)	6.0
C(14)	2486(17)	7732(23)	1372(31)	5.0
S(15)	2728(4)	6780(6)	2995(9)	4.4
C(16)	3544(18)	7230(23)	4330(35)	5.4
C(17)	3692(21)	6761(24)	6041(38)	6.9
O(18)	3821(14)	5590(17)	5520(28)	8.0
C(19)	3981(20)	5057(24)	6994(40)	6.7
C(20)	3824(18)	3902(23)	6449(36)	5.7
O(21)	2894(12)	4183(14)	6271(23)	5.2
C(22)	2634(16)	3252(20)	5973(32)	4.1
C(23)	1805(16)	3314(20)	5296(32)	4.2
C(24)	1705(16)	2232(23)	5290(35)	4.8
C(25)	2490(18)	1507(23)	5813(35)	5.7
C(26)	3114(16)	2114(19)	6281(31)	3.8

a) W.C. Hamilton, *Acta Crystallogr.*, **12**, 609 (1959).

gest that the mercury atoms were coordinated to the ruthenium atom of the ruthenocene nucleus and the sulfur atoms of the macrocyclic moiety.

X-Ray Analyses. The molecular structures of **5**

Table 3. Bond Lengths (l) and Bond Angles (θ) and Torsion Angles (τ) in the Organic Ligand of **5**

1	2	3	4	1-2 l/Å	1-2-3 θ/°	1-2-3-4 τ/°
Tetraoxa-dithia-crown moiety						
O(6)	C(1)	C(2)	C(3)	1.377(5)	121.1(3)	173.3(3)
O(6)	C(1)	C(5)	C(4)		128.6(3)	173.0(3)
C(2)	C(1)	O(6)	C(7)			162.1(3)
C(5)	C(1)	O(6)	C(7)			−24.3(5)
C(1)	O(6)	C(7)	C(8)		116.6(3)	−179.0(3)
O(6)	C(7)	C(8)	O(9)	1.428(5)	105.2(3)	178.1(3)
C(7)	C(8)	O(9)	C(10)	1.500(6)	108.7(3)	−179.1(3)
C(8)	O(9)	C(10)	C(11)	1.420(5)	111.1(3)	178.9(3)
O(9)	C(10)	C(11)	S(12)	1.426(5)	109.5(3)	82.4(4)
C(10)	C(11)	S(12)	C(13)	1.505(6)	116.0(3)	−76.1(3)
C(11)	S(12)	C(13)	C(14)	1.810(4)	103.1(2)	−75.3(3)
S(12)	C(13)	C(14)	S(15)	1.806(4)	111.0(3)	−177.1(1)
C(13)	C(14)	S(15)	C(16)	1.516(6)	113.7(3)	−67.2(3)
C(14)	S(15)	C(16)	C(17)	1.798(4)	100.2(2)	−140.0(3)
S(15)	C(16)	C(17)	O(18)	1.807(5)	110.0(3)	−179.9(1)
C(16)	C(17)	O(18)	C(19)	1.498(6)	106.3(3)	−167.6(3)
C(17)	O(18)	C(19)	C(20)	1.415(5)	113.0(3)	170.8(3)
O(18)	C(19)	C(20)	O(21)	1.419(5)	108.1(3)	−67.1(4)
C(19)	C(20)	O(21)	C(22)	1.491(6)	107.7(3)	171.9(3)
C(20)	O(21)	C(22)	C(23)	1.424(5)	114.6(3)	−164.5(3)
C(20)	O(21)	O(22)	C(26)			18.4(5)
O(21)	C(22)	C(23)	C(24)	1.365(4)	122.5(3)	−176.1(3)
O(21)	C(22)	C(26)	C(25)		128.1(3)	175.9(3)
Cyclopentadienyl ring						
C(1)	C(2)	C(3)	C(4)	1.420(5)	106.6(3)	1.1(4)
C(2)	C(3)	C(4)	C(5)	1.437(3)	108.1(3)	−0.3(4)
C(3)	C(4)	C(5)	C(1)	1.411(5)	109.1(3)	−0.5(4)
C(4)	C(5)	C(1)	C(2)	1.434(5)	106.2(3)	1.2(4)
C(5)	C(1)	C(2)	C(3)	1.418(5)	110.1(3)	−1.4(4)
C(22)	C(23)	C(24)	C(25)	1.418(5)	107.2(3)	−1.0(4)
C(23)	C(24)	C(25)	C(26)	1.421(5)	108.4(3)	0.0(4)
C(24)	C(25)	C(26)	C(22)	1.422(5)	108.9(3)	0.9(4)
C(25)	C(26)	C(22)	C(23)	1.427(5)	106.0(5)	−1.5(4)
C(26)	C(22)	C(23)	C(24)	1.440(5)	109.4(3)	1.6(4)

Table 4. Bond Lengths (l) and Bond Angles (θ) and Torsion Angles (τ) in the Organic Ligand of **6**

1	2	3	4	1-2 l/Å	1-2-3 θ/°	1-2-3-4 τ/°
Hexaoxa-crown moiety						
O(6)	C(1)	C(2)	C(3)	1.32(3)	123(2)	173(2)
O(6)	C(1)	C(5)	C(4)		131(2)	−173(3)
C(2)	C(1)	O(6)	C(7)			−175(2)
C(5)	C(1)	O(6)	C(7)			1(4)
C(1)	O(6)	C(7)	C(8)		115.5(19)	171(2)
O(6)	C(7)	C(8)	O(9)	1.46(3)	104(2)	−177.6(17)
C(7)	C(8)	O(9)	C(10)	1.46(3)	106(2)	−173(2)
C(8)	O(9)	C(10)	C(11)	1.44(3)	113(2)	−168.8(19)
O(9)	C(10)	C(11)	S(12)	1.40(3)	109(2)	−67(3)
C(10)	C(11)	S(12)	C(13)	1.49(4)	113.1(19)	112(2)
C(11)	S(12)	C(13)	C(14)	1.83(3)	103.7(14)	−55(3)
S(12)	C(13)	C(14)	S(15)	1.77(3)	120(2)	−66(3)
C(13)	C(14)	S(15)	C(16)	1.52(4)	114(2)	−78(2)
C(14)	S(15)	C(16)	C(17)	1.85(3)	100.3(13)	167.1(19)
S(15)	C(16)	C(17)	O(18)	1.81(3)	109(2)	50(3)
C(16)	C(17)	O(18)	C(19)	1.51(5)	109(3)	179(2)
C(17)	O(18)	C(19)	C(20)	1.37(4)	114(3)	161(2)
O(18)	C(19)	C(20)	O(21)	1.39(4)	111(3)	−69(3)
C(19)	C(20)	O(21)	C(22)	1.52(4)	107(2)	−174(2)
C(20)	O(21)	C(22)	C(23)	1.46(3)	114(2)	−164(2)
C(20)	O(21)	O(22)	C(26)			17(4)
O(21)	C(22)	C(23)	C(24)	1.36(3)	121(2)	−175(12)
O(21)	C(22)	C(26)	C(25)		127(2)	177(2)
Cyclopentadienyl ring						
C(1)	C(2)	C(3)	C(4)	1.43(4)	109(2)	2(3)
C(2)	C(3)	C(4)	C(5)	1.34(4)	111(2)	0(3)
C(3)	C(4)	C(5)	C(1)	1.43(4)	105(2)	−2(3)
C(4)	C(5)	C(1)	C(2)	1.42(4)	109(2)	4(3)
C(5)	C(1)	C(2)	C(3)	1.42(3)	106(2)	−4(2)
C(22)	C(23)	C(24)	C(25)	1.43(4)	107(2)	−5(3)
C(23)	C(24)	C(25)	C(26)	1.43(4)	107(2)	3(3)
C(24)	C(25)	C(26)	C(22)	1.41(4)	112(2)	−1(3)
C(25)	C(26)	C(22)	C(23)	1.47(4)	102(2)	−2(3)
C(26)	C(22)	C(23)	C(24)	1.45(4)	112(2)	4(3)
Hg coordination						
Ru	HG1	Cl(1)		2.701(2)	129.7(2)	Cl(2′): $1-x, -y, 1-z$
Ru	HG1	Cl(2)			122.6(2)	
Ru	HG1	Cl(2′)			102.4(2)	
Cl(1)	HG1	Cl(2)		2.470(7)	101.1(2)	
Cl(2′)	HG1	Cl(1)		2.792(7)	102.5(2)	
Cl(2)	HG1	Cl(2′)		2.564(7)	88.5(2)	
S(12)	HG2	S(15)		2.576(8)	87.0(2)	
S(12)	HG2	Cl(3)			123.6(3)	
S(12)	HG2	Cl(4)			100.3(3)	
S(15)	HG2	Cl(3)		2.654(8)	127.3(3)	
Cl(3)	HG2	Cl(4)		2.356(9)	121.5(3)	
Cl(4)	HG2	S(15)		2.504(9)	87.2(3)	

and **6** are illustrated in Fig. 1. The final atomic parameters for **5** and **6** are listed in Tables 1 and 2, and bond lengths as well as bond and torsion angles are given in Tables 3 and 4 for **5** and **6**, respectively. The structure of complex **6** differs completely from that of **1** in which the Hg atom of $HgCl_2$ incorporated in the central cavity of the crown ether moiety forms a distorted hexagonal-bipyramidal geometry with an angle of 172.7(2)° (type 1), even though **1** has the same number of crown moieties as **6** and the positions of the two sulfur atoms in **1** and **6** are the only difference between them. Surprisingly, the one Hg(1) atom of $HgCl_2$ in complex **6** is bonded directly to the Ru atom of the ruthenocene nucleus from the opposite side of the crown ether moiety with a distorted trigonal-planar configuration and one Cl(2)′ atom of the adjacent complex also linked by a weak bond to the Hg atom. Therefore, the Hg(1) atom forms a distorted trigonal-pyramidal geometry. The Ru-Hg(1) interatomic distance in **6** is 2.701 Å, which essentially equals the sums (2.68 Å) of the covalent radii of Ru and Hg atoms.[15] However, the value is intermediate between those (2.65 and 2.74 Å) found in the 2:3 $HgCl_2$ complex[16] and the 1:1 $HgBr_2$ complex[16] of ruthenocene. The sum of the three bond angles about the Hg(1) atom is 353.3° and the deviation of the Hg atom from the Cl(1)-Ru-Cl(2) plane is 0.381°. These values are similar to those found in the 1:1 mercury complexes **2** and **3**.[14] The values (2.470(7)

and 2.564(7) Å of the Hg-Cl(1) and Hg-Cl(2) bonds are even smaller than those (2.55 and 2.60 Å) of the corresponding Hg-Cl bonds in the 2:3 complex[16] of ruthenocene with $HgCl_2$. It may be attributed to the difference in the complexing ratios between ruthenocene and $HgCl_2$. Another Hg(2) atom of $HgCl_2$ is also bonded to the two sulfur atoms of the macrocyclic moiety with a distorted tetrahedral geometry. The lengths (2.576(8) and 2.654(8) Å) of S(12)-Hg(2) and S(15)-Hg(2) bonds and the dihedral angle (62.3(2)°) between the planes defined by S(12)-Hg(2)-S(15) and Cl(3)-Hg(2)-Cl(4) is smaller than those found in μ-(1,4,8,11-tetrathiacyclotetradecane-S^1S^4;S^8S^{11})bis[dichloromercury(II)].[17] It is noteworthy that the Cp ring in **6** deviates from planarity, and its tilting angle is 21.1(1)°, although that in the corresponding metal free ligand **5** is only 2.5(2)°. The large tilting in **6** is attributed to the metal-metal (Ru-Hg(1)) bond formation followed by the steric repulsion between the two Cp-rings and $Hg(1)Cl_2$ units. Finally, the difference in the complexing manner of **6** and **3** with $HgCl_2$ seems to be attributable to: (I) the Hg(2) atom is more easily bonded to the S(12) and S(15) atoms in **5** compared to the two sulfur atoms in the metal free ligand **7** of the corresponding complex **3**, because the direc-

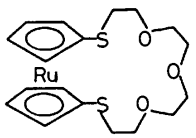

7

tions of the lobes of lone pair electrons of the two sulfur atoms in **5** are more suitable for S-Hg-S bonding compared with those in **7**; (II) the differences of the ring sizes and tilting angles of the two Cp-rings in **5** and **7** are also effected by the complexing manner of the metal free ligands (**5** and **7**) with $HgCl_2$. Therefore, the Hg(2) atom is selectively bonded to the two sulfur atoms in **5** without incorporation into the central cavity of the macrocycle as the linear Cl-Hg-Cl form.

Experimental

Melting points are uncorrected. The ^1H NMR spectra were measured on a JEOL GX400 spectrometer with TMS as the internal standard.

Materials. 1,1′-Diacetoxyruthenocene was prepared according to a method mentioned in a previous paper.[18] The other reagents employed were either commercial or prepared by the usual methods. The solvents were purified by distillation.

1,1′-Bis(6-chloro-1,4-dioxahexyl)ruthenocene (4). 1,1′-Diacetoxyruthenocene (471 mg, 1.36 mmol) was added to 10 ml of potassium hydroxide solution (619 mg, 15.4 mmol) containing catalytic amounts of 18-crown-6 under nitrogen. After the mixture was stirred at reflux temperature, bis(3-chloropropyl) ether (5.488 g, 38.1 mmol) in 10 ml of ethanol was added to the mixture at once. The stirring was continued for 6 h under reflux. The solution was cooled to room temperature, and extracted with three 100 ml portions of ether. The extracts were combined, washed with water, and concentrated in vacuo. The residual oil was chromatographed on silica-gel TLC (hexane : acetone=4 : 1 as eluent). The second band was extracted with acetone at room temperature, followed by filtration and evaporation of the solvent to give **4** as a pale-yellow oil. 73% yield. Found: C, 45.21; H, 5.10%. Calcd for $C_{18}H_{24}Cl_2O_4Ru$: C, 45.38; H, 5.04%. MS(M^+) 476.

1,4,13,16-Tetraoxa-7,10-dithia[16](1,1′)ruthenocenophane (5). A solution of **4** (1.63 g, 3.42 mmol) in THF (120 ml) and a mixture of 1,2-ethanedithiol (1.68 g, 17.8 mmol) and potassium hydroxide (1.46 g, 36.5 mmol) in 120 ml of aqueous ethanol were added to 100 ml of ethanol-THF (1 : 1) solution over 3 h under reflux. The refluxing was continued for 12 h with stirring. The mixture was cooled to room temperature and concentrated in vacuo. The residual oil was chromatographed on silica gel (hexane : acetone=4 : 1 as eluent). The main band was extracted with acetone, and the solution was evaporated in vacuo. Recrystallization of the residue from hexane gave **5** as white needles in 13% yield. Mp 93.0—94.0 °C. Found: C, 48.35; H, 5.55%. Calcd for $C_{20}H_{28}O_4S_2Ru$: C, 48.29; H, 5.63%. ^1H NMR (in DMSO-d_6) δ=4.66 (t, J=1.8 Hz, 4H), 4.27 (t, J=1.8 Hz, 4H), 3.79—3.40 (m, 8H), 3.63 (t, J=6.2 Hz, 4H), 2.80 (s, 4H), 2.70 (t, J=6.2 Hz, 4H). MS (M^+) 497.

Isolation of 1 : 2 Complex of 5 with $HgCl_2$. A solution of **5** (38 mg, 7.6×10^{-2} mmol) in ether (5 ml) was added to a solution containing mercury(II) chloride (26 mg, 9.6×10^{-2} mmol) in 15 ml of ether. As the mixture was concentrated to 10 ml in vacuo, a yellow solid precipitated. Recrystallization of the solid from acetonitrile (2 ml) gave pure mercury complex (**6**) in 47% yield. Mp 159.5—160.5 °C. Found: C, 23.28; H, 2.80%. Calcd for $C_{20}H_{28}O_4S_2Ru(HgCl_2)_2$: C, 23.10; H, 2.69%. ^1H NMR (in DMSO-d_6) δ=4.87 (broad s, 4H), 4.57 (broad s, 4H), 3.78 (t, J=4.6 Hz, 4H), 3.64 (t, J=4.6 Hz, 4H), 3.62 (t, J=6.2 Hz, 4H), 2.86 (s, 4H), 2.75 (t, J=6.2 Hz, 4H).

X-Ray Crystallography of 5 and 6. Crystals of dimensions 0.3×0.3×0.3 mm for **5** and 0.4×0.2×0.1 mm for **6** were used for X-ray crystallography. Lattice constants were determined by a least-squares fit of angular settings of 2θ reflections within the range $15<2\theta<30°$. Intensity data were obtained on a Rigaku AFC-5R diffractometer equipped with graphite-monochromatized Mo $K\alpha$ (λ=0.71069 Å) radiation and using the θ-2θ scan technique ($2\theta<50°$). During data collection, three standards (measured before every 200 reflections) indicated no systematic variation of the intensity with time. Of 3781 and 4928 independent reflections measured, only 3573 and 3999 for **5** and **6**, respectively, were considered as observed on the basis of the criterion $F_o<2\sigma(F_o)$. All intensities were corrected for Lorentz and polarization effects, but not for absorption. Crystal data: **5**, $C_{20}H_{28}O_4S_2Ru$, Mw=497.7. Triclinic, space group $P\bar{1}$, a=11.128(2), b=12.720(2), c=10.196(2) Å, α=113.55(1), β=64.13(1), γ=122.01(1)°, U=1074.1 Å^3, Z=2, D_c=1.54 Mg m^{-3}, μ(Mo $K\alpha$)=0.9 mm^{-1}. **6**, $C_{20}H_{28}O_4S_2RuHg_2Cl_4$, Mw=1040.7. Triclinic, space group $P\bar{1}$, a=16.595(4), b=12.645(3), c=7.401(1) Å, α=104.92(1), β=92.37(1), γ=69.38(2)°, U=1402.4 Å^3, Z=2, D_c=2.46 Mg m^{-3}, μ(Mo $K\alpha$)=12.2 mm^{-1}. The structures of **5** and **6** were solved by the

heavy-atom methods, and refined by the block-diagonal least-squares method. The positions of the hydrogen atoms were estimated using standard geometry. The final refinements with anisotropic temperature factors for the non-hydrogen atoms and isotropic temperature factors for the hydrogen atoms lowered the R values to 0.028 (R_w=0.025, $w=1/\sigma^2(F_o)$) and 0.081 (R_w=0.070, $w=1/\sigma(F_o)$) for **5** and **6**, respectively.[19] Anomalous dispersion corrections were applied to the scattering factors of Hg, Ru, Cl, and S.[20] The complete F_o-F_c data are deposited as Document No. 8904 at the office of the Bull. Chem. Soc. Jpn.

References

1) J. E. Ferguson and K. S. Loh, *Aust. J. Chem.*, **26**, 2615 (1973).
2) M. Zachrissan and K. I. Alden, *Acta Chem. Scand.*, **14**, 994 (1960).
3) P. Biscarini and G. D. Nivellini, *J. Chem. Soc. A*, **1969**, 2206.
4) D. T. McAllen, T. V. Cullum, R. A. Dean, and F. A. Fidler, *J. Am. Chem. Soc.*, **73**, 3627 (1951).
5) C.-I, Branden, *Ark. Kemi*, **22**, 83, 495, 501 (1964).
6) P. J. Hendra and D. B. Powell, *J. Chem. Soc.*, **1960**, 5105.
7) G. Weber, *Acta Crystallogr., Sect. B*, **36**, 2779 (1980).
8) R. Iwamoto and H. Wakao, *J. Am. Chem. Soc.*, **98**, 3764 (1976).
9) R. Iwamoto, *Bull. Chem. Soc. Jpn.*, **46**, 1114 (1973).
10) C. J. Pedersen, *J. Am. Chem. Soc.*, **89**, 7017 (1967).
11) Y. Kawasaki and Y. Matuura, *Chem. Lett.*, **1984**, 154.
12) W. H. Morrison, Jr., and D. V. Hendrickson, *Inorg. Chem.*, **11**, 2912 (1972).
13) S. Akabori, H. Munegumi, Y. Habata, S. Sato, K. Kawazoe, C. Tamura, and M. Sato, *Bull. Chem. Soc. Jpn.*, **58**, 2185 (1985).
14) S. Akabori, S. Sato, K. Kawazoe, C. Tamura, M. Sato, and Y. Habata, *Chem. Lett.*, **1987**, 1783.
15) L. Pauling, "The Nature of the Chemical Bond," 3rd ed Cornell University Press, Ithaca, New York (1960).
16) A. I. Gusev and U. T. Struchkov, *Zh. Strukt. Khim.*, **6**, 1121 (1972).
17) N. W. Alock, N. Herron, and Moore, *J. Chem. Soc., Dalton Trans.*, **1978**, 394.
18) Y. Habata, S. Akabori, and S. Sato, *Bull. Chem. Soc. Jpn.*, **58**, 3540 (1985).
19) T. Asida, "The Universal Crystallographic Computing System: A System of Computer Program for the Automatic Solution of Crystal Structures from X-Ray Diffraction Data," Osaka University (1973).
20) "International Tables for X-Ray Crystallography," Kynoch Press, Birmingham (1974), Vol. IV, pp. 72—98 and 149—150.

Photochromism of 4-Oxazolyl Fulgides[1)]

Hisao SUZUKI,* Akihiko TOMODA,* Mitsuo ISHIZUKA, Akira KANEKO,
Masami FURUI,† and Ryoka MATSUSHIMA†
Basic Research Development Laboratory, Toyooka Plant, Yamaha Co., Toyooka-mura, Iwata-gun 438-01
†Department of Applied Chemistry, Faculty of Engineering, Shizuoka University, Hamamatsu 432
(Received June 15, 1989)

The thermal and photochemical stabilities of 2-[1-(2-phenyl-5-methyl-4-oxazolyl)]alkylidenesuccinic anhydrides (**1**) and (**2**) were studied. These compounds showed good thermal stabilities in PMMA film and low photochemical fatigue (PF $\leq$ 0.03% /cycle) in a dilute toluene solution in the presence of air, compared with 3-furyl fulgide (**3**). Although in PMMA film the photochemical fatigue resistance property of the fulgides was poor, in comparison with that in solution, the addition of an organo-nickel stabilizer improved the property.

In order to use an optical memory device based upon a photochromic system, knowledge concerning the thermal stabilities of the colored and uncolored form (i.e. erase and write modes) is essential.

Heller et al.[2)] reported that heterocyclic fulgides, such as 3-furyl and 3-thienyl derivatives, showed good thermal stabilities. With this as a starting point, the possibility of organic photochromic compounds as data storage media have again been elevated as matters of chemical interest, and various investigations have been initiated.

Recently, Irie[3)] reported that diarylethene derivatives were thermally stable photochromic compounds, and more recently Tamaki and Ichimura[4)] showed that chelation of spiroindolinonaphthoxiazine was effective in improving thermal fatigue resistance.

On the other hand, in a previous paper[5)] we showed that 4-pyrazolyl, 3-indolyl, 4-oxazolyl, and 4-thiazolyl fulgide possesses good thermal and photochemical stabilities in comparison with 3-furyl fulgide **3**. However, it seemed that the photo-responsiveness and/or the conversion of these fulgides to the colored form in the photostationary state were too low, except for 4-oxazolyl fulgide. In this study we report on the responsiveness and the photochemical and thermal fatigue resistances of 4-oxazolyl fulgide in detail, and also on the effect of a long alkyl chain substituent.

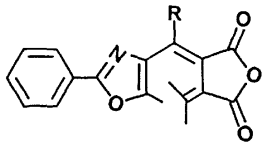

1 R = CH_3
2 R = $C_{17}H_{35}$

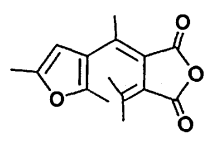

3

Results and Discussion

The absorption spectra of colored and uncolored forms of **1** in dilute toluene solutions (1.0×10^{-4} mol dm^{-3}) and PMMA thin films (ca. 1.0 μm thickness) are illustrated in Fig. 1.

A photostationary state (pss) for coloration, i.e. cyclization reaction, was attained by irradiation with

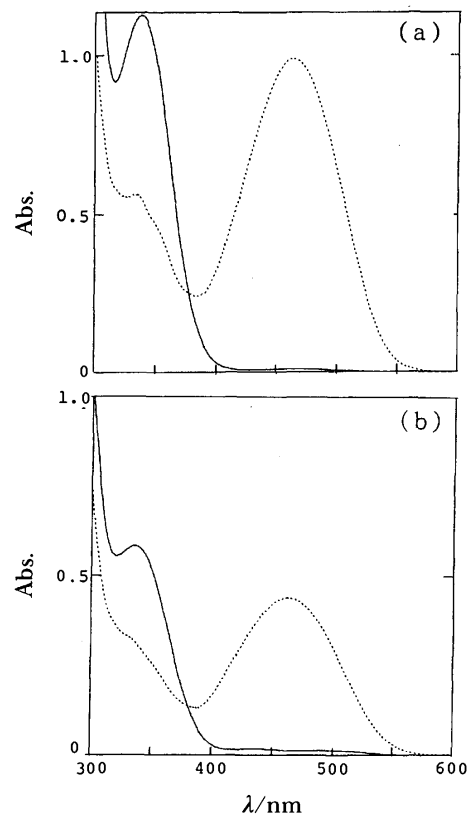

Fig. 1. Absorption spectra of uncolored and colored forms of **1**.
(a) In dilute toluene solutions (1.0×10^{-4} mol dm^{-3}).
(b) PMMA thin films (1.0 μm thickness, 20 wt%).

UV light (366 nm) for 40 s. After subsequent irradiation for 40 s with visible light (>390 nm), it underwent discoloration, i.e. disclosure reaction.

The absorption maximum and its intensity of color are similar, even when a methyl substituent is replaced with a long alkyl chain. Further, 0.20 mol dm^{-3} deuteriochloroform solutions of **1** and **2** in NMR tubes were exposed to UV light. The NMR measurements showed that these were converted nearly quantitatively into colored forms (**1C** and **2C**) in 84 and 91%, respectively.

Photo-responsiveness for coloration and bleaching of **1** and **2** are shown in Fig. 2. It was noticeable that

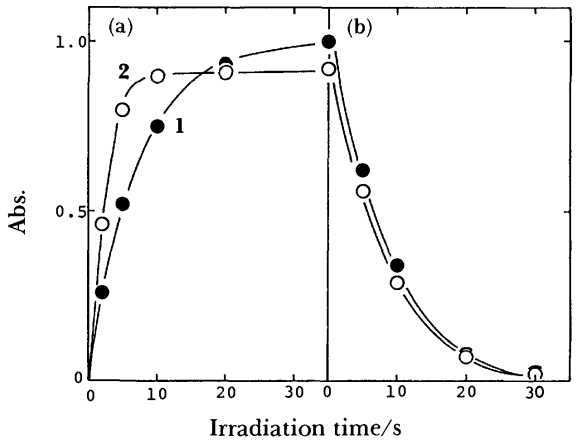

Fig. 2. Photo-responsiveness for coloration (a) and discoloration (b) of **1** and **2** in dilute toluene solutions (1.0×10^{-4} mol dm^{-3}) with UV and visible light irradiation.

fulgide **2** exhibited rapid coloration. The quantum yield (ϕ_c) for coloration of **2** was 0.42. The ϕ_c of **1** was 0.18, which was nearly the same as that for **3**. Kurita et al.[6] reported the relationship between the ϕ_c and the steric interaction for 3-furyl fulgides. According to their study, the introduction of a propyl substituent, instead of a methyl substituent, caused an increase in the ϕ_c, 0.19 to 0.45. They explained that the high efficiency of this cyclization reaction was due to a steric repulsion between the isopropylidene group and the alkyl substituent, which did not favor *E-Z* isomerization.

In our study, the ϕ_c of 3-furyl fulgide substituted with a long alkyl chain was 0.45. These results showed us that the introduction of a bulky alkyl substituent is also effective at improving ϕ_c of oxazolyl fulgide, similar to **3**.

Figure 3 illustrates the photochemical fatigue resistances of **1**, **2** and **3**. 4-Oxazolyl fulgides showed good resistances in a dilute toluene solution in the presence of air. The relative photochemical fatigue PF=$(A_0-A_n)/nA_0$ was evaluated, where A_0 and A_n are the absorbance values at pss attained on the lst and nth cycles of coloration. The values of **1**, **2**, and **3** are 0.03, 0.02, and 0.76%. Similar values were also obtained in an ethyl acetate solution. The photochemical stability of 4-oxazolyl fulgide is attributable to its heteroaromatic structure deactivated by electronegative nitrogen, though photochemical reactions of oxazole, such as photorearrangement[7] or photosensitized oxidation,[8] are known.

Irie et al.[9] evaluated the photochemical fatigue resistances of some photochromic compounds, and indicated that naphthoxazine showed the best stability. It is noteworthly that the excellent durability of naphthoxazine was caused by a slight modification of spiropyran, which showed little resistance. The only structural difference is that C=C bond in the pyran ring is replaced by a C=N bond. This modification improved the resistance remarkably; naphthoxazine could be photo-cyclized more than 2000 times.

As shown in Fig. 3, the replacement of the C=C bond with a C=N bond in the furan ring also improved the fatigue resistance markedly. These facts suggest that the C=N bond plays an important role in reducing photodegradation in a photochromic reaction.

On the other hand, further improvement caused by long alkyl chain substituent seemed to be due to the high ϕ_c of **2**, which reduces the possibility of side reactions.

As shown in Fig. 4, the fatigue resistance in PMMA thin film containing fulgide (20 wt%) was markedly decreased in comparion with that in a dilute solution. The PF values of **1**, **2**, and **3** are 0.63, 0.42, and 2.80%. This undesirable fact suggests the considerable effects of the medium and the concentration of the fulgides on photochemical fatigue.

Chu[10] reported on the photochromic performance

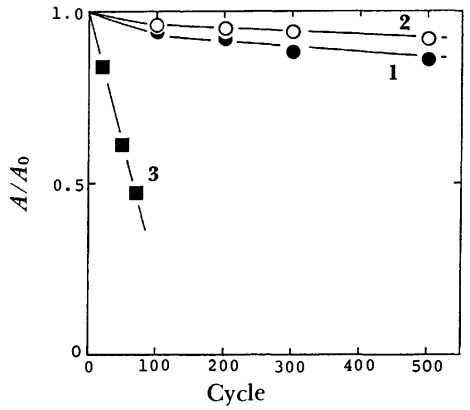

Fig. 3. Photochemical fatigues of fulgides by repeated coloration and discoloration cycles in dilute toluene solutions (1.0×10^{-4} mol dm^{-3}). A_0 and A_n are the absorbance values at pss attained on the 1st and nth cycles of coloration.

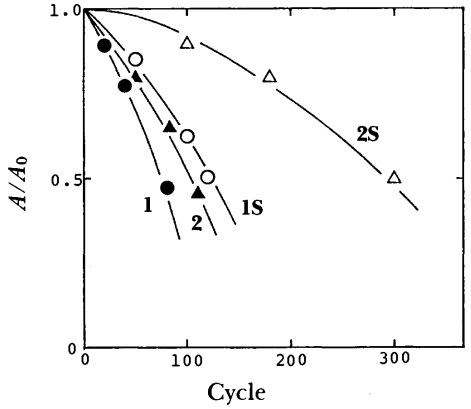

Fig. 4. Photochemical fatigues of fulgides in PMMA thin film (1.0 μm thickness, 20 wt%) and effect of organo-nickel stabilizer. 1 wt% Nickel stabilizer was added into PMMA thin film containing fulgides **1** and **2**; **1S**, **2S**.

of naphthoxazine in plastics. In his study he found that the excellent light fatigue resistance of naphthoxazine could be further improved by an organo-nickel stabilizer. From a practical view point, we also investigated the effect of some nickel stabilizers so as to improve it. Among the various derivatives, the nickel dithiophenolate derivative (bis(1,2,3-trichloro-5,6-dithiophenolate)Ni(II) tetrabutylammonium) which is known as being a light stabilizer for a near-infrared absorbing dye,[11] had the greatest effect on the fatigue resistance. As illustrated in Fig. 4, only 1 wt% of the stabilizer in PMMA film exhibited this effect on the light fatigue resistance.

The thermal degradation of the fulgides in PMMA film at 80 °C in the dark are shown in Fig. 5. Colored forms (**1C** and **2C**) showed good fatigue resistance. Degradation after 11 days was only 7%, and the residues showed a same photochromic performance. Uncolored forms (**1** and **2**) were also investigated. PMMA film containing fulgide had been previously heated for various periods and then irradiated with UV light for coloration. These showed little fatigue, 24% and 18%, respectively, indicating their slight inferiority to colored forms.

Thermal stabilities of fulgide in solution had been investigated in some detail by Heller et al.[12] According to their paper, the colored form of 3-furyl fulgide **3C** was stable below 100 °C. The uncolored form **3** in deuteriochloroform solution (0.20 mol dm^{-3}) on heating at 180 °C turned red, which was not reversible upon exposure to visible light.

As illustrated in Fig. 5, the thermal stability of **3C** in PMMA was much lower than that of **1C** and **2C**, and thermally bleached **3C** showed no photochromism. The uncolored form **3** also showed a similar tendency to the colored form, but thermally colored species were not detected in the absorption spectrum. On the other hand, the photocolorability of **3** in a dilute toluene solution was completely maintained after boiling at 80 °C for 24 h. These facts mean that the degradation in a polymer matrix, such as PMMA, differs from that in solution, and the introduction of a C=N bond is also effective in reducing thermal fatigue in PMMA film because of its higher chemical satability.[12]

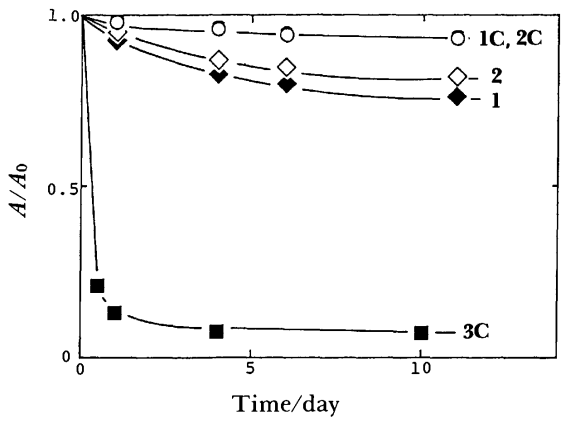

Fig. 5. Thermal degradations of the fulgides in PMMA film at 80 °C in the dark. PMMA films of 1 μm thickness containing fulgides (20 wt%) had been irradiated with UV light leading to the photostationary state for coloration after heating; **1**, **2**. The film had been previously irradiated with UV light for coloration before heating; **1C**, **2C**, **3C**.

Experimental

Materials. 4-Oxazolyl fulgide (**2**). A solution of 5-methyl-2-phenyl-4-stearoyloxazole[13] (4.4 g, 0.010 mol) and diethyl isopropylidenesuccinate (2.7g, 0.012 mol) in *t*-butyl alcohol (10 ml) was added dropwise to a refluxing solution of potassium *t*-butoxide (1.2 g) in *t*-butyl alcohol (15 ml), and the solution was refluxed for 3 h. After removing the solvent, the reaction mixture was poured into water, and extracted with ether. The aqueous layer was acidified, and the liberated half ester was extacted with toluene and dried over anhydrous magnesium sulfate; the solvent was then removed. The residue, yellow oil (6.4 g), was hydrolyzed with 5% ethanolic potassium hydroxide and a solid potassium salt filtered off and acidified. The resulting diacids (4.8 g) were boiled with acetic anhydride. After the solvent was removed, **2** was isolated in 9% yield as *Z*-isomer by column chromatography on silica gel and recrystalized from hexane. Mp 65—67 °C; ^{1}H NMR ($CDCl_3$) δ=0.83 (t, 3H) 1.26 (s, 32H), 2.07 (s, 3H), 2.33 (s, 3H), 2.43 (s, 3H), 7.36—8.13 (m, 5H); mass spectrum, *m/z* 547 (M^+). Calcd for $C_{35}H_{49}NO_4$: C,76.52; H,9.02; N, 2.56; O, 11.68%. Found: C,76.52; H, 9.14; N, 2.61; O, 11.73%.

The *Z*-isomer of this fulgide in toluene solution or PMMA film rapidly isomerized into an *E*-isomer upon UV irradiation.

4-Oxazolyl fulgide (**1**) and 3-furyl fulgide (**3**) were prepared as described above and in the literatures.[2]

Measurements. A mercury lamp (Ushio, 250 W) and a xenon lamp (Ushio, 300 W) were used as light sources for coloration and discoloration reactions. A mercury line, 366 nm (ca. 50 mJ) and visible light beams (>390 nm) were isolated by passing the light through glass filters (Toshiba UV-D36C, UV-35 and L-39). PMMA film (ca. 1.0 μm thickness) was prepared on a glass plate by spin coating a cyclohexanone solution containing fulgide and PMMA (20 : 80 by weight). For the measurement of thermal stability, the surface of the PMMA film was coated with acrylic polymer (SD-17 Dainihon-inki) in 4—5 μm thickness to protect them from sublimation. Quantum yields for coloration were determined by measuring the rate of the photoreaction, which was carried out in a toluene solution (6×10^{-4} mol dm^{-3}) by irradiation of the 311 nm mercury line, using a Quantum Yield Reactor (Model 2001 Applied Photophysics). The light intensity was measured with a potassium iron(II) oxalate actinometer.

The photochemical fatigue of fulgides was investigated by measurements of the absorption spectrums of the colored forms. In the presence of air toluene solution (1×10^{-4} mol dm^{-3}) and PMMA films were irradiated with UV and visible light, alternatively, using a photo-irradiater cycle test system (OMROM).

For evaluating the effect of various organo-nickel stabilizers in improving the fatigue resistance, PMMA films con-

taining 3-furyl fulgide **3** and 4-oxazolyl fulgides **1** and **2** (20 wt%) were used as test samples. These films were prepared as described in the above, except for the addition of the stabilizers to the cyclohexanone solution. Nickel stabilizers such as Cyasorb 1084, AM105 and AM205 (evaluated by Chu) and a nickel dithiophenolate derivative were commercially available from American Cyamid, Ferro. Corp. and Mitsui Toatsu. However, the three stabilizers tested by Chu showed no effect in improving the fatigue resistance of fulgide.

The thermal degradation of PMMA film containing fulgide was carried out in an oven at 80 °C and was monitored by measuring the absorption spectrum of colored forms at room temperature.

UV and ^{1}H NMR spectra were measured with a spectrophotometer (Hitachi U-3200) and 60-MHz spectrometer (JEOL JNM-PMX60 NMR).

References

1) Partially reported in the 58th National Meeting of the Chemical Society of Japan, Kyoto, April 1989, Abst., p. 1878.

2) P. J. Darcy, H. G. Heller, P. J. Strydom, and J. Whittall, *J. Chem. Soc., Perkin Trans. 1*, **1981**, 202; A. P Glaze, S. A. Harris, H. G. Heller, W. Johncock, S. N. Oliver, P. J. Strydom, and J. E. Whittall, *ibid.*, **1985**, 957.

3) M. Irie and M. Mohri, *J. Org. Chem.*, **53**, 803 (1988).

4) T. Tamaki and K. Ichimura, 58th National Meeting of the Chemical Society of Japan, Kyoto, April 1989, Abst., p. 426.

5) A. Kaneko, A. Tomoda, M. Ishizuka, H. Suzuki, and R. Matsushima, *Bull. Chem. Soc. Jpn.*, **61**, 3569 (1988).

6) Y. Yokoyama, T. Goto, T. Inoue, M. Yokoyama, and Y. Kurita, *Chem. Lett.*, **1988**, 1049.

7) M. Maeda and M. Kojima, *Chem. Commun.*, **1973**, 539.

8) H. H. Wasserman, J. R. Scheffer, and J. L. Cooper, *J. Am. Chem. Soc.*, **94**, 4991 (1972).

9) M. Irie, "Hikari-kiroku-gijutsu to Zairyou," CMC, Tokyo (1985), Chap. 13.

10) N. Y. C. Chu, *Solar Energy Materials*, **14**, 215 (1986).

11) K. Nanba, Jpn. Patent 60-118748, 60-118749(1985).

12) I. J. Turchi and M. J. S. Dewar, *Chem. Rev.*, **75**, 389 (1975).

13) A. W. Allan and B. H. Walter, *J. Chem. Soc. C*, **1968**, 1397.

Methanol-Incorporated Photoaddition of *N*-Methyl-9,10-phenanthrenedicarboximide to Alkenes. Addition at Carbonyl and Phenanthrene-Ring Carbon Atoms

Yasuo KUBO,* Mikako NANBA, Etsuko HAYASHI, and Takeo ARAKI†
Department of Chemistry, Faculty of Science, Shimane University, Matsue 690
(Received June 19, 1989)

Irradiation of acetonitrile-methanol (2 : 1 v/v) solutions of *N*-methyl-9,10-phenanthrenedicarboximide (**3**) with alkenes **5a—g** gave methanol-incorporated adducts (**9c—f**) at a carbonyl carbon atom in **3**, those (**10c,f**) at a phenanthrene-ring carbon atom, and a methanol-adduct **11g** to alkene **5g**, together with products **4**, **6b,e—g**, **7b,e—g**, and **8e,f** obtained by the photoreactions in benzene. The concentration effect of alkenes **5e,f** on yields of products **6e,f**, **7e,f**, **8e,f**, **9e,f**, and **10f** showed that both **9e,f** and **10f** arose from a relatively short-lived singlet excited state of **3**. The values of the free-energy change associated with an electron transfer (ΔG_{et}) from alkenes **5a—d,g** to the singlet excited state of **3** and fluorescence quenching rate constants support a photochemical electron transfer mechanism for the methanol-incorporated addition. Both $LiClO_4$ and Bu_4NClO_4 caused only slight decreases in the relative ratios **10c/9c** indicating that both the methanol-incorporated addition at the phenanthrene-ring carbon atom and that at the carbonyl carbon atom might arise from a contact ion pair state. The fact that the methanol-incorporated addition at the arene-ring carbon atom was observed only in the reaction of **3** in a series of *N*-methylarenedicarboximides, possessing a five-membered imide ring, is interpreted on the basis of the spin density of the radical anions of the imides derived from the photochemical electron transfer.

The area of electron transfer photochemistry has received much attention with regard to both synthetic and mechanistic aspects in organic photochemisry.[1] A unique feature of transformations occurring by electron transfer mechanisms is that the key reactive intermediates are radical ion and neutral radical species rather than the initially populated excited states. Consequently, the chemical properties and reactivity profiles of these reactive intermediates have been clarified by investigations on the nature of the reactions.

During the course of investigations of the photochemistry of imides, a wide variety of alcohol (solvent)-incorporated intramolecular cyclization[2] and intermolecular addition reactions[3] in the photoreactions of arenedicarboximide-alkene systems, via an electron transfer process, have been found. The position, at which the alcohol-incorporated addition occurs, largely depends on the arene structures of the arenedicarboximides. Thus, the methanol-incorporated addition has been reported to occur only at the carbonyl carbon atoms of the imide for the reactions of the five-membered imides such as *N*-methylphthalimide (**1**),[3a-e] *N*-methyl-1,2-naphthalenedicarboximide (**2**),[3i] and its 2,3-isomer,[3g] while the addition solely at a naphthalene-ring carbon atom has been observed in the reaction of *N*-methyl-1,8-naphthalenedicarboximide, a six-membered imide.[3f,h] Furthermore, a preferential addition at the sterically more hindered carbonyl carbon atom in the reaction of **2** has been found.[3i] The effect of the arene structures has been explained on the basis of the spin density of the radical anion of the arenedicarboximides derived by the photochemical electron transfer.[3h,i]

Here, we report on the methanol-incorporated photoaddition of *N*-methyl-9,10-phenanthrenedicarboximide (**3**) to alkenes in acetonitrile-methanol (2/1 v/v), in which the first example of the methanol-incorporated addition at an arene-ring carbon atom in the reactions of arenedicarboximides with a five-membered imide ring is observed.

We have already reported the photoreactions of **3** with alkenes in benzene.[4] Thus, photoreaction (>400 nm) of **3** gives the syn-dimer (**4**) (Eq. 1). Photoreactions of **3** with alkenes (**5**) give **4**, insertion products (**6**) of the double bond of the alkenes into the C–N bond of **3**, and cyclobutanes (**7** and **8**) (Eq. 2).

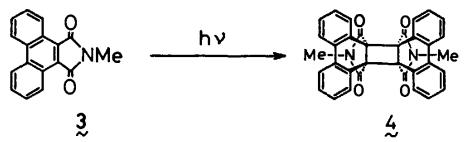

3 **4** (1)

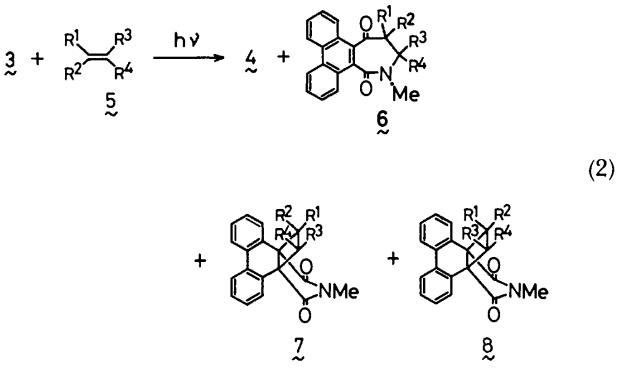

5 **6** (2)

7 **8**

† Present address: Department of Polymer Science and Engineering, Faculty of Textile Science, Kyoto Institute of Technology, Kyoto 606.

The syn dimerization and the insertion occur from the singlet excited state of **3**, and **7** and **8** arises mainly from the triplet excited state of **3** and remarkable heavy atom effect by halides is observed in this system.

Results and Discussion

Results of the photoreactions (>400 nm) of **3** and alkenes **5a—g** in N_2-purged acetonitrile-methanol (2/1 v/v) are summarized in Eq. 3 and Table 1. The

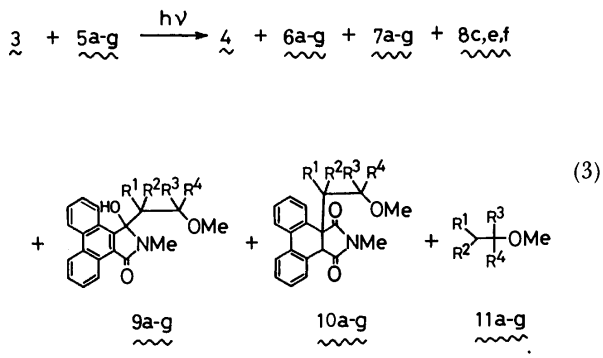

(3)

methanol-incorporated addition was observed in the reactions with ethylenes substituted by more than three alkyl groups, 2-methyl-2-butene (**5c**), 2,3-dimethyl-2-butene (**5d**), as for the reaction with aliphatic alkenes. The fact that the dimerization of **3** to give **4** was only observed in the reaction with 1-hexene (**5a**), an ethylene substituted by one alkyl group, indicates that no interaction occurs between the excited states of **3** and **5a**. Photoreaction with isobutene (**5b**), an ethylene substituted by two alkyl groups, in acetonitrile-methanol and in benzene gave the same products, an insertion product **6b** and a cyclobutane **7b**, as those obtained by the reaction in benzene. The results show that **3** is less reactive on the methanol-incorporated addition than **1** since irradiation of **1** with **5b** gave a methanol-incorporated adduct together with an insertion product.[3d] and **3** has a similar reactivity to **2** because the methanol-incorporated addition was observed in the reactions with the same alkenes **5c,d**.[3i]

Irradiation of **3** with **5c** in acetonitrile-methanol gave a pair of diastereomers of a methanol-incorporated adduct (**9c**, diastereomer ratio=2.8 : 1) at the carbonyl carbon atom of **3** and a pair of diastereomers of a methanol-incorporated adduct (**10c**, diastereomer ratio=1.2 : 1) at a phenanthrene-ring carbon atom with complete quenching of the formation of products **4**, **6c**, **7c**, and **8c** obtained in benzene.[4] The diastereomers of **9c** were isolated as a mixture and those of **10c** were separated by silica-gel column chromatography. The structure of **9c**, including the position of the methyl substituents in the side chain, was supported by the spectral resemblances to the methanol-incorporated adducts obtained by the photoreactions of **1**[3d] and **2**[3i] with **5c**. The structure of **10c** was assigned on the basis of the spectral data: ^{1}H NMR δ=5.07 (s, 1H, CH, for the major diastereomer), 4.35 (s, 1H, CH, for the minor diastereomer); IR 1766 and 1700 (imide moiety for the major diastereomer), 1776 snd 1706 (imide moiety for the minor diastereomer).

Irradiation of **3** with **5d** in acetonitrile-methanol (2/1 v/v) gave no detectable amounts of products. However, irradiation in benzene-methanol (9/1 v/v), a less polar solvent system, gave a methanol-incorporated adduct (**9d**) at the carbonyl carbon atom of **3**. A similar solvent effect was observed in the reactions of **2** with alkenes.[3i]

Irradiation of **3** with styrene (**5e**) in acetonitrile-methanol gave a pair of diastereomers of a methanol-

Table 1. Yields of Photoproducts from *N*-Methyl-9,10-phenanthrenedicarboximide (**3**) and Alkenes **5a—g** in Acetonitrile-Methanol (2/1 v/v)[a]

R^1	R^2	R^3	R^4	5	[5]	Yield[b]/%						
					mM[c]	4	6	7	8	9	10	11
Bu	H	H	H	**5a**	320	90	**6a** 0	**7a** 0	—	**9a** 0	**10a** 0	—[d]
Me	Me	H	H	**5b**	360	16	**6b** 35	**7b** 35	—	**9b** 0	**10b** 0	—[d]
Me	Me	Me	H	**5c**	380	0	**6c** 0	**7c** 0	**8c** 0	**9c** 29[e]	**10c** 41[f]	—[d]
Me	Me	Me	Me	**5d**	320	0	**6d** 0	**7d** 0	—	**9d** 25[g]	**10d** 0	—[d]
Ph	H	H	H	**5e**	190	0	**6e** 17	**7e** 8	**8e** 10	**9e** 25[h]	**10e** 0	**11e** 0
					380		22	6	7	33[h]		
					760		27	5	6	38[h]		
Ph	Me	H	H	**5f**	60	0	**6f** 16	**7f** 7	**8f** 6	**9f** 50[i]	**10f** 3[j]	**11f** 0
					160		19	4	3	55[i]	4[j]	
					310		22	4	2	55[i]	5[j]	
					620		25	3	2	56[i]	5[j]	
Ph	Ph	H	H	**5g**	400	0	**6g** 36	**7g** 8	—	**9g** 0	**10g** 0	**11g** 142

a) Reaction conditions: [**3**]=15 mM, under N_2, $h\nu$ (λ>400 nm). b) Yields were based on consumed **3**. c) 1 M=1 mol dm^{-3}. d) Not checked. e) A mixture (2.8 : 1) of two diastereomers. f) A mixture (1.2 : 1) of two diastereomers. g) In benzene-methanol (9/1 v/v). h) A mixture (1.4 : 1) of two diastereomers. i) A mixture (1.2 : 1) of two diastereomers. j) A mixture (1.3 : 1) of two diastereomers.

incorporated adduct (**9e**) at the carbonyl carbon atom together with products **6e**, **7e**, and **8e** obtained in benzene.[4] Photoreaction with α-methylstyrene (**5f**) afforded a pair of diastereomers of a methanol-incorporated adduct (**9f**) at the carbonyl carbon atom and a pair of diastereomers of a methanol-incorporated adduct (**10f**) at the phenanthrene-ring carbon atom together with products **6f**, **7f**, and **8f** obtained in benzene.[4]

The concentration effect of the alkenes **5e,f** on the yields of the photoproducts was examined in the reactions with **5e,f** to clarify the multiplicity of the excited states of **3** which led to **9e,f** and **10f**. A marked concentration dependency of the yields of products was observed in the reaction of **3** with **5f** in benzene; the yield of **6f** increased and those of **7f** and **8f** decreased with increase of the concentration of **5f**.[4] These results are rationalized by a mechanistic scheme, in which **6f** arises from the relatively short-lived singlet excited state of **3**, and **7f** and **8f** mainly from the relatively long-lived triplet excited state. A similar concentration dependency of the yields of **6e,f**, **7e,f**, and **8e,f** was observed in acetonitrile-methanol (Table 1). At the same time, the yields of **9e,f** and **10f** increased with increase of the concentration of **5e,f**, indicating that **9e,f** and **10f** arose from the relatively short-lived singlet excited state of **3**.

Irradiation of **3** with 1,1-diphenylethylene (**5g**) in acetonitrile-methanol gave 2,2-diphenylethyl methyl ether (**11g**), an anti-Markovnikoff adduct of methanol to **5g**, and products **6g** and **7g** obtained in benzene. No methanol-incorporated adducts of **3** to **5g** were obtained.

A possible mechanism which can interpret the general feature of the methanol-incorporated addition observed in the photoreaction of **3** with alkenes (**5**) is shown in Scheme 1. The initial step of the reaction is the single electron transfer from the alkenes to the singlet excited state of **3**. The singlet multiplicity of the excited state of **3**, which lead to the methanol-incorporated adducts **9** and **10**, is substantiated by the concentration effect of **5e,f**. The electron transfer mechanism is supported by the estimation of the free-energy changes (ΔG_{et}) associated with the electron transfer from alkenes to the singlet excited state of **3** and the fluorescence quenching rate constants (k_q) (vide infra). Concerning the electron transfer mechanism, **11g** by the reaction with **5g** could be one of the typical electron transfer photosensitized products, as reported by Arnold and his co-workers.[5] The electron transfer photo-sensitized addition of methanol to alkenes giving **11** and the methanol-incorporated addition of alkenes to **3** giving **9** and **10** appear to be closely related processes via common intermediates **12**+**14**. Coupling of the two components at the carbonyl carbon atom (C^1) and that at the phenanthrene-ring carbon atom (C^2) of **12** results in the formation of **9** and **10**, respectively, and the back electron transfer

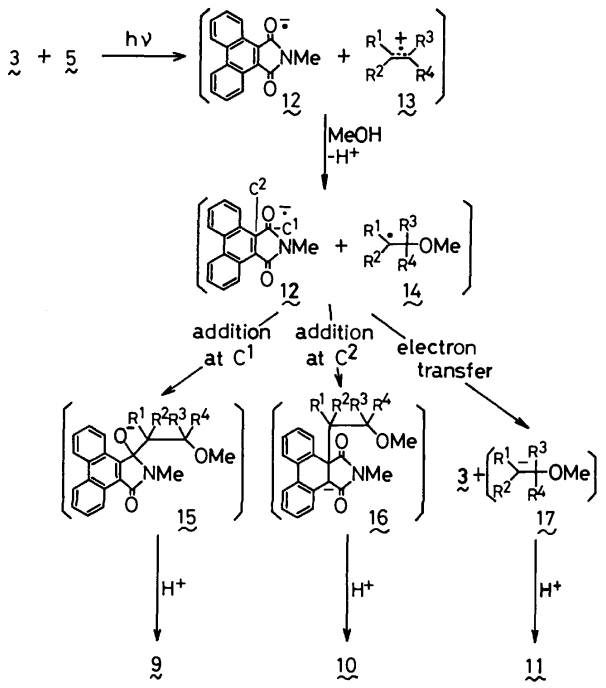

Scheme 1.

from **12** to **14** gives **3** and **11** (Scheme 1).

The values of ΔG_{et} can be estimated by using[6]

$$\Delta G_{et} = 96.49[E(D/D^+) - E(A^-/A)] - \Delta E_{0,0}. \quad (4)$$

In this equation $E(D/D^+)$ is the oxidation potential of the alkenes, $E(A^-/A)$ is the reduction potential of **3**, and $\Delta E_{0,0}$ is the singlet excitation energy of **3**. With these parameters, we can calculate the ΔG_{et} values for reactions with alkenes **5a—d,g** as shown in Table 2, which shows that the methanol-incorporated addition occurs only in the cases having negative ΔG_{et} values, as expected from the electron transfer mechanism.

An addition of alkenes **5b—g** to air-saturated acetonitrile solutions of **3** (1×10^{-5} M) resulted in a reduction of the fluorescence of **3** without varying the shape and the position of the emission. Stern-Volmer plots of the fluorescence quenching by alkenes **5c—g** gave straight lines against concentration of **5c—g**. The values of k_q in acetonitrile calculated from the Stern-Volmer slopes ($k_q\tau$) using the lifetime of the fluores-

Table 2. Calculated Free Energy Changes (ΔG_{et}) Associated with Electron Transfer from Alkenes **5a—d, g** to the Singlet Excited State of *N*-Methyl-9,10-phenanthrenedicarboximide (**3**)

Alkenes	$E(D/D^+)$/V	ΔG_{et}[a]/kJ mol^{-1}
5a	2.64[b]	+64.2
5b	2.39[b]	+40.0
5c	1.79[b]	−17.9
5d	1.63[b]	−33.3
5g	1.48[c]	−47.8

a) Calculated by Eq. 4: $E(A^-/A)$=−1.02 V (in 0.5 M Et_4NClO_4/acetonitrile vs. Ag/0.01 M $AgClO_4$), $\Delta E_{0,0}$= 289 kJ mol^{-1} from Ref. 4. b) Ref. 3b. c) Ref. 7.

Table 3. Fluorescence Quenching Rate Constants (k_q) for *N*-Methyl-9,10-phenanthrenedicarboximide (**3**) and Alkene **5a—g** Systems[a]

Alkenes	$k_q\tau$[b]	k_q[c]	k_q[d]
	M^{-1}	$M^{-1}\,s^{-1}$	$M^{-1}\,s^{-1}$
5a	0	0	0
5b	—[e]	—[e]	—[e]
5c	5.7	3.90×10^{8}	4.0×10^{7}
5d	153	1.05×10^{10}	9.3×10^{7}
5e	11.7	8.01×10^{8}	8.0×10^{7}
5f	16.2	1.11×10^{9}	4.5×10^{8}
5g	22.0	1.51×10^{9}	4.9×10^{8}

a) Conditions: [3]=1×10^{-5} M, at 25 °C. b) Stern-Volmer slopes for the fluorescence quenching in air-saturated acetonitrile. c) Calculated from $k_q\tau$ using the lifetime (τ=14.6 ns) of the fluorescence of **3** in air-saturated acetonitrile. d) In air-saturated benzene from Ref. 4. e) A very low value.

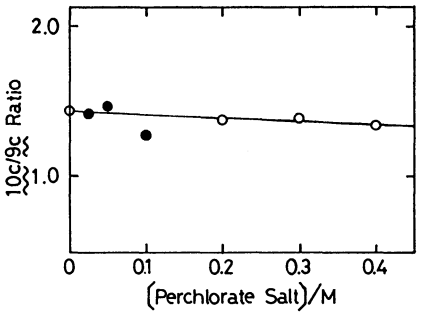

Fig. 1. Methanol-incorporated adducts at a phenanthrene-ring carbon atom to those at the carbonyl carbon atom ratios (**10c**/**9c**) obtained by irradiation of acetonitrile-methanol (2/1 v/v) solutions of *N*-methyl-9,10-phenanthrenedicarboximide (**3**, 1.9 mM) and 2-methyl-2-butene (**5c**, 240 mM) in the presence of varying concentrations of $LiClO_4$ (○) and Bu_4NClO_4 (●).

cence of **3**, together with k_q values in benzene, are shown in Table 3. The k_q values in acetonitrile are larger than those in benzene. The large k_q values in acetonitrile may also support the electron transfer mechanism.

In the area of electron transfer photochemistry, chemistry of ion pairs, involving solvent-separated ion pairs and contact ion pairs, have received much attention in recent years.[1,8] The salt effect was examined in the present system to obtain the information on the ion-pair states involved in the reaction, since the salt effect had been known to play a role in determining preferred ion-pair states of photogenerated radical ions.[9] Thus the relative ratios **10c**/**9c** were determined for the photoreactions of **3** with **5c** in acetonitrile-methanol (2/1 v/v) containing increasing concentrations of $LiClO_4$ and Bu_4NClO_4 in the range of 0—0.4 M. The results are shown in Fig. 1, which indicates that $LiClO_4$ causes only slight decreases in **10c**/**9c** and the effect of Bu_4NClO_4 is similar to that of $LiClO_4$. The lithium cation is known to be a much stronger acceptor than Bu_4N^+ in interactions with oxide anion donors.[9] Thus, $LiClO_4$ should be more capable of intercepting the solvent-separated ion pairs and transforming them to free radical ions, compared with Bu_4NClO_4. The results from the salt effect may indicate that both the methanol-incorporated addition at the phenanthrene-ring carbon atom and that at the carbonyl carbon atom arise from the contact ion pair state.

The variation of the arene structures of arenedicarboximides caused a change in the reaction site at which the methanol-incorporated addition occurred. Thus, the methanol-incorporated addition of **1** and **2** occurs exclusively at the carbonyl carbon atoms,[3a-e,g,i] while that of **3**, possessing a more extended arene structures, occurs both at the arene-ring carbon atom and at the carbonyl carbon stom. Whether the carbonyl carbon atom or the arene-ring carbon atom is attacked may depend on the reactivity of the respective carbons in the imide radical anions toward alkyl radicals such as **14** based on the mechanistic scheme shown in Scheme 1. The relative spin density of the respective carbons in the imide radical anions calculated by the McLachlan method[10] can be used as an index for the reactivity. Of course, other factors such as a steric effect can disturb the reactivity estimated from the spin density.[3i] The spin density of the respective carbons in the radical anions of phthalimide (**18**), 1,2-naphthalenedicarboximide (**19**), and 9,10-phenanthrenedicarboximide (**20**), as model compounds for the radical anions of **1**, **2**, and **3**, respectively, is shown in Fig. 2. In a series of the imide radical anions **18—20** the values of the spin density of

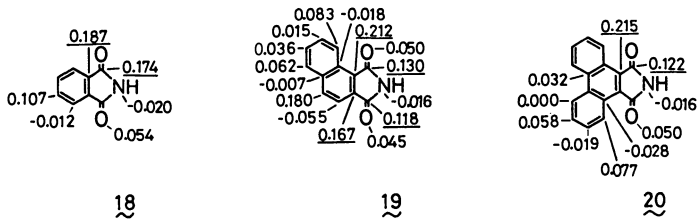

18 19 20

Fig. 2. Spin density of radical anions of phthalimide (**18**), 1,2-naphthalenedicarboximide (**19**), and 9,10-phenanthrenedicarboximide (**20**) calculated by McLachlan method.

the arene-ring carbon atoms shown with underlines in Fig. 2 increased and those of the carbonyl carbon atoms shown with underlines in Fig. 2 decreased from **18** to **20**, although the difference in the relative spin density is not large. Therefore, the methanol-incorporated addition at the arene-ring carbon atom should be favorable in the photoreaction of **3** with alkenes compared with those of **1** and **2** with alkenes, in accord with the fact that the methanol-incorporated addition at the arene-ring carbon atom was observed only in the reaction of **3**.

Experimental

^{1}H NMR spectra were obtained on a JEOL JNM-GX-270 (270 MHz) instrument. Chemical shifts are reported in ppm (δ) relative to internal $SiMe_4$. IR spectra were determined by use of a Hitachi 260-50 spectrometer. Fluorescence spectra and lifetimes were recorded by a Hitachi 850 spectrophotometer and by a Horiba NAES-1100 time-resolved spectrofluorometer, respectively. Melting points were recorded by using a Yanagimoto micro melting point apparatus and are uncorrected. Microanalyses were performed on a Yanagimoto CHN corder MT-2.

Materials. *N*-Methyl-9,10-phenanthrenedicarboximide (**3**) was prepared and purified as described previously.[4] Alkenes **5a**—g were commercially available and purified by distillation of liquid.

General Procedure for Irradiation and Product Isolation. UV irradiation of **3** (15 mM) with alkenes **5a**—g in 25 ml of N_2 purged acetonitrile–methanol (2/1 v/v) was carried out at ambient temperature with an Eikosha EHB-W-300 high-pressure Hg-lamp through a 1-cm path-length aqueous filter, prepared from 27 g of $CuSO_4 \cdot 5H_2O$, 30 g of $NaNO_2$, and 50 ml of concd aqueous ammonia diluted with water to 1000 ml (>400 nm).[11] The reaction was monitored by TLC (Merck, Kieselgel 60 F_{254}) analyses and ^{1}H NMR measurements. After evaporation of the solvent, the residue was subjected to column chromatography (Wakogel C-200). Dichloromethane–ether was used as the eluant for the separation of the products.

Irradiation of 3 with 2-Methyl-2-butene (5c). A mixture (2 : 1) of diastereomers of 3-(1,1-dimethyl-2-methoxypropyl)-3-hydroxy-2-methyl-2,3-dihydro-1*H*-dibenz[*e*,*g*]isoindol-1-one (**9c**): mp 172—180 °C: ^{1}H NMR of the major diastereomer δ=0.42 (s, 3H, CMe), 0.99 (d, *J*=6.4 Hz, 3H, CH**Me**), 1.25 (s, 3H, CMe), 3.23 (s, 3H, NMe), 3.45 (s, 3H, OMe), 4.07 (q, *J*=6.4 Hz, 1H, C**H**Me), 6.46 (s, 1H, OH), 7.5—7.8 (m, 4H, Arom H), 8.6—8.8 (m, 3H, Arom H), 9.3—9.4 (m, 1H, Arom H); ^{1}H NMR of the minor diastereomer δ=0.43 (s, 3H, CMe), 1.19 (d, *J*=6.4 Hz, 3H, CH**Me**), 1.25 (s, 3H, CMe), 3.27 (s, 3H, NMe), 3.54 (s, 3H, OMe), 3.97 (q, *J*=6.4 Hz, 1H, C**H**Me), 6.46 (s, 1H, OH), 7.5—7.8 (m, 4H, Arom H), 8.6—9.0 (m, 3H, Arom H), 9.3—9.5 (m, 1H, Arom H); IR (KBr) 3220 (OH), 1666 (lactam), 1438, 1108, 762, 728 cm^{-1}. Found: C, 75.93; H, 7.04; N, 3.67%. Calcd for $C_{23}H_{25}NO_3$: C, 76.00; H, 6.93; N, 3.85%.

A major diastereomer of 3a-(1,1-dimethyl-2-methoxypropyl)-2-methyl-3a,11b-dihydro-1*H*-dibenz[*e*,*g*]isoindol-1,3(2*H*)-dione (**10c**): mp 229—232 °C; ^{1}H NMR δ=0.60 (s, 3H, CMe), 0.95 (s, 3H, CMe), 1.07 (d, *J*=6.3 Hz, 3H, CH**Me**), 2.96 (s, 3H, NMe), 3.12 (s, 3H, OMe), 3.79 (q, *J*=6.3 Hz, 1H, C**H**Me), 5.07 (s, 1H, CHC=O), 7.2—7.5 (m, 5H, Arom H), 7.7—7.9 (m, 3H, Arom H); IR (KBr) 1766 and 1700 (imide), 1448, 1432, 1380, 1118, 750 cm^{-1}. Found: C, 75.75; H, 6.88; N, 3.77%. Calcd for $C_{23}H_{25}NO_3$: C, 76.00; H, 6.93; N, 3.85%.

A minor diastereomer of **10c**: mp 157—160 °C: ^{1}H NMR δ=0.58 (s, 3H, CMe), 1.04 (d, *J*=6.1 Hz, 3H, CH**Me**), 1.31 (s, 3H, CMe), 2.94 (s, 3H, NMe), 3.01 (s, 3H, OMe), 3.26 (q, *J*=6.1 Hz, 1H, C**H**Me), 4.35 (s, 1H, CHC=O), 7.2—7.5 (m, 5H, Arom H), 7.8—8.0 (m, 3H, Arom H); IR (KBr) 1776 and 1706 (imide), 1440, 1386, 1132, 1118, 760 cm^{-1}. Found: C, 75.84; H, 6.70; N, 3.75%. Calcd for $C_{23}H_{25}NO_3$: C, 76.00; H, 6.93; N, 3.85%.

Irradiation of 3 with 2,3-Dimethyl-2-butene (5d). 3-Hydroxy-3-(2-methoxy-1,1,2-trimethylpropyl)-2-methyl-2,3-dihydro-1*H*-dibenz[*e*,*g*]isoindol-1-one (**9d**): mp 178—180 °C; ^{1}H NMR δ=0.55 (s, 3H, CMe), 1.15 (s, 3H, CMe), 1.27 (s, 3H, CMe), 1.37 (s, 3H, CMe), 3.17 (s, 3H, NMe), 3.40 (s, 3H, OMe), 6.42 (s, 1H, OH), 7.6—7.8 (m, 4H, Arom H), 8.68 (d, 1H, Arom H), 8.71 (d, 1H, Arom H), 8.91 (d, 1H, Arom H), 9.40 (d, 1H, Arom H); IR (KBr) 3300 (OH), 1674 (lactam), 1446, 1078, 724 cm^{-1}. Found: C, 76.51; H, 7.06; N, 3.88%. Calcd for $C_{24}H_{27}NO_3$: C, 76.36; H, 7.21; N, 3.71%.

Irradiation of 3 with Styrene (5e). A mixture (1.2 : 1) of diastereomers of 3-hydroxy-3-(2-methoxy-1-phenylethyl)-2-methyl-2,3-dihydro-1*H*-dibenz[*e*,*g*]isoindol-1-one (**9e**): mp 192—197 °C: ^{1}H NMR δ=3.02 (s, 3H, NMe for the minor diastereomer), 3.31 (s, 3H, NMe for the major diastereomer), 3.43 (s, 3H, OMe), 3.60 (s, 3H, OMe), 3.5—3.7 (m, 2H), 3.8—3.9 (m, 2H), 3.9—4.1 (m, 1H), 4.3—4.5 (m, 1H), 4.92 (s, 1H, OH), 6.18 (s, 1H, OH), 6.4—6.6 (m, 2H, Arom H), 6.7—6.9 (m, 4H, Arom H), 6.9—7.2 (m, 3H, Arom H), 7.4—7.9 (m, 8H, Arom H), 8.5—8.8 (m, 7H, Arom H), 9.0—9.1 (m, 2H, Arom H); IR (KBr) 3300 (OH), 1678 (lactam), 1446, 1086, 766, 706 cm^{-1}. Found: C, 78.29; H, 6.01; N, 3.46%. Calcd for $C_{26}H_{23}NO_3$: C, 78.57; H, 5.83; N, 3.52%.

Irradiation of 3 and α-Methylstyrene (5f). A mixture (1.2 : 1) of diastereomers of 3-hydroxy-3-(2-methoxy-1-methyl-1-phenylethyl)-2-methyl-2,3-dihydro-1*H*-dibenz-[*e*,*g*]isoindol-1-one (**9f**): mp 184—188 °C; ^{1}H NMR δ=1.53 (s, 6H, 2CMe), 3.12 (s, 3H, NMe for the minor diastereomer), 3.27 (s, 3H, NMe for the major diastereomer), 3.56 (s, 3H, OMe), 3.58 (s, 3H, OMe), 3.63 and 4.35 (ABq, *J*=9.3 Hz, 2H, CH_2), 3.85 and 4.00 (ABq, *J*=9.8 Hz, 2H, CH_2), 5.84 (s, 1H, OH), 6.07 (s, 1H, OH), 6.7—7.8 (m, 18H, Arom H), 8.5—8.7 (m, 5H, Arom H), 8.77 (d, *J*=7.1 Hz, 1H, Arom H), 8.99 (d, *J*=9.0 Hz, 1H, Arom H); IR (KBr) 3300 (OH), 1676 (lactam), 1448, 1374, 762, 696 cm^{-1}. Found: C, 78.99; H, 6.35; N, 3.45%. Calcd for $C_{27}H_{25}NO_3$: C, 78.81; H, 6.12; N, 3.40%.

A mixture (1.2 : 1) of diastereomers of 3a-(2-methoxy-1-methyl-1-phenylethyl)-2-methyl-3a,11b-dihydro-1*H*-dibenz-[*e*,*g*]isoindol-1,3(2*H*)-dione (**10f**): mp 242—245 °C; ^{1}H NMR of the major diastereomer δ=1.31 (s, 3H, CMe), 2.90 (s, 3H, NMe), 3.30 (s, 3H, OMe), 3.89 and 4.37 (ABq, *J*=9.5 Hz, 2H, CH_2), 4.74 (s, 1H, CHC=O), 6.8—7.5 (m, 10H, Arom H), 7.62 (d, *J*=7.1 Hz, 1H), 7.84 (d, *J*=6.4 Hz, 1H), 7.92 (d, *J*=8.7 Hz, 1 H); ^{1}H NMR of the minor diastereomer δ=1.73 (s, 3H, CMe), 2.86 (s, 3H, NMe), 3.06 (s, 3H, OMe), 3.33 and 3.72 (ABq, *J*=16.8 Hz, 2H, CH_2), 4.25 (s, 1H, OH), 7.0—7.5 (m, 10H, Arom H), 7.74 (d, *J*=9.0 Hz, 1H, Arom H), 7.80 (d, *J*=7.8 Hz, 1H, Arom H), 7.85 (d, *J*=8.1 Hz, 1H, Arom H); IR (KBr) 1773 and 1698 (imide), 1448, 1382, 1296, 1108 cm^{-1}. Found: C, 78.73; H, 6.03; N, 3.37%. Calcd for $C_{27}H_{25}NO_3$: C, 78.81; H, 6.12; N, 3.40%.

Irradiation of 3 and 1,1-Diphenylethylene (5g). 2,2-Diphenylethyl methyl ether (**11g**) was identical with a sample prepared by irradiation of **5g**, *p*-dicyanobenzene, and phenanthrene (sensitizer) in methanol.[12]

References

1) P. S. Mariano, *Acc. Chem. Res.*, **16**, 130 (1983); S. L. Mattes and S. Farid, *Org. Photochem.*, **6**, 233 (1983); M. Julliard and M. Channon, *Chem. Rev.*, **83**, 425 (1983); G. J. Kavarnos and N. J. Turro, *ibid.*, **86**, 401 (1986); J. J. McCullough, *ibid.*, **87**, 811 (1987); J. Mattay, *Angew. Chem., Int. Ed. Engl.*, **26**, 825 (1987).

2) K. Maruyama, Y. Kubo, M. Machida, K. Oda, Y. Kanaoka, and K. Fukuyama, *J. Org. Chem.*, **43**, 2303 (1978); K. Maruyama and Y. Kubo, *J. Am. Chem. Soc.*, **100**, 7772 (1978); M. Machida, K. Oda, K. Maruyama, Y. Kubo, and Y. Kanaoka, *Heterocycles*, **14**, 779 (1980); K. Maruyama and Y. Kubo, *J. Org. Chem.*, **46**, 3612 (1981); K. Maruyama, T. Ogawa, Y. Kubo, and T. Araki, *J. Chem. Soc., Perkin Trans., 1*, **1985**, 2025; Y. Kubo, N. Asai, and T. Araki, *J. Org. Chem.*, **50**, 5484 (1985).

3) a) K. Maruyama and Y. Kubo, *Chem. Lett.*, **1978**, 851; b) P. H. Mazzocchi, S. Minamikawa, and P. Wilson, *Tetrahedron Lett.*, **1978**, 4361; c) P. H. Mazzocchi and F. Khachik, *ibid.*, **22**, 4189 (1981); d) K. Maruyama and Y. Kubo, *J. Org. Chem.*, **50**, 1426 (1985); e) P. H. Mazzocchi, S. Minamikawa, and P. Wilson, *ibid.*, **50**, 2681 (1985); f) P. H. Mazzocchi, C. Somich, and H. L. Ammon, *Tetrahedron Lett.*, **25**, 3551 (1984); g) Y. Kubo, M. Suto, T. Araki, P. H. Mazzocchi, L. Klingler, D. Shook, and C. Somich, *J. Org. Chem.*, **51**, 4404 (1986); h) C. Somich, P. H. Mazzocchi, and H. L. Ammon, *ibid.*, **52**, 3614 (1987); i) Y. Kubo, M. Mihara, and T. Araki, *Bull. Chem. Soc. Jpn.*, **60**, 241 (1987).

4) Y. Kubo, S. Togawa, K. Yamane, A. Takuwa, and T. Araki, *J. Org. Chem.*, **54**, 4929 (1989).

5) R. A. Neunteufel and D. R. Arnold, *J. Am. Chem. Soc.*, **95**, 4080 (1973).

6) D. Rehm and A. Weller, *Isr. J. Chem.*, **8**, 259 (1970).

7) D. R. Arnold and A. J. Maroulis, *J. Am. Chem. Soc.*, **98**, 5931 (1976).

8) F. D. Lewis, B. E. Zebrowski, and P. E. Correa, *J. Am. Chem. Soc.*, **106**, 187 (1984); W. Hub, S. Schneider, F. Dorr, J. D. Oxman, and F. D. Lewis, *ibid.*, **106**, 708 (1984).

9) J. D. Simon and K. S. Peters, *J. Am. Chem. Soc.*, **104**, 6542 (1982) and **105**, 4875 (1983); E. Hasegawa, W. Xu, P. S. Mariano, U-C. Yoon, and J-U. Kim, *ibid.*, **110**, 8099 (1988).

10) A. D. McLachlan, *Mol. Phys.*, **1**, 233 (1958).

11) A. P. Schaap, G. Prasad, and S. D. Gagnon, *Tetrahedron Lett.*, **24**, 3047 (1983).

12) C. Pac, A. Nakasone, and H. Sakurai, *J. Am. Chem. Soc.*, **99**, 5806 (1977); T. Majima, C. Pac, A. Nakasone, and H. Sakurai, *ibid.*, **103**, 4499 (1981).

Claisen Rearrangements of 5,6-Dideoxy-1,2-*O*-isopropylidene-α-D-*xylo*- and α-D-*ribo*-hept-5-eno-1,4-furanoses with Triethyl Orthoacetate[1)]

Kin-ichi TADANO,* Kei-ichi SHIMADA, Akiko MIYAKE, Jun ISHIHARA, and Seiichiro OGAWA
Department of Applied Chemistry, Faculty of Science and Technology, Keio University, Hiyoshi, Kohoku-ku, Yokohama 223
(Received July 11, 1989)

The (*E*)- and (*Z*)-isomers (**2E** and **2Z**) of 3-*O*-benzyl-5,6-dideoxy-1,2-*O*-isopropylidene-α-D-*xylo*-hept-5-eno-1,4-furanose were subjected to Claisen rearrangement with triethyl orthoacetate. Possible two diastereomers were obtained as a 1 to 1 mixture from both of **2Z** and **2E**, and also from their 3-hydroxy or 3-siloxy derivatives. On the other hand, the rearrangement of the corresponding D-ribo derivative (**13Z**) and its 3-*O*-(*t*-butyldiphenylsilyl) derivative proceeded with a high level of diastereoselectivity. By contrast, the (*E*)-isomer of **13Z** showed no significant stereoselectivity, resulting in the formation of a diastereomeric mixture. The configurations of the introduced stereogenic centers by the rearrangements were unambiguously established by chemical transformations.

Recent extensive studies on [3.3] sigmatropic rearrangements represented by the Claisen-type rearrangement, as one of the promising protocol for stereoselective carbon-carbon bond forming reactions, widen their values through simple access to complex carbon frameworks found in natural products.[2)] In these several years, we focus our efforts on investigation of the ortho ester Claisen (Johnson-Claisen type) rearrangement of the carbohydrate-derived substrates.[3)] As a result, some versatile chiral building blocks, especially for natural products synthesis, are now available.[4)] In the course of pursuit of versatile chirons,[5)] herein, we report the Claisen rearrangement of two 5,6-dideoxyhept-5-eno-1,4-furanoses and some of their derivatives with triethyl orthoacetate. In the present work, the allyl alcohol part of each substrate is involved in the side chain on the furanose ring. These steric environments make the prediction of the stereochemical outcome of the rearrangement more difficult, in comparing with our previous results[3)] obtained by the rearrangements of 3-deoxy-3-*C*-[3-hydroxy-1-propenyl]hexofuranoses with triethyl orthoesters.

Results and Discussion

Rearrangement of Derivatives of 5,6-Dideoxy-α-D-*xylo*-hept-5-eno-1,4-furanose. We pursued first the Claisen rearrangement of some derivatives of 5,6-dideoxy-1,2-*O*-isopropylidene-α-D-*xylo*-hept-5-eno-1,4-furanose, namely, *E* and *Z* isomers of **2**, **3**, and **4**. The allyl alcohols **2E** and **2Z** were prepared from 1,2:5,6-di-*O*-isopropylidene-α-D-glucofuranose (**1**) according to the known procedure.[6)] Compounds **3E** and **3Z** were prepared from **1** by standard functional group manipulation, namely, 1) selective removal of the 5,6-isopropylidene acetal by acid hydrolysis, 2) glycol cleavage with sodium periodate ($NaIO_4$), 3) Wittig olefination with (ethoxycarbonylmethylene)-triphenylphosphorane,[7)] followed by 4) diisobutylaluminum hydride (Dibal-H) reduction.[8)] The *O*-silyl derivatives **4E** and **4Z** were prepared from the 3-*O*-(*t*-butyldimethylsilyl) derivative of **1** by the analogous reaction sequence used for the preparation of **3**. In the preparation of **4**, acid hydrolysis (60% aqueous AcOH) of 3-*O*-(*t*-butyldimethylsilyl)-1,2:5,6-di-*O*-isopropylidene-α-D-glucofuranose was troublesome, and the desired mono isopropylidene derivative was obtained in 12% yield along with substantial amount of 1,2-*O*-isopropylidene-α-D-glucofuranose. We did not optimize the reaction conditions.

The Claisen rearrangement of **2E** with triethyl orthoacetate was performed according to the original procedure.[9)] By repeated silica-gel chromatography of the reaction mixture, two rearrangement products **5S** and **5R** were obtained in 42% and 40% yields, respectively. The unreacted **2E** was also recovered in 8% yield. The *Z* isomer **2Z** was exposed to the same reaction conditions, resulting in the non-stereoselective formation of **5S** (35%) and **5R** (29%) along with recovery of **2Z** (13%). Establishment of the introduced stereogenic centers in diastereomers **5S** and **5R** was achieved by chemical transformation (vide infra). The rearrangements were also explored for **3** and **4**. None of **3E**, **3Z**, **4E**, or **4Z** provided the rearrangement product stereoselectively. In the case of **3E**, two diastereomers **6S** and **6R** were obtained in an approximately 1:1.4 ratio.[10)] Besides, the *Z* isomer **3Z** gave two products in an approximately 1:1 ratio. The silyl ether **4E** gave an approximately 1.4:1 ratio of **7S** and **7R** in a combined yield of 79%,[11)] while the *Z*-isomer **4Z** provided a 55% combined yield of the diastereomeric mixture in an approximately 2:1 ratio with a slightly improved formation of **7S**.

The newly introduced stereogenic centers in **5S** and **5R** were determined by the following transformations. The product with *S*-configuration **5S** was treated with cyclohexene in the presence of $Pd(OH)_2$ on charcoal resulting in the formation of a mixture of **8R** and **9R**. Under these reaction conditions, debenzylation and

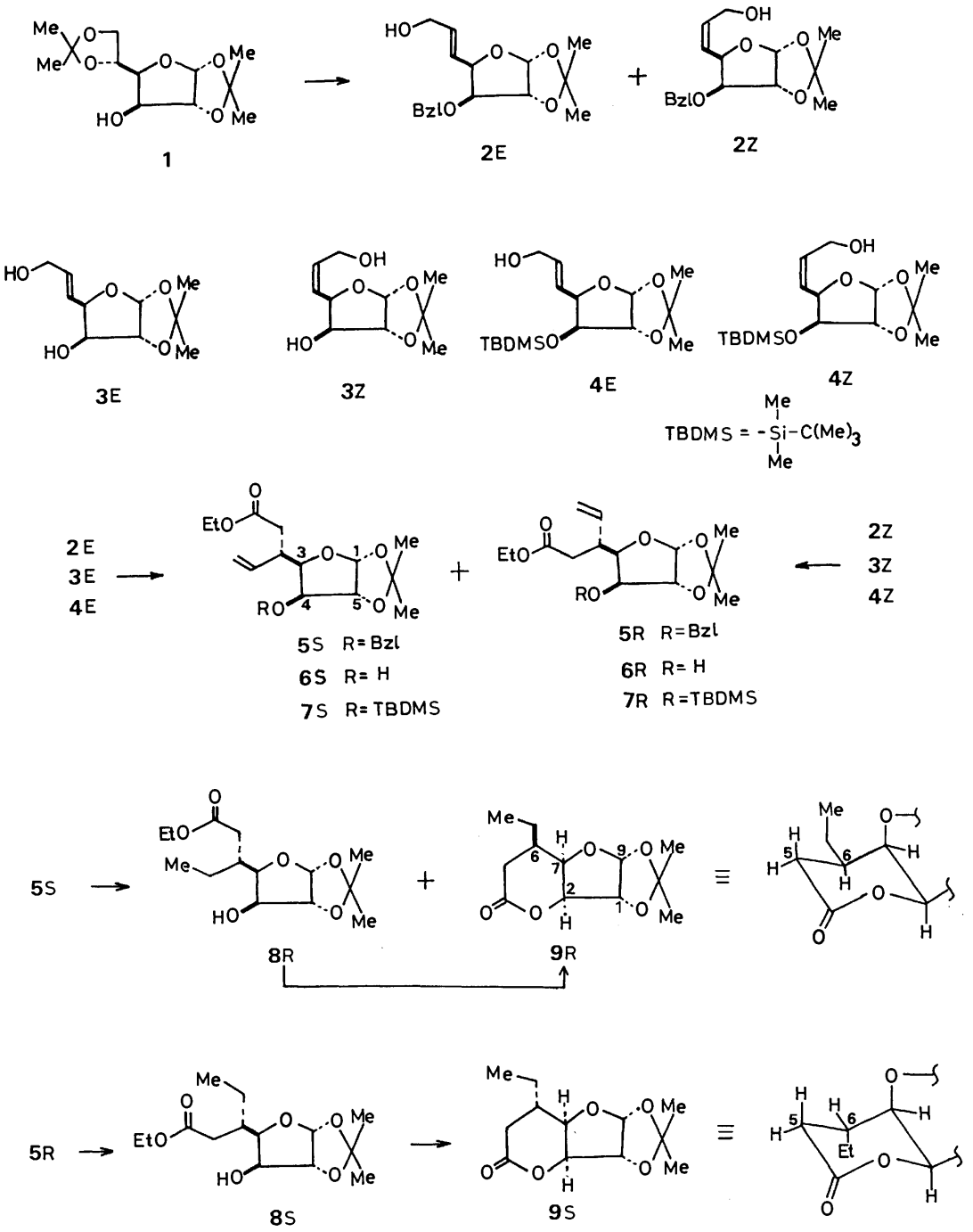

saturation of the double bond took place. δ-Lactonization of **8R** to **9R** was promoted by passage of the mixture through silica gel. The mixture of **8R** and **9R** was treated with silica gel for completion of lactonization. Finally, the tricyclic δ-lactone **9R** was obtained in an overall yield of 66.5%. Analogously, the *R*-diastereomer **5R** was converted into **8S**. Interestingly, no lactonization was observed in this case. Acid (*p*-TsOH) catalyzed lactonization of **8S** smoothly gave the lactone **9S** in 61% from **5R**. Both of ^{1}H NMR spectra (400 MHz) of the tricyclic δ-lactones **9R** and **9S** clarified their structures. The conformations of **9R** and **9S** were also confirmed as depicted. In the ^{1}H NMR spectrum of **9R**, H-5_{ax} and 5_{eq} appeared at δ 2.40 and 2.53 with $J_{5ax,6}$=12.8 Hz, $J_{5eq,5ax}$=17.5 Hz and with $J_{5eq,6}$=5.3 Hz, $J_{5eq,5ax}$=17.5 Hz, respectively. On the other hand, those of **9S** appeared at δ 2.27 and 2.70 with $J_{5ax,6}$=6.8 Hz, $J_{5eq,5ax}$=16.6 Hz, and with $J_{5eq,6}$=5.4 Hz, $J_{5eq,5ax}$=16.6 Hz, respectively. These results indicate that the ethyl groups in **9R** and **9S** are equatorial- and axial-orientations, respectively. Therefore, configurations of the newly introduced stereogenic centers in **5S** and **5R** were unequivocally established.

Rearrangement of Derivatives of 5,6-Dideoxy-α-D-*ribo*-hept-5-eno-1,4-furanose. For pursuit of improving the stereoselectivity, we next executed the rearran-

gement of derivatives of 5,6-dideoxy-α-D-*ribo*-hept-5-eno-1,4-furanose, **13** and **14**. The standard procedures from the known 1,2:5,6-di-*O*-isopropylidene-α-D-allofuranose (**10**)[12] provided efficiently the substrates **13** and **14**. Namely, selective removal of the 5,6-isopropylidene acetal in **10** by acid hydrolysis, glycol cleavage of the 5,6-diol with $NaIO_4$ followed by Wittig reaction with (ethoxycarbonylmethylene)triphenylphosphorane resulted in the formation of α,β-unsaturated esters **11E** and **11Z**, which were readily separated by silica-gel chromatography, in 43% and 31% yields from **10**, respectively.[13] Dibal-H reduction of **11E** and **11Z** provided the allyl alcohols **13E** and **13Z** effectively. Besides, silylation of the *Z*-isomer **11Z** with *t*-butyldiphenylchlorosilane gave the silyl ether **12Z** quantitatively. Silylation was carried

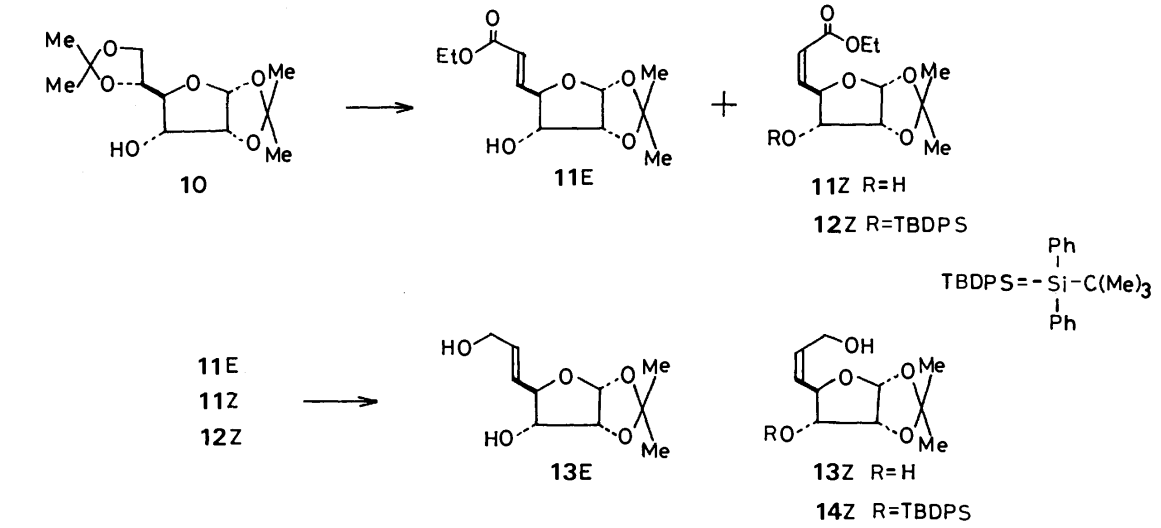

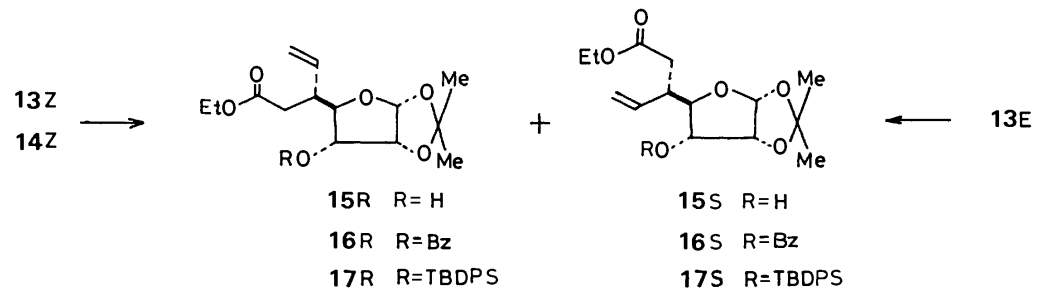

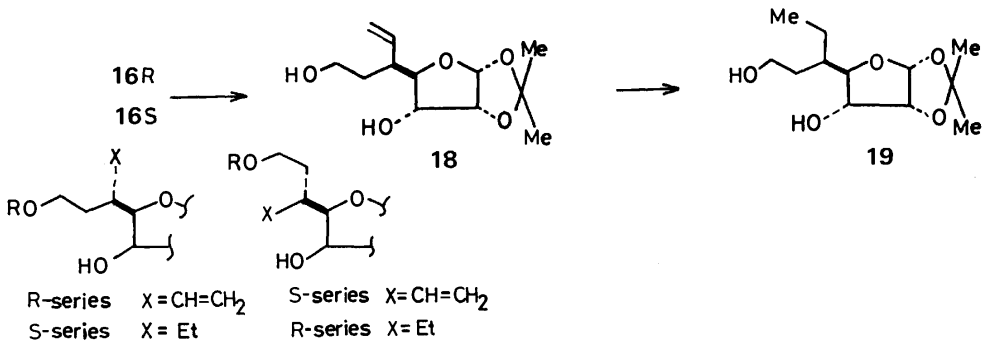

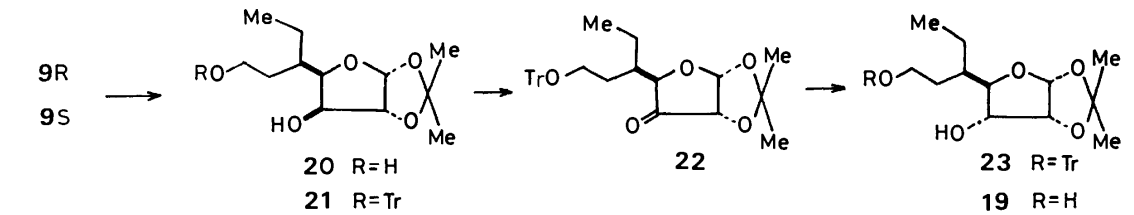

out for *Z*-isomer **11Z** by reason that the rearrangement of the *Z*-isomer **13Z** proceeded with significant stereoselectivity (vide infra). Reduction of **12Z** gave the other substrate **14Z**.

The Claisen rearrangement of **13Z** with triethyl orthoacetate gave an inseparable mixture of **15R** and **15S** in a combined yield of 72%. To determine the ratio of **15R** and **15S** accurately, the mixture was converted into the benzoates **16R** and **16S**, which were readily separated by silica-gel chromatography. From the yields of **16R** and **16S**, the ratio of the rearrangement products **15R** and **15S** was determined to be 11 : 70. On the other hand, *E*-isomer **13E** provided a mixture of **15R** and **15S** in a combined yield of 71% with an approximately 1 : 1.3 ratio. *E*-Isomer **13E** showed no significant stereoselectivity. Furthermore, the rearrangement of the silylated derivative **14Z** proceeded with an improved stereoselectivity to afford an inseparable mixture of **17R** and **17S** in a combined yield of 48%. The ratio (approximately 1 : 8) of **17R** and **17S** was determined by conversion of the mixture into separable **16R** and **16S** by desilylation followed by benzoylation.

The stereochemical assignment of the introduced stereogenic centers in **15R** and **15S** was achieved as follows. Both benzoates **16R** and **16S** were converted into **19S** and **19R** via vinyl-alcohols **18R** and **18S** by $LiAlH_4$ reduction of the ester groups followed by hydrogenation of the vinyl groups. On the other hand, the stereochemically defined δ-lactones **9R** and **9S** were converted into diols **20R** and **20S** by $LiAlH_4$ reduction. Tritylation of **20R** and **20S** under the standard conditions gave mono-trityl ethers **21R** and **21S** quantitatively. Pyridinium chlorochromate (PCC) oxidation[14] of **21R** and **21S** and subsequent $NaBH_4$ reduction of the 3-uloses **22R** and **22S** provided **23R** and **23S**, respectively. As anticipated, the hydride attacks to **22R** and **22S** took place exclusively from the less hindered convex-face to give **23R** and **23S**. Exposure of **23R** to *p*-toluenesulfonic acid provided the detritylated product, which was found to be identical with **19R** by direct comparison (mp, IR, and ^1H NMR). The detritylated product of **23S** was identical with **19S** in all respects. Therefore, the structures of **15R** and **15S** were established.

One of the stereocontrolling factors in the Claisen rearrangement is, in general, a steric environment surrounding the six membered transition state that consists of the intermediary allylic ketene acetal. As concerns the stereochemical outcome of the aforementioned ortho ester Claisen rearrangements, it is most likely that the C-3 substituent of each substrate interacts with the intermediary allylic ketene acetal moiety. It was forecasted that the interactions occurred between the C-3 substituents in **2**, **3**, and **4** and each of the intermediary ketene acetal moiety were more severe than those occurred in the case of substrates **13** and **14**. Unexpectedly, the results of the present work revealed that the C-3 substituent in **2**, **3**, or **4** was not likely to work as a stereocontrolling factor, irrespective of its bulkiness or of the allylic geometry. On the contrary, the C-3 substituents of *ribo*-type substrates possessing *Z*-allyl alcohol part, i.e. **13Z** and **14Z**, seem to contribute largely for outcome of the high-stereoselectivity in their rearrangement reactions. In the case of **13Z** and **14Z**, the transition state (A) shown in Fig. 1, which leads the formation of the major *S*-rearrangement product, seems to be favorable than the alternative transition state (B). This assumption is based on that nonbonded interaction between the C-3 substituent and the ethoxy group in the ketene acetal moiety is not negligible in the case of transition state (B). Furthermore, the influence of this interaction on the stereoselectivity of the rearrangement would be proportional to the bulkiness of the C-3 substituent. In fact, the stereoselectivity was slightly improved when a hydroxy group (i.e. **13Z**) was substituted by a (*t*-butyldiphenylsilyl)oxy group (i.e. **14Z**). Speculation of the transtion state, made by using Dreiding models, also reveals that high-stereoselective formation of either diastereomer is not expected for **13E**. No preferential transition state is considered in this case. Although we have no valid evidence for these explanations, the Claisen rearrangement protocol demonstrated in the present work is a practical access to highly functionalized enantiomerically pure building blocks.

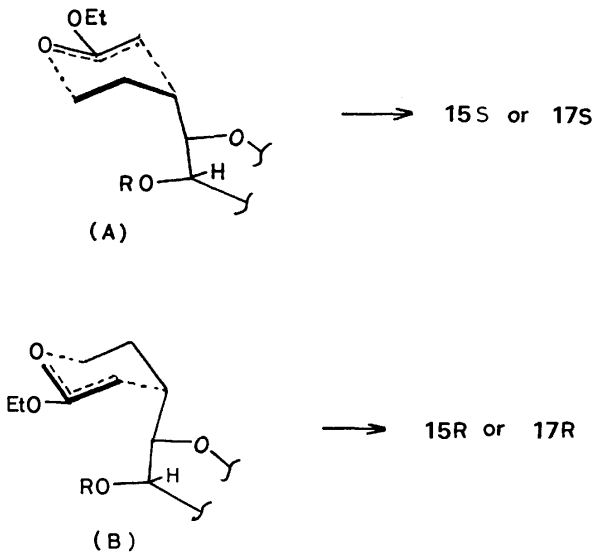

Fig. 1.

Experimental[15]

***E* and *Z* Isomers of 3-*O*-Benzyl-5,6-dideoxy-1,2-*O*-isopropylidene-α-D-*xylo*-hept-5-eno-1,4-furanose (2E and 2Z).** These compounds were prepared according to the reported procedure.[6] **2E**: TLC R_f 0.15 (AcOEt/hexane 1 : 3); $[\alpha]_D^{27}$ −60.9° (*c* 1.22, $CHCl_3$). **2Z**: TLC R_f 0.19 (AcOEt/hexane 1 : 3); $[\alpha]_D^{28}$ −92.9° (*c* 1.10, $CHCl_3$).

***E* and *Z* Isomers of 5,6-Dideoxy-1,2-*O*-isopropylidene-α-D-*xylo*-hept-5-eno-1,4-furanose (3E and 3Z).** 1,2-*O*-Isopropylidene-α-D-glucofuranose (2.39 g), which was obtained by hydrolysis of **1** with 80% aqueous AcOH, was subjected to $NaIO_4$ oxidation (3.0 g in aqueous MeOH, 3 : 5 v/v, 64 ml). The reaction mixture was filtered, and the filtrate was concentrated in vacuo to give an aldehyde, which was used without purification. The aldehyde was dissolved in benzene (50 ml) and (ethoxycarbonylmethylene)triphenylphosphorane (5.0 g) was added. The mixture was stirred for 45 min, and concentrated in vacuo. The residue was chromatographed on silica gel (EtOAc/hexane 1 : 4) to give a mixture of *E*- and *Z*- α,β-unsaturated esters and *Z*-δ-lactone (2.44 g). Dibal-H (1.5 mol dm^{-3} solution in $PhCH_3$, 19 ml) reduction of the mixture in CH_2Cl_2 (40 ml) at −60 °C, and silica-gel chromatographic purification of the reaction mixture (AcOEt/hexane 1 : 1) gave **3E** (509 mg, 22%), **3Z** (356 mg, 15%), and a diastereomeric mixture of the hemiacetals derived from *Z*-δ-lactone (584 mg, 25%). **3E**: mp 70—71.5 °C, TLC R_f 0.43 (AcOEt); $[\alpha]_D^{87}$ −54.1° (*c* 1.53, $CHCl_3$); IR (KBr) ν_{max} 3410, 3230, 2965, 2865, 1630, 1375 cm^{-1}; ^1H NMR (400 MHz, $CDCl_3$) δ=1.32, 1.50 (3H each, 2 s), 3.50, 3.67 (1H each, 2 br s), 4.08 (1H, d, *J*=2.4 Hz), 4.16 (2H, br s), 4.54 (1H, d, *J*=3.7 Hz), 4.68 (1H, dd, *J*=1.0 and 4.8 Hz), 5.78 (1H, ddt, *J*=15.6, 4.8, and 1.0 Hz), 5.94 (1H, d, *J*=3.7 Hz), 6.05 (1H, ddt, *J*=15.6, 4.9, and 1.0 Hz). Found: C, 55.49; H, 7.19%. Calcd for $C_{10}H_{16}O_5$: C, 55.55; H, 7.46%. **3Z:** mp 90.5—92 °C, TLC R_f 0.51 (AcOEt); IR (KBr) ν_{max} 3435, 2990, 2855, 1640, 1460 cm^{-1}; ^1H NMR (400 MHz, $CDCl_3$) δ=1.33, 1.51 (3H each, 2 s), 2.98, 3.20 (1H each, 2 s), 4.12—4.19 (2H, m), 4.30 (1H, dd, *J*=6.8 and 13.1 Hz), 4.57 (1H, d, *J*=3.9 Hz), 4.93 (1H, d, *J*=6.4 Hz), 5.65 (1H, dd, *J*=6.4 and 11.5 Hz), 5.91—5.98 (2H, m). Found: C, 55.54; H, 7.22%. Calcd for $C_{10}H_{16}O_5$: C, 55.55; H, 7.46%.

***E* and *Z* Isomers of 3-*O*-(*t*-Butyldimethylsilyl)-5,6-dideoxy-1,2-*O*-isopropylidene-α-D-*xylo*-hept-5-eno-1,4-furanose (4E and 4Z).** Compound **1** (5.00 g) was silylated with *t*-butylchlorodimethylsilane (4.36 g) in DMF (80 ml) in the presence of imidazole (1.23 g). Extractive work-up and chromatographic purification on silica gel gave the 3-*O*-silyl derivative (6.78 g, 94%) as a colorless oil, TLC R_f 0.18 (AcOEt/hexane 1:30): ^1H NMR (90 MHz, $CDCl_3$) δ=0.13, 0.14 (3H each, 2 s), 0.91 (9H, s), 1.32, 1.40, 1.49 (3H, 3H, 6H, 3 s), 4.04—4.26 (5H, m), 4.34 (1H, d, *J*=3.5 Hz), 5.87 (1H, d, *J*=3.5 Hz).

The 3-*O*-silyl derivative (6.77 g) was hydrolyzed with 60% aqueous AcOH (160 ml) and 1,4-dioxane (10 ml) for 30 min at room temperature. The mixture was concentrated in vacuo, and the residue was chromatographed on silica gel (EtOH/$PhCH_3$ 1:20) to give 3-*O*-(*t*-butyldimethylsilyl)-1,2-*O*-isopropylidene-α-D-glucofuranose (721 mg, 12%) as a colorless oil. This mono-isopropylidene derivative (721 mg) was dissolved in MeOH (26 ml) and $NaIO_4$ (534 mg) in H_2O (4.4 ml) was added. After stirring for 1.5 h, the mixture was filtered. The filtrate was concentrated in vacuo. The residue was dissolved in benzene (25 ml), (ethoxycarbonylmethylene)triphenylphosphorane (1.49 g) was added. The mixture was stirred for 1 h, concentrated in vacuo. The residue was triturated with petroleum ether. The precipitated triphenylphosphine oxide was removed, and the filtrate was concentrated in vacuo. The residue was chromatographed on silica gel (AcOEt/hexane 1 : 60) to give the *E*-α,β-unsaturated ester [407 mg, 51%, TLC R_f 0.59 (EtOH/$PhCH_3$ 1 : 30)] and the *Z*-α,β-unsaturated ester [346 mg, R_f 0.72 (EtOH/$PhCH_3$ 1 : 30)]. Each α,β-unsaturated ester was reduced with Dibal-H at −60 °C. After chromatographic purification of the reaction mixture on silica gel, **4E** (99%) and **4Z** (88%) were obtained. **4E**, TLC R_f 0.26 (AcOEt/hexane 1:3): $[\alpha]_D^{26}$ −42.4° (*c* 0.90, $CHCl_3$); IR (neat) ν_{max} 3425, 2925, 2850, 1470, 1460 cm^{-1}; ^1H NMR (90 MHz, $CDCl_3$) δ=0.06, 0.09 (3H each, 2 s), 0.90 (9H, s), 1.33, 1.55 (3H each, 2 s), 4.09 (1H, d, *J*=2.9 Hz), 4.15, 4.19 (1H each, 2 s), 4.39 (1H, d, *J*=3.7 Hz), 4.61 (1H, dd, *J*=2.9 and 6.4 Hz), 5.81—5.94 (2H, m), 5.92 (1H, d, *J*=3.7 Hz). Found: C, 57.76; H, 8.83%. Calcd for $C_{16}H_{30}O_5Si$: C, 58.15; H, 9.15%. **4Z**, TLC R_f 0.21 (AcOEt/hexane 1 : 5): $[\alpha]_D^{25}$ −63.6° (*c* 1.28, $CHCl_3$); IR (neat) ν_{max} 3460, 2950, 2880, 1480, 1470 cm^{-1}; ^1H NMR (90 MHz, $CDCl_3$) δ=0.07, 0.09 (3H each, 2 s), 0.89 (9H, s), 1.33, 1.51 (3H each, 2 s), 1.93 (1H, s), 4.08 (1H, d, *J*=2.9 Hz), 4.19—4.31 (2H, m), 4.40 (1H, d, *J*=3.6 Hz), 4.91 (1H, dd, *J*=2.9 and 7.4 Hz), 5.51—6.05 (2H, m), 5.93 (1H, d, *J*=3.6 Hz). Found: C, 57.90; H, 8.84%. Calcd for $C_{16}H_{30}O_5Si$: C, 58.15; H, 9.15%.

(1*R*,3*R*,4*S*,5*R*)-4-Benzyloxy-3-[(1*S*)- and (1*R*)-1-(ethoxycarbonyl)methyl-2-propenyl]-7,7-dimethyl-2,6,8-trioxabicyclo[3.3.0]octanes (5S and 5R). From 2E. The reaction was carried out under an argon atmosphere. A solution of **2E** (1.82 g, 5.9 mmol) in freshly distilled triethyl orthoacetate (20 ml) was heated in the presence of 0.013 ml of distilled propionic acid at 135 °C for 5 h. The reaction mixture was then concentrated in vacuo with an aid of $PhCH_3$. The residue was repeatedly chromatographed on silica gel (AcOEt/hexane 1 : 15). The rearrangement products **5S** (940 mg, 42%) and **5R** (901 mg, 40%) were obtained and **2E** (138 mg, 8%) was recovered. **5S**: mp 56—58 °C, R_f 0.21 (AcOEt/hexane 1 : 10); $[\alpha]_D^{28}$ −33.9° (*c* 0.83, $CHCl_3$); IR (neat) ν_{max} 3010, 2960, 2900, 1740, 1650, 1510, 1465, 1380, 1265, 1225 cm^{-1}; ^1H NMR (400 MHz, $CDCl_3$) δ=1.22 (3H, t, *J*=7.3 Hz), 1.31, 1.49 (3H each, 2 s), 2.39 (1H, dd, *J*=10.3 and 15.4 Hz), 2.81 (1H, dd, *J*=4.2 and 15.4 Hz), 3.17 (1H,dddd, *J*=4.2, 7.6, and 10.3 Hz), 3.82 (1H, d, *J*=3.0 Hz), 4.03 (1H, dd, *J*=3.0 and 10.3 Hz), 4.10 (2H, q, *J*=7.3 Hz), 4.47, 4.63 (2H each, 2 d, *J*=11.5 Hz), 4.58 (1H, d, *J*=3.9 Hz), 5.06 (1H, dd, *J*=1.5 and 10.3 Hz), 5.14 (1H, dd, *J*=1.5 and 18.8 Hz), 5.67 (1H, ddd, *J*=7.6, 10.3, and 18.8 Hz), 5.90 (1H, d, *J*=3.9 Hz), 7.28—7.37 (5H, m). Found: C, 66.88; H, 7.36%. Calcd for $C_{21}H_{28}O_6$: C, 67.00; H, 7.50%. **5R:** mp 47.5—49 °C, TLC R_f 0.19 (AcOEt/hexane 1 : 10); $[\alpha]_D^{28}$ −27.1° (*c* 0.98, $CHCl_3$); IR (neat) ν_{max} 2990, 2940, 1735, 1650, 1500, 1460, 1375, 1260 cm^{-1}; ^1H NMR (400 MHz, $CDCl_3$) δ=1.24 (3H, t, *J*=7.3 Hz), 1.32, 1.48 (3H each, 2 s), 2.16—2.28 (2H, m), 3.07—3.15 (1H, m), 3.85 (1H, d, *J*=3.3 Hz), 4.05 (1H, dd, *J*=3.3 and 9.5 Hz), 4.08 (2H, q, *J*=7.3 Hz), 4.46, 4.73 (2H each, 2 d, *J*=11.7 Hz), 4.64 (1H, d, *J*=3.9 Hz), 5.11 (1H, dd, *J*=1.5 and 10.3 Hz), 5.17 (1H, dd, *J*=1.5 and 17.1 Hz), 5.81 (1H, ddd, *J*=7.8, 10.3, and 17.1 Hz), 5.93 (1H, d, *J*=3.9 Hz), 7.30—7.37 (5H, m). Found: C, 66.78; H, 7.27%. Calcd for $C_{21}H_{28}O_6$: C, 67.00; H, 7.50%.

From 2Z. Compoud **2Z** (1.59 g) was subjected to the Claisen rearrangement under the same reaction conditions as above. Silica-gel chromatography of the reaction mixture gave 675 mg (35%) of **5S** and 563 mg (29%) of **5R**, and 202 mg (13%) of **2Z** was also recovered.

Claisen Rearrangement of 3E and 3Z and Successive $LiAlH_4$ Reduction of the Products. From 3E. Compound **3E** (550 mg) was heated at 135 °C in triethyl orthoacetate (5 ml) in the presence of catalytic propionic acid for 5.5 h.

The reaction mixture was concentrated in vacuo, and the residue was chromatographed on silica gel (AcOEt/hexane 1 : 6) to give a mixture of **6S**, **6R**, and their δ-lactone derivatives (472 mg). This mixture (472 mg) was reduced with $LiAlH_4$ (116 mg) in THF (24 ml) for 1 h. The mixture was quenched with H_2O, filtered, and the filtrate was concentrated in vacuo. The residue was chromatographed on silica gel (AcOEt/hexane 1 : 1) to give a diol derived from **6S** (144 mg, 23% from **3E**), a diol derived from **6R** (209 mg, 34%), and a mixture of them (21 mg, 3%). Diol derived from **6S**, TLC R_f 0.59 (AcOEt): $[\alpha]_D^{26}$+12.1° (*c* 1.99, $CHCl_3$); ^1H NMR (90 MHz, $CDCl_3$) δ=1.30, 1.49 (3H each, 2 s), 1.56—2.21 (2H, m), 2.49—2.86 (1H, m), 3.00 (2H, br s), 3.58—4.05 (5H, m), 4.49 (1H, d, *J*=4.0 Hz), 5.15 (1H, dd, *J*=2.7 and 8.4 Hz), 5.22 (1H, dd, *J*=2.7 and 17.8 Hz), 5.65 (1H, dd, *J*=8.4 and 17.8 Hz), 5.89 (1H, d, *J*=4.0 Hz). Diol derived from **6R**, TLC R_f 0.46 (AcOEt): $[\alpha]_D^{26}$=−32.9° (*c* 1.96, $CHCl_3$); ^1H NMR (90 MHz, $CDCl_3$) δ=1.30, 1.48 (3H each, 2 s), 1.42—1.87 (2H, m), 2.44—2.79 (1H, m), 3.34 (2H, br s), 3.47—4.18 (4H, m), 4.50 (1H, d, *J*=3.8 Hz), 5.07—5.24 (2H, m), 5.71 (1H, dd, *J*=9.2 and 17.8 Hz), 5.89 (1H, d, *J*=3.8 Hz).

From 3Z. Rearrangement of **3Z** (327 mg), and successive $LiAlH_4$ reduction of the products as described for **3E** resulted in formation of an approximately 1 : 1 mixture of the diols derived from 6S and **6R** (103.5 mg, 28% from **3Z**). The ratio was estimated based on the ^1H NMR (400 MHz) spectral analysis, though the diastereomers were not separated.

(1*R*,3*R*,4*S*,5*R*)-4-(*t*-Butyldimethylsilyloxy)-3-[(1*S*)- and (1*R*)-1-(ethoxycarbonyl)methyl-2-propenyl]-7,7-dimethyl-2,5,8-trioxabicyclo[3.3.0]octanes (7S and 7R). From 4E. Compound **4E** (376 mg) was heated in triethyl orthoacetate (12 ml) at 135 °C in the presence of catalytic amount of propionic acid for 5 h. Concentration of the reaction mixture, and chromatographic purification of the residue on silica gel (AcOEt/hexane 1 : 25) gave **7S** (202 mg, 44%), **7R** (142 mg, 31%), and a mixture of **7S** and **7R** (16 mg, 4%). **7S:** TLC R_f 0.55 (AcOEt/hexane 1 : 5); $[\alpha]_D^{28}$−27.4° (*c* 1.23, $CHCl_3$); IR (neat) ν_{max} 2990, 2960, 2840, 1740, 1470 cm^{-1}; ^1H NMR (90 MHz, $CDCl_3$) δ=0.08, 0.14 (3H each, 2 s), 0.92 (9H, s), 1.22 (3H, t, *J*=7.2 Hz), 1.31, 1.48 (3H each, 2 s), 2.22—2.78 (2H, m), 2.92—3.25 (1H, m), 3.92—4.11 (2H, m), 4.10 (2H, q, *J*=7.2 Hz), 4.36 (1H, d, *J*=3.7 Hz), 5.04—5.07 (1H, m), 5.15—5.17 (1H, m), 5.23—5.26 (1H, m), 5.85 (1H, d, *J*=3.7 Hz). **7R:** TLC R_f 0.48 (AcOEt/hexane 1 : 5); $[\alpha]_D^{28}$−17.5° (*c* 1.27, $CHCl_3$); IR (neat) ν_{max} 2990, 2960, 2860, 1740, 1640, 1470 cm^{-1}; ^1H NMR (90 MHz, $CDCl_3$) δ=0.13, 0.16 (3H each, 2 s), 0.92 (9H, s), 1.23 (3H, t, *J*=7.1 Hz), 1.30, 1.47 (3H each, 2 s), 2.27—2.40 (2H, m), 2.84—3.21 (1H, m), 3.94—4.13 (2H, m), 4.11 (2H, q, *J*=7.1 Hz), 4.37 (1H, d, *J*=3.7 Hz), 5.05—5.06 (1H, m), 5.18—5.24 (1H, m), 5.67—5.78 (1H, m), 5.88 (1H, d, *J*=3.7 Hz).

From 4Z. As described above, compound **4Z** (114 mg) was subjected to the Claisen rearrangement to give **7S** (44 mg, 32%), **7R** (22 mg, 16%), and a mixture of **7S** and **7R** (9.5 mg, 7%).

(1*R*,2*S*,6*R*,7*R*,9*R*)-6-Ethyl-11,11-dimethyl-3,8,10,12-tetraoxatricyclo[7.3.0.0^{2,7}]dodecan-4-one (9R). A solution of 5S (88 mg, 0.23 mmol) in a mixture of EtOH (3 ml) and freshly distilled cyclohexene (5 ml) was refluxed for 3 h in the presence of 20% $Pd(OH)_2$ on charcoal (133 mg). The catalyst was removed by filtration, washed with EtOH. The combined filtrate and washings were concentrated in vacuo. The residue was chromatographed on silica gel (AcOEt/hexane 1 : 5) to give **9R** (25 mg, 44%) and a mixture of the hydroxy ester **8R** and **9R** (37 mg). The mixture of **8R** and **9R** (37 mg) was dissolved in AcOEt/hexane (1/5 v/v 1.5 ml), then silica gel (0.2 g) was added. The mixture was kept standing at room temperature for 3.5 d. Then, the silica gel was removed by filtration, washed with AcOEt. The combined filtrate and washings were concentrated in vacuo. The residue was chromatographed on silica gel to give **9R** (12.5 mg, total 37.5 mg, 66.5%) as a colorless oil. **9R:** TLC R_f 0.61 (AcOEt/hexane 1 : 2); $[\alpha]_D^{25}$−8.8° (*c* 0.85, $CHCl_3$); IR (neat) ν_{max} 2970, 2950, 2890, 1745, 1460, 1375, 1300, 1220 cm^{-1}; ^1H NMR (400 MHz, $CDCl_3$) δ=0.99 (3H, t, *J*=7.5 Hz), 1.34, 1.52 (3H each, 2 s), 1.44—1.68 (2H, m), 1.97—2.06 (1H, m), 2.40 (1H, dd, *J*=12.8 and 17.5 Hz), 2.53 (1H, dd, *J*=5.3 and 17.5 Hz), 4.42 (1H, dd, *J*=2.0 Hz), 4.68 (1H, d, *J*=3.7 Hz), 4.70 (1H, d, *J*=2.0 Hz), 5.92 (1H, d, *J*=3.7 Hz). Found: C, 59.36; H, 7.26%. Calcd for $C_{12}H_{18}O_5$: C, 59.49; H, 7.49%.

(1*R*,2*S*,6*S*,7*R*,9*R*)-6-Ethyl-11,11-dimethyl-3,8,10,12-tetraoxatricyclo[7.3.0.0^{2,7}]dodecan-4-one (9S). As desdribed for the preparation of **9R**, 119 mg (0.32 mmol) of **5R** was analogously converted into crude **8S** (99.5 mg), which was lactonized directly. The crude **8S** (99.5 mg) was dissolved in benzene (3 ml) and *p*-TsOH (monohydrate, 15 mg) was added. The mixture was stirred at room temperature for 3 h, and saturated aqueous $NaHCO_3$ (2 ml) was added. This was diluted with benzene (15 ml) and washed with H_2O (10 ml×3). The organic phase was dried (Na_2SO_4) and concentrated in vacuo. The residue was chromatographed on silica gel (AcOEt/hexane 1 : 8) to give **9S** (47 mg, 61%), mp 69—70 °C, TLC R_f 0.69 (AcOEt/hexane 1 : 2); $[\alpha]_D^{24}$+28.8° (*c* 1.21, $CHCl_3$); IR (neat) ν_{max} 2970, 2940, 2870, 1730, 1460, 1370, 1250 cm^{-1}; ^1H NMR (400 MHz, $CDCl_3$) δ=1.03 (3H, t, *J*=7.3 Hz), 1.34, 1.52 (3H each, 2 s), 1.36—1.60 (2H, m), 2.09—2.17 (1H, m), 2.27 (1H, dd, *J*=6.8 and 16.6 Hz), 2.70 (1H, dd, *J*=5.4 and 16.6 Hz), 4.30 (1H, dd, *J*=3.4 Hz), 4.66 (1H, d, *J*=3.4 Hz), 4.73 (1H, d, *J*=3.4 Hz), 5.95 (1H, d, *J*=3.4 Hz). Found: 59.54; H, 7.29%. Calcd for $C_{12}H_{18}O_5$: C, 59.49; H, 7.49%.

***E* and *Z* Isomers of Ethyl 5,6-Dideoxy-1,2-*O*-isopropylidene-α-D-*ribo*-hept-5-eno-1,4-furanuronates (11E and 11Z).** A solution of **10**[12] (4.02g, 15.4 mmol) in 60% aqueous AcOH (80 ml) was stirred for 14 h and concentrated in vacuo. The residue [R_f 0.22 (EtOH/$PhCH_3$ 1 : 5)] was dissolved in MeOH (80 ml), and an aqueous solution (15 ml) of $NaIO_4$ (4.01 g, 18.7 mmol) was added. After being stirred for 1 h, insoluble solids were removed. The filtrate was concentrated in vacuo. The residue was triturated with CH_2Cl_2, and insoluble solids were removed. The filtrate was concentrated in vacuo. The residue [R_f 0.52 (EtOH/$PhCH_3$ 1 : 5)] was dissolved in benzene (80 ml) and (ethoxycarbonylmethylene) triphenylphosphorane (8.07 g, 23.2 mmol) was added. The mixture was stirred at room temperature for 1 h and concentrated in vacuo. The residue was triturated with petroleum ether, and insoluble triphenylphosphine oxide was removed. The filtrate was concentrated in vacuo. The residue was chromatographed on silica gel (AcOEt/hexane 1 : 4) to give 1.72 g (43%) of **11E** and 1.24 g (31%) of **11Z** (73 mg of the mixture was also obtained). **11E:** mp 51—52 °C, TLC R_f 0.54 (EtOH/$PhCH_3$ 1 : 5); $[\alpha]_D^{27}$ +33.3° (*c* 1.18, $CHCl_3$); IR (KBr) ν_{max} 3470, 2985, 2950, 1720, 1645, 1465, 1445, 1425, 1385 cm^{-1}; ^1H NMR (90 MHz, $CDCl_3$) δ=1.29

(3H, t, J=7.1 Hz), 1,38, 1.58 (3H each, 2 s), 2.61 (1H, d, J=10.8 Hz), 4.18 (2H, q, J=7.1 Hz), 3.71—4.42 (2H, m), 4.60 (1H, dd, J=4.2 Hz), 5.86 (1H, d, J=4.2 Hz), 6.13 (1H, dd, J=1.5 and 15.8 Hz), 7.00 (1H, dd, J=4.5 and 15.8 Hz). Found: C, 55.80; H, 6.72%. Calcd for $C_{12}H_{18}O_6$: C, 55.81; H, 7.02%. **11Z:** mp 103—105 °C, TLC R_f 0.58 (EtOH/$PhCH_3$ 1 : 5); $[\alpha]_D^{28}$ −23.0° (*c* 1.08, $CHCl_3$); IR (KBr) ν_{max} 3480, 2980, 1720, 1655, 1220 cm^{-1}; ^1H NMR (90 MHz, $CDCl_3$) δ=1.29 (3H, t, J=7.0 Hz), 1.38, 1.62 (3H each, 2 s), 3.41 (1H, d, J=9.0 Hz), 3.75 (1H, ddd, J=4.3, 9.0, and 9.0 Hz), 4.19 (2H, q, J=7.0 Hz), 4.60 (1H, dd, J=4.3 Hz), 5.49 (1H, dd, J=7.1 and 9.0 Hz), 5.80 (1H, d, J=4.3 Hz), 5.99 (1H, d, J=11.8 Hz), 6.22 (1H, dd, J=7.1 and 11.8 Hz). Found: C, 55.95; H, 6.79%. Calcd for $C_{12}H_{18}O_6$: C, 55.81; H, 7.02%.

***Z* Isomer of Ethyl 3-*O*-(*t*-Butyldiphenylsilyl)-5,6-dideoxy-1,2-isopropylidene-α-D-*ribo*-hept-5-eno-1,4-furanuronate (12Z).** A mixture of **11Z** (326 mg, 1.3 mmol), *t*-butylchlorodiphenylsilane (0.66 ml, 2.5 mmol), and imidazole (341 mg) in DMF (6 ml) was stirred at room temperature for 7 h. The mixture was diluted with CH_2Cl_2 (30 ml), wahsed with dilute HCl (30 ml), saturated aqueous $NaHCO_3$ (30 ml), and H_2O (30 ml) successively. The organic phase was dried (Na_2SO_4) and concentrated in vacuo. The residue was chromatographed on silica gel (AcOEt/hexane 1 : 15) to give **12Z** (614 mg, 98%) as a colorless oil: TLC R_f 0.58 (AcOEt/hexane 1 : 4); $[\alpha]_D^{21}$ −30.8° (*c* 0.96, $CHCl_3$); IR (neat) ν_{max} 2985, 2955, 1720, 1650, 1470, 1425, 1380, 1370 cm^{-1}; ^1H NMR (90 MHz, $CDCl_3$) δ=1.04 (9H, s), 1.26, 1.65 (3H each, 2 s), 1.32 (3H, t, J=7.0 Hz), 3.64 (1H, dd, J=4.0 and 8.2 Hz), 3.98 (1H, dd, J=4.0 Hz), 4.20 (2H, q, J=7.0 Hz), 5.55 (1H, d, J=4.0 Hz), 5.68—6.01 (3H, m), 7.29—7.82 (10H, m). Found: C, 67.79; H, 7.10%. Calcd for $C_{28}H_{36}O_6Si$: C, 67.71; H, 7.31%.

***E* and *Z* Isomers of 5,6-Dideoxy-1,2-*O*-isopropylidene-α-D-*ribo*-hept-5-eno-1,4-furanoses (13E and 13Z).** The reaction was carried out under an argon atmosphere. To a solution of **11E** (777 mg, 3.0 mmol) in CH_2Cl_2 (15 ml) was injected Dibal-H (1.5 mol dm^{-3} solution in $PhCH_3$, 7.9 ml, 11.9 mmol) at −78 °C. After being stirred for 90 min, the mixture was quenched with H_2O (0.5 ml). Insoluble solids were removed, washed well with CH_2Cl_2. The combined filtrate and washings were concentrated in vacuo. The residue was chromatographed on silica gel (EtOH/$PhCH_3$ 1 : 15) to give **13E** (514 mg, 79%) as a colorless oil: TLC R_f 0.29 (EtOH/$PhCH_3$ 1 : 5); $[\alpha]_D^{27}$ +31.1° (*c* 1.29, $CHCl_3$); IR (neat) ν_{max} 3400, 2990, 1645, 1375, 1215 cm^{-1}; ^1H NMR (90 MHz, $CDCl_3$) δ=1.33, 1.54 (3H each, 2 s), 2.4—2.7, 2.8—3.0 (1H each, 2 m), 3.52—3.78 (1H, m), 4.07—4.35 (3H, m), 4.53 (1H, dd, J=4.4 Hz), 5.53—5.79 (2H, m), 6.06 (1H, ddd, J=15.6, 4.6, and 4.6 Hz). Found: C, 55.18; H, 7.30%. Calcd for $C_{10}H_{16}O_5$: C, 55.55; H, 7.46%.

As described above, 720 mg of **11Z** was analogously converted into 568 mg (94%) of **13Z**, mp 105—106 °C: TLC R_f 0.34 (EtOH/$PhCH_3$ 1 : 5); $[\alpha]_D^{27}$ +56.6° (*c* 0.86, $CHCl_3$); IR (KBr) ν_{max} 3420, 2995, 1430, 1385, 1250 cm^{-1}; ^1H NMR (90 MHz, $CDCl_3$) δ=1.36, 1.57 (3H each, 2 s), 2.5—2.8, 3.1—3.3 (1H each, 2 m), 3.51—3.75 (1H, m), 4.12—4.19 (2H, m), 4.52—4.70 (2H, m), 5.46—5.67 (1H, m), 5.82 (1H, d, J=4.0 Hz), 5.91—6.12 (1H, m). Found: C, 55.51; H, 7.27%. Calcd for $C_{10}H_{16}O_5$: C, 55.55; H, 7.46%.

***Z*-Isomer of 3-*O*-(*t*-Butyldiphenylsilyl)-5,6-dideoxy-1,2-*O*-isopropylidene-α-D-*ribo*-hept-5-eno-1,4-furanose (14Z).** Compound **12Z** (461 mg, 0.93 mmol) was treated with 5 mol equiv of Dibal-H as described for the preparation of **13E** and **13Z**. By chromatographic purification of the reaction mixture on silica gel, 419 mg (99%) of **14Z** was obtained, mp 92.5—93.5 °C: TLC R_f 0.52 (AcOEt/hexane 1 : 3); $[\alpha]_D^{21}$ +4.7° (*c* 1.33, $CHCl_3$); IR (neat) ν_{max} 3440, 2960, 2900, 1590, 1460, 1430, 1380, 1375, 1250 cm^{-1}; ^1H NMR (400 MHz, $CDCl_3$) δ=1.07 (9H, s), 1.21, 1.60 (3H each, 2 s), 1.79 (1H, d, J=6.1 Hz), 3.65 (1H, dd, J=4.1 and 8.8 Hz), 3.76 (1H, dd, J=4.1 Hz), 4.18—4.25, 4.32—4.38 (2H, m), 4.84 (1H, dd, J=8.8 Hz), 5.36—5.41 (1H, m), 5.50 (1H, d, J=4.1 Hz), 5.89—5.95 (1H, m), 7.35—7.77 (10H, m). Found: C, 68.35; H, 7.20%. Calcd for $C_{26}H_{34}O_5Si$: C, 68.69; H, 7.53%.

(1*R*,3*R*,4*R*,5*R*)-3-[(1*R*)- and (1*S*)-1-(Ethoxycarbonyl)methyl-2-propenyl]-4-hydroxy-7,7-dimethyl-2,6,8-trioxabicyclo-[3.3.0]octanes (15R and 15S). A solution of **13E** (1.32 g, 6.1 mmol) in freshly distilled triethyl orthoacetate (10 ml) was heated at 135 °C for 6.5 h in the presence of catalytic propionic acid. The reaction mixture was concentrated in vacuo. The residue was chromatographed on silica gel (AcOEt/hexane 1 : 5) to give an inseparable mixture of **15R** and **15S** (1.25 g, 71% of combined yield) [TLC R_f 0.58 (EtOH/$PhCH_3$ 1:5)] as a colorless oil.

Analogously, the *Z*-isomer **13Z** (1.18 g) was heated at 135 °C in triethyl orthoacetate (20 ml) in the presence of catalytic propionic acid for 14 h. Concentration of the reaction mixture in vacuo and chromatographic purification of the residue gave the mixture of **15R** and **15S** (1.12 g, 72% of combined yield).

Benzoates 16R and 16S. From the Mixture 15R and 15S Obtained from 13E. The mixture (63 mg, 0.22 mmol) was benzoylated with benzoyl chloride (0.05 ml, 0.43 mmol) in pyridine (2 ml). After being stirred for 30 min, the mixture was concentrated in vacuo. The residue was partitioned between CH_2Cl_2 (20 ml) and H_2O (20 ml). The aqueous phase was extracted with CH_2Cl_2 (20 ml×2). The combined organic phases were dried (Na_2SO_4) and concentrated. The residue was chromatographed on silica gel (Et_2O/hexane 1 : 8) to give 41 mg (48%) of **16S**, 31 mg (36%) of **16R**, and 12 mg (14%) of an approximately 1 : 1 mixture of **16R** and **16S**. **16R:** a colorless oil, TLC R_f 0.20 (Et_2O/hexane 1 : 6); $[\alpha]_D^{23}$ +96.0° (*c* 0.83, $CHCl_3$); IR (neat) ν_{max} 2990, 1725, 1640, 1600, 1450, 1275 cm^{-1}; ^1H NMR (400 MHz, $CDCl_3$) δ=1.21 (3H, t, J=7.1 Hz), 1.31, 1.52 (3H each, 2 s), 2.54 (1H, dd, J=8.8 and 15.6 Hz), 2.63 (1H, dd, J=5.9 and 15.6 Hz), 2.91 (1H, dddd, J=3.7, 5.9, 8.8, and 8.8 Hz), 4.10 (2H, q, J=7.1 Hz), 4.35 (1H, dd, J=3.7 and 9.0 Hz), 4.81 (1H, dd, J=4.9 and 9.0 Hz), 4.91 (1H, dd, J=3.9 and 4.9 Hz), 4.93—5.18 (2H, m), 5.75 (1H, ddd, J=8.8, 10.3, and 17.1 Hz), 5.82 (1H, d, J=3.9 Hz), 7.45—8.08 (5H, m). Found: C, 64.87; H, 6.83%. Calcd for $C_{21}H_{26}O_7$: C, 64.60; H, 6.71%. **16S:** a colorless oil; TLC R_f 0.14 (Et_2O/hexane 1 : 6); $[\alpha]_D^{25}$ +103.9° (*c* 1.08, $CHCl_3$); IR (neat) ν_{max} 2990, 1725, 1640, 1600, 1450, 1375, 1275 cm^{-1}; ^1H NMR (400 MHz, $CDCl_3$) δ=1.23 (3H, t, J=7.1 Hz), 1.31, 1.53 (3H each, 2 s), 2.42 (1H, dd, J=8.8 and 15.1 Hz), 2.71 (1H, dd, J=4.9 and 15.1 Hz), 2.87 (1H, dddd, J=4.9, 7.3, 8.3, and 8.8 Hz), 4.11 (2H, q, J=7.1 Hz), 4.27 (1H, dd, J=7.3 and 8.8 Hz), 4.79 (1H, dd, J=5.2 and 8.8 Hz), 4.92 (1H, dd, J=3.9 and 5.2 Hz), 5.03 (1H, dd, J=1.0 and 10.3 Hz), 5.14 (1H, dd, J=1.0 and 17.1 Hz), 5.76 (1H, ddd, J=8.3, 10.3 and 17.1 Hz), 5.85 (1H, d, J=3.9 Hz), 7.44—8.05 (5H, m). Found: C, 64.79; H, 6.71%. Calcd for $C_{21}H_{26}O_7$: C, 64.60; H, 6.71%.

From the Mixture Obtained from 13Z. The mixture of **15R** and **15S** (491 mg) was benzoylated as described above.

Extractive work-up and silica-gel chromatography of the extracts gave **16R** (76 mg, 11%) and **16S** (466 mg, 70%), which were identical with those obtained above (TLC, IR, and ^{1}H NMR).

Claisen Rearrangement of 14Z and Separation of the Diastereomers as the Benzoates 16R and 16S. Compound **14Z** (211 mg, 0.46 mmol) was heated at 135 °C in triethyl orthoacetate (4 ml) in the presence of catalytic propionic acid for 15 h. Then, the reaction mixture was concentrated in vacuo. The residue was chromatographed on silica gel (AcOEt/hexane 1 : 20) to give an inseparable mixture of **17R** and **17S** (118 mg) as a colorless oil [R_f 0.60 (AcOEt/hexane 1 : 3)].

The mixture (118 mg) was dissolved in THF (3 ml) and tetrabutylammonium fluoride (1.0 mol dm^{-3} solution in THF, 0.49 ml) was added. The mixture was stirred at room temperature for 1 h and concentrated in vacuo. The residue was chromatographed on silica gel (AcOEt/hexane 1 : 5) to give an inseparable mixture of **15R** and **15S** (54 mg).

The mixture (54 mg) was benzolylated as described above. Silica-gel chromatography of the reaction mixture gave 7.8 mg (4.3% yield from **14Z**) of **16R** and 58.2 mg (32.1%) of **16S**.

(1*R*,3*R*,4*R*,5*R*)-4-Hydroxy-3-[(1*R*)- and (1*S*)-1-(2-hydroxyethyl)-2-propenyl]-7,7-dimethyl-2,6,8-trioxabicyclo[3.3.0]-octanes (18R and 18S). A solution of **16R** (30 mg, 0.07 mmol) in THF (2 ml) was stirred in the presence of $LiAlH_4$ (10 mg, 0.27 mmol) for 1 h. To the mixture was added H_2O (0.02 ml). The resulting solids were removed by filtration. The filtrate was concentrated in vacuo. The residue was chromatographed on silica gel (EtOH/$PhCH_3$ 1 : 15) to give **18R** (17 mg, 92%) as a colorless oil: TLC R_f 0.42 (EtOH/$PhCH_3$ 1 : 5); $[\alpha]_D^{23}$ +6.3° (*c* 1.0, $CHCl_3$); IR (neat) ν_{max} 3390, 2940, 1640, 1500, 1455, 1375, 1315, 1220 cm^{-1}; ^{1}H NMR (90 MHz, $CDCl_3$) δ=1.34, 1.55 (3H each, 2 s), 1.62—2.12 (3H, m), 2.37—2.70 (2H, m), 3.46—3.82 (4H, m), 4.49 (1H, dd, *J*=4.3 Hz), 5.02—5.27 (2H, m), 5.74 (1H, d, *J*=4.3 Hz), 5.48—5.93 (1H, m). Found: C, 58.73; H, 8.05%. Calcd for $C_{12}H_{20}O_5$: C, 59.00; H, 8.25%.

Analogously, *S*-diastereomer **16S** (40 mg) was reduced with 3.0 mol equiv of $LiAlH_4$. Silica-gel chromatography of the reaction mixture gave **18S** (23 mg, 92%) as a colorless oil: TLC R_f 0.42 (EtOH/$PhCH_3$ 1 : 5); $[\alpha]_D^{25}$ +53.7° (*c* 1.07, $CHCl_3$); IR (neat) ν_{max} 3390, 2940, 1640, 1455, 1380, 1375, 1240 cm^{-1}; ^{1}H NMR (90 MHz, $CDCl_3$) δ=1.35, 1.56 (3H each, 2 s), 1.63—2.12 (3H, m), 2.28—2.64 (2H, m), 3.42—3.94 (4H, m), 4.53 (1H, dd, *J*=4.1 Hz), 5.02—5.31 (2H, m), 5.65 (1H, d, *J*=4.1 Hz), 5.57—6.00 (1H, m). Found: C, 58.64; H, 8.02%. Calcd for $C_{12}H_{20}O_5$: C, 59.00; H, 8.25%.

(1*R*,3*R*,4*R*,5*R*)-4-Hydroxy-3-[(1*S*)- and (1*R*)-1-ethyl-3-hydroxypropyl]-7,7-dimethyl-2,6,8-trioxabicyclo[3.3.0]octanes (19S and 19R). A solution of **18R** (17 mg, 0.07 mmol) in EtOH (2 ml) was hydrogenated under atmospheric hydrogen gas in the presence of Raney nickel T-4 for 3 h. The catalyst was removed through a Celite pad, washed with EtOH. The filtrate and washings were combined and concentrated in vacuo. The residue was chromatographed on silica gel (EtOH/$PhCH_3$ 1 : 20) to give **19S** (16 mg, 91%) as white crystals, mp 47.5—48.5 °C: TLC R_f 0.43 (EtOH/$PhCH_3$ 1 : 5); $[\alpha]_D^{25}$ +25.0° (*c* 0.76, $CHCl_3$); IR (KBr) ν_{max} 3295, 2980, 2965, 2930, 2870, 1460, 1380, 1370, 1325, 1245, 1235 cm^{-1}; ^{1}H NMR (400 MHz, $CDCl_3$) δ=0.93 (3H, t, *J*=7.6 Hz), 1.37, 1.57 (3H each, 2 s), 1.38—1.85 (5H, m), 2.20 (1H, br s), 2.75 (1H, d, *J*=8.3 Hz), 3.63—3.83 (4H, m), 4.56 (1H, dd, *J*=4.2 Hz), 5.77 (1H, d, *J*=4.2 Hz). Found: C, 58.29; H, 8.71%. Calcd for $C_{12}H_{22}O_5$: C, 58.52; H, 9.00%.

Analogously, compound **18S** (23 mg) was hydrogenated to give **19R** (19.5 mg, 83%) as white crystals, mp 79.5—81 °C: TLC R_f 0.43 (EtOH/$PhCH_3$ 1 : 5); $[\alpha]_D^{23}$ +26.0° (*c* 0.95, $CHCl_3$); IR (KBr) ν_{max} 3425, 2985, 2975, 2955, 2940, 1460, 1380, 1370, 1320 cm^{-1}; ^{1}H NMR (400 MHz, $CDCl_3$) δ=0.95 (3H, t, *J*=7.3 Hz), 1.37, 1.57 (3H each, 2 s), 1.38—1.72 (5H, m), 2.24 (1H, br s), 2.65 (1H, d, *J*=9.8 Hz), 3.62—3.83 (4H, m), 4.56 (1H, dd, *J*=3.9 and 4.9 Hz), 5.78 (1H, d, *J*=3.9 Hz). Found: C, 58.34; H, 8.73%. Calcd for $C_{12}H_{22}O_5$: C, 58.52; H, 9.00%.

(1*R*,3*R*,4*S*,5*R*)-4-Hydroxy-3-[(1*R*)- and (1*S*)-1-ethyl-3-hydroxypropyl]-7,7-dimethyl-2,6,8-trioxabicyclo[3.3.0]octanes (20R and 20S). A solution of **9R** (99 mg, 0.41 mmol) in THF (2 ml) was stirred with $LiAlH_4$ (38.5 mg, 1.0 mmol) for 1 h. The mixture was quenched with H_2O (0.1 ml). The resulting solids were removed, washed with CH_2Cl_2. The combined filtrate and washings were concentrated in vacuo. The residue was chromatographed on silica gel (AcOEt/hexane 1 : 1) to give **20R** (88 mg, 87%) as a colorless oil: TLC R_f 0.26 (AcOEt/hexane 1 : 1); $[\alpha]_D^{27}$ −21.8° (*c* 0.61, $CHCl_3$); IR (neat) ν_{max} 3400, 2960, 2940, 2880, 1460, 1380, 1250, 1220 cm^{-1}; ^{1}H NMR (400 MHz, $CDCl_3$) δ=0.95 (3H, t, *J*=7.5 Hz), 1.31, 1.49 (3H each, 2 s), 1.25—1.89 (5H, m), 2.71 (2H, br s), 3.63—3.69, 3.76—3.82 (1H each, 2 m), 3.93 (1H, dd, *J*=2.4 and 9.8 Hz), 4.11 (1H, d, *J*=2.4 Hz), 4.50 (1H, d, *J*=3.9 Hz), 5.90 (1H, d, *J*=3.9 Hz). Found: C, 58.85; H, 8.78%. Calcd for $C_{12}H_{22}O_5$: C, 58.52; H, 9.00%.

Analogously, 14.5 mg of **9S** was reduced with $LiAlH_4$ to give 12 mg (84%) of **20S** as a colorless oil: TLC R_f 0.55 (AcOEt); $[\alpha]_D^{26}$ −15.6° (*c* 0.61, $CHCl_3$); IR (neat) ν_{max} 3380, 2960, 2940, 2880, 1460, 1370, 1250, 1210 cm^{-1}; ^{1}H NMR (400 MHz, $CDCl_3$) δ=0.93 (3H, t, *J*=7.5 Hz), 1.32, 1.49 (3H each, 2 s), 1.40—1.91 (5H, m), 2.84 (1H, br s), 3.62—3.68, 3.79—3.84 (1H each, 2 m), 3.89 (1H, dd, *J*=2.0 and 11.0 Hz), 4.18 (1H, d, *J*=2.0 Hz), 4.38 (1H, br s), 4.51 (1H, d, *J*=3.7 Hz), 5.90 (1H, d, *J*=3.7 Hz). Found: C, 58.22; H, 8.73%. Calcd for $C_{12}H_{22}O_5$: C, 58.52; H, 9.00%.

Conversion of 20R into 19R via 21R, 22R, and 23R. To a solution of **20R** (20 mg, 0.08 mmol) in pyridine (1 ml) were added trityl chloride (52 mg, 0.19 mmol) and 4-dimethylaminopyridine (5 mg). After being heated at 65 °C for 3.5 h, the mixture was concentrated in vacuo. The residue was partitioned between CH_2Cl_2 (20 ml) and saturated aqueous $NaHCO_3$ (10 ml). The aqueous phase was extracted with CH_2Cl_2 (20 ml). The combined organic phases were dried (Na_2SO_4) and concentrated. The residue was chromatographed on silica gel (AcOEt/hexane 1 : 10) to give **21R** (39 mg, 98%) as a colorless oil: TLC R_f 0.51 (AcOEt/hexane 1 : 2); $[\alpha]_D^{24}$ −11.1° (*c* 1.19, $CHCl_3$); IR (KBr) ν_{max} 3470, 2970, 2940, 2880, 1600, 1490, 1450, 1380, 1220 cm^{-1}; ^{1}H NMR (90 MHz, $CDCl_3$) δ=0.84 (3H, t, *J*=7.2 Hz), 1.24, 1.38 (3H each, 2 s), 1.10—2.10 (6H, m), 3.06—3.25 (2H, m), 3.83 (1H, dd, *J*=2.8 and 9.2 Hz), 4.04 (1H, d, *J*=2.8 Hz), 4.43 (1H, d, *J*=4.1 Hz), 5.79 (1H, d, *J*=4.1 Hz), 7.17—7.49 (15 H, m).

To a solution of **21R** (48 mg, 0.10 mmol) in CH_2Cl_2 (1 ml) were added anhydrous sodium acetate (17 mg), PCC (221 mg, 1.0 mmol), and molecular sieves (4A, powder, 143 mg). The mixture was stirred for 8 h, and charged on silica-gel column (8 g). The column was eluted with Et_2O containing 1% of triethylamine to give 47 mg of **22R** as a colorless oil: TLC R_f 0.80 (AcOEt/hexane 1 : 2); ^{1}H NMR (90 MHz,

$CDCl_3$) δ=0.85 (3H, t, J=7.5 Hz), 1.34, 1.40 (3H each, 2 s), 1.24—2.01 (5H, m), 2.90—3.20 (2H, m), 4.06 (1H, d, J=3.9 Hz), 4.30—4.36 (1H, m), 5.89 (1H, d, J=3.9 Hz), 7.15—7.46 (15H, m).

The crude **22R** (47 mg) was dissolved in EtOH (1 ml), and $NaBH_4$ (10 mg) was added. After being stirred for 50 min, the mixture was neutralized by addition of 50% aqueous AcOH and concentrated in vacuo. The residue was chromatographed on silica gel (AcOEt/hexane 1 : 5 containing 1% of triethylamine) to give **23R** (35 mg, 72% from **21R**) as a colorless oil: TLC R_f 0.59 (AcOEt/hexane 1 : 2); $[\alpha]_D^{20}$ +64.7° (c 1.68, $CHCl_3$); IR (neat) ν_{max} 3500, 2960, 2930, 2870, 1595, 1490, 1450, 1380, 1370, 1215 cm^{-1}; ^1H NMR (90 MHz, $CDCl_3$) δ=0.84 (3H, t, J=7.0 Hz), 1.34, 1.50 (3H each, 2 s), 1.05—2.34 (6H, m), 2.92—3.28 (2H, m), 3.52—3.81 (2H, m), 4.45 (1H, dd, J=4.4 Hz), 5.69 (1H, d, J=4.4 Hz), 7.16—7.49 (15H, m).

A solution of **23R** (28 mg, 0.06 mmol) in MeOH (1 ml) was stirred in the presence of p-toluenesulfonic acid (monohydrate, 10 mg) for 30 min at room temperature. Then, saturated aqueous $NaHCO_3$ (15 ml) was added. This was extracted with CH_2Cl_2 (20 ml×5). The combined organic phases were dried (Na_2SO_4) and concentrated in vacuo. The residue was chromatographed on silica gel (EtOH/$PhCH_3$ 1 : 15) to give **19R** (11 mg, 75%), which was identical with that obtained from **16S** in respects of TLC, mp, $[\alpha]_D$, IR and ^1H NMR.

Conversion of 20S into 19S via 21S, 22S, and 23S. Compound **20S** was converted into **19S** via **21S**, **22S**, and **23S** by the analogous reaction sequence described for **20R**. **21S** (91%): mp 179—180 °C, TLC R_f 0.49 (AcOEt/hexane 1 : 2); $[\alpha]_D^{24}$ +5.8° (c 0.94, $CHCl_3$); IR (KBr) ν_{max} 3440, 2980, 2950, 1620, 1480, 1460, 1380, 1220 cm^{-1}; ^1H NMR (90 MHz, $CDCl_3$) δ=0.86 (3H, t, J=7.5 Hz), 1.29, 1.45 (3H each, 2 s), 1.50—2.03 (5H, m), 2.61 (1H, br s), 3.21 (2H, dd, J=6.2 Hz), 3.85 (1H, dd, J=2.4 and 10.8 Hz), 4.05 (1H, br s), 4.47 (1H, d, J=4.1 Hz), 5.85 (1H, d, J=4.1 Hz), 7.18—7.49 (15H, m). **22S:** a colorless oil, TLC R_f 0.80 (AcOEt/hexane 1 : 2); ^1H NMR (90 MHz, $CDCl_3$) δ=0.83 (3H, t, J=7.7 Hz), 1.39, 1.58 (3H each, 2 s), 1.13—2.25 (5H, m), 3.14 (2H, dd, J=6.2 Hz), 4.19—4.37 (2H, m), 5.96 (1H, d, J=4.5 Hz), 7.20—7.58 (15H, m). **23S** (97% from **21S**): mp 96.5—97.5 °C, TLC R_f 0.62 (AcOEt/hexane 1 : 2); $[\alpha]_D^{21}$ +20.6° (c 1.00, $CHCl_3$); IR (KBr) ν_{max} 3540, 2980, 2960, 1480, 1450, 1400, 1380, 1315, 1260 cm^{-1}; ^1H NMR (90 MHz, $CDCl_3$) δ=0.85 (3H, t, J=7.0 Hz), 1.34, 1.46 (3H each, 2 s), 1.25—2.40 (6H, m), 3.06—3.20 (2H, m), 3.55—3.79 (2H, m), 4.48 (1H, dd, J=4.0 Hz), 5.70 (1H, d, J=4.0 Hz), 7.17—7.50 (15H, m).

Compound **19S** obtained by p-TsOH hydrolysis of **23S** in 58% yield was identical with that obtained from **16R**.

References

1) This work was presented orally at the 58th National Meeting of the Chemical Society of Japan, Kyoto, April 1—4 1989. Abstract 3IL39.

2) A recent leading review on Claisen rearrangement: F. E. Ziegler, *Chem. Rev.*, **88**, 1423 (1988).

3) a) K. Tadano, Y. Idogaki, H. Yamada, and T. Suami, *Chem. Lett.*, **1985**, 1925; b) *idem*, *J. Org. Chem.*, **52**, 1201 (1987). c) K. Tadano, J. Ishihara, H. Yamada, and S. Ogawa, *ibid.*, **54**, 1223 (1989).

4) One of the Claisen rearrangement products obtained in our previous work was efficiently transformed into some natural products: K. Tadano, H. Yamada, Y. Idogaki, S. Ogawa, and T. Suami, *Tetrahedron Lett.*, **29**, 655 (1988). K. Tadano, S. Kanazawa, and S. Ogawa, *J. Org. Chem.*, **53**, 3868 (1988).

5) For a review on the preparation and utility of carbohydrate-derived synthons: S. Hanessian, "Total Synthesis of Natural Products: The Chiron Approach," Pergamon, New York (1983).

6) Y. Kawahata, S. Takatsuto, N. Ikekawa, M. Murata, and S. Omura, *Chem. Pharm. Bull.*, **34**, 3102 (1986).

7) Under the standard reaction conditions (benzene as a solvent at room temperature for 45 min), the formation of three products was detected. These were E- and Z-α,β-unsaturated esters and the δ-lactone derivative derived from the Z-Wittig adduct.

8) Dibal-H reduction of mixture of the E- and Z-α,β-unsaturated esters and the α,β-unsaturated δ-lactone gave the E- and Z-allyl alcohols and a hemiacetal derived from the δ-lactone in 22%, 15%, and 25% yields from **1**, respectively.

9) W. S. Johnson, L. Werthemann, W. R. Bartlett, T. J. Brochsom, T.-T. Li, D. J. Faulkner, and M. R. Petersen, *J. Am. Chem. Soc.*, **92**, 741 (1970).

10) The ratio and stereochemistries of the rearrangement products **6R** and **6S** were determined as follows. The mixture of the rearrangement product was reduced with $LiAlH_4$. The resulting two diols with S- and R-configurations were completely separated by repeated chromatography on silica gel. The ratio of **6S** and **6R** was estimated based on the yields of these diol derivatives. The double bond in each of the diol was then hydrogenated to afford **20R** or **20S**, which were compared with those prepared from structurally defined **9R** and **9S**.

11) The stereochemistries of **7S** and **7R** were confirmed by transformation of them into the diols, which were independently derived from the mixture of **6S** and **6R** (see, Ref. 10), by desilylation follwed by $LiAlH_4$ reduction.

12) J. D. Stevens, *Methods Carbohydr. Chem.*, **6**, 125 (1972).

13) The Wittig reaction was also carried out in MeOH. The ratio of E- and Z-adducts, in this case, was approximately 1 : 1.

14) E. J. Corey and J. W. Suggs, *Tetrahedron Lett.*, **1975**, 2647.

15) For general procedures, see Ref. 3c.

Stereocontrolled Reduction of 2-(*p*-Tolylsulfinyl)cycloalkanones under Basic Conditions: π-Facial Selection in Cyclic Systems Directed by a Chiral Side Chain

Katsuyuki OGURA,* Michio ISHIDA,† and Makoto FUJITA
Department of Synthetic Chemistry, Faculty of Engineering, Chiba University, 1-33 Yayoi-cho, Chiba 260
†Graduate School of Science and Technology, Chiba University, 1-33 Yayoi-cho, Chiba 260
(Received August 8, 1989)

Reduction of a 2-(*p*-tolylsulfinyl)cycloalkanone with sodium borohydride in methanol-triethylamine is accompanied by rapid epimerization at C_2. Under the conditions employed here, the π-facial selectivity of the reduction is directed by the side chain chirality and, among four possible isomers of the corresponding cycloalkanol, one isomer is given with high selectivities up to 85%.

Stereofacial control in nucleophilic additions to cycloalkanones has been recognized as a significant problem for stereoselective construction of cyclic systems.[1] Although the π-facial selection is often controlled by the stereochemistry contained in the cyclic system itself, there are few reports which deal with the selection affected by stereochemistry of the side chain. This may be attributable to the presence of an additional chiral center at the position bonding to this side chain, the configuration of which must be controlled in advance.[2] Recently, an efficient 1,3-asymmetric induction was realized in $NaBH_4$ reduction of α-substituted β-keto sulfoxides under basic conditions: the chirality of the sulfinyl group controls the hydride attack on the β-carbonyl group regardless of the stereochemistry of C_α which rapidly epimerizes under the reaction conditions.[3] This paper describes that the 1,3-stereochemical control accompanied by C_α-epimerization is successfully applied to cyclic systems, i.e., reduction of 2-(*p*-tolylsulfinyl)cycloalkanones with $NaBH_4$ under basic conditions provides a unique method for facial selection directed by the side chain.

Results and Discussion

When a diastereomeric mixture of 2-(*p*-tolylsulfinyl)cyclohexanone (**1a** : **2a**=54 : 46) was reduced with $NaBH_4$ in methanol (Scheme 1),[4] four possible diastereomers (**3a—6a**) of 2-(*p*-tolylsulfinyl)cyclohexanol were formed in a moderately selective manner (**3a** : **4a** : **5a** : **6a**=48 : 12 : 31 : 9). Preferable formation of **3a** and **5a** (total 79%) predicts that this reduction is mainly directed by the stereochemistry of C_2 since **3a** and **5a** have the same stereochemical relationship between C_1 and C_2. Hence, the chirality of the sulfinyl group seems to less reflect on the new chiral center developing on C_1.

In striking contrast, predominant formation of **3a** (72%) was observed when the reaction was carried out under basic conditions (in a 1 : 1 mixture of MeOH-NEt_3).[5] In addition, it is noteworthy that two major isomers (**3a** and **6a**; their total yield 85%) have the same stereochemical relationship between C_1 and S (hereafter, the position of the sulfur atom is represented by a symbol "S"). Thus, the π-facial selection is strongly directed by the side chain chirality.

The same phenomena were observed for the $NaBH_4$ reduction of other 2-(*p*-tolylsulfinyl)cycloalkanones (**1b—d** and **2b—d**) under the basic conditions. The results are summarized in Table 1. In any case, one diastereomer (**3a—d**) is predominantly formed with high selectivities up to 85%.

Under the basic conditions, the C_2 of **1** and **2** might epimerize rapidly during the reduction. In fact, brief treatment of pure **1a**[6] with a 1 : 1 mixture of triethylamine and MeOH (1 h/room temperature) produces **1a** and **2a** in a ratio of 57 : 43. This rapid epimerization allows $NaBH_4$ to attack preferentially from the most favorable face among four possible ones (axial and equatorial faces[7] of **1** and **2**). In this case, the attack from the equatorial face of **1** giving **3** is predominant. Worthy of comment is that the configuration of **3** is in good accordance with that of the major isomer produced in the reduction of acyclic α-sulfinyl ketones.[3] Thus, the reduction of α-sulfinyl ketones might occur via similar stereochemical course in both acyclic and cyclic systems. This is in sharp contrast with the usual addition of a nucleophile to a carbonyl group.[8]

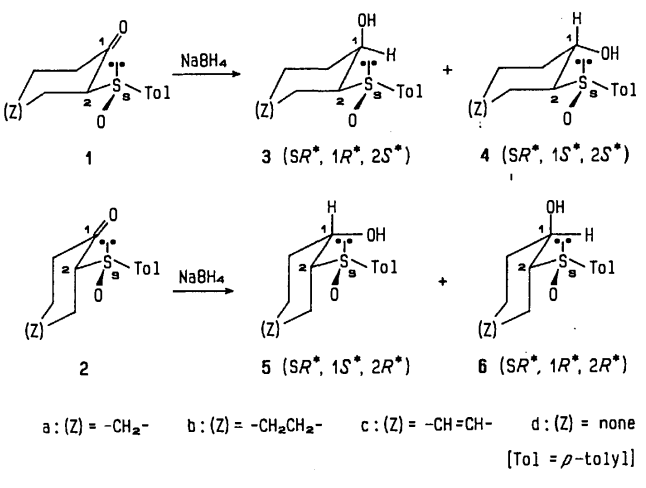

Scheme 1.

Table 1. Stereoselective Reduction of **1** and **2** with $NaBH_4$[a)]

Substrates	(Ratio)	Solvent	Reduction products[b)]	
			Total yield/%	**3**: **4**: **5**: **6**
1a+2a	(54:46)	MeOH-NEt_3 (1:1)	98	72: 6: 9:13
1a+2a	(54:46)	MeOH	99	48:12:31: 9
1a		MeOH	100	65:27: 6: 2
1b+2b	(52:48)	MeOH-NEt_3 (1:1)	97	85: 1:10: 4
1b+2b	(52:48)	MeOH	94	58: 2:35: 5
1c+2c	(53:47)	MeOH-NEt_3 (1:1)	95	75: 4:16: 5
1c+2c	(53:47)	MeOH	95	48: 6:38: 8
1d+2d	(78:22)	MeOH-NEt_3 (1:1)	92	84: 3:12: 1
1d+2d	(78:22)	MeOH	91	78: 4:16: 2

a) Carried out with $NaBH_4$ (1.2—2.0 mol equiv) at 0 °C for ca. 2 h. b) Determined by HPLC analysis (see Experimental section).

Relative configurations of the diastereomers **3**—**6** were assigned as follows. Reduction of 2-(*p*-tolylthio)-cyclohexanone with $NaBH_4$ gave *cis*- and *trans*-2-(*p*-tolylthio)cyclohexanols.[11] In oxidation of *cis*-2-(*p*-tolylthio)cyclohexanol with *m*-chloroperbenzoic acid (*m*-CPBA), a 30:70 mixture of **3a** and **5a** was given. On the other hand, *m*-CPBA oxidation of *trans*-2-(*p*-tolylthio)cyclohexanol resulted in formation of **4a** and **6a** (78:22). Thermolysis of optically active (*SR*)-**3a**, obtainable from a mixture of (*SR*)-**1** and (*SR*)-**2a**,[13] produced (*R*)-2-cyclohexenol. From these facts, the configurations of **3a** and **5a** were assigned to be *SR**, *1R** and *SR**,*1S**,*2R**, respectively.

Since **3a** and **4a** were predominantly given by reduction of one diastereomer (**1a**) in MeOH (Table 1),[15] **4a** has *SR**,*1S**,*2S** configuration. Consequently, the configuration of the final isomer (**6a**) was assigned to be *SR**,*1R**,*2R**.

The stereochemical structure of **5c** was determined by X-ray crystallography. The molecular structure is shown in Fig. 1, which exhibits that **5c** has *SR**,*1S**, *2R** configuration. The configuration of the isomer **3c** was determined to be *SR**,*1R**,*2S**, because both **3c** and **5c** gave the same sulfone (**7**) on oxidation with *m*-CPBA. The structures of the minor products (**4c** and **6c**) were tentatively estimated as depicted in Scheme 1.

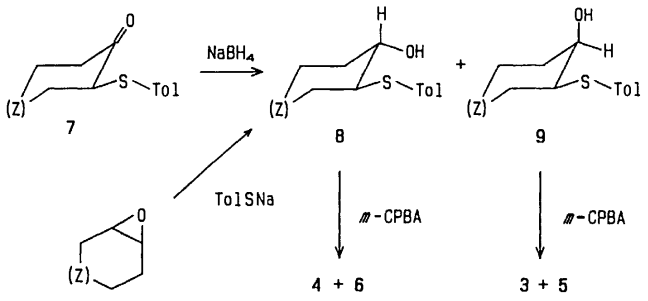

Scheme 2.

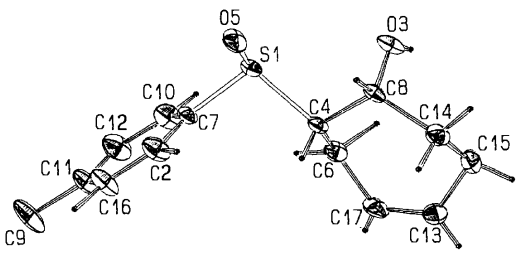

Fig. 1. An ORTEP drawing of **5c**.

Oxidation of *trans*-2-(*p*-tolylthio)cycloheptanol with *m*-CPBA gave **4b** and **6b** in a ratio of 84:16, whereas a 14:86 mixture of **3b** and **5b** was produced by oxidation of *cis*-2-(*p*-tolylthio)cycloheptanol. By considering the analogy between **1b** and **1a** (or **1c**), the configurations of **3b**—**6b** were assigned.

It was also found that *cis*-2-(*p*-tolylthio)cyclopentanol was oxidized with *m*-CPBA to yield **3d** and **5d** (20:80), while the similar oxidation of *trans*-2-(*p*-tolylthio)cyclopentanol resulted in formation of **4d** and **6d** (80:20). By comparision of these facts with oxidation behavior of the corresponding cyclohexanols, the stereochemical structures of **3d**, **4d**, **5d**, and **6d** were tentatively estimated.

In conclusion, a diastereomeric mixture of 2-(*p*-tolylsulfinyl)cycloalkanones can produce (*SR**,*1R**, *2S**)-2-(*p*-tolylsulfinyl)cycloalkanols on reduction with $NaBH_4$ in MeOH-Et_3N, which provides one example for facial selection directed by the side chain.

Experimental

Melting points were determined on a hot-stage microscope apparatus (Yanagimoto) and are uncorrected. ^1H NMR spectra were obtained on Hitachi R-600 (60 MHz), and JEOL JNM-GSX 270 (270 MHz) spectrometers. Infrared spectra were determined with a JASCO A-200 spectrometer. Optical rotations were measured on a JASCO DIP-181 polarimeter. High pressure liquid chromatography (HPLC) analyses were performed with a Hitachi 638-30 using UV detector (270 nm).

2-(*p*-Tolylthio)cycloalkanones. 2-(*p*-Tolylthio)cyclohexanone, 2-(*p*-tolylthio)cyclopentanone, and 2-(*p*-tolylthio)-cycloheptanone are prepared by reaction of an enolate ion of the corresponding cycloalkanones with di-*p*-tolyl disulfide according to the reaction conditions reported for preparing 2-(phenylthio)cycloalkanones.[16]

2-(*p*-Tolylthio)cyclopentanone: A colorless oil; ^{1}H NMR ($CDCl_3$) δ=1.78—2.22 (4H, m), 2.22—2.46 (2H, m), 2.33 (3H, s), 3.49 (1H, t, J=7.9 Hz), 7.10 (2H, d, J=7.9 Hz), and 7.37 (2 H, d, J=7.9 Hz); IR (neat) 1740 cm^{-1}. Found: C, 69.79; H, 6.81%. Calcd for $C_{12}H_{14}OS$: C, 69.86; H, 6.83%.

2-(*p*-Tolylthio)cyclohexanone: A colorless oil; ^{1}H NMR ($CDCl_3$) δ=1.57—2.29 (7H, m), 2.32 (3H, s), 2.91 (1H, m), 3.75 (1H, dt, J=1.3 and 5.6 Hz), 7.10 (2H, d, J=7.9 Hz), and 7.31 (2H, d, J=7.9 Hz); IR (neat) 1710 cm^{-1}. Found: C, 70.53; H, 7.16%. Calcd for $C_{13}H_{16}OS$: C, 70.86; H, 7.31%.

2-(*p*-Tolylthio)cycloheptanone: A colorless oil; ^{1}H NMR ($CDCl_3$) δ=1.23—1.66 (4H, m), 1.71—2.03 (3H, m), 2.16—2.43 (2H, m), 2.32 (3H, s), 2.77 (1H, ddd, J=3.0, 11.9, and 13.2 Hz), 3.67 (1H, dd, J=5.6 and 10.6 Hz), 7.10 (2H, d, J=7.9 Hz), and 7.30 (2 H, d, J=7.9 Hz); IR (neat) 1705 cm^{-1}. Found: C, 71.53; H, 7.74%. Calcd for $C_{14}H_{18}OS$: C, 71.75; H, 7.74%.

Preparation of 2-(*P*-Tolylsulfinyl)cyclohexanone (1 and 2). A Typical Procedure. *m*-Chloroperbenzoic acid (*m*-CPBA) (1.7 g, 9.9 mmol) was added portionwise to a dichloromethane (25 ml) solution of 2-(*p*-tolylthio)cyclohexanone (2.1 g, 9.6 mmol) at 0 °C. After being stirred for an hour at 0 °C and for 3 h at room temperature, the mixture was treated with 20 wt% aqueous K_2CO_3 (40 ml). The aqueous layer was separated and extracted with dichloromethane (40 ml×2). The organic layers are combined, dried over anhydrous $MgSO_4$, concentrated, and subjected to column chromatography (silica gel, benzene-ethyl acetate 6:1) to give 2-(*p*-tolylsulfinyl)cyclohexanone (a 6:4 mixture of **1a** and **2a**) as an oil which soon crystallized. This was identical with an authentic sample (**1a**:**2a**=6:4) which was prepared by intramolecular cyclization of 1-(*p*-tolylsulfinyl)-6-iodo-2-hexanone.[14]

Recrystallization of this diastereomeric mixture from diethyl ether-hexane gave **1a** in a pure form: colorless crystals; mp 99—100 °C: ^{1}H NMR ($CDCl_3$) δ=1.50—1.76 (2H, m), 1.76—2.15 (3H, m), 2.15—2.42 (2H, m), 2.41 (3H, s), 2.42—2.60 (1H, m), 3.37 (1H, ddd, J=1.0, 4.6, and 9.6 Hz), 7.31 (2H, d, J=7.9 Hz), and 7.51 (2H, d, J=7.9 Hz); IR (KBr) 1710 and 1038 cm^{-1}. Found: C, 66.25; H, 6.83%. Calcd for $C_{13}H_{16}O_2S$: C, 66.07; H, 6.82%.

2-(*p*-Tolylsulfinyl)cycloheptanone (1b and 2b): Colorless crystals; 73% yield; mp 104—120 °C (a 52:48 diastereomeric mixture); ^{1}H NMR ($CDCl_3$) δ=1.15—1.65 (4H, m), 1.75—2.10 (4H, m), 2.12—2.28 (1H, m), 2.35—2.53 (1H, m), 2.41 (3H, s), 3.49 and 3.78 (major) [total 1H, dd (J=4.3 and 11.2 Hz) and dd (J=4.3 and 11.9 Hz), respectively], 7.31 (major) and 7.33 (total 2H, d (J=7.9 Hz) and d (J=7.9 Hz), respectively), 7.47 and 7.52 (major) (total 2H, d (J=7.9 Hz) and d (J=7.9 Hz), respectively); IR (KBr) 1700, 1030 cm^{-1}, for the diastereomer mixture. Found: C, 67.17; H, 7.31%. Calcd for $C_{14}H_{18}O_2S$: C, 67.16; H, 7.24%.

2-(*p*-Tolylsulfinyl)cyclopentanone (1d and 2d): A pale yellow oil; 98% yield (a 78:22 diastereomer mixture); ^{1}H NMR ($CDCl_3$) δ=1.70—1.95 (3H, m), 2.05—2.60 (3H, m), 2.41 (3H, s), 3.27 (major) and 3.76 [total 1H, t (J=8.57 Hz) and dd (J=5.77 and 9.07 Hz), respectively], 7.32 (2H, d, J=7.9 Hz), and 7.48 (2H, d, J=7.9 Hz); IR (neat) 1740, 1050, and 1035 cm^{-1}. Found: C, 64.57; H, 6.34%. Calcd for $C_{12}H_{14}O_2S$: C, 64.83; H, 6.34%.

2-(*p*-Tolylsulfinyl)-4-cyclohepten-1-one (1c and 2c): This compound was obtained by a different method from the above one: the reaction of the dianion of (*p*-tolylsulfinyl)acetone with *cis*-1,4-dichloro-2-butene followed by treatment with sodium hydride in DMF.[14]

Reduction of 2-(*p*-Tolylsulfinyl)cyclohexanone (1 and 2) with Sodium Borohydride. (a) Reduction in Methanol: Sodium borohydride (30 mg, 0.81 mmol) was added to a solution involving a 54:46 mixture of **1a** and **2a** (118 mg, 0.50 mmol) in methanol (5 ml) under ice-cooling. After 2 h at 0 °C, water (20 ml) was added and the mixture was extracted with dichloromethane (10 ml×3). The extract was dried ($MgSO_4$), concentrated under reduced pressure, and subjected to column chromatography on silica gel using hexane-ethyl acetate (1:2) as an eluent to give 2-(*p*-tolylsulfinyl)cyclohexanol (117 mg, 99% yield, a mixture of four diastereomers (**3a**:**4a**:**5a**:**6a**=48:12:31:9) as a viscous oil. Found: C, 65.50; H, 7.63%. Calcd for $C_{13}H_{16}O_2S$: C, 65.51; H, 7.61%.

The diastereomer ratio was estimated by HPLC analysis.[17] Retention time (t_R): **3a**, 20 min; **4a**, 31 min; **5a**, 36 min; **6a**, 34 min. In the ^{1}H NMR (270 MHz) of this mixture, the C_1-protons of **3a**, **4a**, **5a**, and **6a** appeared at δ=4.43 (broad s), 3.88 (dt, J=4.7 and 10.4 Hz), 4.32 (broad s), and 4.10 (dt, J=4.6 and 9.9 Hz), respectively.

A single isomer (**1a**) (236 mg, 1.0 mmol) was treated with sodium borohydride (75 mg, 2.0 mmol) in a similar manner to that described above to give a mixture of **3a**, **4a**, **5a**, and **6a** (238 mg, 100% yield), the ratio of which was determined by HPLC analysis to be 65:27:6:2. Found: C, 65.49; H, 7.62%. Calcd for $C_{13}H_{18}O_2S$: C, 65.51; H, 7.61%.

(b) Reduction in Methanol-Triethylamine: A diastereomeric mixture (54:46) of **1a** and **2a** (50 mg, 0.21 mmol) was dissolved in methanol-triethylamine (1:1, 4 ml). Sodium borohydride (10 mg, 0.26 mmol) was added to this solution at 0 °C. After 2 h at 0 °C, brine (20 ml) and water (10 ml) were added and the mixture was extracted with dichloromethane (20 ml×1, 10 ml×3). The extract was dried over anhydrous $MgSO_4$, concentrated under reduced pressure, and subjected to column chromatography on silica gel using benzene-ethyl acetate (2:1) as an eluent to give 2-(*p*-tolylsulfinyl)cyclohexanol (49 mg, 98% yield) as a viscous oil. The diastereomeric ratio (**3a**:**4a**:**5a**:**6a**) was estimated by HPLC analysis to be 72:6:9:13.

From this diastereomeric mixture, **3a** was isolated in a pure form by recrystallization from diethyl ether-hexane: colorless crystals; mp 109—112 °C: ^{1}H NMR ($CDCl_3$) δ=1.07—1.29 (1H, m), 1.32—1.51 (2H, m), 1.62—2.11 (4H, m), 2.43 (3H, s), 2.47 (1H, ddd, J=2.3, 5.0 and 14.6 Hz), 3.32 (1H, broad s, OH), 4.43 (1H, broad), 7.34 (2H, d, J=7.9 Hz), and 7.47 (2H, d, J=7.9 Hz); IR (KBr) 1705 and 1025 cm^{-1}. Found: C, 65.48; H, 7.65%. Calcd for $C_{13}H_{18}O_2S$: C, 65.51; H, 7.61%.

Similarly, a diastereomeric mixture of (*SR*)-2-(*p*-tolylsulfinyl)cyclohexanone (**1a** and **2a**)[8] (435 mg, 1.84 mmol) was treated with sodium borohydride (104 mg, 2.76 mmol) in methanol-triethylamine (1:1, 14 ml) to give a mixture of **3a**, **4a**, **5a**, and **6a** having *R* configuration on the sulfur atom (412 mg, 94%) in a ratio of 72:6:9:13. Recrystallization from diethyl ether-hexane gave (1*R*,2*S*,*SR*)-**3a** in a pure form: colorless crystals; mp 117—117.5 °C; $[\alpha]_D^{22}$ +173.5 (*c* 1, $CHCl_3$) (lit,[18] $[\alpha]_D^{22}$ +174 (*c* 1, $CHCl_3$)). The ^{1}H NMR and IR spectra of this compound were in complete accordance with those of racemic **3a**.

Reduction of 2-(*p*-Tolylsulfinyl)cycloheptanone (1b and 2b). A diastereomeric mixture (52:48) of **1b** and **2b** was subjected to the $NaBH_4$ reduction in methanol in a similar

manner described in reduction of **1a** and **2a** to give a 58:2:35:5 mixture of **3b**, **4b**, **5b**, and **6b** (66 mg: 94% yield) as a colorless solid. Found: C, 66.60; H, 7.81%. Calcd for $C_{14}H_{20}O_2S$: C, 66.63; H, 7.99%.

The diastereomeric ratio was determined by a HPLC analysis[17] (t_R: **3b**, 38 min; **4b**, 59 min; **5b**, 62 min; **6b**, 55 min). The ^1H NMR (270 MHz) of this mixture exhibited the C_1-protons of **3b**, **4b**, **5b**, and **6b** at δ=4.63 (1H, diffused t, J=2.6 Hz), 4.25—4.35 (m), 4.12 (diffused q, J=7.3 Hz), and 4.43 (diffused s), respectively.

Reduction of a 52:48 mixture of **1b** and **2b** in methanol-triethylamine was performed in an analogous manner described in reduction of a mixture of **1a** and **2a**. The total yield of **3b**, **4b**, **5b**, and **6b** was 97%, and its diastereomer ratio was determined by the HPLC analysis to be 85:1:10:4. Recrystallization of this mixture from diethyl ether-hexane gave **3b** in a pure form: colorless crystals; mp 122—123 °C: ^1H NMR ($CDCl_3$) δ=1.20—1.83 (8H, m), 1.92—2.13 (2H, m), 2.42 (3H, s), 2.61 (1H, ddd, J=1.7, 3.6, and 10.9 Hz), 2.73 (1H, broad s, OH), 4.63 (1H, diffused t), 7.33 (2H, d, J=8.2 Hz), and 7.47 (2H, d, J=8.2 Hz); IR (KBr) 3340, 1010, and 990 cm^{-1}. Found: C, 66.80; H, 7.97%. Calcd for $C_{14}H_{20}O_2S$: C, 66.63; H, 7.99%.

Reduction of 2-(*p*-Tolylsulfinyl)-4-cyclohepten-1-one (1c and 2c). In a similar manner described in reduction of **1a** and **2a**, a 53:47 mixture of **1c** and **2c** was reduced with $NaBH_4$ in methanol to give a 48:6:38:8 mixture of **3c**, **4c**, **5c**, and **6c** (95% yield) as a colorless solid; mp 147—169 °C. Found: C, 67.15; H, 7.24%. Calcd for $C_{14}H_{18}O_2S$: C, 67.16; H, 7.24%.

The diastereomeric ratio was determined by a HPLC analysis[17] (t_R: **3c**, 29 min; **4c**, 45 min; **5c**, 53 min; **6c**, 48 min). The ^1H NMR (270 MHz) of this mixture exhibited the C_1-protons of **3c**, **4c**, **5c**, and **6c** at δ=4.66 (broad d, J=4.9 Hz), 4.23 (diffused dt, J=4.3 and 8.6 Hz), 4.46 (diffused s), and 4.27—4.76 (m), respectively.

Pure **5c** was isolated by recrystallization of this mixture from diethyl ether-hexane: mp 158—172 °C: ^1H NMR ($CDCl_3$) δ=1.36—1.52 (1H, m), 1.80—1.97 (2H, m), 2.28—2.40 (1H, m), 2.44 (3H, s), 2.52 (1H, ddd, J=1.7, 2.0, and 11.5 Hz), 2.50—2.63 (1H, m), 3.10 (1H, m), 4.34 (1H, broad d, J=1.7 Hz, OH), 4.46 (1H, diffused s), 5.70—5.82 (1H, m), 5.85—5.97 (1H, m), 7.36 (2H, d, J=7.9 Hz), and 7.54 (2H, d, J=7.9 Hz); IR (KBr) 3275, 1018, and 1005 cm^{-1}. Found: C, 67.15; H, 7.21%. Calcd for $C_{14}H_{18}O_2S$: C, 67.16; H, 7.24%.

A 53:47 mixture of **1c** and **2c** was reduced in methanol-triethylamine (1:1) according to the method described in reduction of **1a** and **2a** in methanol-triethylamine. Chromatography of the crude product gave a 75:4:16:5 mixture of **3c**, **4c**, **5c**, and **6c** (95% yield). Recrystallization of this mixture from diethyl ether-hexane gave pure **3c**: colorless crystals; mp 162—168 °C: ^1H NMR ($CDCl_3$) δ=1.55 (1H, diffused t, J=4.9 Hz), 1.83—2.10 (3H, m), 2.40—2.65 (1H, m), 2.43 (3H, s), 2.56 (diffused dt, J=11.9 and 1.8 Hz), 2.87 (1H, diffused t, J=12.2 Hz), 3.10 (1H, broad s, OH), 5.58—5.70 (1H, m), 5.76—5.90 (1H, m), 7.35 (2H, d, J=7.9 Hz), and 7.48 (2H, d, J=7.9 Hz); IR (KBr) 3275, 1082, and 1015 cm^{-1}. Found: C, 67.10; H, 7.09%. Calcd for $C_{14}H_{18}O_2S$: C, 67.16; H, 7.24%.

Recrystallization of a mixture of **1c** and **2c** from diethyl ether-hexane gave almost pure **1c**. When **1c** (15 mg, 0.060 mmol) was reduced with $NaBH_4$ (3.0 mg, 0.79 mmol) in methanol under ice-cooling, a mixture (15 mg) of **3c**, **4c**, and **5c** was produced. The HPLC analysis of this mixture showed that the product ratio was 87:10:3.

Reduction of 2-(*p*-Tolylsulfinyl)cyclopentanone (1d and 2d). A 78:22 mixture of **1d** and **2d** was subjected to the $NaBH_4$ reduction in methanol in a similar manner described in reduction of **1a** and **2a** to give a 78:4:16:2 mixture of **3d**, **4d**, **5d**, and **6d** in 91% yield as a colorless solid. Found: C, 64.28; H, 7.21%. Calcd for $C_{12}H_{16}O_2S$: C, 64.25; H, 7.19%.

The retention times of **3d**, **4d**, **5d**, and **6d** on an HPLC analysis[17] (the eluent: MeOH-H_2O 35:65) were 44 min, 63 min, 66 min, and 57 min, respectively. The ^1H NMR (270 MHz) of this mixture exhibited the C_1-protons of **3d**, **4d**, **5d**, and **6d** at δ=4.53 (diffused q, J=4.6 Hz), 4.18—4.24 (m), 4.58—4.66 (m), and 4.45 (diffused s), respectively.

When a 78:22 mixture of **1d** and **2d** was reduced with $NaBH_4$ in methanol-triethylamine, total yield of **3d**, **4d**, **5d**, and **6d** was 92%. Its diastereomer ratio was determined by the HPLC analysis to be 84:3:12:1. Recrystallization of this mixture from diethyl ether-hexane gave **3d** in a pure form: colorless crystals; mp 110—111 °C: ^1H NMR ($CDCl_3$) δ=1.39—1.65 (2H, m), 1.70—2.02 (3H, m), 2.21—2.38 (1H, m), 2.41 (3H, s), 2.95 (1H, dt, J=5.6 and 8.6 Hz), 3.12 (1H, broad s, OH), 4.53 (1H, diffused q, J=4.6 Hz), 7.31 (2H, d, J=7.9 Hz), and 7.50 (2H, d, J=7.9 Hz); IR (KBr) 3320, 1020, and 1006 cm^{-1}. Found: C, 64.23; H, 7.12%. Calcd for $C_{12}H_{16}O_2S$: C, 64.25; H, 7.19%.

Thermolysis of (*SR*,1*R*,2*S*)-3a. A mixture of (*SR*,1*R*,2*S*)-**3a** (104 mg, 0.44 mmol) and calcium carbonate (160 mg, 1.60 mmol) was heated at 60 Torr[#]/180 °C in a glass tube oven (Sibata GTO-250RS). The fraction was trapped in a collecting vessel cooled with Dry Ice, and was further distilled under reduced pressure (oven temperature: 120 °C/60 Torr) to give (*R*)-2-cyclohexen-1-ol (32 mg, 75% yield): $[\alpha]_D^{20}$ +115.3° (*c* 0.76, $CHCl_3$) (lit,[18] $[\alpha]_D^{23}$ +67.9 (*c* 0.60, $CHCl_3$)).

Oxidation of 3c and 5c. To a solution of **3c** (137 mg, 0.55 mmol) in dichloromethane (3 ml), was added *m*-CPBA (104 mg, 0.60 mmol) and the resulting mixture was stirred under ice-cooling for 2 h. After addition of aqueous K_2CO_3 solution (20 wt%, 5 ml), the mixture was extracted with dichloromethane (5 ml×2). The combined organic layers were dried ($MgSO_4$), evaporated, and subjected to column chromatography on silica gel using benzene-ethyl acetate (4:1) to afford a sulfone (126 mg: 86% yield): colorless crystals; mp 103—105 °C (from diethyl ether-hexane); ^1H NMR ($CDCl_3$) δ=1.38 (1H, diffused t, J=12 Hz), 1.80—2.03 (2H, m), 2.32—2.74 (2H, m), 2.47 (3H, s), 2.93 (1H, diffused d, J=3.3 Hz), 2.90—2.98 (1H, m), 3.29 (1H, t, J=1.8 Hz, OH),[19] 4.55 (1H, diffused s), 5.65—5.79 (1H, m), 5.82—5.98 (1H, m), 7.39 (2H, d, J=7.9 Hz), and 7.78 (2H, d, J=7.9 Hz); IR (KBr) 3450, 1280, 1160, and 1075 cm^{-1}. Found: C, 63.01; H, 6.81%. Calcd for $C_{14}H_{18}O_3S$: C, 63.13; H, 6.81%.

Similarly, **5c** was oxidized with *m*-CPBA to give a sulfone derivative which was identified (by TLC, IR, and ^1H NMR) with the sulfone derived from **3c**.

Reduction of 2-(*p*-Tolylthio)cyclohexanone. A Typical Procedure. Sodium borohydride (121 mg, 3.21 mmol) was added portionwise to a dichloromethane-methanol (1:2, 15 ml) solution of 2-(*p*-tolylthio)cyclohexanone (426 mg, 1.94 mmol) at 0 °C. The mixture was stirred for 1 h at 0 °C and 11 h at room temperature. Water (10 ml) was added and the whole was extracted with dichloromethane (20 ml×1, 10

[#] 1 Torr=133.322 Pa.

ml×3). The extract was dried over anhydrous $MgSO_4$, condensed under reduced pressure, and subjected to column chromatography (silica gel, benzene-hexane 1:1—2:1) to give *cis*- and *trans*-2-(*p*-tolylthio)cyclohexanols (218 mg and 163 mg, respectively; 88% total yield). *cis*-2-(*p*-Tolylthio)cyclohexanol: a colorless oil; ^{1}H NMR ($CDCl_3$) δ=1.20—1.55 (3H, m), 1.58—1.92 (5H, m), 2.33 (3H, s), 2.49 (1H, broad s, OH), 3.25 (1H, dt, J=2.6 and 5.3 Hz), 3.83 (1H, dt, J=3.0 and 6.4 Hz), 7.11 (2H, d, J=7.9 Hz), and 7.35 (2H, d, J=7.9 Hz); IR (neat) 3450 cm^{-1}. Found: C, 70.04; H, 8.17%. Calcd for $C_{13}H_{18}OS$: C, 70.22; H, 8.15%.

trans-2-(*p*-Tolylthio)cyclohexanol was identified by comparison of its IR and ^{1}H NMR spectra with those of an authentic sample which was prepared by the reaction of cyclohexene oxide with sodium *p*-toluenethiolate.[12]

***cis*- and *trans*-2-(*p*-Tolylthio)cyclopentanols:** These were obtained in a ratio of 65:35 (90% total yield) by reduction of 2-(*p*-tolylthio)cyclopentanone with $NaBH_4$) in methanol. The stereochemistry of *trans*-2-(*p*-tolylthio)cyclopentanol was confirmed by an alternative synthesis of the trans isomer.[12] *cis*-2-(*p*-Tolylthio)cyclopentanol: a colorless oil; ^{1}H NMR ($CDCl_3$) δ=1.55—1.82 (3H, m), 1.82—1.92 (2H, m), 1.97—2.13 (1H, m), 2.32 (3H, s), 2.63 (1H, broad s, OH), 3.39 (1H, ddd, J=4.0, 8.6, and 10.9 Hz), 4.03 (1H,diffused t), 7.10 (2H, d, J=7.9 Hz), and 7.33 (2H, d, J=7.9 Hz); IR (neat) 3400 cm^{-1}. Found: C, 68.85; H, 7.79%. Calcd for $C_{12}H_{16}OS$: C, 69.18; H, 7.74%.

***cis*- and *trans*-2-(*p*-Tolylthio)cycloheptanols:** Similar reduction of 2-(*p*-tolylthio)cycloheptanone gave these compounds in 65% and 31% yields, respectively. *cis*-2-(*p*-Tolylthio)cycloheptanol: a colorless oil; ^{1}H NMR ($CDCl_3$) δ=1.28—1.65 (5H, m), 1.65—2.00 (5H, m), 2.33 (3H, s), 2.55 (1H, broad s, OH), 3.33 (1H, dt, J=3.0 and 9.6 Hz), 3.83 (1H, dt, J=3.0 and 6.4 Hz), 7.11 (2H, d, J=7.6 Hz) and 7.35 (2H, d, J=7.6 Hz); IR (neat) 3450 cm^{-1} Found: C, 70.97; H, 8.46%. Calcd for $C_{14}H_{20}OS$: C, 71.13; H, 8.52%.

***trans*-2-(*p*-Tolylthio)cyclohexanol:** A colorless oil; ^{1}H NMR ($CDCl_3$) δ=1.32—1.80 (7H, m), 1.90—2.15 (3H, m), 2.34 (3H, s), 2.90 (1H, dt, J=3.0 and 9.2 Hz), 2.92 (1H, broad s, OH), 3.52 (1H, ddd, J=3.6, 7.9, and 9.2 Hz), 7.12 (2H, d, J=7.9 Hz), and 7.35 (2H, d, J=7.9 Hz); IR (neat) 3375 cm^{-1}. Found: C, 71.36; H, 8.54%. Calcd for $C_{14}H_{20}OS$: C, 71.13; H, 8.52%.

Oxidation of 2-(*p*-Tolylthio)cyclohexanol with *m*-CPBA. A Typical Procedure: A dichloromethane (5 ml) solution of *cis*-2-(*p*-tolylthio)cyclohexanol (86.7 mg, 0.391 mmol) was cooled at 0 °C. To this solution was added *m*-CPBA (70 mg, 0.40 mmol) and the mixture was stirred for 1 h at 0 °C and for 2 h at room temperature. An aqueous solution (20 wt%, 10 ml) of K_2CO_3 was added and the whole was stirred for a while. The aqueous layer was separated and extracted with dichloromethane (10 ml×2). The organic layers were combined, dried over anhydrous $MgSO_4$, condensed under reduced pressure, and subjected to column chromatography on silica gel using benzene-ethyl acetate (6:1) as an eluent to give a mixture of **3a** and **5a** (82 mg, 88%) in a ratio of 30:70, which was determined by the HPLC analysis.

Similarly, *trans*-2-(*p*-tolylthio)cyclohexanol (89 mg, 0.40 mmol) was treated with *m*-CPBA (70 mg, 0.41 mmol) (1 h at

Table 2. Atomic Positional and Thermal Parameters for **5C**

Atom	*x*	*y*	*z*	*B*
S 1	0.2189(2)	0.2207(2)	0.8257(1)	3.70
C 2	0.4724(7)	0.2238(5)	1.1419(6)	4.40
O 3	−0.1311(4)	0.1123(4)	0.5656(4)	4.30
C 4	0.0536(5)	0.1540(5)	0.8506(5)	3.00
O 5	0.2899(4)	0.0848(5)	0.7587(4)	5.40
C 6	−0.0261(6)	0.2879(5)	0.9255(6)	3.90
C 7	0.3766(6)	0.3075(5)	1.0436(5)	3.40
C 8	−0.0707(6)	0.0387(5)	0.6892(5)	3.30
C 9	0.7792(9)	0.5285(8)	1.5558(7)	8.20
C10	0.4069(7)	0.4622(6)	1.1066(6)	4.60
C11	0.6322(7)	0.4515(6)	1.3722(6)	4.90
C12	0.5359(7)	0.5320(6)	1.2716(7)	5.20
C13	−0.2651(6)	0.1582(6)	0.9180(6)	4.40
C14	−0.2169(6)	−0.0341(5)	0.6901(6)	4.10
C15	−0.3388(6)	0.0691(6)	0.7280(6)	4.50
C16	0.6014(7)	0.2971(6)	1.3086(6)	5.10
C17	−0.1270(6)	0.2530(6)	1.0035(6)	4.20

Table 3. Bond Distances of **5C**

Atom 1 Atom 2	Distance/Å	Atom 1 Atom 2	Distance/Å
S1-C4	1.990(6)	C7-C10	1.400(7)
S1-O5	1.550(4)	C8-C14	1.647(9)
S1-C7	1.836(4)	C9-C11	1.608(7)
C2-C7	1.407(7)	C10-C12	1.433(6)
C2-C16	1.446(6)	C11-C12	1.396(8)
O3-C8	1.426(6)	C11-C16	1.398(8)
C4-C6	1.584(7)	C13-C15	1.523(7)
C4-C8	1.572(5)	C13-C17	1.405(8)
C6-C17	1.593(10)	C14-C15	1.626(9)

Table 4. Bond Angles of **5C**

Atom 2-Atom 1-Atom 3	Angle/°	Atom 2-Atom 1-Atom 3	Angle/°
C4-S1-O5	109.7(2)	O3-C8-C14	107.6(4)
C4-S1-C7	103.9(2)	C4-C8-C14	118.2(4)
O5-S1-C7	101.0(2)	C7-C10-C12	118.8(5)
C7-C2-C16	120.2(4)	C9-C11-C12	122.8(5)
S1-C4-C6	112.1(4)	C9-C11-C16	118.6(5)
S1-C4-C8	110.0(4)	C12-C11-C16	118.6(4)
C6-C4-C8	109.5(4)	C10-C12-C11	122.4(5)
C4-C6-C17	115.6(4)	C15-C13-C17	122.3(6)
S1-C7-C2	122.2(3)	C8-C14-C15	120.8(4)
S1-C7-C10	117.7(4)	C13-C15-C14	109.2(4)
C2-C7-C10	119.9(4)	C2-C16-C11	120.1(5)
O3-C8-C4	106.8(4)	C6-C17-C13	128.0(5)

Table 5. Torsional Angles of **5C**

Atom 3-Atom 1-Atom 2-Atom 4	Angle/°
O5-S1-C4-C6	−178.8(3)
O5-S1-C4-C8	−56.7(4)
C7-S1-C4-C6	74.0(4)
C7-S1-C4-C8	−163.9(3)
C4-S1-C7-C2	77.9(5)
C4-S1-C7-C10	−106.7(4)
O5-S1-C7-C2	−35.7(5)
O5-S1-C7-C10	139.7(4)
C16-C2-C7-S1	175.9(4)
C16-C2-C7-C10	0.6(8)
C7-C2-C16-C11	−0.6(9)
S1-C4-C6-C17	−164.4(4)
C8-C4-C6-C17	73.2(5)
S1-C4-C8-O3	−59.9(4)
S1-C4-C8-C14	178.8(3)
C6-C4-C8-O3	63.7(5)
C6-C4-C8-C14	−57.6(5)
C4-C6-C17-C13	−67.2(7)
S1-C7-C10-C12	−175.7(4)
C2-C7-C10-C12	−0.2(8)
O3-C8-C14-C15	−57.3(6)
C4-C8-C14-C15	63.6(6)
C7-C10-C12-C11	−0.3(9)
C9-C11-C12-C10	178.7(6)
C16-C11-C12-C10	0.3(9)
C9-C11-C16-C2	−178.4(6)
C12-C11-C16-C2	0.1(9)
C17-C13-C15-C14	56.9(7)
C15-C13-C17-C6	1.2(9)
C8-C14-C15-C13	−74.6(6)

0 °C and 2 h at room temperature) to give a mixture of **4a** and **6a** (86 mg, 90%) in a ratio of 78:22, which was determined by the HPLC analysis.

Oxidation of 2-(*p*-Tolylthio)cycloheptanols: The cis isomer gave a mixture of **3b** and **5b** (92% yield) in a ratio of 14:86, while the trans isomer gave a mixture of **4b** and **6b** (83% yield) in a ratio of 84:16.

Oxidation of 2-(*p*-Tolylthio)cyclopentanols: The cis isomer gave a mixture of **3d** and **5d** (85% yield) in a ratio of 20:80, while the trans isomer gave a mixture of **4d** and **6d** (84% yield) in a ratio of 80:20.

X-Ray Crystallography of 5c. Crystal data are as follows: $C_{14}H_{18}O_2S$, F.W.=250.35, triclinic, space group, $P\bar{1}$, a=8.942(2) Å, b=9.592(5) Å, c=9.404(3) Å; α=108.53(5)°, β=118.01(2)°, γ=87.25(4)°; V=670.20 Å^3; D_x=1.116 g cm^{-3}, Z=2. A computer program UNICS III[20] PRG. MULTAN 80[21] run on a HITACHI M680 at Tokyo University was employed for the analysis. The intensity data were collected in the region $3° \leqq 2\theta \leqq 120°$ at a scan rate 4° min^{-1}. 2233 independent reflections with $F(0) > 3\sigma(F_o)$ were used for a structure analysis. The final refined R value was 0.0682. Atomic positional and thermal parameters, bond distances, bond angles, and torsional angles are summarized in Tables 2—5.

The authors are grateful to Dr. Koreharu Ogata of Chemical Analysis Center of Chiba University for the X-ray crystallographic determination.

References

1) a) I. D. Morrison and H. S. Mosher, "Asymmetric Organic Synthesis," Prentice-Hall, Inc., New Jersey; Sect. 3—4; b) π-Facial selection in cyclic systems: D. C. Wigfield, *Tetrahedron*, **35**, 449 (1979); D. Mukherjee, Y. -D. Wu, F. R. Fronczek, and K. N. Houk, *J. Am. Chem. Soc.*, **110**, 3328 (1988), and references cited therein.

2) For example, two diastereomer of (*SR*)-2-(*p*-tolylsulfinyl)cyclohexanone were separated by recrystallization from hexane-acetone, and the major isomer was subjected to reduction with diisopropylaluminium hydride: M. C. Carreño, J. L. G. Ruano, and A. Rubio, *Tetrahedron Lett.*, **28**, 4861 (1987).

3) a) K. Ogura, M. Fujita, T. Inaba, K. Takahashi, and H. Iida, *Tetrahedron Lett.*, **24**, 503 (1983), b) G. Guanti, E. Narisano, and F. Pero, *J. Chem. Soc., Perkin Trans. 1*, **1984**, 189.

4) Although racemic substrates were employed unless noted, one enantiomer is shown for simplicity.

5) $NaBH_4$ reduction in a mixed solvent (MeOH-THF) was reported: K. Soai and K. Ohi, *Bull. Chem. Soc. Jpn.*, **58**, 1601 (1985).

6) Isolated by recrystallization of a mixture of **1a** and **2a** from diethyl ether-hexane (see Experimenatl section).

7) A face for axial (equatorial) attack is defined as the axial (equatorial) face herein.

8) Stereochemical courses for addition of a nucleophile to acyclic and cyclic carbonyl compounds are well-explained in terms of the Felkin[9] and Cieplak[10] models, respectively, both of which predict different mode of facial selection in each other.

9) M. Cherest, H. Felkin, and N. Prudent, *Tetrahedron Lett.*, **1968**, 2199; N. T. Anh and O. Eisenstein, *Nouv. J. Chim.*, **1**, 61 (1977).

10) A. S. Cieplak, *J. Am. Chem. Soc.*, **103**, 4540 (1981).

11) The relative configurations of 2-(*p*-tolylthio)-cycloalkanols were confirmed by an alternative synthesis of the trans isomer from the corresponding cycloalkene oxide and sodium *p*-toluenethiolate[12] (see Experimental section).

12) F. G. Bordwell and R. J. Kern, *J. Am. Chem. Soc.*, **77**, 1141 (1955).

13) Optically active (*SR*)-**3** was obtained by reduction of a mixture of (*SR*)-**1a** and (*SR*)-**2a**,[14] followed by chromatographic separation and recrystallization.

14) K. Ogura, M. Ishida, H. Tomori, and M. Fujita, *Bull. Chem. Soc. Jpn.*, in press.

15) Formation of small amounts of **5a** and **6a** (Table 1) suggests that a part of **1a** epimerized under the reaction conditions.

16) B. M. Trost, T. N. Salzmann, and K. Hiroi, *J. Am. Chem. Soc.*, **98**, 4887 (1976).

17) Stationary phase: Waters Nova Pack C_{18} (3.9 mm×150 mm). Eluent: MeOH-H_2O (45:55 unless noted), 0.3 ml min^{-1}.

18) H. Yamashita and T. Mukaiyama, *Chem. Lett.*, **1985**, 1643. For its enantiomer (*S* configuration), $[\alpha]_D^{20}$ −112° (*c* 0.60, $CHCl_3$): S. Yamada, N. Takamura, and T. Mizoguchi, *Chem. Pharm. Bull.*, **23**, 2539 (1975).

19) In the presence of D_2O, this signal disappeared. The hydroxyl group couples with the C_1 proton and the proton (probably the C_7-proton) which appears at δ=1.38 (diffused t). In the presence of D_2O, this disappeared. This abnor-

mal long-range coupling was supported by the decoupling experimental: By irradiation of the signal at δ=1.38, the hydroxyl proton became a doublet (J=2.0 Hz).

20) T. Sakurai and K. Kobayashi, *Rep. Inst. Phys. Chem. Res.*, **55**, 69 (1979).

21) Following programs were modified: P. Main, M. M. Woolfson, and G. Germain, LSAM "A System of Computer Programmes for the Automatic Solution of Centrosymmetric Crystal Structures;" Univ. of York, York, England and Univ. de Louvain, Louvain, Belgium (1972); P. Main, M. M. Woolfson, and G. German, MULTAN "A Computer Programmes for the Automatic Solution of Crystal Structure," Univ. of York, York, England and Univ. de Louvain, Louvain, Belgium (1971). Also see: A. Furusaki, *Acta Crystallogr., Sect. A*, **35**, 220 (1979).

The Reactivities of Polyaromatic Hydrocarbons in Catalytic Hydrogenation over Supported Noble Metals

Kinya SAKANISHI, Masato OHIRA, Isao MOCHIDA,* Hiroshi OKAZAKI,† and Mahito SOEDA†
Institute of Advanced Material Study, Kyushu University 86, Kasuga, Fukuoka 816
†Nippon Steel Chemical Co., Ltd., Tobata, Kitakyushu 804
(Received July 5, 1989)

The reactivities of several polyaromatic hydrocarbons (pyrene: P, fluoranthene: FL, anthracene: An, fluorene: F, acridine: Ac, and carbazole: C) in the catalytic hydrogenation were studied and compared over supported noble metals (Pt, Pd, Rh, and Ru on a carbon or alumina support). The specific reactivity and selectivity were found to be strongly dependent upon the combination of the catalyst species and the substrate. The catalysts exhibited the activity order of Rh > Pd ≫ Pt > Ru for tricyclic aromatics of An, F, Ac, and C, although the catalysts provided very variable selectivities of the partially hydrogenated products which were produced via both consecutive and competitive routes, apparently according to the type of ring-skeleton and the presence of a nitrogen atom. The reactivity of the starting substrates and intermediates are compared to the quantum chemical reactivity indices, calculated based on MNDO (modified neglect of diatomic overlap). The values of the LUMO electron density, the π-bond order, and the stability of the product appear to govern the reactivity and selectivity of the hydrogenation, depending upon the combination of the catalyst species and the substrate. No hydrogenation of a substrate proceeds when its reactivity indices are less than the threshold value, which is subject to the activity of the catalyst and the reaction conditions defining product selectivity via both competitive and consecutive schemes.

The selective hydrogenation of polyaromatic hydrocarbons including heterocyclic compounds derived from coals and petroleums is one of the important steps in preparing the intermediates for functional molecules and medicines.[1-4]

The present authors have elsewhere reported the selective hydrogenation of pyrene, fluoranthene, acridine, and isoquinoline using noble metal catalysts under rather milder conditions[5-7] than those reported previously.[8-10] The former two substrates were very selectively converted into particular products of the partially-hydrogenated (especially tetrahydro) derivatives; these products could then be used as powerful hydrogen donors and synthetic intermediates.[11-13]

The selective hydrogenation of acridine was also found in a preceding paper to produce some partially hydrogenated acridines.[14] The reaction pathway of such selective hydrogenation was revealed to be competitive as well as consecutive through kinetic simulation, thermodynamic, and stereochemical comparisons of the hydrogenated products by the aid of quantum chemical calculations of the MNDO (modified neglect of diatomic overlap) method[15] and MM2 (molecular mechanics calculations).[16]

In the present study, the reactivities of several polyaromatic hydrocarbons in the catalytic hydrogenation were compared and rather comprehensively studied over typical noble metal catalysts in order to clarify the factors influencing their selective partial hydrogenation, since the specific reactivity and selectivity were found to be strongly dependent upon the combination of the catalyst species and the substrate. The reactivities of the substrates and their intermediates can be correlated to their quantum chemical indices and their stereochemical structures to explain the reaction schemes and to discuss the interaction between the substrates and the catalysts.

Experimental

Materials. Commercially available polyaromatic hydrocarbons (acridine, carbazole, anthracene, fluorene, pyrene, and fluoranthene) and decalin (reaction solvent) of a guaranteed grade were used without further purification in the present study, since sulfur compounds, which are severe poisons for the noble catalysts, were not detected, the sulfur content being less than 0.1%.

Commercial noble metal catalysts of Pd/Al_2O_3, Pd/C, Pt/Al_2O_3, Pt/C, Rh/Al_2O_3, Rh/C, and Ru/C (Metal content: 5 wt%), supplied by the Nippon Engelhalt Co., were used without any pretreatment.

Hydrogenation Procedures and Product Analyses. One of the polyaromatic hydrocarbons (2 g) was placed in an autoclave (50-ml capacity) together with the solvent (10 g of decalin) and one of the catalysts (0.2 g for FL or 0.5 g for the others). The autoclave was flushed with nitrogen three times to replace the air and then filled with pure hydrogen from a cylinder. The initial pressure of hydrogen was adjusted to give a prescribed pressure of 7 MPa at the reaction temperatures. After heating the reactor to a prescribed reaction temperature (373—523 K), magnetic stirring was started when the reaction time was counted. After the prescribed reaction time, the reactor was cooled with a fan to room temperature within 10 min; the reaction mixture (liquid and solid) was then recovered with THF. The catalyst was filtered out, and the liquid product including the solvent was analyzed by a temperature programmed gas chromatograph (column: SE-30, 2 m, heating rate: 10 K min^{-1} from 373 to 498 K). The hydrogenated derivatives were identified with GC-IR ^1H and ^{13}C NMR after the fractional distillation by reference to commercially available samples and/or the literature. The details of the product identification were described in previous papers.[5,6,14] The structures of the substrates and products are illustrated in Fig. 1.

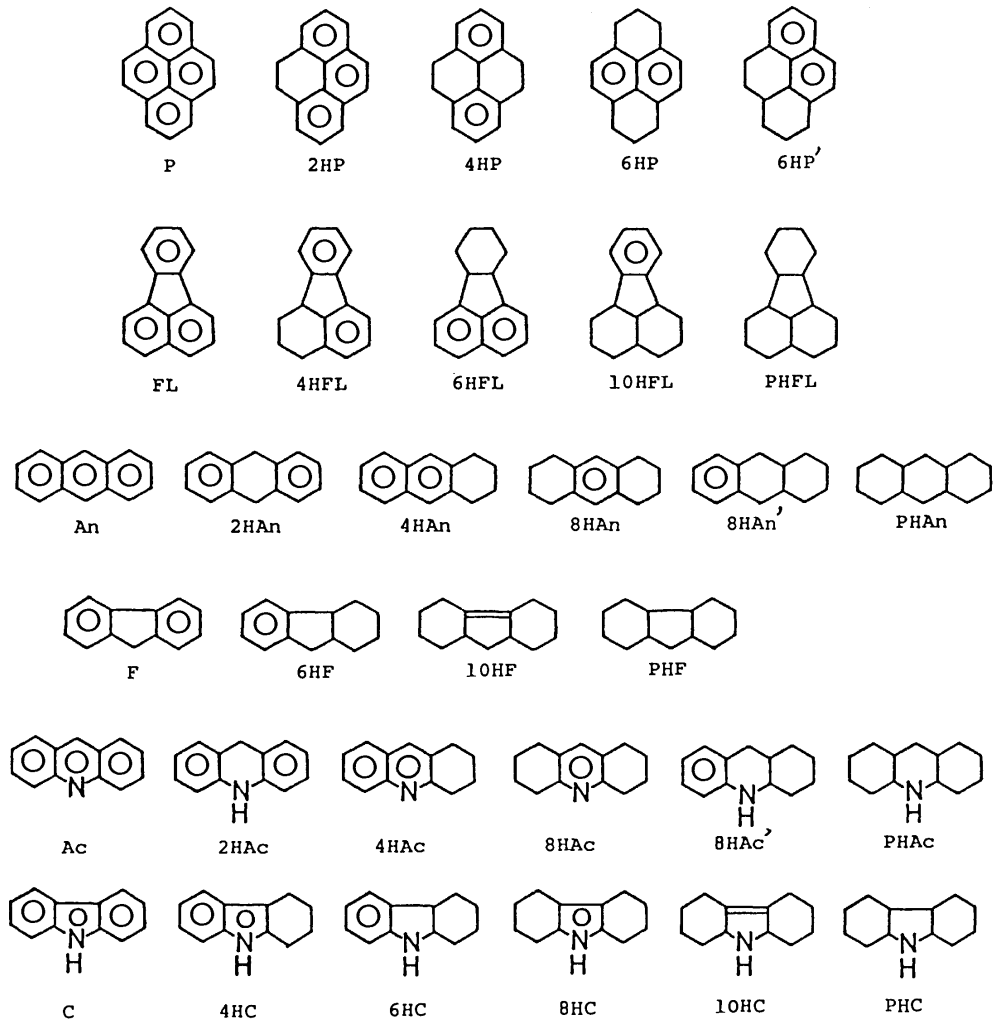

Fig. 1. Structures of the substrates and their hydrogenated products.

Quantum Chemical Calculations. The reactivity indices are calculated by means of the flow diagram shown in Fig. 2. According to the MM2 method,[16] the energetically optimized structures of the respective substrates and their hydrogenated products were determined. The molecular orbitals of the substrates of the determined structure were calculated according to the MNDO method[15] in order to estimate the heats of formation, the electron densities on carbon and nitrogen atoms, and the bond orders of the C-C and C-N bonds. The values thus calculated are more reasonable because the energy calculations are superior to any previously reported.[16]

Results

Hydrogenation Activities of Noble Metal Catalysts on Carbon. Table 1 summarizes the conversions of polyaromatic hydrocarbons in the hydrogenation on various carbon-supporting catalysts under the reaction conditions of 423 K, 7 MPa(H_2), and 30 min. All the catalysts except Ru, which was slightly less active, showed similar activities for pyrene (P) and fluoranthene (FL) of tetracyclic aromatics, although the latter substrate was much more reactive than the former.

The tricyclic aromatics showed very different reactivities, depending greatly on the catalyst used. The activities were in the order of Rh>Pd≫Pt>Ru in anthracene (An), fluorene (F), acridine (Ac), and carbazole (C). It should be noted, however, that the Pt and Ru catalysts exhibited much lower activities particularly for F and C, than did the other two catalysts. Figure 3 illustrates the major products in the hydrogenation of tricyclic aromatics on Rh, Pd, and Pt catalysts. The different selectivities of the catalysts were definite.

Reactivities and Selectivities in the Hydrogenation of Tetracyclic Aromatic Hydrocarbons. The activities and selectivities of the carbon-supported catalysts in the hydrogenations of pyrene (P) and fluoranthene (FL) are summarized in Tables 2 and 3 respectively, where severer and milder conditions than those of Table 1 were selected respectively. Except for Ru, the catalysts again exhibited similar activities under these conditions.

All the catalysts except for Rh/C hydrogenated 70—90% of the pyrene with a similar selectivity under the reaction conditions of 523 K, 5 MPa (H_2), and 6 h,

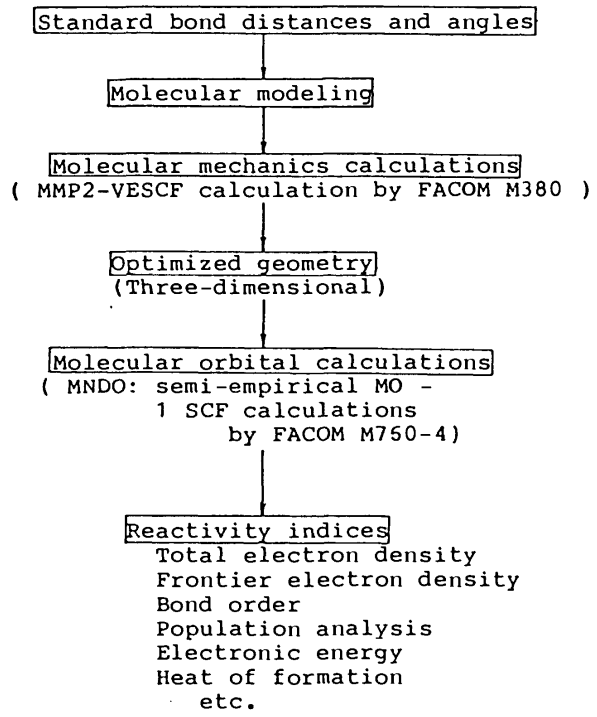

Fig. 2. Calculation diagram of reactivity indices of polyaromatic hydrocarbons.

producing preferentially the dihydro- (2HP) and tetrahydropyrene (4HP) at the selectivities of 40—60% and 30—40% respectively. The consecutive nature of the reaction is definite. The Rh/C catalyst alone produced 1,2,3,6,7,8-hexahydropyrene (6HP) by a considerable selectivity (ca. 30%) at similar conversion levels, suggesting that the competitive reaction may contribute along with the Rh/C catalyst.[5]

Fluoranthene (FL) was more easily hydrogenated than pyrene under the milder conditions of 423 K, 3 MPa (H_2), and 30 min with a smaller amount of the catalyst (0.2 g), as is shown in Table 3. The Pt/C and

Table 1. Hydrogenation Reactivities[a] of Various Polyaromatic Hydrocarbons on Carbon-Supported Catalysts

Substrate	Conversion/%			
	Pt	Pd	Rh	Ru
Pyrene (P)	50	55	52	43
Fluoranthene (FL)	100	100	100	95
Anthracene (An)	19	28	100	10
Fluorene (F)	0	86	100	2
Acridine (Ac)	91	100	100	78
Carbazole (C)	5	72	100	4

a) Reaction conditions: 423 K—7 MPa (H_2), 30 min. catalyst/substrate=1/4 (wt/wt).

Table 2. Screening of Various Noble Metal Catalysts in the Hydrogenation of Pyrene (P)[a]

Catalyst	Conv.	Yield/Selectivity (%)				
	%	2HP	4HP	6HP	6HP′	Others[b]
Pt/C	82	38/46	32/39	6.4/7.7	3.6/4.3	1.8/2.2
Pd/C	87	40/47	35/41	5.5/6.4	3.9/4.6	2.0/2.2
Rh/C	83	31/37	20/25	23/27	4.6/5.6	4.7/5.5
Ru/C	71	43/60	21/30	2.7/3.8	1.6/2.2	2.6/3.7

a) Reaction conditions: 523 K—5 MPa, 6 h. b) Others are more deeply hydrogenated products than the hexahydropyrenes.

Table 3. Screening of Various Noble Metal Catalysts in the Hydrogenation of Fluoranthene (FL)[a]

Catalyst	Conv.	Yield/Selectivity (%)			
	%	4HFL	6HFL	10HFL	PHFL
Pt/C	100	18/18	2.2/2.2	75/75	4.8/4.8
Pd/C	100	0.2/0.2	0/0	99/99	0.4/0.4
Rh/C	92	67/73	5.8/6.3	18/20	0.7/0.8
Ru/C	31	24/78	2.7/8.7	3.7/12	0.4/1.3

a) Reaction conditions: 423 K—3 MPa, 30 min.

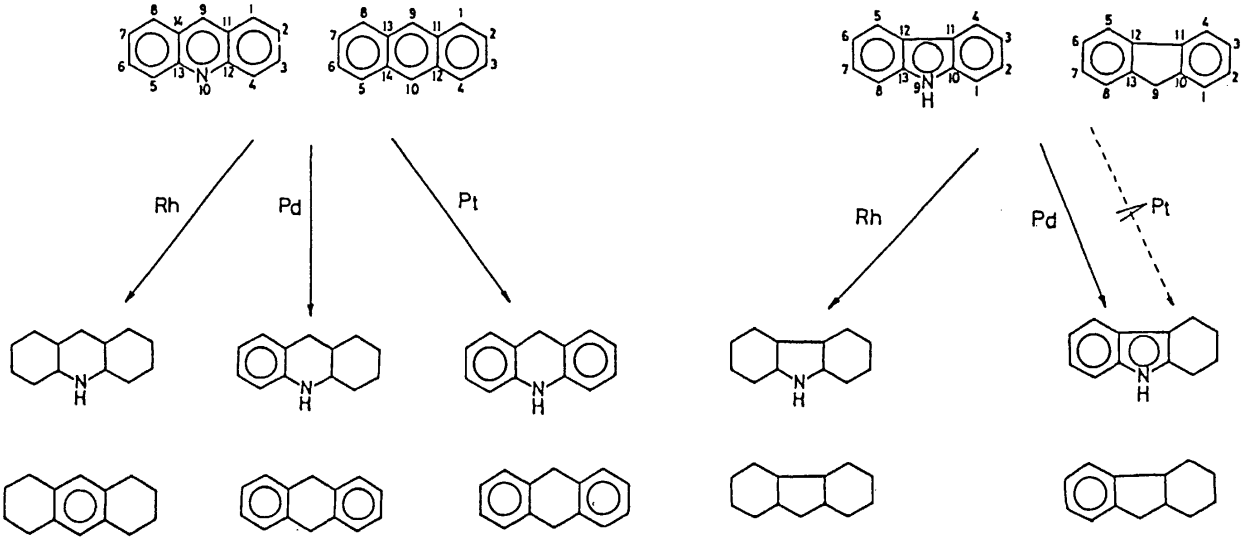

Fig. 3. Main routes in the hydrogenation of tricyclic aromatics on Rh, Pd, and Pt catalysts.

Pd/C catalysts exhibited the highest activity (conversion: 100%), producing 1,2,3,4,5,6,11,12,15,16-decahydrofluoranthene (10HFL) as the major product (selectivity: 75 and 99% respectively). The Rh/C catalyst hydrogenated 92% of the FL, exhibiting the highest selectivity (73%) for tetrahydro FL (4HFL). In marked contrast, the Ru/C catalyst converted only 31% of the FL, mainly into 4HFL (78% selectivity).

Reactivities and Selectivities in the Hydrogenation of Tricyclic Aromatic Hydrocarbons. The reactivities of anthracene (An) and fluorene (F) on alumina-supporting catalysts under some conditions are summarized in Tables 4 and 5 respectively. The Rh catalyst hydrogenated An much faster than the other two catalysts to achieve a 100% conversion within 5 min at 423 K and 7 MPa of H_2, producing principally 1,2,3,4,5,6,7,8-octahydroanthracene (8HAn, 73% selectivity). A minor production of 1,2,3,4,4a,9,9a,10-octahydroanthracene (8HAn') and perhydroanthracene (PHAn) was also observed. The consecutive path of An→4HAn→8HAn→PHAn appears predominant. Dihydro and tetrahydro derivatives were rapidly hydrogenated into octahydro derivatives, which are rather unreactive under these conditions. In contrast, Pd and Pt catalysts produced principally 9,10-dihydroanthracene (2HAn) at a selectivity of 60—70% at the reaction time of 180 min. Tetrahydro derivative (20—30%) was the second major product, the selectivities for the other products being very low.

The Pd and Rh catalysts converted 100% of the fluorene (F) under the conditions of 473 K, 7 MPa (H_2), and 5 min, principally into hexahydrofluorene (6HF, 71% selectivity) and perhydrofluorene (PHF, 72% selectivity). The other products found suggest a consecutive path on both catalysts, although the reaction stopped at their respective products of partial hydrogenation. In contrast, the Pt catalyst exhibited a much lower activity for F under the same conditions, converting only 2.7% of the F into 6HF.

Reactivities and Selectivities in the Hydrogenation of Nitrogen-Containing Aromatics. Tables 6 and 7 summarize the hydrogenation reactivities of acridine (Ac) and carbazole (C) on carbon- and alumina-supporting catalysts respectively. All the catalysts, examined under the conditions of 423 K, 7 MPa, and 10 min, exhibited very high activities against Ac, allowing the conversions of 90—100%. However their selectivities were very different, depending on the metal species, as is shown in Table 6.

The Pd catalyst hydrogenated Ac successively, producing mainly one of 1,2,3,4,4a,9,9a,10-octahydro-Ac (8HAc') via 9,10-dihydro-Ac (2HAc), although the selectivity depended upon the support. The Rh catalysts exhibited the highest activity among the catalysts examined, converting most of the Ac into perhydro-Ac (PHAc) via 1,2,3,4,5,6,7,8-octahydro-Ac (8HAc), regardless of the support.

In contrast, the Pt catalysts exhibited the highest selectivity for 2HAc (59% on Pt/C and 80% on Pt/Al_2O_3), producing very little of the more deeply hydro-

Table 5. Screening of Various Noble Metal Catalysts in the Hydrogenation of Fluorene (F)[a]

Catalyst	Conv.	Yield/%			
	%	6HF	10HF	PHF	Others[b]
Pd/Al_2O_3	100	71	9.5	16	3.6
Rh/Al_2O_3	100	0.7	26	72	1.4
Pt/Al_2O_3	2.7	1.4	0.1	0.1	1.1

a) Reaction conditions: 473 K—7 MPa, 5 min. b) Others are unidentified products.

Table 4. Screening of Various Noble Metal Catalysts in the Hydrogenation of Anthracene (An)[a]

Catalyst	Conv.	Yield/Selectivity (%)					
	%	2HAn	4HAn	8HAn	8HAn'	PHAn	Others[b]
Pd/Al_2O_3	85	57/67	24/28	1.2/1.4	0.7/0.8	1.5/1.8	1.5/1.8
Rh/Al_2O_3	100	1.1/1.1	0.7/0.7	72/73	12/12	13/13	0.8/0.8
Pt/Al_2O_3	58	37/63	17/30	1.0/1.7	0.3/0.5	0.9/1.5	2.2/3.8

a) Reaction conditions: 423 K—7 MPa, 180 min (Pd and Pt); 423 K—7 MPa, 5 min (Rh). b) Others are unidentified products.

Table 6. Screening of Various Noble Metal Catalysts in the Hydrogenation of Acridine (Ac)[a]

Catalyst	Conv.	Yield/Selectivity (%)					
	%	2HAc	4HAc	8HAc	8HAc'	PHAc	Others[b]
Pd/C	95	16/17	1.8/1.9	11/11	44/47	16/16	5.9/6.2
Pd/Al_2O_3	95	44/47	1.6/1.7	4.6/4.9	36/38	2.8/3.0	5.9/6.2
Rh/C	98	0.1/0.1	0.6/0.6	5.2/5.3	0.9/0.9	90/92	1.3/1.3
Rh/Al_2O_3	99	0/0	0.1/0.1	0.9/0.9	0.1/0.1	98/99	0.1/0.1
Pt/C	85	50/59	1.1/1.3	2.8/3.3	12/14	5.8/6.9	13/16
Pt/Al_2O_3	96	77/80	0.5/0.5	1.1/1.2	6.0/6.3	1.9/2.0	9.2/9.6

a) Reaction conditions: 423 K—7 MPa, 10 min. b) Others are unidentified products.

Table 7. Screening of Various Noble Metal Catalysts in the Hydrogenation of Carbazole (C)[a]

Catalyst	Conv.	Yield/Selectivity (%)					
	%	4HC	6HC	8HC	10HC	PHC	Others[b]
Pd/C	82	39/48	3.9/4.7	3.7/4.5	3.8/4.6	25/31	6.3/7.6
Pd/Al_2O_3	71	40/57	4.5/6.4	14/20	1.4/2.0	1.3/1.8	8.7/12
Rh/C	99	0.2/0.2	1.2/1.2	4.1/4.2	0.8/0.8	85/87	6.9/7.0
Rh/Al_2O_3	98	3.1/3.2	2.0/2.0	21/22	6.0/6.1	56/57	10/11
Pt/C	19	7.7/40	2.1/11	4.0/21	0.1/0.5	0.9/4.7	4.4/23
Pt/Al_2O_3	9.2	1.7/19	1.6/17	1.6/17	0.2/2.2	0.7/7.6	3.4/37

a) Reaction conditions: 473 K—7 MPa, 15 min. b) Others are unidentified products.

Table 8. Hydrogenation of Acridine(Ac) on Pt/Al_2O_3 under Variable Conditions

Reaction conditions (K/MPa/min)	Conv.	Yield/%					
	%	2HAc	4HAc	8HAc	HAc′	PHAc	Others[a]
423/7/10	96	77	0.5	1.1	6.0	1.9	9.2
423/7/30	96	79	0.6	1.0	6.5	1.7	7.4
423/7/120	96	68	0.5	0.8	7.1	1.7	18
423/7/240	96	69	0.4	0.6	7.9	1.9	16
473/7/60	96	54	0.5	1.1	17	9.1	15
473/7/180	96	46	0.6	0.7	18	13	19
473/7/300	96	9.5	0.7	1.1	16	55	13
523/7/30	98	8.2	0.8	3.2	17	62	4.9

a) Others are unidentified products.

genated products. It should be noted that the selectivity on the Pt catalysts did not significantly change upon much longer reaction times of 120—240 min at 423 K or even at a higher temperature of 473 K until 180 min, as is shown in Table 8. PHAc became the major product at 473 K and 300 min or at 523 K and 30 min; this suggests that the 2HAc was converted directly to a fully hydrogenated product (PHAc). 2HAc, prepared separately, which was alone converted very slowly into more deeply hydrogenated products at 423 K, as is shown in Table 9, the major product being 8HAc′. Its low reactivity and weak adsorption may stop the reaction at this substrate.

Although alumina- and carbon-supporting catalysts showed much the same activities in the hydrogenation of Ac, as is shown in Table 6, less-hydrogenated 2HAc was more selectively produced on the alumina-supporting Pt and Pd catalysts, much less production of deeply hydrogenated products being observed. PHAc was the principal product on the Rh catalysts.

Tetrahydro-C (4HC) was the principal product with Pd on both supports, although a considerable amount of PHC was also produced with the carbon-supporting one. Both Rh catalysts provided PHC as the major product; however, a considerable amount of 8HC was also produced on the alumina-supporting catalyst. The Pt catalysts a exhibited much lower activity (conversion: 10—20%). No marked selectivity was observed. Thus, carbon-supporting catalysts tend to give more deeply hydrogenated products from nitrogen-containing compounds than do alumina-supporting ones, although the extent of hydrogenation varies with the catalyst species. In contrast, supports exhibited a negligible influence on the hydrogenations of such hydrocarbons as P, FL, An, and F which carry no heteroatom.

Table 9. Hydrogenation of 2HAc on Pt/Al_2O_3 at 423 K and 7 MPa of H_2

Reaction time/min	Composition/%						
	Ac	2HAc	4HAc	8HAc	8HAc′	PHAc	Others[a]
0	5.0	77	0.3	0.7	1.2	0.5	15
30	4.9	54	1.0	3.8	13	4.6	18
240	5.2	39	1.3	4.8	18	6.4	25

a) Others are unidentified products.

Discussion

The present study has revealed that the specific reactivity and selectivity in the hydrogenation on supported noble metals were both strongly dependent upon the combination of the catalyst and the substrate.

The catalytic hydrogenation of polyaromatic hydrocarbons follows competitive-consecutive reaction paths. Hence, the selectivity is governed by both the reaction positions of the first hydrogenation and the extent of successive hydrogenation. Thus, the reactivity of the respective positions of the substrate, the hydrogen reactivity activated by the catalyst, and allowed forms of the adsorbed substrate on the catalyst may define the rate and selectivity of the reaction.

The initial reactivity of the respective position in the substrate may be described appropriately by such quantum chemical indices as the LUMO electron density and the π-bond order.[17] Such indices may reflect the reactivity with hydride or the coordination force to the metal for the adsorption. The higher reactivity of hydrogen may lead to the larger rate of the reaction, but it may be less sensitive to the reactivity differences in the reactive positions. In the consecutive reactions, the hydrogenation may progress or cease, depending upon the stability, reactivity, and adsorbed form of the intermediate product, and also the reactivity of hydrogen, the last two factors being strongly influenced by the catalyst species and the reaction conditions. Based on such considerations, the rate and selectivity of the present study can be discussed.

Rh catalysts always exhibited the highest activity for the hydrogenation of the tricyclic aromatic hydrocarbons examined in the present study, although the selectivity for a specific product was always lower than in the other catalysts. The Rh catalysts may most activate molecular hydrogens, failing to distinguish the specific position of the substrate. Hence, the Rh catalysts are not suitable for a selective hydrogenation, but they can provide a considerable amount of a product which is very minor compared with the other catalysts. The nitrogen atom in the substrates is not so influential in the selectivity on the Rh catalysts, no difference in selectivity between anthracene and acridine being observed.

The Pd catalysts exhibited a moderate activity for the selective hydrogenation of polyaromatic hydrocarbons if the optimum reaction conditions were selected in terms of the reaction temperature and the time. The carbon-supported Pd catalyst selectively hydrogenated pyrene and acridine into tetrahydro and octahydro products respectively at very high yields.[5,6] It should be noted that the Pd catalysts exhibited much different selectivities for acridine and anthracene of the same skeleton, whether or not the nitrogen atom is contained. The Pd catalysts produced 8HAc′ at a rather high yield, although they failed to produce 8HAn′ of the same structure as 8HAc′, indicating that the nitrogen atom is influential on the Pd catalysts.

The Pt catalysts exhibited a very limited activity for the hydrogenations of Ac and An, producing principally 2HAc and 2HAn respectively. Their activity for the hydrogenations of C and F was also very low, producing principally tetra- and hexahydrogenated products respectively. The Pt catalysts hydrogenated preferentially or even exclusively the 9,10-positions of An and Ac. Further hydrogenation proceeded only under severer conditions to give deeply hydrogenated products.

The Ru/C catalyst exhibited the lowest activity of all the substrates examined in the present study, reflecting its smallest ability of molecular hydrogen activation among the four noble metals examined.

In contrast to tricyclic aromatic hydrocarbons, tetracyclic hydrocarbons exhibited much less sensitivity to the catalyst species.

The reactivity and selectivity for the hydrogenation of polyaromatic substrates may be supposed to be controlled by the interactions among the LUMOs and/or all π-orbitals of the substrate and the catalyst, and the HOMO (highest occupied molecular orbital) Frontier electron density of adsorbed hydrogen on the catalyst, which may have a form of hydride to interact with the substrate.[17]

The π-bond order as well as the LUMO electron density, summarized in Table 10, are influential on the hydrogenation reactivity of the tetracyclic aromatics, such as pyrene and fluoranthene. The intermediate product, such as pyrene, hydrogenated initially at the 1 position of the highest LUMO electron density is too unstable under the present conditions to survive as the final product. The hydrogenation of pyrene proceeds initially at the pair of positions 4 and 5, where the LUMO electron density is second highest, but the π-bond order is the largest, as is shown in Fig. 4, thus producing 4HP via 2HP as the major products in the consecutive manner in all case of the present study. Only the Rh/C catalyst provided a considerable amount of 6HP. The active catalyst may rapidly hydrogenate the rather unreactive position 2 as well as

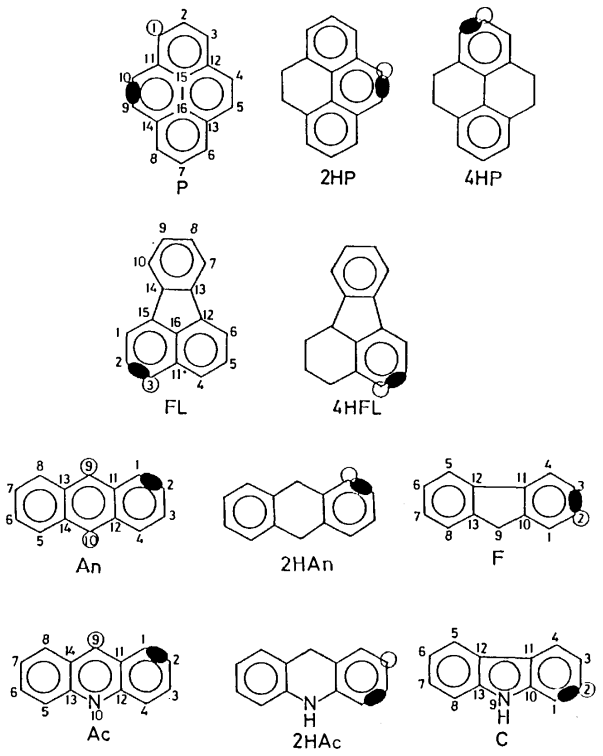

Fig. 4. Reactivity indices of the substrates and some hydrogenated products.
○: Largest LUMO electron density position. ●: Largest π-bond order bond.

Table 10. Largest LUMO Electron Density and π-Bond Order of the Substrates and Some Hydrogenated Products

	Largest LUMO		Largest π-bond order	
	Position	Value	Position	Value
P	C_1	0.25	C_9-C_{10}	0.89
2HP	C_4	0.29	C_4-C_5	0.87
4HP	C_2	0.29	C_1-C_2	0.66
FL	C_3	0.25	C_2-C_3	0.79
4HFL	C_4	0.30	C_4-C_5	0.66
An	$C_{9,10}$	0.39	C_1-C_2	0.84
2HAn	C_1	0.17	C_1-C_2	0.68
F	C_2	0.31	C_2-C_3	0.67
Ac	C_9	0.48	C_1-C_2	0.85
2HAc	C_2	0.28	C_3-C_4	0.68
C	C_1	0.35	C_1-C_2	0.72

the most reactive positions, 1 and 3. Hydrogenation around room temperature is reported to provide 1,6-dihydropyrene (2HP′), which is produced via the hydrogenation of the most reactive positions, 1 and 6, since the product is stable under these conditions.[12]

The large difference in hydrogenation reactivity between pyrene and fluoranthene can be explained by a combination of the effects of the π-bond order and the LUMO electron density. Fluoranthene has the highest π-bond order and LUMO electron density at the same positions of C_2-C_3, while pyrene has those at the different positions, as has been described above. It is the same reason that tetrahydrofluoranthene (4HFL) is more easily and selectively produced from fluoranthene under milder conditions regardless of the catalyst species. 1,2,3,4,5,6,11,12,15,16-decahydrofluoranthene (10HFL) is the major consecutive product, as is to be expected from the reactivity indices of 4HFL. It should be noted that the less active Pt and Pd catalysts provided more of the consecutive product from this particular substrate than did the active Rh. The high reactivity of the substrate may not discriminate the activity of the catalysts.

The reactivity and selectivity in the hydrogenation of tricyclic substrates are very different from those of tetracyclic systems. Anthracene and acridine have a pair of the most reactive 9,10-positions of the highest LUMO electron densities, yielding very selectively the 9,10-dihydro derivatives as the rather stable initial products on the Pt and Pd catalysts, although their π-bond order is never the largest. The hydrogenation of the positions of the largest π-bond order provide the product with the second largest π-bond order. MNDO suggests a large difference in the stability of 2HP′ and 2HAn, the former of which cannot be a stable product. The further hydrogenation of dihydro products is very slow in the consecutive steps, because the maximum LUMO electron density and π-bond order are much reduced to levels which are not large enough to be consecutively hydrogenated at 423 K on Pd or, more especially, Pt catalysts. The successive reaction at a higher temperature overcomes the barrier to produce 8HAn and 8HAc′ selectively.

Although the Rh catalyst provided deeply-hydrogenated products through consecutive reactions, considerable amounts of 8HAn and 8HAc were also produced, indicating that their largest π-bond order positions may be comparatively reactive on Rh catalysts. However, the higher reactivity of Ac than that of An may reflect its larger LUMO electron density, since their largest π-bond order values were much the same.

Fluorene and carbazole have values of the highest π-bond orders (ca. 0.70) at the C_2-C_3 and C_1-C_2 bonds respectively similar to that of the 9,10-dihydro products of anthracene and acridine, as is shown in Table 10 and Fig. 4. It should be noted that such substrates are hardly hydrogenated at all on the Pt catalysts. The π-bond order (ca. 0.70) of these substrates may be a threshold to restrict the hydrogenation on the Pt catalysts under the present conditions.

Pd catalysts could hydrogenate rather selectively one of phenyl groups in these substrates. The C_2-C_3 and C_1-C_2 positions in fluorene and carbazole, where the LUMO electron density and the π-bond order are at their maximum, are hydrogenated first to complete the hydrogenation of the ring. The second phenyl group resists being hydrogenated because of the reduced reactivity caused by the hydrogenation of the pair. The Rh catalyst is very active in hydrogenating every position in an unselective manner. It is interesting that certain amounts of 10HC and 10HF with a double bond between two rings are produced. Highly hindered olefin of the partially hydrogenated products can survive the hydrogenation.

Nitrogen-containing carbazole is again more reactive than fluorene. Nitrogen increases the reactivity indices.

In conclusion, the first hydrogenation of polyaromatic hydrocarbons is found to be principally governed by the LUMO and/or the π-bond order. Such reactivity indices determine the rate and selectivity of the hydrogenation, reflecting the activity of the catalyst. The active catalyst can hydrogenate the positions of a lower reactivity, performing the consecutive reaction to the more deeply hydrogenated product for a substrate and the competitive reactions to lower the selectivity for another substrate.

Hence, selective hydrogenation can be designed by selecting the catalyst and the reaction conditions to match the reactivity of the reaction position in the particular substrate, as predicted on the basis of quantum chemical calculations.

Noble metals' activation ability against molecular hydrogen and their adsorption ability against an aromatic bond are the origins of their catalytic activity; however, no theoretical explanation is available at present. Their empirical classification may, therefore, practical use at present.

References

1) I. Mochida, K. Tamaru, Y. Korai, H. Fujitsu, and K. Takeshita, *Carbon*, **19**, 213 (1981).
2) P. P. Fu, H. M. Lee, and R. G. Harvey, *J. Org. Chem.*, **45**, 2797 (1981).
3) A. Olalde and G. Perot, *Appl. Catal.*, **13**, 373. (1985).
4) I. Amer, H. Amer, R. Ascher, J. Blum, Y. Sasson, and K.P.C. Vollhardt, *J. Mol. Catal.*, **39**, 185 (1987).
5) I. Mochida, M. Ohira, K. Sakanishi, and H. Fujitsu, *Nippon Kagaku Kaishi*, **1986**, 1112.
6) I. Mochida, M. Ohira, K. Sakanishi, H. Fujitsu, and H. Okazaki, *Nippon Kagaku Kaishi*, **1987**, 1033.
7) H. Okazaki, M. Soeda, K. Onishi, and R. Tamura, *Appl. Catal.*, **41**, 99 (1988).
8) S. Friedman, M. L. Kaufman, and I. Wender, *J. Org. Chem.*, **36**, 694 (1971).
9) T. J. Lynch, M. Banah, M. McDougall, and H. D. Kaesz, *J. Mol. Catal.*, **17**, 109 (1982).
10) R. H. Fish, A. D. Thormodsen, and G. A. Cremer, *J. Am. Chem. Soc.*, **104**, 5234 (1982).
11) I. Mochida, K. Otani, Y. Korai, and H. Fujitsu, *Chem. Lett.*, **1983**, 1025.
12) I. Mochida, K. Tamaru, Y. Korai, H. Fujitsu, and K. Takeshita, *Carbon*, **20**, 231 (1982).
13) I. Mochida, H. Hatano, Y. Korai, and H. Fujitsu, *High Temp.- High Press.*, **16**, 439 (1984).
14) K. Sakanishi, M. Ohira, I. Mochida, H. Okazaki, and M. Soeda, *J. Chem. Soc., Perkin Trans. 2*, **1988**, 1769.
15) M. J. S. Dewar and W. Thiel, *J. Am. Chem. Soc.*, **99**, 4899 (1977).
16) N. L. Allinger, *J. Am. Chem. Soc.*, **99**, 8127 (1977).
17) D. Liotta, "Advances in Molecular Modeling," JAI Press., London (1988), Vol. 1.

Behavior of the Enthalpy of Mixing in the Ternary Systems Lead-Antimony-Tin, Bismuth-Lead-Tin, and Bismuth-Cadmium-Tin at 950 K. II. Theoretical Aspects

Walid Ahmad BADAWI
Department of Chemistry, Faculty of Science, Al-Fateh University, Tripoli, Libya
(Received November 9, 1988)

Analysis of the experimental results which have been obtained from our studies on the ternary systems Pb-Sb-Sn, Bi-Pb-Sn, and Bi-Cd-Sn revealed a new effect: deduction of a straight line obtained by interpolation between the pairs Sb-Pb and Sb-Sn at $x_{Pb}=x_{Sn}=0.5$ from the partial enthalpy of mixing of antimony, h^m_{Sb}, yields a remainder quantity, ${}^r h^m_{Sb}$. The minimum of this remainder lies at the section drawing $x_{Pb}/x_{Sn}=1$. Further studies on the systems Bi-Pb-Sn and Bi-Cd-Sn indicated that the present "r-effect" is probably a general property of ternary solutions. The sign of the remainder ${}^r h^m_i$ is opposite to that of h^m of the pair of components existing vis-a-vis a third apex-component in the same ternary system. Systems of strong heteropolar character which indicate Wagner effect overlapped by III—V one could also exhibit r-effectt. Rules for the mixing behavior in binary systems are in some cases not applicable on the corresponding pairs in the ternary solutions.

The theory of liquid solution[1] failed to predict statements for the excess functions behavior in binary systems of metals and metalloids, mainly because only atomic parameters were employed to interpret the data of the excess quantities. Also the specification of the liquid state with the aid of statistical thermodynamic treatments is associated with principle difficulties and thus, these theories are only applicable to simple models. For solutions of complicated behavior of mixing, calorimetric studies seemed to be more appropriate. The results obtained from the enthalpy of mixing measurements (e.g. those by Wittig and coworkers[2-4]) proved to be useful in finding statements for the specification of the effects which could contribute in prediction of the behavior of mixing in binary solutions. These could also shed light on the factors which determine the behavior of mixing in some ternary solutions. However, studies on ternary solutions are required in order that a more definite answer to the question be provided. It is also noteworthy that in some cases, the pairs of components in a ternary system show a behavior of mixing which differs from that one observed in the binary system consisting of the same components as those in the pairs belonging to the ternary one.

In the preceeding paper,[5] the experimental results for the enthalpy of mixing in the ternary system Pb-Sb-Sn have been reported together with results for the systems Bi-Pb-Sn and Bi-Cd-Sn. The results obtained (i.e. level minima of the partial molar enthalpy of mixing of Sb and Bi) pointed out the existence of effects (e.g. the III—V effect and a present one) which contribute in determining the behavior of mixing in the ternary solutions. Our intention now is to predict statements for the behavior of mixing in relation to these effects and other possible ones. Accordingly, we report in this paper the analysis of the experimental results and theoretical approach to the ternary solutions.

Theory

The integral and partial quantities of a system of c components are given by

$$Y_i = Y - \sum_{j\neq i} x_j \cdot \left(\frac{\partial Y}{\partial x_j}\right)_{x_k} ; \; j = 1,\cdots c, \tag{1}$$

where x_i is a dependent nonexplicit variable, Y, a function of all $x_j \neq x_i$. The subscript x_k on the partial derivative means that $x_k \neq x_j$, x_i is constant. Equation 1 is compatible to the following relation:

$$Y_i = Y + (1-x_i) \cdot \left(\frac{\partial Y}{\partial x_i}\right)_{x_j/x_k} ; \; i \neq 1,\cdots c, \; i \neq k, \tag{2}$$

where the subscript x_j/x_k is constant for all j, $k \neq i$. In view of Eq. 1 the partial quantity of the third component in the ternary system is given through the following polynominal function:

$$Y_3 = \sum_{k,l} a_{kl} \cdot x_1^k \, x_2^l \, (1-k-l). \tag{3}$$

Equation 3 depends on the average molar function, $\overline{Y}$, which can be expressed as a polynomial function:

$$\overline{Y} = \sum_{k,l} a_{k,l} \cdot x_1^k \, x_2^l \text{ with } \sum a_{00} = \sum_k a_{k0} = \sum_l a_{0l} = 0 \tag{4}$$

By this procedure, the partial quantities can be calculated from the integral ones. The calculation of Y_1 and Y_2 occurs as follows:

(i) The symmetrical procedure: From the coefficients a_{kl}, the coefficients b_{ij} or c_{ij} corresponding to the variation of the dependent variables x_1, x_2, and x_3, can be calculated and thus we obtain Y_1 and Y_2.

(ii) We can keep x_1 and x_2 as independent variables to determine Y_1 and Y_2 from Y (x_1, x_2). This is only possible when the coefficients a_{kl} are known. Applying this procedure, we obtain

$$Y_1 = \sum_{k,l} a_{kl} \, x_1^k \, x_2^l \, (1-k-l) + a_k x_1^{k-1} \, x_2^l \, k, \tag{5}$$

$$Y_2=\sum_{k,l} a_{kl}\, x_1^k\, x_2^l\,(1-k-l)+a_k\, x_1^k\, x_2^{l-1} l, \quad (6)$$

$$Y_3=\sum_{k,l} a_{kl}\, x_1^k \cdot x_2^l\,(1-k-l). \quad (7)$$

The excess quantity of the enthalpy of mixing is given through the following polynomial function:

$$Y^e=Y^e(x_i, x_j)=\sum_{k,l} a_{kl}\, x_i^k\, x_j^l, \quad (8)$$

where i, j=1,2 or 2,3 or 3,1. In this case, the following condition must be satisfied:

$$\sum a_{00}=\sum a_{k0}=\sum a_{0l}=0.$$

Since the total mole fraction of the three components in the ternary system must equal 1, ($x_1+x_2+x_3=1$), the excess quantities can be expressed in three different pairs of mole fraction. Substitution of the dependent mole fraction occurs as follows:

$$Y^e=Y^e(x_1, x_2)=\sum_{k,l} a_{kl}\, x_1^k\, x_2^l=\sum_{k,l} a_{kl} \cdot x_1^k(1-x_1-x_3)^l$$
$$=Y^e(x_1, x_3)=\sum_{i,j} b_{ij}\, x_3^i\, x_1^j. \quad (9)$$

The calculation of the coefficient b_{ij} occurs from those a_{kl}.

Discussion

From the study[2-4] on binary systems, it was possible to derive appropriate expressions which relate the position of the components in the periodic table to the excess function, Y^e. Accordingly, statements for the expected trends and properties of the excess quantities have been predicted in some noninvestigated systems. In views of these investigations and the results from our studies on a series of ternary systems, we have obtained further conclusions concerning the behavior of the enthalpy of mixing. These results will be discussed here together with those obtained from the present study on the system Pb-Sb-Sn.[5]

In the system Bi-Cd-Sn,[5] the partial molar enthalpies of mixing of bismuth and cadmium, h^m_{Bi}, h^m_{Cd}, showed striking level minima. It was observed that the level minimum of h^m_{Cd} and the bend joined to this minimum disappear rapidly when the mole fraction of Sn increases. At the same time, the bend of h^m_{Bi} becomes larger. Consequently, the partial enthalpy of mixing of Bi takes negative values. This was a somewhat surprising observation since h^m_{Bi} in the pair Bi-Cd showed always positive trends. This behavior could not have been caused by a Wagner effect,[6] since the trend of h^m_{Bi} curve differs from that one belonging to the Wagner effect.[6] It was therefore presumed that a cluster formation (caused by covalent bonds) exists. Indeed, it was not possible to derive a strict concentration interval from which conclusions for stoichiometric relations and electronic arrangements may be obtained. We can therefore suggest a valence electron concentration (C_{ve}) equal 3 for the pair Cd-Sn in the ternary system Bi-Cd-Sn. To check the justness of these presumptions we have been studying the system Bi-Pb-Sn. The partial molar enthalpy of mixing of bismuth showed a level minimum in the region lying between the section drawings $x_{Sn}=0$ and $x_{Pb}/x_{Sn}=6/4$. Also in this system the C_{ve} of the value 3 was presumed for the pair Pb-Sn.

Since the origin of the minima observed is presumed to be caused by the combination of an element (of 5 valence electrons) with comparable pairs of elements belonging to group IIIa and having the same Cve as that of the element, it is expected that the system Cd-Sb-Sn shows similar behavior. However, the study of this system is problematic (high vapor pressure of Cd at the melting point of antimony). The system Sb-Sn-Zn shows in the pair Sb-Zn a striking strong Wagner effect. This would overlap the covalent III—V effect so that no further conclusions from this system could be obtained.

The partial molar enthalpy of mixing of antimony, h^m_{SB}, in the system Pb-Sb-Sn goes through a minimum between the quasi-binary section drawings $x_{Sn}=0$ and $x_{Sn}/x_{Pb}=6/4$. This occurs due to the transfer of electrons from antimony in such a way that the C_{ve} reaches the value of 3 at the tin side. The same behavior could be expected for the system Bi-Pb-Sn where the delivery of electrons occurs by bismuth to yield a C_{ve} of 3 at the lead side. The correct-

Table 1. ζ-Function of Antimony at Quasi-Binary Section Drawings in the System Pb-Sb-Sn Beginning from the Apex Sb in kJ mol^{-1} at 950 K

	Section drawing:										
x_{Sb}	Sn-Pb	1	2	3	4	5	6	7	8	9	Pb-Sb
0.0	−5.50	−4.90	−4.42	−3.98	−3.66	−3.16	−2.71	−2.16	−1.46	−0.66	−0.04
0.1	−5.49	−5.56	−5.58	−5.46	−5.21	−5.21	−4.29	−3.58	−2.67	−1.52	−0.26
0.2	−5.64	−5.96	−6.11	−6.04	−5.77	−5.77	−4.69	−3.90	−2.92	−1.72	−0.31
0.3	−5.72	−6.04	−6.14	−6.00	−5.65	−5.12	−4.44	−3.63	−2.69	−1.58	−0.29
0.4	−5.57	−5.79	−5.79	−5.57	−5.16	−4.60	−3.92	−3.15	−2.29	−1.33	−0.24
0.5	−5.13	−5.23	−5.15	−4.90	−4.50	−3.98	−3.36	−2.67	−1.92	−1.10	−0.17
0.6	−4.40	−4.43	−4.33	−4.12	−3.97	−3.37	−2.86	−2.28	−1.63	−0.89	−0.04
0.7	−3.48	−3.47	−3.40	−3.26	−3.05	−2.75	−2.37	−1.90	−1.32	−0.61	+0.24
0.8	−2.55	−2.48	−2.42	−2.33	−2.19	−1.98	−1.69	−1.29	−0.76	−0.06	+0.82
0.9	−1.86	−1.64	−1.44	−1.25	−1.04	−0.80	−0.48	−0.08	−0.43	+1.07	+1.87

ness of the above cited view will be quantitatively checked through testing the behavior of the ζ-function[7] which in given by

$$\xi = \frac{y_i}{(1-x_i)^2} , \qquad (10)$$

where y_i is the partial molar quantity of the enthalpy of mixing (h^m_{Sb} or h^m_{Bi}) and x_i the mole fraction of the component Sb or Bi.

Using the data for h^m_{Sb} in the system Pb-Sb-Sn,[5] we obtain values for ζ as illustrated in Table 1. From this table, it is evident that the minimum of ζ lies at side of the pair at which h^m_{Sb} takes the more negative value. This is the pair Sn-Sb where the C_{ve} reaches its maximum at the tin side.

The level form of the minima of the enthalpy of mixing of components (belonging to group Va in the periodic table of elements) at the quasi-binary section drawings x_{Bi}=const. and x_{Sb}=const., was presumed to be related to a convalent III—V effect. In fact, the relation between the form of the minima and the enthalpies of mixing of the pairs of components in ternary systems depends on other effect as observed in the present study. This effect may be explained as follows:

Deduction of a straight line (interpolated between the pairs Sb-Pb and Sb-Sn at $x_{Pb}=x_{Sn}=0.5$) from the partial enthalpy of mixing of antimony, h^m_{Sb}, yields a remainder quantity: $^r h^m_{Sb}$. The minimum of $^r h^m_{Sb}$ lies nearly at the section drawing $x_{Pb}/x_{Sn}=1$ (Fig. 1). The same effect (indicated here as r-effect) is expected to be observed in the system Bi-Sb-Sn where the minimum of $^r h^m_{Bi}$ lies at the section drawing $x_{Sb}/x_{Sn}=1$. In both cases, the "r-effect" is probably overlapped by other properties of pairs of components in the ternary systems.

It is possible that the r-effect is a general property of ternary solutions. The properties of ternary solutions are of two origins:

Characteristic effects which have a relevant physical meaning or other ones of trivial nature e.g. the Gibbs-Duhem relation for partial quantities. On the other hand, these properties may be overlapped by a somewhat stronger effect which depends on the type of the ternary system e.g. the expected stronger effect resulting from the substitution of Sn by Zn in the system Pb-Sb-Sn. Such a substitution leads to more heteropolar character and consequently to a Wagner effect. In such cases it would be easy to find a correlation between the position of the component in the periodic table of elements and the Wagner effect.

In order to prove that the above described "r-effect" is not a property of all planes (belonging to the pairs in the ternary system) where these planes satisfy the Gibbs-Duhem relation, the following plane will be discussed:

$$h^m = 1 - x_3 - (1-x_3)^2 + \frac{x_1 x_2}{(1-x_3)}, \qquad (i)$$

where x_1, x_2, and x_3 are the mole fractions of Sb, Pb, and Sn, respectively. This plane has the pair (1,2) and satisfies the Gibbs-Duhem relation.

For x_3=0, we have $h^m(1,2)=x_1 x_2$, and

$$h^m_3 = h^m - (x_3 - 1)\cdot \left(\frac{\partial h^m}{\partial x_3}\right)_{x_1/x_2} = (1-x_3)^2 .$$

For the section drawing x_3=const., h^m_3 is also constant. Despite the existence of the positive pair (1,2), h^m_3 is without $^r h^m_3$. This means that the plane (i) does not indicate r-effect. With this evidence one may conclude that, $^r h^m_3$, with an opposite sign to that one of the enthalpy of mixing corresponding to the pair which exists at the opposite side to the third component in the same ternary system, is not a trivial property which can be derived from the Gibbs-Duhem relation.

To decide that the above described $^r h^m_{x_i}$ is a general property of other ternary systems and to show how this effect takes place, we discuss the behavior of the

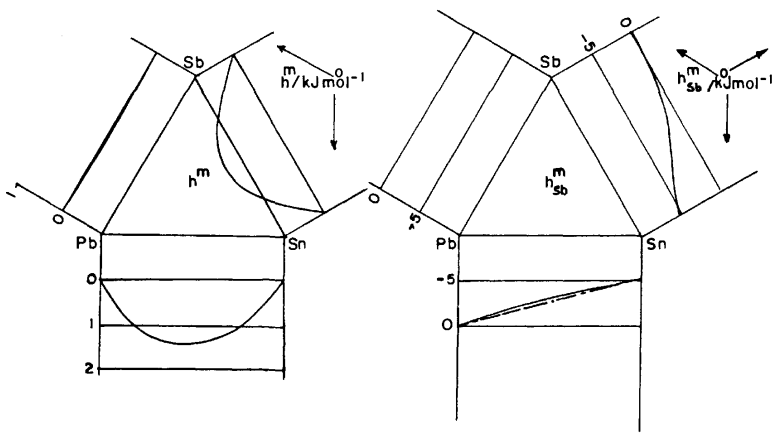

Fig. 1. The molar enthalpy of mixing, h^m, the partial one of antimony, h^m_{Sb}, at the quasi-binary section drawings Sb-Pb and Sb-Sn in the system Pb-Sb-Sn and the "r-effect."

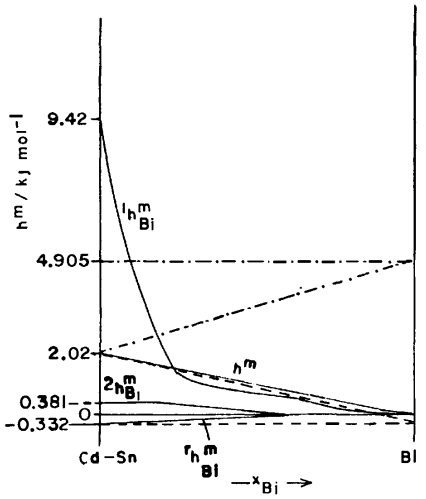

Fig. 2. Representation of the "r-effect" and estimated $^rh^m_{Bi}$ in the system Bi-Cd-Sn.

enthalpy of mixing of bismuth, h^m_{Bi}, using our data for the system Bi-Cd-Sn.[5] The partial molar enthalpy of bismuth is given by

$$h^m_{Bi} = h^m + (1-x_3)\cdot\left(\frac{\partial h^m}{\partial x_3}\right)_{x_1/x_2}, \qquad (11)$$

where x_1, x_2, and x_3 are the mole fractions of Bi, Cd, and Sn, respectively. Figure 2 shows the trends of the partial molar enthalpies of mixing, $^2h^m_{Bi}$ at Sn-Bi and $^1h^m_{Bi}$ at Cd-Bi together with the curve of the molar enthalpy of mixing along the quasi-binary section drawing $x_{Cd}/x_{Sn}=1$ in the ternary system Bi-Cd-Sn.

The partial enthalpies of mixing of bismuth at the spices $x_{Cd}=1$ and $x_{Sn}=1$ are 9.42 and 0.39 kJ mol^{-1}, respectively. From linear interpolation, we can obtain for $x_{Cd}=x_{Sn}=0.5$, the value of 4.91 kJ mol^{-1}. The molar enthalpy of mixing in the system Bi-Cd-Sn at $x_{Cd}=x_{Sn}=0.5$ is 2.02 kJ mol^{-1}. With reference to Eq. 11, the partial enthalpy of mixing of bismuth at this point can reach the average value 4.91 kJ mol^{-1} only when the molar enthalpy of mixing, h^m, starting from 2.88 kJ mol^{-1}, increases. With linear continuous increase where the drop in the value of h^m is, according to $h^m=a(1-x_{Bi})$, proportional to x_{Bi}, the partial molar enthalpy of mixing of bismuth h^m_{Bi} takes, along the whole quasi-binary section drawing $x_{Cd}/x_{Sn}=1$, the value of zero. When h^m without a turning point goes below this straight line, the partial enthalpy of mixing of bismuth, h^m_{Bi}, becomes along the whole quasi-binary section drawing negative. This means that the sign of $^rh^m_{Bi}$ is opposite to that one of the pair which exists at the opposite side of bismuth in the system Bi-Cd-Sn.

On the basis of the above given discussion, we expect that for ternary systems such as Bi-Sb-M (M=metal), in which Bi or Sb exists vis-a-vis a pair with negative enthalpy of mixing, the h^m_{Bi} in the pair Sb-M and h^m_{Sb} in that one Bi-M should have positive $^rh^m_{Bi}$ and $^rh^m_{Sb}$, respectively.

Conclusion

The r-effect is probably a general property of ternary solutions. The level minima of the partial quantities of the enthalpy of mixing in ternary solutions are attributed to the r-effect. Systems of strong heteropolar character which indicate Wagner effect overlapped by III—V effect exhibit also r-effect. Rules for the mixing behavior in binary systems are in some cases not applicable on the corresponding pairs in the ternary solutions.

References

1) I. Prigogine, A. Belleman, and V. Mathot, "The Molecular Theory of Solutions," Longman Green, London (1957).

2) F. E. Wittig and E. Gehring, *Z. Naturforsch.*, **18 a**, 351 (1963).

3) F. E. Wittig, *Z. Elektrochem.*, **63**, 327 (1959).

4) F. E. Wittig and E. Gehring, *Ber. Bunsenges. Phys. Chem.*, **70**, 717 (1966).

5) W. A. Badawi, *Bull. Chem. Soc. Jpn.*, **61**, 1351 (1988).

6) C. Wagner, "Thermodynamics of Alloys," Addison-Wesley, Reading, Mass., (1952).

7) L. S. Darken, "Physical Chem. of Metals," McGraw-Hill Book Co. Inc., New York (1953).

Contribution to the Study of the Dielectric Relaxation Process of 1-Iodoalkanes

José Muñoz Embid,* José Mª Fornies-Marquina,† and Santos Otin*
Departamento de Química Orgánica-Química Fisica, Facultad de Ciencias, Universidad de Zaragoza, 50009-Zaragoza, Spain
†Departamento de Fisica Aplicada, Facultad de Ciencias, Universidad de Zaragoza, 50009-Zaragoza, Spain
(Received April 14, 1989)

A study of the dielectric relaxation process of 1-iodoalkanes (from 1-iodopropane to 1-iodohexadecane) was carried out by measuring their static dielectric constants at 2 MHz and complex dielectric permittivities at 9.23 and 15.05 GHz, in the range of temperature 293.15—343.15 K. The 1-iodoalkanes are classified as belonging to an unsymmetrical distribution of relaxation times of Cole-Davidson type. Activation enthalpies for the relaxation process are obtained by fitting the data of relaxation time as a function of temperature to the Eyring equation. The influence of the aliphatic chain length in the 1-iodoalkane on the characteristic parameters of the relaxation process is discussed.

Systematic studies of the dielectric relaxation parameters for haloalkanes have been reported previously[1-5] for 1-bromoalkanes at several frequencies and as a function of the aliphatic chain length. In the case of other 1-haloalkanes, only a few suitable data are available in the literature.[1-7]

We report measurements of the static dielectric constants at 2 MHz according to the heterodyne beat method, and complex dielectric permittivities at 9.23 and 15.05 GHz, using rectangular waveguides, for eight 1-iodoalkanes (1-iodopropane, 1-iodobutane, 1-iodopentane, 1-iodohexane, 1-iodoheptane, 1-iodooctane, 1-iodododecane, and 1-iodohexadecane) in the temperature range 293.15—343.15 K.

The aim of this work is to study the influence of the aliphatic chain length of the iodoalkane molecules on their characteristic relaxation parameters.

Experimental

The liquids used were: 1-iodopropane and 1-iodobutane (Fluka AG, Buchs, better than 99 mol%), 1-iodopentane, 1-iodohexane, 1-iodoheptane, and 1-iodooctane (Fluka AG, Buchs, better than 98 mol%), 1-iodododecane (Ventron GMBH, Karlsruhe, better than 98 mol%), and 1-iodohexadecane (Merck-Schuchardt, better than 90 mol%).

Dielectric permittivity measurements were performed with a WTW Dipolmeter (model DM01), using a DFL 2 cell at a constant frequency of 2 MHz. The frequency of 2 MHz is well below the dielectric absorption frequency range of similar systems. The cells were thermostated through the outer water jacket using a water thermostat providing a temperature control to ±0.05 K.

The complex permittivities have been measured using rectangular waveguides at 9.23 and 15.05 GHz, described fully elsewhere.[8] The limits of accuracy achieved were 2% in ε' and 5% in ε''.

Refractive index measurements were carried out (at several temperatures) by means of a thermostated Abbé refractometer. Values were obtained for Na-D light. The reproducibility was as good as ±0.00002. Thermoregulation for the complex permittivity and refractive index measurements was the same as that for dielectric constant measurements.

Results

The experimental values of the complex permittivities ε' and ε'' at 9.23 and 15.05 GHz in temperature range 293.15—343.15 K are given in Table 1 along with the static dielectric constants at 2 MHz, ε_s, and ε_∞ assumed to be equal to n^2 (Figs. 1 and 2).

These results let us classify the 1-iodoalkanes as belonging to an unsymmetrical distribution of relaxation times of Cole-Davidson type[9] in which the com-

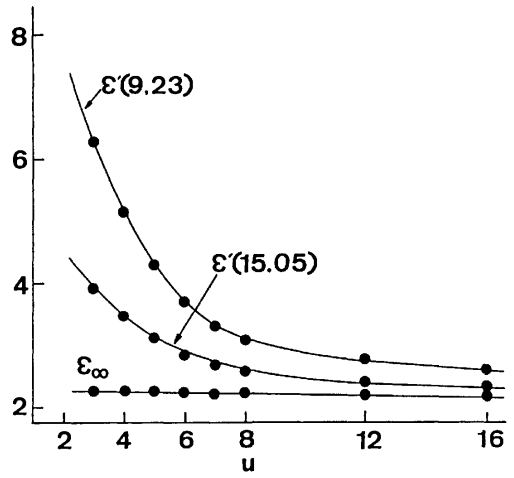

Fig. 1. Plot of ε' (9.23 GHz), ε' (15.05 GHz), and ε_∞ against the number of carbon atoms, u, at 303.15 K in 1-iodoalkanes.

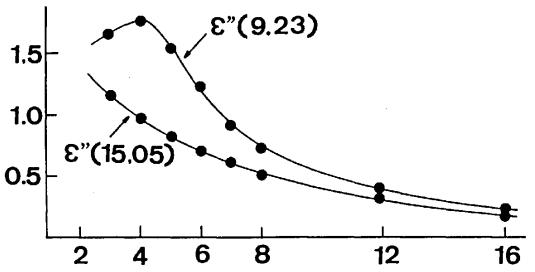

Fig. 2. Variation of ε'' (9.23 GHz) and ε'' (15.05 GHz) with the number of carbon atoms, u, at 303.15 K in 1-iodoalkanes.

Table 1. Measured Values of ε_s, ε', ε'', and ε_∞ for 1-Iodoalkanes

T/K		9.23 GHz		15.05 GHz				9.23 GHz		15.05 GHz		
	ε_s	ε'	ε''	ε'	ε''	ε_∞	ε_s	ε'	ε''	ε'	ε''	ε_∞
	1-Iodopropane						1-Iodobutane					
293.15	7.08	6.23	1.98	3.84	1.19	2.26	6.27	4.99	1.86	3.38	0.97	2.25
298.15	6.96	6.26	1.89	3.89	1.18	2.26	6.17	5.08	1.82	3.43	0.98	2.24
303.15	6.84	6.27	1.80	3.93	1.17	2.25	6.08	5.14	1.77	3.47	0.98	2.23
308.15	6.73	6.26	1.73	3.95	1.15	2.24	5.99	5.18	1.72	3.50	0.97	2.22
313.15	6.62	6.25	1.65	3.97	1.12	2.23	5.90	5.20	1.66	3.53	0.96	2.21
318.15	6.51	6.23	1.58	3.98	1.09	2.22	5.82	5.21	1.60	3.54	0.95	2.21
323.15	6.40	6.21	1.52	3.98	1.06	2.21	5.73	5.20	1.55	3.55	0.93	2.20
328.15	6.30	6.19	1.46	3.96	1.04	2.21	5.65	5.20	1.50	3.56	0.92	2.19
333.15	6.20	6.19	1.40	3.93	1.02	2.20	5.58	5.20	1.46	3.56	0.91	2.18
	1-Iodopentane						1-Iodohexane					
293.15	5.78	4.14	1.53	3.06	0.81	2.24	5.35	3.60	1.17	2.85	0.69	2.23
298.15	5.70	4.23	1.54	3.09	0.81	2.23	5.27	3.66	1.20	2.86	0.69	2.22
303.15	5.62	4.30	1.53	3.12	0.82	2.22	5.20	3.70	1.22	2.87	0.70	2.21
308.15	5.54	4.35	1.52	3.15	0.82	2.21	5.13	3.75	1.23	2.89	0.70	2.21
313.15	5.46	4.39	1.49	3.18	0.82	2.21	5.07	3.78	1.22	2.92	0.71	2.20
318.15	5.38	4.42	1.45	3.20	0.82	2.20	5.00	3.82	1.21	2.94	0.71	2.19
323.15	5.31	4.43	1.41	3.22	0.82	2.19	4.94	3.84	1.18	2.97	0.72	2.19
328.15	5.24	4.43	1.37	3.24	0.81	2.18	4.88	3.86	1.15	2.99	0.72	2.18
333.15	5.17	4.43	1.33	3.24	0.80	2.18	4.82	3.87	1.11	3.02	0.72	2.17
338.15	5.10	4.42	1.29	3.23	0.78	2.17	4.76	3.88	1.07	3.04	0.72	2.16
343.15							4.70	3.87	1.03	3.06	0.72	2.16
	1-Iodoheptane						1-Iodooctane					
293.15	4.99	3.29	0.89	2.73	0.59	2.22	4.72	3.15	0.75	2.66	0.52	2.22
298.15	4.92	3.30	0.91	2.71	0.59	2.21	4.66	3.11	0.72	2.62	0.52	2.21
303.15	4.86	3.32	0.92	2.71	0.59	2.21	4.61	3.08	0.69	2.60	0.51	2.20
308.15	4.80	3.33	0.93	2.71	0.60	2.20	4.55	3.07	0.68	2.60	0.52	2.19
313.15	4.74	3.35	0.93	2.73	0.61	2.19	4.50	3.07	0.67	2.60	0.53	2.19
318.15	4.68	3.38	0.93	2.75	0.62	2.19	4.44	3.09	0.67	2.62	0.54	2.18
323.15	4.62	3.41	0.92	2.78	0.63	2.18	4.39	3.12	0.67	2.65	0.55	2.18
328.15	4.57	3.44	0.90	2.81	0.64	2.17	4.34	3.17	0.68	2.69	0.56	2.17
333.15	4.52	3.49	0.89	2.85	0.64	2.17	4.30	3.22	0.68	2.72	0.57	2.16
338.15	4.46	3.54	0.86	2.89	0.65	2.16	4.25	3.29	0.69	2.77	0.58	2.16
343.15	4.41	3.60	0.84	2.93	0.65	2.15	4.20	3.37	0.70	2.81	0.58	2.15
	1-Iodododecane						1-Iodohexadecane					
293.15	3.96	2.66	0.36	2.30	0.24	2.20						
298.15	3.92	2.74	0.39	2.36	0.27	2.20						
303.15	3.88	2.80	0.41	2.41	0.30	2.19	3.50	2.57	0.23	2.29	0.19	2.18
308.15	3.84	2.85	0.42	2.45	0.32	2.18	3.47	2.59	0.24	2.27	0.19	2.18
313.15	3.80	2.88	0.43	2.47	0.33	2.18	3.44	2.61	0.25	2.27	0.21	2.17
318.15	3.77	2.91	0.44	2.49	0.34	2.17	3.41	2.63	0.26	2.28	0.21	2.17
323.15	3.74	2.92	0.44	2.40	0.34	2.17	3.38	2.64	0.26	2.27	0.22	2.16
328.15	3.70	2.92	0.44	2.49	0.34	2.16	3.35	2.65	0.27	2.28	0.23	2.15
333.15	3.67	2.91	0.44	2.48	0.35	2.16	3.32	2.66	0.28	2.28	0.23	2.15
338.15	3.64	2.90	0.44	2.47	0.35	2.15	3.29	2.69	0.28	2.30	0.25	2.14
343.15	3.61	2.88	0.43	2.45	0.35	2.14	3.27	2.71	0.29	2.31	0.25	2.14

Table 2. Relaxation Times, τ_0/ps, Calculated from Present Data

1-Iodoalkane	$\tau_0(T/\mathrm{K})$/ps										
	293.15	298.15	303.15	308.15	313.15	318.15	323.15	328.15	333.15	338.15	343.15
1-Iodopropane	32	31	29	29	28	28	28	27	27		
1-Iodobutane	34	31	29	28	27	26	26	25	24		
1-Iodopentane	44	40	37	34	32	31	29	29	28	28	
1-Iodohexane	60	53	48	44	41	38	36	34	33	32	32
1-Iodoheptane	78	71	66	60	56	52	48	45	42	39	36
1-Iodooctane	90	93	94	91	85	79	72	65	57	51	44
1-Iodododecane	326	243	191	157	134	118	108	99	93	88	82
1-Iodohexadecane			610	538	456	381	312	259	215	180	149

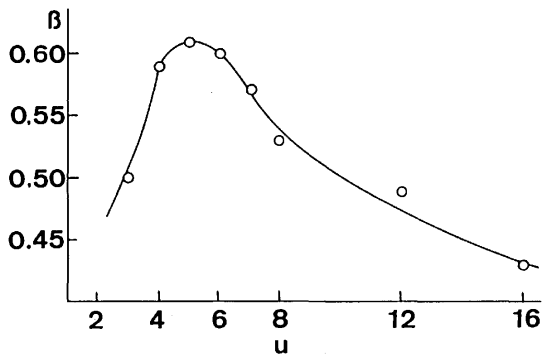

Fig. 3. Variation of β parameter with the number of carbon atoms, u, at 303.15 K in 1-iodoalkanes.

Table 3. Eyring Enthalpy of Activation Associated to the Dielectric Process of 1-Iodoalkanes

1-Iodoalkane	ΔH_E/kJ mol^{-1}
1-Iodopropane	0.8
1-Iodobutane	3.5
1-Iodopentane	5.7
1-Iodohexane	7.8
1-Iodoheptane	10.1
1-Iodooctane	9.8
1-Iodododecane	19.3
1-Iodohexadecane	28.4

plex dielectric permittivity is given by

$$\varepsilon^*=\varepsilon_\infty+\frac{\varepsilon_s-\varepsilon_\infty}{(1+j\omega\tau_0)^\beta} \quad (1)$$

where τ_0 is the value of the most probable macroscopic relaxation time and β the characteristic parameter of the distribution. In Fig. 3 the values of β are plotted against the number of carbon atoms, u, in the molecule of iodoalkane. The obtained results for τ_0 are given in Table 2.

Eyring rate equation was used to study the variation of relaxation times with the temperature

$$\ln(\tau_0 T)=\ln\frac{h}{k}-\frac{\Delta S_E}{R}+\frac{\Delta H_E}{RT} \quad (2)$$

were ΔH_E and ΔS_E are the most probable enthalpy and entropy of activation associated to the dielectric process. The values of ΔH_E are listed in Table 3.

Discussion

Figures 1 and 2 show a plot of the complex permittivities ε' and ε'', respectively, at 9.23 and 15.05 GHz, as a function of the chain length of 1-iodoalkane. As it happens with ε_s, the slopes are higher for 1-iodoalkanes of short chain and, from 1-iodooctane up, they tend to the value of ε_∞. On the other hand, a noticeable influence of the length of chain on the dielectric behavior of a molecule in the region of low frequency is observed, although that influence decreases more and more with increasing frequency and it finally becomes hardly significant.

The influence of number, u, of carbon atoms in 1-iodoalkane on the parameter of distribution, β, is illustrated in Fig. 3. As can be seen, β increases at first with u, shows a maximum value between 1-iodobutane and 1-iodohexane, and then diminishes for larger 1-iodoalkanes. This characteristic behavior of β might be put down to an effect of the high mass of I atom. For 1-iodoalkanes with short aliphatic chain the heteroatom represents a high proportion of the molecular mass, but for progressively longer chains, the center of mass moves increasingly away from I atom. This means that the dielectric behavior of short-chain 1-iodoalkanes is basically determined by both volume and mass of I atom, while for longer molecules the hydrocarbon chain exerts a more significant influence.

As Table 2 shows, relaxation time, τ_0, becomes greater as the chain-length increases, which can be imputed to a parallel increase of both viscosity, and molecular mass and volume. Molecules will move slower with increasing length of their aliphatic chains, leading to increasing values of τ_0. 1-Iodododecane and 1-iodohexadecane show a rather extreme behavior as their freezing points lie very close to our experimental temperature and therefore their molecules will move very slowly; with increasing temperature, rapidly decreasing values of τ_0 are expected, as it, in fact, happens.

A similar explanation emerges from observation of the values of ΔH_E. Attributing the unusual behavior of 1-iodododecane and 1-iodohexadecane to a "quasi-crystalline" structure, ΔH_E changes almost lineary with the length of a 1-iodoalkane between $3 \leqq u \leqq 7$, as if the contribution to ΔH_E by each carbon atom (or each $-CH_2-$ group) were constant. The value for 1-iodooctane seems to be the beginning of a constancy of ΔH_E; however, in the absence of any experimental results concerning molecules between $8<u<12$, no definitive conclusion about that is permitted.

References

1) K. Higasi, K.Bergmann, and C. P. Smyth, *J. Phys. Chem.*, **64**, 880 (1960).
2) F. H. Branin, Jr. and C. P. Smyth, *J. Chem. Phys.*, **20**, 1121 (1952).
3) W. M. Heston, Jr., E. J. Hennelly, and C. P. Smyth, *J. Am. Chem. Soc.*, **70**, 4093 (1948).
4) H. L. Laquer and C. P. Smyth, *J. Am. Chem. Soc.*, **70**, 4097 (1948).
5) E. J. Hennelly, W. M. Heston, Jr., and C. P. Smyth, *J. Am. Chem. Soc.*, **70**, 4102 (1948).
6) F. I. Mopsik and R. H. Cole, *J. Chem. Phys.*, **44**, 1015 (1966).
7) W. P. Conner and C. P. Smyth, *J. Am. Chem. Soc.*, **65**, 382 (1943).
8) F. J. Arcega and J. M. Forniés-Marquina, *J. Phys. D*, **15**, 1783 (1982).
9) D. W. Davidson and R. H. Cole, *J. Chem. Phys.*, **18**, 1417 (1950).

 © 1989 The Chemical Society of Japan Bull. Chem. Soc. Jpn., 62, 4009—4015 (1989)

Kinetics and Mechanisms of Oxidations by Metal Ions. X.[1] Oxidation of Phosphinic and Phenylphosphinic Acids by Tris(polypyridyl)iron(III) Complexes

Kamla SHARMA, Aditya PRAKASH, and Raj N. MEHROTRA*
Department of Chemistry, University of Jodhpur, Jodhpur 342001, India
(Received December 12, 1988)

A kinetic study on the oxidation of phosphinic(hypophosphorous) and phenylphosphinic acids by trispolypyridyliron(III) complexes using excess of either phosphinic or phenylphosphinic acid has been made in perchloric acid. The pseudo first-order rate constant k_{obs}, with respect to iron(III) complex, is independent of $[H^+]$. The results indicated that phenylphosphinic acid is more reactive than phosphinic acid towards any given iron(III) complex. The formation of an intermediate complex is indicated by the kinetics and supported by the spectrophotometry of the reaction mixture. The differences in the observed thermodynamic parameters of this intermediate complex, probably an outer-sphere complex, and those predicted by the Fuoss equation are discussed. It is suggested that the 'inactive' form of either of the acid is reactive towards the iron(III) complexes. It is also shown that the rate of disproportionation of the intermediate complex is not affected by the form of phosphinic or phenylphosphinic acid entering into the complex formation. The values of β_2 and k_1, the equilibrium constant for the formation of the oxidant-substrate complex and the rate limiting constant for its disproportionation respectively, are reported together with respective thermodynamic and activation parameters.

Efforts continue to identify the tautomeric form of oxoacids of phosphorous in their oxidation by metal or metal-complex ions. It had been shown that permanganate[2] and vanadium(V)[3] oxidations of phosphonic (phosphorous) acid involved the 'inactive' form $HP(O)(OH)_2$. However, Ce(IV) in nitric acid[4] oxidized the 'active' $HP(OH)_2$ form of phosphinic acid. The acid dependence in vanadium(V) oxidation of phenylphosphinic acid[5] indicated simultaneous oxidation of 'active' $C_6H_5P(OH)_2$ form by VO_2^+(aq.) (acid independent path) and 'inactive' $C_6H_5PH(O)(OH)$ form by $V(OH)_3^{2+}$ (aq.) (acid dependent path).

A survey of literature indicated that tris(polypyridyl)iron(III) complexes have not been used as oxidants for the oxoacids of phosphorus although it has been extensively used for the oxidations of both inorganic[6] and organic[7] substrates. Yet another reason for undertaking this study was to test the applicability of the Fuoss and Eigen equation[8] which has been applied successfully to several reactions proceeding through the formation of outer-sphere complex.[9] It might be added that an outer-sphere complex was expected in the present case because the tris(polypyridyl)iron(III) complexes are considered substitution inert.

The results indicated that the 'inactive' form of phosphinic and phenylphosphinic acid is the reactive species and the complex formed between tris(polypyridyl)iron(III) and phosphinic acid does not strictly conform to the outer-sphere complex as predicted by the Fuoss-Eigen equation.[8]

Experimental

Reagents. Phosphinic and phenylphosphinic acids (Fluka) were used as received. The stock solutions were standardized by cerimetry.[10] Sodium perchlorate was prepared by the neutralization of a known weight of sodium carbonate (BDH, AnalaR) by standard perchloric acid (E. Merck, GR). The neutralized solution was boiled to remove any dissolved carbon dioxide and made to volume. It was used to adjust the ionic strength. Lithium perchlorate was received from G. F. Smith and used as such. The stock solution of perchloric acid was standardized against a standard alkali. 1,10-Phenanthroline (E. Merck) and 2,2′-bipyridine (BDH) were used as received. Sodium thiosulfate (BDH, AnalaR) was standardized iodometrically against a standard solution of dichromate (BDH, AnalaR) using starch as the indicator. Twice distilled water, once distilled from an all glass still in presence of alkaline permanganate, was used for the preparation of solutions.

Preparation of $[FeL_3]^{3+}$ Complexes. Iron(III) complexes of 1,10-phenanthroline (phen) and 2,2′-bipyridine (bpy), FeL_3^{3+}, were prepared by the interaction of iron(II) sulfate and respective ligand in 1 : 3 ratio. In fact, the ligand was taken in slight excess to ensure complete complexation of Fe(II). The iron(II) complexes were then oxidized by lead dioxide.[11,12] The blue solution of iron(III) complex was filtered through a sintered G4 crucible and the perchlorate salt was precipitated by the addition of minimum quantity of 70% perchloric acid. The solid so obtained was recrystallized from aqueous perchlorate solution.

The standard stock solution of the respective complex was prepared in perchloric acid (10 mol dm^{-3}) by weight and stored in the refrigerator. Although such stock solutions are stated to be stable for at least three months at room temperatures in the dark,[13] the solutions older than 48 hours were discarded. The spectral characteristics of FeL_3^{2+} and FeL_3^{3+} solutions matched well with those reported in the literature.[14]

Stoichiometry. A number of reaction mixtures having different FeL_3^{3+} concentrations and known excess of phosphinic acid were prepared in different $[H^+]$. On complete reduction of the iron(III) complex, the amount of phosphonic acid produced was determined as described below.[15]

The reaction mixtures were suitably diluted or neutralized

to bring down the concentration of perchloric acid to less than 0.1 mol dm^{-3}. A 50 ml of the solution was added to a known solution of iodine in phosphate buffer, and the pH 7.3 was adjusted. After about one hour the solutions in iodine flasks were acidified with 6 mol dm^{-3} acetic acid and immediately titrated for the liberated iodine with a standard thiosulfate solution to a starch-iodine end point. The results of several such estimations indicated that $\Delta[H_3PO_2]/\Delta[FeL_3^{3+}]=0.51\pm0.04$. Hence the stoichiometric equation for the reaction is expressed by Eq. 1.

$$2FeL_3^{3+}+H_3PO_2+H_2O \rightarrow 2FeL_3^{2+}+H_3PO_3+2H^+ \quad (1)$$

Rate Measurements. The rate was measured under pseudo first-order conditions ($[RH_2PO_2]\geq 10[FeL_3^{3+}]$, where R=$C_6H_5$ for phenylphosphinic acid and R=H for phosphinic acid). The reagents, FeL_3^{3+} and phosphinic/phenylphosphinic acid with required concentrations of sodium perchlorate and perchloric acid, were taken separately. These were allowed to attain the thermal equilibrium in a thermostated water bath maintained at the desired temperature with a possible variation of ±0.1 °C. The reaction was initiated by the quick mixing of the desired volumes of FeL_3^{3+} and phosphinic/phenylphosphinic acid solutions.

The kinetics was followed by measuring the absorbance of $Fe(phen)_3^{2+}$ at 510 nm and that of $Fe(bpy)_3^{2+}$ at 520 nm on a Beckman DU-2 spectrophotometer. The quartz cell, 1 cm pathlength, was immediately returned to the cell compartment after the transfer of the reaction mixture. The absorbance of the FeL_3^{2+} complex was quickly measured thereafter.

The slow hydrolysis of $Fe(phen)_3^{2+}$ to free Fe^{2+}(aq.) and 1,10-phenanthroline[16] does not affect the measurements of A_∞ in reactions where the rate of oxidant loss is much faster. It is for this reason that reactions on stopped-flow time scale could be studied for several half lives of the reactions. However, in reactions where the rate of oxidant loss is either of comparable magnitude or slower than the rate of hydrolysis of FeL_3^{2+} there arises a problem both in following the reaction even upto the first half-life and measuring A_∞ because the hydrolyzed product Fe^{2+}, reacting rapidly,[17] vitiates both the kinetics and A_∞. Hence for the measurement of A_∞, the reaction mixture was reduced with a pinch of solid iron(II) sulfate[18] and the absorbance (A_∞) of the resulting solution was immediately recorded.

Since the $t_{1/2}(=0.691/k_{obs})$ with $[H_3PO_2]=0.1$ and $[H^+]=1.0$ mol dm^{-3} at 35 °C approximated to about 4 hours, the rate measurements had to be restricted to the initial 35—40% of the reaction. The plots of $\ln(A_\infty-A_t)$ against time for the mentioned range were linear; where A_∞ and A_t are the absorbance at infinite time and time 't'. The gradient of the linear plots ($=k_{obs}$) was estimated using a computer program based on the method of least squares.

Test for Free Radical. The formation of a free radical during the progress of the reaction was indicated by the polymerization of acrylonitrile added to the reaction mixtures degassed with nitrogen. The individual solutions of FeL_3^{3+} and phosphinic or phenylphosphinic acid, similarly degassed, did not initiate the polymerization of the acrylonitrile monomer.

Spectrophotometry. The visible (450—750 nm) spectra of FeL_3^{3+} and reaction mixtures having FeL_3^{3+} and RH_2PO_2 in the ratios of 1 : 1 and 1 : 10 were recorded on a Shimadzu 240 UV-vis Graphicord spectrophotometer at room temperature (27 °C). The spectra shown in Figs. 1 and 2 are for $Fe(bpy)_3^{3+}$ (8.0×10^{-4} mol dm^{-3}) and phosphinic and phenylphosphinic acids in 2.5 mol dm^{-3} perchloric acid respectively. It is worth noting that absorbance increased with increasing concentrations of oxoacid of phosphorous and a pronounced hump developed near 530 nm for 1 : 10 mixture. The spectra is indicative of the formation of a complex, probably an outer-sphere complex.

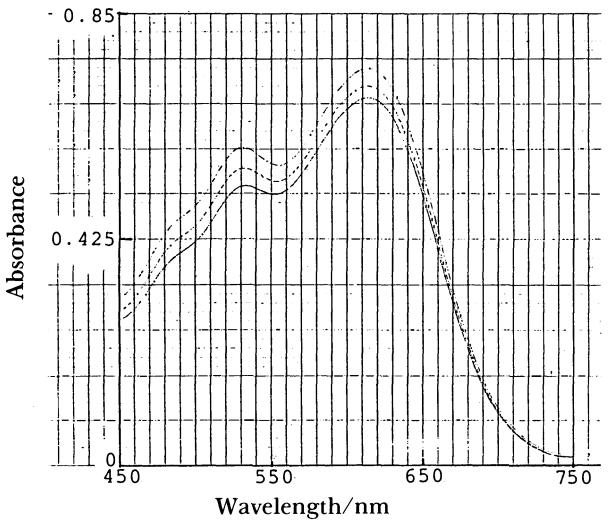

Fig. 1. Visible spectra of the mixtures of $Fe(bpy)_3^{3+}$ and H_3PO_2 at 27 °C in the ratio 1 : 0(——), 1 : 1 (----), and 1 : 10 (—·—) where $[Fe(bpy)_3^{3+}]=8.0\times10^{-4}$ mol dm^{-3}, and $[H^+]=2.5$ mol dm^{-3}.

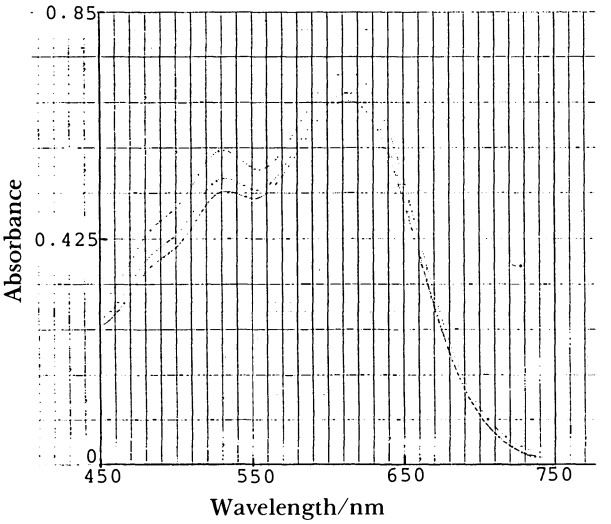

Fig. 2. Visible spectra of $Fe(bpy)_3^{3+}$ and $C_6H_5H_2PO_2$ at 27 °C in the ratio 1 : 0 (——), 1 : 1 (----), and 1 : 10 (—·—) where $10^4[Fe(bpy)_3^{3+}]=8.0$ and $[H^+]=2.5$ mol dm^{-3}.

Results

Dependence on FeL_3^{3+}. The first order reduction of FeL_3^{3+} is confirmed by the invariance of k_{obs} over a ten-fold variation in the initial $[FeL_3^{3+}]$. The results for the oxidation of phenyl phosphinic acid are in

Table 1. Dependence of $k_{obs}(s^{-1})$ on the Initial $[FeL_3^{3+}]$ at 25 °C.

$10^3[C_6H_5H_2PO_2]=3.0$, $[H^+]=0.5$, and $I=1.0$ mol dm^{-3}

$10^5[Fe(phen)_3^{3+}]$	10^5k_{obs}	$10^5[Fe(bpy)_3^{3+}]$	10^5k_{obs}
1.26	10.1	1.46	8.67
5.05	10.0	5.87	8.61
7.58	10.2	8.75	8.77
10.1	9.92	11.7	8.66
12.6	10.1	14.6	8.70

Table 1. The slightly higher k_{obs} value for $Fe(phen)_3^{3+}$ oxidation compared to the value for $Fe(bpy)_3^{3+}$ oxidation is consistent with the higher redox potential of $Fe(phen)_3^{3+}$.

Dependence on [1,10-phenanthroline]. These experiments are designed to know whether the complex between FeL_3^{3+} and oxoacid of phosphorous is formed in accordance with the equilibrium (2). The formation of the complex was indicated by the spectrophotometric studies of the reaction mixtures described earlier.

$$FeL_3^{3+}+nH_3PO_2 \rightleftarrows FeL_{(3-n)}(H_3PO_2)_n^{3+}+nL \quad (2)$$

where n has a maximum value of 1 as indicated by the order of the reaction with respect to phosphinic acid.

A retardation in k_{obs} was expected if $FeL_{(3-n)}(H_3PO_2)_n^{3+}$ is reduced to the products in the rate limiting step. The fact that k_{obs} is independent over more than twelve-fold variation in [1,10-phenanthroline], Table 2, the probability of the formation of an inner-sphere complex is excluded from the purview of any mechanism to be proposed for the reaction.

Dependence on $[Fe(phen)_3^{2+}]$. The rates were measured in terms of disappearance of $Fe(phen)_3^{3+}$ at 360 nm ($\varepsilon_{Fe(phen)_3^{3+}}=5500$ and $\varepsilon_{Fe(phen)_3^{2+}}=1000$ dm^3 mol^{-1}cm^{-1})[19] and then in terms of appearance of $Fe(phen)_3^{2+}$ at 510 nm ($\varepsilon_{Fe(phen)_3^{2+}}=11000$,[20] and $\varepsilon_{Fe(phen)_3^{3+}}=300$ dm^3 mol^{-1}.[21] The values $10^5k_{obs}=5.27$ and 5.37 s^{-1}, obtained at two wavelengths respectively are in agreement with the value $10^5k_{obs}=4.8$ s^{-1} obtained at $[H_3PO_2]=0.10$ mol dm^{-3} in the absence of $Fe(phen)_3^{2+}$ under identical experimental conditions ($10^5[Fe(phen)_3^{3+}]=6.32$, $10^5[Fe(phen)_3^{2+}]=3.16$, $[H_3PO_2]=0.11$, $[H^+]=0.5$ and $I=1.0$ mol dm^{-3} at 36 °C). Hence, reaction (3) or any such other equilibrium has no mechanistic significance.

$$[FeL_3\cdots H_3PO_2]^{3+} \rightleftarrows FeL_3^{2+}+H_3PO_2^+ \quad (3)$$

Dependence on $[H_3PO_2]$. In this study it was noted that k_{obs} did not increase proportionately with $[H_3PO_2]$. The plot between k_{obs} and $[H_3PO_2]$, Fig. 3, is nonlinear. However, the plots between k_{obs}^{-1} and $[H_3PO_2]^{-1}$ are linear with an intercept on the rate ordinate. The results of the temperature dependence study are in Table 3.

Table 2. Dependence of k_{obs} (s^{-1}) on the Initial [1,10-phenathroline] at 30 °C.

$10^5[Fe(phen)_3^{3+}]=6.32$, $[H^+]=0.5$, $[H_3PO_2]=0.1$, and $I=1.0$ mol dm^{-3}

10^5[phen]/mol dm^{-3}	0.5	1.0	2.0	4.0	6.32
$10^5k_{obs}/s^{-1}$	3.45	3.47	3.44	3.46	3.48

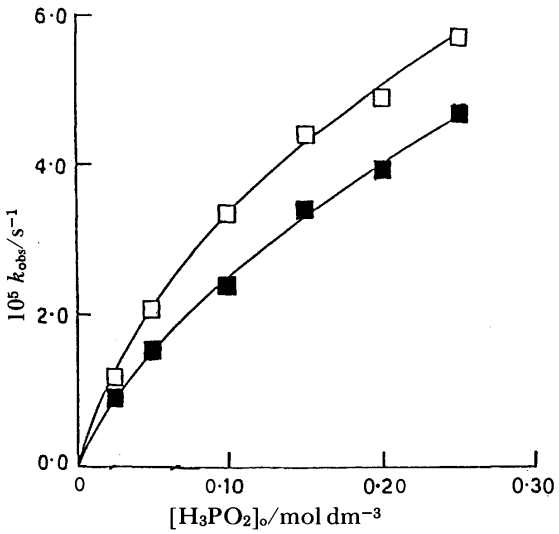

Fig. 3. Plot between $k_{obs}(s^{-1})$ and $[H_3PO_2]$ at 30 °C with $10^4[Fe(phen)_3^{3+}]=0.632$ and $[H^+]=0.5$ and $I=1.0$ mol dm^{-3} (□) and with $10^4[Fe(bpy)_3^{3+}]=0.729$ and $[H^+]=0.5$ and $I=1$ mol dm^{-3} at 30 °C (■).

Dependence on $[H^+]$. The results of the rate measurement at different $[HClO_4]$ between 0.3—3.0 mol dm^{-3} at constant ionic strength are in Table 4.

Table 3. Dependence of k_{obs} on the Initial $[H_3PO_2]$ in the Oxidation by $Fe(phen)_3^{3+}$ at Different Temperatures.

$20^5[Fe(phen)_3^{3+}]=6.32$, $[H^+]=0.5$, and $I=1.0$ mol dm^{-3}

$[H_3PO_2]$	0.025	0.05	0.1	0.15	0.20	0.25
Temp/°C			$10k_{obs}/s^{-1}$			
30	1.23	2.14	3.46	4.40	5.00	5.50
36	1.47	2.80	4.80	6.60	7.84	9.74
40.5	1.80	3.46	6.42	8.95	10.7	13.4
44.5	2.52	4.95	8.80	13.0	17.4	21.7
50	3.42	6.90	11.9	18.6	27.0	32.7

Table 4. Dependence of k_{obs} on the Initial $[H^+]$ at Constant Ionic Strength at 36 °C.

(a) $10^5[Fe(phen)_3^{3+}]=6.32$, $[H_3PO_2]=0.1$, and $I=3.0$ mol dm^{-3}
(b) $10^5[Fe(bpy)_3^{3+}]=7.30$, $[H_3PO_2]=0.09$, and $I=3.0$ mol dm^{-3}

$[H^+]$	$10^5k_{obs}/s^{-1}$		$[H^+]$	$10^5k_{obs}/s^{-1}$	
mol dm^{-3}	(a)	(b)	mol dm^{-3}	(a)	(b)
0.314(0.313)	4.86	3.39	1.703	4.80	3.40
0.509(0.508)	4.88	3.46	2.002	4.80	3.40
0.707(0.706)	4.84	3.40	2.202	4.90	3.35
1.005(1.004)	4.88	3.30	2.502	4.86	3.46
1.304(1.303)	4.80	3.35	3.002	4.94	3.42

Figures in the parentheses are $[H^+]$ calculated for $[H_3PO_2]=0.09$ mol dm^{-3}.

Table 5. Dependence of k_{obs} on the Ionic Strength at 25 °C.

$10^5[Fe(phen)_3^{3+}]=6.32$, $10^3[C_6H_5H_2PO_2]=2.0$, and $[H^+]=0.1$ mol dm^{-3}

$[MClO_4]$/mol dm^{-3}	0.0	0.1	0.3	0.5	0.7	1.0
I/mol dm^{-3}	0.1	0.2	0.4	0.6	0.8	1.1
	.....		10^5k_{obs}/s^{-1}			.....
M=Na	11.7	11.0	10.3	9.85	9.43	9.12
M=Li	11.8	10.2	9.93	9.45	9.05	

The concentration shown under $[H^+]$ in the table is the sum of $[H^+]$ from perchloric acid and dissociation of phosphinic acid. A K_a value=0.051, extrapolated from the data of Espension and Binau[22c] is used to calculate the dissociated $[H^+]$ from phosphinic acid. The conclusion of the study is that k_{obs} is independent of $[H^+]$.

Medium Effects. Redox and substitution reactions are affected by the medium effects[23,24] where uncertainties in hydrogen ion effects may be related to differences in the activity coefficients of the counter ions (Na^+ or Li^+) used as perchlorate salts for adjusting the ionic strength to a constant value while varying the $[H^+]$. These effects are usually absent for intramolecular redox reactions.[25] Indeed the presence of medium effects is confirmed by the fact that k_{obs} values corresponding to Li^+ are consistently lower than the values obtained for the corresponding Na^+. The results are in Table 5.

Effect of Ionic Strength. The results, Table 5, indicate that k_{obs} decreased with increasing ionic strength. The plot of logarithmic value of k_{obs} against $I^{1/2}/(1+I^{1/2})-0.05I$ is linear with the slope value=−0.48 for Na^+ and −0.53 for Li^+ which is much less than the theoretical value expected for the reaction between charged ions involved in the reaction. This discrepancy could be due to the presence of more than one equilibrium before the rate determining step.

Empirical Rate Law. All the above results are summarized by the empirical rate law given in Eq. 4.

$$\frac{-d[FeL_3^{3+}]}{dt}=\frac{d[FeL_3^{2+}]}{dt}=\frac{a[RH_2PO_2]_o[FeL_3^{3+}]_o}{1+b[RH_2PO_2]_o} \quad (4)$$

where a and b are empirical constants and subscript "o" denotes the analytical concentration used.

Discussion

Since the rate of the reaction is independent of $[H^+]$, there is a possibility that two equilibria, which are affected by the H^+ in the opposite directions, are present so that the net effect of H^+ is not noticed. The two such equilibria are considered in Eqs. 5 and 6. The consideration of the equilibrium (5) is influenced by the fact that in the tris (1,10-phenanthroline)iron(III) oxidation of ascorbic acid,[19,26] the pK_{1a} of which is much higher[19,25,26] than that of phosphinic acid[22] and phenylphosphinic acid,[27] both undissociated ascorbic acid and hydrogen ascorbate ion are considered reactive. The equilibrium (6) has been considered in several studies.[19,20,28,29] The concentration of the complex $[FeL_3\cdots RH_2PO_2]^{3+}$, formed through the equilibria (7) and (8), remains stationary under any given $[H^+]$ which explains no effect of H^+on the observed rate of the reaction. The mechanism involving reactions (5)—(10) is considered below.

$$RH_2PO_2 \overset{K_a}{\rightleftarrows} RHPO_2^- + H^+ \quad (5)$$

$$H^+ + FeL_3^{3+} \overset{K_c}{\rightleftarrows} HFeL_3^{4+} \quad (6)$$

$$HFeL_3^{4+} + RHPO_2^- \overset{\beta_1}{\rightleftarrows} [FeL_3\cdots RH_2PO_2]^{3+} \quad (7)$$

$$FeL^{3+} + RH_2PO_2 \overset{\beta_2}{\rightleftarrows} [FeL_3\cdots RH_2PO_2]^{3+} \quad (8)$$

$$[FeL_3\cdots RH_2PO_2]^{3+} \overset{k_1}{\rightarrow} RHPO_2^{\cdot} + FeL_3^{2+} + H^+ \quad (9)$$

$$RHPO_2^{\cdot} + H_2O + FeL_3^{3+} \overset{\text{fast}}{\longrightarrow} RH_2PO_3 + FeL_3^{2+} + H^+ \quad (10)$$

It is thus seen that the formation of the complex $[FeL_3\cdots RH_2PO_2]^{3+}$ in equilibrium (7) involved equilibrium (5) and equilibrium (6) whereas it is also formed through equilibrium (8) alone. The exact path of its formation cannot be stated unambiguously because $\beta_2=\beta_1K_aK_c$. The consideration of the above reactions leads to the rate law in Eq. 11.

$$k_{obs}=\frac{2k_1\beta_2[RH_2PO_2]_o}{(1+K_a[H^+]^{-1})(1+K_c[H^+])+\beta_2[RH_2PO_2]_o} \quad (11)$$

Although the rate law in Eq. 11 is not independent of $[H^+]$, yet with the appropriate assumption that $1+\beta_2[RH_2PO_2]_o \gg K_a[H^+]^{-1}+K_c[H^+]+K_aK_c$ because the values of K_a and K_c are much less than 1; the Eq. 11 is thus reduced to Eq. 12 which is independent of $[H^+]$. The Eq. 12 is identical to the empirical rate law in Eq. 4 where $a=2k_1\beta_2$ and $b=\beta_2$.

$$k_{obs}=\frac{2k_1\beta_2[RH_2PO_2]_o}{1+\beta_2[RH_2PO_2]_o} \quad (12)$$

The Eq. 12 holds in the sense that plots of k_{obs}^{-1} against $[RH_2PO_2]_o^{-1}$, Fig. 4, are linear at all temperatures. From the gradient and intercept of such plots, the values of β_2 and k_1 are derived and are given in Tables 6 and 7 respectively.

Alternate Mechanism. A simple and straight forward mechanism providing a rate law independent of $[H^+]$ could also be described by the reactions (8)—(10). The consideration of these reactions leads to the deduction of the rate law given in Eq. 12. There is no way to differentiate between the mechanisms described by reactions (5)—(10) and the one described by the reactions (8)—(10).

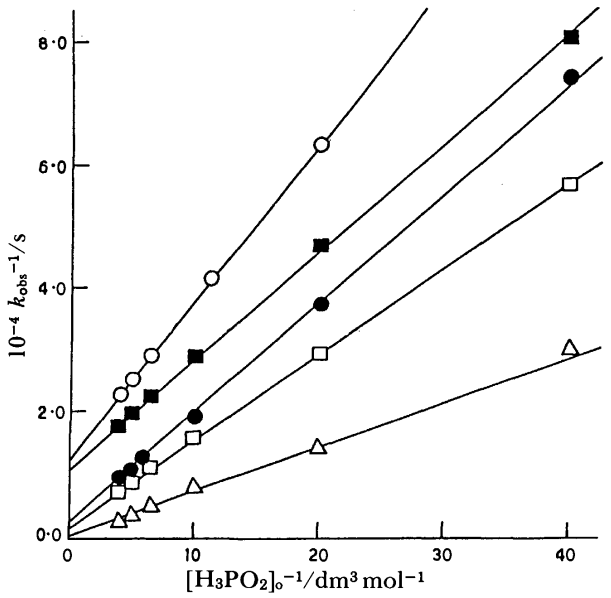

Fig. 4. Plot between k_{obs}^{-1} and $[H_3PO_2]^{-1}$ at different temperatures for the oxidations affected by $Fe(phen)_3^{3+}$ at 30 °C (■), 40.5°C (□), and 50 °C (△) and for the oxidations by $Fe(bpy)_3^{3+}$ at 30 °C (○) and 40.5 °C (●).

Table 6. Values of β_2 for H_3PO_2 at Different Temperatures and the Thermodynamic Parameters

Temp/°C	25[a]	30	36	40.5	44.5	50
Ligand	·····$\beta/dm^3\ mol^{-1}$·····					
phen	11.6	6.4	2.8	1.7	1.1	0.6
bpy	7.1	4.4	3.0	1.1	0.9	0.8

a) Extrapolated value.
$\Delta H°$(phen)=−90±10 kJ mol^{-1}, $\Delta H°$(bpy)=−75±10 kJ mol^{-1}, $\Delta S°$(phen)=−290±40 J K^{-1} mol^{-1}, $\Delta S°$(bpy)=−245±30 J K^{-1} mol^{-1}.

Table 7. Values of the Rate Limiting Constant $k_1(s^{-1})$ at Different Temperatures and Activation Parameters

Temp/°C	30	36	40.5	44.5	50
Ligand	·····$10^5 k_1(s^{-1})$·····				
phen	4.46	11.2	21.1	42.5	128
bpy	4.23	8.06	26.0	42.5	85.5

ΔH^*(phen)=121±5 kJ mol^{-1}, ΔH^*(bpy)=125±6 kJ mol^{-1}, ΔS^*(phen)=70±10 J K^{-1} mol^{-1}, ΔS^*(bpy)=84±12 J K^{-1} mol^{-1}.

The dissociation of ferriin is a first-order reaction[30] in $[H^+]$. Hence in the absence of any dependence of rate on H^+, it is apparent that the dissociation of ferriin is not a part of the mechanism. That there is no dissociation of ferriin is further supported by the results on the effect of variation of 1,10-phenanthroline on the observed rate.

Fuoss equation[8] has been favored as tool to differentiate between an outer-sphere and inner-sphere complex. The Fuoss equation is given in Eq. 13.

$$K_o = \frac{4\pi N_A a^3}{3000} \exp \frac{-z_1 z_2 e^2}{aDkT} + \frac{z_1 z_2 e^2 k}{DkT(1+ka)} \quad (13)$$

where N_A is Avogadro's number, a=the centre to centre separation of the ions at closest approach, e=electronic charge, z_1 and z_2 are the charges on the ions with appropriate sign, D is the dielectric constant, k=Boltzmann's constant, and k the Debye-Hückel parameter.

The approach is based on the theoretical calculation of the association constant and the associated thermodynamic parameters and then these are compared with the experimentally obtained data.

The values of K_o were calculated at different temperatures by considering r=7 Å[16] for $Fe(phen)_3^{3+}$ and 3 Å for phosphinic acid (calculated by the relation $4\pi r^3/3 = M/n_A d$ where M is the molecular weight and d is the density) and a=10 Å and using the value of D at different temperatures.[31] These are given in Table 8 wherein are also reported the calculated thermodynamic parameters. The value of K_o, 4.86 dm^3 mol^{-1}, at 25 °C is somewhat less than the value of β_2 extrapolated to the same temperature. The other differences are (i) K_o increased with the temperature whereas β_2 decreased and (ii) the values of the enthalpy and entropy are positive for K_o whereas these parameters have negative values for β_2. We at this point are not sure whether this is an exception to the applicability of the Fuoss equation or whether the complex formed is an inner-sphere complex. The possibility of the formation of an inner-sphere complex such as proposed in the oxidation of I^- by hexacyanoferrate(III) ion[32] cannot be over ruled. The assignment of an inner-sphere or outer-sphere mechanism to a redox reaction is often difficult.[33]

'Active' vs. 'Inactive' Form. The presence of H^+ in the reaction system requires the consideration of the equilibrium (14). This equilibrium is attractive in the sense that it is independent of $[H^+]$ though the conversion of 'inactive' form to 'active' form is catalyzed by H^+. The active form is thought to be produced as an intermediate in the exchange of phosphorus bonded hydrogen in phosphinic acid with tritium[34] or deuterium.[35] The value of the equilibrium constant is of the order of 10^{-12}.[36]

$$H^+ + H_2P(O)OH \overset{K}{\rightleftarrows} H_2P(OH)(OH^+) \rightarrow H:P(OH)_2 + H^+ \quad (14)$$

Table 8. Values of Outer-Sphere Association K_o, Calculated for $Fe(phen)_3^{3+} \cdots H_3PO_2$ from the Fuoss Equation

Temp/°C	25	30	35	40	45
K_o/dm^3 mol^{-1}	4.86	4.91	4.96	5.01	5.07

$\Delta H°$=1.65 kJ mol^{-1}, $\Delta S°$=18 J K^{-1} mol^{-1}.

The following reactions (15)—(17) duplicate the reactions (8)—(10) and are supposed to have the 'inactive' form as the reactive entity.

$$FeL_3^{3+}+\underset{\text{(inactive)}}{H_2P(O)(OH)} \overset{\beta}{\rightleftarrows} [FeL_3\cdots H_2P(O)(OH)]^{3+} \quad (15)$$

$$[FeL_3\cdots H_2P(O)(OH)]^{3+} \xrightarrow{k} H_2PO_2^{\cdot}+H^+ +FeL_3^{2+} \quad (16)$$

$$FeL_3^{3+}+H_2O+H_2PO_2^{\cdot} \xrightarrow{\text{fast}} H_3PO_3+FeL_3^{2+}+H^+ \quad (17)$$

The consideration of the reactions (14)—(17) and the fact that $1 \gg K$ leads to the rate law in Eq. 18 which is similar to the rate law in Eq. 12.

$$\frac{d[FeL_3^{2+}]}{dt} = \frac{2k\beta[FeL_3^{3+}][H_3PO_2]_o}{1+\beta[H_3PO_2]_o} \quad (18)$$

However, if the 'active' form $H:P(OH)_2$ is reactive then the respective reactions are in Eqs. 14 and 19—21. The rate law based on these reactions, and acknowledging the fact that $1 \gg K$, will have the form given in Eq. 22.

$$FeL_3^{3+}+H:P(OH)_2 \overset{\beta_a}{\rightleftarrows} [FeL_3\cdots H:P(OH)_2]^{3+} \quad (19)$$

$$[FeL_3\cdots H:P(OH)_2]^{3+} \xrightarrow{k_a} :P(OH)_2+H^+ +FeL_3^{2+} \quad (20)$$

$$FeL_3^{3+}+H_2O+:P(OH)_2 \xrightarrow{\text{fast}} HP(O)(OH)_2+H^+ +FeL_3^{2+} \quad (21)$$

$$\frac{d[FeL_3^{2+}]}{dt} = \frac{2k_a\beta_aK[FeL_3^{3+}][H_3PO_2]_o}{1+\beta_aK[H_3PO_2]_o} \quad (22)$$

Thus in the plots between k_{obs}^{-1} and $[H_3PO_2]_o^{-1}$, Fig. 4, the slope and intercept are equivalent to those given in Eq. 23.

$$\text{Slope}=(2k_a\beta_aK)^{-1};\ \text{intercept}=1/2k_a,\ \text{and intercept/slope}=K\beta_a \quad (23)$$

It is thus seen that $k=k_a$ which means that the rate limiting constant for the disproportionation of the complex is not affected by the reactive form of phosphonic acid. However, $\beta=K\beta_a$ so that $\beta_a=\beta/K=10^{12}\beta$ (or $\beta_2=6.4\times10^{12}$ dm^{3}mol^{-1} at 30 °C). Considering that FeL_3^{3+} is inert to substitution this high value of β_a is certainly inadmissible. Hence it is concluded that 'active' form is not the reactive entity thus leaving the 'inactive' form to be the reactive species.

Authors are grateful to CSIR, New Delhi, for the financial support and the award of a Junior Research Fellowship to KS. RNM also thanks Prof. Louis J. Kirschenbaum, Department of Chemistry, University of Rhode Island, Kingston, RI, USA for extending all the facilities in his laboratories where this manuscript was prepared.

References

1) K. Sharma and R. N. Mehrotra, *Trans. Met. Chem.*, **14**, 48 (1989).
2) R. N. Mehrotra, *J. Chem. Soc., Dalton Trans.*, **1984**, 1531.
3) R. N. Mehrotra, *J. Chem. Soc., Dalton Trans.*, **1978**, 681.
4) R. R. Nagori, M. Mehta, and R. N. Mehrotra, *J. Chem. Soc., Dalton Trans.*, **1979**, 216.
5) R. N. Mehrotra, *Can. J. Chem.*, **63**, 663 (1985).
6) D. H. Macartney and A. McAuley, *Can. J. Chem.*, **61**, 103 (1983).
7) M. Kimura and Y. Kaneko, *J. Chem. Soc., Dalton Trans.*, **1984**, 341.
8) R. M. Fuoss, *J. Am. Chem. Soc.*, **80**, 5059 (1958); M. Eigen, *Z. Phy. Chem.*, **1**, 176 (1954).
9) M. R. Hyde and A. G. Sykes, *J. Chem. Soc., Chem. Commun.*, **1972**, 1340; D. P. Deeton and A. G. Sykes, *J. Chem. Soc., Dalton Trans.*, **1972**, 2530; R. K. Wharton, J. F. Ojo, and A. G. Sykes, *J. Chem. Soc., Dalton Trans.*, **1975**, 1526.
10) D. N. Bernhard, *Anal. Chem.*, **26**, 1798 (1951).
11) E. I. Heiba and R. M. Dessau, *J. Am. Chem. Soc.*, **93** 524 (1971).
12) M. Kimura and Y. Kaneko, *J. Chem. Soc., Dalton Trans.*, **1982**, 423.
13) M. Kimura, S. Yamabe, and T. Minato, *Bull. Chem. Soc. Jpn.*, **54**, 1699 (1981).
14) A. A. Schilt, "Analytical Applications of 1,10-Phenanthroline and Related Compounds," Pergamon Press, London (1969).
15) R. T. Jones and E. H. Swift, *Anal. Chem.*, **25**, 1272 (1953).
16) J. E. Dickens, F. Basolo, and H. M. Neuman, *J. Am. Chem. Soc.*, **79**, 1286 (1957). F. Basolo, J. C. Hayes, and H. M. Neuman, *J. Am. Chem. Soc.*, **76**, 3807 (1954).
17) J. E. Dickens, F. Basolo, and H. M. Neumann, *J. Am. Chem. Soc.*, **79**, 1286 (1957).
18) J. S. Littler and I. G. Sayce, *J. Chem. Soc.*, **1964**, 2545.
19) E. Pelizzetti, E. Mentasti, and E. Pramauro, *Inorg. Chem.*, **15**, 2898 (1976).
20) M. Kimura and G. Wada, *Inorg. Chem.*, **17**, 2239 (1978).
21) N. Sutin and B. M. Gordon, *J. Am. Chem. Soc.*, **83**, 70 (1961).
22) a) P. Nylen, *Z. Anorg. Chem.*, **1937**, 230, 385. (K_a=0.076 mol dm^{-3}, 20 °C, I=2 mol dm^{-3}); b) R. O. Griffiths, A. Mckeown, and R. P. Taylor, *Trans. Faraday Soc.*, **36**, 752 (1940). (K_a=0.074, 30 °C, I=1.13 mol dm^{-3}); c) K. M. Masalovich, P. K. Agasyan, and E. R. Nikolaeva, *Russ. J. Chem.*, **1967**, 1074. (K_a=0.12, 20 °C, I=0.2 mol dm^{-3}); d) T. E. Hass and H. D. Gillman, *Inorg. Chem.*, **8**, 1970 (1969). (K_a=0.04, 20 °C, I=1 mol dm^{-3}); e) J. H. Espenson and D. F. Dustin, *Inorg. Chem.*, **8**, 1970 (1969). (K_a=0.135, 25 °C, 1 mol dm^{-3}); f) J. N. Cooper, *J. Phys. Chem.*, **74**, 955 (1970). (K_a=0.101, 25 °C, 1 mol dm^{-3}).
23) C. Lavalee and T. W. Newton, *Inorg. Chem.*, **11**, 2616 (1972).
24) T. J. Kemp and W. A. Waters, *J. Chem. Soc.*, **1964**, 1189.
25) Z. Amjad, A. McAuley, and U. D. Gomwalk, *J. Chem. Soc., Dalton Trans.*, **1977**, 82.
26) M. Kimura, M. Yamamoto, and S. Yamabe, *J. Chem. Soc., Dalton Trans.*, **1982**, 423.
27) L. D. Quin and M. R. Dysart, *J. Org. Chem.*, **27**, 1012 (1962).
28) J. H. Baxendale and N. K. Bridge, *J. Phys. Chem.*, **59**,

785 (1955).
29) P. George and D. H. Irvine, *J. Chem. Soc.*, **1954**, 587.
30) T. S. Lee, I. M. Kolthoff, and D. L. Leussing, *J. Am. Chem. Soc.*, **70**, 3596 (1948).
31) "Handbook of Chemistry and Physics," 43rd ed., (1962), p. 2562.
32) A. Indelli and G. C. Guaraldi, *J. Chem. Soc.*, **1964**, 36.
33) R. G. Wilkins, "The Study of Kinetics and Mechanism of Reactions of Transition Metal Complexes," Allyn and Bacon, London (1976), p. 255.
34) W. A. Jenkins and D. M. Yost, *J. Inorg. Nucl. Chem.*, **11**, 297 (1959).
35) A. Fratiello and E. W. Anderson, *J. Am. Chem. Soc.*, **85**, 519 (1963).
36) J. R. Van Wazer, "Phosphorous and its Compounds," Vol. 1, John Wiley, New York (1958).

3d-Element Coordination Compounds with Bidentate Sulfur-Containing Ligands as Possible Carriers of Non-Silver Photographic Images

O. V. MIKHAILOV* and G. K. BUDNIKOV†
Department of Inorganic Chemistry, Kazan Institute of Chemical Technology, K. Marx Street, 68, 420015, Kazan, USSR
†Department of Analytical Chemistry, Kazan State University, Lenin Street 18, 420008, Kazan, USSR
(Received January 5, 1989)

Complexing processes occurring between reactive matrices obtained from Fe(III), Co(III), Ni(II), Cu(II) hexacyanoferrates(II), and alkaline solutions of various nitrogen-sulfur-containing chelating ligands in thin gelatin layers have been studied. With Fe(III) and Cu(II) hexacyanoferrates, complexing process is found out to proceed according to S_N1 mechanism, while in Co(III) and Ni(II) hexacyanoferrates matrices, S_N2 mechanism is realized. The schemes of the processes proceeding in each of the above matrices are given. The examples of the kinetic curves for particular systems "hexacyanoferrate(II)-ligand" as well as spectral characteristics of thin gelatin layers containing chelate complexes formed as a result of the chelating process are presented. The possibility of practical utilization of complexing processes studied for obtaining non-silver photographic images from light-resistant metallorganic dyes is reported.

Modern chemical photographic industry is known to be one of the largest silver-consuming industries which spends annually about 30% of the total output of this precious metal.[1] One of the ways of overall cutting down the silver consumption in this branch of technology is the so called silver recovery. One of the methods of silver recovery process consists in the following: being a "working material" for the formation of a photographic image, by means of a number of specific chemical reactions, silver is substituted for chelate complexes of 3d-elements having various nitrogen-sulfur-containing ligands intensively absorbing in the visible spectrum region. Due to this process, it becomes possible to form in the initial silver halide photographic material non-silver images characterized by an extremely high light resistance and stability towards detrimental atmospheric attacks (oxygen, sulfuric compounds etc.). From the chemical point of view, the formation of non-silver images with such carriers is nothing but a heterogenous complexing process, and the investigation of the latter presents both academic and practical interest.

In the present paper methods of electron spectroscopy and spectrophotometry were used to investigate the processes of heterogenous complexing occurring in thin layers of various silver halide materials containing previously formed and uniformly dispersed in the gelatin binding agent reactive matrices obtained from Fe(III), Co(III), Ni(II), and Cu(II) hexacyanoferrates(II) upon the reaction with alkaline solutions of chelating ligands of types **I** and **II**:

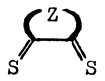

I

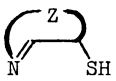

II

(where Z is a closed-ring or open-ring group of various atoms).

Experimental

Matrices containing metal hexacyanoferrates(II) were obtained on the basis of the conventionally formed silver images (by the development and fixation of the silver halide photographic material),[2] by means of the two-stage chemical treatment. The first stage includes oxidation of elemental silver into its hexacyanoferrate(II) or halide, alongside with the co-precipitation of Fe(III), Co(III), Ni(II), and Cu(II) hexacyanoferrates(II) upon the reaction with solutions containing potassium hexacyanoferrate(III), $K_3[Fe(CN)_6]$, and a complex with a corresponding metal ion with a certain oxyacid, according to the following schemes (1—4):[3-6]

$$2Fe_2(HCt)(HTart) + 4[Fe(CN)_6]^{3-} + 4Ag + 3K^+ \rightarrow 3KFe[Fe(CN)_6] + Ag_4[Fe(CN)_6] + [Fe(HTart)_2]^{3-} + 2HCt^{3-} \quad (1)$$

$$4[Co(HCt)_2]^{3-} + 4[Fe(CN)_6]^{3-} + 4Ag + 4Cl^- \rightarrow Co_4[Fe(CN)_6]_3 + 4AgCl + 8HCt^{3-} + [Fe(CN)_6]^{4-} \quad (2)$$

$$6[Ni(HCt)_3]^{7-} + 4[Fe(CN)_6]^{3-} + 4Ag + 4Cl^- \rightarrow 3Ni_2[Fe(CN)_6] + 4AgCl + 18HCt^{3-} + [Fe(CN)_6]^{4-} \quad (3)$$

$$6[Cu(ox)_2]^{2-} + 4[Fe(CN)_6]^{3-} + 4Ag \rightarrow 3Cu_2[Fe(CN)_6] + Ag_4[Fe(CN)_6] + 12ox^{2-} \quad (4)$$

(here H_2ox, H_4Ct, and H_4Tart are oxalic, citric, and tartaric acids, respectively).

The second stage involves the transition of $Ag_4[Fe(CN)_6]$ and AgCl into the solution upon the reaction with an aqueous thiosulfate solution according to schemes (5 and 6) at the expense of the formation of a water-soluble complex:

$$Ag_4[Fe(CN)_6] + 8S_2O_3^{2-} \rightarrow 4[Ag(S_2O_3)_2]^{3-} + [Fe(CN)_6]^{4-} \quad (5)$$

$$AgCl + 2S_2O_3^{2-} \rightarrow [Ag(S_2O_3)_2]^{3-} + Cl^- \quad (6)$$

Between the stages, as well as upon the completion of the second stage, the material comprising a metal hexacyanoferrate(II) matrix was washed by the running water for a few minutes, and then the matrix was processed in alkaline solutions of sulfur-containing ligands such as dithiooxam-

ide NH_2-C(=S)-C(=S)-NH_2, its *N,N'*-diphenyl-substituted derivative, 2,3-quinoxalinedithiol 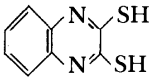 (which can be regarded as a thiol form of a substitution product of two hydrogen atoms for 1,2-phenylene in a dithiooxamide molecule), 8-quinolinethiol 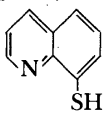 and its 5-chloro- and 5-methylthio derivatives. Ligand concentration in the solution varied in the range of 10^{-3}—10^{-1} mol·dm^{-3}, pH value was maintained at 12.0±0.1, since these parameters provide for the large accumulation of the thiol form of ligands directly involved in heterogenous complexing processes. Besides, a relatively high physicomechanical strength of the gelatin layer is preserved in which a non-silver image is formed. Matrices were kept in alkaline solutions for about 1—10 min at 20 °C. Optical densities of thin layers containing chelate complexes were measured on a "Macbeth TD-504" densitometer (Kodak Co., USA) in the region (0—4) with an accuracy of ±2% (rel.); the absorption spectra were measured on a SPECORD spectrophotometer in the region 10000—30000 cm^{-1} (350—1000 nm). Using the result of the measurements, kinetic curves were plotted in $D=f(D^{Ag})$ coordinates (where D^{Ag} is the density of a thin gelatin layer containing elemental silver. D is the density of a thin layer containing chelate complex formed upon the chemical processing of the gelatin layer having D^{Ag} density) for various time-concentration conditions of heterogenous complexing processes using Fe(III), Co(III), Ni(II), and Cu(II) hexacyanoferrate(II) matrices containing the above mentioned ligands. The examples of such relationships are given in Figs. 1—4. The analysis of these $D=f(D^{Ag})$ relationships enables one to make certain conclusions which are given in the section below.

Results

In case of the systems containing Fe(III) and Cu(II) hexacyanoferrate(II) matrices, heterogenous complexing occurs according to pseudo-S_N1 mechanism where ligand entering the internal coordination sphere is preceded by the decomposition of hexacyanoferrate(II) molecules into the corresponding hydroxides, according to schemes (7,8) and (9), respectively.

$$2KFe[Fe(CN)_6]+6OH^- \rightarrow Fe_2O_3+2[Fe(CN)_6]^{4-}+2K^++3H_2O \quad (7)$$

$$KFe[Fe(CN)_6]+2OH^- \rightarrow Fe(OH)_2+[Fe(CN)_6]^{3-}+K^+ \quad (8)$$

$$Cu_2[Fe(CN)_6]+4OH^- \rightarrow 2Cu(OH)_2+[Fe(CN)_6]^{4-} \quad (9)$$

On a Fe(III) hexacyanoferrate(II) matrix, heterogenous complexing was observed only with type II ligands, with the formation of compounds having metal ion/ligand ratio equal to 1 : 3. The process of their formation, unlike other matrices, occurs in the presence of molecular oxygen and consists of two stages, provided that initially formed Fe(II) chelates are oxidized into Fe(III) chelates, which impart to thin

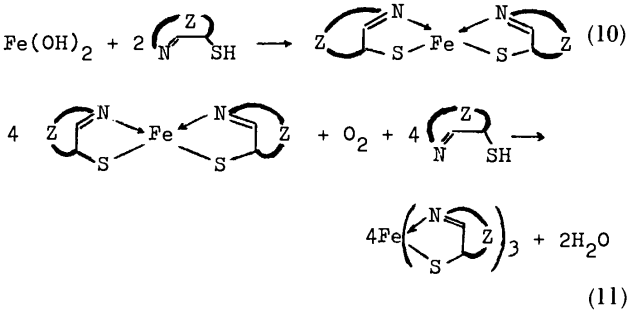

(10)

(11)

gelatin layers different shades of the redbrown color and give absorption in the region of 450—480 nm. For Cu(II) hexacyanoferrate(II) matrices under similar conditions, insoluble 1 : 2 chelates are formed which in a number of cases (e.g. with dithiooxamide or 2,3-quinoxalinedithiol) with an excessive ligand concentration are capable of passing into soluble forms and subsequently diffuse from the thin gelatin layer to a contacting alkaline solution of the respective ligand. The chelates thus formed usually acquire a yellow-brown color or (which is rare) a green-yellow color; absorption spectra of thin gelatin layers containing the above compounds demonstrate the "wings" of intensive bands of charge transfer from the ligand to a metal in the region of 330—370 nm, as well as the bands in the blue (460—490 nm) and the red (620—670 nm) visible spectrum regions. The exception is a dark-green Cu(II) chelate containing dithiooxamide which does not show distinct λ_{max} values. The process of Cu(II) chelate formation can be described by

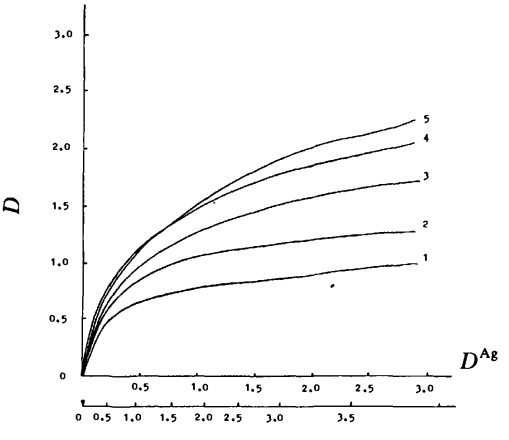

Fig. 1. Kinetic curves in $D=f(D^{Ag})$ coordinates for the system containing $KFe[Fe(CN)_6]$-8-quinolinethiol matrix at the fixed (3×10^{-2} mol·dm^{-3}) ligand concentration in the solution and variable Fe(III) hexacyanoferrate(II) concentrations in the gelatin layer for the complexing process of different durations: 1 min—curve 1; 2 min—2; 4 min—3; 6 min—4; 10 min—5 at 20 °C. Optical densities were measured through the yellow filter with a transmission in the visible spectrum region from its long-wave boundary to 590 nm. C_F is the concentration of hexacyanoferrate(II) in mol·m^2·10^{-2}.

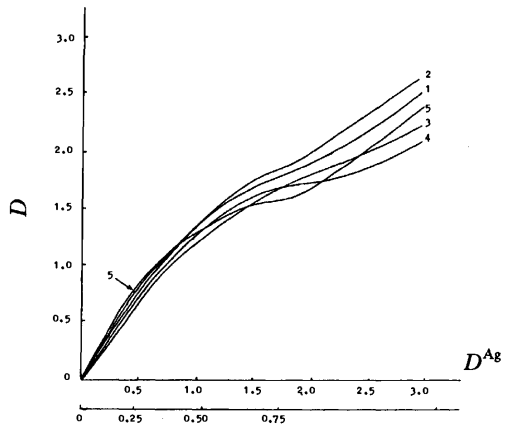

Fig. 2. Kinetic curves in $D=f(D^{Ag})$ coordinates for the system containing $Co_4[Fe(CN)_6]_3$-*N,N'*-diphenyldithiooxamide matrix at the fixed (4×10^{-3} mol·dm^{-3}) ligand concentration in the solution and variable Co(III) hexacyanoferrate(II) concentrations in the gelatin layer for the complexing process of different durations: 1 min—curve 1; 2 min—2; 4 min—3; 6 min—4 and 10 min—5 at 20 °C. Optical densities were measured through the red filter with a transmission maximum at 670 nm.

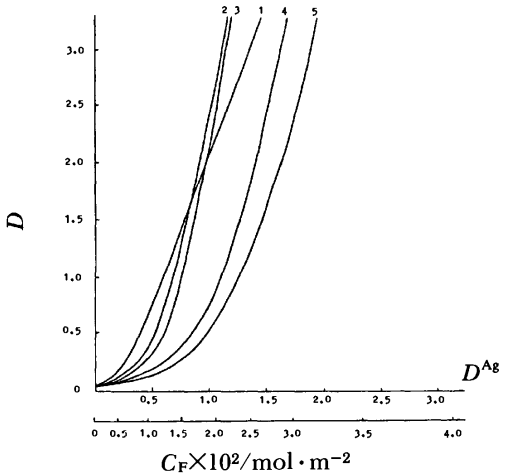

Fig. 3. Kinetic curves in $D=f(D^{Ag})$ coordinates for the system containing $Ni_2[Fe(CN)_6]$-dithiooxamide matrix at the fixed (2×10^{-2} mol·dm^{-3}) ligand concentration in the solution and variable Ni(II) hexacyanoferrate(II) concentrations in the gelatin layer, for the complexing process of different durations: 1 min—curve 1; 2 min—2; 4 min—3; 6 min—4; 10 min—5 at 20 °C. Optical densities were measured through the green filter with transmission maximum at 540 nm.

the equation similar to (10) which for type I ligands acquires the form of (12);

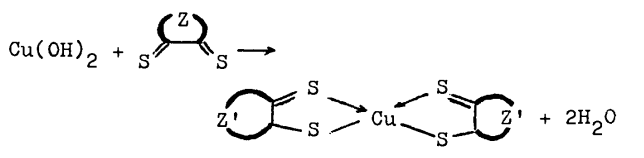

(12)

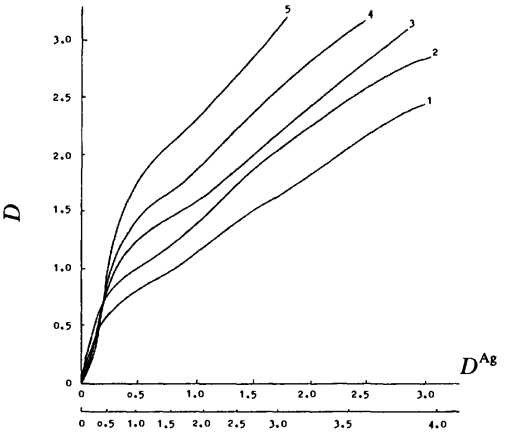

Fig. 4. Kinetic curves in $D=f(D^{Ag})$ coordinate, for the system containing $Cu_2[Fe(CN)_6]$-2,3-quinoxalinedithiol at the fixed (6×10^{-3} mol·dm^{-3}) ligand concentration in the solution and variable Cu(II) hexacyanoferrate(II) concentrations in the gelatin layer, for the complexing process of different durations: 1 min—curve 1; 2 min—2; 4 min—3; 6 min—4; 10 min—5 at 20 °C. Optical densities were measured through the blue filter with transmission maximum at 450 mm.

(Z' is a deprotonated group Z).

In case of $Co_4[Fe(CN)_6]_3$ and $Ni_2[Fe(CN)_6]$ matrices where S_N1 mechanism of ligand addition is realized, quite another way of heterogenous complexing is observed. In Co(III) hexacyanoferrate(II) matrix, a stepwise addition of ligands takes place, together with the formation of compounds having Co(III) ion/ligand ratio of 1 : 1, 1 : 2, and 1 : 3. The above process is accompanied by a somewhat peculiar change in optical densities of the thin gelatin layer which at first tend to increase, then decrease and finally again are observed to increase; this phenomenon is obviously connected with the relation of molar absorption coefficients (ε_{max}), such as $\varepsilon_{1:1}>\varepsilon_{1:2}<\varepsilon_{1:3}$. The chelates thus formed are of yellow, red-brown or brown colors, and they usually have either maximum at 400—460 nm or contain in the visible spectrum only the "wings" of charge transfer intensive bands coming from UV-region. In this case, complexing process can be described by the equations (13—15) (given for the ligands of type **II**):

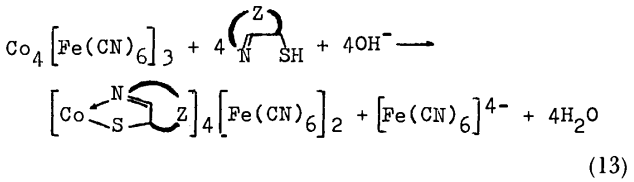

(13)

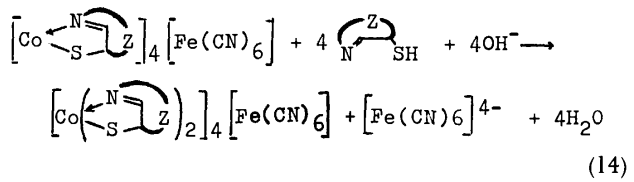

(14)

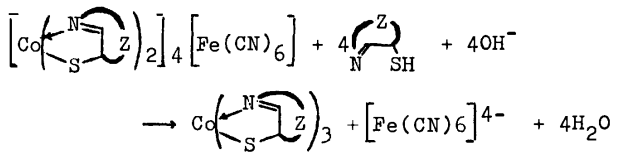

(15)

Of special importance is Ni(II) hexacyanoferrate(II) for which two different types of a ligand-hexacyanoferrate(II) matrix interaction can be distinguished. In the processes of the first type, such as heterogenous complexing in $Ni_2[Fe(CN)_6]$-8-quinolinethiol or its substitutes, insoluble chelates having a metal/ligand ratio of 1:2 with a singly deprotonated form of a ligand are formed. Such chelates do not decompose significantly even under the influence of excessive ligand concentrations in a solution directly contacting the thin gelatin layer. The color of such chelates is usually from pink to violet in the region 500—550 nm. It should be noted that with pH change, these chelates do not change their optical characteristics; for the ligands of type **II**, the formation process can be described by the general Eq. 16

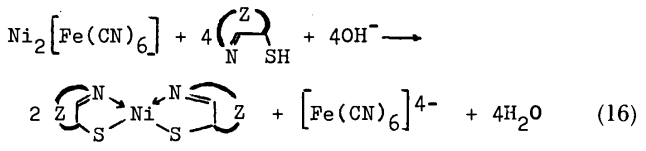

(16)

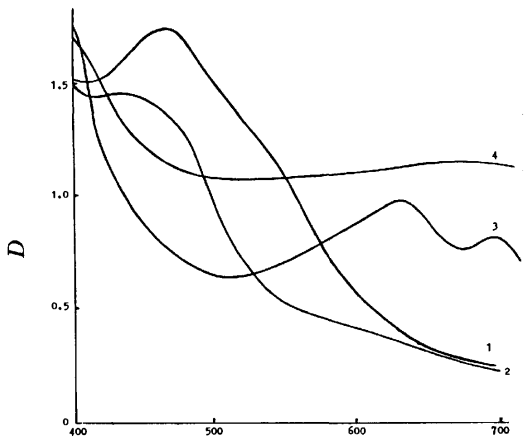

Fig. 5. Spectral characteristics of thin gelatin layers containing: 1—Fe(III) chelate with 8-quinolinethiol (C_F=0.3×10^{-2} mol·m^{-2}, ligand concentration in the solution is 3.0×10^{-2} mol·dm^{-3}, duration of complexing reaction is 2 min at 20 °C); 2—Co(III) chelate with dithiooxamide (C_F=0.4×10^{-2} mol·m^{-2}, ligand concentration in the solution is 1.0×10^{-2} mol·dm^{-3}, duration of complexing reaction is 4 min at 20 °C); 3—Ni(II) chelate with 2,3-quinoxalinedithiol (C_F=3.5×10^{-2} mol·m^{-2}, ligand concentration in the solution is 2.0×10^{-2} mol·dm^{-3}, duration of complexing reaction is 6 min at 20 °C); 4—Cu(II) chelate with dithiooxamide (C_F=4.0×10^{-2} mol·m^{-2}, ligand concentration in the solution is 4.0×10^{-3} mol·dm^{-3}, duration of complexing reaction is 4 min at 20 °C). The thickness of layers is 20000 nm (20 μm).

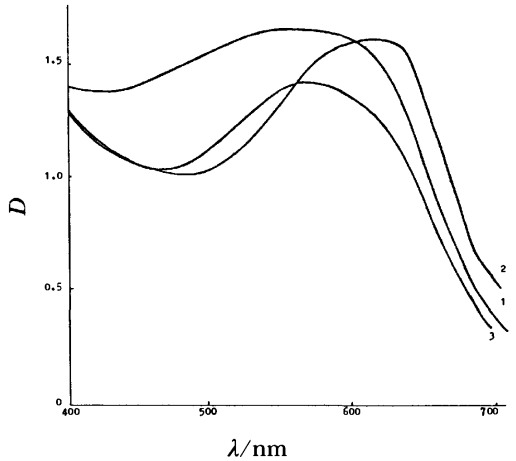

Fig. 6. Spectral characteristics of thin gelatin layers containing: 1—Ni(II) chelate with dithiooxamide of 1:1 ratio comprizing a completely ionized ligand form in the internal sphere (C_F=1.5×10^{-2} mol·m^{-2}, ligand concentration in the solution is 8.0×10^{-3} mol·dm^{-3}, duration of complexing reaction is 6 min at 20 °C); 2—Ni(II) chelate with dithiooxamide of 1:2 ratio (Structure **III**) (C_F=4.0×10^{-2} mol·m^{-2}, ligand concentration in the solution is 4.0×10^{-3} mol·dm^{-3}, duration of complexing reaction is 2 min at 20 °C); 3—Ni(II) chelate with dithiooxamide of 1:1 ratio (Structure **V**) (C_F=4.0×10^{-2} mol·m^{-2}, ligand concentration in the solution is 3.5×10^{-2} mol·dm^{-3}, duration of complexing reaction is 10 min at 20 °C). The thickness of layers is 20000 nm (20 μm).

In a number of cases when a ligand is capable of forming a double-deprotonated form, another variant of heterogenous complexing is possible which can be found in systems containing $Ni_2[Fe(CN)_6]$-dithiooxamide and $Ni_2[Fe(CN)_6]$-2,3-quinoxalinedithiol, where two types of insoluble chelates having a partially or completely deprotonated form of the ligand are obtained. For systems of the first type, at a highly excessive ligand concentration, the initially formed insoluble 1:1 complex can pass into the soluble one diffusing from the gelatin layer into the solution; the process is accompanied by the decrease in optical densities of the thin layer:

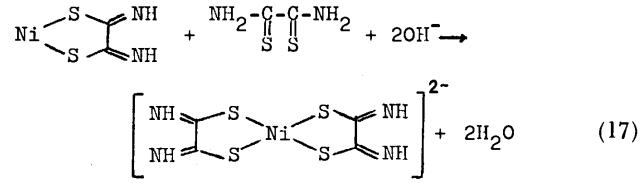

(17)

It is interesting to note that in case of such systems, the transition from the chelate with a completely deprotonated form to that with a partially deprotonated ligand form is also observed; the above mentioned transition can be realized simply by pH decrease in the gelatin layer.

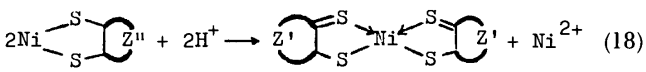

(18)

(Z″ is a double-deprotonated group).

In case of $Ni_2[Fe(CN)_6]$-2,3-quinoxalinedithiol system, the pink color of the thin chelate-containing gelatin layer is changed for the green one, and such color change is accompanied by the shift of absorption maximum from 520 nm up to 630 nm and the emergence of one more band at 700 nm assignable to 1 : 2 chelate.[7] Processing of the gelatin layer containing a cyan chelate results in the reduction of the pink color. In $Ni_2[Fe(CN)_6]$-dithiooxamide system, similar change of colors is observed (from pink-violet into blue) which is accompanied by the bathochromic shift of absorption maximum from 560 nm to 640 nm, but compared to the previously mentioned system, the color change here is found out to be irreversible.[8] The main cause of such differences lies in the structure dissimilarity of "acid" chelates: in case of dithiooxamide, the structure is polymeric **III**, while in 2,3-quinoxalinedithiol it is monomeric **IV**, since steric effects prevent polymer formation. Proton splitting out of the "stiff" polymer structure **III** turns out to be rather difficult and is not observed even at high pH values.

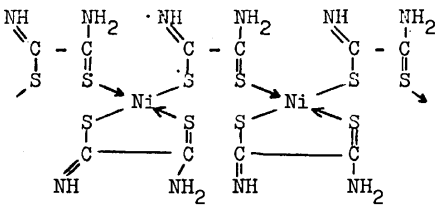

(**III**)

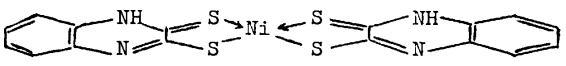

(**IV**)

In the $Ni_2[Fe(CN)_6]$-dithiooxamide system, at high hexacyanoferrate(II) and ligand concentrations, insoluble 1 : 1 chelate complex **V** is also formed having a double-deprotonated ligand form which is uncapable of proton addition; this is associated with the characteristics of a coordination polymer.

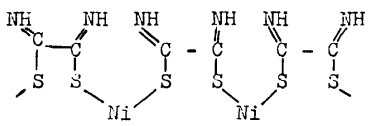

(**V**)

Summarizing the above considerations, it should be noted that testing performed with non-silver images containing metallorganic dyes obtained by heterogenous complexing described in this paper, showed that alongside with silver removal and good storability of images, an increase in photographic sensitivity can also be obtained. In a number of cases (such as in the formation of Co(III) dithiooxamide complexes, the sensitivity increase is an order of magnitude greater than the initial value for the silver photographic image, which is of great practical importance. The process described here can also be used for mono- and polychromatic dyeing of silver images and, in particular, for the production of the "blue slides".[9-11] In the near future, the process can be used in the development of a basically new technique of color photography for obtaining "nonageing" images.

References

1) V. I. Sheberstov, V. L. Zelikman, V. S. Cheltsov et al., "The Foundations of Light-Sensitive Material Technology," Moscow, Chimia (1977), p. 428.

2) K. Mees and T. James, "The Theory of the Photographic Process," Leningrad, Chimia (1973).

3) O. V. Mikhailov and V. K. Polovnyak, Preprint N 901xn-86, ONIITECHIM, Cherkassy (1986).

4) O. V. Mikhailov and V. K. Polovnyak, Preprint N 1334xn-86, ONIITECHIM, Cherkassy (1986).

5) O. V. Mikhailov and V. K. Polovnyak, Preprint N 763xn-86, ONIITECHIM, Cherkassy (1986).

6) O. V. Mikhailov and V. K. Polovnyak, Preprint N 1332xn-86, ONIITECHIM, Cherkassy (1986).

7) V. M. Peshkova and V. M. Savostina, "Analytical Chemistry of Nickel," Moscow, Nauka (1966), p. 118.

8) O. V. Mikhailov, V. K. Polovnyak, and V. K. Kalentyev, Preprint N 1337xn-86, ONIITECHIM, Cherkassy (1986).

9) O. V. Mikhailov, USSR Inventor's Certificate N 1191875 (1985).- Bull. Invent., 42 (1985).

10) O. V. Mikhailov, V. K. Kalentyev, and V. K. Polovnyak, *Bild Ton*, **40**, 10, S. 315 (1987).

11) O. V. Mikhailov, V. K. Kalentyev, and V. K. Polovnyak, *Kép Hangtech.*, **1987**, 183.

 © 1989 The Chemical Society of Japan Bull. Chem. Soc. Jpn., 62, 4021—4032 (1989)

Isomerization in the 1,4,7,10,13,16-Hexaazacyclooctadecanecobalt(III) System [Co(hexacyclen)]$^{3+}$, and Ion-Association Enhancement of the Unstable Facial Isomer

Graeme H. SEARLE
Department of Physical and Inorganic Chemistry, University of Adelaide, Adelaide, S.A. 5001, Australia
(Received March 29, 1989)

The substitution reaction $[Co(NH_3)_5(H_2O)]^{3+}$+hexacyclen·$3H_2SO_4$+6base+charcoal gives *mer*-[Co(hexacyclen)]$^{3+}$ as the major product, and the equilibrium proportion of the *fac* isomer is <1%. The commercial hexacyclen contains linpen (the open chain analogue of hexacyclen, generated by an elimination reaction in the Richman-Atkins cyclization synthesis procedure), so that the synthesis of complex yields [Co(linpen)]$^{3+}$ isomers as co-products which complicate the isolation of the pure [Co(hexacyclen)]$^{3+}$ isomers. Procedures are now given for obtaining the *mer* and *fac* isomers pure. In particular, the unstable *fac* isomer is obtained by isomerization of the *mer* in base in the presence of the strongly associating anion PO_4^{3-}. This yields the new equilibrium mixture *mer*:*fac*:hydrolysis products=71:18:11, wherein the *fac* proportion is enhanced twenty times, enabling the pure *fac* isomer to be obtained in quantity. For the base-catalyzed isomerization reaction *fac* → *mer* in NaOH solutions at 50 °C, procedures are given for following the reaction by analyses of samples using ion-exchange HPLC (Na_2SO_4 elution) and by spectrophotometry. The mechanism must involve intramolecular bond rupture, but the kinetic results are not consistent with a simple SN_1CB mechanism, and a two-step process involving an intermediate is indicated.

The cobalt(III) complex system [Co(hexacyclen)]$^{3+}$ formed by the sexadentate macrocyclic ligand hexacyclen[1] has considerable stereochemical interest since it can exist in several types of isomers (Fig. 1). The ligand can wrap around the cobalt to give the alternative topological arrangements described as *fac* and *mer*. The *fac* has all chelate ring linkages facial and is of approximate symmetry D_{3d}, whereas the *mer* has two meridional linkages and four facial linkages, and has approximate symmetry D_2 in the topological sense (with ring conformations ignored). Thus the *mer* topology is dissymmetric, *Δ* or *Λ*.[2] Additionally for the *mer*, diastereoisomers arise for each of these optical configurations due to the different orientations possible for the N-H bonds at the nitrogen centers coupling the *mer* rings.[2] In acidic conditions where these N-H hydrogen dispositions are prevented from interconverting via hydrogen exchange (and the conformations of the *mer* rings are hence constrained), the effective symmetry of each of the *mer* diastereoisomers is reduced to C_2. Thus there are three geometrically distinct species: the *fac* and the two *mer* racemates *mer*-(*Λδ*/*Δλ*) and *mer*-(*Λλ*/*Δδ*).

This [Co(hexacyclen)]$^{3+}$ system is stereochemically analogous to the $[Co(dien)_2]^{3+}$ system.[1,4] The isomer *sym*-[Co(hexacyclen)]$^{3+}$ corresponds to *sym-fac*-$[Co(dien)_2]^{3+}$. The *mer* isomers of the two complexes are related topologically, as the dien ligands in *mer*-$[Co(dien)_2]^{3+}$ can be coupled together by ethylene bridges in alternative ways to give the *Δ* and *Λ* enantiomeric topologies of *mer*-[Co(hexacyclen)]$^{3+}$. Also, in both of these *mer* complexes the alternative N-H orientations give rise to analogous optical isomerism, in the *δ* and *λ enantiomers* of *mer*-$[Co(dien)_2]^{3+}$, and in the *δ* and *λ diastereoisomers* of each of *Δ* and *Λ mer*-[Co(hexacyclen)]$^{3+}$.

The isomerism of this [Co(hexacyclen)]$^{3+}$ system has been largely elucidated experimentally in previous studies.[5-7] Preparations by substitution reactions between a Co(III)-ammine complex and hexacyclen in the presence of charcoal give all the possible isomers in admixture. The *fac* and *mer* complexes are

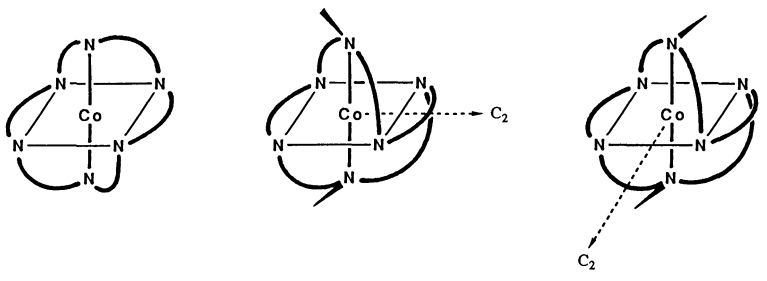

fac (D_{3d}) | Λ-*mer*, δ-NH (C_2) | Λ-*mer*, λ-NH (C_2)

Fig. 1. Isomers and diastereoisomers of [Co(hexacyclen)]$^{3+}$. The *mer* diastereoisomers occur as racemates, *Λδ*/*Δλ* and *Λλ*/*Δδ*, and only one optical form is shown for each.

then separable by chromatography on SP-Sephadex cation-exchange resin,[5,8] and the results show that coordination of this ligand is highly stereospecific: the *mer* topology (both diastereoisomers) occurs at >99% proportion at equilibrium, and the *fac* is barely detectable. SP-Sephadex chromatography under acidic conditions has given a partial separation of the *mer* diastereoisomers (each as racemate) and shows these forms to be in comparable proportions,[5] and the ^{13}C NMR spectrum also shows that the isolated *mer* complex contains the NH diastereoisomers in similar amounts.[6]

Isomerizations of CoN_6^{3+}-type complexes have been studied quite extensively.[9-14] The general catalysis of these reactions by charcoal (heterogeneous reaction) or by base (homogeneous reaction) is well-established, but the mechanisms of these processes have not been settled. Several features of this $[Co(hexacyclen)]^{3+}$ system make it attractive for a study of isomerization within a CoN_6^{3+} framework: (1) the system has only two geometric isomers *fac* and *mer*; (2) the *fac* should isomerize essentially completely to *mer* (>99%) so that only one forward reaction should be observed; and (3) the coupling of all the chelate rings in the macrocyclic ligand should restrict the possible modes of ring movements. The present work thus aimed to establish the occurrence or otherwise of the isomerization between the *fac*- and *mer*-$[Co(hexacyclen)]^{3+}$ isomers, and to determine the base dependence of this reaction, and it was hoped that this base dependence might provide some definite evidence concerning the reaction mechanism.

This work required pure samples of the *fac* and *mer* (diastereoisomer mixture) isomers, but isolation of the *fac* from an equilibrium synthetic mixture (<1%) is clearly an impractical means of obtaining this isomer in quantity. It has been demonstrated with the $[Co(dien)_2]^{3+}$ system that ion-association with phosphate anion can markedly shift the equilibrium position and enhance the proportions of more strongly associating isomers, particularly the *sym-fac*,[15] so that the second aim of the work has been to demonstrate that the ion-association effect can also be applied to the analogous hexacyclen complex system to obtain the unstable *fac* isomer in quantity in an isomerization process.

Royer and co-workers have reported interesting observations on isomerizations from the *mer* isomers of $[Co(hexacyclen)]^{3+}$ (and in two other cobalt(III) systems with analogous symmetrical hexaaza macrocycles).[7] Their work is complementary to our results reported herein.

Experimental

^{13}C NMR Spectra. 20.1-MHz NMR spectra of the complexes, broad-band proton-decoupled, were recorded on solutions in acidified D_2O on a Bruker WP-80 DS spectrometer locked to deuterium. An 8192 data table was used. A capillary of *t*-butyl alcohol provided a reference signal: 618.9 Hz, δ 30.79 for CH_3 downfield from $SiMe_4$. (This reference signal was measured for a *t*-butyl alcohol capillary in $CDCl_3$ against $SiMe_4$ as internal reference). As with other cobalt(III) (3+)-charged complexes previously studied, the chemical shifts of the resonances of the $[Co(hexacyclen)]^{3+}$ isomers showed insignificant variations with different anions (generally <0.1 in δ).

Synthesis of *mer*-[Co(hexacyclen)]$Br_3 \cdot H_2O$. A mixture of $[Co(NH_3)_5(H_2O)](ClO_4)_3$ (1.84 g, 0.004 mol), hexacyclen $\cdot 3H_2SO_4$ (2.32 g, 5% excess; Aldrich 98%), $LiOH \cdot H_2O$ (1.06 g) and freshly ground charcoal (0.2 g) in water (60 ml) was heated over a steam bath for 3 h. The charcoal was filtered off, and the orange solution was applied to a column (4.5 cm diam.×40 cm) of SP-Sephadex C-25 cation-exchange resin.

The column was eluted with 0.1 M Na_3PO_4 (1 M=1 mol dm^{-3}) when bands separated as follows:
(1) a fast-moving barely detectable orange band containing *fac*-$[Co(hexacyclen)]^{3+}$ and a trace of $[Co(linpen)]^{3+}$ (**A**) (See Results);
(2) a second very weak orange band;
(3) the main orange-red band of *mer*-$[Co(hexacyclen)]^{3+}$;
(4) considerable purple material extending down most of the column.

The *mer* effluent from band (3) was collected, diluted two times, and applied directly to a column of Dowex 50W-X2 cation-exchange resin, 200—400 mesh, H^+ form (3×4 cm). The complex was washed on with 0.1 M HBr then washed with 1 M HBr to remove all Na^+, then was eluted off with 3 M HBr. The effluent was rotary evaporated to near dryness, and air was sucked through the flask to remove HBr. A little water was added to dissolve the product, followed by gradual addition of ethanol, and crystallization of the diastereoisomer mixture was encouraged by scratching the flask. The resulting orange crystals were filtered off, washed with ethanol and acetone, and air-dried to constant weight. Yield 1.51 g, 66%. Found: C, 25.2; H, 5.4; Br, 43.5; N, 14.5%. Calcd for *mer*-$[Co(C_{12}H_{30}N_6)]Br_3 \cdot H_2O$: C, 25.1; H, 5.6; Br, 41.7; N, 14.6%. The product may have contained a small amount of isomer $[Co(linpen)]^{3+}$ (**D**), although this was not evident in the ^{13}C NMR spectrum. ^{13}C NMR in D_2O/HBr of the approximately 1:1 NH-diastereoisomer mixture: δ 60.5 (2 carbons), 57.0, 55.8, 55.6, 55.2, 53.2, 52.8*, 51.4, 50.6, 50.1, 49.0. [*δ 52.6 for the nitrate salt].

The *mer* isomer could also be obtained from Dowex resin as the less soluble nitrate salt, and HNO_3 eluent concentration was restricted to 1.5 M maximum to avoid precipitation of complex on the resin. Found: C, 26.8; H, 6.1; N, 23.3%. Calcd for *mer*-$[Co(C_{12}H_{30}N_6)](NO_3)_3 \cdot 2H_2O$: C, 26.7; H, 6.3; N, 23.4%.

The *mer* was also obtained as the perchlorate salt by absorbing the complex on a column of Biorex-70 weak-acid cation-exchange resin, 50—100 mesh, Na^+ form, and eluting off with 0.1 M $HClO_4$. Crystallization from the evaporated solution was completed by the addition of ethanol, and the $NaClO_4$ remained in the mother liquor from filtering off the complex.[6]

The *mer* complex could be separated into the two NH-diastereoisomers (as the racemates $\Lambda\delta/\Delta\lambda$ and $\Lambda\lambda/\Delta\delta$) by chromatography down SP-Sephadex using 0.2 M Na_2SO_4/H_2SO_4 pH 2 as eluent.[5] Under these acidic conditions two

approximately equal but incompletely separated bands were obtained, relative R_x(*mer-1*)/(*mer-2*)=1.24. These were collected and the overlap portion was discarded. The two components were isolated as chlorides using Dowex resin with 3 M HCl elution, and characterized by their ^{13}C NMR spectra in D_2O/HCl: for the first eluted diastereoisomer *mer-1* δ 57.0, 55.6 (2 carbons), 53.2, 50.5, 49.1; for *mer-2* δ 60.4 (2 carbons), 55.2, 52.6, 51.6, 50.1.

The combined effluents of the *fac* isomer from the first weak orange Sephadex band (1) from several preparations were worked up using the Dowex/HCl procedure. The ^{13}C NMR spectrum showed that this band (1) contained *fac*-[Co(hexacyclen)]$^{3+}$ (δ 56.1) together with the [Co(linpen)]$^{3+}$ (**A**) isomer (δ 57.6, 57.2 (2 carbons), 55.4, 42.3), but the total amount obtained was very small.

Preparation of *fac*-[Co(hexacyclen)]Cl$_3$ by Isomerization from *mer*. Two solutions of *mer*-[Co(hexacyclen)]Br$_3$·H_2O in 0.1 M Na_3PO_4 (1.80 g in 80 ml, giving [Co] 0.04 M) in stoppered flasks were heated at 80 °C for 12 h. The solutions were diluted (250 ml) and acidified to pH 2 using 1 M HCl, and were then applied to separate columns (4.5×30 cm) of SP-Sephadex cation-exchange resin. The acidification was necessary to avoid partial elution of the *fac* isomer by PO_4^{3-} during the application. After washing on with water, the columns were eluted with 0.1 M Na_3PO_4, when bands separated in the following order:

(1) (first eluted) light-orange *fac*-[Co(hexacyclen)]$^{3+}$ with a trace of [Co(linpen)]$^{3+}$ (**A**);
(2) very weak yellow;
(3) deep orange-red *mer*-[Co(hexacyclen)]$^{3+}$;
(4) a yellow continuum, containing "*mer*";
(5) pink-carmine;
(6) olive-green precipitate.

The *fac* effluents (1) from the two columns were collected and combined, diluted two times, and acidified to pH 2. This solution was applied to a column of Dowex 50W-X2 resin, 200—400 mesh, H^+ form (3×3 cm). After washing on with 0.1 M then washing with 1 M HCl to remove Na^+, the complex was eluted off with 3 M HCl, and the effluent was evaporated to dryness. Ethanol was added to enable the yellow-orange solid to be removed by filtration. This product was washed with ethanol and acetone, and air-dried to constant weight. Yield 0.43 g, 16%. Found: C, 33.7; H, 7.1; Cl, 25.1; N, 19.6%. Calcd for *fac*-[Co($C_{12}H_{30}N_6$)]Cl$_3$: C, 34.0; H, 7.1; Cl, 25.1; N, 19.8%.

The *mer* effluents band (3) from the columns were combined, diluted, and applied directly (without acidification) to a Dowex 50W-X2 column (3×4 cm). The *mer* was recovered as the bromide salt as described previously. Recovery 2.17 g, 60%.

The two isomers could also be obtained as the nitrate salts, although these are less soluble than the halides, and a lower concentration of HNO_3 had to be used (1.5 M maximum) for the elution from Dowex to avoid precipitation of the complexes on the resin. Yields of nitrates from one isomerizaton run: *fac* 15%, *mer* recovery 60%. Found for *fac*: C, 27.5; H, 6.0; N, 24.2%. Calcd for *fac*-[Co($C_{12}H_{30}N_6$)]-(NO_3)$_3$·H_2O: C, 27.6; H, 6.2; N, 24.2%.

The first-obtained *fac*-[Co(hexacyclen)]Cl$_3$ products contained trace amounts of [Co(linpen)]Cl$_3$ (**A**) as shown by small peaks in the ^{13}C NMR spectrum at δ 57.2 and 42.6. [Co(linpen)]$^{3+}$ (**A**) was not apparent however when *mer*-[Co(hexacyclen)]Br$_3$ which had been recovered from previous isomerization runs was used. Recrystallization of the total *fac*-[Co(hexacyclen)]Cl$_3$ from warm 0.01 M HCl by partial rotary evaporation and addition of some ethanol gave the pure *fac* product, when the [Co(linpen)]Cl$_3$ (**A**) was retained in the mother liquor. Rechromatography of this mother liquor gave a substantial separation of the two components: pale orange *fac*-[Co(hexacyclen)]$^{3+}$ eluted first and was isolated pure from the first portion of the band effluent. The latter portion of the band contained yellow [Co(linpen)]$^{3+}$ (**A**), as the major component (^{13}C NMR peaks from **A** at δ 57.6, 57.3 two carbons, 55.4, 42.6) plus some *fac*-[Co(hexacyclen)]$^{3+}$ (δ 56.1). A trace of the *mer* isomer was also evident in this re-chromatography, this *mer* being formed by re-isomerization.

The material within the yellow continuum (4) seems to be a derivative from *mer*-[Co(hexacyclen)]$^{3+}$. On isolation (Dowex/HCl), this material apparently reverted to *mer* since the ^{13}C NMR spectrum then obtained was identical to that of *mer*-[Co(hexacyclen)]$^{3+}$.

The precipitate (6) seems to form only in the Na_3PO_4 solution, and is deposited at the column head. It dissolves and is eluted if the column is slightly acidified.

Determination of Conditions for Optimum Isomerization of *mer*- to *fac*-[Co(hexacyclen)]$^{3+}$. *mer*-[Co(hexacyclen)]-(NO_3)$_3$·$2H_2O$ was dissolved in 0.1 M Na_3PO_4 (0.408 g of complex, chromatographically pure on SP-Sephadex, in 20 ml giving [Co] ca. 0.04 M). The solution was heated in a stoppered flask at 80±2 °C and samples were removed with a calibrated pipette (2.96 ml) at various times (2, 5, 8, 12, 24 h) and acidified (0.7 ml of 1 M HCl). Acidification was necessary to quench the isomerization and to prevent elution by PO_4^{3-} during application to Sephadex. The samples were eluted down SP-Sephadex columns (1.2×20 cm) using 0.1 M Na_3PO_4, and the effluents of the separated *fac* and *mer* isomers were made up to standard volumes with 0.1 M Na_3PO_4 (*fac* made up to 10 ml, *mer* to 50 ml). Cobalt in these solutions was determined by atomic absorption at 240.7 nm using a dinitrogen monoxide-acetylene flame, against solutions of [Co(en)$_3$](ClO_4)$_3$ in 0.1 M Na_3PO_4 as standards. Moles of total hydrolysis products in the samples were calculated by the difference (initial-final) [Co(hexacyclen)]$^{3+}$.

Kinetics of Isomerization of the *fac* Isomer. (a) HPLC Using Strong-Acid Cation-Exchange. The analytical procedure was developed from that described by Larsen.[16,17] The apparatus comprised a Waters HPLC system (Model 5000 solvent delivery unit, U6K injector, 481 variable-wavelength detector), and chromatograms were recorded and integrated using a Hewlett-Packard integrator model 3380S. The column used for HPLC was a Waters Protein-Pak SP-5PW, of dimensions 7.5 mm i.d.×75 mm, having capacity 300 nmol of 3+ complex.[16] All solutions were prepared with distilled and Milli-Q treated water, and were filtered through an all-glass filter unit fitted with a 0.45 μm membrane (Millipore MF type). The HPLC eluent was 0.2 M Na_2SO_4/pH 2 with H_2SO_4.

Runs were carried out at NaOH concentrations 0.05, 0.1, and 0.5 M (I=1.0 with NaCl). Reaction solutions were prepared of about 0.010 g of *fac*-[Co(hexacyclen]Cl$_3$ in 3 ml of the NaOH solution giving [Co] about 0.007 M, and held at 50.0 °C. Constant samples 0.2 ml were removed at intervals, about ten for each run, using an auto pipette (Gilsen "Pipetman" P200) and placed on small columns (5 mm×15

mm) of SP-Sephadex C25, and washed on with water.

At the completion of the run, all these columns were then eluted totally with 0.2 M Na_2SO_4/pH 2, and each effluent was collected and weighed accurately (ca. 4 g). This prechromatography, which conveniently quenched the samples, was necessary to ensure the removal of any strongly retained complexes prior to the HPLC,[16] and the weighing of the effluents permitted normalization between the samples in each run. Each effluent was filtered through a Millex HV4 filter (using a Pasteur pipette and a dry syringe). Constant samples of the effluents 100 μl (Hamilton syringe) were injected for HPLC. Flow rate was 1.0 ml min^{-1}. Detection was at 480 nm, approximately the band I maxima for *fac* and *mer* (but was also checked at 250 nm when similar results were obtained). Chromatograms were recorded from 0—15 min, with full scale absorption in the range 0—0.1 absorption units. This procedure gave about 40 nmol of [Co(hexacyclen)]$^{3+}$ in each injection.

HPLC elution gave (in general) three completely separated peaks due to the isomers *fac*, *mer-1*, and *mer-2*, with typical retention times 3.9, 8.6, and 11.0 min respectively. The amounts of the *fac* and total *mer* components in the different samples were measured as the products of integrated peak area times mass of Sephadex effluent, where the peaks for the *mer* NH-diastereoisomers *mer-1* and *mer-2* were summed. This procedure normalized the different samples taken over a run.

The optical isomers of *mer*-[Co(hexacyclen)]$^{3+}$ were not separated by this HPLC procedure: there was no sign of any separation of the four diastereoisomeric/optical species using HPLC with 0.15 M sodium di-μ-(*R*,*R*)tartrato(4−)-diantimonate(III)/H_2SO_4 pH 2 eluent.[18] Partial resolutions have however been achieved on Sephadex columns using this eluent or sodium (+)-tartrate.[5,7]

(b) Spectrophotometric Runs. Isomerization runs in 0.1 and 0.5 M NaOH solution at 50 °C (I=1.0 M with NaCl) were followed using a Varian-Cary 219 UV/Vis spectrophotometer with timer, wavelength programmer and cell programmer accessories. Absorbances at wavelengths 520, 478, and 416 nm were measured and stored using the Varian 219/210 spectrophotometer "Master Kinetic Storage Programme" on an Apple IIe computer.

The complex *fac*-[Co(hexacyclen)]Cl_3 was weighed (about 0.008 g) and transferred to an appropriate amount (about 5.4 g) of the NaOH/NaCl solution giving [Co] about 0.0034 M. After dissolution, this solution was transferred to a 1 cm cell in a thermostatted holder 50 °C in the spectrophotometer and the recording cycle was started. Recordings were taken at intervals of 15 min (0.1 M NaOH) or 10 min (0.5 M NaOH) and were continued until the absorptions had reached maxima (at 22 h for 0.1 M NaOH, 11 h for 0.5 M NaOH). Absorbance changes for the run in 0.1 M NaOH at 50 °C were: at 478 nm, 0.25 (ε=71) to 0.94 (ε=274) (cf. in 0.01 M HCl at 20 °C, ε_{478}=62 for *fac*, 241 for *mer*); at 416 nm, 0.13 to 0.47.

Results and Discussion

Possible Pathways for Isomerization in [CoN_6]$^{3+}$ Complexes. In the isomerization of [Co(dien)(medien)]$^{3+}$ on charcoal in water the bis complexes [Co(dien)$_2$]$^{3+}$ and [Co(medien)$_2$]$^{3+}$ are also generated, and this must involve complete dissociation of ligands.[10] However, isomerizations in some other circumstances appear to be exclusively intramolecular: the homogeneous isomerization of [Co(dien)(medien)]$^{3+}$ in base is not accompanied by generation of the bis complexes and thus differs clearly from the charcoal reaction above,[10] and Δ-[Co(pn)$_3$]$^{3+}$ [1] with charcoal racemizes faster than coordinated pn exchanges with pn from the solution.[9] For such intramolecular reactions two alternative mechanisms have been envisaged:[20b] Co-N bond rupture whereby a five-coordinate intermediate is generated in which reattachment can occur at a different position, and a twist process wherein six-coordination is preserved. These alternatives should properly be viewed as the limiting mechanisms of a range.

The experimental observations on isomerizations in a number of [CoN_6]$^{3+}$ systems have been interpreted on the basis of predominantly intramolecular bond-rupture mechanisms: [Co(en)$_3$]$^{3+}$ racemization under both charcoal and homogeneous conditions,[12] [Co(dien)(medien)]$^{3+}$ and [Co(dien)$_2$]$^{3+}$ homogeneous,[10,13] *u-fac*-[Co(daes)$_2$]$^{3+}$ charcoal racemization,[1,11] and [Co(tacd)$_2$]$^{3+}$ homogeneous.[1,14] This bond-rupture mechanism more easily accommodates both the observed base dependence of the isomerization rates for these systems, and the occurrence under some conditions of hydrolytic by-products which have been presumed to be [CoN_6(OH)]$^{2+}$ species.[10]

For the racemization of [Co(en)$_3$]$^{3+}$ in the presence of both charcoal and base, Spiro has deduced that the dominant pathway is through the conjugate base and a five-coordinate intermediate, and it was also shown that a Co(III)-Co(II) electron-exchange process is significant only for solutions containing added [Co(en)$_3$]$^{2+}$ + en.[12] Although this latter pathway is less important than was earlier considered for the [Co(en)$_3$]$^{3+}$ system,[21] such a scheme has to be retained as plausible for the isomerization of [Co(dien)(medien)]$^{3+}$ on charcoal since it can accommodate the complete dissociations of ligands.[10]

As well as the above bond-rupture proposals, twist processes remain an intriguing possibility because there is evidence for their occurrence with isomerizations in some complexes of Cr(III)[22,23] and Cr(I)[24] and Fe(II).[25] Although there is little direct evidence for their occurrence in some other Co(III) systems previously studied,[26-28] an interesting situation has been reported recently with the sexadentate complex [Co(stn)]$^{3+}$ which racemizes homogeneously in base and also in the solid state.[1,29] The catalysis of the homogeneous racemization of this complex by hydroxide indicates that deprotonation at a secondary nitrogen is a first step. A bond rupture as a second step can not be seen to lead to inversion of the absolute configuration about the metal, which has therefore been attributed to a trigonal twist (Bailar twist) process. In this system the racemization has to involve inversion of the absolute configurations of all three

asymmetric nitrogens "simultaneously," so that deprotonation at one nitrogen site initially must precede the twist act.[29,30] However, with tris-bidentate complexes (without such ring-coupling) a purely twist process does not readily accommodate the observed base catalysis and the formation of some hydrolysis co-products in Co(III) systems.

Significance of Isomerization in [Co(hexacyclen)]$^{3+}$. The occurrence or otherwise of isomerization between the *fac* and *mer* [Co(hexacyclen)]$^{3+}$ isomers would seem to be definitive in establishing two aspects of the isomerization mechanism. Firstly, no twist process (of the Bailar or Ray-Dutt types) can be envisaged for the *fac* isomer due to the coupling of the chelate rings,[7] so that any isomerization *fac*$\rightleftarrows$*mer* has presumably to be attributed to a Co-N bond-rupture process. Secondly, if the isomerization is base-catalyzed, as with the other CoN_6^{3+} systems studied, this catalysis should probably be attributable to deprotonation occurring at a *s*-NH center (since hexacyclen has only secondary amine sites). These considerations should be relevant also if the reaction proceeded through a labile Co(II) intermediate, in a redox pathway occcurring under charcoal conditions.

Preparation of *mer*-[Co(hexacyclen)]$^{3+}$. Various preparative procedures for [Co(hexacyclen)]$^{3+}$ were examined in anticipation of obtaining the *fac* isomer in greater proportion than that reported previously, $<1\%$.[5,6] However this was not realized and the *fac* was sometimes barely detectable on the Sephadex among co-products of the reactions (including [Co(linpen)]$^{3+}$ isomers, see below). We therefore sought to isolate from the synthesis only the pure *mer* isomer (both diastereoisomers), and thence to obtain the *fac* by isomerization. The linear hexamine linpen,[1] which is the open-chain analogue of hexacyclen, is a troublesome contaminant of hexacyclen, and additional steps in the isolation procedure for [Co(hexacyclen)]$^{3+}$ are necessary to remove [Co(linpen)]$^{3+}$.

The substitution reaction $[Co(NH_3)_5(H_2O)](ClO_4)_3$+hexacyclen$\cdot 3H_2SO_4$+6LiOH in water with charcoal[5] seemed to give the cleanest product mixture, although considerable hydrolysis by-products were unavoidable.

All the products were then separated by cation-exchange chromatography on SP-Sephadex. We found Na_3PO_4 eluent[6] to be more satisfactory for this preparative work than Na_2SO_4/H^+,[5] as the Na_3PO_4 is highly discriminating[31] and effects the best separation of the *fac*- and *mer*-[Co(hexacyclen)]$^{3+}$ isomers[32] from [Co(linpen)]$^{3+}$ co-products (see below) of the substitution synthesis. Also, in the basic conditions of Na_3PO_4 elution the darkly-colored hydrolysis by-products from the synthesis, or from isomerization reactions for [Co(hexacyclen)]$^{3+}$ as below, elute slowly so that the *mer* (diastereoisomer mixture) can be readily separated ahead of them. (With Na_2SO_4/H^+ elution, the by-products appear mainly as two pink bands between the *fac* and *mer* bands. These same hydrolysis product bands were observed from samples from isomerization reactions carried out in 0.1 M Na_3PO_4 separated on Sephadex with Na_2SO_4/H^+). With Na_3PO_4, the *fac* and *mer* bands are also darkened in color, and we ascribe this to some deprotonation at coordinated nitrogen sites.[17,33] Although the isomerization is base-catalyzed, this was not a problem in the Sephadex/Na_3PO_4 chromatography to obtain the two isomers pure, as we found that the amount of *fac* $\rightarrow$*mer* change occurring in 0.1 M Na_3PO_4 pH 12 was negligible over several hours at room temperature, as samples of *fac* then isolated showed no *mer* by ^{13}C NMR.

From its Sephadex/Na_3PO_4 effluent, the *mer* NH-diastereoisomer mixture could be isolated as its bromide or nitrate salt by using Dowex strong-acid cation-exchange resin.

The *mer* diastereoisomers could be subsequently separated by Sephadex chromatography by using acidic conditions, Na_2SO_4/H^+ eluent.[5,7] Experimentally the diastereoisomers are designated as *mer-1* and *mer-2* according to their elution order from Sephadex, but their identities as ($\Lambda\delta/\Delta\lambda$) or ($\Lambda\lambda/\Delta\delta$) remain unknown.[7]

Preparation of *fac*-[Co(hexacyclen)]$^{3+}$ by Isomerization. The cation-exchange elution order of the isomers *fac*$\gg$*mer* with Na_3PO_4 or Na_2SO_4 indicates that the *fac* associates more strongly with these eluent anions.[8,31] Consequently, under conditions where equilibrations between isomers can occur, i.e. in water with charcoal or base,[10,14] the proportion of *fac* should be enhanced in the presence of associating anions such as PO_4^{3-} or SO_4^{2-}. Such enhancements have been demonstrated previously with *s-fac*-[Co(dien)$_2$]$^{3+}$ [15] and *trans*-[Co(tacd)$_2$]$^{3+}$,[14] and where a less stable isomer preferentially associates with an added anion the shift in equilibrium position may be substantial. Thus in [Co(dien)$_2$]$^{3+}$ the *s-fac* proportion formed in synthesis changed from 8% in water (with counter-anions present Cl^-, NO_3^-, or ClO_4^-, all weakly associating) to 59% with added Na_3PO_4 at 20 °C.[15]

This enhancement effect has now been used in the [Co(hexacyclen)]$^{3+}$ system to obtain the unstable *fac* isomer by allowing the *mer* to isomerize in 0.1 M Na_3PO_4 at 80 °C. The time for optimum conversion was determined from small-scale tests which showed that equilibrium was reached by 12 h. The proportions under these conditions were *mer* : *fac* : hydrolysis products=71 : 18 : 11 (see below), so that ion-association enhances the *fac* proportion by about twenty times. Larger scale mixtures thus isomerized were separated by Sephadex/Na_3PO_4 chromatography, and the recovered *mer* was recycled.

Isomerization in Na_2SO_4+charcoal (pH 5) gave little if any *fac* enhancement. These results suggest that in the equilibrium substitution syntheses on

charcoal,[5,6] the ca. 1% *fac* obtained actually represents an enhancement by ion-association with SO_4^{2-} which was the counter anion present, and which is moderately associating.[15] Thus in the presence of only weakly associating anions, the equilibrium *fac* proportion would be expected to be $\ll$1%.

The Occurrence of [Co(linpen)]$^{3+}$ in [Co(hexacyclen)]$^{3+}$. The complex system [Co(linpen)]$^{3+}$ [1] exists in four topological isomers (Fig. 2). These are designated **A**, **B**, **C**, and **D** according to their elution order on Sephadex, and their geometries have been assigned.[34] Our first-isolated *fac*-[Co(hexacyclen)]$^{3+}$ contained [Co(linpen)]$^{3+}$ (**A**) (identified by its chromatographic elution on SP-Sephadex[8] and by its ^{13}C NMR spectrum being closely similar to those of authentic **A**).

The linpen must have been present as an impurity in the starting hexacyclen·$3H_2SO_4$ material, and indeed the ^{13}C NMR spectrum of the hexacyclen·$3H_2SO_4$ (after conversion to hexacyclen·6HCl) showed a peak (δ 43.7) which can be attributed to the main resonance (three carbons of the five different carbons present) of authentic linpen·6HCl. Our recent work on Richman-Atkins cyclization syntheses of cyclic polyamines[35] has demonstrated how a linear analogue can arise as an elimination reaction co-product during a cyclization synthesis, so that linpen has to be expected as a contaminant in hexacyclen.[36]

In the equilibrium substitution preparation of [Co(hexacyclen)]$^{3+}$ all four isomers **A** to **D** should be formed from the linpen. The isomers **D** (73% proportion[34]) and **C** would contaminate *mer*-[Co(hexacyclen)]$^{3+}$, as these all chromatograph similarly.[8] This **D** would then be expected to isomerize to **A** (9% proportion[34]) during the *mer*→*fac* isomerization, and **A** and *fac* chromatograph similarly. Experimentally, **D** was evident in crude samples of *mer* as a yellowish tail to the orange *mer* band on Sephadex chromatography, and initial samples of *fac* contained **A**. However, samples of *fac* obtained from subsequent isomerizations using recycled *mer* were free of **A**, due to the eventual removal of **D** from *mer* by isomerization.

[Co(linpen)]$^{3+}$ contaminants were thus removed as follows: (1) **A**, **B**, and **D** were separable partially from *mer*-[Co(hexacyclen)]$^{3+}$ by Sephadex chromatography;[8] (2) **D** and **C** were partially removed from *mer* by their isomerization to **A** in Na_3PO_4; (3) fractional recrystallization of the final *mer* and *fac* materials removed (**D**+**C**) and **A** respectively.

Conditions for Optimum Isomerization to *fac*-[Co(hexacyclen)]$^{3+}$. The time and yield for optimum isomerization to *fac* were determined from small-scale runs in which pure *mer*-[Co(hexacyclen)]$(NO_3)_3$ was allowed to isomerize in 0.1 M Na_3PO_4 at 80 °C. The solutions were sampled at various times and analyzed.

The mole proportions of *mer*, *fac*, and hydrolysis products versus time thus determined (Fig. 3) show that the isomerization is slow. The proportion of *fac* rises gradually, to become constant at 18% at about 12 h. Hydrolysis (or decomposition) occurs concomitantly, rising rapidly at first, then levelling out at 11% at about 5—8 h. It is evident that equilibrium is attained between the two isomers and the hydrolyzed species, at *mer*:*fac*:hydrolysis=71:18:11, by 12 h. However, the faster generation of hydrolyzed products (the crossover in the *fac* and hydrolysis curves) suggests that the isomerization process is not simple.

This 18% proportion of *fac* was expected to be near the optimum, since the effect of PO_4^{3-} on enhancing the least stable *s*-*fac*-[Co(dien)$_2$]$^{3+}$ reached maximum at 0.08 M Na_3PO_4.[15] Under the equilibration conditions of Na_3PO_4, hydrolysis to the extent of ca. 11%

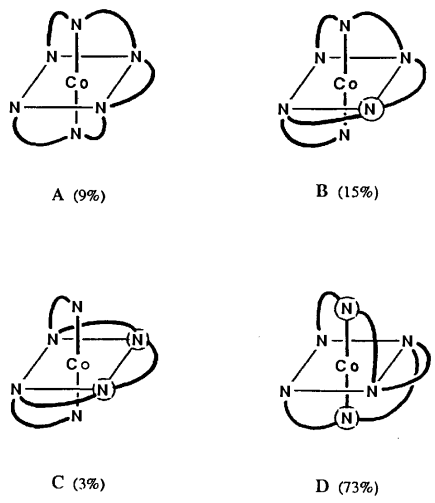

Fig. 2. Topological isomers of Λ-[Co(linpen)]$^{3+}$ and their equilibrium proportions. Diastereoisomers arise from the alternative dispositions (or *R*/*S* configurations) at the circled secondary amines which couple *mer* chelate rings.

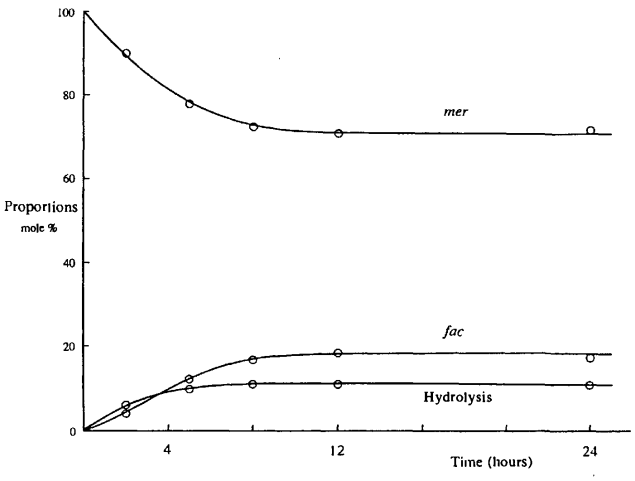

Fig. 3. Isomerization-equilibration of *mer*-[Co(hexacyclen)]$(NO_3)_3$ in 0.1 M Na_3PO_4 at 80 °C. Separation is by Sephadex/Na_3PO_4. Equilibrium mole proportions are *mer*:*fac*:hydrolysis=71:18:11%.

seems to be unavoidable in [Co(hexacyclen)]$^{3+}$.

Kinetic Runs on *fac*→*mer* [Co(hexacyclen)]$^{3+}$ Isomerization. (a) Runs Followed by HPLC Analysis of Samples. The reaction was followed at 50 °C, under the NaOH concentration conditions 0.05, 0.1, and 0.5 M NaOH (I=1.0 M, NaCl). The *fac*-[Co(hexacyclen)]$^{3+}$ complex immediately formed darkish red-brown solutions in base (including 0.1 M Na_3PO_4, as used in elution from Sephadex, see above), giving greater absorption at all wavelengths. These initial darkenings were reversible, so that when the solutions were applied to Sephadex or were acidified, they reverted to pale orange. This conforms to the pattern found with other $[CoN_6]^{3+}$ and $[CoN_4S_2]^{3+}$ systems where very rapid and reversible darkenings occur in base at varying pH values depending on the complex, and we attribute these changes to the formation of darkly colored deprotonated species.[17,33]

In the HPLC procedure, samples from the various solutions removed at intervals were analyzed by HPLC using a strong-acid cation-exchange column. The eluent was Na_2SO_4/H_2SO_4 pH 2, and detection was spectrophotometric. Apparently clean chromatograms were obtained showing completely separated peaks of *fac* and the *mer-1* and *mer-2* diastereoisomers only, over most of the reaction, e.g. up to 12 h for 0.1 M NaOH (Fig. 4).[37] Of the *mer* diastereoisomer products *mer-1* was always observed in slightly greater amount (*mer-1* ≈60—55%, assuming that the two diastereoisomers have similar absorptions), but our kinetic plots were made with respect to *total mer*.

Elution at pH 4 (Na_2SO_4/H_2SO_4) was also tried. Under these conditions the two *mer*-NH diastereoisomers were not completely separated as the absorption recordings did not achieve baseline between the two peaks, and this indicates that the diastereoisomers interconvert at pH 4 over the time scale of the HPLC analysis (although not at pH 2, as above). This is presumably through base-catalyzed N-H exchange involving the deprotonated species, analogously to the racemization of [Co(dien)$_2$]$^{3+}$.[38] However, it seems that the isomerization (pH≥4) in the *mer*-[Co(hexacyclen)$_2$]$^{3+}$ is considerably faster than the analogous racemization (pH>7) of *mer*-[Co(dien)$_2$]$^{3+}$.[38] Although this pH 4 gave similar kinetic plots to those for pH 2, we believe that there are more uncertainties at these higher pH values, as the measured absorptions may have contributions from protonated and deprotonated forms of the two diastereoisomers and from other possible intermediates. In fact, some small shoulders or peaks are evident close to the *fac* peak on the HPLC elution curves, especially in the latter stages of the reactions.

The kinetic plots for disappearance of the *fac* and appearance of the *mer*(total) are irregular for all NaOH concentrations. The amount of *fac* did not decrease in a first order manner, and this was particularly noticeable in the lowest NaOH concentration, 0.05 M, when the *fac* remained nearly constant to about 3 h before decreasing slowly. Also, the 0.1 M NaOH curve for *mer* has a marked hump at 2.5 h (Fig. 5). These observations are consistent with the "*fac*" band in HPLC containing a second species, of a similar *fac* geometry, which builds up slowly, and this is likely to be some longer-lived intermediate.

The irregularities in the *mer* elution kinetic curves

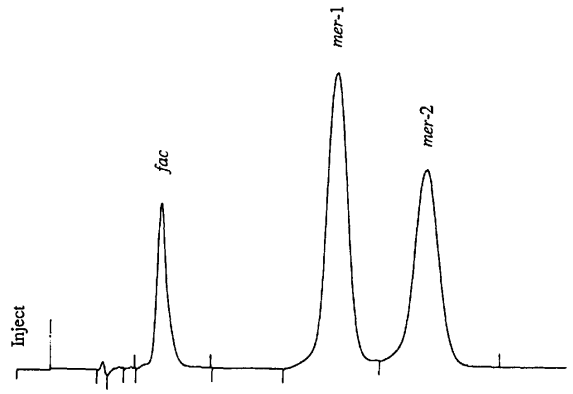

Fig. 4. Typical HPLC chromatogram, Na_2SO_4/H^+ pH 2 elution. (Reaction in 0.1 M NaOH, 50 °C, for 12 h).

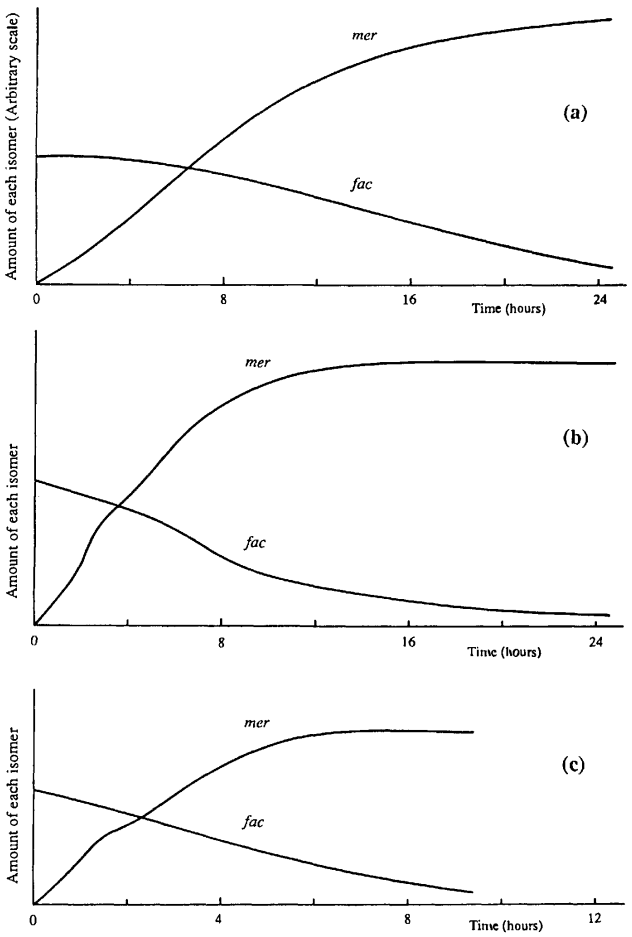

Fig. 5. Kinetic plots from HPLC elutions of isomerization reactions of *fac* at 50 °C: (a) in 0.05 M NaOH; (b) 0.1 M NaOH; (c) 0.5 M NaOH.

were an inflection in the curve for 0.05 M NaOH (≈3 h) and humps for 0.1 M NaOH (≈2.5 h) and 0.5 M NaOH (≈1.5 h) (Fig. 5). Although these irregularities have precluded the precise measurement of reaction rates, the plots of amount of *mer* versus time allow semiquantitative estimates of the rates. For the 0.05, 0.1, and 0.5 M NaOH reactions the half-lives are about 8, 4, and 2 h respectively taking the reactions to be pseudo-first-order, so that there is clearly a base dependence of the rates. The order in hydroxide is approximately first-order, and is in accord with the deprotonation requirement of a bond-rupture process for the *fac*→*mer* isomerization in this system.

(b) Isomerization Followd by Spectrophotometry. Isomerization runs in 0.1 M and 0.5 M NaOH at 50 °C were followed spectrophotometrically. Absorptions were measured at three wavelengths 478 (the λ_{max} for the *mer* isomer where the maximum change occurs), 520, and 416 nm (Fig. 6). Both the initial and the final absorptions were higher at all wavelengths (progressively with increasing OH^- concentration) than those measured in acid (ε_{478} for *fac*: 62 in 0.01 M HCl, initially 71 in 0.1 M NaOH, initially 86 in 0.5 M NaOH). This greater *initial* absorption is attributed to deprotonation.[17,33]

The *subsequent* increases in absorption do not correspond to a single pseudo-first-order reaction, but the absorptions versus time plots show inflections at early stages of the overall reaction. This is particularly clear in the 0.1 M NaOH reaction (Fig. 7), where the inflection in the absorption occurs at 2—3 h. These inflections correspond to the humps on the HPLC versus time plots for the *fac* and the *mer* isomers for the corresponding isomerizations as followed by Sephadex chromatography and HPLC analysis (Fig. 5). With 0.5 M NaOH, irregularities in the absorption versus time plots are evident up to the first 2 h of the reaction as followed both by in-situ spectrophotometry and Sephadex/HPLC chromatography. These plots for the different NaOH concentrations again demonstrate a base dependence of the overall reaction rate.

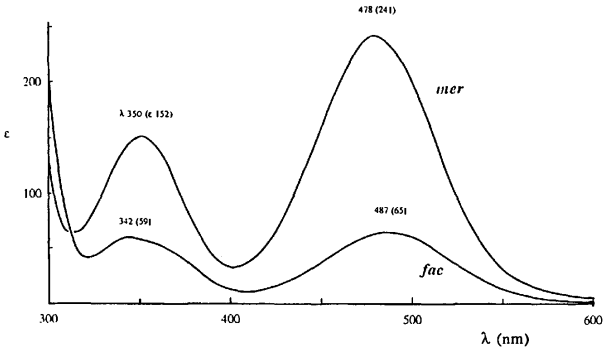

Fig. 6. Absorption spectra in 0.01 M HCl. (a) *mer*-[Co(hexacyclen)]$Br_3 \cdot H_2O$; (b) *fac*-[Co(hexacyclen)]Cl_3.

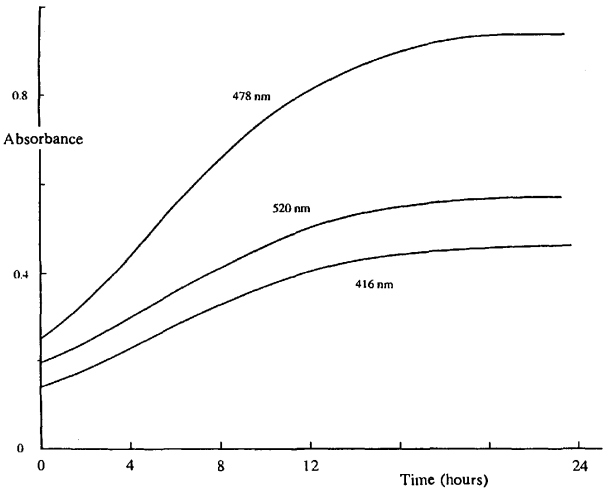

Fig. 7. Absorbance changes during isomerization of *fac* in 0.1 M NaOH at 50 °C.

The occurrence of an inflection (induction period) in the absorbance versus time plots (for different OH^- concentrations and different wavelengths) suggests that the reaction may be described as a series first order scheme **A**→**B**→**C** involving an intermediate **B**.[39] However, plots of the absorbance data as $\log(A_\infty - A_t)$ versus time gave continuous curves having no linear latter sections. We take these results to indicate that the two steps k_1 and k_2 are of comparable rates, or that the overall reaction involves autocatalysis. The steps are not readily analyzed, since the absorbance is a function of at least three varying species.

The Mode of Isomerization. Since a twist is implausible for the *fac*⇄*mer* isomerization, the reaction presumably proceeds by a bond-rupture process. Also, the observed approximately first-order base dependence suggests that a deprotonated intermediate is involved, and the rapid and reversible darkening in base of both isomers is consistent with this proposal.

A scheme of bond rupture and deprotonation steps which can connect all the *fac* and *mer* isomers is shown in Fig. 8. From *fac*, two enantiomeric trigonal-bipyramidal intermediates can arise, and on re-association these could together yield the racemic components ($\Lambda,\delta+\Delta,\lambda$) of *one* the *mer* diastereoisomers. Inversion of configuration at the equatorial nitrogen center in the intermediate (denoted N* in Fig. 8), which is adjacent to the dissociated nitrogen, is required for the detached rings to change their position on re-association to regain octahedral coordination, and the deprotonation thus required at this N* should make the *fac*→*mer* reaction base dependent. Pi-donor bonding to cobalt of this amide group in the trigonal plane could stabilize the five-coordinate intermediate.[20a,40,41] Inversion of configuration is required also at the dissociated nitrogen for the *fac*→*mer* change, but such inversions of free amines are rapid (and should occur within the lifetime of the

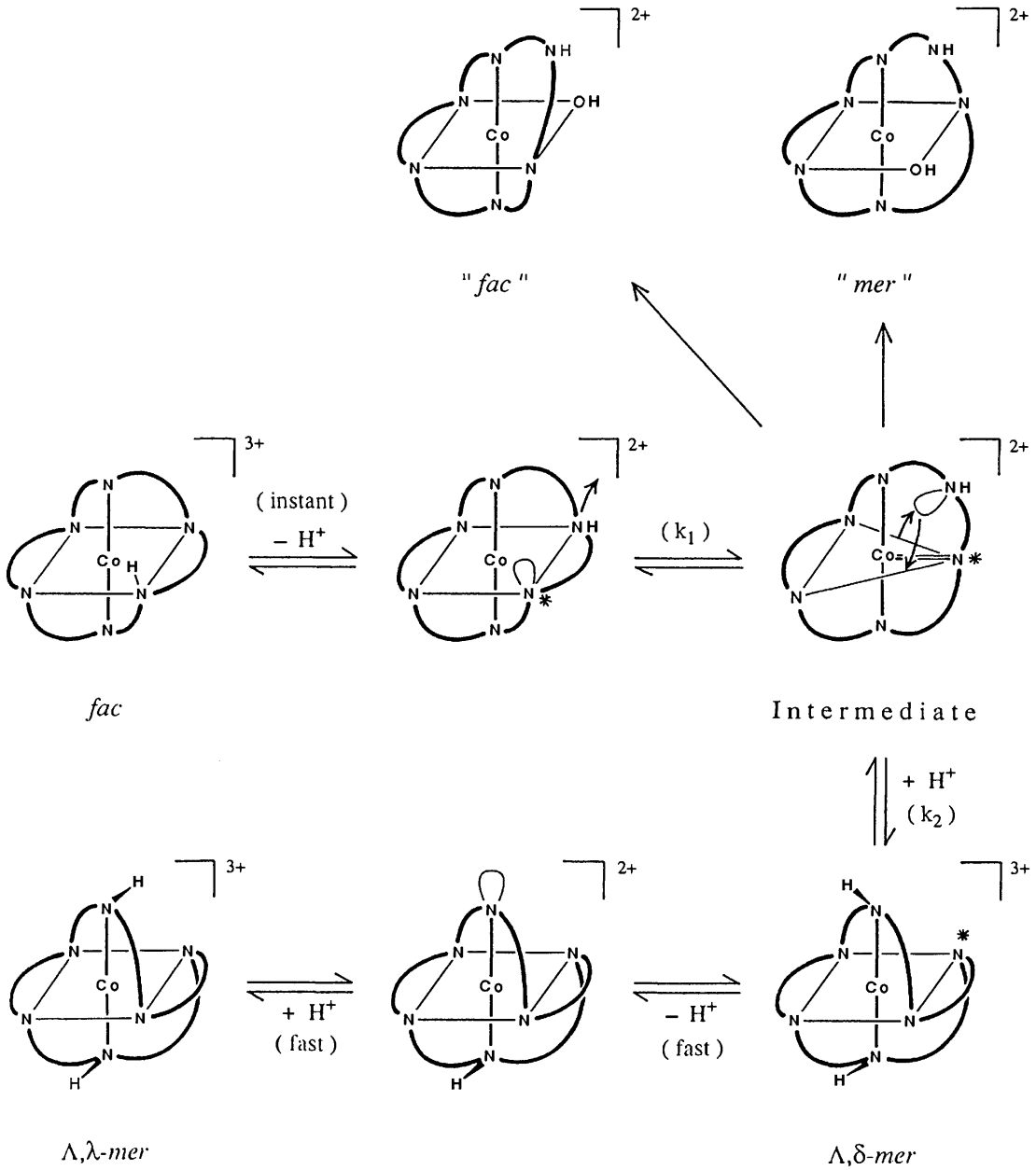

Fig. 8. Bond rupture and deprotonation processes giving *fac* ⇄ *mer* [Co(hexacyclen)]$^{3+}$. Only one enantiomer is shown for the trigonal bipyramid intermediate and for the *mer* diastereoisomers.

trigonal-bipyramid intermediate) and do not exhibit a base dependence.

The HPLC results are consistent with this proposed scheme. The changes in the HPLC "*fac*" peak indicate a slow build up of some intermediate species, since the peak apparently remains constant in magnitude for some time before then decreasing. Also, some residual small peaks (close to the *fac*) become unmasked in the latter stage of reaction when the sharp peak of the octahedral *fac* isomer has largely disappeared. We now identify this intermediate as the proposed trigonal bipyramid, formed slowly by step k_1.

The HPLC *mer* elution versus time plot at 0.05 M NaOH shows an inflection which is consistent with the proposed scheme of consecutive first order reactions involving one intermediate.[39] At the higher NaOH concentrations, however, the *mer* elution curves show in addition humps which indicate that some other species becomes involved under these conditions. It is difficult to see that the hump could be due to an increased amount of the *mer* isomer (irregularly generated, from some other intermediate), and it seems more likely that at these higher NaOH concentrations some other species is formed which elutes similarly to the *mer* so that it is masked, but is detected along with the *mer*.

The spectrophotometric kinetic observations are

also consistent with the proposed consecutive steps scheme, where the rates k_1 and k_2 are indicated to be comparable.

That the isomerization is slow suggests that the trigonal bipyramid intermediate is long-lived, and competition experiments employing strong nucleophiles might be useful to check this. However the present reacting solutions contained Cl^- and OH^- as potential nucleophiles in concentrations greatly exceeding cobalt, and formation of species such as $[Co(hexacyclen)OH]^{2+}$ is plausible (Fig. 8). These may be the species suggested as contributing to the apparent *mer* hump in the HPLC elution curves for the higher NaOH concentration conditions.

The concomitant formation of hydrolysis products (or other substitution products) could be expected, as the proposed five-coordinate intermediate in the *fac*⇄*mer* isomerization (with an uncoordinated amino group) is similar to the intermediate in the generally accepted SN_1CB mechanism for the base hydrolysis of cobalt(III) amine complexes.[40-43] Hydrolysis was especially evident in the isomerization (from *mer*) carried out in phosphate, where the carmine Sephadex band may have contained phosphate-substituted products. It is also relevant that the species *cis*-$[Co(en)_2(mono\text{-}en)(OH)]^{2+}$ is formed as the main product in the base hydrolysis of *cis*-$[Co(en)_2(mono\text{-}enH)Cl]^{3+}$, showing that the free amino group of the monodentate-en ligand does not compete favorably with water for the vacant coordination site in the proposed five-coordinate intermediate.[42] The formation of $[Co(hexacyclen)(OH)]^{2+}$ may be a parallel situation.

With some macrocyclic complex systems closely analogous to $[Co(hexacyclen)]^{3+}$, Royer and coworkers[7] found that equilibrations between *fac* and *mer* isomers were generally facile, and attributed this to the high strain in these macrocyclic structures.[44] We believe that these *fac*→*mer* changes can be accommodated by our proposal of a single Co-N bond rupture, and that the more drastic simultaneous breaking of *two* adjacent Co-N bonds as suggested previously[7] is not necessary.

Although no twist processes are possible for the direct change *fac*→*mer* $[Co(hexacyclen)]^{3+}$, a twist process can be envisaged for direct inversion of one *mer* diastereoisomer, $\Lambda,\lambda \rightleftarrows \Lambda,\delta$ (Fig. 9), and this need not involve deprotonation. Inversion of the other *mer* diastereoisomer Λ,δ does not seem possible directly by a twist, but inversion could occur indirectly through two alternative routes. One path is through the symmetrical *fac* isomer, Λ,δ-*mer*⇄*fac*⇄Δ,λ-*mer*, involving deprotonations and inversions at two nitrogen centers (Fig. 8). The second possible route is through the other diastereoisomer Λ,λ involving one deprotonation and NH inversion step, followed by the twist. We can not envisage direct formation of the $(\Lambda,\lambda/\Lambda,\delta)$-*mer* diastereoisomer from the *fac*, and we

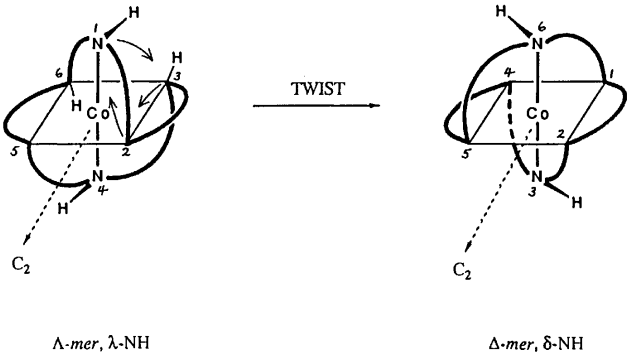

Fig. 9. Possible twist process for *mer*-[Co(hexacyclen)]$^{3+}$ giving inversion around cobalt. The process (as shown) need not involve inversion at a N center, so that it could be independent of pH.

suppose its formation to be via the $(\Lambda,\delta/\Delta,\lambda)$ diastereoisomer (Fig. 8). However, in the present experiments only the total of all the *mer* isomers is calculated, so that the alternative possible routes for the *mer* interconversions are not distinguished.

The present HPLC results show that the interconversion of the *mer* diastereoisomers by NH exchange is rapid, being in evidence at pH 4 over 15 min at 20 °C. The inversion of the *mer* diastereoisomers is of interest, since the relative rates of this inversion and the *mer*→*fac* conversion might provide evidence about the possible *mer* twist process. However, isolation of the *mer* in optically active forms has not yet been achieved. Royer[7] did however obtain a partial resolution of the *mer* material by Sephadex chromatography using acidified 0.3 M sodium (+)-tartrate as eluent, and CD curves were given of two separated fractions, which were both assigned as having the Λ configuration around the cobalt. However, isolation from solution as the perchlorate salt gave only racemic crystals. The structure reported for these was the diastereoisomer $\Lambda,\lambda/\Lambda,\delta$ racemate,[45] but the occurrence of racemization during crystallization precluded identification of this solid with the order of elution of the two *mer* diastereoisomers by Sephadex/Na_2SO_4/H^+ chromatography.

Although the pH conditions used for these experiments were not given, the reported results indicate that inversions of configuration around the cobalt $\Delta \rightleftarrows \Lambda$ in the *mer* geometry are facile.[7] It is difficult therefore to see that these inversions could proceed via the demonstrated slow *mer*→*fac* pathway involving bond rupture, so that a twist process seems likely for these interconversions within the *mer* geometry.

Results obtained recently by Larsen with isomerization of $[Co(aeaps)_2]^{3+}$ in base[1,46] have bearing on the present work. For the reaction of different isomers in 1 M NaOH, a sequential process $A \xrightarrow{k_1\ (fast)} B \xrightarrow{k_2\ (slow)} C$ was found, as deduced herein for the $[Co(hexacyclen)]^{3+}$ system. For this thioether system the individual steps could be separated and were quite slow

($t_{1/2}$=85 s and 23 min at 1 °C) and there seemed to be no evidence (no instant darkening) for a preliminary deprotonation at coordinated amine. The product solution **C** contained at least three species at equilibrium, one of which (20% proportion) was found to be [Co(aeaps)(aeaps-H)]$^{2+}$ [1] involving coordination of a carbanion group on one ligand rather than the thioether sulfur as in the reactants. Although this result is thought provoking, it is likely that this situation of alkyl group coordination is unique to a substrate complex with a six-membered ring having a thioether sulfur donor, and the analogous situation in the [Co(hexacyclen)]$^{3+}$ system seems implausible. Nevertheless, these results clearly show that the isomerization process is not simple and that several products may result.

Finally, cobalt(III) complexes of the types [Co(tetars)X_2]$^{n+}$ [1] and [Co(diars)$_2X_2$]$^{n+}$,[1] each with four tertiary arsine donor centers, are very prone to rapid catalytic substitution and topological equilibration which are supposed to occur via electron transfer with a labile cobalt(II) species.[47,48] These cobalt(II) species are presumed to be produced by spontaneous internal reduction of the cobalt atom and the simultaneous oxidation of the bound ligands X, since the isomerizations occur particularly in concentrated solutions, in reducing solvents like alcohols, and in the presence of excess of X^- where X^- is mildly reducing such as Br^- and NCS^-. These catalytic reactions are characterized by erratic kinetic behavior, such as the non-smooth loss of optical activity in substitution, cis→trans isomerization, or racemization reactions.[47,48] However such involvement of cobalt(II) is expected to be much less with isomerizations in cobalt(III)-amine complexes (amine=NH_3, en, dien, dpt[1]) where spontaneous reductions occur only under forcing conditions.[49,50] Although our work with [Co(hexacyclen)]$^{3+}$ did not involve conditions which were found to favour the catalysis in the arsine systems, there was some evidence of erratic behavior so that the involvement of cobalt(II) in catalytic amounts can not be absolutely excluded in the [Co(hexacyclen)]$^{3+}$ system.[53]

Parts of this work were carried out during leaves at the Departments of Chemistry at University of Otago, Dunedin, New Zealand, and James Cook University, Townsville, Australia. The use of facilities at those Departments and helpful discussions with D. A. Buckingham (Otago) and F. R. Keene (James Cook) are gratefully acknowledged. P. McDuie (Adelaide) kindly assisted with the atomic absorption measurements.

References

1) Ligand abbreviations: hexacyclen=1,4,7,10,13,16-hexaazacyclooctadecane; dien=diethylenetriamine; medien=4-methyldiethylenetriamine, or 2,2′-(methylimino)bis[ethylamine], $H_2NCH_2CH_2N(Me)CH_2CH_2NH_2$; linpen= 3,6,9,12-tetraazatetradecane-1,14-diamine, or "linear pentaethylenehexamine"; pn=1,2-propanediamine; daes=bis(2-aminoethyl) sulfide, $H_2NCH_2CH_2SCH_2CH_2NH_2$; tacd=1,4,7-triazacyclodecane; stn=1,1,1-tris(5-amino-2-azapentyl)ethane, or 5,5′,5″-ethylidynetris[4-azapentan-1-amine]; aeaps=(2-aminoethyl)(3-aminopropyl)sulfide, $H_2N(CH_2)_2S(CH_2)_3NH_2$; aeaps-H=$H_2N(CH_2)_2S(CH^-)(CH_2)_2NH_2$; tetars=$Me_2As(CH_2)_3AsPh(CH_2)_2AsPh(CH_2)_3AsMe_2$; diars=*o*-phenylenebis[dimethylarsine]; dpt=4-azaheptane-1,7-diamine, common name "dipropylenetriamine".

2) The absolute configurations of *mer*-[Co(hexacyclen)]$^{3+}$ are defined in terms of skew pairs of the octahedron edges spanned by chelate rings, Ref. 3. *Λ-mer* has 6*Λ* and 2*Δ* skew pairs. The different relative NH orientations are designated *λ*-NH or *δ*-NH according to their chirality, as with *mer*-[Co(dien)$_2$]$^{3+}$, Ref. 4.

3) IUPAC Commission on Inorganic Chemical Nomenclature, *Inorg. Chem.*, **9**, 1 (1970).

4) F. R. Keene and G. H. Searle, *Inorg. Chem.*, **11**, 148 (1972).

5) Y. Yoshikawa, *Chem Lett.*, **1978**, 109.

6) R. W. Hay, B. Jeragh, S. F. Lincoln, and G. H. Searle, *Inorg. Nucl. Chem. Lett.*, **14**, 435 (1978).

7) D. J. Royer, G. J. Grant, D. G. Van Derveer, and M. J. Castillo, *Inorg. Chem.*, **21**, 1902 (1982).

8) K. Sakakibara, Y. Yoshikawa, and H. Yamatera, *Bull. Chem. Soc. Jpn.*, **52**, 2725 (1979).

9) S. E. Harnung, S. Kallesoe, A. M. Sargeson, and C. E. Schäffer, *Acta Chem. Scand., Ser. A*, **28**, 385 (1974).

10) G. H. Searle, F. R. Keene, and S. F. Lincoln, *Inorg. Chem.*, **17**, 2362 (1978).

11) A. Hammershoi and E. Larsen, *Acta Chem. Scand., Ser. A*, **32**, 485 (1978).

12) P. D. Totterdell and M. Spiro, *J. Chem. Soc., Dalton Trans.*, **1979**, 1324.

13) F. R. Keene, I. A. S. McDonald, and G. H. Searle, *Aust. J. Chem.*, **34**, 1331 (1981).

14) G. H. Searle and M. E. Angley, *Inorg. Chim. Acta*, **49**, 185 (1981).

15) F. R. Keene and G. H. Searle, *Inorg. Chem.*, **13**, 2173 (1974).

16) M. J. Bjerrum and E. Larsen, *Acta Chem. Scand., Ser A*, **39**, 465 (1985).

17) L. R. Gahan, T. W. Hambley, G. H. Searle, M. J. Bjerrum, and E. Larsen, *Inorg. Chim. Acta*, **147**, 17 (1988).

18) Under similar conditions, the optical isomers of each of *u-fac* and *mer*-[Co(dien)$_2$]$^{3+}$ were separable on HPLC, as found also by chromatography on Sephadex columns with this tartrato(4−)diantimonate(III) eluent, Ref. 19.

19) Y. Yoshikawa and K. Yamasaki, *Bull. Chem. Soc. Jpn.*, **45**, 179 (1972); *Coord. Chem. Rev.*, **28**, 205 (1979).

20) F. Basolo and R. G. Pearson, "Mechanisms of Inorganic Reactions," 2nd ed., Wiley, New York (1967). a) p. 174; b) pp. 289—291, 313—322.

21) F. P. Dwyer and A. M. Sargeson, *Nature(London)*, **187**, 1022 (1960); F. P. Dwyer and A. M. Sargeson, *J. Phys. Chem.*, **65**, 1892 (1961).

22) G. A. Lawrance and D. R. Stranks, *Inorg. Chem.*, **16**, 929 (1977).

23) G. A. Lawrance and S. Suvachittanont, *Inorg. Chim. Acta Lett.*, **32**, L13 (1979).

24) W. R. Robinson, D. E. Wigley, and R. A. Walton,

Inorg. Chem., **24**, 918 (1985).

25) L. Christiansen, D. N. Hendricksen, H. Toftlund, S. R. Wilson, and C-L. Xie, *Inorg. Chem.*, **25**, 2813 (1986).

26) S. S. Eaton, J. R. Hutchinson, R. H. Holm, and E. L Muetterties, *J. Am. Chem. Soc.*, **94**, 6411 (1972).

27) S. S. Eaton, G. R. Eaton, R. H. Holm, and E. L. Muetterties, *J. Am. Chem. Soc.*, **95**, 1116 (1973).

28) G. A. Lawrance, S. Suvachittanont, D. R. Stranks, P. A. Tregloan, L. R. Gahan, and M. J. O'Connor, *J. Chem. Soc., Chem. Commun.*, **1979**, 757; *Inorg. Chem.*, **19**, 3443 (1980).

29) K. Tomioka, T. Kashihara, U. Sakaguchi, and H. Yoneda, *Chem. Lett.*, **1984**, 1047.

30) The complex tris(2-pyridylmethyl)-1,4,7-triazacyclononaneiron(II), $[Fe(tptcn)]^{2+}$, has topology analogous to that of $[Co(stn)]^{3+}$ but the ring couplings do not involve secondary amines, and recently this complex was elegantly shown to racemize rapidly and without base catalysis, Ref. 25. This probably occurs by a trigonal twist associated with the high-spin state, since this particular ligand gives a "crossover complex" with Fe(II). Such involvement of the high-spin state with Co(III) systems is much less likely.

31) G. H. Searle, *Aust. J. Chem.*, **30**, 2625 (1977).

32) Relative R_x values *fac/mer*, measured for minimal loadings of the complexes on small columns as in Ref. 31, are 6.2 for 0.1 M Na_3PO_4 and 2.1 for 0.2 M Na_2SO_4/H_2SO_4 pH 2.

33) R. J. Geue, T. W. Hambley, J. M. Harrowfield, A. M. Sargeson, and M. R. Snow, *J. Am. Chem. Soc.*, **106**, 5478 (1984).

34) Y. Yoshikawa and K. Yamasaki, *Bull. Chem. Soc. Jpn.*, **46**, 3448 (1973); Y. Yoshikawa, *ibid.*, **49**, 159 (1976).

35) G. H. Searle and R. J. Geue, *Aust. J. Chem.*, **37**, 959 (1984).

36) T. J. Atkins, J. E. Richman, and W. F. Oettle, *Org. Synth.*, **58**, 86 (1978).

37) Hydrolysis bands which eluted with this Na_2SO_4/H_2SO_4 eluent between the *fac* and *mer* from the isomerizations in Na_3PO_4 at 80 °C (see above) were not evident.

38) G. H. Searle and F. R. Keene, *Inorg, Chem.*, **11**, 1006 (1972).

39) T. W. Moore and R. G. Pearson, "Kinetics and Mechanism," 3rd ed, Wiley, New York (1981), p. 290.

40) M. L. Tobe, in IUPAC, "Coordination Chemistry-20," ed by D. Banerjea, Pergamon, Oxford (1980), p. 47.

41) D. A. Buckingham, P. A Marzilli, and A. M. Sargeson, *Inorg. Chem.*, **8**, 1595 (1969).

42) R. W. Hay and K. B. Nolan, *J. Chem. Soc., Dalton Trans.*, **1975**, 1621.

43) P. Comba and A. M. Sargeson, *J. Chem. Soc., Chem. Commun.*, **1985**, 51.

44) Equilibrations in 1,4,7,10,13,16-tri-(*R,R*)-cyclohexano[*b,h,n*]hexaazacyclooctadecanecobalt(III), $[Co(TC18N6)]^{3+}$, were reported to be facile at pH>7 and pH<1 and were accompanied by decomposition. With 1,4,8,11,15,18-hexaazacycloheneicosanecobalt(III) $[Co(21N6)]^{3+}$ only the one isomer *fac* was apparent in solution and was partially resolved by chromatography. This isomer apparently racemized in solution (conditions not stated), and it isomerized on crystallization to give one of the three possible *mer* diastereoisomers, Ref. 7.

45) This $\Lambda,\lambda/\Lambda,\delta$ diastereoisomer was designated as $\Lambda(\delta\delta\delta)\Lambda(\lambda\lambda\delta)$-*mer*-(1,2) in terms of one enantiomer in Ref. 7.

46) M. J. Bjerrum, M. Gajhede, E. Larsen, and J. Springbϕrg, *Inorg. Chem.*, **27**, 3960 (1988).

47) B. Bosnich, W. G. Jackson, and J. W. McLaren, *Inorg. Chem.*, **13**, 1133 (1974).

48) B. Bosnich, W. G. Jackson, and S. B. Wild, *Inorg. Chem.*, **13**, 1121 (1974).

49) S. Lum, L. Ereshefsky, and C. S. Garner, *J. Inorg. Nucl. Chem.*, **35**, 1591 (1973).

50) Some Co(II) is formed on heating Co(III)-amine complexes: traces of Co(II) are formed on heating $[Co(dien)(en)Cl]Cl_2$ in alcohols,[51] or heating $[Co(en)_3]Cl_3$ in aqueous en;[21,51] substantial Co(II) is generated on heating $[Co(en)_3]Cl_3$[51] or $[Co(en)_2Cl_2]Cl \cdot 2H_2O \cdot HCl$[52] in the solid state.

51) F. P. Dwyer, "Advances in the Chemistry of the Coordination Compounds," (Proceedings Sixth ICCC), ed by S. Kirschner, MacMillan, New York (1961), p. 21.

52) J. Springbϕrg and C. E. Schäffer, *Inorg. Synth.*, **14**, 68 (1973).

53) After heating $[Co(en)_3]Cl_3$ in 0.01 M NaOH at 50 °C for 6 h, the presence of Co(II) was uncertain, being around the detection limit of 2×10^{-4} M. The detection of Co(II) provides no evidence that electron transfer is involved in the mechanism. The test involves acidification with HNO_3, addition of excess KCNS, centrifuging the precipitated $[Co(III)](CNS)_3$, and addition of amyl alcohol to the (pipetted off) supernatant.

The Molecular Structure of the Heterodinuclear Organometallic Complex of Platinum and Tungsten, Phenyl(1,5-cyclooctadiene)platinum-tricarbonyl(η^5-cyclopentadienyl)tungsten

Kunio MIKI,* Nobutami KASAI, Isao ENDO,† and Sanshiro KOMIYA†
Department of Applied Chemistry, Faculty of Engineering, Osaka University, Yamadaoka, Suita, Osaka 565
†Department of Applied Chemistry for Resources, Tokyo University of Agriculture and Technology, Nakamachi, Koganei, Tokyo 184
(Received June 22, 1989)

Synopsis. The structure of the novel heterodinuclear organometallic complex, [(cod)(Ph)Pt-W(CO)$_3$(η^5-C$_5$H$_5$)] has been determined by X-ray crystallography; the Pt-W bond distance is 2.844(1)Å.

Special attention has been drawn recently to heterobimetallic compounds from the viewpoint of their catalytic abilities.[1] Little is so far known, however, about chemistry of heterodinuclear organometallic complexes, especially those containing a direct bond between different transition metals.[2] We have recently reported the preparation of a series of heterodinuclear organometallic complexes containing platinum and tungsten of the type, [(cod)(R)Pt-W(CO)$_3$(η^5-C$_5$H$_5$)] (R=Me, Et, Ph, or tolyl), which show a unique alkyl-transfer reaction from the platinum to tungsten atoms.[3] We describe here the structure of one of these complexes, [(cod)(Ph)Pt-W(CO)$_3$(η^5-C$_5$H$_5$)] established by X-ray crystallography.

Experimental

The title compound was prepared by the method previously reported.[3] The crystals were obtained as deep red plates from dichloromethane-hexane solutions.

Crystal Data. $C_{22}H_{22}O_3PtW$, M=713.4, monoclinic, $P2_1/n$, a=14.291(3), b=12.731(2), c=12.027(3), Å, β=112.48(2)°, U=2021.9(7) Å^3, Z=4, D_c=2.343 g cm^{-3}, μ(Mo $K\alpha$)=133.1 cm^{-1}.

A crystal with approximate dimensions of 0.10×0.50×0.55 mm sealed in a thin-glass capillary under nitrogen was mounted on a Rigaku automated four-circle diffractometer. Accurate unit-cell parameters were determined by the least-squares fit of 2θ values of 25 strong reflections ($21.8<2\theta<29.9°$). Intensity data collection was carried out using Mo $K\alpha$ radiation by the θ-2θ scan mode. The scan speed and range were 4° min^{-1} in 2θ and $\Delta(2\theta)=(1.8+0.7\tan\theta)°$, respectively. The background intensities were measured for 5 s at both ends of a scan. A total of 4413 independent reflections (R_{int}=0.012) were collected with $\sin\theta/\lambda$ up to 0.64. Absorption correction was applied to the intensity data.[4] The minimum normalized transmission factor which was based on intensities obtained by the azimuthal scan of 404 and $\bar{4}0\bar{4}$ reflections was 0.10.

The structure was solved by the heavy atom method and refined by the block-diagonal least-squares procedure using HBLS-V.[5] Non-hydrogen atoms were refined anisotropically except for the C(1), C(20), and O(1) atoms which were refined with the isotropic thermal parameters. All the hydrogen atoms whose positions were estimated from stereochemical consideration were included in the structure factor calculation. At the final stages of refinement, two reflections (200 and 002) were excluded due to the extinction effects. The final R and R_w values are 0.070 and 0.075 for 3778 [$|F_o|>3\sigma(|F_o|)$] reflections. The weighting scheme used in the final refinement cycles is $w=(\sigma_{cs}^2-0.100|F_o|+0.017|F_o|^2)^{-1}$. The atomic scattering factors were taken from the International Tables for X-ray Crystallography.[6] The final atomic parameters are listed in Table 1.§

Table 1. Fractional Atomic Coordinates and (Equivalent) Isotropic Thermal Parameters of Non-H Atoms with e.s.d.'s in Parentheses

Atom	x	y	z	B_{eq}[a]/B**(Å^2)
Pt	0.39951(3)	0.27668(3)	0.27760(4)	2.8
W	0.54984(4)	0.36778(3)	0.20679(4)	3.2
C(1)	0.4527(9)	0.1388(7)	0.2442(11)	3.4(2)**
C(2)	0.5298(9)	0.0870(8)	0.3332(11)	3.8
C(3)	0.5644(11)	−0.0127(8)	0.3077(15)	5.8
C(4)	0.5229(12)	−0.0611(8)	0.2018(16)	6.0
C(5)	0.4386(12)	−0.0079(9)	0.1084(13)	5.4
C(6)	0.4044(9)	0.0907(8)	0.1308(12)	4.1
C(7)	0.2605(9)	0.2010(7)	0.2812(12)	4.1
C(8)	0.3399(9)	0.1957(7)	0.3969(11)	3.7
C(9)	0.3500(11)	0.2640(8)	0.5008(12)	4.7
C(10)	0.3232(10)	0.3822(8)	0.4725(12)	4.3
C(11)	0.3539(9)	0.4209(7)	0.3725(11)	4.1
C(12)	0.2941(10)	0.4253(7)	0.2522(11)	3.9
C(13)	0.1900(10)	0.3806(8)	0.1955(12)	4.7
C(14)	0.1704(9)	0.2797(8)	0.2469(13)	4.5
C(15)	0.6950(12)	0.2772(13)	0.2503(15)	7.9
C(16)	0.7131(14)	0.3843(11)	0.2099(20)	8.9
C(17)	0.6488(14)	0.3911(11)	0.0949(20)	8.5
C(18)	0.5982(15)	0.2994(13)	0.0602(16)	8.6
C(19)	0.6264(11)	0.2280(9)	0.1456(15)	5.7
C(20)	0.5292(10)	0.5176(8)	0.2159(11)	4.1(3)**
C(21)	0.5694(9)	0.3534(6)	0.3781(10)	3.5
C(22)	0.4075(9)	0.3577(7)	0.0932(11)	3.8
O(1)	0.5192(8)	0.6081(6)	0.2247(9)	5.7(2)**
O(2)	0.5957(7)	0.3482(6)	0.4832(8)	4.9
O(3)	0.3303(7)	0.3575(6)	0.0117(9)	5.7

a) As defined by Hamilton.[7]

Computations were done on an ACOS 930 computer at the Research Center for Protein Engineering, Institute for Protein Research, Osaka University.

Results and Discussion

The molecular structure is depicted in Fig. 1 with atomic numbering systems. Bond distances and angles are listed in Table 2. The Pt-W bond distance is 2.844(1) Å, which is corresponding to the sum of

§ Tables for anisotropic temperature factors, for atomic coordinates of hydrogen atoms, and for observed and calculated structure factors are deposited as Document No. 8909 at the Office of the Editor of Bull. Chem. Soc. Jpn.

covalent bond radii of platinum and tungsten [2.85 Å]. This value falls in the range of metal-to-metal bond lengths [2.60—2.90 Å average 2.76 Å] in the platinum-tungsten complexes so far reported[9] but is classified to somewhat long distance among them.

The geometry around the platinum atom is typically square-planar where the carbon (phenyl) atom, the centers of two C=C double bonds of the cod ligand, and the tungsten atom are coplanar to each other [maximum deviation 0.07 Å]. It is noteworthy that the tungsten atom occupies one of four corners of the square-planar geometry, because platinum-tungsten complexes whose structures have been hitherto elucidated[9] always contain bridging μ-ligands between two metal atoms and the arrangement of ligands around the platinum atom is far from square-planer geometry.§§ On the other hand, the geometry around the tungsten atom is square-pyramidal, where the center of the η^5-C_5H_5 ligand is located at an apical position. These geometrical features around both metal atoms are consistent with the d^8 and d^6 electronic configurations of platinum and tungsten, respectively, which are also supported by the spectroscopic results.[3]

Table 2. Selected Bond Distances and Bond Angles for Non-H Atoms with e.s.d.'s in Parentheses

(a) Bond distance/Å			
Pt-W	2.8435(7)	Pt-C(1)	2.014(13)
Pt-C(7)	2.223(14)	Pt-C(8)	2.186(13)
Pt-C(11)	2.381(13)	Pt-C(12)	2.365(14)
Pt-C(21)	2.463(12)	Pt-C(22)	2.488(13)
W-C(15)	2.254(18)	W-C(16)	2.328(24)
W-C(17)	2.314(24)	W-C(18)	2.297(21)
W-C(19)	2.350(18)	W-C(20)	1.940(14)
W-C(21)	1.979(12)	W-C(22)	1.974(13)
C(1)-C(2)	1.38(2)	C(1)-C(6)	1.41(2)
C(2)-C(3)	1.44(3)	C(3)-C(4)	1.33(3)
C(4)-C(5)	1.46(3)	C(5)-C(6)	1.41(3)
C(7)-C(8)	1.42(2)	C(7)-C(14)	1.56(2)
C(8)-C(9)	1.48(2)	C(9)-C(10)	1.56(2)
C(10)-C(11)	1.51(2)	C(11)-C(12)	1.37(2)
C(12)-C(13)	1.49(2)	C(13)-C(14)	1.50(2)
C(15)-C(16)	1.50(3)	C(15)-C(19)	1.41(3)
C(16)-C(17)	1.34(4)	C(17)-C(18)	1.35(4)
C(18)-C(19)	1.31(3)	C(20)-O(1)	1.17(2)
C(21)-O(2)	1.17(2)	C(22)-O(3)	1.16(2)
(b) Bond angle/°			
W-Pt-C(1)	84.8(4)	W-Pt-C(7)	164.9(4)
W-Pt-C(8)	156.5(4)	W-Pt-C(11)	101.9(4)
W-Pt-C(12)	98.8(4)	W-Pt-C(21)	43.1(3)
W-Pt-C(22)	42.8(3)	C(1)-Pt-C(7)	92.0(5)
C(1)-Pt-C(8)	89.5(5)	C(1)-Pt-C(11)	164.1(5)
C(1)-Pt-C(12)	160.4(5)	C(7)-Pt-C(11)	85.1(5)
C(7)-Pt-C(12)	79.6(5)	C(8)-Pt-C(11)	78.6(5)
C(8)-Pt-C(12)	94.2(5)		
Pt-W-C(15)	117.1(5)	Pt-W-C(16)	154.0(6)
Pt-W-C(17)	157.9(6)	Pt-W-C(18)	124.0(6)
Pt-W-C(19)	106.3(5)	Pt-W-C(20)	103.6(4)
Pt-W-C(21)	58.2(4)	Pt-W-C(22)	58.9(4)
C(16)-W-C(20)	94.8(8)	C(16)-W-C(21)	104.5(7)
C(16)-W-C(22)	141.1(7)	C(19)-W-C(20)	149.5(6)
C(19)-W-C(21)	111.0(6)	C(19)-W-C(22)	102.4(6)
C(20)-W-C(21)	89.8(6)	C(20)-W-C(22)	87.9(6)
C(21)-W-C(22)	114.4(6)		
Pt-C(1)-C(2)	120.9(10)	Pt-C(1)-C(6)	119.2(10)
Pt-C(7)-C(8)	69.8(8)	Pt-C(7)-C(14)	111.8(9)
C(8)-C(7)-C(14)	124.0(12)	Pt-C(8)-C(7)	72.6(8)
Pt-C(8)-C(9)	109.8(9)	C(7)-C(8)-C(9)	125.5(12)
C(8)-C(9)-C(10)	116.5(12)	C(9)-C(10)-C(11)	111.6(12)
Pt-C(11)-C(10)	110.2(9)	Pt-C(11)-C(12)	72.6(8)
C(10)-C(11)-C(12)	126.8(12)	Pt-C(12)-C(11)	73.9(8)
Pt-C(12)-C(13)	103.2(9)	C(11)-C(12)-C(13)	125.3(12)
C(12)-C(13)-C(14)	116.7(12)	C(7)-C(14)-C(13)	113.2(12)
W-C(20)-O(1)	178.0(12)	W-C(21)-O(2)	170.1(11)
W-C(22)-O(3)	168.1(12)		

The other remarkable features of the structure are the existences of strong trans-influence on the platinum atom and of the weak interaction between the platinum atom and two CO groups. Firstly, the Pt-C(11) and Pt-C(12) bonds (trans to C(phenyl)) of 2.381(13) and 2.365(14) Å are obviously longer than the Pt-C(7) and Pt-C(8) bonds (trans to W) of 2.223(14) and 2.186(13) Å. This shows stronger trans-influence from the phenyl group than that from the tungsten atom. Secondly, among three carbonyl groups attached to the tungsten atom, two of them (C(21)≡O(2) and C(22)≡O(3)) are located as if attacking the Pt-W bond from both sides. Although the Pt···C(21) and Pt···C(22) distances of 2.463(12) and 2.488(12) Å are much longer than those expected for the Pt-C bond as the μ-CO ligands, the W-C(21) and

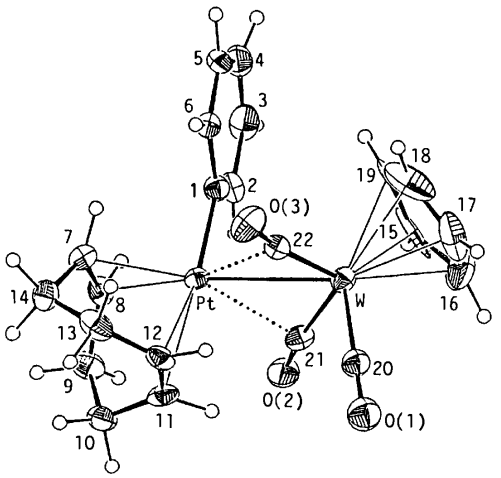

Fig. 1. The molecular structure[8] of [(cod)(Ph)Pt-W(CO)$_3$(η^5-C_5H_5)] together with the numbering scheme (only atomic numbers are shown for carbon atoms). Non-hydrogen atoms are represented by thermal ellipsoids at 30% probability levels, while hydrogen atoms are drawn by spheres with B=1.0 Å^2. Selected coordination angles not appeared in Table 2 are as follows; W-Pt-C(11/12)=100.8, C(1)-Pt-C(7/8)=90.8, C(7/8)-Pt-C(11/12)=83.8 (C(7/8) and C(11/12): midpoints of the C(7)-C(8) and C(11)-C(12) bonds, respectively), CCP-W-Pt=136.5, CCP-W-C(20)=119.9, CCP-W-C(21)=119.4, CCP-W-C(22)=117.9° (CCP: center of gravity of the η^5-cyclopentadienyl ring).

§§ In the hydrido-bridged complex, [(Et$_3$P)$_2$(Ph)Pt(μ-H)W(H)(η^5-C_5H_5)$_2$], the square-planar geometry is apparently observed in case that the bridging hydrido ligand is ignored.[10]

W-C(22) bonds of 1.979(12) and 1.974(13) Å are slightly lengthened and the W-C(21)-O(2) and W-C(22)-O(3) angles of 170.1(11) and 168.1(12)° are slightly bent when compared with those of the other free CO group; W-C(20)=1.940(14) Å and W-C(20)-O(1)=178.0(12)°. These facts simply weak interaction of two CO groups to the platinum atom in spite of the fact that they hardly function as bridging μ-ligands.

The present study was partially supported by the Grant-in-Aids for Scientific Research from the Ministry of Education, Science and Culture (No. 63106006).

References

1) R. M. Bullock and C. P. Casey, *Acc.Chem. Res.*, **20**, 167 (1987) and references cited therein; I. Ojima, M. Okabe, K. Kato, H. B. Kwon, and I. T. Horvath, *J. Am. Chem. Soc.*, **110**, 150 (1988).

2) A. Yamamoto, "Organotransition Metal Chemistry, Fundamental Concepts and Application," John Wiley & Sons, New York (1986).

3) S. Komiya and I. Endo, *Chem. Lett.*, **1988**, 1709.

4) A. C. T. North, D. C. Phillips, and B. W. Matthews, *Acta Crystallogr., Sect. A*, **24**, 351 (1968).

5) T. Ashida, *HBLS*-V, The Universal Crystallographic Computing System-Osaka, The Computation Center, Osaka Univ., (1979), p. 53.

6) International Tables for X-ray Crystallography, Vol. IV, p. 71 (1974).

7) W. C. Hamilton, *Acta Crystallogr.*, **12**, 609 (1959).

8) C. K. Johnson, *ORTEP*-II. Report ORNL-5138. Oak Ridge, National Laboratory, Tennessee, USA, 1976.

9) T. V. Ashworth, J. A. K. Howard, M. Laguna, and F. G. A. Stone, *J. Chem. Soc., Dalton Trans.*, **1980**, 1593; T. V. Ashworth, J. A. K. Howard, and F. G. A. Stone, *ibid.*, **1980**, 1609; J. A. K. Howard, K. A. Mead, J. R. Moss, R. Navarro, F. G. A. Stone, and P. Woodward, *ibid.*, **1981**, 743; J. C. Jeffery, C. Sambale, M. F. Schmidt, and F. G. A. Stone, *Organometallics*, **1**, 1597 (1982); M. R. Awang, G. A. Carriedo, J. A. K. Howard, K. A. Mead, I. Moore, C. M. Nunn, and F. G. A. Stone, *J. Chem. Soc., Chem. Commun.*, **1983**, 964; K. A. Mead, I. Moore, F. G. A. Stone, and P. Woodward, *J. Chem. Soc., Dalton Trans.*, **1983**, 2083; M. R. Awang, J. C. Jeffery, and F. G. A. Stone, *ibid.*, **1983**, 2091; J. C. Jeffery, J. C. V. Laurie, I. Moore, H. Razay, and F. G. A. Stone, *ibid.*, **1984**, 1563; J. C. Jeffery, I. Moore, and F. G. A. Stone, *ibid.*, **1984**, 1571; J. C. Jeffery, I. Moore, H. Razay, and F. G. A. Stone, *ibid.*, **1984**, 1581; E. D. Morrison, A. D. Harley, M. A. Marcelli, G. L. Geoffroy, A. L. Rheingold, W. C. Fultz, *Organometallics*, **3**, 1407 (1984); J. Powell, J. F. Sawyer, and S. J. Smith, *J. Chem. Soc., Chem. Commun.*, **1985**, 1312; M. R. Awang, R. D. Barr, M. Green, J. A. K. Howard, T. B. Marder, and F. G. A. Stone, *J. Chem. Soc., Dalton Trans.*, **1985**, 2009; G. P. Elliott, J. A. K. Howard, C. M. Nunn, and F. G. A. Stone, *J. Chem. Soc., Chem. Commun.*, **1986**, 431; M. R. Awang, J. C. Jeffery, and F. G. A. Stone, *J. Chem. Soc., Dalton Trans.*, **1986**, 165.

10) A. Albinati, R. Naegell, A. Togni, and L. M. Venanzi, *Organometallics*, **2**, 926 (1983).

Synthesis and Characterization of a 3-Thio-2,4-pentanedionate Pt(II) Complex; Bis(dimethylphenylphosphine)[2,4-pentanedione-3-thiolato(2−)-*O*,*S*]-platinum(II) Prepared by S-S Bond Cleavage of 2,3-Dithio-1,1,4,4-tetraacetylbutane

Shinsaku YAMAZAKI,* Tomoharu AMA,† Masashi HOJO,† and Tamio UENO††
Chemistry Laboratory, Kochi Gakuen College, 292 Asahi Tenjin-cho, Kochi 780
†Department of Chemistry, Faculty of Science, Kochi University, 2-5-1 Akebono-cho, Kochi 780
††Department of Agriculture, Kyoto University, Oiwake-cho Kita-Shirakawa, Sakyo-ku, Kyoto 606
(Received May 5, 1989)

Synopsis. 3-Thio-2,4-pentanedionate (tac) complex of platinum(II), [Pt(tac)(PMe_2Ph)$_2$], has been prepared by treating [PtCl(PMe_2Ph)$_3$][PF_6] with 2,3-dithio-1,1,4,4-tetraacetylbutane in a KOH/methanol-acetone mixed solution. This complex has been characterized by IR, ^{1}H, ^{13}C, and ^{31}P NMR, secondary ion mass and ESR spectroscopy and cyclic voltammetry.

Linkage modes of 1,1,2,2-tetraacetylethane(dahd= 3,4-diacetyl-2,4-hexadiene-2,5-diol) to Rh(I) and Pd(II) as well as Pt(II) as bifunctional O_2-chelates and a (C^3,O')-chelate, respectively, have been formerly established.[1-3] The dahd dianion in acidic condition favors symmetrical O-bonding bifunctional chelation, while in basic condition it prefers the (C^3,O')-chelate. In them, the metal-carbon bonded [Pt(dahd-C^3,O')(SEt_2)$_2$] exhibits its unusual behavior.[3] An inversion of one sulfur atom arranged at the trans position to C^3 accompanies a bond dissociation the rearrangement of which may proceed via an intermolecular pathway. An extention of these previous findings has been investigated for the linkage mode of its dithio derivative: 2,3-dithio-1,1,4,4-tetraacetylbutane. A basic treatment of the sulfur compound gave an S-S bond cleavaged product, 3-thio-2,4-pentanedionate dianion (tac^{2-}), whose bonding mode to platinum(II) is, however, unknown so far.

This paper deals with a convenient synthesis of the 3-thio-2,4-pentanedionate Pt(II) complex, [Pt(tac)-(PMe_2Ph)$_2$], by an alkaline treatment of 2,3-dithio-1,1,4,4-tetraacetylbutane with [PtCl(PMe_2Ph)$_3$][PF_6]; the complex has been characterized using ^{1}H, ^{13}C, ^{31}P NMR and SIMS spectroscopy.

Experimental

2,3-Dithio-1,1,4,4-tetraacetylbutane (H_2dttb): H_2dttb was prepared by a method described in the literature.[4] Found: C, 45.28; H, 5.14%. Calcd for $C_{10}H_{14}O_4S_2$: C, 45.79; H, 5.38%. IR(Nujol mull): ν(C=O)+ν(C=O) 1548(br). ^{1}H NMR ($CDCl_3$): δ_{Me}=2.37, δ_{OH}=17.00.

[PtCl(PMe_2Ph)$_3$][BF_4] and Its PF_6^- Salt: 1.7 g of *cis*-$PtCl_2$-(PMe_2Ph)$_2$[5] was dissolved in acetone (partial suspension), and 0.62 g of $AgBF_4$ was added to the solution, producing AgCl (0.4 g; 94% per Pt atom). After filtration of AgCl, the solution was evaporated to give a pale-orange oil, which was dried in vacuo (1.5 g; 84%). Found: C, 32.91; H, 3.69%. Calcd for $C_{16}H_{22}ClP_2BF_4Pt$: C, 32.37; H, 3.74%. 0.6 g of the [Pt_2Cl_2(PMe_2Ph)$_4$][BF_4]$_2$ product was dissolved in acetone, and 0.13 g of PMe_2Ph was added to the solution. This solution was then evaporated to give an orange oil, which was dried in vacuo (0.72 g; 100%). Found: C, 38.34; H, 4.51%. Calcd for $C_{24}H_{35}OClBF_4Pt$ with a solvation of H_2O: C, 38.44; H, 4.71%. ^{31}P{^{1}H} NMR($CDCl_3$) shows a typical AB spin system: δ_A=16.86, δ_B=−3.94 ppm with J(A-B)=21.8, J(^{195}Pt-A)=3496.8 and J(^{195}Pt-B)=2310.9 Hz. An analogous PF_6 salt was prepared by reacting *cis*-$PtCl_2$(PMe_2Ph)$_2$ (1.0 g) with PMe_2Ph (0.3 g) and NH_4PF_6 (0.3 g) in a methanol-acetone solution (yield: 1.4 g; 93%).

Bis(dimethylphenylphosphine)(2,4-pentanedione-3-thiolato)platinum(II), [Pt(tac)(PMe_2Ph)$_2$]: 1.7 g of [PtCl-(PMe_2Ph)$_3$][PF_6] was dissolved in acetone; to the solution a methanol solution of KOH 0.25 g and H_2dttb 0.57 g were added as the pale-yellow solution turned orange. The solution was stirred for 30 minutes under N_2 as a white solid precipitated (0.5 g: 200% per Pt atom as a summation of KCl and KPF_6 salts). After filtration, the solution was developed by TLC (silica) in CH_2Cl_2–acetone. A yellow band was eluted and recrystallized from CH_2Cl_2–hexane (0.79 g; 61%). Found: C, 41.84; H, 4.81%. Calcd for $C_{21}H_{28}$-O_2P_2SPt: C, 41.93; H, 4.69%. M.W. (CH_2Cl_2) 664(602). The other species, showing orange and brown layers (TLC), have not been characterized.

Dipotassium 3-Thio-2,4-pentanedionate, K_2tac(CH_3OH): 1 g of H_2dttb was dissolved in CH_3OH and to the solution 0.43 g of KOH in CH_3OH was added as the solution turned orange. The solution was reduced in volume under reduced pressure to about 5 cm^3. The addition of diethyl ether to the residual solution, by allowing it to stand in a refrigerator overnight, gave a pale-orange solid (ca. 0.5 g). The product was further reprecipitated from methanol-diethyl ether (the product was moisture sensitive, and a slight weight loss was accompanied in its elemental analysis). Found: C, 28.62; H, 4.34%. Calcd for $C_6H_{11}O_{3.5}SK_2$ with a solvation of CH_3OH and H_2O: C, 28.89; H, 4.45%. IR(Nujol mull): ν(C=O)+ν(C=C)1580(vs) cm^{-1}. ^{1}H NMR (CD_3OD): δ_{Me}=2.08 .

Cyclic Voltammetry of [Pt(tac)(PMe_2Ph)$_2$]: A cyclic voltammograph of [Pt(tac)(PMe_2Ph)$_2$] was produced in acetone [1.16 and 1.74 mM (1 M=1 mol·dm^{-3})], 0.1 M TEAP at a platinum electrode or a glassy carbon electrode using a BAS voltammograph CV-27 and a Ag/AgCl reference electrode. An irreversible oxidation wave was observed, in which the corresponding cathodic wave was small. The anodic peak potential at 100 mV s^{-1} for the wave was E_p=+0.46 V. Controlled-potential coulometry at +0.60 V using a YANACO Potentiostat Model V8 revealed that a total of 0.94 electrons was involved in this oxidation. The nature of the reaction, via an electrochemical reaction, is not known at this time.

Elemental analyses were performed at the Micro Analytical Center, Kyoto University. IR spectra were recorded on a Hitachi 260-10 infrared spectrometer. ^{1}H NMR spectra at 90 MHz, ^{13}C at 22.66 MHz, and ^{31}P{^{1}H} at 36.36 MHz were recorded on a Hitachi R-90H FT NMR(90.04 MHz) operating in the Fourier transform mode. The SIMS spectrum was produced using a Hitachi M-80 mass spectrometer and

Table 1. IR, ^1H and $^{31}P\{^1H\}$ NMR Data of $[Pt(tac)(PMe_2Ph)_2]$

Chracteristic bands (IR)[a]			^1H[b]					^{31}P[c]		
ν(C=C) or ν(C=C)	ν(C-O)	ν(C-S)	δ_{Me}(tac)	J(P-H)	δ_{Me}(PMe_2Ph)	J(P-H)	$J(^{195}Pt-H)$	(PMe_2Ph)	J(Pt-P)	J(P-P)
1621(s)	1488(vs)	1262	2.42	1.8	1.74	12.5	39	−6.88(d)	2790.8	26.4
	1475(vs)		2.48	1.8	1.64	13.0	26	−26.52(d)	3354.0	

a) Measured in CH_2Cl_2. b) Measured in $CDCl_3$. Chemical shifts are relative to Me_4Si at 0.00.
c) Measured in $CDCl_3$. Chemical shifts are relative to 85% H_3PO_4 at 0.00.

Table 2. $^{13}C\{^1H\}$ NMR datum of $[Pt(tac)(PMe_2Ph)_2]$ and 2,3-Dithio-1,1,4,4-tetraacetylbutane ($dttb\text{-}H_2$)[a]

	tac					PMe_2Ph		
	C^1	C^2	C^3	C^4	C^5	C^1	$C^{1'}$	C^2
H_2-dttb	24.51	197.60	106.19					
$[Pt(tac)(PMe_2Ph)_2]$	25.66	194.66	109.76	179.96	29.79	16.04	15.96	12.71
	(4.84)	(3.46)	(8.29,	(9.33,		(43.53)	(44.22)	(35.93)
	[59.42]	[28.56]	2.77)	3.11)		[37.31]	[36.62]	[20.39]

a) Measured in $CDCl_3$. Chemical shifts are relative to Me_4Si at 0.00. J(P-C) and $J(^{195}Pt-C)$ are in parentheses and bracket respectively.

3-nitrobenzylalcohol or glycerin as a matrix and Xe gas as the first ion source. The molecular weight was obtained using a CORONA Molecular Weight Apparatus M-117 (vapor pressure osmometry) at 30 °C in CH_2Cl_2. The ESR spectra of the solid were recorded on a Varian E Line Century Series EPR spectrometer, and the diamagnetism of the complex was affirmed.

Results and Discussion

2,3-Dithio-1,1,4,4-tetraacetylbutane (H_2dttb) in solution has a dienolic form (Experimental section). The crystal structure of its tri-thio analog, 2,3,4-trithio-1,1,5,5-tetraacetylpentane, has been established by X-ray diffraction studies[4] to have a dienolic form, which is in analogy with 1,1,2,2-tetraacetylethane (H_2dahd). These previous findings may give rise to a question concerning its linkage mode to the metal: whether it may be stabilized in a form of bifunctional O_2-chelates or another, for example (S,O)-chelates. Unexpectedly, an alkaline treatment of $[PtCl(PMe_2Ph)_3][PF_6]$ with H_2dttb in methanol-acetone gave a diamagnetic 2,4-penatanedione-3-thiolato Pt(II) complex, $[Pt(tac)(PMe_2Ph)_2][tac(2-)$=3-thio-2,4-pentanedionate], which was produced via a S-S bond cleavage of the dttb dianion.

^1H, $^{31}P\{^1H\}$ NMR and IR spectral data of $[Pt(tac)(PMe_2Ph)_2]$ are shown in Table 1, and $^{13}C\{^1H\}$ NMR datum in Table 2. ^{31}P NMR shows an AB spin system with $J(^{195}Pt-P_A)$=3354 and $J(^{195}Pt-P_B)$=2791 Hz. These values are apart from a trans configuration, but rather close to cis configuration for the two phosphorous atoms.[6,7] Me-protons of PMe_2Ph appeared as two resonances, showing that the structure of the complex has low symmetry. Me protons of the tac also appear as two resonances with doublet patterns respectively, which may arise from a coupling with phosphorous nuclei at their trans positions. Its ^{13}C NMR spectrum shows that the circumstances around one acetyl group is distinct from the other. Resonances at 24.5 and 19.7 are due to C^1 and C^2, and each resonance appears as a doublet pattern accompanying ^{195}Pt satellites. The resonance pattern is in accordance with those observed for $[Pt(dahd\text{-}C^3,O')(PMe_2Ph)_2]$ and is consistent with one carbonyl in an enol-form being bound to Pt(II). However, resonance at 180.0 arising from C^4 is in a region close to that of ketonic carbonyl;[8,9] it appeared as a quartet pattern which may arise from a long-range coupling with two phosphorous nuclei. A single resonance at 29.8 is due to C^5. In both resonances no ^{195}Pt satellites could be observed, indicating that the ketonic carbonyl is liberated from the metal. IR bands at 1488 and 1475 cm^{-1} can be assigned to ν(C-O) and 1262 cm^{-1} to ν(C-S), the latter of which is in a region close to that found in the thiolato complex.[10] A

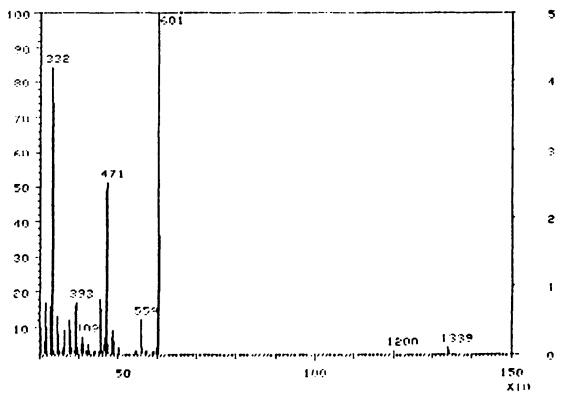

Fig. 1. SIMS spectrum of $[Pt(tac)(PMe_2Ph)_2]$: M^+= 601, $[M-tac]^+$=471, $[M-tac-PMe_2Ph]^+$=332.

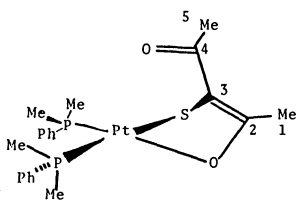

Fig. 2. Supposed structure of $[Pt(tac)(PMe_2Ph)_2]$.

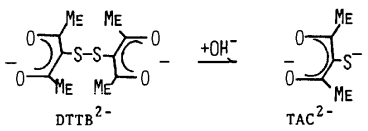

$DTTB^{2-}$ TAC^{2-}

$$[PtCl(PMe_2Ph)_3][PF_6] + K_2\text{-tac} \longrightarrow [Pt(tac)(PMe_2Ph)_2] + KCl + KPF_6 + PMe_2Ph \quad (1)$$

$$[PtCl(PMe_2Ph)_3][PF_6] + H_2\text{-dttb} + KOH \longrightarrow \tfrac{1}{2}[Pt_2(dttb)(PMe_2Ph)_4][PF_6]_2 + KCl + PMe_2Ph$$
$$\tfrac{1}{2}[Pt_2(dttb)(PMe_2Ph)_4][PF_6]_2 + KOH \longrightarrow [Pt(tac)(PMe_2Ph)_2] + KPF_6 \quad (2)$$

Scheme 1.

band at 1621 cm^{-1} can, therefore, be assigned to ν(C=O) or ν(C=C), which is in a lower frequency region than the 1600—1700 region found in metal carbon bonded Pt(II) and Pd(II) complexes of β-diketone.[11,12] Its SIMS spectrum shows an explicit basal peak at M/Z=601 corresponding to the molecular ion (Fig. 1). The result of a molecular weight measurement was consistent with this SIMS data. These spectral data are in accordance with a square planar structure in which 3-thio-2,4-pentanedionate bonds Pt(II) with (*S,O*)-chelate, as shown in Fig. 2. Any other conceivable structure for [Pt(tac)-(PMe_2Ph)$_2$], in which tac may retain an (O-H) or (S-H) group, can be neglected, since no corresponding ^1H NMR resonances have been observed in the region 0—20 ppm. It is also quite unlikely, judging from a molecular model, that the ketonic carbonyl may have any interaction with the metal from the apical site of the coordination tetragonal plane. In fact, by varying the temperature (20—50 °C), we did not observe any spectral change which should correspond to a coordination site exchange, as observed for five-coordinate complexes.[13,14]

[Pt(tac-*S,O*)(PMe_2Ph)$_2$] produced via an S-S bond cleavage[15] of the dttb dianion may be given by supposing two reaction paths: first, the dttb dianion by an attack of OH^- cause an S-S bond cleavage to form the tac dianion and a following metathesis of the complex; second, a dinuclear dttb complex, such as [Pt_2(dahd)(PMe_2Ph)$_4$][BF_4]$_2$, is formed and a subsequent S-S bond cleavage occurs by and attack of the nucleophile OH^-, as attributed in Scheme 1. By treating H_2dttb with KOH in methanol, K_2tac could be obtained. By reacting [$PtCl(PMe_2Ph)_3$][PF_6] with K_2tac, we have also obtained [Pt(tac)(PMe_2Ph)$_2$]. No isolation of a dinuclear complex, such as [Pt_2-(dttb)(PMe_2Ph)$_4$][PF_6]$_2$, have yet succeeded. Another likely type of cleavage for the reaction is via the S-C bond of the dttb dianion. Yet, its details are uncertain at this time.

An author (Shinsaku Yamazaki) appreciate Dr. Hideki Yamagata (Department of Physics, Faculty of Science, Kochi University) for obtaining ESR spectra.

References

1) S. Yamazaki, *Polyhedron*, **5**, 1183 (1986).
2) S. Yamazaki, T. Ama, and Z. Taira, *Polyhedron*,**7**, 353 (1988).
3) S. Yamazaki and T. Ama, *Bull. Chem. Soc. Jpn.*, **62**, 931 (1989).
4) D. H. Dewar, J. E. Fergusson, R. P. Hentschell, C. J. Wilkins, and P. P. Wiliams, *J. Chem. Soc.*, **1964**, 688: L. F. Power and R. D. Jones, *Acta. Crystallogr. Sect. B*, **27**, 181 (1971).
5) R, Favez, R. Roulet, A. A. Pinkerton, and D. Schwarzenbach, *Inorg. Chem.*, **19**, 1356 (1980).
6) J. J. Macdougall, J. H. Nelson, and F. Mathey, *Inorg. Chem.*, **21**, 2145 (1982).
7) J. G. Verkade and L. D. Quin, "Phosphorous-31 NMR Spectroscopy in Stereochemical Analysis-Organic Compounds and Metal Complexes," VCH Publisher (1987).
8) T. Ito, T. Kiriyama, Y. Nakamura, and A. Yamamoto, *Bull. Chem. Soc. Jpn.*, **49**, 3257 (1976).
9) H. Tanaka, K. Isobe, S. Kawaguchi, and S. Okeya, *Bull. Chem. Soc. Jpn.*, **57**, 1850 (1984).
10) C. Sleelatha, D. K. Srivastava, and V. P. Gupta, *J. Chem. Soc., Dalton Trans.*, **1988**, 407.
11) D. Gibson, J. Lewis, and C. Oldham, *J. Chem. Soc. A*, **1970**, 72: J. Hills, J. Francis, M. Ori, and M. Tsutsui, *J. Am. Chem. Soc.*, **96**, 4800 (1974).
12) N. Yanase, Y. Nakamura, and S. Kawaguchi, *Inorg. Chem.*, **19**, 1575 (1980).
13) S. Yamazaki, *Bull. Chem. Soc. Jpn.*, **60**, 1155 (1987). T. Sakai, Z. Taira, S. Yamazaki, and T. Ama, *Polyhedron*, in press.
14) S. Okeya, T. Miyamoto, S. Ooi, Y. Nakamura, and S. Kawaguchi, *Bull. Chem. Soc. Jpn.*, **57**, 395 (1984).
15) M. Hojo and T. Sawyer, *Inorg. Chem.*, **28**, 1201 (1989).

Formation of a Hydrogen Insertion Compound of Hydrated Molybdenum Oxide from Hydrogen Molybdenum Bronze

Kazuo EDA* and Noriyuki SOTANI
College of Liberal Arts, Kobe University, Tsurukabuto, Nada, Kobe 657
(Received May 15, 1989)

Synopsis. It was found that hydrogen molybdenum bronze, $H_{0.3}MoO_3$, turns into a hydrogen insertion compound of hydrated molybdenum oxide in a 1M HCl aqueous solution at 353 K. It was predictable that the compound has a composition of $H_{0.15}MoO_3 \cdot 0.88H_2O$ and is identical with $Mo_8O_{15}(OH)_{16}$ or a similar compound.

Hydrogen molybdenum bronzes are interesting materials and have been studied extensively.[1-6] The authors have studied the stability of bronzes and have found that one member, $H_{0.3}MoO_3$, changes into a new compound upon treatment at 353 K in a 1M HCl aqueous solution (1 M=1 mol dm^{-3}). In the present study, a characterization of this compound was achieved.

Experimental

Preparation. The sample was prepared from $H_{0.3}MoO_3$ in a 1M HCl aqueous solution at 353 K for one week. It was filtrated, washed by water, and then vacuum dried.

Measurements. Powder X-ray diffraction patterns were obtained by using a RIGAKUDENKI GEIGER D-1 FLEX diffractometer with Cu$K\alpha$ radiation. Samples for X-ray diffraction measurements were mixed with an internal standard (ca. 5 wt% Si powder). The IR spectra were recorded at room temperature by using a JASCO 701G spectrophotometer. Samples for this measurement were pressed into disks (ca. 0.5 wt% in KBr). TG-DTA was carried out on a MAC SCIENCE TG-DTA 2000 at a heating rate of 10 K min^{-1}. The sample weight for the measurement was ca. 20 mg. The hydrogen contents of the samples were determined chemically by Choain and Marion's method.[7]

Results and Discussion

The prepared sample was powder with a bluish gray color. The X-ray diffraction pattern and IR spectrum of the sample are shown in Figs. 1 and 2, respectively. The observed diffraction peaks in Fig. 1 and the IR bands in Fig. 2 are clearly different from those of $H_{0.3}MoO_3$. Those marked with the symbol ★ in these Figures correspond to those of MoO_3. The diffraction peaks with the symbol ○ correspond to those of $Mo_8O_{15}(OH)_{16}$, which have been synthesized from a mixture of $MoO_3 \cdot 2H_2O$ and Mo metal by Glemser and Lutz.[8] According to chemical analysis, the sample contained 0.10 hydrogen atom/Mo atom. Figure 3 shows a TG-DTA curve of the sample. Endothermic peaks appear at 429 and 477 K, and an exothermic peak appears at 621 K. Both endothermic peaks are followed by a large weight loss, which corresponds to 4.2 and 2.6 wt%, respectively. The peak temperature of 429 K is comparable to the releasing temperature of hydrate-water in yellow $MoO_3 \cdot H_2O$.[9] By H-NMR a Pake-doublet (r=0.15 nm) can be observed. Thus, the peaks can be attributed to the release of two kinds of hydrate-water, and a gradual weight loss continues until 573 K after their release. The exothermic peak at 621 K is followed by a weight gain (0.2 wt%). The peak might be attributed to the oxidation of the sample. The structural change at each DTA peak has been investigated. The results by X-ray diffraction and IR spectroscopy measurements are also shown in Figs. 1 and 2. With the release of two kinds of hydrate-water, the diffraction peaks and IR bands without the symbol ★ exhibit apparent changes. On the other hand, those with the symbol exhibit no or little change below 573 K. After the exothermic peak, the sample perfectly changes into MoO_3. The hydrogen contents of the samples heated at 448, 493, 573, and 673 K were 0.09, 0.07, 0.04, and 0.00 H atom/Mo atom, respectively. This shows that a large portion of the inserted hydrogen atoms are released in the temperature region which corresponds to a gradual TG loss. Thus, the release of hydrogen may be associated with a gradual TG loss. On the basis of the above results, the authors propose that the newly found compound by an HCl treatment of $H_{0.3}MoO_3$ is a hydrogen insertion compound of

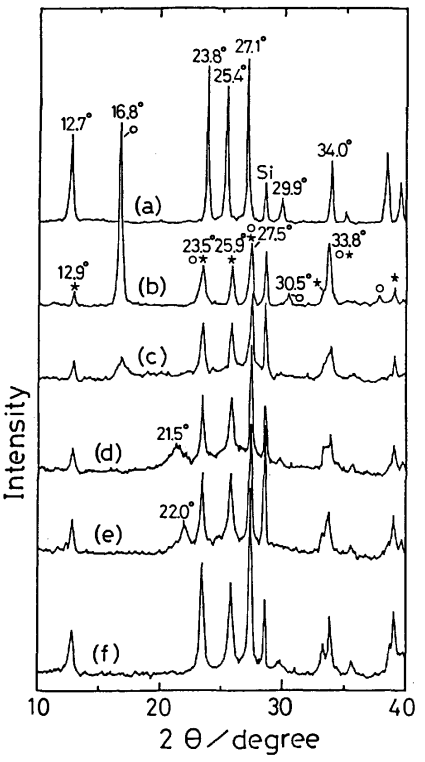

Fig. 1. Powder X-ray diffraction patterns of $H_{0.3}MoO_3$ (a), the sample as prepared (b), the sample heated in air at 448 K (c), at 493 K (d), at 573 K (e), and at 673 K (f).

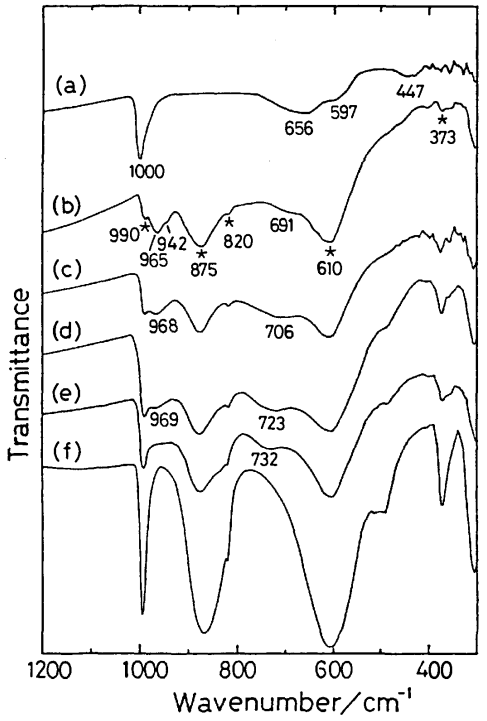

Fig. 2. IR spectra of $H_{0.3}MoO_3$ (a), the sample as prepared (b), the sample heated in air at 448 K (c), at 493 K (d), at 573 K (e), and at 673 K (f).

hydrated molybdenum oxide. However, it is also concluded that the sample is not single phase and contains MoO_3.

The total composition of the as-prepared sample was $H_{0.10}MoO_3(H_2O)_{0.59}$. This composition corresponds to a formula of $0.36MoO_3+H_{0.15}MoO_3 \cdot 0.88H_2O$ ($0.36MoO_3+0.08Mo_8O_{15.40}(OH)_{15.95}$). This formula means that the content of MoO_3 is 33.5 wt%. On the other hand, the content of MoO_3, by an estimation from the change in the intensity ratio of the characteristic diffraction peak at 25.9° by adding known amounts of commercial MoO_3 to the sample, has been 50 wt%, although the intensity of the peak at 25.9° for MoO_3 is appreciably small than that of the peak at 16.8° for the new compound. The real content might deviate from the estimated value to some extent because of the uncertainty of the assumption regarding the estimation that MoO_3 in the sample had

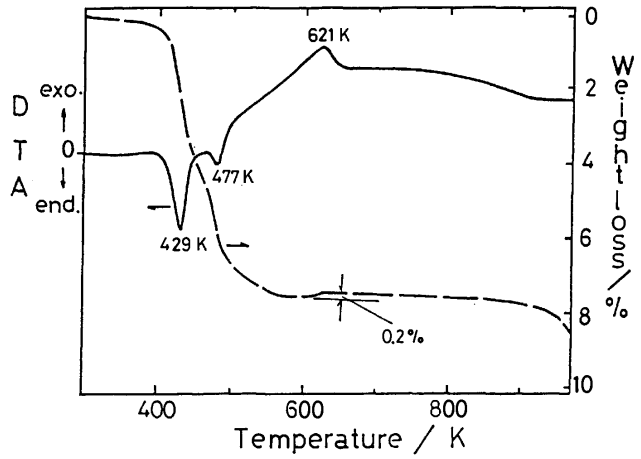

Fig. 3. TG-DTA curve of the sample as prepared.

the same diffraction peak intensity as the commercial one. It is therefore considered that the estimated value supports the above-mentioned large content of MoO_3 (33.5 wt%). On the basis of this discussion and the similarity in the X-ray diffraction pattern, the compound can be predicted to be $H_{0.15}MoO_3 \cdot 0.88H_2O$ which is identical with $Mo_8O_{15}(OH)_{16}$ or a similar compound. A synthesis of the compound as a single phase is in progress.

References

1) P. A. Sermon and G.C. Bond, *J. Chem. Soc., Faraday Trans. 1*, **76**, 889 (1980).
2) N. Sotani, N. Yoshida, Y. Yoshioka, and S. Kishimoto, *Bull. Chem. Soc. Jpn.*, **58**, 1626 (1985).
3) R. C. T. Slade, T. K. Halstead, and P. G. Dickens, *J. Solid State Chem.*, **34**, 183 (1980).
4) Cl. Ritter, W. Müller-Warmuth, and R. Schöllhorn, *J. Chem. Phys.*, **83**, 6130 (1985).
5) S. J. Hibble and P. G. Dickens, *Ber. Bunsenges. Phys. Chem.*, **90**, 702 (1986).
6) N. Sotani, K. Eda, M. Sadamatsu, and S. Takagi, *Bull. Chem. Soc. Jpn.*, **62**, 903 (1989).
7) C. Choain and F. Marion, *Bull. Soc. Chim. Fr.*, **1963**, 212.
8) O. Glemser and G. Lutz, *Z. Anorg. Allgem. Chem.*, **264**, 17 (1951).
9) N. Sotani, U. Saitou, M. Oita, and M. Hasegawa, *Nippon Kagaku Kaishi*, **1974**, 673.

Crystal Structure and Magnetic Property of Cubane Tetranuclear Copper(II) Complex with Ferromagnetic Coupling

Naohide MATSUMOTO,* Takashi KONDO, Masahito KODERA, Hisashi ŌKAWA, and Sigeo KIDA
Department of Chemistry, Faculty of Science, Kyushu University, Hakozaki, Higashi-ku, Fukuoka 812
(Received June 19, 1989)

Synopsis. The magnetic susceptibility measurement down to the liquid helium temperature and the single-crystal X-ray analysis of alkoxo-oxygen bridged tetranuclear copper(II) complex $[CuL]_4$ have been performed, where H_2L is a tridentate ligand derived from condensation of 3-ethoxymethylene-2,4-pentanedione and 2-aminoethanol. The magnetic data demonstrated that the four unpaired electrons of the four copper(II) ions are ferromagnetically coupled, the ground spin state of the cubane molecule being $S=2$. The structural analysis has confirmed several structural features, i.e., the distorted Cu_4O_4 cubane structure, the square pyramidal coordination geometry, nearly perpendicular arrengement between adjacent basal coordination planes, and inequivalent Cu-O bond distances.

Studies on discrete dinuclear or oligonuclear metal complexes with ferromagnetic spin coupling are fundamental requirement not only for elucidation of the structural and electronic factors governing magnetic interaction between paramagnetic centers but also for developing ferromagnetic materials.[1-4] However, such complexes are relatively rare, while a large number of polynuclear metal complexes with antiferromagnetic interaction have been known.[5]

Previously some of the present authors[6] synthesized copper(II) complex with a tridentate ligand derived from condensation of 3-ethoxymethylidene-2,4-pentanedione and 2-aminoethanol, and measured the magnetic susceptibility in the temperature range 80—300 K. The magnetic susceptibility obeys the Curie-Weiss law ($\chi_A=C/(T-\theta)$) with positive Weiss constants suggesting a ferromagnetic interaction between copper(II) ions. In this study, in order to detect the spin ground state of the molecule and elucidate the structural factors causing ferromagnetic coupling, the complex has been subjected to the magnetic susceptibility measurement down to the liquid helium temperature and the single-crystal X-ray analysis.

Experimental

Synthesis. The complex was prepared according to the method reported previously[6] and recrystallized twice from dichloromethane/methanol solution. Calcd for [CuL], $CuO_3NC_8H_{11}$: C, 41.29; H, 4.76; N, 6.02%. Found: C, 41.16; H, 4.86; N, 5.99%.

Physical Measurements. Elemental analyses were performed at the Elemental Analysis Center of Kyushu University. Magnetic susceptibilities were obtained at 4.2—100 K by use of a HOXAN HSM-D SQUID magnetometer in the magnetic field 0.5 T and at 80—300 K by a Faraday balance designed in our laboratory. The data were corrected for magnetization of the sample holder and for the diamagnetism of the component atoms by the use of Pascal's constants. The molar effective magnetic moment was calculated by the equation $\mu_{eff}=2.828(\chi_A T)^{1/2}$.

X-Ray Crystallography. Reflection data were measured on a Rigaku Denki AFC-5 automated four-circle diffractometer with graphite-monochromatized Mo $K\alpha$ radiation at room temperature. The details of data collection and crystallographic data are summarized as follows: $[CuL]_4$, formula=$Cu_4O_{12}N_4C_{32}H_{44}$, FW=930.91, triclinic, space group $P\bar{1}$, a=12.330(2) Å, b=13.766(4) Å, c=11.109(3) Å, α=97.44(2)°, β=92.05(2)°, γ=85.09(2)°, V=1862.3(7) Å^3, D_m=1.64 g cm^{-3} (by floatation method in aqueous KI solution), D_x=1.66 g cm^{-3} (Z=2), crystal size 0.3×0.3×0.4 mm, μ(Mo $K\alpha$)=23.23 cm^{-1}, scan mode θ-2θ, scan range 2.5—52°, scan width (1.2+0.35 tan θ)°, octant measured $+h$, $\pm k$, $\pm l$, number of observed reflections with $|F_o|>3\sigma(|F_o|)$ 5516, R=4.20%, R_w=5.01%, highest peak on the final D-Fourier 0.4 e Å^{-3}.

The intensity data were corrected for Lorentz and polarization effects but not for absorption and extinction effects. The structure was solved by the standard heavy-atom method and refined by the block-diagonal least-squares method, in which the function minimized is $\sum w(|F_o|-|F_c|)^2$ and the equal weight w=1 was adopted for all the reflections. The atomic scattering factors were taken from Ref. 7. All computations were performed on a FACOM M 780 computer at the Computer Center of Kyushu University using the UNICS III program system.[8] The final atomic coordinates are given in Table 1. Tables of observed and calculated structure factors, listings of atomic positional and anisotropic thermal parameters, and complete lists of bond distances and angles with their estimated standard deviations have been deposited as Document No. 8905 at the Office of the Editor of Bull. Chem. Soc. Jpn.

Results and Discussion

Magnetic Property. The magnetic susceptibilities have been measured in the 4.2—300 K temperature range. Figure 1 shows the result of $[CuL]_4$, in the forms of the χ_A vs. T, the $1/\chi_A$ vs. T, and the μ_{eff} vs. T plots, where χ_A is the magnetic susceptibility per copper atom, μ_{eff} the effective magnetic moment per copper atom, and T the absolute temperature. The numerical values of the magnetic susceptibilities are given as supplementary materials.

The $1/\chi_A$ vs. T plot follows the Curie-Weiss law ($\chi_A=C(T-\theta)$) above 50 K with a Weiss constant 20 K, suggesting a ferromagnetic interaction. The effective magnetic moment at room temperature is 1.84 μ_B/Cu, which is close to the spin-only value (1.72 μ_B). As the temperature is lowered, the magnetic moment increases from 1.84 μ_B at 297.8 K, reaches a maximum value of 2.49 μ_B at 13 K, and finally decreases to 2.41 μ_B at 4.5 K. The maximum value (2.49 μ_B/Cu=4.98 μ_B/4Cu) agrees well with the spin-only value (4.90 μ_B expected for S=2 spin state effected by a ferromagnetic spin coupling of four unpaired electrons. The decrease of μ_{eff} below 13 K is attributable to either the intermolecular effect or the zero-field splitting of the S=2 ground state. The result clearly demonstrates that a ferromagnetic spin-exchange coupling is oper-

ating within a molecule and the spin ground state of the cubane molecule is $S=2$ and is fully populated below 13 K.

Structural Description. The ORTEP drawing of $[CuL]_4$ with the atom numbering scheme is shown in Fig. 2. The selected bond distances and angles with their estimated standard deviations are available in Table 2. The complex has a cubane-type alkoxo-oxygen bridged tetranuclear structure. The distances of Cu1-Cu3 and Cu2-Cu4 are 3.337(1) Å and 3.316(1) Å, respectively, which are longer than the other four Cu-Cu distances (3.092(1)—3.126(1) Å), indicating a distortion from the ideal cubane struc-

Table 1. Positional Parameters of Non-Hydrogen Atoms ($\times 10^4$)

Atom	x	y	z	B_{eqv}
Cu1	2301(1)	3048(0)	4214(1)	2.8
Cu2	622(1)	1528(1)	3427(1)	2.7
Cu3	2712(1)	1293(0)	1869(1)	2.6
Cu4	1203(1)	3184(1)	1680(1)	2.7
O1	2109(3)	1634(3)	3996(3)	2.8
O2	1144(3)	1467(3)	1749(3)	2.8
O3	2691(3)	2731(3)	2119(3)	2.6
O4	890(5)	3243(3)	3402(3)	2.9
O5	2608(4)	4400(3)	4446(4)	4.0
O6	3701(6)	5865(4)	7674(6)	8.3
O7	62(3)	1397(3)	4980(4)	3.8
O8	−3643(4)	1169(3)	3996(4)	5.6
O9	2794(3)	−109(3)	1418(4)	3.6
O10	5549(4)	−2062(3)	1337(5)	5.4
O11	1409(4)	3134(3)	−33(4)	3.9
O12	−927(6)	3610(5)	−2718(5)	9.1
N1	3391(4)	2744(3)	5393(4)	2.7
N2	−741(4)	1305(3)	2640(4)	2.9
N3	4243(4)	1325(3)	1884(4)	2.9
N4	−233(4)	3810(4)	1524(4)	3.4
C1	2588(5)	1215(4)	5010(6)	3.4
C2	3619(5)	1676(4)	5382(5)	3.1
C3	3744(5)	3359(4)	6240(5)	3.0
C4	3583(5)	4405(4)	6321(5)	3.3
C5	3933(7)	4981(5)	7430(7)	4.8
C6	4609(10)	4502(7)	8370(8)	8.3
C7	3092(5)	4854(4)	5337(6)	3.4
C8	3145(7)	5921(5)	5218(7)	5.3
C9	448(5)	910(4)	961(5)	3.3
C10	−728(5)	1247(5)	1299(5)	3.4
C11	−1651(5)	1282(4)	3158(6)	3.2
C12	−1802(5)	1357(4)	4450(5)	2.9
C13	−2957(5)	1404(5)	4752(6)	3.5
C14	−3321(6)	1827(6)	6008(7)	4.9
C15	−915(5)	1325(4)	5268(5)	3.1
C16	−981(6)	1134(5)	6566(6)	4.3
C17	3695(5)	3010(4)	1709(6)	3.2
C18	4599(5)	2310(4)	2162(5)	3.1
C19	4945(5)	557(4)	1712(5)	2.8
C20	4710(5)	−442(4)	1447(5)	2.9
C21	5648(6)	−1191(4)	1370(5)	3.6
C22	6780(6)	−861(5)	1369(7)	4.7
C23	3638(5)	−721(4)	1265(5)	3.2
C24	3364(6)	−1745(5)	803(6)	4.4
C25	94(6)	4058(5)	3691(6)	3.9
C26	−787(5)	3993(5)	2723(6)	4.1
C27	−746(5)	3955(5)	547(6)	3.7
C28	−353(6)	3731(4)	−662(6)	3.8
C29	−1112(7)	3912(5)	−1662(7)	5.4
C30	−2188(8)	4480(7)	−1409(8)	6.8
C31	732(6)	3339(5)	−859(6)	3.8
C32	1200(7)	3148(6)	−2110(6)	5.5

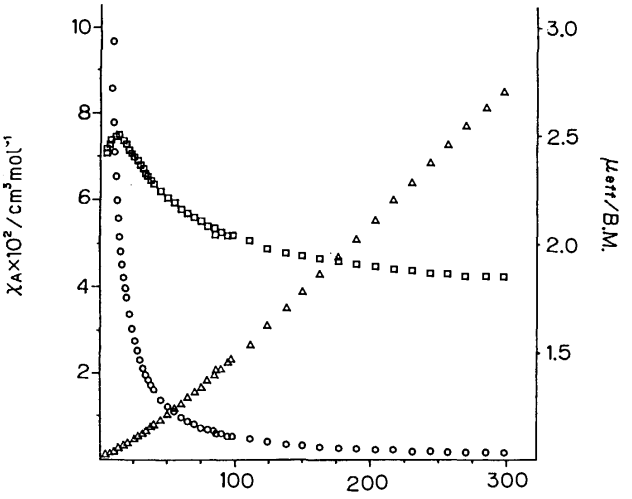

Fig. 1. The plots of χ_A vs. T (○), $1/\chi_A$ vs. T (△), and μ_{eff} vs. T (□) for $[CuL]_4$.

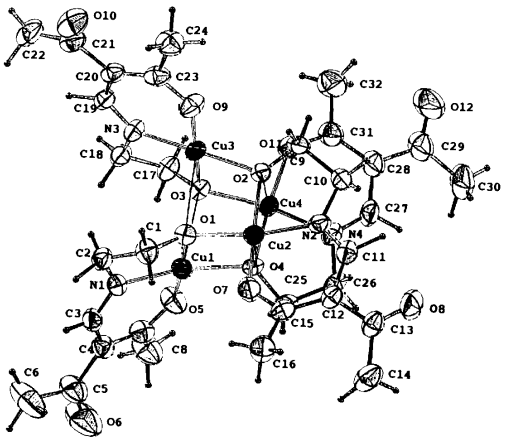

Fig. 2. Molecular Structure of Cubane-like Tetranuclear Copper(II) Complex $[CuL]_4$ with the atom numbering scheme.

Table 2. Selected Bond Distances(Å) and Angles(deg)

(a) Bond distance/Å			
Cu1-Cu2	3.092(1)	Cu1-Cu3	3.337(1)
Cu1-Cu4	3.100(1)	Cu2-Cu3	3.126(1)
Cu2-Cu4	3.316(1)	Cu3-Cu4	3.094(1)
Cu1-O1	1.963(4)	Cu2-O1	1.929(4)
Cu2-O2	1.983(4)	Cu3-O2	1.930(4)
Cu3-O3	1.961(4)	Cu4-O3	1.952(4)
Cu4-O4	1.955(4)	Cu1-O4	1.945(4)
Cu1-O3	2.370(4)	Cu2-O4	2.414(4)
Cu3-O1	2.477(3)	Cu4-O2	2.382(4)
(b) Bond angle/deg			
Cu1-O1-Cu2	105.2(2)	Cu2-O2-Cu3	106.0(2)
Cu3-O3-Cu4	104.5(2)	Cu4-O4-Cu1	105.3(2)
Cu1-O1-C1	108.9(3)	Cu2-O1-C1	124.4(3)
Cu2-O2-C9	108.3(3)	Cu3-O2-C9	127.4(3)
Cu3-O3-C17	108.7(3)	Cu4-O3-C17	128.6(3)
Cu4-O4-C25	107.1(4)	Cu1-O4-C25	125.8(4)

ture. The coordination geometries of the four copper(II) ions are best described as a square pyramid. The apical positions of the square pyramids of Cu1, Cu2, Cu3, and Cu4 are occupied by O3, O4, O1, and O2, respectively, where the Cu-O(apical) bond distances fall in the range 2.370(4)—2.477(3) Å. The basal coordination sites of each copper(II) ion are occupied by the NO_2 donor set of the tridentate ligand L and an alkoxo-oxygen atom of the neighbouring ligand, where the bond distances are in the range 1.892(5)—1.983(4) Å. Adjacent copper(II) ions are bridged by two alkoxo-oxygen atoms inequivalently. For example, Cu1 and Cu2 atoms are doubly bridged by two alkoxo-oxygen atoms O1 and O4 with the bond distances of Cu1-O1 1.963(4) Å, Cu2-O1 1.929(4) Å, Cu1-O4 1.945(4) Å, and Cu2-O4 2.414(4) Å, indicating that one Cu-O bond among the four Cu-O bonds in Cu_2O_2 unit is elongated. The dihedral angle between the basal coordination planes of Cu1 and Cu2 is 78.7°, that of Cu2 and Cu3 94.9°, that of Cu3 and Cu4 92.6°, and that of Cu4 and Cu1 93.4°. Thus, the basal coordination planes are nearly perpendicular to each other.

References

1) O. Kahn, "Structure and Bonding," 68, Springer-Verlag, Berlin Heidelberg (1987), pp. 89—167.
2) C. J. Cairns and D. H. Busch, *Coord. Chem. Rev.*, **69**, 1 (1986).
3) P. J. Hay, J. C. Thibeault, and R. Hoffmann, *J. Am. Chem. Soc.*, **97**, 4884 (1975).
4) A. Caneschi, D. Gatteschi, A. Grand, J. Laugier, and P. Rey, *Inorg. Chem.*, **27**, 1031 (1988).
5) U. Casellato, P. A. Vigato, and M. Vidali, *Coord. Chem. Rev.*, **23**, 31 (1977).
6) N. Matsumoto, T. Tsutsumi, A. Ohyoshi, and H. Okawa, *Bull. Chem. Soc. Jpn.*, **56**, 1388 (1983).
7) "International Tables for X-Ray Crystallography," Vol. IV, Kynoch Press, Burmingham, England (1974).
8) T. Sakurai and K. Kobayashi, *Rikagaku Kenkyusho Houkoku*, **55**, 69 (1979); S. Kawano, *Rep. Comput. Cent. Kyushu Univ.*, **13**, 39 (1980).

Complexation Reactions of Copper(II) Ions with 16-Membered and 18-Membered Monocyclic Dioxopolyamines in an Aqueous Solution

Mutsuo KODAMA,* Hideki ANAN,† Tohru KOIKE,† and Eiichi KIMURA†
Department of Chemistry, College of General Education, Hirosaki University, Bunkyo, Hirosaki 036
†Department of Medical Chemistry, Hiroshima University School of Medicine, Kasumi, Hiroshima 734
(Received July 10, 1989)

Synopsis. The equilibria of complexation reactions of dioxo[16]aneN$_5$, dioxo[18]aneN$_6$, and their related compounds with copper(II) ions were determined potentiometrically. Making a sharp contrast to the 13—15-membered monocyclic dioxotetramine system, they interact with copper(II) ions in their neutral and doubly deprotonated forms, L and $H_{-2}L^{2-}$, yielding stable CuL^{2+} and $CuH_{-2}L^0$ complexes.

In earlier studies on the complexation of 13—15-membered monocyclic dioxotetramines,[1,2] it was demonstrated that these potential quadridentate macrocycles only form square planar N_4 complexes, $MH_{-2}L^0$, with Cu(II) and Ni(II) ions as a result of a double deprotonation of the amides. The binding of the metal(II) is assumed to take place first at the amide group, followed by imidiate amide deprotonation and coordination. The latter coorperative action might occur more readily in the macrocycles than in the linear tripeptides, particularly in those having rigid planarity and suitable cavity sizes for the small metal ions having a stronger tendency to square-planar coordination like Cu(II) and Ni(II) ions.

As a continuation of our equilibrium study concerning the complexation reactions of macrocyclic dioxopolyamines, we have now determined the equilibria of copper(II) complex formations of dioxo[16]aneN$_5$, dioxo[18]aneN$_6$, and their related compounds. Comparisons of the present findings with those for the 13—15-membered macrocyclic dioxotetramines and the relevant linear tripeptides might shed more light on the ligating properties of macromonocyclic dioxopolyamines, leading to an explanation of their useful applications.

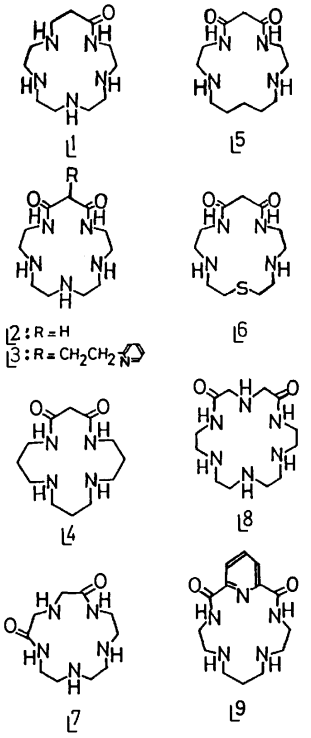

Chart 1.

Experimental

The macrocyclic dioxopolyamines used were prepared according to methods described in the literature[1-4] (Chart 1). The salt $CuSO_4 \cdot 5H_2O$ was an analytical grade chemical and its solutions were standardized by EDTA titration.[5]

The pH-metric titrations were performed with a Mettler automatic titrator[6,7] under a nitrogen or an argon atmosphere at 25±0.2 °C. All of the experimental conditions and procedures employed have been mentioned previously.[6] The values of $-\log[H^+]$ were estimated by applying a correction of −0.13 pH unit to the pH readings.[7] The mixed protonation constants (K_i's) were determined potentiometrically.[4] The mixed protonation constants ($\log K_i$'s) of a new ligand, L^7, were 8.35, 4.85, and ca. 2.6 and those of L^9, 8.73 and 6.22.

Results and Discussion

The equimolar mixture solution of copper(II) and L^4, L^5, L^6, or L^9 in its fully protonated form (H_2L^{2+}) gave titration curves with a buffer region at the titration point $4>a>0$, which fitted to the theoretical equation (16) in Ref. 1 derived for the formation of $CuH_{-2}L^0$ in the dioxotetramine system ($C_M=C_L$). Therefore, the cumulative formation constants, $K_{CuH_{-2}L}(=[CuH_{-2}L^0]\cdot[H^+]^2/[Cu^{2+}]\cdot[L])$, were determined similarly in a graphic way.[1]

In sharp contrast with these ligand systems, the titration curve of an equimolar mixture of Cu(II) and L^2 (dioxo[16]aneN$_5$) in its fully protonated form (H_3L^{3+}) gave two buffer regions at titration points $3>a>0$ and $5>a>3$ (Fig. 1). Two breaks, one occurring at $a=3$ and the other at $a=5$ suggest the complexation equilibria (1) and (2) for the titration points $3>a>0$ and $5>a>3$, respectively. The K_{CuL} value was determined in an analogous way to that described for the complexation of the macromonocyclic triamine with copper(II) ions.[8] The K^{-2H} value was then estimated from the gradient of the straight line between

$$Cu^{2+} + L = CuL^{2+},\ K_{CuL} = [CuL^{2+}]/[Cu^{2+}]\cdot[L] \quad (1)$$

$$CuL^{2+} = CuH_{-2}L^0 + 2H^+,\ K^{-2H} = [CuH_{-2}L^0]\cdot[H^+]^2/[CuL^{2+}] \quad (2)$$

the $(\alpha'/2)/(C_L-\alpha'/2)$ and $[H^+]^{-2}$ (Fig. 2). Here, α' is

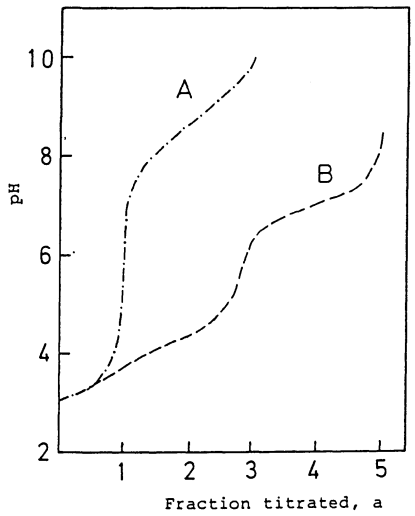

Fig. 1. Titration curves of 1.00 mM dioxo[16]aneN$_5$ (3HCl salt).
Ionic strength (I)=0.20 M, 25 °C, (A) dioxo[16]aneN$_5$ only, (b) dioxo[16]aneN$_5$+1.00 mM Cu(II), sample solution 50.0 ml with 0.100$_0$ M tetraethylammonium solution.

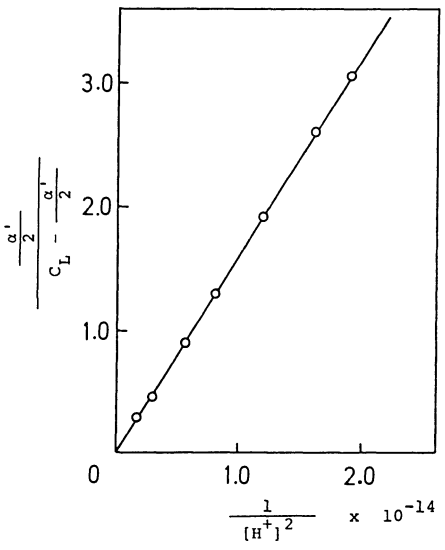

Fig. 2. Plots of $(\alpha'/2)/(C_L-\alpha'/2)$ against $1/[H^+]^2$.
[Cu(II)]=1.00 mM, [dioxo[16]aneN$_5$ 3HCl]=1.00, mM, I=0.20 M, 25 °C.

defined as $(a-3)C_L+[H^+]$, and $(\alpha'/2)/(C_L-\alpha'/2)$ corresponds to the $[CuH_{-2}L^0]/[CuL^{2+}]$ ratio. This also turned out to be the case for the 1:1 Cu(II)-dioxo[18]aneN$_6$(L^8) mixture solution ($4>a>0$, $6>a>4$). The K_{CuL} and K^{-2H} values for the Cu(II) complex of dioxo[18]aneN$_6$ were also estimated in a quite similar way.

In the case of a Cu(II)-monooxo[16]aneN$_5$(L^1, H_4L^{4+}) system, two breaks occurring at a=3 and 5 suggest the formation of $CuHL^{3+}$ and $CuH_{-1}L^+$. The K_{CuHL} (=$[CuHL^{3+}]/[Cu^{2+}]\cdot[HL^+]$ value was determined by using the following equation (3) derived in an identical manner as that employed for the complexation of macromonocyclic pentamines with Zn(II) ions ($C_M=C_L$).[8]

$$\frac{K_{CuHL}\cdot[H^+]}{K_4}(3C_L-\alpha)^2(\alpha_H)_L = (\alpha(\alpha_H)_L-\beta_H C_L)\cdot(3(\alpha_H)_L-\beta_H). \quad (3)$$

Here, K_4 means the 4-th dissociation constant of H_4L^{4+}. As in the case of the dioxo[16]aneN$_5$ system, the K^{-2H} (=$[CuH_{-1}L^+]\cdot[H^+]^2/[CuHL^{3+}]$) value was determined from the gradient of the straight line between the $(\alpha'/2)/(C_L-\alpha'/2)$ (=$[CuH_{-1}L^+]/[CuHL^{3+}]$) value and $[H^+]^{-2}$. The titration of an equimolar mixture of Cu(II) and dioxo[15]aneN$_5$ (L^7, H_3L^{3+}) also gave two breaks at a=4 and 5, suggesting the formation of $CuH_{-1}L^+$ and $CuH_{-2}L^0$. The $K_{CuH_{-1}L}$ (=$[CuH_{-1}L^+]\cdot[H^+]/[Cu^{2+}]\cdot[L]$) and $K^{-H}_{CuH_{-1}L}$ (=$[CuH_{-2}L^0]\cdot[H^+]/[CuH_{-1}L^+]$) values for the Cu(II)-L^7 complex were determined in an identical manner as that previously applied to the Cu(II)-dioxo[12]aneN$_4$ complex formation.[2] All of the equilibrium constants determined in this study are listed in Table 1.

The equimolar mixture solution of Cu(II) ion and dioxo[16]aneN$_5$ at pH 4—5 (at titration point $a<3$) is blue, greatly differing from the pink (λ_{max}=505 nm) shown by the square-planar Cu(II)-dioxo[14]aneN$_4$ complex $CuH_{-2}L^0$,[2,9] However, it turns to violet at pH's higher than 7.0, indicating a certain change in the coordination mode of dioxo[16]aneN$_5$ to the Cu(II) ion. In light of the similarity between the visible spectra of the blue complex and $[Cu(dien)(OH_2)_3]^{2+}$ (λ_{max} for the blue complex is 610 nm and that for the $[Cu(dien)(OH_2)_3]^{2+}$ complex is 611 nm[10]), the tetragonally distorted octahedral structure, where the three amino nitrogen donors and one H_2O stay at

Table 1. Equilibrium Constants of Copper(II) Complexes.
Ionic Strength (I)=0.20, 25 °C

Ligand	K_{CuHL}	K_{CuL}	$K_{CuH_{-1}L}$	$K_{CuH_{-2}L}$	K^{-2H}
Monooxo[16]aneN$_5$(L^1)	(1.1±0.1)×10^7	—	(2.8±0.5)×10^3	—	(2.5±0.2)×10^{-4}
Dioxo[16]aneN$_5$(L^2)	—	(9.8±1.0)×10^{11}	—	(1.6±0.5)×10^{-2}	(1.6±0.3)×10^{-14}
Pyr-dioxo[16]aneN$_5$(L^3)	—	(1.1±0.1)×10^{14}	—	(2.6±0.7)×10^{-2}	(2.5±0.4)×10^{-16}
Dioxo[16]aneN$_4$(3,3,3,3)(L^4)	—	—	—	(4.4±0.6)×10^{-11}	—
Dioxo[16]aneN$_4$(3,2,5,2)(L^5)	—	—	—	(1.3±0.2)×10^{-5}	—
Dioxo[16]aneN$_4$S(L^6)	—	—	—	(1.5±0.2)×10^{-3}	—
Dioxo[15]aneN$_5$(L^7)	—	—	(7.3±0.8)×10^2	(3.0±0.8)×10^{-6}	(4.1±0.6)×10^{-9}[a]
Dioxo[18]aneN$_6$(L^8)	—	(3.6±0.5)×10^{10}	—	(9.4±1.5)×10^{-6}	(2.6±0.4)×10^{-16}
Dioxopyo[16]aneN$_5$(L^9)	—	—	—	(1.4±0.2)×10^{-2}	—

a) $K^{-H}_{CuH_{-1}L}$.

the basal positions, would be assumed for the blue complex. In fact, a Dreiding molecular model study shows that the Cu(II) ion in this complex can have a coordination environment of three amino nitrogen donors and one carbonyl oxygen of L^2 in plan with two H_2O molecules above and below, completing the distorted octahedral coordination. The formation constant, K_{CuL}, determined in this study is slightly larger than that of the copper(II)-diethylenetriamine (dien) complex ($\log K_{CuL}=10.01$).[11] This finding also lends a strong support to the above explanation.

As in the case of the nickel(II)-dioxo[16]aneN$_5$ complex, $NiH_{-2}L^0$,[4] the doubly-deprotonated dioxo[16]aneN$_5$ anion for the violet complex, $CuH_{-2}L^0$, which is formed at pH's higher than 7.0, would encircle the Cu(II) ion in a square-pyramidal configuration with two deprotonated amide nitrogen donors staying at the basal positions, along with the two amino nitrogens, probably completing the distorted octahedral coordination. The 16-membered dioxotetramine, dioxo[16]aneN$_4$ (3,3,3,3)(L^4), forms solely $CuH_{-2}L^0$. Its violet aqueous solution displays visible spectra ($\lambda_{max}=550$ nm) similar to those for the dioxo[16]aneN$_5$ complex, $CuH_{-2}L^0$. Hence, for this complex the distorted octahedral coordination including water molecules must be likely. A molecular model examination shows that the ligand in this complex can encircle the Cu(II) ion with two amino and two deprotonated amide nitrogens staying at the basal positions with two H_2O molecules at the axial coordination sites. The other 16-membered dioxotetramine, L^5, also afforded the $CuH_{-2}L^0$ complex. Its aqueous solution, however, is pink and gives visible spectra quite similar to those of Cu(II)-13—15-membered dioxotetramine complexes.[2,4] This implys that the structure of the Cu(II)-L^5 complex can be described as an extremely flattened tetrahedron or a square-planar geometry.[12] L^9 and L^6 also yielded only stable $CuH_{-2}L^0$ under the present experimental conditions. The significant difference in the magnitude of $K_{CuH_{-2}L}$ value between L^4 and L^5 complexes clearly suggests that the presence of the dioxo-[2.3.2]tetramine moiety is essentially required for the formation of stable doubly-deprotonated $CuH_{-2}L^0$ (Table 1), because the doubly-deprotonated dioxo-[2.3.2]tetramine frame can adapt most easily to the achievement of the rigid square-planar geometry.

As demonstrated by the $K_{CuH_{-2}L}$ values in Table 1, the sulfur and pyridine nitrogen donors incorporated within the 16-membered macrocyclic frame also assist in stabilizing the complex. Dioxo[18]aneN$_6$, L^8, also forms blue CuL^{2+} at pH 3.5—6.0, and mauve doubly-deprotonated $CuH_{-2}L^0$ at pH's higher than 7.5. The fact that dioxo[16]aneN$_5$ and dioxo[18]aneN$_6$ can form CuL^{2+} as well as $CuH_{-2}L^0$, but L^5 gives only $CuH_{-2}L^0$ clearly suggests that neutral dioxopolyamines can encircle the copper(II) ion in their macrocyclic cavity only when three or more amine nitrogens are available for the complexation.

References

1) M. Kodama and E. Kimura, *J. Chem. Soc., Dalton Trans.*, **1979**, 325.
2) M. Kodama and E. Kimura, *J. Chem. Soc., Dalton Trans.*, **1981**, 694.
3) I. Tabushi, H. Okino, and Y. Kuroda, *Tetrahedron Lett.*, **1976**, 4339.
4) E. Kimura, R. Machida, and M. Kodama, *J. Am. Chem. Soc.*, **106**, 5497 (1984).
5) G. Schwarzenbach, "Complexometric Titrations," Interscience Publishers, New York (1957).
6) E. Kimura, T. Koike, and M. Kodama, *Chem. Pharm. Bull.*, **32**, 3569 (1984).
7) M. Kodama and E. Kimura, *Bull. Chem. Soc. Jpn.*, **62**, 3093 (1989).
8) M. Kodama and E. Kimura, *J. Chem. Soc., Dalton Trans.*, **1978**, 1081.
9) E. Kimura, T. Koike, R. Machida, R. Nagai, and M. Kodama, *Inorg. Chem.*, **23**, 4181 (1984).
10) C. K. Jorgensen, *Acta Chem. Scand.*, **10**, 887 (1956).
11) D. W. Margerum, B. L. Powell, and J. A. Luthy, *Inorg. Chem.*, **7**, 800 (1968).
12) B. J. Hathway, *Coord. Chem. Rev.*, **41**, 423 (1982).

The Magnetic Properties of Copper(II) 3- and 4-Substituted Benzoate Adducts with Quinoline and 4-Methylquinoline

Shuji EMORI,* Satoru MATSUNAGA, and Miyako GOTO
Department of Chemistry, Faculty of Science and Engineering, Saga University, Honjo-machi, Saga 840
(Received July 12, 1989)

Synopsis. Various copper(II) 3- and 4-substituted and 3,5-disubstituted benzoate adducts with quinoline and 4-methylquinoline have been prepared, and characterized by means of magnetic susceptibility and IR spectroscopy measurements. The variation of their magnetic moments is discussed in terms of the acidities of their parent acids and the resonance effects of 4-substituents.

Most copper(II) carboxylates have bridged dinuclear structures and exhibit strong antiferromagnetic coupling between the pairs of copper(II) ions. With the intention of elucidating the mechanism of the spin-exchange coupling, an attempt has been made to relate the strength of the coupling to the acidity of the parent carboxylic acid.[1-3] While such a correlation has been confirmed for various alkanoate series,[3-5] it remains obscure for arenecarboxylates.[6-8] This is supposed to reflect the versatility of coordination polymerism in arenecarboxylates.[9,10] Besides, their magnetic properties may also be affected by the steric and resonance effects of substituents, as would be expected from the Hammett equation.[11] In order to investigate the resonance effects, we have prepared the quinoline (quin) and 4-methylquinoline (4-Mequin) adducts of a series of copper(II) 3- and 4-substituted benzoates with the substituents of CH_3, Cl, NO_2, CF_3, CH_3O, and CN.

The quinoline adducts of copper(II) 4-substituted benzoates, except 4-cyanobenzoate, were prepared according to the general procedure[9] and recrystallized from *N*,*N*-dimethylformamide containing excess quinoline. The remaining compounds were prepared by treating the ethanol solution of appropriate benzoic acid with a chloroform solution of the quinoline adduct of copper(II) propionate. In most cases the fine green crystals precipitated within a few hours; when this was not the case, the mixture was evaporated under reduced pressure. The effective magnetic moments of these compounds (Table 1) were evaluated from the room-temperature magnetic susceptibilities (χ_M) using the equation $\mu_{eff}=2.83[(\chi_M-\chi_{dia}-N\alpha)T]^{1/2}$. The diamagnetic corrections (χ_{dia}) were estimated from Pascal constants[12] and the temperature-independent paramagnetic contribution ($N\alpha$) was taken as 60×10^{-6} (1 emu$=4\pi\times10^{-6}$ m^3). For the quinoline adducts of copper(II) 3-nitrobenzoate and 3,5-dinitrobenzoate, the temperature dependence of their magnetic susceptibilities was measured in the temperature range of 80—300 K in order to confirm their dinuclear structures. The result agreed well with the Bleaney-Bowers equation,[13] using the parameters of $g=2.17$ and $2J=-276$ cm^{-1} for the 3-nitrobenzoate and $g=2.18$ and $2J=-259$ cm^{-1} for the 3,5-dinitrobenzoate. The IR spectra of the solid compounds show bands characteristic of bridging carboxylate due to unsymmetric and symmetric carboxyl stretching vibrations.[14] The magnetic and IR spectral data indicate that the present compounds have a bridged dinuclear structure, similar to that of copper(II) acetate monohydrate.[15,16]

From an analogy to plots for the corresponding alkanoates,[4,5] the room-temperature magnetic moments (in BM) of the present compounds, together with literature data concerning the corresponding pyridine adducts,[7,16] are plotted in Fig. 1 against $pK_a-0.068pK_a'$ values, where pK_a and pK_a' are the acidities of the parent benzoic acid and the conjugate acid of the addend *N*-heteroaromatic donor. The points for the 3-substituted and 3,5-disubstituted benzoates give a straight line which has the same slope as that for the alkanoates:[4]

$$\mu_{eff}=-0.052(pK_a-0.068pK_a'-4.00)+1.37_1. \quad (1)$$

The variation of the singlet-triplet separation energies (e.g. $-2J=280$, 276, and 259 cm^{-1} for the quinoline adducts of benzoate,[17] 3-nitrobenzoate, and 3,5-dinitrobenzoate, respectively, and $-2J=309$, 307, and 292 cm^{-1} for the pyridine adducts of copper(II) 3-methylbenzoate,[7] benzoate,[18] and 3-bromobenzoate,[7] respectively) is consistent with this equation. Similarly, the carboxyl frequencies (in cm^{-1}) for these compounds show systematic shifts against the acidities of the parent benzoic acids ($\tilde{\nu}_{unsym}=1683-15.0(pK_a-0.068pK_a')$ and $\tilde{\nu}_{sym}=1406+4.9(pK_a-0.068pK_a')$). These relationships indicate that the magnetic properties of the 3-substituted and 3,5-disubstituted benzoates are influenced unambiguously by the inductive effects of substituents. On the other

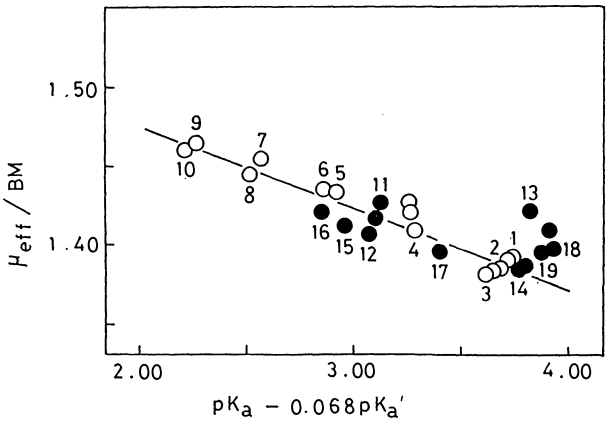

Fig. 1. The magnetic moments at 20 °C plotted against the acidities of the ligands for the copper(II) 3-substituted (○) and 4-substituted (●) benzoate adducts with pyridine, quinoline, and 4-methylquinoline.

Table 1. Analytical Data and Effective Magnetic Moments at 20 °C

Compound		Found(Calcd)/%				μ_{eff}/BM
		Cu	C	H	N	
$Cu(3\text{-}CH_3C_6H_4COO)_2 \cdot quin$	(1)	13.85 (13.73)	64.37 (64.86)	4.65 (4.57)	2.96 (3.03)	1.39
$Cu(3\text{-}CH_3C_6H_4COO)_2 \cdot 4\text{-}Mequin$	(2)	13.52 (13.32)	65.34 (65.47)	4.74 (4.86)	2.87 (2.94)	1.39
$Cu(C_6H_5COO)_2 \cdot 4\text{-}Mequin$	(3)	14.17 (14.15)	63.89 (64.21)	4.15 (4.27)	3.06 (3.12)	1.38
$Cu(3\text{-}ClC_6H_4COO)_2 \cdot quin$	(4)	12.62 (12.61)	54.67 (54.83)	2.98 (3.00)	2.70 (2.78)	1.41
$Cu(3\text{-}NO_2C_6H_4COO)_2 \cdot quin$	(5)	11.87 (12.11)	52.48 (52.63)	2.81 (2.88)	7.89 (8.00)	1.43
$Cu(3\text{-}NO_2C_6H_4COO)_2 \cdot 4\text{-}Mequin$	(6)	11.45 (11.79)	53.31 (53.49)	3.11 (3.18)	7.65 (7.80)	1.44
$Cu(3,5\text{-}Cl_2C_6H_3COO)_2 \cdot quin$	(7)	11.10 (11.10)	47.82 (48.24)	2.46 (2.29)	2.35 (2.45)	1.46
$Cu(3,5\text{-}Cl_2C_6H_3COO)_2 \cdot 4\text{-}Mequin$	(8)	11.04 (10.83)	48.93 (49.13)	2.51 (2.58)	2.32 (2.39)	1.44
$Cu[3,5\text{-}(NO_2)_2C_6H_3COO]_2 \cdot quin \cdot CHCl_3$	(9)	8.89 (8.65)	39.13 (39.26)	1.89 (1.92)	9.47 (9.54)	1.46
$Cu[3,5\text{-}(NO_2)_2C_6H_3COO]_2 \cdot 4\text{-}Mequin \cdot CHCl_3$	(10)	8.64 (8.49)	39.98 (40.13)	2.30 (2.15)	9.33 (9.36)	1.46
$Cu(4\text{-}CF_3C_6H_4COO)_2 \cdot quin$	(11)	11.45 (11.13)	52.63 (52.59)	2.67 (2.65)	2.55 (2.45)	1.43
$Cu(4\text{-}CF_3C_6H_4COO)_2 \cdot 4\text{-}Mequin$	(12)	10.87 (10.86)	53.48 (53.39)	2.97 (2.93)	2.43 (2.39)	1.41
$Cu(4\text{-}CH_3C_6H_4COO)_2 \cdot quin$	(13)	13.62 (13.73)	65.04 (64.86)	4.61 (4.57)	3.27 (3.03)	1.40
$Cu(4\text{-}CH_3C_6H_4COO)_2 \cdot 4\text{-}Mequin$	(14)	13.19 (13.32)	65.59 (65.47)	4.93 (4.86)	2.99 (2.94)	1.38
$Cu(4\text{-}NCC_6H_4COO)_2 \cdot 4\text{-}Mequin \cdot C_2H_5OH$	(15)	11.96 (11.66)	61.33 (61.70)	3.97 (4.25)	7.79 (7.71)	1.42
$Cu(4\text{-}NO_2C_6H_4COO)_2 \cdot 4\text{-}Mequin$	(16)	11.88 (11.79)	53.57 (53.49)	3.31 (3.18)	7.85 (7.80)	1.43
$Cu(4\text{-}ClC_6H_4COO)_2 \cdot 4\text{-}Mequin$	(17)	11.99 (12.27)	55.88 (55.67)	3.45 (3.31)	2.85 (2.70)	1.41
$Cu(4\text{-}CH_3OC_6H_4COO)_2 \cdot quin \cdot (CH_3)_2NCHO$	(18)	11.47 (11.19)	60.70 (59.20)	4.80 (4.97)	4.75 (4.93)	1.40
$Cu(4\text{-}CH_3OC_6H_4COO)_2 \cdot 4\text{-}Mequin$	(19)	12.36 (12.48)	61.53 (61.35)	4.59 (4.55)	2.83 (2.75)	1.40

hand, the magnetic moments of the present 4-substituted benzoates are rather independent of the acidities of the parent acids (Fig. 1). This discernible trend has already been pointed out for the magnetic properties of the copper(II) 4-substituted benzoate adducts with 1-butanol, since their singlet-triplet separation energies are insensitive to the nature of the substituents.[6] It is plausible that the resonance and inductive effects of 4-substituent[11,19] tend to be cancelled out. For cases where the perturbation on the π-electron density of the carboxyl group may not be disregarded, using $\Delta\mu_\pi$ to represent this correction term, we can write

$$\mu_{eff} = -0.052(pK_a - 0.068pK_a' - 4.00) + \Delta\mu_\pi + 1.37_1. \quad (2)$$

Previously, we have pointed out that the $\Delta\mu_\pi$ term may be correlated with $R-0.38F$,[5] where R and F are the resonance and field constants of Swain and Lupton.[20] The $\Delta\mu_\pi$ values evaluated by the use of Eq. 2 are plotted, in Fig. 2, against $R-0.38F$. The apparent linear correlation indicates that the resonance effect takes a role in determining the magnetic properties of the 4-substituted benzoates. The magnitude of the resonance effect is estimated to be about $-0.03_5(R-0.38F)$, e.g., 0.00_4, 0.01_5, and 0.02_3 BM for

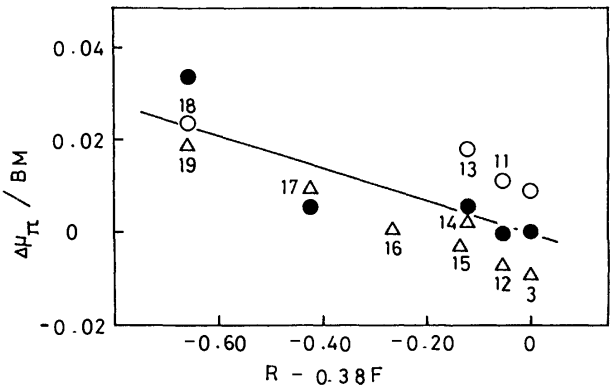

Fig. 2. The correction values $\Delta\mu_\pi$ for the 4-substituted benzoate adducts with pyridine (●), quinoline (○), and 4-methylquinoline (△) plotted against the substitutent constants $R-0.38F$.

the CH_3, Cl, and CH_3O substituents, respectively. These values are much smaller than those found in the case of copper(II) (substituted formate)s.[5] This refers perhaps to the torsion between the planes of the carboxylate and phenyl groups (the dihedral angles of 0.2—27.2°),[21-24] in adition to the long separation between the bridging carboxylato and substituent groups.

References

1) J. Lewis and R. C. Thompson, *Nature (London)*, **200**, 468 (1963).
2) A. Earnshaw and K. S. Patel, *J. Inorg. Nucl. Chem.*, **27**, 1805 (1965).
3) M. Melnik, *Coord. Chem. Rev.*, **42**, 259 (1982); and references therein.
4) S. Emori, K. Ohishi, H. Kurihara, and Y. Muto, *Bull. Chem. Soc. Jpn.*, **61**, 4439 (1988).
5) S. Emori and H. Kondo, *Bull. Chem. Soc. Jpn.*, **62**, 3368 (1989).
6) W. E. Hatfield, C. S. Fountain, and R. Whyman, *Inorg. Chem.*, **5**, 1855 (1966).
7) F. G. Herring, B. Landa, R. C. Thompson, and C. F. Schwerdtfeger, *J. Chem. Soc. A*, **1971**, 528.
8) N. Kumar, B. L. Kalsotra, and R. Sachar, *J. Indian Chem.*, **60**, 715 (1983).
9) J. Lewis, Y. C. Lin, L. K. Royston, and R. C. Thompson, *J. Chem. Soc.*, **1965**, 6464.
10) M. Melnik, *J. Inorg. Nucl. Chem.*, **41**, 779 (1979).
11) L. P. Hammett, "Physical Organic Chemistry," McGraw-Hill Book Co., New York (1940).
12) G. Foex, "Constants Sélectionées, Diamagnétisme et Paramagnétisme," Masson, Paris (1957).
13) B. Bleaney and K. D. Bowers, *Proc. R. Soc. London, Ser. A*, **214**, 451 (1952).
14) L. J. Bellamy, "The Infrared Spectra of Complex Molecules," 3rd ed., Chapman and Hall, London (1975).
15) J. N. van Niekerk and F. R. L. Schoening, *Acta Crystallogr.*, **6**, 227 (1953).
16) G. M. Brown and R. Chidambaram, *Acta Crystallogr., Sect. B*, **29**, 2393 (1973).
17) A. Bencine, C. Benelli, D. Gatteschi, and C. Zanchini, *J. Am. Chem. Soc.*, **102**, 5820 (1980).
18) J. Lewis and F. Mabbs, *J. Chem. Soc.*, **1965**, 3894.
19) R. A. Zelonka and M. C. Baird, *Inorg. Chem.*, **11**, 134 (1972).
20) C. G. Swain and E. C. Lupton, Jr., *J. Am. Chem. Soc.*, **90**, 4328 (1968).
21) A. Bencini, D. Gatteschi, and C. Mealli, *Cryst. Struct. Commun.*, **8**, 305 (1979).
22) B. T. Usubaliev, E. M. Movsumov, F. N. Musaev, G. N. Nadzafov, I. R. Amiraslanov, and H. S. Mamedov, *Koord. Khim.*, **6**, 1091 (1980).
23) I. Bkouche-Waksman, C. Bois, G. A. Popovitch, and P. L'Haridon, *Bull. Soc. Chim. Fr.*, **1—2**, 69 (1980).
24) M. Melnik, M. Dunaj-Jurco, and M. Handlovic, *Inorg. Chim. Acta*, **86**, 185 (1984).

Synthesis and Four Isomers of 5-Arylamino-3-isopropyl-6-methyl-6-phenyl-1,2,4-trioxanes

Hiroshi YAMAMOTO,* Takehiko NISHIO,† Masatoshi HIRAYAMA,†† Masamoto AKUTAGAWA,††† and Choji KASHIMA†
Faculty of Education, Ibaraki University, Bunkyo, Mito 310
†Department of Chemistry, The University of Tsukuba, Tsukuba, Ibaraki 305
††Department of Chemistry, Ibaraki University, Bunkyo, Mito 310
†††Faculty of Education, Kumamoto University, Kumamoto 860
(Received April 21, 1989)

Synopsis. 5-Arylamino-3-isopropyl-6-methyl-6-phenyl-1,2,4-trioxanes were synthesized by autoxidation of imines in the presence of isobutyraldehyde. Their four isomers have been identified and the anomerization of 5-arylamino-1,2,4-trioxanes has been detected by the ^{13}C NMR spectra in chloroform-*d*.

The 1,2,4-trioxanes have attracted the attention of researchers since they play an active role in sesquiterpene Arteannuin,[1] an antimalarial remedy. Several methods for the synthesis of 1,2,4-trioxanes have been reported,[2] while we obtained 5-arylamino-1,2,4-trioxanes **4** and **5** through reactions of arylamines **1** and aldehydes **2** and **3** in the presence of oxygen (Scheme 1).[3] The structures of both the cis($3R^*,5S^*$) and trans ($3R^*,5R^*$) isomers of **4** became apparent based on X-ray crystal-structure analyses;[4] the distinction between these two isomers were established on the basis of ^{13}C NMR chemical shifts.[5] Trioxanes **4** and **5** are composed of an arylamine and two molecules of aldehyde incorporated in the same ring. We now report on the synthesis of trioxanes in which two different kinds of aldehydes are incorporated. The structures of four isomers of trioxanes, thus produced, are characterized.

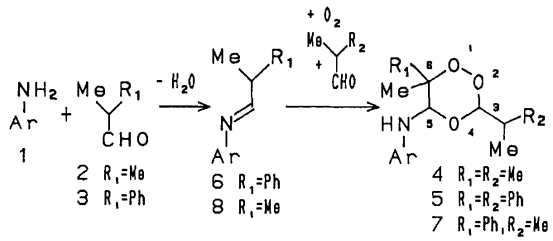

Ar = a; *p*-tolyl b; *o*-tolyl c; phenyl d; 2-chlorophenyl e; 2,4-xylyl f; 4-chlorophenyl g; *m*-tolyl h; 2,6-xylyl i; mesityl.

Scheme 1.

Results and Discussion

Imines **6**, easily obtained from **1** and **3**, were autoxidized in the presence of **2** for a few days (Scheme 1). After the resulting mixture was separated into five products by HPLC (high-performance liquid chromatography), products were characterized by the use of a mass spectrometer. In the case of **6a**, the product corresponding to the first peak was assigned to be trioxane **4a** (*m/z* 265, M^+) in which two molecules of isobutyraldehyde are incorporated. The other four products showed the same parent ion peaks for new trioxane (*m/z* 327, M^+). A similar tendency in the reaction of imines **6b—g** was also observed by means of HPLC. On the other hand, imines **6h,i** bearing a 2,6-disubstituted phenyl moiety gave only one product. From these mixtures, colorless crystallines of trioxanes **7a—i** were obtained by column chromatography and recrystallization from hexane; they gave satisfactory spectral data (NMR, IR, MS).

Since imine **8** was partly interconverted into imine **6** during autoxidation with **3**, the oxidation of imines **8** in the presence of **3** gave a number of products. In the case of **8a**, these products consisted of **4a**, two isomers of **5a** and four isomers of **7a** on the basis of HPLC and mass spectra. We could not isolate any pure crystallines from these reaction mixtures.

Four isomers of **7** ($3R^*,5S^*,6R^*$, $3R^*,5R^*,6R^*$, $3R^*,5S^*,6S^*$, $3R^*,5R^*,6S^*$) and another four equatorial-axial interconversion conformers are expected by analogy with the case of 1,2,4-trisubstituted cyclohexanes.[6] Since a previous X-ray analysis of **4** suggested that the isopropyl group at C-3 is bonded at an equatorial position, **7** may exists in four isomers which have an isopropyl group bonding at an equatorial position (Fig. 1). ^{13}C NMR was the established method for the conformational analysis of **4**. Therefore, a conformational analysis of **7** was attempted by ^{13}C NMR.

Since the ^{13}C signal of C-3 of **7e,f** appeared at δ 99.8—99.9, the anilino nitrogen at C-5 is located γ-gauche to C-3 and the conformation at C-5 has been determined to be R^*. Since the methyl at C-6 is γ-

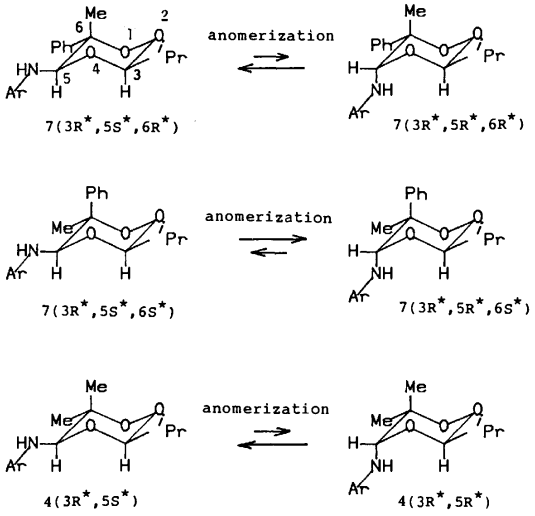

Fig. 1. Four possible isomers of **7** and two isomers of **4**.

Table 1. ^{13}C NMR Chemical Shifts of **7** in $CDCl_3$ at 25 °C (δ/ppm from Me_4Si)[a]

	C-3	CH	Me	Me	C-5	C-6	Me	Me-Ar
7a(3*R**,5*S**,6*R**)	107.2	31.1	17.0		86.8	82.6	16.3	20.4
(3*R**,5*R**,6*R**)	(99.9)	(30.6)			(83.0)		(25.7)	
7b(3*R**,5*S**,6*R**)	107.1	31.1	16.9		87.0	82.7	16.3	17.0
(3*R**,5*R**,6*R**)	(99.9)	(30.7)			(83.4)		(24.9)	
7c(3*R**,5*S**,6*R**)	107.2	31.0	17.0		86.4	82.6	16.3	—
(3*R**,5*R**,6*R**)	(99.9)	(30.6)			(82.6)		(25.6)	
7d(3*R**,5*S**,6*R**)	107.1	31.0	17.0		86.1	82.5	16.2	
(3*R**,5*R**,6*R**)	(99.6)	(30.6)			(83.7)		(25.2)	
7e(3*R**,5*R**,6*R**)	99.8	30.7	16.9		83.6	82.8	25.0	16.5, 20.4
(3*R**,5*S**,6*R**)	(107.1)	(31.1)			(87.5)		(16.3)	
7f(3*R**,5*R**,6*R**)	99.9	30.6	16.9		82.4_9	82.5_2	25.6	
(3*R**,5*S**,6*R**)	(107.2)	(31.1)			(86.5)		(16.2)	
7g(3*R**,5*R**,6*S**)	99.5	30.4	16.6		79.7	84.1	25.8	21.6
(3*R**,5*S**,6*S**)	(107.6)	(31.1)			(87.6)		(22.9)	
7h(3*R**,5*S**,6*R**)	106.9	31.1	16.7, 16.6		90.9	83.6	14.7	18.0
7i(3*R**,5*S**,6*R**)	106.7	31.2	16.7		91.1	83.6	14.6	17.9, 20.5
	C-3	CH	Me	Me	C-5	eq. Me	C-6	ax. Me
4f(3*R**,5*S**)[b]	107.2	31.0	16.8		86.4	21.8	79.8	17.4
(3*R**,5*R**)	(99.5)	(30.6)			(81.2)	(22.4)	(79.7)	(23.6)

a) Newly appeared signals in solution are given in parenthese. b) Typical trioxane of **4**, (3*R**,5*S**)-5-(4-chloroanilino)-3-isopropyl-6,6-dimethyl-1,2,4-trioxane, from Ref. 5).

trans to the nitrogen, from the ^{13}C shift value for this carbon at δ 25.0—25.6, the conformation at C-6 has been determined to be *R**. It may, therefore, be considered that the structure of **7e,f** is **7** (3*R**,5*R**,6*R**). When $CDCl_3$ solutions of **7e,f** were allowed to stand for a few days new ^{13}C signals appeared in lower fields where trioxanes of **7a—d** had shown signals. Similarly, when $CDCl_3$ solutions of **7a—d** were allowed to stand new ^{13}C signals were observed in the higher fields, where those of **7e,f** had appeared. These new signals are shown in parentheses in Table 1. Since these spectral changes can be ascribed to anomerization at C-5 of the 1,2,4-trioxane ring between **7** (3*R**,5*R**,6*R**) and **7** (3*R**,5*S**,6*R**), by analogy with the case of **4**[5] the structure of **7a—d** seems to be **7** (3*R**,5*S**,6*R**). The ^{13}C chemical shifts of C-3 (δ 107.1—107.2) and the methyl carbon (δ 16.2—16.3) support this conformation.

The ^{13}C NMR signals for **7g** were notable for C-5 and C-6 at δ 79.7 (the highest field) and at δ 84.1 (the lowest field), respectively. Since the nitrogen is located γ-gauche to C-3 from its value δ 99.5, the conformation of C-5 has been determined to be *R**. The ^{13}C signal for the methyl carbon at C-6 of this isomer (δ 25.8) was close to that of the anomeric isomer (δ 22.9). This may suggest that the methyl group in each isomer occupies an equatorial position of the trioxane ring and that the conformation of C-6 is *S**. Therefore, the structure of **7g** seems to be **7** (3*R**,5*R**,6*S**) and the anomeric isomer to be **7** (3*R**,5*S**,6*S**). Attempts to analyze **7g** by X-rays were unsuccessful because of the rapid intensity decrease of the reflections during measurement. However, an analysis with a technically insufficient number of reflections may support the 3*R**,5*R**,6*S** conformation of **7g**.[7]

Table 2. Equilibration of **7** in $CDCl_3$ at 25 °C

3*R**,5*S**,6*R** isomer/%		$\Delta G^{oa)}$/kJ mol^{-1}
7a	62±1	1.2±0.1
7b	62±2	1.2±0.2
7c	61±3	1.1±0.3
7d	71±1	2.2±0.1
7e	62±1	1.2±0.1
7f	57±1	0.7±0.1
3*R**,5*R**,6*S** isomer/%		$\Delta G^{ob)}$/kJ mol^{-1}
7g	81±5	3.7±0.8

a) $\Delta G^\circ = G^\circ_{3R^*,5R^*,6R^*} - G^\circ_{3R^*,5S^*,6R^*}$. b) $\Delta G^\circ = G^\circ_{3R^*,5S^*,6S^*} - G^\circ_{3R^*,5R^*,6S^*}$.

The ^{13}C NMR spectra of **7h,i** were very similar to those of **7a—d**, except for the C-5 signal which shifted to lower field (δ 90.9—91.1). It may, thus, be considered that the structure of **7h,i** is **7** (3*R**,5*S**,6*R**) and that the C-5 signal appeared at a low field owing to an anisotropic effect of the twisted aryl group.

The free-energy difference of anomerization was evaluated from the molar fractions of isomers derived from the average intensity of ^{13}C signals at equilibrium (Table 2). These values were smaller than those of trioxane **4**. The phenyl substitution of the ring causes a smaller free-energy differences between the anomeric isomers.

Experimental

Melting points are all uncorrected. Spectral characterizations were carried out with the following instruments: ^{13}C NMR, JEOL JNM-GSX400 spectrometer; ^1H NMR,

Hitachi R-20A spectrometer; MS, JEOL JMS-DX300 mass spectrometer; and IR, Hitachi 215 spectrometer. HPLC was performed by using a JASCO 800 liquid chromatograph with a SIL C18T column (7.2×250 mm, 90% methanol aq as eluent).

General Preparation of Trioxanes 7. The mixture of arylamine **1** (15 mmol) and 2-phenylpropionaldehyde (**3**) (15.5 mmol) was heated in an oil bath (110 °C) under nitrogen for 30 min. A solution of the crude imine **6** and isobutyraldehyde (**2**) (30 mmol) in hexane (25 ml) was autoxidized in a 100 ml Erlenmyer flask at room temperature. After about 2 to 4 days, the solvent and excess **2** were removed under reduced pressure and the residue was chromatographed on silica gel to give the corresponding trioxane **7**.

(3*R,5*S**,6*R**)-3-Isopropyl-6-methyl-6-phenyl-5-(*p*-toluidino)-1,2,4-trioxane (7a):** prisms from hexane (yield 13%), mp 83—85 °C (decomp); IR(Nujol) 3450, 1300, 1255, 1145, and 1055 cm^{-1}. ^1H NMR ($CDCl_3$) δ=0.99 (6H, d, J=6.5 Hz), 1.87 (3H, s), 2.19 (3H, s), ca. 1.9 (1H, m), 3.87 (1H, d, J=10 Hz), 5.14 (1H, d, J=10 Hz), 5.18 (1H, d, J=5.5 Hz), and 6.3—7.5 (9H, m); DI-MS m/z (%) 327 (M^+, 0.3), 136 (90), and 135 (100); Found: C, 73.27; H, 7.74; N, 4.26%. Calcd for $C_{20}H_{25}NO_3$: C, 73.36; H, 7.69; N, 4.27%.

(3*R,5*S**,6*R**)-3-Isopropyl-6-methyl-6-phenyl-5-(*o*-toluidino)-1,2,4-trioxane (7b):** prisms from hexane (yield 10%), mp 111—115 °C (decomp); IR (Nujol) 3460, 1300, 1260, 1175, 1145, and 1050 cm^{-1}; ^1H NMR ($CDCl_3$) δ=1.04 (6H, d, J=6.5 Hz), 1.93 (3H, s), 2.05 (3H, s), ca. 2.0 (1H, m), 3.88 (1H, d, J=9 Hz), 5.14 (1H, d, J=9 Hz), 5.26 (1H, d, J=5.5 Hz), and 6.5—7.6 (9H, m); DI-MS m/z (%) 327 (M^+, 0.2), 136 (100), and 135 (63); Found: C, 73.44; H, 7.70; N, 4.24%. Calcd for $C_{20}H_{25}NO_3$: C, 73.36; H, 7.69; N, 4.27%.

(3*R,5*S**,6*R**)-5-Anilino-3-isopropyl-6-methyl-6-phenyl-1,2,4-trioxane (7c):** prisms from hexane (yield 13%), mp 97—98 °C (decomp); IR (Nujol) 3450, 1305, 1250, 1155, and 1050 cm^{-1}; ^1H NMR ($CDCl_3$) δ=1.00 (6H, d, J=6.5 Hz), 1.88 (3H, s), ca. 1.9 (1H, m), 4.00 (1H, d, J=9.5 Hz), 5.16 (1H, d, J=9.5 Hz), 5.20 (1H, d, J=5.5 Hz), and 6.5—7.8 (10H, m); DI-MS m/z (%) 313 (M^+, 1.5), 122 (83), and 121 (100); Found: C, 72.58; H, 7.40; N, 4.48%. Calcd for $C_{19}H_{23}NO_3$: C, 72.81; H, 7.39; N, 4.46%.

(3*R,5*S**,6*R**)-5-(2-Chloroanilino)-3-isopropyl-6-methyl-6-phenyl-1,2,4-trioxane (7d):** prisms from hexane (yield 6%), mp 116—118 °C (decomp); IR (Nujol) 3460, 1325, 1255, 1175, 1120, and 1050 cm^{-1}; ^1H NMR ($CDCl_3$) δ=1.01 (6H, d, J=6.5 Hz), 1.87 (3H, s), ca. 2.0 (1H, m), 4.79 (1H, d, J=9.5 Hz), 5.19 (1H, d, J=9.5 Hz), 5.28 (1H, d, J=5.0 Hz), and 6.5—7.6 (9H, m); DI-MS m/z (%) 349, 347 (M^+, —, 0.2), 156 (49), 155 (25), and 120 (100); Found: C, 65.44; H, 6.45; N, 4.02%. Calcd for $C_{19}H_{22}NO_3Cl$: C, 65.60; H, 6.37; N, 4.02%.

(3*R,5*R**,6*R**)-3-Isopropyl-6-methyl-6-phenyl-5-(2,4-xylidino)-1,2,4-trioxane (7e):** prisms from hexane (yield 7%), mp 103—105 °C (decomp); IR (Nujol) 3450, 1295, 1265, 1150, and 1055 cm^{-1}; ^1H NMR ($CDCl_3$) δ=0.97 (6H, d, J=6.5 Hz), 1.54 (3H, s), 1.96 (3H, s), ca. 1.9 (1H, m), 2.19 (3H, s), 3.95 (1H, d, J=6 Hz), 5.13 (1H, d, J=6 Hz), 5.47 (1H, d, J=5.5 Hz), and 6.7—7.4 (8H, m); DI-MS m/z (%) 341 (M^+, 0.2), 150 (24), 151 (56), and 105 (100); Found: C, 73.84; H, 8.09; N, 4.06%. Calcd for $C_{21}H_{27}NO_3$: C, 73.87; H, 7.97; N, 4.10%.

(3*R,5*R**,6*R**)-5-(4-Chloroanilino)-3-isopropyl-6-methyl-6-phenyl-1,2,4-trioxane (7f):** prisms from hexane (yield 2.2%), mp 69—70 °C (decomp); IR (Nujol) 3440, 1310, 1290, 1250, 1150, and 1050 cm^{-1}; ^1H NMR ($CDCl_3$) δ=0.95 (6H, d, J=6.5 Hz), 1.91 (3H, s), ca. 1.9 (1H, m), 4.18 (1H, d, J=6.5 Hz), 5.15 (1H, d, J=6.5 Hz), 5.32 (1H, d, J=5.5 Hz), and 6.3—7.4 (9H, m); DI-MS m/z (%) 349, 347 (M^+, —, 3.6), 156 (61), and 155 (100); Found: C, 65.60; H, 6.41; N, 4.05%. Calcd for $C_{19}H_{22}NO_3Cl$: C, 65.60; H, 6.37; N, 4.02%.

(3*R,5*R**,6*S**)-3-Isopropyl-6-methyl-6-phenyl-5-(*m*-toluidino)-1,2,4-trioxane (7g):** prisms from hexane (yield 4.7%), mp 84—85 °C (decomp); IR (Nujol) 3430, 1320, 1260, 1210, 1170, 1150, and 1050 cm^{-1}; ^1H NMR ($CDCl_3$) δ=0.67 (6H, d, J=6.5 Hz), 1.38 (3H, s), ca. 1.7 (1H, m), 2.29 (3H, s), 4.90 (1H, d, J=10 Hz), 5.66 (1H, d, J=10 Hz), 5.26 (1H, d, J=4.5 Hz), and 6.5—7.3 (9H, m); DI-MS m/z (%) 327 (M^+, 0.4), 134 (37), 135 (67), and 105 (100); Found: C, 73.28; H, 7.67; N, 4.28%. Calcd for $C_{20}H_{25}NO_3$: C, 73.36; H, 7.69; N, 4.27%.

(3*R,5*S**,6*R**)-3-Isopropyl-6-methyl-6-phenyl-5-(2,6-xylidino)-1,2,4-trioxane (7h):** prisms from hexane (yield 27%), mp 86—88 °C (decomp); IR (Nujol) 3390, 1285, 1260, 1215, 1065, and 1025 cm^{-1}; ^1H NMR ($CDCl_3$) δ=0.96 (6H, d, J=6.5 Hz), 1.89 (6H, s), 1.94 (3H, s), ca. 1.95 (1H, m), 3.32 (1H, d, J=10 Hz), 4.58 (1H, d, J=10 Hz), 5.05 (1H, d, J=5.0 Hz), and 6.7—7.6 (8H, m); DI-MS m/z (%) 341 (M^+, 0.05), 150 (100), and 149 (83); Found: C, 74.00; H, 7.90; N, 4.12%. Calcd for $C_{21}H_{27}NO_3$: C, 73.87; H, 7.97; N, 4.10%.

(3*R,5*S**,6*R**)-3-Isopropyl-5-mesitylamino-6-methyl-6-phenyl-1,2,4-trioxane (7i):** prisms from hexane (yield 41%), mp 116—117 °C (decomp); IR (Nujol) 3410, 1230, 1165, 1070, and 1020 cm^{-1}; ^1H NMR ($CDCl_3$) δ=0.94 (6H, d, J=6.5 Hz), 1.83 (6H, s), 1.93 (3H, s), ca. 1.9 (1H, m), 2.14 (3H, s), 3.23 (1H, d, J=11 Hz), 4.54 (1H, d, J=11 Hz), 5.03 (1H, d, J=4.5 Hz), and 6.6—7.6 (7H, m); DI-MS m/z (%) 355 (M^+, 0.07), 164 (100), and 163 (68); Found: C, 74.36; H, 8.22; N, 3.92%. Calcd for $C_{22}H_{29}NO_3$: C, 74.33; H, 8.22; N, 3.94%.

The authors gratefully acknowledge the help of Dr. Tadashi Sato and Dr. Takatoshi Kawai of Eisai Co. Ltd. for X-ray analysis of **7g**, and are also indebted to Mr. Mamoru Sekine of Ibaraki University for ^1H and ^{13}C NMR spectra.

References

1) J.-M. Liu, M.-Y. Ni, J.-F. Fan, Y.-Y. Tu, Z.-H. Wu, Y.-L. Wu, and W.-S. Chou, *Acta Chimica Sinica*, **37**, 129 (1979).

2) G. B. Payne and C. W. Smith, *J. Org. Chem.*, **22**, 1682 (1957); W. Adam and A. Rios, *J. Chem. Soc., Chem. Commun.*, **1971**, 822; R. M. Wilson, E. J. Gardner, R. C. Elder, R. H. Squire, and L. R. Florian, *J. Am. Chem. Soc.*, **96**, 2955 (1974); V. Subramanyam, C. L. Brizuela, and A. H. Soloway, *J. Chem. Soc., Chem. Commun.*, **1976**, 508; M. Miura, M. Nojima, and S. Kusabayashi, *J. Chem. Soc., Chem. Commun.*, **1981**, 581; C. W. Jefford, D. Jaggi, J. Boukouvalas, and S. Kohmoto, *J. Am. Chem. Soc.*, **105**, 6497 (1983); C. W. Jefford, J. Boukouvalas, and S. Kohmoto, *Helv. Chim. Acta*, **66**, 2615 (1983); C. W. Jefford, J. Boukouvalas, and S. Kohmoto, *J. Chem. Soc., Chem. Commun.*, **1984**, 523.

3) H. Yamamoto, M. Akutagawa, H. Aoyama, and Y. Omote, *J. Chem. Soc., Perkin Trans. 1*, **1980**, 2300.

4) A. Takenaka, Y. Sasada, and H. Yamamoto, *Acta Crystallogr., Sect. B*, **33**, 3564 (1977); H. Yamamoto, I. Nakai, C. Kashima, Y. Omote, and M. Akutagawa, *Chem. Lett.*, **1983**, 1841.

5) H. Yamamoto, M. Hirayama, M. Akutagawa, T. Nishio, C. Kashima, and Y. Omote, *Bull. Chem. Soc. Jpn.*, **61**, 2678 (1988).

6) T. Suami, "Ritsutai-haiza Kaiseki," Tokyo Kagaku Douzin, Tokyo (1980), p. 86.

7) The structure with non-hydrogen atoms was obtained, though at R=0.14, and showed both the phenyl and *m*-toluidino groups occupying and axial position.

Stereoselective Bromination of Acetylenes with Bromine in the Presence of Graphite

Mitsuo KODOMARI,* Takaaki SAKAMOTO, and Suehiko YOSHITOMI
Department of Industrial Chemistry, Shibaura Institute of Technology, Shibaura, Minato-ku, Tokyo 108
(Received May 27, 1989)

Synopsis. Acetylenes were stereoselectively brominated with molecular bromine adsorbed on graphite in dichloromethane to produce (*E*)-α,β-dibromoalkenes; isomerization of the *E*-isomer to the *Z*-isomer, usually catalyzed by bromine, did not occur in the presence of graphite.

The use of inorganic solid supports has been attracting widespread interest in organic synthesis.[1,2] Significant improvements of reagent activity or regioselectivity has been achieved in a wide variety of organic reactions by the use of supported reagents formed by the adsorption of reagent molecules onto the surface of a solid support. However, only a few studies on stereoselective control using supported reagents have been reported.[3] In a previous paper,[4] we reported that graphite inhibits the bromine-catalyzed isomerization of (*E*)-α,β-dibromostyrene to the *Z*-isomer, and that the addition of bromine to phenylacetylene produces (*E*)-α,β-dibromostyrene exclusively in the presence of graphite. We further found that the addition of graphite is also effective in the bromination of several other acetylenes. In the present paper we describe these recent results.

Results and Discussion

The bromination of acetylenes with bromine usually produces a mixture of two isomeric dibromoalkenes due to the reversible addition of a halogen atom to the double bond.[5-7] Thus, the *E*/*Z* ratio depends on the reaction conditions; namely, the *E*/*Z* ratio decreases when a prolonged reaction time, higher temperature, and a higher molar ratio of bromine relative to acetylenes are employed. We found, however, that acetylenes are stereoselectively brominated by molecular bromine adsorbed on graphite in dichloromethane to give (*E*)-α,β-dibromoalkenes. The *E*/*Z* ratio in the products mixture was almost independent of the reaction conditions. The results are summarized in Table 1. For example, the treatment of propargyl bromide with 0.5-equiv of bromine in dichloromethane at 20 °C gave a mixture of two isomeric 1,2,3-tribromo-1-propene; the *E*/*Z* ratio was 76/24, and with 1.1-equiv of bromine, the *E*/*Z* ratio was 46/54. In contrast, an appreciable difference in the isomer ratio between a reaction with 0.5-equiv and 1.1-equiv of bromine was hardly observed when the reaction was carried out in the presence of graphite under similar conditions. (*E*)-1,2,3-Tribromo-1-propene was obtained in high yield stereoselectively. The *E*/*Z* ratio was 96/4. The rate of bromination in the presence of graphite was slower than that without graphite. The electron-withdrawing group (*R*) decreased the reactivity of the acetylenes toward bromine as follows:

$$C_6H_5- > HOCH_2-,\ CH_3C(OH)H- > CH_3OOC-.$$

The results show that the bromine-catalyzed isomerization of (*E*)-α,β-dibromoalkenes to the *Z*-isomer does not occur in the presence of graphite.[7] To make sure of the role of graphite, the bromine-catalyzed isomerization of (*E*)- or (*Z*)-α,β-dibromoalkenes was carried out in the presence or in the absence of graphite. Both bromine-catalyzed isomerization of the *E*- to the *Z*-isomer and the *Z*- to the *E*-isomer in dichloromethane readily occurred. In contrast, neither the *E*- nor the *Z*-isomer was isomerized in the presence of graphite under similar conditions. The results are summarized in Table 2. We previously explained the role of graphite on the basis of a heterogeneous reaction on the surface of a solid support. Recently, however, we observed that the photostimulated bromination of toluene with bromine in the presence of

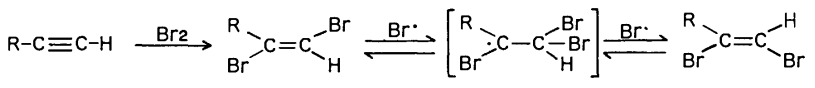

Scheme 1.

Table 1. Stereoselective Bromination of Acetylenes with Bromine[a]

H-C≡C-R (**1**)	Temp/Time (°C/h)	Composition/%[b] With graphite *E*-**2**:*Z*-**2**	Composition/%[b] Without graphite *E*-**2**:*Z*-**2**
R: C_6H_5	20/2	94:6	20:80
CH_2Br	20/4	96:4	46:54
CH_2OH	20/2	100:0	91: 9
$CH(OH)CH_3$	20/2	100:0	66:34
$COOCH_3$	30/10	97:3	12:88

a) The molar ratio of bromine/acetylenes was 1.1. b) Yields were almost quantitative.

Table 2. Bromine-Catalyzed Isomerization of α,β-Dibromoalkenes[a)]

RBrC=CHBr (2)		Temp/Time (°C/h)	Composition/%	
			With graphite *E*-2 : *Z*-2	Without graphite *E*-2 : *Z*-2
E-, R:	C_6H_5	20/2	100 : 0	36 : 64
E-,	$CH(OH)CH_3$	20/2	100 : 0	66 : 34
E-,	CH_2OH	20/2	100 : 0	67 : 33
Z-,	CH_2OH	20/2	0 : 100	65 : 35
E-,	CH_2Br	20/4	100 : 0	48 : 52
Z-,	CH_2Br	20/4	0 : 100	47 : 53
E-,	$COOCH_3$	30/5	100 : 0	58 : 42
Z-,	$COOCH_3$	30/5	0 : 100	55 : 45

a) All reactions were carried out in dichloromethane. The molar ratio of bromine/**2** was 0.2.

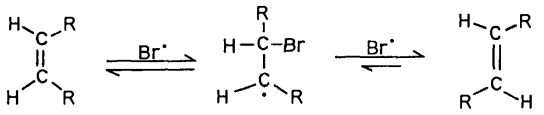

R = C_6H_5, CH_3OOC.

Scheme 2.

graphite occurs by electrophilic substitution rather than free-radical substitution.[8)] This observation suggests that a bromine radical may not be generated in the presence of graphite. Therefore, the inhibition of the isomerization by graphite is more likely to be due to the fact that no bromine radical is generated in the presence of graphite, rather than to a restriction of the rotation around the C-C bond in the radical intermediate adsorbed on graphite, as was previously presumed. Isomerization of (*Z*)-stilbene to the *E*-isomer and dimethyl maleate to dimethyl fumarate are usually catalyzed by bromine. These bromine-catalyzed isomerizations are attributed to the reversible addition of a bromine radical to the double bond. If graphite inhibites the formation of a halogen atom, bromine-catalyzed isomerization of (*Z*)-stilbene and dimethyl maleate as well as α,β-dibromoalkenes may not occur. In fact, these bromine-catalyzed isomerizations did not proceed at all in the presence of graphite.

Experimental

(*E*)-1,2,3-Tribromo-1-propene. General Procedure for Bromination of Acetylenes. Graphite (5 g) was added to a solution of bromine (11 mmol, 1.76 g) in dichloromethane (50 ml), and stirred at room temperature for 0.5 h. To the resulting mixture was added a solution of propargyl bromide (10 mmol, 1.19 g) in dichloromethane (10 ml), and stirring was continued at 20 °C for 4 h. Aqueous sodium thiosulfate was then added, and the mixture was filtered. The organic layer was separated, washed with water and dried. The residue, after evaporation of the solvent, was analyzed by GLC and ^{1}H NMR. The yield of 1,2,3-tribromo-1-propene was 98%, the *E* : *Z* ratio 94 : 6.

Isomerization of (*E*)-1,2,3-Tribromo-1-propene: General Procedure for Isomerization of α,β-Dibromoalkenes. Graphite (5 g) was added to a solution of (*E*)-1,2,3-tribromo-1-propene (0.66 mmol, 0.184 g) in dichloromethane (20 ml), and stirred at 20 °C for 0.2 h. To the resulting mixture was added a solution of bromine (0.132 mmol, 0.02 g) in dichloromethane (10 ml), and stirring was continued at 20 °C for 4 h. Aqueous sodium thiosulfate was added, and the mixture was filtered. The organic layer was separated, washed with water and dried. The residue, after evaporation of the solvent under reduced pressure, was analyzed by ^{1}H NMR.

Isomerization of Dimethyl Maleate. The isomerization was carried out as above using dimethyl maleate (1 mmol, 0.144 g) and bromine (0.1 mmol, 0.016 g) in dichloromethane (30 ml) with or without graphite (5 g) at 50 °C for 5 h under a nitrogen atmosphere and irradiation with a tungsten lamp (30 W). Isomerization without graphite gave dimethyl fumarate in 98% yield; graphite dimethyl maleate was recovered quantitatively.

Isomerization of (*Z*)-Stilbene: (a) Without Graphite. A mixture of (*Z*)-stilbene (1 mmol, 0.180 g) and bromine (0.2 mmol, 0.050 g) in hexane (30 ml) was stirred at 50 °C for 3 h. Aqueous sodium thiosulfate was then added in order to removed bromine. The organic layer was separated, washed with water and dried. The residue, after evaporation of the solvent under reduced pressure, was analyzed by GLC. The *E* : *Z* ratio of the isomers was 86 : 14.

(b) With Graphite. The isomerization was carried out as described above using graphite (5 g). (*Z*)-Stilbene was recovered in 97% yield after 5 h.

References

1) G. H. Posner, *Angew. Chem., Int. Ed. Engl.*, **17**, 487 (1978).

2) A. Mckillop and D. W. Young, *Synthesis*, **1979**, 401, 481. For graphite intercalation compounds as reagents in organic synthesis, see R. Setton and F. Beguin, *Synth. Met.*, **4**, 299 (1982).

3) K. Takahashi, T. Nishizawa, and H. Iida, *Tetrahedron Lett.*, **22**, 2389 (1981).

4) M. Kodomari, N. Tanaka, S. Yamamura, and S. Yoshitomi, *J. Chem. Soc., Chem. Commun.*, **1987**, 1850.

5) C. Walling, "Free Radical in Solution," Chapman and Hall, New York (1957), pp. 302—304.

6) S. W. Benson, K. W. Egger, and D. W. Golden, *J. Am. Chem. Soc.*, **87**, 468 (1965).

7) S. G. Levine, K. D. Barbroiak, and H. S. Cho, *J. Chem. Educ.*, **65**, 79 (1988).

8) Bromination of toluene (10 mmol) with bromine (5 mmol) in carbon tetrachloride was carried out at 50 °C for 1 h in the presence of graphite (5 g) under irradiation with a tungsten lamp (30 W), and bromotoluene was obtained in 84% yield (p/o=2.6). The reaction without graphite under similar conditions gave benzyl bromide in 87% yield.

(2-Pyridylmethoxy)calixarenes: New Versatile Ionophores for Metal Extraction

Seiji SHINKAI,* Toshio OTSUKA, Koji ARAKI, and Tsutomu MATSUDA
Department of Organic Synthesis, Faculty of Engineering, Kyushu University, Fukuoka 812
(Received June 16, 1989)

Synopsis. (2-Pyridylmethoxy)calix[*n*]arenes (*n*=6,8) were newly synthesized. It was shown in two-phase solvent extraction that they can extract not only alkali metal cations but Cu^{2+}, Ag^{+}, and UO_2^{2+} and are stable even at high pH. The results indicate that disadvantages of calixarene esters, which were previously developed as calixarene-based ionophores, can be improved by using the pyridyl group.

"Calixarenes" are cyclic oligomers made up of benzene units.[1,2] It has been expected, therefore, that introduction of appropriate ionophoric groups would append, like that of crown ethers, a new function as ionophores to calixarenes. Several groups have reported on the ionophoric properties of calixarenes which were obtained by introducing ester, ether, and amide groups into the edge of the cylindrical architecture.[3-9] Among them ester derivatives (**1***n*) have been studied most extensively.[3-7] We noticed through our work,[7,10] however, that there exist two inevitable disadvantages about **1***n*: (i) cannot be used at high pH region because of basic hydrolysis of the ester groups and (ii) **1***n* can extract only "hard" metal cations because of the "hard" ionophoric nature. We considered that the defects might be removed by introducing nitrogen base (instead of oxygen base) through the ether linkage (instead of the ester linkage). In order to use them at neutral pH region, aromatic amines with low pK_a values are recommended rather than aliphatic amines with high pK_a values. We thus designed new ionophores **2***n* in which 2-pyridylmethyl groups are appended to the calixarene cavity. We have found that **2***n* can extract not only alkali metal cations but other heavy metal cations and are stable even at high pH.

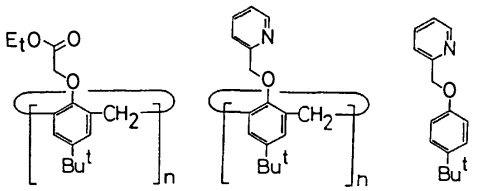

1*n* **2***n* **3**

Experimental

37,38,39,40,41,42-Hexakis(2-pyridylmethoxy)-*p*-*t*-butylcalix[6]arene (2₆). *p*-*t*-Butyl calix[6]arene (1.0 g; 1.0 mmol), 2-chloromethylpyridine hydrochloride (2.1 g; 13 mmol), and powdered K_2CO_3 (7.0 g) were mixed in 70 mL of anhydrous *N*,*N*-dimethylformamide (DMF), and the mixture was heated at 60—70 °C for 14 h under a nitrogen stream. The solution was diluted with water, the precipitate being collected by filtration. This was dissolved in 100 mL of chloroform and washed with water. The chloroform solution was concentrated in vacuo and the residual oil was crystallized from methanol. Finally, the product (**2₆**) was recrystallized from chloroform–methanol; mp (decomp) 268 °C, yield 45%; IR (Nujol) no ν_{OH}, $\nu_{C=N}$ 1565 cm^{-1}. ^1H NMR ($CDCl_3$): δ=1.05 (9H, s, *t*-Bu), 3.9 (2H, broad s, $ArCH_2Ar$), 4.84 (2H, s, OCH_2), 7.0, 7.3, 8.3 (6H, broad, benzene and pyridine protons). Found: C, 79.87; H, 7.47; N, 5.43%. Calcd for $(C_{17}H_{19}NO)_6$: C, 80.60; H, 7.56; N, 5.53%.

49,50,51,52,53,54,55,56-Octakis(2-pyridylmethoxy)-*p*-*t*-butylcalix[8]arene (2₈). This compound was synthesized from *p*-*t*-butylcalix[8]arene in a manner similar to that described for **2₆**; mp 151—152 °C, yield 24%; IR (Nujol) no ν_{OH}, $\nu_{C=N}$ 1565 cm^{-1}. ^1H NMR ($CDCl_3$): δ=1.03 (9H, s, *t*-Bu), 4.05 (2H, s, $ArCH_2Ar$), 4.74 (2H, s, OCH_2), 6.99 (2H, s, benzene protons), 6.81, 7.00, 7.11, 8.28 (1H each, q, d, q, and d, respectively, pyridine protons). Found: C, 79.90; H, 7.55; N, 5.34%. Calcd for $(C_{17}H_{19}NO)_8$: C, 80.60; H, 7.56; N, 5.53%. The reaction of *p*-*t*-butylcalix[4]arene and 2-chloromethylpyridine under the same reaction conditions afforded di-substituted *p*-*t*-butylcalix[4]arene and no tetra-substituted product. This is attributed to steric crowning in a small calix[4]arene ring. Thus, subsequent extraction experiments were carried out about **2₆** and **2₈**.

The methods of two-phase solvent extraction were described previously.[3-5,11] The detailed extraction conditions were recorded in footnotes to Table 1. In some cases we determined both the concentration of extracted metal cations (by atomic absorption spectroscopy) and that of extracted picrate anion (by absorption spectroscopy). At acidic to neutral pH region the concentration of picrate anion was always higher than those of metal cations. This shows that picrate anion is extracted, in part, as a counteranion of pyridinium cation. In contrast, these two values showed a good agreement (error less than 4%) in extraction from 0.1 M MOH aqueous solution.

The stability of **1₆** and **2₆** against basic hydrolysis was evaluated as follows. A CH_2Cl_2 solution containing **1₆** or **2₆** (2.5×10^{-4} M†) was shaked at 25 °C for one day with a same amount of an aqueous 0.1 M NaOH solution. The CH_2Cl_2 solution containing **2₆** separated clearly from the aqueous phase. We could recover **2₆** (>99%) from the CH_2Cl_2 solution. On the other hand, a considerable amount of white precipitates was formed at the interface between water and **1₆**-containing CH_2Cl_2. They were collected by filtration, acidified by 0.1 M HCl , and extracted with $CHCl_3$. This compound turned out to be 37,38,39,40,41,42-hexakis(carboxymethoxy)-*p*-*t*-butylcalix[6]arene[11] (yield 5%). From the CH_2Cl_2 phase we recovered **1₆** (90%).

Results and Discussion

We first compared the stability of **2***n* and **1***n* in solvent extraction from a strongly basic aqueous phase. It was shown that **2₆** is totally stable against basic hydrolysis whereas **1₆** is hydrolyzed to the carboxylate derivative. Thus, calixarene esters **1***n* are recommended only for the short-period extraction. Interestingly, we could not recover any partly-hydrolyzed carboxylate derivatives from **1₆**. This implies that once the hydrolysis takes place at one

† 1 M=1 mol dm^{-3}.

ester unit, subsequent hydrolysis in the same calixarene ring occurs acceleratively. Presumably, partly-hydrolyzed carboxylate derivatives, which are less soluble in CH_2Cl_2, are adsorbed at the water-CH_2Cl_2 interface and subsequent hydrolysis occurs rapidly thereabout.

In order to estimate the "basicity" of **2**$_n$ and **3** (*p*-(2-pyridylmethoxy)-*t*-butylbenzene: used as a reference compound) at a water-CH_2Cl_2 interface, we carried out picrate extraction as a function of pH. Since sodium picrate was not extracted by **2**$_n$ under the conditions employed (see a caption to Fig. 1), the concentration of extracted picrate anions should be equal to that of protonated pyridine (i.e., pyridinio) units. As shown in Fig. 1, pH-Ex% curves for **2**$_n$ shift to higher pH region than that for **3** (4.1 pH unit for **2**$_6$ and 2.5 pH unit for **2**$_8$) Thus, the "basicity" of **2**$_n$ is considerably strengthened because of the cyclic architecture. This suggests that calixarenes **2**$_n$, in which basic pyridine groups are arranged on the lower rim of the calixarene cavity, have a character of proton cryptates.

Results of two-phase solvent extraction of alkali picrates are summarized in Table 1. Under the present extraction conditions (0.1 M MOH in the aqueous phase) the concentration of extracted picrates was equal to that of M^+ ions, which was confirmed by the separate determinations of [picrate] by absorption spectroscopy and [M^+] by atomic absorption spectroscopy. The previous extraction study with **1**$_n$ established that (i) **1**$_6$ has the extraction ability greater than **1**$_8$ for alkali metal cations and (ii) the order of the ion selectivity is $Cs^+>K^+>Na^+$ for **1**$_6$ and $Cs^+\approx K^+>Na^+$ for large, flexible **1**$_8$.[3,5] Examination of Table 1 reveals that both **2**$_6$ and **2**$_8$ are Cs^+-selective and **2**$_6$ gives the greater Ex% than **2**$_8$ Thus, the size effect operating in **2**$_n$ is basically comparable with that operating in **1**$_n$. As expected, calixarenes **2**$_n$ are capable of extracting heavy metal cations such as Ag^+ and Cu^{2+}. In particular, extraction of Cu^{2+} is ascribed to the affinity of Cu^{2+} with pyridine nitrogens.

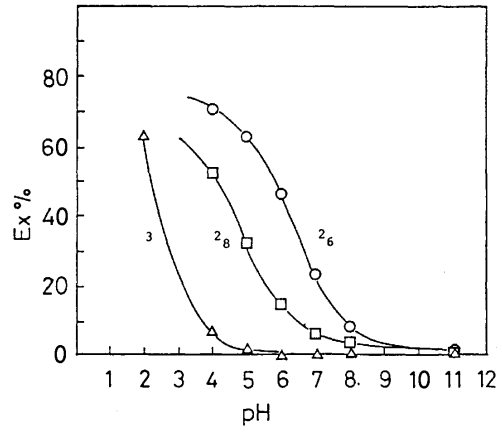

Fig. 1. Extraction of picrate anion by **2**$_n$ and **3** at 25 °C: 2.5×10^{-4} M **2**$_n$ or 2.0×10^{-3} M **3** (=8·[**2**$_n$]) in CH_2Cl_2, 2.5×10^{-4} M picric acid and [Na^+]=0.02 M in water. pH of the aqueous phase was adjusted by 0.02 M acetate buffer for pH 4—5, 0.02 M phosphate buffer for pH 6—8, and NaOH for pH 11. Under the conditions Na^+ was not extracted into the CH_2Cl_2 phase (confirmed by the analysis of the CH_2Cl_2 phase by atomic absorption spectroscopy).

Table 1. Extraction (%) of Metal Picrates in CH_2Cl_2 at 25 °C[a]

Metal	Calixarene	
	2$_6$	**2**$_8$
Na^+[b]	12.7	9.3
K^+[b]	26.7	7.5
Cs^+[b]	51.0	18.2
Ag^+[c]	21.2	24.0
Cu^{2+}[c]	3.3	1.8
UO_2^{2+}[d]	0	5.4
UO_2^{2+}[d] (at 100 °C)	82.1	76.8

a) 2.5×10^{-3} M calixarene in CH_2Cl_2. Extraction time 30 min. b) 2.5×10^{-4} M picric acid in aqueous 0.1 M MOH and 0.5 M MCl. Extractability denotes the percentage of picrate anion extracted by **2**$_n$. c) 2.5×10^{-3} M picric acid in aqueous 5×10^{-4} M metal nitrates at pH 11 (with 1.00×10^{-2} M NH_3) for Ag^+ and at pH 8.0 (with 1.00×10^{-2} M Bis-Tris) for Cu^{2+}. Extractability denotes the percentage of metal cations extracted by **2**$_n$ (determined by atomic absorption spectroscopy). d) 1.0×10^{-4} M calixarene in *o*-dichlorobenzene. 2.0×10^{-5} M $UO_2(CH_3COO)_2$ in aqueous buffer solution (pH 8.0 with 0.01 M *N*-tris(hydroxymethyl)methyl-3-amino-1-propanesulfonate). Extractability denotes the percentage of UO_2^{2+} extracted by **2**$_n$ (calculated by the analysis of UO_2^{2+} remaining in the aqueous phase with Arsenazo III): for details of the extraction method see Ref. 11.

We previously found that among calix[*n*]arenes (*n*=4, 5, and 6) calix[5]arene and calix[6]arene derivatives complex UO_2^{2+} selectively.[11,12] The finding is quite complementary with the X-ray crystallographic data that UO_2^{2+} complexes adopt either a pseudo-planar pentacoordinate or hexacoordinate structure.[11,12] This implies that the structure of these calixarenes is well pre-organized for selective complexation of UO_2^{2+}. We applied **2**$_n$ to solvent extraction of UO_2^{2+}. The rate of UO_2^{2+} extraction was slow at 25 °C. In particular, **2**$_6$ scarcely extracted UO_2^{2+} (see Table 1). On the other hand, efficient UO_2^{2+} extraction took place at 100 °C. It is known that the association of cyclic ligands with large, rod-like UO_2^{2+} ion occurs very slowly because of steric hindrance.[13-15] In the present system the ring structure of **2**$_6$ is expected to be rigid because of six pyridyl groups incorporated into the narrow lower rim of calix[6]arene. This view is supported not only by Corey-Pauling-Koltun molecular models but also by the broadened ^1H NMR spectrum (see Experimental). This suggests that the extraction speed with **2**$_6$ would be fairly slow at room temperature. On the other hand, **2**$_6$ and **2**$_8$ served as excellent neutral uranophiles at high temperature. This is related to the increase in the thermal molecular motion of these calixarenes. The high extractability observed for **2**$_6$ is rationalized in terms of the pre-organized structure suitable for the binding of hexacoordinate UO_2^{2+}. Although **2**$_8$ does not possess such a pre-organized structure, the ring is flexible enough to employ either a pentacoordinate or

a hexacoordinate structure. Presumably, the UO_2^{2+} affinity observed for $\mathbf{2}_8$ is accounted for by "induced-fit" complexation with the large calixarene ring. In fact, the ^1H NMR peaks for $\mathbf{2}_8$ are mostly sharp (see Experimental) supporting the flexible nature of the $\mathbf{2}_8$ ring. Under the identical extraction conditions $\mathbf{1}_n$ (n=4, 6, and 8) could not extract even a trace amount of UO_2^{2+}.

In conclusion, it has been established that new calixarene-based ionophores $\mathbf{2}_n$ display versatile affinity not only for alkali metal cations but also for Ag^+, Cu^{2+}, and UO_2^{2+} and are recommended for solvent extraction from strongly basic aqueous solutions.

We are indebted to Mr. Yoshiharu Shirahama for the determination of Ex% for UO_2^{2+}.

References

1) C. D. Gutsche, *Acc. Chem. Res.*, **16**, 161 (1983).
2) C. D. Gutsche, *Top. Curr. Chem.*, **123**, 1 (1984).
3) M. A. McKervey, E. M. Seward, G. Ferguson, B. Ruhl, and S. J. Harris, *J. Chem. Soc., Chem. Commun.*, **1985**, 388.
4) G. Ferguson, B. Kaitner, M. A. McKervey, and F. M. Seward, *J. Chem. Soc., Chem. Commun.*, **1987**, 584.
5) S.-K. Chang and I. Cho, *J. Chem. Soc., Perkin Trans. 1*, **1986**, 211.
6) A. Arduini, A. Pochini, S. Reverberi, and R. Ungaro, *Tetrahedron*, **42**, 2089 (1986).
7) S. Shinkai, S. Edamitsu, T. Arimura, and O. Manabe, *J. Chem. Soc., Chem. Commun.*, **1988**, 187.
8) H. Taniguchi and E. Nomura, *Chem. Lett.*, **1988**, 1773.
9) H. Funada, Y. Nakamoto, and S. Ishida, *Polym. Prepr. Jpn.*, **34**, 368 (1985).
10) T. Arimura, M. Kubota, T. Matsuda, O. Manabe, and S. Shinkai, *Bull. Chem. Soc. Jpn.*, **62**, 1674 (1989).
11) S. Shinkai, Y. Shirahama, H. Satoh, O. Manabe, T. Arimura, K. Fujimoto, and T. Matsuda, *J. Chem. Soc., Perkin Trans. 2*, **1989**, 1167.
12) S. Shinkai, H. Koreishi, K. Ueda, T. Arimura, and O. Manabe, *J. Am. Chem. Soc.*, **109**, 6371 (1987) and references cited therein.
13) P. Fux. J. Lagrange and P. Lagrange, *J. Am. Chem. Soc.*, **107**, 5927 (1985).
14) K. Kawano, K. Araki, S. Shinkai, and T. Matsuda, to be submitted.
15) I. Tabushi, A. Yoshizawa, and H. Mizuno, *J. Am. Chem. Soc.*, **107**, 4585 (1985).

Detailed Dynamic NMR Study of a Molecular Gear, 1-Methoxy-9-(3,5-dimethylbenzyl)triptycene

Gaku YAMAMOTO
Department of Chemistry, Faculty of Science, The University of Tokyo, Bunkyo-ku, Tokyo 113
(Received June 29, 1989)

Synopsis. Stereodynamics of the title compound was studied by dynamic NMR spectroscopy. The "isolated" rotation of the aryl group was found to have a lower barrier than the correlated gear rotation.

In 1979, we reported a dynamic NMR study of 9-(3,5-dimethylbenzyl)triptycene derivatives,[1] which behave as molecular gears composed of a two-toothed wheel and a three-toothed one.[2] We pointed out the presence of two fundamental processes, gear rotation (GR), in which the correlated disrotation of the aryl group (Ar) and the triptycene moiety (Tp) occurs, and "isolated" rotation (IR) of the Ar group without rotation of the Tp moiety. At that time, the NMR spectra were measured on a 60-MHz CW spectrometer and the analysis was made by an approximate method, in which only the rate constant at the coalescence temperature was obtained. Thus some of the data were somewhat unreliable and the conclusion drawn therefrom was simplistic. We therefore decided to reinvestigate this topic, by obtaining variable temperature NMR spectra of a typical derivative, 1-methoxy-9-(3,5-dimethylbenzyl)triptycene (**1**), at 270 MHz in the FT mode and analyzing the data by total lineshape analysis.

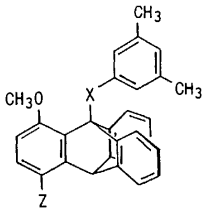

1 X=CH_2, Z=H
2 X=O, Z=OCH_3

The possible dynamic processes exhibited by the molecules of **1** are shown in Scheme 1. Three sites are available about the Tp-CH_2 bond, i.e. *ap*, $+sc$, and $-sc$, and thus six conformers should be considered if the two *m*-methyl groups are differentiated. Processes shown at the periphery in the Scheme constitute a gear rotational circuit, which comprises two kinds of primary steps; GR(H) in which the aryl group passes over a peri-hydrogen, and GR(Y) in which the aryl group passes over the peri-substituent Y. In each

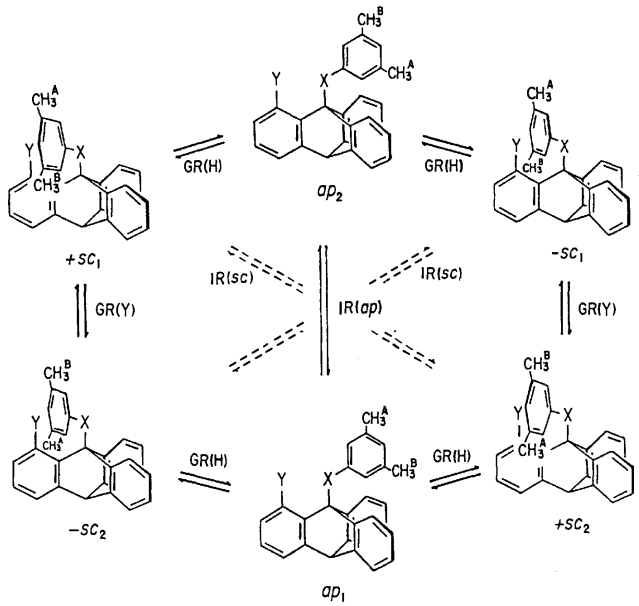

Scheme 1.

step the edge of the aryl rotor interchanges; each *m*-methyl group points inside and outside alternatively. Two other motions should be taken into account; isolated rotations of the aryl group at the *ap* and $\pm sc$ sites, designated as IR(*ap*) and IR(*sc*), respectively. Isolated rotation of the Tp moiety may be neglected because the plausible transition state of this process, in which the aryl group and one of the benzene ring of the triptycene skeleton becomes coplanar, is highly unlikely. Transition states of these processes are schematically shown as Newman projections along the Tp-X bond axis in Scheme 2. Therefore, four independent rate constants are necessary to describe the whole processes exhibited by the molecule at a given temperature.

At −98.1 °C, the lowest attainable temperature, internal rotation of both the Tp-CH_2 and Ar-CH_2 bonds is frozen and two isomers, *ap* and $\pm sc$, are separately observed in the ^1H NMR spectrum in CD_2Cl_2 (Fig. 1). The major isomer present in 70% at

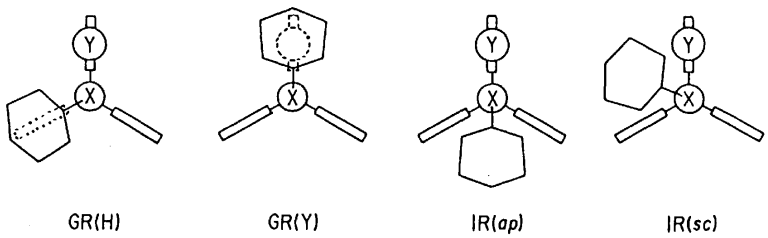

Scheme 2.

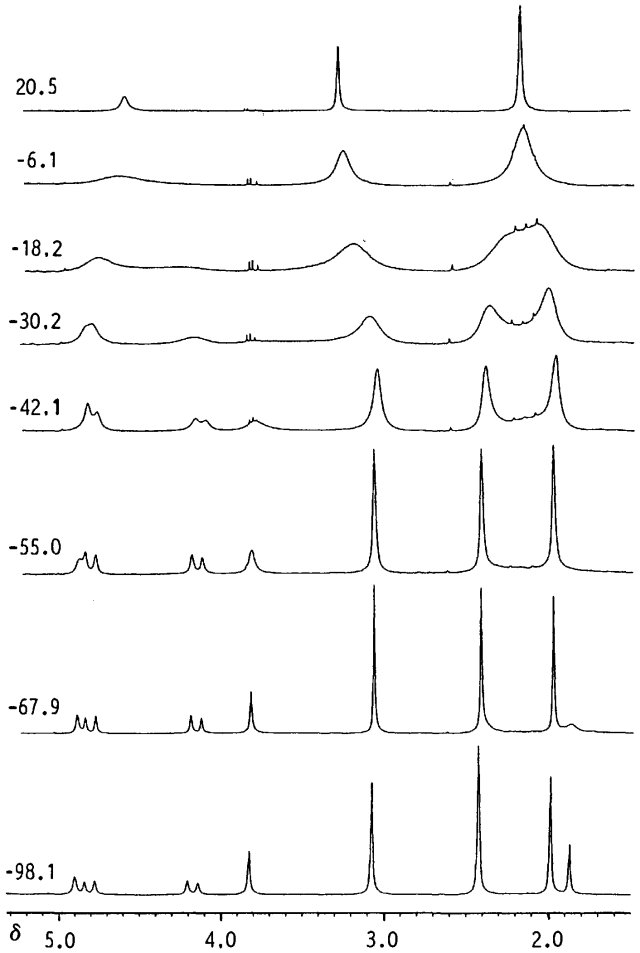

Fig. 1. ^{1}H NMR spectra of **1** in CD_2Cl_2 at several temperatures (°C). Impurity peaks are seen at δ 2.1—2.3, ca. 2.6, and 3.8—3.9 regions.

this temperature is assigned as ±*sc*; the methylene protons give an AB-quartet signal (δ 4.17 and 4.80, J=17.4 Hz) and the methoxyl proton signal appears at a high field of δ 3.07 because of the ring current effect of the benzylic aryl group. The minor isomer assigned as *ap* gives a singlet at δ 4.90 for the methylene protons and a singlet for the methoxyl protons at a normal position of δ 3.82. The *m*-methyl protons of the benzylic aryl group appear as a pair of singlets for each isomer, although the low-field peaks are overlapped (*ap*: δ 1.87 and 2.42; ±*sc*: δ 1.98 and 2.42). The two higher-field singlets are reasonably assigned to the methyl groups pointing inside (CH_3^B in ap_1 and ±sc_1 and CH_3^A in ap_2 and ±sc_2).

The signals broaden and coalesce as the temperature rises, and a broad singlet is observed for each of the methyl, methoxyl and methylene protons at room temperature.

The dynamic NMR behavior of the 1-methoxyl proton signal, in which two unequally intense singlets at low temperature coalesce into a single peak, corresponds to the *ap*⇄±*sc* interconversion which occurs by the GR(H) process and is described by a single rate constant, $k(ap \rightarrow \pm sc)$, which we refer to as $k_{GR(H)}$. The rate constant for the reverse process, $k(\pm sc \rightarrow ap)$, is related to $k_{GR(H)}$ by the equilibrium constant K. Line-shape analysis of the spectra at nine temperatures between −6 and −55 °C as a one-spin two-site system using the DNMR5[3] and/or DNMR3K[4] program affords the best-fit values of $k_{GR(H)}$ and the kinetic parameters for the GR(H) process (Table 1).

Table 1. Kinetic Parameters Obtained from DNMR

Compd	Process	$\Delta H^{\ddagger}$	$\Delta S^{\ddagger}$	$\Delta G^{\ddagger}_{200}$
		kcal mol^{-1}	cal mol^{-1} K^{-1}	kcal mol^{-1}
1	GR(H)[a]	10.6±0.1	−4.1±0.5	11.5±0.1
	GR(Y)			>12.7
	IR(*ap*)	9.6±0.2	−3.1±0.8	10.2±0.1
	IR(*sc*)			>12.7
2[b]	GR(H)			<7.7[c]
	GR(Y)	11.8±0.2	−0.9±0.7	12.0±0.2
	IR(*ap*)			>12.0
	IR(*sc*)			≫12.0

a) The kinetic parameters refer to the *ap*→*sc* process. b) Ref. 2c. c) Reinvestigated. No splitting down to −100 °C at 500 MHz.

The methylene proton signal is composed of a singlet due to *ap* and an AB-quartet due to ±*sc*. The line-shape is controlled by two independent rate constants. The one is $k_{GR(H)}$ and the other describes the direct interconversion between +*sc* and −*sc* corresponding to the GR(Y) process. Careful examinations revealed that the observed spectra are excellently reproduced with $k_{GR(Y)}$ of zero and $k_{GR(H)}$ obtained from the analysis of the methoxyl signal, suggesting that $k_{GR(Y)}$ is very small relative to $k_{GR(H)}$. Actually, incorporation of $k_{GR(Y)}$ larger than one twentieth of $k_{GR(H)}$ distinctly deviates the calculated spectrum from the observed one. Therefore, the GR(Y) process has a free energy barrier of at least 1.3 kcal mol^{-1} (1 cal= 4.184 J) higher than that of GR(H).

The dynamic NMR behavior of the *m*-methyl proton signal is somewhat complex. Four singlets (apparently three because of the overlap) at low temperature coalesce into a single peak. In the DNMR5 program, the case is treated as a one-spin four-site system. Four sites represent *ap*-in, *ap*-out, *sc*-in, and *sc*-out. The *ap*-in⇄*sc*-out and *ap*-out⇄*sc*-in motions correspond to GR(H) and *ap*-in⇄*ap*-out to IR(*ap*). The *sc*-in⇄*sc*-out conversion may occur either by GR(Y) or by IR(*sc*) and the dynamic NMR analysis can not predict which is actually occurring. *ap*-in⇄*sc*-in and *ap*-out⇄*sc*-out are assumed to be negligible. Detailed analysis of the spectra shows that only two non-zero rate constants corresponding to GR(H) and IR(*ap*) are required to reproduce the observed spectra. Line-shape analysis of the spectra at seven temperatures between −42 and −80 °C using the extrapolated values of $k_{GR(H)}$ obtained as described above affords the best-fit values of $k_{IR(ap)}$ and the kinetic parameters for the IR(*ap*) process (Table 1).

The *sc*-in⇄*sc*-out process and hence both of GR(Y) and IR(*sc*) have again free energy barriers of at least 1.3 kcal mol^{-1} higher than that of GR(H).

It is interesting to compare the present results with

those previously reported for the corresponding ether analog, 1,4-dimethoxy-9-(3,5-dimethylphenoxy)triptycene (**2**).[2c] We assume that the 4-methoxyl group in **2** has no significant effect on the dynamic processes discussed here.

In the ^{1}H NMR spectra of **2**, the 1-methoxyl signal appears as a sharp singlet in the whole temperature range studied, and the methyl protons give a singlet at room temperature but two equally intense singlets below −18 °C.[2c] This indicates that the GR(H) barrier is very low (<7.7 kcal mol^{-1}) and the observed dynamic process should be explained by either GR(Y), IR(*ap*), or IR(*sc*) as the rate-determining step. Molecular mechanics studies by MM2 revealed that GR(Y) has the lowest barrier and therefore the observed process was assigned to GR(Y) as shown in Table 1.[2c]

The results given in Table 1 show that **1** has higher barriers for the GR processes than **2** but lower barriers for the IR processes. This is understood in terms of the differences in valencies (tetravalent in **1** and divalent in **2**) and in bond lengths (1.49—1.55 Å for C-C and 1.36—1.42 Å for C-O), as discussed in detail in the previous papers.[2b,c] The valency effect would predominate over the bond length effect at the GR transition states, where the eclipsing interactions occur at three sites in **1** and at only one site in **2**. Meanwhile the bond length effect would predominate at the IR transition states, where the ortho hydrogens of the Ar group are closer to the Tp skeleton in **2** than in **1**.

In conclusion, in compound **1** the gear rotation is not the minimum energy process while in the ether analog **2** the meshed gearing is the most favorable process.

Experimental

Synthesis of **1** has been described.[1]

Variable temperature ^{1}H NMR spectra were obtained on a JEOL GX-270 spectrometer operating at 270.17 MHz in the FT mode using a ca. 4% (w/v) solution of **1** in CD_2Cl_2. Temperatures were calibrated using a methanol sample and are reliable to ±0.5 °C.

Line-shape analysis was performed either on a Hitac M-680H computer system at the Computer Center of the University of Tokyo using the DNMR5 program[3] or on a NEC PC-9801F personal computer equipped with a Graphtec MIPLOT II plotter using the DNMR3K program.[4] Temperature dependence of the rotamer populations, chemical shift differences, and T_2 values was properly taken into account.

References

1) G. Yamamoto and M. Ōki, *Chem. Lett.*, **1979**, 1251; *Bull. Chem. Soc. Jpn.*, **54**, 473 (1981).

2) a) G. Yamamoto, *J. Mol. Struct.*, **126**, 413 (1985) and references cited therein. b) G. Yamamoto and M. Ōki, *Chem. Lett.*, **1984**, 97; *Bull. Chem. Soc. Jpn.*, **58**, 1953 (1985). c) *idem, ibid.*, **59**, 3597 (1986).

3) D. S. Stephenson and G. Binsch, *QCPE*, No. 365.

4) A modified version of the DNMR3 program[5] converted for use on personal computers by Dr. H. Kihara of Hyogo University of Teacher Education.

5) D. A. Kleier and G. Binsch, *QCPE*, No. 165.

Homologation of the Side Chain of 2-Nitrotoluene. Synthesis of a Tryptophan Precursor

Hideo TANAKA, Yasuo MURAKAMI, and Sigeru TORII*
Department of Applied Chemistry, Faculty of Engineering, Okayama University, Okayama 700
(Received July 3, 1989)

Synopsis. 2-(2-Nitrophenyl)-1,3-propanediol (**2**) was selectively converted to 2-(2-nitrophenyl)propenal (**3**) by the use of a mixture of dicyclohexylcarbodiimide (DCC) and dimethyl sulfoxide in benzene, while 2-nitrobenzoic acid was obtained by the oxidation of the diol **2** with sodium periodate in the presence of a catalytic amount of ruthenium dioxide or with chromic acid. The enal **3** was subjected to further transformation to afford a potent tryptophan precursor and some useful indole derivatives.

A continuing interest in the tryptophan synthesis has led to the development of novel synthetic methodologies.[1] Among them, a straightforward route to tryptophan has been achieved by the homologation of the side chain of 2-nitrotoluene (**1**) followed by the reductive cyclization.[2] The transformation involves a two carbon homologation of the side chain of **1** by a successive treatment with *N,N*-dimethylformamide dimethyl acetal[3] and formaldehyde, leading to 2-(2-nitrophenyl)propenal (**3**) (atropaldehyde). In the previous paper, we reported a facile double hydroxymethylation of 2-nitrotoluene (**1**) with formaldehyde promoted by an electrochemically generated base (EG-base), affording 2-(2-nitrophenyl)-1,3-propanediol (**2**).[4] This finding prompted us to investigate an alternative access to the key intermediate **3** by the oxidative dehydration of **2**. Herein, we describe a selective oxidation of 2-(2-nitrophenyl)-1,3-propanediol (**2**) leading to either the aldehyde **3** or 2-nitrobenzoic acid (**4**) by choosing oxidizing agents.

In the transformation of the diol **2** into the desired enal **3**, one hydroxyl group may serve for the aldehyde group and the other for the olefinic one. After examination of various oxidizing agents, a combination of dicyclohexylcarbodiimide (DCC) and dimethyl sulfoxide (DMSO)[5] was found to be suitable for the present purpose; thus, the oxidative dehydration of **2** to afford **3** took place smoothly (97% yield) by the action of DCC and DMSO in benzene containing pyridine and trifluoroacetic acid at room temperature.

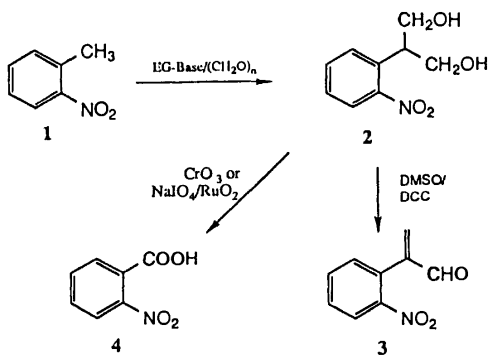

Scheme 1.

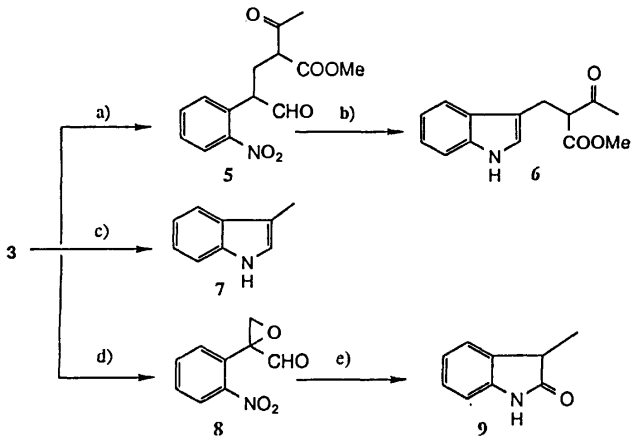

(a): $CH_3COCH_2CO_2Me$, NaOMe (0.1 eqiv), MeOH. (b): H_2, Pd/C, MeOH. (c): H_2, PtO_2, MeOH. (d): H_2O_2, aq. NaOH, MeOH. (e): H_2, PtO_2, Ac_2O.

Scheme 2.

Notably, upon oxidation of **2** with chromic acid in acetone (Method A), a completely different reaction occurred to afford 2-nitrobenzoic acid (**4**) in 96% yield. A similar result was obtained by the oxidation of **2** with sodium periodate and a catalytic amount of ruthenium dioxide (Method B). The EG-base-promoted double hydroxymethylation followed by the oxidation (Methods A and B) may offer an access to 2-nitrobenzoic acid (**4**) which has not been prepared by the direct oxidation of **1** efficiently.[6]

2-(Nitrophenyl)propenal (**3**) is an intriguing starting candidate for the indole synthesis. The Michael addition of methyl acetoacetate to the enal **3** in methanol containing a catalytic amount of sodium methoxide afforded adduct **5** (90%). Subsequently, the hydrogenative cyclization of **5** over palladium on charcoal in methanol furnished methyl 2-acetyl-3-(3-indolyl)propionate (**6**, 95%), a potent tryptophan precursor.[7] Under similar hydrogenation conditions, the enal **3** provided 3-methylindole (**7**) which would arise from the hydrogenation of both the olefin and nitro groups. On the other hand, the epoxidation of **3**, leading to **8**, followed by the hydrogenation in acetic anhydride afforded lactam **9**. Although the reaction mechanism is still unclear, the lactam **9** might arise from some mutual interaction between the formyl and the nitro groups.

Experimental

IR spectra were recorded on a JASCO IRA-1 grating spectrometer. ^1H NMR spectra were measured at 60 MHz with a Hitachi R-24 spectrometer. Chemical shifts are expressed in parts per million downfield from Me_4Si used as

an internal reference. Melting and boiling points are uncorrected. Column chromatography was carried out with Merck Kieselgel 60 (silica gel) using hexane–EtOAc as an eluent. Elementary analyses were performed in our laboratory. 2-(2-Nitrophenyl)-1,3-propanediol (**2b**) was prepared by the electrolysis of 2-nitrotoluene (**1**) in a $(CH_2O)_n$–DMF–Et_4NOTs (Pt electrode) system.[4]

2-(2-Nitrophenyl)propenal (3). To a mixture of **2** (592 mg, 3.0 mmol), benzene (10 ml), and DMSO (10 ml) were successively added pyridine (0.24 ml, 3 mmol), trifluoroacetic acid (0.12 ml, 1.5 mmol), and DCC (1.5 g, 7.3 mmol) at room temperature. After stirring at room temperature for 2 h, benzene (20 ml) was added and the precipitates (dicyclohexylurea) were removed by filtration and washed with benzene. The filtrates and washings were combined, washed three times with 20 ml portions of water, dried (Na_2SO_4), and concentrated. The residue was chromatographed to give **3** (516 mg, 97%): mp 53—54 °C (lit,[2] mp 54.5—56 °C).

2-Nitrobenzoic Acid (4). Method A. To a solution of **2** (98.5 mg, 0.5 mmol) in acetone (4 ml), was added dropwise the Jones reagent (0.7 ml, 2.2 mmol) at 0 °C over a period of 30 min. After stirring at room temperature for 6 h, most of the solvent was evaporated and the residue was taken up in CH_2Cl_2. The CH_2Cl_2 solution was washed with aqueous $NaHCO_3$. The aqueous layers were acidified with aqueous 10% HCl, extracted with EtOAc, washed with brine, and dried (Na_2SO_4). After evaporation of the solvent, the residue was chromatographed to afford **4** (83.6 mg, 96%): mp 143—146° (lit,[8] mp 146—148 °C), whose IR and ^1H NMR spectra data were fully identical with those reported.[9]

Method B. To a mixture of **2** (105 mg, 0.53 mmol), EtOAc (2.5 ml), water (4 ml), and RuO_2 (4 mg, 0.02 mmol) was added portionwise $NaIO_4$ (706.7 mg, 3.57 mmol) at room temperature over a period of 10 h. After being stirred for additional 10 h, the reaction mixture was worked up in a similar manner as described above to afford **4** (83.6 mg, 90%).

Methyl 2-Acetyl-4-formyl-4-(2-nitrophenyl)butyrate (5). A mixture of 2-(2-nitrophenyl)propenal **3** (101.3 mg, 0.57 mmol) and methyl acetoacetate (79.2 mg, 0.68 mmol) in MeOH (2 ml) containing NaOMe (3 mg, 0.06 mmol) was stirred for 1 h at −5 °C and for 2 h at room temperature. After being neutralized with aqueous 5% HCl, the mixture was concentrated under reduced pressure, extracted with EtOAc, washed with brine and dried (Na_2SO_4). After evaporation of the solvent, the residue was chromatographed to afford **5** (151 mg, 90%): IR (neat) 3400, 2940, 1740, 1720, 1528, 1435, 1350, 1240, 1000, 990, 782, 743 cm^{-1}; ^1H NMR ($CDCl_3$) δ=2.18—2.27 (m, 3H, $COCH_3$), 3.16—3.23 (m, 3H, CO_2CH_3), 2.5—4.8 (m, 4H, $CHCH_2CH$), 7.2—8.1 (m, 4H, ArH), 9.67 (s, 1H, CHO); Found: C, 57.20; H, 5.21; N, 5.18%. Calcd for $C_{14}H_{15}NO_6$: C, 57.34; H, 5.16; N, 5.05%.

Methyl 2-Acetyl-3-(3-indolyl)propionate (6). A mixture of **5** (150 mg, 0.51 mmol) and 5% Pd/C (5 mg) in MeOH (5 ml) was stirred at room temperature under H_2 (1 atm) for 5 h. After the catalysts were removed by filtration, the solvent was evaporated under reduced pressure, the residue was chromatographed to afford **6** (119mg, 95%):[7] IR (neat) 3375, 2943, 1735, 1710, 1458, 1435, 1360, 1218, 1150, 1098, 743 cm^{-1}; ^1H NMR ($CDCl_3$) δ=2.07 (s, 3H, $COCH_3$), 3.23—3.98 (m, 3H, $CHCH_2$), 3.59 (s, 3H, CO_2CH_3), 6.8—8.3 (m, 6H, C=CH, NH, ArH).

3-Methylindole (7). A mixture of **3** (32.0 mg, 0.18 mmol) and PtO_2 (3.0 mg) in MeOH (2 ml) was stirred at room temperature under H_2 (1 atm) for 3 h. After the catalysts were removed by filtration, the solvent was evaporated under reduced pressure and the residue was chromatographed to afford 3-methylindole (**7**) (9.6 mg, 40%): mp 92—94 °C (lit,[10] mp 95 °C).

2,3-Epoxy-2-(2-nitrophenyl)propionaldehyde (8). To a mixture of **3** (94.4 mg, 0.53 mmol) and aqueous 31% H_2O_2 (120 mg, 1.1 mmol) in MeOH (2.0 ml) was added dropwise aqueous 24% NaOH (0.03 ml, 0.18 mmol) at −5—0 °C over a period of 30 min. The reaction mixture was stirred for additional 1 h at 10 °C. The usual workup followed by chromatography gave 2,3-epoxy-2-(2-nitrophenyl)propionaldehyde (**8**) (95.7 mg, 93%): mp 64—66 °C; IR ($CHCl_3$) 3050, 2900, 1735, 1530, 1340, 910, 860, 720, 695 cm^{-1}; ^1H NMR ($CDCl_3$) δ=3.36 (d, J=5.0 Hz, 1H, CH), 3.64 (d, J=5.0 Hz, 1H, CH), 7.5—8.3 (m, 4H, ArH), 8.98 (s, 1H, CHO); Found: C, 55.88; H, 3.58; N, 7.33%. Calcd for $C_9H_7NO_4$: C, 55.96; H, 3.65; N, 7.25%.

3-Methyl-2-oxoindoline (9). A mixture of **8** (51.0 mg, 0.26 mmol) and Pd/C (10 mg) in acetic anhydride (2 ml) was stirred at room temperature under H_2 (1 atm). After the catalysts were removed by filtration, the mixture was concentrated under the reduced pressure. The residue was taken up with EtOAc, washed with aqueous 5% HCl, brine, and dried (Na_2SO_4). Evaporation of the solvent followed by chromatography afforded 3-methyl-2-oxoindoline **9** (20.6 mg, 53%): mp 117—120 °C (lit,[11] mp 122.5—123.5 °C).

References

1) For example, see: J. P. Greenstein and M. Winitz, "Chemistry of the Amino Acids," Wiley, New York (1961), Vol. 3, pp. 2316—2347; "Aminosan Kogyo, Gosei to Riyo," ed by T. Kaneko, Y. Izumi, I. Chibata, and T. Itoh, Kodansha Scientific, Tokyo (1973), p. 214.

2) U. Hengartner, A. D. Batcho, J. F. Blount, W. Leimgruber, M. E. Larscheid, and J. W. Scott, *J. Org. Chem.*, **44**, 3748 (1979).

3) A. D. Batcho and W. Leimgruber, *Org. Synth.*, **63**, 214 (1985); R. D. Clark and D. B. Repke, *Heterocycles*, **22**, 195 (1984).

4) S. Torii, Y. Murakami, H. Tanaka, and K. Okamoto, *J. Org. Chem.*, **51**, 3143 (1986).

5) K. E. Pfitzner and J. G. Moffatt, *J. Am. Chem. Soc.*, **85**, 3027 (1953); K. E. Pfitzner and J. G. Moffatt, *J. Am. Chem. Soc.*, **87**, 5661, 5670 (1965); J. G. Moffatt, *Org. Synth.*, Coll. Vol. 5, 242 (1973).

6) C. Hakanson and M. Nilsson, *Acta Chem. Scand.*, **21**, 1978 (1967); R. Hasegawa and Y. Kamiya, *Bull. Chem. Soc. Jpn.*, **51**, 1490 (1978).

7) D. O. Holland and J. H. C. Nayler, *J. Chem. Soc.*, **1953**, 280; D. O. Holland, Brit. Patent 723986 (1955); *Chem. Abstr.*, **50**, P8741d (1956).

8) "1988—1989 Aldrich Catalog Handbook of Fine Chemicals," Aldrich Chemical Co., Inc., Milwaukee (1988), p. 1108.

9) "The Aldrich Library of Infrared Spectra," Aldrich Chemical Co., Inc., Milwaukee (1970), p. 713E; "The Aldrich Library of NMR Spectra," Aldrich Chemical Co., Inc., Milwaukee (1974), Vol. VI, p. 145B.

10) F. E. King and P. Lecuyer, *J. Chem. Soc.*, **1934**, 1903; "Aldrich Library of NMR Spectra," Aldrich Chemical Co., Inc., Milwaukee (1974), Vol. VIII, p. 51C.

11) A. S. Endler and E. I. Becker, *Org. Synth.*, Coll. Vol. 4, 657 (1963).

Reaction of Iminophosphoranes with a Diazonium Salt: Synthesis of Wholly Aromatic Aminophosphonium Salts

Makoto TAKEISHI* and Naoyuki SHIOZAWA
Department of Polymer Chemistry, Yamagata University, Yonezawa, Yamagata 992
(Received July 17, 1989)

Synopsis. *N*-Phenyliminotriphenylphosphorane reacts with benzenediazonium tetrafluoroborate to form wholly aromatic *N,N*-diphenylaminotriphenylphosphonium tetrafluoroborate. This synthetic method can be applied to prepare a cationic polymer having the aminophosphonium structure.

Highly polarized iminophosphoranes undergo a variety of nucleophilic reactions.[1] Several decades ago, Staudinger found that they react with alkyl halides to yield aminophosphonium halides.[2] This nucleophilic substitution has been applied for the preparation of *N,N*-dialkylaminotriphenylphosphonium salts,[3,4] and the hydrolysis of these aminophosphonium salts has been investigated to prepare amines carrying bulky alkyl groups.[5] Since aryl halides do not react with iminophosphoranes, no *N,N*-diarylaminophosphonium salt can be synthesized by this method, and no other reaction has been reported for the preparation of wholly aromatic aminophosphonium salts. We report in the present paper that *N*-phenyliminotriphenylphosphorane reacts with a benzenediazonium salt to give such an aromatic aminophosphonium salt.

Results and Discussion

Phosphonium ylids, i.e., Wittig reagents couple directly with diazonium salts: methoxycarbonylmethylenetriphenylphosphorane reacts with benzenediazonium tetrafluoroborate to yield a phosphonium salt which can be converted into a phenylazo-substituted new ylid upon treatment with an aqueous base.[5] Cyclopentadienylidenetriphenylphosphorane also reacts with benzenediazonium chloride, but electrophilic aromatic substitution of the phenylazo group takes place on the cyclopentadienyl ring.[6]

$$(C_6H_5)_3P{=}NC_6H_5 + C_6H_5N_2^{\oplus}BF_4^{\ominus} \longrightarrow (C_6H_5)_3P^{\oplus}N(C_6H_5)_2BF_4^{\ominus} + N_2$$

We have found that *N*-phenyliminotriphenylphosphorane reacts with benzenediazonium tetrafluoroborate with an elimination of nitrogen to afford wholly aromatic *N,N*-diphenylaminotriphenylphosphonium tetrafluoroborate (Table 1). In polar solvents, such as acetonitrile or DMF, the reaction proceeded homogeneously, while the reaction was heterogeneous in benzene because both the diazonium salt and the phosphonium salt formed are less soluble in the solvent. The reaction, however, occurred readily even in the less polar benzene and the IR and NMR spectra of the products were identical with those of the products obtained in the polar solvents. When the orange-colored aminophosphonium salt was dissolved in methanol together with dimethoxybenzene, the spectrophotometric observation showed no definite evidence for the formation of a charge-transfer complex. The results suggest that the positive charge is not dispersed over the aminophosphonium molecule but, rather, localized on the phosphorus atom.

A few polymers carrying phosphonium structures have been reported,[7,8] whereas a number of anion-exchange resins with ammonium structures are available. Therefore, the above-mentioned reaction was applied in order to introduce the aminophosphonium structure into a polymer: poly(*N*-phenylimino-*p*-styryldiphenylphosphorane (P-1) was converted into a

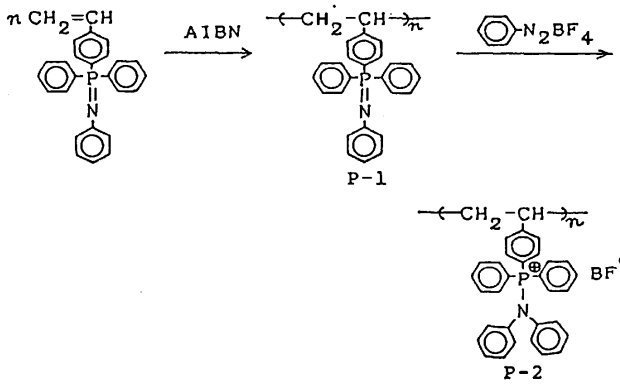

Table 1. Reaction of *N*-Phenyliminotriphenylphosphorane with Benzenediazonium Tetrafluoroborate[a]

Run	Solvent(condition)[b]	Reaction time/h	Yield/%
1	Acetonitrile(homo)	23	83
2	DMF (homo)	19	51
3	Benzene (hetero)	13	79
4	Benzene (hetero)	24	84

a) The reaction conditions are described in the experimental section. b) The reaction mixtures are homogeneous(homo) or heterogeneous(hetero).

Table 2. Reaction of P-1 with Benzenediazonium Tetrafluoroborate[a]

Run	Solvent	Temp/°C	Reaction time/h	Conversion/%
1	DMF	40	26	82
2	DMF	60	24	79
3	Benzene	60	24	72
4[b]	Benzene	60	20	70

a) The reaction conditions are described in the experimental section. b) The concentration of reactants was half compared with that for the other runs.

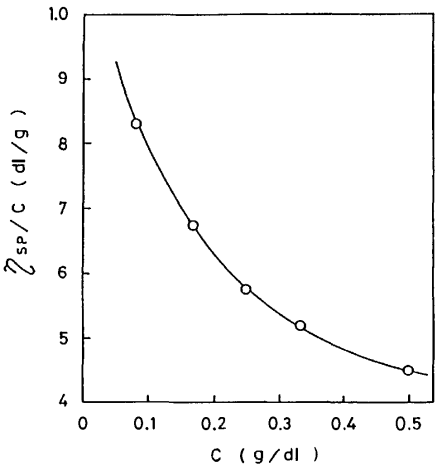

Fig. 1. Solution viscosity of P-2 (Run 3 in Table 2). The viscosity was measured in methanol at 30 °C.

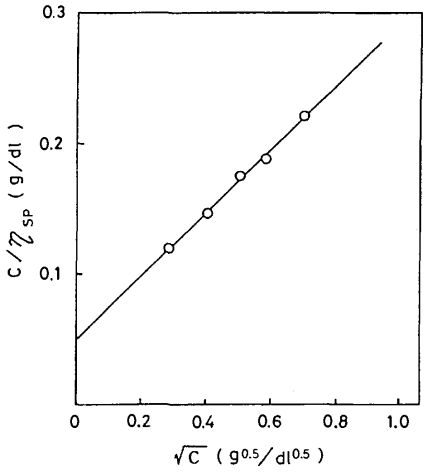

Fig. 2. The Fouss plot of the data of Fig. 1.

polymeric phosphonium salt (P-2) by the reaction with benzenediazonium tetrafluoroborate. The reaction proceeded in less polar benzene as well as in DMF (Table 2). Fig. 1 shows the solution viscosity behavior of P-2 (Run 3 in Table 2), suggesting the characteristic of ionic polymers. The linearity of the Fuoss plot[9] indicates that the physicochemical properties of the polymer are very similar to those of typical ionic polymers (Fig. 2). We previously reported the introduction of the iminophosphorane structure into cross-linked polystyrene beads, which can be utilized to prepare a phosphonium resin whose affinity for anions is different from that of ammonium resins. P-2 is therefore of interest from the viewpoint of chromatografic anion-selectivity.

Experimental

Materials. All reagent grade chemicals were used without further purification. *N*-Phenyliminotriphenylphosphorane and *N*-phenylimino-*p*-styryldiphenylphosphorane were synthesized by the reaction of the corresponding phosphines(*p*-styryldiphenylphosphine was kindly supplied by Hokko Chemical Industry Ltd.) and phenyl azide,[11,12] and freshly prepared benzenediazonium tetrafluoroborate was used.

Diphenylaminotriphenylphosphonium Tetrafluoroborate. Homogeneous Reaction. A solution of benzenediazonium tetrafluoroborate (2 mmol) in acetonitrile (10 ml) was added dropwise to a solution of *N*-phenyliminotriphenylphosphorane (2 mmol) in the solvent (10 ml). The solution turned red with the evolution of nitrogen at room temperature. After the solution was kept at 60 °C for 23 h, the solvent was removed by evaporation and benzene was added to solidify the only residue. The solid product was collected by filtration (yield 83%, Run 1 in Table 1) and was recrystallized from benzene. The IR spectrum of the product was identical with that of the product obtained by the heterogeneous reaction described below.

Heterogeneous Reaction. Benzenediazonium tetrafluoroborate (5 mmol) was added to a solution of *N*-phenyliminotriphenylphosphorane (5 mmol) in benzene (20 ml). The heterogeneous mixture was kept at 60 °C with stirring for 24 h, turning red with evolution of nitrogen. After the reaction mixture was cooled and kept at room temperature for 4 h, the precipitated product was collected (yield 84%, Run 4 in Table 1) and recrystallized from benzene, mp 170 °C. Found: C, 69.4; H, 5.0; N, 3.0; P, 6.2%. Calcd for $C_{30}H_{25}BF_4NP$: C, 69.7; H, 5.0; N, 2.7; P, 6.0%.

Poly(*N*-phenylimino-*p*-styryldiphenylphosphorane)(P-1). *N*-Phenylimino-*p*-styryldiphenylphosphorane (3.2 mmol) was polymerized with α,α'-azobis(isobutyronitrile)(AIBN) (1.6×10^{-5} mol) in benzene (4 ml) at 65 °C for 6 h; the polymer formed was precipitated in methanol and collected by filtration, conversion 71%. Found: C, 82.2; H, 5.8; N, 3.7; P, 8.0%. Calcd for $C_{26}H_{22}NP$: C, 82.3; H, 5.8; N, 3.7; P, 8.2%.

Poly(diphenylamino-*p*-styryldiphenylphosphonium tetrafluoroborate) (P-2). Homogeneous Reaction. A solution of benzenediazonium tetrafluoroborate (1.4 mmol) in DMF (10 ml) was added dropwise to a solution of P-1 (1.4 mmol, based on the monomer unit) in the solvent (10 ml). The evolution of nitrogen was observed and the solution turned red at room temperaure as in the case of monomeric compounds described above. After the solution was kept at 60 °C for 24 h, the phosphonium polymer formed was precipitated in a large excess of ether. The conversion into the phosphonium structure in P-2 was determined on the basis of a conductometric titration with silver nitrate in DMF-H_2O (9 : 1): 79% (Run 2 in Table 2).

Heterogeneous Reaction. Benzenediazonium tetrafluoroborate (1.4 mmol) was added to a solution of P-1 (1.4 mmol, based on the monomer unit) in benzene (10 ml). The heterogeneous mixture was kept at 60 °C for 24 h, turning red with evolution of nitrogen. After the reaction mixture was cooled to room temperature, the precipitated polymer was filtered and purified by reprecipitation from DMF/ether, conversion 72% (Run 3 in Table 2).

References

1) For example, see: A. W. Johnson, "Ylid Chemistry," Academic, New York (1966), Chap. 6.
2) H. Staudinger and E. Hauser, *Helv. Chim. Acta*, **4**, 861 (1921).
3) L. Horner and A. Gross, *Justus Lebigs Ann. Chem.*, **591**, 117 (1955).
4) H. Zimmer and G. Singh, *J. Org. Chem.*, **28**, 483 (1963).
5) G. Markl, *Tetrahedron Lett.*, **1961**, 807.
6) F. Ramirez and S. J. Levy, *J. Am. Chem. Soc.*, **79**, 6167 (1957).
7) N. V. Stamicarbon, U. S. Patent 2713038 (1955).

8) E. B. Trostyanskaya, I. P. Losev, A. S. Tevlina, S. B. Makarova, G. Z. Nefedova, and L. J. Zhao, *J. Polym. Sci.*, **59**, 379 (1962).
9) R. M. Fuoss and U. P. Strauss, *J. Polym. Sci.*, **3**, 246 (1948).
10) M. Takeishi, M. Tadano, and S. Hayama, *Makromol. Chem., Rapid Commun.*, **3**, 871 (1982).
11) H. Staudinger and J. Meyer, *Helv. Chim. Acta*, **2**, 635 (1919).
12) J. E. Leffler and R. D. Temple, *J. Am. Chem. Soc.*, **89**, 5235 (1967).

A New Preparative Method of 4-Hydroxybenzofuran-2-carboxylic Acid Derivatives

Seiji YAMAGUCHI,* Ken-ichi YAMAMOTO, Toshinori UEDA, Tetsuya MORIKAWA, and Yoshiyuki KAWASE*
Department of Chemistry, Faculty of Science, Toyama University, Gofuku 3190, Toyama 930
(Received July 17, 1989)

Synopsis. 4-Oxo-4,5,6,7-tetrahydrobenzofuran-2-carboxylic acid was prepared from 1,3-cyclohexanedione and ethyl bromopyruvate. Dehydrogenation of this acid or its methyl ester gave 4-hydroxybenzofuran-2-carboxylic acid derivatives.

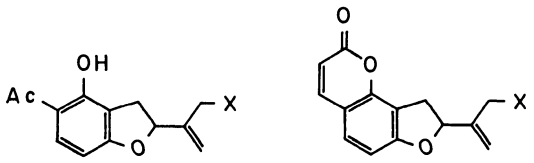

1a X = H
1b X = OCOCH(CH$_3$)$_2$
1c X = OCOCH(CH$_3$)C$_2$H$_5$

2a X = H
2b X = OH

Chart 1.

We reported the synthesis of some natural dihydrobenzofuran derivatives from optically active 2,3-dihydrobenzofuran-2-carboxylic acid.[1] For a similar synthesis of some natural dihydrobenzofuran derivatives having an *O*-functional group at the 4 position, such as **1a**,[2] **1b**, **1c**,[3] **2a**,[4] and **2b**,[5] 4-hydroxy-2,3-dihydrobenzofuran-2-carboxylic acid (**6**) might be a key compound. However, no effective preparation of 4-hydroxybenzofuran-2-carboxylic (**4**) and **6** has been reported. We now describe a new preparative method of **4** and its conversion to **6**.

A methanolic solution of 1,3-cyclohexanedione and ethyl bromopyruvate was refluxed with sodium methoxide; acidification of this mixture gave 4-oxo-4,5,6,7-tetrahydrobenzofuran-2-carboxylic acid (**3a**) in 76% yield. This acid **3a** was readily converted to the corresponding methyl ester **3b** with methanol-*p*-toluenesulfonic acid (76%) or diazomethane (69%).

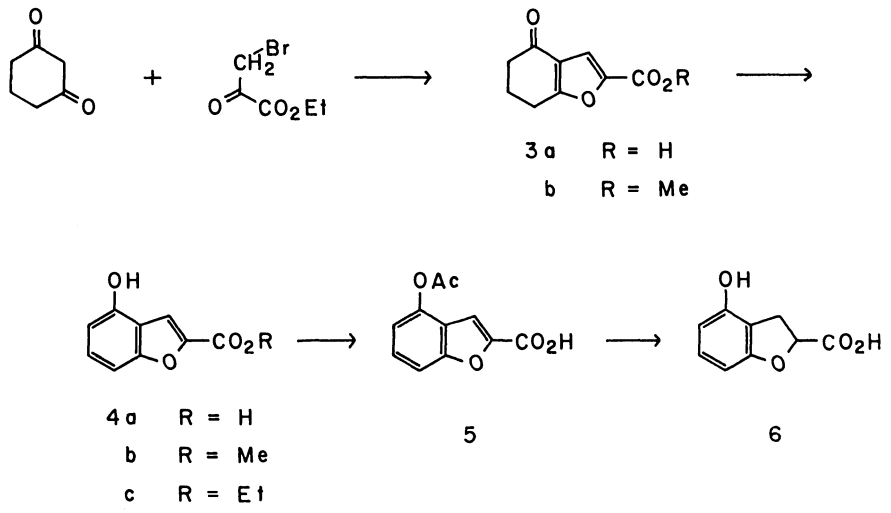

3a R = H
b R = Me

4a R = H
b R = Me
c R = Et

5

6

Chart 2.

Table 1. Dehydrogenation Reactions of **3a** and **3b**

Substrate	Reagent[a]	Conditions		Product	Yield/%
		Temp/°C	Time/h		
3a	A	250	1	—	0
3b	A	250	3	**4a**	13
3a	B	AcOEt-CHCl$_3$[b]	1	**4a**	9
3a	B	AcOEt-CHCl$_3$[b]	5	**4c**	23
3a	B	AcOMe-CHCl$_3$[b]	5	**4b**	28
3a	B	EtOH[b]	2	**4c**	38
3a	B	MeOH[b]	2	**4b**	56
3a	B	THF[b]	2	**4a**	16
3b	B	MeOH[b]	2	**4b**	38
3a	C	Benzene[b]	4	**4a**	5
3b	C	Benzene[b]	4	**4b**	5

a) A: sulfur, B: copper(II) bromide, C: DDQ. b) Refluxing temp.

Table 2. Some Physical Data and Elemental Analyses of New Benzofuran-2-carboxylic Acid Derivatives

Compound	Mp °C	IR ν_{CO} /cm^{-1}	UV λ_{max}(log ε) /nm	MS (*m/z*)	Elemental analyses Found (%)	Calcd (%)	
3a	146—147	1730 1630	264 (3.70)	180 152 136	C 59.70 H 4.72	C 60.00 H 4.48	for $C_9H_8O_4$
3b	108.5—109	1735 1655	256 (3.84)	194 166 163	C 61.71 H 5.22	C 61.85 H 5.19	for $C_{10}H_{10}O_4$
4a	200—202	1695	230 (4.32) 260sh (3.96) 287 (3.79)	178 160 132	C 60.77 H 3.48	C 60.68 H 3.40	for $C_9H_6O_4$
4b	87—89	1675	229 (4.04) 275 (3.50)	192 160 132	C 62.34 H 4.36	C 62.50 H 4.20	for $C_{10}H_8O_4$
4c	67—68	1670	231 (3.75) 275 (3.24)	206 160 132	C 64.15 H 4.97	C 64.07 H 4.89	for $C_{11}H_{10}O_4$
5	202—203	1750 1670	250 (3.82) 278sh (2.90)	220 178 160	C 60.04 H 3.56	C 60.00 H 3.66	for $C_{11}H_8O_5$
6	142—143.5	1700	274 (3.26) 280.5 (3.21)	180 178 160	C 59.94 H 4.49	C 60.00 H 4.48	for $C_9H_8O_4$

Table 3. ^{1}H NMR Data of Benzofuran-2-carboxylic Acid Derivatives

Compound	(solvent)	Chemical shifts data/ppm
3a	($CDCl_3$)	2.4 (2H, m, *J*=6 Hz) 2.7 (2H, t, *J*=6 Hz) 3.1 (2H, t, *J*=6 Hz) 8.3 (1H, s) 13.4 (1H, s)
3b	(CCl_4)	2.2 (2H, m, *J*=6 Hz) 2.6 (2H, t, *J*=6 Hz) 2.9 (2H, t, *J*=6 Hz) 3.9 (3H, s) 7.9 (1H, s)
4a	(acetone-d_6)	6.9 (1H, dd, *J*=8 and 2 Hz) 7.3 (1H, dd, *J*=8 and 2 Hz) 7.5 (1H, t, *J*=8 Hz) 8.7 (1H, s)
4b	(CCl_4)	3.8 (3H, s) 6.7 (1H, dd, *J*=8 and 2 Hz) 6.9 (1H, dd, *J*=8 and 2 Hz) 7.2 (1H, t, *J*=8 Hz) 8.0 (1H, s) 9.7 (1H, s)
4c	(CCl_4)	1.4 (3H, t, *J*=7 Hz) 4.4 (2H, q, *J*=7 Hz) 6.7 (1H, dd, *J*=8 and 2 Hz) 6.8 (1H, dd, *J*=8 and 2 Hz) 7.1 (1H, t, *J*=8 Hz) 8.0 (1H, s) 9.8 (1H, s)
5	($CDCl_3$)	2.3 (3H, s) 7.1 (1H, dd, *J*=6 and 3 Hz) 7.3 (1H, t, *J*=6 Hz) 7.5 (1H, dd, *J*=6 and 3 Hz) 7.5 (1H, s) 8.3 (1H, s)
6	($CDCl_3$)	4.5 (1H, dd, *J*=14 and 8 Hz) 4.7 (1H, dd, *J*=14 and 7 Hz) 4.9 (1H, dd, *J*=8 and 7 Hz) 6.4 (2H, d, *J*=8 Hz) 7.0 (1H, t, *J*=8 Hz) 9.3 (2H, broad s)

The dehydrogenation of **3a** and **3b** was attempted by the following three methods: A) heating with sulfur,[6] B) bromination with copper(II) bromide followed by dehydrobromination,[7] and C) heating with 2,3-dichloro-5,6-dicyano-1,4-benzoquinone (DDQ)[8] (summarized in Table 1). In some cases with copper(II) bromide, trans-esterification or esterification was observed. The dehydrogenation of **3a** was most effective with copper(II) bromide in refluxing methanol for 2 h. Interestingly, esters **4b** and **4c** showed a lower carbonyl band than acid **4a** regarding their IR spectra.

4-Hydroxy-2,3-dihydrobenzofuran-2-carboxylic acid (**6**) was obtained by a sodium amalgam reduction of 4-acetoxybenzofuran-2-carboxylic acid (**5**) in 56% yield, which was prepared from **4a** by acetylation with acetic anhydride.

Experimental

The melting points were uncorrected. The IR spectra were measured on a Hitachi EPI-S2 spectrophotometer in KBr disks, and the UV spectra were taken on a Hitachi 220A spectrophotometer in ethanol. The ^{1}H NMR spectra were recorded on a JEOL PMX-60Si NMR spectrometer in CCl_4, $CDCl_3$, or acetone-d_6 and the mass spectra were recorded on a JEOL JMS-OISG-2 mass spectrometer. The yields, some physical data, and elemental analyses are summarized in Tables 1, 2, and 3.

Preparation of 4-Oxo-4,5,6,7-tetrahydrobenzofuran-2-carboxylic Acid (3a). To a methanolic solution of sodium methoxide, prepared from sodium metal (2.8 g, 122 mmol) and abs. methanol (45 ml), 1,3-cyclohexanedione (14.5 g, 129 mmol) was added. Then, a solution of ethyl bromopyruvate[9] (25.0 g, 128 mmol) in abs. methanol was added to the mixture with stirring. After refluxing for 4 h, the mixture was allowed to stand for 20 h at room temperature. The solvent was removed under reduced pressure, and the residue was diluted with water and acidified with 10% hydrochloric acid. The mixture was allowed to stand for 2 d to complete cyclization and crystallization. The crystals were collected and recrytsallized from ethanol to give 4-oxo-4,5,6,7-tetrahydrobenzofuran-2-carboxylic acid (**3a**) (16.6 g, 76%) as colorless needles. A similar reaction of 1,3-cyclohexanedione and ethyl bromopyruvate with equivalent potassium hydroxide in water-methanol also gave **3a**, but in

poorer yield (31%).

Preparation of Methyl 4-Oxo-4,5,6,7-tetrahydrobenzofuran-2-carboxylate (3b). To a solution of **3a** (2.11 g, 11.7 mmol) in methanol (100 ml) was added a small amount of *p*-toluenesulfonic acid; the mixture was refluxed for 24 h. After removing the methanol, the residue was diluted with benzene. The benzene layer was washed with sat. sodium hydrogencarbonate solution and then with sat. sodium chloride solution, and dried over anhydrous sodium sulfate. After removing the solvent, the residue was crystallized from cyclohexane to give methyl 4-oxo-4,5,6,7-tetrahydrobenzofuran-2-carboxylate (**3b**) (1.72 g, 76%) as colorless plates. This methyl ester **3b** was also obtained by esterification of **3a** with an excess of diazomethane ethereal solution in 69%.

Dehydrogenation of 3a or 3b. A) With Sulfur:[6] A mixture of **3b** (903 mg, 4.65 mmol) and sulfur powder (152 mg, 4.74 mmol) was heated at ca. 250 °C on a metal bath for 3 h. After cooling, the mixture was treated with benzene and the benzene solution was extracted with a 5% sodium hydroxide solution. The alkaline aqueous solution was acidified with 10% hydrochloric acid and re-extracted with benzene. The benzene layer was washed with sat. sodium chloride solution and dried over anhydrous sodium sulfate. After removing the solvent, the residue was crystallized from benzene to give 4-hydroxybenzofuran-2-carboxylic acid (**4a**) (105 mg, 13%). A similar heating of acid **3a** with sulfur generated an odour of hydrogen sulfide, but did not give **4a**.[10]

B) With Copper(II) Bromide:[6] To a solution of **3a** (1.93 g, 10.7 mmol) in methanol (50 ml) was added copper(II) bromide (4.60 g, 20.6 mmol), and the mixture was refluxed for 2 h. After cooling, the precipitates of copper(I) bromide were filtered off and washed with benzene. The filtrate and the washings were combined and concentrated at reduced pressure. The residue was diluted again with benzene, and the precipitates of copper(II) bromide were filtered off. After removing the benzene, the residue was crystallized from methanol to give methyl 4-hydroxybenzofuran-2-carboxylate (**4b**) (1.15 g, 56%) as colorless plates. Similar treatments of **3a** or **3b** with copper(II) bromide gave **4a**, **4b**, or **4c**, depending on the solvent used. Ester **4c** was purified by recrystallization from ethanol and obtained as colorless wooly crystals. Acid **4a** was purified by sublimation (150—180 °C at 16 mmHg[11]), followed by recrystallization from benzene, and obtained as colorless wooly crystals. The yields and some physical data are summarized in Tables 1, 2, and 3.

C) With DDQ:[7] To a solution of **3a** (588 mg, 3.27 mmol) in benzene (30 ml) was added 2,3-dichloro-5,6-dicyano-1,4-benzoquinone (DDQ)(763 mg, 3.36 mmol), and the mixture was refluxed for 4 h. After cooling, the precipitated hydroquinone was filtered off and washed with benzene. The filtrate and the washings were combined and extracted with a sodium hydrogencarbonate solution. The alkaline extract was acidified with 10% hydrochloric acid and re-extracted with benzene. The benzene layer was dried over anhydrous sodium sulfate and concentrated. The residue was sublimed to give **4a** (29 mg, 5%). A similar treatment of **3b** (513 mg, 2.64 mmol) with DDQ (711 mg, 3.13 mmol) in benzene (30 ml) for 4 h gave **4b** (26 mg, 5%) as a sodium hydroxide extract, which was purified by crystallization from methanol.

4-Acetoxybenzofuran-2-carboxylic Acid (5). A solution of **4a** (1.02 g, 5.73 mmol) in acetic anhydride (5 ml) was heated on a water bath for 3 h. After removing the solvent, the residue was treated with water and the precipitates were collected and recrystallized from benzene to give 4-acetoxybenzofuran-2-carboxylic acid (**5**) (0.92 g, 74%) as colorless needles.

4-Hydroxy-2,3-dihydrobenzofuran-2-carboxylic Acid (6). To a solution of **5** (1.01 g, 4.59 mmol) in an aqueous potassium hydroxide solution (containing 0.5 g of potassium hydroxide in 10 ml of water) was added 2% sodium amalgam (0.32 g of sodium metal in 17 g of mercury); the mixture was stirred for one night. The alkaline aqueous layer was acidified with 10% hydrochloric acid and extracted with ether. After removing the solvent, the residue was recrystallized from benzene to give 4-hydroxy-2,3-dihydrobenzofuran-2-carboxylic acid (**6**) (450 mg, 56%) as colorless crystals.

References

1) S. Yamaguchi, S. Kondo, K. Shimokawa, O. Inoue, M. Sannomiya, and Y. Kawase, *Bull. Chem. Soc. Jpn.*, **55**, 2500 (1982).

2) F. Bohlmann, J. Jakupovic, R. M. King, and H. Robinson, *Phytochemistry*, **21**, 161 (1982). But, the structure was revised to 4-acetyl-2-isopropenyl-2,3-dihydrobenzofuran-5-diol in our paper; S. Yamaguchi, A. Saitoh, and Y. Kawase, *Bull. Chem. Soc. Jpn.*, **59**, 3983 (1986).

3) F. Bohlmann and C. Zdero, *Tetrahedron Lett.*, **1970**, 3575.

4) Angenomalin: K. Hata, M. Kozawa, and Y. Ikeshiro, *Yakugaku Zasshi*, **87**, 1118 (1967). F. Bohlmann and H. Franke, *Chem. Ber.*, **104**, 3229 (1971). Majurin: E. A. Ab-mustafa, F. K. A. El-bay, and M. B. E. Fayez, *Tetrahedron Lett.*, **1971**, 1967. Masquin: E. Agullo Martinez, R. Esteves Reyes, A. G. Gonzalez, and F. Rodrigez and Luis, *An. Quim.*, **63**, 205 (1967).

5) Discophoridin: W. Bottomley, *Aust. J. Chem.*, **16**, 143 (1963). Sachalinin: G. K. Nikonov and M. G. Pimenov, *Khim. Prir. Soedin.*, **1**, 73 (1965). G. K. Nikonov, *Khim. Prir. Soedin.*, **6**, 623 (1970).

6) H. Stetter and E. Siehnhold, *Chem. Ber.*, **88**, 271 (1955).

7) L. C. King and G. K. Ostrum, *J. Org. Chem.*, **29**, 3459 (1964).

8) A. B. Turner, *J. Chem. Soc.*, **1968**, 2568.

9) A. A. Golberg and W. Kelly, *J. Chem. Soc.*, **1947**, 1372.

10) High reaction temperature probably caused decarboxylation and polymerization.

11) 1 mmHg = 133.322 Pa.

Oxidation of Aromatic *s*-Alcohols with Cobalt(III) Acetate in the Presence of Sodium Bromide

Masao HIRANO and Takashi MORIMOTO*
Department of Applied Chemistry, Faculty of Technology,
Tokyo University of Agriculture and Technology, Koganei, Tokyo 184
(Received July 26, 1989)

Synopsis. The title oxidation in acetic acid resulted in a selective formation of the corresponding ketones in excellent yields under mild conditions.

Oxidative transformation of alcohols to the corresponding carbonyl compounds constitutes an important part of synthetic chemistry. Thus, a wide variety of metal oxidants have been used for the stoichiometric and/or catalytic oxidation of alcohols. Extensively studied examples are those with lead(IV) acetate,[1] chromium(VI) compounds,[2-4] active manganese(IV) dioxide,[5-7] aluminum alkoxides (Oppenauer oxidation),[8] potassium ferrate(IV),[9] cerium(IV) ammonium nitrate,[10] etc. In economical and environmental terms, however, these procedures are not entirely satisfactory, because of the inherently hazardous toxicity and rather high cost of the reagents. In addition, from an experimental point of view, some limitations, viz. a lack of generality, manipulative complications, low yield of the product etc., have reduced the utility of the reagents for this purpose.

Cobalt salts are potent reagents and have wide applications for the oxidation of various functional groups, especially for the oxidation of alkylaromatics[11-13] and olefins.[14-16] However, there has hitherto been only a small amount of data on the oxidation of alcohols,[17,18] and it is apparent that these are not adequate for estimating the full validity of the reagent for this objective. We have found that cobalt(III) acetate in acetic acid is an efficient reagent for the oxidation of 1,2-glycols;[19-21] this fact prompted us to examine the oxidation of a variety of alcohols. The present paper describes the oxidation of aromatic *s*-alcohols using a cobalt(III) acetate-NaBr system, since this procedure can be expected to overcome the drawbacks attendant on conventional methods.

Results and Discussion

Oxidation of 1-phenylethyl alcohol (**1**) in acetic acid with stoichiometric cobalt(III) acetate [2 equiv per mol of **1**] was performed under an inert atmosphere in order to exclude any influence of autoxidation, since an alcohol has a rather high sensitivity to cobalt(III)-catalyzed autoxidation.[17] After heating the reaction mixture at 60 °C for 2 h in the absence of NaBr, a GLC analysis showed that a considerable amount of unreacted **1** (38%) and only 49% of acetophenone (**2**), along with ca. 7% of 1-phenylethyl acetate (**3**) were involved in the reaction mixture. Upon the addition of a small amount of NaBr ([NaBr]/[Co(III)]=0.05; mole ratio), the conversion of **1** was markedly increased to roughly 94%, whereas **3** decreased to a trace amount. Consequently, NaBr contributes not only to facilitate the reaction, but to inhibit any side reaction. The yield of **2** was independent of the concentration of NaBr in the range [NaBr]/[Co(III)]=0.05—0.5.

Various inorganic bromides (KBr, LiBr, and $MgBr_2$) were also examined. All of the bromides were effective, and there was no marked difference in efficacy between NaBr and them. Thus, subsequent reactions were carried out using NaBr, since the reagent is inexpensive and easy to handle, as compared with the other bromides.

The oxidation of 1-phenylethyl alcohols and diarylmethanols was conducted under comparable conditions and the results are summarized in Table 1. As with the case of **1**, the addition of NaBr commonly resulted in the promotion of the reaction and also in the predominant formation of the corresponding ketones. When the oxidation was carried out with stoichiometric cobalt(III) acetate, the formation of a small amount of the corresponding acetate, possibly due to competitive acetylation of unreacted alcohol, was observed in some cases. Therefore, the experiments were performed with a small excess of the oxidant for the completion of the reaction in such cases. Depending on the conditions used, a concomitant formation of some unidentified by-products was also observed in the oxidation of phenyl-*o*-, -*m*-, and -*p*-tolylmethanol and *o*-methyldiphenylmethanol. This might be partly attributable to the susceptibility of the methyl side chain towards cobalt(III) acetate[11,12] and/or the Co(III)-NaBr system.[13] Thus, the other reaction conditions (temperature, time, and concentration of NaBr) were selected on the basis of the reactivity of alcohol as well as the yield and selectivity of the ketone.

The influence of the position of the substituents on the benzene-ring on the yield of the ketones was investigated (Entries 2—4, 6—8, 9—11, 15—17, and 20—22); interestingly, however, there was no significant difference in the yields of the ketones.

In order to clarify an active species, the independent oxidations of **1** and diphenylmethanol with bromine were carried out in acetic acid under comparable conditions (60 °C, 2 h), since bromine might be formed by the possible interaction of bromide ion with cobalt(III) acetate. Indeed, bromine itself can oxidize the alcohols, but afforded only lower yields of **2** and benzophenone (23 and 18%, respectively). In these reactions acetylation of the alcohols (65 and 64%, respectively) was predominant, showing little contribution of bromine in the present reaction. Moreover, when cobalt(III) acetate was heated without the addition of a substrate under "standard conditions" (60 °C

Table 1. Oxidation of Aromatic *s*-Alcohols with Cobalt(III) Acetate in the Presence of Sodium Bromide[a)]

$X\text{-}C_6H_4\text{-}CH(OH)\text{-}R \longrightarrow X\text{-}C_6H_4\text{-}C(=O)\text{-}R$

Entry No.	Alcohols			Temp	Time	NaBr[b)]	Co(III)[b)]	Ketones[c)]
	X		R	°C	h	Co(III)	Sub	%
1	H		Me	60	2	0.05	2.0	91
2	Me	*o*-	Me	50	2	0.05	2.5	84
3		*m*-	Me	50	2	0.05	2.5	97
4		*p*-	Me	50	2	0.05	2.2	86
5	OMe	*p*-	Me	60	2	0.25	2.2	96
6	Br	*o*-	Me	60	1.5	0.05	2.5	93
7		*m*-	Me	60	1.5	0.05	2.5	96
8		*p*-	Me	60	2	0.25	2.2	90
9	Cl	*o*-	Me	60	1	0.05	2.5	96
10		*m*-	Me	60	2	0.05	2.5	95
11		*p*-	Me	60	2	0.25	2.2	93
12	F	*p*-	Me	60	2	0.25	2.2	90
13	NO_2	*p*-	Me	70	2	0.25	2.2	84
14	H		Ph	60	2	0.25	2.0	94
15	Me	*o*-	Ph	60	2	0.05	2.5	92
16		*m*-	Ph	60	1	0.05	2.5	95
17		*p*-	Ph	60	1	0.05	2.0	93
18	OMe	*p*-	Ph	60	1.5	0.05	2.5	97
19	Br	*p*-	Ph	60	1.5	0.25	2.5	93
20	Cl	*o*-	Ph	60	1	0.05	2.5	93
21		*m*-	Ph	60	1	0.05	2.5	96
22		*p*-	Ph	60	2	0.25	2.0	91
23	NO_2	*p*-	Ph	70	2	0.05	2.5	93
24	Benzoin			60	2	0.25	2.0	83

a) Under argon, $[Co(OAc)_3]=0.2703$ mol dm^{-3}; 0.50 g of alcohols were used in every run.
b) Mole ratio. c) Isolated yield.

for 2 h) in both the presence and absence of NaBr ([NaBr]/[Co(III)]=0, 0.15, 0.25, 0.35, and 0.5), we observed that the concentration of a cobaltic species remained essentially unchanged within the experimental error; the ratios of concentration of remained Co(III) vs. initial concentration of Co(III) were 1, 0.995, 0.974, 0.989, and 0.979, respectively. Based on these observations and on earlier studies,[13,22)] the reacting species is thought to be acetoxybromocobalt(III), formed from a reaction of cobalt(III) acetate with bromide ion. The species, so generated, is presumed as a highly active mononuclear complex.[23)] Its

$$Co(OAc)_3 + Br^- \rightarrow (AcO)_2CoBr + AcO^-$$

highly reactive nature is very consistent with the marked rate enhancement observed in the present reactions. The cobaltic species could abstract the α-hydrogen atom of an alcohol in a radical manner,[22)] finally giving the corresponding ketone by the following oxidation of the resultant carbon radical with cobalt(III) acetate.

Experimental

^{1}H NMR spectra were measured with a JEOL model PMX-60 spectrometer for solutions in carbon tetrachloride. IR spectra were recorded for thin films or KBr disks on a JASCO DS-403G spectrophotometer. GLC was carried out on a Shimadzu GC-6A or GC-4CM instrument with a 2 m column packed with 5% PEG-20M or 1.5% OV-17, respectively, on Chromosorb GAW-DMCS, with temperature programming.

Materials. Cobalt(III) acetate in acetic acid was prepared according to lit.[24)] The concentration was determined by adding an excess of Fe(II) and back-titration with Ce(IV) ion. 1-Phenylethyl alcohol, diphenylmethanol, phenyl-*o*-tolylmethanol and phenyl-*p*-tolylmethanol, *p*-chlorophenyl-phenylmethanol, and benzoin were commercially available. The other alcohols were synthesized by reductions of the corresponding ketones, either with $NaBH_4$ in 90% aqueous EtOH, with $LiAlH_4$ in dry ether, or with aluminum isopropoxide in 2-propanol. All of the alcohols, thus prepared, were purified by distillation or by recrystallization just before use. The commercial inorganic bromides were used without any treatment.

Oxidation Procedures. The following procedures are representative. To a mixture of **1** (0.50 g, 4.10 mmol) and 0.05 mole equiv of NaBr in a round-bottomed flask was added a stoichiometric cobalt(III) acetate (2 mole equiv) in acetic acid (30 ml). The flask was flushed with dry argon, and the reaction was carried out at a controlled temperature in a thermostat with magnetic agitation. After a given period, the reaction mixture was poured into brine and extracted three times with ether. The combined extract was successively washed with brine, 10% aqueous sodium carbonate, and brine and then dried ($MgSO_4$). Removing the ether on a rotary evaporator gave a pale-yellow oil, which was chromatographed on silica gel (hexane–ethyl acetate).

All products so formed were known compounds and their identities were confirmed by comparisons of their NMR and IR spectra with those of authentic samples.

References

1) G. M. Rubottom, "Oxidation in Organic Chemistry," Part D, ed by W. S. Trahanovsky, Academic Press, N. Y. (1982), p. 2.
2) S. Kanemoto, K. Oshima, S. Matsubara, K. Takai, and H. Nozaki, *Tetrahedron Lett.*, **24**, 2185 (1983).
3) E. J. Corey, E.-P. Barrett, and P. A. Magriotis, *Tetrahedron Lett.*, **26**, 5855 (1985).
4) K. B. Wiberg, "Oxidation in Organic Chemistry," Part A, ed by K. B. Wiberg, Academic Press, N. Y. (1965), p. 69.
5) C. A. Buehler and D. E. Pearson, "Survey of Organic Synthesis," John Wiley & Sons, N. Y. (1971), p. 546.
6) L. F. Fieser and M. Fieser, "Reagents for Organic Synthesis," John Wiley & Sons, N. Y. (1967), p. 636.
7) L. A. Carpino, *J. Org. Chem.*, **35**, 3971 (1970).
8) C. Djerassi, "Organic Reactions," Vol. 6, (1951), p. 207.
9) R. J. Audette, J. W. Quail, and P. J. Smith, *Tetrahedron Lett.*, **1971**, 279.
10) W. S. Trahanovsky, L. B. Young, and G. L. Brown, *J. Org. Chem.*, **32**, 3865 (1967).
11) E. I. Heiba, R. M. Dessau, and W. J. Koehl, Jr., *J. Am. Chem. Soc.*, **91**, 6830 (1969).
12) Y. Kamiya and M. Kashima, *J. Catal.*, **25**, 326 (1972).
13) Y. Kamiya and M. Kashima, *Bull. Chem. Soc. Jpn.*, **46**, 905 (1973).
14) M. Hirano, K. Nakamura, and Morimoto, *J. Chem. Soc., Perkin Trans. 2*, **1981**, 817.
15) M. Hirano and T. Morimoto, *J. Chem. Soc., Perkin Trans. 2*, **1984**, 1033.
16) M. Hirano and T. Morimoto, *J. Chem. Soc., Perkin Trans. 2*, **1985**, 1105.
17) R. Kawai and Y. Kamiya, *Nippon Kagaku Kaishi*, **1973**, 1533.
18) M. Hirano, T. Morimoto, and K. Itoh, *Bull. Chem. Soc. Jpn.*, **61**, 3749 (1988).
19) T. Morimoto and M. Hirano, *J. Chem. Soc., Perkin Trans. 2*, **1982**, 1087.
20) T. Morimoto and M. Hirano, *J. Chem. Soc., Perkin Trans. 2*, **1983**, 123.
21)T. Gunji, M. Hirano, and T. Morimoto, *J. Chem. Soc., Perkin Trans. 2*, **1985**, 1827.
22) T. Morimoto, M. Hirano, M. Wachi, and T. Murakami, *J. Chem. Soc., Perkin Trans. 2*, **1984**, 1949.
23) R. A. Sheldon and J. K. Kochi, "Metal-Catalyzed Oxidation of Organic Compounds," Academic Press, N. Y. (1981), p. 127.
24) S. S. Lande, C. D. Falk, and J. K. Kochi, *J. Inorg. Nucl. Chem.*, **33**, 4101 (1971).

One-Pot *C*-Arylmethylation of Active Methylene Compounds with Aromatic Aldehydes Induced by a Me_3SiCl-NaI-MeCN Reagent

Takashi SAKAI,* Kazuyoshi MIYATA, Sadao TSUBOI, and Masanori UTAKA*
Department of Applied Chemistry, Faculty of Engineering, Okayama University, Tsushima, Okayama 700
(Received August 4, 1989)

Synopsis. Reaction of active methylene compounds with aromatic aldehydes in the presence of chlorotrimethylsilane-sodium iodide-acetonitrile reagent gave *C*-arylmethylated products, the reduced condensation products, although the reaction either with aliphatic primary aldehydes or with isobutyraldehyde afforded alkylidenation products or dihydrofurans.

C-Arylmethylation at α-position of ketonic active methylene compounds is a fundamental and important process in organic synthesis. However the conventional method with arylmethyl halides under basic conditions often suffered from dialkylation and/or self-condensation of the ketonic substrates especially in the case of 1,3-diketones.[1] For example, acetylacetone is required to be converted to a cobalt complex for *C*-benzylation with benzyl bromide. Moreover, the yield remained moderate due to the formation of by-products.[2] In order to avoid the problems, sequential reactions of the Knoevenagel condensation with aromatic aldehyde followed by reduction of the resulting carbon-carbon double bond is sometimes forced to take.[3] In this paper, we describe a development of one pot method for the *C*-arylmethylation by use of aromatic aldehydes and a chlorotrimethylsilane-sodium iodide-acetonitrile reagent.[4] Meanwhile, we recently reported that the reagent can be used for reduction of carbon-carbon double bond of conjugated enones[5a] and for deoxygenation of benzylic alcohols.[5b] On the other hand, chlorotrimethylsilane has been known to catalyze the Knoevenagel condensation.[6] The present reaction is of a successful combination of these reactions and simplified the classical stepwise procedure, although it is not suitable for aliphatic aldehydes. Primary aliphatic aldehydes gave merely Knoevenagel condensation products and isobutyraldehyde yielded dihydrofurans and/or γ-lactones.

In a typical reaction, ethyl acetoacetate (**1a**) (1 mol) was allowed to react with benzaldehyde (**2a**) (1 mol) in the presence of the Me_3SiCl-NaI-CH_3CN reagent (5 mol) in acetonitrile at room temperature to 60 °C for 16 h to give benzylated product **3a** in an 82% yield (Scheme 1, Table 1). The reaction with acetylacetone (**1b**) gave product **3e** quantitatively, much increasing the yield as compared with that in the cobalt complex method (53% yield).[2] Interestingly, methyl ethyl ketone (**1c**), acetophenone (**1d**) and acetone (**1e**) also gave the corresponding benzylated compounds **3h** (67%), **3i** (76%), and **3j** (17%), respectively. The results using various aldehydes are summarized in Table 1.

A possible mechanism is depicted in Scheme 2. Condensation of enol or enol silyl ether **4** with iodinated silyl ether **5**[7] gives β-iodo ketone intermediate **6**,[8,9] which would be readily reduced to ketone **3** by in situ generated HI in a similar manner to that discussed previously.[5] The reaction, thus, requires two moles of the reagents, which are consumed to give hexamethyldisiloxane and iodine. The mechanism is supported by the fact that the reaction of **1a** with **2a** carried out at lowered temperature (0 °C—room temperature) gave ethyl 2-benzylidene-3-oxobutanoate (**7**) (45% yield), exclusively, by elimination of HI from **6**. In addition, ethyl 2-(α-iodobenzyl)-3-

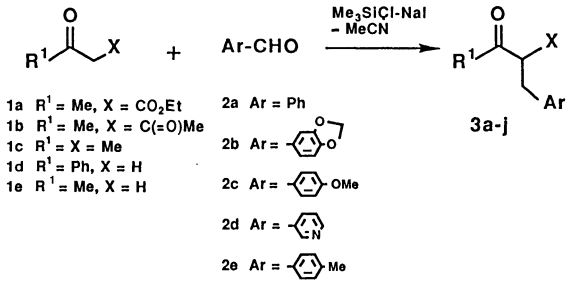

Scheme 1.

Table 1. *C*-Arylmethylation of Active Methylene Compounds **1** with Aromatic Aldehydes **2**

Substrate	Aldehyde	Product[a]				
1	**2**	**3**	R^1	X	Ar	Yield/%
1a	**2a**	**3a**	Me	CO_2Et	Ph	82
1a	**2b**	**3b**	Me	CO_2Et	3,4-(Methylenedioxy)phenyl	73
1a	**2c**	**3c**	Me	CO_2Et	*p*-Methoxyphenyl	60
1a	**2d**	**3d**	Me	CO_2Et	3-Pyridyl	29
1b	**2a**	**3e**	Me	C(=O)Me	Ph	100
1b	**2c**	**3f**	Me	C(=O)Me	*P*-Methoxyphenyl	80
1b	**2e**	**3g**	Me	C(=O)Me	*P*-Tolyl	100
1c	**2a**	**3h**	Me	Me	Ph	67
1d	**2a**	**3i**	Ph	H	Ph	76
1e	**2a**	**3j**	Me	H	Ph	17

a) Known compounds.

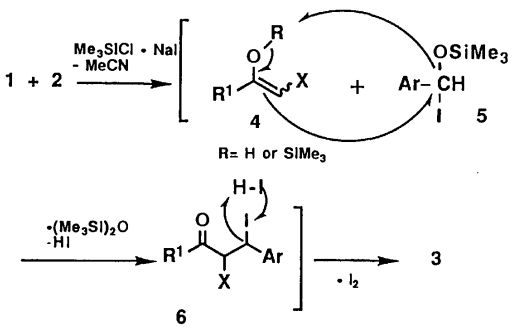

Scheme 2.

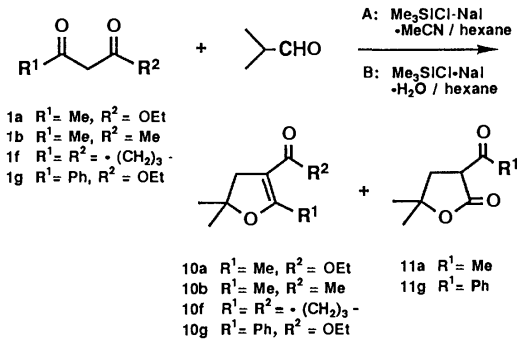

Scheme 3.

oxobutanoate (**9**) could be isolated (68% yield) by changing the solvent to ether.

Application of the present reaction to hexanal gave a mixture of unidentified products, while the reaction using ether as a solvent in place of acetonitrile at 0 °C—room temperature yielded merely a condensation product **8**.

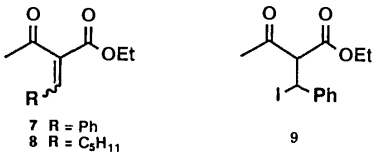

In contrast, the reaction of **1b** with isobutyraldehyde in hexane at reflux temperature provided 4-acetyl-2,2,5-trimethyl-2,3-dihydrofuran (**10b**) in a 33% yield (Scheme 3, Table 2). The yield was markedly improved up to a quantitative one by replacing acetonitrile with the same mole of water. Favorably, the reaction can be done at room temperature. Herein, the water would be consumed to generate anhydrous HI, which may be a promoter of the reaction. The reaction is applicable to 1,3-cyclohexanedione (**1f**), giving **10f**, although the yield was moderate. The present dihydrofuran synthesis also simplified the conventional stepwise method, which involves the Knoevenagel condensation and an acidic (HCl or H_2SO_4) cyclization.[10a] Moreover, the reaction applied to β-keto esters **1a** and **1g** afforded dihydrofurans **10a**, **g** together with γ-lactone derivatives **11a**, **g** in moderate to low yields.

Table 2. Reaction of Active Methylene Compounds with Isobutyraldehyde in the Presence of Me_3SiCl–NaI

Substrate	Reactn. Condn.[a]	Product(s) (Yield/%)[b]	
		Dihydrofuran **10**	Lactone **11**
1a	A	**10a**[c] (23)	**11a**[c] (21)
1b	A	**10b**[c] (33)[d]	
	B	**10b** (100)[d]	
1f	A	**10f**[e] (17)	
	B	**10f** (45)	
1g	A	**10g**[c] (13)	**11g**[f] (41)

a) A: Reaction with Me_3SiCl–NaI–MeCN (5 mol equivalents) in hexane under reflux for 24 h; B: Reaction with Me_3SiCl–NaI–H_2O (5 mol equivalents) in hexane at room temperature for 24 h. b) Isolated by preparative TLC (hexane-acetone, 3:1). c) Spectral data were consistent with those reported. See Ref. 10a. d) Purified by distillation (bp 115—120 °C (28 mmHg, 1 mmHg=133.322 Pa.)). e) See Ref. 10b. f) New compound.

Experimental

General. IR spectra were taken on a JASCO A 102 spectrometer. ^1H NMR spectra (60 MHz) were measured with a JEOL JNM-PMX60 SI spectrometer. Chemical shifts are reported in value (ppm) down field from tetramethylsilane. Preparative TLC was done on silica gel (E. Merck, Kiesel gel 60 PF_{254}). Elemental analyses were performed by Mr. Eiichiro Amano of our laboratory using a Yanagimoto MT-3 CHN recorder. All active methylene compounds **1a—e** and aldehydes **2a—e** are commercially available.

General Procedure for the Reaction of Active Methylene Compounds 1 with Aromatic Aldehydes 2. To a stirred mixture of Me_3SiCl (1.28 ml, 10 mmol), NaI (1.50 g, 10 mmol), **1** (2 mmol), and MeCN (10 ml) was added **2** (2 mmol) at 0 °C. The mixture was stirred for 6 h at room temperature and then for additional 10 h at 60 °C. After addition of water, the organic layer was extracted with ether, washed with aqueous $Na_2S_2O_3$ to remove liberated iodine and then with brine, dried over $MgSO_4$, and concentrated under reduced pressure. The residual oil was purified by preparative TLC on silica gel (hexane-ether, 3:1) or by vacuum distillation to give product **3**. Compounds **3a**[11a] and **3j** were identified by comparison of the spectral data with that reported in the literature[11a] and with that of authentic sample, respectively. IR and ^1H NMR spectral data, which are not given in the literatures, are shown below.

Ethyl 4-Piperonyl-3-oxobutanoate (3b):[11b] IR (neat) 1745, 1720, 1645, 1613 cm^{-1}; ^1H NMR (CCl_4) δ=1.20 (3H, t, J=7 Hz, CH_3), 2.04, 2.10 (3H, two s with a similar intensity), 2.97 (2H, d, J=7 Hz), 2.60 (1H, dd, J=6 and 7 Hz), 4.08 (2H, q, J=7 Hz), 5.83 (2H, s), 6.57 (3H, s).

Ethyl 2-(*p*-Methoxyphenyl)methyl]-3-oxobutanoate (3c):[11c] IR (neat) 1735, 1712, 1620, 1610, 1600, 1580 cm^{-1}; ^1H NMR (CCl_4) δ=1.13 (3H, t, J=7 Hz), 2.15 (3H, s), 2.95 (2H, d, J=7 Hz), 3.60 (1H, dd, J=6 and 7 Hz), 3.76 (3H, s), 4.12 (2H, q with shoulder, J=7 Hz), 6.50—7.10 (4H, m), 12.80 (s, trace, enol OH).

Ethyl 3-Oxo-2-(3-pyridylmethyl)butanoate (3d):[11d] IR (neat) 1740, 1715, 1595, 1575 cm^{-1}, ^1H NMR (CCl_4) δ=1.23 (3H, t, J=7 Hz), 2.19 (3H, s), 3.10 (2H, d, J=7 Hz), 2.70 (1H, dd, J=6 and 8 Hz), 4.13 (2H, q, J=7 Hz), 6.95—8.65 (4H, m).

3-Benzyl-2,4-pentanedione (3e):[11e] IR (neat) 1730, 1705, 1605 cm^{-1}; ^1H NMR (CCl_4) δ=1.96 (3H, s), 1.99 (3H, s), 3.02 (1.2H, d, J=7 Hz), 3.57 (0.8H, s, $PhC\underline{H}_2$- of enol form), 3.58 (0.6H, t, J=7 Hz), 7.07 (5H, s), 16.69 (0.4H, s, enol OH).

3-[(*p*-Methoxyphenyl)methyl]-2,4-pentanedione (3f):[11f] IR (neat) 1728, 1700, 1612, 1591 cm^{-1}; ^1H NMR (CCl_4) δ=2.00 (6H, s), 2.97 (1.3H, d, J=7 Hz), 3.72 (0.7H, s, $PhC\underline{H}_2$ of enol form), 3.69 (3H, s), 3.78 (0.65H, t, J=7 Hz), 6.50—7.20 (4H, m), 16.64 (0.35H, s, enol OH).

3-(*p*-Tolylmethyl)-2,4-pentanedione (3g):[11g] IR (neat) 1735, 1705, 1605 cm^{-1}; ^1H NMR (CCl_4) δ=2.00 (6H, s), 2.27 (3H, s), 3.00 (1.4H, d, J=7 Hz), 3.55 (0.6H, s, $PhCHPhC\underline{H}_2$ of enol form), 3.81 (0.7H, t, J=7 Hz), 6.94 (5H, s), 16.66 (0.3H, s, enol OH).

3-Methyl-4-phenyl-2-butanone (3h):[11h] IR (neat) 1715 cm^{-1}; ^1H NMR (CCl_4) δ=1.02 (3H, d, J=7 Hz), 1.93 (3H, s), 2.17—3.33 (3H, m), 7.09 (5H, m).

1,3-Diphenyl-1-propanone (3i):[11i] IR (neat) 1680, 1596, 1575 cm^{-1}; ^1H NMR (CCl_4) δ=3.62—2.70 (4H, m), 6.90—8.10 (10H, m).

Ethyl 2-Benzylidene-3-oxobutanoate (7):[12] The reaction was carried out in the presence of Me_3SiCl-NaI-MeCN (5 mol equivalents) in ether at 0 °C—room temperature for 7 h and worked up in a usual manner to give **7** in a 45% yield. The IR and ^1H NMR were consistent with those reported.[12]

Ethyl 2-Acetyl-2-octenoate (8).[13] The reaction was carried out in a manner described above to give **8** (48% yield): IR (neat) 1735, 1680, 1640, 1620 cm^{-1}; ^1H NMR (CCl_4) δ=0.8—1.6 (9H, m), 2.20, 2.24 (3H, s), 2.0—2.5 (2H, m), 4.16, 4.22 (2H, q, J=7 Hz), 6.67, 6.75 (1H, t, J=8 Hz).

Ethyl 2-(α-Iodobenzyl)-3-oxobutanoate (9). The reaction was done at 0—5 °C in a similar manner to that of foregoing experiment. Recrystallization from hexane-ether (10:1) gave crystalline product **9** (67% yield): mp 68.2—70.0 °C; IR (KBr) 1735, 1710, 1275 cm^{-1}; ^1H NMR (CCl_4) δ=0.89, 1.34 (3H t, J=7 Hz), 1.90, 2.35 (3H, s), 3.84, 4.22 (2H, q, J=7 Hz), 4.22, 4.49 (1H, d, J=12 Hz), 5.45, 5.54 (1H, d, J=12 Hz), 7.23 (5H, m). Found: C, 45.37; H, 4.14%. Calcd for $C_{13}H_{15}O_3I$: C, 45.11; H, 4.37%.

3,5,6,7-Tetrahydro-2,2-dimethyl-4(2*H*)-benzofuranone (10f):[10b] IR (neat) 1725, 1625 cm^{-1}; ^1H NMR (CCl_4) δ=1.41 (6H, s), 2.15 (6H, m), 2.52 (2H, m).

3-Benzoyl-5,5-dimethyl-4,5-dihydro-2(3*H*)-furanone (11g): IR (neat) 1765, 1685 cm^{-1}; ^1H NMR (CCl_4) δ=1.36 (3H, s), 1.42 (3H, s), 1.92—2.80 (2H, m), 4.06 (1H, m), 7.36 (3H, m), 7.89 (2H, m). Found: C, 71.35; H, 6.45%. Calcd for $C_{13}H_{14}O_3$: C, 71.54; H, 6.47%.

References

1) C. Weizmann, E. Bergmann, and M. Sulzbacher, *J. Org. Chem.*, **15**, 918 (1950).

2) J. Marquet and M. M.-Mańas, *Synthesis*, **1979**, 348, and literatures cited therein.

3) For example: H. Yokotani, T. Murata, and M. Miyamoto, Ger. Offen, 2035334 (1971); *Chem. Abstr.*, **74**, p87624f (1971).

4) G. A. Olah, S. C. Narang, B. G. B. Gupta, and R. Malhotra, *J. Org. Chem.*, **44**, 1247 (1979).

5) a) T. Sakai, K. Miyata, M. Utaka, and A. Takeda, *Bull. Chem. Soc. Jpn.*, **60**, 1063 (1987); b) T. Sakai, K. Miyata, M. Utaka, and A. Takeda, *Tetrahedron Lett.*, **28**, 3817 (1987).

6) S. I. Zav'yalov, O. V. Dorofeeva, and O. K. Taganova, *Izu. Akad. Nauk SSSR, Ser. Khim.*, **1985**, 495.

7) M. E. Jung, A. B. Mossman, and M. A. Lyster, *J. Org. Chem.*, **43**, 3698 (1978).

8) a) A. H. Schmidt and M. Russ, *Chem. Ztg.*, **102**, 26 (1978); b) *idem, ibid.*, **102**, 65 (1978); c) *idem, ibid.*, **103**, 285 (1979); d) *idem, ibid.*, **103**, 183 (1979).

9) G. A. Olah and S. C. Narang, *Tetrahedron*, **38**, 2225 (1982).

10) a) R. Verhé, N. D. Kimpe, D. Courtheyn, L. D. Buyck, and N. Schamp, *Tetrahedron*, **38**, 3649 (1982); b) E. I. Heiba and R. M. Dessau, *J. Org. Chem.*, **39**, 3456 (1974).

11) a) D. Wrovel, R. Tacke, U. Wannagat, and U. Harder, *Chem. Ber.*, **115**, 1694 (1982); b) I. Yanagisawa, M. Ohta, and T. Takagi, Eur. Pat. Appl., EP86647 (1982); *Chem. Abstr.*, **100**, p6543j (1984); c) L. M. Gnanadoss and D. Kalaivani, *J. Org. Chem.*, **50**, 1174 (1985); d) R. P. Pioch, U. S. Patent, US 4468399 (1984); *Chem. Abstr.*, **102**, P6535z (1985); e) M. Boya, M. M.-Mańas, and M. Prior, *Tetrahedron Lett.*, **1975**, 1727; f) A. González, F. Güell, J. Marquet, and M. M.-Mańas, *ibid.*, **26**, 3735 (1985); g) W. Chen, Y. Wang, and H. Hu, *Gaodeng Xuexiao Huaxue Xuebao*, **5**, 57 (1984); *Chem. Abstr.*, **100**, 209292z (1984); h) L. E. Hightower, L. R. Glasgow, K. M. Stone, D. A. Albertson, and H. A. Smith, *J. Org. Chem.*, **31**, 1881 (1970); i) K. Nakamura, M. Fujii, A. Ohno, and S. Oka, *Tetrahedron Lett.*, **25**, 3983 (1984).

12) P. A.-Robertson and J. A. Katzenellenbogen, *J. Org. Chem.*, **48**, 5288 (1983).

13) P. Mastagli, P. Lambert, and N. Andric, *Bull. Soc. Chim. Fr.*, **1956**, 796.

Synthesis of a 24-Epimeric Mixture of 24-Methyl-19,29-dinorlanost-9(11)-en-3-one[1)]

Tetsuya MAKINO, Tatsushi MURAE, Takahiko TSUYUKI,* and Takeyoshi TAKAHASHI
Department of Chemistry, Faculty of Science, The University of Tokyo, Hongo, Bunkyo-ku, Tokyo 113
(Received August 8, 1989)

Synopsis. A 24-epimeric mixture of 24-methyl-19,29-dinorlanost-9(11)-en-3-one was synthesized from 24-methylenecycloartanol. The synthesis comprises acid-cleavage of the cyclopropane ring, 4β-demethylation, the Barton reaction of the 3-nitrile, dehydration of the 11β-hydroxy derivative, and oxidation of the 19-hydroxy derivative followed by photolysis.

As an authentic sample for identification of a triterpene isolated from the plant fossile,[2)] a 24-epimeric mixture of 24-methyl-19,29-dinorlanost-9(11)-en-3-one (=4α,14α,24-trimethyl-19-norcholest-9(11)-en-3-one) (**1**) was prepared from 24-methylene-9,19-cyclo-lanostan-3β-yl acetate (=24-methylenecycloartenyl acetate) (**2**). The synthetic route is given in Fig. 1.

Experimental[3)]

Isolation of the Starting Compound (2). Rice bran oil contains phenolic compounds, named oryzanol A and C, which were reported to be cycloartenyl ferulate and 24-methylenecycloartenyl ferulate, respectively.[4)] Alkaline hydrolysis of a powdery oryzanol mixture[5)] (16 g) followed by acetylation yielded a mixture (10 g), which was shown to be a 1 : 1 mixture of **2** and 9,19-cyclolanost-24-en-3β-yl acetate (cycloartenyl acetate) (**3**) by the gas chromatography-mass spectrometry (GC-MS)[6)] and the proton nuclear magnetic resonance (^{1}H NMR) spectrometry. Since the mixture (**2** and **3**) showed a single spot on the thin-layer chromatography (TLC), the mixture (40.0 g) in CH_2Cl_2 (800 ml) was subjected to selective epoxidation and the reaction was mon-

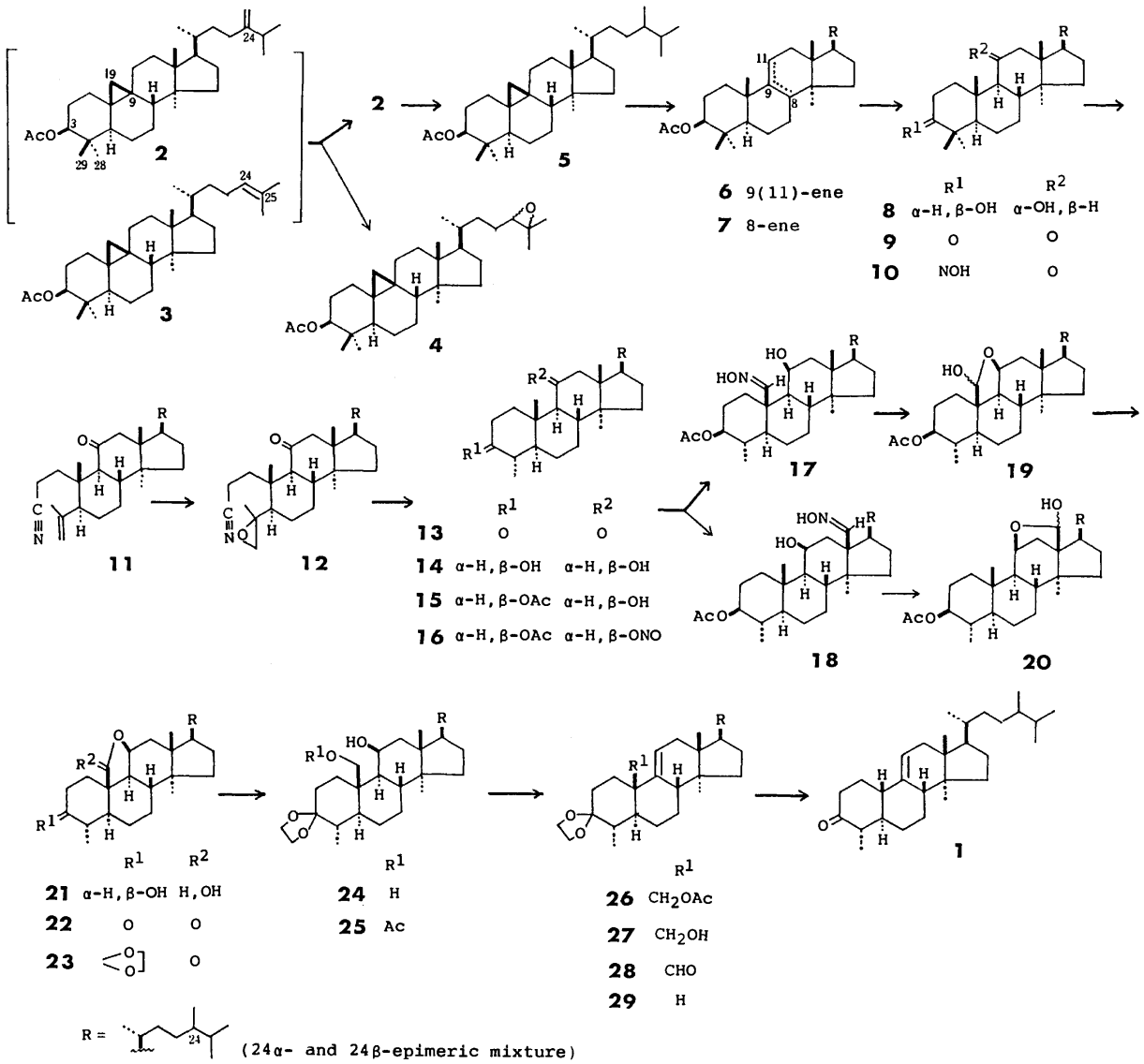

Fig. 1.

itored by GC. The epoxidation with *m*-chloroperbenzoic acid (mCPBA; 80%, 12.3 g) at −40 °C for 6 h gave an epoxide (**4**; 20.1 g) and the unchanged **2** (19.7 g) after column chromatography (SiO_2; 4—40% Et_2O in hexane). **2**: mp 108—109 °C (lit,[4] 116—117 °C); ^1H NMR δ=4.43—4.77 (3H, m; 3α-H and $C_{(24)}$=CH_2).

Hydrogenation of 2. The 24-methylene derivative (**2**; 29.2 g) in ether (1 l) was subjected to catalytic hydrogenation to give a 24-epimeric mixture of 24-methyl-9,19-cyclolanostan-3β-yl acetate[7] (**5**; 29.3 g), mp 125—126 °C; ^1H NMR; δ=0.34 (1H, d, J=4 Hz; 19-H), 0.59 (1H, d, J=4 Hz; 19′-H), 0.75 (3H, s; Me), 0.87—0.93 (6×Me), 0.97 (3H, s; Me), 2.04 (3H, s; OAc), and 4.43—4.70 (1H, m; 3α-H); MS m/z (%) 484 (M^+; 21), 469 (13), 444 (12), 424 (100), 409 (46), 385 (20), 382 (22), 356 (20), 302 (37), and 296 (32).

24-Methyllanostane-3,11-dione (9). Dry hydrogen chloride was introduced into a solution of **5** (11.5 g) in $CHCl_3$ (300 ml) for 2 h.[8] The usual work-up gave a mixture (11.2 g) of 24-methyl-9(11)-lanosten-3β-yl acetate (**6**) and its 8-ene isomer (**7**) in a ratio of 7 : 3, ^1H NMR δ=0.64—1.07 (9×Me), 2.04 (3H, s; OAc), 4.33—4.60 (1H, m; 3α-H), and 5.11—5.30 (0.7H, m; 11-H of **6**).

To a solution of the mixture (65.4 mg) in THF (4 ml) kept at 0 °C, diborane in THF (1.1 mmol^{-1}ml, 0.15 ml) was added and the solution was stirred for 2 d at 40 °C. After addition of water (3 ml), 3 M (1 M=1 mol dm^{-3}) NaOH (0.2 ml), and 30% H_2O_2 (0.2 ml), the reaction mixture was worked up as usual to afford 24-methyllanostane-3β,11α-diol (**8**; 26.5 mg), mp 202—204 °C; ^1H NMR δ=0.75 (3H, s; Me), 0.82—0.92 (6×Me), 0.98 and 1.01 (each 3H, s; Me), 3.08—3.35 (1H, m; 3α-H), and 3.73—4.12 (1H, m; 11β-H); MS m/z (%) 460 (M^+; 11), 442 (29), 427 (30), 424 (14), 409 (31), 399 (13), 238 (86), 223 (100), and 84 (>100).

A solution of **8** (8.45 g) in acetone (500 ml) was treated with Jones reagent (10 ml) for 5 min at 0 °C. The reaction mixture was worked up and chromatographed (SiO_2; 5% Et_2O in C_6H_6) to yield 24-methyllanostane-3,11-dione (**9**; 7.10 g), mp 158—159 °C; ^1H NMR δ=0.75—0.83 (4×Me), 0.89 (3H, s; Me), 1.05—1.09 (3×Me), 1.20 (3H, s; Me), and 2.78—3.13 (1H, m); MS (%) 456 (M^+; 100), 442 (8), 428 (44), 413 (18), 317 (96), and 219 (100).

4β-Demethylation of 9 According to the Pinhey's Procedure.[9] The dione (**9**) was converted into 24-methyl-29-norlanostane-3,11-dione (**13**) by the same procedure as before[1] through 3-hydroxyimino-24-methyllanostan-11-one (**10**), 24-methyl-11-oxo-3,4-secolanost-4(29)-ene-3-nitrile[10] (**11**), and 4,29-epoxy-24-methyl-11-oxo-3,4-secolanostane-3-nitrile[10] (**12**) in 48% overall yield. **10:** mp 215.5—216 °C; IR (KBr) 3320, 1700, and 930 cm^{-1}; ^1H NMR δ=0.73—0.90 (5×Me), 1.07 (6H, s; 2×Me), 1.13 and 1.17 (each 3H, s; Me); MS m/z (%) 471 (M^+; 76), 454 (46), and 140 (100). **11:** as a pale yellow oil, IR (neat) 2250, 1700, 890, and 680 cm^{-1}; ^1H NMR δ=0.75—0.89 (5×Me), 1.10 (6H, s; 2×Me), 1.73 (3H, br s; Me), 4.69 and 4.90 (each 1H, br s; C=CH_2); MS m/z (%) 453 (M^+; 100), 439 (14), 413 (15), and 372 (49). **12:** as a pale yellow oil, IR (neat) 2250, 1700, 820, and 660 cm^{-1}; ^1H NMR δ=0.75—0.89 (5×Me), 1.05, 1.14, and 1.28 (each 3H, s; Me), 2.43, and 2.68 (each 1H, br s); MS m/z (%) 469 (M^+; 43), 455 (12), 441 (100), 370 (55), 317 (42), 291 (53), and 264 (49). **13:** an amorphous solid, IR (KBr) 1710 and 1700 cm^{-1}; ^1H NMR δ=0.76—0.83 (4×Me), 0.90 (3H, s; Me), 0.99 (3H, d, J=6.5 Hz), 1.09, 1.26 (each 3H, s; Me), and 3.05 (1H, ddd, J=13, 6, and 3 Hz); MS m/z (%) 442 (M^+: 100), 428 (13), 414 (11), 317 (40), 288 (23), 274 (27), 221 (29), and 205 (100).

Photolysis of 3β-Acetoxy-24-methyl-29-norlanostan-11β-yl Nitrite (16). The 3,11-dione (**13**; 236 mg) in ether (100 ml) was reduced with LAH (200 mg) to yield 24-methyl-29-norlanostane-3β,11β-diol (**14**; 148 mg), mp 208—209 °C; ^1H NMR δ=0.78—0.93 (6×Me), 1.01, 1.11 (each 3H, s; Me), 2.83—3.25 (1H, m; 3α-H), and 4.10—4.31 (1H, m; 11α-H); MS m/z (%) 464 (M^+; 11), 428 (33), 413 (21), 410 (7), 274 (69), 238 (100), and 208 (78). Acetylation of the diol (**14**; 148 mg) gave 11β-hydroxy-24-methyl-29-norlanostan-3β-yl acetate (**15**; 150 mg), mp 170—171 °C; ^1H NMR δ=0.78—0.87 (6×Me), 0.98, 1.10 (each 3H, s; Me), 2.00 (3H, s: OAc), and 4.07—4.55 (2H, m; 3α-H and 11α-H); MS m/z (%) 488 (M^+; 11), 470 (65), 455 (80), 410 (17), 395 (53), and 238 (100).

A solution of the hydroxy acetate (**15**; 250 mg) in pyridine (25 ml) was treated with NOCl at −30 °C and worked up in the usual manner to afford 3β-acetoxy-24-methyl-29-norlanostan-11β-yl nitrite (**16**; 261 mg) as a pale yellow oil, IR (neat) 1735, 1630, 1600, 1250, 820, 775, and 755 cm^{-1}; ^1H NMR δ=0.77—0.88 (8×Me), 2.02 (3H, s; OAc), 4.12—4.53 (1H, m; 3α-H), and 5.83—6.05 (1H, m; 11α-H); MS m/z (%) 487 (M^+−NO; 2), 470 (7), 455 (20), 433 (9), 426 (15), 395 (20), 249 (23), and 95 (100).

A solution of the nitrite (**16**; 567 mg) in toluene (40 ml) and *t*-butylamine (2 ml) was photoirradiated with a 400 W high-pressure mercury lamp for 10 min under nitrogen. The usual work-up and chromatographic separation (SiO_2; 4% Et_2O in C_6H_6) gave a mixture (246 mg) of 11β-hydroxy-19-hydroxyimino-24-methyl-29-norlanostan-3β-yl acetate (**17**) and its 18-hydroxyimino isomer (**18**) together with **15** (248 mg). The mixture showed two singlet signals due to olefinic protons attached to carbon bearing hydroxyimino groups at δ=7.75 (0.7H) and δ=7.43 (0.3H), the major product being the 19-hydroxyimino isomer (**17**).[11] MS of the mixture: m/z (%) 517 (M^+; 1), 499 (23), 440 (91), and 57 (100).

24-Methyl-3-oxo-29-norlanostan-19,11β-olide (22). The mixture (159.2 mg) of **17** and **18** in acetone (10 ml) was stirred with concd HCl (4 drops) overnight at room temperature. The reaction product was chromatographed (SiO_2; 4—10% Et_2O in hexane) to give 11,19-epoxy-19-hydroxy-24-methyl-29-norlanostan-3β-yl acetate (**19**; 62.4 mg) and its 11,18-epoxy-18-hydroxyimino isomer (**20**; 30.9 mg). **19:** IR (KBr) 1740 and 1250 cm^{-1}; ^1H NMR δ=0.70 (3H, s; Me), 0.76—0.90 (5×Me), 1.04 (3H, s; Me), 2.06 (3H, s; OAc), 4.07—4.27 (1H, m; 11α-H), 4.27—4.64 (1H, m; 3α-H), and 5.35 and 5.63 (total 1H, br s; 19-H's of 19-epimeric mixture of **19**); MS m/z (%) 502 (M^+; 0.4), 484 (1.6), 469 (1.3), 456 (23), 441 (14), 396 (100), and 381 (38). **20:** IR (KBr) 1730 and 1260 cm^{-1}; ^1H NMR δ=0.77 (3H, s; Me), 0.82—1.00 (6×Me), 2.04 (3H, s; OAc), 4.13—4.51 (1H, m; 3α-H), 4.42 (1H, d-like, J=6 Hz; 11α-H), 5.10 (0.7H, d, J=6 Hz; 18-H), and 5.48 (0.3H, d, J=5 Hz; 18-H of the other epimer); MS m/z (%) 484 (M^+ −H_2O; 28), 469 (8), 456 (42), 441 (14), 381 (12), 356 (11), 329 (100), 269 (46), and 207 (82).

The acetate (**19**; 156 mg) in EtOH (50 ml) containing KOH (600 mg) was refluxed for 3 h to afford a hemiacetal, 11,19-epoxy-24-methyl-29-norlanostane-3β, 19-diol (**21**; 161 mg), MS m/z (%) 442 (M^+ −H_2O; 100), 428 (22), 425 (11), 415 (38), 400 (35), 397 (51), 387 (15), and 382 (32). The hemiacetal (**21**; 161 mg) in acetone (30 ml) was treated with Jones reagent (2 ml) and the reaction product was chromatographed (SiO_2; 5% Et_2O in C_6H_6) to afford 24-methyl-3-oxo-29-norlanostan-19,11β-olide (**22**; 86.8 mg), mp 209—210 °C; IR (KBr) 1750 and 1730 cm^{-1}: ^1H NMR δ=0.73—0.94 (6×Me), 1.00 (3H, d, J=6 Hz), 3.30—3.77 (1H, m), 4.67—4.83 (1H, m; 11α-H); MS m/z (%) 456 (M^+; 100), 442 (21), 428 (5), 412 (15), and 397 (6).

3,3-Ethylenedioxy-24-methyl-29-norlanost-9(11)-en-19-al (28). The keto lactone (**22**; 19 mg) was converted into the ethylenedioxy derivative (**23**; 20 mg), mp 211—212 °C, IR (KBr) 1755 cm^{-1}; ^1H NMR δ=0.76—0.92 (7×Me), 2.60—3.05 (1H, m), 3.93 (4H, br s; -OCH_2CH_2O-), and 4.56—4.78 (1H, m; 11α-H); MS m/z (%) 500 (M^+; 16), 485 (2), 472 (8), 100 (100), and 99 (>100). The lactone (**23**; 56.1 mg) in THF (20 ml) was treated with LAH (47 mg) to afford 3,3-ethyl-

enedioxy-24-methyl-29-norlanostane-11β,19-diol (**24**; 60.7 mg), mp 174—175 °C; ^{1}H NMR δ=0.75—0.90 (6×Me), 1.04 (3H, s; Me), 3.58 and 3.91 (2H, ABq, J=12 Hz; 19-H$_2$), 3.95 (4H, br s; -OCH$_2$CH$_2$O-), and 4.17 (1H, m; 11α-H); MS m/z (%) 504 (M$^+$; 0.5), 486 (4), 468 (15), 385 (68), 100 (100), and 99 (>100).

The diol (**24**; 60.7 mg) was acetylated to give 3,3-ethylenedioxy-11β-hydroxy-24-methyl-29-norlanostan-19-yl acetate (**25**; 43.3 mg), mp 105—107 °C; IR (KBr) 3470, 1735, and 1260 cm^{-1}; ^{1}H NMR δ=0.77—0.84 (4×Me), 0.88 (6H, s; 2×Me), 1.00 (3H, s; Me), 2.05 (3H, s; OAc), 3.94 (4H, br s; -OCH$_2$CH$_2$O-), 4.07—4.28 (1H, m; 11α-H), and 4.37 (2H, br s; 19-H$_2$); MS m/z (%) 546 (M$^+$; 10), 528 (4), 486 (32), 454 (15), 444 (48), 385 (100), 384 (>100), and 99 (>100).

The 11β-hydroxy acetate (**25**; 54.1 mg) in pyridine (10 ml) was treated with phosphoryl chloride (0.05 ml) under nitrogen. After the solution was heated at 80 °C for 3 h, the reaction product was chromatographed (SiO$_2$; 5% Et$_2$O in C$_6$H$_6$) to give 3,3-ethylenedioxy-24-methyl-29-norlanost-9(11)-en-19-yl acetate (**26**; 45.6 mg), mp 170—171 °C; IR (KBr) 1745 and 1240 cm^{-1}; ^{1}H NMR δ=0.60 (3H, s; Me), 0.77—0.89 (6×Me), 1.97 (3H, s; OAc), 3.95 (4H, br s; -OCH$_2$CH$_2$O-), 4.27 (2H, br s; 19-H$_2$), and 5.28—5.48 (1H, m; 11-H). Alkaline hydrolysis of **26** (4.8 mg) gave 3,3-ethylenedioxy-24-methyl-29-norlanost-9(11)-en-19-ol (**27**; 4.3 mg), mp 154—155 °C; ^{1}H NMR δ=0.66 (3H, s; Me), 0.75—0.90 (6×Me), 3.56 and 3.74 (2H, ABq, J=11 Hz; 19-H$_2$), 3.95 (4H, br s; -OCH$_2$CH$_2$O-), and 5.37—5.53 (1H, m; 11-H); MS m/z (%) 486 (M$^+$; 11), 471 (9), 455 (42), 441 (9), and 99 (100).

To the Collins reagent prepared from CrO$_3$ (35 mg) and pyridine (0.12 ml) in CH$_2$Cl$_2$ (6 ml) was added **27** (29.3 mg) in CH$_2$Cl$_2$. After the usual work-up, chromatographic separation (SiO$_2$; 5% Et$_2$O in C$_6$H$_6$) afforded 3,3-ethylenedioxy-24-methyl-29-norlanost-9(11)-en-19-al (**28**; 29.0 mg), mp 131—133 °C; IR (KBr) 1720 cm^{-1}; ^{1}H NMR δ=0.57 (3H, s; Me), 0.77—0.90 (6×Me), 3.93 (4H, br s; -OCH$_2$CH$_2$O-), 5.50—5.73 (1H, m; 11-H), and 9.11 (1H, br s; CHO); MS m/z (%) 484 (M$^+$; 3), 469 (2), 455 (85), 441 (12), 411 (4), 393 (12), and 99 (100).

Photo-decarbonylation of 28. Photo-decarbonylation of homoallylic aldehydes was carried out according to the procedure described in literatures.[12a,b] A solution of **28** (29.0 mg) in EtOH (50 ml) was photoirradiated for 30 min using a 400 W-high-pressure mercury lamp. Evaporation of the solvent followed by chromatography (SiO$_2$; C$_6$H$_6$) afforded 3,3-ethylenedioxy-24-methyl-19,29-dinorlanost-9(11)-ene (**29**; 25.9 mg), mp 153—154 °C; ^{1}H NMR δ=0.67 (3H, s; Me), 0.77—0.92 (6×Me), 3.93 (4H, br s; -OCH$_2$-CH$_2$O-), and 5.13—5.33 (1H, m; 11-H); MS m/z (%) 456 (M$^+$; 100), 441 (26), 427 (7), 412 (9), 394 (49), 380 (18), 100 (92), and 99 (>100).

24-Methyl-19,29-dinorlanost-9(11)-en-3-one (1). A solution of **29** (24.3 mg) in acetone was treated with p-TsOH (30 mg) overnight and the reaction product was chromatographed (SiO$_2$; C$_6$H$_6$) to give 24-methyl-19,29-dinorlanost-9(11)-en-3-one (**1**; 16.3 mg), mp 126—128 °C; $[\alpha]_D^{25}$ +70° (c 0.2, CHCl$_3$); $[\theta]_{290}$ +5350 (peak); IR (KBr) 1715 cm^{-1}; ^{1}H NMR (Brucker AM-500, 500 MHz, CDCl$_3$) δ=0.70 (3H, br s), 0.755 (3H, s), 0.786 (3H, d, J=6.9 Hz), 0.790, 0.811 (total 3H, each d, J=6.8 Hz), 0.857, 0.860 (total 3H, each d, J=6.8 Hz), 0.884, 0.893 (total 3H, d, J=6.5 Hz), 1.03 (3H, d, J=6.5 Hz), 2.34—2.50 (3H, m), and 5.30 (1H, d, J=4.5 Hz); MS m/z (%) 412 (M$^+$; 73), 397 (100), 383 (14), 285 (29), 271 (8), 258 (12), 243 (20), 229 (23), 217 (33), and 149 (36); Found: m/z 412.3692. Calcd for C$_{29}$H$_{48}$O: M, 412.3703.

References

1) The previous papers: M. Naora, T. Murae, T. Tsuyuki, and T. Takahashi, *Bull. Chem. Soc. Jpn.*, **59**, 1767 (1986); M. Yamashita, M. Naora, T. Murae, T. Tsuyuki, and T. Takahashi, *ibid.*, **60**, 1383 (1987).

2) T. Murae, M. Namikawa, K. Hosokawa, H. Miyazaki, M. Ishibashi, T. Tsuyuki, and T. Takahashi, "21st Symposium on the Chemistry of Natural Products," Sapporo 1978, Symposium paper, p.568.

3) General procedures were the same as those described in Ref. 1. ^{1}H NMR spectra were measured using a JEOL FX90 (90 MHz, FT) in CDCl$_3$ solution unless otherwise stated. Gas chromatography was carried out on a Shimadzu GC-6A.

4) G. Ohta, *Chem. Pharm. Bull.*, **8**, 5 and 9 (1960).

5) The authors wish to express their thanks to Boso-yushi Co. Ltd. for generous gift of the powdery oryzanol mixture.

6) T. Itoh, T. Tamura, and T. Matsumoto, *Steroids*, **27**, 275 (1976); H. E. Audier, R. Berugelwans, and B. C. Das, *Tetrahedron Lett.*, **1966**, 4341.

7) All 24-methyl derivatives obtained by the preparation described below in this paper refer to 24-epimeric mixtures, respectively.

8) D. S. Irvine, J. A. Henry, and F. S. Spring, *J. Chem. Soc.*, **1955**, 1316.

9) K. F. Cohen, R. Kazluskas, and J. T. Pinhey, *J. Chem. Soc. D*, **1971**, 1419.

10) The carbon number at C-29 was given tentatively.

11) D. H. R. Barton, R. P. Budhiraja, and J. F. McGhie, *J. Chem. Soc. C*, **1969**, 336.

12) a) C. W. Shoppee, J. C. Coll, and R. E. Lack, *J. Chem. Soc. C*, **1968**, 1581. b) J. Iriarte, J. Hill, K. Schaffner, and O. Jeger, *Proc. Chem. Soc.*, **1963**, 114.

Selective Dimerization of Alkyl Crotonates Catalyzed by Iron(0) Complexes Having 1,2-Bis(dimethylphosphino)ethane Ligands

Sanshiro KOMIYA,* Naohiko OYASATO, and Tomoyuki FURUKAWA
Department of Applied Chemistry, Tokyo University of Agriculture and Technology, 2-24-16 Nakamachi, Koganei, Tokyo 184
(Received August 11, 1989)

Synopsis. Highly selective dimerization of alkyl crotonates has been performed in the presence of a catalytic amount of $FeHNp(dmpe)_2$ or $FeH_2(dmpe)_2$/UV irradiation at room temperature.

Although metal-catalyzed dimerizations of olefins having functional groups under mild conditions have been expected to have wide applications to organic syntheses, only limited examples are known so far such as dimerizations of methyl acrylate[1] and acrylonitrile[2] by comparison with well known metal-catalyzed dimerizations of simple olefins or dienes.[3] Unfortunately the most of these dimerizations in fact are not sufficiently selective and their yields are considerably low, in spite of their severe reaction conditions. We wish to report iron-catalyzed selective dimerization of alkyl crotonates under ambient conditions.

When methyl crotonate was treated with a catalytic amount of $FeHNp(dmpe)_2$, **1** (1 mol%)[4] at room temperature, a methyl crotonate dimer was smoothly obtained in high yield in 2 h (dmpe=1,2-bis(dimethylphosphino)ethane, Np=2-naphthyl). $FeH_2(dmpe)_2$,[5] **2** also catalyzed the dimerization under irradiation of UV light. Results of the catalytic dimerization of alkyl crotonates under various conditions are summarized in Table 1.

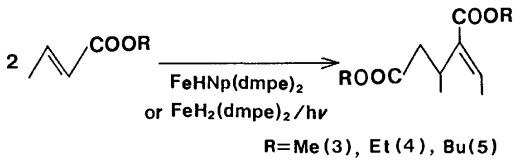

The dimerization is selective with high conversion. ^{1}H NMR, GC, and GCMS analyses reveal that the dimer consists of an only head-to-tail dimer (*E* isomer). Trace amounts of trimer and tetramer were detected in the reaction mixture (see experimental). The rate of the catalytic dimerization slightly decreased in the order of methyl, ethyl, and butyl esters, as shown in the time-yield curve of the reactions (Fig. 1). Unfortunately dimerization of other types of unsaturated esters such as methyl acrylate, methyl 3-butenoate and methyl methacrylate has failed.[6] Addition of 1,2-bis(dimethylphosphino)ethane ligand (1 mol/**1**) severely retarded the reaction, suggesting that the formation of a coordinatively unsaturated intermediate such as $[Fe(dmpe)_2]$ is a key step in the catalytic dimerization. Such a coordinatively unsaturated species has been previously proposed in the C-H bond activations by **1**[4] or by **2** under UV irradiation.[5] Rate of the reaction was not significantly affected by changing the solvent from hexane to DMF, excluding the formation of ionic species as reaction intermediates. Thus, for the present catalytic Michael type

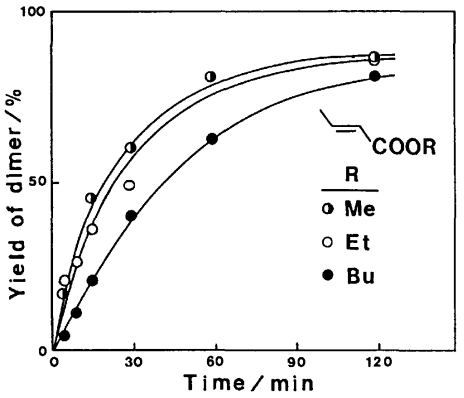

Fig. 1. Time-yield curve of the dimerization of alkyl crotonates by **1** (1 mol%) at r.t.

Table 1. Catalytic Dimerization of Alkyl Crotonates Promoted by Iron Complexes[a]

Catalyst /mol%		Solvent	MeCH=CHCOOR /mmol	Conversion /%	Yield /%
$FeH_2(dmpe)_2$	(1.0)[b]	None	R=Me(2.95)	93	89
	(5.0)[b]	None	(2.86)	99	95
$FeHNp(dmpe)_2$	(1.0)	None	(2.89)	92	87
	(5.0)	None	(2.85)	98	93
	(1.0)[c]	None	(3.72)	36	36
	(0.4)	DMF	(2.95)	81	73
	(0.4)	Hexane	(2.76)	80	78
	(1.0)	None	R=Et (2.72)	88	85
	(1.0)	None	R=Bu(2.28)	84	83

a) All the reactions were carried out for 2 h under N_2 at room temperature. b) UV irradiation with high-pressure Hg lamp. c) An equimolar amount of dmpe ligand (0.0372 mmol) per Fe was added.

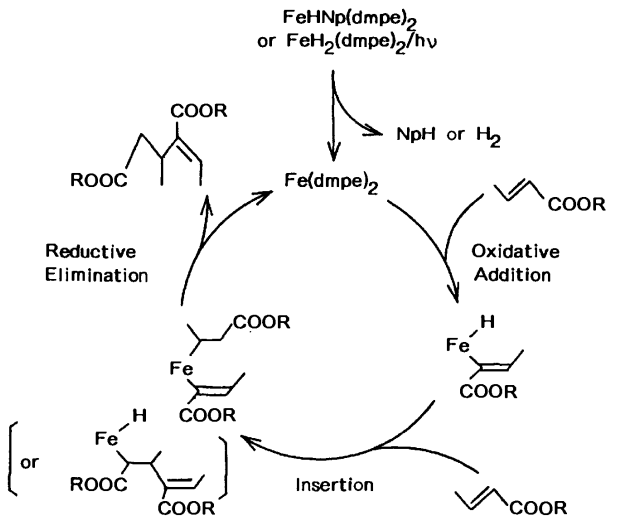

Scheme 1. A possible mechanism for the iron-catalyzed dimerization of alkyl crotonates.

dimerization, the following concerted mechanism involving C-H bond oxidative addition followed by insertion of alkyl crotonate and reductive elimination of the dimer has been proposed (Scheme 1).[7] The vinylic C-H bond oxidative addition process as an initial step is reasonable, since the hydrido-(vinyl)-metal complexes were isolated from the reactions of zero-valent iron and ruthenium complexes with alkyl methacrylates.[5,8]

Experimental

General. All the reactions were carried out under nitrogen. Solvents used were dried by usual procedure, distilled, and stored under nitrogen. Reagent grade of unsaturated esters were dried with CaH_2 and distilled before use. $FeH_2(dmpe)_2$ and $FeHNp(dmpe)_2$ were prepared according to the literature methods.[4,5]

Dimerization of Methyl Crotonate. A typical procedure of the dimerization is described below: $FeHNp(dmpe)_2$ (14.0 mg, 0.0289 mmol) was placed in a Schlenk tube under nitrogen and a settled amount of methyl crotonate (0.304 cm^3, 2.89 mmol) was added by using a microsyringe. After stirring the solution for 2 h, the solution was analyzed by GC and GCMS. The results were summarized in Table 1. The dimer was purified by column chromatography (alumina/hexane) and characterized mainly by NMR. **3**, GCMS: m/z=200, ^1H NMR ($CDCl_3$): δ=1.20 (Me, d, 7.1 Hz), 1.85 (Me, d, J=7.3 Hz), 2.59 (H, dd, J=7.1, 15.4 Hz), 2.75 (H, dd, J=7.8, 15,4 Hz), 3.30 (H, ddq, J=7.1, 7.8, 7.1 Hz), 3.63 and 3.72 (OMe, s), 6.83 (H, q, J=7.3 Hz). Traces of trimers (m/z=300, yield=0.7%) and tetramers (m/z=400, yield=2.8%) were also detected, but the detail structure of these oligomers was not characterized. Other reactions were performed analogously. **4**, ^1H NMR ($CDCl_3$): δ=0.93 (Me, t, J=7.2 Hz), 0.97 (Me, t, J=7.1 Hz), 1.28 (Me, d, J=7.1 Hz), 1.57 (Me, d, J=7.3), 2.63 (H, dd, J=6.8, 15.4 Hz), 2.94 (H, dd, J=8.1, 15.4 Hz), 3.37 (H, ddq, J=6.8, 8.1, 7.1 Hz), 3.92 (CH_2, q, J=7.2 Hz), 3.99 (CH_2, q, J=7.1 Hz), 6.84 (H, q, J=7.3 Hz); **5**, δ=0.92 (Me, t, J=7.1 Hz), 0.95 (Me, t, J=7.1 Hz), 1.21 (Me, d, J=7.1 Hz), 1.3—1.7 (CH_2, m), 1.84 (Me, d, J=7.3 Hz), 2.57 (H, dd, J=7.3, 15.4 Hz), 2.74 (H, dd, J=8.1, 15.4 Hz), 3.30 (H, ddq, J=8.1, 7.3, 7.1 Hz), 4.03 (CH_2, t, J=5.6 Hz), 4.12 (CH_2, t, J=6.6 Hz), 6.82 (H, q, J=7.3 Hz). When $FeH_2(dmpe)_2$ was used as a catalyst, UV irradiation with a high-pressure Hg lamp was applied during the reaction. In these cases hydrogen gas was detected in the gas phase after the reaction.

Authors are grateful to a support by a Grant-in-Aid for Scientific Research on Priority Areas from the Ministry of Education, Science and Culture.

References

1) T. Alderson, E. L. Jenner, and R. V. Lindsey, Jr., *J. Am. Chem. Soc.*, **87**, 5638 (1965); R. J. Mckinney and M. C. Colton, *Organometallics*, **5**, 1080 (1986) and references cited therein.

2) A. Misono, Y. Uchida, M. Hidai, and H. Kanai, *Chem. Commun.*, **1967**, 357.

3) P. A. Chaloner, "Handbook of Coordination Catalysis in Organic Chemistry," Butterworths, London (1986); J. P. Collman, L. S. Hegedus, J. R. Norton, and R. G. Finke, "Principles and Applications of Organotransition Metal Chemistry," University Science Books, Mill Valley (1987) and references cited therein.

4) C. A. Tolman, S. D. Ittel, A. D. English, and J. P. Jesson, *J. Am. Chem. Soc.*, **100**, 4080 (1978); J. Chatt and H. R. Watson, *J. Chem. Soc.*, **1962**, 2545.

5) D. H. Gerlach, W. G. Peet, and E. L. Muetterties, *J. Am. Chem. Soc.*, **94**, 4545 (1972); M. V. Baker and L. D. Field, *ibid.*, **109**, 2825 (1987).

6) In these reactions unreacted esters were recovered. In the reaction of $FeH_2(dmpe)_2$ with methyl acrylate and methyl methacrylate under UV irradiation, stable hydrido-(alkenyl)- and/or methyl(carboxylato)iron complexes, which are not catalytically active and are tentatively characterized by only in situ ^1H NMR (in C_6D_6), were formed. FeH(CH=CHCOOMe)(dmpe)$_2$: 10.3 ppm (d of qui, J(HH)=18.3 Hz, J(PH)=7.3 Hz, FeC<u>H</u>=CH-), 6.26 (d, J(HH)=18.3 Hz, FeCH=C<u>H</u>-), −16.76 (qui, J(PH)=45.2 Hz, FeH). FeH(CH=C(Me)COOMe)(dmpe)$_2$: 10.18 (br, FeCH=), −12.91 (d of q, J(PH)=42, 55 Hz). FeMe(O-COC(Me)=CH_2)(dmpe)$_2$: 5.06 and 5.56 (br, CH_2), −3.23 (qui, J(PH)=7.3 Hz, FeMe). Other signals are obscured due to extensive overlapping with the signals of large free ester.

7) At present we prefer the above mechanism involving C-H bond oxidative addition followed by insertion of methyl crotonate into Fe-H bond, since other mechanisms involving successive insertion into Fe-H bond and β-elimination are not suitable for interpreting the high selectivity of the reaction.

8) S. Komiya, T. Ito, M. Cowie, A. Yamamoto, and J. A. Ibers, *J. Am. Chem. Soc.*, **98**, 3874 (1976).

The Adsorption Equilibria of Organic Vapors on Activated Carbon at High Temperatures

Hajime HORI,* Isamu TANAKA, Takashi AKIYAMA, and Yasuhiko ARAI†
Department of Environmental Health Engineering, Institute of Industrial Ecological Sciences, University of Occupational and Environmental Health, Japan, 1-1 Iseigaoka, Yahatanishi-ku, Kita-kyushu 807
†Department of Chemical Engineering, Faculty of Engineering, Kyushu University, 6-10-1 Hakozaki, Higashi-ku, Fukuoka 807
(Received July 3, 1989)

Synopsis. Nitrogen gas containing organic vapor was introduced into a column packed with activated carbon at high temperatures up to 200 °C, and the amounts of the solvents adsorbed were measured. The adsorption equilibrium data for single- and bi-component systems could be correlated by the Freundlich and extended Freundlich isotherms respectively.

The measurement of the adsorption equilibrium is very important to understanding the basic adsorption and desorption characteristics of organic vapor on activated carbon. For example, the vapor in the work environment is collected using a charcoal tube and the amount adsorbed is measured by a thermal desorption method to determine the vapor concentration, the equilibrium data at the desorption temperature are necessary to estimate the thermal desorption efficiency. Although many kinds of organic compounds are used as solvents in work places, there are very few data available on organic vapor-activated carbon systems at high temperatures, because the desorption has usually not been carried out by the thermal-desorption method, but by an extraction method using a harmful organic desorbent such as carbon disulfide.[1] In particular, we have not found out any data for a multicomponent organic vapor system, although most of the organic solvents used in work places are multicomponent ones.

In this paper, we measured the adsorption equilibria of single- and bi-component organic vapor-activated carbon systems at high temperatures up to 200 °C and correlated the data using Freundlich and extended Freundlich isotherms.

Experimental

The adsorption column is made by using a Pyrex glass tube (4 mm in inner diameter), which is inserted into a brass block heated by a band heater. Organic vapors were obtained by means of a generator developed by the authors.[2] PCB Pittsburgh activated carbon (Calgon Co., 12/30 mesh), which is commonly used for the measurement of organic vapor in a work environment, was used as the adsorbent. Before the experiments, the carbon particles were heated at 250 °C for 24 hours under a nitrogen gas flow. The column temperature was measured by the use of a thermocouple and was controlled within ±0.5 °C by means of a relay-controller and a temperature-regulator.

One hundred milligrams of activated carbon particles were put into the heated column, and then pure nitrogen gas was introduced. After steady-state conditions had been obtained, the gas was changed to nitrogen gas containing organic vapor. A part of the column outlet gas was sampled periodically by the use of an auto-gas sampler (Gasukuro Kogyo, GS-5000A), while the vapor concentrations were determined by the use of a gas chromatograph (CC, Shimadzu GC-6A) equipped with a flame-ionization detector. After carbon particles had been recognized from the breakthrough curve as being fully saturated with the solvents, the particles were put into a vial and 2 ml of carbon disulfide was added. After having been kept for about 1 hour to insure the desorption of the adsorbed solvents, a part of the solution was injected into the GC and the amount adsorbed was determined.

Results and Discussion

Single-Component System. Figure 1 shows a Freundlich plot of toluene at various temperatures. The data are expressed by the following Freundlich equation:

$$q = A\,C^{\beta} \tag{1}$$

where C is the vapor concentration, q is the adsorption capacity in equilibrium with C per unit of weight of the activated carbon (equilibrium adsorption capacity), and A and β are constants. The equilibrium adsorption capacity decreased, and the value of β increased with the increase in the temperature. These findings show that the effect of the temperature on the adsorption capacity becomes larger at lower vapor concentrations. Figure 2 shows the isotherms for benzene, toluene, *o*-xylene, and methyl isobutyl ketone (MIBK) at 200 °C. They are commonly used in work places as solvents, but their thermal-desorption efficiencies are relatively low.[3] The experimental data can also be expressed by the Freundlich isotherm.

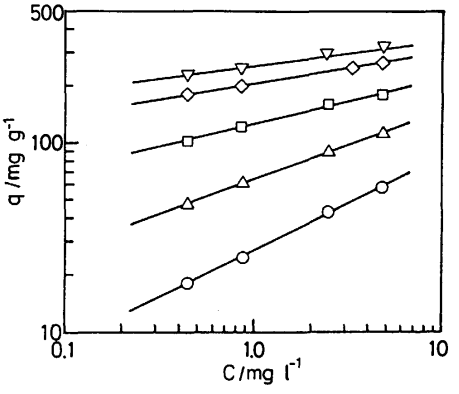

Fig. 1. Adsorption isotherm of toluene. O: 200 °C, △: 150 °C, □: 100 °C, ◇: 50 °C, ▽: 25 °C.

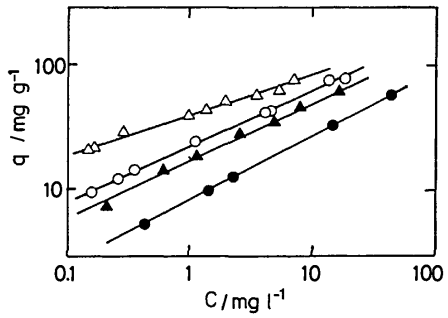

Fig. 2. Adsorption isotherm of organic solvent vapors on activated carbon at 200 °C. ○: toluene; $q=22.5C^{0.45}$, ●: benzene; $q=7.90C^{0.53}$, △: *o*-xylene; $q=42.0C^{0.35}$, ▲: MIBK; $q=17.7C^{0.47}$.

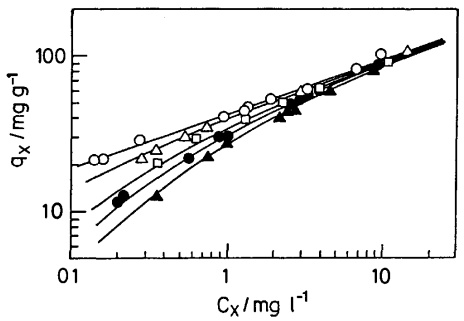

Fig. 4. Adsorption isotherm of *o*-xylene for MIBK–*o*-xylene system at 200 °C. ○: MIBK concentration=0.0 mg l^{-1}, △: 0.9 mg l^{-1}, □: 4.3 mg l^{-1}, ●: 7.0 mg l^{-1}, ▲: 12.5 mg l^{-1}, solid line: estimated by Eq. 2 and Table 1.

The equilibrium adsorption capacity depends on the adsorption affinity, which is itself dominated by the van der Waals force,[4] but it is difficult to obtain the quantitative relationship between the kind of material and the equilibrium adsorption capacities. In our experiment, the component which had the higher saturation vapor pressure tended to have the smaller adsorption capacity. The reason for this is that the higher vapor-pressure component is hard to condense in the pores of the adsorbent. As the saturate vapor pressure depends greatly on the temperature, the adsorption capacity may also be decreased with the temperature, as is shown in Fig. 1.

Bi-Component System. Figures 3 and 4 show the Freundlich plots of the MIBK-*o*-xylene system at 200 °C. The isotherms are shown as convex curves except when the vapor concentration of the co-adsorbed component is zero. This result indicates that the effect of the vapor concentration of the co-adsorbed component becomes larger as the vapor concentration of one component decreases. The equilibrium adsorption capacity of MIBK remarkably decreased with the increase in the *o*-xylene concentration, but the effect of MIBK on the adsorption capacity of *o*-xylene was small. The reason for this is that the MIBK which was adsorbed on activated carbon was easily desorbed and replaced by *o*-xylene because the adsorption affinity of MIBK is weaker than that of *o*-xylene, as can be predicted from the fact that the saturate vapor pressure of MIBK is larger than that of *o*-xylene.

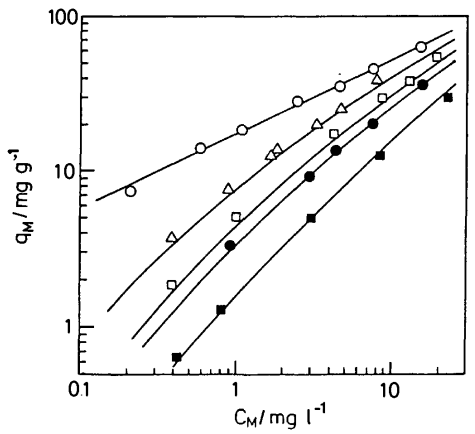

Fig. 3. Adsorption isotherm of MIBK for MIBK(M)–*o*-xylene(X) system at 200 °C. ○: *o*-xylene concentration=0.0 mg l^{-1}, △: 0.55 mg l^{-1}, □: 2.2 mg l^{-1}, ●: 3.9 mg l^{-1}, ■: 14.9 mg l^{-1}, solid line: estimated by Eq. 2 and Table 1.

As the Freundlich isotherm could be applied to the adsorption equilibrium data for the single-component system, we tried to correlate the bi-component adsorption equilibrium data using the following Freundlich isotherm empirically extended.

$$q_1=\frac{A_1C_1^{\beta_1}}{C_1^{\alpha_1}+B_1C_2^{\gamma_1}}\ ,\qquad q_2=\frac{A_2C^{\beta_2}}{C_2^{\alpha_2}+B_2C_1^{\gamma_2}} \tag{2}$$

where A_i, B_i, α_i, β_i, and γ_i (i=1, 2) are constants, and where C_1 and C_2, and q_1 and q_2 are the vapor concentrations and the equilibrium adsorption capacities of Components 1 and 2 respectively. In this paper, Component 1 is the weaker-adsorption-affinity component.

The parameters in Eq. 2 could be determined by Fritz and Schlüender's method.[5] Table 1 shows the values of these parameters for several systems. The values of A_1 and A_2, and $\beta_1-\alpha_1$ and $\beta_2-\alpha_2$, are the same as those of A and β in Eq. 1 respectively. The second term of the denominator indicates the effect of the co-adsorbed component. When the vapor concentration of one component is small, the second term is neglected and Eq. 2 is reduced to Eq. 1. We can know the relative strength of the adsorption affinity from the ratio of B_1 to B_2. Usually, B_1 is larger than B_2, for the effect of C_2 on q_1 is larger than that of C_1 on q_2, but if the adsorption affinities of both components

Table 1. Parameters of the Extended Freundlich Isotherm

	B-T		T-X		M-X	
i	1	2	1	2	1	2
α_i	0.74	0.47	0.50	1.55	0.66	0.79
β_i	1.27	0.92	0.95	1.90	1.13	1.14
γ_i	0.72	0.49	0.86	1.64	0.62	0.82
A_i	7.90	22.5	22.5	42.0	17.7	42.0
B_i	1.36	0.242	1.80	0.055	1.91	0.068

B: benzene, T: *o*-toluene, X: *o*-xylene, M: MIBK.

are almost the same, B_1 may be close to B_2. The lines estimated by means of Eq. 2 and Table 1 are also shown in Figs. 3 and 4. They were in good agreement with the experimental data.

Equations 1 and 2 are empirical equations. However, as the form of these equations are simple, they can be used to estimate the thermal desorption efficiencies of organic solvents from activated carbon. These equations should thus prove useful in future investigations.

References

1) "NIOSH Manual of Analytical Method," 3rd ed., National Institute for Occupational Safety and Health, Cincinnati (1984).

2) H. Hori, I. Tanaka, and T. Akiyama, *Am. Ind. Hyg. Assoc. J.*, **49**, 1 (1988).

3) H. Hori, I. Tanaka, and T. Akiyama, *Nippon Kagaku Kaishi*, **1986**, 1241.

4) H. Yanai,"Kyuchaku Kogaku Youron," Kyoritsu Shuppan, Tokyo (1977), Chap. 2.

5) W. Fritz and E. U. Schluender, *Chem. Eng. Sci.*, **29**, 1279 (1974).

Liquid-Crystalline Behavior and Configuration Change of Polyitaconates with Methoxyazobenzene as Mesogens

Kohei SHIRAISHI, Kazuo SUGIYAMA,* and Takayuki OTSU†
Department of Industrial Chemistry, Faculty of Engineering, Kinki University, Hirokoshinkai, Kure, Hiroshima 737-01
†Department of Applied Chemistry, Faculty of Engineering, Osaka City University, Sugimoto, Sumiyoshi-ku, Osaka 558
(Received July 3, 1989)

Synopsis. Nematic polyitaconates having 4-methoxyazobenzene moieties as mesogen in the side chain were prepared. Thermal properties, polymer composition, and the photoinduced configuration change have been examined to suggest a possible use of the polymers for photosensitive liquid-crystalline materials.

During the last decade, the side chain type of liquid crystalline polymers (LCPs) have been widely investigated on their chemical and physical properties as well as potential application. In these polymers, the mesogenic groups examined were flexible polysiloxanes[1] and different types of vinyl backbone such as polyacrylates,[2,3] polymethacrylates,[2,4] and polyitaconates.[5] In the course of our study on thermotropic behavior and potential uses of LCPs,[6-8] nematic polyitaconates, poly[ethyl ω-[4-(4-methoxyphenylazo)phenoxy]alkyl itaconate]s, Poly**2**, were prepared and their configuration changes were photochemically studied.

Experimental

4-[4-(ω-Hydroxyalkoxy)phenylazo]anisole, **1**: 4-[4-(6-hydroxyhexyloxy)phenylazo]anisole, **1a**, and 4-[4-(11-hydroxyundecyloxy)phenylazo]anisole, **1b** were prepared from the *O*-alkylation of 4-(4-hydroxyphenylazo)anisole with ω-halo-1-alkanol in the presence of KOH and KI according to the method used in the preparation of 4-(ω-hydroxyalkoxy)-benzoic acids.[9]

1a (n=6): 51.0% yield; mp 122—123 °C; ^{1}H NMR ($CDCl_3$) δ=1.13—1.30 (t, J=4 Hz, 3H, -CH$_3$), 1.43—2.17 (m, 8H, HOCH$_2$(CH$_2$)$_4$CH$_2$O-), 3.79 (s, 3H, -OCH$_3$), 3.22—4.15 (m, 4H, HOCH$_2$(CH$_2$)$_4$CH$_2$O-), and 6.55—7.97,(m, 8H, aromatic).

1b (n=11): 65.1% yield; mp 86—87 °C; ^{1}H NMR ($CDCl_3$) δ=1.27—2.28 (m, 18H, HOCH$_2$ (CH$_2$)$_9$CH$_2$O-), 3.42 (s, 3H, -OCH$_3$), 3.68—4.51 (m, 4H, HOCH$_2$ (CH$_2$)$_9$CH$_2$O-), and 7.37—8.66 (m, 8H, aromatic).

Ethyl 3-chloroformyl-3-butenoate: Ethyl 3-chloroformyl-3-butenoate from ethyl 3-carboxy-3-butenoate and thionyl chloride. 85% yield; bp 86—86.5 °C/8 mmHg (1 mmHg≈ 133.322 Pa).

Ethyl ω-[4-(4-methoxyphenylazo)phenoxy]alkyl itaconate, **2**: 0.05 mol of **1** was dissolved in 300 mL of chloroform and 0.10 mol of triethylamine. Then a trace of 1,4-benzoquinone was added with stirring and cooling at 0 °C, and a 0.10 mol portion of ethyl 3-chloroformyl-3-butenoate was dropped into the solution. After stirring for 4 h at 60 °C, ca. 200 mL of water was added to the reaction mixture. The chloroform layer was then washed with water and evaporated to dryness, and the residual solid was recrystallized from ethanol.

4-Ethyl 1-[6-[4-(4-methoxyphenylazo)phenoxy]hexyl] 2-methylenesuccinate, **2a** (n=6): 60.2% yield; mp 82 °C; ^{1}H NMR ($CDCl_3$) δ=1.13—1.30 (t, 3H, J=4 Hz, -CH$_3$), 1.43—2.17 (m, 8H, -OCH$_2$(CH$_2$)$_4$CH$_2$O-), 4.00 (s, 3H, -OCH$_3$), 4.10—4.28 (q, 2H, -CH$_2$-), 4.28—4.64 (m, 4H, -OCH$_2$(CH$_2$)$_4$CH$_2$O-), 5.87—6.06 (m, 1H, H-CH=), 6.55—6.74 (m, 1H, H-CH=), and 7.16—8.52 (m, 8H, aromatic).

Found: C, 67.10; H, 6.23; N, 5.98%. Calcd for $C_{24}H_{30}O_6N_2$: C, 66.94; H, 6.48; N, 6.00%.

4-Ethyl 1-[6-[4-(4-methoxyphenylazo)phenoxy]undecyl] 2-methylenesuccinate, **2b** (n=11): 59.4% yield; mp 64 °C; ^{1}H NMR ($CDCl_3$) δ=0.94—2.11 (m, 18H, -OCH$_2$(CH$_2$)$_9$-CH$_2$O-), 3.25 (s, 2H, -CH$_2$-), 3.78 (s, 3H, -OCH$_3$), 3.79—4.34 (m, 6H, -OCH$_2$(CH$_2$)$_9$CH$_2$-, -CH$_2$-), 5.46—5.61 (m, 1H, H-CH=), 6.06—6.24 (m, 1H, H-CH=), and 6.63—7.84 (m, 8H, aromatic).

Found: C, 70.09; H, 6.35; N, 5.32%. Calcd for $C_{31}H_{40}O_6N_2$: C, 70.31; H, 6.28; N, 5.29%.

Polymerization: The polymerization procedure was the same as that described by Sugiyama.[10] Polymers were reprecipitated twice from benzene and methanol. The copolymerization products from monomer **2** and styrene were analyzed by ^{1}H NMR for the phenyl protons of monomer **2** and styrene. The intrinsic viscosity (dL·g^{-1}) of the polymer was determined in benzene at 30 °C by a Ubbelohde viscometer.

Measurements: The phase-transition temperature was determined by means of differential scanning calorimeter, using a Rigaku Thermoflex DSC 8230B. Microscopic observation was performed by an Olympus microscope with temperature controlling heating stage. The cis-trans isomerization of polymers was carried out as follows: a known amount of the polyitaconate in THF was put in a quartz tube, which was placed on a merry-go-round Rayonet photochemical reactor Model-RMA-400 equipped with 4 RPR-253.7 nm lamps. The distance between the tube and lamps was 10 cm. After irradiating the sample for a given time, an aliquot of the solution was taken for UV measurement by a Shimadzu UV 200S spectrophotometer.

Results and Discussion

Thermal Properites: Monomers **2** are yellow crystals and showed no mesophase. It was found that monomer **2** can polymerize by a free radical reaction to give homopolymers, [Poly**2**] with low intrinsic viscosity as shown in Scheme 1. Poly**2** with various intrinsic viscosity values were prepared by changing the polymerization conditions. All of Poly**2** turned into mesophase, which showed the Schlieren texture and were confirmed to be a nematic phase by observation and polarization microscopy of thin samples. The phase-

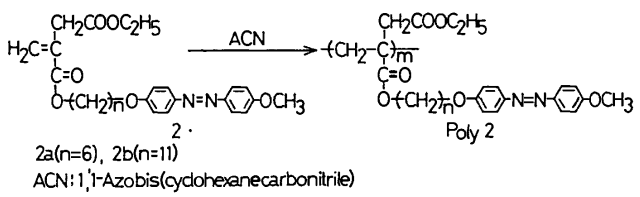

Scheme 1.

Table 1. Radical Polymerization of **2** and Characterization of Poly **2**

	2	Initiator×10^2	Yield	$[\eta]^{c)}$×10^2	Phase transition temp$^{d)}$/°C	
	mol	mmol	%	dL·g^{-1}	T_m	T_i
2a[a)]	2.12	4.20	11.6	5.6	45	78
	2.12	6.78	13.5	5.3	48	76
	2.12	10.17	19.1	5.2	52	71
	2.12	13.56	22.2	4.9	50	68
	2.12	17.00	26.6	4.4	38	61
2b[b)]	1.77	1.77	24.5	6.2	67	127
	0.23	1.15	31.1	6.0	54	120
	0.27	2.51	54.0	5.2	52	118

a) Polymerized with 2,2′-azobisisobutyronitorile (AIBN) in benzene (1g of **1a**/2 mL of benzene) at 60 °C for 24 h. b) Polymerized with 1,1′-azobis(cyclohexanecarbonitrile)(ACN) in bulk at 100 °C for 7 days. c) Measured in benzene at 30 °C. d) Determined by means of DSC thermogram on heating cycle (rate, 5 K·min^{-1}).

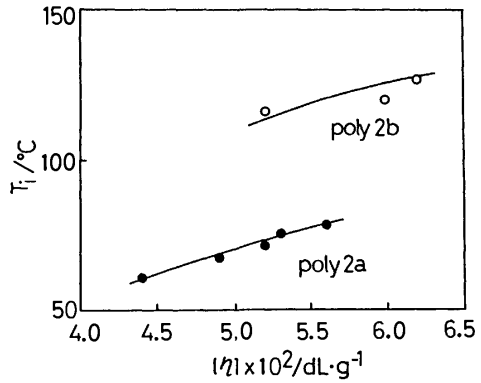

Fig. 1. Relationship between T_i and $[\eta]$ for Poly **2a**.

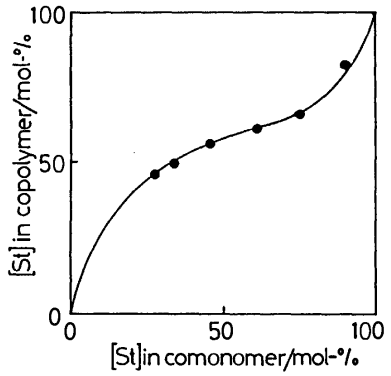

Fig. 2. Composition curve for the polymerization of the monomer **2a** (M_1) and styrene (M_2).

transition temperature determined by DSC was in good agreement with that obtained from the polarization microscopic measurement. The results are listed in Table 1. From the data in Table 1, it can be seen that the phase transition temperature of Poly**2** is influenced by the length of methylene spacer groups as well as intrinsic viscotiy of the polymer. Figure 1 shows the dependence of isotropization temperature (T_i) on intrinsic viscosity of Poly**2**. T_i values of both Poly**2a** and Poly**2b** increase gradually with the increase of intrinsic viscosity values. In general, the phase behavior of LCPs depends on their molecular weight and this influence is strong for low molecular weight,[9,11] for instance, T_i values of liquid crystalline polyacrylates increase with the increase in $[\eta]$ below 0.1.[12]

Copolymerization: Since monomer **2** showed low polymerization reactivity, monomer **2a** (M_1) was radically copolymerized with styrene (M_2) in order to know the monomer reactivity ratio of monomer **2**. Figure 2 shows the composition curves for the copolymerization of monomer **2a** with styrene initiated by AIBN in benzene at 60 °C. Applying the data in Fig. 2 to the curve-fitting method,[13] r_1 and r_2 were calculated to be 0.11 and 0.44, respectively. Monomer **2a** was then found to copolymerize alternatively with styrene. Sato et al.[14] reported that r_1=0.36 and r_2=0.40 for the copolymerization of methyl phenethyl itaconate (4-methyl 1-phenethyl 2-methylenesuccinate) (M_1) and styrene (M_2). The r_1 of monomer **2a** is smaller than that of methyl phenethyl itaconate. This is explained by the bulkiness of mesogenic group in monomer **2a**. From either DSC or polarization microscopic measurements, none of the copolymers exhibited liquid crystalline behavior.

Cis-Trans Isomerization: The photoinduced configuration change due to a cis-trans isomerization of the chromophore such as azobenzene is known to control the permeation of water, ion, etc. through the membrane.[15,16] The configuration change of Poly**2** was photochemically studied for the purpose of applying the polymer to practical separation. The progressive spectral change for Poly**2a** due to the isomerization from *trans*- to *cis*-azobenzene was observed during the irradiation of 253.7 nm light. From a decline of the absorption of trans-azobenzene chromophore (λ_{max}=365 nm) in THF, the first-order rate constant was, estimated to be 0.021 s^{-1} according to the method described by Sugiyama et al.[17] These nematic polyitaconates will have the possibility of use for a photoresponsive membrane material.

References

1) H. J. Coles and R. Simon, *Polymer*, **26**, 1801 (1985).
2) R. V. Talrose, S. G. Kostromin, V. P. Shibaev, N. A. Platé, H. Kresse, K. Sauer, and D. Demus, *Makromol. Chem., Rapid Commun.*, **2**, 305 (1981).

3) M. Eich and J. H. Wendorff, *Makromol. Chem., Rapid Commun.*, **8**, 467 (1987).
4) G. R. Meredith, J. G. VanDusen, and D. J. Williams, *Macromolecules*, **15**, 1385 (1982).
5) P. Keller, *Macromolecules*, **18**, 2337 (1985).
6) K. Sugiyama, A. Sakamoto, Y. Murata, K. Shiraishi, and T. Otsu, *Nippon Kagaku Kaishi*, **1987**, 1064.
7) K. Shiraishi, A. Sakamoto, and K. Sugiyama, *Nippon Kagaku Kaishi*, **1988**, 946.
8) K. Shiraishi, K. Sugiyama, A. Sakamoto, and T. Otsu, *Bull. Chem. Soc. Jpn.*, **61**, 783 (1988).
9) M. Portugall, H. Ringsdorf, and R. Zentel, *Makromol. Chem.*, **183**, 2311 (1982).
10) K. Sugiyama, *J. Macromol. Sci.-Chem.*, **A23**, 1155 (1986).
11) R. Zentel and H. Ringsdorf, *Makromol. Chem., Rapid Commun.*, **5**, 393 (1984).
12) S. G. Kostromin, R. V. Talrose, V. P. Shibaev, and N. A. Platé, *Makromol. Chem., Rapid Commun.*, **3**, 803 (1982).
13) R. W. Tidwell and G. A. Mortimer, *J. Polym. Sci.*, **A2**, 645 (1964).
14) T. Sato, K. Morino, H. Tanaka, and T. Ota, *Makromol. Chem.*, **188**, 2951 (1987).
15) A. Kumano, O. Niwa, T. Kajiyama, M. Takayanagi, T. Kunitake, and K. Kano, *Polym. J.*, **16**, 461 (1984).
16) K. Okuyama, H. Watanabe, M. Shimomura, K. Hirabayashi, T. Kunitake, T. Kajiyama, and N. Yasuoka, *Bull. Chem. Soc. Jpn.*, **59**, 3351 (1986).
17) K. Sugiyama, T. Nakaya, and M. Imoto, *Makromol. Chem.*, **163**, 185 (1973).

Electrical Conduction in Some Ternary Metallo-Organic Solid Complexes of Biological Importance and Compensation Effect

Biswanath MALLIK
Department of Spectroscopy, Indian Association for the Cultivation of Science, Jadavpur, Calcutta: 700032, India
(Received March 13, 1989)

Synopsis. The electrical conduction in some ternary solid complexes of Cu(II) with 2,2′-bipyridyl/1,10-phenanthroline and several amino acids (e.g., α-alanine, leucine, tryptophan, glycine, and norvaline) is studied as a function of temperature. These materials show semiconductivity. Results suggest that true compensation effect is valid for most of the materials studied. Importance of characteristic temperature (T_o) in biological process is pointed out.

Investigations on the electrical conduction properties in biologically important solid materials may bring significant contribution[1,2] to the field of 'bioenergetics'. In general, ternary complexes (mixed ligand complexes) of different metal ions play an important role in biolgical system.[3,4] Copper is one of the essential trace elements[3] present in living organism and in general copper exists in complexed form either with small molecules like amino acids or with macromolecules such as proteins. Several ternary complexes of Cu(II) containing amino acids have been detected recently in human serum.[5-7] The ternary complexes of Cu(II) formed by the interaction of one amino acid and a nonionized ligand like 2,2′-bipyridyl, 1,10-phenanthroline are typical examples[8-11] of such complexes present in biological systems.[3] Such complexes are expected to take part actively in the biological process[12] involving (i) electron transport and (ii) dioxygen transport and metabolism. In spite of the importance of metallo-organic complexes in biological process scant attention has been paid to the measurment of their electrical properties. Therefore, it was though worthwhile to study the electrical properties of some ternary solid metallo-organic complexes. This present paper concerns the validity of compensation rule[13-15] in the electrical conduction process in some ternary solid complexes of Cu(II) with 2,2′-bipyridyl/1,10-phenanthroline and amino acids.

In case of some organic semiconductors as reported[13-15] earlier the different values of activation energy (E) obtained by adsorption of vapors on semiconductor powders and the specific conductivity $\sigma(T)$ at a temperature T are related by the three constant expression

$$\sigma(T)=\sigma_o' \exp(E/2kT_o)\exp(-E/2kT) \quad (1)$$

where k is the Boltzmann constant and the parameters σ_o' and T_o are constants for a particular semiconductor. Thus, the pre-exponential factor σ_o in the usual semiconduction expression

$$\sigma(T)=\sigma_o \exp(-E/2kT) \quad (2)$$

is related to the activation energy (E) by the expression

$$\sigma_o=\sigma_o' \exp(E/2kT_o) \quad (3)$$

As evidenced from expression (3), $\log\sigma_o$ is linearly related to E which is known as compensation effect (or rule). The origin of this effect and the physical significance of T_o is not yet clear. In this paper it is shown that the true compensation effect is valid for some ternary complexes of Cu(II) containing amino acids. The origin of this effect in this case and the possible role of T_o in biological system are discussed.

Experimental

The ternary metallo-organic solid complexes used in this investigation are of the type [Cu(II)·A.L]Cl·H_2O where A represents 2,2′-bipyridyl/1,10-phenanthroline and LH=α-alanine, leucine, tryptophan, glycine, and norvaline. These complexes were synthesized and characterized by usual procedure.[10,11] The reagent chemicals used were of AR or GR quality (E.Merck, BDH, LOBA). This synthesis work was carried out by Prof. M. C. Saxena and his co-workers in the Deptt. of Chemistry, Dr. H. S. Gour University, Sagar: 470003, India. These samples were dried under vacuum before use. The finely powdered sample pressed in a sandwich cell[13,16] between a conducting glass and a stainless steel electrode at moderate pressure by spring clips. The separation between the electrodes was maintained by a two mil (1 mil=0.00254 cm) thick Teflon spacer. The sample cell was then placed in a suitably designed conductivity chamber[13,16] made of brass and fashioned with Teflon. A dc voltage of 27 volts from a dry battery pack was applied across the sample cell. The dark conductivity was measured in vacuum [10^{-3} Torr (1 Torr=133.322 Pa)] using an electrometer, model no. 617, of Keithley Inst. Inc., U.S.A. The thermo emf was measured by a digital panel meter, model no. HIL: 2301, India. Details of the experimental arrangement is similar to that described earlier.[13,16]

Results and Discussion

The electrical conductivity of the materials under investigation was studied in the temperature range 298 K to 345 K. In all the cases an increase in conductivity with increasing temperature was observed which indicates that these materials behave like semiconductors. Each measurement was repeated several times in vacuum. All the measurements gave consistent results. The $\log\sigma$ vs. $1/T$ plots for some complexes under study are shown in Fig. 1. It is seen that all the linear plots intersect the ordinate at wide variety of positions but all they meet at a point of intersection corresponding to a fixed tempereture (307 K) showing that the conductivity at this temperature is same for all these meterials. The linear plots for the complexes containing (bipy·α-ala) and (1,10-phen·leu) are not included in Fig. 1 as the corresponding linear plots do not pass through the common point of intersection.

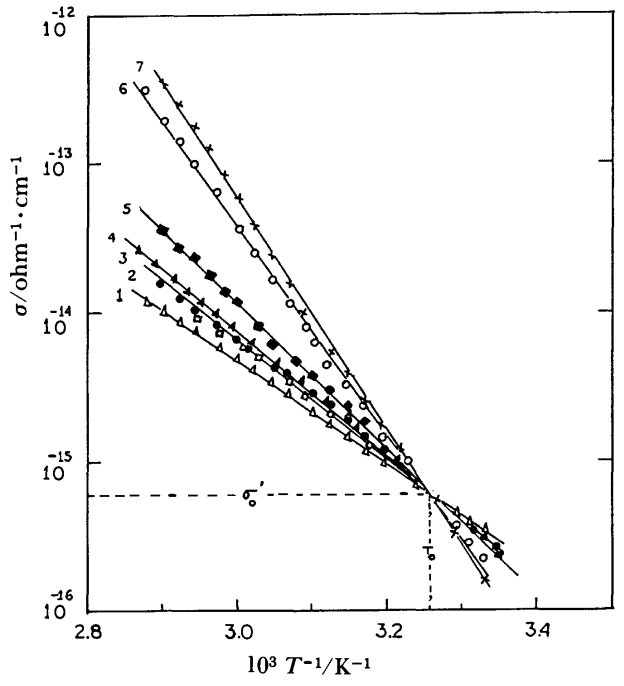

Fig. 1. Plot of $\log\sigma$ value vs. $1/T$ for some ternary solid complexes†† of Cu(II) with 2,2′-bipyridyl/1,10-phenanthroline and several amino acids.
The line (1) for [Cu(II)·1,10-phen·ala]Cl·H_2O [—△—]; (2) for [Cu(II)·bipy·trp]Cl·H_2O [—□—]-this almost overlaps with (3); (3) for [Cu(II)·bipy·leu]Cl·H_2O [—●—]; (4) for [Cu(II)·bipy·norval]Cl·H_2O [—▲—]; (5) for [Cu(II)·1,10-phen·trp]Cl·H_2O [—■—]; (6) for [Cu(II)·1,10-phen·gly]Cl·H_2O [—○—]; and (7) for [Cu(II)·bipy·gly]Cl·H_2O [—×—].
These lines were fitted by the method of least squares. For each linear plot at least 20 data points were considered. To avoid overcrowding of data points (particularly near T_o) only few representative data points are shown for each complex.
The value of T_o=307 K; $\sigma_o'=6.2\times10^{-16}$ $(\Omega\cdot cm)^{-1}$.
††Standard abbreviations used.

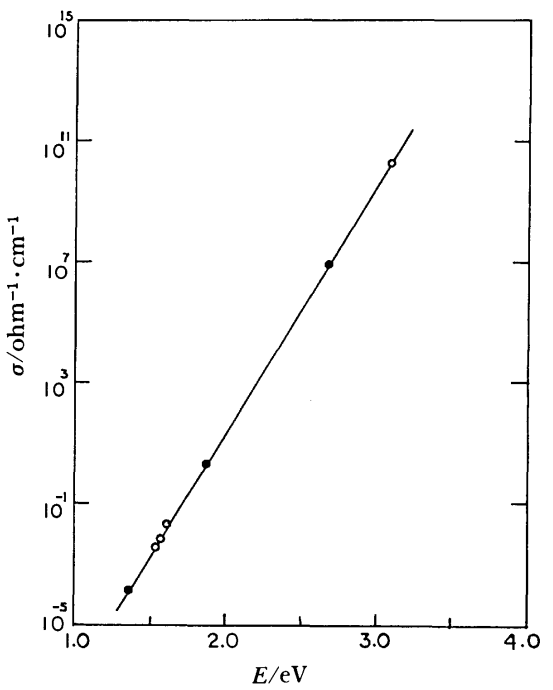

Fig. 2. Plot of $\log\sigma_o$ value vs. E for some ternary solid complexes of Cu(II) with 2,2′-bipyridyl/1,10-phenanthroline and several amino acids.
—○— for complexes with 2,2′-bipyridyl and amino acids; —●— for complexes with 1,10-phenanthroline and amino acids. Value of T_o=307 K; $\sigma_o'=7.55\times10^{-16}$ $(\Omega\cdot cm)^{-1}$.

The reason for this anomally is discussed latter on. The values of E and measured values of σ_o for the complexes are shown in Table 1. The temperature where all the materials show equal conductivity, $\sigma(T_o)$, is known as characteristic or compensation temperature (T_o). The value of σ at T_o gives σ_o' value. The values of T_o and σ_o' obtained from the $\log\sigma$ vs. $1/T$ plots are 307 K and 6.2×10^{-16} $(\Omega\cdot cm)^{-1}$ respectively. To test the validity of compensation effect $\log\sigma_o$ was plotted against E and a linear plot as expected from expression (3) is shown in Fig. 2.

The compensation effect is thought[17] to arise from the existence of a linear relationship between the activation energy and activation entropy of the system. It has been pointed out by Johnston and Lyons[17] that if a true linear free energy relationship (LFER) does hold for a dark conduction process a definite point of intersection for the Arrhenius plots of the experimental data must exist as we have observed in Fig. 1. In the experiment of Johnston and Lyons[17] the $\log\sigma_o$ vs. E plot was linear, but a very poor correlation between $\log\sigma$ and E was observed in one component crystal of anthracene by changing its purity and doping with tetracene. On the basis of that experimental results it was concluded that a simple linear relation between $\log\sigma_o$ and E is not sufficient for judging the validity of compensation effect. However, in the present case it is clearly seen that the true compensation effect is valid.

There are number of theses (models) as mentioned in earlier communications[13,14] about the mechanism

Table 1. The Values of E and σ_o for Some Ternary Solid Complexes[a] of Cu(II) with 2,2′-Bipyridyl/1,10-Phenanthroline and Several Amino Acids

Complexes studied	E / eV	Measured value of $\sigma_o/\Omega^{-1}\cdot cm^{-1}$
[Cu(II)·bipy·leu]Cl·H_2O	1.53	3.54×10^{-3}
[Cu(II)·bipy·trp]Cl·H_2O	1.57	6.41×10^{-3}
[Cu(II)·bipy·norval]Cl·H_2O	1.61	1.64×10^{-2}
[Cu(II)·bipy·ala]Cl·H_2O[b]	1.63	4.25×10^{-2}
[Cu(II)·bipy·gly]Cl·H_2O	3.07	1.71×10^{10}
[Cu(II)·1,10-phen·ala]Cl·H_2O	1.35	1.07×10^{-4}
[Cu(II)·1,10-phen·trp]Cl·H_2O	1.86	1.72
[Cu(II)·1,10-phen·leu]Cl·H_2O[b]	1.88	5.84
[Cu(II)·1,10-phen·gly]Cl·H_2O	2.66	7.72×10^{6}

a) Standard abbreviations used. b) Compensation effecct is not valid for this complex.
(The samples are arranged separately for each primary ligand in order of increasing E-value).

of conduction in organic semiconductors leading to compensation effect. The applicability of different models has already been discussed.[13,14] A models depending on the interaction between the electrons and the vibrational motion[18] of the molecules appears suitable[13] to give a possible mechanism behind such compensation effect in case of some polyene[13,14] and nitroaromatic[15] semiconductors.

It has been reported by Sigel et al.[19] that the ternary metal complexes under investigation exist predominantly in a 'folded form'. Similar to common biopolymers (peptides, proteins, DNA), these complexes posses defined conformation[20] in their normal state. In the normal condition each atom performs thermally excited movements around its mean position. Also several energetically similar positions may be occupied by the same groups with comparable probability. Any change of external parameters such as temperature, pressure, electric field etc. will influence this dynamics and flexibility of the structure which may lead to changes[20] of conformations. The particular electronic properties of a complex in its normal state will obviously change with the change in its precise conformation. A change in electronic state (as involved in transport) gives rise to an activation entropy[18] because of a change in vibrational frequencies associated with the conformatinal changs. Each compound possesses a definite value of activation entropy arising from the temperature-dependent conformational changes in the temperature range under consideration. The variation in both the electronic energy gap (E_g) and activation entropy (S) can account for compensation effect if the changes in these parameters are given by[18]

$$E_g = E_{g_o} + nE_{g_1} \text{ and } S = S_o + nS_1$$

where n is a definite number for each compound and E_{g_o}, E_{g_1}, S_o, and S_1 are same for all the compounds. In this case the characteristic temperature is given by

$$T_o = E_{g_1}/(2S_1).$$

Unfortunately due to the fact that the nature of these complexes is not precisely known at present, the activation entropy S (hence S_1) is a relatively obscure quantity and any quantitative estimate of T_o could not be done.

The compensation behavior depends on the molecular property[13-15] of the complexes/materials involved and T_o plays an important role in dark conduction process. Though attempts have been made to understand the compensation behavior as mentioned in the earlier communications,[13,14] the factors on which the value of T_o depends is not yet clear. It should be mentioned here that compensation effect is not valid for the ternary complexes of Cu(II) with 2,2′-bipyridyl and alanine; and 1,10-phenanthroline and leucine ligands possibly due to different types of conformational changes in these complexes on thermal agitation. Such anomaly has also been observed[15] previously in some nitroaromatics on adsorption of several vapors related to an experiment on compensation effect.

The observed value of T_o in most of the reported data is either much higher[13] or lower[14,15] than physiological tempereture. It is interesting to note that the characteristic tempereture for the materials under investigation is near the physiological temperature. Since at this temperature (T_o) the collective electronic properties of these materials are significantly changed, the presence of these materials in a biological system may have some important role in the biological processes involving transfer of electrons (charges) near physiological temperature. Investigation with complexes containing other amino acids as well as other metal ions could be of much interest but unfortunately such experiment could not be performed as the materials were not available at this moment.

The author is thankful to Prof. M. C. Saxena, Department of Chemistry, Dr. H. S. Grour University, Sagar: 470003, India for a generous gift of these ternary Cu(II) solid complexes. Thanks are also due to Prof. T. N. Misra of this department for his constant encouragement.

References

1) F. Gutmann, H. Keyzer, and L. E. Lyons, "Organic Semiconductors," Robert E. Krieger Publishing Co., Malabar, Florida (1983), p. 319.
2) D. G. Nicholls, "Bioenergetics," Academic Press, London, New York (1982).
3) H. Sigel, "Metal Ions in Biological Systems," Marcel Dekker, Inc., (1973), Vol. 2, p. 2.
4) Ref. 3, Vol. 12 (1981), p. 233.
5) Ref. 4, p. 141.
6) B. Sarkar and T. P. A. Kruck, *Can. J. Biochem.*, **45**, 2066 (1967).
7) T. P. A. Kruck and B. Sarkar, *Can. J. Chem.*, **51**, 3555 (1973).
8) R. Griesser and H. Sigel, *Inorg. Chem.*, **9**, 1238 (1970).
9) M. V. Chidambaram and P. K. Bhattacharya, *J. Inorg. Nucl. Chem.* **32**, 3271 (1970).
10) R. L. Dutta and D. De, *J. Indian Chem. Soc.*, **46**, 74 (1969).
11) M. V. Chidambaram, and P. K. Bhattacharya, *J. Inst. Chem.*, **64**, 144 (1972).
12) Ref. 4, p. 2.
13) B. Mallik, A. Ghosh, and T. N. Misra, *Bull. Chem. Soc. Jpn.*, **52**, 2091 (1979).
14) B. Mallik, A. Ghosh, and T. N. Misra, *Phys. Stat. Sol.(a)*, **62**, 267 (1980).
15) A. Ghosh, K. M. Jain, B. Mallik, and T. N. Misra, *Jpn. J. Appl. Phys.*, **20**, 1059 (1981).
16) B. Mallik, A. Ghosh, and T. N. Misra, *Proc. Indian Acad. Sci.*, **88A**, 25 (1979).
17) G.R. Johnston and L. E. Lyons, *Aust. J. Chem.*, **23**, 2187 (1970).
18) T. A. Kaplan and S. D. Mahanti, *J. Chem. Phys.*, **62**, 100 (1975).
19) H. Sigel and C. F. Naumann, *J. Am. Chem. Soc.*, **98**, 730 (1976).
20) J. Engel, "Biophysics," ed by W. Hoppe, W. Lohmann, H. Markl, and H. Ziegler, Springer Verlag, Berlin, Heidelberg, New York, Tokyo (1983), p. 234.

On the Existence of $NaC_2O_4^-$ Ion Pair Complex

Raj Pal SINGH
Central Analytical and Materials Characterization Laboratories, Metrology Standards and Meterial Division, The Research Institute, King Fahd University of Petroleum and Minerals, Dhahran 31261, Saudi Arabia
(Received March 6, 1989)

Synopsis. Existence of $NaCO_4^-$ ion pair complex formation in solutions has been further documented through the solubility measurements of calcium oxalate monohydrate in sodium chloride, magnesium chloride, and mixtures of sodium and magnesium chlorides.

In a recent publication Berland et al.[1] have argued against the existence of alkali metal oxalate ion pair complexes, such as $NaC_2O_4^-$, in urine. However, the evidence for the nonexistence of such ion pairs, presented by them does not seem to be appropriate since using Hammarsten's data[2] of calcium oxalate monohydrate (COM) solubility in sodium chloride, Finlayson et al.[3,4] have computed a value of about 13 $dm^3 mol^{-1}$ as the stability constant of $NaC_2O_4^-$ ion pair. Further, regarding the conductivity measurements on sodium oxalate solutions, indeed 17% of the oxalate will be bound in a 30 mmol dm^{-3} sodium oxalate solution but only 8.5% of the total sodium ion will participate in the complexation. Since $NaC_2O_4^-$ is also charged, the overall decrease in the equivalent conductivity will be 8.5%. The decrease in equivalent conductivity at lower sodium oxalate concentrations, however, would be even smaller and that might be the reason why a substantial change between measured and calculated conductivity values was not observed.

The existence of alkali metal oxalate ion pair complexes in solutions has also been reported in the literature by other workers. For example, Daniele et al.[5] have used potentiometric titration method to determine the stability constants of sodium and potassium oxalate complexes and found a value of about 10 $dm^3 mol^{-1}$ for $NaC_2O_4^-$ and 9 $dm^3 mol^{-1}$ for $KC_2O_4^-$ at 37 °C. An spectral evidence for the existence of $LiC_2O_4^-$, $KC_2O_4^-$, and $CsC_2O_4^-$ ion pairs has been presented by Kanamori et al.[6] after measuring the Raman spectra of aqueous solutions of lithium, potassium, and caesium oxalates.

Because of high concentrations of sodium and potassium ions in urine, correction for $NaC_2O_4^-$ and $KC_2O_4^-$ ion pairs will be important in the computation of urine supersaturation with respect to COM.[7] This reference has further clarified the presence of such ion pairs in urine snd synthetic solutions containing alkali metals and oxalate.

Experimental

Reagent grade calcium chloride dihydrate, magnesium chloride hexahydrate, and sodium chloride (Merck and B. D. H. Chemical companies) were used. Solutions were prepared using doubly distilled, deionized water (Nanopure II) and standardized by analyzing for chloride with Mettler's Memotitrator system (Model DL-40RC). Standard solution of oxalate at 1000 mg dm^{-3} was made from analytical grade oxalic acid purchased from Baker Chemical Co. Calcium oxalate monohydrate used for solubility measurements was received in powdered form from B. D. H. Chemical Co.

Solubility measurements were carried out by equilibrating approximately 20 mg of COM in 20 cm^3 solulion maintained at 37 °C for over 50 h, to ensure complete equilibrium. After that, samples were filtered and diluted immediately to prevent from any precipitation which could result due to the attainment of supersaturation with respect to COM at lower temperature. Diluted solutions were then analyzed for calcium and oxalate using ion chromatography, and solubility was reported as the mean of four determinations.

Ion-chromatographic measurements were made on a Dionex ion chromatograph model 2120i fitted with conductivity detector. The separation of oxalate was achieved on a Dionex AG4 guard column and an AS4 separator. Calcium was analyzed on a Dionex CS1 separator and a CG1 guard column using a mixture of 0.0025 mol dm^{-3} ethylenediamine and 0.005 mol dm^{-3} hydrochloric acid. The eluent for anion chromatography consisted of a mixture of 0.003 mol dm^{-3} sodium hydrogen carbonate and 0.0024 mol dm^{-3} sodium carbonate. The flow rate in both instances was maintained at 2.0 $cm^3 min^{-1}$. Peak heights were integrated on a Dionex 4217 integrator.

The concentrations of different ionic species in the equilibrated COM solutions were calculated from mass balance and electroneutrality expressions.[8] The corrections for $CaC_2O_4^0$ and $NaC_2O_4^-$ ion pairs when needed, were made by using their respective stability constant values of 2746 $dm^3 mol^{-1}$ [3,4] and 13.2 $dm^3 mol^{-1}$.[3,4] Since the Debye-Hückel equation is inaccurate at high ionic strengths, well adopted extended form of the Debye-Hückel equation[9-11] as proposed by Davies,[12] was used to calculate the activity coefficients at high ionic strengths.

Results and Discussion

The results of solubility of COM in water and different concentrations of sodium chloride are summarized in Table 1. The mean solubility product, $(3.347\pm0.18)\times10^{-9}$ $mol^2 dm^{-6}$, obtained from the solu-

Table 1. Results of Solubility Determinations of COM in Water and Sodium Chloride Solutions at 37 °C

NaCl / mol dm^{-3}	Solubility $Ca^{2+}=C_2O_4^{2-}$ / 10^{-4} mol dm^{-3}	K_{sp}[a] / 10^{-9} $mol^2 dm^{-6}$	K_{so}[b] / 10^{-9} $mol^2 dm^{-6}$
0.00	0.564±0.010	2.18	2.18
0.05	1.364±0.015	3.39	2.20
0.10	1.610±0.020	3.15	2.18
0.15	1.890±0.025	3.50	2.18

a) K_{sp}=Solubility product of COM corrected for ionic strength and $CaC_2O_4^0$ ion pair. b) K_{so}=Thermodynamic solubility product of COM corrected for ionic strength and, $NaC_2O_4^-$ and $CaC_2O_4^0$ ion pairs.

bility values at three different sodium chloride concentrations after $CaC_2O_4^0$ ion pair and ionic strength correction is in good agreement with the value, $(3.289\pm0.03)\times10^{-9}$ mol^2 dm^{-6}, computed by Berland et al.[1] from Hammarsten's data. However, as can be seen from the last column of Table 1, both of the above values are about 50% higher than the corresponding thermodynamic solubility product, K_{so}. The K_{so} was calculated from the solubility of COM in water and sodium chloride solutions following the corrections of both $CaC_2O_4^0$ and $NaC_2O_4^-$ ion pairs, and ionic strength. The marked difference in K_{sp} and K_{so} values (the latter is a constant at a given temperature) clearly emphasizes the importance of taking into account $NaC_2O_4^-$ ion pair correction when calculating the thermodynamic solubilily product from COM solubility in sodium chloride solutions. The mean K_{so}, $(2.185\pm0.01)\times10^{-9}$ mol^{2}dm^{-6}, thus obtained from the solubility results in Table 1, compared well with 2.244×10^{-9} mol^{2}dm^{-6}, the value computed by Finlayson and co-workers from Hammarsten's data of COM solubility in water.[3,4]

Table 2 contains the results of COM solubility in different magnesium chloride solutions, and in the mixtures of magnesium chloride and 0.15 mol dm^{-3} sodium chloride. Magnesium concentrations were kept the same in both instances. The stability constants of $MgC_2O_4^0$ ion pair were calculated from different solubility values and reported in the last two columns of the Table 2. Closely similar values of stability constants (K_1) were obtained from the solubilities of COM in pure magnesium chloride solutions with a mean value of 4037 ± 138 dm^3 mol^{-1}, following $CaC_2O_4^0$ ion pair and ionic strength correction. The mean value of K_1 at 2446 ± 129 dm^3 mol^{-1} obtained from the COM solubilities in the mixtures of magnesium and sodium chlorides after ionic strength and, only $CaC_2O_4^0$ ion pair correction, was found to be approximately 40% lower then the above mentioned value. However, after additional correction of $NaC_2O_4^-$ ion pair, the mean K_1 at 2446 ± 129 dm^3 mol^{-1} changed to 4001 ± 189 dm^3 mol^{-1} (reported as K_2 in the last column of Table 2) and compared excellently well ($p>0.25$) with 4037 ± 138 dm^3 mol^{-1}. A value of approximately 4000 dm^3 mol^{-1} for the stability constant of $MgC_2O_4^0$ ion pair has also been reported by other workers using different methods.[13,14]

In conclusion, the existence of $NaC_2O_4^-$ ion pair in solulion containing sodium and oxalate ions (Tables 1 and 2) has been further confirmed from the results of COM solubility measurements. Direct observations, obtained from Raman spectroscopy by Kanamori et al.,[6] together with the results of potentiometry[5] and COM solubility measurements in different media, all indicated the existence of $NaC_2O_4^-$ or $KC_2O_4^-$ ion pairs in urine or synthetic solutions containing sodium/potassium and oxalate ions. In the light of above it is, therefore, suggested that the correction for these ion pairs should be made when calculating the supersaturation of calcium oxalate phases in synthetic solutions, containing alkali metal and oxalate ions, and urine.

The support of the research Institute, King Fahd University of Petroleum and Minerals and permission to publish the results is greatly appreciated.

References

1) Y. Berland, M. Olmer, M. Gandvuillemin, H. E. Lundager Madsen, and R. Boistelle, *J. Cryst. Growth*, **87**, 494 (1988).
2) G. Hammarsten, *Comp. Rend. Traveaux Lab. Carlsberg*, **17**, 1 (1929).
3) B. Finlayson, R. A. Roth, and L. G. Dubois, "Urinary Calculi," ed by L. Cifuentes Delatte, A. Rapado, and A. Hodgkinson, Karger, Basel (1973).
4) B. Finlayson and R. A. Roth, *Urology*, **1**, 142 (1973).
5) P. G. Daniele, C. Rigano, and S. Sammartano, *Thermochim. Acta*, **46**, 103 (1981).
6) K. Kanamori, M. Mihara, and K. Kawai, *Bull. Chem.*

Table 2. Results of Solubility Determinations of COM in Magnesium Chloride and in the Mixtures of Magnesium Chloride and 0.15 mol dm^{-3} Sodium Chloride at 37 °C

NaCl / mol dm^{-3}	$MgCl_2$ / mmol dm^{-3}	Solubility $Ca^{2+}=C_2O_4^{2-}$ / mmol dm^{-3}	γ_2	K'	K_1	K_2
0.0	1.0	0.119	0.7936	2658	4220	—
0.0	2.0	0.154	0.7114	2054	4058	—
0.0	4.0	0.207	0.6312	1582	3970	—
0.0	8.0	0.285	0.5416	1144	3900	—
Mean					4037	
SD					138	
0.15	1.0	0.208	0.3193	237	2325	3825
0.15	2.0	0.233	0.3182	241	2380	3901
0.15	3.0	0.276	0.3160	245	2458	4019
0.15	4.0	0.349	0.3119	255	2621	4257
Mean					2446	4001
SD					129	189

K'=conditional stability constant of MgC_2O^0 ion pair. K_1=stability constant of $MgC_2O_4^0$ ion pair corrected for $CaC_2O_4^0$ ion pair and ionic strength. K_2=stability constant of $MgC_2O_4^0$ corrected for both $CaC_2O_4^0$ and $NaC_2O_4^-$ ion pairs, and ionic strength. γ_2=activity coefficient for bivalent ion.

Soc. Jpn., **52**, 2205 (1979).
7) P. G. Werness, C. M. Brown, L. H. Smith, and B. Finlayson, *J. Urology*, **134**, 1242 (1985).
8) R. P. Singh, S. S. Gaur, M. E. Sheehan, and G. H. Nancollas, *J. Cryst. Growth*, **87**, 318 (1988).
9) W. G. Robertson, "Biological Mineralization and Demineralization," ed by G. H. Nancollas, Springer-Verlag, Berlin (1982).
10) W. E. Morf, "The Principles of Ion-Selective Electrodes and of Membrane Transport," Elsevier Scientific Publishing Co., Amsterdam (1981), pp. 13 and 24.
11) G. Sposito and S. J. Traina, *J. Environ. Qual.*, **16**, 80 (1987).
12) C. W. Davies, "Ion Association," Butterworth, London (1962).
13) B. Finlayson, A. Smith, and L. Dubois, *Investigetive Urology*, **13**, 20 (1975).
14) P. G. Daniele and M. Marangella, *Ann. Chim.*, **72**, 25 (1982).

A New Crystalline Form of Bis(1,2-diphenyl-1,2-ethenedithiolato)nickel: Asymmetric β-Ni(dpedt)2

Michel MEGNAMISI-BELOMBE* and Bernhard NUBER†
Department of Inorganic Chemistry, Faculty of Science, P.O. Box 812,
The University of Yaoundé, Yaoundé, Cameroon
†Anorganisch-Chemisches Institut der Universität, Im Neuenheimer Feld 270,
D-6900 Heidelberg 1, West Germany
(Received March 24, 1989)

Synopsis. The full structure of a new crystalline form of bis(1,2-diphenyl-1,2-ethenedithiolato)nickel, β-Ni(dpedt)$_2$, has been determined by single crystal X-ray diffraction at room temperature. The structure was refined by full matrix least-squares to a final R_w=0.038. Comparison of this triclinic ($P\bar{1}$) structure with the monoclinic ($P2_1/n$) α-form established previously reveals that the difference between the two structures is basically due to a different conformation of the phenyl rings, which gives rise to *dissymmetry* in β-Ni(dpedt)$_2$.

Since the discovery of Ni(dpedt)$_2$,[1] bis-dithiolato complexes of transition metals have attracted a great deal of scientific interest in inorganic chemistry. Synthetic and experimental findings[2] as well as structural systematics[3,4] of these materials have been reviewed, and an extensive theoretical treatment has been presented.[5] We recently introduced a new concept[6] for preparing a wide range of stacking solids made up of alternated square planar sulfur (S)-containing, and square planar nitrogen (N)-containing complexes. In an attempt to fabricate solids of this type, we have employed, on the one hand, α-Ni(dpedt)$_2$[3] as the S-containing component and, on the other hand, either bis(1,2-diphenylethanedione dioximato)cobalt(II), Co(dpg)$_2$, or bis(butanedione dioximato)copper(II), Cu(dmg)$_2$, as the N-containing components. Although we failed to produce the desirable stacking materials with so-called pseudo-(SN)$_x$ bundle-structure,[6] we interestingly obtained, in both cases, the novel asymmetric β-Ni(dpedt)$_2$, which may be regarded as a potentially versatile optically active solid system. We therefore have determined its full structure and have compared it with the previously known α-modification,[3] as we report in the following.

Experimental

Material Preparation. Single crystals of β-Ni(dpedt)$_2$ were obtained in two different preparations. In a first preparation, analytical grade Co(dpg)$_2$ (100 mg) was dissolved in a mixture of warm methyl cyanide and chloroform (50 ml+50 ml) and filtered (brown solution). Analytical grade α-Ni(dpedt)$_2$[1,3] (100 mg) was dissolved similarly and filtered (blue-green solution). The two solutions were mixed together and refluxed for 15—20 min. The mixture was filtered warm, and the dark-green filtrate was left to concentrate by slow evaporation at ca. 40 °C. When the solvent volume was reduced to 150 ml, shiny long crystals appeared. They grew larger as concentration of the solution progressed until the volume was reduced to about 50 ml. The long black crystals were separated by filtration, washed with some 100 ml of high purity diethyl ether (sparingly soluble with green color). The yield was 70 mg of slightly dichroic prisms. The density determined by flotation in a mixture of dibromomethane and 1,3,5-trimethylbenzene was D_m=1.44 Mg m^{-3}. The second preparation was carried out in a closely similar manner by using analytical grade Cu(dmg)$_2$ (30 mg) dissolved in warm chloroform (40 ml), and α-Ni(dpedt)$_2$ (55 mg) dissolved in chloroform (40 ml).

Table 1. Experimental and Computational Details

Crystal shape	Prismatic
Crystal size /mm^3	0.2×0.3×0.3
Possible indep. reflections	3878
Reflections observed $I>2.5\sigma(I)$	3256
Reflections for ψ-scans	6
2θ range /°	3—60
Min. transmission (max.=1)	0.90
μ(Mo $K\alpha$)/mm^{-1}	1.094
R_{int} (from merging)	0.014
parameters for least-squares	250
R_w, R	0.038, 0.044
Goodness-of-fit	2.59
Max. shift/error	0.07
Extremes in diff. Fourier/e Å^{-3}	+0.28, −0.32

Structure Determination. A suitable crystal from each batch was analyzed independently by X-ray diffraction at room temperature. Crystal data were collected on a Siemens-Stoe AED 2, or on a Syntex R3, four-circle automatic diffractometer equipped with graphite-monochromated Mo $K\alpha$ radiation (λ=0.7107 Å).

Crystal Data. Virtually identical data were obtained for both batches of crystals. $C_{28}H_{20}NiS_4$, M_r=543.4, triclinic, space group $P\bar{1}$, a=10.135 (2) Å, b=10.212 (1) Å, c=12.631 (1) Å; α=79.53 (3)°, β=89.08 (3)°, γ=82.02 (3)°; V=1273.02 Å^3; Z=2; D_c=1.42 Mg m^{-3}, D_m=1.44 Mg m^{-3}.

Table 1 summarises further experimental and computational details. The structure was solved by the Patterson methods and completed by Fourier syntheses. It was refined by full matrix least-squares, based on F with weight $w=\sigma(|F|)^{-2}$. The phenyl rings were refined as rigid groups. The calculations were carried out on an Eclipse S140 computer with SHELXTL program[7] which uses scattering factors from "International Tables",[8] and takes anomalous dispersion into account.[9] The final refinement with anisotropic thermal parameters for non-hydrogen atoms, and isotropic parameters for hydrogen atoms yielded R (R_w)=0.044 (0.038). An empirical absorption correction (μ(Mo $K\alpha$)=1.094 mm^{-1}) was applied using ψ-scans of 6 reflections (8<2θ<43°).

Results and Discussion

The purpose of this note is to highlight the structural divergence that exists between the two phases of

the same chemical compound, Ni(dpedt)$_2$. Final atomic coordinates with their equivalent isotropic thermal parameters for the β-phase elucidated here are listed in Table 2. Figure 1 displays a molecular view of this phase with atom labeling scheme. For both crystalline forms, such a molecular entity consists of two specific structural cores, namely, the chelate plane NiS_4C_4 (comprising the four non-benzenic C atoms), and the four phenyl rings. Comparison of these molecular spheres between the two modifications reveals rather nicely matching values in terms of corresponding bond distances and angles. For the β-phase, the following bond lengths are observed: Ni-S 2.120—2.127 (1) Å; C=C 1.404—1.424 (6) Å; S-C 1.695—1.701 (4) Å; C-C_{Ph} 1.474—1.488 (5) Å; average $(C\text{-}C)_{Ph}$ 1.395 (0) Å; the following angles are measured: S1-Ni-S3 91.1 (1)° S1-Ni-S4 88.0 (1)° S2-Ni-S4 91.3 (1)° S2-Ni-S3 89.5 (1)° C-S-Ni 105.9—106.1 (2)° S-C=C 117.9—118.9 (3)°.

Angles between selected planes for the β-phase are listed in Table 3. By comparison with the previously established α-phase,[3] it is seen that the basic difference between the two structural modifications arises as a result of different conformations of the phenyl groups.

Table 2. Final Atomic Coordinates ($\times 10^5$) and Their Equivalent Isotropic Thermal Parameters ($\times 10^4$)[a]

Atom	X	Y	Z	B_{eq}/Å^2
Ni1	6135(6)	26386(6)	4182(5)	511(2)
S1	25928(12)	16483(13)	6853(9)	542(5)
S2	−14242(11)	34844(12)	1951(9)	498(4)
S3	6301(11)	33241(12)	19081(9)	526(5)
S4	6170(12)	19169(13)	−10571(10)	596(5)
C1	−9612(42)	23588(41)	−15623(33)	457(16)
C2	−19242(40)	30523(38)	−9529(31)	417(15)
C3	21621(41)	26797(41)	24840(32)	430(16)
C4	30556(39)	18903(40)	19163(31)	417(15)
C11	24233(25)	30379(28)	35408(23)	449(16)
C12	36785(25)	33287(28)	37782(23)	530(10)
C13	39138(25)	36833(28)	47671(23)	668(22)
C14	28938(25)	37471(28)	55186(23)	740(24)
C15	16386(25)	34563(28)	52812(23)	702(23)
C16	14033(25)	31017(28)	42923(23)	544(10)
C21	44014(29)	12078(25)	22985(17)	426(16)
C22	54953(29)	13936(25)	16311(17)	523(10)
C23	67630(29)	7570(25)	19756(17)	606(20)
C24	69368(29)	−654(25)	29875(17)	596(20)
C25	58429(29)	−2512(25)	36549(17)	543(10)
C26	45752(29)	3855(25)	33104(17)	482(17)
C31	−12209(27)	20170(21)	−26176(23)	451(16)
C32	−18589(27)	29939(21)	−34345(23)	522(17)
C33	−20654(27)	26775(21)	−44424(23)	630(21)
C34	−16340(27)	13841(21)	−46335(23)	656(22)
C35	−9960(27)	4072(21)	−38167(23)	604(21)
C36	−7895(27)	7237(21)	−28087(23)	511(18)
C41	−33628(26)	33423(23)	−12302(20)	411(15)
C42	−40508(27)	46144(23)	−11923(20)	443(16)
C43	−54195(26)	48791(23)	−13963(20)	510(10)
C44	−61004(26)	38716(23)	−16381(20)	603(20)
C45	−54125(26)	25995(23)	−16760(20)	586(20)
C46	−40437(26)	23349(23)	−14721(20)	530(10)

a) Equivalent isotropic B_{eq} defined as one-third of the trace of the orthogonalized B_{ij} tensor. Last significant esd digits for each term are given in parentheses.

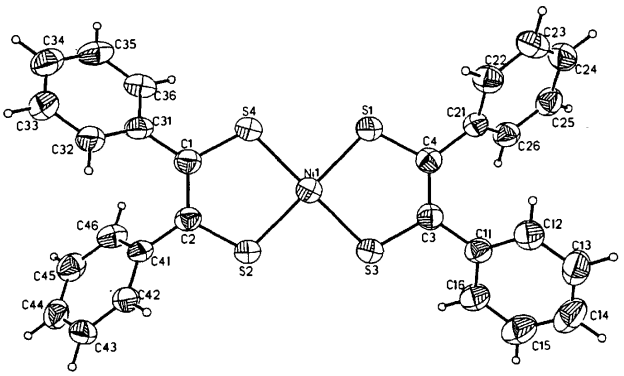

Fig. 1. A molecule of β-Ni(dpedt)$_2$ with atom labeling, seen onto the Ni,S1-S4,C1-C4 plane.

In the α-phase, the conformation allows for the molecule to possess a $\bar{1}$ symmetry; in the β-phase, by contrast, the conformation is such that the molecule totally lacks reflection symmetry, as clearly revealed by Table 3. Thus, β-Ni(dpedt)$_2$ is a *disymmetric* molecule, and is expected to exhibit optical activity. This finding obviously adds a new dimension to the scientific and technological relevance of this chemical compound, which now may be viewed as a potentially versatile chiroptical system in its β-phase.

One may reasonably assume that the stabilization of the phenyl librational energy into this dissymmetric conformation is influenced, during material preparation, by the presence of the Co(dpg)$_2$ or Cu(dmg)$_2$ complexes. It seems rather hard to say, however, *why* and *how* this influence could actually be brought about!

Michel Mégnamisi-Bélombé wishes to thank "Stiftung Volkswagenwerk" (West Germany) for partial support of this work via its "Partnership Program".

We thank Dr. H. Pritzkow, Heidelberg, for his help with a set of diffraction data.

References

1) G. N. Schrauzer and V. P. Mayweg, *J. Am. Chem. Soc.*, **84**, 3221 (1962).
2) J. A. McCleverty, *Prog. Inorg. Chem.*, **10**, 49 (1963).
3) D. Sartain and Mary R. Truter, *J. Chem. Soc. A*, **1967**, 1264.
4) R. Eisenberg, *Prog. Inorg. Chem.*, **12**, 295 (1970).
5) S. Alvarez, R. Vincente, and R. Hoffmann, *J. Am. Chem. Soc.*, **107**, 6253 (1985).
6) a) M. Mégnamisi-Bélombé, *J. Phys. (Paris), Colloq.*, **44**, C3-717 (1983). b) M. Mégnamisi-Bélombé, *Synth. Met.*,

Table 3. Angles (°) between Selected Planes (e.s.d.'s of Planes: −0.1043—+0.0902)

Plane	Defined by	Angles to planes 1	2	3	4	5
1	Ni1,S1-S4,C1-C4					
2	C11-C16	34.0				
3	C21-C26	52.7	53.5			
4	C31-C36	45.5	79.5	71.1		
5	C41-C46	51.0	62.8	103.6	59.6	

18, 605 (1987).

7) G. M. Sheldrick, SHELXTL. An integrated system for solving, refining and displaying crystal structures from diffraction data, University of Göttingen, FRG (1983). (Revision 5.1, Eclipse 32K Version, 1985).

8) International Tables for X-ray Crystallography, Vol. IV, Kynoch Press, Birmingham (1974). Present distributor: D. Reidel, Dordrecht, The Netherlands.

9) Observed and calculated structure factors (20 pages), atomic parameters of hydrogen atoms and anisotropic thermal parameters have been deposited as Document No. 8898 at the Office of the Editor of Bull. Chem. Soc. Jpn.